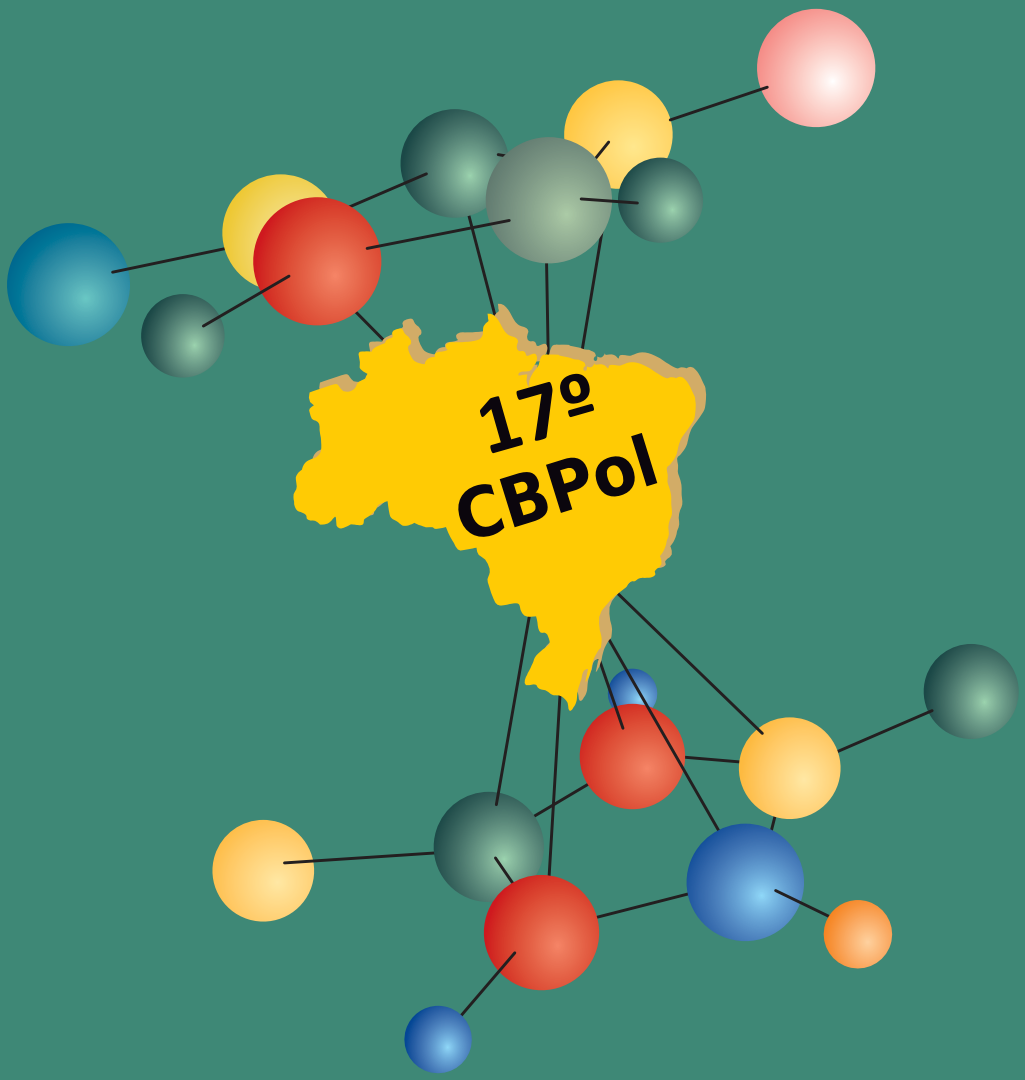

17º Congresso Brasileiro de Polímeros

29 de Outubro a 02 de Novembro de 2023

Joinville - SC

ANAIS

Associação Brasileira de Polímeros

Associação Brasileira de Polímeros

Anais do 17° Congresso Brasileiro de Polímeros

Joinville, SC
2023

Copyright © 2023 para os autores

Revisão textual e gramatical: Resposanbilidade dos respectivos autores.

Todos os direitos reservados 2023
A reprodução não autorizada desta publicação, no todo ou em parte,
constitui violação de direitos autorais (Lei 9.610/98).

Dados Internacionais de Catalogação na Publicação (CIP)
(Câmara Brasileira do Livro, SP, Brasil)

Congresso Brasileiro de Polímeros (17. : 29 out. - 2 nov. 2023 : Joinville, SC)
Anais do 17° Congresso Brasileiro de Polímeros [livro eletrônico] / organização Associação Brasileira de Polímeros. -- Joinville, SC : Aptor Software, 2023.

PDF

Vários colaboradores.
ISBN 978-85-63273-55-0

1. Polímeros 2. Polímeros e polimerização 3. Química - Congressos I. Título.

24-188263 CDD-540

Índices para catálogo sistemático:

1. Química : Congressos 540

Eliane de Freitas Leite - Bibliotecária - CRB 8/8415

Foreword

The 17th Brazilian Polymer Congress (CBPol 2023) was held between 29 October - 2 November 2023, in Joinville, Santa Catarina, Brazil, the “City of Flowers” and “Capital of Dance in Brazil”. This was the seventeenth of a series of conferences that takes place biennially in Brazil, intended to provide a forum for the presentation and discussion of the latest research and technology in the field of polymer science and technology.

The conference, promoted by the Brazilian Polymer Association (ABPol) with the support of the Santa Catarina State University (UDESC), University of the Region of Joinville (Univille), Federal University of Santa Catarina (UFSC), Federal University of Technology – Parana (UTFPR) and Federal University of Rio Grande do Sul (UFRGS), marked the return to in-person format, after the difficult period that the Brazilian polymer community went through due to the COVID-19 pandemic, a moment that everyone was waiting for to have the opportunity to meet and celebrate.

The CBPol 2023 focused on 10 technical topics, touching on the currently crucial points of circularity and innovation involving polymer science and technology, and highlighting the strength of the women who are part of our polymer community. Six plenary lectures were delivered by scientists of international prestige and representatives of the Brazilian industry, along with twenty-eight key lectures given by renowned Brazilian and foreign researchers, addressing topics of interest to academia, industry and society. Furthermore, 20 companies were exhibiting their products and making connections with new researchers and potential customers during the event.

Around 800 delegates participated in this event, 476 of whom were undergraduate and graduate students. In this Proceedings you will find more than 850 scientific and technical works, in the form of short and extended abstracts, which have been approved and presented as oral or poster communications during the conference. The publications are in the areas of Polymerization reactions and polymer chemistry, Polymer physics and characterization, Polymer nanostructures and nanocomposites, Blends, composites and polymer networks, Processing and materials design, Rubber and Elastomers, Recycling and environmental issues associated with polymers, Biomedical applications of polymers, Polymers in agriculture and special industrial applications, and Innovation and management in polymers and education.

The members of the CBPol Organizing Committee would like to express their deep appreciation to all the speakers and delegates for their contribution and participation, as well as the invaluable support of sponsors, Brazilian agencies (in especial CAPES and FAPESC) and colleagues for the successful and joyful event in Joinville.

We are also grateful to all authors, reviewers and participants for the present publication.

We look forward to seeing you at the 18th CBPol!

Prof. Dr. Sérgio H. Pezzin - UDESC
Conference Chair

Prof. Dr. Palova Santos Balzer - Univille
Conference Vice-Chair

Prof. Dr. Daniela Becker – UDESC
Scientific Coordinator

Organizing Committee

Sergio Henrique Pezzin (UDESC) - Chair

Palova Santos Balzer (UNIVILLE) - Vice-Chair

Marco Aurélio De Paoli (UNICAMP) - ABPol President

Antonio José Felix de Carvalho (USP) - ABPol Events Director

Ana Paula Testa Pezzin (UNIVILLE)

Carla Damolin (UDESC)

Claudia Sayer (UFSC)

Daniela Becker (UDESC)

Fernando Lafratta (UDESC)

Guilherme Mariz de Oliveira Barra (UFSC)

Juliana Kloss (UTFPR)

Noeli Sellin (UNIVILLE)

Rosmary Nichele Brandalise (UCS)

Sandro Campos Amico (UFRGS)

Wagner Pachekoski (UFSC)

Scientific Committee

Daniela Becker (UDESC) – Coordinator

Amanda Dantas de Oliveira (UFPel)

André Mello Guimarães Mautone (ABTB)

André Ricardo Fajardo (UFPel)

Carlos Henrique Scurachio (UFSCar)

Cesar Liberato Petzhold (UFRGS)

Denise Freitas Siqueira Petri (USP)

Derval dos Santos Rosa (UFABC)

Edcleide Maria Araújo (UFCG)

Edson Cocchieri Botelho (UNESP)

Fábio Roberto Passador (UNIFESP)

Fernando Antônio Ribeiro (BASF)

Hélio Wiebeck (USP)

José Carlos Costa da Silva Pinto (UFRJ)

Juliana Kloss (UTFPR)

Juliano Marini (UFSCar)

Kingston Soares (IFES)

Lidiane Cristina Costa (UFSCar)

Marcelo Aparecido Chinelatto (USP)

Marcelo Silveira Rabello (UFCG)

Marcia Margarete Meier (UFSC)

Marly Maldaner Jacobi (UFRGS)

Palova Santos Balzer (UNIVILLE)

Renato Ditomaso (Braskem)

Rodrigo Lambert Oréfice (UFMG)

Roselena Faez (UFSCar)

Sebastião Vicente Canevarolo Jr (UFSCar)

Tatianny Soares Alves (UFPI)

Walter Ruggeri Waldmann (UFSCar)

International Committee

Fernando Duarte (University of Minho - Portugal)

James Njuguna (Robert Gordon University - Reino Unido)

Jerusa Roeder (Braskem - Alemanha)

João Pedro Lourenço Gil Nunes (University of Minho - Portugal)

Katharina Landfester (Max Planck Institute for Polymer Research - Alemanha)

Luis Prado (Capgemini - Alemanha)

Maria C. Paiva (University of Minho - Portugal)

Miguel Nóbrega (University of Minho - Portugal)

Olga Sousa Carneiro (University of Minho - Portugal)

Ricardo Oliveira (2D Materials Pte Ltd - Singapura)

Sami Halila (Cermav - CNRS – Université Grenoble Alpes - França)

Sergey Shishatskiy (Helmholtz-Zentrum Hereon - Alemanha)

Siva Irulappasamy (Kalasalingam University - India)

Suzana Pereira Nunes (King Abdullah University of Science and Technology - Arábia Saudita)

Area coordinators

Amanda Dantas Oliveira

Carlos Henrique Scuracchio

César Liberato Petzhold

Daniela Becker

Fabio Roberto Passador

Juliana Regina Kloss

Kinglston Soares

Marcelo Chinelatto

Marcelo Silveira Rabello

Marcia Margarete Meier

Roselena Faez

Referees

Adriana de Campos Pastre

Adriana Martinelli Catelli Souza

Adriane Gomes Simanke

Adriano Gonçalves Viana

Alex Carvalho Alavarse

Alexandre Luis Parize

Ana Maria Furtado de Sousa

Ana Pacheli Heitmann

Ana Paula Testa Pezzin

Ana Rita Morales

Andre Luis Marcomini

André Ricardo Fajardo

Antonio Aprigio da Silva Curvelo

Aparecido Junior de Menezes

Augusto C.C. Peres

Benjamim de Melo Carvalho

Bluma Guenther Soares

Breno Rocha Barrioni

Bruna Louise Silva

Carla Cristina Schmitt Cavalheiro

Carlos Henrique Scuracchio

Carolina Lipparelli Morelli

Cesar Augusto Gonçalves Beatrice

César Liberato Petzhold

Claudia Sayer

Clemens Kilian Weiss

Clodoaldo Saron

Cristiane Medina Finzi-Quintão

Daniel Eiras

Daniela Becker

Denise Freitas Siqueira Petri

Douglas Alexandre Simon

Douglas Cardoso Dragunski

Douglas Gamba

Éder José Siqueira

Edson Cocchieri Botelho

Edson Noriyuki Ito

Eduardo Henrique Backes

Edvânia Trajano Teófilo

Eliane Trovatti

Elisangela Corradini

Elizabeth Grillo Fernandes

Fabio Herbst Florenzano

Fabio Roberto Passador

Felipe Nunes Linhares

Fernando Carlos Giacomelli

Fernando Gomes de Souza Junior

Francisco de Assis Avelino de Figueredo Sobrinho

Francys Kley Vieira Moreira

Giuliano Siniscalchi Martins

Guilherme Mariz de Oliveira Barra

Guilhermino José Macedo Fechine

Heitor Ornaghi Junior

Hélio Wiebeck

Henrique Finocchio

Hernane da Silva Barud

Ivana Lourenço de Mello Ferreira

Izabel Cristina Riegel Vidotti

Janaina Cecília Oliveira Villanova

Jane Maria Faulstich de Paiva

Jeanny da Silva Maciel

Jorge Amim Junior

José Maria Marlet

José Ricardo Tarpani

Juliana Bonametti Olivato

Juliana Regina Kloss

Juliano Elvis Oliveira

Juliano Marini

Kássio André Lacerda

Kátia Cecília de Souza Figueiredo

Katia Monteiro Novack

Larissa Nardini Carli

Larissa Stieven Montagna

Laura Hecker de Carvalho

Leonardo Zborowski Sobrinho

Liane Lucy de Lucca Freitas

Liliane Cristina Battirola

Lísias Pereira Novo

Luiz Claudio Pardini

Marcelo Chinelatto

Marcelo Silveira Rabello

Márcia Cristina Branciforti

Marcia Margarete Meier

Márcio Yee

Marco Aurelio De Paoli

Marcos Lopes Dias

Marcos Yukata Shiino

Maria de Fátima Vieira Marques

Maria Lucia Caetano Pinto da Silva

Marindia Decol

Marly Maldaner Jacobi

Mateus Ferrer

Merces Coelho da Silva

Michelle Leali Costa

Nádya Pesce da Silveira

Nelson Marcos Larocca

Otávio Bianchi

Paulo Henrique de Souza Picciani

Paulo Rodrigo Stival Bittencourt

Regina Célia Monteiro de Paula

Regina Célia Reis Nunes

Reinaldo Yoshio Morita

Renata Barbosa

Renate Wellen

Renivaldo José dos Santos

Ricardo Jorge Espanhol Andrade

Rita de Cassia Mendonca Sales

Rômulo Maziero

Roniérik Pioli Vieira

Rosane Michele Duarte Soares

Roselena Faez

Rosmary Nichele Brandalise

Ruth Marlene Campomanes Santana

Sami Halila

Sandra Maria da Luz

Sandro Campos Amico

Sebastião Vicente Canevarolo Jr.

Sergio Henrique Pezzin

Silmara França Buchviser

Soraia Zaioncz

Tales da Silva Daitx

Tatianny Soares Alves

Tomás Jeferson Alves Mélo

Valdir Soldi

Veronica Maria de Araújo Calado

Vilásia Guimarães Martins

Viviane Muniz Fonseca

Wagner Mauricio Pachekoski

Walter Ruggeri Waldman

Poster Evaluation Committee

Juliana Kloss (UTFPR) - Coordinator

Ana Paula Cysne Barbosa (UFRN)

André Ricardo Fajardo (UFPel)

Claudia Sayer (UFSC)

Daniela Becker (UDESC)

Denise Freitas Siqueira Petri (USP)

Derval dos Santos Rosa (UFABC)

Fábio Roberto Passador (UNIFESP)

Lidiane Cristina Costa (UFSCar)

Tales da Silva Daitx (UFPel)

Sandro Campos Amico (UFRGS)

Wagner Pachekoski (UFSC)

Walter Ruggeri Waldmann (UFSCar)

Platinum Sponsor

KRONA TUBOS E CONEXÕES

Palladio Sponsor

CREA-SC

Gold Sponsor

INSTRON

TA Instruments

Silver Sponsor

dp UNION

Zwick / Roell

Senior Sponsor

nano

PerkinElmer For the Better

NETZSCH Proven Excellence.

ReoTerm

SHIMADZU Excellence in Science

Master Sponsors

Anton Paar

Plásticos Máquinas Técnicas Ltda.

DOW

HSENSOR

KCEN

ROYAL SOCIETY OF CHEMISTRY

Junior Sponsors

CCDM DEMa/UFSCar

IOTO INTERNATIONAL

GRUPO WORTEX

Support

abtb

CAPES

fapesc

INCT Polissacarídeos

Joinville e Região Convention & Visitors Bureau

Plástico virtual

RHEIN

UDESC

univille

UNIVERSIDADE FEDERAL DE SANTA CATARINA

UFRGS UNIVERSIDADE FEDERAL DO RIO GRANDE DO SUL

UTFPR UNIVERSIDADE TECNOLÓGICA FEDERAL DO PARANÁ

Summary

PLENARY LECTURES	**1**
BRASKEM'S INNOVATION JOURNEY TO IMPLEMENT THE CIRCULAR ECONOMY	2
DEVELOPING STRATEGIES FOR POLYMER REDESIGN AND RECYCLING USING REACTION PATHWAY ANALYSIS	3
GELS FOR ENVIRONMENTAL REMEDIATION: FROM AEROGELS TO NANOSPONGES	4
NATURAL FIBER AND HYBRID COMPOSITES: SCIENCE AND TECHNOLOGY	5
POLYMERS AND AGRICULTURE: PRESENT AND PROMISING TECHNOLOGICAL FUTURE	6
TWO DECADES OF POLYMER NANOCOMPOSITES RESEARCH: FROM ACADEMIA TO INDUSTRY	7
POLYMERIZATION REACTIONS AND POLYMER CHEMISTRY	**8**
POLYURETHANES-NIOBIUM COMPOUNDS WITH POTENTIAL APPLICATION FOR THE TREATMENT OF DYES	9
SYNTHESIS AND EVALUATION OF POLYMERIC SCALE INHIBITORS PREPARED BY RAFT POLYMERIZATION	10
ASSESSING THE CURING PROCESS OF LIMONENE DIOXIDE USING DSC ANALYSIS	11
CELLULOSE ALKYLATION IN THE DMSO/DBU/CO_2 SOLVENT SYSTEM	15
DEVELOPMENT OF A NOVEL BIOREFINERY PROCESS FOR PRODUCING PHOSPHYLATED-LIGNIN FROM COCONUT WASTES	20
ON THE CURING AND DEGRADATION OF BISPHENOL A DIGLYCIDYL ETHER AND EPOXIDIZED SOYBEAN OIL COMPOUNDS CURED WITH ITACONIC AND SUCCINIC ACIDS	25
SYNTHESIS OF POLY(BUTYLENE SUCCINATE)-CO- GLUTAMIC ACID MICROPARTICLES VIA SUSPENSION AND MINIEMULSION POLYMERIZATION	30
EVALUATION OF CARBOXYMETHYL-KAPPA-CARRAGEENAN AS A SCALE AND CORROSION INHIBITOR: A THEORETICAL AND EXPERIMENTAL APPROACH	35
FORMALDEHYDE MIGRATION STUDY IN POLYOXYMETHYLENE FROM COSMETICS INDUSTRY PACKAGING COMPONENTS BY EXTRACTABLE TESTING AND GCMS	36
INCORPORATION OF RENEWABLE CARBONS VIA FORMAMIDE REACTIVITY FOR NOVEL BIOBASED POLYMERS	37
SYNTHESIS OF ALKYNE-FUNCTIONALIZED CELLULOSE FOR ATTACHMENT OF BIOMOLECULES BY THIOL-YNE CLICK CHEMISTRY	38
SYNTHESIS OF STAR-SHAPED DIBLOCK POLY(AMINO ACIDS) BY RING-OPENING POLYMERIZATION OF N-CARBOXYANHYDRIDES	39
CHEMICAL GRAFTING OF BACTERIAL CELLULOSE WITH AMINOPROPYLTRIETHOXYSILANE	40
CUSTOMIZING BIOBASED RESINS OF EPOXIDIZED SOYBEAN OIL AND ISOSORBIDE WITH ALUMINIUM TRIFLATE AS A CATALYST	45
EFFECT OF PHENOLIC AND HYDROXYLAMINE-BASED ADDITIVES ON THE STABILIZATION OF POLYPROPYLENE EXPOSED TO UV-C RADIATION	50
EVALUATION OF STARCH PROCESSING STEPS WITH ADDED CITRIC ACID	55
EVALUATION OF THE EFFECT OF SYNTHESIS VARIABLES ON THE MORPHOLOGICAL CHARACTERISTICS OF PUF/ENB MICROCAPSULES USING FRACTIONAL DESIGN.	60
EVALUATION OF THE THERMOPLASTIC STARCH PROPERTIES: REACTION WITH STRUCTURALLY DISTINCT CARBOXYLIC ACIDS	65
FATTY ACID-BASED DIISOCYANATE SYNTHESIS FOR THE PRODUCTION OF GREEN POLYURETHANES	69
FULLY BIO-BASED NOVOLAC RESINS FROM AGROINDUSTRIAL RESIDUES FOR APPLICATION IN ANTICORROSIVE COATINGS	74
INFLUENCE OF TEMPERATURE ON THE SYNTHESIS OF OCTYL OLEATE USING IMMOBILIZED PANCREATIC LIPASE ON MAGNETIZED PARTICLES OF POLY(STYRENE-CO-DIMETHACRYLATE TRIETHYLENE GLYCOL)	79

PHOTODEGRADATION INVESTIGATION OF ALOE VERA AS A PHOTOPROTECTOR FOR POLY(LACTIC ACID) 84
POLYMERIZATION OF POLY-DL-LACTIC ACID (PDLLA) BY RING-OPENING POLIMERIZATION FOR POTENTIAL APPLICATION IN TISSUE ENGINEERING 90
POLY(N-VINYLCAPROLACTAM) POLYMERIZATION BY ULTRAVIOLET RADIATION 95
PRODUCTION OF METHACRYLATED GELATIN: A STUDY ON THE BUFFER EFFECT 100
PVOH HYDROGELS CROSSLINKED BY ORGANIC ACIDS. PART II: KINETICS OF CONTROLLED DYE RELEASE 105
PVOH HYDROGELS CROSSLINKED BY ORGANIC ACIDS. PART I: SWELLING-KINETICS STUDY 110
SYNTHESIS AND PHYSICOCHEMICAL CHARACTERIZATION OF STYRENE/LIMONENE/CASTOR OILCOPOLYMER OBTAINED BY RADICAL POLYMERIZATION 115
SYNTHESIS, CURING, AND DEGRADATION KINETICS OF POLYURETHANES BASED ON POLY(ETHYLENE GLYCOL), ISOSORBIDE, AND PENTAMETHYLENE DIISOCYANATE 119
SYNTHESIS OF HYDROGELS BASED ON PRODUCTS OBTAINED FROM RENEWABLE SOURCES APPLIED ON THE REMOVAL OF CRYSTAL VIOLET DYE. 124
SYNTHESIS OF LYSINE DERIVATIVE SURFACTANTS AND APPLICATION IN POLYSTYRENE EMULSION POLYMERIZATION 129
SYNTHESIS OF STYRENE-TMPTA ACIDIC RESIN AND ITS APPLICATION AS A CATALYST IN THE GLYCEROL ACETYLATION 134
THERMAL DEGRADATION KINETICS OF TWO BRAZILIAN WOOD SPECIES: PART 1. THERMOGRAVIMETRY AND FWO METHOD 139
THERMAL DEGRADATION KINETICS OF TWO BRAZILIAN WOOD SPECIES: PART 2. SOLID-STATE REACTIONS 144
TUNG OIL AND ITACONIC ACID AS GREEN PLATFORMS FOR THE PRODUCTION OF MONOMERS AND POLYESTERS 149
24 FACTORIAL DESIGN OF SBS BLOCK COPOLYMER SULFONATION 154
APPLICATION OF HS-GCMS ON THE EVALUATION OF STYRENE MIGRATION FROM COSMETIC PACKAGING BASED ON SAN AND ABS 155
CHEMICAL MODIFICATION OF POLY(PROPYLENE GLYCOL) BIS(2-AMINOPROPYL ETHER) WITH SATURATED DIMER FATTY ACID: EVALUATION OF APPLICABILITY IN SYNTHETIC DRILLING FLUIDS 156
EFFECT OF THE DEGREE OF SUBSTITUTION ON THE RHEOLOGICAL PROPERTIES OF HYDROPHOBICALLY MODIFIED CARBOXYMETHYLCELLULOSE 157
EFFECTS OF GRAFTING DEGREE ON THE PROPERTIES OF CARBOXYMETHYLCELLULOSE-*G*-OLIGO(PROPYLENE OXIDE-*CO*-ETHYLENE OXIDE) 158
ENZYMATIC SYNTHESIS OF BIO-BASED POLYESTERS CONTAINING LEVOGLUCOSAN UNIT. 159
ENZYMATIC SYNTHESIS OF POLY(GLOBALIDE) AND CROSSLINKING VIA THIOL-ENE POST-MODIFICATION 162
FUNCTIONALIZATION OF “BOTTLEBRUSH” POLYDIENES 167
GRAFTING OF POLY(N-VINYLCAPROLACTAM) ON POLYURETHANE BY GAMMA RADIATION 168
INFLUENCE OF THE CATALYST ADDITION PROCEDURE AND INITIAL MOLECULAR WEIGHT ON THE SOLID-STATE POLYMERIZATION OF POLY (LACTIC ACID) 169
INFLUNCE OF SURFACTANT AND COSTABILIZER INTERACTIONS IN THE KINETICS OF IN-SITU POLYSTYRENE/BASO4 NANOCOMPOSITES OBTAINED VIA MULTIPLE SEQUENCIAL MICROEMULSIONS 170
INSIGHTS INTO THE BACKBITING REACTION IN ACRYLIC ACID POLYMERIZATION: A MODELING APPROACH 171
LINEAR POLYGLYCEROL FROM CHLOROPROPANOL: NEW SYNTHETIC ROUTES. 172
LUMINESCENT PROPERTIES OF THE EU 3+ COMPLEX IN POLYURETHANE FOAM 173
MODIFICATION OF EUDRAGIT S100 POLYMER USING UGI MULTICOMPONENT REACTION 174
PERFORMANCE OF THE BACTERIAL CELLULOSE HYDROPHOBIZATION PROCESS FOR APPLICATION IN FOOD PACKAGING 175

PREPARATION AND CHARACTERIZATION OF RIGID POLYURETHANE FOAMS WITH AGROINDUSTRIAL RESIDUES 176
PREPARATION AND CHARACTERIZATION OF RIGID POLYURETHANEFOAM WITH ORANGE PEEL 177
PRODUCTION OF HIGH-PERFORMANCE ACETOSOLV COCONUT FIBER LIGNIN-INCORPORATED DGEBA CURED WITH APROTIC IONIC LIQUID 178
RADICAL POLYMERIZATION OF HYDROPHOBICALLY MODIFIED WATER-SOLUBLE POLYACRYLAMIDE HAVING OLIGO(LACTIC ACID) AS HYDROPHOBIC MACROMONOMER 179
RIGID POLYURETHANE FOAM WITH BENTONITE CLAY MODIFIED WITH NIOBIUM FOR PHOTODEGRADATION OF RHODAMINE B 180
STRUCTURE ASSESSMENT OVER TIME OF HYDROXYPROPYLATED STARCH GRANULES 181
SYNTHESIS AND CHARACTERIZATION OF MONOMERS: A POSSIBLE SUBSTITUTE FOR BPA FREE POLYMERS 182
SYNTHESIS AND CHARACTERIZATION OF POLI(BUTYL ACRYLATECO-FARNESENE) OBTAINED VIA EMULSION POLYMERIZATION 183
SYNTHESIS OF EUGENOL EPOXY FOR VITRIMERIC POLYMERS 184
SYNTHESIS OF PH-RESPONSIVE NANOPARTICLES FOR THE DEVELOPMENT OF STARCH-BASED SMART PACKAGING 185
SYNTHESIS OF POLY(GLOBALIDE) BY ENZYMATIC RING-OPENING POLYMERIZATION USING GERANIOL AS INITIATOR 186
THIOL-ENE PHOTOPOLYMERIZATION OF (R)-(+)-LIMONENE IN MINIEMULSION: A GREEN APPROACH FOR SYNTHESIZING POLYMERIC NANOPARTICLES 187
POLYMER PHYSICS AND CHARACTERIZATION 188
POLYETHYLENE RHEOLOGY ADDITIVED WITH THERMOCHROMIC PIGMENTS 189
REFLECTIONS ON TEACHING AND PROFESSIONAL PRACTICE IN POLYMERS. HOW TO COMBINE THEORY AND PRACTICE? 194
ASSESSMENT OF THE RELAXATION TIME OF POLYSTYRENE UNDER CONTROLLED SHEAR FLOW BY RHEO-OPTICAL TECHNIQUES 195
CROSSLINKED PVA NANOFIBERS WITH ANTIMICROBIAL ACTION 200
EFFECT OF STORAGE TIME ON RETROGRADATION OF EXTRUDED THERMOPLASTIC STARCH 201
EVALUATION OF THE DEGRADATION OF OXO-BIODEGRADABLE PP BY THE ACTION OF NATURAL WEATHERING 206
EVALUATION OF THE THERMAL PROPERTIES OF BACTERIAL CELLULOSE FILMS ADDED WITH EXTRACT OF *CAESALPINIA FERREA MART.* 211
HIGH STRAIN RATE COMPRESSIVE BEHAVIOR OF BALLISTIC POLYCARBONATE: EXPERIMENTAL AND NUMERICAL MODELLING 216
THERMAL, RHEOLOGICAL AND MECHANICAL PROPERTIES OF EPOXY RESIN FORMULATIONS 221
BIOPOLYMERIC COATINGS FOR FOOD PRESERVATION: CHARACTERIZATION STUDY 226
EVALUATION OF PHENOLIC FOAM'S TOXICITY USED IN FLORAL ARRANGEMENTS 227
INFLUENCE OF POLYMER GELATION GRADE ON THE PERFORMANCE OF PLASTICIZED PVC FILMS USED IN COATED FABRICS 228
PERFORMACE OF RESVERATROL AS AN ADDITIVE IN POLY (LACTIC ACID) 229
TENSILE AND INDENTATION ANALYSIS OF THERMOPLASTIC POLYMERS: PP AND ABS 230
ADHESION STUDY OF PRINTING INKS ON ANIMAL FEED MULTILAYER PACKAGING MADE WITH MIXTURE OF PETROCHEMICAL LDPE AND GREEN LDPE IN THE OUTER LAYER 235
AGAR CHARACTERIZATION TECHNIQUES: A VERSATILE POLYSACCHARIDE 240

ANALYSIS OF ULTRAVIOLET EXPOSURE IN SYNTHETIC FIBERS OF POLYESTER AND HIGH MODULUS POLYETHYLENE 245
ANALYSIS OF WATER SORPTION ISOTHERM IN CASSAVA STARCH PACKAGING WITH TOMATO PEEL 250
APPLICATION OF THERMAL ANALYSIS FOR IDENTIFICATION OF FKM TYPES 1 AND 2 IN RUBBER COMPOSITES 253
COMPARISON BETWEEN THE RESULTS OF DIGITAL IMAGE CORRELATION (DIC) AND THE STRAIN GAUGES IN A SPLIT HOPKINSON PRESSURE BAR (SHPB) TEST 258
DEVELOPMENT OF NON-STICK SURFACES FOR RIGID PACKAGING 263
DYNAMIC MECHANICAL CHARACTERISTICS OF RIGID POLYURETHANE FOAMS DERIVED FROM KRAFT LIGNIN 268
EFFECT OF THE CROSSLINK CONDITIONS ON THE THERMAL PROPERTIES OF A POLY(VINYL ALCOHOL)-BASED MEMBRANE 272
EFFECT OF YERBA MATE EXTRACT AND MALIC ACID ON THE PHYSICAL PROPERTIES OF POTATO STARCH FILMS 277
EVALUATION OF JUTE FIBRE IN REACTION WITH FURFURYL ALCOHOL TOWARD PROSPECTIVE PREPREG APPLICATION 282
EVALUATION OF MECHANICAL BEHAVIOR OF OFFSHORE MOORING POLYESTER FIBERS BY HYDROLYSIS PROCESS 286
EVALUATION OF THE EFFECTS OF A SUPERABSORBENT POLYMER ON THE GRANULOMETRIC AND CHEMICAL DISTRIBUTIONS OF AN IRON ORE 291
EVALUATION OF THE MECHANICAL AND OPTICAL PROPERTIES OF LDPE INJECTION-MOLDED WITH BENZOIN IN HDPE MASTERBATCH 296
EVALUATION OF THE PLASTICIZERS CONTENT IN THE RHEOLOGICAL AND PHYSICAL PROPERTIES OF TPS THROUGH FACTORIAL DESIGN 301
INFLUENCE OF THE ADDITION OF POLYPHENOLS EXTRACTED FROM WINE WASTE ON THE PROPERTIES OF POLYLACTIC ACID 306
INFLUENCE OF THE AVERAGE DIAMETER OF THERMOCROMIC MICROCAPSULES ON THE FLUIDITY AND VISUAL APPEARANCE OF POLY (METHYL METHACRYLATE) 307
NATURALLY LM PECTINS FROM CHARDONNAY GRAPE POMACE EXTRACTED UNDER DIFFERENT CONDITIONS FORM GELS BY ADDITION OF CA^{2+} 311
PERFORMANCE OF PE WAXES ON EPS NUCLEATION AND RELATIONSHIP WITH THEIR THERMAL TRANSITIONS 316
PHYSICOCHEMICAL EVALUATION OF OAT SHELLS BY DIFFERENT CHARACTERIZATION TECHNIQUES 321
PRELIMINARY STUDY OF THE EXTRACTION OF WATER-SOLUBLE POLYSACCHARIDES FROM MACAW PALM 326
STRESS CRACKING EM RESINA EPÓXI 331
A MULTISCALE APPROACH TO EVALUATE UV-C PHOTODEGRADATION IN POLYPROPYLENE 336
ANALYSIS OF EARLY FAILURE OF THE TOPCOAT SYSTEM USED IN PVC COATED FABRICS FOR MARINE UPHOLSTERY 337
ANTHOCYANIN EXTRACT COVALENTLY INCORPORATING POLYMERIC FILMS FOR APPLICATION IN INTELLIGENT FOOD PACKAGING. 338
A TECHNIQUE TO INVESTIGATE NON-UNIFORM OXIDATION DURING RUBBER AGING 339
BENDING TEST OF PLA/CARBON FIBER ELEMENTS PRODUCED BY FDM. 340
CHARACTERIZATION AND COMPARISON OF LIGNINS FROM BANANA PSEUDOSTEM ISOLATED BY DIFFERENT TREATMENTS 341
COMPARATIVE ANALYSIS OF DIFFERENT FILL PATTERNS ON TENSILE STRENGTH IN ASTM D638 TEST SPECIMENS PRODUCED BY ADDITIVE MANUFACTURING 342

DETERMINATION OF EPOXY RESIN CURING CYCLE USING TWO TYPES OF HARDENERS 343
DETERMINATION OF THE SPECIFIC HEAT OF MANUFACTURED PARTS BY FDM USING CONDUCTIVE POLYMER, THROUGH THE INVERSE PROBLEMS TECHNIQUE 344
EFFECT OF TEMPERATURE ON THE PROPERTIES OF THE PVDF COMPOSITE AND COMMERCIAL LIGHT-CURING RESIN MATRIX 349
ENHANCEMENT OF ANTIMICROBIAL PROPERTIES IN (BIO)POLYMER AND SEMICONDUCTOR SYSTEMS THROUGH PLASMA MODIFICATION 350
EVALUATION OF THE MECHANICAL RESPONSE OF RIGID PLATES BASED ON UHMWPE SUBJECTED TO HIGH STRAIN RATES 351
EXPERIMENTAL EVALUATION OF ABRASION IN POLYAMIDE FIBERS FOR DIFFERENT SOAKING AND LOAD CONDITIONS 352
EXPERIMENTAL TEST OF THE EFFECT OF TEMPERATURE ON CREEP TEST IN HMPE MULTIFILAMENTS 353
EXTRACTION OF LOW MOLAR MASS KERATIN FROM FEATHER MEAL 354
FUEL CELL PERFORMANCE OF ACRYLAMIDE BASED HYDROCARBON PROTON EXCHANGE MEMBRANES 355
GALACTOMANNAN-BASED COPOLYMER NANOPARTICLES : EFFECT OF CHARGE ON PHYSICAL-CHEMICAL PROPERTIES 356
IMPREGNATION OF GREEN PROPOLIS IN PLLA COMPOSITES WITH SUPERCRITICAL CO2 FOR ACTIVE FOOD PACKAGING 357
INSIGHTS INTO MORPHOLOGICAL AND MECHANICAL PROPERTIES: POLY(ETHYL BENZENE-1,4-DICARBOXYLATE) RECYCLED FIBER SUPPORTS FOR ENZYME IMMOBILIZATION 358
MECHANICAL BEHAVIOR IN POLYESTER FIBER RUPTURE FOR DIFFERENT STRAIN RATES 359
MECHANICAL BEHAVIOR OF POLY(ACRYLONITRILE-CO-METHACRYLIC ACID) ELECTROSPUN MEMBRANES IN FUNCTION OF ACID CONTENT 360
PHYSICOCHEMICAL PROPERTIES OF CHITOSAN-BASED FILMS INCORPORATED WITH INVERTASE ENZYME 361
RHEOLOGICAL PARAMETERS OF PLA/EGGSHELL DETERMINED BY TORQUE RHEOMETRY 362
RHEO-OPTICAL CHARACTERIZATION OF THE SHEAR-INDUCED NON-ISOTHERMAL CRYSTALLIZATION OF POLIAMIDE 6 363
SHEAR STRENGTH IN THE GLUE LINE TO EVALUATE THE USE OF THE ADHESIVE EXTRACTED FROM THE SWIMMING BLADDER OF THE BLACK HAKE (MACRODON ANCYLODON) 364
STARCH/CHITOSAN BIOFILMS USING 4-HYDROXYCHALCONE 365
STUDY OF EVA/BENTONITE CLAY-NIOBIUM PENTOXIDE HYBRID SYSTEMS BY DRX AND TD-NMR 366
STUDY OF SURFACE MODIFICATION OF BACTERIAL CELLULOSE BY ATMOSPHERIC PLASMA JET 367
STUDY OF THE DEGRADATION OF POLY(METHYL METHACRYLATE) (PMMA) IN CONTACT WITH BRAKE FLUID 368
SYNTHESIS, CHARACTERIZATION AND EVALUATION OF PNVCL THERMORESPONSIVENESS BY DIFFERENT TECHNIQUES 369
THE EFFECT OF ACCELERATED PHOTOAGING ON THE MORPHOLOGICAL, PHYSICAL AND CHEMICAL PROPERTIES OF POLYETHYLENE TEREPHTHALATE (PET) MICROPLASTIC 370
THE INFLUENCE OF SYNTHESIS CONDITIONS ON THE CHARACTERISTICS OF POLY(N-ISOPROPYLACRYLAMIDE) 371
BIODEGRADABLE ELECTROSPUN NANOFIBERS CONDUITS FOR NERVE REGENERATION 372
ENZYMATIC RING OPENING COPOLYMERIZATION OF LACTONES FOR THE PREPARATION OF FUNCTIONALIZED ELECTROSPUN SCAFFOLDS 373
IMPROVING THE MECHANICAL PROPERTIES OF HEMICELLULOSE BY ADDING POLYLACTIC ACID (PLA) 374
MICROWAVE ABSORBING MATERIALS BASED ON MULTILYERED POLYMERIC COMPOSITES 379
TUNING PROPERTIES OF POLYURETHANES BY CHAIN EXTENDERS 380

B-CYCLODEXTRIN FUNCTIONALIZED WITH CARBON QUANTUM DOTS AS ADSORBENT SENSORS OF METALLIC SPECIES IN AQUEOUS ENVIRONMENTS 381
BIMODAL EVA FOAMS REINFORCED WITH CELLULOSE NANOFIBERS 386
DEVELOPMENT OF ACTIVE STARCH BIOFILMS REINFORCED WITH NANOSILICA FOR FOOD PACKAGING 391
DEVELOPMENT OF NANOCOMPOSITES BASED ON CASSAVA STARCH FOR THE PRODUCTION OF BIO-PACKAGING MATERIALS 396
FABRICATION OF PHOTOACTIVE NANOFIBERS OF CROSSLINKING POLYVINYL ALCOHOL AND PHOTOSENSITIZERS FOR COMBATING WOUND INFECTION 401
IMPROVING THE OPTICAL AND MECHANICAL PROPERTIES OF PVA POLYMER THROUGH THE INCORPORATION OF CARBON DOTS. 406
INFLUENCE OF GRAPHENE AND GLASS FIBER ADDITIONS ON MECHANICAL AND RHEOLOGICAL PROPERTIES OF POLYPROPYLENE COPOLYMER 411
PHBV NANOCOMPOSITES WITH KAOLIN NANOPARTICLES MODIFIED WITH OREGANO ESSENTIAL OIL FOR APPLICATION IN FOOD PACKAGING 416
PRODUCTION OF ACID HETEROGENEOUS CATALYST BASED ON GRAPHITE–CELLULOSE NANOFIBERS AEROGEL COMPOSITES 421
SURFACE BIOMODIFICATION OF COTTON FABRIC WITH CHITOSAN NANOPARTICLES CONTAINING ESSENTIAL OILS 426
THERMAL, MECHANICAL AND MORPHOLOGICAL CARACTERIZATION OF THE PLA-TIO_2-MWCNT FOR 3D PRINTING FILAMENTS 431
USE OF LIPASES IN THE (BIO)MODIFICATION OF POLYESTER FOR THE INCORPORATION OF CHITOSAN NANOPARTICLES 436
APPLICATION OF GRAPHENES IN LDPE FOR FILMS: STUDY OF PARTICLE SIZE AND MECHANICAL PROPERTIES 441
BIODEGRADABLE POLYMERIC NANOCOMPOSITES BASED ON POLY(3-HYDROXYBUTYRATE-CO-3-HYDROXYVALERATE) (PHBV) AND GRAPHENE OXIDE (GO) 442
FEW-LAYER GRAPHENE PRODUCTION THROUGH GRAPHITE EXFOLIATION IN PRESSURIZED CO_2 443
INTERVENTIVE CONSERVATION OF RIGID POLYURETHANE FOAM BY MEANS OF TITANIUM DIOXIDE-BASED NANOCOATING 444
MODIFICATION OF SYNTHESIS ROUTE AND AGGREGATION ANALYSIS OF SILICA NANOPARTICLES FOR CORE-SHELL STRUCTURE 445
ORGANIC-INORGANIC PHOTOPOLYMERIZABLE NANOCOMPOSITES FOR 3D PRINTING WITH ANTIVIRAL ACTIVE SURFACES 446
PLASMA-FUNCTIONALIZED CARBON NANOTUBES FOR THE ADSORPTION OF RHODAMINE-B IN WATER 447
REUSABLE CELLULOSE NANOFIBRILS-BASED NANOCOMPOSITE AEROGELS FOR MALACHITE GREEN DYE REMOVAL 448
SYNTHESIS AND CHARACTERIZATION OF GELATIN AND STARCH NANOPARTICLES FOR INTELLIGENT MICROGELS PREPARATION 449
SYNTHESIS OF ELECTROSPUN POLYSTYRENE MEMBRANES COATED WITH GRAPHENE OXIDE AND POLYPYRROLE: STUDY OF THE REMOVAL OF ERIOCHROME BLACK T FROM AQUEOUS MEDIA 450
TENSILE AND INDENTATION TESTS ON CARBON NANOSTRUCTURES AND EPOXY RESIN COMPOSITES 451
TERMOPLASTIC STARCH NANOCOMPOSITES REINFORCED WITH NANOFIBRILLATED CELLULOSE: PLASTICIZATION WITH GLYCEROL IN THE PRESENCE OF WATER AS PROCESS PLASTICIZER 456
AMMONIA GAS SENSOR BASED ON RGO/PVDF NANOFIBERS 457
CELLULOSE NANOCRYSTALS FROM BANANA FIBER: EXTRACTION AND APPLICATION IN DENTAL MATERIALS 462
CHARACTERIZATION OF HEMICELLULOSE FILMS AS A CONDUCTIVE FLEXIBLE SUBSTRATE FOR APPLICATION IN SENSORS 467

CHARACTERIZATION OF REDUCED GRAPHENE OXIDE: CHALLENGES IN DETERMINING OF ELECTRICAL CONDUCTIVITY FOR APPLICATION IN CONDUCTIVE INKS 472
DEVELOPMENT OF ELECTROPUN MEMBRANES OF TPU/MWCNTS FOR APPLICATION IN WEARABLE SENSORS FOR HUMAN MOTION MONITORING 477
DEVELOPMENT OF MULTIFUNCTIONAL ELECTROSPUN POLYMERIC MEMBRANES FOR FACE MASKS: INCORPORATION OF ZINC OXIDE NANOPARTICLES 482
DEVELOPMENT OF NANOCOMPOSITES BASED ON DIFFERENT PHOTOSENSITIVE RESINS AND GRAPHENE OBTAINED VIA 3D PRINTING FOR DENTAL USE 487
DEVELOPMENT OF POLYMERIC FILMS OF POLYETHYLENE MODIFIED BY CLAY NANOPARTICLES AND GRAPHENE NANOPANELS FOR APPLICATION IN FOOD PACKAGING 492
ECOLOGICAL PANELS PRODUCED FROM AÇAI FIBER AND COPPER NANOPARTICLES 497
EFFECT OF HYDROTALCITE NANOPARTICLES ON THE ANTIOXIDANT PERFORMANCE OF STARCH/TANNIC ACID PACKAGING FILMS 502
EFFECT OF THE ADDITION OF SIO2 NANOPARTICLES ON THE COMPATIBILITY OF IMMISCIBLE POLYMERIC SYSTEMS BASED ON POLYETHYLENE AND POLYAMIDE 11 FROM OFFSHORE PLATFORMS 506
EFFECT OF THE GRAPHENE NANOPLATELETS ON FLEXIBLE PVC 511
EFFECT OF THE INCORPORATION OF MODIFIED SILICA IN A COMPOSITE WITH NANOFIBRILLATED CELLULOSE 516
EFFECTS OF SINGLE-WALLED CARBON NANOTUBE ADDITION ON THE MECHANICAL PROPERTIES OF CARBON FIBER STRUCTURAL COMPOSITE 521
EVALUATION OF B-PHASE ENHANCEMENT OF PVDF-TRFE NANOCOMPOSITES WITH GRAPHENE OXIDE PROCESSED BY EXTRUSION 526
EVALUATION OF PBAT/CUMBARU FIBER/ORGANOCLAY NANOCOMPOSITES FOR FOOD PACKAGING APPILICATION 531
EVALUATION OF THE ANTICORROSION POTENTIAL OF POLYMER NANOCOMPOSITE COATINGS WITH REDUCED GRAPHENE OXIDE FOR THE OIL INDUSTRY 536
EVALUATION OF THE CATALYTIC PROPERTIES OF POLYMER COMPOSITES CONTAINING NIOBIUM OXYHYDROXIDES 541
EVALUATION OF THE DEGRADATION OF POLY(ETHYLENE TEREPHTHALATE) WITH THE ADDITION OF CHAIN EXTENDERS AND GRAPHENE NANOPLATELETS AFTER PROCESSING 545
EVALUATION OF THE INFLUENCE OF NANOPARTICLE ADDITIVES ON THE MECHANICAL PROPERTIES OF EPOXY ADHESIVES 550
EVALUATION OF THERMAL, RHEOLOGICAL AND MECHANICAL PROPERTIES OF POLYPROPYLENE COMPOSITES AND GRAPHENE NANOPLATELETS WITH DIFFERENT NUMBER OF LAYERS 555
EXPLORING THE RHEOLOGICAL PROPERTIES OF WATERBORNE POLYURETHANE/CARBON QUANTUM DOTS NANOCOMPOSITES WITH PHOTOACTIVE CHARACTERISTICS 560
FUNCTIONALIZATION OF CLAY NANOPARTICLES BY PLASMA FOR APPLICATION IN ACTIVE PACKAGING 565
GRAPHENE OXIDE/COPPER, COPPER OXIDE AS HEAT CONDUCTIVE ADDITIVES FOR ENGINE OIL, PAINTS & POLYMERS 570
GRAPHENE OXIDE DEPOSITION ON METALLIC AND POLYMERIC SUBSTRATE VIA ELECTROPHORETIC DEPOSITION 575
HYBRID MATERIALS BASED ON CHITOSAN/MAGNETITE/SILVER NANOPARTICLES FOR ADSORPTION AND DEGRADATION OF DYES. 580
HYDROPHOBICITY EVALUATION OF POLYSTYRENE/STEARIC ACID ELECTROSPUN MEMBRANES 585
IMPACT BEHAVIOR OF UNSATURATED POLYESTER RESIN TOUGHENED BY CELLULOSE NANOCRYSTALS 590
INCORPORATION OF SILVER NANOPARTICLES INTO POLYESTER FABRICS 595
INFLUENCE OF GRAPHITE AND GRAPHENE INCORPORATION IN POLYURETHANE FOAMS OIL SORBENTS 600

INFLUENCE OF PROCESSING IN THE DRUM BALL MILL ON OBTAINING CELLULOSE NANOFIBERS 605
INFLUENCE OF THE ADDITION OF MONTMORILLONITE CLAY NANOFILLERS ON THE PROPERTIES OF ACRYLIC RESIN COMPOSITES APPLIED TO THE DEVELOPMENT OF OCCLUSAL PLATES BY ADDITIVE MANUFACTURING 609
MAGNETICALLY ENHANCED ADSORPTION OF PHARMACEUTICALS FROM AQUEOUS MEDIUM USING MAGNETIC ALGINATE/POLYPYRROLE/ZNFE2O4 BEADS 614
MAIN PROCESS PARAMETERS AND ANTIVIRAL PROPERTIES OF MELALEUCA OIL PICKERING EMULSION STABILIZED WITH NANOCELLULOSE 619
MONODISPERSE NANOPARTICLES PREPARED BY MICROEMULSION POLYMERIZATION 624
MORPHOLOGICAL INFLUENCE ON THE INCORPORATION OF NANOCELLULOSE INTO DE MEMBRANES POLYVINYLIDENE FLUORIDE (PVDF) 629
MORPHOLOGICAL STUDY OF COCONUT FIBERS MODIFIED BY MECHANICAL AGITATION IN AQUEOUS SOLUTION AND COMPARATION WITH ULTRASONIC AGITATION 634
MULTIFUNCTIONAL MONTMORILLONITE CLAY/SILVERNANOPARTICLES COATINGS FOR MEDICAL TEXTILES 639
NANOCELLULOSE MODIFICATION USING MODIFIED-DTPA TO REMOVE METALLIC IONS INTO WATER 644
NANOPARTICLES FILLED WITH VETIVER ESSENTIAL OIL SYNTHESIZED BY NANOPRECIPITATION AND IONIC GELATION METHODS FOR DERMOCOSMETIC 649
PHYSICAL AND RHEOLOGICAL CHARACTERIZATION OF RECYCLED PP NANOCOMPOSITE WITH MONTMORILLONITE CLAY 654
PLA/HNT NANOCOMPOSITES: INFLUENCE OF HNT CONTENT ON THERMAL, RHEOLOGICAL AND MECHANICAL PROPERTIES 659
POLI(LACTIC ACID-CO-GLYCOLIC ACID)/POLY(VINYL ALCOHOL) CORE-SHELL ELECTROSPUN FIBERS 664
POLYETHERSULPHONE/ATTAPULGITE FLAT MEMBRANES AND THEIR PERMEATION PROPERTIES 669
POLY(LATIC ACID) (PLA)/POE-G-GMA NANOCOMPOSITES REINFORCED WITH MWCNT FOR ANTISTATIC APPLICATION 670
PREPARATION AND CHARACTERIZATION OF NANOSTRUCTURED HYDROGELS BASED ON KAPPA-CARRAGENAN AND CLOISITE-NA+ 671
RHEOLOGICAL BEHAVIOR OF MELALEUCA OIL PICKERING EMULSIONS WITH CELLULOSE NANOFIBRILS 675
STUDY OF A SIPN APPLICABILITY AS A SOLID ELECTROLYTE FOR FUEL CELLS 680
SURFACE-MODIFIED MICROFIBRILLATED CELLULOSE FROM EUCALYPTUS SAWDUST FOR POTENTIALLY TOXIC ELEMENTS REMOVAL FROM CONTAMINATED WATER 685
SYNTHESIS AND PHYSICOCHEMICAL CHARACTERIZATION OF NANOFIBERS FROM BIOCELLULOSE WASTE 690
SYNTHESIS OF SBS/POLYPYRROLE FLEXIBLE FILMS: EVALUATION AS STRAIN SENSORS 695
TENSILE PROPERTIES OF SELF-HEALING EPOXY COMPOSITES REINFORCED WITH GRAPHENE NANOPLATELETS 700
TITANIUM DIOXIDE NANOPARTICLES OBTAINED BY GREEN ROUTE AS AN UV-BLOCKER ADDITIVE IN POLYMERS 705
WATER ADSORPTION BEHAVIOR IN CARBON NANOTUBES PLASMA-FUNCTIONALIZED WITH MALEIC ANHYDRIDE AND UREA 710
ALGINATE FILAMENTS REINFORCED WITH CELLULOSE NANOCRYSTALS FROM TEXTILE COTTON WASTE 715
ANALYSIS OF NANOCOMPOSITES WITH PIEZOELECTRIC PROPERTIES COMPOUNDS OF POLY(VINYLIDENE FLUORIDE) AND GRAPHENE OXIDE 716
ANALYSIS OF THE MECHANICAL PROPERTIES OF NANO COMPOSITE OF PLA POLYMERIC MATRIX WITH VEGETABLE FIBER AND NANO PARTICLE SUBMITTED TO 3D PRINTING 717
APPLICATION OF PANI/TITANIA HYBRIDS IN ELECTRORHEOLOGICAL FLUIDS 718
APPLICATION OF ZNO NANOPARTICLES IN THE DEVELOPMENT OF ACRYLIC RESIN-BASED PAINT WITH ANTIFOULING PROPERTIES 719

CELLULOSE ACETATE/TIO2 BIOCOMPOSITES FOR WATER TREATMENT BY PHOTOCATALYSIS 720
CONDUCTIVE FILMS BASED ON CARBON NANOTUBES AND CELLULOSE NANOFIBERS FOR SUPERCAPACITOR APPLICATION 721
CONTROLLING IPMC ACTUATOR IN HIGH HUMIDITY ENVIRONMENT 722
COTTON ANTIBACTERIAL ACTIVITY EVALUATION AFTER PLASMA FUNCTIONALIZED TIO2 AND ZNO DEPOSITION 723
DEVELOPMENT OF CORE-SHELL PVC/PMMA/PANI MEMBRANES BY COAXIAL ELECTROSPINNING 724
DEVELOPMENT OF ELECTROSPUN MEMBRANES OF PVDF/SILICA FUNCTIONALIZED WITH IONIC LIQUID FOR EFFLUENT TREATMENT 725
EFFECT OF CARBON NANOTUBE CONCENTRATION ON THE ELECTRICAL, THERMAL AND MECHANICAL PROPERTIES OF NTC/EPOXY NANOCOMPOSITES 726
EFFECT OF CELLULOSE NANOCRYSTALS ON WATER ABSORPTION OF SULFONATED SBS BASED IONIC POLYMER METAL COMPOSITE 727
EFFECT OF CURING ON THE GLASS TRANSITION TEMPERATURE OF THE EPOXY/GNP SYSTEM 728
EFFECT OF GRAPHENE CONCENTRATION ON POLYCAPROLACTONE ELETROSPUN MEMBRANES 733
EFFECT OF GRAPHENE MORPHOLOGY ON THE PROPERTIES OF PBAT/GRAPHENE NANOCOMPOSITES FOR APPLICATION IN PACKAGING 734
ELECTROSPINING IN THE MANUFACTURE OF ZNO AND PVB NANOCOMPOSITES TO CONTROL THE PROLIFERATION OF MICROORGANISMS 735
ELECTROSPUN MATS WITH ALIGNED FIBERS, BASED ON POLY(LACTIC ACID) CONTAINING CARBON NANOTUBES AND IONIC LIQUID 736
ENCAPSULATION AND SUSTAINED RELEASE OF NATURAL LARVICIDE FROM POLYURETHANE/PIPERINE NANOPARTICLES 737
ENCAPSULATION OF ESSENTIAL OILS ON CHITOSAN NANOPARTICLES WITH ANTIMICROBIAL PROPERTIES FOR FUNCTIONALIZATION OF FABRICS 738
ENHANCED SCALE INHIBITION PERFORMANCE BY POLYPHOSPHATE ENCAPSULATION IN POLYELECTROLYTE COMPLEXES 739
ENHANCING ELECTROSPINABILITY OF CHITOSAN: THE INFLUENCE OF PEO BLEND 740
EVALUATION OF AC AND DC ELECTRICAL PROPERTIES OF NATURAL RUBBER NANOCOMPOSITES WITH MWCNTS 741
EVALUATION OF AC AND DC ELECTRICAL PROPERTIES OF VULCANIZED NATURAL RUBBER NANOCOMPOSITES WITH MWCNTS: AN ANALYSIS BY MEANS OF THE ELECTRICAL MODULUS 742
EVALUATION OF ACID CONCENTRATION ON OBTAINING NANOCRYSTALS CELLULOSE AND SURFACE MODIFICATION BY SILANE 743
EVALUATION OF LDPE/GRAPHENE NANOCOMPOSITE IN ROTATIONAL MOULDING 744
EVALUATION OF POLYDIMETHYLSILOXANE (PDMS) WITH ZINC OXIDE NANOSTRUCTURES AS AN ENCAPSULANT IN PHOTOVOLTAIC MODULES 745
EVALUATION OF THE ANTIMICROBIAL EFFECT OF ZINC OXIDE MASTERBATCH ON HIGH DENSITY POLYETHYLENE 746
EVALUATION OF THE INCORPORATION OF BORON NITRIDE MICROPARTICLES AND NANOPARTICLES IN POLY(VINYL CHLORIDE) COMPOUND 747
EXTRACTION AND CHARACTERIZATION OF NANOCRYSTALS FROM PROCESS WASTES FOR APPLICATION IN TECHNOLOGICAL MATERIALS 748
FABRICATION AND CHARACTERIZATION OF POLYPYRROLE NANOCOMPOSITES WITH CARBON QUANTUM DOTS 749
FLUORESCENCE EMISSION FROM GELATIN CARBON DOT UNDER X-RAY FLUORESCENT IRRADIATION 750

FORMULATION OF HIGH THERMAL PERFORMANCE XLPE NANOCOMPOSITE 751
FRACTAL TYPE SELF ASSEMBLY FORMED BY CARBON QUANTUM DOTS INDUCED BY ELECTRIC FIELD IN POLYPYRROLE MATRIX 752
FUNCTIONALIZED LEATHER FOR ELIMINATING THE SARS-COV-2 VIRUS 753
GALACTOMANNAN AS A CARRIER FOR A-BISABOLOL-LOADED NANOCAPSULES INTENDED FOR BIOMEDICAL APPLICATION 754
HYBRID MULTIFUNCTIONAL NANOCOMPOSITES BASED ON POLYAMIDE 10.10 AND TWO-DIMENSIONAL MATERIALS 755
INFLUENCE OF MINERAL FILLERS IN CARBON BLACKS TRIMODAL MIXTURE ON THE COLORIMETRIC PROPERTIES AND MECHANICAL BEHAVIOR OF LOW-DENSITY POLYETHYLENE FILM: PART 3 756
INFLUENCE OF NITROGEN DOPING ON THE CONDUCTIVE PHASE IN CONDUCTIVE HYDROGELS 757
INFLUENCE OF OPERATIONAL PARAMETERS ON THE COLORING OF POLIAMIDE TEXTILES USING CURCUMIN/POLYMER NANOPARTICLES 758
MANUFACTURE OF FIBROUS BANDAGES BY ELECTROSPINING WITH BACTERICIDAL EFFECT FOR PHOTODYNAMIC THERAPY 759
MECHANICAL PROPERTIES OF POLYPROPYLENE/CALCIUM CARBONATE MICRO AND NANOCOMPOSITES 760
MICROFIBRILLATED CELLULOSE DRYING TECHNIQUES AND MATERIAL PROPERTIES 761
MIXED LIPOSOMES INCORPORATED WITH CURCUMIN AND SILVER NANOPARTICLES FOR PHOTODYNAMIC THERAPY 762
NANOCOMPOSITES OF MESO-PORPHYRINS DERIVED FROM CARDANOL AND VANILLIN FOR APPLICATION IN ANTICORROSIVE ORGANIC COATINGS. 763
NANOCOMPOSITES OF POLYSTYRENE/PSEUDOBOEHMITE TREATED WITH OCTADECYLAMINE 764
NANOENCAPSULATION OF THE OILY EXTRACT OF CHENOPODIUM AMBROSIOIDES L. IN LIGNIN USING AN ANTISOLVENT METHOD 765
NATURAL GUM FILMS AND SILVER NANOPARTICLES FOR EVALUATION OF ANTIBACTERIAL PROPERTIES 766
PHOTOSTABILIZATION OF HYBRID NANOCOMPOSITES BASED ON EPDM RUBBER, CARBON BLACK AND GRAPHENE OXIDE 767
POLYCAPROLACTONE/AMINO-MODIFIED SODIUM ALGINATE ELECTROSPUN CORE-SHELL FIBERS 768
POLYMER NANOCOMPOSITES BASED ON ACRYLONITRILE BUTADIENE STYRENE (ABS) COPOLYMER, GRAPHENE NANOPLATELETS AND HEXAGONAL BORON NITRIDE 769
POLYURETHANE WASTE AS A REDUCING AGENT OF SILVER NANOPARTICLES 770
PREPARATION AND CHARACTERIZATION OF NANOPARTICLES FOR POTENTIAL APPLICATION IN TREATMENT OF CONTAMINATED WATER 771
PREPARATION AND CHARACTERIZATION OF NANOSTRUCTURED HYDROGELS BASED ON CALCIUM ALGINATE AND MONTMORILLONITE. 772
PREPARATION AND CHARACTERIZATION OF SOLUTION BLOWN PVA/CNCS NANOBIOCOMPOSITE FIBERS 776
PROCESSING AND MECHANICAL PROPERTIES OF MICROFIBRILLATED CELLULOSE REINFORCED POLYPROPYLENE COMPOSITES 777
PVDF NANOFIBERS WITH ZNO NANOSTRUCTURES FOR APPLICATION IN GAS SENSORS 778
"DEVELOPMENT OF SILOXANE-PMMA AND SILOXANE-PEO-PMMA HYBRID MATERIALS FOR FUTURE APPLICATIONS OF PROLONGED RELEASE OF PENICILLIN G" 779
RECOVERY OF THE MECHANICAL PROPERTIES OF POST-CONSUMER ABS COPOLYMER BY INCORPORATION OF GRAPHENE OXIDE (GO) AND GRAPHENE 780
REPLACEMENT OF ETHYLENE VINYL ACETATE (EVA) LAYER BY POLYDIMETHYLSILOXANE COMPOSITES (PDMS) WITH GRAPHENE NANOSTRUCTURES IN PHOTOVOLTAIC MODULES 781
SINGLE WALL CARBON NANOTUBES AND ITS INFLUENCE ON PROPERTIES OF POLYMER NANOCOMPOSITES 782

STUDY OF ELECTROSPUN MATS OF POLY(ACID LACTIC) WITH GRAPHENE NANOPLATELETS AND CHOLINE BITARTRATE FOR USE IN NERVE TISSUE ENGINEERING 783
STUDY OF THE INCORPORATION OF CARBON NANOTUBES ON WATER-BASED EPOXY INK 784
STUDY OF THE INFLUENCE OF THE SHAPE OF CARBON BLACK NANOPARTICLE AGGREGATES ON THE PROPERTIES OF NANOCOMPOSITES WITH AND WITHOUT BLOCK COPOLYMER 785
STUDY ON THE INFLUENCE OF MATERIAL PARAMETERS IN ELECTROSPUN NANOMEMBRANES FROM AQUEOUS PVA SOLUTIONS 786
SUPERHYDROPHOBIC COATINGS BASED ON EPOXY RESIN CONTAINING ORGANICLY MODIFIED SILICA (ORMOSIL) 787
SYNERGISTIC COMBINATION OF NATURAL RUBBER LATEX AND LIGNIN FOR SUSTAINABLE WATER-BASED ADHESIVES 788
SYNERGISTIC EFFECT OF ADDING GRAPHENE NANOPLATES AND CARBON NANOTUBES IN PLA/PHBV BLENDS 789
SYNTHESE OF NANOPARTICLES BY ELECTROSPINNING 790
SYNTHESIS AND DEPOSITION BY SLOT DIE COATING OF WATER BASED P3HT AND P3HT:PCBM NANOPARTICLES 791
SYNTHESIS AND STABILIZATION OF SILVER NANOPARTICLES IN COPOLYMERIC MICELLES COMBINED WITH ROSE BENGAL COMBINED FOR PHOTODYNAMIC THERAPY 792
SYNTHESIS OF ALGINAT BEADS WITH FUNCTIONALIZED CLAYMINERAL APPLIED TO CHROMIUM REMOVAL 793
SYNTHESIS OF POLYANILINE IN BACTERIAL CELLULOSE OBTAINED FROM KOMBUCHA TEA FERMENTATION 794
THERMAL PROPERTIES CHARACTERIZATION OF PBAT NANOCOMPOSITES WITH GRAPHENE OXIDE AND CARBON BLACK 795
TITANIUM NANOPARTICLES ENCAPSULATED WITH ZWITTERION AND USE IN ELECTRORHEOLOGICAL FLUIDS 796
USE OF POLYSTYRENE/POLYPYROLE/ORGANOPHILIC MONTMORILLONITE MEMBRANE AS A HUMIDITY SENSOR 797
BLENDS, COMPOSITES AND POLYMER NETWORKS 798
ALL-POLYSACCHARIDE IN SITU FORMING HYDROGEL OF CARBOXYMETHYL CHITOSAN AND ALDEHYDE-FUNCTIONALIZED HYDROXYETHYL CELLULOSE 799
ANTIMICROBIAL ACTIVE BIOCOMPOSITE USING PBAT, CACTUS FIBER AND CLOVE ESSENTIAL OIL 804
INFLUENCE OF COMPATIBILIZER AGENT ON THE PROPERTIES OF GREEN POLYETHYLENE COMPOSITES REINFORCED WITH BAMBOO FIBER 809
INVESTIGATION OF AGING IN EPOXI-MATRIX COMPOSITES 814
RECYCLING OF THERMOSET CARBON FIBER COMPOSITES FOR AUTOMOTIVE SECTOR 815
WOOD PLASTICS COMPOSITES BASED ON PVC REINFOCED WITH NATURAL FIBERS: COMMERCIAL APPLICATION S FOR PROFILES 816
ARTESANAL HYBRID TECHNICAL TEXTILES REINFORCED POLYESTER COMPOSITES 822
COMPARATIVE STUDY OF METHODS FOR PRODUCING STARCH/PVA BLEND FILMS BY CASTING 827
DIFFERENT MOLAR MASS OF PEG-B-PPG-B-PEG TRIBLOCK COPOLYMER: EFFECT ON THERMOSETTING SYSTEMS 832
EFFECT OF PH ON THE ADSORPTION OF METHYLENE BLUE IN PECTIN/MONTMOROLINITE COMPOSITE HYDROGEL 837
EFFECT OF THE INCORPORATION OF LIGNIN ON STARCH/PVA BLEND FILMS PRODUCED BY CASTING 842
ELECTROSPRUN NANOFIBERS BLENDS PREPARED FROM POLYVINYL ALCOHOL /LIGNIN MIXTURES 847
EVALUATION OF GRAPHENE INCORPORATION FOR MECHANICAL PROPERTIES OF POLYPROPYLENE COMPOSITES 852

EVALUATION OF THE PHYSICAL AND MECHANICAL PROPERTIES OF POLYMERIC BLENDS WITH RESIDUES OF POLYPROPYLENE MASKS 857
IMPACT EVALUATION OF GLASS FIBER / POLYESTER WATERPROOF COMPOSITE SUBJECTED TO TEMPERATURA AND ACID ENVIRONMENT 862
INFLUENCE OF CURE CONDITIONS ON CROSSLINKG AND DYNAMIC MECHANICAL BEHAVIOR OF EPOXY 866
MODIFICATION AND CHARACTERIZATION OF LUFFA CYLINDRICA FIBERS WITH ZINC NANOFERRITE 871
STATISTICAL EVALUATION OF ELECTROMAGNETIC ABSORPTIVITY OF PDMS/CNT/GNP COMPOSITES 876
STRUCTURAL PERFORMANCE OF HYBRID FIBER-METAL LAMINATES WITH NATURAL AND SYNTHETIC FIBERS 881
THERMAL, MECHANICAL, RHEOLOGICAL, AND MORPHOLOGICAL CHARACTERIZATION OF THE EXTRUDED PLA/PE-G-MA/CNC SYSTEM WITH AND WITHOUT CONTROLLED ELONGATIONAL FLOW DEVICE. 886
THERMOPLASTIC CORN STARCH/VISCOSE YARN WASTE BIOCOMPOSITES PROCESSED BY EXTRUSION-COMPRESSION MOLDING 891
TRANSMITTANCE AND THERMAL STABILITY OF REGENERATED CELLULOSE FILMS WITH SILVER NANOPARTICLES AND PLASTICIZERS 896
ANTIOXIDANT PROPERTIES OF BIOPOLYMERIC ONION (ALLIUM CEPA L.) FILMS MODIFIED WITH LAPONITE CLAY 901
A STUDY OF MIXED-MATRIX POLYSULFONE-RECAM® FILTRATION MEMBRANE MORPHOLOGY 902
DEVELOPMENT AND CHARACTERIZATION OF UPCONVERSION COMPOSITE FILMS OF CELLULOSE ACETATE-BUTYRATE/$NAYF_4$:YB^{3+}, ER^{3+} FOR LUMINESCENT THERMOMETRY APPLICATIONS 903
EFFECT OF NATURAL-BASED PLASTICIZERS ON PROPERTIES OF POLYHYDROXYBUTYRATE FILMS 904
EFFECTS OF ELECTROPHORETIC DEPOSITION OF CARBON NANOTUBES ON JUTE FIBERS 905
ESTIMATION OF CREEP AND FATIGUE LONG TERM BEHAVIOR OF A GLASS-FIBER/POLYPROPYLENE COMPOSITE USING SHORT TERM DATA 906
EXTRUSION SEQUENCE FOR ENHANCED DISPERSION OF MICROFIBRILLATED CELLULOSE IN PLA/PCL BLENDS: IMPACT ON MORPHOLOGY AND MECHANICAL PROPERTIES 907
INTERFACIAL IMPROVEMENT OF JUTE FIBRE EPOXY COMPOSITE USING INTERMITTENT HIGH VOLTAGE PULSED ELECTROPHORESIS DEPOSITION 908
ON THE PEG-B-PCL MULTIBLOCK COPOLYMER LOCALIZATION IN PLA/PCL BLENDS VIA AFM-IR 909
PLASMA FUNCIONALIZATION OF ZINC OXIDE THROUGH ORGANIC COMPOUNDS 910
PRODUCTION OF POLYSULPHONE/ALUMINE HOLLOW FIBER MEMBRANES FOR WASTEWATER TREATMENT 911
SPECTROSCOPIC, ELETRICAL AND MORPHOLOGICAL CHARACTERIZATIONS OF CONDUCTIVE POLYMER HYDROGELS FOR APPLICATION IN HYBRID SUPERCAPACITORS 912
SYNTHESIS AND CHARACTERIZATION OF FLAT MEMBRANES FROM POLYMERIC BLENDS 913
ACCELERATED WEATHERING ENVIRONMENT: INFLUENCE ON MECHANICAL AND THERMAL PROPERTIES OF CF/PA6 COMPOSITES 914
ANALYSIS OF THE PROJECT OF AN AUTOMOTIVE CRANKCASE USING THE PC/ABS BLEND 915
ANALYSIS OF THERMAL AND MORPHOLOGICAL PROPERTIES OF PVA/CHITOSAN BLENDS INCORPORATED WITH PITAYA EXTRACT 920
BIODEGRADABLE COMPOSITES OF SUGARCANE BAGASSE AND POLYURETHANE 925
BRAZIL NUT BUR PARTICLES REINFORCED POLYPROPYLENE COMPOSITE 929
CHEMICAL AND THERMAL EVALUATION OF A COMPOSITE FOAM BASED ON CASSAVA STARCH, CLAY AND RAMIE FIBERS 934
CHITOSAN-BASED MULTILAYER FILM INCORPORATED WITH BIOACTIVE COMPOUNDS FROM JABOTICABA PEEL 939

COMPARISON BETWEEN LLDPE COMPOSITES CONTAINING RESIDUES OF BACURI MESOCARP (BM) AND BACURI SEED (BS) 944
COMPATIBILITY BETWEEN PBAT AND SWEET POTATO STARCH: INFLUENCE OF THE COMPATIBILIZING AGENT 949
COMPOSITE AEROGELS CONTAINING NANOCELLULOSE: NANOCELLULOSE ON CROSSLINKING AND CADMIUM REMOVAL 954
COMPOSITES OF POLYESTER RESIN WITH DIFFERENT COMBINATIONS OF FIBERGLASS REINFORCEMENTS OBTAINED BY PULTRUSION 959
DEVELOPMENT OF CHITOSAN HYDROGELS FOR METAL REMOVAL IN CONTAMINATED WATER 963
DEVELOPMENT OF CORN STARCH HYDROGELS FOR SORPTION OF POTENTIALLY TOXIC METALS 968
DEVELOPMENT OF HIGH-DENSITY POLYETHYLENE COMPOSITES WITH MACAIBA BARK 973
DEVELOPMENT OF MAGNETIC COMPOSITES OF POLYPROPYLENE (PP) AND MAGNETITE MICROPARTICLES (FE3O4) 978
DEVELOPMENT OF SYNTHETIC COMPOSITE WITH RECYCLED HIGH DENSITY POLYETHYLENE (HDPE) MATRIX AND FIBERGLASS REINFORCEMENT 983
EFFECT OF BACURI SEED (BS) NATURAL FILLER ON PBAT 984
EFFECT OF INCORPORATING RECYCLED FLEXOGRAPHIC PHOTOPOLYMER PLATE PARTICLES INTO AN EPOXY MATRIX 989
EFFECT OF NON-HALOGENATED FLAME RETARDANT ON ABS/PC BLEND PROPERTIES 994
EFFECTS OF LONG-TERM HYGROTHERMAL AGING ON THE MECHANICAL BEHAVIOR OF CARBON FIBER/EPOXY COMPOSITE 998
EVALUATION OF BARRIER PROPERTIES AND COMPATIBILITY OF EVA/THERMOPLASTIC STARCH BLENDSFOI ALTERADO PARA EVALUATION OF BARRIER THE WATER VAPOR PROPERTIES AND COMPATIBILITY OF EVA/THERMOPLASTIC STARCH BLENDS 1003
EVALUATION OF BENDING PROPERTIES OF POLYESTER COMPOSITES AND PLANT FIBERS COATED WITH INVERTED SUCROSE 1007
EVALUATION OF RECYCLED POLYPROPYLENE PROPERTIES WITH BANKNOTE-REINFORCED 1012
EVALUATION OF SODIUM ALGINATE MEMBRANES INCORPORATEDWITH RED ARAÇÁ (PSIDIUM CATTLEYANUM SABINE) EPICARPEXTRACT 1017
EVALUATION OF THE EFFECT OF DIFFERENT LEVELS OF CITRIC ACID ON THE PHYSICOCHEMICAL PROPERTIES OF CASSAVA STARCH/POLY(BUTYLENE SUCCINATE) BLENDS 1021
EVALUATION OF WEAR RESISTANCE OF LLDPE/UHMWPE BLENDS 1026
EXPANDED GRAPHITE AS REINFORCEMENT OF POLYPROPYLENE 1031
FLOW BEHAVIOR AND DEGRADATION OF HIGH DENSITY POLYETHYLENE (HDPE) AND ULTRA HIGH MOLAR MASS POLYETHYLENE (UHMWPE) BLENDS 1036
FOAM COMPOSITES REINFORCED WITH MDF POWDER: EFFECTS ON MECHANICAL PROPERTIES AND SUSTAINABILITY 1041
FRACTOGRAPHIC ANALYSIS OF RECYCLED CF/PPS COMPOSITES 1046
HYBRID BIOCOMPOSITE BASED ON BACTERIAL CELLULOSE WITH HYDROXYAPATITE PARTIALLY SUBSTITUTED BY MG/ZN AND MG/SR FOR GUIDED BONE REGENERATION 1047
HYDROPHOBIC AND FLEXIBLE POLYURETHANE FOAMS REINFORCED WITH MICROCRYSTALLINE CELLULOSE FIBERS FOR OIL SPILL CLEAN UP 1052
INFLUENCE OF DIFFERENT ORGANIC ACIDS AS COUPLING AGENTS ON THE THERMAL PROPERTIES OF HDPEPC/CURAUA FIBER COMPOSITE 1057
INFLUENCE OF NATURAL EXPOSURE ON CASTOR OIL BASED POLYURETHANE REINFORCED WITH MACADAMIA RESIDUES 1062

INFLUENCE OF SODIUM BENTONITE CLAY CONCENTRATION ON THE PROPERTIES OF BIOCOMPOSITES BASED ON BABASSU COCONUT MESOCARP STARCH AND ALGINATE 1067
INFLUENCE OF THE ADDITION OF PEG-B-PPG-B-PEG AND PPG-B-PEG-B-PPG TRIBLOCK COPOLYMERS IN THERMOSETTING SYSTEMS 1072
INFLUENCE OF THE INCORPORATION OF AGAVE ANGUSTIFOLIA FIBERS VAR. MARGINATA (FAAM) IN THE MECHANICAL AND THERMAL PROPERTIES OF THE COMPOSITE UNSATURATED POLYESTER/FAAM 1077
INFLUENCE OF THE MODIFICATION OF BREWER'S SPENT GRAIN FIBERS ON CONTACT ANGLE MEASUREMENTS OF THERMOPLASTIC STARCH COMPOSITES 1082
INFLUENCE OF THE MODIFICATION OF BREWER'S SPENT GRAIN FIBERS ON THE BIODEGRADABILITY OF THERMOPLASTIC STARCH COMPOSITES 1086
INFLUENCE OF UV SENSITIVITY ON STAB RESISTANCE OF KEVLAR® FABRICS IMPREGNATED WITH SHEAR THICKENING FLUIDS (STFS) 1091
LUFFA CYLINDRICA GRAFTED WITH POLYETHYLENEIMINE: A POTENTIAL ADSORBENT TO TREAT POST-COVID-19 WASTEWATER 1096
MAGNESIUM POWDER REINFORCED CASTOR OIL FOAMS: PHYSICAL AND MORPHOLOGY ANALYSES 1101
MECHANICAL BEHAVIOR AND GEL CONTENT OF POLY(VINYLIDENE FLUORIDE)/ THERMOPLASTIC POLYURETHANE BLENDS DYNAMICALLY CROSS-LINKED WITH AMINE. 1106
MIXED MATRIX FILMS BASED ON PEBAX® FILLED WITH LAYERED DOUBLE HYDROXIDES 1111
MODIFICATION OF LUFFA CYLINDRICA WITH B-CYCLODEXTRIN FOR THE ADSORPTION OF EMERGING CONTAMINANTS IN AQUEOUS MEDIUM 1116
MORPHOLOGY AND MECHANICAL PROPERTIES OF A COMPOSITE FOAM BASED ON CASSAVA STARCH, CLAY AND RAMIE FIBERS 1121
NANOCELLULOSE AEROGELS FROM EUCALYPTUS WASTES: MECHANICAL PERFORMANCE AND CADMIUM REMOVAL 1126
PAAM/RHA HYDROGELS AS AN INTERNAL CURING AGENT IN MORTARS AND CONCRETES 1131
PBAT BIOCOMPOSITES WITH BRAZIL NUT SHELL FIBERS (CP) 1136
PBAT BIOCOMPOSITE WITH BACURI MESOCARP (BM) RESIDUE 1141
POLY(BUTYLENE-ADIPATE-CO-TEREFTALATE) BIOCOMPOSITES WITH CORN STRAW FOR FOOD PACKAGING 1146
PRODUCTION OF BIODEGRADABLE PACKAGING FROM RENEWABLE SOURCES 1151
PROTON CONDUCTING MEMBRANES BASED ON SODIUM ALGINATE AND PROTIC IONIC LIQUIDS 1156
REMOVAL OF METHYLENE BLUE DYE BY PVDF/RGO MICRO/NANOSTRUCTURAL MEMBRANES PRODUCED BY AIRBRUSHING 1161
REVALORIZATION PINECONE RESIDUES REINFORCED ACRYLONITRILE BUTADIENE STYRENE (ABS) COMPOSITE FILAMENTS FOR 3D-PRINTING BY FDM 1166
RICE HUSK FILLED PLA/PBAT COMPOSITES FOR FOOD CONTAINERS: PROCESSABILITY, RHEOLOGICAL AND THERMAL PROPERTIES 1171
SELF-HEALABLE MULTI-NETWORK HYDROGELS OF POLY(ACRYLIC ACID)/POLY(VINYL ALCOHOL) AND FE^{3+} IONS: DESIGN, CHARACTERIZATION AND SELECTIVE ADSORPTION OF CATIONIC DYE 1176
SORPTION KINETICS OF CATIONIC DYES IN PECTIN-CLAY MINERAL COMPOSITE HYDROGELS 1181
STARCH-BASED COMPOSITE HYDROGEL ENHANCED BY ACTIVATED CARBON FROM THE BANANA PEEL: MORPHOLOGICAL, CHEMICAL AND THERMAL PROPERTIES 1185
STUDY, CHARACTERIZATION AND ANALYSIS OF POLYETHYLENE POLYMER COMPOSITES (HDPE) WITH FIBERS FROM THE BABASSU PALM (ARECACEAE) 1190
STUDY OF THE PLASTICIZER EFFECT OF CASTOR OIL DERIVATIVES IN THE PREPARATION OF FLEXIBLE PHBV FILMS 1195

SUSTAINABLE ALTERNATIVES FOR PACKAGING: EXPLORING THE HIGROSPICITY OF BIODEGRADABLE MATERIALS BASED ON PLA, PBAT, AND RICE HUSK 1200
SUSTAINABLE POLYURETHANE FOAM WITH RICE HUSK ASH RESIDUES WITH POTENTIAL APPLICATION IN THE ADSORPTION OF PESTICIDES IN WATER FOR HUMAN CONSUMPTION 1205
SYNTHESIS AND CHARACTERIZATION OF BACTERIAL CELLULOSE MEMBRANES INCORPORATED WITH ZINC OR SILVER NANOPARTICLES 1210
SYNTHESIS OF HYDROGEL BASED ON MODIFIED PECTIN AND POLY (VINYL ALCOHOL) FOR IMMOBILIZATION OF METALLIC NICKEL FOR CATALYTIC APPLICATIONS 1215
SYNTHESIS, SPECTROSCOPIC AND THERMAL STUDY OF NETWORKS CONTAINING POLY(STYRENE-CO-MALEIC ANHYDRIDE) 1220
THE CO-COMPATIBILIZATION EFFECT OF NANOFILLERS IN IMMISCIBLE SYSTEMS BASED ON POLYETHYLENE AND POLYESTER FROM OFFSHORE PLATFORMS 1225
THE EFFECTS OF AGING ON GLASS FIBER-EPOXY COMPOSITES WITH IMPACT DAMAGE. 1230
THE EFFECTS OF COPPER POWDER ON THE PROPERTIES OF ABS 1231
THERMAL AND MECHANICAL PROPERTIES OF ARAMID FIBER REINFORCED POLYPROPYLENE 1236
THE STUDY OF THE BEHAVIOR OF TE PP/PS BLEND UNDER STRESS CRACKING 1241
UV-VIS, PHOTOLUMINESCENCE AND ANTIOXIDANT PROPERTIES OF OF PVA/CHITOSAN BLENDS MODIFIED WITH PITAYA EXTRACT 1242
ACTIVE COMPOSITE FILMS- CARBOXYMETHYLCELLULOSE/ CURCUMIN AND EGG-SHELL POWDER COMPLEX 1247
BIOCOMPOSITES BASED ON PBAT AND SPENT COFFEE GROUNDS: EVALUATION OF BIODEGRADATION IN SOIL AND SIMULATED MARINE ENVIRONMENT 1248
BIOPOLYMER-BASED HYDROGELS FOR CD2+ ION REMOVAL IN AQUEOUS MEDIUM 1249
CATALYSTS IN POLYHIDROXYESTER BASED VITRIMERS 1250
CHARACTERIZATION OF NATURAL RUBBER-BASED FIBROUS BIOCOMPOSITE REINFORCED WITH BIOACTIVE GLASS-CERAMIC PARTICLES FOR BIOMEDICAL APPLICATIONS 1251
COCONUT FIBER TREATED AS A FUNCTION OF TIME WITH METAKAOLIN AND INDUSTRIAL ASH SOLUTION 1252
COMPARATIVE STUDY OF THE EXTRACTION OF SOLUBLES FROM COCONUT FIBER IN AQUEOUS ALKALINE SOLUTION UNDER SHAKING AND REST 1257
COMPOSITES BASED ON BACTERIAL CELLULOSE/AG3PO4 WITH POTENTIAL ANTIMICROBIAL ACTION 1262
CONSOLIDATION AND CHARACTERIZATION OF CARBON FIBER/SNAP CURE EPOXY RESIN LAMINATES PRODUCED BY PREPREG HOT PRESSING 1263
DEVELOPMENT OF FILTERING SYSTEMS BASED ON POLYSACCHARIDES BY ELECTROSPINING 1264
DEVELOPMENT OF SULFONATED PEEK IONIC POLYMER METAL COMPOSITES: ELECTROMECHANICAL CHARACTERIZATIONS 1265
DYNAMICAL-MECHANICAL PROPERTIES OF RECYCLED POLYMER FROM MULTILAYER FILMS AFTER STRUCTURAL CHANGE BY HIGH SHEAR RATE.RECYCLING, MULTILAYER FILMS, LDPE, SHEAR RATE, DMA. 1266
EFFECT OF ALGINATE ADDITION ON THE PHYSICOCHEMICAL PROPERTIES OF CHITOSAN FILMS 1267
EFFECT OF CARBOXYMETHYL CELLULOSE (CMC) CONCENTRATION AND GLYCEROL PLASTICIZER VARIATION ON THE PRODUCTION OF PLASTIC FILMS VIA CASTING METHOD 1268
EFFECTS OF ACCELERATED AGING ON A GLASS FIBER - EPOXY COMPOSITE WITH SELF-HEALING AGENT FOR PIPELINE REPAIR IN THE OIL INDUSTRY 1269
EFFECTS OF DIFFERENT CURING AGENT TYPES AND STOICHIOMETRY RATIO ON THE CROSSLINKING GRADE AND ITS CORRELATION WITH THE YELLOWING RATE OF WATER-BASED EPOXY CLEAR COATINGS 1270
EVALUATION OF COMPATIBILIZATION IN RECYCLABLE BLENDS AND COMPOSITES FROM THE AMAZON 1275
EVALUATION OF THE EFFECTS OF USING COMPATIBILIZERS IN HDPE COMPOSITES WITH TREATED COCONUT FIBER 1276

EVALUATION OF THE MECHANICAL PROPERTIES OF POLYMERIC BLENDS PRODUCED FROM EXPANDED POLYSTYRENE (EPS) AND WASTE TIRE RUBBER (WTR). 1277
EXPLORING THE USE OF A THERMOMECHANICAL ANALYZER TO ASSESS THE AGING OF PROPELLANTS 1278
FRACTOGRAPHIC ANALYSIS OF FATIGUE FAILURE IN CFRP COMPOSITE WITH PA6 MATRIX 1279
GREEN COCONUT (*COCOS NUCIFERA*) LONG FIBER POLYMERIC BIOCOMPOSITE WITH NATURAL BIOACTIVE COMPOUNDS 1280
GREEN TPV BASED ON PE RECICLABLE AND WASTE TYRE 1281
IMPREGNATION OF POLYCARBONATE/POLY(L-LACTIC ACID) BLENDS WITH CLOVE EXTRACT ASSISTED BY SUPERCRITICAL CO2 1282
IMPRESSIVE MECHANICAL AND BIOLOGICAL PROPERTIES OF FILMS OF QUATERNIZED CHITOSAN 1283
INACTIVATION OF SARS-COV-2 IN POLYELECTROLYTE FILM BASED ON PECTIN/POLY(DIALLYLDIMETHYLAMMONIUM CHLORIDE) 1284
INFLUENCE OF MIXING SEQUENCE ON THE SELECTIVE LOCALIZATION OF CELLULOSE NANOCRYSTALS IN POLY(LACTIC ACID)/POLY(Ɛ-CAPROLACTONE) BLENDS 1285
INFLUENCE OF THE WASHING PROCESS ON THE PROPERTIES OF CHITOSAN-ALGINATE COMPOSITE FILMS 1286
INFLUENCE OF UNTREATED AND ALKALI-TREATED BARLEY BAGASSE ON MECHANICAL PROPERTIES OF POLYESTER RESIN COMPOSITES 1287
LECITHIN MODIFIED KAPOK FIBER/HYDROXYPROPYL METHYLCELLULOSE/GRAPHITE COMPOSITES: THERMAL AND ACOUSTIC PROPERTIES 1288
MECHANICAL AND THERMAL PROPERTIES ANALYSIS OF GLASS FIBER-REINFORCED POLYAMIDE 9T COMPOSITES FOR ENGINEERING 1289
MORPHOLOGICAL, MECHANICAL AND THERMAL CHARACTERIZATION OF CARBON FIBER REINFORCED PETG AND PLA AFTER MANUFACTURING PROCESS WITH THE FFF TECHNIQUE 1290
MORPHOLOGY AND MECHANICAL PROPERTIES OF PBAT/PLA BIOCOMPOSITES WITH CELLULOSE IMPROVED BY DISC REFINING 1291
MORPHOLOGY CHARACTERIZATION OF SULFONATED POLY(STYRENE-B-BUTADIENE-B-STYRENE) 1292
NANOCELLULOSE HYDROGELS DERIVED FROM PALM SHEATHS: SYNTHESIS AND CHARACTERIZATION 1293
OBTAINING AND CHARACTERIZING PVDF-HFP/PVA/CLAY COMPOSITES FOR THE REMOVAL OF ORGANIC CONTAMINANTS IN AQUEOUS MEDIUM 1294
OXYALKYLATED LIGNIN POLYOL FOR POLYURETHANE SYSTEMS: RHEOLOGY AND CURE KINECTICS 1295
PHOTOCATALYST IMMOBILIZATION ON ELECTROSPUN FIBERS FOR THE DEGRADATION OF THE DRUG PARACETAMOL 1296
POLYURETHANE-TYPE MATRICES SYNTHESIZED FROM LIGNOSULFONATE AS POLYOL: FORMATION OF COMPOSITES REINFORCED BY LIGNOCELLULOSIC FIBERS SIMULTANEOUSLY WITH SYNTHESIS 1297
PREPARATION AND CHARACTERIZATION OF POLYETHERIMIDE/CLAY MEMBRANES 1298
PROCESSING PARAMETERS AS POTENTIAL VARIABLES TO TPS/PVOH BLENDS SENTIVITY TO WATER 1299
PRODUCTION AND CHARACTERIZATION OF A SIMPLE AND LOW-COST BACTERIAL CELLULOSE/SILICA GEL COMPOSITE 1300
PRODUCTION OF BIOCIDAL POLYMERIC COATINGS BASED ON ALKYLATED POLYETHYLENEIMINE AND PMMA BLENDS 1301
PRODUCTION OF CELLULOSE-POLYACRILICACID HYDROGELS 1302
PRODUCTION OF CELLULOSE/PVOH/CHONDROITIN SULFATE MEMBRANES AND POTENTIAL APPLICATIONS AS A TRANSDERMAL MEMBRANE 1303
PROPERTIES OF ALGINATE CAPSULES: A COMPARATIVE STUDY USING DIFFERENT CROSSLINKERS 1304
REACTIVE COMPATIBILIZATION OF PEBD/PP BLENDS USING NATURAL CLAY 1305

REDOX-RESPONSIVE HYDROGELS OF THIOLATED PECTIN: POTENTIAL VEHICLES FOR DRUG RELEASE 1306
RESPONSE SURFACE METHODOLOGY TO MAXIMISE THE SWELLING OF STARCH AND ACRYLIC ACID BASED HYDROGELS 1307
RHEOLOGICAL CHARACTERIZATION AND STUDY OF MECHANICAL AND THERMAL PROPERTIES OF NATURAL RUBBER AND POLYBUTADIENE BLENDS WITH ADDITION OF POLYURETHANE RESIDUE 1308
STUDY OF POLYMERIC COMPOSITES FROM LDPE/NATURAL FIBERS FROM THE AMAZON 1309
STUDY OF THE TRIBOLOGICAL PROPERTIES OF PARTS OBTAINED BY 3D PRINTING USING PET FILAMENT WITH CARBON FIBER 1310
SYNTHESIS OF COMPOSITES MEMBRANES BASED ON SPEEK/SGO FOR APPLICATION IN PEMFC 1311
SYNTHESIS OF KRAFT LIGNIN-IRON NANOPARTICLES AND ITS APPLICATION ON POLYSULPHONE MEMBRANES FOR BIOGAS PURIFICATION 1312
SYNTHESIS OF POLYURETHANES FROM THERMALLY DEGRADED VEGETABLE OIL POLIOS DOPED WITH LIGNIN FROM MALTE BASCASSE 1313
TANNIN COMPATIBILIZING ACTION IN BAMBOO FIBER REINFORCED GREEN LOW DENSITY POLYETHYLENE COMPOSITES 1314
TENSILE PROPERTIES OF RECYCLED ABS/RECYCLED CARBON FIBER FABRIC/JUTE FABRIC COMPOSITES 1315
THE EFFECT OF CONDUCTIVE MIXTURES OF EVA/PP/CNT ON ELECTROMAGNETIC PROPERTIES 1316
THE INFLUENCE OF MAGHEMITE ON CALCIUM ALGINATE BASED BIOHYDROGEL FORMATION 1317
THERMO-OXIDATIVE DEGRADATION ANALYSIS OF A POLYMER BLEND COMPOSED OF HDPE, EVOH AND PA-G-MA APPLIED IN THE AUTOMOTIVE 1322
THERORICAL PREDICTION OF H-BN AND SI_3N_4 NANOPARTICLES FINAL LOCALIZATION IN PP/EOC POLYMER BLEND NANOCOMPOSITES AND ITS IMPACT IN THERMAL CONDUCTIVITY 1323
USE OF CELLULOSE AND ALGINATE BEADS WITH MAGNETITE NANOPARTICLES FOR ADSORPTION OF CADMIUM IONS 1324
PROCESSING AND MATERIALS DESIGN 1325
ADDITIVE MANUFACTURING OF BIOACTIVE COMPOSITES 1326
NEW TOOLS FOR PROCESSING BIOBASED MATERIALS 1327
EXPLORING MECHANICAL PROPERTIES OF 3D PRINTING FILAMENTS : A COMPREHENSIVE STUDY OF BRAZILIAN MARKET PRODUCTS 1328
STUDY OF 3D PRINTED BILAYERD PLA HONEYCOMB COMPONENTS FOR MICROWAVE ABSORBING APPLICATIONS 1333
THE USE OF NATURAL CLAY AS A FILLER IN POLYPROPYLENE COMPOSITES FOR 3D PRINTING PURPOSES 1338
INFLUENCE OF PRINT ORIENTATION ON THE MECHANICAL PROPERTIES OF 3D-PRINTED PLA AND PETG MATERIALS 1343
INJECTION OVERMOLDED POLYMER-METAL HYBRID STRUCTURES 1344
POLYPROPYLENE MEMBRANE COATED WITH POLY (1-VINYLPYRROLIDONE-CO-VINYL-ACETATE) ELECTROSPUN FOR RESPIRATORY FACE MASKS 1345
A NEW COATING METHOD FOR PRODUCING CONDUCTIVE POLYMER COMPOSITES FILLED WITH NANO-EXPANDED GRAPHITE 1346
CHEMICAL AND MECHANICAL EVALUATION OF COMPOSITE FILAMENTS FOR 3D PRINTING 1351
COMPARATIVE ANALYSIS OF ROTOMOLDING AND INJECTION PROCESSES FOR THE MANUFACTURE OF HDPE PRODUCTS 1356
DEPOSITION OF STAINLESS-STEEL FILMS ON EPOXY FIBERGLASS REINFORCED COMPOSITE BY MAGNETRON SPUTTERING 1361
DEVELOPMENT AND IMPROVEMENT OF THE QUALITY OF PULTRUDED COMPONENTS AND INSPECTION REQUIREMENTS 1366

EFFECT OF FILLING PERCENTAGE ON THE TENSILE STRENGTH OF PARTS PRINTED BY FDM 1371
EFFECT OF ULTRA HIGH MOLAR MASS POLYETHYLENE (UHMWPE) ON HIGH DENSITY POLYETHYLENE (HDPE) PROCESS PARAMETERS 1376
EFFECTS OF 3D FDM PRINTING PARAMETERS ON MECHANICAL PROPERTIES OF POLY(LACTIC ACID) FOR UPPER LIMB ORTHOSES 1380
EVALUATION OF MECHANICAL PROPERTIES OBTAINED BY ADDITIVE MANUFACTURING CORRELATED WITH INJECTION MOLDING 1385
EVALUATION OF THE FEASIBILITY OF RECONDITIONING ABS SAMPLES MANUFACTURED BY 3D PRINTING 1389
INJECTION OVERMOLDED POLYMER-WOOD HYBRID STRUCTURE 1394
POROUS DEVICES FOR WATER DECONTAMINATION MANUFACTURED BY 3D PRINTING AND RICE HUSK SILICA 1399
STUDIES ON PLA STRUCTURES USING 3D PRINTING FOR RADAR ABSORBING PROPERTIES 1403
THE INFLUENCE OF PRESSURE IN ELECTRICAL RESISTANCE WELDING OF CARBON FIBER/POLY(ARYL ETHER KETONE) THERMOPLASTIC COMPOSITE 1408
3D-PRINTED ELECTRODES: THE CASE OF IMMUNOSENSOR FOR THE EARLY DIAGNOSIS OF PARKINSON'S DISEASE 1413
ASSESSMENT OF SHAPE MEMORY PROPERTIES IN COMPOSITE 4D PRINTING FILAMENTS OF PLA/TPU 1414
CORRELATION BETWEEN UV-CURING INKJET ADHESION AND AIR PLASMA TREATMENT IN POLYURETHANE COATING 1415
DEGRADATION UNDER PROCESSING OF A PLA/EGGSHELL 1416
DEVELOPMENT OF BIODEGRADABLE COMPOSITES FOR ADDITIVE MANUFACTURING USING POLY(BUTYLENE SUCCINATE) AND COCOA RESIDUES 1417
ELECTROSTATIC CHARGED FUNCTIONAL 3D PRINTED POLYMERS 1418
MELT MIXING PROCESS PARAMETER ANALYSIS OF PVDF/EVA FILLED WITH GNP TO INSURE BEST PROPERTIES 1419
NIOBIUM OXIDE (NB2O5) AS A FILLER FOR PLA FILAMENTS: 3D PRINTING IN BIOMEDICAL APPLICATIONS 1420
SUSTAINABLE DEVELOPMENT OF PLA/COFFEE GROUNDS FILAMENTS AT DIFFERENT CONTENTS: EVALUATION OF MECHANICAL STRENGTH 1421
SUSTAINABLE GRAPHENE OXIDE-CHITOSAN FILTER ELEMENTS 1422
RUBBER AND ELASTOMERS 1423
USE OF ELASTOMERS IN THE MANUFACTURE OF MECHANICAL SENSORS AND ACTUATORS : FLEXIBLE ELECTRODES AND BEYOND 1424
EFFECT OF THE USE OF RICE HUSK ASH (RHA) AS A NON-CONVENTIONAL FILLER IN NITRILE RUBBER (NBR) COMPOSITIONS 1425
STUDY OF THE DEGRADATION BY HYDROLYSIS OF POLYMERS USED AS DAMPING PARTS 1430
EVALUATION OF THERMOMECHANICAL AND WEAR PROPERTIES OF RUBBER PADS USED IN HEAVY MILITAR VEHICLES 1435
NATURAL RUBBER NANOCOMPOSITES FOR SENSING APPLICATIONS 1436
PAYNE EFFECT IN NR COMPOUNDS WITH SUSTAINABLE FILLERS USING DYNAMIC MECHANICAL CHARACTERIZATION 1437
EFFECT OF PEPTIZER ON NATURAL RUBBER AND CHLOROBUTYL RUBBER 1438
EFFECT OF SOYBEAN POLYOL CONTENT ON PHASE SEPARATION OF THERMOPLASTIC POLYURETHANE OBTAINED BY REACTIVE EXTRUSION 1443
ELASTOMERS AND CHAOS: AN UNCONVENTIONAL PERSPECTIVE ON ELECTROMECHANICAL COUPLING AND ITS RELATIONSHIP WITH FAILURE FORECASTING 1447

EVALUATION OF THE INTERACTION BETWEEN BIOCHAR AND ELASTOMERS OF DIFFERENT POLARITIES FOR APPLICATION OF BIOCHAR AS REINFORCEMENT FILLER 1450
EVALUATION OF THE MECHANICAL PROPERTIES AND ADHESIVE STRENGTH OF POLYCHLOROPRENE-BASED ADHESIVES 1455
MAGNESIUM OXIDE AS ACTIVATOR FOR NITRILE RUBBER COMPOUNDS: VULCANIZATION KINETICS AND CROSS-LINK DENSITY 1460
RHEOMETRIC, RHEOLOGICAL AND MECHANICAL PROPERTIES OF ELASTOMERIC COMPOUNDS CONTAINING SBR AND GRAPHENE NANOPLATELETS 1465
STUDY OF THERMO-OXIDATIVE AGING OF FLUORINATEDGASKETS (FKM) USED IN PLATE HEAT EXCHANGERS 1469
THERMAL BEHAVIOR OF NBR VULCANITES ACTIVATED WITH PLANT-EXTRACT-DERIVED MAGNESIUM OXIDE 1474
VULCANIZATION AND MECHANICAL PROPERTIES OF NR/CIIR BLENDS 1479
A STEP TOWARDS UNDERSTANDING THE INTERACTION BETWEEN RUBBER CARBOXYL GROUPS AND LIGNIN THROUGH ATR-FTIR AND DMA 1484
CHARACTERIZATION OF NATURAL RUBBER COMPOUNDS WITH PRECIPITATED RICE HUSK SILICA 1485
DEVELOPMENT OF MATERIAL BASED ON NATURAL RUBBER LATEX FOR BIOMEDICAL APPLICATIONS 1486
EFFECT OF ACCELERATED AGEING ON THE PHYSICAL AND MECHANICAL PROPERTIES OF THE RUBBER COVER COMPOUND OF A CONVEYOR BELT 1487
EFFECT OF MIXTURE OF ACCELERATORS AND ADDITION SEQUENCE OF ADDITIVES ON THE PROPERTIES OF NATURAL RUBBER (NR) AND STYRENE-BUTADIENE COPOLYMER (SBR) ELASTOMERIC MATRIX 1488
EVALUATION OF ANTIOXIDANT AND ANTIOZONANT PROTECTIVE AGENTS ON THE MECHANICAL PROPERTIES OF EPDM 1489
EVALUATION OF PHYSICAL-MECHANICAL PROPERTIES OF ELASTOMERIC MIXTURES 1490
EXAMINING THE DISPERSION OF ACAI RESIDUE AS A FILLER IN NATURAL RUBBER MATRIX USING RHEOMETRY, SEM-EDX, AND TENSILE STRENGTH IN THE PRODUCTION OF ECO-FRIENDLY BIOCOMPOSITE 1491
INFLUENCE OF ACCELERATED AGING IN WEATHEROMETER CHAMBER ON THE ADHESION OF A FABRIC-REINFORCED CONVEYOR BELT 1492
INFLUENCE OF PROCESSING ON THE DISPERSION OF CARBON NANOTUBES IN RUBBER COMPOSITES 1493
MORPHOLOGICAL AND MECHANICAL PROPERTIES OF HYBRID EPDM/GRAPHENE NANOCOMPOSITES 1494
PREDICTION OF CURE CHARACTERISTICS OF RUBBER COMPOUNDS WITH RECOVERED CARBON BLACK USING ARTIFICIAL NEURAL NETWORKS 1499
PRODUCTION OF COMPOSITES BASED ON NATURAL RUBBER/SYNTHETIC RUBBER: RHEOMETRICAL AND MECHANICAL PROPERTIES 1500
PROPERTIES OF CONVEYOR BELT RUBBER COVERS USED IN MINING 1501
STEEL CORD CONVEYOR BELT ADHESION AFTER ACCELERATED AGING 1502
STUDY OF REINFORCMENT PROPERTIES OF DRACAENA TRIFASCIATA FIBERS IN NATURAL RUBBER COMPOSITES 1503
THE EFFECT OF LIGNIN ON SELF-HEALING AND SHAPE MEMORY OF CARBOXYLATED NITRILE RUBBER WITH DIFFERENT CARBOXYL GROUP CONTENT 1504
RECYCLING AND ENVIRONMENTAL ISSUES ASSOCIATED WITH POLYMERS 1505
AN OVERVIEW OF THE GAPS IN MICROPLASTIC RESEARCH THAT POLYMER SCIENCE CAN HELP TO FILL 1506
PCR(PP AND PE) SOURCES CHARACTERISTICS AVAILABLE FOR PRODUCTS AND APLICATIONS DEVELOPMENTS: A CONCEPT CHALLENGE 1507
RECYCLING OF POLYMERIC WASTE AIMING EDUCATION FOR SUSTAINABLE DEVELOPMENT 1508
STRATEGIES, TECHNOLOGIES AND MATERIALS FOR REDUCING THE ENVIRONMENTAL IMPACT OF OCEAN PLASTIC WASTE 1513

WHEN NANOCELLULOSE MEETS MICROORGANISMS: TO KILL OR NOT TO KILL?	1515
ASPECTS OF HIGLY MICROPLASTIC CONTAMINATION IN THE ATLANTIC FOREST ESTUARY	1516
DEVELOPMENT OF POLYLACTIC ACID MEMBRANE BY PHASE INVERSION ROUTE WITH HIGH POROSITY AND HYDROPHOBICITY	1520
EVALUATION OF THE BACTERIAL CELLULOSE DEGRADATION OF MEMBRANES IN NATURAL ATMOSPHERE OF THE SERTÃO REGION	1525
MECHANICAL BEHAVIOR OF CASSAVA STARCH BIOFILMS WITH WINE INDUSTRY BY-PRODUCTS PARTICLES.	1530
POROUS CHITOSAN BIOPOLYMER MEMBRANES BY ACETONE ADDITION AS A TUNABLE NON-SOLVENT COMPONENT	1535
"BEYOND SYNTHESIS: HOW ECOTOXICOLOGY CAN HELP DEVELOP SUSTAINABLE POLYMERIC MATERIALS"	1540
REGENERATED CELLULOSE FILAMENTS OBTAINED FROM TEXTILE COTTON WASTE RECYCLING USING IONIC LIQUID	1544
SYNTHESIS OF NEW SUSTAINABLE POLYESTER-TYPE HYDROGELS FROM CHEMICAL RECYCLED POLY(ETHYLENE TEREPHTHALATE) APPLIED IN THE REMOVAL OF INDIGO CARMINE DYE.	1549
TGA MONITORING OF THE GLYCOLYSIS OF HIGH TENACITY POLYESTER FIBER FROM MOORING LINES	1554
UV BLOCKING PROPERTIES OF POLYCAPROLACTONE-TRIOL-BASED POLYURETHANE FILMS INCORPORATED WITH CITRUS PEEL EXTRACTS	1559
CHEMICAL RECYCLING OF POLY(3-HYDROXYBUTYRATE-CO-3-HYDROXYVALERATE) (PHBV) SOLUTION BLOW SPUN FIBERS THROUGH HYDROLYSIS	1564
COMPARISON OF MANUAL PROCESSES WITH NEW TECHNOLOGIES FOR SEPARATING AND REUSING PLASTICS FROM MUNICIPAL SOLID WASTE	1565
DEVELOPMENT OF A METHODOLOGY FOR EVALUATING BIODEGRADATION OF FLEXOGRAPHIC INKS	1566
DOES THE DEGRADATION LEVEL INTRODUCE BIASES IN MICROPLASTIC ANALYSIS? (SPOILER: YES…)	1567
EVALUATION OF PLASTIC DEGRADATION UNDER SEMI-CONTROLLED ENVIRONMENTAL CONDITIONS	1568
GLYCOLYSIS OF PET BY MICROWAVE-ASSISTED HYDROTHERMAL METHOD USING A CLOSED SYSTEM	1569
INCORPORATION OF BIO-BASED MATERIALS IN COMERCIAL POLYMERS: STUDY OF POLY(BUTYLENE-ADIPATE-CO-TEREPHTHALATE)/WHEY PROTEIN ISOLATE BLENDS	1570
POLYAMIDE 6 TEXTILE RECYCLING: AN EVALUATION OF THE USE OF CARBODIIMIDE	1571
POLYSACCHARIDES AND ECO-FRIENDLY PACKAGING: TRENDS AND INNOVATIONS	1572
RECYCLING OF FACE SHIELD HEADBANDS BASED ON PP/SGF COMPOSITE: INFLUENCE OF REPROCESSING CYCLES ON RHEOLOGICAL AND MECHANICAL BEHAVIOR	1573
SUPERCRITICAL CO_2 FOAMING AND DEGRADATION BEHAVIOR OF PBAT/PLA BLENDS FOR ENHANCING LIGHTWEIGHT BIOPOLYMER	1574
THE ROLE OF CARBODIIMIDE IN BIOPOLYMER RECYCLING AND ITS EFFECT ON FOOD SAFETY	1575
UPCYCLING BANANA PEELS: TRANSFORMING WASTE INTO BIOPLASTIC FILMS WITH SPECIAL PROPERTIES	1576
ADSORPTION STUDY OF PHENATHRENE FROM AQUEOUS SOLUTION BY POLYMERIC RESINS CROSSLINKED WITH DIVINYLBENZENE	1577
A NEW BIOPOLYURETHANE COATING BASED ON BIO OIL	1582
ANTIOXIDANT ACTIVITY AND THERMAL DEGRADATION OF BIOFILMS INCORPORATED WITH GRAPE RESIDUES	1586
BARRIER AND MECHANICAL PROPERTIES OF PACKAGING FILMS FOR MEAT PRODUCTS WITH MALEIC ANHYDRIDE-BASED COMPATIBILIZER	1591
BIOCHAR DERIVED FROM BRAZILIAN-PINE FRUIT SHELL AND AGAROSE HYDROGEL COMPOSITES FOR ENVIRONMENTAL ANALYSIS	1597
BIODEGRADABLE ACTIVE MATERIALS BASED ON STARCH AND BLACKBERRY DRY RESIDUE	1598

CELLULOSE HYDROGELS WITH LIGNIN BIOCHAR FOR REMOVAL OF HEAVY METAL IONS 1603
COMPOSITE HYDROGEL BASED ON ALGINATE-G-POLY(ACRYLAMIDE)/CARBON NANOTUBES FOR SOLID PHASE EXTRACTION OF METALS FROM CORN CEREAL SAMPLES 1608
DEVELOPMENT AND CHARACTERIZATION OF STARCH-BASED COMPOSITE FILMS CONTAINING BREWERS' SPENT GRAIN EXTRACT 1613
DEVELOPMENT OF BIODEGRADABLE FILM OF THERMOPLASTIC STARCH AND YERBA MATE WASTE 1618
ECO-AUDIT ANALYSIS AND IMPACT OF DIFFERENT END-OF-LIFE FOR PLASTIC BOTTLES 1623
EFFLUENT CHEMICAL INDUSTRY WASTEWATER TREATMENT BY MEMBRANE DISTILLATION USING COMMERCIAL MEMBRANES 1628
EVALUATION OF COMPOSTING AND VERMICOMPOSTING IN THE DEGRADATION OF HDPE FILMS 1633
EVALUATION OF COMPOSTING AND VERMICOMPOSTING IN THE DEGRADATION OF PLA/TPS BLEND FILMS 1639
EVALUATION OF USING KRAFT LIGNIN-BASED BIOCHAR IN THE ADSORPTION OF METHYLENE BLUE DYE 1644
EXTRACTION, PURIFICATION AND APPLICATION OF BREWER’S SPENT GRAIN IN STARCH-BASED COMPOSITES 1649
GREEN SYNTHESIS OF TITANIUM DIOXIDE NANOPARTICLES FOR APPLICATION IN PHOTOVOLTAIC DEVICES 1654
INFLUENCE OF DRYING CONDITIONS ON THE MELT FLOW INDEX OF POLYBUTYLENE SUCCINATE (PBS) AFTER LONG TIME STORAGE 1658
INFLUENCE OF FEEDSTOCK COMPOSITION ON CHEMICAL RECYCLING OF PLASTIC WASTES VIA PYROLYSIS 1662
LIPASE NS-40116 INCORPORATED IN BACTERIAL CELLULOSE MODIFIED WITH ZEIN 1667
MECHANICAL PROPERTIES OF CELLULOSE FILAMENTS REGENERATED FROM COLORED COTTON WASTE USING IONIC LIQUID/COSOLVENTS SYSTEM 1672
METAL IONS REMOVAL EFFICIENCY USING GREEN CELLULOSE HYDROGEL ADSORBENT 1677
OIL SPILL RECOVERY FROM SEAWATER USING POST-CONSUMER POLYURETHANE FOAM HYDROPHOBIZED WITH PALMITIC ACID: A KINETIC STUDY 1681
POST-CONSUMER PET/HDPE INJECTION AND EXTRUSION REPROCESSING 1686
REDUCTION, RECYCLING, AND REUSE OF POLYURETHANE MATTRESSES FOR RECOVERING OILS SPILLED IN SEAWATER: KINETICS AND SURFACE PHENOMENA STUDY 1691
REMOVAL OF METHYLENE BLUE DYE FROM AQUEOUS SOLUTION USING POLYURETHANE FOAM SYNTHESIZED WITH ORANGE PEEL AS ADSORBENT 1696
REMOVAL OF POTENTIALLY TOXIC METALS BY HYDROGELS CONTAINING MICROCELLULOSE WASTE FROM EUCALYPTUS SAWDUST 1701
STUDY OF BIODEGRADATION OF A POLYELECTROLYTE COMPLEX: SPECTROSCOPIC AND MORPHOLOGICAL ASPECTS 1706
SYTHESIS AND PROPERTIES OF POLYURETHANE COATINGS BASED ON BIOPOLYOLS: LIQUEFIED MACAÚBA ENDOCARP MIXED WITH CNSL 1711
THERMAL DECOMPOSITION OF DIFFERENT KRAFT LIGNINS THROUGH THERMOGRAVIMETRIC ANALYSIS 1716
THERMAL DEGRADATION AND BIODEGRADABILITY OF POTATO STARCH FILMS WITH YERBA MATE EXTRACT AND MALIC ACID 1721
THE ROLE OF ISOCYANATE IN THE PROPERTIES FOR RECYCLABLE POLYURETHANE FOAMS 1726
USE OF ACRYLONITRILE BUTADIENE STYRENE (ABS) WASTE FROM ELECTRICAL AND ELECTRONIC EQUIPMENT (WEEE) IN OBTAINING FILAMENTS FOR 3D PRINTING 1731
ABIOTIC DEGRADATION OF OXO-DEGRADABLE BAGS: POTENTIAL SOURCES OF MICROPLASTICS 1736
ACID HYDROLYSIS OF WASTE PET (POLYETHYLENE TEREPHTHALATE) AND PA (POLYAMIDE) MIX 1737
ACTION OF THE ANIONIC SURFACTANT SSO ON THE WATER VAPOR PERMEABILITY OF FILMS CONSISTING OF CASSAVA STARCH 1738

ADDITION OF TITANIUM DIOXIDE NANOPARTICLES IN ECOVIO® BIODEGRADABLE POLYMER FOR UV RADIATION BARRIER 1739
ADSORPTION OF CHLORPYRIFOS ON PHOTODEGRADED AND NON-PHOTODEGRADED MICROPLASTICS 1740
ADSORPTION OF THE ORGANOPHOSPHATE PESTICIDE ON PHOTODEGRADED POLYETHYLENE MICROPLASTICS 1741
A FACILE WAY TO RECYCLE EPOXY/CF RESIN COMPOSITES 1742
APPLICATION OF BACTERIAL CELLULOSE IN THE PRODUCTION OF A PAPER PACKAGING 1743
A PRELIMINARY STUDY OF ELECTROSPUN POLY (LACTIC ACID) (PLA)/ POLY (BUTYLENE ADIPATE-CO-TEREPHTHALATE) (PBAT) FIBERS FOR AIR FILTERS APPLICATION 1744
BACTERIAL CELLULOSE PRODUCTION USING ERYTHRINA MULUNGU TEA AS A GROWTH MEDIUM 1745
BIODEGRADABLE FILMS BASED ON CASSAVA STARCH AND RICE HUSK WITH IMPROVED PROPERTIES 1746
BIODEGRADABLE POLYMER MATERIAL FROM MACROALGAE 1747
BIODEGRADATION OF MODIFIED POLY(ETHYLENE TEREPHTHALATE) FILMS UNDER ANAEROBIC CONDITIONS 1748
BIOPOLYMER-BASED TIO_2 FOR ENVIRONMENTAL REMEDIATION PROCESSES 1749
CARBOXYMETHYL CELLULOSE/MORINGA OLEIFERA SEED HUSK ADSORBENTS FOR THE TREATMENT OF UNDERGRADUATE LABORATORY WASTE 1750
CASSAVA GUM HYDROGEL FOR ADSORPTION OF ORGANIC DYE 1751
CHARACTERIZATION OF POST-INDUSTRIAL PET WASTE FOR USE IN THE TEXTILE INDUSTRY 1752
CHARACTERIZATION OF THE FRACTION OF SOLID LIGNOCELLULOSIC RESIDUES OBTAINED AFTER ENZYMATIC HYDROLYSIS AND EVALUATION OF ITS POTENTIAL APPLICATIONS IN POLYMERIC MATERIALS 1753
COMPOSITION ANALYSIS, RECYCLING AND REDESIGN PROPOSAL OF DISPOSABLE FACE MASKS 1754
DEVELOPMENT AND CHARACTERIZATION OF BACTERIAL CELLULOSE REINFORCED WITH COCONUT FIBER 1755
DEVELOPMENT OF A STARCH-BASED POLYMER BLENDED WITH PET RECYCLING BY-PRODUCTS FOR THE SLOW RELEASE OF FERTILIZER 1756
DEVELOPMENT OF CHITOSAN HYDROGELS WITH CARBON NANOTUBES FOR ADSORPTION OF COPPER IONS FROM INDUSTRIAL EFFLUENTS 1757
DEVELOPMENT OF SUSTAINABLE PRODUCTS WITH RECYCLED POLYMER COMPOSITES AND SILICA PARTICLES FROM FOUNDRY SAND 1758
EFFECT OF CELLULOSE ACETATE ADDITION ON THE BARRIER PROPERTIES OF BROKEN BEAN FLOUR FILMS 1759
EFFECT OF CORN ZEIN ON THE PHYSICAL PROPERTIES OF BEAN FLOUR FILMS 1760
ENHANCING SUSTAINABLE PACKAGING POTENCIAL: INVESTIGATION OF HIGH CALCIUM CARBONATE CONTENT VIA INJECTION MOLDING AS AN ALTERNATIVE TO FOSSIL-BASED PLASTICS 1761
ENZYMATIC SYNTHESIS OF ALLYL-(METH)ACRYLATE MONOMERS FOR BIODEGRADABLE THIOL-ENE BASED POLYMERS 1766
EVALUATION OF ENVIRONMENTAL IMPACTS AND PRODUCTION PROCESSES OF CHITOSAN DERIVED FROM SHRIMP EXOSKELETONS 1767
EVALUATION OF THE INFLUENCE OF COLORATION ON THE YIELD OF PET DEPOLYMERIZATION BY HYDROLYSIS 1768
EVALUATION OF THERMAL BEHAVIOR IN POLYMERIC BLENDS OF EXPANDED POLYSTYRENE (EPS) AND WASTE TIRE RUBBER (WTR) 1769
FULL FACTORIAL EXPERIMENTAL DESIGN ON EXTRACTION PROCESS OF TAMARIND SEED GUM (*TAMARINDUS INDICA L.*) 1770
INFLUENCE OF DYES AND ADDITIVES USED IN POLYETHYLENE TEREPHTHALATE (PET) BOTTLE CAPS ON CHEMICAL RECYCLING VIA PYROLYSIS. 1771

INTEGRATION OF TEXTILE WASTE IN THE PRODUCTION CHAIN: STUDY OF EPOXY MATRIX COMPOSITES	1772
LOW COST HETEROGENEOUS CATALYST FOR BIODIESEL PRODUCTION	1773
IN SILICO ANALYSIS POLYURETHANASE FROM *SERRATIA LIQUEFACIENS* WITH DIFFERENT POLYURETHANE MONOMERS AND TETRAMERS	1774
MECHANICAL PROPERTIES OF LDPE AND LDPE/PP BLENDS AFTER STRUCTURAL CHANGE BY HIGH SHEAR RATE	1775
MICROSPHERES OF NATURAL POLYMER PROMOTE LESS IMPACT ON THE ENVIRONMENT	1776
MODIFICATION OF WHEY PROTEIN ISOLATE WITH SURFACTANT AND PLASTICIZER	1777
PLASTICIZATION OF CITRUS PULP: INFLUENCE OF WASHING METHODOLOGY AND GLYCEROL CONCENTRATION	1778
PLASTIC PYROLYSIS VAPORIZATION	1779
POLYMERS COMBINED WITH GEOLOGICAL MATERIAL AS A HUMAN LEGACY IN EARTH'S RECORD.	1780
POLYURETHANES BIODEGRADATION BY *STAPHYLOCOCCUS WARNERI* ISOLATED FROM THE GUT OF LARVAE OF *GALLERIA MELLONELLA*	1781
PREPARATION OF NEW SUSTAINABLE HYDROGELS FROMCHEMICAL RECYCLED POLY(ETHYLENE TEREPHTHALATE) ANDAPPLICATION ON THE REMOVAL OF CRYSTAL VIOLET DYE	1782
PREPARATION OF SODIUM ALGINATE HYDROGELS FOR ADSORPTION OF COPPER IONS FROM INDUSTRIAL WASTEWATER	1783
PRODUCTION AND CHARACTERIZATION OF BIODEGRADABLE ACTIVE FILMS FOR COSMETIC APPLICATIONS	1784
PRODUCTION AND PHYSICAL-CHEMICAL ANALYSIS OF WOOD, PET, AND HDPE ECO-COMPOSITES FOR COATINGS	1785
PRODUCTION AND REUSE OF KOMBUCHA WASTE FOR CELLULOSE PRODUCTION FROM DIFFERENT PLANTS EXTRACT	1786
RECYCLING MDF WASTE AS A NEW COMPOSITE MATERIAL AS AN ALTERNATIVE FOR INDUSTRY	1787
RECYCLING OF AEROSPACE COMPOSITES: NEW COMPOSITES OF PROTECTIVE POLYETHYLENE FILM REINFORCED WITH CF/PAEK WASTE	1788
REMEDIATION OF HEAVY METAL CONTAMINATED WATER ASSOCIATED WITH THE COLLAPSE OF MINING DAMS IN MINAS GERAIS BY USING A NANOCOMPOSITE-BASED POLYURETHANE FOAM	1789
REMEDIATION POTENTIAL OF CONTAMINED SOILS BY LUBE OIL USING SODIUM POLYACRILATE	1790
SEPARATION AND IDENTIFICATION OF POLYMERS BY SELECTIVE DISSOLUTION AND PRECIPITATION TECHNIQUE AND FTIR FOR MULTILAYER PACKAGING RECYCLING	1791
STUDY OF POLYURETHANE FOAMS BASED ON WASTE COOKING OIL USING PYROLISIS CARBON AS FILLER	1792
STUDY OF THE ADSORPTION OF CHROME AND DYES BY POLYMERIC MATRIXES	1793
STUDY OF THE BIODEGRADATION OF CASSAVA STARCH PACKAGING WITH THE ADDITION OF TOMATO PEELS (LYCOPENE): A SUSTAINABLE APPROACH FOR REDUCING ENVIRONMENTAL IMPACT	1794
STUDY OF THE CONTAMINATION OF SAMPLES OBTAINED VIA PYROLYSIS OF VIRGIN POLYMERS AND PLASTIC WASTE RICH IN POLYOLEFINS	1795
STUDY OF THE PROPERTIES OF A COMPOSITE OFEXPANDED POLYSTYRENE WITH MDF	1796
SYNTHESIS AND CHARACTERIZATION OF NANOCELLULOSE FROM INDUSTRIAL LAUNDRY	1797
SYNTHESIS OF A RENEWABLE MONOMER DERIVED FROM 10-UNDECENOIC ACID	1798
THE INFLUENCE OF SALT (NACL) ON THE PYROLYSIS OF POLYPROPYLENE AND MARINE LITTER (REAL WASTE)	1799
THE REFLUX INFLUENCE ON CHEMICAL RECYCLING OF VIRGIN AND WASTE POLYETHELENE PYROLYSIS	1800
THE USE OF NATURAL POLYMER AS STRATEGIES TO IMPROVE THE PROPERTIES OF ZNO	1801

USE OF LIGNIN-BASED HYDROGEL EXTRACTED FROM THE PEEL OF TINGUI (*MAGONIA PUBESCENS A. ST. - HIL.*) FOR DYE ADSORPTION 1802
UTILIZING POLYURETHANE WASTE IN THE PRODUCTION OF RIGID FOAMS:CHARACTERIZATION AND PROPERTIES 1803
XEROGEL OF LIGNOCELLULOSE EXTRACTED FROM COFFEE HUSKS AND CALCIUM PEROXIDE FOR THE CONTROLLED RELEASE OF O_2 1804
BIOMEDICAL APPLICATIONS OF POLYMERS 1805
BIOMATERIALS & NANOTECHNOLOGY: THE CHALLENGE IN MODIFYING NANOPARTICLE SURFACES 1806
NATURAL POLYMERS: DEVELOPMENT OF ADVANCED MATERIALS AND DELIVERY SYSTEMS 1807
RECENTLY DEVELOPED POLYMERIC BIOMATERIALS AT GMPC/UEM AND LIMAV/UFPI 1808
DEVELOPMENT OF CHITOSAN-BASED NANOPARTICLES FOR DOUBLE ENCAPSULATION OF 5-FLUOROURACIL AND METHOTREXATE 1809
GELATIN-ALGINATE-BASED FILMS CONTAINING 1,4-ANHYDROUS-4-SELENE-D-THALITOL (SETAL) AS AN APPROACH FOR THE TREATMENT OF ATOPIC-DERMATITIS 1814
IN VITRO RELEASE AND IN VIVO PHARMACOKINETICS OF PRAZIQUANTEL LOADED IN PMMA-CO-DEAEMA SMART MICROPARTICLES 1819
3D PRINTING OF POLY(Ɛ-CAPROLACTONE) METHACRYLATED/ SILANIZED-NANO-HYDROXYAPATITE RESIN BASED: SYNERGY IN MORPHOLOGY AND FUNCTIONALIZATION 1824
ALGINATE/HYDROXYAPATITE FILMS WITH ANTIMICROBIAL PROPERTY AS A WOUND DRESSING 1825
COMPOSITE MEMBRANES OF POLY (GLYCEROL SEBACATE) WITH CALCIUM PHOSPHATES FOR BONE TISSUE REGENERATION 1826
DEVELOPMENT OF COPOLYMER FILAMENT FOR 3D PRINTING BASED ON POLY(L-LACTIC ACID-CO-TRIMETHYLENE CARBONATE) 1827
EXTRUSION OF POLYCAPROLACTONE AND F18 BIOACTIVE FILLER COMPOSITES 1828
INFLUENCE OF DEGRADATION OF PLA/ZNO BIOCOMPOSITES ON SCAFFOLD CELL VIABILITY 1829
MECHANICAL CHARACTERIZATION OF HYDROGELS ENVISIONING ITS APPLICATION IN NEURAL NICHE 1830
SYNTHESIS, CHARACTERIZATION AND ANTIMICROBIAL PROPERTIES OF CHITOSAN-SILVER NANOPARTICLES FOR COATING MEDICAL DEVICES 1831
SYNTHESIS OF POLYMERIC RESVERATROL PRODRUGS 1832
ANTIMICROBIAL ACTIVITY OF SILVER NANOPARTICLES PRODUCED BY GREEN SYNTHESIS FROM ENDOPHYTIC FUNGI PENICILLIUM SPP 1833
CHITOSAN/GELATIN 3D PRINTED ANTIMICROBIAL HYDROGELS 1838
COATING SCAFFOLDS "MG FOAMS" SURFACES WITH COLLAGEN SOLUTIONS TO EVALUATE CORROSION VELOCITY IN A SIMULATED ENVIRONMENT OF PHYSIOLOGICAL CONDITIONS 1843
CONTROLLED RELEASE AND CELL VIABILITY OF MEGLUMINE ANTIMONIATE INCORPORATED INTO POLYMERIC MATRICES OF PEG 4000 1849
DESIGN AND PHARMACEUTICS ANALYSIS OF IN SITU FILM-FORMING SOLUTIONS CONTAINING POMEGRANATE PEEL EXTRACT FOR MASTITIS PROPHYLAXIS 1854
DEVELOPMENT OF BACTERIAL CELLULOSE INCORPORATED WITH ESSENTIAL OILS FOR WOUND TREATMENT 1859
FABRICATION AND CHARACTERIZATION OF VANILLIN CROSSLINKED CHITOSAN FILMS WITH MODULATED MECHANICAL PROPERTIES AND SURFACE TOPOGRAPHY FOR CELLULAR ATTACHMENT 1864
FLUORESCENCE INTERACTION STUDIES BETWEEN CURCUMIN AND PIPERINE: TARGETING INCORPORATION INTO POLYMERIC NANOCARRIERS 1869
HUMAN IMMUNOGLOBULIN G ADSORPTION WITH DIFFERENT RATES OF STIRRING ONTO FIBROIN MICROPARTICLES 1874

IMMOBILIZATION OF LACCASES ON STY-DVB COPOLYMERS CONTAINING DIAZONIUM GROUPS	1879
PHYSICAL-CHEMICAL ANALYSIS OF PVA-BASED POLYMERIC FILMS BY ADDITION OF POMEGRANATE EXTRACT	1884
POLY(VINYL ALCOHOL) MEMBRANES OBTAINED BY ELECTROSPINNING CONTAINING 5-AMINOLEVULINIC ACID FOR PHOTODYNAMIC THERAPY OF SKIN CANCER	1889
PRODUCTION AND CHARACTERIZATION OF BIODEGRADABLE WOUND DRESSINGS CONTAINING ZEOLITE SILVER PARTICLES	1893
PVA/CHITOSAN FIBERS PRODUCED BY ELECTROSPINNING: STRUCTURAL, THERMAL, MORPHOLOGICAL, ANTIBACTERIAL AND CYTOTOXYC PROPERTIES	1898
ROTARY JET SPUN MEMBRANE BASED ON POLY(CAPROLACTONE),HYDROXYAPATHITE AND SILVER NANOPARTICLES	1903
WET-SPUN FILAMENTS BASED ON ALGINATE AND CHITOSAN WITH DRUG RELEASE	1907
BIOPOLYMERIC FILMS FOR CONTROLLED RELEASE OF HYDROCORTISONE: POTENTIAL DEVICES FOR MANAGING CHRONIC SKIN CONDITIONS	1912
CERIUM OXIDE NANOPARTICLE DEPOSITION ON PLA/TCP SCAFFOLDS VIA ACTIVE SCREEN PLASMA	1913
CHARACTERIZATION OF PBAT NANOFIBERS WITH ANTIMICROBIAL ESSENTIAL OIL PRODUCED BY SOLUTION BLOW SPINNING	1914
CHITOSAN/ZN^{2+}-CURCUMIN OR CU^{2+}-CURCUMIN ANTIMICROBIAL MEMBRANES FOR PHOTODYNAMIC THERAPY	1915
CONTROLLED RELEASE FROM POLY-3-HYDROXYALKANOATE MICROPARTICLES CONTAINING NANOMAGNETITE	1916
CONTROLLING THE DEGRADATION OF PLA/ZNO COMPOSITE THROUGH FILLER SURFACE MODIFICATION	1917
DEVELOPMENT AND CHARACTERIZATION OF 3D PRINTED BIOCOMPOSITES BASED ON PLA/PBAT/BIOSILICATE®	1918
DEVELOPMENT OF BIOMATERIALS REINFORCED WITH BIOMIMETIC COMPONENTS AND SCAFFOLD PRODUCTION VIA 3D PRINTING APPLIED TO BONE TISSUE ENGINEERING	1919
DEVELOPMENT OF BIOPOLYMERIC SYSTEMS FOR ENCAPSULATION OF BARBATIMÃO EXTRACT	1920
DEVELOPMENT OF CITRAL NANOEMULSIONS COATED WITH N-SUCCINYL CHITOSAN FOR THE TREATMENT OF ORAL MUCOSAL DISEASES	1921
DEVELOPMENT OF CRYOGEL SYSTEMS FOR BIOMEDICAL APPLICATIOINS	1922
DEVELOPMENT OF MEMBRANES BASED ON KAPPA-CARRAGEENAN AND MICROFIBRILLATED CELLULOSE	1923
DEVELOPMENT OF PMMA-BASED BONE CEMENT LOADED WITH QUATERNIZED POLYETHYLENEIMINE (QPEI)	1924
DEVELOPMENT OF TPS/PVA/NCC FILMS FOR THE RELEASE OF COPPER OXIDE NANOPARTICLES - POTENTIAL APPLICATION AS TRANSDERMAL DRESSINGS	1925
ENCAPSULATION OF INDOCYANINE GREEN PHOTOSENSITIZINGAGENT IN POLYGLOBALIDE NANOPARTICLES FOR COMBINED CANCER PHOTOTHERAPY	1926
ENCAPSULATION OF PHOTOPROTECTIVE COMPOUNDS INTO STARCH PARTICLES	1927
ENGINEERING HIGHLY POROUS 3D ARCHITECTURES BASED ON NANOCELLULOSE THROUGH IN VIVO BIOFABRICATION	1928
EVALUATION OF THE ANTIBACTERIAL ACTIVITY OF CHLORHEXIDINE ASSOCIATED WITH CASSAVA GUM HYDROGEL	1929
GREEN TECHNIQUES FOR MODIFYING CASSAVA STARCH TO IMPROVE FEASIBILITY IN PRINTED BONE SCAFFOLDS PRODUCTION	1930
IMPROVEMENT OF THE MECHANICAL PROPERTY AND COEFFICIENT OF FRICTION OF THE HIGH-DENSITY POLYETHYLENE/HYDROXYAPATITE NANOPARTICLE COMPOSITE (HDPE/HA) BY ADDING THE ERUCAMIDE-MONTMORILLONITE (EU/MMT) NANOCOMPOSITE	1931

STUDY OF THE CONTROLLED RELEASE OF VITAMIN B12 AND CYTOTOXICITY ASSAYS OF HYDROGELS BASED ON XANTHAN GUM 1932
TANNIN DERIVATIVES AS VENUE FOR NEW BIOMATERIALS 1933
USING BURITI (MAURITIA FLEXUOSA L.) OIL TO OBTAIN POLYURETHANES 1934
POLYMERS IN AGRICULTURE AND SPECIAL INDUSTRIAL APPLICATIONS 1935
POLYSACCHARIDE-BASED MATERIALS FOR ENHANCED EFFICIENCY FERTILIZERS: PERSPECTIVES FOR THE SUSTAINABLE DEVELOPMENT GOALS 1936
SYNTHESIS AND APPLICATIONS OF GLYCO-AMPHIPHILES 1937
BACTERIAL CELLULOSE FILMS FOR BIODEGRADABLE PACKAGING WITH ESSENTIAL OILS 1938
BIODEGRADATION OF POLYELECTROLYTE COMPLEXES IN ULTISOL CONDITIONING: PHYSICOCHEMICAL AND MICROBIOLOGICAL MONITORING 1943
COTTON FABRIC FUNCTIONALIZED WITH CHITOSAN AND NEEM SEED OIL AIMING REPELLENT TEXTILE APPLICATIONS 1948
ENCAPSULATION OF COPAIBA ESSENCIAL OIL AND JOJOBA VEGETABLE OIL IN BIOPOLYMERIC NANOPARTICLES 1953
THE EFFECT OF HUMIDIFICATION WITH SALINE SOLUTION ON IMPEDANCE MEASUREMENTS OF ELETROSPUN PVC/CNT MEMBRANES 1958
EFFECTS OF A CHITOSAN/GELATIN AND POMEGRANATE (*PUNICA GRANATUM* L.) PEEL EXTRACT COATING ON THE PHYSICOCHEMICAL AND SHELF-LIFE OF PAPAYA (*CARICA PAPAYA* L.) FRUITS 1959
FUNCTIONALIZATION OF TEXTILE SUBSTRATE WITH CONDUCTIVE POLYMER 1960
FUNCTIONAL POROUS MATERIALS FROM LIGNOCELLULOSE 1961
POLYETHERIMIDE MEMBRANES FOR SEPARATION OF SYNTHETIC EFFLUENT 1962
SYNTHESIS OF POLYANILINE ON PLASMA TREATED CARBON FIBER TEXTILE FOR SUPERCAPACITOR APPLICATIONS 1963
ANTIOXIDANT PERFORMANCE OF NATURAL ANTIOXIDANT-LOADED GELATIN FILMS PRODUCED BY SOLUTION CASTING METHODS 1964
CHITOSAN FILMS FOR THE STABILIZATION OF ENZYMES IN AQUEOUS SOLUTIONS 1969
EFFECT OF NANOCLAY ADDITION IN POLY(LACTIC ACID) (PLA)/POLY(BUTYLENE ADIPATE-CO-TEREPHTHALATE) (PBAT) BLENDS IN AGROINDUSTRY SECTOR APPLICATION 1974
EFFECT OF STORAGE CONDITIONS ON THE MECHANICAL RESISTANCE OF HIGH-DENSITY POLYETHYLENE AS GASOLINE-ETHANOL BLEND PACKAGING 1979
EFFECTS OF INTERACTIONS OF B-D-GALACTOSIDASE WITH CHITOSAN FILMS AND EVALUATION BY FACTORIAL DESIGN 1984
FTIR AND AFM CHARACTERIZATION OF ZEIN/LIGNIN NANOPARTICLES AS GEOPROPOLIS CARRIERS FOR THE TREATMENT OF AGROECOLOGICAL SEEDS 1989
PECTIN EDIBLE FILM OBTAINED FROM ORANGE PEEL: FABRICATION AND APPLICATION TO EXTEND THE SHELF LIFE OF MINIMALLY PROCESSED APPLES 1994
PERFORMANCE ASSESSMENT OF BACTERIAL CELLULOSE FILMS FROM KOMBUCHA IN CONSERVATION OF STRAWBERRIES IN NATURA 1999
SYNTHESIS AND CHARACTERIZATION OF FATTY AMIDES WITH POTENTIAL FOR BIOLUBRICANT 2004
THE INFLUENCE OF IONIZING RADIATION ON THE PHYSICAL PROPERTIES OF POLYESTER MULTIFILAMENTS 2009
ACTIVE FILMS WITH JAMBOLAN EXTRACT (SYZYGIUM CUMIN) BASED ON ALGINATE/XANTHAN: CHARACTERIZATION AND ANTIOXIDANT ACTION 2013
ALGINATE-BASED HYDROGEL FOR ENCAPSULATION OF PLANTGROWTH-PROMOTING BACTERIA 2014
ANALYSIS THE INFLUENCE OF THE DRYING METHOD ON THE BACTERIAL CELLULOSE MEMBRANES PROPERTIES 2015

A NEW METHOD FOR DETERMINATION OF GLYCEROL IN BIODIESEL USING CELLULOSE MONOLITH SORPTIVE STIR BAR 2016
ANGICO GUM HYDROGEL: INFLUENCE OF POLYSACCHARIDE PURIFICATION ON WATER ABSORPTION AND TOXICITY 2017
ANTIOXIDANT ACTIVITY OF BOVINE GELATIN FILMS ADDED OF A LIPID EXTRACT FROM OLIVE GROWING RESIDUES 2018
ANTIOXIDANT ACTIVITY OF SODIUM ALGINATE FILMS FUNCTIONALIZED WITH PURPLE ONION PEEL AND BLUE FLOUR EXTRACT 2019
APPLICATION OF PAAM/CMC-NANOCLAY NANOCOMPOSITES TO IMPROVE THE SOIL PROPERTIES 2020
BABASSU MESOCARP HYDROGEL FOR MACRONUTRIENT RELEASE 2021
BIODEGRADATION EVALUATION IN THE SOIL OF AN ENHANCED EFFICIENCY FERTILIZER COMPOSED OF POLY(VINYL ALCOHOL) AND STARCH MICROSPHERES. 2022
CHEMICALLY MODIFIED CELLULOSE NANOFIBRILS AS A MACRONUTRIENT-CARRYING VEHICLE 2023
DEVELOPMENT, CHARACTERIZATION, AND APPLICATION OF BIOFILM IN BRAZIL NUT USING PECTIN EXTRACTED FROM ORANGE ALBEDO FROM MARABÁ/PA JUICE INDUSTRIES 2024
DEVELOPMENT OF BIODEGRADABLE MICROCAPSULES CONTAINING BACILLUS AMYLOLIQUEFACIENS BS01 FOR BIOLOGICAL CONTROL 2026
DEVELOPMENT OF BIOPOLYMERIC BEADS FOR APPLICATION IN THE CONTROLLED RELEASE PROCESS OF POTASSIUM IN THE SOIL 2027
DEVELOPMENT OF CROSSLINKED BIOFILMS FOR APPLICATION IN CONTROLLED NUTRIENT RELEASE SYSTEMS 2028
DEVELOPMENT OF POROUS FIBROIN MEMBRANES AND APPLICATION AS A POTENTIAL ADSORBENT FOR REMOVAL OF ORGANIC DYES 2029
DEVELOPMENT OF STARCH/XANTHAN GUM/NANOEMULSION OF CINNAMON ESSENTIAL OIL BASED FILM FOR EDIBLE COATING 2030
EFFECT OF HYDROLYSIS ON THE QUANTIFICATION OF SULFONATED POLYACRYLAMIDE BY SEC-UV 2031
ELECTROCHEMICAL PROPERTIES OF POLYANILINE SYNTHETIZED ON PLASMA TREATED CARBON FIBER TEXTILE FOR SUPERCAPACITOR APPLICATIONS 2032
ENCAPSULATION OF THE UREA FERTILIZER IN LIGNIN NANOCAPSULES 2033
ETHYL HYDROXYETHYL CELLULOSE (EHEC) FILMS CONTAINING ALFA-TOCOPHEROL: EFFECTS ON STABILITY, RELEASE IN VITRO AND PROPERTIES OF THE FILM 2034
EVALUATION OF THE INFLUENCE OF OXYPROPYLATED CELLULOSE NANOFIBRILS ON THE MECHANICAL AND MORPHOLOGICAL PROPERTIES OF POLYURETHANE FOAM 2035
GENERATION OF 3D PRINTING FILAMENTS FOR CONTROLLED RELEASE FERTILIZER UTILIZING PLA, UREA, AND ROCK POWDER 2036
NANOCOMPOSITE HYDROGELS OF CASHEW TREE GUM WITH LAPONITE TO CONTROL WATER RELEASE 2037
PEBAX®/POLYDOPAMINE BLEND MEMBRANES WITH HIGH CO_2/N_2 SELECTIVITY. 2038
PEBAX®/ZIF-67 MIXED MATRIX MEMBRANES FOR CO_2/N_2 SEPARATION. 2039
PHOTOSTABILITY STUDY OF ANGICO GUM HYDROGEL 2040
PHYSICOCHEMICAL PERFORMANCE OF AN ECO-FRIENDLY AGRICULTURAL COMMERCIAL PRODUCT: EVALUATION OF PHEROGEN® INTERACTION ON SOY LEAVES UNDER SIMULATED ENVIRONMENTAL CONDITIONS 2041
POLYANILINE COATING ON COPPER AND ITS CORROSION PROTECTION IN ACID MEDIUM 2042
POLY(TMPTA-CO-EDMA-CO-MAA) MOLECULARLY IMPRINTED WITH N-NITROSODIMETHYLAMINE AS A MONOLITHIC SORBENT FOR DISPOSABLE PIPETTE EXTRACTION 2043
PRODUCTION OF WOOD PLASTIC COMPOSITE USING EUCALYPTOS WITH VULCANIZED NATURAL RUBBER 2044

STUDY OF THE THERMAL STABILITY OF A GRANULATED ORGANOMINERAL FERTILIZER BASED ON LIGNOCELLULOSIC RESIDUE BY THERMOGRAVIMETRIC ANALYSIS 2046
SUPERABSORBENT HYDROGELS BASED ON ALGINATE/POLYACRYLATE AND POLYACRYLAMIDE AS WATER RETAINER 2047
SYNTHESIS AND CHARACTERIZATION OF CASHEW GUM (ANACARDIUM OCCIDENTALE L) HYDROGELS CONTAINING MODIFIED PHOSPHATES 2048
SYNTHESIS OF ANIONIC SCALE INHIBITOR WITH DENDRITIC STRUCTURE BY AZA-MICHAEL ADDITION OF ETHYLENEDIAMINE TO A,B-UNSATURATED COMPOUNDS 2049
SYNTHESIS OF BIOCHAR-HYDROGEL COMPOSITE AS ECO-FRIENDLY ALTERNATIVE FOR AGRICULTURAL APPLICATIONS WITH CONTROLLED WATER ABSORPTION AND NUTRIENTS RELEASE 2050
THE USE OF CASSAVA GUM (MANIHOT ESCULENTA) HYDROGEL FOR STORAGE AND RELEASE OF MACRONUTRIENTS IN AGRICULTURAL 2051
USE OF POLYSULFIDES FROM INVERSE VULCANIZATION AS STRATEGIC MATERIALS FOR AGRICULTURE 2052
INNOVATION AND MANAGEMENT INVOLVING POLYMERS AND EDUCATION 2053
CIRCULAR ECONOMY TRENDS ABOUT THE REUSE OF SYNTHETIC FIBER WASTE FROM THE OIL INDUSTRY 2054
CLAY-BASED POLYMERIC NANOCOMPOSITES: BIBLIOMETRIC AND VISUAL ANALYSIS OF RESEARCH TRENDS USING VOSVIEWER 2060
USE OF ASSOCIATION RULES FOR EVALUATION OF STRESS CRACKING IN POLYMERS 2065
AN EXPERIENCE OF DEVELOPMENT OF HDPE/NATURAL FIBER COMPOSITES IN HIGH SCHOOL TO PROMOTE RECYCLING 2070
CHALLENGES AND OPPORTUNITIES FOR PLASTIC RECYCLING DURING THE COVID-19 PANDEMIC: A CASE STUDY IN SÃO PAULO STATE, BRAZIL 2071
POLYMERS AND PEPTIDES: WORLDWIDE TECHNOLOGICAL INTEREST 2072

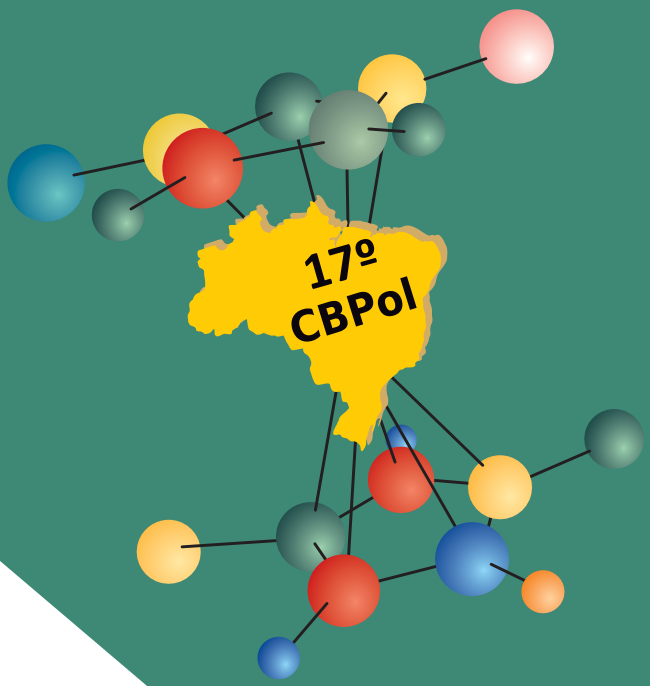

Plenary Lectures

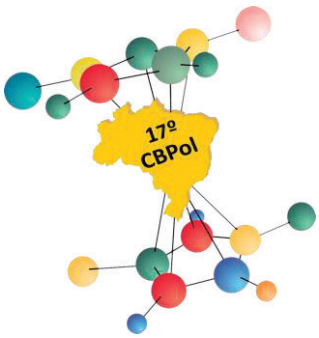

BRASKEM'S INNOVATION JOURNEY TO IMPLEMENT THE CIRCULAR ECONOMY

Fabiana Quiroga Garbin[1]*

1 – Circular Economy Director in South America, Braskem, Brazil
fabiana.quiroga@braskem.com

Abstract - The speaker will share Braskem's transformation journey in implementing a Carbon Neutral Circular Economy, highlighting the challenge of plastic waste in a linear economy, going through the established commitments and goals, and detailing concrete actions for the development of mechanical and chemical recycling for offer sustainable solutions with recycled content to its customers. In addition to technological and product innovations, it will present society engagement actions and the importance of design in packaging design to leverage circularity and reduce impacts on the environment.

Keywords: *innovation, circular economy, plastic waste, recycling.*

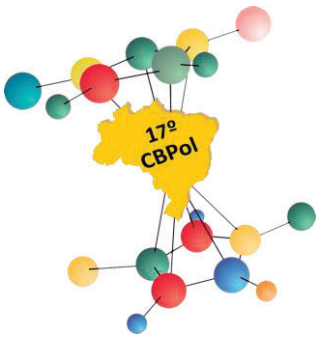

DEVELOPING STRATEGIES FOR POLYMER REDESIGN AND RECYCLING USING REACTION PATHWAY ANALYSIS

Linda J. Broadbelt[1]*

1 – Department of Chemical and Biological Engineering, Northwestern University, Evanston, IL 60208, USA
broadbelt@northwestern.edu

Abstract - The current lack of sustainability of and the limited portfolio of recycling processes for synthetic polymers have posed serious threats to the environment. Approximately 90% of plastics are produced via fossil fuels, and over 150 million tonnes of plastics have been discarded in the ocean. Annual production of plastics is expected to reach over 1 billion tons in 2050, but the current manufacturing, consumption, and disposal schemes of fossil-based polymers follow an unsustainable framework. Using reaction pathway analysis, we are pursuing a portfolio of strategies for redesign and recycling of polymers for sustainability. Pyrolysis is a promising method for resource recovery from plastic waste that is compatible with current petrochemical infrastructure that thermally converts polymers in the absence of oxygen into valuable chemical feedstocks and monomer. To provide further insight into polymer pyrolysis, a greater understanding of the mechanistic and kinetic details of the underlying reaction network is needed. To handle the complexity of mechanistic modeling of polymer degradation, we have developed both continuum and kinetic Monte Carlo (kMC) models. We have applied these approaches to study the degradation of polystyrene, polypropylene, polyisoprene, polystyrene peroxide and binary mixtures, and we are able to capture diverse experimental measures, including yields of individual low molecular weight products, as a function of reaction conditions. In order to solve the large models that are created, values of the rate coefficients for O(10^5) reactions are typically required. The approach that we have developed to specify rate coefficients is hierarchical, based on a combination of literature values, estimation methods, and computational chemistry. Alternatively, redesign efforts focusing on polymers that can be reused and recycled to monomers can lead to sustainable solutions for the plastics waste problem. One pathway to success is to identify bioprivileged molecules, biology-derived chemical intermediates that can be efficiently converted to a diversity of chemical products, including both novel molecules and drop-in replacements, and molecules emanating from them that can be used as monomers leading to recyclable polymers. We have developed a framework for molecule discovery and reaction pathway design that is automated and flexible and can be used to screen for bioprivileged candidates and target molecules. The application to discovery of known and novel monomers for poly(hydroxyurethanes) that are derived from biobased molecules and lead to recyclable materials will be discussed, and computational methods to evaluate the recyclability of different polymers will be outlined.

Keywords: *polymer redesing, recycling, pyrolysis, reaction pathway analysis.*

GELS FOR ENVIRONMENTAL REMEDIATION: FROM AEROGELS TO NANOSPONGES

Artur J. M. Valente[1]*

1 – Department of Chemistry, CQC, University of Coimbra, 3004-535 Coimbra, Portugal
avalente@ci.uc.pt

Abstract - Since the industrial revolution, several industrial processes have emitted biodegradable and non-biodegradable organic and inorganic pollutants into air, soil, and water. Some harmful wastes have long resident times and remain in the environment for decades, producing imbalances in specific ecosystems. Anthropogenic pollution includes: municipal wastewater, which carries detergents, organic matter, inorganic compounds present in everyday personal care products, and urban runoff that contains contaminants originating from tires and engines; wastewater from agriculture and livestock activities, which includes pesticides, fertilizers, antibiotics, and other synthetic products; and industrial wastewaters, which varies depending on the origin: from hydrocarbons (oil refineries) to dyes (textile industry) passing by metal ions (surface treatment industries and mining). Several physical, chemical, and biological treatment methods have been studied and applied for the removal/degradation of organic/inorganic compounds from water and soil. However, the large majority have significant drawbacks. In the last decades, Sorption processes and materials have wakened great attention being straightforward in application and often reusable, showing good efficiency and advantageous cost effectiveness. In the last decade we have been developed research on the development of materials for sorption of a large variety of pollutants: including hydrocarbons, dyes, metal ions, antibiotics, and pesticides. Different gel architectures and synthetic routes can be used to ensure specificity in the adsorption of different pollutants. Polysaccharides (e.g., chitosan), oligosaccharides (cyclodextrins, see Fig 1) and silica allow the synthesis of highly versatile materials for sorption of different pollutants. Additionally, the synthesis of new porous organic polymers with dual function (pollutant adsorption and catalysis) will also be presented and discussed.

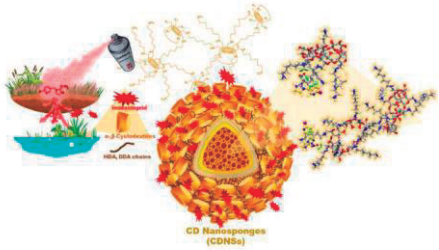

Figure 1 – Schematic representation of adsorption of pesticides by cyclodextrin nanosponges.

Keywords: *gels, environmental remediation, aerogels, nanosponges.*

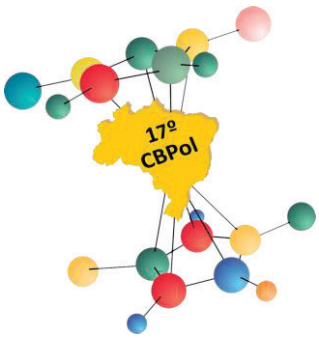

NATURAL FIBER AND HYBRID COMPOSITES: SCIENCE AND TECHNOLOGY

Sandro Campos Amico[1]*

1 – Department of Materials Engineering, Federal University of Rio Grande do Sul (UFRGS), Porto Alegre, RS, Brazil
amico@ufrgs.br

Abstract - This lecture will start with a short overview of the current composites market, including materials, sectors, market value and share by region/country, and post-pandemic situation. This will be followed by basic concepts on natural fibers (types, composition, production, reinforcement architecture, new developments, challenges), and their use in composites (chronology, properties, research topics, opportunities and applications in WPC, automotive and other sectors).
The hybrid concept will then be exploited, focusing on the combination of natural fibers with other reinforcements, especially synthetic fibers. Previous work of the group on intermingled and interlaminated hybrids, and on sandwich panels will then be presented. The final remarks will summarize the addressed concepts and present some expected trends in this field.

Keywords: *composites, hybrid composites, natural fibers, sandwich panels.*

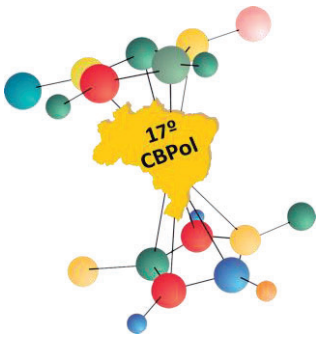

POLYMERS AND AGRICULTURE: PRESENT AND PROMISING TECHNOLOGICAL FUTURE

Luiz H.C. Mattoso[1]*

1 – Embrapa Instrumentation, National Laboratory of Nanotechnology for Agribusiness, São Carlos, SP, Brazil
luiz.mattoso@embrapa.br

Abstract - There is enormous technological potential for growth in the development of materials from renewable sources, which meet the concepts of green chemistry, bioeconomy, sustainability, and circularity sought worldwide. This lecture will present new approaches for the development of polymeric materials from a renewable source for applications of high technological potential, such as packaging and biodegradable products, films and edible coatings for food, sensors, biosensors, and electronic devices, systems for the controlled release of pesticides, fertilizers, and drugs, tissue engineering, among others.

Fundings: FAPESP – proc. 2018/22214-6.

Keywords: *polymers, agriculture, sustainability, circularity, green chemistry.*

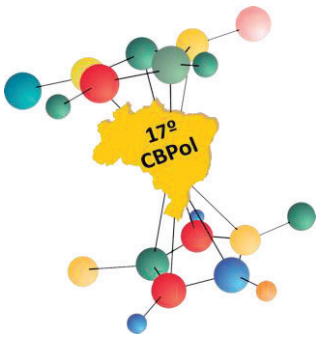

TWO DECADES OF POLYMER NANOCOMPOSITES RESEARCH: FROM ACADEMIA TO INDUSTRY

Ricardo V. B. de Oliveira[1]*

1 – 2D Materials Pte Ltd (2DM), Singapore
ricardo.oliveira@2dmsolutions.com

Abstract - The lecture will address Dr. Ricardo Oliveira's academic career in nanocomposites and nanotechnology, highlighting the importance of these fields. The challenges and opportunities for researchers who wish to dedicate themselves to these promising areas will be discussed. The need for solid training, interdisciplinary collaborations and engagement with industry will be explored. In addition, inspiring events will be presented in the speaker's career, ranging from the generation of knowledge in academia, technology transfer, the creation of companies and new businesses and some future projects. The speaker will emphasize the relevance of continuous investments in research and innovation, aiming for significant advances and practical applications of nanostructured materials that will drive technological evolution and its positive impact on society and industry.

Keywords: *polymer nanocomposites, graphene, industry, innovation.*

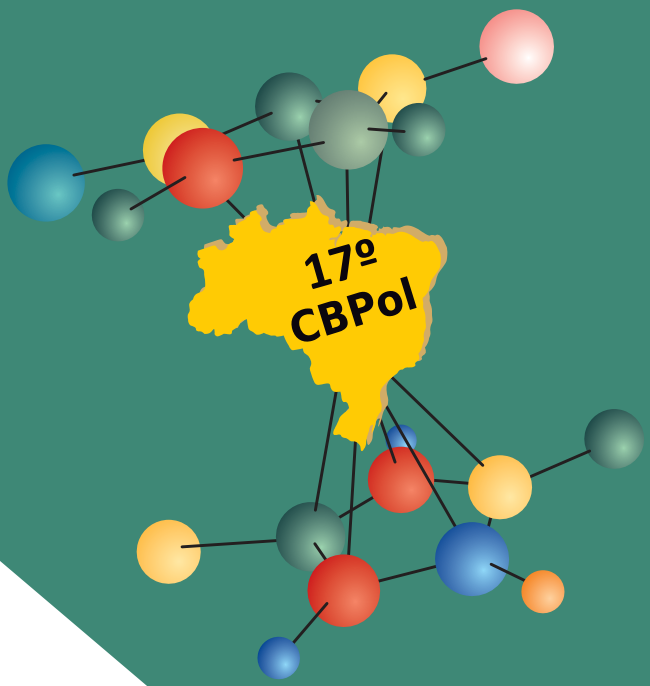

Polymerization reactions and polymer chemistry

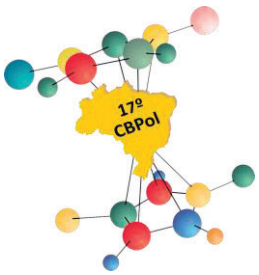

POLYURETHANES-NIOBIUM COMPOUNDS WITH POTENTIAL APPLICATION FOR THE TREATMENT OF DYES

Juliana Kloss

Academic Department of Chemistry and Biology, Federal University of Technology – Paraná (UTFPR), Curitiba, PR, Brazil

Dyes are widely used in the pharmaceutical, printing, plastics, cosmetics, food and textile industries. In turn, population and industrial growth have led to an increase in waste generation, contributing to the contamination of water resources. In addition, the presence of these organic contaminants can be detected even in low concentrations, a fact that markedly alters the coloration of rivers and consequently prevents light from penetrating the aquatic environment, reducing the amount of dissolved oxygen and making the process of photosynthesis difficult. As a result, interest in studying and developing new systems for treating industrial effluents has been growing in recent decades. Polyurethane compositions with supported niobium compounds or polyurethane/clay/niobium stand out because they are not widely explored and act as heterogeneous catalysts, which are capable of oxidizing and transforming toxic agents into products with reduced environmental impact, since they offer greater specific area, giving the material greater porosity and making it easier to obtain a system on an industrial scale, combined with a low economic cost, offering promising results for application in remediation processes.

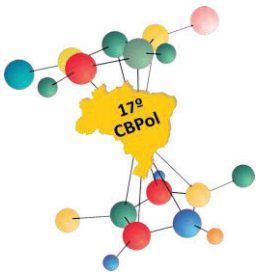

SYNTHESIS AND EVALUATION OF POLYMERIC SCALE INHIBITORS PREPARED BY RAFT POLYMERIZATION

Bisatto, R.[1,2], Picoli, V.M.[1] and Cesar L. Petzhold[1*]

1 – Department of Organic Chemistry, Federal University of Rio Grande do Sul (UFRGS), Porto Alegre, RS, Brazil
petzhold@iq.ufrgs.br
2 – Research, Development, and Innovation (RD&I), Dorf Ketal Brasil LTDA, Nova Santa Rita, RS, Brazil

Abstract - This study focuses on the synthesis of polymeric scale inhibitors produced via radical polymerization in solution. It compares two preparation methods: the conventional approach and RAFT (reversible addition-fragmentation chain transfer polymerization), with the primary goal of developing novel block polymeric materials.The process began by selecting potential monomers, which were then used to create homopolymers through conventional techniques. These homopolymers exhibited diverse functional groups (sulfonic, carboxylic, and phosphonic) and molecular weights ranging from 1,000 to 43,100 Da. Static and dynamic efficiency tests yielded outstanding results for the sulfate condition, especially with the monomer sodium styrene sulfonate (NaSS), which had an average numeric molecular weight of 13,000 Da. It demonstrated exceptional performance in multiple scale inhibition scenarios. For RAFT polymerization conditions, initial experiments utilized homopolymers as a starting point. The most favorable outcomes were achieved using 4-cyano-4-(phenylcarbonothioylthio)pentanoic acid as the RAFT agent and DMSO as the solvent, at a ratio of [CTA]/[I] = 5.0. These conditions led to conversions of up to 65% and a dispersity of less than 2.0. In the case of RAFT homopolymers using 2,2'-[carbonothioylbis(thio)]bis[2-methylpropanoic acid] as RAFT agent, superior results were obtained in an aqueous system (sometimes combined with methanol), with conversions reaching up to 95% and a dispersity close to 2.0.Building upon the knowledge gained from the homopolymers (both conventional and RAFT-produced), new di- and ABA-triblock copolymers were synthesized with conversions nearing 100% and an average numeric molecular weight close to 3,500 Da. These materials displayed distinct anti-scale behavior dependent on their architectural composition.The diblock copolymer (acrylic acid / sodium styrene sulfonate) exhibited a preference for the dispersive inhibition mechanism, while the triblock copolymers (acrylic acid / sodium styrene sulfonate) and (acrylic acid / 2-acrylamido-2-methylpropane sulfonic acid) were more inclined to delay nucleation mechanisms.

References

1. Zhou, M.; Gu, Y.; Yi, R.; Han, H. *J. Polym. Res*. 2020, 27 (10). https://doi.org/ 10.1007/s10965-020-02270-7.
2. R. Bisatto; V. M. Picoli; C. L. Petzhold *J. Petr. Sci. Eng.* 2022, *213,* 110331. https://doi.org/10.1016/j.petrol.2022.110331.
3. M. F. Mady; P. Bayat; M. A. Kelland *Ind. Eng. Chem. Res.* 2020, *59,*. https://doi.org/10.1021/acs.iecr.0c01636.

Fundings: The authors acknowledge the PPGQ (Programa de Pós-Graduação em Química) from UFRGS (Universidade Federal do Rio Grande do Sul) and DORF KETAL BRASIL LTDA company for the support on analysis.

Keywords: *Scale inhibitor, RAFT polymerization, blockcopolymer, calcium carbonate, barium sulphate.*

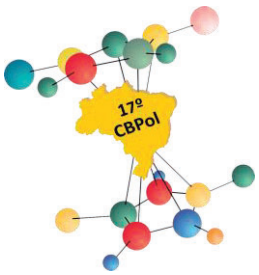

ASSESSING THE CURING PROCESS OF LIMONENE DIOXIDE USING DSC ANALYSIS

Maurício C. D. F. Xavier[1], Otávio Bianchi[1], Sandro C. Amico[1] and Cesar Petzhold[2]

1 – Department of Materials Engineering, Federal University of Rio Grande do Sul (UFRGS), Porto Alegre, RS, Brazil
carpe.diem@ufrgs.br

2 – Department of Organic Chemistry, Federal University of Rio Grande do Sul (UFRGS), Porto Alegre, RS, Brazil

Abstract – In this study, we present the findings of a brief investigation into the curing process of limonene dioxide (LDO) using three different hardeners: phthalic anhydride (PA), 4,4'-methylenediamine (MDA), and tetramethylenetriamine (TETA). The cured systems were characterized by measuring their glass transition temperatures (T_g) through differential scanning calorimetry (DSC). The observed T_g values ranged from -2 to 81 °C, indicating a significant variation in thermal properties among the cured systems. Furthermore, we preliminary optimized the epoxidation process for limonene using Oxone® and acetone.

Keywords: Epoxy resin, Bio-based epoxy, Limonene, Epoxidation, DSC
Fundings: The present work was funded by the Foundation for Research Support of the State of Rio Grande do Sul (FAPERGS), INOVA TECHNOLOGICAL CLUSTERS Edict, process 02/2022.

Introduction

The development of bio-based epoxy resins with mechanical and thermal properties comparable to commercial bisphenol A-based epoxies is a challenging goal pursued by researchers in academic and industrial fields [1]. The global need for advanced materials derived from renewable sources is necessary to sustain the production and advancement of such products. While bio-based epoxy resins are available in the market, they are predominantly used for applications that do not require high thermal resistance, typically up to around 100 °C. A substantial body of research publications and patents describe various bio-based epoxy resins. The terpene *R*-limonene has promising features, particularly its availability, low toxicity, and ease of handling [2]. Moreover, current methods for epoxidizing limonene are relatively inexpensive and mild [2]. However, limonene presents challenges when applied to epoxy resins, such as its hindered chemical structure and the fully saturated nature of the molecule after epoxidation, making it challenging to achieve resins with high glass transition temperatures (T_g) [3]. One of the few examples of limonene being used for bio-based resin involves solvents and a complex iron catalyst [4].

In this study, our objective was to determine the T_g of a bio-based epoxy resin called limonene dioxide (LDO), cured with three different hardeners that have not been previously reported for LDO curing. Additionally, we aimed to investigate potentially more cost-effective conditions for synthesizing LDO using Oxone® and acetone in a Shi-type epoxidation reaction.

Experimental

Materials

All reagents were used directly without further purification. Their structure and supplier are presented in Table 1.

Table 1: Materials suppliers

Material	Purity (%)	Supplier
R-Limonene	97	Local supplier
Acetone	98	Synth
Oxone®	98	Sigma-Aldrich
$NaHCO_3$	98	Sigma-Aldrich
PA	98	Sigma-Aldrich
MDA	97	Sigma-Aldrich
TETA	96	Sigma-Aldrich

Synthesis of limonene dioxide

The procedure used for the epoxidation of *R*-limonene was based on previously described methods [2]. In a 250 mL round bottom flask containing $NaHCO_3$ (51 mmol, 4,3 g), *R*-limonene with 97% purity (10 mmol, 0,14 g) in acetone (20 mL) was added and mechanical stirring (400 rpm) was applied while the temperature was kept at 25 °C. Then, a potassium monopersulphate (Oxone®) solution in water is added to the system at 1 mL/min. After 4 h, agitation ceased, and ethyl acetate (40 mL) and water (20 mL) were added to the system. Liquid-liquid extraction was performed by washing the aqueous phase three times with ethyl acetate. The solvent was removed by evaporation under reduced pressure. LDO structure was confirmed by ^{1}H NMR analysis comparing with reported spectra [2]. The conversion of *R*-limonene to LDO was above 99%. This is in accord with the base reference.

Differential scanning calorimetry

The glass transition temperature (T_g) of the LDO-Hardener systems was using a TA Instruments Q2000 calorimeter. Samples (~10 mg) were placed inside hermetically-sealed aluminum crucibles and subjected to the following thermal cycle under nitrogen atmosphere (50 mL min^{-1}): heating from -80 °C to 210 °C at 20 °C/min.

Results and Discussion

Initially, a set of variations on the quantities of reagents used in the base epoxidation protocol was employed to evaluate if lower amounts of reagents could lead to a similar conversion of limonene to LDO. Maximum amounts were chosen as the ones already reported, while the minimum amount of Oxone® and $NaHCO_3$ was determined based on the reaction stoichiometry. It was observed that in every set of conditions in which the amount of $NaHCO_3$ was the minimum, epoxide ring opening took place as observed by ^{1}H Nuclear Magnetic Resonance (^{1}H NMR) of signals of ROH hydrogens at ~4,7 ppm and of aldehyde at 9.6 ppm, and almost no LDO remained after the reaction time. A plausible explanation for this result is that epoxide ring opening quickly occurs under pH > 7.

Regarding cases with the maximum amount of base, lower conversion rates were observed when the amounts of Oxone® and acetone were minimized. The average conversion to LDO was 88% under these conditions. However, when acetone was minimized while the other two reagents were maximized, the conversion rate matched when all reagents were maximized, resulting in a 99% conversion. This modification led to a 50% reduction in the amount of acetone used in the protocol (Table 2, entry 4). Additionally, we conducted a final experiment using an intermediate amount of base, which yielded an 82% conversion to LDO. Scaling up the conditions from entry four did not alter the conversion to LDO.

Table 2: Optimization of conditions for LDO synthesis.

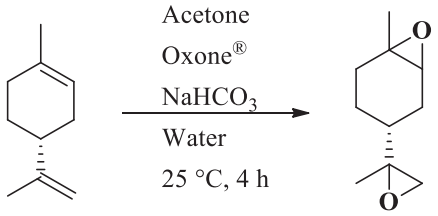

***R*-limonene** **LDO**

Entry	Acetone (mL)	Oxone® (mmol)	$NaHCO_3$ (mmol)	Conversion to LDO (%)[a]
1[b]	2	2.2	2.2	>01
2	2	2.2	5.1	88
3[b]	2	2.8	2.2	>01
4	2	2.8	5.1	99
5[b]	4	2.2	2.2	>01
6	4	2.2	5.1	99
7[b]	4	2.8	2.2	>01
8	4	2.8	5.1	99
9	2	2.4	3.8	82

[a]Conversion determined by integrating limonene vinylic hydrogens and LDO epoxide ring hydrogens in ^1H NMR. Each condition was performed in duplicate. [b]Epoxide ring opening subproducts observed in ^1H NMR.

The subsequent stage involved investigating the curing of LDO using hardeners that have not been previously reported in the literature. The results revealed that a combination of LDO with phthalic anhydride (PA) yielded a polymer with a T_g of 82°C. When 4,4'-methylenediamine (MDA) was employed as the hardener, the observed T_g was 61°C. Notably, the same sample was subjected to a temperature of 110°C for 7 days, and the T_g remained relatively high at 81°C. However, when the molar ratio of MDA was doubled, the T_g dropped to 23°C, indicating that the NH_2 groups only reacted once with the oxirane groups present in LDO. In the case of tetramethylenetriamine (TETA), the resulting polymer displayed a T_g of -2°C (Table 3).

Table 3. Curing protocols and T_g

Hardenecer	LDO: Hardener molar ratio	T_g (°C)
PA	1:1	82
MDA	1:1	61 (81)[a]
MDA	2:1	23
TETA	1:1	-2

[a]After DSC analysis, the sample was placed in a kiln at 110 °C for 7 days, and then the T_g was measured again by DSC.

These findings offer valuable insights into the impact of various hardeners on LDO's glass transition temperature (Tg), contributing to the development of bio-based epoxy resins. Furthermore, by exploring different hardeners, we better understand how they influence the thermal properties of the cured LDO polymer. This knowledge is crucial for advancing the field of bio-based materials and facilitating the design of epoxy resins with desirable characteristics.

Conclusions

A slight improvement to the epoxidation of limonene using Oxone® and acetone was developed, which can be helpful in processes for synthesizing LDO on an industrial scale. As for the T_g, we observed that using PA or MDA as hardeners were compatible with applications such as

adhesive, vacuum infusion, and coatings. Nonetheless, further investigations and characterizations are being conducted to obtain more complete data regarding LDO as a bio-based epoxy resin. These efforts deepen our understanding and provide a more comprehensive assessment of LDO's properties and potential applications.

Acknowledgments
The present work was funded by the Foundation for Research Support of the State of Rio Grande do Sul (FAPERGS), INOVA TECHNOLOGICAL CLUSTERS Edict, process 02/2022.

References

1. A) G. M Roudsari; A. K. Mohanty; M. Misra *ACS Sustain. Chem. Eng.* 2017, 5, 9528−9541. https://doi.org/10.1021/acssuschemeng.7b01422. B) Tsuneo Koike *Polym. Eng. Sci*. 2012, *52*, 701-717. https://doi.org/10.1002/pen.23119. C) H. Sukanto; W. W. Raharjo; D. Ariawan; J. Triyono; M. Kaavesina *Open Engineering*. 2021, *11*, 797-814. https://doi.org/10.1515/eng-2021-0078.

2. L. Charbonneau; X. Foster; D. Zhao; S. Kaliaguine *ACS Sustainable Chem. Eng.* 2018, *6*, 5115. https://10.1021/acssuschemeng.7b04782.

3. A) E. Louisy; S. Olivero; V. Michelet; A. Mija *ACS Sustainable Chemistry & Engineering*. 2022, *10*, 7169-7179. https://doi.org/10.1021/acssuschemeng.2c01553. B) L. Schutz; F. Kazemi; E. Mackenzie; J-Y. Bergeron; E. Gagnon; J. P. Claverie *J. Polym. Sci.* 2021, *59*, 321–328.

4. L. P. Carrodeguas; C. Martín; A. W. Kleij *Macromolecules*. 2017, *50*, 5337–5345. https://doi.org/10.1021/acs.macromol.7b00862.

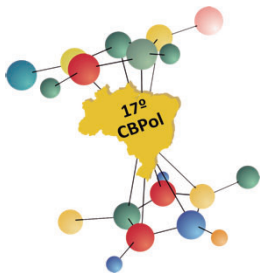

CELLULOSE ALKYLATION IN THE DMSO/DBU/CO_2 SOLVENT SYSTEM

Matheus F. Flores[1]* and Antonio A. S. Curvelo[1]

1 – São Carlos Institute of Chemistry, University of São Paulo (USP), São Paulo, SP, Brazil
matheus.flores@usp.br

Abstract - Despite the development of numerous products and processes in cellulose solid-state modification, its dissolution has become a topic of great scientific interest, as it enables the production of more homogeneous products. In 2005, Jessop et al. introduced the DMSO/DBU/CO_2 solvent system for organic synthesis, which has recently been optimized for cellulose dissolution, allowing chemical modification of cellulose under milder conditions. Building upon this, the present study aimed to explore the insertion of carbon chains of different lengths into cellulose. Linear alkyl halides with chains ranging from 4 to 12 carbons were used as precursors to produce these cellulose derivatives. Infrared spectroscopy and X-ray diffraction analyses confirm the success of the reaction by the appearance of a symmetrical stretching band C=O at 1740 cm^{-1} and the disappearance of the crystalline pattern of the cellulose. Further confirmation of the cellulose derivative's structure was obtained through ^{1}H and ^{13}C NMR spectra.

Keywords: *Carbon dioxide, Cellulose carbonate, Switchable solvent, S_N2 reaction, Renewable polymer.*

Fundings: National Council for Scientific and Technological Development (CNPq; grant # 131146/2021-1).

Introduction

The study and application of renewable resources, particularly in the field of chemistry and polymer engineering, has increased considerably in recent years due to the depletion of fossil resources. Among these, cellulose, the most abundant macromolecule on the planet, has become a topic of interest due to its biocompatibility, biodegradability, low cost, and thermal and mechanical stability. However, the extensive hydrogen bonds in the cellulose structure presents challenges for its processing, including lack of thermal transition and insolubility in water and conventional organic solvents [1]. Two strategies can be adopted to overcome these challenges and make cellulose more processable: (1) the use of solvents that can break or disrupt hydrogen bonds, and (2) the chemical modification of the -OH groups present in cellulose [2].

Some examples for the first case include processes using N,N-dimethylacetamide/lithium chloride (DMAc-LiCl), dimethylsulfoxide/tetrabutylammonium fluoride (DMSO-TBAF), and N-methylmorpholine N-oxide (NMMO) which is used industrially and known as the Lyocell process [3,4]. However, these solvents have limitations in terms of sustainability, as they are difficult to recover and highly toxic. Ionic liquids such as 1-butyl-3-methylimidazolium chloride (BMIMCl) have desirable characteristics for a more sustainable route, but they are expensive and require high reaction temperatures.

For the chemical modification of cellulose, two routes can be used: heterogeneous and homogeneous. The heterogeneous route is commonly used in the industry to produce cellulose esters, ethers, and silyl ethers as it is easy to carry out and does not require dissolving the cellulose in the process [5]. However, strong acids or bases are needed to activate the cellulose chains, and

there is a lack of control over the degree of substitution obtained. The homogeneous route offers better control over the structure of the obtained cellulose derivatives, but the solubilization step preceding the modification is challenging. In addition to the previously mentioned solvents for dissolving cellulose, there are solvents called derivatives which, through a pre-functionalization of cellulose, allow its solubilization. One of the best-known examples is the viscose process, which was developed in the 19th century and still dominates the means of production for the manufacture of regenerated cellulose films and yarns [6]. However, the viscose process has high toxicity and workers have reported diseases caused by exposure to carbon disulfide.

In 2005, Jessop et al. [7] proposed a new solvent system for cellulose dissolution that is less toxic and more recyclable than the viscose process. This system involves the derivatization of -OH groups in a carbonate anion that is soluble in DMSO using CO_2 and a superbase like DBU. Several studies have since reported successful dissolution of cellulose under mild conditions using this system. However, due to product instability, there was no conclusive evidence of in situ cellulose carbonate formation.

Onwukamike et al. [8] optimized the process and achieved complete cellulose solubilization within 10-15 minutes using low CO_2 pressures (2-5 bar) and a temperature of 30 ºC. They indirectly proved the formation of cellulose carbonate through substitution reactions between alkyl halides with the obtained solution and the capture of carbon dioxide in the structure of the formed cellulose derivative.

Recent studies have shown that solubilizing cellulose in the DMSO/DBU/CO_2 system can improve its ability to be modified under mild conditions. Various derivatizations have been carried out in this system, such as acylation with anhydride, grafting with polylactic acid and polyesters, transesterification with oils plants, substitution reactions with fluorescent alkyl halides and the synthesis of O-cellulose thiocarbamate [9,10]. However, there is no comparative study available in the literature that investigates the impact of carbon chains with different sizes on the behavior of the modified cellulose. Therefore, this study aims to provide a better understanding in this context. The formation reaction of cellulose carbonate and alkyl cellulose carbonate is depicted in Figure 1.

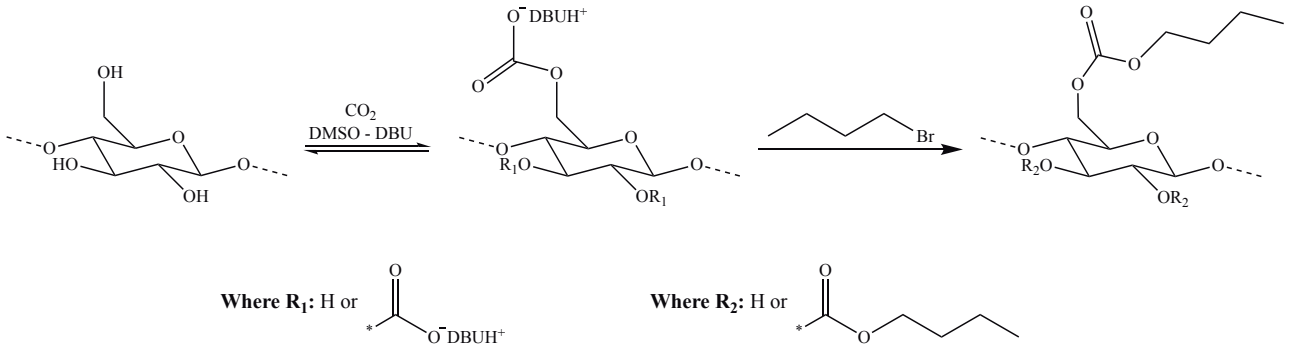

Figure 1 – Cellulose solubilization in DBU/DMSO/CO_2 and subsequent alkylation with 1-bromobutane.

Experimental

Materials

Microcrystalline cellulose PH-102 was purchased from Sigma-Aldrich. It was dried at 100 °C for 24 h under vacuum to remove free water before use. The following chemicals were also purchased from Sigma Aldrich and were used without further purification: deuterated dimethyl sulfoxide (DMSO-d6), dimethyl sulfoxide (DMSO), 1,8-diazabicyclo[5.4.0]undec-7-ene (DBU), 1-bromobutane, 1-bromohexane, 1-bromooctane, 1-bromodecane, 1-bromododecane, and methanol. Carbon dioxide (CO_2 mixture of air-liquid in a cylinder with dip tube) was high grade purity and no refining was needed.

General Procedure for the Synthesis of Alkyl Cellulose Carbonates

The methodology for carrying out this study comprised four stages: the dissolution of cellulose from the formation of cellulose carbonate, the reaction of the carbonate with the alkyl halides, the precipitation and isolation of the formed products and the characterization of these products. An illustrated summary is presented in Figure 2.

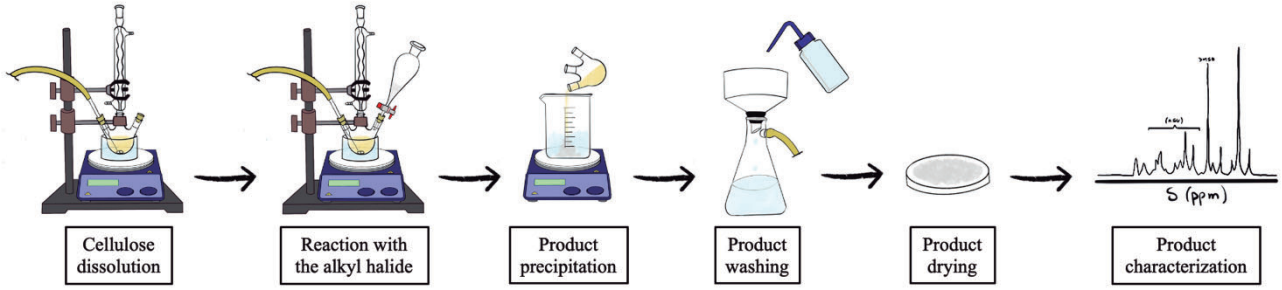

Figure 2 – Experimental procedure scheme.

The DMSO/DBU/CO_2 system was used to dissolve cellulose by following the experimental conditions reported in literature [10]. First, 2.00 g (12.33 mmol) of cellulose was suspended in 60 mL of DMSO in a round-bottom flask. Next, 1,8-diazabicyclo[5.4.0]undec-7-ene (5.5 mL, 37.00 mmol, 3.0 eq. per anhydroglucose unit) was added dropwise. After applying a CO_2 flow through the solution for 20 minutes at 40°C, a clear solution was obtained. Then, one of the alkyl halides mentioned in the *Materials* section was added dropwise to the solution (6.0 eq. per AGU), which was then stirred for 2 hours until a homogeneous solution was achieved. Subsequently, the solution was added dropwise into 300 mL of water under vigorous stirring to precipitate the alkyl cellulose carbonate. It was then vacuum filtrated and washed with water (3 × 50 mL) and methanol (3 × 50 mL). The obtained precipitate was dried under vacuum for 24 h.

Measurements

– X-ray diffraction (XRD): X-ray diffraction patterns were collected on a Bruker D8 Advance diffractometer. The samples were analyzed in the form of powder and the measurements were made between the 2θ angles from 5º to 60º with a step of 0.020 degrees and an irradiation time of 0.5 s.

– Infrared spectroscopy (IR): Infrared spectra of all samples were recorded on a IRAffinity-1S (Shimadzu) using ATR technology within the range from 4000 to 650 cm^{-1}.

– Nuclear magnetic resonance spectroscopy (NMR): ^{1}H NMR spectra were recorded using an Agilent 500/54 Premium Shielded spectrometer operating at 500 MHz at 80 ºC (DMSO-d_6) with 1024 scans and a time delay d_1 of 1 s. ^{13}C NMR spectra were also recorded using an Agilent 500/54 Premium Shielded spectrometer operating at 125 MHz at 80 ºC with 6000 scans and a time delay d_1 of 2 s. All products were dissolved with the concentrations of 10-20 mg/mL.

Results and Discussion

The codes used for microcrystalline cellulose, regenerated cellulose and each one of the reaction products are summarized in Table 1. Confirmation of the success of the reactions was achieved through infrared spectroscopy analysis (Figure 3a), which showed the appearance of a carbonate ester's symmetrical stretching band C=O at 1740 cm^{-1} and a symmetrical absorption band of C-O at 1256 cm^{-1}. The presence of these bands indicates the incorporation of CO_2 into the cellulose derivative's structure. Additionally, an increase in the intensity of the asymmetric deformation bands of C-H bonds at 2926 cm^{-1} and 2853 cm^{-1} was observed, being greater for the longer added chains.

Table 1 – Codes used.

Sample Code	Description
Cel MCC	Microcrystalline cellulose
Cel II	Regenerated cellulose (Cellulose II)
CelBr4	Reaction product with 1-bromobutane
CelBr6	Reaction product with 1-bromohexane
CelBr8	Reaction product with 1-bromooctane
CelBr10	Reaction product with 1-bromodecane
CelBr12	Reaction product with 1-bromododecane

Figure 3b presents the X-ray diffraction results obtained for both cellulose and the reaction products. It can be observed that after the dissolution and chemical modification of cellulose, the characteristic peaks for Cellulose I and Cellulose II disappeared, being replaced by a broad signal around 2θ = 20°. The increase in the amorphous portion is an indication that the compounds inserted into the cellulose chain prevented its reorganization in the form of the thermodynamically more stable polymorph, Cellulose II.

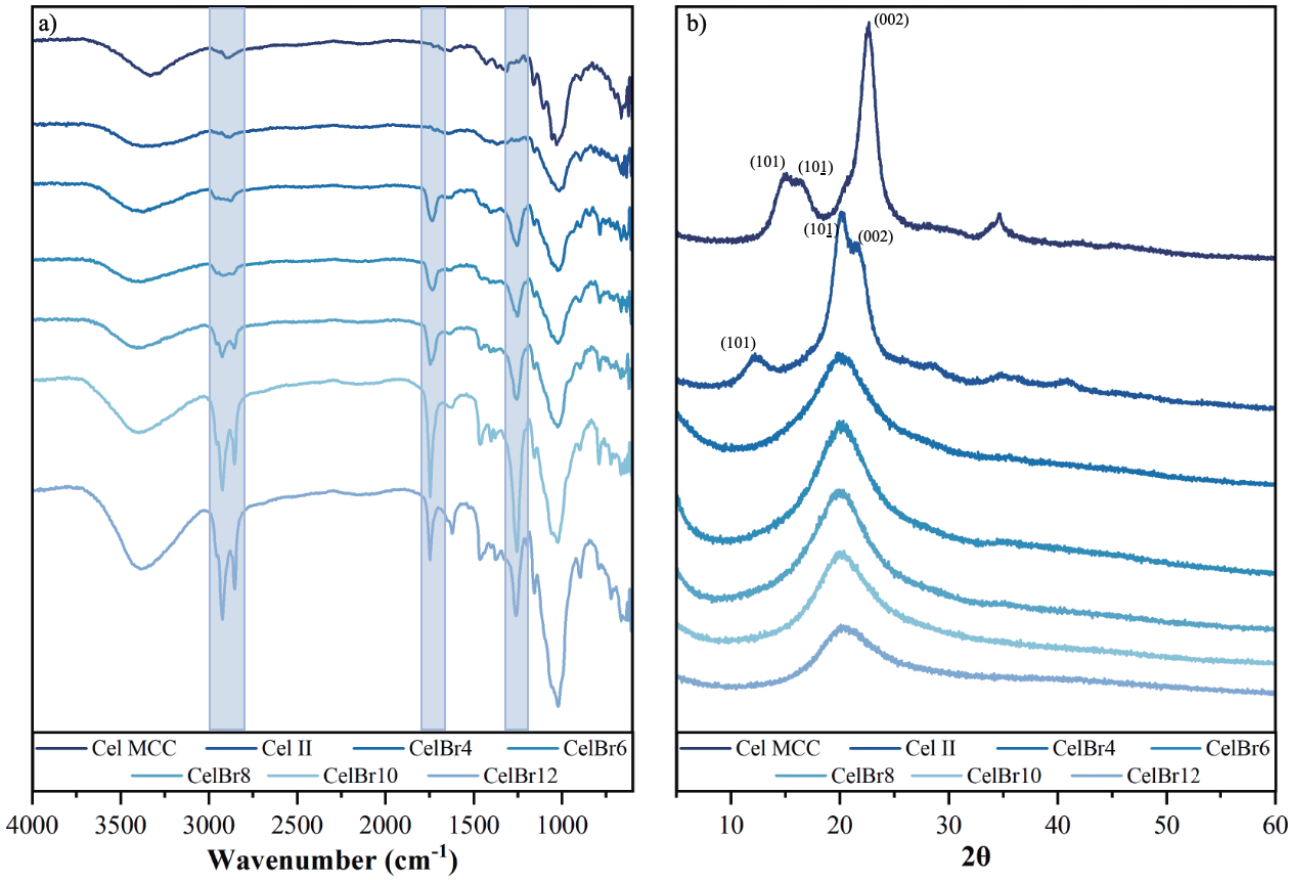

Figure 3 – (a) FT-IR spectra and (b) X-ray diffraction patterns of microcrystalline cellulose, regenerated cellulose, and its derivatives.

Further confirmation of the structure of the products was obtained from ^{1}H and ^{13}C NMR. As an example, the NMR results for the experiment performed with 1-bromobutane alkyl halide are presented (Figure 4). Determining the degree of substitution of the products obtained is difficult due to the H_2O observed at a chemical shift of 3.1 ppm in ^{1}H NMR and the protons next to the

carbonate group at a chemical shift of 4.2 ppm, which signs are located among the protons of the cellulose backbone ones (between 5.3 and 3.0 ppm).

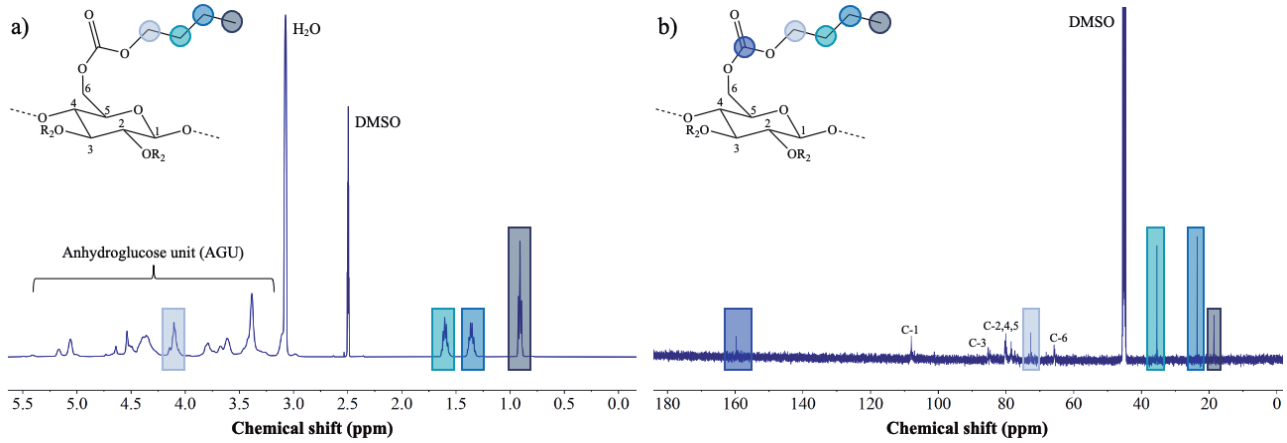

Figure 4 – ^{1}H (left, 500 MHz) and ^{13}C (right, 125 MHz) NMR (DMSO-d_6) at 80 ºC for CelBr4.

Conclusions

During this study, cellulose derivatives were obtained through a homogeneous and more sustainable route than those described in the literature. Cellulose solubilization was achieved within 20 min at 40°C. Subsequent alkylation took place within 2 h at the same temperature. Due to the difficulty in determining the degree of substitution, in the future we intend to perform 31P NMR to overcome this difficulty. In addition, mechanical and contact angle tests are interesting for future characterization of the material.

Acknowledgements

São Carlos Institute of Chemistry (IQSC/USP) and National Council for Scientific and Technological Development (CNPq).

References

1. Y. Habibi; L. Lucia; O. Rojas. *Chemical Reviews* 2010, 110, 3479. https://doi.org/10.1021/cr900339w.
2. B. Medronho; B. Lindman; *Advances in colloid and interface science* 2015, 222, 502. https://doi.org/10.1016/j.cis.2014.05.004.
3. T. Heinze; R. Dicke; A. Koschella; A. Kull, E. Klohr; W. Koch. *Macromolecular Chemistry and Physics* 2000, 201, 627. https://doi.org/10.1002/(SICI)1521-3935(20000301)201:6%3C627::AID-MACP627%3E3.0.CO;2-Y.
4. H. Fink; P. Wigel; H. Purz; J. Ganster. *Progress in Polymer Science* 2001, 26, 1473. https://doi.org/10.1016/S0079-6700(01)00025-9.
5. D. Klemm; B. Heublein; H. Fink; A. Bohn. *Angewandte chemie international edition* 2005, 44, 3358. https://doi.org/10.1002/anie.200460587.
6. T. Heinze; A. Koschella. *Polímeros* 2005, 15, 84. https://doi.org/10.1590/S0104-14282005000200005.
7. P. Jessop; D. Heldebrant; X. Li; C. Eckert; C. Liotta. *Nature* 2005, 436, 1102. https://doi.org/10.1038/4361102a.
8. K. Onwukamike; T. Tassaing; S. Grelier; E. Grau; H. Cramail; M. Meier. *ACS Sustainable Chemistry & Engineering 2018*, 6, 1496. https://doi.org/10.1021/acssuschemeng.7b04053.
9. Q. Cao; J. Dai; X. Bao; Z. Zhang; F. Liu; Y. Feng; H. Na; J. Zhu. *Cellulose* 2021, 28, 10373. https://doi.org/10.1007/s10570-021-04184-z.
10. J. Wolfs; M. Meier. *Green Chemistry* 2021, 23, 4410. 10.1039/D1GC01508G.

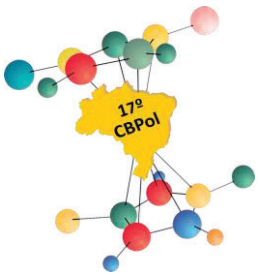

DEVELOPMENT OF A NOVEL BIOREFINERY PROCESS FOR PRODUCING PHOSPHYLATED-LIGNIN FROM COCONUT WASTES

Lucas de Sousa Nascimento[1], Rogério J. Melo Nascimento[2], Allann Karlos Alves da Mata[1], Vinícius Taveira Andrade Felipe[1], Rayanne Ferreira Araújo[1], Luiz Carlos Alves Bezerra[1], Jéssica Silva Almeida[3], Adriano Lincoln Albuquerque Mattos[4], Daniel Esdras Andrade Uchoa[5], Leice Milla Ribeiro de Novais[6], Caroline Da Ros Montes D'Oca[6], Francisco Avelino[1*]

1 – Departament of Research, Extension and Production, Federal Institute of Ceará (IFCE), Iguatu, CE, Brazil
francisco.avelino@ifce.edu.br
2 – Departament of Metallurgical and Materials Engineering, Federal University of Ceará (UFC), Fortaleza, CE, Brazil
3 – Departament of Chemical Engineering, Federal University of Ceará (UFC), Fortaleza, CE, Brazil
4 – Embrapa Tropical Agroindustry, CNPAT, Fortaleza, CE, Brazil
5 – Departament of Organic and Inorganic Chemistry, Federal University (UFC), Fortaleza, CE, Brazil
6 – NMR Lab, Departament of Chemistry, Federal University of Paraná (UFPR), Curitiba, PR, Brazil

Abstract
This work aimed to develop a phosphorous-based biorefinery process for obtaining phosphorylated lignocellulosic fractions in a one-pot protocol from coconut fiber. Natural coconut fiber (NCF) was mixed with 85 % m/m H_3PO_4 at 70 ^oC for 1 hour to yield the modified coconut fiber (MCF), aqueous phase (AP), and coconut fiber lignin (CFL). CFL structure was evaluated by FTIR, ^{31}P NMR, and P content and was compared to that of milled wood lignin (MWL). It was observed that CFL was phosphorylated during the pulping (0.23 % wt.). The phosphorylation of CFL was proved by spectroscopic analyses, which presented characteristic absorption bands or peaks related to monoester phosphate groups. The results show that a platform of functional materials such as biosorbents, biofuels, flame retardants, and biocomposites can be created through an eco-friendly, simple, fast, and novel biorefinery process.
Keywords: *Agrowastes; biomass valorization; lignin valorization; phosphorylation; chemical modification.*
Fundings: This work was funded by Fundação Cearense de Apoio ao Desenvolvimento Científico e Tecnológico (FUNCAP) under the grants numbers FUNCAP BP4-0172-00159.01.00/20 and BP5-00197-00113.01.00/22.

Introduction

The lignocellulosic biomass has a great potential for generating valuable building blocks through different biorefinery processes due to its rich chemical composition, mainly by celulose, hemicellulose and lignin. Among the different classes of lignocellulosic biomasses, agricultural wastes stand out due to its huge production and underutilization. One of the main crops produced worldwide is coconut which had a world production of 63.68 Mt in 2021 (FAOSTAT, 2022). Brazil is one of the biggest producers of agroindustrial wastes in the world, being the 4th biggest world coconut producer with a production of 2.46 Mt in 2021 (FAOSTAT, 2022).

As resulting of such production for yielding edible products from copra, considerable amount of solid wastes is generated from coconut processing, such as coconut shell, coir, and mesocarp, representing a potential source of environmental pollution. In addition, part of those residues is burned in industrial furnaces, representing an underutilization of the material, since it presents elevated cellulose, hemicellulose, and lignin contents that can be properly valorized for noble applications.

The valorization of the lignocellulosic fractions requires their previous isolation from the biomass (KANT et al., 2020). In this sense, several types of processes can be used, and the chemical ones such as acid hydrolysis are the most used for promoting the deconstruction of lignocellulosic biomass (AHMAD et al., 2019). A common approach is the utilization of concentrated or diluted phosphoric acid (H_3PO_4) as a pre-treatment step. However, the literature does not report any insights about the occurrence of phosphorylation in none lignocellulosic componentes, which can be valuable for obtaining phosphorylated lignocellulosic fractions that can be used for several applications. Based on this background, it is urgent the development of a biorefinery process that uses H_3PO_4 for promoting biomass fragmentation and the phosphorylation of the lignocellulosic fractions in a one-pot process, in order to create a phosphorous-based platform of functional materials with a wide range of technological applications.
The aim of this work was to develop *for the first time* a phosphorous-based biorefinery process for promoting the isolation and phosphorylation of the lignin concomitantly from natural coconut fibers through a simple, fast, and sustainable methodology, evaluating its potential applications by a deep structural characterization.

Experimental

1. Materials

All the chemicals were used as received. Natural coconut fibers (NCF) were gently donated by Iapacoco Nordeste S/A (Paraipaba – CE, Brazil).

2. Milled-wood lignin (MWL) extraction from NCF

MWL was extracted from NCF to serve as a standard for structural comparisons to the phosphorylated lignin obtained in the present work. MWL was isolated according to the protocol previously described by Guerra et al. (2004) and Holtman et al. (2006) (GUERRA et al., 2004; HOLTMAN et al., 2006).

3. Phosphorous-based biorefinery process

NCF (ϕ = 2.0 mm) (10 g) was mixed with 100 mL of concentrated phosphoric acid (85 % w/v) in a beaker and the system was kept at 70 ºC for 1 hour under atmospheric pressure. After the end of the reaction, the system cooled down at room temperature. The cellulosic pulp was separated from the black liquor by vacuum filtration, which was exhaustively washed with distilled water (DW) at room temperature (≈ 23 °C) until the pH of the filtrate reached that of the DW. Then, the washed cellulosic pulp was oven-dried at 65 ºC for 24 hours, yielding the modified coconut fiber (MCF). The black liquor obtained in the previous step was used for isolating lignin through acid precipitation. Therefore, DW at 70 ºC was added to the black liquor in a liquor/DW ratio of 1:5 (mL/mL). The mixture was kept resting at room temperature for 24 hours, and subsequently, vacuum filtered to separate the aqueous phase from the isolated lignin. The first filtrate (aqueous phase) was collected and stored in a refrigerator at 2 – 8 ºC for further characterization. The isolated lignin was exhaustively washed with DW at room temperature (≈ 23 °C), following the same procedure described for the cellulosic pulp. Lignin was oven-dried at 65 ºC for 24 hours, weighed, and stored in a glass flask.

4. Physicochemical and structural characterization of the lignocellulosic fractions obtained from the biorefinery process

Fourier Transform Infrared Spectroscopy (FTIR) analyses were carried out using a spectrometer (Perkin Elmer, FT-IR/NIR FRONTIER) using an attenuated total reflectance (ATR) accessory with ZnSe crystal surface. The spectra were acquired in the wavelength range from 4000 to 550 cm^{-1} with a resolution of 4 cm^{-1} and a number of scans (NS) of 16.

Thermogravimetric and derivative thermogravimetric analyses (TGA and DTG) were carried out using Mettler-Toledo TGA/SDTA851e analyzer using 5.0 mg of sample. The measurements were performed from 30 to 800 ºC at a heating rate of 10 ºC min^{-1} under inert and oxidative atmospheres (N_2 and synthetic air, respectively) at a flow rate of 50 mL min^{-1}.
The quantification of the phosphorous present in the lignin was performed by wet chemical analysis combined with UV-Vis spectroscopy according to the methodology described by Ure and Mutus (2020) (URE; MUTUS, 2020).
The ^{1}H-decoupled ^{31}P NMR spectra were recorded on a Bruker AVANCE 400 MHz spectrometer, operating at 161.97 MHz ^{31}P frequency, at 298 K. The experiment was performed with a spectral width of 464.1942 ppm; an acquisition time of 0.218 s, a number of points of 32768, and a number of scans of 2048. About 30 mg of lignin was dissolved in 600 µL of a freshly prepared mixture of anhydrous pyridine and chloroform deuterated (1.6:1, v/v). The mixture was transferred into a 5 mm NMR tube, and 100 µL of chromium (III) acetylacetonate solution (Cr(acac)3; 5 mg/mL) was added to proceed with the analysis. The chemical shifts were related to the external reference of the phosphoric acid signal (85% in D_2O), at δ 0.0 ppm.

Results and Discussion

1. Phosphorous content by UV-Vis quantification

It is important to evaluate if the phosphorous-based biorefinery process was capable of inserting phosphate groups on coconut fiber lignin (CFL) structure since it would represent a useful platform for phosphorylated functional materials such as bio-based flame retardants. In this sense, the amount of phosphorous in CFL was compared to the native lignin (MWL) from NCF. The spectrophotometric quantification data of phosphorous on CFL are presented in **Table 1**.

Table 1 – Phosphorous content on MWL and CFL obtained by spectrophotometric quantification.

Sample	Phosphorous concentration (% wt.)
MWL	0.08 ± 0.005
CFL	0.23 ± 0.02

Table 1 shows that the proposed biorefinery process promoted the phosphorylation of CFL concomitantly to its extraction from NCF since its phosphorous content is three times higher than that of MWL. It is important to highlight that the low amount of phosphorous in MWL can be attributed to the presence of this nutrient on NCF. Therefore, as shown by **Table 1** the contribution of phosphorous already present in NCF is minor, since MWL (native lignin) has presented a very low concentration of the element.
This finding represents an alternative and one-pot methodology to obtain phosphorylated lignin for several applications, including bio-based flame retardants (ILLY et al., 2015; MARCIANO et al., 2022; PRIEUR et al., 2016, 2017). For such purposes, generally, a certain type of technical lignin is submitted to a phosphorylation reaction, which adds an extra step in the lignin valorization chain.
The phosphorous content reported by the aforementioned authors was significantly higher than that shown in **Table 1**. However, it is worth mentioning that in the current work, the phosphorylation of CFL was performed in a one-pot process and has competed with the acid hydrolysis (lignin extraction) of NCF.
Considering the high acidity of the medium it is also necessary to take into account other possible side reactions, such as depolymerization and repolymerization of lignin, which can also contribute to the low phosphorous incorporation in comparison to (PRIEUR et al., 2016).

2. Fourier infrared transform spectroscopy (FTIR)

The grafting of phosphate groups in CFL was evaluated by analyzing their functional groups by FTIR and comparing them to those of protolignin (MWL). The full spectra and the fingerprint region of each spectrum were analyzed, to identify the appearance and/or disappearance of specific

absorption bands, **Figure 1**. The main absorption bands were assigned according to previous reports in the literature.

Figure 1 – (A) Full FTIR spectra; (B) fingerprint region of MWL, CFL and H_3PO_4.

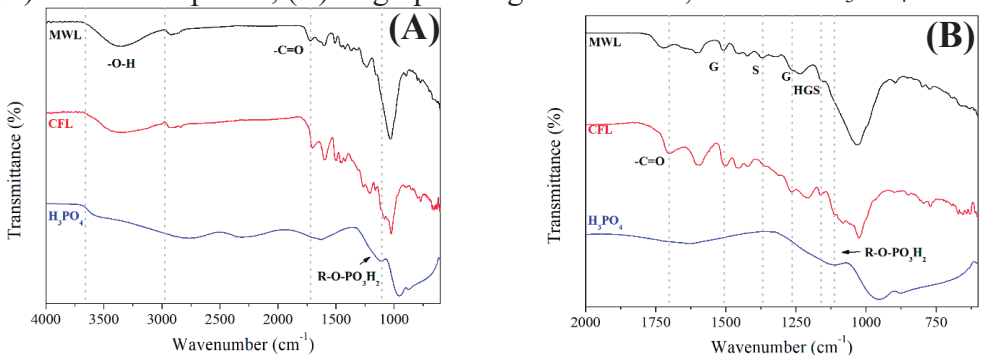

Figure 1(A) shows a notorious decrease in the intensity of the absorption band at 3368 cm^{-1} that is related to the stretching of O – H bonds and could be attributed to the grafting of phosphate groups of aliphatic and phenolic hydroxyl groups present in the lignin structure. Another remarkable difference between MWL and CFL is the displacement of the band related to C = O stretching to lower frequency regions, specifically from 1729 to 1704 cm^{-1}. This fact is indicative of the oxidative effect caused by the pulping process.

Figure 1(B) also shows the appearance of a band at 1109 cm^{-1} in CFL, which is absent in the MWL spectrum, that is characteristic of P – O – R groups and indicates the grafting of phosphorous in the form of phosphate monoester groups as a result of the parallel reaction occurred during the pulping process. Similar results regarding the decrease of the band at 3368 cm^{-1} and the appearance of the band at 1109 cm^{-1} were also reported by Marques et al. (2021) and Prieur et al. (2016) (MARQUES et al., 2021; PRIEUR et al., 2016).

3. ^{31}P NMR

The confirmation of the successful phosphorylation of CFL during the phosphorous-based biorefinery process and the elucidation of the type of phosphorous functional group grafted on its structure were performed by ^{31}P HR-MAS NMR. The ^{31}P NMR spectrum is shown in **Figure 2** and the chemical shifts are reported considering phosphoric acid as a reference.

Figure 2 – ^{31}P HR-MAS spectrum of CFL.

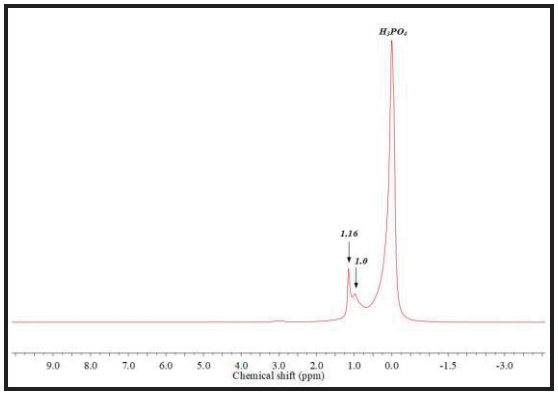

Figure 2 clearly shows the appearance of two signals at 1.0 and 1.16 ppm on ^{31}P NMR of CFL, indicating that the phosphorylation reaction occurred concomitantly to the acid hydrolysis during the pulping process. This structural feature corroborates with those previously observed by UV-Vis quantification, FTIR, and ^{1}H NMR analyses, which already suggested the grafting of phosphorous on CFL.

Furthermore, according to the literature, signals between 0 – 10 ppm on the ^{31}P NMR spectrum are related to phosphate monoester (R-O-PO_2H_2) groups (SANNIGRAHI; INGALL, 2005). This is consistent with the result shown in **Figure 2**. This outcome was already expected since the phosphorylation agent used during the pulping process was phosphoric acid and the proposed mechanism involves a bimolecular nucleophilic substitution (SN_2) on hydroxyl groups of lignin, as reported by (MARCIANO et al., 2022).
The proposed mechanism can also explain the appearance of two signals, which could be related to the grafting of phosphate groups on phenolic and aliphatic groups. It is worth mentioning that Marciano et al. (2022) also reported a broad signal at ^{31}P NMR spectra of phosphorylated acetosolv coconut shell lignin ranging from 0 to 5.0 ppm, which was also classified as phosphate monoester groups (MARCIANO et al., 2022).

Conclusions

The development of a sustainable, fast, simple, and one-pot biorefinery process allowed the obtainment, *for the first time*, of phosphorous-containing lignin from coconut fiber creating a wide platform of functional materials with several potential technological applications. Phosphorylated lignin was obtained in the present work and constitute an interesting building block to be explored in the future years for producing biosorbents, composites, bacterial cellulose, biofuels, additives, antioxidants, and many other bioproducts.

Acknowledgements

The authors acknowledge Brazilian agency FUNCAP (BP4 – 0172 – 00159.01.00/20) for the financial support, Prof. Diego Lomonaco and Prof. Selma Mazzetto from Laboratório de Produtos e Tecnologia em Processos (LPT) at UFC; Central Analítica-UFC/CT-INFRA/MCTI-SISNANO/Pró-Equipamentos; Centro Nordestino de Uso e Aplicação da Ressonância Magnética Nuclear (CENAUREMN) at UFC and Laboratório Multiusuário de Ressonância Magnética Nuclear (LabRMN) at UFPR and Prefeitura Especial de Gestão Ambiental at UFC.

References

AHMAD, F. B. et al. The outlook of the production of advanced fuels and chemicals from integrated oil palm biomass biore fi nery. **Renewable and Sustainable Energy Reviews**, v. 109, p. 386–411, 2019.

FAOSTAT. **Food and Agriculture Organization of the United Nations - Statistics Division, http://www.fao.org/faostat/en/#data/QC (accessed 10.01.2023)FAOSTAT**. [s.l: s.n.].

GUERRA, A. et al. Structural Characterization of Lignin during Pinus taeda Wood Treatment with Ceriporiopsis subvermispora. **Applied and Environmental Microbiology**, v. 70, n. 7, p. 4073–4078, 2004.

HOLTMAN, K. M. et al. Quantitative 13C NMR characterization of milled wood lignins isolated by different milling techniques. **Journal of Wood Chemistry and Technology**, v. 26, n. 1, p. 21–34, 2006.

ILLY, N. et al. Phosphorylation of bio-based compounds: The state of the art. **Polymer Chemistry**, v. 6, n. 35, p. 6257–6291, 2015.

KANT, S. et al. Recent developments in pretreatment technologies on lignocellulosic biomass : Effect of key parameters, technological improvements, and challenges. **Bioresource Technology**, v. 300, p. 122724, 2020.

MARCIANO, S. J. et al. Microwave-assisted phosphorylation of organosolv lignin: new bio-additives for improvement of epoxy resins performance. **Biomass Conversion and Biorefinery**, v. 12, n. 1, p. 619–631, 2022.

MARQUES, J. F. et al. Performance of phosphorylated tannin-based intumescent coatings in passive fire protection. **Journal of Coatings Technology and Research**, v. 18, n. 3, p. 899–910, 2021.

PRIEUR, B. et al. Phosphorylation of lignin to flame retard acrylonitrile butadiene styrene (ABS). **Polymer Degradation and Stability**, v. 127, p. 32–43, 2016.

PRIEUR, B. et al. Phosphorylation of lignin: characterization and investigation of the thermal decomposition. **RSC Advances**, v. 7, n. 27, p. 16866–16877, 2017.

SANNIGRAHI, P.; INGALL, E. Polyphosphates as a source of enhanced P fluxes in marine sediments overlain by anoxic waters: Evidence from 31P NMR. **Geochemical Transactions**, v. 6, n. 3, p. 52–59, 2005.

URE, D.; MUTUS, B. The removal of inorganic phosphate from water using carboxymethyl cellulose-iron hydrogel beads. **Journal of Chemical Technology and Biotechnologyogy**, v. 96, n. 1, p. 38–47, 2020.

On the curing and degradation of bisphenol A diglycidyl ether and epoxidized soybean oil compounds cured with itaconic and succinic acids

José Vinícius Melo Barreto[1], Ananda Karoline Camelo de Albuquerque[1*], Nicholas Guimarães Jacques[1*], Renate Maria Ramos Wellen[1*, 2]

[1]Materials Engineering Department, Federal University of Paraiba, João Pessoa 58051-900, Brazil
[2]Academic Unit of Materials Engineering, Federal University of Campina Grande, Campina Grande 58249-140, Brazil
wellen.renate@gmail.com*

Abstract - This work investigated the curing of compounds made with 1:1 of bisphenol A diglycidyl ether (DGEBA) and epoxidized soybean oil (ESO), cured with itaconic acid (ITA) and succinic acid (SUC), coded as EP/ITA and EP/SUC. Complex peaks observed in DSC are mostly due to the catalyzed curing and homopolymerization. FTIR spectra suggest that the curing follows the SN_2 reaction mechanism for both compounds. Lower activation energies of curing were verified for EP/ITA compared to the EP/SUC, mainly due to their greater reactivity with the epoxy matrix at temperatures below the acids structures and melting points.

Keywords: *Activation energy. Biobased materials. Curing kinetics. Dicarboxylic acids. Thermosets polymers.*
Fundings: CNPq - Conselho Nacional de Desenvolvimento Científico e Tecnológico.

Introduction

Short-chain dicarboxylic acids (DCAs), such as itaconic acid (ITA) and succinic acid (SUC), can be produced by sustainable routes. ITA can be obtained from microorganisms and through citric acid present in several natural resources [1], mainly through the carbohydrate fermentation promoted by Aspergillus terreus strains [2]. Succinic acid is mainly obtained from bacterial fermentation. Itaconic and succinic acids have the same main chain length, however, itaconic acid has a branch characterized by C=C unsaturation at the secondary carbon.

The reported ideal COOH/Epoxy molar ratio (R) is 0.7 for the preparation of systems with high cross-linking density [3,4]. It was reported that the increase in the chain length induces a decrease in the glass transition temperature (T_g) and elongation at the break of cured ESO/DCA, while the tensile strength and Young's modulus increase; this behavior is associated with the decrease of the cross-linking density, and an increase of the density of ester bonds.

In this work, the curing kinetics of EP/ITA and EP/SUC was investigated. Suggested cross-linking schemes were presented based on Fourier transform infrared spectroscopy (FTIR). The curing was followed using differential scanning calorimetry (DSC) while the degradation was investigated by thermogravimetry (TG). The kinetic modeling was performed using Friedman and Vyazovkin's isoconversional models, which provided the curing activation energy (E_{ac}). The degradation activation energy (E_{ad}) of investigated systems was determined using the Kissinger-Akahira-Sunose (KAS) and Ozawa-Flynn-Wall (OFW) models, in addition to other kinetic parameters such as the pre-exponential factor (A) and the reaction order (n). Additionally, the DCA branching influence on cross-linking was systematically reported using DCA molar ratios of 0.4 and 0.7.

Experimental

Bisphenol A diglycidyl ether (DGEBA) (DER 383) with epoxide equivalent weight EEW_{DGEBA} = 182g/eq was supplied by Olin Corporation (Brazil). Epoxidized soybean oil (Vikoflex 7170) with epoxide equivalent weight EEW_{ESO} = 239g/eq was supplied by Arkema. The cross-linkers itaconic acid ($C_5H_6O_4$) (≥99.0%) and succinic acid ($C_4H_6O_4$) (≥99.0%) were purchased from Sigma Aldrich (United States). Isopropyl alcohol was purchased from Neon (Brazil).
The EP/DCA compounds were prepared with the ESO:DGEBA mass ratio of 1:1, the amount of added dicarboxylic acid was evaluated based on the molar ratios $\frac{-COOH}{Epóxi} = 0.4 \text{ and } 0.7$. The dicarboxylic acid was initially solubilized in isopropyl alcohol (IPA) until homogenization, then added to ESO:DGEBA, the reagents were mixed using a magnetic stirrer at 800 rpm for 5 min at 80°C. Afterwards, the samples remained in the exhaust to evaporate the solvent for 24 hours.
Spectra were collected in the wavenumber range 4000-600 cm^{-1}, with 16 scans and 4 cm^{-1} resolution, applying ATR mode. The equipment used was a Perkin Elmer Spectrum 400 (Waltham, Massachusetts, USA) and data modeling was done in the Spectrum software.
DSC scans were computed using DSC SDT 650 from TA Instruments (USA) using a standard closed aluminum pan under a synthetic air gas flow of 50 mL/min. The samples were heated from 25 to 400°C, using the heating rates of 10, 15, 20, and 25°C/min.

Results and Discussion

Figure 1 shows the scheme of the cross-linking reaction on the ESO network and the DGEBA network initiated by dicarboxylic acid. The cross-linking of EP/DCA systems, i.e., the reaction between the DCA and the epoxy oxirane groups, is a nucleophilic substitution reaction type 2 (S_N2) [5]. The oxygen of the -OH bond of the -COOH carboxylic group acts as a nucleophile on the carbon of the C-O-C bond of the epoxy group, breaking the C-O bond and forming the cross-linked network. The negatively charged oxygen due to the breakage of the C-O bond allows a bond with the hydrogen that belongs to the acid molecules in the system, forming hydroxyls along the cross-linked network.
Compared with the SUC, the ITA has one more resonance structure (three in total) due to the unsaturated bond with the alpha carbon of the dicarboxylic acid, which contributes to the higher nucleophilic behavior. Based on this, the compounds EP/ITA showed higher reactivity conducting the cross-linking reaction. For both compounds, the unimolecular mechanism is not favored due to the formation of an unstable carbonation.

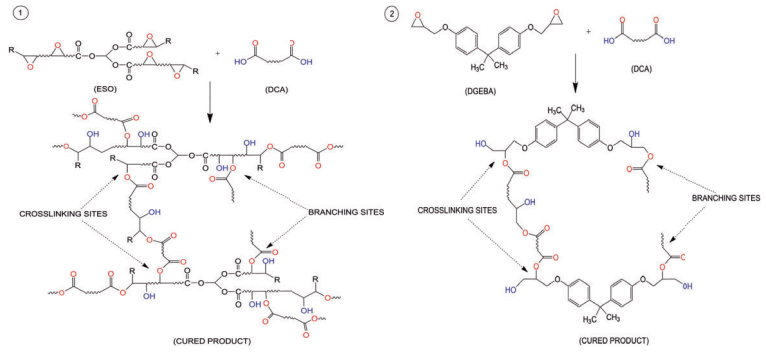

Figure 1 – (1) Suggested scheme for ESO matrix curing, (2) Suggested scheme for DGEBA matrix curing.

Figure 2 displays the FTIR spectra of EP/DCA compounds collected at indicated temperatures. For all the investigated compounds, the epoxy ring characteristic band (915cm^{-1}) decreased with the temperature increase, which confirms the epoxy ring-opening through the nucleophilic attack from the DCA. The gradual increase in the hydroxyl bands (-OH) during the curing is observed at 3450 cm^{-1}, characteristic of the ring-opening reaction, due to the nucleophilic attack on the epoxide groups.

As the cross-linking progressed, the bands at 1190cm^{-1} (corresponding to C-O-C bonds of ethers and esters vibrations) and 1732cm^{-1} (characteristic of the carbonyl group) gradually increased, resulting from ester formed during curing. All compounds, i.e., (A), (B), (C), and (D), displayed similar trends.

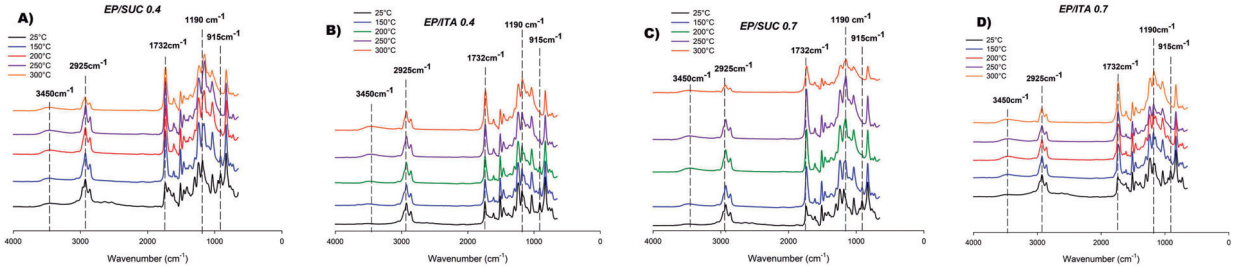

Figure 2: FTIR spectra of EP/SUC 0.4 (A), EP/ITA 0.4 (B), EP/SUC 0.7 (C) and EP/ITA 0.7 (D). Spectra collected at indicated temperatures.

Figure 3 shows DSC scans for compounds cured at 10°C/min. It was observed on the first heating, an exothermic peak associated with the epoxy's cross-linking reaction, with further kinetic modeling and activation energy calculations. Furthermore, there is no evidence of an exothermic peak during the second heating indicating the maximum epoxy conversion was achieved in the first heating According to DSC scans, it is verified that the exothermic peaks are shifted to higher temperatures upon heating rates increase.

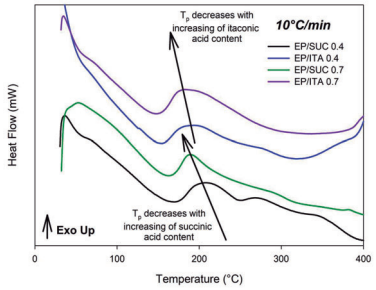

Figure 3: DSC scans acquired using the heating rate of 10°C/min, compositions indicated.

Regarding the sigmoids plots by integration of DSC scans presented in Figure 4, EP/ITA 0.7 presented onset and end at lower temperatures, that is, $T_{0.01}$: 160 °C and $T_{0.99}$: 275 °C, while EP/ITA 0.4 $T_{0.01}$: 164°C and $T_{0.99}$: 288°C. Regarding the curing rate EP/ITA 0.7 showed C_{max}: 0.1325 min^{-1} and ΔT: 115 °C, while EP/ITA 0.4 C_{max}: 0.1350 min^{-1} and ΔT: 124 °C were computed, that is, despite higher maximum curing rate, the cross-linking took place at wider temperature range. The compound EP/SUC 0.7 showed $T_{0.01}$: 180 °C and $T_{0.99}$: 311 °C while EP/SUC 0.4 $T_{0.01}$: 181 °C and $T_{0.99}$: 306 °C were computed. Regarding the curing rate, EP/SUC 0.7 presented higher values, being C_{max}: 0.1503 min^{-1} and ΔT: 130 °C, while EP/SUC 0.4 C_{max}: 0.1402 min^{-1} and ΔT: 125 °C. Overall, EP/SUC compounds displayed onset and end at higher temperatures, at both molar concentrations.
The excess of cross-linking agent, i.e., R = 0.7, made the cross-linking easier due to the greater reactive groups availability, that is, EP/ITA and EP/SUC enthalpies of 299.0 J/g and 361.5 J/g were computed. Exothermic cross-linking events follow endothermic DCA melting events, i.e., ITA $T_m \approx$ 166°C and SUC $T_m \approx$ 185°C. The temperature range ΔT ≈ 20°C as computed using DSC and FTIR are associated with the melting points of the acids used in this work, clarifying the higher reaction kinetics observed for EP/ITA related to EP/SUC. Although the ITA shows the highest reactive than SUC, SUC has higher $C_{máx}$ and higher enthalpy (ΔH), indicating the epoxy with SUC has higher cross-linking density.

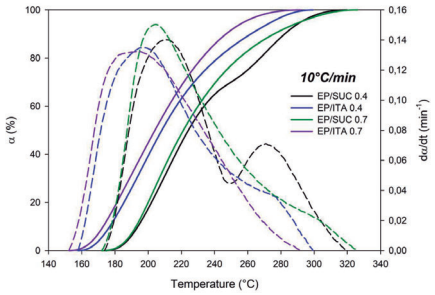

Figure 4: Degree of curing (α) and curing rate (dα/dt) as temperature function for the investigated compounds using the heating rate of 10°C/min.

The conversion rate of a chemical reaction is commonly written as the product of a temperature-dependent rate constant k(T) and a conversion function f(α) characteristic of the reaction mechanism, as shown in Eq. 1:

$$\frac{d\alpha}{dt} = k(T)f(\alpha) \quad (1)$$

The conversion rate assuming a constant rate k(T) defined by Arrhenius is shown in Eq. 2:

$$k(T) = Aexp^{-\frac{E_{ac}}{RT}} \quad (2)$$

The isoconversional model-free method assumes that the activation energy (E_{ac}) and the pre-exponential factor are functions of the degree of curing. In this work, E_{ac} was determined using the Friedman method, based on the logarithmic form of the curing rate as shown in Eq. 3:

$$ln\left(\frac{d\alpha}{dt}\right) = ln\,[A.f(\alpha)] - \frac{E_{ac}(\alpha)}{RT} \quad (3)$$

Vyazovkin developed an advanced nonlinear procedure that performs integrations in small conversion intervals, Δα ≈ 0.01, where E_{ac} is considered constant. Then, for a series of n experiments at different heating rates, E_{ac} is determined for each interval as the value that minimizes the function given by Eq. 5. Systematic errors associated with the main integrations are then minimized by this method:

$$J[E_{ac}, T(t_\alpha)] = \int_{t_\alpha - \Delta\alpha}^{t_\alpha} \exp\left(\frac{-E_{ac}}{RT(t)}\right) dt \quad (4)$$

$$\sum_{i=1}^{n}\sum_{j\neq i}^{n} \frac{J[E_{ac}, T_i(t_\alpha)]}{J[E_{ac}, T_j(t_\alpha)]} \quad (5)$$

E_{ac} of EP/DCA compounds were plotted as a function of the curing degree (α) through the Friedman and Vyazovkin methodologies as shown in Figure 5, these kinetic models displayed good R^2, 0.96528 to 0.99325. Related to EP/ITA compounds, increasing the molar ratio from R = 0.4 to R = 0.7 decreased the E_{ac} i.e., 42.5 kJ/mol and 34.5 kJ/mol for α = 50%. EP/ITA 0.4 displayed an increase in E_{ac} from α = 40%. It is supposed that this behavior is associated with epoxy homopolymerization due to the lower availability of acid groups for the curing. In the final curing stages, E_{ac} decreased in EP/ITA compounds, suggesting that the curing is controlled by diffusion. Concerning the EP/SUC compounds, E_{ac} of EP/SUC 0.7 was higher than for EP/SUC 0.4 for the range α < 55%, i.e., 65kJ/mol and 59kJ/mol at α = 50%. EP/SUC 0.4 showed a considerable increase in E_{ac} from α = 55% mostly due to the epoxy homopolymerization, as also observed for EP/ITA. At α = 70% for EP/SUC 0.4 and EP/SUC 0.7, E_{ac} was 98.5kJ/mol and 72.0kJ/mol respectively; the decrease in E_{ac} in the final stage of curing also suggests a change in the reaction mechanism to a diffusion-controlled reaction. Associating the kinetic modeling with the data

computed using DSC, EP/ITA compounds displayed lower E_{ac} due to a higher reactivity. The matrix of EP/ITA compounds showed a higher rate of epoxy ring consumption versus EP/SUC systems as computed by FTIR in lower temperatures.

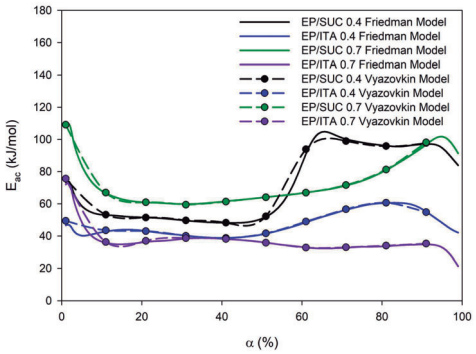

Figure 5: E_{ac} as function of the degree of curing evaluated using Friedman and Vyazovkin methods

Conclusions

EP/ITA and EP/SUC compounds were successfully produced; the evaluation of the curing were investigated using FTIR and DSC. The results demonstrated that increasing the DCA molar ratio results in a greater degree of cross-linking. EP/ITA 0.7 showed a higher rate of oxirane group consumption, while EP/SUC 0.7 showed a higher maximum curing rate. The activation energy of curing, computed using Friedman and Vyazovkin, showed that curing was more favorable for EP/ITA, however, EP/SUC showed higher cross-linking densities. The effect of branching, resonance structures, and the lower melting point of ITA in relation to SUC favored faster cross-linking. It can be concluded that the applied methodology offers alternatives in the epoxies cross-linking in order to precisely define the degree of cross-linking as well as the thermal stability for applications in several technological sectors.

Acknowledgements

The authors would like to thank to CNPq for the funding and Fraunhofer Institute for Environmental, Safety and Energy Technology (UMSICHT) for their kindly supporting.

References

1. Zhao, M., Lu, X., Zong, H., Li, J., & Zhuge, B. (2018). Itaconic acid production in microorganisms. Biotechnology letters, 40(3), 455-464. https://doi.org/10.1007/s10529-017-2500-5.
2. El-Imam, A. A., & Du, C. (2014). Fermentative itaconic acid production. J Biodivers Biopros Dev, 1(1), 1-8. doi:10.4172/2376-0214.1000119.
3. Mustata, F., & Tudorachi, N. (2017). Curing kinetics and thermal characterization of epoxy resin cured with amidodicarboxylic acids. *Applied Thermal Engineering*, *125*, 285-296. https://doi.org/10.1016/j.applthermaleng.2017.07.037
4. Chen, Y., Xi, Z., & Zhao, L. (2017). Curing kinetics of bio-based epoxy resin based on epoxidized soybean oil and green curing agent. *AIChE Journal*, *63*(1), 147-153. https://doi.org/10.1002/aic.15486
5. Zeng, R. T., Wu, Y., Li, Y. D., Wang, M., & Zeng, J. B. (2017). Curing behavior of epoxidized soybean oil with biobased dicarboxylic acids. Polymer Testing, 57, 281-287. 10.1016/j.polymertesting.2016.12.007

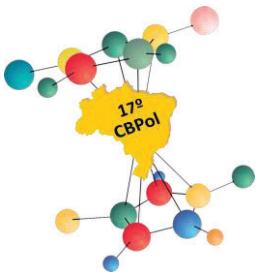

SYNTHESIS OF POLY(BUTYLENE SUCCINATE)-CO- GLUTAMIC ACID MICROPARTICLES VIA SUSPENSION AND MINIEMULSION POLYMERIZATION

Luciana Dutra[1]*, Jéssica Bentes[2], Martina C. C. Pinto[1], Milena Ferreira[3], Marcio Nele[3], José Carlos Pinto[1]

1 – Chemical Engineering Program (PEQ/COPPE), Federal University of Rio de Janeiro (UFRJ), Rio de Janeiro, RJ, Brazil
ldutra@eq.ufrjbr
2 – Nanotechnology Program (PENT/COPPE), Federal University of Rio de Janeiro (UFRJ), Rio de Janeiro, RJ, Brazil
3 – Chemical School (EQ), Federal University of Rio de Janeiro (UFRJ), Rio de Janeiro, RJ, Brazil

Abstract - Renewable monomers such as succinic and glutamic acid can produce biodegradable materials for biomedical applications. Besides, combining these monomers polymers presenting distinct properties may be synthesized. In this way, microparticles were made via polycondensation exploring suspension and miniemulsion methods. The suspension method produced well-defined microparticles with an average size of 250 µm for both poly(butylene succinate) and copolymers, containing 2.5% w/w and 5% w/w of glutamic acid. The 10% w/w glutamic acid copolymer showed greater polydispersion, and an average size higher than 520 µm. On the other hand, miniemulsion method produced particles with an average particle diameter smaller than 100 µm for copolymers with 5% w/w and 10% w/w of glutamic acid. Microparticles' hydrophobicity was also determined by contact angle. Glutamic acid increased the biodegradability of the copolymers, more significantly in the miniemulsion system. Thus, the addition of glutamic acid as a functional comonomer not only preserved the polymeric microparticle formation, but also increased their biodegradability.
Keywords: *Microparticles, glutamic acid, biodegradable, PBS, poly(butylene succinate)*

Fundings: FAPERJ (Fundação Carlos Chagas Filho de Apoio à Pesquisa do Estado do Rio de Janeiro) (project numbers E-26/204.566/2021, E-26/204.567/2021, E-26/201.246/2021, and E-26/202.251/2018). CAPES (Coordenação de Aperfeiçoamento de Pessoal de Nível Superior)

Introduction

The biotech industry is advancing in new fermentation processes to generate multifunctionalized organic acids [1]. Succinic acid (SA), in particular, is noteworthy due to its potential cost-effectiveness compared to its petrochemical counterpart. It can be obtained from glucose with a theoretical yield greater than 100%, It consumes CO_2 during production and is a raw material for several chemical compounds, forming a chemical platform from a renewable source, dispensing with the use of oil in its manufacture [2].
Additionally, SA can be used to produce poly(butylene succinate) (PBS), which is a biodegradable aliphatic polyester obtained from succinic acid and 1,4-butanediol. It has favorable characteristics for biomedical applications, including high water resistance, good thermal and mechanical properties, and non-toxic degradation products. PBS is a sustainable biomaterial option [3].
In addition to succinic acid, which can be produced from renewable sources and used to make biodegradable PBS, glutamic acid is another functionalized acid derived from biomass that can be

utilized in biodegradable and biocompatible materials for various biomedical applications. Glutamic acid has been employed in the production of antimicrobial complexes, vaccine adjuvants, and materials for cancer therapy. By incorporating the -NH2 group in glutamic acid into the PBS chain, the material's affinity with proteins and cells can be improved, and covalent or ionic interactions with drugs, antibodies, or DNA can be facilitated, resulting in a more efficient release of drugs and genes [4-5].

Polymeric microparticles range in size from 1 to 1000 μm and are classified as microspheres or microcapsules. They find applications in biomedical and cosmetic fields and may or may not contain active ingredients. Functional groups on their surface can promote bioconjugation with biomolecules [6-7]. Spray drying, solvent evaporation, coaxial electrospray, microfluid dynamics, and dispersion in supercritical CO2 are some of the common methods used for their production. While these methods use a polymeric solution to form the particles, polymer synthesis occurs simultaneously in the reactor for emulsion and suspension polymerizations, eliminating a production step [8].

Dutra et al [2,9] recently developed a suspension polycondensation process for manufacturing microparticles in a single step. Their work demonstrated the successful production of microparticles of poly (butylene succinate) (PBS) through polycondensation in suspension of succinic acid and 1,4-butanediol. This method can be applied to obtain microparticles from different polymer matrices, offering the potential to obtain various particles from renewable, biodegradable sources.

To promote the development of eco-friendly materials, it is essential to explore biodegradable materials that produce non-toxic intermediates during the depolymerization process. The objective of this study is to produce biodegradable microparticles of PBS copolymer with glutamic acid, through the comparison of suspension and miniemulsion production processes. The miniemulsion approach aims to achieve smaller particle sizes, and the influence of sonication in the polycondensation process will be evaluated. Additionally, the biodegradability of the resulting particles will also be investigated.

Experimental

Materials

Succinic acid (SA) was obtained from Sigma Aldrich (Rio de Janeiro, Brazil), 1,4-butanediol (1,4-BD) was supplied by MERCK (Darmstadt, Germany), and L-glutamic acid (AG) was provided by Dinâmica (Indaiatuba, Brazil) both used as monomers. SPAN 80 (sorbitan monooleate) was obtained from FLUKA (Mexico City, Mexico), and Tween 80 was supplied by Sigma Aldrich (Rio de Janeiro, Brazil), both used as surfactants. Corn oil, obtained from Bunge Alimentos (Santa Catarina, Brazil) as a food-grade material, was used as a suspending medium in some of the polymerization trials. All reagents were of analytical grade and high purity and were used as received without further purification.

Production of Poly(butylene succinate-co-glutamate) (PBS-AG) microparticles

Polymeric microparticles of poly(butylene succinate-co-glutamate) (PBS-AG) were prepared using suspension and miniemulsion polymerization techniques. The method for suspension polycondensation was based on the methodology described by Dutra et al. (2019) [9], whilst the method for polycondensation in miniemulsion was based on the method by Alves et al. (2022) [10]. The main difference between the two methods was the inclusion of a sonication step in the miniemulsion procedure (as shown in Figure 1).

The ratio of the disperse phase to continuous phase was 30:70 for all runs, and the content of glutamic acid varied from 2.5% to 10% w/w in relation to the total carboxylic acid content. In the

first step, the monomers (succinic acid, glutamic acid, and 1,4-butanediol) were dissolved in a solution containing 50% w/w water and the surfactant Tween 80 (1% w/w in relation to the monomeric phase). Meanwhile, the solution containing the surfactant (SPAN 80 10% w/w in relation to the disperse phase) and the continuous phase (plant oil) was prepared, and both solutions were stirred for approximately 20 minutes. For the miniemulsion procedure, the dispersed phase and the continuous phase were mixed and then homogenized using a sonicator provided by Branson (Branson 450, Marshall Scientific, Hampton, USA) at an amplitude of 40% (equivalent to 160 W) for 3 minutes. After the homogenization step, the miniemulsion was added to the reactor. For the suspension method, the solubilized monomers were added to a 100 ml glass reactor (EasyMax 102, Mettler Toledo, Ohio, USA) containing the continuous phase. In both cases, the reaction occurred under stirring at 900 rpm and a temperature of 160°C. The final step includes washing the material with acetone, performing vacuum filtration, and subsequently drying it, for the suspension methodology. For the miniemulsion methodology, the final step involves washing with acetone and centrifugation.

The resulting PBS-AG microparticles were characterized using various techniques, including, particle size distribution analysis, determination of hydrophobicity degree, gel permeation chromatography and biodegradability.

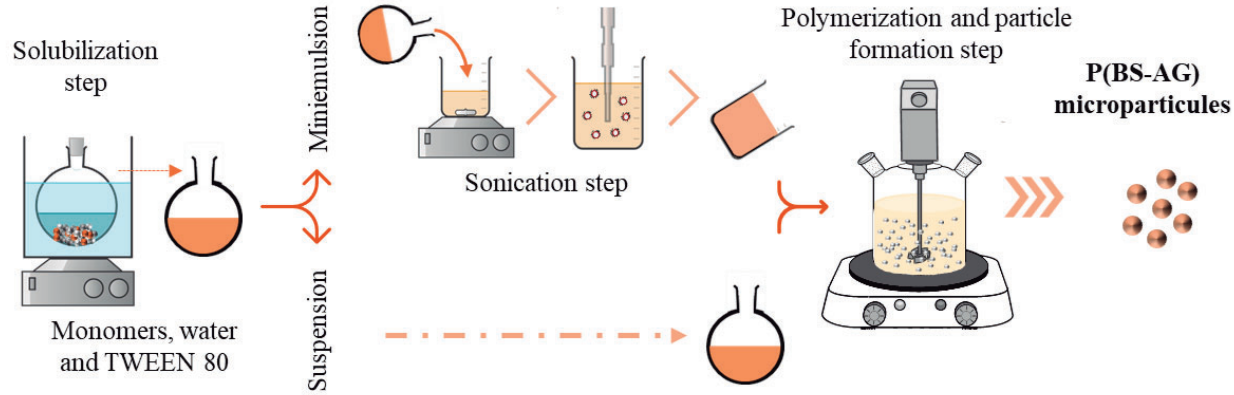

Figure 1 - Scheme showing the stages of the suspension and miniemulsion polymerization process

Results and Discussion

Polymeric microparticles based on biodegradable poly(butylene succinate-co-glutamate) copolymers were prepared via polycondensation in suspension and miniemulsion. Glutamic acid was added at concentrations of 2.5%, 5%, and 10% w/w in order to produce the biodegradable microparticles. The introduction of chemical groups into the polymer structure allows the modification of beads' surface and interface properties, leading to changes in the material's physical, chemical, or biological properties [11].

The main objective of this study was to produce microparticles of biodegradable PBS copolymers with glutamic acid, which proved to be a challenging task due to the difficulty of stabilizing the microparticles. The particles obtained in suspension presented molar masses in the magnitude of 3 x 10^3 Da, whereas the miniemulsion particles exhibited molar masses in the magnitude of 7 x 10^3 Da. Interestingly, the molar mass of the particles produced in the suspended system did not vary significantly with the formation of the copolymer, as shown in Table 1. In contrast, the particles produced in the miniemulsion system presented higher molar masses, suggesting that the sonication step, which generates high energy, may have favored chain growth.

Figure 2 presents the particle size distributions of the produced microparticles. The microparticles produced in suspension exhibited a well-defined size distribution, with an average size of approximately 250 µm for both PBS and the copolymers with 2.5% and 5% of glutamic acid.

However, the copolymer with 10% of glutamic acid exhibited greater polydispersion, with average sizes of approximately 520 µm, as demonstrated in Table 1. In contrast, the miniemulsion reactions showed multimodal size distributions, but shifting the particles sizes towards lower values, suggesting that particle agglomeration might be occurring during the reaction and drying process.

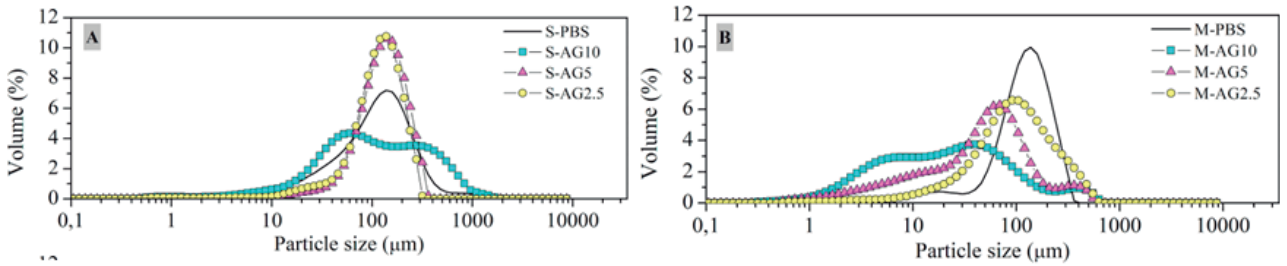

Figure 2 – Particle size distribution of biodegradable microparticles produced with 2.5%, 5% and 10% w/w of glutamic acid.

Table 1. Characterization of the produced particles.

	Samples	Contact angle [°]	Particle size (µm)	Molar mass			Weight loss (%)	
				Mn (Da)	Mw (Da)	Mw/ Mn	7 days	30 days
Suspension	PBS-AG 2,5%	63.5 ± 5.8	226	2686	2760	1.03	6.7 ± 0.5	9.0 ± 3.6
	PBS-AG 5%	56.5 ± 6.1	246	2678	2746	1.02	6.5 ± 0.5	6.7 ± 0.8
	PBS-AG 10%	68.4 ± 3.6	520	2,699	2775	1.03	7.5 ± 0.9	12.8± 3.3
	PBS	71.1 ± 3.4	296	2412	2318	0.9	3.3 ± 2.4	6.0 ± 1.7
Mini emulsion	PBS-AG 2,5%	77.8 ± 5.9	125	6101	10601	1.7	28.1 ± 3.1	27.9 ± 5.0
	PBS-AG 5%	65.3 ± 0.3	72	5002	7143	1.4	30.3 ± 0.5	29.2 ± 2.1
	PBS-AG 10%	68.0 ± 11.6	55	6120	8288	1.3	35.4 ± 6.9	33.9 ± 1.4
	PBS	63.2 ± 5.6	128	140	887	6.3	3.2 ± 1.4	5.4 ± 1.5

The hydrophobicity level of the produced microparticles were evaluated by measuring their contact angle with water (Table 1). The amount of glutamic acid in the copolymer was expected to affect the overall hydrophobicity, as PBS is a hydrophobic polymer and glutamic acid is a polar and hydrophilic amino acid. Thus, adding low amounts of glutamic acid, the copolymer would remain predominantly hydrophobic, exhibiting only a few hydrophilic areas, in which the glutamic acid was present. On the other hand, adding high amounts of glutamic acid, the copolymer would become more hydrophilic and polar, with limited hydrophobic areas. The microparticles containing up to 10% w/w of glutamic acid did not show a statistically significant change in contact angle in relation to the glutamic acid content for both suspension and miniemulsion systems. However, this surface phenomenon is currently being investigated in more detail to better understand the influence of glutamic acid on the cristalinity and degree of hydrophobicity of the material, as well as the possible effect of the microparticle synthesis process.

The synthesized microparticles are currently undergoing biodegradation tests in a neutrum medium (pH of 7.4), simulating the pH of blood. As shown in Figure 3, the presence of glutamic acid increased the biodegradability of the material, particularly in the miniemulsion system. Glutamic acid, a natural amino acid, probably promotes enzymatic degradation, leading to the breakdown of microparticles. Thus, the accelerated biodegradation is due to the susceptibility of glutamic acid to enzymatic attack, gradually eroding the microparticles. Even in the suspension system, in which the degradation is less efficient than in the miniemulsion system, mass losses occur compared to pure PBS microparticles. This indicates that including glutamic acid in the copolymer increases the materials' biodegradability, regardless the formulation method.

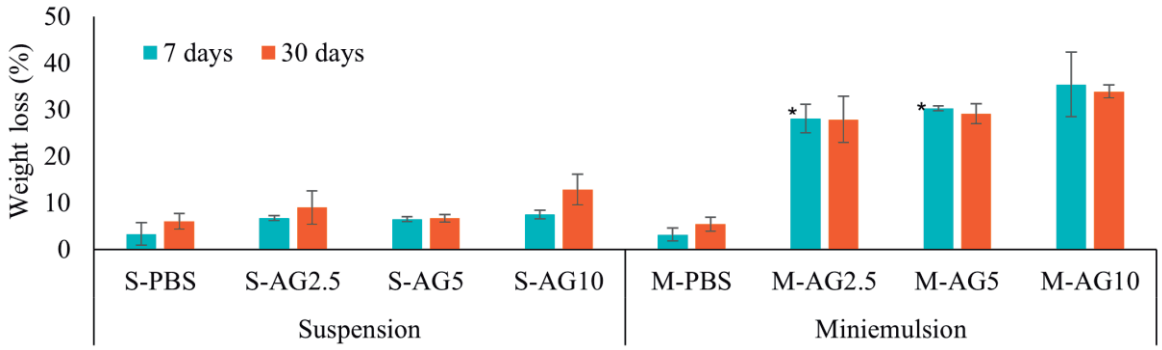

Figure 3 – Weight loss for degradation tests in medium with pH 7.4.
*this samples was collected with 14 days.

Conclusions

The findings of this study reveal that the addition of glutamic acid as a functional comonomer presents minimal impact on the formation system of polymeric microparticles, enabling the production of particles of varying sizes. The miniemulsion process alters the particle size distribution, resulting in a multimodal behavior, whereas the suspension process produces well-defined distributions. Furthermore, the miniemulsion process generates particles with a higher molar mass, implying that the sonication process has a favorable effect on chain growth. Thus, the addition of glutamic acid as a functional comonomer not only preserved the polymeric microparticle formation, but also increased their biodegradability.

Acknowledgements

Authors thank CNPq (Conselho Nacional deDesenvolvimento Científico e Tecnológico), CAPES (Coordenação de Aperfeiçoamento de Pessoal de Nível Superior) and FAPERJ (Fundação Carlos Chagas Filho de Apoio à Pesquisa do Estado do Rio de Janeiro).

References

1. G.T. Tsao; N.J. Cao; J. Du; C.S. Gong in *Recent Progress in Bioconversion of Lignocellulosics.*, Springer, Heidelberg. 1999.
2. T.M. Joseph; A.B. Unni; K.S. Joshy; D. Kar Mahapatra; J. Haponiuk; S. Thomas Journal of Carbon Research 2023, 9, 30. https://doi.org/10.3390/c9010030.
3. L. Dutra; M. Nele; J. C. Pinto Macromolecular Symposia, 2018, 381, 1, 1800118. https://doi.org/10.1002/masy.201800118
4. C. Deng; G. Rong; H. Tian; Z. Tang; X. Chen; X; Jing Polymer, 2005 46, 653–659. https://doi.org/10.1016/j.polymer.2004.11.100.
5. J. Hulsbosch; L. Claes; D. Jonckheere; D. Mestach; D. E. De Vos; RSC Advances, 2018, 8, 8220–8227. https://doi.org/10.1039/c8ra00060c
6. E. Jabbari; M. Khakpou; Biomaterials, 2000, 21, 2073-2079. https://doi.org/10.1016/S0142-9612(00)00135-6
7. GUAN, J.; CHAKRAPANI, A.; HANSFORD, D. J. Polymer Microparticles Fabricated by Soft Lithography. [s. l.], n. 13, p. 6227–6229, 2005.
8. L. Dutra; M. Nele; J. C. Pinto Journal of Polymers and the Environment, 2021, 29, 219-229. https://doi.org/10.1007/s10924-020-01869-7
9. L. Dutra; M. Nele; J. C. Pinto Macromolecular Reaction Engineering, 2018, 12, 6, 1800039. https://doi.org/10.1002/mren.201800039
10. J. B. Alves, Ph. D. Thesis, Universidade Federal do Rio de Janeiro, 2022.
11. S. Park; M. Sung; H. Uyama; D.K. Han. Progress in Polymer Science, 2021, 113, 101341. https://doi.org/10.1016/j.progpolymsci.2020.101341

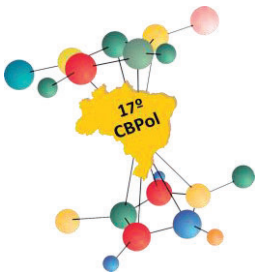

EVALUATION OF CARBOXYMETHYL-KAPPA-CARRAGEENAN AS A SCALE AND CORROSION INHIBITOR: A THEORETICAL AND EXPERIMENTAL APPROACH

Rafael S. Fernandes*, Onézimo F. M. Neto, Kallyne F. Damasceno, Miguel Angelo F. de Souza, Elessandre Alves de Souza, and Rosangela C. Balaban

Institute of Chemistry (IQ), Federal University of Rio Grande do Norte (UFRN), Natal, RN, Brazil

rafael.fernandesqa@gmail.com

Abstract – Chemical modification of polysaccharides is an important route to improve, develop or change the properties of these biopolymers. In this work, kappa-carrageenan (KC) was modified (carboxymethylation, CM) and applied as a scale and corrosion inhibitor (CMKC). For the carboxymethylation reactions, κ-carrageenan and monochloroacetic acid were used in an alkaline medium (NaOH), under heating at 55 ºC and reflux. The chemical characterization of the materials was performed by infrared spectroscopy. The dynamic efficiency test, used to determine the efficiency and the minimum effective concentration (MEC) of the CMKC as a scale inhibitor, was performed based on the NACE standard TM31105-2005 (capillary precipitation test) using the Differential Scale Loop equipment (DSL 4025) from PSL Systemtechnik, Germany. The efficiency of CMKC as a corrosion inhibitor was determined by gravimetric mass loss test and conductimetry. Theoretical calculations were performed to support the experimental evidence of the inhibitor. Density functional theory (DFT) calculations were performed using the B3LYP-D3/6-311+G(2df,p)//6-31+G(d,p). The results of the chemical characterization demonstrated that the strategy used for the carboxymethylation of KC was efficient. The appearance of the band at 1594 cm^{-1} (C = O) confirms the addition of a carboxyl group to the KC molecule. Dynamic tests revealed that the inhibitor was effective when applied at concentrations of 100 mg/L (MEC) and 120 mg/L. The results indicate that the carboxyl group interacts with the fouling cation (Ca^{2+}) and prevents the formation of $CaCO_3$ scale.[1,2] Corrosion tests have shown that the addition of CMKC significantly reduces the corrosion rate. DFT calculations suggest that the mechanism of action of the inhibitor, through the carboxyl group, occurs through complexation with the encrusting cations.[3] Finally, the results indicate that the inhibitor CMKC can be an alternative for the simultaneous prevention of scale and corrosion formation.

References

1. Wang, Y.; Li, A.; Yang, H. ;Desalination 2017, 408, 60.
2. Hasson, D.; Shemer, H.; Sher, A. ;Ind. Eng. Chem. Res. 2011, 50, 7601.
3. Gutierrez, M. E.; Gaona, S. J.; Calvete, F. E.; Botett, J. A.; Ferrari, J. V. ;Proc. - SPE Int. Symp. Oilf. Chem. 2019, 2019.

Fundings: The authors are thankful to Petróleo Brasileiro S.A. – PETROBRAS for financial support.

Keywords: *Scale inhibitor, corrosion inhibitor, carrageenan, polysaccharides, biopolymers.*

FORMALDEHYDE MIGRATION STUDY IN POLYOXYMETHYLENE FROM COSMETICS INDUSTRY PACKAGING COMPONENTS, BY EXTRACTABLE TESTING AND GC-MS

Guilherme M. Menegasso[1], Jonathan Dos Santos[2], Letícia B. Cerqueira[2], Leandro C. Gonçalves[2], Fernanda G. Henning[2], Desirée C. Schuck[2], Márcia P. P. Dos Santos[2]*

1 – Euvaldo Lodi Institute, Curitiba, PR, Brazil
2 – Cencoderma Institute, São José dos Pinhais, PR, Brazil
mporto@grupoboticario.com.br

Abstract - Polyoxymethylene (POM) is an engineering polymer, known as Polyacetal or Acetal Resin. It features elevated mechanical resistance to fatigue, which brings its advantages on several applications, including packaging, automotive parts and industrial equipment. However, POM may be questionable for some purposes, such as in direct contact with some cosmetic formulations, due to the raw material used in the production process. There are two main variations of POM for industrial uses: homopolymer and copolymer. The homopolymeric one is produced from the polymerization of formaldehyde, a substance considered as carcinogenic by IARC (International Agency for Research on Cancer) and by Proposition 65 from California. The copolymeric POM is produced from 1, 3, 5-Trioxane and a cyclic ether, as Methylene Oxide, Propylene Oxide or 1, 4-Dioxane, they also present carcinogenic potential. To identify the presence of formaldehyde extracted from POM components, the applied methodology was based in gas chromatography coupled with mass spectrometry (GC-MS), using the derivatization agent 2, 4-Dinitrophenylhydrazine (2, 4 DNPH). A liquid lipstick stick was taken as a sample, and immersed in isododecane (Permethyl 99A®), which acted as an extracting agent. For analysis, three sample takings were conducted, 2 mL, 4 mL and 6 mL, besides the blank and a contaminated matrix with 2 mL of formaldehyde 37%, those were injected into GC-MS. After the runs, the chromatograms were analyzed and it was observed that the samples with aliquots presented defined and gradual peaks in 19.05 min and, in comparison with the contaminated sample, it was possible to detect the presence of formaldehyde in the extracting agent. The result obtained leads to the conclusion about the presence of free formaldehyde in the polymer sample, simulating a potential migration of the molecule in formulation with high concentrations of isododecane or similars.

References:

1. F. A. Lobo; T. M. O. Santos; K. M. Vieira; V. M. Osório; J. G. Taylor. Drug Testing and Analysis, 7, 2015, 1808. https://doi.org/10.1002/dta.1808.
2. W. Yuniati; T. Amelia; S. Ibrahim; S. Diamayanti. ACS Omega, 6, 2021, 28403. https://doi.org/10.1021/acsomega.1c04792.
3. B. D. A. D. Daoudy; M. A. Al-Khayat; F. Karabet; M. A. Al-Mardini. Journal of Analytical Methods in Chemistry, 2018, 2018, 4526396. https://doi.org/10.1155/2018/4526396.
4. A. De Souza; I. C. M. Cunha; J. O. Chagas; E. B. P. Carlos; L. L. Santos; T. R. Campos e Figueiredo; L. A. L. Machado; V. M. Osório; K. M. Vieira; F. A. Lobo. InTech, 2017, 68922. https://dx.doi.org/10.5772/intechopen.68922.

Keywords: *Polyoxymethylene, cosmetic packaging , formaldehyde, chromatography, polyacetal*

INCORPORATION OF RENEWABLE CARBONS VIA FORMAMIDE REACTIVITY FOR NOVEL BIOBASED POLYMERS

Bianca C. Rocha[1], Isabela H. Dourado[1], Noemi S. P. Kimura[1], Priscila H. Cordeiro[1], Luiz H. Catalani[1] and Leandro H. Andrade[1]*

1 – Department of Chemistry, University of São Paulo (USP), São Paulo, SP, Brazil
leandroh@iq.usp.br

Motivated by the great importance of polymers in our society, this work aims to develop a new synthetic approach to produce biobased polymers in which all their carbons come from renewable sources. The first step of this work proposes the exploration of formamide reactivity with vinylic esters. Formamide ($HCONH_2$) can be produced from carbon dioxide (CO_2).[1] The first step of this work involved the synthesis of monomers from the reaction of vinyl esters with the carbamoyl radical ($\bullet CONH_2$), under a continuous flow system, using TBADT (tetrabutylammonium decatungstate) as a photocatalyst.[2] (Fig 1a). In the second step of this work, the monomer prepared from itaconic ester was polymerized with biobased diols,[3] originating a new polyester with nitrogen in its structure (Fig 1b). For the polycondensation, a reaction sequence was proposed in which a thermal cyclization, esterification, and subsequent opening of the succinimide ring allowed the growth of the oligomer chain, leading to a highly branched polymer structure.

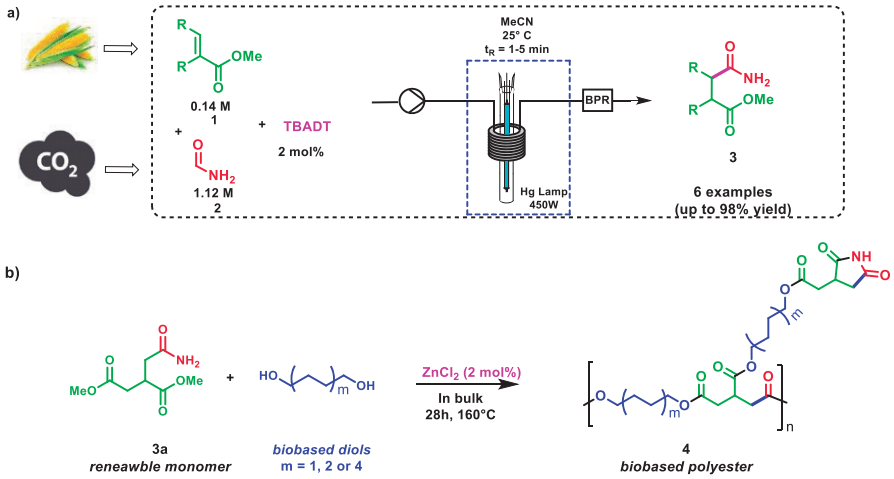

Figure 1: a) Synthesis of the monomers, b) Reaction of Polymerization.

References

1. Schaub, T.; Paciello, R.; Pazicky, M.; Fachinetti, G.; Preti, D. US Patent 2013/0102807A1, 2013; BASF SE
2. Angioni, S.; Ravelli, D.; Emma, D.; Dondi, D.; Fagnoni, M.; Albini, A. *Advanced Synthesis & Catalysis*. 2008, 350, 2209-2214. DOI: 10.1002/adsc.200800378.
3. Zhang, Q.; Song, M.; Xu, Y.; Wang, W.; Wang, Z.; Zhang, L. *Progress in Polymer Science*. 2021, 120, 101430.

Fundings: FAPESP (2021/12555-3 and 2022/15898-1)
Keywords: *renewable monomers, biobased polymer, polyester, nitrogen, formamide*

SYNTHESIS OF ALKYNE-FUNCTIONALIZED CELLULOSE FOR ATTACHMENT OF BIOMOLECULES BY THIOL-YNE CLICK CHEMISTRY

Marcos V. Ferreira[1]*, Anizio M. de Faria[1,2], Rodrigo B. Panatieri[1,2], Brent S. Sumerlin[3], Rosana M. N. Assunção[1,2]

1 – Institute of Chemistry, Federal University of Uberlândia, Uberlândia, MG, Brazil
marcosferreira@ufu.br
2 – Institute of Exact and Natural Sciences of Pontal, Federal University of Uberlandia, Ituiutaba, MG, Brazil
3 – George & Josephine Butler Polymer Research Laboratory, Department of Chemistry, University of Florida, Gainesville, FL, USA

Abstract - To expand the applications of cellulose for protein/enzyme immobilization and biocompatible reactions such as thiol-yne click reactions, it is essential to incorporate an alkyne into the cellulose support. In this work, we developed a methodology for the synthesis of a derivative intermediate, tosyl-cellulose (MCC-Tos), through the optimization of the reaction conditions (i.e., time, temperature, and the anhydroglucose unit/tosyl chloride molar equivalent) using a Doehlert Matrix of statistical design. The degree of substitution of the tosyl groups (DS_{tos}) was quantitatively determined by analyzing specific bands in the infrared (IR) spectra: ν_{simSO2} at 1174 cm^{-1} from the tosyl group and νC1-O-C5 at 1056 cm^{-1} from the cellulose backbone. The optimized product exhibited a DS_{tos} value of 0.81. MCC-Tos was subsequently reacted with propargylamine, and the progress of the reaction was monitored by periodic analysis of the IR spectra. The IR spectra showed a decrease in the intensities of the bands associated with the tosyl groups, indicating the progress of the reaction. Equilibrium was reached after 48 h (Fig. 1A). Additionally, the DS_{tos} value demonstrated a decrease of approximately 50% in the initial number of tosyl groups (Fig. 1B). Thermogravimetric analysis (TGA/DTG) indicated a reduction in tosyl groups, as evidenced by an increase of about 30 °C in the thermal stability of the resulting aminopropargyl cellulose (MCC-P_{NH}). The presence of alkyne groups on MCC-P_{NH} was further investigated by attaching an azide-functionalized coumarin by copper(I)-catalyzed alkyne-azide cycloaddition (CuAAC), followed by quantification with UV spectroscopy. The degree of substitution for the aminopropargyl group was estimated to be 0.21. In conclusion, the synthesis of the alkyne-functionalized cellulose was successful, enabling opportunities for further investigation into the reaction conditions required for protein attachment via the thiol-yne click reaction.

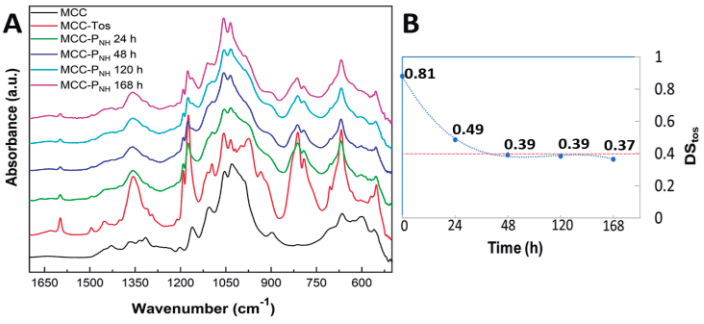

Figure 1. A) IR spectra of the cellulosic samples. B) DS_{tos} as a function of propargyl reaction time.

References

1. Rahn, K.; Diamantoglou, M.; Klemm, D.; Berghmans, H.; Heinze, T. *Angewandte Makromolekulare Chemie* 1996, *238*, 143–163. https://doi.org/10.1002/apmc.1996.052380113

Fundings: The authors would like to thank CAPES, CAPES-PrInt, PROPP, FINEP (INFR13 01.13.0371.00), the University of Florida, and the National Science Foundation (NSF).

Keywords: *Cellulose Derivatives, Tosylation, Alkyne-functionalization, Click Chemistry.*

Título: Síntese de poliaminoácidos dibloco com arquitetura estrela por polimerização por abertura de anel de N-carboxianidrido

Autores: Daniel José da Silva[1], Raphael Colonese Vlasman[1], Luiz Henrique Catalani[1]

[1] Instituto de Química, Universidade de São Paulo, Av. Lineu Prestes, 748, CEP 05508-000, São Paulo, SP, Brasil.

Resumo:

A síntese de poliaminoácidos (PAAs) através de polimerização por abertura de anel (ROP) de N-carboxianidridos (NCAs) é uma alternativa vantajosa quando sequências definidas de aminoácidos (AAs) não são exigidas. Através da ROP é possível obter poliaminoácidos com arquitetura tipo estrela projetados para oferecer uma rota barata para materiais biocompatíveis para engenharia de tecidos e sistema de entrega de fármacos, além de apresentar outras propriedades interessantes para diferentes aplicações que envolvam comportamento pseudoplástico, respostas a estímulos externos e capacidade de automontagem. Neste trabalho, copolímeros em bloco em forma de estrela contendo um centro de núcleo hidrofílico de L-lisina e um invólucro hidrofóbico de L-fenilalanina ou L-leucina foram sintetizados por ROP. A estrutura química dos polímeros foi confirmada por ressonância magnética nuclear de ^{1}H. Dicroísmo circular indicam que os PAAs formam estruturas secundárias dependendo do pH do meio e do comprimento do bloco hidrofóbico. O aminoácido hidrofóbico influência no teor das estruturas secundárias e no comportamento reológico dos PAAs em solução aquosa.

Palavras-chave: poliaminoácidos, reologia, polimerização, polímeros responsivos, carboxianidridos.

Title: Synthesis of star-shaped diblock poly(amino acids) by ring-opening polymerization of N-carboxyanhydrides

Authors: Daniel José da Silva[1], Raphael Colonese Vlasman[1], Luiz Henrique Catalani[1]

[1] Institute of Chemistry, University of São Paulo, Av. Lineu Prestes, 748, CEP 05508-000, São Paulo, SP, Brazil.

Abstract:

The synthesis of poly(amino acids) (PAAs) via ring-opening polymerization (ROP) of N-carboxyanhydrides (NCAs) is a promising alternative when defined sequences of amino acids (AAs) are not required. Through ROP, it is possible to obtain star-shaped PAAs designed to offer a cheap route to biocompatible materials for tissue engineering and drug delivery systems. They also present other interesting properties for different applications involving responses to external stimuli, pseudo-plasticity and self-assembly capacity. In this work, star-shaped block copolymers containing a L-lysine hydrophilic core center and a hydrophobic shell based on L-phenylalanine or L-leucine were synthesized by ROP. The chemical structure of the polymers was confirmed by ^{1}H nuclear magnetic resonance. Circular dichroism indicates that PAAs form secondary structures depending on the pH of the medium and the hydrophobic block length. The hydrophobic amino acid influences the secondary structure content and the rheological behavior of the star-shaped block PAAs in an aqueous solution.

Keywords: poly(amino acids), rheology, polymerization, responsive polymer, carboxyanhydrides.

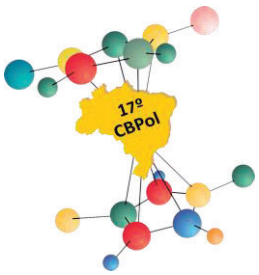

CHEMICAL GRAFTING OF BACTERIAL CELLULOSE WITH AMINOPROPYLTRIETHOXYSILANE

Ketlin C. B. Mancinelli[1]*, Victoria Mendes[2], Marcia M. Meier[3], Ana Paula T. Pezzin[4] and Gilmar S. Erzinger[1]

1 – Post-graduation Program in Health and Environment, University of Joinville Region (Univille), Joinville, SC, Brazil ketlin.cb@gmail.com
2 – Department of Chemical Engineering, University of Joinville Region (Univille), Joinville, SC, Brazil
3 – Department of Chemistry, Santa Catarina State University (UDESC), Joinville, SC, Brazil
4 – Post-graduation Program in Process Engineering, University of Joinville Region (Univille), Joinville, SC, Brazil

Abstract - Bacterial cellulose (BC) is biosynthesized primarily by acetic acid bacteria, the most common belonging to the *Komagataeibacter* genus. Many applications of BC are related to its porous structure composed of randomly arranged extremely fine fibrils that can be compromised by drying and chemical modification processes. The objective of this study was to obtain amine-grafted BC with aminopropyltriethoxysilane without significantly compromising the porous structure of BC. The efficiency of grafting was confirmed by Fourier transform infrared spectroscopy by the presence of new bands in the region of 1600 cm^{-1} attributed to the NH_2 groups and confirmed by X-ray photoelectron spectroscopy. Scanning electron microscope images showed that amine-grafted BC membranes demonstrated changes in porosity, but maintained the typical 3D network structure of BC. The water contact angle increased in amine-grafted BC due to the covalent linkage with hydrophobic aminoalkylsilane groups.

Keywords: *Bacterial cellulose, Aminoalkylsilane group, Chemical modification.*

Introduction

The chemical grafting reaction of aminoalkyl groups on cellulose surfaces normally involves 3 stages: a) hydrolysis of the silane derivative to form silanol; b) adsorption of hydrolyzed species on BC nanofibrils by hydrogen bonding between silanol and cellulosic OH and c) chemical condensation reaction leading to siloxane bridges (Si−O−Si) and grafting on the surface of BC nanofibrils through Si−O−C bonds. The siloxane bridges resulting from self-condensation contribute to the formation of a polysiloxane network on the surface of BC nanofibers [1,2]. This grafting reaction of aminoalkyl groups can be realized in order to intend to mimic the intrinsic antimicrobial properties of chitosan. Fernandes et al. [1] devolved novel grafted bacterial cellulose membranes using 3-aminopropyltrimethoxysilane that were lethal against *S. aureus* and *E. coli* and nontoxic to human adipose-derived mesenchymal stem cells with potential for biomedical applications. Shao et al. [3] obtained functionalized BC membranes prepared using aminoalkylsilane that displayed effective antibacterial and antifungal activities against *E. coli*, *S. aureus*, *S. subtilis*, and *C. albicans* with great potential applications in biomedical applications. BC can be also functionalized using aminosilane to provide better interaction with different biopolymers. BC can be also functionalized using aminosilane to provide better interaction with different biopolymers and is considered the most suitable choice for chemical grafting on the BC membrane due to their well-known potential for the surface modification of hydroxyl-containing surfaces [4]. Then aldehyde groups can be covalently bonded to cellulose by the reaction between

the NH_2 from the functionalized cellulose and the aldehyde or carboxyl groups of the cross-linkers by the formation of a Schiff base [5]. Hamedi et al. [6] developed a novel hydrogel composed of BC and schizophyllan (SPG) biopolymers. BC was first functionalized using 3-aminopropyl triethoxysilane to provide better interaction with SPG and glutaraldehyde was employed as a cross-linking agent. Amine-grafted BC/SPG exhibited moderate antibacterial activity and stimulated the proliferation of normal human fibroblast cells. Therefore, this study proposes to obtain the amino-functionalized BC with 3-aminopropyl triethoxysilane (APTES) without compromising its structure.

Experimental

BC membranes were produced using the *Komagataeibacter hansenii* (ATCC 23769). The cell activation and culture medium was in HS medium [7]. BC membranes were produced in static conditions for 12 d culture. These membranes were washed in NaOH at 80 °C in order to remove bacteria and then several times in water, until neutral pH. The wet BC membranes were autoclaved in distilled water at 121 °C for 20 min at 1 atm and stored at 4 °C. The chemical grafting reaction of aminoalkyl groups on wet BC was based on Frone et al. [5] with adaptations. Firstly, 0.5 g of APTES was pre-hydrolyzed in a 90/10 vol% ethanol/water mixture (50 mL) at room temperature for 2 h. Glacial acetic acid (99.8%) was used to adjust the silane solution to pH 4 and the solution was continuously stirred. After pH stabilization, a number of 20 wet BC membranes were added to the silane solution and stirred at RT for 2 h. The mixture was heated under reflux at 110 °C for 2 h to perform the chemical reaction. In the final grafting step, BC membranes (M1) were washed thoroughly by Soxhlet extraction with solvent (ethanol) for 10 h and grafted membranes were finally freeze-dried. The methodologies were optimized and adapted throughout the study, varying the proportion of ethanol/water, APTES, the concentration of the solution, the number of membranes, and the type of washing to remove residual APTES (Table 1). Methodology optimized: An amount of APTES was pre-hydrolyzed in a 90/10 vol% ethanol/water mixture (100 mL) at RT for 2 h. A number of 5 wet BC membranes were added to the silane solution and stirred at RT for 24 h. The wet membranes were removed from the silane solution and lyophilized in order to avoid the collapse of the pores of the amine-grafted BC. Then, amine-grafted BC membranes were heated in an oven at 110 °C for 2 to promote reaction condensation. Amine-grafted BC membranes were washed in an ultrasonic bath in ethanol. Especially in methodology n. 6, washing was conducted in steps using ultrasonic baths every 10 min. In the 1st step, the membranes were immersed in ethanol/water (30/70%), in ethanol/water (70/30%), and in ethanol (100%). In the 2nd step, rehydration was performed in ethanol/water (70/30%), ethanol/water (30/70%), and distilled water (100%) (overnight). FTIR was used to characterize the chemical structure of the BC and the amine-grafted BC membranes. The FTIR - Attenuated Total Reflectance (ATR) of the BC and amine-grafted BC membranes were recorded on Spectrum One equipment (Perkin- Elmer) in the range of 4000–600 cm^{-1} at a resolution of 4 cm^{-1}. Membrane surface morphologies were analyzed by scanning electron microscope JEOL (model JSM-6701F). The samples were prepared by coating them with a layer of gold. Images of 5,000 times were obtained. XPS measurements were carried out with a K-Alpha spectrometer (Thermo Scientific) using Al Ka radiation (1486.6 eV) and a base pressure of 10^{-8} mBar. Thermal gravimetric analysis (TGA) was performed on a thermal analyzer (TA Instruments, Q50). Samples were heated from room temperature to 1000 °C at a scanning rate of 10 °C/min under a nitrogen atmosphere. Static water contact angles were measured using the sessile drop method with a goniometer (Ramé-Hart Inst. Co. model 250-F1).

Table 1. Variations in the methodologies used in this study.

Method	ethanol/water (vol%)	APTES (g)	Solution (mL)	Number of membranes	Type of Washing
1	90/10	0.5	50	20	Soxhlet/etanol
2	90/10	1	100	5	Ultrasonic /Ethanol
3	10/90	1	100	5	Ultrasonic /Ethanol
4	10/90	0.1	100	5	Ultrasonic /Ethanol
5	10/90	0.5	100	5	Ultrasonic /Ethanol
6	10/90	1	100	5	Ultrasonic /Ethanol and water

Results and Discussion

Fig. 1 shows the evolution of BC according to the applied methodology. The visual analysis demonstrated that amine-grafted BC membranes tend to collapse (M1-5). The M6 not revealed collapse, maintaining characteristics similar to BC.

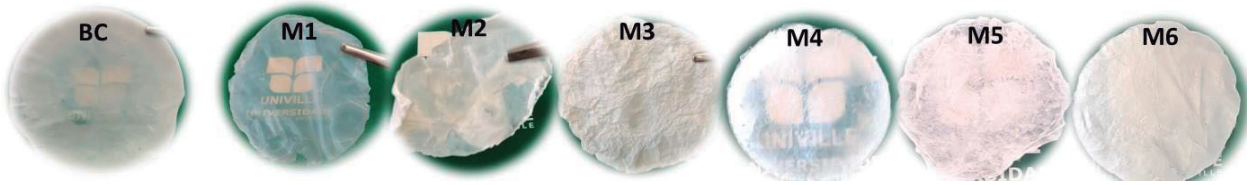

Figure 1. Evolution of modification methodologies and visual aspect of grafted BC membranes.

Fig. 2a shows the FTIR spectra of BC and amine-grafted BC membranes. Amine-grafted BC membranes showed a spectrum profile similar to BC. The peak at around 3400 cm^{-1} is attributed to the −OH stretching vibration. In some spectra, the −OH peak becomes broader, attributed to the overlap with the NH_2 stretching vibration [6,8]. An increment of the band around 2900 cm^{-1} can be associated with the CH_2 vibrations of the propyl moiety of the silane moiety [1,4]. M3 (both sides) presented bands at 1560 cm^{-1} and 1480 cm^{-1} attributed to the bending of NH_2 groups [1,4-6]. However, FTIR should be evaluated compared with other techniques because bands close to these regions may be characteristic of structures of proteins (amino acids), lipids, metabolites, and some residual biomass of bacteria or compounds of the culture medium trapped between the fibrils of BC [9]. Other bands around 870-897 cm^{-1} appear in the spectra (M3) and can be attributed to the wagging of amino groups (NH_2) [6]. The presence of Si−O−cellulose and −Si−O−Si−bridges that correspond to the condensation of the hydroxyl groups of the silane derivative with the hydroxyl groups of BC and of those silanols that react with themselves, respectively, are not easily identified by FTIR, since the typical vibrations of these moieties occur around 1150 and 1135 cm^{-1}, and are overlapped by the large and intense cellulose C−O−C vibration bands (1162-1034 cm^{-1}) [1]. M1, M3, and M6 were selected for further study. Table 2 shows the TGA and the corresponding differential thermogravimetry (DTG) profiles of BC and amine-grafted BC membranes. M1 and M3 showed two thermal events in the range of 25-150 °C. A major degradation step was observed for all the samples, at 334 °C (BC), 326 °C (M1), 295 °C (M3), and 329 °C (M6). Amine-grafted BC (M1-5) showed a loss in thermal stability compared to BC. The residue at 1000 °C was 1.6% for BC and higher for amine-grafted BC (M1-5), corresponding to an increase of 92% (M3) that is indicative of the successful chemical grafting reaction of the BC with aminosilane considering that the increment in the inorganic residue is mainly due to SiO_2 [1]. M6 did not present an increase in the inorganic residue observed at ∼1000 °C and can be associated with no successful modification. Therefore, M6 was selected because of its good aspect visual and to confirm the FTIR and TGA results. XPS analysis was performed to confirm the FTIR results (Fig. 2b). The survey spectra showed of BC showed two major peaks at 286.08 and 533.08 eV, corresponding to C 1s and O 1s adsorption, respectively, indicating that the main components in BC were C and O [10]. For M3

two main peaks at 285.08 eV and 531.08 eV were detected due to C 1s and O 1s adsorptions, respectively, and three additional news peaks, one at 399.08 eV in the N 1s region and two peaks at 102.08 eV and 153.08 eV corresponding to the binding energies of Si 2s and 2p, respectively [3]. XPS results confirm the presence of APTES only on M3.

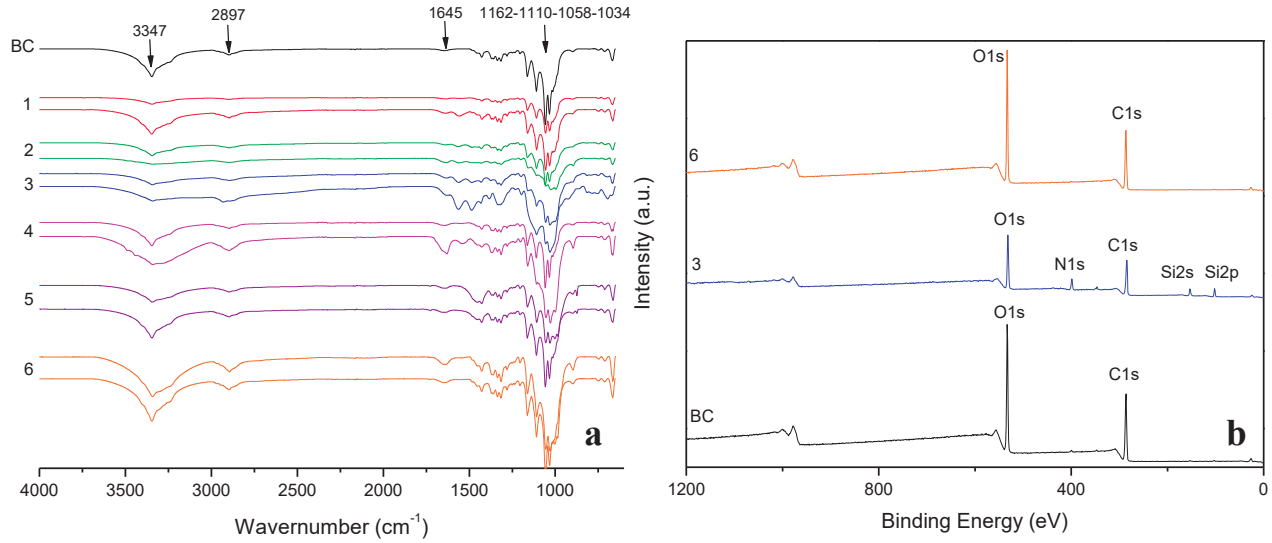

Figure 2. a) FTIR spectra of BC and APTES grafted BC membranes (M1-6), b) XPS survey spectra of BC and grafted BC membranes (M3 and M6).

Table 2. Important values from TG curves of BC and grafted BC membranes.

Membranes	Thermogravimetric data			
	T_{onset} °C	T_{max} °C	Weigth lost %	Residue % at 1000 °C
BC	333.99	361.66	86.46	1.60
M1	325.91	369.08	72.48	10.83
M3	295.06	350.17	48.37	19.41
M6	328.62	359.22	81.41	0.41

The surface morphology of BC showed an organized 3D and porous network structure characteristic of freeze-dried BC (Fig. 3a) [11,12]. Therefore, for M3 (Fig. 3b) the nanofibrils are thicker because of the coverage with silane associated with the formation of Si−O−Si bridges [1,3]. M6 (Fig. 3c) presented a more homogeneous fibril profile compared to BC. The high hydrophilicity and porosity of the membranes determine the absorption of water droplets during the contact angle (CA) measurements [13]. CA measurements for BC were difficult to obtain due to the complete spreading of the water drop over the BC surface. In the literature, CA measurements are found between 30° to 48° [3,10,13]. M3 showed a CA value of about 58° due to covalent bonding with hydrophobic aminoalkylsilane groups.

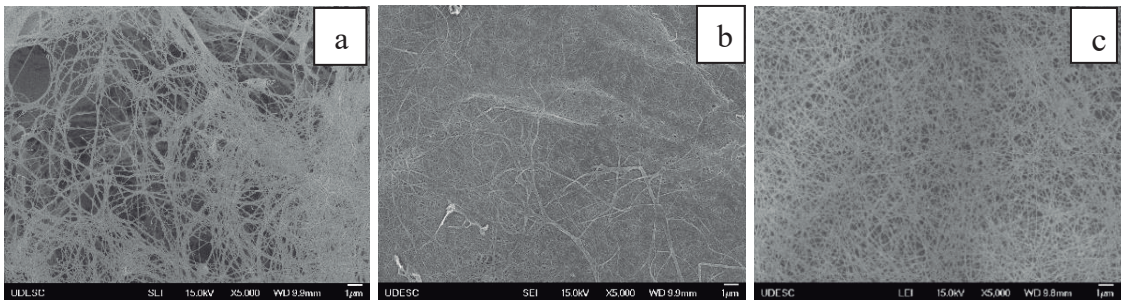

Figure 3. SEM surface micrographs for BC (a), M3 (b) and M6 (c).

Conclusions

Amine-grafted BC membranes were obtained using a higher concentration of distilled water without pH adjustment. SEM images revealed a loss in porosity that influenced the wettability of membranes. It was observed that membrane washing (M6) interfered with surface functionalization with APTES. FTIR analyses showed differences in absorption according to the side of the sample. This characteristic must be considered.

Acknowledgements

One of the authors (K. C. B. Mancinelli) gratefully acknowledges the scholarship offered by the Coordenação de Aperfeiçoamento de Pessoal de Nível Superior – Brasil (CAPES). The authors are also indebted for the financial support of Univille Research Support Fund (FAP/Univille) and sincerely grateful to Santa Catarina State University (UDESC) for XPS, SEM, and AC analyses.

References

1. S.C.M. Fernandes; P. Sadocco; A. Alonso-Varona; T. Palomares; A. Eceiza; A.J.D. Silvestre; I. Mondragon; C.S.R. Freire ACS Applied Materials and Interfaces 2013, 5(8), 3290–3297. https://doi.org/10.1021/am400338n
2. J. Meng; X. Zhang; L. Ni; Z. Tang; Y. Zhang; Y. Zhang; W. Zhang Desalination 2015, 359, 156–166. http://dx.doi.org/10.1016/j.desal.2014.12.032
3. W. Shao; J. Wu; H. Liu; S. Ye; L. Jiang; X. Liu Carbohydrate Polymers 2017, 178, 270–276. http://dx.doi.org/10.1016/j.carbpol.2017.09.045
4. S. Saini; M.N. Belgacem; J. Bras Materials Science and Engineering C 2017, 75, 760–768. http://dx.doi.org/10.1016/j.msec.2017.02.062
5. A.N. Frone, D.M. Panaitescu; C.A. Nicolae; A.R. Gabor; R. Trusca; A. Casarica; P.O. Stanescu; D.D Baciu; A. Salageanu Materials Science and Engineering C 2020, 110, 110740. https://doi.org/10.1016/j.msec.2020.110740
6. S. Hamedi; S. A. Shojaosadati; V. Najafi; V. Alizadeh Carbohydrate Polymers 2020, 229, 115383. https://doi.org/10.1016/j.carbpol.2019.115383
7. S. Hestrin; M. Schramms Biochemical Journal 58(2), 345–352. https://doi.org/10.1042/bj0580345
8. Hamedi; S. A. Shojaosadati Cellulose, 2021, 28(14), 9269–9282. https://doi.org/10.1007/s10570-021-04119-8
9. N.F. Vasconcelos; F.K. Andrade; L. de A.P. Vieira; R.S. Vieira; J.M. Vaz; P. Chevallier; D. Mantovani; M. de F. Borges; M. de F. Rosa Cellulose 2020, 27(6), 3055–3083. https://doi.org/10.1007/s10570-020-02966-5
10. W. He; Z. Zhang; Y. Zheng; S. Qiao; Y. Xie; Y. Sun; K. Qiao; Z. Feng; X. Wang; J. Wang Journal of Biomedical Materials Research - Part A 2020, 108(5), 1086–1098. https://doi.org/10.1002/jbm.a.36884
11. J. Kim; Z. Cai; H.S. Lee; G.S. Choi; D.H. Lee; C. Jo Journal of Polymer Research 2011, 18, 739–744.
12. M.L. Cacicedo; G. Pacheco; G.A. Islan; V.A. Alvarez; H.S. Barud; G.R. Castro International Journal of Biological Macromolecules 2020, 147, 1136–1145. https://doi.org/10.1016/j.ijbiomac.2019.10.082
13. A.N. Frone; D.M. Panaitescu; I. Chiulan; C.A. Nicolae; A. Casarica; A.R. Gabor; R. Trusca; C.M. Damian; V. Purcar; E. Alexandrescu; P.O. Stanescu Coatings 2018, 8, 221.

CUSTOMIZING BIOBASED RESINS OF EPOXIDIZED SOYBEAN OIL AND ISOSORBIDE WITH ALUMINIUM TRIFLATE AS CATALYST

I. D. S. Silva[1*], M. F. Souza[1], P. Moerbitz[2] , I. Bretz[2], A. Ries[3], R. Wellen[1,4]

1 – Department of Materials Engineering, University of Campina Grande (UFCG), Campina Grande, PB, Brazil
2 –Fraunhofer Institute for Environmental, Safety and Energy Technology (UMSICHT), Oberhausen, Germany
3 – Multidisciplinary Center for Technological Investigations, National University of Asunción, San Lorenzo University Campus, San Lorenzo 1039, Paraguay
4 – Department of Materials Engineering, Federal University of Paraíba (UFPB), João Pessoa, PB, Brazil

*Ingrydy.dayane@gmail.com**

Abstract - Synthesis of thermosetting resin (ESOISO) based on isosorbide (ISO) and Epoxidized Soybean Oil (ESO) catalyzed by aluminium triflate ($Al(OTf)_3$) was performed. Cross-linked ESOISO was obtained, and the curing kinetics was followed via Fourier transform infrared spectroscopy (FTIR) and differential scanning calorimetry (DSC). The resins ESOISO 0.07 mol% and ESOISO 0.1 mol% showed 80% conversion at 180 min, while ESOISO 0.05 mol% was approximately 60% of conversion as verified by FTIR. The curing peak temperature (T_p) of ESOISO 0.1 mol% ranged from 80 to 115°C, depending on the heating rate. ESOISO 0.07 mol% displayed lower activation energy (E_a) during curing as modeled using Friedman model, showing a constant plateau within the conversion range of $0.1 < \alpha < 0.6$, subsequently decreasing in the range $\alpha > 0.6$ to 60.59 kJ/mol. Rheological experiments supported the hypothesis that the gelation process affects the apparent viscosity evolution. $Al(OTf)_3$ addition produced ESOISO with higher viscosity and shear stress due to gel or cross-linking structures. These results support the evidence of $Al(OTf)_3$ reactivity as a catalyst for epoxidized soybean oil and isosorbide resins.
Keywords: epoxidized soybean oil, isosorbide, aluminium triflate ($Al(OTf)_3$), curing kinetics
Funding: Coordenação de Aperfeiçoamento de Pessoal de Nível Superior (CAPES), Conselho Nacional de Desenvolvimento Científico e Tecnológico (CNPq), Fundação de Apoio à Pesquisa do Estado da Paraíba (FAPESQ).

Introduction

Isosorbide (ISO) is a green platform chemical that may be produced from glucose through hydrogenation to sorbitol and two-fold dehydration via sorbitan. ISO itself provides versatile possibilities for applications as monomeric segments in new polymers [1, 2]. Epoxidized soybean oil (ESO), consisting of glycerol esters with three long-chain fatty acids, is a promising feedstock for producing bio-based polyols or resins conferring to the polymer products' strong mechanical strength, design flexibility, and solution processability [3].

ESOs can be polymerized by a cationic mechanism or Lewis acid-catalyzed ring opening photo-polymerization. However, acids are mostly toxic and/or corrosive and generate many side reactions. Aluminium triflate ($Al(OTf)_3$), a Lewis acid catalyst, has been used as a catalyst in organic synthesis for reactions such as the ring opening of epoxides in the presence of alcohols or amines. However, challenges associated with the mechanisms and curing kinetics of these systems acquired by non-isothermal polymerization remain in the literature [4-6].

The present work aimed to synthesize bio-based ESO resin modified with ISO using $Al(OTf)_3$. The exothermal curing was followed using differential scanning calorimetry (DSC), kinetics and thermodynamic parameters were evaluated, while chemical conversion was tracked using Fourier-

transform infrared spectroscopy (FTIR). The rheological properties of uncured resins (before the complete curing, after 2 hours of reaction) were analyzed.

Experimental

Epoxidized soybean oil (ESO) was supplied by HOBUM. D-Isosorbide was purchased from Thermoscientific (Germany), and Aluminium triflate or $Al(OTf)_3$ was purchased by Sigma Aldrich (Germany). The reaction took place in a three-necked 100 mL round-bottomed flask equipped with a magnetic stirrer, in nitrogen-gas atmosphere, and an outlet connected to the condenser. ISO was heated to 100°C and left stirring for 20 min under distillation. A stock solution of the catalyst in acetone was prepared (0.021 M) to take the necessary volumes to reach the required molar percentage: 0.05, 0.07, and 0.1 mol%. ESO and $Al(OTf)_3$ were added to the flask and stirred under a nitrogen atmosphere.

Differential Scanning Calorimetry (DSC) was performed uisng a DSC 8000 from PerkinElmer, over the temperature range from 25 to 250°C at 2, 5, 10, 15, and 20°C/min under nitrogen atmosphere (100 mL/min). Experiments were performed using specimens with 5-7 mg.

Fourier Transform Infrared Spectroscopy (FTIR) spectra were captured considering the wavenumber range 4000-350 cm^{-1}, 16 scans per spectrum, and 16 cm^{-1} resolution. The equipment used was Bruker Tensor 27 (Germany).

The rheology test was carried out using an Anton Paar MCR-302 with a parallel plate measuring system with a diameter of 25 mm at 60°C with 1mm of gap between the disks. The measurement was made with a rotational movement with a shear rate of 0.1 to 100 1/s.

Results and Discussion

The infrared spectra of ESOISO are shown in Fig. 1. Accordingly, the spectra display a very intense band at 3429 – 3464 cm^{-1} due to the vibration peak of hydroxyl groups (–OH). The presence of the band at 1100 – 1200 cm^{-1} and 1097 cm^{-1} are assigned to the C–O–C stretching from ester groups. ESO and ISO show a characteristic band at 820 – 830 cm^{-1}, related to the epoxy ring band absorption for ESO and furan ring vibration for ISO. It is observed that the reaction time under 60°C leads to a reduction of the bands intensities attributable to the oxirane ring in ESO (820 – 830 cm^{-1}), no absorption changes were verified in the region of –OH stretching, and absorption increase in the region of stretching vibrations of C–O–C ether bonds at 1097 cm^{-1}, which indicates an interaction of ester bonds with oxirane groups or –OH groups of ISO. This interaction began to be noted at 60 min of reaction and increased until 180 min of reaction at 60°C [7-8].

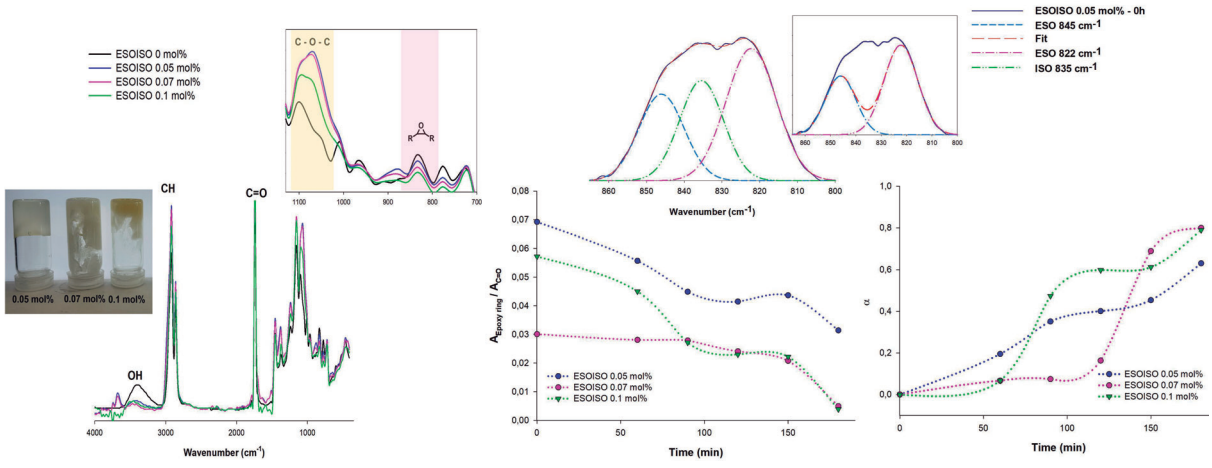

(a) (b)

Figure 1 – (a) FTIR spectra of ESOISO, (b) decay of the relative absorbance ($A_{Epoxy}/A_{C=O}$) and degree of conversion estimated using Beer-Lambert Law at 60°C for 180 min.

The region of the epoxy ring (820 – 830 cm^{-1}) was deconvoluted with Gaussian−Lorentzian functions using Fityk software, and the epoxy conversion was quantified based on the Beer-Lambert law. The spectra were deconvoluted, the area of the epoxy ring band, and the conversion versus time are displayed in Fig. 1b. For the compositions ESOISO 0.07 mol% and ESOISO 0.1 mol%, the

conversion reached 80% of conversion at 180 min, while for ESOISO 0.05 mol%, with less catalyst amount, it was approximately 60% of conversion. [8, 9].
Aliquots of the mixtures were run using the DSC to investigate the polymerization, and curing kinetics, based on the thermodynamical analysis for directly assessing the heat energy uptake during the reaction. DSC scans acquired under a dynamic environment of ESOISO containing different amounts of catalyst (0, 0.05, 0.07, and 0.1 mol%) are shown in Fig. 2. An endothermic peak at a low-temperature range (around 60°C) was first observed for all samples, ascribed to ISO melt. Subsequently, a broad exothermic peak results from the epoxy group ring-opening.
There was no exothermic peak of ESOISO crosslinking in the DSC scans for ESOISO 0 mol% (without catalyst). Adding $Al(OTf)_3$ to ESOISO an exothermic peak was verified related to the epoxy rings opening due to the functionalization of ESO with ISO and, consequently, homopolymerization of ESO, with peak temperatures (T_p) at around 80 - 115 °C, depending on the heating rate and catalyst content [5]. $Al(OTf)_3$ addition shifted T_p to lower temperatures, suggesting an increased curing rate, accelerating the curing process. Adding 0.1 mol% of $Al(OTf)_3$ decreased the T_p and enabled the curing to finish at the temperature range of 109.56 - 156.16 °C, depending on the heating rate.
The heating rate also influences the curing of ESOISO. The exothermic peak was shifted to higher temperature as the heating rate increased. This behavior is a direct consequence of the reaction kinetics and it is assigned to the time lag effect.
Fig. 2b shows the degree of conversion versus temperature of ESOISO systems at indicated heating rates and the sigmoidal shape for the degree of conversion versus temperature was observed for all systems.Through the DSC thermograms, mainly for the compositions with higher catalyst content, the heating rates of 10 and 15°C/min had similar behavior. The mechanism was not sensitive to the heating rate at 15°C/min. Once the degree of conversion is calculated based on DSC scans, it is possible to observe the overlap in the conversion curves at rates of 10 and 15°C/min.

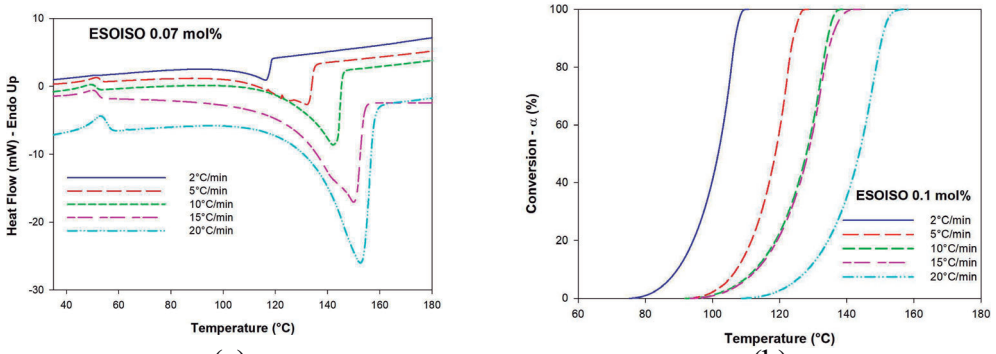

(a) (b)

Figure 2 – (a) DSC scans of ESOISO 0.07 mol%, (b) degree of conversion versus temperature for ESOISO 0.1 mol%.

Thermodynamics and kinetic parameters computed from DSC are graphically displayed in Fig 3a. C_{max} increased with the heating rates and $Al(OTf)_3$ addition, suggesting that ESOISO with higher content of catalyst has the highest curing rate, in other words, faster curing.

The apparent activation energy (E_a) of ESOISO was evaluated using Friedman model, Eq. 1 and the plot is displayed in Fig. 3b.

$$ln\left(\beta\frac{d\alpha}{dT}\right) = lnA + lnf(\alpha) - \frac{E_a}{RT} \quad (1)$$

Where: α is degree of conversion, f(α) is the function of α, which depends on the mechanism; A is the pre-exponential factor (s^{-1}); E_a is the activation energy (J mol^{-1}), β is the heating rate (K min^{-1}); R is the gas constant (8.314 J mol^{-1} K^{-1}) and T is the absolute temperature of reaction (K). It is clearly observed that ESOISO presented a different energy trend according to the catalyst content.

In the first curing stage, α < 0.2, ESOISO 0.05 mol% and ESOISO 0.1 mol% followed the same tendency, low energy consumption was verified which increases with the degree of conversion and increases slowly. Within the conversion range of 0.2 < α < 0.6, there is a plateau that subtly increases with a maximum at 71.10 kJ/mol, afterward decreasing in the range α > 0.6 to 61.26 kJ/mol. ESOISO 0.07 mol% presented a decreased Ea α < 0.1, and a constant plateau within the conversion range of 0.1 < α < 0.6, subsequently, decreasing in the range α > 0.6 to 60.59 kJ/mol. These results confirm those obtained by DSC about the reactivity of the epoxy rings under the catalyst presence.

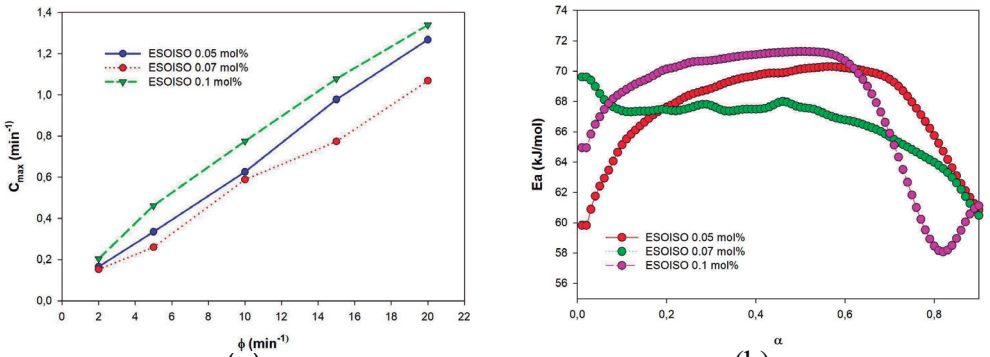

(a) (b)

Figure 3 – (a) Effect of the heating rates and composition on C_{max}, (b) Activation energy during ESOISO curing. Data modeled using Friedman model.

Viscosity plots and shear stress against the shear rate were obtained for the uncured ESOISO after 180 min under 60°C with different catalyst content, as shown in Fig.4. A decrease in viscosity and boost-up in shear stress with the rise in shear rate was observed for all samples. The relaxation mechanism of the polymeric chains from the entanglements determines the dependence of the viscosity on the shear rate. For uncured ESOISO (gel structure) this dependence reveals the non-Newtonian flow, shear-thinning (n < 1), with decreasing viscosity during shear rate increase. Similar analyses were reported in the literature for polymeric gels [10].

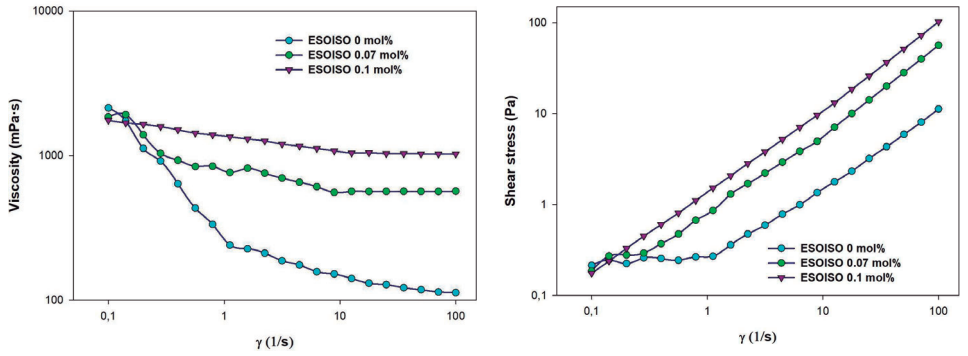

(a) (b)

Figure 4 – (a) Change in the viscosity versus temperature and (b) shear stress of ESOISO.

The viscosity of ESOISO 0.1 mol% and ESOISO 0.07 mol% was higher than that of ESOISO 0 mol% at the same shear rate. Adding $Al(OTf)_3$ as catalyst led to the homopolymerization of ESO through the ring-opening reaction of epoxidized soybean oil, producing a gel or networking (cross-linking), depending on the degree of conversion. Consequently, it has high molecular weight (i.e., high viscosity). With increasing chain size, entanglement occurs by randomly coiling the polymer chains. The lowest shear stress was observed for the ESOISO 0 mol%, which may be due to the absence of polymerization reaction or non-functionalization of ESO with ISO ensuing short polymer chains compared with ESOISO with catalyst. Under shear, the polymer chains of ESOISO 0 mol% without catalyst content (hence less molecular weight) are more deformed, which increases their disentanglement. This behavior leads a less flow resistance, resulting in shear-thinning flow behavior with decreasing viscosity values at higher shear rates.

Conclusions

Fully sustainable ESOISO resins catalyzed by $Al(OTf)_3$ were successfully prepared by open-ring epoxy reactions. The curing was followed using FTIR and DSC and indicated that the curing rate of ESOISO increased with the catalyst, efficiently accelerating the curing rate of the system. $Al(OTf)_3$ addition produces ESOISO with higher viscosity and shear stress due to gel or cross-linking structures. The presented results in this work provide reliable evidence of $Al(OTf)_3$ reactivity as a catalyst for epoxidized soybean oil and isosorbide resins.

Acknowledgements

The authors would like to thank to Coordenação de Aperfeiçoamento de Pessoal de Nível Superior (CAPES), Conselho Nacional de Desenvolvimento Científico e Tecnológico (CNPq), and Fundação de Apoio à Pesquisa do Estado da Paraíba (FAPESQ) for the funding and Fraunhofer Institute for Environmental, Safety and Energy Technology (UMSICHT) for their kindly supporting. Professor Renate Wellen is CNPq fellow (Number: 303426/2021-7).

References

1. F. Aricó. Current Opinion in Green and Sustainable Chemistry, 2020 21, 82-88. https://doi.org/10.1016/j.cogsc.2020.02.002
2. H. Blache, F. Méchin, A. Rousseau, E. Fleury, J. P. Pascault, P. Alcouffe, R. Saint-Loup. Industrial Crops and Products, 2018, 121, 303-312. https://doi.org/10.1016/j.indcrop.2018.05.004
3. C. Zhang, T. F. Garrison, S. A. Madbouly, M. R. Kessler. Progress in Polymer Science, 2017, 71, 91-143. https://doi.org/10.1016/j.progpolymsci.2016.12.009
4. Y. M. Terblans, J. J. Huyser, M. Huyser, M. J. Green, D. A. Young, M. S. Sibiya. Canadian journal of chemistry, 2005, 83(6-7), 854-861. https://doi.org/10.1139/v05-098
5. E. D. Márquez, E. V. Santiago, S. H. López. Physical Chemistry, 2019, 9(1), 1-7. 10.5923/j.pc.20190901.01
6. D. Bradley, G. Williams and M. Lawton. Organic and Biomolecular Chemistry, 2005, 3, 3269–3272. https://doi.org/10.1039/B508924G
7. J. Zhang, J. Jun Tang, J. X. Zhang. International Journal of Polymer Science, 2015, 529235.http://dx.doi.org/10.1155/2015/529235
8. X. Pan, Y.Tian, J. Li, Q. Tan, J. Ren. Chemical Engineering Science, 2022 264, 118152. https://doi.org/10.1016/j.ces.2022.118152
9. L. H. Fan, C. P. Hu, Z. P. Zhang, S. K. Ying, J . Journal of applied polymer science, 1996, 59(9), 1426. https://doi.org/10.1002/(SICI)1097-4628(19960228)59:9<1417::AID-APP9>3.0.CO;2-E
10. I. Ali, L. A. Shah. Polymer Bulletin, 2021, 78, 1275–1291. https://doi.org/10.1007/s00289-020-03163-x

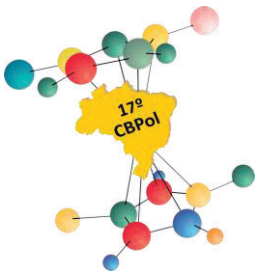

EFFECT OF PHENOLIC AND HYDROXYLAMINE-BASED ADDITIVES ON THE STABILIZATION OF POLYPROPYLENE EXPOSED TO UV-C RADIATION

Marcos V. Basaglia[1,2]*, Lucas H. Staffa[2], Jessica C. F. Gimenez[3], Sandra A. Cruz[3], Manoel G. P. Homem[3], Silvia H. P. Bettini[1,2]

1 – Graduate Program in Materials Science and Engineering (PPGCEM), Federal University of São Carlos (UFSCar), São Carlos, SP, Brazil

2 – Department of Materials Engineering (DEMa), Federal University of São Carlos (UFSCar), São Carlos, SP, Brazil

3 – Department of Chemistry (DQ), Federal University of São Carlos (UFSCar), São Carlos, SP, Brazil

marcosbasaglia@estudante.ufscar.br

Abstract

The exposure of polymeric materials to UV-C radiation (200-280 nm) can result in degradation and may shorten their useful life. The use of additives is an alternative to minimize degradative effects, but the chemical groups present in their structure can act to absorb radiation. In this study, the degradative effects and performance of different stabilization systems containing phenolic (Irganox 1010) and hydroxylamines-based stabilizers (Irgastab FS 301 FF) were analyzed. For this purpose, polypropylene films were exposed to UV-C radiation for 24, 48, and 96 hours (doses equivalent to 155, 310, and 620 J.cm^{-2}). Degradation levels were measured regarding rheological properties, infrared spectroscopy (FTIR), and elongation at break. After exposure, it was shown that hydroxylamine is more efficient in initial exposure times, while the phenolic class is more effective for longer periods. After 96 hours, the PP starts to exhibit fragile behavior.

Keywords: Photod*egradation; polypropylene; UV-C radiation; stabilization systems.*

Introduction

UV-C radiation is a range of the electromagnetic spectrum with wavelengths between 200 and 280 nm. This range of radiation gained notoriety after proving to be an efficient method to inactivate several microorganisms [1] and may be an alternative for disinfecting objects and surfaces. The most accessible source of UV-C radiation is low-pressure mercury lamps which emit specific wavelengths of 254 nm.

In addition to damage caused to microorganisms, ultraviolet radiation can also interact with polymeric materials. If any species present in the material has binding energy equal to the energy of the incident photon, this photon will be absorbed, possibly resulting in the formation of free radicals, which, in turn, can trigger degradation reactions [2,3].

Polypropylene (PP) is a polymer widely used in medical and hospital settings and can be subjected to disinfection processes and, consequently, degradation processes [4]. There are some reports in the literature about the UV-C degradation in polypropylene, in which color changes, reduction of elongation at break, and formation of carbonyl groups are reported. In addition, chances in the crystallinity and formation of cracks on the surface are reported due to the chemi-crystallization [5,6].

The use of stabilizing additives is a way to minimize and delay the degradation process. Phenolic antioxidants are the most used additives for stabilization during the processing and service of polyolefins. Its mechanism of action involves the donation of labile hydrogen from the phenolic

group to stabilize a free radical. Then, its structure is modified through the internal delocalization of electrons, allowing the trapping of a free radical in the para-position of the phenolic group [7]. However, quinone groups are formed during this mechanism of action, which can absorb radiation in the region of UV-C wavelength.

Hydroxylamine-based antioxidants are an alternative class of phenol-free additives that can act without forming quinone groups. Its mechanism of action involves the donation of the labile hydrogen bonded to oxygen to a free radical, forming aminoxyl radicals. Then, there is a divergence in the literature about the subsequent stages of action of this class of additives, but the occurrence of internal conversion reactions that allow the capture of free radicals is in common agreement [2,8].

However, few studies address the effectiveness of these additives for degradation by UV-C radiation. Thus, this study aimed to evaluate the performance of two classes of antioxidant additives, based on phenols and hydroxylamine, about the stabilization capacity of polypropylene when exposed to different doses of UV-C radiation.

Experimental

Materials

The polymer used was a polypropylene homopolymer with code DP 5000 SCPV, without any additives, supplied by Braskem. For the stabilization system, three different types of additives supplied by BASF were used: Irganox 1010, a phenolic primary antioxidant, Irgafos 168, a secondary antioxidant phosphite-based and Irgastab FS 301 FF, a blend of Irgafos 168 and Irgastab FS 042, in a 1:1 ratio, being the last one a primary antioxidant and free radical scavenger based on hydroxylamine. For the study, four formulations were prepared, the first being composed of non-additive polypropylene and the other three containing a 1:2 weight ratio of primary antioxidants about secondary antioxidants, for which the secondary antioxidant content was fixed in 1,000 ppm, and the primary antioxidants were varied between phenolics and hydroxylamine, maintaining the proportion, as shown in Table 1.

Table 1 – Composition of prepared formulations (ppm)

Sample	Irganox 1010 (AO1)	Irgastab FS 042 (NOH1)	Irgafos 168 (AO2)
Neat PP	0	0	0
PP + AO1/AO2	500	0	1,000
PP + NOH1/AO2	0	500	1,000
PP + AO1/NOH1/AO2	250	250	1,000

Processing

The samples were processed in a Haake Rheomix 600 internal mixer, with counter-rotating rotors, at 200°C and 100 rpm. The additives were added to the system after 30 seconds of mixing, with the polymer already in the molten state. The total residence time in the mixer was 2 minutes. Once prepared, the formulations were pressed in a hydraulic press at a temperature of 190°C and a pressure of 1 kgf, resulting in films approximately 180 µm thick. The films were shaped in the format of tensile specimens according to ASTM D1708-18.

Exposure to UV-C radiation

The prepared specimens had both sides exposed to UV-C radiation (254nm) in a chamber of two T5/G5 type 4 W low-pressure mercury lamps. The chamber was also composed of a ventilation system to remove ozone. The specimens were placed 10 cm apart from the lamps for 24, 48, and 96 hours, resulting in nominal doses equivalent to 155, 310, and 620 $J.cm^{-2}$.

Characterization

The levels of degradation caused by UV-C radiation were measured in terms of rheology, carbonyl groups, and elongation at break. The rheological tests were carried out in a rotational rheometer of controlled deformation of the TA Instruments model AR-G2, in parallel plates geometry and steady state, with a distance between plates of 0.5 mm. Fourier Transform Infrared Spectroscopy (FTIR) tests were performed on Nicolet 6700 equipment, in transmission mode, with 64 scans and a resolution of 4 cm^{-1}. For this test, carbonyl indices (CI) were calculated from the ratio between the area of the band referring to the stretching of the C=O bond (between 1660 and 1800 cm^{-1}) and the area of the band referring to the axial deformation C-C (between 1125 and 1200 cm^{-1}). Finally, uniaxial tensile tests were performed in a Universal Testing Machine, model Instron 5569, following the ASTM D1708-18 standard, with a test speed of 1mm.min^{-1}.

Results and Discussion

Table 2 presents the viscosity values at zero shear rates (η_0) obtained in the rheological tests in a steady state.

Table 2 – Zero shear viscosity of samples for different exposure times to UV-C radiation

Sample	Zero shear viscosity (Pa.s)			
	0 h	24 h	48 h	96 h
Neat PP	1,300	280	200	90
PP + AO1/AO2	5,200	2,300	1,400	340
PP + NOH1/AO2	4,500	2,200	700	170
PP + AO1/NOH1/AO2	5,000	2,100	800	200

As can be seen, the exposure of the specimens to UV-C radiation reduces η_0 values, which occurs more pronouncedly with the increase in exposure time. This fact is a consequence of photo-oxidative degradation reactions, which mostly involve chain scission for polypropylene. It can also be seen that the non-irradiated samples have different values of η_0 due to the thermo-oxidative degradation during processing in the internal mixer, in which different stabilization systems provided different stabilities. Relative comparison between the η_0 values allows a better relationship of the degradative effects due to UV-C radiation.

From this point of view, for exposure times up to 24 hours, the presence of hydroxylamine in the formulations provided greater retention of η_0 values, indicating better stabilization of this additive in initial times. In comparison, for more than 24 hours, the formulation containing only the primary antioxidant of the phenolic type (PP + AO1/AO2) proved to be more efficient in stabilizing UV-C radiation.

An explanation may be related to the mobility of the additives. The phenolic antioxidant has a steric hindrance, while the hydroxylamine has higher mobility, which may provide greater efficiency in trapping the free radicals. This behavior is reversed by increasing the exposure time due to the total capacity of trapping radicals from the first one being greater than the second one.

The carbonyl index values for the irradiated samples are presented in Table 3.

Table 3 – Carbonyl index of samples for different exposure times to UV-C radiation

Sample	Carbonyl index			
	0 h	24 h	48 h	96 h
Neat PP	0.041 ± 0.002	0.085 ± 0.008	0.136 ± 0.009	0.352 ± 0.016
PP + AO1/AO2	0.035 ± 0.001	0.061 ± 0.004	0.096 ± 0.007	0.298 ± 0.007
PP + NOH1/AO2	0.037 ± 0.001	0.057 ± 0.006	0.107 ± 0.005	0.305 ± 0.010
PP + AO1/NOH1/AO2	0.036 ± 0.002	0.062 ± 0.004	0.103 ± 0.008	0.310 ± 0.009

During the photo-oxidation process of polypropylene, occurs the formation of carbonyl groups, identified in wavenumbers between 1660 and 1800 cm^{-1}, referring to ketones, carboxylic acids, aldehydes, esters, and lactones, also identified in other works in the literature for degradation of polypropylene subjected to ultraviolet radiation [6,9].

An increase in the carbonyl index can be seen for initial irradiation times, which increase more pronounced for longer exposure times, in agreement with the rheological results. The carbonyl groups, products of photo-oxidative reactions, act as chromophores initiating new reactions and accelerating the degradative process as their concentration in the material increases. In addition, it can be seen that the PP without additives showed higher rates for all exposure times, indicating the action of the additives.

Finally, the degradative effects were compared in terms of mechanical properties. The property of greatest interest in this test was elongation at break. The values presented in Figure 1 are presented as retention results, that is, the measured value of elongation at break was divided by the elongation at break of the respective non-irradiated sample. Each formulation was tested using five specimens.

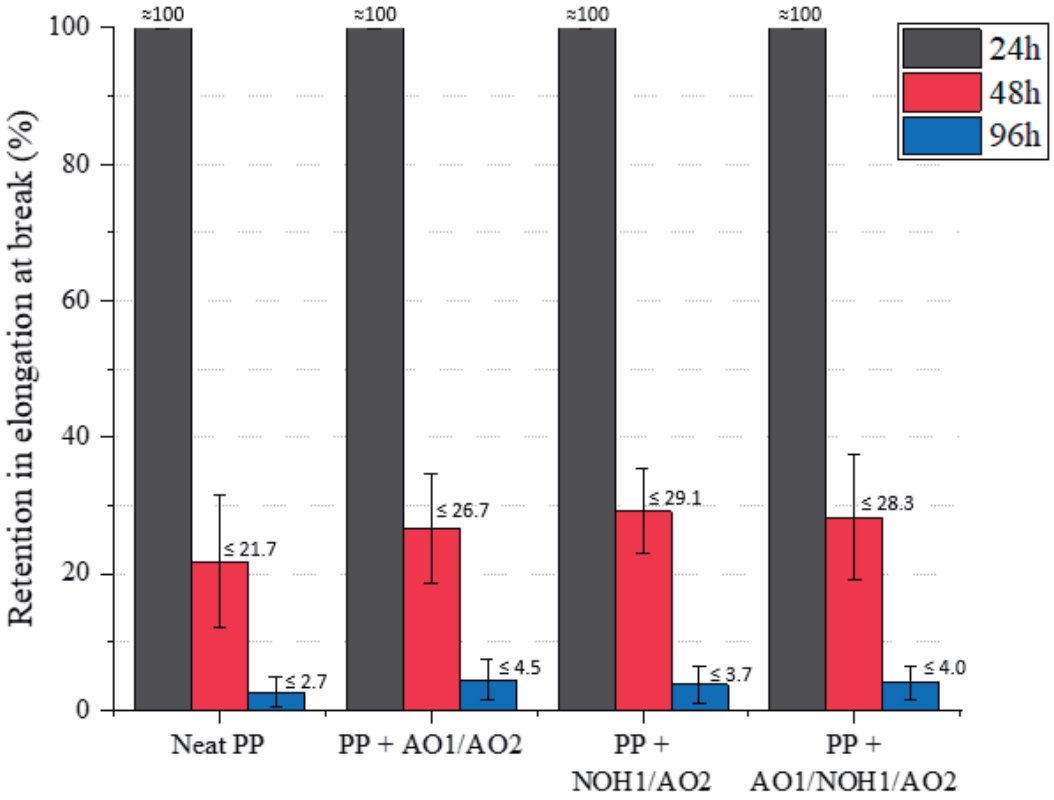

Figure 1 – Retention in Elongation at break of samples in the function of the exposure time to UV-C radiation

Exposure of samples to UV-C radiation for up to 24 hours did not affect this property under the test conditions used, in which all samples exceeded 300% deformation without fracture, resulting in retention considered to be close to 100%. The exposure of the test specimens for 48 hours resulted in a decrease in the elongation at break, for which the retention was lower than 21,6% for the non-additive PP and lower than 29% for the other additive formulations. However, the standard deviation does not allow differentiation between the samples.

After 96 hours of exposure, the specimens start to show brittle fracture behavior, with relative values of retention in elongation at break lower than 2,7% for samples without additives

and lower than 4,5% for the samples containing additives. Again, there is no distinction between the samples due to the standard deviation.

This behavior can be mainly associated with the decrease in the molecular weight of PP, resulting from chain breaks during the degradation process, which were evidenced by the decrease in viscosity at zero shear rates. Furthermore, stabilization systems containing only primary and secondary antioxidants were insufficient to maintain this property for times longer than 24 hours.

Conclusions

Levels of degradation of polypropylene films subjected to UV-C radiation were evaluated using stabilization systems based on phenols and hydroxylamines. Degradation levels were observed for all exposure times analyzed under the exposure conditions, which were more pronounced for longer exposure times. Changes in elongation at break were only verified after 48 hours. After 96 hours, all samples showed brittle behavior. It is possible to notice the performance of the stabilizing additives, but these were not enough to avoid the PP embrittlement. Finally, the hydroxylamine-based antioxidant was more effective for the initial exposure times, while the phenolic antioxidant was more effective for prolonged times.

Acknowledgements

This study was financed in part by the Coordenação de Aperfeiçoamento de Pessoal de Nível Superior - Brasil (CAPES) - Finance Code 001. The present work was carried out with the support of the National Council for Scientific and Technological Development – Brazil (CNPq) (Process 161111/2021-1).

References

1. T.P. Coohill, J.L. Sagripanti Photochemistry and Photobiology, 2008, 1084 http://dx.doi.org/10.1111/j.1751-1097.2008.00387.x.
2. H. Zweifel, Stabilization of Polymeric Materials, Springer, Berlin, 2012.
3. M.A. De Paoli, Degradação e Estabilização de Polímeros, Artliber Editora, São Paulo, 2009.
4. W, Kowalski, Ultraviolet Germicidal Irradiation Handbook, Springer, Berlin, 2009.
5. A.d.S.M. de Freitas, et al., Jornal of Polymer Research 2022, 29, 506. https://doi.org/10.1007/s10965-022-03357-z.
6. S. Aslanzadeh, M Haghighat Kish, Fibers and Polymers, 2010, 11, 710 https://doi.org/10.1007/s12221-010-0710-8.
7. N.S. Allen, M. Edge, S. Hussain, Polymer Degradations and Stability 2022, 201, 109977. https://doi.org/10.1016/j.polymdegradstab.2022.109977.
8. Y. Ohkatsu, R. Baba, K. Watanabe, Journal of the Japan Petroleum Institute 2011, 54. https://doi.org/10.1627/jpi.54.15.
9. S. Fernando, et al., Polymer Degradation and Stability 2008, 92, 2163. https://doi.org/10.1016/j.polymdegradstab.2007.01.032.

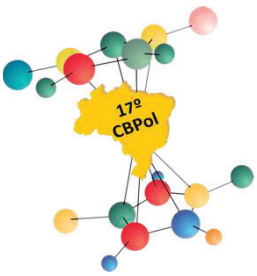

EVALUATION OF STARCH PROCESSING STEPS WITH ADDED CITRIC ACID

Ítalo R. Coura[1] and Patrícia S. O. Patricio[1]*.

1 – Department of Chemical, Federal Center for Technological Education of Minas Gerais (CEFET-MG), Belo Horizonte, MG, Brazil
italorochac@gmail.com

Abstract – Since the 1990s, researchers have been conducting studies to enhance starch properties through chemical or structural modifications in its polymeric chains. Glycerin, acting as a plasticizer, is the primary modifying agent enabling the thermal processing of starch. As a result, it is extensively used in most publications on modified starch. Another commonly employed chemical compound in starch modification is citric acid, which is low-cost and non-toxic. However, it is important to note that the specific interactions and reaction mechanisms between starch and its polymer chains, particularly in the presence of citric acid, still require further exploration, as these aspects are not extensively discussed in current literature. Starch citrate based polymers were obtained by simple dry method and their processing steps were analyzed. The organoleptic observations demonstrated that there was a reaction between the native starch and the citric acid, with the formation of new polymeric structures, indicated by the change in color and opacity. High proportions of citric acid can promote reactions prior to extrusion and the residual acid can react in subsequent procedures, suggesting that it is possible to obtain different materials by changing processing variables.
Keywords: *Starch; starch citrated; thermoplastic starch*

Introduction

A report has been conducted on the issue stemming from the disposal of post-consumer plastics and their subsequent accumulation in the oceans. The findings reveal that despite implementing public policies over the years to raise awareness and promote recycling and responsible plastic consumption, the environmental, social, and economic damage has continued to escalate. Certain countries have introduced legislation to regulate the use of disposable plastic products to mitigate the problem. However, alternative approaches, such as using environmentally-friendly polymers, categorized as (i) green polymers and (ii) oxo-biodegradable polymers, have proven ineffective in addressing the issue. Concerns have been raised regarding negative consequences associated with post-consumption. The first category of polymers mentioned persists in the environment due to its structural similarity to conventional polymers. On the other hand, the second category generates microparticles, which are recognized as pollutants with a significant environmental impact. Consequently, the use of oxo-biodegradable plastics was prohibited in European Union countries in 2019. Thus, the call for environmental action presents an opportunity to develop innovative biodegradable and non-toxic (eco-friendly) materials.[1; 2]

Environmentally friendly polymers can be derived from either synthetic or natural sources. However, synthetic biodegradable materials tend to have higher prices than conventional polymers, while natural polymers often possess undesirable physicochemical properties that limit their ability to replace traditional polymers. Therefore, extensive research is needed to explore alternative solutions and overcome these challenges. Among natural polymers, starch has emerged as a prominent option in Brazil due to the favorable conditions for cultivating various starch-rich raw materials. Since the 1990s, researchers have been conducting studies to enhance starch properties through chemical or structural modifications in its polymeric chains. Glycerin, acting as a plasticizer, is the primary modifying agent enabling the thermal processing of starch. As a result, it is extensively used in most publications on modified starch. Another commonly employed chemical compound in starch modification is citric acid, which is low-cost and non-toxic. However, it is important to note that the specific interactions and reaction mechanisms between starch and its polymer chains, particularly in the presence of citric acid, still require further exploration, as these aspects are not extensively discussed in current literature.[3; 4; 5; 6]

In this context, investigating methodologies that can help elucidate and guide the reactions occurring in starch, in the presence of citric acid and glycerin under various reaction conditions is of great interest. Such research benefits the scientific community and holds potential value in the consumer market. The general objective of this work is to develop polymeric, biodegradable, low-cost materials based on starch, in addition to contributing to the elucidation of the chemical species formed in the reaction medium between the modifying agents and cassava starch. Cassava starch was submitted the extrusion processing. The material produced was studied by organoleptic and thermal analysis. The main objective of this study is to develop polymeric, biodegradable, and cost-effective materials based on cassava starch while also contributing to the understanding of the chemical species formed in the reaction medium between the modifying agents and cassava starch.

Experimental

Modified starches were produced using citric acid (CA) content of 0.0%, 3.0%, and 10.0 %wt, while the glycerin content was set at 30 %wt relative to the native starch (NS). To prepare the samples, cassava starch (commercial brand, native starch) and anhydrous citric acid PA (NEON) were added to three polyethylene containers, according to Table 1, the proportions were defined based on the results of previous works by the research group. The mixtures were manually homogenized and then poured into aluminum trays. These trays were placed in an oven (Thoth Equipment's, model Th-510-100) and heated at 120.0 °C for 1 hour to facilitate drying. After drying, the samples were named AA-00, AA-03, and AA-10. Next, 30 %wt Glycerin PA ACS (Anhydrol) was added to each mixture and manually homogenized using a moldable container, ensuring no direct contact with the mixture. The materials were poured into their respective trays and returned to the oven at 100.0 °C for 1 hour. These materials were identified as AAG-00, AAG-03, and AAG-10. Then, the materials were extruded into filaments and identified as $ATP_{M1}00$, $ATP_{M1}03$ and $ATP_{M1}10$. Plates of these materials were also produced in a hydraulic press with heating.

Qualitative organoleptic analyzes of the filaments and thermal analysis of all products were carried out. Thermogravimetric analysis (TGA) was performed in an atmosphere of N_2, scanning from room temperature to 600 °C at a rate of 10 °C/min.

Table 1. Mass content of precursor materials for each sample.

CA (%)	NS (g)	CA (g)	Glycerin (g)	Total (g)
00	70	-	30	100
03	70	2.2	30	102
10	70	7.8	30	108

Results and Discussion

Table 2 presents the characteristics observed during the analysis of the filaments. The tactile response, when in contact with water, average diameter, color, opacity, rigidity, and visual aspect were evaluated.

Table 2. Organoleptic characteristics of the materials produced.

Sample	$ATP_{M1}00$	$ATP_{M1}03$	$ATP_{M1}10$
Diameter (mm)	3.3±0.1	3.3±0.1	2.9±0.1
Color	Yellow	Soft pink	Dark pink
Opacity	Translucent	opaque	opaque
Hardness	soft	soft	soft
Aspect	Smooth	Smooth	Rough
water sensitivity*	09	09	10

*Scale from 0 to 10 where 0 is a material that does not change with washing and 10 is a material that exhibits an adhesive character due to moisture.

Figure 1a shows the TGA curves of the materials without CA for observation of the processing effect. Table 2 presents the values of the thermal events. Before extrusion, the curves presented thermal events separated from the components: (i) humidity; (ii) glycerin; (iii) starch. After extrusion, the materials showed a continuous mass loss over a wide temperature range during initial heating. A peak was observed close to the main event, this signal may be related to the degradation of glycerin bound to starch (by esterification reaction or by intermolecular interactions in the amorphous phase). Glycerin acts as a thermal barrier, hindering the diffusion of heat in the phase of greater thermal stability of starch, since the continuous loss after the main event is less intense than in pure starch, resulting in a greater residual mass at 600 °C, except for the film, which indicates glycerin exudation due to pressing.

Figure 1b shows the materials with CA before and after extrusion, 4 thermal events were observed: from 30 to 140 °C, 140 to 250 °C, present in the materials before extrusion, related to (i) moisture loss and (ii) the glycerin that has less interaction with the starch chains; respectly, 250 to 300 °C, related to the loss of (iii) smaller molecules such as glycerine oligomers, smaller starch chains or chain-bound reagents (esterification or graphitization); (iv) 270 to 370 °C, main event of starch thermal degradation. The materials produced showed high levels of moisture, which can generate hydrolysis during extrusion. The highest proportion of CA promoted modifications before extrusion, indicated by the presence of the third event and less mass loss in the second event. The extrusion of the materials resulted in higher starting temperatures in the main event. More accentuated by the lower concentration, which suggests that 10% by mass represents excess CA, which can generate degradation reactions in addition to esterification reactions.

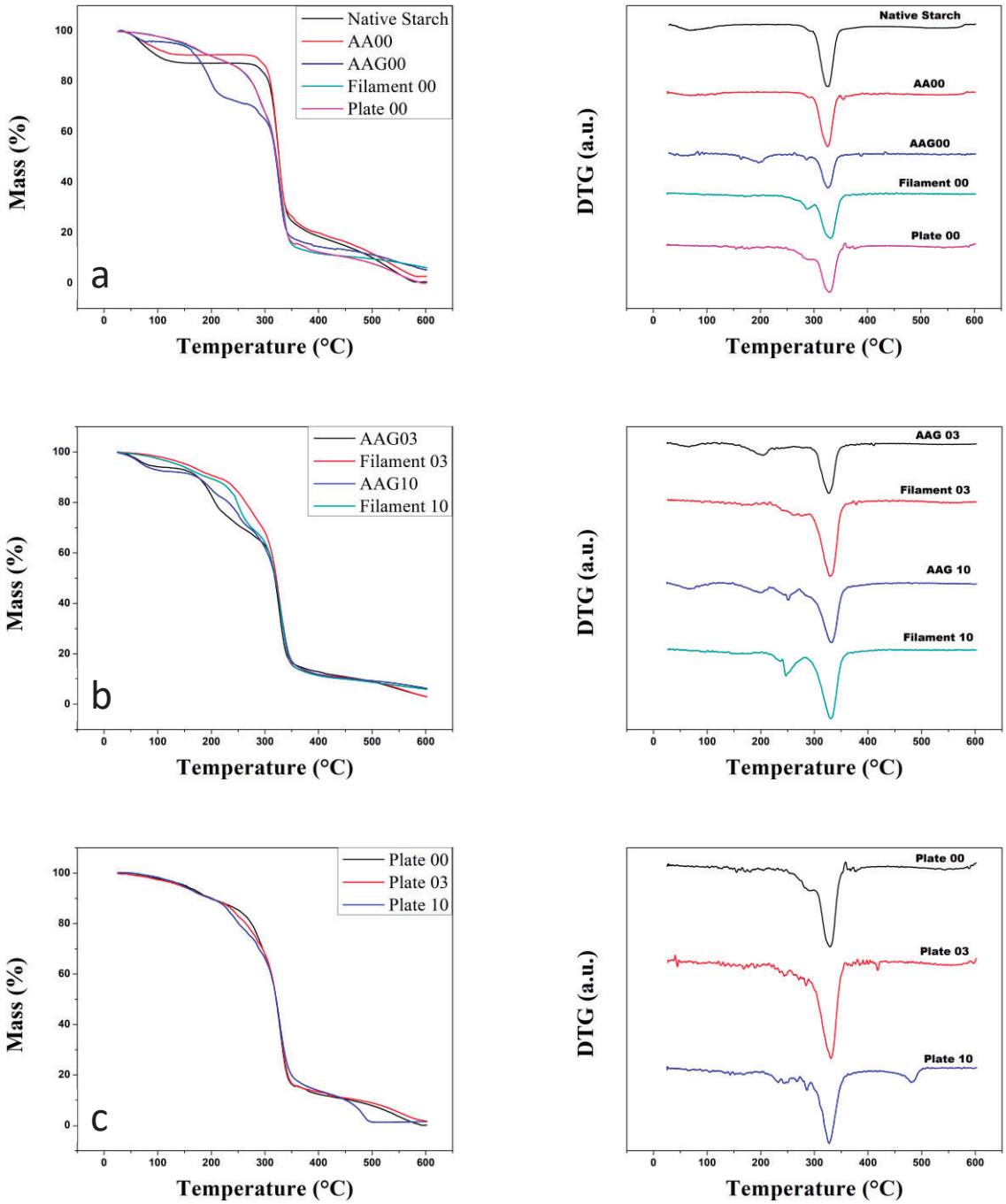

Figure 1 – TGA (right) and DTG (left) curve of processing steps without AC (a), effect of AC reactive extrusion (b) and effect of AC content in plates (c).

Plate production is a processing step that involves high pressure and constant temperature, the TGA curves are shown in Figure 1c. The plates produced showed differences when compared to their respective filaments, which suggest the continuation of the reaction with citric acid: the material with 3% wt CA became more homogeneous, coupling the events in a single step with lower initial temperature. While the material with 10% wt presented a thermal event at high temperatures, approximately 440 °C. One hypothesis is the formation of a structure of greater thermal stability in

an approximate proportion of 9% wt, possibly the reticulated or branched structure. This result is corroborated by WEERAPOPRASIT and PRACHAYAWARAKORN (2019)[7] who observed the thermal degradation of modified starch obtained from cassava and methacrylic acid. The authors observed three mass loss events in all materials associated with the release of: (i) glycerol used as a plasticizer, at temperatures between 170 and 180 °C; (ii) starch that suffered partial degradation during processing, at temperatures between 245 and 268 °C; (iii) starch not degraded by processing, at temperatures between 300 and 330 °C, however, the cross-linked materials showed one more event, around 500 °C, associated with the degradation of the co-polymer produced, which has greater thermal stability.

Conclusions

Starch citrate based polymers were obtained by simple dry method and their processing steps were analyzed. The organoleptic observations demonstrated that there was a reaction between the native starch and the citric acid, with the formation of new polymeric structures, indicated by the change in color and opacity.

Chemical reactions occur preferentially by reactive extrusion, however, high proportions of citric acid can promote reactions prior to extrusion and the residual acid can react in subsequent procedures, suggesting that it is possible to obtain different materials by changing processing variables. New analyzes such as HPSEC and NMR should clarify the reaction processes so that they can be directed and facilitate the achievement of environmentally friendly polymers with more opportunities to replace the usual polymers.

Acknowledgements

INCT-Midas and FAPEMIG.

References

1 **From Pollution to Solution: A global assessment of marine litter and plastic pollution**. Nairobi: United Nations Environment Programme (UNEP), 2021.

2 BRITO, G. F. et al. **Biopolímeros, Polímeros Biodegradáveis e Polímeros Verdes**. Revista Eletrônica de Materiais e Processos. 6.2**:** 127-139 p. 2011.

3 LIU, H. et al. Thermal processing of starch-based polymers. **Progress in Polymer Science,** v. 34, p. 1348–1368, 2009.

4 MA, X. F.; YU, J. G.; MA, Y. B. Urea and formamide as a mixed plasticizer for thermoplastic wheat flour. **Carbohydrate Polymers,** v. 60, p. 111-116, 2005.

5 REDDY, N.; YANG, Y. Citric acid cross-linking of starch films. **Food Chemistry,** v. 118, p. 702-711, 2010.

6 SHI, R. et al. Characterization of citric acid/glycerol co-plasticized thermoplastic starch prepared by melt blending. **Carbohydrate Polymers,** v. 69, p. 748–755, 2007.

7 WEERAPOPRASIT, C.; PRACHAYAWARAKORN, J. Characterization and properties of biodegradable thermoplastic grafted starch films by different contents of methacrylic acid. **International Journal of Biological Macromolecules,** v. 123, p. 657-663, 2019.

EVALUATION OF THE EFFECT OF SYNTHESIS VARIABLES ON THE MORPHOLOGICAL CHARACTERISTICS OF PUF/ENB MICROCAPSULES USING FRACTIONAL DESIGN

Maria Paula de Carvalho Freire[1], Ygor Matheus Pereira de Paula[1], Ana Leticia Fernandes dos Santos[1], José Daniel Diniz Melo and Maria Carolina Burgos Costa[2]

1 - Graduate Program in Materials Science and Engineering (PPGCEM), Federal University of Rio Grande do Norte (UFRN), Natal, RN, Brazil maria.paula.freire.110@ufrn.edu.br , ygor.pereira.087@ufrn.edu.br , analeticiaferds30@gmail.com

2 - Materials Engineering Department, Federal University of Rio Grande do Norte (UFRN), Natal, RN, Brazil daniel.diniz@ufrn.br , carolina.nascimento@ufrn.br

Abstract – The study of self-healing materials has grown in the recent decades due to the need for materials to have a longer lifetime. In this work, microcapsules of poly(urea-formaldehyde) (PUF) containing 5-ethylidene-2-norbonene (ENB) were obtained through the *in situ* polymerization technique. These experiments are part of a sequential strategy of experimental design, in which a 2^{4-1} fractional experimental design was performed to evaluate the influence of the effect of the variables of the synthesis process on the morphological characteristics of microcapsules obtained, where the output variable analyzed was the diameter of the microcapsules and the encapsulated content. Some variables of synthesis as the molar ratio of monomers urea/formaldehyde (U/F), the ammonium chloride and the resorcinol were kept constant, once these parameters do not exert a significant effect on the results evaluated, a fact verified in previous design. From the responses obtained in the statistical analysis using the program Protimiza, it was possible to affirm that the agitation speed and poly(ethylene-alt-maleic) (EMA) content are the variables of the synthesis that should be selected to obtain a complete experimental design to be performed later, considering the polymerization yield.

Keywords: *self-healing; polymeric microcapsules;* 2^{4-1} *factorial design, in situ polymerization*

Introduction

The products and structures are susceptible to damages due to several factors during use, where the material is exposed to mechanical stresses, chemical deteriorations, and others. Materials are capable of being damaged extending from the micro to the macro level. Inspired by the biological concept of healing, self-repair methods refer to the ability of a material to regenerate after incurring damage, where the self-healing technology may mitigate damage at the molecular level [1,2].

Self-healing materials are divided between different methods that depends on their mechanism, these are: intrinsic, microvascular and microcapsules. The microcapsules synthesis occurs from the encapsulation of liquid or solid particles, where the material is involved by a shell. The development of polymers that are able to repair their damage autonomously and quickly is highlighted in the importance of safety factors and product performance [3].

The work of [4] reports that microcapsules between 60 and 69 µm are appropriate for self-healing systems and coating applications, where the wall thickness around 4 µm is adequate to resist the processing of microcapsules with polymer matrix, where they rupture only when the self-healing process is initiated. According to [5], microcapsules with satisfactory characteristics as thermal stability, high encapsulated content and reduced surface defects can be achieved when the microcapsules have an average diameter of 75 µm, thus allowing the obtaining of thicker walls. In this work, microcapsules with diameters around this value were obtained in the PUF/ENB 4

condition, where a satisfactory yield (78.79%), and a high encapsulated content (94.8%) were achieved.
The work of [6] emphasizes the need for understanding the influence of synthesis variables and how they affect the morphological characteristics of polymeric microcapsules obtained by *in situ* polymerization. The parameters analyzed include agitation speed, pH, EMA content, U/F ratio, ammonium chloride content, resorcinol content, and 1-octanol droplets. In recognition of the importance of selecting the parameters properly, in this work, part of a sequential factorial design strategy to optimize the synthesis conditions of PUF filled with ENB microcapsules are synthesized by in situ polymerization. To select the most significant parameters on the morphology of the microcapsules, a 2^{4-1} fractional experimental design was prepared.

Experimental

Experimental design

In agreement with the literature, the variables involved in the synthesis process influence in morphological characteristics of the microcapsules. To evaluate the effect of these synthesis parameters on the different conditions of synthesis of the microcapsules, a fractional factorial design was elaborated, continuing the work developed by [6], aiming to optimize the synthesis conditions of polymeric microcapsules of PUF/ENB. The statistical analysis was performed by using the software Protimiza Experimental Design. The fractional factorial design matrix is shown in Table 1.

Table 1 – Fractional 2^{4-1} experimental design matrix.

FRACTIONAL FACTORIAL DESIGN 2^{4-1}				
Experiments	**Agitation speed**	**pH**	**EMA**	**1-Octanol**
PUF/ENB 1	300	3	0.425	1
PUF/ENB 2	300	3	0.825	3
PUF/ENB 3	700	3	0.425	3
PUF/ENB 4	700	3	0.825	1
PUF/ENB 5	300	4	0.425	3
PUF/ENB 6	300	4	0.825	1
PUF/ENB 7	700	4	0.425	1
PUF/ENB 8	700	4	0.825	3
PUF/ENB 9	500	3.5	0.625	2
PUF/ENB 10	500	3.5	0.625	2
PUF/ENB 11	500	3.5	0.625	2

The U/F ratio was kept at 1:1.9, and ammonium chloride and resorcinol were kept at 0.25 g and 0.25 g, respectively.

PUF/ENB microcapsules synthesis

The synthesis of microcapsules was supported by the studies of [7,8], and were performed under different conditions, according to Table 1. The PUF/ENB synthesis system was prepared using a heating mantle, a three-neck flask, a mechanical stirrer, and a thermometer. The synthesis flowchart (Fig. 1) illustrates the synthesis steps. Initially, the EMA was dissolved in 25 mL of deionized water. Then, the urea, the ammoniun chloride and resorcinol were dissolved in 100 mL of deionized water and right after, the dissolved EMA was added. Then, the pH of the synthesis was adjusted according to the experimental condition of the design, followed by transfer to the three-neck flask, addition of

the dispersed phase (ENB), the 1-octanol droplets and formaldehyde (mL). Finally, the synthesis was performed fixing the temperature at 55 ºC for 4 hours, under mechanical agitation. Aiming to validate the experimental design, the experiments were also performed in three central points.

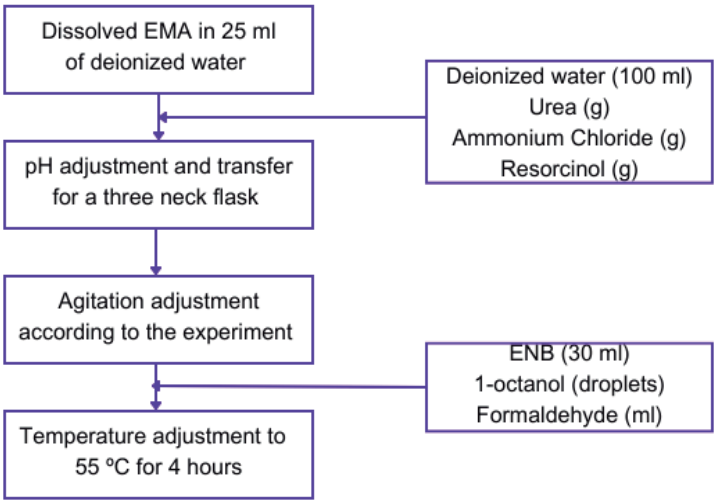

Figure 1 – Synthesis of microcapsules of PUF/ENB flowchart

Microcapsules characterization method

The microcapsules morphology was observed using a scanning electron microscopy (Hitachi Tabletop Microscope – TM-3000), and the software TM3000. To obtain the normal distribution of the microcapsules diameter, the images were analyzed using Image J software, and for each specimen result, at least one hundred measurements were done.

Results and Discussion

SEM images analysis

To evaluate quantitatively and qualitatively the microcapsules, measurements and editions were obtained through ImageJ software, with the contribution of SEM images. In aiming to observe the most significant microcapsules (PUF/ENB 3, 4, and 8), Fig. 2 showed the SEM images, as also the histogram with the normal distribution of the microcapsules.

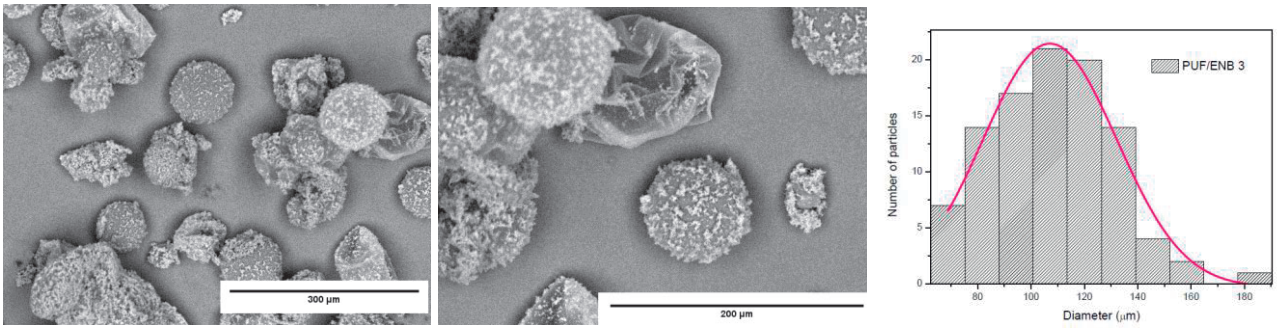

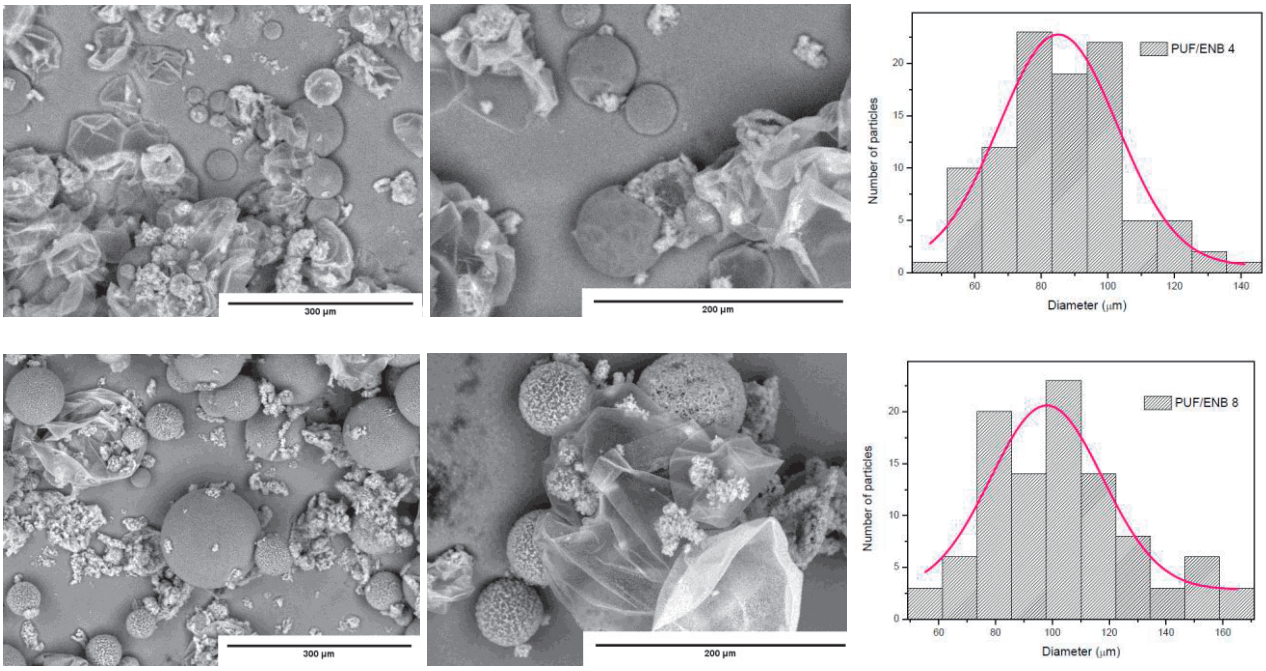

Figure 2 – Morphology observations in SEM images: (a) PUF/ENB 3 microcapsules; (b) PUF/ENB 4 microcapsules and (c) PUF/ENB 8 microcapsules

In Fig. 2 it is shown microcapsules having superior characteristics, including a few residues of U/F, smoother walls, distribution of the mean diameter tightest, as well as symmetrical and regular spheres. Therefore, the SEM analyses helped in establishing the best synthesis conditions in the fractional design that evidently resulted in microcapsules with more uniform morphological characteristics.

Average diameter of microcapsules

To determinate the average diameter, one hundred measurements were made for each sample. After the analysis, it was observed that most of the microcapsules presented average diameter about 150 µm. The PUF/ENB 4 and 8 samples showed an average diameter of 78.79 and 54.28 µm, respectively. The Fig. 3 shows the Pareto chat for the average diameter of microcapsules.

Figure 3 – Pareto chart for average diameter for a confidence level of 90% [9]

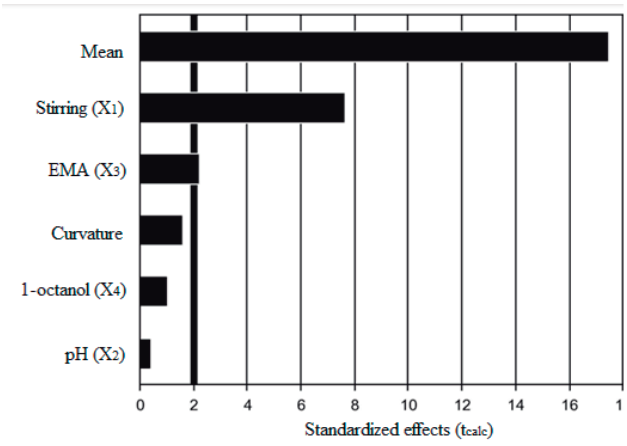

It was observed that variables X_1 and X_3 (stirring and EMA content) are statistically significant for a 90% confidence level. According to [6], it is expected that stirring rate and EMA content, a emulsifier, exerts significant effect on the microcapsules diameter, as well as their morphology. It is possible to affirm that when the agitation rate and the EMA content increase, microcapsules with smaller diameters are obtained, as was seen in the PUF/ENB 4 and 8 samples in Fig. 2. The increased agitation rate promotes the formation of microcapsules with smaller diameters [7,8,10]. And the higher EMA content contributes to the stability and dispersion of the emulsion, also enhancing the formation of the microcapsules.

Conclusions

From the analyzed parameters, the EMA content and stirring rate exerted more significant effects on the response variable, for a confidence level of 90%. Microcapsule samples with satisfactory properties such as particle symmetry, less U/F residue, uniform shell, tight diameter distribution, were found out of the central points. To obtain the optimal conditions of the synthesis process, it is necessary to develop the complete design with the variables that exerted significant effect in the fractional design.

Acknowledgements

This work was supported by CAPES – Coordination for the Improvement of Higher Education Personnel. The authors acknowledge the support of UFRN – Federal University of Rio Grande do Norte and technical support from LIME – Institutional Laboratory of Metrology and Microscopy.

References

1. Y. Zhu. et al. *ACS Applied Materials and Interfaces* 2019, 11, n. 36, 9b10737. https://doi.org/10.1021/acsami.9b10737
2. N. N. F. N. M. N. Kahar. et al. *Polymers* 2021, 13, n. 8, 13081194. https://doi.org/10.3390/polym13081194
3. S. M. F. Salehuddin. et al. *Chemical Engineering Transactions* 2019, 72, 1972073. https://doi.org/10.3303/CET1972073
4. A. C. M. de Carvalho. Ph. D. Thesis. Universidade Federal do Rio Grande do Norte, 2017.
5. T. M. A. M. de Melo. Ph.D. Thesis, Universidade Federal do Rio Grande do Norte, 2021.
6. T. M. A. Marinho. et al. *Journal of Polymer Research* 2021, 28, n. 136, 021024941. https://doi.org/10.1007/s10965-021-02494-1
7. S. R. White. et al. *Nature* 2001, 409, 35057232. https://doi.org/10.1038/35057232
8. E. N. Brown; N. Sottos; S. R. White. *Experimental Mechanics* 2002, 42, n. 4, 02412141. https://doi.org/10.1007/BF02412141
9. Protimiza Software. *Protimiza experimental design* 2017. https://experimental-design.protimiza.com.br/. Accessed 10 Apr 2023.
10. E. N. Brown. et al. *Journal of Microencapsulation* 2003, 20, 0265204031000154160. https://doi.org/10.1080/0265204031000154160

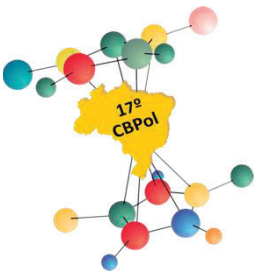

EVALUATION OF THE THERMOPLASTIC STARCH PROPERTIES: REACTION WITH STRUCTURALLY DISTINCT CARBOXYLIC ACIDS

Luan M. Santos [1]*, Ítalo R. Coura[1] Patricia S. O. Patrício[1]

1 –Federal Center for Technological Education of Minas Gerais (CEFET) Belo Horizonte - MG
luan.mendonca@ufvjm.edu.br

Abstract:

Given the significant environmental impact caused by fossil-based polymers, it is essential to explore ways to minimize this impact by studying and developing products that can reduce damage to the environment. In addition to investigating important properties to ensure competitiveness with materials already present in the market, enabling their possible substitution. From this perspective, this study aims to use environmentally friendly compounds to investigate the modification of biodegradable polymers. Commercial cassava starch, glycerin, and different types of organic acids, Citric, Tartaric, and Succinic, were used to modify starch through reactive extrusion. The results obtained from structural and thermal characterizations suggest that starch esterification occurred, and new chemical bonds were formed between the chains.

Keywords: Modified *starch, reaction extrusion, biodegradables polymers*

Introduction:

For over 100 years, synthetic polymers have been devolved from fossil sources. These compounds have contributed to expanding the petrochemical industry, offering a wide range of uses and applications. Due to their low cost, low density, rapid processing, acceptable optical, mechanical, and barrier properties, as well as various functionalities, these materials have excelled in the market and proven extremely useful in multiple sectors. However, despite their advantages, these materials have caused a significant environmental impact, particularly on a large scale, creating financial challenges for their reuse and taking extended periods to degrade in the environment. From this perspective, employing and developing materials that minimize environmental harm becomes necessary, contributing to a more sustainable and environmentally conscious society [1].

Starch is a natural polymer and, therefore, biodegradable. Moreover, it is widely available and cost-effective, making it an attractive candidate for replacing fossil-based polymers. Adding plasticizers is necessary to process starch, resulting in the formation of thermoplastic starch (TPS). Thermoplastic starch is considered a biodegradable material, and its production involves modifications in both intramolecular and intermolecular interactions. However, its mechanical properties are still deemed insufficient for broad applicability. As a result, extensive research has focused on chemically modifying this material through acid reactions using natural organic acids or those derived from metabolic pathways, intending to obtain a material with improved physical, chemical, and mechanical properties. The objective is to use these polymers in a biodegradable, ecological and sustainable way. Such structural modifications can alter chemical properties, aiming at mechanical improvement and resistance to solubility [2].

This study aims to assess the impact of chemical reactions occurring during the extrusion process, in the presence of structurally different organic acids, on the properties of thermoplastic starch. Thermoplastic starch modified by three different acids commonly used in the food industry was produced, and its structural and thermal properties were evaluated.

Experimental

For the production of TPS and the respective modified starches, commercial cassava starch, citric acid (analytical grade), tartaric acid (analytical grade), succinic acid (analytical grade), and glycerin (analytical grade) from the brand Synth were used.

The starch was dried in an oven at 120 °C for 2 hours and then transferred to a low-density polyethylene envelope. Mass percentages of 1%, 3%, 7%, and 15% of the organic acids were added. After homogenization, 30% glycerin was added. Subsequently, the formed mass was manually mixed until it detached from the container walls. The process was conducted separately for each type of organic acid and their respective concentrations. A Thermo Scientific single-screw extruder, Haake Polylab model, was utilized. The extruder operated at a torque of 30 rpm and temperatures of 100 °C, 120 °C, 120 °C, and 110 °C in the four heating zones.

FTIR analyses were conducted for the samples of modified TPS with citric acid (TPSC), succinic acid (TPSS), and tartaric acid (TPST). The infrared spectroscopy was performed with the Shimadzu IRPrestige-21 Spectrophotometer with an ATR accessory. Thirty scans were performed at room temperature between 4000 and 400 cm^{-1}.

To analyze the thermal stability of the polymers obtained, thermogravimetric curves were generated in synthetic air flow, varying the ambient temperature up to 600 ºC and heating rate of 10 ºC min-1 in the DTG- 60H from Shimadzu with an average mass of 8 mg.

Results and discussion

The spectra show a broad and intense absorption in the range between 3292 cm^{-1} and 3282 cm^{-1}, characteristic of the -OH stretching vibrations present in the starch structure. The bands appearing in the spectrum around 2930 cm^{-1} and 2880 cm^{-1} are related to the axial deformations of the primary and tertiary -C-H bonds, respectively. For the TPSS spectra, a prominent absorption can be observed at 1418 cm^{-1}, which may be associated with the coupling of angular deformation in the plane of the -O-H bond and the axial deformation of -C-O from the carboxylic acid derived from the succinic acid structure. The absorption bands between 1200 cm^{-1} and 1244 cm^{-1} and 1005 cm^{-1} and 1011 cm^{-1} are associated with the stretching vibrations of the -C-O-C- group from unsaturated esters from a starch structure.

The band appearing between 1730 cm^{-1} and 1690 cm^{-1} is associated with stretching the carbonyl -C=O bond from the ester present in the chemical structure of carboxylic acids and absent in starch. This absorption band can be shifted to lower energy regions due to intra- or intermolecular chemical group interactions. The relative intensity of the band with the increases within the content of all carboxylic acids used can be observed in Figure 01. In order to verify if this band could be associated with the presence of carboxylic acids on the surface due to the excess acid added, samples of all materials were immersed in distilled water and dried in an oven. FTIR spectra were obtained again, and no significant changes were observed, indicating that the additives may not function as crosslinking agents or plasticizers.

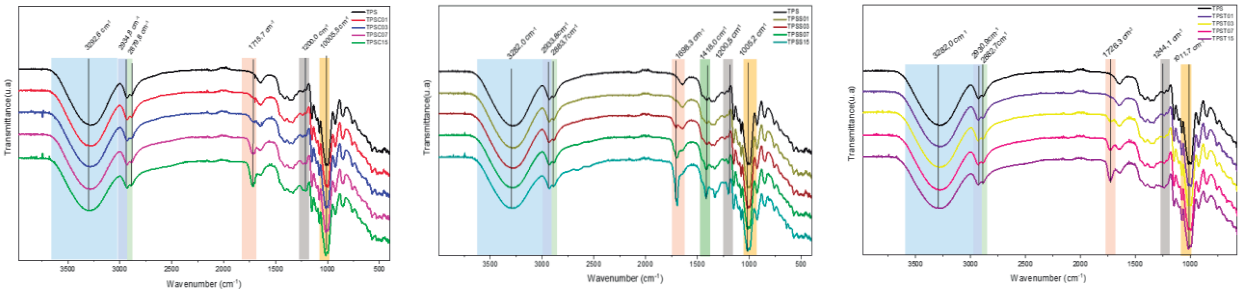

Figure 1: FTIR spectra obtained for the modified starch samples, TPSC, TPSS, and TPST.

Figure 2 shows TGA curves obtained to thermoplastic starch after and before modification with citric acid (TPSC), succinic acid (TPSS), and tartaric acid (TPST). In general, TGA curves of TPS, the three modified starch, TPSS, TPST, and TPSC, present a similar profile whit a four-step mass loss in addition to the first stage of mass loss related to the elimination of moisture and low molecular weight molecules.

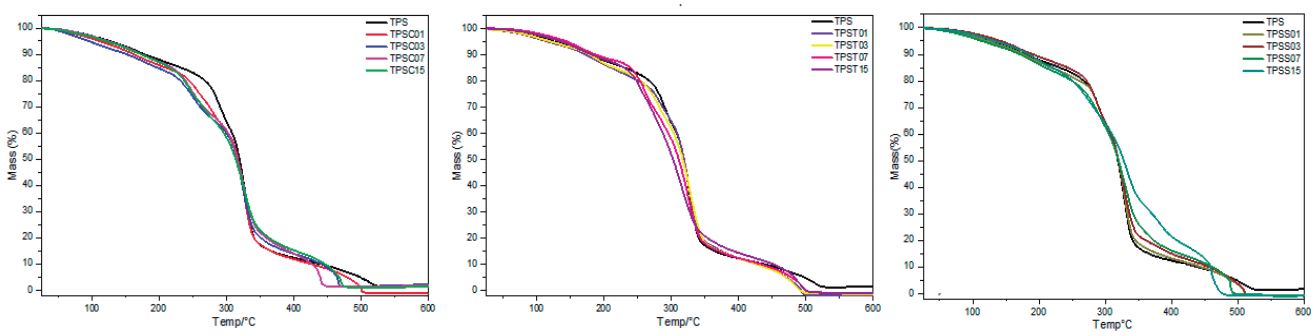

Figure 2: TGA curves modified starch TPSC, TPSS, TPST (respective percentages of acid) and TPS.

For the modified samples TPSC,TPSS and TPST it was observed the occurrence of 5 events. The first and second have coupled outputs related to moisture loss as well as the output of smaller molecules contributing to the degradation of glycerin.

A third event may be related to the decomposition of low molar mass chains resulting from the esterification and glycosidation reaction, facts that are observed in the FTIR analyses. The decompositions referring to the fourth and fifth event occur in a similar way to what was observed for the third and fourth event for the TPS sample, being related to starch degradation, as well as its residues.

It was observed that the materials modified with acids with higher amounts of carboxylic functionalities showed lower thermal stability than the others. this fact may be linked to the fact that these molecules are more likely to undergo hydrolysis, reversing the polymerization reaction and facilitating decomposition [2]

Conclusion

Studies show the effectiveness of starch esterification due to evidence of possible structural changes. In the spectroscopy analysis in the infrared region (FTIR), it was possible to observe the formation of carbonyl groups, from the appearance of bands in the region close to 1700 cm^{-1}. It can be suggested the occurrence of modification by chemical esterification reactions involving the hydroxyl groups of the starch and carboxyls of the acid.

As for the thermogravimetric analysis, it was possible to observe the occurrence of thermal events that are not seen in the starting materials, suggesting that the reactive extrusion promoted the formation of chemical bonds between the chains of starch, glycerin, and their respective acids. Structural and mechanical studies are in the testing phase and may provide more conclusive evidence for the processed material.

Acknowledgment

CNPq and FAPEMIG (INCT-Midas).

References

1. G. A. Gebresas; T. Szabó; K. Marossy Journal of Molecular Structure 2023, 1277, 134886. https://doi.org/10.1016/j.molstruc.2022.134886

2. H. L. C. Pulgarin; C. Caicedo; E. F.López Heliyon 2022,8,10833. https://doi.org/10.1016/j.heliyon.2022.e10833

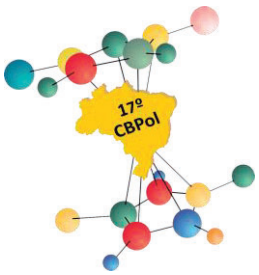

FATTY ACID-BASED DIISOCYANATE SYNTHESIS FOR THE PRODUCTION OF GREEN POLYURETHANES

Ângela G. L. L. Andrade[1*], Sérgio H. Pezzin[1]
1 –Department of Chemistry, Santa Catarina State University (UDESC), Joinville, SC, Brazil
angela.lechinski@gmail.com

Abstract – Aiming to the development of new synthetic routes for polyurethanes (PU) from raw materials exclusively from renewable sources, a 'green' synthesis of 1,8-diisocyanatooctane (DIO) was carried out from fatty acid derivatives by a method without the use of phosgene. The three-step synthetic route started from dimethyl sebacate, with the preparation of decanedihydrazide and decanedioyl diazide as intermediates, under nitrogen atmosphere. FTIR and ^{1}H NMR analyses confirmed the structure of the diisocyanate, which is a promising 'green' alternative to be used in the production of more sustainable polyurethanes by reaction with suitable polyols from biomass.
Keywords: Isocyanate, fatty acids, renewable sources, green synthesis.

Introduction

Polyurethanes (PU) are the result of the reaction between polyols and di- or poly-isocyanates. Due to its chemical versatility, it is possible to adapt to many structures, by selecting the most suitable polyol or isocyanate for the desired purpose. Sometimes, its synthesis is carried out through chemical routes that do not consider its adverse consequences, using raw materials derived from fossil products and substances harmful to health, for example [1]. However, the search for potential raw materials from renewable sources that resemble or exceed the efficiency of these materials, mainly from the oil industry, has gained great prominence in the scientific community [2]. In the literature, there are numerous attempts to replace materials from the petrochemical industry or create new materials from renewable sources [3-4].

The preparation of isocyanates to produce PU can occur in numerous ways, although the most used method on an industrial scale involves the reaction between gaseous phosgene ($COCl_2$) with amines or their corresponding salts [5]. The high toxicity, combined with the growing environmental appeal, has led to the development of new routes for the preparation of isocyanates without the use of phosgene. Lossen, Curtius and Hoffmann rearrangements, and the use of phosgene equivalents such as di and triphosgene, for example, are some of the alternative methods employed for its replacement. In this perspective, there are fatty acids, such as sebacic acid, which is a naturally occurring dicarboxylic acid, which is still little explored for obtaining isocyanates [6]. Studies have shown that isocyanates from fatty acids, when reacted with a suitable polyol, can improve the thermal properties of PU [3,7].

Therefore, in this work we propose the synthesis and characterization of an isocyanate from a renewable source from sebacic acid derivatives, for the production of 1,8-diisocyanatooctane (DIO).

Experimental

Dimethyl sebacate synthesis

Dimethyl sebacate was produced according to the procedure described by Kunkuma et al. [8]. In a 200 mL kitassato, 15 g (74 mmol) of sebacic acid 99% (Sigma Aldrich), 2 mL of sulfuric acid 95 – 97% (Biotec) and 100 mL of methyl alcohol 99,8% (Honeywell) were added at 65 °C for 5 hours. At the end of the reaction, the reaction mixture was cooled to room temperature, being extracted with ethyl acetate 99,5% (Reatec) (200 mL). The organic phase was successively washed with water (4 times of 50 ml) until neutral pH. Anhydrous sodium sulfate 99% (Dinâmica) was used for drying the organic phase. With the rotary evaporator, the solvent was removed. Purification was carried out on a silica gel column, using a mixture of hexane and ethyl acetate 99,5% (Reatec) (v/v, 95:5) as eluent, resulting in the end dimethyl sebacate in liquid form. Final mass obtained: 16.8 g. Yield: 99%.

Fattty acid based isocyanate synthesis

The isocyanate synthesis route was based on the produced reported by More et al. [3], involving three steps to obtain 1,8-diisocyanatooctane (DIO) (Figure 1).

Step 1: Synthesis of decanedihydrazide (DDH)

In a round bottom flask were added dimethyl sebacate (32 g, 138.94 mmol), hydrazine hydrate 99% (Sigma Aldrich) (34.77 g, 694.74 mmol) and ethanol 96% (Honeywell) (150 mL). The reaction mixture was stirred at 35°C for 48 hours under a nitrogen atmosphere. At the end, the rotary evaporator was used to evaporate the excess of solvent, obtaining a white powdery solid.

Step 2: Synthesis of decanedioyl diazide (DDD)

In step 2, dihydrazinedecane (4 g, 17.39 mmol) was reacted in a beaker kept cooling at 0 °C with a solution of concentrated hydrochloric acid 37% (Reotec) (6.34 g, 173.91 mmol) and acetic acid 98% (Cinética) (10 mL). Soon after 30 mL of dichloromethane 99,9% (Scharlau) were added. Then, under vigorous stirring, an aqueous solution of sodium nitrite 97% (Dinâmica) (6.48 g, 93.91 mmol + 15 mL of water) was slowly dropped onto the reaction mixture. After the completion of the addition, the reaction mixture was kept under stirring for 30 minutes at 0 °C. In the next step, the organic phase was separated and washed with a 0.1 $mol \cdot L^{-1}$ aqueous solution of sodium hydrogencarbonate 99,7% (Dinâmica) (twice), followed by a 0.1 $mol \cdot L^{-1}$ solution of sodium chloride. Finally, drying was performed with anhydrous sodium sulfate. The solvent was evaporated with the rotary evaporator at room temperature.

Step 3: Synthesis of 1,8-Diisocyanatooctane (DIO)

In the third and last step, the previously prepared DDD (3 g, 11.60 mmol) was mixed in a round bottom flask with tetrahydrofuran 99% (Dinâmica) (40 mL) under a nitrogen atmosphere for 6 hours. After completion of the reaction, the solvent was removed using a rotary evaporator. Then, 10 mL of petroleum ether was added to the compound and passed through a silica gel column to purify the substance. Finally, the compound was rotary evaporated to evaporate the solvent.

Characterization

Fourier transform infrared spectroscopy (FTIR) has been performed in a Bruker INVENIO-S equipment. The samples were measured in transmission mode at 4 cm^{-1} resolution, from 450 to 4,000 cm^{-1}.

Proton nuclear magnetic resonance (^1H NMR) was measured in a Bruker AVANCE III HD 400MHz spectrometer, using deuterated chloroform ($CDCl_3$) as a solvent.

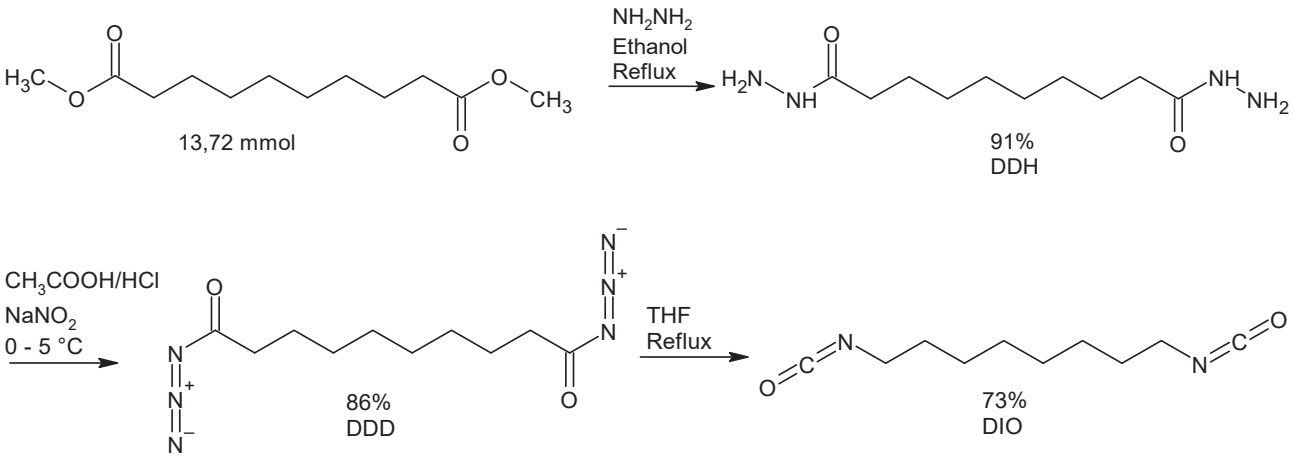

Figure 1 – Synthesis route for DIO production.

Results and Discussion

Initially, the characterization of the synthesized dimethyl sebacate was carried out, a necessary reagent for the synthesis of diisocyanate. FTIR and ^{1}H NMR spectra were performed and compared with a commercially available dimethyl sebacate standard (Sigma Aldrich). The main absorption bands related to the main functional groups present in the structure of the molecule were observed, such as -C=O and -C-O- ester bonds. The ^{1}H NMR spectra also allowed the identification of the hydrogens present in the dimethyl sebacate structure. Kunkuma et al. (2013) in their studies for the synthesis of dimethyl sebacate, reported the same trends observed in the FTIR and ^{1}H NMR spectra for both the synthesized and the commercially available molecule, indicating success in the synthesis.

The FTIR spectra (Figure 2) show the absorption bands of the synthesized diisocyanate. In the initial stage of DDH formation, two absorption bands with moderate intensity are observed at 3310 and 3291 cm^{-1} related to the presence of the -NH_2 and -NH functional groups, while at 1629 cm^{-1} there is a strong absorption typical of amide carbonyl. For the DDD formation stage, at 2135 cm^{-1} the appearance of a strong band can be observed, which can be attributed to the presence of azide (N_3) in the molecule. At 1706 cm^{-1} a band of strong intensity is due to the presence of the carboxyl that directly performs a chemical bond with the azide (-CON_3). Finally, for the spectrum of obtaining octane 1,8-diisocyanate (DIO) at 2256 cm^{-1}, a strong absorption relative to the formation of the isocyanate bond (NCO) in the molecule is observed. More et al. [3] describe similar results for the synthesis of DIO regarding the formation of absorption bands, corroborating the spectral profiles obtained.

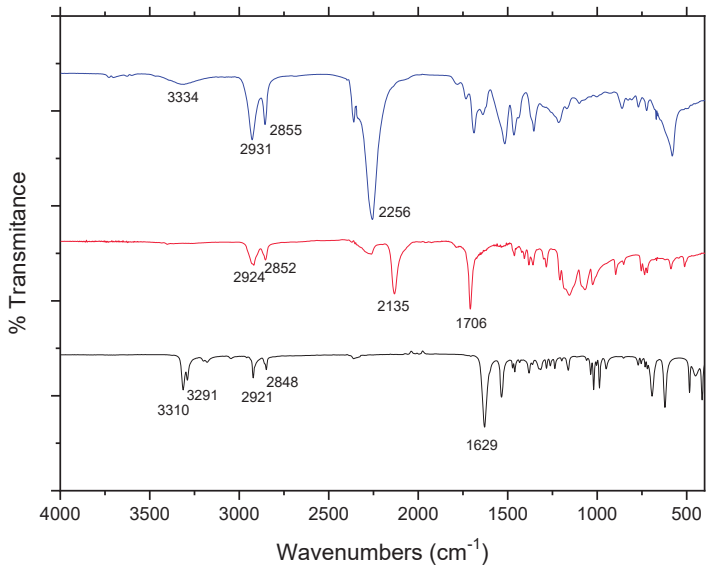

Figure 2 – FTIR spectrum for the synthesized isocyanate: 1,8-diisocyanatooctane (blue), decanediol diazide (red) and dihydrazinedecane (black).

Figure 3 shows the ^{1}H NMR spectrum for the synthesis of DIO performed in DMSO-d6. For the stage of obtaining the DDH, the chemical shift relative to hydrogen (-NH-) of the amide bond is observed at 8.92 ppm (s, CH_2-$CONHNH_2$). At 4.15 ppm (s, CH_2-$CONHNH_2$) shifts of the primary hydrogens (-NH_2-) of the amide are formed. The chemical shift of 1.98 ppm (t, J = 7.75 Hz, CH_2-CO) is attributed to the neighboring hydrogens of the carboxyl present in the DDH structure. It is also observed the formation of a peak between 1.35 – 1.55 ppm (m, CH_2-CH_2CO) attributed to the chemical displacement of the distant hydrogens in two chemical bonds of the amide carboxyl. Finally, at 1.10 – 1.25 ppm (m, CH_2) the formation of a peak is seen relative to the hydrogens internal to the chain, which consequently are further away from the -C=O- bonds of the amide, suffering less influence in their chemical shift values.

Also in Figure 3, the ^{1}H NMR spectrum for DDD, which was carried out in $CDCl_3$, can be seen. This shows at 2.26 ppm (t, J = 7.13 Hz, CH_2CO) a chemical shift attributed to the neighboring hydrogens of the azide carboxyl. The region around 1.40 – 1.60 ppm (m, CH_2-CH_2CO) refers to hydrogens separated by two carboxyl bonds. Peaks at 1.10 – 1.30 ppm (m, CH_2) are attributed to the main chain methylenes, which suffer less influence from the carbonyl in their chemical shifts.

Finally, for the DIO spectrum (Figure 3), which was performed in $CDCl_3$. It is observed at 3.23 ppm (t, J = 6.83 Hz, CH_2NCO), the appearance of a small peak related to the chemical shift attributed to the neighboring hydrogens to carboxyl. At 1.40 – 1.60 ppm (m, CH_2-CH_2CO) we have the chemical shift relative to the distant hydrogens in two carboxyl chemical bonds. In the region of 1.10 – 1.30 ppm (m, CH_2), we observe the formation of peaks related to the -CH_2- bonds internal to the chain, which suffer less influence from the carboxyl in their chemical shifts.

The patterns of ^{1}H NMR chemical shifts are similar to those obtained in the work developed by More et al. (2013) for the synthesis of new isocyanates based on fatty acids, where the authors synthesized DIO following a synthetic route similar to that described here.

For the three stages of synthesis to obtain DIO, it was observed that the generated spectra presented coherent and characteristic chemical shifts for each of the synthesized compounds, which were very similar to the studied literature. Based on this, it is possible to state that the isocyanate of interest for this work was successfully synthesized.

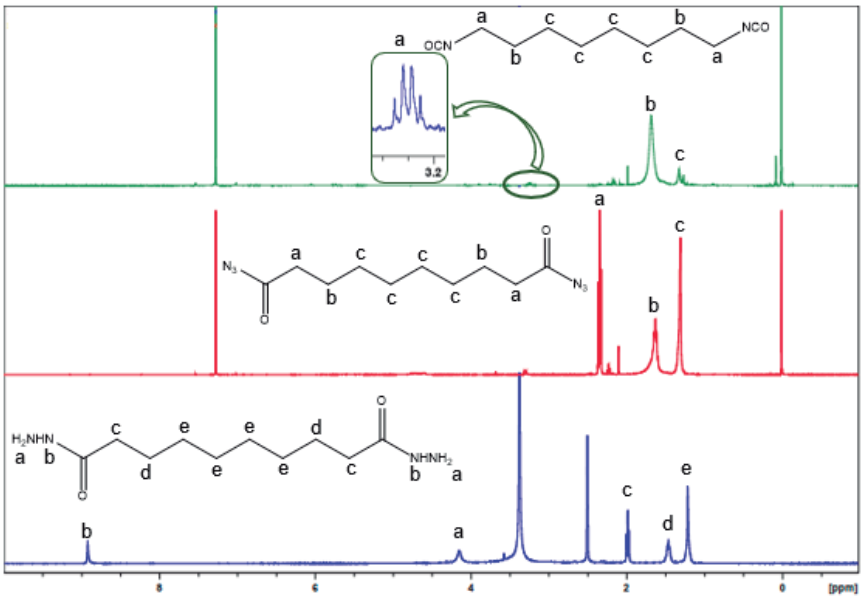

Figure 3 – ^{1}H NMR spectra for the synthesized isocyanate: DDH (blue), DDD (red) and DIO (green).

Conclusions

The synthesis of octane 1,8-diisocyanate was successfully performed from renewable raw material, without the use of phosgene, by a 'green' synthesis using fatty acid via diacyl hydrazine intermediate. The presence of the main functional groups in the diisocyanate structure can be observed through FTIR spectroscopy. ^{1}H NMR spectra confirmed that DIO had formed. The synthesized diisocyanate presents itself as a promising 'green' alternative to be used in the synthesis of polyurethanes.

Acknowledgements

This work was supported by FAPESC (2019TR582), FINEP and UDESC/CCT. We would like to thank Prof. Rogério A. Gariani for the ^{1}H NMR analyses.

References

1. J. B. Zimmerman et al. Science, 2020, 367, 6476, 397. https://doi.org/10.1126/science.aay3060

2. A. E. Coman et al. European Polymer Journal 2021, 149, 110363. https://doi.org/10.1016/j.eurpolymj.2021.110363

3. A. S. More et al. European Polymer Journal 2013, 49, 4, 823. http://dx.doi.org/10.1016/j.eurpolymj.2012.12.013

4. Y. Song et al. Applied Catalysis A 2023, 651, 119017. https://doi.org/10.1016/j.apcata.2022.119017

5. B. W. Ellis, *Ullmann's Encyclopedia of Industrial Chemistry*. Wiley-VCH Verlag GmbH, Weinheim, Germany, 1999.

6. Z. Wei, et al. RSC Advances, 2015, 53, 42777. https://doi.org/10.1039/C5RA04761G

7. A. G. L. L. Andrade; S. H. Pezzin Macromolecular Symposia 2022, 406, 202200051. http://dx.doi.org/10.1002/masy.202200051

8. V. L. Kunkuma et al. European Journal Of Lipid Science And Technology, 2013, 115, 8, 921. http://dx.doi.org/ 10.1002/ejlt.201200195

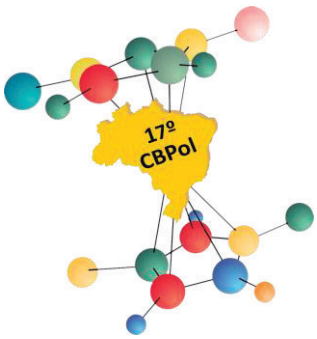

FULLY BIO-BASED NOVOLAC RESINS FROM AGROINDUSTRIAL RESIDUES FOR APPLICATION IN ANTICORROSIVE COATINGS

Sara J. Marciano[1*], Maria A. C. Monteiro[2], Maycon M. Vasconcelos[1], Walney S. Araújo[1], Selma E. Mazzetto[2], Diego Lomonaco[2]

1 – Department of Metallurgical and Materials Engineering, Federal University of Ceará (UFC), Fortaleza, CE, Brazil
sarajessica@alu.ufc.br
2 – Department of Organic and Inorganic Chemistry, Federal University of Ceará (UFC), Fortaleza, CE, Brazil

Abstract
In recent years, there has been an increasing trend of replacing the use of petrochemical derivatives with bio-based alternatives. In this study, the objective was to develop entirely bio-based novolac resins from cashew nutshell liquid (CNSL) as alternative anticorrosive coatings for steel. CNSL and furfural were reacted using a solvent-free method to create the bio-based polymers. The coating preparation involved combining the CNSL-based novolac resin with a commercial epoxy resin (DGEBA), along with 1-methylimidazole as an accelerator. The resulting coatings were characterized in terms of their crosslink density, thermal stability, and anticorrosive properties. The results indicated that the coatings exhibited a high impedance module. These findings demonstrate the promising potential of the developed bio-based novolac coating as a partial replacement for the commercial resin used in corrosion protection applications.

Keywords: o*rganic coating; bio-based coating; corrosion protection; CNSL; agrowaste.*

Introduction

Corrosion is one of the biggest problems related to the use of metals and causes major problems to industries. Organic coatings are one of many strategies used to protect the metal from corrosion, acting as a physical barrier isolating the metal from corrosive media and extending their useful life [1]. In this context, epoxy resins are a class of thermosetting polymer widely used in the largest part of the coating market. Epoxy resins have an excellent combination of mechanical properties, high chemical resistance, adhesion capacity, thermal stability and easy processability [2]. Despite all these advantages, the commercially available epoxy resins (bisphenol A diglycidyl ether - DGEBA) are synthesized and involve a phenolic precursor derived from petrochemical resources (bisphenol A - BPA) and studies have shown that BPA can cause severe risks to human health and the environment [3-4].

The scientific community has been prospecting different types of compounds that have the capability to act as precursors in the development of partially/fully biobased thermoset polymers that may reduce and/or replace the use of BPA with good properties. Among them, CNSL has attracted the attention of scientists due to its abundance in nature and rich chemical composition composed mainly of phenolic structure. From the vast possibilities of chemical modifications to

obtain new materials from CNSL, the production of phenolic resins stands out. Phenolic resins are obtained through the condensation reaction between phenol and formaldehyde, and CNSL is one of potential substitutes in the synthesis. Also, due to their excellent properties, they are widely used as adhesives for wood, in plastic production, insulation materials, composites and coatings [5]. In this context, there are works in the literature that present the use of CNSL and its constituents as an alternative in the production of resins for application as an organic coating [6-8] and as a substitute for DGEBA [6] in the production of coatings and which has shown excellent potential for this use.

Therefore, the aim of this work was the direct use of CNSL without prior separation of its components, for novolac resin production to evaluate the effects caused by replacing partially DGEBA as anticorrosive protective coating for steel surfaces.

Experimental

The reaction from CNSL and furfural novolac resins was performed according to the methodology described by Srivastava et al. [9] with some modifications as shown in Fig. 1.

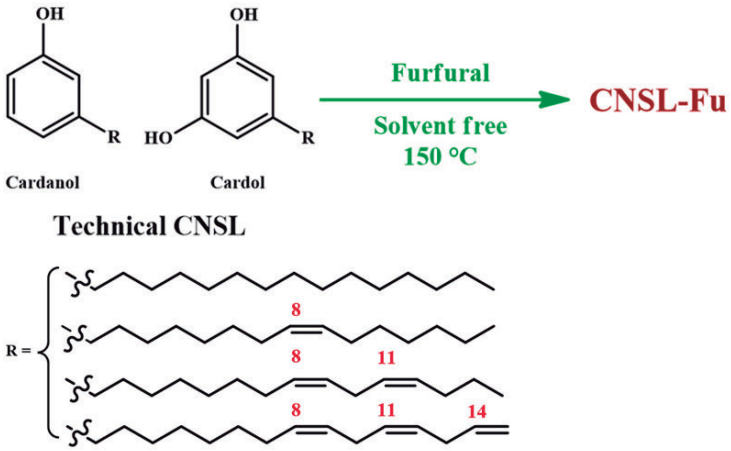

Figure 1. Reaction scheme of CNSL-Fu novolac resin synthesis.

Novolac-based resins coatings were prepared from a mixture of CNSL-Fu, DGEBA and 1-methylimidazole (1-MIM), using toluene as solvent. The preparation of the novolac-based resin involved the solubilization of CNSL-Fu and DGEBA using toluene as co-solvent, and a certain amount of 1-MIM as a catalyst.

Table 1 shows the quantity of reagents used in the preparation of novolac/epoxy coatings. Preparation of coatings was performed by adding varying amounts of novolac resin (20 to 50% w/w) to the epoxy resin and 1-MIM (5% w/w in relation to DGEBA) under mechanical stirrer.

To evaluate resin properties such as polymeric coating, carbon steel plates were coated with this formulation and then curing was done by controlled temperature program: 80, 100, 120 °C for 1 h. The coated substrates were submitted to a post curing process at 150 °C for 1h and 160 °C for 2h. The cured samples were conditioned at room temperature for 24 h and then were characterized as to their chemical resistance, density of crosslinks (ASTM D2765) [10], thermal stability (TGA) and anticorrosive properties.

Table 1. Reagents used in the production of coatings.

Coating	Mass of novolac (g)	Mass of DGEBA (g)	Volume catalyst (µl)	Volume toluene (µl)
DGEBA/Nov20%	0,6	2,4	115,9	170
DGEBA/Nov30%	0,9	2,1	101,4	170
DGEBA/Nov40%	1,2	1,8	86,9	170
DGEBA/Nov50%	1,5	1,5	72,4	170

Results and Discussion

Table 2 shows the results of the chemical resistance tests presented by the thermosetting polymers obtained from bio-based resin (DGEBA/CNSL-Fu), when subjected to tetrahydrofuran (THF).

Table 2. Gel content ant thermal properties of DGEBA/Nov coatings.

Sample Name	Gel content (%)	T_{onset}	$T_{d30\%}$	CY (%)
DGEBA/IPDA	99	359	370	7,0
DGEBA/Nov20%	100	402	412	9,1
DGEBA/Nov30%	97	406	417	9,1
DGEBA/Nov40%	96	403	416	9,5
DGEBA/Nov50%	94	403	416	8,5

Table 2 shows that the insertion of novolac in the resin had significant effect on the chemical resistance of the polymer obtained. These results also suggest that partial replacement of DGEBA by novolac resin affected the formation of crosslinks between polymeric chains, despite the fact that novolac has reactive functional groups that can catalyze the opening of oxirane rings and the decrease of this valor might be a greater portion of novolac in relation to the others, was not crosslinked. Thus, the insertion of a phenolic molecule such as novolac structure in the epoxide group could confer interesting properties to the final material, such as rigidity and chemical resistance, due to the high amount of aromatic structures present in the final material.

The thermal behavior was performed for cured polymers to investigate the thermal stability of materials under nitrogen atmospheric conditions by thermogravimetric analysis and the results are shown in Fig. 2.

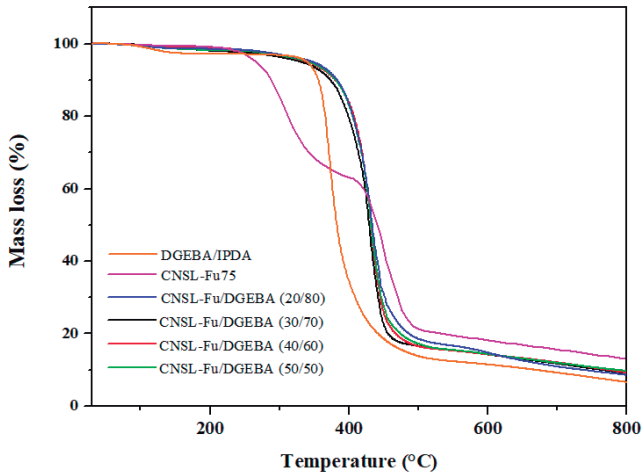

Figure 2. Thermal degradation profile of CNSL-Fu uncured and polymers under inert atmosphere conditions.

It is possible to observe that the partial replacement of DGEBA by novolac resin causes an increase in thermal stability, as observed by the values of initial degradation temperature (T_{onset}) showed in Table 2. The system epoxy/novolac provided a high crosslinking density of novolac resin, which in turn is more stable at high temperatures compared to the uncured resin. Also, it is possible to notice that the insertion of novolac causes a considerable increase in the final pyrolysis residue at 800°C. This behavior is due to the density of the aromatic ring, which undergo recondensation reactions at high temperatures, forming a high amount of carbonaceous material, which prevents the diffusion of heat between the polymer and the environment, delaying its emission. This property is extremely interesting for this class of resins, as epoxy resins are highly

flammable and, therefore, the addition of bio-based novolac to these resins, in addition to increasing hydrophobicity, can provides flame retardancy.

Electrochemical impedance spectroscopy (EIS) was performed to evaluate the anticorrosive potential of the coatings on the 1020 steel surface. The impedance measurements obtained after 38 days of immersion in 3,5% NaCl solution at room temperature are shown in Fig. 3. The values of modulus of impedance obtained from the Bode diagram at the lowest frequency are presented in Table 3. The thicknesses of all coatings were measured in the range of 80-100 µm.

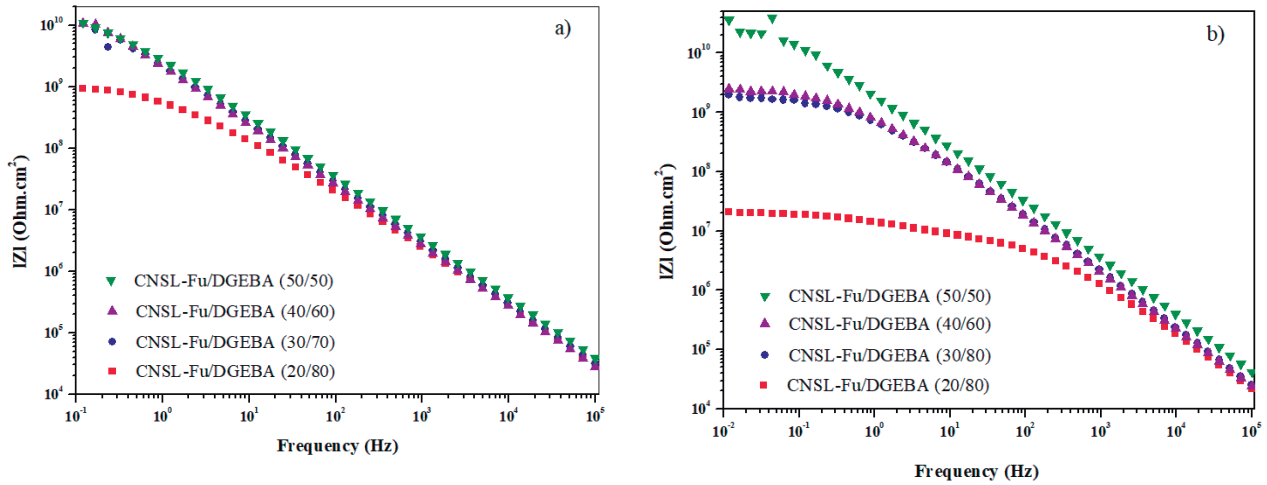

Figure 3. Evaluation of degradation over time by Bode plot: a) start immersion; b) after 38 days immersed in NaCl 3.5% at room temperature.

Table 3. Corrosion parameter of coatings.

Coating	Coating Resistance (ohm.cm^2) start immersion	Coating Resistance (ohm.cm^2) After 38 days of immersion
DGEBA/IPDA[11]	5,19 x 10	-
DGEBA/20%Nov	7,98 x 10^8	2,21 x 10^7
DGEBA/30%Nov	8,07 x 10^8	2,01 x 10^9
DGEBA/40%Nov	1,01 x 10^{10}	2,31 x 10^9
DGEBA/50%Nov	1,85 x 10^{10}	3,08 x 10^{10}

It is evident that the impedance value, represented by the coating resistance (Rc) is higher for the commercial coating (DGEBA/IPDA) when compared to the bio-based novolac coating. This behavior indicates that the insertion of novolac in the epoxy resin causes a considerable decrease in the capacity of the coating to act as a physical barrier. This may be due to the presence of the long aliphatic side chain in the cardanol molecule. However, the novolac-based coating exhibits comparable values to the commercial resin and still can hindering the transfer of charge between the metal and the solution, preventing its oxidation. This study revealed that all coatings presented values of Rc higher than 10^6, which is indicative the paint is viewed as being a good organic coating [12]. Therefore, such results indicate the potential of epoxy resin incorporated with bio-based novolac as an anticorrosive polymeric coating.

Conclusions

This study makes a noteworthy contribution to the research and advancement of sustainable materials by investigating the utilization of CNSL as a promising substitute for petrochemical

phenol in the production of novolac phenolic resins. Furthermore, the feasibility of furfural as a replacement for formaldehyde was explored using a straightforward approach. These discoveries advocate for an alternative framework in the development of bio-based resins, which holds significant significance in the realm of sustainable materials.

Acknowledgements
Universidade Federal do Ceará (UFC), Laboratório de Produtos e Tecnologia em Processos (LPT), Laboratório de Pesquisa em Corrosão (LPC). CNPq, CAPES e FUNCAP for the financial support.

References

1. Y. Wu, J. Yu, W. Zhao, C. Wang, B. Wu, G. Lu, Prog. Org. Coat. 2019, 133, 8–18. https://doi.org/10.1016/j.porgcoat.2019.04.028.
2. Zhi, Maoyong; Yang, Xiong; Fan, Rong; Yue, Shan; Zheng, Lingling; Liu, Quanyi; He, Yuanhua, Polymer Degradation and Stability 2022, 201, 109976. https://doi.org/ 10.1016/j.polymdegradstab.2022.109976.
3. A. Ramaswami, R.G. Luthy, Environ. Sci. Technol. 1997, 31, 8, 2268–2276. https://doi.org/10.1021/es9608508.
4. A.C.L. Chiovatto, et al., Mar. Pollut. Bull 2021, 166, 112221. https://doi.org/10.1016/j.marpolbul.2021.112221.
5. Liu, X., Li, Y., Xing, X., Zhang, G., & Jing, X., Polymer 2021, 229. https://doi.org/10.1016/j.polymer.2021.124022.
6. L. R. R. da Silva, F. Avelino, O. B. F. Diogenes, V. D. O. F. Sales, K. T. da Silva, W. S. Araujo, S. E. Mazzetto, D. Lomonaco, Prog. Org. Coat. 2020, 139, 105449. https://doi.org/10.1016/j.porgcoat.2019.105449.
7. Da Silva, Kássia Teixeira; Oliveira, Beatriz S.; Da Silva, Lucas R.R.; Mattos, Adriano L.A.; Mazzetto, Selma E.; Lomonaco, Diego, Journal of Applied Polymer Science 2023, 140, 13, 1–13. https://doi.org/10.1002/app.53661.
8. R. Srivastava, D. Srivastava; J. Polym. Environ. 2015, 23, 283. https://doi.org/10.1007/s10924-014-0659-6.
9. R. Srivastava, D. Srivastava; Int. J. ChemTech Res. 2013, 5, 2575.
10. American Society for Testing Materials. ASTM D 2765 - Standard Test Methods for Determination of Gel Content and Swell Ratio of Crosslinked Ethylene Plastics. In Annual Book of ASTM Standards, 2011. https://doi.org/10.1520/D2765-16.
11. O. B. F. Diogenes, D. R. de Oliveira, L. R. R. da Silva, Í. G. Pereira, S. E. Mazzetto, W. S. Araujo, D. Lomonaco; Prog. Org. Coat. 2021, 161, 1. https://doi.org/10.1016/j.porgcoat.2021.106533.
12. A. Amirudin, D. Thieny; Prog. Org. Coat. 1995, 26, 1–28. https://doi.org/10.1016/0300-9440(95)00581-1.

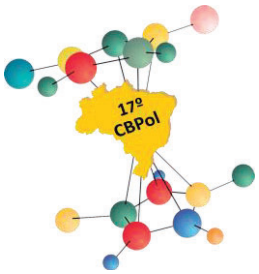

INFLUENCE OF TEMPERATURE ON THE SYNTHESIS OF OCTYL OLEATE USING IMMOBILIZED PANCREATIC LIPASE ON MAGNETIZED PARTICLES OF POLY(STYRENE-CO-DIMETHACRYLATE TRIETHYLENE GLYCOL)

Gabrielle P. de Assis[1], Vinicius S. Silva[1], Barbara L. A. de Albuquerque[1], Mateus V. Silva[1], Larissa de Freitas [1]

1 – Departament of Chemical Engineering, University of São Paulo (USP), Lorena, SP, Brazil
larissafreitas@usp.br

Abstract - The study aimed to synthesize the emollient ester octyl oleate via an enzymatic route using immobilized pancreatic lipase on a magnetized polymeric support composed of styrene and triethylene glycol dimethacrylate. The copolymer synthesis process was carried out through suspension polymerization with the addition of Fe^{2+} and Fe^{3+}, and the lipase was immobilized using the physical adsorption technique. The ester syntheses were performed using an equimolar mixture of alcohol:acid as the substrate and 10% w/w of biocatalyst in a temperature range of 35-55 ºC. Various analyses were conducted to quantify enzymatic activity, resulting in values of 389.94 ± 61.27 U g^{-1} for the synthesis of ethyl oleate and 1262.53 ± 19.74 U g^{-1} for the hydrolysis of olive oil. The results demonstrated that the maximum conversions of oleic acid were achieved at temperatures of 50 and 55ºC (82% and 64%, respectively), confirming the suitability of the copolymer used as a support and the immobilization method employed, as the temperature range of lipase activity was expanded.

Keywords: *Magnetized copolymer; immobilization; pancreatic lipase; emollient ester.*

Introduction

The demand for new technologies and environmentally sustainable industrial processes has driven the development of innovations employing enzymatic methods for the production of pharmaceuticals, food, cosmetics, among other products. It is estimated that by the year 2028, the global enzyme market will experience a growth of 6.5% when compared to the 2021 market, which was valued at approximately US$ 11 [1-3].

Enzymatic processes employing lipases as biocatalysts, enzymes belonging to the class of hydrolases, have become promising technological sources, as they can be used in a variety of application possibilities, such as esterification, transesterification, interesterification, and hydrolysis of oils and fats. Lipases demonstrate high efficiency, high selectivity and specificity, generating products with high quality and yield compared to conventional catalysts, in addition to the possibility of recovery and reuse at the end of the bioprocess when immobilized [1,4].

The use of magnetized copolymer based on styrene as a support for lipase immobilization has become a promising approach, as they are highly hydrophobic matrices, which is suitable for immobilizing this lipase. Additionally, the recovery of

the biocatalyst at the end of the reaction is easier, as it can be recovered through magnetic force, thus avoiding the need for filtration, centrifugation, or column separation [5-6].

Therefore, the present study aimed to synthesize octyl oleate via esterification using immobilized pancreatic lipase on magnetized poly(styrene-co-triethylene glycol dimethacrylate) (LPP-STY-TEGDMA-M), evaluating the influence of temperature on the yield of this bioprocess.

Experimental

The synthesis of the magnetized copolymer was performed using the suspension polymerization technique in a jacketed reactor (Fig. 1) with a capacity of 500 mL. The polymeric matrix consisted of two phases, organic and aqueous. The organic phase comprised styrene (base monomer), triethylene glycol dimethacrylate (TEGDMA) crosslinking agent, toluene (high-affinity solvent), and heptane (low-affinity solvent), while the aqueous phase consisted of a 1% solution of polyvinyl alcohol (PVA 88% hydrolyzed) dissolved in 400 mL of ultrapure water. Purified azobisisobutyronitrile (AIBN) initiator was also used, and the synthesized and modified magnetite was employed as described by Bento *et al*. (2017).

Figure 1 – *Experimental system used in the polymeric supports synthesis.*

The polymerization reaction was carried out for 6 hours, with the first two hours conducted under an inert atmosphere (N_2) at a mechanical stirring rate of 310 rpm and 70°C. After synthesis, the copolymer was washed, dried, and classified granulometrically using Tyler mesh sieves (24 - 80) in a sieve shaker. The moisture content of the support was also measured to ensure it was below 10%. Subsequently, pancreatic lipase immobilization was performed using the physical adsorption technique, forming the LPP-STY-TEGDMA-M complex.

Enzymatic activities of the biocatalyst were evaluated through the synthesis of ethyl oleate as described by Pinto *et al*. (2014), quantified by linearizing the consumption of oleic acid, and the hydrolysis of olive oil, as proposed by Soares *et al.* (1999), quantified according to Equation 1. For the synthesis of octyl oleate, a molar ratio (acid/alcohol) of 1:1 and a biocatalyst concentration of 10% (w/v) were established. The syntheses were conducted in batch mode in agitated flasks, under stirring at 150 rpm and temperatures ranging from 35 to 55°C. The acid consumption was quantified by titration using a 0.04 mol L^{-1} KOH solution and phenolphthalein as an indicator (Equation 2).

$$Hydrolytic\ activity\ (U\ g^{-1}) = \frac{(V_a - V_b)\ x\ M\ x\ 1000}{(t\ x\ m)}$$

(1)

$$Carboxylic\ Acid\ (g.L^{-1}) = \frac{V*M*MM}{v}$$

(2)

Where: V_a is the volume of KOH used in the titration in mL, V_b is the volume of KOH in the blank titration, M is the concentration of KOH in mol L^{-1}, t is the time in minutes, m is the mass of biocatalyst used in grams, V is the volume of KOH in mL, MM is the molar mass of the carboxylic acid in g mol^{-1}, and v is the volume of the collected aliquot.

Results and Discussion

Characteristics of the support and enzymatic activity of the biocatalyst

The characteristics of the support and the quantification of the catalytic activity of the LPP-STY-TEGDMA-M biocatalyst are presented in Table 1.

Table 1: *Characteristics of the polymeric support and the LPP-STY-TEGDMA-M biocatalyst.*

Analysis	Values
Esterification activity (U g^{-1})	389,94 ± 61,27[a]
Hydrolytic activity (U g^{-1})	1262,53 ± 19,74[a]
Hysteresis (emu g^{-1})	4,79[b]
Pore volume ($cm^3\ g^{-1}$)	0,15 [b]
Average pore diameter (nm)	9,90 [b]
Surface area ($m^2\ g^{-1}$)	44,00 [b]
Swelling degree (%)	3,58 [b]

[a] – author own
[b] - Rosa, 2019

The polymeric support synthesized in the present work (STY-TEGDMA-M) was also studied by Rosa, 2019, who analyzed the optimal synthesis conditions and characterized it, highlighting some parameters, as shown in Table 1.

In a study conducted by Zou et al. (2010), where mesoporous silica was used as an immobilization support for pancreatic lipase, a hydrolytic activity of 975 U g-1 was obtained, which is lower than the activity of the LPP-STY-TEGDMA-M biocatalyst (1262.53 ± 19.74 U g-1) developed in this work. Thus, the suitability of the polymeric matrix and immobilization method used in the present study for pancreatic lipase immobilization can be confirmed.

Influence of temperature on the synthesis of octyl oleate

Figure 2 shows the conversion profile obtained for the synthesis of octyl oleate at different temperatures using pancreatic lipase immobilized in magnetized copolymer as the biocatalyst.

Figure 2 – *Conversion profile of oleic acid in the esterification reaction for the synthesis of octyl oleate in the temperature range of 35-55 ºC.*

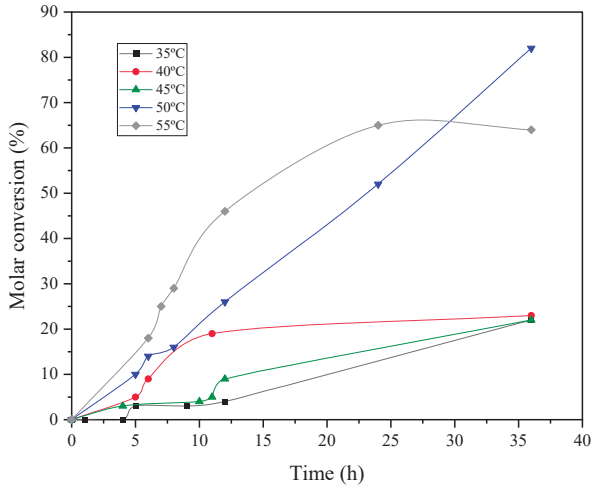

According to Figure 2, it can be observed that the highest conversions were obtained at temperatures of 50 and 55ºC, reaching 82% and 64% respectively. These results show the efficiency of the support and the method adopted, considering that the optimal temperature range for free pancreatic lipase is 35-45 ºC [10], indicating that the immobilization of this lipase on the STY-TEGDMA-M support provided greater stability to the enzyme, allowing its catalytic activity at higher temperatures.

Lei et al. (2009) immobilized LPP on magnetized polymeric microspheres to catalyze the synthesis of hexyl acetate at 50ºC in a solvent medium and achieved maximum conversions of 83%. This demonstrates the high efficiency of the biocatalyst tested in this study, as the syntheses conducted in the current research did not involve the use of solvents.

However, a decrease in conversion was observed in the synthesis conducted at 55ºC after 24 hours of reaction. This observation may be related to a possible decrease in the stability of the biocatalyst when exposed for a longer period of time at this temperature. An alternative to overcome this obstacle would be the use of covalent immobilization techniques, which could result in a more stable biocatalyst at higher temperatures.

Conclusions

The results obtained in this study demonstrated the feasibility of using immobilized pancreatic lipase in magnetized copolymer for the synthesis of octyl oleate ester, as significant reaction yields were achieved. It is noteworthy that the use of

pancreatic lipase as a biocatalyst is of high interest, as its cost is more affordable compared to other commercially available lipases.

Furthermore, the suitability of the support used for immobilization can be observed, as the synthesized biocatalyst exhibited good performance at higher temperatures compared to the optimal range of the free lipase. The use of covalent binding immobilization method is suggested to enhance the stability of the immobilized enzyme at higher temperatures.

Acknowledgements

The authors would like to thank Coordenação de Aperfeiçoamento de Pessoal de Nível Superior (CAPES) – Funding Code 001, Fundação de Amparo à Pesquisa do Estado de São Paulo (FAPESP 2016/10636-8) and Unified Scholarship Program of the University of São Paulo (PUB-USP, project code number 1068) for their financial support.

References

1. A. S. Pereira; A. H. de Souza; J. L. Fraga; P. Villeneuve; A. G. Torres; P. F. F. Amaral, Catalysts 2022, *12*, 88. https://doi.org/10.3390/catal12010088.
2. C. S. Sampaio; J. A. F. Angelotti; R. Fernandez-Lafuente; D. B. Hirata International Journal of Biological Macromolecules 2022, 215, 434-449. https://doi.org/10.1016/j.ijbiomac.2022.06.139
3. R. A. Sheldon; D. Brady Catalysts 2022, 13, 303. https://doi.org/10.1002/cssc.202102628.
4. Q. D. Utama; A. B. Sitanggang; D. R. Adawiyah; P. Hariyadi.Food Technology and Biotechnology 2019, 57, 3, 305. doi: 10.17113/ftb.57.03.19.6025.
5. M. V. C. Silva; L. G. Aguiar; C. M. R. Rosa; H. F. Castro; L. Freitas Chemical Engineering Communications 2020, 207, 9, 1329–1336. DOI:10.1080/00986445.2019.1647179.
6. C. M. R. Rosa; M. V. C. Silva; L. G. Aguiar; H. F. Castro; L. Freitas Journal of Applied Polymer Science 2020, 137, 41. https://doi.org/10.1002/app.49258.
7. H. B. S. Bento; H. F. Castro; P. C. Oliveira; L. Freitas Journal of Magnetism and Magnetic Materials 2017, 426, 95–101. https://doi.org/10.1016/j.jmmm.2016.11.061
8. M. C. C. Pinto; D. M. G. Freire; J. C. Pinto Molecules 2014, 19, 8, 12509–12530. https://doi.org/10.3390/molecules190812509.
9. C. M. F. Soares; H. F. Castro; F. F. Moraes; G. M. Zanin Applied Biochemistry and Biotechnology 1999, 77-9, 745-757. https://doi.org/10.1385/ABAB:79:1-3:745.
10. A. A. Mendes; P. C. Oliveira; H. F. Castro Journal of Molecular Catalysis B: Enzymatic 2012, 78, 119-134. https://doi.org/10.1016/j.molcatb.2012.03.004.
11. L. Lei; Y. Bai; Y. Li; L. Yi; Y. Yang; C. Xia. Journal of Magnetism and Magnetic Materials 2009, 321, 4, 252–258. https://doi.org/10.1016/j.jmmm.2008.08.047.
12. B. Zou;Y. Hu; D. Yu; J. X; S. Tang; W. Liu; E. Huang. Biochemical Engineering Journal 2010, 53, 150-153. https://doi.org/10.1016/j.bej.2010.09.005.
13. ROSA, C. M. R. Dissertação (Mestrado em Ciências) – Escola de Engenharia de Lorena, Universidade de São Paulo, Lorena, 2019, 130.

PHOTODEGRADATION INVESTIGATION OF ALOE VERA AS A PHOTOPROTECTOR FOR POLY(LACTIC ACID)

Pedro H. M. Nicácio[1*], Ananda K. C. Albuquerque[1], M. F. Souza[1],Andreas Ries[2], Jana Kolbe[3], Renate M. R. Wellen[1,4]

1 – Department of Materials Engineering, University of Campina Grande (UFCG), Campina Grande, PB, Brazil
2 – Multidisciplinary Center for Technological Investigations, National University of Asunción, San Lorenzo University Campus, San Lorenzo 1039, Paraguay
3 – Fraunhofer Institute for Manufacturing Technology and Advanced Materials, Wiener Straße 12, 28359 Bremen, Germany
4 – Department of Materials Engineering, Federal University of Paraíba (UFPB), João Pessoa, PB, Brazil

henrinicaicoeq@gmail.com*

Abstract - Among renewable polymers, poly (lactic acid) (PLA) has emerged due to its biodegradable character and proper performance similar to the engineering resins. In this work, we investigated the effect of Aloe Vera (AV) as a photoprotective agent for PLA, since AV has polysaccharides and anthraquinones, such as acemannan and aloin, respectively, able to absorb and dissipate the innocuous energy generated by UV radiation. PLA/AV biocomposites were photodegraded in an aging chamber for 112 days. Biocomposites with 10% AV displayed higher stability to photodegradation and a 96% reduction in the content of photodegraded material as evidenced by FTIR measurements. It is suggested that hydrogen bonds between PLA and AV contribute to the photoprotective effect. Photodegraded PLA/AV presented reasonable thermal stability, which is supposed to be influenced by PLA crosslinking. Acquired results point to AV as a proper candidate as a photoprotective agent for PLA, being environmentally friendly, as they are products from a renewables source.
Keywords: PLA, Aloe Vera, Photodegradation, Thermal degradation
Fundings: CAPES – Coordenação de Aperfeiçoamento de Pessoal de Nível Superior.

Introduction

Poly(lactic acid) (PLA) is a thermoplastic and biodegradable biopolymer, which has stood out as a substitute for petroleum-based polymers [1]. It presents a wide range of applications, due to its ability to be processed using most polymer processing equipment [2]. PLA can be thermally crystallized and additionally modified using additives and copolymers [3]. Nevertheless, PLA is sensitive to ultraviolet (UV) radiation, due to its C=O chromophore group [2].

The Aloe Vera extract (AV) (inner part of the leaf) is a renewable and low-cost resource, which appears as a viable alternative to be used as filler in PLA, reducing costs and environmental impacts, in addition to contributing to better PLA performance, i.e., increase in mechanical strength [4], greater biocompatibility for application in tissue engineering [5], improvement in optical properties [6]. AV also displays antimicrobial and UV protection properties, which encourages investigations of its contributions to polymeric compounds.

The UV power protection of AV is attributed to polysaccharides and aloin, which is due to the harmful UV radiation (UVC, UVB, and UVA) absorption and the dissipation of innocuous thermal energy, that is, intramolecular excited state transfer through very fast internal conversion [7]. Although AV has potential UV absorption, so far no studies have been found reporting its use in the

photodegradation of PLA/AV biocomposites, which is a gap in the literature and technological applications that are worth investigating.
The main objective of this work was to obtain photostable PLA biocomposites with 1, 5 and 10% by weight of Aloe Vera; the biocomposites were extruded and the specimens injection molded. The photodegradation exposure took place in accelerated aging chambers with radiation, humidity, and temperature control. The chemical and thermal behavior ware investigated, were investigated using Fourier transform infrared spectroscopy (FTIR) and thermogravimetry (TG).

Experimental

Poly(lactic acid) Biopolymer 3251, extrusion grade 2003D was purchased from NatureWorks Ingeo™, Minnesota— USA. Freeze-dried Aloe Vera powder with an average diameter of 44.02μm was provided by Engenharia das Essências Comercial LTDA, São Paulo, Brazil. The PLA/AV biocomposites, with 1, 5 and 10% of AV, were prepared using a PolyLab Haake torque rheometer (Massachusetts, EUA), with roller rotors, at 180 °C, 60 rpm, and 10 min. Afterwards, the material was ground in a knife mill and the specimens were injection molded using an Arburg Allrounder 270C Golden Edition (Radevormwald, Germany), with temperatures in the mold, feed section, cylinder, and nozzle of 20, 170, 180, and 185 °C, respectively. The injection and hold pressures were 900 bar and 600 bar with an operation time of 8 s.
The exposure to photodegradation was performed with UVA340 Lightex lamps, purchased from Elétrica Paulista, São Paulo-Brazil. The specimens were photodegraded at intervals of 0, 7, 14, 28, 56 and 112 days, using an aging chamber, model C-UV Standard from Adexim Comexim-Brazil. The cycles between light (with temperature of 46.3±1.6 °C and humidity of 19.4% ± 1.9%) and dark (with temperature of 36.5±1.3 °C and humidity of 37.6% ± 2.6%) of 4 h, controlled according to ASTM G-154 [8].
Fourier Transform Infrared Spectroscopy tests were performed using a Perkin Elmer Spectrum 400 Series spectrometer (Waltham, Massachusetts, USA) in the infrared range, with wavelengths ranging from 4000 to 650 cm^{-1}, with the Attenuated Total Refectance (ATR) accessory, under a spectral resolution of 16 cm^{-1} and 32 scans.
Thermogravimetry tests carried out using a Perkin Elmer TGA Pyris-1 equipment (Waltham, MA, USA), samples weighing approximately 4.5 mg were tested in a platinum crucible, heated from room temperature (~ 23 °C) to 700 °C with a heating rate of 10 $°C.min^{-1}$, under an inert atmosphere (N_2) with a gas flow of 20 $mL.min^{-1}$.

Results and Discussion

Figure 1 displays AV spectrum with a band at 3283 cm^{-1} referring to OH, which may be associated with phenolic groups of anthraquinones, such as aloin and aloe emodin, or with the mannose stretching. At 2929 cm^{-1} belonging to the C–H bonds elongation, in 1635 and 1570 cm^{-1} possibly associated with C=O and C=C bonds, respectively, present in aloin and acemannan. In 1351 cm^{-1} due to axial deformation of C–H, at 1142 and 1010 cm^{-1} there are axial deformations of C=O and C–O–C groups due to the ether bonds (ROR) of acemannan [4].
PLA spectrum shows bands at 3008–2853 cm^{-1} associated with the elongation of CH bond in CH_2 and CH_3 groups, at 1746 cm^{-1} due to the C=O elongation vibration of ester carbonyl group, at 1458-1267 cm^{-1} related to CH bond (CH_2 and CH_3) of symmetric angular deformation (scissors), at 1151 cm^{-1} and 1058 cm^{-1} which are associated with C=O and C–O–C elongations, respectively, and at 874–704 cm^{-1} referring to the OH deformation.
PLA/AV biocomposites spectra present bands similar to PLA, without identification of sudden variations; both have similar chemical groups, whereas bands overlapping is supposed to take place. It is suggested that this behavior may be associated with possible interactions, such as hydrogen bonds, of hydroxyl groups between AV and PLA carbonyl, as indicated in Fig. 1 (b, c). These secondary bonds can help to protect PLA against UV radiation, as acemannan polysaccharide and

aloin anthraquinone can absorb harmful UV radiation and dissipate innocuous thermal energy, preventing photodegradation of PLA/AV biocomposites.

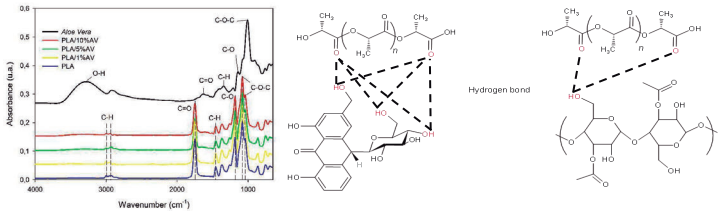

(a) (b) (c)

Figure 1 – FTIR spectra of PLA/AV compounds, collected before photodegradation (a), Hydrogen bonds between PLA and Aloin (b) and PLA and acemannan (c).

As previously reported, PLA photodegradation occurs according to the Norrish II mechanism [2]. A new peak at 1830 cm^{-1} referring to anhydride groups, RO=COC=OR, which is characteristic of photodegradation and/or photo-oxidation processes in PLA, being more evident for neat PLA. AV addition acts to decrease this band intensity, suggesting that AV can reduce the damage caused by UV radiation in PLA/AV. AV photo-protection is supposed to be associated with the UV radiation absorption added to the secondary interactions as indicated in Fig. 1 (b, c) [6]. Aiming at a deeper understanding of the anhydride groups' origin during photodegradation, deconvolution of the absorption band at 1830 cm^{-1} was performed using the Fityk software. The acquired peaks for PLA and PLA/10%AV at 0, 56, and 112 days are shown in Fig. 2.

Instability, intensity variation, and complex profile are observed for this band along with the photodegradation for both compositions, ranging from 1809 to 1843 cm^{-1} for PLA, and from 1825 to 1842 cm^{-1} for PLA/10%AV, being more evident in PLA. It is suggested that the photodegradation chamber moisture also contributes to its decay, as anhydride groups are unstable/reactive with water, in addition to having two carbonyls in its structure, which are also reactive in the UV radiation incidence.

In neat PLA, the absorption intensity, referring to the anhydride group, reaches a maximum of 0.0009, while under the addition of 10%AV its intensity is 0.0005, both at 1825 cm^{-1} after the period of 56 days. Therefore the addition of 10% AV represents an intensity decrease of 45% in the anhydride groups' peak, which corroborates the speculations that Aloe Vera presents potential protection in PLA/AV biocomposites against UV radiation.

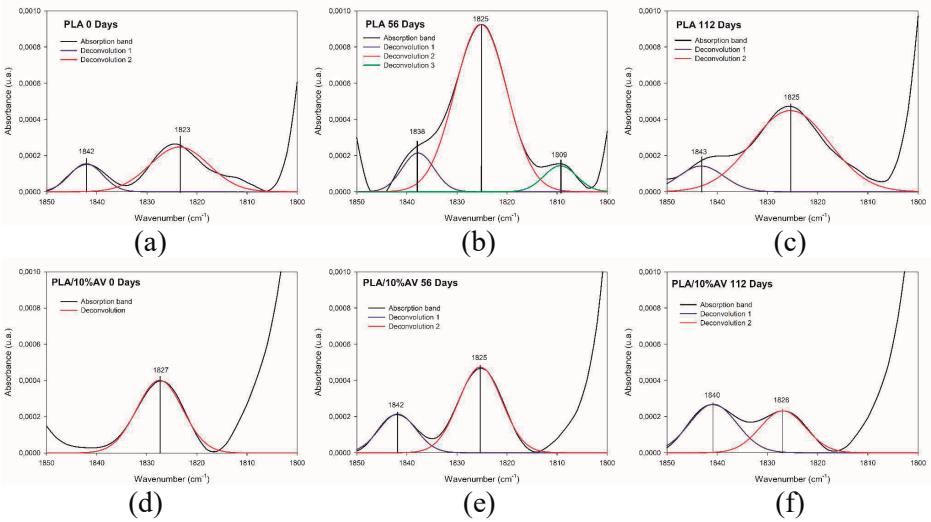

(a) (b) (c)

(d) (e) (f)

Figure 2. Deconvoluted FTIR spectra – absorption band referring to the anhydride group formation due to the PLA photodegradation. Compositions and photodegradation periods indicated.

Eq. 1 was used to assess the degree of photodegradation, adopting the reference band, 1458 cm^{-1} $(I_R)_{0\rightarrow t}$, and the photodegradation marker band, 1746 cm^{-1} $(I_C)_{0\rightarrow t}$. The bands were integrated using Fityk software, and acquired plots are shown in Fig. 3.

$$\alpha = \left(1 - \left(\frac{\left(\frac{I_C}{I_R}\right)_t}{\left(\frac{I_C}{I_R}\right)_0}\right)\right) * 100 \quad (1)$$

Where $(I_C)_t$ is the band intensity associated with the functional group of interest at time t and $(I_R)_t$ is the reference band intensity (a functional group that remains practically unchanged throughout the investigated reaction).

For PLA, there are variations in the degree of photodegradation ranging among 16.7 %, 25.4 %, 25.5 %, and 28.6 % which are observed between 7 to 56 days, reaching 29.9 % of the degree of photodegradation after 112 days, it is suggested that this behavior is related to the fact that photodegradation starts in the amorphous regions of PLA, promoting the formation of caboxyl groups, thus, acidifying the material, and inducing PLA to autocatalysis [2].

PLA/1%AV presented a degree of photodegradation of 0.5 % in 7 days and 3.9 % in 28 days, reaching 8.9 % in 56 days and 13.2 % in 112 days of photodegradation. The biocomposite with 5 % of AV presented a degree of photodegradation of 1.0 % in 14 days, 3.0 % in 28 days, and 4.4 % in 56 days. PLA/10%AV showed no significant decomposition during the investigated UV exposure time, reaching only 1.10 % of photodegradation after 112 days of photodegradation.

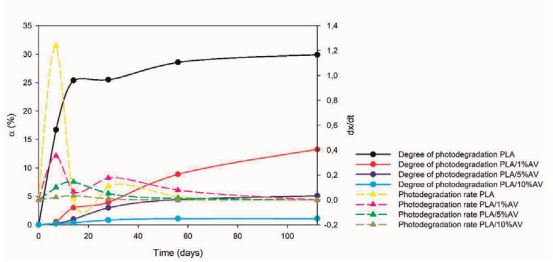

Figure 3. Degree and rate of photodegradation computed from FTIR spectra using the Eq. 2. Compounds indicated.

Presented data indicates that the AV addition and increased concentration provided photoprotection to PLA. It is important to clarify that for 112 days, based on the calculations using Eq. 2, only 1% of AV was able to reduce 55.7% of photodegradation when compared to neat PLA and that 10% of AV could reduce the degree of photodegraded PLA by up to 96.3%.

$$X_{PAV} = 100 - \frac{X_{dB} * 100}{X_{dP}} \quad (2)$$

Where, X_{PAV} is the protective power of AV in the investigated biocomposite, X_{dP} is the photodegradation degree of PLA at 112 days and, X_{dB} is the photodegradation degree of the investigated biocomposite at 112 days.

Fig. 4 displays the weight loss plots for neat PLA (a) and PLA/10%AV biocomposite (b), photodegraded for 0, 28, 56 and 112 days. After 28 days of photodegradation, the weight loss range shifted to higher temperatures, going from 283 to 365 °C in 0 days to from 308 to 398 °C in 28 days on neat PLA, and from 290 to 368 °C in 0 days to from 314 to 396 °C in 28 days on PLA/10%AV, suggesting that photodegradation generates active sites in PLA chain able of rearrangement, promoting the crosslinking thus increasing the thermal stability.

After 56 days, neat PLA displayed weight loss in the range from 299 to 389 °C. Suggesting that, even after the supposed cross-linking of the macromolecular chain (28 days), UV radiation induces PLA scission in the macromolecule. As predicted in the FTIR section (Fig. 3), indicating that photodegradation promoted carboxylic acid formation at PLA chain ends, inducing autocatalytic reactions and consequently breaking the macromolecular chain, which justifies the decrease in

thermal stability for photodegraded PLA at 56 days. The same behavior is observed at 112 days of photodegradation for PLA, where the weight loss takes place in the range from 298 to 378 °C.
PLA/10%AV thermal stability was kept almost unchanged after 28 days of photodegradation. Weight loss events were observed in the range from 290 to 368 °C for 0 days, from 314 to 396 °C for 28 and 56 days, and, from 314 to 389 °C for 112 days; corroborating FTIR results (Fig. 3), where composition with the highest AV content showed better chemical stability and lower content of photodegraded material, consequently inducing greater thermal stability.

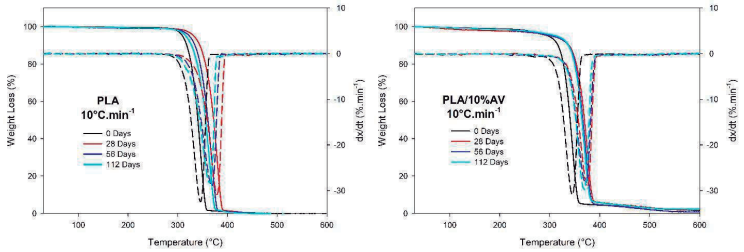

(a) (b)

Figure 4. Weight loss plots (solid line) and DTG (dashed line). Nitrogen atmosphere. Photodegradation times and compositions indicated.

Conclusions

PLA/AV biocomposites with 1%, 5% and 10% of Aloe Vera were produced by mixing PLA and AV in the molten state using a torque rheometer. Hydrogen bonds between AV and PLA were proposed based on FTIR spectra, promoting secondary interactions in PLA, where PLA/10%AV was chemically more stable during the whole photodegradation period. 10% of AV could reduce the degree of photodegraded PLA by up to 96%. TG thermograms showed that UV radiation promoted an increase in thermal stability until 28 days of exposure, probably due to crosslinking, however, longer UV exposure times decreased the decomposition temperature of PLA, without affecting PLA/10% AV. AV addition presented satisfactory results reaching the main objective of this work, acting as a photoprotective agent for PLA. PLA/AV biocomposites showed weight loss starting at 250 ºC, therefore, being interesting for outdoor applications due to the photo-protective properties.

Acknowledgements

The authors would like to acknowledge the financial support from the Coordenação de Aperfeiçoamento de Pessoal de Nível Superior (CAPES), from Conselho Nacional de Desenvolvimento Científico e Tecnológico (CNPq), Fundação de Apoio à Pesquisa do Estado da Paraíba (FAPESQ) (Concession term: 017/2019) and from the Laboratório de Avaliação e Desenvolvimento de Biomateriais do Nordeste (CERTBIO) for the kind support. Professor Renate Wellen is CNPq fellow (Number: 303426/2021-7).

References

1. Mülhaupt R. Macromolecular Chemistry Physics 2013, 214, 159–174. https://doi.org/10.1002/macp.201200439
2. Castro-Aguirre E, Iñiguez-Franco F, Samsudin H, et al. Advanced Drug Delivery Reviews 2016, 107, 333–366. https://doi.org/10.1016/j.addr.2016.03.010
3. Henton DE, Gruber P, Lunt J, Randall J. "Polylactic acid technology." *Natural Fibers, Biopolymers, and Biocomposites*. CRC Press, Florida - EUA, pp 527–577, 2005
4. Chaitanya S, Singh I. International Journal of Precision Engineering and Manufacturing-Green Technology 2018, 5, 143–150. https://doi.org/10.1007/s40684-018-0015-8
5. Komatsu D, Mistura D V., Motta A, et al. Journal of Biomaterials Applications 2017, 32, 311–320. https://doi.org/10.1177/0885328217719854
6. Shen Y, Huang Y, Jiang L, Dan Y. Reactive and Functional Polymers 2020, 148, 104–486. https://doi.org/10.1016/j.reactfunctpolym.2020.104486

7. Rodrigues D, Viotto AC, Checchia R, et al. Photochemical and Photobiological Sciences 2016, 15, 334–350. https://doi.org/10.1039/c5pp00409h
8. G-154 A (2016) ASTM G-154 Operating Fluorescent Light Apparatus for UV Exposure of Nonmetallic Materials. West Conshohocken, PA 1–11

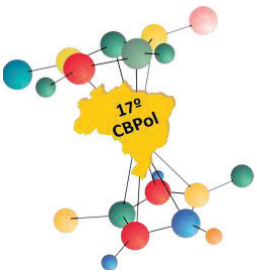

POLYMERIZATION OF POLY-DL-LACTIC ACID (PDLLA) BY RING-OPENING POLIMERIZATION FOR POTENTIAL APPLICATION IN TISSUE ENGINEERING

Geraldine D. Bazan[1]*, and Maria V. Carranza-Oropeza[1]

1 – Department of Chemical Engineering, Major National University of San Marcos (UNMSM), Lima, Perú
geraldinebazanpanana@gmail.com

Abstract - Poly(lactic acid) has been studied as an important material for biomedical applications. The aim of this research was to determine the optimal parameters in the synthesis of PDLLA to obtain a polymer of high molecular weight, so that it can be used in the development of scaffolds. The synthesis of PDLLA was carried out in three stages: polycondensation, depolymerization, and ring-opening polymerization of lactide, using a rotary evaporator coupled with a two-stage pump in the presence of nitrogen gas. As a result, it was demonstrated that carrying out the oligomerization reaction for 6 hours and, using stannous octoate as catalyst and 1-octanol as initiator, both at 1%, for 4 hours, a high molecular weight polymer can be obtained. The existence of the polymer was verified by FTIR. The yield of the synthesis was 18%. The molecular weight of the obtained PDLLA polymer was determinated by viscometry method, resulting in 117 kDa, making the resulting PDLLA useful for tissue engineering.
Keywords: *PDLLA, ROP, FTIR, viscometry method, tissue engineering*
Fundings: Research projects with funding for UNMSM Research Groups Year 2022 - PCONFIG 2022.

Introduction

Poly(lactic acid) (PLA) is a completely biodegradable polymer that is highly versatile, biocompatible, non-toxic, and has excellent mechanical properties, making it especially attractive for biomedical applications [1,2]. Scaffolds based on this biomaterial can guide the development of new bone tissue, in a context where biocompatible alternatives are currently being sought in the bone replacement market, since the repair of bone defects has been and continues to be one of the most important challenges in clinical practice and has created a high demand for bone repair materials [3,4].

To produce devices with high mechanical strength, it is necessary to use high molecular weight PLA. Generally, there are two methods that can be used to produce high molecular weight PLA of approximately 100 kDa: (a) azeotropic dehydration condensation, and (b) lactide ring-opening polymerization (ROP) [5].

The azeotropic dehydration condensation method does not use adjuvants during PLA synthesis, but the disadvantage of this method is that organic solvents are used in the reaction while the catalyst remains, such as xylene or diphenyl ether [2,6-7].

Ring-opening polymerization (ROP) is the most common route to achieve high molecular weight [5]. This process involves opening the ring of the cyclic dimer of lactide in the presence of a catalyst. The process consists of three steps: polycondensation, depolymerization, and ROP [8]. Lactide polymerization by this method requires a catalyst but results in high molecular weight PLA. Studies have found that the use of tin(II) produces fewer impurities during the synthesis of high molecular weight poly(lactic acid), resulting in the purest poly(lactic acid). For example, tin(II) dioctoate has high catalytic activity, low toxicity, and was approved by the FDA and is a very

suitable initiator [2], in addition to providing high reaction rate, high conversion rate, and high molecular weight, even under mild polymerization conditions [9].

At the laboratory level, several authors have attempted to obtain high molecular weight PLA using the solvent-free ROP method, and as it contrasts with the literature, it could not be achieved under these conditions. Boua-In et al. conducted poly(lactic acid) synthesis via ROP and achieved a maximum molecular weight of 50.5 kDa [10]. Pholharn et al. synthesized PLLA with molecular weights below 15 kDa [11]. Horváth et al. synthesized PLLA with a molecular weight of 3.8 kDa, concluding that exceeding a catalyst volume of 1 mass/% had a detrimental effect on molecular weight due to the lactide/catalyst ratio being one of the key factors for successful ROP process in high molecular weight PLA synthesis [12]. On the other hand, Chen et al. successfully obtained high molecular weight PLA via ROP, surpassing 400 kDa. However, they employed tin octoate as the catalyst along with N,N-dimethylformamide dimethylacetal (DMF-DMA) solvent [13].

It is for the reasons mentioned above that this research seeks to define the optimal parameters that allow the synthesis of PDLLA with a molecular weight greater than 100 kDa, which will allow for its use in tissue engineering.

Experimental

Materials

DL-lactic acid (85% purity) was supplied by from Sigma-Aldrich. As for catalysts, tin(II) chloride dihydrate (98% purity) was purchased from HIMEDIA, and stannous octoate from Sigma-Aldrich was imported from Brazil. The ring-opening initiator, 1-octanol, was acquired from Sigma-Aldrich.

A DLAB rotary evaporator was used, with a temperature range from room temperature to 180 ºC, with a temperature control precision for oil of ±3, and a rotation speed range from 20 to 200 rpm. A two-stage pump from VALUE, model VE245N and with a power of ½ HP, was coupled to this equipment. An SI-Analytics Typ 530 10/I Ubbelohde viscometer.

Synthesis of high molecular weight PDLLA

The synthesis of PDLLA by the ring opening method was carried out in three stages: polycondensation, thermal depolymerization or cracking, and ring opening polymerization (ROP). During the synthesis, the working pressure was 15 microns and continuous stirring was maintained at 100 rpm. Additionally, it was necessary to use oil in the heating bath, since temperatures higher than 100°C were employed, and an inert atmosphere of N_2 was essential in order to provide an oxygen- and moisture-free environment to prevent oxidation or decomposition of the product.

Stage 1: Polycondensation of lactic acid. 50 mL of DL-lactic acid was added to a round bottom flask. The dehydration reaction was carried out to remove the water content of the monomer. An initial temperature of 80 ºC was chosen and gradually increased to 120 ºC carefully, without exceeding the boiling temperature of lactic acid (122 ºC). Subsequently, the temperature was increased to 160 ºC to form oligomers, with reaction times of 4 and 6 hours. The reaction product was dissolved with 25 mL of acetone and precipitated in 150 mL of distilled water with vigorous stirring at 700 rpm. Then, the precipitate was recovered by vacuum filtration using Whatman 42 filter paper and stored in a desiccator for 24 hours to eliminate moisture.

Stage 2: Depolymerization of the oligomer. The obtained oligomer from Stage 1 was heated in a round-bottom flask at a temperature of 180 °C for 7 hours, with the addition of $SnCl_2{\cdot}2H_2O$ 1% w/w as a catalyst. Then, lactide was purified by recrystallization using 30 mL of ethyl acetate at its boiling point (77.2 °C) as a solvent. After cooling the solution, the crystals were isolated by vacuum filtration and dried at 40 °C for 24 hours.

Stage 3: Polymerization by the ring-opening method of lactide (ROP). High molecular weight PDLLA was obtained via ROP, using stannous octoate catalyst (1% and 2% w/w) and 1-octanol (1% w/w) as initiator. The lactide obtained in Stage 2, the catalyst, and the initiator were added to a round-bottom glass flask with a reaction temperature of 140 °C for 4 and 6 hours. After completing

the synthesis, the PDLLA acid obtained was dissolved in 25 mL of chloroform and precipitated in 80 mL of methanol, then separated by vacuum filtration, and finally dried in an oven at 60 °C for 12 hours.

Characterization of PDLLA

In order to characterize the obtained PDLLA, two analyses were performed. The first was Fourier-transform infrared spectroscopy (FTIR), which determined if it was PDLLA, as the characteristic absorption peaks appeared at 3000, 1750, 1450, and 1180 cm^{-1}. The second was the molecular weight determination by viscometry, using chloroform as the solvent and polymer solutions of different concentrations to determine the reduced viscosity, which allowed for the calculation of the molecular weight.

Results and Discussion

When 4 hours were used for oligomerization, the resulting consistency was watery, rather than a thick gel, indicating that something had gone wrong. This was confirmed when attempting to dissolve the oligomer in acetone and failing to obtain the desired consistency. Additionally, when precipitating in distilled water, no precipitate formed, confirming the hypothesis. In contrast, with 6 hours of oligomerization, a gel-like consistency was obtained, and a compact precipitate formed during precipitation for recovery by vacuum filtration. However, in the third stage of synthesis, with a polymerization time of 6 hours, the product turned out to be very dark in color, different from what was expected, and this was negatively influenced by a 2% concentration of catalyst. On the other hand, with a shorter 4-hour oligomerization time, the product remained clear and dissolved well in chloroform, forming a compact precipitate in distilled water. The results at the end of each stage are shown in Fig 1. The synthesis yield was 18%, which means that for each 100g of DL-lactic acid used, 18g of polymer can be synthesized.

Figure 1 – PDLLA oligomer / Lactide crystals / PDLLA of high molecular weight.

The optimal parameters for polymer synthesis are shown in Table 1.

Table 1 – Optimal parameters for PDLLA synthesis.

Stage	Time (h)	Temperature (°C)	Catalyst-Initiator (%)
Polycondensation (Dehydration)	1	80-120	---
Polycondensation (Oligomerization)	6	160	---
Depolymerization	7	180	1
ROP	4	140	1-1

To confirm that the produced material was PDLLA, FTIR technique was used. The FTIR spectrum showed characteristic absorption peaks of the obtained polymer, representing the functional groups that make up the internal structure of PLA, thus confirming the formation of the product. The peaks observed were the -CH tension of the alkane group at 3000 cm^{-1}, the carbonyl group of the ester at 1755 cm^{-1}, the $-CH_3$ of the alkane group at 1456 cm^{-1}, and the alkoxy group of the ester at 1182, 1130 and 1097 cm^{-1}. Using the OPUS software, designed for processing information from the

BRUKER ALPHA II equipment, it was possible to compare the spectrum of PDLLA obtained with the standard PDLLA (CAS 26969-66-4), as shown in Fig 2.

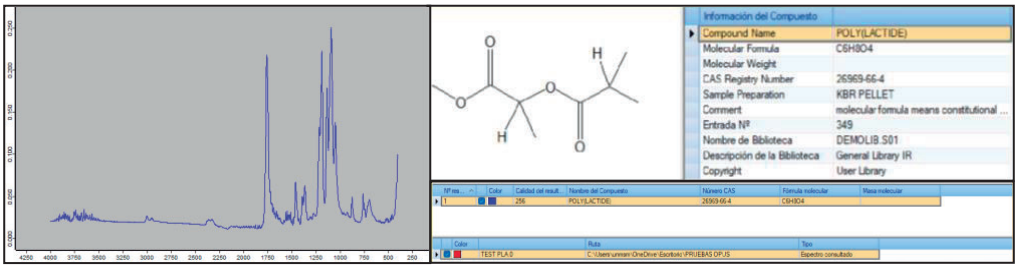

Figure 2 – FTIR spectra of PDLLA.

There is an alternative indirect method based on rheology that can be employed to obtain reliable results. This method is since the viscosity of polymer solutions is strongly influenced by the concentration and length of polymer chains, which is represented by their molecular weight. Polymeric solutions were prepared at concentrations of 0.7%, 0.5%, and 0.3% using chloroform at 25°C, and the times taken for the viscometer to traverse were recorded. Using Eq. 1, the reduced viscosity respect to concentration was calculated.

$$\eta_{red} = \frac{t_1 - t_0}{t_0 \cdot c} \qquad (1)$$

The data collected from the method are shown in Table 2, and graphically, in Fig 3, from which the value of intrinsic viscosity was obtained, which is equivalent to the reduced viscosity when concentration tends to 0.

Table 2 – Results related to the capillary viscometry technique.

Concentration (%)	Cp (g/mol)	Flow time	Reduced viscosity (mol/g)
0.7	0.007	47.8	18.57
0.5	0.005	46.1	17.97
0.3	0.003	44.5	17.34
C → 0	Cp → 0	42.3	

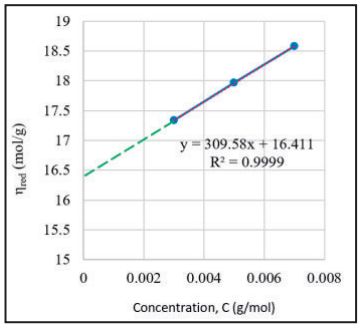

Figure 3 – Graphical determination of intrinsic viscosity of PDLLA.

Then, using the Mark-Houwink relations, which is shown in Eq. 2, and its rearranged form in Eq. 3, the molecular weight of the PDLLA obtained by synthesis was determined to be 117 kDa. The constants "K" and "a" were obtained from the Polymer Data Handbook, with K=0.0066 and α=0.67.

$$[\eta] = K \cdot M^{\alpha} \qquad (2)$$

$$M = \sqrt[\alpha]{\frac{[\eta]}{K}} \qquad (3)$$

Conclusions

A high molecular weight PDLLA polymer can be obtained by the lactide ring opening method using 6 hours for oligomerization reaction, 4 hours for polymerization, and 1% concentration of tin(II) octoate catalyst. A synthesis yield of 18% was achieved. Analysis of the FTIR spectrum confirmed the synthesis of PDLLA by the presence of characteristic peaks of the biomaterial. The molecular weight obtained by the synthesis was 117 kDa, making it useful for application in the biomedical field, such as tissue engineering.

Acknowledgements

This work was possible thanks to the fact that the National University of San Marcos (UNMSM) and the Center for Technological, Biomedical and Environmental Research (CITBM) provided access to their research laboratories.

This research was supported by Research projects with funding for UNMSM Research Groups Year 2022 - PCONFIG 2022.

References

1. Z. Jing; X. Shi; G. Zhang; J. Li; J, Li; L. Zhou; H. Zhang Polymer 2016, 92, 210-221. https://doi.org/10.1016/j.polymer.2016.04.001.
2. G. Li; M. Zhao; F. Xu; B. Yang; X. Li; X. Meng; L. Teng; F. Sun; Y. Li Molecules 2020, 25(21), 5023. https://doi.org/10.3390/molecules25215023.
3. L. Albrecht; S. Sawyer; P. Soman 3D Printing and Additive Manufacturing 2016, 3(2), 106-112. http://doi.org/10.1089/3dp.2016.0006.
4. B. Zhang; L. Wang; P. Song; X. Pei; H. Sun; L. Wu; C. Zhou; K. Wang; Y. Fan; X. Zhang Materials and Design 2021, 201, 109490. https://doi.org/10.1016/j.matdes.2021.109490.
5. R. Auras; L. Lim; S. Selke; H. Tsuji *Poly(lactic acid): Synthesis, Structures, Properties, Processing, and Applications*, John Wiley & Sons, New Jersey, 2005.
6. K. Kim; S. Woo Macromolecular Chemistry and Physics, 2002, 203(15), 2245-2250. https://doi.org/10.1002/1521-3935(200211)203:15<2245::AID-MACP2245>3.0.CO;2-3.
7. Y. Maryanty, Y; S. Hadiantoro; K. Widjajanti; D. Putri; L. Nikmah IOP Conference Series: Materials Science and Engineering 2021, 1053, 012043. https://doi.org/10.1088/1757-899X/1053/1/012043.
8. M. Singhvi; S. Zinjarde; D. Gokhale Journal of Applied Microbiology 2019, 127(6), 1612-1626. https://doi.org/10.1111/jam.14290.
9. R. Mehta; V. Kumar; H. Bhunia; S. Upadhyay Journal of Macromolecular Science, Part C: Polymer Reviews 2005, 45(4), 325–349. https://doi.org/10.1080/15321790500304148.
10. K. Boua-In; N. Chaiyut; B. Ksapabutr Optoelectronics and Advanced Materials – Rapid Communications 2010, 4(9), 1404-1407.
11. D. Pholharn; Y. Srithep; J. Morris IOP Conference Series: Materials Science and Engineering 2017, 213 http://doi.org/10.1088/1757-899X/213/1/012022.
12. T. Horváth; K. Marossy; T. Szabó Journal of Thermal Analysis and Calorimetry 2022. https://doi.org/10.1007/s10973-020-10540-1.
13. H. Chen; H. Fang; Y. Chen; S. Hsu; Y. Lai; H. Ou; W. Peng; Y. Chang; Y. Tsou; T. Wu; H. Chung; Y. Chen; T. Huang; B. Wu Journal of Polymer Science, Part A: Polymer Chemistry 2012, 50(16), 3286-3294. https://doi.org/10.1002/pola.26108

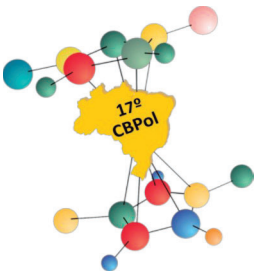

POLY(N-VINYLCAPROLACTAM) POLYMERIZATION BY ULTRAVIOLET RADIATION

Djalma A. de Oliveira[1], Grazielle R. Cerqueira[1], Tulio L. Pedrosa[2], Renato E. Araujo[2], Michelle F. de Andrade[3], Yêda M. B. de Almeida[1,3] and Carolina L. Morelli[1,4]*

1– Materials Science Program, Federal University of Pernambuco (UFPE), Recife, PE, Brazil
2 – Department of Electronics and Systems, Federal University of Pernambuco (UFPE), Recife, PE, Brazil
3 – Department of Chemical Engineering, Federal University of Pernambuco (UFPE), Recife, PE, Brazil)
4 – Department of Mechanical Engineering, Federal University of Pernambuco (UFPE), Recife, PE, Brazil
carolina.morelli@ufpe.br

Abstract – Poly(N-vinylcaprolactam) is a thermoresponsive polymer synthesized from the N-vinylcaprolactam monomer, which has a phase transition temperature close to the physiological temperature. The use of this polymer has been studied in numerous areas, from industrial to biological. In the present work, the polymerization of poly(N-vinylcaprolactam) was studied by ultraviolet radiation in the UV-A range. Polymerization was evidenced by infrared spectroscopy, as well as by obtaining a continuous polymeric film formed by casting. The synthesized polymer had its thermoresponsiveness confirmed through cloud point analysis, with a transition temperature from hydrophilic to hydrophobic behavior equal to 35°C. The glass transition temperature observed by differential scanning calorimetry was 178°C, and the onset temperature of thermal degradation evaluated by thermogravimetry was 390°C. The presented polymerization methodology proved to be simple and low cost, resulting in a thermoresponsive polymer.

Keywords: *Poly(N-vinylcaprolactam); Ultraviolet radiation; Thermoresponsive polymers; Synthesis; Smart polymers.*

Introduction

Thermoresponsive polymers are those that can exhibit change of properties with temperature. Examples of these polymers include: poly(N-vinylcaprolactam) (PNVCL) [1-3], poly(N-isopropylacrylamide) (PNIPAAm) [4], poly(N,N-diethylacrylamide) (PDEAAm) [5], poly(methyl vinyl ether) (PMVE) [5] among others.

The PNVCL presents its lower critical solution temperature (LCST), in which the transition from hydrophilic to hydrophobic behavior occurs, close to the physiological temperature, between 32 ºC and 35 ºC [6]. In addition, the advantage of not producing toxic by-products when undergoing hydrolysis expands its possibilities of application in the biomedical area. It has been considered for applications as drug delivery systems, wound dressings, scaffolds for cell growth, tissue engineering, orthodontic treatments, and also in smart windows, sensors, cosmetics, among others [1-2, 5]. PNVCL is an amorphous polymer whose glass transition temperature (Tg) can vary considerably according to the purity of the material, its molar mass and polydispersity, the presence of water between the chains and the molecular arrangements in the polymeric structure [7].

The PNVCL is synthesized from the monomer N-vinylcaprolactam (NVCL), which is an organosoluble substance with amphiphilic character [2], being soluble in polar and apolar solvents. Its synthesis occurs through free radical polymerization with the breaking of the double bond usually induced by initiators of the azo-compound type, such as (2,2-azobis(isobutyronitrile) (AIBN) [8], 4,4'-azobis(4-cyanopentanol) and azobisisobutyric acid dinitrile [2]); peroxide initiators (potassium persulfate, tert-butylperoxide, benzoylperoxide) [2] or photoinitiators (irgacure 184 [3], irgacure 651 [9], irgacure 2959 [2] and benzophenone [10]).

In the present work, the polymerization of PNVCL was carried out through ultraviolet radiation, using benzophenone as a photoinitiator. When irradiated by UV light, benzophenone enters a

singlet excited state, followed by a triplet state, in which it is able to abstract hydrogen atoms from the reaction medium [9-10], leading to the formation of free radicals in monomers and subsequent growth of the polymeric chain. The termination of the synthesis occurs by removing the UV radiation, causing the excited molecules of benzophenone to return to their fundamental state of lower energy, with no formation of new radicals in the reaction.

The use of UV radiation is advantageous due to its low cost and simplicity [10]. Ultraviolet radiation comprises a wavelength range that varies from 400-100 nm, and can be classified into UV-A, UV-B and UV-C according to its emitting source. In the range of 400-320 nm (UV-A), radiation is not enough to induce degradation, but it is enough to generate excitation states that provoke the formation of free radicals. At UV-C wavelengths, from 280-100 nm, degradation and breakdown of primary bonds occur [11]. The UV-B range, which comprises wavelengths between 320-280 nm, is considered a medium wave that can already efficiently cause photodamage in synthetic polymers [11-12].

In the present work, the polymerization of PNVCL by ultraviolet radiation in the UV-A range was studied. The present study aims to contribute to the dissemination of simple and alternative techniques for the polymerization of PNVCL. Different synthesis routes can impact PNVCL thermoresponsive properties, diversifying its field of application.

Experimental

The materials used were: i) monomer N-vinylcaprolactam (98% and MM=139.19g.mol^{-1}), purchased from Sigma-Aldrich, purified through recrystallization in hexane to remove its inhibitor, ii) benzophenone (99% and MM=182.22g.mol^{-1}), used as photoinitiator of the synthesis, purchased from Sigma-Aldrich, iii) hexane P.A. (98.5%, d=0.66g.cm^{-3}) acquired from Dynamics/Brazil.

In a glass petri dish, 1g of NVCL and 1%wt. of benzophenone in relation to the monomer were solubilized in 2 mL of hexane. The solution was positioned at a distance of 4 cm from the UV-A light source in the chamber. The chamber used had three UV-A lamps, with nominal power of 20 W each and measured optical power of 3.03 mW, resulting in a total intensity of 3.86 mW.cm^{-2}.

Radiation was maintained for 8, 18 and 24 hours at room atmosphere. At the end of this time, the sample was washed by pouring the solution into hot water in order to remove unreacted monomer and dried for two days in a hood at room temperature.

The polymers obtained at different times of radiation and the monomer were characterized by attenuated total reflectance Fourier transform infrared spectroscopy (FTIR-ATR) in a Spectrum 400 spectrometer (Perkin Elmer), in the range of 4000-500cm^{-1}, with 16 scans and a resolution of 4cm^{-1}.

Thermogravimetric analysis (TGA) was carried out using the TGA 2 Star and System equipment (Mettler Toledo), in the range of 30 to 800°C, at a rate of 10°C.min^{-1}, in a nitrogen atmosphere.

Differential scanning calorimetry (DSC) was performed in the DSC 1 Stare System (Mettler Toledo), with a heating, cooling and a second heating cycle from 25 to 300 °C, at a rate of 10°C.min^{-1}, in a nitrogen atmosphere with a flow rate of 50 mL.min^{-1}.

The cloud point analysis was performed to verify the transition temperature from hydrophilic to hydrophobic behavior of the polymer, given by the turbidity of the solution. This analysis was carried out in an aqueous solution containing 12.5%wt. of PNVCL, heated in a water bath with a temperature ranging from 20 ºC to 50 ºC.

A continuous polymeric film was obtained through the solvent casting technique. For this purpose, the polymeric solution containing 12.5%wt. of PNVCL in water was poured into a 4 cm diameter PTFE plate and left at room temperature for two days for solvent evaporation.

Results and Discussion

FTIR

Fig. 1 exhibits FTIR results of the samples irradiated for 8, 18 and 24 h, as well as the monomer and the dry film obtained by casting.

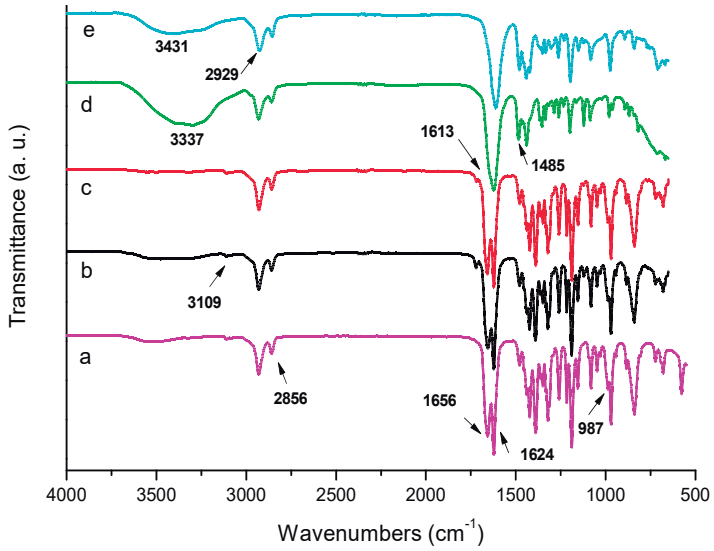

Figure 1: FTIR of: (a) monomer; solution irradiated for (b) 8h, (c) 18h and (d) 24h; (e) dry film of PNVCL.

Table 1 shows the wavenumbers corresponding to the peaks of the spectra, and related to the main functional groups present in the monomer and polymer structures.

Table 1: FTIR wavenumbers of samples.

Funcional groups	Wavenumbers (cm^{-1})	
	NVCL	PNVCL
C=C	1656	-
Aliphatic groups C-H	2929, 2856	2929, 2856
=CH, $=CH_2$	3109, 987	-
C=O	1624	1613
O-H	-	3300-3500
C-N	1485	1485

Source: [3, 7, 13].

As can be seen in Table 1 and Fig 1, the bands at 3109, 1656 and 987 cm^{-1}, characteristic of the double bond in the monomer (curve a), still remain in samples irradiated for shorter times (curves b and c). Nonetheless, these bands disappear in the sample irradiated for 24 h (curve d) and also in the dry polymeric film obtained by casting (curve e), confirming PNVCL synthesis. Another band that PNVCL presents (samples d and e) and is absent in NVCL is the broad band between 3300-3500 cm^{-1}, referring to the elongations of the O–H bond, characteristic of PNVCL due to its high hydrophilicity [3, 6, 15]. These results confirm the polymerization of PNVCL through UV radiation after 24 h.

Thermal analyses

The glass transition temperature (Tg) of the PNVCL was determined through Differential Scanning Calorimetry (DSC). This transition temperature can be affected by the presence of water between the chains, the purity of the material, its molar mass as well as the dispersivity of the molecular arrangement in the polymeric structure [7]. The Tg value of PNVCL was determined in the DSC second heating curve, to remove the effect of the presence of moisture in the sample. It was around 178ºC, as shown in Fig. 2A. This value of the polymer obtained through UV radiation was very

close to the Tg of 177ºC found by Moraes et al [7] for their PNVCL synthesized by RAFT/MADIX technique.

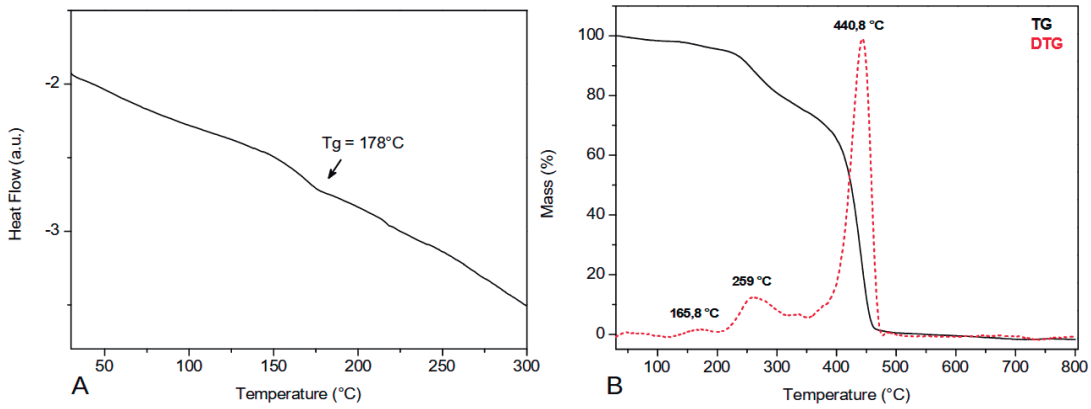

Figure 2: A) DSC curve of PNVCL e B) TGA e DTG do PNVCL.

PNVCL thermal stability was determined from thermogravimetric analysis (TGA) and its first derivative (DTG), as shown in Fig. 2B. The first mass loss, around 6%, occurred up to about 220ºC (TGA curve), with a maximum mass loss rate at 165.8ºC (DTG first peak). This mass decrease refers to the loss of moisture and crystalline water trapped in the polymeric chain, due to PNVCL hydrophilicity [6, 15]. The second and third mass losses show a maximum rate at 259°C and 440.8°C, respectively, reducing the mass to zero. These can be attributed to the depolymerization of the PNVCL, as also reported by Kozanoğlu, Özdemir, Usanmaz [13] and Usanmaz, Özdemir, Polat [15].

Cloud point analysis

The obtained polymer was solubilized in water at 20ºC, and subjected to gradual heating until the turbidity of the solution (Fig. 3A), which occurs due to the precipitation of the polymer resulting from the passage to a hydrophobic state, proving its thermoresponsiveness.

The solution cloud point occurred at 35°C. This result is in agreement with that found in the works of Medeiros et al. [8] and Halligan et al. [3], whose transition temperatures were found to be 36°C and 34°C, respectively.

By continuing to heat the solution up to 50°C (Figure 3Ac), the formation of large agglomerates of the polymer was verified, as well as its deposition on the glass walls. After decreasing the temperature to 5ºC, there was complete resolubilization of the polymer, showing the reversibility of the thermoresponsive behavior. This homogeneous solution was poured into a petri dish and dried under a hood for two days, resulting in a homogeneous film with 4 cm of diameter, as seen in Fig. 3B. The achievement of a continuous film is another confirmation of obtaining a polymer through the UV radiation conditions employed.

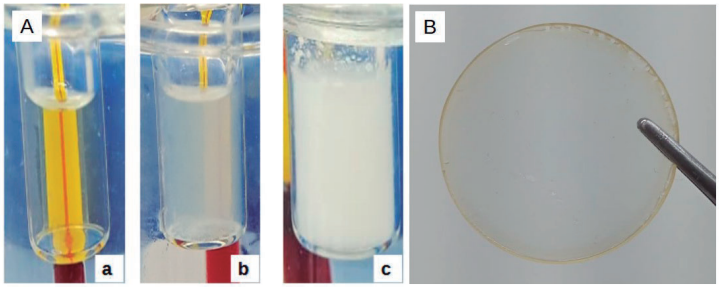

Figure 3: A) PNVCL in the solution below (a) and above the phase transition temperature ("b" and "c") e B) PNVCL film obtained by casting.

Conclusions

In the present work, it was possible to synthesize the thermoresponsive polymer PNVCL through ultraviolet radiation after 24 h of exposure to the UV-A source. Polymerization was evidenced by FTIR and also by obtaining a continuous polymeric film by casting. The synthesized polymer had its thermoresponsiveness confirmed through cloud point analysis, with a transition temperature from hydrophilic to hydrophobic behavior equal to 35°C. In addition, the observed glass transition temperature was 178ºC, and the polymer chain thermal degradation onset temperature was 390ºC. The present study aims to contribute to the dissemination of simple and alternative techniques for the polymerization of PNVCL with suitable properties for several applications.

Acknowledgements

The authors are grateful for the financial support provided by the National Council for Scientific and Technological Development (CNPq) governed by process: 163900/2021-3.

References

1. E. R. Camargo, A. M. Kubo, R. L. Sala. Archives of Nanomedicine Open Acess Journal. 1 (2018) 4. DOI: 10.32474/ANOAJ.2018.01.000102
2. N. A. Cortez-Lemus, A. Icea-Claverie. Progress in Polymer Science. 53, (2016) 1. DOI: 10.1016/j.progpolymsci.2015.08.001
3. S. C. Halligan, M. B. Dalton, K. A. Murray, Y. Dong, W. Wang, J. G. Lyons, L. M. Geever. Materials Science and Engineering: C. 79 (2017) 130. DOI: 10.1016/j.msec.2017.03.241
4. H. Chen, J. Cheng, X. Cai, J. Han, X. Chen, L. You, C. Xiong, S. Wang. ACS Appl. Mater. Interfaces. 14 (2016) 16. DOI: 10.1021/acsami.2c00580
5. K. M. Rao, K. S. V. K. Rao, C. Ha. Gels. 2 (2016) 6. DOI: 10.3390/gels2010006
6. G. R. Cerqueira, MSc Dissertação, Universidade Federal de Pernambuco, BR, 2022.
7. R. M. Moraes, L. T. Carvalho, G. M. Alves, S.F. Medeiros, E. Bourgeat-Lami, A. M. Santos. Polymers. 12 (2020) 1252. DOI: 10.3390/polym12061252
8. S. F. Medeiros, J. C. S. Barboza, M. I. Ré, R. Giudici, A. M. Santos. Journal of Applied Polymer Science. 118 (2010) 229. DOI: 10.1002/app.32204
9. W. Tomal, J. Ortyl. Polymers, 12 (2020) 1073. DOI:10.3390/polym12051073
10. M. H. Gutiérrez-Villarreal, J. G. Guzmán-Moreno. Journal of Polymer Research. 20 (2013) 149. DOI: 10.1007/s10965-013-0149-x
11. A. Martínez-Romo, R. González-Mota, J. J. Soto-Bernal, I. Rosales-Candelas. Journal of Spectroscopy. 1 (2015) 6. DOI:10.1155/2015/586514
12. C. Ignacio, Doc Tese, Universidade Federal de Minas Gerais, Belo Horizonte, BR, 2009.
13. S. Kozanoğlu, T. Özdemir, A. Usanmaz. Journal of Macromolecular Science, Part A. 48 (2011) 467. DOI:10.1080/10601325.2011.573350
14. F. Loyer, A. Combrisson, K. Omer, M. Moreno-Couranjou, P. Choquet, N. D. Boscher. ACS Applied Materials & Interfaces. 1 (2018) 49. DOI:10.1021/acsami.8b14806
15. A. Usanmaz, T. Özdemir, Ö. Polat. Journal of Macromolecular Science, Part A: Pure and Applied Chemistry. 46 (2009) 597. DOI:10.1080/10601320902851868

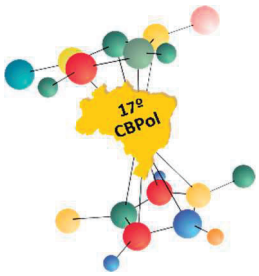

PRODUCTION OF METHACRYLATED GELATIN: A STUDY ON THE BUFFER EFFECT

Angelita R. Krama[1] and Marcia M. Meier[1]

1 – Department of Chemistry, Santa Catarina State University (UDESC), Joinville, SC, Brazil
marcia.meier@udesc.br

Abstract – Methacrylated gelatin (GelMA) is a product of the reaction between methacrylic anhydride (AM) and gelatin and is widely used in tissue engineering. To achieve higher degree of methacrylation (DM) during the reaction pH needs to be controlled. Thus, the use of a pH buffer within the isoelectric point of gelatin is essential for a good reaction yield. The objective of this work is to present a study on the strength of the pH buffer during the reaction of insertion of methacrylic groups in gelatin to find the best concentration to obtain higher DM than described in the literature. Different concentrations of reagents and pH buffer were evaluated, and the reaction product was analyzed by ^{1}H NMR. The results showed that the carbonate buffer with a concentration of 0.6 M maintained the pH stable in the isoelectric point range and produced GelMA with 95% of DM.

Keywords: *gelatin, methacrylic anhydride, carbonate buffer, GelMA.*

Fundings: Fundação de Amparo à Pesquisa e Inovação do Estado de Santa Catarina (FAPESC, TO 2021TR1222).

Introduction

Photopolymerizable hydrogels such as methacrylated gelatin (GelMA) form a three-dimensional macromolecular network filled with water or other fluids, generating scaffolds available for cell culture, which are important in tissue engineering. Methacrylic anhydride (MA), a bifunctional molecule, is often used in the preparation of GelMA. Its anhydride function can form bonds with different active functional groups of gelatin, and its methacrylate function enables radical gelatin crosslinking [1]. The product of this functionalization is known as methacrylated gelatin (GelMA), a material capable of photocrosslinking and has been widely studied in tissue engineering.

There are many methods to prepare GelMA hydrogels, the most common is the reaction between the hydroxyl and amine groups of gelatin with methacrylic anhydride. Primary amine and hydroxyl groups are mainly involved in this substitution reaction, where methacryloyl groups are introduced into gelatin, which is usually carried out in phosphate or carbonate buffer at 50°C [2–3], as illustrated in Fig. 1a.

During the the functionalization reaction, by-products, such as methacrylic acid, reduce the pH, which in turn causes the gelatin amino groups to become protonated, inhibiting the reaction with methacrylic anhydride (MA). Thus, maintaining a stable pH can contribute to the efficiency of the gelatin reaction with MA owing to the greater reactivity of deprotonated amino groups, as shown in Fig. 1b, which demonstrates how the functional groups of gelatin undergo protonation and deprotonation depending on the pH of the reaction medium.

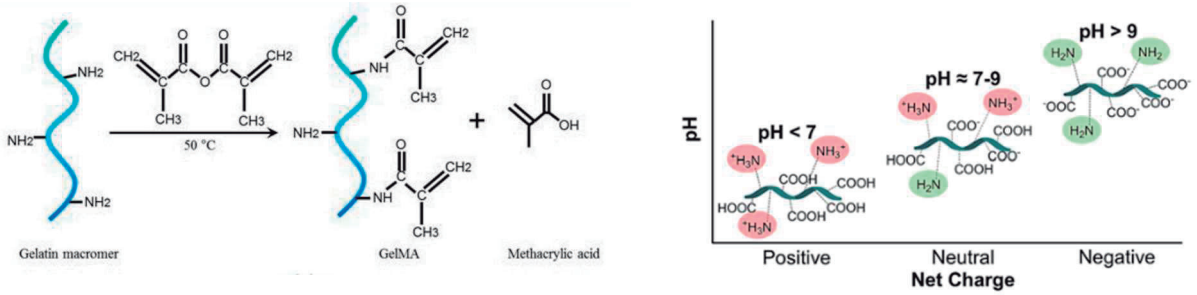

(a) (b)

Source: Adapted from Krishnamoorthy et al. [4] e Lee et al.[5].

Figure 1 - (a) Synthesis of methacrylated gelatin (GelMA). (b) Effect of pH on ionization of gelatin functional groups.

Therefore, understanding the effect of the pH of the reaction medium is essential for optimizing the procedure to obtain a higher degree of methacrylation.

Experimental

The gelatin functionalization procedure with methacrylic anhydride was adapted from the optimized literature procedure [5], as briefly described in Fig. 2, with a thin film as the final product.

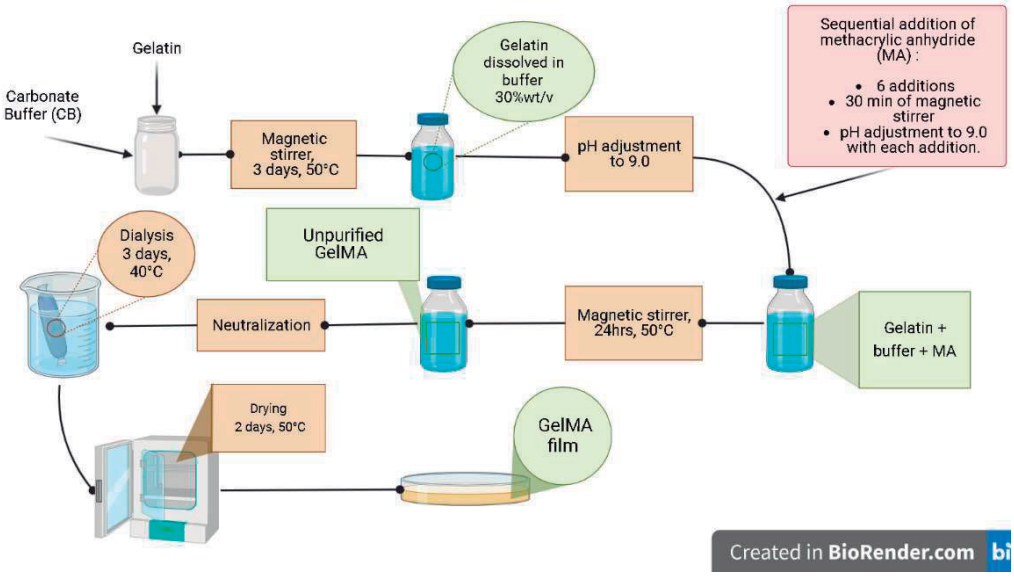

Figure 2 - Schematic of the experimental procedure to produce methacrylated gelatin (GelMA) films.

Before the addition of each MA aliquot, the pH was determined and later adjusted to 9.0 with 6 M NaOH(aq). The final product was characterized by ^{1}H NMR spectroscopy (Bruker, Ascend 400). The identification of each experimental group and concentrations evaluated are presented in Table 1.

Table 1. Sample abbreviations and descriptions of gelatin and MA content corresponding to each evaluated group.

Sample name	Methacrylic anhydride content ($mL.g^{-1}$ of gelatin)	Gelatin content (% wt in water)
GelMA-0.05 10%	0.05 $mL.g^{-1}$	10%
GelMA-0.10 10%	0.10 $mL.g^{-1}$	10%
GelMA-0.20 10%	0.20 $mL.g^{-1}$	10%
GelMA-0.05 30%	0.05 $mL.g^{-1}$	30%
GelMA-0.10 30%	0.10 $mL.g^{-1}$	30%
GelMA-0.20 30%	0.20 $mL.g^{-1}$	30%

Results and Discussion

Fig. 3 (left) shows the overlapping of the ^{1}H NMR spectra of gelatin and GelMA in water. There was a decrease in the intensity of the peak at 2.98 ppm, attributed to lysine that underwent reaction, and new peaks have emerged between 6.0 and 5.3 ppm associated to hydrogen atoms of the methacrylate groups. The relationship between the areas of lysine peaks in gelatin before and after the reaction allowed determination of the degree of substitution.

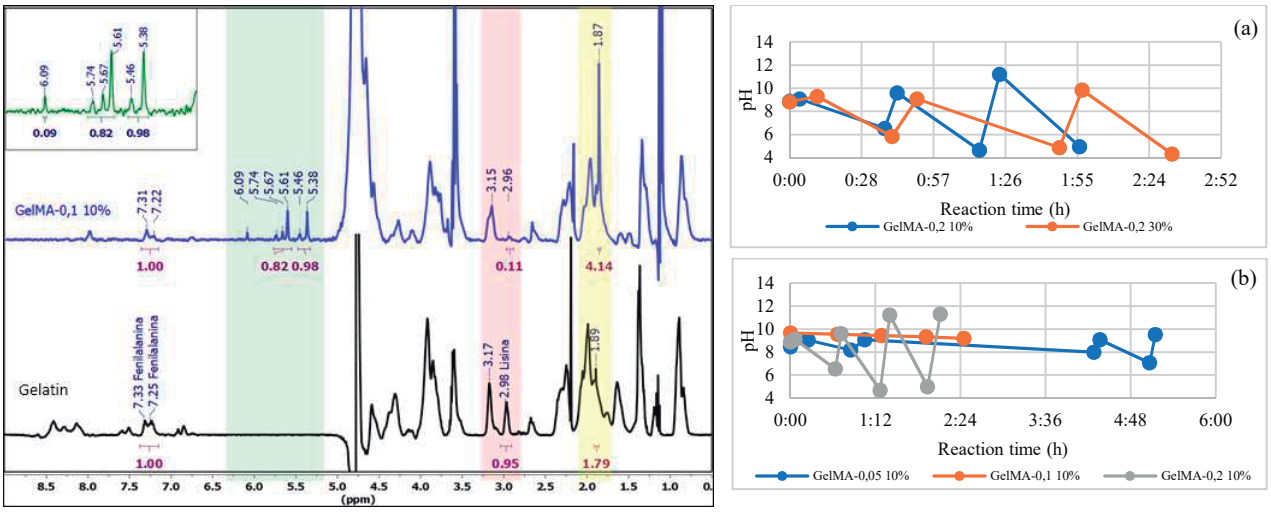

Figure 3 - Left ^{1}H NMR spectra of pure gelatin (black) and 10% GelMA-0.1 10% (blue) in 0.1 M carbonate buffer medium. Upper left corner: magnified view of the green region. On the right, (a) pH variation in relation to the concentration of solubilized gelatin in a solution with 0.1 M carbonate buffer, (b) pH variation as a function of the MA/gelatin ratio in 0.1 M carbonate buffer.

The evaluation of the pH effect during the reaction occurred in two ways: 1) varying the gelatin content in the solution (10% and 30%, Fig. 3a) and 2) varying the MA/gelatin ratio (Fig. 3b).
In Fig. 3a, it is observed that for both assays, after the addition of each aliquot of MA, a pH reduction occurred. Thus, the pH was always adjusted to 9.0 before adding the next MA aliquot. This behavior suggests that the buffer strength´s was not enough to stabilize the pH during the reaction. With the pH decrease, protonated species are occurring, that are less reactive, compromising the degree of substitution.
In turn, when analyzing the effect of higher amount of MA/gelatin ratio (0.05, 0.10 and 0.2 $mL.g^{-1}$) (Fig. 3b), significant changes at pH are observed at higher MA contend, caused by methacrylic acid as byproducts.

Thus, there was a considerable decrease at the reaction pH, which should be controlled by the strength of the buffer. At the highest ratio of MA/gelatin (GelMA-0.2 10%), the pH exceeded the isoelectric point of gelatin (pH 7–9), which can impair the efficiency of the reaction.
In view of this, different strengths of carbonate buffer (0.10, 0.3, and 0.6 M) were evaluated. The pH values during the reaction are shown in Fig. 4.

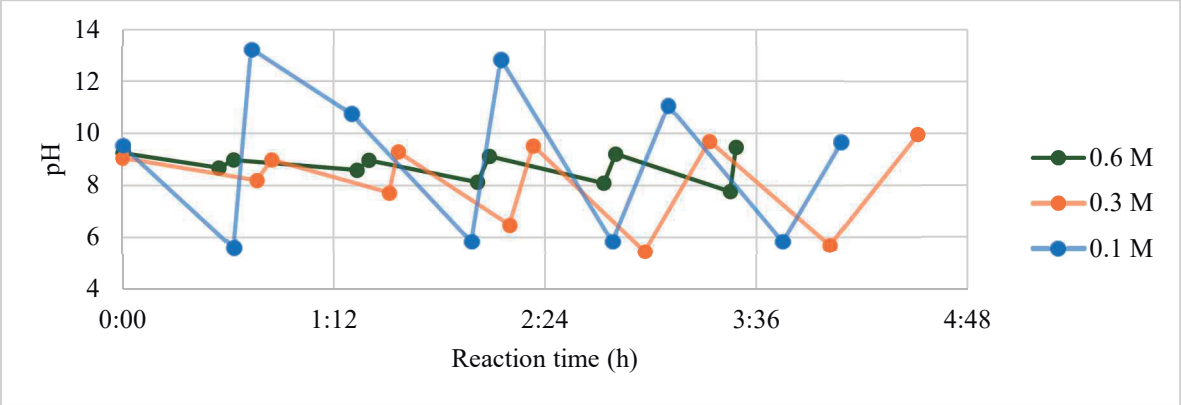

Figure 4 - Effect of carbonate buffer strength on the GelMA-0.2 30% synthesis reaction.

The gelatin used in this work is derived from collagen type 2, with an isoelectric point between pH 7 to 9. As shown in Fig. 1, a pH below 7.0 promotes the protonation of the amine groups, making them unavailable for the reaction, so the ideal buffer concentration is the one that keeps the amine groups available for nucleophilic attack by the methacrylates groups during the reaction. The 0.1 M of carbonate buffer, indicated by the literature, does not maintained the pH over the isoelectric point of the reactions with MA/gelatin contents of 0.2 $mL.g^{-1}$. As shown in Fig. 4, many times the pH of the reaction reached values below 6.0. Similar behavior occurred in 0.3 M carbonate buffer, specially in prolonged reaction time. On other hand, the 0.6 M carbonate buffer maintained the pH between 7.0 and 8.0, allowing the deprotonation of the functional groups necessary for the nucleophilic attack, promoting a more efficient reaction.
Later tests showed the efficiency of the 0.6 M carbonate buffer for lower anhydride/gelatin ratios, as shown in Fig. 5. In all reactions, the pH was maintained between 8.0 and 9.0. The last pH value was registered after the reaction neutralization.
The DM is determined using the integrals of lysine via ^{1}H NMR spectroscopy as described by Claaßen et al. [6]. The proportion of functionalization for lysine using a carbonate 0.1 M buffer was 89% while using a 0.6 M carbonate buffer achieved 95%. Thus, adjusting the buffer strength improved the efficiency of the reaction.

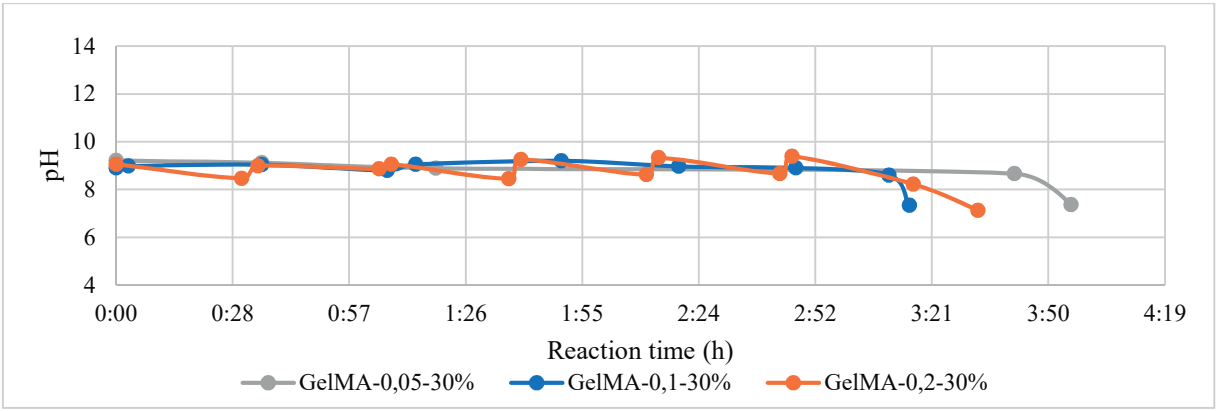

Figure 5 - pH variation as a function of the MA/gelatin ratio in 0.6 M carbonate buffer.

Conclusions

Preliminary studies showed that the buffer (0.1 M) commonly used in the literature is only applicable to reactions with low MA/gelatin ratios, producing GelMA with a lower degree of substitution.
Tests with higher concentrations of carbonate buffer maintained the pH above the isoelectric point, even at high concentrations of gelatin and MA, which were significantly higher than those described in the literature. Thus, this study optimized the gelatin methacrylation reaction without affecting the stability of the functional groups required for the reaction.

Acknowledgements

Thanks to Gelnex Indústria e Comércio Ltda for donating the gelatin used in this work and to DN Prime Ltda for donating the particle to be used in the next stages of the research. This study was financed in part by the Coordenação de Aperfeiçoamento de Pessoal de Nível Superior – Brasil (CAPES) – Finance Code 001 and Fundação de Amparo à Pesquisa e Inovação do Estado de Santa Catarina (FAPESC, TO 2021TR1222) .

References

1. Z. Dong; Q. Yuan; K. Huang; W. Xu; G. Liu; & Z. Gu RSC Advances 2019, 9, 31. https://doi.org/10.1039/C9RA02695A.

2. A. G. Kurian; R. K. Singh; K. D. Patel; J.-H. Lee; & H.-W. Kim Bioactive Materials 2022, 8, 2021. https://doi.org/10.1016/j.bioactmat.2021.06.027.

3. S. Xiao; T. Zhao; J. Wang; C. Wang; J. Du; L. Ying; J. Lin; C. Zhang; W. Hu; L. Wang; & K. Xu Stem Cell Reviews and Reports 2019, 15, 5. https://doi.org/10.1007/s12015-019-09893-4.

4. S. Krishnamoorthy;B. Noorani;& C. Xu International Journal of Molecular Sciences 2019 , 20, 20. https://doi.org/10.3390/ijms20205061.

5. B. H. Lee; H. Shirahama; N. J. Cho;& L. P. Tan RSC Advances 2015, 5,128. https://doi.org/10.1039/c5ra22028a.

6. C. Claaßen; M. H. Claaßen; V. Truffault; L. Sewald; G. E. M. Tovar; K. Borchers;& A. Southan Biomacromolecules 2018, 19, 1. https://doi.org/10.1021/acs.biomac.7b01221.

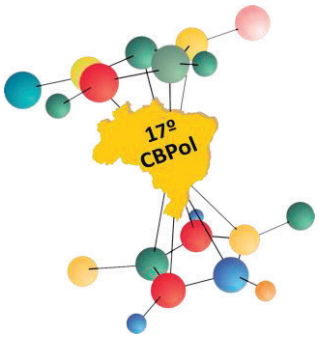

PVOH HYDROGELS CROSSLINKED BY ORGANIC ACIDS. PART II: KINETICS OF CONTROLLED DYE RELEASE

Dione P. de Castro* **and Ruth Marlene C. Santana**

Department of Materials Engineering, Federal University of Rio Grande do Sul (UFRGS), Porto Alegre, RS, Brazil
**dione.castro@ufrgs.br*

Abstract - In the present study, poly (vinyl alcohol) (PVOH) hydrogels have been synthesized using organic acids - OA (malic and tartaric) as a crosslinker agent. The hydrogels were characterized by Flory-Rehner theory to crosslink degree and migration dye time parameters. Methyl red was used as a model dye for the diffusion experiments, and the diffusion of dyes into hydrogel was monitored over time, using a UV-VIS analysis. The effects of OA type and time of synthesis on the equilibrium swelling have been investigated. With OA content and time of the synthesis, the swelling capacity decreases, due to the crosslink PVOH matrix, while the tartaric acid had good migration dye times compared with the malic acid, with more PVOH chain chemical flexibility. Flory-Rehner was applied to the crosslinking ratio of hydrogels to explain the mass transfer mechanism and specify swelling kinetic-chemical parameters with the water uptake. The swelling parameters such as equilibrium swelling capacity, and swelling rate constant, have been evaluated. The results obtained show that the incorporation of malic and tartaric acids is a good option for the development of PVOH hydrogels and the dye released controlled showed different results in both samples, with a highlight on malic acid for more control dye release. Was observed also that both acids have chemical and dimensional stability for use in hydrogels crosslink.

Keywords: *PVOH hydrogels, organic acids, Flory-Rehner theory, dye release.*

Funding: National Council for Scientific and Technological Development (CNPq) [grant number: 141265/2020-5].

Introduction

Hydrogels are widely studied in the synthesis of novel scaffolds and controlled release systems [1-3]. Due to their water absorption and retention properties, however, hydrogels can suffer a phenomenon called migration, which is the displacement of the polymer to regions of higher solute concentration, swelling it [3,4]. Flory-Rehner theory is a mathematical model [1,5-7] used to describe the behavior of polymers in solutions, considering the interaction between the polymer and the solvent, and the interaction/migration of these dyes to the medium [4]. However, this migration may affect the efficiency of its application, and an unwanted release of dyes or degradation of the hydrogel may occur.

Thus, several studies have been conducted to investigate the migration of dyes/pigments in PVOH hydrogels [1,4,8,9]. Another study, published in 2020 [8], investigated the incorporation of tomato-derived pigments into PVOH and polyol hydrogels. The results showed that the natural pigments extracted did not influence the biofilms' malleability but confirmed their aesthetic impact in coloring the biofilm matrices regardless of the presence of polyols, and lower transparency

values compared with control biofilms (without vegetal pigments). However, the study of migration in PVOH hydrogels and the Flory-Rehner theory are important concepts for understanding the behavior in aqueous solutions [1,4,6,7,9]. The study of migration and diffusion of dyes in hydrogels has shown that migration can be controlled by several factors including dye concentration, immersion time, pH of the medium, and incorporation of other materials [8,9].

This work aims to investigate the chemical crosslinking of hydrogels by dye migration kinetic and its importance for the development of new materials incorporated as essential oils and control release systems.

Experimental

Initially, a solution of distilled water (~494 mL) and PVOH (~26g) was solubilized at 85°C for 40 min to make a casting solution. For the synthesis of hydrogels, the PVOH solution was mixed with ~114g of distilled water and 1% (w/w) of specific organic acids used in the total volume final solution and HCl was used (1M, 4mL) as a catalyst [10-13]. The mixture was stirred continuously for 20 min, 1 h, 2 h, and 3 h, following a previous method [2].

The methods used in the preparation of PVOH hydrogels are described in detail in the manuscript *Part I: Swelling-kinetics study*, and the nomenclature of the PVOH hydrogels is shown in Table 1.

Table 1 - Nomenclature of the PVOH hydrogels and your reaction times used

Organic acid	PVOH Hydrogels crosslinking time			
	20 min	1 h	2 h	3 h
Malic acid	PVOH-AM (-AM)	PVOH-AM1 (-AM1)	PVOH-AM2 (-AM2)	PVOH-AM3 (-AM3)
Tartaric acid	PVOH-AT (-AT)	PVOH-AT1 (-AT1)	PVOH-AT2 (-AT2)	PVOH-AT3 (-AT3)

1 - Flory-Rehner theory

Theoretical evaluation of the yield of the reactions under the different cross-linking agent's mechanisms and catalyst/time studied were modeled using Flory-Rehner theory [2,7,14], in which the rate of the degree of swelling of the hydrogel chain is directly linked to the degree of chemical crosslinking (*GX*) promoted by organic acids. Flory-Rehner's theory is described in detail with the swelling volume ratio (v_{2m}) from Eq. 1.

$$v_{2m} = \frac{V_p}{V_g} = \frac{V_g - V_w}{V_g} = 1 - \frac{m_w\,\rho_g}{\rho_w\,m_g} \quad (1)$$

Where V_p is the volume of the dry polymer (hydrogel); V_g (gel) is the volume in the equilibrium state, Vw is a volume of water inside the hydrogel; ρ_g is the density of the swollen hydrogel at equilibrium, ρ_w is the density of the water, m_g is the mass of the swollen polymer at equilibrium and m_w is the mass of water present in the swollen polymer. After the v_{2m} value, the *GX* is calculated using Eq. 2.

$$GX = \frac{V_1\,[(v_{2m})^{\frac{1}{3}} - (\frac{2}{f}\,v_{2m})]}{-[\ln(1 - v_{2m}) + v_{2m} + x1\,(v_{2m})^2]} \quad (2)$$

Where $x1$ is the Flory-Huggins solvent-polymer interaction parameter (0.49) [2], V_1 is the molar volume of water as solvent (18 $cm^3\ mol^{-1}$) [7] and f is the functionality of available hydroxyl groups

[7] of the organic acids for crosslink formation, In this case: AM = 3 and AT = 4. The relationship between *GX* and *v* is assigned by the following Equation:

$$GX = \frac{\rho_p}{v} \tag{3}$$

Where *GX* is a polymer molecular weight between crosslinked bonds (g/mol); ρ_p is the polymer density (g/cm^3); *v* is the hydrogel crosslinking density (mol/cm^3).

2 - Migration dye in hydrogels

Hydrogels were prepared and incorporated with an aqueous solution containing the dye methyl red (Neon®) at a concentration of 0.05 µM, following an adapted methodology [9]. The solution was added at the end of each synthesis reaction (5 min remaining) to the hydrogels to avoid early degradation and change of physical-chemical behavior. Hydrogels were placed in Erlenmeyer's containing 100 mL of distilled water and submitted to different controlled release times (1, 2, 3, 5, 8, 10, and 24 h) with constant stirring of 96.5 rpm and temperature of 27.5°C using a Shaker® incubator. Aliquots of liquid containing the dye released from the hydrogels were separated and the evolution time of the dye concentration released was monitored using UV-VIS spectrophotometry, with the wavelength of maximum absorbance obtained (λ_{max} 513 nm) for accurate and reliable results, thus obtaining the final calibration equation ($y = 0.0003e^{1.7733x}$ / $R^2 = 0.9924$) for the dye methyl red. After the analysis, the samples were dried in an oven at 65°C for 24h to evaluate the dye migration.

Results and Discussion

Fig. 1-a and 1-b show the migration-kinetics range for the PVOH hydrogels with AM, AT, and their reaction time variations.

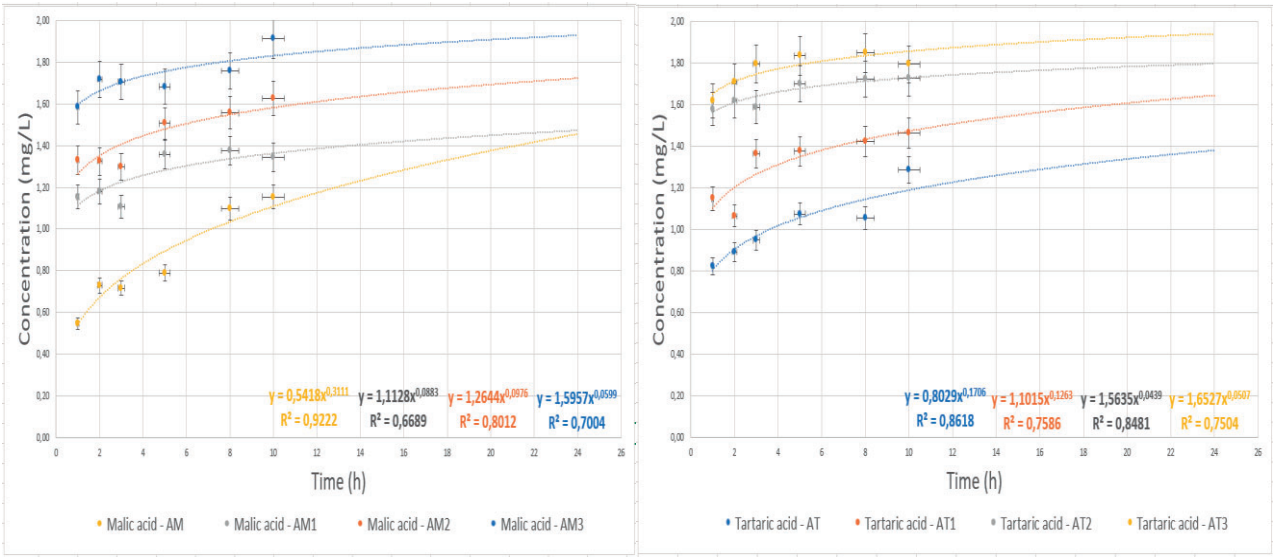

Figure 1 – Migration-kinetics for hydrogels PVOH-based: Malic acid (left) and Tartaric acid (right)

The results show that the migration of dye used, increased with the synthesis time, being that with lower times obtained a greater chemical crosslinking for the hydrogels constituted of malic acid and consequently lower release. The release process occurred exponentially and was based on the factors approximately calculated and described in the figures above. The samples -AM and -AT obtained better release results (20 min/1 h reaction) when compared with the other times employed,

the sample -AM having a slower release when compared with tartaric acid, due to the chemical interaction promoted by specifical functionalization from hydroxyls (-OH) [2,15]. For the AM and AT samples the concentration (mg/L) at 3 h had approximate values due to a faster dye release because of a lower degree of crosslinking promoted at the end of the 3 h reaction.

In a more recent study, the researchers investigated the migration of dyes in hydrogels using models and migration theories [4,9,10]. The results indicated that dye migration was influenced by concentration, temperature, dye molecular size, and polymer matrix support. In addition, it was observed that dye migration increased with increasing temperature.

Fig. 2 and 3 show the migration stages and crosslinking density (*GX*) applied for the PVOH hydrogels with AM and AT and their reaction time variations in crosslinked molar mass function in the reaction synthesis time for comparison.

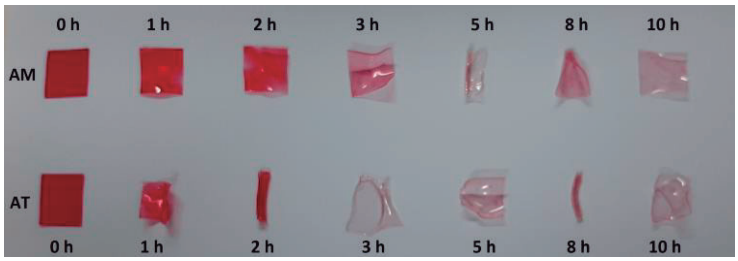

Figure 2 – Migration stages for PVOH-AM and PVOH-AT hydrogels in function on the time

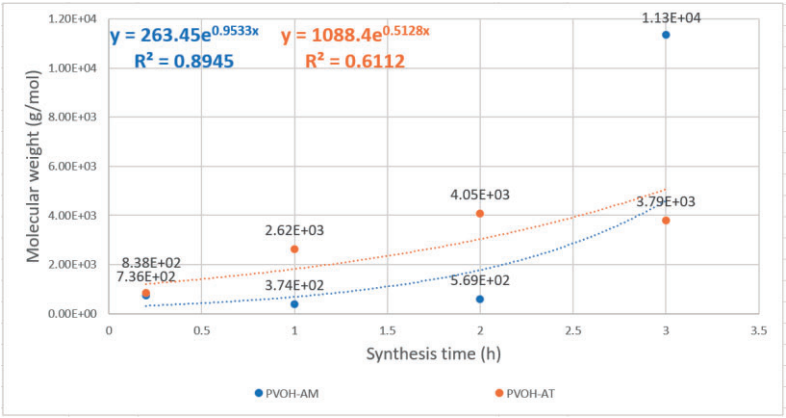

Figure 3 – Crosslinking density for PVOH-AM and PVOH-AT hydrogels

The average *GX* obtained from the hydrogels was analyzed using the Flory-Rehner theory [5]. For analysis, the values were assigned to the respective swelling rate determined at 1 h for the -AM hydrogels and 2 h for the -AT. Also, the Flory-Rehner was applied to each time selected (20 min, 1, 2, and 3 h) to show the changes for each synthesis studied and show the influence of the synthesis time on the mass weight obtained.

The results obtained for the hydrogels of -AM and -AT, show that the reactions with a shorter time, generated more chemically esterified hydrogels with average *GX* of $7.36x10^2$; $3.74x10^2$; $5.69x10^2$ and $1.13x10^4$ $g.mol^{-1}$ for -AM and $8.38x10^2$; $2.62x10^2$; $4.05x10^2$ and $3.79x10^3$ g/mol for -AT hydrogels respectively. For the Flory-Rehner theory, the samples composed of malic acid obtained the highest average crosslinking indexes, having the maximum crosslinking value (g/mol) for the time of 20 min of reaction. Thus, the decrease in molar mass between the PVOH chemical structure and consequently an increase in the average density between the acids used (higher for malic acid compared to tartaric acid) formed more esterified hydrogels with higher *GX* in a shorter proposed synthesis time [15]. The increase of chemical reactivity induced by malic acid compared to tartaric acid is evidenced from the initial times of the chemical reaction until the 3 h of

reaction with the decrease of *GX* of all hydrogels, over the reaction time due to the reagents to consumption (organic acids) from the starting of the reaction. It is observed that with the increase of the crosslinked molar mass of the hydrogel, there is a lower release of the dye over the reaction time in comparison to the migration graphs. This event is shown after the synthesis has been shifted during the reaction and shown in the collated data for the 3 h of the reaction due to the lower degree of crosslinking as seen in Figure 3.

Conclusions

The dyes used were incorporated, obtaining a good dispersion in the middle of the crosslinked polymeric networks of the hydrogels. With the evaluation of the migration of the dye using UV-VIS spectroscopy, a suitable time and synthesis of 20 min up to 2 h is observed for a controlled release with optimization of the synthesis time. For the Flory-Rehner theory, the samples composed of malic acid obtained the highest average crosslinking indexes, having the maximum crosslinking value (g/mol) for the time of 20 min of reaction. Thus, hydrogels based on malic and tartaric acids can be used to immobilize higher amounts of dyes or essential oils systems and a higher proportion (reaction low times) of them remained mobile after the analysis time.

Acknowledgments

The authors would like to thank LAPOL/UFRGS and the Institute of Chemistry (UFRGS) for the infrastructure used in this work and CNPq, PPGE3M/UFRGS-CAPES for financial support.

References

1. Ganji F, Vasheghani-Farahani S, Vasheghani-Farahani E. Theoretical Description of Hydrogel Swelling: A Review. Iranian Polymer Journal. 2010;19(5):375-398.
2. Sonker AK, Verma V. Influence of crosslinking methods toward poly(vinyl alcohol) properties: Microwave irradiation and conventional heating. Journal of Applied Polymer Science. 2018;135(14):8.
3. Vasile C, Pamfil D, Stoleru E, Baican M. New Developments in Medical Applications of Hybrid Hydrogels Containing Natural Polymers. Molecules. 2020;25(7):68.
4. Vyroubal D, Klucakova M, Ltd T. DIFFUSION OF DYES IN BIOPOLYMERIC HYDROGELS. 12th International Conference on Nanomaterials - Research & Application (Nanocon 2020). 2021:379-384.
5. Borges FTP, Papavasiliou G, Teymour F. Characterizing the Molecular Architecture of Hydrogels and Crosslinked Polymer Networks beyond Flory-Rehner-I. Theory. Biomacromolecules. 2020;21(12):5104-5118.
6. Richbourg NR, Peppas NA. The swollen polymer network hypothesis: Quantitative models of hydrogel swelling, stiffness, and solute transport. Progress in Polymer Science. 2020;105:14.
7. Hoti G, Caldera F, Cecone C, et al. Effect of the Cross-Linking Density on the Swelling and Rheological Behavior of Ester-Bridged beta-Cyclodextrin Nanosponges. Materials. 2021;14(3):20.
8. Mitrea L, Calinoiu LF, Martau GA, et al. Poly(vinyl alcohol)-Based Biofilms Plasticized with Polyols and Colored with Pigments Extracted from Tomato By-Products. Polymers. 2020;12(3):19.
9. Klucakova M, Havlikova M, Mravec F, Pekar M. Diffusion of dyes in polyelectrolyte-surfactant hydrogels. Rsc Advances. 2022;12(21):13242-13250.
10. Kim SJ, Lee KJ, Kim IY, Lee YM, Kim SI. Swelling kinetics of modified poly(vinyl alcohol) hydrogels. Journal of Applied Polymer Science. 2003;90(12):3310-3313.
11. Dlamini DS, Wang JW, Mishra AK, Mamba BB, Hoek EMV. Effect of Cross-Linking Agent Chemistry and Coating Conditions on Physical, Chemical, and Separation Properties of PVA-Psf Composite Membranes. Separation Science and Technology. 2014;49(1):22-29.
12. Zhang QY, Huang XY, Zhang L, Jin ZX. Isothermal Titration Calorimetry Directly Measures the Selective Swelling of Block Copolymer Vesicles in the Presence of Organic Acid. Acs Omega. 2022;7(12):10580-10587.
13. Omidian H, Park K. Introduction to Hydrogels. In: Park K, Okano T. Biomedical Applications of Hydrogels Handbook. 1 ed. ed: Springer; 2010.
14. Uyanga KA, Daoud WA. Green and sustainable carboxymethyl cellulose-chitosan composite hydrogels: Effect of crosslinker on microstructure. Cellulose. 2021;28(9):5493-5512.
15. Gautam L, Warkar SG, Ahmad SI, Kant R, Jain M. A review on carboxylic acid cross-linked polyvinyl alcohol: Properties and applications. Polymer Engineering and Science. 2022;62(2):225-246.

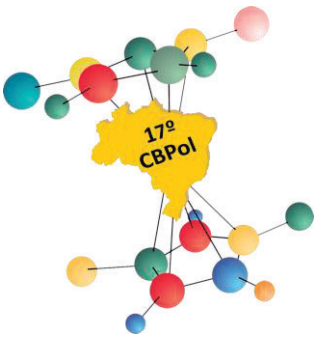

PVOH HYDROGELS CROSSLINKED BY ORGANIC ACIDS. PART I: SWELLING-KINETICS STUDY

Dione P. de Castro*, Vanessa Z. Kieffer and Ruth Marlene C. Santana

Department of Materials Engineering, Federal University of Rio Grande do Sul (UFRGS), Porto Alegre, RS, Brazil
**dione.castro@ufrgs.br*

Abstract - In the present research, poly (vinyl alcohol) (PVOH) hydrogels have been synthesized using organic acids (citric, malic and tartaric) as a crosslinker agent. The hydrogels were characterized by water uptake analysis and kinetics-chemical parameters. The effect of organic acids and time of synthesis on the equilibrium swelling has been investigated. With organic acids (malic and tartaric) contents, the swelling capacity increases, due to a degree of swelling promoted, while the citric acid used causes a disintegration of the hydrogel after the swelling times are extended. Fick's law was applied to the swelling ratio of hydrogels to explain the mass transfer mechanism and specify kinetic-swelling parameters. The swelling parameters such as equilibrium swelling capacity, and swelling rate constant, have been evaluated. The results obtained show that the incorporation of citric acid, due to its chemical functionalization, did not obtain dimensional stability, contributing to the disintegration of the hydrogels after a while. The incorporation of malic and tartaric acids shows good kinetics for both, especially for malic acid with a rate n and k elevated in comparison with the tartaric acid, bringing sustainable options for the development of PVOH hydrogels with a release control system.

Keywords: *PVOH hydrogels, organic acids, kinetic-swelling study.*

Funding: National Council for Scientific and Technological Development (CNPq) [grant number: 141265/2020-5].

Introduction

Hydrogels are efficient to absorb large amounts of water and organic solutions, thus, the absorption of large amounts of aqueous solution brings a potential for applications in different fields [1]. PVOH is a water-soluble polymer containing a large number of hydroxyl groups because it has many advantages such as low cost and high chemical stability for hydrogel synthesis [1]. Chemical crosslinking forms chemical bonds between the polymeric chains of PVOH. Various carboxylic acids such as dicarboxylic, polycarboxylic and their derivatives are used as good crosslinking agents due to their reactive sites that form a stable and high-density crosslinked network in PVOH through esterification reactions and different forms of intermolecular/intramolecular bonds [2,3].

One of the most important characteristics of hydrogels is their capacity for absorption and retention of liquids, which can be high performance or not depending on the parameters used [3,4]. One of these parameters considered is the water absorption kinetics that can be estimated and calculated by the linear derivation of Fick's law [1,4]. This work aims to investigate the swelling and the individual performance data of the hydrogel samples with different organic acids when submitted to the swelling-kinetics test to evaluate the uptake systems.

Experimental

Materials

Poly(vinyl alcohol) (PVOH) (87% hydrolyzed) and citric acid (AC) were supplied from Neon®; Malic acid (AM) was obtained from Êxodo Científica®; tartaric acid (AT) was obtained from Synth® and hydrochloric acid catalyst (HCl) (37% w/w) was obtained from Química Moderna®. All chemicals were used as received without further purification.

Preparation and characterization of Organic acids/PVOH hydrogels

Initially, a solution of distilled water (~494 mL) and PVOH (~26g) was solubilized at 85°C for 40 min to make a casting solution. For the synthesis of hydrogels, the PVOH solution was mixed with ~114g of distilled water and 1% (w/w) of specific organic acids used in the total volume final solution and HCl was used (1M, 4mL) as a catalyst [5-7]. The mixture was stirred continuously for 20 min, 1 h, 2 h and 3 h, following a previous method [8]. Subsequently, hydrogel aliquots were weighed and placed in Petri dishes and dried in an oven at 65°C for 24 h and stored in a desiccator for 6 days for the final curing process following an adapted methodology [9]. The nomenclature of the PVOH hydrogels, as prepared, is presented in Table 1.

Table 1 - Nomenclature of the PVOH hydrogels and your reaction times used

Organic acid	PVOH Hydrogels crosslinking time			
	20 min	1 h	2 h	3 h
Citric acid	PVOH-AC (-AC)	PVOH-AC1 (-AC1)	PVOH-AC2 (-AC2)	PVOH-AC3 (-AC3)
Malic acid	PVOH-AM (-AM)	PVOH-AM1 (-AM1)	PVOH-AM2 (-AM2)	PVOH-AM3 (-AM3)
Tartaric acid	PVOH-AT (-AT)	PVOH-AT1 (-AT1)	PVOH-AT2 (-AT2)	PVOH-AT3 (-AT3)

The kinetic profiles of swelling of the hydrogels by sample size studied were modelled using Fick's law, in which the rate of the degree of relaxation of the hydrogel chain is directly linked to the degree of chemical crosslinking promoted by organic acids. These mechanisms of water absorption in the three-dimensional structure of a hydrogel have been described by diffusion and macromolecular relaxation or only by macromolecular relaxation in the literature [1]. In Eq. 1 the parameters of swelling kinetics including the diffusion exponent (n) and diffusion constant (k) were calculated [1,4].

$$\frac{M_t}{M_{eq}} = kt^n \tag{1}$$

Where: t is time; k is the diffusion constant of the studied hydrogel and the swelling medium; n is the solvent diffusion exponent; M_t and M_{eq} are the hydrogel mass at a defined swelling time and the equilibrium state, respectively.

Results and Discussion

Fig. 1 to 3 show the swelling-kinetics plots for the PVOH hydrogels with AC, AM and AT and their reaction time variations. The graphs were plotted to have the reaction kinetics defined by a linear

trend line, where the values of *n* and *k* were assigned for the intumescence kinetics and the solvent diffusion coefficient respectively. The error of the applied model was assigned to R^2.

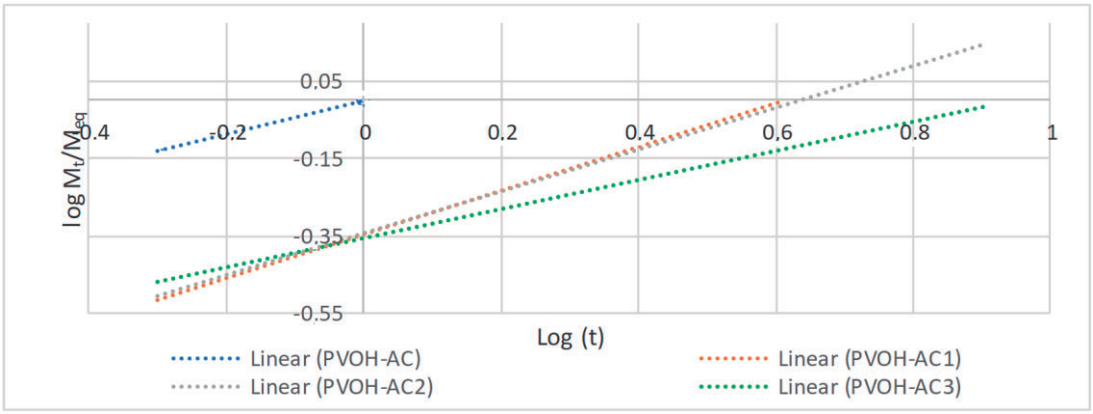

Figure 1 – Swelling-kinetics for PVOH-AC hydrogels

The PVOH-AC sample had a shorter reaction time compared to the others due to its reaction kinetics (n = 0.4399). The samples of hydrogels with -AC1 (n = 0.5637) and -AC2 (n = 0.5396) had similar reaction kinetics and percentages of swelling, besides having suffered mass disintegration in the same time scale. The sample -AC3 obtained more stable kinetics and consequently presented dimensional stability in the swelling test, due to the crosslink PVOH partial after the time synthesis applied (3 h), but with gradual mass loss. This behaviour is a result of a decrease in the final dimensional strength of the hydrogel and its disintegration due to high interaction with water hydrolysis, depending on the elaborate reaction kinetics and the time for hydrogel crosslinking [4,8]. It can be seen that the swelling ratio of a hydrogel is affected by both the concentration of citric acid and the final pH medium (3.5) of the solution in the swelling medium, through the conversion of carboxylic molecules (-COOH) into protonated acids that can result in a reduction of swelling [1,10].

In Fig. 2 it is observed that the hydrogel samples with -AM had similar reaction kinetics which resulted in dimensional and chemical stability, however with lower values of intumescence (n = 0.1344 to n = 0.1465). This behaviour is presented previously in the swelling test. It is also described in the literature that the pH of the solution also influences the intumescence of the samples and consequently in its swelling kinetics [1]. This interaction of the organic acids [3] of the protonated hydrogels in the aqueous conditions of acidic pH, resulted in the reduction of the swelling rate [1].

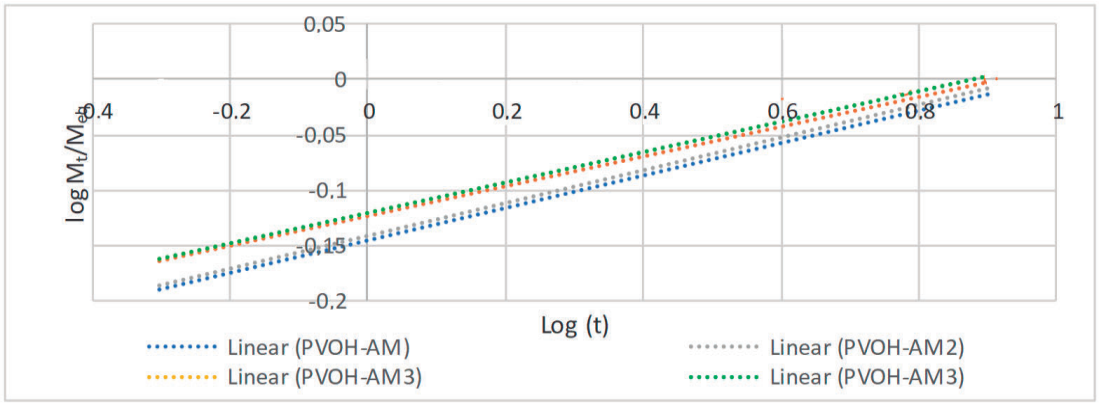

Figure 2 – Swelling-kinetics for PVOH-AM hydrogels

The samples of hydrogels with -AT (Fig. 3) had the second highest values of the kinetics of swelling (n = 0.2198 - 0.3170) and the sample -AT3 (n = 0.3170) that obtained this highest percentage due to the end of the reaction kinetics of the sample, shown by the swelling test and its dimensional stability by 8 h of the test. The behaviour of its swelling kinetics occurred due to the intumescence being dependent on the pH (3.5) obtained experimentally from the crosslinked hydrogels via chemical catalysis (HCl) and the presence of unreacted free -COOH group of the tartaric acid. This behaviour was also studied and observed by Kanmaz et al. [1].

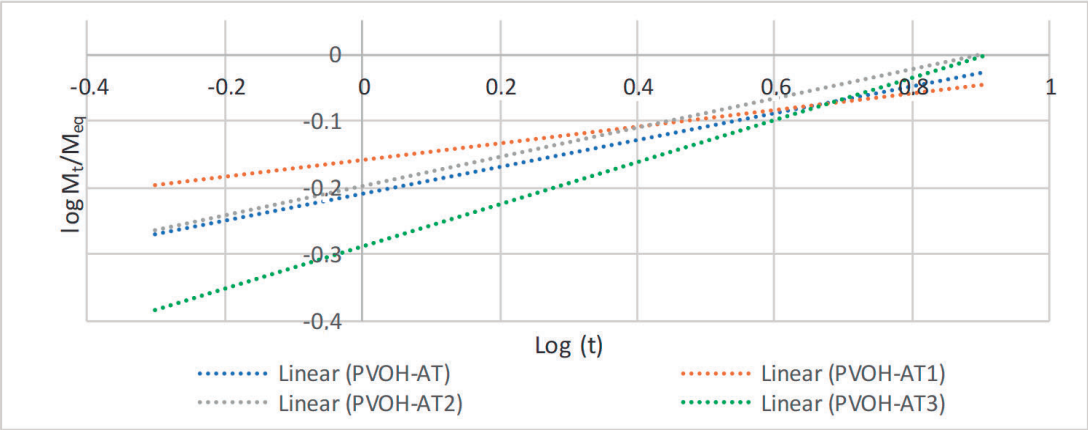

Figure 3 – Swelling-kinetics for PVOH-AT hydrogels

Table 1 shows the values of the swelling-kinetic constants of n and k for the hydrogels, obtained from the graphs of log $(\frac{M_t}{M_{eq}})$ vs log (t) and were calculated from the slope and intercept of the lines of the previous graphs, with a value of n as 0.5 being a description of Fickian mass transfer, and between 0.5 and 0.89 showing a non-Fickian transport mechanism [1,4]. The evaluation of data for the calculation of swelling kinetics was assigned in the time interval from 0.5 to 8 h of the test.

Table 1 - Values of n and k to swelling-kinetic

Hydrogel	*n*	*k*	Model error (%)
PVOH-AC	0.4399	1	1
PVOH-AC1	0.5637	0.4501	0.3184
PVOH-AC2	0.5396	0.4525	0.5893
PVOH-AC3	0.3768	0.4402	0.1861
PVOH-AM	0.1465	0.7160	0.1463
PVOH-AM1	0.1344	0.7537	0.0985
PVOH-AM2	0.1485	0.7219	0.1186
PVOH-AM3	0.1364	0.7575	0.1001
PVOH-AT	0.2004	0.6194	0.0733
PVOH-AT1	0.1248	0.6934	0.0340
PVOH-AT2	0.2198	0.6329	0.1572
PVOH-AT3	0.3170	0.5146	0.1360

The values of n were below 0.5 for all hydrogels which are attributed to higher kinetics of solvent swelling for the hydrogels studied, and the samples of PVOH-AC (n = 0.4399);

PVOH-AM2 (n = 0.1485) and PVOH-AT3 (n = 0.3170) obtained the highest values in their respective groups. This is attributed to the higher reaction kinetics for swelling of these samples and partially converges with the swelling data shown in other studies submitted by this group [11]. Kanmaz et al. [1] describe that hydrogels may have sufficient chemical mobility to allow solvent diffusion and this model can be expressed as Fickian mass transfer. The PVOH-AC hydrogel sample, by having the highest swelling kinetics, showed the highest percentage, while the other samples consisting of -AM2 and -AT3 due to chemical crosslinking and had dimensional stability and did not reach higher diffusion plateaus than -AC.

Conclusions

This investigated the synergistic effect of organic acids (OA) and time of synthesis on PVOH to obtain a good swelling hydrogel. The embedding of OA into PVOH the crosslink groups were addicted and the swelling capacity of the hydrogel was increased effectively. It was also found that the use of the malic and tartaric acids exhibited the best results for uptake properties with interconnected narrow bonds, which made it more attractive for water diffusion calculated by Fick's law. Insertion of citric acid into the network, loading ratios caused a peak in swelling values up to nearly 0.5396 and n = 0.5637, respectively. Malic and tartaric acids embedded hydrogels showed a good response to uptake/swelling properties. Finally, it is concluded that OA incorporated in hydrogels can be tuned to serve as water uptake/swelling for essential oils released systems.

Acknowledgements

The authors would like to thank LAPOL/UFRGS for support in this work, and CNPq, PPGE3M/UFRGS-CAPES for financial support.

References

1. Kanmaz N, Saloglu D, Hizal J. Humic acid embedded chitosan/poly (vinyl alcohol) pH-sensitive hydrogel: Synthesis, characterization, swelling kinetic and diffusion coefficient. Chemical Engineering Communications. 2019;206(9):1168-1180.
2. Awada H, Daneault C. Chemical Modification of Poly(Vinyl Alcohol) in Water. Applied Sciences-Basel. 2015;5(4):840-850.
3. Gautam L, Warkar SG, Ahmad SI, Kant R, Jain M. A review on carboxylic acid cross-linked polyvinyl alcohol: Properties and applications. Polymer Engineering and Science. 2022;62(2):225-246.
4. Karoyo AH, Wilson LD. A Review on the Design and Hydration Properties of Natural Polymer-Based Hydrogels. Materials. 2021;14(5):35.
5. Kim SJ, Lee KJ, Kim IY, Lee YM, Kim SI. Swelling kinetics of modified poly(vinyl alcohol) hydrogels. Journal of Applied Polymer Science. 2003;90(12):3310-3313.
6. Dlamini DS, Wang JW, Mishra AK, Mamba BB, Hoek EMV. Effect of Cross-Linking Agent Chemistry and Coating Conditions on Physical, Chemical, and Separation Properties of PVA-Psf Composite Membranes. Separation Science and Technology. 2014;49(1):22-29.
7. Zhang QY, Huang XY, Zhang L, Jin ZX. Isothermal Titration Calorimetry Directly Measures the Selective Swelling of Block Copolymer Vesicles in the Presence of Organic Acid. Acs Omega. 2022;7(12):10580-10587.
8. Sonker AK, Verma V. Influence of crosslinking methods toward poly(vinyl alcohol) properties: Microwave irradiation and conventional heating. Journal of Applied Polymer Science. 2018;135(14):8.
9. Omidian H, Park K. Introduction to Hydrogels. In: Park K, Okano T. Biomedical Applications of Hydrogels Handbook. 1 ed. ed: Springer; 2010.
10. Sabzi M, Afshari MJ, Babaahmadi M, Shafagh N. pH-dependent swelling and antibiotic release from citric acid crosslinked poly(vinyl alcohol) (PVA)/nano silver hydrogels. Colloids and Surfaces B-Biointerfaces. 2020;188:10.
11. Pittol L. C. Obtenção e caracterização de hidrogéis de PVA reticulados com ácidos orgânicos. 2021. Dissertation. (Master in Mining, Metallurgical and Materials Engineering) - Federal University of Rio Grande do Sul, Porto Alegre, 2021. Available em: <https://www.lume.ufrgs.br/>.

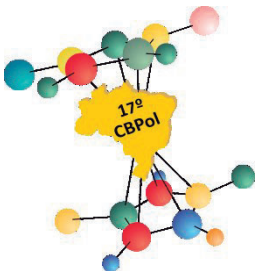

SYNTHESIS AND PHYSICOCHEMICAL CHARACTERIZATION OF STYRENE/LIMONENE/CASTOR OIL COPOLYMER OBTAINED BY RADICAL POLYMERIZATION

Enoar Dipp[1], Alex Sanches Torquato[1], Ivan José S. Junior[1], Kassia E. Bortoloso[2], Marília Gabriela S. de Souza[2], Paulo Rodrigo S. Bittencourt[1]

1 – Department of Chemistry (DAQUI), Universidade Tecnológica Federal do Paraná (UTFPR), Medianeira, PR, Brazil

paulob@utfpr.edu.br

2 – Department of Food Engineering (DAALM), Universidade Tecnológica Federal do Paraná (UTFPR), Medianeira, PR, Brazil

Abstract - The production of polymers based on vegetable oils is a way of preserving the environment by replacing non-biodegradable materials with raw materials that are more biodegradable. Vegetable oils represent a renewable and low-cost option. Castor oil has a homogeneous composition, with 85-95% ricinoleic acid. The reaction of castor oil with maleic anhydride forms castor oil maleate (MOMA). D-limonene is a natural substance that has been studied for use as a green monomer. This work proposes the synthesis of a new polymeric material, using limonene and castor oil with styrene in radical polymerization as renewable sources in the copolymer synthesis. The obtained materials were analyzed by infrared spectrometry (FTIR) and thermogravimetry (TG). The analysis results of the copolymers show that the proportion of comonomers used significantly interfere in the thermal properties of the obtained material.
Keywords: *Green Chemistry, Sustainability, Thermogravimetry, Infrared Spectrometry*

Introduction

Currently there is much discussion in society about the environmental problems caused by the accumulation of non-biodegradable materials in the ecosystem, linked to this, the growing interest in green chemistry has made the replacement of renewable raw materials become an increasingly common habit in the chemical industry [1-4] and several studies have found the synthesis or production of biodegradable polymers and ways to replace them with commercial plastics. Therefore, the search for alternative renewable resources has become more explored, with this the enormous potential of vegetable oils as a raw material in obtaining plastics has been evidenced, since its production cost becomes lower, it has higher availability and biodegradability [5-8].

The synthesis of polymers with vegetable oils shows that the products can be used as raw material for several products [9-10]. The synthesis of maleinized castor oil (MOMA) has been extensively studied in the production of a green comonomer and, due to the presence of hydroxyl groups at C12 of the ricinoleate molecule and its replacement by the maleate group, a very efficient product can be synthesized in a radical polymerization reaction. MOMA Copolymers with styrene, divinylbenzene, vinyl toluene and methyl methacrylate are much discussed in the literature [11], the products obtained are varnishes, resins, paints and materials with excellent biocompatibility for medical applications.

Limonene is a terpenoid of plant origin present in citrus fruits such as oranges and lemons. This substance, as well as terpenes, have already been used in the synthesis of some copolymers of vinylic monomers, which were prepared in the presence of free radical initiators, such as

azobisisobutyronitrile (AIBN) and benzoyl peroxide (BPO) [8], however, polymerizations with limonene, even effective, results in low conversion and low molecular weight [12-15].

The present work presents the synthesis and thermal and spectrometric characterization in the infrared region of a polymeric material, using styrene, limonene and castor oil as precursors of a copolymer.

Experimental

Synthesis of castor oil maleate (MOMA).

Castor oil ≥99.5%); Maleic anhydride (≥99%); Benzoyl peroxide (≥99%) were purchased from SigmaAldrich.

In a 500 mL Erlenmeyer were placed 100 mL of castor oil (0.644 mol), 63.15 g of Maleic Anhydride (0.644 mol) and 2.5 g of Benzoyl Peroxide (0.10% by mass). The reaction was maintained at a temperature of 60 °C under stirring for 2 hours. The maleinized castor oil (MOMA) obtained was vacuum filtered and placed in a vacuum oven at 80 °C for 4 hours in order to remove residual water.

Copolymerization

The monomers MOMA, Styrene (≥99% - SigmaAldrich) and d-Limonene (≥99.8% - SigmaAldrich) were copolymerized by AIBN 0.2 mol L^{-1} (Azobisisobutyronitrile - SigmaAldrich), in this work indicated in the nomenclature of the samples ending in A, or Benzoyl Peroxide (≥99% - SigmaAldrich), indicated with ending B, both 0.10% by mass. The amounts used for the synthesis, as well as the nomenclature used can be observed in table 1.

Table 1 - Nomenclature and composition of samples in relation to the mass of polymers and copolymers.

Nomenclature	Mass ratio MOMA:Styrene:d-Limonene
PS-A ou PS-B	0:1:0
PL-A ou PL-B	0:2:1
PM-A ou PM-B	1:2:0
PLM-A ou PLM-B	1:1:1

The monomers mixture and initiators were homogenized using a 25 Hz ultrasonic bath (Ultrassonique) for 3 minutes and placed in an oven at a temperature of 80 °C for 4 hours for synthesis.

FTIR-ATR.

The FTIR spectrum of the samples was performed in a PerkinElmer spectrometer, Model Frontier, with an accessory of total attenuated reflectance (ATR) using a crystal of zinc selenide (ZnSe), with accumulation of 4 scans in the range of 650 to 4000 cm^{-1} and resolution of 4 cm^{-1}.

Thermogravimetric Analysis (TG)

The thermogravimetric curves were performed by a simultaneous thermal analyzer PerkinElmer, model STA6000, in a platinum crucible with 10 mg of sample, heated in a

temperature range between 50 and 550 ºC. The heating rate used will be 20 ºC min^{-1}, conducted under a nitrogen atmosphere (N_2 5.0 – White Martins) with a flow rate of 20 mL min^{-1}.

Results and Discussion

Fig. 1 and 2 show, respectively, the FTIR spectra and thermogravimetric curves of the compounds obtained by synthesizing with AIBN and benzoyl peroxide used as initiator, among the FTIR spectra of compounds with the same composition using different initiators apparently not there were significant differences, spectra still under analysis, except in the case of the synthesis of the 3 copolymers.

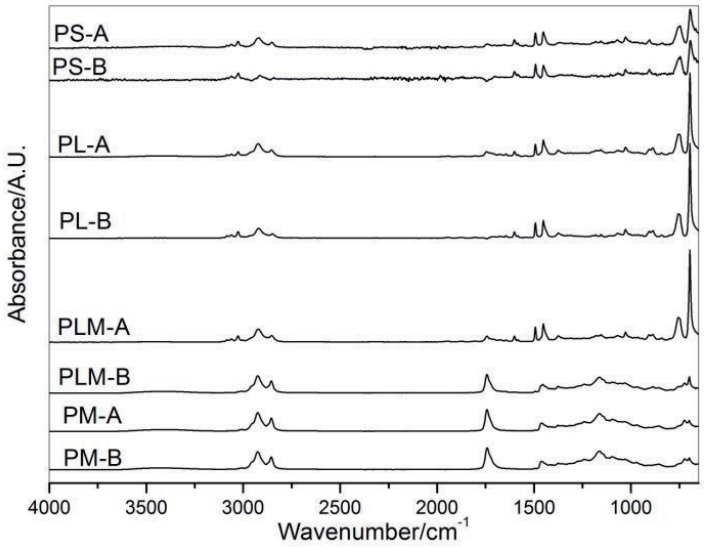

Figure 1 – FTIR spectra obtained from the reaction product of limonene with maleinized castor oil (MOMA and styrene, in different proportions), initiated by AIBN and benzoyl peroxide.

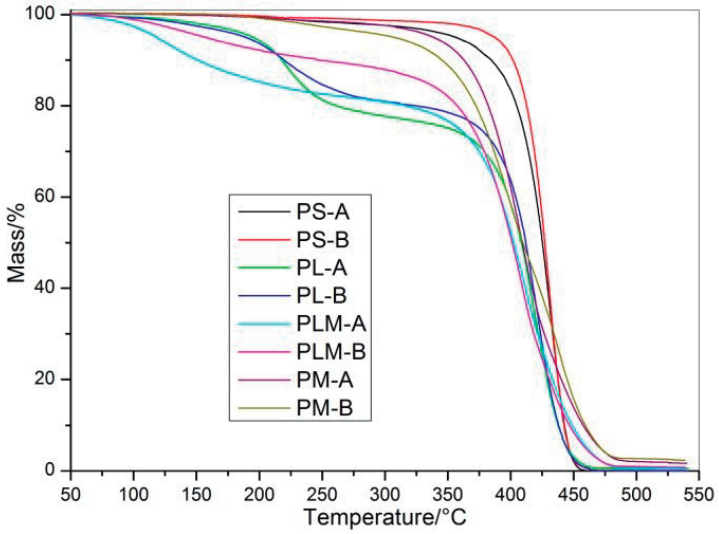

Figure 2 – Thermogravimetric curves of the reaction product of limonene with maleinized castor oil (MOMA and styrene, in different proportions), initiated by AIBN and benzoyl peroxide.

Some limonene-containing compounds had an initial mass loss of up to 20% due to unreacted d-limonene mass. PLM-A and PLM-B compounds had lower degradation temperatures than pure PS, but still above 325 °C. Thermogravimetry shows that the reactions initiated with benzoyl peroxide formed more thermally stable compounds, with the possible formation of macromolecules with relatively longer chains than those formed by initiation with AIBN, again

with the exception of the MOMA/styrene/limonene system, whose material with the formation of an apparent solid.

Conclusions

Despite still being in progress, the work presented demonstrates physical-chemical differences of the synthesized macromolecules, however the proportions of the reagents used are still being stoichiometrically evaluated to obtain a product with superior mechanical and thermal properties, with better use of renewable comonomers d- limonene and castor oil.

Acknowledgements

The authors would like to thank the National Council for Scientific and Technological Development (CNPq) and National Council for Scientific and Technological Development Coordination for the Improvement of Higher Education Personnel (CAPES) for financial support, Laboratory of Thermal Analysis and Spectrometry of Fuels and Materials (LATECOM) and CEANMED - Central Analítica Multiusuário of the Federal University of Technology - Campus Medianeira, Paraná State, Brazil, by the thermal analyzes performed.

References (Times New Roman 12, bold)

1. A. Ashothaman; J. Sudha,; N. Senthilkumar Materials Today: Proceedings 2021 80, 2829-2839 https://doi.org/10.1016/j.matpr.2021.07.047.
2. V. Fernández-González; J. M. Andrade-Garda; P. López-Mahía; S. Muniategui-Lorenzo Analytica Chimica Acta 2021, 1142, 179–188. https://doi.org/10.1016/j.aca.2020.11.002.
3. L. Manfra; V. Marengo; G. Libralato; M. Costantini; F. De Falco; M. Cocca Journal of Hazardous Materials 2021, 416, 125763. https:// doi.org/10.1016/j.jhazmat.2021.125763.
4. S. Wendels; L. Avérous Bioactive Materials 2021, 6(4), 1083–1106. https:// doi.org/10.1016/j.bioactmat.2020.10.002.
5. C. Meiorin; M.I. Aranguren; M.A. Mosiewicki European Polymer Journal. Elsevier Ltd 2015, 67, 551–560. https:// doi.org/10.1016/j.eurpolymj.2015.01.005.
6. B. Zong; B. Sun; S. Cheng; X. Mu; K. Yang; J. Zhao; X. Zhang; W. Wu Engineering 2017, 3, 379–384. https:// doi.org/10.1016/J.ENG.2017.03.003.
7. H. Kim; J. Choi; W. Won Journal of Cleaner Production 2020, 277, 124072. https:// doi.org/10.1016/j.jclepro.2020.124072.
8. S. Valentina; M. Palenzuela; J. Damián; M.E.G. Mosquera Polymer 2020, 210, 1–7. https:// doi.org/10.1016/j.polymer.2020.123003.
9. G. Capiel; E. Hernández; N.E. Marcovich; M.A. Mosiewicki European Polymer Journal 2020, 132, 109740. https:// doi.org/10.1016/j.eurpolymj.2020.109740.
10. X. Huang; M. Panahi-Sarmad; K. Dong; R. Li; T. Chen; X. Xiao Composites Part A: Applied Science and Manufacturing 2021, 147, 106444. https:// doi.org/10.1016/j.compositesa.2021.106444.
11. R.S. Alves; D.L.H. Maia; F.A.N. Fernandes; F.X. Feitosa; H.B. de Sant'Ana Fuel 2020, 269, 117429. https:// doi.org/10.1016/j.fuel.2020.117429.
12. S. Sharma; A.K. Srivastava European Polymer Journal 2004, 40(9), 2235–2240. https:// doi.org/10.1016/j.eurpolymj.2004.02.028.
13. C. Gutiérrez; J.F. Rodríguez; I. Gracia; A. de Lucas; M.T. García Journal of Supercritical Fluids 2014, 88, 92–104. https:// doi.org/10.1016/j.supflu.2014.02.002.
14. C. Li; R.J. Sablong; C.E. Koning European Polymer Journal 2015, 67, 449–458. https:// doi.org/10.1016/j.eurpolymj.2015.01.003.
15. C. Li; S. van Berkel; R.J. Sablong; C.E. Koning European Polymer Journal 2016, 85, 466–477. https:// doi.org/10.1016/j.eurpolymj.2016.10.053.

SYNTHESIS, CURING, AND DEGRADATION KINETICS OF POLYURETHANES BASED ON POLY(ETHYLENE GLYCOL), ISOSORBIDE, AND PENTAMETHYLENE DIISOCYANATE

Amanda M. Araújo[1], José Vinícius M. Barreto[1], Pedro Henrique M. Nicácio[2], Ananda Karoline C. de Albuquerque[1], Ingridy Dayane dos S. Silva[1], M. F. Souza[1], Andreas Ries[3], Renate Maria R. Wellen[1, 2]*

[1]Materials Engineering Department, Federal University of Paraíba, João Pessoa 58051-900, Brazil
[2]Academic Unit of Materials Engineering, Federal University of Campina Grande, Campina Grande 58249-140, Brazil
[3] Multidisciplinary Center for Technological Investigations, National University of Asunción, San Lorenzo University Campus, San Lorenzo, Paraguay

*wellen.renate@gmail.com

Abstract - Polyurethane (PU) synthesis based on poly(ethylene glycol) (PEG) with isosorbide (ISO) and pentamethylene diisocyanate (PDI) was carried out targeting PUs from renewable sources. Compounds with ISO content between 0-70% were produced and investigated using Fourier transform infrared spectroscopy (FTIR), differential scanning calorimetry (DSC), and thermogravimetry (TG). DSC scans displayed exotherms between 100-200 °C, related to cross-linking. ISO addition accelerated the curing, with 91 °C for the compound with 70% ISO. FTIR spectra confirmed the interaction between OH (ISO/PEG) and NCO (PDI) groups, with total NCO consumption (band at 2267 cm^{-1}). TGs presented weight loss at 146 °C, due to ISO degradation in PU/70%ISO. Curing and degradation kinetics were modeled using Friedman (FR), Kissinger-Akahira-Sunose (KAS), and Ozawa-Flynn-Wall (OFW). Overall, ISO accelerated the curing rate and increased the degradation activation energy, suggesting high thermal stability for PUs with intermediate ISO contents, i.e., 30 – 50%.

Keywords: *Isosorbide, poly(ethylene glycol), pentamethylene diisocyanate, biobased polyurethane, curing and degradation kinetics*
Fundings: Coordenação de Aperfeiçoamento de Pessoal de Nível Superior (CAPES), Conselho Nacional de Desenvolvimento Científico e Tecnológico (CNPq), Fundação de Apoio à Pesquisa do Estado da Paraíba (FAPESQ) and Federal University of Paraíba (UFPB).

Introduction

Polyurethanes (PU) based on renewable sources such as bio-based polyols and diisocyanates are being synthesized with the objective to replace PUs from non-renewable sources such as petroleum, and to reduce the use of toxic isocyanates. The synthesis of bio-based PUs from alternative resources such as glucose has been growing considerably due to its potential to modify the mechanisms of curing and degradation, providing greater chemical and physical stability [1-4]. PUs synthesis takes place through urethane bonds by the polymerization of flexible segments (polyether or polyester), known as polyols, which have one or more OH groups, and rigid segments (diisocyanates) which have two or more NCO groups. Additionally, seeking the synthesis of high-performance PUS, poly(ethylene glycol) (PEG) can be used, as it has advantages such as good biodegradability and excellent biocompatibility. Aiming at providing a PU with higher thermal stability, isosorbide (ISO) addition was successfully employed [1-2], providing reticulation, curing, and variations in the degradation mechanism.

One of the found obstacles for PUs processing through PEG and pentamethylene diisocyanate (PDI) synthesis is the low reactivity of the molecules responsible for cross-linking, with no curing reactions. The three reactive groups (NCO) of PDI have great potential for chemical interaction with OH groups on both sides of PEG and ISO molecular chain, providing urethane bonds by forming a three-dimensional network (thermosetting polyurethane).
This work aimed at the synthesis of PUs through the polymerization of PEG and PDI with ISO content addition between 10 and 70% of the weight. The curing was followed using DSC, and FTIR with spectra collected at room temperature, during and after curing, while the thermal stability was investigated by TG. Modeling of curing and degradation was performed using the Friedman (FR), Kissinger-Akahira-Sunose (KAS), and Ozawa-Flynn-Wall (OFW) models.

Experimental

Poly(ethylene glycol) (PEG) and Isosorbide (1.4:3.6-Dianhydro-D-sorbitol) (ISO) were purchased from Sigma-Aldrich. Pentamethylene diisocyanate (PDI) a 70 % bio-based trimer – commercially DESMODUR® eco N 7300 was supplied by Solution Center Covestro, Germany. The reaction took place in a 250 mL round bottom flask equipped with a magnetic stirrer in a vacuum system with an outlet connected to a condenser. ISO was heated to 60 °C and left stirring for 20 min under distillation. Simultaneously, PEG and PDI (1.1:NCO/1:OH) were mixed using magnetic stirring for 10 minutes at 60 °C, i.e., until complete homogenization. Afterwards, ISO was added to the system in different ratios. The mixture was kept under magnetic stirring at 60 °C for 10 min under vacuum.
Fourier Transform Infrared Spectroscopy (FTIR) spectra were captured considering the wavenumber range 4000-650 cm^{-1}, 32 scans per spectrum, and 16 cm^{-1} resolution. The equipment used was Perkin-Elmer Spectrum 400 FT-IR/FT-NIR Spectrometer (USA) in ATR mode.
DSC scans were acquired using the Perkin Elmer DSC 8500 (Waltham, MA, USA), with samples of approximately 4 mg. The samples were heated in the range from -20-250 °C at a rate of 10 °C/min, cooling from 250-25 °C at a rate of 20 °C/min and second heating from 25-250 °C at the rate of 10 °C/min, under nitrogen atmosphere (50 mL/min).
Thermogravimetric analyzes were carried out using the Perkin-Elmer Pyris 1 TGA (Waltham, MA, USA), at the heating rates of 5, 10, 15, and 20 °C/min in the temperature range from 30-800 °C under nitrogen atmosphere (20 ml/min). Experiments were performed using 4 mg.

Results and Discussion

Fig. 1 shows the FTIR spectra acquired at room temperature and after curing for the investigated compounds, with ISO content ranging among 10, 30, 50 and 70%. At 30 °C, 3370 cm^{-1} flexible diol segment (OH) stretching bands are observed, the bands at 2944-2867 cm^{-1} are asymmetric and symmetric stretching of C-H bonds. The band at 2267 cm^{-1} is attributed to the NCO stretching vibration, corresponding to PDI diisocyanate. The carbonyl group (C=O) is observed in the region of 1687 cm^{-1} and the amide group III (CN) of PDI is observed in 1352 cm^{-1}. The band at 1114-997 cm^{-1} is attributed to the aliphatic ether group (C-O-C), referring to ISO. After curing, bands at 3347 cm^{-1} are verified, which correspond to the stretching vibrations of NH groups, and at 1670 cm^{-1} there is the stretching of C=O bonds. These spectra indicate the urethane bonds (NHCOO) development, which become more intense increasing the ISO content from 30% upwards, due to the hydroxyl groups present in the diol.
The band at 3347 cm^{-1} of NH stretching vibration is attributed to hydrogen bonding with C=O groups and with C-O-C groups. The disappearance of NCO bands at 2267 cm^{-1} of 50% and 70% ISO evidences the occurrence of polymerization reactions between (NCO) group of PDI diisocyanate and the flexible hydroxyl groups of polyols (OH) of PEG and ISO, promoting the crosslinks.

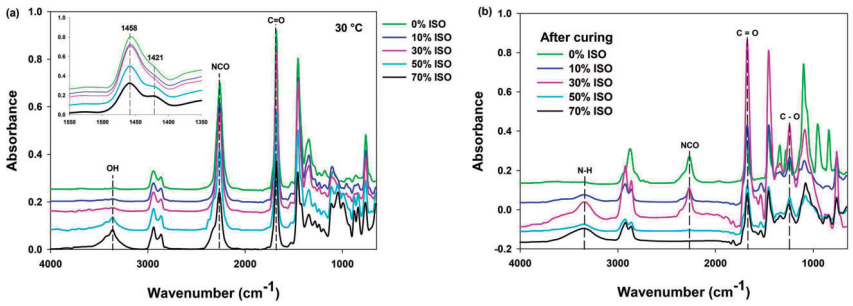

Figure 1 – FTIR spectra for PU and ISOPUs compounds collected at (a) room temperature and (b) after curing.

DSC scans in Fig. 2 illustrate the endothermic melting peaks of PEG and ISO, the exothermic curing peaks and the effect of the heating rates and ISO content on degree of curing (α) of ISOPUs. Curing reactions and peak intensities are dependent on PU compositions and heating rates. In the ISOPUs scans for the rate of 10 °C/min, in addition to two melting peaks, there are exothermic peaks due to the curing as verified in the range from 100 to 200 °C. For the compound with 0% ISO no exothermic peak was observed indicating that the curing was not developed during the heating.

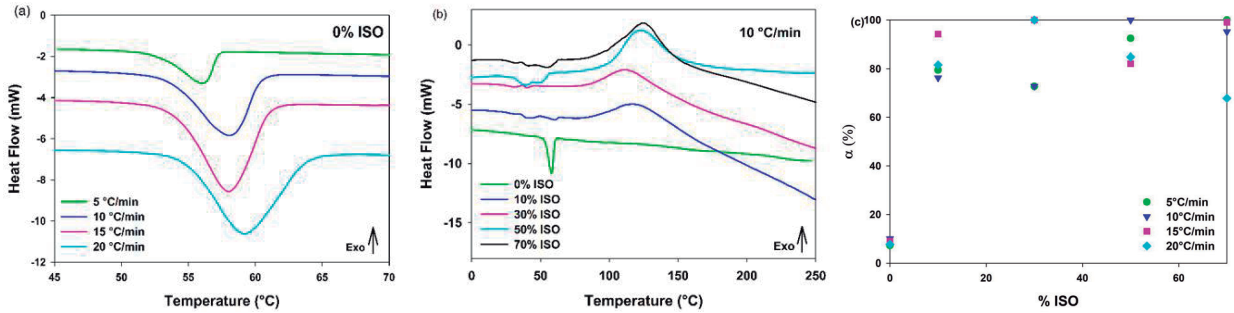

Figure 2 – DSC scans (a) of 0% ISO at indicated heating rates and (b) at 10 °C/min, compounds indicated. (c) Effect of the heating rate on degree of conversion (α) of investigated ISOPUs.

ISO addition provided changes in the reaction mechanisms, leading to crosslinks among the functional groups of diisocyanate (NCO) and PEG (OH). The increase in the ISO content contributed to the peak shifting to higher temperatures, which started to cure at $T_{0.01}$ = 91 °C for 70% ISO, while for 10% ISO $T_{0.01}$ = 86 °C. The real conversion (α) (Fig. 2 (b)) is presented as function of the ISO content for the four applied heating rates. Upon ISO addition the synthesis reaches higher values of curing conversion, i.e., 80-100% of α from 50% of ISO on. For 70% ISO α data are close to 95-100%.

Fig. 3 (a) displays the weight loss plots and the weight loss derivative at 10 °C/min and (b) the plot for maximum degradation rate (D_{max}) versus heating rates, for all compounds. ISO addition shifted the PU weight loss plots to the right, increasing the thermal stability, i.e., $T_{0.01}$ from 245 °C (0% ISO) to 277 °C (70% ISO) at the rate of 10 °C/min. The thermal stability for the rate 10 °C/min follows the trend: 30% ISO > 10% ISO > 50% ISO > 70% ISO > 0% ISO. The initial weight loss of the compounds with 50 and 70% ISO were, respectively, 151 and 146 °C. The displacement of the degradation beginning of compounds with higher ISO contents to lower temperature values is most due to the water evaporation events and ISO degradation, due to the ISO excess in the compounds.

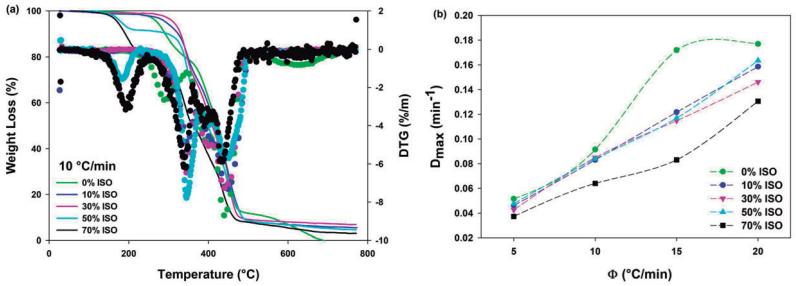

Figure 3 – (a) Weight loss and degradation rate for investigated PU and ISOPUs at 10 °C/min. N_2 atmosphere. (b) Degradation rates for PU and ISOPUs as a function of the ISO content and heating rates.

PU presented 4 stages of weight loss. The first stage with 18.64% of weight loss corresponds to the degradation of urethane bonds into polyols and diisocyanates. The second and third stages, 23.86 and 44.00% of weight loss, respectively, are associated with the decomposition of polyol stable segments [5]. The fourth stage corresponds to 11.36% of weight loss and it is related to the decomposition of residues into volatile compounds, occurring after 500 °C. In general, ISO addition increased the thermal stability, and the compound with 30% ISO presents the highest initial degradation temperature. The thermal stability of ISOPUs with 10 and 30% ISO ($T_{0.01}$ = 282 °C and $T_{0.01}$ = 308 °C), is higher than that of PU and ISOPUs with 50 and 70% ISO.

D_{max} increases upon increase in heating rate, ISO addition promoted a decrease in D_{max}, suggesting that at lower rates and in compositions with higher ISO content degradation occurs slowly. Although high ISO content compounds display weight loss stages at lower temperatures than low ISO content compounds and neat PU, the maximum degradation rate is slower.

There are two possible degradation mechanisms that describe the behavior of low stability for ISOPUs with higher amounts of ISO (Fig. 4). The first mechanism refers to the attack of terminal hydroxyl group of ISO to the carbonyl of urethane bond, with formation of two macroradicals. The second mechanism occurs less frequently and is the β-elimination of the carbonate bond with bond-breaking reactions in the molecular chain with production of two macroradicals and carbon dioxide. The propagation reactions of degradation by attack of hydroxyl group in excess, as seen in the FTIR spectra for 50 and 70% ISO (Fig. 1), often contribute to the degradation of PU and are terminated when the reactive end groups are consumed [6]. Therefore, it can be considered that high amounts of ISO reduce the thermal stability of the compounds, despite the high degree of curing for these compounds (50 and 70% ISO) observed in Fig. 2 (c), which start to degrade at low temperatures when compared to PU and ISOPUs with low contents of ISO.

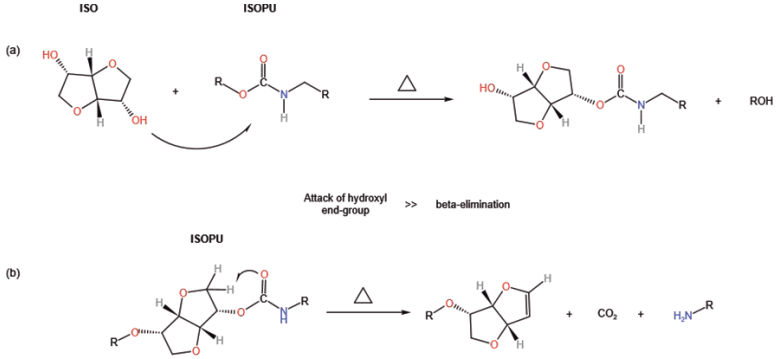

Figure 4 – Degradation mechanism (a) attack of hydroxyl end-group and (b) β-elimination for 50 and 70% ISO compounds.

Fig. 5 presents the E_{ad} for all investigated compounds computed using the Friedman (FR) (a), Kissinger-Akahira-Sunose (KAS) (b) and Ozawa-Flinn-Wall (OFW) (c) models according to Eq. 1, 2 and 3, respectively.

$$ln\left(\frac{d\alpha}{dT}\right) = ln\left(\beta\frac{d\alpha}{dT}\right) = ln\left[Af(\alpha)\right] - \frac{E_{ad}}{RT} \quad (1)$$

$$ln\,ln\left(\frac{\beta}{T^2}\right) = \left[ln\,ln\left(\frac{AR}{E_{ad}}\right) - lnG(\alpha)\right] - \frac{E_{ad}}{RT} \quad (2)$$

$$ln\,\beta = ln\frac{AE_{ad}}{RG(\alpha)} - 5.331 - 1.052\frac{E_{ad}}{RT} \quad (3)$$

In general, the three models showed similar behavior, where E_{ad} increases with degradation. In the range of $20 < \alpha < 60$, the E_{ad} for 10% ISO is superior to the other compositions, with a range of 200-327 kJ/mol, indicating that at this stage 10% ISO is more thermally stable. From $\alpha > 90$, a decrease in E_{ad} is observed for all compositions. This behavior reveals that the effect of the relative degree of conversion on the activation energy in this step is independent of the ISO amount in PU. For the compounds with 10 and 30% there was a considerable improvement in stability compared to the PU without ISO, showing the highest values of E_{ad}, while PU with 70% ISO presented the lowest E_{ad} values for the three models (FR, KAS and OFW). Although higher amounts of ISO show lower thermal stability, PUs with lower contents are promising for higher degree of crosslinking, as well as increasing thermal stability providing PU for higher performance applications.

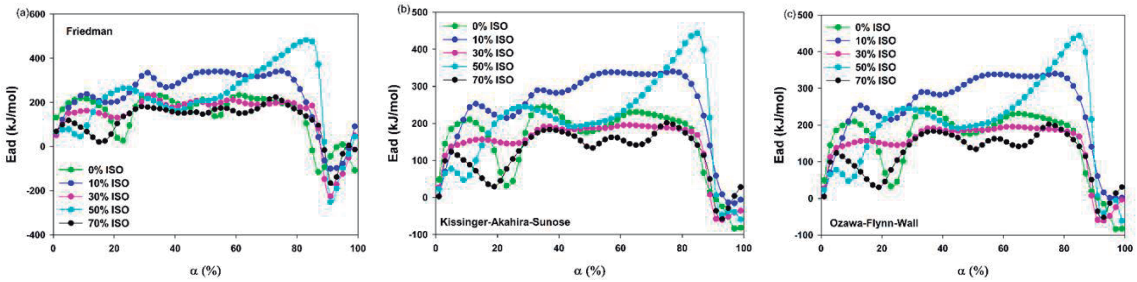

Figure 4 – Activation Energy (E_{ad}) during degradation at indicated compounds. Data modeled using (a) FR, (b) KAS and (c) OFW models.

Conclusions

Polyurethanes based on isosorbide, poly(ethylene glycol) and pentamethylene diisocyanate were synthesized. PUs curing was confirmed through FTIR spectra upon NCO bands consumption and exothermic peaks in DSC scans. It was evidenced that the curing was accelerated upon ISO addition while higher thermal stability was verified. Nevertheless, compounds with 50 e 70% ISO demonstrated easier degradation.

Acknowledgements

The authors are deeply grateful to Professor Marcus Vinícius Lia Fook and coordinators of CERTBIO (Northeast Biomaterials Assessment and Development Laboratory) for the DSC, FTIR and TGA analyses.

References

1. HS. Park; MS. Gong; JC. Knowles. J Mater Sci: Mater Med 2013, 24, 281–294. https://doi.org/10.1007/s10856-012-4814-0.
2. DE. Almeida; AKC. de Albuquerque; ID. dos Santos Silva; R. Andreas; RMR. Wellen. Polym Adv Technol 2022, 33(8), 2434- 2447. https://doi.org/10.1002/pat.5699.
3. Z. Schnepp. Angew Chem Int Ed 2013, 52, 1096-1108. https://doi.org/10.1002/anie.201206943.
4. JP. Latere Dwan'isa; AK. Mohanty; M. Misra; LT. Drzal; M. Kazemizadeh. Journal of materials Science 2004, 39, 2081-2087. https://doi.org/10.1023/B:JMSC.0000017770.55430.fb.
5. V. Besse; R. Auvergne; S. Carlotti; G. Boutevin; B. Otazaghine; S. Caillol; JP Pascault; B. Boutevin. Reactive and Functional Polymers 2013, 73(3), 588-594. https://doi.org/10.1016/j.reactfunctpolym.2013.01.002
6. S. Yan; G. Wu. Polymer Degradation and Stability 2022, 202, 110028.

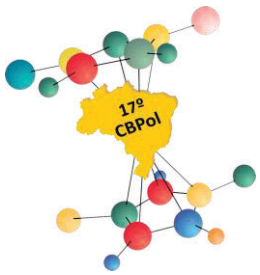

SYNTHESIS OF HYDROGELS BASED ON PRODUCTS OBTAINED FROM RENEWABLE SOURCES APPLIED ON THE REMOVAL OF CRYSTAL VIOLET DYE

Bibiana Bitelo[1*], Cesar L. Petzhold[1], Douglas Gamba[1] and Tales da Silva Daitx[1*]

1 – Institute of Chemistry, Federal University of Rio Grande do Sul (UFRGS), Porto Alegre, RS, Brazil.
bibibitelo@hotmail.com, tales.daitx@ufrgs.br

Abstract - The objective of this work was to synthesize hydrogels based on products derived from renewable and/or sustainable sources and evaluate their capacity to adsorb the cationic dye crystal violet in aqueous medium, aiming its application in wastewater treatment of the textile industry. For this, hydrogels were synthesized from renewable source polyester obtained from the reaction between oligoglycerol and malic acid under acid conditions, which were subsequently crosslinked with different amounts of citric acid, in order to study their influence on the water uptake and dye adsorption. All materials were characterized by spectroscopic and thermal techniques, confirming the synthesis of the intermediates and hydrogels. In relation to the water uptake capacity, the hydrogels showed values between 167% to 888%, depending on the citric acid content used for crosslinking step. In terms of dye adsorption, the hydrogels were able to almost completely adsorb the dye from the solution, according to a pseudo-second-order mechanism, indicating that contact time and hydrogel structure influence the adsorption.

Keywords: *bioproducts, Sustainability, Adsorption, cationic dye, Wastewater treatment textile.*

Introduction

Currently, the industry accounts for 22% of the world's water consumption, and wastewater treatment is an ally in its recovery and reuse [1]. In this scenario, the development of new polymeric materials for the removal of industrial contaminants has the potential to solve this problem. Polymeric hydrogels are attracting attention in this area due to their high-water absorption capacity resulting from the galleries formed by crosslinking, and their ability to adsorb contaminants such as dyes and heavy metals [2,3].

In recent years, green chemistry has been in evidence, where the use of renewable reagents and/or derived from plant sources in the synthesis of biodegradable and eco-friendly polymers is becoming increasingly popular. Among these, are the polyester-based hydrogels, where various types of structures can be modulated from different monomers such as polyfunctional alcohols or carboxylic acids. These hydrogels are particularly interesting because they have many applications, such as in medical chemistry due to their biocompatibility, and in wastewater treatment, where they can also be biodegraded after disposal [4,5].

The adsorption of dyes by polyester-type bio-based hydrogels is an excellent option for the treatment of textile effluents, due to their ability to interact with the dye, which occurs in a way that the ions present on the polymer chains interact with the ions of the dye, leading to an electrostatic interaction [6]. In this perspective, the objective of this work is the synthesis of hydrogels based on products derived from renewable and/or sustainable sources and evaluates their capacity to adsorb the cationic dye crystal violet in aqueous medium, aiming their application in effluent treatment of the textile industry.

Experimental

Synthesis and characterization of poly(oligoglycerol maleate) precursor

Previously to the synthesis of poly(oligoglycerol maleate), the macromonomer oligoglycerol was synthesized. The reaction was carried out in a microwave reactor operating a maximum power of 200 W at 100 °C for 20 min under catalysis of 1 wt.% of sodium carbonate, as shown in Fig 1. Afterwards, the oligoglycerol obtained was reacted with malic acid and 2 mol% of tin (II) chloride to obtain the hydrogel precursor (Fig 1). In a first moment, the reaction was conducted in an oil bath at 150 °C for 3 h under a nitrogen atmosphere, followed by a step of reduced pressure of 100 mbar for 4 h. The macromonomer and precursor were characterized to determine their structures by hydrogen nuclear magnetic resonance (^{1}H NMR) and Fourier-transform infrared spectroscopy (FTIR).

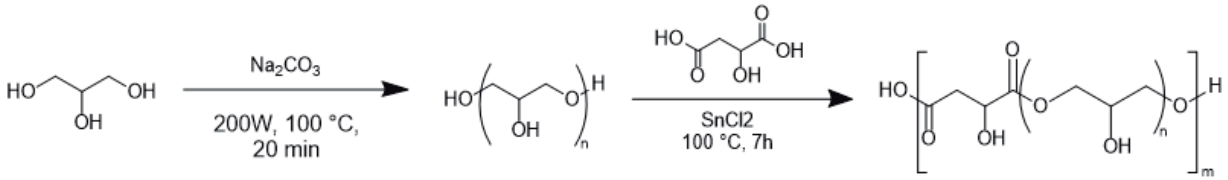

Figure 1. Scheme of the synthesis of oligoglycerol and poly(oligoglycerol maleate) precursor.

Synthesis and characterizations of hydrogels

In a round bottom flask, poly(oligoglycerol maleate) and different amounts of citric acid (10, 15 and 20 mmol/g of precursor) were reacted using tin (II) chloride as a catalyst. The reaction was carried out in an oil bath heated to 150 °C for 3 h under a nitrogen atmosphere. After this period, the system pressure was reduced to approximately 100 mbar and the reaction was continued until the product vitrified. The resulting hydrogels were obtained as yellowish rigid solids, which were subsequently washed with deionized water and lyophilized to remove the soluble content. The hydrogels were structurally characterized through FTIR and in relation to their water uptake capacity and soluble content values. The hydrogels were nominated PMO-CA20, PMO-CA15 and PMO-CA10, in relation to the concentration of citric acid used.

Evaluation of crystal violet dye adsorption capacity

The crystal violet dye adsorption experiments were conducted to investigate the capacity of the synthesized hydrogels to remove cationic compounds from aqueous solutions. For this purpose, approximately 0.2 g of hydrogel were immersed in different solutions of crystal violet dye (CV) with a concentration of 10 ppm. At specific time intervals, the residual concentration of the dye was measured by ultraviolet-visible spectroscopy (UV-Vis). These measurements made it possible to determine the percentage of cationic dye adsorbed by the hydrogels. Furthermore, the adsorption kinetics was evaluated using a pseudo-second order mathematical model. (Eq. 1)

$$\frac{t}{Q_t} = \frac{1}{k_2 {Q_e}^2} + \frac{t}{Q_e} \quad (1)$$

where t is contact time, Qt is the amount of dye adsorbed at time t, Qe is the amount of dye adsorbed at equilibrium and k_2 is the pseudo-second order adsorption rate constant.

Results and Discussion

Synthesis and characterization of poly(oligoglycerol maleate) precursor

The synthesis of oligoglycerol macromonomer and the precursor were successfully conducted. The macromonomer was obtained with good yield and the purity of the compounds allowed their use in the polymerization reactions for the hydrogels preparation. Analyzing the ^{1}H NMR spectra it is

possible to confirm the synthesis of the two compounds (Fig. 2). For the oligoglycerol macromonomer, signals in 3.64-3.60 ppm for $1H_a$, in 3.50 ppm for $2H_{a,c}$, in 3.40 ppm for $2H_{a,c}$. As for the poly(oligoglycerol maleate) precursor, there are observed signals in 4.53 ppm for H of terminal group derived from malic acid, in 4.49 for $1H_e$, in 4.14-3.95 ppm and in 3.84-3.78 ppm for H of terminal group derived from oligoglycerol linked to malic acid, in 3.59 ppm for $6H_b$, in 3.51-3.41 ppm for H of terminal group derived from oligoglycerol, 3.46 ppm for $12H_{a,c}$, in 3.37 ppm for $12H_{a,c}$, in 2.82 ppm for H of terminal group derived from malic acid and in 2.75 for $2H_d$, confirming the synthesis.

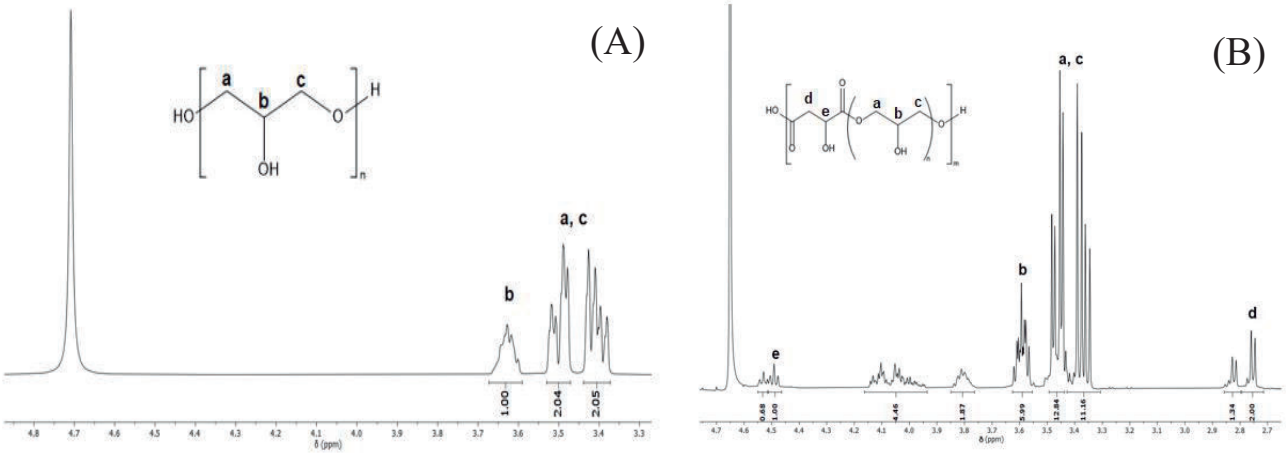

Figure 2. ^{1}H NMR spectra for the oligoglycerol macromonomer (A) and poly(oligoglycerol maleate) precursor (B).

Synthesis and characterizations of hydrogels

In relation to the synthesis of hydrogels, the Fig. 3 shows the FTIR spectra for the different samples, which exhibit similar spectral profiles. An intense and broad band at around 3400 cm^{-1} is attributed to the stretching vibration of the -OH bond, characteristic of the presence of hydroxyl groups. The stretching vibration of the C=O bond can be observed at approximately 1730 cm^{-1}, while the C-C bond stretching vibration is observed at 1190 cm^{-1}. These observations suggest that there was a structural change in relation to the polyester, as evidenced by modifications in the band patterns. Furthermore, a decrease in the intensity of the hydroxyl band is observed due to crosslinking between the polyester chains, which is carried out through the free -OH groups present in the precursor structure, proving the crosslinking reactions.

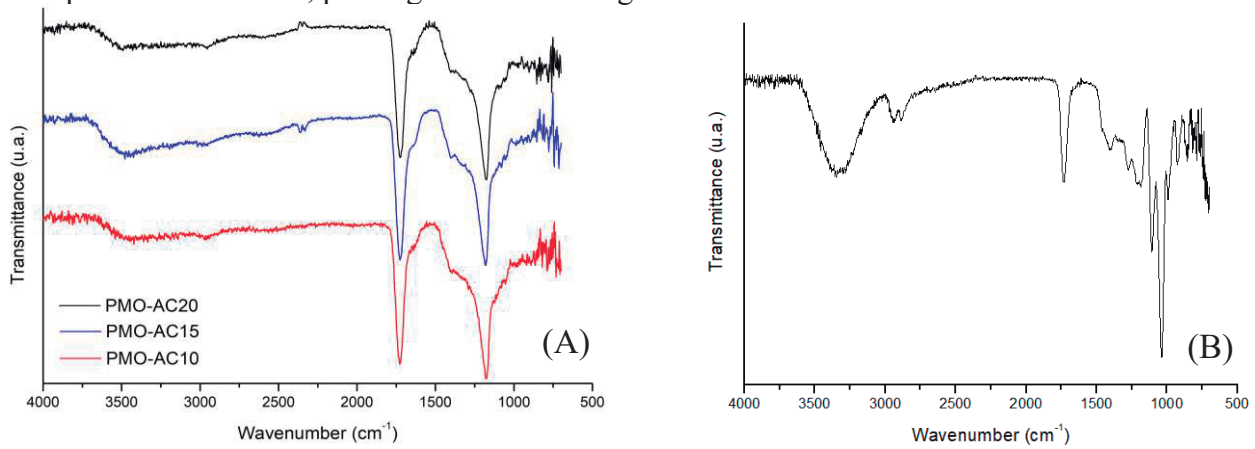

Figure 3. IV-ATR spectra for PMO-AC20, PMO-AC15 and PMO-AC10 hydrogels (A), and poly(oligoglycerol maleate) (B).

The water uptake capacity and the soluble content of the hydrogels also were evaluated, and the Table 1 presents the results for the different hydrogels. As the proportion of crosslinker used

increases, the water absorption content also increases, indicating that the presence of carboxylate ions is important for this effect. On the other hand, the soluble content also increases, since the excess of citric acid in the medium is higher, and the unreacted crosslinker solubilize in water during the washing step.

Table 1. Water uptake capacity and soluble content for the PMO-AC20, PMO-AC15, and PMO-AC10 hydrogels.

Sample	Crosslinker ratio (mmol citric acid/g polyester)	Water uptake content (%)	Soluble content (%)
PMO-AC20	20	888.7 ± 53.7	37.8 ± 1.2
PMO-AC15	15	615.1 ± 40.1	25.2 ± 6.1
PMO-AC10	10	187.2 ± 57.8	17.6 ± 0.3

In addition, the different hydrogels were evaluated in relation to their ability to adsorb ionic dyes, in order to simulate their applicability in the treatment of textile industrial effluents. For this purpose, each hydrogel was put into contact with solutions of the cationic crystal violet (VC) dye and analyzed over time using UV-Vis technique. The obtained adsorption values are presented in Table 2 and Fig 4a.

Table 2. Percentage of VC dye adsorption at 5 h and 24 h for the PMO-AC20, PMO-AC15, and PMO-AC10 hydrogels.

Hydrogel	Adsorption in 5 h (%)	Adsorption in 24 h (%)
PMO-AC20	67.0 ± 12.9	84.3 ± 10.3
PMO-AC15	74.8 ± 9.6	90.4 ± 5.8
PMO-AC10	86.7 ± 1.2	94.2 ± 0.6

The adsorption data indicate that almost 100% adsorption occurs in 24 h. The behavior can be explained by the fact that the dye is cationic and undergoes a strong interaction with the citrate portion present in the hydrogel. Regarding the adsorption mechanism, it is observed that the behavior is very similar among the different samples, where at the eighth hour of the assay, a plateau is reached. Furthermore, when comparing the different hydrogels, they present a similar performance, but the hydrogel with the best result is PMO-AC10, which has both the highest proportion of VC adsorption and the fastest mechanism. This may be mainly related to its low water uptake, with less competition within the hydrogel channels and with carboxylate ions.

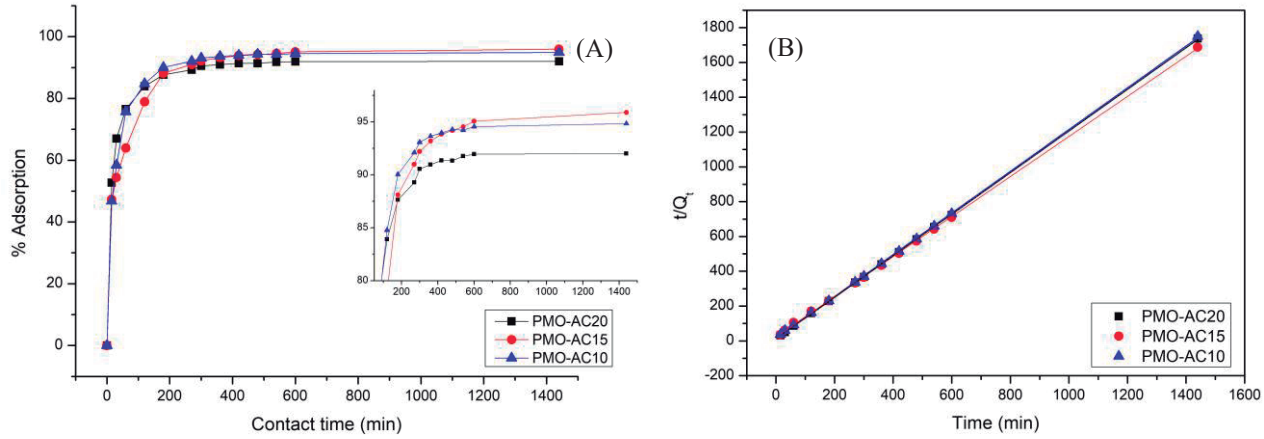

Figure 4. Adsorption profile of the cationic dye VC obtained from the kinetics as a function of contact time with the hydrogels (A) and pseudo-second order kinetic fitting for different hydrogels in contact with VC dye (B).

Additionally, a kinetic study was performed in order to determine the mechanism of adsorption of the hydrogel. For this, a pseudo-second order model was employing, and the results are presented in Table 3 and Fig 4b.

Table 3. Data obtained for pseudo-second order kinetic adjustment for PMO-AC20, PMO-AC15, and PMO-AC10 hydrogels and VC dye.

Hydrogel	k_2 (g mg.min^{-1})	R^2	Q_e theoretical (mg g^{-1})	Q_e experimental (mg g^{-1})
PMO-AC20	0,12317	0,99994	0,83718	0,82902
PMO-AC15	0,05750	0,99979	0,86875	0,85306
PMO-AC10	0,09547	0,99989	0,83396	0,82328

For the VC dye, the hydrogels behave according to a pseudo-second order mechanism, as they present R^2 values very close to unity and theoretical Q_e values also very close to experimental values. In this mechanism, the limiting step is the chemical adsorption, where there are intermolecular forces between the dye and the hydrogel. This theory supports the proposal that the cationic dye interacts with the citrate portion of the hydrogel, thus forming ionic bonds between the species and adsorbing the dye to a greater extent. Furthermore, the contact time and chemical structure also influenced the adsorption process.

Conclusions

In this work, a family of sustainable hydrogels with potential applicability on the removal of the cationic dye crystal violet, which is commonly used in the textile industry, was efficiently developed. Different bio-based monomers and a natural crosslinking agent were used to obtain a low-cost material with high added value. The hydrogel crosslinked with 20 mmol of citric acid showed the highest water uptake capacity and soluble content. However, an inverse behavior to water absorption was observed for dye adsorption, where the hydrogel with the highest water absorption capacity showed the lowest dye adsorption. The hydrogel crosslinked with 10 mmol of citric acid was capable of adsorbing 94% of the cationic dye VC present in the solution. Regarding the adsorption kinetics, the determined mechanism was pseudo-second order, where the contact time and the chemical structure influenced the adsorption.

Acknowledgements

The authors are grateful to Conselho Nacional de Desenvolvimento Científico e Tecnológico (CNPq) and Fundação de Amparo à Pesquisa do estado do Rio Grande do Sul (PRONEX/FAPERGS - Finance Code 16/2551-0000470-6) for financial support.

References

1. UNESCO. *The United Nations World Water Development Report 2018: Nature-Based Solutions for Water*; United State Environmental Protection Agency: Paris, France, 2018.
2. Ahmed, Enas M; Journal of Advanced Research, 2015, 6, 105-121. https://doi.org/10.1016/j.jare.2013.07.006
3. Mendonça, Fernanda; Menezes, Izadora; Silva, Ingrid; Lago, Rochel; New Journal of Chemistry, 2021, 45, 2410-2416. https://doi.org/10.1039/D0NJ06138G
4. Chyzy, Adam; Plonska-brzezinska, Marta E; Molecules, 2020, 25, 5795. https://doi.org/10.3390/molecules25245795
5. Asadi, Safoura; Eris, Setareh; Azizian, Saeid; ACS Omega, 2018, 3, 15140-15148. https://doi.org/10.1021/acsomega.8b02498
6. Van tran, Vinh; Park, Duckshin; Lee, Young-Chul. Environmental Science and Pollution Research, 2018, 25, 24569-24599. https://doi.org/10.1007/s11356-018-2605-y

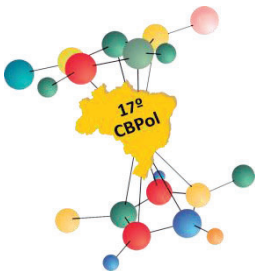

SYNTHESIS OF LYSINE DERIVATIVE SURFACTANTS AND APPLICATION IN POLYSTYRENE EMULSION POLYMERIZATION

Leonardo Zborowski, Cesar Liberato Petzhold

Department of Organic Chemistry, Institute of Chemistry, Federal University of Rio Grande do Sul
leonardo.zborowski@gmail.com; petzhold@iq.ufrgs.br

Abstract – Amino-acid based surfactants present several advantages such as possibility of using renewable resources and similar chemical structures to natural surfactants. These chemicals can be applied in a plenty of uses, including particles synthesis. This work reported the synthesis of lysine-derivative surfactants and their use in emulsion polymerization of styrene. Chemicals from renewable resources was employed for the synthesis of surfactants. The most important barrier in the proposed synthetic route is the amidation of lysine with stearic acid, which conversion was 80%. In emulsion polymerization, monomer conversion was higher when used stearyl-lysinate sodium salt as surfactant. The formulation with stearyl-lysinate ester presented higher difficulty to dispersion and, consequently, lower particle formation. Through SEC measurements, both polystyrene obtained with lysine-surfactants exhibited broader molar-mass distribution than SDS one.
Keywords: *Fatty Amides, Renewable Resources, Lysine Surfactant, Emulsion Polymerization.*

Introduction

As the demand for ecologic routes to obtain chemicals increased, one option that expanded in last decades is use of renewable resources, including aminoacid surfactants. This possibility was opened due to the similarity of the chemical structure of these surfactants with natural surfactants, in addition to the availability and variety of raw materials for their production [1] Aminoacids surfactants can be obtained via chemical and/or biochemical processes and present applications in agriculture, medicine, drug delivery, cosmetics, antimicrobiant agent, food industry [2-5]. Besides, a potential application of this sort of surfactant includes particle synthesis [6-8]. There are a reduced number of reports related to use of amino-acid-based surfactants in polymerization process. In order to reduce this lack, this work reported the use of lysine-derivative surfactants in emulsion polymerization of styrene.

Experimental

Materials

Lysine monochloridrated from Dinâmica Química, stearic acid from Synth, ethanol from Química Moderna, hydrochloric acid from Neon, sodium hydroxide from Nuclear, sodium fluoride from Merck, aluminium oxide from ACROS Organics, styrene from INNOVA, sodium dodecyl sulphate from Sigma-Aldrich, ammonium persulphate from TCI, deionized water.

Synthesis of Lysine Surfactants

2.50 g (13.687 mmol) of Lysine was esterified with ethanol and addition of hydrochloric acid in order to warranty reaction of aminoacid carboxylic group to protect this group. After the first reaction, esterified lysine was reacted with sodium hydroxide in ethanol to deprotonate the amine

groups and conditionate them to promote amidation with stearic acid. Amidation parameters: 110°C, 6 hours, inert atmosphere, sodium fluoride as catalyst, aluminium oxide to absorb water which is amidation subproduct, based on literature [9]. After this, stearyl-lisinate ester reacted with sodium hydroxide ethanolic solution. Scheme with the reactions sequence is exhibited in Fig.1.

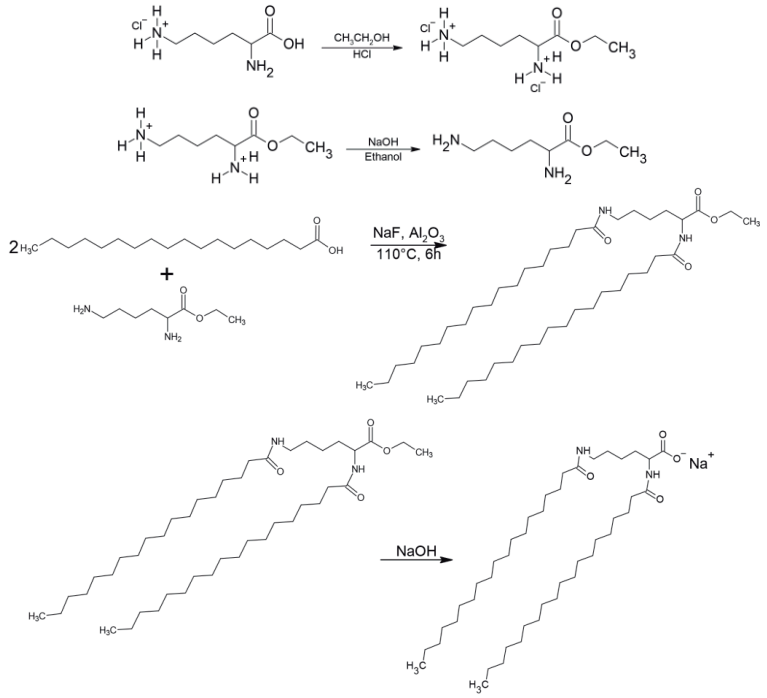

Figure 1 – Synthesis of Lysine surfactants.

Emulsion Polymerization

Emulsion Polymerization was carried in an EasyMax 102 minireactor from Mettler Toledo. Formulation included deionized water, initiator, surfactant and monomer. In all formulations, surfactant amount was equivalent to six times the necessary to obtain solution concentration equal to critical micelar concentration (CMC). Furthermore, initiator quantity was 0.050 g (0.2191 mmol), styrene volume was 15 mL and deionized water, 60 mL. Firstly, at room temperature, it was prepared solution with water, initiator and surfactant. After this step, solution was fed to the minireactor with monomer and the mixture was stirred at 400 rpm without heating during 10 minutes, at inert atmosphere, in order to start the dispersion. Then, minireactor was heated up to 80°C and the reaction time, 4 hours, started to be accounted. After the reaction time, minireactor temperature was reduced up to 25°C to interrupt the polymerization.

Characterization of lysine surfactants, lattices and polymer

Conversion from L-lysine to lysine surfactants was detrermined gravimetrically. Lysine surfactants were characterized in their critical micellar concentrations (CMC) via K6 tensiometer, from Krüss. Lattices were characterized in terms of conversion via solids content measurement and mean particle diameter. Solids content was measured gravimetrically, according to literature [10]. Mean particle diameter measurements were obtained using a DLS BrookHaven Instruments spectrophotometer (BI) 9000. After lattices characterization, solid polymer of each used formulation was analyzed via SEC, using a Viscotek GPC, model VE2001, with Viscotek TDA 302 triple detector array, Shodex pre-column (KF-G 4A) and four Shodex columns (KF806).

Results and Discussion

In lysine-derivative surfactants synthesis, the step which was revealed as main barrier to reagents conversion is amidation. This reaction conversion was 80%. In all other reactions, conversion was higher than 95%. Table 1 shows CMC values of synthesized surfactants. It is observed that sodium salt surfactant presented higher CMC value than ester surfactant. This occurs due to the existing electrostatic work due to the ionic polarity of these molecules [11]. Thus, CMC value order is: stearyl-lisinate ester < Stearyl-lisinate sodium salt < Sodium Dodecyl Sulphate.

Table 1 – CMC values of sodium dodecyl sulphate and synthesized lysine-derivative surfactants.

Surfactant	CMC (M)
Sodium Dodecyl Sulphate	8.10×10^{-3}
Stearyl-lisinate ester	1.76×10^{-5}
Stearyl-lisinate sodium salt	3.10×10^{-4}

Solids content measures, indirectly, monomer conversion to polymer. Table 2 presents values of solids content of the formulations used in this report. The highest value was obtained when the surfactant in the formulation was sodium dodecyl sulphate. It is observed that the increase on the monomer conversion follows the trend of CMC values increase. Besides lower solids content, lattice of stearyl-lisinate ester formulation exhibited lower stability, possibly due to electrostatic forces in the ionic surfactant which increment emulsion stability. One detail is lower monomer conversion of both formulations with lysine-derivatives surfactant in comparison to sodium dodecyl sulphate formulation.

Table 2 – Solids content and styrene conversion.

Surfactant	Solids content	Conversion (%)
Sodium Dodecyl Sulphate	18	99
Stearyl-lisinate ester	5	27
Stearyl-lisinate sodium salt	11	62

Table 3 showed mean diameter particles distribution of the lattices. It has been noticed an inverse order on mean particle order. Lattice with formulation using lowest value of CMC surfactant presented largest particle diameter. This fact can indicate higher difficulty on particles formation related to a non-ionic surfactant and reduced dispersion capacity of stearyl-lisinate ester surfactant in comparison to stearyl-lisinate sodium salt surfactant. It was also noticed that both lysine-derivative surfactants showed more difficulty in particles formation than sodium dodecyl sulphate.

Table 3 – Mean diameter particles of the particles diameter.

Surfactant	Diameter (nm)
Sodium Dodecyl Sulphate	64
Stearyl-lisinate ester	707
Stearyl-lisinate sodium salt	524

SEC chromatograms (Fig. 3) demonstrated a broader molar mass distribution for polystyrene obtained from lattice formulation with lysine-derivative surfactants in comparison to the obtained from sodium dodecyl sulphate formulation. In the case of polystyrene from stearyl-lisinate sodium salt formulation, polydispersity index value surpassed 20. One fact that can justify reduction of initiator efficiency is the presence of two hydrophobic tails on lysine-derivative surfactants, which tends to interact with styrene and only one hydrophilic head, independently of ionic character of the surfactant. Thus, free radicals generated in aqueous phase tend to remain in the water. On the other

hand, it is more difficult to radicals penetrate in the micelle. This behavior can be evidenced by solids content and molecular-weight distribution curves. However, there is possibility of increase monomer conversion, $\overline{M_n}$ and reduce polydispersity index via optimization of reaction processes, such as surfactant and initiator content.

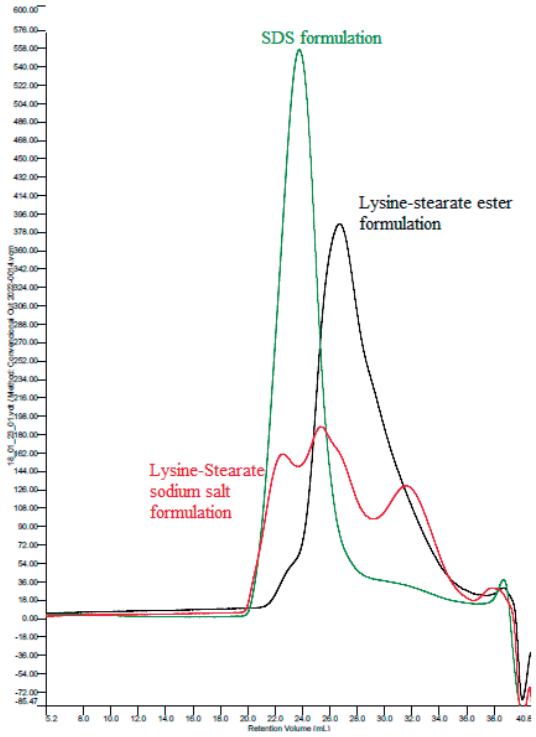

Figure 2 – SEC chromatograms of resulting lattices.

Table 4 – Molecular weight of resulting polymer of formulations.

Surfactant	$\overline{M_n}$ (Da)	$\overline{M_w}$ (Da)	PDI
Sodium Dodecyl Sulphate	316000	767000	2.4
Stearyl-lisinate ester	20000	104000	5.2
Stearyl-lisinate sodium salt	19000	494000	26.4

Conclusions

Lysine-derivative surfactants were synthesized in a chemical route used reagents which can be obtained from renewable resources. After synthesis, they were employed in emulsion polymerization of styrene. Stearyl-lisinate sodium salt was more efficient in formulation than stearyl-lisinate ester. Although polymerization occurred, it is necessary improve process parameters in order to obtain polystyrene with higher value of $\overline{M_n}$ and narrower molecular weight distribution.

Acknowledgements

Authors would like to acknowledge Laboratory of Mineral and Environmental Technology of UFRGS for permission of use of tensiometer.

References

1. R. Bordes, K. Holmberg Adv. Colloid Interface Sci. 2015, 222, 79-91. https://doi.org/10.1016/j.cis.2014.10.013

2. D. B. Tripathy, A. Mishra, J. Clark, , T. Farmer C. R. Chimie 2018, 21, 112 – 130. https://doi.org/10.1016/j.crci.2017.11.005
3. M. Zhang, S-X. Zhao, B. Ding, Y-Q. Zhang Drug Delivery 2020, 27, 482 – 490. https://doi.org/10.1080/10717544.2020.1742250
4. C. Faustino, T. Martins, N. Duarte, M. H. Ribeiro, J. Surfact. Deterg. 2020, 23, 581 – 593. https://doi.org/10.1002/jsde.12391
5. J. Coronel-León, A. Pinazo, L. Pérez, M. J., Espuny, A. M., Marqués, A., Manresa Colloids Surf. B Biointerfaces 2017, 149, 38 – 47. https://doi.org/10.1016/j.colsurfb.2016.10.008
6. E-M. Rosenbauer, A. I. Triftaridou, S Karpati, F. Tournilhac, L. Leibler, S. Auguste, J-M. Pernot Polym. Chem. 2012, 3, 2178 – 2185. 10.1039/c2py20278f
7. L. C. Preiss, M. Wagner, Y. Mastai, K. Landfester, R. Muñoz-Espí Macromol.Rapid Commun. 2016, 37, 1421 – 1426. 10.1002/marc.201600210
8. N. Judge, D. Pavlović, E, Moldenhauer, P. Clarke, R. Brannigan, A. Heise Polym. Chem. 2022, 13, 2822 – 2830. 10.1039/d2py00331g
9. S.M.S. Hussain, M. S. Kamal, T. Solling, M. Murtaza, L. T. Fogang, RSC Adv., 2019, 9, 30154 – 30163. 10.1039/c9ra06577f
10. L. Zborowski, D. Porto, J. R. Taparelli, L. H. I. Mei Chem. Res. J. 2020, 5, 35-42.
11. F. K. G. Santos, J. V. A. Alves, T. N. C. Dantas, A. A. Dantas Neto, T. D. Dutra Jr., E. L. Barros Neto in Proceedings of 4th PDPETRO, Campinas, 2007, Vol. 2.1.72, 1-9.

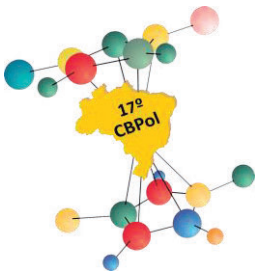

SYNTHESIS OF STYRENE-TMPTA ACIDIC RESIN AND ITS APPLICATION AS A CATALYST IN THE GLYCEROL ACETYLATION

William M. Godoy[1], Giovanna C. Lima[1], Leandro G. Aguiar[1]*, Nuno A. B. S. Graça[2] and Alírio E. Rodrigues[2]

1 – Department of Chemical Engineering, Engineering School of Lorena, University of São Paulo (USP), São Paulo, SP, Brazil Corresponding author: williammendes@usp.br
2 – LSRE-LCM, Associate Laboratory ALiCE, Department of Chemical Engineering, Faculty of Engineering, University of Porto (FEUP), 4200-465 Porto, Portugal

Abstract – The aim of this work was to study the influence of the synthesis of different formulations of STYRENE-TMPTA and assess its applications as a catalyst in the glycerol acetylation reaction. To synthesize the resins and evaluate their structure, a factorial design was proposed, varying the percentage of crosslinker (2, 6 and 10%) and the crosslinker feed time (30, 150 and 270 minutes). The methodology used consisted, firstly, in synthesizing the copolymer particles, sulfonating them, finding the ion exchange capacity and performing catalytic tests. The resin with the lowest crosslinking percentage (2%) and the longest TMPTA feeding time (270 minutes) achieved the highest glycerol conversion (90%) and highest catalytic efficiency (206), thus demonstrating that the structure of the catalyst (a consequence of the formulation and procedure) affects its catalytic activity. Based on the obtained results, it is concluded that, despite the synthesized resin presents a low ion exchange capacity, the polymeric particles formed with low concentrations of TMPTA, favored the use of this resin as a catalyst in the glycerol acetylation reaction.

Keywords: resins, *TMPTA, copolymer, catalysis and catalytic efficiency*

Fundings: This research was financially supported by the São Paulo Research Foundation (FAPESP) under grant numbers 2020/08631-3 and 2021/10350-5, and also by LA/P/0045/2020 (ALiCE), UIDB/50020/2020 and UIDP/50020/2020 (LSRE-LCM), funded by national funds through FCT/MCTES (PIDDAC).

Introduction

In recent decades, ion exchange resins have been applied as catalysts in various organic reactions, such as esterification [1], etherification [2], acetylation [3], transesterification [4], among others. Among the most used polymeric resins, one can mention resins formulated from styrene cross-linked with divinylbenzene, as shown by the commercial lines such as Amberlyst and Dowex [5]. However, recent studies have shown that resins formulated from styrene with divinylbenzene present certain regions containing inaccessible sites to the reaction medium, causing a loss of catalytic performance of the resins [6]. On the other hand, according to the literature, resins with low densities of divinylbenzene present greater flexibility in their polymeric structure, favoring the morphology of the resin for catalytic applications [7], as this allows for a greater number of catalytic sites to be accessible to the reaction medium. This study consisted of an experimental design to investigate the influence of trimethylolpropane triacrylate (TMPTA) as a cross-linker and the effect of cross-linking density on the resin catalytic efficiency in the glycerol acetylation.

Experimental

Catalyst synthesis

For the catalyst synthesis, the system of suspension copolymerization was carried out according to a procedure described in the literature [8,9], with modifications. The crosslinker was fed at specific reaction times. Suspension copolymerization was performed in a 1 L jacketed glass reactor at 80 °C and 350 rpm for 6 h. The reactor was fed with a mixture of organic (11.5 vol%) and aqueous (88.5 vol%) phases. The aqueous phase consisted of a solution of polyvinyl alcohol (0.0038% w/v) in water. The solution was purged with nitrogen gas (15 mL min-1) for 1 h, and then the organic phase was fed into the reactor. The organic phase consisted of a mixture of 1 mol% benzoyl peroxide (initiator) relative to the monomer mixture (styrene + TMPTA), different fractions of TMPTA in the monomer mixture (0.02, 0.06 and 0.10), 30 vol% monomers in the organic phase, and 50% toluene in the solvent mixture (toluene + heptane). The cross-linker (TMPTA) was fed into the reactor at pre-defined times.

After resin synthesis, the sulfonation process was carried out according to the literature [3,10]. Ten grams of dried resin was added to concentrated sulfuric acid (140 mL) at 57 ◦C, and the content was kept under stirring at 175 rpm for 1 h. Subsequently, the mixture (resin + sulfuric acid) was diluted in distilled water at 25 °C and filtered. The sulfonated resin was extensively washed to remove all residual acid and oven-dried at 50 °C to constant weight. All procedure for synthesis and application of catalyst, are explained in the scheme below.

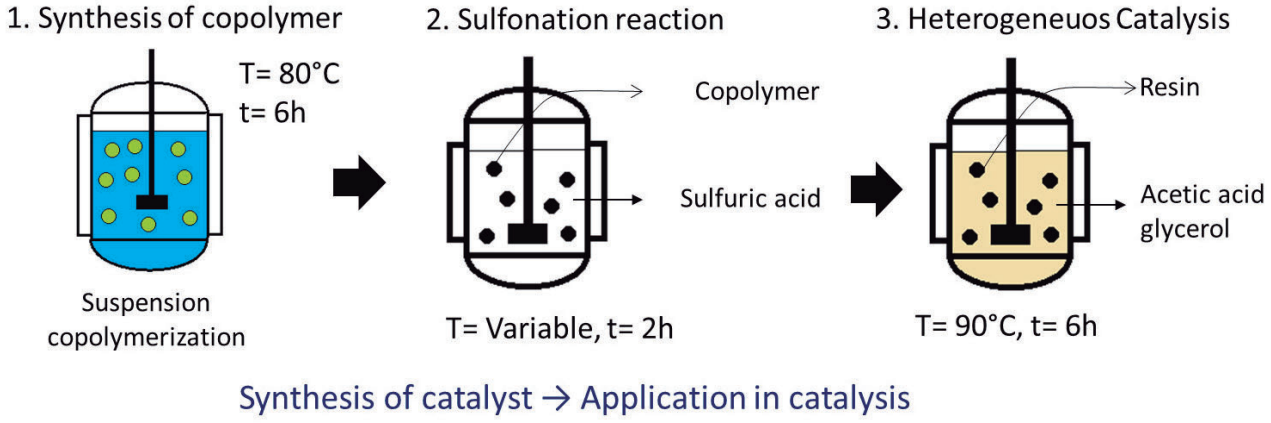

Figure 1 - Process for synthesis and application of a polymer catalyst. The glycerol acetylation was carried out with 4:1 of acetic acid / glycerol molar ratio, 40 g L^{-1} of catalyst concentration, at 90 °C under magnetic stirring for 6 hours.

After the studies in the batch reactor, a fixed bed reactor was tested with the synthesized catalyst. The reactor dimensions are: 20 cm of length and 3 cm of diameter. The results and experimental conditions are detailed in Fig.3

Catalysts characterization

To characterize the synthesized catalysts, three analysis methods were adopted, namely: ion exchange capacity, swelling index and turnover number, as described in literature [9,11].

For ion exchange capacity, 0.5 grams of dry resin was weighed and placed in contact with nitric acid (8 mL, 1M) for 4 hours. Subsequently, the resins were filtered and taken to the oven until constant mass was obtained. After constant mass, the resins were placed in contact with 30 mL of NaOH solution (0.1M), remaining in contact for 24 hours. At the end of 24 hours, the NaOH solution was titrated with HCl solution (0.1M). The titrated volume was calculated and then the ion exchange capacity was found.

For swelling index, the calculation was based on the moister mass of resin, in the end of reaction, divided by dry mass in the beginner of reaction.

The catalytic efficiency was calculated by the number of mols of consumed glycerol divided by amount of catalytic sites of resins (ion exchange capacity multiplied by the mass of catalyst) at a determined time.

Results and Discussion

After the synthesis resins, proposed analysis was performed and the resins was tested as a catalyst in the glycerol acetylation reaction. Results are presented in Table 1.

Table 1 - Glycerol conversion and catalytic effciency of polymer resins.

Resin	Y_{TMPTA}	T_{TMPTA} (min)	IEC (mmol g^{-1})	X_G (%)	Ton (min^{-1})
S1	0.10	30	0.585	86	98
S2	0.10	150	0.540	66	90
S3	0.10	270	0.540	63	87
S4	0.06	30	0.418	78	173
S5	0.06	150	0.641	72	83
S6	0.06	270	0.537	88	181
S7	0.02	30	0.357	64	147
S8	0.02	150	0.413	34	84
S9	0.02	270	0.411	90	206

Y_{TMPTA}, cross-linker content; T_{TMPTA}, cross-linker feed time; IEC, ion-exchange capacity. Conversions and turnover number calculated from glycerol content at 1 h of reaction. Reaction conditions (acetic acid/glycerol molar ratio of 4:1, 90 °C, and 40 g L^{-1} catalyst).

Analyzing Table 1, it is possible to verify that experiments S1, S6 and S9 presented higher conversions at 1 hour of reaction. However, the calculation of catalytic efficiency shows us which resins provided better catalytic performances. Considering the results of catalytic efficiency, it is possible to verify that experiment S9 presented better catalytic performance, since it was the experiment with the lowest ion exchange capacity and the highest glycerol conversion (90%).

In order to assess the behavior of catalytic efficiency on the limit crosslinker percentages (2 and 10 %), the catalytic efficiencies along the reaction time of experiments S3 and S9 were compared, as shown Fig. 2.

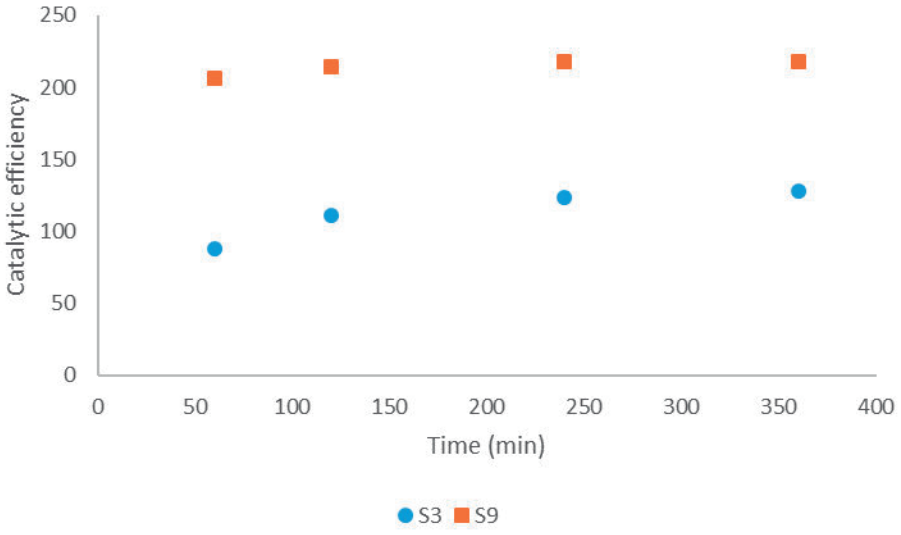

Figure 2 - Catalytic efficiency along the reaction time of experiments S3 and S9.

According to Fig.2 it is possible to verify the effect of polymeric structure on the catalytic efficiencies of resins, since polymer network with higher crosslinker (TMPTA) contents tend to present tighter structure [12], consequently reducing the accessibility to catalytic sites. Such behavior shows that the structure of the copolymer affects the catalytic performance of resin.
Regarding the swelling index of the resins, around 1.32, there was no considerable variation, thus demonstrating that the crosslinking fraction under these conditions was not an influential factor for this analysis.
In order to assess the behavior of the resins on industrial experimental condition simulation, a new catalyzed reaction was carried out in a tubular reactor with recycle. The chosen's resin was S9 that presented better catalytic performance in the batch reactor. The results are shown in Fig.3.

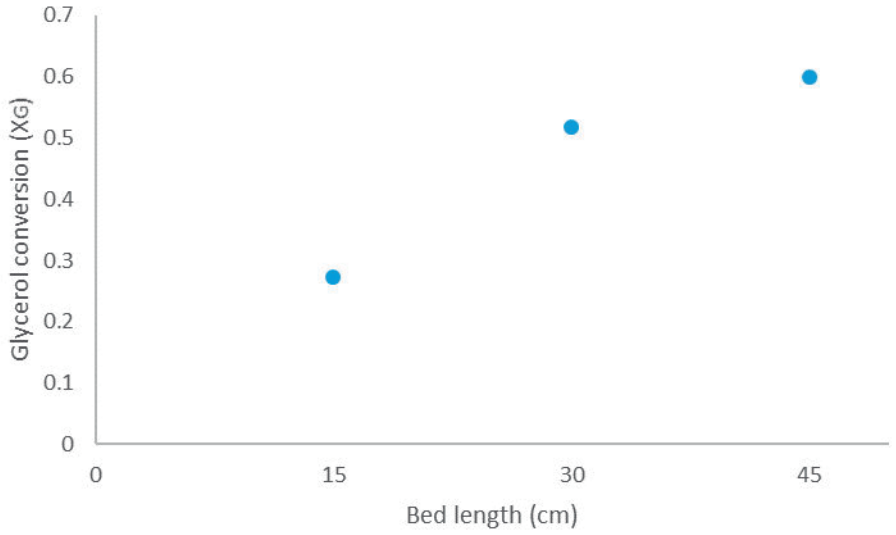

Figure 3 - Glycerol acetylation with resin S9 at 90 ° in a tubular reactor with recycle. Experimental conditions: 46 grams of catalyst; 25 mL / min of flow rate; 425 mL of reactor volume and 3 – 5 mm particle size.

Fig. 3 shows an expected behavior for reactions carried out in a tubular reactor. With the first pass of the reaction medium, the glycerol conversion, around 15 cm of bed length, reaches equilibrium with 27% of conversion. In the second cycle of the reaction medium (second pass), the glycerol conversion reaches a level around 52% of conversion considering 30 cm of bed length. In the interval from 30 to 45 cm (third pass), the conversion still increases gradually reaching, as in the first passes, a new level of conversion, around 60% of glycerol conversion.
Considering the residence time of each step (around 17 minutes) and the glycerol conversion reached (27, 52 and 60 %) for each cycle, these results lead to concluded that this type of resin and reaction medium is viable for industrial application, since continuous equipment is attractive for industrial field.

Conclusions

Acidic resins were synthesized from styrene-TMPTA under different percentages and crosslinker feed times (TMPTA) and tested as catalysts in the glycerol acetylation reaction. A factorial design was carried out for the synthesis of the resins and the resin that presented the best results was the one formulated with the smallest fraction of crosslinker (2%) fed in the time of 270 minutes. It was found, according to the results presented, that the catalytic efficiency decreased with the increase in the crosslinking percentage, which was expected, since denser resins tend to be more rigid, hindering the flow of compounds (reagents and products), consequently, hindering the accessibility to the catalytic sites. The swelling index, in this study, did not vary significantly with the variation

in the percentage of TMPTA, nor with the feeding time of the crosslinker to the reactor. Catalytic tests were carried out in a tubular reactor and the results found were satisfactory, with 60% of glycerol conversion around 51 minutes of reaction time. Despite the low ion exchange capacities produced under the sulfonation conditions studied herein, styrene-TMPTA resins show attractive accessibility when applied as catalysts.

References

1. Dalla Costa, B.O.; Decolatti, H.P.; Legnoverde, M.S.; Querini, C.A. Influence of Acidic Properties of Different Solid Acid Catalysts for Glycerol Acetylation. *Catal. Today* **2017**, *289*, 222–230, doi:10.1016/j.cattod.2016.09.015.
2. Bagheri, S.; Julkapli, N.M.; Yehye, W.A. Catalytic Conversion of Biodiesel Derived Raw Glycerol to Value Added Products. *Renew. Sustain. Energy Rev.* **2015**, *41*, 113–127, doi:10.1016/j.rser.2014.08.031.
3. Godoy, W.M.; Carpegiani, J.A.; Pereira, F.M.; Guimarães, D.H.P.; Aguiar, L.G. Kinetic Modeling of Glycerol Acetylation Catalyzed by Styrene–Divinylbenzene and Styrene-Trimethylolpropane Triacrylate Sulfonated Resins. *React. Kinet. Mech. Catal.* **2022**, *135*, 233–245, doi:10.1007/s11144-021-02141-2.
4. Witoon, T.; Bumrungsalee, S.; Vathavanichkul, P.; Palitsakun, S.; Saisriyoot, M.; Faungnawakij, K. Biodiesel Production from Transesterification of Palm Oil with Methanol over CaO Supported on Bimodal Meso-Macroporous Silica Catalyst. *Bioresour. Technol.* **2014**, *156*, 329–334, doi:10.1016/j.biortech.2014.01.076.
5. Chandane, V.S.; Rathod, A.P.; Wasewar, K.L.; Sonawane, S.S. Esterification of Propionic Acid with Isopropyl Alcohol over Ion Exchange Resins: Optimization and Kinetics. *Korean J. Chem. Eng.* **2017**, *34*, 249–258, doi:10.1007/s11814-016-0249-5.
6. Aguiar, L.G.; Godoy, W.M.; Nápolis, L.; Faria, R.P. V.; Rodrigues, A.E. Modeling the Effect of Cross-Link Density on Resins Catalytic Activities. *Ind. Eng. Chem. Res.* **2021**, *60*, 6101–6110, doi:10.1021/acs.iecr.1c00695.
7. Tejero, M.A.; Ramírez, E.; Fité, C.; Tejero, J.; Cunill, F. Applied Catalysis A : General Esterification of Levulinic Acid with Butanol over Ion Exchange Resins. *"Applied Catal. A, Gen.* **2016**, *517*, 56–66, doi:10.1016/j.apcata.2016.02.032.
8. Carpegiani, J.A.; Godoy, W.M.; Guimarães, D.H.P.; Aguiar, L.G. Glycerol Acetylation Catalyzed by an Acidic Styrene-Co-Dimethacrylate Resin: Experiments and Kinetic Modeling. *React. Kinet. Mech. Catal.* **2020**, doi:10.1007/s11144-020-01788-7.
9. Godoy, W.; Castro, G.; Nápolis, L.; Carpegiani, J.; Guimarães, D. Synthesis of Sulfonated Poly [Styrene-Co- (Trimethylolpropane Triacrylate)] and Application in the Catalysis of Glycerol Acetylation. **2020**, *1900169*, 1–7, doi:10.1002/masy.201900169.
10. Aguiar, L.G.; Moura, J.O.V.; Theodoro, T.R.; Neto, T.G.S.; Lopes, V.M.P.; Dias, J.R. Prediction of Resin Textural Properties by Vinyl/Divinyl Copolymerization Modeling. *Polymer (Guildf).* **2017**, *129*, 21–31, doi:10.1016/j.polymer.2017.09.042.
11. Boudart, M. Heterogeneous Catalysis by Metals. *J. Mol. Catal.* **1985**, *30*, 27–38, doi:10.1016/0304-5102(85)80014-6.
12. Godoy, W.M.; Aguiar, L.G.; Graça, N.A.B.S. Synthesis of Vinyl – Trivinyl Acidic Resins for Application in Catalysis : Statistical Study and Site Accessibility Assessment. **2023**, 1–14.

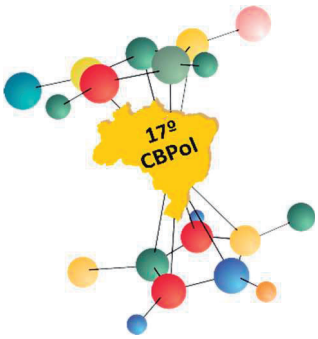

THERMAL DEGRADATION KINETICS OF TWO BRAZILIAN WOOD SPECIES: PART 1. THERMOGRAVIMETRY AND FWO METHOD

Matheus P. Andrade[1], Matheus Poletto[1], Ademir J. Zattera[1]

1 – PGEPROTEC, University of Caxias do Sul (UCS), Caxias do Sul, RS, Brazil mpandrade@ucs.br

Abstract - The thermal degradation kinetics of two Brazilian wood species have been studied, using three different heating rates (5, 10 and 15 °C.min^{-1}) under nitrogen atmosphere. Thermogravimetric analysis was performed and showed that *Andira surinamensis* (ASU) initiate its degradation at 276 °C and has its maximum degradation at 352 °C, while *Tabeuia ocracea* (TOC) presents its temperatures at 285 °C and 362 °C, respectively, showing a slightly higher thermal stability than ASU. Flynn-Wall-Ozawa (FWO) method were applied to evaluate the thermal degradation behavior of both wood species Through FWO method, ASU and TOC apparent activation energy (E_a) was determined, ranging 141-168 kJ.mol^{-1} and 168-189 kJ.mol^{-1} respectively. The results indicated that, TOC may need more energy to degrade than ASU, as showed by FWO method, being a more thermally stable material.
Keywords: Thermal degradation, FWO, kinetics, wood.

Introduction

Biomass has been one of the materials that has been receiving most attention from materials industry and researchers in the last few years [1–3]. One of the major reasons to this, is evolution of the global environmental awareness associated to the circular economy principle. Nevertheless, some biomass such as wood, have always played a key role on our economic model, but now the interest has grown. For instance, wood presents a good mechanical properties and relative low density, besides, can be a cheap and abundant waste from several industrial processes. Due to the large number of wood species, alongside with the fact of being a natural material, its properties can vary a lot, so knowing the properties of different species is fundamental to choose the right wood for each application [4–6].

With that, wood thermal properties can be a limiting depending on the desired application, so the understanding of the wood performance on higher temperatures as well as the thermal degradation behavior, is a subject of great importance [7–9]. Lignocellulosic materials have a heterogenic structure, mostly composed by three components: cellulose, hemicellulose, and lignin. Each one of them have specific characteristics and play a different role on wood properties [10,11]. Thermogravimetric analysis can help to understand the degradation of wood and its components, and with the aid of some auxiliar methodologies, such as the isoconversional method, with Flynn-Wall-Ozawa (FWO), Kissinger-Akahira-Sunose (KAS) and Friedman being some of the most popular in the literature [1,7,8]. With those methods the apparent energy activation (E_a) can be determined, however, FWO method enable the E_a calculation for each conversion (α), differently from the other two methods, that calculates only a general E_a.

Finally, the degradation kinetics of few wood species are well known and studied. However, for most of them, still not documented. In this work, the composition and degradation kinetics of two Brazilian

wood species, namely *Andira surinamensis* (ASU) and *Tabebuia ochracea* (TOC), were performed through termogravimetric analysis and an isoconversional method, namely FWO.

Experimental

Composition

The composition content of tree wood samples was measured. Wood extractives were determined based on TAPPI T204 cm-97 standards on an ethanol/benzene 1:2 solution. The Klason lignin were determined according to TAPPI T222 om-02. Humidity, cellulose, and hemicellulose for instance were determined based on Van Soest method.

Thermogravimetric Analysis

In the present work, two Brazilian wood species will be evaluated, *Andira surinamensis* (ASU) and *Tabebuia ochracea* (TOC). Samples of both wood species were provided by Madeireira Bianchi, Garibaldi/RS.

The samples were subjected to the thermogravimetric analysis (TGA). TGA were performed in a Shimadzu TGA-50 equipment, using a nitrogen atmosphere with flow of 50 $mL.min^{-1}$, starting from 25°C up to 800°C, with three different heating rates 5, 10 and 15 $°C.min^{-1}$.

Degradation Kinetics

The determination of the apparent energy activation was performed using Flynn-Wall-Ozawa (FWO) method, following Equation 1.

$$log\beta = \log\left[\frac{AE_a}{g(\alpha)R}\right] - 2.315 - 0.4567\frac{E_a}{RT} \quad (1)$$

Where β is the heating rate, A is the pre-exponential factor, g(α) is the function of the degree of conversion, R is the gas constant and E_a is the apparent activation energy. Also, there is a linear relationship when plotting log β vs 1/T for different β values. With the slope of the straight line, the apparent activation energy is calculated.

Results and Discussion

The composition of the studied woods is presented on Table *1*. Those species presented an evident difference in its composition. Cellulose content for example is around 46.8% whereas TOC presented a much lower cellulose content, around 27.9 %, this can be important, because in some cases the cellulose content is closely related to mechanical properties of lignocellulosic materials. Lignin content can be another very important component and impact some important wood characteristics. ASU lignin content was around 32.1 % whereas TOC was 48.9%. Lignin is an amorphous biopolymer and have a complex structure compared to the other wood components. Due to its complexity takes more energy do degrade, so lignin is generally correlated with antioxidant properties [1].

Table 1 - Composition of *Andira surinamensis* (ASU) and *Tabeuia ochracea* (TOC)

Sample	Cellulose (%)	Hemicellulose (%)	Lignin (%)	Extractives (%)	Ashes (%)
ASU	46.8 ± 1.4	6.9 ± 3.2	32.1 ± 2.7	1.62 ± 0.6	2.15 ± 0.4
TOC	27.9 ± 2.9	9.7 ± 2.3	48.9 ± 0.9	4.98 ± 0.1	0.28 ± 0.0

Thermogravimetric analysis can help to analyze the thermal stability and the thermal degradation behavior of wood. In Figure 1 TGA (a) and DTG (b) of *Andira surinamenses* samples are displayed and three major degradation steps can be identified. Up to 100 °C there is a mass loss that is related to the water content due to the hygroscopic character of the wood, it can absorb a high percent of water , also to the naturally chemically bonded water present in the wood [7,12]. The first degradation step starts around 200 °C and is attributed to some components with low molecular weight and to

hemicellulose, which is the component with the lower thermal stability among the principal components of wood [7]. To compare the thermal stability between the evaluated species, the temperature when 5 % of mass loss occurs (T_5) were measured, for a heating rate of 10 °C.min^{-1}. For *Andira surinamenses*, T_5 was 250 °C. The temperature where the sample reach its maximum degradation rate (T_{max}) was 351 °C. This degradation step is visible also on Fig. 1 (b) where a shoulder around 295 °C can be identified and is correspondent to hemicellulose [13]. A second step take places around 370 °C and is tightly bonded to the first step, so the hemicellulose degradation still occurring. Now, cellulose degradation is the main event, its thermal degradation firstly occurs in the amorphous phase, and the degradation get to the crystalline phase as the temperature still raises. Finally, tightly bonded to cellulose degradation process, from 400 °C and going to all the remaining degradation process, the lignin is the main degraded component. Due to its very complex structure, composed by benzene-propane units, being heavily cross-linked and having high molecular weight, lignin requires a much higher energy to degrade when compared to hemicellulose and cellulose [7,13]. From the above explanation. is possible to observe that the wood degradation reactions are concurrent, so at the same time as the extractives are degrading, hemicellulose starts its on degradation process and when temperature rise a few degrees cellulose degradation as well takes place, and that is the main reason behind the superimposed peaks observed on DTG. The variation on heating rate, from 5 until 15 °C.min^{-1}, shift the degradation process to higher temperature zone for a few degrees. For instance, the T_{max} is shifted from 342 °C to 359 °C for 5 and 15 °C.min^{-1} heating rates, respectively.

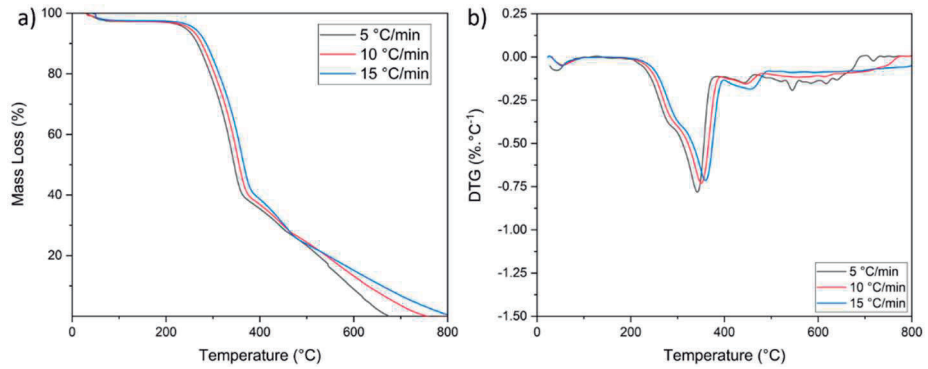

Figure 1 - TGA (a) and DTG (b) of *Andira surinamenses* samples, at 5, 10 and 15 °C.min^{-1} heating rate.

Tabebuia ochracea TGA (a) and DTG (b) curves are shown in Fig. 2. The general behavior observed is the same as the *Andira surinamenses*. The first step begins around 202 °C, T_5 occurs at 264 °C, and T_{max} at 362 °C, displaying a very similar thermal stability at this point. Some aspects of wood and lignocellulosic materials can be responsible for its thermal stability.

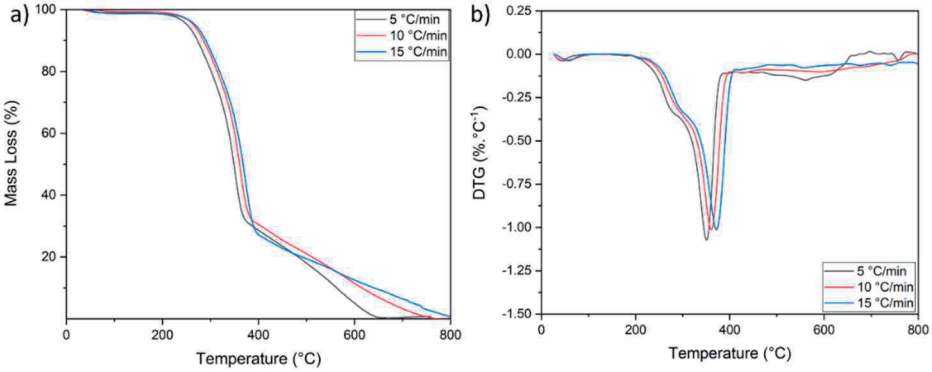

Figure 2 - TGA (a) and DTG (b) of *Tabebuia ochracea* samples, at 5, 10 and 15 °C.min^{-1} heating rate.

The mass fraction ratio of its components generally has a major role in this aspect and can be determinant whether a material is more stable thermally than the other. When the material presents a

high ratio of extractives and hemicellulose, the material can degrade prior to the one that present lower ratio. Also, the lignin has a complex structure that demands higher energy to degrade, so, if the lignocellulosic material has a high fraction of lignin, it may present higher thermal stability as well [3,9,14]. As observed on ASU TGA, with the increase of the heating rate, there is a shift of T_{max} to higher temperatures, ranging from 350 until 372 °C for 5 and 15 °C.min^{-1} respectively.
With the TGA results, the next step was to apply Flynn-Wall-Ozawa method to determinate the apparent activation energy for those samples. Fig. 3 show ASU (a) and TOC (b) FWO plots.

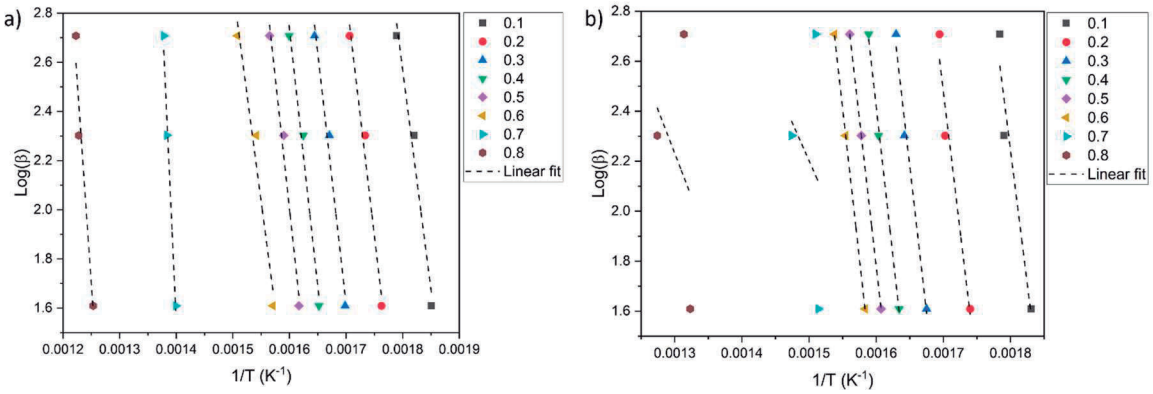

Figure 3 - FWO plot for *Andira surinamenses* (a) and *Tabeuia ochracea* (b)

From FWO plot, the slope of every linear fit was extracted, and the apparent activation energy was calculated as shown on Table 1.

Table 2 - Slope, R^2 and E_a for *Andira surinamenses* and *Tabeuia ochracea*

α	*Andira* surinamenses (ASU)			*Tabeuia ochracea* (TOC)		
	R^2	E_a (kJ.mol^{-1})	Temperature (°C)	R^2	E_a (kJ.mol^{-1})	Temperature (°C)
0.1	0.97	141.2 ± 22.0	276.2	0.93	168.9 ± 43.4	285.4
0.2	0.98	154.6 ± 20.7	303.7	0.96	176.7 ± 36.8	314.2
0.3	0.98	161.2 ± 21.2	325.5	0.98	185.7 ± 20.7	335.9
0.4	0.98	165.4 ± 20.8	342.4	0.99	189.8 ± 9.7	350.5
0.5	0.98	168.1 ± 21.7	355.8	1.00	186.4 ± 0.2	360.6
0.6	0.96	137.6 ± 26.4	375.6	0,99	189.9 ± 2.9	370.3
0.7	0.98	397.6 ± 43.9	449.8	0.05	48.1 ± 195	405.2
0.8	0.94	261.4 ± 60.1	541.4	0.11	55.1 ± 159	511.7

ASU wood initially presents activation apparent energy (E_a) ranging from 141 until 394 kJ.mol^{-1}. Conversion (α) presents a good fitting all the way from 0.1 to 0.8. with a $R^2 > 0.9$. Above 0.6 R^2 begins a slightly decrease in the fitting. However, when $\alpha \geq 0.7$ the E_a is much higher than the predecessors, although R^2 show a good fitting, that may be related to a change in degradation mechanism, or it is due to lignin degradation, that takes place in that range of conversion [14,15].
TOC presents a very good linear fitting from a conversion of 0.1 until 0.6 and E_a ranging from 168 up to 189, on this α range. That means that TOC need more energy do degrade than ASU, what is supported by the main temperatures analyzed on TGA, where TOC presented a higher T_5 and T_{max}, showing a higher thermal stability. Is possible that the lignin content may be the most important factor that explain that difference in thermal stability observed on TGA and the discrepancy on E_a. Since lignin degrade under higher temperatures, as explained in TGA curves, it can be elevating the thermal stability of TOC.

Conclusions

Both woods presented similar trends on the behalf of their thermal degradation steps. However, TGA showed a higher thermal stability for *Tabeuia ochracea* (TOC) with higher T_5 and T_{max}. *Andira*

surinamensis (ASU) presented an E_a from 141 up to 168 kJ.mol^{-1} and *Tabeuia ochracea* (TOC) apparent energy activation where higher, starting from 168 until 189 kJ.mol^{-1}, for conversion (α) in the range from 0.1 to 0.6. These results are probably due to the specimen composition, since TOC presented a higher lignin content, who is generally related to thermal stability.

References

1. Nawaz A, Kumar P. Pyrolysis behavior of low value biomass (Sesbania bispinosa) to elucidate its bioenergy potential: Kinetic, thermodynamic and prediction modelling using artificial neural network. Renew Energy. Pergamon; 2022;200:257–70.
2. Magalhaes D, Kazanc F. Influence of biomass thermal pre-treatment on the particulate matter formation during pulverized co-combustion with lignite coal. Fuel. Elsevier; 2022;308:122027.
3. Sen S, Singh A, Bera C, Roy S, Kailasam K. Recent developments in biomass derived cellulose aerogel materials for thermal insulation application: a review. Cellulose 2022 29:9 [Internet]. Springer; 2022 [cited 2023 Feb 26];29:4805–33. Available from: https://link.springer.com/article/10.1007/s10570-022-04586-7
4. Lee SH, Lum WC, Boon JG, Kristak L, Antov P, Pedzik M, et al. Particleboard from agricultural biomass and recycled wood waste: a review. Journal of Materials Research and Technology. Elsevier; 2022;20:4630–58.
5. Kromoser B, Reichenbach S, Hellmayr R, Myna R, Wimmer R. Circular economy in wood construction – Additive manufacturing of fully recyclable walls made from renewables: Proof of concept and preliminary data. Constr Build Mater. Elsevier; 2022;344:128219.
6. Liu F, Zhang H, Jiang F, Wang X, Guan C. Variations in Orthotropic Elastic Constants of Green Chinese Larch from Pith to Sapwood. Forests 2019, Vol 10, Page 456. Multidisciplinary Digital Publishing Institute; 2019;10:456.
7. de Prá Andrade M, Piazza D, Poletto M. Pecan nutshell: morphological, chemical and thermal characterization. Journal of Materials Research and Technology. 2021;13:2229–38.
8. Kumar M, Mishra PK, Upadhyay SN. Thermal degradation of rice husk: Effect of pre-treatment on kinetic and thermodynamic parameters. Fuel. Elsevier; 2020;268:117164.
9. Poletto M, Zattera AJ, Santana RMC. Thermal decomposition of wood: Kinetics and degradation mechanisms. Bioresour Technol. 2012.
10. Vaghetti JCP, Lima EC, Royer B, da Cunha BM, Cardoso NF, Brasil JL, et al. Pecan nutshell as biosorbent to remove Cu(II), Mn(II) and Pb(II) from aqueous solutions. J Hazard Mater. 2009;162:270–80.
11. Wang J, Minami E, Kawamoto H. Thermal reactivity of hemicellulose and cellulose in cedar and beech wood cell walls. Journal of Wood Science [Internet]. Springer; 2020 [cited 2022 Jul 28];66:1–10. Available from: https://jwoodscience.springeropen.com/articles/10.1186/s10086-020-01888-x
12. Martínez-Casillas DC, Mascorro-Gutiérrez I, Arreola-Ramos CE, Villafán-Vidales HI, Arancibia-Bulnes CA, Ramos-Sánchez VH, et al. A sustainable approach to produce activated carbons from pecan nutshell waste for environmentally friendly supercapacitors. Carbon N Y. 2019;148:403–12.
13. Quiles-Carrillo L, Montanes N, Sammon C, Balart R, Torres-Giner S. Compatibilization of highly sustainable polylactide/almond shell flour composites by reactive extrusion with maleinized linseed oil. Ind Crops Prod. 2018;
14. Andrade M de P, Piazza D, Poletto M. Pecan nutshell: morphological, chemical and thermal characterization. Journal of Materials Research and Technology. Elsevier; 2021;13:2229–38.
15. Ornaghi HL, Poletto M, Zattera AJ, Amico SC. Correlation of the thermal stability and the decomposition kinetics of six different vegetal fibers. Cellulose. 2014;21:177–88.

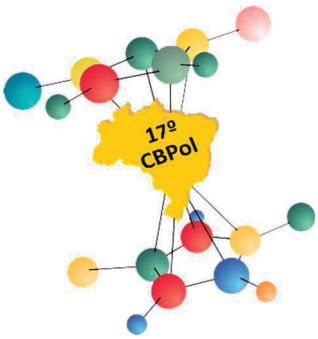

THERMAL DEGRADATION KINETICS OF TWO BRAZILIAN WOOD SPECIES: PART 2. SOLID-STATE REACTIONS

Matheus P. Andrade[1], Matheus Poletto[1], Ademir J. Zattera[1]

1 – Engineering of Processes and Technologies Post-Graduate Program (PGEPROTEC), University of Caxias do Sul (UCS), Caxias do Sul, RS, Brazil mpandrade@ucs.br

Abstract – The solid-state degradation mechanism of two Brazilian wood species have been studied. From Flynn-Wall-Ozawa (FWO) isoconversional method, apparent activation energy was calculated and applied to the Criado method. The main degradation mechanism of both species was determined as being diffusion mechanism. ASU degrades under a three-dimensional mechanism whereas TOC degrades under one-dimensional mechanism.

Keywords: Thermal degradation, Master Curves, solid state degradation mechanism, kinetics, wood.

Introduction

Thermal degradation kinetics of biomass materials is a subject of great importance. With that, it is possible to make assumptions on how the material going to behave when exposed to temperature over time and kinetic predictions can be done around the material. Isoconversional methods, help us to evaluate the kinetic triplets, activation energy (E_a), pre-exponential factor (A) and reaction model ($f(\alpha)$). There are a great variety of isoconversional methods, such as Friedman [1], Flynn-Wall-Ozawa (FWO) [2], Kissinger-Akahira-Sunose (KAS) [3], Starink [4], Vyazovkin [5] and many others. Those methods are the so-called model-free methods, because they do not rely on an explicitly model to determinate the kinetic triplet.

Many authors tend to investigate the reaction mechanisms through which the material is thermally degraded, combining the model-free methods and the application of master plots, such as the method described by Criado [6]. One very common way to achieve this, is to apply an isoconversional method, such as FWO and with the obtained E_a values apply Criado method to determinate material reaction mechanism. So, combining isoconversional and a master plots methods, enables one to describe very technically the thermal kinetics degradation of a material, knowing all the way of kinetic triplet. So, Criado master plots method, is often used by many authors to determinate the degradation mechanism of a material such as lignocellulosic ones and can help to understand if one degrades under a unique or multi degradation mechanisms [6,7].

This approach is very well established for wooden materials, as reported by many authors [8–10]. Cavinato and Poletto (2021) performed the kinetic analysis using FWO method and solid-state reaction of three wood species. In this study, they found out that three-dimensional diffusion was the most prominent degradation mechanism associated to the woods.

In this work, two Brazilian wood species, *Andira surinamensis* (ASU) and *Tabebuia ochracea* (TOC) solid-state reaction mechanism were determined, through master plots from Criado method.

Experimental

Thermogravimetric Analysis

In the present work, two Brazilian wood species will be evaluated, *Andira surinamensis* (ASU) and *Tabebuia ochracea* (TOC). Those woods were provided by Madeireira Bianchi.

The samples were grounded and subjected to the thermogravimetric analysis (TGA). TGA were performed in a Shimadzu TGA-50 equipment, using a nitrogen atmosphere with flow of 50 mL.min^{-1}, starting from 25 °C up to 800°C, with three different heating rates 5, 10 and 15 °C.min^{-1}.

Degradation Kinetics

From part 1 achieved results, using Flynn-Wall-Ozawa (FWO) calculated apparent activation energy (heating rate of 5 °C.min^{-1}), was possible to perform Criado method. The FWO calculations were performed using the Eq. 1, as follows:

$$log\beta = \log\left[\frac{AE_a}{g(\alpha)R}\right] - 2.315 - 0.4567\frac{E_a}{RT} \quad (1)$$

Where β is the heating rate, A is the pre-exponential factor, g(α) is the function of the degree of conversion, R is the gas constant and E is the apparent activation energy. Also, there is a linear relationship when plotting log β vs 1/T for different β values. With the slope of the straight line, the apparent activation energy is calculated. The three different heating rates were used as recommended by International Confederation of Thermal Analysis and Calorimetry (ICTAC), since with at least three heating rates is possible to identify non-Arrhenius temperature dependence and reduce errors. Through this method, is possible to determinate the main degradation kinetics mechanism. Eq. 2 is used to determine the reaction mechanism in a solid-state reaction process, as follows:

$$Z(\alpha) = \frac{\left(\frac{d\alpha}{dt}\right)}{\beta}\pi(x) \quad (2)$$

where $x = Ea/RT$ and $\pi\ (x)$ is an approximation of the temperature integral. From Eq. 3 the master curves can be obtained.

$$Z(\alpha) = f(\alpha)g(\alpha) \quad (3)$$

Equation 4 is used to plot $Z(\alpha)$ vs α curves for the theoretical models.

$$Z(\alpha) = \frac{d\alpha}{dT}\frac{E_\alpha}{R}e^{\frac{E_\alpha}{RT}}P(x) \quad (4)$$

Results and Discussion

From part 1 results, apparent activation energy (Ea) for *Andira Surinamensis* (ASU) and *Tabebuia ochracea* (TOC) were displayed on Figure 1.

As seen on the previous work, from a 0.6 conversion (α), the confidence (R^2) of FWO results begins to drop, and as can be verified at Figure 1, E_a displays a very different behavior when compared to 0.1-0.6 α range, due to a probably change on reaction mechanism, due to that low confidence, E_a for conversions higher than 0.6 were not used [7].

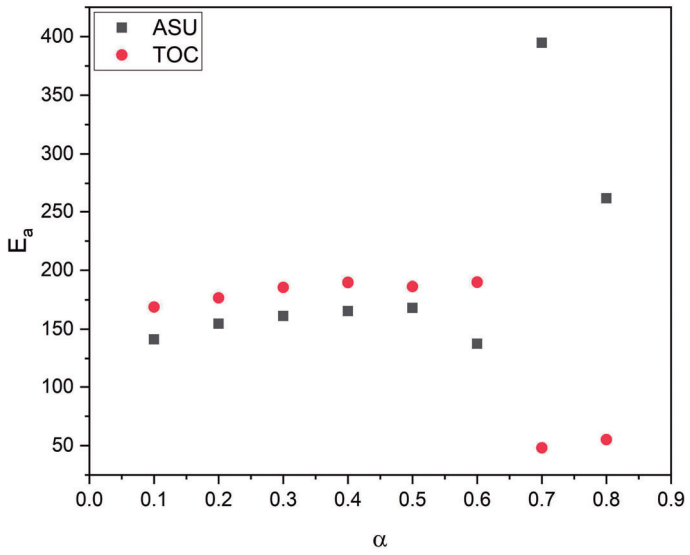

Figure 1 – Theoretical curves of solid-state degradation mechanism

From these results and following Criado method, Z(α) was calculated for *Andira surinamensis* (ASU) and *Tabebuia ochracea* (TOC) samples and the plots are shown in Figure 2. Is possible to observe that until conversion (α) of 0.5, ASU main degradation mechanism is controlled by a diffusion mechanism. Since the calculated Z(α) may overlap more than one model and to verify which model had better fit to the calculated Z(α), the error between each model and the value was calculated and is displayed at Figure 3 (a). Some models were removed from the visualization to have a better visualization of the model that presented better fitting. So, it is possible to verify that the main degradation mechanism for ASU is a three-dimensional (D3), since it presented the lower error compared to the model. Diffusion mechanism are expected degradation mechanisms for lignocellulosic materials, as reported by many authors [11–13]. The same behavior is observed in Ornaghi [7] research, when the authors have observed that six different vegetal fibers degraded under diffusion mechanism, at least from 0.1-0.5 conversion range.

TOC experimental present a very similar trend to ASU sample, where diffusion is the main degradation mechanism. Still, TOC has a better fit to D3, until a conversion of 0.6, as that can be seen in Figure 3 (b).

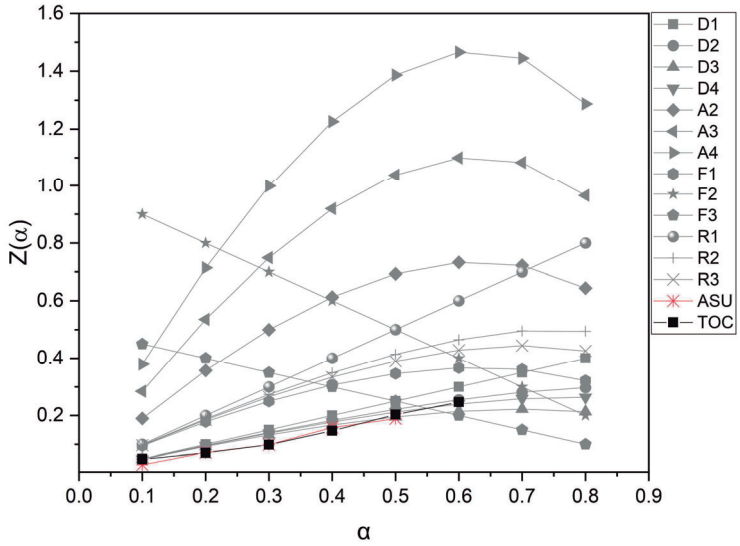

Figure 2 - Experimental curves of solid-state degradation mechanism for ASU and TOC samples

Diffusion degradation is generally associated to the cellulose and hemicellulose fraction of ASU and TOC samples. The diffusion process occurs on most between crystal lattices and can occur between molecules as well. For TOC sample with a predominantly observed D3 mechanism, degradation take place on three dimensions, possibly on a boundary between two phases, that can be for example a gas and solid [11,13].

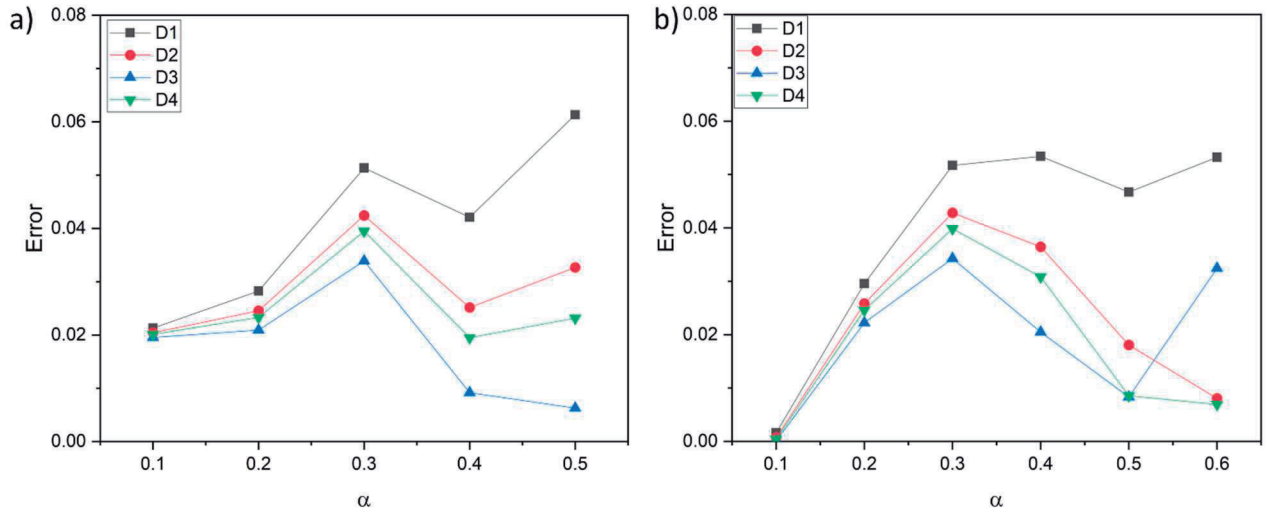

Figure 3 - Calculated Z(a) error for ASU and TOC, compared to the models.

From a α of 0.6 to the limit, the reaction mechanism begins to change, and the fitting to the curves is poor, and that is the reason why they were not plotted, for better visualization. That behavior is probably related to a mix of chemical reaction and lignin degradation, who is in place at this range of temperatures, since for ASU 0.5 conversion is correspondent to the temperature of 355 °C. Lignin has a more complex structure than cellulose and hemicellulose, so its degradation mechanism is also more complex, besides, is possible that other components, such dense aromatic structures are degrading at the same time. Generally, lignin can degrade trough F-mechanism (random nucleation), but on lignocellulosic materials, the material components are bonded [11]. When lignin is beginning its degradation process, cellulose has not finished all of it, so in some conversion ranges, is possible that various degradation mechanism are occurring at the same time, and that is reflect on Figure 2, when the mechanism is changed at 0.6, and is also visible on FWO results, when r-square for the same conversions starts do decay for low confidence intervals [14]. Also, lignocellulosic materials present a series of condensed aromatic structures, that degrades under a slow rate, and that may be one reason why the fitting on those conversion range are no good fitted to master curves as well. Finally, lignocellulosic materials are very heterogeneous, so the degradation kinetics may not follow exactly a model, but in general will follow a trend [7,15].

Conclusions

This study demonstrates that ASU and TOC degrade mostly through diffusion processes, until conversion of 0.6. However, ASU will degrade over three-dimension mechanism and TOC as well. For conversion higher than 0.6 the degradation mechanism begins to change and is possible that diffusion mechanism and other mechanism, such random nucleation, can be occurring at the same time, while cellulose and lignin are degrading.

References

1. Friedman HL. Kinetics of thermal degradation of char-forming plastics from thermogravimetry. Application to a phenolic plastic. Journal of Polymer Science Part C: Polymer Symposia [Internet]. 1964 [cited 2023 Apr 15];6:183–95. Available from: https://onlinelibrary.wiley.com/doi/full/10.1002/polc.5070060121
2. Flynn JH, Wall LA. General Treatment of the Thermogravimetry of Polymers. J Res Natl Bur Stand A Phys Chem [Internet]. 1966 [cited 2023 Apr 15];70A:487. Available from: /pmc/articles/PMC6624709/
3. Akahira T, Sunose T. Method of determining activation deterioration constant of electrical insulating materials. Res Rep Chiba Inst Technol. 1971;16,.
4. Starink MJ. The determination of activation energy from linear heating rate experiments: a comparison of the accuracy of isoconversion methods. Thermochim Acta. 2003;404:163–76.
5. Vyazovkin S, Sbirrazzuoli N. Isoconversional Kinetic Analysis of Thermally Stimulated Processes in Polymers. Macromol Rapid Commun [Internet]. 2006 [cited 2023 Apr 15];27:1515–32. Available from: https://onlinelibrary.wiley.com/doi/full/10.1002/marc.200600404
6. Criado JM, Málek J, Ortega A. Applicability of the master plots in kinetic analysis of non-isothermal data. Thermochim Acta. 1989;
7. Ornaghi HL, Poletto M, Zattera AJ, Amico SC. Correlation of the thermal stability and the decomposition kinetics of six different vegetal fibers. Cellulose. 2014;21:177–88.
8. Guida MY, Lanaya S, Rbihi Z, Hannioui A. Thermal degradation behaviors of sawdust wood waste: pyrolysis kinetic and mechanism. J Mater Environ Sci [Internet]. 2019 [cited 2023 Sep 15];10:742–55. Available from: http://www.jmaterenvironsci.com
9. Cavinato CD, Poletto M, Cavinato CD, Poletto M. Kinetic analysis of thermal degradation of Cedrela odorata, Marmaroxylon racemosum and Tectona grandis from timber industry. Maderas Ciencia y tecnología [Internet]. 2021 [cited 2023 Sep 15];23:1–10. Available from: http://www.scielo.cl/scielo.php?script=sci_arttext&pid=S0718-221X2021000100446&lng=es&nrm=iso&tlng=en
10. Poletto M, Zattera AJ, Santana RMC. Thermal decomposition of wood: Kinetics and degradation mechanisms. Bioresour Technol. 2012;126:7–12.
11. Ornaghi HL, Ornaghi FG, Neves RM, Monticeli F, Bianchi O. Mechanisms involved in thermal degradation of lignocellulosic fibers: a survey based on chemical composition. Cellulose [Internet]. 2020 [cited 2023 Apr 17];27:4949–61. Available from: https://link.springer.com/article/10.1007/s10570-020-03132-7
12. Açıkalın K. Determination of kinetic triplet, thermal degradation behaviour and thermodynamic properties for pyrolysis of a lignocellulosic biomass. Bioresour Technol. 2021;337:125438.
13. Cavinato CD, Poletto M, Cavinato CD, Poletto M. Kinetic analysis of thermal degradation of Cedrela odorata, Marmaroxylon racemosum and Tectona grandis from timber industry. Maderas Ciencia y tecnología [Internet]. 2021 [cited 2023 Apr 17];23:1–10. Available from: http://www.scielo.cl/scielo.php?script=sci_arttext&pid=S0718-221X2021000100446&lng=es&nrm=iso&tlng=en
14. Shen DK, Gu S, Jin B, Fang MX. Thermal degradation mechanisms of wood under inert and oxidative environments using DAEM methods. Bioresour Technol. 2011;102:2047–52.
15. Poletto M. Assessment of the thermal behavior of lignins from softwood and hardwood species. Maderas Ciencia y tecnología [Internet]. 2017 [cited 2023 Apr 30];19:63–74. Available from: http://www.scielo.cl/scielo.php?script=sci_arttext&pid=S0718-221X2017000100006&lng=en&nrm=iso&tlng=en

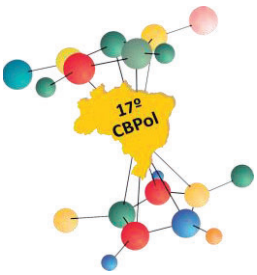

TUNG OIL AND ITACONIC ACID AS GREEN PLATFORMS FOR THE PRODUCTION OF MONOMERS AND POLYESTERS

Julio Antonio Conti Silva[1,2], Rafael Lopes Quirino[2] and Talita Martins Lacerda[1]*

1 – Department of Biotechnology, University of São Paulo (USP), Lorena, SP, Brazil talitalacerda@usp.br
2 – Chemistry Department, Georgia Southern University, Statesboro, GA, USA

Abstract – Environmental concerns related to the utilization of petroleum-based raw materials for the production of polymers have prompted the development of materials derived from renewable resources. In this work, tung oil and itaconic acid were used for the synthesis of poly-functional monomers and polyesters. In a first step, a Diels-Alder reaction between methyl α-eleostearate and dimethyl itaconate allowed the production of trifunctional monomers. For the sake of comparison, a petroleum-based molecule, *n*-butyl methacrylate, was used instead of dimethyl itaconate to produce a bifunctional monomer. The synthesized monomers were submitted to step-growth polymerization reactions with either glycerol or ethylene glycol. Spectroscopic analyses of the polymers detected the disappearance of methyl groups characteristic signals, implying that the polymerization reactions were successful to some extent. With some improvements, this method could be utilized to produce novel bio-based polymers.
Keywords: *tung oil; itaconic acid; Diels-Alder reaction; polyesters*
Fundings: This research was funded by Coordenação de Aperfeiçoamento de Pessoal de Nível Superior – Brasil (CAPES) – Finance Code 001, and FAPESP (São Paulo Research Foundation, Grant 2022/12451-6).

Introduction

The wide use of petroleum-based raw materials for the synthesis of polymers have raised environmental concerns over the last decades, and the urge for alternatives is already a reality. In this context, vegetable oils became protagonists due to their versatility and abundance [1]. Tung oil has a major fatty acid composition of α-eleostearic acid (80-85%), which contains three conjugated carbon-carbon double bonds that can undergo free-radical and cationic polymerizations, or react with dienophiles in Diels-Alder *click* reactions to produce step-growth monomers and polymers [2-4]. Another interesting bio-based molecule that has received attention is itaconic acid, an unsaturated di-carboxylic acid with a chemical structure resembling acrylic and methacrylic acids. Progress have been made on the free and controlled radical polymerization of itaconic acid and its derivatives, originating materials that can be exploited in terms of drug delivery, antimicrobial activity, among other potential applications [5,6]. Herein, methyl α-eleostearate was reacted with dimethyl itaconate through Diels-Alder reaction, leading to polyfunctional monomers which were later reacted with glycerol or ethylene glycol via step-growth polymerization. The strategy aims at contributing with the development of original polymers from renewable resources.

Experimental

Synthesis of polyfunctional monomers via Diels-Alder reaction

Methyl α-eleostearate (ME), was synthesized and characterized as previously described [7]. The Diels-Alder reaction was performed by stirring methyl α-eleostearate with dimethyl itaconate (DI) or *n*-butyl methacrylate (BM) (25 mol %) in a three-necked round-bottom flask equipped with a condenser under N_2 atmosphere and reflux (BP of DI = 208 °C; BP of BM = 163 °C) for 5 h. The

products were characterized by Proton Nuclear Magnetic Resonance Spectroscopy (^{1}H-NMR), Gas Chromatography-Mass Spectrometry (GC-MS), and Fourier-Transform Infrared Spectroscopy (FTIR). The products were denominated DA1, for the reaction with dimethyl itaconate, and DA2, for the reaction with *n*-butyl methacrylate.

Synthesis of polyesters

Polyesters were synthesized by reacting DA1 or DA2 with glycerol or ethylene glycol, in the presence of 1 wt. % H_2SO_4. Potassium acetate and 1,5,7-triazabicyclo[4.4.0]dec-5-ene (TBD) were also used as catalysts in preliminary tests, but the reaction yields were inferior than the acid-catalyzed polymerization, therefore only the higher yield results are shown here. Table 1 shows the combinations of monomers and sample names. Monomers and catalyst were added to a round bottom flask equipped with a distillation setup and kept under stirring for 20.5 h at 150 °C. The comonomers were added in stoichiometric amounts, i.e., if both monomers were tri- or bi-functional, they were added in a 1:1 molar ratio, whereas if one of them was tri-functional and the other was bi-functional, they were added on a 2:3 molar ratio of tri-:bi-functional monomer. The final product was neutralized with pyridine, and then submitted to Soxhlet extraction with dichloromethane for 2 h, in case of a branched product, or precipitated in cold methanol, in case of a linear product. After either the extraction or precipitation, the products were dried in a vacuum oven at 70 °C for 24 h, and the reaction conversions were calculated by dividing the actual weight of the polymers by the expected weight predicted by the stoichiometry. The polymers were characterized by FTIR, Thermogravimetric Analysis (TGA), and Differential Scanning Calorimetry (DSC), and the linear polymer was also characterized by ^{1}H-NMR spectroscopy and Gel Permeation Chromatography (GPC).

Table 1 – Combinations of polymerization reactions and sample names.

Monomer 1	Monomer 2	Product
DA1	Glycerol	P1
DA1	Ethylene glycol	P2
DA2	Glycerol	P3
DA2	Ethylene glycol	P4

Characterization

FTIR spectra were collected using a Thermo Nicolet iS10 FTIR spectrometer (Thermo Scientific, Waltham, MA, USA) with an attenuated total reflectance (ATR) accessory. The spectra were obtained in the 400-4000 cm^{-1} spectral region, with 32 scans, and 4 cm^{-1} resolution. The ^{1}H-NMR spectra were acquired on an Agilent MR400DD2 spectrometer (Santa Clara, CA, USA) operating at 400 MHz. All samples were dissolved in deuterated chloroform. GC-MS analyses were made on a Shimadzu GC–2030 gas chromatograph equipped with a mass spectrometer detector Shimadzu GCMS-QP2020NX (Kyoto, Japan) using a 30 m Rtx-5MS column (Restek, Bellefonte, PA, USA) with an internal diameter of 0.25 mm and a film thickness of 0.25 μm. Samples were dissolved in acetone, leading to an approximate concentration of 5% (v/v). Helium was used as the carrier gas at a total (column + split) flow rate of 50 mL/min. The temperature was initially kept at 70 °C for 2 min, then increased to 300 °C at a heating rate of 15 °C/min, and finally kept at 300 °C for 13 min.
The molecular weight distribution was determined via GPC, with a LC-20AD liquid chromatograph from Shimadzu (Tokyo, Japan), equipped with a SIL-20A HT autosampler, and a RID-20A refractive index detector, operating on THF at 40 °C with a flow rate of 1 mL/min. The column system comprised five Phenogel main columns (5 μm, 300 mm × 7.80 mm, 500-10^6 Å) and a Phenogel pre-column (5 μm, 50 mm × 7.80 mm), from Phenomenex (Torrance, CA, USA). The calibration curve was created using polystyrene standards (Sigma-Aldrich, Saint Louis, MO, USA), ranging from 2500 to 50000 Da. TGA tests were performed in a Q50 TGA instrument (TA

Instruments, New Castle, DE, USA), under air or N_2 atmosphere. Approximately 10 mg of sample were heated in platinum pans from room temperature to 650 °C at a rate of 10 °C/min. DSC experiments were conducted with a Q20 DSC instrument (TA Instruments, New Castle, DE, USA). Around 10 mg of sample were placed in aluminum pans and cooled to -60 °C, then heated to 250 °C, cooled to -60 °C again, and heated to 250 °C one more time, at a constant rate of 10 °C/min under N_2 atmosphere.

Results and Discussion

Synthesis of polyfunctional monomers via Diels-Alder reaction

To calculate the conversion of the Diels-Alder reactions, samples were submitted to ^{1}H-NMR spectroscopy, and the results are presented in Fig 1. Signals that should be present only on the dienophile spectra were chosen for the calculations. For DI, the signal around 6.30 ppm, denominated "a" (Fig 1) was selected for the calculations, whereas for BM, the signal around 5.51 ppm, denominated "c" (Fig 1) was chosen, both related to hydrogens linked to one of the sp^2 carbons. Since during the Diels-Alder reactions a π bond is converted into a σ bond, the corresponding ^{1}H-NMR signals should be shifted upfield within the spectra. Therefore, whatever is left at the aforementioned chemical shifts represent a non-reacted dienophile. The conversion of the reactions was calculated by Eq. 1, where A_i is the intensity of the non-reacted dienophile signals, and A_j is the intensity of signals of hydrogens from methyl groups selected as a reference. The conversion of DI to DA1 was approximately 88%, whereas of BM to DA2 was around 55%, suggesting that DI, a bio-based molecule, is more reactive than the petroleum-based BM at the investigated conditions.

$$Conversion\ (\%) = 100 * \left(1 - \frac{15A_i}{4A_j}\right) \quad (1)$$

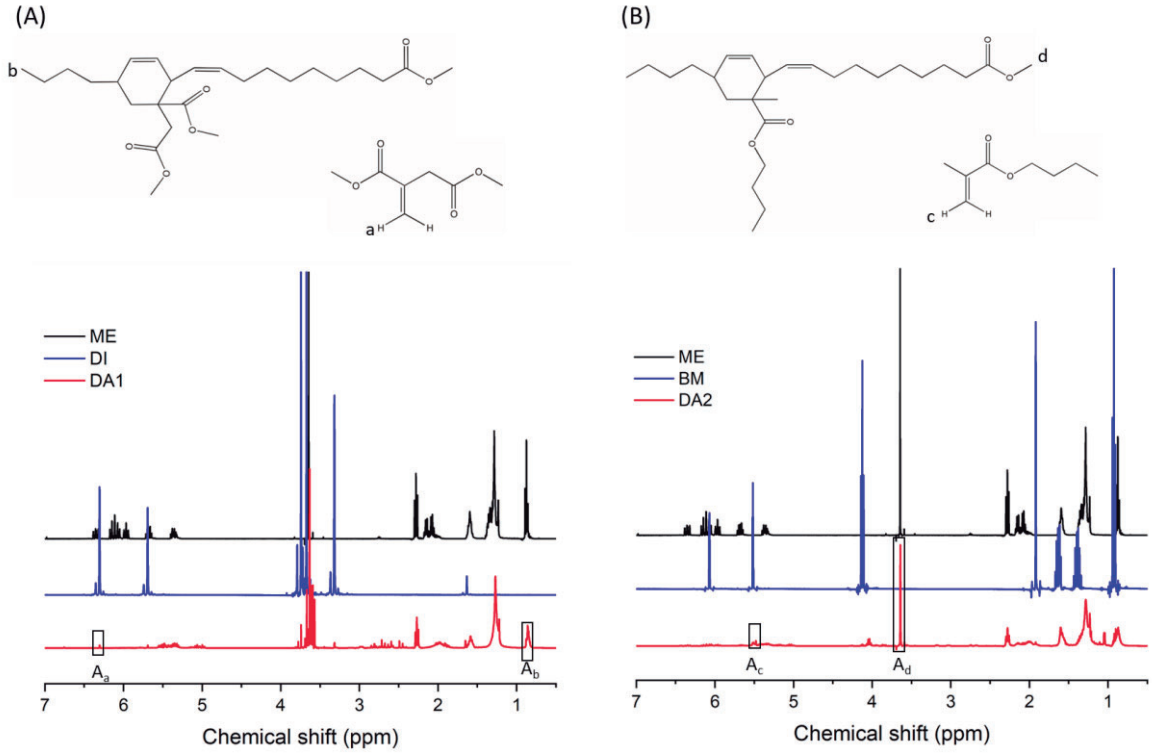

Figure 1 – ^{1}H-NMR spectra of (A) ME, DI, and DA1, and (B) ME, BM, and DA2.

Fig 2 represents the GC chromatograms of ME, DA1, and DA2. Several peaks were eluted at different retention times, ranging from 14.3 to 20.9 min, in ME chromatogram. This result was expected, since tung oil is composed of a variety of fatty acid chains. Thus, ME is composed of methyl esters of all those fatty acids, which contain distinct molecular weights, and should have

different retention times on GC. Since only methyl α-eleostearate can undergo Diels-Alder reaction, the different fatty acid methyl esters of were still present in the Diels-Alder products, and consequently, in their chromatograms. However, new peaks at retention times of 21.6 min for DA1, and 21.4 min for DA2 were observed. Their molecular weights, calculated by MS, were 450 and 434 g/mol, respectively, which are precisely the molecular weights of the predicted Diels-Alder products, suggesting that the reactions were successful.

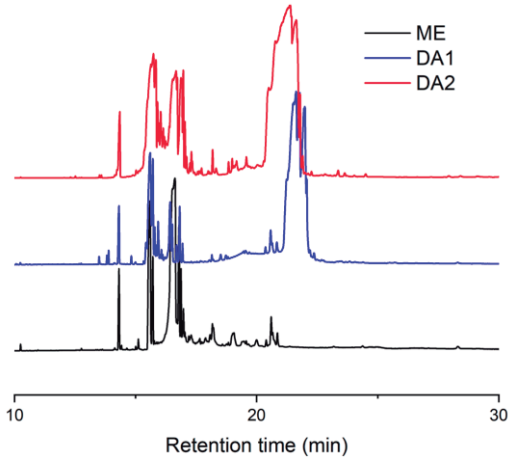

Figure 2 - GC chromatograms of ME, DA1 and DA2.

Synthesis of polyesters

A combination of different comonomers was studied, and the results are presented in Table 1. Only three of the four studied reactions yielded a final product at the applied conditions, being P1, P3, and P4. P3, however, yielded only 8% conversion, whereas P1 yielded 56%, and P4 yielded 75%. Due to the low conversion, P3 was chosen not to be characterized. P1 was a branched solid polymer, while P4 was a linear polymer, having a very viscous aspect.

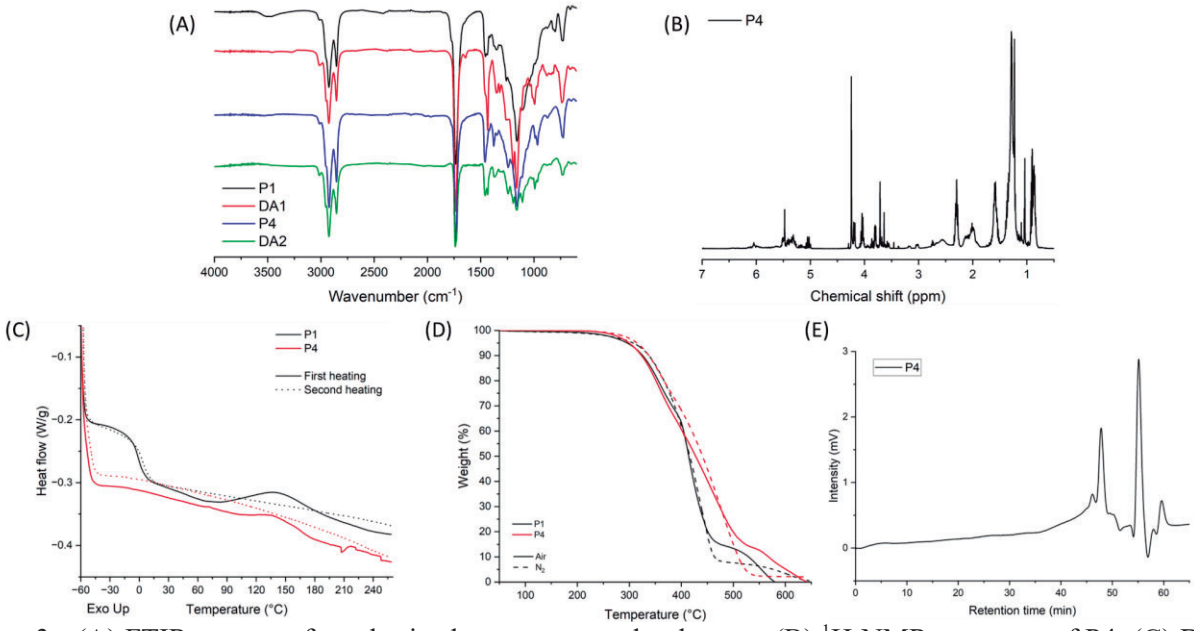

Figure 3 - (A) FTIR spectra of synthesized monomers and polymers; (B) ^{1}H-NMR spectrum of P4; (C) DSC thermograms of synthesized polymers; (D) TGA thermograms of synthesized polymers; (E) GPC chromatogram of P4.

FTIR spectroscopy (Fig 3A) showed that all spectra presented bands (cm^{-1}) at around 3014, 1735, which correspond to sp^2 C-H stretch, and C=O stretch, respectively. A peak at 1429 cm^{-1}, related to

vibrations of the C-H bonds of the methyl ester group, was observed in both monomers, but was less intense or did not appear in the case of polymers. The polymerization reaction is a transesterification reaction, i.e., the methyl and butyl groups of the monomers should be replaced by the glycol chains. Therefore, the vanishing of the 1429 cm^{-1} band suggests the reaction took place [8]. ^{1}H-NMR spectrum of P4 (Fig 3B) indicated that the signal at around 3.6 ppm, present in DA2 (Fig 1B), related to the protons of methyl groups, was shifted downfield, probably due to the polymerization reaction replacing the methyl groups with larger chains from the glycol. This is a good indication that the reaction happened at some extent. The DSC thermograms (Fig 3C) showed a small exothermic peak around 140 °C on the first heating, but not in the second, suggesting that the reactions were not complete, and were finished inside the instrument. P1 presented a baseline change at around 0 °C, which is most likely the glass transition temperature. These results suggest that the reaction conditions should still be optimized in order to obtain fully polymerized products. The presence of a second order transition, however, is a good indicative that the reaction took place, even though it was not complete. TGA thermograms (Fig 3D) showed that the polymers have similar thermal stabilities, which is not surprising since they are chemically similar. Both polymers barely present any weight loss before 280 °C, which means that there is no residual solvent or absorbed moisture in the final product. Under air atmosphere the polymers are slightly less stable and are completely degraded, probably due to oxidation reactions, whereas under N_2 some ashes remain, which is expected for products of step-growth polymerizations. GPC chromatograms of P4 (Fig 3E) showed two distinct peaks with retention times at 46.144 min and 47.813 min, with Mw equal to 2218 and 1423 Da, respectively, which indicates that the reaction occurred at some extent, but still needs tuning to achieve more homogenous polymer chains.

Conclusions

In this work, novel bio-based polyesters derived from tung oil and itaconic acid were successfully polymerized. This synthesis still needs some improvements in order to achieve full conversion. However, the results obtained so far seem promising, and they open new possibilities of using this route to produce fully or partially bio-based polymers.

Acknowledgements

CAPES, FAPESP (São Paulo Research Foundation, Grant 2022/12451-6), Chemistry Department at Georgia Southern University, Department of Biotechnology at Engineering College of Lorena.

References

1. A. Gandini; T. M. Lacerda; A. J. F. Carvalho; E. Trovatti Chemical Reviews 2016, 116, 1637-1669. https://doi.org/10.1021/acs.chemrev.5b00264.
2. J. A. C. Silva; L. M. Grilo; A. Gandini; T. M. Lacerda Polymers 2021, 13, 1722. https://doi.org/10.3390/polym13111722.
3. S. Yang; H. Fang; H. Li; F. Shen; X. Chen; Y. Hu; Z. Yang Progress in Organic Coatings 2022, 170, 106967. https://doi.org/10.1016/j.porgcoat.2022.106967.
4. Y. Ma; Y. Bei; M. Zhang; F. Song; F. Hu; Z. Kou; L. Hu; Y. Zhou; P. Jia Industrial Crops and Products 2022, 188, 115646. https://doi.org/10.1016/j.indcrop.2022.115646.
5. B.-E. Teleky; D. C. Vodnar Polymers 2021, 13, 3574. https://doi.org/10.3390/polym13203574.
6. L. Solka; K. Lienkamp Macromolecular Rapid Communications 2021, 42, 2000546. https://doi.org/10.1002/marc.202000546.
7. C. Meiorin; M. I. Aranguren; M. A. Mosiewicki European Polymer Journal 2015, 67, 551-560. https://doi.org/10.1016/j.eurpolymj.2015.01.005.
8. T. M. Lacerda; A. Gandini Industrial Crops and Products 2020, 157, 112886. https://doi.org/10.1016/j.indcrop.2020.112886.

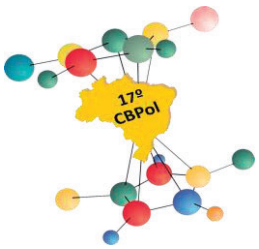

2^4 FACTORIAL DESIGN OF SBS BLOCK COPOLYMER SULFONATION

Matheus Saccardo[1*], Ariel Zuquello[2], Rafael Barbosa[1], Roger Gonçalves[1], Kaique Tozzi[3], Guilherme Blanco[1], and Carlos Scuracchio[1]

1 – Department of Materials Engineering (DEMa), Federal University of São Carlos (UFSCar), São Carlos, SP, Brazil
matheusaccardo@hotmail.com
2 – Community University of Chapecó Region. Polytechnic School, Chapecó, Santa Catarina, Brazil
3 – Univ. Grenoble Alpes, Univ. Savoie Mont Blanc, CNRS, Grenoble INP, LEPMI, UMR5279, 38000 Grenoble, France

Abstract – Block copolymer sulfonation to develop amphiphilic block copolymers has attracted considerable attention for its potential in proton exchange membrane applications [1]. It has been demonstrated that charged-neutral block copolymers, such as sulfonated styrene-butadiene-styrene block copolymer (s-SBS), can present mechanical resistance, flexibility and higher proton conductivity than random ionic copolymers and homopolymers [2]. Although there are many sulfonation techniques, for each polymer, there is an ideal reaction condition so that commonly observed problems such as degradation through oxidation [3], chain scission and sulfoxide crosslinks [4], incomplete polymer sulfonation [5], and aggregation in solution [6] could be avoided. For this reason, it is essential to establish a sulfonation protocol for each polymer. Since many variables and problems are associated with this type of reaction, a 2^4 factorial design of the sulfonation process was performed on commercial SBS copolymer samples. A standard sulfonation procedure was adopted for the SBS styrenic domains, in which the copolymer is solubilized, the temperature of the solution is maintained constant, the sulfonating agent is added, and the reaction proceeds over time. Thus, the main variables were considered: i) temperature, ii) time, iii) sulfonating agent (H_2SO_4/Ac_2O) ratio, and iv) copolymer morphology. The individual and interaction effects of those variables were analyzed. Samples with a sulfonation degree between 2% and 26% were obtained, and it was observed that the linear terms (H_2SO_4/Ac_2O ratio and time) and the quadratic terms ([H_2SO_4/Ac_2O ratio]^2 and [time]^2) were the most relevant for sulfonation. For this reason, sulfonation does not increase linearly with these factors. However, there is a point at which sulfonation is maximum, which occurs after 60 minutes and an H_2SO_4/Ac_2O ratio of 1:1.7. With this study, it was possible to verify the best conditions to obtain a certain degree of sulfonation of SBS block copolymer.

References

1. J. Mays et al., *Soft Matter*, 2012, 8, 3036X. doi:10.1039/c2sm07223h.
2. E. Garcia, B. Jung. *Membrane Journal*, 2019, 29, 252-262. doi.org/10.14579/membrane_journal.2019.29.5.252
3. A. Theodoropoulos et al., *Polymer* 1993, 34, 18, 3905-3910. doi.org/10.1016/0032-3861(93)90518-F
4. H. Roth, *Industrial and Engineering Chemistry,* 1957, 49, 11, 1820-1822. doi.org/10.1021/ie50575a022
5. D. Baigl et al., *Macromolecules,* 2002, 35, 6, 2318–2326. doi.org/10.1021/ma011707o
6. J. Li et al., *Polymer Journal*, 2010, 42, 609-625. doi.org/10.1038/pj.2010.59

Fundings: This study was financed in part by the Coordenaçao de Aperfeiçoamento de Pessoal de Nível Superior - Brasil (CAPES) - Finance Code 001. The authors would also like to thank the CNPq and FAPESP (process #2020/02696-6) funding agencies.

Keywords: *SBS, block copolymer, Sulfonation, Factorial Design, Ionic copolymers.*

APPLICATION OF HS-GCMS ON THE EVALUATION OF STYRENE MIGRATION FROM COSMETIC PACKAGING BASED ON SAN AND ABS

Guilherme M. Menegasso[1], Letícia B. Cerqueira[2], Jonathan Dos Santos[2] Leandro C. Gonçalves[2], Fernanda G. Henning[2], Desirée C. Schuck[2], Márcia P. P. Dos Santos[2]*

1 – Euvaldo Lodi Institute, Curitiba, PR, Brazil
2 – Cencoderma Institute, São José dos Pinhais, PR, Brazil
mporto@grupoboticario.com.br

Abstract - Several applications employ the use of products arised from the petrochemical industry, such as styrene, derived from ethylbenzene. This substance can be applied in a considerable variety of materials, like PS (Polystyrene), ABS (Acrylonitrile-Butadiene-Styrene), SAN (Styrene-Acrylonitrile copolymer) and EPS (Expanded Polystyrene). Materials such as these are versatile, applied in packaging for food and cosmetics, personal care products and industrial uses. Despite the versatility of its materials, since 2016, styrene is classified by PROP65 (Proposition 65) from the state of California as a substance that causes cancer. The IARC (International Agency for Research on Cancer), classifies it as potentially carcinogenic, and in Europe, it is listed as a harmful substance by REACH (Registration, Evaluation, Authorisation and Restriction of Chemicals) regulation. Although there are no regulations for its prohibition or approval in sectors, as cosmetics, styrene in materials is liable to migration, even though there aren't enough evidences to concretize this characteristic, studies indicate that cosmetic products conditioned in packaging made of styrene are susceptible to demonstrate its presence on the composition. The presented study comes with the purpose of understanding in practical uses this potential migration occurrence, due to all context and positioning of some agencies. An evaluation were made on the main usages in cosmetics packaging and included two materials for analysis, one of them is made of SAN and the other in a blend of SAN and ABS, and for both, it was practiced the evaluation by headspace gas chromatography coupled with mass spectrometry (HS-GCMS). The implemented method allowed to quantify the migrated styrene. Besides the indicative of the migration, the found quantity indicates that its usage can be considered safe, however more studies and regulatory organizations definitions about this subject are necessary, so that the directive for industry is better established.

References:

1. A. Ajaj; S. J'Bari; A. Ononogbo; F. Buonocore; J. C. Bear; A. G. Mayes; H. Morgan. Foods, 2021, 10, 10051136. https://doi.org/10.3390/foods10051136.
2. V. Guazzotti; A. Ebert; A. Gruner; F. Welle. Journal of Consumer Protection and Food Safety, 2020, 16, http://dx.doi.org/10.1007/s00003-020-01308-8.
3. V. Guazzotti; A. Gruner; V. Hendrich; A. Störmer. F. Welle. International Symposium on Food Packaging, 2022, 7, http://dx.doi.org/10.13140/RG.2.2.18708.99202.
4. P. Dawson; A. C. Seydim; D. Hirt. Journal of Food Research, 2020, 9. https://doi.org/10.5539/jfr.v9n3p39.

Keywords: *ABS, SAN, cosmetic packaging, migration, styrene*

CHEMICAL MODIFICATION OF POLY(PROPYLENE GLYCOL) BIS(2-AMINOPROPYL ETHER) WITH SATURATED DIMER FATTY ACID: EVALUATION OF APPLICABILITY IN SYNTHETIC DRILLING FLUIDS

Aline N. Vasconcelos[1*], Elessandre A. de Souza[2], Rosangela de C. Balaban[1]

1 – Laboratório de Pesquisa em Petróleo, University of Rio Grande do Norte (UFRN), Natal, RN, Brazil
aline-n.vasconcelos@hotmail.com
2 - Centro de Pesquisa e Desenvolvimento Leopoldo Américo Miguêz de Mello – CENPES/PETROBRAS, Rio de Janeiro, RJ, Brazil

Abstract - The stability of synthetic drilling fluids in the deepwater fields has been acquired from the development of chemical additives that promote the maintenance of rheological properties with variations in temperature (flat rheology systems). In this context, fatty amide was synthesized via condensation reaction between saturated dimer fatty acid and poly(propylene glycol) bis(2-aminopropyl ether). The product was characterized by Fourier Transform Infrared spectroscopy (FTIR), and the result confirmed that the fatty amide was successfully synthesized due to the presence of the band of amide carbonyl group, at 1624 cm^{-1}. The performance of the hydrophobic product was evaluated in a synthetic drilling fluid through electrical stability, volume of filtration under high-temperature and high-pressure, and viscosity in the temperature range from 4 to 49ºC. The drilling fluid containing the fatty amide showed electrical stability values above 200 V, and a volume of filtrate below the required specifications by the Standard API RP 13B-2 (Table 1) [1]. In addition, the viscosity curves showed minimal variation in the selected temperature range (Figure 1), indicating that the poly(propylene glycol) derivative can attribute flat rheological properties [2] to synthetic drilling fluids.

Table 1. Electrical stability and Filtrate volume

Sample	Electrical stability (Volts)	Filtrate volume (mL)
Fatty amide	233	4.9

Fig. 1. Viscosity curve of the Fatty amide

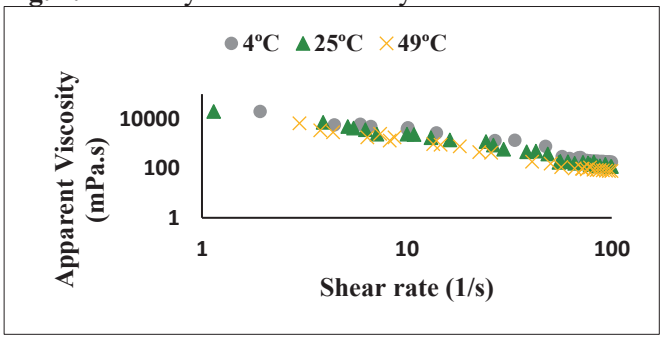

References

1. API Recommended Practice 13B-2 in American Petroleum Institute, Washington, 2019, Vol. 5, 141.
2. V. Gupta, S. Indulkar, M. Asrani, A. Patel, S. Ramane, A. Sarase, S. Thakur, A.K. Singh. *SPE International Conference on Oilfield Chemistry, 2019,* SPE-193618-MS. https://doi.org/10.2118/193618-MS.

Keywords: *Fatty amide; Flat-Rheology; Drilling Fluids*

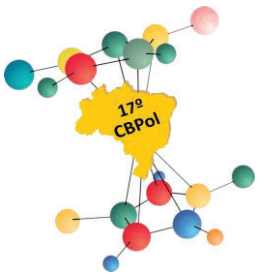

EFFECT OF THE DEGREE OF SUBSTITUTION ON THE RHEOLOGICAL PROPERTIES OF HYDROPHOBICALLY MODIFIED CARBOXYMETHYLCELLULOSE

Bruna L. B. Lima[1], Nívia N. Marques[1], Elessandre A. Souza[2], Rosangela. C. Balaban[1*]

1 – Laboratório de Pesquisa em Petróleo (LAPET), Instituto de Química, Universidade Federal do Rio Grande do Norte (UFRN), Natal, RN, Brasil
rosangela.balaban@ufrn.br
2 – Centro de Pesquisas e Desenvolvimento Leopoldo Américo Miguêz de Mello (CENPES), PETROBRAS, Rio de Janeiro, RJ, Brasil

Abstract - Hydrophobically modified water-soluble polymers consist of hydrophilic polymer chains that carry a small number of alkyl chains. These alkyl groups tend to associate in aqueous solution forming intra and intermolecular bonds [1]. Particularly in enhanced oil recovery, hydrophobically modified polymers can be added to the injection water in order of thickening the brine that pushes the oil from the reservoir to the producing well, promoting greater displacement efficiency and, thus, greater oil production [2]. In this study, hydrophobically modified carboxymethylcellulose (CMC) with different degrees of substitution (DS) (1.0 and 1.87) was obtained from the reaction between the carboxylic acid groups from CMC and the amine group from dodecylamine (DDA), via carbodiimide coupling. Structural characterization was performed by Fourier transform infrared spectroscopy (FTIR) and the properties were evaluated through rheological measurements in brine (NaCl 3.0 mol.L^{-1}) with polymer concentration of 1.0 g.L^{-1} at 25 °C. FTIR confirmed that reaction was successfully done, by the presence of amide I (1651 cm^{-1}) band. Rheological measurements showed pseudoplastic behavior for all samples, i.e., there is a decrease in the apparent viscosity with the increase in the shear rate, due to the disruption of entanglements and associations and orientation of macromolecules in the flow direction. The values of DS led to differences of viscosity values, due to the changes of hydrophilicity of the products. The hydrophobic derivative with lower DS (1.0) also exhibited the highest pseudoplastic behavior and the highest viscosity in brine because of its higher hydrophobic character compared to others, favoring more associations between polymer chains. These results reveal that the hydrophobically modified CMC could be good candidates for enhanced oil recovery applications.

References

1. D. Charpentier; G. Mocanu; A. Carpov; S. Chapelle; L. Merle and G. Muller *Carbohydrate Polymers* 1997, *33*, 177. https://doi.org/10.1016/S0144-8617(97)00031-3.
2. A. Maia; R. Borsali; R. Balaban *Materials Science and Engineering C* 2009, *29*, 505. https://doi.org/10.1016/j.msec.2008.09.018.

Keywords: *Carboxymethylcellulose, Polysaccharide, Degree of substitution, Rheology.*

EFFECTS OF GRAFTING DEGREE ON THE PROPERTIES OF CARBOXYMETHYLCELLULOSE-*g*-OLIGO(PROPYLENE OXIDE-*co*-ETHYLENE OXIDE)

Nívia do N. Marques[1], Sami Halila [2], Redouane Borsali [2] and Rosangela de C. Balaban [1*]

1 – Laboratório de Pesquisa em Petróleo (LAPET), Instituto de Química, Universidade Federal do Rio Grande do Norte (UFRN), Natal, RN, Brazil
rosangela.balaban@ufrn.br
2 – Centre de Recherches sur les Macromolécules Végétales (CERMAV), Université Grenoble Alpes, CNRS, Grenoble, France

Abstract – In this work, graft copolymers were prepared by combining carboxymethylcellulose (CMC) and the thermoresponsive oligomer Jeffamine® M-600 (propylene oxide/ethylene oxide – PO/EO = 9/1) via coupling reaction with 1-ethyl-3-[3-(dimethylamino)-propyl]carbodiimide hydrochloride (EDC) and *N*-hydroxysuccinimide (NHS) [1]. The grafting reaction was confirmed by Fourier-Transform Infrared (FTIR) and Proton Nuclear Magnetic Resonance (^{1}H NMR). Grafting degree (GD) increased from 9 (CP1) to 16% (CP2) when the amount of the oligomer was increased on the reactional feed (Table 1). The second virial coefficient (A_2) was positive for CMC, CP1 and CP2, indicating good polymer-solvent interactions. CP2 exhibited higher weight-average molar mass (M_w) and radius of gyration (R_g) (0.1M $NaNO_3$) than CP1 and CMC. Also, cloud point temperature was only observed for CP2. This behavior can be attributed to the higher amount of the Jeffamine® M-600 on CP2, promoting greater interactions among the thermoresponsive grafts on saline medium, and leading to the clouding temperature at 85 °C in 0.5 M NaCl. This associative performance is interesting for enhanced oil recovery applications [2].

Table 1 – Stoichiometric amount of reactants, grafting degree (GD), weight-average molar mass (M_w), radius of gyration (R_g), second virial coefficient (A_2) and cloud point temperature (CPT)

Sample	COO^-:Jeffamine® M-600:EDC:NHS	GD* (%)	M_w ($g.mol^{-1}$)**	A_2 ($mol.L.g^{-2}$)**	R_g (nm)**	CPT (°C)***
CMC	-	-	9.0×10^4	9.1×10^{-6}	43.1	-
Jeffamine® M-600	-	-	-	-	-	44
CP1	1:0.5:4:2	9	2.7×10^5	1.4×10^{-6}	68.5	-
CP2	1:2:4:2	16	6.0×10^5	1.7×10^{-6}	99.0	85

*GD was obtained by ^{1}H NMR; **M_w, R_g and A_2 were obtained by static light scattering (SLS) in 0.1 M $NaNO_3$; ***CPT was obtained by ultraviolet-visible (UV-Vis) in 0.5 M NaCl.

References

1. N. do N. Marques; R. de C. Balaban; S. Halila; R. Borsali *Carbohydrate Polymers* 2018, *184*, 108. https://doi.org/10.1016/j.carbpol.2017.12.053
2. S. Wang; P. Xiong; X. Liu; F. Meng; Q. Ma; C. Song; Q. Zhang; Y. Che *Energy Fuels* 2022, *36*, 2488. https://doi.org/10.1021/acs.energyfuels.1c03699

Keywords: *carboxymethylcellulose, Jeffamine® M-600, cloud point temperature*

ENZYMATIC SYNTHESIS OF BIO-BASED POLYESTERS CONTAINING LEVOGLUCOSAN UNIT.

Davi Boaventura[2], Jonathan Bassut1, Kifah Nasr[1,3], Philippe Zinck[1], Jean-Marie Raquez[3], Audrey Favrelle-Huret[1], Robert Wojcieszak[1] and Ivaldo Itabaiana Jr.[1,2]

1- *Univ. Lille, CNRS, Centrale Lille, ENSCL, Univ. Artois, UMR 8181-UCCS-Unité de Catalyse et Chimie du Solide, 59000 Lille, France.*
2- *Department of Biochemical Engineering, School of Chemistry, Federal University of Rio de Janeiro, Rio de Janeiro 21941-910 Rio de Janeiro, Brazil*
3- *Laboratory of Polymeric and Composite Materials (LPCM), University of Mons, Place du Parc 23, 7000 Mons, Belgium*

Corresponding author: ivaldo@eq.ufrj.br

Abstract - Levoglucosan (LGA) is an anhydrous sugar obtained from the fast pyrolysis of lignocellulosic biomass. In this work, LGA was reacted with diethyl adipate/sebacate and α,ω-diols to give terpolymers with up to 35% of LGA content (related to the α,ω-diol content), number-average molecular weights (Mn) of up to 7900 g·mol−1, and up to 94% yield. It was observed that the amount of LGA in the polymer structure affects the crystallinity, hydrophilicity, and melting point of the polymers. We also evaluated the effect of LGA loading and the comonomer's size on yields, molecular weight, and the incorporation of LGA in the polymer structure. High loads of LGA lead to a decrease in the yield, but a higher molecular weight and higher extent of LGA incorporation in the polymer could be obtained.

KEYWORDS: biomass, levoglucosan,**Keywords**: biomass valorization, biopolymers, levoglucosan, lipases, polyesters

Fundings: Este projeto é financiado pela FAPERJ (jovem cientista do nosso estado, processos E26/201.367/2022 e E26/203.267/2017, CAPES e CNRS (França).

Introduction

Levoglucosan (1,6-anhydro-β-D-glucopyranose; LGA) is an anhydrous sugar obtained from the fast pyrolysis of cellulose fraction of lignocellulosic biomass [1]. In recent years, biomass has emerged as an important renewable source for the production of green chemicals and materials [2]. As one of the recently most attractive use for biomass, biopolymers have been developed as environmentally friendlier alternative to petroleum-based polymers, presenting similar properties to their oil-based counterparts and a broad range of potential applications in food, cosmetic and pharmaceutical areas. Thus, new polyesters and polyamides have been produced from biomass-derived monomers, such as itaconic acid, furan-2,5-dicarboxylic acid, bio-olefins, terpenes, and others via biocatalysis [3]. In this context, LGA has a peculiar structure, presenting three hydroxyl groups disposed in trans-positions on a pyranose ring, which might confer unique properties to a new biopolymer. As far as we know, levoglucosan has not been yet employed as a monomer for polymers production. In this work, we report the production of terpolymers containing incorporated levoglucosan units via lipase-catalyzed polycondensation reactions.

Experimental

Experimental conditions: Diester (diethyl sebacate or diethyl adipate; 1 mmol), LGA (0.25-0.5

mmol), diol (1,4-butanediol, 1,5-pentanediol, 1,8-octanediol, or 1,12-dodecanediol; 0.5-0.75 mmol), and Novozyme 435 (Candida antartica Lipase B immobilized on acrylic resin; 20%wt of total monomers) were added into schlenk tubes. Then, 1mL of diphenyl ether was added (if applicable). A two-stage polymerization method was employed. 1st stage: 100 °C, 1 atm, 2 hours; 2nd stage: 100 °C, vacuum (10-50 mbar), 24 hours. Yield was obtained by weight; LGA content was calculated by 1H NMR; Size Exclusion Chromatography (SEC) in tetrahydrofuran at 40 °C at a flow rate of 1 mL.min-1. Mn and Đ were determined from the Refractive Index (RI) signal using a calibration curve based on polystyrene (PS) standards from Polymer Standards Service, on a Waters apparatus equipped with Waters Styragel columns HR2, HR3, HR5 and HR5E.

Results and Discussion

For diethyl adipate, yields were similar in diphenyl ether or bulk. Comparing similiar conditions, the increase of LGA feed led to lower yields, but higher LGA content in polymers structure. LGA content was limited to 14%. Diol chain-length affects yield and LGA content.

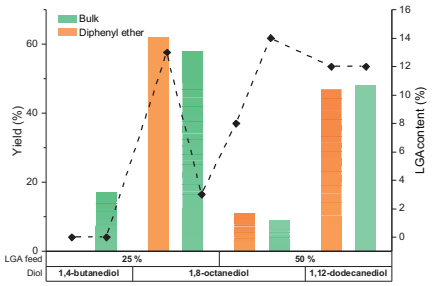

Fig 1. Diethyl adipate (m= 4)

When diethyl sebacate was employed, higher yields and LGA content were achieved. Reactions in diphenyl ether led to better yields and LGA content than in bulk. As for diethyl adipate, increase of LGA feed led to lower yields. Up to 35% of LGA content was reached with high yields.

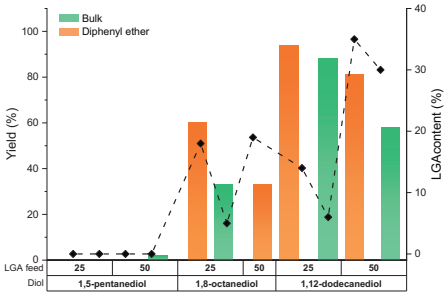

Fig 2. Diethyl sebacate (m= 8)

NUMBER AVERAGE MOLECULAR WEIGHT (M_n):

Increase of both diol chain-length and LGA feed seems to decrease polymer molecular weight. On the other hand, increasing diester chain-length gave high molecular weight of polymers. Although, for diethyl adipate, reactions in bulk gave higher M_n polymers, for diethyl sebacate increase of M_n was observed.

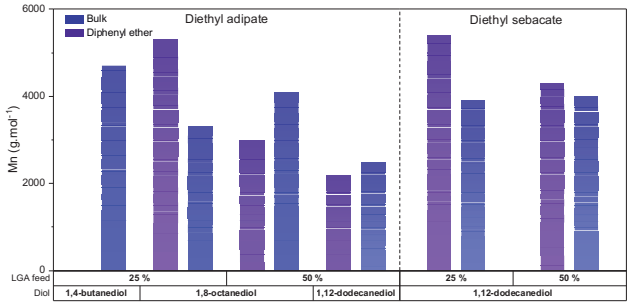

Fig 3.

DSC ANALYSIS: EFFECT OF LEVOGLUCOSAN CONTENT:

The glass transition temperature (T_g) for high content LGA polymer was 31°C, but no T_g was detected for the low content LGA polymer. High levoglucosan content polymer showed lower melting temperature and crystallinity than low LGA content polymer. Also, high LGA content polymer presents multiple melting endotherms, due to multiple crystalline forms.

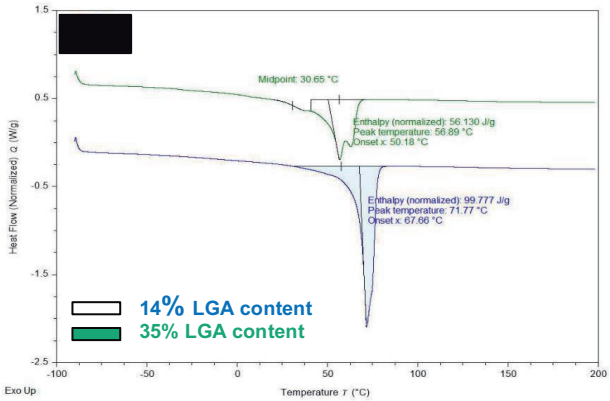

Fig 4. Glass transition for new biopolymers containing 14% and 35% of LGA.

Conclusions

Concerning LGA content and yields, best results were achieved when diethyl sebacate and long chain-length diols were employed. Reactions in diphenyl ether led to higher yields and LGA content than in bulk when diethyl sebacate was used, but no difference was observed for diethyl adipate. When 1,4-butanediol and 1,5-pentanediol were used, poor results were obtained and levoglucosan was not observed in the polymer structure. Polymers of up to 5,500 g.mol-1 were obtained and up to 35% of levoglucosan were observed in polymer structure.

Acknowledgements (Times New Roman 12, bold)

The authors would like to thank the French government through the Programme Investissement d'Avenir (I-SITE ULNE/ANR-16-IDEX-0004 ULNE) managed by the Agence Nationale de la Recherche. LIA CNRS France-Brazil "Energy & Environment" and Métropole Européen de Lille (MEL) for "CatBioInnov" project are also acknowledged. In Brazil, authors would like to thank FAPERJ, CNPq and CAPES.

References

1. I. Itabaiana Junior; M.A. do Nascimento; R.O.M.A. de Souza; A. Dufour; R. Wojcieszak; *Green Chemistry,* **2020**, 22, 5859–5880.
2. F.H. Isikgor, C.R. Becer. *Polymer Chemistry*. **2015**, 6, 4497–4559.
3. K. Nasr, J. Meimoun, A. Favrelle-Huret, J. de Winter, J-M. Raquez, P. Zinck. Polymers. **2020**, 12, 1907: Y. Jiang ; K Loos ; *Polymers*, **2016**, 8, 243.
4. M.A. do Nascimento, L.E. Gotardo, E.M. Bastos, F.C.L. Almeida, R.A.C. Leão, R.O.M.A de Souza, R. Wojcieszak, I. Itabaiana Junior. *Sustain*. **2019**, 11, 1–15.

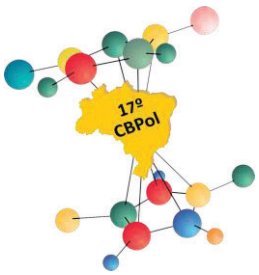

ENZYMATIC SYNTHESIS OF POLY(GLOBALIDE) AND CROSSLINKING VIA THIOL-ENE POST-MODIFICATION

Felipe O. Lima[1], Thiago O. Machado[1,2], Pedro H. H. Araujo[1] and Claudia Sayer[1]

1 – Department of Chemical Engineering and Food Engineering, Universidade Federal de Santa Catarina (UFSC), Florianópolis, SC, Brazil
felipe.ol@posgrad.ufsc.br
2 – School of Chemistry, University of Birmingham, Birmingham, United Kingdom

Abstract - Poly(globalide) (PGl) is a polyester that has gained significant interest in the biomedical field due to its non-toxicity and biodegradability. Its unsaturation in the chain backbone provides a versatile tool for diverse functionalization reactions that can be useful for tuning its properties. Enzymatic ring-opening polymerization (e-ROP) of unsaturated macrolactone globalide was performed in solution. PGl was characterized in relation to molecular weight and distribution, chemical structure, and thermal properties and then modified via thiol-ene reaction using 2,2′-(ethylenedioxy)diethanethiol (EDDT) as a crosslinking agent in the presence of thermal initiator azobisisobutyronitrile (AIBN) in solution in different molar ratios of thiol:ene. The thermal properties of the resulting crosslinked polymers (PGl-EDDT) of the materials were significantly changed, mainly exhibiting a decrease in crystallinity as theoretical crosslinking increased. In summary, PGl modification was able to change chemical characteristics and modulate the material's thermal properties.

Keywords: *macrolactone, globalide, enzymatic ring-opening polymerization, crosslinking, thiol-ene reaction.*
Fundings: Coordenação de Aperfeiçoamento de Pessoal de Nível Superior (CAPES) and Conselho Nacional de Desenvolvimento Tecnológico (CNPq).

Introduction

In polymer science, upcoming challenges hinge on the discovery of novel synthetic components and approaches that can enhance functionalities, customize properties, reduce costs, and mitigate environmental impacts[1]. Applying biodegradable polymers in the biomedical and pharmaceutical fields represents a natural solution to address several challenges in modern medicine. These polymers can be utilized as sutures, bone screws, tissue engineering scaffolds, and drug delivery systems, offering potential benefits in terms of degradability and functionality[2].

Ring-opening polymerization of lactones is a well-established method for producing aliphatic polyesters with diverse applications[2]. The choice of initiators and catalysts determines the polymerization mechanism, including cationic, anionic, coordination-insertion, organocatalytic, and enzymatic polymerization[3]. Enzyme-catalyzed polymerization reactions have gained significant attention due to their greener nature, specificity, efficiency, reusability, low toxicity, and mild reaction conditions[4]. Macrolactones, particularly those with more than 12 atoms, have seen increased demand for manufacturing hydrophobic polyesters derived from fatty acids, with applications in industries such as fragrances and pharmaceuticals[5,6].

Polyglobalide (PGl) is an unsaturated poly(macrolactone) known for its biocompatibility and non-toxicity. It is synthesized from globalide, a macrolactone with a double bond at the 11 or 12 positions[6]. The unique features and modification potential of globalide have been explored in various studies for biomedical materials synthesis[7]. However, the semicrystalline nature and hydrophobicity of PGl represents challenges for its degradation in biomedical applications[3,6].

The thiol-ene "click reaction" offers a promising approach for modifying PGl due to its versatility and cost-effectiveness[8]. This 'click' reaction occurs under mild conditions and results in high yields of polymer with unharmful byproducts[9]. Thiol-ene polymerization and post-modification allow for the customization of polymer characteristics, including reduced crystallinity and increased hydrophilicity, while maintaining non-cytotoxic properties[8]. Understanding the nature of each process is crucial for achieving the desired application, as the range of polymer synthesis, modification, and properties enables the tailoring of materials for various biomedical uses.
In that sense, the present work proposes to develop a modification process of promising polyester poly(globalide) using 2,2′-(ethylenedioxy)diethanethiol (EDDT) as a crosslinking agent and AIBN as a thermal initiator. Understanding this process is helpful to tailor PGl or other similar materials' properties to fulfill specific application requirements and overcome related challenges.

Experimental

Materials

Globalide (Gl) was kindly donated by Symrise. Toluene P.A was purchased from Dinâmica Química Contemporânea LTDA (Brazil). Dichloromethane P.A 99.8% (DCM), ethanol (EtOH) P.A 99,8, methanol (MetOH) P.A 99,5 and tetrahydrofuran P.A. 99,9% (THF) were purchased from Neon Química (Brazil) and used as received. Novozym 435 (N435 – commercial lipase B from Candida antarctica immobilized on polyacrylate beads was a kind gift from Novozymes). Azobisisobutyronitrile 98% (AIBN) and 2,2′-(ethylenedioxy)diethanethiol (EDDT) were acquired from Vetec Química (Brazil). Gl and Nz435 were previously dried for 24h at 60ºC under vacuum and stored desiccator over silica and 4 Å molecular sieves and AIBN was recrystallized before reactions.

Synthesis of poly(globalide) via enzymatic ring-opening polymerization

The synthesis of PGl was carried out in a sealed glass vial in a 2:1 monomer (Gl): solvent (toluene) ratio. Enzyme and molecular sieves concentrations were 5 wt.% and 0.5 wt.%, respectively, in relation to the monomer. Monomer, solvent, enzyme, and molecular sieves were directly weighted in the reaction vial on an analytical precision balance. The reaction was conducted under magnetic stirring at 65ºC for 2h in a sand bath. These conditions were based on the previous works of the group that involved globalide polymerization and other similar polyesters[2,4].
Enzymes and molecular sieves were separated by filtration with the addition of dichloromethane (DCM), and PGl was precipitated in cold methanol. In sequence, the polymer was placed in petri dishes and dried overnight at 60ºC. Yield was measured gravimetrically, reaching 75%. A schematic representation of e-ROP of Gl is showed in Fig. 1.

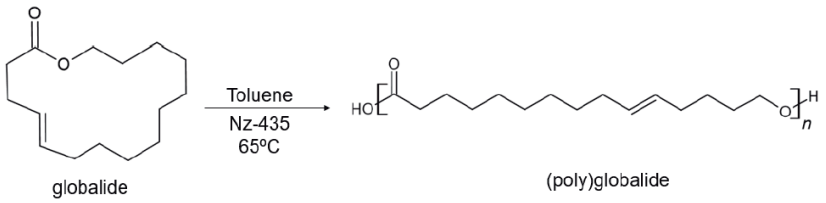

Figure 1:Schematic representation of PGl synthesis via e-ROP

Thiol-ene crosslinking reaction of poly(globalide) with EDDT

Crosslinking of PGl was conducted using a one-pot procedure in solution. The study aimed to investigate the reaction behavior by testing different thiol to ene ratios and varying the amount of the initiator (AIBN) in relation to the thiol. Four formulations (F1, F2, F3, and F4) were prepared with specific ratios and initiator concentrations. Reactants PGl, AIBN, and EDDT were weighed and placed in vials and in sequence THF, the reaction system was purged with nitrogen, sealed, and

subjected to continuous magnetic stirring at 70ºC for 8 h in a sand bath. Table 1 presents the formulations, and Fig. 2 depicts a schematic representation of the crosslinking reaction. After crosslinking, the samples were purified by precipitation in cold ethanol, followed by drying at 60ºC for 48 h to eliminate any residual solvent or unreacted EDDT. The purified samples were then stored for further analysis.

Table 1 – Formulations of crosslinking of PGl via thiol-ene reactions with EDDT.

Entry	PGl (mg)	EDDT (mg)	AIBN (mg)	THF (mL)
F1 (2:1, 1%)	242	92	1	4.4
F2 (2:1, 5%)	238	93	5	4.4
F3 (1:1, 1%)	239	182	2	5.6
F4 (1:1, 5%)	243	180	10	5.6

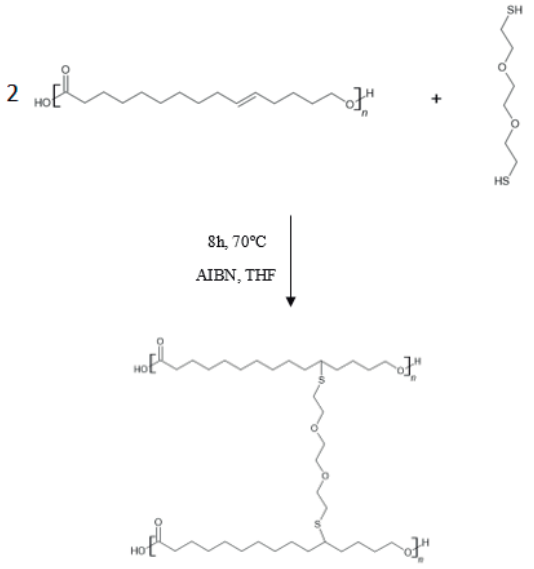

Figure 2: Crosslinking of PGl with EDDT

Polymer characterization

Number average molecular weight (M_n), weight average molecular weight (M_w), and dispersity (Đ) were determined by Gel Permeation Chromatography (GPC) using THF as eluent and calibration against polystyrene standards. Fourier transform infrared (FT-IR/ATR) spectroscopy was performed to identify the chemical structure characteristics PGl and crosslinked polymers. The analysis was determined by Attenuated Total Reflectance (ATR) on thin solid samples Cary 600 model (Model: Agilent Technologies CARY 600) spectrometer with ZnSe window Transmission infrared spectra were recorded in a wavenumber range of 650-4000 cm^{-1}. Thermal properties were determined by differential scanning calorimetry (DSC) using a Perkin-Elmer JadeDSC equipment, under inert atmosphere (N_2, 50 $mL \cdot min^{-1}$), from -30 to 120 °C at a heating rate of 10 $°C \cdot min^{-1}$. Thermal history was removed, and the melting temperatures (T_m) were taken from the second heating runs and melting enthalpies (ΔH_m) and areas from first heating curves. Crosslinked samples crystallinity was estimated using their ΔH_m and ΔH_m of a standard of 100% crystalline poly(ω-pentadecalactone) (PPDL) using Eq 1:

$$T_m^0(X) = \left[\frac{\Delta H(T_m^0, X)}{\Delta H(T_m^0)}\right] T_m^0 \qquad (1)$$

where $\Delta H(T_m^0, X)$, $\Delta H(T_m^0)$, $T_m^0(X)$ and T_m^0 are the melting enthalpies and melting temperature of the crosslinked polymer and homopolymer respectively [2,10].

Results and Discussion

The number (M_n) and weight (M_w) average molecular weights of PGl determined by GPC were 16,700 g·mol^{-1} and 44,926 g·mol^{-1}, respectively, resulting in a dispersity Đ of 2.69.

FT-IR/ATR spectra (Fig. 3a) indicated PGl modification with the appearance of C-S-C stretch (1095 cm^{-1}) present in 2,2′-(ethylenedioxy)diethanethiol (EDDT) ratifying crosslinking agent incorporation in the modified samples.

DSC thermograms (Fig. 3b) suggest that PGl tends to become less crystalline upon cross-linking as the melting peaks area decrease as thiol and initiator concentration increase. These result is in line with previous works that approached crosslinking of PGl[7,11]. The degree of crystallinity in the materials were estimated by Eq. 1 using the value of a PPDL sample as reference. PGl homopolymer displayed highest crystallinity (49.54%) confirming its semicrystalline characteristic (Table 2). Also, the theoretically more crosslinked sample (F4, with the highest thiol and initiator concentrations) presented a complete disappearance of its melting peak and, therefore its T_m could not be determined, indicating a completely amorphous feature as Fig. 3b shows. Regarding melting temperatures, neither significant variation nor pattern were observed with the peaks broadening.

Table 2 – Thermal properties determined by DSC analysis for PGl and crosslinked samples (ΔH_m: melting enthalpy; T_m: melting temperature peak; X_C: degree of crystallinity, calculated from the fusion enthalpy value of a PPDL 100% crystalline sample[2,10].

Sample	ΔH_m(J/g)	T_m (C°)	X_C (%)
PGl	91.49	46.54	49.54
F1	62.00	47.50	33.56
F2	46.41	42.50	25.12
F3	9.53	44.24	5.16
F4	2.78	-	1.50

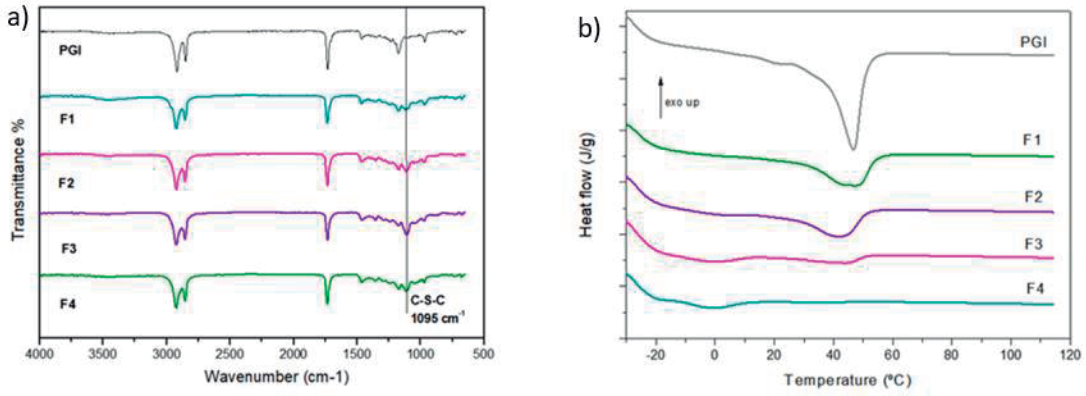

Figure 3: a) FTIR spectra and b) DSC thermograms of PGl and crosslinked samples using different thiol ene ratios and AIBN concentrations.

Conclusions

Enzymatic ring opening polymerization of globalide was carried out obtaining a polymer with Mw and Mn of 44,926 g·mol^{-1} and 16,700 g·mol^{-1}, respectively, and polydispersity Đ of 2.69. In addition,

thiol-ene crosslinking modification of resulting poly(macrolactone) poly(globalide) was studied in solution varying thiol:ene ratios and initiator concentration. PGl and crosslinked PGl were chemically characterized by FTIR/ATR confirming their structure change. Thermal properties of the materials were significantly changed mainly exhibiting a decrease in crystallinity as theoretical crosslinking increased. The results of this study suggest that PGl can be adjusted to meet specific requirements by introducing crosslinking agents into the polymer structure.

Acknowledgements
The authors acknowledge the financial support from Coordenação de Aperfeiçoamento de Pessoal de Nível Superior - Brasil (CAPES) and Conselho Nacional de Desenvolvimento Tecnológico (CNPq) and Symrise for providing the monomer.

References

1. Resetco, C., Hendriks, B., Badi, N., & Du Prez, F. (2017). Thiol–ene chemistry for polymer coatings and surface modification – building in sustainability and performance. *Mater. Horiz.*, *4*(6), 1041–1053. https://doi.org/10.1039/C7MH00488E
2. Guindani, C., Dozoretz, P., Veneral, J. G., da Silva, D. M., Araújo, P. H. H., Ferreira, S. R. S., & de Oliveira, D. (2017). Enzymatic ring opening copolymerization of globalide and ε-caprolactone under supercritical conditions. *Journal of Supercritical Fluids*, *128*(April), 404–411. https://doi.org/10.1016/j.supflu.2017.06.008
3. Lecomte, P., & Jérôme, C. (2012). Recent developments in ring-opening polymerization of lactones. In *Advances in Polymer Science* (Vol. 245, pp. 173–218). Springer New York LLC. https://doi.org/10.1007/12_2011_144
4. Polloni, A. E., Chiaradia, V., Figura, E. M., De Paoli, J. P., de Oliveira, D., de Oliveira, J. V., de Araujo, P. H. H., & Sayer, C. (2018). Polyesters from Macrolactones Using Commercial Lipase NS 88011 and Novozym 435 as Biocatalysts. *Applied Biochemistry and Biotechnology*, *184*(2), 659–672. https://doi.org/10.1007/s12010-017-2583-4
5. Chiaradia, V. (2019). *Unsaturated macrolactone polymerization followed by its modification and crosslinking via click chemistry-based reactions*.
6. Wilson, J. A., Ates, Z., Pflughaupt, R. L., Dove, A. P., & Heise, A. (2019). Polymers from macrolactones: From pheromones to functional materials. *Progress in Polymer Science*, *91*, 29–50. https://doi.org/10.1016/j.progpolymsci.2019.02.005
7. Van Der Meulen, I., De Geus, M., Antheunis, H., Deumens, R., Joosten, E. A. J., Koning, C. E., & Heise, A. (2008). Polymers from functional macrolactones as potential biomaterials: Enzymatic ring opening polymerization, biodegradation, and biocompatibility. *Biomacromolecules*, *9*(12), 3404–3410. https://doi.org/10.1021/bm800898c
8. Beltrame, J. M., Guindani, C., Novy, M. G., Felipe, K. B., Sayer, C., Pedrosa, R. C., & Hermes De Araújo, P. H. (2021). Covalently Bonded N-Acetylcysteine-polyester Loaded in PCL Scaffolds for Enhanced Interactions with Fibroblasts. *ACS Applied Bio Materials*, *4*(2), 1552–1562. https://doi.org/10.1021/acsabm.0c01404
9. Machado, T. O., Sayer, C., & Araujo, P. H. H. (2017). Thiol-ene polymerisation: A promising technique to obtain novel biomaterials. *European Polymer Journal*, *86*, 200–215. https://doi.org/10.1016/j.eurpolymj.2016.02.025
10. Crescenzi, V., Manzini, G., Calzolari, G., & Borri, C. (1972). Thermodynamics of fusion of poly-β-propiolactone and poly-ϵ-caprolactone. comparative analysis of the melting of aliphatic polylactone and polyester chains. *European Polymer Journal*, *8*(3), 449–463. https://doi.org/10.1016/0014-3057(72)90109-7
11. Chiaradia, V., Hanay, S. B., Kimmins, S. D., de Oliveira, D., Araújo, P. H. H., Sayer, C., & Heise, A. (2019). Crosslinking of electrospun fibres from unsaturated polyesters by bis-triazolinediones (TAD). *Polymers*, *11*(11). https://doi.org/10.3390/polym11111808

FUNCTIONALIZATION OF "BOTTLEBRUSH" POLYDIENES

Geilza A. Porto[1], Nelson N. dos Santos[2,3], Mariana M. V. M. Souza[2] and Marcos L. Dias[1]*

1 – Institute Professor Eloisa Mano of Macromolecules, Federal University of Rio de Janeiro (UFRJ), Rio de Janeiro, RJ Brazil mldias@ima.ufrj.br
2 – School of Chemistry, Federal University of Rio de Janeiro (UFRJ), Rio de Janeiro, RJ Brazil
3– Federal Institute of Education, Science and Technology of Rio de Janeiro (IFRJ), Rio de Janeiro, RJ Brazil

Abstract - Polyfarnesenes are "bottlebrush" polymers that retain three alkene moieties per repeating unit[1,2]. The addition of polar groups to alkenes enables further nucleophilic substitutions, making these biobased, super-soft and rubberish materials versatile building blocks for several polymer specialties. In this work, we report the hydrochlorination[3] of an oligomer (85% 1,4-cis and 15% 3,4-enchainment, with about ten monomer units) with tosylic acid and $CaCl_2$ in CH_2Cl_2/acetic acid medium at room temperature for 17 hours. The aliphatic region of ^1H NMR spectra of the polymers (Fig. 1) showed a higher reactivity for less hindered C10-C11 double bond. The Fig. 1b exhibits two broad peaks at 1.73 ppm and 1.53 ppm, assigned to C10 and C9 methylene groups. Noteworthy, the integration area between 1.85-2.10 ppm (CH_2 bound to alkene) decreased from 11.8 to 6.7 (43%) indicating hydrochlorination of C6-C7 bond. The olefin protons are not shown in Fig. 1.

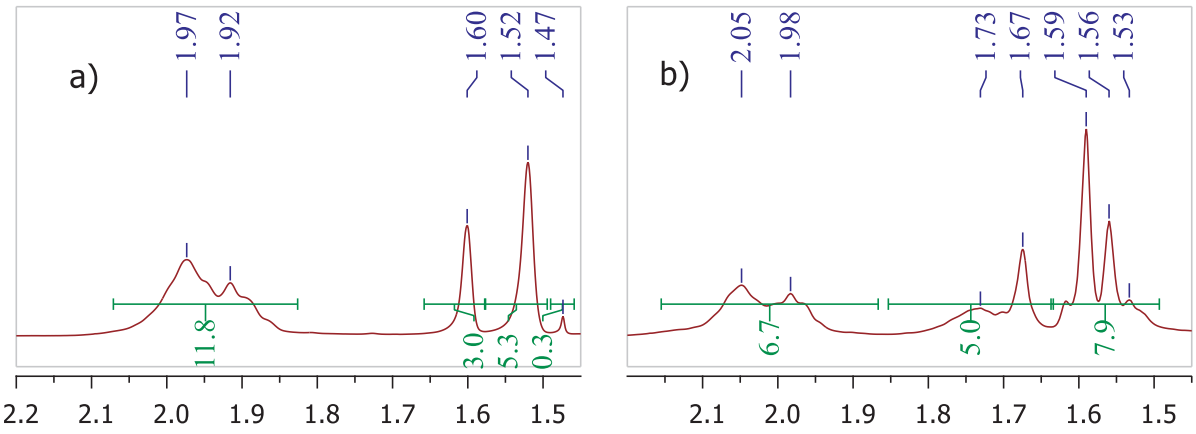

Figure 1. NMR spectra of original (a) and hydrochlorinated (b) polyfarnesenes.

References.
1. X. Liu; P. M. Claesson *Polymers* 2022, *14*, 2724. https://doi.org/103390/polym14132724.
2. D. J. McPhee U.S. Patent 8 217 128 B2, 2012.
3. X. Bertrand; P. Paquin; L. Chabaud; J.-F. Paquin *Synthesis* 2022, *54*, 1413. https://doi.org/10.1055/s-0040-1719856.

Keywords: p*olyfarnesenes, alkene functionalization, hindrance.*

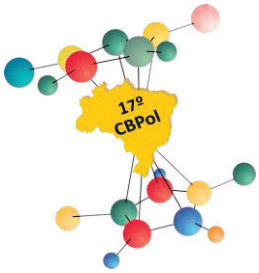

GRAFTING OF POLY(N-VINYLCAPROLACTAM) ON POLYURETHANE BY GAMMA RADIATION

Grazielle R. de Cerqueira[1*], Rhodivam L. M. Feitosa[1], Mariana A. Henrique[1], Michele F. Andrade[1], Felipe C. S. Trindade[2], Elmo S. Araujo[3], Armando Navarro-Vázquez[1,2], Wilson B. Junior[4], Glória M. Vinhas[1,5], Yêda M. B. Almeida[1,5], Carolina L. Morelli[1,6]

1 - Materials Science Program, Federal University of Pernambuco (UFPE), Recife, PE, Brazil
grazielle.rozendo@ufpe.br
2 - Department of Fundamental Chemical (DQF), Federal University of Pernambuco (UFPE), Recife, PE, Brazil
3 - Department of Nuclear Energy (DEN), Federal University of Pernambuco (UFPE), Recife, PE, Brazil
4 - Department of Physics (DF), Federal University of Pernambuco (UFPE), Recife, PE, Brazil
5 - Department of Chemical Engineering (DEQ), Federal University of Pernambuco (UFPE), Recife, PE, Brazil
6 - Department of Mechanical Engineering (DEM), Federal University of Pernambuco (UFPE), Recife, PE, Brazil

Abstract - Poly(N-vinylcaprolactam) (PNVCL) is a thermoresponsive, biocompatible, non-toxic polymer with a phase transition temperature from hydrophilic to hydrophobic state (T_{pt}) close to the physiological temperature. In this work, PNVCL homopolymers were synthesized, as well as PNVCL was grafted onto thermoplastic polyurethane (TPU) films using gamma radiation at doses of 5 and 20 kGy. Fourier transform infrared spectroscopy (FTIR) and thermogravimetry (TGA) results confirmed PNVCL polymerization as well as the grafting of PNVCL on TPU films. The T_{pt} of homopolymers determined by cloud point method and rheological analysis was around 30ºC. PNVCL grafting provided thermoresponsive features to the TPU films as observed by the variation in hydrophilicity of film surfaces with temperature as measured by the contact angles with water. The present work contributed to the development of a thermoresponsive graft copolymer, with the innovation of grafting PNVCL on TPU films using gamma radiation.

References

1. L. Marsili, M. D. Bo, G. Eisele, I. Donati, F. Berti, G. Toffoli *Polymers* 2021, *13*, 2639. https://doi.org/10.3390/polym13162639.
2. I. V. Nieuwenhove, S. Maji, M. Dash, S. V. Vlierberghe, R. Hoogenboom, P. Dubruel *Polymer Chemistry 2017, 8*, 2433-2437. https://doi.org/10.1039/C6PY02224C.
3. Q. Zhang, C. Weber, U. S. Schubert, R. Hoogenboom *Materials Horizons* 2017, *4*, 109-116. https://doi.org/10.1039/C7MH00016B.
4. A. Usanmaz, T. Özdemir, Ö. Polat *Journal of Macromolecular Science Part A* 2009, *46*, 597–606, https://doi.org/10.1080/10601320902851868.

Keywords: *Poli(N-vinylcaprolactama, polyurethane, gamma radiation, grafting, thermoresponsive polymers.*

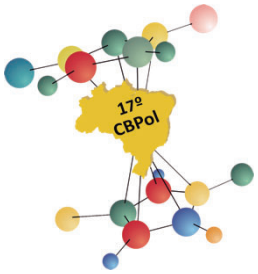

INFLUENCE OF THE CATALYST ADDITION PROCEDURE AND INITIAL MOLECULAR WEIGHT ON THE SOLID-STATE POLYMERIZATION OF POLY (LACTIC ACID)

Lívia M. G. Gonçalves[1]*, Rosario E. S. Bretas[1] and Sílvia H. P. Bettini[1]

1 – Graduate Program in Materials Science and Engineering, Federal University of São Carlos (UFSCar), São Carlos, SP, Brazil
liviagarciagoncalves@gmail.com

Abstract – *Solid-state polymerization* is a known method applied to polycondensation polymers such as poly (ethylene terephthalate) PET, particularly for recycling post-consumer material, to recover the molecular weight reduction caused by degradation. However, the literature provides few references for its use on poly (lactic acid) (PLA), a promising biodegradable alternative, mainly as a synthesis route. This study aims to study the influences of the process of incorporating catalyst systems on the pre-polymer and the molecular weight of this pre-polymer on the conversion of the solid-state polymerization of commercial poly (lactic acid) previously hydrolyzed. PLA Ingeo 3100HP (NatureWorks LLC) was hydrolyzed in distilled water at 60°C for 24, 48, 72 or 96 h. After hydrolysis, a catalytic system composed of 0,5% in weight of $SnCl_2.2H_2O$ and an equimolar proportion of p-toluenesulfonic acid (p-TSA) was added to the polymer by two different means: via solubilization of the polymer in chloroform, adding the catalyst and evaporating the solvent; or via mixing in the polymer melt. The samples were then pressed, and heat treated to crystallization. After crystallization, samples were submitted to SSP and then characterized by size exclusion chromatography (SEC) for molecular weight evaluation, and their acidity percentage was determined via titration. Adding a catalyst is necessary for the molecular weight increase during SSP; however, due to the acidity of the catalysts, degradation of the starting material is caused. The addition process via solubilization causes higher degradation, i.e., molecular weight decreases more than the process via melting. The molecular weight increase obtained after SSP is also less significant in the samples produced in the solvent. Concerning the influence of the initial molecular weight on the SSP process, the higher the molecular weight of the pre-polymer, the higher the molecular weight achieved after the reaction.

Fundings: This study was financed in part by the Coordenação de Aperfeiçoamento de Pessoal de Nível Superior - Brasil (CAPES) - Finance Code 001. The authors also thank to the Fundação de Amparo à Pesquisa do Estado de São Paulo, process number 2020/07633-2.

Keywords: *poly (lactic acid), solid state polymerization*

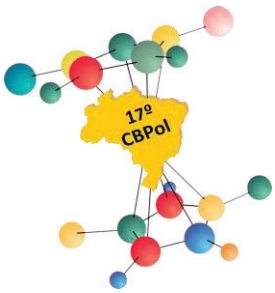

INFLUNCE OF SURFACTANT AND COSTABILIZER INTERACTIONS IN THE KINETICS OF IN-SITU POLYSTYRENE/BASO4 NANOCOMPOSITES OBTAINED VIA MULTIPLE SEQUENCIAL MICROEMULSIONS

Rafael C.J.P.S. Salvato[1*], Amilton M. Santos[1]

1 – Department of Chemical Engineering, Lorena Engineering School, University of São Paulo, Lorena, SP, 12602-810, Brazil. Corresponding author: rafaelcaetano@usp.br

Abstract - Polymer/inorganic nanocomposites have received considerable attention of academic and industrial research as the incorporation of nanofillers within a polymer matrix often leads to materials with enhanced mechanical, thermal, or barrier properties, even at low inorganic contents [1]. However, obtaining these nanoparticles as well as stabilizing them proves to be a particularly challenging task, mainly via heterophase polymerization in aqueous media. In many papers in the literature miniemulsion polymerization have been reported as an alternative to overcome these drawbacks, however using specific equipment with clear limitations of scale-up to industrial end-use, what severely limited their adoption by the main targeted applications [2]. Furthermore, this process frequently relies on complex interactions such as surfactant adsorption onto polymeric and inorganic particles, as well as on control variables which influences the surfactant-oil-water system likewise temperature, ionic strength, and pH [3]. Data-driven and semi phenomenological modeling such as Hansen solubility parameters (HSP) have been recently used to understand better polymer-surfactant-nanoinorganic particle interactions [4]. In this report, a comparative evaluation involving polymerization kinetics and component affinity assessment via HSP theory was done for polystyrene/barium sulfate (Sty/$BaSO_4$) hybrid latices obtained via in-situ synthesis of both inorganic and polymeric nanoparticles through the sequential processing of multiple (mini)emulsions. As variables in this two-step radical polymerization approach, were considered: the process intensification technique (phase inversion temperature and rotor stator mixers), the technical-grade surfactant architecture (linear lauryl fatty and branched oxo hydrophobic tails) and costabilizer chemical nature (hexadecane and lauryl fatty alcohol). Experimental results from the kinetic study (conversion and dynamic light scattering data) indicates that surfactant and costabilizer compatibility matters (same fatty tail shown best results) and the affinity predictions for surfactant-costabilizer pairs via HSP theory correlate with it.

References

1. A. Bhat et al, Smart polymeric nanocomposites: synthesis and applications, Nanotechnology Reviews (2021). doi: 10.1515/ntrev-2021-0018
2. J.M Asua, Challenges for industrialization of miniemulsion polymerization. Progress in Polymer Science (2014). doi: 10.1016/j.progpolymsci.2014.02.009S.
3. V. V. Ginzburg. Mesoscale Modeling of Micellization and Adsorption of Surfactants and Surfactant-Like Polymers in Solution: Challenges and Opportunities *Industrial & Engineering Chemistry Research* (2022). doi: 10.1021/acs.iecr.2c01512
4. S. Abbott. Solubility, similarity, and compatibility: A general-purpose theory for the formulator. *Current Opinion in Colloid & Interface Science*, 2020, *48*, 65-76. Doi: 10.1016/j.cocis.2020.03.007

Keywords: *miniemulsion polymerization, phase inversion emulsification, polymer nanocomposite, HSP*

INSIGHTS INTO THE BACKBITING REACTION IN ACRYLIC ACID POLYMERIZATION: A MODELING APPROACH

Victor A. Salles[1]*, Reinaldo Giudici[1]

1 – Department of Chemical Engineering, University of São Paulo (USP), São Paulo, SP, Brazil
(vsalles@usp.br)

Abstract - This study focuses on modeling the polymerization of acrylic acid considering the backbiting reaction. By analyzing the kinetics and properties of the resulting polymers, the aim is to understand the impact of this reaction during the polymerization process. The polymerization of acrylic acid in aqueous media is widely used in industry due to its favorable cost-effectiveness. However, the presence of partial charges and dipole moments in the acrylic acid molecule can interact with water and deviate from the usual polymerization behavior. This study specifically addresses the backbiting reaction that can occur during the polymerization. The modeling of the polymerization process was carried out, considering the characteristics of acrylic acid and the influence of the backbiting reaction. Utilizing kinetic modeling methods, equations were developed to describe the monomer consumption rate, initiator decomposition, and polymer formation. Through the analysis of the kinetic equations, valuable insights into the kinetics of acrylic acid polymerization considering the occurrence of the backbiting reaction were obtained. The kinetic parameters were estimated using nonlinear regression analysis, providing a better understanding of the polymerization process. The results revealed that the backbiting reaction significantly influences the kinetics and properties of the resulting polymers. This information is crucial for optimizing polymerization processes and assisting in the development of tailored polymeric products. In summary, this study focuses on the modeling of acrylic acid polymerization with a particular emphasis on the backbiting reaction. The utilization of kinetic modeling allows for the establishment of equations that accurately describe the process. The findings contribute to a deeper understanding of the behavior of acrylic acid polymerization, enabling improvements in industrial processes and the development of customized polymeric products.

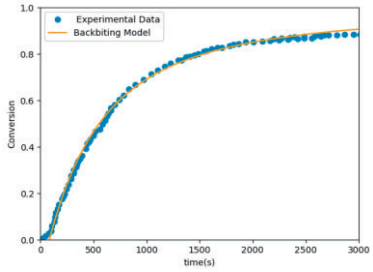

Fig 1 – Conversion per time for backbiting model

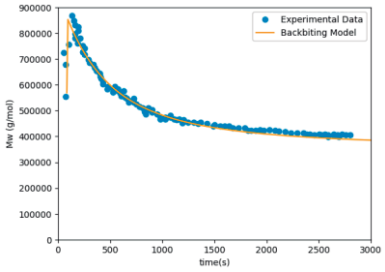

Fig 2 – Molar weight per time for backbiting model

References

1. R. J. Minari; G. Caceres; P. Mandelli; M. M. Yossen; M. Gonzalez-Sierra; J. R. Vega; L. M. Gugliotta *Macromol. React. Eng. 2011, 5, 223-231*. https://doi.org/10.1002/mren.201000059
2. G. M. Araújo, *Synthesis of a superabsorbent polymer and homopolymerization study of acrylic acid*, University of São Paulo, 2021.
3. G. Odian, *Principles of Polymerization*, John Wiley & Sons, New Jersey, 2004.

Keywords: *Acrylic polymerization, Backbiting, Kinetic modeling, Polymer properties, Reaction mechanisms.*

LINEAR POLYGLYCEROL FROM CHLOROPROPANOL: NEW SYNTHETIC ROUTES

Ticiane V. P. Souza[1], Angelo R. S. Oliveira[1], Valéria G. Costa[2], Maria Aparecida F. César-Oliveira[1]*

1 – LEQUIPE – Department of Chemistry, Federal University of Paraná (UFPR), Curitiba, PR, Brazil
mafco@ufpr.br
2 – LAMAP – National Institute of Technology (INT-MCTI), Rio de Janeiro, RJ, Brazil

Abstract – This work presents a new synthetic route to obtain a majority of a linear polyglycerol (PG), with control of the molar mass values for the obtained products, from step-by-step polymerization of 3-chloropropane-1,2-diol (MCPD) in presence of a basic salt. It also explores the use of halogenated starting materials that are derived by chemical modification of glycerol, a raw material abundant and low cost, obtained from a renewable source. This work used a mild reaction condition, with low temperatures, avoiding the formation of toxic by-products, such as acrolein, for example. To achieve these goals, a methodology was developed based on the etherification reaction, inspired by the reaction conditions of the Williamson Synthesis, but applied to the polymerization of MCPD. The reaction is carried out in three steps, using K_2CO_3 as a catalyst, and this process was submitted to a patent application, for this reason, the experimental procedure cannot be presented in detail. The first stage was carried out in an inert atmosphere (N_2) in the range of 140-160 °C, for 2-4 h; the second step was carried out at 180-200 °C (2-4 h); and the third step, the residual products were removed under reduced pressure. The PG obtained was separated by solubilization in methanol and filtered. The purification was carried out by cooling the solution below 10 °C, followed by filtration and solvent removal by evaporation. The PG was characterized by ^{1}H and $^{13}C\{^{1}H\}$ NMR, FTIR, and MALDI-TOF. Which presented molar mass values around 520-580 g mol^{-1} of PG, obtained as a pure product, with average yields of 92%.

Table 1 – Molar mass (M_n and M_w values) from MALDI-TOF, for polyglycerols synthesized from MCPD.

Reaction time in different conditions (h)		MCPD	
140-160 ºC, N_2	180-200 ºC, N_2	M_n	M_w
8	2	568	582
6	2	540	568
4	2	506	524

Figure 1 – ^{1}H NMR (DMSO-d6, 400 MHz) and $^{13}C\{^{1}H\}$ (100 MHz) representative spectra, respectively, of synthesized polyglycerols.

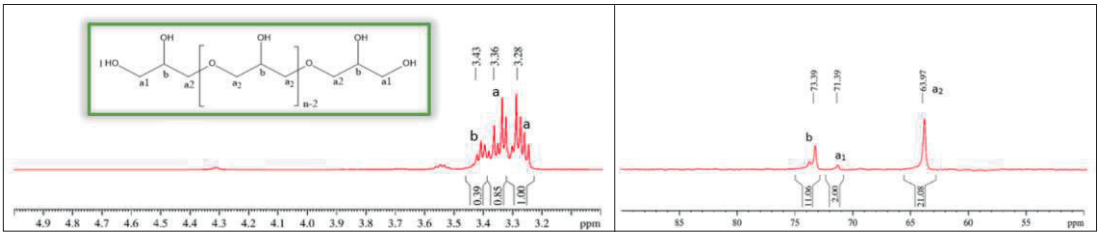

References:
1. C, CHONG,. *et al*. *Environmental Technology and Innovation* 2020, 19. 100859.
2. M., IONESCU, Z. S. PETROVIC *Eur. J. Lipid Sci. Technol.* 2018, 120, 1800004.

Keywords: *Linear polyglycerol, Chloropropanol, Glycerol, Hydroxylated polyether, Molar-mass control.*

LUMINESCENT PROPERTIES OF THE EU $^{3+}$ COMPLEX IN POLYURETHANE FOAM

Taissa T. de Deus[1]*, Samanta, T. Medeiros[1] , Mariana Passarin[1] , Juliana R. Kloss[1] and Renata D. Adati[1]

Academic Department of Chemistry and Biology, Federal University of Technology – Paraná (UTFPR), Curitiba, PR, Brazil taissa@alunos.utfpr.edu.br

Abstract - Optical sensors devices are often used to detect physical and/or chemical changes by measuring the intensification or suppression of the emission process. The synergic properties from hybrid europium ion (Eu^{3+}) coordination compounds dispersed in a polyurethane (PU) matrix overcome disadvantages such as low thermal stability, chemical reactivity, and energy transfer processes. This work objective to synthesize and characterize, through structural and optical properties, the luminescent complex hybrid $[Eu(tta)_3(H_2O)_3]$, where tta= tenoyltrifluracetone and rigid polyurethane foam. The complex was added to the foam at 1:3 and 5 % (w/w) proportions. The Eu^{3+} complex $[Eu(tta)_3(H_2O)_3]$ was prepared by adding the pre-linker Htta. The hybrid was obtained through the reaction between the formulated polyol-polyester, 4,4' diphenylmethane diisocyanate and $[Eu(tta)_3(H_2O)_3]$ complex. The material was characterized by Fourier transform infrared spectroscopy (FTIR), UV-Vis absorption spectroscopy, and photoluminescence measurements. In the spectra obtained by FTIR, the presence of the characteristic bands from the PUs matrix from ν(NH) group at 3300 and 1530 cm^{-1}, ν(CH) at 2900 cm^{-1} and ν(C=O) at 1750 cm^{-1}, revealing the successful polymer formation. The UV-Vis spectrum exhibits absorption at 260 and 330 nm confirming that the PU matrix and tta ligand act as an efficient antenna. It was found that (f-f) transitions intensities change according to the higher complex concentration in the matrix. Preliminary results suggest that the luminescent complex is homogenously distributed into the PU matrix to obtain hybrid materials, which exhibit monochromatic emission in the red region of the electromagnetic spectrum, and, therefore the study has potential for applications in the identification and monitoring of metal ions, such as Cu^{2+} present in aqueous solution.

References

1. GAO, Lijun et al. *Journal of Luminescence 2019,* 212, 328-333. https://doi.org/10.1016/j.jlumin.2019.02.055
2. UTOCHNIKOVA, V. V. *Coordination Chemistry Reviews*, 2019, 398, 113006. https://doi.org/10.1016/j.ccr.2019.07.003
3. CLEMENTINO, F. C. et al. *Applied Clay Science*, 2022, 227, 106591. https://doi.org/10.1016/j.clay.2022.106591

Keywords: *rigid foam, polymer, Eu $^{3+}$ complex, photoluminescence, hybrid compound.*

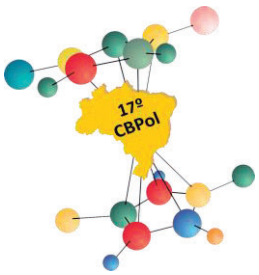

MODIFICATION OF EUDRAGIT S100 POLYMER USING UGI MULTICOMPONENT REACTION

Taylor F. da Paz Gomes[1*], Cassia Almeida Brito[1] e Marcos Lopes Dias[1]

1 – *Instituto de Macromoléculas Professora Eloisa Mano* (IMA), *Universidade Federal do Rio de Janeiro* (UFRJ), Rio de Janeiro, RJ, Brasil

taylorferreira@ima.ufrj.br

Abstract - Eudragit S100 (ES100) is an anionic copolymer of methacrylic acid and methyl methacrylate (poly(methacrylic acid-co-methyl methacrylate)), which has 27-30% acidic groups in its structure and is marketed as a solid in the form of a white powder[1]. Multicomponent reactions have been widely used in the synthesis of new molecules, but it was only in 2011 that the first work was published, in which multicomponent reactions were used, both for the synthesis and modification of polymers[2]. Among these reactions, the Ugi Reaction has been used to modify polymers, because in this type of reaction there is no need to use a catalyst, the vast majority of reactions being possible at room temperature, with high economy of atoms and high yield[3]. In this work, Eudragit S 100 was modified with p-chloro-aniline, through the Ugi reaction, at room temperature. The reaction was carried out using formaldehyde and tert-butyl isocyanide as reagents and methanol as solvent, not requiring the use of an inert atmosphere. For the structural and physical-chemical characterization of the modified polymer, nuclear magnetic resonance (1H NMR), thermogravimetric analysis (TGA), Fourier transform infrared spectroscopy (FTIR) and Differential Scanning Calorimetry (DSC) were used. The structural evaluation of the modified polymer by 1H NMR demonstrated that the spectrum presents peaks between 6.69 and 7.21 ppm, characteristic of aromatic compounds substituted in the para-position, confirming the formation of polymer containing pendant p-chloro-phenyl fragments to the polymeric chain.

1. DOS SANTOS, Juliana et al. Eudragit®: A versatile family of polymers for hot melt extrusion and 3D printing processes in pharmaceutics. **Pharmaceutics**, v. 13, n. 9, p. 1424, 2021.
2. KREYE, Oliver; TÓTH, Tommy; MEIER, Michael AR. Introducing multicomponent reactions to polymer science: Passerini reactions of renewable monomers. **Journal of the American Chemical Society**, v. 133, n. 6, p. 1790-1792, 2011.
3. Wen, Y. Chen, X. Liu, Z. Zhu, Q. Li, Z. He, G. Yan, H. Lin,Q . Hydrophobically Modified Alginate Derivatives via the Ugi Multicomponent Reaction for the Development of Hydrophobic Pharmaceutical Formulations. Chemistry Select, v. 6, n. 40, p. 10965–10973, 2021.

Keywords: *Polymer modification, Ugi reaction, Acrylic polymer.*

PERFORMANCE OF THE BACTERIAL CELLULOSE HYDROPHOBIZATION PROCESS FOR APPLICATION IN FOOD PACKAGING

Maryana M. Frota[1]*, Kelvi W. E. Miranda[2], Tiago M. de Souza[2]; Vitória S. Marques[1]; Maria do S. R. Bastos[3]; Lucicléia B. Vasconcelos[1]

1 – Department of Food Engineering, Federal University of Ceará (UFC), Fortaleza, CE, Brazil
mary.m.frota@gmail.com
2 – Department of Chemical Engineering, State University of Amapá (UEAP), Macapá, AP, Brazil
3 - Embrapa Tropical Agroindustry, Brazilian Agricultural Research Company, Fortaleza, CE, Brazil

Abstract - Bacterial cellulose (BC) is considered one of the most promising polysaccharides, presenting a unique three-dimensional structure, nanomorphology and mechanical properties of great interest. Such characteristics draw the attention of the food industry to its use in packaging. However, due to its high hydrophilicity, its application is limited. Thus, the present work aimed to functionalize BC with silane groups, aiming to increase its hydrophobicity for later application in food packaging. The purified BC membranes were defibrillated in a colloid mill to obtain bacterial cellulose nanofibers (BCNF) suspended in a carboxymethylcellulose solution (0.1% w/v). BCNF modification occurred with acidification of the suspension with lactic acid (2 M), pH 3.0, 3.5, 4.0 and 4.5. Then, a suspension in water of 1% (w/v) of silicon dioxide (SiO_2) was added at a ratio of 1:1 and subsequent stirring for 2 hours. Obtaining the dry functionalized cellulosic material (s-BCNF) was obtained by lyophilization. From infrared spectra, it was possible to confirm the functionalization of BC/SiO_2. Likewise, at pH 4.5, there was a greater interaction between the BC hydroxyl groups and the SiO_2 silanol groups, with an increase in the intensity of the bands, in relation to the other treatments. The morphology of s-BCNF at pH 4.5 showed SiO_2 nanoparticles attached to the fibers, forming microsized agglomerates. Such conformation favors BCNF functionalization and reduction of the hydrophilic profile of the material, as can be seen by the larger contact angles for s-BCNF at this pH, on average 41.4° ± 1.7, differing significantly from BCNF, with a contact angle of 20.6° ± 1.88. This functionalization method provides a new and promising way to hydrophobize BCNF from bacterial cellulose, developed from a simple method of surface modification and using safe materials for use in food application.

References

1. A. L. S. Pereira; J. P. A Feitosa; J. P. S Morais; M. de F Rosa. Bacterial cellulose aerogels: Influence of oxidation and silanization on mechanical and absorption properties. *Carbohydrate Polymers* 2020*, 250*, 116927. https://doi.org/10.1016/j.carbpol.2020.116927

2. X. Hu; B. Yang; M. Hao; Z. Chen; Y. Liu; S. Ramakrishna; X. Wang; J. Yao. Preparation of high elastic bacterial cellulose aerogel through thermochemical vapor deposition catalyzed by solid acid for oil-water separation. *Carbohydrate Polymers* 2023, *305*. https://doi.org/10.1016/j.carbpol.2023.120538

Fundings: This work was financially supported by CNPq/MCTI/FNDCT n.18/2021 Universal (404638/2021-0).

Keywords: *Bacterial cellulose; Silanes; Silicon dioxide*

PREPARATION AND CHARACTERIZATION OF RIGID POLYURETHANE FOAMS WITH AGROINDUSTRIAL RESIDUES

Jessica C. Burda[1*], Flávia F. Guimarães[2], Maraísa L. Menezes [2], Adriano G. Viana[3] and Juliana R. Kloss[1]

1 – Academic Department of Chemistry and Biology, Federal University of Technology – Paraná (UTFPR), Curitiba, PR, Brazil
**Jessicaburda@alunos.utfpr.edu.br*
2 – Coordination of Chemical Engineering, Federal University of Technology – Paraná (UTFPR), Apucarana, PR, Brazil
3 – Department of Chemistry, State University of Ponta Grossa (UEPG), Ponta Grossa, PR, Brazil

Resulting from industrial interest, the synthesis of polyurethanes (PU) has grown in recent decades because of its versatility. However, there are environmental implications related to its production and the inadequate disposal of this class of material. Thus, the use of agroindustrial waste in the composition of polymeric materials has been studied since the beginning of this century, aiming to replace petrochemical reagents, helping to improve thermal and morphological properties besides expanding sustainable applications in civil construction and in the process of contaminant removal, adding value to agroindustrial waste and contributing to the reduction of environmental impacts related to its disposal. The present research objective to prepare, characterize and compare the properties of PU foams with different proportions of passion fruit, tamarind and pine nut shells, replacing part of the polyol-polyester in the formulations. They were characterized through particle size, *Fourier*-transform infrared spectroscopy (FTIR) and X-ray diffraction (XRD), and the compositions were evaluated by FTIR, XRD and Scanning electron microscopy (SEM). According to the results obtained, an average particle size of 0.180 mm was verified for passion fruit peel, 0.920 mm for tamarind and 0.125 mm for pine nut. The FTIR analysis revealed in the compositions the presence of groups of polyurethane foams, indicating the formation of the polymer, and the lignocellulosic compounds present in the different shells. The XRD data showed a peak at 2θ= 21º related to the crystalline fraction of the cellulosic, and the SEM showed the interconnected cells of the foam. Thus, the presence of the shells in the foam formulations did not interfere in the formation of the polymer in question, demonstrating promising future applications. Moreover, the substitution of part of the polyol by cellulosic materials reduced the consumption of petrochemical reagents in accordance with one of the principles of Green Chemistry.

References

1. R. Beran; L. Zarybnicka; D. Machova; *Journal of Applied Polymer Science* 2020, *137,* 49095. https://doi.org/10.1002/app.49095
2. A. R. Carmona; H. A. C. Lopera; *Journal of the Mechanical Behavior of Biomedical Materials* 2022, *126*, 105064. https://doi.org/10.1016/j.jmbbm.2021.105064
3. K. M. Al-Qahtani; *Journal of Taibah University for Science* 2015, *10,* 700. https://doi.org/10.1016/j.jtusci.2015.09.001
4. M. L. Meneses, PhD. Thesis, State University of Maringa, 2010.

Keywords: *Expanded polymer, fruit peels, cellulose, waste.*

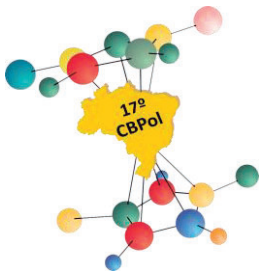

PREPARATION AND CHARACTERIZATION OF RIGID POLYURETHANE FOAM WITH ORANGE PEEL

Tobias C. Negrão[1], Lucila A. A. Coral[1], Paulo R. S. Bittencourt[2] and Juliana R. Kloss[1*]

1 – Academic Department of Chemistry and Biology, Federal University of Technology – Paraná (UTFPR), Curitiba, PR, Brazil
2 – Academic Department of Chemistry (DAQ), Federal University of Technology – Paraná (UTFPR), Medianeira, PR, Brazil
tobiasnegrao@alunos.utfpr.edu.br

Abstract - Polyurethane (PU) foams make up a significant portion of the synthetic polymers produced worldwide, with applications mainly in civil construction[1]. Research indicates that polyurethane foams and agricultural residues of lignocellulosic composition, such as fruit waste and vegetable fibers, can be combined to improve the physical, mechanical and chemical properties of the material, promote the economy of petrochemical reagents and add value to a waste generated in high quantity as a by-product of the food industry[2]. This work aimed to prepare and characterize rigid polyurethane foam compositions with powdered orange peel (OP). For the synthesis of the foams, 4,4'-diphenylmethane diisocyanate (MDI),formulated polyester-polyol and orange peel in the proportions of 7 % (PUCS7), 10 % (PUCS10) and 14 % (PUCS14), replacing (m/m) the polyol. Foam preparation was performed with a mechanical stirrer for 30 seconds at 600 RPM. The characterization of samples of precursor reagents, OP and PU foams was performed using Fourier transform infrared spectroscopy (FTIR), thermogravimetry (TGA) and scanning electron microscopy (SEM). In the infrared spectrum of OP samples, characteristic bands of groups present at cellulose, pectin and lignin were identified at 3285 cm^{-1} (O–H groups), 2919 cm^{-1} (C–H bonds in CH_2 groups) and 1733 cm^{-1} (C=O)[3]. For PU and PUCS7, characteristic bands were found at 3278 cm^{-1} (NH), 1710 cm^{-1} (C=O) and 1593 cm^{-1} (NH_2), showing that the urethane bonds were formed[4]. SEM analyses showed that the foam morphology was altered by the progressive addition of the OP load, increasing the organization of cells[5]. The TGA analysis revealed that the decomposition of the foams occurs in one step after the loss of water and that the addition of CL increased the thermal stability of the polymer[4].

References

1. D. Naldzhiev, D. Mumovic, M. Strlic. *Building and Environment* 2020, 169, 106559. https://doi.org/10.1016/j.buildenv.2019.106559
2. E. S. Ali, S. Ahmad. *Composites Part B: Engineering* 2012, 43, 04043. https://doi.org/10.1016/j.compositesb.2012.04.043
3. C. M. Santos, L. C. de Morais. *Quím. Nova 2015*, 38, 488-492. http://dx.doi.org/10.5935/0100-4042.20150026
4. A. Sittinun, P. Pisitsak, S. Ummartyotin. *Composites Communications* 2020, 20, 100351. https://doi.org/10.1016/j.coco.2020.04.017
5. S. Czlonka, A. Strakowska, A. Kairyté. *Polymer Testing* 2020, 87, 106534. https://doi.org/10.1016/j.polymertesting.2020.106534

Keywords: *Polymers, materials, residues, citrus fruit.*

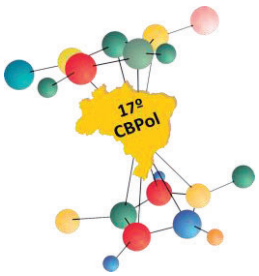

PRODUCTION OF HIGH-PERFORMANCE ACETOSOLV COCONUT FIBER LIGNIN-INCORPORATED DGEBA CURED WITH APROTIC IONIC LIQUID

Vinícius Taveira[1], Jéssica Marques[2], Mauro Silveira[2], Carlos Arthur[2], Selma Mazzetto[3], Diego Lomonaco[3], Francisco Avelino[1*]

1 – Department of Research, Extension and Production (DPEP), Federal Institute of Ceará (IFCE), Iguatu, CE, Brazil, francisco.avelino@ifce.edu.br
2 – LAPOL/PPGEM, Federal University of Rio Grande do Sul, Porto Alegre, RS, Brazil
3 – Department of Organic and Inorganic Chemistry, Federal University of Ceará (UFC), Fortaleza, CE, Brazil

Abstract - Lignin valorization constitutes a chemical platform for several segments of the chemical industry. The aim of this work was to evaluate the potential of acetosolv coconut fiber lignin (ACFL) as an additive to bisphenol A diglycidyl ether (DGEBA), curing it using an aprotic ionic liquid (IL) ([BMIM][PF_6]) and characterize the obtained thermosetting materials. ACFL was obtained by mixing coconut fiber with 90 % v/v acetic acid and 2 % HCl v/v at 110 °C for 1 hour under reflux and atmospheric pressure. ACFL was characterized by Fourier transform infrared spectroscopy (FTIR), thermogravimetric analysis (TGA), and nuclear magnetic resonance (^{1}H NMR). The formulations were fabricated by mixing DGEBA and ACFL at different concentrations (0 – 50 % wt.). The curing parameters and [BMIM][PF_6] concentrations were optimized by differential scanning calorimetry (DSC) analyses. The cured ACFL-incorporated epoxy resins were characterized by gel content (GC), TGA, microscale combustion calorimetry (MCC), and chemical resistance in different media. ACFL has undergone selective partial acetylation that favored its miscibility with DGEBA. DSC analyses have shown that the IL was able to catalyse the curing reaction, being its optimized concentration 10 % wt, since it caused a significant decrease in onset polymerization temperature (T_{onset}) and peak temperature (T_{peak}). High GC values were obtained in different organic solvents (chloroform and methyl ethyl ketone) at high curing temperatures and ACFL concentration. The crescent ACFL concentration did not affect the T_{onset} of the thermosetting materials significantly, and produced thermosetting materials with high char yield (26 – 45 %) and limiting oxygen index (LOI) (27.9 – 35.5) values, suggesting a potential for flame retardancy. ACFL has increased the resistance of DGEBA to combustion and different chemical media. ACFL has shown great potential to be used as a bio-additive for enhancing the chemical, termal, and combustion properties of high-performance materials.

Fundings: This work was funded by Fundação Cearense de Apoio ao Desenvolvimento Científico e Tecnológico (FUNCAP) under the grants numbers FUNCAP BP4-0172-00159.01.00/20 and BP5-00197-00113.01.00/22.

Keywords: *agrowaste; biomass valorization; lignin valorization; thermosetting materials*

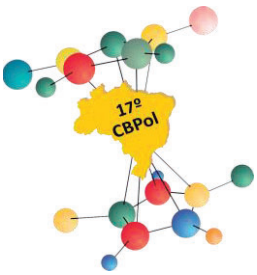

RADICAL POLYMERIZATION OF HYDROPHOBICALLY MODIFIED WATER-SOLUBLE POLYACRYLAMIDE HAVING OLIGO(LACTIC ACID) AS HYDROPHOBIC MACROMONOMER

Larissa R. Rabaioli[1], Vanessa M. Picoli[2] and Cesar L. Petzhold[3]

1 – Organic Chemistry Department, Federal University of Rio Grande do Sul(UFRGS), Porto Alegre, RS, Brazil
larissa.rabaioli@ufrgs.br
2 – Organic Chemistry Department, Federal University of Rio Grande do Sul(UFRGS), Porto Alegre, RS, Brazil
vanessapicoli@yahoo.com.br
3 – Organic Chemistry Department, , Federal University of Rio Grande do Sul(UFRGS), Porto Alegre, RS, Brazil
petzhold@iq.ufrgs.br

The control and modification of the viscosity of polyacrylamide incorporated with hydrophobic monomer has proven to be of great interest in recent years due to their low cost and consequent feasibility for application in enhanced oil recovery[1,2]. Polyacrylamide copolymer hydrophobically modified with oligo(lactic acid) was synthesized using two methods, micellar and heterogeneous radical polymerization, to investigate which would provide the highest hydrophobic incorporation content. Synthesis of the oligo(lactic acid) macromonomer was performed by ring opening polymerization of the lactide. Macromonomers containing four (M4), five (M5), seven (M7) and eleven (M11) repetitive units, as determined using hydrogen nuclear magnetic resonance (^{1}H NMR), were prepared. Micellar radical polymerization in aqueous medium was used to synthesize C5 and C11 copolymers with 2.5% mol content of M5 and M11. Heterogeneous radical polymerization was performed in methanol and water mixture (1:1) and employed to obtain the copolymers C4 and C7 with 2.5% mol content of M4 and M7. For C4, C5, C7 and C11, the ^{1}H NMR spectra confirmed the experimental incorporation and conversion (mol incorporation|conversion), being: 1.48%|97% for C4, 1.02%|75% for C5, 1.63%|86% for C7 and 0.90%|60% for C11. Through size exclusion chromatography it was observed that the molar masses of the copolymers were on the order of 10^5 g mol^{-1}. Therefore, it is noted that the incorporation of the macromonomer into acrylamide is more effective when performed by the heterogeneous radical copolymerization method.

1. Bhut PR, Pal N, Mandal A. Characterization of Hydrophobically Modified Polyacrylamide in Mixed Polymer-Gemini Surfactant Systems for Enhanced Oil Recovery Application. ACS Omega. 2019 Nov 19;4(23):20164-20177. doi: 10.1021/acsomega.9b02279. .
2. Chen, Q., Zhang, S., Wang, Z., Ye, Z., Lai, N., *J. Appl. Polym. Sci.* 2023, 140(15), e53734. https://doi.org/10.1002/app.53734 .

RIGID POLYURETHANE FOAM WITH BENTONITE CLAY MODIFIED WITH NIOBIUM FOR PHOTODEGRADATION OF RHODAMINE B

Samanta T. Medeiros[1]*, Maria Eduarda S. R. de Souza[1], Laís J. da Cruz[1], Marcus V. de Liz[1], Elenice H. C. Lacerda[2], Juliana R. Kloss[1]

1 – Academic Department of Chemistry and Biology, Federal University of Technology – Paraná (UTFPR), Curitiba, PR, Brazil samantamedeiros@alunos.utfpr.edu.br
2 – Department of Chemistry, Federal University of Santa Catarina (UFSC), Florianópolis, SC, Brazil

Abstract – Polyurethane (PU) is obtained by the polymerization reaction between polyol and isocyanate, that can be used in photodegradation of textile dyes. In this work, rigid PU foams were synthesized with addition of different proportions of bentonite clay modified with niobium pentoxide (Nb_2O_5), being 5, 7 and 9 wt.%, aiming at the photodegradation of the textile dye rhodamine B in a concentration of 10 mg L^{-1}, under the conditions: 100 mg of pre-ground foam, 300 mL of dye solution, using a mercury vapor lamp as a source of radiation. The synthesized foams and modified clay were characterized by *Fourier*-transform infrared spectroscopy (FTIR), X-ray diffraction (XRD) and scanning electron microscopy with energy dispersive spectroscopy (SEM-EDS). The FTIR results showed characteristic bands of urethane bonds. Fig 1 shows crystalline peaks in the XRD, referring to the clay modified with Nb_2O_5 and the amorphous region referring to PU. In the SEM-EDS images, it was possible to see the presence of Nb_2O_5 particles on the bentonite clay and the dispersion of the modified clay in the PUF. The results of a photodegradation test for samples of 5, 7 and 9 wt.% showed discoloration efficiency of 40, 45 and 60 %, respectively, after one hour of reaction. In conclusion, the system composed of PUF and Nb_2O_5-modified clay was compatible with each other, without interfering in the polyurethane polymerization process and the results were promising in the degradation of the rhodamine B dye.

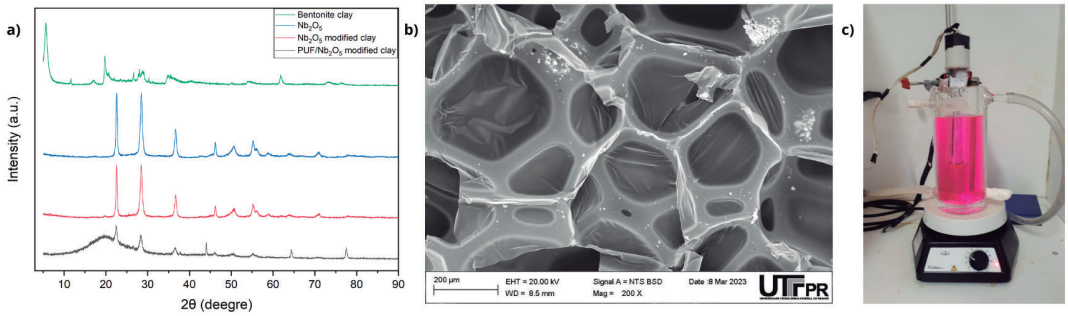

Figure 1 – a) XRD, b) SEM of the PUF/Nb_2O_5-modified clay and c) photodegradation system.

References

1. E. Lacerda; F. Monteiro; J. Kloss; S. Fujiwara. *Journal of Photochemistry and Photobiology A: Chemistry* 2020, 388, 112084. https://doi.org/10.1016/j.jphotochem.2019.112084

2. Y. Meng; Y. Wang; C. Wang. *Polymers* 2021, 13, 283. https://doi.org/10.3390/polym13020283

Keywords: *heterogeneous catalysis, remediation, bentonite clay, textile dye, Nb_2O_5 supported*

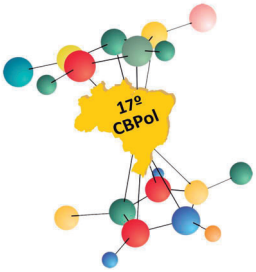

STRUCTURE ASSESSMENT OVER TIME OF HYDROXYPROPYLATED STARCH GRANULES

Henrique Solowej Medeiros Lopes[12], Daniel Komatsu[23], Alain Dufresne[4], Aparecido Júnior de Menezes[1]*

1 - Graduate Program in Material Science (PPGCM), Federal University of São Carlos (UFSCar), Sorocaba, SP, Brazil
2 – Technological College of Sorocaba (Fatec), Sorocaba, SP, Brazil
3 - Pontifical Catholic University of Sao Paulo (PUC-SP), Sorocaba, SP, Brazil
4 – The International School of Paper, Print Media and Biomaterials, Grenoble Institute of Technology, Saint Martin d'Hères, France
jrmenezes@ufscar.br

Abstract – Starch bioplastics is one of the most promising alternatives for replacing conventional polymers in various market segments, such as short-term packaging, mulch films and many others [1]. Nevertheless, starch intrinsic properties limit its application. Sensitivity to moisture combined with retrogradation results in poor mechanical properties and low processability, which often difficult its use as films or packaging [2]. A possibility is to blend starch with other biodegradable polymer [2], modify starch granules [3] and/or reinforce a starch matrix with natural fibers [4], among others, to improve starch materials' properties. In this work, we propose to modify starch granules by hydroxypropylation in an autoclave reactor to obtain hydroxypropylated starch (HPS) matrix. A design of experiment (DOE) was carried out to obtain materials with different molar ratios, temperature and time. Obtained films by thermopressing were investigated regarding its structure by time in X-Ray Diffraction (XRD), Scanning Electron Microscopy (SEM) and Differential Scanning Calorimetry (DSC). Fourier Transform Infrared Spectroscopy (FTIR) were performed to evaluate the chemical modification and Dynamic Mechanical Thermal Analysis (DMTA) to assess its mechanical properties over temperature changes. As expected, parameters variations in the modification process produced different starch materials, reflecting in its structure changes over time and, consequently, in mechanical properties. Further analysis would confirm the proper route to obtain HPS capable of different applications, with the possibility to be reinforced with lignocellulosic fibers.

References

1. P. Halley; L. Avérous. *Starch Polymers: from genetic engineering to green applications,* Elsevier, California, 2014.
2. M. Dammak; Y. Fourati; Q. Tarrés; M. Delgado-Aguilar; P. Mutjé; S. Boufi. *Industrial Crops & Products 2020, 144, 112061.* https://doi.org/10.1016/j.indcrop.2019.112061.
3. A. J. de Menezes; D. Pasquini; A. A. S. Curvelo; A. Gandini. *Biomacromolecules 2007, 8, 7. 10.* https://doi.org/1021/bm070389j.
4. S. Collazo-Bigliardi; R. Ortega-Toro; A. Chiralt. *Food Packaging and Shelf Life 2019, 22, 100383.* https://doi.org/10.1016/j.fpsl.2019.100383.

Fundings: This study was financed in part by the Coordenação de Aperfeiçoamento de Pessoal de Nível Superior - Brasil (CAPES) - Finance Code 001 and São Paulo Research Foundation (FAPESP) – nº 2022/11062-6.

Keywords: *Starch, retrogradation, hydroxypropylation.*

SYNTHESIS AND CHARACTERIZATION OF MONOMERS: A POSSIBLE SUBSTITUTE FOR BPA FREE POLYMERS

Gustavo S. Corrêa[1], Marcia M. Meier[1] and Rogério A. Gariani[1]*

1 – Department of Chemistry, Santa Catarina State University (UDESC), Joinville, SC, Brazil
rogerio.gariani@udesc.br

Abstract - Based on the increasing number of studies on new dental materials with superior physicochemical properties[1] and considering the current interest in finding materials free of bisphenol A (BPA)[2] and derivatives due to their potential toxicity[3], the present work sought to study the synthesis and the properties of a new monomer free of BPA moiety, starting from easily accessible precursors and simple synthesis. One of the synthesized compounds was TDA (N,N'-(thiobis(4,1-phenylene))bis(2-methylacrylamide)) at 38% overall yield, according to the synthetic route shown in Fig 1.

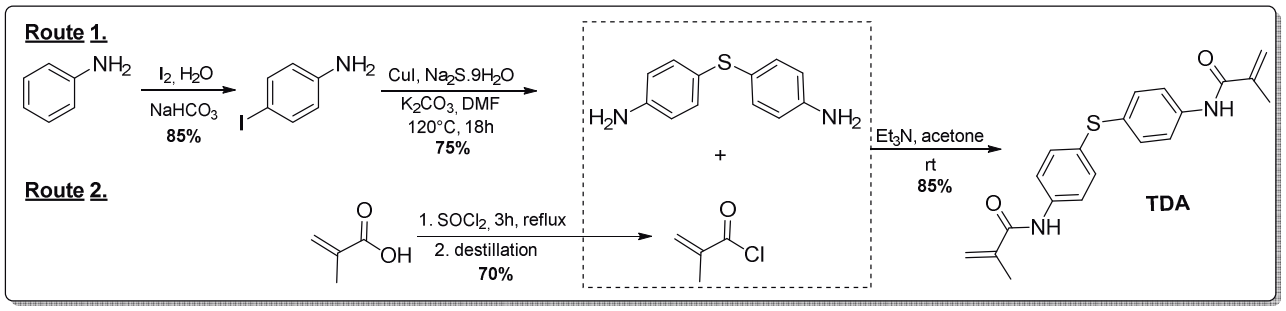

Figure 1. Monomer synthetic route to produce TDA.

The monomer characterizations were carried out from NMR, GC-MS, and IR analyses. To evaluate the effect of the chemical structure of the monomer on the polymer properties, specimens of TDA and BisGMA (bisphenol A-glycidyl methacrylate) copolymers containing HEMA (2-hydroxyethyl methacrylate) were prepared and characterized in terms of mechanical properties such as flexural strength and microhardness. Its physicochemical properties were also studied, such as solubility, water absorption and degree of conversion. Both copolymers showed similarities in the analyzed properties.

References

[1] J. Ferracane, *Dental Materials*, 2011, 29, https://doi.org/10.1016/j.dental.2010.10.020.
[2] A. M. Nelson, T. E. Long, *Polym Int.*, 20121, 1485, https://doi.org/10.1002/pi.4323.
[3] W. Qiu, H. Zhan, J.Hu, T. Zhang, H. Xu, M. Wong, B. Xu, C. Zheng, *Ecotoxicol. Environ. Saf., 2019, 173,* 192, https://doi.org/10.1016/j.ecoenv.2019.01.114.

Fundings: PAP-FAPESC-2021TR964
Keywords: *Dental Resins, BPA, New Monomers, bisphenol free.*

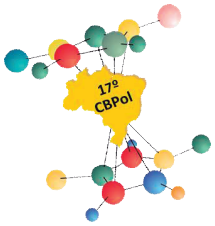

SYNTHESIS AND CHARACTERIZATION OF POLI(BUTYL ACRYLATE-*CO*-FARNESENE) OBTAINED VIA EMULSION POLYMERIZATION

Lina D. A. Rodrigues[1] and Maurício P. Oliveira[1]*

1 – Laboratory of Polymer Synthesis and Process, Department of Science and Technology, Federal University of São Paulo (Unifesp), São José dos Campos, SP, Brazil
lina.dayse@unifesp.br; mauricio.pinheiro@unifesp.br

Abstract – Development of sustainable materials and products has grown, especially polymers derived from bio-based monomers containing, at least, one C=C bond[1,2]. On the other hand, bio-based monomers copolymerization via free radical polymerization normally led to their lower conversion due to lower reactivity ratio. In this report, copolymerization of the bio-based *trans*-*β*-farnesene (Far), obtained from the fermentation of sugar cane, with *n*-butyl acrylate (Bu) was investigated to make bio-based materials. Latexes were prepared by semi-batch emulsion copolymerization of Bu with various ratios of Far (100/0, 80/20 and 50/50). The effect of Far/Bu ratios on the properties of the latexes and copolymers were investigated. The latexes were prepared using deionized water, surfactant (sodium diphenyl oxide disulfonate) and ammonium persulfate as initiator. No chain transfer agent was used in the polymerizations. Monomer mixture (Bu/Far) was added dropwise to the reactor over a period of 4 h at 85ºC. Latexes were characterized in terms of solids content (SC), overall monomer conversion (Xg), particle diameter (Dp), coagulum concentration (CC), pH and viscosity (η). Copolymers were evaluated in terms of gel content and tensile strength (maximum tension and elongation). Table 1 shows the values obtained from the characterizations of the latexes and copolymers. Overall monomer conversion decreases with Far increase due to the lower reactivity ratio of Far. The pH mostly remained constant and the particle size slightly decreased with increased Far concentration. Content of the gel increased and the elongation of the films decreased due to possible copolymer cross-linking[3]. In the polymerization of Bu (100/0) no gel formation was observed. Finally, the resulting films showed good mechanical properties performance, which are comparable to that of a petroleum-based copolymer.

Table 1 – Properties of the latexes and copolymers with different contents of Bu/Far (100/0, 80/20,50/50).

Polymerizations	Bu/Far (wt/wt)	SC (%)	Xg (%)	Dp (nm)	DTP	CC (ppm)	pH	η (cPs)	Gel cont. (%)	$\sigma_{máx}$ (MPa)	δ (%)
1	100/0	33.8	94.7	132.2	0.02	8.3	1.5	2	0	1.5	998.3
2	80/20	32.7	91.5	136.8	0.06	10.6	1.5	1	78.3	1.8	96.8
3	50/50	30.9	86.6	124.3	0.06	11.2	1.5	1	80.5	1.2	45.3

Note: Theoretical solid content = 35.7%; SC = solid content; DTP = particle size distribution; $\sigma_{máx}$ = maximum stress; δ = elongation.

References

1. Luk, S. B., & Maríc, M. *ACS Omega,* 2021*, 6(7), 4939–4949.* doi:10.1021/acsomega.0c05992.
2. Sahu, P. & Oh, J. S. Ind. & Eng. Chem. Res., 2022, 61(42), *11815-1182*. doi:10.1021/acs.iecr.2c01917.
3. L. D. A. Rodrigues. Thesis, Federal University of São Paulo, 2022.

Fundings: The authors gratefully acknowledge the financial support of CAPES and FAPESP (grant 2022/07165-4).

Keywords: Emulsion polymerization, *trans*-*β*-farnesene, latex, adhesive, bio-based nomonomer.

SYNTHESIS OF EUGENOL EPOXY FOR VITRIMERIC POLYMERS

Angela B. Lovera[1], Marcos L. Dias[1], Diego H. S. Souza[1]

1 – Institute of Macromolecules Professora Eloisa Mano – IMA, Federal University of Rio de Janeiro
angela.becerra@ima.ufrj.br

Abstract - Bio-based vitrimers are a group of sustainable and high-performance materials, which have thermostable, mechanical and thermal properties, combined with high malleability, self-healing capacity, reprocessability and recyclability, which emerge as an option that can help improve the durability of thermoset materials, reducing their environmental impact[1]. Eugenol is an abundant bio-based renewable raw material with low toxicity which can improve the thermal and mechanical properties of polymeric materials for its rigid aromatic structure, functional diversity, and reactive functional groups, making it an ideal candidate for the synthesis of vitrimers[2]. With the objective of obtaining an epoxy resin based on eugenol for the development of a bio-based vitrimer, a two-stage approach was made: (1) eugenol-derived diene made through the Williamson ether synthesis between dibromoethane and the phenolic group of eugenol to produce an intermediate that contains two double bonds, with 90% yield; and (2) epoxidation of the allyl groups to produce a symmetrical eugenol diepoxide. The methodology was based on the use of Oxone® (potassium peroxymonosulfate) in a system composed of a mixture of acetyl acetate/acetone, chosen due to its ecological character as a non-chlorinated oxidizing agent and the improvement in atom economy[3] (Figure 1). The product obtained (3^3,8^2-dimethoxy-4,7-dioxa-1,10(2)-dioxirana-3,8(1,4)-dibenzenadecaphane) was a yellow powder, the yield, of the reaction was 50%, and the evaluation by Nuclear magnetic resonance (NMR) showed the formation of the epoxy ring. ^{1}H NMR ($CDCl_3$; δ, ppm): 6,91–6,77 (m, 6H, Ar– H), 4,24–4,17 (d, 2H, OCH_2 -CH_2O), 3,77–3,72 (s, 6H, −O–CH_3), 2,50–2,42 (m, 2H, O−CH_2- CH_2−O), 2,57–2,52 (dd, 2H, −CH–CH_2 –O), 2,78–2,62 (m, 6H, Ar–CH_2 – and −CH–CH_2–O). The Fourier-transform infrared spectroscopy FTIR spectrum confirmed the structure of the epoxy eugenol with bands in 3400, 1374, 1259, 1165, 1064, 860cm^{-1}.

Figure –

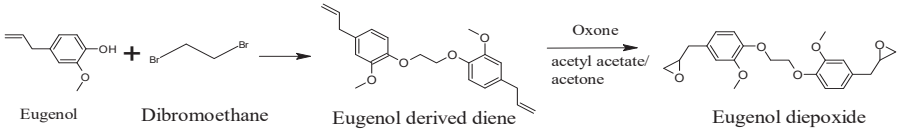

Figure 1. Synthesis of eugenol diepoxide

References –

1. X. Yang; L. Guo; X. Xu, S. Shang; H. Liu *Materials & Design* 2020, *186*, 108248. https://doi.org/10.1016/j.matdes.2019.108248
2. C. Ocando; Y. Ecochard; M. Decostanzi; S. Caillol; L. Avérous *European Polymer Journal* 2020, *135*, 109860. https://doi.org/10.1016/j.eurpolymj.2020.109860
3. D. Guzmán; A. Serra; X. Ramis; X. Fernández-Francos; S. De la Flor *Reactive and Functional Polymers* 2019, *136*, 153. https://doi.org/10.1016/j.reactfunctpolym.2018.12.024

Fundings: *Conselho Nacional de Desenvolvimento Científico e Tecnológico* (CNPq), and *Coordenação de Aperfeiçoamento de Pessoal de Nível Superior* (CAPES).
Keywords: Bio-based vitrimer, eugenol, epoxidation.

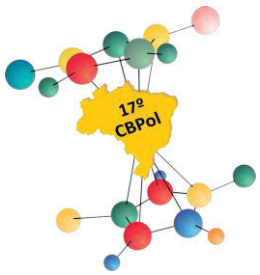

SYNTHESIS OF PH-RESPONSIVE NANOPARTICLES FOR THE DEVELOPMENT OF STARCH-BASED SMART PACKAGING

Emmanuelle G. David[1*], Douglas Gamba[1] and Tales S. Daitx[1]

1 – Institute of Chemistry, Federal University of Rio Grande do Sul (UFRGS), Porto Alegre, RS, Brazil
emmannu2009.ed@gmail.com, tales.daitx@ufrgs.br

Abstract – Smart packaging is an important solution for the industry and final consumers, as it can increase the shelf life of a product or act as a sensor indicative of freshness [1]. This work aims to synthesize nanoparticles based on bentonite and kaolinite clay minerals modified with the natural dye anthocyanin and poly(ε-caprolactone) for the production of pH-responsive starch nanocomposites that can be used on this application [2]. For this, the different nanoparticles were synthesized through an initial microwave reaction between each clay mineral with e-caprolactone, where PCL chains were grafted onto their surfaces in the presence of tin (II) chloride for 10 min at 150 °C and 200 W. Subsequently, the residual monomer and the ungrafted chains were extracted with dichloromethane and the modified clays were recovered by centrifugation and dried. Afterwards, the dye was incorporated into the structures by mixing it with each modified clay in aqueous media. The mixtures were stirred for 1 h at room temperature and after this period the excess of dye was removed by successive washes with water and centrifugation. Then the starch nanocomposites were prepared using 3% and 5% of the modified mineral clays. The samples were prepared by casting process, where the nanoparticles were first dispersed in a solution of starch, water and glycerol using ultrasound. The resulting suspensions were then heated at 85 °C for 30 min for gelatinization of the starch and then dispersed on glass plates for evaporation of residual water and obtention of the final nanocomposites. The modified clay minerals and polymeric films were characterized through Fourier transform infrared spectroscopy, thermogravimetric analysis and in relation to colorimetric modification in environments that simulate food decomposition. All results indicate the modification of nanoparticles and showed that the films are sensitive to food degradation processes, evidencing their potential as smart packaging.

References

1. R. C. da Costa; T. S. Daitx; R. S. Mauler; N. M. da Silva; M. Miotto; J. S. Crespo; L. N. Carli *Food Packing and Shelf Life* 2020, *26*, 100602. https://doi.org/10.1016/j.fpsl.2020.100602
2. X. Zheng; X. Xu; C. Liu; Y. Sun; Z. Lin; H. Liu *Separation and Purification Technology* 2013, *104*, 17. https://doi.org/10.1016/j.seppur.2012.11.011

Fundings: The authors are grateful to Conselho Nacional de Desenvolvimento Científico e Tecnológico (CNPq) and Fundação de Amparo à pesquisa do estado do Rio Grande do Sul (PRONEX/FAPERGS - Finance Code 16/2551-0000470-6) for financial support.

Keywords: *Anthocyanin, Bentonite, Kaolinite, Nanocomposites, Smart Packaging.*

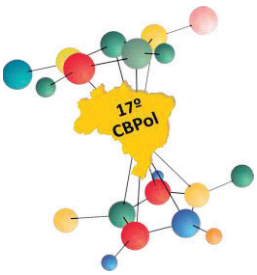

SYNTHESIS OF POLY(GLOBALIDE) BY ENZYMATIC RING-OPENING POLYMERIZATION USING GERANIOL AS INITIATOR

Amanda V. Farias[1], Gustavo Giovanardi[1], Tamara Agner[1], Pedro H. H. de Araújo[1] and Claudia Sayer[1]*

1 – Department of Chemical Engineering and Food Engineering (EQA), Federal University of Santa Catarina (UFSC), Florianópolis, SC, Brazil
claudia.sayer@ufsc.br

Abstract - Poly(globalide) (PGL) is a biodegradable and non-toxic polymer obtained by the polymerization of globalide (GL). Enzymatic ring-opening polymerization (e-ROP) is a green approach to the synthesis of this polyester using enzymes that are considered green catalysts and enable milder reaction conditions. The use of different alcohols as initiators in the e-ROP allows to obtain polymers with an infinity of terminal groups, providing changes in the final properties of the polymer. Furthermore, the initiator allows molecular weight control by varying the ratio of initiator (I) to monomer (M). In this study, e-ROP of GL was performed in solution (toluene) using geraniol as initiator, and Novozymes 435 as biocatalyst. Before each reaction, the enzyme (Novozyme 435, immobilized lipase B from Candida antarctica) was dried at 40 °C in a vacuum oven for 24 h in the presence of molecular sieves. The I/M ratio was 1:20 and the e-ROP was performed under N_2 atmosphere and magnetic stirring for 1 h at 65 °C. The polymer was precipitated with an excess of cold methanol for 24 h, vacuum filtered, and dried at 30 °C for 24 h. Polymer formation, molecular weight, and chemical structure assignment were determined using ^{1}H-NMR. The characteristic peaks of the repeating units (2H, δ = 3.63–3.68 ppm) and for geraniol end-groups (2H, δ = 4.57–4.61 ppm) were identified. The reactions showed yields of around 70% and molecular weights of up to 4200 g/mol. The results also indicate that, even with humidity control, the water content in the enzymes influences the chain initiation and final molecular weight of the polymer.

References

1. N. U. Kaya; Y. A. Guvenilir *International Journal of Polymer Science* 2015, 458756. https://doi.org/10.1155/2015/458756.
2. A. E. Polloni; V. Chiaradia; E. M. Figura; J. P. de Paoli; D. de Oliveira; J. V.de Oliveira; P. H. H. de Araujo; Claudia Sayer *Applied Biochemistry and Biotechnology* 2017, *184*, 659–672. https://doi.org/10.1007/s12010-017-2583-4.
3. P. Olsén; T. Borke; K. Odelius; A.-C. Albertsson *Biomacromolecules* 2013, *14,* 2883–2890. https://doi.org/10.1021/bm400733e.

Fundings: We thank Coordenação de Aperfeiçoamento de Pessoal de Nível Superior (CAPES) and Conselho Nacional para o Desenvolvimento Científico e Tecnológico for the financial support.

Keywords: *e-ROP, poly(globalide), geraniol*

THIOL-ENE PHOTOPOLYMERIZATION OF (R)-(+)-LIMONENE IN MINIEMULSION: A GREEN APPROACH FOR SYNTHESIZING POLYMERIC NANOPARTICLES

Luiz P. S. Pereira, Yasmin M. de Aguiar, Tamara Agner, Pedro H. H. de Araújo, and Claudia Sayer*

Department of Chemical Engineering and Food Engineering (EQA), Federal University of Santa Catarina (UFSC), Florianópolis, SC, Brazil
claudia.sayer@ufsc.br

Abstract - Brazil is the largest orange producer in the world, accounting for about 30% of global production[1]. Most of the oranges are used to make orange juice, which results in orange peels as a by-product[2]. The essential oil extracted from these orange peels consists mainly of (R)-(+)-limonene (85-95%), a natural terpene that is abundant, inexpensive, and widely available[3]. The chemical structure of (R)-(+)-limonene, with two double bonds, makes it an ideal monomer for use in thiol-ene polymerizations[4]. Miniemulsion polymerization is a highly efficient technique for producing polymeric nanoparticles used in several applications, including drug delivery systems[5]. In this study, thiol-ene miniemulsion photopolymerizations using limonene and a bifunctional thiol (2,2′-(ethylenedioxy)diethanethiol) were conducted within a UV chamber at 40 °C and average luminous intensity of 3.83 mW cm^{-2} under magnetic stirring at 150 rpm. 2,2-dimetoxi-2-fenilacetofenone was used as photoinitiator. Polymerizations resulted in polymer particles with an intensity average size of 130 nm and narrow size distribution (polydispersity index - PdI < 0.13) as determined by Dynamic Light Scattering. The weight average molar mass of these nanoparticles was 7300 g mol^{-1} (measured by Gel Permeation Chromatography) and the yield was above 90%. Thus, this study provides an efficient and interesting method for producing polymeric nanoparticles using miniemulsion photopolymerization of (R)-(+)-limonene as a renewable monomer, with potential application in sustained drug delivery systems.

References

1. United States Department of Agriculture Foreign Agricultural Service – USDA, *Citrus: World Markets and Trade*, January 2023. https://apps.fas.usda.gov/psdonline/circulars/citrus.pdf
2. R. Ciriminna; M. Lomeli-Rodriguez; P. Demma Carà; J. A. Lopez-Sanchez; M. Pagliaro *Chemical Communications* 2014, *50*, 15288. https://doi.org/10.1039/C4CC06147K
3. M. Firdaus; M. A. R. Meier *Green Chemistry* 2013, *15*, 370. https://doi.org/10.1002/ejlt.201300206
4. M. Claudino; M. Jonsson; M. Johansson *RSC Advances* 2013, *3*, 11021. https://doi.org/10.1039/C3RA40696B.
5. T. O. Machado; C. Sayer; P. H. H. Araujo *European Polymer Journal* 2017, *86*, 200. http://dx.doi.org/10.1016/j.eurpolymj.2016.02.025.

Fundings: The authors would like to thank the financial support provided by Coordenação de Aperfeiçoamento de Pessoal de Nível Superior (CAPES) and Conselho Nacional de Desenvolvimento Científico e Tecnológico (CNPq).

Keywords: *Renewable monomer, thiol-ene photopolymerization, miniemulsion.*

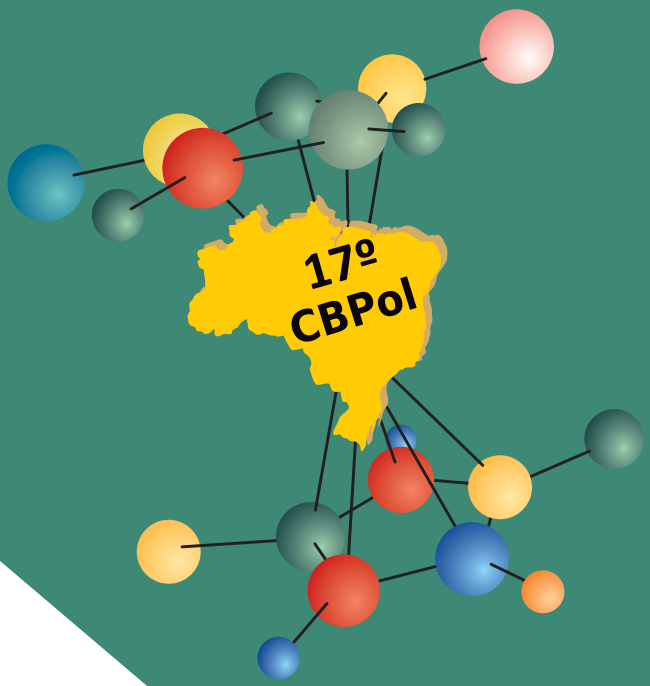

Polymer physics and characterization

POLYETHYLENE RHEOLOGY ADDITIVED WITH THERMOCHROMIC PIGMENTS

Carla L. S. C. Costa[1,6], Alice C. Silva[2], Carlos H. R. Miltont[2], Adriano L.A. Mattos[3], Juciklécia S. Reinaldo[4], José I. Medeiros[5], Edson Noriyuki Ito[6*]

1 – Graduate Program in Textile Engineering, Federal University of Rio Grande do Norte, Natal, RN, Brazil carlalaize@yahoo.com.br
2 – Graduate Program in Materials Science and Engineering, Federal University of Rio Grande do Norte, RN, Brazil alice.silva.111@ufrn.edu.br; henrique.milfont@gmail.com
3 –Embrapa Tropical Agroindustry, Fortaleza, CE, Brazil adriano.mattos@embrapa.br
4 – Higher School of Technology, State University of Amazonas, Manaus, AM, Brazil jreinaldo@uea.edu.br
5 –Textile Engineering Department, Federal University of Rio Grande do Norte, Natal, RN, Brazil ivan.medeiros@ufrn.br
6 – Materials Engineering Department, Federal University of Rio Grande do Norte, Rio Grande do Norte, RN, Brazil edson.ito@ufrn.br

Abstract - The influence of the addition of encapsulated thermochromic pigments on the rheological behavior in the linear viscoelastic region of high density polyethylene (HDPE) was investigated. The materials added with 0.5, 1.0 and 2.0 wt% of thermochromic pigments were mixed and homogenized in a corotational twin-screw extruder and test specimens were produced by injection molding. The analysis of the visual appearance of the samples indicated an efficient mixture in a twin screw extruder, maintaining the physical integrity and promoting a good dispersion of the pigments in the HDPE matrix. The rheological characterization performed at low frequencies in the linear viscoelasticity region indicated changes in the storage modulus (G'), loss modulus (G") and complex viscosity (η^*) of HDPE due to the presence of pigments.

Keywords: *HDPE, additives, thermochromic pigment, extrusion.*

Introduction

Smart materials are those that can modify their physical properties as a response to an external mechanical or physical stimulus. Within this class, chromic materials are of industrial interest because they allow color changes in certain situations, such as variations in hydrogen potential (pH), temperature, light and electric current [1].

Thermochromic materials are those that have the ability to undergo a reversible color change when subjected to temperature variation, and this ability is promoted by the presence of multicomponent microencapsulated pigments. These pigments, in turn, are mainly used in body thermometers, paint formulation, food packaging, electronic circuits and in the textile industry [2].

Zhang et al. [3] incorporated thermochromic pigments in a polypropylene (PP) polymeric matrix in order to obtain filaments for textile applications through the extrusion process. The results obtained indicated that the obtained filaments presented a good visual appearance, good resistance to friction and maintenance of the thermochromic characteristics of the pigment, which maintained its color reversibility capacity even after processing in an extruder.

Cheng et al. [4] produced polylactic acid (PLA) films added with thermochromic pigments through the extrusion-blow process for application in packaging. The rheological, mechanical and barrier properties were measured and the results indicated a reduction in the viscosity of the melt, an increase in elongation at break and a reduction in the water vapor permeability of the films when the pigment was incorporated up to a concentration of 7 wt%. This work aimed to evaluate the influence of the concentration of thermochromic pigments on the visual appearance and rheological properties of HDPE.

Experimental

Materials

High-density polyethylene (HDPE), grade GE 7252 from Braskem, with a flow index of 2.0g/10min (190 °C/2.6 Kg) and thermochromic pigments from CSY Paint Store in purple and orange (T = 23°C) in color were used. The thermochromic activation temperature is 31 °C with mean diameters of the purple and orange microcapsules are 2.4 and 3.4 μm, respectively. Table 1 shows the formulations developed in this work.

Table 1 – Materials and formulations.

Materials	Composition (phr)
HDPE	100/0
HDPE/Purple Pigment	100/0.5
	100/1.0
	100/2.0
HDPE/Orange Pigment	100/0.5
	100/1.0
	100/2.0

Methods

Extrusion and injection molding

A co-rotational twin screw extruder from AX Plásticos Máquinas Técnicas, with a diameter of 16 mm and l/d of 40, was used to mix the materials, with a temperature profile of 91/150/185/190/195/203/195/203 °C from feed to die, a screw speed of 240 rpm, using a die for pellet production. After the extrusion mixing the materials, all materials were injection molded (mold disc-type specimens with 25 mm in diameter and 1.5 mm thick) using a Thermo Scientific HAAKE MiniJet II injection molding machine with a gun temperature of 210 ◦C, pressure of 640 bar and mold temperature of 50°C.

Visual aspect

The change in color of the specimens as a function of temperature was carried out considering the activation temperature of thermochromic pigments (31°C). The samples were kept at temperatures below (5°C) and above (60°C) the thermochromic activation temperature for a period of 30 minutes,

and then a simple digital camera was used, maintaining the luminosity and fixed focal length, to capture digital images of the surface of the samples.

Rheological characterization

The injection molded discs were used for rheological analysis using a rotational rheometer of the Thermo Scientific company Haake Mars model with parallel plates (d = 25mm), in the region of linear viscoelastic behavior at a temperature of 190°C and a tension of 350 Pa.

Results and Discussion

Fig 1 presents the visual aspects of the injection molded samples subjected to temperatures below and above the thermochromic activation temperature of the pigments and shows a color variation due to the increased proportion of orange and purple pigments when compared to pure HDPE (beige color). The samples with 0.5 wt% of purple and orange pigments had a uniform color change to blue and yellow, respectively, when subjected to temperatures above 31°C and the increase in the proportion of pigments intensified the color of the samples showing more intense coloring (solid). The color change observed also indicates that the mixture in a twin-screw extruder was efficient, maintaining the physical integrity and promoting the dispersion of pigment microcapsules within the polymeric matrix.

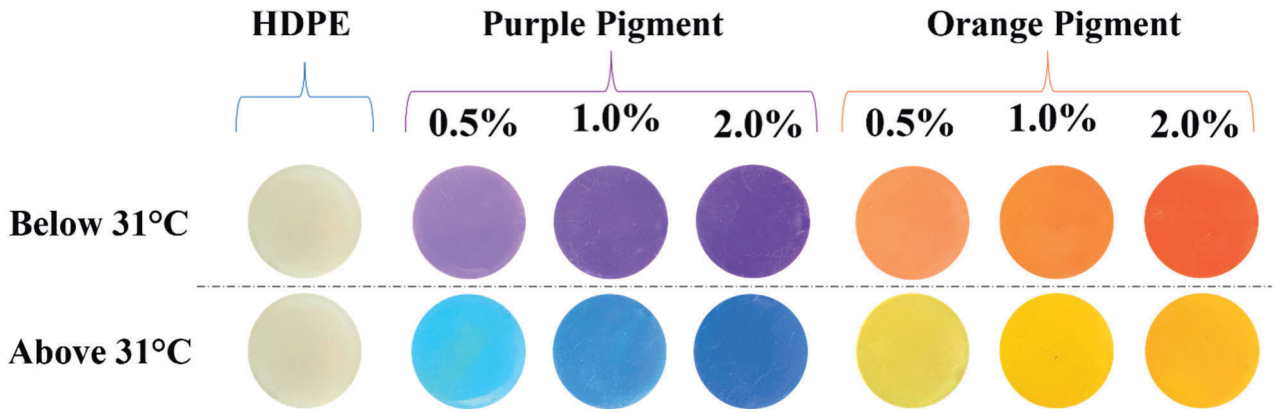

Figure 1 – Visual appearance of injected materials under controlled temperature conditions.

Fig 2 shows the linear viscoelastic rheological behavior of HDPE and formulations containing thermochromic pigments and indicates that the addition of pigments promoted changes in the storage modulus (G') and loss modulus (G"). It is observed in Fig 2a that HDPE presents values of G' and G", in the terminal zone, of 159.4 and 688.5 Pa, respectively, and the addition of 0.5% of purple pigment promoted a reduction of these values while the same amount of orange pigment had the opposite effect. The addition of 1 and 2 wt% (Fig 2b and c) of both pigments, in turn, promoted the same effect by reducing the values of G' and G", reaching values of 106.8 and 586.8, respectively , at a concentration of 2 wt% of orange pigment. According to Wo and Tanner [5], the increase in G' and G" values observed in HDPE with the addition of 0.5% orange pigment may be associated with an increase in the degree of crystallinity of the material, while the reduction of values, as observed in the other formulations, may indicate an increase in the flexibility of the HDPE polymeric chains, indicating an increase in the fluidity of the material.

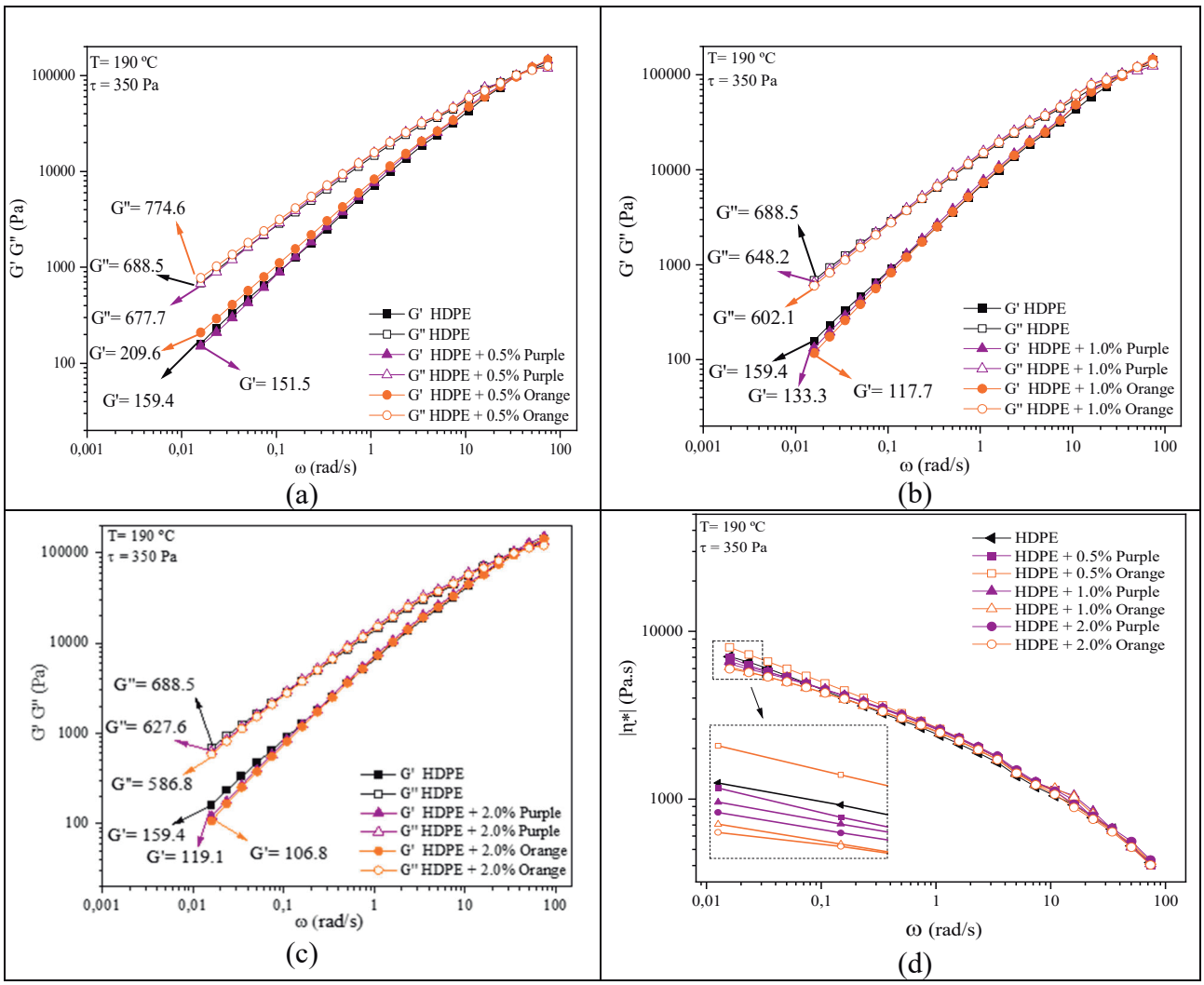

Figure 2 – Curves of the rheological behavior of HDPE and HDPE with different concentrations of thermochromic pigments (purple and orange). (a) G' versus G" for HDPE with 0.5 wt% of pigments. (b) G' versus G" for HDPE with 1.0 wt% of pigments. (c) G' versus G" for HDPE with 2.0 wt% of pigments. (d) Complex viscosity versus angular frequency.

Fig 2d presents the graph of log η* versus log ω for HDPE and HDPE with thermochromic pigments. It is observed that the addition of 0.5 wt% of orange pigment promoted an increase in the complex viscosity of HDPE in the terminal zone of the test, while for the addition of 0.5 wt% of purple pigment and 1.0 and 2.0 wt% of both pigments a reduction in the complex viscosity in the terminal zone was observed, this reduction being more pronounced for the orange pigment, which may be associated with the size of the pigment microcapsules. The results observed in Fig 2d corroborate those presented for G' and G" and indicate a possible plastification effect of the pigments in the HDPE matrix when added at concentrations of 1.0 and 2.0 wt%.

Conclusions

The results indicated that the mixture in a twin-screw extruder was efficient and promoted the dispersion of microcapsules of thermochromic pigments in the polymeric matrix. The analysis of the linear viscoelasticity region showed evidence that the addition of thermochromic pigments with different sizes of microcapsules provided changes in the rheological behavior of HDPE.

Acknowledgements

The authors are grateful to CAPES and CNPq for granting financial support.

References

1. R. M. Christie, in *Chromic materials for technical textile applications*, Advances in the Dyeing and Finishing of Technical Textiles. M.L. Gulrajani, Ed. Woodhead Publishing, Edimburgo 2013.
2. M. S. Tözüm; S. A. Aksoy; C. Alkan International Journal of Energy Research 2021, 7018. https://doi.org/10.1002/er.6287
3. Y. Zhang; Z. Hu; H. Xiang; G. Zhai; M. Zhu Dyes and Pigments, 2019 162, 705 https://doi.org/10.1016/j.dyepig.2018.11.007.
4. Z. Cheng; Z. Chen; B. Zhao; H. Liao; T. Yu; Y. Li International Journal of Biological Macromolecules, 2022, 220 238 https://doi.org/10.1016/j.ijbiomac.2022.08.070.
5. D. L. Wo; R.I. Tanner Rheol Acta, 2010, 49, 78 https://doi.org/10.1007/s00397-009-0388-2

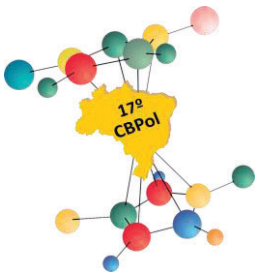

REFLECTIONS ON TEACHING AND PROFESSIONAL PRACTICE IN POLYMERS. HOW TO COMBINE THEORY AND PRACTICE?

Marcelo Silveira Rabello

Department of Materials Engineering, Federal University of Campina Grande, PB, Brazil.
marcelo.rabello@ufcg.edu.br

Teaching and learning are always a big issue at the university environment. To what extent do students acquire sufficient learning experience to be able to face the challenges of the professional life? Are the lecturers fully involved in the teaching process to provide the students the tools to become capable professionals? Are both students and lecturers committed to this proposal? Actually, there are some gaps in the teaching-learning process that must be faced. The world has changed significantly but the academic procedures seem to be stuck to the past, though some good experiences are shown with inverted classes and active methodologies. The new generation of students are very fast learners but like to appeal to shortcuts in order to gain information or to solve academic problems. Truly, the era of Google and ChatGPT made the life much easier for all of us! However, when the student becomes a professional, he/she must be involved with industry problems, and is frequently "the" decision maker. In this situation, the work is not separated by disciplines like at the university. The contents are "entangled" and he/she are demanded even for topics that no one taught. In an industry of polymer processing, for example, he/she must be capable of solving problems or being innovative, creating new materials or new products. In this case, the "shortcuts" are not necessarily clear! Can the way of doing the job be anticipated or trained at the university? This is a meaningful question! This presentation describes the experience gained with the discipline "Structure and Properties of Polymers" over many years, which turned into a didactic book[1], to help the learning process. The book intended to mirror the actual classes, enhancing the relevance of the information to the practice of the future professional. For example, when dealing with crystallization of polymers, less time is consumed with the (complicated) equations, and more emphasis is given to industrial consequences of a slow or fast crystallization process. The useful properties of a product can be predicted based on the type of polymer, grade, physical structure, environmental exposure, etc., i.e., based on the theory of polymer science. Hence, the presentation of the theory is rather important, but must necessarily be connected to the practical use of it. Otherwise, it will be vanished in the vast amount of information that the students are exposed to. The title of this presentation contains a question mark ("How to combine theory and practice?"), therefore it is very far from being a definitive statement!

References.

1. M.S. Rabello, *Estrutura e Propriedades de Polímeros,* Ed. do autor, Campina Grande, 2023. ISBN 978-65-00-69331-7.

Keywords: *education, teaching, learning, professional practice.*

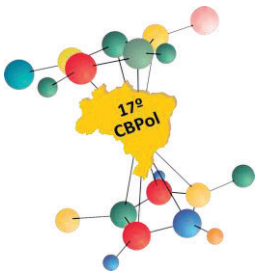

ASSESSMENT OF THE RELAXATION TIME OF POLYSTYRENE UNDER CONTROLLED SHEAR FLOW BY RHEO-OPTICAL TECHNIQUES

Felipe O.C. Bernardo[1]* and Sebastião V. Canevarolo[2]

1 – Graduate Program in Materials Science and Engineering (PPGCEM), Federal University of São Carlos (UFSCar), São Carlos, SP, Brazil
felipeocb@hotmail.com
2 – Department of Materials Engineering (DEMa), Federal University of São Carlos (UFSCar), São Carlos, SP, Brazil

Abstract - An attempt has been made to study the relaxation characteristics of polystyrene (PS) during a controlled shear flow. In polymers, optical properties can be used to estimate morphological changes under flow and, for this reason, being a trustful tool to evaluate relaxation time. The experiments consisted of varying the shear rate imposed on the polymer system while collecting the light signal isothermally at distinct temperatures. Then, birefringence was evaluated via an own built optical sensor by measuring the transmitted light intensity with crossed polarizers. Shear rates between 3 and 180 s^{-1} were imposed. The relaxation time was directly influenced by temperature and shear rate, increasing for higher shear and temperatures. For all samples, the relaxation time values found with our optical apparatus were validated by rheometric measurements found in literature. The values in both techniques were very similar, showing the effectiveness of the proposed technique.

Keywords: *Rheo-optical characterization; Relaxation time; Birefringence; Shear rate; Optical Microscopy;*

Fundings: This study was financed in part by the Coordenação de Aperfeiçoamento de Pessoal de Nível Superior - Brasil (CAPES) - Finance Code 001 scholarship (00889834001-08).

Introduction

The morphology of polymer mixtures during thermal processing results from different mechanical processes, namely phase deformation by shear and stretching stresses, relaxation, coalescence and, eventually, freezing [1]. All of them are highly dependent on processing parameters such as shear rate, in which higher levels of shear increase the level of dispersion resulting in more uniform morphologies and, consequently, more attractive to the market [2,3], and melting temperature, that strongly affects polymers' viscosity and their relaxation's capability.

Relaxation time on polymers is commonly measured by DMTA, rheometry, spectroscopy or microscopy. Extensive fundamental studies have been published on these aspects. Liao et al. [4] used DMTA analysis to evaluate the relaxation time differences of PMVS/LDPE blends. LDPE-rich blends have higher viscoelasticity and longer relaxation time than the PMVS-rich blends. Silva et al. [5] used scanning electron microscopy (SEM) to show the existence of one relaxation time and non-deformed droplets for an immiscible blend, and two relaxation times and deformed droplets for compatibilized ones, being the second relaxation more pronounced for higher compatibilizer contents. Sharma et al. [6] evaluated the influence of moisture distribution effects on the relaxation time and stiffness of polyamide 6, for this, a thermodynamically coupled model within the framework of mixture theory was developed. Zare et al. [7] develops two equations for relaxation

time of biopolymer nanocomposites at unlike frequency ranges. The author correlated the relaxation time to zero complex viscosity, yield stress, K constant and power-law index for a model proposition.

Optical phenomena such as birefringence, due to optical anisotropy caused by molecular orientation, can be used in the evaluation of these main parameters that directly affect the morphology of a polymer mixture [8]. The use of optical properties to characterize polymers' morphology has great advantages, such as not disturbing the system during the data acquisition process and for exhibiting high sensitivity and accuracy [9]. Nevertheless, these properties are still receiving little consideration from researchers due to the relative complexity of current detection systems.

Building on this development, this work aims to use optical properties for the evaluation of relaxation time in polymers. In other words, the use of rheo-optical techniques by means of birefringence is proposed as a new tool to measure the impact of shear flow on the relaxation time of PS/PA6 mixtures. Different temperatures and shear flow rates were evaluated. The assembly used in this work consists of a polarized light optical microscope, a device to control shear and temperature and a home-made rheo-optical detector to measure birefringence in real-time [10].

Experimental

Materials

A commercial grade of a general-purpose polystyrene, PS (N2560, manufactured by Innova, Triunfo, Brazil), with MVR of 3.8 cm^3/10 min (5.0 kg, 200 °C) was used in this work.

PLOM procedure

All measurements were performed on a polarized light optical microscope (PLOM), model DMRXP from Leica with a Cambridge Shearing System (CSS450), from Linkam Scientific Instruments. The CSS450 consists of two parallel plates with a quartz window each through which light is transmitted. Temperature and shear are controlled by the Linkam's software. Objective lens of 5X were used to perform the analysis.

The rheo-optical experiments were conducted at five established temperatures (°C): 180, 190, 200, 210 and 220, with a gap of 400 μm between the CSS450 plates. Variations in the rotation speed of the bottom quartz window, programmed by a LabVIEW 8.6 software, were done to achieve shear rates between 3 and 180 s^{-1} to polymer samples of about 0.5 g. A water pumping system was used to cool down the CSS450 plates throughout all experiments.

Samples of about 0.5 g were heated at 30 °C/min from room temperature to 230 °C and kept isothermally for 3 min, then cooled down to one of the five experiments' temperatures. After that, the shear profile presented on Table 1 was executed and any deviation on the transmitted light intensity automatically collected by LabVIEW. More details of the rheo-optical system used to measure the transmitted light intensity can be found elsewhere [10,11].

Table 1. Shear profile applied for all rheo-optical measurements.

#	1	2	3	4	5	6	7	8	9	10	11	12
Shear rate (s^{-1})	3	5	7	10	15	20	30	50	75	100	150	180
Time (s)	60	60	60	60	60	60	60	60	60	60	60	60

Results and Discussion

Rheo-optical characterization

The cross-polarized transmitted light intensity (I^B) measured by the optical detector can be normalized to a dimensionless value (I^B_N) set between zero and one, using the minimum intensity while the polarizers are crossed (I_C) and the maximum intensity while parallel (I_P), as defined by:

$$I^B{}_N = \frac{I^B - I_C}{I_P - I_C} \quad (1)$$

$I^B{}_N$ is related to the optical path difference (OPD) of an anisotropic material placed between crossed polarizers and oriented at 45° with respect to their optical axes by a simplified version of Malus' law [11]:

$$I^B{}_N = \sin^2\frac{\delta}{2} = \sin^2\left(\frac{\pi\, OPD}{\lambda}\right) \quad (2)$$

where λ is the wavelength of the light source (taken as 550 nm for visible light) and δ is the relative retardation of the polarized light ray.

Fig. 1 shows curves of normalized cross-polarized transmitted light intensity ($I^B{}_N$) as a function of shear rate for each temperature for samples of PS. Dashed lines are the quadratic sinusoidal fitting predicted by Eq. 2.

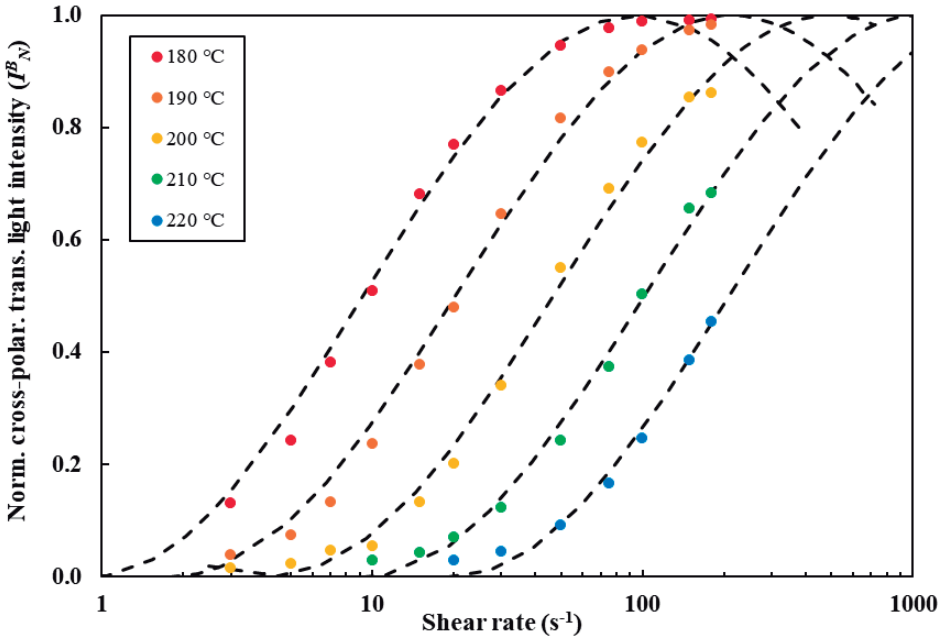

Figure 1. Normalized cross-polarized transmitted light intensity ($I^B{}_N$) of PS as a function of shear rate at the temperatures: 180 °C, 190 °C, 200 °C, 210 °C and 220 °C. Also shown the calculated curves from the theoretical Malus' Law, a quadratic sinusoidal fitting for each polymer system.

The normalized cross-polarized transmitted light intensity for PS at 220 °C is considerably lower than that measured for PS at 180 °C. The reason is the high reduction in viscosity which is reflected in lower orientation of the polymer chains under flow. Thus, even testing at the maximum practical shearing speed that the Linkam CSS450 can apply without loosen the sample out of the shearing plates, the first maximum at the highest evaluated temperatures is far from being reached, even though the quadratic sinusoidal behavior is present. For 180 °C, shear rates up to 75 s^{-1} are sufficient to achieve the half order maximum, which are values smaller than the range of 100 s^{-1} normally achieved in extrusion process.

A closer look of the fitted sinusoidal curves on the experimental points reveals that the fitting works very well. This effect is easier to be seen after calculating the total birefringence, Δn, shown in Fig. 2. Starting from the measured $I^B{}_N$, the optical path difference can be calculated by rearranging Eq. 2. It follows that, by knowing that the microscope gap (sample's thickness, t) is 400 μm, birefringence for PS can be calculated applying Eq. 3:

$$\Delta n = \frac{OPD}{t} \tag{3}$$

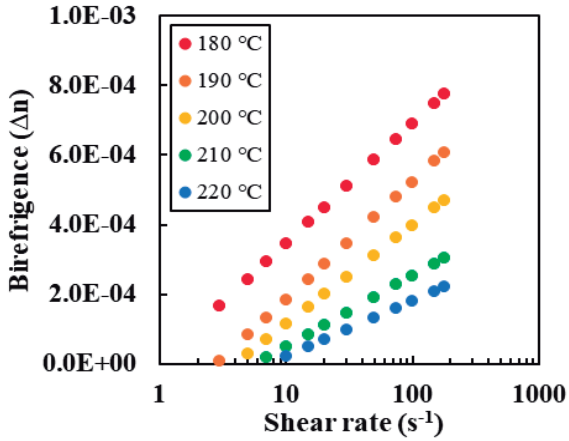

Figure 2. Birefringence of PS (derived from the cross-polarized transmitted light intensity curves of Fig. 1) as a function of shear rate at the temperatures: 180 °C, 190 °C, 200 °C, 210 °C and 220 °C.

Fig. 2 shows the calculated birefringence of PS as a function of shear rate for all temperatures. Because the measured cross-polarized transmitted light intensity is the result of all optical effects, the calculated birefringence is the total birefringence. While no shear rate is applied to the sample in the molten state, the polymer chains are in a random coil conformation, being optically isotropic and therefore no birefringence occurs ($\Delta n = 0$). When a shear rate is applied, the velocity gradient will orientate the random coils in the flow direction, if the chain deformation is faster than its relaxation. This happens above a minimum critical shear rate, when the random coils start to unwind, causing anisotropy in its refractive indexes and leading to a measurable birefringence. For pure polymers, the only type of birefringence present in these conditions is flow birefringence, as the result of the orientation of the polymer chains. As seen in Fig. 2, this effect increases linearly with the logarithm of the shear rate, for the range up to 180 s^{-1}. Here, an interesting consequence from the curves of Fig. 2 is the possibility to extrapolate the fitted linear curves to zero birefringence finding shear rate values that give information related to the stress relaxation time of the PS chains. With this assumption, for all experimental temperatures, the fitted linear curves from Fig. 2 were extrapolated until zero to evaluate the relaxation time. Fig. 3 shows the results.

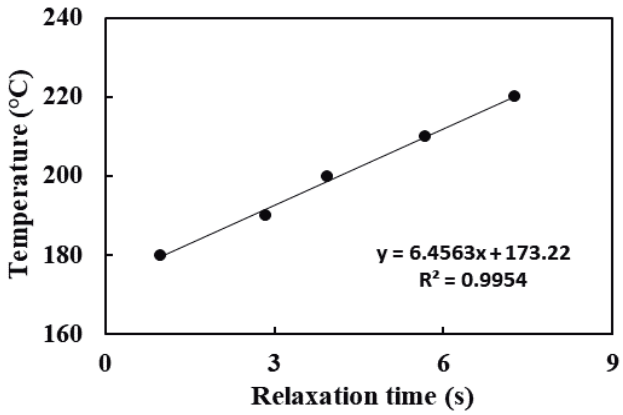

Figure 3. Relaxation time (s) as a function of temperature (°C) for PS.

Fig. 3 indicates that the stress relaxation of the PS chains is in the order of 1 s at 180 °C and follows an increasing behavior until reaching the mark of 7.27 s at 220 °C. At this temperature, the

relaxation time is more than seven times bigger than the small temperature of measure, reinforcing the influence that temperature causes on relaxation time.

The relaxation time spectrum obtained by our developed rheo-optical technique are in good agreement with former works found in the literature. West [12] obtained relaxation times in the order of 10 s for polystyrenes of narrow molecular weight at 227 °C with a cone-and-plate system. Caro et al. [13] used a laser diffraction particle size analyzer to measure the relaxation spectra for neat PS, neat PA6 and PS/PA6 80/20 blend at 230 °C achieving a relaxation peak at 6.6 s for the PS, a little low comparing to the results showed in Fig. 3, but still in the same range considering both works' differences.

Conclusions

This work used birefringence signal's changes for the evaluation of relaxation time in polystyrene while being sheared. The polymer (PS) was deformed under a controlled shear flow, while the normalized transmitted light intensity was measured with crossed polarizers by an own built optical sensor. Measurements of birefringence indicates the dynamic of orientation in the dispersed phase droplets during shear flow. The relaxation time is influenced by the shear level, increasing with its percentage, and increasing for higher temperatures. Decent agreement with available theoretical predictions was found. The entire measurement apparatus presented proved to be reliable and handy for a fast obtainment of the relaxation time spectrum of polymers without the need to face complex calculations, being, therefore, considered a useful tool in industrial processes.

Acknowledgements

The authors acknowledge the Federal University of São Carlos and the Graduate Program in Materials Science and Engineering for providing the laboratorial facilities.

References

1. S. Bärwinkel; A. Seidel; S. Hobeika; R. Hufen; M. Mörl; V. Altstädt. Materials 2016, 9. http://doi:10.3390/ma9080659.
2. F. Bernardo; J. A. Covas; S. V. Canevarolo. Polymers 2022, 14, 1152. http://doi:10.3390/polym14061152.
3. H. Li; U. Sundararaj. Macromolecular Chemistry and Physics 2009, 210, 852–863. http://doi:10.1002/macp.200800543.
4. H. Y. Liao. Academic Journal of Polymer Science 2020, 3. http://doi:10.19080/AJOP.2020.03.555621.
5. J. Silva; A. V. Machado; J. Maia. Rheologica Acta 2007, 46, 1091–1097. http://doi:10.1007/s00397-007-0201-z.
6. P. Sharma; S. Diebels. Continuum Mechanics and Thermodynamics 2021, 33, 1891–1905. http://doi:10.1007/s00161-021-01019-x.
7. Y. Zare; K. Y. Rhee. Journal of Materials Research and Technology 2021, 12, 500–511. http://doi:10.1016/j.jmrt.2021.03.016.
8. W. Becker; V. Guschin; I. Mikonsaari; U. Teipel; S. Kölle; P. Weiss. Analytical and Bioanalytical Chemistry 2017, 409, 741–751. http://doi:10.1007/s00216-016-0038-3.
9. C. W. Macosko, *Rheology Principles, Measurements and Applications*, Wiley-VCH, New York, USA.
10. R. L. Vasconcelos; S. V. Canevarolo. Polymer Testing 2020, 90, 1–8. http://doi:10.1016/j.polymertesting.2020.106737.
11. G. H. Meeten, *Optical Properties of Polymers*, Elsevier Science Publishing, New York, USA.
12. G. West. Polymer Journal 1969, 10, 751–758. http://doi:10.1016/0032-3861(69)90103-7.
13. A. S. Caro; T. Parpaite; B. Otazaghine; A. Taguet; J. M. Lopez-Cuesta. Journal Rheology 2017, 61, 305–310. http://doi:10.1122/1.4975334.

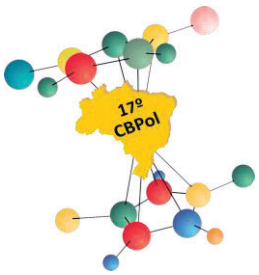

CROSSLINKED PVA NANOFIBERS WITH ANTIMICROBIAL ACTION

Gabriel N. Fraga[1]*, Douglas C. Dragunski[1,2]

1 – Department of Chemistry, State University of Maringá (UEM), Av. Colombo, 5790 - Zona 7, Maringá - PR, 87020-900, Brazil

2 – GIPeFEA, Department of Chemistry, State University of West Paraná (Unioeste), Toledo, PR, Brazil

gabrielnardi1@hotmail.com

Human skin is our most important organ and is our first protection mechanism against microorganisms. It is a vulnerable organ that is subject to damage to its continuity. Due to its importance, it is essential to ensure ideal protection for the skin when damaged, providing a physical barrier against bacterial contamination and promoting an adequate microenvironment that guarantees cell growth resulting in effective healing [1,2]. Electrospun polymeric membranes are a class of materials that meet the characteristics of modern dressings. Electrospinning is a simple, easy-to-apply and low-cost technique capable of obtaining membranes formed by polymeric nanofibers. These membranes stand out for having a high surface to volume ratio and high porosity. Therefore, obtaining nanofibers containing active compounds capable of preventing infections is of great interest for tissue engineering [3]. This work aimed to obtain bioactive dressings formed from polyvinyl alcohol (PVA) nanofibers through electrospinning, crosslinked with citric acid (CA) and/or glutaraldehyde (GLA), containing the antibiotic chloramphenicol (CLF) for the treatment of injuries. According to the SEM images, it can be seen that it was possible to obtain homogeneous nanofibers with diameters between 600 and 700 nm. DSC, XRD and FTIR analyses showed an increase in the crystallinity of PVA promoted by crosslinking, presenting a linear correlation with the increase in fusion enthalpy ΔH_{melt}, crystallinity also ends up influencing the release of the drug since the greater the crosslinking, the more rigid the structure decreasing the mobility of the drug [4]. The release of CLF followed the Weibull model typical for matrix systems, showing an instantaneous release within 30 min [5]. Disk diffusion assays showed antimicrobial activity against the strains S. aureus, S. epidermidis and P. aeruginosa, in addition to the membranes showing hemocompatibility, making them promising for application in dressings with anti-infective activity.

References

1. F. Zeighampour, F. Alihosseini, M. Morshed, A.A. Rahimi, J. Appl. Polym. Sci. 135 (2018) 1–13. https://doi.org/10.1002/app.45794.
2. T. Mirmajidi, F. Chogan, A.H. Rezayan, A.M. Sharifi, Int. J. Pharm. 596 (2021) 120213. https://doi.org/10.1016/J.IJPHARM.2021.120213.
3. T.B. Alberti, D.S. Coelho, M. de Prá, M. Maraschin, B. Veleirinho, J. Mater. Sci. 55 (2020) 9712–9727. https://doi.org/10.1007/s10853-020-04502-z.
4. X.H. Qin, S.Y. Wang. J. Appl. Polym. Sci. 109 (2008) 951–956. https://doi.org/10.1002/APP.28003.
5. S. Kajdič, O. Planinšek, M. Gašperlin, P. Kocbek, J. Drug Deliv. Sci. Technol. 51 (2019) 672–681. https://doi.org/10.1016/J.JDDST.2019.03.038.

Fundings: CAPES.

Keywords: *PVA, electrospinning, dressing, crystallinity.*

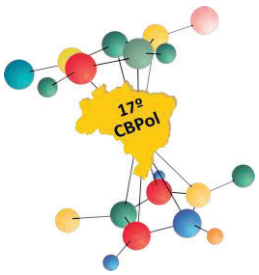

EFFECT OF STORAGE TIME ON RETROGRADATION OF EXTRUDED THERMOPLASTIC STARCH

Kelly L. Lizano[1]*, Antonio A. S. Curvelo[2] and Antonio J. F. Carvalho[1]

1 – Department of Materials Engineering, University of São Paulo (USP), São Carlos, SP, Brazil
klucasl@usp.br
2 – Instituto de Química de São Carlos, Universidade de São Paulo (USP), São Carlos, SP, Brazil

Abstract - The great development of thermoplastic starches (TPS), for biodegradable film applications, is still limited due to the already known disadvantages of the material. However, retrogradation, an inevitable and often undesirable process, has been little explored in the field of TPS and basically depends on storage conditions. In fact, retrogradation really limits the storage time and average life of starch-based thermoplastic materials. Thus, extruded thermoplastic starch samples plasticized with glycerol were characterized to identify possible structural changes due to retrogradation and its relationship with storage time. The rheological properties of TPS were measured in relation to storage time, and accompanied by other characterization techniques XRD, FTIR and DSC to verify the occurrence of retrogradation at different levels of ordering. Regarding storage time, the results showed the relative increase in viscosity at low shear rates and the increase in crystallinity, which became more evident around 10 days of storage. Furthermore, the FTIR signals in the 1050 – 950cm^{-1} range of the FTIR spectrum gradually increased over time. The ratio of signals 1022 and 995 cm^{-1} were used to measure retrogradation, and showed a relative increase with storage time. Meanwhile, the results by DSC did not show short-range molecular ordering after 30 days of storage. Thus, in general, the rheology, XRD and FTIR results were consistent with the possible structural changes, with a discrete retrogradation process of the extruded TPS samples. These results evidenced the slight change in the behavior of the TPS after its storage, at room temperature, due to the formation of more orderly structure.

Keywords: *Starch retrogradation, thermoplastic starch, storage time, TPS, extrusion.*

Fundings: This study was financed in part by the Coordenação de Aperfeiçoamento de Pessoal de Nível Superior – Brasil (CAPES) – Finance Code 001 – Process 88887.510940/2020-00.

Introduction

Starch is a naturally carbohydrate mainly composed of amylose and amylopectin, and is a widely available polysaccharide used for energy storage in plants [1]. It offers low-cost, biodegradable, renewable, and processable properties, making it highly attractive for applications like biodegradable packaging [2]. Starch-based polymers, or thermoplastic starch (TPS), are formed through the irreversible gelatinization of starch granules [3]. Upon cooling and storage, gelatinized starch undergoes retrogradation, leading to the formation of a distinct ordered structure [4]. Therefore, gelatinized starch, an amorphous state, returns to an insoluble, aggregate or crystalline condition [5], which is understood as a nonequilibrium, thermos-reversible and recrystallization process.

Starch-based polymers (TPS) have limitations compared to fossil-based plastics. TPS materials are hydrophilic with limited mechanical properties and thermal stability. The main limitation is retrogradation [6], an undesirable process and not well studied in TPS that affects the mechanical properties over time. It leads to film breakage, reduced elongation, and decreased optical clarity due to increased crystallinity [7]. Retrogradation also increases viscosity and firmness in gelatinized starch pastes during storage [8]

Starch retrogradation involves two stages: short-term and long-term. Short-term retrogradation entails rapid crystallization of amylose, while long-term retrogradation involves slower crystallization of amylopectin. The branched structure of amylopectin limits chain mobility, taking more time for the development of an ordered structure [9]. Starch retrogradation in starch-based food products is influenced by internal factors (starch composition, moisture content, etc.) and external factors (processing and storage conditions) [4], [9], [10]. The main components react differently to retrogradation based on their mobility. The degree of structural reconstruction depends on their content (amylose:amylopectin ratio) and molecular structure (molecular size and chain length distribution) [11]. Amylose content has a significant impact on retrogradation in starch thermoplastics [12]. Environmental factors like temperature, time, and cooling rates during storage also affect retrogradation. These factors can induce changes in the properties of TPS films [13].
The measurement of short-range order in starch-based materials involves Fourier Transform Infrared Spectroscopy (FTIR), while X-ray diffraction (XRD) is used to assess long-range order [4], [10]. Relative crystallinity is employed to quantify the degree of long-range ordering [7]. Structural changes caused by retrogradation impact the rheological properties of starch-based thermoplastics, commonly studied using capillary rheometer [14], [15]. Differential Scanning Calorimetry (DSC) is utilized to identify first-order endothermic transitions, providing insights into short-range molecular ordering, such as melting and crystallization [3].
Retrogradation is a challenging aspect in the industrial production of thermoplastic starch (TPS). While significant progress has been made in studying retrogradation, particularly in starch-based food products involving excess of water [4], [9], there is a lack of research on starch-based thermoplastic materials. Consequently, a more comprehensive understanding of the effects of retrogradation on TPS is necessary, including its impact on both extruded TPS and final products. The changes that occur in TPS due to retrogradation significantly affect their rheological and mechanical properties, and these changes are primarily influenced by storage conditions. Thus, a potential trend towards the formation of ordered structures in the TPS matrix, and therefore possible changes in the properties of extruded TPS as a function of storage time, may influence the processing parameters involved in obtaining starch-based plastic products.
In this study, TPS samples plasticized with glycerol were produced in a single screw extruder. Thus, the present work aims to study the effect of storage time on the retrogradation performance of extruded TPS. The results will help to identify the occurrence of possible changes on properties related to retrogradation. Rheological behavior, crystallinity, infrared spectroscopy and DSC were used to evaluate retrogradation during different storage periods. In this way, contribute to the study of the retrogradation of TPS.

Experimental

Materials – Regular native maize starch (30% amylose, 11% moisture content) and glycerol (Synth, 99,5%). Glycerol was used as plasticizer.
Preparation of TPS samples (Extrusion) – A mixture of starch and glycerol was fed into a single screw extruder (AX-Plásticos, Brasil), with a single screw of 16 mm in diameter and L/D ratio of 26. The rotation speed used was 40 rpm. The temperature profile of the heating zones along the extruder barrel was 115, 125 and 120°C from the feed zone to the die.
Characterization – To study the effect of storage time on the retrogradation process, samples were conditioned at 53% relative humidity (RH) and 23°C before the measurements. Extruded TPS was cut into particles to be characterized by capillary rheology. Cross sections of TPS extrudates were evaluated by XRD, FTIR and DSC. Retrogradation studies were used to monitored changes in properties since leaving the extruder (0 days) and during 30 days after extrusion.
The rheological behavior was obtained using an Instron capillary rheometer, model CEAST SR20 at 120°C. Power-law index (n) and consistency (K) were calculated. Diffractograms XRD were recorded in a Bruker X-ray diffractometer, model D8 Advance, equipped with a Cu source (Kα =

1.5418 Å). Scattered radiation was detected in the Bragg-angle (2θ) range of 5-60°. To calculate the degree of crystallinity, the area of the signals corresponding to the crystalline and amorphous phases was used. FTIR analyzes were performed on Perkin Elmer equipment, model Spectrum 100, using the attenuated total reflectance (ATR) accessory. The ratio of the signals at 1047/1022 and 1022/995 were used to measure retrogradation. DSC was carried out in a Perkin Elmer DSC 8000. Samples were placed in aluminum pans. The analyses were performed under a nitrogen flow (20ml/min), from -30 to 180°C, at a heating rate of 10°C/min.

Results and discussion

Capillary rheology

In Figure 1(a) it can be relatively observed that the longer the storage time, the higher the viscosity in the range of shear rates between 10-100s^{-1}, which reveals possible structural differences and formation of ordered structures incorporated in the viscoelastic amorphous phase of TPS [15], due to retrogradation. Those ordered structures can be assumed as reinforcements in the TPS matrix, which cause a slight increase in viscosity in relation to storage time at low shear rates, as some authors have reported the present of short-range residual ordering due to the rapid retrogradation in starch gels during storage at 4°C [8]. However, comparatively and in relation to storage time, there were no significant changes in viscosity from shear rates greater than 1000s^{-1}, due to the loss of those possible ordered structures throughout the test. Finally, in relation to the storage time, retrogradation hypothesis is also supported by the increasing results of the consistency index (K) of the power law as it is showed in Figure 1(b). Those results indicated differences in the behavior of the TPS, that involve formation of ordered structures and in greater quantity in the amorphous matrix of TPS when given 10 days of storage and thereafter.

XRD

The results of the DRX spectra (Figure 1(c)) showed that the crystalline structure of the native starch (A-type) was destroyed during extrusion, and subsequently the process of slow recrystallization occurred. Changes in TPS crystallinity over time were monitored and quantified as shown in Figure 1(d). Quantitatively, little considerable changes were achieved over time. However, after 10 days of storage, the (relatively) maximum degree of crystallinity was reached. An increasing of at least 8% was achieved. Some previous studies have shown that crystallinity is not always a measure of retrogradation over time.

FTIR

The FTIR technique is used to identify structural changes at a short-range molecular level [4], [10]. Figure 1(e) shows the FTIR spectra of native starch and TPS samples prepared and stored up to 30 days after extrusion. Signals between 1050 and 950 cm^{-1} indicate the formation of hydrogen bonds between the starch and the plasticizer [16]. Conformation changes due to retrogradation during storage can be monitored by the analysis of intensity of the bands in the mentioned region [10]. In native starch, the peak at 1047 cm^{-1} represents the crystalline region of the starch, whereas the peak at 1022 cm^{-1} corresponds to the amorphous region. However, the 1047cm^{-1} signal disappears with the disruption of the starch, as seen in the FTIR spectra of the TPS due to plasticization and the extrusion process. The spectral band at 995 cm^{-1} is sensitive to water content [4]. As is showed in Figure 1(e), FTIR curves were normalizing to compare signals. It was found a slight increase in intensity of the signal after 30 days of storage.

According to the report by Wang *et al.*, on retrogradation, ratios of 1047/1022 and 1022/995 cm^{-1} are assumed to represent organization in crystalline regions and the state of organization of the double helices localized inside crystallites, respectively. In that way, they were used to measure and evidence potential crystals formed as a result of the retrogradation process [4], [17]. There was a slight relative increment in the ratios 1022/995 during storage, indicating a progressive and intensified degree of starch reorganization, providing evidence of retrogradation occurrence, as is showed in Figure 1(f), while the ratios at 1047/1022 exhibited a tendency to remain constant.

DSC

No obvious melting behavior could be observed in the studied temperature range for all samples stored up to 30 days, indicating that there were no detectable crystals using the DSC technique. It was possible to have weak endothermic signal to be detected.

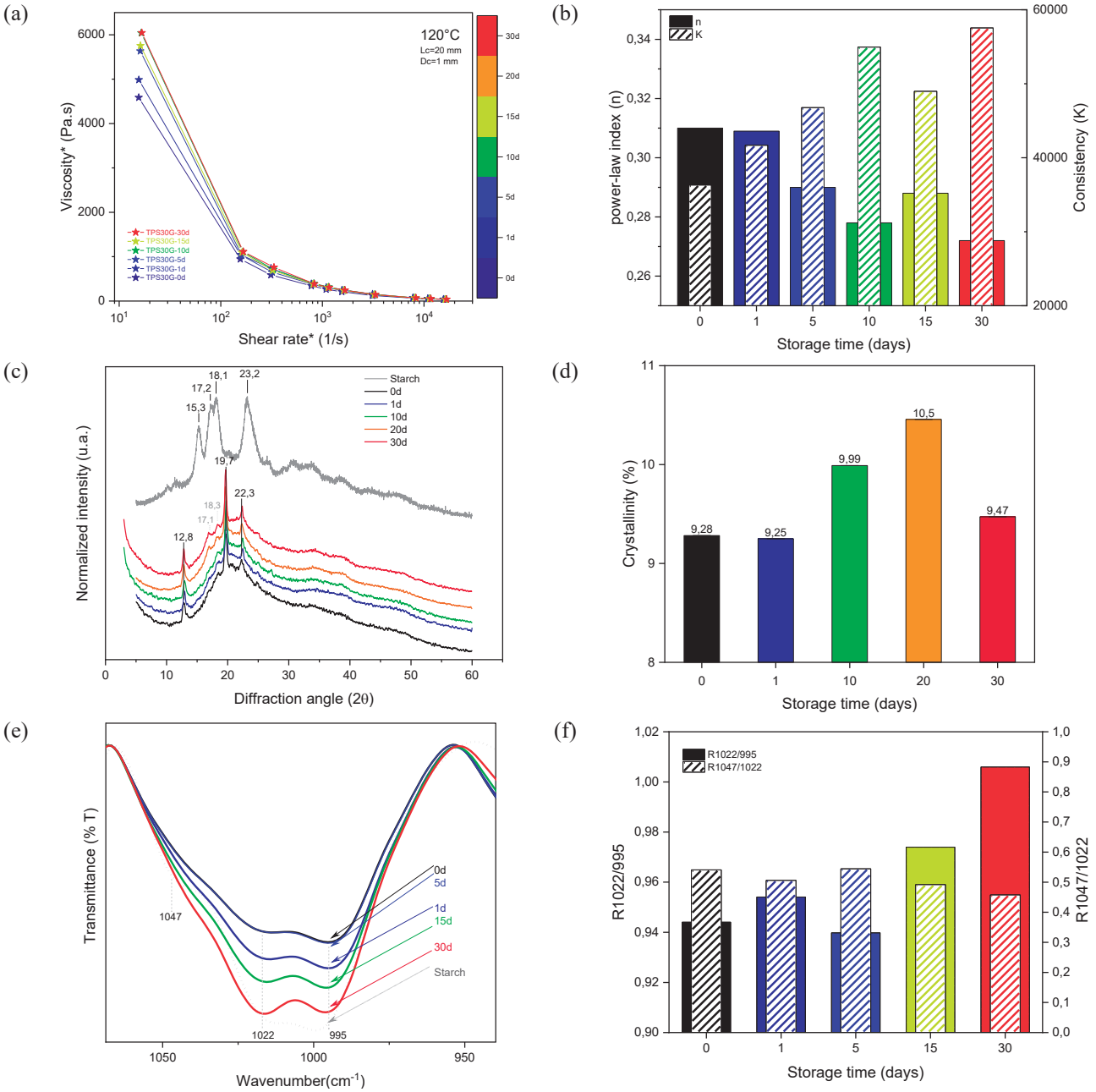

Figure 1 – Characterization of TPS samples after 30 days of storage at 23°C and 53% relative humidity. (a) Capillary rheology curves versus shear rate (120°C, Lc/Rc=40) and (b) Rheological parameters of the Power-Law model; (c) XRD spectra and (d) Crystallinity from XRD spectra, (e) Comparison of normalized FTIR spectra in the range 1050 – 950cm^{-1}, and (f) FTIR ratios at 1022/995 and 1047/1022, during storage.

Conclusions

The study involved the search for changes in the properties of extruded TPS conditioned at 53% RH and 23°C, specially related to the potential formation of ordered or crystalline structures in the amorphous matrix of TPS due to starch retrogradation. Thus, it was possible to identify, quantify, and evaluate the effect of storage time on TPS through comparative rheology, X-ray diffraction

(DRX), and Fourier-transform infrared spectroscopy (FTIR) analyses among samples during storage. Comparing results of low shear rate viscosities and crystallinities obtained through XRD showed congruence between them. After 10 days of storage, a maximum difference in rheological and structural behavior was observed. This was because these techniques are more sensitive to long-range ordering. However, FTIR is more sensitive to short-range ordering. FTIR has revealed the occurrence and increased retrogradation with respect to storage time. In contrast, it was not possible to determinate features of crystalline structures by the presence of endothermic signal by DSC. This study has provided a contribution into TPS retrogradation, which are relevant for industrial production and applications of starch-based plastic materials.

Acknowledgements
The authors thank Ricardo Gomes and Luiz Ramos for their help with technical support related to the processing and characterization of polymeric materials at the Department of Materials Engineering and at Instituto de Química de São Carlos, respectively, at the University of São Paulo, São Carlos.

References

1. A. Gandini and M. N. Belgacem, in *Monomers, Polymers and Composites from Renewable Resources*, 1st ed, Elsevier, 2008, chapter 1, 1–16.
2. A. J. F. Carvalho, in *Monomers, Polymers and Composites from Renewable Resources*, Elsevier, 2008, chapter 15, 321–342.
3. C. G. Biliaderis, in *Starch: Chemistry and Technology*, 3er Ed., J. N. BeMiller and R. Whistler, Eds. Elsevier, 2009, chapter 8, 293–372.
4. S. Wang, *et al.*, *Comprehensive Reviews in Food Science and Food Safety*, 2015, 14(5), 568–585. https://doi.org/10.1111/1541-4337.12143.
5. L. A. Bello-Pérez, *et. al*, *Journal of Agricultural and Food Chemistry, 2005*, 53(4), 1081–1086, Feb. 2005. https://doi.org/10.1021/jf0488581
6. A. M. Nafchi, *et al.*, *Starch - Stärke*, 2013, 65(1-2), 61–72. https://doi.org/10.1002/star.201200201.
7. K. Frost, *et al.*, *Carbohydrate Polymers, 2009*, 78(3), 543–548. https://doi.org/10.1016/j.carbpol.2009.05.018.
8. X. Liu, *et al., Food Hydrocolloids*, 2021, 120, 106914. https://doi.org/10.1016/j.foodhyd.2021.106914.
9. Q. Chang, *et al.*, *International Journal of Biological Macromolecules,* 2021, 186, 163–173. https://doi.org/10.1016/j.ijbiomac.2021.07.050.
10. A. A. Karim, M. H. Norziah, and C. C. Seow, *Food Chemistry*, 2000, 71(1), 9–36. https://doi.org/10.1016/S0308-8146(00)00130-8
11. V. Vamadevan and E. Bertoft, *Food Hydrocolloids*, 2018, 80, 88–96. https://doi.org/10.1016/j.foodhyd.2018.01.029.
12. N. Fujita, *in Starch: Metabolism and Structure*, 2015, Y. Nakamura Ed., chapter 10, 335–369.
13. R. Thakur, *et al.*, *International Journal of Biological Macromolecules*, 2019, 132, 1079–1089. https://doi.org/10.1016/j.ijbiomac.2019.03.190.
14. H. Liu, *et al.*, *Progress in Polymer Science*, 2009, 34(12), 1348–1368. https://doi.org/10.1016/j.progpolymsci.2009.07.001.
15. F. Xie, P. J. Halley, and L. Avérous, *Progress in Polymer Science*, 2012, 37(4), 595–623. https://doi.org/10.1016/j.progpolymsci.2011.07.002.
16. C. E. Montilla-Buitrago, *et al.*, *Starch - Stärke*, 2021, 73(9–10), 2100060. https://doi.org/10.1002/star.202100060.
17. A. Flores-Morales, M. Jiménez-Estrada, and R. Mora-Escobedo, *Carbohydrate Polymers*, 2012, 87(1), 61–68. https://doi.org/10.1016/j.carbpol.2011.07.011.

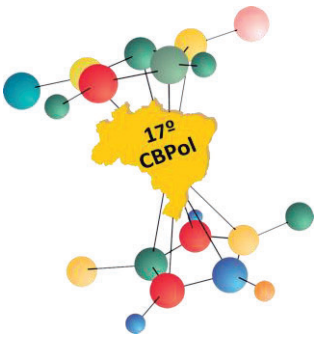

EVALUATION OF THE DEGRADATION OF OXO-BIODEGRADABLE PP BY THE ACTION OF NATURAL WEATHERING

João A. O. Brandão[1*], Francisco Gehlen[1], Edson L. Francisquetti[2] and Ruth M. C. Santana[1]
1 –Departamento de Engenharia de Materiais, Universidade Federal do Rio Grande do Sul (UFRGS), Porto Alegre, RS, Brasil
jaobrandao@yahoo.com.br
2 – Instituto Federal do Rio Grande do Sul, Campus Farroupilha, Farroupilha, RS, Brasil

Abstract – Polypropylene (PP) is one of the most used polymers in the world, especially in packaging. As the recycling of these items is still unfeasible, an alternative to favour its decomposition is to process PP with pro-degradant additive, which will favour its abiotic and biotic degradation. In this work, benzoin was used to obtain oxo-biodegradable PP, and the properties of the injection-molded PP were evaluated before and after 30 days of natural aging. It was evidenced that the benzoin favoured the thermo-oxidation of the PP in the processing, reducing its molar mass and increasing its MFI, but with little influence on its mechanical properties, evaluated by tensile and Izod impact tests. After 30 days of aging, it was observed that benzoin favours photooxidation, with a significant reduction of the molar mass of the additived PP, accompanied by a significant increase of the MFI. The losses of mechanical properties were similar for PP with and without additive.
Keywords: PP, thermo-oxidation, photooxidation, mechanical properties, molar mass

Introduction

Benzoin proved to be effective as a promoter of the degradation by thermo-oxidation [1] and photooxidation [2] of polyethylene (PE) in previous studies, indicating that, in the future, it may be used in obtaining oxo-biodegradable PE. Considering that the mechanism of degradation by thermo-oxidation and photooxidation of PE and polypropylene (PP) are similar [3], since they are polyolefins, it is convenient to think that benzoin can also be used to obtain oxo-biodegradable PP, an alternative to solve the problem involving the accumulation of polymeric material in the environment, a result of the incorrect disposal, especially of packaging, which does not present attractive recycling. Currently, however, the pro-degradant additives are based on organic salts of transition metals [4], whose use could lead to a second problem: the accumulation of metals where, normally, their presence would not be observed. Benzoin, on the contrary, is a biodegradable and non-toxic substance (according to EC Regulation No. 1907/2006).

In this work, it was sought to obtain oxo-biodegradable PP from the addition of benzoin in the processing. Besides evaluating the acceleration of thermo-oxidation and photooxidation, the changes in the mechanical properties of PP with and without the additive were evaluated, before and after exposure to natural weathering. Injection-molded specimens were obtained, with 0, 2, 4 and 6% of masterbatch produced in PP matrix, which was characterized by dilute solution viscometry, with subsequent determination of the viscosity average molar mass; determination of MFI, to confirm the reduction of chain size due to degradation; besides the evaluation of mechanical properties by Izod impact and tensile strength tests.

Experimental

Materials
In this work, PP grade H-605, with MFI of 2.1 g/cm3 (230 ºC/2.160 kg) and density of 0.905 g/cm3, produced by Braskem Brasil; benzoin, with purity degree higher than 99%, produced by Merck KGaG, were used.

Benzoin masterbatch production in PP matrix (pro-degradant additive)
The masterbatch was obtained from the mixture of PP with benzoin in a Haake thermokinetic mixer, model RheoDrive 7, at a temperature of 190 ºC. The initial 6 minutes were to guarantee the melting of the PP. After that, the benzoin mass was added, with an effective mixing time of 4 minutes. Therefore, the total process lasted 10 minutes. A masterbatch with a mass ratio of 3:1 (PP/benzoin) was obtained. The mixture was cut with the help of pliers into granules with dimensions like those of PP pellets. Fig 1 shows the produced masterbatch.

Figure 1 – Benzoin masterbatch after cutting with pliers, with dimensions like PP pellets.

Obtaining the injection-molded specimens
Specimens with 0, 2, 4 and 6% (w/w) of benzoin masterbatch were produced and therefore were named as: PP_0%, PP_2%, PP_4% and PP_6%, respectively. All were obtained in Thermo Scientific Haake MiniJet II at 190 ºC, with injection pressure at 400 bar and withdrawal pressure at 350 bar. The mixture of the masterbatch with the virgin PP was previously done in the thermokinetic mixer, as it is a piston type injection molding machine. Besides guaranteeing a good diffusion of the additive in the PP, the process simulated the usual processing in the thermoplastic industry, in which the material would pass through a screw for later injection. Five specimens were obtained for each one of the different samples to be tested for tensile strength and Izod impact.

Natural weather ageing in Porto Alegre/RS
The specimens were naturally aged in Porto Alegre/RS. The specimens were placed on a 45º inclined stand, specifically located in front of the State Center for Research and Remote Sensoring and Meteorology (UFRGS) with their phases facing north. They were evaluated before and after 30 days of exposure. The experiment was performed from 21 November 2022 to 21 December 2022. (ASTM 1435-13). Fig 2 shows the specimens exposed to natural weathering on the first day.

Figure 2 – PP specimens, with and without benzoin, exposed to natural weathering in Porto Alegre/RS.

Determination of the average viscosimetric molar mass of PP ($\overline{Mv}$)

The intrinsic viscosity ([Ƞ]) of PP in the samples was determined by dilute solution viscometry, for subsequent calculation of $\overline{Mv}$. Solutions with concentrations of 0.7; 0.5; 0.39; 0.32; 0.27 and 0.23 g/dL were used. The flow times of the initial solution and other dilutions were measured at a temperature of 135 ± 0.1ºC in a Cannon-Ubbelohde viscometer for diluted solutions (nº 50). From the flow times of the solutions and solvent (decalin) the relative (η_{rel}), specific (η_{esp}), and reduced specific ($n_{esp.red}$) viscosities were determined. The intrinsic viscosity ([Ƞ]) of PP was obtained from the graph of $n_{esp.red}$ versus concentration by extrapolation of the linear regression of the curve when the concentration tends to zero. Through the Mark-Howink-Sakurada equation (Eq. 1) the $\overline{Mv}$ of PP was determined. The constants α and k used for the polymer-solvent were 0.8 and 1.05 x 10^{-4} dL/g, respectively [5] (ASTM D446 and D445).

$$[\eta] = k.(\overline{Mv})^{a} \qquad (1)$$

Determination of the MFI of PP in injection-molded specimens

The melt flow indexes (MFI) of PP, with and without the additive, were obtained in a CEAST model 7026.000 modular plastomer. The conditions were: 230 ºC/ 2.160 kg, with 240 seconds of residence time (ASTM D1238).

Tensile test

Universal equipment Instron, model 4200, was used, using a load cell of 5 kN and removal speed of 25 mm/min (ASTM D638-10).

Izod impact test

Ceast equipment, model Impactor II, was used. The specimens were notched, and a 0.5 J hammer was used for impact, at room temperature (ASTM D638-10).

Results and Discussion

The PP specimens were characterized before and after exposure to natural weathering. Fig 3 presents the values determined by dilute solution viscometry. The $\overline{Mv}$ at t=0 indicates that, the higher the content of benzoin added, the higher the rate of thermos-oxidation in processing. In natural aging, it was possible to observe that the higher the benzoin content, the higher the degradation rate, mainly induced by photooxidation (caused, in turn, by the incidence of UV radiation). Such results show the pro-degradation action of benzoin, which favoured the degradation process in a similar way to the pro-degradants based on organic salts of transition metals on polyolefins [6].

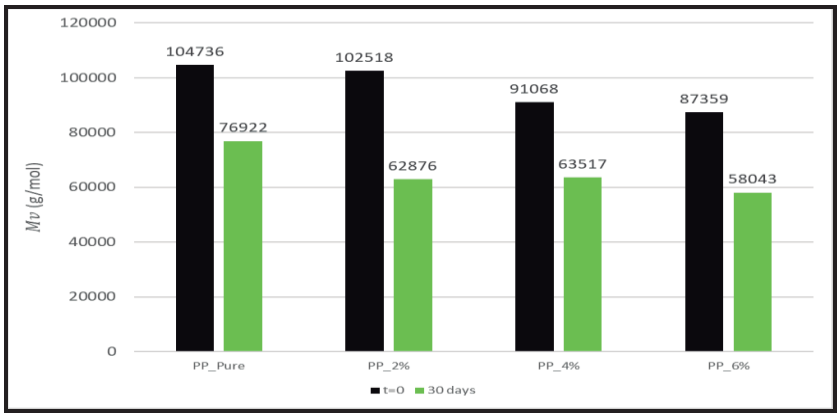

Figura 3 – $\overline{Mv}$ do PP nos corpos de prova injetados, antes e após a exposição ao intemperismo natural.

The MFI values, before and after exposure to natural weathering, are presented in Fig 4. At t=0, it was possible to observe that there was an increase in MFI, indicating greater ease of flow of the melt, possibly due to the reduction of chain size, corroborating the results obtained from $\overline{Mv}$, which strongly evidences the higher rate of thermo-oxidation for the injection-molded specimens with benzoin. After processing, the samples PP_4% and PP_6% presented an increase of 70% in MFI compared to PP_0%. The same occurred after exposure to natural weathering, and it was possible to observe that the photooxidation was more favored with the addition of benzoin, because when exposed to solar radiation, the increase in MFI was 154% for PP_6% compared to PP_0%. The increase is also consistent with the reduction in molar mass. These results are consistent with those verified in other studies in which the degradation of polyolefins processed with metallic pro-degradants and subjected to natural aging was evaluated [7].

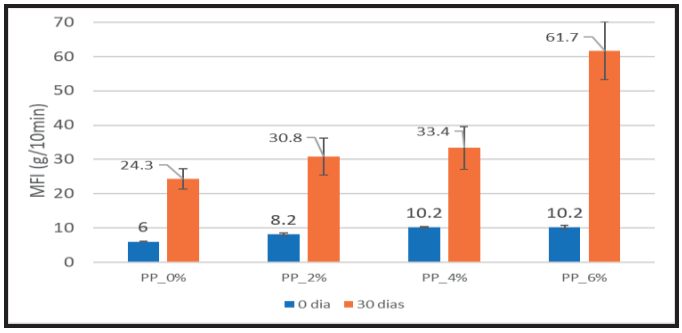

Figure 4 – MFI of the injection-molded specimens before and after exposure to natural aging.

The results of the Izod Impact test are presented in Fig 5, and it is possible to observe that, at t=0, the values found were statistically similar, allowing predicting that the addition of benzoin does little alter this mechanical property of PP. However, due to the acceleration of the photooxidative degradation process, part of this property is lost in natural aging. On average, it is possible to observe a reduction of the mechanical resistance to impact, although, considering the experimental error, the values for PP_4 and PP_6% are similar to the value found for PP_0%.

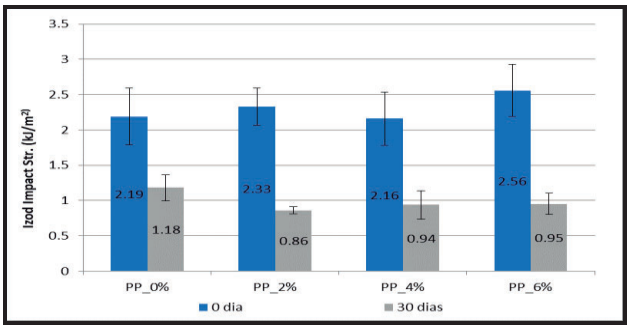

Figure 5 – Impact strength of the specimens, before and after natural aging.

Fig 6 presents the results of the tensile tests. The results of the elongation at rupture of the specimens will be discussed. At t=0, only PP_2% presents an average deformation below 430%. However, considering the experimental error, all of them have similar tensile, i.e., benzoin had little effect on this property of PP after processing, a behaviour similar to the one observed in impact strength. Regarding the elongation observed in the specimens after 30 days of aging, an accentuated reduction was observed in all samples. However, PP_2%, PP_4%, and PP_6% presented elongation values, on average, 50% lower than PP_0%. The results of this study are similar to those found in other scientific research in which the oxo-biodegradable PP, obtained from metallic organic salts, also showed reduced loss of mechanical properties compared to unadditivated polymer [8].

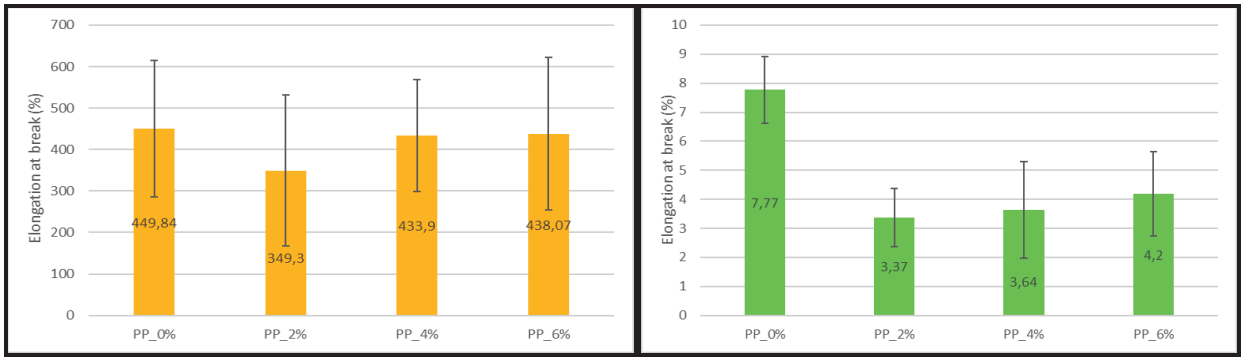

(a) (b)

Figure 6 – Elongation at break of the injection-molded specimens, (a) before and (b) after 30 days of aging.

Conclusions

According to the results found in this study, it was evidenced that benzoin also acts as a pro-degradant of PP, as occurs with PE, accelerating its abiotic degradation by thermo-oxidation and photooxidation. The higher the concentration of the additive, the higher the thermos-oxidation rate in injection-molding process. Similarly, the higher the concentration of the additive, the higher the photooxidation rate caused by the incidence of UV radiation from sunlight during exposure to natural weathering.

However, despite the reduction in the molar mass and increase in the MFI of the samples, the mechanical properties are weakly altered due to the addition of benzoin, indicating that, when used as a pro-degradation additive, it will little affect the quality of the items manufactured with oxo-biodegradable PP.

Acknowledgements

Thanks to Capes-Proex for the financial support.

References

1. J.A.O. Brandão; F.D.P. Morisso; E. L. Francisquetti; R.M.C. Santana. Polímeros 2021, 31, e2021029. https://doi.org/10.1590/0104-1428.20210058.

2. J.A.O. Brandão; F.D.P. Morisso; E. L. Francisquetti; R.M.C. Santana. Heliyon 2022, 8, e10217. https://doi.org/10.1016/j.heliyon.2022.e10217.

3. X. Liu; C. Gao; P. Sangwan; L. Yu; Z. Tong. Journal of Applied Polymer Science 2014, 131, 40750. https://doi.org/10.1002/app.40750.

4. A. Benitez; J.J. Sánchez; M.L. Arnal; A.J. Müller, O. Rodríguez; G. Morales. Polymer Degradation and Stability 2013, 98, p. 490-501. https://doi.org/10.1016/j.polymdegradstab.2012.12.011.

5. S. Gupta; X. Yuan; T.C.M. Chung; M. Cakmak; R.A. Polymer 2016, 107, p. 223-232. https://doi.org/10.1016/j.polymer.2016.11.027.

6. J.L. Pablos; C. Abrusci; I. Marín; J. López-Marín; F. Catalina; E. Espí; T. Corrales. Polymer Degradation and Stability 2010, 95, p. 2057 - 2064. https://doi.org/10.1016/j.polymdegradstab.2010.07.003.

7. P.K. Roy; P. Surekha; C. Rajagopal; V. Choudhary. Polymer Degradation and Stability 2006, 91, p. 1980-1988. https://doi.org/10.1016/j.polymdegradstab.2006.02.007.

8. T. Jachowicz; T. Garbacz; A. Tor-Swiatek; I. Gajdos; A. Czulak. International Journal of Polymer Analysis and Characterization 2015, 20, p.307-315 https://doi.org/10.1080/1023666X.2015.1016788.

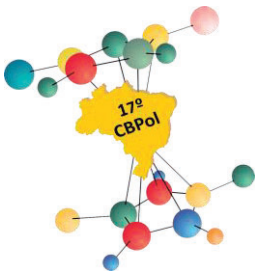

EVALUATION OF THE THERMAL PROPERTIES OF BACTERIAL CELLULOSE FILMS ADDED WITH EXTRACT OF *CAESALPINIA FERREA MART.*

Viviane F. Caetano[1*], Amanda C. O. Diniz[2], Alice C. A. de Lima[1], Angela M. M. Santos[2], Ivo D. L. Silva[1], Michelle F. de Andrade[1] and Glória M. Vinhas[1]

1 – Department of Chemical Engineering, University of Pernambuco (UFPE), Recife, PE, Brazil
viviane.caetano@ufpe.br
2 – Postgraduate Program in Material Science, University of Pernambuco (UFPE), Recife, PE, Brazil

Abstract - Bacterial cellulose (BC) is a biopolymer that has great potential to be used in plastic packaging. In this work, the thermal properties of BC films were added with *Caesalpinia Ferrea Mart.* the extract was produced and evaluated. The ethanolic extract was obtained from the stem bark, using the Soxhlet method for 6 hours. For BC production, 5 mL of the inoculum (100 mL of saline medium1, 30 g/L of glucose, 1 mL of ethanol; and 0.6 $g.L^{-1}$ of the bacterium (*Gluconacetobacter hansenii*) were transferred to systems in duplicates (50 mL of the saline medium; 0.5 mL of ethanol; 30 g/L of glucose) containing different extract doses (0.18, 0.27 and 0.45 g/L). Thermal analyzes were performed using the Mettler Toledo TGA-2 equipment. These results show that increasing the concentration of this extract in the culture medium causes a decrease in the material's thermal stability but does not compromise its use as food packaging.

Keywords: *Bacterial cellulose, Caesalpinia Ferrea Mart., Thermal properties*

Introduction

Due to the growing environmental problems caused by the improper disposal of plastic packaging, there is a need for new polymer alternatives that are sustainable and renewable. In this context, there is bacterial cellulose (BC), which is a biopolymer produced extracellularly by gram-negative bacteria and which has excellent characteristics, such as high porosity, high water retention capacity, high mechanical strength hydrated or not, low density, biocompatibility, and biodegradability [1-3].

The incorporation of natural additives to the bacterial cellulose matrix can change its physicochemical and mechanical properties and provide bioactive properties, such as antioxidant and/or antimicrobial [4]. Among the natural additives, there are plant extracts, such as the extract of *Caesalpinia Ferrea Mart.*, popularly known as "pau ferro" or "jucá, that can be incorporated into the BC polymeric matrix, providing it with bioactive properties. This extract is obtained from the Fabaceae family tree. Several parts of this tree, such as bark, stems, and leaves, have bioactive properties, such as anti-fungal, anti-ulcer, and anti-inflammatory [5]. These properties are due to the presence of flavonoids, tannins, saponins, and steroids in their chemical composition [6].

The combination of bacterial cellulose with *Caesalpinia Ferrea Mart.* extract is a promising alternative for the active packaging sector and an ecologically correct and sustainable option. In this work, bacterial cellulose films are incorporated with *Caesalpinia Ferrea Mart.* extract was developed and thermally evaluated, aiming at applications such as active packaging with bioactive properties.

Experimental

Materials

To produce bacterial cellulose, the bacteria *Gluconacetobacter hansenii*, deposited in the Culture Bank of the Department of Antibiotics at UFPE, was used as a producer of bacterial cellulose. For the preparation of the culture medium and inoculum, the saline medium patented by SOUZA et al., 2020 [7] was used, using glucose as a carbon source in both. The extract of *Caesalpinia Ferrea Mart.* was obtained from stem bark purchased at a local market in the city of Serra Talhada - PE.

Extraction of Caesalpinia Ferrea Mart

The extract from *Caesalpinia Ferrea Mart*. was obtained from the Soxhlet method. The extraction was carried out for a period of 6 hours, using ethanol as solvent. The experiments were performed in duplicates.

Bacterial cellulose production

The inoculum was prepared using 100 mL of saline medium containing 30 g/L of glucose as a carbon source; 1 mL of ethanol; and 0.6 $g.L^{-1}$ of the bacterium *Gluconacetobacter hansenii* in static culture for 3 days. At the end of this period, the inoculum was transferred to several static systems, previously sterilized in an autoclave for 15 min at 120ºC, in duplicate to start the pulp production process. Initially, 5 mL of inoculum were transferred to each Erlenmeyer system containing 50 mL of saline medium each, 0.5 mL of ethanol, and using glucose as a carbon source at a concentration of 30 g/L. Different amounts (0; 0.18; 0.27; and 0.45 g/L) of *Caesalpinia Ferrea Mart*. extract was added to each system. Bacterial cellulose membranes were produced over a total period of 20 days in static culture. After the end of this period, the membranes were washed in running water for 1 minute, wet weighed, and placed in an Erlenmeyer flask containing distilled water. After this step, the membranes were sterilized in an autoclave for 15 min at 120°C. Subsequently, they were dried at a temperature of 2°C.

Acquisition of MIR spectra

The medium infrared spectra (MIR) of the films were recorded using a Spectrum 400 FT-IT/FT-NIR spectrometer from the Perkin Elmer brand, with an attenuated total reflection accessory (Attenuated Total Reflectance –ATR), in the following conditions: spectral region of 4000 to 650 cm^{-1}, with 4 cm^{-1} resolution and 32 scans.

Thermogravimetric analysis

The dry membranes were subjected to thermogravimetric analysis using the equipment of the Mettler Toledo model TGA-2 under the following conditions: temperature range from 30 to 600 °C; heating rate of 10 to 10 °C/min under nitrogen atmosphere. The sample weights were in the range of 2 to 3 mg of dry bacterial cellulose.

Results and Discussion

Getting the extract

For the extraction of *Caesalpinia Ferrea Mart.* bark powder, an average mass of 20.0145 ± 0.0125 g was used, respectively. The average yield obtained after extraction performed in duplicate was 18 g/L.

Bacterial cellulose films

Table 2 shows the average yields of the wet and dry masses as well as the percentage loss of water from the cellulose membranes incorporated with the *Caesalpinia Ferrea Mart.* extract in different amounts. Codes BCPF1, BCPF2, and BCPF3 refer to films produced in culture media with iron extract at concentrations of 0.18 g/L, 0.27 g/L, and 0.45 g/L.

Table 2. Results of wet and dry mass yields of bacterial cellulose and water loss.

System	Wet mass (g)	Dry mass (g)	Water loss (%)
BCPF1	12.153±0.070	0.189±0.021	98.44±0.16
BCPF2	15.923±0.781	0.238±0.033	98.51±0.13
BCPF3	16.372±0.067	0.254±0.019	98.45±0.11

From the results, it is observed that there was an increase in the cellulose mass due to the increase in the concentration of the extract in the culture medium. There was water loss greater than 98% in all situations evaluated. The films showed similar macroscopic characteristics such as opacity, homogeneity, thickness, and diameter. This shows that the procedure used in the production of bacterial cellulose was effective and reproducible. The dry films had an average thickness of 0.158±0.005 mm and an average diameter of 5.7 cm.

Middle infrared spectrum

Fig. 1 illustrates the representative spectra of bacterial cellulose films produced from 0 g/L, 0.18 g/L, 0.27 g/L, and 0.45 g/L amounts of *Caesalpinia Ferrea Mart*. extract which correspond to BC, BCPF1, BCPF2 and BCPF3, respectively. The extract of Caesalpinia Ferrea *Mart*. was represented by the code PF.

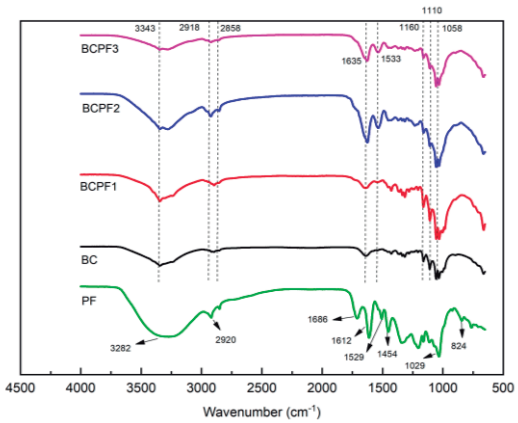

Figure 1. Representative spectra of pure bacterial cellulose (BC) and BC films produced in media containing different amounts of *Caesalpinia Ferrea Mart* extract (PF).

The spectra of the bacterial cellulose films were similar, only with different intensities in the maximum peaks in some spectral regions, probably due to the overlapping of characteristic bands of the cellulose and the extract. The maximum peaks of the bands found in bacterial cellulose films are in accordance with the literature. The maximum peaks of the bands found were 3343; 2918; 2858; 1738; 1631; 1160 and 1110; and 1033 cm^{-1} which refer to the vibrational stretching of the hydroxyl groups (OH), asymmetrical vibrational stretching of the methylene bridges (-CH2-), symmetrical

vibrational stretching of the methyl groups (-CH3-), angular deformation C-C, axial deformation of carbonyl group C=O, elongation of the CO and C-OH groups and elongation of the COC and C-OH bonds, respectively [8-9]. Regarding the representative spectrum of the *Caesalpinia Ferrea Mart.* extract, the maximum peaks were found for 3282, 2920, 1696, 1612, 1529, 1454, 1029, and 854 cm^{-1}, which refer to the presence of functional groups, such as ethanol, acids carboxylic and carbohydrates; asymmetric and symmetric elongation of ethane; elongation of the carbonyl group (C=O) due to the possible presence of flavonoids and lipids; C=C vibrations belonging to the aromatic rings of chemical compounds present in plant extracts, such as phenolic classes; C-O elongation and -OH deformation of tertiary alcohols; and the deformation of the C-H bonds in the aromatic ring of the compounds [10].

Thermogravimetric analysis

Fig. 2 illustrates the thermogravimetric curves, TGA and DTG, referring to bacterial cellulose films incorporated with *Caesalpinia Ferrea Mart.* extract. in amounts of 0.18 g/L, 0.27 g/L and 0.45 g/L which refer to the BCPF1, BCPF2 and BCPF3 systems, respectively.

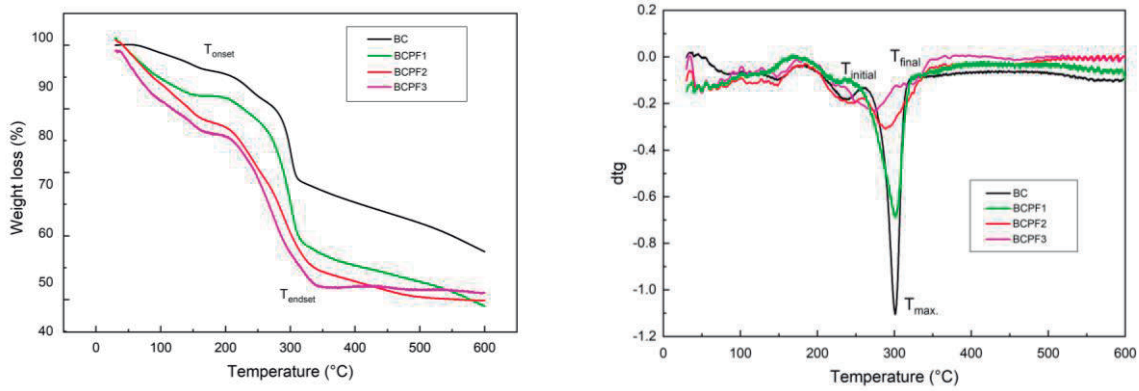

Figure 2. TGA and DTG thermogravimetric curves of the films obtained from the culture medium containing *Caesalpinia Ferrea Mart.* extract.

From the curves, it is possible to verify the four stages of mass loss. The first stage refers to the evaporation of residual water in the range of 40°C to 100°C. The second and third stages refer to the degradation of the components of the culture medium present in the cellulose films. The fourth stage refers to the thermal decomposition of cellulose (Table 2), with less mass loss of 50,49 %.

Table 2. Onset, endset and maximum temperatures of the pulp degradation and mass loss event.

System	4rd Stage			
	T_{onset}	T_{endset}	$T_{max.}$ (°C)	Mass loss (%)
BC	262,43	316,29	301,46	50,49
BCPF1	244,67	316,29	301,46	71,47
BCPF2	261,85	335,51	290,24	69,20
BCPF3	234,27	345,59	271,75	68,35

From the results, it was verified that there was a decrease in the T_{onset} with the increase of the extract concentration in the culture medium, except for the BCPF2 sample which proved to be thermally stable. This shows that for this composition, the insertion of the extract did not affect substantially the intermolecular forces present in the polymer. Regarding T_{endset}, there was an increase in this variable with the increase in the extract concentration in the culture medium. The T_{onset} and T_{endset} refer to the extrapolations of the beginning and end of the thermal decomposition

process, respectively. In relation to the maximum degradation temperature ($T_{max.}$), it appears that there was a more substantial decrease for the sample with the highest concentration of extract.

Conclusions

From the results, it was verified that the extract was incorporated into the polymeric matrix of bacterial cellulose and that its insertion in greater quantity interferes with the stability of the material due to the decrease in intermolecular forces, except for the addition of 0.27 g/L of extract that did not have substantial changes in its thermal stability. In general, the decrease in thermal stability for some evaluated compositions is not a factor that prevents the use of this material as food packaging since the extract has great potential for bioactive properties.

Acknowledgements

Foundation for Science and Technology Support from Pernambuco (FACEPE) for research grants.

References

1. A. P. C. Almeida; J. N. Saraiva; G. Cavaco; R. P. Portela; C. R. Leal; R. G. Sobral; P. L. Almeida European Polymer Journal 2022, 177, 111438. https://doi.org/10.1016/j.eurpolymj.2022.111438

2. V. M Bergottini; D. Bernhardt D. Mater Today Commun, 2023, 35, 105975. https://linkinghub.elsevier.com/retrieve/pii/S2352492823006669

3. G. F. Picheth; C. L. Pirich; M. R. Sierakowski; M. A. Woehl; C. N. Sakakibara; C. F. de Souza; A. A. Martin; R. da Silva; R. A. de Freitas International Journal of Biological Macromolecules, 2017, 104, 97–106. https://doi.org/10.1016/j.ijbiomac.2017.05.171

4. P. P. Nadira; V. M. A. Mujeeb; P. M. Rahman; K. Muraleedharan Carbohydrate Polymer Technologies and Applications, 2022, 3, 100191. https://doi.org/10.1016/j.carpta.2022.100191

5. M.I. Gallão; L. O. Normando; Í. G. P. Vieira; F. N. P. Mendes; N. M. P. S. Ricardo; E. S. de Brito Industrial Crops and Products, 2013, 47, 58–62. https://doi.org/10.1016/j.indcrop.2013.02.035

6. Indriani D, Elya B, Didier Noviani A. Pharmacognosy Journal, 2018, 10(6). https://doi.org/10.5530/pj.2018.6.202

7. K. C. Souza, *et al*. Patent BR 102014027203-8 A2, 2020.

8. Almeida do Nascimento H, Pedrosa Amorim J, José Galdino da Silva Júnior C, D'Lamare Maia de Medeiros A, Fernanda de Santana Costa A, Carla Napoleão D, et al. Influence of gamma irradiation on the properties of bacterial cellulose produced with concord grape and red cabbage extracts. Current Research in Biotechnology, 2022, 4, 119-128. https://doi.org/10.1016/j.crbiot.2022.02.001

9. P. Rachtanapun P; P. Jantrawut; W. Klunklin; K. Jantanasakulwong; Y. Phimolsiripol; N. Leksawasdi; P. Seesuriyachan; T. Chaiyaso; C. Insomphun; S. Phongthai; S. R. Sommano; W. Punyodom; A. Reungsang; T. M. P. Ngo Polymers (Basel), 2021, 13(3), 348. https://doi.org/10.3390/polym13030348

10. T. K. Patle,; K. Shrivas; R. Kurrey; S. Upadhyay; R. Jangde; R. Chauhan Spectrochimica Acta Part A: Molecular and Biomolecular Spectroscopy, 2020, 242, 118717.

HIGH STRAIN RATE COMPRESSIVE BEHAVIOR OF BALLISTIC POLYCARBONATE: EXPERIMENTAL AND NUMERICAL MODELLING

Rafael Rodrigues Dias[1], Iaci Miranda Pereira[1]

1-Brazilian Army Technological Center, Materials Laboratory, Brazil, rrodrigues083@gmail.com

Abstract – The dynamic compression properties of ballistic polycarbonate (PC) was evaluated at this paper through Split Hopkinson pressure bar (SHPB) tests. For that, four different high strain rates were examined. True strain-stress relations and the mechanical properties evolution as function of strain rate were obtained and evaluated. The experimental data was used to feed explicit simulations on Ansys LS-Dyna. The accomplished numerical model results were then compared to a particular experimental case.

Keywords: *high strain rate; split Hopkinson pressure bar; polycarbonate; explicit simulation*

Introduction

The polycarbonate (PC) is a thermoplastic polymer recognized by its transparency and high impact resistance, been widely used on shielding application where visibility is mandatory. Since it can have ballistic properties, PC can be used alone, as a visible part of a riot shield or in a google eyewear, where its use is limited to a certain range of impact velocity; or as a part of a system, as a bullet-proof glass, where it is used in a multi-ply laminate along with glass [1]. The high strain rate behavior of PC is, therefore, of great interest for defense applications.

Materials' compressive dynamic behavior under high strain rates are mostly studied using SHPB [2]. The SHPB apparatus comprises of three bars, with a specimen sandwiched between an incident bar and a transmitted bar, as exhibited in Fig.1. The strike bar travels to the end of the incident bar while being propelled forward by an instantaneous release of gas. The striker's collision with the incident bar generates an incident wave (ε_I). This wave is partially reflected (ε_R) at the interface incident bar/sample, while the remaining portion is transmitted up to the transmission bar (ε_T).

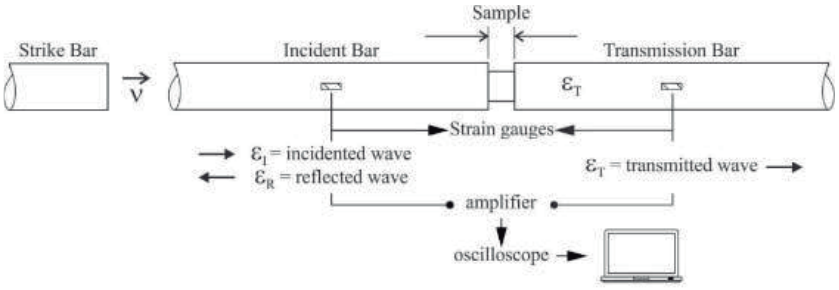

Figure 1 - Split Hopkinson pressure bar main parts [3]

The signals are captured by strain-gauges and recorded by an oscilloscope, which transmits them to an amplifier system, creating results of Voltage (mV) vs. Time (ms). The specimen true stress-strain

and strain rate-time relationships are derived from the recorded signals using the one-dimensional elastic wave theory [3], resulting in the following equations, Eq.1 to 3 [2-4]:

$$\sigma = E\frac{A}{2A_s}(\varepsilon_T) \quad (1) \qquad \varepsilon = \frac{C_B}{L}\int_0^L(\varepsilon_R) \quad (2) \qquad \varepsilon' = \frac{C_B}{L}(\varepsilon_R)dt \quad (3)$$

In this paper, the main goal is to study the dynamical behavior of ballistic polycarbonate in SHPB and understand the evolution of its properties with respect to the strain rate. With that, develop a trustable explicit numerical model.

Experimental

Materials

The compact polycarbonate plate 2 m x 2 m x 0.04 m Poli 25 was acquired from Bold® company. This specific grade was design to have high impact resistance with application in security as shielded windows against impacts up to 200 m/s [5].

Compressive Tests

A SHPB, from REL Inc., MI, USA, with an oscilloscope from Pico Technology, TX, USA (PicoScope 5000 Series) and a signal conditioning amplifier system from Vishay Micro-Measurements, NC, USA (2300 System) was used to execute the tests. The 7075-T6 aluminum incident, transmission and strike bar has Young´s Modulus of 69 GPa. All bar have 9,5 mm diameter. Both incident and transmission bar have 1830 mm length, while the the strike bar, 308.4 mm. SHPB cylindrical samples with smooth parallel surfaces were cut on water jet, 4 mm thick and 8 mm diameter, having a thickness/diameter ratio, H/D, of 0.50, according to 0.5<H/D<1 recommended for polymer materials. Table 1 resumes the parameters applied in this paper, presenting the applied pressure (kPa) and the respective average strain rates (ε').

Table 1 - Hopkinson bar's parameters.

Samples Group	Pressure (kPa)	ε' (s^{-1})
ε_1'	62,05	1000
ε_2'	82,74	2500
ε_3'	117,21	4500
ε_4'	144,79	5500

Numerical Modelling

Ansys LS-Dyna, which is an explicit finite element analysis software used to highly nonlinear models, was chosen to create the numerical modelling because of its broad platform of constitutive models appliable to thermoplastic polymers [6,7]. Concerning the constitutive models chosen to represent the dynamic behavior of the materials, the bars were all modelled using *MAT_ELASTIC (MAT01). As the aluminum bars should not reach plastic deformation, the selection is sufficient. The parameters of the model were density ρ = 2.73 g/cm^3, Elastic Modulus E = 69 GPa and Poisson's ratio ν = 0.33. For the polycarbonate sample, *MAT_PLASTIC_POLYMER (MAT89) was employed. The MAT89 is appliable to an elasto-plastic material behavior, in which the elastic and plastic zones are not as easily determined as it is for metals [8]. The models contemplates strain hardening and strain rate dependency, by the entrance of Cowper-Symonds parameters (C,P) and an empirical stress-strain curve [8,9]. For the sake of simplicity, only the SHPB test at ε_3' was chosen to establish comparison between experimental and simulation results. One was chosen for its proximity to the rate impose by a ballistic impact [1]. Table 2 summarizes the entrance data for PC as MAT89.

Table 2 - PC MAT89 parameters

	ρ (g/cm³)	ν	E (MPa)
Quasi-Static compressive properties	1,20	0,32	1.450
	C		P
Cowper-Symonds parameter	89.025		3,89
Load Curve	average of experimental PC ε_3' stress-strain curve		

Cowper-Symonds parameters can easily be calculated by linearization of the function relating yield stress (σ_y) and strain rate (ε'), Eq. 4 [8,9].

$$\sigma = \left(\sigma_y + B\varepsilon^n\right)\left[1 + \left(\frac{\varepsilon'}{C}\right)^{1/P}\right] \quad (4)$$

where σ is the yield stress of the material, σ_y is the quasi-static yield stress, B and n are the strain hardening constant, $\varepsilon_{plastic}$ is strain at plastic region, C and P are the strain rate sensitivity constants and ε', the strain rate.

Results and Discussion

Experimental Results

Fig.2(a) shows PC dynamic true stress-strain plots, along with a 0,5 s^{-1} quasi-static compressive true stress-strain plot (dashed line), tested at a INSTRON 5969 universal machine. The quasi-static test was executed to obtain properties to feed the numerical modelling, serving in this plot only as reference. Fig.2(b) and Fig.2(c) presents the dynamical properties as a function of strain rate.

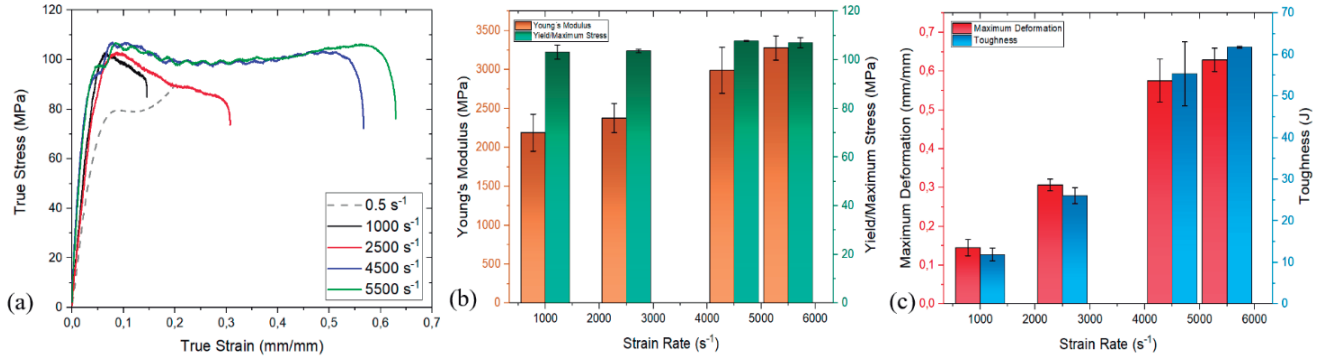

Figure 2 - Experimental results at SHPB (a) true stress-strain curves; properties as function of strain rate (b) Young's Modulus (MPa) and Yield/Maximum Stress (MPa) and (c) Maximum Deformation (mm/mm) and Toughness (J)

One can note that, although it exists a considerable strain hardening, specially from ε_1' to ε_3', the material strain rate sensitivity is considerably low (which was observable by the large Cowper-Symonds 'C' value). Fig.2(b) shows no significant variation in the Yield/Maximum Stress and a sectorized increase in the Young's Modulus, where only from ε_2' to ε_3' a statistical substantial escalation was detected. Fig.2(c) shows the correlation between the PC maximum deformation and its tenacity, which presents an almost linear evolution, with a slight asymptotic form between the two higher strain rates.

Numerical Modelling Results

A full 3D split Hopkinson pressure bar of solid elements was modeled at Ansys LS-Dyna. All experimental parameters were preserved (diameter and lengths of the bars and sample). Mostly hexahedral elements were employed to enhance the mesh aspect ratio. As the sample undergoes large deformation, the so call under-integrated elements (*SECTION_SOLID; ELFORM=1) were chosen

as best choice [10]. Consequently, it is most likely to occur hourglass deformation as error source, which is an non-physical behavior of solid elements. Thus, an hourglass control was imposed (*CONTROL_HOURGLASS; hourglass type IHQ=2, with hourglass coefficient QM=0.1). Fig.3 is an image of the model, where it can be seen incident bar, the sample and transmission bar, the impact oriented at Y-axis.

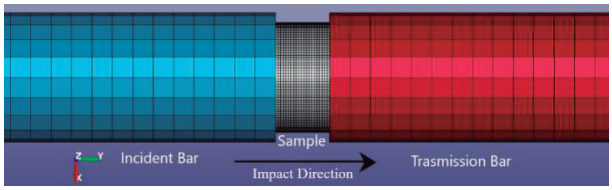

Figure 3 - Split Hopkinson pressure bar model.

Boundary conditions were employed to the three bars, restricting dislocation and momentum at any direction other than the impact direction. All the contacts interfaces (strike bar/incident bar; incident bar/specimen and specimen/transmission bar) were defined applying *CONTACT_SURFACE_TO_SURFACE frictionless (i.e. neglecting all forces other than the ones at Y-axis). To remain as close as possible to the experimental event, the only initial condition imposed was the strike bar velocity, replicating the ones input on the experimental events (V_{sb} = 25.75 m/s). Before interpreting the results, as a good simulation practice, the model is post-processed [10]. It must be observed, at this stage, the hourglass/internal energy relation, which must have a maximum of 10%. Fig.4 is a plotting of internal energy and hourglass energy of the PC sample, showing that the hourglass energy is quite lower than 10% of the internal energy. This means that the interference on the system energy by an unphysical, although exist, is in an acceptable scope.

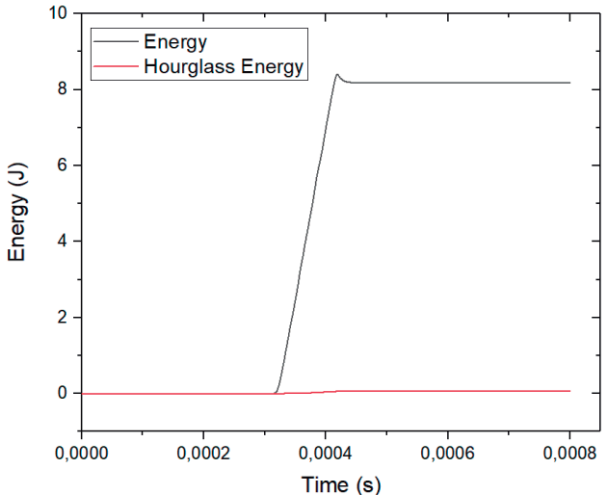

Figure 4 - Post-processing plots Internal vs Hourglass Energies.

After ensured the model correctness, the results can be studied. Fig.5 shows a 4500 s^{-1} SHPB test experimental vs numerical comparison, while Fig.5(a) is the Strain Rate vs Time and Fig.5(b) is the True Stress-Strain. One can note, in Fig.5(a), that the simulation's achieved rate is considerably close to that obtained in the tests, although less intense and with shorter duration. Nonetheless, the contrast between empirical and numerical is reasonable approximated. Fig.5(b) delivers the comparison between experimental and numerical procedure. It is valid to point out that many polymers show a more brittle response at higher strains rates, as seen for PC at the SHPB experimental results. The MAT 89 constitutive model, however, predicts that. Hence, the stress-strain curve is permitted to have sections steeper (i.e. stiffer) than the inserted [9]. So, the quasi-static modulus is conformed to the high strain rate one and the elastic region is achieved with greater precision.

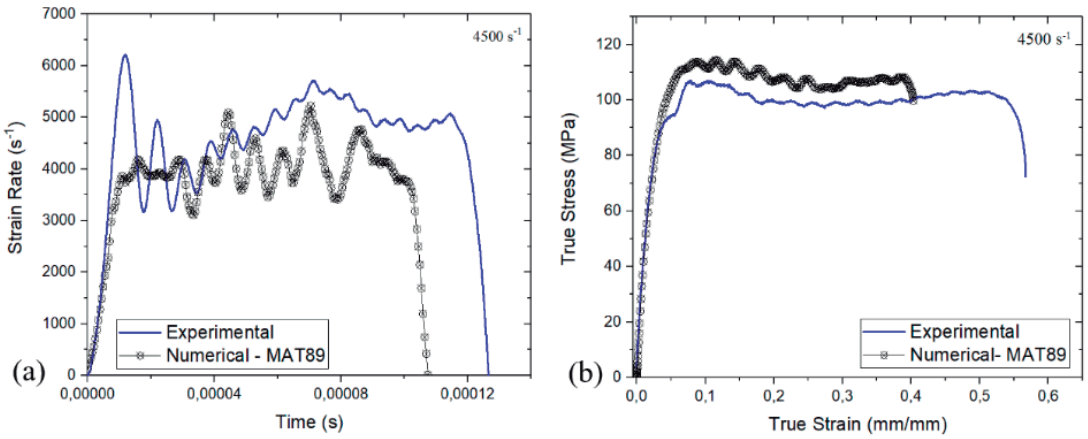

Figure 5 - Experimental vs simulation comparison (a) Strain Rate vs Time, (b) True Stress-Strain

Differences were detected on the plastic region, displaying lightly higher values of stress and appreciably lower value of maximum deformation. As the PC has noticeably large deformation, it must be included on the numerical model some control parameters to avoid simulation errors. One common case is the "Negative Volume in Solid Element", which occurs when the element deformation is so high that the element gets extremely distorted, returning a negative volume (which is physically unfeasible) [8,10]. In large scale, this leads the simulation to be interrupted. To avoid it, a series of control parameters are inserted on the model to stiff the solid elements that composes the thermoplastic, preventing it from reach negative volume, yet interfering in the result. From that, it is perfectly reasonable that the simulation shows a conservative result in terms of deformation/toughness and one can affirm that MAT89 constitutive model is accurate.

Conclusions

The PC samples were tested at SHPB and presented extensive strain hardening, but limited strain rate sensitivity as function of strain rate. Thus, the main mechanism of energy absorption to PC under high strain rate compression is deformation. A numerical model was built in LS-Dyna using the empirical properties. The numerical simulations used the MAT 89, with rate dependency represented using the Cowper-Symonds model. Overall, the numerical simulations provided an accurate prediction of the behavior observed in the actual testing.

Acknowledgements

The authors thanks the FAPERJ for its continuous financial support.

References

1. I. Crouch, *The Science of Armour Materials*, 1st ed., Sydney: Elsevier, 2017
2. W. W. Chen and B. Song, *Split Hopkinson (Kolsky) Bar*, 1st ed., New York: Springer, 2011.
3. B. A. Gama, S. L. Lopatnikov, J. W. Gillespie, Appl. Mech. Rev. 2004, 57, 223
4. R.R. Dias; I.M. Pereira; B.G. Soares; Global Journal of Researches in Engineering (J) 2019, XIX, V. https://doi.org/10.1016/j.polymer.2022.125406.
5. Datasheet*:* Dados Técnicos do Policarbonato Compacto Poli 25, 2020.
6. P.A. Du Bois et al. in LS-DYNA Anwendenforum, Bamberg, Germany 2005.
7. P. Reithofer et al. in 15th International LS-DYNA® Users Conference, Detroit, USA, 2018.
8. LS-DYNA® Theory Manual, California: LST-Ansys, 2019.
9. LS-DYNA® Keyword User's Manual. Vol.II, California: LST-Ansys, 2019.
10. LS-DYNA® Aerospace Working Group (AWG), "*Modeling Guidelines Document*", PA, 2021.

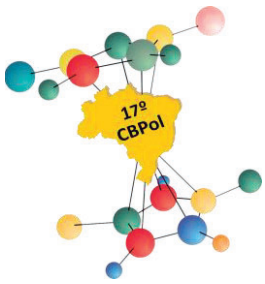

THERMAL, RHEOLOGICAL AND MECHANICAL PROPERTIES OF EPOXY RESIN FORMULATIONS

Tainá Klein[1,*], Cristiane Fonseca[1], Daiane Romanzini[2], Otávio Bianchi[1], Sandro Campos Amico[1]

1 – Department of Materials Engineering, Federal University of Rio Grande do Sul (UFRGS), Porto Alegre, Brazil
taina.klein@ufrgs.br
2 - Postgraduate Program in Materials Technology and Engineering (PPGTEM), Federal Institute of Rio Grande do Sul (IFRS), Feliz, Brazil

Abstract
This study aimed at identifying the most suitable combination of epoxy and hardener for filament winding composite manufacturing. The curing behavior of formulations prepared with a combination of epoxy resins (called E1 and E2) and hardeners (called H1 and H2) were investigated by non-isothermal differential scanning calorimeter analysis, rheometry, and Fourier-transform infrared (FTIR) spectroscopy. Post-cured formulations were also characterized using thermal (DMA, TGA) and mechanical (tensile strength) analyses. The E2 resin formulations showed higher glass transition temperature, higher storage modulus, and thermal stability. In addition, the viscosity of E1 and E2 at 60 ºC were similar. Higher storage modulus results were found for the E2H1 sample, although both E2H1 and E2H2 showed similar glass transition temperatures. In all, the E2H1 formulation showed the most suitable overall performance.

Keywords: *Epoxy, rheology, thermal analysis, glass transition temperature.*

Fundings: FAPERGS Inova Clusters Tecnológicos (Project 22/2551-0000839-9).

Introduction

Epoxy resins are thermosetting polymers usually obtained by reacting epichlorohydrin with bisphenol, and characterized by two or more epoxy groups per molecule through which the crosslinking reaction (curing) takes place. The final polymer properties depend on the hardener, the curing conditions, and the degree of conversion achieved [1]. The hardener determines the mechanism of the curing reaction and consequently influences the curing kinetics, the processing cycle (viscosity as a function of time), and the gelation and properties of the cured material [2, 3]. Examples of hardeners for epoxy resins are: amines, amides, anhydrides, imidazoles, boron trifluoride complexes, phenols, and metallic oxides [4,5].

Due to their excellent thermal and mechanical properties, epoxy resins stand out due to their various applications such as: coatings, paints, and composite materials. Several processes work with epoxy for manufacturing composite materials [1], including filament winding, where performance, material qualification, and product consistency are paramount requirements for aerospace components, pipes, tubes etc. Many thermosets applied in composites are cured using complex cure cycles to optimize the tradeoff between processing time and final product properties. Thus, understanding the viscoelastic properties of a thermoset resin is essential. It is also vital to monitor viscosity, gel temperature, onset and peak curing temperature, degree of curing, and glass transition temperature to optimize the manufacturing [6].

This study aimed at identifying the most suitable combination of epoxy and hardener for filament winding composite manufacturing. The curing behavior of formulations prepared with a combination

of epoxy resins (called E1 and E2) and hardeners (called H1 and H2) were investigated , along with various analyses of the cured resin systems.

Experimental

Materials

Two diglycidyl ether of bisphenol A (DGEBA)-based epoxy resins, called E1 and E2, with viscosity at 25 ºC (ISO 3219) of 1300-1500 and 7000-10000 mPa.s, respectively, and two anhydride-based hardeners, called H1 and H2, with viscosity at 25 ºC (ISO 3219) of 90-100 and 150-300 mPa.s, respectively, were studied. All materials were donated by Olin Corporation.

Methods

Four different formulations were produced with the available materials, named E1H1, E1H2, E2H1, and E2H2. For example, E1H1 sample was prepared with epoxy E1 and hardener H1.The epoxy:hardener ratio was 1:1. Samples for DSC and rheometry were prepared by mixing epoxy and hardener just prior to the analysis. The other samples were prepared by casting the mixture into a silicon mold, and curing in an oven for 24 h at 60 °C, followed by post-curing for 1-2 h at 90 °C and 4-6 h at 140 ºC as per the manufacturer datasheet.

Rheological analysis (Anton Par rheometer, MCR 101) was carried out at 60 °C in the shear-rate of 1 $Hz.s^{-1}$, at a rotation speed of 60 rpm (ASTM D2983), with a cone-plate geometry. In the rheological analysis, the viscosity at 60 °C was measured and the gel time was taken as that corresponding to the change in slope of the two linear parts of the curve. Fourier-transform infrared spectroscopy (FTIR) was performed using the ATR technique in a Perkin Elmer, Spectrum 1000 in the 450-4000 cm^{-1} range. For each sample (neat resins, neat hardeners, and post-cured formulations), 32 scans were recorded with a resolution of 4 cm^{-1}. Differential scanning calorimetry (DSC) analysis was conducted in a TA Instruments Q20 calorimeter under a nitrogen atmosphere with a flow-rate of 50 $mL.min^{-1}$. Each formulation (~10 mg) was subjected to the following cycle: heating from room temperature to 200 ºC (to measure enthalpy of curing), cooling to 25 ºC, and heating to 200 ºC (to measure the T_g of the cured sample). All heating and cooling rates were of 10 $ºC.min^{-1}$. Dynamic-mechanical analysis (DMA) was performed in a TA Instruments TA2980 equipment using dual cantilever mode, dimensions of (35 × 12.6 × 4) mm, with a frequency of 1 Hz and 4.4 μm (linear viscoelastic region) of amplitude, using a heating rate of 1 $ºC.min^{-1}$, from room temperature to 250 °C. Thermogravimetric analysis (TGA) was performed in a TA Instruments Q50 equipment on the post-cured samples (~10 mg), under nitrogen gas flow (50 $mL.min^{-1}$), at a heating rate of 10 $ºC.min^{-1}$, from room temperature to 900 ºC.

Results and Discussion

Fig. 1 shows the FTIR results for neat resins, hardeners and post-cured formulations. In Fig. 1A, in both resins (E1 and E2), it is possible to verify the presence of oxirane groups (915 cm^{-1}), the ether group (1185 cm^{-1}), alkane group (between 2960–2850 cm^{-1}), and C=C bonds in aromatic rings (1600 and 830 cm^{-1}). It is also possible to verify for the hardeners bands of different intensities within 1730-1780 cm^{-1} referring to the C=O group, as well as in the 1300-900 cm^{-1} region referring to the C-O group.

Fig. 1B presents the FTIR spectra of the post-cured formulations. The non-appearance of band 915 cm^{-1} indicates complete cure. The attenuation of the C=O band of the carboxylic groups (1720-1700 cm^{-1}) indicates that the crosslinking reactions occurred, as well as the band at 1180 cm^{-1} of the C-O bonds in the chain [7,8].

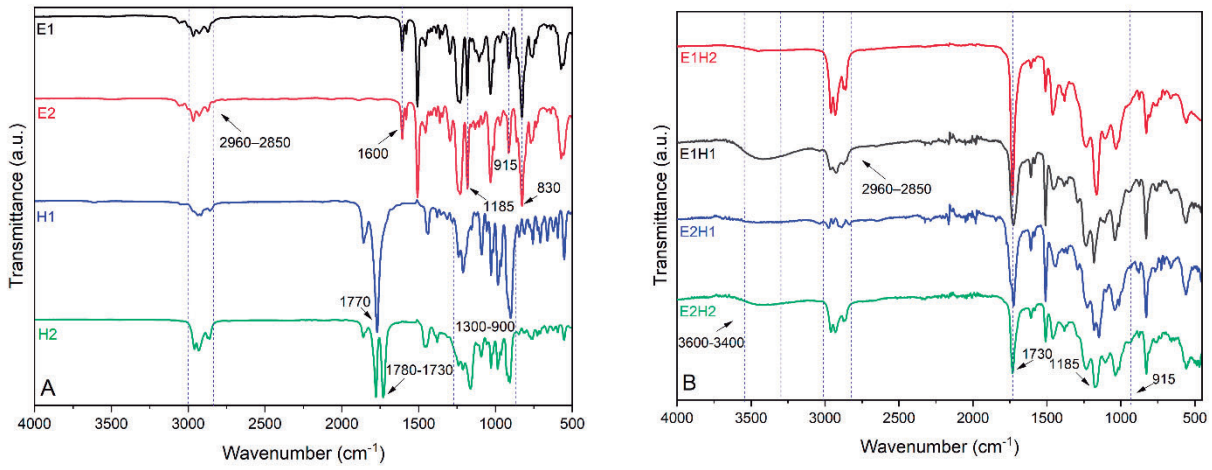

Figure 1. FTIR spectra of neat resins and hardeners (A)and the post-cured formulations (B).

Table 1 summarizes the data from DSC relative to peak temperature (T_{peak}), enthalpy of curing (ΔH), and the glass transition temperature (T_g). In all formulations, an exothermic peak was found around 143 °C, indicating similar crosslinking reactions [8]. However, the enthalpy varied, with the highest value (219 J/g) found for the E1H2 sample, indicating a greater release of energy in the curing reaction. This agrees with the FTIR results, which presented a weaker band in the region of the oxirene group (915 cm^{-1}). The T_g results from the second heating scan occurred within 90-110 °C. The E2H2 formulation showed higher T_g (110 °C), indicating greater mobility resistance of the polymeric chains in the rubbery state [9].

Table 1. DSC, DMA and TGA results for the studied formulations.

Sample	T_{peak} (°C) (DSC)	ΔH (J/g) (DSC)	T_g (°C) DSC	T_g (°C) DMA (tan delta)	T_{peak} (°C) (loss modulus)	E'g @50 °C (MPa)	E'r @140 °C (MPa)	E" @25 °C (MPa)	$T_{10\%}$ (°C) (TGA)
E1H1	143	167	90	105	67	1190	1.6	118	320
E1H2	143	219	100	106	67	1307	4.2	118	390
E1H1	143	205	95	119	88	1506	4.8	145	350
E2H2	142	186	110	119	77	939	2.5	73	380

The T_g was also determined from the the tan delta data of the DMA analysis, and it is shown in Table 1 along with the storage modulus in the glassy (E'_g) and in the rubbery (E'_r) region, and the loss modulus (E") at 25 ºC. The E2H1 formulation obtained higher E' in the glassy and rubbery regions, indicating greater crosslinking, constituting a three-dimensional network, and higher T_g. Some difference in the T_g results from DSC and DMA analyses is seen because each analysis is sensitive to a specific region, and the DSC analysis has a lower sensitivity in the glassy region, compared with DMA, making DMA more accurate for T_g determination.

From TGA analyses of the post-cured formulations, similar mass loss behavior can be observed, and the onset of thermal decomposition occurred at ~250 °C, with mass losses ranging from 3% to 5% for all samples. Degradation occurs in one step, with the maximum weight loss temperature at ~ 420 ºC. However, the temperature for 10% mass loss ($T_{10\%}$), shown in Table 1, varied for the samples. The H2 hardener, compared to H1, increased the thermal stability of the formulations, and the E1H2 sample presented better thermal stability based on the $T_{10\%}$.

Fig. 2 displays viscosity curves over time. The resin system E2H2 exhibits a more pronounced viscosity increase, while the E1H2 and E2H1 systems show similar behavior, and E1H1 took longer to show a significant increase. The initial viscosity rise is associated with chain size and growth. Due to its higher molar mass, the E2 resin displays greater viscosity changes in the early stages [4].The

viscosity increase after a specific temperature is associated with the early crosslinking stages (formation of the three-dimensional network). All resins showed overall similar behavior, and the lowest viscosity was found for E1H1 formulation.
The estimated gel time was 120, 110, 109, and 90 min for E1H1, E1H2, E2H1, E2H2 systems, respectively. The longer the gel time, the longer the processing window at this temperature.

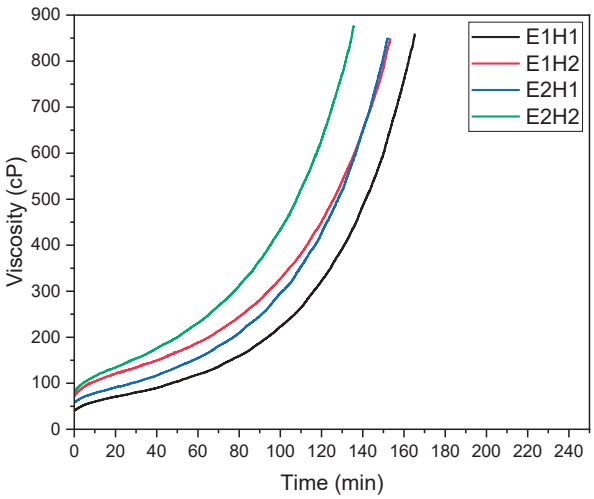

Figure 2. Curing progression in terms of viscosity *vs* time for the studied formulations at 60 ºC.

Fig. 3 shows the tensile strength and modulus results for the studied formulations. For the tensile strength, the highest mean value was found for the E2H2, and the lowest for the E1H1 sample, while E1H2 and E2H1 showed similar results. As for modulus, the E2H1 and E2H2 showed higher mean values, with a significant difference found for the E2H1 sample only.

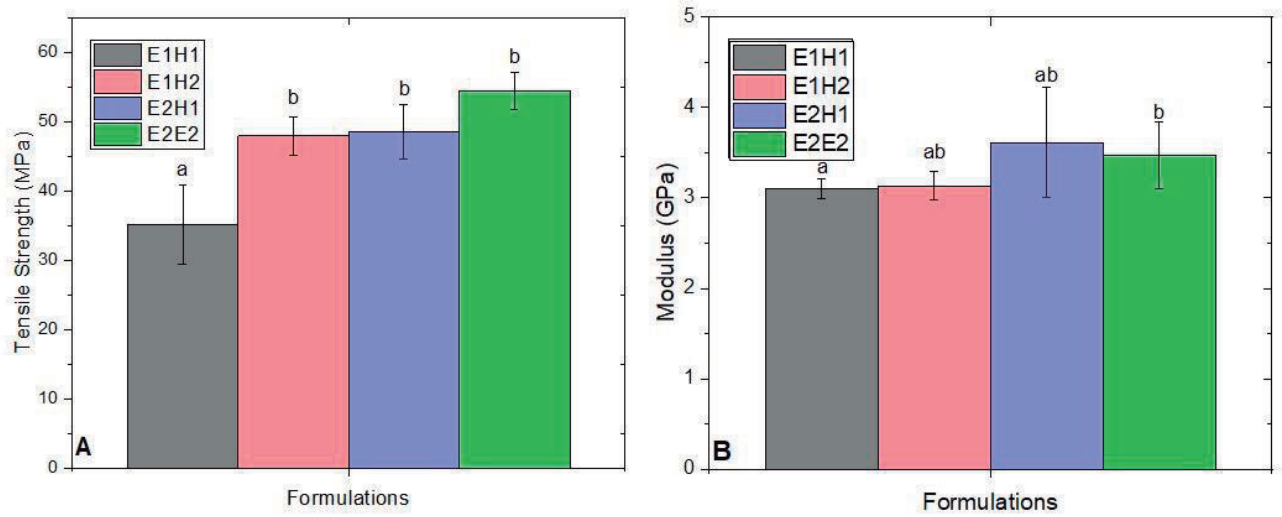

Figure 3. Tensile strength and modulus for the studied formulations.

Conclusions

DGEBA epoxy resin formulations with anhydride-based hardeners were characterized targetting filament winding composite manufacturing. For all systems, the consumption of the oxirane ring band (915 cm^{-1}) was observed during curing. The highest curing enthalpy was found for the E1H2 formulation, while the exothermic peak temperature was similar for all samples (143 °C). Thermal stability was improved with the H2 hardener. The E2H1 formulation exhibited higher loss modulus temperature (T_{peak} at 88 °C) compared to other formulations (67 - 77 °C), and the tan delta T_g was higher for the E2 epoxy formulations (119 °C).

Additionally, viscosity at the processing temperature (60 °C) was slightly lower for the E1 resin. In DMA analysis, the E2H1 and E2H2 samples exhibited similar glass transition temperatures, but significant modulus differences were observed between the E2 resin formulations. The E1H1 sample showed the lowest tensile strength (~35 MPa), while the E2H1 and E2H2 samples showed slightly higher modulus (~3.5 GPa). Despite its higher viscosity at room temperature, the E2 resin performed similarly to other formulations at the processing temperature, demonstrating higher glass transition temperature, storage modulus, and thermal stability. In all, the E2H1 formulation was chosen as the best overall performance for the intended application.

Acknowledgment
The authors are grateful to FAPERGS and CAPES for sponsoring this work. Also, the support of the Federal Institute of Education, Science, and Technology of Rio Grande do Sul (IFRS), and Olin Corporate for material donation.

References
1. X. Zhang; Y. Wu; J. Wei; J. Tong; X. Yi. Sci China Tech Sci 2017, 60, 9. https://doi.org/10.1007/s11431-016-9029-y.
2. S. G. Nunes. Ph.D Thesis, Universidade Federal do Rio Grande do Sul, 2018.
3. M. Çelik; T. Noble; F. Jorge; R. Jian; C. M. Ó Brádaigh; C. Robert. J. Compos. Sci. 2022, 6, 75. https://doi.org/10.3390/jcs6030075.
4. G. T. Toso. Master Thesis, Universidade Federal do Rio Grande do Sul, 2014.
5. J. C. Capricho, B. Fox, N. Hameed Polymer Reviews 2020, 60, 1. https://doi.org/10.1080/15583724.2019.1650063.
6. S. M. Silva; C. P. N. Silva; T. C. Silva; M. C. Rezende; E. C. Botelho; M. L. Costa. Eclética Química Journal 2022, 47, 2. https://doi.org/10.26850/1678-4618eqj.v47.2SI.2022.p83-99.
7. S. Meure, D. Wu, S. Furman. Vibrational Spectroscopy 2010, 52, 1. https://doi.org/10.1016/j.vibspec.2009.09.005.
8. E. Fonseca; V. Demétrio da Silva; J. S. Klitzke; H. S. Schrekker; S. C. Amico. Polymer Testing 2020, 87, 106556. https://doi.org/10.1016/j.polymertesting.2020.106556.
9. M. M. S. P. Abreu. Master Thesis, Universidade de São Paulo, 2008.

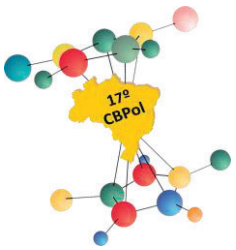

BIOPOLYMERIC COATINGS FOR FOOD PRESERVATION: CHARACTERIZATION STUDY

Vitória S. Marques[1,3]*; Maryana M. Frota[1,3]; Kelvi W. E. Miranda[1,3]; Maria G. S Coutinho[2,3]; Adriano L. A. Mattos[3], and Maria S. R. Bastos[3]

1 – Department of Food Engineering, Federal University of Ceará (UFC), Fortaleza, CE, Brazil
vitoriasmarques78@gmail.com
2 – Science and Technology Center; Ceara State University (UECE), Fortaleza, CE, Brazil
3 – Embrapa Tropical Agroindustry, Brazilian Agricultural Research Company, Fortaleza, CE, Brazil

Abstract - Biopolymer coatings are considered a potentially effective technology for preserving food, most commonly fresh food, as it regulates respiratory rates and reduces moisture loss. It is already possible to see some fruits using coatings to improve post-harvest quality, however few commercial alternatives for this product are found, opening the possibility of testing some materials for this purpose. In this perspective, this study aimed to produce and characterize biopolymeric coatings of 1% (w/v) of chitosan (Cs), 2% (w/v) of commercially modified starch (MSc) and 1% (w/v) of sodium alginate (SA) through optical morphology, visual stability, rheological parameters, and wettability profile. The gelatinized MSc granules showed a spherical shape with variations in size, confirming that the gelatinization time and temperature were insufficient to cause granule rupture. On the other hand, the Cs coating showed homogeneity in its solution, with good solubility in the solvent used, the same was observed for the SA. The data corroborate the stability profile of the samples. The Cs and SA coatings remained stable throughout the observed period, difference of the MSc, that presented phase separation. The rheological profile of the polymeric solutions shows that there is a difference in the modulus of storage (G') and energy loss (G") as a function of the shear stress of the MSc, being lower in relation to the others. As well as the viscosity that presents a Newtonian behavior, unlike the solutions of SA and Cs, having a pseudoplastic behavior. All coatings were hydrophilic, which indicates good interaction between the polymeric suspensions and most food surfaces. The results indicate that it is possible to apply biopolymer coatings for food preservation associated with characteristics that suit the food application.

References

1. H.H.S. Abdel-Naeem, N.E.R. Zayed, H.A. Mansour. *LWT* 2021, *150*, 111928. H.H.S. Abdel-Naeem, N.E.R. Zayed, H.A. Mansour. *LWT* 2021, *150*, 111928.
https://doi.org/10.1016/j.lwt.2021.111928
2. W. Oyom; H. Xu; Z. Liu; H. Long; Y. Li; Z. Zhang; Y. Bi; R. Tahergorabi; D. Prusky. *LWT* 2022, *153,* 112475.
https://doi.org/10.1016/j.lwt.2021.112475
3. D.P. Singh; G. Packirisamy. *Food Chemistry: Molecular Sciences* 2022, 4, 100085.
https://doi.org/10.1016/j.fochms.2022.100085

Fundings: The authors would like to thank CNPq for financial support and Embrapa.

Keywords: *Alginate; Chitosan; Conservation; Starch.*

EVALUATION OF PHENOLIC FOAM'S TOXICITY USED IN FLORAL ARRANGEMENTS

Bianca S. de Sousa[1*], Laís M. de Brito[1], Wanessa A. Ramsdorf[1], Adriane M. de Freitas[1] and Juliana R. Kloss[1]

1 – Academic Department of Chemistry and Biology, Federal University of Technology Paraná (UTFPR), Curitiba, PR, Brazil biancasousa@alunos.utfpr.edu.br

Abstract - Phenolic foams, commonly found in floral arrangements, are made from phenolic resin with free phenol content between 5 and 8%, which makes this material sterile, an advantage for the preservation of flowers. However, phenol is a highly toxic substance, and if the disposal of the residue is inadequate, there is the possibility of an aquatic contamination that can affect the local biota. In view of this, the objective of this work is to characterize and evaluate the toxicity of phenolic foam used in floral arrangements. The sample was characterized using thermogravimetric analysis (TGA), *Fourier* transform infrared spectroscopy (FTIR) and scanning electron microscopy (SEM). To evaluate the toxicity, tests were conducted on *D. magna*, with vacuum filtered leachate from the macerated foam at an initial concentration of 50 $g.L^{-1}$ with dilutions of 40, 30, 20 and 10 $g.L^{-1}$ and readout in 24 and 48h. Regarding the results obtained in the characterization of the foam (Fig 1), absorbance peaks were observed at 3500 to 3300, 1610 and 1010 cm^{-1} referring to the vibration of the O-H bond, C=C of the benzene ring and hydroxymethyl, respectively, the open cells of the foam, besides the high degradation at 535ºC indicating the decomposition of the main chain by the breakdown of the methylene bridge, data that are in agreement with those found in the literature. Regarding the toxicity test, the acute exposure provided an EC_{50} value of 15.43 ± 2.69 $g.L^{-1}$. Further tests on lettuce seeds are in progress, as well as the quantification of free phenol by gas chromatography (GC). In view of the studies already conducted it can be concluded that floral foam presents toxicity and may be a cumulative risk that surrounds the population invisibly.

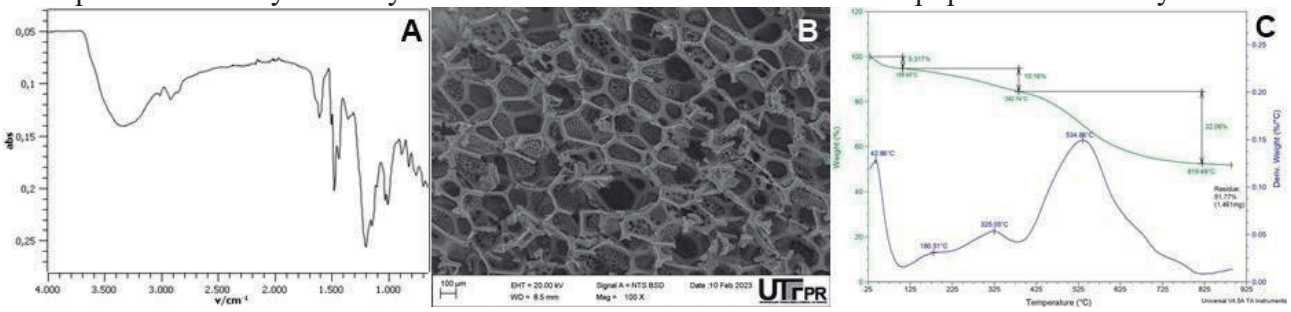

Figure 1 – FTIR spectrum (A), SEM image (B) and thermogravimetric analysis (C) of the phenolic foam.

References

1. C. Trestrail et al *Science of the Total Environment* 2020, *705,* 135826. https://doi.org/10.1016/j.scitotenv.2019.135826
2. H. Hu et al *Polymers and Polymer Composites* 2022, *30*, 11. https://doi.org/10.1177/09673911221102114
3. K. Tang et al *Polymer Testing* 2022, *111*, 107626. https://doi.org/10.1016/j.polymertesting.2022.107626
4. L. Ravindran et al *Polymer Composites* 2022, *43*, 8602. https://doi.org/10.1002/pc.27059

Keywords: *rigid foam; phenolic resin; ecotoxicology; D. magna; characterization.*

INFLUENCE OF POLYMER GELATION GRADE ON THE PERFORMANCE OF PLASTICIZED PVC FILMS USED IN COATED FABRICS

Paula Pinto*, Gabriel Peláez, Juliana Lasprilla-Botero, Ricardo Santana

Grupo de Investigación en Polímeros y Recubrimientos Textiles (GINPRETEX), Proquinal S.A.S. Calle 11A 34-50, Bogotá, Colombia. paula.pinto@spradling.group

Abstract – Plasticized poly vinyl chloride (pPVC) is a popular polymer used in the coated fabric industry because it is a cost-effective and versatile approach to get an imitation leather look with superior thermal, mechanical and chemical resistance. However, achieving good compatibility between the plasticizer and PVC, which is affected by the polymer gelation grade (GG) attained during the PVC film production, is one of the important criteria to achieving the aforesaid properties. To quantify this GG, there are different kind of methods including rheological, thermal, optical, and mechanical measurements, and their results can be combined to produce a reliable concept of when the gelation is complete. Poor GG results in low mechanical performance, low chemical resistance and significant plasticizer migration, all of which have an impact on the overall performance of the coated fabrics. This study aims to determine the GG of pPVC formulas used in the coated textile sector, and the consequences on the plastisol procesability and final product performance. Two kinds of plasticizers (DOTP and DPHP) were used in the formulations, and pPVC films were produced under varied conditions (temperatures and heating times), determined by using parallel rheometry on plastisol. These films were characterized by differential scanning calorimetry, mechanical tensile resistance, and plasticizer migration quantification that was performed using high-performance liquid chromatography (HPLC). The results allowed to identify that DOTP films have a wider temperature range of gelation (150 °C – 180 °C) compared to DPHP formulations (>145°C). This can be a significant parameter as lower temperatures are easier to adjust in processing and lead to better GG.

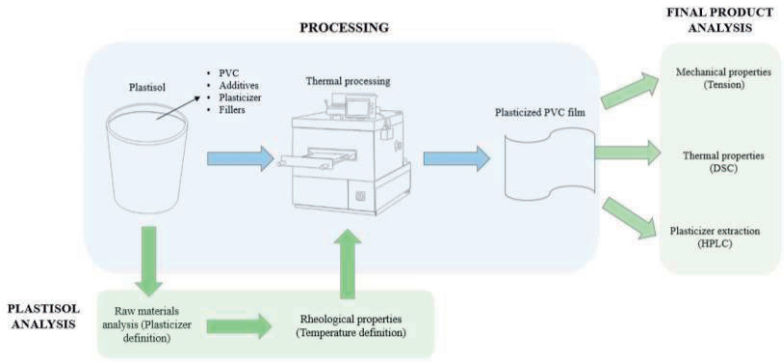

Fig 1. Experimental procedure

References

1. Chen, Y., Zhou, S., Pan, S. et al. Methods for determination of plasticizer migration from polyvinyl chloride synthetic materials: a mini review. J Leather Sci Eng 4, 8 (2022). https://doi.org/10.1186/s42825-022-00081-8
2. Wang, G.Q. and Chen, Y.T. (1991) Test Methods for Gelation of PVC Plastisol. Polymer Testing, 10, 315-324. http://dx.doi.org/10.1016/0142-9418(91)90025-S

Keywords: Gelation grade, plasticized PVC, coated fabrics, PVC films

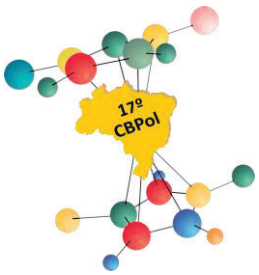

PERFORMACE OF RESVERATROL AS AN ADDITIVE IN POLY (LACTIC ACID)

Michele Roberta Fischer[1]; Wagner Maurício Pachekoski[2]

1 – Department of Materials Engineering, University of Santa Catarina (UFSC), Joinville, SC, Brazil
michelefischer2005@hotmail.com
2 – Department of Materials Engineering, University of Santa Catarina (UFSC), Joinville, SC, Brazil
pwmp1583@gmail.com

Abstract - The search for the use of raw materials from renewable sources and the use of biodegradable products is a reality today, as they are alternatives for reducing environmental impact. Among the materials with such characteristics is poly (lactic acid), also known as PLA, a polymer biodegradable. It is made from using lactic acid and which can be synthesized from the fermentation of sustainable resources[1]. With properties similar to petroleum-based polymers, PLA has applications in the medical, textile and packaging industries, being also very promising in 3D printing[2]. However, one of PLA's limitations is thermal degradation and consequent effect on the processability of the polymer, this limitation being the object of study in several researches[3]. One of the hypotheses for reducing thermal degradation of PLA is the use of an additive based on resveratrol, which is a natural polyphenol found in grape skin. With antioxidant properties, resveratrol can aid in PLA thermal stability, improving its processability and mechanical properties. This study aims to evaluate the addition of resveratrol to PLA at concentrations of 1, 3, 5 and 10% (w/w) and its effect on processability, thermal and mechanical properties in the PLA. Analytical characterization of the samples by melt index there was a gradual increase and at the 10% concentration it increased 4 times when compared to pure PLA. Regarding the thermal properties, in the Thermogravimetry (TGA), the initial degradation temperature is 330 °C for pure PLA and 329 °C for the 10% additive. In the Differential Scanning Calorimetry (DSC), the Tg had an increase of only 1 °C and the Tm and crystallinity decreased. Hardness test evaluated the mechanical properties, with a slight increase. In the analysis of infrared by Fourier transform (FTIR) there was an increase in the intensity of the bands.

References:

1. S. Koltzenburg; M. Maskos; O. Nuyken in *Polymer Chemistry*, Springer, 2017, 547.
2. A. P. Gupta; V. Kimar. *European Polymer Journal*, 2007, 4053-4074. http://dx.doi.org/10.1016/j.eurpolymj.2007.06.045.
3. H. Nushida. *Poly (Lactic Acid): synthesis, structures, properties, processing, and applications,* R. Auras, *et al,* Ed.; John Wiley & Sons, Inc., 2010, 401-412.

Keywords: *Thermal stability, PLA, Additive, Biopolymer*

TENSILE AND INDENTATION ANALYSIS OF THERMOPLASTIC POLYMERS: PP AND ABS

K. Sales de Oliveira[1*], S.M. da Luz[1], T. Doca[1]

1 – Department of Mechanical Engineering, Faculty of Technology, University of Brasilia, Asa Norte, Brasilia, 70.910-900, DF, Brazil

karoline.oliveira@aluno.unb.br

Abstract – Thermoplastic polymers are extremely important due to their versatility and wide range of applications. In this study, two commonly used thermoplastics, PP and ABS, are selected for their excellent chemical resistance, lightweight, and remarkable remolding capabilities. The materials underwent standard tensile tests and indentation tests using hemispherical indenter and flat specimens controlled for thickness and roughness. The tests aim the determination of elasticity modulus, hardening parameters, ultimate stress, yield stress and indentation resistance of each polymer.

Keywords: *Thermoplastic polymers, Mechanical properties, PP, ABS.*

Introduction

Thermoplastic polymers are widely employed by several industrial applications due to their unique properties and versatility. It is a type of polymer that can be melted and re-molded multiple times without any significant degradation in its properties. This feature makes them an ideal choice for various industrial applications, including packaging, automotive, medical, and construction [1,2] [1,2].

The viscoelasticity of a thermoplastic polymer is defined as the phenomenon whereby there is a viscous behavior as a liquid superimposed on an elastic behavior as a solid. The elastic fraction of deformation occurs due to variations in the angle and distance of bonds between atoms, both in the main chain and in the side groups. The plastic fraction occurs due to friction between the main polymeric chains and side groups [2]. In addition to the influence of temperature, the loading rate also has a major influence on tensile tests on polymers. The lower the applied loading rate, the greater the observed plasticity due to the time the polymer chains have to organize themselves, and this is also related to viscosity.

Furthermore, as the degree of crystallinity grows, the modulus of elasticity, yield strength and hardness increase, this effect can be seen by comparing the stress-strain behavior of Polyethylene (PE) of different densities [3]. As for Polypropylene (PP), in the same way as for PE, the modulus of elasticity increases linearly with the increase in density and crystallinity of the material. Therefore, any variation in the procedure for its preparation and processing or post-treatment, such as slow cooling or subsequent heat treatment, which provides an increase in density and crystallinity, will also increase the modulus of elasticity and rigidity[4–6]. A similar behavior is expected from the Acrylonitrile Butadiene Styrene (ABS).

In order to better understand the behavior of these materials in compression, in this work, the behaviors of thermoplastic polymers were analyzed with the aid of the indentation test, this test commonly analyses the hardness of material in different types of scales, it is a common technique used to evaluate the mechanical properties of polymers. In this method, a small indenter is pressed into the surface of the material, and the resulting deformation is measured provide important information on the mechanical behavior of polymers, including their hardness, elastic modulus and viscoelastic properties [7,8] .

Recent studies have focused on the development and application of indentation testing for polymers. Researchers have used nanoindentation to study the mechanical behavior of thin polymer films and coatings[9,10]. This technique allows for precise measurements of mechanical properties at small scales and can provide valuable insights into the structure-property relationships of polymers[11].

Herein, an assessment of PP and ABS tensile monotonic and compression behaviors is presented. Tests are carried out using standard specimens carefully controlled for dimension and surface finish. Monotonic tests are executed at two displacement rates (2 mm/min and 5 mm/min) and their results are used for the identification of the material's ultimate stress, elastic modulus and yield stress. The indentation tests are executed and their results showed compressive strength of the studied materials.

Experimental

The methodology employed in this study involves five main steps for the analysis of thermoplastic polymer samples:

Specimen evaluation and quality control
Specimens were prepared following ASTM D638 guidelines. Before indentation testing, the specimens were polished and controlled for a specific thickness, flatness, and surface roughness.

Mounting setup
Tests were conducted using a servo-hydraulic system with a load-cell capacity of 5 kN. The specimens were mounted in a flat clamp system with diamond-shaped grooves to ensure optimal restraining. The contact pressure and distance between clamps were standardized to maintain the same usable section in all specimens, and the room temperature was carefully monitored.

Monotonic tensile tests
Four monotonic tensile tests were performed for each type of material, two for each displacement rates (2 mm/min and 5 mm/min). A clip gauge extensometer was used up to 10% strain, and the test continued up to 30% strain, considering the observed loss of stiffness without rupture. Data collected during the tests included axial displacement, axial force, axial deformation and time.

Indentation tests:
Indentation tests were conducted using the Zwick/Roell ZHU 250 Universal Hardness Machine with a 5mm tungsten carbide spherical indenter. Two specimens for each material were tested in loading ranges of 100N to 400N, resulting in a total of eight specimens. The diameter and depth of indentation marks were measured using confocal laser scanning microscopy. The indentation marks have been made at the clamping zone of untested tensile specimens.

Microscopic analysis
Microscopic analysis was performed using confocal laser scanning microscopy (Olympus LEXT OLS4100) to observe the indentation marks and gather additional data on the materials' responses to indentation.

Microscopic inspection
An Olympus LEXT OLS4100 confocal laser microscope was used to create a three-dimensional profile of marks on a specimen surface after each test. The microscope's software was used to measure the diameter, depth and volume of the damage marks, and the markings' characteristics were assessed based on intensity, color, or height spectra. The indentation data provided values into the stress-strain behavior of polymeric materials under compression, using loads ranging from 100 N to 400 N with a

5mm diameter indenter. These experimental conditions helped identify unique characteristics indicating the nature of materials in the inelastic phase.

To start this analysis, with the data obtained from the measurements made in the confocal microscope, the stress and strain values were calculated [12]. For the stress, the calculation of the maximum stress was used Eq.(1):

$$p_0 = \frac{3F}{2\pi a^2} \tag{1}$$

where a corresponds to the radius of the indentation measured in the microscope confocal. The non-dimensional strain can be expressed mathematically, as follows,

$$\varepsilon_{ind} = \frac{a}{R_i} \tag{2}$$

The non-dimensional strain in Johnson's expression is determined using Tabor's classical equation for the indentation strain, Eq.(2). In a more recent study, Bhat et al. [12] proposed a new definition for the indentation strain, given by:

$$\varepsilon_{ind} = \frac{4}{3\pi} * \frac{h_t}{a} \approx \frac{h_t}{2.36a} \tag{3}$$

where h_t represents the total depth of indentation and a is the contact radius.

Results and Discussion

Monotonic tensile tests The comparison between displacement rates in tensile tests for PP and ABS provides valuable information about the mechanical behavior of these polymers, considering their degree of crystallinity and how the displacement rate influences their mechanical properties and are presented in Figure 1:

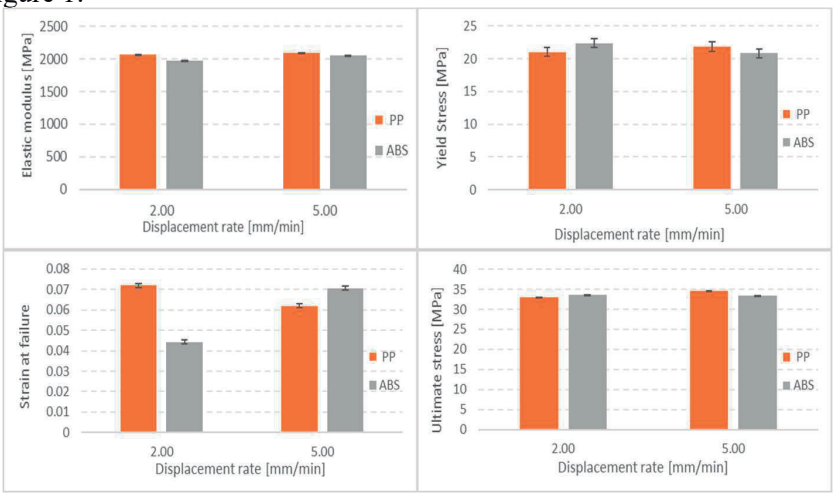

Figure 1- PP and ABS properties measured at displacement rates of 2 mm/min and 5 mm/min.

The comparison between PP and ABS polymers reveals that their mechanical properties are influenced by the degree of crystallinity. PP exhibits higher stiffness and greater deformation at failure due to its higher crystallinity, while ABS shows higher yield strength and resistance to plastic deformation despite its lower crystallinity. Both polymers display similar ultimate stress behavior, suggesting that other factors may contribute to this mechanical property. These findings emphasize the importance of considering the displacement rate during the development and selection of

polymeric materials to ensure optimal performance for specific project requirements in various applications.

*Indentation tests and microscopic inspection*The indentation test data consists of an indentation performed on a polymeric material (ABS and PP) using a tungsten carbide indenter with 5 mm. The contact relationship is considered as a sphere-on-plane contact. The data obtained includes the load applied (in Newtons), the depth of the indentation mark (in micrometers), the average of the x and y diameters (in micrometers) and the hardness of the material. Fig. 2 shows that increasing the load from 100 N to 200 N doubles the indentation depth, for ABS and PP. Beyond 200 N, these incremental decreases. This increase in indentation depth in PP, as well as in ABS, is due to inelastic deformation caused by the greater force applied by the indenter. However, the relationship between load and indentation depth is not strictly linear, and non-linear behavior can occur due to factors such as strain hardening or strain rate effects. These polymers also exhibit viscoelastic properties, which can affect the measured indentation depth, influenced by factors such as relaxation time and creep behavior.

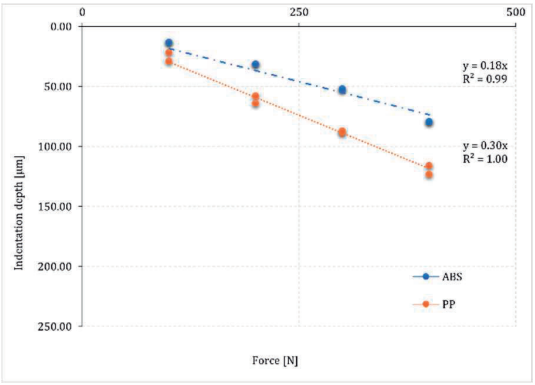

Figure 2 -Indentation depth versus applied load.

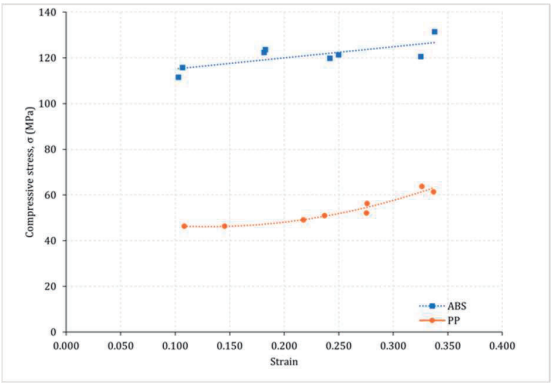

Figure 3 - Relationship between compressive stress and strain.

The compression behavior of ABS and PP polymers differs significantly. ABS exhibits a linear stress-strain relationship with stress values ranging from 115 to 132 MPa, while PP shows a quadratic stress-strain relationship with stress values varying between 50 and 60 MPa. These dissimilar behaviors can be attributed to the viscoelastic properties of the materials, indicating a predominant elastic response for ABS and a more significant influence of viscous properties for PP. The viscoelastic behavior is influenced by factors such as molecular structure, chain branching, cross-linking density, and degree of crystallinity, which are crucial for understanding and predicting the mechanical performance of these polymers in various industrial applications.

Conclusions

This study investigated the mechanical properties of two widely used thermoplastic polymers, ABS and PP, through tensile and indentation tests. Both polymers showed an increase in elastic modulus with higher displacement rates, indicating their ability to withstand greater tensile loads. PP exhibited slightly higher elastic modulus values than ABS, attributed to its higher crystallinity. Despite ABS having higher yield stress values due to better resistance to plastic deformation, PP maintained acceptable strength levels, making it promising for diverse applications. In terms of strain at failure, polypropylene displayed higher deformation capacity at both displacement rates, typical of semicrystalline materials. Both polymers exhibited similar ultimate stress values before failure, suggesting comparable strengths. Indentation tests revealed distinct viscoelastic properties, with ABS displaying a linear stress-strain relationship and PP showing a quadratic relationship, reflecting

different elastic and viscous influences. This analysis provides valuable insights into the mechanical characteristics of ABS and PP, aiding their effective utilization in engineering and manufacturing applications.

Acknowledgements

The authors gratefully acknowledge the financial support provided by the Brazilian National Council for Scientific and Technological Development (CNPq), the Brazilian Federal Agency for Support and Evaluation of Graduate Education (CAPES) and the Foundation for the Support of Research in the Federal District (FAP-DF).

References

[1] Van Den Oever M, Peijs T. Continuous-glass-fibre-reinforced polypropylene composites II. Influence of maleic-anhydride modified polypropylene on fatigue behaviour. Compos Part A Appl Sci Manuf 1998;29:227–39. https://doi.org/10.1016/S1359-835X(97)00089-4.

[2] Canevarolo JR S V. Ciência dos polímeros: um texto básico para tecnólogos e engenheiros. vol. 24. São Paulo: 2002.

[3] Amjadi M, Fatemi A. Tensile behavior of high-density polyethylene including the effects of processing technique, thickness, temperature, and strain rate. Polymers (Basel) 2020;12. https://doi.org/10.3390/POLYM12091857.

[4] Canevarolo S V., De Candia F, Russo R. Stereoblock polypropylene/isotactic polypropylene blends. II. Mechanical behavior. J Appl Polym Sci 1995;55:387–92. https://doi.org/10.1002/app.1995.070550302.

[5] Strapasson R, Amico SC, Pereira MFR, Sydenstricker THD. Tensile and impact behavior of polypropylene/low density polyethylene blends. Polym Test 2005;24. https://doi.org/10.1016/j.polymertesting.2005.01.001.

[6] Li J, Zhu Z, Li T, Peng X, Jiang S, Turng LS. Quantification of the Young's modulus for polypropylene: Influence of initial crystallinity and service temperature. J Appl Polym Sci 2020;137. https://doi.org/10.1002/app.48581.

[7] Amitay-Sadovsky E, Wagner HD. Evaluation of Young's modulus of polymers from Knoop microindentation tests. Polymer (Guildf) 1998;39. https://doi.org/10.1016/S0032-3861(97)00550-8.

[8] Rocha JR, Yang KZ, Hilbig T, Brostow W, Simoes R. Polymer indentation with mesoscopic molecular dynamics. J Mater Res 2013;28:3043–52. https://doi.org/10.1557/jmr.2013.307.

[9] Lei M, Xu B, Pei Y, Lu H, Fu YQ. Micro-mechanics of nanostructured carbon/shape memory polymer hybrid thin film. Soft Matter 2015;12. https://doi.org/10.1039/c5sm01269d.

[10] Lu YC, Shinozaki DM. Effects of substrate constraint on micro-indentation testing of polymer coatings. Materials Science and Engineering A 2005;396. https://doi.org/10.1016/j.msea.2004.12.045.

[11] Rocha JR, Yang KZ, Hilbig T, Brostow W, Simoes R. Polymer indentation with mesoscopic molecular dynamics. J Mater Res 2013;28:3043–52. https://doi.org/10.1557/jmr.2013.307.

[12] Bhat A, Neu RW. An improved methodology for extracting uniaxial stress–strain curves from spherical indentation data. Mechanics of Materials 2022;174. https://doi.org/10.1016/j.mechmat.2022.104459.

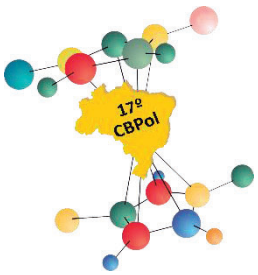

ADHESION STUDY OF PRINTING INKS ON ANIMAL FEED MULTILAYER PACKAGING MADE WITH MIXTURE OF PETROCHEMICAL LDPE AND GREEN LDPE IN THE OUTER LAYER

Kelin C. Hau[1]*, Matheus V. G. Zimmermann[2], Noeli Sellin[1]

*[1, 2] Graduate Program in Process Engineering, University of Joinville Region (UNIVILLE), Joinville, SC, Brazil, *aspkelincarvalho@gmail.com*

[3]Graduate Program in Materials Science and Engineering, University of the Extreme South of Santa Catarina (UNESC), Criciúma, SC, Brazil

Abstract - Failures in packaging coding, due to the lack of adhesion between the printing inks and the outer surface of the packaging, occur frequently and cause economic and environmental impacts throughout the production chain. In this study, the evaluation of the factors that influence the adhesion of three types of Ink Jet inks on the surface of multilayer packaging with mixture of low-density polyethylene from petrochemical origin (pLDPE) and green LDPE from sugar cane (gLDPE) on the outer layer treated and untreated by corona discharge was carried out. The samples were characterized by DSC, FTIR/ATR, XPS, contact angle, surface tension, and AFM. Among the evaluated factors, it was verified that the corona discharge treatment did not cause significant alterations on the surface morphology and chemical structure of the packaging with mixtures of pLDPE and gLDPE in the outer layer, and this problem was recurrent, causing failure in the coding and environmental and economics impacts due to returned packaging. An alternative to solve coding failures caused by corona discharge and its impacts is to improve operating conditions or use laser printing.
Keywords: *Packaging coding, ink adhesion, multilayer films, laser printing.*

Introduction

The National Health Surveillance Agency (ANVISA) supervises the labeling of products in Brazil and determines whether they are suitable for consumption, such definition is based on regulations that indicate requirements for a product to circulate legally in the market. Among the requirements is the obligation to present the manufacturing and expiration date legible to the consumer on the packaging [1, 2, 3]. To encode the manufacturing and expiration date, continuous inkjet printing (CIJ) technology is used, which is considered the most widespread in the world [4]. In this context, it is important that the manufacturing and expiration date printed with CIJ technology are durable, for this it is necessary to know the substrate of the packaging and the ink used in the coding [5].

The packaging most used for food are the multilayer packaging that have a greater protection barrier promoted by the combination of different polymers [6]. Among the materials used, PET is one of the most used in packaging production, due to the ease of adhesion of inks on its surface, as it has high surface tension [7, 8].

Due to the growing demand for more sustainable packaging, many companies have replaced polyethylene terephthalate (PET) packaging by others made of high-density polyethylene (HDPE) in the inner layer and a mixture of pLDPE and gLDPE in the outer layer [9]. However, mixtures of pLDPE and gLDPE have lower surface tension when compared to PET and require surface treatment to improve the adhesion of inks used in coding [10]. One of the treatments used for this is corona discharge [11]. Failures in packaging coding can be due to several factors, such as chemical incompatibility between the ink and the polymer surface, inefficient corona treatment, surface dirt

(dust particles, oils, greases, etc.), among others. These failures can cause significant economic and environmental impacts and are often identified only by end consumers. Aiming to contribute to the minimization of the economic and environmental impacts caused by failures in packaging coding, this work evaluated the main factors that can influence the adhesion of printing inks in multilayer packaging for animal feed, composed of HDPE (in the inner layer) and a mixture of pLDPE and gLDPE (in the outer layer).

Experimental

In this study, the factors that could affect the adhesion of inkjet inks on multilayer packaging composed of HDPE in the inner layer and of mixture of pLDPE and gLDPE in the outer layer were investigated, and it was found that the most likely factor for failures in packaging coding was corona discharge treatment, which was investigated in this work.
The polymeric films of the packaging were produced with HDPE resins HD5000N and LDPE TX8079 resins mixed with green LDPE resin SEB853/72, produced by Braskem. According to the manufacturer, the composition of the LDPE mixture varies greatly, being 40 to 80% of pLDPE resin TX8079 (petrochemical) and 15 to 40% of gLDPE resin SEB853/72 (green). The packaging samples were provided by an animal feed packaging company.
The surface of the outer layer (mixture of pLDPE and gLDPE) of packaging untreated and treated by corona discharge were coded with Linx ink 1014, Linx ink 3203 and Linx ink 1063 using a Linx Inkjet printer. The adhesion quality of the paints was evaluated by the tape peel test, using a 3M 810 Scotch Magic Tape, which was applied under the surface and then peeled off. The result obtained was classified according to the FINAT FTM21 standard, based on the degree of ink removal from the surface of the samples.
To evaluate the effectiveness of corona discharge, the external surface of the packaging (mixtures of pLDPE and gLDPE) treated and untreated were characterized by:
- *X-Ray Induced Photoelectron Spectroscopy (XPS):* it was used to evaluate the chemical groups on the surface, using an X-ray spectrometer, model Scienta-Omicron ESCA, equipped with a monochromator. The analysis was carried out in an ultra-high vacuum environment, with pressure in the range of 10-8 Torr, using Al Kα X-ray source, with energy of 1486.6 eV (hν) and power of 65 W.
- *Atomic Force Microscopy (AFM):* it was used to evaluate the surface morphology and average roughness of samples using a Shimadzu model SPM-9700 equipment, operating in intermittent contact mode. Images of 10 μm x 10 μm were obtained and 15 average roughness measurements were performed in each sample.
- *Contact angle and surface tension:* a Ramé-Hart model 590 goniometer was used to measure the contact angles with deionized water (polar component) and diiodomethane (dispersive component) and using the DROP Image Advanced software, the surface tension of the samples was calculated. For the measurements, 10 drops of 5 μL of each liquid were deposited on the surface and 10 contact angle measurements were performed on each drop, totaling 60 measurements, with an interval of 1 s between each measurement. Surface tension was also determined using pens with surfactant liquids (from 30 to 56 dynes/cm), according to ISO 8296 (2003).

Results and Discussion

Evaluation of the adhesion of the inks on the packaging surface

Fig. 1 and 2 show the images of the packaging surfaces, treated and untread by corona discharge, respectively, which were coded with the three inks, before and after the adhesion test (tape peel test) and the respective tapes torn off. It can be seen by visual inspection that the coding are well adhered and visible on the surface of the packaging, however, after the adhesion test, the ink applied to the surface of the material was removed, that is, it remained on the tape when it was removed. Visually, it can be verified that removal was greater than 60%, that is, almost complete, classifying it as grade

5. Comparing the samples, a small reduction in coding failures after stripping was observed, however this reduction was not enough to change the degree of removal. Under these conditions, the packaging cannot be sold, as it is in violation of Law 8137/1990 of the Federal Senate [2] and Resolution 259/2002 of ANVISA [3].

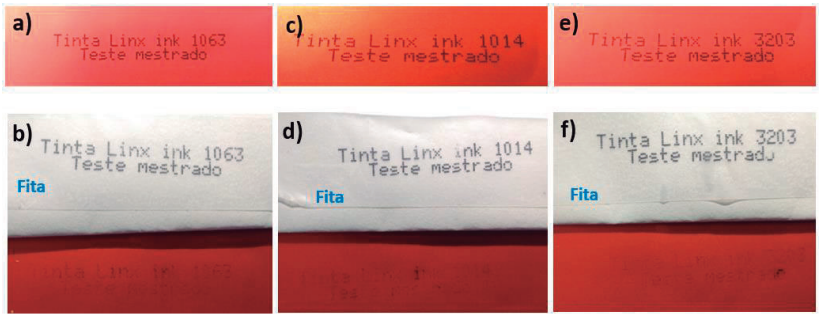

Figure 11: Coding of packaging without corona treatment, (a) ink 1063, (c) ink 1014 and (e) ink 3203, all before applying the tape; and (b) ink 1063, (d) ink 1014 and (f) ink 3203, all accompanied by their respective tapes removed

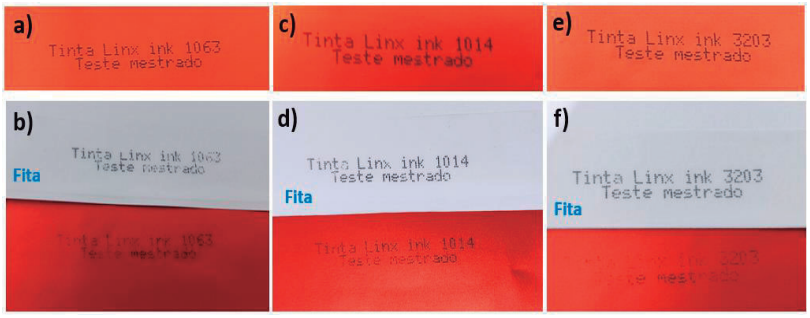

Figure 2: Coding of packaging with corona treatment, (a) ink 1063, (c) ink 1014 and (e) ink 3203, all before applying the tape; and (b) ink 1063, (d) ink 1014 and (f) ink 3203, all accompanied by their respective tapes removed

Evaluation of chemical groups on the packaging surface

Table 1 shows the atomic concentrations of C, O and N obtained by XPS of the samples surface treated and untreated by corona discharge.

Table 1: Atomic concentration of surface packaging treated and untread by corona discharge

	Atomic concentration (%)		
Sample	**C**	**O**	**N**
Treated	88.9	8.56	8.90
Untreated	86.8	14.9	8.90

The sample treated by corona discharge showed a slight decrease in the atomic concentration of carbon, of 2.4%, while the atomic concentration of oxygen increased by 74% and of nitrogen did not change. The increase in oxygen concentration was not sufficient to promote the adhesion of inks to the polymer surface, as observed by the tape adhesion test. Other authors observed an increase of up to 397% in oxygen concentration after surface treatment of LDPE films by corona discharge [11].

Evaluation of the morphology and roughness of the packaging surface

Fig. 3 shows AFM images and average roughness of the samples surface untreated and treated by corona discharge.

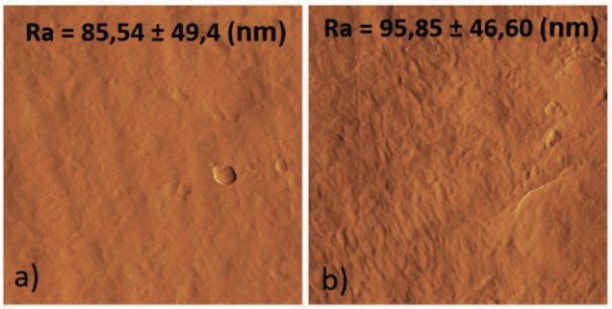

Figure 3: AFM Images and average roughness of the samples surface (a) treated and (b) untreated by corona discharge.

It is observed that the untreated sample had a smooth surface, with some small imperfections arising from the stages of the industrial process of packaging manufacturing (extrusion, lamination, and movement of films). After corona treatment, a slight increase in average surface roughness of ~12% was observed. The corona treatment breaks chemical bonds on the surface of the material, promoting the formation of pores, indentations and roughness, which contribute to the mechanical anchoring of the ink and its adhesion to the surface. Thus, it appears that the corona discharge did not cause significant changes on the surface of the samples to promote adhesion. Other authors observed an increase of 378% in roughness after treating LDPE samples by plasma [12].

Evaluation of wettability and surface tension of packaging

Table 2 shows the contact angle and surface tension of the samples treated and untread by corona discharge.

Table 2: Contact angle and surface tension of the samples treated and untread by corona discharge

Sample	Water contact angle (°)	Diiodomethane contact angle (°)	Surface tension (dinas/cm)
Untreated	99.6 ± 0.2	63.2º ± 0.3	29.9 ± 0.6
Treated	91.8 ± 2.5	57.8º ± 4.3	31.9 ± 3.7

After corona treatment, the samples showed a slight decrease in the contact angle with water, which may have occurred due to surface oxidation observed by XPS. However, the surface remained hydrophobic, as the contact angles remained close to 90°. There was no significant change in the surface tension obtained through measurements of the contact angle of the samples after corona treatment and this result is confirmed by the test with pens with different surface-active liquids, which indicated a surface tension of 30 dynes/cm for the sample without corona treatment and of 34 dynes/cm for the treated sample. According to the manufacturer of the inks analyzed in this study, for good adhesion of the inks, the surface tension on the substrate must be greater than 35 dynes/cm, which was not achieved by the corona treatment in the operating conditions employed by the industry.

Conclusions

Among the possible factors that may influence the quality of adhesion of the three inks tested on the surface of packaging composed of mixtures of pLDPE and gLDPE on the outer layer, it was verified that the corona discharge treatment contributed to the failures in the coding of the packaging, as evidenced by the analyzes carried out. To solve this problem, it is necessary to evaluate and adjust the corona discharge operating conditions for the packaging evaluated in this study. However, every time packaging materials are replaced, these procedures must be carried out by the company. Another alternative would be to carry out the coding using a laser printer, which does not require corona treatment and can also be used for other types of polymeric substrates, preventing the problem from

recurring in the future, thus minimizing the economic and environmental impacts caused by the return and disposal of packaging with coding failures.

References

1. DELGADO, J. S. Regulação sanitária: atribuição da agência nacional de vigilância sanitária em prol da saúde pública. Direito e Desenvolvimento, v. 6, n. 2, 2015.
2. SENADO FEDERAL. Lei nº 8.137, de 27 de dezembro de 1990. Define crimes contra a ordem tributária, econômica e contra as relações de consumo. Brasília/DF, 1990.
3. ANVISA - Agência Nacional de Vigilância Sanitária. Ministério da Saúde. Resolução RDC nº 259, de 20 de setembro de 2002. Aprova o Regulamento Técnico sobre Rotulagem de Alimentos Embalados. Brasília/DF: Diário Oficial da União, 2002. Disponível em: https://bvsms.saude.gov.br/bvs/saudelegis/anvisa/2002/rdc0259_20_09_2002.html. Acesso em: 15 mai. 2023.
4. LUO, X. Application of inkjet-printing technology in developing indicators/sensors for intelligent packaging systems. Current Opinion in Food Science, v. 46, p. 100868, 2022.
5. FREIRE, E. M. *Ink jet printing technology* (CIJ/DOD). In: Digital Printing of Textiles. [s.l.] : Elsevier, 2006. p. 29-52.
6. LANDIM, A. P. M.; BERNARDO, C. O.; MARTINS, I. B. A.; FRANCISCO, M. R.; SANTOS, M. B.; MELO, N. R. Sustentabilidade quanto às embalagens de alimentos no Brasil. Polímeros, v. 26, n. spe, p. 82-92, 2016.
7. SOARES, C. T. de M.; EK, M.; ÖSTMARK, E.; GÄLLSTEDT, M.; KARLSSON, S. Recycling of multi-material multilayer plastic packaging: Current trends and future scenarios. Resources, Conservation and Recycling, v. 176, p. 105905, 2022.
8. PELAGADE, S. M.; SINGH, N. L.; QURESHI, A.; RANE, R. S.; MUKHERJEE, S.; DESHPANDE, U. P.; GANESAN, V.; SHRIPATHI, T. Investigation of surface properties of Ar-plasma treated polyethylene terephthalate (PET) films. Nuclear Instruments and Methods in Physics Research Section B: Beam Interactions with Materials and Atoms, v. 289, p. 34-38, 2012.
9. ABBADE, E.B. Food loss/waste and logistics performance: an analysis of the brazilian scenario. Revista Gestão da Produção, Operações e Sistemas, v. 14, n. 5, p. 328-350, 2019.
10. RICHARD, M. Coding onto PE and PP plastics. 2016. Disponível em: <https://www.linxglobal.com/en-gb/blog/posts/2016/may/coding-onto-pe-and-pp-plastics/>. Acesso em: 25 ago. 2022.
11. ABUSRAFA, A.E; HABIB, S.; KRUPA, I.; OUEDERNI, M.; POPELKA, A. Modification of Polyethylene by corona treatment. Coatings, v. 9, n. 2, p. 145, 2019.
12. PASCUAL, M.; SANCHIS, R.; SÁNCHEZ, L.; GARCÍA, D.; BALART, R. Surface modification of Low-Density Polyethylene (LDPE) film using corona discharge plasma for technological applications. Journal of Adhesion Science and Technology, v. 22, n. 13, p. 1425-1442, 2008.

AGAR CHARACTERIZATION TECHNIQUES: A VERSATILE POLYSACCHARIDE

Luiz Paulo B. Barbosa[1], Marcia P. M. da Costa[1] and Ivana L. M. Ferreira[1]*

[1]Instituto de Química, Universidade do Estado do Rio de Janeiro, Rua São Francisco Xavier, 524, PHLC, sala 310, Maracanã, Rio de Janeiro, RJ, 20550-900
**ivanamello@uerj.br; ivanalmello@pq.cnpq.br*

Abstract: Agar is a hydrocolloid extracted from red marine algae, agarophytes, consisting of a heterogeneous mixture of two polysaccharides, *agarose* and *agaropectin*. It is a linear galactan, hydrophilic colloid which has ability to form reversible gels simply by cooling a hot aqueous solution. It is composed of alternating 1,3-linked D-galactose and 1,4-linked 3,6 anhydro-L-galactose units. In this work, agar was studied by physical and chemical analysis. The gelling temperature of agar samples were around 38 °C. The samples were characterized by X-ray diffraction (XRD), thermogravimetric analysis (TGA) and infrared spectroscopy (FTIR). The XRD showed that the gels presented amorphous behavior. The FTIR spectrum showed the presence of characteristic bands for polysaccharide. The main objective of this work was the investigation of this biopolymer, a versatile polysaccharide with application in areas such as biology and chemistry.

Keywords: *polysaccharide; agar; X-ray diffraction; gelling temperature.*

Introduction

In the development of new materials, the use of natural polymers, as a renewable source, has gained space [1]. The great advantage of using natural polymers, in addition to being non-toxic and hydrophilic, there is no need for organic solvents for their solubilization, consequently, they are very attractive due to their biodegradability and biocompatibility [2,3]. Some polysaccharides and their derivatives have gained attention due to the sustainability in which they are applied industrially. Agar-agar is a hydrocolloid with a repeating structure of alternating 1,3-linked β-d-galactopyranose and 1,4-linked 3,6-anhydro-α-l-galactopyranose; it also contains sulfate, methoxyl and pyruvate esters (Fig. 1) [11]. Agars are widely employed in many fields, including the food business, dentistry, bacteriology, and biotechnology. In order to predict the high product of agar in each application, it is necessary to better understand the diversity of its commercial goods and its physical and chemical properties. This biopolymer is extracted from seaweed and is used in industries such as food, medicine and cosmetics [13].

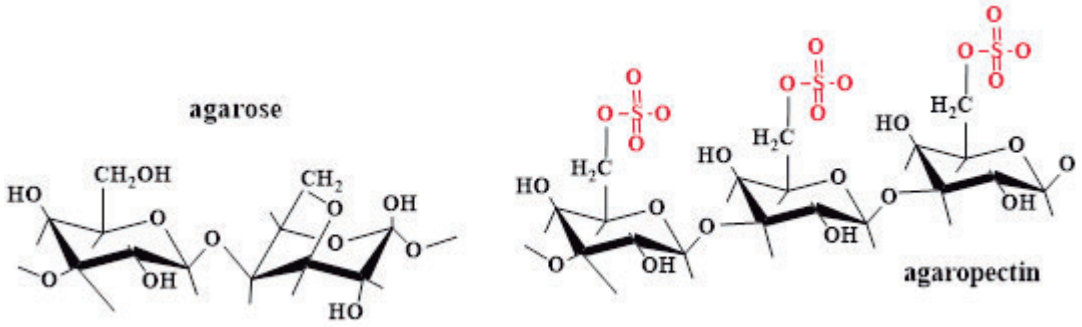

Figure 1 – Molecular structure of agar-agar

Agar has great versatility, in addition to serving as a culture medium, it can be mixed with clays, metallic nanoparticles and nanocellulose, improving the chemical, physical and mechanical properties of the materials developed as for example in dye decontamination [8,9]. The composition and structure of the agar is directly interconnected with growth conditions and extraction procedures, mention is made of the relationship between high and low levels of sulfate of 3,6-anhydrous-α-l-galactose, which originate a low-quality agar [10]. Therefore to verify these characteristics, there is a need for characterization to increase the added value of the material and indicate some trends. Therefore, the main objective of this work was to study the physicalchemical properties of agar in order to elucidate the relationship between the biological properties and the macromolecular structure of this biopolymer, with the purpose of being used in mixtures with other biopolymers and being application in different fields.

Experimental

Preparation of the polysaccharide solution

Agar solution (Sigma-Aldrich) was prepared at a concentration of 1% at a temperature of 90°C in the first hour, and after that it was maintained stirring for 23 hours.

Characterization

An elemental analyzer model VARIO MACRO CHNS in a combustion temperature of 1150◦C was used to determine and quantify the elemental composition of the agar. The chemical composition of the agar samples was performed on a Perkin Elmer spectrum 1000 FTIR spectrometer, being analyzed in the spectral range of 4000 – 400 cm^{-1}. At this frequency, infrared radiation, when absorbed, is converted into molecular vibration energy, making it possible to identify the functional groups present in the structure of the material. The crystalline/amorphous structures of the biopolymer were analyzed in a Bruker D8 X-ray diffractometer (XRD) with CuKα, radiation source, at 40 kV and operating at a wavelength of 1.542Å. The thermal degradation behavior of the biopolymer was analyzed using a TA instruments thermogravimetric analyzer (TGA), model TGA Q50, series 0050-0390. The analysis was performed in the range of 50 to 800°C with a heating rate of 20°C/min.

Results and Discussion

CHNS analysis

Aiming to analyze the chemical composition of the agar, elemental analysis measurements were performed. The elemental composition of the agar was carbon (38.14%), hydrogen (7.22%) and nitrogen (2.02%) and súlfur (0,87%). The results presented showed a small percentage of sulfur, characteristic of the structural formation of agaropectin

FTIR spectroscopy

The FTIR spectrum for agar is shown in Fig. 2. The band at 3291 cm^{-1} is associated with OH groups, the absorbance

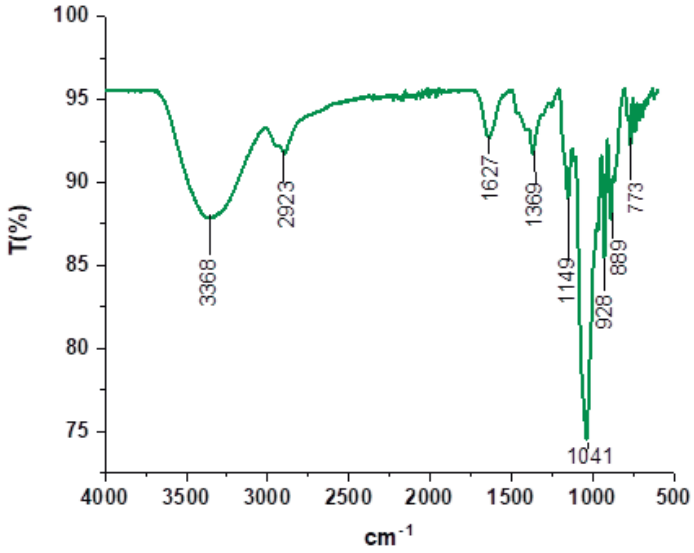

Figura 2. FTIR ágar

Characteristic agarose absorption bands were observed at 3368 cm^{-1} (-OH stretching of the hydroxyl group), and 928 cm^{-1} (3,6-anhydrous-L-galactopyranose C-O-C bridge vibration) [4]. The peaks at 1149 and 1041cm^{-1} were attributed to C–C and C–O stretching vibrations in the pyranose ring, respectively [12]. Furthermore, the agar bands at 1627 cm^{-1} (C = O stretching peak) [5], 928 cm^{-1} (C-O-C bend of 3,6-anhydro-L-galactopyranose), 1149 cm^{-1} (S = O of sulfate esters) absorption indicated by agaropectin. [4]. The bands at 773 cm^{-1} and 889cm^{-1}, correspond to the presence of 3,6-anhydrogalactose-2-sulfate and galactose-4-sulfate, respectively [6].

X-ray diffraction (XRD)

The agar is a semicrystalline polysaccharide. The Figure 3 shows X ray diffraction patterns obtained for the agar. The scan for agar powder shows peaks at 2θ ~ 14.0°, ~19.0°, and ~27.0°. The first peak was observed around at 2θ ~14.0° narrower and with lower intensity. The second peak at 2θ ~ 19.0° is wider and more intense, evidencing the semicrystalline behavior of agar. In addition to being shown a third shoulder of low intensity and higher angle at ~27.0° [14].

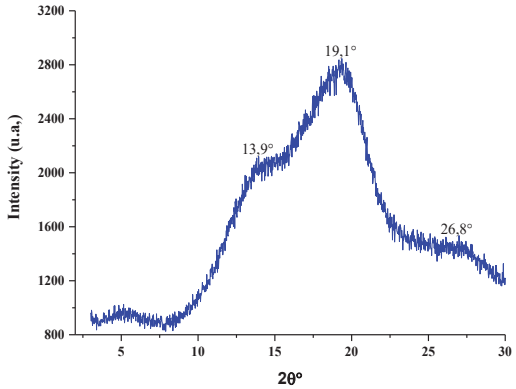

Figure 3 - X-ray diffraction profile of agar powder.

Thermal stability analysis

The TGA was performed to evaluate the thermal stability of the biopolymer. Fig.4 shows the agar TG-DTG curves. The T_{onset} around 262 ◦C relate the beginning of degradation of the polymerics chains. The degradation profile of the DTG curve shows that the agar presented three stages of

decomposition, the first stage around 40 to 130°C evidence the hydrophilicity of the polysaccharide, referring to the evaporation of water [6]. The second and third stages around 282°C and 325°C, respectively, refer to the degradation of the polymeric chain [7].

.

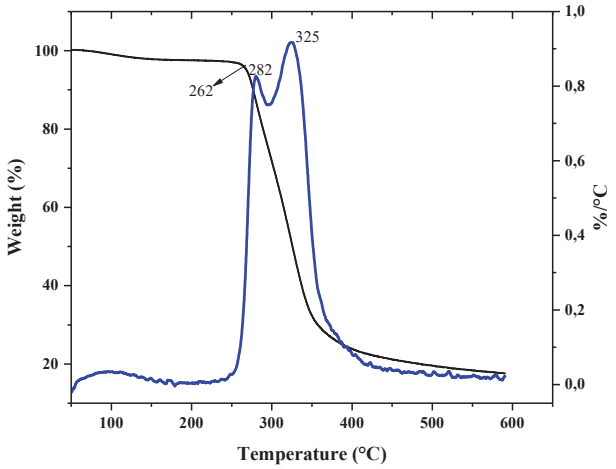

Figura 4 – TGA and DTG curves.

Conclusions

Experimental data show that agar is a very versatile material, usually applied in biology, but can be applied in scientific work in chemistry. The FTIR tests showed -OH stretching of the hydroxyl group, S = O of sulfate esters, glycosidic linkage, 3,6-anhydrogalactose-2-sulfate, galactose-4-sulfate and vibration of the - C-O-C bridge 3,6 anhydrous -L-galactopyranose that are characteristic of this polysaccharide XRD test shows a high degree of crystallinity indicated by a peak at 19.1°Θ and a slight shoulder at 13.9°Θ. The thermal stability showed that this polysaccharide has a good thermal stability, which makes it a biopolymer applicable in various areas.

Acknowledgements

The authors would like to thank the Carlos Chagas Filho Foundation for Research Support in the State of Rio de Janeiro (FAPERJ) and the National Council for Scientific and Technological Development (CNPq), for financial support.

References

[1] B. Munro, P. Conrad, S. Krämer, H. Schmidt, P. Zapp. Solar Energy Materials and Solar Cells 1998, 54, 131-137. https://doi.org/10.1016/S0927-0248(98)00063-4

[2] T. R. Hoare, D. S. Kohane. Polymer 2008, 49, 1993-2007.https://doi.org/10.1016/j.polymer.2008.01.027

[3] O. B. G. Assis; V. L. Silva. Polímeros: Ciência e Tecnologia 2003, 13, 223-228.

[4] P. Guerrero, et al. Carbohydrate Polymers 2014, 99, 491-498. https://doi.org/10.1016/j.carbpol.2013.08.049.

[5] A. L. L. Aguiar, et al. Algal Research 2023, 69, 102920. https://doi.org/10.1016/j.algal.2022.102920.

[6] Y. Freile-Pelegrín, et al. Polymer Degradation and Stability 2007, 92, 244–252. https://doi.org/10.1016/j.polymdegradstab.2006.11.005.

[7] L Wei, et al. Carbohydrate Polymers 2023, 243, 116416. https://doi.org/10.1016/j.carbpol.2020.116416.

[8] N. Sarkar, G. Sahoo, S. K. Swain. Nano-Structures and Nano-Objects 202, 23, 100507. https://doi.org/10.1016/j.nanoso.2020.100507.

[9] G. Boopathi, *et al*. Ionics 2017, 23, 2781–2790. https://doi.org/10.1007/s11581-016-1876-x.
[10] S. G. Pereira, et al. Innovative Food Science and Emerging Technologies 2023, 84, 103306. https://doi.org/10.1016/j.ifset.2023.103306
[11] C. Araki. Bulletin of the Chemical Society of Japan 1956, 29, 543-544. https://doi.org/10.1246/bcsj.29.543
[12] D. AN, *et al.* Food Hydrocolloids 2021, 113, 106520. https://doi.org/10.1016/j.foodhyd.2020.106520
[13] Y. Pandya, et al. The Pharma Innovation Journal 2022, 6, 151–1157. https://dx.doi.org/10.22271/tpi
[14] K. Sharma, V. Kumar, C. Swart-Pistor, B. Chaudhary, C.H. Swart. Journal of Bioactive and Compatible Polymers 2017, 32, 74-91. https://doi.org/10.1177/0883911516653148

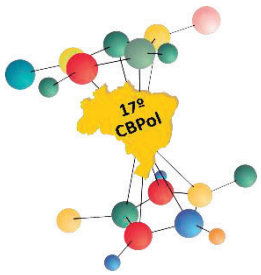

ANALYSIS OF ULTRAVIOLET EXPOSURE IN SYNTHETIC FIBERS OF POLYESTER AND HIGH MODULUS POLYETHYLENE

Daniel Magalhães da Cruz[1, 3, *], Marcelo de Ávila Barreto[2, 3], Larissa Basei Zangalli[3], Felipe Tempel Stumpf[1], Carlos Eduardo Marcos Guilherme[2], Ivan Napoleão Bastos[4] and Ana Lúcia Nazareth da Silva[5]

1 – Department of Mechanical Engineering (DEMEC), Federal University of Rio Grande do Sul (UFRGS), Porto Alegre, RS, Brazil
** Corresponding author: daniel.cruz@ufrgs.br*
2 – School of Engineering (EE), Federal University of Rio Grande (FURG), Rio Grande, RS, Brazil
3 – Tecnofibers Desenvolvimento e Tecnologia Ltda., Itajaí, SC, Brazil
4 – Polytechnic Institute (IPRJ), Rio de Janeiro State University (UERJ), Nova Friburgo, RJ, Brazil
5 – Institute of Macromolecules Professora Eloisa Mano (IMA), Federal University of Rio de Janeiro (UFRJ), Rio de Janeiro, RJ, Brazil

Abstract
Polyester (PET) and high modulus polyethylene fibers (HMPE) are currently the most common fibers used in the manufacture of ropes for offshore operation. Several studies have been carried out in an analytical, experimental, and numerical field, addressing diverse conditions related to traction, fatigue, creep, and environmental and exposition conditions that can influence the behavior. This work presents data referring to an experimental study of resistance to rupture in semi-finished products of PET and HMPE fibers subjected to different exposure times of ultraviolet radiation. Experimental procedure includes ultraviolet exposure, with subsequent rupture testing based on ISO 2062. The results showed that degradation by UV exposure occurs in a monotonic way for PET while HMPE presents some stability. Future studies can be carried out with longer times for complement the data, or even new similar studies at lower levels as multifilaments, or at higher construction levels as subropes.

Keywords: *Experimental characterization, Polymeric fibers, Ultraviolet degradation, Strength at break, Offshore mooring.*

Introduction

In the 1990s, Del Vecchio proposed the used of polymeric fiber mooring systems [1]. This represented a significant change in technique, moving away from steel catenaries and adopting Taut-Leg systems with synthetic fibers. With advances in the offshore industry, polymeric fibers have become a widely used material, rather than an alternative one [2-5]. As a result, these materials are extensively studied using analytical, numerical, and experimental approaches [6-9].

Synthetic ropes are commonly used for anchoring, mooring, towing and other marine applications. Polyester ropes dominate the market due to their low cost, simple processability, easy blending with other fibers, and recyclability. However, high-modulus polyethylene (HMPE) has shown promising results on terms of evolution towards ultra-deep waters.

Numerous studies aim to experimentally investigate polymeric fibers, such as polyester, HMPE, aramid, polyamide, liquid crystal Polymer, etc. These studies address various tests, such as monotonic loads, fatigue cycles, abrasion, impact, among others [10-13]. The current study aims to experimentally analyze the effect of ultraviolet radiation on synthetic polymeric polyester fibers and HMPE intended for offshore use, in the tensile strength test.

Experimental

Materials

The materials tested are semi-finished products (SFP), made out of polyester (PET) and high modulus polyethylene (HMPE).

The characteristics of the SFP samples for polyester are: 19 multifilaments with a linear density of 2200 dtex were used. Each multifilament with 192 strands. Its coding is polyester SFS5202 2200dtex/192f. And for high modulus polyethylene they are: 7 multifilaments with a linear density of 1760 dtex were used. Each multifilament has 480 strands. Described by the manufacturer as high modulus polyethylene JX99 1600D/480f. The results of the Test Report referring to both multifilaments materials are shown in Table 1.

Table 1 – Test Report results for multifilament of base of the semi-finished product.

	PET		HMPE	
	Technical standard	Testing Results	Technical standard	Testing Results
Linear density / dtex	2240	2261.9	1777	1769
Force at break / N	≥180	188.5	≥551.1	597.9
Elongation at break / %	14.0	13.9	≤4.0	3.5
Tenacity / cN/dtex	≥8.2	8.3	≥31	33.8

The semi-finished products (SFP) made from polyester SFS5202 and high modulus polyethylene JX99 are specifically designed for use in the offshore industry. While cost is a critical consideration for these materials, it is also important to compare their performance and characteristics quantitatively.

According to literature [8-9,12] and the presented certificate of analysis, polyester typically exhibits elongation at break values between 12 and 15 percent, whereas high modulus polyethylene usually has values lower than 4%. This lower elongation in HMPE fibers produces shorter platform displacement for offshore mooring. In addition, high modulus polyethylene has higher rupture values and lower linear density, resulting in linear tenacity values (strength to linear density ratio) up to four times higher than that of polyester.

High modulus polyethylene has another important characteristic, its buoyancy, due to its density being lower than that of water. Given that mooring systems are being used in increasingly deeper waters, high modulus polyethylene is promising for mooring systems in ultra-deep waters.

Ultraviolet Exposure

The UV exposure was conducted at the Polytechnic Institute, Rio de Janeiro State University in Nova Friburgo. The experiment used an ultraviolet lamp, No. UVA-340 Q-Lab, which emits radiation with a wavelength of 340 nm. Fig 1 shows the device used to hold the samples and their length. Areas outside the analysis region were covered with aluminum foil to block UVA (ultraviolet A) radiation. The Fig 1 also depicts the UV exposure process, where the distance between the lamp and the samples was 150 mm. The study involved exposure times of 0, 14, 28, 42, 56, 70, and 84 days. The samples were rotated at half of the exposure time to ensure uniform exposure.

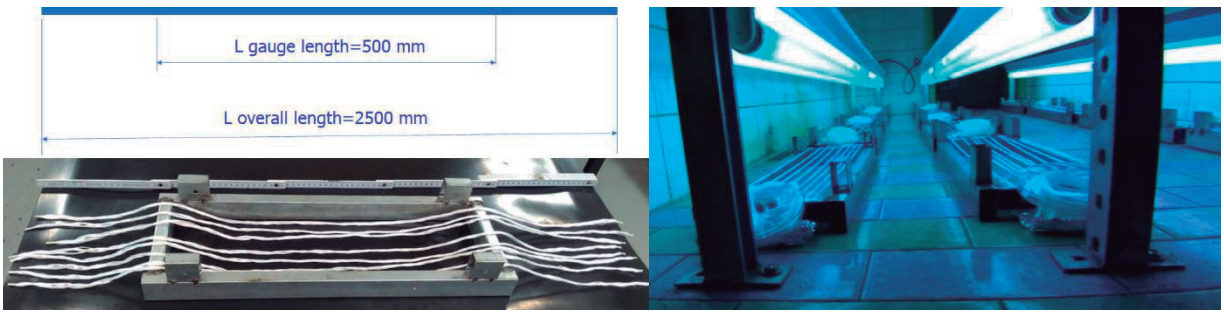

Figure 1 – Support detail and UV exposure.

Mechanical Characterization

The mechanical characterization is done through linear density tests, rupture tests and obtaining linear tenacity, was conducted at the Policab Stress Analysis Laboratory, Federal University of Rio Grande. The titer test procedure (linear density) is standardized by ASTM D1577 [14] and complies ISO 139 [15]. Linear density testing was performed for 10 samples without UV exposure. Linear density is not changed by exposure (due to the law of conservation of mass), so it would not be necessary to perform an exposure and then take the mass readings by length. The basic details are given below:

- 10 standard samples with a length of 1000 mm;
- Weighing each sample on precision balance, 9 minutes of stabilization;
- Application of statistical criteria for possible exclusion of outliers.

Although the material is a semi-finished product and does not have a specific standard norm for breaking, it is considered the standard for yarns and multifilaments. The rupture test procedure is standardized by ISO 2062 [16] and ISO 139 standard [15]. The length of 2500 mm was chosen to ease the handling of the sample and especially for clamping the samples in the grips of the equipment. The useful test length is 250 mm. The basic details are given below:

- 5 samples with a length of 2500 mm, for each sample group;
- Torsion of 60 turns/meter in each sample;
- Test performance with force and elongation recording in the Instron 8801 equipment, with tested useful length of 250 mm, and constant extension rate of 250 mm/min;
- Application of statistical criteria for possible exclusion of outliers.

Linear tenacity is a dependant result on both the linear density test and the Yarn Breaking Load test. With the results, the ratio of breaking strength in Newtons by linear density in tex can provide the linear tenacity of the SFP.

Results and Discussion

For the linear density results, are presented the results for the mass per length for both polyester (PET) and high modulus polyethylene (HMPE) in Table 2. The results presented linear density average for polyester at 3647 ± 12 tex and for high modulus polyethylene 1220 ± 3 tex.

Table 2 – Linear density of SFP polymers.

PET / g/m		HMPE / g/m	
3.630	3.623	1.223	1.226
3.658	3.660	1.218	1.220
3.649	3.646	1.219	1.217
3.658	3.643	1.219	1.217
3.650	3.655	1.221	1.223
Average	3.647	Average	1.220
SD	0.012	SD	0.003

The breaking test results for polyester samples are presented in summarized form in Table 3, which compiles the average and standard deviation data for each group. Similarly, the results for HMPE samples are presented in Table 4.

Table 3 – Average and Standard Deviation mechanical properties at break of PET.

UV days	Force / N	Elongation / mm	Strain / %
0	2911 ± 226	129 ± 20	52 ± 8
14	2737 ± 83	106 ± 3	43 ± 1
28	2481 ± 155	100 ± 5	40 ± 2
42	2288 ± 149	92 ± 6	37 ± 3
56	2159 ± 39	84 ± 2	34 ± 1
70	1978 ± 32	80 ± 4	32 ± 2
84	1797 ± 25	74 ± 1	30 ± 1

Table 4 – Average and Standard Deviation mechanical properties at break of HMPE.

UV days	Force / N	Elongation / mm	Strain / %
0	3474 ± 346	52 ± 3	21 ± 1
14	3407 ± 233	60 ± 14	24 ± 6
28	3210 ± 242	58 ± 6	23 ± 2
42	3391 ± 229	56 ± 6	23 ± 3
56	3224 ± 299	53 ± 4	21 ± 2
70	2922 ± 369	48 ± 3	19 ± 1
84	3146 ± 194	55 ± 8	22 ± 3

The results are depicted in Fig 2 for PET and in Fig 3 for HMPE.

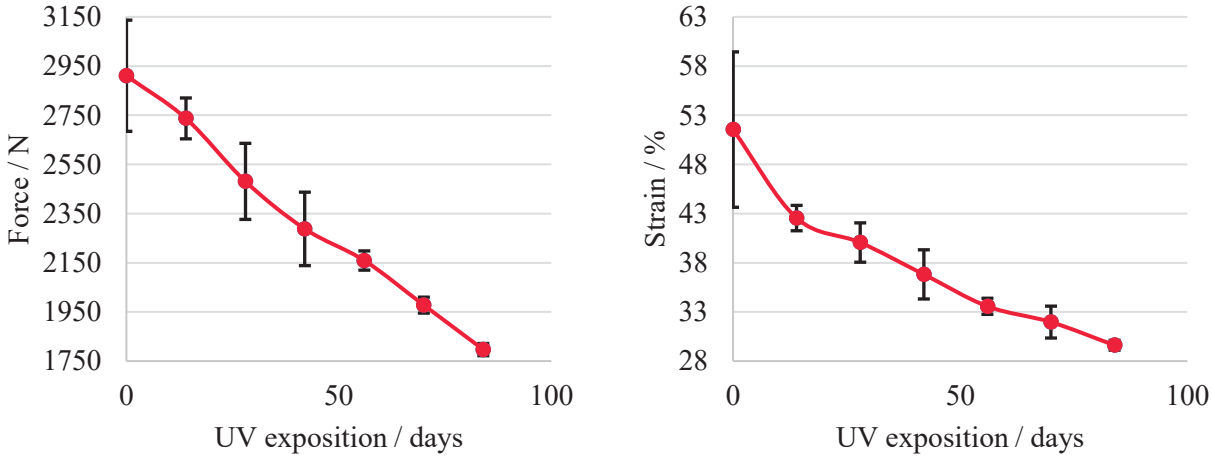

Figure 2 – PET: Force vs. UV exposition and Strain vs. UV exposition.

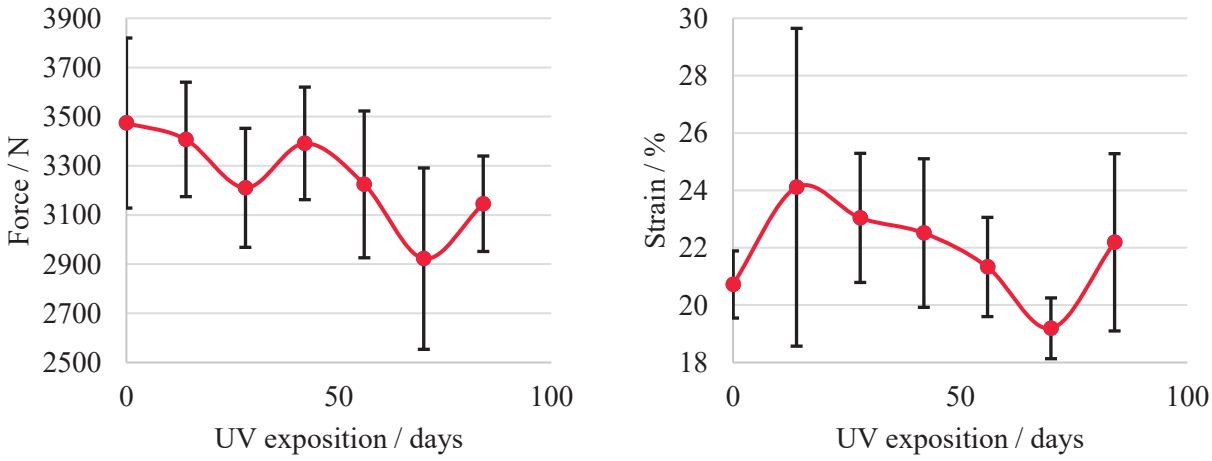

Figure 3 – HMPE: Force vs. UV exposition and Strain vs. UV exposition.

As mentioned before, the linear tenacity values are determined through the mathematical procedure in a ratio of the rupture value in Newtons divided by the linear density value in tex. For this linear tenacity value reference, the break value without UV exposure is considered, Table 5.

Table 5 – Linear tenacity results.

Material	Force at break / N	Linear Density / tex	Linear Tenacity / N/tex
PET	2911 ± 226	3647 ± 12	0.80 ± 0.06
HMPE	3474 ± 346	1220 ± 3	2.85 ± 0.29

Conclusions

The results reveal significant differences between two polymers, high modulus polyethylene (HMPE) and polyester (PET), concerning ultraviolet (UV) exposure. As the UV exposure time increases, polyester exhibits a reduction in both breaking value and strain value, whereas high modulus polyethylene does not show a statistically significant reduction.

Even though HMPE's highest rupture value is obtained without UV exposure, the material shows a certain level of stability to ultraviolet exposure. If we consider the standard deviations, the values remain approximately constant within a certain range, unlike polyester's behavior, which shows a monotonic decrease. The plot of rupture force versus exposure time provides evidence to support this conclusion, resulting in a reduction slope of 13.26 N/day for PET submitted to 340 nm UV radiation and a strain reduction slope of 0.26 %/day. Therefore, the UV simultaneously reduces the strength and tenacity of polyester.

Still regarding the results, it is noteworthy that each rupture has a set of data acquired in terms of force and elongation. It is possible to plot the rupture graph of each UV exposure for verify if constitutive behavior change as the UV exposure time increases.

References

1. C. J. M. Del Vecchio, Ph.D. Thesis, University of Reading, 1992.
2. K. Huang; M. Y. Lee in Proceedings of Offshore Technology Conference, Houston, 1998, OTC-8770-MS. https://doi.org/10.4043/8770-MS.
3. J. F. Flory; S. P. Banfield; D. J. Petruska in Proceedings of Offshore Technology Conference, Houston, 2004, OTC-16151-MS. https://doi.org/10.4043/16151-MS.
4. L. F. Haach; D. T. Poitevin; M. B. Bastos in Proceedings of Rio Oil & Gas Expo and Conference, Rio de Janeiro, 2010, IBP2745_10.
5. S. D. Weller; L. Johanning; P. Davies; S. J. Banfield, Renewable Energy 2015, 83, 1268-1278. https://doi.org/10.1016/j.renene.2015.03.058.
6. H. Liu; Y. Lian; L. Li; Y. Zhang, Journal of Offshore Mechanics and Artic Engineering 2015, 137(6), 061401. https://doi.org/10.1115/1.4031392.
7. K. Naresh; K. A. Khan; R. Umer; A. Vasudevan, Polymers 2020, 12(8), 1700. https://doi.org/10.3390/polym12081700.
8. F. T. Stumpf; C. E. M. Guilherme; D. M. da Cruz; A. H. M. F. T. da Silva; M. B. Bastos, Ships and Offshore Structures 2022. https://doi.org/10.1080/17445302.2022.2116766.
9. D. M. da Cruz; F. M. Clain; C. E. M. Guilherme, Acta Polytechnica 2022, 62(5), 538-548. https://doi.org/10.14311/AP.2022.62.0538.
10. P. Smeets; M. Jacobs; M. Mertens in Proceedings of MTS/IEEE Oceans, Honolulu, 2001, 685-690. https://doi.org/10.1109/OCEANS.2001.968205.
11. C. Humeau; P. Davies; P. Smeets; T. A. P. Engels; L. E. Govaert; M. Vlasblom; F. Jacquemin, Polymer Testing 2018, 65, 497-504. https://doi.org/10.1016/j.polymertesting.2017.12.014.
12. D. M. da Cruz; C. E. M. Guilherme; F. T. Stumpf; M. B. Bastos in Proceedings of Offshore Technology Conference, Houston, 2022, OTC-31906-MS. https://doi.org/10.4043/31906-MS.
13. E. S. Belloni; A. H. M. F. T. da Silva; F. M. Clain; C. E. M. Guilherme, Polymers and Polymer Composites 2022, 30, 09673911221103934. https://doi.org/10.1177/09673911221103934.
14. American Society for Testing and Materials, ASTM D1577, 2008, West Conshohocken.
15. International Organization for Standardization, ISO 139, 2005, Geneva.
16. International Organization for Standardization, ISO 2062, 2009, Geneva.

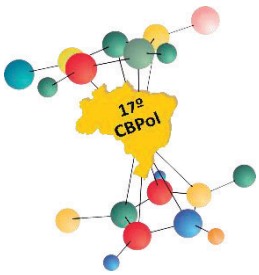

ANALYSIS OF WATER SORPTION ISOTHERM IN CASSAVA STARCH PACKAGING WITH TOMATO PEEL

Anômora A.R.S. Cotta[1,2], Laura F. Fonseca[1], Sorais V. Borges[2], Bruna S. Nascimento[2], Alexandre A.C. Cotta[3], Marali V. Dias[1,2]

1 – Graduate Program in Biomaterials Engineering., Federal University of Lavras (UFLA), Lavras, MG, Brazil
arianerochido@gmail.com
2 – Graduate Program in Food Engineering, Federal University of Lavras (UFLA), Lavras, MG, Brazil
3 - Graduate Program in Physical Engineering, Federal University of Lavras (UFLA), Lavras, MG, Brazil

Abstract - This study focuses on the development of sustainable packaging technologies as an alternative to fossil-based packaging materials. Specifically, biodegradable active packaging made from natural polymeric sources and natural antioxidants, such as lycopene, were investigated. The objective of this research was to analyze the water sorption isotherms of these active biodegradable packages. Water sorption isotherms describe the relationship between water activity and the equilibrium moisture content of the material. The packages were subjected to different temperature and relative humidity conditions until reaching a constant weight to obtain the water sorption isotherms. The experimental data was fitted to the Guggenheim-Anderson-de Boer (GAB) mathematical model, which provided accurate estimations of the monolayer moisture content as temperature increased. The results demonstrated a general increase in the monolayer moisture content with rising temperature. These findings are crucial for understanding the behavior of active biodegradable packaging in relation to moisture and contribute to the development of more effective packaging solutions for preserving product quality. Furthermore, the utilization of biodegradable packaging derived from natural sources and natural antioxidants presents a promising alternative to mitigate the environmental and resource-related challenges associated with conventional packaging materials. This study emphasizes the significance of biodegradable materials and water sorption studies in advancing sustainable packaging technologies. By reducing the negative environmental impact of traditional packaging materials, these research efforts contribute to the development of efficient and environmentally friendly packaging solutions. As part of the ongoing commitment to promoting sustainable practices, scientists continue to explore innovative solutions that can replace fossil-based packaging materials with more eco-friendly alternatives.

Keywords: *Biodegradable packaging; Active packaging; Water sorption isotherm.*

Introduction

Petrochemical-based packaging is widely used in the food industry but raises environmental concerns due to waste generation and its low degradation rate. To address this issue, biodegradable packaging made from natural polymers such as starch is being studied as a more sustainable alternative [1]. However, starch has limitations in its mechanical and moisture barrier properties. Researchers are investigating packaging made from cassava starch with the addition of lycopene to improve these properties and make them suitable for food applications [2].

In the food industry, the technique of water sorption isotherm analysis is widely employed to assess the water adsorption capacity of packaging materials. Water adsorption refers to the material's ability to attract and retain water molecules on its surface, which can have a significant impact on the quality and shelf life of packaged food. The water sorption isotherms describe the relationship between water activity and equilibrium moisture content of the material at a constant temperature and are graphically represented within a range of relative humidity [3].

These isotherms provide crucial information about the interaction between the packaging and ambient humidity, enabling proper selection of materials that prevent issues such as moisture migration, food

deterioration, and growth of undesirable microorganisms [4]. Understanding the water adsorption capacity of the packaging is essential to ensure the quality, safety, and durability of food over time. Therefore, the aim of this study was to investigate the water sorption isotherms in packaging made from cassava starch with tomato peel (lycopene), in order to better understand their thermodynamic properties and evaluate their effectiveness in the preservation and protection of food.

Experimental

This study aimed to determine the water sorption isotherms of packaging materials. The samples were subjected to a drying process in a vacuum oven for 24 hours at 60 ºC. After drying, the samples were carefully distributed in glass containers with airtight lids, containing saturated solutions of specific salts such as magnesium chloride ($MgCl_2$), potassium carbonate (K_2CO_3), magnesium nitrate ($Mg(NO_3)_2$), sodium chloride (NaCl), potassium chloride (KCl), and potassium sulfate (K_2SO_4). These saline solutions were strategically selected to cover a wide range of water activity at each studied temperature. The containers were placed in an air-circulating oven of the D.O.B brand, at different temperatures: 5 ºC, 15 ºC, and 25 ºC, representing the cooling and ambient temperature conditions of food. During this period, periodic weighings were performed using high-precision analytical balances with an accuracy of 0.001 g until the samples reached a constant weight, indicating equilibrium with the environment. These weighings allowed determining the adsorbed moisture content of the packaging materials. The obtained results provided valuable information about the water sorption properties of the packaging materials under different temperature and water activity conditions, contributing to the development of more efficient and suitable packaging for food preservation [4] and [5].

Results and Discussion

Sorption isotherm

After analyzing the results, it was found that the GAB model was the most suitable for describing the sorption isotherms at different temperatures (5°C, 15°C, and 25°C) and for the different packaging materials studied. Figure 1 - a, b, and c shows the second-order polynomial sorption curves of the GAB model, which were fitted to the experimental data for the three mentioned temperatures.

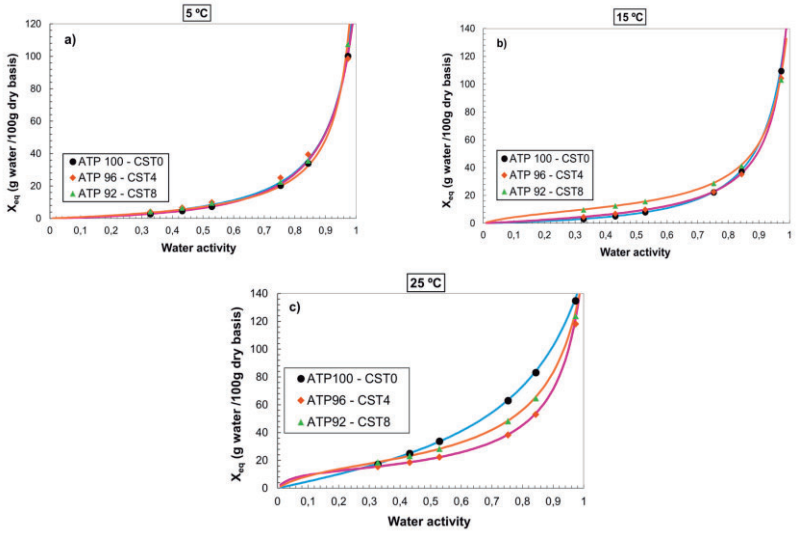

Figure 1 - Graphical representation of sorption isotherms at three different temperatures: a) 25°C, b) 15°C, and c) 5°C.

The curves presented follow the classification of Type II, according to the categorization by Brunauer et. al. [6]. This type of behavior is common in food products with a high protein content, as mentioned by Goula et. al. [7]. In the multilayer sorption region, there is a gradual and slow increase in the equilibrium moisture content for all packaging samples at water activities below 0.6, followed by a rapid and steep increase at water activities above 0.7. In this region, water molecules are weakly bound to the product matrix, making them available for chemical and microbiological reactions.
Furthermore, it is observed that the equilibrium moisture content (X_{eq}) of the packaging increases with increasing water activity while maintaining a constant temperature. However, for a given temperature, the equilibrium moisture content slightly decreases with an increase in lycopene concentration in the polymeric matrix. This effect can be attributed to the lower affinity of water for antioxidant films, likely due to a reduction in the number of active sites available for water binding and the formation of stronger bonds between starch and the chemical structure of lycopene.

Conclusions

In conclusion, the obtained results demonstrated that the GAB (Guggenheim-Anderson-de Boer) model was the most suitable for describing the experimental data of the isotherm. This model accurately represented the three temperature ranges studied and the different packaging formulations. Furthermore, it was observed that the monolayer moisture content (X_m) generally increased with increasing temperature. This indicates that as the temperature rises, the packaging's ability to retain moisture also increases.
These findings are important for understanding the behavior of the packaging in relation to moisture and provide valuable insights for the development of more efficient packaging for moisture-sensitive products. In the future, these findings can be applied to improve packaging and develop appropriate storage strategies to ensure the quality and durability of products.

Acknowledgements

To Brazilian Agencies Coordenação de Aperfeiçoamento de pessoal de Vível Superior (Finance Code 001) and Conselho Nacional de Desenvolvimento Científico e Tecnológico (CNPq, Brazil).

References

1. T. P. Haider, C. Völker, J. Kramm, K. Landfester, F. R. Wurm. *Angewandte Chemie* v. 58, n. 1, p. 50–62, 2019.
2. H. Onyeaka, K. Obileke, G. Makaka, N. Nwokolo. *Polymers*, v. 14, n. 6, p. 1126, 2022
3. B. R. B. Lara, M. V. Dias, M. G. Junior, P. S. Andrade, B. S. Nascimento, L. F. Ferreira, M. I. Yoshida. *Food Hydrocolloids Journal*, v. 103, 2020.
4. Y. Tao, Y. Wu, J. Yang, N. Jiang, Q. Wang, D.-T. Chu, Y. Han, J. Zhou. *Powder Technology*, v. 323, p. 208–218, 2018.
5. L. Greenspan. *Journal of Research of the National Bureau of Standards- a. physics and chemistry,* v. 81, n. 1, 1977.
6. S. Brunauer, L. S. Deming, W. E. Deming, and E. Teller. *Journal of the American Chemical Society*, v. 62, n. 7, p. 1723–1732, 1940.
7. A. M. Goula, T. D. Karapantsios, D. S. Achilias, K. G. Adamopoulos. *Journal of Food Engineering*, v. 85, n. 1, p. 73–83, 2008.

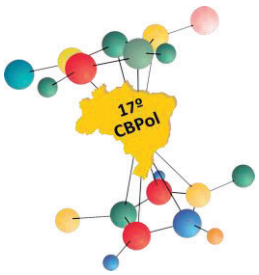

APPLICATION OF THERMAL ANALYSIS FOR IDENTIFICATION OF FKM TYPES 1 AND 2 IN RUBBER COMPOSITES

Christine R. Nascimento[1], Daniele R. de Lima[1,3], Janaina F. M. de Almeida[1], Ana Lúcia N. da Silva[1,2], Ana Maria F. de Sousa[3], Mônica Regina C. M. Calderari[3], Fernando R. da Cunha[4] and Cristiane X. S. Campo[4]

1 - Professora Eloisa Mano Macromolecules Institute, Federal University of Rio de Janeiro (IMA/UFRJ), Rio de Janeiro, RJ, Brazil.
2 - Environmental engineering Program, Federal University of Rio de Janeiro (PEA/UFRJ), Rio de Janeiro, RJ, Brazil.
3 - Chemistry Institute, State University of Rio de Janeiro , Rio de Janeiro, RJ, Brazil.
4 - Leopoldo Américo Miguez de Mello Research, Development, and Innovation Center (CENPES/PETROBRAS), Rio de Janeiro, RJ, Brazil.

Abstract.
Fluororoelastomers (FKM) are materials employed as seals in the chemistry and oil and gas industries under harsh working conditions. The most common FKM types are 1 and 2, but distinguishing between them is not a simple task. The main difference between types 1 and 2 is that type 2 contains tetrafluoroethylene, which increases its thermal and chemical strength. Thermogravimetric analysis is an ideal method for determining the thermal stability of polymers; thus, in this study, several FKM formulations were analyzed using two distinct methodologies and the results were compared. The identification of the two types was better performed with the method in which an isothermal temperature was applied at 455 °C in comparison with the temperature ramp method.

Keywords: *FKM, thermogravimetry, pyrolysis, fluoroelastomer, characterization*.

Fundings: This work was supported by CENPES/PETROBRAS and Conselho Nacional de Desenvolvimento Científico e Tecnológico (CNPQ) [PQ-2:309461/2021-9 received by Ana Maria Furtado de Sousa and PQ-2: 307889/2022 received by Ana Lúcia Nazareth da Silva].

Introduction

Fluororoelastomers (FKM) are a class of materials with high thermal and chemical strength that are indicated to be applied in hard operational environments. Due its high cost, FKM is used in the oil and gas industry in applications where common elastomers would fail [1].
Fluoroelastomers are vinylidene fluoride (VDF) copolymers, where the other monomers are added to contribute to the achievement of specific requirements for the material's end application. In this context, five FKM types are classified in ASTM D1418 [2] according to their monomeric composition.
The most widely used FKM are types 1 and 2. FKM type 1 is a vinylidene fluoride (VDF) and hexafluoropropylene (HFP) copolymer. HFP units contribute to FKM flexibility, and, in the case of FKM 1 and 2, at least 20% mol of HFP must be added to assure that an amorphous polymer will be

obtained [3,4]. The FKM type 2 is a terpolymer of VDF, HFP, and tetrafluoroethylene (TFE), so this type has the thermal and chemical strength improved by TFE unit addition.
In terms of distinguishing FKM types 1 and 2 using standard characterization techniques, the complexity of this goal increases significantly in the case of a cured rubber compound due to its insolubility and interference caused by fillers and other compounds added. On the other hand, from a practical standpoint, identifying the elastomer contained in a formulation is far more important than identifying it as a raw elastomer, because all useful products are elastomer compositions.
As the main difference between FKM types 1 and 2 is the TFE units, and thermal stability is a key property to differentiate them, the purpose of this study is to explore pyrolysis experiments and thermogravimetric analysis for the identification of FKM types 1 and 2. The comparison of the two test protocols and the influence of formulation were discussed.

Experimental

Materials

FKM Type 1 (DHP-201NC) and FKM Type 2 (DHP-356F) elastomers were used. The formulated compositions are shown in Table 1.

Table 1. FKM types 1 (T1) and 2 (T2) formulations

Compounds	T1 F1		T1 F2		T2 F1		T2 F2	
	phr	%	phr	%	phr	%	phr	%
Raw FKM Type 1*	100	75.2	100	75.2	-	-	-	-
Raw FKM Type 2*	-	-	-	-	100	79.4	100	79.4
MgO	3	2.2	3	2.2	3	2.4	3	2.4
$Ca(OH)_2$	-	-	-	-	3	2.4	3	2.4
Carbon Black N900	30	22.6	15	11.3	20	15.8	10	7.9
BaSO4	-	-	15	11.3	-	-	10	7.9

* The cure system was inserted by the manufacturer

Pyrolysis Experiment

Pyrolysis was carried out in triplicate using a fixed-bed reactor inserted in a vertical oven (Figure 1) with a temperature controller of a maximum capacity of 550 °C.

Figure 1. Pyrolysis System and fixed bed reactor (LABTAM-UERJ)

Stainless steel reactors were used with holders for the samples. A condenser was attached to the bottom of the reactor, below the oven, to collect the pyrolytic oil. The experiments were carried out

under a constant flow of 50 mL.min^{-1} of nitrogen, for 25 min at 455 °C. The amount of sample used was 1 g of raw FKM and 2.5 g of formulated composites. After the pyrolysis, both solid residue and pyrolytic oil were weighed. The gas mass was calculated as the difference of the mass balance.

Thermogravimetric analysis

Thermogravimetric analysis was performed on TA Instruments Thermal Analysis TGA Q500 equipment under a nitrogen atmosphere. The nitrogen flows in the balance and in the sample were, respectively, 40 and 60 mL/min. Two test protocols were used, as described below:

A- Temperature scan test protocol: a heating ramp from room temperature to 650 °C, heating rate of 10 °C/min.

B- Isothermal test protocol: a fast-heating ramp (200°C/min) from room temperature to 455 °C and an isothermal at 455°C for 60 min.

For each sample, five replicates of 5.0 ± 0.5 mg were analyzed. The equipment software (Universal V4.5A) was used to calculate mass loss, temperature, and time at the maximum point of the derivative and residue amount.

Results and Discussion

Table 2 shows the mass balance results of the pyrolysis carried out at 455°C. It can be noticed that all samples of FKM type 2 showed solid residue significantly higher than type 1, despite the fact that the amount of filler and inorganic compounds added in FKM type 2 formulations was smaller than that added in FKM type 1 samples. So, it's very probable that this difference is due to the TFE units, which did not degrade at pyrolysis temperature.

Table 2. Mass balance of raw and formulated FKM types 1 (T1) and 2 (T2) samples

Residue	Type 1			Type 2		
	Raw	T1 F1	T1 F2	Raw	T2 F1	T2 F2
Solid (%)	26.5 ± 1.7	45.0 ± 0.9	46.9 ± 1.3	52.5 ± 0.9	66.9 ± 0.5	67.6 ± 1.5
Liquid (%)	73.5 ± 2.0	51.3 ± 0.8	49.5 ± 0.7	45.9 ± 1.5	31.4 ± 1.1	31.3 ± 0.4
Gas (%)	0	3.7 ± 0.6	3.6 ± 0.6	1.6 ± 1.1	1.7 ± 0.6	1.5 ± 1.3

The thermal stability is commonly associated with the degradation temperature, calculated as the maximum point of the derivative curve obtained in thermogravimetric analysis using a temperature scan (test protocol A). An alternative test protocol B, applying an isothermal at a temperature just below the degradation temperature, can also be used to compare samples with different thermal stabilities. Figure 2 shows the typical curve results of an isothermal analysis (test protocol B). The mass loss observed in an isothermal condition shows a maximum point at derivative curve, which also can be associated with the degradation kinetics and, which in turn, is related to comonomer structure and the formulation used. The more stable the FKM sample is, the longer will be the observed time at the maximum point of the derivative curve.

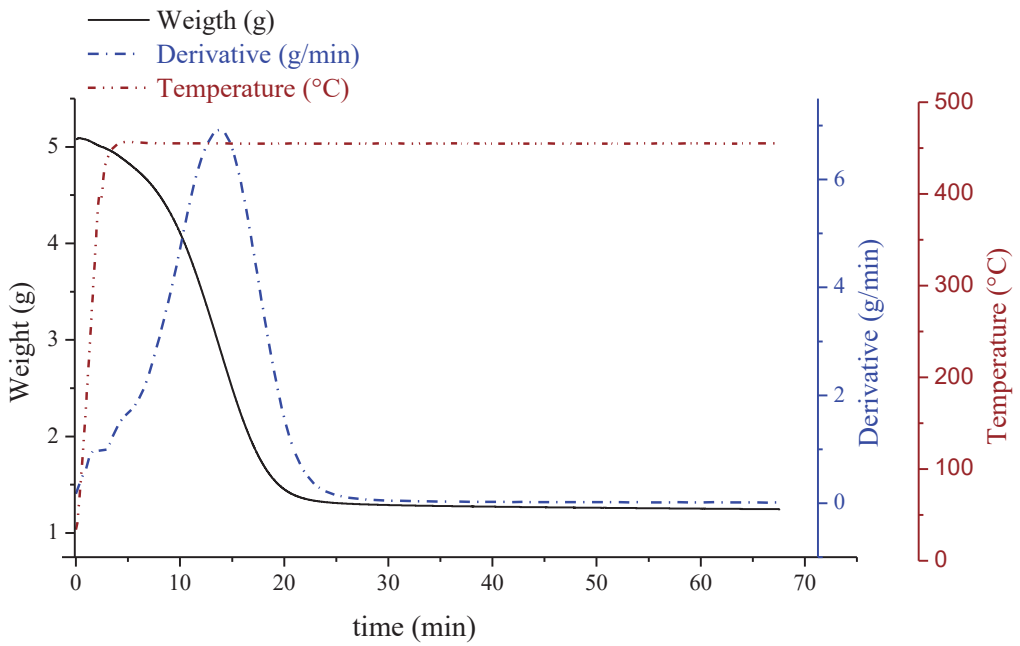

Figure 2. TGA curves of isothermal analysis of a FKM type 2 composition sample (test protocol B)

As the thermal stability is impacted both by the macromolecular structure and the formulation used, it is ideally required that the variability of formulations does not influence it to the extent that it masks the effect of comonomer type. In this way, the greater the influence of the comonomer over the formulation, the more accurate the methodology will be for differentiating the types of FKM. Figure 3 shows the comparison of FKM formulations related to the degradation temperature and derivative maximum, obtained, respectively, by test protocols A and B.

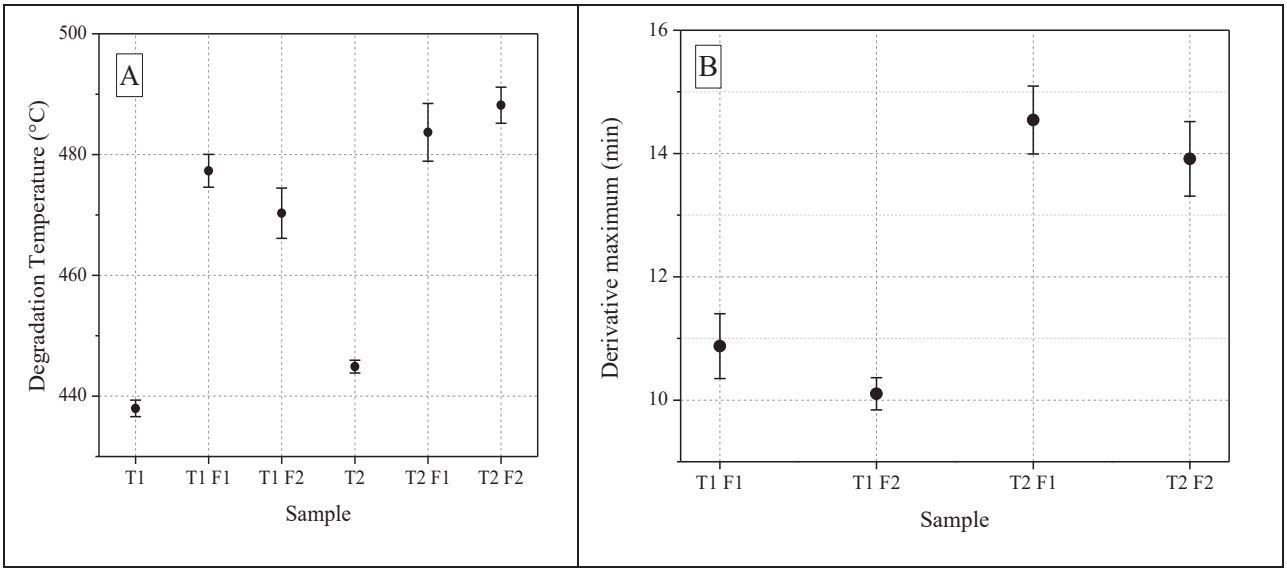

Figure 3. Degradation temperature obtained from temperature scan analysis [A] and Derivative maximum from isothermal analysis [B].

As expected, the degradation temperature values shown in Figure 3A reveal that FKM type 2 is more thermal stable than FKM type 1. In addition, composites were more stable than neat-FKMs, with FKM type 2 composites exhibiting greater thermal resistance than type 1 composites. However, considering the measurement uncertainty, the distinction of FKM types was best achieved using test protocol B (Figure 3B), since the differences between the two types are less influenced by

the deviation of the results. It is worthy to note that, as shown in Figure 3B, protocol B is not applicable in the case of raw rubbers since the temperature of 455 °C exceeds the degradation temperature of these materials (437–444 °C)..

Conclusions

Regarding the differentiation by thermogravimetry of types 1 and 2 of FKM rubber formulations, the test protocol in which a constant temperature is applied, just below the degradation temperatures, proved to be suitable. The protocol using an isothermal seems to be more accurate and less sensitive to formulation changes when compared to one using temperature scan.

Acknowledgements

Our acknowledgements to CENPES/PETROBRAS, CNPq and CAPES for all the support given to this research.

References

1. Farrow P, Merli F. New low-temperature FKM for effective sealing in the chemical industry. Seal Technol. 2010, 1, 8.
2. ASTM D-1418-17 Standard Practice for Rubber and Rubber Latices—Nomenclature (2017).
3. B. Ameduri Progress in Polymer Science 2022, 133, 101591. https://doi.org/10.1016/j.progpolymsci.2022.101591
4. A. L. Logothetis Progress in Polymer Science 1989, 14, 251. https://doi.org/10.1016/0079-6700(89)90003-8

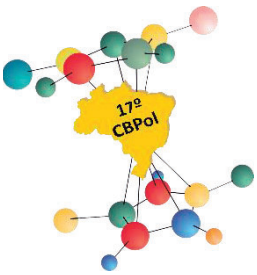

COMPARISON BETWEEN THE RESULTS OF DIGITAL IMAGE CORRELATION (DIC) AND THE STRAIN GAUGES IN A SPLIT HOPKINSON PRESSURE BAR (SHPB) TEST

Matheus S Domingos[1], Iana C Carvalho[1], Rafael R Dias[1], Iaci M Pereira[1]

1 – Laboratório de Materiais, Centro Tecnológico do Exército (CTEx), Rio de Janeiro, RJ, Brazil. dasilva.domingos@eb.mil.br
1 – Laboratório de Materiais, Centro Tecnológico do Exército (CTEx), Rio de Janeiro, RJ, Brazil. iana.carvalho@eb.mil.br
1 – Laboratório de Materiais, Centro Tecnológico do Exército (CTEx), Rio de Janeiro, RJ, Brazil. rodrigues.dias@eb.mil.br
1 – Laboratório de Materiais, Centro Tecnológico do Exército (CTEx), Rio de Janeiro, RJ, Brazil. iacipere@gmail.com

Abstract – In this work, a Split Hopkinson Pressure Bar compression test (SHPB) was conducted on a ballistic vest sample, and the results obtained by processing the data acquired from the bar's strain gauges were compared with the results obtained from the analysis of Direct Image Correlation (DIC-2D) of images captured during the test by a high-speed Phantom TMX-7510 camera. The results obtained by the DIC technique allowed for an analysis of the deformation wave propagation across the entire surface area of the tested sample, as well as the determination of the deformation wave propagation velocity in the sample and the identification of regions within the samples that exhibited different responses to the deformation wave passage. The use of the DIC-2D technique during SHPB tests can validate the results obtained from the bar's strain gauges and provide additional information for the study of the behavior of the tested samples under high deformation rates. For the tested sample, the discrepancies between the results of the two methods were shown to be significative.

Keywords: *SHPB, DIC, Ballistic Armor.*

Introduction

Materials used in ballistic applications can be studied using laboratory tests that simulate events with high deformation rates (similar to ballistic impacts) under more controlled and reproducible conditions. One example of a test in this context is the Hopkinson bar compression test.

The Split Hopkinson Pressure Bar (SHPB) investigates the dynamic-mechanical properties of samples submitted to high strain rates, ranging from 10^2 s^{-1} to 10^4 s^{-1}. The Hopkinson bar test consists of a boosting a strike bar, using a gas propulsion system, toward to the free end of an incident bar, causing a compressive deformation wave that travels along the incident bar and reaches the sample on the other extreme of the bar. Part of the wave is reflected and part travel along the transmission bar [1]. The test utilizes the data provided from strain gauges glued to the incident and transmission bars to calculate the forces and deformation that a sample is subject to during the test, this processing of the data considers many simplifying hypotheses, such as the unidirectional propagation of the deformation wave and parallelism of the faces of the samples. The test does not differentiate between parts and segments of the sample. When testing a multilayered composite armor, for example, to obtain information related to each layer, a technic such as Direct Image Correlation (DIC) must be employed.

This technique involves recording with a high-speed camera capable of observing the movement of the deformation wave front and analyzing its effects across the entire surface of the

sample and in different layers or materials that make up the sample. It compares subsequent images to calculate deformations and deformation rates.

Experimental

Sample preparation

The investigated material was a ballistic vest of Ultra-High Molecular Weight Polyethylene (UHMWPE) fiber from the brand 4GATE (imported material for use in the Brazilian Army). The test samples were extracted from the rigid plates used in the vest. The extraction was done using a water jet cutter, with cutting parameters set to obtain a cylindrical sample with a final diameter of approximately 16mm. After cutting, the sample was kept inside a climatic chamber at a temperature of 40°C and 10% humidity for 5 days.

Split Hopkinson Pressure Bar compression test (SHPB)

Dynamic compression tests were conducted using a compression Hopkinson bar provided by the American company REL Inc. The data from the strain gauges were amplified using a Vishay Micro-Measurements signal conditioner and amplifier (2300 System), and the data were recorded by a Pico Technology oscilloscope (PicoScope 5000 Series). The impacting, incident, and transmitted bars used were made of maraging steel C-350, with a Young's modulus of 200 GPa. The incident and transmitted bars were 2 meters long and had a diameter of 19.05 mm, while the impacting bar was 203.2 mm long and had a diameter of 19.05 mm.

Direct Image Correlation (DIC)

The preparation of the sample surfaces for DIC involved applying thin layers of gray primer to the entire surface of the samples. Subsequently, a black ink pen with a 0.3 mm diameter tip, specifically the PIGMA MICRON 003 model, was used. The high-speed camera used in the tests was the monochromatic Phantom TMX 7510 provided by Vision Research. The camera was manually triggered and positioned transversely to the bar, aiming at the sample position. Images were captured using a Canon 100mm macro lens at a frame rate of 875,000 fps. The GOM Correlate software from Zeiss was used to analyze the images. The analysis focused on obtaining values for the deformation rate and the velocity of the deformation wave front in the sample.

Results and Discussion

SHPB compression test

The sample size shown in Table 1, in addition to the data collected by the strain gauges, are parameters used to calculate the strain gauge results given in Table 2.

Table 1 - Size of the tested sample and the pressure parameter for the test

Sample	Length (mm)	Thickness (mm)	Pressure (psi)
4GATE	17.45	17.1	12

Table 2 - Strain gauge results for the tested samples

Sample	ε_{Total} (mm/mm)	U_{max} (J/m^3)	σ_{max} (MPa)	$\dot{\varepsilon}$ (mm/mm/s)
4GATE	9.3 %	4.8	81.1	1201

These results are primarily used for characterization and performance comparison between samples.

4GATE sample results

A notable difference between both techniques is that the strain gauge data necessarily considers the whole extension of the sample, while the DIC analysis was performed for the first half (F), second half (S) and the whole extension of the sample separately, as shown in Figure 1.

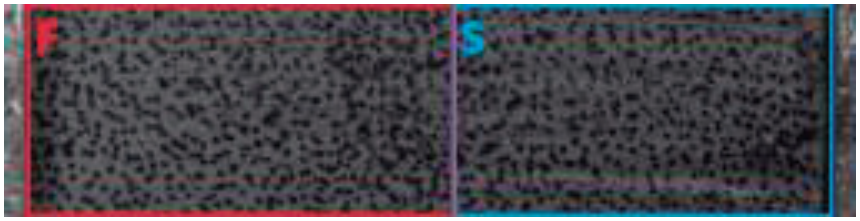

Figure 1 –Image of the 4GATE sample denoting the regions of interest of the sample, F stands for first half of the sample and S for second half of the sample.

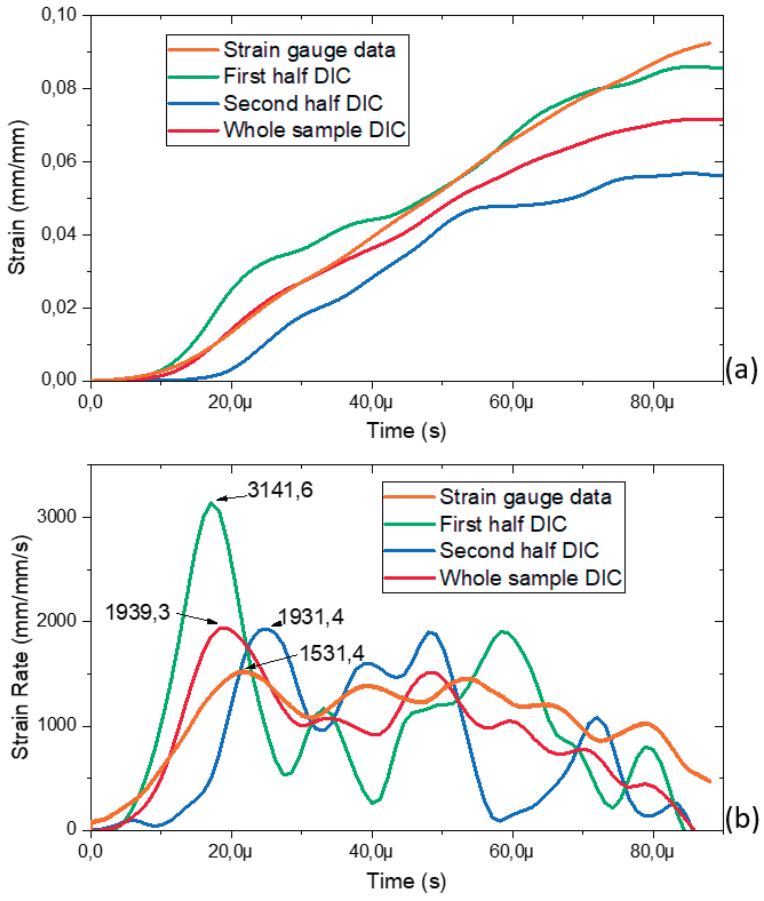

Figure 2 – DIC and strain gauges results for the 4GATE sample. Strain (a) and strain rate (b) per time.

The total strain data quantified with the aid of the extensometer and described by the camera are similar up to approximately 40 µs (shown by the red and orange lines on Fig 2a). Beyond this

value, the DIC analysis starts to show progressively smaller deformation values for the entire sample. It can be said that the error accumulates over time because, starting from 40 µs, the difference between the deformation values obtained by the extensometer and the values obtained by the camera is 10.8%, and at 80 µs, the error increases to 24.1%. It is expected that compression will be much more pronounced in the regions of the sample that are first subject to the impact, this effect can be seen comparing the green and blue lines on Fig 2a, where the first half of the sample is subject to a maximum deformation of 0.086 and the second half of the sample to 0.056, representing a difference of 53.6%.

Furthermore, upon analyzing the Fig 2b, a higher peak of deformation is observed in the initial part of the sample, reaching 3140 s^{-1}, while the second half of the sample was subject to lower peak deformation rate of 1931 s^{-1}, and the effect of considering the sample as a whole also evened out the higher deformation rate of the first half of the sample and resulted in a peak deformation rate of 1939 s^{-1}. From this information, it can be inferred that the region closest to the impact undergoes most of the total deformation of the sample.

The strain gauges perform an indirect measurement of the properties of the sample based on the incident, reflected, and transmitted deformation waves that propagate through the bar, which may lead to deviations if the simplifying assumptions required for the test are not met [2]. The strain gauge data reaches a peak deformation rate of 1531 s^{-1}, representing only 48.7% of the actual peak deformation rate that the initial part of the sample is subject to. The geometry of the sample did not fully satisfy these assumptions, as it did not have perfect parallelism between its two flat faces, which caused the given deviations. Nevertheless, the strain gauge result is more in line with the peak deformation rate calculated for the whole sample via DIC, where it represents 78.9% of the value.

The DIC analysis obtains its data directly from the sample and can provide the "true" deformation and deformation rate for the whole sample or for specific regions of interest, which can be more accurate than the strain gauge data, if done correctly [3]. From these results the strain gauge data underestimates the peak deformation rates for the samples when compared to the DIC data. On the other hand, even though the peak deformation rates are underestimated in the strain gauge data, the deformation rate is consistently higher for the strain gauge data throughout the time, which leads to the higher maximum deformation of the sample, as stated for Fig 2a.

Deformation wave velocity

The propagation velocity of the deformation wave was determined by analyzing the deformation wave front and its average advancement in the sample as a function of the test time. In Fig 3, the advancement of the deformation front (shown in red) can be observed. The calculation of the propagation velocity used the highlighted intervals in the images, along with the measurement of the wave advancement distance, using the Eq. 1.

$$V_m = \frac{\Delta L}{\Delta t} \tag{1}$$

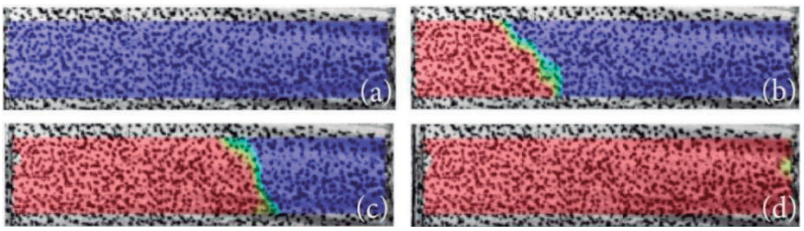

Figure 3 – The advancement of the deformation wave front for the 4GATE sample is as follows: (a) 0 s, (b) 5,8 µs, (c) 11,6 µs, e (d) 17,4 µs.

Due to a slight misalignment in the parallelism of the cylindrical faces of the sample caused by the cutting process to obtain the specimen, it is observed that the wave propagation is not perfectly perpendicular to the axis of the sample. The analysis of the deformation wave front velocity data is shown in Fig 4.

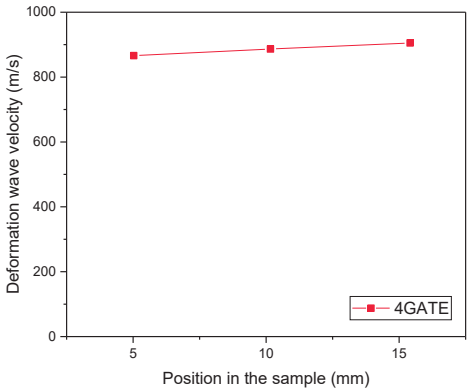

Figure 4 - Speed of the deformation wave in the UHMWPE sample (4GATE).

An average velocity of 886 ± 20 m/s was obtained for the wave propagating through the 4GATE sample, representing the wave velocity through the composite layers. It is interesting to note that the 4GATE is a Type III ballistic vest, which means that the armor protects against 7.62 mm ammunitions at 838 m/s, according to NIJ 0101.04. Therefore, the SHPB impose the same velocity of a rifle ammunition and the DIC technique was able to observe its propagation through the sample.

Conclusions

The results obtained by the DIC technique allowed for an analysis of the deformation wave propagation across the entire surface area of the tested sample, as well as the determination of the deformation wave propagation velocity in the sample and the identification of regions within the samples that exhibited different responses to the passage of the deformation wave.

As a direct measurement technique, the use of the DIC-2D analysis during SHPB tests can validate the results obtained from the strain gauges and indicate if the characteristics of the sample are in line with the simplifying assumptions used to process the data from the strain gauges. For the tested sample, the results between the two methods indicate that the discrepancies between the data is significative.

The limitations of using the technique are related to the high cost of the high-speed cameras capable of achieving around 1 million fps or more with enough resolution to analyze the whole surface of the sample, and to the additional sample preparation steps for the surface of the sample.

References

1. R. R. Dias; I. M. Pereira; B. G. Soares. Fracture Analysis of UHMWPE Ballistic Hard Armor Tested at Split Hopkinson Pressure Bar. 15h Brazilian Polymer Conference. 2019.
2. (Gama) Haque, Bazle & Gillespie Jr, John. Hopkinson bar experimental technique: A critical review. Applied Mechanics Reviews. 2004.
3. P. Lava, S. Cooreman, S. Coppieters, M. De Strycker, D. Debruyne, Assessment of measuring errors in DIC using deformation fields generated by plastic FEA, Optics and Lasers in Engineering. 2009.

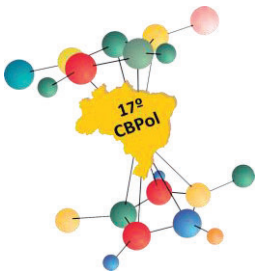

DEVELOPMENT OF NON-STICK SURFACES FOR RIGID PACKAGING

Marina Kauling de Almeida[1], Matheus Vinicius Gregory Zimmermann[1]

1 – Programa de Pós-Graduação em Engenharia e Ciência dos Materiais. Universidade do Extremo Sul Catarinense (UNESC), Av. Universitária, 1105, Criciúma, Santa Catarina CEP 88806-000, Brazil marinakauling.a@gmail.com

Abstract - The use of rigid packaging is present in several moments of life and, therefore, there is a need for packaging with specific characteristics for each use, such as the need for non-stick packaging to assist in the complete use of products. In this work, the surface modification of three substrates (metal, glass and polymer) was evaluated in order to reduce the adhesion of polar and non-polar liquid media. Five surface modifying agents based on organosilanes and fluoropolymer were used to obtain non-stick surfaces. Samples were analyzed for wettability and adherence properties. Significant increase in hydrophobicity was observed with the application of the modifiers Resysil 263, Resysil 902 and Resyfluor 2308 forming non-adherent surfaces in relation to water. It was observed that the use of coatings on substrates increased their oleophobicity, reaching higher values of contact angles.

Keywords: *Non-stick, organosilanes, fluoropolymer, wettability, hydrophobic.*

Introduction

The packaging market grows daily, as these are present in products used in everyday life, whether ceramic, metallic or polymeric. Packaging has always been present in humanity and has helped in the development of commerce and cities, its main function is to protect and enable the transport and storage of the product [1,2]. Currently, packaging has acquired new functions such as self-sales, so the visual aspects of packaging are becoming more important in manufacturing.

However, concerns with the aesthetic and functional characteristics of the product also influence the financial aspect, in high viscosity products, such as sunscreens, nail polishes and bases, mechanisms with lids or suction pumps are used to facilitate the removal of the product, the which increases the cost of packaging. Thus, if the material used in the packaging assists in removing the entire product contained in the container, it becomes possible to discard some of these mechanisms and, thus, reduce the cost of the final product. In addition, the residues of products that remain inside the packaging make it difficult to completely clean and subsequently recycle [3].

Surface modification is the process of altering the physical, chemical or biological characteristics of the surface, which may be roughness, wettability, surface energy and biocompatibility characteristics that, when altered, can help in the removal of the product [4].

A surface modification consolidated and present in everyday life are the frying pans/pans with non-stick coating of polytetrafluoroethylene (PTFE), known by its widely spread trade name Teflon®. This polymer has characteristics arising from its molecular structure formed by fluorine linked to a long carbon chain, which result in low adhesion of food to the material, facilitating the subsequent cleaning of the utensil [5].

Surface modifications can be applied in different ways, with the sol-gel method presented by Carneiro, Ferreira and Houmard (2018) [6] and Sacilotto (2015) [7] being quite widespread. In this method, hydrolysis and condensation reactions form a colloidal suspension of solid particles in a fluid that is deposited on the surface of interest by methods such as dip-coating, where the substrate

is immersed vertically in the solution and then dried to obtain of the desired properties. Kehrwald (2009) [8] used a simpler method for deposition, where the organosilanes to be used were mixed with water and then poured over the desired surface, after the water present had evaporated, the samples were cured in an oven. Another method used by researchers is vaporization, where the organosilane is kept in liquid condition in a container that will be covered with the surface to be covered, in which case both are isolated from the environment and will go to the oven, generating steam from the organosilane that will adhere the surface of interest [9].

Adhesion is the permanent union of two bodies through the contact of their surfaces, this phenomenon can occur by different mechanisms such as: thermodynamic, electrostatic, diffusion and mechanical. The mechanical adhesion mechanism occurs due to surface roughness such as pores and grooves that make breaking difficult. Thermodynamic adhesion is related to surface molecular forces, thus being linked to surface free energy [8].

Several studies [7,8,10-12] point to the use of organosilanes to produce superhydrophobic and non-stick surfaces. Kehrwald (2009) [8], studied the behavior of the polymeric coating based on fluorosilane and identified that the presence of CFx groups in the structure made the material hydrophobic and oleophobic. Sacilotto (2015) [7] obtained hydrophobic films based on vinyltriethoxysilane silane (VTES) on AISI 204 stainless steel sheets, which helped to protect the metal against corrosion. Cellulose/nanocellulose fibers have been the subject of studies to transform the material into a hydrophobic one, given that they are biodegradable and can be used to separate oil and water in oil spills at sea [10-12].

In more recent studies Jianliang, et al (2022) [13] used organosilanes to modify the seaweed Enteromorpha so that it became hydrophobic and maintained the oleophilic characteristic, being able to absorb oil spills in the ocean. Meanwhile, Usman et al (2020) [14] during a study analyzed the use of organosilanes for the modification of ceramic membranes used in the recovery of oil in waters arising from the extraction of oil and natural gas.

Thus, the present work aims to evaluate the surface alteration of metallic, ceramic and polymeric substrates using different coatings based on organosilanes and fluoropolymers being applied through the immersion method.

Experimental

Materials

Surface modifiers based on organosilanes and fluoropolymers have been used to change adhesion on metallic, polymeric and ceramic substrates. The modifiers Resysil 263 (organosilane), Resysil 902 (organosilane), Resyfluor 2308 (fluoropolymer), Resysil 2003 (fluoropolymer + organosilane) were provided by the company PG Química and the organosilane GPTMS (3-0 n-789-Glycidoxypropyltrimethoxysilane) was purchased from company Sigma-Aldrich (Merk). As a substrate, sandblasted AISI 1020 steel plates, glass and poly(methyl methacrylate) – PMMA, commercial and popular name for acrylic, were used for the deposition of surface modifying agents. The plates used are 70 mm X 50 mm in size. As substances for the adherence and contact angle tests, water and multipurpose apolar lubricating oil from King were used. According to the manufacturer, the oil has the following characteristics: density from 0.850 to 0.860 g/cm^3, kinematic viscosity at 40 ºC from 9 to 11 Cst and main application as a multipurpose lubricant. Composition based on petroleum derivatives.

Methods

In this work, the application method of surface modifiers by immersion was used. However, before application, all plates were cleaned with acetone to avoid possible contaminants. Initially, the GPTMS modifying agent was first hydrolyzed. 96 mL of 48° alcohol in 250 mL beaker was added, then 4 mL of the modifying agent was added. Under stirring, the pH of the solution was adjusted to 4.0 by adding acetic acid. The solution was kept at rest for 24 h [7]. To avoid oxidation of the AISI

1020 steel substrate, the plates were covered with Acrilex primer. Afterwards, the plates of all substrates were immersed in the GPTMS solution and other modifying agents for 2 min and then taken to an oven for 3 hours at 150°C for drying and curing of the modifying agents. The modifiers Resysil 902, Resysil 263, Resyfluor 2308, Resysil 2003 are commercialized ready for use, not being necessary to make any modification of composition for application.

Characterizations

The wettability on a surface can be analyzed through the contact angle formed between the drop of fluid and the surface of the analyzed material, depending on the angle formed it is possible to determine whether the material is hydrophilic/oleophilic or hydrophobic/oleophobic [6,7,11,15]. This characteristic is verified with the contact angle technique, where the characteristics of the deposition of a drop on the surface of the material are observed at times 0 and after 5 min of the application of drops of water and lubricating oil on the plates. The drops were deposited using a dropper, for greater uniformity, and the images were obtained through photos taken at 20 cm from the analyzed sample. Using the Surftens software, the contact angle was analyzed to determine the wettability of the material.

The verification of the adhesion of liquids (water and oil) on the plates was analyzed using the method developed by the authors, in which the plate to be tested is at an angle of 60° with a straight surface. At the top of the plate, a drop of the sample to be tested is placed with the aid of a dropper (the mass varies with the variation in the density of the liquid), and at the lower end of the plate in contact with the surface, the amount of sample collected is collected. it ran over the surface in 5 s and it is checked whether all the sample deposited at the top is contained at the end of the process, as described in Eq. 1. For this test, water and lubricating oil were used as samples. Eq. 2 was used to verify the occurrence of increase or reduction in adhesion compared to plates without coating. Fig 1 presents specifications of the method assembly and the equations used.

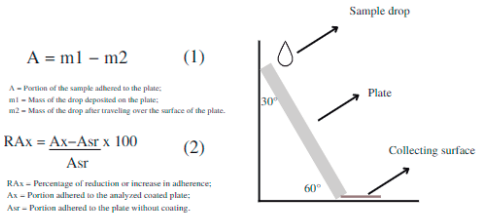

Figure 1 – Illustration of the scheme used for the adherence test. Source: From the Authors, 2022.

Results and Discussion

Fig 2 shows the photographic images and the contact angle using water as a liquid medium. It is observed that all surfaces after coating with the different modifying agents suffered an increase in the contact angle when compared to the uncoated surface. When the angle was greater than 90°, the liquid tends not to wet the surface of the solid, and the material is considered hydrophobic. If the angle is less than 90°, the liquid is considered to wet the solid and the material is considered hydrophilic. If the angle is 0°, there is complete wettability. However, only samples coated with Resysil 902 on glass and acrylic plates, Resysil 263 on acrylic plates and Resyfluor 2308 on metal plates, reached angles greater than 90° and remained above 5 min after drop deposition, configuring hydrophobic surfaces with greater stability. The magnitude of the contact angle is not independent of time, as it can change in seconds or minutes, depending on the liquid used and the nature of the solid.

On the glass plates, only the surface coated with the agent Resysil 902 remained hydrophobic, with a contact angle of 97.1° at t=0 and 91.2° at t=5. On acrylic, two modifying agents deposited generated hydrophobic surfaces, namely Resysil 263, with 92.5° at t=0 and 91.6° at t=5, and also Resysil 902, with 94.7° at t=0 and 94.3° at t=5. For metallic plates, hydrophobicity was achieved with the Resyfluor 2308 coating, where the value of the angle at t=0 was 98.7° and at

t=5 97.6°, these being the highest contact angle values found during rehearsals. Thus, the best modifying agent for water analysis was Resyfluor 2308 on the metal sample.

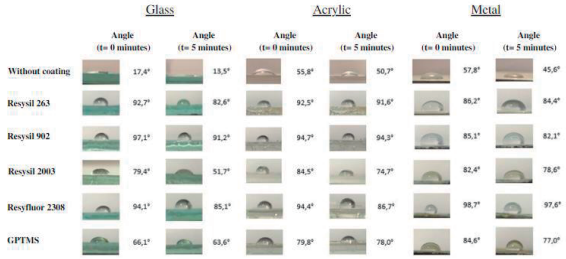

Figure 2 - Photographic images and measurements of the contact angle for the different substrates with and without modification, using water as the means of analysis. Source: From the Authors, 2022.

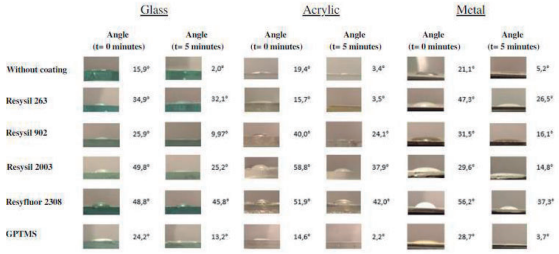

Figure 3 - Photographic images and measurements of the contact angle for the different substrates with and without modification, using oil as the means of analysis. Source: From the Authors, 2022.

The contact angle of the samples tested with lubricating oil increased for the coated surfaces, however the values obtained remained below 90° as can be seen in Fig 3. According to Polak (2010) [16], the term oleophobicity is broader, and no strict definition can be found in the literature, as oils tend to spread over surfaces, therefore, they have a much smaller contact angle than those found with water. A surface with high oleophobicity needs a structure that contains micro and nano-roughness, making production difficult [17].

It is observed that after coating there was an increase in the contact angle for all samples, except for the GPTMS coating which, after 5 min, on the acrylic and AISI 1020 steel plates, had a lower contact angle than the uncoated plate. This result indicates that these coatings present an increase in the oleophobic behavior of the materials.

Tables 1 and 2 present the results for the analysis of water and oil adherence on the surface of the substrates before and after application of the modifying agents. The weight of a drop of water is equivalent to 0.050 g, while that of a drop of lubricating oil weighs 0.016 g, this difference is a result of the difference in the density of liquids. The measurement of adherence used the variation of the initial and final weight of the drop, as previously mentioned.

In the test with water, all the boards tested showed a reduction in the adherence of the liquid to its surface when it was covered by some modifying agent (Table 1). On glass plates there were adhesion reductions of up to 76.9%, on acrylic 94.4% and on metal up to 100%. For glass and acrylic plates, the best coating was Resysil 902, while for metal, the best agent was Resyfluor 2308.

Table 1 – Adherence of water on the plates with and without coating.

Sample	Glass		Acrylic		Metal	
	Adhered portion (g)	Reduction (%)	Adhered portion (g)	Reduction (%)	Adhered portion (g)	Reduction (%)
Without coating	0,013 ± 0,001	-	0,018 ± 0,004	-	0,019 ± 0,002	-
Resysil 263	0,004 ± 0,003	-69,2	0,005 ± 0,003	-72,2	0,001 ± 0,001	-94,7
Resysil 902	0,003 ± 0,005	-76,9	0,001 ± 0,001	-94,4	0,002 ± 0,002	-89,5
Resysil 2003	0,004 ± 0,003	-69,2	0,002 ± 0,003	-88,9	0,006 ± 0,004	-68,4
Resyfluor 2308	0,004 ± 0,004	-69,2	0,002 ± 0,003	-88,9	0	-100
GPTMS	0,004 ± 0,003	-69,2	0,002 ± 0,002	-88,9	0,001 ± 0,001	-94,7

Source: From the Authors, 2022.

Table 2 – Adherence of oil on the plates with and without coating.

Sample	Glass		Acrylic		Metal	
	Adhered portion (g)	Reduction (%)	Adhered portion (g)	Reduction (%)	Adhered portion (g)	Reduction (%)
Without coating	0,003 ± 0,000	-	0,004 ± 0,000	-	0,004 ± 0,001	-
Resysil 263	0,004 ± 0,002	33,3	0,004 ± 0,002	0,0	0,005 ± 0,001	25,0
Resysil 902	0,005 ± 0,002	66,7	0,005 ± 0,001	25,0	0,004 ± 0,001	0,0
Resysil 2003	0,002 ± 0,001	-33,3	0,003 ± 0,001	-25,0	0,006 ± 0,001	50,0
Resyfluor 2308	0,002 ± 0,001	-33,3	0,004 ± 0,001	0,0	0,002 ± 0,001	-50,0
GPTMS	0,003 ± 0,001	0,0	0,003 ± 0,003	-25,0	0,004 ± 0,001	0,0

Source: From the Authors, 2022.

Observing the data in Table 2, on boards where the adhesion of lubricating oil was tested, it is noted that in some cases there was a reduction in adhesion, while in others there was an increase, with increases of up to 66.7% and reductions of up to 50 ,0%. The agents Resysil 2003 and Resyfluor 2308 generated a greater reduction in the adhesion of oil on the glass, in acrylic the improvement occurred with Resysil 2003 and GPTMS and in metal with the agent Resyfluor 2308.

For the metal plates, the modifying agent that resulted in the decrease in the adhesion of both oil and water was Resyfluor 2308, but in the other plates, the agents that caused the decrease in adhesion were different for each of the tested samples.

Conclusions

This study showed the possibility of modifying hydrophobic and oleophobic surfaces through treatment with modifying agents based on organosilanes and fluoropolymers, with results of a contact angle of 98.7° on metallic plates with the agent Resyfluor 2308 for water. When treated with oil, an increase in the oleophobicity of the plates coated with modifying agents was observed, reaching angles greater than those of the uncoated plates, with values of up to 58.8° in the acrylic plates with Resysil 2003. Furthermore, it was possible to demonstrate the relationship between the contact angle, adhesion and surface roughness of the material, proving that, with the increase in roughness, there is an increase in the contact angle and a decrease in adhesion, generating more hydrophobic and repellent surfaces (reduction in adhesion).

References

1. BORGHI, Aparecido. “Design de embalagem: mais que estética, uma estratégia empresarial”, Embalagem marca,2022.
2. BARRETO, Emiliano. “A influência da embalagem de produtos de consumo sobre a tomada de decisão de compra pelo consumidor”, Curitiba, 2008.
3. OLIVEIRA, Kamila R.; MOTTIN, Artur C. “Design de embalagens: Aplicação de superfícies super-hidrofóbicas na redução de resíduos”, CONGRESSO BRASILEIRO DE PESQUISA E DESENVOLVIMENTO EM DESIGN, 2014.
4. RAMANATHAN, Rajajeyaganthan. WEIBEL, Daniel E. “Novel liquid–solid adhesion superhydrophobic surface fabricated using titanium dioxide and trimethoxypropyl silane”, Applied Surface Science, 2012.
5. STRABELLI, Patrícia G. et al. “Influência de variáveis de sinterização na microestrutura de peças de PTFE moldadas por prensagem isostática”, Polímeros, 2014.
6. CARNEIRO, Andreia R. C.; FERREIRA, Fabio A. S.; HOUMARD, Manuel. “Easy functionalization process applied to develop super-hydrophobic and oleophobic properties on ASTM 1200 aluminum surface”, Surface And Interface Analysis, 2018.
7. SACILOTTO, Daiana G. “Obtenção e caracterização de revestimento hidrofóbico utilizando viniltrietoxisilano (VTES) como precursor em solução sol-gel sobre aço inoxidável AISI 204 por dip-coating”, Porto Alegre, 2015.
8. KEHRWALD, André M. et al. “Comportamento hidrofóbico e oleofóbico de revestimento polimérico a base de fluorsilano”, CONGRESSO BRASILEIRO DE POLÍMEROS, 2009.
9. LAZZARI, Lídia K. et al. “A study on adsorption isotherm and kinetics of petroleum by cellulose cryogels”, Cellulose, 2018.
10. ZANINI, Márcia et al. “Producing aerogels from silanized cellulose nanofiber suspension”, Cellulose, 2016.
11. LAZZARI, Lídia K. et al. “Sorption capacity of hydrophobic cellulose cryogels silanized by two different methods”, Cellulose, 2017.
12. ZANINI, Márcia et al. “Obtaining Hydrophobic Aerogels of Unbleached Cellulose Nanofibers of the Species Eucalyptus sp. and Pinus elliottii”, Journal Of Nanomaterials, 2018.
13. JIANLIANG, Xue et al. “Durable hydrophobic Enteromorpha design for controlling oil spills in marine environment prepared by organosilane modification for efficient oil-water separation”, Journal Of Hazardous Materials, 2022.
14. USMAN, Jamilu et al. “Impact of organosilanes modified superhydrophobic-superoleophilic kaolin ceramic membrane on efficiency of oil recovery from produced water”, Journal Of Chemical Technology & Biotechnology, 2020.
15. SINDERSKI, Luís G. Z. “Ângulo de Contato e Rugosidade de Madeiras, uma breve revisão”, Revista Ciência da Madeira, 2020.
16. POLAK, Peter L. “Processamento por plasma de polímeros para Aplicações eletroquímicas”, São Paulo, 2010.
17. ALLEGRO, Clara M. C. S. “Aplicação de revestimentos hidrofóbicos e oleofóbicos obtidos por sol-gel em têxteis”, Coimbra, 2015.

DYNAMIC MECHANICAL CHARACTERISTICS OF RIGID POLYURETHANE FOAMS DERIVED FROM KRAFT LIGNIN

Kelvin T. Barbosa[1]*, Silvia H.F. Da Silva[2], Darci A. Gatto[2], Rafael Beltrame[2], Rafael A. Delucis[2] e Sandro C. Amico[1]

1 - Graduate Program in Mining, Metallurgical and Materials Engineering, Federal University of Rio Grande do Sul (UFRGS), Porto Alegre, Brazil.
kelvintecherabarbosa@gmail.com
2 - Graduate Program in Materials Science and Engineering, Federal University of Pelotas (UFPEL), Pelotas, Brazil.

Abstract - Residues leftover from cellulose and paper production are mostly burned to generate energy, despite having potential to be transformed into high-value products. The purpose of this study was to produce and characterize rigid polyurethane (PU) foams derived from Kraft lignin polyols using different contents of acid catalyst (H_2SO_4). The liquefaction process (polyol production) was carried out using a commercial lignin powder from black liquor. This process followed optimized parameters from a previous study of the group, and the catalyst contents employed were 0%, 3%, and 6% in relation to the amount of lignin. The PU foams rose by free expansion and later subjected to dynamic-mechanical analysis (DMA). The results indicated that the addition of the acid catalyst yielded PU foams with more fine, uniform and solid cell structure.

Keywords: DMA; *Kraft lignin liquefaction; lignin-based polyol; bio-based polyurethane foam.*

Funding: CNPq.

Introduction

The worldwide production of pulp and paper from cellulose generates around 50-60 million tons of lignin per year in the form of a black liquor [1]. Lignin has a highly branched and aromatic structure rich in various reactive functional groups, enabling the production of advanced products through its chemical or thermochemical conversion. However, the majority of black liquor (over 95%) is primarily used as fuel for energy production. Therefore, it is essential to develop efficient strategies for converting lignin into high-value-added products, which can benefit the entire wood production chain.

There have been recent studies on the liquefaction of residual lignin or lignin obtained from the black liquor to synthesize bio-based polyols [2]. In the liquefaction process, the use of an acid catalyst plays a crucial role in facilitating the depolymerization and conversion of the lignin complex structure into smaller molecules that can be further reacted to form polyols [3]. Indeed, the acid catalyst enhances the overall efficiency and yield of the liquefaction process. It can also enable the utilization of lignin for the production of polyurethane foams [4], although this still demands further studies, especially on the effect of the acid content in relation to the other compounds.

To understand the properties of the foam produced from lignin, and its suitability for specific applications, dynamic-mechanical analysis can be used. This technique can provide valuable insight into key properties of these foams including glass transition temperature, storage modulus, loss modulus, and damping properties, which can be used to optimize formulations, tailor the properties, and ensure quality and suitability in various applications.

Thus, the objective of this study is to perform the dynamic-mechanical characterization of polyurethane (PU) foams produced from Kraft lignin polyols obtained from liquefaction using different contents of acid catalyst (sulfuric acid).

Experimental

The liquefaction procedure (production of polyols) was carried out based on a previous study by the group [5] on a Kraft lignin powder, precipitated through the Lignoboost® method from the black liquor of Suzano S/A company. In brief, 120 g of polyethylene glycol (PEG-400), 30 g of PA glycerin used as a solvent, and different contents (0%, 3%, and 6% in relation to the lignin) of sulfuric acid (H_2SO_4), used as a catalyst, were put in a round-bottomed volumetric flask (500 mL). This flask was connected to a condenser and the mixture was magnetically stirred under reflux and heating using a mantle until it reached 160 °C, which took about 1 h. Then, 15 g of Kraft lignin was added and the mixture refluxed for another hour under the same conditions. The resulting polyol was cooled to room temperature (~20 °C) with a water bath.

The rigid PU foams were produced by free expansion. Kraft lignin polyol was preheated to 60 °C and chain extender and surfactant were added to it, which were then mechanically stirred at 1000 rpm for 60 s and left to degas for 2 min. Next, a pre-polymer of 4,4'-diphenylmethane diisocyanate (p-MDI), for an NCO/OH ratio of 1.2 was added along with the catalyst, and manually mixed for further 20 s. Immediately afterwards, the mixture was poured into an open wooden mould, previously lined with brown paper. After complete expansion, the final foams were cured in an oven at 60 °C for 2 h and post-cured at 25 °C for 20 days. The whole procedure after polyol heating was described in a recent study of the research group [6].

The dynamic mechanical analysis (DMA) of the foams was carried out to obtain storage modulus (E'), loss modulus (E''), delta tan (δ) and Cole-Cole curves, using a 2980 equipment (TA Instruments) operating under compression. The analysis was carried out using cylindrical samples (15 mm diameter × 10 mm height) and an inert N_2 atmosphere, with a frequency of 1 Hz, 10% strain, 1 N preload, and heating from -50 °C to 100 °C at a heating rate of 3 °C.min^{-1}.

Results and Discussion

Storage modulus, loss modulus, and tan δ data as a function of the temperature are given in Fig. 1A–C. The main results are also compiled in Table 1. The Log E' curves are similar to previous studies on PU foams obtained using single cantilever or compression [7] modes. There are three distinct stages in the E' curves, a glassy region followed by a glass transition region and then a rubbery region. Below the glassy region (-50 to -45 °C), there is a glass transition region (-45 to 0 °C) where the storage modulus gradually decreases, while in the range of (0-100 °C) presents a rubbery phase is almost constant. The PU components are highly immobile and tightly packed in the glassy region (frozen phase), resulting in a higher storage modulus. As the temperature increases, their mobility increases and the packed configuration is lost, decreasing the storage modulus [8,9].

The foams prepared with acid catalyst (LPF3% and LPF6%) exhibited higher levels of storage modulus (E') compared to the foam without catalyst (LPF0%) in the temperature range from -40 °C to -20 °C. The acid-catalyzed liquefaction process facilitates the breakdown of lignin into smaller molecules potentially resulting in polyols with higher molecular weights and/or enhanced crosslinking, leading to a stiffer foam [10]. However, the LPF0% foam showed a higher storage modulus than the catalysed foams due to unreacted components which may contribute to its higher stiffness. The catalysed foams (LPF3% and LPF6%) may have undergone more extensive depolymerization reactions due to the use of acid, resulting in inferior storage modulus.

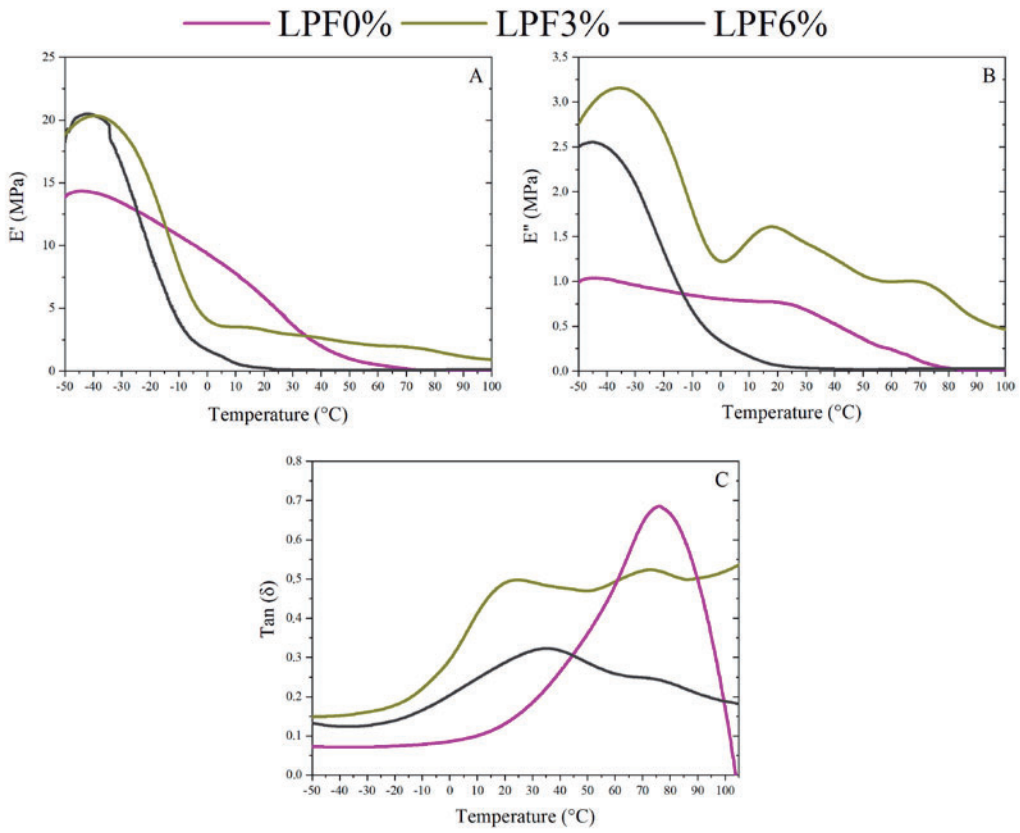

Figure 1 - DMA curves for the studied PU foams: storage modulus (A), loss modulus (B), tan δ (C).

Table 1 - Values of storage modulus (E') related to the different regions of behavior.

	Glassy region range (-50/-45 °C) [MPa]	Glass transition region range (45/0 °C) [MPa]	Rubbery region range (70/100 °C) [MPa]
LPF0%	14.30	9.37	0.20
LPF3%	19.90	4.10	1.90
LPF6%	20.41	1.80	0.18

In all cases, there was a prominent peak in the storage modulus curve between -50 °C and 20 °C, indicating a significant (glass) transition or relaxation process in this temperature range [11]. The specific effects of the acid catalyst on these transitions still require further investigation and analysis.

Regarding the loss modulus (E''), LPF3% stood out, displaying higher values than the other foams throughout the entire range (-50 °C to 100 °C). This can be attributed to the formation of polyols with a higher degree of branching or a greater number of reactive functional groups. These characteristics contribute to increased intermolecular interactions and enhanced energy dissipation in the foam, resulting in higher loss modulus values. However, LPF6% only surpassed LPF0% in the -50 °C to -10 °C range, perhaps because the acid catalyst at high concentration (6%) led to excessive crosslinking or increased rigidity of the foam, limiting its ability to dissipate energy and resulting in lower loss modulus values compared to LPF3%. Similar to storage modulus, the loss modulus curve of the foams produced with acid-catalyzed polyols exhibited a prominent peak within -50 °C and 20 °C. In contrast, the foam without catalyst showed nearly constant values in this range. This suggests that the LPF0% foam may have a different structural arrangement or a lower degree of crosslinking. As for the tan delta results, LPF3% and LPF6% foams exhibited two prominent peaks around 10-20 °C and 70-80 °C, while LPF0% showed a single large peak at 70-80

°C. These peaks indicate temperature regions where significant energy dissipation or relaxation processes occur, as explained before. This again suggests that the liquefaction in the absence of the acid catalyst may result in a different foam structure with a distinct relaxation behavior, perhaps a lower degree of crosslinking or a different arrangement of polymer chains, leading to a single dominant relaxation process.

Conclusions

The use of an acid catalyst during the liquefaction process of lignin influenced the dynamic-mechanical behavior of the resulting PU foams. The acid catalyst enhanced the storage modulus and loss modulus within certain temperature ranges, suggesting changes in the foam mechanical behavior. The observed peaks in storage modulus, loss modulus, and tan δ curves suggest specific temperature regions structural transitions or relaxation processes occur. These findings provide insight for optimizing the formulation and performance of lignin-based polyurethane foams.

Acknowledgements

We would like to thank CNPq for the financial support.

References

[1] M. Brodin; M. Vallejos; M.T. Opedal; M.C. Area; G. Chinga-Carrasco J. Clean. Prod. 2017, 162, 646–664. https://doi.org/10.1016/j.jclepro.2017.05.209.
[2] S. Zhu; K. Chen; J. Xu; J. Li; L. Mo , RSC Adv. 2018, 8, 15754–15761. https://doi.org/10.1039/C8RA01089G.
[3] I. Singh; S.K. Samal; S. Mohanty; S.K. Nayak Eur. J. Lipid Sci. Technol. 2020, 122 . https://doi.org/10.1002/ejlt.201900225.
[4] X. Zhang; Y. Kim; I. Elsayed; M. Taylor; T.L. Eberhardt; E.B. Hassan; R. Shmulsky Ind. Crops Prod. 2019, 141. https://doi.org/10.1016/j.indcrop.2019.111797.
[5] S.H.F. Silva; P.S.B. Dos Santos; D.A. Gatto; M.A. Andres; I. Egüés; J. Renew. Mater. 2019 7, 527–534. https://doi.org/10.32604/jrm.2019.04291.
[6] R.D.A. Delucis; W.L.E. Magalhães; C.L. Petzhold; S.C. Amico; W. Luiz; E. Magalhões Polym. Compos. 2018, 39, E1770–E1777. https://doi.org/10.1002/pc.24784.
[7] L. Chang; Y.U. Xue; F. Hsieh , J. Appl. Polym. Sci. 2001, 81, 2027–2035.
[8] A. Albertin; I. Jos; D. Araújo; A. Clara; M. Miranda; A. Manes; S. Campos , Mater. Today Commun. 2022, 32, https://doi.org/10.1016/j.mtcomm.2022.104021.
[9] M. Jawaid; H.P.S.A. Khalil; O.S. AlattasCompos. Part A. 2012, 43, 288–293. https://doi.org/10.1016/j.compositesa.2011.11.001.
[10] Z. Wu; L. Hu; Y. Jiang; X. Wang; J. Xu; Q. Wang; S. Jiang Biomass Convers. Biorefinery. 2023, 13,519–539. https://doi.org/10.1007/s13399-020-00976-8.
[11] R. Mohammadpour; G. Mir Mohamad Sadeghi J. Polym. Res. 2020, 27. https://doi.org/10.1007/s10965-020-02334-8.

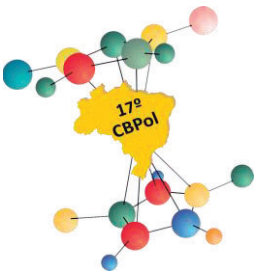

EFFECT OF THE CROSSLINK CONDITIONS ON THE THERMAL PROPERTIES OF A POLY(VINYL ALCOHOL)-BASED MEMBRANE

Camila S. Raota[1]*, Janaina da Silva Crespo[1], Camila Baldasso[2], Marcelo Giovanela[1]*

[1] Postgraduation Program in Materials Science and Engineering (PPGMAT), University of Caxias do Sul (UCS), Brazil
[2] Postgraduation Program in Process Engineering and Technologies (PGEPROTEC), University of Caxias do Sul (UCS), Brazil
** Corresponding authors: csraota@ucs.br; mgiovan1@ucs.br*

Abstract – Membrane technology uses poly(vinyl alcohol) (PVA) due to its sustainable reputation, even though its hydrophilicity is challenging for water treatment. The control of PVA solubility occurs *via* crosslink through an esterification reaction, usually accelerated by heat treatment. Thus, crosslink parameters are relevant factors in membrane properties. In this sense, this work aimed to investigate the effect of time and temperature on the crosslink of PVA membranes with citric acid. For this, an experimental design determined the factors' combinations, and the crosslinked membranes were then characterized using differential scanning calorimetry. The results showed the crosslink conditions influenced the crystallinity and temperatures of glass transition and fusion, even without statistical significance. Moreover, the crosslink reduced chain mobility and time was the experimental parameter that most impacted the membrane crystallinity. Overall, the study indicated significant aspects of the crosslinking effect on PVA properties and conveyed contributions for further investigation.
Keywords: *PVA, citric acid; esterification; differential scanning calorimetry; crystallinity.*
Fundings: This work was supported by the *Coordenação de Aperfeiçoamento de Pessoal de Nível Superior* (CAPES Brazil – Finance Code 001) through the scholarship PROEX.

Introduction

Poly(vinyl alcohol) (PVA) is a synthetic polymer obtained from the hydrolysis of poly(vinyl acetate), with application in food packaging [4,5], membrane technology [6,7], and biomedical [8-10] fields. As a membrane, PVA has excellent chemical resistance and good mechanical and thermal properties, renowned for its easy processing, flexibility, transparency, and anti-fouling characteristics [1, 2]. However, the intense water solubility limits its application in aqueous media, requiring hydrophilicity control through crosslink methods [3, 4].

Crosslink is an established method to create a polymer network by linking chains [5, 6]. In the case of PVA, the reaction occurs on the hydroxyl groups from the polymer backbone, thus consuming them and reducing the interaction sites that promote hydrophilicity [6, 7]. Additionally, the mobility restrictions imposed interfere with the crystallinity and swelling, besides mechanical, chemical, and thermal properties [2, 6, 8]. The control of crosslink parameters can tune the impact on PVA properties [6, 9], finding a balance between reducing the water solubility without losing flexibility, selectivity, and permeate production [2, 4, 10]. Crosslink reactions using carboxyl acids (especially citric acid) are preferred since they are considered green crosslinkers due to the properties of non-toxicity, biodegradability, and availability [6]. The reaction occurs through esterification, in which the carboxyl groups react with PVA hydroxyl groups under temperature [6]. Thus, the comprehension of crosslink parameters on the thermal properties can contribute to membrane optimization for specific separation processes.

In this sense, the present work aimed to evaluate the effect of time and temperature on the thermal properties of a PVA-based membrane crosslinked with citric acid. For this purpose, the membranes were crosslinked accordingly to an experimental design and characterized using differential scanning calorimetry (DSC), and the crystallinity (X_c) and glass transition (T_g) and fusion (T_f) temperatures were statistically analyzed to evaluate which factors had statistical significance on the membrane properties.

Experimental

Reagents

Poly(vinyl alcohol) (PVA, hydrolysis > 99%, MW 85,000–124,000 kDa) was achieved from Sigma-Aldrich – Brazil, anhydrous citric acid (2-hydroxypropane-1,2,3-tricarboxylic acid, ≥ 99.5%) from Cinética Ltda – Brazil, glycerol (propane-1,2,3-triol, ≥ 99.5%) from Vetec Química Fina Ltda – Brazil, and silver nitrate (≥99.0%) from Merck – Germany.

Preparation of the poly(vinyl alcohol) membranes

For the membranes' preparation, 0.32 g of anhydrous citric acid, and 1.6 g of glycerol were incorporated into 32 mL of PVA 10% m/v (pre-dissolved in distilled water at 80°C for 24 h). After mixing for 30 min at 50 °C, 8 mL of silver nanoparticles (AgNPs), green synthesized following the procedure published elsewhere [11]) was incorporated to this solution. The membrane composition was optimized in preliminary experiments. After bubbles removal (ultrasonic bath for 30 min), the solution was spread on a glass sheet with a glass blade producing a wet film of ~1.0 mm. The membrane dried at room temperature (23±2 °C) for ~24 h, and then the crosslink occurred in an oven (model AGSEDT, DeLeo, Brazil) following the conditions of time and temperature determined by the experimental design.

Experimental design of experiments for the membrane crosslink

The time and temperature of crosslink are relevant for the esterification reaction of PVA and citric acid, and its combined effect is worthy of investigation [12]. For this, a central composite rotational design (CCRD) of experiments used time and temperature as factors. The initial condition of the esterification reaction (called centre point, '0,0') was carried out at 60 min and 130 °C (pre-optimized by a 2^3 experimental design in previous works [13]). Higher and lower axial points corresponded to 30 and 90 min for time and 120 and 140 °C for temperature, plus four points at a distance $\alpha = \sqrt{2}$ from the centre for quadratic effects analysis [14]. The thermal data collected from DSC thermograms were analyzed statistically using *Statistica 10* software [14]. Table 1 shows the design of experiments and the coding for each membrane ("M" + "time"_"temperature").

Table 1 Design of experiments using the time (factor x_1) and temperature (factor x_2) for the crosslink of a PVA-based membrane.

x_1	x_2	Time (min)	Temperature (°C)	Membrane
+1	+1	90	140	M90_140
+1	–1	90	120	M90_120
–1	+1	30	140	M30_140
–1	–1	30	120	M30_120
–√2	0	18	130	M18_130
+√2	0	102	130	M102_130
0	–√2	60	116	M60_116
0	+√2	60	144	M60_144
0	0	60	130	M60_130

Differential scanning calorimetry analysis

DSC analyses were performed in a DSC-60 (Shimadzu – Japan) using ~10 mg of each sample in aluminum pans, with a heating rate of 10 °C min^{-1} under a nitrogen atmosphere (50 mL min^{-1}), from

room temperature (~23±2 °C) until 225 °C. Thermal events were obtained from the results of the first run to avoid interfering with the effect of the crosslinking temperature on the esterification reaction. Crystallinity (X_c, %) was calculated using Eq. 1 [15], where ΔH_f is the sample fusion enthalpy (J g^{-1}) normalized by PVA content in the membrane (95.9%), and $\Delta H_{f,\ 100\%}$ is the theoretical fusion enthalpy of PVA hypothetically 100 % crystalline (162 J g^{-1} [16]).

$$X_c = (\Delta H_f / \Delta H_{f,\ 100\%}) \cdot 100 \quad (1)$$

Results and Discussion

Thermal characterization using differential scanning calorimetry

The results of the thermal characterization of the membranes crosslinked accordingly to the experimental design are presented in Figure 1 and Table 2. T_g varied from 42.1 to 62.6 °C, while for pure PVA these values were between 74.0–86.0 °C [17, 18]. The overall reduction of T_g on the crosslinked membranes compared to pure PVA can be associated with the plasticizing effect of glycerol on unreacted PVA, which facilitates the chain mobility by reducing the cohesive attraction forces [19, 20]. Among the membranes, the higher temperatures tended to reduce T_g due to the inhibited chain movement caused by crosslinks [19]; a similar effect was also observed in mild temperatures combined with extended time. It was not possible to differentiate the fusion of crystalline phase and crosslinked regions of the membrane [21]; thus, T_f and ΔH_f refer to both membrane components. Nataraj *et al*. (2020) [22] attributed the increase in molecular weight of crosslinked PVA to the requirement of more thermal energy to melt, reflecting on more elevated T_f. However, the diverse crosslink conditions had not a relevant impact on the fusion temperature, varying from 201.7 °C (M18_130) to 215.9 °C (M90_120). In contrast, mild temperatures for an extended time and higher crosslink temperatures manifested increased crystallinity. Shi *et al*. (2015) reported a similar thermal behavior, but measured the crystallinity with X-ray diffractometry [23], and Zeng *et al*. (2023) related the reduction in crystallinity with high crosslink degree due to the limitation on available hydroxyl groups for hydrogen bondings [3]. In addition, the higher crystallinity of the membranes (in comparison with pure PVA, 35% [17]) can be related to the presence of AgNPs that act as points of nucleation for the crystalline regions [24].

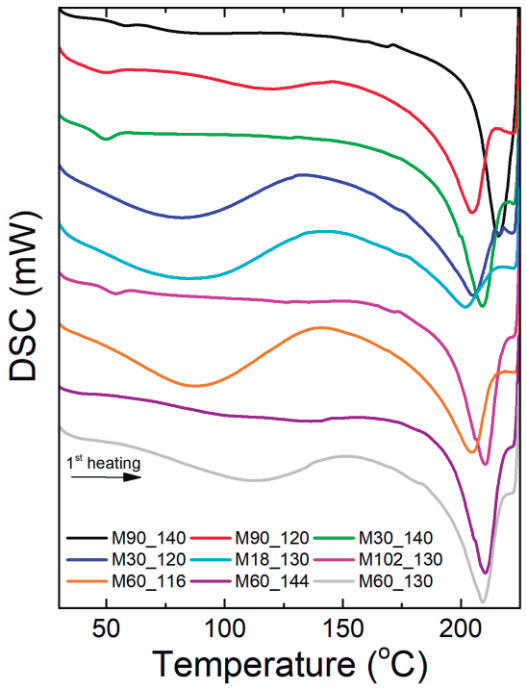

Figure 1 DSC thermograms of the membranes crosslinked according to the experimental design. Conditions: 10 mg of sample, nitrogen atmosphere (50 mL min^{-1}), heating rate of 10 °C min^{-1} from room temperature (23±2 °C) until 225 °C.

Table 2 Thermal events of the crosslinked membranes obtained from DSC thermograms: T_g = temperature of glass transition, T_f = temperature of fusion, ΔH_f = variation of fusion enthalpy, and X_c = crystallinity.

Membrane	T_g (°C)	T_f (°C)	ΔH_f (J g^{-1})	X_c (%)
M90_140	42.1	204.4	75.5	46.4
M90_120	53.7	215.9	83.9	51.6
M30_140	44.6	208.9	83.9	51.6
M30_120	45.8	205.2	80.7	49.7
M18_130	46.2	201.7	56.4	34.7
M102_130	49.6	210.4	81.5	50.1
M60_116	45.1	204.4	75.4	46.3
M60_144	62.6	210.3	75.3	46.3
M60_130	60.9	209.2	75.2	46.2

Statistical analyses of the thermal data from the crosslinked membranes

Surprisingly, none of the factors or combination of factors had a significant effect on the thermal behavior of the crosslinked membranes, considering a 95% confidence interval (p = 0.05) for the ANOVA analysis of variance. Specifically, the variations of factors (time and temperature) were not enough to produce modification statistically relevant to the thermal characteristics of the crosslinked membranes. Nonetheless, it is possible to observe some trends when the surface responses are analyzed (Figure 2).

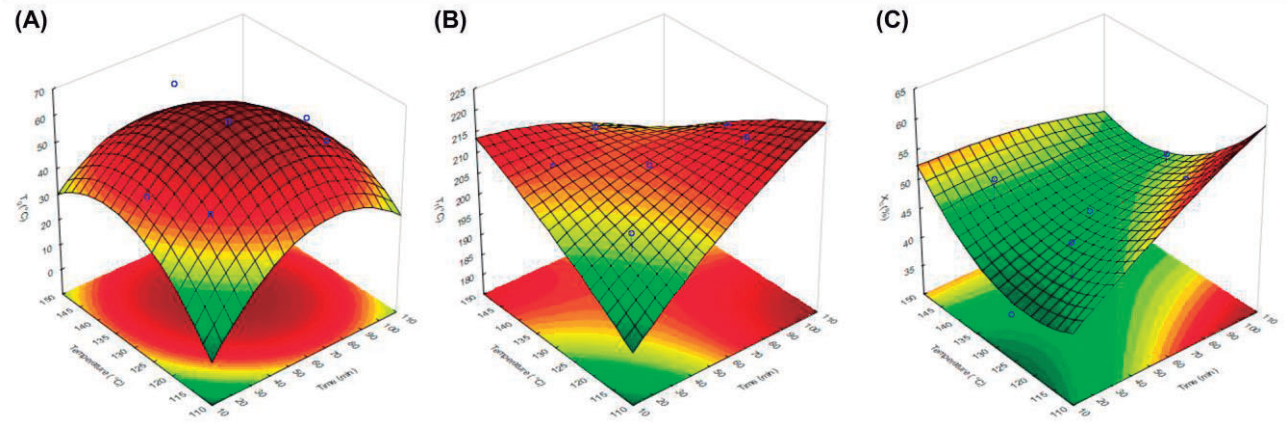

Figure 2 Response surfaces obtained using the software *Statistica 10* for the effect of time and temperature of crosslink on the thermal characteristic of the membranes: **(A)** temperature of glass transition (T_g), **(B)** temperature of fusion (T_f), and **(C)** crystallinity (X_c).

Figure 2A shows that mild temperatures during medium crosslinking times affected the polymer mobility, which can be associated with more crosslinks among PVA chains [19]. Conversely, T_f increased more intensively when the membrane was crosslinked for a longer time (Figure 2B), meaning that more energy was required to melt organized regions of the membrane, crosslinked or crystallized. This behavior was observed in Figure 2C, pointing out the membrane had more time to accommodate unreacted chains and form crystalline regions. A similar tendency was observed by Miraftab *et al*. (2015), in which PVA thermally treated increased the crystallinity from 46 to 54 % when the crosslink time changed from 30 min to 8 h [25]. Overall, it is visible that the time and temperature of the esterification reaction have varied effects on T_g, T_f, and X_c, enabling the tuning of PVA thermal properties through its crosslink.

Conclusions

In general, DSC results and the analysis using surface responses graphs showed that the crosslink influenced the polymer chain mobility and, consequently, the membrane crystallinity. The factors

analyzed (time and temperature of crosslink) were not statistically relevant for the thermal events, even though some trends could be observed. The time seemed to have influenced the membrane crystallinity by providing time for the chain's accommodation, which also affected membrane fusion. The T_g, on the other hand, suffered the most impact on mild conditions of time and temperature, which can be attributed to better esterification and consequently limiting PVA chain mobility. In conclusion, the data set contributed to understanding the crosslink conditions of PVA with citric acid and pointed topics for further investigation.

References

[1] K. Razmgar, M. Nasiraee, Polymer Engineering & Science, 62 (2022) 25-43. 10.1002/pen.25846
[2] A.A. Sapalidis, Symmetry, 12 (2020) 960. 10.3390/sym12060960
[3] H. Zeng, F. Sun, J. Zhang, Y. Wang, S. Yang, D. Xing, Journal of Membrane Science, 675 (2023) 121548. 10.1016/j.memsci.2023.121548
[4] A. Michele, P. Paschkowski, C. Hänel, G.E.M. Tovar, T. Schiestel, A. Southan, Journal of Applied Polymer Science, 139 (2022) 51606. 10.1002/app.51606
[5] A.K. Sonker, K. Rathore, R.K. Nagarale, V. Verma, Journal of Polymers and the Environment, 26 (2018) 1782-1794. 10.1007/s10924-017-1077-3
[6] L. Gautam, S.G. Warkar, S.I. Ahmad, R. Kant, M. Jain, Polymer Engineering & Science, 62 (2022) 225-246. 10.1002/pen.25849
[7] F.C. do Nascimento, L.C.V. de Aguiar, L.A.T. Costa, M.T. Fernandes, R.J. Marassi, A.d.S. Gomes, J.A. de Castro, Polymer Bulletin, 78 (2021) 917-929. doi.org/10.1007/s00289-020-03142-2
[8] E. Rynkowska, K. Fatyeyeva, S. Marais, J. Kujawa, W. Kujawski, Polymers, 11 (2019) 1799. 10.3390/polym11111799
[9] B. Bolto, T. Tran, M. Hoang, Z. Xie, Progress in Polymer Science, 34 (2009) 969-981. 10.1016/j.progpolymsci.2009.05.003
[10] R.R. Choudhury, J.M. Gohil, K. Dutta, Polymers for Advanced Technologies, 32 (2021) 4175-4203. 10.1002/pat.5431
[11] C.S. Raota, A.F. Cerbaro, M. Salvador, A.P.L. Delamare, S. Echeverrigaray, J. da Silva Crespo, T.B. da Silva, M. Giovanela, Journal of Environmental Chemical Engineering, 7 (2019) 103383. 10.1016/j.jece.2019.103383
[12] S. Sau, S. Pandit, S. Kundu, Surfaces and Interfaces, 25 (2021) 101198. 10.1016/j.surfin.2021.101198
[13] J.Z. Merck, C.S. Raota, J. Duarte, C. Baldasso, J.d.S. Crespo, M. Giovanela, Revista Eletrônica em Gestão, Educação e Tecnologia Ambiental, 24 (2020) e5. 10.5902/2236117062660
[14] D.C. Montgomery, Design and analysis of experiments, 8 ed., John Wiley & Sons, 2013.
[15] S.V. Canevarolo Júnior, Ciência dos polímeros: um texto básico para tecnólogos e engenheiros, Artiiber, São Paulo, Brasil, 2006.
[16] C. Birck, S. Degoutin, N. Tabary, V. Miri, M. Bacquet, Express Polym. Lett., 8 (2014) 941-952. 10.3144/expresspolymlett.2014.95
[17] W. Yang, X. He, F. Luzi, W. Dong, T. Zheng, J.M. Kenny, D. Puglia, P. Ma, International Journal of Biological Macromolecules, 161 (2020) 617-626. 10.1016/j.ijbiomac.2020.06.082
[18] A. Fattoum, M. Arous, R. Pedicini, A. Carbone, C. Charnay, Polymer Science Series A, 57 (2015) 321-329. 10.1134/S0965545X15030049
[19] R. Shi, J. Bi, Z. Zhang, A. Zhu, D. Chen, X. Zhou, L. Zhang, W. Tian, Carbohydrate Polymers, 74 (2008) 763-770. 10.1016/j.carbpol.2008.04.045
[20] P. Mandal, K. Stokes, G. Hernández, D. Brandell, J. Mindemark, ACS Applied Energy Materials, 4 (2021) 3008-3016. 10.1021/acsaem.0c02051
[21] L. Wen, Y. Liang, Z. Lin, D. Xie, Z. Zheng, C. Xu, B. Lin, Polymer, 230 (2021) 124048. 10.1016/j.polymer.2021.124048
[22] D. Nataraj, R. Reddy, N. Reddy, European Polymer Journal, 124 (2020) 109484. 10.1016/j.eurpolymj.2020.109484
[23] J.J. Shi, E.L. Yang, Journal of Nano Research, 32 (2015) 32-42. 10.4028/www.scientific.net/JNanoR.32.32
[24] M. Sabzi, M.J. Afshari, M. Babaahmadi, N. Shafagh, Colloids and Surfaces B: Biointerfaces, 188 (2020) 110757. 10.1016/j.colsurfb.2019.110757
[25] M. Miraftab, A.N. Saifullah, A. Çay, Journal of Materials Science, 50 (2015) 1943-1957. 10.1007/s10853-014-8759-1

EFFECT OF YERBA MATE EXTRACT AND MALIC ACID ON THE PHYSICAL PROPERTIES OF POTATO STARCH FILMS

Magali Canton Casagranda[1]*, Renan Borges da Silva[1] and Ruth Marlene Campomanes Santana[1]

1 - Department of Materials Engineering, Federal University of Rio Grande do Sul (UFRGS), Porto Alegre, RS, Brazil
magalicanton@gmail.com

Abstract - Yerba mate extract at different concentrations (1%, 10% and 20%) was incorporated into a potato starch-based matrix. In order to enhance the barrier properties of the films, malic acid was added as a comparative. The samples were evaluated for moisture absorption parameters in saturated solutions of sodium chloride (75%) and potassium sulfate (98%), revealing a decrease in the moisture absorption rate and water content in the films containing malic acid. The addition of yerba mate extract also seemed to improve the barrier properties of the starch films, as well as increase their contact angle, indicating a decrease in hydrophilicity.
Keywords: *Starch films; potato starch; yerba mate; malic acid; moisture absorption; wettability*

Introduction

The growing concern for the environment preservation has driven a great interest in replacing synthetic polymers with biodegradable materials. In this sense, starch has become an interesting alternative for the polymeric films production, due to its high availability, low cost, renewability and edible characteristics [1]. However, the high solubility of starch in water, important for its biodegradability, leads to insufficient barrier properties [2]. Polycarboxylic acids, such as malic acid, are used as additives to crosslink the starch matrix, aiming to improve its stability against water permeability [3].

The incorporation of extract of yerba mate (*Ilex paraguariensis*), a plant of great importance to the economy of the southern states of Brazil, was studied as a modifier of the polymeric matrix. The average consumption of processed yerba mate in Rio Grande do Sul state is around 70,000 tons per year and its waste has not found viable alternatives for reuse yet [4-5].

Therefore, this work proposes to study the incorporation of yerba mate extract in potato starch films, as well as to evaluate the malic acid addition in order to improve its physical properties.

Experimental

Materials

Potato starch was supplied by Federal Institute of Rio Grande do Sul (IFRS). Glycerol P.A./ACS (NEON) was used as plasticizer and malic acid (DL) P.A. (Êxodo Científica) was used as crosslinking agent. Yerba mate (*Ilex paraguariensis*) extract was simulated using commercial yerba mate purchased at a local market in Porto Alegre, Brazil.

Preparation of the yerba mate extract

The yerba mate extract was prepared by infusing 3 g of sifted yerba mate in 100 g of distilled water at an initial temperature of 80 °C, under agitation [6-7]. After 5 minutes, the liquid was filtered and cooled to room temperature.

Preparation of the potato starch films

The polymeric matrix was developed by mixing 5 g of potato starch (PS) in glycerol (1 g) and distilled water (94 g). For samples containing yerba mate extract (YM), a fraction of distilled water was replaced by the desired concentration of extract (1 g, 10 g and 20 g). The systems were homogenized under constant agitation at 100 °C until complete starch gelatinization. Subsequently, about 30 g of each filmogenic solution was poured into individual polymeric plates. After casting, the solutions were oven-dried at 30 °C for ~24 h under ventilation in order to form polymeric films. The same method was followed to prepare samples containing 0.5% malic acid (MA) (wt/vol), with a proportional decrease in the distilled water fraction. The samples produced are described in Table 1.

Table 1 – Composition of potato starch (PS) films with yerba mate extract (YM), with and without malic acid (MA).

Film specimen	Composition
PS	100% potato starch
PS1YM	Potato starch + 1% yerba mate extract
PS10YM	Potato starch + 10% yerba mate extract
PS20YM	Potato starch + 20% yerba mate extract
MA	100% potato starch + 0.5% malic acid
MA1YM	Potato starch + 1% yerba mate extract + 0.5% malic acid
MA10YM	Potato starch + 10% yerba mate extract + 0.5% malic acid
MA20YM	Potato starch + 20% yerba mate extract + 0.5% malic acid

Characterization

The moisture absorption of the films was evaluated by exposing five samples of each formulation to sodium chloride and potassium sulfate saturated solutions in order to simulate environments with 75% and 98% relative humidities, respectively. The solutions were prepared based on the E 104-02 standard and the film specimens were weighted as a function of time. The data obtained was fitted according to a mathematical model suggested by Peleg [8] (Eq. 1).

$$M(t) = M_0 + (t/(k_1 + k_2 t)) \quad (1)$$

Where M(t) is the moisture at the time t (h), M_0 is the initial moisture content, k_1 is the rate constant of Peleg [h/(g water/g solids)] and k_2 is the Peleg capacity constant (g solids/g water).

The surface wettability was determined according to ASTM D 7334-08 standard, considering the contact angle formed between a droplet of water and the films surface. The angles were measured after 3 s and 180 s and an average of six measurements for each sample was considered. The contact angle was determined by *Surftens* software.

Results and Discussion

Due to their hydrophilic nature, starch-based films tend to absorb high amounts of water under elevated relative humidity (RH) conditions [9]. Therefore, the moisture absorption kinetics of the film specimens were studied under 75% RH (sodium chloride solution) and 98% RH (potassium sulfate solution). The measured data was mathematically fitted to the Peleg's equation (Eq. 1) to obtain information about the water interaction with the film components. The Peleg's parameters are shown in Table 2.

As k_1 is inversely proportional to mass transfer, it can be seen that the films containing malic acid tend to absorb moisture more slowly, even in a saturated environment at 98% RH. Whereas the parameter k_2, which is inversely proportional to the amount of absorbed moisture, suggests that the

reference specimen, PS, absorbed overall more water and also more rapidly. At a relative humidity of 75%, films with malic acid showed higher values of k_1 and k_2, demonstrating an increased stability against water permeability. Values of r^2 close to 1 indicate that the mathematical model was reliable to predict the moisture content of the films.

Table 2 – Peleg constants (k_1 and k_2) related to the absorption kinetics of films.

Film specimen	NaCl (75%)			K_2SO_4 (98%)		
	k_1	k_2	r^2	k_1	k_2	r^2
PS	0,0129	0,0136	0,9939	0,0214	0,0141	0,9994
PS1YM	0,0193	0,0257	0,9961	0,0261	0,0148	0,9974
PS10YM	0,0163	0,0222	0,9955	0,0180	0,0156	0,9999
PS20YM	0,0233	0,0186	0,9997	0,0239	0,0133	0,9996
MA	0,0288	0,0220	0,9931	0,0273	0,0145	0,9999
MA1YM	0,0330	0,0379	0,9978	0,0369	0,0140	1,0000
MA10YM	0,0407	0,0344	0,9979	0,0345	0,0116	1,0000
MA20YM	0,0255	0,0334	0,9972	0,0282	0,0149	0,9938

Fig. 1 represents the percentage of moisture absorption in starch-based films with increasing levels of yerba mate extract in their formulation, with and without malic acid as an additive. Initially, a high absorption rate is observed; however, this tendency slows down in subsequent measurements.

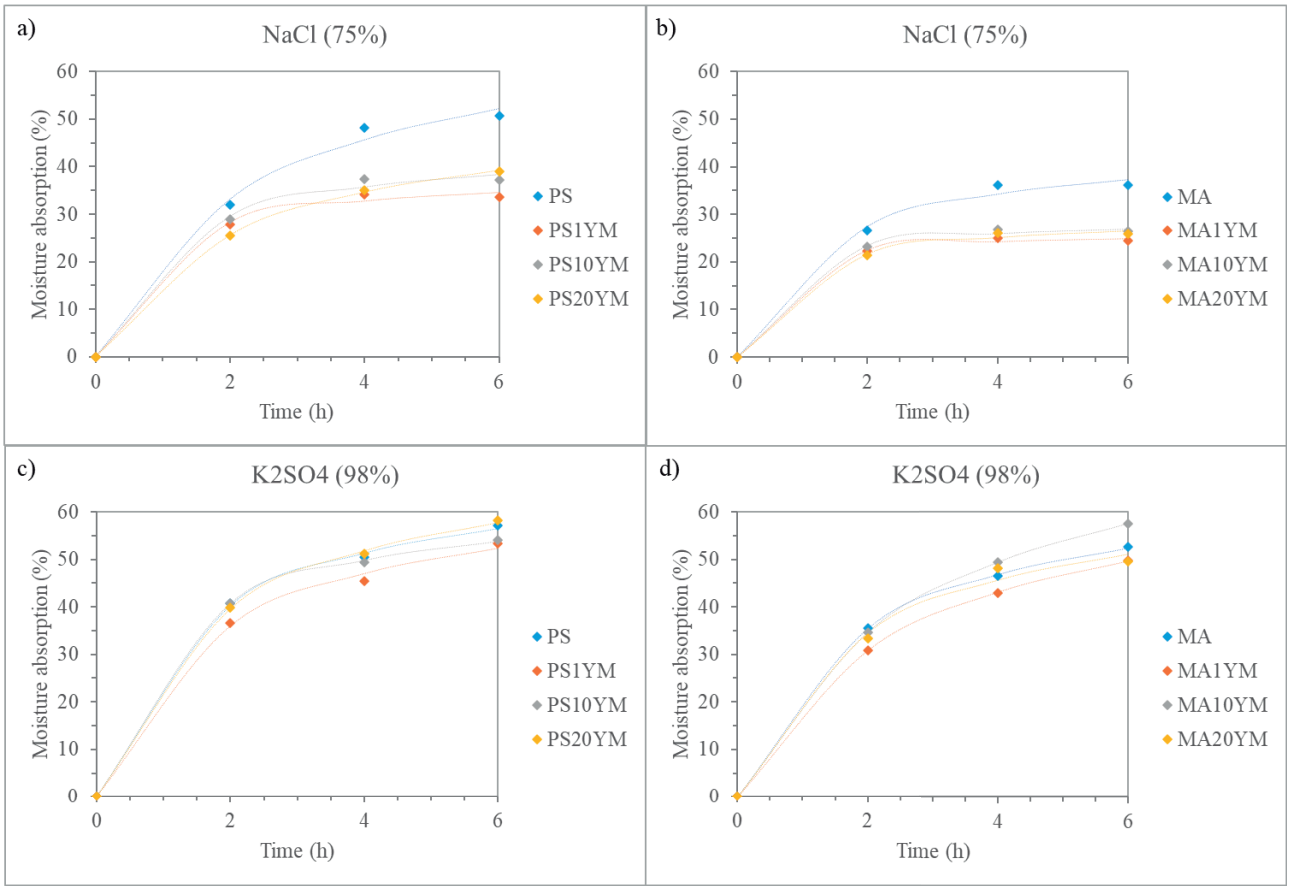

Figure 1 – Moisture kinetics related to exposure time in (a) 75% RH, films without malic acid; (b) 75% RH, films with malic acid; (c) 98% RH, films without malic acid; (d) 98% RH, films with malic acid. Lines represent the Peleg's model.

The comparison between the curves shows a significant increase in moisture absorption in specimens exposed to 98% RH (Fig. 1-c and Fig. 1-d). Over the period of 6 hours, an increase of more than 50% of their initial mass was seen. Under these conditions, no considerable differences were observed in the moisture content of different formulations. In the same way, the constant related to water absorption capacity (k_2) also showed similar values for all compositions, which was lower than those found in the 75% RH environment (Table 2).

However, for 75% RH (Fig. 1-a and Fig. 1-b), the addition of malic acid significantly decreased the moisture absorption capacity of the films, as shown in Fig. 1-b and predicted by Table 2. This is an expected result, as the crosslinks from malic acid are capable of interconnecting starch molecules through covalent bonding, increasing their molecular weight and improving their physical properties [3, 10-11].

It is important to highlight that the incorporation of yerba mate extract also appeared to contribute to lower moisture content values, as can be seen in Fig. 1-a and Fig 1-b. In this case, the increase in extract concentration (1-20%) did not seem to influence this behavior, indicating that a concentration of 1% of the extract was already sufficient to modify the barrier properties of the starch matrix. Yerba mate contains a high content of phenolic compounds, which are miscible with the amylose in potato starch, enabling the formation of hydrogen bonds between starch and water. The covalent interactions between polysaccharides and phenolic compounds can limit the availability of hydrogen groups to form hydrophilic bonds with water, leading to a decrease in the films' affinity for moisture [6].

To evaluate the hydrophilicity of the material, contact angle measurements were performed between a water droplet and the surface of each system. Table 3 shows the variations in the measured contact angle for each formulation. For all evaluated samples, the contact angles reached their maximum values at the beginning of the test (3 s) and decreased with increasing time (180 s). In particular, the specimens containing malic acid exhibited a higher contact angle kinetics (CA) compared to those without the additive.

Table 3 – Contact angle kinetics for potato starch (PS) films with yerba mate extract (YM), with and without malic acid (MA), measured after 3 s and 180 s of contact.

Film specimen	3 s	180 s	ΔCA
PS	65,80° ± 2,46	57,56° ± 4,02	8,24°
PS1YM	62,67° ± 0,89	53,78° ± 2,02	8,89°
PS10YM	74,72° ± 2,10	68,67° ± 3,99	6,05°
PS20YM	76,33° ± 1,45	69,10° ± 1,19	7,23°
MA	45,69° ± 0,75	36,50° ± 1,71	9,19°
MA1YM	44,00° ± 1,49	34,68° ± 3,65	9,32°
MA10YM	54,97° ± 2,35	38,27° ± 2,02	16,70°
MA20YM	67,74° ± 2,69	53,52° ± 2,88	14,22°

A proportional increase in the contact angle was observed with the addition of yerba mate extract. The films formulated with malic acid showed remarkably lower values, indicating a higher hydrophilic character. This can be explained by the relationship between the surface roughness of the material and its hydrophobicity. A rough morphology can increase the fraction of trapped air on the material surface, resulting in an increased contact angle by reducing the contact area between the water droplet and the surface [12]. On the other hand, malic acid provides a smoother texture to the films.

Images of the sample surfaces after 3 seconds of contact with the water droplet can be seen in Fig. 2. It is noticeable that the droplet has a spherical shape on the films without the presence of malic

acid (Fig. 2-a and Fig. 2-b), while the samples with malic acid spread more easily on the polymeric surface (Fig. 2-c and Fig. 2-d).

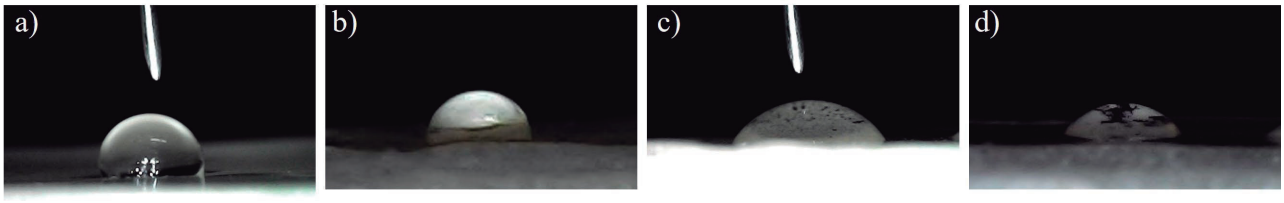

Figure 2 – Drop of water deposited on the surface of: (a) PS; (b) PS20YM; (c) MA; (d) MA20YM.

Conclusions

Starch-based films were successfully produced by casting using potato starch matrix and different levels of yerba mate extract. The addition of malic acid was responsible for reducing the mass transfer kinetics of the samples and decreasing their moisture absorption, suggesting an improvement in their barrier properties. The incorporation of yerba mate extract also resulted in a decrease in water absorption and reduced hydrophilicity of the films. However, the contact angle of the samples with malic acid was significantly lower compared to the specimens without this additive. This could be attributed to the reduction in surface roughness of the material, which facilitates water spreading on its surface.

Acknowledgements

The authors would like to thank to CAPES-PROEX for supporting the research, the Laboratory of Polymeric Materials (LaPol) from Federal University of Rio Grande do Sul (UFRGS) for the infrastructure provided and the Federal Institute of Rio Grande do Sul (IFRS) for donating the potato starch.

References

1. M. A. Knapp et al. Journal of Food Processing and Preservation 2019, 43, 1-12. https://doi.org/10.1111/jfpp.13897
2. L. C. de Azevedo et al. ACS Applied Polymer Materials 2020, 2, 2160-2169. https://doi.org/10.1021/acsapm.0c00124
3. T. G. Dastidar; A. N. Netravali. Carbohydrate Polymers 2012, 90, 1620-1628. https://doi.org/10.1016/j.carbpol.2012.07.041
4. J. P. Lima et al. Journal of Agricultural and Food Chemistry 2016, 64, 2361-2370. https://doi.org/10.1021/acs.jafc.6b00276
5. B. Gullón et al. Industrial Crops and Products 2018, 113, 398-405. https://doi.org/10.1016/j.indcrop.2018.01.064
6. C. M. Jaramillo et al. Starch-Stärke 2015, 67, 780-789. https://doi.org/10.1002/star.201500033
7. D. Piñeros-Hernandez et al. Food Hydrocolloids 2017, 63, 488-495. https://doi.org/10.1016/j.foodhyd.2016.09.034
8. M. Peleg. Journal of Food Science 1988, 53, 1216. https://doi.org/10.1111/j.1365-2621.1988.tb13565.x
9. S. Mali et al. Carbohydrate Polymers 2005, 60, 283-289. https://doi.org/10.1016/j.carbpol.2005.01.003
10. N. Thessrimuang; J. Prachayawarakorn. Journal of Polymers and the Environment 2019, 27, 234–244. https://doi.org/10.1007/s10924-018-1340-2
11. M. Majzoobi et al. Starch-Stärke 2013, 66, 491-495. https://doi.org/10.1002/star.201300188
12. S. I. Kim et al. Macromolecular Research 2014, 22, 1229-1237. https://doi.org/10.1007/s13233-014-2168-9

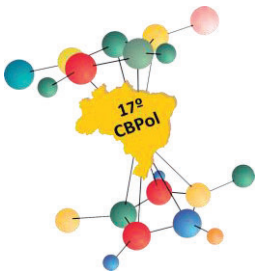

EVALUATION OF JUTE FIBRE IN REACTION WITH FURFURYL ALCOHOL TOWARD PROSPECTIVE PREPREG APPLICATION

Cristiane da Silva Fonseca[1*], Andrey Pereira Acosta[1], Rafael de Avila Delucis[2], Sandro Campos Amico[1]

1 – Department of Materials Engineering, Federal University of Rio Grande do Sul (UFRGS), Porto Alegre, Brazil
cristiane.fonseca@ufrgs.br
2 - Postgraduate Program in Materials Science and Engineering (PPGCEM), Technology Development Center, Federal University of Pelotas (UFPel), Pelotas, Brazil

Abstract
This study aimed to measure and understanding the reaction behavior of jute fibres at different intervals with furfuryl alcohol (FA). The furfurylation process occurred by the addition of FA and maleic anhydride (MA), used as a catalyst. The samples were prepared by the hydrolysis method consisted of inserting 200 mL of FA and 30 g of jute fibre into a closed flask. Then, the samples were washed with acetone at an interval of 1, 7, 14 and 28 days, respectively and were investigated by Fourier-transform infrared (FTIR) spectroscopy and scanning electron microscopy (SEM). The SEM micrographs reveal that the degradation of the surface the fibre increased of the more period of contact with the FA. Thus, this study aimed to measure and understand the reaction behavior of jute fibres at different intervals with AF, for further evaluation of the potential in the manufacture of prepregs.

Keywords: *natural fibres; surface degradation; hydrolysis.*

Introduction

Prepreg denotes a type of material that is a combination of fibre strands such as carbon, glass or aramid with a resin formulation that is usually thermosetting or thermoplastic. These materials show excellent performance in terms of mechanical properties and are widely used in the manufacture of composite materials, mainly for purposes where a high percentage of fibre is required, for naturally higher mechanical performance. However, these types of materials are generally manufactured using raw materials of non-renewable origin and do not present an idea of sustainability. In some exceptions, such as Evopreg® and EcoRein®, which use natural fibre, but still require the use of non-renewable epoxy resin [1, 2].

Thus, in recent years, there is a growing interest of studies that include the development of materials that apply renewable compositions, such as natural fibres and resins extracted from bio-based sources [2]. Lignocellulosics materials such as sisal, coconut, banana, curaua and jute fibres used as reinforcement in composites is related to its low cost, lower density than syntetic fibres, in addition to being widely available in the national territory [3, 4].

Similarly, the use and development of resins of renewable origin, such as furfuryl alcohol (FA), derived from sugarcane bagasse, have been widely studied due to its high thermal performance, good mechanical and chemical properties for use as a matrix in reinforced composites [5, 6]. However, the polycondensation reaction of furfuryl alcohol (PFA) is extremely exothermic and an excess of water is released during the reaction which may induce hydrolysis of the lignocellulosic material [7, 8].

Nevertheless, it is necessary to understand the effect of these parameters on the combination of natural fibres, such as jute fibre, and AF for further evaluation of the potential in the manufacture of

prepregs. Thus, this study aimed to measure and understand the reaction behavior of jute fibres at different intervals with AF.

Experimental

Materials

Jute fabrics (areal density of 239 g.m^{-2}) were purchased from Castanhal textile company (Para/Brazil). The high-purity (98 wt%) furfuryl alcohol (FA) was acquired from Sigma Aldrich and maleic anhydride (MA) was acquired from Sigma Aldrich.

Methods

The furfurylation process occurred by the addition of FA and maleic anhydride (MA), used as a catalyst, at a concentration of 1.5 wt% in relation to the FA weight. Before the hydrolysis process the jute fibre was washed with acetone to verify possible modification on the surface of the fibre and analyzed by Fourier-transform infrared (FTIR) spectroscopy was performed using attenuated total reflection (ATR) technique in a Perkin Elmer, Spectrum 1000 in the 500-4000 cm^{-1} range with 32 scans were recorded at a scan interval of 4 cm^{-1}. The acetone was chosen due to no reaction with the lignocellulosic materials and good solubility in FA. In order to verify the hydrolysis process, a solution of ~200 mL of FA and ~30 g of jute fibre was inserted into a closed flask. Then, the samples were washed with acetone at an interval of 1, 7, 14, 21 and 28 days, respectively and analyzes by FTIR. The surface of the fibres was analyzed by scanning electron microscopy (SEM) in MA10 equipment (Zeiss Evo brand, Oberkochen/Germany) operating at 3 kV. For each day, the hydroxyl index was measured by a ratio between the values of ~3500 cm^{-1} (OH) and ~1350 cm^{-1} (conjugated C-H), this peak was chosen regarding the no alteration of the hydrolysis process. Fig. 1 shows the experimental methodology of preparation of the jute fibre impregnation with the FA.

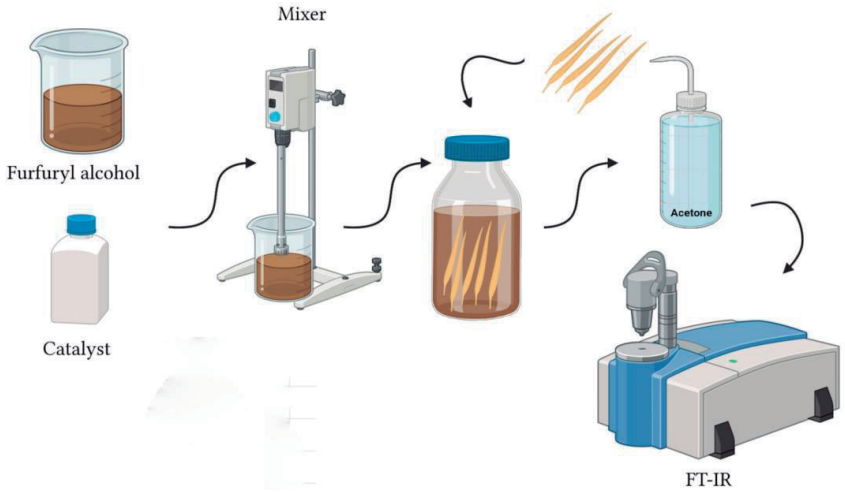

Figure 1. Scheme of experimental methodology.

Results and Discussion

Fig. 2 shows the FTIR results for jute fibre with acetone and jute fibres in different intervals of 7, 14, and 28 days. All the samples of jute fibre presented similarly shaped FTIR spectra. It is possible to verify the broad peak at ~3300 cm^{-1} can be associated with O-H groups that is in the surface of the fibre. A ~2.50 times increase in hydroxyl content can also be noticed. Probably this is associated to the homolytic scission in the ether bond type (1-4) of the holocellulose present in the fibre, caused by the residual water from the natural polymerization process of the furfuryl alcohol in the presence of the catalyst [9]. Some studies point out that the hydrolysis process in natural fibre may impair the interfacial adhesion between the matrix and the fibre, weakening the transmission of

tension to support mechanical loads [10, 11]. For use as prepregs this can be detrimental, compromising the shelf life of the product.

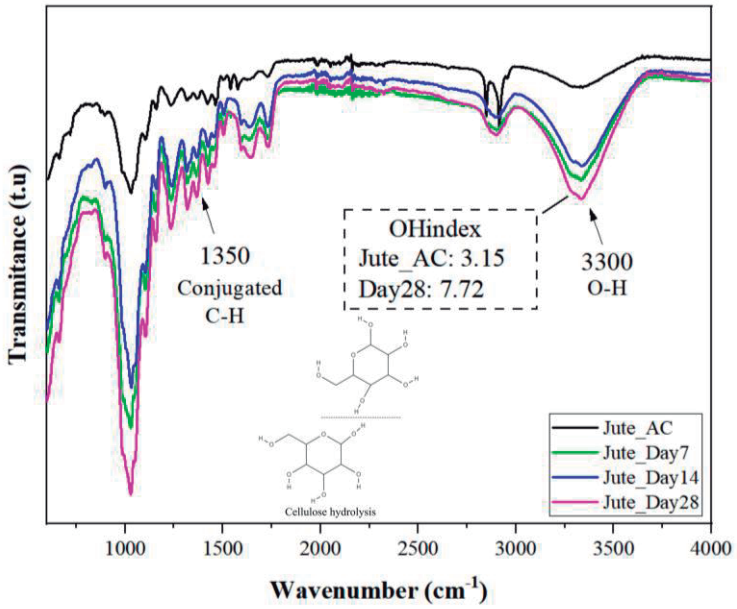

Figure 2. FTIR spectra of jute fibre at intervals of 7, 14, 21 and 28 days.

The Fig. 3 shows the SEM micrographs for jute fibre with acetone and jute fibres at different intervals of days. In Fig. 3-A is presents the jute fibre washed with acetone and is possible to verify no degradation on the surface of the fibre, indicating no reaction with the lignocellulosic materials. In contrast, Fig. 3-B show the jute fibre at the interval of 1 day in contact with FA and it was possible to verify some alteration on the surface. As shown in Fig. 3-C and 3-D, most areas of jute fibres surfaces exhibit some degraded regions caused by the hydrolyzes reaction in -interval of 7 and 14 days, respectively. It can be seen greater exposure of cellulose fibrils at the 28 days of reaction, the surface of the fibre appearance a higher degradation, as depicted in Fig. 3-E, due to more time of the contact of the FA with the fibre and the presence of reaction with OH groups at the surface of the fibre. This degradation areas indicates that the hydrolyzes reaction by the PFA causes breaking down cellulose generating hydroxyl groups.

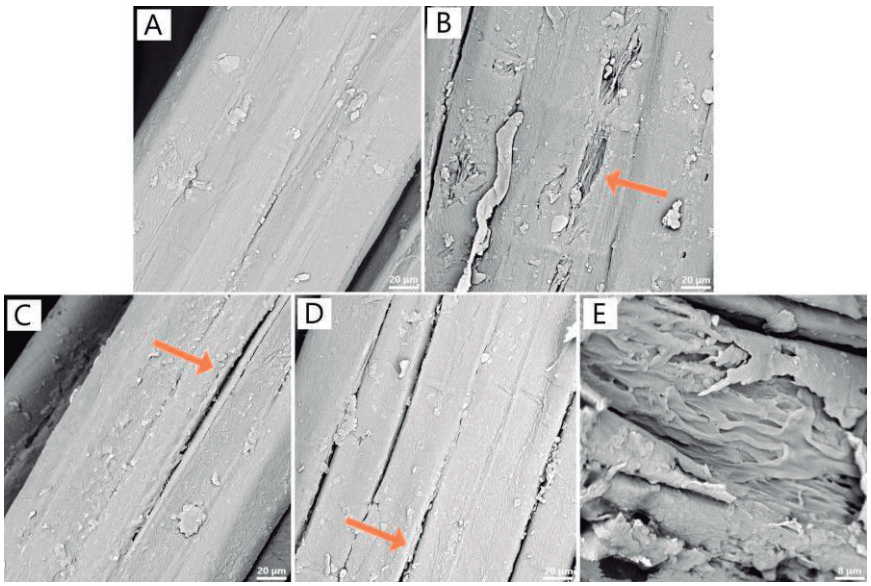

Figure 3. SEM micrographs of jute fibre with acetone (A), jute fibre at interval of 1 day (B), 7 days (C), 14 days (D) and 28 days (E), respectively.

Conclusions

It was possible to see that the furfuryl alcohol hydrolyzed the lignocellulosic material, as expected, mainly in the ether bonds present in the halocellulose. The microscopies proved a severe interfacial degradation to the fibre, mainly due to the acid character of the resin. However, some alterations in the resin and fibre formulation will be made in further studies, as for example: changing the pH of the resin to reduce the hydrolytic process. Thermal treatment of the fibres to reduce the percentage of holocellulose, susceptible to hydrolysis.

Acknowledgements

The authors are thankful to the financial support of Coordination of Superior Level Staff Improvement – CAPES for the research productivity scholarship.

References

1. A. R. Pouladvand; M. Mortezaei; H. Fattahi, I. A. Amraei. Composites Part A, 2020, 132. https://doi.org/10.1016/j.compositesa.2020.105852.
2. A. P. Acosta; R. Beltrame; A. L. Missio; S. C. Amico; R. A. Delucis; D. A. Gatto. Biomass Conv. Bioref. 2022. https://doi.org/10.1007/s13399-022-02821-6.
3. A. Flores; A. Albertin; R. A. Delucis; S. C. Amico. Journal of Natural Fibers. 2023, 20. https://doi.org/10.1080/15440478.2023.2178586.
4. V. D. Libera Junior; L. A. Teixeira, S. C. Amico; S. M. Luz. Polymers and Polymer Composites. 2022, 30, https://doi.org/10.1177/09673911221087591.
5. M. C. R. Coimbra; T. R. Brazil; G. F. M. Morgado; E. F. Martins; E. G. R. Anjos; I. Monteiro; C. Oyama; J. S. Rodrigues; V. R. Botaro; L. S. Montagna; M. C. Rezende. Matéria, 2022, 27. https://doi.org/10.1590/1517-7076-RMAT-2022-0054.
6. M. C. R. Coimbra. Master Thesis, Universidade Federal de São Paulo, 2022.
7. E. M. Lems; S. Winklehner; C. Hansmann; W. G. Almutter; S. Veigel. Cellulose. 2019, 26. https://doi.org/10.1007/s10570-019-02348-6.
8. A. P. Acosta; A. B. Aramburu; R. Beltrame; D. A. Gatto; S. C. Amico; J. Labidi; R. A. Delucis; Polymers. 2022, 14. https://doi.org/10.3390/polym14245510.
9. T. E. Motaung; Z. Gqokoma; L. Z. Linganiso; M. J. Hato. Polymer composites, 2016, 37. https://doi.org/10.1002/pc.23428.
10. A. Mtibe; Y, Mandlev; L. Z. Linganiso; R. D. Anandjiwala. Journal of Biobased Materials and Bioenergy, 2015, 9. https://doi.org/10.1166/jbmb.2015.1531.
11. L. Pranger; R. Tannenbaum; Macromolecules, 2008, 41, 22. https://doi.org/10.1021/ma8020213.

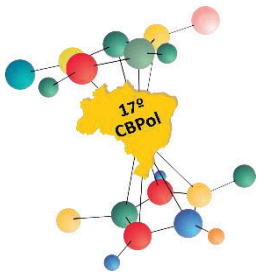

EVALUATION OF MECHANICAL BEHAVIOR OF OFFSHORE MOORING POLYESTER FIBERS BY HYDROLYSIS PROCESS

Ignácio Melito[1], Daniel Magalhães da Cruz[2,*], Aleones José da Cruz Júnior[3], Ivan Napoleão Bastos[4], Ana Lúcia Nazareth da Silva[5], Jakson Manfredini Vassoler[2], Fernanda Mazuco Clain[1] and Carlos Eduardo Marcos Guilherme[1]

1 – School of Engineering (EE), Federal University of Rio Grande (FURG), Rio Grande, RS, Brazil
2 – Department of Mechanical Engineering (DEMEC), Federal University of Rio Grande do Sul (UFRGS), Porto Alegre, RS, Brazil
** Corresponding author: daniel.cruz@ufrgs.br*
3 – Federal Institute of Education, Science and Technology of Goiano, Trindade, GO, Brazil
4 – Polytechnic Institute (IPRJ), Rio de Janeiro State University (UERJ), Nova Friburgo, RJ, Brazil
5 – Institute of Macromolecules Professora Eloisa Mano (IMA), Federal University of Rio de Janeiro (UFRJ), Rio de Janeiro, RJ, Brazil

Abstract
High-performance polymeric fibers have been used in the recent decades for offshore mooring, such as polyester (PET), which is used due to its low cost, high strength, ease of processing, and recyclability. The application in the offshore branch promove a series of studies with the PET fibers, whether analytical, experimental, or numerical studies, and with different load, exposure and environmental conditions. This work experimentally studies the breaking behavior of different polyester fibers that go through a hydrolysis process at different temperatures. Methodology applied is hydrolysis with sea water in an appropriate tank, followed by rupture tests for varied withdrawal. As a result, it is evident that the hydrolysis process decreases the strength performance of all PETs. For some temperature groups, it shows a gradual decrease in strength with increasing hydrolysis time. As future study, more data should be collected to capture behavior and represent it by mathematical models.

Keywords: *Mechanical characterization, Synthetic yarns, Hydrolysis reaction, Sea water, Tensile test.*

Introduction

In recent decades, the offshore sector has advanced into deeper waters, even replacing traditional systems in steel ropes and catenaries, and adopting an approach with ropes made of high tenacity polymeric materials [1].

The challenges in the offshore area led to the development of the use of polymeric synthetic fibers in anchoring systems. From the point of view of materials, there is a wide variety of options for synthetic polymeric fibers to be used: polyester, polyethylene, high modulus polyethylene (HMPE), aramid, polyamide, polyethylene, liquid crystal polymer (LCP), among others. In the present work, attention was given to polyester, polyethylene terephthalate (PET) [2].

Considering mooring ropes, the structures operate in severe environments: sea water, bioencrustation, wind action, wave and tidal movements, which can lead to significant changes in their mechanical properties. This context is an incentive for several research activities related to offshore branch, whether in samples of ropes, sub-ropes or multifilaments, or even in numerical or experimental analytical approaches [3-6].

One of the main aging phenomena that occurs in some polymers in service in the oil field is hydrolysis [7], in which the polymer chains are broken when in contact with water, resulting in a

rapid decrease in molecular weight and subsequent deterioration of some properties, such as mechanical properties, especially tensile strength [8-11].

The objective of this work is to evaluate samples of polyester multifilament supplied by three different manufacturers, in terms of performance at break by hydrolysis process in different temperatures, 60°C, 65°C and 70°C, during around 100 days of exposure.

Experimental

Materials

Three polyester fibers from different manufacturers were used, and all these fibers are used specifically for making cores for offshore mooring ropes. The names of the manufactures cannot be disclosed, so they are called polyester A, B and C. Polyester A and Polyester B has a linear density indication of 2200 dtex, and Polyester C has a linear density of 3300 dtex.

Hydrolysis test

The hydrolysis process is carried out on the polyester samples in a temperature- and level-controlled tank. It is noteworthy, through the specific application of the fibers for the offshore sector, that the hydrolysis was carried out with water collected from the sea, this is not saline water reproduced in the laboratory, but authentically seawater.

The hydrolysis test was performed with different temperatures: 60°C, 65°C and 70°C. For the three polyesters, the withdrawal times were slightly different, but the total time of hydrolysis test is close to 100 days. The hydrolysis tank is shown in Fig 1, and withdrawal times for each polyester are given in Table 1.

Figure 1 – Hydrolysis tank.

Table 1 – Hydrolysis withdrawal times for each temperature condition.

For 60°C	For 65°C	For 70°C
0	0	0
14	19	19
28	33	26
42	47	33
56	61	40
70	82	47
84	96	54
98		61
		68
		82
		89
		103

Note: Withdrawal times are not exactly the same because of technical difficulties, related to the operation of the tank and also to sample quantities.

Yarn Breaking Load

After the immersion time (hydrolysis), 20 samples for each group were broken in a rupture test, to acquire the Yarn Breaking Load (YBL), following the ISO 2062 [12] procedure. The specimens were twisted at a rate of 60 turns per meter for homogenization before the rupture, and then the test followed with recording of force and elongation in the Instron 3365 test equipment where the extension rate was set at 250 ± 5 mm/min. The length of the samples is 1000 ± 2 mm for clamping the samples in the grips of the equipment, the useful test length being 500 mm.

Rupture test procedure is performed in standard atmosphere described in ISO139 [13].

Results and Discussion

As a first result to be considered, the YBL test was performed on samples without exposure hydrolysis condition. The results are presented in Table 2.

Table 2 – Reference data for fibers (without hydrolysis).

Polyester A			Polyester B			Polyester C		
Linear density [dtex]	Breaking strenght [N]	Strain [%]	Linear density [dtex]	Breaking strenght [N]	Strain [%]	Linear density [dtex]	Breaking strenght [N]	Strain [%]
2200	173.77	15.58	2200	174.44	16.40	3300	261.15	13.58

Tables 3, 4 and 5 show the rupture results for the polyester samples analyzed in the hydrolysis process.

Table 3 – YBL results for hydrolysis at 60°C.

	PET A		PET B		PET C	
days	Force [N]	Dimensionless [%]	Force [N]	Dimensionless [%]	Force [N]	Dimensionless [%]
0	173,77	100,00	174,44	100,00	261,15	100,00
14	165,53	95,26	172,70	99,00	256,73	98,31
28	159,83	91,98	169,32	97,07	248,30	95,08
42	156,72	90,19	167,19	95,85	241,93	92,64
56	160,63	92,44	165,54	94,90	248,45	95,14
70	158,50	91,21	165,63	94,95	244,32	93,56
84	157,39	90,58	169,53	97,18	242,27	92,77
98	159,11	91,56	164,43	94,26	242,48	92,85

Table 4 – YBL results for hydrolysis at 65°C.

	PET A		PET B		PET C	
days	Force [N]	Dimensionless [%]	Force [N]	Dimensionless [%]	Force [N]	Dimensionless [%]
0	173,77	100,00	174,44	100,00	261,15	100,00
19	166,58	95,86	173,60	99,52	257,41	98,57
33	162,27	93,38	163,98	94,01	254,88	97,60
47	154,80	89,08	158,84	91,06	250,86	96,06
61	152,03	87,49	155,86	89,35	251,03	96,13
82	147,44	84,85	151,24	86,70	246,57	94,42
96	146,45	84,28	147,00	84,27	239,17	91,58

Table 5 – YBL results for hydrolysis at 70°C.

	PET A		PET B		PET C	
days	Force [N]	Dimensionless [%]	Force [N]	Dimensionless [%]	Force [N]	Dimensionless [%]
0	173,77	100,00	174,44	100,00	261,15	100,00
19	162,66	93,61	170,78	97,90	245,05	93,83
26	165,85	95,44	173,55	99,49	248,73	95,24
33	164,02	94,39	171,08	98,07	247,06	94,60
40	161,98	93,22	167,32	95,92	248,64	95,21
47	165,59	95,29	171,28	98,19	246,60	94,43
54	162,58	93,56	166,41	95,40	247,94	94,94
61	161,18	92,76	171,71	98,44	246,63	94,44
68	160,69	92,48	166,85	95,65	244,56	93,65
82	163,28	93,96	167,94	96,28	244,01	93,43
89	160,65	92,45	170,28	97,62	249,62	95,58
103	164,90	94,90	166,36	95,37	244,02	93,44

Figures 2, 3 and 4 show the data presented in Tables 3, 4 and 5, graphically, for better evaluation.

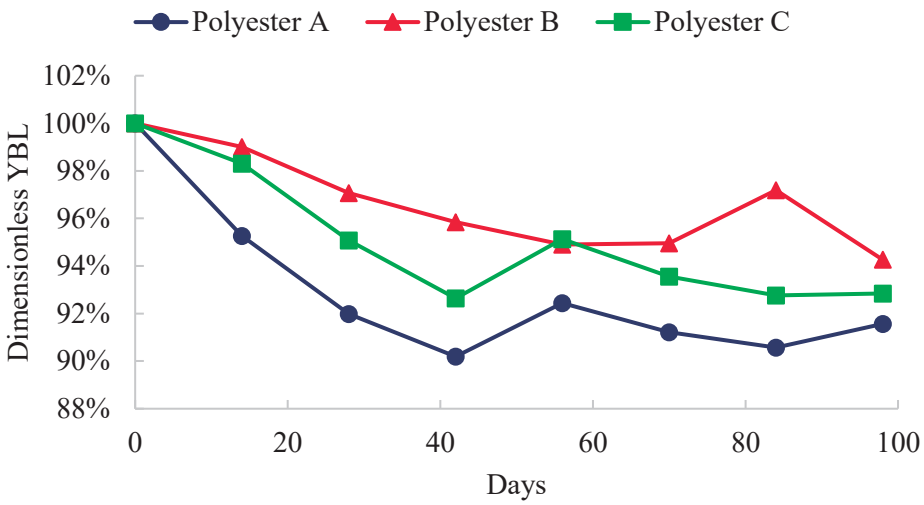

Figure 2 – Dimensionless rupture *versus* hydrolysis time, 60°C.

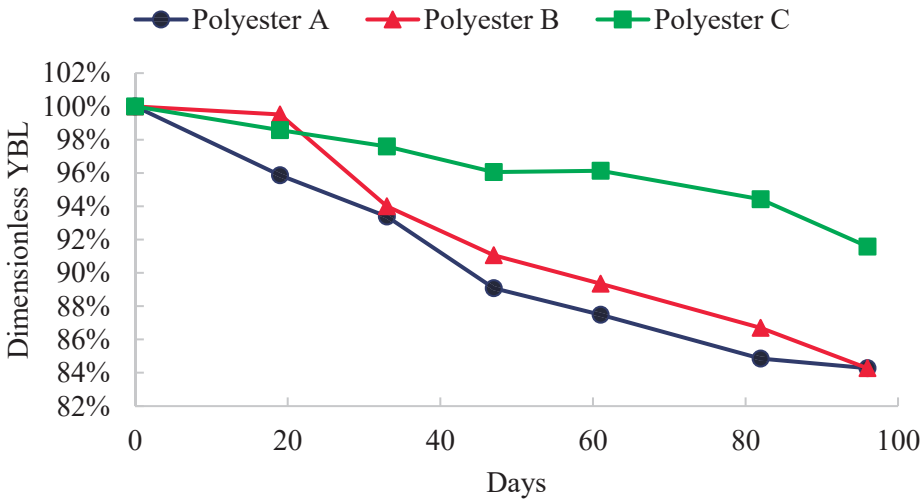

Figure 3 – Dimensionless rupture *versus* hydrolysis time, 65°C.

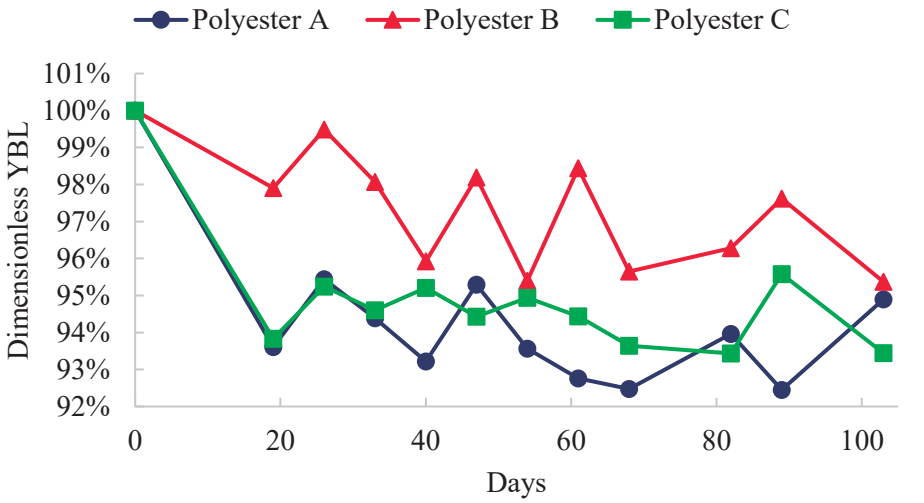

Figure 4 – Dimensionless rupture *versus* hydrolysis time, 70°C.

As can be seen from the curves, the hydrolysis process reduces the tensile strength property for all polyesters and groups tested. It is also noted that for 70°C there is a more abrupt drop in the resistance values for the first withdrawal when compared to the other temperature groups, however in the continuation of the withdrawals, 70°C presents more stabilized values, while in 60°C and 65 °C there is a decreasing tendency as time in hydrolysis evolves. Thus, in the 60°C and 65°C groups, the drop by hydrolysis occurs gradually with longer hydrolysis times, giving a characteristic to the gradual decay curve within the range tested.

It is observed for PET A and PET B samples, at 60°C and 70°C temperatures, the curves showed a more stable behavior; while at 65°C, the property values drop, showing the lowest values of breaking strength. For PET C, a more homogeneous behavior can be observed in the whole hydrolysis conditions analyzed.

Conclusions

The mechanical degradation caused by hydrolysis in polyester multifilaments is notorious. The performance related to materials from different manufactures was not a determining factor, no manufacturer stood out for its resistance to the hydrolysis process.

In addition, data grouping presents different behaviors for temperature groups and also hydrolysis times. The continuation of the study should be done considering longer hydrolysis times with regular withdrawals and other temperature groups, both higher and lower. Perhaps a more complete database will enable the use of mathematical modeling to describe phenomena such as Krigeage surfaces, Arrhenius equation, among other techniques.

References

1. C. J. M. Del Vecchio, Ph.D. Thesis, University of Reading, 1992.

2. E. Chailleux; P. Davies, Mechanics of Time-Dependent Materials 2005, 9(2-3), 147-160. https://doi.org/10.1007/s11043-005-1082-0.

3. M. Rudman; P. W. Cleary, Ocean Engineering 2016, 115(15), 168-181. https://doi.org/10.1016/j.oceaneng.2016.02.027.

4. Z. Liu; Y. Lu; W. Wang; G. Qian, Applied Sciences 2019, 9(6), 1075. https://doi.org/10.3390/app9061075.

5. D. M. da Cruz; A. Penaquioni; L. B. Zangalli; M. B. Bastos; I. N. Bastos; A. L. N. da Silva, Applied Ocean Research 2023, 134, 103513. https://doi.org/10.1016/j.apor.2023.103513.

6. E. S. Belloni; F. M. Clain; C. E. M. Guilherme, Acta Polytechnica 2021, 61(3), 406-414. https://doi.org/10.14311/AP.2021.61.0406.

7. B. Jacques; M. Werth; I. Merdas; F. Thominette; J. Verdu, Polymer 2002, 43(24), 6439-6447. https://doi.org/10.1016/S0032-3861(02)00583-9.

8. P. D. Calvert, British Polymer Journal 1986, 18(4), 278-278. https://doi.org/10.1002/pi.4980180422.

9. I. Melito; F. M. Clain; C. E. M. Guilherme; A. H. M. F. T. da Silva in Proceedings of 25th ABCM International Congress of Mechanical Engineering, Uberlândia, 2019, COBEM-0883.

10. N. V. Nadalín; I. Melito; C. E. M. Guilherme; F. M. Clain in Proceedings of 25th ABCM International Congress of Mechanical Engineering, Uberlândia, 2019, COBEM-0913.

11. J. P. Duarte; C. E. M. Guilherme; A. H. M. F. T. da Silva; A. C. Mendonça; F. T. Stumpf, Polymers and Polymer Composites 2019, 27(8), 518-524. https://doi.org/10.1177/0967391119851386.

12. International Organization for Standardization, ISO 2062, 2009, Geneva.

13. International Organization for Standardization, ISO 139, 2005, Geneva.

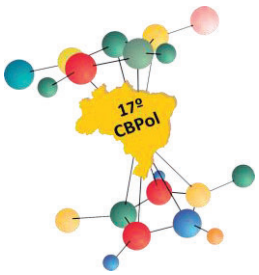

EVALUATION OF THE EFFECTS OF A SUPERABSORBENT POLYMER ON THE GRANULOMETRIC AND CHEMICAL DISTRIBUTIONS OF AN IRON ORE.

Kátia Monteiro Novack[1], Cláudio Gouvea dos Santos[2] and Mariana Babilone De Souza Ferreira[3]

1 – Department of Chemistry, University of Ouro Preto(UFOP), Ouro Preto, MG, Brazil
knovack@ufop.edu.br
2 – Department of Chemistry, University of Ouro Preto(UFOP), Ouro Preto, MG, Brazil
claudio@ufop.edu.br
3 – Redemat, University of Ouro Preto(UFOP), Ouro Preto, MG, Brazil
mariana.babilone@aluno.ufop.edu.br

Abstract – Superabsorbent polymers (PSAs) have been employed in a wide range of applications due to their absorption and retention capacity, which is of interest for the processing of iron ore, since most of the transported ores occurs in the presence of water and this excess free water generates several productivity, quality and even safety problems for the iron ore processing chain. This work aimed to evaluate the effects of using a superabsorbent polymer commercially used in contact with an iron ore containing phosphorus. Evaluation of the granulometric characteristics indicated that the presence of PSA causes an increase in the size of iron ore particles. As for the chemical characteristics before and after PSA treatment, no significant changes were observed in the parameters.

Keywords: *superabsorbent polymer, iron ore, granulometry, moisture.*

Introduction

Superabsorbent polymers (PSA's) have been investigated as an alternative for application in the processing of iron ore, with the aim of reducing the moisture content presented by iron ore.[1] Most of the ores transported, mainly the iron ore fines (IOF), are not shipped dry. These products contain water due to the stages of ore processing and/or rain and inclement weather during the transport and storage of this material. [2] The excess moisture of the iron ore compromises the quality of the product, being undesirable even for the customer, since it hinders the subsequent processes in the steel industry. Thus, the control of the moisture content in the ore proves to be an important factor, both in terms of the volume of ore to be transported as well as the operability of the process, which is directly impacted by excess water. [3] An alternative that has been recently studied and applied is the use of superabsorbent polymers (PSAs). These polymers, used in the form of gel, have as their main characteristic the absorption and retention of large amounts of water and/or aqueous solution in up to a thousand times their own mass. They are hydrophilic, partially cross-linked, high-molecular-weight materials capable of absorbing several hundred times their own

mass of water and expanding in size, but preserving the individual identity of the particles. [4] The opportunity then arises to evaluate the effects of a superabsorbent polymer on the granulometric distribution of iron ore and also to evaluate possible chemical changes that the ore could undergo after the polymer dosage.

Experimental

The tests carried out in this work focused the behavior of a superabsorbent polymer in contact with a sample of iron ore, by evaluating the granulometric distribution of the mixture, possible chemical changes after the interaction between the superabsorbent polymer and the ores and the ability of the polymer to act in the reduction of the humidity of the iron ore. The materials used in this work for the production were:

- Iron Ore Concentration Phosphor (IOCP)
- Commercial superabsorbent polymer KURISAT KE-0806

The iron ore sample was prepared according to ISO 3082:2017 - Iron ores — Sampling and Sample Preparation procedures, being separated and weighed up to 2.5kg of each sample, considering the determination of moisture according to ISO 3087:2011 - Iron ores — Determination of the Moisture Content of a lot, where the sample presented humidity of 9.7%. Subsequently that sample was homogenized with as spoon for five minutes.

Polymer Dosage

The polymer dosage in the sample was performed with the aid of a glass dropper. To define the amount of drops for each test, the polymer was weighed and the mass, in grams, converted to drops. The range of polymer/sample ratio used in the bench test was the same as suggested by the manufacturer, 0.27kg/ton, and the necessary weighings were performed until the proportion for samples of 2.5 kg was reached. After the polymer was measured, a new homogenization was performed by continuously stirring the mixture of iron ore and superabsorbent polymer in all directions for 5 minutes.

Sample size determination

The determination of the sample size was performed based on ISO 4701:2019 - Iron ores and direct reduced iron — Determination of Size Distribution by sieving. Sieves of size 12.5mm, 9.5mm, 6.3mm, 3.35mm, 2mm, 1mm, 0.500mm, 0.300mm, 0.212mm, 0.150mm were used for this analysis.

Chemical Analysis

Ore characterizations were performed by Chemical Analysis (XRF), based on ISO 9516-1:2003 - Iron ores — Determination of various elements by X-ray fluorescence spectrometry and ISO 11536:2015 - Iron ores - Determination of Loss On Ignition - Gravimetric method.

Results and Discussion

The samples were analyzed by X-ray Fluorescence (XRF) before polymer dosage, as shown in Table 1. The Size Distribution Analysis – Before Dosing is presented in Table 2.

Elements	IOCP (%)
Fe	61.73
SiO_2	6.78
Al_2O_3	1.52
Mn	0.50
P	0.058
CaO	0.02
MgO	0.07
TiO_2	0.10
LOI	2.5
H_2O	9.7

Table 1: Chemical Analysis (XRF) of the Iron Ore after dosing.

Sieve (mm)	IOCP (g)
12.5	0
9.5	3.3
6.3	12.8
3.35	28.7
2.0	41.3
1.0	53
0.5	60.9
0.3	66.6
0.212	71.5
0.150	77.6

Table 2: Size Distribution of the Iron Ore after dosing.

To evaluate the effect of the polymer on the IOCP sample, acceptable deviations according to ABNT NBR ISO 11535:2011 were applied for each chemical parameter analyzed. These acceptable deviations were applied in the analysis of the samples without polymer addition, generating a content range for each parameter. Subsequently, the analyses of the samples were made with the addition of the polymers, within this range, indicating that the polymers did not affect the chemical results analyzed. From these considerations, it was not possible to assert the influence of the addition of polymers in the parameters, since no clearly defined behavior for all parameters outside the range was observed.

Comparison between the chemical analyses before and after the addition of the polymer (Figure 1) indicated differences in composition greater than those accepted in reproducibility of analyses. A priori, from such random behavior it was not possible to infer any kind of correlation. The granulometric distribution before the polymer dosage is shown in Figure 2. Some difficulties were experienced during sieving, as the material collapsed into the finest sieves. Blinding of sieves from the 1mm mesh was observed when the particle size analysis of the sample with an initial humidity was performed after polymer dosage. This blinding was overcome by drying the sample. As yet we do not know the effect of the drying temperature (105º C) on the polymer.

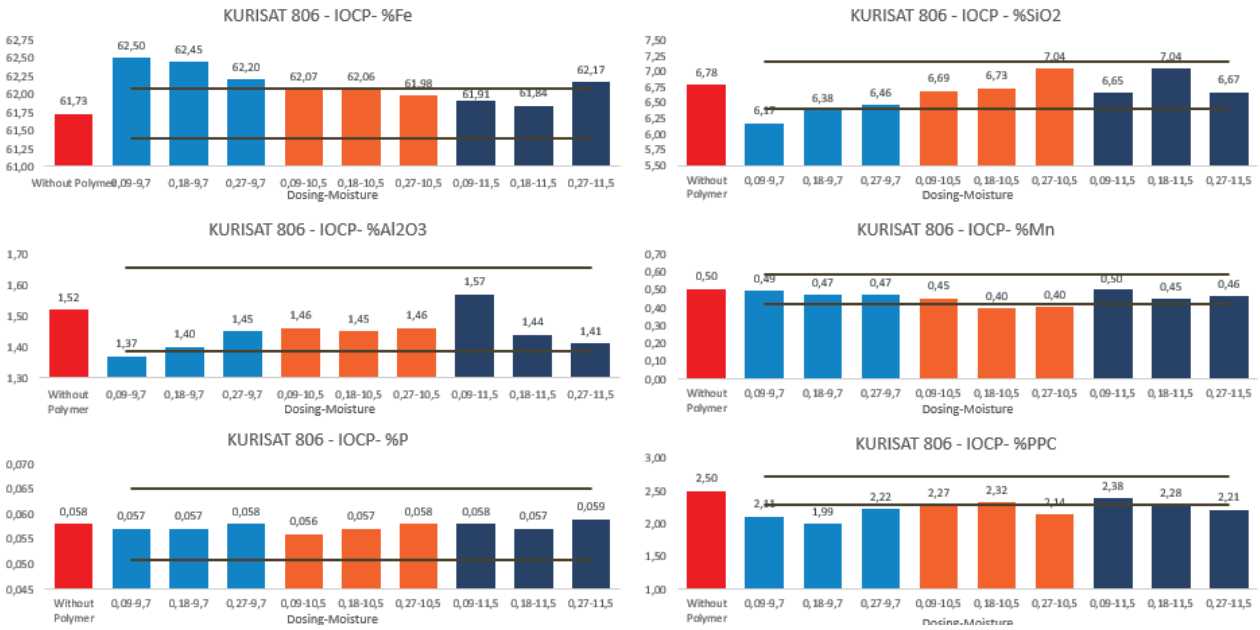

Figure 1: Chemical analyses before and after the addition of the superabsorbent polymer to IOCP ore

It is possible to observe that the average grain size is smaller before the polymer dosage. When the sample presents 9.7% of humidity, upon treatment with the superabsorbent polymer, an increase in particle size is observed, demonstrating the efficiency of the polymer in order to increase the agglomeration of iron ore particles. Finally, after the sample dries, it is possible to observe a superior behavior in relation to the effect of the polymer in relation to the agglomeration of the particles and consequently, in the average particle size.

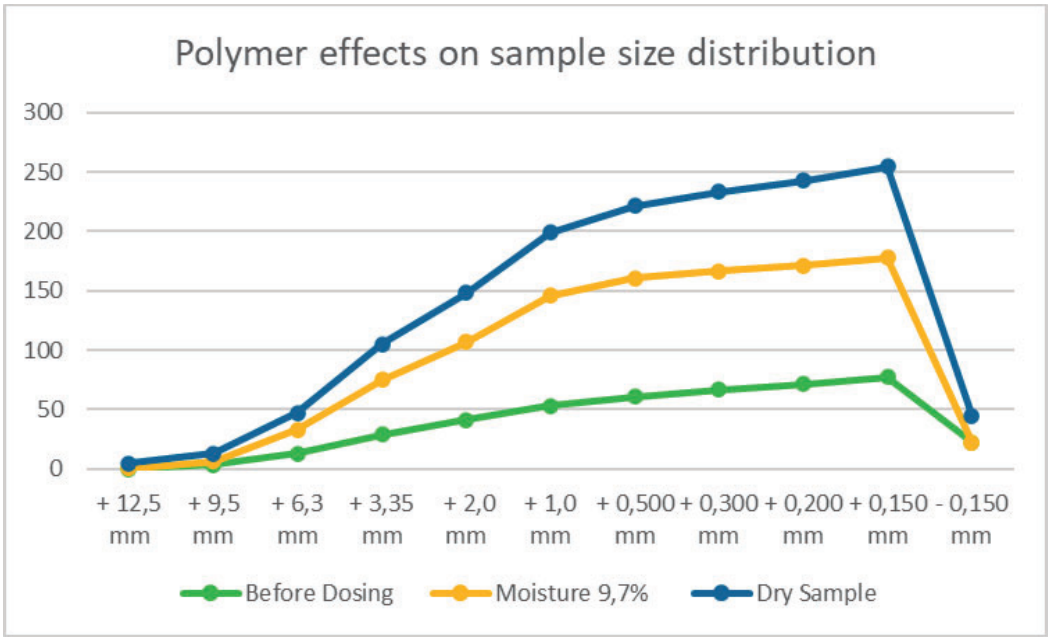

Figure 2: Effects of the polymer on the sample size distribution.

Conclusions

The comparison between the chemical analyses before and after the addition of the polymer indicate differences in results in the elements greater than those accepted in reproducibility of analyses. A priori, the behavior is random, and it is not possible to determine any kind of correlation. Thus, we can conclude that the use of the superabsorbent polymer does not directly interfere in the chemical composition of the polymer. Regarding the effects of the polymer on the distribution of sample sizes, it is possible to observe that the polymer affects the agglomeration of the particles, as expected, generating an increase in the size of the samples, especially after drying the material. These encouraging results support further studies with the use of PSA in order to improve the processing of iron ore, by reducing its moisture content and contributing to the increase of productivity, quality and safety in the processes related to this material.

Acknowledgements
Support from CSN, FAPEMIG, REDEMAT and PROPPI-UFOP is gratefully acknowledged.

References

1. SRIKAKULAPU, N. G., CHEELA S. S., MAKHIJA D., SHARMA, N. (2020). Improved flowability of iron ore using superabsorbent polymers. Powder Technology 364 321–331.
2. Fontanelli SA, Lima VMA. Análise do domínio no contexto da mineração no Brasil [Internet]. In: Organização do conhecimento responsável: promovendo sociedades democráticas e inclusivas. Belém: Ed. da UFPA; 2019. [citado 2023 maio 25] Available from: https://www.eca.usp.br/acervo/producao-academica/003045227.pdf
3. PINTO, T. C. S.; JUNIOR, D. M.; LIA L. R. B.; FILHO, L. S. L. (2015) Mecanismos de Secagem Visando a Redução de Umidade em Sinter Feed de Minério de Ferro. Abm Week. Rio de Janeiro, nº45. P. 1016 -1024
4. BUCHHOLZ FL, GRAHAM AT. *Modern Superabsorbent Polymer Technology*. Wiley-VCH, New York. 1998

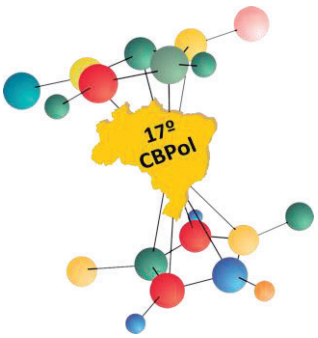

EVALUATION OF THE MECHANICAL AND OPTICAL PROPERTIES OF LDPE INJECTION-MOLDED WITH BENZOIN IN HDPE MASTERBATCH

João A. O. Brandão[1*], Pedro Tonom Martin[1], Edson L. Francisquetti[2] and Ruth M. C. Santana[1]
1 –Department of Materials Engineering, Federal University of Rio Grande do Sul (UFRGS), Porto Alegre, RS, Brazil
jaobrandao@yahoo.com.br
2 – Federal Institute of Rio Grande do Sul, Farroupilha Campus, Farroupilha, RS, Brazil

Abstract – The incorporation of additives to polymers needs to be well evaluated, since, in general, it changes the matrix properties. The pro-degradant additives also accelerate the thermo-oxidation of polyolefins, therefore, this degradation is already observed in the processing, when the polymer is subjected to high temperatures, in addition to shear stress. In this work, the mechanical and optical properties of LDPE injection-molded specimens with benzoin were evaluated using a masterbatch in an HDPE matrix to compensate for the reduction of molar mass caused by thermo-oxidation and possible loss of properties. The MFI of the samples indicated that the use of HDPE causes some compensation in the chain size. Statistically, the Izod impact and tensile test results indicated that adding HDPE minimizes the impact of the loss of mechanical properties. The colorimetry, however, indicated that the benzoin acts in the oxidation of the LDPE, causing their yellowing.
Keywords: *polyethylene, oxo-biodegradable, mechanical properties, yellowing, thermo-oxidation.*

Introduction

The accumulation of polymeric waste, mainly from single-use packaging, is an environmental problem observed all over the world. The use of pro-degradant additives to obtain oxo-biodegradable polymers is a reality in facing this problem. Such additives are characterized by favouring the abiotic degradation of polyolefins, accelerating the thermo-oxidation and photooxidation of these macromolecules so that, subsequently, the oxygenated fragments can be used as nutrients by microorganisms [1].
Benzoin, a biodegradable organic compound free of transition metals, proved to be a promising pro-degradation additive in previous studies since it accelerated the thermo-oxidation [2] and photooxidation [3] of HDPE/LDPE films. However, thermo-oxidation was observed already during the processing of the films, when the polymer was exposed to temperatures that exceeded its melting point, easily reaching 200 ºC.
In this work, LDPE (low density polyethylene) injection-molded specimens with benzoin were studied. However, to compensate for the reduction of the molar mass and possible loss of mechanical and optical properties (yellowing) due to the thermo-oxidation accelerated by benzoin in the processing, the additive was incorporated from a masterbatch produced in a matrix of HDPE (high density polyethylene), known for its greater thermal stability, if compared to other polyethylenes (PE). Injection-molded specimens were produced with 0, 2, 4 and 6% of the masterbatch, which was characterized by MFI (melt flow index), to assess possible changes in the polymer chain sizes of the compound; colorimetry, to assess changes in colour and gloss, which

may be associated with the thermo-oxidation suffered during processing; Izod impact and tensile tests to assess changes in mechanical properties.

Experimental

Materials

In this work, LDPE grade EB-853, with MFI of 2.7 g/10 min (190 ºC/ 2.160 kg) and density of 0.923 g/cm3; and HDPE grade HE-150, with MFI of 1.0 g/10 min (190 ºC/ 2.160 kg) and density of 0.948 g/cm3, both manufactured by Braskem Brazil, were used. Benzoin, with a purity grade of over 99%, is produced by Merck KGaG.

Benzoin masterbatch production in HDPE matrix (pro-degradation additive)

The *masterbatch* was obtained from the mixture of HDPE with benzoin in a Haake thermokinetic mixer, model RheoDrive 7, at a temperature of 160 ºC. The first 6 minutes were to guarantee the melting of the HDPE. After that, the benzoin mass was added, with an effective mixing time of 4 minutes. Therefore, the total process lasted 10 minutes. A masterbatch with a mass ratio of 3:1 (HDPE/benzoin) was obtained. The mixture was cut with the help of pliers into granules with dimensions like those of LDPE pellets. Fig 1 shows the produced masterbatch.

Figure 1 – Benzoin masterbatch after cutting with pliers, with dimensions like LDPE pellets.

Obtaining the injection-molded specimens

The samples were obtained in a Thermo Scientific Haake MiniJet II injection molding machine at 145 ºC, with injection pressure set at 600 bar and set back pressure at 400 bar. The samples, with 0, 2, 4, and 6% (w/w) of masterbatch of the pro-degradation additive, were named PE_0%, PE_2%, PE_4%, and PE_6%, respectively. Because it is a piston type injection molder, the mixture of LDPE with the masterbatch was previously performed in the thermokinetic mixer, for 6 minutes and at a temperature of 160 ºC. In addition to ensure a good diffusion of the additive in the LDPE, a way to establish similar conditions to those observed in industrial processes was sought, in which the material would pass through a screw for subsequent injection. Five specimens were obtained for tensile and Izod impact tests for each of the additive concentrations. The specimens are presented in Fig 2.

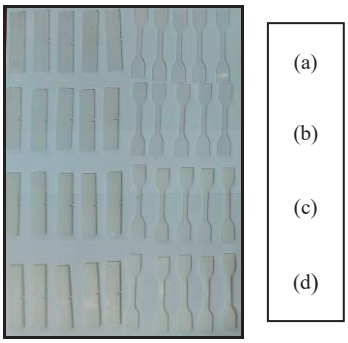

Figure 2 – Injection-molded specimens: (a) PE_0%, (b) PE_2%, (c) PE_4% and (d) PE_6%.

Determination of the melt flow index (MFI) of the injected specimens
The tests to determine the melt flow index (MFI) of the different samples, with and without the additive, were performed in CEAST modular plastomer, model 7026.000, according to ASTM D1238 standard procedures. The conditions used were 190 ºC/ 2.160 kg, with a residence time of 240 seconds.

Colorimetric test
The colorimetric test was performed using the CIE L*a*b System. In addition, the brightness was also determined. A BYK - Gardner instrument, model Spectro-guide 45/0 gloss/ Spectro-guide sphere gloss was used. In the CIE L*a*b system, it is stated that **"L"** is the luminance axis, which refers to the human perception of luminosity (on a scale from 0 to 100, where 0 is absolutely black and 100 is white); **"a"** is the axis that goes from green to red, with negative values tending to maximum green and positive values tending to maximum red; and **"b"** is the axis that goes from blue to yellow, with negative values tending to blue and positive values tending to yellow.

Tensile test
The tensile tests were performed in a universal equipment Instron, model 4200, following the procedure of ASTM D638-10, using a load cell of 5 kN and a retraction speed of 10 mm/min.

Izod Impact Test
Izod impact test was determined in Ceast equipment, model Impactor II, according to procedures described in ASTM D256-10. The specimens were notched, and a 0.5 J hammer was used for impact at room temperature.

Results and Discussion

To evaluate the thermo-oxidative degradation of macromolecules, the MFI of PE was determined in the injection-molded specimens, whose values are presented in Fig 3. Evaluating the results, it is possible to observe an increase of approximately 20% among the additivated samples, if compared to PE_0%, suggesting that the benzoin promoted the thermo-oxidation of the PE with consequent reduction of the chains, facilitating the melt flow [2, 4]. However, the MFI value remained with statistically similar values for samples PE_2%, PE_4%, and PE_6%, indicating that the reduction in the average chain size was compensated by the addition of HDPE.

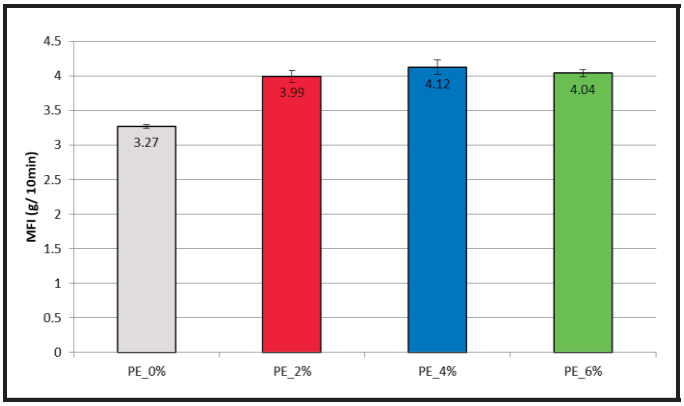

Figura 3 – MFI of PE in the injection-molded spicemens with 0, 2, 4 and 6% masterbatch.

Subsequently, to evaluate the thermo-oxidation degradation suffered by the samples, a colorimetric test was performed, whose results are presented in Table 1. It is possible to observe that there is a

progressive increase in the value of **"b"**, indicating a possible formation of polymeric oxygenated fragments (containing carbonyl) and unsaturated, responsible for the yellowing of the PE [5]. The data obtained confirm the increase in the rate of LDPE thermo-oxidation in the processing with benzoin. The addition of HDPE, however, left the samples with a whiter tone (L factor), which was confirmed by the increase in the opacity of the samples (Gloss), which was expected, since the HDPE presents high crystallinity, making the thick samples more matte.

Table 1 – L*a*b and Gloss values of the PE samples obtained by colorimetric test.

Sample	L	A	b	Gloss
PE_0%	69.13 ± 0.94	0.10 ± 0.03	-1.84 ± 0.03	11.78 ± 3.20
PE_2%	67.62 ± 0.80	-1.02 ± 0.09	0.92 ± 0.19	1.68 ± 0.09
PE_4%	70.11 ± 0.77	-2.20 ± 0.20	1.77 ± 0.29	1.72 ± 0.28
PE_6%	74.02 ± 0.92	-2.69 ± 0.23	1.73 ± 0.43	2.24 ± 0.73

The results obtained in the Izod impact tests are shown in Fig 4. It can be observed that there was a reduction of approximately 8% in the strength of samples PE_4% and PE_6%, but this is not significant, showing that the addition of HDPE had a possible positive influence on the samples. The maintenance of the mechanical properties, according to Ojeda and collaborators [6], is a premise for pro-degradant additives. Thus, the masterbatch of the pro-degradant with HDPE polymer matrix is an alternative to prevent the loss of impact strength of the samples due to thermo-oxidation of LDPE.

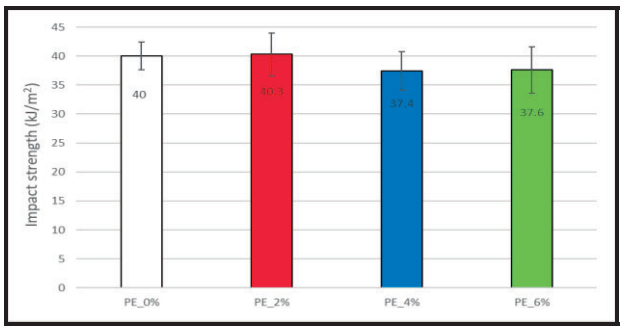

Figure 4 – Impact strength of injection-molded specimens submitted to the Izod Impact test.

Finally, Fig. 5 shows the elongation at the break of injection-molded specimens with benzoin. It can be observed that the additive may have influenced the results. It was expected that the increasing concentration of benzoin in the samples would lead to a reduction of the strain at the break due to the higher rate of thermos-oxidation of LDPE caused by the processing. But the results showed an increase in tensile strength around 10% for PE_2% and 20% for PE_4% and PE_6% compared to PE_0%. This was possibly due to the addition of HDPE, as it is known that, compared to LDPE, it has better mechanical properties [7].

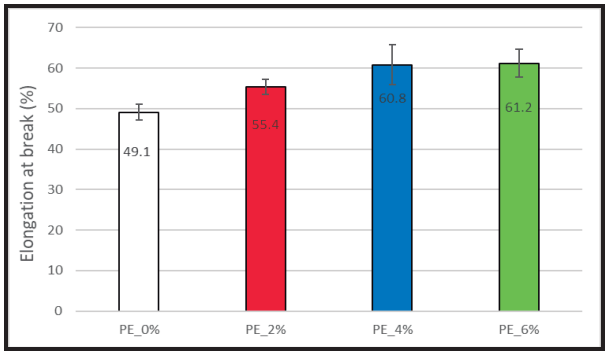

Figure 5 – Elongation at break of injection-molded specimens submitted to the tensile test.

Conclusions

Benzoin promoted LDPE thermo-oxidation, as demonstrated by the increase of MFI and the increase of the "b" value index, in the colorimetric test. However, the addition of the organic compound in HDPE matrix compensated, in parts, the degradation suffered by LDPE by thermo-oxidation and, therefore, the specimens injected with increasing concentrations of the pro-degradant masterbatch showed similar MFI values.

The addition of the additive in a matrix of HDPE maintained or even improved the mechanical properties of LDPE, proven by the results of Izod impact and tensile tests. The addition of the Masterbatch produced in this work compensates for the thermo-oxidation of LDPE macromolecules. However, the polymer is still oxo-biodegradable, being the addition of benzoin in HDPE matrix masterbatch as an alternative to reduce the loss of properties by thermo-oxidation in processing, either by extrusion or injection.

Acknowledgements

Thanks to Capes-Proex for the financial support.

References

1. M. Rujnic-Sokele; A. Pilipovic. Waste Management & Research 2017, 35, p. 132-140. https://doi.org/10.1177/0734242X16683272.
2. J.A.O. Brandão; F.D.P. Morisso; E. L. Francisquetti; R.M.C. Santana. Polímeros 2021, 31, e2021029. https://doi.org/10.1590/0104-1428.20210058.
3. J.A.O. Brandão; F.D.P. Morisso; E. L. Francisquetti; R.M.C. Santana. Heliyon 2022, 8, e10217. https://doi.org/10.1016/j.heliyon.2022.e10217.
4. P.K. Roy; P. Surekha; C. Rajagopal; V. Choudhary. Journal of Applied Polymer Science 2008, 108, p. 2726-2733. https://doi.org/10.1177/0734242X16683272.
5. H. Bockhorn; A. Hornung; U. Hornung; D. Schawaller. Journal of Analytical and Applied Pyrolysis 1999, 48, p. 93-109. https://doi.org/10.1016/S0165-2370(98)00131-4.
6. T.F.M. Ojeda; E. Dalmolin; M.M.C. Forte; R.J.S. Jacques; F.M. Bento; F.A.O. Camargo. Polymer Degradation and Stability 2009, 94, p. 965-970. https://doi.org/10.1016/j.polymdegradstab.2009.03.011.
7. F.M.B. Coutinho, I.L. Mello, L.C.S. Maria. Polímeros: Ciência e Tecnologia 2003, 13, p. 1-13. https://doi.org/10.1590/S0104-14282003000100005.

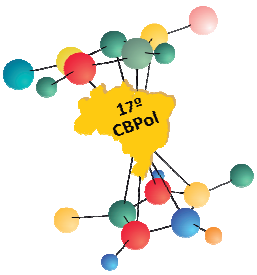

EVALUATION OF THE PLASTICIZERS CONTENT IN THE RHEOLOGICAL AND PHYSICAL PROPERTIES OF TPS THROUGH FACTORIAL DESIGN

Ariel L.V. Cordeiro[1], Carlos H. R. Milfont[2], Alice C. Silva[2], Juciklécia S. Reinaldo[3] and Edson N. Ito[4]*

1 – Undergraduate Course in Materials Engineering, Federal University of Rio Grande do Norte, Natal, RN, Brazil arielavinia@gmail.com
2 – Graduate Program in Materials Science and Engineering, Federal University of Rio Grande do Norte, Natal, RN, Brazil henrique.milfont@gmail.com, alice.silva.111@ufrn.edu.br
3 – Higher School of Technology, State University of Amazonas, Manaus, AM, Brazil jreinaldo@uea.edu.br
*4 – Materials Engineering Department, Federal University of Rio Grande do Norte, Natal, RN, Brazil *edson.ito@ufrn.br*

Abstract – The aim of this work was to evaluate the effect of glycerol and water content, as plasticizers, on the rheological and physical properties of thermoplastic starch (TPS) using a 2^2 full factorial design for the formulation of the experiments and showing a response surface to visualize the results. The results of measurements of flow index (MFI) of the samples indicated a greater influence of the glycerol concentration, which provided an increase in fluidity when incorporated at 55 wt%. X-ray diffraction indicated that increasing water concentration increased the degree of crystallinity, while glycerol had the opposite effect. The results of the water absorption test showed a greater absorption capacity of TPS with a higher content of plasticizers. The experimental design response surfaces obtained were useful for understanding the results and facilitated the correlation between the results.

Keywords: *Thermoplastic starch, plasticizer, extrusion, full factorial design.*

Introduction

The use of starch as a raw material for the production of a biodegradable polymeric material has been gaining prominence in recent decades as an alternative for replacing polymers from the petrochemical industry. Starch in its native form does not have the characteristics of an industrially applicable thermoplastic polymer, and it is necessary to break the original semicrystalline structure of the granules to obtain a homogeneous and amorphous polymeric matrix that can be processed by traditional polymer processing techniques and, obtain the thermoplastic starch (TPS) [1].

Breaking the semicrystalline structure of starch granules is achieved with the use of plasticizing additives, which act by reducing intermolecular interaction and increasing the mobility of the polymeric chains present in the starch. Glycerol and water are two plasticizers widely used to obtain TPS since they have hydroxyl in their respective structures, which makes them soluble and compatible with starch [2].

Recent studies [3, 4] have shown that small changes in the concentration of glycerol used as a starch plasticizer can significantly affect the morphological characteristics, the glass transition temperature (Tg), crystallinity and mechanical properties of TPS films. Giuri et al. [3] in their study observed that the increase in the concentration of glycerol, used as a plasticizer of TPS, can increase the water absorption of TPS, mainly affecting the mechanical properties, that is, making the application of this material difficult. Thus, this work aimed to evaluate the influence of different

concentrations of plasticizers on the physical and rheological properties of the obtained thermoplastic starch.

Experimental

Materials

Commercial cassava starch (Yoki Alimentos S/A), glycerol p.a. from Dinâmica Contemporânea Ltda. with a degree of purity of 99.5% and distilled water.

Methods

Experimental Design

2^2 full factorial design with 3 central points was used, with glycerol concentration (G) and water concentration (W) as analyzed factors, and mathematical models and response surfaces were obtained using the Statistica 12 software. Table 1 shows the experimental matrix used.

Tabela 1 - 2^2 full factorial design with 3 central points.

Experiment	Formulation	Codification		Variables	
		Glycerol	Water	Glycerol (%)	Water (%)
1	35G10W	-1	-1	35	10
2	55G10W	+1	-1	55	10
3	35G20W	-1	+1	35	20
4	55G20W	+1	+1	55	20
5		0	0		
6	45G15W	0	0	45	15
7		0	0		

Premixes

Premixes were carried out in an orbital mixer of the Cadence BAT508 brand with 400W of power at maximum speed for a time of 10 minutes.

Extrusion Processing

Co-rotational twin-screw extruder from AX Plásticos Máquinas Técnicas Ltda, a screw with diameter of 16 mm and length-to-diameter ratio (L/D) of 40 was used to prepare the TPS under the same conditions, i.e., a temperature profile of 50/60/110/110/120/120/130/130/135 °C from feed to die with screw rotation speed of 180 rpm, using a die for filament production.

After mixing in a twin screw extruder, tapes were produced in a single screw extruder from AX Plásticos Máquinas Técnicas Ltda, a screw with a diameter of 16mm and a length-to-diameter ratio (L/D) of 26. The temperature profile was set at 120/130/140 °C from feed to the die with screw rotation of 40 rpm.

Melt Flow Index

Melt index measurements were performed in a Ceast Melt Flow, Modular Liner at a temperature of 150 °C and a weight of 5 kg.

X Ray Diffraction

The X-ray diffraction pattern of the TPS was obtained using a Shimadzu diffractometer (model XRD-7000) with CuKα radiation (λ = 1.5418 Å) at 40 kV and 30 mA with speed of 1º (2θ)/min. The test was performed in the 2θ range of 2.5 to 60º at room temperature. The degree of crystallinity was calculated based on the method proposed by Kaminski et al [5].

Water Absorption

Water absorption measurements were performed based on ASTM D570, using rectangular specimens. Initially, the materials were dried in a vacuum oven at temperature of 60 °C for 24 hours and then the samples were weighed on an analytical balance and immersed in distilled water at 23 °C, where these samples were weighed at na interval of 20 minutes up to maximum time of 6 hours. The measurement of water absorption was obtained from the Eq. 1:

$$WA\ (\%) = \frac{M_1 - M_0}{M_0} * 100\ (1)$$

Where M1 is the mass of the specimen (in grams) after immersion times in water and M0 is the mass of the sample before immersion in water.

Results and Discussion

The results of the melt index measurements for the TPS processed in a twin-screw extruder are shown in Fig. 1a. The concentrations with 35 and 45 wt% of glycerol showed low fluidity. According to Edhirej [6], this indicates the presence of strong intermolecular interactions, reducing the mobility of the polymeric chains present in the starch, thus increasing the viscosity and, consequently, reducing the fluidity of the TPS. On the other hand, the high fluidity of the TPS was observed for the 55 wt% of glycerol concentration, showing that the intermolecular interactions were reduced, thus increasing the macromolecular mobility and, facilitating the fluidity of the material.

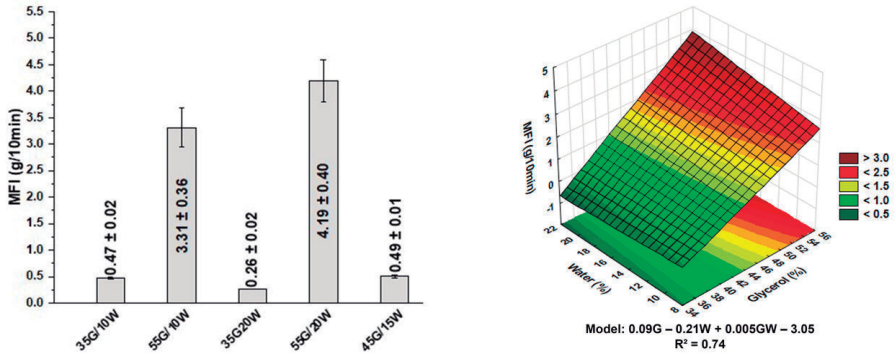

(a) **(b)**

Figure 1 – Experimental and statistical results. (a) Measurements of flow index of TPS. (b) Experimental design response surfaces.

Water showed an indication of reducing the fluidity of TPS at the same glycerol concentration, as in the 35G/10W and 35G/20W formulations. The increase in water concentration reduced the fluidity of the TPS, making it more viscous. According to Vieira et al [7], because the water molecule has a low molecular weight, the molecules tend to be incorporated into the starch. Water molecules tend to volatilize when the material is subjected to high temperatures, thus increasing the viscosity of the TPS. The influence of glycerol and water on the MFI of the TPS is illustrated in the response surface shown in Fig 1b, making it possible to observe that the increase in the fluidity of the material is mainly due to the presence of glycerol as a plasticizer.

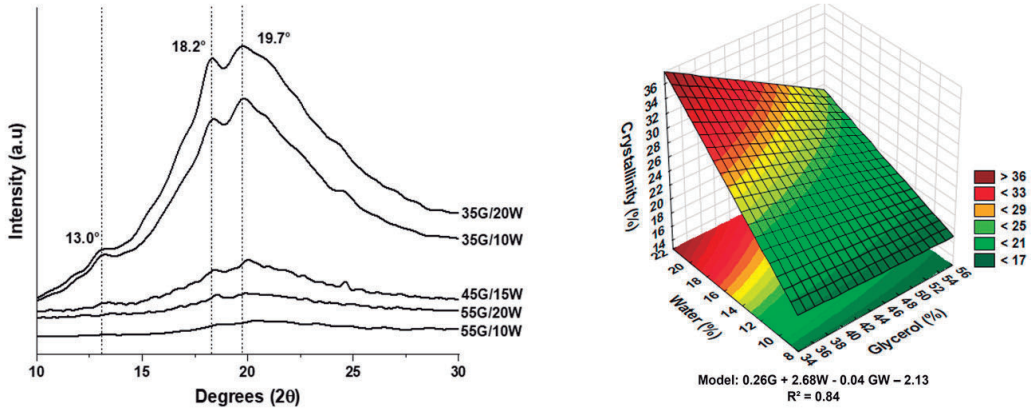

(a) **(b)**

Figure 2 – Experimental and statistical results. (a) TPS X-ray diffractograms. (b) Crystallinity response surface.

The TPS diffractograms are presented in Fig 2a and show that the 35G/20W and 35G/10W formulations presented characteristic peaks of high intensity at 13, 18.2° and 19.7° (2θ) indicating that such formulations presented a higher degree of crystallinity. According to González et al. [8] these peaks are characteristic of a crystalline structure known as type V, which is formed by the molecules of plasticizers used with the macromolecules present in starch (amylose-glycerol/water).

Increasing the glycerol concentration reduces the formation of the V-type crystalline structure (Fig 2a), since the diffractogram for the formulations containing 45 and 55% glycerol did not show well-defined or high-intensity peaks. The increase in water concentration promoted a slight increase in TPS crystallinity, showing that the water molecule can remain in the starch structure, favoring the formation of the V-type structure.

The response surface presented in Fig 2b indicates the tendency of TPS crystallinity to decrease with increasing glycerol concentration, which can be visualized by observing the green color region.

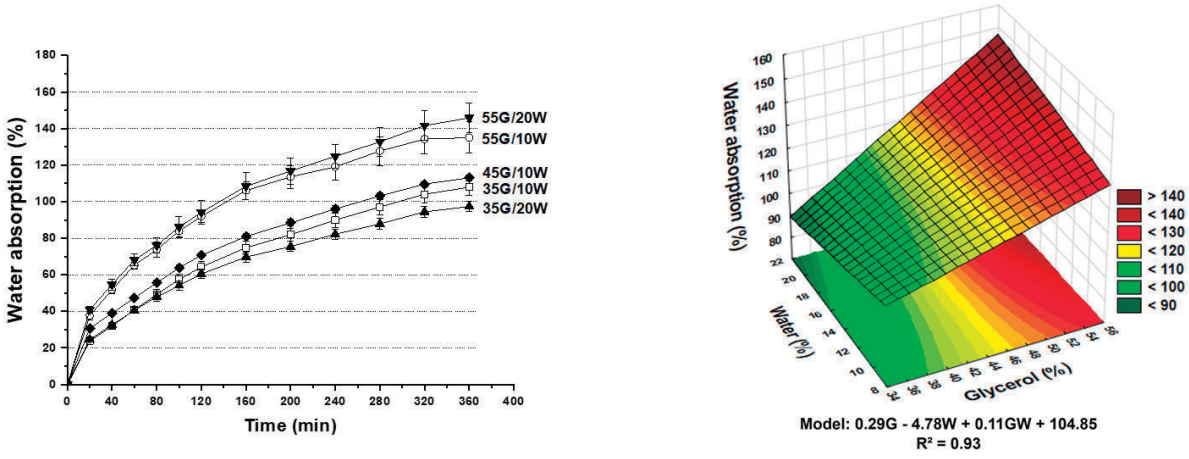

(a) **(b)**

Figure 3 – Experimental and statistical results. (a) TPS water absorption. (b) Water absorption response surface after 6 hours immersion.

The TPS water absorption curves are shown in Fig 3a and indicate that over time the samples that showed the highest glycerol concentration were those that showed the highest degree of water absorption. According to the literature [4,7], glycerol molecules have more hydroxyl groups when compared to water, allowing greater interaction with the macromolecules present in

starch and, as a consequence, increasing the intermolecular spacing, that is, facilitating the penetration of water molecules in the material.

The formulations that showed the lowest degree of water absorption were those with low concentration of glycerol (35G/10W and 35G/20W), showing that evidence that the greater crystallinity of the material hinders the diffusion of water molecules to the nucleus of the material. Comparing the crystallinity response surfaces (Fig 2b) with the water absorption response surface (Fig 3b), it is verified that the increase in the glycerol concentration reduces the crystallinity and causes an increase in water absorption, while for the water the relationship is opposite.

Conclusions

In view of the results presented in this work, it was possible to observe, through the measurement of flow index, X-ray diffractogram and water absorption test, an influence of the concentration of plasticizers on the rheological and physical properties of the TPS obtained. The increase in the mass concentration of glycerol provided an improvement in the fluidity and provided a reduction in the degree of crystallinity of the TPS, while the increase in the mass concentration of water proportional to the reduction of the water absorption of the material. Response surfaces were an important tool to visualize the plasticizer concentration relationship and the properties obtained.

Acknowledgements

The authors are grateful to CAPES and CNPq for granting financial support.

References

1. A. S. Giroto; R. H. S. Garcia; L. A. Colnago; A. Klamczynski; G. M. Glenn; C. Ribeiro Int. J. Biol. Macromol. 2020, 144, 143. https://doi.org/10.1016/j.ijbiomac.2019.12.094
2. A. C. Correa; V. B. Carmona; J. A. Simão; L. H. Capparelli Mattoso; J. M. Marconcini, Carbohydr. Polym. 2017, 167, 177 https://doi.org/10.1016/j.carbpol.2017.03.051
3. A. Giuri; S. Colella; A. Listorti; A. Rizzo; C. E. Corcione Journal of Thermal Analysis and Calorimetry, 2018, 134, 549 https://doi.org/10.1007/s10973-018-7404-7
4. C. E. Montilla-Buitrago; R. A. Gómez-López; J. F. Solanilla-Duque; L. Serna-Cock; H. S. Villada-Castillo, Starch - Stärke 2021, 73, 2100060. https://doi.org/10.1002/star.202100060
5. K. Frost; d. Kaminski; G. Kirwan; E. Lascaris; R. Shanks Carbohydr. Polym. 2009, 78, 543 https://doi.org/10.1016/j.carbpol.2009.05.018
6. A. Edhirej; S.M. Sapuan; M. Jawaida; N.I. Zahari Starch – Stärke 2017, 69: 1500366. https://doi.org/10.1002/star.201500366
7. M. G. A. Vieira, M. A. Da Silva, L. O. Dos Santos, M. M. Beppu, Eur. Polym. J. 2011, 47, 254 https://doi.org/10.1016/j.eurpolymj.2010.12.011
8. K. González, L. Iturriaga, A. González, A. Eceiza, N. Gabilondo, Eur. Polym. J. 2020, 123, 109415. https://doi.org/10.1016/j.eurpolymj.2019.109415

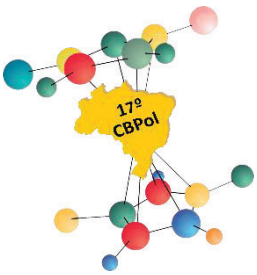

INFLUENCE OF THE ADDITION OF POLYPHENOLS EXTRACTED FROM WINE WASTE ON THE PROPERTIES OF POLYLACTIC ACID

Beatriz Luize de Souza[1*], Wagner Mauricio Packekoski[1]

1 – Department of Engineering and Mechanical Sciences, University of Santa Catarina (UFSC), Joinville, SC, Brazil
*beatriz.luize@posgrad.ufsc.br

Abstract – Polylactic acid (PLA) is a promising biopolymer that can be synthesized from first-and second-generation raw materials, such as corn straw and bagasse [1]. Characteristics such as biocompatibility, recyclability and non-toxicity make it attractive as a material for biomedical and medicinal applications. However, the high price, the fragility of the mechanical properties and its low temperature of thermal deformation limit its wider applications in the industrial field and, therefore, many efforts have been dedicated to the improvement of its mechanical and thermal properties [2]. In parallel, grapes are one of the most cultivated, demanded, and valued fruits globally. Utilizing by-products from grape production can address ecological and economic issues. One approach to the use of these materials is the use of fractions recovered from the waste to be used as natural additives for polymers [3]. The antioxidant activity is considered one of the most remarkable bioactivities of the phenolic compound of grape pomace, this is dependent on the number of hydroxyl groups present in the molecule [4]. These antioxidant compounds are intended for use in polymers to interrupt the radical degradative reaction of the chains [3]. This study aims to evaluate the application of wine production by-products as natural additives for PLA, optimizing processing and improving thermal properties while maintaining biodegradability and mechanical properties. The expectation of the results is successful polyphenol extraction and a significant polyphenol presence. The tests should prove the efficiency of the natural oxidative potential of the polyphenols obtained from the grape pomace in the thermal properties, with no substantial improvement in mechanical properties. Degradation tests should show increased weight loss over time in samples with grape seed extract (GSE).

References

1. V. Aryan; D. Maga; P. Majgaonkar; R. Hanich *Resources, Conservation And Recycling* 2021, 172, 105670. http://dx.doi.org/10.1016/j.resconrec.2021.105670.
2. T. Albuquerque; J. Marques Júnior; L. Queiroz; A. Ricardo; M. Rocha *International Journal Of Biological Macromolecules* 2021, 186, 933-951. http://dx.doi.org/10.1016/j.ijbiomac.2021.07.074.
3. A. Nanni; D. Battegazzore; A. Frache; M. Messori *Polymer Degradation And Stability* 2019, 165, 49-59. http://dx.doi.org/10.1016/j.polymdegradstab.2019.04.020.
4. T. Ilyas; P. Chowdhary; D. Chaurasia; E. Gnansounou; A. Pandey; P. Chaturvedi *Environmental Technology & Innovation* 2021, 23, 101592. http://dx.doi.org/10.1016/j.eti.2021.101592.

Fundings: The authors are grateful to Conselho Nacional de Desenvolvimento Científico e Tecnológico (CNPq) and and Coordenação de Aperfeiçoamento de Pessoal de Nível Superior/Fundação de Amparo à Pesquisa e Inovação do Estado de Santa Catarina (FAPESC/CAPES).

Keywords: *Grape pomace, Polylactic acid, Polyphenols, Antioxidant, Electrospinning.*

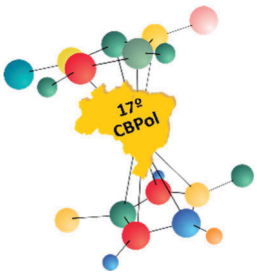

INFLUENCE OF THE AVERAGE DIAMETER OF THERMOCROMIC MICROCAPSULES ON THE FLUIDITY AND VISUAL APPEARANCE OF POLY (METHYL METHACRYLATE)

Silviane B. Silva[1], Alice C. Silva[2], Carlos H. R. Miltont[2], Carla L. S. C. Costa[4], Juciklécia S. Reinaldo[3], Edson N. Ito[4*]

1 – Undergraduate Course in Materials Engineering, Federal University of Rio Grande do Norte, Rio Grande do Norte, RN, Brazil silvianebsilva@gmail.com
2 – Graduate Program in Materials Science and Engineering, Federal University of Rio Grande do Norte, Rio Grande do Norte, RN, Brazil alice.silva.111@ufrn.edu.br; henrique.milfont@gmail.com
3 – Higher School of Technology, State University of Amazonas, Manaus, AM, Brazil jreinaldo@uea.edu.br
4 – Materials Engineering Department, Federal University of Rio Grande do Norte, Rio Grande do Norte, RN, Brazil carlalaize@yahoo.com.br; edson.ito@ufrn.br

Abstract

The objective of this work was to evaluate the influence of the average diameter of thermochromic microcapsules on the melt flow index measurements (MFI) and visual appearance of poly(methyl methacrylate) (PMMA). The purple and orange thermochromic pigments (Tamb = 23°C) were incorporated into the PMMA in the proportions of 0.1, 0.25 and 0.5 wt% using a twin-screw co-rotational extruder and then specimen were produced by injection moulding. The results of MFI showed an increase in fluidity in relation to PMMA and an increase in fluidity as a function of increasing the average diameter of thermochromic microcapsules, purple and orange, respectively. The visual aspect results indicated that the concentration above 0.25 wt% in both pigments and above the thermochromic activation temperature, the added polymers showed changes in color from darker to lighter. It was concluded in this work that the size of the microcapsules and the type of polymers influence the fluidity and optical properties.

Keywords: *PMMA*, *thermochromic pigment, average diameter, extrusion.*

Introduction

Pigments are coloring additives that can be added to a polymer to change the way the material interacts with light, imparting shades of color. These pigments are insoluble and are physically dispersed in the polymeric matrix and do not significantly affect its molecular structures, but they can influence the processability and final properties of polymeric materials [1,2].

For applications that require color changes, thermochromic pigments can be a great option, as they are compounds with high refractive power, low tincture power, and are insoluble. These pigments are additives that have the property of reversibly changing color when subjected to different temperatures, having a significant potential for the functional and aesthetic design of various polymeric materials [3].

Thermochromic materials have been widely applied in areas such as security printing, thermometers, food packaging, medical thermography, electronic circuits, pharmaceutical industry and in the textile sector. Currently, several works are reported in the literature that aim at the incorporation of thermochromic pigments in different polymeric materials, among them poly(methyl methacrylate) (PMMA) [4].

Poly (methyl methacrylate) (PMMA) is a thermoplastic, rigid, transparent and amorphous material, considered one of the most versatile polymeric materials in terms of properties and

applications [2]. This study aims was evaluate the incorporation of thermochromic pigments in purple and orange colors, in the melt flow measurements and optical properties compared to the pure PMMA, produced by extrusion in the molten state.

Experimental

Materiais

Poly (methyl methacrylate) (PMMA) from Unigel AS with a melt flow index of 4.14 g/10 min (230 °C/3.80 kg) and thermochromic pigments from CSY Paint Store was used. The thermochromic activation temperature of the purple and orange pigments is 31 °C and the average diameter of the microcapsules is 2.4 and 3.4 µm, respectively, as verified by Costa [5]. Table 1 shows the materials developed in this work.

Table 1- Materials used

Materials	Compositions (phr)
PMMA	100
PMMA/Orange Pigment	100/0.1
	100/0.25
	100/0.5
PMMA/Purple Pigment	100/0.1
	100/0.25
	100/0.5

Methods

Extrusion and injection processing

A co-rotational twin screw extruder from AX Plásticos Máquinas Técnicas, with a diameter of 16 mm and l/d = 40, was used to plasticized and homogenized the materials, with a temperature profile of 110/160/180/200/210/220/220/200ºC ºC from the feed to the die, a screw speed of 220 rpm, using a die for pellets production.

After the extrusion mixing, the materials were dried at 60°C/12h and subsequent injection molded (test specimens, ASTM D638 type I). Injection molding was carried out using an Arburg Allrounder 270S equipment with a temperature profile of 220/230/220/210/200 ºC from the feed to the injection nozzle. The mold temperature was 50 °C with a cooling time of 50s.

Visual aspects of injection molding specimens

The color change was observed by keeping the materials in two temperature conditions (5 and 60°C) for a period of 30 min and then simple digital camera was used, maintaining the luminosity and fixed focal length, to capture digital images of the surface of the samples.

Melt flow index (MFI)

Melt flow index measurements of the materials were calculated using a CEAST melt flow modular line equipment at 230 °C/3.80Kg (ASTM D1238).

Results and Discussion

Fig 1 presents the results of the melt flow index measurements obtained after mixing by extrusion for mixtures with increased concentration of microcapsules in purple and orange color. The addition of both pigments increased the fluidity of PMMA, with the microcapsules with a smaller average diameter (2.4 µm) presenting a lower fluidity than the microcapsules with a larger average diameter (3.4 µm) in all compositions studied, acting as a plasticizing agent in the mixture as a function of a critical microcapsule size.

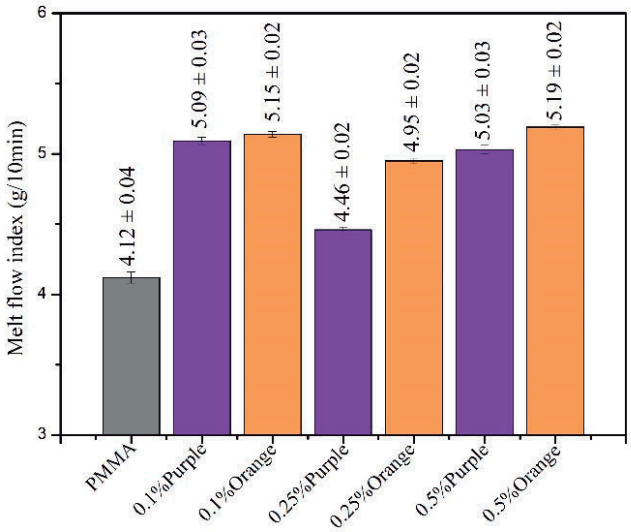

Figure 1 - Melt flow index measurements as a function of thermochromic microcapsules concentration.

Fig 2 shows the visual aspects of injection molded samples when subjected to a temperature of 5 and 60 °C. Pure PMMA is transparent and the addition of 0.1 wt% of both pigments promoted a color change in the matrix, however, the thermochromic activation of the pigments was not observed when the materials were subjected to heating. The addition of 0.25 and 0.5 wt% of the purple pigment, promoted a slight color change, starting from a dark blue color to a light blue color at 0.5 wt%, when heated, with the same behavior observed for the incorporation of the pigment orange, that is, a change in color from dark yellow to light yellow.

A color change after activation of the pigments from purple and orange to blue and yellow, respectively, was expected, which was not observed. This could be due to a possible disruption of pigment microcapsules during extrusion mixing. Another factor that may have influenced the color change of the materials, according to Mathur and Sharma [6], is the low thermal conductivity of PMMA, which makes it difficult to heat and cool the material evenly.

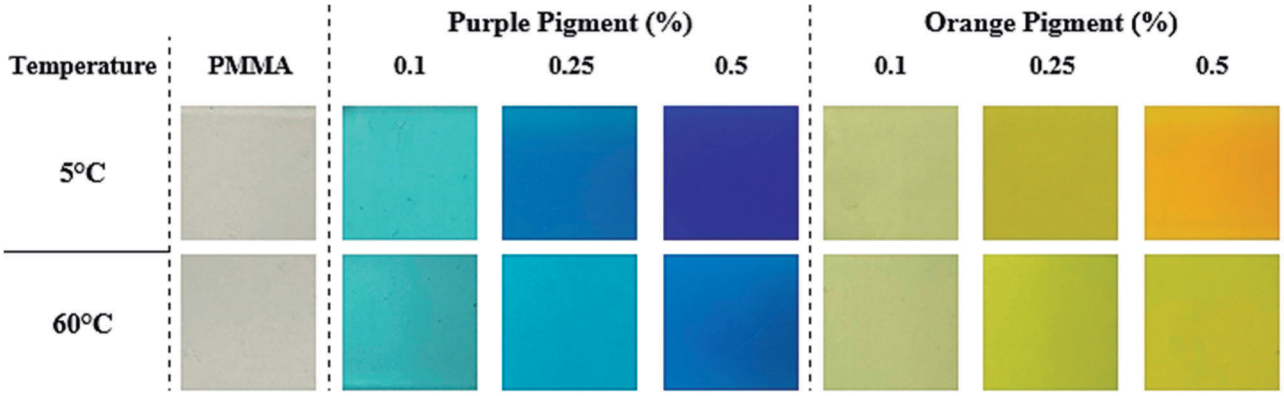

Figure 2 - Visual appearance of injection molded materials.

Conclusions

It was concluded in this work that the size of the microcapsules and the type of polymers influence the fluidity and optical properties. The incorporation of 0.5 wt% of pigments is sufficient to visualize the change in color of materials when subjected to heating for both microcapsules used.

Acknowledgements

The authors are grateful to UFRN, CAPES and CNPq for granting financial support.

References

1. S. V. Canevarolo Jr. *Ciência dos Polímeros*. Ed.: Artliber, São Paulo, 2006.
2. W. H. Brendley; R. D. Bakule Applied Polymer Science 1985, 285, 1031. https://doi.org/10.1021/bk-1985-0285.ch042.
3. X. Tao. *Smart Fibres, Fabrics and Clothing*. Ed.: Woodhead, Cambridge, 2001.
4. M. S. Tözum; S. A. Aksoy; C. Alkan Fibers and Polymers 2018, 19, 3, 660 https://doi.org/10.1007/s12221-018-7801-3.
5. C. L. S. C. Costa, MSc. Dissertation, Federal University of Rio Grande do Norte, 2022.
6. V. Mathur; K. Sharma Heat Mass Transfer 2016, 52, 2901. https://doi.org/10.1007/s00231-016-1779-4.

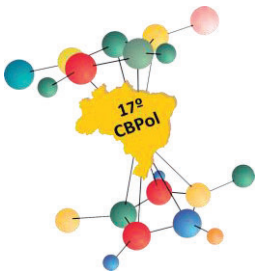

NATURALLY LM PECTINS FROM CHARDONNAY GRAPE POMACE EXTRACTED UNDER DIFFERENT CONDITIONS FORM GELS BY ADDITION OF Ca $^{2+}$

Cristiane Colodel[1], Carmen Lúcia de Oliveira Petkowicz[2]

1 – Department of Structural, Molecular and Genetic Biology, State University of Ponta Grossa (UEPG), Ponta Grossa, PR, Brazil criscolod@gmail.com
2 – Department of Biochemistry and Molecular Biology, Federal University of Parana (UFPR), Curitiba, PR, Brazil

Abstract - Pectins are widely used hydrocolloids due to their ability to form gels under specific conditions, which directly depend on their structural characteristics, mainly their degree of methyl-esterification (DM). Commercially available pectins are extracted from citrus peel and apple pomace. However, these materials originate only high DM (HM) pectins, requiring additional chemical treatments to produce low DM (LM) pectins. Furthermore, the growing demand for this hydrocolloid has made it necessary to search for new sources of pectins with good gelling properties. In this work, naturally occurring LM pectins were extracted from grape pomace using 0.5% ammonium oxalate at 25°C/4h (CSPC) and 100°C/2h (CSPH). Pectins were structurally characterized and showed a GalA content >65%, meeting commercial requirements, and DM < 18%. Both formed gels by adding Ca^{2+} and showed good stability over time, maintaining their viscoelastic properties for 60 days.

Keywords: *LM pectins; grape pomace; pectin gels; gel stability; oscillatory rheology*

Introduction

Pectins are one of the main biopolymers in plant cell walls, varying in quantity and structure depending on the species, plant tissue and developmental stage [1]. Structurally, pectins are the most complex of plant cell wall polysaccharides and correspond to a group of biopolymers, classified as homogalacturonan (HG), ramnogalacturonan I (RG I) and ramnogalacturonan II (RG II), with HG, followed by RG I, being the most common and abundant in plant tissues [1, 2, 3, 4].

HG comprise the smooth domain of pectins and are linear structures formed by repetitive residues of →4(α-D-GalA)1→, in which carboxyl group at C-6 may be free or methyl-esterified. Acetyl groups may also be present, attached at the O-2 and/or O-3 positions. The presence of methyl and acetyl groups strongly influences the physicochemical properties of pectins [1, 3, 4].

RG-I and RG-II constitute the hairy domains of pectins. RG I is formed by the repetition of the →4(α-D-GalA)1→2(α-L-Rha)1→ dyad, in which the rhamnose units may contain arabinan, galactan and/or arabinogalactan side chains of variable lengths attached at O-4. RG-II is the most complex pectic domain, composed of a short, partially methyl-esterified HG main chain substituted by 5 different types of complex side chains O-2- or O-3 linked, containing up to 13 different types of monosaccharides, including unusual monosaccharides. [1, 3, 4].

Pectins attract great industrial interest due to their physicochemical properties, especially by forming gels under specific conditions [2, 3]. Its gelation mechanism is closely related to the degree of methyl-esterification (DM); when more than 50% of the GalA units are methyl-esterified, pectin is classified as HM and form gels at low pH (< 3.5) at high concentration of soluble solids (>55%). When less than 50% of the GalA units are methyl-esterified, pectin is classified as LM and forms

gels by adding divalent ions. However, the gelation process is not so simple and the formation and quality of the formed gel also depends on other factors, such as molar mass, distribution of carboxyl/methyl-ester groups and presence of acetyl groups. Thus, pectins with differences in structural parameters can form gels with different properties or even not be able to gel [2, 3].

The main sources of industrially extracted pectins for commercial use are citrus peel and apple pomace, both residues from the juice industry, and both produce HM pectins. For commercial production of LM pectins, it is necessary to undergo HM pectins to additional de-esterification processes. Therefore, LM pectins are more valuable and search for plant sources of naturally LM pectins can be of great interest to the pectin industry [1, 2].

Grape pomace is the residue from wine production and is one of the possible non-conventional sources of pectins. Grapes are one of the most cultivated fruit species worldwide, with a world production of more than 70 million tons in 2021 [5]. Around 80% of all the grapes produced are used for winemaking [6]. For wine production, grapes are pressed and the pomace remains as waste, which corresponds to about 20% of the fruit mass [7]. It represents around 11 million tons of grape pomace produced worldwide per year [8], which means that grape pomace is a widely available raw material, distributed in different regions of the world.

In this work, grape pomace was investigated as a possible source of naturally LM pectins and the ability of forming gels by addition of Ca^{2+}, as well the properties of the gels formed were evaluated.

Experimental

Plant material

Chardonnay grape pomace (CGP) was kindly provided by Vinícola Araucária, in São José dos Pinhais, Parana, Brazil. The whole fruits were pressed to obtain the juice for production of white wine and the CGP, composed of skins, seeds and stalks, was immediately collected after pressing. CGP was then frozen, lyophilized, milled and sieved (1 mm × 1 mm). The dried and powdered CGP was then treated with boiling ethanol (1:10 w/v) under reflux for 20 min. The resulting alcohol insoluble residue (AIR) was dried at room temperature and used for extraction of pectins.

Pectin extraction

Extractions were performed in duplicate using 0.5% (w/v) ammonium oxalate (pH 6.43) under two different conditions: at 25 ºC for 4 h under mechanical stirring, yielding the fraction CSPC, and at 100 ºC for 2 h under reflux, yielding the fraction CSPH. In both extractions the solvent was employed at a solid-liquid ratio of 1:25 g/ml. After the extraction, each extract was centrifuged, filtered and dialyzed against distilled water until the presence of oxalate not be detected by addiction of $AgNO_3$. Then, the extracts were concentrated to 50% of initial volume by rotative evaporation and so pectins were precipitated by addition of ethanol 2:1 (v/v). After refrigeration for 4 ºC overnight, pectins were recovered by filtration, washed with ethanol and lyophilized.

Monosaccharide composition

The monosaccharide composition was determined by gas-chromatography of alditol acetates, as described by [9].

High pressure size exclusion cromatography

HPSEC analyses and the calculus of average molar mass were performed as described by [9].

Acetyl content

The acetyl content was determined by Hestrin method [10], using galactose pentaacetate as standard, and the degree of acetylation (DA) was calculated as described by [9].

Fourier-transform infrared

The Fourier-transform infrared (FT-IR) spectra of pectic fractions were collected at the absorbance mode in the frequency range of 4000–400 cm^{-1} using a Vertex 70 spectrophotometer (Bruker, Germany), at 4 cm^{-1} resolution and 32 scans. Spectroscopic grade KBr powder was used and discs were prepared using a 99:1 salt/sample proportion. The degree of methyl-esterification was calculated as the ratio between the integration area of the methyl-esterified band (1749 cm^{-1}) and the sum of the areas of methyl-esterified (1749 cm^{-1}) and non-esterified (1630 cm^{-1}) bands.

Rheological analysis of pectin gels

Pectins were dissolved in deionized water at the desired concentration (0.5 – 2% w/v), poured into a dialysis cellulose membrane (cut-off 1 KDa) and placed against 1 M $CaCl_2$ solution at 4 ºC for 24 h. The gel formed was recovered from the dialysis membrane and a gel disk of 20 mm (diameter) × 5 mm (height) was employed for rheological analysis. The rheological characterization of gels was performed using a Thermo Scientific HAAKE MARS II rheometer (Haake GmbH, Germany) coupled to a HAAKE K15 thermostatic water bath, a HAAKE DC5 heating control and HAAKE UTMC unit. Data were collected and analyzed using the software RheoWin 4. Graphs were generated using the software GraphPad Prism. The gels were characterized by oscillatory experiments, that were carried out at 25 ºC using a P20 TiL parallel plate geometry. First, stress sweeps were performed under a range of 0.01–10 Pa at constant frequency of 1 Hz, in order to determine the viscoelastic region of samples. Thereafter, frequency sweeps were performed applying a frequency range of 0.01–100 Hz, under shear stress within the linear viscoelastic region, previously determined. To assess the stability of the gels over time, after the rheological analysis on the day the gels were prepared, the disks were stored in 1M CaCl2 solution at 4ºC and the analyzes were repeated after 15, 30 and 60 days.

Results and Discussion

Table 1 presents a comparative data concerning the chemical composition and some structural parameters of CSPC and CSPH.

Table 1 Comparison of yield, composition and structural characteristics of CSP and CSPH

		CSPC	**CSPH**
	Yield (%)	2.2 ± 0.4	6.9 ± 0.8
Monosaccharide composition (%)	Rha	3.0 ± 0.2	1.5 ± 0.1
	Fuc	0.4 ± 0.3	0.1 ± 0.0
	Ara	12.8 ± 0.8	6.8 ± 0.0
	Xyl	1.9 ± 0.0	0.5 ± 0.0
	Man	2.5 ± 0.0	0.8 ± 0.0
	Gal	8.9 ± 0.4	4.0 ± 0.0
	Glc	4.5 ± 0.1	2.9 ± 0.0
	GalA	65.7 ± 0.7	83.4 ± 2.3
	DM	9.3 ± 0.6	17.7 ± 0.7
	Acetyl content (%)	2.1 ± 0.4	2.2 ± 0.03
	DA (%)	15.4 ± 0.4	10.8 ± 0.2
	HG (%)	62.7	81.9
	RG-I (%)	27.7	13.8
	(Ara+Gal)/Rha	7.2	7.2
	M_w (g/mol)	9.777×10^4 (±0.6%)	5.077×10^5 (±0.6%)
	dn/*dc*	0.129	0.146
	Polydispersity (M_n/M_w)	6.874±0.113	32.859±0.691

The extraction conditions applied extraction tested affected the yield, since hot extraction resulted in yield of 6.9%, more than three times higher than cold extraction.

Regarding the GalA content, both pectins had >65%, complying with commercial requirements, but the GalA content was notably higher in CSPH (83.4%). It results in a higher HG ratio in CSPH (81.9%) compared to CSPC (62.7%). As a result, CSPC was richer in neutral sugars, mainly arabinose and galactose.

Although they are very different in relation to the proportion of HG and RG-I that compose their structures, CSPC and CSPH presented exactly the same ratio (Ara+Gal)/Rha, which acts as an indicator of the average size of the branches in the RG-I domain . For both, the average length of the side chains was 7.2 residues.

CSPC and CSPH was both characterized as naturally LM pectins, with DM of 9.3% and 17.7%, respectively. Both pectins presented low acetyl content, of 2.1 and 2.2%, which is a desirable parameter, since acetyl content above 3.5% tends to hinder the gelation of pectins [11].

The average molar mass of CSPC was 9.777×10^4 g/mol, about 5 times smaller than the average molar mass of CSPH, 5.077×10^5 g/mol, suggesting that higher temperatures are more prone to breaking bonds and interactions between larger biopolymers in the plant cell wall and solubilizing them upon extraction. However, CSPC showed a polydispersion value almost 5 times lower than CSPH, suggesting a structurally more homogeneous pectin.

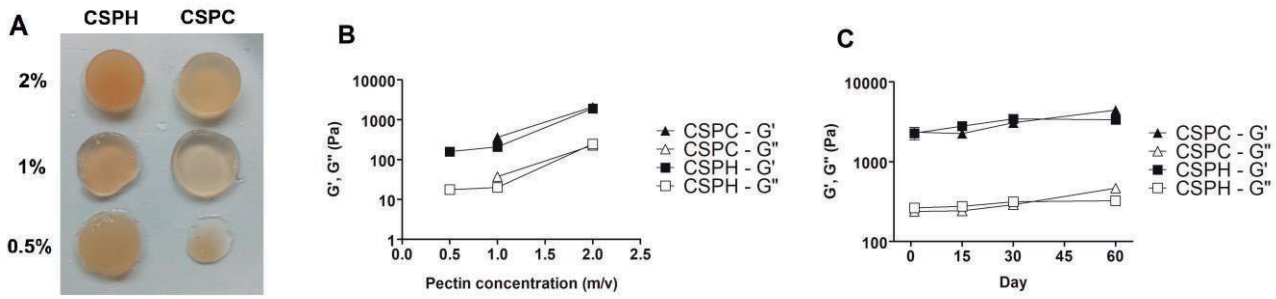

Figure 1– Gel formation of CSPC and CSPH at different concentrations (A), viscoelastic response at 0.1 Hz of gels at different concentrations (B) and time stability of gels over 60 days at 2% (m/v) and 0.1 Hz (C).

Fig. 1-A shows that there was satisfactory gel formation at all concentrations tested, except for CSPC at a concentration of 0.5%, where microgel formation was observed [12].

The graph shown in Fig 1-B shows the dependence of the viscoelastic properties of the gels on the pectin concentration used. The results show that the increase in pectin concentration leads to an increase in elastic (G') and viscous (G") modulus, characterizing the formation of stronger and more consistent gels. Although the two pectins showed great structural differences, the viscoelastic behavior of the gels was very similar.

At Fig 1-C, the graph shows the viscoelastic properties of gels prepared at 2% (m/v) of pectins stored and evaluated over 60 days. The graph shows that the gels prepared with the two pectins were stable for 60 days, maintaining the values of G' and G" throughout the analysis time. The formation of stable gels is a desirable characteristic for pectins, since that this property is related to the shelf life of products made with this biopolymer.

Conclusions

Naturally LM pectins can be obtained from Chardonnay grape pomace by extraction using ammonium oxalate solution under different conditions. These pectins have structural parameters comparable to commercial pectins, particularly with GalA content > 65%. Although CSPH showed more favorable structural parameters, such as high GalA content, low neutral sugar content and

higher molar mass, CSPC showed lower polydispersion. Both pectins were able to form gels in the presence of Ca^{2+} and showed similar viscoelastic properties and good stability for 60 days of storage. The results obtained suggest that Chardonnay grape pomace can be a good industrial source of naturally LM pectins.

Acknowledgements
The authors thanks to the Brazilian agency CNPq for financial support and especially to Mr. Adolar Adur and Joel Ferrari from Vinicola Araucaria that kindly provided the grape pomace material.

References

1. L. H. S. Reichembach; C. L. O. Petkowicz 2021. Food Hydrocolloids, 118, 106824. https://doi.org/10.1016/j.foodhyd.2021.106824
2. R. Ciriminna *et al.* 2022. Food Hydrocolloids, 127, 107483. https://doi.org/10.1016/j.foodhyd.2022.107483
3. S. Y. Chan *et al.* 2017. Carbohydrate Polymers, 161, 188-139. http://dx.doi.org/10.1016/j.carbpol.2016.12.033
4. D. Mohnen 2008. Current Opinion in Plant Biology, 11, 266-277. https://doi.org/10.1016/j.pbi.2008.03.006
5. FAOSTAT 2022. Available in https://www.fao.org/faostat/en/#data/QCL/visualize, accessed March 23, 2023.
6. R. G. Maroun *et al* in *Handbook of grape processing by-products – Sustainable solutions,* C.M. Galanakis, Ed., Academic Press, London, 2017; 155-181.
7. J. García-Lomillo; M. L. González-Sanjosé, 2017. Compreensive Reviews in Food Science and Food Safety. 16, 3-22. https://doi.org/10.1111/1541-4337.12238
8. J. Domínguez; J. C. Sanchez-Hernandez; M. Lores in *Handbook of grape processing by-products – Sustainable solutions*, C.M. Galanakis, Ed., Academic Press, London, 2017; 55-78.
9. L. H. S. Reichembach; C. L. O. Petkowicz 2020. Carbohydrate Polymers, 245, 116473. https://doi.org/10.1016/j.carbpol.2020.116473
10. S. Hestrin 1949. Journal of Biological Chemistry, 180, 249–261. https://doi.org/10.1016/S0021-9258(18)56740-5
11. E. L. Pippen; R. M. McReady; H. S. Owens 1950. Journal of American Chemical Society, 72, 813-816. https://doi.org/10.1021/ja01158a043
12. C. Garnier; M. A. V. Axelos; J. F. Thibault 1993. Carbohydrate Research, 240, 219-232. https://doi.org/10.1016/0008-6215(93)84185-9

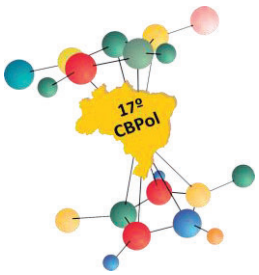

PERFORMANCE OF PE WAXES ON EPS NUCLEATION AND RELATIONSHIP WITH THEIR THERMAL TRANSITIONS

Jéssica F. T. C. Petry, Rafael Guzatto, Vinicius S. Leite, Andreia Ossig

Innova, Triunfo, RS, Brazil
jessica.petry@iinova.com.br

Abstract – Polyethylene (PE) waxes are used in the production of expandable polystyrene (EPS) as nucleating agents, directly influencing the formation of the cellular structure formation of expanded polystyrene foam. The performance of the material in its final application depends on the homogeneity of the expanded bead cells. The characteristics of each wax affect nucleation in different ways, which can lead to collapsed, heterogeneous or porous beads, indicating poor cell nucleation. This work aims to understand how the chemical and physicochemical characteristics of PE waxes influence the nucleation process during EPS expansion. These evaluations were carried out by DSC analyzes and pilot line tests. PE waxes with around 2,000 g mol^{-1} molar weight and narrow polydispersity index showed better results as nucleating agents for EPS.
Keywords: polyethylene waxes, expandable polystyrene, differential scanning calorimetry, nucleating agents, thermal behavior

Introduction

Polyolefin waxes are ethylene oligomers formed as by-products in ethylene polymerization processes with molecular weight below 10,000 g mol^{-1}. The accumulation of polyethylene waxes in the reaction system is undesirable and therefore needs to be removed. In addition, olefinic waxes can also be obtained through direct monomer synthesis or thermal degradation of polyolefins.[1]
The properties of polyethylene waxes change according with process parameters such as amount of hydrogen, amount of comonomer or type of catalyst. These characteristics change according to the wax application. They can be used in fertilizers production, textile and electrotechnical industry, plastics processing and thermoplastic foams production.[2-4]
Thermal properties of waxes are crucial in determining their application as they are related to the need for modifications to improve their performance. The modifications commonly made involve both chemical and physical modifications, the most common of which is oxidation reaction. One of the most used methods to determine the thermal properties of materials is Differential Scanning Calorimetry (DSC). Through this analysis it is possible to quickly determine thermal transitions of the material.[5,6]
Polyethylene waxes are used as nucleating agents in EPS production. EPS is a lightweight, closed-cell, rigid foam plastic material produced from polystyrene. The most common uses are for packaging and construction.[7] The most important step in manufacturing EPS is to create the correct foam structure, which are homogeneously distributed and with similar cell size. Nucleating and blowing agents play the main role to control cell formation sites. The performance of the expanded material in its final application depends on the homogeneity of the expanded bead cells. The characteristics of each wax affect nucleation in different ways, which can lead to collapsed, heterogeneous or porous beads when poor nucleation occurs.[8] This work aims to understand how

the chemical and physicochemical characteristics of PE waxes influence the nucleation process during EPS expansion. These evaluations were carried out by DSC analysis and processing tests (expansion and molding) of EPS produced in a pilot line.

Experimental

Polyethylene waxes
Polyethylene waxes from different sources were tested in this work. Waxes' physical and chemical properties are shown in Table 1, according to each supplier information.

Table 1 - Physical and chemical characteristics of waxes.

Wax	Mw (g mol^{-1})	Viscosity (cP) ASTM D3236	Drop Melting Point (°C) ASTM D127/D3954	ρ (g cm^3) ISO 1183	Penetration 25 °C (10^{-1} mm) ASTM D1321
Wax 1	2,000	49-55	126	0,97	0,5
Wax 2	2,000	35-55	125	-	1
Wax 3	2,300	40-80	125-130	0,97	-
Wax 4	2,000	80	126	0,97	-
Wax 5	1,000	< 600	120-130	-	1
Wax 6	1,000	12-15	113	0,96	1
Wax 7	1,100	13	117	-	1
Wax 8	1,000	450	112	0,92	-
Wax 9	-	370-475	112-117	0,93-0,95	1

Thermal behavior - Differential scanning calorimetry DSC
Differential scanning calorimetry was carried out on a DSC25 TA Instruments thermal analyzer in nitrogen atmosphere and operating at a gas flow rate of 50 mL/min. Samples were heated from 20 °C to 100 °C at a heating rate of 10 °C min^{-1} and cooled at the same rate, after which the cycle was repeated. Thermal properties such as melting and crystallization temperatures, and enthalpies were determined from the second scan.

Nucleating agents – Pilot line EPS production and expansion
Expandable polystyrene beads were obtained by extruding polystyrene (GPPS – general purpose polystyrene) with expansion agent impregnation in the melt. Polystyrene matrix, nucleating agent PE wax and other additives are mixed in a co-rotating twin-screw extruder before pentane injection in a pressure-controlled system. After that, the melt passes through a series of static mixers before an underwater micropelletizing cutting system to obtain the EPS beads.
EPS beads were dried, added surface additive to improve posterior processing and let rest for some days. After maturation, EPS granules were expanded in an Erlenbach expander with wet steam pressure to evaluate the nucleation efficiency.

Results and Discussion

Thermal behavior - Differential scanning calorimetry DSC
Thermal behavior of the waxes was analyzed by DSC and transition temperatures are summarized in Table 2 and Table 3. Thermograms with melting endotherms e crystallization exotherms are presented in Figure 1 and Figure 2.
Through thermograms it is possible to observe that higher molecular weight waxes showed melting endotherms at higher temperatures. Waxes with narrow polydispersity indexes presented narrow thermal transitions. Melting and crystallization temperatures follow closely the molecular weights

of the waxes, with lower molecular weight waxes melting sooner and crystallizing at lower temperatures. Broad thermograms observed for some waxes can be attributed to the increased heterogeneity in this wax in terms of chain length, branching frequency and therefore defects in the crystal structure.

DSC thermograms curves for second heating cycle and second cooling were interpreted and obtained reviewed data were compared among studied waxes. To better understand waxes behavior, results were separated in two groups. One of them including waxes with molecular weight around 1,000 g mol^{-1} and the other containing waxes with molecular weight around 2,000 g mol^{-1}.

Table 2 - Thermal behavior from waxes with molecular weight around 2,000 g mol^{-1} for second heating cycle.

Waxes	Temperature onset (°C)	Peak Temperature (°C)	Peak width at half heignt (°C)	Enthalpy (J/g)
Wax 1	119,08	124,48	5,35	205,63
Wax 2	119,14	123,27	4,41	130,56
Wax 3	116,88	124,04	6,2	220,70 bimodal
Wax 4	117,91	124,35	6,49	238,19 bimodal
Wax 5	104,17	111,87	10,92	244,51 bimodal

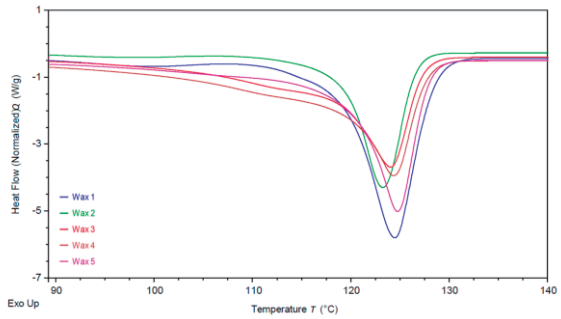

Figure 1 – Thermogram for second heating cycle from waxes with molecular weight around 2,000 g mol^{-1}.

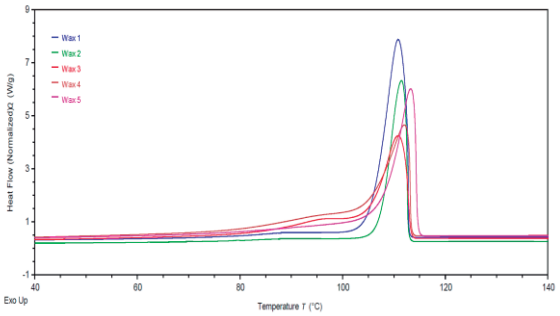

Figure 2 – Thermogram for second cooling cycle from waxes with molecular weight around 2,000 g mol^{-1}.

Through second heating thermograms shown in Figure 1, it is possible to observe the width variation for melting peak at lower temperatures, trending bimodal profiles, more pronounced according to the increase of waxes polydispersity index. Broad molecular weight distribution leads to non-uniform nucleation, causing defects in bead and impairing its mechanical properties. Among the studied waxes, Wax 1 and Wax 2 presented more similar thermal behavior with narrower peaks, proving their narrow polydispersity index. Exothermic process related to waxes crystallization follow melting behavior, as shown in Figure 2. Wax 1 and Wax 2 presented narrow crystallization peaks and absence of bimodal profile.

Thermal characteristics for waxes with 1,000 g mol^{-1} molecular weight are presented in Table 3. These waxes showed thermal behavior more distant from each other. Wide transitions peaks and

bimodal profiles became more pronounced in these waxes. Wax 1 was used as standard and compared as desirable behavior.

Table 3 - Thermal behavior waxes with molecular weight around 1,000 g mol^{-1} for second heating cycle.

Waxes	Onset temperature (°C)	Peak temperature (°C)	Peak width at half height (°C)	Enthalpy (J/g)
Wax 1	119,08	124,48	5,35	205,63
Wax 6	104,16	111,87	10,92	244,28 bimodal
Wax 7	80,97	100,76 / 112,66	25,89	230,39 bimodal
Wax 8	100,01	106,43 / 110,01	12,94	118,52 bimodal
Wax 9	107,01	112,3	6,41	145,5 bimodal

Thermograms for second heating and second cooling cycle are shown in Figure 3 and Figure 4. For both graphs, thermal behavior stayed the same. Waxes showed different range for melting and crystallization transitions, although all of them presented bimodal profiles. DSC analyzes proved that studied waxes with lower molecular weight own thermal behavior distant for Wax 1 when it comes to temperature range and profile. And these characteristics lead to different conduct as nucleating agent.

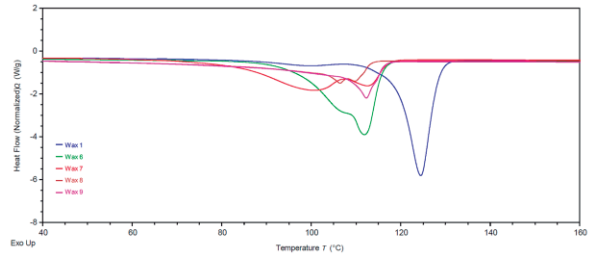

Figure 3 – Thermogram for second heating cycle from waxes with molecular weight around 1,000 g mol^{-1}.

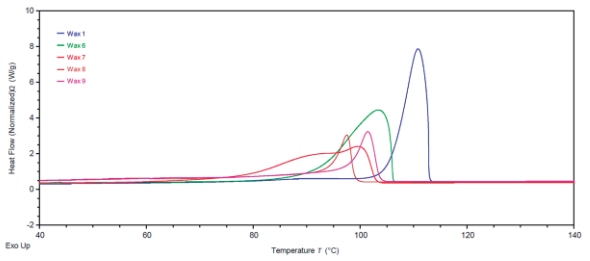

Figure 4 – Thermogram for second cooling cycle from waxes with molecular weight around 1,000 g mol^{-1}.

Nucleating agents – Pilot line test producing EPS

In order to better understand how the results referring to the thermal behavior affect the nucleation properties, tests in a pilot line were carried out. EPS was produced using studied waxes and analyzed about the expansion process. Table 4 presents the comparative data for the analyzes and waxes behavior. Wax 2 which has molecular weight of 2,000 g mol^{-1} and narrow polydispersity index showed excellent performance. However, Wax 5 which has molecular weight around 2,300 g mol^{-1}, a slight increase compared to Wax 1, showed a deviation in the maximum peak of crystallization and, consequently, the nucleating action of the wax.

Table 4 – Comparative results from DSC analyzes and pilot line tests.

Waxes	Pilot line results	DSC results		
		Profile	Tc (°C)	Peak width at half height (°C)
Wax 1	Standard wax	Low polydispersity index	111	4,7
Wax 2	Similar to Wax 1	Low polydispersity index	111	3,5

Wax 3	Shiny beads	Bimodal profile (High polydispersity index)	111	5,5
Wax 4	Shiny and heterogeneous beads	Wide molecular weight distribution, bimodal profile	112	5,7
Wax 5	Collapsed beads, bad nucleation and high density	Narrow molecular weight distribution, although bimodal profile	113	4,3
Wax 6	Couldn't expand	Wide molecular weight distribution	103	9,1
Wax 7	High density	High polydispersity index	100	16,7
Wax 8	Shiny and heterogeneous beads	Narrow molecular weight distribution, although bimodal profile	98	2,9
Wax 9	Shiny and collapsed beads	Narrow molecular weight distribution, although bimodal profile	101	3,6

Conclusions

Comparing DSC thermograms and pilot line tests, it is possible to observe a better performance trend for waxes that have a maximum crystallization peak temperature between 110 and 112 °C. Furthermore, waxes with narrow molar weight distribution (polydispersity index) presented better bead nucleation performance. Molecular weight also directly affects waxes behavior. Using the same expansion conditions for every sample, Wax 2 was the only to achieve similar performance from the standard Wax 1. Both presents same molecular weight (2000 g mol^{-1}) and narrow polydispersity index.

References

1. G. Marszałek; J. Zielinski; W. Ciesinska Przem Chemiczny 2011, 90, 1264. https://doi.org/10.1007/s10973-016-5706-1.
2. M. Mngomezulu; A. Luyt; I. Krupa Polymer Composites 2011, 32, 1155. https://doi.org/10.1002/pc.21134.
3. Y. Edwards; Y. Tasdemir; U. Jsacsson Energy Fuels 2005, 19, 2519. https://doi.org/10.1021/ef050166r.
4. J. Hadiya; A. Shukla Journal of Thermal Analysis and Calorimetry 2016, 124, 1511. https://doi.org/10.1007/s10973-016-5276-2.
5. S. Yetgin European Journal of Technique 2020, 10, 489. https://doi.org/10.36222/ejt.718423.
6. E.J. Lee; J.K. Park; Y.S. Lee Korean Journal of Chemical Engineering 2010, 27, 524. https://doi.org/10.1007/s11814-010-0113-y.
7. A. Ellouze; D. Jesson; R. Cheikh Polymer Engineering & Science 2020, 60, 2710. https://doi.org/10.1002/pen.25502.
8. J. Shea *Polymeric foams: mechanisms and materials [Book review],* IEEE Electrical Insulation Magazine 2005, 21, 56. https://doi.org/10.1109/MEI.2005.1412232.

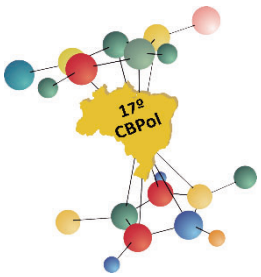

PHYSICOCHEMICAL EVALUATION OF OAT SHELLS BY DIFFERENT CHARACTERIZATION TECHNIQUES

Raphael Valle Ferreira[1], Ivana Lourenço de Mello Ferreira[1*] e Marcia Parente Melo da Costa[1].

1 – Instituto de Química, Universidade do Estado do Rio de Janeiro (UERJ), Rio de Janeiro, RJ, Brasil.
*ivanalmellof@gmail.com ; ivanamello@uerj.br

Abstract – Oat shells (or hulls) are considered to be agricultural waste from the production of oats, usually as food. This material was pressed through different meshes, with size of 200 chosen as a reference for the physicochemical analyses. The procedures aimed to identify which substances were contained in the samples studied, seeking the best possible applicability. FTIR was used to identify the main compounds present in the shells; SEM was applied to observe whether the porosity is sufficient for the material to act as an adsorbent; TGA was used to evaluate the thermal stability of the material; and XRD was used to identify the elements composing the sample and the crystallinity degree. The results provided insights into the possibility of using oat shells for various purposes as alternatives to conventional materials, which are often toxic and non-biodegradable.

Keywords: *Oat shell; characterization; microscopy; biodegradable.*

Introduction

In the midst of the 21st century, the world is experiencing a growing number of techno-scientific innovations related to electronic devices, medicinal and therapeutic treatments and food processing, among other advances. However, this progress must pay heed to the growing global concern for the environment. The disposal of wastes and byproducts, which are often ignored, is an environmental concern due to their possible toxic nature. Scientific development must be accompanied by a critical look at what is being produced and how it is being produced.

In this work, oat hulls, a primary residue, were investigated with the objective of determining their physical-chemical composition and identifying possible properties that can be applied in the development of final products. Although there are no official data related to environmental harm caused by out shells, adding value to this waste is important for combating environmental pollution [1, 2].

Oats, a cereal consumed all over the world, have high fiber content - about 88% in the husks. In Brazil, the South region is the main producer [3, 4]. However, only the grains are used and the husks are discarded. These husks correspond to 25% to 30% [3-6] of the weight of oats, so adding value to this agricultural residue is one of the fundamental tasks to avoid its accumulation and the corresponding environmental impact.

Understanding the composition of oat hulls opens up a range of possibilities for new alternatives. Because it is a biodegradable material, with high availability and low cost, it can have high environmental value [7]. Two aspects are involved: improvement of the environmental impact caused by improper disposal; and possible development of new technologies to protect the environment.

Experimental

A sample of fresh oat hulls was used as received, kindly donated by Dubai Alimentos.

The oat hulls were ground in an Arno Power Max 1000 W blender and then sieved with a sieve shaker (Retsch AS 2000 Basic) using sieves with different meshes (200, 270 and 325), with the aim of obtaining sample fractions with homogeneous size.

Fourier-transform infrared spectroscopy (FTIR) was performed with a PerkinElmer Frontier MIR/FIR spectrometer. The sample was previously prepared to keep it dry and the air was dehumidified. After being placed in a suitable support, the compartment was quickly closed to prevent carbon dioxide and water vapor from the environment from interfering with the sample. The blank used for this analysis was atmospheric air itself. This result was obtained in the range of 4000 - 600 cm^{-1}, with an attenuated total reflectance (ATR) accessory.

For scanning electron microscopy (SEM) analysis, we used a Thermo Scientific 6742A-1UUS-SN microscope. The sample was coated with a thin layer of gold to improve electrical conductivity. The applied voltage was 20 kV.

The thermogravimetric analysis (TGA) relied on a TA Instruments Q50 analyzer. The sample was placed in platinum capsules and heated in an inert nitrogen atmosphere so that the stages of degradation could be evaluated. Degradation onset temperatures (Tonset) were calculated by extrapolating the baseline with the TG decay line.

Finally, for the X-ray diffraction (XRD) analysis, we used a Bruker D8 Advance diffractometer. The sample was placed on a rotating support inside the device using copper as an emitting source, sweeping the sample at angles ranging from 10º to 60º. With this technique, it was possible to verify the crystallinity of the sample through Bravais networks.

Results and Discussion

Fourier-transform infrared spectroscopy (FTIR)

Oat hulls ground to 200 mesh were chosen for characterization because they were obtained in the largest quantity. Fig. 1a shows the infrared spectrum of oat hulls, in terms of transmittance, where it is possible to follow the chemical composition. A broad peak related to the stretching of the O-H bond was observed, both intermolecularly and intramolecularly, in the region between 3400-3200 cm^{-1}; along with a narrow peak (1152 cm^{-1}), indicating the stretching of the common C-O-C bond in cyclic ethers and stretching of the open-chain ether C-O bond near the region between 1140-1070 cm^{-1} and between 1150-1050 cm^{-1}, respectively. These are characteristic of the structures of cellulose and lignin [7-9]. We observed symmetric and asymmetric stretching of the C-H bond in the region between 2970-2950 cm^{-1}, while in the region between 1680-1620 cm^{-1} there was vibration of the C=C bond of the aromatic ring, related to lignin [10]. The stretching of the C-O-C, C-O and C-H bonds are characteristic of carbohydrates such as cellulose, hemicellulose and lignin, present in various biomasses [11]. We also noted the presence, in the same range of lignin C=C vibration, of deformation of the C-O-H bond of the glucose ring present in the starch and stretching of the C-O bond also of the starch close to 1022 cm^{-1} [11, 12].

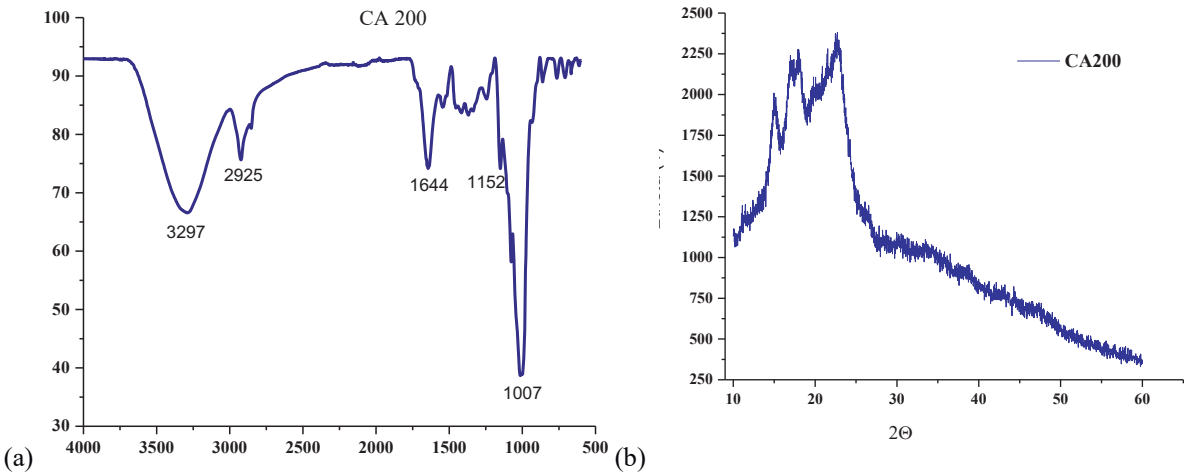

Figure 1 - Composition analysis of oat hulls: (a) FTIR spectrum and (b) XRD diffractogram.

X-ray diffraction (XRD)

This technique can predict the presence of crystalline compounds in the sample. The peaks of the diffractograms indicate the crystallographic planes according to the concepts of Bravais networks. According to previous data found in the literature [7, 13, 14] and the diffractogram shown in Fig. 1b, oat hulls have crystallinity relative to the presence of type I cellulose, in crystallographic planes of the monoclinic type.

The crystallinity of the sample means it can be used as a source of reinforcement for other matrices, such as structural reinforcement of food packages.

Scanning electron microscopy (SEM)

The ground oat waste consists mainly of hulls, trichomes and starch granules [11]. These constituents can be seen in Fig. 2a and 2b. The surface is heterogeneous, with a rounded shape and irregularities (circled in blue), which facilitate the adsorption process. This enables there use to remove liquid contaminants.

Furthermore, when ground and sieved, oat hulls have spherical shape with small diameter and a high contact surface, which facilitates their adsorptive process or its incorporation into mixtures with other materials.

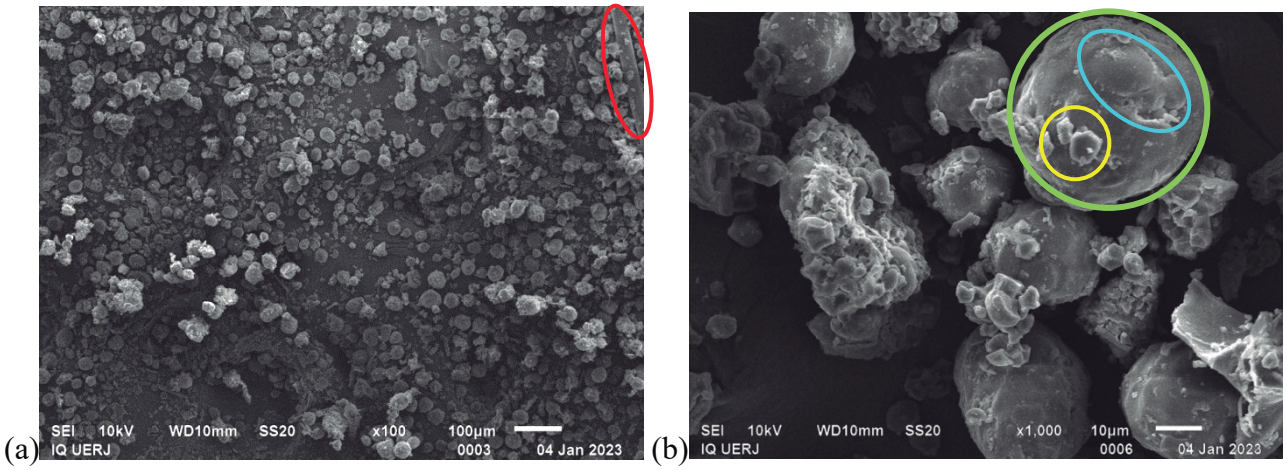

Figure 2 – SEM images of oat hulls at magnification: (a) 100X with the presence of trichomes (structures circled in red) and (b) 1000X with the presence of cavities (blue circle) and starch (structure circled in yellow) on top of the oat shell (spherical structure circled in green).

Thermogravimetric analysis (TGA)

Fig. 3 shows the thermogravimetry curves (TG) and derivatives (DTG), indicating the stages of mass loss found in the oat hull sample. From this curve it is possible to observe the initial stage of mass loss at a temperature close to 100 ºC (T1), related to the loss of water to levels lower than 10%.

The second stage of mass loss begins at a temperature close to 300 ºC (Tonset = 275.7 ºC) where the degradation of the polymeric chains present in the oat hulls occurs, with the rupture of the glycosidic bonds in a depolymerization process [15]. This value is close to those found in the literature, such as Tonset of glucose around 310 ºC [7, 15, 16], hemicellulose around 256 ºC [12] and lignin, which due to its large structure and greater stability presents a wide range of decomposition temperatures, ranging from 100 ºC to 800 ºC [7].

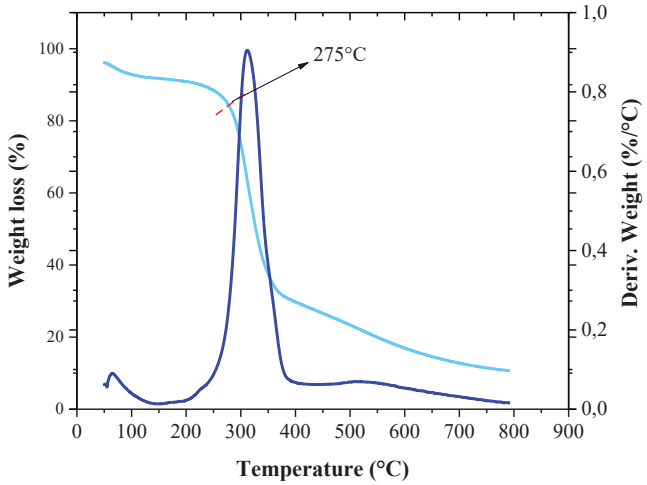

Figure 3 – TG and DTG curves of the oat hull sample.

Conclusion

From the physical-chemical analyses of the material, it can be inferred that this biomass can be very useful for the production of biofuel, due to its high degradation temperature. Its components, identified through FTIR, can also be extracted for use to reinforce other materials or as an adsorbent material, since the SEM revealed irregular surface, facilitating linkage with other materials.

Acknowledgements

We are grateful to Fundação Carlos Chagas Filho de Amparo à Pesquisa do Estado do Rio de Janeiro (FAPERJ) and Conselho Nacional de Desenvolvimento Científico e Tecnológico (CNPq) for financial support. This study was also partly financed in Coordenação de Aperfeiçoamento de Pessoal de Nível Superior (CAPES), Finance Code 001.

References

1. D. C. Doehlert; S. Simsek; D. Thavarajah; P. Thavarajah; J. B. Ohm Cereal Chemistry 2013, 90, 6. http://dx.doi.org/10.1094 / CCHEM-09-12-0111-R

2. J. P. de Oliveira; G. P. Bruni; S. L. M. el Halal; F. C. Bertoldi; A. R. G. Dias; E. R. Zavareze Internacional Journal of Biological Macromolecules 2019, 124. https://doi.org/10.1016/j.ijbiomac.2018.11.205

3. C. Tamanini; E. V. Canettieri; M. G. A. Felipe; M. C. O. Hauly; F. P. Bernardi in Proceedings of Brazilian Congress of Science and Technology in Waste and Sustainable Development, Florianópolis, 2004, Vol. 1.

4. J. B. Olivato; A. P. Bilck; F. Yamashita; M. V. E. Grossmann in Proceedings of 12th Brazilian Congress of Polymers, Florianópolis, 2013, Vol. 1.

5. D. Dziki; W. Tarasiuk; U. G. Dziki Materials 2021, 14, 5443. https://doi.org/10.3390/ma14185443

6. F. Demirel; M. Germec; H. B. Coban; I. Turhan Cellulose 2018, 25. https://doi.org/10.1007/s10570-018-2022

7. S. Dehkhoda; M. Bagheri; M. Heydari; S. Rabieh Internacional Journal of Biological Macromolecules 2022, 212. https://doi.org/10.1016/j.ijbiomac.2022.05.125

8. A. B. D. Nandiyanto, R. Oktiani, R. Ragadhita Indonesian Journal of Science & Technology 2019, 97, 118. http://dx.doi.org/10.17509/ijost.v4i1.15806

9. D. Watkins, Md. Nuruddin, M. Hosur, A. Tcherbi-Narteh, S. Jeelani Journal of Materials Research and Technology 2015, 4. http://dx.doi.org/10.1016/j.jmrt.2014.10.009

10. J. S. De Oliveira, M.Sc. Thesis, Federal University of Bahia, 2015.

11. R. Sandrin, M.Sc. Thesis, Federal University of Santa Catarina, 2013.

12. B. Li, Y. Wang, L. Zhu, C. Huang, Y. Zhang, Y. Zhao, G. Wu, L. Tan Food Hydrocolloids 2022, 123, 107145. https://doi.org/10.1016/j.foodhyd.2021.107145

13. Z. Qazanfarzadeh, M. Kadivar International Journal of Biological Macromolecules 2016, 91. http://dx.doi.org/10.1016/j.ijbiomac.2016.06.077

14. J. P. de Oliveira, G. P. Bruni, S. L. M. el Halal, F. C. Bertoldi, A. R. G. Dias, E. R. Zavareze International Journal of Biological Macromolecules 2019, 124. https://doi.org/10.1016/j.ijbiomac.2018.11.205

15. L. Ravindran, S. M.S., S. Thomas International Journal of Biological Macromolecules 2019, 131. https://doi.org/10.1016/j.ijbiomac.2019.03.134

16. Md. Nuruddin, M. Hosur, Md. J. Uddin, D. Baah, S. Jeelani Journal of Applied Polymer Science, 2016. https://doi-org.ez83.periodicos.capes.gov.br/10.1002/app.42990

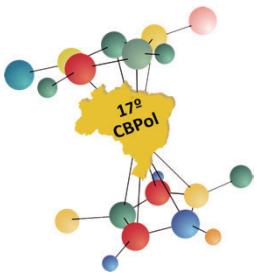

PRELIMINARY STUDY OF THE EXTRACTION OF WATER-SOLUBLE POLYSACCHARIDES FROM MACAW PALM

Ludmyla B. Lacerda[1], Marcela O. Ferreira[1], Nívia do N. Marques[2], Rosangela de C. Balaban[2] and Ana M. S. Maia[1]*

1 – Course of Bioproces Engineering and Biotechnology, Federal University of Tocantis (UFT), Gurupi, TO, Brazil
anamaia@uft.edu.br
2 – Chemistry Institute, Federal University of Rio Grande do Norte (UFRN), Natal, RN, Brazil

Abstract - The fruits of the palm popularly known as macaúba are studied mainly for the oils that can be extracted from them. However, its mesocarp is also rich in soluble and insoluble fibers. Insoluble fibers have already been studied for several applications. However, there are few studies on water-soluble polysaccharides. Due to its high oil content, it is necessary to degrease the mesocarp before extracting the polysaccharides. Therefore, in this work, the degreasing of macaúba mesocarp was evaluated using n-hexane and ethanol as extracting solvents. The results obtained indicate n-hexane as being more suitable for its degreasing. From the defatted pulp, four fractions of water-soluble compounds were extracted. And two of them were characterized by infrared spectroscopy.

Keywords: *Macaúba; cerrado palm; degreasing; water-soluble polysaccharides; deproteinization.*

Fundings: The authors are grateful to PETROBRAS S/A (SAP 4600580022 and 4600568098) and Conselho Nacional de Desenvolvimento Científico e Tecnológico (CNPq grant 304339/2019-9) for their financial support.

Introduction

Macaúba or bocaiúva, belonging to the genus *Acrocomia*, is a palm tree native from Latin America. It is widely distributed in Brazilian territory, with greater predominance in the Cerrado biome [1, 2]. Its fruits are spherical or slightly flattened and have a smooth skin. When mature, they are brittle, with a yellowish-brown color, and their pulp is yellow or whitish (Fig. 1). The endocarp that covers the almond is rigid and dark in color. The pulp, rich in oil, fibers and mucilage, and the almond, rich in oil, are edible [1, 3, 4].

Figure 1 – Macaúba palm tree and its fruit with and without the bark

There are studies that report the presence of structural and reserve polysaccharides in macaúba pulp, such as cellulose, hemicellulose and starch [5, 6, 7, 8]. However, more detailed research on the water-soluble polysaccharides present in this pulp is scarce, being located an article in which the characterization of a galactomannan is made [9].

Therefore, this study is the first part of a project to characterize water-soluble polysaccharides from macaúba pulp. Its objective was to optimize the pulp degreasing process, to facilitate the extraction of polysaccharides, since the oil present in the pulp makes the purification steps after polysaccharides extraction difficult.

Experimental

Materials

The fruits of macaúba (*Acrocomia* sp) were purchased at the local market in the city of Montes Altos/MA. Ethanol, n-hexane, chloroform, and butanol PA, were purchased from Cromoline, Quimex, respectively. Distilled water was used in all experiments.

Mesocarp degreasing

The fruits were peeled and the pulp manually removed, dried in an oven at 40 °C to constant weight and crushed. The pulps were defatted at a pulp:solvent ratio of 1:5 for 9 hours, being named DH and DE, as they were defatted with *n*-hexane or ethanol, respectively. The mixtures were filtered through a common filter paper to separate the organic phases of the defatted cake. They were dried at room temperature for 24 hours, to remove the solvents. The degreasing efficiency (Def) was calculated from Eq. 1, where M0 is the mass of the dried pulp and M1 is the mass of the defatted pulp.

$$Def = (M0 - M1)\, x\, 100/M0 \qquad (1)$$

Extraction of water-soluble compounds from the mesocarp

The DH cake was subjected to successive aqueous extractions at temperatures of 4 and 28 °C, both for 24 hours. The cake:water ratio was 1:6. The crude extracts obtained were named EDH1-4 and EDH1-28, respectively.

Purification of water-soluble polysaccharides

The EDH1-4 and EDH1-28 extracts were centrifuged at 572 G for 5 minutes. Their precipitates (REDH1-4 and REDH1-28) were dried and their supernatants (EDH2-4 and EDH2-28) were deproteinized by the Sevag method [10] with some changes. The tubes were vortexed for 20 minutes and then centrifuged at 572 G for 10 minutes. The supernatants and precipitates obtained

were named EDH3-4, EDH3-28, REDH3-4 and REDH3-28. All were dried at room temperature to constant weight. The EDH3-4 supernatant and the REDH3-4 precipitate were crushed.

Infrared spectroscopy

Samples EDH3-4 and REDH3-4 were characterized in the infrared using the KBr pellet method. Spectra were obtained between 4500 – 400 wavenumbers per centimeter using the Fourier method.

Results and Discussion

The dried pulp was crushed to increase the contact surface with the solvent, facilitating mass transport, as the oil removal can be by simple dissolution when present in the crushed sample and by diffusion when present inside intact cells [11].

The efficiency of degreasing was 24.1% and 0.06% for DH and DE, respectively. The lower efficiency calculated for ethanol indicates that lipophilic compounds were still present in the DE sample, showing that a solvent with lower polarity is more suitable for degreasing macaúba pulp. In this way, only the pulp defatted with hexane was used in the following steps.

Aqueous extraction at 4°C followed by the one at 28 °C aimed to fractionally extract the water-soluble compounds present in the defatted pulp. In this way, the EDH1-4 should have the molecules that are more easily soluble in cold water, whereas in the EDH1-28 only the molecules that were not cold-extracted remained.

From the dehydrated mass after the aqueous extractions, it was found that the extracted water-soluble compounds correspond to 54.4% of the initial dried pulp. Probably most of them being composed of low molar mass sugars [12].

It was observed that the aqueous extracts still had traces of oil, so it was necessary to subject them to centrifugation to remove residual oil. In addition to the removal of residual oil, this centrifugation led to the precipitation of water-soluble polysaccharides with higher molar mass, extracted at temperatures of 4°C and 28°C, which have been labeled REDH1-4 and REDH1-28.

The supernatants obtained after centrifugation were subjected to a deproteinization step. At the end of this step, materials were only obtained from supernatant EDH2-4. This result indicates that extraction at 4 °C removed most of the water-soluble compounds present in macaw palm pulp. And that the compounds extracted at 28 °C sedimented with centrifugation.

The spectra obtained for samples EDH3-4 and REDH3-4 are shown in Fig. 2. Comparing with spectra in the literature [13], it is possible to verify that they do not correspond to galactomannan.

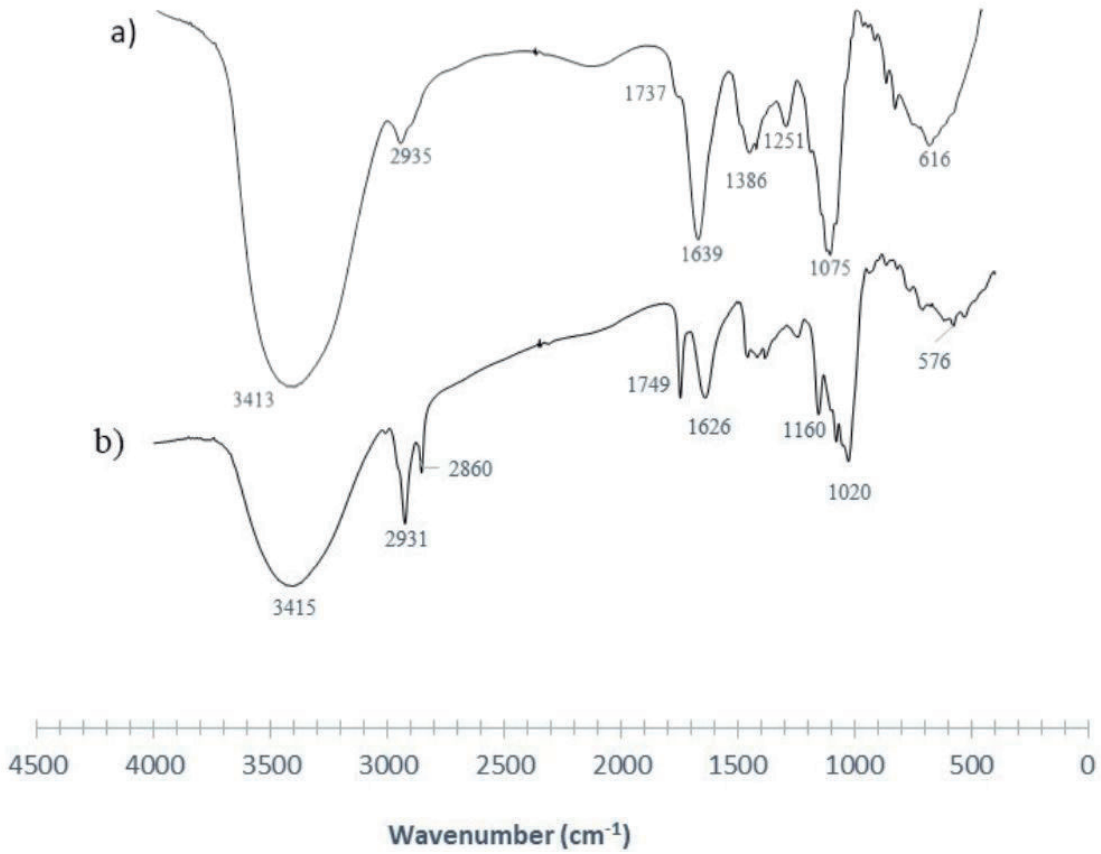

Figure 2 – IR spectra of samples a) EDH3-4 and b) REDH3-4.

Conclusions

Hexane is a more suitable solvent for degreasing macaúba pulp, probably due to the presence of lipids with long alkyl chains. Although, the degreasing process using hexane has not yet been optimized, considering that traces of oil were detected in the sample during the aqueous extraction. However, the obtained results indicate that the successive extraction using different temperatures was adequate for the fractionation of the water-soluble polysaccharides.

Acknowledgements

The authors thank professors Talita P. S. Ferreira, Vanessa M. Chapla, Melissa B. Rodrigues and Raimundo Wagner de S. Aguiar for the necessary structure for the development of the research, and professor Lucas S. S. Santos for the analyzes in the IR.

References

1. B. G. D. Hernandez. Ph.D. Thesis, State University of Campinas, 2020.
2. F. G. Aquino; M. R. Silva; J. A. Ratter, J. F. Ribeiro; M. F. Vilela. M. C. Oliveira in Proceedings of IX Simpósio Nacional Cerrado, Brasília, 2008.
3. S. A. Vianna; L. H. C. Berton; A. Pott; S. M. C. Guerreiro; C. A. Colombo International Journal of Biology 2017, 9, 2017. https://doi.org/10.5539/ijb.v9n3p78
4. C. F. Costa. Ms. Thesis. Instituto Agronômico, 2009.
5. M. I. L. Ramos; M. M. Ramos Filho; P. A. Hiane; J. A. Braga Neto; E. M. A. Siqueira Food Science and Technology, Campinas, 2008; vol. 28, 90-94.
6. C. Z. P. Revello. Ph.D. Thesis, Federal University of Grande Dourados, 2014.
7. I. C. A. Bolina; C. Contigli; M. Santos; E. C. Cren in Proceedings of Brazilian Congress of Chemical Engineering, Fortaleza, 2016, Vol. 1.

8. A. C. Corrêa; V. B. Carmona; J. A. Simão; F. Galvani; J. M. Marconcini; L. H. C. Mattoso. Polymers 2019, 11, 1785. http://dx.doi.org/10.3390/polym11111785
9. B. P. da Silva; G. de M. Silva; J. P. Parente. Carbohydrate Polymers 2009, 75, 380. https://doi.org/10.1016/j.carbpol.2008.09.031
10. G. Huang; F. Chen; W. Yang; H. Huang. Trends in Food Science & Technology 2021, 109, 564. https://doi.org/10.1016/j.tifs.2021.01.038
11. S. H. T. Silva; L. B. Silva; S. B. Mittermaier; P. Eisner in Proceedings of 8th International Conference on Dietary Fiber, Leuven, 2022.
12. A. da Fonseca. Ms. Thesis, Federal University of Minas Gerais, 2016.
13. H. B. M. Frota; J. E. S. A. Menezes; S. M. C. Siqueira; N. M. P. Ricardo; T. G. Araújo; C. A. G. Souza; P. N. Bandeira; H. S. dos Santos. Química Nova 2018, 41, 544. http://dx.doi.org/10.21577/0100-4042.20170214.

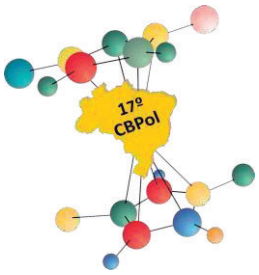

STRESS CRACKING IN EPOXY RESIN

Silva E.S [1], C. Barbosa, A. P[1]

1 – Department of Materials Engineering, Federal University of Rio Grande do Norte (UFRN), Natal, RN, Brazil
emanuela.santos.077@ufrn.edu.br

Abstract - Epoxy resin is often used as matrix in glass fiber-reinforced composite materials for coating and pipeline fabrication in the presence of a large variety of fluids. The simultaneous action of an aggressive fluid and mechanical stresses in polymeric materials generates a phenomenon called environmental stress cracking (ESC), which is associated with the appearance and development of microcracks in the structure of the material. As there are few studies in the literature that investigate environmental stress cracking in epoxy resin and glass fiber composites, the purpose of this work is to evaluate the development of environmental stress cracking (ESC) in epoxy resin, under static and dynamic conditions, in contact with agressive fluids. For this, the mechanical behavior in the presence of NaCl solution (5 wt.%) and NaOH solution (5 wt.%) was investigated through tensile tests. Fatigue tests were also carried out with 70% and 90%of the maximum yield stress of the resin in order to evaluate its behavior in dynamic conditions. The static results showed that the mechanical behavior of the epoxy resin is affected by the alkaline environment (NaOH) and by exposure to the saline environment (NaCl). FTIR analysis suggest a slight change in 915 cm^{-1}, in the spectra of the samplesto which aggressive fluid was applied. The fracture surface analysis using SEM did not show significant differences among the studied materials.

Keywords: *epoxy, pipelines, stress cracking, aggressive fluids*

Introduction

Composite materials have been frequently used in applications exposed to environmental, mechanical, and chemical factors, which can induce damage to the material [1]. Some of this damage can be difficult to detect or repair (for example microcracks and delamination) and can result in a shorter material life. The damage caused to the material may be the result of a phenomenon known as environmental stress cracking (ESC) [2]. The term environmental stress cracking is generally used to describe product cracking resulting from contact with certain types of fluids accepted by the polymer. It is a phenomenon not yet completely understood, but it happens when there is a simultaneous action of a surface-active agent (liquid or steam) and mechanical stress (external or internal) [3]. Thus, this work will contribute to the study of the mechanical behavior of epoxy resin, which is used as a matrix in composites reinforced with glass fiber, used in coatings and pipelines in the oil and gas industry, under conditions of environmental stress cracking (ESC) under static and dynamic conditions.

Experimental

Materials

The epoxy system employed was a mixture of 100:32 parts per hundred (ppc) of Araldite LY 1564 from Huntsman and curing agent Aradur 3489 from Huntsman. In order to study the development of the stress cracking phenomenon in the epoxy resin, the samples were subjected to three different types of conditioning: ambient, aqueous NaCl solution (5 wt.%) and aqueous NaOH solution (5 wt.%), according to previous studies in literature [4].

Methods

For the preparation of the specimens, epoxy resin plates were made using a metallic mold. The plates were prepared by mechanical mixing between Araldite LY 1564 Resin and Aradur 3489 (100:32). Subsequently, the mixture was subjected to degassing process and the curing process was carried out at room temperature and for 24 hours according to the resin manufacturer's instructions. After the plates were produced, the specimens were cut to the dimensions established by Standard ASTM D638.

Study of Stress Cracking for Epoxy Resin in static tests

Static tests of resistance to environmental stress cracking (ESC) were conducted in a tensile testing machine, and with an ambient temperature of 22°C, according to ASTM D 638. According to previous studies, the strain rate interferes with the ESC behavior of the polymer. Therefore, a strain rate of 5 mm/min was chosen. Tests were performed with and without fluid. The fluids were applied to one of the surfaces of the specimen with the aid of a moistened cottonswab, from the moment the tensioning began. With the test it is possible to obtain information regarding the mechanical properties of the tested polymer in the absence and presence of ESC agents. For each ESC agent tested, 6 specimens were used.

Fatigue Behavior of epoxy resin

Stress and strain levels are below the proportional limits of the material where strains and stresses are relatively elastic. The method was used from procedure A, fatigue testing tension in accordance with ASTM D7791, Standard Test Method for Uniaxial Fatigue Properties of Plastics.

Scanning Electron Microscopy (SEM)

Scanning electron microscopy (SEM) analysis were carried out to investigate the fracture surface of the samples before and after the phenomenon of environmental stress cracking, in order to understand the emergence and development of cracks in the simultaneous presence of stress and aggressive fluid. Microscopic analyzes will be performed in a Hitachi scanning electron microscope (SEM), model Hitachi Tabletop Microscope TM -3000.

Fourier-Transform infrared (FTIR) spectroscopy

FTIR analysis was carried out to investigate alterations in epoxy resin which was in contact with aggressive fluid under environmental stress cracking conditions. The spectrometer used for analysis was a Fourier transform infrared spectrometer model Frontier by PerkinElmer.

Results and Discussion

Stress Cracking in Static Conditions

The results presented in this first stage of the work confirmed what the literature had pointed out in previous studies [4]. The epoxy resin is considerably attacked by the action of the NaOH solution and even more so by the action of the NaCl solution under static conditions. According to the results presented in Table 1, The maximum tension of the epoxy resin without the fluid is 50,3 MPa, reducing to 48,3 MPa in the presence of NaOH and to 42,4 in the presence of NaCl. The results of the tensile test are shown in Fig 1.

Table 1 - Mechanical Behavior - Environmental Stress Cracking (ESC).

	τ_{max} (MPa)
No fluid	50,3 ± 1,6
ESC NaOH	48,3 ± 0,7
ESC NaCl	42,4 ± 3,1

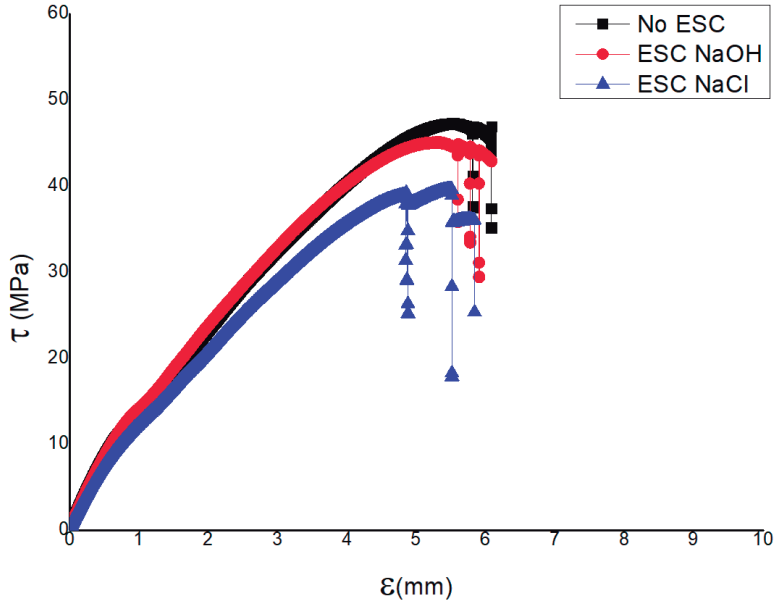

Figure 1 - Stress Cracking of Epoxy Resin (a) 5% NaOH and (b) 5% NaCl.

Fatigue behavior of epoxy resin

The test showed the behavior of the resin up to approximately 100.000 cycles for 90% of the maximum yield stress in relation to the values obtained in the static test and 125.000 cycles for 70% of the maximum reference yield stress. The S-N curve is described in Fig 2.

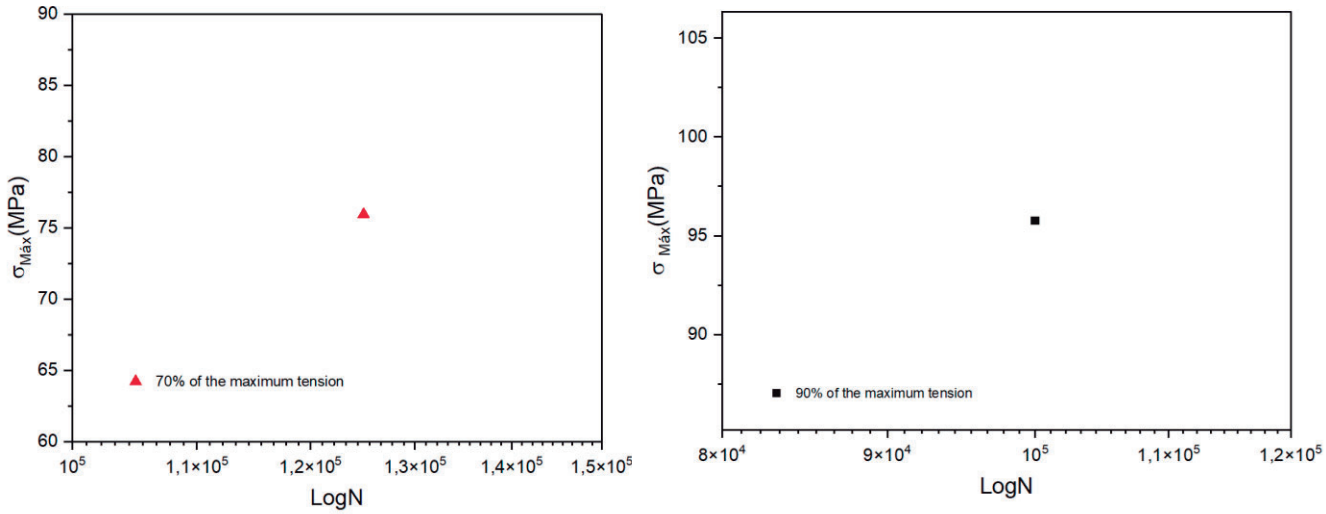

Figure 2 - Fatigue behavior of the epoxy resin. (a) 70% of maximum stress, (b) 90% of maximum stress.

FTIR analysis

The FTIR spectroscopy analysis of the material evaluated possible chemical alterations in the samples and the functional groups present in the epoxy resin used, before and after environmental stress cracking (ESC), Fig 3.

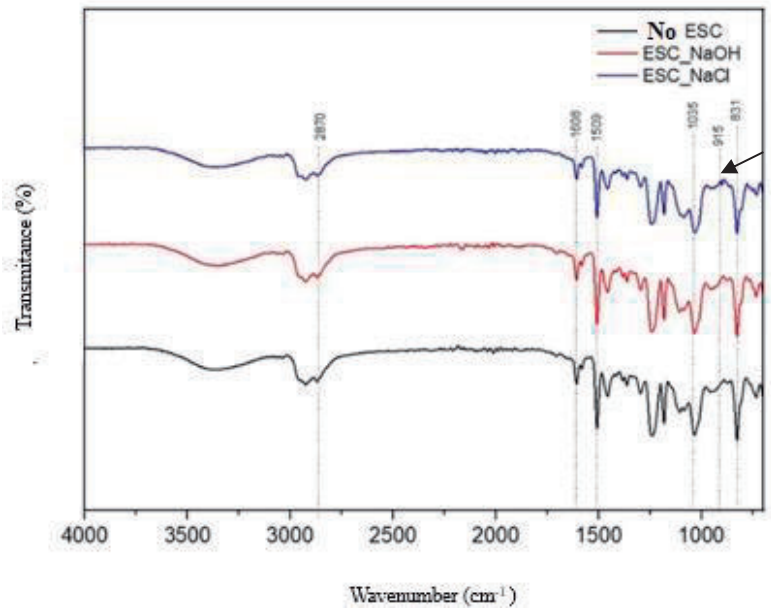

Figure 3 - FTIR spectra of samples without environmental stress cracking (ESC) and with ESC.

The range between 2965 and 2873 - 2870 cm-1 is related to the C-H elongation of aromatic and aliphatic CH2 and CH. The characteristic peak at 1608 cm-1 is attributed to the C=C elongation of aromatic rings. At 1509 cm-1 the peak is related to the ether group with stretching (epoxy resin) between the rings [5]. The characteristic peak at 831 cm-1 is attributed to C-O-C elongation of the oxirane group [5]. At 915 cm^{-1}, a slight alteration is observed in the spectra of the samples submitted to ESC in the presence of NaCl, indicating that there are chemical alterations as compared to the unmodified epoxy.

Scanning Electron Microscopy (SEM)

The results obtained in the scanning electron microscopy analysis compare the fracture surfaces of the samples with and without ESC, Fig 4. As observed in a), b) and c) the analysis of the fracture surface by SEM did not show significant differences between the epoxy resin with and without fluid.

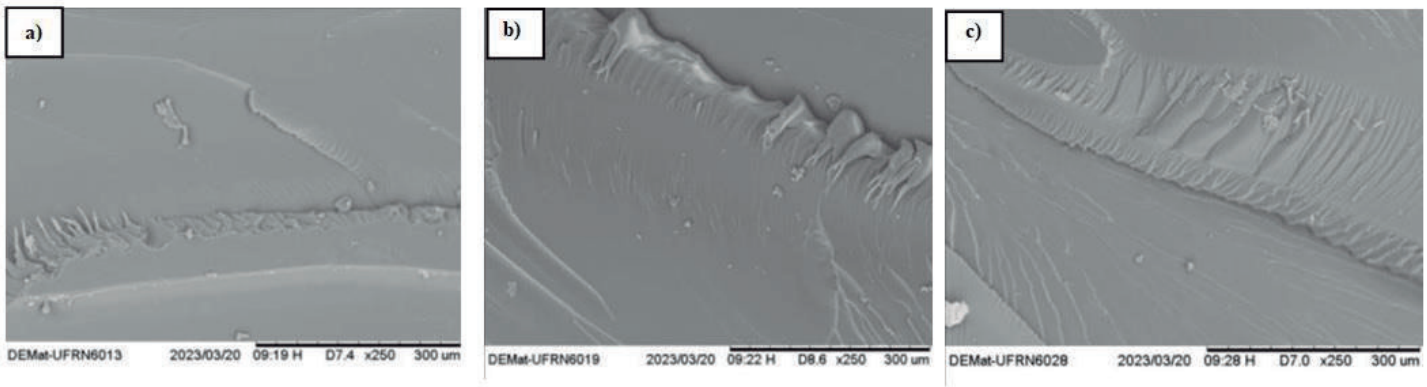

Figure 4 - Scanning electron microscopy (a) Epoxy resin fracture surface without the presence of the aggressive fluid. (b) Fracture surface of epoxy resin in the presence of NaOH and (c) Fracture surface of epoxy resin in the presence of NaCl.

Conclusions

As stated in the literature, there are indications that the two fluids investigated are fluids that are aggressive to epoxy resin, due to changes in the mechanical behavior of the resin in the presence of both NaOH and NaCl, in static conditions. Initial fatigue results were inconclusive as the trial was stopped. The phenomenon will be more deeply understood with development of the following steps, which involve more fatigue tests of the material and investigation of ESC in glass fiber-epoxy composites.

Acknowledgements

This study was financed in part by the Coordenação de Aperfeiçoamento de Pessoal de Nível Superior - Brasil (CAPES) - Finance Code 001.

References

[1] D. Y. Wu, S. Meure, and D. Solomon, Progress in Polymer Science (Oxford) 2008, vol. 33, no. 5, pp. 479–522. https://doi.org/10.1016/j.progpolymsci.2008.02.001.
[2] J. A. Jansen, Advanced Materials & Processes 2004, 50-53.
[3] E. J. Moskala, Polymer 1998, vol. 39, no. 3, pp. 675–680. https://doi.org/10.1016/S0032-3861(97)00312-1.
[4] R. S. Chen, Y. H. Muhammad, and S. Ahmad, Polymer Testing 2021, vol. 96, p. 107088. https://doi.org/10.1016/j.polymertesting.2021.107088.
[5] GONZÁLEZ, M. G.; CABANELAS, J. C.; BASELGA, J. Ed.: Theophile, T. Infrared Spectroscopy - Materials Science, Engineering and Technology, Intech, Croatia, 2012.

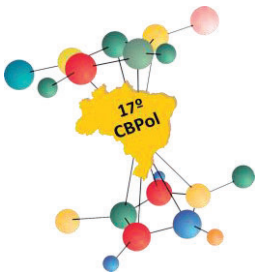

A MULTISCALE APPROACH TO EVALUATE UV-C PHOTODEGRADATION IN POLYPROPYLENE

Jessica C. F. Gimenez [1], Marcos V. Basaglia[2], Sophia H. F. Bonatti [1], Lucas H. Staffa[2], Silvia H. P. Bettini[2], Manoel G. P. Homem[1], Sandra A. Cruz[1*]

1 – Department of Chemistry (DQ) , Federal University of São Carlos (UFSCar), São Carlos, SP, Brazil
sandra.cruz@ufscar.br
2 – Department of Materials Engineering (DEMa), Federal University of São Carlos (UFSCar), São Carlos, SP, Brazil
(Times New Roman, 10, italic, centered paragraph, single space)

Abstract – In order to avoid the possibility of cross contamination [1], the UV-C light became a tool to sterilize, disinfect, and clean surfaces at hospitals in Brazil [2]. However, even though UV-C light has a well-known germicide activity, it also has enough energy to break chemical bonds in wood, paper, and polymers such as polypropylene. In this work, the polypropylene was irradiated with UV-C light (245 nm) in different times, using a chamber developed by the group. The ozone produced during this process was removed using a fan. The extent of photodegradation was investigated by FTIR, water contact angle, SEM and rheology using frequency sweep and, time sweep. The methyl index (MI) was more efficient in monitoring the early stages of photodegradation compared to the classical carbonyl index (CI) [3]. Rheology data indicated that from 24 hours onwards a continuous reduction in molar mass is observed with increasing exposure time. However, from 384 hours, an increase in this property is observed, which may lead to the hypothesis of crosslinking or branching. The time sweep mode were performed to verify this result. These results show that understanding degradation on UV-C sterilised surfaces is of paramount importance and, in this context, monitoring it even at early stages is essential to understand the extent of photooxidation.

References

1. W. J. Wiersinga; A. Rhodes; A. Cheng; S. J. Peacock; H. C. Prescott *JAMA - J. Am. Med. Assoc.* 2020, 324, 782-793. 10.1001/jama.2020.12839.
2. E. Alisson, *Agencia FAPESP Jornal da USP* 2021, 2-5. https://agencia.fapesp.br/startup-desenvolve-equipamento-para-esterilizacao-remota-de-ambientes/35301/
3. C. Roullion; P. Bussiere; E. Desnoux ; S, Collin; C. Vial; Therias, S; J. L. Gardette, *Polymer Degradation and Stability* 2016, 128, 200-208. http://dx.doi.org/10.1016/j.polymdegradstab.2015.12.011

Fundings: The authors would like to thank the financial funding given by Coordination of Higher Education Personnel – CAPES (001) and São Paulo Research Foundation – FAPESP

Keywords: *UV-C light, Polypropylene Photooxidation, Rheology*

ANALYSIS OF EARLY FAILURE OF THE TOPCOAT SYSTEM USED IN PVC COATED FABRICS FOR MARINE UPHOLSTERY

Mauricio Acelas*, Cristina Combariza, Paula Pinto, Gabriel Peláez, Natalia Zapata, Ricardo Santana & Juliana Lasprilla-Botero.

Grupo de Investigación en Polímeros y Recubrimientos Textiles (GINPRETEX), Proquinal S.A.S. Calle 11A 34-50, Bogotá, Colombia. mauricio.acelas@spradling.group

Abstract

PVC-coated fabrics are frequently used in marine upholstery applications since they are a cost-effective and a versatile way to get an imitation leather look with outstanding durability to outdoor environments [1]. However, due to the rigid nature of PVC, the use of plasticizers for this kind of flexible application is required, as these substances could migrate and compromise the integrity of the finished product. A typical PVC-coated fabric construction includes PVC-based skin, foam and adhesive layers applied to a polyester textile, followed by a thin layer of a topcoat system that offers further resistance properties and unique haptics to the surface (Fig 1) [2].

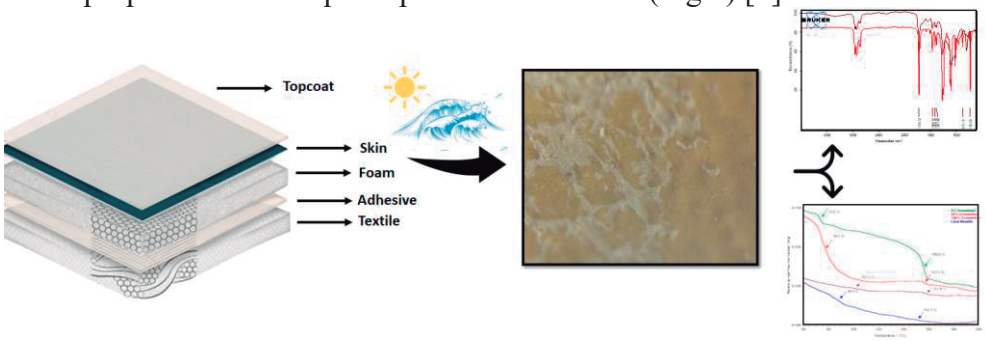

Figure 1. PVC-based synthetic leather construction and topcoat failure

The COVID-19 pandemic forced consumers to acquire harsher cleaning habits. Thus, PVC-leather producers had to adapt their top-coating systems within a short time to fulfill these new requirements. However, some of these modifications resulted in a lower outdoor resistance and affected the appearance of some products only a few months after installation. To determine the root cause of this failure, several topcoat system configurations were characterized using DSC, FTIR, surface energy and HPLC. All samples were exposed to UV radiation, high temperature, and salt fog conditions to imitate real marine environments. FTIR analyses of the damaged layer revealed a shift in the carbonyl band to lower wavenumbers, as well as the evolution of signals that matched the plasticizer's vibrational profile. Also, the T_g values of the affected film were lower when compared to a reference topcoat, suggesting a plasticization phenomenon. Assessment of all assembled product configurations allowed us to discover adhesion issues across layers as confirmed by surface energy measurements and HPLC plasticizer migration quantification [3]. All these findings served as the foundation to enhance the resistance of topcoat systems for future product developments.

References

1. L.S. Sutherland. *Composite Structures* 2022, *188*, 512–518. https://doi.org/10.1016/j.compstruct.2018.01.042
2. M. Bautista; J. Lasprilla-Botero; J. Mendez; J. Álvarez; A. Forero; R. Santana. *Revista Colombiana De Materiales*, 2020, *15*, 1–7. https://doi.org/10.17533/udea.rcm.342050
3. A. P. Tüzüm Demir; S. Ulutan. *J. Appl. Polym. Sci*. 2013, *128*, 1948-1961. https://doi.org/10.1002/app.38291

Keywords: *PVC coated fabrics; topcoat failure analysis; polymer characterization; coated fabrics; plasticizer migration; marine upholstery.*

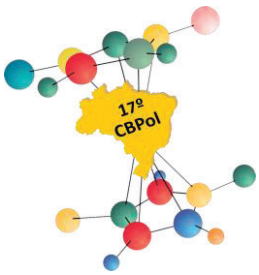

ANTHOCYANIN EXTRACT COVALENTLY INCORPORATING POLYMERIC FILMS FOR APPLICATION IN INTELLIGENT FOOD PACKAGING.

Amanda F. Bambinetti[1], Ismael C. Bellettini[1] and Patrícia B. Brondani[1]

1 – Department of Nanoscience, Advanced Processes, and Materials, Federal University of Santa Catarina (UFSC), Blumenau, SC, Brazil amanda_bambinetti@hotmail.com

Abstract – Intelligent packaging has become a focus of extensive research due to its high efficiency in the food industry. In the search for new technology, freshness, pH, and temperature indicators are incorporated into packaging as a new concept to alert consumers about the condition of the food[1]. In this sense, packaging composed of films containing anthocyanins can be an interesting option. Anthocyanins are natural compounds found in fruits and vegetables that have the ability to change color in different pH environments. In several studies, only polymeric films performing a coating with anthocyanin are presented, that is, a mixture of anthocyanin extract on the surface of the polymeric film[1]. The objective of this study is covalently incorporate anthocyanins derived from raspberries into a polymeric film for use in the development of intelligent food packaging. The covalent bond could enhance the stability of the anthocyanin expanding the utility of the film. The extraction of anthocyanins was performed using purple-colored raspberries, an extracting solvent (15:85 HCl/ethanol) at a temperature of 50°C in an ultrasonic bath[2]. A polymeric film of Ethyl Hydroxyethyl Cellulose (EHEC) polymer cross-linked with glyoxal was produced and the surface of this film was incorporated with the crude anthocyanin extract in acetone, dicyclohexylcarbodiimide (DCC), 4-dimethylaminopyridine (DMAP). The covalently incorporated anthocyanin EHEC film was evaluated by Fourier-transform infrared spectroscopy (FTIR) the anthocyanin-EHEC film proved to be pH-responsive and the colored response was reversible. The characterization of polymeric film incorporating covalently anthocyanin was performed by FTIR analysis, where it was observed the appearance of a band was observed at 1733 cm-1 referring to C=O, when compared to the polimeric film without anthocyanins. The film was also analyzed by UV-VIS, which showed maximum absorption at 530 nm, indicating the incorporation of cyanindin-3-glucosíde anthocyanin at polymeric film[3].

References

1. TIRTASHI, Fahimeh Ebrahimi et al. Biological Macromolecules. 2019, p. 920-926. https://doi.org/10.1016/j.ijbiomac.2019.06.148
2. CHEN, Fang; SUN, Yangzhao; ZHAO, Guanghua; LIAO, Xiaojun; HU, Xiaosong; WU, Jihong; WANG, Zhengfu. Ultrasonics Sonochemistry, 2007, v. 14, n. 6, p. 767-778. http://dx.doi.org/10.1016/j.ultsonch.2006.12.011.
3. SINGH, Mamatha Chandra; PRICE, William E.; KELSO, Celine; CHARLTON, Karen; PROBST, Yasmine. Food Chemistry, 2022, v. 386, p. 132855. http://dx.doi.org/10.1016/j.foodchem.2022.132855.

Keywords: *Packaging.. Intelligent packaging. Anthocyanins. pH indicators. Raspberries.*

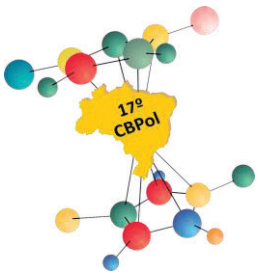

A TECHNIQUE TO INVESTIGATE NON-UNIFORM OXIDATION DURING RUBBER AGING

Elias L. de Souza[1], Gabriel B. Dutra[2], Guilherme M. O. Barra[1], Mateus S. Zanzi[1*], Rafael S. Ribeiro[2]

1 – Mechanical Engineering Department, Federal University of Santa Catarina (UFSC), Santa Catarina, Brazil
mateus_zanzi@hotmail.com
2 – Department of Mobility Engineering, Federal University of Santa Catarina (UFSC), Santa Catarina, Brazil

Abstract - Rubbers are polymeric materials based on elastomers with certain crosslinking levels in their entangled chains. These characteristic structures give specific mechanical properties. Therefore, during service or aging of the rubber in the presence of oxygen and elevated temperatures, these properties are deteriorated by oxidation (crosslinking and chain scission reactions). However, in determined conditions, these reactions can occur at different rates along the material cross-section, especially crosslinking, which promotes the rubber molecular structure stiffness. This phenomenon is known as the DLO (Diffusion-Limited Oxidation) effect and affects the mechanical rubber behavior and its properties during aging. Considering this effect, indentation tests can be realized along the cross-section of rubbers to investigate non-uniform aging in determined conditions. As a result, surface stiffness mapping was obtained and expressed in terms of a relation between force and displacement at each point along the cross-section. Based on this, it is possible to monitor the increase in stiffness and, from there, estimate the behavior of the evolution of the reticulation density along the cross-section of the rubber. With this support technique, it is possible to investigate and qualitatively predict the operating conditions to which known materials will be subject to different oxidation rates (DLO effect). Furthermore, it is possible to define which polymers and blends are subject to the DLO effect under specified conditions.

Keywords: *Rubber. Non-Uniform Oxidation. DLO effect. Indentation modulus profile.*

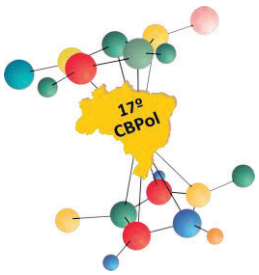

BENDING TEST OF PLA/CARBON FIBER ELEMENTS PRODUCED BY FDM.

Reinaldo S. J. Júnior[1], Erica C. Almeida[2], Clecia S. Borges[3], Maria E. A. C. Alves [4]

1 – Department of engineering and computing (DEC), State University of Santa Cruz (UESC), Ilhéus, BA, Brazil
rsjovita.egm@uesc.br

The polylactic acid (PLA), it's a thermoplastic produced based on renewable sources of raw materials, like beet, corn, and similar ones, being easily recycled. The PLA/Carbon fiber its PLA with addition of a dispersed phase, carbon fiber, so, carbon fiber it's the reinforcement of PLA being able to change a few properties of polylactic acid, making it harder and increasing the resistance. Therefore, with the purpose of better understanding the material features and infer possibilities of practical applications and them viabilities, there were made three points bending tests with 30 test bodies (TB) using the universal test machine with a few tweaks. The TB were made of by additive manufacturing, through FDM (Fused deposition modeling), via a 3D (three dimensional) printer model Ender 3 Pro, changing the elements infill begging the process with 20% of infill and doubling up the value until 80% of infill is achieved, the same way with the layer height, initiating with 0,15mm and doubling up the value. After the tests were performed, it was noticed that the carbon fiber promotes changes in the mechanical properties of the material (PLA). While the bending resistance of PLA is given by 70 MPa, PLA/Carbon Fiber has about 89 MPa, although we note greater flexural rigidity of PLA/Carbon Fiber compared to conventional, we realize that the reinforcement delays the sudden fracture of the material. As for the viability of the material, we must analyze the printing process, extruder nozzles with diameters smaller than 0.6mm suffer from obstruction of the hole, making it difficult to flow the filament to the heated table. Thus, PLA/carbon fiber, has potential for small-scale structural applications, apart from tight tolerance operations.

Keywords: Bending test, PLA, Carbon fiber, 3D printing.

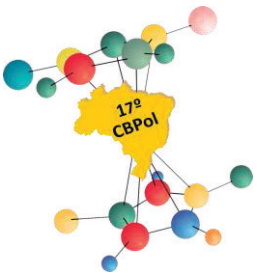

CHARACTERIZATION AND COMPARISON OF LIGNINS FROM BANANA PSEUDOSTEM ISOLATED BY DIFFERENT TREATMENTS

Rosangela Almeida Maia[1] , Adilson Roberto Gonçalves[1], Gustavo Ventorim[2]

1 – Institute of Bioenergy Research, São Paulo State University (UNESP), Rio Claro, SP, Brazil
rosangela.maia@unesp.br

2 – São Paulo State University (UNESP), Itapeva, SP, Brazil

Abstract - Lignin, a complex heterogenous structure, is formed by phenylpropane units[1]. Due to its wide availability, high-energy density and intrinsic aromatic-based structure, lignin exhibits great potential for the production of fuels, value-added chemicals, and functional materials. There are several methods for lignin extraction, although each method significantly affects the structural and chemical properties of lignin. Alkaline hydrolyses are common methods used for biomass delignification, promoting the solubilization of lignin and hemicellulose[2]. In this study, the concept of biorefinery was employed to valorize residues from the banana plant. Lignin from pseudostem was isolated from two different alkaline methods. All lignin samples were prepared and characterized from black liquor obtained through pulping processes. The findings demonstrate that pretreatment of biomass (acid and hydrothermal) has a favorable effect on lignin extraction. However, the high quantity of extractives in the pseudostem negatively affects lignin extraction in the absence of pretreatment. All lignin fractions exhibit band at 1600, 1517, and 1461 cm^{-1}, characteristic of lignin, as well as a distinct absorbance around 830 cm^{-1}, corresponding to *p*-hydroxyphenyl structures. Comparatively, lignin fractions obtained from both pulping processes with hydrothermal pretreatment showed a lower molecular weight average (Mw) than those processes with acid pretreatment. Additionally, elemental analysis demonstrates that the soda process is more effective for lignin extraction, with higher content of carbon and oxygen when compared to the lignin from Kraft process. In conclusion, lignin fractions extracted from pulping processes without pretreatment exhibited higher impurities, hindering accurate characterization. Lignin fractions extracted with hydrothermal pretreatment exhibited lower lignin condensation during the pulping process. For better comprehension and the potential applications of this kind of lignin, we will study the removal of extractives from biomass, and then repeat the steps of lignin extraction adjusting the temperature and quantity of reagents used.

References.

1. Isikgor FH, Becer CR. Lignocellulosic biomass: a sustainable platform for the production of bio-based chemicals and polymers. *Polym Chem*. 2015;6(25):4497-4559. doi:10.1039/C5PY00263J

2. Schutyser W, Renders T, Van Den Bosch S, Koelewijn SF, Beckham GT, Sels BF. Chemicals from lignin: an interplay of lignocellulose fractionation, depolymerisation, and upgrading. *Chem Soc Rev*. 2018;47(3):852-908. doi:10.1039/C7CS00566K

Fundings: São Paulo Research Foundation (FAPESP).
Keywords: *Biorefinery, characterization, lignin, pseudostem.*

COMPARATIVE ANALYSIS OF DIFFERENT FILL PATTERNS ON TENSILE STRENGTH IN ASTM D638 TEST SPECIMENS PRODUCED BY ADDITIVE MANUFACTURING

Alexandre Aparecido Neves[1], Carlos Eduardo Carvalho de Jesus[2], Filipe Gaspar Thomé[3], Vinicius Malveze[4], Vitor Lopes Zillig Gonçalves[5]

1 – Department of Mechanical Engineering, University Anhembi Morumbi, São Paulo, SP, Brazil
alexandre.aparecido@animaeducacao.com.br
2 – Department of Mechanical Engineering, University Anhembi Morumbi, São Paulo, SP, Brazil
carloseduardocj1002@gmail.com
3 – Department of Mechanical Engineering, University Anhembi Morumbi, São Paulo, SP, Brazil
fthome2000@gmail.com
4 – Department of Mechanical Engineering, University Anhembi Morumbi, São Paulo, SP, Brazil
viniciusmalveze@gmail.com
5 – Department of Mechanical Engineering, University Anhembi Morumbi, São Paulo, SP, Brazil
vitorlopeszillig@gmail.com

Abstract - The objective of this study is to present an analysis of the fill pattern of a unique geometry arranged in four different ways on the printing bed. The pattern used is the lightning pattern, a more recent option available in the Ultimaker Cura 5.0 software. The test specimens were fabricated using PLA material with two different fill densities, 10% and 40%, and a tensile test was conducted following the ASTM D638 standard. The purpose was to evaluate whether there are differences in strength between the fill densities and the angles of arrangement on the printing bed, as well as to investigate potential material savings. Currently, there is a scarcity of studies on the lightning fill pattern. Therefore, this research allows for the examination of the tensile strength of each test specimen at angles of 0°, 45°, 90°, and 135° in additive manufacturing, across the same geometry. The methodology involved dividing the prints among each fill pattern for production, optimizing the process. After manufacturing the test specimens, they underwent tensile tests, which demonstrated that the is a real difference between the use of on fill pattern or another. Moreover, the lightning pattern resulted in material savings, exhibited greater strength compared to the cross pattern, and had a resistance very close to that of the triangle pattern.

References

1. MATHIAS, Rainer Fernando et al. Análise experimental de amostras produzidas por manufatura aditiva em PLA através de ensaio de tração. 2019.
2. DOMINGOS, Caroline Maciel et al. Análise comparativa das propriedades do poliácido láctico PLA de fornecedores distintos para aplicações em manufatura aditiva: uma avaliação dos parâmetros de impressão na busca da otimização do processo de impressão 3D via fabricação filamento fundido (FFF). 2022.
3. AMATO, Mário. Estudo comparativo de corpos de prova poliméricos (ABS), fabricados por extrusão, injeção e DDM baseado em ensaios de tração. 2018.
4. GOLDSHIMIDT, Benjamin. Cura & Infill: os melhores padrões de preenchimento. Disponível em: <Cura & Infill: os melhores padrões de preenchimento | All3DP>. Access: 25 May 2023.
5. LOVO, João Fiore Parreira; FORTULAN, Carlos Alberto. Estudo de propriedades mecânicas e anisotropia em peças fabricadas por manufatura aditiva tipo FDM. I Simpósio Do Programa de Pós-Graduação Em Engenharia Mecânica Da EESC-USP (SiPGEM/EESC-USP), v. 1, p. 2-8, 2016.

Keywords: *Manufacturing, Additive, Tensile, Fill, PLA.*

DETERMINATION OF EPOXY RESIN CURING CYCLE USING TWO TYPES OF HARDENERS

Maikon S. Santos[1], Larissa S. Montagna[1] and Fabio R. Passador[1]*

1 – Department of Science and Technology, Polymer and Biopolymer Technology Laboratory (TecPBio), Federal University of São Paulo (UNIFESP), 330 Talim, São José dos Campos, São Paulo 12231-280, Brazil
maikon.stefan95@gmail.com

Abstract - Epoxy resin is one of the most common thermosetting resins and is used in aerospace and automotive industries due to its high performance such as high tensile strength, high stiffness, and chemical resistance [1,2,3]. To use epoxy resin in a wide variety of applications, it is also necessary to make use of the hardener, which when added to the epoxy resin has the purpose of cross-linking with the reactive groups to result in a cured polymer. The present study aims to determine the curing cycle of epoxy resin by viscosity analysis and differential scanning calorimetry (DSC) using two types of hardeners, Aradur HY 951 and Aradur 2963, and the same ratio epoxy/hardener (88/12). The viscosity was performed on a Brookfield digital viscometer (DV2T) coupled a thermosel system that's provide control of sample temperature. The analysis was carried out with a temperature variation of 10 °C ranging from 30 °C to 70 °C. DSC analyses were performed using TA Instruments equipment (Q2000 model) from 0 ºC to 150 ºC (rate 10 ºC/min). Tensile specimens were prepared using the chosen curing condition and tensile tests were performed on MTS equipment (Criterion 45). For the two curing agents used it was observed exponential growth of the curve was at the temperature of 70 ºC and by the variation of tan δ of these curves it is possible to obtain the gel time, which is the time required for the solidification of the material to occur and for the reaction to become irreversible [4]. It was possible to conclude the gel time at 70 °C for the two hardeners used, with this result it was defined that the process of making the samples should cure the resin at a controlled temperature for 24 h at 25 °C and then finish it for 1 h at 70 °C in an oven to obtain the total cure of the material. The Aradur HY 951 hardener made it possible to reach the mechanical properties according to the manufacturer's datasheet.

References

1. Liu, S., Chevali, V.S., Xu, Z., Hui, D., Wang, H. A review of extending performance of epoxy resins using carbon nanomaterials. Composites Part B: Engineering. 136, 197-214, 2018. https://doi.org/10.1016/j.compositesb.2017.08.020

2. Pascault, J-P., Williams, R.J.J. Chapter 1 - Overview of thermosets: Present and future. Thermosets (Second Edition) - Structure, Properties, and Applications. 3-34, 2018. https://doi.org/10.1016/B978-0-08-101021-1.00001-0

3. Jin, J-L., Li, X., Park, S-J. Synthesis and application of epoxy resins: A review. Journal of Industrial and Engineering Chemistry. 29, 1-11, 2015. https://doi.org/10.1016/j.jiec.2015.03.026

4. Costa, M.L.; Paiva, J.M.F.; Botelho, E.C.; Rezende, M.C. Thermal and rheological evaluation of a carbon/epoxy prepreg cure cycle. Polímeros: Ciência e Tecnologia, vol. 13, nº 3, p. 188-197, 2003. https://doi.org/10.1590/S0104- 14282003000300009

Fundings: Capes.

Keywords: *Epoxy resin; Curing cycle; Viscosity; Thermosets, Composites.*

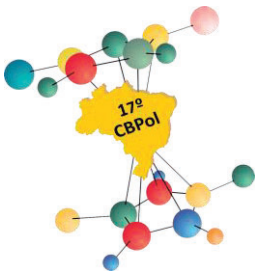

DETERMINATION OF THE SPECIFIC HEAT OF MANUFACTURED PARTS BY FDM USING CONDUCTIVE POLYMER, THROUGH THE INVERSE PROBLEMS TECHNIQUE

Dr. José C. Camargo[1], Dr. Antônio José da Silva Neto[2], Dr. Diego C. Knupp[3], Dr. Luiz A. da Silva Abreu[3], Iago Silva da Cruz[4]

1 - Professor of the Computational Modeling postgraduate program (PPGMC) and Associate Professor in the Mechanical Engineering course at UESC- State University of Santa Cruz, Ilhéus, BA, Brazil.
jccamargo@uesc.br
2 – Full Professor at the Polytechnic Institute of UERJ- State University of Rio de Janeiro, Nova Friburgo, RJ, Brazil.
3 – Associate Professor at the Polytechnic Institute of UERJ- State University of Rio de Janeiro, Nova Friburgo, RJ, Brazil.
4 - Student of the Mechanical Engineering course at UESC- State University of Santa Cruz, Ilhéus, BA, Brazil.

Abstract – This research proposes a theoretical/experimental investigation, with inverse problems, for the thermal characterization of parts printed using the Fused Deposition Modeling (FDM) process, using conductive ABS polymer as the raw material. The experimental data was obtained by heat transfer conducted through a resistance between the plates. The temperature values were measured using an infrared thermographic camera. The mathematical model proposed for solving the direct problem was transient heat conduction. On the other hand, the inverse problem of heat transfer by conduction was formulated aiming to use stochastic methods, which seek to estimate a set of parameters considered optimal through an objective function. A routine was developed to estimate the specific heat for each of the filling patterns and validated using a material with known properties. As the FDM process is anisotropic, meaning that the thermal properties vary according to the established process parameters, it is of fundamental importance that these methods are well understood and utilized, as they replace traditional methods that use heat transducers.

Keywords: *FDM process, thermal characterization, inverse problems, infrared thermography.*

Introduction

Additive manufacturing (AM) can be defined as a manufacturing process consisting of adding material in successive flat layers. This technology is ideal for manufacturing items with complex forms that could not be created using a conventional machining process. One of the available AM technologies is the fused deposition modelling (FDM) process. One of the FDM processes is the 3D printing, used to create 3D components from data obtained directly from the geometrical model generated in a CAD system. This process begins by electronically "slicing" the 3D model of the item in the CAD to obtain 2D curves (XY orientation) that will define where material must be added in each layer (Z orientation) [1].

However, recently, researchers have been exploring the capability of FDM to produce conductive polymers, opening new possibilities for applications in flexible electronics, sensors, medical devices, and many other fields. Conductive polymers are organic materials that exhibit electrical properties like metals or semiconductors. They have a special molecular structure in which the conduction of electric charges is enabled by the presence of conjugated bonds or functional groups capable of carrying electrons. These properties make conductive polymers highly attractive for device manufacturing flexible electronics, as they can be printed in different shapes and sizes, enabling the creation of electronic circuits on flexible and lightweight materials. These

characteristics pave the way for the development of customized electronic devices such as flexible sensors, integrated circuits, and even implantable medical devices. Printing conductive polymers using the FDM process also presents significant challenges. The proper selection of materials and printing parameters is crucial to achieve consistent conductivity properties and satisfactory performance. Additionally, the development of new formulations of conductive polymers compatible with the FDM process is necessary, taking into consideration changes in mechanical [1], physical, electrical, and thermal properties [2-3].

This research proposes a theoretical/experimental investigation, with inverse problems, for the thermal characterization (specific heat) of parts printed using the Fused Deposition Modeling (FDM) process, using conductive ABS polymer as the raw material. Understanding the progress and obstacles in this field is crucial to further propel the development of innovative and functional electronic devices manufactured through 3D printing.

Transient heat transfer

The proposed problem consists of a pair of plates manufactured by the Fused Deposition Modeling (FDM) process and using conductive ABS as the raw material, along with a heater, forming a sandwich-type configuration (plate-heater-plate). The assembly is heated with a thermal flux (q''), supplied by a heater, until it reaches a steady-state condition (Fig. 1).

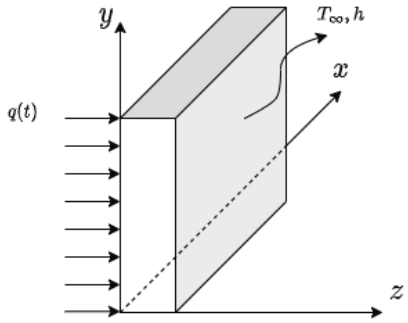

Figure 1 – A schematic representation of the experiment

The following assumptions were considered: perfect thermal contact between the heater and the plate assembly, constant properties, negligible heat source within the plates, heat exchange through natural convection on the external surfaces, ambient temperature (T_∞), and constant heat transfer coefficient (h).

The average temperature of the plate as a function of time during heating, for the direct problem, is given by Eq. 1 and Eq. 2.

$$T_m(Z,t) = T_\infty + \frac{q^{"} A_1}{h\, A_2}\left[1 - \exp\left(\frac{-h\, A_2 t}{\rho_{abs} V\, Cp_{abs}}\right)\right] \quad (1)$$

$$T_m(0) = T_{ini} \quad (2)$$

Where A_1 is the cross-sectional area of the plate, A_2 is the area of the plate in contact with the air, V is the volume of the plate, T_{ini} is the initial average temperature of the plate, and Cp_{abs} is the specific heat of the conductive ABS material. The measurement of temperature T as a function of time, as described, was carried out using an infrared thermographic camera, model *FLIR_A645_SC*.

Inverse problems (IP)

Inverse Problems (IP) appear in various branches of engineering, physics, chemistry, and mathematics and have been the subject of study by several researchers [3]. They are typically used to estimate parameters that govern the physical behavior of a problem based on experimental measurements, which may come with inherent errors that affect the accuracy of the solution. This work is based on the study of heat transfer in a conductive ABS plate, heated by a thermal flux (q''). The objective is to analyze the correlation between the thermal parameters involved in the problem, such as heat flux (q''), mass density (ρ_{abs}), and specific heat (Cp_{abs}), through a sensitivity analysis

that indicates which parameters can be estimated simultaneously. The centered finite difference method (Eq. 3) was used for this purpose.

$$J_{ij} = P_i \frac{\partial T_i}{\partial P_i} \qquad (3)$$

Furthermore, the value of Cp_{abs} (for each filling pattern) will be estimated from experimental data using the methods of Differential Evolution (DE), Firefly algorithm (FA), and Hybrid (Firefly/Luus-Jaakola (FLJ)) [4].

In order to estimate the Cp_{abs} parameter was adopted as the objective function, given by (Eq. 4):

$$Q(Cp_{abs}) = \sum_{i=1}^{N_d} \frac{[Tm_i(Cp_{abs}) - Tm_i^{exp}]^2}{[Tm_i^{exp}]^2} \qquad (4)$$

Where N_d is the number of experimental data points, $Tm_i(Cp_{abs})$ is the average temperature obtained from the direct problem using the estimated value for Cp_{abs} and Tm_i^{exp} is the experimentally obtained average temperature.

Experimental

The conductive ABS plate, manufactured for each filling pattern, was produced with dimensions of 40 x 40 x 1.2 mm and the following printing parameters: orientation = flat (CP position parallel to the print bed), extruder diameter = 0.40 mm, layer height = 0.20 mm, number of top and bottom layers = 1, number of perimeter lines = 2, raster (internal and external) filling patterns: rectilinear, grid, triangular, wiggle, fast and fullhoneycomb. The infill percentage was set to 100%. The extruder temperature was 235°C, print bed temperature was 60°C, extruder travel speed was 2000 mm/min, filament diameter was 1.75 mm, and density was 1.04 g/cm^3.

Results and Discussion

A computational routine was developed to analyze the results obtained experimentally and using the methods described above. Validation was performed using a material with well-known characteristics (Aluminum). The average specific heat calculated by the routine was 914.022196 J/(Kg.°K), while the value indicated in the main datasheets was 903 J/(Kg.°K). Thus, the error between the value estimated by the routine and the actual value was 1.206%.

Sensitivity Analysis

A sensitivity analysis was conducted on the discussed parameters to evaluate if there is correlation between them. Small absolute values of the sensitivity coefficients indicate that large variations in the parameters, P_i, have little influence on the values of T_i.

The Fig. 2 presents a graph with the sensitivity analysis conducted for the rectilinear filling pattern. It can be observed that the curves corresponding to ρ_{abs} and Cp_{abs} are overlapped and tend towards zero after t=400s. This indicates a linear dependence between them, where it is not possible to estimate them simultaneously. On the other hand, the coefficient related to q'', appears to be linearly independent of the other two parameters, indicating that it can be estimated simultaneously with either of the two parameters.

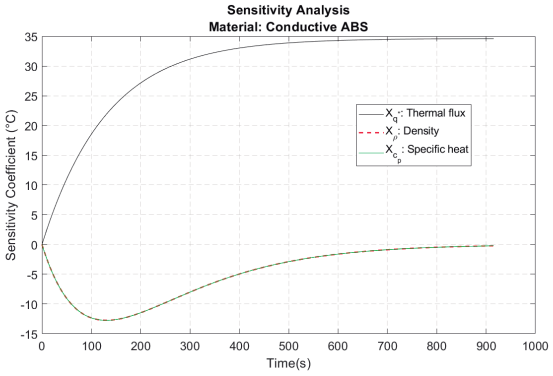

Figure 2 – Sensitivity Analysis

Estimation of specific heat using the differential evolution method.

In this method, the analyses were performed using a population of 5 and 10 individuals. A total of 46 combinations were tested, varying the disturbance factor F with values of 0.2, 1.0, and 1.2, and the number of generations with values of 10, 30, 40, and 50. From these 46 combinations, the maximum, minimum, and two values around the mean were also extracted to present the histogram of the results according to the parameters inserted in each of the graphs. All the histograms were related to the rectilinear filling pattern. From the performed analyses, the lowest average value was 1445.9969 J/(Kg.°K), the highest was 1454.4533 J/(Kg.°K), and the mean was 1449.1383 J/(Kg.°K). The average standard deviation was 1.1990. With the extreme values and two around the mean, a histogram of the value distribution was generated with 100 repetitions (Fig. 3a, 3b, 3c, 3d).

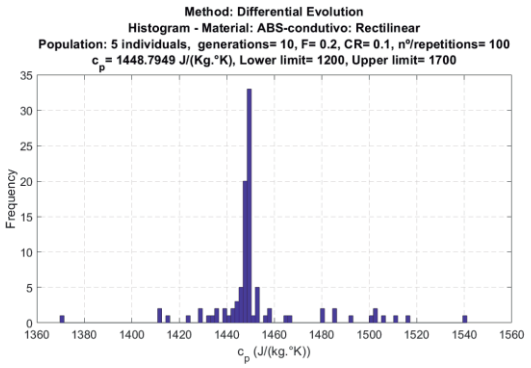

Fig. 3a: P=5, ger.=10, F=0.2 e CR=0.1

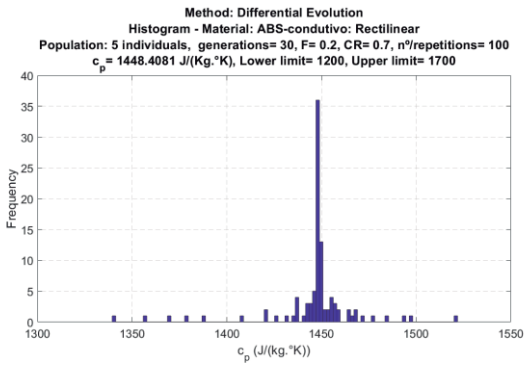

Fig. 3b: P=5, ger.=30, F=0.2 e CR=0.7

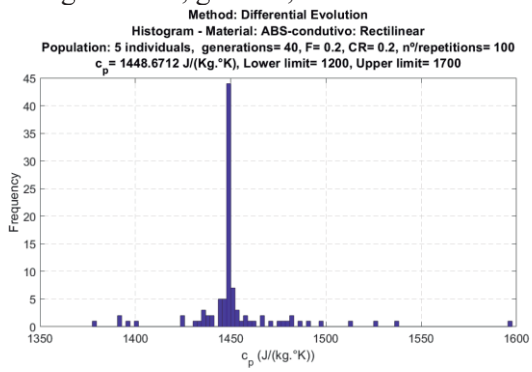

Fig. 3c: P=5, ger.=40, F=0.2 e CR=0.2

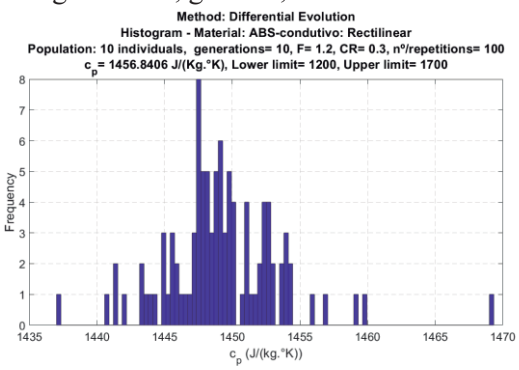

Fig. 3d: P=10, ger.=10, F=1.2 e CR=0.3

Estimation of specific heat using the Firefly method

The parameters adopted by this method were: number of fireflies = 100, precision: 1E-06, absorption coefficient, γ = 0.01, and attractiveness rate, α = 1. The maximum number of repetitions was set at 1000. The estimation routine for C_p will be processed until a convergence value is reached with the established precision or the maximum number of repetitions. With these parameters, the calculated specific heat value was 1448.6726 J/(Kg.°K), and the standard deviation was 0.2162 (values achieved after 468 iterations) - Fig. 4a,4b and 4c.

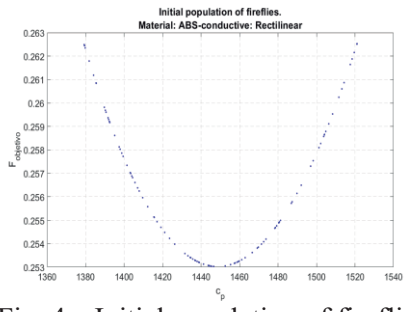

Fig. 4a: Initial population of fireflies

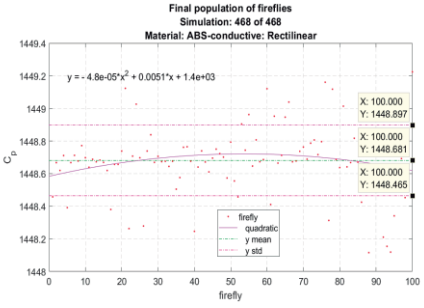

Fig. 4b: Final population of fireflies

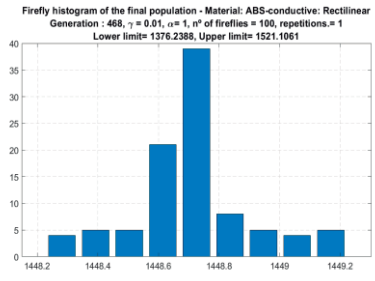

Fig. 4c: Fireflies histogram of the final population

Estimate of specific heat by the hybrid method (Firefly and Luus-Jaakola)

The hybrid method initially used the firefly method to determine the best candidate, and then this best candidate was exported to be processed by the Luus-Jaakola method. For this method, the same parameters as the firefly method (initial estimate) were used, and for Luus-Jaakola, the parameters were: Contraction coefficient = 0.1, number of internal iterations = 100, and number of external iterations = 15. With these parameters, the calculated value of specific heat was 1448.6724 J/(Kg·°K).

Compilation of results for all filling patterns

Table 1 compiles the values of specific heat calculated for the filling patterns: rectilinear, grid, triangular, wiggle, full honeycomb, and fast honeycomb. The values were estimated using the Differential evolution, Firefly, and hybrid (Firefly/Luus-Jaakola) methods.

Table 1 – Estimated specific heat values for each of the methods

Patterns	Differential Evolution	Firefly algorithm	Hybrid (Firefly/Luus-Jaakola)	Average value
Full honeycomb	1075.6820	1062.4691	1062.4694	1066.8735
Fast honeycomb	1138.5148	1131.4974	1131.4975	1133.8366
Grid	1214.9022	1206.0495	1206.0497	1209.0005
Triangular	1287.1276	1284.2150	1284.2757	1285.2061
Wiggle	1419.5689	1419.0071	1419.0070	1419.1943
Rectilinear	1449.1383	1448.6726	1448.6724	1448.8278

It can be observed, according to Table 01, that the specific heat values for each of the infill patterns are different. Among the various reasons, we can point out:

Porosity distribution: Porosity can vary in FDM-printed parts, even though the infill percentage in these experiments was 100%. Different infill patterns can result in different levels of porosity in the final part. The presence of porosity affects the material's ability to store and conduct heat, which can lead to variations in specific heat.

Layer orientation: In the FDM process, parts are built in successive layers. The orientation of the layers can affect the thermal properties of the part. The layer orientation was kept constant; however, the alignment of the raster depends heavily on the infill pattern.

Variation in crystal structure: During the 3D printing process, the rapid cooling of the material can affect the crystal structure of conductive ABS. Different infill patterns can result in different cooling rates in different regions of the part, resulting in variations in the crystal structure. The crystal structure can affect the thermal properties of the material, including specific heat.

References

1. J.C. Camargo, A.R. Machado, E.C. Almeida, E.F.M.S. Silva, 2019, Mechanical properties of PLA-graphene filament for FDM 3D printing. The International Journal of Advanced Manufacturing Technology. ISSN 0379-6779. https://doi.org/10.1007/s00170-019-03532-5.
2. J.C. Camargo, A.R. Machado, E.C. Almeida V.H. M. de Almeida, 2022, Mechanical and electrical behavior of ABS polymer reinforced with graphene manufactured by the FDM process. The International Journal of Advanced Manufacturing Technology, ISSN 0379-6779. L https://doi.org/10.1007/s00170-021-08288-5.
3. P. Roudný, T. Syrový, 2022, Thermal conductive composites for FDM 3D printing: A review, opportunities and obstacles, future directions, Journal of Manufacturing Processes, ISSN 1526-6125, https://doi.org/10.1016/j.jmapro.2022.09.026.
4. A. J. Silva neto, J. C. Becceneri, H. F. C. Velho, Inteligência Computacional Aplicada a Problemas Inversos em Transferência Radiativa, Ed. UERJ, Rio de Janeiro, 2015.

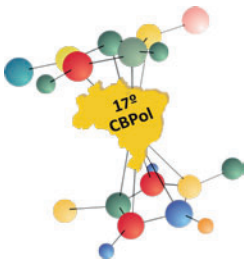

EFFECT OF TEMPERATURE ON THE PROPERTIES OF THE PVDF COMPOSITE AND COMMERCIAL LIGHT-CURING RESIN MATRIX

Júnio A. R. Pasqual[1] and Carla C. Schmitt[2] *

1 – Department of Materials Engineering, USP-São Carlos, São Carlos, SP, Brazil
junio.pasqual@usp.br
2 – Department of Physics and Chemistry - USP-São Carlos, São Carlos, SP, Brazil

Abstract – The development of new materials is a way of filling gaps linked to certain functions to which a finished product will be applied. When talking about biomaterial applications, biocompatibility and biofunctionality are some of the fundamental properties, considering the final application. With this focus in mind, different materials can be developed so that the final properties of a product are satisfactory. Polyvinylidene fluoride (PVDF) is a polymer that can be used as a biomaterial due to its piezoelectric behavior and biocompatibility, among other properties, as can also be observed in the hydroxyapatite (HAp) case, making possible the use of this materials in different bioapplications as 3D printing. In the present study, two types of PVDF (PVDF1015/1001 and PVDF6008/0001) in 10% for each sample, HAp (1%) and commercial biocompatible light-cured resin were analysed with a view to using the formed composite as a product for bone regeneration. Shore A hardness, Fourier Transform Infrared Spectroscopy (FTIR) and X-Ray Diffraction (XRD) analysis were carried out to observe the behaviour of these materials when three different temperatures (25°C, 45°C and 60°C) are applied during the PVDF solubilization process in a solution containing solvent (Dimethylacetamide – DMAc), nanometric HAp and the commercial resin. After the analyses, it was possible to verify significant hardness increasing related to temperature changes and HAp presence. A greater intensity of acrylate groups due to the increase in temperature and a decrease on the PVDF betha-phase formation was also observed due to the increase in temperature. These results make it possible to observe more suitable conditions when mixing PVDF and HAp in commercial light-curing acrylic resin. More studies are being carried out to better understand this parameter in the properties of the proposed composite.

References

1. A. Carter, K. Popowski, K. Cheng, A. Greenbaum, F. S. Ligler, and A. Moatti, “Enhancement of Bone Regeneration Through the Converse Piezoelectric Effect, A Novel Approach for Applying Mechanical Stimulation,” Bioelectricity, vol. 3, no. 4, p. 255, Dec. 2021, doi: 10.1089/BIOE.2021.0019.
2. Song, H., Li, H., & Lim, S. (2021). Fast 3D Digital Light Process Printing of PVDF-HFP Composite with Electric In Situ Poling System for Piezoelectric Applications. Macromolecular Materials and Engineering, 306(10). https://doi.org/10.1002/mame.202100266
3. Webb, B., & Doyle, B. J. (2017). Parameter optimization for 3D bioprinting of hydrogels. Bioprinting, 8(July), 8–12. https://doi.org/10.1016/j.bprint.2017.09.001

Fundings: CAPES, CNPq, FAPEPS and Rhodia Solvay.

Keywords: Biomaterials, polymers, filler dissolution, composites, *bone regeneration.*

Enhancement of Antimicrobial Properties in (Bio)polymer and Semiconductor Systems through Plasma Modification

Isabelly, Bertochi Veroneze[1], Letícia Akemi Onoue de Jesus[1], Maciel Lima Barbosa[1], Lara Kelly Ribeiro[1], Mariana Ottaiano Gonçalves[2], Marcelo Assis[3], Elson Longo[1], Cristina Paiva Sousa[2], Sandra Andrea Cruz[1]*

[1]*Department of Chemistry, Exact Sciences and Technology Centre (CCET), Federal University of São Carlos (UFSCar), Rodovia Washington Luís, Km 235, 10 SP-310, São Carlos, Brazil*

2Morphology and Pathology Department (DMP - UFSCar), Biotechnology Graduation Program (PPGBiotec – UFSCar) São Carlos 13565-905, SP, Brazil

3Department of Analytical and Physical Chemistry, University Jaume I (UJI), Castelló 12071, Spain

*Corresponding Author E-mail: *sandra.cruz@ufscar.br*

ABSTRACT

Recently, the world has faced numerous microbial infections and a viral pandemic, resulting in significant losses and fatalities. In this context, there has been a growing focus on the development of novel materials capable of combating these potentially pathogenic microorganisms. Nanocomposite materials, comprising a polymer matrix and nanoscale inorganic fillers, have garnered considerable attention for biomedical applications, particularly for the creation of antimicrobial device. Silver-based semiconductors have shown potential as promising materials with high biocidal activity. Thus, the mixture of (bio)polymers with semiconductors seems to be an interesting alternative for the reduction of possible cross-contamination of various pathogens. This property can be significantly improved if the semiconductor particles are more exposed on the surface, which can be achieved by plasma modification. In this study, semiconductor-based polymer composites were subjected to oxygen plasma treatment to improve of antimicrobial properties. The chemical modifications induced by plasma treatment were analyzed through contact angle measurement, Fourier-transform infrared spectroscopy (FTIR-ATR), and X-ray photoelectron spectroscopy (XPS). The morphological modifications on the surface of the films caused by plasma exposure were analyzed by atomic force microscopy (AFM) and scanning electron microscopy (SEM). Finally, the antimicrobial activity of the nanocomposite was confirmed. Moreover, it was verified that the plasma treatment acts as a potentiator of the antimicrobial effect by exposing the particles on the surface.

Keywords: polymer, plasma, semiconductor, pathogenes.

Biography: Professor Sandra Andrea Cruz has a PhD in Materials Science and Engineering from the Department of Materials Engineering, UFSCAR, Brazil. Today, she is a full professor at the Department of Chemistry, Federal University of São Carlos, Brazil, SP. As a polymer scientist, she researches the recycling, modification, and stabilization of polymeric materials. Her investigations are on the quality of recycled materials with focus on their modification and property improvement. The degradation, stabilization and modification of polymers are used to make them meet market applications such as packaging, health care and equipment.

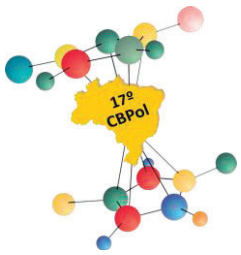

EVALUATION OF THE MECHANICAL RESPONSE OF RIGID PLATES BASED ON UHMWPE SUBJECTED TO HIGH STRAIN RATES

Iana C Carvalho[1], Matheus S Domingos[1], Amanda L S M Andrezo[1], Rafael R Dias[1], Iaci M Pereira[1]

1 – Materials Laboratory, Army Technological Center (CTEx), Rio de Janeiro, RJ, Brazil. iana.carvalho@eb.mil.br
1 – Materials Laboratory, Army Technological Center (CTEx), Rio de Janeiro, RJ, Brazil. dasilva.domingos@eb.mil.br
1 – Carbon Materials Technology Section, Centro Tecnológico do Exército (CTEx), Rio de Janeiro, RJ, Brazil. amandaluizamartins@gmail.com
1 – Materials Laboratory, Army Technological Center (CTEx), Rio de Janeiro, RJ, Brazil. rafael.dias@eb.mil.br
1 – Materials Laboratory, Army Technological Center (CTEx), Rio de Janeiro, RJ, Brazil. iacipere@gmail.com

Abstract - This study focuses on evaluating the mechanical response and failure mechanisms occurring in a composite ballistic plate made of ultra-high molecular weight polyethylene (UHMWPE) during dynamic compression testing. The material under evaluation is the rigid plate of the bulletproof vest used by the Brazilian Army, designed to withstand Level III impacts according to the NIJ 01.01.06 standard when used in conjunction with the complete set (rigid + flexible). In the literature, one way to characterize a material under high strain rates, similar to ballistic impact, is through the compression Hopkinson bar test, which provides the mechanical properties of the material (Strain, Maximum Compression Stress, Toughness). Therefore, in order to characterize the mechanical behavior of this rigid plate under different dynamic conditions, a compression Hopkinson bar test was conducted at two different strain rates, ε1' = 647±49 and ε2' = 791±46 (mm/mm/s). Additionally, in order to investigate the fracture mechanisms occurring during the test and compare them with non-impacted samples, scanning electron microscopy (SEM) images were obtained. Analysis of the Compression Stress (MPa) vs. Strain (mm/mm) curves from the dynamic compression tests revealed variations in the mechanical properties of the composite with increasing strain rate, which is a common behavior in polymer composites. For the higher strain rate ε2', the values of Maximum Stress, Toughness, and Maximum Strain of the material increased, particularly in terms of maximum stress and toughness, which increased by 188% and 247% respectively. SEM analysis showed that the "as received" samples, obtained by waterjet cutting, already exhibited some defects in their structure, such as sheared end fibers, surface undulations, and delamination. In the case of samples subjected to a high strain rate, the micrographs revealed the appearance of new failure modes, such as matrix rupture, defibrillation, and fiber splitting.

References

1. R. R. Dias; I. M. Pereira; B. G. Soares. Fracture Analysis of UHMWPE Ballistic Hard Armor Tested at Split Hopkinson Pressure Bar. 15h Brazilian Polymer Conference. *2019.*
2. R. R. Dias et.al. Effect of molecular structures on static and dynamic compression properties of clay and amphiphilic clay/carbon nanofibers used as fillers in UHMWPE/composites for high-energy-impact loading. Journal of applied polymer science. 2019.
3. G. Guo; S. Alam; L. D. Peel. An investigation of deformation and failure mechanisms of fiber-reinforced composites in layered composite armor. Elsevier. 2021.

Keywords: SHPB, Composite Ballistic, UHMWPE, Failure Mechanisms, Polymer Fibers.

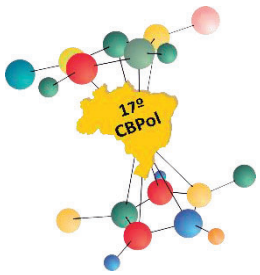

EXPERIMENTAL EVALUATION OF ABRASION IN POLYAMIDE FIBERS FOR DIFFERENT SOAKING AND LOAD CONDITIONS

Marcelo de Ávila Barreto[1, 3, *], Daniel Magalhães da Cruz[2, 3], Larissa Basei Zangalli[3], Stephane Pires de Souza[1], Fernanda Mazuco Clain[1] and Carlos Eduardo Marcos Guilherme[1]

1 – School of Engineering (EE), Federal University of Rio Grande (FURG), Rio Grande, RS, Brazil
** Corresponding author: marcelobarretobm@gmail.com*
2 – Department of Mechanical Engineering (DEMEC), Federal University of Rio Grande do Sul (UFRGS), Porto Alegre, RS, Brazil
3 – Tecnofibers Desenvolvimento e Tecnologia Ltda., Itajaí, SC, Brazil

Abstract – Offshore mooring systems have evolved since the first propositions to replace steel catenaries with Taut-leg systems made with synthetic fibers [1]. Although polyester is main fiber, others have gained prominence such as high modulus polyethylene, polypropylene, polyamide, aramid. Among these, polyamide stands for its high elongation values, and for ability to absorb dynamic parcels. These characteristics, associated with wave mechanics, enable moorings in shallow waters, such as FOWT [2]. Although it is possible to approach theoretical, analytical, experimental, and numerical studies, the experimental knowledge of the material is important, as the observational can provide understanding of the behavior of the material even to subsidize other approaches. In addition, several mechanical tests can be contemplated, rupture, creep, fatigue, abrasion, impact. The aim this work is the experimental evaluation of abrasion in polyamide multifilaments, for 5 different soaking conditions and for 3 load groups. The methodology follows with the initial characterization of the fiber in terms of rupture [3] and linear density [4], and with the abrasion test following ASTM [5] and CI [6] standards. As a result, the initial characterization of the fiber is obtained, and for the abrasion data, a curve of the number of cycles that resisted in abrasion is plotted to compare each load link and immersion time. By analyzing the results obtained, it is evident that the increase in load to perform the Yarn-on-Yarn test decreases the number of cycles resistant to abrasion. The immersion time of polyamide multifilaments in water increases the number of cycles in abrasion test. This increase is observed in all loads with greater impact on smaller ones. Therefore, the immersion condition provides an improvement in the abrasion behavior, as future studies it is necessary to observe the effect of water absorption for other groups and other fibers used for mooring offshore structures.

References

1. C. J. M. Del Vecchio, Ph.D. Thesis, University of Reading, 1992.
2. Y. Chevillotte, Y. Marco, G. Bles, K. Devos, M. Keryer, M. Arhant, P. Davies, *Ocean Engineering* 2020, *199*, 107011. https://doi.org/10.1016/j.oceaneng.2020.107011.
3. International Organization for Standardization, ISO 2062, 2009, Geneva
4. American Society for Testing and Materials, ASTM D1577, 2008, West Conshohocken.
5. American Society for Testing and Materials, ASTM D6611, 2016, West Conshohocken.
6. Cordage Institute, CI 1503, 2019, Wayne.

Keywords: S*ynthetic fibers, Experimental characterization, Yarn-on-yarn test, Water immersion, Polyamide.*

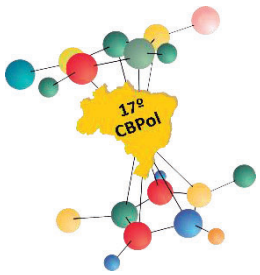

EXPERIMENTAL TEST OF THE EFFECT OF TEMPERATURE ON CREEP TEST IN HMPE MULTIFILAMENTS

Marcelo de Ávila Barreto[1, 3, *], Daniel Magalhães da Cruz[2, 3], Larissa Basei Zangalli[3], Aleones José da Cruz Júnior[4], Tales Luiz Popiolek Júnior[1], Fernanda Mazuco Clain[1] and Carlos Eduardo Marcos Guilherme[1]

1 – School of Engineering (EE), Federal University of Rio Grande (FURG), Rio Grande, RS, Brazil
** Corresponding author: marcelobarretobm@gmail.com*
2 – Department of Mechanical Engineering (DEMEC), Federal University of Rio Grande do Sul (UFRGS), Porto Alegre, RS, Brazil
3 – Tecnofibers Desenvolvimento e Tecnologia Ltda., Itajaí, SC, Brazil
4 – Federal Institute of Education, Science and Technology of Goiano, Trindade, GO, Brazil

Abstract – Polymeric fibers for mooring revolutionized the offshore area [1]. The rise of polyester also provided the study and application of other fibers, including high modulus polyethylene (HMPE), that has a tenacity up to four times greater than polyester, has a lower specific mass and linear density than polyester, and is buoyant in water. The elongation at break of the HMPE close to 3% stands out, which may allow advance in installation depths. Some studies have been carried out around its use in MODU systems (Mobile Offshore Drilling Units) and experimental investigations of mechanical tests on high modulus polyethylene [2, 3]. On the other hand, HMPE has lower creep performance than when compared to polyester [4]. Although there are studies in this area, there is still much to be done in the characterization of the creep of HMPE studies. Therefore, the objective of this work is to evaluate the creep behavior of HMPE multifilaments in two temperature ranges: ambient temperature (22ºC) and oceanic temperatures (15ºC). The methodology includes an initial characterization of the fiber in terms of linear density [5] and rupture [6], and subsequent creep test [7] for 50% of the Yarn Break Load (YBL). The results of the initial characterization yield linear density, breaking value, elongation at break and linear tenacity, observing compliance with the norm that the HMPE fiber must have a linear tenacity greater than 2.5 N/tex. Creep result is observed that the decrease in temperature "locks" the creep mechanism causing the curve to have another characteristic of longer duration in creep before rupture, but with a maximum elongation value close to the group with the highest temperature. A continuation of the study should be proposed for other fibers e.g. polyester and polyamide, and also advancing to deep water temperatures (4°C).

References

1. C. J. M. Del Vecchio, Ph.D. Thesis, University of Reading, 1992.
2. S. Leite, J. Boesten in Proceedings of the OTC Brasil, Rio de Janeiro, 2011, OTC-22486-MS.
3. E. S. Belloni, F. M. Clain, C. E. M. Guilherme, *Acta Polytechnica* 2021, *61(3)*, 406-414.
4. Y. Lian, H. Liu, W. Huang, L. Li, *Applied Ocean Research* 2015, *52*, 234-244.
5. American Society for Testing and Materials, ASTM D1577, 2008, West Conshohocken.
6. International Organization for Standardization, ISO 2062, 2009, Geneva.
7. International Organization for Standardization, ISO 18692-3, 2020, Geneva.

Keywords: *Mechanical characterization, Creep behavior, Ocean temperature, High modulus polyethylene, Synthetic fibers.*

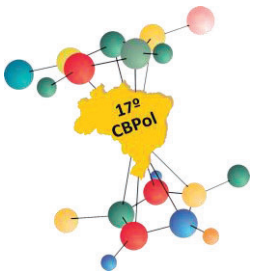

EXTRACTION OF LOW MOLAR MASS KERATIN FROM FEATHER MEAL

Guilherme Emanuel de Queiros Souza[1,2*], Glaucia Regina Medeiros Burin[1], Rilton Alves de Freitas[3], Graciela Inês Bolzon de Muniz[2], Helton José Alves[1,2]

1 – Laboratory of Materials and Renewable Energy (LABMATER), Federal University of Paraná (UFPR), Palotina-PR, Brazil - gui.emanuel97@gmail.com
2 – Central Laboratory of Nanotechnology (LCNano), Federal University of Paraná (UFPR), Curitiba-PR, Brazil
3 - Department of Pharmacy, Federal University of Paraná (UFPR), Curitiba-PR, Brazil

The advance of industrial poultry farming has led to a significant increase in the amount of waste generated, such as feathers, eggshells, carcasses, blood, and wastewater [1]. Globally, it is estimated that more than 8.5 million tons of feathers are produced annually as a byproduct of this activity [2]. However, poultry feathers are composed of approximately 91% keratin protein [3]. From economic and environmental points of view and considering the composition of poultry feathers, the development of efficient processes for the extraction of keratin is highly desirable. This work presents an alternative for the extraction of low molar mass keratin from chicken feather meal, an industrial byproduct rich in poultry feathers. The keratin was obtained by an alkaline extraction process at a temperature of 15 °C, NaOH concentration of 2 M, and extraction time of 90 min, resulting in an extraction yield of 20%. After keratin milling, the samples were analyzed by Dynamic Light Scattering (DLS), being possible to observe the presence of particles with diameters ranging from 5 to 200 nm. According to the literature, β-keratin (the main conformation of the keratin protein in poultry feathers) has a molar mass of approximately 10 g mol^{-1} [4]. The results of Gel Permeation Chromatography (GPC) analysis showed that β-keratin from feather meal had a molar mass of approximately 9 g mol^{-1}. Scanning Electron Microscopy (SEM) analysis revealed the existence of particles with diameters ranging from 5 to 15 nm, corroborating DLS results. Keratin particles of low molar mass in the nanometer size range were successfully extracted from feather meal. This study represents an important advance for the poultry industry, providing an alternative reuse of poultry feathers and the extraction of keratin from feather meal.

References

1. E. Chowdhury, *Journal of Applied Poultry Research*, 2019; Vol. 4, 791-800.
2. T. Mcgauran, *Journal of Cleaner Production*, 2021; Vol. 291, 125948.
3. S. Yadav, *Studies in Chemical and Environmental Engineering*, 2021; Vol. 4, 100114.
4. T. Fujii, *Journal of Biological Macromolecules*, 2008; Vol. 8, 48-55.

Keywords: *Agro-industrial byproduct, alkaline hydrolysis, β-keratin, protein.*

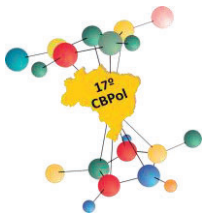

FUEL CELL PERFORMANCE OF ACRYLAMIDE BASED HYDROCARBON PROTON EXCHANGE MEMBRANES COMPOUNDS

João Henrique L. Moura[1]*, Letícia G. Trindade[1] , Emilse M. A. Martini[1] and Cesar L. Petzhold[1]

1 – Department of Organic Chemistry, Federal University of Rio Grande do Sul (UFRGS), Porto Alegre, RS, Brazil
2 – Chemistry Dept., Federal University of São Carlos, P.O. Box 676, 13560-970 São Carlos, SP, Brazil
jhlingner@hotmail.com

Abstract –Fuel Cells equipped with Proton Exchange Membranes (PEM have received increasing attention as one of the most promising alternatives to mitigate the dependency on fossil fuels, mainly in the automotive industry.).. Typically PEMs are based on sulfonated perfluorinated polymers (Nafion type) which combine hydrophilic and hydrophobic domains granting high proton conductivity and stability in the fuel cells aqueous media. Nonetheless, some features of these membranes including high costs, complex production technology, generation of toxic fluorine radicals and reduced performance above 80ºC still limit their use on a larger scale[1,2]. In face of these disadvantages many researches have proposed the synthesis of new PEMs, using, for example, different components in order to match all the required properties for application in fuel cells[3]. Herein is described the evaluation of novel multicomponent PEMs based on non-fluorinated hydrocarbon monomers. For that, a new membrane class was synthesized by radical copolymerization in aqueous media, using monomers with proton conductive groups such as 2-acrylamide-2-methyl-1-propanesufonic acid (AMPS), crosslinking sites such as 2-hydroxyethyl acrylamide (HEA), and hydrophobic domains – N-isopropylacrylamide (NIPAM). The membranes were obtained by crosslinking the copolymers with glutaraldehyde and evaluated for their conductivity, oxidative stability, dynamic mechanical properties (DMA) and performance in fuel cells. The produced membranes showed conductivity values comparable to those of commercial Nafion® membranes. While the presence of sulfonated groups were important to ensure a high conductivity, the presence of crosslinking sites and hydrophobic moieties were crucial for the stability of the membranes in the Fuel Cell environment. Among the tested samples the one with that best combined such properties, the membrane MHAN-2/1.6G-60C containing 48.8 % HEA, 5% AMPS and 46.2% NIPAM which showed the best performance in the Fuel Cell tests.

References

1. PINHEIRO, Daniela et al. Non-pre-treated sulfonated poly (ether ether ketone) membrane as an efficient alternative for Nafion in acidic aqueous organic redox flow batteries. **Journal of Energy Storage**, v. 57, p. 106201, 2023.
2. SABA, Beenish. Graphene-Based Membranes for Proton Exchange Membrane Fuel Cells. **Proton Exchange Membrane Fuel Cells: Electrochemical Methods and Computational Fluid Dynamics**, p. 17-31, 2023.
3. MOURA, João Henrique Lingner et al. Multi-component polymeric membranes based on acrylamide monomers for fuel cells. **Solid State Ionics**, v. 391, p. 116128, 2023.

Fundings: This work was supported by Coordenação de Aperfeiçoamento de Pessoal de Nível Superior, Brazil (CAPES), [finance code 001]. The authors acknowledge the PPGQ (Programa de Pós-Graduação em Química) from UFRGS (Universidade Federal do Rio Grande do Sul).

Keywords: *PEM, Fuel Cell, Copolymerization, Acrylamide monomers.*

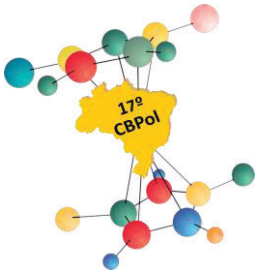

GALACTOMANNAN-BASED COPOLYMER NANOPARTICLES : EFFECT OF CHARGE ON PHYSICAL-CHEMICAL PROPERTIES

Cláudio B. A. Paula[1], Raelle F. Gomes[1], Irisvan S. Ribeiro[1], Regina C. M. de Paula[1*]

1 – Department of Organic and Inorganic Chemistry, Federal University of Ceará (UFC), Fortaleza, CE, Brazil
rpaula@dqoi.ufc.br

Abstract - Thermal responsive materials can be used in different areas of science, including biomedicine, sensors, catalysts, and textiles. Copolymer of polysaccharide and poly-isopropylacrylamide (PNIPAM) has been reported to self- assembling into nanoparticle and show pH and thermal responsiveness [1-3]. In this work we used galactomannan (GM) extract from seeds from *Delonix regia* and its carboxymethylated derivative (GMCM) to form copolymers with PNIPAM. The GM carboxymethylation reaction was carried out with monochloroacetic, acid in basic medium, with degree of carboxymethylation of 0.35 (GMCM-1) and 0.60 (GMCM-1). Copolymers of GM and GMCM were synthesized via radical copolymerization of N-isopropylacrylamide (NIPAM) monomers (CP-GM; CP-GMCM-1; CP-GMCM-2). The synthesis of the copolymers was confirmed by FT-IR and ^{1}H NMR. The % of PNIPAM increases with increasing of charge in the galactomannan chain. Copolymers showed critical association concentration (CAC) at 25 and 50 °C. The increase of charge in CP-GMCM leads to an increase of CAC in comparison with non-charged galactomannan (GM). The increase in charge do not affect the transition temperature of the copolymers, where a sharp decrease in particle size is observed at 35°C for all copolymers. The nanoparticles showed sizes of 219, 341 and 356 nm at 37 °C for CP-GMCM-1, CP-GMCM-2, and CP-GM, respectively. Thus, CP-GMCM-1 is the most suitable material for the incorporation of drugs, as it has a nanoparticle size of less than 300 nm.

References

1. M. Constantin; S. Bucătariu; I. Stoica; G. Fundueanu. *International Journal of Biological Macromolecules* 2017, 94, 698-78. https://doi.org/10.1016/j.ijbiomac.2016.10.064
2. M. Kumar, P. S. Gehlot; D. Parihar; P. K. Surolia; G. Prasad. *European polymer jornal* 2021, 152, 110448. https://doi.org/10.1016/j.eurpolymj.2021.110448
3. R. F. Gomes; L. R. Lima; J. P. Feitosa; H.C. Paula; R. C. de Paula. *International Journal of Biological Macromolecules* 2020, 156, 446-453. https://doi.org/10.1016/j.ijbiomac.2020.04.004

Fundings: FUNCAP, CAPES, CNPq, INCT/ Polysaccharide.
Keywords: *galactomannan; carboxymethylation; N-isopropylacrylamide; copolymer; nanoparticle.*

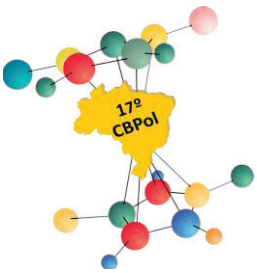

IMPREGNATION OF GREEN PROPOLIS IN PLLA COMPOSITES WITH SUPERCRITICAL CO_2 FOR ACTIVE FOOD PACKAGING

Gisele de C. Ferreira[1]*, Mathilde J. G. Champeau[1]

1 – Center for Engineering, Modeling and Applied Social Sciences, Universidade Federal do ABC (UFABC), Santo André, SP, Brazil

campos.gisele@ufabc.edu.br

Abstract - Supercritical CO_2-assisted impregnation is a process that enables to load molecules into a polymer. CO_2 is a transfer agent that can solubilize the molecules and carry them in the polymer when it is above its critical point (Tc= 31,1 °C; P_C= 73,8 bar). After depressurizing the system, functional polymers are recovered free of solvent, making this process adequate for developing food packages. This process is efficient for impregnating poly(L-lactic acid) (PLLA), which is a biodegradable polymer used in the food industry [1]. The objective of this project it to develop a film with antioxidant activity that can protect the food from photodegradation [2]. The green propolis extract has been selected for its efficient antioxidant actions and its high polyphenolic content [3] to increase the food shelf life. In this project, we applied a design of experiment to investigate the influence of temperature (35 to 60 °C) and pressure (10 to 30 MPa) on the impregnation yield of green propolis in PLLA. The interaction between the extract and PLLA is observed by Fourier Transform Infrared spectroscopy. Differential Scanning Calorimetry and Scanning Electron Microscopy aims to probe the extract's influence on the PLLA microstructure.

References

(1) Milovanovic, S.; Lukic, I.; Horvat, G.; Novak, Z.; Frerich, S.; Petermann, M.; García-González, C. A. Green Processing of Neat Poly(Lactic Acid) Using Carbon Dioxide under Elevated Pressure for Preparation of Advanced Materials: A Review (2012–2022). *Polymers* 2023, *15* (4), 860. https://doi.org/10.3390/polym15040860.

(2) Črešnar, K. P.; Zamboulis, A.; Bikiaris, D. N.; Aulova, A.; Zemljič, L. F. Kraft Lignin/Tannin as a Potential Accelerator of Antioxidant and Antibacterial Properties in an Active Thermoplastic Polyester-Based Multifunctional Material. *Polymers* 2022, *14* (8), 1532. https://doi.org/10.3390/polym14081532.

(3) Machado, B. A. S.; Silva, R. P. D.; Barreto, G. de A.; Costa, S. S.; da Silva, D. F.; Brandão, H. N.; da Rocha, J. L. C.; Dellagostin, O. A.; Henriques, J. A. P.; Umsza-Guez, M. A.; Padilha, F. F. Chemical Composition and Biological Activity of Extracts Obtained by Supercritical Extraction and Ethanolic Extraction of Brown, Green and Red Propolis Derived from Different Geographic Regions in Brazil. *PLoS ONE* 2016, *11* (1), e0145954. https://doi.org/10.1371/journal.pone.0145954.

.

Fundings: Capes - financing code 001.

Keywords: *Biodegradable polymer. Polyphenolic content. Food shelf life.*

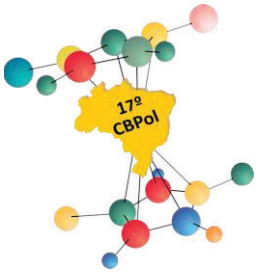

INSIGHTS INTO MORPHOLOGICAL AND MECHANICAL PROPERTIES: POLY(ETHYL BENZENE-1,4-DICARBOXYLATE) RECYCLED FIBER SUPPORTS FOR ENZYME IMMOBILIZATION

Ellaine C. G. Silva[1], Ricardo S. Cunha[1], Daniela Bresolin[1], and Sergio Y. G. González[1]*

1 – Chemical and Food Engineering Department, Federal University of Santa Catarina (UFSC), University Campus, Postal Box 476, ZIP 88040-900, Florianópolis, SC, Brazil
sergio.gomez@ufsc.br

Abstract

Enzymes are considered as alternatives to conventional chemical catalysts due to their high specificity. However, their free usage is limited by susceptibility to inactivation from various factors during application and storage. The immobilization of enzymes on solid supports has emerged as a promising strategy to enhance their operational stability. In this context, the utilization of recycled Poly(ethyl benzene-1,4-dicarboxylate) - PET fibers as a support for enzyme immobilization is of great interest, due to its low degradability, cost competitiveness, ease of processing, and favorable mechanical properties. This study focused on the manufacturing of PET fibers through the electrospinning process at different concentrations (10%, 20%, and 30% w/w) using trifluoroacetic acid (TFA) as a solvent. Moreover, the influence of operational parameters such as volumetric flow rate, applied voltage, and distance between the collector and needle was analyzed regarding the morphology and diameter of the fibers. The morphology and diameter were examined through Scanning Electron Microscopy (SEM), while Fourier Transform Infrared Spectroscopy (FTIR) was employed to investigate the chemical properties, and uniaxial tensile tests were conducted to evaluate the mechanical properties. The analysis of chemical composition, morphology, and diameter distribution of the fibers revealed their potential for applications in enzyme immobilization and PET recycling.

Keywords: *Enzyme immobilization, Supports, Recycled PET fibers, Morphology, Mechanical properties*

MECHANICAL BEHAVIOR IN POLYESTER FIBER RUPTURE FOR DIFFERENT STRAIN RATES

Stephane Pires de Souza[1,*], Marcelo de Ávila Barreto[1,2], Daniel Magalhães da Cruz[2], Larissa Basei Zangalli[2], Fernanda Mazuco Clain[1] and Carlos Eduardo Marcos Guilherme[1]

1 – School of Engineering (EE), Federal University of Rio Grande (FURG), Rio Grande, RS, Brazil
** Corresponding author: stephane.pires@outlook.com.br*
2 – Tecnofibers Desenvolvimento e Tecnologia Ltda., Itajaí, SC, Brazil

Abstract – Synthetic ropes are used for offshore anchoring, mooring, towing and other marine applications. Del Vecchio [1] implemented polyester fibers in a Taut-Leg system to replace steel catenaries. Polyester is still the main fiber for offshore mooring systems [2]. As offshore mooring ropes are subjected to heavy loads and adverse conditions, it is necessary to study as much as possible about the best mechanical performance of ropes/multifilaments. Considering that, this abstract addresses the study of the mechanical behavior of a polyester multifilament, as the main fiber characterization test, the tensile strength test, for different speeds (extension rate). The material is a polyester multifilament, manufactured in Europe, with a linear density of 3300 dtex. Breaking tests were carried out based on the standard norm for Yarn Break Load [3], varying for 8 different speeds: 0.5mm/min; 1mm/min; 10mm/min; 50mm/min; 100mm/min; 150mm/min; 200mm/min; 250mm/min. For each group, 20 samples were broken, with the useful length of the specimen being 500 mm, and a twist of 60 turns/meter is applied. The test was conditioned during its performance with temperature and humidity according ISO139 [4]. With the data acquired, it is possible to create tables and graphs with the average data that express the values of rupture and deformation for each condition, Fig 1. In addition, the behavior of force by deformation for each group can be plotted to verify whether the different velocities modify the constitutive behavior of the material. The results achieved indicate that there is a velocity range that optimizes the rupture force (approximately 50~100mm/min) and that all tested velocities do not significantly modify the stress-strain constitutive behavior. As a future study, should be proposed to increase the database for other speeds, and complementing it for other fibers.

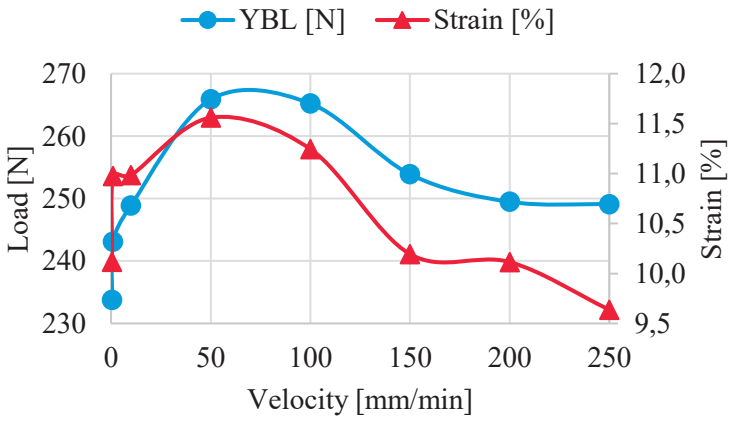

Figure 1 - Average Load and Strain results.

References

1. C. J. M. Del Vecchio, Ph.D. Thesis, University of Reading, 1992.
2. L. F. Haach; D. T. Poitevin; M. B. Bastos in Proceedings of Rio Oil & Gas Expo and Conference, Rio de Janeiro, 2010, IBP2745_10.
3. International Organization for Standardization, ISO 2062, 2009, Geneva.
4. International Organization for Standardization, ISO 139, 2005, Geneva.

Keywords: *Extension rate, Yarn Break Load, Polyester fibers, Experimental characterization, Velocity.*

MECHANICAL BEHAVIOR OF POLY(ACRYLONITRILE-CO-METHACRYLIC ACID) ELECTROSPUN MEMBRANES IN FUNCTION OF ACID CONTENT

Luiz Guilherme Abreu de Paula[1]*, Geilza Alves Porto[1] and Marcos Lopes Dias[1]*

1 – Macromolecules Institute Professora Heloisa Mano IMA, Federal University of Rio de Janeiro (UFRJ),Rio de Janeiro, RJ, Brazil luizguilhermeacm@ima.ufrj.br

Abstract – The development of acrylonitrile copolymers for electrospinning applications requires a comprehensive understanding of their mechanical behavior to determine the most suitable applications [1]. Acid comonomers have the potential to influence the mechanical properties of nanofibrous membranes made from polyacrylonitrile (PAN), making it important to investigate their stiffness and fracture profile. This study aims to evaluate the mechanical behavior of nanofibrous membranes made from poly(acrylonitrile-co-methacrylic acid) (PANCMAA) with different comonomer content. PANCMAA membranes were synthesized using an aqueous suspension method [2], with two variations: PANCMAA1, which has a lower acid content, and PANCMAA2, which features a higher acid content. The mechanical properties of the PAN and PANCMAA membranes were evaluated through stress-strain analysis, while the fracture profile was examined using scanning electron microscopy (SEM) at a magnification of 1000x in fractured membranes after stress-strain. Tensile tests revealed that the Young's modulus of the membranes demonstrated a specific threshold of acid comonomer content. Beyond this threshold, the stiffness of the membranes increased, thereby enhancing their mechanical resistance. Moreover, the addition of acid comonomer led to a decrease in the elongation at breaking stress. SEM micrographs depicted aligned fibers in the axial direction across all samples, with no discernible differences among the various membranes.

Keywords: *Copolymers, mechanical properties, stiffness, methacrylic acid, acrylonitrile*

References

1. Bigogno RG, Dias ML, Manhães MBN, Sanchez Rodriguez RJ (2022) Integrated Treatment of Mining Dam Wastewater with Quaternized Chitosan and PAN/HPMC/AgNo3 Nanostructured Hydrophylic Membranes. J Polym Environ 30:1228–1243. https://doi.org/10.1007/s10924-021-02273-5

2. Bajaj P, Paliwal DK, Gupta AK (1993) Acrylonitrile–acrylic acids copolymers. I. Synthesis and characterization. J Appl Polym Sci 49:823–833. https://doi.org/https://doi.org/10.1002/app.1993.070490508

Fundings: Authors acknowledge the Coordenação de Aperfeiçoamento de Pessoal de Nível Superior (CAPES), Conselho Nacional de Desenvolvimento Científico e Tecnológico (CNPq) (Grant 307364/2018-6), FAPERJ (Grants E-26/202.538/2019 and SEI-260003/000311/2023) and Project nº 022019 Nanotechnology Research Networks Program in the State of Rio de Janeiro (grant E-26/010.000979/2019) for financial support.

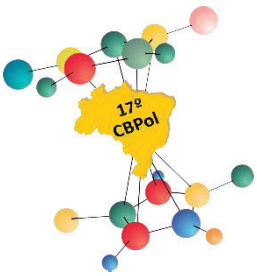

PHYSICOCHEMICAL PROPERTIES OF CHITOSAN-BASED FILMS INCORPORATED WITH INVERTASE ENZYME

Joyce F. G. Motta[1*], Alex F. Almeida[2], Glêndara A. S. Martins[2] and Soraia V. Borges[1]

1 – Department of Food Science, Universidade Federal de Lavras – UFLA, Lavras, MG, Brasil
joycefgmotta@hotmail.com
2 – Laboratory of Kinetics and Process Modeling, Universidade Federal do Tocantins – UFT, Palmas, TO, Brasil

Abstract – Invertase has been used in bulk candy to prevent crystallization during storage. Due to possible reactions with the ingredients and minimization of the enzymatic effect, it is interesting to develop active packages containing this enzyme. Research on the use of biopolymers for the production of active packaging has increased considerably due to the lower negative impact that these materials cause on the environment, such as chitosan (Negm et al., 2020; Aranaz et al., 2021). Thus, this study aimed to produce films based on chitosan incorporated with the invertase enzyme (0, 1 e 10%) and characterize them in terms of thickness using a micrometer, opacity in a spectrophotometer and solubility using a gravimetric method. Part of the chitosan polymeric solution had its pH adjusted to 5 with 10 M NaOH (optimum pH for invertase enzymatic activity), the other part did not, and the films were produced by the casting method (Santos et al., 2021). The films that presented greater thickness ($p<0.05$) were those that had pH adjustment in their composition, possibly due to the 10 M NaOH having hindered the evaporation of the solvent. Among the films with pH adjustment, the incorporation of invertase was not enough to interfere with its thickness. As for opacity, the films, in general, were not very opaque and both the pH adjustment and the insertion of the invertase enzyme were not enough to interfere with this property. Regarding the solubility test, the films that did not have pH adjustment were less soluble than those that had adjustment, due to the fact that NaOH is a very soluble base. Regarding the different concentrations of the invertase enzyme, there was no significant difference in solubility. In conclusion, only the pH adjustment was able to influence these characteristics analyzed in this package.

References

I. Aranaz; A. R. Alcántara; M. C. Civera; C. Arias; B. Elorza; A. H. Caballero; N. Acosta *Polymers* 2021, *13*, 3256. https://doi.org/10.3390/polym13193256

N. A. Negm; H. H. H. Hefni; A. A. A. Abd-Elaal; E. A. Badr; M. T. H. Abou Kana *International Journal of Biological Macromolecules* 2021, *152*, 681-702. 10.1016/j.ijbiomac.2020.02.196

T. A. Santos; B. R. Cabral; A. C. S. Oliveira; M. V. Dias; C. Oliveira; S. V. Borges *Journal of Food Processing and Preservation* 2021, *45*, 15900. https://doi.org/10.1111/jfpp.15900

Fundings: Federal University of Lavras (UFLA), Federal University of Tocantins (UFT), Coordination for the Improvement of Higher Education Personnel (CAPES) - funding code 001, PROCAD, and National Council for Scientific and Technological Development (CNPq).

Keywords: *Active packaging; crystallization; environment*

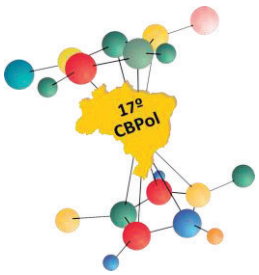

RHEOLOGICAL PARAMETERS OF PLA/EGGSHELL DETERMINED BY TORQUE RHEOMETRY

Daniella S. C. Andrade[1]*, Lara M. M. Oliveira[2], Renata Barbosa[3], Tatianny S. Alves[3] and Yêda M. B. de Almeida[1]

1 – Materials Science Program, Federal University of Pernambuco (UFPE), Recife, PE, Brazil
daniella.andrade@ufpe.br
2 – Department of Chemical Engineering, Federal University of Pernambuco (UFPE), Recife, PE, Brazil
3 – Graduate Program in Materials Science and Engineering, Federal University of Piauí (UFPI), Teresina, PI, Brazil

With technological advances focused on sustainability, the use of biodegradable polymers has been valid to reduce the environmental impact caused by plastics derived from petroleum, a fossil and non-renewable source. Another attractive factor to the environmental theme is the use of waste such as chicken eggshell as filler in biodegradable polymers, which are still expensive. Parameters involving the processing of polymers are factors that influence the characteristics of the final product and the manufacturing industry is always looking for better properties. The objective of this work was to evaluate the rheological characteristics of the composite poly(lactic acid) (PLA) and chicken eggshell in different contents by torque rheometry. The composites were processed in an internal mixer under different temperatures and rotation speeds and later characterized by torque rheometry to obtain the rheological parameters. The index of dependence of temperature with viscosity for PLA and the index of pseudoplasticity was verified for all studied systems. The results indicated that pure PLA has a lower pseudoplasticity index than the other compositions. It was observed that the higher the rotor speed, the higher the final processing temperature. Among the compositions studied, the composite with 5% eggshell stood out due to the rapid stabilization of torque and temperature during processing. The incorporation of eggshell powder increased the viscosity of the PLA matrix.

1. T. S. Alves; J. E. Silva Neto; L. H. Carvalho; E. L. Canedo. *Polymer Testing* 2015, 50.
2. D. S. C. Andrade; E. L. Canedo; L. H. Carvalho; R. Barbosa; T. S. Alves. *Materials Research* 2021, 24.
3. E. S. B. Ferreira; C. B. B. Luna; D. D. Siqueira; E. A. Santos Filho; E. M. Araujo; R. Wellen. *Sustainability*, 2021, 13.
4. M. Barletta; M. Puopolo. *Journal of Manufacturing Process* 2020, 56.

Fundings: The authors are grateful to CAPES (Coordination for the improvement of Higher Education Personnel) and FACEPE (Foundation for the Support of Science and Technology of the State of Pernambuco) for the financial support.

Keywords: *PLA, eggshell, torque rheometry, rheology, processing.*

RHEO-OPTICAL CHARACTERIZATION OF THE SHEAR-INDUCED NON-ISOTHERMAL CRYSTALLIZATION OF POLIAMIDE 6

Sebastião V. Canevarolo[1]* and Felipe O.C. Bernardo[2]

1 – Department of Materials Engineering - DEMa, Federal University of São Carlos (UFSCar), São Paulo, SP, Brazil
*caneva@ufscar.br
2 – Graduate Program in Materials Science and Engineering (PPGCEM), Federal University of São Carlos (UFSCar), São Carlos, SP, Brazil

Abstract - A rheo-optical detector system was used to evaluate the shear-induced non-isothermal crystallization of PA6 diluted in a polypropylene (PP) matrix. A Cambridge Shearing System CSS450 from Linkam Scientific Instruments was fitted to a polarized light optical microscope from Leica, model DMRXP, to impart controlled shear and varying temperature to the samples. Photos of the optical morphology and interference colors were obtained with an AxioVision system accoupled to the system. The thermal transformations during non-isothermal analysis were measured with a specially built quantitative optical plate, set in the analyzer slot of the microscope. The experiments consisted of shearing the polymer system while collecting the cross-polarized transmitted light intensity response by a LabVIEW software. Shear rates up to 180 s^{-1} were applied to all samples. Data above 100 s^{-1} are difficult to get because the polymer melt tends to come out of the shearing glass plates. Quiescent crystallization was obtained with a DSC, used as reference technique and with the rheo-optical system. Next the dynamic crystallization of PA6 during shear flow was studied. Under shear-induced non-isothermal condition the crystallization degree of dispersed PA6 phase in a PP molten matrix is affected increasing with the increase of the shear rate. Even moderate shear rates are capable to affect the morphology of the crystallized PA6 dispersed phase. These results suggest that the moving molten polymer matrix can transfer the stress to the dispersed phase, deforming them and consequently partially orienting the PA6 chains, leading to a crystallization morphology which is spherulitic when no external shear is present, and as shear increases another population of PA6 crystals of a fibrillar type is formed. Their preferential orientation along the flow direction increases the birefringence, measured as cross-polarized transmitted light intensity.

Fundings: This study was funded by the Coordenação de Aperfeiçoamento de Pessoal de Nível Superior-Brasil (CAPES) - Finance Code 001 scholarship (00889834001-08) and the authors would also acknowledge the Programa de Pós-Graduação em Ciência e Engenharia de Materiais (PPG-CEM) of Federal University of São Carlos for providing the laboratorial facilities.

Keywords: *Rheo-optical characterization; Shear-induced crystallization; Non-isothermal; Polyamide 6;*

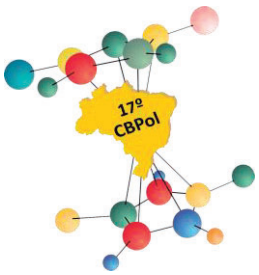

SHEAR STRENGTH IN THE GLUE LINE TO EVALUATE THE USE OF THE ADHESIVE EXTRACTED FROM THE SWIMMING BLADDER OF THE BLACK HAKE (MACRODON ANCYLODON)

Vera L. D. da Silva[1*], Syme R. S. Queiroz[1], Rosemary M. P. Coutinho[1] and Luiz Fernado S. Mendes[1]

1 – Department of Chemistry, Federal Institute of Education, Science and Technology of Pará (IFPA), Belém, PA, Brazil vera.silva@ifpa.edu.com.br

Abstract - The current production of wood panels depends mainly on formaldehyde-based adhesives or have formaldehyde and other volatile components in their formulation. These resins are produced from non-renewable resources, and there are some ongoing environmental issues with possible risks to human health due to the emission of organic solvents. The objective of this research was to produce an adhesive, extracted in an acidic medium, from the swim bladder of gó hake (Macrodon ancylodon), for use in wood substrate, for non-structural use and internal use in building works and the furniture industry. The bladders were solubilized in an acidic medium to produce the natural adhesive and later applied to glue plywood samples. Shear strength tests were carried out in the glue line, according to ASTM D2339, NBR ISO 12466- 1:2012 and EN 314-1: 1993 standards. The two ways of extracting the natural adhesive reached an average shear strength of 1, 10 and 1,11 MPa higher than the reference adhesive, traditional Cascola contact adhesive, and equal stress values in relation to joints bonded with polyvinyl acetate (PVA) adhesive.

References

1. ASSOCIAÇÃO BRASILEIRA DE NORMAS TÉCNICAS. NBR ISO 12466-1:2012: Madeira compensada – Qualidade de colagem. Rio de Janeiro, 2012. 9 p. Angles, M. N.; Dufresne, A.; *Macromolecules* 2000, 33, 8344.
2. BIANCHE, J. J. TEXEIRA, A. P.M., et al. Cisalhamento na Linha de Cola de Eucalyptus sp. Colado com Diferentes Adesivos e Diferentes Gramaturas, Floresta e Ambiente. Viçosa/MG, Brasil, v. 24, p. 9, 2017. Disponível em < https://doi.org/10.1590/2179-8087.077114>. Acesso em: 18 dez. 2019. CANTERI, M. H. G.; MORENO, L.; WOSIACKI, G.; SCHEER, A. P. Pecta: da matéria-prima ao produto fal. *Polímeros*, v. 22, p. 149-157, 2012.
3. PIZZI, A.; MITTAL, K. L. Handbook of Adhesive Technology. 2ª. ed. New York: MARCEL DEKKER, INC., 2003. 999 p. Acesso em: 20 jan. 2020. SRIAMORNSAK, P., KENNEDY, R. A. Swelling and diffusion studies of calcium polysaccharide gels intended for film coating. *International Journal of Pharmaceutics*, v.358, p.205-213, 2008.
4. WILCZAK, L. Avalição do comportamento mecânico do adesivo poliuretano derivado do óleo de mamona utilizado na produção de painéis compensados. 2014, 79 p. Trabalho de conclusão de curso (Engenharia de Produção Civil), Universidade Tecnológica Federal do Paraná - (UTFPR). Curitiba - PR, 2014.

Keywords: Wood Panels. Swim bladder. Gó hake. Shear strength

STARCH/CHITOSAN BIOFILMS USING 4-HYDROXYCHALCONE

Jonathan F. Ricardo[1], Luís A. Pinheiro [2,] Adriano G. Viana[1] and Barbara C. Fiorin[1]

1 - Departamento de Química, Universidade Estadual de Ponta Grossa, UEPG, PR, Brasil
2 - Departamento de Engenharia de Materiais, Universidade Estadual de Ponta Grossa, UEPG, PR, Brasil
jonathanfelipericardo@gmail.com

This work shows the development of starch/chitosan biofilms (SCB) using 4-hydroxychalcone (4-OH-Chal) for the treatment of skin diseases caused by fungi and/or bacteria. This chalcone is reported in the literature as good antifungal, antimicrobial, antiviral and antiproliferative agent.[1] Polysaccharides have consolidated antifungal and antiviral activities.[2] Biofilms were developed with 80% polysaccharides (72.5% starch and 7.5% chitosan) and 20% glycerol (w/w). [3,4] The methodology used in the development of biofilms was adapted from the work of Shi et al. (2013), starch films were prepared in the proportion of 5% solid concentration (w/V).[5] Starch was gelatinized in distilled water for a temperature of 100°C, adding an anhydrous alcoholic solution of 4-OH-Chal, to achieve good dispersion of the active principle. The characterization of the biofilms was carried out by means of an infrared spectroscopic analysis, where it is evident that the 4-OH-Chal were added to the film, due to the broadening of bands in the spectrum region between 1651 and 1467 cm^{-1}. The 4-OH-Chal was submitted to thermal analysis up to 100°C for 30 minutes, and later characterized by Nuclear Magnetic Resonance (^{1}H NMR and ^{13}C NMR). In the spectra, we can identify important signals, such as the unsaturation doublets between the α and β carbons in ^{1}H NMR and the carbonyl signal at 190 ppm in ^{13}C NMR. Furthermore, the melting point was determined and is in agreement with the literature (186 -188°C). These spectroscopic and physical data indicate that 4-OH-Chal was not degraded due to the high temperature of biofilm synthesis.

References

1. Elkanzi, N. A. A. *et al.* **Synthesis of Chalcones Derivatives and Their Biological Activities: A Review**. ***ACS Omega*** vol. 7 27769–27786 Preprint at https://doi.org/10.1021/acsomega.2c01779 (2022).
2. Xu, S. Y., Huang, X. & Cheong, K. L. **Recent advances in marine algae polysaccharides: Isolation, structure, and activities**. ***Marine Drugs*** vol. 15 Preprint at https://doi.org/10.3390/md15120388 (2017).
3. Ávila-Salas, F. *et al.* **Film dressings based on hydrogels: Simultaneous and sustained-release of bioactive compounds with wound healing properties**. ***Pharmaceutics*** **11**, (2019).
4. Nuñez, Y. A. R. *et al.* **Preparation of hydrogel/silver nanohybrids mediated by tunable-size silver nanoparticles for potential antibacterial applications**. ***Polymers*** *(Basel)* **11**, (2019).
5. Shi, A. M., Wang, L. J., Li, D. & Adhikari, B. **Characterization of starch films containing starch nanoparticles Part 1: Physical and mechanical properties**. ***Carbohydr Polymers*** **96**, 593–601 (2013).

Fundings: CAPES.

Keywords: *biofilms, starch, chitosan, 4-hidroxichalcone.*

STUDY OF EVA/BENTONITE CLAY-NIOBIUM PENTOXIDE HYBRID SYSTEMS BY DRX AND TD-NMR

Heliton Barra[1], Reinaldo Y. Morita[2], Roberta C. P. Rizzo-Domingues[1]and Juliana R. Kloss[1]

*1 – Department Academic of Chemistry and Biology, Federal University of Technology – Paraná (UTFPR), Curitiba, PR, Brazil *helitoon@hotmail.com*
2 – Coordination of Bioprocess and Biotechnology Engineering, Federal University of Technology – Paraná (UTFPR), Dois Vizinhos, PR, Brazil

The latest technologies require materials with more robust and diversified properties, which are usually not found in conventional materials, so hybrid structures formed by the dispersion of inorganic fillers in polymeric matrices may be an alternative. Poly(ethylene vinyl acetate) (EVA), can also be used as a building block for polymeric hybrid composites. In this sense, the objective of this work was to study hybrid EVA/clay systems modified with niobium pentoxide (Nb_2O_5), using the low-field nuclear magnetic resonance (TD-NMR) and X-ray diffraction (XRD) technique. The bentonite clay was modified with niobium pentoxide (Nb_2O_5) as described by E. Lacerda *et al* 2020[1], then the compositions were prepared using an intensive homogenizer, at EVA/clay-Nb_2O_5 in the proportions of 3, 5 and 7 % (m/m), at 3600 rpm for 15s, followed by injection molding, using the following parameters: temperatures between 160 and 180°C and pressure of 300 bar. During injection processing, it was possible to observe that the addition of the inorganic fillers made the material more viscous, making it necessary to change the injection pressure to 250 bar and the temperatures between 188 and 227°C. The compositions were analyzed by X-ray diffraction and low-field nuclear magnetic resonance. The XRD results for the compositions showed peaks for EVA (21.1° and 23.3°), bentonite clay (7°) and Nb2O5 (23° and 29°). The degree of crystallinity calculated for the compositions showed changes, being proportional to the increase in the fraction of inorganic filler added. Through the analysis of the longitudinal relaxation curves, obtained by TD-NMR, it was possible to investigate the importance and the effect of the addition of the modified clay in the polymeric matrix, and this study of hybrid systems is promising for future applications in the treatment of contaminants in water bodies.

a) 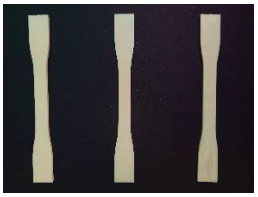 b) c) 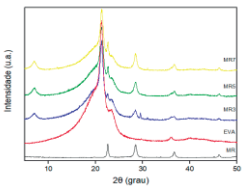

Figure 1 - a) EVA/Nb_2O_5-modified clay compositions, b) TD-NMR and c) XRD of the EVA/Nb_2O_5-modified clay.

References

1. E. Lacerda; F. Monteiro; J. Kloss; S. Fujiwara. *Journal of Photochemistry and Photobiology A: Chemistry* 2020, 388, 112084. https://doi.org/10.1016/j.jphotochem.2019.112084
2. E. Beyou; E. Lami. Progress in polymer Science, p.1-31, 2020. https://doi.org/10.1016/j.progpolymsci.2021.101434.

Keywords: Poly(ethylene vinyl acetate); polymer, inorganic filler, niobium; crystallinity.

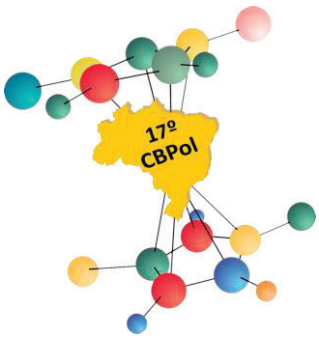

STUDY OF SURFACE MODIFICATION OF BACTERIAL CELLULOSE BY ATMOSPHERIC PLASMA JET

Aline R. Almeida[1]*, Bianca Fusinato[1], Cristiane Stegemann[2], Henrique de Souza Medeiros[2], Julio César Sagás[1] and Daniela Becker[1]

1 – Laboratory of Plasmas, Films and Surfaces, Santa Catarina State University (UDESC), Joinville, SC, Brazil
alinerosaufpr@gmail.com
2 –DuMeio – Inovação Sustentável (Startup), Jaraguá do Sul, SC, Brazil

Bacterial cellulose (BC) is a polymer that has a three-dimensional structure formed by pure cellulose nanofibers, synthesized by some bacteria and organized as a coherent network. Its biodegradability, biocompatibility and mechanical properties have aroused interest for use in various applications, such as food packaging, regenerative system, sensor base, cosmetics, filter media, fabric and leather substitute. However, BC presents challenges to be overcome, with the hydrophilicity and porosity of BC being some of the most relevant, as they hinder the application in several segments. Thus, the objective of the study is to evaluate the effect of treatment with atmospheric air plasma jet on the wettability of BC. The CB used was provided by the startup DuMeio – Inovação Sustentável, being used dry. The plasma jet was generated from a dielectric barrier discharge in atmospheric air with laminar flow rate of 2.0 NL/min, voltage frequency of 8.0 kHz, providing a voltage pulse with a width of 100 μs, interspersed by zero voltage intervals and voltage amplitude around 15 kV. The distance between the reactor outlet and the sample was 4 mm, varying the time of exposure of the sample to the plasma jet in 0, 10, 20, 30, 40, 50, 60 and 70 seconds. The results were promising to improve the hydrophobicity of the material, with 70 seconds of treatment the contact angle increased from 58.0 ± 0.4 and 43.5 ± 0.3 in the untreated sample to 93.1 ± 0.7 and 68.9 ± 0.5 after 0 and 15 seconds of surface contact with the water drop, respectively. This change suggests that the treatment may have acted on the OH groups of BC, modifying the affinity with water on the surface of the samples without changing the appearance characteristics.

References

1. F. Sederavičiūtė, P. Bekampienė, J. Domskienė. *Polymer Testing* 2019, 78. https://doi.org/10.1016/j.polymertesting.2019.105941.
2. I. Sulaeva, et al. *Biotechnology Advances* 2015, 33, 8, 1547–1571. http://dx.doi.org/10.1016/j.biotechadv.2015.07.009.
3. J. Wang; J. Tavakoli; Y. Tang. *Carbohydrate Polymers* 2019, 219, 63–76. https://doi.org/10.1016/j.carbpol.2019.05.008

Fundings: This study was partially funded by the National Council for Scientific and Technological Development-Brazil (CNPq)-Financial Code n°. 350722/2022-6.
Keywords: *Contact angle; Bacterial cellulose, Wettability.*

STUDY OF THE DEGRADATION OF POLY(METHYL METHACRYLATE) (PMMA) IN CONTACT WITH BRAKE FLUID

Joaquim S. de Oliveira[1], Woodley T. A. da Silva[1 #], Juciklécia S. Reinaldo[1*]

1 – Department of Materials Engineering, Superior School of Technology, University of Amazonas State (EST-UEA), Manaus, AM, Brazil [1]jso.emt18@uea.edu.br [#]wtads.emt19@uea.edu.br, [*]jreinaldo@uea.edu.br,

Abstract – The PMMA is a polymer of the methacrylate class that presents greater possibilities for technological applications. Some of the most important characteristics of PMMA are transparency and ability to reflect light, being widely used in panels, signs and automotive applications. In this work we investigated the effects of the degradation caused by exposure of PMMA to a solvent (brake fluid) and increasing of temperature. Samples were exposed to fluid contamination and subjected to heating in a circulating air oven at 50°C for 1 hour. Fractography analysis of the samples were performed by optical and scanning electron microscopy (SEM). We observed that the increase in temperature intensified the signs of *Environmental Stress Cracking* (ESC), promoting nucleation of cracks (crazing), in addition to degradation (opacity) of the surface exposed to the solvent and temperature at 50°C for 1 hour, demonstrating the fragility and susceptibility to degradation of PMMA in contact with brake fluid and temperature variation.

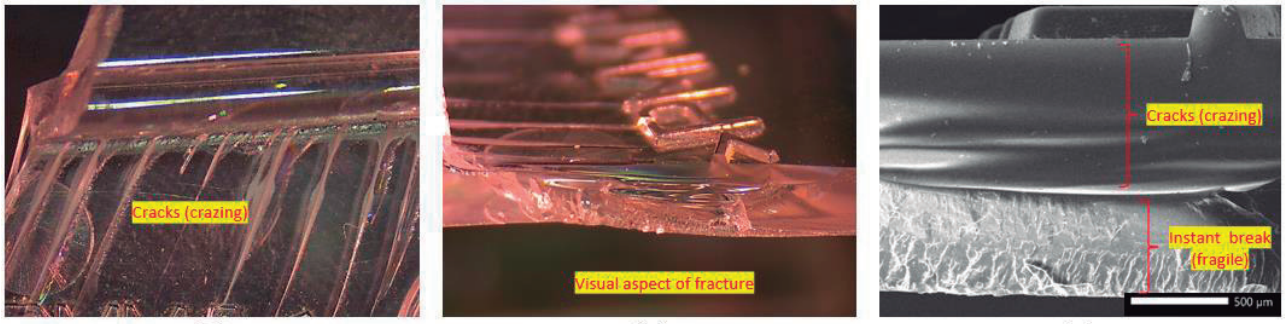

Fig 1 – Fractography analyzed samples. Cracks detected on the surface of samples after test (a). Macro aspect of fracture surface (b) and fractography analyzed by SEM (c).

References

1. A. Turnbull; A. S. Maxwell; S. Pillai *Polym. Test.* 2000**,** *19,* 117.

2. Rabello, M; De Poli, M.A. Aditivação de Termoplástico. Editora Artliber, São Paulo – SP, 2013.

Keywords: *PMMA, solvents, temperature, degradation, Environmental Stress Cracking.*

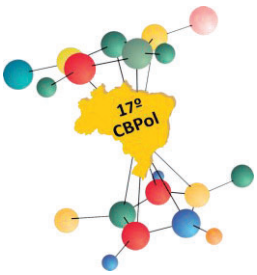

SYNTHESIS, CHARACTERIZATION AND EVALUATION OF PNVCL THERMORESPONSIVENESS BY DIFFERENT TECHNIQUES

Rhodivam Lucas Mendes Feitosa [1*], Grazielle Rozendo de Cerqueira [1], Alessandra de Sousa Lima [1], Cecilãne Regina Dioclecia da Silva Ribeiro de Assis [1], Elmo Silvano Araujo [3], Armando Navarro-Vázquez [1,2], Fernando Hallwass [1,2], Yêda Medeiros Bastos de Almeida [1,2], Carolina Lipparelli Morelli [1,4]

[1] Materials Science Program, Federal University of Pernambuco (UFPE), 50670-901, Recife, PE, Brazil
rhodivam.lucas@ufpe.br
[2] Department of Fundamental Chemistry, Federal University of Pernambuco (UFPE), 50670- 901, Recife, PE, Brazil
[3] Department of Nuclear Energy, Federal University of Pernambuco (UFPE), 50740- 545, Recife, PE, Brazil
[4] Department of Mechanical Engineering, Federal University of Pernambuco (UFPE), 50670- 901, Recife, PE, Brazil

Abstract - Poly N-vinylcaprolactam (PNVCL) is a thermoresponsive material of great interest in medical applications due to its biocompatibility. This work presents a study of methodologies for the synthesis of Poly N-vinylcaprolactam (PNVCL), with and without a chain transfer agent (CTA), as well as the evaluation of the thermoresponsive behavior of the polymer through different techniques: cloud point, relaxometry and differential scanning calorimetry. Infrared spectroscopy (FTIR) and nuclear magnetic resonance (NMR) analyses confirmed the polymerizations. Molecular masses determined by viscometry were 170,000 g·mol^{-1} for PNVCL and 73,000 g·mol^{-1} for the PNVCL synthetized with CTA (PNVCL-COOH). The phase transition temperatures found by DSC were 24 and 30.5 ºC, for PNVCL-COOH and PNVCL, respectively. The cloud point of solutions occurred between 32 and 33 ºC for both polymers. In the relaxometry analysis, the hydrophilic/hydrophobic phase transition of polymers was indicated between 31 and 33 °C, related to the change in the mobility of water molecules in the system. Relaxometry is a non-destructive technique that represents an important alternative tool for evaluating the behavior of smart polymers.

References -

1. L. Marsili, M. D. Bo, G. Eisele, I. Donati, F. Berti, G. Toffoli Polymers 2021, 13, 2639. https://doi.org/10.3390/polym13162639
2. Y. Li, X. Li, C. Chen, D. Zhao, Z. Su, G. Ma, R. Yu. Carbohydrate Polymers 2016, 13, 1251-1260. http://dx.doi.org/10.1016/j.carbpol.2016.06.054
3. L. Shao, M. Hu, L. Chen, L. Xu, Y. Bi. Reactive & Functional Polymers 2012, 11, 407-413. http://dx.doi.org/10.1016/j.reactfunctpolym.2012.04.002

Keywords: *Poli(N-vinylcaprolactama); relaxometry; thermoresponsive polymers; synthesis.*

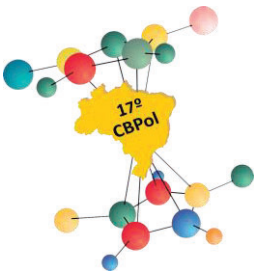

THE EFFECT OF ACCELERATED PHOTOAGING ON THE MORPHOLOGICAL, PHYSICAL AND CHEMICAL PROPERTIES OF POLYETHYLENE TEREPHTHALATE (PET) MICROPLASTIC

Kelven G. A. Conceição[1*], Eric M. Silva[1], Gabriela Z. Diaz[1], Thais B. O. Costa[1], Diego Q. Melo[2] and Carla B. Vidal[1]

1 – Department of Chemistry & Biology, Federal University of Technology - Paraná (UTFPR), Curitiba, PR, Brazil
2 - Federal Institute of Education, Science, and Technology of Sertão Pernambucano (IFSertão), Petrolina, PE, Brazil
*kelvengabriel@alunos.utfpr.edu.br

Abstract - The pollution caused by plastics has been increasing every day, especially in marine environments. Once discarded in the environment and exposed to natural processes such as UV radiation degradation and physical fragmentation, plastic can break down into smaller particles (<5mm), defined as microplastics (MPs). Based on the above, studies investigating the effect of MP photodegradation using accelerated artificial aging and its effects on morphological and physicochemical properties are essential for a better understanding of the dynamics of these pollutants in the environment. Polyethylene terephthalate (PET) microplastics were irradiated in a UV-B accelerated aging chamber, where 10g of MPs were placed on 4 petri dishes 30 cm distance from the lamps during 1h, 4h, 6h, and 8h exposure times. Scanning electron microscopy (SEM) was used to obtain photomicrographs of the surface physical structure of the PETs before and after aging, at various magnifications. In addition, Energy-Dispersive X-ray Spectroscopy (EDS) analysis allowed a qualitative estimation of the MPs chemical composition. X-ray diffraction (XRD) analysis was performed to determine the degree of crystallinity in the adsorbent materials. The results of the SEM and EDS characterization revealed few morphological alterations on the material's surface, with the appearance of small pores only in the MPs exposed to longer irradiation times. Through the XRD technique, a reduction in the degree of crystallinity (%): PET *in natura* (28.97), PET-1h (18.32), PET-4h (17.37), PET-6h (20.34) and PET-8h (16.86) was observed, likely due to the alteration in the chemical structure of the photodegraded MPs. It can be concluded that PET MPs, when subjected to photodegradation processes, change their chemical structure, which can impact the dynamics of this plastic in the aquatic environment.

References

1. DUARTE, Luciana Tavares et al. Thermally sprayed coated carbon steel produced using PET powder obtained in different grinding conditions, v. 13, p. 198-204, 2003. https://doi.org/10.1590/S0104-14282003000300010
2. Fechine, G.J.M., Souto-Maior, R.M. & Rabello, M.S. Structural changes during photodegradation of poly(ethylene terephthalate). Journal of Materials Science 37, 4979–4984 (2002). https://doi.org/10.1023/A:1021067027612
3. Mitrano, D.M., Wagner, M. A sustainable future for plastics considering material safety and preserved value. Nat Rev Mater 7, 71–73 (2022). https://doi.org/10.1038/s41578-021-00406-9
4. PLASTICS EUROPE. Plastics - the Facts. 2021

Keywords: *Polyethylene terephthalate, photoaging, characterization, microplastic*

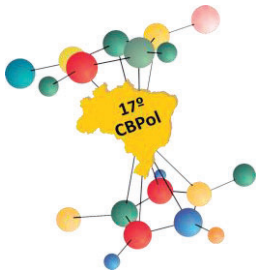

THE INFLUENCE OF SYNTHESIS CONDITIONS ON THE CHARACTERISTICS OF POLY(N-ISOPROPYLACRYLAMIDE)

Maíra Theisen[1], Maria C. S. Durigon[2], Heloise R. de Barros[1], Leandro Piovan[2] and Izabel C. R. Vidotti[1]

1 – Research Group on Macromolecules and Interfaces (GPMIn), Department of Chemistry, Federal University of Paraná (UFPR), Curitiba, PR, Brazil
theisen.maira@gmail.com
2 – Chemical and enzymatic synthesis Laboratory (LaSQuE), Department of Chemistry, Federal University of Paraná (UFPR), Curitiba, PR, Brazil

Abstract – Responsive polymers are a category of intelligent materials that exhibit the ability to react to external stimuli, such as changes in pH and temperature [1]. Among these, poly(N-isopropylacrylamide) (PNIPAm) stands out as one of the extensively studied temperature-responsive polymers. Specifically, thermoresponsive polymers undergo conformational changes at a specific temperature. In the case of PNIPAm, the polymeric chains change from extended to collapsed conformation (coil-to-globule transition) around 32 °C [2], being a viable option for different applications. Our study focuses on the synthesis and characterization of PNIPAm. Free-radical polymerization was employed as the method for polymer formation, in which synthesis parameters, such as temperature, reaction time, presence of accelerator, and solvent quantity, were varied to produce two distinct polymers with unique characteristics. The confirmation of polymer formation was carried out through Nuclear Magnetic Resonance (NMR) and Fourier-transform infrared spectroscopy (FTIR). In both cases, the products were obtained with good yields (exceeding 75%). Size-exclusion chromatography (SEC) was used to determine the molecular weight and polydispersity, revealing that one of the synthesis methods yielded a more polydisperse polymer. To investigate the thermoresponsive behavior, the polymers were subjected to a heating-cooling cycle and studied through dynamic light scattering (DLS) and turbidimetric measurements. Notably, temperature values of 31.5 °C and 33.5 °C were identified during turbidimetry. In summary, in this study, the PNIPAm was successfully synthesized, characterized and is suitable for applications that depend on polymer transition.

References:

1. M. A. Ward; T. K. Georgiou *Polymers* 2011, 3(3), 1215. https://doi.org/10.3390/polym3031215
2. A. Halperin; M. Kröger; F. M. Winnik *Angew. Chem. Int. Ed.* 2015, 54, 15342. https://doi.org/10.1002/anie.201506663

Fundings: CAPES

Keywords: *Poly(N-isopropylacrylamide), thermoresponsive polymers, free-radical polymerization*

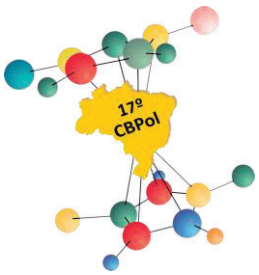

BIODEGRADABLE ELECTROSPUN NANOFIBERS CONDUITS FOR NERVE REGENERATION

Claudia Merlini [1]

1 – Materials Engineering Special Coordination, Universidade Federal de Santa Catarina (UFSC), Blumenau 89036-002, SC, Brazil
claudia.merlini@ufsc.br

Peripheral nerve injuries affect the quality of life of people worldwide and despite advances in materials development in this area, nerve repair remains a challenge. Nowadays some nerve conduits are available for clinical use and appear as an alternative to the autograft. Nevertheless, they still need to be optimized concerning the degradation time and microstructure, for better functional nerve response. In order to overcome these challenges, conductive conduits made from electrospun nanofibers are an interesting alternative. The electrospun nanofibers displays several important properties in this application, such as high surface area, porosity, and structural flexibility. Furthermore, they may have some similarity to the hierarchical structures of natural biological tissues, because they can be manufactured with different geometries. The use of different biodegradable polymers associated with conductive nanofillers makes it possible to obtain conduits with an adequate degradation profile and electrical conductivity, in order to enhance nerve regeneration. Moreover, aligned fibers can guide physical cell growth and can promote superior cell maturation compared to randomly distributed fibers. In this context, this work proposes to analyze the development of aligned electrospun nerve conduits with electrical activity, in order to provide electrical stimulation and guide axon growth, facilitating nerve regeneration and functional recovery. In this context, the development of electrospun mats with aligned nanofibers based on biodegradable and bioabsorbable polymers containing conductive nanofillers such as carbon nanotubes (NTC) and intrinsically conductive polymers (PICs) will be discussed. Thus, morphology and mechanical performances, hydrolytic degradation, and cytotoxicity will be outlined in order to develop nerve conduits.

References

1. For articles: V.O.Castro; C.Merlini. *Artificial Organs.* 2021; 00:1–6. https://doi.org: 10.1111/aor.13942.
2. V.O.Castro; Ph.D. Thesis, Federal University of Santa Catarina, 2022.

Keywords: *nanofibers, nerve conduits, tissue engineering, conductive fillers; electrospinning.*

ENZYMATIC RING OPENING COPOLYMERIZATION OF LACTONES FOR THE PREPARATION OF FUNCTIONALIZED ELECTROSPUN SCAFFOLDS

Heloísa B. Madalosso[1], Camila Guindani[2], Bianca C. Maniglia[3], Pedro H. H. Araújo[1], Claudia Sayer[1*]

1- Chemical Engineering and Food Engineering Department (EQA), Federal University of Santa Catarina (UFSC), Florianópolis, SC, Brazil, claudia.sayer@ufsc.br
2- Chemical Engineering Program/ COPPE, Federal University of Rio de Janeiro (UFRJ), Rio de Janeiro, Brazil
3- São Carlos Institute of Chemistry, University of São Paulo (USP), São Carlos, Brazil

Abstract – The development of biomaterials of polymers derived from macrolactones has gained attention due to their suitable and tunable properties, such as biocompatibility and biodegradability[1-3]. Besides, green synthesis approaches, such as enzymatic catalysis, enable to obtain polyesters with high molecular weight via ring-opening polymerization. However, the application of these polymers to design biomedical devices still faces drawbacks, such as poor bioresorbability and high hydrophobicity. In this sense, the copolymerization and further functionalization of macrolactones via click chemistry allow designing functional biomaterials with improved properties favoring specific interactions with biological systems. Thus, this work involves the synthesis and functionalization of the copolymer poly(globalide-co-ω-pentadecalactone) via enzymatic ring-opening polymerization (e-ROP), aiming to design biomaterials suitable for applications in tissue engineering for bone regeneration. Results evidence that it is possible to tune the copolymer properties by varying the monomer ratios and that the increase of the PDL content led to an increase in molecular weight, dispersity, melting temperature, and crystallinity. In sequence, the conformation of the copolymers via electrospinning resulted in homogeneous fibers and the formed scaffolds proved to be non-toxic and improved cell growth of osteoblasts and mineralization. Finally, the functionalization with cysteine via a thiol-ene click reaction and the conjugation with collagen via EDC/NHS chemistry hugely reduced polymer crystallinity and turned the surfaces of the designed scaffolds hydrophilic. Tests with pre-osteoblast cells revealed an increase of up to 85% in cell viability for the PGlPDL-collagen scaffolds and also increased in 75% the mineralization compared to the raw fibers.

References

1. C. L. Savin; C. Peptu; M. Popa.; J. Mosnáček,. *Biomacromolecules* 2018, *19*, 3331–3342. https://doi.org/10.1021/acs.biomac.8b00634.
2. J. Zhang; H. Shi; D. Wu; Z. Xing; A. Zhang; Y. Yang; Q. Li. *Process Biochem*. 2014, *49*, 797–806. https://doi.org/10.1016/j.procbio.2014.02.006.
3. Z. Jiang; H. Azim; R. A. Gross; M. L. Focarete; M. Scandola. *Biomacromolecules* 2007, *8*, 2262–2269. https://doi.org/10.1021/bm070138a.

Fundings: The authors would like to thank the financial support provided by Coordenação de Aperfeiçoamento de Pessoal de Nível Superior (CAPES), Conselho Nacional de Desenvolvimento Científico e Tecnológico (CNPq) and FAPERJ (Fundação Carlos Chagas Filho de Amparo à Pesquisa do Estado do Rio de Janeiro).

Keywords: *E-ROP, Polyester, Scaffolds, Bioconjugation*

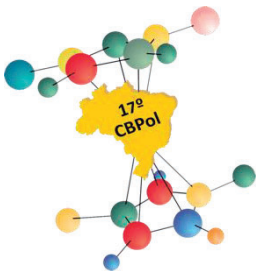

IMPROVING THE MECHANICAL PROPERTIES OF HEMICELLULOSE BY ADDING POLYLACTIC ACID (PLA)

Michaella S. B. Fialho *, Layse M. Diniz, Linconl A. Teixeira and Sandra M. Luz
Mechanical Sciences Graduate Program, University of Brasília (UnB), CEP: 70910-900 – Brasília, DF - Brazil
** michaella.socorro@gmail.com*

Abstract - Biodegradable polymers extracted from natural sources such as hemicellulose have been extensively sought to replace synthetic plastics. The polymeric films of hemicellulose had low mechanical properties, limiting their applications as materials. However, some strategies can be used to improve the mechanical properties, for example, blending with other biodegradable polymers. Therefore, this study developed polymer blends of polylactic acid (PLA) and hemicellulose extracted from jute fiber. To prepare the blends, the hemicellulose was solubilized at 5, 15, and 25% (w/w), concerning PLA weight, in distilled water, and 10% (w/w) of citric acid was added. Then, the PLA was solubilized in chloroform, blended with hemicellulose solutions, and molded into films using solvent casting. The blends' mechanical performance was studied using tensile tests and dynamic mechanical analysis (DMA). Tensile properties show the blends are improved tensile strength compared to the pure PLA and hemicellulose film. However, the elongation at the break of the blends was substantially smaller than pure PLA. The hemicellulose content decreased the elastic and storage modulus of the films. From these results, it can be concluded that the PLA blending improved the mechanical properties of hemicellulose film.

Keywords: *polymer blends, dynamical and mechanical properties, hemicellulose, polylactic acid.*

Introduction

Studies of biomass polymers gained interest in development-friendly plastics in the last few years. The packaging industry has developed new materials from renewable sources with a short degradation period, such as hemicellulose. Hemicellulose is a polysaccharide found in plant cell walls that can be extracted using light alkaline treatments [1]. One of the main advantages of hemicellulose processing is its ability to form flexible films, making it attractive as an ecologically correct material in several applications [2]. However, some characteristics, such as low mechanical properties and sensitivity to humidity, can limit its broad applicability in the industry [2].

PLA is currently one of the most widely studied sustainable polymers that exhibit biodegradability and good thermal and mechanical properties. Glass transition temperatures between ~60 °C, tensile strength ranging from 15~150 MPa, and an elastic modulus 2.7 GPa are strongly affected by molecular weight (Mw) [3]. Therefore, due to these characteristics, blending hemicellulose into a semicrystalline and thermoplastic polymer, such as PLA, can be an option to improve its properties.

Although, due to the hydrophilic character of hemicellulose and the hydrophobic portion of PLA, an incompatibility between the polymers is expected. Thus, it becomes necessary to incorporate plasticizers and/or compatibilizers to facilitate the interaction between the polymers. For example, citric acid has been used as a compatibilizer for polysaccharides, as the carboxyl groups of its structure interact with the hydroxyl groups of hemicellulose, resulting in an esterification reaction that can improve compatibility with other polymers [4]. In this study, the solvent casting technique prepared PLA/hemicellulose polymeric films using citric acid as a compatibilizer. And then, the

influence of hemicellulose content at 5, 15, and 25% (w/w) blended with PLA on mechanical properties using tensile and dynamic mechanical tests were studied.

Experimental

Materials

The jute fibers (*Corchorus capsularis*) were provided by Sisalsul Industry and Commerce LTDA for hemicellulose extraction. The polylactic acid pellets provided by NatureWorks are semi-crystalline, with a melting temperature of 145 °C and a glass transition temperature of 55 °C.

Obtaining the hemicellulose

The hemicellulose extraction methodology was adapted from [1]. About 10 g of raw jute fibers were soaked in 200 mL of distilled water at 25 ºC for 1 h to remove impurities from the fibers and facilitate hemicellulose extraction. Then, the fibers were added to 200 mL KOH 10% (w/v) solution under mechanical stirring at a constant 50 rpm and orbital shaking 250 rpm for 3 h at 25 ºC. The liquor was filtrated, and the pH was adjusted to 4.8 using acetic acid. After 24 h, the solution was centrifuged at 4000 rpm for 5 min. A 250 mL glacial acetic acid and ethanol 1:10 (v/v) were added to the liquor to precipitate the hemicellulose. Subsequently, the resulting solution was filtered, and the hemicellulose portion was washed with distilled water (200 mL) three times and dried at room temperature for 24 h.

Obtaining the blends of films

The films were obtained by solvent casting technique [5]. First, PLA was solubilized at a concentration of 10% (m/v) with chloroform and hemicellulose in distilled water at a proportion of 33% (m/v) under constant magnetic stirring for approximately 2 h, and molded into a glass plate of 15 x 15 cm. To prepare the blends films, the hemicellulose (5, 15, and 25% w/w) was first solubilized in distilled water at a concentration of 33% (w/v) with magnetic stirring at 35 °C and incorporated citric acid (CA) (10% w/w) to the solution for 1 h at 85 °C. Then, PLA pellets (90, 88, and 70% w/w) were dissolved to 10% (w/v) of chloroform with magnetic stirring for 2 h. After completely dissolved polymers, the solutions were mixed with 5% (w/w) of glycerol under constant magnetic stirring for 2 h. Finally, the solution was casting a glass plate and dried at room temperature until the complete evaporation of the solvent for 24 h to remove the film from the glass plate. The sample codes were identified as 5HEMI/90PLA, 15HEMI/80PLA, and 25HEMI/70PLA, where the first number refers to the proportion of hemicellulose (abbreviation: HEMI), and the following number to the percentage of PLA.

Blends characterization

Uniaxial tensile test followed the ASTM D882-91 standard method for tensile tests on polymeric films. The test was performed in MTS 810 Material Test System machine, coupled to a 2.5 kN load cell and a 5 mm/min speed at room temperature. Three specimens with dimensions 100 x 15 x 0.30 mm were analyzed for each film composition. Statistical analysis was performed using SPSS 20.0 to compare the mechanical test results. Dunnett's test considered all blends compared to the neat hemicellulose film.

Film samples dimensions of 10 × 5 x 0.30 mm were also evaluated Dynamic Mechanical Thermal Analysis by using a NETZSCH DMA model 242 E Artemis equipment, from 20 °C to 120 °C at a heating rate of 3 °C/min and a frequency of 1 Hz.

Results and Discussion

Tensile Stress-strain and DMA curves results are shown in Fig. 1. The tensile test provided Tensile strength (MPa), elongation (%), and Elastic modulus results; and the dynamic mechanical

analysis provided information regarding the storage modulus (E') and damping (tan δ) for neat PLA, neat hemicellulose and blends films, detailed in number in Table 1.

Tensile strength, % elongation at break, and elastic modulus of neat PLA were 13.4 MPa, 80%, and 1026.0 MPa, respectively, which agrees with the PLA fragility and results of previous studies produced by solvent casting technique [6]. A neat film of hemicellulose was essentially brittle, showing 12.2 MPa, 1.2%, and 13.7 MPa, respectively. The poor mechanical properties of hemicellulose films are due to their low molecular weight and low degree of polymerization [7].

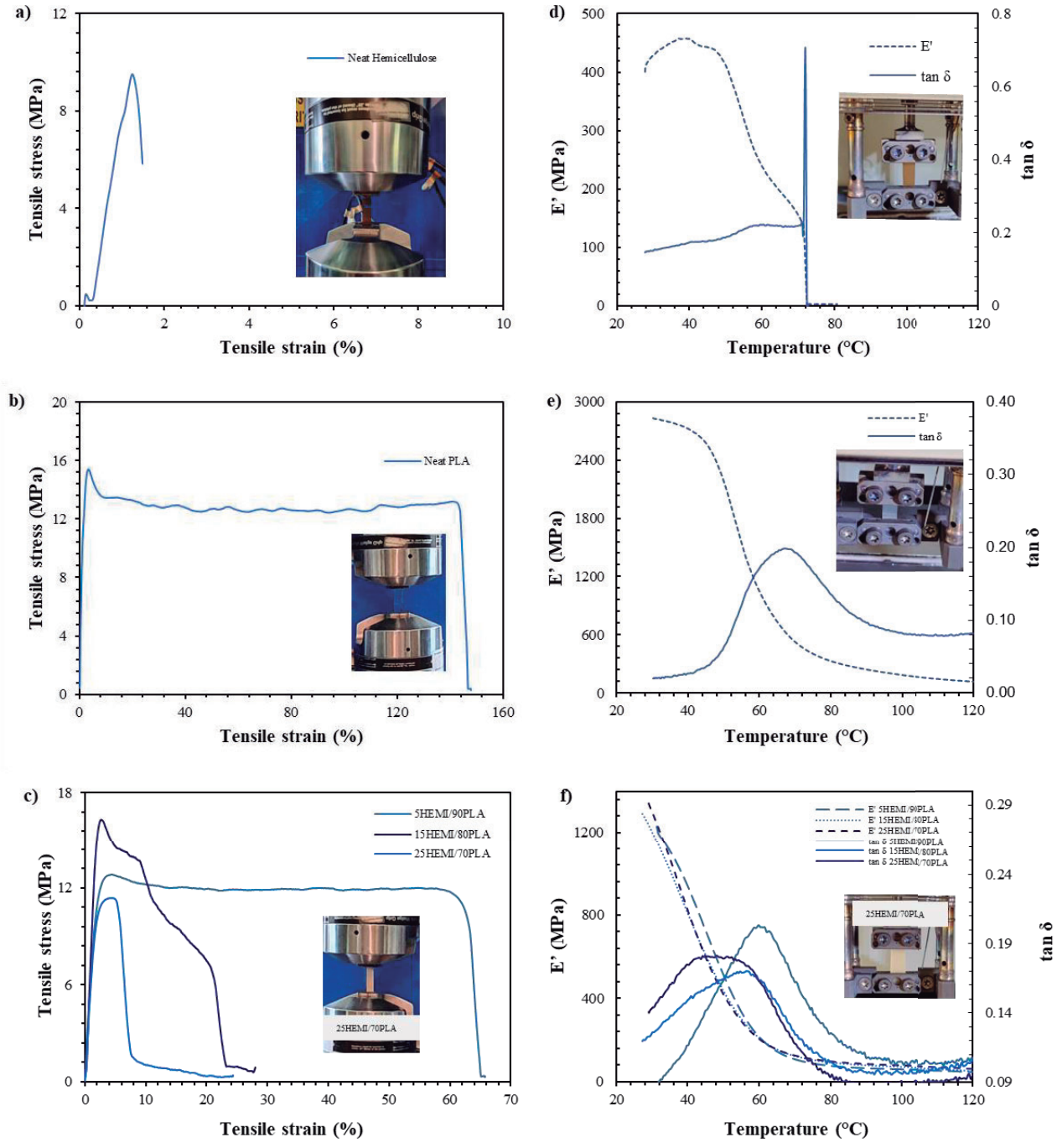

Figure 1 – Stress-strain curves of (a) neat hemicellulose, (b) neat PLA (c) blends films; DMA curves for d) neat hemicellulose, e) neat PLA, and f) blends films.

For the blends, the tensile strength of 5HEMI/90PLA and 15HEMI/80PLA has improved by approximately 40% compared to the neat PLA and 54% to the neat hemicellulose film (Table 1). This behavior can be attributed to the incorporation of citric acid in the blends, which resulted in the esterification reaction of the hemicellulose [2], which led to better compatibility between the polymers, slightly affecting the tensile strength. However, for the highest amount of hemicellulose content, 25% (w/w), the tensile strength decreases by approximately 46% compared to the blends. The decrease in tensile properties has also been reported in blends of PLA and other polysaccharides, in which higher starch levels resulted in a lower tensile strength [8,9]. A gradual decrease in the % elongation and elastic modulus can also be observed as the hemicellulose content increases. For example, the % elongation of neat hemicellulose was 99% lower than neat PLA.

Regarding the hemicellulose content in the blends, the elongation at break was 59.1, 46.8, and 20.7% for the films with 5, 15, and 25 wt%, respectively, indicating a flexibility drop in the blends. The hemicellulose film is less rigid, with a lower modulus of elasticity of 13.7 MPa. The blend 5HEMI/90PLA showed the highest modulus of elasticity of approximately 1032 MPa, while neat PLA is 1026 MPa. The blends' elasticity modulus decreases with the hemicellulose and CA addition. The CA can increase the flexibility of the PLA chains [8,9]. The statistical evaluation (Dunnett's test) of the mechanical properties showed no significant difference in tensile strength between neat hemicellulose and the blends. Besides, the hemicellulose influenced a decrease in % elongation and Elastic modulus, demonstrating a substantial difference between the neat hemicellulose and the blend films.

Table 1 – Mechanical properties of neat PLA, hemicellulose, and blends.

Blend films	Tensile strength (MPa)	% Elongation	Elastic modulus (MPa)	$E'_{30°C}$ (MPa)	$E'_{50°C}$ (MPa)	Tan δ peak	T_g (°C)
Neat PLA	13.4 ± 3.6	152.6 ± 6.4	1026.0 ± 28.8	2829.7	2180.8	0.20	67.1
Neat hemicellulose	12.2 ± 1.7	1.2 ± 0.3	13.7 ± 0.7	428.5	412.1	0.18	-
5HEMI/90PLA	18.9 ± 6.2	59.1 ± 5.9*	1032.0 ± 104.5*	1303.4	513.7	0.20	59.8
15HEMI/80PLA	18.70 ± 1.2	46.8 ± 7.4*	880.6 ± 94.7*	1195.0	429.1	0.17	56.4
25HEMI/70PLA	10.2 ± 10.2	20.7 ± 3.31*	615.6 ± 66.5*	1228.3	416.9	0.18	48.10

*Significant difference between the neat film of hemicellulose and blend films by Dunnett's test.

Fig 1 is shown the storage modulus (E') and tan δ of neat PLA, neat hemicellulose, and the blends as a function of temperature. Table 1 shows the values referring to the storage module defined in the 30-50°C temperature range and the tan δ peaks corresponding to the glass transition temperature. Neat hemicellulose showed a low storage modulus at 30 °C of 428.5 MPa, and a rapid decrease occurs at ~70 °C. The δ tan peak is related to identifying the T_g of polymers. Observing the T_g of hemicellulose is impossible because it occurs between 150~220°C [10]. The neat PLA and the blend curves exhibit an amorphous characteristic typical of the drop in storage modulus at the glass transition temperature. Three different regions can be observed, the glassy region (~40 °C), the glass transition region (between 45 and 80 °C), and the rubbery plateau (~80 °C).

From the tan δ curves, neat PLA exhibited a glass transition (T_g) at 67.1 °C, and showed a high E' at 30 °C of 2829.7 MPa with a sharp drop at 50 °C of 2180.8 MPa. The intensity of the tan δ peak can indicate the compatibility of the blend's polymers. The sample 5HEMI/90PLA did not

exhibit peak value variation for tan δ compared to pure PLA. As for the 25HEMI/70PLA, the peak value for tan δ decreased by 10%. This result may infer partial compatibility between the polymers because T_g decreased to 59.8, 56.4, and 48.10 °C for hemicellulose contents in 5, 15, and 25wt%, respectively [11].

Adding hemicellulose decreases the storage modulus in the glassy and rubbery regions compared to the pure PLA film with increasing temperature. The storage modulus is an indication of the elastic response of a material. Therefore, blend films become approximately 57% less rigid at 30 °C. At 50 °C, the storage modulus for 5HEMI/90PLA increased by approximately 46% compared to neat hemicellulose film. For higher hemicellulose content in the blends, there was no significant difference in the value of the storage modulus, probably due to the effect of adding citric acid, which increased the mobility of the PLA chain resulting in poor interfacial adhesion of hemicellulose to PLA. This behavior is also reported in blends of PLA/starch and decreases a T_g [12].

Conclusions

This study aimed to investigate the influence of hemicellulose content on the mechanical properties of hemicellulose/PLA blends. The tensile strength of blends was higher than the neat PLA and hemicellulose, indicating improved mechanical properties. However, the hemicellulose addition decreased the % Elongation and the Elastic modulus compared to neat PLA. Also, the blends' storage modulus and glass transition temperature decreased with hemicellulose content, increased by the flexibility of the PLA chains. These results encourage further investigations into the use of hemicellulose in blends.

Acknowledgments

The authors thank CAPES, DPG/UnB, FAPDF, and CNPq for their support.

References

1. L. Kataoka; M. Hidalgo; S. Luz J Nat Fibers 2021, 8; 18:1-13. https://doi.org/10.1080/15440478.2021.1934934.
2. H. Shao; H. Sun; Y. Zhang RSC Adv 2019, 9(5), 2395-401. https://doi.org/10.1039/C8RA09937E.
3. E. Rezvani; F. Khosravi; A. Saedi; RE. Dai; F. Foroughi Polymers (Basel), 2021, 13(11), 1–16. https://doi.org/10.3390/polym13111854.
4. X. Cui; A. Ozaki; T. Asoh; H. Uyama Polym Degrad Stab 2020, 175, 109118. https://doi.org/10.1016/j.polymdegradstab.2020.109118.
5. P. Anbukarasu; D. Sauvageau; A. Elias Sci Rep 2016, 17884. https://doi.org/10.1038/srep17884.
6. S. Sousa; A. Costa; A. Silva; R. Simões Polymers (Basel), 2019, 11(1), 66. https://doi.org/10.3390/polym11010066.
7. M. Oliveira; L.Diniz; A. Elias; S. Luz Polymers (Basel) 2022, 14(15), 2999. https://doi.org/10.3390/polym14152999.
8. N. Ibrahim; M. Kahar. A. Wahab; D. Uyan; H. Ismail BioResources, 2017, 12(2), 3076–87. https://doi.org/10.15376/biores.12.2.3076-3087.
9. E. Murillo Macromol Res 2023, 31, 157–169. https://doi.org/10.1007/s13233-023-00127-8.
10. I. Mendes; M. Fialho; R. Leão; E. Silveira; S. Luz Materials Research, 2023, 26, e20220390. https://doi.org/10.1590/1980-5373-MR-2022-0390.
11. Z. Liu; H. Lu; H. Zhang; L. Li J Appl Polym Sci. 2021, e51204. https://doi.org/10.1002/app.51204.
12. R. Awale; F. Ali; A. Azmi; N. Puad; H. Anuar; A. Hassan Polymers (Basel), 2018, 10(9), 977. https://doi.org/10.3390/polym10090977.

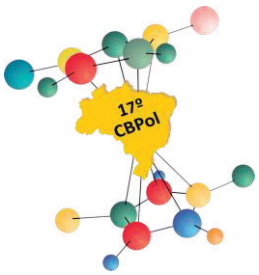

MICROWAVE ABSORBING MATERIALS BASED ON MULTILYERED POLYMERIC COMPOSITES

Juliana M. Farias da Silva[2], Debora Schmitz[2], Bluma G. Soares[1,2]*

1 – Universidade Federal do Rio de Janeiro, Departmento de Engenharia Metalúrgica e de Materiais Rio de Janeiro, RJ, Brazil bluma@metalmat.ufrj.br
2 – Universidade Federal do Rio de Janeiro, Instituto de Macromoléculas, Rio de Janeiro, RJ, Brazil

Abstract - The development of sophisticated and high performance wireless devices caused enormous electromagnetic (EM) pollution, since the emitted EM wave (EMW) by these devices can negatively affect the operation of other sensitive electronic equipments, as well as on human health [1]. Therefore, several works have been focused on the development of lightweight microwave absorbing (MWA) materials. In this context, polymer composites loaded with dielectric (nanocarbon materials, conducting polymers) [2] have been extensively studied due to their easy processability, flexibility, cost effective production, corrosion resistance and low weight. Another requirement for attaining good MWA performance is the use of hollow/porous structure [3-4].
Thus, the present work focuses on the evaluation of MWA properties of structures constituted by multilayered structures including honeycomb sandwiched by two layers constituted by polymeric conducting composite. The honeycomb was built using the additive manufacture technology and poly(lactic acid). The MWA properties were evaluated in the X- and Ku-band frequency range. The best combination of minimum reflection loss and broad frequency bandwidth with EM attenuation higher than 90% was achieved by using multi-layered structure with the less conductive layer at the top of the stacked structure and the higher conducting layer at the bottom.

References

1. S.M. Zachariah, Y. Grohens, N. Kalarikkal, S. Thomas. Polym. Compos. 43 (2022) 2507.
2. B.G. Soares, G.M.O. Barra, T. Indrusiak, J Compos Sci 5 (2021) 173.
3. P. Song, H. Qiu, L. Wang, X. Liu, Y. Zhang, J. Zhang, J. Kong, J. Gu. **Sustainable Mater. Technol. 24 (**2020) e00153
4. D. P. Schmitz, B.G. Soares, G.M.O. Barra, L. Santana. Polym. Compos. 44 (2023) 2250.

Fundings: CNPq; FAPERJ..

Keywords: *absorbing materials; multilayered structure; honeycomb; conducting composites; carbon nanomaterials.*

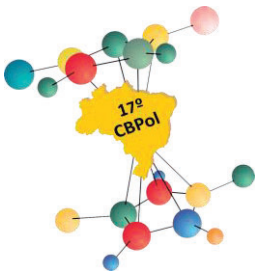

TUNING PROPERTIES OF POLYURETHANES BY CHAIN EXTENDERS

Otávio Bianchi[1]*

1 – Department of Materials Engineering, Federal, University of Rio Grande do Sul (UFRGS), Porto Alegre, RS, Brazil
otavio.bianchi@ufrgs.br or otavio.bianchi@gmail.com

Abstract – Polyurethanes (PU) stand as some of the most versatile polymers available, thanks to their highly adaptable structure that depends on the composition of their monomers. The synthesis of polyurethanes typically involves step reactions between alcohols (-OH) and isocyanates (-NCO) groups. Achieving specific physical-mechanical properties often necessitates using chain extenders (CEs), which are low molecular weight diols or diamides. CEs play a crucial role in influencing phase separation and the formation of segmented phases while also reducing solubility between flexible phases formed by high molar mass diols and rigid phases formed by isocyanates. This research sheds light on various aspects of phase separation effects and the physical-mechanical properties of polyurethanes synthesized through different methods, including reactive extrusion, casting, and solution processes. We will showcase practical examples of how CEs can be strategically employed to engineer polyurethane materials with customizable properties for various applications, including transparent materials, waterborne polyurethanes, and more [1-6].

References

1 . D. Favero, V. Marcon, C.A. Figueroa, C.M. Gómez, A. Cros, N. Garro, M.J. Sanchis, M. Carsí, O. Bianchi, Effect of chain extender on the morphology, thermal, viscoelastic, and dielectric behavior of soybean polyurethane, *Journal of Applied Polymer Science*, 2021, 138, https://doi.org/10.1002/app.50709.
2 . J.R. Ernzen, C.H. Romoaldo, C. Gommes, J.A. Covas, A. Marcos-Fernández, R. Fiorio, O. Bianchi, Tuning Thermal, Morphological, and Physicochemical Properties of Thermoplastic Polyurethanes (TPUs) by the 1,4-Butanediol (BDO)/Dipropylene Glycol (DPG) Ratio, *Polymers*, 2022, 14,
3 . D. Favero, V. Marcon, L.D. Agnol, C.M. Gómez, A. Cros, N. Garro, M.J. Sanchis, M. Carsí, C.A. Figueroa, O. Bianchi, Effect of chain extenders on the hydrolytic degradation of soybean polyurethane, *Journal of Applied Polymer Science*, 2022, 139, https://doi.org/10.1002/app.52623.
4 . L. Dall Agnol, F.T.G. Dias, O. Bianchi, Photoactive coating based on waterborne polyurethane and carbon quantum dots as a prevention strategy for bacterial resistance, *Progress in Organic Coatings*, 2023, 179, https://doi.org/10.1016/j.porgcoat.2023.107492.
5 . H.L. Ornaghi, A. Nohales, M. Asensio, C.M. Gómez, O. Bianchi, Effect of chain extenders on the thermal and thermodegradation behavior of carbonatodiol thermoplastic polyurethane, *Polymer Bulletin*, 2023, 10.1007/s00289-023-04812-7.
6 . L. Dall Agnol, H.L. Ornaghi, J.R. Ernzen, F.T.G. Dias, O. Bianchi, Production of a sprayable waterborne polyurethane coating with silver nanoparticles for combating SARS-CoV-2, *Journal of Coatings Technology and Research*, 2023, 10.1007/s11998-023-00788-1.

Fundings: CNPq - grant numbers 308567/2018-8 and 305814/2021-4; FAPERGS - grant: 19/2551-0001843-6

Keywords: *PUs, TPUs, WPU, structure-properties, chain extenders*

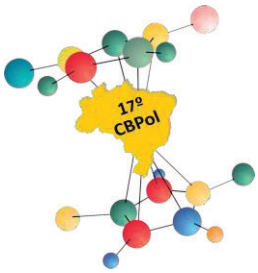

β-CYCLODEXTRIN FUNCTIONALIZED WITH CARBON QUANTUM DOTS AS ADSORBENT SENSORS OF METALLIC SPECIES IN AQUEOUS ENVIRONMENTS

Emilly Silva,[1,2*] Charlie Gomes[1], João Pina[2], Artur Valente[2], André Fajardo[1]

1 – Laboratório de Tecnologia e Desenvolvimento de Compósitos e Materiais Poliméricos (LaCoPol), Universidade Federal de Pelotas (UFPel), Campus Capão do Leão, Pelotas-RS, Brazil.
2 – Departamento de Química, Universidade de Coimbra (UC), Portugal
emillycruzds@gmail.com

Abstract – Waste dumped by industries is rich in heavy metals that have properties highly harmful to living beings. Carbon quantum dots (QDs) appear as a good proposal as detection materials and can be immobilized on hosts like β-cyclodextrins, which provide stability, support, and maintain their luminescent properties. In this communication, we describe the manufacture of an adsorbent composed of β-cyclodextrins functionalized with carbon quantum dots applied in the adsorption and immediate detection via fluorescence of Cd, Cu, Ni, and Pb species. The experimental design was constructed to achieve the best adsorption conditions, this results the best system to observe changes in the fluorescence of the material after interaction with the metal species. It was possible to perceive the greater adsorption capacity of the materials containing QDs, which was favorable to the detection process. The material detected and adsorbed 96% of Ni, 95% of Cu, 86% of Cd, and 87% of Pb.
Keywords: Supramacromolecules, quantum dots, bifunctional compounds, detection, adsorption, metals

Fundings: Emilly C. Silva thanks for scholarship CAPES/PRINT - Edital UFPel nº 41/2017. The authors are thankful to CNPq and to the Coimbra Chemistry Centre, which is supported by the FCT, through Projects UIDB/00313/2020 and UIDP/00313/2020.

Introduction

The waste dumped by industries is rich in organic and inorganic pollutants [1], among which, it is possible to mention heavy metals that have toxic properties and are highly harmful to living beings. Species of most concern include Arsenic (As), Lead (Pb), Copper (Cu), Cadmium (Cd), Chromium (Cr), Nickel (Ni), and Mercury (Hg). These species come from dyes, fertilizers, pesticides, bleaching agents, and some alloys [2]. The adsorption process becomes the most advantageous because it does not have by-products; the adsorbent material has a high rate of reuse and reapplication; it has profitable operating conditions and high efficiency. Adsorption has a notorious space in the literature because it offers flexibility in the application system. Besides, many materialsand mediums can be tested for different compounds. The detection of potentially toxic metals has great potential for monitoring the environment and surroundings of industrial facilities, assessingthe influence of these contaminations, and quantifying, characterizing, and removing these metals from aquatic environments [3]. So, it becomes interesting to develop methods and probes for immediate and real-time detection of these metals, making it possible to save cost and work. To optimize the adsorption capacity, selectivity, and removal of heavy metals from water, several adsorbents are being reported in the literature. In this current scenario, more materials need to be proposed for adsorption processes and simultaneous detection of these species. Carbon quantumdots (QDs) appear as a good proposal as detection materials, a current generation of carbonaceous

materials sizing from 0 to 10 nanometers, well-defined structures, and photoluminescent properties. The assembly of quantum dots in other materials is explored in the literature mainly in sensing applications that require greater stability for these materials. QDs can be immobilized on binders that provide stability, support, and maintain their luminescent properties [4]. For this, QDs functionalized in β-cyclodextrin can be an attractive material because cyclodextrins are well-known hosts of a range of materials in their cavities, it presents adsorbent properties, thus forming a stable and efficient composite for adsorption and detection of metallic species. In this research, we describe the manufacture of an adsorbent composed of β-cyclodextrins functionalized with carbon quantum dots applied in the adsorption and immediate detection via fluorescence of Cd, Cu, Ni, andPb ions. The entire experimental design was constructed to obtain the best study conditions through detailed graphs of the response surface, in addition to studies on selectivity and counter-ion effects were evaluated, demonstrating a more complete study on the adsorption of heavy metals and the influence that the concentration of these metals can affect the fluorescence properties of the detectorproduced.

Experimental

Polyethylene glycol (PEG-400) (5 mL) was dissolved in deionized water (45 mL) in a beaker. The solution was transferred into a 150 mL Teflon-lined stainless-steel autoclave and heated at 120 ºC for 24 h and then cooled to room temperature. The obtained solution was subjected to dialysis (24 h, changing the deionized water every 4 h). Finally, a yellow aqueous solution containing C-dots was obtained and named QDs. Crosslinked β-CD was obtained by reacting Citric Acid (CA) with β-CD pure, named β-CD(P) according to the esterification-polycondensation method using KH_2PO_4 as a catalyst. CA (0.5 g), β-CD (1 g), KH_2PO_4 (0.25 g) and 25 mL of deionized water were mixed in a round bottom flask and stirred in a water bath. The mixture was transferred to a Petri dish and heated in a drying oven (100 °C) for 4 h. After cooling, the raw product was purified by soaking and washing with deionized water several times, then suction filtered and vacuum dried at 50 °C overnight, this material was named β-CD(C). For the preparation of the material called β-CD-g- QDs, the same process was reproduced by replacing the solvent, deionized water, with the quantum dot solution. The synthesis process of both materials was summarized in Fig. 1.

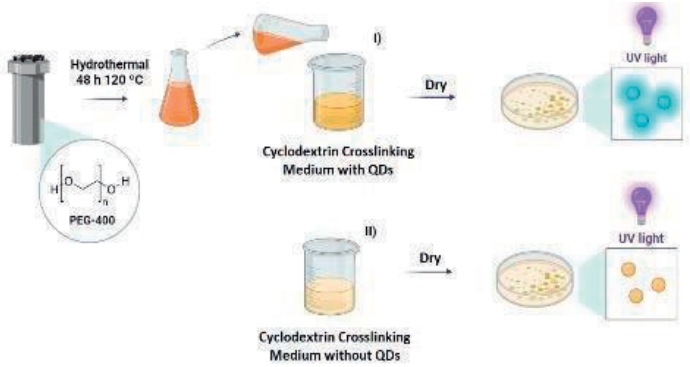

Fig. 1. Representative scheme of the preparation of the fluorescent adsorbents.

The effect of some parameters on the adsorption of Cd, Cu, Ni, and Pb on CD/QDs was investigated using a central composite design (CCDR), 2^3 x 2 with 3 central points and 6 axial points, totaling 31 experiments. Three independent variables were evaluated: contact time between adsorbent and adsorbate (1–24 h), adsorbent dosage (1–20 mg), and medium pH (2–5). The variables and levels used in the factorial design are presented in Table 1. To determine the maximum and minimum values for each variable in the factorial design, the following aspects were taken into consideration: i. Adsorption time: The adsorption time was determined based on preliminary kinetic tests; ii. Adsorbent dose: The adsorbent dose was determined by considering the maximum value that would not have an adverse effect on the adsorption capacity of the material; and ii. pH range: The pH range was chosen to be below the precipitation pH of metallic salts used in the research. This decision was made to prevent the formation of insoluble precipitates that could interfere with the adsorption process.

Table 1. Variables and levels in factorial design to evaluate the adsorption of Cd, Cu, Ni, and Pb species on CD/QDs hydrogels.

	-1.68	**-1**	**0**	**1**	**1.68**
Contact time (h)	2.8	6.7	12.5	18.2	22.2
Adsorbent (mg)	1.5	5	10.0	15.0	18.4
pH	2.3	2.7	3.5	4.3	4.8

Results and Discussion

Here we present an extensive study about a fluorescent adsorbent material. From β-CD produced a supramolecular adsorbent that, when combined with PEG-400 quantum dots, acquired modulable fluorescent properties in the presence of different metallic species. This material was tested to adsorb and detect Cd, Cu, Ni, and Pb species. For this process, the factorial design helped to findthe optimal adsorption condition for the material towards all the mentioned species and to evaluate the change in fluorescence of the adsorbent in systems containing metals. The quantum dots were characterized by Transmission Electron Microscopy and Fluorescence Emission techniques, and the β-CD(P), β-CD(C) materials, and the β-CD-g-QDs adsorbent were largely characterized by morphological analysis. (SEM), chemical analysis (FTIR, EDS, DLS), thermal analysis (TG), and spectroscopic analysis (UV-VIS, Fluorescence). In this abstract, we will bring a brief overview of the results that were obtained through this research. To understand the chemical composition of the prepared samples, we performed the FTIR spectra of the formation of quantum dots from PEG-400, as can be seen in Fig. 2(A) some major changes can be cited as an increase in the intensity of the band at 3435 cm^{-1} which may be related to the increase in O–H groups, as these tend to reach the surface during the passivation of CDs [5]. At 2866 cm^{-1}, the band related to the stretching of the C–H bond showed a reduction in intensity that can be related to a more structured and tensioned chemical bond, as reported by Mohamed et al. [6]. This trend is due to the high pressure and temperature synthesis process made for the passivation of PEG-400. After obtaining the quantum dots, they were incorporated into the β-CD during the crosslinking process, as described in the experimental section. The β-CD(C) spectrum in Fig. 2(B) showed the appearance of the band at 1718 cm^{-1}, referring to the carbonyl band formed by crosslinking process with CA. The β-CD-g- QDs spectrum, exhibited the characteristic bands of QDs and β-CD; however, changes were observed in the bands related to stretching of O–H and C–O bonds. The grafting of the QDs in the β-CD increased the amount of oxygen-containing groups, which explain these changes.

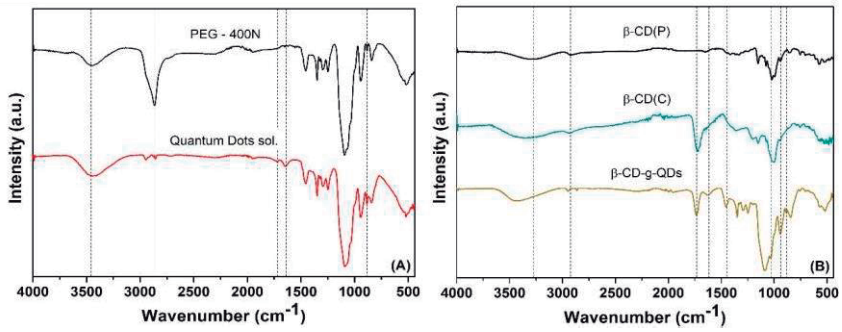

Fig. 2. FTIR spectra of (A) QDs formation and (B) β-CD(P), β-CD(C) and (C) β-CD-g-QDs.

Other altered characteristics of the β-CD(C) for the β-CD-g-QDs material were observed such as increased porosity and morphological alteration where the β-CD-g-QDs material has cavities on its surface and a non-uniform morphology. In addition, properties such as Zeta potential and swelling capacity were studied for a better understanding of the adsorptive process. The adsorption tests followed the factorial design and indicated that the optimum adsorption condition, that is, for all

metals, were pH 4.3 and contact time of 15.8 h, respectively (see Fig. 3). Experiments evaluating solid-liquid ratio and counterion effect were performed separately. To explain some properties of compounds the adsorption kinetics processes and isotherms were evaluated and the models that best fit the results were the pseudo-second order kinetics and the Langmuir-Freundlich adsorption model for the isotherms. Based on these models, a chemisorption relationship between the adsorbent and the adsorbate occurred.

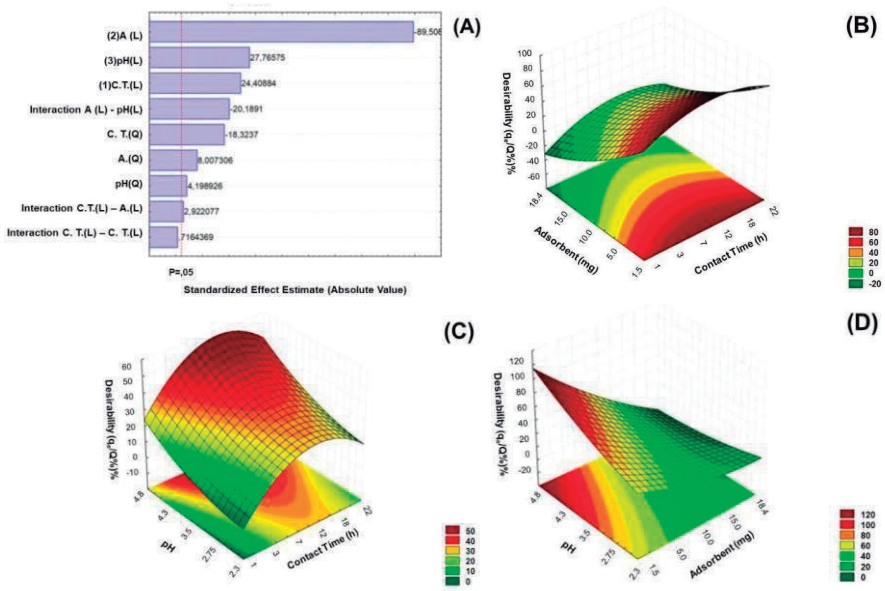

Fig. 3. Statistical data obtained for the best overall condition of adsorption of all studied species onto β-CD-g-QDs adsorbent (A) Pareto charts of standardized effects, (B) Surfaces responses plots for the effect of adsorbent dosage and contact time, (C) pH and contact time and (D) pH and adsorbent dosage.

After obtaining the optimal interaction conditions between the β-CD-g-QDs material and the metallic species, detection studies were done. Among the conventionally used basic characterizations, the absorption characteristics are analyzed for the identification of electronic transition bands with the aid of UV-visible absorbance spectroscopy, emission spectra, and PL excitation, as these are the basic parameters necessary for optical detection in carbon-based nanomaterials. The absolute/relative quantum yield was measured using an integration sphere/comparing the fluorescence intensity with another sample with known quantum yield, forthis material the obtained quantum yield was 0.009 φ_F. The fluorescence decay of the sample was well fitted with a bi-exponential decay law with fluorescence lifetimes of 2 and 6.9 ns. Regarding the detection of species, the material was placed in contact with different concentrations of metallic species, as can be seen in Fig. 4. It is possible to notice that there is a suppression of the fluorescence of the β-CD-g-QDs adsorbent proportionally to the increase in the concentration of metals. Fluorescence quenching is the decrease in the quantum yield of fluorescence from a fluorophore, induced by a variety of molecular interactions with quencher molecules [5]. There are two types of extinction processes: static extinction and collisional extinction. In static quenching,the complex is formed through interactions between fluorescent molecules (QDs) and quencher molecules (analytes). Fluorescent molecule (QD) and quencher molecule form a complex by strong coupling reaction, where it is possible to notice the suppression of the material's fluorescence.

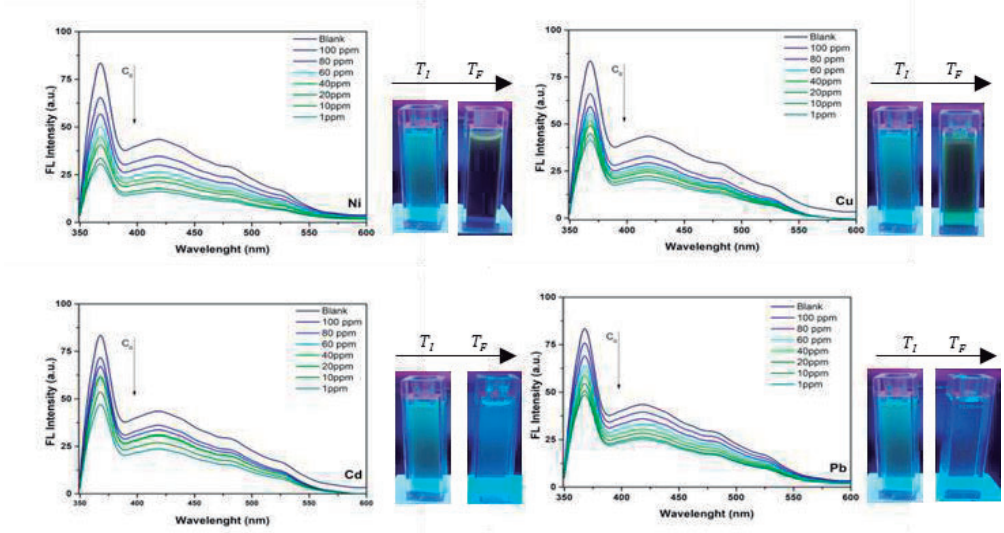

Fig. 4: Fluorescence intensity of a solution derived from β-CD-g-QDs materials after contact with different concentrations of Ni, Cu, Cd, and Pb.

In addition to this expanded abstract of the observed results, it is possible to note, also through Fig. 4 that there is a greater detection capacity, in the form of fluorescence suppression, of some metals to the detriment of others. The detection capacity followed the order Ni > Cu > Cd > Pb, which was the same observed in the adsorption capacity of the material β-CD-g-QDs. This result indicates that the greater the interaction of the species with the adsorbent, the better the detection efficiency. Several aspects of the adsorbent/adsorbate interaction were evaluated and explained these results, such as the ionic radius of metals, species charge, porosity of the material, among others.

Conclusions

Supramacromolecules of β-CD-g-QDs were successfully prepared. The materials demonstrate distinct morphological, chemical, and optical properties. The β-CD-g-QDs material showed higher adsorption than the β-CD(C) and both were better suited to the Langmuir-Freundlich isothermal model. The QDs optimized the adsorption capacity of the polymer and conferred fluorescence capacity that allowed the detection of different concentrations of the tested metals, where detection was higher in the following order Ni > Cu > Cd > Pb.

References

1. Alengebawy, A., Abdelkhalek, S. T., Qureshi, S. R., & Wang, M.-Q. (2021). *Toxics*, *9*(3), 42. https://doi.org/10.3390/toxics9030042
2. Badsha, M. A. H., Khan, M., Wu, B., Kumar, A., & Lo, I. M. C. (2021). *Journal of Hazardous Materials*, *408*, 124463. https://doi.org/10.1016/j.jhazmat.2020.124463
3. Fan, R.-J., Sun, Q., Zhang, L., Zhang, Y., & Lu, A.-H. (2014). *Carbon*, *71*, 87–93. https://doi.org/10.1016/j.carbon.2014.01.016
4. Fernando, K. A. S., Sahu, S., Liu, Y., Lewis, W. K., Guliants, E. A., Jafariyan, A., Wang, P., Bunker, C. E., & Sun, Y.-P. (2015). *ACS Applied Materials & Interfaces*, *7*(16), 8363–8376. https://doi.org/10.1021/acsami.5b00448
5. Gao, X., Du, C., Zhuang, Z., & Chen, W. (2016). *Journal of Materials Chemistry C*, *4*(29), 6927–6945. https://doi.org/10.1039/C6TC02055K

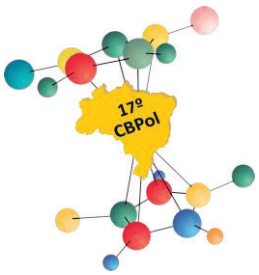

BIMODAL EVA FOAMS REINFORCED WITH CELLULOSE NANOFIBERS

Matheus Vinicius Gregory Zimmermann, Ademir José Zattera[2], Ruth Marlene Campomanes Santana[3]

1 – Programa de Pós-Graduação em Engenharia e Ciência dos Materiais. Universidade do Extremo Sul Catarinense (UNESC), Av. Universitária, 1105, Criciúma, Santa Catarina CEP 88806-000, Brazil
2 – Universidade Federal do Rio Grande do Sul (UFRGS), Av. Bento Gonçalves, 9500, CEP 91501-970, Porto Alegre – Brazil.
3 – Universidade de Caxias do Sul (UCS), R. Francisco Getúlio Vargas, 1130, CEP 95070-560, Caxias do Sul – Brazil
matheus.vgz@gmail.com

Abstract - Cellulose nanofibers are promising materials in the development of polymeric foams, because they act as heterogeneous nucleation sites for the growth of cells during foaming. In this research, we studied the incorporation of cellulose nanoparticles in poly(ethylene-co-vinyl acetate)-EVA foams. The foams were produced with different fiber contents. The main results indicate that with the addition of only 1% of cellulose nanofibers, cell density significantly reduces when compared with the pure EVA foams. On the other hand, by increasing the cellulose content, the agglomeration of nanofibers also increases, which results in heterogeneous cell sizes and bimodal foam formation.

Keywords: *foams, EVA, nucleation, cellulose, bimodal foam*

Introduction

The insertion of fillers in polymeric foams is generally associated with reducing the cost of the final artifact, as well as modifying some specific property, such as, for example, increased stiffness, increased thermal stability, greater cell nucleation (smaller cells and in greater amount), facilitate the opening of pores, act as a flame retardant or change some surface characteristic in the polymeric wall, in the contour of the cells [1-2]. Currently, the fillers most used in the formulation of polymeric foams consist of inorganic materials, but, recently, the use of organic materials, such as vegetable fibers, has aroused interest due to the fact that they are less abrasive and lighter when compared to inorganic materials [2].

Cell nucleation is a term for a process that induces the formation of a bubble in the polymer matrix. Considering a polymer melt already completely saturated with a blowing agent, with a phase change, either by temperature or pressure induction, the system becomes supersaturated. Therefore, the gassed polymer solution tends to form small bubbles in order to re-establish a steady state of low energy. The theory of classical cell nucleation in polymeric materials classifies cell nucleation into two types: homogeneous nucleation and heterogeneous nucleation [3-6].

In homogeneous nucleation, with the phase change, the spontaneous formation of small air bubbles occurs randomly within the polymeric matrix, and when a bubble reaches a critical size, the other bubbles, of smaller size, tend to migrate to this region, coalescing and propagating the growth of this unit. The existence of small voids in the polymeric matrix is also attributed, which favor the migration of gas from the expanding agent to this region.

In heterogeneous nucleation, it is suggested that the gas is dispersed in a heterogeneous environment, with at least two distinct phases. Among the heterogeneous elements attributed to this theory, the use of fillers, different polymer matrices and also crystals (in the case of semi-crystalline polymers) stand out. During cell formation, the gas tends to migrate to the region of lower energy. In a heterogeneous system with charges, the lowest energy region is preferably found in the charge

interface region, that is, in the contact area of the polymer with the charge. The manipulation of this interface region, either by content or by the size of the filler, can impact the variation in the cellular morphology of the foam in formation [6,7].

Changing cell morphology has a great impact on their properties. Cell size and density directly influence the physical and mechanical properties of polymeric foams. In general, microcellular foams (cell size 1-300 μm) have superior mechanical properties (compression), greater rigidity, greater wear resistance and superior thermal and acoustic properties, while conventional foams (cell size >300 μm) have greater resilience, physical-mechanical structure with greater flexibility and greater capacity for cushioning and absorbing impacts [8].

In this way, the manipulation of the shape and size of the cells, in order to combine microcellular and conventional cells in a foam, with a bimodal cellular structure, has been a great challenge from the technological point of view. According to Qiu et al., (2020) [9] it is more difficult to produce and stabilize the morphology of foams with a bimodal cell structure when compared to foams with a uniform cell structure. The use of a bimodal structure of cells allows the combination of superior mechanical properties, high resistance to abrasion with impact cushioning capacity, an ideal condition for use in footwear.

Experimental

Materials

The EVA copolymer (trade name EVATENO 3019 PE) was provided by Braskem S.A. It contains 19% vinyl acetate and a density of 0.940 g/cm^3, a MFR (190 °C/2.16 Kg) of 2.5 g/10 min and a melting temperature of 86 °C. The chemical blowing agent azodicarbonamide (ACA), activated with zinc oxide (ZnO), was supplied by Inbra Industria Química Ltda. Dicumyl peroxide, grade DCP 40 SAP, was supplied by Retilox Química Especial Ltda. The vegetal oil-based lubricant (trade name OLVEX 51) was supplied by SGS Polímeros. The silicon-based surfactant (trade name NIAX L-595) was supplied by Momentive Performance Materials, Inc. The microcrystalline cellulose (MC) grade Sigmacell type 20 mm (cod. S3504) was supplied by Sigma Aldrich S.A.

Methods

Production of Nanocellulose by Mechanical Grinding. Ultrafine grinding of MC was performed using a Masscolloider Masuko Sangyo, model MKCA6 – 2J wheel mill. Milling was performed in a suspension containing water and 3% MC. The equipment was coupled to a recirculating pump and the milling time was 4 h at a speed of 2000 rpm. After grinding, the cellulose suspension was centrifuged using a centrifuge Novatecnica, NT820 model, at a speed of 5000 rpm for 30 min. The phases were separated and the solid/water relation was measured and stabilized at a solids ratio for all samples of approximately 20% cellulose.

Preparation of Foams

The incorporation of the suspensions 20% of cellulose nanofibers (CN) in the EVA was carried out in a mixing chamber (torque rheometer) at a temperature of 120 °C with a rotor speed of 100 rpm during 600s. The cellulose was added to the EVA at concentrations of 1%, 2% and 3%. Dispersant additives were added to the cellulose suspension with high solids content, 1 g oil (Olvex 51), 1 g of n-heptane and 1 g of surfactant (Niax Silicone L-595) to facilitate dispersion during the incorporation of nanocellulose. The content of the additives was kept constant regardless of the cellulose content added to the polymer and the cellulose suspension was added dropwise during the processing period. Thereafter, the material was pressed into a 1 mm plate using a thermal press SCHULZ at 120 8C for 2 min. The plates were placed in a thermal oven with vacuum at 60 °C for 24 h to promote the oil migration to the composite surface.

Additives to produce the EVA foams were added to the composite in the same torque rheometer at 120 °C, with 100 rpm during 250s. The content of the additives was kept constant for

all formulations: azodicarbonamide (3 parts hundred resin – phr); dicumyl peroxide (2 phr) and zinc oxide (0.5 phr). After the mixing, the material was molded into a preform, by using a heat press at 120 °C for 2 min. The expansion of EVA foams was carried out in a thermal press at 170 °C at constant pressure, by using a method in which the sample is compressed by a period of 10 min with 7.000 kgf of closing force, and the expansion of the foam occurs when the mold is opened.

Characterizations

Cellulose was evaluated by transmission electron microscopy (TEM) using a Jeol Jem 2010 equipment. Uranyl acetate was used as contrast and the analysis was applied at a voltage of 120 kV. The morphology of the fractured surface of the foams was evaluated by scanning electron microscopy (SEM) using a Tescan Mira3 equipment. All samples were previously coated with Au. The observation area in all foams was analyzed in cross section (horizontal direction) of the expanded sample. The software used to measure the cell size was ImageJ. The cell population density per unit volume of the foamed composites (Nf) was determined from the SEM micrographs using eqs. (1) and (2).

$$Vf = 1 - \frac{\rho f}{\rho p} \quad (1)$$

$$Nf = \left(\frac{nM^2}{A}\right)^{3/2} \cdot \left(\frac{1}{1-Vf}\right) \quad (2)$$

Where *Vf* is the void fraction (%), qf is the density of the foam (g cm^{-3}), qp is the unfoamed polymer density (g cm^{-3}), Nf is the cell density (cell cm^{-3}), A is the area of the micrograph (cm^2), M is the magnification factor for micrograph, n is the number of bubbles in the SEM micrograph (cells). The cell size was measured by the Ferret diameter

Results and Discussion

Figure 1 shows the TEM micrographs after the mechanical defibrillation of nanocellulose. NC presented dimensions of approximately 50 nm referring to the nanoscale thickness after the mechanical defibrillation.

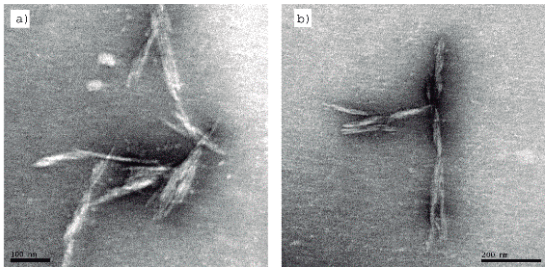

Figure 1. TEM micrograph of CN.

Figure 2 show the SEM images of the cross-sections and the cells size distribution graphs of the EVA foams and reinforced EVA foams with different contents of NC. All foams exhibited predominantly closed-cell morphologies. With the insertion of nanocellulose, all samples decreased in cell size and increased in cell density when compared with non-reinforced EVA foams, mostly because nanocellulose acts as a nucleating agent.

Doroudiani and Kortschot [10] and Lee et al.[11] relate that different cell morphologies can be obtained depending on the type, size, shape, distribution and concentration of the nucleating agent used in the composition of polymeric foams. In addition, depending on the obtained morphology, different properties can be attributed to the foams. The cell density (number of cells per unit area) is affected by the content and by the size/diameter of the filler. In general, fillers act as nucleation sites for the formation of cells. However, the existence of micropores or voids in the polymer-filler interface cause the migration of gas generated from the blowing agent to these

regions, and consequently cells spread and grow. With the reduction in fiber size, there is an increase in the contact area of fibers with the polymeric matrix, which can lead to the formation of a larger amount of nucleation sites for the formation of cells, considering an equal filler content. According to Chen et al.,[12] larger particles contain more trapped air (greater contact area considering a single fiber) and promote the formation of larger cells. By decreasing the particle size and keeping the content constant, there is a greater concentration of smaller fibers, resulting in the formation of a larger number of cells, and thus an increase in cell density.

However, considering the data shown in Figure 2, by increasing the CN content, the presence of large cells increases, and on the contour of these large cells the presence of a large amount of small cells is observed. Foams with the presence of two different groups of cells, that is, of two sizes, is discussed by Duan et al.[12] and are defined as bimodal foams.

As previously discussed, cellulose nanofibers act as nucleating agents for the formation of cells. However, during the incorporation of the fibers into the polymeric matrix, the agglomeration and aggregation of these cellulose fibers can occur, and this phenomenon can promote the formation of larger cells. A larger interface (contact area between the fiber and polymeric matrix) favors the formation of large cells, since the gas from the blowing agent tends to migrate to the least resistant region and propagate their growth from this point. Thus, with the dimorphism on the size between nanometric and micrometric agglomerated particles, the formation of a bimodal foam is favored. By increasing the cellulose fiber content, the probability of obtaining agglomerated particles is higher, as well as the probability of obtaining a bimodal foam.

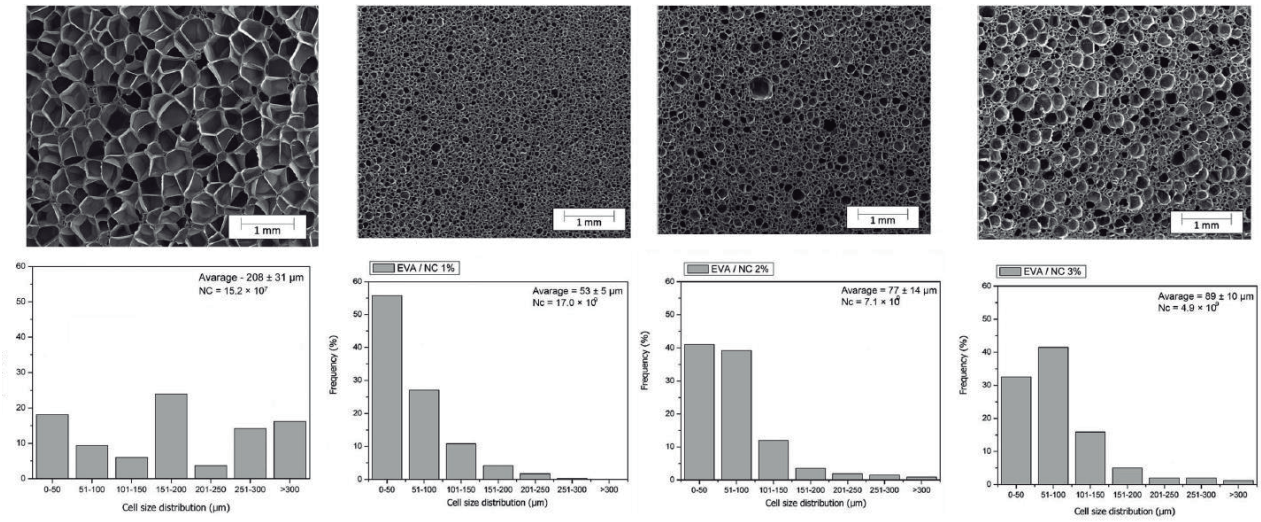

Figure 2: SEM micrographs of EVA foams and EVA foam reinforced with NC.

Figure 3 shows the variation of the arrangement of the CN in the EVA foams. An individualized nanofiber is observed in Figure 3(a), and agglomerated fibers are shown in Figure 3(b).

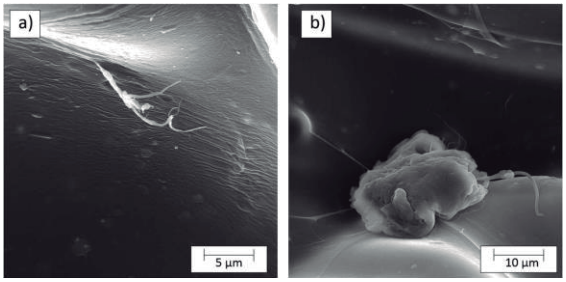

Figure 3: SEM micrograph of an EVA reinforced foam, with (a) an individualized fiber and (b) an agglomerated fiber.

Conclusions

The incorporation of cellulose nanofibers in EVA foams modifies the morphology of cells during the foam expansion process, because the fillers act as nucleating agents. The gas from the blowing agent, during the decomposition, tends to migrate to the lowest possible energy region located at the fiber polymer interface. The most efficient nucleation, observed by the cell size uniformity, was observed with 1% of NC. By increasing the content of NC, nanofibers agglomerate, affecting in the formation of heterogeneous cell sizes, with the presence of bimodal cell foams. Morphologically, compared with the EVA foams without NC, all reinforced foams showed a lower cell size and a higher cell density, that is, the number of cells per unit area.

References

1. Wu, W.; Cao, X.; Zhang, Y.; He, G. J. Appl. Polym. Sci. 2013, 130, 443.
2. Shan, C.W.; Izwana, M.I.; Ghazali, M.I. Study of Flexible Polyurethane Foams Reinforced with Coir Fibres and Tyre Particles. International Journal of Applied Physics and Mathematics, v. 2(2), 2012.
3. Park, C.B.; Baldwin, D.F.; Suh, N.P. Effect of the Pressure Drop Rate on Cell Nucleation in Continuous Processing of Microcellular Polymers. Polymer Engineering and Science, v. 35(5), p. 432-440, 1995.
4. Jones, S.F.; Evans, G.M.; Galvin, K.P. Bubble Nucleation from Gas Cavities – A Review. Advances in Colloid and Interface Science, v. 80(1), p. 27-50, 1999.
5. Throne, J.L. Thermoplastic Foam Extrusion: An Introduction. Ed. Carl Hanser Verlag, Munich, 2004.
6. Leung, S.N.S. Mechanisms of Cell Nucleation, Growth, and Coarsening in Plastics Foaming: Theory, Simulation, and Experiment. PhD Thesis. Department of Mechanical and Industrial Engineering, University of Toronto, 2009.
7. Zimmermann, M.V.G. Espumas poliméricas reforçadas com celose. Tese de Doutorado. Programa de Pós Graduação em Engenharia de Minas, Materiais e Metalurgia. Universidade Federal do Rio Grande do Sul (UFRGS), 2016.
8. Kord, B.; Varshoei, A.; Chamany, V. Influence of Chemical Foaming Agent on the Physical, mechanical, and morphological properties of HDPE/Wood flou/nanoclay composites. Journal of Reinforced Plastics and Composites, v. 30, p. 1115-1124, 2011.
9. Sefadi, J. S.; Luyt, A. S. J. Thermoplast. Compos. Mater. 2012, 27, 895.Doroudiani, S.; Kortschot, M. T. J. Thermoplast. Compos. Mater. 2004, 17, 13.
10. Lee, L. J.; Zeng, C.; Cao, X.; Han, X.; Shen, J.; Xu, G. Compos. Sci. Technol. 2005, 65, 2344.
11. Chen, L.; Rende, D.; Schadler, L.; Ozisik, R. J. Mater. Chem. 2013, 1, 3837.
12. Duan, Z.; Ma, J.; Xue, C.; Deng, F. J. Cell. Plast. 2014, 50, 263.

DEVELOPMENT OF ACTIVE STARCH BIOFILMS REINFORCED WITH NANOSILICA FOR FOOD PACKAGING

Maria Augusta Corrêa Martins[1], Rosa Maria Vercelino Alves[2*]
1 – School of Chemical Engineering, State University of Campinas, Campinas, São Paulo, Brazil.
2 – Packaging Technology Center, Institute of Food Technology, Campinas, São Paulo, Brazil
*rosa.cetea@gmail.com

Abstract - The active starch biofilms reinforced with nanosilica (S/SiO_2) were prepared in four samples of different concentrations (0, 2, 4 and 6 wt% of nano-SiO_2/starch) through the casting method. The thickness increased from 20% to 50% in the biofilms, as the reinforcement was added. The tensile strength was elevated up to 54%. Towards the modulus of elasticity, higher results were observed in the reinforced samples with concentrations of 2% and 6% of nanosilica in comparison to the control films. The reinforced biofilms showed poorer plasticizing properties, as the ones with 2% and 4% of nano-SiO_2 did not differentiate statistically from the control and as the sample with 6% presented lower results. The water vapor permeability indicated that the biofilms with 2% and 4% of reinforcement became more permeable, as their average permeability rose expressively in relation to the control sample. The transmittance was lower at the reinforced films, mainly at the visible and infrared regions. At last, the Fourier transform infrared test indicated strong intermolecular interactions occurred between the starch and the nanosilica.
Keywords: *active films, nanosilica, starch biofilms, sustainability, biopolymers*

1. Introduction

Food packages made from plastic are of big importance to the food industry, since they are versatile, cheap, very moldable and a great chemical and biological barrier; they also have good mechanical properties for this purpose [1]. Thus, the usage of food plastic packages was widespread in the food sector and throughout the world [2]. Consequently, the excessive usage of food plastic packages led to bigger and bigger impacts: daily generation of tons of non-recyclable and of low degradation trash, shortage of places destined to the correct garbage disposal, microplastic formation and chemical pollution of soils; besides that, conventional plastics are made from components of fossil origin, which is another factor to be avoided [2-4].

On the other hand, starch biofilms are a sustainable option to be used as food packages. The main component of these films, the starch, presents high availability in nature, elevated rate of renovation, low-cost and great properties of forming films [6,7]. However, starch biofilms also present disadvantages: fragility, high solubility in water and inferior mechanical properties [5]. To bypass some of the cited problems, the objective of this research was to synthesize starch biofilms reinforced with nanosilica at the concentrations ($m_{nanosilica}/100\ g_{starch}$) of 2%, 4% and 6% of nanosilica (S/SiO_2 2%, S/SiO_2 4% and S/SiO_2 6% respectively), and to analyze their mechanical and optical properties. Improvements were verified in comparison to the control film (S).

2. Experimental

Materials: The materials used in the preparation of the biofilms were: nanosilica AEROSIL ® 200 F, CAS [112945-52-5, 7631-86,-9], corn products; glycerol, CAS [56-81-5]; soluble starch, CAS [9005-84-9]; distilled water.

Preparation of the biofilms: The preparation of the biofilms occurred through the casting method and the quantities of each material used was shown in Table 1 [5]. Firstly, the water was heated up to 40 °C and the nanosilica was dispersed in it for 1 min with Ultra-Turrax (model T25, IKA ® - Staufen, Germany) at 7000 rpm. Then, the glycerol and the starch were carefully added in the mixture, being agitated for 5 min at 7000 rpm. After, the solution was heated under stirring (3000 rpm) until it reached 80 °C. Maintaining this temperature, the solution was dispersed more intensely for 15 min at 10000 rpm to get a better homogeneity. The solution was taken off the heating and agitated for 5 min at 7000 rpm. To eliminate bubbles, the film solution was placed in the ultrasound (model Q335D, Quimis Ltda. - SP, Diadema, St. Gema 292) for 15 min. The solution was then separated in portions of 60 g on petri plates (140 mm diameter) and dried for 24 h at 40 °C in a forced air circulation oven (Ethik Technology, Vargem Grande Paulista/SP, Brazil) for 24 h at 40 °C to form the films. All the samples followed the described process. The only difference was towards the control sample (S), which did not require the nanosilica dispersion step.

Table 1: Quantities of the materials used for each sample

Components	**S**	**S/SiO_2 2%**	**S/SiO_2 4%**	**S/SiO_2 6%**
Starch (g)	35,0	35,0	35,0	35,0
Glycerol (g)	10,5	10,5	10,5	10,5
Nanosilica (g)	-	0,7	1,4	2,1
Water (g)	700	700	700	700

Characterization

The thickness of the biofilms was determined following the ISO 4593 (1993). They were conditioned at 25 °C and 75% RH (relative humidity) at the acclimatizing camera (Pharma 1300, Weiss Technik ® - Reiskirchen, Germany). The measurements were done with a digital micrometer (Mitutoyo Co, Kawasaki-Shi, Japan).

The mechanical tests followed the method ASTM D882 (2012). The specimens were cut on the precision guillotine (RDS-100-C, ChemInstruments, OH, USA) and the tests were done with the universal test machine (Instron, 5966-E2, Norwood, USA).

The water vapor permeability (WVP) tests were based on the method ASTM E96/E96 (2016). The biofilms were conditioned in an air-conditioned chamber Pharma 1300 (Weiss Technik, Reiskirchen, Germany). It was used the precision scale (Mettler Toledo ®, Columbus, Ohio, EUA). To obtain the results of WVTR (water vapor transmission rate) and WVP, the Eq. 1 and Eq. 2 were used respectively. The T regarded the average thickness (10^{-6} m) of the film; P_s was the saturated pressure (23,756 mmHg at 25 °C); the RH was the relative humidity (75%).

$$WVTR = \frac{angular\ coefficient}{permeable\ area} \quad (1)$$

$$WVP = \frac{WVTR \times T}{P_s \times RH} \quad (2)$$

The optical properties were determined by the norm ASTM E1348 (2015) with the spectrophotometer (model Cary 60, Agilent Technologies, Santa Clara, California, USA).

The Fourier transform infrared analysis was realized with the spectrometer (PerkinElmer Spectrum, PerkinElmer ®, version 10.4.00, Waltham, Massachusetts, USA).

The statistical analysis was done through the Analysis of Variance (ANOVA), by the Tukey test at a confidence level of 95% ($p<0,05$). The PAST program (version 3.26, 2019) was used.

3. Results and Discussion

Thickness and mechanical properties

As showed in Table 2, the thickness increased from 20% to 50% ($p<0,05$). The control sample (S) presented the lowest thickness (126,7 ± 18,1 μm), while the sample with 4% of reinforcement presented the highest average (168,4 ± 21,2 μm). The significant increase of this parameter was due to the addition of the nanosilica: an hygroscopic and hydrophilic material [4]

The addition of nano-SiO_2 changed ($p<0,05$) the TS, tensile strength, of the biofilms analyzed (Table 2). The growth of the strength reached up to 54% and the sample S/SiO_2 2% showed the bigger increase (7,2 ± 0,5 MPa). The higher resistance to traction of the reinforced biofilms, compared to the control sample (5,0 ± 0,4 MPa), was related to the intermolecular interactions between the nanoparticles of SiO_2 and the polymeric matrix formed by the starch. These interactions possibly occurred by hydrogen bonds, which permitted the better distribution of physical stress through the film structure [8]. However, the increase of the TS did not happen linearly as the nano-reinforcements were added: 6,1 ± 0,4 MPa and 6,7 ± 0,4 MPa were the results obtained from the S/SiO_2 4% and S/SiO_2 6% respectively.

The results of S (42,7 ± 3,2 %), S/SiO_2 2% and S/SiO_2 4% towards the EAB (elongation at break) did not differ statistically ($p<0,05$) from each other (Table 2). It was noticeable a significant decrease in the EAB of the sample S/SiO_2 6% (29,0 ± 8,8 %). Therefore, the expected role of plasticizer of the nano-reinforcement was not observed [8]. These results could be related to the insufficient dispersal of the nano-SiO_2, which troubled the intermolecular interactions between the polymeric chains and their rearrangement as the mechanical stress was developed [8].

Finally, the modulus of elasticity (ME) was an important parameter to determine the stiffness of the biopolymers (Table 2). The control sample (S) resulted in 189,3 ± 25,3 MPa and the S/SiO_2 4% did not differ statistically from this interval ($p<0,05$). Regarding the films reinforced with 2% and 6%, it was observed the significant increase of the ME (405,9 ± 64,9 MPa and 316,0 ± 28,4 MPa) compared to the not reinforced biofilms. Therefore, it was concluded that the addition of nano-SiO_2 led to higher modulus of elasticity, but in a non-linear pattern.

Table 2: Thickness, TS, EAB and ME of each sample of the biofilms.

Sample	Thickness (μm)	TS (MPa)	EAB (%)	ME (MPa)
S	126,7 ± 18,1 ^{b}	5,0 ± 0,4 ^{c}	42,7 ± 3,2 ^{a}	189,3 ± 25,3 ^{b}
S/SiO_2 2%	155,7 ± 29,0 ^{a}	7,2 ± 0,5 ^{a}	43,6 ± 10,3 ^{a}	405,9 ± 64,9 ^{a}
S/SiO_2 4%	168,4 ± 21,2 ^{a}	6,1 ± 0,4 ^{b}	47,5 ± 12,6 ^{a}	256,9 ± 42,0 ^{bc}
S/SiO_2 6%	135,9 ± 22,1 ^{a}	6,7 ± 0,4 ^{ab}	29,0 ± 8,8 ^{b}	316,0 ± 28,4 ^{c}

The data was obtained for the average of the mechanical results of 5 repetitions more or less their standard deviation. The same index in the same column indicates that the difference is not statistically significant ($p<0,05$).

Water vapor permeability

The results towards the WVP and WVTR (water vapor transmission rate) were showed in Table 3. The control sample (1,7 ± 0,3 g mm m^{-2} day^{-1} $mmHg^{-1}$) did not have a different result ($p<0,05$) from the sample reinforced with 6% of nanosilica. The biofilms S/SiO_2 2% and S/SiO_2 4% (4,9 ± 0,8 g mm m^{-2} day^{-1} $mmHg^{-1}$ and 4,5 ± 0,3 g mm m^{-2} day^{-1} $mmHg^{-1}$ respectively) presented an increase compared to S and to S/SiO_2 6%. This phenomenon was possibly due to the non-establishment of stronger interactions between the matrix and the nano-reinforcement: an opposite situation reported on other researches, who highlighted the decrease of WVP as the films were increasingly reinforced [8]. These weaker formation of bonds and interactions might have

favored the accumulation of water, as the nano-SiO_2 has a hydrophilic nature [8]. Thus, the addition of nanosilica increased the permeability to water vapor of the starch biofilms studied.

Table 3: Results of WVP and WVTR of the samples.

Sample	WVP (g mm m^{-2} day^{-1} $mmHg^{-1}$)	WVTR (g day^{-1} m^{-2})
S	1,7 ± 0,3 [b]	226,5 ± 29,0 [b]
S/SiO_2 2%	4,9 ± 0,8 [a]	482,5 ± 95,5 [a]
S/SiO_2 4%	4,5 ± 0,3 [a]	436,4 ± 34,1 [a]
S/SiO_2 6%	1,8 ± 0,3 [b]	185,2 ± 19,7 [b]

The data was obtained for the average of the mechanical results of 5 repetitions more or less their standard deviation. The same index in the same column indicates that the difference is not statistically significant ($p<0,05$).

Optical properties

The spectroscopic scanning analysis of the biofilms occurred on the interval of 200-800 nm (Fig. 1a). The films showed a similar light transmission initially (200-230 nm). However, the sample S/SiO_2 2% had lower results of transmittance compared to the cited biofilms, mainly after 315 nm. The sample S/SiO_2 6% indicated a decrease ($p<0,05$) of light transmission at transmittance above 230 nm. These results implied that the addition of nano-SiO_2 caused lower light transmission through the films, mostly at the visible region and infrared region: this result represented the potential to delay food deterioration, as the lipid oxidation rate would be reduced [8].

Fourier transform infrared spectroscopy (FT-IR)

The resulting graphic of the FT-IR was presented in Fig. 1(b). The peaks from 3283 cm^{-1} to 3271 cm^{-1} and from 2929 cm^{-1} to 2931 cm^{-1} were typically from the stretching of the groups O-H and C-H of the starch's polysaccharide chains [8, 9]. The lower intensity of the first band of S/SiO_2 6% could indicate that the intermolecular interactions (hydrogen bonds) between the polymeric chains and the reinforcement were established in a stronger way, when compared to the sample reinforced with 2% and 4% of SiO_2. The nano-SiO_2 showed stretching peaks at 1076 cm^{-1} and at 760 cm^{-1} of the Si-O-Si formations [8]. The higher transmittance, from 1076 cm^{-1} to 997 cm^{-1}, could be attributed to the stretching of the groups C-O and C-C, besides the deformation of pyranose rings (typical hexagonal rings of saccharides) [8]. Therefore, it was possible to highlight important intermolecular interactions between the components of the biofilms, such as the hydrogen bonds, as well as the expected functional groups of the substances used in the research.

(a) (b)

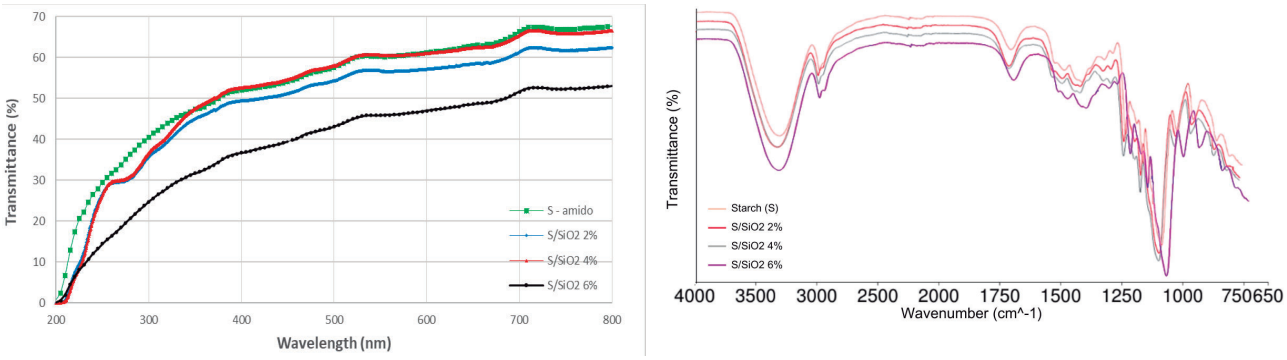

Figure 1: The resulting graphics of the spectroscopic analysis (a) and of the FT-IR (b).

4. Conclusions

The study indicated advantages and disadvantages towards the addition of nanosilica as a reinforcement of starch biofilms destined to be used as food packages. The reinforcement of the films led to higher values of TS, which improved their capacity of resistance to traction up to 54%, when the control film and the S/SiO_2 2% were compared. The modulus of elasticity of the biofilms also presented higher results in the reinforced samples S/SiO_2 2% and S/SiO_2 6% (405,9 ± 64,9 MPa and 316,0 ± 28,4 MPa in order) in comparison to S (189,3 ± 25,3 MPa). Regarding the optical properties, it was observed lower light transmission in the biofilms with nano-SiO_2, mainly in the S/SiO_2 6% sample: this was an improvement towards a film that could delay lipid oxidation of foods and, as a consequence, its deterioration. On the other hand, the EAB presented lower results, as S/SiO_2 6% (29,0 ± 8,8 %) was compared to the other samples; thus, the addition did not show the plasticizing properties of the nanosilica. The WVP tests indicated that the biofilms had their permeability increased with the addition of the nano-SiO_2, as the samples with 2% and 4% (4,9 ± 0,8 g mm m^{-2} day^{-1} $mmHg^{-1}$ and 4,5 ± 0,3 g mm m^{-2} day^{-1} $mmHg^{-1}$ respectively) presented higher results compared to the control films (1,7 ± 0,3 g mm m^{-2} day^{-1} $mmHg^{-1}$). Furthermore, the thickness increased as the reinforcement was incorporated and the FT-IR indicated intermolecular interactions between the reinforcement and the matrix of the biofilms.

Acknowledgements

This research was possible thanks to the infrastructure and resources of Cetea (Ital) and to the research scholarship promoted by the CNPq (*Conselho Nacional de Desenvolvimento Científico e Tecnológico*).

References

1. L. P. Viégas, Master. Master's thesis, Universidade Estadual do Norte Fluminense Darcy Ribeiro, 2016.

2. A. L. L. Fortuna, Graduated. Dissertation, Universidade Federal do Rio de Janeiro, 2020.

3. C. Silva; G. Santos; L. Silva. A. REGET 2013, 2236-1170. http://dx.doi.org/10.5902/223611708248.

4. Y. Liu; Z. Cai; L. Sheng; M. Ma; Q. Xu. A. Carbohydrate Polymers 2019, 0144-8617. https://doi.org/10.1016/j.carbpol.2019.02.079.

5. L. M. Júnior; C. R. Fozzatti; E. Jamróz; R. P. Vieira; R. M. V. Alves. A. Materials 2022, 3881. https://doi.org/10.3390/ma15113881.

6. J. F. Da Silva, Graduated. Dissertation, Universidade Tecnológica Federal do Paraná, 2015.

7. P. Sappakul; J. Miltz; K. Sonneveld; S. W. Bigger. A. Concise Reviews and Hypotheses in Food Science 2003, 1365-2621. https://doi.org/10.1111/j.1365-2621.2003.tb05687.x.

8. X. Hou; Z. Xue; Y. Xia; Y. Qin; G. Zhang; H. Liu; K. Li. A. International Journal of Biological Macromolecules 2018, 0141-8130. https://doi.org/10.1016/j.ijbiomac.2018.09.109.

9. E. Sholichah; B. Purwono; P. Nugroho. A. IOP Publishing 2017, 1755-1315. https://doi.org/10.1088/1755-1315/101/1/012018.

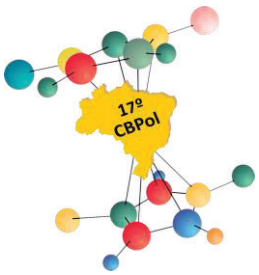

DEVELOPMENT OF NANOCOMPOSITES BASED ON CASSAVA STARCH FOR THE PRODUCTION OF BIO-PACKAGING MATERIALS

Danieli Mützenberg [1], Douglas Alexandre Simon[1], Eveline Bischoff[1] *

1 – Instituto Federal do Rio Grande do Sul (IFRS), Farroupilha, RS, Brazil
**eveline,bischoff@farroupilha.ifrs.edu.br*

Abstract This study focuses on the development of films using cassava starch as the main component, aiming to replace traditional polymer-based packaging materials. Various additives, including glycerol, Kaolinite (Kal), Halloysite Nanotubes (HNT), and Layered Double Hydroxides (LDH), were incorporated into the starch-glycerol matrix to improve the properties of the films. The thermal stability, water vapor permeability, and degradation behavior of the films were investigated. Results showed that the addition of Kal and HNT led to reduced water vapor permeability, indicating improved barrier properties. However, the inclusion of LDH did not significantly enhance the barrier performance. Thermal analysis revealed the temperature range of degradation for each sample was very similar. These findings demonstrate the potential of using cassava starch-based films with suitable additives as sustainable alternatives for food packaging, offering enhanced barrier properties and thermal stability. Further optimization of the film composition and processing conditions is necessary to maximize their performance and commercial viability.

Keywords: *Starch-based materials, thermal stability, water vapor permeability.*

Introduction

The widespread use of polymers in the protection and preservation of food, cosmetics, medications, and chemicals has raised concerns due to their low biodegradability. This has led to the accumulation of non-degradable waste in landfills and the release of microplastics, posing risks to human health and the environment. To address this issue, the development of biodegradable materials as alternatives to traditional polymers has gained significant attention. While synthetic polymers like polylactic acid (PLA), polyvinyl alcohol (PVA), polycaprolactone (PCL), poly(butylene succinate-co-adipate) (PBSA), and poly(butylene adipate-co-terephthalate) (PBAT) have been extensively studied, natural polymers such as proteins, polysaccharides, and lipids have also emerged as promising candidates [1].

Starch-based materials have attracted considerable interest as biodegradable alternatives due to their abundance, renewability, low cost, and biocompatibility [2]. Starch, the primary carbohydrate in human diets and found in various plant sources, consists of long glucose chains (amylose and amylopectin) with varying properties depending on the source. However, pure starch films have limitations in terms of mechanical and barrier properties when compared to traditional polymers like polyethylene. To overcome these limitations, the incorporation of clays such as halloysite nanotubes (HNTs), kaolinite (Kal) and layered double hydroxides (LDH) has been explored [3].

However, achieving proper dispersion of clays in starch-based polymers remains challenging due to their cohesive structure [4]. The objective of this study is to evaluate the final properties of starch-based nanocomposite films reinforced with clays in order to develop a material

with satisfactory performance as a food packaging material, able to replace traditional oil-based polymers packaging.

Experimental

Materials

- Commercially available cassava starch in powder form.
- Glycerol, commercially available from Nuclear.
- Halloysite nanotubes, commercially available from Sigma Aldrich.
- Kaolinite, commercially available from Sigma Aldrich.
- Layered double hydroxides, commercially available from Kisuma Chemicals.
- Citric acid (CA), commercially available from Nuclear.

Method

The cassava starch-based films were prepared using the casting method. The film-forming solutions were heated from 30 to 95°C and maintained at 95°C for 10 minutes. Then, the clay particles were added to the solution, and cooled to 50°C with the assistance of a mechanical stirrer to aid in dispersion. After 60 minutes, the film-forming solution was poured onto Teflon plates and dried in a circulating air oven with air renewal at 40°C for 24 hours.

The content applied and the sample codes of the starch-based films are specified in Table 1.

Table 1 – Samples concentrations

Samples	Starch (%)	Glycerol (%)	CA (%)	HNT (%)	Kal (%)	LDH (%)
Starch-Glycerol	80	20	-	-	-	-
Starch-Glycerol-HNT	77	20	1	2	-	-
Starch-Glycerol-Kal	77	20	1	-	2	-
Starch-Glycerol-LDH	77	20	1	-	-	2

Prior to analysis, the films were stored in desiccators under controlled conditions with magnesium nitrate to maintain a relative humidity of 57% and a temperature of 30°C, creating an artificial environment that ensures stable moisture conditions for the films.

Characterization

The thermal stability of the films were investigated using thermogravimetric analysis (TGA) using a Perkin Elmer instrument (model TG 4000), in order to determining the degradation steps and final weight after 750 °C (residue) and also the maximum degradation temperature (DTG). Approximately 6 mg samples of the films were heated from 30°C to 800°C at a heating rate of 20°C.min^{-1} under a nitrogen atmosphere.

The water vapor permeability of the films was tested according to ASTM E96/00 standard, with some adaptations. The analysis were performed in triplicate using test specimens with a diameter of 60 mm and an average thickness obtained from four measurements. The samples were conditioned at 64% relative humidity for 48 hours prior to the analysis.

In the experimental setup, the film was positioned at the opening of the permeation cell and fixed using silicone grease. The interior of the cell was filled with a saturated solution of Magnesium Chloride, and the prepared capsule will be placed in a desiccator containing a saturated solution of Sodium Nitrite. Weighings were performed successively every 12 hours for a period of 7 days. The mass gain (m) was plotted against time (t), and the slope of the linear regression line was determined to obtain the angular coefficient. The water vapor permeability rate (WVP) was calculated using Equation 1:

$$WVP = \frac{m}{t} + \frac{1}{A} \qquad \text{Eq.1}$$

Results and Discussion

Thermal Stability

The results obtained from the TGA data are presented in Figure 1 and compiled in Table 2 provided valuable insights into the degradation behavior of the films at different temperature ranges. Initially, a mass loss was observed in all samples up to 200 °C, which was attributed to the evaporation of surface and inner moisture, commonly known as free water.

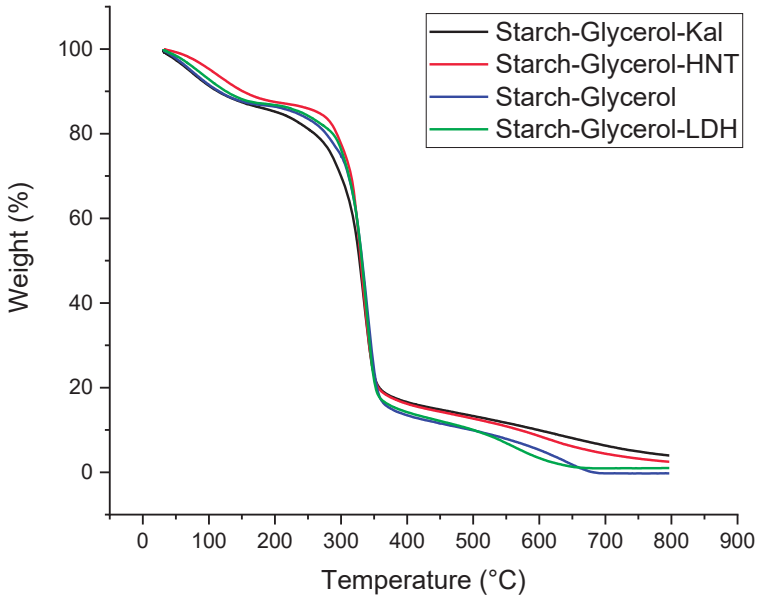

Figure 1 - Thermogravimetry analysis

Between 200 and 480 °C, the starch-based polymer exhibited degradation, as indicated by the recorded DTG values. Interestingly, a slight decrease in degradation temperature was observed in samples containing HNT or Kal, suggesting that the presence of these components may have an impact on the degradation process.

During the third degradation phase, occurring between 480 and 700 °C, a thermal event was observed due to dihydroxylation of the hydroxyl groups (-OH) from the clay particles or other components present in the film samples. Previous studies have reported a similar phenomenon in the temperature range of 500 to 700 °C, corresponding to the dehydroxylation of clay sheets [5]. Further investigation is required to determine the exact mechanisms behind this phenomenon.

Table 2 – TGA data of Starch-Glycerol samples

Samples/Weight Loss (%)	First Step 30-200 °C	Second Step 200-480 °C	Third Step 480-750 °C	Residue < 750 °C	DTG (°C)
Starch-Glycerol	12.4	75.5	10.8	1.3	341
Starch-Glycerol-HNT	12.1	73.7	10.1	4.1	330
Starch-Glycerol-Kal	14.1	70.9	8.9	6.1	336
Starch-Glycerol-LDH	12.4	75.5	10.0	2.1	340

At temperatures above 680 °C, the samples of starch-glycerol and starch-glycerol-LDH showed no significant weight changes. In contrast, samples containing HNT or Kal reached a near plateau around 750 °C. Consequently, the residue measurement was performed at 750 °C. The absence of any clay component resulted in an expected residue of 1.3%. However, the addition of LDH led to an increase of 0.8% in undegraded matter. Remarkably, the presence of HNT and Kal seemed to disrupt the third degradation phase, with a rapid decomposition around 580-620 °C transitioning to a steady decrease in mass, ultimately resulting in higher amounts of residue.

Water Vapor Permeability

The water vapor permeability (WVP) values provide important information about the barrier properties of the film samples and it presented in Figure 2. A lower WVP value indicates that the film has a lower permeability to water vapor, which is desirable for packaging materials aiming to maintain the freshness and quality of food products.

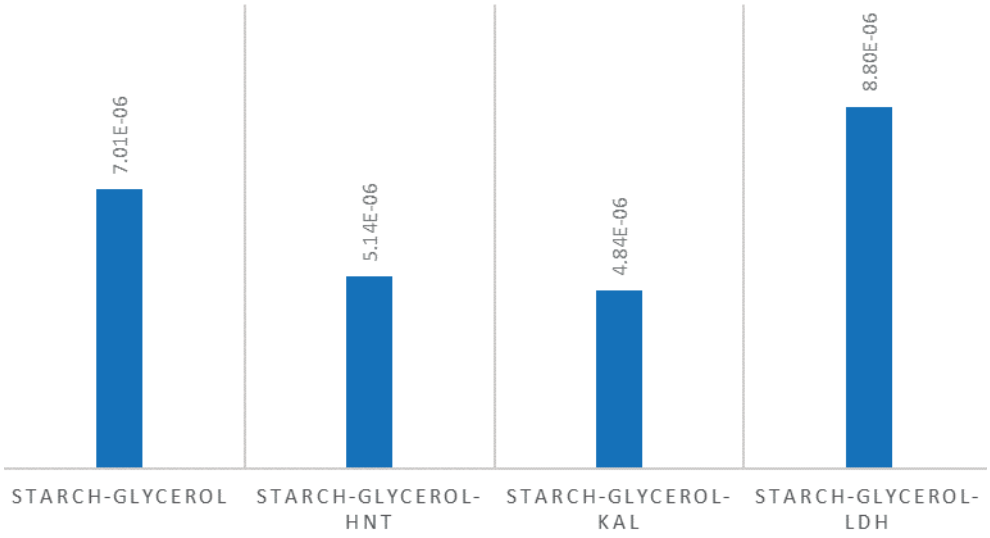

Figure 2 - Water Vapor Permeability of the Films

Comparing the WVP values of the different samples, we can observe that the Starch-Glycerol-Kal sample has the lowest WVP value of $4.84E^{-06}$, indicating a relatively better barrier performance compared to the other samples. This suggests that the incorporation of Kaolinite (Kal) into the starch-glycerol matrix improves the resistance to water vapor transmission.

On the other hand, the Starch-Glycerol-HNT sample also exhibits a relatively lower WVP value of $5.14E^{-06}$, indicating that the inclusion of Halloysite Nanotubes (HNT) in the film composition contributes to the reduction of water vapor permeability. However, it is worth noting that the Starch-Glycerol-Kal sample shows a slightly lower WVP value, suggesting a potentially superior barrier performance.

The Starch-Glycerol and Starch-Glycerol-LDH samples have higher WVP values of $7.01E^{-06}$ and $8.80E^{-06}$, respectively, indicating relatively higher permeability to water vapor compared to the other samples. This suggests that the addition of Layered Double Hydroxides (LDH) in the Starch-Glycerol-LDH sample did not significantly improve the barrier properties in terms of water vapor transmission. In a similar study by Schmidt et al. [6], a WVP value of $5.81E^{-07}$ was reported for a comparable Starch-Glycerol composition, potentially attributed to variations in chain distribution and the final polymer network, resulting in lower values by incorporating a fatty acid to increase hydrophobicity.

Conclusions

These findings highlight the complex thermal behavior of the starch-based polymer films and emphasize the influence of various components, such as HNT, Kal, and LDH, on the degradation process. The results suggest that the addition of these components can significantly impact the thermal stability and residue formation of the films.

Also, the results indicate the potential of incorporating clays such as Kaolinite and Halloysite Nanotubes in starch-glycerol-based films to enhance their barrier properties and reduce water vapor permeability. Further research and optimization of the film composition and processing conditions could lead to even better barrier performance, making these materials viable alternatives to traditional polymer-based packaging materials.

Acknowledgements

This study was supported by the Instituto Federal de Educação, Ciência e Tecnologia do Rio Grande do Sul (IFRS).

References

1. J.-W. Rhim; H.-M. Park and C.-S. Ha Progress in polymer science 2013, 38, 1629-1652. https://doi.org/10.1016/j.progpolymsci.2013.05.008.
2. A. Fadeyibi; Z. D. Osunde; G. Agidi; P. Idah and E. C. Egwim Journal of Food Processing & Technology 2016, http://dx.doi.org/10.4172/2157-7110.1000591.
3. M. Avella; J. J. De Vlieger; M. E. Errico; S. Fischer; P. Vacca and M. G. Volpe Food chemistry 2005, 93, 467-474. https://doi.org/10.1016/j.foodchem.2004.10.024.
4. A. Arora and G. Padua Journal of Food science 2010, 75, R43-R49. https://doi.org/10.1111/j.1750-3841.2009.01456.x.
5. H. Liu; P. Yuan; Z. Qin; D. Liu; D. Tan; J. Zhu and H. He Applied Clay Science 2013, 80, 398-406. https://doi.org/10.1016/j.clay.2013.07.005.
6. V. C. R. Schmidt; L. M. Porto; J. B. Laurindo and F. C. Menegalli Industrial Crops and Products 2013, 41, 227-234. https://doi.org/10.1016/j.indcrop.2012.04.038.

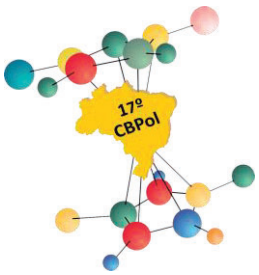

FABRICATION OF PHOTOACTIVE NANOFIBERS OF CROSSLINKING POLYVINYL ALCOHOL AND PHOTOSENSITIZERS FOR COMBATING WOUND INFECTION

Ariane R. S. Rossin[1,2]*, Fabiana S. L. Cardoso[1,2], Josiane Caetano[2], Hueder P. M. de Oliveira[3], Charles B. Silva[3], Alessandro F. Martins[4], Suellen P. Facchi[4], Eduardo Radovanovic[1] , Wilker Caetano[1] and Douglas C. Dragunski[1,2]

1 – Department of Chemistry, State University of Maringá (UEM), Maringá, PR, Brazil, ariane.rossin@gmail.com
2 – Center of Engineering and Exact Sciences, State University of West Paraná (Unioeste), Toledo, PR, Brazil
3- Center of Natural and Human Sciences, Federal University of the ABC (UFABC), Santo André, SP, Brazil
4-Laboratory of Materials, Macromolecules, and Composites, Federal University of Technology-Paraná (UTFPR), Apucarana, PR, Brazil

Abstract – Infected wounds can progress to chronic, causing great concern and costs for treatment. Electrospun membranes in union with photodynamic therapy can provide satisfactory and less invasive results, causing less suffering to the patient. Also, facilitators for drug delivery such as Pluronic® F127 can be triggered, further increasing positive results to the treatment. Therefore, this work aims to obtain electrospun membranes from crosslinked polyvinyl alcohol and Pluronic® F127, with the addition of erythrosine B and methylene blue for photoantimicrobial activity. The methods of characterization of the material were scanning electron microscopy, emission of phosphorescence and amicrobial activity with evaluating the adhesion and proliferation of *Staphylococcus aureus*. The fibers had an average of 250 nm and showed the formation of reactive species The study of adhesion and proliferation demonstrated that when illuminated the membranes cause the death of the microorganisms with more satisfactory results for methylene blue. The fiber characteristic is lost when the membrane is placed in solution, but the results are Important being able to accredit the material for medical application in wounds.
Keywords: *Electrospinning, Photodynamic Inactivation, Methylene Blue, Erythrosine B, Citric Acid.*

Introduction

Untreated wounds can become a public health problem when bacterial infection leads to non-healing, suffering to the patient, hospitalization and more severe complications. Nanomaterials come as an alternative for drug delivery and holiday protection [1]. Among the nanomaterials, electrospun membranes (EM) provide satisfactory results by simulating the structure of the extracellular matrix and provide breathability, high surface area and gas exchange, promoting tissue regeneration of the skin [2]

Electrospinning is based on the use of electrostatic forces for the spinning of ultrafine fibers of different polymers, as in the case of polyvinyl alcohol (PVA). In the medical field, PVA is used as a biomaterial because it presents biocompatibility, bioadhesives, and swelling and for not present toxicity and carcinogenic characteristics [3].

A inserção de agentes antimicrobiano podem ser utilizadas para resultados mais satisfatórios frente a microrganismos. Photodynamic therapy (PDT) is highly selective chemotherapy with the use of biocompatible photosensitizers (PS) that do not cause microbial resistance and are suitable for the treatment of wound infections [4].

PS delivery can be improved for improved infection control results with the insertion of Pluronic®. Pluronic® F-127 (F127) It is a triblock, non-ionic amphiphilic copolymer that tends to

self-assemble in micelles, forming a support network of active drugs. It presents promising results when applied in a drug delivery system by providing the system with improvements in biopharmaceutical, pharmacodynamic and pharmacokinetic properties [5].

Therefore, this work aims to use the electrospinning methodology to obtain EM based on crosslinked PVA with the addition of F127 and methylene blue (MB) and erythrosine B (Ery) photosensitizers to formulate nanofibers with photosensitive characteristics to fight wound infections.

Experimental

Initially, the mass of PVA (Mw 186 KDa) fixed at 8% m/v with GH and 87-88% was solubilized in a bath with continuous agitation at 80°C for approximately 8 hours. After the dissolution of PVA, 10% citric acid (CA) crosslinking mass was added to the PVA mass and left under agitation at room temperature. Thin films of F127 were prepared following the methodology proposed by Da Silva et al. [6]. For this, 1% (m/v) of F127 and 0.8% of erythrosine B (Ery) or methylene blue (MB) were dissolved in ethanol and rotated at 50°C until the formation of a solid film and left in a desiccator for 24 hours. Finally, the aqueous solution of PVA/CA was poured into the F127 film and stirred in a bath at 40°C until complete miscebilization.

The PVA solution was spun from optimal conditions already reported by Rwei & Huang [7] (2012). The solution was placed in a plastic syringe and connected to a metal needle with a straight tip. As wiring parameters were used voltage of 20 kV, flow of 0.5 mL/h and collection system with rotation of 325 cm/s, ambient temperature of 26°C ± 4°C and relative humidity of 45 %. The fibers were deposited in an aluminum foil covered over the collector. At the end of the process, the electrospun matrices were placed on glass plates and taken to the oven at 100°C for the cross-linking reaction to occur.

The surface morphology of the polymer matrices was evaluated by scanning electron microscopy. The equipment used was the FEI brand of the QUANTA 250 series line. To make the samples electrically conductive they were metalized with gold up to a thickness of 30 nm. The images were obtained by applying an electron acceleration voltage ranging from 12 to 20 kV at different magnifications.

Fluorescence emission spectra were recorded on a PicoQuant FluoTime 300 Fluorescence Lifetime Spectrometer using a 1 cm path-length quartz cuvette at room temperature. Fluorescence lifetimes (τ_F) and phosphorescence decay curves at 1270 nm were recorded on a PicoQuant FluoTime 300 Fluorescence Lifetime Spectrometer. Fluorescence lifetimes ($\tau_{F)}$ were recorded using a time-correlated single-photon counting setup (TCSPC). The decays were analyzed using PicoQuant FluoFit Global Fluorescence Decay Analysis Software. Phosphorescence decay curves at 1270 nm were recorded in the equipment with a near-infrared photomultiplier tube (NIR PMT) Hamamatsu, model H10330B. Photo-irradiations were done using a picosecond pulsed diode laser (LDH-P-635 driven by PDL 800-B, 635 nm, 80 MHz repetition rate, 72 ps pulse width, PicoQuant GmbH).

The bactericidal and non-stick properties of electrospun membranes containing MB, Ery EryMB and pure were evaluated as previously described by Facchi et al.[8] with some changes. The bacterial culture *S. aureus* (ATCC® 25923) as well as the Mueller-Hinton solution at 1.0×10^7 CFU mL^{-1} (500 µL) were sown in membranes previously packed in a 48-well culture plate. The experiment was carried out in duplicate, where one of the plates after sowing was illuminated for 15 minutes with a white LED. After 24 h, the supernatants were aspirated and the samples containing the adhered bacteria were fixed. Subsequently, the membranes containing the bacteria were processed n serial dehydration with ethanol for 10 min each before being subjected to a reduced-pressure oven (25 °C, 8h) until moments before SEM imaging

Results and Discussion

The morphology of the membranes electrospun with or without the addition of FS was evaluated by SEM and can be observed in Figure 1. The formation of homogeneous fibers occurs

with the presence of few beads for all the solutions studied. The average diameter of the membranes is PVA/F127/CA 212±35 nm, PVA/F127/CA/Ery 289±47 nm, PVA/F127/CA/MB 251±73 nm and PVA/F127/CA/EryMB 248±41 nm.

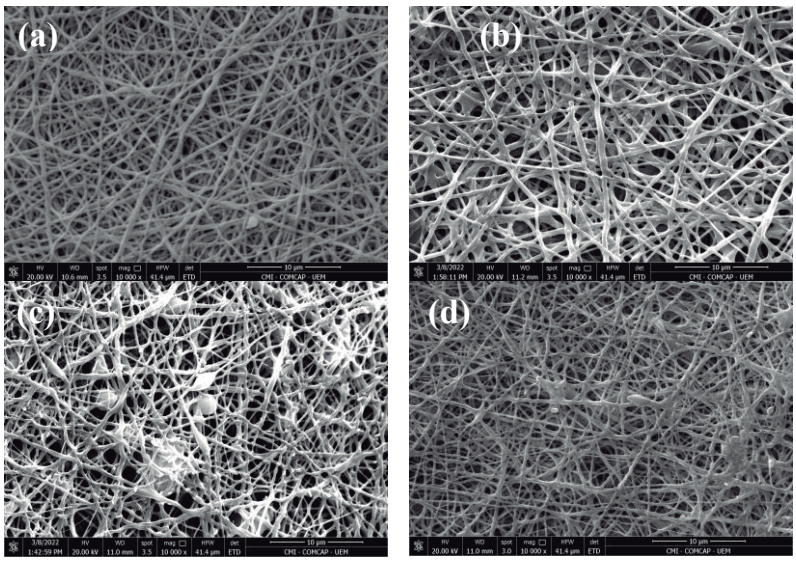

Figure 1. Morphology of electrospun matrices for (a) PVA/F127/CA, (b) PVA/F127/CA/Ery, (c) PVA/F127/AC/MB and (d) PVA/F127/AC/EryBM.

The detection of $^1O_2$ can be performed by the physical method of emission of phosphorescence at 1270 nm from the transition $^1\Delta_g(0) \rightarrow {}^3\sum_g^-(0)$ [9]. For all membranes studied can be observed in Figure 2 the formation of $^1O_2$, highlighting the membrane containing Ery. Ery when compared to MB already has a quantum yield of singlet oxygen ($\Phi_\Delta{}^1O_2$) with a value of 0.62 [10] against 0.22 [11] in water. The FS used in this study and immobilized in nanofibers have not yet been reported $\Phi_\Delta{}^1O_2$ using this technique. It can also be observed that contrary to what was expected there was no synergistic effect of the joining of the two PS.

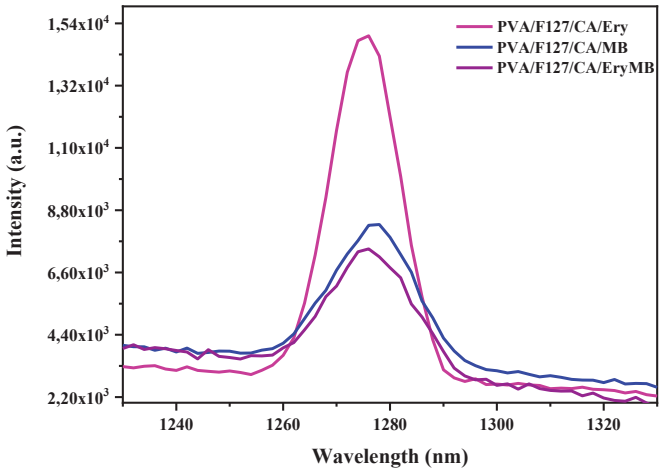

Figure 2. Emission of singlet oxygen phosphorescence to electrospun membranes containing MB, Ery and EryMB – 0.8% w/v.

The adhesion (ADE) and proliferation (PROF) of microorganisms with *S. aureus* in the dark and illuminated to the studied membranes are shown in Figure 3. For PVA/F127/CA control (Figure 3 (a) and (e)) a large ADE of microorganisms with intrigue structure and large PROF is observed even with the incidence of light, indicating that the pure material is a growth vector for the microorganism. The same factor was observed for the membrane with the addition of Ery without

illumination Figure 3(b). With illumination (Figure 3(f)), the incidence of microorganisms was greatly decreased in both PROF and ADE characters. For the addition of AM, the ADE and PROF of the microorganisms were almost non-existent already in the dark Figure 3(c). For the same material after illumination is no longer denoted any microorganism with integrated structure. The EryMB membrane (Figure 3(d)), also provides ADE and PROF of the microorganism without illumination. However, when compared to the control of pure PVA, ADE and PROF are less expressive. This fact can be attributed to the presence of MB in the fibers since the results demonstrate its antimicrobial activity in the dark. With the lighting, the Figure 3(h) the ADE and PROF are drastically reduced. A synergistic effect of PS was also not observed, these data following the phosphorescence results for $^1O_2$ (Figure 2). Given these data, the anti-stick/anti-adhesive power of the studied materials can attest, it can be classified with antimicrobial power as follows: F127/CA/Eri < F127/CA/EryMB < F127/CA/MB. Still, it is worth mentioning that the reduction of microorganisms comes from the generation of $^1O_2$ by all materials when illuminated, causing photodynamic inactivation of these.

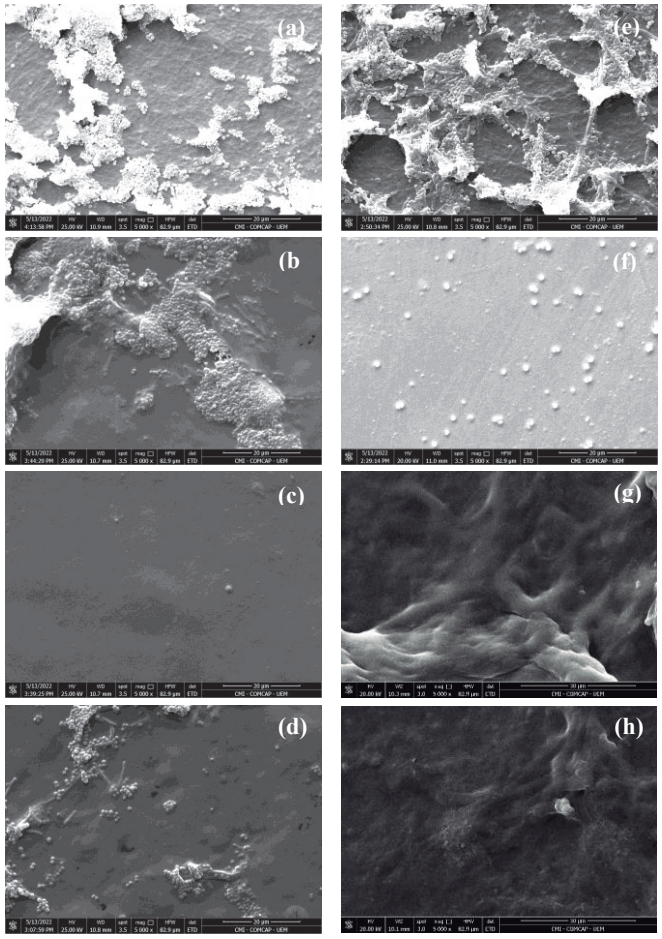

Figure 3. ADE and PROF of the *S. Aureus* for(a) and (e) PVA/F127/CA, (b) and (f) PVA/F127/CA/Ery, (c) and (g) PVA/F127/CA/MB e (d) e (h) PVA/F127/CA/EryMB, where (a)-(d) are controls in the dark and (e)-(h) illuminated for 15 minutes.

A fact observed in the microscopies of Figure 3 For all electrospun membranes is the loss of fibrous characteristics after immersion in solution. Contrary to what is reported by 10% mass of AC was not sufficient for crosslinking at the temperature used and molar mass of PVA used in this work. The temperature chosen for crosslinking took into account the decomposition temperatures of MB and Ery already reported in the literature by Salimi & Roosta [12]. Another bridge that should be investigated is the interaction of the competitive type between PS and the CA and with the PVA

groupings. Therefore, new approaches should be employed to maintain the fibers with the greater mass addition of the crosslinker and new temperatures.

Conclusions

The results presented are satisfactory in the antimicrobial power by photodynamic inactivation of the material even with the disruption of the fibers. The maintenance of the photophysical properties of the FS employed and the formation of reactive species should be emphasized. The property of inhibition in the dark by MB brings advantages in the application of dressings since they offer extra protection. Therefore, MB is considered the best PS to be used in union with PVA.

Acknowledgments

The authors would like to thank the Nucleus for Research in Photodynamic Systems (NUPESP–UEM) and the Interdisciplinary Group for Photochemical and Electrochemical Environmental Research (GIP&FEA–Unioeste). ARSR acknowledges Coordenação de Aperfeiçoamento de Pessoal de Nível Superior (CAPES–Brazil) for her Ph.D. fellowship.

References

[1] Pan, F., Giovannini, G., Zhang, S., Altenried, S., Zuber, F., Chen, Q., ... & Ren, Q. Acta Biomaterialia, 2022, 145, 172-184.

[2] Sylvester, M. A., Amini, F., & Tan, C. K. Materials Today: Proceedings, 2020, 29, 1-6.

[3] Baker, M. I., Walsh, S. P., Schwartz, Z., & Boyan, B. D. Journal of Biomedical Materials Research Part B: Applied Biomaterials, 2012, 100(5), 1451-1457.

[4] Sun, L., Song, L., Zhang, X., Zhou, R., Yin, J., & Luan, S. Materials Science and Engineering: C, 2020, 113, 110936.

[5] Nascimento, M. H. M., Franco, M. K. K. D., Yokaichyia, F., De Paula, E., Lombello, C. B., & De Araujo, D. R. International journal of biological macromolecules, 2018, 111, 1245-1254.

[6] da Silva Junior, R. C., Campanholi, K. D. S. S., de Morais, F. A. P., dos Santos Pozza, M. S., dos Santos, G. T., Hioka, N., & Caetano, W. Dyes and Pigments, 2019, 167, 204-215.

[7] Rwei, S. P., & Huang, C. C. Fibers and polymers, 2012, 13(1), 44.

[8] Facchi, S. P., de Oliveira, A. C., Bezerra, E. O., Vlcek, J., Hedayati, M., Reynolds, M. M., ... & Martins, A. F. European Polymer Journal, 2020,130, 109677.

[9] Jarvi, M. T., Niedre, M. J., Patterson, M. S., & Wilson, B. C. Photochemistry and photobiology, 2006, 82(5), 1198-1210.

[10] Pellosi, D. S., Estevão, B. M., Semensato, J., Severino, D., Baptista, M. S., Politi, M. J., ... & Caetano, W. Journal of Photochemistry and Photobiology A: Chemistry, 2012, 247, 8-15.

[11] Shahinyan, G. A., Amirbekyan, A. Y., & Markarian, S. A. Spectrochimica Acta Part A: Molecular and Biomolecular Spectroscopy, 2019, 217, 170-175.

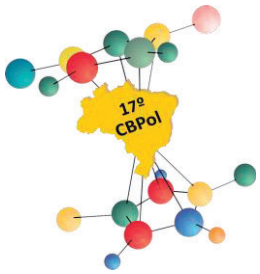

IMPROVING THE OPTICAL AND MECHANICAL PROPERTIES OF PVA POLYMER THROUGH THE INCORPORATION OF CARBON DOTS.

Arthur Hegermann Ferreira[1], Everton Luiz de Paula[2], Rafael Barbosa de Rezende[1], Fabiano Vargas Pereira[1]*.

1 – Department of Chemistry, Federal University of Minas Gerais (UFMG), Belo Horizonte, MG, Brazil
2 - Department of EaD, Federal University dos Vales do Jequitinhonha e Mucuri, Diamantina, MG, Brazil
arthurhegerfer@gmail.com

Abstract - This study investigates the impact of carbon dots (C-Dots), a type of fluorescent carbon nanoparticle, used as filler, on the optical and mechanical properties of Polyvinyl alcohol (PVA) polymer matrix. The C-Dots were synthesized by a simple and cost-effective hydrothermal method and characterized using spectroscopic techniques. The C-Dots were then incorporated into PVA polymer at different concentrations via solution casting method. The optical properties of the resulting PVA/C-Dots films were analyzed using UV-Vis spectroscopy, and the mechanical properties were assessed using tensile strength and Young's modulus measurements. The results demonstrate that the incorporation of C-Dots into PVA polymer leads to a significant improvement in both the optical and mechanical properties. Specifically, the PVA/C-Dots films exhibit enhanced optical absorption in the ultraviolet region, and a fluorescent emission in visible light. Also, an increased tensile strength and Young's modulus were observed, indicating improved mechanical stability. The study provides valuable insights into the potential applications of PVA-C-Dots polymer for various optical and mechanical devices.

Keywords: *Carbon Dots; PVA polymer, Optical Properties; Mechanical Properties.*

Funding: CNPq.

Introduction:

Polyvinyl alcohol (PVA) is a widely used polymer due to its excellent mechanical and chemical properties, as well as its biodegradability. However, to further expand its applications, it is necessary to enhance its properties. One potential approach to achieve this is through the use of carbon dots (C-Dots) as fillers [1-2]. C-Dots are a type of fluorescent carbon nanoparticle with unique optical and chemical characteristics, which have been extensively investigated for their potential in various applications such as bioimaging, sensing, and optoelectronics.
In recent years, there has been growing interest in exploring the use of C-Dots as fillers in polymer matrices to enhance mainly their mechanical properties. In this study, we investigate the impact of the C-Dots incorporation on the optical and mechanical properties of PVA polymer [3]. The C-Dots were synthesized by a simple and cost-effective hydrothermal method, using ammonium citrate and succinic acid as precursors. Finally, they are incorporated into PVA polymer at different concentrations via solution casting method. The optical and mechanical properties of the resulting PVA/C-Dots films were analyzed using UV-Vis spectroscopy, tensile strength, and Young's modulus measurements.

Experimental:

Synthesis of C-dots

The C-Dots were synthesized using the hydrothermal method. A stainless-steel Teflon-lined hydrothermal autoclave was used, into which a 1:1 molar ratio of succinic acid (0.51 g) and ammonium citrate (0.98 g) were added along with 30 mL of deionized water and allowed to react for 8 hours. After the reaction was complete, the resulting mixture was dried in a vacuum drying oven to yield a dark-brown powder, which was named CSA 1-1.

Preparation of Composites

The PVA composites were prepared via solution casting, using water as the solvent. To achieve the desired concentrations of C-Dots in the final composite (2.5%, 5.0%, and 7.5%), and a pure PVA matrix, an appropriate amount of the C-Dots dispersion was added to a PVA solution with the same solvent. The resulting samples were named PVA, PVA 2.5%, PVA 5.0%, and PVA 7.5%, depending on their C-Dots content.
After mixing the solutions for 2 hours, they were poured onto a Teflon® plate and left for slow evaporation of the solvent for 18 hours. The resulting films were then further dried under vacuum for 8 hours.

Instrumental Analysis

The optical properties of the carbon dots were evaluated using UV-Vis and fluorescence spectroscopy. Specifically, the UV-Vis absorption spectra were measured on a Shimadzu UV-2550 spectrometer, with suspensions of the C-Dots being placed in quartz cuvettes with a pathlength of 1.0 cm. Similarly, fluorescence spectra were recorded on a Varian Cary Eclipse Fluorescence spectrometer using quartz cuvettes with an optical path of 1.0 cm.
The mechanical properties of the samples were evaluated using tensile testing, which was conducted using an EMIC-DL500 miniature material tester equipped with a 1000 N load cell and a cross head speed of 2 mm/min. The length between the gaps was set to 60 mm, and three samples were tested for each material.

Results and Discussion:
Figure 1 shows the results of fluorescence and UV-Vis spectroscopy for the obtained C-Dots and photographed under 365 nm UV lamp.

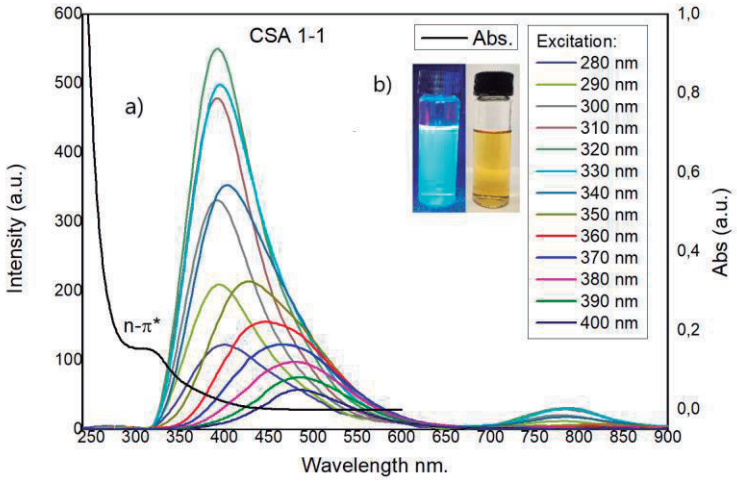

Figure 1: a) Intensity for different wavelengths and absorption in UV-vis for the C-dot used in the polymer. **b)** Photographs under 365 nm UV lamp.

The UV-VIS absorption spectra of the CSA 1-1 sample exhibit absorption bands with a maximum at around 320 nm. These bands are attributed to n → π* of C=O transitions originating from various functional groups. Photoluminescence spectra of the sample were obtained using different

excitation wavelengths, revealing a prominent and broad fluorescence emission peak ranging from approximately 300 nm to 600 nm. Additionally, a weaker broad emission peak was observed in the 700 nm to 900 nm range. Importantly, the position of the primary peak varied depending on the excitation wavelength used.

Figure 2 shows luminescent composite films derived from C-Dots and PVA that emitted single white light at different concentrations under the excitement.

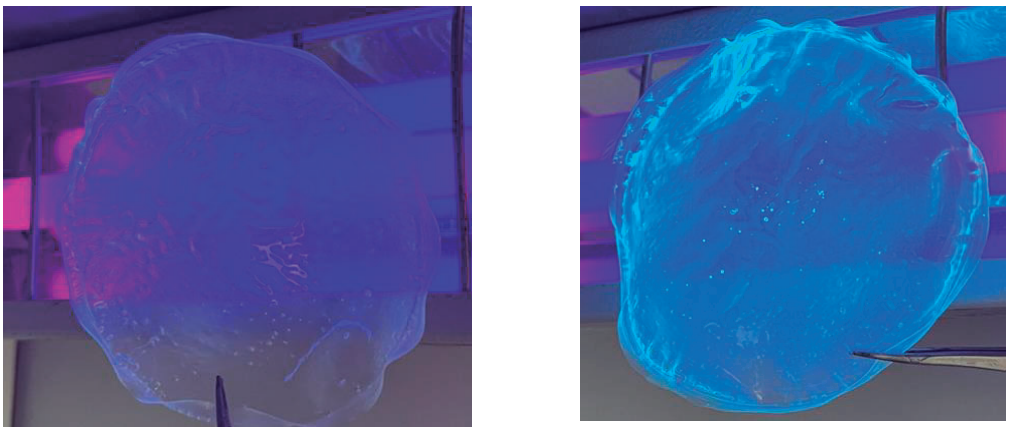

a) **b)**

Figure 2 – Polymeric films under UV light (365 nm): (a) PVA pure e (b) PVA 5.0%.

The optical properties of all films were assessed by measuring their UV-Visible absorption and transmittance. The aim was to investigate the films' ability to block ultraviolet light, comparing both the pure polymer and the prepared compounds. Figure 3 presents a summary of the results obtained for the absorbance and transmittance:

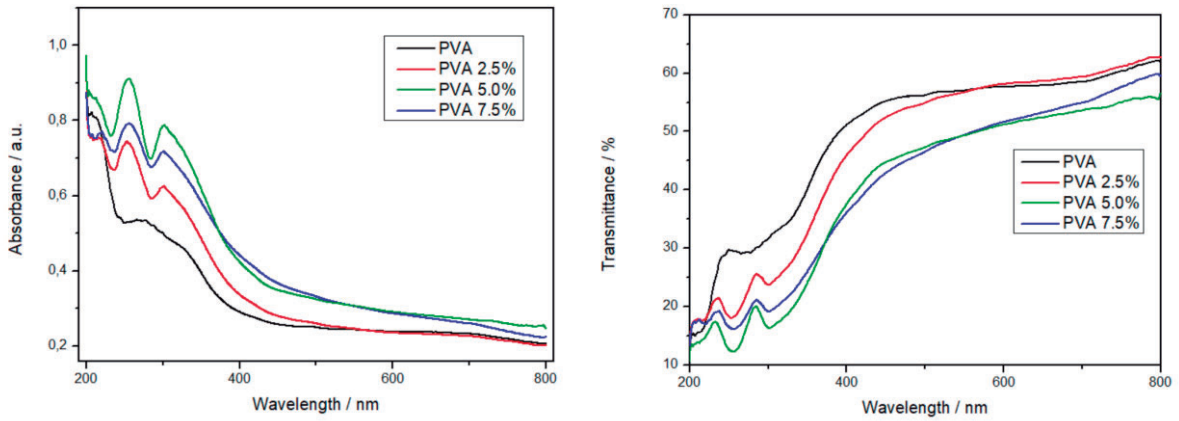

a) **b)**

Figure 3 - UV–Visible absorbance(a) and transmittance (b) spectra of PVA and composite films.

The UV-blocking percentage of UV-A, UV-B, UV-C and visible light transmittance was calculated using the following equation [4]:

$$UV\ Blocking\ percentage\left(B_{UV(A-B-C)}\right)=100-\frac{\int_a^b T(\lambda)d\lambda}{\int_a^b d\lambda}\ldots\ldots\ldots\ldots(1)$$

where, a and b are the limits of the UVA, UVB and UVC spectrum range. In this study we calculated using the range (230-280 nm) for the UVC, (280-315 nm) for the UVB, (315-400 nm) for UVA and (400-800 nm) for the visible light. For the visible light, only the 'light transmittance' is calculated and not the blocking percentage. Table 1 summarize the results:

Sample	B_UVC %	B_UVB %	B_UVA %	T_Visible %
PVA	71.4	68.6	57.7	57.5
PVA 2.5%	79.7	75.3	64.8	57.8
PVA 5%	85.1	82.2	73.2	50.1
PVA 7.5%	82.2	79.9	72.1	50.6

Table 1: Blocking percentages of different ranges of UV radiation for PVA and PVA composites prepared with C-Dots.

The findings of the study suggest that the addition of C-Dots into PVA polymer can lead to a significant improvement in the ability of PVA films to block UV light. According to the data presented in Table 1, the optimal concentration for achieving superior optical performance was found to be 5%, which resulted in blocking 85.1% of UV-C, 82.2% of UV-B, and 73.2% of UV-A light. As the concentration of C-Dots in the PVA matrix was increased, the transmittance of visible light decreased from 57.5% to 50.1%. The incorporation of C-Dots into the PVA polymer matrix can enhance the light absorption in the UV region. This is due to the unique optical properties of C-Dots, including strong light absorption and tunable photoluminescence. Incorporating C-Dots into the PVA matrix can enable the absorption, scattering, and emission of light in different wavelengths, leading to improved optical properties of the composite material. These characteristics can be fine-tuned to create a UV filter polymer with PVA-C-Dots.

To evaluate the mechanical properties of composites, the Stress-Strain curves were obtained for the different concentrations of the C-dot on the polymer and show Figure 4:

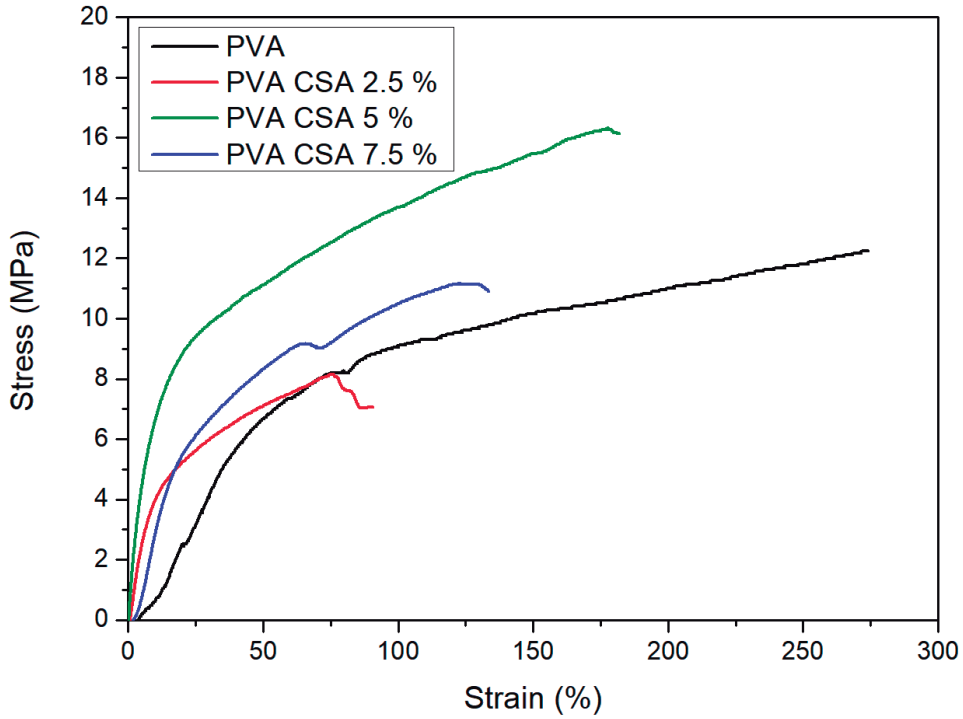

Figure 4 - Tensile curves for PVA and composites with different C-Dots contents.

Sample	Resistance to traction (MPa)	Modulus of elasticity (MPa)	Deformation (%)
PVA	12.23	0.1680	276.8
PVA 2.5%	8.138	0.6126	91.64
PVA 5.0%	16.30	1.406	193.7
PVA 7.5%	11.18	0.3851	133.2

Table 2: Mechanical properties of PVA/C-Dots composites.

The data in Table 2 shows that the mechanical properties of the polymer matrix are significantly improved at concentration of 5%. The incorporation of C-Dots into the PVA matrix can enhance the mechanical properties of the composite material by creating a strong interfacial bonding between the filler and matrix, resulting in increased load transfer efficiency and interfacial adhesion. The high surface area of the C-Dots can also effectively distribute the applied stress throughout the matrix and resist deformation. Furthermore, the small size of the C-Dots can improve the mobility of the polymer chains and enhance the packing density of the nanocomposites, leading to further improvements in mechanical properties. These findings demonstrate the potential of PVA-C-dot nanocomposites as high-performance materials in various applications.

Conclusions:

In summary, this study aimed to create a nanocomposite material by combining C-Dots and PVA polymer through a simple casting process using water as the solvent. The focus was to investigate how the addition of C-Dots as a filler would affect the optical and mechanical properties of the PVA matrix. The results indicated that the incorporation of 5% of C-Dots showed the most significant enhancement in both the optical absorbance in the UV region and the tensile strength and elastic modulus of the PVA-C-Dots films.

Finally, the study demonstrated that the incorporation of C-Dots into the PVA polymer matrix can be an effective way to enhance its properties, with potential applications in fields such as optoelectronics, sensors, and packaging.

Acknowledgements:
This work was supported by CNPq.

References:

1. Y. Hu; R. Guan; S. Zhang; X. Fan, W. Liu, K. Zhang; X. Shao; X. Li; Q. Yue, Food Chemistry, 2022, 372, 131287. https://doi.org/10.1016/j.foodchem.2021.131287.

2. Hu, M., Gu, X., Hu, Y., Deng, Y., & Wang, C. Macromolecular Materials and Engineering, 2016, 301, 1352. https://doi. org/10.1002/mame.201600248.

3. Z. He; C. Zhang; J. Zhang. Et al. Journal of Materials Science. 2022, 57, 1069. https://doi.org/10.1007/s10853-021-06606-6

4. N. P Klochko NP, Barbash VA, Klepikova KS, et al. Solar Energy, 2021, 220, 852. https://doi.org/10.1016/j.solener.2021.04.014

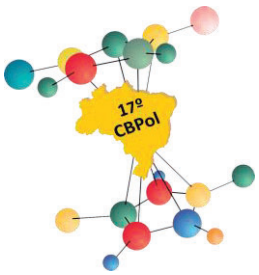

INFLUENCE OF GRAPHENE AND GLASS FIBER ADDITIONS ON MECHANICAL AND RHEOLOGICAL PROPERTIES OF POLYPROPYLENE COPOLYMER

Charles A. Ost[1]*, Artur S. C. Rego[2,3], Monique C. R. Camargo[2], Rodrigo D. O. Polkowski[2], Ricardo F. C. Albuquerque[2], Diego Piazza[1], Ademir J. Zattera[1]

1 – Postgraduate Program in Engineering of Processes and Technologies (PGEPROTEC), Universidade de Caxias do Sul (UCS), Caxias do Sul, RS, Brazil caost@ucs.br
2 – Ford Motor Company, Camaçari, BA, Brazil
3 – Instituto Euvaldo Lodi (IEL), Salvador, BA, Brazil

Abstract – The present study examines the effects of graphene and glass fiber (GF) additions on the mechanical and rheological properties of a CP442XP PP copolymer. Graphene concentrations of 0.125 % and 1 % by mass were used, and 10 % GF was added to both mixtures. Test specimens were prepared using extrusion and injection molding processes, followed by mechanical and rheological testing according to ASTM standards. Results demonstrated that graphene increased tensile rupture elongation in mixtures without GF, with the 1 % graphene sample showing the highest improvement. The addition of GF led to increased Young's modulus in tensile and flexural tests, while graphene enhanced tenacity in non-GF samples. However, GF caused a significant reduction in elongation, with graphene presence influencing tensile toughness and Young's modulus in GF-containing samples. The addition of GF generally increased material viscosity. In conclusion, incorporating graphene and GF into the PP copolymer can have varied effects on mechanical and rheological properties, providing insights into potential applications and processing requirements for these composites.

Keywords: *Graphene, Glass Fiber, Polypropylene Copolymer, Mechanical Properties, Rheological Properties.*

Introduction

The unique properties of graphene, one of which is its large surface area at the nanoscale, have attracted significant attention across various fields, revealing a wide range of potential applications. One such promising area is in polymer matrix nanocomposites, where the addition of graphene can enhance properties such as heat conduction, mechanical strength, and fluidity in the molten state [1-5]. Polypropylene (PP), a widely used thermoplastic in industries such as automotive, piping, and packaging, faces limitations in terms of its thermal and mechanical properties, which restricts its application as an engineering material [2,4]. However, by incorporating a small amount of graphene particles into polymer matrices like PP, the material's mechanical and thermal properties can be improved [4]. Graphene exhibits exceptional mechanical, thermal, and electrical properties, including an elastic modulus of approximately 1100 GPa. Graphene nanoplatelets (GNPs) are multi-layered graphite nanocrystals held together by van der Waals forces [2]. Despite their multiple layers, they have the desired properties of graphene and are less expensive to produce compared to single-layer graphene. [1].

The percentage and geometry of graphene can significantly impact the thermal [1-3, 5], mechanical [2-6], and rheological [4] properties of the resulting nanocomposite. It's worth highlighting that the

rheological properties and crystallinity are particularly significant in processes such as component injection.

Glass fibers (GF) are a commonly used material, since they can quite efficiently reinforce most polymeric matrices due to their high stiffness and strength, their outstanding fatigue performance, and low cost. However, the GF presence leads to an undesirable increase in density, decreased melt flow, increased brittleness, and reduced processability. One strategy to further enhance the properties of the PP composites, or counterbalance some of the above-mentioned disadvantages of GF fillers, is the use of a filler mixture where two or more reinforcements are used in combination [1, 7].

The present study aims to investigate the effect of graphene and glass fiber on the mechanical and rheological properties of a polypropylene copolymer. The findings of this study could provide valuable insights into developing high-performance composites with tailored properties suitable for specific applications.

Experimental

The PP used in this study is a copolymer, CP442XP produced by Braskem. The graphene used is the UGZ 4003, they are nanoplatelets with a thickness between 10 and 20 layers, produced by UCS Graphene. The GF used on the materials is from Owens Corning Fiberglass. The PP was then processed with graphene loadings of 0.125 % (PP0125GNP) and 1 % (PP1GNP) by mass. In a sequence, those materials were given a fiber load of 10 % GF. Three samples with graphene mixed with GF are (PP10GF, PP0125GNP10GF and PP1GNP10GF). The Graphene mixture process occurred in a twin screw, where the screws have a diameter of 20 mm and an L/D ratio of 46. The model of the twin-screw extruder is COR 20-32-LAB, and the temperature profile used in the extrusion process was 100 °C, 160 °C, 170 °C, 174 °C, 180 °C, 180 °C, 185 °C, 190 °C, and -a screw rotation speed set to 200 rpm. The mixtures were extruded and cut into pellets with a diameter of 3 mm and length of 4 mm. The glass fiber mixture was conducted in a single screw extruder SEIBT model ES 35FR with a profile temperature of 170°C, 180°C and 190°C, and screw rotation speed of 70 rpm. The material was then extruded and manually cut in pellets with diameter a 3 mm and length 40 mm.

The mixtures were injected to obtain specimens for mechanical testing. The injection occurred in an LHS 150-80 injector, with a temperature profile of 170 °C, 180 °C and 190 °C, at a pressure of 94 MPa. Tensile and flexural test samples were produced. Those tests were performed on an EMIC DL 2000 universal testing machine with a 200 kgf load cell and a maximum speed of 50 mm/min following ASTM D638 and D790 standards, respectively. To determine the tenacity modulus of each sample, the area under the stress-strain curve was calculated using the tensile testing machine output data. This method allowed us to quantify the material's ability to withstand deformation and absorb energy before failure [8].

To measure the viscosity at each shear rate, capillary rheology was performed. The test was carried using a Ceast SR 20 equipment with a capillaries of size 20/1 mm for the samples with no GF, and 40/2 mm for samples with GF, at a temperature of 190 °C. The shear rates used in the test were 10, 30, 50, 100, 300, 500 and 1000 s^{-1}. The sample was loaded into the capillary, and the flow was allowed to stabilize before the measurements were taken. The shear rate was then increased incrementally, and the viscosity recorded.

Results and Discussion

The mechanical properties obtained on the tensile tests and flexure tests are presented in Table 1. Tensile strength exhibited minor variations across the samples with no graphene. Materials with GF presented an increase of around 10% in tensile strength compared to the samples with no GF among

other properties that also changed, providing a more comprehensive understanding of the materials' behavior. Tensile rupture elongation, which indicates a material's ability to stretch before breaking, showed significant improvement with the addition of graphene. The PP1GNP sample, containing 1 % graphene, displayed the highest elongation, more than double that of the pure PP sample. However, the addition of 10 % GF in subsequent samples led to a drastic reduction in elongation values.

The tensile Young's modulus, which reflects a material's stiffness in response to tensile, exhibited a slight increase with the addition of 1 % graphene (PP1GNP) compared to the pure PP sample. The incorporation of 10 % GF resulted in a more pronounced increase in tensile Young's modulus for all three GF samples, highlighting the reinforcing effect of glass fiber.

Flexural strength and flexural Young's modulus, which characterize a material's resistance to bending and stiffness during bending, respectively, demonstrated improvement with the addition of graphene and GF. The samples containing both graphene and GF (PP0125GNP10GF and PP1GNP10GF) exhibited the highest values for flexural strength and flexural Young's modulus, in comparison with the PP10GF sample, suggesting a synergistic effect between graphene and glass fiber on the mechanical performance of the polypropylene copolymer.

Table 1 – Table of mechanical properties of the tested mixtures.

Sample	Tensile Strength (MPa)	Tensile Rupture Elongation (%)	Tensile Young's Modulus (MPa)	Flexural Strength (MPa)	Flexural Young's Modulus (MPa)
PP	20.76 ±0.16	197.8 ±99.1	503.5 ±11.9	22.15 ±0.55	893.1 ±55.2
PP0125GNP	22.27 ±0.41	362.8 ±188.3	508.6 ±16.1	25.78 ±0.93	934.0 ±52.6
PP1GNP	21.16 ±0.68	557.9 ±186.4	529.6 ±11.6	25.15 ±0.70	889.5 ±79.5
PP10GF	24.18 ±0.62	58.44 ±22.5	658.4 ±34.18	30.79 ±0.43	1451 ±19.7
PP0125GNP10GF	25.98 ±0.44	20.40 ±1.4	788.0 ±19.28	28.03 ±0.32	1602 ±48.5
PP1GNP10GF	25.55 ±0.38	17.41 ±9.8	712.3 ±127.5	29.14 ±0.92	1552 ±31.2

The area under the deformation curve was used to calculate the tensile toughness, which represents the material's ability to withstand deformation and absorb energy before failure. The results showed that the addition of graphene, led to a significant increase in tensile toughness The PP0125GNP and PP1GNP samples exhibited mean tensile toughness values of 63.21 N.mm.mm^{-2} and 96.96 N.mm.mm^{-2}, respectively. This result, combined with the elongation data, demonstrates that graphene may be capable of enhancing the amount of energy a material, in this case a copolymer, can absorb during deformation. This behavior deviates from the findings reported in previous studies [3, 5, 9, 11]. However, Liu, et al. 2021, used a three-layer graphene in conjunction with isotactic polypropylene and observed similar behavior. The authors justified that graphene nanosheets can serve as stress transfer and reinforcement agents when the composites are exposed to external forces. The remarkable elongation at break observed in the PP/graphene composites suggests effective stress transfer at the interfaces, which may be attributed to the two-dimensional structure and favorable dispersibility of graphene in PP in that work. As the composite is subjected to external forces, the macromolecular chains of the matrix and graphene nanosheets align along the force direction. Since crack propagation direction is roughly perpendicular to this alignment, graphene nanosheets can bridge the crack ends, effectively inhibiting crack propagation [6]. In contrast, the presence of GF in the composites resulted in a reduction in tenacity, as the stiffening effect of the fibers restricted the mobility of the polymer chains and thus reduced the material's ability to withstand deformation and absorb energy before failure [1, 7, 9, 10]. The PP10GF sample showed a mean tensile toughness of 11.17 N.mm.mm^{-2}. The PP0125GNP10GF and PP1GNP10GF samples exhibited mean tensile toughness values of 4.38 N.mm.mm^{-2} and 4.90 N.mm.mm^{-2}, respectively. In this case, graphene addition showed a restraining effect in conjunction with the

glass fiber, in comparison with the sample without graphene (PP10GF). These findings provide valuable insights into the potential applications and processing requirements for graphene-based composites in engineering and industrial contexts.

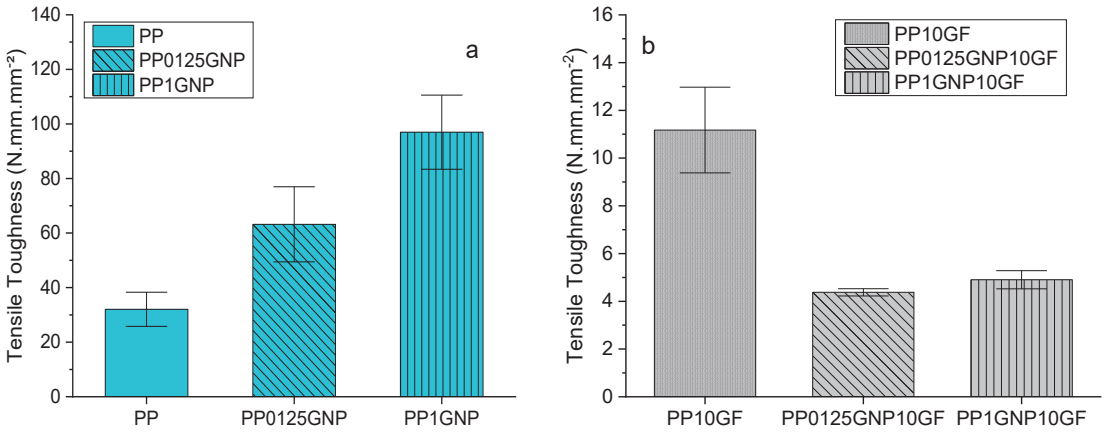

Figure 1 – Tensile Toughness plot of the samples. Samples without glass fiber (a) and with glass fiber (b).

The rheological properties of the samples, presented as Viscosity Rabinovich (Pa.s) versus shear rate (s^{-1}), were evaluated using capillary rheology, with the results presented in Figure 2. At most shear rates tested, the addition of GF led to a significant increase in viscosity for all samples. The viscosity of the molten state can be increased by the presence of GF, which creates a network of fibers within the material. This network hinders the flow of the material and increases its resistance to deformation [7]. The samples with graphene still exhibited a higher viscosity than the unmodified PP, but the increase in viscosity was less pronounced compared to the samples with GF. At higher shear rates, the viscosity of all samples, including those with GF, drops slightly. Although the presence of particles in a molten flow typically increases viscosity, in this particular study, it was found that the incorporation of graphene particles did not significantly alter the polymer's viscosity [4].

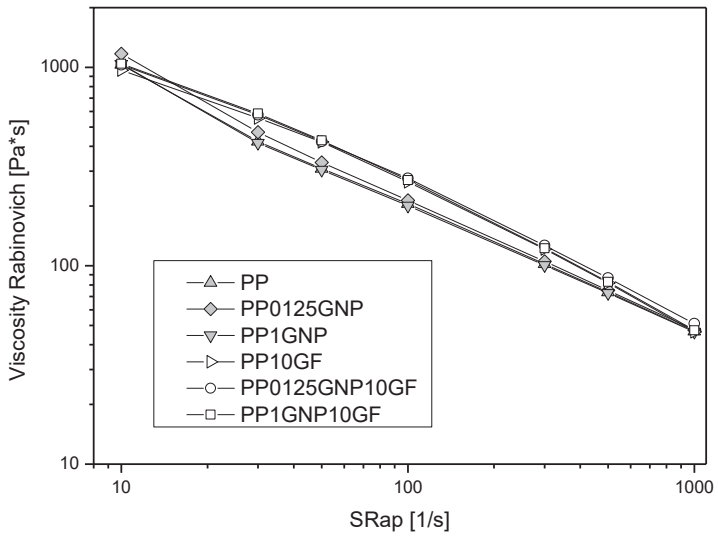

Figure 2 – Plot of capillary rheology for each sample.

Conclusions

The study reveals that adding graphene and glass fiber to a polypropylene copolymer significantly impacts its mechanical properties. Graphene enhances tensile rupture elongation, while glass fiber increases Young's modulus, flexural strength, and flexural Young's modulus. These findings offer valuable insights for tailoring polypropylene copolymer properties to suit specific applications and processing requirements. Additionally, the incorporation of graphene can also increase the tenacity modulus of the polypropylene copolymer. Moreover, rheological analysis revealed that small amounts of graphene slightly increase viscosity of the material in its molten state, while glass fiber was observed to have a more pronounced increase in the viscosity of the material. These findings offer valuable insights into how graphene and glass fiber can affect the material behavior in processes like injection molding, but further optimization is necessary for specific industrial applications.

Acknowledgements

The authors would like to thank Ford Motor Company, UCS, and CNPq for their financial support.

References

1. E. Tarani, G. Z. Papageorgiou, D. N. Bikiaris, K. Chrissafis, Molecules 2019, 24. https://doi.org/10.3390/molecules24101984.
2. H. Sutar, B. Mishra, P. Senapati, R. Murmu, D. Sahu, J. Compos. Sci. 2021, 5, 24. https://doi.org/10.3390/jcs5010024.
3. C. K. Abuoudah, A. Z. Abuibaid, Y. E. Greish, H. M. A. Ehmann, B. M. Iqbal, J. Polym. Res. 2022, 29, 247. https://doi.org/10.1007/s10965-022-03100-8.
4. F. P. Mantia, V. Titone, A. Milazzo, M. Cerualo, L. Botta, Nanomaterials 2021, 11, 3058. https://doi.org/10.3390/nano11113058.
5. O. E. Ezenkwa, A. Hassan, S. A. Samsudim, Polym. Compos. 2022, 43, 1852-1863. https://doi.org/10.1002/pc.26503.
6. J. Liu, H. Liang, Thermochim. Acta 2021, 699, 178916. https://doi.org/10.1016/j.tca.2021.178916.
7. N. D. Sansone, Z. Razzaz, M. Salari, A. V. Tuccitto, R. Aguiar, M. Leroux, P. C. Lee, ACS Appl. Mater. Interfaces 2022, 14, 40232−40246. https://doi.org/10.1021/acsami.2c11231.
8. Y. Xing, D. Sun, M. Zhang, G. Shu, Polymers 2023, 15, 2059. https://doi.org/10.3390/polym15092059.
9. J. Wang, F. Song, Y. Ding, M. Shao, Materials and Design 2020, 195, 109073. https://doi.org/10.1016/j.matdes.2020.109073.
10. N. Ning, W. Zhang, J. Yan, F. Xu, T. Wang, H. Su, C. Tang, Q. Fu*, Polymer 2013, 54, 303-309. http://dx.doi.org/10.1016/j.polymer.2012.11.045.
11. P. Song, Z. Cao, Y. Cai, L. Zhao, Z. Fang, S. Fu, Polymer 2011, 52, 4001-4010. https://doi.org/10.1016/j.polymer.2011.06.045.

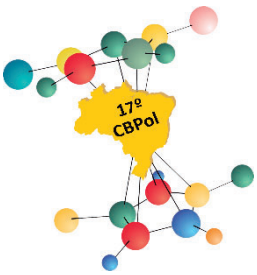

PHBV NANOCOMPOSITES WITH KAOLIN NANOPARTICLES MODIFIED WITH OREGANO ESSENTIAL OIL FOR APPLICATION IN FOOD PACKAGING

Pâmela R. Oliveira[1,2], Renata C. da Costa[2], Janaina S. Crespo[3], Tales S. Daitx[4], Marilia Miotto[5], Daiane M. Bobermin[5], Cristiano S. Teixeira[1], Ismael C. Bellettini[1], Larissa N. Carli[1]*

1 – Centro Tecnológico, de Ciências Exatas e Educação, CTE, Universidade Federal de Santa Catarina (UFSC), Blumenau, SC, Brasil
larissa.carli@ufsc.br
2 – Programa de Pós-Graduação em Ciência e Engenharia de Materiais, Universidade Federal de Santa Catarina (UFSC), Florianópolis, SC, Brasil.
3 – Área de Conhecimento em Ciência Exatas e Engenharias, Universidade de Caxias do Sul (USC), Caxias do Sul, RS, Brasil.
4 – Instituto de Química, Universidade Federal do Rio Grande do Sul (UFRGS), Porto Alegre, RS, Brasil.
5 – Departamento de Ciência e Tecnologia de Alimentos, Universidade Federal de Santa Catarina (UFSC), Florianópolis, SC, Brasil.

Abstract – This research aimed to modify kaolin nanoparticles with oregano essential oil (OEO) for application in poly(hydroxybutyrate-*co*-hydroxyvalerate) (PHBV) in the production of active packaging with antimicrobial properties. The halloysite (Hal) and kaolinite (Kaol) were modified with OEO by sonication process and characterized. The best result was obtained with Hal modified with OEO, with 45% OEO incorporation efficiency and low OEO evaporation rates at 25°C. The nanocomposite films were produced by melt processing. The nanocomposite produced with modified Hal with addition of OEO presented the lowest oxygen permeability and allowed a controlled OEO release, resulting in an antibacterial activity against the *E. coli* close to the satisfactory value required by JIS Z 2801:2000, being promising for application in active packaging.
Keywords: *Organic modification. Biodegradable polymers. Polymer nanocomposites. Antibacterial activity. Active packaging.*
Fundings: Conselho Nacional de Desenvolvimento Científico e Tecnológico (CNPq - Processes 435650/2018-1 and 313599/2018-1) and Coordenação de Aperfeiçoamento de Pessoal de Nível Superior/Fundação de Amparo à Pesquisa e Inovação do Estado de Santa Catarina (CAPES/FAPESC).

Introduction

Active food packaging contains active components that aim to maintain food quality and extend its shelf life. Among the active compounds, essential oil has stood out for being able to present molecules with antimicrobial and antioxidant properties[1-2]. However, its high volatilization makes its application in food packaging difficult.

Clay minerals can act as nanocarriers, trapping the active compounds in its lumen or basal spacing, thus avoiding their volatilization and providing a controlled release[1-3]. In addition, clay minerals present high surface area and can act as reinforcing fillers, improving the thermal and barrier properties of the polymeric matrix [2-4]. In this case, the formation of the PHBV nanocomposites might improve its properties and has been considered as an alternative to increase the competitiveness of PHBV regarding conventional materials [2,4]. In this study, Hal and Kaol were modified with OEO and compared according to their physicochemical characteristics. PHBV

nanocomposites were also prepared and evaluated by their thermal, oxygen barrier, and antimicrobial properties, aiming their application in active food packaging.

Experimental

Organic modification of clay mineral

Hal and Kaol were modified with OEO by an adapted sonication process [3]. The mixture (1:10 clay:OEO mass ratio) was sonicated (Elma S40H, Elmasonic) for 30 min in an ice bath. The resulting dispersion was vacuumed for 30 min at room temperature and then subjected to atmospheric pressure for 10 min. This procedure was repeated twice to increase loading efficiency. The modified clay mineral was centrifugated at 7000 rpm for 5 min and dried for 4 d at room temperature in a desiccator.

Characterization of the nanoparticles

The SEM analysis was carried out using a field emission scanning electron microscope (FEG/SEM Mira3 LMU) at 20 kV acceleration. Thermogravimetric analyses (TGA) were carried out using PerkinElmer TGA 8000 from 30 to 900 °C at a heating rate of 20 °C min^{-1} under argon atmosphere (20 mL min^{-1}). The incorporation efficiency (IE) was calculated as the percentual mass difference between the theoretical and volatilized oil up to 240 °C. For evaporation tests, 60 mg of each sample were weighed in Petri dishes in duplicate. The changes in mass were monitored for 11 d at 25 °C (a suitable temperature for fungal growth) and 32 h at 37 °C (a suitable temperature for bacterial growth).

Melt processing and films production

PHBV nanocomposite films were prepared by melt processing using a Roller-Rotors R600, Rheomix 6002C mixer [2]. The PHBV and raw Hal were previously dried at 80 °C for 6 h. The processing was performed at 170 °C or 165 °C for the compositions without and with oil, respectively, at 100 rpm for 6 min. The materials (Table 2) were milled in a knife mill (SL-32, Solab Equipamentos) and compression molded in an electrically heated hydraulic press (SL-11, Solab Equipamentos) at 1 ton and 190 °C for 2 min.

Table 1: Composition of the films.

Samples	PHBV (g)	Hal (g)	OEO (g)	Hal:OEO (g)
PHBV	50.0	-	-	-
PHBV/OEO	46.0	-	4.0	-
PHBV/Hal/OEO	44.5	1.5	4.0	-
PHBV/Hal:OEO	47.3	-	-	2.7[a]
PHBV/Hal:OEO/OEO	44.5	-	2.8[b]	2.7

[a] Equivalent amount of 1.5 g of clay mineral (3 wt%), considering 45% of incorporation of OEO.
[b] Added to a total of 4.0 g of OEO in the mixture (8 wt%).

Characterization of the nanocomposites

Thermal stability of the nanocomposites was evaluated by TGA as previously described. The oxygen permeability analyses were carried out at 23 °C with 100 cm^3 min^{-1} oxygen flow, according to ASTM D1434 in an L100-5000 Systech Illinois equipment. The release rate of OEO was analyzed using 3% (v/v) acetic acid as food simulant solution. The samples (150 mg) were immersed in 30 mL of simulant and stirred at 100 rpm and 25 °C for 72 h in a MK1210 – TR orbital shaker. The OEO release (%) was determined by UV-Vis spectrophotometry in a Shimadzu UV-Vis 1800 at 272 nm. The antibacterial activity of the films was evaluated according to the JIS Z 2801:2000 [5], against the Gram-negative bacteria *Escherichia coli* (*E. coli* ATCC 25922). The antibacterial activity was calculated according to Eq (1), where *R* is the value of antibacterial

activity (%), A is the mean of bacterial counts in the control sample after 24 h (inoculum) (CFU mL^{-1}), and B is the mean of bacterial counts of the test sample after 24 h (CFU mL^{-1}).

$$R(\%) = ((A - B)/A) \times 100 \qquad (1)$$

Results and Discussion

Characterization of the nanoparticles modified with OEO

Hal:OEO and Kaol:OEO showed a high incorporation efficiency (45% and 43%, respectively). The sonication process might increase the dispersion of particles through cavitation, which is auxiliary in the process of the deagglomeration of nanoparticles and consequently the increase of the specific area [6]. Furthermore, the application of vacuum might allow the diffusion of molecules from the more concentrated medium (OEO) to the less concentrated one (lumen of clay nanoparticles)[7].

The tubular structure of raw Hal (Fig 1 (a)) was maintained after modification and the diameter increased from 85 – 113 nm to 87 – 169 nm (Fig 1 (b)). This increase suggests the adsorption of OEO both on the external surface and in the lumen of the clay mineral promoted by the modification process used [7]. The raw Kaol (Fig 1 (c)) exhibited a laminar structure in a pseudo-hexagonal shape, with stacked plates interacting by strong secondary interactions [8]. For Kaol:OEO (Fig 1 (d)), the OEO did not cause significant changes on the surface of Kaol.

Figure 1: SEM images of (a) Hal, (b) Hal:OEO, (c) Kaol, and (d) Kaol:OEO.

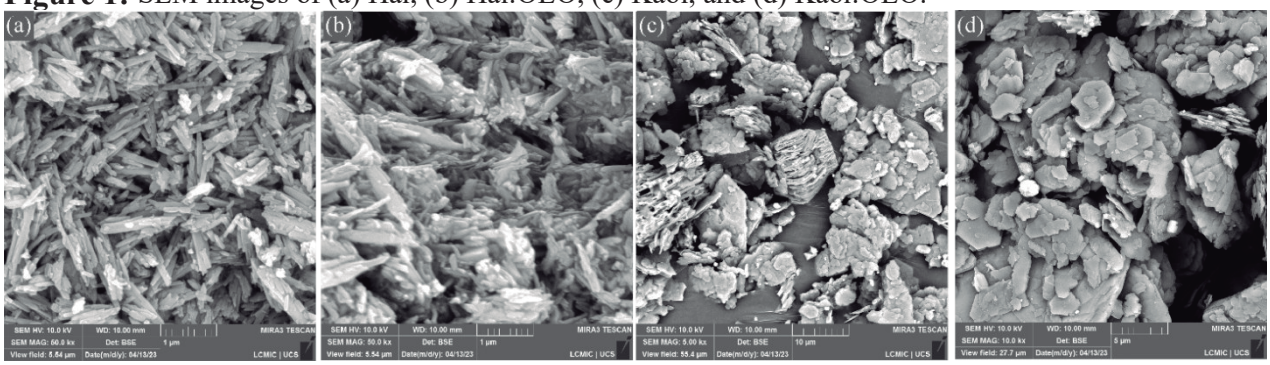

The evaporation of OEO in the free form at 25 °C and 37 °C (Fig 2) was approximately 50% higher than in the adsorbed form. The effects at 37 °C (Fig 2 (b)) were similar for both clays. However, the Hal:OEO showed better OEO retention at 25 ºC (Fig 2 (a)) probably due to the greater interaction of the oil with the surface of Hal and immobilized at the lumen of Hal. Therefore, Hal:OEO sample was selected to be incorporated into the PHBV matrix.

Characterization of the nanocomposites

All nanocomposites showed similar thermal properties (Fig 3(a)), with a first mass loss up to 240 °C referred to the volatilization of OEO and a second mass loss at 270 °C – 320 °C, associated with the degradation of PHBV.

The release of OEO from the films in a simulating medium was gradual (Fig 3 (b)), with a faster release exhibited by PHBV/OEO. The slower release was achieved by nanocomposites containing Hal modified with OEO (PHBV/Hal:OEO e PHBV/Hal:OEO/OEO), where the higher proportion of OEO might be immobilized in the surface and trapped within the lumen of the Hal. Furthermore, the organophilic characteristic of Hal might have improved clay mineral dispersion in the matrix, thus inhibiting the diffusion of OEO from the polymer to the medium. These results were corroborated by the Korsmeyer-Peppas kinetic model, with higher release rates (k) for PHBV/OEO and PHBV/Hal/OEO (5.98 and 5.34, respectively) compared to 4.24 and 4.02 for PHBV/Hal:OEO and PHBV/Hal:OEO/OEO, respectively. The diffusion exponent (n) was lower than 0.5, indicating that the OEO release occurred predominantly by Fickian diffusion, where the polymer chain relaxation time is longer than the OEO diffusion [9].

Figure 2:Evaporation profile of OEO incorporated in Hal and Kaol and in free form at (a) 25 °C for 11 d and (b) 37 °C for 32 h.

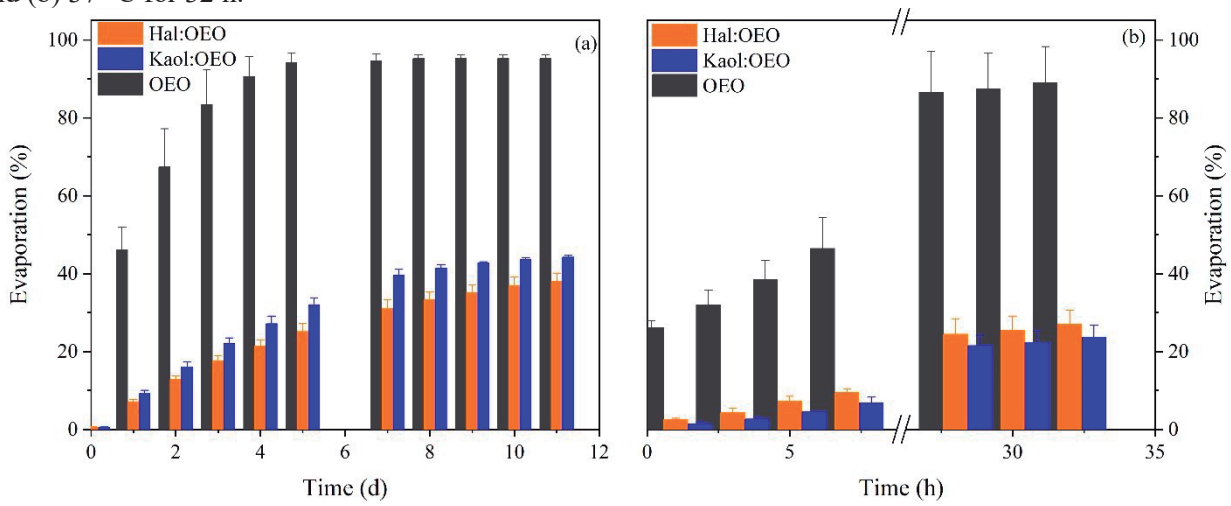

Figure 3: (a) TGA and DTG curve of the PHBV nanocomposite e (b) Release of OEO from PHBV compositions in 3% acetic acid (v/v) at 25°C (experimental data – dashed lines) and predicted concentration of OEO released by Korsmeyer-Peppas model (lines).

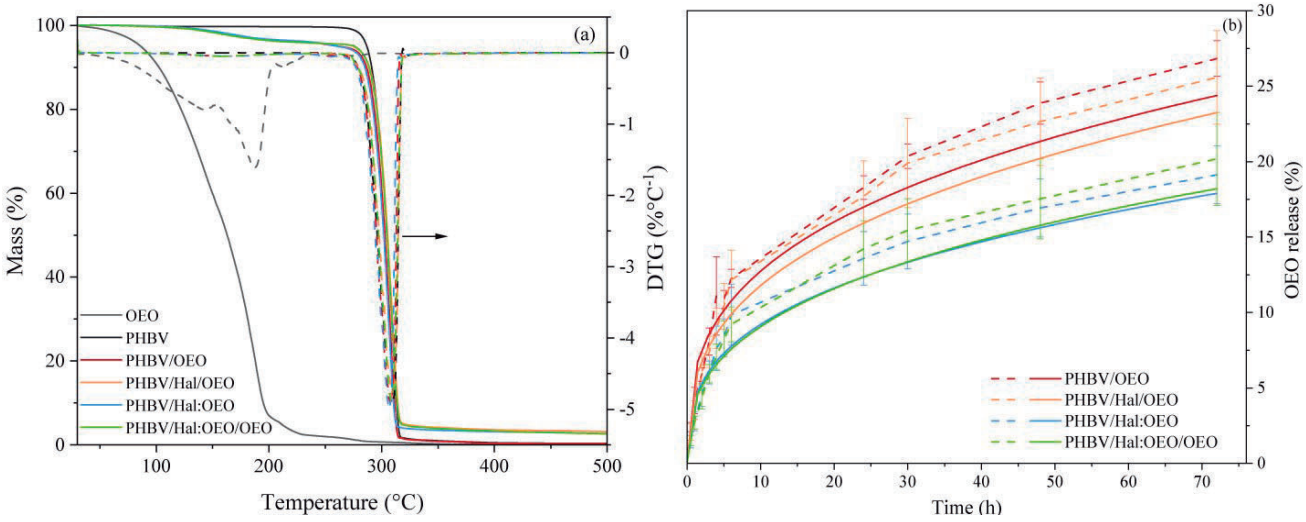

Oxygen is responsible for nutrient deterioration, oxidation, changes in color and flavor, and also contributes to microbial growth during food storage and handling [10]. Therefore, packaging production with an adequate oxygen barrier may help to improve the quality and extend the shelf life of the products. The improvement in the barrier property in PHBV compositions (Table 2) might be related to the distribution of polar OEO within the free volume of the polymer, thus hindering the diffusion of non-polar O_2 molecules. For PHBV nanocomposites, the tortuous path created by clay minerals contributes to the improvement in the barrier property of the material [2].
The antimicrobial activity against *E. coli* was also evaluated (Table 2). The PHBV/OEO showed a satisfactory reduction of 99.8%, and this inhibition was greater for PHBV/Hal/OEO. These results might be related to the diffusion of the oil to the medium with a slight delay caused by the crystallinity of PHBV and the presence of Hal. The PHBV/Hal:OEO composition did not show a significant reduction in bacterial count. Besides the reduced amount of OEO in this composition, all OEO content was entrapped in the clay mineral, which caused a delay in its diffusion to the medium.

Table 2: Oxygen permeability and antimicrobial activity, calculated by direct contact assay against *E. coli*, on PHBV films containing OEO.

Sample	O_2 permeability mL mm m^{-2} day^{-1}	Antibacterial activity (*E. coli*)		
		After inoculation (CFU mL^{-1})	After de 24 h (CFU mL^{-1})	R (%)
Reference*	860.6 ± 0.0	1.6×10^4	5.5×10^7	-
PHBV/OEO	111.1 ± 4.8	-	1.3×10^5	99,8
PHBV/Hal/OEO	349.2 ± 27.5	-	9.0×10^{-1}	100,0
PHBV/Hal:OEO	232.4 ± 15.2	-	9.0×10^6	83,6
PHBV/Hal:OEO/OEO	127.6 ± 4.6	-	8.3×10^5	98,5

*Control film of PHBV without antimicrobial agent.

Conclusions

The best OEO incorporation result was obtained by Hal:OEO (45%), with the OEO adsorbed on the outer surface of the material. In addition, the Hal:OEO showed higher retention of the incorporated oil. When incorporated into the PHBV matrix, Hal:OEO contributed to a higher oxygen barrier property. The clay modification with OEO provided a greater organophilic characteristic that resulted in a better interaction with the polymer and, consequently, an improved dispersion. The composition in which the modified Hal was used with the addition of free OEO during processing (PHBV/Hal:OEO/OEO) was the most promising one, exhibiting a slow and gradual release of the oil in a food simulant medium. Furthermore, this composition showed a bacterial inhibition close to a value considered satisfactory. Therefore, an adjustment in the free oil content would allow a faster and greater release in the period of the first 24 h. As it contains OEO immobilized in its structure, this effect could be prolonged, thus increasing the shelf life of the product.

Acknowledgements

The authors are grateful to CNPq and CAPES/ FAPESC for financial support, and Laboratório Central de Microscopia Prof. Israel Baumvol (LCMIC) from UCS.

References

1. A. A. Oun, A. Y. Bae, G. H. Shin, M. Park, and J. T. Kim. *Appl Clay Sci* 2022, 224, 106522. https://doi.org/10.1016/j.clay.2022.106522.
2. R. C. da Costa *et al. Food Packag Shelf Life* 2020, 26, 100602. https://doi.org/10.1016/j.fpsl.2020.100602.
3. S. Hendessi, E. B. Sevinis, S. Unal, F. C. Cebeci, Y. Z. Menceloglu, and H. Unal, *Prog Org Coat* 2016, 101, 253–261. https://doi.org/10.1016/j.porgcoat.2016.09.005.
4. S. D. F. Brandolt, T. S. Daitx, R. S. Mauler, H. L. Ornaghi Junior, J. S. Crespo, and L. N. Carli. *Polym Compos* 2019, 40, 3835–3843. https://doi.org/10.1002/pc.25242.
5. JIS Z 2801:2000. Antimicrobial products – Test for antimicrobial activity and efficacy.
6. A. Kaboorani, B. Riedl, and P. Blanchet. *J Nanomater* 2013, 2013, 1–9. https://doi.org/10.1155/2013/341897.
7. E. Abdullayev and Y. Lvov. *J Nanosci Nanotechnol* 2011, 11, 10007–10026. https://doi.org/10.1166/jnn.2011.5724.
8. G. K. Dedzo and C. Detellier. *Appl Clay Sci* 2016, 130, 33–39. https://doi.org/10.1016/j.clay.2016.01.010.
9. J. Siepmann and N. A. Peppas. *Adv Drug Deliv Rev* 2012, 64, 163–174. https://doi.org/10.1016/j.addr.2012.09.028.
10. R. Sothornvit and N. Pitak. *Food Research International* 2007, 40, 365–370. https://doi.org/10.1016/j.foodres.2006.10.010.

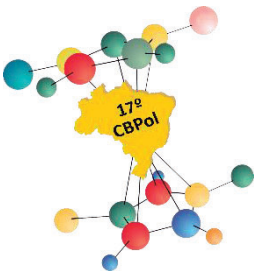

PRODUCTION OF HETEROGENEOUS ACID CATALYST BASED ON GRAPHITE-CELLULOSE NANOFIBER AAIRGEL COMPOSITES

Érica Rost [1] *, Gabriela Ciribelli Santos Pompêu [1], Daniel Pasquini [1]

1 – Institute of Chemistry , Federal University of Uberlândia (UFU), Uberlândia , MG, Brazil
erica.rost@ufu.br

Summary - This study had as a goal to produce a catalyst composite polymeric heterogeneous in the form of an airgel of cellulose nanofibers coated with graphite sulfonated. the graffiti he was rusty by TIME and sulphonate per three sulfonation methodologies, using _ respectively i) 4-benzenediazonium sulfonate ii) acid sulfuric acid, and iii) sodium dodecylbenzenesulfonate. To the suspension of cellulose nanofibers, he added graphite sulfonated, a proportion of 50% in the dough, and the mixture was submitted to the lyophilization process, resulting in the catalyst in the form of an airgel. The efficiency of the graphite sulfonation step _ was evaluated through analysis of FTIR, RAMAN, exchange capacity ionic and zeta potential. You aerogels were characterized by SEM, TGA, and viscosimetric molar mass. It was possible to obtain grade materials _ a satisfactory form of sulfonation, which, when incorporated into the nanofibers, resulted in aerogels with characteristics suitable for applications in Law Suit catalytic.
Keywords: *Cellulose nanofiber, graphite _ sulfonate, airgel, composite, catalyst heterogeneous.*

Introduction

The cellulose nanofibers _ they are bottom materials _ cost, easy to functionalize, have high availability, biocompatibility, renewability, biodegradability, high rigidity, good resistance mechanical, thermal, and tensile, and low density. In the form of airgel – a solid and highly porous – nanocellulose has the characteristics of discharge expected _ surface area, good flexibility, high porosity, low conductivity thermal and liquid sorption _ in big quantities [1]. In that sense, one hypothesis raised is that if we deposit other components at the surface of these fibers in the form of airgel, we hope to obtain a material with properties like the nanocellulose airgel, mainly regarding sorption and high _ porosity, mainly at the case of catalysts heterogeneous, because they are characteristics that can speed up the reactions involved. In addition, Furthermore, this material can to present characteristics of nanofibers that result in good resistance thermal, mechanical, and tensile necessary to withstand the temperatures and pressures involved in some processes, like biodiesel production reactions by _ catalysis acidic heterogeneous, by example. The main advantage of heterogeneous catalysts is to facilitate the separation and the possibility of reuse, and specifically in the production of biodiesel, it has the advantage of recovering glycerin free of ions. Disadvantages include the frequent need to activate active sites, which can sometimes be leached or covered by organic deposition, and the need for high temperatures and oil/alcohol ratios [2]. Compared with homogeneous acid catalysts, heterogeneous acid catalysts have mild reaction conditions and lower corrosivity and toxicity. The limitations involved are high-temperature requirements, longer reaction times and higher catalyst loading. In esterification and transesterification processes, the large pore structure combined with the high or moderate density of active sites helps the catalyst to resist mass transfer from the carbon chains of triglycerides and is also important to achieve high reaction rates [3]. The mechanism of action of Brönsted -Lowry solid acid catalysts – a species capable of donating

a proton – is the protonation of the carbonyl of fatty reagents, formation of carbocations, and increased susceptibility to the nucleophilic attack of alcohol. In this sense, it is known that these properties are found in the sulfonic groups of sulfonated materials, which in many cases are produced in the form of sulfonated activated carbons but can also be produced by the sulfonation routes of graphite. Thus, this work presents results of the production and characterization of a heterogeneous acid catalyst, combining the properties of cellulose nanofibers with those of sulfonated graphite, to obtain a material with acidic sites and high surface area, which has potential for applications in catalyzed heterogeneous reactions by acids, and which, therefore, have potential for application in esterification and transesterification reactions for biodiesel production. Its main expected advantages are biocompatibility and the greater contact surface, due to the use of airgel as support, high activity, stability, and the possibility of reusing the product.

Experimental

TIME-mediated oxidation of graphite

The oxidation of graphite (from the company Nacional graphite) was mediated by the free radical 2,2,6,6-Tetramethylpiperidine 1-oxila (TEMPO). TEMPO and sodium bromide (NaBr) were added to 100 mL of water containing 1g of graphite in the ratio Graphite:NaBr: TEMPO = 1.0:0.5:0.1 (w/w/w). An aqueous solution of sodium hypochlorite (NaClO) (NaClO Graphite = 1:1, w/w) was added to start graphite oxidation and the obtained mixture was stirred for 4 h at room temperature. The pH of the system was maintained between 10 and 11 by careful addition of 2M NaOH solution. Oxidation was stopped by the addition of 0.5 mL of ethanol, which resulted in the total consumption of NaClO. At the end of the reaction, the oxidized graphite (GO) was initially separated by centrifugation. Finally, the material was subjected to dialysis against water for 3 days and subsequent sonication for 5 min. The suspensions obtained were adjusted to 1.5% solids [4]. In the subsequent sulfonation steps, the processes were carried out with samples of pure graphite (GP) and oxidized graphite (GO).

Sulfonation of graphite samples with sulfanilic acid

In this procedure, 15g of sulphanilic acid was dispersed in 300 mL of 1M HCl. The temperature of the solution was maintained at 5°C with continuous stirring. Subsequently, 90 mL of 1M $NaNO_2$ was added dropwise. After adding all the $NaNO_2$, a clear solution was obtained and the mixture was stirred for another 1 h, maintaining the temperature. Then, the mixture was allowed to stand and the white precipitate of 4-benzenediazonium sulfonate (4-BDS) formed was filtered and washed to remove impurities. The precipitate was mixed with 200 ml of aqueous solution containing the graphite samples (1.5% concentration, i.e. 3 g of GP or GO) and 60 ml of ethanol, and the temperature was maintained between 3 and 5 °C. Then 100 mL of 30 wt% H_3PO_2 was added and stirred for 30 min. Then, another 50 mL of H_3PO_2 was added and left to stir for another 1 h. The resulting sulfonated graphite samples were filtered, washed, and dried in an oven for 12 h [5]. The resulting samples in this step were named GP - sulphanilic acid and GO - sulphanilic acid.

Sulfonation of graphite samples with sulfuric acid

Sulfonation was performed by direct reaction with concentrated sulfuric acid (98%) at a solid /liquid ratio of 1:10 (w/w), a temperature of 160ºC (in an oil bath), and a reaction time of 2 h. After the end of the reaction time, the graphite samples were centrifuged to reduce the acidity to pH 6.0, to ensure that all remaining sulfuric acid was removed and that the acidity of the material resulted from the incorporation of sulfonic groups. Subsequently, the samples were dried in an oven at 105 °C for 12 hours [6]. The resulting samples in this step were named GP - sulfuric acid and GO - sulfuric acid.

Sulfonation of graphite samples with sodium dodecylbenzenesulfonate (SDBS)

The graphite sample (2 g) was dispersed in a 500 mL beaker containing 100 mL of water. To this solution was added 100 mL of 0.1 M SDBS solution and the mixture was stirred for 3 days at room temperature. Then, the samples were filtered and washed several times with water until reaching pH 6. Finally, they were left to dry in an oven at 60 °C [7]. The resulting samples in this step were named GP – SDBS and GO – SDBS.

Characterization of graphite samples

The occurrence of oxidation and sulfonation processes was evaluated by Fourier Transform Spectroscopy (FTIR) (Shimadzu, IR PRESTIGE-21), in the infrared region, between 4000 and 500 cm^{-1}, Raman Spectroscopy (LabRAM HR Evolution, HORIBA) with 532 nm excitation laser, reading of 3 accumulations of the spectrum in the region from 1000 to 3500 cm^{-1}, Ion Exchange Capacity (ITC) and Zeta Potential (Litesizer, 500), at a temperature of 25 ± 1 °C and dissolution of 0.01 g/ mL of the sample in aqueous medium.

Preparation of graphite-cellulose nanofiber airgel composites

nanofiber (CNF) suspensions (supplied by SUZANO) were used as received, which had a concentration of 3.0% by weight. The aerogels were prepared with the addition of 50% by weight of graphite samples in relation to the dry weight of CNF. In 20 g of CNF suspension, 0.3 g of graphite samples were added, under mechanical agitation, until complete homogeneous dispersion of the graphite samples in the mixture. Finally, the mixtures were subjected to the lyophilization process to obtain aerogels [8].

Characterization of aerogels

airgel samples were characterized for morphology by Scanning Electron Microscopy (SEM) (Tescan, VEGA 3 LMU), for thermal stability by Thermogravimetric Analysis (TGA) (Shimadzu, DTG-60H) at a heating rate of 10 ° C/min and 50 mL/min airflow from 25 ° to 700 °C. Additionally, the integrity of the cellulose structure was evaluated by determining its viscosimetric molar mass obtained through flow measurements in an Ostwald.

Results and discussion

Characterization of graphite samples

Through the FTIR spectra (not shown here), the occurrence of oxidation of the samples was verified, evidenced by the appearance of polar groups such as hydroxyl with a band around 3450 cm^{-1}, carboxyl with a peak around 1650 cm^{-1} and CO with a peak around 1100 cm^{-1}. The insertion of sulfonic groups in all samples was verified by the appearance of peaks in the region from 1280 to 1080 cm^{-1} referring to the asymmetric elongation of the SO^{3-} groups, by the peak at 1080 cm^{-1} referring to the symmetrical elongation of the SO^{3-} groups and, also, by the increase in the intensity of the band at 3400 cm^{-1} referring to the hydroxyls present in the SO_3H group. Specifically in the samples with SDBS insertion, an increase in peaks was observed in the region from 3000 to 2800 cm^{-1}, referring to the stretching of the CH groups that make up the SDBS molecule. Thus, it can be successfully affirmed that there was oxidation and later sulfonation of the graphite, with a gain of sulfonic groups.

From the results presented in Table 1, it is possible to verify the modification performed in the graphite samples with the insertion of oxidized and sulfonic groups and corroborate the insertion of chemical modifications on the GP surface observed in the FTIR analysis. The results of the Zeta Potential analysis showed the changes in the electric charge environment. An increase in the negative charge of the samples was observed, mainly, for functionalization using SDBS, demonstrating that this composite was the most stable in suspension, being less prone to flocculation or sediment. By the CTI analysis, it was noticed that the greatest increase in the total acidity content was observed in the sulfonation process with sulphanilic acid, which increased the SO_3H content by 0.38 mmol/g for GO – sulphanilic acid and 0, 21 mmol/g for GP – sulfanilic acid, such increase is due to the incorporation

of sulfonic groups to the initial sample. The Raman spectra (not shown here) showed a less intense signal in the D band and more intense in the G band for all tested samples; this is due to the high degree of crystallinity of the rhombohedral structure of powdered graphite used as raw material in this study. Due to the intensity of the D and G peaks, a peak ID/IG ratio value of 0.1546 was obtained for the GP sample. This value decreased by 0.1388 in the GO sample, and this reduction is a consequence of the decrease in the G band and the increase in the intensities of the D band, which indicate an increase in the disorder of the graphite structure due to oxidation. In some sulphonated samples, the reduction in ID/IG was more pronounced in the GP samples than in the GO samples. For the values of the degree of disorganization of the sulfonated GO samples, it was noted that after going through the functionalization, they had a small increase in the qualitative degree of disorder of the structure, thus indicating the existence of the sulfonation process, without, however, resulting in the loss of symmetry of the carbonic chain, considerably [9].

Table 1 - Zeta Potential data, Raman D/G peak intensities ratio, total acidity, and group content sulfonic obtained by the CTI tests, for the GP, GO and their respective samples sulfonated.

Sample	Zeta Potential (mV)	D/G	Total acidity	SO3H (mmol /g)
GP	-27.2532 ± 0.39	0.1546	0.02	-
GO	-27.7875 ± 0.63	0.1388	0.04	-
GP - sulphanilic acid	-28.8264 ± 0.98	0.1331	0.23	0.21
GO - sulphanilic acid	-20.4396 ± 0.37	0.1546	0.42	0.38
GP - sulfuric acid	-31.6529 ± 0.23	0.0561	0.05	0.03
GO - sulfuric acid	-25.6278 ± 1.54	0.1171	0.11	0.07
GP – SDBS	-54.7977 ± 0.84	0.0852	0.05	0.03
GO - SDBS	-58.6732 ± 0.31	0.1116	0.08	0.04

Characterization of aerogels

From the thermograms _ obtained by TGA (not shown here), it is observed that pure CNF has two stages of degradation, the first with a T_{onset} of 286 °C for the decomposition of polysaccharides and a second with a T_{onset} of 396 °C for the decomposition of structures carbonic resulting from the decomposition of the first phase. For the modified CNF samples, it is observed that with the incorporation of groups sulfonics, such as analogs sulfonated with acid sulphanilic acid _ sulfuric acid and SDBS, there was one small alteration in the decomposition temperatures of the first stage, attributed to the presence of groups sulfonics that reduce The CNF stability, however, for the second stage, there was an increase in the degradation temperatures starting from T, attributed to the presence of graphite. the biggest stability increase _ reached 428 °C for the GO sample - acid sulphanilic.

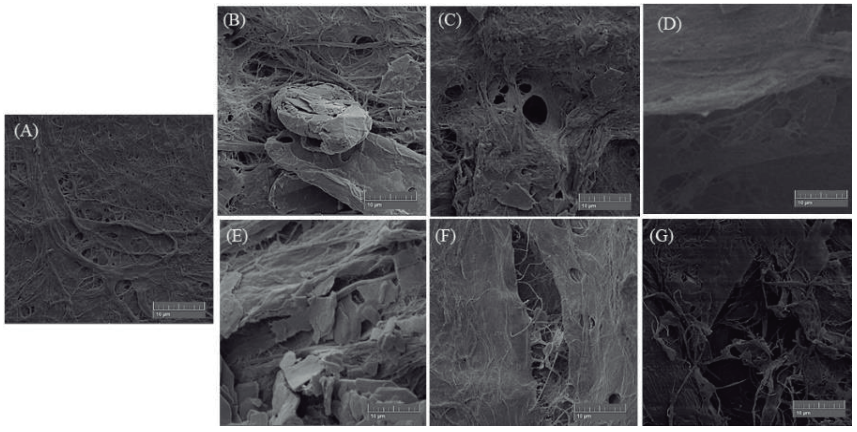

Figure 1 – SEM images of airgel samples: (A) CNF, (B) CNF with GP - sulphanilic acid, (C) CNF with GP - sulfuric acid, (D) CNF with GP - SDBS, (E) CNF with GO - acid sulphanilic, (F)CNF with GO - acid sulfuric and (G)CNF with GO – SDBS. Magnification 5000X.

He is the nanofiber network is evidently typical of CNF and which results in one structure porous. Adding samples _ GP and GO sulphonates apparently, no affects the fibers, however, it is possible to observe that the particles are distributed among the fibers. This distribution was Apparently uniform per all the structures of aerogels, and they seem to have generated more airgel structures open and with pores larger, which can result in bigger permeation of reagents in application cases _ of these materials as catalysts.
The integrity of cellulose nanofibers _ was evaluated per viscosimetry measures, evaluating the viscosimetric molar mass of the cellulose that composes your aerogels. The viscosimetric molar mass (Mv) of CNF was 79,580 g.mol $^{-1}$ with a degree of polymerization (DP) of 941. Samples containing graphite sulfonated presented a reduction us DP and Mv values. The reduction value corresponds to a smaller nanofiber mass _ at a mixture composed of _ around 66.6%, which leads to a decrease in cellulose molecules _ at the solution and consequently _ _ smaller viscosity. So, we can conclude that the presence of groups of sulfonics not significantly affected the structure of cellulose nanofibers. _

Conclusions
It was possible to functionalize the graphite by oxidation and sulfonation with different routes. It was verified that the degree of sulfonation depended on the modifier used, obtaining the highest degree of sulfonation for the samples with sulphanilic acid. Also, it was possible to produce composite aerogels from the mixture of samples of CNF and sulfonated graphite, obtaining a structure with preservation of the structure of cellulose and CNF, with thermal stability for application as catalysts in reactions catalyzed by acids, as is the case of reactions of esterification and transesterification for biodiesel production, highlighting the high temperature of functionalized graphitic stability of sulphanilic acid, which reached 428 °C.

Thanks
You authors thank FAPEMIG, CAPES, CNPQ, and FINEP for the support financial.

References
1. M. Zanini. *Hydrophobic aerogels of cellulose nanofibers.* Dissertation, University of Process Engineering, 2016.
2. IMR Fattah; HC Ong; TMI Mahlia ; M. Mofijur ; AS Silitonga ; SMA Rahman; A. Ahmad. Frontiers in Energy Research, 8. https://doi.org/ 10.3389/fenrg.2020.00101.
3. DW Lee; KY Lee. Asia Catalysis Research, 18. https://doi.org/ 10.1007/s10563-014-9166-y.
4. J. Araki ; Y. Hida . Celulose, 2018, 25. https://doi.org/10.1007/s10570-017-1640-z.
5. Lean; CY Yes; YL Pang ; KH Wong. sains Malaysiana, 2020, 390. https://doi.org/10.1016/j.jhazmat.2019.121532 .
6. AC Fraga. *Valorization of residual raw materials: generation of adsorbents and catalysts.* 2013.119p. Dissertation, Federal University of Rio de Janeiro, 2013.
7. S. Zhou; D. Wei; H.Shi; X. Feng; K.Xue; F. Zhang; W. Song. Talanta, 2013, 107. https://doi.org/10.1016/j.talanta.2013.01.041.
8. P. Zhu; Y. Kuang ; Y. Wei; F.Li ; H. Or; F. Jiang; G Chen. Chemical Engineering Journal 2021, 404, 127105. https://doi.org/10.1016/j.cej.2020.127105.
9. AEF Oliveira; AC Pereira; GB Bettio ; CRT Tarley . Virtual Magazine of Chemistry Síntese, 2019, 11, 3. https://doi.org/10.21577/1984-6835.20190060.

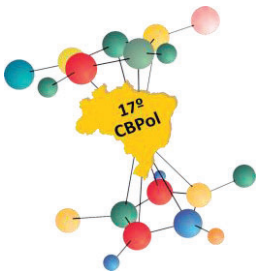

SURFACE BIOMODIFICATION OF COTTON FABRIC WITH CHITOSAN NANOPARTICLES CONTAINING ESSENTIAL OILS

Fernanda C. da Rosa*[1], Pedro G. V. Silva[1], Amanda C. R. G. Melo[1], Patrícia B. Brondani[2], Larissa N. Carli[1]

1 – Coordenadoria Especial de Engenharia de Materiais,Universidade Federal de Santa Catarina (UFSC), Blumenau, SC, Brazil rosa.fernandacris@gmail.com
2 – Departamento de Ciências Exatas e Eucação, Universidade Federal de Santa Catarina (UFSC), Blumenau, SC, Brazil

Abstract – Cotton is one of the most used fibers in the textile sector and, as a natural fiber, it is susceptible to the proliferation of microorganisms. The encapsulation of essential oils as antimicrobial agents in natural polymers such as chitosan and its incorporation into a cotton matrix is a promising approach for obtaining a functional fabric. With the aim of promoting the superficial oxidation of cellulose and improving its interaction with nucleophilic groups of chitosan, a system using laccase and TEMPO was employed. FTIR and TEM analyses confirmed the successful encapsulation of the essential oil into spherical and nanosized chitosan particles. FTIR characterization confirmed the oxidation of cellulose to some extent. The functionalization of the oxidized fabric exhibited better results with nanoparticle concentrations of 25% and 35%. The FEG-SEM analysis showed that the impregnation of the nanoparticles in the fabric fibers was successful.
Keywords: Laccase, TEMPO, Biooxidation, Antimicrobial property, Functional cotton fabric

Introduction

Natural fibers, such as cotton, have high applicability in the textile industry due to their many advantages such as low cost, biodegradability, versatility, and breathability [1, 2]. However, the porosity and hydrophilicity of these fibers create an environment suitable for the proliferation of microorganisms [3, 4]. Thus, with the aim of increasing the competitiveness of cotton in the market, several chemical treatments have been used to improve pre-existing properties, as well as to assign new functionalities to these products [3, 5].

Chitosan is one of the polymers satisfactorily used in the functionalization of cotton due to the presence of reactive amino and hydroxyl groups. [6-8]. Some active agents can be as well applied in the surface modification to confer interesting properties, such as essential oils – natural substances obtained from aromatic plants which have several biological properties [9]. The most effective treatment methods use chitosan to encapsulate the essential oil, thus controlling its volatilization and release and extending its bioavailability [9, 10].

Among the methods that can be used to modify cotton with chitosan nanoparticles, the formation of covalent bonds gives the material more stability [6, 11]. One of the most common routes is the surface oxidation of the CH_2OH groups of cellulose to carboxylic acids or aldehydes [12, 13]. However, oxidation methodologies can be quite drastic, and a good strategy to overcome this problem is the use of enzymes, such as laccases, known to oxidize cellulose-based materials [12]. Thus, the aim of this work is to biooxidize cellulose of cotton fabric by using different laccases and post-treatments to obtain a more efficient process and incorporate the synthesized chitosan nanocapsules containing eucalyptus essential oil. Finally, it is intended to study the properties of the materials obtained after the optimization of all processes.

Experimental

Synthesis of nanoparticles

Chitosan nanoparticles containing eucalyptus essential oil (EEO-NPs) were prepared through a two-step process: oil-in-water emulsification followed by ionic gelation, which was adapted from Hosseini *et al.* (2013) [14]. For oil-in-water emulsification, the aqueous phase was prepared with a chitosan solution (1% w/v) in acetic acid (1% v/v) and Tween 80 as surfactant; the oil phase was prepared by dissolving the essential oil in ethanol. The latter was slowly added to the aqueous phase during homogenization at 13,000 rpm in the Ultra-Turrax® IKA disperser to form an oil-in-water emulsion. A sodium tripolyphosphate (TPP) solution (0,4% w/v) was added dropwise to the emulsion in the ionic gelation step for the formation of NPs. The obtained EEO-NPs were collected by centrifugation, washed with deionized water, and freeze-dried.

Cotton biooxidation

The Biooxidation process was carried out by the reaction between the laccase enzyme and mediator, followed by a post-treatment with NaOH to potentiate the oxidation. To study the best condition of the process, four different laccases – immobilized or not – and two mediators were tested: TEMPO (2,2',6,6'-tetramethylpiperidine-N-oxyl) and ABTS (2,2-azinobis (3-ethylbenzothiazoline-6-sulfonic acid).

Cotton functionalization

Previously oxidized fabrics were impregnated with chitosan nanocapsules (EEO-NPs) through a methodology adapted from Liu *et al.* (2001) [15] and Specos *et al.* (2010) [16]. This methodology consists of immersing the samples in 25 mL of a dispersion containing the EEO-NPs at concentrations (w/v) 5%, 15%, 25%, and 35%, with constant stirring for 2 h. Then, the fabric was immersed in 25 mL of deionized water with agitation for 24 h. The samples were dried to obtain the modified cotton fabric.

Characterizations

The EEO-NPs were characterized by Fourier transform infrared spectroscopy (FTIR) and transmission electron microscopy (TEM) to evaluate the chemical structure and morphology, and by encapsulation efficiency [14]. The functionalized fabric was characterized by FTIR and scanning electron microscopy (FEG-SEM) analyses. In addition, dyeing tests were carried out with acid orange 7 dye to determine the concentration of nanocapsules that led to the most effective impregnation.

Results and Discussion

Synthesis of nanoparticles

Fig. 1(a) presents a comparison between the FTIR spectra of eucalyptus essential oil (EEO), pure chitosan (CHI), and EEO-NPs. The EEO spectrum presented two characteristic bands: between 1440 and 1460 cm^{-1}, associated with the stretching vibration of the C=C bond of the olefinic groups, and at 3484 cm^{-1}, corresponding to the stretching of the O-H components of EEO. The latter is most likely overlaid by the asymmetric chitosan band between 3500 and 2600 cm^{-1}. Furthermore, a band at 2900 cm^{-1} can be seen when comparing CHI and EEO-NPs spectra, with an overlap of N-H and O-H bands. This could be the result of the intense band related to the stretching of the methylene group of eucalyptus essential oil [17, 18]. Through Fig. 1 (b, c) it can be observed that the EEO-NPs obtained have a spherical shape and follow the expected structure for a nanocapsule: the outer layers of the wall formed by chitosan, and the inner layer containing the essential oil. In addition, the obtained particles showed a nanometric size, smaller than 20 nm.

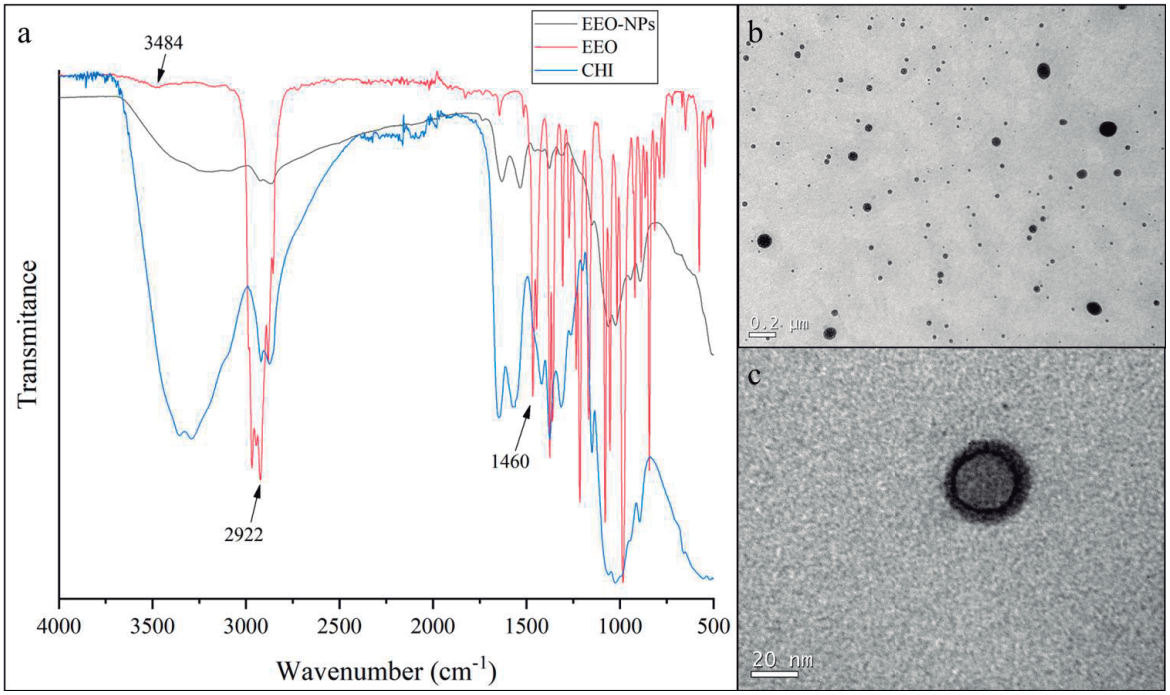

Figure 1. Characterization of chitosan nanoparticles containing eucalyptus essential oils: (a) Comparative FTIR spectra: eucalyptus essential oil (EEO), pure chitosan (CHI) and chitosan nanoparticles containing the essential oil (EEO-NPs); (b) and (c) TEM image of EEO-NPs

Encapsulation efficiency

The nanoparticles were synthesized with chitosan:essential oil ratio of 1:0.4 (w/w). At this concentration, the encapsulation efficiency was 61.18%, a much higher percentage compared to the literature, whose efficiency was 8.53 ± 0.94 at the same concentration [14].

Cotton biooxidation

The best result in terms of the percentage of oxidation was obtained using laccase from *Pleurotus ostreatus* and TEMPO as mediator. FTIR analysis indicated some changes in the spectrum that confirmed the successful oxidation (Fig. 2), as the appearance of two bands at 1725 cm^{-1} e 1550 cm^{-1} attributed to the carbonyl group that indicates the oxidation of the hydroxyl groups of the cellulose to carboxylic acid groups [12, 13].

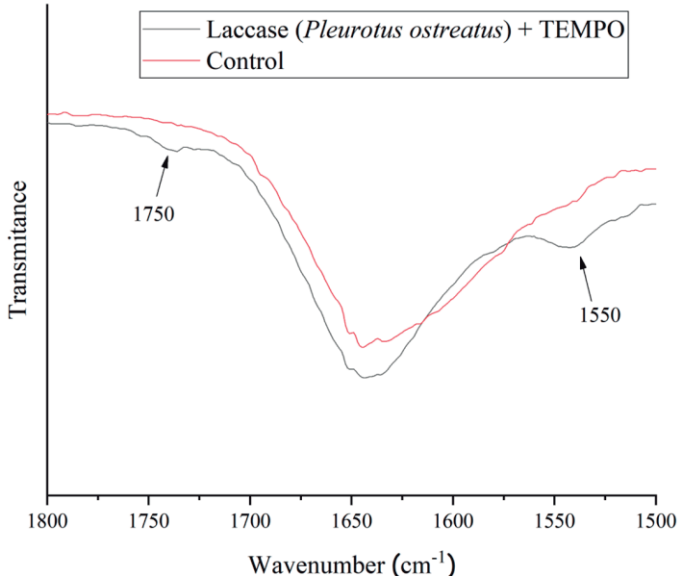

Figure 2. Comparative FTIR spectra between the control and the oxidized sample.

Cotton functionalization

In order to perform the quantification of the impregnation of the nanoparticles into cotton fabric, an acid dye test (Fig. 3(a, b, c, d, e)). The dyeing test aimed to identify the presence of chitosan in the material by the interaction of the dye with the amine group (NH_2) of chitosan. Therefore, the more intense the fabric color, the more chitosan nanoparticles are present and, consequently, the more efficient the impregnation process was. It can be observed in Fig. 3 that the samples impregnated with the 25% and 35% solutions presented the strongest staining. The scanning electron microscopy (FEG-SEM) analysis (Fig. 3(f)) was also performed. FEG-SEM images of the fabric impregnated with nanoparticles (15%) indicate that the impregnation process was successful, being possible to notice the presence of nanoparticles in the cotton fibers surface.

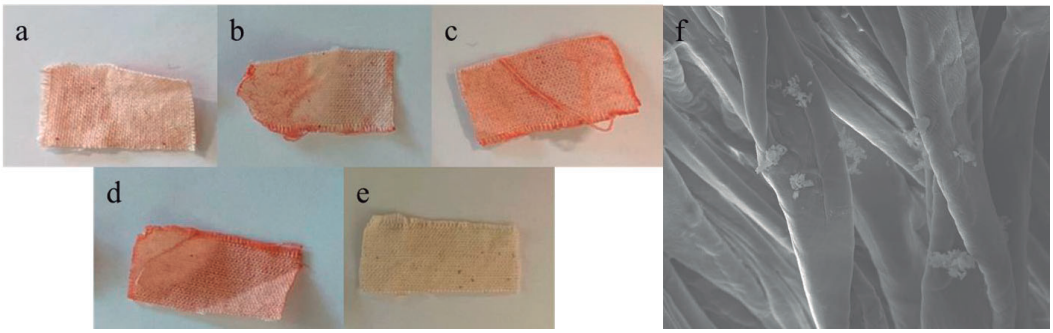

Figure 3. Dyeing test results with different concentrations of nanoparticles: (a) 5%, (b) 15%, (c) 25%, (d) 35% and (e) control; and (e) FEG-SEM image in which it is possible to observe small clusters of nanoparticles in the cotton fibers surface.

Conclusions

Chitosan nanoparticles containing essential oil were successfully synthesized, obtaining as a spherical shaped particles with nanometric size, and excellent encapsulation efficiency. Among the variations of the biooxidation methodology employed, the optimized condition was obtained with the laccase from *Pleurotus ostreatus* using TEMPO as a mediator. The functionalization of oxidized cotton with nanoparticles containing essential oil showed the highest incorporation tax applying the nanoparticles dispersions at concentrations of 25% and 35% and, as can be seen in the image obtained by the SEM-FEG analysis, the impregnation of the nanoparticles in the cotton fabrics was successful.

References

1. Rahman Bhuiyan, M. A. *et al*. Journal of Polymers and the Environment 2017 v. 25, n. 2, p. 334–342. https://doi.org/10.1007/s10924-016-0815-2.
2. Albinante, S. R.; Pacheco, E. B. A. V.; Visconte, L. L. Y. Quimica Nova 2013, v. 36, n. 1. https://doi.org/10.1590/S0100-40422013000100021.
3. Javid, A. *et al*. Journal of Microencapsulation 2014, v. 31, n. 5, p. 461–468. https://doi.org/10.3109/02652048.2013.879927
4. Yilmaz, F. Journal of the Textile Institute 2021, v. 112, n. 2, p. 341–345. https://doi.org/10.1080/00405000.2020.1753394
5. Vigneshwaran, N.; Arputharaj, A. in *Advances in functional finishing of textiles*, Shahid, M.; Adivarekar, R. Springer Nature Singapore Pte Ltd, 2017, cap. 2, p. 43–56.
6. Cheng, X. *et al*. Surface Science 2014, v. 309, p. 138–143. https://doi.org/10.1016/j.apsusc.2014.04.206
7. Arias, M. J. L. *et al*. Journal of Biomedical Science and Engineering 2021, v. 14, n. 03. doi:10.4236/jbise.2021.143012

8. Saleh, S. N. *et al*. International Journal of Biological Macromolecules 2021, v. 183, p. 23–34. https://doi.org/10.1016/j.ijbiomac.2021.04.059
9. Asbahani, A. E. *et al*. International Journal of Pharmaceutics 2015, v. 483, n. 1–2, p. 220–243. https://doi.org/10.1016/j.ijpharm.2014.12.069
10. Ghayempour, S.; Montazer, M. Journal of Microencapsulation 2016, v. 33, n. 6, p. 497–510. https://doi.org/10.1080/02652048.2016.1216187
11. Eid, B.M.; Ibrahim, N.A. Journal of Cleaner Production 2021, Volume 284, 15 February 2021, 124701. https://doi.org/10.1016/j.jclepro.2020.124701
12. Jaušovec, D.; Vogrinčič, R.; Kokol, V. Carbohydrate Polymers 2015, v. 116, p. 74–85. https://doi.org/10.1016/j.carbpol.2014.03.014
13. Yu, Y. *et al*. Carbohydrate Polymers 2016, v. 137, p. 549–555. https://doi.org/10.1016/j.carbpol.2015.11.026
14. Hosseini, S. F. *et al*. Carbohydrate Polymers 2013, v. 95, n. 1, p. 50–56. https://doi.org/10.1016/j.carbpol.2013.02.031
15. Liu, X. D. *et al*. Carbohydrate Polymers 2001, v. 44, n. 3, p. 233–238. https://doi.org/10.1016/S0144-8617(00)00206-X
16. Specos, M.M.M. *et al*. Transactions of the Royal Society of Tropical Medicine and Hygiene 2010, v. 104, n. 10, p. 653–658. doi: 10.1016/j.trstmh.2010.06.004.
17. Kringel, D. H. *et al*. of Food Science 2017, v. 82, n. 11, p. 2598–2605. https://doi.org/10.1111/1750-3841.13923
18. Branca, C. *et al*. Polymer 2016, v. 99, p. 614–622. https://doi.org/10.1016/j.polymer.2016.07.086.

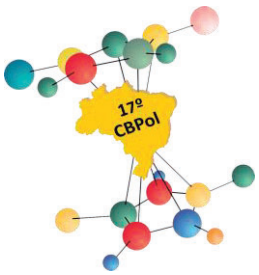

THERMAL, MECHANICAL AND MORPHOLOGICAL CHARACTERIZATION OF THE PLA-TIO2-MWCNT SYSTEM FOR 3D PRINTING FILAMENTS

Milena M. Nogueira[1], Bruno A.B. Cordova[1] and Benjamim de M. Carvalho[1]

1 – Department of Materials Engineering (DEMA), State University of Ponta Grossa (UEPG), Ponta Grossa, PR, Brazil

mimacedo8@gmail.com

Abstract – In the present study, filaments for the PLA-MWCNT-TiO_2 system were produced and characterized in order to develop formulations with bactericidal properties. However, in this first stage, morphological characterizations were performed using electron microscopy with EDS, thermal characterization using DSC, and mechanical characterization using tensile testing to evaluate the effect of the fillers on the PLA matrix. There was no significant effect of TiO_2 and MWCNT fillers on the crystallinity of the extruded filaments. Regarding the cooling crystallization in DSC, it was observed that MWCNTs significantly increased ΔHc and crystallinity compared to pure extruded PLA. The pure extruded PLA with elongational flow exhibited higher tensile strength than the commercially available pure PLA filament, likely due to the greater molecular orientation promoted by the elongational flow. EDS analysis revealed that the concentration of TiO_2 on the surface of the produced filaments is higher than in the core. This characteristic can be important when aiming for a bactericidal effect.

Keywords:*Polylactic acid,, 3D printing, titanium dioxide, carbon nanotube, extrusion.*

Fundings: Coordination for the Improvement of Higher Education Personnel (CAPES).

Introduction

Additive manufacturing, also known as 3D printing, is a manufacturing technology that has gained increasing prominence in recent years. It allows the creation of three-dimensional objects from digital models using a variety of materials, including polymers, metals, ceramics, and even biological tissues. This technology began in the 1980s with stereolithography, a process that uses a laser to solidify (photopolymerize) liquid resins in successive layers. Since then, 3D printing has evolved with the emergence of new techniques and materials, expanding its possibilities. Its applications range from producing prototype parts for industry and engineering to creating decorative objects, jewelry, and medical prosthetics and orthotics, as well as mass production of automotive and aircraft components [1,2].

Polylactic acid (PLA) is one of the most used polymer filaments in 3D printing. Under suitable conditions of temperature, light, oxygen, humidity, nutrients, and microorganisms, it undergoes biodegradation. It is produced from renewable sources such as corn and sugarcane starch, making it a more sustainable material compared to others like Acrylonitrile Butadiene Styrene (ABS) terpolymer. However, in the field of 3D printing, PLA is widely used not only for its biodegradable nature but also for its ease of printing and excellent visual quality. Additionally, it is an excellent material for 3D printing in the medical field, allowing the production of biocompatible and biodegradable parts, thereby reducing the risk of rejection in the human body [2,3].

Titanium dioxide (TiO_2) is a chemical compound widely used as a white pigment. Due to its photocatalytic effect, it has also been employed in the development of polymers with bactericidal properties. Carbon nanotubes can be considered one of the most promising materials for producing polymer matrix nanocomposites due to their properties, such as high mechanical strength, electrical conductivity, and thermal conductivity. Hybrid polymer systems incorporating TiO_2 and carbon nanotubes have been utilized in studies aiming to achieve microbicidal properties [4,5].

The present work corresponds to the first stage of the project and aims to characterize the thermal, mechanical, and morphological properties of 3D printing filaments produced through extrusion with elongational flow using the PLA-TiO_2-MWCNT system.

Experimental

Extrusion of filaments

For the extrusion of the filaments in this study, the following materials were used: Natural-colored PLA filament provided by 3DLab©, produced with PLA from NatureWorks©; Titanium dioxide powder with a particle size fraction of 50-500 nm; Multi-walled carbon nanotubes (MWCNT) supplied by the company Nanocyl© under the trade name NC7000, average diameter: 9.5 nm. The PLA in the form of commercial filaments from 3Dlab was cut using a BGM granulator. Prior to the extrusion of the formulations, the materials were dried in an oven at 60°C for 24 hours. The polymer and particle pre-mixture was manually performed by tumbling. The extrusion process took place using a homemade single-screw mini-extruder with three temperature zones. To aid in the dispersion of nanoparticles, 5 pairs of elongational flow rings were used in the matrix. Each pair consisted of a ring with a 2mm channel diameter followed by another ring with a 4mm channel diameter. The screw rotation was set to 20 rpm. The temperature profile was 180°C, 200°C, and 200°C for the feeding, compression/metering, and elongational matrix zones, respectively. The produced filaments for each composition had approximate diameters of 1.75mm. Table 1 presents the compositions of the produced filaments.

Table 1- Compositions of the produced filaments.

Composition nomenclature	PLA (% m/m)	TiO_2	NTC
Pure PLA	100%	-	-
Extruded pure PLA	100%	-	-
PLA/0.5 NTC	99.5%	-	0.5%
PLA/1.0 NTC	99.0%	-	1.0%
PLA/2.5 TiO_2	97.5%	2.5%	-
PLA/5.0 TiO_2	95.0%	5.0%	-
PLA/2.5 TiO_2/0.5 NTC	97.0%	2.5%	0.5%
PLA/4.0 TiO_2/1.0 NTC	95.0%	4.0%	1.0%

The term "pure PLA" refers to the pure polymer in the form of commercial filament as received from 3DLab. This commercial filament was used as a reference in various characterizations.

Field Emission Gun (FEG) and Energy *Dispersive Spectroscopy (EDS)*

The filaments were cut using blades, and the surfaces of the cross-sections were characterized. The samples were metallized with gold and then analyzed using a FEG Tescan/Mira 3 Scanning Electron Microscope (SEM) with Energy-Dispersive X-ray Spectroscopy (EDS). The FEG SEM with EDS microanalysis was used to analyze the dispersion/location of the particles in the matrix, allowing for the determination of the percentage of each particle in the extruded filament.

Differential Scanning Calorimetry (DSC)

The thermal characterization using Differential Scanning Calorimetry (DSC) was conducted following ASTM D3418 standard. A Shimadzu DSC 60 instrument was used, and the analyses were performed under a nitrogen atmosphere. The initial test temperature was set at 30°C, with heating up to 220°C at a rate of 10°C/min, followed by an isothermal hold of 3 minutes. After this time, the sample was cooled down to 50°C at a rate of 5°C/min, with an isothermal hold of 3 minutes, and the same thermal cycle was repeated. This methodology was applied to all filament compositions in duplicate. The crystallinity of PLA in the formulations was calculated using the following expression: $Xm(\%)=[(\Delta Hm-\Delta Hcc)/f*\Delta Hm^{\infty}]*100$. Xm (%) is the percentage of crystallinity, ΔHm is the fusion enthalpy obtained from the DSC analysis, ΔHcc is the cold crystallization enthalpy

obtained, f is the mass fraction of PLA in the mixture, and ΔHm∞ is the standard enthalpy for 100% crystalline PLA, which is tabulated as 93.6 J/g. [6].

Tensile test

The tensile test was performed using a Shimadzu Autograph AGS universal testing machine with a 10 kN load cell. Ten samples measuring 15 cm in length were tested for each filament composition. The gauge length between the grips was set to 5 cm, and the test speed was set to 5 mm/min.

Results and Discussion

Field Emission Gun (FEG) and Energy *Dispersive Spectroscopy (EDS)*

Both the filaments and the powder particles were subjected to FEG and EDS analysis. Fig. 1 shows the images of the MWCNT and TiO_2 particles.

Figure 1 - FEG of the particles: a) and b) MWCNT; c) and d) TiO_2

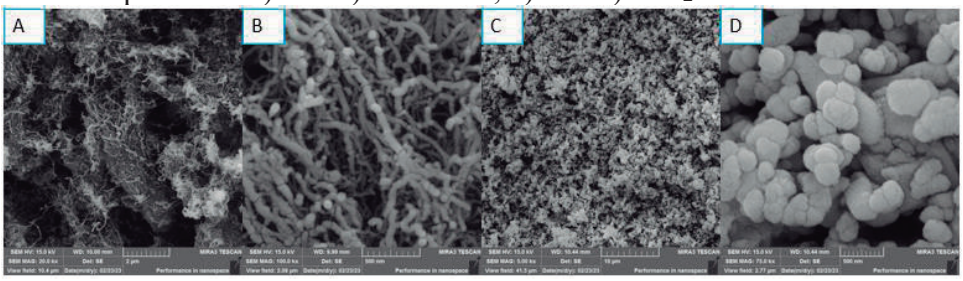

By analyzing the images, it was possible to observe the morphology and confirm the nanoscale size of the MWCNT and TiO_2 particles. Fig. 2 presents the images obtained for each filament composition.

Figure 2 - FEG of the filaments: a) Pure PLA; b) Extruded pure PLA; c) PLA/0.5 MWCNT; d) PLA/1.0 MWCNT; e) PLA/2.5 TiO_2; f) PLA/5.0 TiO_2; g) PLA/2.5 TiO_2/0.5 MWCNT; h) PLA/4.0 TiO_2/1.0 MWCNT.

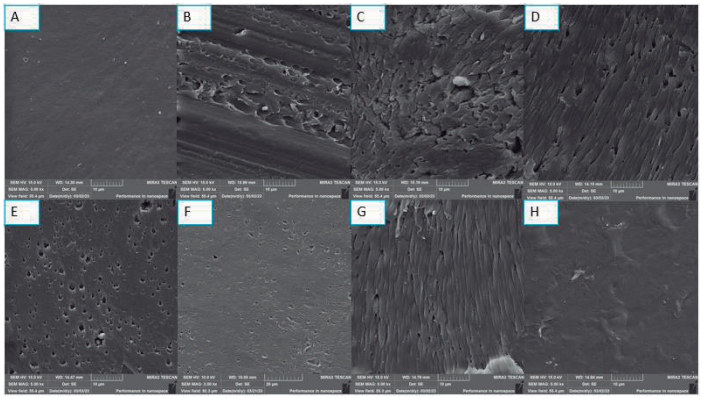

From the images, it was possible to visualize the cross-sectional surface of the filaments. It can be observed that the surface of pure PLA differs the most from the others, appearing flatter and free from heterogeneities, as seen in the other images. No particle clusters were observed in filaments with additives. However, they are present on the surfaces. Confirmation was done through EDS analysis. Table 2 presents the amount of TiO_2 obtained via EDS in the center and on the surface of filaments containing this particle.

Table 2 - Mass % of TiO_2 obtained via EDS in the filaments

Filament composition	TiO_2 surface content (%)	TiO_2 center content (%)
PLA/2.5 TiO_2	1.31	2.66

PLA/5.0 TiO_2	3.59	5.30
PLA/2.5TiO_2/0,5 NTC	0.17	2.56
PLA/4.0 TiO_2/1.0 NTC	0.36	3.77

It can be observed that the distribution of titanium in the filament is not homogeneous. For both filaments, the amount of Ti in the center is lower than at the edge. The % of Ti at the edge is consistent with the filament composition. The other detected chemical elements were carbon and oxygen. However, carbon is present in both the PLA and MWCNT chemical structures. Therefore, it is not possible to precisely measure the % of carbon from the MWCNT using this technique. Another important factor to consider is the dispersion of particles in the PLA matrix during the extrusion process, with the presence of controlled extensional flow. Goes (2022) observed better dispersion of MWCNT in the polymer matrix during extrusion with elongational flow, as well as a reduction in the size of MWCNT clusters. [7].

Differential Scanning Calorimetry (DSC)

The values of Cold Crystallization Temperature (Tcc), Cold Crystallization Enthalpy (ΔHcc), Melting Temperature (Tm), Melting Enthalpy (ΔHm), Crystallization Temperature from Melt (Tc), Crystallization Enthalpy on Cooling (ΔHc), and Crystallinity of the extruded filaments (Xm) are presented in Table 3.

Table 3 – DSC data for the compositions.

Compositions	Tcc(°C)	ΔHcc (J/g)	Tm (°C)	ΔHm (J/g)	Tc (°C)	ΔHc (J/g)	Xm(%)
Pure PLA	100.1	-13.8	181.1	40.0	107.6	-2.7	28.0 ± 0.5
Extruded pure PLA	99.2	-21.5	178.3	43.5	103.3	-9.7	23.5 ± 3.8
PLA/0.5 NTC	95.8	-21.2	178.4	47.7	102.9	-28.1	28.2 ± 4.5
PLA/1.0 NTC	95.2	-21.2	177.5	47.8	103.7	-28.8	28.1 ± 0.4
PLA/2.5 TiO_2	95.6	-16.4	178.9	41.7	102.8	-28.6	26.3 ± 4.9
PLA/5.0 TiO_2	100.6	-28.2	178.1	51.8	102.8	-18.9	23.9 ± 4.6
PLA/2.5 TiO_2/0.5 NTC	94.8	-15.2	178.3	42.7	102.5	-23.8	28.5 ± 3.8
PLA/4.0 TiO_2/1.0 NTC	96.4	-23.9	178.4	49.1	106.4	-32.9	25.5 ± 0.6

It was observed that the pure PLA (commercial filament without re-extrusion) showed higher values of Tcc, Tm, and Tc compared to the extruded pure PLA. The addition of MWCNT or TiO_2 resulted in a decrease in Tcc compared to the extruded pure PLA but did not increase ΔHcc. The extruded pure PLA exhibited a decrease in crystallinity compared to the pure PLA. However, considering the margin of error, there was no significant effect of the fillers on the crystallinity of the extruded filaments. For the cooling crystallization in DSC, it was observed that MWCNT significantly increased ΔHc and crystallinity compared to the extruded pure PLA. Literature values for the crystallinity of PLA range from 20-45%, with the values strongly dependent on the cooling rates in DSC and processing conditions. The obtained crystallinity values fall within this range.

Tensile test

The results obtained in this mechanical test, ultimate tensile strength and elongation at break, are presented in Table 4

Table 4 – Tensile test data of the filaments compositions.

Composition	σ máx (MPa)	ε máx (%)
Pure PLA	57.0 ± 1.62	6.1 ± 0.70
Extruded pure PLA	63.5 ± 2.88	4.5 ± 0.43
PLA/0.5 NTC	57.39 ± 3.31	4.41 ± 0.48
PLA/1.0 NTC	55.05 ± 3.45	5.19 ± 0.95

PLA/2.5 TiO_2	51.19 ± 3.13	5.55 ± 0.93
PLA/5.0 TiO_2	61.26 ± 3.62	3.71 ± 0.40
PLA/2.5 TiO_2/0.5 NTC	54.07 ± 4.13	4.38 ± 0.23
PLA/4.0 TiO_2/1.0 NTC	51.81 ± 0.99	4.53 ± 0.65

Based on the obtained data, a statistical test using the Tukey Method was conducted, identifying outliers and result clusters. The extruded pure PLA with elongational flow exhibited an increase in the ultimate tensile strength (σ max) compared to the pure PLA (commercial filament as received). This effect is likely attributed to the molecular orientation due to elongational flow, as its crystallinity is slightly lower. Therefore, for the pure materials, the extrusion process contributed to increase tensile strength of PLA. There was a decrease in the tensile strength of the other compositions with the addition of fillers. The addition of MWCNT indeed weakened the material, but the added quantity did not show statistical significance. The addition of TiO_2 did not follow a linear pattern in terms of increased tensile strength, as the lower quantity decreased the ultimate tensile strength, while the higher quantity increased it. Statistically, the extruded pure PLA and the composition with the highest quantity of TiO_2 are equivalent in terms of tensile strength. For the hybrid compositions, no statistical differences were observed among the results. The maximum deformation (ε max) did not show statistical differences in any of the compositions. The elastic modulus was not calculated due to the unavailability of an extensometer in the testing equipment.

Conclusions

It was observed that the TiO_2 content on the surface of the filaments is higher than in the center. This characteristic is beneficial when aiming to develop filaments with bactericidal effects. The next step of the study is to investigate the microbicidal activity of the loaded filaments. There was no significant effect of the fillers on the crystallinity of the extruded filaments. Regarding the cold crystallization in DSC, it can be observed that MWCNT significantly increased ΔHc and crystallinity compared to the extruded pure PLA. The extruded pure PLA with elongational flow exhibited higher tensile strength than the commercially obtained pure PLA filament, likely due to the increased molecular orientation promoted by the elongational flow used.

Acknowledgements

The authors are grateful to CAPES, Fundação Araucária, Complexo de laboratórios multiusuários (C-LABMU) and Maria Eduarda Teleginski by the support in the extrusion of the filaments.

References

1. A. Parihar; V. Pandita; A. Kumar; D. S. Parihar; N. Puranik; T. Bajpai; R. Khan Regenerative Engineering and Translational Medicine 2022, 8, 173-199. https://doi.org/10.1007/s40883-021-00219-w.
2. D. Garlott. J. Polymers 2001, 9, 63-84. https://doi.org/10.1023/A:1020200822435.
3. A. Aimar; A. Palermo; B. Inoccenti J. of Healthcare Engineering 2019. https://doi.org/10.1155/2019/5340616.
4. C. L. Dicastillo; M.G. Correa; F.B. Martínez; C. Streitt; M.J Galotto Appl. Sci. 2021, 11, 4623. https://doi.org/10.3390/app11104623.
5. J. N. Coleman; U. Khan; W. J. Blau; Y.K. Gun'ko Carbon 2016, 44, 1624-1652. doi:10.1016/j.carbon.2006.02.038.
6. W. Y. Jang; B. Y. Shin; T. J. Lee; R. Narayan J. Ind. Eng. Chem 2007, 13, 457-464. https://www.cheric.org/PDF/JIEC/IE13/IE13-3-0457.pdf.
7. M. A Goes; J. P. F Santos; B. M. Carvalho. Polímeros: Ciência e Tecnologia 2022, 32(2). https://doi.org/10.1590/0104-1428.20210116.

USE OF LIPASES IN THE (BIO)MODIFICATION OF POLYESTER FOR THE INCORPORATION OF CHITOSAN NANOPARTICLES

Wendhy C. Vicente[1], Larissa N. Carli[1] and Patrícia B. Brondani[1]*

1 – Technological Center of Exact Sciences and Education, Federal University of Santa Catarina (UFSC), Blumenau, SC, Brazil p.b.brondani@ufsc.com.br

Abstract - Polyester synthetic fiber (PET) is considerably interesting to be functionalized due to its properties such as high resistance, low shrinkage, and roughness, that's a low-cost material with less need for maintenance. However, PET has a hydrophobic nature that causes several processing difficulties and is flammable. One way to improve the PET properties is by performing covalent surface modification. The lipases can hydrolyze the PET ester groups, improving their hydrophilicity in a mild process, and leaving reactive sites on the surface. Chitosan nanoparticles (ChiNps) are attractive candidates to be combined with modified PET due to their biological properties. In this sense, we proposed the study of several lipases to perform the superficial hydrolysis of PET with subsequent impregnation of ChiNps to the fiber. The new materials are expected to have properties, such as antimicrobial action, ultraviolet protection, and flame retardancy, in an eco-friendly process.

Keywords: Polyester, Enzymatic hydrolysis, Biocatalysis, Nanotechnology, Textile Materials.

Fundings: CAPES- DS.

Introduction

PET is composed of poly(ethylene terephthalate) and is one of the most popular and widely produced fibers, therefore it is an interesting material to incorporate functions. In addition, it requires low maintenance, has high durability, low cost, and excellent physical properties, such as high resistance to wear or stretching, low shrinkage, and roughness. [1-3]. In general, conventional textiles are functionalized by manipulating the surface characteristics of the fiber, this can be performed by electrostatic interaction or by covalent bond formation.

One way to generate the most stable covalent bond on PET surface is to hydrolyze the ester groups. The most usual way to modify PET is an alkaline treatment, which affects directly the fiber strength. Other disadvantages would be the high amount of sodium hydroxide and high operating temperature. Enzymatic hydrolysis of synthetic fibers to improve some of their undesired properties, such as hydrophobicity, low dyeability, and insufficient washability, is of high interest, as it leads to a reduction in the use of hazardous chemicals, energy consumption, and production cost, resulting in an ecologically friendly methodology. Studies showed that PET ester groups can be hydrolyzed by lipases [1-3, 6-8]. Under ideal conditions, the enzymatic treatment of polyester using a lipase can lead to the hydrolysis of surface ester groups transforming them into carboxyl groups (-COOH) and/or hydroxyl groups (-OH). Subsequently, the formed -COOH groups can be reacted with nucleophilic functional groups for further modification [1-3].

The surface modification can be combined with nanotechnology and such processes have already resulted in products with all the advantages and characteristics of nanomaterials, being able to acquire antimicrobial action, thermoregulatory effect, ultraviolet (UV) protection, electrical conductivity, and flame retardancy, among others, but without compromising the comfort,

flexibility, and durability of the substrates. This way, a wide range of uses for these materials is generated for areas such as fashion, sports, health, military, and agriculture [4-6].

Among several materials, chitosan is an example of a polysaccharide that has been satisfactorily used in such processes. Based on its biological potential, several reports already confirm that these nanoparticles (ChiNps) can confer antimicrobial activity on textiles, improve dyeing processes, and increase the strength and durability of fabrics. Other studies also point to a positive effect concerning UV protection and flame-retardant properties [4-6].

The most adopted strategy for synthesizing ChiNps is ionic gelation with a sodium tripolyphosphate (TPP) crosslinker. It is a simple and controllable technique, which can be performed in mild environmental conditions, has low residual toxicity, and is free of organic solvents [7.8].

After hydrolyzing the PET surface applying lipases and reducing the hydrophobic properties of this fiber ChiNps can be covalently incorporated into PET simply by immersing the fabrics in a solution containing the nanoparticles [7]. It was also found that it is possible to enhance the impregnation of ChiNps by the incidence of UV radiation that causes dehydroxylation and dehydrogenation on the chitosan surface, generating free radicals in its nitrogen and oxygen atoms, making them available for the coupling of more nanoparticles [8].

Although the superficial degradation of PET through the action of some lipases is known, as well as the reaction of impregnation of chitosan to the fiber, the combination of biocatalysis and the covalent impregnation of ChiNps was not already performed. Besides that, a complete study with several lipases taking into account a complete optimization of the hydrolysis step was not found for the modification of PET. Based on these highlights, this project proposes a study of PET hydrolysis catalyzed by nineteen lipases for the development of a new methodology for obtaining modified PET, followed by the reaction with ChiNps producing a functionalized PET. The proposed process would reduce production costs and environmental pollution associated with conventional textile processes.

Experimental

Chemicals

100% polyester fabric has been used to evaluate the effect of enzyme treatment. The following textile auxiliary products were used: the emulsifying agent Coloremulg EMG 441, the dispersing agent Colorsperse DI650 and the dye Brilliant Blue Colorpes S-EBL 200%, both from Color Química and Apolo's Orange Triacet RN Acid dye.

Tris (hydroxymethyl) amino methane (0.05 mol L^{-1}, pH 7.0, Vetec, TRIS) and acetate (0,1 mol L^{-1}, pH 5,0) were used as a buffer. The pH was adjusted using 1 mol L^{-1} HCl, 1 mol L^{-1} CH_3COOH or 0,1 mol L^{-1} NaOH. Chitosan from Sigma-Aldrich with medium molar mass was used to synthesize the nanoparticles. The 0.1% TPP solution was prepared using the commercial reagent Dinâmica with a molar mass of 367.86 g mol^{-1} in distilled water.

Enzymes

Eighteen commercial enzymes were available for carrying out the project, namely: Lipase from *Rhizomucor miehei* (immobilized in Duolite-type ion exchange resin, Lipozyme RM-IM), Lipase from *Candida antarctica B* (in solution, Lipozyme CAL-B L), Lipase from *Aspergillus oryzae* (in solution, Lipolase 100L), Lipase PS (Amano) from *Burkholderia cepacia* (immobilized on ceramics, PS-C), Lipase from *Candida antarctica B* (immobilized on acrylic resin, Novozyme 435), Lipase from *Candida antarctica B* (immobilized on ion exchange resin, Lipozyme 435), Lipase from *Thermomyces Ianuginosus* (immobilized on silica, Lipolase 100T), Lipase from *Candida rugosa* type VII (lyophilized), Lipase PS (Amano) from *Burkholderia cepacia* (immobilized on diatomite, PS-D), Lipase from *Porcine pancreas* type II (lyophilized), Lipase A (Amano) from *Aspergillus niger* (lyophilized), Lipase PS (Amano) from *Burkholderia cepacia* (

immobilized on silica), Lipase from *Rhizomucor miehei* (in solution, Novozyme 388), Lipase from *Thermomyces Ianuginosus* (sol-gel), Lipase from *Thermomyces Ianuginosus* (lyophilized), Lipase F-AP15 (Amano) from *Rhizopus oryzae* (lyophilized), Lipase M (Amano) from *Mucor javanicus* (lyophilized) and Lipase PS (Amano) from *Burkholderia cepacia* (lyophilized, PS-SD).

Lipase enzyme treatment

At first, the fabrics were subjected to washing to eliminate the presence of impurities. PET was immersed in 2.0 gpl emulsifying and dispersing agents at 95°C and treated for 40 min to liquor ratio (LR) of 1:20 [1] using a dyeing machine (TEXCONTROL IR DYER TC 2200).

Each fabric sample was cut into 4x4 cm dimensions and weighed ~0.3 g. Depending on pH (6.0, 7.0, and 8.0), temperature (25, 40, and 60°C), amount of enzyme (15, 30, and 45 mg), and treatment time (45, 60 and 90 min), the PET was treated with lipases in Tris buffer solution. All the lipase treatments were performed at 150 rpm using a shaking bath (Shaker SL-22). To ensure the reproducibility of the results, the reactions were done in duplicate. In addition, the procedure was also performed once without PET sample to make a control solution that will be called blank [1-3].

The lipase-treated samples were thoroughly washed with water and dried at room temperature (r.t). Then, an aliquot of 8 mL of the treatment bath was inactivated with 20 mL of ethanol in a beaker and 4 drops of phenolphthalein were added. Later, the solution was titrated with NaOH. The volume used in the titration was recorded to calculate the enzymatic activity of lipase enzyme on PET, using Eq. (1).

$$\text{Enzymatic activity (mL/g)} = (Vs - Vb) / Wf \times 100 \quad (1)$$

where Vs and Vb are volumes of NaOH consumed in mL for the sample treated and blank titration, respectively. Wf is the weight of the PET sample treated.

The mass loss was measured based on the percent ratio of PET weight before and after treatment. To check the carboxyl and hydroxyl groups on the surface of PET, each sample was dyed using 0.5% (owf) disperse dye and 1 g/L dispersing agent in a shaking bath (150 rpm for 20 min at 60 °C). After this period, the analysis of the dyebath of each sample was performed in UV-Vis (Shimadzu UV-1800, UVProbe 2.42) and the results were obtained in terms of absorbance (λ= 800 to 200 nm) for comparison. The enzymatic activity and absorbance values found were used to determine the best enzyme and the best reaction condition [1-3].

ChiNps synthesis

The ChiNps were synthesized via ionic gelation method [7,8]. 1% m/v chitosan solution in acetate buffer pH 5 was stirred for at least 60 min, the solution was centrifuged at 2500 rpm and then vacuum filtered. Then, 0.1% TPP solution was added dropwise to the chitosan solution in a LR 3:1 Chitosan:TPP (v/v) under stirring at r.t. After this, homogenization by Ultra-Turrax® IKA (T 18 DI with dispersion element S 18 N) was performed at 13000 rpm for 10 min in an ice bath. The chitosan nanoparticles prepared were kept in solution under refrigeration at approximately 4°C.

ChiNps incorporation

After the surface modification of the fiber, ChiNps was impregnated by immersing the PET in a solution containing the nanoparticles. The fabric sample was cut into 1x1 cm dimensions and weighed ~0.06 g. Then, 20% (w/w) of ChiNps solution:PET was produced in acetate buffer. The incorporation was performed at 150 rpm using a shaking bath (120 min at 60°C). At the end of the treatment, the samples were washed with 20 mL of distilled water at r.t for 24 h [7,8].

UV light exposure

To increase the incorporation tax of ChiNps, previously impregnated PET samples were placed in beakers containing 18 mL of acetate buffer solution and left under UV radiation (λ= 254

nm) in a UV cabin. Samples were produced with exposure times varied at 480, 360, 240, 120, and 60 min to assess the best condition to increase impregnation. Subsequently, in each beaker, 2 mL of ChiNps in solution was added and the incorporation procedure in the shaking bath was repeated, followed by washing [8].

Characterization of ChiNps incorporation

The incorporation of ChiNps into PET was confirmed through dye yield using acid dye. Each sample of PET incorporated with ChiNps was dyed using the shaking bath (150 rpm for 30 min at 30°C) in a solution of 100 µL of 1:100 orange acid dye solution in 50 mL of distilled water, with pH adjusted to pH 3 with HCl. After this period, the analysis of the dyebath of each sample was performed in UV-Vis (Shimadzu UV-1800, UVProbe 2.42) and the results were obtained in terms of absorbance (λ= 800 to 200 nm) for comparison [1,5-6].

Results and discussion

The eighteen commercial lipases, immobilized or not, were tested. But only the lipases that showed higher activity were highlighted in Fig 1, which describes the values of enzymatic activities, accompanied by the percentage of mass loss. One should note that the enzymatic activity values coincide with those found in the literature, which range from 0.1 to 0.6 mL/g [1-3].

Figure 1 - Graphs of enzymatic activity and mass loss

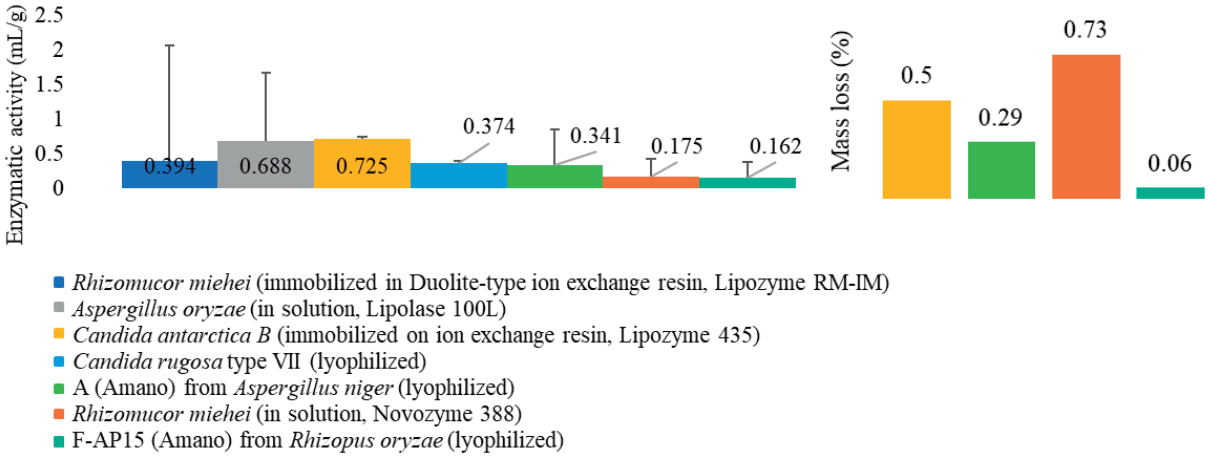

In the literature, the mass loss value found in PET modified by alkaline hydrolysis is 18.5%, while the one modified by lipases is 0.35%, which also coincides with those obtained in the tests (Fig 1) [1-3]. After the preliminary tests applying titration, the result was confirmed by the disperse dyeing assay, by measuring the remaining dye in the solution using UV-Vis spectrophotometry. Lipase A (Amano) of *Aspergillus niger* (lyophilized) was selected because of its considerable activity, low mass loss, and absorbance value in disperse dyeing assay. After the selection of the lipase, the other parameters were evaluated (pH, temperature, and reaction time) and the best condition for the PET hydrolysis was found at pH 7, 40°C, and 90 min.

The incorporation of ChiNps, was performed directly in acetate buffer pH 5, in the presence of urea as cross-link agent, or after the exposition to UV (254 nm) light. The results were evaluated by the acid dyeing assay, visually, and by the measured absorbance values [5-9]. Assuming that after incorporating ChiNps into PET, the NH_2 groups become available on the fabric surface and are capable of electrostatically binding to an acid dye, the more intense the sample staining, the more ChiNps were incorporated (Fig 2). In this sense, it is possible to notice that UV light exposure increased the incorporation tax, dependent on exposure time, which varied at 480, 360, 240, 120,

and 60 min. Preliminarily, the best condition to increase impregnation is applying one round of direct impregnation in pH 5, 120 min at 60°C, followed by 480 min UV light exposure, and a second round of impregnation under the same conditions. It's important to notice that, performing the same optimized condition without UV light exposure, leads to low tax of impregnation, meaning that UV light plays an important role in the process.

Figure 2 - Acid dyeing test for the modified PET samples.

(a)PET sample (b) ChiNps modified PET sample (c) ChiNps modified PET sample with 480 min UV exposure.

Conclusions

The change in the PET surface by the action of lipases proved to be an efficient alternative compared to traditional processes. The Lipase A (Amano) from *Aspergillus niger* (lyophilized) successfully hydrolyzed PET fiber in a mild condition (pH 7, 40°C, and 90 min). The low mass loss indicates no effects on fiber strength. The incorporation methodology applying one round of direct impregnation in pH 5, followed by UV exposure, and a second round of impregnation showed the best results so far. The acid dyeing assay confirmed the excellent results in ChiNps incorporation on PET fibers. But other characterizations will also be carried out to evaluate characteristics such as the morphology of synthesized ChiNps, and changes in the hydrophobicity on the PET surface. The antimicrobial activity, flame retardancy, and UV protection will be studied using the AATCC methods for the textile industry.

References

1. J. A. Kumar; M. S. Kumar. AUTEX Research Journal 2020, 20, 0030. https://doi.org/10.2478/aut-2019-0030
2. H. R. Song; W. S. Song. Fibers and Polymers 2008, 7, 0068-3. https://doi.org/10.1007/s12221-008-0068-3
3. R. Ramasamy; R. B. Subramanian. Environmental Science and Pollution Research 2022, 21467-5. https://doi.org/10.1007/s11356-022-21467-5
4. M. Fernandes; J. Padrão; A. I. Ribeiro; R. D. Fernandes; L. Melro; T Nicolau; B. Mehravani; C. Alves; R. Rodrigues; A. Zille. Nanomaterials 2022, 12, 1006. https://doi.org/10.3390/nano12061006
5. A. Javid; Z. A. Raza; T. Hussain; A. Rehman. Journal of Microencapsulation 2015, 31, 879927. https://doi.org/10.3109/02652048.2013.879927
6. M. T. Abate; A. Ferrib; J. Guanc; G. Chenc; J. A. Ferreira; V. Nierstrasza. The Journal of Supercritical Fluids 2019, 147, 08.015. https://doi.org/10.1016/j.supflu.2008.08.015
7. Z. A. Raza; F. Anwar; S. Abid. Polymer Bulletin 2019, 76, 2523-7. https://doi.org/10.1007/s00289-018-2523-7
8. D. Alonso; M. Gimeno; R. Olayo; H. Vázquez-Yorres; J. D. Sepúlveda-Sánchez; K. Shirai. Carbohydrate Polymers 2009, 77, 01.027. https://doi.org/10.1016/j.carbpol.2009.01.027

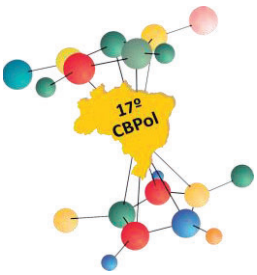

APPLICATION OF GRAPHENES IN LDPE FOR FILMS: STUDY OF PARTICLE SIZE AND MECHANICAL PROPERTIES

Neuma M. Pereira[1], Giuliana D. M. Luiz[1], Irina M. Factori[1], Ana Clélia B. Ferreira[1], Anderson Maia[1], Gustavo S. G. de Almeida1, Pamela S. Garcia[2]*, Josué M. O. Cremonezzi[2] and Valdirene S. T. Peressinotto[2]

1 – SENAI Institute for Innovation in Advanced Materials and Nanocomposites, São Bernardo do Campo, SP, Brazil
2 – Gerdau Graphene, São Paulo, SP, Brazil
pamela.garcia@gerdaugraphene.com

This abstract discusses an innovative project carried out by the partnership between Gerdau Graphene and ISI Advanced Materials, which aims to explore the properties of graphene in low density polyethylene (LDPE) tubular films for packaging applications. In this project two types of graphene were used: particles smaller than 30 µm and larger than 80 µm. The effects of the particle's sizes on the films' mechanical properties and processing parameters were verified. Graphene is an extremely thin and strong carbon material with outstanding mechanical and electrical properties [1]. Its incorporation into polymeric matrices, such as LDPE, offers the possibility of significantly improving the characteristics of tubular films used in packaging [2]. The results indicated that the addition of graphene in LDPE films provided improvements in mechanical properties, such as tensile strength and stiffness. Graphene with 30 µm particles showed a more pronounced increase in tensile strength compared to 80 µm. Also, it was observed that the 80 µm graphene films required lower electric current during processing compared to the 30 µm. This suggests that the larger particle size graphene may promote higher energy efficiency during the production of the films, which may be associated with the lubricity effect [3]. Based on the promising results of this project, it is possible to envision a future use of LDPE films with graphene in packaging. These films could offer improved mechanical properties such as strength and stiffness, as well as reduced energy consumption during the manufacturing process.

1. Sandeep N. Tripathi, G. S. Srinivasa Rao, Ajit B. Mathur and Rakshvir Jasra. *RSC Adv*., 2017, *7*, 23615. https://doi.org/10.1039/C6RA28392F
2. Nunes, MABS, de Matos, BR, Silva, GG, Ito, EN, de Melo, TJA, Fechine, GJM. *Polymer Composites*. 2021; 42: 661– 677. https://doi.org/10.1002/pc.25856
3. Eder H. C. Ferreira, Angela A. Vieira, Lúcia Vieira, Guilhermino J. M. Fechine. Polymers 2021, 13, 2237. https://doi.org/10.3390/polym13142237

Fundings: Brazilian Company for Industrial Research and Innovation (Embrapii)

Keywords: *Graphene, Polyethylene, Film.*

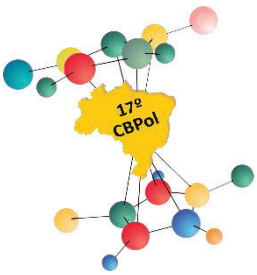

BIODEGRADABLE POLYMERIC NANOCOMPOSITES BASED ON POLY(3-HYDROXYBUTYRATE-CO-3-HYDROXYVALERATE) (PHBV) AND GRAPHENE OXIDE (GO)

Giovanna C. Silva[1,2], Patrícia, M. S. Souza[1,2], Guilhermino J. M. Fechine[1,2*]

1- School of Engineering, Mackenzie Presbyterian University, São Paulo, Brazil
2 - MackGraphe (Mackenzie Institute for Research in Graphene and Nanotechnologies), São Paulo SP, Brazil
**guilherminojmf@mackenzie.br*

Poly(3-hydroxybutyrate-co-3-hydroxyvalerate) (PHBV) is a bio-based and a biodegradable polymer, a material that has gained interest as one of the solutions for environmental problems arising from the accumulation of plastics. However, some of its characteristics end up limiting the expansion of its use. This project aims to develop a biodegradable polymeric nanocomposite, PHBV/graphene oxide (GO) system, through the melt mixing technique using a twin-screw extruder, since it is one of the most utilized methods in industry. Therefore, seeking to improve the mechanical performance, thermal stability and better processability, without losing the biodegradable properties of the nanocomposites. GO was synthesized through the Hummers methodology using a bench reactor [1]. The deposition of the nanoparticles in PHBV followed the solid-solid deposition (SSD) technique [2] to produce masterbatches, with 2 wt% of GO. The final content of GO for the nanocomposites obtained by extrusion were 0.1 wt%, 0.3 wt% and 0.5 wt%. Differential Scanning Calorimetry (DSC), during heating, did not show significant changes in the melting peak for neat PHBV and nanocomposites. The crystallization temperature increased in approximately 12% for a content of 0.5 wt%, possible due to nucleating agent of GO. So, the polymer chains in contact with the GO sheets are capable of organize themselves at higher temperatures. In mechanical impact tests, the nanocomposites with 0.1 wt% of GO showed a 25.5 % increase in impact strength, indicating a high level of dispersion as well as good interaction between the filler and the polymeric matrix. This result was also observed by Field Emission Gun Scanning Electron (FEG-SEM), with the fracture surface being rougher when compared to neat PHBV. Thus, it is possible to infer that the incorporation of GO to PHBV maintained the crystal organization, allowing it to occur at higher temperatures, and increased the mechanical performance.

References

1. C. S. Andrade, *et al. Nanomaterials* 2022, *261*, 1975. https://doi.org/10.3390/nano11081975.
2. P. A. R. Muñoz, *et al.* eXPRESS Polymer Letters 2018, 12, 930-945. DOI: 10.3144/expresspolymlett.2018.79

Fundings: This project is supported by FAPESP (2022/06541-2 and 2022/07054-8) and CAPES/PROSUC program.

Keywords: *PHBV, graphene oxide, biodegradable polymer nanocomposite, mechanical properties*

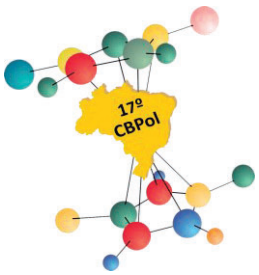

FEW-LAYER GRAPHENE PRODUCTION THROUGH GRAPHITE EXFOLIATION IN PRESSURIZED CO_2

Thuany G. Maraschin[1]*, Raiane V. Gonçalves[4], Marina C. Vargas[2], Nara R. de S. Basso[1], Eduardo Cassel[1], Griselda B. Galland[3]

1 – Program in Materials Engineering and Technology (PGETEMA), Pontifical Catholic University of Rio Grande do Sul (PUCRS), Porto Alegre, RS, Brazil
thuany.maraschin@edu.pucrs.br
2 – Polytechnic School, Pontifical Catholic University of Rio Grande do Sul (PUCRS), Porto Alegre, RS, Brazil
3 – Institute of Chemistry, Federal University of Rio Grande do Sul (UFRGS), Porto Alegre, RS, Brazil
4 – Department of Chemical Engineering, Federal University of Rio Grande do Sul (UFRGS), Porto Alegre, RS, Brazil

Abstract – Direct liquid-phase exfoliation (LPE) of graphite has emerged as an alternative method for producing graphene. LPE offers several advantages over oxidation methods, such as low cost, simplicity, high yield, and scalable industrial graphene production, striking a balance between quality and cost [1-3]. A fast route for obtaining few-layer graphene using the LPE of graphite powder will be presented. This innovative approach utilizes a naturally derived surfactant called cardanol. Initially, the graphite flakes were pre-exfoliated through tip ultrasonication for 10, 20, and 30 minutes in a system containing an aqueous solution of 20% ethanol and variations of surfactant concentration (2.4×10^{-4} and 4.8×10^{-4} mol.L^{-1}). Subsequently, the stable dispersion of the exfoliated graphite was heated at 40 °C with constant stirring and underwent pressurization into the CO_2 cell, operating at 150 bar for 30 minutes. Afterward, the reaction cell was depressurized, and the gray-colored suspensions were collected. The concentration of dispersed exfoliated graphite was assessed by UV-vis. Morphological and structural characterizations were investigated using TEM-SAED, AFM, XRD and RAMAN. Promising results were achieved by employing a cardanol specific concentration of 2.4×10^{-4} mol.L^{-1}. The resulting graphene exhibits excellent structural quality, low defect density, and small stacking, with an average size below 15 nm. Notably, the sample treated with pressurized fluid and 20 minutes of ultrasonication demonstrates a significant percentage of graphene stacking smaller than 5 nm, aligning with the typology known as few-layer graphene. This technological advancement has the potential to transform cost-effective materials into high-value products, with a particular focus on applications in polymer composites and advanced materials.

References

1. Z. Li et al., *ACS Nano* 2020, *14*, 10976–10985. https://doi.org/10.1021/acsnano.0c03916.
2. Z. Sun, Q. Fan, M. Zhang, S. Liu, H. Tao, J. Texter, *Advanced Science* 2019, *6*, 1901084. https://doi.org/10.1002/advs.201901084.
3. S. Lund et al., *Carbon* 2021, *174*, 123–131, https://doi.org/10.1016/j.carbon.2020.11.094.

Keywords: *Graphene production; Few-layer graphene; Liquid-phase exfoliation; Advanced materials.*

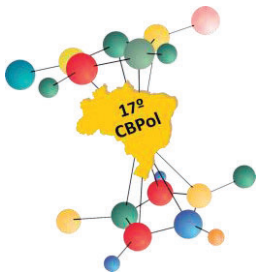

INTERVENTIVE CONSERVATION OF RIGID POLYURETHANE FOAM BY MEANS OF TITANIUM DIOXIDE-BASED NANOCOATING

Diana B. D. Simões[1*], Raquel S. Mauler[1] and Tales S. Daitx[1*]

1 – Institute of Chemistry, Federal University of Rio Grande do Sul (UFRGS), Porto Alegre, RS, Brazil
diana.bulcao@ufrgs.br, tales.daitx@ufrgs.br

Abstract - Polyurethane (PUR) rigid foams have been used since the 20th century as a material for art and design. However, as its deterioration processes occurs in around 20-30 years depending on the environment in which they are exposed, it is of interest in the cultural heritage field the development of methods and materials to aid its conservation. Since the main PUR deterioration agents are temperature, relative humidity (RH) and ultraviolet radiation (UV), the objective of this work is to develop a nanocoating based on titanium dioxide (TiO_2) modified with different organosilanes, in order to protect and consolidate the PUR samples without altering its sensorial characteristics [1, 2]. For this, TiO_2 nanoparticles were modified using different proportions of 3-aminopropyl(triethoxisilane) (APTES) and *n*-octyl(triethoxysilane) (OTES) (100/0, 75/25, 50/50, 25/75 and 0/100 APTES/OTES) [3]. The reagents were stirred and heating under toluene reflux during 24 h. After the period, the samples were centrifuged and oven-dried at 65°C to constant weight. The nanoparticles were characterized by Fourier-transform infrared spectroscopy (FTIR) and thermogravimetric analysis (TGA), confirming the insertion of organic groups on the surface of the TiO_2. After the modification steps, the nanoparticles were applied on the PUR samples. For this, each nanoparticle was dispersed in ethanol with a concentration of 5% (w/v) and the solutions poured on the samples, followed by air-dry for 48 h. The PUR samples were then submitted to a climatic chamber at 50% RH, 75-90°C and UV radiation for 3 weeks, in order to simulate extreme degradation conditions. After treatment, the samples were evaluated through FTIR, TGA, dynamic-mechanical analysis (DMA) and scanning electronic microscopy (SEM). The results indicated that the coatings have a positive effect on the conservation of the samples, where the levels of degradation compared to the uncoated sample were minimized.

References

1. A. P. Kanth; A. K. Soni *Journal of Cultural Heritage* 2023, *59*, 120. https://doi.org/10.1016/j.culher.2022.11.010
2. M. Baglioni; G. Poggi; D. Chelazzi; P. Baglioni *Molecules* 2021, *26*, 3967. https://doi.org/10.3390/molecules26133967
3. C. Daher; I. Fabre-Francke; N. Balcar; G. Barabant; S. Cantin; O. Fichet; H. Chéradame; B. Lavédrine; A. L. Derieux *Polymer Degradation and Stability* 2018, *158*, 92. https://doi.org/10.1016/j.polymdegradstab.2018.10.029

Fundings: The authors are grateful to Conselho Nacional de Desenvolvimento Científico e Tecnológico (CNPq), Coordenação de Aperfeiçoamento de Pessoal de Nível Superior (CAPES), Fundação de Amparo à Pesquisa do estado do Rio Grande do Sul (PRONEX/FAPERGS - Finance Code 16/2551-0000470-6) and Programa de Pós-Graduação em Ciência dos Materiais (PPGCIMAT/UFRGS) for financial support.

Keywords: Art and design, Deterioration, Nanoparticles, *Organosilane, Rigid polyurethane foam.*

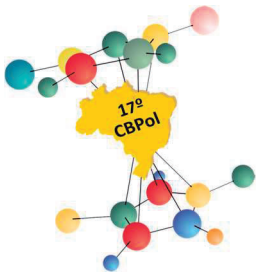

MODIFICATION OF SYNTHESIS ROUTE AND AGGREGATION ANALYSIS OF SILICA NANOPARTICLES FOR CORE-SHELL STRUCTURE

Giulia S. Vieira[1*], Grazielle Lopes[1] and Luciana S. Spinelli[1,2]

1 – Macromolecules Institute (IMA), Federal University of Rio de Janeiro (UFRJ), Rio de Janeiro, RJ, Brazil
giuliasilvares@nano.ufrj.br
2 – Nanotechnologie Engineering Program (PENt), Posgraduated and Research Institute Alberto Luiz Coimbra (COPPE), Federal University of Rio de Janeiro (UFRJ), Rio de Janeiro, RJ, Brazil

Abstract - Silica nanoparticles (SNPs) are extremely important and represent growing interest in several science fields. The original synthesis route was developed by Stöber *et al* in 1968. However, the search for methodology modifications to obtain particles with different sizes and functionalities is common and varies with the desired application. Given that, this work aims to test three different silica nanoparticles synthesis methodologies, to obtain a size range that will be applied in a core-shell structure with a terpolymer. For that, the following methodologies were used: classic Stöber method, Moon *et al* method and modified Stöber method, as described in Table 1. DLS analyses demonstrated that the obtained particles presented, respectively, medium approximate sizes: 160 nm, 650 nm and 134 nm. Also, was possible to verify that the SNPs tended to agglomerate more in aqueous media in comparison with alcoholic media. In brief, is possible to conclude that both Stöber methods (original and modified) were efficient, providing smaller size ranges, that are appropriate for the future synthesis of different core-shell structures.

Table 1 – Silica nanoparticles (SNPs) synthesis methodologies

Methodology	H_2O (mL)	Etanol (mL)	NH_4OH (mL)	TEOS (mL)	Temperature (°C)	Time (Minutes)
Traditional Stöber	40	160	6	0,6	27	270
Moon *et al*	3.2	20	2	2	35	240
Modified Stöber	1	30	2	5	24	180 (sonication)

References

S. Moon, K. J. Lee *Advanced Powder Technology* 2017, *2914–2920.* http://dx.doi.org/10.1016/j.apt.2017.08.019
W. Stöber, A. Fink *Journal of Colloid and Interface Science 1968*, *62–69.* https://doi.org/10.1016/0021-9797(68)90272-5

Fundings: ANP, PRH16.1, CAPES, CNPQ

Keywords: *Silica, Nanoparticles, Core-shell, Synthesis*

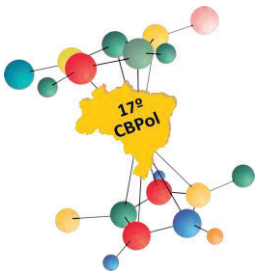

ORGANIC-INORGANIC PHOTOPOLYMERIZABLE NANOCOMPOSITES FOR 3D PRINTING WITH ANTIVIRAL ACTIVE SURFACES

Tamires S. Lima*, Karina M. S. Silva, Ivani Malvestiti and Petrus A. Santa-Cruz

Department of Fundamental Chemistry (DQF), Federal University of Pernambuco (UFPE), Recife, PE, Brazil
tamires.lima@ufpe.br

Abstract – We report on the development of hybrid organic-inorganic photopolymerizable nanocomposites based on soybean oil resins with embedded metal/metal oxide nanoparticles to produce 3D prints with self-decontaminating surfaces by MSLA (Masked Stereolithography Apparatus) technology. Approaches that exploit the synergistic effects of nanoparticles and polymers have the potential to create new technologies and functional active materials [1]. Printable nanocomposites of silver nanoparticles, with emphasis on antibacterial mechanisms, have already been reported by our group [2] and, in this work, focused on viral decontamination, we report the development of a self-decontaminating material based on copper nanoparticles (CuNP) and copper oxide nanoparticles (CuONP). The contamination through contact with contaminated surfaces (fomites) has been presented as a secondary route of the viruses spread with a high level of transmissibility [3]. As nanostructured materials and their antiviral mechanisms show effectiveness in surface treatments for a significant group of viruses [4], the production of these photopolymerizable nanocomposites for 3D printing aims to inhibit virus propagation. Nanostructured materials with self-decontaminating properties can act in an active-passive manner for viral inactivation [5]. Allying bioinspiration, these materials allow the exploration of different hierarchical structures by 3D printing technology through active-passive mechanisms [6]. Here the active phase of the nanocomposites, CuNP and CuONP, were synthesized by two methodologies: chemical reduction via L-ascorbic acid and mechanochemistry and presented average sizes of 18.3 nm and 8.3 nm respectively. The nanocomposites were characterized by UV-vis, FTIR, DRX, SEM, TGA, and DSC. Antiviral tests were performed in collaboration with FIOCRUZ-PE, initially with a model virus (Zika), in an NB-2 biosafety level environment. The nanocomposites show good formation, stabilization, and uniform distribution of the nanoparticles in the polymeric phase, with good interface adhesion between the two components. Through the antiviral activity tests, it was verified that the nanocomposites were able to inactivate the analyzed virus.

References

1. P. D. Rakowska et al. Commun Mater. 2021, 2, 53. https://doi.org/10.1038/s43246-021-00153-y
2. N. Barrera et al. PLoS One, 2018, *13* https://doi.org/10.1371/journal.pone.0200918
3. E. Toledo et al. *PLoS ONE*, 2022, *17*, 8. https://doi.org/10.1371/journal.pone.0272307
4. A. Bhatti; R. K. Delong *ACS Pharmacol. Transl. Sci*. 2023, *6*, 2. https://doi.org/10.1021/acsptsci.2c00195
5. A. P. Mouritz et al. *Nano Select* 2021, *2*, 2061. https://doi.org/10.1002/nano.202100078
6. P. A. Santa-Cruz et al. in Proceedings of XX Brazil MRS Meeting, Foz do Iguaçu, 2022.

Fundings: This work was supported by the Coordenação de Aperfeiçoamento de Pessoal de Nível Superior (CAPES) RIMA Project - Edital Capes 09/2020 and CNPq Brazilian Agencies.

Keywords: p*hotopolymerizable nanocomposites; self-decontaminating; copper nanoparticles; 3D printing; antiviral activity.*

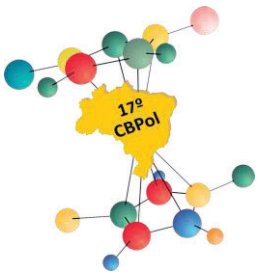

PLASMA-FUNCTIONALIZED CARBON NANOTUBES FOR THE ADSORPTION OF RHODAMINE-B IN WATER

Julya F. Lima*, Mirlene P. Vitorino, Teresa T. Steffen, Luis C. Fontana, Alexandre T. Paulino and Daniela Becker.

Center for Technological Sciences, UDESC, Joinville, Santa Catarina, Brazil.

julyaflima1@gmail.com*

Abstract – Water pollution is a serious problem that can be mitigated by treatments using adsorbent solid materials. Efficient adsorption processes occur via physical-chemical interactions between adsorbent material surfaces and pollutants [1]. Carbon nanotubes (CNT) can be used as adsorbents for the adsorption of dyes in water, including Rhodamine-B (RhB), since their properties agree with those required in adsorption studies, i.e., high surface area and adsorption capacity [2]. In this work, CNT and urea were solid-mixed and then treated in a capacitively coupled plasma reactor, powered by radiofrequency. The plasma parameters were established according with a previous work [3], so samples were treated by 30 minutes at 35 W, using ultrapure argon gas. After the CNT surface modification on plasma, the samples were filtered with the aim of removing unreacted urea. CNT and functionalized CNT were characterized by Fourier-transform infrared (FTIR) spectroscopy, thermogravimetric analysis (TGA), X-ray photoelectron spectroscopy (XPS), Brunauer-Emmett-Teller (BET) analysis and point of zero charge (pH_{PZC}). The CNT surface was modified after plasma-treatment in presence of urea. Experimental results revealed that the urea- functionalized CNT has pH_{PZC} ~6.2. As the pH value of RhB in aqueous solution is ~4.0, the surface charge of the functionalized CNT in this medium would be positive, adsorbing anionic RhB species [4]. Overall, this work indicates that the urea-functionalized CNT can be used as adsorbent of RhB in water. Future assats of adsorption will be performed for confirming the best conditions for the adsorption of RhB on the functionalized CNT surface.

References

1. T. G. Kebede, S. Dube, M. M. Nindi. Science of the total environment 2020, 738, 140282. https://doi.org/10.1016/j.scitotenv.2020.140282.
2. S. Zghal, et al. Materials 2023, 16, 1015. https://doi.org/10.3390/ma16031015.
3. T. T. Steffen, et al. Applied Surface Science 2022, 583, 152493. https://doi.org/10.1016/j.apsusc.2022.152493
4. M.A Silva, H. P. Felgueiras, M. T. P. Amorim. Cellulose 2020, 27, 1497-1516. https://doi.org/10.1007/s10570-019-02861-8

Fundings: The authors would like to thank PROMOP/UDESC, CAPES, CNPq and FAPESC for the financial support. The authors are also thankful for the Multi-User Facility infrastructure of the Technological Sciences Center of the Santa Catarina State University.

Keywords: *Carbon nanotube; urea; Rhodamine B; functionalization; plasma; adsorption.*

REUSABLE CELLULOSE NANOFIBRILS-BASED NANOCOMPOSITE AEROGELS FOR MALACHITE GREEN DYE REMOVAL

Amanda A. D. Maia[1], Pedro I.C. Claro[1], Marcos V. Lorevice[1] and Rubia Figueredo Gouveia[1,2]*

1 – Brazilian Nanotechnology National Laboratory (LNNano), Brazilian Center For Research in Energy and Materials (CNPEM), Campinas, SP, Brazil
2 – Center for Natural and Human Sciences, Federal University of ABC, Santo André, São Paulo, Brazil.
rubia.gouveia@lnnano.cnpem.br

Abstract – Cellulose nanofibrils (CNF)-based porous materials from sugarcane bagasse for water remediation have recently received attention due to their high specific surface area, ultralow density, and cellulose intrinsic properties (renewability, low cost, and biodegradability)[1]. Although aerogels based on this biopolymers have reached comparable or, in some cases, superior adsorption capacity, when compared with commercial adsorbents, the aerogel reuse still needs to be clarified. In this context, the present work shows a reusability study (adsorption/desorption) of aerogel comprising CNF and natural rubber latex (NRL) in a malachite green dye (MGD) solution. The CNF and CNF/NRL aerogels were obtained through an ice-templating approach[2]. The reusability study consisted of several adsorption/desorption cycles with different initial concentrations (0.5-5 mg· L^{-1}) of MGD. The reuse performance was evaluated by considering the MGD removal (%) and adsorption capacity (mg· g^{-1}). The CNF/NRL and CNF aerogels presented efficient adsorption of MGD, about 89 to 92 % of MGD removal and 375 to 424 mg · g^{-1} of adsorption capacity, respectively. Regarding adsorption mechanisms, the adsorption data were analyzed considering pseudo 1st and 2nd order. Pseudo-2nd presented a high correlation coefficient of R^2 (0.99), indicating a chemisorption process, possibly promoted by carboxyl and phospholipids groups of CNF and NRL, respectively. Aerogels also presented reuse properties, and MGD removal remained practically constant over the cycles, ranging from 80 to 94 %. These results confirm the potential of these CNF-based renewable, cost-effective, and promising porous materials for water remediation.

References

1. M.V. Lorevice;P.I.C Claro; N. A. Aleixo; L.S. Martins; M. T. Maia; A. P. S. Oliveira; D. S. T. Martinez; R. F. Gouveia.. *Chemical Engineering Journal* 2023, 462, 142166. doi:10.1016/j.cej.2023.142166.
2. M.V. Lorevice; E.O. Mendonça; N.M. Orra; A.C. Borges; R.F. Gouveia ACS *Applied Nano Materials* 2020, 3, 10954–10965. https://doi. org/10.1021/acsanm.0c02203.

Fundings: This study was financed in part by the Coordenação de Aperfeiçoamento de Pessoal de Nivel Superior - Brasil (CAPES). Finance Code 001. National Council for Scientific and Technological Development. Grants 380312/2020-4 and 380173/2022-0. Grant #2020/08651-4 São Paulo Research Foundation (FAPESP)
Keywords: *Cellulose nanofibrils. Water remediation. Green malachite dye. Adsorption study.*

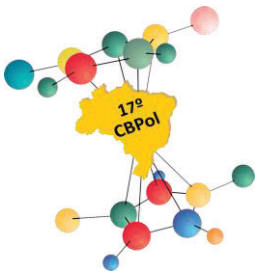

SYNTHESIS AND CHARACTERIZATION OF GELATIN AND STARCH NANOPARTICLES FOR INTELLIGENT MICROGELS PREPARATION

Nádya Pesce da Silveira[1*], Roberta Zucatti[1] and Daiani Canabarro Leite[2]

1 – Institute of Chemistry, Federal University of Rio Grande do Sul (UFRGS), Porto Alegre, RS, Brazil
2 – Physics Department, Federal University of Santa Maria (UFSM), Santa Maria, RS, Brazil
nadya@iq.ufrgs.br

Nanoparticles based on corn starch polymers (SNPs) and type-B gelatin (GNPs) were synthesized to produce, in the future, intelligent microgels. The SNPs were prepared by nanoprecipitation technique,[1] using absolute ethanol as non-solvent and a polymeric solution consisting of 2% (w/v) starch in 0,5 M KOH. The polymeric solution/absolute ethanol ratio was fixed at 1:20 (v/v), and different starch types were evaluated (Table 1). The GNPs were synthesized by the two-step desolvation method using acetone,[2] with and without the incorporation of synthesized polypyrrole nanospheres, crosslinked with 1-ethyl-3-(3-dimethylaminopropyl)carbodiimide (EDC) or glutaraldehyde. Dynamic light scattering (DLS) analyses showed the impact of surfactant and starch type on the formation of SNPs (Table 1), and the different GNPs crosslinking protocols resulted in samples with modulated diameters ranging between 280 - 600 nm. Scanning electron microscopy images revealed the SNPs. Further studies are being conducted to synthesize intelligent microgels (responsiveness to pH, temperature, and electric stimuli) based on the nanoparticles produced.

Table 1 – Typical SNPs sample parameters and the average diameters determined by DLS.

Sample	Corn starch type (H, R and W)	Tween 80 % (v/v) (TW 1, 3 and 5%)	Mean diameter (D_h/nm)	Polydispersity Index
SNP-H	High amylose	0	439,7 ± 18,1	0,076 ± 0,023
SNP-H-TW1%	High amylose	1	282,1 ± 1,9	0,219 ± 0,006
SNP-H-TW3%	High amylose	3	192,6 ± 1,0	0,303 ± 0,010
SNP-H-TW5%	High amylose	5	208,8 ± 2,3	0,117 ± 0,035
SNP-R	Regular	0	655,5 ± 2.2	0,128 ± 0,023
SNP-R-TW1%	Regular	1	414,1 ± 19,1	0,196 ± 0,040
SNP-W-TW1%	Waxy	1	331,6 ± 3,1	0,031 ± 0,026

* Mean values (n= 3) ± standard deviation. The waxy starch did not form SNPs in the absence of surfactant.

References

1. H. Marta; D. I. Rizki; E. Mardawati; M. Djali; M. Mohammad; Y. Cahyana. *Polymers 2023*, *15*(5), 19–25. https://doi.org/10.3390/polym15051167
2. F. Milano; A. Masi; M. Madaghiele; A. Sannino; L. Salvatore; N. Gallo. *Pharmaceutics 2023*, 15, 1499. https://doi.org/10.3390/ pharmaceutics15051499

Fundings: CAPES fellowship. LNNano (SEM images).
Keywords: *starch nanoparticles; amylose; amylopectin; gelatin nanoparticles; intelligent polymer.*

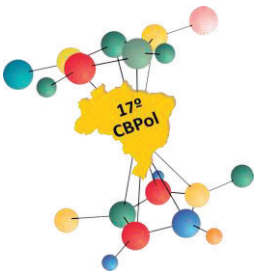

SYNTHESIS OF ELECTROSPUN POLYSTYRENE MEMBRANES COATED WITH GRAPHENE OXIDE AND POLYPYRROLE: STUDY OF THE REMOVAL OF ERIOCHROME BLACK T FROM AQUEOUS MEDIA

Lúcio Flávio M. Cavalcanti[1*], Winnie Q. Brandão[2], Andressa N. R. Leal[3], Maurício F. de Aguiar[1], Celso P. de Melo[2,4], Braúlio S. Barros[1] and Kleber G. B. Alves[1]

1 – Department of Mechanical Engineering, University of Pernambuco (UFPE), Recife, PE, Brazil
lucio.moreira@ufpe.br
2 –Materials Science graduate program, Federal University of Pernambuco (UFPE), Recife, PE, Brazil
3- Department of Chemical Engineering, Federal University of Pernambuco (UFPE), Recife, PE, Brazil
4 - Department of Physics, Federal University of Pernambuco (UFPE), Recife, PE, Brazil

Abstract – The presence of dyes in industries' wastewater reveals the inefficiency of the technologies used in the treatment of effluents and the need for new methodologies to mitigate environmental impacts. Given this perspective, this work consists of synthesizing polystyrene (PS) membranes through electrospinning and coating it with functionalized graphene oxide (GOf) and polypyrrole (PPy) and the evaluation of this composite membrane on the removal of eriochrome black T (EBT) dye. The obtained membranes were characterized by scanning electron microscopy (SEM) and Fourier-Transform infrared (FTIR). From the SEM images we observed that the fibers presented a homogeneous appearance, without beads and ruptures, as well as the incorporation of GOf and PPy on the PS fibers surface. Through FTIR spectra it was observed the functional groups characteristic of PS, GOf, and PPy. A first evaluation of the removal of EBT was carried out. Then, we evaluated the effect of pH on the removal and the removal kinetics. In regards to pH, we verified that the dye removal increases as pH decreases. As for the kinetics, we realized that the time to remove approximately 75% of the dye was obtained after a period of 4 hours. Finally, we conclude that our PS/GOf/PPy composite membranes appears promising on the removal of dye from aqueous media.

References

1. M.F. de Aguiar; A.N.R. Leal; C.P. De Melo; K.G.B. Alves, Polypyrrole-coated electrospun polystyrene films as humidity sensors, Talanta 2021, 234, 122636. https://doi.org/10.1016/j.talanta.2021.122636
2. L.M.S. de Farias; M.G. Ghisland; M.F. de Aguiar; D.B.R.S. Silva; A.N.R. Leal; F.A.O. Silva; T.J.M. Fraga; C.P. De Melo; K.G.B. Alves, Electrospun polystyrene/graphene oxide fibers applied to the remediation of dye wastewater, Materials Chemistry and Physics 2022, 276, 125356. https://doi.org/10.1016/j.matchemphys.2021.125356

Keywords: *Polystyrene. Graphene oxide. Polypyrrole. Dye removal.*

TENSILE AND INDENTATION TESTS ON CARBON NANOSTRUCTURES AND EPOXY RESIN COMPOSITES

H. R. F. M. Guimarães[1], K. Sales de Oliveira[1], T. Doca[1],J.A. da Cruz [2],S. C. Amico [2].

1 – Department of Mechanical Engineering, University of Brasília (UnB), Brasília, DF, Brazil
190029404@aluno.unb.br
2 – Laboratório de Materiais Poliméricos, Universidade Federal do Rio Grande do Sul, 91501-970, Porto Alegre, Rio Grande do Sul, Brasil.

Abstract – Carbon nanostructures have been employed as reinforcements due to their lightweight and high mechanical resistance. Although theoretical properties for these materials are presented as promising, manufacturing errors (e.g., misalignment of fibers or bad interface adhesion) often compromise the composite's properties. This work aims to describe the mechanical behavior of epoxy resin matrices reinforced with either graphene nanoplatelets or carbon nanotubes. Tensile tests are carried out for the evaluation of traction resistance, while spherical indentation tests are employed for the assessment of compressive properties. For each nanostructure, three concentrations are analyzed: 0% (pure epoxy), 0.5% and 1.0%. It is observed that the reinforcements do not lead to meaningful improvement in tensile properties, with 1% CNT presenting a reduction of 29% in ultimate stress. However, higher compression resistance is noted for some configurations, although 0.5% CNT decreases stiffness in 26%.
Keywords: *epoxy, carbon nanotubes, graphene nanoplatelets, mechanical properties.*
Funding: Brazilian National Council for Scientific and Technological Development (CNPq) and Foundation for the Support of Research in the Federal District (FAP-DF).

Introduction

Carbon-based nanoparticles have been explored as reinforcements for polymers due to their advantageous theoretical properties. These particles can present different geometrical configurations, such as carbon nanotubes (CNT) and graphene nanoplatelets (GNP). CNT has a theoretical elasticity modulus of up to 1 TPa and outstanding thermal and electric conductivity. Moreover, its low density makes it a lightweight alternative for various applications [1]. As for the GNP, studies on its mechanical properties demonstrate that this material balances manufacturing costs and mechanical resistance [2].

Composites' properties rely on good adhesion between reinforcement and matrix. Epoxy resin, a thermoset brittle polymer, is widely used in association with carbon fiber in aeronautic applications [3]. Carbon nanoparticles-epoxy resin systems have the potential to display good matrix-filler compatibility. However, errors in the manufacturing process affect the properties of the resulting composite. Carbon particles tend to agglutinate, and poor filler dispersion will effectively weaken the material. Treatments to mitigate this behavior can damage the filler's surface, compromising its mechanical performance. Moreover, poor interface adhesion and fiber orientation have a significant impact on mechanical resistance, and these problems have been previously identified in this type of composite [4].

This work aims to evaluate the behavior of epoxy resin-carbon nanofiller composites in tensile and indentation tests. Elasticity modulus, yield and ultimate stress, and strain at failure, and

are compared. In indentation tests, indentation diameter and depth are evaluated, to analyze compression strength. It will then be possible to assess the effectiveness of filler in improving mechanical performance.

Experimental

Materials

Epoxy resin AR260 was mixed with hardener triethylenetetramine (TETA) HY 951 at a mass ratio of 100:13. The resin was degassed for five minutes and cured at room temperature for 24 hours. Post-curing followed, for 3 hours at a temperature of 100°C. The two types of specimens (Fig. 1) are made by casting in a silicon mold.

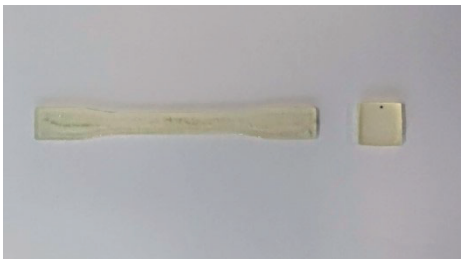

Figure 1 – Specimen types.

The fillers are manufactured by STREM Chemicals. Graphene platelets have a thickness of 6-8 nm. Multiwalled Carbon nanotubes, with a diameter of 140 nm and a length of 7 μm, have been used. The composites' fabrication followed standard procedure: the filler(CNT or GNP, at concentration 0.5% or 1%) was mechanically stirred into the resin at 13000 rpm for 30 minutes in an ice bath. After that, the mixture underwent a sonication process (60% amplitude, pulses on/off, 60 s/60 s) to improve dispersion. The curing process followed, under the same conditions as the pure epoxy resin specimens. All specimens were later polished to control flatness and thickness (5.00±0.05 mm).

Tensile tests

The tensile tests are performed using a MTS Landmark Servohydraulic Test Systems according to ASTM D638 – 14, using Type I specimens[5]. The tests are controlled for displacement, and three displacement rates are adopted (0.5, 1.0 and 2.0 mm/min). A clip gauge extensometer is used to acquire the axial strain data.

Indentation tests

The indentation tests are performed using the Zwick/Roell ZHU 250 Universal Hardness Machine, with a 5 mm diameter spherical tungsten carbide indenter. The goal is to evaluate and compare the plastic deformation behavior of the materials when under compressive stress. Normal forces of 600 N, 700N, 800 N, and 900 N are applied. The diameter and depth of the indentation marks are measured using confocal laser scanning microscopy (CLSM).

Results and Discussion

Tensile Tests

Elasticity modulus, yield stress, ultimate stress, and strain at failure are displayed in Fig. 2. Displacement rates had little influence on yield stress and elasticity modulus for most configurations. Failure likely occurs due to slip and detachment between matrix and filler. It induces stress concentration, which, allied to the loss of structural integrity, results in sudden and

quick failure. Breton *et al.* [6] reached a similar conclusion for multi-walled CNTs at higher volumetric percentages of filler. Hence, it can be concluded that CNT and GNP increased the polymer's brittleness.

Elasticity modulus improved for some configurations, especially at higher displacement rates. The error bars, particularly for the 1% CNT configuration, indicated material's behavior under tensile stress varied depending on specimen properties, which may change due to filler dispersion and orientation. It evidences the influence of the manufacturing process on mechanical performance.

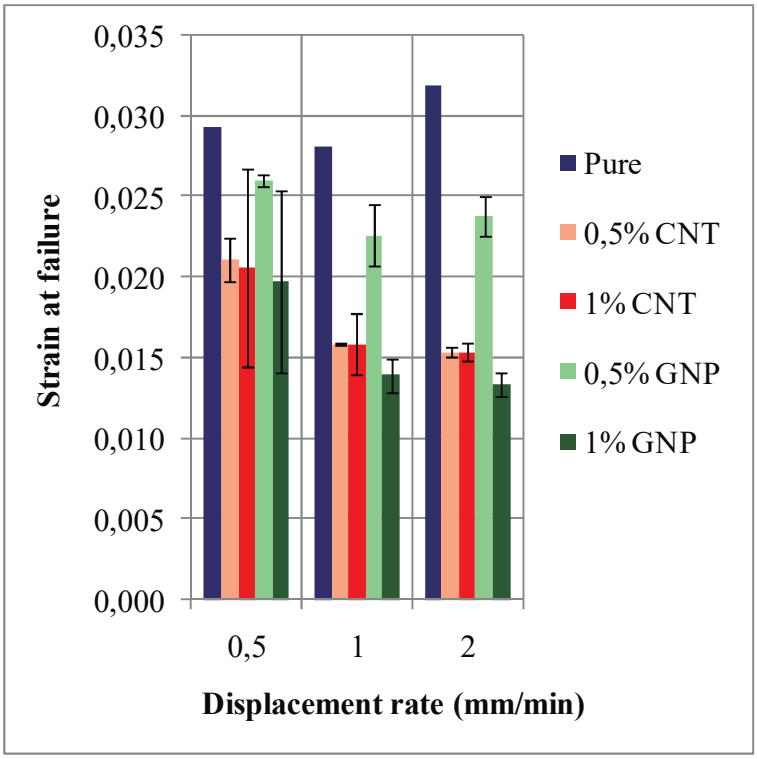

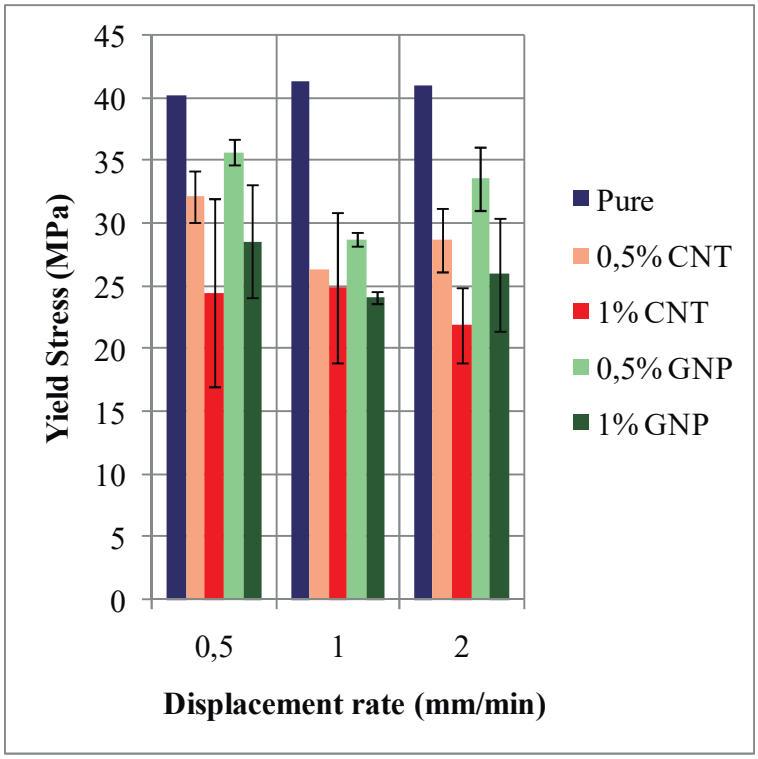

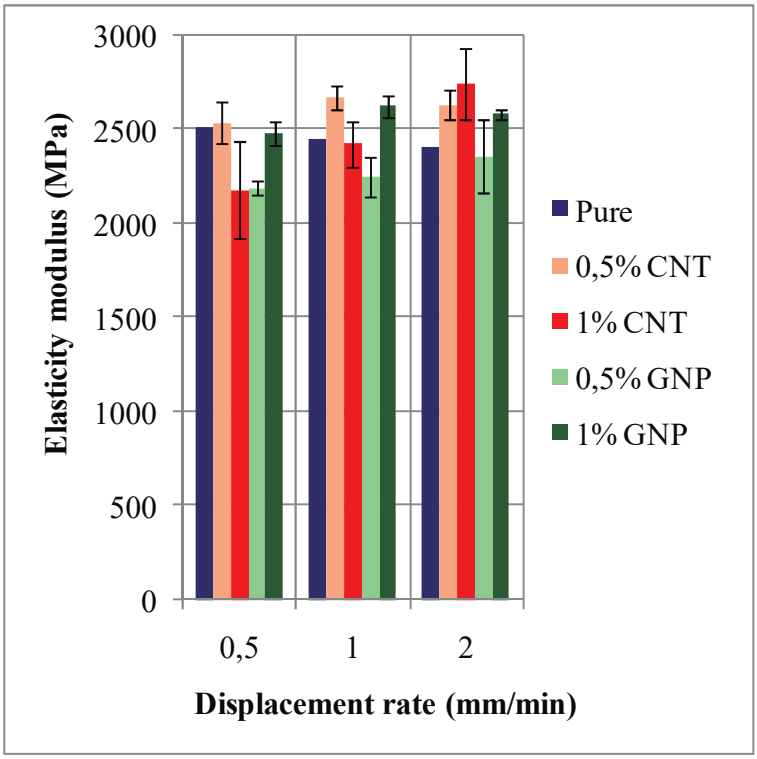

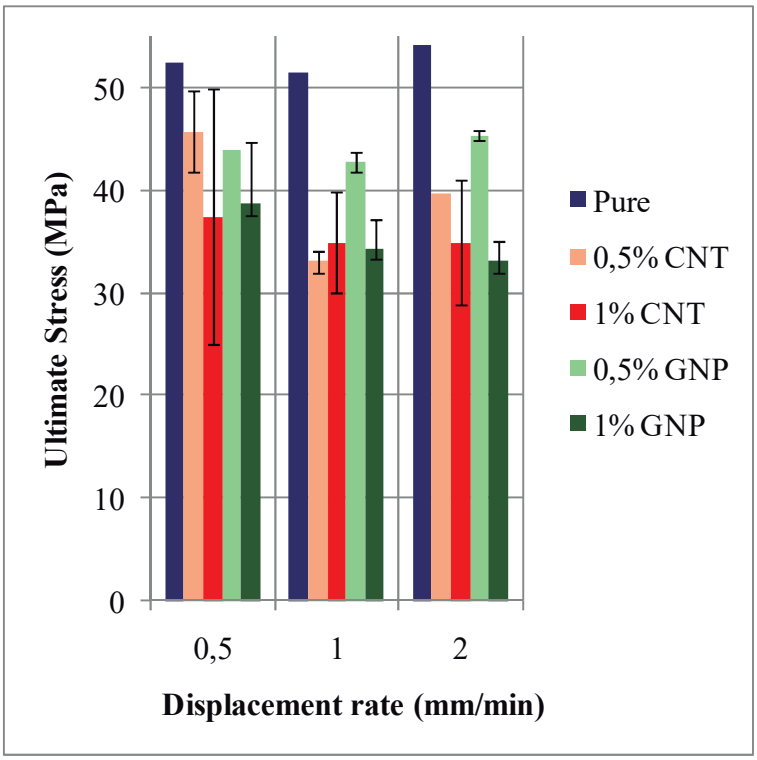

Figure 2 – Strain at failure, elasticity modulus, yield stress and ultimate stress for the different composite configurations and displacement rates.

Indentation Tests

Depth and diameter measurements were taken from 2D profiles. Bartier [7] indicates indentation marks grow in three stages: elastic, contained plastic and uncontained plastic. Upon establishing contact, the indenter applies the load. It initially creates an elastic deformation field beneath the free surface. As the stress increases, yielding starts. Plastic deformation is observed, first under the surface, and then expanding outward [8].

At the loading conditions analyzed, no visible crack formation has been observed. Low *et al.* [9] observed a similar behavior for pure epoxy resin under compressive stress. It can be inferred then that the fillers did not reduce the critical load for crack initiation. The indentation diameter for both carbon nanostructures remained similar to the one observed in the reference configuration.

Fig. 3 presents the mean value of the indentation depth for the different configurations. The 0,5% GNP specimens followed pure epoxy resin plastic deformation behavior. At 1%, the material presents a reduction of about 9% in stiffness. It is possible that the GNP might be suppressing the polymer's viscoelastic recovery, observed in the pure epoxy resin specimens.

At 0.5% concentration, CNT has shown a decrease in mechanical performance (approx.-26%). At 1% CNT, however, the CNT nearly matched the behavior of pure epoxy resin. Measurements presented high dispersion for the 0.5% CNT configuration due to the influence of local properties. This effect is reduced at a 1% filler concentration.

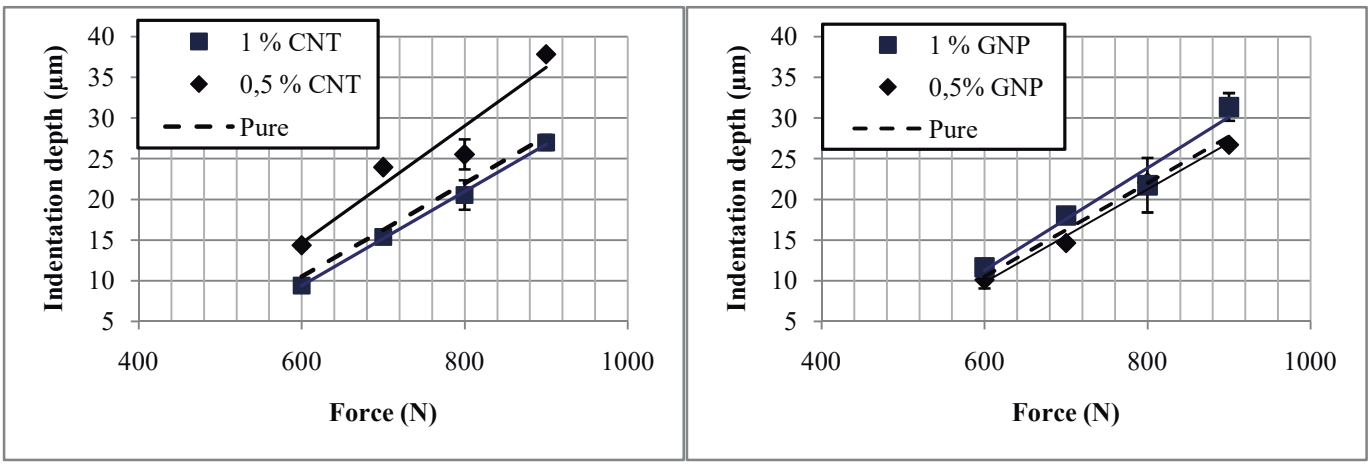

Figure 3 – Indentation depth.

The presence of filler also affected the morphology of the 2D profiles for all polymer configurations. The presence of the carbon nanostructures lessened pile-up. This phenomenon results from a difference in elasticity caused by the hardening of the deformed material when compared to the material in the indent's immediate vicinity. When the load is removed, the border tends to recover more than the plastically deformed center [10]. It is possible to assume the filler would reduce this effect by deforming elastically instead of allowing the residual stresses to dissipate into the matrix.

Conclusions

This study evaluated the mechanical properties of epoxy resin composites. Five configurations of epoxy and carbon nanostructures (pure epoxy resin, 0.5% GNP, 1.0% GNP, 0.5% CNT, and 1.0% CNT) underwent tensile and indentation tests. From the tensile tests, elasticity

modulus, strain at failure, ultimate stress, and yield stress are measured. The presence of filler caused no meaningful improvement in the polymer's mechanical performance under tensile stress. From the indentation tests, GNP and CNT presented different effects on indentation depth. GNP's effect on plastic deformation was negligible. The addition of 0.5% CNT led to slightly worse mechanical resistance. However, at 1% CNT behaved similarly to the reference configuration. As for profile morphology, the nanofillers seemed to have inhibited material pile-up. Another set of tests, for all material configurations, is to be performed to confirm these findings.

Acknowledgements
The authors gratefully acknowledge the financial support provided by the Brazilian National Council for Scientific and Technological Development (CNPq) and the Foundation for the Support of Research in the Federal District (FAP-DF).

References

1. I. A. Kinloch; J. Suhr; J. Lou; R. J. Young; P. M. Ajayan *Science* 2018, *362*, 6414. https://doi.org/10.1126/science.aat7439.
2. U. Kilic; M. M. Sherif; O. E. Ozbulut*Polymer Testing* 2019, *76*. https://doi.org/10.1016/j.polymertesting.2019.03.028.
3. P. D. Mangalgiri*Bulletin of Materials Science* 1999, *22*, 3. https://doi.org/10.1007/bf02749982.
4. S. G. Advani, Ed., *Processing and properties of nanocomposites*. World Scientific, Singapore, 2006.
5. ASTM D638-14 (2014) Standard Test Method for Tensile Properties of Plastics. ASTM International, West Conshohocken. http://www.astm.org.
6. Y. Breton; G. Desarmot; J. P. Salvetat; S. Delpeux; C. Sinturel; F. Beguin; S. Bonnamy*Carbon* 2004, *42*, 12026. https://doi.org/10.1016/j.carbon.2003.12.026.
7. Olivier Bartier; X. Hernot*International Journal of Solids and Structures* 2012. *49*, 2015–2026. https://doi.org/10.1016/j.ijsolstr.2012.04.005.
8. L. Q. Machado and L. Malcher*Journal of The Brazilian Society of Mechanical Sciences and Engineering* 2019, *41*. https://doi.org/10.1007/s40430-019-1976-4.
9. I. M. Low; G. Paglia; and C. Shi.*Journal of Applied Polymer Science* 1998, *70*, 2349–2352. https://doi.org/10.1002/(SICI)1097-4628(19981219)70:12%3C2349::AID-APP6%3E3.0.CO;2-T.
10. B. Taljat; and G. M. Pharr. *International Journal of Solids and Structures* 2004, *41*, 3891–3904. https://doi.org/10.1016/j.ijsolstr.2004.02.033.

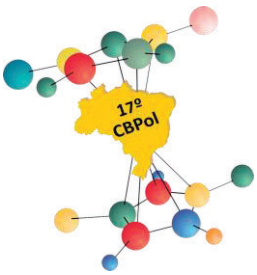

TERMOPLASTIC STARCH NANOCOMPOSITES REINFORCED WITH NANOFIBRILLATED CELLULOSE: PLASTICIZATION WITH GLYCERAL IN THE PRESENCE OF WATER AS PROCESS PLASTICIZER

Annette D. C. Lipa[1*], Kelly L. Lizano[1], Antonio J. F. Carvalho[1]

1 – Department of Materials Engineering, University of São Paulo (USP), São Paulo, SP, Brazil
annette.cochon@usp.br

Abstract –In this work, it was described the preparation of thermoplastic starch (TPS) reinforced with nano-fibrillated cellulose (NFC), being plasticized with glycerol and as a process plasticizer the residual water of the semidried suspension of NFC. The materials were prepared with corn starch and glycerol in the proportion of 70:30 and eucalyptus NFC. Different concentrations 0%, 2.5%, 5% and 10% of NFC were employed, and the mixtures, along with the suspension and the other components were dried in order to control the residual water content to 15%. The composites were prepared in a single screw extruder (16mm, L/D26) with temperature profile from feeding to matrix of 115°C, 120°C and 110°C. The extruded composites were hot pressed to 2mm thick films. Mechanical tension tests were performed with samples conditioned in 53% relative humidity for at least one week. To evaluate the presence of fiber agglomerates, it was performed optical microscopy of thin films with approximately 0.5 mm of thickness. Water content was performed by thermogravimetry (TGA). The results showed that a higher amount of NFC resulted in a higher young's modulus, indicating that the material is more resistant to deformation. The tensile modulus for the composites with 0%, 2.5%, 5%, 10% was respectively of 38.08, 52.35, 84.18 and 122.14 MPa and water absorption at 53% relative humidity for the composites of 0% and 10% was 2.25% and 0.91%, and in 2.5%, 5% and 7.5% lost water in 2.20%, 1.21% and 5.06%. The process in the presence of 15% residual water showed homogeneous materials with no sign of degradation due to overheating and the mechanical properties showed the effect of fiber reinforcement. The presence of residual water also decreases the melt viscosity and allows processing at lower temperatures.

References

1. A. J. F. Carvalho, A. A. S. Curvelo, *Carbohydrate Polymers*. 2001, 45, 183-188. https://doi.org/10.1016/S0144-8617(00)00314-3.
2. A. J. F. Carvalho, *Monomers, Polymers and Composites from Renewable Resources*, Ed.: N.M. Belgacem & A. Gandini. 2008; Chapter 15, 321–342.
3. S. Jayarathna,M. Andersson and R. Andersson. *Recent Advances in Starch-Based Blends and Composites for Bioplastics Applications*. 2022, 14, 4557. https://doi.org/10.3390/polym14214557.
4. D. Klemm., F. Kramer, S. Moritz, T. Lindstrom, M. Ankerfors, D. Gray and A. Dorris, *Nanocelluloses: A New Family of Nature-Based Materials.* 2011, 50, 5438 – 5466. https://doi.org/10.1002/anie.201001273
5. R.A. Ilyas, S.M. Sapuan, M.R. Ishak, E.S. Zainudin, S.N. in Proceedings of 5th International Conference on Applied Sciences and Engineering (ICASEA), Malaysia, 2018.

Acknowledgments: We thank CAPES and CNPQ for financial support. Thanks to Ricardo Gomes for his help in the experiments.
Fundings: This field is optional. Indicate fundings if there is any.

Keywords: *TPS, cellulose nanofibers, nanocomposites thermoplastic starch, reinforcing agents, process plasticizer.*

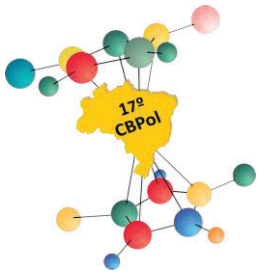

AMMONIA GAS SENSOR BASED ON rGO/PVDF NANOFIBERS

Beatriz M. Carvalho[1], Vitor H. U. F. Mingroni[1], Bruno H. S. Gois[1], Lucas M. Martins[2], Luiz C. S. Filho[2], Clarissa A. Olivati[1], Deuber L. S. Agostini[1]

[1]*Departamento de Física, Faculdade de Ciências e Tecnologia, Universidade Estadual Paulista "Júlio de Mesquita Filho" (FCT-Unesp), Presidente Prudente, SP, Brazil*
beatriz.carvalho@unesp.br
[2]*Departamento de Química, Faculdade de Ciências, Universidade Estadual Paulista "Júlio de Mesquita Filho" (FC-Unesp), Bauru, SP, Brazil*

Abstract: The electrospinning technique allows the development of nanofibers with high surface area, porosity and flexibility. Poly(vinylidene fluoride) (PVDF) is a fluoropolymer that has a piezoelectric effect, interesting for technological applications. Reduced graphene oxide (rGO) is a derivative of graphene and can be obtained from the thermal or chemical reduction of graphene oxide. Thus, PVDF nanofibers with rGO were produced for application in gas sensors. For this, a solution of pure PVDF and PVDF with 6% rGO were prepared to analyze the influence of rGO on the sensor response. The membranes were morphologically characterized by scanning electron microscopy (SEM) and as an ammonia gas sensor, resulting in graphs of current (*I*) measurements by time (t) in the presence of the gas. Through the results obtained, it was determined that the rGO allowed greater sensitivity in the detection of ammonia gas than in pure PVDF nanofibers, proving to be a good additive for this application.
Key words: *polymeric nanofibers, reduced graphene oxide, electrospinning, gas sensor.*

Introduction

With the advancement of the areas of nanoscience and nanotechnology over the years, the search for the development of nanomaterials with improved properties has been growing, and with that the interest in the use of techniques that allow their production. In this sense, electrospinning stands out for being a simple and versatile technique capable of producing fibers with varied composition, morphology, and diameters ranging from nanometers to micrometers [1]. Electrospun nanofibers have wide applications in technological, environmental, and biomedical areas, due to their high surface area to low volume ratio, porosity, flexibility, mechanical performance, processing simplicity, and relatively low cost [2]. Among the materials that can be used to produce fibers, polymeric materials stand out due to their low development cost, easy preparation, and relatively simple functionalization properties [3]. The poly(vinylidene fluoride) (PVDF) is a semi-crystalline thermoplastic polymer, soluble in organic solvents, with thermal stability, mechanical, chemical, and aging resistance, and good processability, in addition to being light and flexible [4]. Reduced graphene oxide (rGO) is a graphene derivative and can be obtained from the thermal or chemical reduction of graphene oxide (GO). rGO is used in gas sensors because the absorption of the gas molecule induces a change in the electrical conductance of graphene, so it can detect some molecules present in the environment, including ammonia [5]. In this work, PVDF nanofibers with rGO were produced for application in gas sensors. For this, solutions of pure PVDF and PVDF with 6% were prepared. After the nanofibers were prepared using the electrospinning technique, the membranes were analyzed by scanning electron microscopy (SEM) and as a gas sensor, so the response of the sensor in the presence of ammonia gas was observed through the variation of the electric current in the gas for a certain time.

Experimental

Materials

In this work, poly(vinylidene fluoride) (PVDF) with a molar mass of 534,000 g/mol, from the brand Arkema Kynar, was used. As a solvent, we used dimethylformamide (DMF) (99.8%), sold by Synth. As an additive, reduced graphene oxide (rGO) was used, synthesized by the group of Professor Luiz Carlos da Silva Filho from the São Paulo State University (Unesp), campus in Bauru – SP.

Methods

Two samples were prepared, one of pure PVDF and one of PVDF varying the concentration of the rgo additive in 6%. PVDF solutions in DMF were prepared at a concentration of 15% (m/m), and the solutions were under magnetic stirring for 2 h at 70 °C, as seen in Fig 1. The rGO solution were prepared at concentrations of 6%, remaining in an ultrasonic bath for 2 h. After the solution preparation time, the rGO solution were mixed with the PVDF solution, remaining under magnetic stirring for 30 min at room temperature (25 ºC).

Figure 1: PVDF solution under magnetic stirring (Carvalho, 2022).

After preparing the solutions, the nanofibers were produced using the electrospinning technique. Electrospinning involves an electrohydrodynamic process, during which a drop of liquid is electrified to generate a jet, followed by stretching and elongation to generate fibers [6]. As can be seen in Fig 2, for this process to occur it is necessary to have a polymeric solution, which is a mixture of a polymer and a solvent, placed in a syringe equipped with a needle, which must be connected to a high voltage source, which varies from 0 to 30 kV, and a collector that is responsible for collecting the nanofibers.

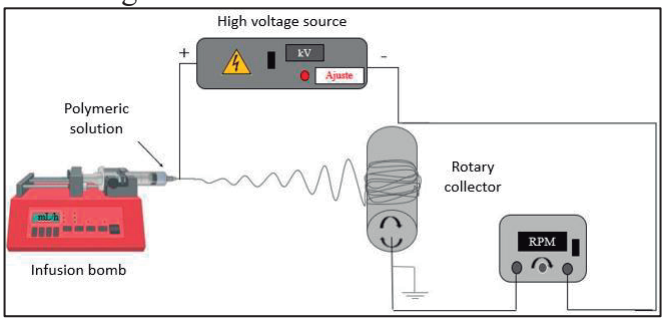

Figure 2: Electrospinning system [6].

Thus, PVDF and rGO/PVDF solution were placed in a 5 mL syringe equipped with a metallic needle measuring 1.60x40 mm (16G) in diameter. The syringe was inserted into the infusion pump, then the needle was connected to the high-voltage source, with a positive charge output and the metallic rotary collector being grounded at the negative output, thus generating a field between the tip of the needle and the collector, due to the applied potential difference, which

was maintained at 10 kV. The distance between the needle and the collector was 15 cm, the flow rate was 0.3 mL/h and the collector was rotated at 400 rpm. Thus, the solutions were ejected from the needle towards the rotating collector.
For analysis as a gas sensor, the nanofibers deposited on the interdigitated gold electrodes (IDE) were placed in the sample holder in Fig 3, thus a nitrogen flow was applied for a time of 2 min, and ammonia gas for 1 min, 5 exposure cycles were performed interspersing gas exposure. Thus, it was possible to analyze the influence of the organ on the sensitivity of the nanofibers in detecting the presence of ammonia gas.

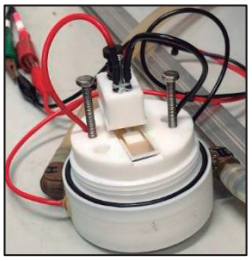

Figure 3: Sample holder for EDIs and realization of electrical and gas measurements. (Carvalho, 2022).

Results and Discussion

From the SEM images shown in Fig 4, it is observed that the nanofibers have good morphology and there is the presence of beads as the concentration of rGO increases, this is because rGO tends to form aggregates due to Van der Waals forces [7], causing the material to accumulate at these points. But with the additive the fibers became thinner, this is observed in the graphs of the variation of diameters, and for the pure polymer, the average diameter is 326 nm, and with the additive the average diameter decreases to 175 nm with 6% rGO, this is due to the increase in the ionic conductivity of the solution with the addition of rGO, resulting in greater mobility of the ions in the solution, thus, with the application of an external electric field the charges are oriented allowing the drop to undergo greater stretching or mechanical stretching during the electrospinning process, favoring the formation of fibers with reduced diameter [8].

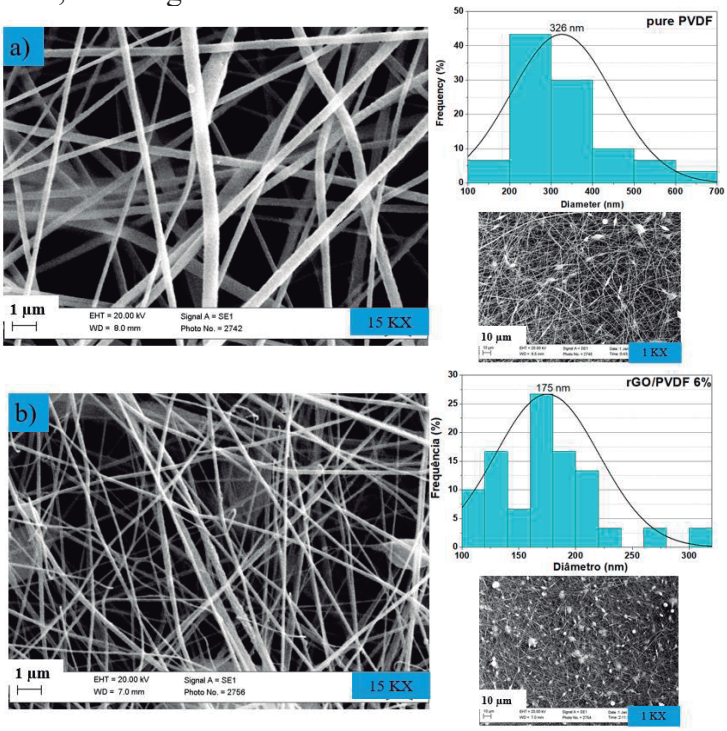

Figure 4: SEM images of nanofibers from a) pure PVDF and b) PVDF with 6% rGO.

It is observed from the graphs in Fig 5 that the nanofibers containing rGO provided gas detection responses in all exposure cycles and this was not observed for the nanofibers containing only pure PVDF, this because the absorption of the gas molecule induces a change in the electrical conductance of graphene [5].

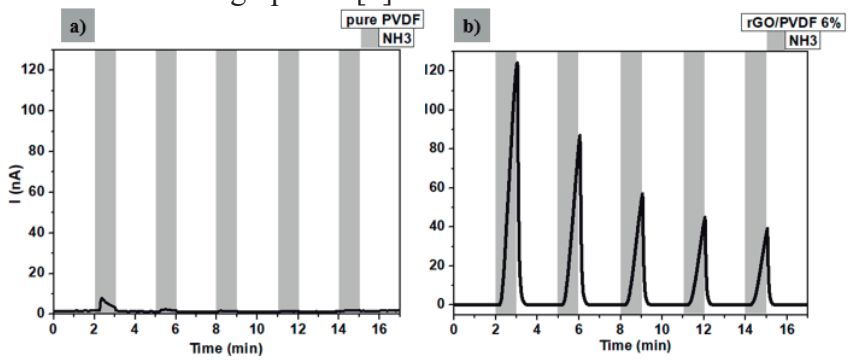

Figure 5: Gas measurements for samples a) pure PVDF and b) PVDF with 6% rGO.

Futhermore, it is observed in Fig 6 that the nanofibers containing rGO allowed a faster gas detection (10 s) than the pure PVDF nanofibers (15 s). The time of 40 s observed in the nanofibers with organ after the gas exposure time (180 s or 2 min) refers to the time that nitrogen took to clean the membrane surface for the next exposure cycle to occur.

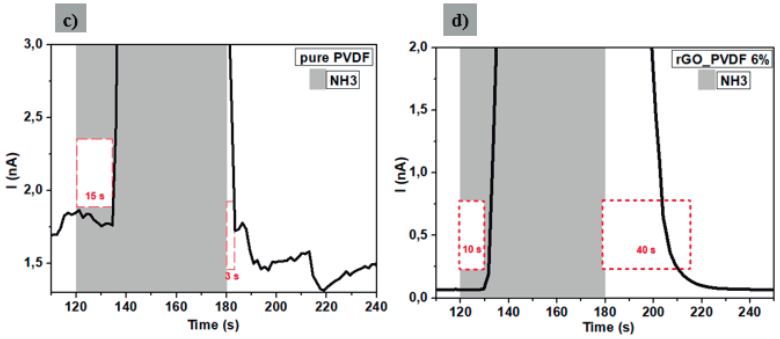

Figure 6: Graphs displaying the ammonia gas detection time for nanofibers of c) pure PVDF and d) PVDF with 6% rGO.

Conclusions

We can conclude that it is possible to produce PVDF nanofibers with the rGO additive. The rGO allowed the formation of thinner fibers. For gas sensor applications, rGO proved to be an efficient additive for ammonia gas detection, exhibiting higher current variation values and faster detection.

Acknowledgements

The authors would like to thank CNPq, LabMEV–FCT/UNESP, INEO and FAPESP. CAPES-PRINT-UNESP 2022 - Unesp Network for the development of organic and flexible electronics – ORGFLEX. This research used facilities of the Brazilian Nanotechnology National Laboratory (LNNano), part of the Brazilian Centre for Research in Energy and Materials (CNPEM), a private non-profit organization under the supervision of the Brazilian Ministry for Science, Technology, and Innovations (MCTI). The (NNano staff is acknowledged for the assistance during the experiments (20230903).This study was financed in part by the Coordenação de Aperfeiçoamento de Pessoal de Nível Superior - Brasil (CAPES) - Finance Code 001.

References

[1] L. Mercante; R. Andre; J. Macedo; A. Pavinatto; D. Correa. Química Nova 2021, 6, 44, 717-736. https://doi.org/10.21577/0100-4042.20170721

[2] M. Tebyetekerwa; S. Ramakrishna. Matter 2020, 2, 279-283. https://doi.org/10.1016/j.matt.2020.01.004
[3] B. Adhikari; S. Majumdar. Elsevier 2004, 7, 29, 669-766. https://doi.org/10.1016/j.progpolymsci.2004.03.002
[4] J. Zhang et al. Elsevier 2013, Vol 448, 81-92. https://doi.org/10.1016/j.memsci.2013.07.064
[5] L. Wen, F. Rao, L. Dong. Graphene Sensors: Interlayered. In Dekker Encyclopedia of Nanoscience and Nanotechnology, 2014.
[6] J. Xue; T. Wu; Y. Dai; Y. Xia. ACS Publications, 2019, 119, 8, 5298-5415. https://doi.org/10.1021/acs.chemrev.8b00593
[7] M. Bastiurea; M.S. Rodeanu; D. Dima; M. Murarescu; G. Andrei. Thermal and mechanical properties of polyester composites with graphene oxide and graphite, 2015.
[8] R. Costa; C. Ribeiro; L. Mattoso. Ingenta Connect 2010, 2, 2, 157-162. https://doi.org/10.1166/sam.2010.1065

CELLULOSE NANOCRYSTALS FROM BANANA FIBER: EXTRACTION AND APPLICATION IN DENTAL MATERIALS

Jamille Bazzo Scurupa[1], Marcia Margarete Meier[1]*

1 – Department of Chemistry, Santa Catarina State University(UDESC), Santa Catarina, SC, Brazil
marcia.meier@udesc.br

Abstract - The high aspect ratio and surface reactivity of cellulose nanocrystals (NCC) make its application quite versatile as a reinforcement particle, due to the potential to chemically modify its surface. Considering this context and the abundance of plant fibers from Brazilian agribusiness, the objective of this work was to develop NCC extraction strategies from a lignocellulosic source abundant in Santa Catarina, banana tree fiber, and functionalize its surface with γ-methacryloxypropyltrimethoxysilane (MPS) and evaluate its compatibility with methacrylate polymers, commonly used in dental materials. Thus, the NCC were extracted under different conditions according to a 2^3 factorial design with a central point to establish the optimized conditions. Nanocomposites containing 0.5 and 2.0% of NCC in methacrylate polymer indicate a significant increase in microhardness and elastic modulus, as a result of the compatibilization caused by MPS.

Keywords: cellulose nanocrystals (NCC), dental, nanocomposite, methacryloxypropyltrimethoxysilane

Fundings: This is study was supported by FAPESC (2021TR000654) and CAPES (Coordenação de Aperfeiçoamento de Pessoal de Nível Superior – Código de Financiamento 001).

Introduction

Dental caries is one of the most common bacterial infections, which promotes demineralization and consequent loss of dental tissue that is replaced by dental composites, also called resins. The composite consists of a polymer matrix based on hydrophobic methacrylate monomers, inorganic fillers as reinforcement and a coupling agent such as an organosilane to link the two phases.

In turn, cellulose nanocrystals (NCC) have a needle shape, high crystallinity, abundance of hydroxyl groups along the surface that confer a hydrophilic character to the nanoparticle. The surface reactivity makes it possible to functionalize the NCC with different molecules, making the nanoparticle compatible with different polymer matrices, acting as a reinforcing structure [1, 2].

Plant fibers are an important source of NCC. In this context, the cultivation of banana trees is a highlight within Brazilian production, and the high production also causes a high generation of waste due to the commercial use of the fruit alone. From this residue it is possible to extract nanocrystals and nanofibers with application in the personal care, cosmetics, paints, composites, medical care industry, among others [3]. Fig 1 illustrates the extraction process of the crystalline region of cellulose by acid hydrolysis.

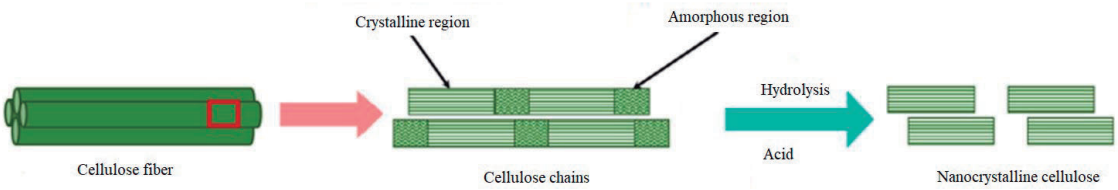

Figure 1 – Scheme representing the extraction of crystalline nanocellulose by acid hydrolysis.

Unlike conventional composites, nanocomposites have a low filler content that is well dispersed in the matrix, not requiring the incorporation of a large amount, and with the addition of approximately 5% good mechanical properties are already obtained [4,5].

Faced with the abundance of lignocellulosic raw material in Brazil, combined with the need to increase and added value of agribusiness waste, this project proposes the extraction of cellulose nanocrystals from banana fiber and its functionalization with MPS in order to make nanoparticles compatible with the polymer matrices used in dental restoration materials.

Experimental

The NCC were extracted from the banana pseudostem using different conditions of sulfuric acid concentration, temperature and time, according to a 2^3 factorial design with a central point to establish the optimized conditions, aiming at higher extraction yield and crystallinity. The NCC were characterized according to their morphological appearance (FEG, Jeol, DSM940A, and TEM, Jeol, JEM2100), crystallinity by X-ray diffractometry (DRX, Shimadzu, XRD-600) and thermal stability by thermogravimetric analysis (TG, TGA 449C, Netzsch, under synthetic air flow atmosphere and 10ºC.min^{-1}). NCC functionalized with MPS were characterized by X-ray photoelectron spectroscopy (XPS), TG and infrared spectroscopy (FTIR, Bruker, Invenio-S) by ATR.

The nanocomposites were prepared by dispersing 0.5 and 2.0 wt% of functionalized (RNCCMPS0.5 and RNCCMPS2.0) and non-functionalized (RNCC0.5 and RNCC2.0) NCC in a polymeric matrix composed of BisGMA resins (bisphenol A-glycidyl methacrylate) and TEGDMA (triethyleneglycol) (50/50 wt%) containing 0.6% of camphorquinone, 1.2 wt% of ethyl-4-dimethylaminobenzoate and 0.05 wt% of butyl hydroxytoluene. Specimens were prepared by light curing the resin for 50s/face with a curing light (Schuster LED, λ_{max} = 468 nm). The composites were characterized in terms of flexural strength and modulus of elasticity (EMIC DL50, 20x2x2 mm), Vickers microhardness (Shimadzu HMV-2T) and degree of conversion (FTIR).

Results and Discussion

The result obtained from the factorial design indicates a strong interaction between sulfuric acid concentration and temperature on the NCC extraction yield. Thus, the extraction of NCC performed with 55% sulfuric acid, 45ºC and for 75 minutes generated nanocrystals with higher yield (45%), in the form of rods and nanometric dimensions (122 ± 26 nm by 4 ± 1 nm, with a ratio of aspect of 31 ± 8), as shown in the micrograph shown in Fig 2.

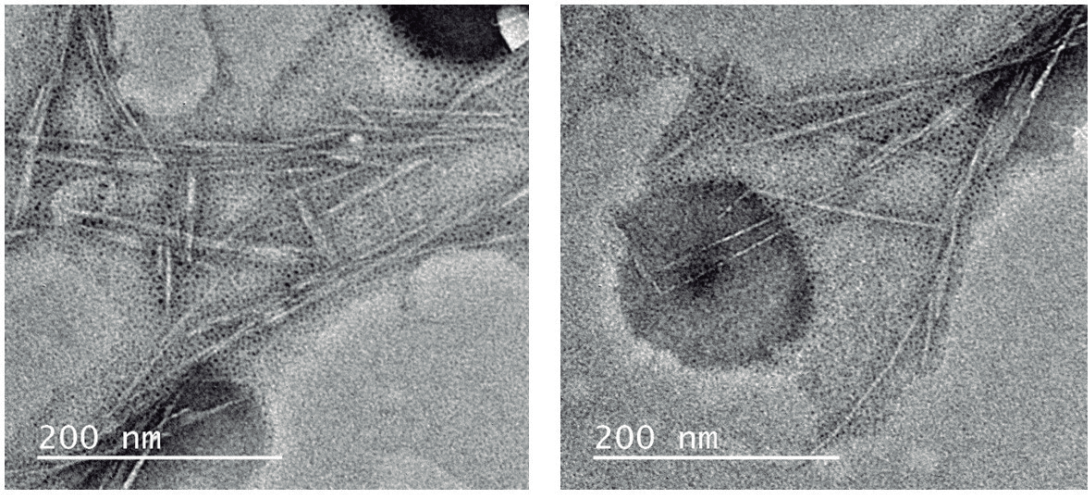

Figure 2 - TEM micrographs of NCC extracted from banana fiber and stained with 2% m/v phosphotungic acid.

Spectroscopic data (FTIR, Fig.3) indicate the presence of a signal associated with the C-O-S bond at 811 cm^{-1}, suggesting the insertion of sulfate groups by sulfuric acid during the hydrolysis process. Hydrolysis also caused a reduction in the thermal stability of cellulose, whose degradation peak temperature decreased from 361ºC (bleached fiber) to 317ºC after acid hydrolysis and generation of NCC. The NCC obtained showed 86% of crystallinity, a result similar to other authors [5].

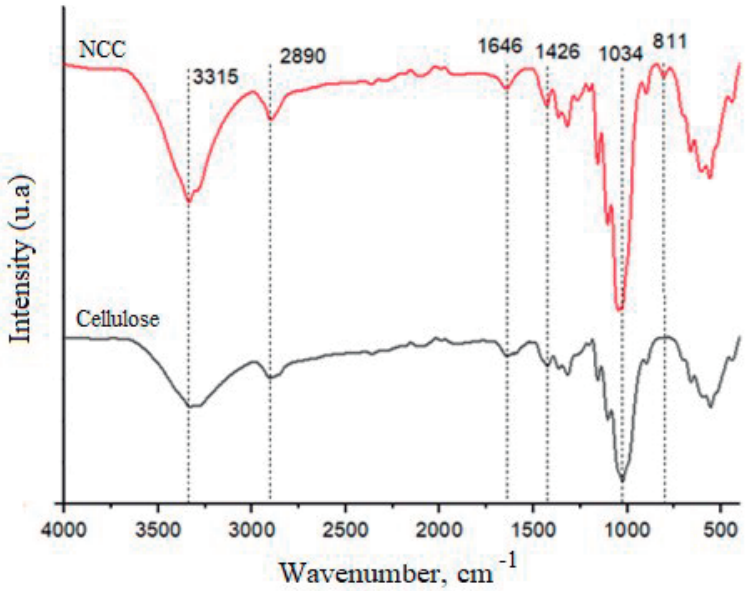

Figure 3: FTIR spectra of cellulose after bleaching and NCC.

The chemical modification of NCC by the insertion of MPS groups was confirmed by the increase of the sample residue above 700ºC, after TG analysis under synthetic air flow. There was an increase in residue from 7.21% to 18.4%, caused by the presence of silicon atoms that did not generate volatile by-products during the analysis. Atomic composition data obtained by XPS indicate an increase in the content of silicon atoms from 2.0 to 8.9% after functionalization with MPS.

The nanocomposites showed a statistically similar degree of conversion to each other, with values ranging from 27.7 to 31.9%. On the other hand, the dispersion of 0.5% NCC-MPS caused an increase in the contact angle of the sample surface from 63.2 (polymer only) to 73.5%, indicating a change in the polarity of the composite due to the presence of the nanoparticle modified.

Fig 4 presents the Vickers microhardness results of the nanocomposites. The different letters between the groups indicate a statistically significant difference (ANOVA, $p<0.05$) between the groups, with the RNCCMPS0.5 and RNCCMPS2.0 groups presenting higher values, suggesting that the functionalization of the NCC surface with MPS contributed to the increase in microhardness due to the formation of a covalent bond between the nanofiller and the polymeric matrix, mediated by the MPS molecule.

On the other hand, the addition of NCC to the polymer matrix caused a reduction in the flexural strength of the nanocomposites (Fig 5a) and consequently an increase in the modulus of elasticity (Fig 5b).

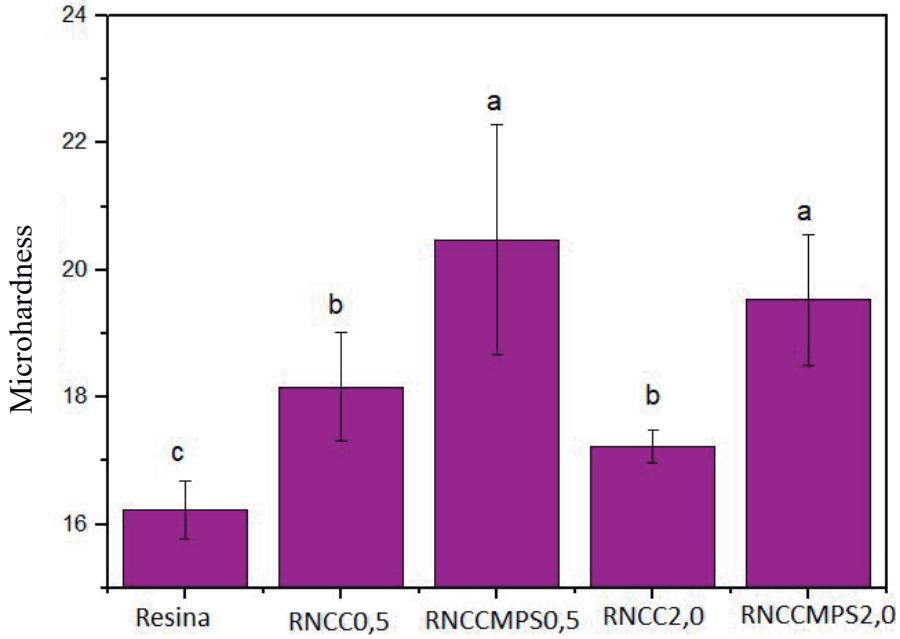

Figure 4 - Vickers microhardness of polymerized resin (BisGMA and TEGDMA copolymer) and nanocomposites containing NCC, n=3. Different letters indicate statistically significant difference between groups (ANOVA, $p<0.05$).

The flexural strength of the nanocomposites decreased when compared to the unfilled copolymer (Fig 5a). This behavior may also be associated to a tendency of the NCC agglomerates due to hydrogen interactions from the remaining hydroxyl groups on their surface. The mechanical properties are influenced by the particle size distribution, but also by how these filler particles are dispersed in the polymer structure [6]. This can be observed by the group containing 2.0% of NCC which presented lower flexural strength compared to the group containing 0.5% NCC, likely due to NCC agglomeration at higher levels [5, 6].

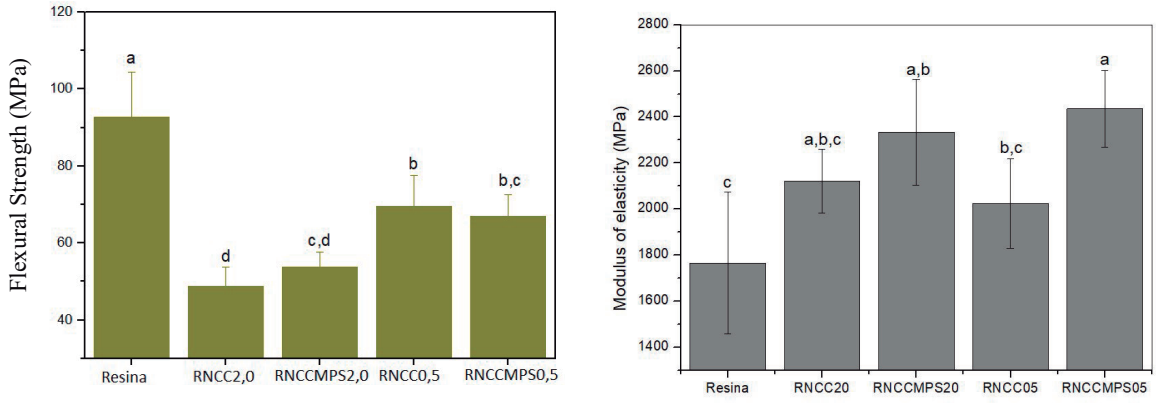

Figure 5 - Flexural strength (left) and modulus of elasticity (right) of polymerized resin (copolymer of BisGMA and TEGDMA) and nanocomposites containing NCC, n=5. Different letters indicate statistically significant difference between groups (ANOVA, $p<0.05$).

Nanocomposites prepared with NCC functionalized with MPS show an increase in elastic modulus, increase of 38% for RNCCMPS0.5 and approximately 32% for RNCCMPS2.0 compared to the control group (Resin), which suggests better interfacial adhesion between the nanocrystals and the matrix. Therefore, the incorporation of functionalized NCC at low concentrations, such as 0.5%, may reflect significant increases in the modulus of elasticity. In this case, the advantage of functionalized composites over non-functionalized ones resides in the covalent bonds formed between the nanoparticles and the polymeric matrix.

Conclusions

It is possible to extract NCC from banana pseudostem with adequate yield. The chemical modification of the surface of NCC by MPS mediated the formation of covalent bonds between the surface of the nanoparticle and the polymeric matrix, increasing the microhardness of the nanocomposites and the modulus of elasticity, acting as a reinforcement nanofiller.

Acknowledgements

The authors thank UDESC, FAPESC (FAPESC, TO 2021 TR000654) and CAPES.

References

1. R. SILVA et al. Materials Science and Engineering C 2016, 58, 389–395. https://doi.org/10.1016/j.msec.2015.08.041
2. Q. YU et al. Carbohydrate Polymers 2019, 217, 168–177. https://doi.org/10.1016/j.carbpol.2019.04.049
3. M. RAJINIPRIYA et al. ACS Sustainable Chemistry and Engineering 2018, 6, 2807–2828. https://doi.org/10.1021/acssuschemeng.7b03437
4. A. PEREIRA et al., Carbohydrate Polymers 2014, 112, 165–172. https://doi.org/10.1016/j.carbpol.2014.05.090
5. G. SIQUEIRA; J. BRAS; A. DUFRESNE Polymers 2010, 2, n. 4, 728–765. https://doi.org/10.3390/polym2040728
6. M. HOSSEINALIPOUR; J. JAVADPOUR; H. REZAIE Journal of Prosthodontics 2010, 19, 112–117. https://doi.org/10.1111/j.1532-849X.2009.00530.x

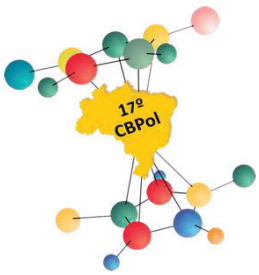

CHARACTERIZATION OF HEMICELLULOSE FILMS AS A CONDUCTIVE FLEXIBLE SUBSTRATE FOR APPLICATION IN SENSORS

Layse Mendes Diniz[1]*, Lays Furtado de Medeiros Souza Kataoka[1], Michaella Socorro Bruce Fialho[1], Wladymyr J. B. de Sousa[2] and Sandra Maria da Luz[1]

1 – Department of Mechanical Engineering, University of Brasilia (UnB), Brasília, DF, Brazil.
laysemendis@hotmail.com

2 - Graduate Program in Materials Engineering, Federal University of Campina Grande (UFCG), Campina Grande, PB, Brazil.

Abstract - The use of polymers by society has grown constantly, as these polymers are mostly artificial and take years to degrade in the environment, causing various environmental impacts. Research on natural polymers has become prominent in the scientific community to alleviate this situation. In addition to being obtained from renewable energy sources, natural polymers are polymers that degrade more quickly in nature. An example of a natural polymer is hemicellulose, among the most abundant biopolymers in nature. Hemicellulose is extracted from plant fibers, and because it is a biodegradable material, interest in using it has increased. Among the possible applications for hemicellulose, we can mention its use as a flexible conductive substrate due to its low cost, low density, flexibility, and the possibility of recycling. Therefore, this work aims to develop conductive hemicellulose films with silver nanoparticles and thus evaluate their potential use as a conductive flexible substrate. First, the hemicellulose was extracted from the jute fiber with KOH 10% w/v. Then polymeric films of pure hemicellulose and nanocomposites of hemicellulose with different silver nanoparticles (AgNPs) content (0.25 to 5 wt%) were manufactured using the water casting technique. After. the films were characterized using TGA (Thermogravimetry), DSC (Differential Scanning Calorimetry), FTIR (Spectroscopy in the Infrared Region with Fourier Transform), benchtop multimeter, and hot plate. The hemicellulose and silver nanoparticle films showed thermal stability at 170°C and thermal degradation at 262°C. Hemicellulose films with 5.0 wt% AgNPs showed the best conductivity result at room temperature. By increasing the temperature, all films showed a lower conductivity. It can be concluded that the hemicellulose films showed good characteristics to be used as a conductive flexible substrate in sensors, and the films with 5.0 wt% AgNPs were the ones that presented the best performance for such use.

Keywords: *conductive flexible substrate, hemicellulose, films, temperature sensor.*

Introduction

Technological advances and the demand for electronic sensors in the most diverse areas and applications, such as humidity, pressure, voltage, vibration, movement, temperature, energy, pH, and chemical compounds sensors [1], have stimulated the development of flexible conductive components that can be obtained from environmental friendly materials and that are produced in large scale and at low cost.

In this sense, the high demand for raw materials for producing these conductive components inevitably lead to severe environmental problems. To minimize negative environmental impacts, increase economic viability, and meet energy efficiency requirements, natural polymers are being increasingly explored as candidates to replace some conventional materials in the manufacture of these devices.

These polymers occur widely in nature or are extracted from plants or animals. Among the various existing natural polymers, hemicellulose can be highlighted. It can be extracted from plant fibers or lignocellulosic fibers, which are made up of three main components (percentage by weight): cellulose (40-60%), hemicellulose (20-40%), and lignin (10-25%) [2], depending on the source.

Hemicellulose polymers are branched, totally amorphous, partially soluble in water, and hygroscopic [3]. Because it is a biodegradable material and renewable source, there has been an increase in interest in using hemicellulose for a variety of applications. Despite having these good qualities, hemicellulose is still little studied compared to other natural polymers, such as cellulose.

Therefore, this research proposes an innovative and simplified study of using hemicellulose as a flexible substrate for application as a sensor. The main objective is to know the electrical behavior of substrates based on hemicellulose aggregated with silver nanoparticles, thus evaluating the viable possibilities for its application in manufacturing flexible temperature sensors.

Experimental

Hemicellulose Extraction and Obtaining Films

The hemicellulose extraction procedures were performed according to [4]. About 10 g of fibers were immersed in 200 mL of distilled water for 1 h and filtered. The fibers were added to the 10% KOH solution (w/v), remaining under orbital agitation at 250 rpm and mechanical agitation at 50 rpm for 3 h. They were then filtered, and the liquor obtained had its pH adjusted to 4.8 using acetic acid. After 24 h, the liquor was centrifuged for 5 min at 4000 rpm. A solution (1:10 acetic acid and ethanol) was added to the liquor to precipitate the hemicellulose. The resulting solution was filtered, and a portion of hemicellulose was obtained. Afterward, a film was produced using the "water casting" technique, in which the material was molded using water as a solvent. For this, the hemicellulose was solubilized in distilled water at a concentration of 33% (w/v) under magnetic stirring for 2 h at 35°C. Afterward, the solution was centrifuged at 4000 rpm for 10 min and poured onto a glass plate (30 x 40 cm), allowing the film to dry at 25°C. Different concentrations of AgNPs (0.25, 0.50, 1, and 5 wt%) were incorporated to prepare conductive flexible substrates from the hemicellulose. Then, the solution was under magnetic stirring for 10 min at 25°C. And finally, the solution was deposited on a glass plate (15 x 15 cm), until drying at room temperature and film formation.

Characterization of Nanocomposites

Thermogravimetry (TGA) and Differential Scanning Calorimetry (DSC) tests were carried out for hemicellulose films and their nanocomposites in a simultaneous thermal analyzer TGA/DSC, model SDT Q600 (TA Instruments), in an alumina crucible, under N_2 atmosphere with a flow of 50 mL/min, at a heating rate of 10°C/min, starting at room temperature up to 950°C.

Fourier Transform Infrared Spectroscopy (FTIR) was performed for hemicellulose films and their nanocomposites using a Thermo Scientific Nicolet iS10 spectrometer with the transmittance accessory. Spectra were collected in the 400 to 4000 cm^{-1} range, with a resolution of 4 cm^{-1} and 64 scans.

An ET-1649-Minipa digital multimeter and a heating plate were used to obtain the conductivity of these films. By varying the temperature, the electrical voltage and electrical current were measured. The electrical conductivity was calculated using the 1st and 2nd Ohm's Law, following Equations [1], [2] and [3].

$$\mathbf{U=R.I} \quad [1] \qquad \mathbf{R=\rho.L/A} \quad [2] \qquad \boldsymbol{\rho} = 1/\boldsymbol{\sigma} \quad [3]$$

Where: U = Electric voltage in V, R= Electric resistance in **Ω**, I= Electric current in A, $\boldsymbol{\rho}$ = Resistivity in **Ω**.m, L = conductor length in m, A= conductor cross-sectional area in m2, $\boldsymbol{\sigma}$ = Conductivity in **S/m**.

Results and Discussion

Fig 1 presents the FTIR spectra for the hemicellulose and nanocomposite films. Absorption bands are attributed to functional groups of hemicellulose cell wall components. A more intense stretching band is observed at approximately 3302 cm^{-1}, referring to the hydroxyl groups (OH) present in the hemicellulose in the residual water in the sample [5]. At 2915 cm^{-1} there is a band corresponding to the stretching vibration of the CH group, symmetrical and asymmetrical in hemicellulose components [6]. The short band at 1664 cm^{-1} is associated with absorbed moisture. The band at 1533 cm^{-1} represents vibrations of CH and OH groups in hemicellulose. At 1410 cm^{-1}, the C-H ester band refers to partial acetylation of hydroxyl groups in hemicellulose [7]. And a band at 1045 cm^{-1} is due to the elongation of side groups (C-OH) and glycosidic bonds (C-O-C) of hemicellulose [7].

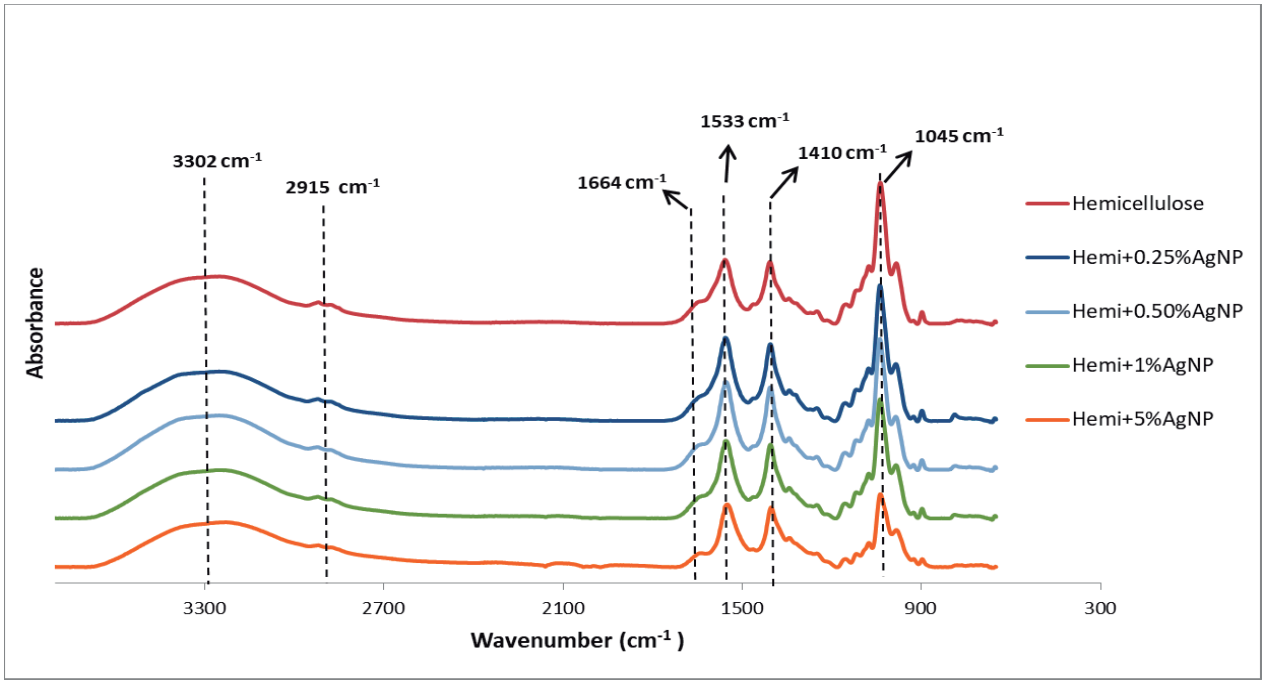

Figure 1- FTIR spectrum of Hemicellulose films and their nanocomposites.

Fig 2 illustrates the thermal characterization of hemicellulose and nanocomposite films by TG and DSC. In Figure 2(a) it is observed that there are four weight loss stages. The first peak, of lesser intensity, which occurred at 48°C, is the beginning of hemicellulose moisture loss, with dehydration and cleavage of its side chains, and belongs to the first weight loss stage. The second degradation peak occurred at 216°C and the third one at 263°C. The third peak showed a higher intensity of degradation compared to the second peak. Both peaks belong to the second stage, referring to hemicellulose degradation. The fourth peak occurred at 442°C and the fifth at 810°C and referred, respectively, to portions of lignin and residues of the KOH solution with its possible conversion into oxide. The thermal degradation of lignin occurs in the temperature range between 225ºC and 450ºC [8]. The thermal stability shown was an average of 170°C. And hemicellulose residue content was 8.4%.

As shown in Fig 2(b), four main thermal events were detected for Hemicellulose films and nanocomposites. The first is endothermic and has low energy, occurring around 50°C and is related to moisture loss; a second endothermic event is related to the glass transition temperature (Tg) of the hemicellulose, occurring at 191ºC; the third event is exothermic, at 262°C and corresponds to the degradation of hemicellulose [9]; and in the fourth event, the occurrence of broad and poorly defined endothermic undulations is observed, without characterizing peaks, attributed to the degradation of the cellulosic portion present in the samples. Other events, such as an endothermic peak at 758°C, can also be observed, which may be related to lignin pyrolysis. And another exotherm at 803°C refers to the residual potassium oxides in the extraction solution.

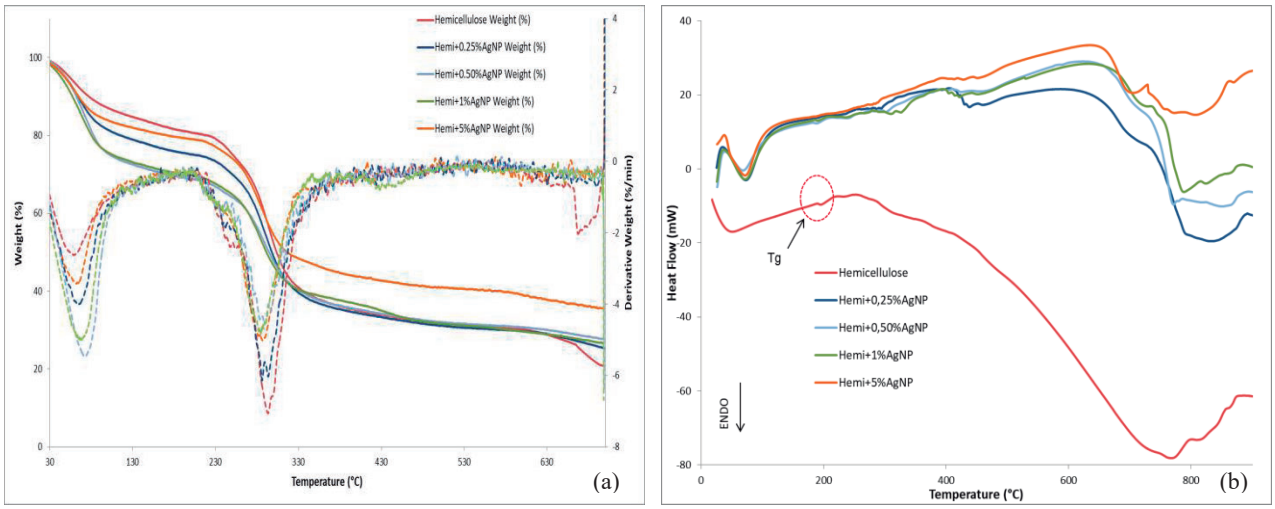

Figure 2 - (a) TG and DTG (dotted curves), and (b) DSC curves of hemicellulose films and their nanocomposites.

Table 1 shows the electrical resistance and conductivity values for hemicellulose and nanocomposite films. From the values found for electric current and voltage, Eq. 1, 2, and 3 calculate the electrical resistance values, resistivity, and, consequently, its conductivity.

Table 1 - Electrical resistance and conductivity results for hemicellulose and hemicellulose films with 0.25, 0.50, 1.0, and 5.0 wt% of silver nanoparticles (AgNPs).

	HEMICELLULOSE		HEMICELLULOSE+ 0.25%AgNP		HEMICELLULOSE+ 0.50%AgNP		HEMICELLULOSE+ 1%AgNP		HEMICELLULOSE+ 5%AgNP	
Temperature (°C)	**Electrical resistance (Ohm)**	**Conductivity(S/m)**	**Electrical resistance (Ohm)**	**Conductivity(S/m)**	**Electrical resistance (Ohm)**	**Conductivity(S/m)**	**Electrical resistance (Ohm)**	**Conductivity(S/m)**	**Electrical resistance (Ohm)**	**Conductivity(S/m)**
25	183.68	0.16	164.37	0.17	125.95	0.23	92.42	0.31	84.43	0.34
30	194.94	0.15	169.21	0.17	113.47	0.25	107.02	0.27	104.28	0.27
35	224.63	0.13	205.31	0.14	171.30	0.17	121.14	0.23	115.34	0.25
40	389.09	0.07	360	0.08	285.93	0.10	111.27	0.25	122.43	0.23
45	1251.67	0.02	412.5	0.07	303.82	0.09	156.87	0.18	138.05	0.21
50	1007.14	0.03	200	0.14	331.33	0.08	207.14	0.14	208.78	0.14

It is observed that the samples with 0.25% of silver nanoparticles showed conductivities lower or similar to those of the hemicellulose film. It can be inferred that in these situations there was not a good dispersion of the nanoparticles in the hemicellulose polymeric matrix, so this makes conduction by means of electrons more difficult.

As expected, the results showed that at room temperature (25ºC), the higher the percentage of AgNPs in the nanocomposite composition, the greater the resulting electrical conductivity since a greater amount of conductive nanoparticles is dispersed in the film, facilitating the conduction of

electrons. In the Hemicellulose+5%AgNP sample, a lower electrical resistance and, consequently, a higher conductivity (0.34 S/m) was observed compared to the other samples. It can be inferred that the amount of silver nanoparticles was sufficient to disperse well in the matrix and conduct electrons. Noble metals like silver are generally good candidates as conductive agents due to their excellent conductivities [10].

By increasing the temperature of the samples, it is observed that there is a decrease in the conductivity value. It may be related to the disorderly movement of electrons. For example, when there is disorderly movement between the electrical charges present in a conductor, this disorganization of movement happens without creating an electric field within that conductor, causing its free electrons to develop a disordered movement [11], thus not presenting good conductivity.

Conclusions

In the present work, we verified good thermal stability for hemicellulose films and their nanocomposites. When producing hemicellulose films with different percentages of silver nanoparticles (AgNPs), it was verified that the samples with the highest nanoparticles content induced a significant increase in the electrical conductivity of the film. A probable hypothesis for the results obtained is that these nanoparticles were well dispersed in the hemicellulose matrix, with 5.0 wt% being the most appropriate for use as a sensor. It was also verified that the higher the temperature to which the films were submitted, the lower the electrical conductivity values found.

Acknowledgments

The authors thank CAPES, DPG/UnB, FAPDF, and CNPq for their support.

References

1. S. Fan; L. Dan; L. Meng; W. Zheng; A. Elias; X. Wang. Nanoscale 2017, 9,1615-1621. http://dx.doi.org/10.1039/c7nr05218a.
2. M. Spinacé; C. Lambert; K. Fermoselli; M. De Paoli. Carbohydrate Polymers, 2009, 77, 47-53. http://dx.doi.org/10.1016/j.carbpol.2008.12.005.
3. X. Li; L.Tabil; S. Panigrahi. Journal of Polymers and the Environment, 2007, 15, 25-33. http://dx.doi.org/10.1007/s10924-006-0042-3.
4. L. Kataoka; M. Hidalgo; S. Luz. Journal of Natural Fibers, 2021, 1-13. http://dx.doi.org/10.1080/15440478.2021.1934934.
5. X. Zhao; T. Tong; H. Li; H. Lu; J. Ren; A. Zhang; et al. Carbohydrate Polymers, 2017, 156, 333-339. http://dx.doi.org/10.1016/j.carbpol.2016.09.041
6. A. AbdulkhanI; A. Mazhar; S. Hedjazi; Y. Hamzeh. Polymer Bulletin, 2020, 77, 6227-6239. https://doi.org/10.1007/s00289-019-03075-5.
7. M. Oliveira; L. Diniz; A. Elias; S. Luz. Polymers, 2022, 14, 2999. https://doi.org/10.3390/polym14152999.
8. M. Figueroa; P. Moraes. Ambiente Construído, 2009, 9, 157-174. 10.1590/s1678- https://doi.org/86212009000400525.
9. S. Hanim; A. Akma. Polymer science research advances, pratical applications and educational aspects, 2016, 404-411.
10. X. Du; Z. Zhang; W. Liu; Y. Deng. Nano Energy, 2017, 35, 299-320. https://doi.org/10.1016/j.nanoen.2017.04.001.
11. J. Stewart. Electric current, 2020. https://doi.org/10.1036/1097-8542.215700.

CHARACTERIZATION OF REDUCED GRAPHENE OXIDE: CHALLENGES IN DETERMINING OF ELECTRICAL CONDUCTIVITY FOR APPLICATION IN CONDUCTIVE INKS

Ygor Matheus Pereira de Paula[1]*, Maria Paula de Carvalho Freire[1], Ana Letícia Fernandes dos Santos[1], Maria Carolina Burgos Costa[2]

1 – Graduate Program in Materials Science and Engineering (PPGCEM), Federal University of Rio Grande do Norte (UFRN), Natal, RN, Brazil ygor.pereira.087@ufrn.edu.br; maria.paula.freire.110@ufrn.edu.br; analeticiaferds30@gmail.com*

2 – Department of Materials Engineering (DEMat), Federal University of Rio Grande do Norte (UFRN), Natal, RN, Brazil carolina.nascimento@ufrn.br

Abstract - Currently, one of the most viable synthesis routes to obtain graphene is the chemical exfoliation, followed by reduction of the product obtained, allowing the production of a larger amount of reduced graphene oxide (rGO). The reduction step is essential in this process, because it allows the partial elimination of oxygenated functional groups inserted in the material and thus recover its conductive properties. The results obtained by the electrical conductivity test showed that the rGO is a conductive material, but the GO (insulating material) also expressed electrical conductivity, being even higher than the rGO. It is known that this factor is linked to the solubility of these materials in water, GO being soluble, allows the uniform measurement of its conductivity, unlike the rGO, whose removal of functional groups prevents the formation of chemical bonds between this material and the water used, negatively affecting the evaluation of the product obtained.

Keywords: *Reduced graphene oxide; Chemical exfoliation; Conductive inks.*

Introduction

The discovery of graphene and its properties was a milestone in materials science, given its great emerging potential [1] cited by [2]. As cited, the properties of this material brought with it the wide interest of researchers, since, a high surface area, high intrinsic mobility, high Young's modulus and good thermal and electrical conductivity, are properties obtained by using graphene [3]. Obtaining graphene in the laboratory is something that has been studied hard by experts, several synthesis routes have been developed, but producing it in large quantities is still a problem. Chemical exfoliation allows the conversion of graphite into GO, by incorporating oxygenated functional groups between its chains, pulling them apart. Through this method, larger quantities of rGO can be obtained after the reduction of the material [4].

The addition of the functional groups in the structure of GO, makes this material an electrical insulator [5]; [6]; cited by [7]. In view of this, its conductivity can be improved by removing these groups, through a procedure called chemical reduction [8]; [9]; [10]; [11] cited by [7]. In another perspective, thermal reduction, besides being much faster than chemical reduction, also ensures the partial removal of oxygenated groups and the possibility of applying rGO in scenarios that target the electrical properties of graphene, by allowing it to be obtained in dry powder form [12]; [13] cited by [14]. The synthesis parameters directly affect the properties of the

material, one of them being the particle size of the graphite used, impacting the surface area and electrical conductivity of the synthesized rGO [4]. It is important to highlight that there is a great challenge in the characterization of the electrical conductivity of graphene in solution (conductive inks). Thus, in addition to focusing on the synthesis of graphene in the laboratory, this work aims to analyze the electrical conductivity of graphene in aqueous solution to solve challenges related to this method in future works. It is not clear in the literature the best way to determine the electrical conductivity of conductive inks, since their composition can also influence this characterization.

Conductive paints are based on the incorporation of a conductive component in the solution that constitutes the respective paint, in view of this, the search for new formulations tends to increasingly move the market. Finally, this paper aims to study and report the synthesis process used to obtain rGO, assigning it to a possible application in a conductive paint, as well as to identify the challenges encountered during the evaluation of the electrical conductivity of the material in solution.

Experimental

To start the oxidation of graphite, 192.6 ml sulfuric acid (H_2SO_4) and 21.4 ml phosphoric acid (H_3PO_4) were added to a large beaker. In view of the high exothermic character of the following reactions, the solution needs to be exposed to an ice bath in order to control the temperature and avoid further problems. The next step was to add 1.2 g of graphite powder, always aiming to use a material with the smallest possible granulometry, which was then left in magnetic stirring for 30 minutes.

After 30 minutes, 8.6 g of potassium permanganate ($KMnO_4$) were added and the solution was then gradually heated up to 40 °C, so, upon reaching thermal equilibrium, the solution was left in magnetic stirring for a period of 6 hours. Fig 1 represents the solution and its greenish coloration, after the addition of potassium permanganate. Soon after this period, 500 ml of distilled water was added in order to finish the reaction, avoid the formation of MnO_2 and consume the residual potassium permanganate. Next, 30 ml of hydrogen peroxide (H_2O_2) was added, and then the solution was stirred for a period of 1 hour. After this period, 400 ml of hydrochloric acid (HCl) was added to the solution and then the solution was stirred for 1.5 hours. At the end of this step, the solution was left to stand for 15 hours for decantation.

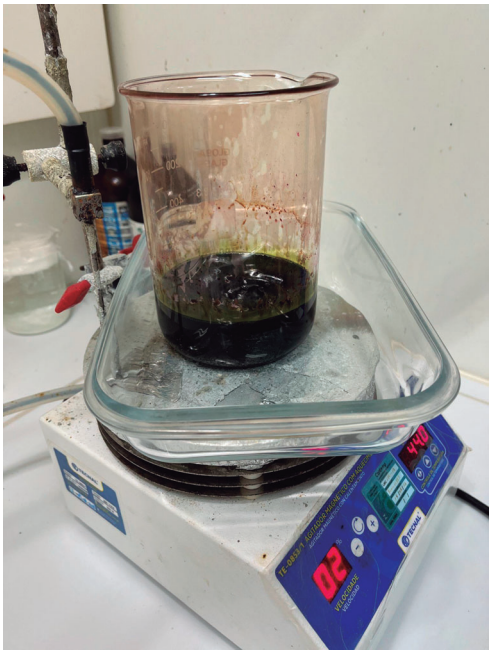

Figure 1 - Solution after the addition of $KMnO_4$

After 15 hours and with successful decantation, the liquid phase was discarded. With the resulting product, the sample was washed via centrifugation in order to neutralize the pH of the solution. Four washes were performed, using 1 L of deionized water for each of the samples. Table 1 describes the washing procedure in detail. After the washes, the obtained GO was placed in petri dishes, covered with aluminum foil and left in an oven at 90 °C to dry.

Table 1 - Washing specifications

Lavagem	Tempo (min)	Rotação (rpm)	PH
1	10	5500	1
2	10	5500	1
3	10	5500	3
4	10	5500	5

The next step is based on the reduction of GO to obtain rGO. To perform the thermal reduction procedure, a porcelain mortar embedded in a heating mantle was used. The temperature chosen for the process was 260 °C and as a result, rGO was obtained, a black colored powder and even smaller granulometry than GO [15].

Results and Discussion

Through scanning electron microscopy (SEM), performed on the obtained rGO sample, it was verified that individual sheets of graphene were obtained, as shown in Figure 2. The regions that present wrinkling are present due to the thermal reduction step, an abrupt process that can lead to other structural defects in the material if not well controlled.

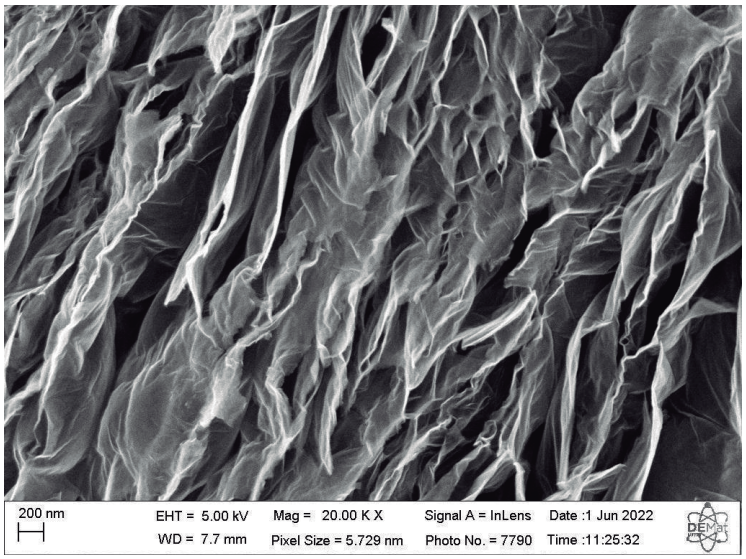

Figure 2 - SEM image of rGO sample at 20 K X magnification

X-ray diffraction (XRD) showed that both GO and rGO were satisfactorily obtained. Figure 3 and Figure 4 represent the XRD results for GO and rGO respectively. It is evident the

displacement and the reduction of the characteristic peak intensity when we relate the two images, these variations occur due to the reduction of the interplanar distance, ensuring the effectiveness of the reduction process [16].

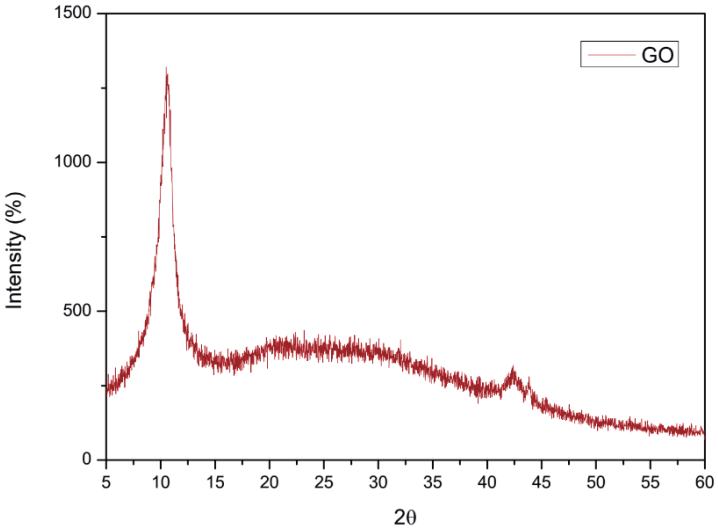

Figure 3 - XRD results for GO

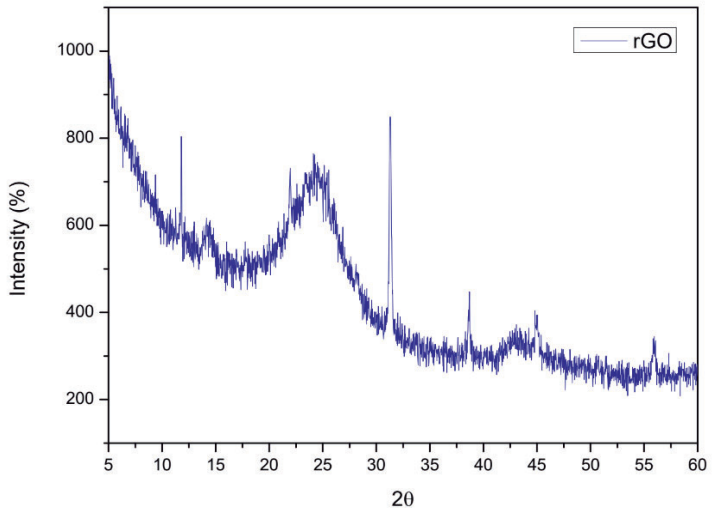

Figure 4 - XRD results for rGO

Two samples were produced, the first containing GO and water and the second, rGO and water, in order to test the conductivity of both solutes. The electrical conductivity tests performed using a conductivimeter, indicated that the conductivity of rGO was theoretically lower than that of GO, 277.20 (µS/cm) and 876.80 (µS/cm), respectively. Therefore, as GO has more oxygenated functional groups than rGO, and is consequently soluble in water, the conductivity meter detector was not able to calculate the conductivity of rGO as it was insoluble in aqueous medium and remained in suspension during the analysis.

Conclusions

In view of the SEM results obtained, it can be inferred that, despite being wrinkled, individual sheets of graphene were obtained. The interplanar separation and rapprochement was verified via XRD, proving the addition and later partial removal of functional groups. On the other hand, the electrical conductivity tests indicated results out of the expected standard, and although

rGO is a conductive material and very promising in terms of its applicability in this field, the outcome of the work entails the need to find the best method to analyze the conductivity of the materials produced in this work.

Acknowledgements

This work was supported by capes (Coordination for the Improvement of Higher Education Personnel), UFRN (Federal University of Rio Grande do Norte) and LIME (Institutional Laboratory of Metrology and Microscopy).

References

1. K, S. Novoselov; A. K. Geim; S. V. Morozov; D. Jiang; Y. Zhang; S. V. Bubonos; I. V. Grigorieva; A. A. Firsov. Science 2004, 306, 1102896. http://dx.doi.org/10.1126/science.1102896.
2. S. Eigler; A. Hirsch. Angewandte Chemie International Edition 2014, 53, 201402780. http://dx.doi.org/10.1002/anie.201402780.
3. Y. Zhu; S. Murali; W. Cai; X. Li; J. W. Suk; J. R. Potts; R. S. Ruoff. Advanced Materials 2010, 22, 201001068. http://dx.doi.org/10.1002/adma.201001068.
4. T. D. Dao; H. M. Jeong. Materials Research Bulletin 2015, 70, 201505038. http://dx.doi.org/10.1016/j.materresbull.2015.05.038.
5. H. P. Boehm; A. Clauss; G. Fischer; U. Hofmann. Proceedings Of The Fifth Conference On Carbon 1962, 9780080097077500133. http://dx.doi.org/10.1016/b978-0-08-009707-7.50013-3.
6. H. P. Boehm; A. Clauss; G. Fischer; U. Hofmann. Zeitschrift FÜR Anorganische Und Allgemeine Chemie 1962, 316, 19623160303. http://dx.doi.org/10.1002/zaac.19623160303.
7. S. Stankovich; D. A. Dikin; R. D. Piner; K. A. Kohlhaas; A. Kleinhammes; Y. Jia; Y. Wu; S. T. Nguyen; R. S. Ruoff. *Carbon* 2007, 45, n. 7, 200702034. http://dx.doi.org/10.1016/j.carbon.2007.02.034
8. A. B. Bourlinos; D. Gournis; D. Petridis; T. Szabó; A. SzeriS; I. Dékány. Langmuir 2003, 19, 026525. http://dx.doi.org/10.1021/la026525h.
9. N. A. Kotov; I. Dékány; J. H. Fendler. Advanced Materials 1996, 8, 19960080806. http://dx.doi.org/10.1002/adma.19960080806.
10. P. Xiao; M. Xiao; P. Liu; K. Gong*. Carbon 2000, 38, 0008622300000051 http://dx.doi.org/10.1016/s0008-6223(00)00005-1.
11. U. Hofmann; A. Frenzel. Kolloid-Zeitschrift 1934, 68, 01451376. http://dx.doi.org/10.1007/bf01451376.
12. C. Botas; P. Álvarez; P. Blanco; M. Granda; C. Blanco; R. Santamaría; L. J. Romasanta; R. Verdejo; M. A. López-Manchado; R. Menéndez. Carbon 2013, 65, 201308009. http://dx.doi.org/10.1016/j.carbon.2013.08.009.
13. M. J. Mcallister; J. L. LI; D. H. Adamson; H. C. Schniepp; A. A. Abdala; J. Liu; M. Herrera-Alonso; D. L. Milius; R. Car; CAR; R. K. Prud'homme. Chemistry Of Materials 2007, 37, 0630800. http://dx.doi.org/10.1021/cm0630800.
14. T. G. Maraschin. Dissertation. Pontifícia Universidade Católica do Rio Grande do Sul, 2016.
15. A. G. M. R. de Albuquerque. Dissertation. Universidade Federal do Rio Grande do Norte, 2021.
16. A. G. B. A. M. Oliveira; A. M. Lima; W. A. Pinheiro in 74th Congresso Anual da ABM, São Paulo, 2019, Vol. 74, 74.

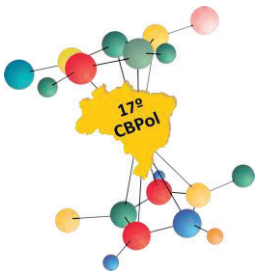

DEVELOPMENT OF ELECTROPUN MEMBRANES OF TPU/MWCNTs FOR APPLICATION IN WEARABLE SENSORS FOR HUMAN MOTION MONITORING

Bruna Caldas de Sousa [1], Johnny de Nardi Martins[2] and Claudia Merlini [2*]

1 - Mechanical Engineering Department, Federal University of Santa Catarina (UFSC), Florianópolis, SC, Brazil
2 - Engineering Special Coordinating, Federal University of Santa Catarina (UFSC), Blumenau, SC, Brazil
claudia.merlini@ufsc.br

Abstract – Piezoresistive sensors, which transform a mechanical traction effort into an electrical signal, with a change in the electrical resistivity of the sensor, have been studied for their ability to monitor various activities and health problems of the human body, and an ideal traction sensor can monitor activities such as the movement of joints in different parts of the body. In this work, electrospun membranes were produced with aligned fibers of Thermoplastic Polyurethane (TPU) with different weight concentrations of carbon nanotubes (CNT) through the electrospinning process. The produced membranes were analyzed by Scanning Electron Microscopy (SEM), electrical conductivity and tensile test. With the membranes produced, piezoresistive traction sensors were obtained, which were tested on the finger to monitor human movement. Through the SEM it was noticed that there was an alignment of the fibers with the electrospinning parameters used and despite the noise in the sensor, it was possible to observe an increase of the electrical resistivity of the sensor when bending the finger.
Keywords: *Piezoresistive sensors, electrospinning, thermoplastic polyurethane, carbon nanotubes.*

Introduction

Currently, there is a growing interest in employing wearable and highly flexible sensors in the fields of human health, robotics, prosthetics, electronic skins, among others. These sensors can be used for monitoring movement and human health, being placed on clothes, helmets, accessories and directly on the skin to detect different important physiological parameters, without influencing daily life or restricting the user's movements, informing him at all times that there is an abnormal condition [1]. Several types of wearable sensors with excellent detection performance, highly flexible and good response reproducibility are being developed with different structures and transduction mechanism [2, 3]. Among these devices, piezoresistive sensors, which transform the mechanical stimulus into an electrical signal, changing the electrical resistivity of the sensor, have been widely used because of their simple detection mechanism, ease of construction and simple structure. Among the piezoresistive sensors, the traction sensors have been widely used for monitoring human movement. However, it remains a challenge to simultaneously achieve high sensitivity, wide detection range, excellent mechanical stability, fast response/recovery for prolonged use during monitoring [3]. Wearable sensors can be obtained from conductive polymeric composites constituted by conductive fillers, dispersed in a polymeric matrix [4]. In order to obtain a wearable sensor with high performance and high sensitivity of response, it is necessary that the materials and the manufacturing process are properly selected. As a conductive filler in composites for wearable sensors, a good alternative would be carbon nanotubes (MWCNT), because they have a high aspect ratio (ratio between length and diameter), high modulus of elasticity, high tensile strength [5], enabling a good sensitivity and response reproducibility for the sensor. As a polymeric matrix in conductive polymeric composites for application in wearable sensors, a good alternative

would be thermoplastic polyurethane (TPU), because it presents an elastic behavior, having a good shape memory with small mechanical hysteresis. An interesting process for obtaining materials for application in wearable traction sensors is the electrospinning process. In this process, fibrous membranes with a three-dimensional porous structure and high surface area are obtained, giving the sensor good flexibility and extensibility, and good response sensitivity, due to the greater contact of conductive additives, the aligned fibers give the membranes greater tensile strength [6]. In view of the great importance of using wearable sensors in monitoring human movement and the challenges of obtaining a sensor with good flexibility and at the same time having durability and good response sensitivity, in this work electrospun membranes were developed with aligned fibers of a TPU polymeric matrix with conductive fillers of carbon nanotubes (MWCNTs) for application in wearable traction sensors for monitoring human movement.

Experimental

Materials

The Thermoplastic Polyurethane (TPU) used in the work is based on ether (Elastollan 1180 A10) and based on diphenylmethane diisocyanate (MDI), manufactured by Basf. The Carbon Nanotubes (NTC) (NC7000) used to obtain the electrospun membranes are manufactured by the company Nanocyl. The solvents that will be used are Tetrahydrofuran (THF) and Dimethylformamide (DMF), manufactured by Sigma Aldrich, which will be used as supplied.

Electrospinning of TPU/MWCNT mats

To obtain the electrospun mats, TPU (10 wt.%) was dissolved in 10 mL of DMF:THF [1:1] under stirring until the polymer was completely dissolved for approximately 1 hour. Subsequently, different weight fractions (wt.%) of MWCNT, 0,25, 0,5, 0,75 and 1,0 wt.% were incorporated at room temperature and the dispersion was carried out in the solution through an Ultrasonic Processors VCX 500 Disperser, at temperature of 20 °C and amplitude of 35%, for 8 minutes. An adequate amount of the solution was added to a 5mL syringe with a needle of internal diameter of 0.8mm. The solution was pumped through an infusion pump at a flow rate of 2 mL h^{-1}. The fibers were collected in a fixed collector (120 mm diameter) consisting of an aluminum plate covered with aluminum foil. The electric field was generated from a high voltage power supply (INSTOR), capable of generating a voltage of 0 - 30 kV. The positive pole was connected to the syringe needle and the negative pole to the collector. The electrospun mats were obtained using electrical voltages of 21 kV for membranes with 0.25, 0.5, 0,75 and 1,0 wt.% of MWCNT. The distance used between the needle and the collector was 25 cm and the solution feed rate was 2 ml/h.The process was carried out with the rotating collector at a speed of 2.300 r.p.m. to obtain membranes with aligned fibers.

Development of wearable sensory device

To obtain the piezoresistive traction sensor, samples of electrospun membranes produced with dimensions of approximately 60x10 mm were prepared and copper tapes with silver ink were attached to the tips of these samples, with a distance of 30 mm between them. To monitor human movements, this sensor was placed on the finger to measure the difference in electrical resistivity of the sensor when the finger was bent.

The obtained traction sensors were mounted on finger joints to monitor human movement. The sensor electrodes were connected to an electrometer (Keithley 6517A), and by bending the fingers, the electrical resistivity variation as a function of time was calculated.

Characterizations

Scanning Electron Microscopy (SEM) was performed on samples of electrospun TPU/MWCNT membranes, with different concentrations of nanocharges, in a JEOL microscope, model JSM-6390LV. This analysis was carried out to evaluate the morphology of the samples, verify the dispersion and distribution of conductive additives in the polymeric matrix.

The electrical conductivities of the TPU/MWCNT electrospun mats, with low conductivities from 10^{-17} to 10^{-7}, were obtained by the 2 probe method. Analyzes were performed according to ASTM D-257 on circular specimens of 90 mm of diameter, using a Keithley 6517A electrometer connected to a Keithley 8009 testing device.

Tensile tests were carried out on electrospun membranes to verify the influence of conductive additives on the tensile strength of the produced membranes. The tests were carried out in a dynamic-mechanical analysis equipment model Q-800, from TA Instruments, equipped with the sample holder for film traction, from the Materials Laboratory (LABMAT) of the Federal University of Santa Catarina. 3 samples were prepared, with a size of 10 x 70 mm, using a force rate of 0.05 $N.min^{-1}$, until the samples rupture, preload of 0.001 N, at room temperature.

Results and Discussion

The SEM micrographs obtained for the electrospun membranes with the aligned TPU/NTC fibers in Fig. 1. From the micrographs obtained, it can be observed that the fibers are aligned in a preferred orientation and the they did not show agglomerates or defects, indicating that the electrospinning parameters used provided a good morphology, with a good uniformity of the fibers to the membranes and the speed of the rotating collector of 2.300 r.p.m. was enough for fiber alignment to occur.

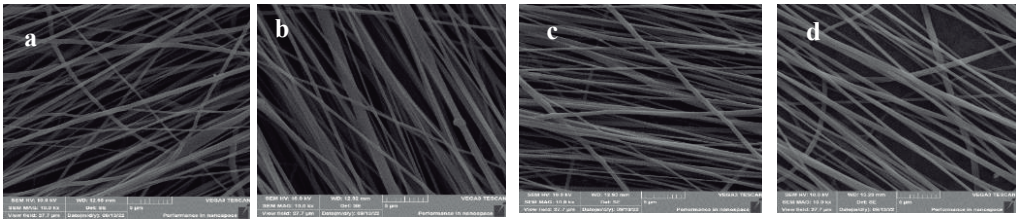

Figure 1 - SEM micrographs and histogram with the distribution of fiber diameters of TPU membranes obtained with different concentrations of MWCNTs. a) TPU/0,25MWCNT, b) TPU/0,5MWCNT, c) TPU/0,75MWCNT, d) TPU/1,0MWCNT.

Table 1 presents the electrical conductivity values obtained for the aligned TPU/MWCNT electrospun membranes with different MWCNT mass fractions. It can be seen that there was an increase in the electrical conductivity of the TPU/MWCNT electrospray membranes in relation to the pure TPU electrospun membrane. As expected, there was also an increase in the electrical conductivity of the membranes with the increase in the mass fractions of the MWCNT, indicating that the MWCNTs act as conductive fillers, due to the formation of conductive paths with the contact of the MWCNTs in the fibers. Only for the weight concentration of 1.0 wt.% of MWCNT that there was no increase in electrical conductivity in relation to the other membranes, probably due to the MWCNT agglomeration.

Table 1 - Electrical conductivity values for TPU/MWCNT electrospun mats with different concentrations of MWCNTs.

Samples	Electrical conductivity (S cm^{-1})
TPU	$(5.12 \pm 0.02)x10^{-13}$
TPU/0,25MWCNT	$(8.45 \pm 1.02)x10^{-13}$
TPU/0,5MWCNT	$(1.24 \pm 0.02)x10^{-12}$
TPU/0,75MWCNT	$(6.86 \pm 9.70)x10^{-8}$
TPU/1,0MWCNT	$(4.39 \pm 2.9)x10^{-13}$

Fig. 2 shows the stress versus strain curves obtained for the aligned electrospun membranes of pure TPU and TPU/MWCNT with 0,25, 0,5, 0,75 and 1,0 wt.%, with the samples being pulled parallel to the orientation of the fibers. From the stress versus strain curves, it can be seen that there was an increase in the tensile strength of the membranes with the increase in the mass fraction of MWCNT, indicating that the conductive nanocharge increased the mechanical resistance of the membranes, and they withstood a greater stress than the than pure TPU before rupture occurs.

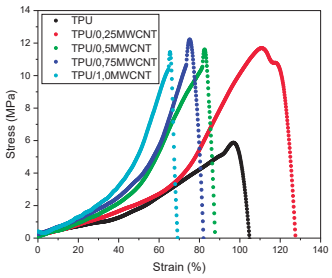

Figure 2 - Stress x strain curve for electrospun pure TPU and TPU/MWCNT membranes with 0,25, 0,5, 0,75 and 1,0 wt.% aligned, pulled parallel to the fiber orientation.

To monitor human movement, the obtained wearable sensors were placed under the glove to monitor finger movement. The response of the TPU/MWCNT wearable sensor with different concentrations of MWCNT, showing the variation of the electrical resistivity of the sensor when bending and stretching the finger and the sensor mounted under the glove to monitor the movement of the finger are represented by Fig. 3. There was an increase in the electrical resistivity of the sensor due to the removal of the MWCNT charges when bending the finger, despite the small variation in electrical resistivity, but the response was very noisy.

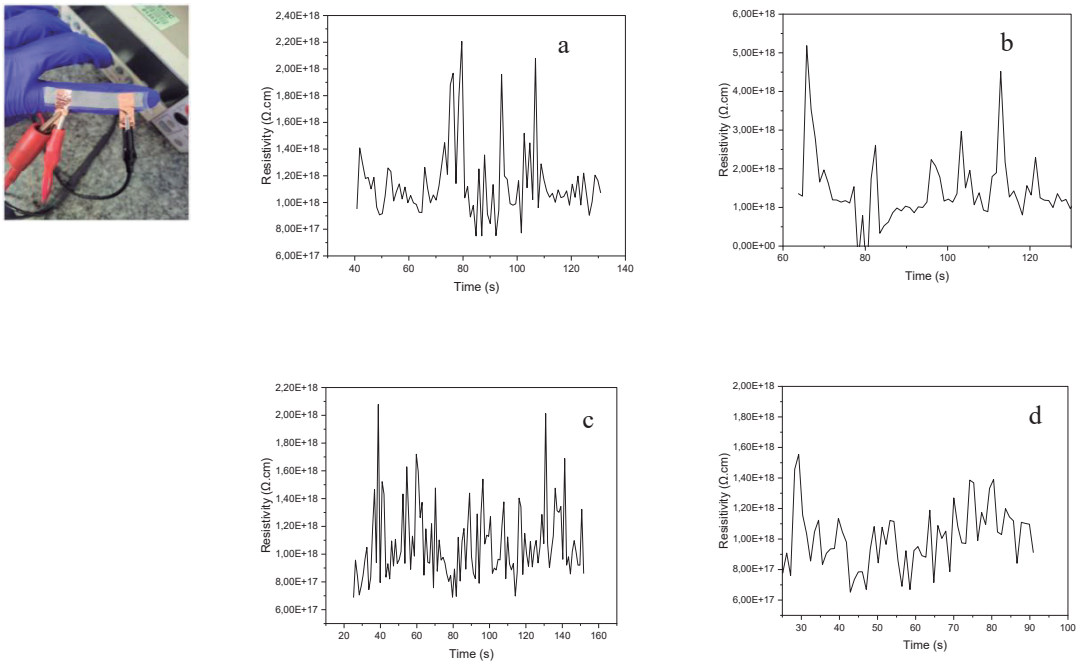

Figure 3 – Response of TPU/MWCNT sensors with different MWCNT fractions when monitoring finger movement – a) TPU/0,25MWCNT, b) TPU/0,5MWCNT, c) TPU/0,75MWCNT, d) TPU/1,0MWCNT.

Conclusions

It can be concluded that there was an increase in electrical conductivity of the TPU/MWCNT electrospun membranes with the addition of MWCNT. Moreorver, there was an increase in the tensile strength of the electrospun TPU/MWCNT membranes in relation to the pure TPU membrane. The wearable sensor obtained by electrospinning TPU/MWCNT membranes showed a response when tested on the finger, with variation in electrical resistivity, but the response showed a lot of noise. Further experiments must to be performed in order to improve the quality of the response.

Acknowledgements

To the Central Laboratory of Electron Microscopy (LCME) of the Federal University of Santa Catarina (UFSC), to the Research Center for Ceramic and Composite Materials (CERMAT), to CAPES for financial support.

References

1. S. Nasiri; M. R. Khosravani. Sensors and Actuators A 2020, 312, 112105. https://doi.org/10.1016/j.sna.2020.112105.
2. J. He; Y. Zhang; R. Zhou; L. Meng; T. Chen; W. Mai; C. Pan. Journal of Materiomics 2020, 6, 01.009. https://doi.org/10.1016/j.jmat.2020.01.009.
3. Y. Wang; M. Chao; P. Wan; L. Zhang. Nano Energy 2020, 70, 104560. https://doi.org/10.1016/j.nanoen.2020.104560
4. T. Li; J. Li; A. Zhong; F. Hanc; R. Sunb; C. Wong; F. Niue; G. Zhang; Y. Jin. Sensors and Actuators A: Physical 2020, 306, 111959. https://doi.org/10.1016/j.sna.2020.111959.
5. X. Gao; A. I. Isayev; C. Yi. Polymer 2016, 84, 12.051. http://dx.doi.org/10.1016/j.polymer.2015.12.051.
6. K. Qi; Y. Zhou; K. Ou; Y. Dai; X. You; H. Wang; J. He; X. Qin; R. Wang. Carbon 2020, 170, 07.042. https://doi.org/10.1016/j.carbon.2020.07.042.

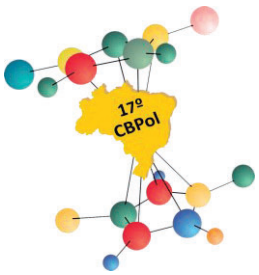

DEVELOPMENT OF MULTIFUNCTIONAL ELECTROSPUN POLYMERIC MEMBRANES FOR FACE MASKS: INCORPORATION OF ZINC OXIDE NANOPARTICLES

Matheus C. Hemkemaier[1], Cristiano Binder [2], and Claudia Merlini[1]

1 – Graduate Program in Nanoscience, Processes and Advanced Materials (PPGNPMat), University of Santa Catarina – Blumenu Campus (UFSC), Santa Catarina, SC, Brazil
matehus.c.hemkemaier@gmail.com.br, cristiano.binder@ufsc.br, claudia.merlini@ufsc.com.br
2 – Department of Mechanical Engineering, University of Santa Catarina – Florianópolis Campus (UFSC), Santa Catarina, SC, Brazil

Abstract - The COVID-19 pandemic has significantly increased the demand for non-pharmacological measures, including the use of face masks to reduce the spread of the virus. However, the high consumption of face masks has resulted in a large volume of waste, posing a risk to the environment and public health. To address this problem, it is necessary to develop new filtering media that meet the basic functionalities of face masks. The inclusion of new functionalities in the membranes applied to face masks can further improve their efficacy in disease transmission prevention and reduce the environmental impact after disposal. This work aims to develop composite polymeric nanofibers of polylactic acid (PLA) with zinc oxide nanoparticles (nZnO) to produce functional, biodegradable, and antiviral face masks. The electrospinning technique allows producing micro and nanofibers, with the need to control the process parameters and the methodology used for the dispersion and distribution of nZnO in a 10% polymeric solution in organic solvents, and the incorporation of loads in mass ratios of 1% and 2%. Dispersion methods were evaluated, with the use of a tip sonicator proving to be the most efficient. The polymeric solutions, with and without nZnO, were subjected to electrospinning under constant parameters. The obtained membranes were characterized by scanning electron microscopy (SEM) for morphological analysis and fiber diameter distribution, thermal stability, and contact angle. Preliminary results showed that the addition of zinc oxide nanoparticles significantly affected the morphology, leading to a trend of decreasing fiber diameter and decreasing defects in the membranes. The hydrophobicity of the membrane was maintained with the addition of nZnO, while the thermal stability was reduced due to the presence of the nanoparticles.

Keywords: electrospinning; face masks; zinc oxide nanoparticles; polylactic acid.

Introduction

Despite exponential human development, humans remain vulnerable to external agents, particularly infectious diseases that afflict communities worldwide. The recent COVID-19 pandemic has highlighted the need for non-pharmacological measures to effectively combat airborne transmission of diseases. Universal mask-wearing has proven to be an effective strategy in reducing disease spread, including the transmission of the SARS-CoV-2 virus [1]. However, the increased consumption of facial masks has led to improper disposal and the generation of substantial waste, posing environmental concerns and the potential for disease transmission through contaminated biological waste. The American Chemical Society estimates that approximately 129 billion masks are consumed worldwide each month during the COVID-19 pandemic [2-3]. To address this issue, the development of disposable masks with functionalities beyond standard technical requirements, such as particle retention and breathability, is of great interest. The focus is on incorporating

biodegradable materials along with additives and/or fillers to achieve functionalities such as antiviral, antibacterial, and self-cleaning properties. Biopolymers such as chitosan, cellulose, gelatin, and starch, as well as synthetic polymers like poly(lactic acid) (PLA), are among the raw materials used to ensure biodegradability in polymeric matrices for facial masks [1]. PLA, a synthetic biopolymer derived from corn starch, sugarcane, or other plant sources, is particularly noteworthy. It can be processed using various production techniques, including extrusion, injection molding, and electrospinning. Electrospinning is particularly attractive for producing micro and nanofibers by randomly depositing fibers from a polymer solution under an electric field between a metallic needle and a collector. This makes PLA a versatile material for the production of face masks [4].Incorporating nanomaterials into PLA-based masks offers additional multifunctionalities. The focus is on antimicrobial and/or antiviral properties. Among the nanoparticles evaluated, silver oxide, titanium dioxide, and zinc oxide (ZnO) have shown promising results. ZnO stands out as a highly promising material for medical applications due to its antibacterial, antifungal, and antiviral properties. It has demonstrated effectiveness against common pathogens such as Staphylococcus aureus and Escherichia coli. Recent studies have also shown its antiviral activity, including against the SARS-CoV-2 virus, with low cytotoxicity to the human body [5]. This study aims to understand the interactions between the polymer matrix (PLA) and zinc oxide nanoparticles (ZnO) in the production of electrospun membranes for potential use in multifunctional face masks.

Experimental

To prepare the PLA polymer solutions, 0.8233 g of polymer granules were weighed to achieve a polymer concentration of 10%wt in 6 ml of a mixture of DCE and DMF in a volume ratio of 3:1, respectively. The solutions were uniformly dissolved under magnetic stirring and heated at approximately 50 °C for 12 hours. This process was performed for subsequent electrospinning and collection of pure PLA control samples. To incorporate the nanoparticles and obtain solutions containing nZnO, different mass fractions of 1% and 2%wt relative to the mass of PLA were used. The nanoparticles were incorporated after 12 hours of magnetic stirring at 50 °C, following dispersion procedures. Two methodologies were employed to evaluate the effectiveness of dispersion: i) ultrasound bath, ii) dispersion using an ultrasound probe, as indicated in Figure 1(a), for subsequent electrospinning procedures.

Figure 1 – Experimental procedure for obtaining PLA/ZnO membranes, dispersion methods (a), and electrospinning process (b).

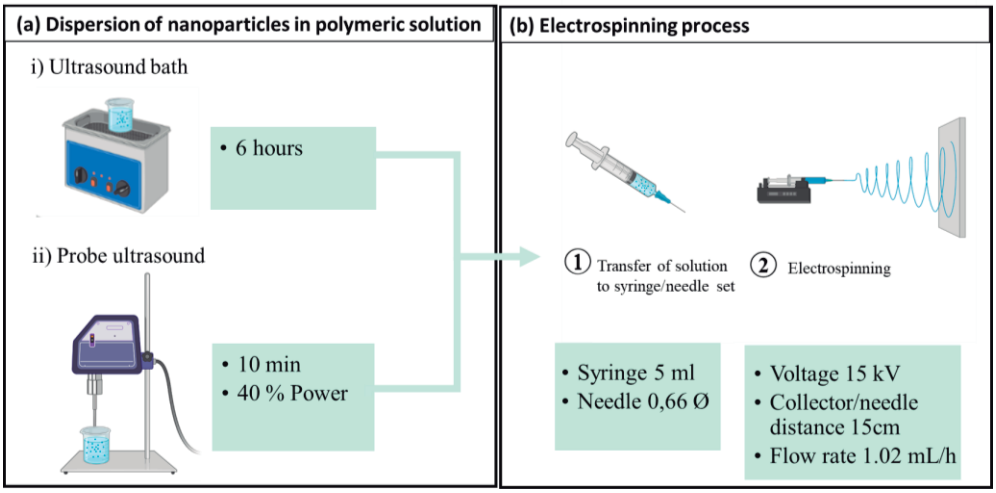

The PLA, PLA/1%ZnO, and PLA/2%ZnO solutions obtained were transferred to 5 mL glass syringes, and the electrospinning process was subsequently performed. The electrospinning parameters described in Figure 2(b) were kept constant throughout the experimental procedures, while the ambient parameters of temperature and humidity were monitored. The electrospinning process lasted approximately 2 hours. The obtained samples were subjected to morphological analysis of the fibers through transmission electron microscopy (TEM), thermogravimetric analysis (TGA), and contact angle measurement.

Results and Discussion

Preliminary SEM results, Figure 2, indicate that the use of the ultrasonic probe as a dispersion method is more efficient compared to the ultrasonic bath, due to the low incidence of defects in the membrane fibers.This difference can be attributed to the intensity and application of ultrasonic energy. In the case of the ultrasonic bath, the ultrasonic energy is applied gently and uniformly throughout the liquid, which may not be sufficient to fully disperse the nanoparticles, especially when they are agglomerated. This can result in inadequate dispersion and the presence of defects in the fibers during the electrospinning process (Figure 2 (b)). On the other hand, the use of the ultrasonic probe provides more targeted and intense ultrasonic energy at a specific point in the solution. This allows for more effective dispersion of the nanoparticles, even when they are agglomerated, resulting in a significant reduction in fiber defects (Figure 2(c)). Additionally, the ultrasonic probe can deliver ultrasonic energy at higher frequencies and with greater amplitude, contributing to a more efficient dispersion of the nanoparticles. These combined factors result in better outcomes in obtaining fibers with a more uniform morphology and lower incidence of defects. Therefore, based on the preliminary results, the utilization of the ultrasonic probe as a dispersion method for ZnO nanoparticles has proven to be more suitable for attaining membranes with superior fiber quality and reduced defects. Consequently, for the subsequent research endeavors, solely the ultrasonic dispersion method will be employed.

Figure 2 – SEM micrographs of electrospun PLA membranes (a), and PLA/ZnO dispersed in ultrasonic bath (b) and ultrasonic probe (c).

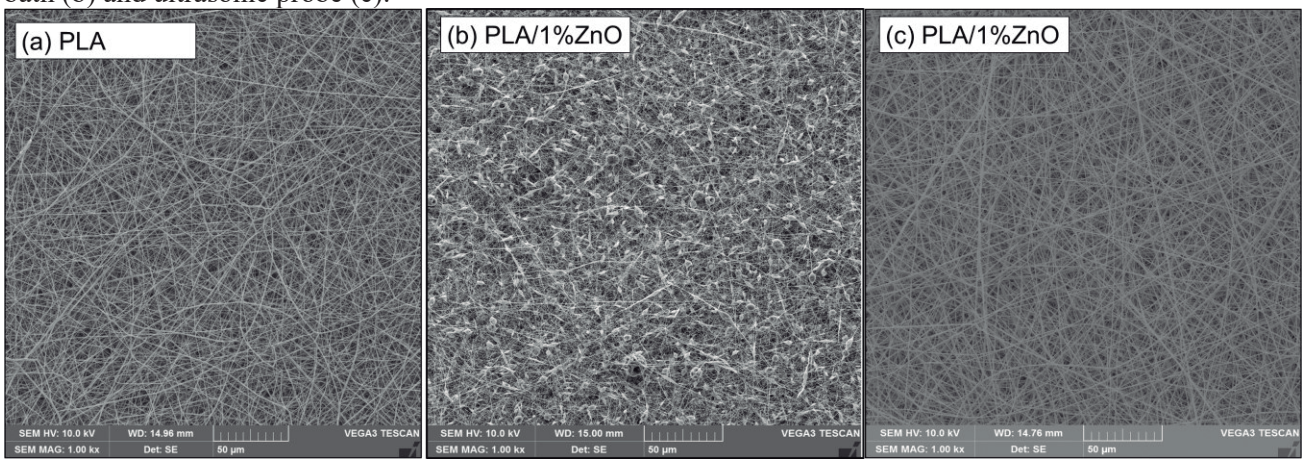

Furthermore, the presence of nanoparticles can not only cause morphological changes but also decrease the thermal stability of the polymer due to catalyzed hydrolysis mechanisms. Studies have reported that ZnO has the ability to bind to the terminal groups of the PLA chemical structure, which can catalyze polymer hydrolysis processes, resulting in a reduction in molecular weight and, consequently, a decrease in thermal stability [6]. The results of TGA for the membranes support these findings. The analysis of thermogravimetric (TGA) and derivative thermogravimetric (DTGA) curves, as shown in Figure 2, reveals a reduction in thermal stability with the incorporation

of nanoparticles. However, it is important to note that in their potential application in facial masks, the maximum usage temperature does not exceed 40°C, ensuring the stability of the system under usage conditions. The incorporation of ZnO nanoparticles causes a significant reduction in the thermal stability of PLA. The degradation temperature of pure PLA is approximately 325°C. However, with the addition of 2% ZnO nanoparticles, the degradation temperature decreases to 300°C, and with 1% ZnO nanoparticles, the degradation temperature is further reduced to 275°C.

Figure 2 – Análise termogravimétrica (TGA) de membranas de PLA e PLA/ZnO.

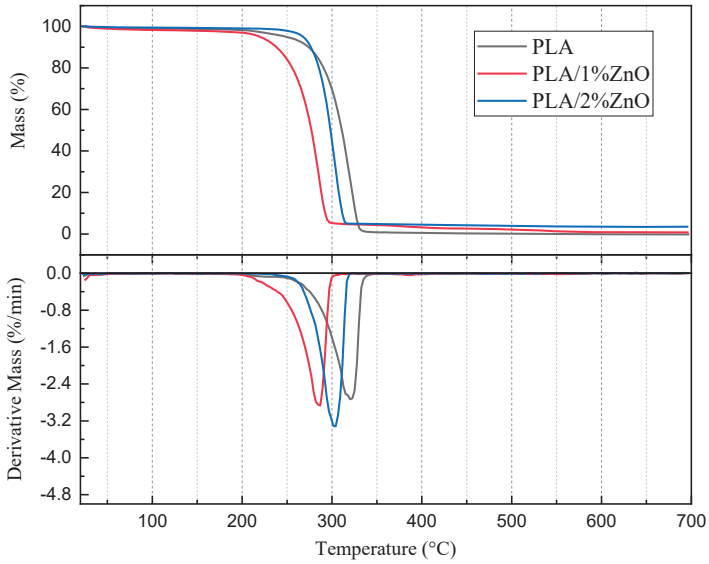

The contact angle test demonstrates that the hydrophobic nature of the PLA membranes is maintained after the incorporation of nZnO, as shown in Figure 12. The red line on the graph represents the angle value of 90°, indicating that the material exhibits hydrophobic characteristics above this value, while below this value, the material exhibits hydrophilic characteristics, showing an affinity for polar liquids.

Figure 3 – Contact angle test on electrospun membrane.

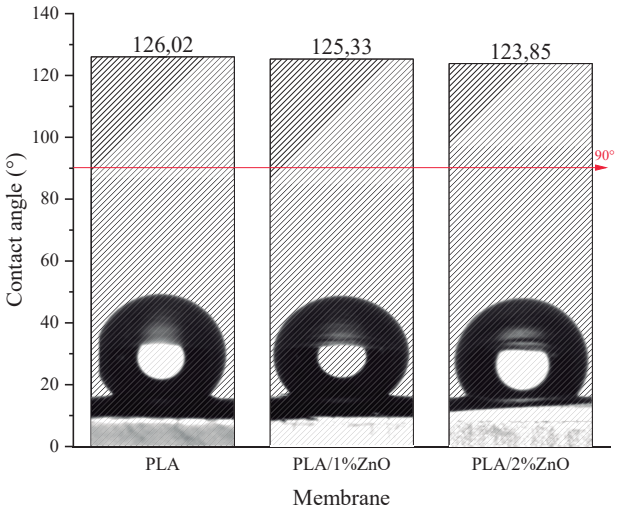

The hydrophobic nature of the membrane can be attributed to its morphology, which consists of micro and nanofibers, resulting in a surface roughness that enhances hydrophobicity. Generally,

electrospinning can produce membranes with a fibrous and porous structure, which can increase the specific surface area.

Conclusions

Electrospinning is a highly promising technique for the production of polymeric membranes with unique properties, such as high permeability, large surface area, and flexibility. Through this technique, it is possible to obtain microfibers with a uniform morphology and a low incidence of defects, as demonstrated by Scanning Electron Microscopy (SEM) analysis. The results obtained indicate that the incorporation of nanoparticles requires a more intense process, such as the use of ultrasonic energy, to ensure proper dispersion of the particles in the polymer solution. Additionally, the produced membranes exhibit a hydrophobic character, which is desirable for mask applications. The presence of nanoparticles can negatively affect the thermal stability, lowering the material's degradation temperature.

Acknowledgements

Thanks to PPGNPMat (Postgraduate Program in Nanostructures and Polymeric Materials), CNPq (National Council for Scientific and Technological Development) and CAPES (Coordination for the Improvement of Higher Education Personnel) for the academic and financial support provided for the realization of this study. To the research group on Polymeric Nanofibers and Nanocomposites, for collaboration and support during the research process, as well as for collaborations and partnerships between the Materials Laboratory (LABMAT) and the Microstructural Characterization Laboratory (LCM), fundamental contributions to the development this work.

References

1. G. PULLANGOTT, et al. A comprehensive review on antimicrobial face masks: An emerging weapon in fighting pandemics. RSC Advances, v. 11, n. 12, p. 6544–6576, 2021.
2. X. CHEN, et al. Used disposable face masks are significant sources of microplastics to environment. Environmental Pollution, v. 285, p. 117485, 15 set. 2021.
3. A. W. H CHIN; L. L. M. POON. Stability of SARS-CoV-2 in different environmental conditions – Authors' reply. The Lancet Microbe, v. 1, n. 4, p. e146, 1 ago. 2020.
4. M. W. NUGRAHA, et al. Electrospun polylactic acid/ tungsten oxide/ aminofunctionalized carbon quantum dots (PLA/WO3/N-CQDs) fibers for oil/water separation and photocatalytic decolorization. Journal of Environmental Chemical Engineering, v. 9, n. 5, p. 106033, 1 out. 2021.
5. S. M. EL-MEGHARBEL, et al. Utilizing of (Zinc oxide nano-spray) for disinfection against "sars-cov-2" and testing its biological effectiveness on some biochemical parameters during (covid-19 pandemic)—"zno nanoparticles have antiviral activity against (sars-cov-2)". Coatings, v. 11, n. 4, 2021.
6. M. QU, et al. Zinc oxide nanoparticles catalyze rapid hydrolysis of poly(lactic acid) at low temperatures. Journal of Applied Polymer Science, v. 131, n. 11, p. 1–7, 2014.

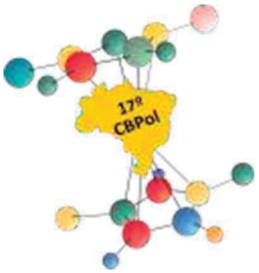

DEVELOPMENT OF NANOCOMPOSITES BASED ON DIFFERENT PHOTOSENSITIVE RESINS AND GRAPHENE OBTAINED VIA 3D PRINTING FOR DENTAL USE

Maria Eduarda P. Goulart[1], Lilian V. R. Beltrami[1], Thiago O. Gamba[2] e Ademir J. Zattera[1*]

1–Postgraduate Program in Engineering of Processes and Technologies (PGEPROTEC), Universidade de Caxias do Sul (UCS), R. Francisco Getúlio Vargas, 1130, Caxias do Sul, Rio Grande do Sul, RS, Brazil*
ademirjzattera@gmail.com

2 – Postgraduate Program in Health Science, University of Caxias do Sul (UCS), R. Francisco Getúlio Vargas, 1130, Caxias do Sul, Rio Grande do Sul, RS, Brazil

Abstract – The present work evaluated the influence of the addition of graphene nanoplatelets (NGPs) in two photosensitive resins for 3D printing, commercially available, especially on their mechanical properties, in order to develop composites for 3D prototyping for the field of Dentistry. The concentration of NGPs used was 0.250 wt%. The specimens were printed using 3D printing, which uses digital light processing technology. The addition of graphene considerably increased the compressive strength of the resins in relation to the pure resins, especially in the PRIZMA PROV_NPG resin, where an increasing of about 50% was observed. However, the values of the modulus of elasticity of the pure resins were higher, being considered more rigid materials compared to the resins with the addition of NPGs, which are more flexible, and consequently deformed considerably more in relation to the pure resins.

Keywords: *Resins, graphene nanoplatelets, dentistry, 3D printing.*

Introduction

Research involving nanocomposites has shown constant growth due to the wide application of these nanomaterials in several areas, also present in the dental area. In general, graphene is among the most investigated nanomaterials today, because it has the potential to improve or modify the characteristics and properties of other materials [1,2].

One of the most used polymeric materials in dental practice is polymethylmethacrylate (PMMA), with several applications, with the aim of replacing lost teeth and hard and soft tissues, presenting a good cost-benefit ratio, versatility, acceptable aesthetics, in addition to allowing ease of handling and repair [3,4,5]. Polymethylmethacrylate is a polymer obtained by a polymerization reaction, however, during this polymerization reaction, there is no total conversion of monomers into polymers. Residual monomers, when in contact with the oral cavity, can lead to biodegradation of the material, giving rise to biological responses such as irritation, hypersensitivity and even allergic reactions. In addition, the presence of residual monomers can affect the mechanical properties of thematerial, which can increase the possibility of failure [4, 6].

3D printing is an increasingly evident reality in dentistry, allowing dentists to diagnose and treat faster and more accurately through three-dimensional planning. This manufacture method involves the production of structures layer by layer of resin giving rise to materials printed materials, which have several dental applications, whether for the production of dental models, surgical guides, orthodontic and bite guides, bruxism plates and even the manufacture of dental prostheses [7-10].

In an attempt to improve the characteristics and properties of polymethylmethacrylate, studies have incorporated nanoplatelets in different forms and concentrations in resins, including graphene and

its derivatives, which have emerged as a new class of nanomaterials, and may be an alternative to improve the properties of composites to PMMA base [3, 9-11]. Graphene-based materials have become popular in dentistry due to their excellent properties, such as conductivity, large surface area, low bulk density and ease of chemical modification [5,11].
The aim of this work was to evaluate the influence of the addition of graphene nanoplatelets (NPGs) on the mechanical properties of two 3D printing resins in order to develop 3D prototyping polymeric composites for dental application.

Experimental

Samples preparation

For the development of the composites, 0.250 wt% of graphene nanoplatelets UGZ-1004, from UCSGRAPHENE company, were incorporated into the photosensitive resins Prizma 3D Bio Splint and Prizma 3D Bio Prov, from dOne 3D company, by the probe sonification method with temperature control. A Sonics Vibra-Cell sonifier was used with an amplitude of 40% for 15 minutes in an ice bath. The samples were put into a closed place so as not to be exposed to external light sources.
The samples were printed on a printer model Flashforge 3D Printer, from the company dOne 3D, which uses stereolithography technology of digital light processing, after printing they were placed in a vat with isopropyl alcohol P.A., where according to the manufacturer's recommendation of the two resins, the samples were immersed for 3 to 5 minutes in isopropyl alcohol to remove the resin on the surface. It is important to emphasize that the printing parameters were not changed after the addition of the nanoplatelets, they remained constant for the production of pure resin samples and samples with graphene addition. The dried samples were submitted to the post-cure process in a 72W UV chamber purchased from the company dOne 3D, being cured by ultraviolet light for 10-20minutes according to the manufacturer for the Prizma 3D Bio Prov resin, the Prizma 3D Bio Splint resin requires a post-curing time of 10-15 minutes. Table 1 shows some differences in the characteristics of the two resins used in the present study.

Table 1 - Differences in the characteristics of the two resins

Resin	Characteristics
Prizma 3D Bio Prov	Resin curable by UVA/UVB light, developed for 3D printing of teeth and temporary crowns. Provides a 3D print with excellent definition, high resolution and low shrinkage. It can be used in DLP and SLA printers with a wavelength between 385 and 405 nm. It has A1 color.
Prizma 3D Bio Splint	Resin curable by UVA/UVB light, indicated for 3D printing of retainers and myorelaxing plates. It is a transparent 3D printing material, can be used in DLP / SLA printers and provides a 3D printing with high strength and hardness.

Mechanical tests

Compressive strength: this test was carried out on eight specimens with dimensions of 12.7 mm in diameter x 25.4 mm, in accordance with ASTM D695-15 standards, using a universal testing machine EMIC DL 2000 from the Polymer Laboratory of University of Caxias do Sul (UCS).
Young's modulus for compression: was used as an indicator of the rigidity of the material when flexed, the test was carried out in accordance with the ASTM D695-15 standard, using a load cell of 100 kgf and a speed of 1.5 mm/min^{-1}, using a universal testing machine EMIC DL 2000. Five specimens were used, with dimensions of 127 x 12.7 x 2.9 mm (according to standard ASTM D695-15), which remained for 48 h in a closed environment at a temperature of 23 °C (± 2 °C) and humidity of 50% (± 10%). All tests were performed in the Polymer Laboratory (LPOL) at the University of Caxias do Sul (UCS).

Results and Discussion

Compressive Strength

Fig. 1 shows the average compressive strength values of pure resins and resins with NPGs added.

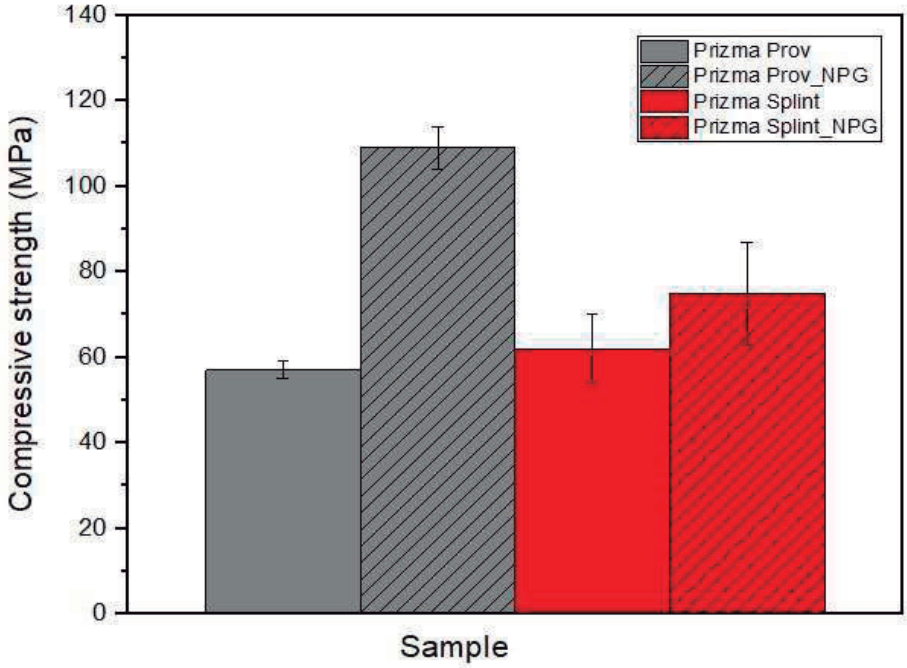

Figure 1- Graph of the compressive strength of pure resins and resins with 0.250 wt% NPGs addition.

The addition of graphene considerably increased the compressive strength values of the material in relation to pure resins, since the sample that presented the highest compressive strength was Prizma Prov_NPG around 110 MPa, while for the pure resin sample Prizma Prov this value was around 55 MPa. An increase in compressive strength was also obtained in the Prizma Splint resin when graphene was added, since the strength was around 70 MPa, whereas for the pure resin this value was 60 MPa. The restorative materials used in dentistry must have a minimum capacity to withstand masticatory resistance, especially for patients who have parafunctional habits, such as bruxism, who require greater occlusal needs, and may suffer material breakage during use, if they do not present certain resistance. In this way, this essay provides important information to dentists in the selection of dental materials, assisting in planning and more complex treatments.

Young's modulus for compression

According to Fig. 2, the sample that presented the highest Young's modulus for compression was the Prizma Splint around 1300 MPa, followed by the Prizma Prov sample around 1100 MPa. It can be observedthat the pure resin samples showed a higher Young's modulus for compression in relation to the resins with the addition of nanoplatelets, since they presented values of 1000 MPa for the Prizma Prov_NPG resin and around 900 MPa for Prizma Splint_NPG.

A high Young's modulus for compression means a greater resistance of the material to deformation, that is, greater ease for the material to return to its original state when the load being applied is removed, characterizing itself as an elastic material.

Figure 2- Graphic of the Young's modulus for compression of pure resins and resins with the addition of 0.250 wt% NPGs.

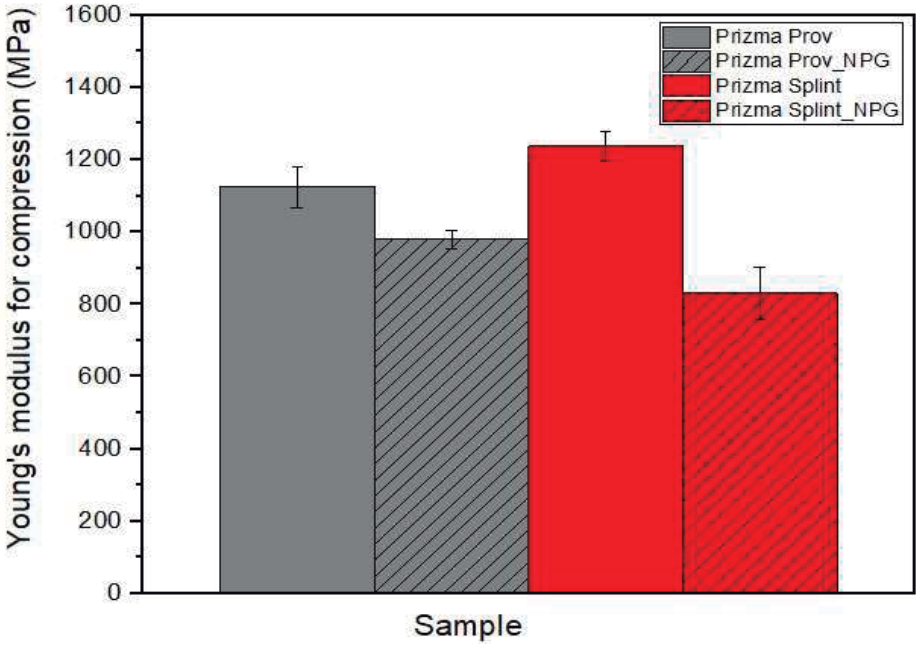

Deformation maximum for compression

The deformation maximum for compression of pure resins and resins with the addition of NPGs is shown in Fig. 3.

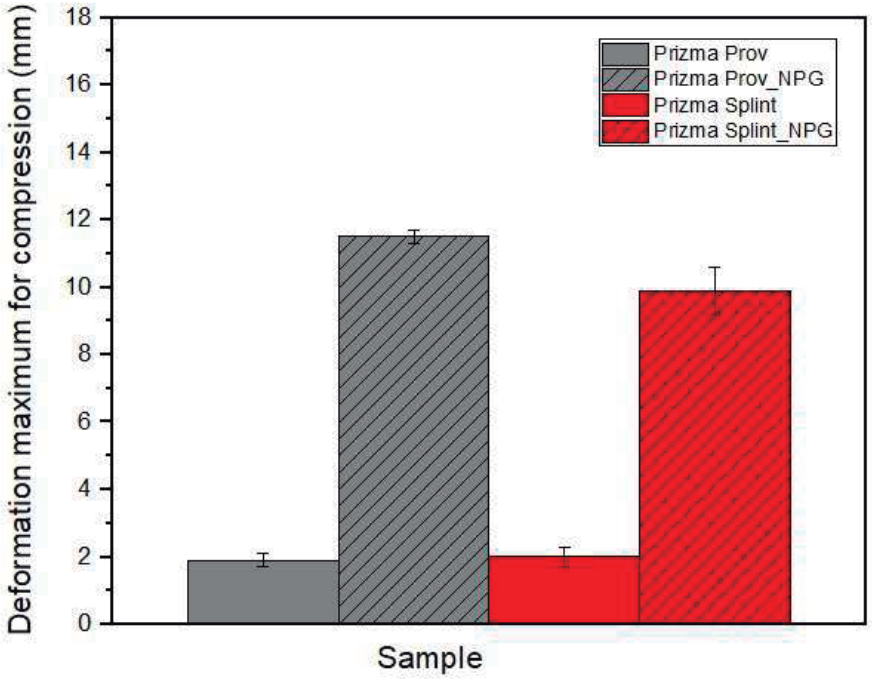

Figure 3- Graph of deformation maximum for compression of pure resins and resins with the addition of 0.250 wt% NPGs.

The two samples with the addition of graphene Prizma Prov_NPG and Prizma Splint_NPG showed significantly higher values in relation to the pure resins, around 12 mm and 10 mm respectively, while the pure resin samples Prizma Prov and Prizma Splint had values around 2 mm, which means a better resistance to deformation of the resins with the addition of the nanoload in relation to the pure resins. The increase in the values of deformation maximum test for compression of the resins with the addition of graphene is due to the low modulus of elasticity of the material presentedabove.

In general, dental materials, especially restorative materials, should not undergo permanent

deformation during use. In some cases, such as prostheses, it is necessary to use materials that are more rigid and difficult to deform. In other cases, such as restorative materials, ideally, the material should not be too rigid, so that the restorative material is more likely to deform as the tooth deforms.

Conclusions

This work evalluated the effect of graphene incorporation in two commercial photosensitive resins for 3D printing and the results obtained showed that the addition of the nanoplatelets promoted several changes in the mechanical properties.

A significant increase in the mechanical property of resistance to compression with the addition of 0.250 wt% graphene in relation to pure resins. However, the modulus of elasticity decreased with the addition of the nanoplatelets, making the resins less rigid. Furthermore, the maximum compressive strain of the resins increased when NPGs were added, corroborating the decrease in the modulus of elasticity.

The results obtained so far indicate that more investigations need to be done to develop nanocomposites for 3D printing with competitive costs and performance in the market.

Acknowledgment

The authors would like to thank CAPES, CNPQ and FINEP for granting grants and funds for research and the University of Caxias do Sul for providing the infrastructure and materials.

References

1. R. Guazzo; C. Gardin; G. Bellin; L. Sbricoli; L. Ferroni; F. S. Ludovichetti; A. Piatelli; J.
2. Antoníaco; E. Bressan; B. Zavan Nanomaterials 2018, 8(5):349. https://doi: 10.3390/nano8050349
3. V. Srimaneepong; H. E. Skallevold; Z. Khurshid; M. S. Zafar; D. Rokaya; J. Sapkota J. Int. J. Mol. Sci. 2022, 23(1):499. https://doi.org/10.3390/ijms23010499
4. M. M. Gad; R. Abualsaud; A. Rahoma; A. M. Al-Thobity; K. S. Al-Abidi; S. Akhtar Int J Nanomedicina 2018, 13: 283–292. https://doi.org/10.2147/IJN.S152571.
5. M. L. P. D. Engler; JF. Güth; C. Keul; K. Erdelt; D. Edelhoff; A. Liebermann Clin Oral Investiga 2020, 24(1):277-284. htps://Doi: 10.1007/S00784-019-02947-4
6. S. Aati; A. Chauhan; B. Shrestha; S. M. Rajan; H. Aati; A. Fawzy Dental Materials 2022, 1921–1933. https://doi.org/10.1016/j.dental.2022.10.001
7. C. Keul; J. Seidl; JF. Güth; A. Liebermann Clin Oral Investig. 2020, 24(12):4519-4530. https://doi: 10.1007/s00784-020-03317-1
8. CH. Lin; YM. Lin; YL. Lai; SY. Lee The Journal of Prosthetic Dentistry 2020, 123(2):349-354. https://doi.org/10.1016/j.prosdent.2019.05.002
9. E. Bayarsaikhan; JH. Lim; SH. Shin; KH. Park; YB. Park; JH. Lee; JE. Kim; Polymers. 2021, 13(8):1180. https://doi.org/10.3390/polym13081180
10. S. Helena; A. T. P. C. Gomes; A. S. Duarte; J. M. F. Ferreira; C. Fernandes; M. H. Figueiral; P. Mesquita Biomedicines 2022, *10*(10), 2607.https://doi.org/10.3390/biomedicines10102607
11. A. Scarano; Orsini. T; F. Carlo; L. Valbonetti; F. Lorusso Int. J. Mol. ciência 2021, *22* (3), 1441; https://doi.org/10.3390/ijms22031441

DEVELOPMENT OF POLYMERIC FILMS OF POLYETHYLENE MODIFIED BY CLAY NANOPARTICLES AND GRAPHENE NANOPANELS FOR APPLICATION IN FOOD PACKAGING

Renata G. da Conceição[1], Cleide Borsoi[2], Lílian V. R. Beltrami[1], Ademir J. Zattera[1]

1 – Graduation Program of Processes Engineering, University of Caxias do Sul (UCS), Rio Grande do Sul, RS, Brazil
ajzatter@ucs.br
2 - Ciências Exatas e Engenharia, Universidade do Vale do Taquari -Univates, Lajeado, RS, Brazil

Abstract – The flexible food packaging industry is constantly growing and, as a result, numerous research studies are being conducted to develop new materials and combinations that meet the industry's demands. The incorporation of different nanocarriers, such as clay and graphene, enables the production of materials with superior properties for use in flexible packaging. Therefore, the objective of this study was to evaluate the addition of clay and graphene nanocarriers in high-density linear polyethylene (HDPE) films and the properties of the resulting materials. The parameters of crystallinity, oxygen permeability, and tensile strength were analyzed. The 30B clay and UCSGraphene graphene samples showed the highest degree of crystallinity at 59%, with a mass concentration of 2.5% for both. Regarding permeability, the 30B clay sample with a mass concentration of 5% showed a higher value than pure polyethylene, while the other samples exhibited lower values. The sample with a mass concentration of 1% UCSGraphene showed the most significant reduction, reaching around 69%. With respect to tensile strength, the samples with clay showed superior performance to those with graphene.

Keywords: *Food packaging; nanoclay; graphene nanoplatelets; flexible packaging.*

Introduction

Food packaging is a fundamental element in preserving the quality and safety of food during storage and transportation [1]. Various polymers are used in packaging, with high-density polyethylene (HDPE) and low-density polyethylene (LDPE) being the most common. HDPE is commonly used for applications that require greater mechanical strength. Technological advancements have brought new opportunities to improve the properties of packaging, including the addition of clay and graphene nanocarriers. These materials are considered nanomaterials due to their reduced dimensions, with structures on a nanoscale, which give them unique properties [2]. Clay is a mineral found abundantly in nature that can be used in various applications, including food packaging. The incorporation of clay nanocarriers into packaging can improve its mechanical properties, such as tensile and tear strength, as well as provide a more effective barrier against gases, moisture, and light [4]. Graphene is a material composed of a single layer of carbon atoms, with a nanoscale structure that imparts it with unique properties. These include high thermal and electrical conductivity and high mechanical strength, all while being a lightweight and flexible material. The addition of graphene nanoplatelets to composites can improve their mechanical properties, increasing their tensile and compression strength, as well as provide similar barrier effects to the ones previously described [5]. Therefore, the use of clay and graphene nanoloads in food packaging can bring significant benefits, such as improving the quality and safety of food, as well as reducing waste and losses [2].

Experimental

To carry out this work, the following materials were used: high-density polyethylene (Braskem, Brazil), montmorillonite clay of the Cloisite® 20A and Cloisite® 30B types (Southern Clay Products, USA), polybond® 3029 compatibilizing agent (Addivant, USA), and graphene nanoplatelets from Strem Chemicals (USA) and UCSGraphene (Brazil). Polyethylene films with the addition of nanoloads were produced according to the formulations presented in Table 1. The twin-screw extrusion process was utilized, with a pelletizer attached to the end part of the process to form homogenized pellets that were subsequently processed by single-screw blow extrusion to form polymeric films of different compositions. Fig. 1 shows the visual aspect of the developed samples.

Table 1 – Composition and identification of the developed film samples.

Samples	HDPE (%)	Cloisite® 20A (%)	Cloisite® 30B (%)	Polybond ® 3029 (%)	Strem Chemicals (%)	UCSGraphene (%)
PE	100	-	-	-	-	-
PE-20A_5	95	5	-	-	-	-
PE-20A_2.5	97.5	2.5	-	-	-	-
PE-20A_1	99	1	-	-	-	-
PE-30B_5	93	-	5	2	-	-
PE-30B _2.5	95.5	-	2.5	2	-	-
PE-30B _1	97	-	1	2	-	-
PE-NPG-S_2.5	97.5	-	-	-	2.5	-
PE-NPG-S_1	99	-	-	-	1	-
PE-NPG-U_2.5	97.5	-	-	-	-	2.5
PE-NPG-U_1	99	-	-	-	-	1

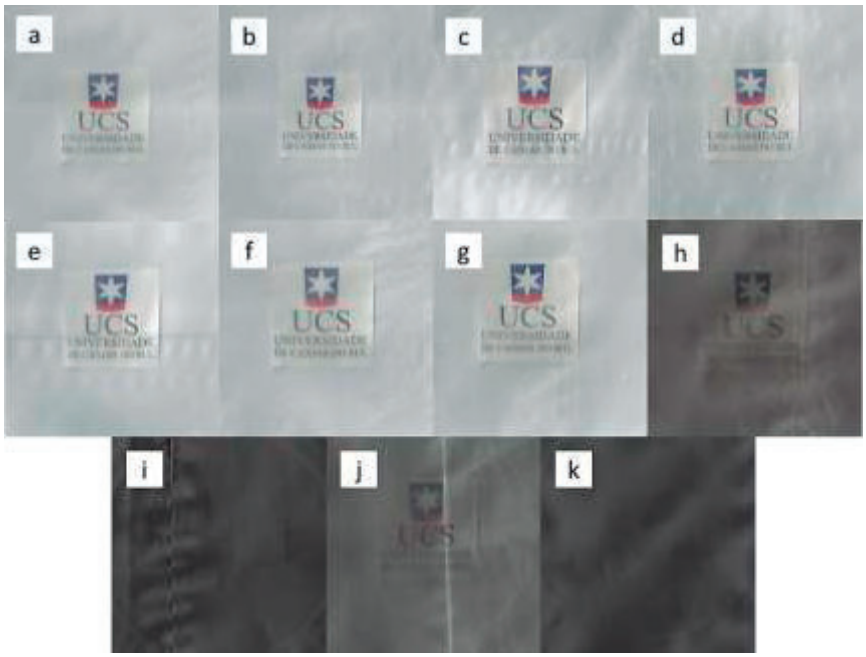

Figure 1 - Samples of (a) polyethylene film, (b) PE-20A_1, (c) PE-20A_2.5, (d) PE-20A_5, (e) PE-30B_1, (f) PE-30B_2.5, (g) PE-30B_5, (h) PE-NPG-S_1, (i) PE-NPG-S_2.5, (j) PE-NPG-U_1, and (k) PE-NPG-U_2.5.

The differential scanning calorimetry (DSC) analysis was conducted at the Polymer Laboratory (USC, Brazil) using the DSC-60 Shimadzu equipment, with approximately 10 mg of sample and a heating rate of 10 °C.min^{-1}, utilizing a N_2 flow rate of 50 mL.min^{-1}, and temperature variation of 23 to 250 °C, following ASTM D3418-21. Two heating runs and one cooling run were

performed. The crystallinity index of the samples was calculated using Eq. 1, where X_c is the crystallinity, ΔH_c is the measured melting enthalpy, % load is the percentage of nanoloads present in the sample, and ΔH_m is the melting enthalpy of HDPE, considered as 293 $J.g^{-1}$ as per Bortoncello (2021).

$$X_C = \frac{\Delta H_C}{(1-\%\, load) \cdot \Delta H_m} \cdot 100 \quad (1)$$

Barrier property analyses were carried out using an L100-5000 instrument according to ASTM F1927-07. Measurements were conducted at a temperature of 23 °C and oxygen flow rate of 100 cm^3. The oxygen permeability coefficient ($P'O_2$) was calculated using Eq. 2, where $P'O_2$ is the permeability coefficient, PO_2 is the oxygen permeation ($cm^3\ m^{-2}\ day^{-1}$), and l is the thickness of the sample (m).

$$P'O_2 = PO_2 \cdot l \quad (2)$$

Tensile strength tests were performed using an EMIC DL2000 universal testing machine with a testing speed of 50 mm/min. Both the barrier properties and tensile strength analyses were carried out in quintuplicate.

Results and Discussion

Table 2 shows the results of the DSC analysis for the developed samples.

Table 2 - Data and values obtained by calculating the crystallinity index for the samples for the first and second peak.

Sample	Enthalpy ($J.g^{-1}$)	X_{C1} (%)	Enthalpy ($J.g^{-1}$)	X_{C2} (%)
PE	154	52	165	56
PE-20A_1	150	52	158	54
PE-20A_2.5	141	49	154	54
PE-20A_5	139	50	158	57
PE-30B_1	146	50	154	53
PE-30B_2.5	150	52	168	59
PE-30B_5	139	50	160	57
PE-NPG-S_1	151	52	160	55
PE-NPG-S_2.5	148	52	164	57
PE-NPG-U_1	142	49	168	58
PE-NPG-U_2.5	149	52	170	59

The crystallinity values ranged from 53 to 59%, with the PE-NPG-U_2.5 sample having the highest value and PE-30B_1 having the lowest. The PE-30B_2.5 clay-added film showed higher crystallinity values compared to pure PE and 20A clay. Similarly, UCSGraphene had higher crystallinity values than pure PE. Sample PE-NPG-U_2.5 had the highest melting enthalpy value, while PE-20A_2.5 and PE-30B_1 had the lowest values. Regarding the clays, samples with 20A clay performed better in terms of melting enthalpy; in comparison with the graphenes, however, UCSGraphene showed better results. The oxygen permeability calculation was performed according to the values obtained for oxygen permeation in the polymer films, and the results are presented in Table 3.

Table 3 - Values obtained for oxygen permeability of the samples are presented in Table 3.

Sample	P'O2*10^{10} (mL.cm.cm^{-2}.s^{-1}.cmHg^{-1})
PE	86.84 ± 1.99
PE-20A_1	59.76 ± 1.75
PE-20A_2.5	54.12 ± 3.39
PE-20A_5	70.38 ± 5.36
PE-30B_1	53.07 ± 3.99
PE-30B_2.5	42.16 ± 3.63
PE-30B_5	89.20 ± 2.58
PE-NPG-S_1	49.67 ± 2.72
PE-NPG-S_2.5	35.93 ± 4.78
PE-NPG-U_1	27.19 ± 1.88
PE-NPG-U_2.5	60.45 ± 4.55

All the developed film samples exhibited better oxygen barrier properties than pure PE films, indicating that the incorporation of nanoloads leads to the formation of a more tortuous path, resulting in lower O_2 gas permeability. The sample with 1% by weight of UCSGraphene showed the lowest oxygen permeability values, indicating the best barrier performance. However, no clear pattern was observed for the concentrations of the employed loads.
The results obtained from the tensile strength analyses are shown in Figure 2.

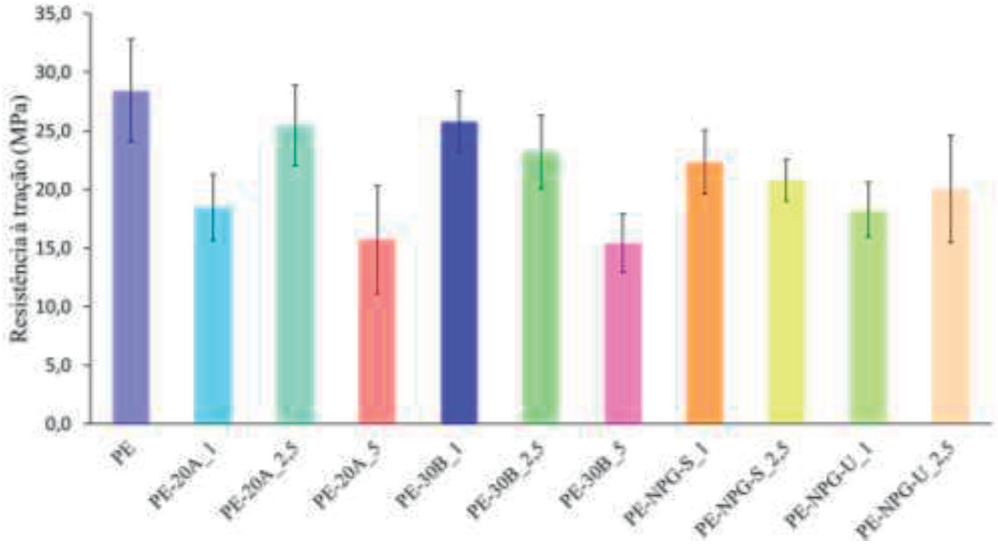

Figure 2 - Tensile strength of PE, PE-20A, PE-30B, PE-NPG-S and PE-NPG-U samples, with their respective concentration variations.

The tensile strength results were similar among the different types of clay used in the polyethylene films, with values of 25.5 MPa for PE-20A_2.5, 25.8 MPa for PE-30B_1, and 23.2 MPa for PE-30B_2.5. Both 20A and 30B clays showed slightly lower tensile strength compared to the pure PE sample. The tensile strength values of the graphene films were similar, with PE-NPG-S_1 presenting the highest value (22.3 MPa) and PE-NPG-U_1 the lowest (18.3 MPa). The sample with clay showed a superior performance compared to graphene due to better interaction between the phases of the composite.

Conclusions

According to the evaluation of the films developed with polyethylene and clay or graphene nanoplatelets, the PE-30B_1 sample exhibited the best mechanical properties in terms of tensile strength, while the PE-NPG-U_1 sample stood out in terms of permeability. In general, clay-incorporated films presented better mechanical properties, while the incorporation of graphene nanoplatelets showed better permeability and crystallinity properties.

Acknowledgements

The authors would like to thank the financial support from CAPES and Universidade de Caxias do Sul.

References

1. Q. Jiang; T. Horozov; A. Bismarck Polymer 2022, 261, 125406. https://doi.org/10.1016/j.polymer.2022.125406.
2. T. Anukiruthika; P. Sethupathy; A. Wilson; K. Kashampur; J. A. Moses; C. Anandharamakrishnan *Comprehensive Reviews In Food Science And Food Safety* 2020, 19, 1156-1186. https://doi.org/10.1111/1541-4337.12556.
3. S. N. Tripathi; G. S. S. Rao; A. B. Mathur; R. Jasra Rsc Advances 2017, 7, 23615-23632. http://dx.doi.org/10.1039/c6ra28392f.
4. T. Mumladze; S. Yousef; M. Tatariants; R. Krisnkiene; V. Makarevicius; S. Lukolinte; R. Bendikiene; G. Denafas *Green Chemistry* 2018, 20, 3604-3618. https://doi.org/10.1039/C8GC01062E
5. L. Komatsu; W. Oliani; A. Lugao; D. Parra *Radiation hysics and Chemistry* 2014, 97, 233-238. https://doi.org/10.1016/j.radphyschem.2013.12.004
6. F. Bellucci *Panorama tecnológico grafeno: contexto brasileiro e sua demanda por financiamento*. Rio de Janeiro: Finep, 2021. 86 p.
7. I. Bortoncello *Estudo da adição de nanocargas de argila e grafeno em filmes de pead*. Caxias do Sul: UCS, 2021. 79 p.

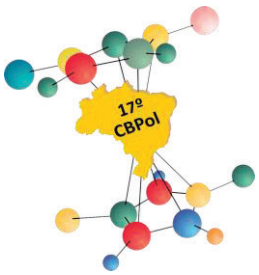

ECOLOGICAL PANELS PRODUCED FROM AÇAI FIBER AND COPPER NANOPARTICLES

Antônio de Lima Mesquita[1], José Costa de Macedo Neto[1], Júlio Simonetti Junior [1], Renato Moreira Teixeira Junior[1], Zaqueu Dias de Freitas[2] and Nubia Mireya Garzón Barrero[2]*

1 – Department of Materials Engineering, University of the State of Amazonas (UEA), Manaus – AM, Brazil;
mesquita@uea.edu.br; jmacedo@uea.edu.br; jsmj.emt20@uea.edu.br; rmtj.mec@uea.edu.br

2 – Department of Zootechnics and Food Engineering of USP, Pirassununga, SP, Brazil;
eng.zaqueu@gmail.com; nubiagarzonbarrero@yahoo.com

Abstract – MDF is a medium-density fiber panel, made from wood fiber agglutination with synthetic resins with joint application of temperature and pressure, is primarily intended for the furniture industry. Concerns about sustainability and the search for more environmentally sound alternatives have led to a growing demand for sustainable building and decoration materials, including natural fibers from the Amazon. Among them are the fiber of the acai fruit and copper nanoparticles. Copper is an antimicrobial agent that helps prevent the proliferation of microorganisms and increases the resistance of the panel to moisture and wear. The use of acai fiber in its production reduces the need to cut trees for the production of panels, reducing the environmental impact, the natural resins that exist in wood are not enough to aggregate in the manufacture of these plates, so it is necessary to add some bonding element. The adhesive used in the production of these medium density fiberboard (MDF) plates was a mixture of bi-component resin components and nanoparticles in the proportions (0,1%, 0,4%, 0,6%, and 0,8%), respectively, where 0.6% was the most effective in both physical and mechanical tests.

Keywords: *Acai, nanocomposites, copper, natural fiber, MDF.*

Introduction

Non-biodegradable synthetic materials have a major environmental impact and an alternative is the use of environmentally friendly materials such as biodegradables. The medium density fiberboard (MDF) is an example of biodegradable materials, as the material comes from reforestation wood, such as eucalyptus [1].

The MDF particulate panel is a medium-density wooden sheet, made from an agglutination of wooden fibers with synthetic resins and joint temperature and pressure applications. For the production of fibers, the wood is cut into small pieces that are subsequently crushed by equipment called defibrillators [2]. The MDF is mainly intended for the furniture and civil industries such as thin floors, footplates, door pads, divisories and beams. MDF can be reused as it is a material from biodegradable waste. This is a practice that generates a number of social, economic and ecological advantages for the development of Brazil.

Adding metal nanoparticles such as Ag, TiO_2, ZnO and Cu to polymeric materials can improve mechanical, electrical, magnetic and virucidal properties [4]. The addition of metal nanoparticles to particulate panels is a solution for improving mechanical and virucidal properties.

Some studies have already addressed the production of particulate panels (ecopaineals) in which lignocellulose particles and nanoparticles have been used. Y. Liu et al. [5] produced particulate panels with waste wood particles and TiO_2 nanoparticles and montmorylonite clay and formaldehyde urea as cluster resin. In this study they investigated the influence of processing on the

mechanical properties of particulate panels. In the work of Rangavar and Hoseiny [6] it investigates the effect of adding copper nanoparticles to a urea-formaldehyde resin on the physical and mechanical properties of clustered panels made from tamareira waste (tamareira is a type of fruitful palm, very important in the history and culture of the Middle East). Another study conducted by Taghiyari and Bibalan [7] showed the effect of the size of copper nanoparticles mixed with urea-formaldehyde resin and ammonia chloride and rest álamo (large-size tree, call populus spp) spheres on the production of particulate panels. They studied the physical and mechanical properties and permeability.
The article was intended to present a study on the ecopainels produced from the fiber of the acai fruit and copper nanoparticles (nanoCu). In this study the mechanical properties were obtained by three-point flexion test and physical properties.

Materials and Methods

Obtaining and preparation of the fibers

The waste fiber of acai berries collected was collected from the agro-industrial in Belém in the state of Pará, Brazil. The natural fibers were washed with de-ionized water and dried in a 60 °C greenhouse to a moisture of 8% and then grind and sift with 8 mm mesh.

Mixed resin + nanoparticles

The preparation of the resin was carried out with the mixture of components of the bi-component resin and copper nanoparticles (Hongwu International Group, China) in the proportions (0,1%, 0,4%, 0,6%, and 0,8%) by weight. The image obtained by scanning electron microscopy (MEV-EDS) (Jeol-IT500 HR, Jeol, Japan) shows the size and chemical composition of 80nm nanoparticles (Fig 1). For the preparation of the mixtures, the resin and the catalyst were weighed in the proportion of 1 part of polyol (alcohol containing multiple hydroxyl groups) to 1 portion of the polymer based on mammon oil in the ratio of 15% of the dry mass of the waste in relation to the dry massa of the residue (85%).

Mixture of resin with fibers

The compressed air homogenization process consists of the application of polyurethane resin and copper nanoparticles to the fibers, using air-compressed devices. This methodology is the simulation of an industrial process of mixing resin with lignocellulose fibers. After application, the homogeneous distribution and adhesion of the fibers with the resin will be checked, for the conformation process, the organic compound isocyanate was not used.

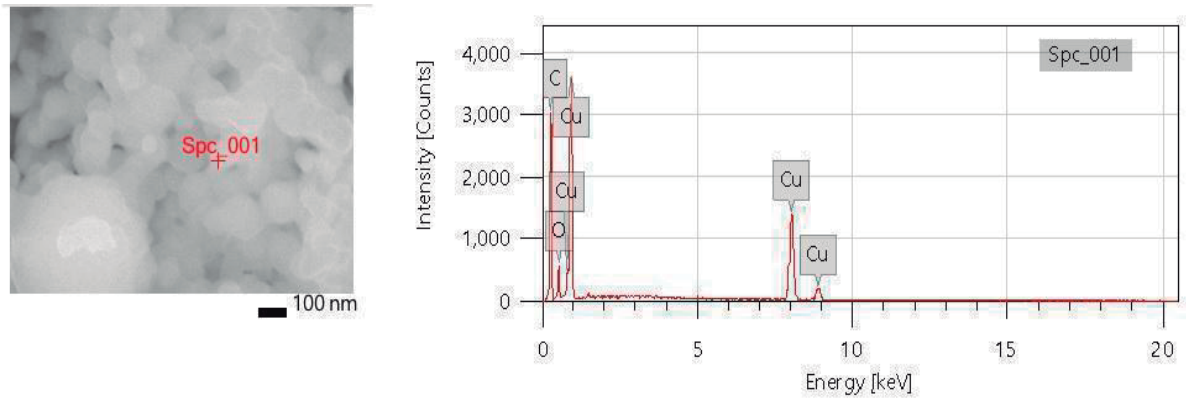

Figure 1. MEV-EDS of nanoparticles used for the production of ecopanels (nanocomposites).

Pressure and conditioning

At this stage, the mattress was pressed in a heated hydraulic press with a pressure of 5 MPa and a temperature of 100 °C. The produced panels remained for 72 hours in the process of stabilizing and cutting the test bodies.

Mechanical characterization

For this test it was carried out by three-point static flexion using a universal test machine. The samples showed dimensions 270 x 50 mm and the test was carried out at a test speed of 7 mm/min according to the standard [5].

Absorption of water

This physical property was determined based on technical standards of NBR 9778 (2009). As the fibers were weighed and dried to the constant mass, determining a water absorption by the equation %A = (MO – MF/MO) x 100, where %A corresponds to the moisture absorptions percentage, MO is the initial mass before drying, MF is the final mass after drying; D = CP density in kg/m³.

Density

This property was determined on panel test bodies (50 x 50 mm) using a scale (Modelo, Toledo, Brasil). D = (M/V) X 100,000; D = CP mass in g; V = CP volume in mm³ according to the standard [5].

Results and Discussion

The results showed the mechanical and physical behaviors of acai ecopainels (without nanoparticles) and the eco panels produced by adding copper nanoparticle (ecopainel-0,1%nanoCu), (ecopainel-0,4%nano Cu), (ecopainel-0,6%NanoCu) and (ecopainel-0.8%nano CU).

The results of three mechanical flexion tests for the reference ecopainel (without nanoparticles) and with nanoparticle (ecopainel/nanoCu) were obtained after 10 days of production. The reference panel (no nanoparticles) showed a breakdown module (MOR) and total specific energy (EE) close to the do (ecopainel-0,6%nanoCu). Ecopainels with amounts of 0.1, 0.4 and 0.8% in weight of nanoCu presented lower MOR and EE than the reference ecopainel as shown in the (Figura 2a).

These results show that the use of copper nanoparticles led to a better and faster heat transfer from one face to the core of the plates during the hot-pressing process [6], and this affected resin polymerization (harp healing) by increasing MOR and EE [7]. Ecopainel nanocomposites with amounts of 0.1, 0.4 and 0.8% in weight of nanoCu presented lower MOR and EE than pure ecopainel and nanocomposite (ecopaineel-0,6%nanoCu). It is likely that NanoCu particles have a negative effect on the bonds between wood and resin particles resulting in a reduction in MOR and EE [8]. It is noted that the MOR and EE were smaller for the ecopainel-0,8%nanoCu this behavior was due to this amount of nanoparticles that reduced molecular mobility and thus reducing the elasticity of the material [5].

It is noted that the reference ecopainel presented a higher elastic modulus (MOE) and limit of proportionality (LOP) than the nano composites. Ecopainel-0,1%nanoCu and ecopainell-0,6%NanoCu presented near and larger elastic MOE and LOP than the ecopaineel-0.4%nano Cu and ecoopainelle-0,8%naneCu (Fig 2b). One study conducted [8] showed that adding copper nanoparticles to MD plates resulted in increases in MOR and LOP values. Copper nanoparticles can improve adhesion between wood particles and resin, strengthening the structure of the material and increasing its mechanical strength [8].

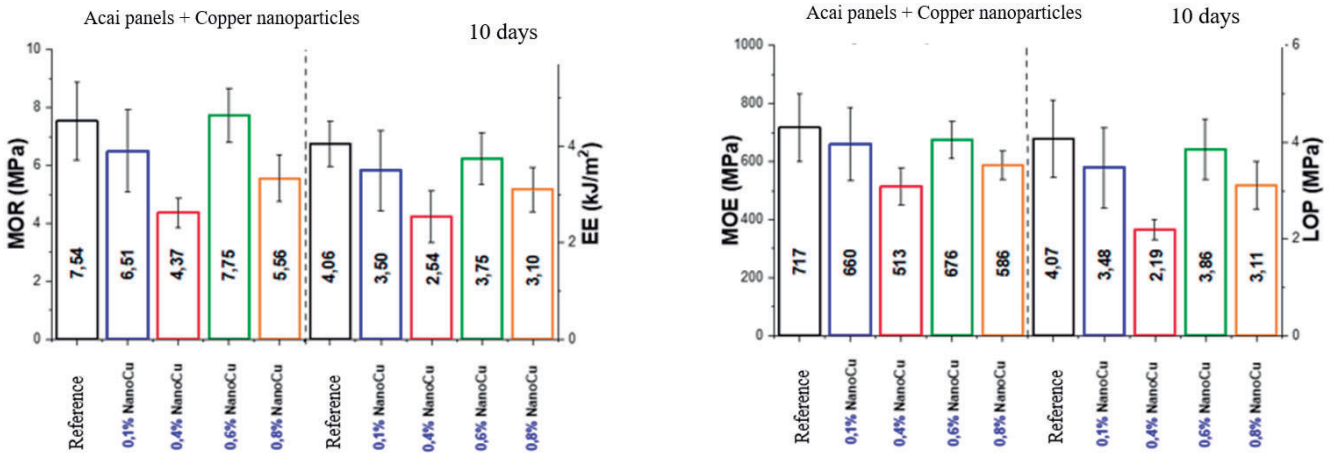

Figure 2. Mechanical properties (a) (MOR and EE) and (b) (LOP and MOR) obtained from mechanical flexion testing.

By Fig 3a it is observed that the water absorption was greater for the ecopanels with the nanoCu (ecopainel-nanoCu) compared to the reference ecopainel. This behavior shows a negative effect of copper nanoparticles [7] as the hydroxyl group of water adsorbs onto the surface of the copper nano particles [10]. The ecopainels ecopainel-1%nanoCu and Ecopaineel-6%namoCu showed lower water absorption than the ecopainels ecopainenel-4%natoCu and ecopainedel-8%nadoCu. The amount of 1 and 6% of nanoCu has shown better distribution in the resin and which has caused a twisted pathway layer for water transport, and thus resulted in a reduction in water diffusiveness [9]. On the other hand, the ecopainels ecopainel-4%nanoCu and Ecopaineel-8%NanoCu may have shown clumping of copper nanoparticles in the pores and increasing water absorption [10]. It is also observed by Fig 3a that the ecopainels with copper presented a higher density than the reference density. The quantity of nanoparticles dispersed from the resin caused the increased density. From Fig 3b it is observed that all ecopainels-nanoCu exhibited moisture and swelling higher than the reference ecopanel. Copper nanoparticles can react with oxygen to form copper oxide and then react to water which increases the moisture and swelling of the ecopainels-nanoCu relative to the reference ecopainel [11].

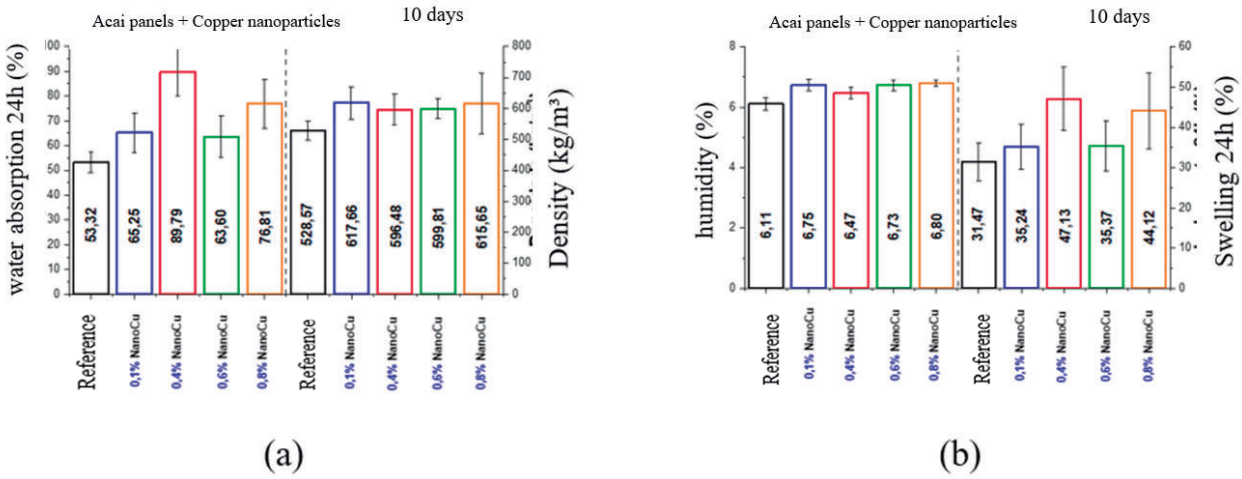

Figure 3. Physical properties of the ecopanel and its nanocomposites and (MOE and LOP).

Conclusions

With the results obtained with the physical and mechanical tests with the MDF of acai fiber and copper nanoparticles and a research in the literature on MDF nanoparticles, it is observed that the eco-acai panel with copper nano-particles is a viable option, since the echo panel with the composition of 0.6% of copper Nanoparticles comes to equal with the conventional, recalling that the places from which the fibers were harvested, is widely discarded in the State of Pará - PA, thus reducing the disposal in sanitary landfills and generating a sustainable process.

References

1. BNDES. Setorial: Painéis de madeira no Brasil: panorama e perspectivas 2008, Rio de Janeiro, p.121-156.
2. NBR 15316-3: Chapas de fibras de media densidade. Parte 3: Métodos de ensaios 2006, Rio de Janeiro.
3. A. M. Bauinain; M. O. Batalha. Cadeia produtiva de madeira. Brasília, 2007.
4. A. Ingle; N. Duran; M. Rai. Microbiol Biotechnol 2014, 98, 1001. https://doi.org/10.1007/s00253-013-5422-8
5. Y. Liu; J. Shen; X. D. Zhu 2015, Eur. J. Wood Prod. 2015, 73, 449. https://doi.org/10.1007/s00107-015-0910-4
6. H. Rangavar; M. S. Hoseiny Fard, Mech Compos Mater 2015, 51, 119–126. https://doi.org/10.1007/s11029-015-9482-y
7. H. R. Taghiyari; O. F. Bibalan European Journal of Wood and Wood Products 2013, 71, 69. https://doi.org/10.1007/s00107-012-0644-5.
8. M. Ghofrani, A. Ashori, R. Mehrabi, Polym Test 2017, 60, 153, https://doi.org/10.1016/j.polymertesting.2017.03.028.
9. X. Cai, B. Riedl, S.Y. Zhang, H. Wan, Compos Part A Appl Sci Manuf 2008, 39, 727. https://doi.org/10.1016/j.compositesa.2008.02.004
10. L. Zhou; S. Wang; H. Ma; S. Ma; D. Xu; Y. Guo 2015, 36. http://dx.doi.org/10.1016/j.cherd.2015.04.004.
11. H. Cong; H. Michels; J. R. Scullya. Journal of The Electrochemical Society 2009, 115, C16. http://dx.doi.org/10.1149/1.2999351.

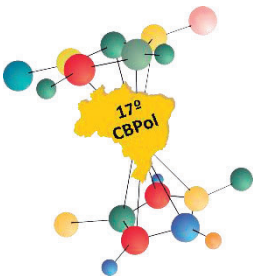

EFFECT OF HYDROTALCITE NANOPARTICLES ON THE ANTIOXIDANT PERFORMANCE OF STARCH/TANNIC ACID PACKAGING FILMS

Matheus L. Pavão[1], Bruno R. Luchesi[2,1], Fábio R. Passador[3], Juliano Marini[1], Luiz H. C. Mattoso[2] and Francys K V Moreira[1,*]

[1]Multifunctional Packaging group (GEF[m]), Department of Materials Engineering (DEMa), Federal University of São Carlos (UFSCar), São Carlos (SP), Brazil. [*]francys@ufscar.br
[2]National Nanotechnology Laboratory for Agriculture (LNNA), Embrapa Instrumentation, São Carlos (SP), Brazil.
[3]Biopolymers & Polymer Technology Laboratory, Federal University of São Paulo (UNIFESP), São José dos Campos (SP), Brazil.

Abstract - This study aimed to evaluate the antioxidant performance of biodegradable starch films loaded with tannic acid (TA) and hydrotalcite (HT) nanoparticles for active packaging applications. The films were produced via continuous solution casting (CSC) from film-forming solutions (FFS) obtained as per two mixing protocols (Pre-M and Post-M), so the effect of component interactions on the antioxidant activity of films was assessed. The results showed that starch/TA/HT films with better antioxidant performance were achieved with Post-M (EC_{50} = 2 g/L) rather than with Pre-M. The HT nanoparticles reduced the antioxidant activity of the starch/TA films most likely due to acid-base reaction between HT and TA or adsorption of TA molecules on the HT particle surface. This study reveals the potential of CSC for the staged production of antioxidant, multifunctional starch films for several food packaging applications.
Keywords: *Antioxidant packaging, nanotechnology, mixing protocol, DPPH.*
Fundings: PIBITI/CNPq/UFSCar/Nº 164260/2022-6.

Introduction

The recent decades have witnessed deep research into biodegradable films made up from natural polymers with the aim to replace non-biodegradable synthetic plastics [1]. Among biopolymers, starch have received special attention due to its abundance, excellent filmogenic capacity, low cost, and fast biodegradation [1-2].

Incorporation of bioactive agents in starch films is a trend in research whether for applications as multifunctional edible films, coatings, and flexible packaging [3]. In this context, tannic acid (TA) has attracted much attention as a component of biodegradable films due to its low cost, antioxidant capacity and broad antimicrobial activity [4]. TA is a plant-derived compound widely found in nature likewise starch. However, starch films are brittle, consequently their application becomes limited. The drawback of starch films has been overcome with the use of plasticizers, typically glycerol, but this leads to a reduction in their mechanical strength, also reducing their feasibility compared to conventional petroleum-based plastics [5].

A possible strategy to counterbalance the plasticizer effect in starch films is the formation of nanocomposites, once nanofillers can significantly reinforce a polymer matrix when included at low contents [5,6]. In the scope of this study, the nanofiller to be studied is hydrotalcite (HT), a layered double hydroxide (LDH) with formula ($Mg_6Al_2CO_3(OH)_{16}{\cdot}4H_2O$). HT is the most abundant LDH in nature, is edible, relatively simple to synthesize, and has been attracting interest for nanotechnologies, not only due to its reinforcing effect, but also due to its flame-retardant characteristics, possibility of

intercalation with organic molecules and biomineralization [7]. Prior to assess the mechanical reinforcement in starch/TA/HT nanocomposite films, it is utmost importance to evaluate whether HT nanoparticles can influence on the antioxidant capacity imparted by TA.
The present study was aimed at evaluating the influence of HT nanoparticles on the antioxidant performance of starch/TA films intended for biodegradable, antioxidant packaging applications. To assess the effect of component interactions (HT and TA structures are illustrated in Figs. 1A and 1B), the film-forming solutions (FFS) were prepared as per two different mixing protocols. Films were produced by continuous solution casting at 12 cm min^{-1} to extend the perspective of developing active starch packaging at a pilot-scale [8]. The antioxidant capacity of films was assessed by the classical diphenyl picryl hydrazyl (DPPH) free radical (Fig. 1C) scavenging assay.

Experimental

Materials

Food-grade cassava starch was purchased at a local market in São Carlos (SP). Tannic acid (TA) was purchased from Sigma-Aldrich (USA). Hydrotalcite (HT) (PURAL® MG 61 HT) with average particle diameter of 150 ± 63 nm was kindly donated by Sasol – Germany GmbH [9]. Glycerol (CAS No. 56-81-5) with purity of 99.5 % was used as a plasticizer. All solutions were prepared with ultrapure water obtained from a Milli-Q system.

Film-forming solution (FFS) preparation

Two different mixing procedures regarding the production of the starch/HT/TA films by CSC were evaluated in this study, namely, Pre-mixing (Pre-M) and Post-mixing (Post-M). In the Pre-M method, HT and TA were added to ultrapure water and sonicated at 70% amplitude (Branson 450 sonifier, pitch horn 1 /2″ tip diameter) for 10 min. This ensuing dispersion was added to an aqueous starch/glycerol suspension (30 wt.%) and further mechanically stirred at 1000 rpm under heating at 75 - 85°C for 30 min until starch was completely gelatinized. The Post-M method was carried out by first gelatinizing starch likewise followed by the addition of the HT/TA dispersion which obtained in a similar manner as that of Pre-M. All FFS were homogenized mechanically at 500 rpm for 30 min before the CSC process. The HT, TA, and glycerol contents used herein were 5 wt%, 1 wt%, and 22.5 wt.%, respectively, on a starch mass basis.

Continuous solution casting (CSC)

The starch/HT/TA films were prepared by CSC in a KTF B labcoater machine (Werner Mathis AG, Switzerland). In brief, the FFS were poured onto the moving substrate in the coating device, where a wet layer with a thickness of 1.2 mm was formed using a B-type doctor blade. The wet layer was dried through conveyance at speed of 12 cm min^{-1} by an IR pre-dryer with 42% emission potency and consecutive through two air circulating ovens equilibrated at 120 °C [8,9]. Dried films were then collected at the oven outlet and stored in plastic bags prior to use.

Determination of antioxidant activity

The antioxidant capacity was determined for each film using the standard DPPH free radical scavenging method, as reported elsewhere [10,11].

Results and Discussion

The results of the DPPH tests for the starch/HT/TA films obtained by the Pre-M and Post-M methods are illustrated in Fig. 1D e 1E. Comparing the 5% HT-loaded films, it can be seen that the larger antioxidant activity was achieved with Post-M (Fig. 1D) rather than with Pre-M (Fig. 1E). This becomes clear when 2g/L of Post-M film concentration is analyzed, at which the DPPH absorbance reduced by 34 % over the same concentration related to the Pre-M film. This trend is also verified in starch/TA films without HT (0% HT). Also taking the 2 g/L concentration as a reference, the Post-M

method resulted in films capable of reducing the DPPH absorbance at a higher extent than those obtained by Pre-M.
The difference observed between Post-M and Pre-M regarding the antioxidant performance of films could be ascribed to the fact that TA is not exposed to the starch gelatinization step in the Post-M method, whereas the prolonged heating needed to gelatinize starch may also have oxidized TA at some extent during the Pre-M method [4].
In addition, it is observed that the addition of HT nanoparticles reduced the antioxidant activity of the starch/TA films. This fact may have occurred due to a possible acid-base reaction between HT and TA. It is also possible that some TA molecules adsorbed on the HT particle surface or, less likely, were intercalated within the HT galleries, reducing the antioxidant performance of the starch/HT/TA films. Probe of such mechanisms is in progress.

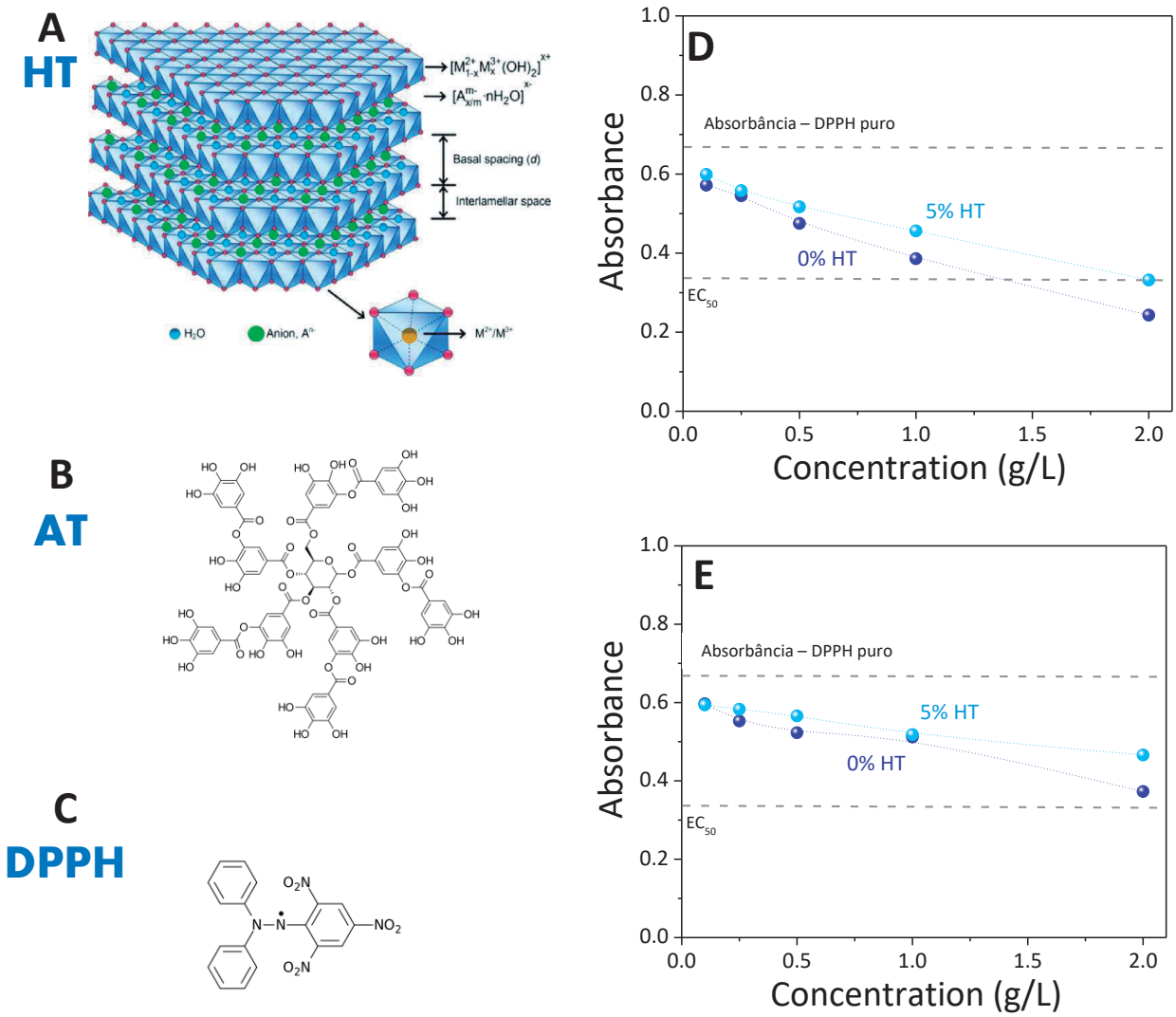

Figure 1: (A) Crystalline structure of HT [12] (B) Molecular structure of TA [13] (C) Molecular structure of DPPH [14]; DPPH absorbance variation as a function of starch/TA/HT film concentration (g/L). Films were produced following the (D) Post-mixing and (E) Pre-mixing methods. Pure DPPH absorbance (A = 0.668) was added as a reference for null antioxidant activity.

Overall, it was found that the starch/HT/TA films produced by CSC had a good antioxidant capacity, suggesting that TA did not lose its bioactive properties due to the processing at 120 °C. TA is considered an effective antioxidant due to its sterically hindered polyphenolic structure, as illustrated in Fig. 1B, that reacts directly with DPPH or any other free radical in a similar manner to primary

antioxidants used in polymers (Irganox® and so on). An important parameter obtained from the DPPH scavenging test is the Ec_{50} (sample concentration capable of reducing the initial DPPH absorbance by 50%). According to Figs. 1D-E, the EC_{50} was reached only with the Post-M starch/HT/TA films at 2 g/L approximately.

Conclusions

Eco-friendly starch/TA films loaded with HT nanoparticles were successfully produced on a pre-pilot scale by CSC. The mixing protocol used to prepare the FFS plays a role in the final antioxidant performance of films. Ideally, the maximum antioxidant capacity can be reached by adding TA or any other antioxidant as the final FFS component. Overall, this study highlights the potential of CSC for the staged production of multifunctional films containing antioxidant properties for various applications. The starch/TA/HT films developed herein can be used as monolayers or coatings in flexible paper packaging.

Acknowledgements

The authors thank the support provided by DEMa/UFSCar, Embrapa Instrumentation, National Network of Laboratories for Nanotechnology (SisNANO), CNPq Universal Program (Project nº 407288/2021-0) and Coordination of Superior Level Staff Improvement - Brazil (CAPES) - Finance Code 001.

References

1. Liu, F.; Chiou, B.; Avena-Bustillos, R. J.; Zhang, Y.; Li, Y.; McHugh, T. H.; Zhong, F. Food Hydrocolloids, 2017, 65, 1 – 9. http://dx.doi.org/10.1016/j.foodhyd.2016.10.004
2. MacArthur Foundation, *The New Plastics Economy: Rethinking the future of plastics*, Ellen MacArthur Foundation, 2017.
3. Campos, C. A.; Gerschenson, L. N.; Flores, S. K. Food and Bioprocess Technology, 2011, 4(6), 849–875. http://dx.doi.org/10.1007/s11947-010-0434-1
4. Leite, L. S. F.; Pham, C.; Bilatto, S.; Azeredo, H. C. M.; Cranston, E. D.; Moreira, F. K.; Mattoso, L. H. C.; Bras, J. ACS Sustainable Chemistry Engineering, 2021, 9, 8539−8549. https://doi.org/10.1021/acssuschemeng.1c01774,
5. Alcântara, A.C.S; Darder, M.; Aranda, P.; Ayral, A.; Ruiz-Hitzky, E. Journal of Applied Polymer, 2016, 133(2), 42362. http://dx.doi.org/10.1002/APP.42362
6. Mishraa, G.; Dasha, B.; Pandey, B.; Applied Clay Science, 2018, 153, 172–186, http://dx.doi.org/10.1016/j.clay.2017.12.021.
7. Leroux, F.; Besse, J. Chemistry of Materials, 2001, 13, 3507-3515 http://dx.doi.org/10.1021/cm0110268
8. Leite, L. S. F.; Ferreira, C. M.; Corrêa, A. C.; Moreira, F. K. V.; Mattoso, L. H. C. Carbohydrate Polymers, 2020, 238, 116198. http://dx.doi.org/10.1016/j.carbpol.2020.116198.
9. Munhoz, D. R.; Bernardo, M. P.; Malafatti, J. O. D.; Moreira, F. K. V.; Mattoso, L. H. C. International Journal of Biological Macromolecules, 2019, 141, 504–510. https://doi.org/10.1016/j.ijbiomac.2019.09.019
10. Do, M.; Rufino, S. M.; Alves, R. E.; De Brito, E. S. *Metodologia Científica: Determinação da Atividade Antioxidante Total em Frutas pela Captura do Radical Livre DPPH Introdução*. Embrapa, ISSN 1679-6535, 2007.
11. Sánchez-Moreno, M. Food Science and Technology International, 2002, 8(3), 121–137. https://doi.org/10.1106/108201302026770.
12. Cavani, F.; Trifirb, F.; Vaccari, A. Catalysis Today, 1991, 11, 173–301. https://doi.org/0920-5861/91.
13. Tannic acid. Available at: https://en.wikipedia.org/wiki/Tannic_acid
14. DPPH structure. Available at: https://commons.wikimedia.org/wiki/File:DPPH_radical.svg

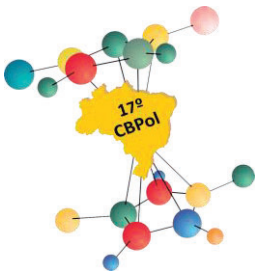

EFFECT OF THE ADDITION OF SIO_2 NANOPARTICLES ON THE COMPATIBILITY OF IMMISCIBLE POLYMERIC SYSTEMS BASED ON POLYETHYLENE AND POLYAMIDE 11 FROM OFFSHORE PLATFORMS

Joyce B. Camargo[1*], Ana Lucia N. Da Silva[1,2], Gisele Cristina V. Iulianelli[1], Christine Rabello Nascimento[3]

1 – Instituto de Macromoléculas Professora Eloisa Mano (IMA), Universidade Federal do Rio de Janeio (UFRJ), Rio de Janeiro, RJ, Brazil
2 – Programa de Engenharia Ambiental (PEA), Universidade Federal do Rio de Janeio (UFRJ), Rio de Janeiro, RJ, Brazil
3- Universidade Federal do Rio de Janeiro, Programa de Engenharia Metalúrgica e de Materiais (COPPE/UFRJ), CEP: 21941-972, Rio de Janeiro, RJ, Brazil.
joycecamargo@ima.ufrj.br

Abstract - In the present study, immiscible polymeric systems based on high density polyethylene (HDPE) and post-consumer polyamide 11 (PA11) from offshore platforms were produced and their properties were evaluated. HDPE/PA11 (80/20, wt.%) blend containing 1.5 wt.% of polyethylene grafted with maleic anhydride (HDPE-g-MA) were obtained by melt processing, using a twin-screw extruder. Silicon dioxide nanoparticles (n-SiO_2) were added to the blend at 2 and 4 wt.%. The effect of this nanofiller on the HDPE/PA11 blend, containing or not containing HDPE-g-MA as compatibilizer, was studied by thermogravimetric analysis (TGA), melt flow index (MFI), tensile test and morphologically by FEG-SEM. The results showed that SiO_2 nanoparticles at lower content, had a synergic effect when traditional compatibilizer was added, providing improvement on the elastic modulus and on the thermal stability. The flow behavior of systems containing HDPE-g-MA and SiO_2 nanoparticles was reduced, confirming a synergic effect in the interaction between the immiscible phases. In addition, this composition presented the better balance between thermal and mechanical properties.
Keywords: *Immiscible polymeric blend; compatibility processes; nanocomposites; SiO_2 nanoparticles*

Introduction

Ternary hybrid blends composed by two polymers and a mineral nanofiller have been developed in order to respond to several industrial demands, such as improving the properties of pure polymers, reusing recycled materials and reducing the cost of the final product. However, many polymeric systems do not have good miscibility between phases, which can compromise their application as a final product. Among the effects of mineral nanofillers used in immiscible blends, one can cite is the improvement of the interaction between polymeric phases. The literature presents new technologies for reducing phases domains in immiscible polymeric blends [1-5].

The aim of this work was to develop immiscible systems based on high density polyethylene (HDPE) and polyamide 11 (PA11) from offshore flexible pipes in the ratio of 80:20 (w/w) and to evaluate the effect of adding a traditional compatibilizer, high density polyethylene grafted with maleic anhydride (HDPE-g-AM) (1.5, wt.%). In addition, it was evaluated the effect of adding silicon dioxide nanoparticles (n-SiO_2) (2 and 4 wt.%), as a compatibilizer or co-compatibilizer for HDPE/PA11 blends.

Experimental

Materials

The commercial materials used in this study were: High Density Polyethylene (HDPE) provides by Braskem S/A; silicon dioxide (SiO_2) chemically modified with hydrophobic dimethyldichlorosilane (DDS) Aerosil® R972 provided by Evonik Operations GmbH, specific area 110 ± 20 m^2/g and average particle size 16 nm and high-density polyethylene-grafted maleic anhydride (HDPE-g-MA) with 0.4 wt.% of maleic anhydride, Mw 15,000 g/mol supplied by Sigma Aldrich.

The post-consumer PA11, from an offshore flexible pipe pressure barrier (Fig.1) donated by PRIMAPLAST was mechanically cut and subsequently ground in a knife mill, with prior immersion in liquid nitrogen.

Figure 1 – PA11 post-consumer from a pressure barrier of a flexible pipe (left) and PA11after milling (right). Source: own authorship.

Methodology

Systems based on HDPE/PA11 were melt processing in a co-rotational twin screw extruder, according to the following processing conditions: temperature profile: 90 ºC / 160 ºC/ 170 ºC/ 180 ºC/ 190 ºC / 190 ºC / 190 ºC / 190 ºC / 200 ºC / 200 ºC and screw speed of 400 rpm. The HDPE:PA11 ratio was fixed at 80:20 (wt.%). HDPE-g-MA, as traditional compatibilizer, was added at 1.5, wt.% and SiO_2 nanoparticles (n-SiO_2) at 2 and 4 wt.%. Table 1 shows the different HDPE/PA11 compositions produced.

Table 1- Compositions prepared.

Sample Code	Composition
1	HDPE/PA11
2	HDPE/ HDPE-g-AM / PA11
3	HDPE/ HDPE-g-AM / PA11+ 2% n-SiO_2
4	HDPE/ HDPE-g-AM / PA11+ 4% n-SiO_2
5	HDPE/PA11 + 2% n-SiO_2
6	HDPE/PA11 + 4% n-SiO_2

Characterization

The obtained blends were characterized by thermogravimetric analysis (TGA), melt flow index (MFI), tensile test and scanning electron microscopy (SEM) according to the following experimental conditions: TGA: initial temperature (Ti): 30 ºC; final temperature (Tf): 700°C; heating rate: 10°C/min; under nitrogen atmosphere (N_2); MFI test: ASTM D1238 (2013) standard; conditions of 235ºC/5 kg; Tensile test: ASTM D638-10 (2014) standard. Equipment: EMIC model

DL3000. The test specimens were prepared by injection molding in the Arburg machine model 270S with a temperature profile of 210/220/240/250/260 ºC, 1600 bar injection pressure, mold temperature of 30 °C, and cooling time of 30 s. The SEM analysis was carried out in a Mira equipment, with electron emission of FEG Schottky, using 10 KeV of voltage and 10,000X of magnification. The specimens were cryogenically fractured, and the surfaces were evaluated.

Statistical Analysis

The statistical analysis of the results was performed using STATISTICA 6 software. Analysis of variance (ANOVA) was applied to test the significant differences between means. The residuals normality and homogeneity of variances (Cochran C) were tested before univariate tests of significance and Fisher's least significant difference (LSD) test, using a significance level of $\alpha = 0.05$.

Results and Discussion

Table 2 shows the results of the thermal ($T_{Máx}$ values), rheological (MFI values) and mechanical properties of the analysed compositions.

Table 2 – Results of the thermal, rheological and mechanical properties of the HDPE/PA11 compositions.

Material	Composition	$T_{Máx}$ (°C)	MFI (± 0,05) (g/10 min)	Tensile strength (MPa) **	Stress at break (MPa)*	Elastic Modulus (MPa)*
1	HDPE/PA11	467	0,96	21,0	9,00	667
2	HDPE/ HDPE-g-AM / PA11	461	0,84	20,9	9,32	649
3	HDPE/ HDPE-g-AM / PA11+ 2% n-SiO_2	482	0,75	21,8	11,7	746
4	HDPE/ HDPE-g-AM / PA11+ 4% n-SiO_2	479	0,82	22,3	11,2	751
5	HDPE/PA11 + 2% n-SiO_2	479	1,04	21,8	12,0	713
6	HDPE/PA11 + 4% n-SiO_2	466	1,08	22,1	11,5	695

*The Values had verified by perform ANOVA and a confidence interval of 0.95 was applied.
** Value corresponding to Ultimate tensile strength.

From Table 2, it was seen that n-SiO_2 addition led to an increase on the thermal stability, especially when n-SiO_2 was added with the traditional compatibilizer. The HDPE/HDPE-g-AM/PA11 composite containing the lowest n-SiO_2 content (2 wt.%) presented a lower MFI value, indicating that in this composition, the restrict to flow is more pronounced. Probably this behaviour is due to the efficiency of the interaction between n-SiO_2 nanoparticles and HDPE/PA11 matrix in the presence of the compatibilizer, inhibiting the flow of the polymeric chains. Furthermore, a reduction in the viscosities (high MFI values), $T_{Máx}$, elastic modulus and tensile stregth values was observed in compositions without the compatibilizer, indicating a poor interaction between nanoparticles and polymeric matrix.

From mechanical properties evaluated by the tensile test, it was seen that the values of tensile strength, stress at break and elastic modulus, increased with the addition of the nanofiller in the matrix. Based on Fisher LSD test, whose data indicates whether the data are “statistically equal” or “statistically different”, the results showed that tensile strength and stress at break of the samples with the nanofiller are statistically similar to each other. While when compared to the matrix, they are statistically different, that is, the addition of n-SiO_2 in the presence or absence of the traditional compatibilizer (HDPE-g-AM) increased these mechanical properties. Regarding elastic modulus property, it was shown, from the statistical analysis, it was observed that the compositions HDPE/PA11 and HDPE/HDPE-g-AM/PA11 are statistically equal to the other samples, except for the composition HDPE/PA11 with 4 wt.% of n-SiO_2. The elastic modulus value for this material is statistically similar to the HDPE/PA11 sample and to the HDPE/PA11 with 2 wt.% of n-SiO_2

sample; while HDPE/PA11 with 2 wt.% of n-SiO_2 is statistically different comparing to PEAD/PA11. It was possible to conclude that the addition of 2 wt.% nSiO_2 in the blend promoted a better balance in relation to mechanical properties.

Images obtained by SEM for different compositions are shown in Figure 2.

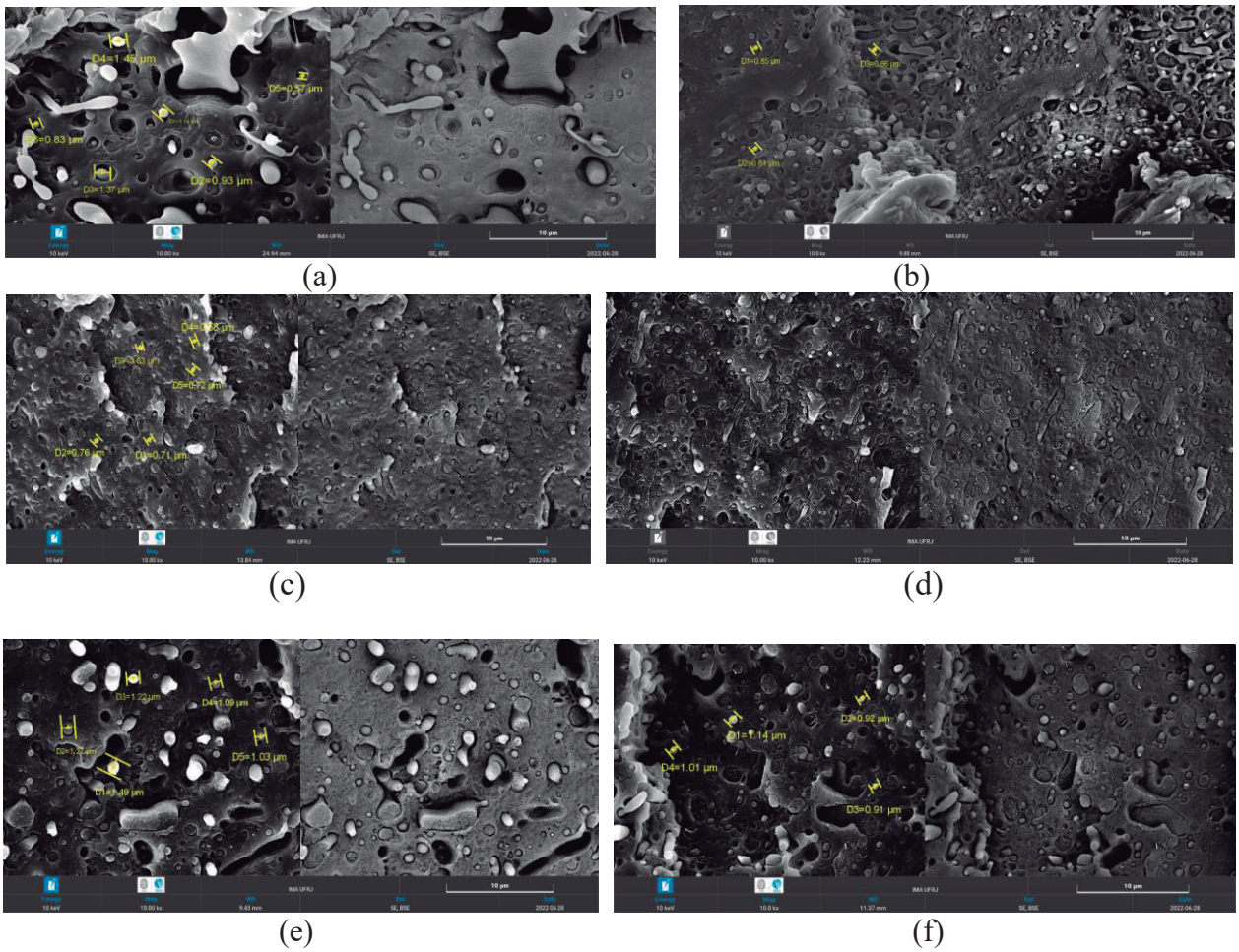

Figure 2 – SEM micrographs of (a) HDPE/PA11; (b) HDPE/HDPE-g-MA/PA11; (c) HDPE/HDPE-g-MA/PA11/n-SiO_2 (2 wt.%); (d) HDPE/HDPE-g-MA/PA11/n-SiO_2 (4 wt.%); (e) HDPE/PA11/n-SiO_2 (2 wt.%) and (f) HDPE/PA11/n-SiO_2 (4 wt.%)

According to Fig. 2a, HDPE/PA11 binary blend has typical island-sea type morphology, where irregular droplets are dispersed in HDPE matrix (sea phase of HDPE). When the compatibilizer (HDPE-g-MA) was added to the HDPE/PA11 binary blend (Fig. 2b), the droplets, which represent the dispersed phase of PA11, decreased, became more uniform, and well dispersed into HDPE matrix, indicating an improvement in the interaction between the HDPE and PA11 phases. The change of the blend morphology of HDPE/HDPE-g-MA/PA11, compared to the HDPE/PA11, can be attributed to reduction of interfacial tension between HDPE and PA11 phases, caused by addition of the compatibilizer agent. However, no improvement was observed in the thermal and mechanical properties of the HDPE/HDPE-g-MA/PA11 blend compared to the HDPE/PA11 system. When SiO_2 nanoparticles were added, the morphology changed significantly. PA11 domains reduced in size, especially with lower n-SiO_2 content (2 wt.%), and a greater interaction between HDPE and PA11 seems to have occurred. In the compositions without the presence of the compatibilizer, the PA11 domains became larger again and a poor interaction between HDPE and PA11 seems to occur. These morphologies suggest the synergistic effect of the SiO_2 nanoparticles

and HDPE-g-MA on the interaction between the immiscible phases. These evaluations corroborate the previously discussed results (Table 2), indicating that n-SiO_2 can act as a co-compatibilizer in the HDPE/PA11 blend.

Conclusions

The present study evaluated the effect of n-SiO_2 as a "co-compatibilizer", improving the HDPE-g-MA compatibilizing action in the blends based on HDPE and PA11 from offshore flexible pipes. The morphological results showed that the HDPE/PA11 binary blend presented a typical island-sea type morphology, where irregular droplets of the minor phase (PA11) are dispersed in the HDPE matrix. The addition of the compatibilizer agent, HDPE-g-MA, contributed to decrease in the size of the PA11 droplets; however, no improvement on the thermal and mechanical behavior was observed for both blends. When n-SiO_2 was added, PA11 domains reduced in size, especially with lower n-SiO_2 content (2 wt.%). In addition, there seems to have been a greater interaction between HDPE and PA11, showing that the nanoparticles affected the level of interaction between HDPE and PA11 phases. This composition also presented the best balance between thermal and mechanical properties.

Acknowledgments

The authors acknowledge the Conselho Nacional de Desenvolvimento Científico e Tecnológico (CNPQ) (307889/2022) and Coordenação de Aperfeiçoamento de Pessoal de Nível Superior - CAPES.

References

1. MAZINANI, S. ; DARVISHMANESH, S. ; RAMAZANI, R ; VAN, B.. Reactive and Functional Polymers, 2017, 111, 88–101. DOI: 10.1016/j.reactfunctpolym.2016.12.010.
2. SADIK, W.; EL DEMERDASH, A.; ABBAS, R.; BEDIR. A.; Journal of Polymers and the Environment. 2021, 29, 1600–1615. DOI: 10.1007/s10924-020-01983-6.
3. MARTINS, M.; CARTER, M.; ROUSE, S.; RUSSELL, D. Marine Policy. 2023, 152, 105629, ISSN 0308-597X. DOI: https://doi.org/10.1016/j.marpol.2023.105629.
4. FERREIRA, A.; ROCHA, E.; JANDORNO JR, J.; SOUSA, A.; DA SILVA, A. Polymer bulletin. 2023. v. Online,. p. 1,. DOI: https://doi.org/10.1007/s00289-023-04819-0
5. ZORZANELLI, L.; SALIMENA, L.; PEREIRA, E..; PACHECO, E..; SILVA, A.; BERTOLINO, L.; BASTOS, M.; SOUSA, A.; SILVA, A. Fibers and polymers. 2023. v. online, p. 1, DOI: https://doi.org/10.1007/s12221-023-00079-x.

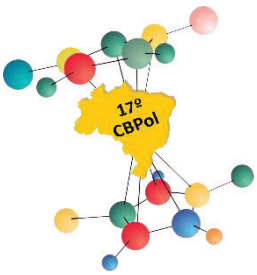

EFFECT OF THE GRAPHENE NANOPLATELETS ON FLEXIBLE PVC

Daniela M. Cecatto[1], Tarcisio S. Sene[2], Lilian V. R. Beltrami[1] and Ademir J. Zaterra[1]*

1 – Graduate Program in Process and Technology Engineering, University of Caxias do Sul (UCS), Caxias do Sul, RS, Brazil
dmcecatto@ucs.com.br
2 – Department of Materials Engineering (Grendene SA, Farroupilha, RS, Brazil)

Abstract - Polyvinyl chloride is one of the most used thermoplastics in the world, and there are currently several researches in the application of nanocomposites in polymeric matrix, especially with graphene, which has been receiving more attention due to its properties. In this research, it was carried out the dispersion of graphene ia a flexible PVC compound. The raw materialswere mixed in a Henschel mixer, extruded in a twin-screw extruder and pelletized, then injected into a sample mold and spiral flow mold, the latter aiming to evaluate the influence of graphene nanoplatelets on flexible PVC flow. Five compositions were then obtained for evaluation, standard PVC with plasticizer, and the incorporation of 0.05%, 0.01%, 0.1%, 0.2% and 0,5% of graphene nanoplatelets. It was also possible to observe about 1 cm of flow increment in spiral mold, all the concentrations reduced the coefficient of friction in the sliding test. It can be concluded that despite the low levels used, it was possible to notice the influence of the incorporation of the nanomaterial on some of the properties evaluated.

Keywords: *Graphene nanoplatelets, Vinyl polychloride, nanocomposite, properties*

Introduction

In recent years, nanocomposites have been applied in various sectors of industry, due to their characteristics of increasing the properties of the matrices that they are applied, one of which is graphene, has been receiving even more attention. Graphene is one of the allotropic forms of carbon and is made up of a single two-dimensional layer of sp^2 hybridized carbons, aligned hexagonally [1] This material was discovered in 2004 by Andre Geim and Konstantin Novoselov, who reproduced it by applying adhesive tape over a layer of graphite and removing it from this material several times. This process is called mechanical exfoliation and allows to prepare films.[3].

Graphene is characterized by having tensile strength and elasticity. In addition, it can be noted that because of its nanometric particles, it has a large surface area and has antibacterial properties. Due to all these properties, this material has been studied to enable its application in several areas, such as equipment and electronic parts, in the automotive and medical industries, as well as in several areas of chemistry, as it still has catalytic properties [8].

Polyvinyl chloride (PVC) is obtained through the polymerization of vinyl chloride monomer, which is one of the most consumed thermoplastics in the world. It is estimated that in 2017 the average consumption of this plastic was around 43 million tons. In Brazil, consumption reached 1 million tons of polymer, equivalent to 5 kg of PVC per citizen per year.[2] The additives responsible for altering the hardness of PVC, making it flexible, are called plasticizers. Another prominent feature of PVC is that it is inert and non-toxic. When choosing additives with these same features, its application is further expanded to food packaging and objects for hospital use [4].

In addition, the recyclability of PVC is also a positive factor for this material. Its compounds are usually thermoplastic, which can be molded after heated in a molden state. After cooling, it can be be reshaped if heated again [9]. The mechanical properties of flexible PVC materials are of extreme importance, always attracting the attention of academic and industrial researchers. Some fillers, such as calcium carbonate, clay, and silica, have been added to improve the mechanical properties of PVC [5].

Nanocomposites can be defined by hybrid compounds, in which at least one of these materials has nanometric dimensions. In this work, the polymer compound is the matrix in which the graphene will be dispersed as a reinforcing phase [7]. Regarding the interaction between nanoparticles (such as graphene), it is challenging to disperse and keep it dispersed in a molten polymer matrix. Agglomerated nanoparticles may act as stress concentrators, which may fail under stresses lower than the original matrix would tolerate [6].

This work aimed to evaluate the behavior of graphene nanoparticles dispersed in the polymeric matrix of PVC, studying its influence on the mechanical properties of the polymer.

Experimental

Materials:

The flexible PVC compound for this work used a suspension PVC with a K value of 71. All additives, plasticizers and fillers used are from closed formulations by the company Grendene SA. The dispersed material, the graphene nanoplatelets, were produced by UCSGraphene (ZEXTECNANO) through exfoliation in liquid phase. The commercial name of this material is Graphene UGZ-1001.

Nanocomposite preparation

To manufacture the nanocomposite pellets, a dry blend was initially prepared, mixing the resin, plasticizers, additives, and graphene nanoplatelets (0.005% to 0.5% m/m). The samples were mixed in a Henschel-type mixer (Mecanoplast ML 9 RH 20),with rotation of 2500 rpm, until reaching 100 ºC, when the plasticizer dosage begins. Then, each mixture is released into a cooler mixer, where they will be stirred until they reach 30 °C. Afterwards, the nanocomposites were extruded, using a modular twin-screw Co-rotating extruder, with 18 mm in diameter, L/D 32, from the Coperion SZK 18 ML, at 300 rpm, with temperature profiles of 135 °C , 140 °C, 145 °C, 150 °C, 155 °C, 155 °C, 160 °C.

Nanocomposite injection

The injection of the test specimens was carried out in a Golden Eagle GEK-220injection machine, with 220 tons of clamping force and a screw diameter of 55 mm. The specimens relevant to the mechanical analysis. The specimens for mechanical analysis and spiral flow length were injected in Grendene S.A. The temperature profile for injection molding was 180 ºC – 175 °C – 160 ºC, with a injection rate of 25 cm3.s^{-1}. For the spiral mold flow, samples were injected until the flow stabilized, maintaining a constant speed of 70% in the injector, with pressure in the injector varying from 70% and 55% for each of the samples. The mold has markings inside the cavity indicating the flow length in centimeters. The nomenclature adopted to the samples was: blank PVC for the flexible standard PVC formulation from Grendene SA; and G1, G2, G3, G4, G5 for the samples with graphene, with respectively 0,005%, 0,01%, 01%, 0,2% and 0,5% (m/m) of the UCSGraphene nanoplatelets.

Tensile test

The tensile test was carried out in a universal testing machine, Instron 34TM-5, with a load cell of 5 kN, at a speed of 50 mm/min, using an extensometer with a distance of 25 mm between grips, according to the ASTM standard. D-638:2014. The values of tensile strength, elastic modulus at 100% deformation, elastic modulus at 20% deformation were obtained.

Slip resistance test

The sliding test was carried out in a Gester static slip resistance test equipment, model GT-KB43, with a 400-grit silicon carbide sliding surface, on a circular specimen, 12.7 mm in diameter and thickness between 5.08 mm and 6.35 mm, according to ASTM F609.

Results and Discussion

Spiral mold flow injection

Injection in a spiral flow mold, whose data are shown in Fig. 1, took place at two injection pressures. The first at 70%, represented in black, and the second at 55%, represented in gray, both with constant injection speed.

Samples G1 and G2, at 70% pressure, presented smaller flow lengths in relation to the standard sample. Samples G3 and G4 presented a greater flow, and G4 presented almost 2 cm more in the injected part, which can be attributed to a possible lubricating effect of the proportion of 0.2% of graphene. However, when adding the highest content of graphene(G5), there is a reduction in the injected flux in centimeters. A hypothesis for this feature is that the viscosity increases due to the interaction of the graphene with the matrix, compensating the possible effect of lubrication.

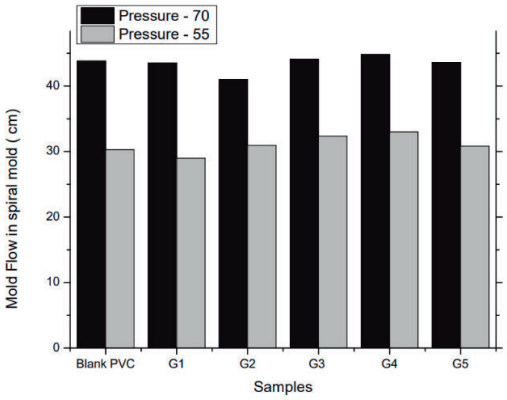

Figure 1 - Spiral mold flown injection in cm.

Tensile test

Fig. 2 represents the graphs of the tensile test representing the results related to tensile strength (A) and tensile modulus at 20% elongation (M20)(represented in the graph in black) and 100% elongation (represented in the graph in gray) (B), showing the average values obtained for the five samples comparing them to the standard sample.

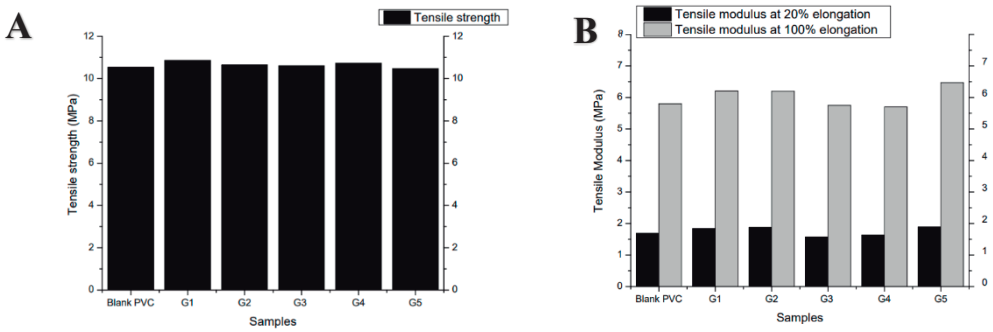

Figure 2- Tensile strength (A); Tensile modulus at 20% and 100% elongation (B).

The addition of graphene slightly increased the elastic modulus at the lowest contents, these being samples G1 and G2, with respectively 0.005% graphene and 0.01% graphene. However, samples G3 and G4, containing 0.1% and 0.2% slightly reduced their elastic moduli in both degrees of deformation, 20% and 100%. In sample G5, with the highest concentration, an increase in the elastic modulus is again noted.

Therefore, it can be considered that for the samples of lower concentration, G1 and G2, the standard deviation overlaps the values obtained, not being possible to observe an increase in the elastic modulus of the material, in G3 and G4. The G5 sample presents greater rigidity compared to the other compositions, , due to the higher elastic modulus value in both evaluated deformations, due to a larger interaction of the higher content of graphene with the matrix.

As for the tensile strength, the reference sample showed the lowest value, while when graphene is added, the value increases, going from 10.5 MPa, in the blank PVC, to 10.86 MPa, in the G1 sample, however, the deviation also increases pattern of results. By increasing the graphene content, the tensile strength decreases, however in G4, it increases again. Sample G5, on the other hand, presents lower values for yield strength, with a higher standard deviation.

Sliding test

The results of the slip resistance test are presented in Fig. 3. When graphene is added, the values in the slip test decrease, that is, less force is required for this material to slip in relation to the standard sample. The values fall gradually from sample G1 to G3; however, it increases again in sample G4 by 0.15 kgF in relation to sample G3. In sample G5, the value drops again, showing a tendency to decrease the coefficient of friction with the addition of graphene, only showing point G4, with 0.2% of graphene as an exception.

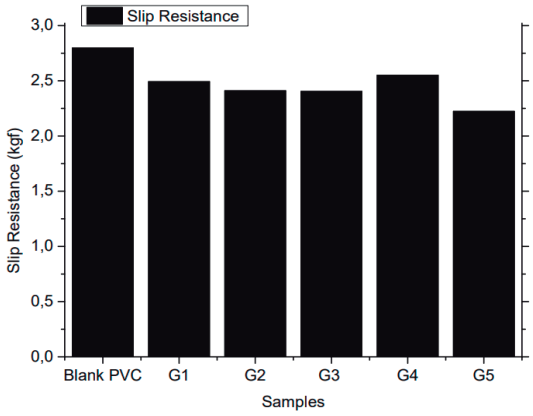

Figure 3 – Slip resitance

Conclusions

In this study, it was possible to evaluate the influence of graphene on different mechanical properties of flexible PVC. Regarding the tensile mechanical properties, graphene tends to increase the tensile strength, but reduces the elongation at rupture. Regarding stress at 20% and 100% strain, the changes were subtle, being more noticeable at 20% strain. Samples G1 and G2 and G5 showed increasing trends, while samples G3 and G4 showed lower values. These similar results are attributed to the low alteration of graphene contents in the samples. For sliding, it was noted that less force is needed for sliding to occur with the addition of graphene, thus representing a lower coefficient of friction.

In view of all the results obtained, with the techniques used in the methodology and the samples evaluated, the formula that presents the best performance and can be used in some applications would be the G5 sample. The requirements for the material must always be observed,, as its resistance to fatigue can be harmed.

Acknowledgements

The authors acknowledge CAPES, FAPERGS and CNPq for the financial support and grants as well as that to the University of Caxias do Sul (UCS) for all analysis presented in this paper.

References

1. H Saalem.; M, Haneef.; H. Y Abbasi. *Synthesis route of reduced graphene oxide via thermal reduction of chemically exfoliated graphene oxide*. Materials Chemistry and Physics, 204, p. 1–7, 2018. https://doi.org/10.1016/j.matchemphys.2017.10.020

2. A. Rodolfo; L, Nunes. *Tecnologia do PVC*., Braskem, Brasil, 2002.

3. K. S Novoselov. et al. *Two-dimensional gas of massless Dirac fermions in graphene*. Nature, v. 438, n. 7065, p. 197–200, 2005. https://doi.org/10.1038/nature04233

4. A. M. Souza. et al. *Nanocompósitos de Poli(Cloreto de Vinila) (PVC)/Argilas Organofílicas*., 2006

5. Wang, H., Xie, G., Ying, Z., Tong, Y., & Zeng, Y. (2015). *Enhanced mechanical properties of multi-layer graphene filled poly(vinyl chloride) composite films*. Journal of Materials Science and Technology, 31(4), 340–344. https://doi.org/10.1016/j.jmst.2014.09.009

6. Hasan, M., & Lee, M. (2014). *Enhancement of the thermo-mechanical properties and efficacy of mixing technique in the preparation of graphene/PVC nanocomposites compared to carbon nanotubes/PVC.* Progress in Natural Science: Materials International, 24(6), 579–587. https://doi.org/10.1016/j.pnsc.2014.10.004

7. A.C. Esteves.; A. Barros, T. Trindade *Nanocompósitos de matriz polimérica: estratégias de síntese de materiais híbri*dos Quim. Nova. 2004.

8. Wilczewski, S., Skórczewska, K., Tomaszewska, J., Lewandowski, K., Szulc, J., & Runka, T. (2020). *Manufacturing homogenous PVC/graphene nanocomposites using a novel dispersion agent*. Polymer Testing, 91. https://doi.org/10.1016/j.polymertesting.2020.106868

9. D. C. dos Santos. *Inferências sobre o uso de grafeno em materiais compósitos com ênfase em materiais à base de polipropileno*. Revista Ibero-Americana de Humanidades, Ciências e Educação, v. 7, n. 10, p. 992–1024, 2021.

EFFECT OF THE INCORPORATION OF MODIFIED SILICA IN A COMPOSITE WITH NANOFIBRILLATED CELLULOSE

Adriana A. Silva[1*], Veronica Calado[1], Bluma G. Soares[2]

1 – Chemistry School, Federal University of Rio de Janeiro (UFRJ), Rio de Janeiro, RJ, Brazil
anjosadriana@eq.ufrj.br
2 – Macromolecules Institute (IMA, Federal University of Rio de Janeiro (UFRJ), Rio de Janeiro, RJ, Brazil

Abstract
Nanofibrillated cellulose (NCF) was modified by the addition of silica filler to obtain composite materials. The sol gel process of silica preparation was carried out in situ in the NCF, starting from the aqueous solution under different conditions of the reaction medium, adjusted by the addition of acid (HCl) or base (NH_4OH). Organically modified silica (ORMOSIL) was obtained with octylsilane. The presence of silica reduced the NCF crystallinity and increased the thermal stability of the NCF by shifting to higher degradation temperatures, regardless of the composite preparation conditions. The silica modification contributed to increase the organophilic character of NCF for water contact angle (WCA) values above 140^0.

Keywords: *Nanofibrillated cellulose (CNF), silica, ORMOSIL, hidrophobicity*

Introduction

Silica is extensively used to obtain hybrid material with a polymeric matrix, due to the possibility of adjusting the size of SiO2 particles [1], thermal stability and chemical inertness, high mechanical strength, high modulus and extensive surface area [2]. Such characteristics come from the Si-OH groups on the surface, and the versatile surface modifications on the silica surface, which can form multifunctional materials [3,4]. Silica is extensively used in several fields, such as reinforcing filler in composite materials and coatings, because of their low cost, ease of fabrication, ease of functionalization and low density compared to other nanoparticles [5]. Silica is easily obtained by several synthesis routes of the sol-gel process [6], under different reaction medium conditions: neutral, acidic [7] and basic [8]. However, silica is easily aggregated due to its high surface energy, which results in property damage. To overcome this limitation of silica in composites, modification with alkylsillanes is commonly performed, and thus, by the sol-gel process, the organically modified silica particle, (ORMOSIL) is prepared [9]. Obtaining organic-inorganic hybrid particles improves the distribution of ORMOSIL, promotes high silica dispersion, and consequently improves properties, through the synergism of the characteristics of the composite's constituents.

Additionally, the proper selection of the organosilane makes it possible to adjust the silica properties, such as hydrophobicity [10]. Several researchers mimic these types of natural superhydrophobic features on artificial surfaces to utilize their benefits for various applications, such as anti-corrosion, anti-oxidation, water drag reduction, anti-soiling and anti-icing [11-14]. Furthermore, hydrophobic silica can be a constituent of filter elements to prevent the permeation of hydrophilic aqueous fluids.

Hydrophobicity is also required in materials containing Nanofibrillated cellulose (NCF) [15], because its functional groups have the ability to form hydrogen bonding interactions [16]. NCF has

many important characteristics, such as natural abundance [17], biocompatibility [18], and therefore great interest in cellulosic composites [19,20]. The preparation of NFC composites with silica [21,22] combines characteristics of both components [23], such as high aspect ratio and adhesion by interfacial interaction, which promote the improvement of mechanical [24], flexibility and thermal properties [25,26]. Chemical interactions between cellulose and organosilane have been widely studied [27,28]. Researches show that several mechanisms are involved between NFC and alkylsilane: i) physisorption, the adsorption of silanol groups on to the hydroxyl groups of cellulose surfaces; ii) hydrolysis, the alkoxy groups of the silane are catalyzed in acid conditions forming silanol; iii) condensation, giving rise to the chemical sorption/grafting, as the bond Si-O-Cellulose [29,30], iv) self condensation Si-O-Si [31]. can be achieved by incorporating ORMOSIL obtained with octylsilane in order to prepare filter elements.

Experimental

Composites preparation

The preparation of silica particles was obtained by homogenizing tetraeoxysilane (TEOS) with ethanol and water, in a 4:1 molar ratio, at 1000 rpm for 10 minutes, and at room temperature. Then, the aqueous suspension of nanofibrillated cellulose (NCF) was added in a 1:2 NCF:silica mass ratio. The NCF modification was carried out at 1000rpm, 60°C, for 24 hours. Subsequently, the composite (NCF-Si) was obtained by lyophilization and compression at 5 bar, 60^0C, for 5min.

ORMOSIL was prepared by adding triethoxyoctylsilane:TEOS in a molar ratio of 1:2. Subsequently, the reaction conditions were adjusted to acid (pH:4) and basic (pH:11), by adding HCl and NH_4OH, to obtain ORMOSIL particles: OS-a and OSi-b, respectively. The methodology for preparing ORMOSIL and the composites was similar to that described above, with the following samples being obtained: NCF-OS-a, NCF-OS-b and NCF-OS-n.

Characterization

FT-IR analysis (Chemical characterization). The IR spectra were taken via FT-IR with an attached ATR (atten-uated total reflectance). X-ray diffraction (XRD) was observed in the 2<theta> range of 10–60◦, using Cu-Kα radiation. The water contact angle (WCA)was measured with 5 μL de-ionized water droplet at ambient tem-perature by using Contact Angle Meter (goniometer). Thermal analysis. Thermogravimetric analysis (TGA) was performed device equipped with a thermal analysis data.

Results and Discussion

Absorption spectroscopy in the IR region was used to characterize the functional groups on the surface of the NCF-Si composite and to evaluate the surface modification of the NCF. The Fig 1 shows that the absorption peaks characteristic of NCF remained in the composite spectra. One of the absorption bands at 3400cm-1, which refers to the O-H stretching vibration in the NCF structure; the absorption band at 2976cm-1 relative to the stretching vibration of the CH2 C-H bond; the absorption peak at 1640cm-1 related to the H-O-H strain vibration, which is an indication of the water adsorbed by the NCF; and the absorption peak at 1055cm-1, which is attributed to the C-O stretching vibration of the OH groups in the NCF structure [32]. Compared to NCF, new vibrations characteristic of the silane appeared in the composite spectra, such as the vibration at 1278cm-1 of the C-H bond of the methyl group; the stretching vibration at 905cm-1 of the Si-OH group; and the asymmetric stretching vibration of Si−C and Si−O−Si at 1080 and 800 cm−1. The presence of these new absorption peaks was reported by Gupta et al [33] confirming that the NCF was modified. Furthermore, the characteristic peak of the Si-OH bond at 967 cm-1 disappears after surface modification, which means that the silanol group has been replaced by the Si-O-Si(CH3) group (900 cm-1) in the structure of the ORMOSIL. The low intensity of the Si-C and –CH3 bands in the composite spectra is due to the small amount of silane agent added in the preparation of

ORMOSIL. However, the difference in the nature of silica and ORMOSIL prepared in different media did not show a significant change in the position of the absorption bands.

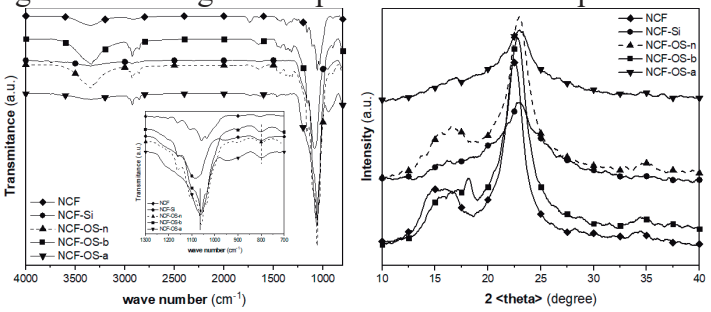

Figure 1 – FT-IR and XRD spectra of the NCF, NCF-Si and NCF-OS composites.

X-Ray Diffraction was used to evaluate the degree of crystallinity of the NCF in the composites. In the Fig 1 The diffractogram of the NCF is shown and the presence of shoulders and diffraction peaks, at angles of 2θ of 14.8° and 16.5°, peak at 2θ = 22.2° and shoulder at 2θ = 34.5°. According to the literature, these diffraction peaks correspond to the crystallographic planes (1 $\bar{1}$ 0), (1 1 0), (2 0 0) and (0 0 4) of cellulose I, respectively [34]. Diffraction peaks are an indication that NCF remains as a crystalline structure of cellulose after freeze-drying and pressure-forming the samples. The cellulose crystalline structure remained in the composites as observed by the cellulose I diffraction peaks, which corroborates the infrared spectroscopy results. However, the intensity of the diffraction peaks decreased in the diffraction patterns of the composites, as observed by the reduction in the intensity of the crystal plane peak (200). Therefore, the incorporation of silica into NFC was determined by quantifying the crystallinity index (Ic), according to the equation Ic= [(I200-Iam)/I200]x100, where I200 is the value of the maximum intensity of the peak of the plane (2 0 0), located at the diffraction angle 2θ = 22.5°, and Iam is the intensity of the valley between the peaks corresponding to planes (20 0) and (1 1 0), at the diffraction angle of 2θ = 18° [35]. The Ic determined for NCF was 77%, and decreased to 63% with the incorporation of silica. This result was similar to that reported for modification of NCF by the introduction of methyltrimethoxysilane by sol-gel process, studied by Liu et al [36]. The silica precursor is an amorphous molecule, and the hydroxyl groups on the surface of NCF have been replaced by the alkyl chain of the silane, which results in the opening of cellulose chains linked by intermolecular hydrogen bonding interaction and the formation of new amorphous regions, which reduced the total crystallinity [37].

The wettability of the water drop on the surfaces of NCF and silica based materials results in water contact angle (WCA) values below 900 [38]. This behavior is related to the presence of abundant hydroxyl groups (–OH) on both surfaces of NC fibers and silica particles, indicating the hydrophilic characteristic of materials containing pure NCF and Silica. The Fig 2 shows WCA values of composites prepared with silica and ORMOSIL.

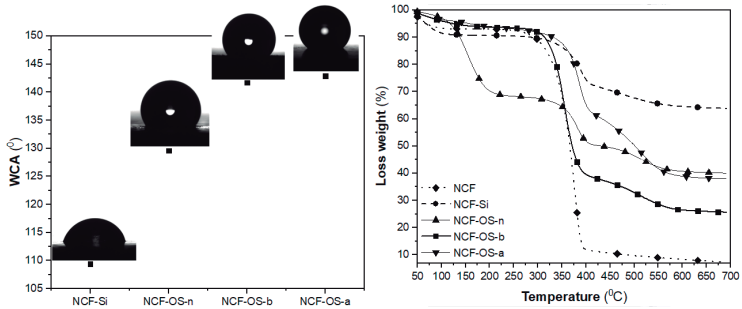

Figure 2 – WCA and TGA curves of the NCF, NCF-Si and NCF-OS composites.

The modification of silica with octylsilane modified the shape of the water drop, which became stable and spherical on the surface of the composites. This change in the surface wettability of the composites demonstrates that the hydrophilic OH groups of NCF have been replaced by the

hydrophobic octyl group on the cellulose surface. The terminal octyl groups in the ORMOSIL structure have low surface energy, contributing to the formation of a rough and hydrophobic structure. Silica nanoparticles increase the roughness and porosity of materials [39]. Furthermore, alkylsilanes are used as hydrophobic modifying agents to reduce the surface energy of cellulose nanofibers and silica nanoparticles [39]. Additionally, the influence of the reaction medium conditions on the wettability of the composites was evaluated. It is known that the surface microstructure of a solid can be destroyed under severe acidic and basic conditions. The wettability of the hydrophobic surface of composites prepared under acidic and basic pH conditions was improved by increasing the WCA to approximately 143^0. The composite prepared with ORMOSIL at acidic pH showed a higher WCA value, due to the synergistic effect of the small size of the ORMOSIL particles and the low surface energy of octylsilane on the surface. However, the composite containing ORMOSIL prepared at basic pH showed a slight decrease in WCA. This result may be associated with the possibility of hydrophobicity deterioration under the caustic condition. Similar result was achieved by Zhou et al. [39] for composites of NCF with silica submitted in reaction medium with pH above 12.

The mass loss curves for NCF and composites are shown in Fig 2. Three main mass loss events were observed in the thermograms. The first two degradation events (between 25 and 100^0C) were related to the evaporation of water adsorbed on the NCF fibers and volatile compounds. The third thermal event, between 225 and 370 °C, refers to the thermal depolymerization of cellulose [40].

The incorporation of silica in composites caused the displacement of thermal events to higher temperatures. The residue percentage of the NCF, at 600^0C, was approximately 8%, while in the NCF-Si composite, the residual material was about 65% due to the incorporation of the silica particle in the NCF fibers. On the other hand, the percentage of residue decreased to 27 and 40% for the composites containing ORMOSIL, due to the organic portion of octylsilane, which to the layer formed onto the surface to protect NFC. This behavior has been observed in other alkyl, as with γ-aminopropyltriethoxysilane (APS) [41], (3-chloropropyl)triethoxysilane (CPTES) [42], γ-methacryloxypropyltrimethoxy (MPS) [43], and glycidylsilane [44] . However, the smaller residue obtained for the composite containing ORMOSIL prepared under conditions of basic pH, corroborates with the slight decrease in the hydrophobicity of this composite. The condition of the basic medium may have been impaired, allowing the dissociation of the functional group (octyl) on the surface of the hydrophobic composite. The interaction between the hydrophobic surface and water is a crucial factor influencing most applications of hydrophobic cellulosic materials.

Conclusions (Times New Roman 12, bold)

Hydrophobic NCF-silica composites can be prepared by an in situ methodology and under different conditions of the reaction medium. The hydrophilic surface of the NCF was transformed into a hydrophobic one due to the low surface energy of the alkylsilane octylsilane agent. The highest WCA value of the composites was 143^0 for the composite prepared in a reaction medium in acid (low pH). The incorporation of silica and ORMOSIL also favors the improvement of the thermal stability of the composites..

Acknowledgements

CNPQ, FAPERJ and UFRJ.

References (Times New Roman 12, bold)

1. S. Shi, Y. Zhao, Z. Zhang, L. Yu. Prog Org Coat 132 (2019) 227-34
2. M. Kothmann, R. Zeiler, A. Anda, A. Brückner, V. Altstadt. Polymer 60 (2015) 157-63
3. Y. Zhang, X. Liu, J. Huang. Appl. Mater. Interfaces 3 (2011) 3272–3275.

4. M. Porgham Daryasari, M. Dusti Telgerd, M. Hossein Karami, A. Zandi-Karimi, H. Akbarijavar, M. Khoobi, E. Seyedjafari, G. Birhanu, P. Khosravian, F. SadatMahdavi,. Nanomed., and Biotech. 47 (2019) 4020–4029.
5. K. Sharma, A. Hooda, M.S. Goyat, R. Rai, and A. Mittal. Ceram. Int., 2022, 48, p 5922– 5938.
6. L. L. Hench and J. K. West, Chemical Reviews, Vol. 90, No. 1, 1990, pp. 33-72. http://dx.doi.org/10.1021/cr00099a003
7. S.D. Wang, S.S. Luo.. Appl. Surf. Sci. 258 (2012) 5443–5450.
8. A.M. Buckley, M. Greenblatt. J. Chem. Educ. 71 (7) (1994) 599.
9. ZHANG, Xinxiang; XIAO, Fuchuan; FENG, Qifan; et al.. Progress in Organic Coatings, v. 138, p. 105384, 2020.
10. Mahmood, MH, Sopyan, I Journal of Engineering and Applied Sciences, 10 (22) 17252–17255 (2015)
11. A. Hooda, M.S. Goyat, J.K. Pandey, A. Kumar, and R. Gupta. Coatings, Prog. Org. Coat., 2020, 142, p 105557.
12. H. Qiu, K. Feng, A. Gapeeva, K. Meurisch, S. Kaps, X. Li, L. Yu, Y.K. Mishra, R. Adelung, and M. Baum. Prog. Polym. Sci., 2022, 127, p 101516.
13. I. Ho¨lken, M. Hoppe, Y.K. Mishra, S.N. Gorb, R. Adelung, and M.J. Baum, Complex Shaped ZnO Nano- and Microstructure Based Polymer Composites: Mechanically Stable and Environmentally Friendly Coatings for Potential Antifouling Applications, Phys. Chem. Chem. Phys., 2016, 18(10), p 7114–7123.
14. M. Sharma, M. Joshi, S. Nigam, D.K. Avasthi, R. Adelung, S.K. Srivastava, and Y.K. Mishra Appl. Mater. Today, 2019, 17, p 130–141.
15. Y. Habibi Chem. Soc. Rev. 43 (2014) 1519–1542.
16. N. M. Julkapli, S. Bagheri,. Funct. Polym. 112 (2017) 9–21.
17. M. A. El-Fattah, A. M. Hasan, M. Keshawy, A. M. El Saeed, O. M. Aboelenien, Carbohydr. Polym. 183 (2018) 311–318.
18. S. Saini, N. Belgacem, J. Mendes, G. Elegir, J. Bras, Contact antimicrobial surface obtained by chemical grafting of microfibrillated cellulose in aqueous solution limiting antibiotic release, ACS Appl. Mater. Interfaces 7 (2015) 18076–18085.
19. C. Shi, F. Tao, Y. Cui, Evaluation of nitriloacetic acid modified cellulose film on adsorption of methylene blue, Int. J. Biol. Macromol. 114 (2018) 400–407.
20. S. Sayen, M. Ortenbach-L´opez, E. Guillon, Sorptive removal of enrofloxacin antibiotic from aqueous solution using a ligno-cellulosic substrate from wheat bran, J. Environ. Chem. Eng. 6 (2018) 5820–5829.
21. [21] Garusinghe UM, Raghuwanshi VS, Garvey CJ, Varanasi S, Hutchinson CR, Batchelor W et al (2017) Assembly of nanoparticles–polyelectrolyte complexes in nanofiber celulose structures. Colloids Surf A 513:373–379
22. [22] Varanasi S, Low Z-X, Batchelor W (2015) Cellulose nanofibre composite membranes—biodegradable and recyclable UF membranes. Chem Eng J 265:138–146
23. [23] Krol LF, Beneventi D, Alloin F, Chaussy D (2015) Microfibrillated cellulose-SiO2 composite nanopapers produced by spray deposition. J Mater Sci 50(11):4095–4103
24. [24] J.C.H. Wong, H. Kaymak, P. Tingaut, S. Brunner, M.M. Koebel, Mechanical and thermal properties of nanofibrillated cellulose reinforced silica aerogelcomposites, Micropor. Mesopor. Mat. 217 (2015) 150–158.
25. [25] A. Mabrouk, H. Kaddami, S. Boufi, F. Erchiqui, A. Dufresne, Cellulosicnanoparticles from alfa fibers (Stipa tenacissima): Extraction procedures andreinforcement potential in polymer nanocomposites, Cellulose 19 (2012)843–853.
26. G. Siqueira, J. Bras, A. Dufresne, Cellulose whiskers versus microfibrils:influence of the nature of the nanoparticle and its surface functionalization onthe thermal and mechanical properties of nanocomposites,Biomacromolecules 10 (2009) 425–432.
27. K. Xie, Y. Yu, Y. Shi, Synthesis and characterization of cellulose/silica hybridmaterials with chemical crosslinking, Carbohyd. Polym. 78 (2009) 799–805.
28. [28] M. Abdelmouleh, S. Boufi, M. N. Belgacem, A. Dufresne, A. Gandini, Modification of celulose fibers with functionalized silanes:effect of the fiber treatment on the mechanical performances of cellulose-thermoset composites, J.Appl.Polym.Sci.98 (2005)974–984.
29. [29] A. S. Singha, A. K. Rana, Effect of aminopropyltriethoxysilane (APS) treatment on properties of mercerized lignocellulosic Grewia optiva fiber, J.Polym.Environ.21 (2013)141–150.

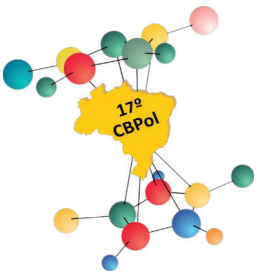

EFFECTS OF SINGLE-WALLED CARBON NANOTUBE ADDITION ON THE MECHANICAL PROPERTIES OF CARBON FIBER STRUCTURAL COMPOSITE

Rafael L. Costa[1], Gerson Marinucci[1] and Leonardo G. de Andrade e Silva[1]*

1 – Instituto de Pesquisas Energéticas e Nucleares (IPEN), São Paulo, SP, Brazil rafaellcosta@gmail.com

Abstract – Different concentrations of single-wall carbon nanotubes were added to a carbon fiber composite with an epoxy matrix to evaluate its mechanical properties. The dispersion of the nanoparticles exhibited good quality and the flexural strength in the 90-degree direction showed an increase of over 10% with a concentration of only 0.0087% of nanotubes in the composite.

Keywords: Carbon Nanotube, Nanocomposite, Carbon Fiber Composite, Hierarchical Composite, Filament Winding

Introduction

Material strength is one of the technological limitations of various projects, where performance is constrained by the strength-to-mass ratio. As a result, the demand for materials with higher strength and lower density will remain constant in many industries.

One example of this is wind turbine blades, where larger dimensions result in higher energy generation efficiency [1]. By utilizing materials with greater mechanical strength and lower density, it becomes possible to manufacture larger blades. Thus, the advancement of materials is directly related to the viability of wind energy generation.

For many applications in industries such as aerospace, automotive, chemical, oil and gas, several components are transitioning to composite materials, which offer the best strength-to-mass ratios. Therefore, improving the properties of current composites enables technological advancements in various sectors.

Although composite materials, by definition, involve the multifaceted combination of any material classes, including two or more materials from the same class [2, 3], this study will specifically delve into polymer matrix composites reinforced with ceramic fibers, particularly those reinforced with carbon fibers (CFRP - Carbon Fiber Reinforced Polymer).

CFRP composites are commonly utilized in applications demanding high performance. In these composites, epoxy resin-based matrices are the predominant choice, which will be the focus of the study. Given that carbon fiber and epoxy resin are widely used in the market this study holds significant relevance for both the scientific community and industry.

Among the various potential failures that occur in composites, one of the most frequent and severe is interlaminar fracture (or delamination), which essentially refers to matrix failure between layers of fibers with different orientations. This failure occurs precisely in a region considered one of the "weak points" of laminated composites [2].

Carbon fibers and polymer matrices used in CFRP composites possess significantly different mechanical strengths. For example, Toray T300 carbon fiber has a tensile strength of 3500 MPa,

while the epoxy resin-based matrix Huntsman™ GY260 has a tensile strength close to 50 MPa, according to manufacturer data. Consequently, regions of the composite where the matrix experiences higher loads become potential areas of failure.

Therefore, methods that increase the matrix's stress limits are essential for enhancing the strength of a composite, thereby enabling technological advancements limited by the strength of existing materials. Increasing the matrix strength is one of the objectives of developing composites with dispersed nanoparticle additions in addition to traditional reinforcements.

The technology of CFRP composites with nanoparticles is still in its early stages, recently transitioning from specific structural applications such as wind turbines and high-performance aircraft to more mainstream products, as evidenced by their adoption by major automobile manufacturers. A significant expansion is expected in the coming years [4].

Given that delamination failure is very common in composites, the development of methods to prevent or at least reduce its occurrence is of great relevance. In this study, nanoparticles were tested to reinforce the matrix and enhance resistance to delamination.

Experimental

Test specimens were fabricated using a polymer matrix consisting of the following Huntsman™ products: epoxy diglycidyl ether bisphenol A (DGEBA) resin LY 5052, methyl tetrahydrophthalic anhydride (MTHPA) hardener HY 2918, and benzyl dimethyl amine-based accelerator DY 062, reinforced with Tenax™ HTA40 carbon fiber without the addition of nanotubes, to be used as a reference, using the filament winding process (Fig.1), set to a high ratio of carbon fiber. The curing process was carried out according to the following cycle: a plateau at 100°C for one hour, a ramp from 100°C to 145°C over 3 hours, a plateau at 145°C for 8 hours and cooling from 145°C to 25°C over 4 hours. The resulting sheet was used to produce specimens according to ASTM D7264/D7264M-21 standard.

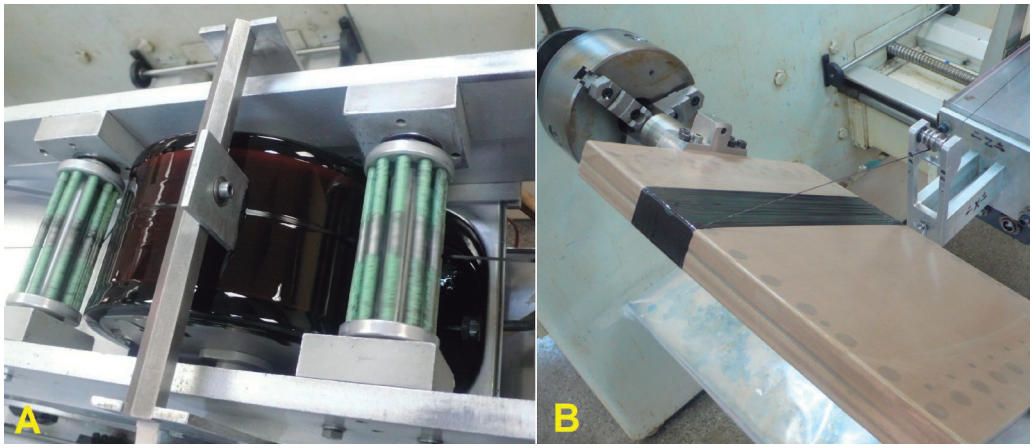

Figure 1 – Filament winding process: (A) Resin bath and (B) rotating mold

Subsequently, test specimens were fabricated and characterized under conditions similar to the reference samples, with the addition of the commercial product TUBALL™ MATRIX 301 (a compound pre-dispersed with 10% single-walled carbon nanotubes in epoxy matrix) at concentrations of 0.046% and 0.087%, using a Thinky Mixer ARE310 planetary mixer. The final composition of the specimens are presented in Table 1.

Table 1 – Composition of specimens

Specimen	Carbon fiber	Resin LY 5052	Hardener HY 2918	Accelerator DY 062	TUBALL™ MATRIX 301
0 wt% TUBALL™ MATRIX 301	718.1 g (77.00 wt%)	100.0 g (10.72 wt%)	114.0 g (12.22 wt%)	0.5 g (0.05 wt%)	-
0,046 wt% TUBALL™ MATRIX 301	719.5 g (77.00 wt%)	100.0 g (10.70 wt%)	114.0 g (12.20 wt%)	0.5 g (0.05 wt%)	0.428 g (0.046 wt%)
0,087 wt% TUBALL™ MATRIX 301	763.5 g (78.00 wt%)	100.0 g (10.22 wt%)	114.0 g (11.65 wt%)	0.5 g (0.05 wt%)	0.856 g (0.087 wt%)

The quality of dispersion was assessed using an FESEM JEOL JSM-7401F scanning electron microscope, a Discovery.V8 stereomicroscope and a simple method recommended by the manufacturer by depositing the dispersed resin on white paper (Fig. 2).

Figure 2 – Simple method recommended by the manufacturer: (A) Quality control procedure / (B) Example of poor quality dispersion / (C) Example of good quality dispersion (source: TUBALL™ MATRIX 300 series Processing Guide)

The mechanical property was evaluated using a flexural mechanical test, following the ASTM D7264/D7264M-21 standard (Fig. 3), which is a suitable method for assessing the strength of laminated composite matrices [5-7].

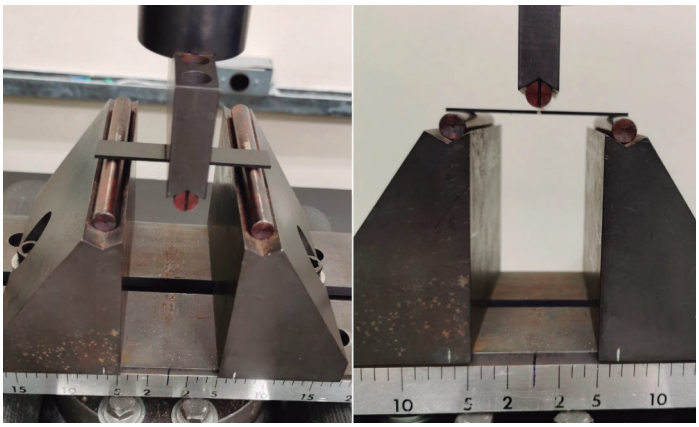

Figure 3 – Flexural mechanical test according to ASTM D7264/D7264M-21 standard

Results and Discussion

The duration of 30 minutes at 2000 rpm in the Thinky Mixer ARE310 proved to be suitable for dispersing the nanotubes in the epoxy resin matrix.

Small agglomerates were observed in the dispersion of TUBALL™ MATRIX 301 in the LY 5052 resin (without the addition of hardener and accelerator) using the stereo microscope (Fig. 4).

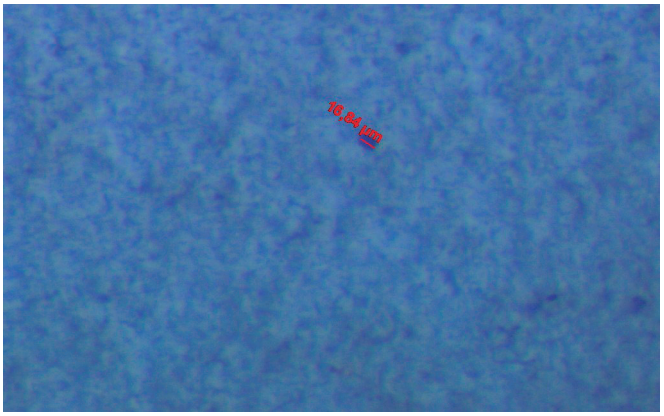

Figure 4 – Dispersion of TUBALL™ MATRIX 301 in LY 5052 resin: a cluster measuring 16.84 µm was identified (magnification 80X)

As observed in Figure 4, the dispersion of nanotubes, which is a critical step in the fabrication of nanocomposites [8-9], exhibited only small and rare clusters, indicating excellent dispersion quality.

Dispersion was evaluated using the method recommended by the manufacturer. As shown in Figure 5, the dispersion pattern is deemed suitable, according to the manufacturer's manual (Fig. 2).

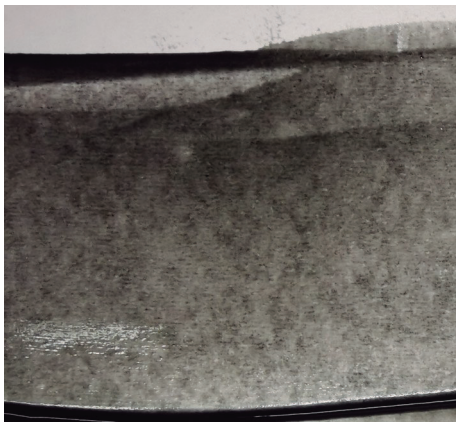

Figure 5 – Result of simple test recommended by the manufacturer: a high-quality dispersion is observed

The detail of the dispersed nanotube can be observed in the image obtained from the FESEM JEOL JSM-7401F scanning electron microscope (Fig. 6), on the fracture surface of the specimen containing carbon nanotubes.

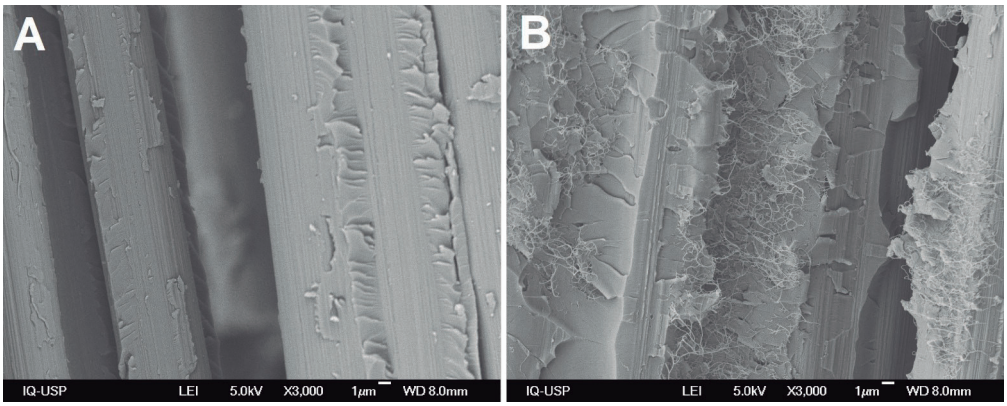

Figure 6 – Fracture surface observed using an FESEM JEOL JSM-7401F scanning electron microscope: (A) with 0 wt% TUBALL™ MATRIX 301 and (B) with 0.087% wt% TUBALL™ MATRIX 301, showing the nanotubes well dispersed in surface

The flexural test with the carbon fiber oriented at 90 degrees yielded the following results (Table 2).

Table 2 – Results of the flexural tests

Composition (details on Table 1)	Flexural strength (MPa)	Number of Specimens
0% wt% TUBALL™ MATRIX 301	93±4	10
0.046 wt% TUBALL™ MATRIX 301	101±2	9*
0.087 wt% TUBALL™ MATRIX 301	103±4	9*

* One outlier specimen was discarded

As can be seen in Table 2, the addition of 0.046% of TUBALL™ MATRIX 301, which corresponds to 46 ppm of carbon nanotubes, increased the transverse flexural strength from 93 to 101 MPa, representing an 8.6% improvement. The addition of 0.087% of TUBALL™ MATRIX 301, which corresponds to 87 ppm of carbon nanotubes, increased the strength from 93 to 103 MPa, corresponding to a 10.7% increase. The improved mechanical properties achieved corroborate the behavior already established in the literature [4, 8-10].

Conclusions

The presented results demonstrate that the commercial product TUBALL™ MATRIX 301 can be successfully dispersed in the resin using a planetary mixer. The addition of 0.046% of the product increased the transverse flexural strength by 8.6%, while the addition of 0.087% resulted in a 10.7% increase. This suggests a nonlinear relationship between the nanotube concentration and strength enhancement but tests are needed on additional compositions to confirm this hypothesis.

References

1. M. Caduff, M. A. J. Huijbregts, H. J. Althaus, A. Koehler, S. Hellweg Environmental Science & Technology 2012, 46(9), 4725–4733. https://doi.org/10.1021/es204108n.
2. G. Marinucci, *Materiais Compósitos Poliméricos – Fundamentos e Tecnologia*, Artliber, São Paulo, 2011.
3. W. D. Callister Júnior; D. G. Rethwisch, *Ciência e engenharia de materiais: uma introdução*, LTC – Livros Técnicos e Científicos Editora Ltda, Rio de Janeiro, 2012.
4. F. Valorosi; E. De Meo; T. Blanco-Varela; B. Martorama; A. Veca; N. Pugno; I. A. Kinloch; G. Anagnostopoulos; C. Galiotis; F. Bertocchi; J. Gomez; E. Treossi; R. J. Young; V. Palermo Composites Science and Technology 2019, Art. 107848. https://doi.org/10.1016/j.compscitech.2019.107848.
5. D. F. Adams; T. R. King; D. M. Blackketter Composites Science and Technology 1990, 39(4), 341–353. https://doi.org/10.1016/0266-3538(90)90080-O.
6. D. M. Blackketter; D. Upadhyaya; T. R. King Polymer Composites 1993, 14(5), 437–446. https://doi.org/10.1002/pc.750140511.
7. C. M. Arndt; N. V. Carvalho; M. W. Czabaj Composites Science and Technology 2020, 54(23), 3297–3312. https://doi.org/10.1177/0021998320914065.
8. C. Zhang; G. Zhang; X. Shi; X. Wang Journal of Materials Science 2022, 57(4), 2388–2410. https://link.springer.com/article/10.1007%2Fs10853-021-06734-z.
9. M. L. Gupta; S. A. Sydlik; J. M. Schnorr; D. J. Woo; S. Osswald; T. M. Swager; D. Raghavan Journal of Polymer Science Part B: Polymer Physics 2012, 51(6), 410–420. https://doi.org/10.1002/polb.23225.
10. J. Karger-Kocsis; H. Mahmood; A. Pegoretti Composites Science and Technology 2019, Art. 107932. https://doi.org/10.1016/j.compscitech.2019.107932.

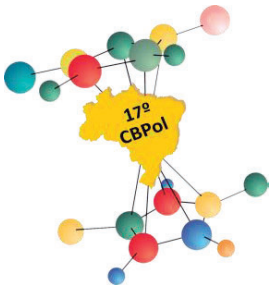

EVALUATION OF β-PHASE ENHANCEMENT OF PVDF-TrFE NANOCOMPOSITES WITH GRAPHENE OXIDE PROCESSED BY EXTRUSION

Fábio E. Jorge[1], Thiago B. de Abreu[1] and Maria de F. V. Marques[1]*

1 – Instituto de Macromoléculas professor Eloísa Mano, Federal University of Rio de Janeiro (UFRJ), Rio de Janeiro, RJ, Brazil fmarques@ima.ufrj.br

Abstract – Humanity is facing an increasing energy demand. With the need to replace fossil fuels, renewable energy sources will be considered essential to solving the energy crisis in the future, and research into clean energy harvesting is needed. The electromagnetic and piezoelectric transduction methods are the most promising research in energy harvesting compared to other methods due to the generation of electric current through a simple mechanical voltage application. The materials most used for these applications are ceramics due to their high piezoelectric coefficient. However, as their mechanical properties are not equally high, their replacement by polymeric materials that compensate for this limitation has been studied. Fluorinated polymers such as poly(vinylidene fluoride) and its copolymers are the most investigated for this application due to the ease of polarization of one of the crystalline phases (β-phase). Polymer nanocomposites have been studied to obtain materials with the properties of piezoceramics and the advantages of polymers. Oxygen incorporation into graphite was successful, with a maximum incorporation of 43.15%, impacting on the increase of the β-phase of the corresponding nanocomposite by 22.86%
Keywords: *Extrusion, Clean Energy, PVDF, β-Phase, Graphene Oxide.*

Introduction

Due to the growing search for clean and renewable energy sources, techniques for exploiting this type of energy to transform it into electrical energy have been evaluated. This capture can come from sources available in the environment, usually kinetic energy (wind, waves, and vibrations), thermal (solar, geothermal, and combustion), chemical (biofuels and biomass), photovoltaic or atomic (nuclear) [1, 2].

The electromagnetic and piezoelectric transduction methods are the most promising research in the capture of kinetic energy, and vibration transducers with piezoelectric technology are more intensively studied, with a high number of ongoing research and effective publications, demonstrating that the piezoelectric materials are potentially suitable candidates to efficiently convert mechanical voltage into electrical energy, without any additional source, besides having flexibility as to the type of piezoelectric material to be used [3, 4].

Among the naturally piezoelectric materials, quartz and tourmaline crystals can be mentioned, as well as lead titanate-zirconate (PZT), barium titanate, and Rochelle salt ceramics. These materials have a polarized geometry in the form of dipoles, and precisely this natural polarization of their crystals is mainly responsible for the induction of surface charges. Besides these materials, there is the possibility of inducing the formation of dipoles in polymers that do not necessarily have a natural molecular polarization, in such a way as to generate a polymeric material with piezoelectric properties, as in the case of poly(vinylidene fluoride) (PVDF), and the copolymer of hexafluoropropylene-tetrafluoroethylene (FEP) [5-8].

Ceramic materials, such as PZT, have high piezoelectric coefficient values but have disadvantages, such as high lead toxicity and low mechanical strength in the final device. Polymers are more flexible and easier to produce than ceramics but have disadvantages such as the difficulty of polarization and low piezoelectric constant. To overcome these obstacles, the formulation of ceramic/polymer composites have been studied, which are ceramic materials dispersed in a polymeric matrix, and the mechanical properties of polymers make the material have improvements where traditional ceramics are not effective, such as flexibility and mechanical strengths and, in return, increases the piezoelectric coefficient of the material and its polarization ability [9, 10].

Polymers such as PVDF offer several advantages, such as low dielectric constant, low density, and flexibility. Therefore, although they have low piezoelectric coefficients when compared to PZT, their elastic coefficient is large, having better applicability. On the other hand, polymers have disadvantages such as difficulty in polarization and low piezoelectric constant. PVDF is a polymer composed of carbon, hydrogen, and fluorine atoms, presenting molecular formula $-(CH_2CF_2)_n-$ as the repetitive unit of the polymer chain. Its chains can be organized into four types of crystalline structures, which are called α, β, γ, and δ phases. These crystalline phases result from conformational changes in the polymer chains, which depend on the method of obtaining the polymer, thermal or mechanical treatments, in addition to electrical polarization and pressure. Each crystalline phase configures different characteristics, providing PVDF with great application versatility [11, 12, 13].

Among these phases, the β-phase is of great technological interest for presenting piezo and pyroelectric properties that are fundamental in applications such as sensors and transducers. Studies to promote this phase are mostly done by using organic solvents to dissolve the material and further processing (casting, electrowinning, and others), which also causes environmental problems due to the toxicity of the substances used for the solubilization of the polymer, i.e., the effort to reduce PZT-based materials becomes in vain [14, 15]. Therefore, it is necessary to use processing methods with lower environmental impact, which can have higher β-phase rates, thus increasing their piezoelectric properties. An alternative material studied is the PVDF nanocomposite with graphene because the oxidation of graphene synergistically induces the polar phase of PVDF due to the interaction between the oxygenated group with the CF_2 of the polymer, but with a possible reduction of crystallinity of the material and as a result, reduces some of the mechanical properties. Thus, oxidized graphene is a strong candidate for composite applications with PVDF as a result of these interactions [16].

In the present work, aiming the β-phase improvement of poly(vinylidene fluoride-co-trifluoroethylene), P(VDF-TrFE), and, consequently, the piezoelectric behavior of the material, a polymeric mixture of this matrix with graphene oxide nanoparticles at different levels of oxidation was carried out to obtain better piezoelectric properties. Natural graphite, chemically treated by the modified Hummers method, was used to obtain the graphene oxide. The nanocomposites were obtained using melt mixing techniques in the double-threaded extruder.

Experimental

Synthesis of Graphene Oxide (GrO) nanoparticles

3 g of natural graphite were added into an Erlenmeyer flask (250 mL) containing a mixture of concentrated sulfuric acid and nitric acid in a ratio of 4:1 v/v, respectively. The reaction occurred under magnetic stirring for 30 min. After this time, 0.5 g of potassium permanganate was added, leaving the system in agitation for a given time (2 h, 24 h, and 120 h). After neutralizing, washing, and drying, 50 mg of the obtained GO were added to a 250 mL Erlenmeyer flask containing 100 mL of distilled water and treated with ultrasound for 48 h. The obtained material (GrO) was dried in an oven at 100°C [17].

Producing of P(VDF-TrFE) nanocomposites by extrusion

The P(VDF-TrFE) nanocomposites were prepared in a Haake Minilab Rheomex (CTW5) twin-screw counter-rotating extruder, as shown in Fig 1. Before processing, the following procedures were performed: 1) Drying of the ground material at 80ºC overnight to remove possible humidity; 2) Mixture between P(VDF-TrFE) and GrO nanoparticles synthesized at concentrations of 0.5%, 1.0%, and 2.0 wt.% for further analysis.

This mixture was added to the extruder with a fixed feed of 6 g for 10 min, the processing temperature of 220 °C, and the screw speed was 100 rpm. Pure P(VDF-TrFE) was also extruded under the same conditions for comparison.

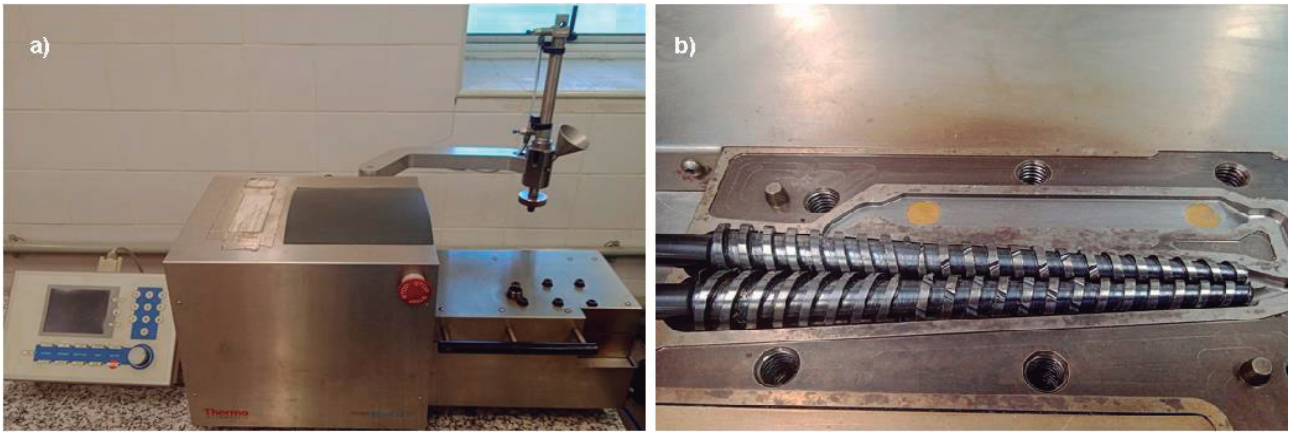

Figure 1: Haake Minilab Rheomex Mini-extruder. A) External structure of the equipment. B) View of the double counter-rotating screw.

Results and Discussion

In the diffractogram analysis in Fig 2a, it was observed that the characteristic peaks of the GrO nanoparticles at 26.46º (GrO 2h), 26.49º (GrO 24h), and 26.59º (GrO 120h) have different intensities due to the oxygen content on the nanoparticles, being the one with higher oxidation state (GrO 120h) with the highest peak intensity. In the analysis of the FTIR spectra presented in Fig. 2b, the wide bands around 3426 cm^{-1} are assigned to the O-H bond of the hydroxyl group, the bands around 1639 cm^{-1} are attributed to the C=O bond of carbonyl, and the bands around 1057 cm^{-1} correspond to C-O bond, being these functional groups present after the oxidation of graphite.

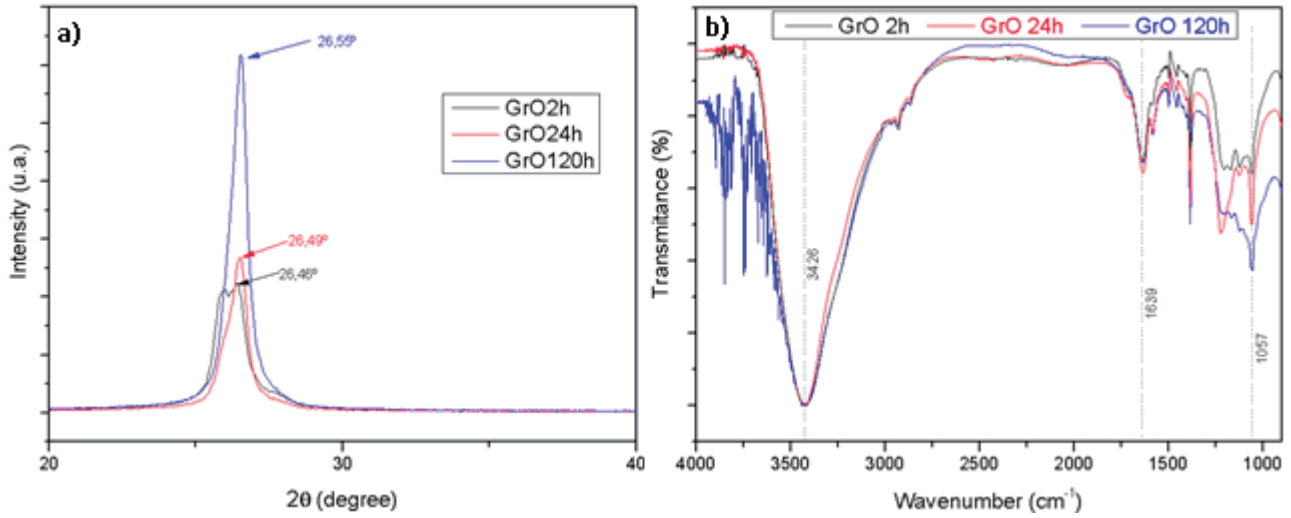

Figure 2: a) Diffractograms of the GrO 2h, GrO 24h and GrO 120h nanoparticles; b) FTIR spectra of the GrO 2h, GrO 24h and GrO 120h nanoparticles.

The thermograms of the nanoparticles in Fig. 3 show the mass loss of the GrO nanoparticles related to the production of CO and CO_2, resulting from the decomposition of carboxylates, carbonyls, epoxides and hydroxyls present on the surface of the graphite. It is observed that the longer the reaction time, the greater the mass loss (43.15%), i.e., the greater the amount of oxygen in the nanoparticle.

The pure P(VDF-TrFE) exhibited α-phase bands at 975, 763 and 613 cm^{-1} and the β-phase bands at 1276 and 840 cm^{-1}. The bands between 4000-1500 cm^{-1} and those at 1178, 1067 cm^{-1} and 871 cm^{-1} correspond to the CH_2 bonds [18-20]. FTIR spectra can be used to quantify the phase contents of PVDF. The absorption of FTIR follows the Lambert-Beer law if the absorption coefficients, K_α and K_β, were calculated in the respective wave number of 763 and 840 cm^{-1} [21]. We can observe in Fig. 4 the α-phase bands at 763 cm^{-1} and the β-phase bands at 840 cm^{-1} of nanocomposites of P(VDF-TrFE)/GrO.

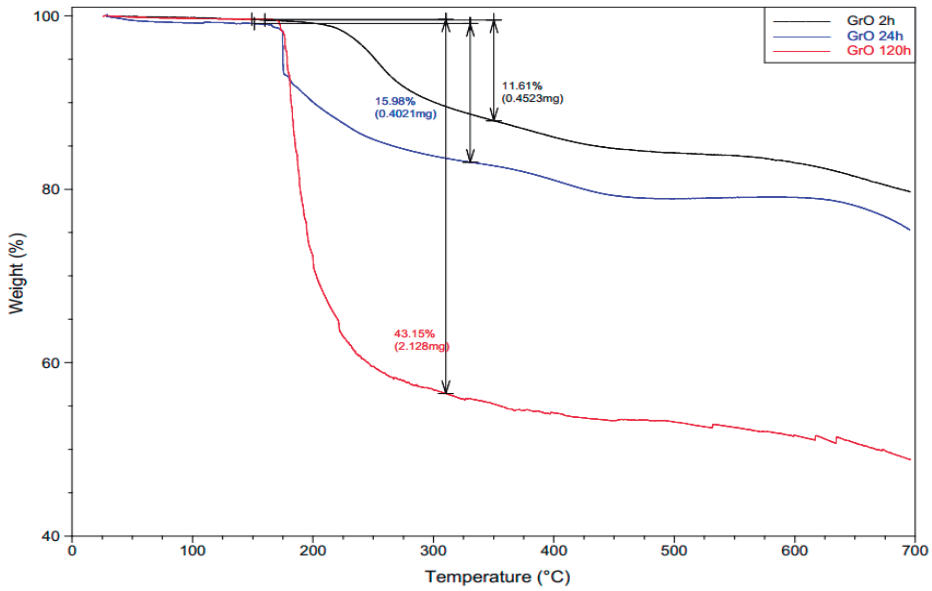

Figure 3: Thermogram of the GrO 2h, GrO 24h and GrO 120h nanoparticles.

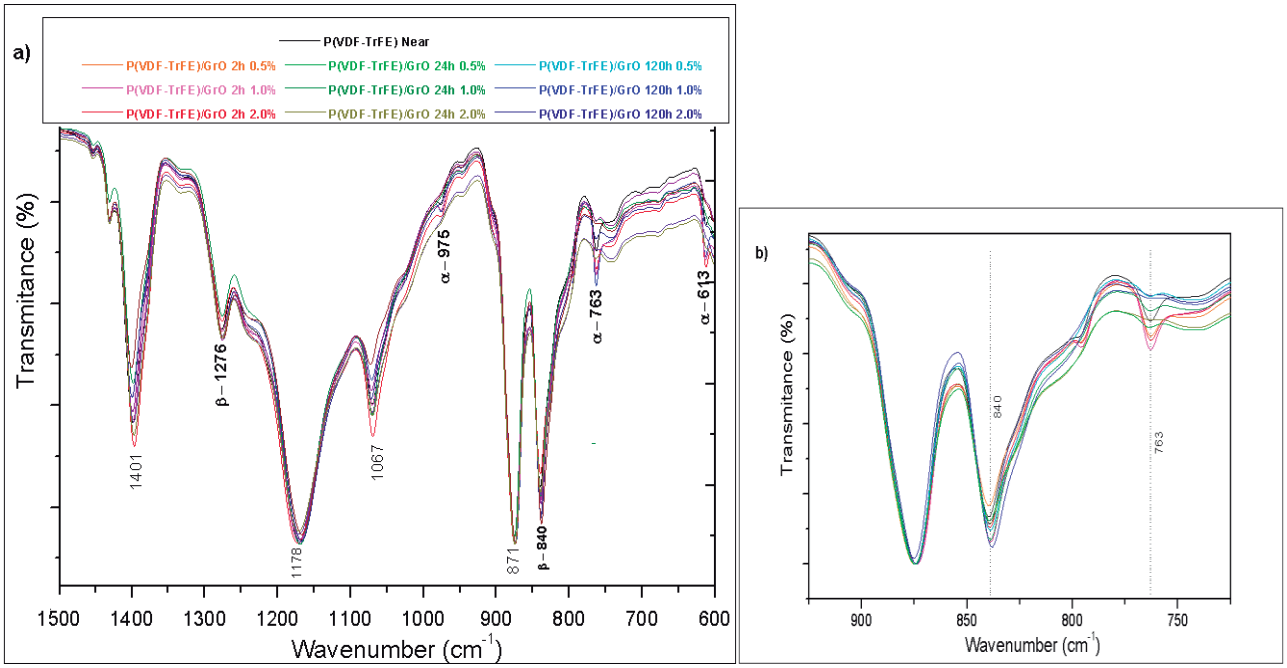

Figure 4: FTIR spectra of the nanocomposites. a) Area where the incidence of the bands is observed (1500-600 cm^{-1}). b) Area used to calculate the fractions F(β) and F(α) (950-725 cm^{-1}).

Table 1 shows the result of the fractions F(β) and F(α) in each nanocomposite. The nanocomposite of P(VDF-TrFE)/GrO 120h 1.0% had the highest β-phase content among all analyzed samples, with 88.45%.

Table 1: F(β) and F(α) in nanocomposites obtained GO

Sample	F(α) (%)	F(β)(%)	Sample	F(α) (%)	F(β)(%)
Pure P(VDF-TrFE)	28.01	71.99	P(VDF-TrFE)/GrO 24h 1.0%	13.68	86.32
P(VDF-TrFE)/GrO 2h 0.5%	18.49	81.51	P(VDF-TrFE)/GrO 24h 2.0%	13.35	86.65
P(VDF-TrFE)/GrO 2h 1.0%	14.64	85.36	P(VDF-TrFE)/GrO 120h 0.5%	13.03	86.97
P(VDF-TrFE)/GrO 2h 2.0%	15.13	84.87	P(VDF-TrFE)/GrO 120h 1.0%	11.55	**88.45**
P(VDF-TrFE)/GrO 24h 0.5%	14.71	85.29	P(VDF-TrFE)/GrO 120h 2.0%	15.33	84.67

Conclusions

It is concluded that the synthesis of the nanoparticles with higher oxygen contents was successful due to the longer reaction time and with the more oxygenated sample (GrO 120h), greater promoted the beta phase in the final nanocomposite (P(VDF-TrFE)/GrO 120h 1.0%)

Acknowledgments

Acknowledgment to CAPES, CNPQ and FAPERJ for the investment in the research.

References

1. R. F. Rangel, MSc. Dissertation, UFPB/CEAR, 2014.
2. K. K. Kar; C. Gayner. Progress in Materials Science 2016, 83, 330-382. https://doi.org/10.1016/j.pmatsci.2016.07.002.
3. D. Singh; F. L. Deepak; A Garg. Physical Chemistry Chemical Physics 2017, 19, 7743-7750. https://doi.org/10.1039/C7CP00275K.
4. S. Mohammadpourfazeli; S. Arash; A. Ansari; S. Yang; K. Mallick; R. Bagherzadeh. RSC Advances 2023, 13, 370-387. https://doi.org/10.1039/D2RA06774A.
5. S. Gupta; M. Kumar; G. Singh; A. Chanda. Advances in Electrical Engineering, Electronics and Energy 2023, 3, 100-115. https://doi.org/10.1016/j.prime.2023.100115.
6. J. Hao; W. Li; W. Zhai; H. Chen. Materials Science & Engineering 2019, 135, 1–57. https://doi.org/10.1016/j.mser.2018.08.001.
7. Y. Ting; C. W. Chiu; H. E. Gunawan. Journal of Applied Polymer Science 2018, 135, 46677-46687. https://doi.org/10.1002/app.46677.
8. C. Chen; L. Wang; X. Liu; W. Yang; J. Lin; G. Chen; X. Yang. Polymers 2019, 11, 1-12. https://doi.org/10.3390/polym11020310.
9. S. Zhukov; D. Eder-goy; C. Biethan; S. Fedosov; B. X. Xu; H. Seggern. Smart Materials and Structures 2017, 27, 015017. https://doi.org/10.1088/1361-665X/aa9a63.
10. K. K. Sappati; S. Bhadra. Sensors 2018, 18, 1-30. https://doi.org/10.3390/s18113605.
11. S. Begum; H. Ullah; A. Kausar; M. Siddiq; M. A. Aleem. Composites Science and Technology 2018, 167, 497-506. https://doi.org/10.1016/j.compscitech.2018.08.041.
12. J. Li; C. Zhao; K. Xia; X. Liu; D. Li; J. E. Han. Applied Surface Science 2019, 463, 626-634. https://doi.org/10.1016/j.apsusc.2018.08.266.
13. R. Tu; E. Sprague; H. A. Sodano. ACS Applied Materials & Interfaces 2020, 12, 58081. https://doi.org/10.1021/acsami.0c16207.
14. F. Algarni; G. Zapsas; N. María; J. Maiz; A. J. Müller; N. Hadjichristidis. Macromolecular Chemistry and Physics 2023, 224 2200268. https://doi.org/10.1002/macp.202200268.
15. M. Zhang; C. Liu; B. Li; Y. Shen; H. Wang; K. Ji; X. Mao; L. Wei; R. Sun; F. Zhou. Nanoscale Advances 2023, 5, 1043-1059. https://doi.org/10.1039%2Fd2na00773h.
16. P. Xu; W. Fu; Z. Cui; Y. Ding; Applied Physics Letters 2018, 112, 63910. https://doi.org/10.1063/1.5011051.
17. F. E. Jorge; L. G. P. Tienne; M. F. V. Marques. Materials Science and Engineering: B 2021, 263, 114851. https://doi.org/10.1016/j.mseb.2020.114851.
18. T. Chowdhury; N. D'Souza; Y. H. Ho; N. Dahotre; I. Mahbub. Sensors 2020, 20, 3053. https://doi.org/10.3390/s20113053.
19. E. Brunengo; M. Castellano; L. Conzatti; G. Canu; V. Buscaglia; P. Stagnaro. Journal of Applied Polymer Science 2020, 137, 48871. https://doi.org/10.1002/app.48871.
20. A Thakur; S. Dam; D. Nath; N.V. C. Shekar; G. Amarendra; S. Hussain. Polymer 2020, 186, 122074. https://doi.org/10.1016/j.polymer.2019.122074.
21. N. Momenzadeh; H. Miyanaji; T. A Berfield. International Journal of Advanced Manufacturing Technology 2019, 103, 4713–4720. https://doi.org/10.1007/s00170-019-03978-7.

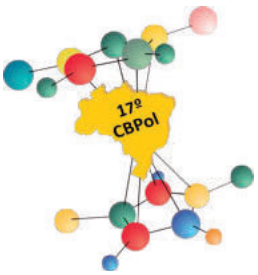

EVALUATION OF PBAT/CUMBARU FIBER/ORGANOCLAY NANOCOMPOSITES FOR FOOD PACKAGING APPILICATION

Mário Lucas S. Carvalho[1], Regina Felipe do Ó[1], Paula de Miranda C. Maciel[2], Gisele C. Valle Iulianelli[1*]

1 – Instituto de Macromoléculas Professora Eloisa Mano, Universidade Federal do Rio de Janeiro (IMA/UFRJ), Rio de Janeiro, RJ, Brazil
2- Instituto Federal do Rio de Janeiro (IFRJ), Rio de Janeiro, RJ, Brazil
gisele@ima.ufrj.br

Abstract

To improve the general properties of biodegradable materials for food packaging application, and reduce their cost through incorporation of low-cost materials, in this work nanocomposites films using poly(butylene adipate-co-terephthalate) (PBAT) as matrix, lignocellulosic cumbaru endocarp as filler at 10 wt% and organoclays Viscogel B8 and S4 at 1, 3 and 5 wt% as nanofiller were developed. The nanocomposites, were obtained by a twin-screw extruder at 140 °C and 50 rpm and characterized by Thermogravimetric Analysis (TGA), Differential Scanning Calorimetric (DSC), X-ray Diffraction (XRD) and Contact Angle measurement. The results revealed that, although cumbaru filler has reduced thermal stability of PBAT, the addition of both organoclays, regardless of the proportion used, restored this property. XRD analysis showed that PBAT/CBR/S4 at 1wt% and PBAT/CBR/B8 at 3 wt% presented a higher degree of crystallinity, which represent a better barrier property, important to food packaging application. From contact angle measurement it was observed a trend of progressive increase in the contact angle with increasing organoclays addition and that all PBAT/CBR/B8 nanocomposites presented a hydrophobic character, with contact angle greater than 90º, which is also an advantage for food packaging. In conclusion, it was seen that the biodegradable materials produced using agroindustry residue and low cost nanofiller such as clays presented great potential for use as food packaging, reducing the final cost of biodegradable matrices and not compromising and/or improving some import properties for this purpose.

Keywords: *Nanocomposite; Food Packaging; Clay; PBAT; Cumbaru*

Introduction

Food packaging is used to protect and preserve food, ensuring consumer safety and food quality, against physical, chemical and biological damage. In addition, they maintain visual attributes of food, avoiding loss of market value. [1-5]. Nowadays, it is common to use packaging consisting of petrochemical products, mainly produced by non-biodegradable polymers [1-3]. However, these products have caused harm to the ecosystem, intoxicating animals, plants, water bodies and therefore human society in the end, due to its inappropriate disposal, degradation products and permanence in the environment [1-4].

In view of this, researchers have sought developed new material from biodegradable polymers with good physical-chemical and mechanical properties that are suitable for use in food packaging. Among these polymers, poly (butylene adipate-co-terephthalate) (PBAT) has shown growing interest. PBAT is a biodegradable polymer, which has been used in many applications,

including biomedicine, tissue bioengineering, increasing the biodegradability of other polymers and more recently studies are being directed to food packaging [1,2,4].

Although promising, the use of biopolymers, such as PBAT is still restricted due to their higher prices and less efficient mechanical and gas barrier properties compared to its conventional polymeric competitors from petrochemical sources [1-4]. Therefore, current researches aim to implement the use of biodegradable polymers, reducing their cost from insertion of low-value fillers in its composition such as lignocellulosic fillers from agriculture waste, while adding reinforcing characteristics [1-4]. Another strategy to improve the general properties of biodegradable polymers is to use nanotechnology knowledge, developing nanocomnposites materials.

Cumbarú, baru or coconut bean (*Dipteryx alata Vogel*) is a fruit native to Brazil and South American countries, and belongs to the drupe family. This fruit have a fleshier part (mesocarp) and a woody core (endocarp) inside, rich in lignocellulosic material, which protects the seed. The cumbarú seed tastes close to that of peanuts, and this characteristic makes it widely used as a substitute for the product in regions of the Brazilian Midwest. In addition to being used as supplementary feed and water source for cattle in times of drought, producing large amounts of woody endocarp. As it is a lignocellulosic material, cumbaru endocarp has great potential for use as a reinforced filler in biodegradable polymers such as PBAT, which would promote greater added value for this agroindustry residue.

Another strategy to improve the biodegradable polymers properties is the use of particles on the nanometric scale, which constitutes the field of Nanotechnology, widely used in recent decades to confer new properties and improve existing characteristics in materials without modifying their density too much [5]. Organoclay nanoparticles are commonly introduced into polymeric composites in order to improve mechanical and barrier properties [5].

Considering the above information, in this work new nanocomposites containing PBAT as matrix, cumbaru endocarp fiber as filler and two types of organoclays were developed.

The obtained nanocomposites were characterized by Thermogravimetric Analysis (TGA), Differential Scanning Calorimeter (DSC), X-Ray Diffraction (XRD) and Contact Angle measurement.

Experimental

Materials

PBAT Ecoflex® F Blend C1200 was provided by BASF (Ludwigshafen, SE, Germany). Cumbaru fruit was supplied by Universidade Federal do Mato Grosso. Organoclay Viscogel® S4 and B8 were provided by Laviosa Chimica Mineraria SA, Italy.

Preparation of films

Cumbarú endocarp filler and PBAT were ground and then dried in an oven for 48 hours at 50 ºC before melting process. The nanocomposites were prepared using PBAT, a biodegradable polymer as matrix, cumbaru fiber (40-80 mesh) at 10 wt% as filler, and organoclays B8 and S4 at 1, 3 and 5 wt% as nanofiller. The materials were processed in a mini extruder Thermo Scientific HAAKE MiniLab II with a counter-rotating twin-screw operating at 140 °C, 50 rpm for 10 min of cycling (mixing). For the characterizations, films by compressing molding at 140 ºC for 5 min were prepared.

Characterization of PBAT/cumbaru/organoclays nanocomposites

PBAT and its nanocomposites were characterized by Thermogravimetric Analyzer (TGA) and Differential Scanning Calorimeter (DSC). For the TGA analysis, a Thermogravimetric Analyzer TA Instruments model Q500 was used, under a temperature range of 30 °C to 700 °C with

heating rate of 10 °C/min, in an inert atmosphere of N_2. For DSC, a TA Instruments, model Q1000 was used. DSC runs were carried out following analysis conditions: Heating from -60 °C to 200 °C, with heating rate of 20 °C/min and cooling from 200 °C to -60 °C, with a cooling rate of 20 °C/min.

X-ray diffraction (XRD) was performed for cumbaru powder and fiber, pure PBAT, and its nanocomposites using a Rigaku Miniflex 600 diffractometer, with 2θ scanning in the range from 2° to 60° at a rate of 1°/min and step of 0.05º.

The sessile drop method was employed to evaluate the wettability of the samples from measurement of the contact angle θ of the water on the surface of the analyzed films. The measurements were performed using the OCA-15EC equipment (Dataphysics Instruments, Germany), and the results were based on the average of five repeated measurements.

Results and discussion

PBAT/cumbaru/organoclays nanocomposites

Thermal analyzes

Pure PBAT, cumbaru (CBR), PBAT/CBR fiber 10 wt% (PBAT/CBR10) and PBAT/cumbaru10 containing organoclays S4 and B8 at 1, 3 and 5 wt% were examined. From TGA analysis, Tonset temperature and Tmax temperature were determined and from DSC, glass transition temperature (Tg), crystallization temperature (Tc) and melting temperature (Tm) were obtained. According to the results, shown in Table 1, it was possible to verify that addition of cumbaru to the PBAT decreased the thermal stability of the system by 6 ºC. However, when both organoclays were added, at all proportions tested, the thermal stability was restored. Thermal transition temperatures obtained from DSC remained virtually unchanged.

Table 1 - Results obtained from TGA and DSC analyzes

Samples	Tonset (ºC)	Tmax (ºC)	Tg	Tc	Tm
PBAT	373	399	-31	79	122
CBR	239	279	-	-	-
PBAT/CBR10	367	398	-30	80	123
PBAT/CBR10/S4 1	374	402	-30	96	123
PBAT/CBR10/S4 3	372	399	-31	96	120
PBAT/CBR10/S4 5	373	402	-32	93	122
PBAT/CBR10/B8 1	373	402	-32	96	122
PBAT/CBR10/B8 3	370	400	-31	96	122
PBAT/CBR10/B8 5	375	404	-30	101	123

X-ray diffraction (XRD)

X-ray diffraction patterns obtained for all studied samples are shown in Figure 1. XRD diffractogram of the pure PBAT, organoclays S4 and B8 and cumbaru exhibited characteristics peaks indicating semicrystalline structures, as expected. Compared to pure PBAT, PBAT containing 10 wt% of cumbaru presented an increase in the degree of crystallinity, as observed by the increase in intensity and area of the crystalline peaks. For the systems containing S4, the degree of

crystallinity decreased considerably when 3 wt% of this organoclay was added while the system containing 1 wt% presented a greater increment in this profile. For PBAT/cumbaru systems containing B8, the behavior was the opposite. A lower degree of crystallinity was observed for the formulation containing 1 wt% of this organoclay and a higher degree of crystallinity was observed for PBAT/CBR/B8 at 3 wt%.

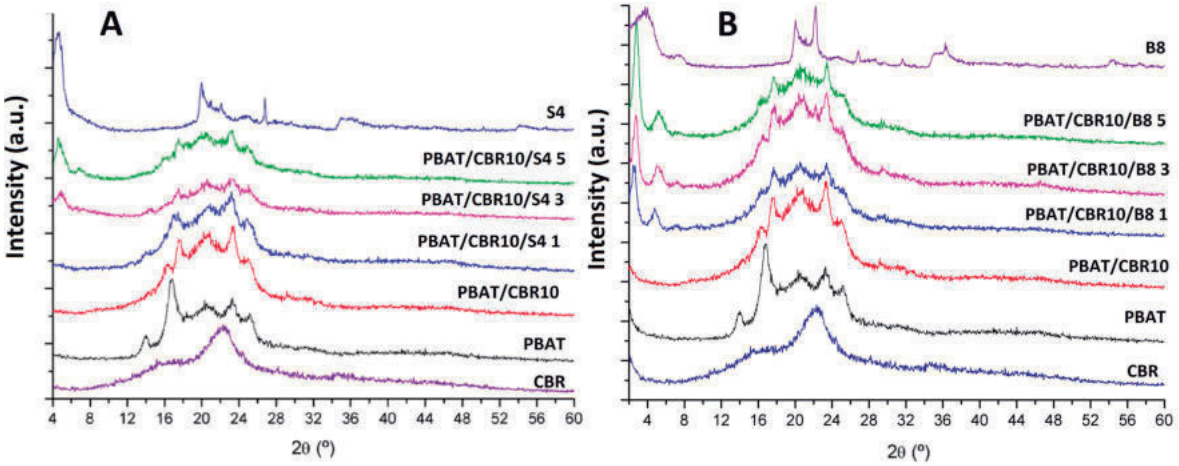

Figure 1 - DRX diffractogram obtained for PBAT, S4, B8 and PBAT/CBR/S4 (A) and PBAT/CBR/B8 (B) systems.

Contact Angle

Table 2 presents the values found from contact angle measurements for pure PBAT, PBAT/CBR10 and its nanocomposites. The values represent the average of five measurement. The respective standard deviations for each sample also are presented. For both organoclays studied, S4 and B8, a progressive tendency of increasing hydrophobicity with increasing organoclay proportions was observed. The organoclay B8 increased more significantly the hydrophobicity as can be seen from the increase in contact angle. Considering that contact angle above 90º characterize a material as hydrophobic, the results found from this analysis showed that the nanocomposites prepared with B8 at 1, 3 and 5 wt% presented a hydrophobic character.

Table 2 - Contact Angle measurement

Samples	θ	Dp
PBAT	81.73	5.76
PBAT/CBR10	83.94	3.01
PBAT/CBR10/S4 1	83.37	3.73
PBAT/CBR10/S4 3	84.43	6.29
PBAT/CBR10/S4 5	87.42	3.10
PBAT/CBR10/B8 1	93.33	6.55
PBAT/CBR10/B8 3	100.38	9.01
PBAT/CBR10/B8 5	101.57	7.39

Conclusions

The results found in this study, showed that cumbaru filler reduced the thermal stability of PBAT, however the addition of both organoclays studied restored this property. Furthermore, cumbaru filler and organoclays S4 and B8 did not cause changes on the thermal transition temperatures. Concerning XRD, the organoclays presented different influence, for systems containing S4 the highest degree of crystallinity was found for formulation containing 1 wt% and for systems containing B8, the highest value was found for system containing 3 wt%. Contact angle measurement showed that both organoclays increased the hydrophobicity of the PBAT, however B8, regardless of the proportion inserted, promoted a more important influence, providing a hydrophobic character to the obtained systems. The compiled results found in this study, showed that the systems obtained using low cost filler and nanofiller, mainly the formulations containing B8 as nanoclay, exhibited promising characteristics to be used as food packaging.

Acknowledgements (Times New Roman 12, bold)
The authors thank the Instituto de Macromoléculas Professora Eloisa Mano (IMA/UFRJ).

References

1. J. Xie; Z. Wang; Q. Zhao; Y. Yang; J. Xu, G. I. N. Waterhouse; K. Zhang; S. Li; P. Jin and G. Jin. ACS Omega**,** 2018, *3* (1), pg.1187-1196. https://doi.org/10.1021/acsomega.7b02062.
2. S.J. Xiong; B. Pang; S.J. Zhou; M.K. Li; S. Yang; Y.Y. Wang; Q. Shi, S.F. Wang; T.Q. Yuan; R.Q. Sun; ACS Sustainable Chemistry & Engineering 2020 *8* (13), 5338-5346, https://doi.org/10.1021/acssuschemeng.0c00789.
3. A. Bhardwaj; T. Alam; V. Sharma; et al. J Package Technol Res, 4, 205–216 (2020). https://dx.doi.org/10.4314/tjs.v47i5.6.
4. H. Moustafa, A. M. Youssef, N. A. Darwish; A. I. Abou-Kandil; Composites Part B: Engineering, Volume 172,2019, Pages 16-25, ISSN 1359-8368, https://doi.org/10.1016/j.compositesb.2019.05.048.
5. Falcão, G.A.M.; Vitorino, M.B.C.; Almeida, T.G; et al. Polym. Bull. 74, 4423–4436 (2017). https://doi.org/10.1007/s00289-017-1966-6.

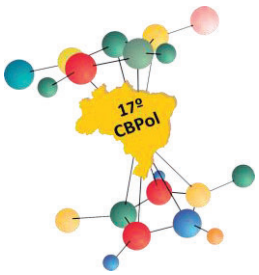

EVALUATION OF THE ANTICORROSION POTENTIAL OF POLYMER NANOCOMPOSITE COATINGS WITH REDUCED GRAPHENE OXIDE FOR THE OIL INDUSTRY

Ana Leticia F. dos Santos[1]*, Maria Paula de C. Freire[1], Ygor Matheus P. de Paula and Maria Carolina B. Costa[2]

1 – Graduate Program in Materials Science and Engineering (PPGCEM), Federal University of Rio Grande do Norte (UFRN), Natal, RN, Brazil
analeticiaferds30@gmail.com
2 – Department of Materials Engineering (DEMat), Federal University of Rio Grande do Norte (UFRN), Natal, RN, Brazil

Abstract - This work aims to correlate the results obtained for epoxy nanocomposite coatings with reduced graphene oxide (rGO), indicating its possible anticorrosive behavior. X-ray diffraction (XRD), Fourier transform infrared spectroscopy (FTIR) and scanning electron microscopy (SEM) analyses were performed. Nanocomposite coatings were prepared with 0.1%wt, 0.3%wt and 0.5%wt of rGO. The SEM analyses for the applied coatings showed that there was a decrease in the number of defects on the surface of the samples with increasing rGO concentration up to 0.3%wt in the coatings. The anticorrosion behavior of some coatings was evaluated by electrochemical impedance spectroscopy (EIS), which showed that the addition of rGO in the polymer matrix improves the corrosion protection of the anticorrosion coating by increasing the diffusive path of corrosive agents. Furthermore, the high potential of the prepared nanocomposite coatings for improving corrosion resistance was noted.
Keywords: *Graphene; Coating; Nanocomposite; Corrosion*.
Fundings: Resource Program Humans of the National Agency of Petroleum, Natural Gas and Biofuels.

Introduction

Corrosion is a natural phenomenon that affects several industries that make use of metallic materials in their metallic materials in their industrial plants, including the oil industry. This problem affects the structural properties and the useful life of the equipment susceptible to corrosion, and can generate economic losses, environmental damage, and general safety risks [1, 2]. The metal pipes, which transport and distribute substances generated by this industry that are economically important, are one of the equipment with high sensitivity to corrosion [3].

Thus, there is considerable effort in developing new strategies to minimize the effects caused by corrosion. Among these, the development of new classes of organic corrosion protection coatings is gaining popularity due to their scalability and ease of application. In the last decades, several materials have been tested as alternative for synthesis of coatings, such as polymeric ones [4].

One of the most commonly used polymers in this case are epoxy resins, which combine their anticorrosive nature, chemical resistance, fatigue resistance, and excellent adhesion to various substrates. However, there is a limitation in their long-term applicability due to hydrolytic degradation. With this, it is necessary to add other materials to its composition to improve its anticorrosive properties, and nanoparticulate materials are an excellent alternative [1]. Among the nanoparticles used, graphene has attracted immense research interest in recent years due to its high mechanical strength, high thermal conductivity, and high surface area. However, due to its difficulty in production, its derivatives, graphene oxide (GO) and reduced graphene oxide (rGO),

are more studied. Of these, rGO has properties close to those of pure graphene, which has made it widely accepted for obtaining graphene-like materials. Despite this, its application in the oil and gas industry is still recent [5, 6].

Therefore, the objective of this work was to correlate the results obtained for the synthesized materials, indicating the possible anticorrosion behavior of the epoxy nanocomposite coatings with rGO synthesized in the laboratory. These coatings were applied to metallic piping substrates used in the oil industry, aiming to increase corrosion resistance.

Experimental

The nanocomposite coatings were produced by solution mixing using ethanol as the solvent for dispersing the rGO. The solvent was evaporated by heating while it was stirred. The coatings were produced with 0.1%wt, 0.3%wt and 0.5%wt of rGO (EP/0.1rGO, EP/0.3rGO and EP/0.5rGO respectively), and samples containing the pure epoxy resin were prepared for comparison of the results. The coatings were applied using a high-pressure paint gun, and they were cured at room temperature for 24 h. Prior to the application of the coatings, the metal substrates used were cut, sanded, cleaned and dried. The substrates were a section of an API X65 steel metal pipe.

The rGO used was obtained by thermal reduction of graphene oxide (GO). GO was synthesized from the chemical exfoliation of graphite powder (99% with grain size < 20 µm from SigmaAldrich) based on the improved graphene oxide synthesis method [7]. This method is performed in a solution with dr 9:1 sulfuric acid (H2SO4) and 21.4 ml phosphoric acid (H3PO4), using graphite powder as precursor and potassium permanganate (KMnO4). For reduction of this material and production of rGO, the procedure performed was by the thermal reduction method at 225 °C [8].

X-ray diffraction (XRD), Fourier transform infrared spectroscopy (FTIR) and field emission scanning electron microscope (FE-SEM) analyses were performed. In addition, the surface of the nanocomposite coatings applied to the metal substrate were analyzed via FE-SEM. Electrochemical impedance spectroscopy (EIS) assay in 0.5 M NaCl solution was performed on the pure epoxy coatings and with 0.1%wt and 0.5%wt added. The measurements were performed at open circuit potential until stabilization, applying AC amplitude of 10mV, with frequency range from 10-2 Hz to 105 Hz in an Autolab PGSTAT302N potentiostat. The area of the samples exposed to the solution was 1 cm2, and it was limited with the use of durepox in the remaining areas. The results obtained were analyzed with the help of Nova 1.1 software.

Results and Discussion

X-ray diffraction (XRD)

The diffractograms of GO and rGO are shown in Fig 1a, and it is possible to observe the characteristic intensity peak of GO around 2θ = 9.82°, which disappears in the diffractogram of rGO. Moreover, when comparing the result of the XRD analysis of the rGO sample with the diffractogram of the pure graphite (Fig 1b) used as raw material in the synthesis, it is noted that the specific peak of rGO (in the range of 2θ = 24.10°) is located close to the largest peak of pure graphite (around 2θ = 26.18°), but of much lower intensity and broader. This shows that the material has an amorphous characteristic, and that GO has been fully reduced [9].

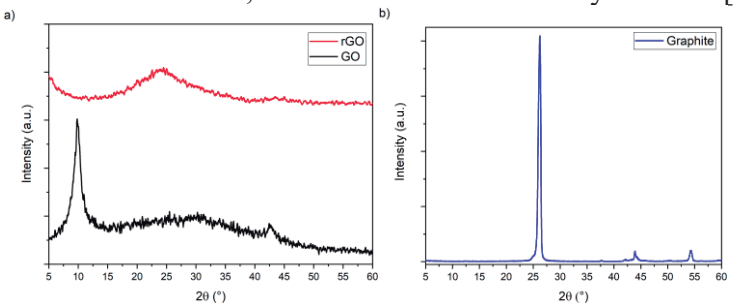

Figure 1 – XRD spectra of samples of a) GO and rGO and b) pure graphite.

Fourier transform infrared spectroscopy (FTIR)

The FTIR spectra of GO and rGO are shown in Fig 2. In the case of GO, characteristic valleys can be observed at approximately 1040 cm^{-1}, 1615 cm^{-1} and 1705 cm^{-1} that correspond to the presence of alkoxy groups (C - O), the atomic vibration of sp^2 domain bonds of the aromatic ring (C = C) and existence of carbonyl groups (C = O) in the basal plane of carbons, respectively. In addition, a broad absorption band is seen at approximately 3270 cm^{-1} that represents the bond stretching vibrations of the hydroxyl groups (O - H) present in the material [9]. When compared to the rGO spectrum, we see that the valleys are of much lower intensity, or even disappear. This shows that the thermal reduction step was efficient in removing the functional groups from the basal plane of carbons for the proper formation of rGO.

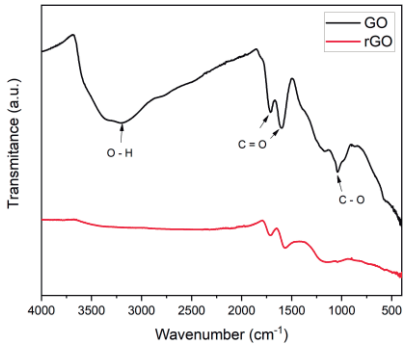

Figure 2 – FTIR spectra of GO and rGO.

Field emission scanning electron microscope (FE-SEM)

The morphological analysis of the synthesized materials (Fig 3) shows the overlapping and highly agglomerated rGO sheets. Also, in the image at higher magnification (Fig 3b), it is observed a 3D structure with well exfoliated layers, as already seen in other studies on the thermal reduction of GO [8]. However, they still have points of connections between these layers preventing their complete separation.

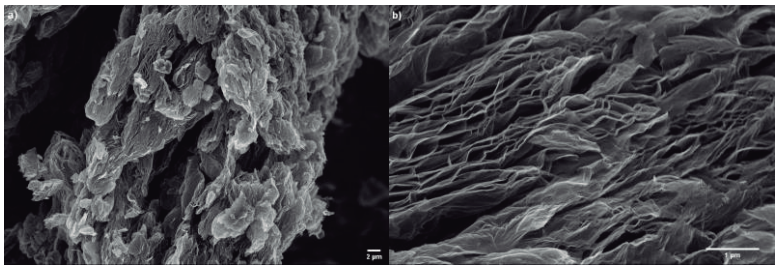

Figure 3 – SEM images of rGO at a) 2000x and b) 16000x magnification.

Since the protection against corrosion of epoxy coatings occurs by preventing the transport of corrosive agents to the metal substrate to be protected, the visualization of defects in them is important to understand how these coatings will behave with the addition of nanoparticles. Thus, from the SEM analysis performed on the coatings, it is possible to see the decrease in the amount of defects and pores on their surface with the increase in the percentage of rGO up to 0.3% by mass. This is due to the fact that the addition of this nanomaterial in the polymeric matrix causes its particles to move in place of these defects and pores, enabling the increase of the diffusive path of the corrosion agents to the metal. However, with the addition of the highest percentage of rGO in the epoxy coating (EP/0.5rGO), these defects increase in relation to the other coatings probably due to the high tendency of agglomeration of the rGO particles [10]. The defects are identified in Fig 4, which shows in addition to the presence of pores also the existence of runoff type defects, stains and impregnation of solid materials [11].

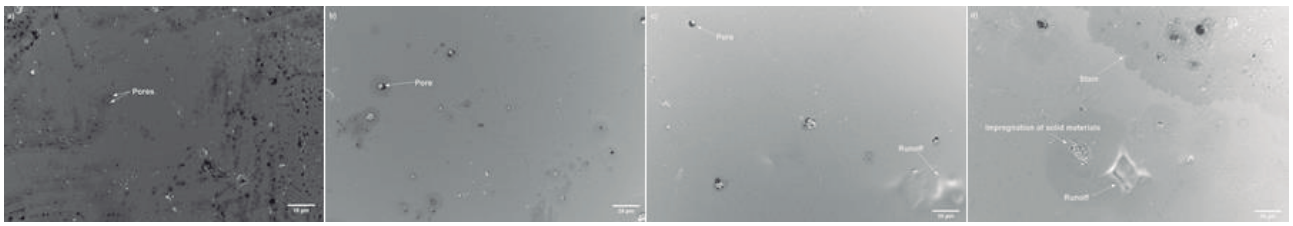

Figure 4 – SEM images with 500x magnification of coating surfaces a) epoxy pure, b) EP/0.1rGO, c) EP/0.3rGO and d) EP/0.5rGO.

Anticorrosive behavior

Electrochemical impedance spectroscopy (EIS) measurements were displayed in the form of Nyquist (Fig. 5a) and Bode (Fig. 5b) diagrams as a function of rGO contents, for the samples immersed for 4 h in a 0.5M NaCl solution, for the pure epoxy samples and nanocomposite coatings with 0.1%wt and 0.5%wt rGO.

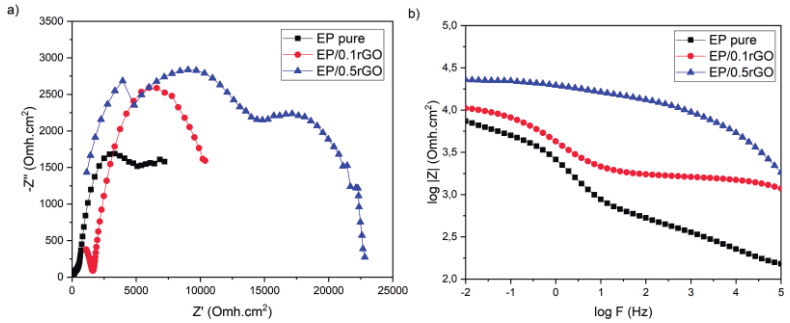

Figure 5 – a) Nyquist and b) Bode diagram for pure epoxy and nanocomposite coatings immersed for 4 h in a 0.5M NaCl solution.

As shown in the Nyquist diagram, both coatings showed a kind of characteristic impedance semicircle controlled by charge transfer during the test. Since the radius of this semicircle is the sum of the charge transfer resistance and the solution resistance, the higher its value, the higher the corrosion resistance of the material [10]. Thus, it is possible to verify the increase of the capacitive arc with the addition of rGO in the coating, indicating that the addition of the nanoparticulate material improves the corrosion resistance of the coating used.

The low value of $|Z|_{0.01Hz}$ for the pure epoxy coating indicates its low performance of physical barrier protection, allowing electrolyte diffusion to the metal substrate. The nanocomposite coatings show values of $|Z|_{0.01Hz}$, indicating their better efficiency in blocking the passage of corrosive agents through the coating and consequently have better corrosion protection performance. Of the nanocomposite coatings, the addition of the highest concentration of rGO (0.5% by weight) resulted in better test results. This is due to the presence of defects and pores in the pure epoxy coating (as already seen in the SEM images), limiting its corrosion protection. With the addition of rGO, the diffusive path of corrosive agents is increased causing this metal surface protection to be improved [10]. It is worth mentioning that the method of sample preparation chosen to perform the test was not ideal, once the samples were left immersed for a longer time for visual analysis it was possible to observe electrolyte infiltration through the durepox, thus interfering in the results obtained.

Nevertheless, one study [12] showed that the addition of different concentrations of rGO in epoxy effectively improved the corrosion resistance of the polymeric material. The coatings in this case were prepared with 0.5%wt, 1.0%wt, 2.0%wt, and 4.0%wt of rGO applied to a metallic substrate of an N80 steel pipeline. This preparation was similar to that shown in this paper, with the mixing being via solution. The surface morphology of the coatings was evaluated by SEM and their corrosion behavior was carried out by EIS tests.

Conclusions

Epoxy nanocomposite coatings with reduced graphene oxide (rGO) were prepared and applied on API X65 steel metal substrates. FE-SEM analyses were performed on the surfaces of the applied

coatings, making it possible to observe the decrease in the number of defects and pores on their surface with increasing percentage of rGO added up to 0.3%wt. Furthermore, the correlation of this work with a study carried out for epoxy nanocomposite coatings with up to 4.0%wt of rGO, showed the high potential for improving the corrosion resistance of the prepared coatings.

Acknowledgements
The development of this work was only possible from the financial support of the Human Resources Program of the National Agency of Petroleum, Natural Gas and Biofuels - PRH-ANP, supported with resources from the investment of oil companies qualified in the P, D&I Clause of ANP Resolution No. 50/2015, and the permission to use the infrastructure of the Laboratory of Environmental and Applied Electrochemistry (LEAA) of UFRN for measurement of the corrosion test.

References

1. GEORGE, J. S.; VIJAYAN P, P.; PADUVILAN, J. K.; SALIM, N. et al. Advances and future outlook in epoxy/graphene composites for anticorrosive applications. Progress in Organic Coatings, 162, p. 106571, 2022/01/01/ 2022.
2. SPEIGHT, J. G. Chapter 5 - Corrosion in Other Systems. In: SPEIGHT, J. G. (Ed.). Oil and Gas Corrosion Prevention. Boston: Gulf Professional Publishing, 2014. p. 93-107.
3. VANAEI, H. R.; ESLAMI, A.; EGBEWANDE, A. A review on pipeline corrosion, in-line inspection (ILI), and corrosion growth rate models. International Journal of Pressure Vessels and Piping, 149, p. 43-54, 2017.
4. OTHMAN, N. H.; CHE ISMAIL, M.; MUSTAPHA, M.; SALLIH, N. et al. Graphene-based polymer nanocomposites as barrier coatings for corrosion protection. Progress in Organic Coatings, 135, p. 82-99, 2019.
5. MEHMOOD, A.; MUBARAK, N. M.; KHALID, M.; WALVEKAR, R. et al. Graphene based nanomaterials for strain sensor application—a review. Journal of Environmental Chemical Engineering, 8, n. 3, p. 103743, 2020.
6. NEUBERGER, N.; ADIDHARMA, H.; FAN, M. Graphene: A review of applications in the petroleum industry. Journal of Petroleum Science and Engineering, 167, p. 152-159, 2018.
7. MARCANO, D. C.; KOSYNKIN, D. V.; BERLIN, J. M.; SINITSKII, A. et al. Improved Synthesis of Graphene Oxide. ACS Nano, 4, n. 8, p. 4806-4814, 2010/08/24 2010.
8. HUSSEIN, A.; SARKAR, S.; KIM, B. Low Temperature Reduction of Graphene Oxide Using Hot-plate for Nanocomposites Applications. Journal of Materials Science & Technology, 32, n. 5, p. 411-418, 2016.
9. AUNKOR, M. T. H.; MAHBUBUL, I. M.; SAIDUR, R.; METSELAAR, H. S. C. The green reduction of graphene oxide. RSC Advances, 6, n. 33, p. 27807-27828, 2016. 10.1039/C6RA03189G.
10. POURHASHEM, S.; RASHIDI, A.; VAEZI, M. R.; YOUSEFIAN, Z. et al. The effect of polycrystalline graphene on corrosion protection performance of solvent based epoxy coatings: Experimental and DFT studies. Journal of Alloys and Compounds, 764, p. 530-539, 2018.
11. FREIRE, L. N. S. V.; LEITE, R. S. A tecnologia das tintas na proteção anticorrosiva na indústria de óleo e gás offshore. 2021. 109 f. Monografia (Bacharel em Engenheira Química) - Departamento de Engenharia Química de Petróleo, Universidade Federal Fluminense, Niterói.
12. ZHU, L.; FENG, C.; CAO, Y. Corrosion behavior of epoxy composite coatings reinforced with reduced graphene oxide nanosheets in the high salinity environments. Applied Surface Science, 493, p. 889-896, 2019/11/01/ 2019.

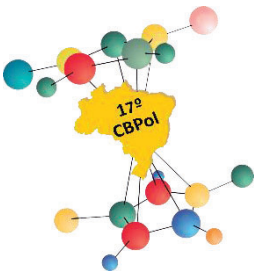

EVALUATION OF THE CATALYTIC PROPERTIES OF POLYMER COMPOSITES CONTAINING NIOBIUM OXYHYDROXIDES

Maria Eduarda Soares Pinheiro[1*], Ana Pacheli Heitmann[2], Patterson Souza[1], Patrícia Patricio[1]

1 - Federal Center for Technological Education of Minas Gerais (CEFET-MG), Av. Amazonas, 5253, Nova Suiça, Belo Horizonte, MG, Brazil
2 - Federal University of Minas Gerais (UFMG), Av. Antônio Carlos, Pampulha, Belo Horizonte, MG, Brazil

Abstract – In this study, the photocatalytic degradation of the organic dye methylene blue was investigated using the PBAT/S_2/UV system, which is a nanomaterial obtained by dispersing niobium oxyhydroxide (S_2) in a poly(butylene adipate co-terephthalate) (PBAT) polymeric matrix activated by UV light. Degradation tests were performed using spectrophotometry to analyze parameters such as the catalyst concentration and its distribution in the polymeric matrix. Chemical interactions between PBAT and S2 were observed using FTIR-ATR. The composite exhibited high catalytic activity for removing methylene blue dye during photocatalysis.

Keywords: *PBAT*, *photocatalysis, niobium oxide.*

Introduction

A significant portion of colorant usage is associated with industrial processes, with approximately 15% of global dye production being lost during the dyeing process and subsequently released into effluents. The treatment of this waste necessitates multiple stages, thereby demanding the development of diverse methodologies for removing these substances from river matrices [1]. Recent research indicates that non-conjugated polymers offer several advantages for this application. They have emerged as photocatalysts in recent years owing to their distinctive properties, particularly their capacity to absorb light within the visible spectrum and act as mediators of intermediate charge transport. Non-conjugated polymers, such as biodegradable polyesters, facilitate more effective electron migration from vacancies generated by light absorption on the surface of photocatalytic or photoelectrochemical materials, thereby enabling their participation in chemical degradation reactions [2,3].

PBAT, a non-conjugated polymer, exhibits ease of processing and molding and is relatively cost-effective compared to similar products. Moreover, PBAT, a thermoplastic polyester, demonstrates exceptional mechanical and thermal properties. Additionally, PBAT can be easily synthesized from renewable raw materials and possesses compostability, making it viable for transformation into organic compost for soil fertilization [3] and biodegradability. To enhance the photocatalytic efficiency in dye degradation, inorganic catalysts such as niobium oxide have been investigated due to their catalytic activity, akin to TiO_2 [4]. The research group has studied the catalytic material based on niobium oxide and polyhydroxy butyrate. It has proven effective for the photooxidative degradation of methylene blue dye in an aqueous environment [6]. From this perspective, the present study aims to develop a composite based on the PBAT polymer and niobium oxyhydroxide as an alternative for photocatalyst development while investigating its catalytic activity in removing methylene blue dye from an aqueous medium under ultraviolet radiation.

Experimental

For the synthesis of niobium oxyhydroxide (S_2), the work of HEITMANN et al. (2018) was used as a reference, starting with 46.2 mmol of the ammonium oxalate niobium as precursor salt ($NH_4NbO(C_2O_4)_2(H_2O)n$) (CBMM). The niobium salt was dissolved in 100 mL of distilled water at 90°C. After the complete dissolution of the salt, NH_4OH (5 mol L^{-1}) was slowly added to the solution until reaching pH 7 to precipitate niobium oxyhydroxide. The suspension was then continuously stirred for 12 hours for aging. Finally, the resulting white solid was filtered, washed, and dried in an oven at 60°C for 12 hours. This material (300 mg) added 4 mL of 30% hydrogen peroxide and 80 mL of water at 25°C. The yellow solid was filtered, washed with distilled water, and dried at 60°C for 12 hours.

The PBAT/S_2 catalytic materials were obtained from poly(butylene adipate co-terephthalate) (PBAT) as pellets. A variation of 100 e 95% wt of the polymer and 1 to 5% wt of niobium oxyhydroxide was used during the mechanical processing. The mixtures were placed in a single-screw extruder (Thermoscientific- HAAKE - PolyLab QC) at a speed of 50 rpm and a temperature of 100°C in zones 1 and 4 and 120°C in zones 2 and 3. The produced pellets were pressed using a hydraulic press. In the materials referred to as (surface), during the pressing step, niobium oxide was added to the surface after processing.

Characterization and Catalytic test

The produced materials were characterized using an IRPrestige-21 Spectrophotometer, Shimadzu, with an ATR accessory. FTIR data were obtained from spectra collected from 4000 to 400 cm^{-1} with 30 scans.

Catalytic tests were conducted at 25°C using a 15mL solution of methylene blue (20 mgL^{-1}). The specific quantity of the polymeric materials was used with magnetic stirring at 330 rpm for - 60 to 120 minutes. A UV lamp (λ= 254 nm) with a power of 15W was employed. The oxidation efficiency was monitored using a UV-Vis spectrophotometer at 664 nm.

Results and Discussion

FTIR spectra of the PBAT and catalytic material are shown in Figure 1.

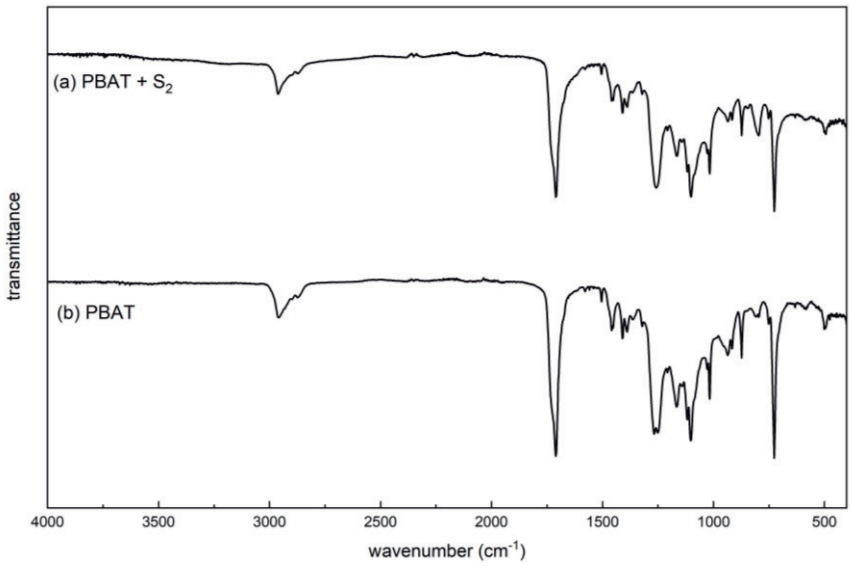

FTIR spectra of the PBAT and PBAT/S_2.

The FTIR spectra of PBAT and PBAT/S_2 reveal absorption bands of the polymer in the regions of 1715 and 1475 cm^{-1}, corresponding to the stretching of the carbonyl group C=O (νC=O) and the stretching of C=C bonds in aromatic rings (νC=C), respectively. Additionally, bands in the

range of 1300 to 1000 cm^{-1}, centered at 1267 and 1106 cm^{-1}, are observed, which are associated with the stretching of the -C-O bond in the ester group (νC-O)) [5]. The addition of the catalyst did not cause significant changes in the bands associated with the polymeric matrix. No significant bands or the formation of new bands related to the polymeric matrix were observed upon the addition of the catalyst [6]. However, the changing C-O band profile indicated the possibility of interaction through the carboxylic group.

The range of -60 to 120 minutes represents the dye adsorption time by the matrix. During this interval, the UV light remained off to prevent dye degradation. At time zero of the reaction, the light is turned on, initiating the photocatalytic reaction. Figure 2 represents the dye removal by the polymeric compound associated with the catalyst. The removal of methylene blue by adsorption is small compared to the investigated systems.

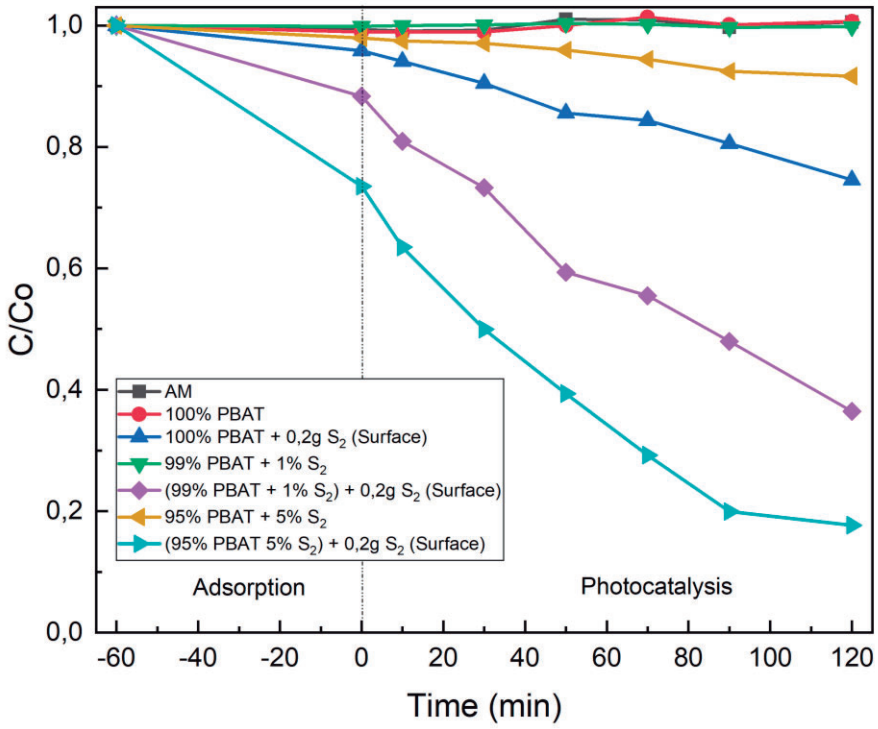

Figure 2. Graphic of methylene blue concentration reduction in aqueous medium as a function of time using the polymeric matrix PBAT and nanocomposites (S_2) with varying concentration and distribution.

The removal of methylene blue by adsorption becomes significant when incorporating S_2 into the polymer, regardless of how the compound is produced, reaching 30% dye adsorption using 95% PBAT 5% S_2 + 0.2g S_2 (surface). By incorporating the catalyst on the surface of the polymer and catalyst mixture (95% PBAT 5% S_2 + 0.2g S_2 (surface)), the dye removal was superior to the material in which the catalyst is only mixed with the polymer (95% PBAT + 5% S_2) where the removal was 30 and 3%, respectively.

A similar behavior was observed in the removal of methylene blue by photocatalysis, when the catalyst S_2 is incorporated into the medium of the polymeric matrix. In the compounds 99% PBAT + 1% S_2 and 95% PBAT + 5% S_2, the photocatalysis is low and the methylene blue removal is around 1 and 8%, respectively. This is probably due to the method of mixing the catalyst into the polymer, since mixing in the Termo haake can lead to partial or total coverage of S_2 by the PBAT. Similar results were presented by HEITMANN et al. (2018) who associated the lack of contact of the catalyst with the dye solution and UV radiation with the reduction of the photocatalytic activity of the material [7].

In Figure 2, it is evident that the incorporation of the catalyst into the polymeric matrix through mechanical processing, as well as its distribution on the film surface, as demonstrated in the cases of 99% PBAT 1% S_2 + 0.2g S_2 (surface), 95% PBAT 5% S_2 + 0.2g S_2 (surface), and 100% PBAT + 0.2g S_2 (surface), leads to a significant increase in dye removal, with removal percentages of 60%, 80%, and 20%, respectively, after 120 minutes of reaction. Moreover, it is noteworthy that the concentration of the S_2 catalyst in the polymer impacts the efficacy of methylene blue removal through photocatalysis. Higher concentrations of S_2 are associated with more efficient color removal.

When incorporated into the polymer and distributed on the film surface, niobium oxyhydroxide retains its catalytic activity, facilitating the photocatalytic reaction. Consequently, the material becomes more exposed within the polymeric matrix, enhancing the likelihood of interaction between the catalyst and dye molecules. This interaction generates electron-hole pairs that diffuse to the surface of the catalytic system, resulting in a higher rate of methylene blue discoloration.

Conclusions

In this work, nanocomposites containing PBAT and niobium oxyhydroxide (S_2) with different percentage of it were developed. From the results, important characteristics were observed, the nanocomposites are more effective for removing the methylene blue dye in the aqueous medium in the presence of UV radiation via photocatalysis, and when they are incorporated into the surface of the PBAT. The 95% PBAT 5% S2 + 0.2g S_2 (surface) system showed the best performance among the studied systems, removing 80% of dye in 120 minutes. Therefore, the concentration of catalyst S_2 and the method for obtaining the compounds determine the way the catalyst disperses in the polymer, determining the performance of the material in removing the dye by photocatalysis.

Acknowledgements

CNPq and FAPEMIG.

References

1. A. Houas, et al. Applied Catalysis B: Environmental, 2001, 2/31, 145. https://doi.org/10.1016/S0926-3373(00)00276-9.
2. Z. WEI, et al. Journal of the American Chemical Society, 2020, 52/142, 21899. https://doi.org/10.1021/jacs.0c11057.
3. J. Jian; Z. Xiangbin; H. Xianbo. Advanced Industrial and Engineering Polymer Research, 2020, 1/3, 19. https://doi.org/10.1016/j.aiepr.2020.01.001.
4. A. Nogueira; T. Ramalho; L. Oliveira. Topics in Catalysis, 2011 54, 270. https://doi.org/10.1007/s11244-011-9641-x.
5. R. COSTA, et al. 2020, 10/12, 2317. https://doi.org/10.3390/polym12102317.
6. A. Heitmann, et al. Journal of Applied Polymer Science, 2018, 7/135, 5836. https://doi.org/10.1002/app.45836.
7. K. Tennakone; C. Tilakaratne; I. Kottegoda. Journal of Photochemistry and Photobiology A: Chemistry, 1995, 2/87, 177. https://doi.org/10.1016/1010-6030(94)03980-9.

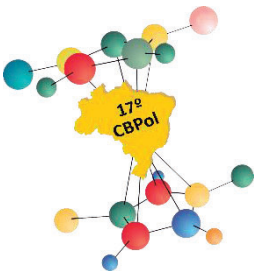

EVALUATION OF THE DEGRADATION OF POLY(ETHYLENE TEREPHTHALATE) WITH THE ADDITION OF CHAIN EXTENDERS AND GRAPHENE NANOPLATELETS AFTER PROCESSING

Daiane Torani[1], Diego Piazza[1], Rosmary N. Brandalise[1*], Nathan R. V. Albino[2], Renato G. F. Neto[2], Raphael B. M. Bergamini[2]

*1 – Graduate Program in Materials Science and Engineering (PPGMAT), University of Caxias do Sul (UCS), Caxias do Sul, RS, Brazil, *rnbranda@ucs.br.*

2 – Senai - Technology Center of Chemical and Textile Industry (CETIQT), Rio de Janeiro, RJ, Brazil.

Abstract - Poly(ethylene terephthalate) (PET) is the most consumed polyester in the world, as it is mainly used for carbonated beverage packaging and textile fiber production. Due to the different processes that occur during the production of textile fibers, they can show a loss of properties. The aim of this study was to evaluate the effect of the dianhydride chain extender 1,2,4,5-benzenetetracarboxylic acid (PMDA) and graphene nanoplatelets (NPs) on the properties of PET after the different processes. First, the virgin PET (PETv) was processed in a single-screw extruder, and then it was extruded in a twin-screw extruder with PMDA and NPs added as additives. The chemical and thermal properties of PETv samples and samples processed in single-screw and twin-screw extruder with additives were characterized based on the chemical and thermal properties. Compared with PETv, the samples processed in the single-screw and twin-screw extruders showed a degradation principle demonstrated by the techniques, except for the use of PMDA. The NPs acted as processing aids.

Keywords: *PET, PMDA, extrusion, graphene nanoplatelets, degradation.*

Introduction

The most consumed polyester in the world is poly(ethylene terephthalate) (PET), as it is used in the production of bottles for carbonated drinks and in the production of textile fibers. It also has good mechanical properties and high resistance to chemical agents. physical and chemical materials combined with relatively low cost [1]. PET can be easily reprocessed because it melts when heated and can be reshaped [2]. In evaluating degradation and stabilization, many of the homopolymers contain small concentrations of comomers that provide different properties.

Intrinsic viscosity is often used to evaluate degradation based on the behavior of the molar mass PET [3]. The use of extrusion for the processing of PET leads to a strong reduction of the properties after three processing cycles. In these cases, the intrinsic viscosity decreases by 23%, making it impossible to use it in applications similar to those of untreated polymer. To address the deficiency caused by the reduction in intrinsic viscosity, chain lengthening is encouraged. The selection of a chain extender must take into account the presence of at least two functional groups that promote addition reactions with the terminal hydroxyl or carboxyl groups of the polyester [2,4].

NPs are widely used as nanofillers in polymer matrices, concrete, metals, and others. Their incorporation in polymer matrices improves the mechanical behavior, increases the chemical resistance and thus the lifetime of the artifact [5,6]. In view of this, the objective of this work was to evaluate the degradation of PET, to which PMDA and NPs were added, after several processes.

Experimental

The raw materials used in this study were: PET from Indorama Ventures Fibras, PMDA extender from Sigma-Aldrich Chemistry, graphene nanoplatelets in the form of a PET masterbatch, 2 wt% Znano Grafeno. The codes and compositions of the developed blends are listed in Table 1.

Table 1 - Coding and composition of the study samples

Coding	Composition and description of the samples
PET_v	Virgin PET pellet
M-PET_v	100 wt% of PET_v processed in single screw extrusion
D-PET_v	100 wt% of PET_v processed in twin-screw extrusion
D-PET_{vPMDA}	100 wt% of PET_v processed in twin screw extrusion + 0.2 wt% of PMDA
D-PET_{vNPs}	100 wt% of PET_v processed in twin screw extrusion + 0.4 wt% of NPs
D-$PET_{vPMDA/NPs}$	100 wt% of PET_v processed in twin screw extrusion + 0.2 wt% of PMDA + 0.4 wt% of NPs

The preparation of the blends in this work was carried out in 2 stages, where in stage 1 the PETv was extruded in a single screw, and in stage 2 the composition obtained in stage 1 was extruded in a twin screw, with the addition of PMDA and NPs, followed by characterization of the chemistry by Fourier transform infrared spectroscopy (FTIR) and differential scanning calorimetry (DSC) and thermogravimetry (TGA).

Characterization of PETv and mixtures from Steps 1 and 2

The PET_v and the mixtures prepared in steps 1 and 2 were characterized in pellet form by their chemical properties using attenuated total reflectance (ATR) FTIR in a Spectrum 100 FTIR spectrophotometer from Perkin Elmer (USA) with 9 scans in the scan range of 400 to 4000 cm^{-1}. Thermal analysis by TGA in a TGA instrument, model Q5000 from TA Instruments (USA), at a heating rate of 10 ºC.min^{-1}, ranging from 25 °C to 810 °C, under a nitrogen flow of 50 mL.min^{-1}, in a platinum crucible, and also by DSC, in a model Q200 instrument from TA Instruments (USA), at a heating rate of 10 °C.min^{-1}, under a nitrogen flow of 50 mL.min^{-1} , where one run is considered to be a warm-up followed by a cool-down.

Single-screw extrusion and characterization of the mixture from Step 1

The PET_v was dried in a Marconi oven, model MA 035/5 (Brazil), at a temperature of 80 °C for 5 hours before entering the single-screw extrusion process. The M-PET_v compound was produced in a single-screw extruder from Seibt Máquinas para Plásticos Ltda, model ES 35 (Brazil). The temperature profile was 228 °C in zone 1, 237 °C in zone 2, 245 °C in zone 3, and 192 °C in the matrix. The mixture was taken in an open matrix for grinding process in a Primotecnica knife mill, model 1001, with a screen size of 10 mm diameter at the outlet. Characterization of the M-PET_v mixture was performed by DSC, TGA and FTIR.

Twin-screw extrusion and characterization of the mixture from Step 2

The M-PET_v mixture in the form of pellets was prepared in an M.H. Plant, model MH-COR - 20-32- LAB (Brazil), with a temperature profile of 124 °C in zone 1, 200 °C in zone 2, 210 °C in zone 3, 224 °C in zone 4, 229 °C in zone 5, 240 °C in zone 6, 240 °C in zone 7, 253 °C in zone 8, 246 °C in zone 9, 261 °C in zone 10, 250 °C in zone 11, and 225 °C in zone 12, a speed of 200 rpm, and a feed rate of 100 g.min^{-1}. At the exit of the extruder, the temperature was 229 °C and was removed with the die open. The extruded material was ground in a knife mill. In this step, the PMDA and NP additives were incorporated into the PET_v and the characterization of the blends was performed by DSC, TG and FTIR.

Results and Discussion

Fig. 1 shows the FTIR of PET_v and mixtures from Steps 1 and 2.

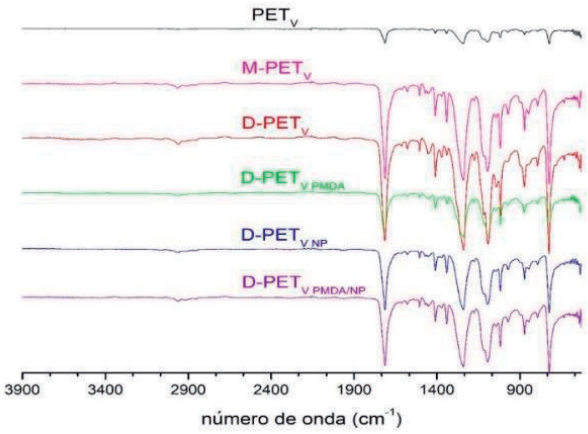

Figure 1 - FTIR of PET_v, M-PET_v and mixtures from Step 2 produced in the twin screw with and without additive.

FTIR showed the characteristic bands of PET, namely at 1240 cm^{-1} and 1114 cm^{-1} the axial deformation of the terephthalate group, at 1096 cm^{-1} and 1041 cm^{-1} the methylene group and the vibration through the ester bond. The bands at 1250 cm^{-1} and 1095 cm^{-1} correspond to the stretching of the C–O–C group by the ether groups. The band at 723 cm^{-1} indicates the occurrence of polar interactions between ester groups and aromatic rings. The absorption range between 3800 cm^{-1} and 3200 cm^{-1} is characteristic of the stretching vibrations of the O–H group of carboxylic acids and alcohols [7-9]. The band with the absorption maximum at 1720 cm^{-1} corresponds to the stretching of the bond of the carbonyl group (C=O), which may be intrinsic in the ester segments of the PET polymer chain or generated by the degradation process in the polymer chain. [8,10]. The band at 3100 cm^{-1} was attributed to the absorption of hydroxyl groups, while in the range from 2900 cm^{-1} to 2800 cm^{-1} the C–H stretching of the PET ethylene unit occurred [9].

Compared to the M-PET_v and D-PET_v samples, the use of PMDA resulted in a decrease in the intensity of the hydroxyl absorption band. According to Bimestre and Saron (2012) [11], this can be explained by the mechanism of the chain extension reaction, in which the hydroxyl group reacts with the active sites of PMDA. In this way, the hydroxyl groups are converted into other groups, such as ethers or esters, which link the PMDA molecule to the polymer chain.

In the M-PET_v and D-PET_v spectra, the formation of two new bands at 2925 cm^{-1} and 2850 cm^{-1} was evident after two PET_v extrusion processes, which could be attributed to the asymmetric and symmetric deformation of the methylene and ethylene glycols as dimers. The dimerization could be related to the possible presence of linear and cyclic oligomers formed during the hydrolytic degradation of PET. This phenomenon was also observed by Gouissem; Douibi; Benachour (2014) [7] in his study.

When evaluating the spectra in terms of degradation, it is noted that there were changes in terms of PET_v. There is a clear increase in the bands between 3000 cm^{-1} and 2850 cm^{-1} (CH_2 grouping) and an increase in the intensity of the band at 1720 cm^{-1} (carbonyl), also there is a small increase at 3400 cm^{-1}, the region of the hydroxyl group. According to Silva *et al.* (2018) [12] and Pacheco *et al*. (2021) [13], these changes in the spectra indicate PET degradation, similar events were also observed in their studies.

Incorporation of NPs did not change the spectrum compared to D-PET_v. This could be due to insufficient dispersion or poor interaction of NPs in the polymer matrix. Good dispersion of nanofillers in polymer matrices is important to obtain the desired properties. Care should also be taken when using graphene, as agglomeration and poor dispersion can occur when incorporated into the matrix [14, 15].

Fig. 2 shows the DSC curves of the samples processed in the twin screw, in addition to PET_v and M-PET_v.

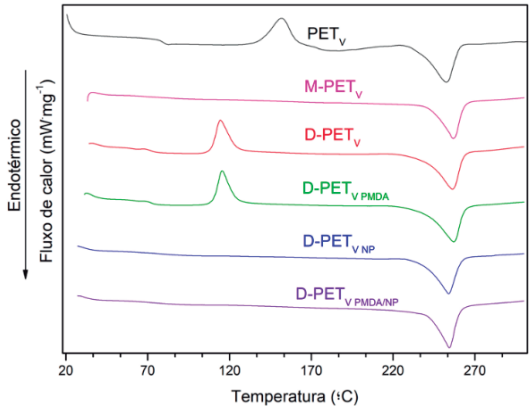

Figure 2 – DSC curves of the samples processed in the double screw in addition to PET_v and M-PET_v.

The evaluation of the PET_v curve demonstrated the occurrence of three thermal events, the first at T_g at 79.8 °C, a second exothermic event of crystallization at about 152.1 °C, due to the rapid cooling there was no time for crystallization in the cooling phase, this phenomenon is called cold crystallization. The last endothermic event, which started at about 252.5 °C, was attributed to the crystal melting temperature of the polymer, which according to the literature can range from 250 to 265 °C [16].

To evaluate the effects of the proposed processes and the use of additives, it was found that the melting temperature (T_m) had similar values among the samples. The presence of additives did not lead to changes in the thermal transitions, suggesting that the additives did not alter the processing parameters.

The T_g of the samples, evident from the DSC curves, showed lower values than the T_g of the PET_v. The decrease in T_g values was attributed to the different processes imparted to the samples, which may have triggered degradation processes, as they indicate T_g shifts to lower values. The T_g is related to the mobility of the polymer chains in the amorphous phase. When the polymer has disordered chains at low temperatures and heating occurs, the chains acquire mobility and a certain degree of freedom, which leads to a change in their heat capacity, resulting in a shift in the baseline of the DSC curve without peak values [16]. This has also been demonstrated for some samples.

Fig. 3 shows the TGA curves of the investigated samples. Two thermal events can be seen in Fig. 3, the first attributed to the degradation of the polymer chain initiated by the end groups, while the second corresponds to the degradation of the products formed during the first decomposition process [17].

Mixtures with additives did not lead to significant changes in the TGA curves, as shown in Fig. 3.

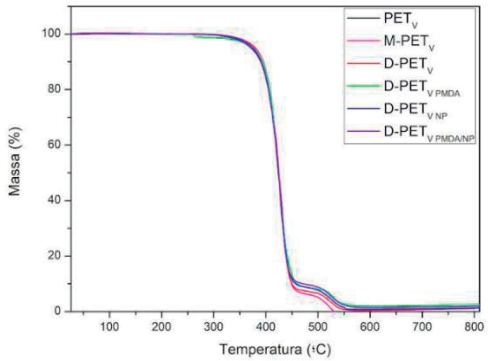

Figure 3 - TGA curves of samples processed in the twin-screw extruder in addition to PET_v and M-PET_v

Azman *et al*. (2021) [18] studied the incorporation of NPs in PET nanocomposites in the proportions of 0.1 and 0.5%. In the analysis TG the authors found an improvement in the thermal stability of the composites with NPs. This improvement was attributed to the two-dimensional planar structure of graphene, which acts as a protective layer and prevents the thermal degradation of PET. This phenomenon was not observed in this study, although the NP content used was 0.4 mass percent, which was within the limits used by the authors.

Conclusions

Compared to PET_V, the samples with one and with two screws showed the principle of degradation, which was confirmed by FTIR, DSC and TGA. The addition of additives did not improve the thermal stability of the samples studied, and FTIR showed bands related to degradation.

Acknowledgements

The authors thank Senai CETIQT, the company Znano Grafeno and the University of Caxias do Sul.

References

1. J. Fabia *et al*. Polymer 2020, 12. https://doi.org/10.3390/polym12040774.
2. F. Awaja; F. Daver. Polymer Engineering and Science 2004, 44. https://doi.org/10.1002/pen.20155.
3. S. D. Mancini; I. G. Matos; R. F. Almeida. Polímeros: Ciência e Tecnologia 2004, 14. https://doi.org/10.1590/S0104-14282004000200008.
4. M. A. S. Spinacé; M. A. De Paoli. Journal of Applied Polymer Science 2001, 80. https://doi.org/10.1002/1097-4628(20010404)80:1<20::AID-APP1069>3.0.CO;2-S.
5. A. Jiménez-Suárez, A; S. G. Prolongo. Applied Sciences 2020, 10. https://10.3390/app10051753.
6. C. Arribas *et al*. Polymer Degradation and Stability 2019, 170. https://doi.org/10.1016/j.polymdegradstab.2019.109003.
7. L. Gouissem; A. Douibi; D. Benachour. Polymer Science Series A 2014, 56. https://10.1134/S0965545X14060157.
8. J. M. M. Vidales. Construction and Building Materials 2014, 65. https://dx.doi.org/10.1016/j.conbuildmat.2014.04.114.
9. A. P. S. P. Pereira *et al*. Materials Research 2017, 20. https://doi.org/10.1590/1980-5373-MR-2017-0734.
10. Y. Chen *et al*. Polymer Composites 2020, 42. https://10.1002/pc.25814.
11. B. N. Bimestre; C. Saron. Materials Research 2012, 15. https://10.1590/S1516-14392012005000058.
12. D. D. Silva *et al*. Revista Matéria 2018, 23. https://doi.org/10.1590/S1517-707620170001.0320.
13. J. A. L. Pacheco *et al*. Brazilian Journal of Development 2021, 7. https://10.34117/bjdv7n2-509.
14. R. R. R. Cecci *et al*. Journal of Materials Science and Engineering B 10 2020, 3. https://10.17265/2161-6221/2020.3-4.002.
15. E. Nilson *et al*. Journal Applied Polymer Science 2013, 130. https://doi.org/10.1002/app.39480.
16. G. Bannach *et al*. Química Nova 2011, 34. https://doi.org/10.1590/S0100-40422011001000016.
17. R. R. Chowreddy; K. Nord-Varhaug; F. Rapp. Journal of Materials Science 2018, 53. https://doi.org/10.1007/s10853-018-2014-0.
18. N. F. I. Azman. Journal of Nanomaterials 2021, 2021. https://doi.org/10.1155/2021/6633604.

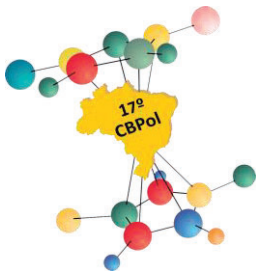

EVALUATION OF THE INFLUENCE OF NANOPARTICLE ADDITIVES ON THE MECHANICAL PROPERTIES OF EPOXY ADHESIVES

Elton J. Sehnem[1], Rafael Beck[1], Daniela Becker[1] and Ricardo De Medeiros[1]*

1 – Department of Mechanical Engineering, Santa Catarina State University (UDESC), Joinville, SC, Brazil
ricardo.medeiros@udesc.br

Abstract - This paper presents an analysis of the effect of nanoparticles on the mechanical properties of epoxy adhesives, aiming to enhance their strength and stiffness. Two types of nanoparticles, namely carbon black and carbon nanotubes, are investigated. The nanoparticles were incorporated into the pure adhesive resin matrix at a mass concentration of 1%. Tensile tests were conducted on the specimens following the ASTM D638 standard. Transmission electron microscopy (TEM) was employed to examine the formation of clusters. The results demonstrate that the addition of nanoparticles generally leads to a reduction in the stiffness of the epoxy resin. The use of carbon nanotubes exhibits a lower level of dispersion in the resulting curves compared to carbon black. These findings offer valuable insights into the influence of nanoparticles on the mechanical behaviour of epoxy adhesives. This research contributes to the understanding of how nanoparticles can effectively enhance the mechanical properties of epoxy adhesives, enabling improved performance and reliability in various composite bonded joints, including the Double Cantilever Beam (DCB), Single Lap Joint (SLJ), and End Notched Fracture (ENF) standard tests. Finally, it was discussed the potential and limitations of nanoparticles in adhesive engineering and advancing the field of nanocomposite adhesives.

Fundings: The authors acknowledge the financial support of the Santa Catarina State Research and Innovation Funding Agency (FAPESC grant: 2017TR1747, and 2021TR843). As well as, Coordination for the Improvement of the Higher-Level Personnel (CAPES Finance Code 001). Ricardo De Medeiros acknowledges the financial support of the National Council for Scientific and Technological Development (CNPq process number: 304795/2022-4).

Keywords: *Nanoparticles, Mechanical properties, Epoxy adhesives, Composite bonded joints, Carbon nanotubes.*

Introduction

In industries where component weight plays a crucial hole, such as aeronautics and aerospace, there is an increasing focus on analysing and developing materials that meet the specific requirements while offering a high strength-to-weight ratio [1]. Fibre-reinforced composite materials have emerged as a highly promising alternative capable of replacing traditional material in complex and advanced applications. For example, the Boeing 787 commercial plane utilizes carbon fibre composites for 50% of its structure, resulting in a 20% reduction in fuel consumption compared to similar-size aircraft. Additionally, this application extends the maintenance interval for the fuselage from 6 to 12 years [2]. The growing use of composite materials has led to greater geometric and dimensional complexity in component manufacturing, often requiring the integration of multiple parts to form a cohesive structure. The joining process for composites differs from the methods employed with metallic materials, such as welding or riveting. Post-manufacturing riveting, for example, can lead to fibre breakage and initiate delamination, thereby compromising the strength of the material in the fastening region. An alternative approach that overcome these issues is adhesive bonding. This method involves applying a polymeric material between the composite parts, which,

upon solidification, promotes adhesion between the parts and ensures a more uniform stress distribution within the joint region [3,4].

In recent years, there has been growing interest in incorporating nanoparticles into adhesives to enhance their mechanical characteristics. Nanoparticles are particles with at least one dimension smaller than 100 nanometres, possessing distinct physical and chemical properties compared to their large counterparts [5,6]. The addition of nanoparticles in adhesives facilitates tailoring their properties to fulfil specific requirements, such as increased strength, stiffness, toughness, and durability. However, the ultimate response of the material depends on several factors, including nanoparticle type, size, morphology, and others [7]. However, a crucial factor to consider is the proper dispersion of nanoparticles within the epoxy matrix. This aspect was demonstrated in [8], where silica nanoparticles were integrated into an epoxy resin for coating applications. In [9,10], the addition of graphene in small proportions resulted in a significant increase of up to 31% in the modulus of elasticity and a 41% increase in the maximum stress of the epoxy resin. Similarly, the inclusion of carbon nanotubes led to approximately 3% and 14% respective increase in these properties. Furthermore, there was a 53% increase in fracture energy in mode I for samples with graphene and a 20% increase for samples with carbon nanotubes. In both cases, particular attention was paid to the process of mixing the nanoparticles into epoxy matrix, employing solution processes, ultrasonic agitation, and shear mixing. This is essential because agglomerates of nanoparticles act as stress concentrators, promoting the crack propagation and reducing the tensile strength of the material. These cracks tend to follow the path of least resistance, often aligning with the lines of the agglomerates, thereby impeding the material's ability to uniform distribute and dissipate stress. This underscores the critical significance of the chosen mixing method during the sample preparation. Nevertheless, the introduction of functionalized graphene resulted in only marginal improvements in the mechanical properties, which was due to loss of cross-links between the nanoparticle and the adhesive. Regrettably, this led to an increased brittleness of the material in both instances [11].

Considering the aforementioned aspects, this study aims to investigate the influence of nanoparticles on the mechanical properties of epoxy resin adhesive used in the manufacturing of composite bonded joints. Carbon black and carbon nanotubes were incorporated into the pure adhesive resin matrix at mass concentration of 1%. Tensile tests were conducted on the specimens following the ASTM D638 standard, with the specimens positioned in flat orientations. To analyse the observed differences in strain characteristics under uniaxial tensile load, digital image correlation (DIC) was employed. The mechanical properties were assessed through tensile testing, enabling the acquisition of stress-strain curves and extraction of elastic modulus, ultimate tensile stress, and Poisson's ratio. After the tensile test, a transmission electron microscope (TEM) was utilized to examine not only the adhesion and clusters, but also the possible failure modes. Finally, the effects of varying nanoparticle concentrations and geometries on the mechanical properties were discussed, alongside potential alterations in the adhesive efficiency of the compositions.

Experimental Analysis

To compare the pure matrix with the matrix containing nanoparticles, an experimental analysis was conducted using monotonic tensile tests. The study focused on Type I specimens (according to the ASTM D638 Standard) fabricated from pure epoxy resin and epoxy resin infused with carbon black and carbon nanotubes. The resin matrix chosen was epoxy AR-345, along with hardener AH-345, supplied by Barracuda Advanced Composites (Rio de Janeiro, Brazil). The epoxy resin and catalyst were thoroughly mixed, and once a uniform mass was achieved, it was carefully introduced into the silicone moulds. The test specimens were allowed to cure for a minimum of 24 hours before undergoing testing. The study involved incorporating a nanoparticle addition of 1% by mass. The crosshead velocity, as recommended by ASTM D638, was set to 2 mm/min. The elongation and Poisson ratio were obtained by monitoring transversal and longitudinal displacements using a DIC

Dantec Q-400 apparatus. DIC enables a comprehensive understanding of the strain field across the entire specimen surface. Based on the stress versus strain curve, it is possible to determine the Modulus of Elasticity, ultimate tensile strength, and strain at rupture. The Modulus of Elasticity measures the material's stiffness within the linear region of the curve. The ultimate tensile strength represents the maximum load sustained by the specimen during the test, while the strain at rupture indicates the maximum strain endured by the specimen. Poisson's coefficients were obtained by correlating the data of maximum and minimum principal strains, which are mutually perpendicular. Finally, a transmission electron microscopy (TEM) analysis was conducted to examine the presence of clusters in the specimens.

Results and Discussion

The stress-strain curves for the pure, carbon black, and carbon nanotubes specimens are shown in the Fig 1. It is evident from the graph that the incorporation of carbon black and carbon nanotubes led to a decrease in the stiffness of the specimens, as evidenced by the lower modulus of elasticity compared to the specimens made by pure resin. The reduction amounted to approximately 12% for the specimens containing carbon black and 18.4% for those incorporating carbon nanotubes. Table 1 present the properties obtained from the stress versus strain curves.

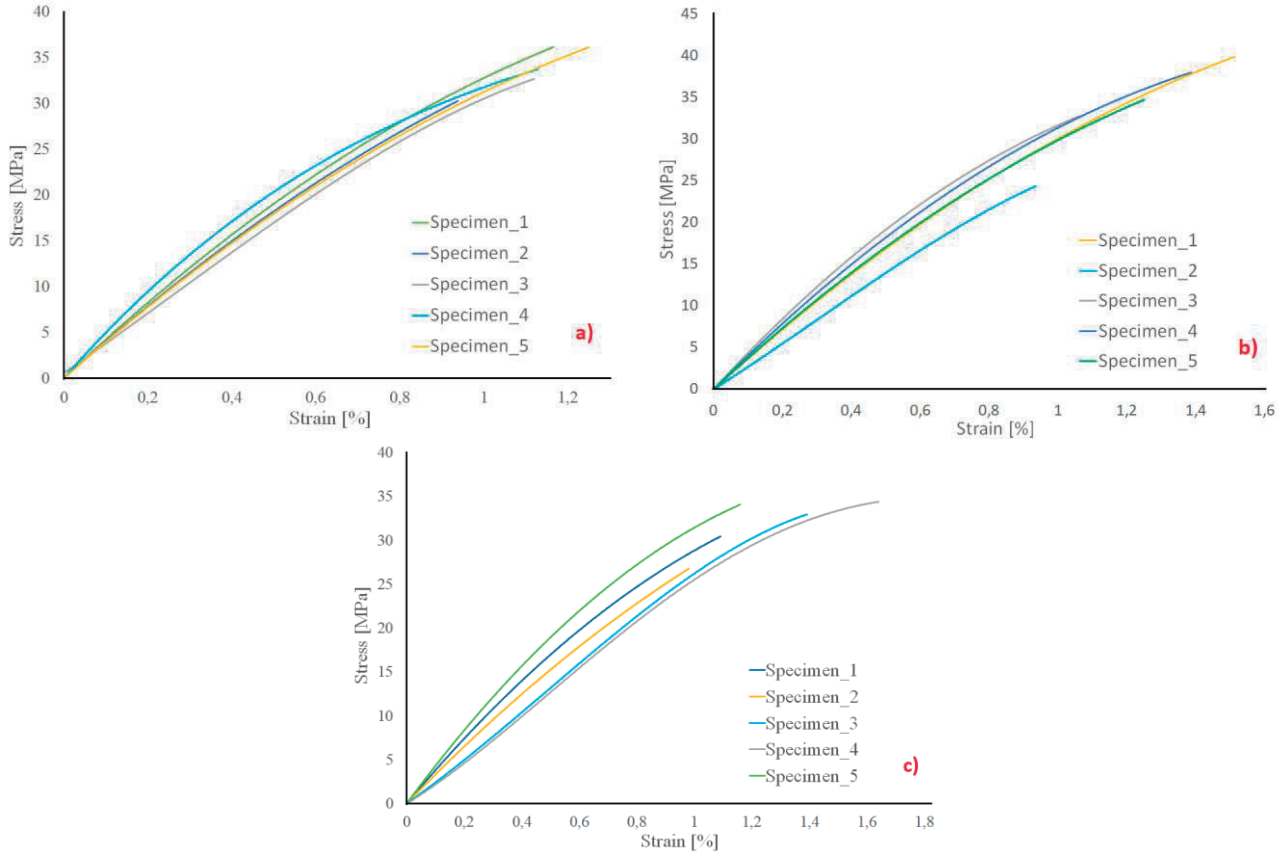

Figure 1 –Stress-strain curves. Pure Resin (a), Resin-Carbon Black (b) and Resin-Carbon Nanotubes (c)

Table 1 – Mechanical properties – mean values.

Specimen	Elastic Modulus [MPa]	Maximum Stress [MPa]	Poisson's Ratio
Pure Resin	3,844.0±273.8	34.1±2.6	0.351±0.094
Resin-Carbon Black	3,384.9±381.5	33.6±5.7	0.368±0.072
Resin-Carbon Nanotubes	3,134.4±534.5	31.9±3.4	0.361±0.104

One possible explanation for this decrease in stiffness can be attributed to the manual mixing of the nanoparticles, which may have led to the formation of random clusters of nanoparticles in certain regions and internal voids within the epoxy resin matrix, as highlighted in red in Fig 2, which the presence of these clusters is clearly visible. In this context, the internal voids within the epoxy resin matrix can weaken the material's cross-section against external forces, while the random clusters of nanoparticles can act as stress concentrators, promoting the initiation of internal fractures in those specific areas.

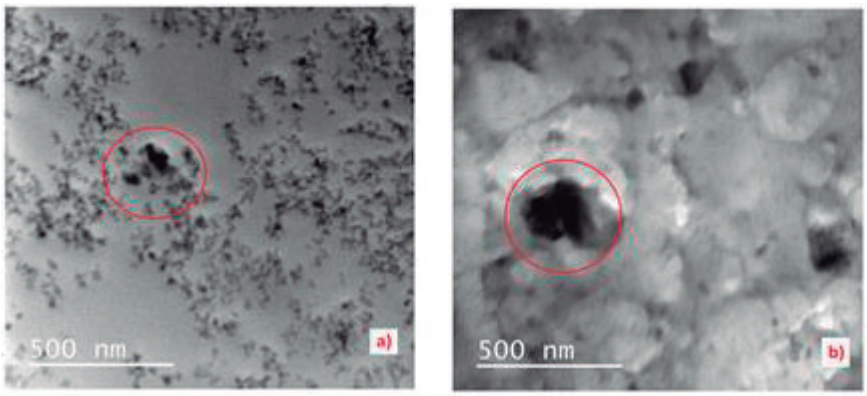

Figure 2: Carbon black clusters (a) and Carbon nanotubes clusters (b).

The decrease in the modulus of elasticity was accompanied by an increase in its dispersion, as indicated by the standard deviation values. Table 1 clearly demonstrates that the dispersion increased for the resin samples loaded with carbon black, and this dispersion was further amplified in the epoxy resin samples incorporating carbon nanotubes. The proposed hypothesis for the increase in dispersion is based on the manual mixing process, which tends to create voids and randomly distributed nanoparticle concentrations within the epoxy resin matrix. In the case of the pure resin, the dispersion was attributed specifically to limitations in the manual moulding process used to manufacture the test specimens. To address this issue, future efforts will focus on increasing the number of specimens and improving the moulding technique.

Regarding mechanical strength, the results suggest a slight reduction. This finding aligns with existing literature indicating a decrease in mechanical strength associated with the addition of nanoparticles to pure epoxy resin. Furthermore, this decrease is accompanied by an increased dispersion in the maximum resistance values. However, when comparing the dispersion of values between the samples containing carbon nanotubes and those containing carbon black, it is observed that the dispersion in the samples with carbon nanotubes was lower. This could be attributed to the more regular morphology and uniform size of carbon nanotubes compared to carbon black. Finally, the results for the Poisson coefficient indicate that the presence of nanoparticles induces an increase in the relationship between longitudinal and transverse strain in the samples. However, the dispersion of values for this property remained consistent, regardless of whether the sample contained nanoparticles or not. These preliminary findings still require a more comprehensive evaluation, including an increased number of samples and a detailed study of the matrix and nanoparticle agglomerates.

Conclusions

The preliminary results demonstrate that the incorporation of nanoparticles leads to a reduction in the stiffness of the adhesive epoxy resin. This decreases in stiffness is accompanied by an increase in the dispersion of the elasticity modulus, which may be attributed to the manual manufacture process. The manual mixing of nanoparticles within the epoxy resin matrix during this procedure can result in the formation of voids and clusters, thus diminishing the strength in localized regions.

Moreover, the results indicate a decrease in the maximum stress value, along with an increased dispersion in the samples incorporating nanoparticles. However, when comparing the dispersion between samples containing carbon nanotubes and carbon black, it is evident that the samples with carbon black exhibit greater dispersion. This difference can be attributed to the more irregular morphology and size of carbon black in comparison to carbon nanotubes. Additionally, the results concerning the Poisson's coefficients reveal that the addition of nanoparticles to the epoxy resin enhances the correlation between longitudinal and transverse deformations of the samples, while maintaining an equivalent standard deviation of the Poisson's coefficient values across the three tested materials. Nevertheless, further tests will expand the number of specimens an provide a more comprehensive insight. Also, exploring mechanized nanoparticle mixing methods and investigating the hypotheses regarding void formation in the resin matrix and the formation of random clusters will contribute to a deeper understanding of the impact of nanoparticles on the mechanical properties of epoxy resin-based adhesives.

References

1. McIlhagger A, Archer E, McIlhagger R 2020, 3. Processos de fabricação de materiais compósitos e componentes para aplicações aeroespaciais, pp59–81.
2. Engenharia FEG. Aplicação de Fibra de Carbono na Indústria Aeronáutica. http://engenhariafeg.com.br/2011/seminarios/a2/a2.pdf.
3. Banea MD, da Silva LFM, Juntas adesivas em materiais compósitos: uma visão geral. Proc Institut Mech Eng Part LJ Mater Des Appl, 2009, 223(1):1–18
4. Jeevi G, Nayak SK, Abdul Kader M, Revisão sobre juntas adesivas e sua aplicação em estruturas compostas híbridas. J Adhesion Sci Technol 2019, 33(14):1497–1520.
5. Kreuter, Jörg. Nanoparticles—a historical perspective. International journal of pharmaceutics, v. 331, n. 1, p. 1-10, 2007. doi:10.1016/j.ijpharm.2006.10.021
6. Santos, Cátia SC et al. Industrial applications of nanoparticles–a prospective overview. Materials Today: Proceedings, v. 2, n. 1, p. 456-465, 2015. doi:10.1016/j.matpr.2015.04.056
7. Eslami-Farsani, Reza, et al. "Recent trend in developing advanced fiber metal laminates reinforced with nanoparticles: a review study." Journal of Industrial Textiles 51.5_suppl (2022): 7374S-7408S. DOI: 10.1177/1528083720947106
8. Allahverdi, Ali, et al. "The effect of nanosilica on mechanical, thermal and morphological properties of epoxy coating." Progress in Organic Coatings 75.4 (2012): 543-548.
9. Rafiee, Mohammad A., et al. "Enhanced mechanical properties of nanocomposites at low graphene content." ACS nano 3.12 (2009): 3884-3890.
10. Singh, S.; Srivastava, V. K.; Prakash, R. Mater Sci Tech**.** v. 29, p. 1130-1134, 2013.
11. Ejaz, Hassan, et al. "Effect of functionalised and non-functionalised GNPs addition on strength properties of high viscous epoxy adhesive and lap shear joints." Polymer Testing 113 (2022): 107680. https://doi.org/10.1016/j.polymertesting.2022.107680.

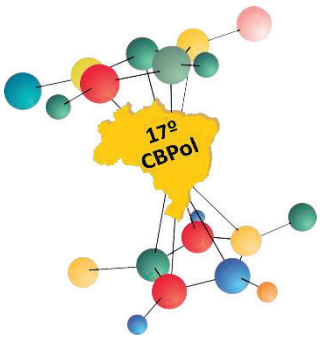

EVALUATION OF THERMAL, RHEOLOGICAL AND MECHANICAL PROPERTIES OF POLYPROPYLENE COMPOSITES AND GRAPHENE NANOPLATELETS WITH DIFFERENT NUMBER OF LAYERS

Giovani B. Berti[1], Diego Piazza[1,2], Bruna F. Bortoli[3], Gabriel G. de Lima[3], Monique C.R. de Camargo[3], Rodrigo D. O. Polkowski[3], Ricardo F. C. de Albuquerque[3], Rosmary N. Brandalise[1*]

1 – Graduate Program in Process and Technology Engineering (PGPROTEC), University of Caxias do Sul (UCS), Caxias do Sul, RS, Brazil

2 – UCSGraphene, Universidade de Caxias do Sul, RS, Brazil

3 – Ford Motor Company, Camaçari, BA, Brazil

*rnbranda@ucs.br

Abstract – In this work, the use of graphene nanoplatelets (GNP) as nanofillers was investigated to improve the properties of commercially available polymer materials, especially polypropylene (PP). Two types of GNP (20 and 40 layers on average) were evaluated in the production of composites, which were added to PP at a mass content of 0.125% by a twin-screw extrusion process and molded by injection molding. The thermal, mechanical and rheological properties were analyzed using techniques such as thermogravimetry (TG), differential scanning calorimetry (DSC), thermal deflection temperature analysis (HDT), flow index (MI), impact strength, tensile and flexural stress. The results show that the different GNP sizes showed different responses to the analyzed properties. Regarding PP, an improvement in the properties of the composite was observed with GNP with an average of 20 layers, such as tensile strength, which increased by 7.1%, 12% of elastic modulus in tension, 7.5% in HDT, 2.2% in MI and increased crystallinity. The GNP sample with 40 layers of media showed improvements of 4.9% in HDT, 13.3% in melt index, and increased crystallinity. Samples with 20-layer nanoplates showed improvements in tensile strength, tensile elastic modulus, HDT, and increased crystallinity compared to samples with 40-layer nanoplates. Samples with 40-layer nanoplatelets showed higher MI and impact strength compared to samples with 20-layer nanoplatelets.

Keywords: *graphene nanoplatelets, polypropylene, nanocomposites.*

Fundings: Conselho Nacional de Desenvolvimento Científico e Tecnológico (CNPq), Ford Motor Company Brasil, Universidade de Caxias do Sul (UCS)

Introduction

Polymers play an important role in today's society because they are an economical and easy-to-process option compared to other materials, such as metals. Nevertheless, their physical properties limit their use in some applications. Reinforcing polymers with fillers of different sizes makes it possible to overcome these limitations and expand their applications [1,2].

The use of graphene and its derivatives such as graphene nanoplatelets (GNPs) is being investigated in composite materials. In particular, GNPs are the subject of research due to their electrical conductivity, large specific surface area, and robust mechanical properties, as well as ease and cost of fabrication and processing compared to other graphene variants [3,4].

Due to the fast and economical process, the melt-mixing process is an industrially useful technique for the production of thermoplastic-based nanocomposites. This has significant implications for the decoupling of the polymer chains in the molten state, allowing the polymer chains to move freely and mix with the discontinuous phase of the composite. The polymer nanocomposites prepared by mixing by extrusion (twin screw) exhibit satisfactory dispersion of the fillers and are suitable for nanocomposites with low weight fractions of nanofillers (below 9.2% w/w) [1,2].

In this context, two different types of graphene nanoplatelets (with different average number of layers) are incorporated and evaluated in polypropylene matrices in this work, with the aim of obtaining composites with improved properties compared to conventional polymer matrices.

Experimental

Materials and manufacturing

Polypropylene copolymer CP 442XP supplied by Braskem® (density 0.895 g.cm^{-3} and melt flow index (MFI) 6.0 g.10 min^{-1}. Nanoplatelets UGZ-1004 supplied by UCSGraphene® (20 GNP layers, specific surface area 26.09 m^2.g^{-1} and carbon mass > 95%) Nanoplatelets UGZ-1001 supplied by UCSGraphene® (40 GNP layers, specific surface area 11.25 m^2.g^{-1} and carbon mass > 90%).

The PP/GNP composites were prepared as indicated in Table 1 in an interpenetrating co-rotating twin screw extruder model MH-COR -20-32- LAB (MH Equipamentos). The extruder was operated at a speed of 200 rpm and a temperature profile of 160 to 190°C. The material was then pelletized and injected into test samples using a LH 150-80 (Himaco) injection molding machine at a temperature profile of 170 to 190°C. Table 1 describes the samples and their respective formulations.

Table 1. Composition and coding of nanocomposites

Sample	PP (% weight)	GNP 20 (% weight)	GNP 40 (% weight)
PP/GNP0	99.875	0.0	0.0
PP/GNP20	99.875	0.125	0.0
PP/GNP40	99.875	0.0	0.125

Characterization Methods

Prior to testing, samples were stored at 23°C and 50% relative humidity for 48 hours.

Thermogravimetry (TG) evaluation was performed in the TGA-50 apparatus (Shimadzu) according to the ASTM E1131-20 standard, with heating from 23 to 800°C and a heating rate of 10°C.min^{-1} in nitrogen atmosphere.

For differential scanning calorimetry (DSC) analyses, the ASTM D3418-21 standard was used, with a DSC50 model (Shimadzu) with an N_2 flow of 50 mL.min^{-1} and a heating rate of 10°C.min^{-1} from 23 to 250°C. The crystallinity index of the samples was determined using Eq. 1, where $\Delta Hf_{100\%}$ is the enthalpy of fusion of 100% crystalline PP, which corresponds to 209 J.g^{-1} [5], and ΔHf is the enthalpy of fusion of the standardized polymer relative to its content in the mixture in J.g^{-1}.

$$Xc = \left(\frac{\Delta Hf}{\Delta Hf\ 100\%}\right) x\ 100\% \qquad (1)$$

The heat deflection temperature (HDT) was evaluated according to ASTM D468-18 up to a deflection of 0.25 mm and a load of 1.8 MPa. The instrument used is the VICAT model (CEAST). Three samples of each sample were examined. The melt flow index (MFI) was determined according to procedure A of ASTM D1238-20 in a plastomer with balance, model AS200 (Dynisco).

The flexural strength tests were carried out according to the ASTM D790-17 standard with a load cell of 2000 kgf and a speed of 50 mm.min^{-1}. Five specimens of each sample were examined. Tensile strength tests were performed according to ASTM D638-14 standard with a speed of 50 mm.min^{-1} and a carding cell of 2000 kgf in the equipment already mentioned. Five specimens of each sample were evaluated. Both tests were performed in a DL200 (Emic) type equipment.

Based on the ASTM D256-10 standard, the impact tests were performed with IZOD notch in a CEAST device with a 4 J pendulum at a speed of 3.46 m.s^{-1}. For each sample, 10 specimens were tested.

Results and Discussion

Fig. 1(a) illustrates the results of the thermogravimetric curves. It was found that the maximum degradation temperatures for the samples PP/GNP0, PP/GNP20 and PP/GNP40 were 465.0, 447.5 and 469.2 °C, respectively. Compared to sample PP/GNP0, sample PP/GNP20 showed a decrease in maximum degradation temperature by 21.7 °C, while sample PP/GNP40 showed an increase in maximum degradation temperature by 3.3 °C.

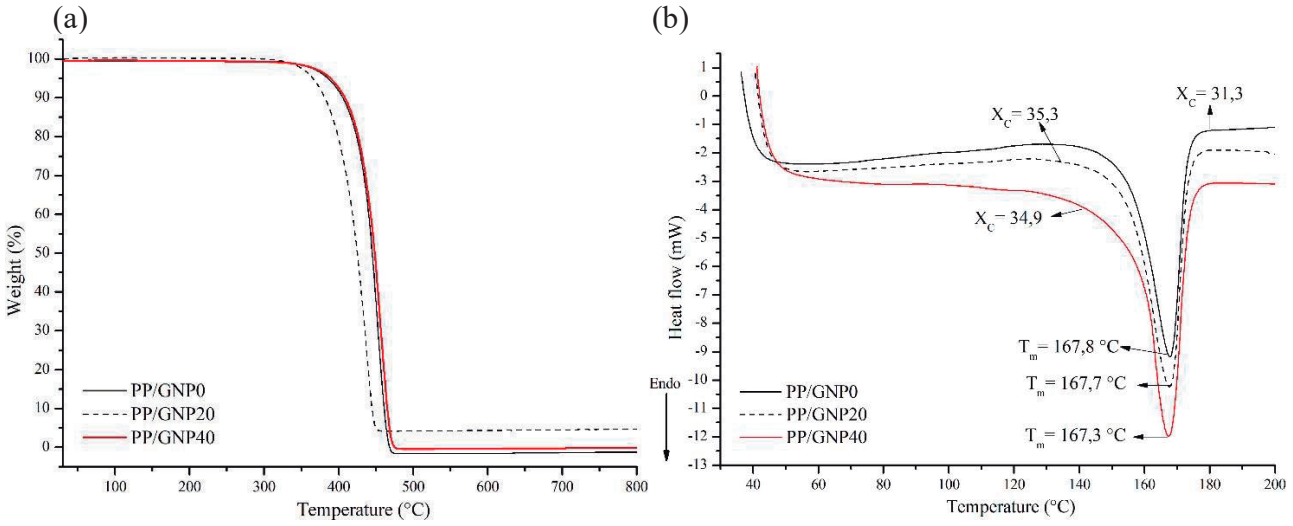

(c)

Sample	HDT (°C)	MI (g.10min^{-1})
PP/GNP0	49,3±0,9	4,5±0,1
PP/GNP20	53,0±1,0	4,6±0,1
PP/GNP40	51,7±0,6	5,1±0,1

Figure 1. (a) TG curve, (b) DSC, (c) HDT and MI of the samples PP/GNP, PP/NP20 and PP/GNP40.

From the DSC analyzes shown in Fig. 1(b), the samples were found to have no changes in melting temperatures (T_m), with 167.8 °C, 167.7 °C, and 167.3 °C for samples PP/GNP0, PP/GNP 20, and PP/GNP40, respectively. However, the crystallinity index showed an increase compared to the sample PP/GNP0. Samples with GNP showed a wider melting event compared to PP/GNP0, which can be attributed to the fact that the GNP surface affects the formation and different sizes of PP crystals [2,6].

The HDT and MI results of the composites are shown in Fig. 1(c). It was observed that the flowability increased with the use of nanoplatelets, as did the HDT. This increase is related to the high inherent stiffness of the nanoplatelets, their dispersion between the polymer chains, and the interfacial interaction between the GNP and the PP matrix. It is important to point out that the GNP type used in the PP/GNP20 sample has a specific surface area of 26.09 $m^2.g^{-1}$, while the PP/GNP40 sample has a specific surface area of 11.25 $m^2.g^{-1}$, which favors the matrix/GNP interaction.

As for the results of MI analyzes, as expected, it was confirmed that the incorporation of GNP into the nanocomposite decreases its flow resistance and increases the MI value. For GNP with 40 layers and smaller specific surface area, its activity as a processing aid is more evident [6-8].

The results of tensile strength and elastic modulus under stress are shown in Fig. 2(a).

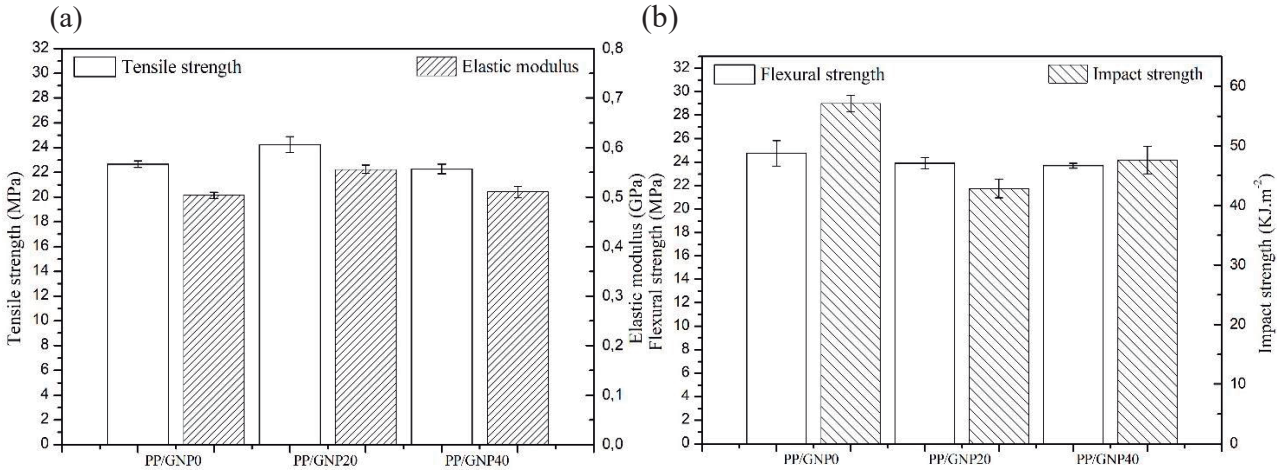

Figure 2. (a) Tensile strength and (b) flexural and impact strength of the study samples.

It was found that the tensile strength values for samples GNP0, GNP20, and GNP40 were 22.6 MPa, 24.2 MPa, and 22.3 MPa, respectively. This pattern was also observed in the tensile modulus, which was 0.50 GPa, 0.56 GPa, and 0.51 GPa, respectively. The 7.1% increase in tensile strength and 12.0% increase in elastic modulus for the GNP20 sample compared to PP/GNP0 is related to the interaction between the filler and the matrix and the specific surface area of this nano loading. While for the PP/GNP40 sample, the 1.3% decrease in tensile strength and 2.0% increase in elastic modulus compared to PP/GNP0 is due to the type of GNP used, whose specific surface area is smaller compared to GNP20, the interaction between the filler and the PP matrix was reduced [3,9].

The results of flexural strength and impact strength are shown in Fig. 2(b). It was found that the flexural strength did not differ among the samples and was 24.7 MPa, 23.9 MPa and 23.7 MPa for GNP0, GNP20 and GNP40, respectively. On the other hand, the impact strength values were 57.1, 42.84 and 47.58 KJ.m^{-2} for GNP0, GNP20 and GNP40, respectively, which may be inversely related to the stiffness of the materials. This result suggests that the better interaction between the load and the matrix reduces the absorption and dispersion of the impact energy. Thus, the sample containing GNP with an average of 20 layers showed better interaction with the continuous phase, which is related to its larger specific surface area while occupying less space, than the sample containing GNP with an average of 40 layers [3,9].

Conclusions

In this work, differences in properties were presented when graphene nanoparticles with an average of 20 and 40 layers were incorporated into PP. As for the thermal properties, the crystalline melting temperature did not change, but the shape of the melting process changed with the GNP, as well as the crystallinity index was higher for the PP/GNP20 sample. The thermal bending temperature and melting index increased with the incorporation of GNP. The incorporation of GNP with 20 layers was more efficient for the tensile strength, the same was observed for the modulus of elasticity, while the impact strength decreased.

Acknowledgements

National Council for Scientific and Technological Development (CNPq), Ford Motor Company Brazil, University of Caxias do Sul (UCS).

References

1. S. J. Lee; S. J. Yoon; I. Y. Jeon Polymer 2022, 14, 4733. https://doi.org/10.3390/polym14214733.
2. S. Fu; Z. Sun; P. Huang; Y. Li; N. Hu Nano Materials Science 2019, 1, 1. https://doi.org/10.1016/j.nanoms.2019.02.006.

3. K. Bilisik; M. Akter; Journal of Industrial Textiles 2022, 51, 3. https://doi.org/10.1177/15280837211024252.
4. K. Yee; M. H. Ghayesh International Journal of Engineering Science 2023, 186, 103831. https://doi.org/10.1016/j.ijengsci.2023.103831.
5. H. Barangizi; A. Pawlak; Polymers 2022, 254, 125049. https://doi.org/10.1016/j.polymer.2022.125049.
6. X. Zhao; D. Huang; C. M. Ewulonu; M. Wu; C. Wang; Y. Huang e-Polymers 2021, 21, 1. https://doi.org/10.1515/epoly-2021-0039.
7. Y. F. Zhang; X. F. Lin; H. Hu Polymers for Advanced Technologies 2020, 31, 10. https://doi.org/10.1002/pat.4950.
8. N. H. Md Said; W. W. Liu; C. S. Khe; C. W. Lai; N. N. Zulkepli; A. Aziz Polymer Composites 2021, 42, 3. https://doi.org/10.1002/pc.25922.
9. F. Wang; L. T. Drzal; Y. Qin; Z. Huang Journal of Materials Science 2015, 50. https://doi.org/10.1007/s10853-014-8665-6.

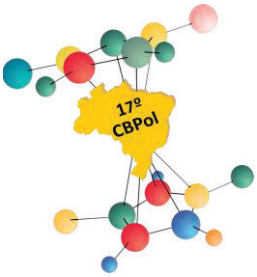

EXPLORING THE RHEOLOGICAL PROPERTIES OF WATERBORNE POLYURETHANE/CARBON QUANTUM DOTS NANOCOMPOSITES WITH PHOTOACTIVE CHARACTERISTICS

Lucas Dall Agnol[1]*, Fernanda T. G. Dias[2] and Otávio Bianchi[1,3]

1 – Postgraduate Program in Materials Science and Engineering (PGMAT), University of Caxias do Sul (UCS), Caxias do Sul, RS, Brazil
agnol.lucasdall@gmail.com and otavio.bianchi@gmail.com
2 – Department of Organic Chemistry, Institute of Chemistry, Federal University of Rio Grande do Sul (UFRGS), Porto Alegre, RS, Brazil
3 – Department of Materials Engineering (DEMAT), Federal University of Rio Grande do Sul (UFRGS), Porto Alegre, RS, Brazil

Abstract: Incorporating carbon quantum dots (CQDs) into waterborne polyurethane (WPU) can significantly impact its rheological behavior, which is crucial for optimizing its performance in applications such as surface coating. This study investigated the effect of adding 1.0 wt.% of CQDs on the rheological behavior of WPU. Oscillatory shear measurements were conducted at different temperatures (110–180 °C), and the resulting master curves revealed a shear-thinning behavior for the materials. Furthermore, both the nanocomposite containing 1.0 wt.% CQDs (WPU1) and the neat polymer (WPU0) exhibited practically identical flow activation energy (~ 80 kJ/mol), despite the higher molar mass of WPU1 due to CQDs' polyfunctionality. The slight reduction in the system's viscosity due to CQDs' presence can be attributed to the sliding effect of small particles (<10 nm) on polymer nanocomposites, seeming not to compromise its application as a functional coating.

Keywords: *waterborne polyurethane; carbon quantum dots; photoactive coating; viscosity; flow activation energy.*

Introduction

Photoluminescent materials have attracted attention for sensing due to their distinct advantages over solution-based probes, including excellent stability, ease of transport, storage, recycling, non-invasive nature, and tunable shape and size. The potential application of CQDs in developing these photoluminescent materials has already been demonstrated [1]. These materials' surface hydroxyl and carboxyl groups provide excellent solubility in water and organic solvents but hinder their deposition as thin films by conventional methods. Moreover, in environments where they are insoluble, these nanostructures lose their photoactivity in the solid-state [2]. Using a polymer matrix as support can facilitate the application of CQDs and prevent their photoluminescence loss, also providing mechanical resistance and catalytic stability to the final material. In this context, WPU emerges as an option for CQDs support due to its exceptional mechanical, chemical, and adhesion properties and low emission of organic volatiles [3]. Also, the excellent transparency of polyurethane makes it an ideal matrix for producing suitable fluorescent materials [1]. WPU is soluble in water, contributing to CQDs distribution in the matrix and preserving their photoluminescence activity. During synthesis, the polyurethane chains can be chemically linked at the surface of the embedded CQDs to form a slightly crosslinked network structure, improving nanocomposite properties [1]. It is known that the presence of CQDs can influence the rheological behavior of polymer nanocomposite. At low concentrations, the CQDs may not significantly affect WPU rheology. At higher concentrations, however, small particles can form aggregates that alter the viscosity of polymer systems. Most works and patents on WPU/CQDs mainly report the industrial applications of these systems [4, 5], without

deeply investigating the relationship between structure, rheological behavior, and coating performance of such materials under their typical service conditions [1].

Thus, the current work aims to investigate the effect of incorporating only 1.0 wt.% of CQDs on the rheological behavior of the WPU. The film's rheological investigation involved small-amplitude oscillatory shear measurements at different temperatures, determination of flux activation energy (E_a), and generation of master curves capable of predicting material's performance under particular conditions. Indeed, this information will contribute to optimizing processing conditions and designing WPU/CQDs nanocomposites with tailored properties that could be applied as functional coatings. We need to understand how the addition of CQDs can affect the nanocomposite's flow properties.

Experimental

Synthesis of CQDs: The CQDs were produced by microwave-assisted pyrolysis of an aqueous solution of citric acid (CA; 98.5% purity, Sigma Aldrich) and ethylenediamine (EDA; ≥ 99.5% purity, Sigma Aldrich) (1:1 molar ratio) according to [1]. Briefly, the mixture was first ultrasonicated for 2 min (20 MHz) and then irradiated for 6 min in a domestic microwave oven (650 W). The resulting red-brown solid was purified by dialysis in ultrapure water (MWCO membrane of 1000 Da) for 3 days. Then, the CQDs were vacuum-dried at 65 °C (reaction yield was about 78 %).

Synthesis of WPU/CQDs nanocomposites: The WPU/CQDs dispersion was initially prepared by an oil heating flask reaction of hexamethylene diisocyanate (HDI, ≥ 99% purity, Sigma Aldrich) and polycarbonate diol (PCD, 2000 g/mol; UBE Corporation Europe) for 4 h at 80 ºC under nitrogen atmosphere. Then, 2,2-bis(hydroxymethyl)propionic acid (DMPA, 98% purity, Sigma Aldrich) was incorporated into the –NCO-terminated prepolymer by reaction at 80 ºC for 2 h. Acetone was added to control the reaction medium viscosity. Subsequently, the reaction temperature was reduced to 45 ºC, and triethylamine (TEA, ≥ 99.5% purity, Sigma Aldrich) was added (~45 min) to neutralize the carboxyl groups in the prepolymer. Finally, the prepolymer was dispersed in aqueous solutions containing 1.0 wt.% CQDs under vigorous stirring (1100 rpm) for 30 min. The stoichiometric ratio of HDI/PCD/DMPA/TEA was 3:1:1:1.2. The residual solvents were removed by distillation under reduced pressure (60 ºC for 1 h). The dispersion's solids content was about 30% by weight. For characterization, WPU/CQDs films were prepared on a Teflon substrate by dispersions drying in an oven. Two samples were prepared, one without CQDs, named WPU0 and the other with 1.0 wt.% CQDs, named WPU1. This CQDs content was chosen based on the best results of [1].

Chemical structure and photoluminescence: The chemical structure, thermal and mechanical properties and photoluminescence behavior of WPU/CQDs nanocomposite was shown and discussed in detail in Dall Agnol *et al*. [1]. Here, only the main findings will be punctuated, whose information is relevant to understanding the rheological data of these materials.

Rheological behavior: All rheological measurements were performed on the materials films obtained after water evaporation (0.5 mm thickness) in an Anton Paar MCR 101 rheometer (parallel plates geometry, 25 mm diameter, 0.5 mm gap) under a nitrogen atmosphere. Small-amplitude oscillatory shear measurements were evaluated at 100–180 °C, using angular frequency sweep mode (0.1–500 rad/s) and strain amplitude of 1% (linear viscoelastic regime). The zero-shear viscosity (η_0) was calculated by fitting the complex viscosity (η^*) *vs.* angular frequency (ω) data to the Cross model [1]. After fitting the η^* *vs.* ω experimental data, the flux activation energy was calculated using the Arrhenius equation (Equation 1). This equation is a phenomenological model that relates the reaction rate's temperature dependence to the reaction's activation energy (*Ea*). It can be expressed as:

$$\eta_0^* = A.e^{-\frac{E_\alpha}{RT}} \quad (1)$$

where η_0^* is the zero shear/frequency viscosity obtained by Cross model fit, A is the pre-exponential factor, E_a is the activation energy, R is the gas constant, T is the absolute temperature, and e is the exponential function. By taking the logarithm of the expression and plotting $ln(\eta_0^*)$ *vs*. $1/T$, the E_a can be determined from the slope of the resulting straight line. In this case, the Arrhenius equation was

used to calculate the flux activation energy, which measures the energy required for the flow of the molten WPU/CQDs nanocomposite. From carrying out the rheological experiments at various temperatures, it was possible to generate a set of master curves based on the relationship between experimental data and a particular reference temperature. Master curves allow the prediction of material behavior under temperatures different from those tested, enabling a better understanding of material performance in a variety of conditions:

$$\eta^*(\omega, T, p) = \eta_0^{**}[1 + A_1(\eta_0^*\omega)^{\alpha} + A_2(\eta_0^*\omega)^{2\alpha}]^{-1} \quad (2)$$

where, A_1, A_2 and α are fitted parameters. In this case η_0^{**} is the value of the zero shear/frequency viscosity obtained by the master curve.

Results and Discussion

The CQDs as-synthesized presented carboxyl, hydroxyl, and amino surface groups capable of interacting strongly with the flexible and rigid segments of WPU, which has been characterized in [1, 2]. This work investigated the effect of incorporating CQDs on the molten state rheological properties of WPU. Fig. 1 shows the dependence of η^* as a function of ω for WPU0 and WPU1. Complex viscosity (η^*) decreases with the addition of CQDs, especially at low frequencies, which may be related to the lubrication caused by nanoparticles [6]. Table 1 shows the rheological parameters obtained by fitting Cross's equation to the experimental data. The viscoelastic behavior of WPU0 and WPU1 was pseudoplastic, as evidenced by a decrease in viscosity with increasing oscillation frequency. The Cross-model adjustments yielded correlation coefficients above 0.9. The incorporation of CQDs caused a reduction in the λ values. A high λ value indicates that a relatively high oscillatory shear is required to cause structural failure. In contrast, a low λ value corresponds to a weaker structure that can be disrupted at lower shear rates (frequencies). Consequently, the Newtonian plateau transition occurs at lower frequencies due to the increased viscous dissipation induced by CQDs.

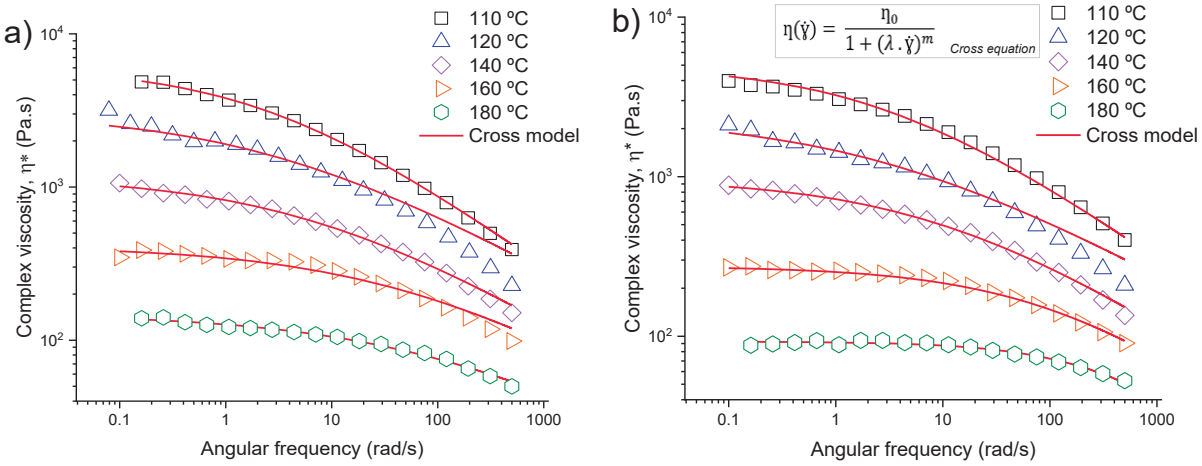

Figure 1 – Dependence of complex viscosity (η^*) as a function of angular frequency (ω) for (a) WPU0 and (b) WPU1

Table 1 – Rheological parameters obtained by fitting the Cross equation for WPU0 and WPU1

Sample	T (ºC)	η_0^* (Pa.s)	λ (s)	m	R^2	Sample	T (ºC)	η_0^* (Pa.s)	λ (s)	m	R^2
WPU0	110	6120	0.370	0.49	0.9988	WPU1	110	4491	0.300	0.48	0.9992
	120	3661	0.300	0.40	0.9799		120	2630	0.300	0.38	0.9788
	140	1178	0.140	0.42	0.9955		140	975	0.090	0.43	0.9982
	160	411	0.018	0.40	0.9888		160	271	0.007	0.50	0.9906
	180	148	0.009	0.37	0.9886		180	93	0.001	0.66	0.9648

η_0^*: complex viscosity at zero frequency; λ: time-dependent parameter associated with the transition from the Newtonian *plateau*; m: dimensionless (m → 1 = pseudoplastic behavior, m → 0 = Newtonian fluid behavior); R^2: correlation coefficient.

As expected, the η_0^* values decreased with increasing temperature for both WPU0 and WPU1 systems. However, the WPU1 system exhibited lower viscosities than neat WPU0, despite having a higher molar mass according to SEC data (M_n, WPU0 = 26,476 g/mol and WPU1 = 27,066 g/mol, polydispersion ~2 for both [1]). This could be attributed to the sliding effect caused by the CQD particles, which can favor the polymer chains' flow and reduce the system's overall viscosity. The flux activation energy was estimated using Eq. 1 (Fig. 2).

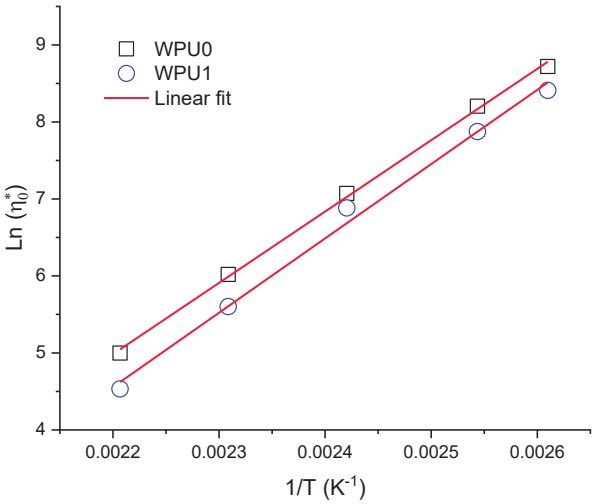

Figure 2 – Linear fit slope of $ln(\eta_0^*)$ *vs.* $1/T$ data for *Ea* determination

The WPU0 exhibited a flux E_a of 77 kJ/mol, whereas the addition of CQDs led to a slightly higher value of 80 kJ/mol for WPU1. This result was unexpected, considering that SEC analyses showed an increase in the molar mass of the system with CQDs. However, the polyfunctionality of the CQDs had a negligible effect on the flow activation condition. This phenomenon could be attributed to the small size of the particles, which could cause a reduction in viscosity as previously reported by [1, 6]. In conclusion, CQDs did not significantly affect the flux *Ea*, despite the larger molar mass of WPU1. Fig. 3 (a) and (b) schematically illustrate the master curve derived from η^* data that depends on oscillatory shear (WPU0 and WPU1). To obtain a dimensionless number, $log\ \eta/\eta_0$, viscosity is divided by viscosity at zero shear or frequency. Parameter $log\ \eta/\eta_0$ approaches zero when the viscosity is shear-independent (Newtonian plateau) and becomes negative in the shear-thinning region.

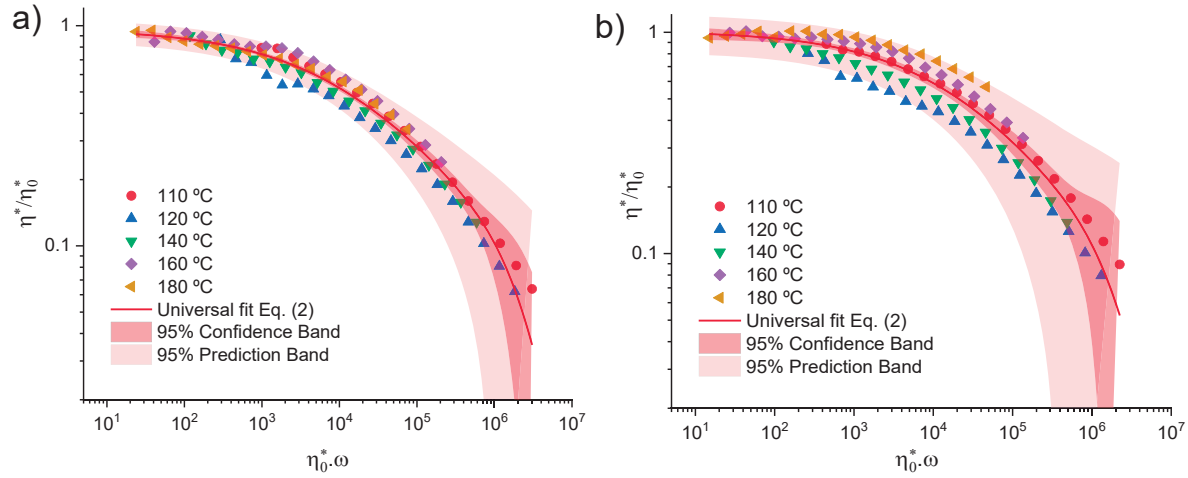

Figure 3 –Master curve from η^* data for a) WPU0 and b) WPU1

Regarding the master curve adjustment, both samples showed a smaller dispersion of experimental points at lower frequencies. The parameters of Eq. 2 were adjusted with R^2 greater than 0.9 for both samples. The following parameters were obtained for WPU0 ($A_1 = 0.013$, $A_2 = 3.54 \times 10^{-12}$, $\alpha = 0.45$, and $\eta_0 = 0.96$) and WPU1 ($A_1 = 0.008$, $A_2 = 3.58 \times 10^{-12}$, $\alpha = 0.47$, and $\eta_0 = 1.01$). Assuming that $\alpha =$

1-*n*, where *n* is the power index, it can be inferred that both systems exhibit a shear-thinning behavior. However, the sliding effect caused by the small particles alters the transition region of the Newtonian plateau for the polymeric chain [6].

Conclusions

Here, we explored the effect of photoluminescent CQDs on the rheological behavior of a waterborne polyurethane nanocomposite synthesized by *in situ* polymerization. The WPU1 nanocomposite (containing 1 wt.% CQDs) and the neat polymer showed the same flux activation energy (E_a). Furthermore, a master viscosity function was obtained, indicating a shear-thinning behavior for WPU0 and WPU1. Interestingly, the addition of small particles such as CQDs (<10 nm [1]) leads to a reduction in the polymer nanocomposite viscosity despite the increase detected in its molar mass. Other studies also observed a viscosity reduction of the polymer matrix by incorporating C-dots [7, 8]. Some mechanisms for this nanocomposite viscosity reduction were pointed out in these works, such as the nanoparticles' radius of gyration and polymer molar mass, polymer degradation induced by nanoparticles, adsorption of polymers on nanoparticles' surface, free volume effect and particle agglomeration, changes in the entanglement density of polymer chains, and the sliding effect caused by nanoparticles with favored chains' flow, which is the mechanism suggested by the authors for the WPU/CQDs system. From the results, the incorporation of only 1.0 wt.% CQDs caused a slight change in the polymer matrix rheology, both in viscosity and flow activation energy, indicating that this nanoparticle content would not affect the WPU/CQDs nanocomposite performance as a functional coating. Besides the promising luminescent characteristics of this nanocomposite, it was essential to investigate its rheological behavior for applications under high temperatures or thermal cycles conditions.

Acknowledgements

The authors acknowledge Brazilian Agency Coordenação de Aperfeiçoamento de Pessoal de Nível Superior (CAPES, Brazil) and Fundação de Amparo à Pesquisa do Estado do Rio Grande do Sul (FAPERGS, Brazil; grants: 19/2551-0001843-6).

References

1. L. Dall Agnol, F.T.G. Dias; O. Bianchi, *Prog. Org. Coat.* 2023, 179. https://doi.org/10.1016/j.porgcoat.2023.107492.
2. Y. Zhang; X. Liu; Y. Fan; X. Guo; L. Zhou; Y. Lv; J. Lin, *Nanoscale* 2016, *8*, 15281. https://doi.org/10.1039/C6NR03125K.
3. L. Dall Agnol; F.T.G. Dias; H.L. Ornaghi; M. Sangermano; O. Bianchi, *Prog. Org. Coat.* 2021, 154. https://doi.org/10.1016/j.porgcoat.2021.106156
4. R. Duarah; Y.P. Singh; P. Gupta; B.B. Mandal; N. Karak, *Biofabrication* 2016, *8*, 045013. https://doi.org/10.1088/1758-5090/8/4/045013.
5. M. Kovacova; Z.M. Markovic; P. Humpolicek, *et al*., *ACS Biomater. Sci. Eng.* 2018, *4*, 3983. https://doi.org/10.1021/acsbiomaterials.8b00582.
6. O. Bianchi; H.L. Ornaghi; J.N. Martins; C. Dal Castel; L.B. Canto, *Polym. Eng. Sci.* 2020, *60*, 2272. https://doi.org/10.1002/pen.25469.
7. M.A. Haruna; Z. Hu; H. Gao; J. Gardy; S.M. Magami; D. Wen, *Fuel* 2019, *248*, 205. https://doi.org/10.1016/j.fuel.2019.03.039.
8. G. Yao; J. Zhao; M.A. Haruna; D. Wen, *RSC advances* 2021, *11*, 26037. https://doi.org/10.1039/D1RA03935K.

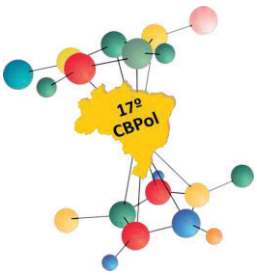

FUNCTIONALIZATION OF CLAY NANOPARTICLES BY PLASMA FOR APPLICATION IN ACTIVE PACKAGING

Pamela X. Mendoza[1], Pâmela R. Oliveira[2], Renata C. da Costa[2], Cesar Aguzzoli[3], Janaina S. Crespo[3], Larissa N. Carli[1]*

1 – Centro Tecnológico, de Ciências Exatas e Educação, Universidade Federal de Santa Catarina (UFSC), Blumenau, SC, Brasil

larissa.carli@ufsc.br

2 – Programa de Pós-Graduação em Ciência e Engenharia de Materiais, Universidade Federal de Santa Catarina (UFSC), Florianópolis SC, Brasil.

3 – Área de Conhecimento em Ciência Exatas e Engenharias, Universidade de Caxias do Sul (UCS), Caxias do Sul, RS, Brasil

Abstract - In this work, Halloysite (Hal) nanoparticles were submitted to plasma treatment under varying conditions – different gases (N_2, O_2, Ar and Ar/H_2), power and treatment time – and subsequently modified with oregano essential oil (OEO) as antioxidant and antimicrobial compound. The modified clay nanoparticles were incorporated in a biodegradable matrix of poly(hydroxybutyrate-*co*-hydroxyvalerate) (PHBV) for the production of active packaging. The OEO incorporation efficiency was higher (61.9%) for the sample treated with N_2 at 200 W for 2 h. The formation of nanocomposites did not significantly change the thermal and mechanical properties of PHBV, but resulted in a more controlled release profile, which may be interesting for application in active packaging, which might extend the antioxidant and antimicrobial effects of the active compound.

Keywords: *Clay nanoparticles. Plasma treatment. Biodegradable polymers. Organic modification. Active packaging.*

Introduction

In a scenario where the production of disposable packaging corresponds to about 30% of the production of polymeric solid waste, the use of biodegradable polymers becomes a promising alternative for this application. By combining it with compounds that present antimicrobial properties, it is possible to produce active packaging that can interact with food in order to increase its shelf life due to the antioxidant and antimicrobial properties [1].

Oregano essential oil (OEO) is a substance of natural origin that possess antioxidant and antibacterial characteristics. When added to a biodegradable polymer, it can bring new properties to the packaging. However, as a highly volatile substance, its controlled release becomes a challenge to maintain the concentration necessary to act as an antioxidant in food and inhibit microbial growth. Therefore, the immobilization of this compound in clay nanoparticles might overcome these challenges.

Halloysite is a clay mineral with tubular shape and high specific area that allows the incorporation of OEO molecules in its structure [2,3]. Additionally, a previous surface treatment by plasma might insert new functional groups on its surface in order to favor the Hal-OEO and Hal-PHBV interaction and, consequently, promote better properties and a more controlled release of the active compound to the food packaging [4].

Experimental

Plasma treatment and characterization of nanoparticles

Hal nanoparticles were subjected to plasma treatment under different conditions (Table 1). The plasma was generated by a radiofrequency (RF) power source and the discharge caused the hollow cathode effect on the samples. The treated nanoparticles were characterized by Fourier transform

infrared spectroscopy (FTIR) in a PerkinElmer Frontier equipment from 4000 to 450 cm^{-1} with 4 cm^{-1} resolution and 16 scans.

Organic modification and characterization

Plasma treated and untreated nanoparticles were modified for the immobilization of OEO. The clay nanoparticles were mixed with OEO in a 1:4 (w:w) ratio and subjected to an ultrasound process in an ice bath followed by the application of the vacuum (two cycles), centrifugation, and drying in a desiccator [3]. The modified samples were analyzed by the incorporation efficiency through the analysis of OEO volatilization in an oven at 200 °C and by their chemical characteristics by FTIR. Evaporation tests were also carried out at 25 °C and 37 °C (ideal temperatures for the growth of fungi and bacteria, respectively) [5].

Nanocomposites preparation and characterization

The PHBV and nanocomposites were prepared by melt mixing in a Haake Roller-Rotors R600 mixer with 8%m OEO and 3%m of Hal [6] at 170 °C and 165 °C for PHBV and the formulations containing OEO, respectively. The obtained material was milled and compression molded into films and was characterized by differential scanning calorimetry (DSC) in a Netzsch 214 Polyma equipment in the range of 40 ºC to 200 ºC at 10 ºC/min under nitrogen atmosphere (40 mL/min). Tensile strength tests were performed in accordance with ASTM D638 (Type IV) in a universal testing machine (EMIC 23-100, INSTRON), with a grip separation of 10 mm/min at 25 °C [7]. For the OEO release tests, 150 mg of each film composition was immersed in 30 mL of 50% ethanol (v/v) medium, in order to simulate foods with a lipophilic character and which can extract lipophilic as alcoholic beverages, canned fruits and vegetables, fermented milk, cream, canned cheese and others [6]. The system was maintained under continuous stirring in an orbital shaker MK1210 – TR at 25 ºC for 96 h. The amount of OEO released was analyzed by UV-Vis spectrophotometry in a Shimadzu UV-1800 equipment. After 96 h, an aliquot of 1.6 mL was removed and mixed with 0.4 mL of a 2,2-diphenyl-1-picrylhydrazyl radical (DPPH•) solution (0.1 mmol/L in ethanol) in the dark for 30 min at room temperature, for determination of the antioxidant activity (AA). The test was performed in triplicate and the AA was calculated by the difference between absorbance of the DDPH solution and the sample, divided by the absorbance of DPPH solution, at 523 nm (determined by UV-Vis spectrophotometry) [8].

Results and Discussion

Characterization of nanoparticles

The higher incorporation efficiency of OEO was found for the Hal sample treated with nitrogen at 200 W for 1.5 h (Hal_N_2_200_1.5) (Table 1).

Table 1. Plasma process conditions applied and incorporation efficiency of OEO (IE).

Sample	Gas/Atmosphere	Power (W)	Time (h)	IE (%)
mHal_N_2_90_1	Nitrogen (N_2)	90	1	54.4
mHal_N_2_90_2		90	2	53.1
mHal_N_2_200_1.5		200	1.5	61.9
mHal_O_2_150_1	Oxygen (O_2)	150	1	45.0
mHal_O_2_200_2		200	2	46.7
mHal_Ar_200_1.5	Argon (Ar)	200	1.5	48.8
mHal_Ar_H_2_200_1.5	50/50 Argon/Hydrogen (Ar/H_2)	200	1.5	45.2
mHal	-	-	-	64.0

This sample was selected for the production of PHBV nanocomposites. The FTIR spectra for pure and plasma treated Hal (Fig. 1(a)) exhibits two bands between 3730 cm^{-1} and 3560 cm^{-1} related to hydroxyl (OH) from its inner surface. A weak band at 2980 cm^{-1} corresponds to the CH bond of CH_2

groups and it was found in Hal samples treated with N_2 and O_2. Furthermore, weak bands were also observed at 1370 cm^{-1} indicating the angular deformation of Si-CH bonds. A band at 1645 cm^{-1}, related to the adsorbed water (H_2O) was also observed in all samples except those treated with Ar, which might indicate the removal of residual moisture in this case [9,10]. In the spectra related to the nanoparticles modified with OEO (Fig. 1(b)), the band at 3400 cm^{-1} found in modified samples corresponds to the OH group form OEO, and the bands in the region from 3110 to 2780 cm^{-1} are assigned to the stretching vibration of CH group from OEO, thus evidencing the presence of oil in organically modified Hal.

Figure 1. FTIR spectra of a) pure Hal and plasma treated Hal nanoparticles, and b) Hal selected samples after modification with OEO.

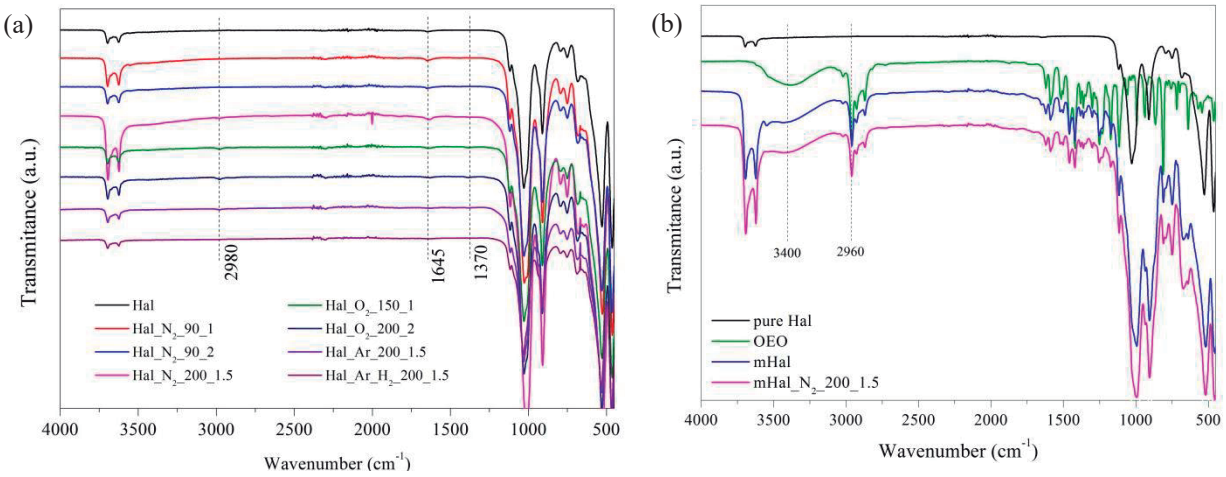

In the evaporation tests at 25 ºC and 37 ºC, slight differences were found between the samples, where the treatment of Hal with O_2 at 200W for 2 h resulted in a lower evaporation rate. This result might be related to the insertion of functional groups at the surface of Hal that interacted stronger with OEO. The sample selected for incorporation into the polymer was the one that, combined with the highest percentage of incorporation, showed a faster release in the beginning of the test, since this characteristic might be important for microbial inhibition and antioxidant properties during application.

Figure 2. Evaporation test at a) 37 ºC and b) 25 ºC for Hal samples treated with plasma and modified with OEO.

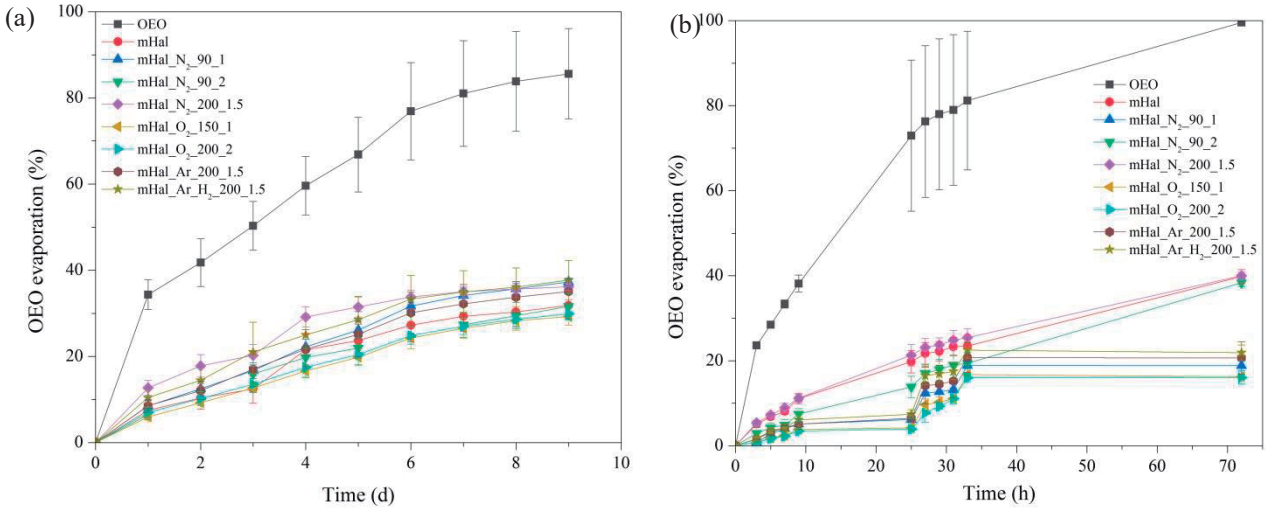

Nanocomposites characterization

The incorporation of OEO promoted a reduction in melting (Tm) and crystallization (Tc) temperatures and in the degree of crystallinity (Xc) of PHBV. Mechanical properties were also affected by the plasticizing effect of OEO, with a reduction in modulus and tensile strength for all compositions.

Table 2: Thermal and mechanical properties of PHBV compositions.

Sample	Tm (ºC)	Tc (ºC)	Xc (%)	Elongation at break (%)	Tensile strength (MPa)	Modulus (GPa)
PHBV	174	83	59	1.7 ± 0.1	25.6 ± 2.8	1.75 ± 0.28
PHBV/OEO	167	72	55	2.0 ± 0.2	18.8 ± 1.5	1.36 ± 0.09
PHBV/OEO/Hal	168	74	54	2.0 ± 0.2	20.1 ± 1.0	1.18 ± 0.05
PHBV/OEO/mHal	168	75	54	2.4 ± 0.2	20.7 ± 2.0	1.34 ± 0.07
PHBV/OEO/mHal_N_2_200_1.5	168	72	54	2.1 ± 0.4	18.8 ± 2.8	1.33 ± 0.08

Release of OEO and antioxidant activity

All compositions containing OEO were evaluated by the release kinetics in a simulating medium of foods with lipophilic character (ethanol 50% v/v) [11]. All compositions exhibited a gradual and controlled release (Figure 3), especially when plasma-treated halloysite was used (PHBV/OEO/mHal_N2_200_1.5 composition). This is interesting for the proposed application for the food preservation, thus avoiding its oxidation and the growth of bacterial population for extended periods [12].

Figure 3. OEO release in 50% v/v ethanol solution.

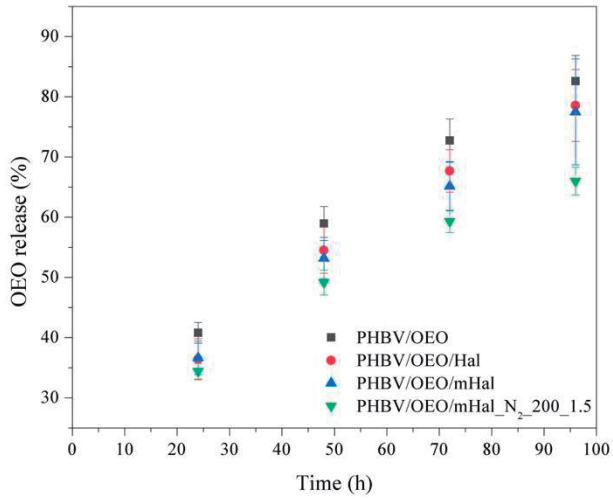

The high antioxidant activity (AA) of OEO is mainly related to the presence of phenolic compounds such as carvacrol and thymol [8]. In this study, this AA was confirmed by values between 47% for PHBV/OEO and 53% for PHBV/OEO/mHal composition. Although PHBV/OEO/mHal_N_2_200_1.5 composition presented the slower release profile, its AA was similar to other formulations (48%). This result evidence the effectiveness of the OEO released and its prolonged effect due to the higher affinity of OEO and Hal provided by the plasma treatment.

Conclusions

In this work, the influence of surface treatment with plasma on halloysite nanoparticles was evaluated by the incorporation efficiency of oregano essential oil and its effect on the properties of PHBV for the production of biodegradable active packaging. Plasma treatment was effective in inserting functional groups on the surface of nanoparticles, influencing the kinetics of oil volatilization due to different interfacial interactions. The addition of nanoparticles to PHBV did not change its thermal and mechanical properties significantly, but indicated that it is possible to adjust the kinetics of oil release in a food simulant medium, an important factor to optimize and extend the antimicrobial and antioxidant properties of the compositions.

Acknowledgements

The authors are grateful to Conselho Nacional de Desenvolvimento Científico e Tecnológico (CNPq), Universidade Federal de Santa Catarina (UFSC) and Universidade de Caxias do Sul (UCS).

References

1. J. Rhim; H. Park; C. Ha. Progress in Polymer Science 2013, 38, 1629–1652. https://doi.org/10.1016/j.progpolymsci.2013.05.008.
2. P. R. Oliveira, Master. Dissertation, Universidade Federal de Santa Catarina, 2022.
3. S. Hendessi; E. B. Sevinis; S. Unal; F. C. Cebeci; Y. Z. Menceloglu; H. Unal. Progress in Organic Coatings 2016, 101, 253–261. https://doi.org/10.1016/j.porgcoat.2016.09.005.
4. R. Scaffaro; A. Maio. Polymer Testing 2012, 31, 889–894. https://doi.org/10.1016/j.polymertesting.2012.06.006.
5. A. Bernardos; M. Bozik; S. Alvarez; M. Saskova; E. Perez-Esteve; P. Kloucek, et al. Flavour and Fragrance Journal 2019, 34, 151–162. https://doi.org/10.1002/ffj.3488.
6. R. C. da Costa; T. S. Daitx; R. S. Mauler; N. M. da Silva; M. Miotto; J. S. Crespo; L. N. Carli. Food Packaging and Shelf Life 2020, 26, 100602. https://doi.org/10.1016/j.fpsl.2020.100602.
7. S. Torres-Giner; L. Hilliou; B. Melendez-Rodriguez; K. J. Figueroa-Lopez, et al. Food Packaging and Shelf Life 2018, 17, 39–49. https://doi.org/10.1016/j.fpsl.2018.05.002.
8. A. A. Oun, A. Y. Bae, G. H. Shin, M. Park, J. T. Kim. Applied Clay Science 2022, 224, 106522. https://doi.org/10.1016/j.clay.2022.106522.
9. Y. Zhang; X. He; J. Ouyang; H. Yang. Scientific Reports 2013, 3, 2948. https://doi.org/10.1038/srep02948.
10. P. Yuan; P. D. Southon; Z. Liu; M. E. R. Green, et al. The Journal Physical Chemistry C 2008, 112, 15742–15751. https://doi.org/10.1021/jp805657t.
11. Commission Regulation (EU) No 10/2011 of 14 January 2011 on plastic materials and articles intended to come into contact with food, 2011.
12. P. R. Oliveira, R. C. da Costa, D. S. Malvessi, T. S. Daitx, R. S. Mauler, M. Miotto, D. M. Bobermin, J. S. Crespo, C. S. Teixeira, I. C. Bellettini, L. N. Carli. Applied Clay Science 2023, 241, 107004. https://doi.org/10.1016/j.clay.2023.107004.

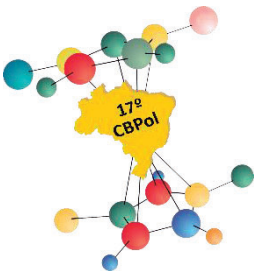

GRAPHENE OXIDE/COPPER, COPPER OXIDE AS HEAT CONDUCTIVE ADDITIVES FOR ENGINE OIL, PAINTS & POLYMERS

Maysa C. Marques*[1,2], Maria F. X. Pinto[2], Maria E. Leyva[1,2], Adhimar F. Oliveira[1] and Estácio T. W. Neto[2]

1 – Institute of Physics and Chemistry (IFQ), Federal University of Itajubá (UNIFEI), Itajubá, MG, Brazil
maysa.candido@unifei.edu.br
2 – Institute of Electrical Systems and Energy (ISEE) High Voltage Laboratory (LAT), Federal University of Itajubá (UNIFEI), Itajubá, MG, Brazil

Abstract – Develop heat conductive additives (HCA) for engine oil, paints and polymers is important to electrical and electronic industry. The main objective of this work is prepared a new HCA based on graphene oxide (GO) and copper, using a simple preparation route. The GO was prepared by electrochemical exfoliation of graphite. Then GO/copper composite was prepared by electrochemical reduction of Cu^{2+} from GO aqueous dispersion. The product was characterized by UV-vis spectroscopy, Fourier transform infrared (FTIR) spectroscopy, thermogravimetric analysis (TG), X-ray diffraction (XRD), scanning electron microscopy (SEM) and studies of thermal conductivity. The UVvis, FTIR and SEM confirmed the electrosynthesis of Cu/Cu_xO. XRD results reveled that Cu was oxidated to Cu_2O. TG reveled that GO allow the reaction between Cu and nitrogen, at high temperature.
Keywords: *Graphene oxide, Copper, Copper oxide (I), Nanocomposite, Heat conductive additives.*
Fundings: CAPES, Coordination for the Improvement of Higher Education Personnel.

Introduction

Paints and polymer thermally insulating are important to improve the thermal performance of materials used in electrical or electronic applications [1, 2]. Engine oil is a conventional fluid with lubricant and heat transfer properties employed in various industrial sectors [3]. The growth of the miniaturization in the electronic industry makes an increase in the amount of heat generated per unit volume. Therefore, is needed to make materials that allow an adequate heat dissipation. In between the metals the Copper (Cu) has higher values of thermal conductivity (TC). But the TC is an anisotropic property and to Cu its values differ little in different directions. Therefore, the objective of researchers is used different fillers, such as graphite, graphene oxide and graphene to enhance the anisotropy of the thermal conductivity of Cu. Graphene/Cu composites are the more interest due to higher values of anisotropic thermal conductivity of Graphene, in-plane of 4000–5000 W/mK and 5-20 W/mK through plane [4, 5].

In this paper, we realized a new and efficient route of preparation of graphene oxide/copper composite as a heat conductive additive for engine oil, paint, and polymer compound. Firstly, of graphene oxide (GO) is prepared by electrochemical exfoliation of graphite. Then, is realized the electrochemical reduction of Cu^{2+} to Cu, in the presence of aqueous dispersion of GO. The GO, Cu/Cu_xO, and $GO/Cu,Cu_xO$ nanocomposites were characterized by physical chemistry methods, such as, UV-vis spectroscopy, Fourier transform infrared (FTIR) spectroscopy, thermogravimetric analysis (TG), X-ray diffraction (XRD), scanning electron microscopy (SEM) and studies of thermal conductivity.

Experimental

Preparation of GO by electrochemical exfoliation

The graphene oxide was prepared by electrochemical exfoliation of graphite using anodic method. Graphite (density 2.45 g/cm^3, of commercial source) was use as anode and cathode of electrolytical cell. The electrodes were immersed in 0.5 M sulfuric acid electrolyte solution. Exfoliation occurred by applying a direct current voltage of +3 V for 10 minutes, using a Power Supply Mod. FA-3005 1-channel digital. Then the voltage was increased to +2 V for 5 minutes and step by step increased (staying 5 minutes each voltage) up to +7V. The yield of graphene oxide (GO) produce was determinate by mass difference of electrolytical cell before and after electrochemical exfoliation. The aqueous dispersion of graphene oxide was kept under ultrasonic bath during 6h to increase efficiency the exfoliation of graphite oxide to GO. Finally, GO dispersion solution was filtered to gravity, and it was broadly washed with distilled water until pH=7. The GO powder was dried in an oven with forced air circulation at a temperature 100° (Venticell brand).

Preparation of GO/Cu, Cu_xO nanocomposites

The powder of GO was physical blend to different amount of copper sulfate heptahydrated ($CuSO_4$ $7H_2O$) (from Sigma Aldrich). The different concentrations GO/Cu (wt/wt) was prepared considering the mass of Cu in $CuSO_4.7H_2O$, 100/0, 70/30, 60/40, 50/50, 30/70, 20/80, 15 /85, 10/90, 5/95 & 0/100. The GO/Cu, Cu_xO nanocomposite was realized by electrochemical reduction of Cu^{2+} to Cu in the presence of GO using two wire platinum Pt electrode as anode and cathode under magnetic agitation 900 rpm. The electrochemical reduction was realized at constant current 50 mA using a Power Supply Mod. FA-3005 1-channel digital, for 1 hour. After electrochemical reduction the GO/Cu, Cu_xO dispersion solution was filtered to gravity and broadly washed with distilled water. The GO/Cu, Cu_xO nanocomposite powder was dried in an oven with forced air circulation at a temperature 100° (Venticell brand).

Physical Chemical characterization of GO and GO/Cu nanocomposites

The GO, Cu and GO/Cu,Cu_xO nanocomposite were characterized by UV-Vis, FTIR, TG and XRD. A Cary 50 Varian UV-Vis spectrometer was used in the characterization of aqueous dispersion of GO, Cu and GO/Cu, Cu_xO composite. The UV-Vis was carried out in quartz cells the spectra were collected from 250 to 500 nm. All samples were analyzed through FTIR Shimadzu IRTracer 100 spectrometer by KBr pellet method. The FTIR spectrum was obtained on absorbance mode and was scanned registering the spectrum with 30 scans at a resolution of 8 cm^{-1}, from 4000 to 650 cm^{-1}. TG measurements were carried out using a TGA-60, Shimadzu at a constant heating rate of 10 °C min^{-1} from 25 to 1000 °C under nitrogen atmosphere (25 mL.min^{-1}).

Powder X-ray diffractograms were collected at room temperature (25 ºC) using a X'Pert PRO, Malvern Panalytical, Cu Kα radiation (λ = 1.5417 Å) source, operating at 40 kV and 40 mA. Powder diffractograms were collected over an angular 2θ range between 5° and 90° (2θ) with a step size of 0.02° and scanning speed of 2 sec/step. SEM was conducted by EVO MA15 (Zeiss), operating at 20 kV.

Results and Discussion

The results obtained show the reactivity of Cu obtained with the oxygen generated during water electrolysis. The Table 1 shows comparatively the amount ratio of GO/Cu prepared and the concentration ratio GO/Cu,Cu_xO nanocomposite obtained by way electrochemical.

The UVvis spectrum of GO/Cu composite dispersed in distilled water is show in the Fig 1a. The UVvis spectrum of GO shows a maximum at 267 nm attributed to the electronic transition of the molecular orbitals $\pi \rightarrow \pi*$, present in the graphene [6]. The $\pi \rightarrow \pi*$ electronic band is observed in the GO/Cu composite at lower wavelength. The UVvis spectrum of Cu/Cu_xO composite shows a broad band. This band is due to overlapping between the plasmon resonance band of nanoparticle and

interband transition. The interband transition is accept as the band electronic transition from 3d to 4s orbital [7].

Table 1. Values of mass initial of GO to 0.005g of Cu in $CuSO_4*7H_2O$ and amount (g) of GO/Cu composite obtained by electrolysis.

GO (g)	GO/Cu (g)	Concentration of Cu,Cu_xO (%) wt/wt	Nomenclature of samples
0.0000	0.6624	100.00	Cu, Cu_xO 100
0.0026	0.6333	99.59	GO / Cu 99.6
0.0056	0.4900	98.86	GO / Cu 98.9
0.0088	0.4829	98.18	GO / Cu 98.2
0.0125	0.4819	97.41	GO / Cu 97.4
0.0214	0.505	95.76	GO / Cu 95.8
0.0500	0.6152	91.87	GO / Cu 91.9
0.0750	0.5573	86.54	GO / Cu 86.5
0.1164	0.5924	80.35	GO / Cu 80.4

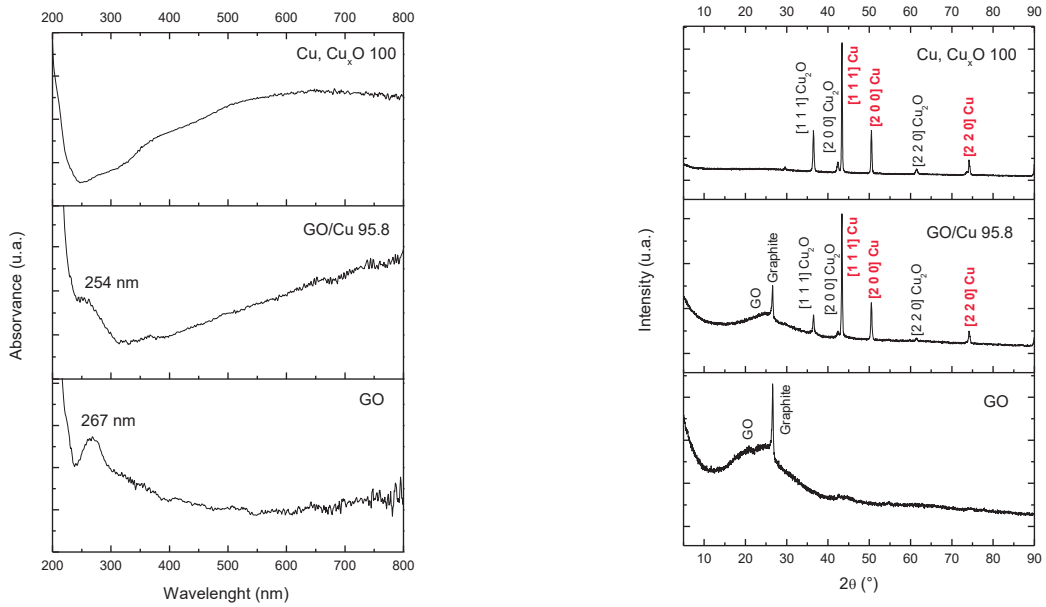

(a) (b)

Figure 1. UVvis spectrum (a) and XRD (b), of samples GO, GO/Cu 95.8 & Cu,Cu_xO

The XRD patterns of the GO (Fig. 1b) exhibits broad peak near 2θ ~22,5° assigned to sheets of graphene [8]. The peak in 2θ ~26,6° correspond to graphite phase. The XRD patterns of GO/Cu 95.8 nanocomposite show the characteristics peak of GO & Graphite phases and the diffraction peaks of Cu and Cu_2O [9, 10].

The SEM image of GO (Fig 3a) exhibits regions like sheets with wavy folds and other regions of higher density relatives to sheets stacked [8]. Fig 3b shows Cu and Cu_2O with morphologies of grains aggregates on surface of sheets stacked of GO. The SEM image of Cu, Cu_2O nanocomposite (Fig 3c) exhibits great aggregates of grains and fine dendritic structure with branches of about 1-2µm [11].

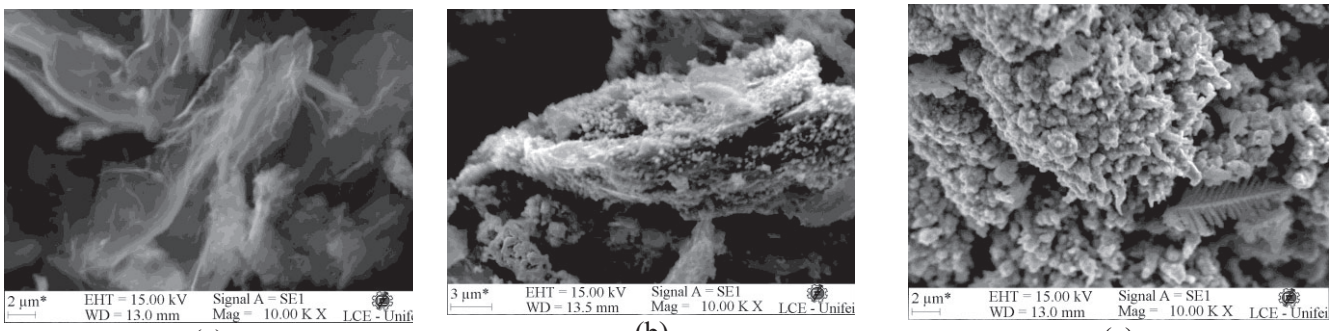

(a) (b) (c)

Figure 3. SEM images of GO (a), GO/Cu 95.8 (b) & Cu, Cu_xO.

Conclusions

We can conclude that electrosynthesis method was satisfactory to obtained cupper & Cu_2O nanoparticles, as confirmed by UVvis and FTIR. The XRD pattern shows that jointly to Cu is obtained Cu_2O. The SEM images shows a dendritic structure to Cu nanoparticle and a homogeneous distribution of Cu and Cu_2O on sheets stacked of GO. TG analysis shows the reaction between Cu and gaseous nitrogen in the presence of GO.

Acknowledgements

This research project to thank to the Coordination for the Improvement of Higher Education Personnel (CAPES) and the Financial Support of Minas Gerais Research Funding Foundation (Fapemig) through the project APQ-02676-16.

References

1. A. Simpson, R. Fitton, I.G. Rattigan, A. Marshall, G. Parr, W. Swan Bismarck Energy and Buildings 2019. 197. 196. https://doi.org/10.1016/j.enbuild.2019.04.027.
2. T. Morishita, M. Matsushita Carbon 2021. 184. 786. https://doi.org/10.1016/j.carbon.2021.08.058.
3. A. Fazlali, V. Ghalehkhondabi, and F. Alahyarpur Petroleum Science and Technology 2022. 40. 803. https://doi.org/10.1080/10916466.2021.2006705.
4. 4. F. Nazeer, Z. Ma, Y. Xie, L. Gao, A. Malik, M. A. Khan, F. Wang, and H. Li RSC Adv. 2019. 9. 17967. https://doi.org/10.1039/c9ra03743h.
5. K. Jagannadham Metallurgical and Materials Transactions B 2012. 43B. 316. https://doi.org/10.1007/s11663-011-9597-z.
6. T. Zhang, G-Y. Zhu, C-H. Yu,Y. Xie, M-Y. Xia, B-Y. Lu, X. Fei1 and Q. Peng. Microchimica Acta. 2019. 186. 207. https://doi.org/10.1007/s00604-019-3329-5.
7. H. Wang, F. Tam, N. K. Grady, and N. J. Halas Journal Physical Chemistry B, 2005. 109. 18219. https://doi.org/10.1021/jp053863t.
8. S. S. Shojaeenezhad, M. Farbod, I. Kazeminezhad Journal of Science: Advanced Materials and Devices 2017. 2. 470. https://doi.org/10.1016/j.jsamd.2017.09.003.
9. R. Phul, C. Kaur, U. Farooq, T. Ahmad Material Science & Engineering International Journal 2018. 2. 90. https://doi.org/10.15406/mseij.2018.02.00040.
10. Q. He, Y. Tian, Y. Wu, J. Liu, G. Li, P. Deng, D. Chen Biomolecules 2019. 9. 176. https://doi.org/doi:10.3390/biom9050176.

11. Z. B. Hoffman, T. S. Gray, Y. Xu. Q. Lin, T. B. Gunnoe, G. Zangari, ChemSusChem 2019. 12. 231 https://doi.org/10.1002/cssc.201801708.

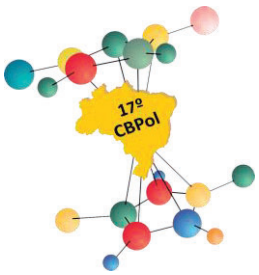

GRAPHENE OXIDE DEPOSITION ON METALLIC AND POLYMERIC SUBSTRATE VIA ELECTROPHORETIC DEPOSITION

Bruna Segat[1], Luis G. S. Rosa[1] and Daniela Becker[1]*

1 – Graduate in Materials Science and Engineering Program, Santa Catarina State University (UDESC), Joinville, SC, Brazil
brusegat@gmail.com

Abstract - Electrophoretic deposition (EPD) is an important coating technique that has stood out for being more economical and more ecological than other techniques. This technique has been used to deposit graphene oxide (GO) on several substrate types, mainly on conductive metallic substrates. Polymeric substrates have been little explored. Thus, this work aimed to deposit GO on a copper substrate (Cu) and polypropylene (PP) substrate using EPD with direct current. The samples were characterized by optical microscopy (OM) and Fourier Transform Infrared spectroscopy (FTIR). The OM analysis showed that the deposition on Cu was more effective than on the polymeric substrate, which had only punctual deposits. In FTIR, some characteristic GO bands appeared in the Cu sample, and only one band appeared in the PP sample. Thus, the deposition on the conductive substrate, although not homogeneous, formed a better deposit on the surface. For the PP sample, the deposition was not successful.
Keywords: *Electrophoretic deposition. Graphene oxide. Copper. Polypropylene.*
Fundings: The authors acknowledge the financial support provided by FAPESC and CAPES.

Introduction

Electrophoretic deposition (EPD) is an important technology for coating surfaces with thin films from suspensions. In EPD, charged particles suspended in a liquid medium are attracted and deposited on a conductive substrate of opposite charge in applying an electric field, usually direct current (DC) [1]. This technique is more viable and ecological than other deposition processes since it is possible to conduct it using aqueous solutions [2]. Thus, it is widely used to prepare GO thin films for various applications such as coating against corrosion, improvement of tribological properties, and hydrogen storage [3-5]. Thus, by associating graphene derivatives with substrates of different materials through EPD, it is possible to obtain a substrate with improved and even different properties.

Furthermore, it is essential to emphasize that the choice of substrate depends on the applications, and it is expected that the deposition is homogeneous so that there is consistency of properties throughout the entire film, which has good adhesion and stability. Regarding substrates, conductive metallic substrates are the most exploited in EPD depositions.

One of the most widely used substrates is copper (Cu). In addition to being an excellent thermal and electrical conductor, copper is used in several applications, mainly in the manufacture of electrical products and industrial equipment [6]. Thus, GO is deposited as a thin film on its surface for various purposes, mainly as an anti-corrosion agent [3,6]. In this way, GO can prevent the diffusion of harmful materials to the metallic surface or even promote the generation of a passivation layer [7].

Thinking about exploring other substrate possibilities within this area, the EPD process for polymeric substrates was analyzed. Polypropylene (PP) was chosen due to its wide range of applications. PP is a polymer widely used industrially, as it has a good balance between general properties, processability and cost [8]. In addition, it has good resistance to pH, thermal, chemical and solvent stability [9]. PP has been widely used as a dielectric material in organic thin-film capacitors due to its high breakdown strength, low dielectric loss and self-healing capability [10]. However, little has been studied about its coating with GO, mainly through the EPD technique.
Thus, this work aimed to conduct an initial study of the behavior of GO deposition on different substrates, one conductor and one non-conductor, using the EPD technique with direct electric current. For this purpose, the homogeneity of GO deposition on Cu substrate (CuOG) and on PP (PPOG) was evaluated. This work seeks to contribute to the deposition step. Once this step is successful, other works can explore the applications of combining the substrate with a GO film on the surface.

Experimental

Electrophoretic deposition

Before the deposition, the graphene oxide suspension was prepared in deionized water at 1 mg/mL. Then, the solution was homogenized in a sonicator tip (*Sonics VCX 750*) for 1 h and 20 min. The conductivity and pH of the suspension were measured. The materials used in the electrophoretic deposition were PP film and Cu plate with dimensions of 4.5 x 3.5 cm each. The PP film was prepared from pellets pressed with 2 tons in a hydraulic press heated to 180 °C for 2 min e 30 s. For the deposition, the *Supplier DC Power Source* was used. The reactor consisted of two graphite electrodes spaced 4 cm apart. The deposition was carried out under direct electric current (DC), with a voltage of 50 V for 5 min. The entire deposition process was conducted using an ultrasonic bath at 30 kHz to promote agitation of the suspension. In addition, a digital oscilloscope was used to monitor current and voltage. After deposition, substrates were dried at room temperature for 24 h and then characterized. Fig. 1 shows a schematic diagram of the EPD setup.

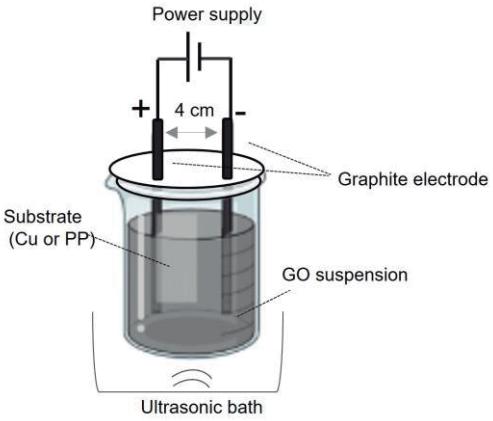

Figure 1 – Schematic diagram of the EPD setup.

Optical microscopy (OM)

Optical microscopy aimed to verify the surface of the substrate before and after deposition to verify the deposition of GO, as well as its homogeneity and possible points without deposition.

Fourier Transform Infrared Spectroscopy (FTIR)

Fourier Transform Infrared Spectroscopy analysis was performed on the GO, on the PP film and on the substrates after deposition to verify possible changes in the leading bands and verify the GO deposition. The spectra were performed with 32 scans from 4000 to 400 cm^{-1}, with a resolution of 4 cm^{-1} and in transmittance mode.

Results and Discussion

Electrophoretic deposition

The graphene oxide suspension was successfully prepared. Some measurements were performed to determine the solution's behavior before the EPD process. The measured suspension conductivity was 109.89 μS/cm, the pH was 5.40, and the suspension temperature was 25 °C. After 1 h and 20 min of sonication of the suspension, an apparently stable suspension was obtained. The suspension temperature remained constant throughout the process. After deposition, the samples were washed with deionized H_2O to remove excess GO and the nanoparticles that were not well adhered. Fig. 2 shows the Cu substrate before the EPD process (Fig. 2A), after the EPD process (Fig. 2B), after washing with deionized H_2O (Fig. 2C) and the PP substrate before and after the EPD process (Fig. 2D-E).

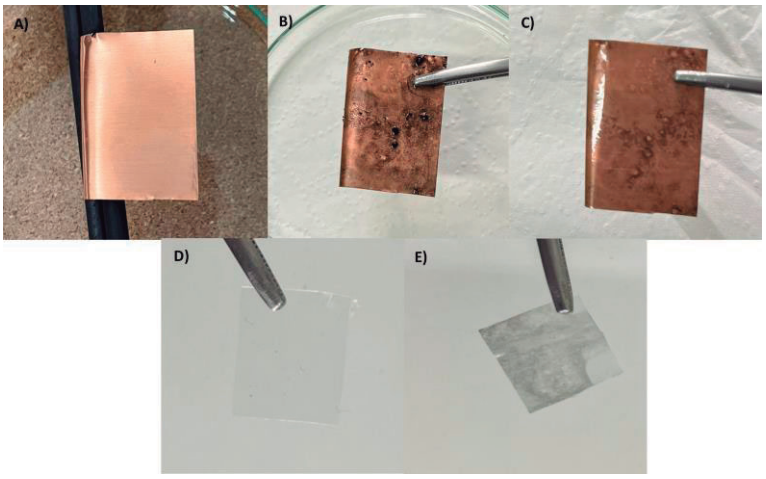

Figure 2 –Cu substrate A) before the EPD process, B) After the EPD process, C) After washing, D) PP substrate before the EPD process and E) After the EPD and washing process.

Analyzing Fig.2, it is possible to see that after washing the sample with water, there was a reduction in the presence of GO on the surface. The same behavior was observed for the PP samples. This indicates that the GO deposited on the surface was not fully adhered to the substrate. It is also observed that the deposition was neither homogeneous nor robust.

Optical microscopy (OM)

Fig. 3 shows the surface of Cu before deposition (Fig. 3A), after deposition (Fig. 3B), and the surface of PP after deposition (Fig. 3C). The surface of PP before deposition was not shown as it is transparent.

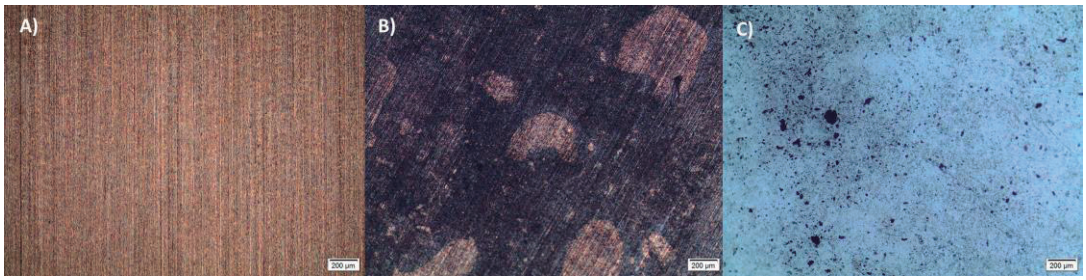

Figure 3 – Microscopy image of A) Cu substrate before deposition, B) After deposition and C) PP substrate after deposition.

For the Cu sample (Fig. 3B), it is observed that there are spaces in which there was no deposition, that is, the deposition was not homogeneous. This is believed to have been caused by water hydrolysis during deposition. Using voltages above the thermodynamic oxidation and reduction voltages of water, electrochemical reactions occur at the electrodes and generate O_2 and H_2 gases,

so these gas bubbles can be incorporated into the deposit and result in damaged coatings and poor quality [2]. Studies carried out by Chávez-Valdez *et al.* (2012) [11] deposited TiO_2 nanoparticles in aqueous suspensions on stainless steel foils by EPD. They found that the coating suffered damage due to the formation of gas bubbles, even using a voltage of 5 V for 1 min. Another factor that may have hindered the deposition is the distance between the electrodes of 4 cm, while the literature works with 1 cm [3,11]. The greater the distance between the electrodes, the smaller the electrical force.

Regarding the polymeric substrate, the deposition was not successful. It is observed in Fig. 3C that there were some punctual deposits, although visually, it seems that the deposition was on the entire surface (Fig.2E), it did not form a film. In this case, it is believed that it is linked to the conductivity of the substrate, as PP is not conductive. Substrate conductivity is a critical parameter for EPD deposition quality; thus, low conductivity leads to non-uniform film and slow deposition [1].

Fourier Transform Infrared Spectroscopy (FTIR)

FTIR analyses for GO (Fig.4A), the copper substrate after deposition (Fig.4A), PP (Fig.4B) and PP after deposition (Fig.4B) are shown below.

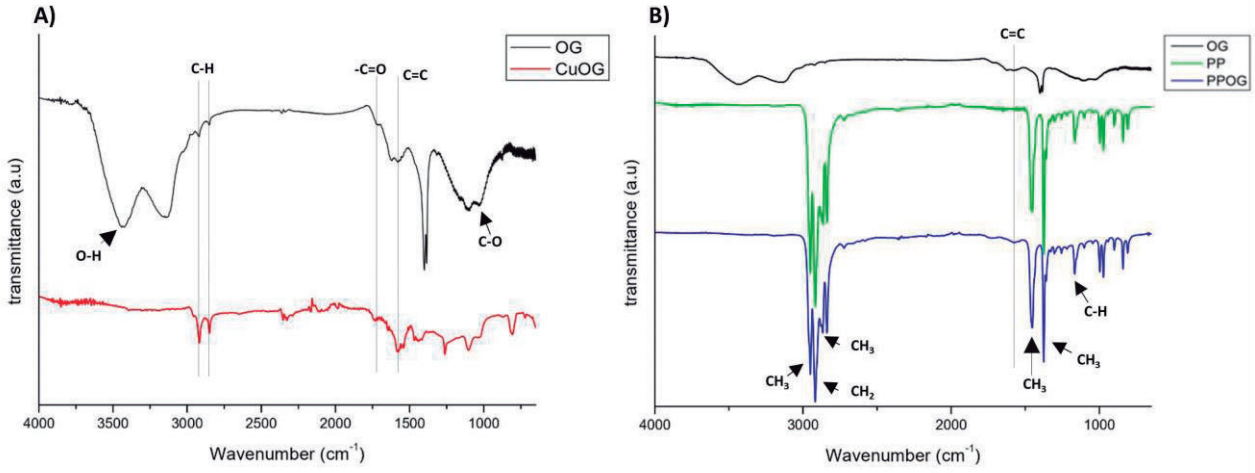

Figure 4 – FTIR spectrum of A) graphene oxide and copper substrate after deposition and B) graphene oxide and polypropylene before and after deposition.

The FTIR for GO showed a broad absorption band at 3437 cm^{-1} that can be attributed to the O-H stretching vibration, furthermore, the presence of water molecules interspersed between the layers of GO broadens this band [12, 14]. Another bands showed for GO are the C-H stretching that shows two sharp peaks at 2922 cm^{-1} and 2850 cm^{-1}, a band at 1719 cm^{-1} is attributed to the -C=O vibration modes of carboxyl groups that were linked in the surface of nanoparticles after oxidation, a band at 1578 cm^{-1} is associated with vibrations of non-oxidized regions (C=C) and a band at 1070 cm^{-1} corresponds to C-O stretching [6, 12-14]. The presence of oxygen functional groups confirms that graphene was oxidized. Furthermore, the curve profile was similar to the literature's [14]. For the Cu sample (Fig.4A), some characteristic bands of OG appeared, such as two sharp peaks at 2917 cm^{-1} and 2847 cm^{-1} related to C-H stretching, the band 1719 cm^{-1} assigned to the -C=O vibration modes and the band at 1575 cm^{-1} associated with the C=C vibrations. This can be indicative of the presence of GO on the surface, corroborating with the OM analysis that indicates the presence of GO on the surface.

For PP and PPOG samples (Fig.4B), the characteristic bands of PP appeared at 2950 cm^{-1} and 2875 cm^{-1} representing, respectively, asymmetric CH_3 stretching and CH_3 stretching, a band at 2918 cm^{-1} representing asymmetric stretching CH_2 and flexion symmetric CH_3 at 1377 cm^{-1} [15]. For the PPOG sample, there was the appearance of a very subtle band at 1575 cm^{-1}, which can be

attributed to the C=C vibrations present in the GO sample. However, the deposition of GO in PP was punctual, therefore, some regions in which there was not a large amount of deposit could have been analyzed, but in any case, this result was expected since the deposition was not effective.

Conclusions

From the visual analysis of the samples after deposition, it is possible to verify that some deposition occurred since, even after washing, there was GO on the surface. The OM analysis corroborated with the previous analysis, however, from it, it was possible to verify that the deposition on the PP was only punctual, it did not form a film on the surface, indicating problems in the adherence of the GO by the surface. The lack of conductivity of the PP substrate may have caused this. As for the Cu substrate, the deposition was better, however, not homogeneous, possibly resulting from water hydrolysis or the electrodes distance. In the FTIR analysis, some bands characteristic of the GO in the Cu sample appeared, while for the PP, there was only the appearance of a subtle band. Thus, the deposition on Cu was more successful, it is believed that it is crucial to explore the process parameters to improve the deposition, as for the PP substrate, the deposition was not as expected, so it is believed that it is necessary to replace it, by a conductive polymeric substrate.

Acknowledgements

The authors are thankful for the Multi-User Facility infrastructure from Santa Catarina State University's Technological Sciences Center.

References

1. L. Besra; M. Liu Progress in Materials Science 2007, 52, 1-61. https://doi.org/10.1016/j.pmatsci.2006.07.001.
2. M. Ammam RSC Advances 2012, 2, 7633-7646. https://doi.org/10.1039/C2RA01342H
3. E. Hares; A. H. El-Shazly; M. F. El-Kady; A. S. Hammad Arabian Journal of Science and Engineering 2019, 22, 5559-5569. https://doi.org/10.1007/s13369-019-03872-0
4. X. Miao; S. Liu; L. Ma; Y. Yang; J. Zhu; Z. Li; J. Wang Tribology International 2022, 167, 107361. https://doi.org/10.1016/j.triboint.2021.107361
5. S. S. Y. Bonab; H. Kouzehgar; A. T. Tabrizi; H. Aghajani International Journal of Hydrogen Energy 2022, 47, 2491-2499. https://doi.org/10.1016/j.ijhydene.2021.10.158.
6. N. U. Kiran; S. Dey; B. P. Singh; L. Besra Coatings 2017, 7, 214. https://doi.org/10.3390/coatings7120214
7. A. T. Smith; A. M. LaChance; S. Zeng; B. Liu; L. Sun Nano materials Science 2019, 1, 31-47. https://doi.org/10.1016/j.nanoms.2019.02.004
8. J. Balart; V. Fombuena; J. M. España; L. Sánchez-Nácher; R. Balart Materials and Design 2012, 33, 1-10. doi:10.1016/j.matdes.2011.06.069.
9. D. Hua; T. Chung Carbon 2017, 122, 604-6013. https://doi.org/10.1016/j.carbon.2017.07.011
10. C. Lee; C. Chang Journal of composites Science 2021, 5, 52. https://doi.org/10.3390/jcs5020052.
11. A. Chávez-Valdez; M. Herrmann; A. R. Boccaccini Journal of colloid and Interface Science 2012, 375, 102-105. https://doi.org/10.1016/j.jcis.2012.02.054.
12. A. Nekahi; P. H. Marashi; D. Haghshenas Applied Surface Science 2014, 295, 59-65. http://dx.doi.org/10.1016/j.apsusc.2014.01.004
13. S. Ghasemi; R. Hosseinzadeh; M. Jafari International Journal of Hydrogen Energy 2015, 40, 1037-1046. http://dx.doi.org/10.1016/j.ijhydene.2014.11.072.
14. R. H. Bello, Master Thesis, Santa Catarina State University, 2015.
15. J. Fang; L. Zhang; D. Sutton; X. Wang; T. Lin Journal of nanomaterials 2012, 16, 1-9. https://doi.org/10.1155/2012/382639.

HYBRID MATERIALS BASED ON CHITOSAN/MAGNETITE/SILVER NANOPARTICLES FOR ADSORPTION AND DEGRADATION OF DYES.

Ana L. de Andrade[1], Andressa L. Ratajk[1], Ismael C. Bellettini[1], Cristiano S. Teixeira[1], Larissa N. Carli[1]*

1–Centro Tecnológico, de Ciências Exatas e Educação, CTE, Universidade Federal de Santa Catarina (UFSC), Blumenau, SC, Brasil
larissa.carli@ufsc.br

Abstract – The aim of this work is to produce and characterize hybrid materials based on chitosan (CHI), magnetite (Fe_3O_4), and silver nanoparticles prepared by different methodologies and the use of those materials in the adsorption and (photo)degradation of methyl violet 2B (MV 2B) dye from aqueous solution. The synthesis of the hybrids was successful and confirmed by FTIR with the appearance of characteristic bands of the components. The hybrids were applied to the adsorption and degradation of MV 2B dye in aqueous solution in combination with hydrogen peroxide (H_2O_2) and ultraviolet (UV) radiation, and the remaining amount of dye in solution was analyzed by UV-Vis spectrophotometry. The results showed a high efficiency of the hybrids, mainly when combined with H_2O_2 and UV radiation. Based on the preliminary results, hybrids can be highlighted as a promising material for the proposed application, which can be enhanced when used in conjunction with agents that promote the degradation of dyes.

Keywords: Chitosan. Hybrid materials. Adsorption. Photocatalysis. Dyes.

Introduction

The presence of dyes in water and wastewater is a significant environmental problem, as these substances can persist in the environment for long periods and cause adverse effects on human health and aquatic ecosystems. Dyes are often used in industrial processes including textiles, paper production, and inks, being released in the effluents and polluting rivers, lakes, and oceans [1]. The presence of dyes in water can affect the penetration of sunlight, gas exchange, and oxygenation, as well as alter the chemical composition of water, impairing the survival of aquatic species and reducing water quality. Therefore, it is essential to develop water and wastewater treatment technologies that can remove or degrade these substances to protect the environment and ensure public health [2].

Numerous methods have been developed to mitigate such damages. These methods can be divided into three categories: physical, chemical, and biological. Currently, the most applied method is through the adsorption of the dye using activated carbon, but other adsorbents such as chitosan are gaining attention due to its versatility, high efficiency, and cost-effectiveness. Chitosan is obtained from chitin, a natural polymer found in crustaceans, and is essentially a low-toxicity, biocompatible, and biodegradable polysaccharide with a high potential for dye removal. When combined with magnetite (Fe_3O_4, or MGT) and silver nanoparticles (AgNPs), the obtained material might exhibit a higher specific area [3] due to the presence of nanoparticles on its surface, magnetic properties that facilitates its recovery after use, and photocatalytic activity to promote degradation of dyes [4].

In this work, these hybrids materials – combined or not with hydrogen peroxide (H_2O_2) and UV radiation – were applied in adsorption and (photo)degradation tests for the methyl violet 2B (MV 2B) dye with the aim of analyzing and compare their efficiency.

Experimental

Synthesis of magnetite

The synthesis of MGT was based on the method of Duan et al [5]. Two 50 mL solutions were prepared, one with 0.507 g of $FeCl_2$ and 0.504 g of $FeCl_3$. Both solutions were mixed under argon atmosphere and magnetically stirred for 2 h. After this time, the flask was placed in a glycerol bath at 50 °C for 30 min. Then, 13 mL of NaOH 1 mol/L solution were added and the mixture was stirred for 30 min at 90 °C. The flask was removed from the bath and cooled to room temperature. Finally, the magnetite was centrifuged for 10 min and washed with distilled water until neutral pH. Finally, magnetite was dried at 50 °C for 24 h in an oven.

Preparation of the hybrids

The production of CHI, MGT, and AGNPs hybrids was divided into two methods, proposed by Yeamsuksawat, Zhao, and Liang et al. (2012) [6] and Torezan et al. (2023) [7]. Method 1 (M1) begins with the dispersion of 0.4 g of MGT in 30 mL of the previously prepared CHI solution (1.5% w/v) in acetic acid (5% v/v). Then, this solution was dripped into 60 mL of mineral oil and 1 mL of Tween 80, and stirred for 10 min, followed by the addition of 6 mL of 25% (v/v) glutaraldehyde and stirred for 1 h. The particles were then washed with petroleum ether, sodium bisulfite, and acetone. For the synthesis and impregnation of AgNPs, 0.75 g of the hybrids were dispersed in 15 mL of DMF at 50 °C for 10 min. Then, a solution of 10 mL of DMF with 1.8 g of glucose was added and stirred for 1 h. Then, 10 mL of DMF with 0.06 g of $AgNO_3$ were added at 10 min intervals in increments of 2 mL. The hybrids obtained were washed with distilled water and ethanol and dried in an oven at 50 °C for 24 h. For Method 2 (M2), firstly 0.0072 g of $AgNO_3$ were added to 0.6 mL of distilled water. This solution was added to the chitosan solution (1.5%) and stirred at 50 °C for 10 min. Then, 0.0288 g of glucose in 0.6 mL of distilled water were added. After 10 min, a solution of NaOH 0.005 mol/L was added, and the solution was stirred for 25 min. Then, 0.4 g of magnetite was dispersed in 30 mL of CHI/AgNPs dispersion. After this stage, the M2 hybrid was crosslinked following the procedure described for M1.

Characterization of the hybrids

The hybrids obtained were characterized by their chemical characteristics through the determination of the pH at the point of zero charge (pH_{pzc}) [8] and Fourier transform infrared spectroscopy (FTIR) analysis. For the pH_{pzc} test, 0.01 g of each material was placed into 10 falcon tubes with 5 mL of NaCl solution with initial pH values from 2 to 11 (adjusted with HCl and NaOH). After 24 h stirring, the final pH was determined. FTIR analysis was performed in a PerkinElmer Frontier equipment with a resolution of 4 cm^{-1} and 16 scans from 4500 cm^{-1} to 450 cm^{-1}.

Adsorption and (photo)catalytic activity

For the adsorption tests, 40 mg of hybrids were added to 10 mL of dye solution (35 mg/mL). For the degradation tests, 10 mL of dye solution was mixed with 40 mg of hybrids and 0.7 mL of hydrogen peroxide, in the presence or absence of UV light. All these preliminary tests were performed for 15 min at room temperature. For the removal efficiency, UV-Vis spectrophotometry analyses were performed in a Shimadzu 1800 equipment.

Results and Discussion

Characterization of the hybrids

The determination of pH_{pzc} was aimed to understand how the hybrids interact with the adsorbate (dye) and how the surface charge of the materials affects its adsorption. When the pH is above the point of zero charge, the surface carries a negative net charge, and below the point of zero charge, the net charge is positive. This occurs because the electric charge on the surface of particles or solid

surfaces is determined by the functional groups present on the surface, which can be ionized in solution [8]. From Fig. 1, it is possible to observe that the pH_{pzc} of pure chitosan (8.0) decreased to 5.3 for the hybrids produced by M1 and to 1.8 for M2. These results indicate that the preparation procedure and the distribution and organization of MGT and AgNPs in the hybrids interfere in its surface characteristics. Further studies should be carried out to clarify the effect of each constituent in the material's surface characteristics.

Figure 1: pH_{pzc} results for (a) pure chitosan, (b) M1 hybrids, and (c) M2 hybrids.

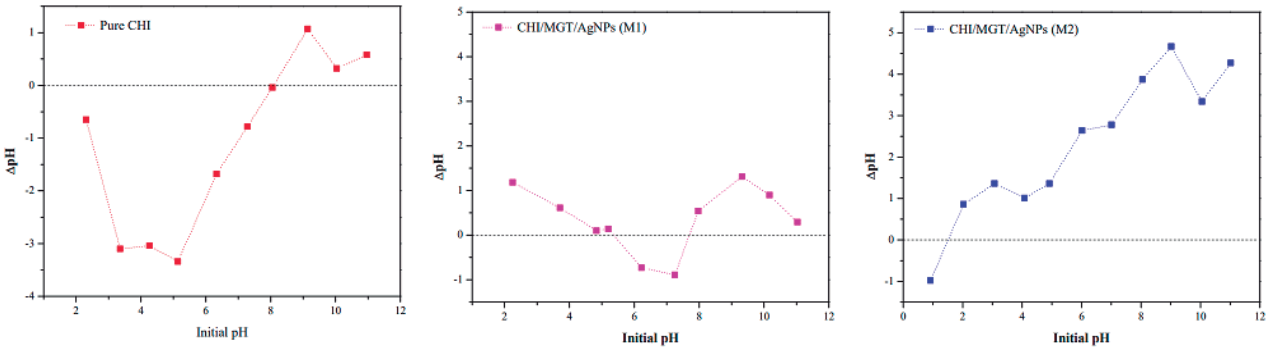

FTIR analysis was used to identify the characteristic bands of the main compounds of the hybrids. From Fig. 2, the characteristic bands of each material could be observed: an intense band around 1650-1655 cm^{-1} attributed to the angular deformation of amide I (C=O) [4] characteristic of CHI, a band at 1730 cm^{-1} for crosslinked materials due to the C=N bond with glutaraldehyde, and the band around 580-590 cm^{-1} attributed to the vibration of the Fe-O bond characteristic of MGT [10]. However, the AgNPs did not show any band because it cannot adsorb the infrared region [6].

Figure 2: FTIR spectra (a) pure CHI, CHI (M1), CHI/AgNPs (M1) and CHI/AgNPs (M2), and (b) CHI (M1), CHI/MGT (M1), CHI/MGT/AgNPs (M1) and CHI/MGT/AgNPs (M2) .

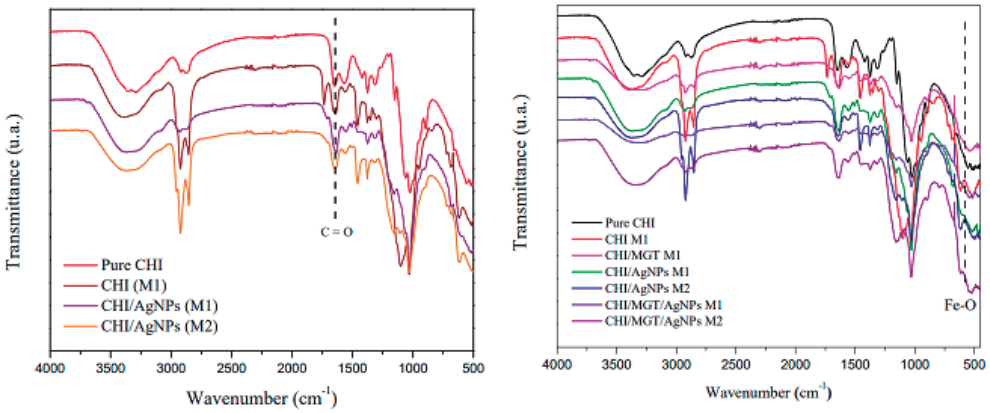

Adsorption and (photo)catalytic activity

Initially, the various combinations of materials were compared by their removal efficiency by using the combination of H_2O_2 and UV radiation (Fig. 3 (a)). Adsorption tests were also conducted by applying UV, H_2O_2, and the combination of both to a dye solution (Fig. 3 (b)) without the use of any material, with the aim of analyzing the need for the application of the hybrids. It was possible to infer that the combination of chitosan with MGT or AgNPs (used individually) provided interesting results (even better than hybrid M1). However, the materials without MGT presented some limitations regarding their recovery from the aqueous solution after treatment. Therefore, hybrids M1 and M2 were selected for further studies.

In Fig.4, one can analyze the use of hybrids under different conditions, where the best result was obtained with the application of the complete set, that is, the combined use of UV light and

hydrogen peroxide. An adsorption test was also performed, which obtained the lowest removal efficiency compared to other tests.

Figure 3: (a) Photodegradation tests using varying combinations of materials. (b) Photodegradation tests using UV, H_2O_2 and UV + H_2O_2

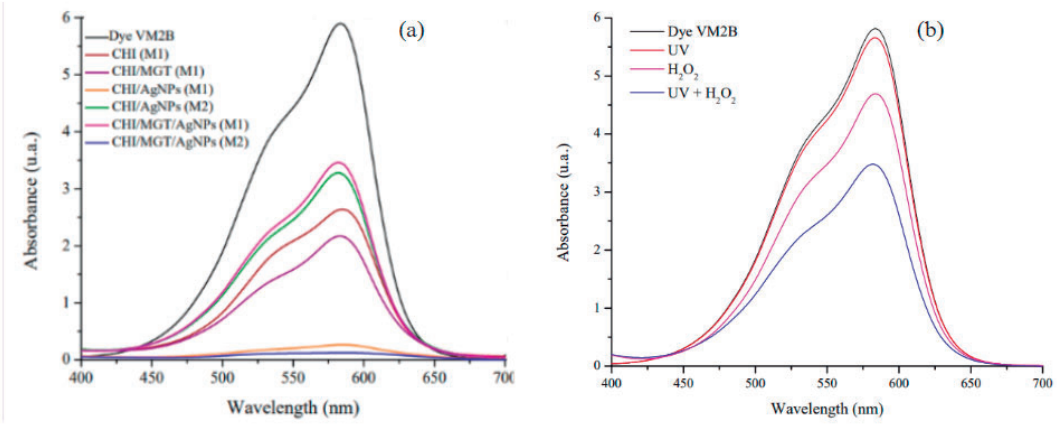

Figure 4: Dye removal tests using M1 and M2 hybrids under different conditions.

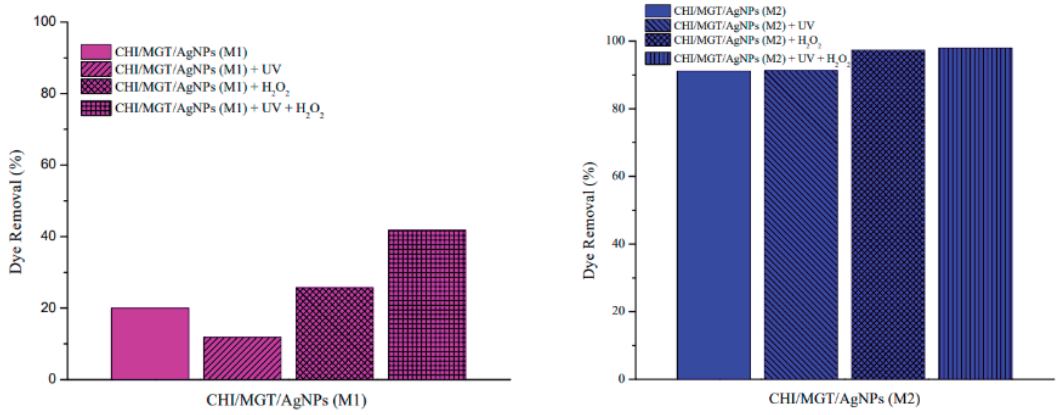

In Fig.5, the dye removal efficiency was evaluated through the reuse of the hybrids. For these tests, the materials were collected, washed with distilled water and ethanol, and dried for further reuse. M1 hybrid presented similar removal efficiency up to two reuse cycles, whereas M2 hybrid had a decrease after the first reuse, reaching similar removal levels of M1 hybrid after four cycles.

Figure 5: Dye removal efficiency after reuse cycles.

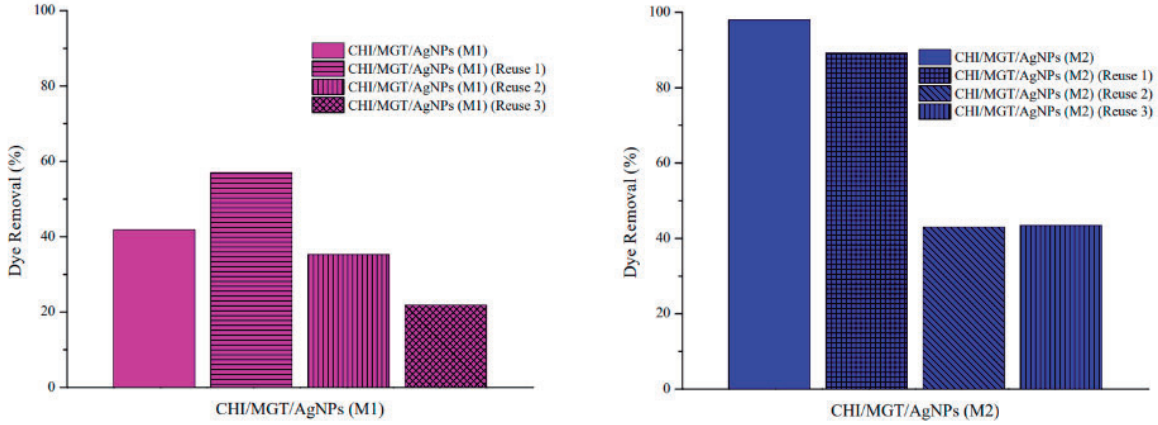

Conclusions

The synthesis of hybrid materials based on chitosan, magnetite, and silver nanoparticles was successful. The quantity, the order of addition of reactants, and the organization of them in the hybrids promoted changes in their surface characteristics, especially in the pH_{pzc}. The preliminary tests regarding the adsorption and (photo)catalytic activity showed that all combinations of chitosan had good efficiency in removing MV 2B from aqueous solution. However, hybrid materials present the advantage of easy recovery after treatment through the application of an external magnetic field. Furthermore, the M2 hybrid exhibited removal rates above 98% and maintained a good efficiency after the first use. New tests will be carried out for the optimization of the process and the determination of the removal kinetics. Nevertheless, the hybrid materials show promising characteristics for applications in water and wastewater treatment.

Acknowledgements
The authors are grateful to Conselho Nacional de Desenvolvimento Científico e Tecnológico (CNPq) and Universidade Federal de Santa Catarina.

References
1. T. ROBINSON, et al. Bioresource technology 2001, 77, 8524(00)00080-8. https://doi.org/10.1016/S0960-8524(00)00080-8
2. L. ARDILA-LEAL, et al. Molecules 2021, 26 (13), 3813; https://doi.org/10.3390/molecules26133813
3. D. REDDY; S. LEE. Advances In colloid and interface science 2013, 201, 10002; https://doi.org/10.1016/j.cis.2013.10.002
4. B. CAGLAR, et al. Solid State Sciences 2018, 83; https://doi.org/10.1016/j.solidstatesciences.2018.07.013
5. J. DUAN, et al. Desalination 2012, 293; https://doi.org/10.1016/j.desal.2012.02.022
6. T. YEAMSUKSAWAT; H. ZHAO; J. LIANG. C Materials Today Communications 2021, 28, 102481; https://doi.org/10.1016/j.mtcomm.2021.102481
7. L. TOREZAN, et al. Journal of Dispersion Science and Technology 2023, 44, 2008420; https://doi.org/10.1080/01932691.2021.2008420
8. V. AGHAZADEH.; S. BARAKAN; E. BIDARI. Journal of Molecular Structure 2020, 1204, 127570; https://doi.org/10.1016/j.molstruc.2019.127570
9. V. M. BISPO, dissertação de mestrado, Universidade Federal de Minas Gerais, 2004.

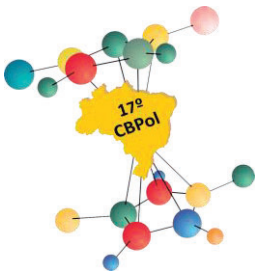

HYDROPHOBICITY EVALUATION OF POLYSTYRENE/STEARIC ACID ELECTROSPUN MEMBRANES

Andressa N. R. Leal[1*], Maurício F. de Aguiar[2], Lúcio F. M. Cavalcanti[2], Winnie Q. Brandão[4], Kleber G. B. Alves[2], Celso P. de Melo[3], Yêda M. B. Almeida[1].

1 – Department of Chemical Engineering, Federal University of Pernambuco (UFPE), Recife, PE, Brazil
andressa.nathally@ufpe.br
2 – Department of Mechanical Engineering, Federal University of Pernambuco (UFPE), Recife, PE, Brazil
3 – Department of Physics, Federal University of Pernambuco (UFPE), Recife, PE, Brazil
4 – Materials Science graduate program, Federal University of Pernambuco (UFPE), Recife, PE, Brazil

Abstract – In this work, we enhanced the hydrophobicity of polystyrene (PS) electrospun membranes through the incorporation of stearic acid (SA). Once the electrospun parameters of PS (flux of 1 mL/h, distance of 14 cm, 19 kV) were optimized for a rotary collector, we added SA on varying mass proportions (10%, 20%, and 30%) to the PS solution. All samples were characterized through scanning electron microscopy (SEM), Fourier Transform Infrared (FTIR), X-ray diffraction (XRD), thermogravimetric analysis (TGA), and contact angle. The membrane with the highest hydrophobicity was the one with 20% of SA

Keywords: *Polystyrene. Stearic acid. Electrospinning. Hydrophobicity.*

Introduction

Electrospinning is a technique where polymer fibers are produced after an electrical field is applied to a polymeric solution [1]. This methodology has attracted the attention of the scientific community for allowing the simple and economical preparation of flexible membranes with a high surface area [2]. Polystyrene (PS) is an interesting material to electrospun since it can lead to low-cost hydrophobic fibers that exhibit good mechanical properties [3]. In addition, the PS fibers can be easily modified through the incorporation of organic materials, such as stearic acid, resulting in fibers with reduced surface energy and increased hydrophobicity [4, 5].

Stearic acid (SA) is a cheap, simple, and environmentally friendly organic material that presents a high hydrophobicity. When dissolved in an aqueous medium, SA causes physical and chemical changes in the liquid-air interface, lowering the surface energy and increasing its hydrophobicity [3]. In this work, we aimed to prepare and characterize stearic acid-containing (PS/SA) polystyrene membranes, evaluate their hydrophobicity, and examine their use in the removal of non-polar organic contaminants.

Experimental

The composite membranes of polystyrene (Sigma-Aldrich, USA) and stearic acid (Dinâmica, Brazil) were synthesized by electrospinning. For this, we first dissolved PS in dimethylformamide (DMF) (Química Moderna, Brazil), resulting in a 20% w/v solution. Then, we incorporated different concentrations of SA (10%, 20%, and 30% w/v) on the solution and kept it stirring for 5 hours at room temperature. Afterward, we placed each solution in a syringe with 18G stainless steel needle (Beckton Dickinson, USA) and allowed the electrospinning process to occur

for 3 hours, which resulted in the PS_10%SA, PS_20%SA, and PS_30%SA membranes. We adopted the following operational parameters: a 1 mL/h flux provided by a NE-4000 syringe pump (New Era, USA), 19 kV voltage supplied by a homemade power source, a distance of 14 cm from the needle to a rotary collector, the temperature of 18 °C, and relative humidity close to 50%. The materials were characterized by a MIRA3 scanning electron microscope (TESCAN, CZ), Fourier Transform Infrared (FTIR) (Shimadzu, Japan), X-ray diffraction (XRD) (Rigaku, Japan), TGA2 thermogravimetric analysis (TGA) (Mettler Toledo, Switzerland), and a CAM 200 contact angle meter (KSV, Finland).

Results and Discussion

The morphology of PS, PS_10%SA, PS_20%SA, and PS_30%SA membranes can be seen in the scanning electron microscopy (SEM) images shown in Fig. 1, where it is possible to observe the presence of beads and an increase in the fiber roughness, as a result from the incorporation of SA. In addition, it can be also noted the absence of defects and ruptures along the length of the fibers.

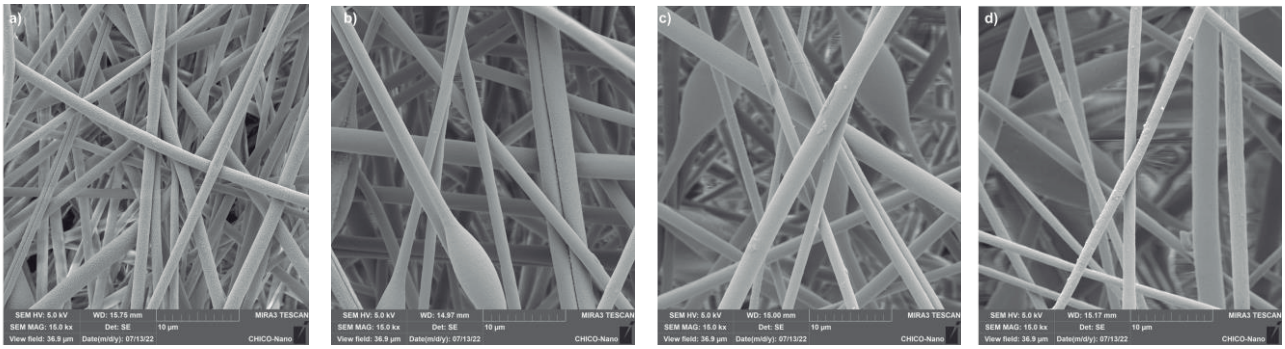

Figure 1 – SEM images of the PS (a), PS_10%SA (b), PS_20%SA (c), and PS_30%SA (d) membranes.

We measured the water (at natural pH) contact angle of the membranes to assess their wettability. As can be observed in Fig. 2, the incorporation of SA on the electrospun membranes leads to an increase in the contact angle as a result of a synergistic effect between the fatty acid and the polymer, which reduces the surface energy of the material and increases its roughness. Therefore, the incorporation of SA causes an enhancement of the hydrophobic character of the PS membranes. It can be observed that all samples have a hydrophobic character since the contact angle is higher than 90° [6]. In addition, the highest degree of hydrophobicity is achieved by PS_20%SA. Due to an inefficient incorporation of SA into the fibers at higher concentrations, the membrane hydrophobicity reduced slightly [7]

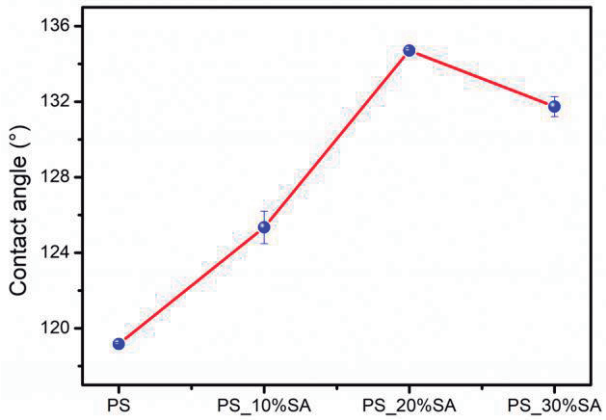

Figure 2 – Contact angle of the PS, PS_10%SA, PS_20%SA, and PS_30%SA membranes.

The FTIR spectrum of the PS, SA, PS_10%SA, PS_20%SA, and PS_30%SA membranes are shown in Fig. 3. In the PS spectra (Fig. 3a), one can observe the characteristic bands at 3022 cm^{-1}, 2920 cm^{-1} and 2850 cm^{-1}, which corresponds to the C-H stretching vibration of the aromatic ring, CH_2 symmetric and asymmetric stretching vibration, respectively [8]. In addition, the C=C aromatic ring stretching is observed at 1600 cm^{-1} [9]. On the other hand, for the SA spectrum (Fig. 3b), one can identify the bands at 1700 cm^{-1} and 1290 cm^{-1}, which are due to C-O stretching and carboxyl (-COOH) bending vibration [10]. As for the composite membranes (Fig. 3c-3e), one can observe bands that are characteristic of both PS and SA, corroborating the presence of these two components.

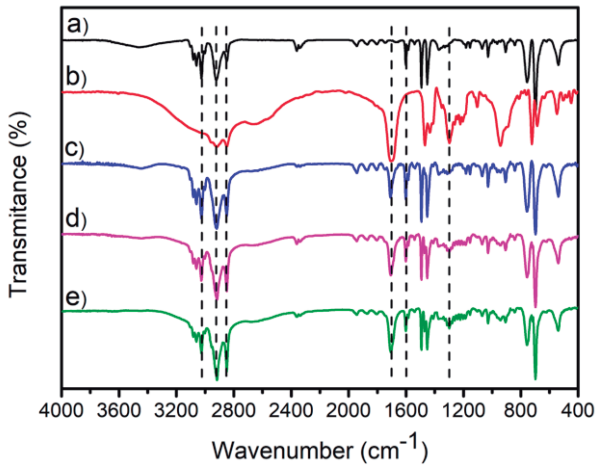

Figure 3 – FTIR spectrum of the PS (a), SA (b), PS_10%SA (c), PS_20%SA (d), and PS_30%SA (e) membranes.

The XRD diffractogram of SA and the PS membranes are shown in Fig. 4. In the pristine PS curve, one can observe an amorphous band at 19.4°, which corresponds to the van der Waals distance between adjacent polymer chains [11, 12]. On the other hand, peaks related to regular crystallization at 21.5° and 24.0° are observed on the SA spectrum [13, 14]. As for the composite membranes, one can observe the presence of bands of both materials, confirming the presence of PS and SA.

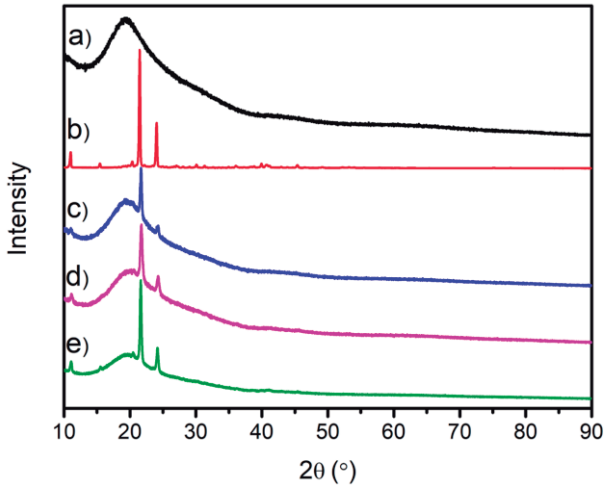

Figure 4 – XRD spectrum of PS (a), SA (b), PS_10%SA (c), PS_20%SA (d), and PS_30%SA (e).

In Fig. 5, we show the thermal decomposition of PS, SA, and the composite membranes containing both materials. Through the analysis of the TGA and DTG curves, one can observe that

the decomposition of the SA and PS membranes begin at 200 °C and 330 °C, respectively [9, 10], with the maximum rate occurring at 273 °C and 415 °C, for each case. Concerning the composite membranes, they exhibit a similar thermal behavior since both stages of mass loss are observed. The first stage, which corresponds to the presence of SA, has a maximum degradation rate at 226 °C and the decomposition extends to 300 °C. The second stage corresponds to the degradation of PS, in which the thermal decomposition starts at 345 °C, with the maximum rate observed at 415 °C, and ends at 450 °C. Therefore, it can be concluded that for the PS_10%SA, PS_20%SA, and PS_30%SA membranes, the first thermal degradation corresponds to 10%, 20%, and 30% of SA mass, respectively. For all membranes, the remainder of the mass is PS.

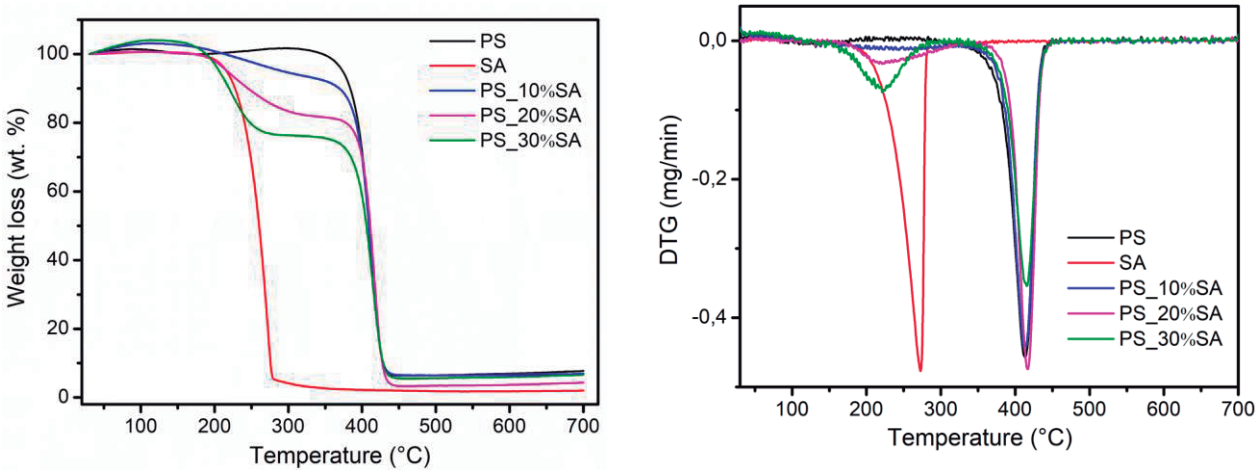

Figure 5 – TGA and DTG results of PS, SA, PS_10%SA, PS_20%SA e PS_30%SA

Conclusions

The results confirm that it was possible to enhance the hydrophobicity of a polystyrene membrane through the incorporation of stearic acid into the solution before the electrospinning process. This methodology to produce membranes was chosen for allowing the preparation of flexible membranes with high porosity in a fast, cheap, and simple manner. Although the pristine PS membrane already presented a hydrophobic character, this characteristic was enhanced after the incorporation of SA with varying concentrations (10%, 20%, and 30% w/v of SA). We have determined that the membrane prepared with a 20% SA concentration exhibited the highest contact angle. This is a relevant result because SA is a cheap and environmentally friendly compound, which has a noticeable effect in reducing the surface energy of the membrane.

References

1. T. J. Sill; H. A. Von Recum. *Biomaterials*, 2008, v. 29, n. 13, p. 1989–2006. https://doi.org/10.1016/j.biomaterials.2008.01.011
2. D. Han; A. J. Steckl. *ChemPlusChem*, 2019, v. 84, n. 10, p. 1453–1497. https://doi.org/10.1002/cplu.201900281
3. A. Patti et al. *Journal of Industrial and Engineering Chemistry*, 2021, v. 96, p. 1–33. https://doi.org/10.1016/j.jiec.2021.01.024
4. C. Loos et al. *Beilstein Journal of Nanotechnology*, 2014, v. 5, p. 2403–2412. https://doi.org/10.3762/bjnano.5.250
5. X. Mao et al. *Journal of Materials Science*, 2023, v. 58, n. 1, p. 3–33. https://doi.org/10.1007/s10853-022-07945-8
6. M. Cui et al. *Thin Solid Films*, 2018, v. 657, p. 88–94. https://doi.org/10.1016/j.tsf.2018.05.008
7. M. Yang et al. *ACS Applied Electronic Materials*, 2021, v. 3, n. 5, p. 2067–2078. https://doi.org/10.1021/acsaelm.1c00076

8. Y. A. Sihombing et al. *Heliyon*, 2022 v. 8, n. 8, p. e10113. https://doi.org/10.1016/j.heliyon.2022.e10113
9. L. M. S. de Farias et al. *Materials Chemistry and Physics*, 2022, v. 276, p. 125356. https://doi.org/10.1016/j.matchemphys.2021.125356
10. N. Zhang et al. *Chemical Engineering Journal*, 2018, v. 354, p. 245–253. https://doi.org/10.1016/j.cej.2018.07.184
11. N. Bhardwaj; S. C. Kundu. *Biotechnology Advances*, 2010, v. 28, n. 3, p. 325–347. https://doi.org/10.1016/j.biotechadv.2010.01.004
12. N. Wu et al. *Journal of Materials Chemistry*, 2012, v. 22, n. 33, p. 17254–17261. https://doi.org/10.1039/C2JM33114D
13. C. Li et al. *Sustainable Cities and Society*, 2019, v. 44, p. 458–464. https://doi.org/10.1016/j.scs.2018.10.041
14. B. Xie et al. *Solar Energy*, 2020, v. 204, p. 624–634. https://doi.org/10.1016/j.solener.2020.05.004

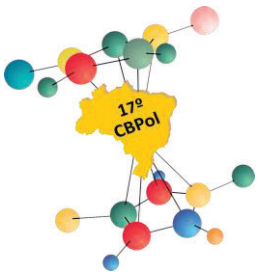

IMPACT BEHAVIOR OF UNSATURATED POLYESTER RESIN TOUGHENED BY CELLULOSE NANOCRYSTALS

Arthur B. Aramburu[1*], Rafael A. Delucis[2] and Sandro C. Amico[1]

1 – Postgraduate Program in Mining, Metallurgical and Materials Engineering, Federal University of Rio Grande do Sul (UFRGS), Porto Alegre, RS, Brazil
arthuraramburu@gmail.com
2 – Postgraduate Program in Materials Science and Engineering, Federal University of Pelotas (UFPEL), Pelotas, RS, Brazil

Abstract – Unsaturated polyester resin (UPR)/cellulose nanocrystals (CNC) composites were studied in an attempt to improve the impact strength of the polymer. 2 wt% of CNC was dispersed in the UPR using a lab-scale ultrasonic processor. The results showed that the incorporation of 2 wt% of CNC yielded nanocomposites with increased toughness, as well as decreased tensile strength and modulus. These effects were attributed to the high CNC content and long ultrasonic dispersion process, which potentially led to styrene volatilization. Interestingly, these changes also positively influenced the impact properties since the CNC-based nanocomposite displayed higher impact strength compared to the neat UPR.

Keywords: *CNC, Celluforce NCC®; Izod impact; tensile.*

Fundings: This work was supported by National Council for Scientific and Technological Development (CNPq) (140229/2022-1) and by FAPERGS Inova Clusters Tecnológicos (22/2551-0000839-9)

Introduction

Cellulose nanocrystals (CNC) have gained attention in the field of nanocomposites due to interesting properties including high surface area, low density, good mechanical behavior, renewability and biodegradability [1]. These CNCs, with 100-1000 nm length, have been extensively evaluated as reinforcing agents of polymeric nanocomposites with matrices such as polyester [2]. Indeed, the addition of CNC can improve various properties, e.g., reducing crack propagation and enhancing overall toughness [1], enabling their wider use.

Unsaturated polyester resin (UPR) is widely employed in composites. Its properties include good strength and modulus, water resistance, room temperature curability, transparency, and low cost [3]. However, the use of the UPR is limited by its brittle behavior and low toughness, especially when subjected to impact loads. This issue has been sometimes tackled by incorporating elastomeric particles into the resin. Although it increases toughness, the addition of elastomers unavoidably diminishes the stiffness and strength of the UPR. Thus, this study aims at investigating a CNC reinforcement to increase the toughness of UPR, while retaining its stiffness and strength.

Experimental

Materials selection and characterization

A low viscosity orthophthalic polyester resin with a high content of styrene monomer (41-47%) supplied by Embrapol (Brazil) was used. Methyl ethyl ketone peroxide (MEKP, Butanox

M50) was used as initiator. Cellulose nanocrystals (CNC), commercially called Celluforce NCC®, were acquired from Celluforce. According to the manufacturer, the CNC was obtained through acid hydrolysis using a high sulfuric acid concentration of 64% applied at 45 °C for 25 min followed by sonication for 15 min, and spray-dried.

The CNC was analyzed by X-ray diffraction (XRD) using a Rigaku model system. The diffracted intensity of the Cu K-α radiation (40kV/17mA) was measured in the 10º - 90º range with 0.02 step. The crystallinity index was determined by integrating the crystalline peaks in relation to all peaks. Moisture, volatile matter and residue content were obtained by thermogravimetry (TG) at a heating rate of 10 °C min^{-1} using a TA Instruments (model Q50) equipment under N_2 atmosphere. The chemical structure was analyzed by Fourier-transform infrared (FTIR) spectroscopy coupled with attenuated total reflection device (ATR) in a Perkin Elmer Spectrum (model 400) equipment using 32 scans in the 400–4000 cm^{-1} range at 4 cm^{-1} resolution.

Manufacturing and mechanical testing of the nanocomposites

The CNCs (2 wt%) were dispersed in the UPR using an ultrasonic processor (Vibracell), at 40% amplitude and 500W for 10 min, in an ice bath. To prevent styrene volatilization, 1-min on and 1-min off cycle was used. The CNC-UPR mixture was cooled to room temperature, the initiator (1.5 wt%) was added and the solution was mechanically stirred at 1000 rpm for 2 min. The mixture was casted into a silicon mold, cured at room temperature for 24 h and post-cured at 60 ºC for 4 h.

Neat resin (UPR) and CNC-UPR nanocomposites were analyzed with Fourier-transform infrared (FTIR) spectroscopy. Tensile testing was carried out using a 3382 Instron Universal Testing Machine at a cross-head speed of 5 mm/min, according to ASTM D638. Izod impact test was performed according to ASTM D256 in a CEAST 9050 Impactor II equipment using a 2.75 J hammer at room temperature. The mechanical tests were conducted using 10 samples per group and the means compared using ANOVA tests. Tukey post hoc test tests were conducted at a significance level of 0.05.

Results and Discussion

CNC characteristics

FT-IR spectra of the CNC (Fig. 1A) showed typical chemical groups of lignocellulosic materials. OH groups were represented by the 3451 cm^{-1} band, indicating high hydrophilicity [4]. The prominent 1382 cm^{-1} band is typically associated with the bending vibrations of the CH_3 groups in the cellulose structure, whereas the 1060 cm^{-1} band corresponds to C-O stretching vibrations of the CNC, which may vary depending on cellulose source, crystallinity, and sample preparation [5]. The band at 2901 cm^{-1} is attributed to C–H stretching and can be related to the degree of crystallinity [4], degree of polymerization and presence of other functional groups in the cellulose structure, while the band at 1644 cm^{-1} is due to O–H vibration in adsorbed water [6]. The high intensity in these bands can be related to the well-known high crystallinity of CNCs.

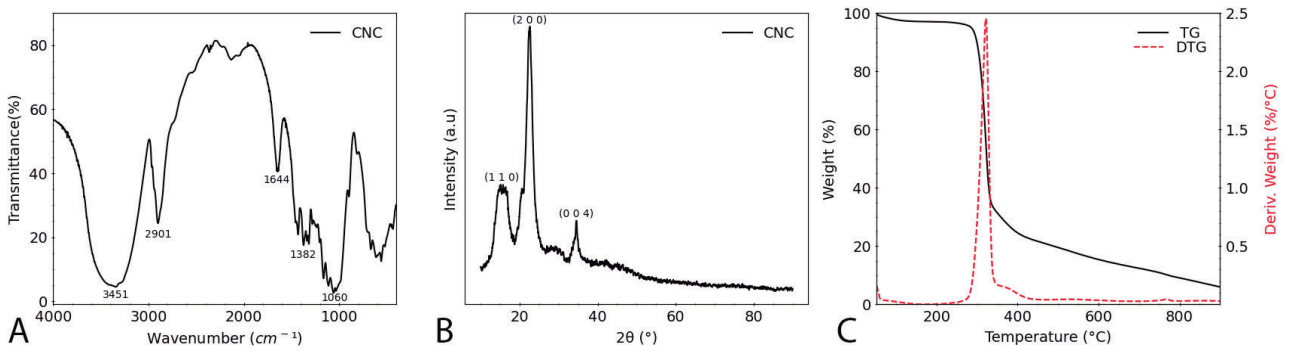

Figure 1 – FT-IR spectra (A), XRD diffractogram (B) and TG/DTG curves (C) of the neat CNC.

In the XRD diffractogram (Fig. 1B), the peaks at 2θ of 16.5º and 22.5º are attributed to the (1 1 0) and (2 0 0) planes, respectively. They correspond to the cellulose I structure, suggesting that the pristine cellulose crystals remain unaffected after the conversion of the lignocellulosic material into CNC [7]. A high crystallinity of 66.9% was calculated. Thermogravimetric curves of the CNC showed a two-stage degradation pattern (Fig. 1C). There is an initial loss (below 100 ºC) related to moisture adsorbed on the cellulose surface and volatile compounds. Within 280 - 400 ºC, a significant weight loss is seen, indicating degradation of structural chemical groups from cellulose polymer chains and release of volatile decomposition products, including water, carbon dioxide, and organic compounds [8].

UPR/CNC nanocomposites

Fig. 2 shows the FT-IR spectra of the neat UPR and CNC-UPR composite. The small peak at 2960 cm^{-1} for neat UPR increased for CNC-UPR, attributed to the elongation of C–H bonds in cellulose [8]. The peak at 1720 cm^{-1} indicates the presence of carbonyl groups (C=O) and the peaks around 1260 cm^{-1} the stretching vibrations of C–O–C bonds connected to aliphatic groups [5]. The 800 cm^{-1} peak may be associated with cellulose-specific vibrations such as C–O–C glycosidic linkages or C–H bending modes. The band at 800 cm^{-1} in the CNC-UPR group is related to an out-of-plane bending absorption of N-H groups, perhaps due to interactions between UPR and CNC. The aforementioned peaks showed higher intensity in the CNC-UPR sample, which could be related to the crystallinity of CNC [5,6].

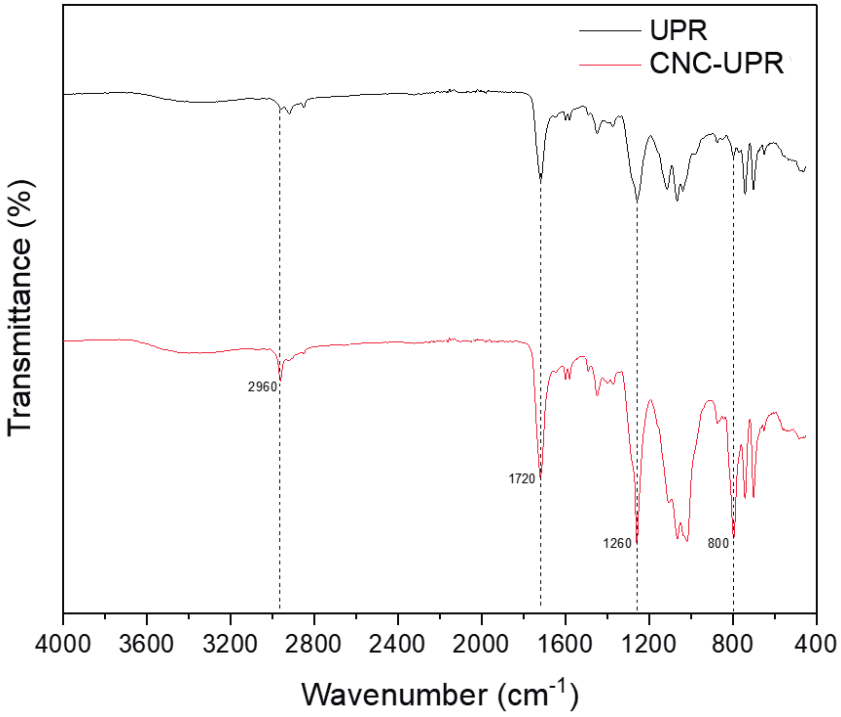

Figure 2 – FT-IR spectra of UPR and CNC-UPR samples.

The effect of the incorporation of 2 wt% CNCs in tensile properties of the UPR matrix is presented in Fig. 3. The stress vs. strain curves (Fig. 3A) show greater deformation in the CNC-UPR samples, suggesting higher toughness. However, a significant decrease was observed in both tensile modulus ($F= 282.94$; $p < 0.01$) (Fig. 3B) and tensile strength ($F= 92.49$; $p < 0.01$). In fact, the tensile strength of the UPR group was 43.99 (± 2.71) MPa, while a reduction of 30% in this property was observed for the CNC-UPR group (30.72 ± 1.49 MPa). This may be related to the hydrophilicity of CNCs, in turn poor interfacial adhesion with the hydrophobic matrix, and the relatively high nanomaterial content (2 wt%), wherein CNC agglomerations may occur and impair

an effective filler/matrix dispersion and bonding [6]. Moreover, prolonged ultrasonic dispersion times may cause damage in the chemical structure of the UPR accompanied of styrene volatilization. In fact, the loss of styrene has been reported to justify changes in nanocomposite mechanical properties [2,3].

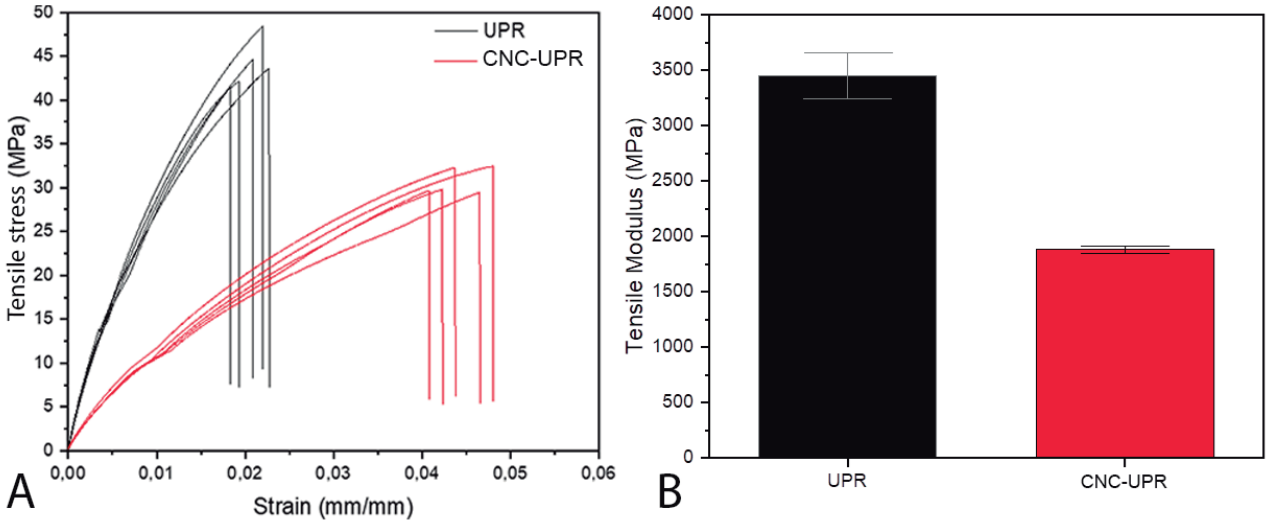

Figure 3 – Stress *vs.* strain curves (A) and tensile modulus (B) of UPR and CNC-UPR.

Fig. 4 shows the impact strength results for the UPR and CNC-UPR samples, wherein the nanocomposite exhibited a higher impact strength (≈80%). The significant improvement in impact strength can be attributed to interactions between nanofiller and matrix, since CNC particles exhibit strong hydrogen bonds, which enhances the ability of the composite system to absorb energy during fracture propagation [5]. The toughening mechanism in the nanocomposites can be explained by crack trapping and crack pinning. As the crack propagates, it bows out between the reinforcing particles, while remaining pinned at these particles. This pinning of the crack at the particles appears to be the dominant toughening mechanism. The presence of CNC particles with a large specific area increases the interfacial interaction with the matrix, which contributes to energy absorption [9].

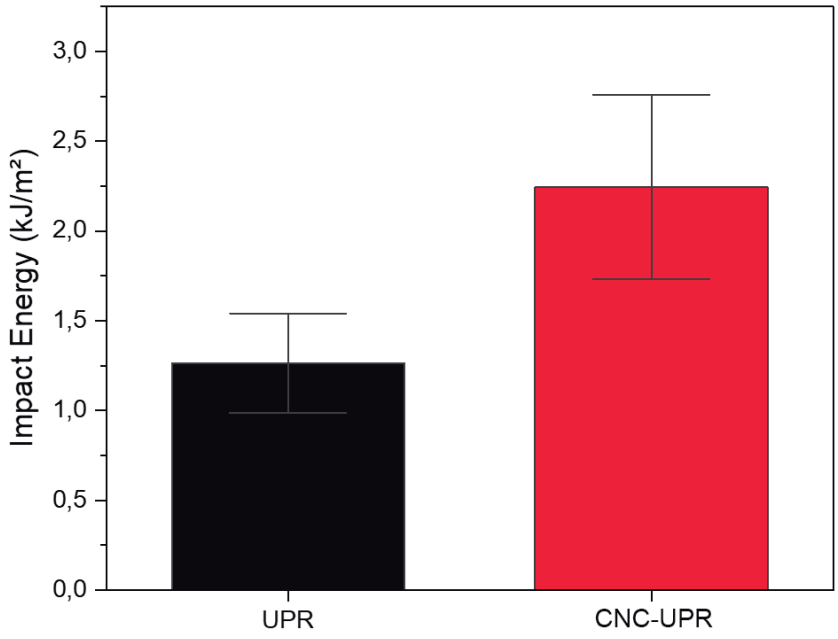

Figure 4 – Impact strength of UPR and CNC-UPR.

Conclusions

FTIR results revealed that the incorporation of 2 wt% CNC did not significantly alter the chemical structure of the polyester matrix, however, the observed increase in the peaks indicated some degree of CNC interaction. Furthermore, CNC addition increased toughness and decreased tensile strength and modulus compared to the neat polyester, probably due to an exaggerated CNC addition and a long ultrasonic dispersion process, which may have caused styrene volatilization. This effect may also be related to the hydrophilicity of CNCs, which is usually modified chemically or physically to achieve the desired interfacial adhesion with the hydrophobic matrix. Finally, improvement of ≈80% in Izod impact strength was obtained with the CNC addition. Further investigations are needed to comprehensively understand the underlying mechanisms behind these observed effects to achieve the desired mechanical properties in CNC-reinforced UPR composites.

Acknowledgements

The authors would like to thank the National Council for Scientific and Technological Development (CNPq) (140229/2022-1) and FAPERGS Inova Clusters Tecnológicos (22/2551-0000839-9) for the financial support.

References

1. Shojaeiarani, J.; Bajwa, D.S.; Chanda, S. *Compos. Part C Open Access* 2021, *5*, 100164, doi:10.1016/j.jcomc.2021.100164.
2. Kargarzadeh, H.; Sheltami, R.M.; Ahmad, I.; Abdullah, I.; Dufresne, A. *Polymer (Guildf).* 2015, *71*, 51–59, doi:10.1016/j.polymer.2015.06.045.
3. Kargarzadeh, H.; Sheltami, R.M.; Ahmad, I.; Abdullah, I.; Dufresne, A. *Ind. Crops Prod.* 2015, *72*, 125–132, doi:10.1016/j.indcrop.2014.12.052.
4. Sain, M.; Panthapulakkal, S. *Ind. Crops Prod.* 2006, *23*, 1–8, doi:10.1016/j.indcrop.2005.01.006.
5. Maradini, G. da S.; Oliveira, M.P.; Carreira, L.G.; Guimarães, D.; Profeti, D.; Dias Júnior, A.F.; Boschetti, W.T.N.; Oliveira, B.F. de; Pereira, A.C.; Monteiro, S.N. *Polymers (Basel).* 2021, *13*, 1–11, doi:10.3390/polym13111878.
6. Kargarzadeh, H.; Sheltami, R.M.; Ahmad, I.; Abdullah, I.; Dufresne, A. *Polymer (Guildf).* 2015, *56*, 346–357, doi:10.1016/j.polymer.2014.11.054.
7. Lv, J.; Zeng, D.; Wei, C. *Adv. Polym. Technol.* 2015, *34*, 1–8, doi:10.1002/adv.21483.
8. Lavoratti, A.; Scienza, L.C.; Zattera, A.J. *Carbohydr. Polym.* 2015, *136*, 955–963, doi:10.1016/j.carbpol.2015.10.008.
9. Johnsen, B.B.; Kinloch, A.J.; Mohammed, R.D.; Taylor, A.C.; Sprenger, S. *Polymer (Guildf).* 2007, *48*, 530–541, doi:10.1016/j.polymer.2006.11.038.

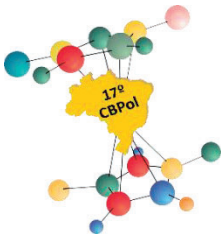

INCORPORATION OF SILVER NANOPARTICLES INTO POLYESTER FABRICS

Vania Sonda[1], Diego Piazza[1], Edson L. Francisquetti[2], Mara Z. Anadrade[2], Ana M.C. Grisa [1,2]

1-Universidade de Caxias do Sul, Caxias do Sul,RS, Brasil.1

2 –Instituto Federal de Ciência e Tecnologia (IFRS), Campus Farroupilha, Farroupilha, RS, Brasil

Abstract - Due to technological and environmental reasons, the search for materials with well-defined and pre-established properties is increasing. In this regard, the textile industry is advancing by creating fabrics for various purposes with antimicrobial properties that do not harm the environment, while retaining the characteristics of virgin tissue. In this study, the application of silver nanoparticles as a chemical treatment on polyester fabrics was investigated, with an evaluation of their morphological, chemical, physical, mechanical, and biological properties. The incorporation of silver nanoparticles into the fabric was carried out using a foulard equipment. The polyester fabric was assessed in its original state and after treatment with silver nanoparticles, both before and after exposure to UV radiation. The presence of silver nanoparticles in the polyester fiber was found to have no impact on fiber distribution, morphology, and chemistry. Following the UV exposure test, samples treated with silver nanoparticles exhibited a greater degree of surface degradation, as observed through scanning electron microscopy (SEM).

Keywords: **nanotechnology, silver nanoparticles, polyester fabric.**

Introduction

Nowadays, the use of nanostructured materials is becoming increasingly widespread. Over the last few decades, there has been significant interest from transformation industries in inputs with bactericidal properties, particularly in the textile sector [1]. Silver nanoparticles (NPSAg) have garnered substantial attention due to their remarkable properties, including high surface area and excellent microbial activity [2]. They are also considered as alternatives for reducing bacterial adhesion [3]. These nanoparticles exhibit activity against various types of bacteria, including multidrug-resistant strains, and can be easily incorporated into diverse materials [4]. The inherent properties and structure of textile fibers provide a suitable environment for the growth of harmful microorganisms, especially exacerbated by humidity and high temperatures [5]. One approach to incorporating bactericidal agents into textile fibers involves immersing the fabric in a solution containing the additive [6]. Silver, known for its antiseptic properties, becomes even more effective in nanoparticle form, where its contact surface area is significantly enhanced [7]. Medical research has demonstrated silver's ability to eliminate more than 650 pathogenic organisms [8]. Therefore, this study involves the application of a chemical treatment using silver nanoparticles for textile processing. The aim is to provide not only antimicrobial properties but also an enhancement in the characteristics of polyester fabrics.

Experimental

Materials

The material employed in this study is a 100% polyester curtain fabric supplied by Indústrias Têxteis H Milagre - IT (Farroupilha/RS), adhering to Engineering Specification

EME REV013/00. The antimicrobial additive employed was a colloidal silver dispersion in an aqueous medium, consisting of silver nanoparticles stabilized with organic molecules. This dispersion, known commercially as NpAg_925, was sourced from TNS (Brazil) nano.

Production of PL tissue/ NPSAg impregnation

The procedure for producing the polyester fabric with the integration of nanoparticles involves several steps. These steps include yarn production, warping (which involves assembling thousands and hundreds of yarns onto a reel), weaving (the interlacing of weft and warp yarns), scouring (the removal of paraffins and oils introduced during spinning and weaving), heat setting (a stage of thermal fixation), dyeing (altering the fiber color), another round of heat setting, the application of nanoparticles, and a final heat setting. The infusion of silver nanoparticles into the fabric was conducted at ITM - Indústrias Têxteis H. Milagre S.A. As shown in Figure 1, the process of applying silver nanoparticles onto the fabric is illustrated. The incorporation of nanoparticles into the polyester fabric took place using a Folard equipment at the ITM company.

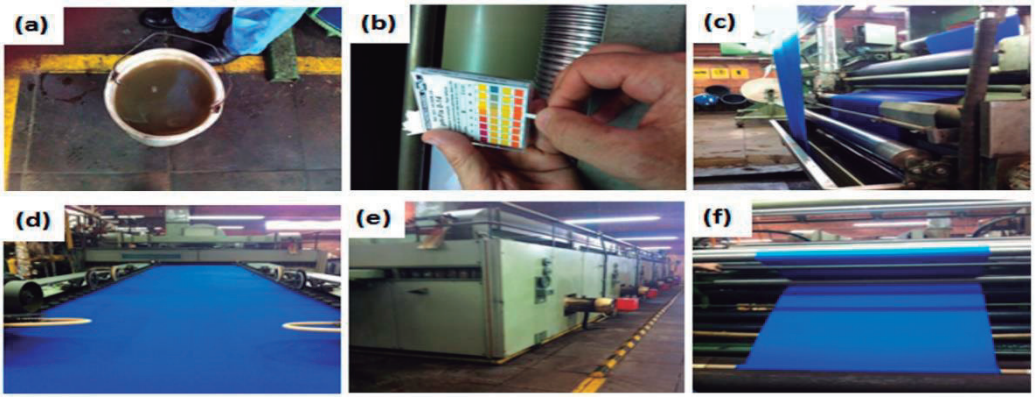

Figure 1 - Antimicrobial fabric preparation steps: (a) preparation of the bath (dilution of the antimicrobial additive); (b) pH correction of the bath; (c) incorporation of nanoparticles; (d) correction of fabric weft; (e) drying; and (f) finished fabric.

The polyester fabric samples were subjected to a series of controlled environmental conditions involving repeated cycles of light and humidity exposure. Each cycle lasted for 4 hours, with 4 hours of UV exposure followed by 4 hours of condensation exposure. This sequence was maintained for a total duration of 120 hours, which is equivalent to approximately 3 months of real-world environmental exposure. The testing procedure was conducted using the C-UV Comexim System Accelerated Aging equipment for Non-Metallic materials, situated in the Polymer Laboratory of the University of Caxias do Sul.

Characterization

The morphological characterization of the fabrics was carried out using a SHIMADZU SSX-550 Superscan scanning electron microscope, operating at an acceleration voltage of 5 kV, under a voltage of 12 V and a current of 22. The samples were analyzed by FTIR, in a Nicolet Impact IS10 Transmission spectrophotometer, using the attenuated total reflection (ATR) technique, in the spectral range of 4000 to 400 cm^{-1}.

Results and Discussion

Figure 2 shows SEM micrographs of untreated and silver nanoparticle-treated polyester fabric surface.

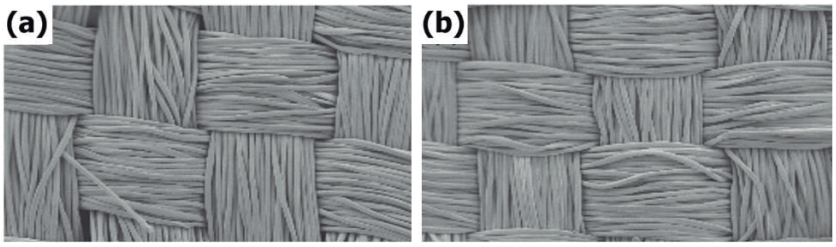

Figure 2 -SEM micrographs of polyester fabric (a) without treatment and (b) with silver nanoparticle treatment, at a magnification of 70x.

In the analysis of the morphology of the untreated and silver nanoparticle-treated polyester fabric, it was observed that the impregnation of silver nanoparticles is not visible at 70 times magnification and does not interfere with the arrangement of the polyester fibers in the weft and warp directions. Figure 3 illustrates the SEM micrograph of the polyester fabric at 500x magnification with and without silver nanoparticle treatment.

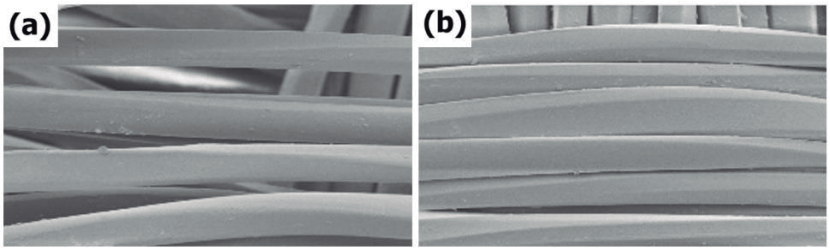

Figure 3 -SEM micrograph of the polyester fabric (a) untreated polyester fabric; (b) silver nanoparticle treated polyester fabric, with a magnification of 500x.

It was possible to observe that the fibers have a rough appearance where dirt may have adhered (Figure 3a) and in Figure 3(b) the adhesion of silver nanoparticles on the surface of polyester fibers was observed. Perera et al. [12] observed the adhesion of silver nanoparticles on the surface of cotton fibers treated with silver nitrate ($AgNO_3$). Figure 4 shows the SEM micrograph of polyester fabric with and without silver nanoparticle treatment with a magnification of 10,000x. In Figure 4b, the presence of spherical domains on the surface of the untreated polyester fabric samples was observed, which may have originated during the impregnation of silver nanoparticles. In untreated fabrics (Figure 4a), a smooth and uniform surface was observed. The adhesion of aggregates formed on the surface of the fabric fibers originates from weak van der Waals forces with lower binding energy.

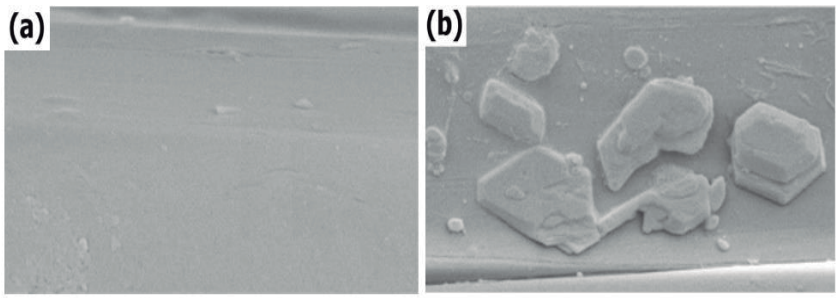

Figure 4 -SEM micrograph of polyester fabric (a) untreated polyester fabric; (b) silver nanoparticle-treated polyester fabric, with a magnification of 10,000x.

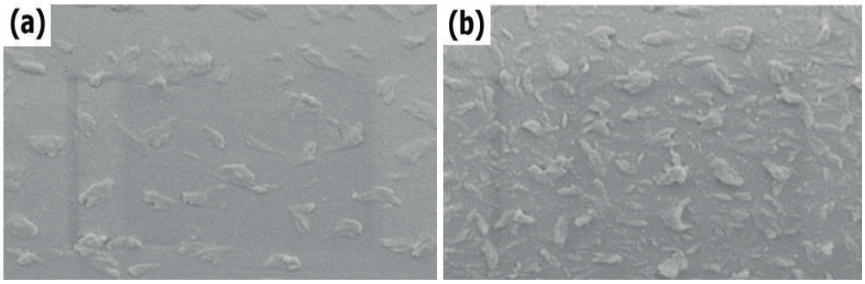

Figure 5 - SEM micrograph of polyester fabric after accelerated aging under UV radiation (a) untreated polyester fabric; (b) polyester fabric treated with silver nanoparticles, magnification of 10,000x.

The Figure 5 shows the SEM micrographs of polyester fabric after 120 hours of UV radiation exposure accelerated aging under UV radiation: (a) untreated polyester fabric and (b) polyester fabric treated with silver nanoparticles, with a magnification of 10,000x. In the SEM image, it is possible to observe that the particles adsorbed on the surface are silver nanoparticles. A more significant physical change (deterioration) was observed on the surface of the UV-treated material, exhibiting a higher concentration of dirt. This might be attributed to the elevated radiation intensity in these samples, which could be amplified by the presence of silver nanoparticles situated on the sample's surface. This alteration could potentially stem from the degradation of polyester, leading to hydrolytic degradation [13]. The chemical structure of the polyester fabrics with and without silver nanoparticle treatment, before and after exposure to UV radiation, can be identified through the absorption bands in the FTIR spectrum, represented in the Figure 6. The FTIR spectrum shows characteristic peaks of the untreated polyester fabric samples, like those observed by Assis (2012) [13]: at 1090-1150 cm^{-1}, stretching mode of C-O bonds; at approximately 1730 cm^{-1}, a band attributed to vibrations of the ester carbonyl group; and at 2850-3000 cm^{-1}, absorption bands referring to the symmetrical stretching vibration of C-H bonds.

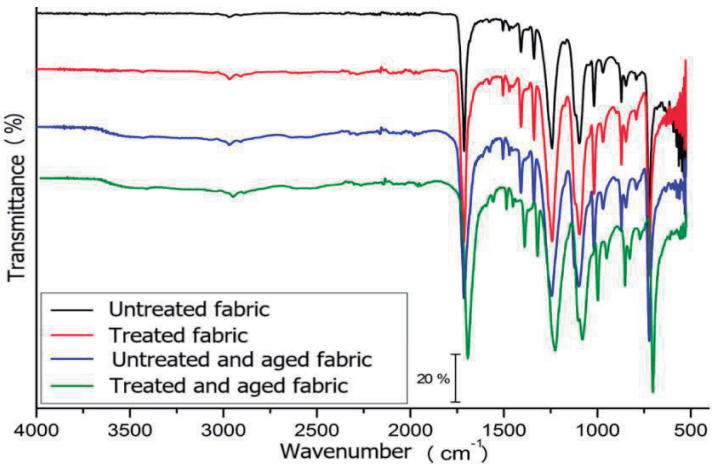

Figure 6 - FTIR spectroscopy of silver nanoparticle treated and untreated polyester fabrics before and after UV exposure.

There were no significant changes in the absorption bands for the silver nanoparticle-treated untreated polyester fabric samples, thus showing that the silver nanoparticles are located on the surface of the fibers. In the FTIR spectra (Figure 6) for samples with and without treatment after exposure to UV radiation, bands were observed near 3500 cm^{-1} (hydroxyl groups (-OH), related to carboxylic acid (-COOH) with low intensity, which may be associated with exposure to UV radiation, causing bond breakage leading to

polyester degradation [13,14]. Polyester undergoes degradation through hydrolysis, as evidenced in the spectra following UV exposure. There may be a noticeable increase in the intensity of the band at 3400 cm-1, corresponding to the stretching and deformation of the O-H group (Batista et al., 2001).

Conclusion

The foulard process and parameters adopted in this study were efficient and kept the nanoparticles on the surface of the fibers without damaging the fabric structure, as verified by MEV. No changes in the chemical structure were observed in the polyester fabric treated with silver nanoparticles, proving that the nanoparticles are only adhered to the surface of the fabric. After exposure to UV radiation, the polyester degraded due to the breakage of its bonds. The biological assays of the samples treated with NPSAg, both with and without UV irradiation, were conducted by the microbiology laboratory at UCS. The results were positive for *Escherichia coli and Bacillus*. However, they are currently being redone due to contamination.

Acknowledgements

The authors appreciate support the University of Caxias do Sul – Brazil, Instituto Federal de Ciência e Tecnologia do RS (IFRS), CNPq and FAPERGS.

References

1. H. Y. Kim; S. C. Kwon; S. H. Jeong*; Journal of Materials Science*, 2017, 42, 8020–8024.
2. F. S. Antunes; N. Dal'acqua; C.P. Bergann; M. Giovanela; *Estud. Tecnol. Eng*. 2013, 9(1):20-26.2013. https://doi.org/2013.9103.
3. A.A. Pereira; E.A. Araújo; L. Ribeiro; F.R. Passos; D.A. Botre;. N.J.D. Andrade, Biosci. *J. Online* 2013, 29,506-515.
4. M. A. Rodrigues; R. Ruggiero; W. Guerra;*Boletim da Sociedade Portuguesa de Química*, 2009,115, 25-30.
5- H. J. Lee; S. Y. Yeo ; G S. H. Jeong, *Journal of Materials Science*, 2003,38, 2199 – 2204. https://doi.org/10.1023/A:1023736416361
6. M Gorensek; J. P. Recel; *Research Journal*, 2017 77, 138–141; https://doi.org/10.1177/0040517507076329
7. K Yoon; J. H. Byeon; J. Park; J. Hwang; – Susceptibility constants of Escherichia coli and Bacillus subtilis to silver and copper nanoparticles, *Science of the Total Environment*, 2007, 373, 572–575. https://doi.org/ 10.1016/j.scitotenv.2006.11.007.
8. L. Geranio; M. Heuberger; B. Nowack; *Environ. Sci. Technol*., 2009,1,8113-8. https://doi.org/10.1021/es9018332.
12.S. Perera; B.Bhushan; R.Bandara;G.Rajapakse;S.Rajapakse;C.Bandara*; Colloids and Surfaces A: Physycochemical and Engineering Aspects*, 2013.436, 975-989. https://doi.org/10.1016/j.colsurfa.2013.08.038Get rights and content.
13. A. H. C. PH.D. - Universidade Federal do Paraná, Curitiba, 2012.
14- M. A. J. Batista; Congresso Brasileiro de Polímeros, Gramado, 2001.

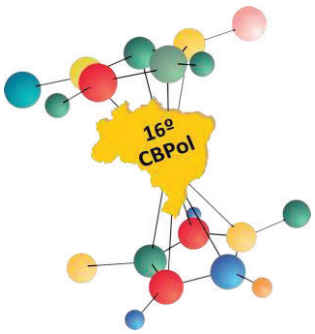

INFLUENCE OF GRAPHITE OR GRAPHENE INCORPORATION IN POLYURETHANE FOAMS OIL SORBENTS

Tiago Mari[1*], Bruna Rossi Fenner[2], Matheus V. G. Zimmermann[3], Camila Baldasso[1], Ademir José Zattera[1]

1 – Postgraduate Program in Engineering of Processes and Technologies (PGEPROTEC), Universidade de Caxias do Sul (UCS), R. Francisco Getúlio Vargas, 1130, Caxias do Sul/RS.

2 – Postgraduate Program in Mining, Metallurgical, and Materials Engineering (PPGE3M), Universidade Federal do Rio Grande do Sul (UFRGS), Av. Paulo Gama, 110 - Bairro Farroupilha - Porto Alegre/RS.

3 – Postgraduate Program in Materials Science and Enginnering (PPGCEM), Universidade do Extremo Sul Catarinense (UNESC), Av. Universitária, 1105 – Bairro Universitário, Criciúma/SC.

Abstract

The improper disposal of oily effluents can cause serious problems for the environment. Consequently, the use of sorbents, such as polyurethane foam (PU), emerges as an alternative for the treatment of these effluents. However, the sorption process using PU foams may prove to be inefficient due to the presence of both polar and non-polar regions within the PU polymeric chain. It needs to undergo modification processes to enhance the hydrophobicity of PU foam. Thus, this study aimed to develop modified PU foams by directly incorporating graphite or graphene into the formulation. The samples were characterized through morphological, hydrophobicity, and mechanical and thermal strength analyses. The results indicate a slight increase in selectivity for apolar fluids, improvements in compressive strength, and unchanged thermal properties.

Keywords*: oily effluents, sorbent, polyurethane foam, modification.*

Introduction

Oily wastewater, originating from both domestic and industrial sources, poses serious environmental risks when discarded into the environment without proper treatment [1–3]. In this sense, polyurethane foam (PU), a 3D porous material with low density, high porosity, mechanical flexibility, and high sorption and reuse capacity, has emerged as an attractive alternative for oil sorption in effluent treatment.

However, the presence of both polar (oxygen and nitrogen atoms) and apolar (carbon and hydrogen bonds) regions within PU polymeric chains means that PU foams present wettability by both oil and water when this sorbent is used in oil-in-water mixtures [4].

To achieve the desired characteristics of a hydrophobic and oleophilic material, modification processes are necessary to reduce surface energy and enhance surface roughness at the

nano/microscale (rough surface) [5-7]. However, surface modification of the PU foam alone does not guarantee efficient oil sorption. Other factors, such as capillary forces and pore connectivity, are also important for the foam to achieve maximum oil sorption [8]. In addition to efficient oil sorption, another desirable characteristic of an oil sorbent foam is reusability, i.e. the ability of the foam to maintain its sorbent properties even after several cycles of sorption, saturation, and compression [9].

Thus, the objective of this work is to develop PU foams with the direct incorporation of graphite or graphene into the formulation and evaluate their morphology, hydrophobicity, and mechanical and thermal properties.

Experimental

Materials

Voranol Polyol^{TM} 3010, toluene diisocyanate (TDI) Voranate^{TM} T-80, triethylenediamine Dabco 33-LV, tin (II) octoate LIOCAT® 29 and urethane grade methylene chloride were provided by Herval Indústria de Móveis, Colchões e Espumas LTDA. The surfactant Niax silicone L-95, produced by Momentive Performance Materials Inc. was provided by Flexível Indústria e Comércio Ltda. Pure powder graphite (140 mesh) from Êxodo Científica was purchased and graphene nanoplatelets (6 – 8 nm thick x 5 microns wide) from Strem Chemicals Inc. were provided by the Polymer Laboratory of UCS.

Methods

A polyurethane foam with a theoretical density of 8 kg.m^{-3} (PU8) was produced, based on the methodology described by Zimmermann *et al*. (2016) and Macedo (2015) [10-11]. The free expansion method with mechanical mixing was used. A Fisatom mixer, model 715, with a speed of 1000 rpm, was used to produce the foam. Graphite and graphene nanoplatelets were incorporated in the foam formulation at concentrations of 0.5% and 1.0 wt% by mass of polyol. Fig. 1 demonstrates the flowchart of the methodology used.

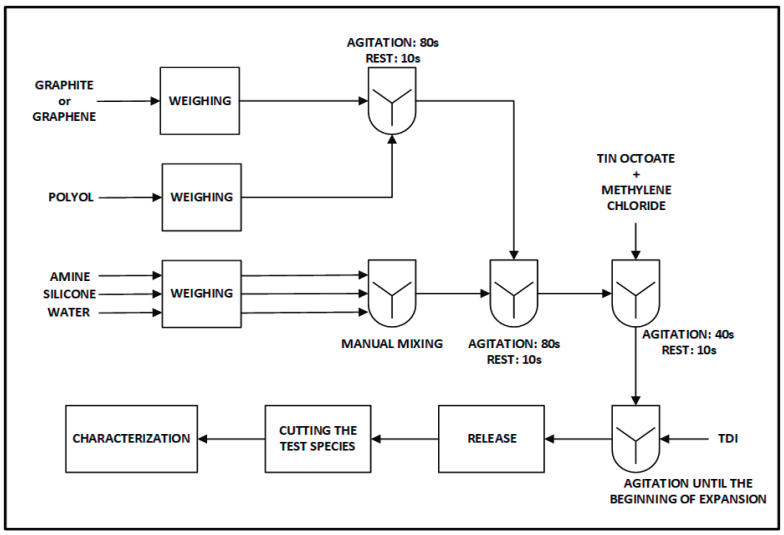

Figure 1 - Methodology for the production of PU foams.

Characterizations

The specific mass of the foams was determined according to ASTM D3574-11(A). The morphology of the samples was evaluated using Field Emission Scanning Electron Microscopy (SEM-FEG), with the aid of Tescan equipment, model FEG Mira 3, operating at a voltage of 15 kV. Before imaging, the samples were coated with a layer of gold. The thermal behavior and the influence

of graphite and graphene in the PU foams were determined by thermogravimetric analysis (TGA), conducted using Shimadzu equipment, model TGA-50, with a heating rate of 10°C.min^{-1}. The temperature range for the analysis (heating ramp) was from 23 to 700 °C under a nitrogen atmosphere (N^2) with a flow rate of 50 mL.min^{-1}. The hydrophobic characteristics of the coated foams were evaluated through partition coefficient tests (water-heptane mixture) and contact angle measurements. Compressive strength tests were performed using universal testing equipment, EMIC model DL 2000. The compression speed was set at 50 mm.min^{-1}, based on ASTM D3574-11(C), and the permanent deformation to compression (DPC) was assessed based on ASTM D395-16(B) at a temperature of 70 ± 2°C.

Results and Discussion

The calculated specific masses for the foams produced are shown in Table 1.

Table 1 – Experimental specific masses of the different foams produced.

Sample	PU8	PUGT0.5%	PUGT1%	PUGN0.5%	PUGN1%
Specific Mass (kg.m^{-3})	9.13 ± 0.12	9.05 ± 0.32	10.92 ± 0.75	11.40 ± 1.33	12.18 ± 1.86

The experimentally calculated specific mass of PU8, with a value of 9.13 ± 0.12 kg.m^{-3}, showed a slight variation from the theoretical value. This discrepancy could be attributed to variations in reagent measurements and timings in the stages of the process of development and stirring of the mixture. The addition of 0.5% graphite did not result in an increase in specific mass compared to the PU8 sample. However, with the addition of 1% graphite and 0.5% and 1% graphene nanoplatelets, a slight increase in specific mass was observed.

The morphological analysis of the foams, according to Fig. 2, revealed that the produced foam presented a 3D integrated network structure containing both open and closed cells. This is interesting for the sorption process: the open cells promote proper interconnection between chambers of the foam, while the closed cells provide a larger contact surface area with the effluent and hinder the escape of the already sorbed oil.

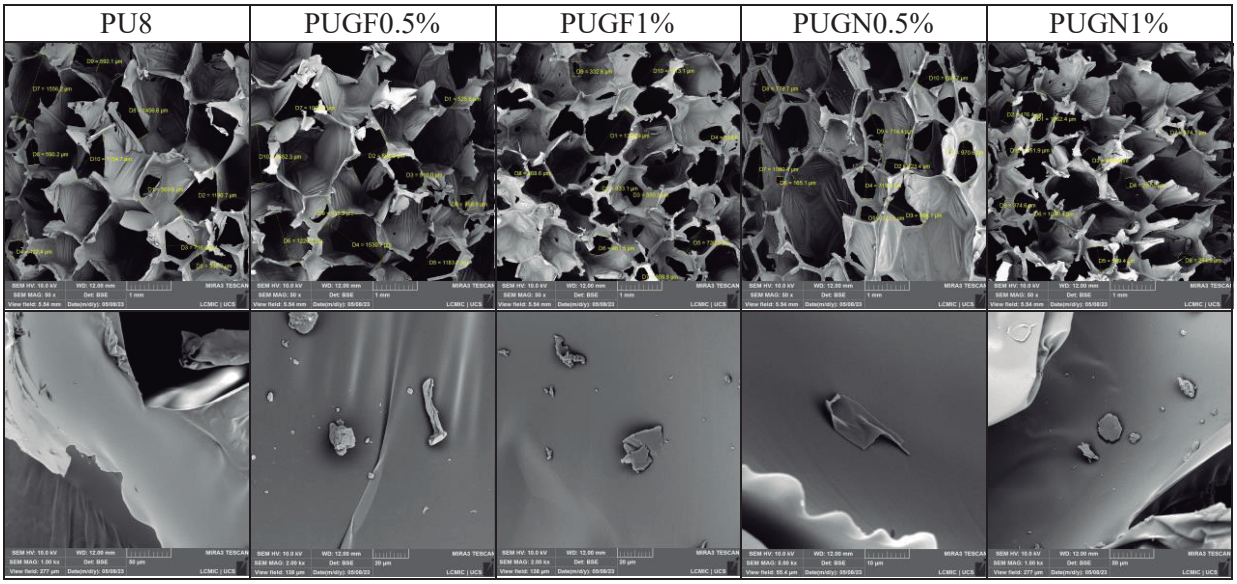

Figure 2 – Micrographs of PU8, PUGF0.5%, PUGF1%, PUGN0.5% and PUGN1% samples.

Table 2 – Results of the contact angle measurements of the different PU foams produced.

Sample	PU8	PUGT0.5%	PUGT1%	PUGN0.5%	PUGN1%
WCA	106.2° ± 3.2	113.4° ± 3.8	105.9° ± 2,3	113.2° ± 5,5	114.2° ± 6.9

However, despite the contact angles of the foams with water being below 150°, all of them exhibited complete deposition in the heptane phase (apolar solvent) during the partition coefficient test, confirming the selectivity of the foams for apolar fluids, such as oils present in wastewater.

Table 3 shows the mechanical properties of compressive strength and permanent deformation under compression of the developed foams. It is noticed that with the addition of carbon structures in the polymeric matrix served a reinforcement function, increasing the compressive strength of the foams. On the other hand, the addition of graphite or graphene did not significantly affect the permanent deformation under compression of the foams at a temperature of 70°C.

Table 3 – Results of the compressive strength analysis of the different PU foam samples at 50 and 80% deformation and permanent deformation under compression (PDC) at 70°C.

Sample	PU8	PUGT0.5%	PUGT1%	PU8GN0.5%	PUGN1%
Stress (kPa) Def. 50%	30.17 ± 2.70	42.50 ± 4.33	36.47 ± 4.46	44.96 ± 7.82	46.90 ± 4.25
Stress (kPa) Def. 80%	75.53 ± 6.34	182.5 ± 22.78	82.80 ± 13.16	115.90 ± 49.18	110.90 ± 10.32
PDC (%)	50.73 ± 0.59	53.60 ± 2.03	53.50 ± 0.24	48.35 ± 1.85	50.31 ± 0.69

Upon analyzing the data from the TGA curves presented in Table 4, two events of mass loss characteristic of polyurethane were observed. The first refers to the breakdown of the links between isocyanate and alcohols, while the second event corresponds to the degradation of the flexible segments of polyol [13]. It was observed that the addition of graphite and graphene to the foams did not result in significant changes in their thermal behavior.

Table 4 – TGA analysis results of the different PU samples produced.

Date	PU8		PUGT0.5%		PUGT1%		PU8GN0.5%		PUGN1%	
	1st event	2nd event	1st event	2nd event	1st event	2nd event	1st event	2nd event	1st event	2nd event
T_{onset} (°C)	265.25	341.88	262.27	344.59	264.48	351.66	257.91	344.62	261.17	343.68
T_{endset} (°C)	318.48	401.99	318.98	408.41	323.41	413.14	317.61	410.35	318.90	409.07
T_{max} (°C)	302.32	384.91	302.69	376.52	305.89	382.01	299.15	377.72	303.46	378.53

Conclusions

In summary, hydrophobic polyurethane foam was developed by directly incorporating graphite or graphene into the formulation. The addition of graphite or graphene led to a slight increase in the specific mass of the foam. Morphological analysis revealed that all foams exhibited a 3D integrated network structure of open and closed cells, as well as the presence of graphite or graphene on their surface. The addition of carbon structures caused a slight increase in the contact angle of samples

PUGT0.5%, PUGN0.5%, and PUGN1% with water, suggesting an increase in hydrophobicity, which was further confirmed using the partition coefficient test, in which the foams remained completely in the heptane phase. Moreover, the incorporation of carbon structures promoted an increase in the compressive strength of all samples, indicating the strengthening of the polymeric matrix. The thermal stability of the PU foams did not undergo significant changes with the incorporation of the carbon structures in the formulation. Overall, the results demonstrate that the incorporation of graphite or graphene nanoplatelets in polyurethane foams can improve the selectivity of the material for apolar fluids, such as oils present in effluents.

Acknowledgments

The authors would like to thank CNPq and CAPES for the financial support and the Laboratories of the University of Caxias do Sul (UCS) for all the analyses reported in this work.

References

1. M. Kish, W. J. Böckel *Est. Cient.* 2017, 7, 61. https://doi.org/10.18468/estcien.2017v7n3.p61-69.
2. L. Wang, B. Zhang, B. Zhao, A. Yang, K. Wu, J. Sun, C. Hu *J. Environ. Sci.* 2022, 118, 171. https://doi.org/10.1016/j.jes.2021.12.018.
3. R. M. Bande, B. Prasad, I. M. Mishra, K. L. Wasewar *Chem. Eng. J.* 2008, 137, 503. https://doi.org/10.1016/j.cej.2007.05.003.
4. Y. Liu, J. Ma, T. Wu, X. Wang, G. Huang, Y. Liu, H. Qiu, Y. Li, W. Wang, J. Gao *ACS Appl. Mater Interfaces* 2013, 5, 10018. https://doi.org/10.1021/am4024252.
5. M. S. Selim, S. A El-Safty, N. A. Fatthallah, M. A. Shenashen *Prog. Org. Coat.* 2018, 121, 160. https://doi.org/10.1016/j.porgcoat.2018.04.021.
6. J. Tan, W. Li, C. Ma, Q. Wu, Z. Xu, S. Liu *Materials* 2018, *11*, 1106. https://doi.org/10.3390/ma11071106.
7. B. Lin, J. Chen, Z. Li, F. He, D. Li *Coat. Technol*. 2019, 359, 216. https://doi.org/10.1016/j.surfcoat.2018.12.054.
8. J. Pinto, A. Athanassiou, D. Fragouli *J. Phys. D*. 2016, 49, 14. http://iopscience.iop.org/0022-3727/49/14/145601.
9. S. M. Hailna, D. Ponnamma, I. Krupa *Polymers*, 2021, 13, 4142. https://doi.org/10.3390/polym13234142.
10. M. V. G. Zimmermann, A. J. Zattera, R. M. C. Santana *Rev. Mater*. 2016, 24, 2. https://doi.org/10.1590/S1517-707620190002.0692.
11. V. Macedo, Mestrado. Dissertação, Universidade de Caxias do Sul, 2015.
12. D. D. Ejeta, C. F. Wang, C. H. Lin, S. W. Kuo, J. K. Chen, H. C. Tsai, W. S. Hung, C. C. Hu, J. Y. Lai *Sep. Purif. Technol.* 2021, 263, 118387. https://doi.org/10.1016/j.seppur.2021.118387.
13. R. Gu, M. M. Sain *J. Polym. Environ.* 2013, 21, 30. https://doi.org/10.1007/s10924-012-0538-y.

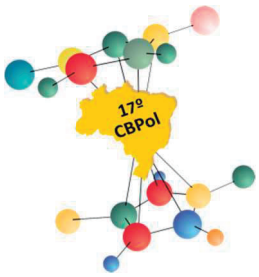

INFLUENCE OF PROCESSING IN THE DRUM BALL MILL ON OBTAINING CELLULOSE NANOFIBERS

Tendy C. S. Saar, Celso C. M. Fornari Junior*

1 – Department of Engineering and Computer, State University of Santa Cruz (UESC), Ilhéus, BA, Brazil
corresponding_celso@uesc.com.br

Abstract

Energy consumption has progressively increased as a result of world population growth. In the same situation, energy and material resources have been increasingly scarce and valued. In the technology for obtaining cellulose nanofibers, new materials with better properties, greater efficiency and more environmentally friendly are expected. However, obtaining cellulose nanofibers undergoes processes that involve high consumption of energy and time, in addition to the additional cost of waste. In this search for more efficient and productive processes, many works have demonstrated viable alternatives. This work was dedicated to evaluate the productivity in the modification of coconut fibers. The results demonstrated that the process time is proportional to the generation of micronized fibers and reached the production of nanofibers.

Keywords: *Coconut fiber, nanofiber, Process.*

Introduction

Cellulose is a natural and abundant polymer, with ecologically correct production, and that presents interesting properties. Cellulose nanofiber has resistance a few times greater than steel, promising the construction of composites with high mechanical performance. Due to the promising properties, many works have been dedicated to investigating the application of cellulosic fibers. [1-5]. The application of cellulose fibers by the industry must be such that the properties of the fiber are associated with the materials in use or in the creation of new materials.

The processing of plant fibers for the production of composites, nanofibers or other interest, involves chemical and/or mechanical action, requiring process time and energy. The most crucial point in our age involves energy consumption. World energy consumption has increased with population growth and will continue to do so. Data has shown that in 2019, the world consumption of crude oil was 4.45 billion metric tons compared to 3.6 billion metric tons consumed in 2001 [6].

This real scenario led our society to drastic changes in consumption habits. From the use of biofuels to the improvement of technologies and improvement of recycling processes, in order to adjust to the new growing reality of energy consumption and demand. In this context, many works have investigated cellulose fibers for applications that replace materials from non-renewable sources and reduce energy consumption in production processes [7].

Interestingly, cellulose nanofibers are materials with high mechanical properties and have already been applied in numerous technological processes, such as: conductive composites, proton

exchange membranes, electronics, energy storage devices, piezoelectric sensors, biomedical products, adhesives, supercapacitors, textile fibers, food coating, antimicrobial films, special printing paper, cosmetics [8,9].

The need to search for technological alternatives for the exploitation of cellulosic fibers in the production of nanofibers has been more deeply analyzed. Many treatments have been combined in order to reduce energy consumption in the pulp industry. Among the various treatments, combined physical and chemical processes have shown interesting results in relation to obtaining nanocellulose [10-12]. The ball milling technique is promising and considered effective in terms of producing nanocellulose, as it can break the axis of the polymer structure. In this way, the crystallinity is reduced and the nanofibers are separated. Compared with other mechanical equipment, the ball mill has a high energy production/consumption ratio, and can operate at ambient temperature and pressure. This work was dedicated to evaluate the productivity of coconut fiber processing in drum ball mill associated with treatment in alkaline solution. The results revealed that the production increases in relation to the process time and that plant fiber nanoparticles were produced.

Experimental

Coconut fibers were conditioned in an oven at 130 ± 5 ºC for 120 min. before and after processing. The work used an analytical scale with four decimal places to carry out the gravimetric evaluation of the fibers, before and after processing. Coconut fibers were processed in a planetary ball mill. For 5 g of fibers 35 balls of diameter 20 mm were used. In each processing, an aqueous solution of 8% w/w of sodium bicarbonate was used. Each processing was conducted in steps of 60 minutes. Thus, the processing (A – 60 min.), (B – 120 min) successively until (F – 360 min) was carried out in a ball mill at 100 rpm. After each processing, the balls were removed and the solution and fibers were filtered through an 80 mesh sieve, dried in an oven and evaluated by gravimetry, as described. Figure 1 presents a sequence of images of processing in a drum ball mill.

Figure 1 - Sequence of drying (1), loading (2), milling of coconut fiber (3)

Results and Discussion

The studies evaluating the modification of coconut fibers used the ball mill methodology to promote the alteration of the fibers. Ball mill processing has the advantages of easy handling and processing, and strong mechanical action. In this work, coconut fibers were processed in ball mills in combination with alkaline chemical action and their modification with respect to processing time was evaluated. The results revealed that as the processing time increases, the micronized particles increase. During the unitary grinding operation using the ball mill, a strong mechanical stress occurs on the fibers. The centrifugal force makes the system of jug, balls and fibers preferentially remain on the walls of the jug up to a certain limit where the force of gravity overcomes the centrifugal force, initiating the fall of the balls. When the balls precipitate from a height approximately equal to half the diameter of the pitcher, they project onto the fibers then placed. In this way, the impact that will

occur will be mostly absorbed by the fibers and the drum wall. This mechanical energy proved to be sufficient to partially destroy the fibrous structures, transforming the fiber into fine particles, as observed in studies in the literature [13,14]. Fig. 2 shows the residual volume of ground and decanted fibers after each ball mill processing. At each processing step, the results showed that the fibers separate into micronized particles (decanted residue).

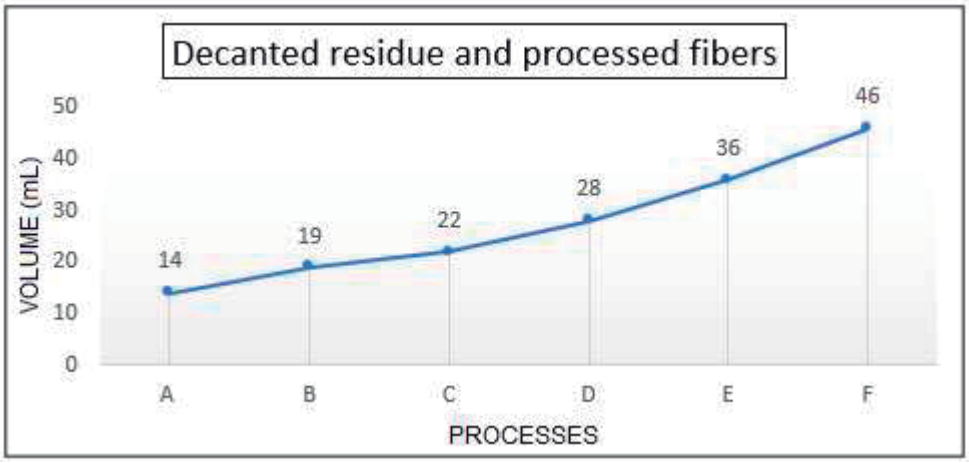

Fig. 2 - Amount of decanted waste after each processing

After one hour of processing, 14 mL of fine particles were obtained and after six hours of processing there was an increase of approximately 300%. Evidently, the greatest mechanical impact request transforms the physical structure of the vegetable fiber, fragmenting the original fiber by mechanical action.

However, this processing took place in aqueous solution, which considerably modifies the behavior of the vegetable fiber. It is important to remember that vegetable fiber is fragile when in the dry condition, which promotes the rupture of its structure more easily. The work used alkaline aqueous solution for the operation of the milling process, which considerably promotes the plastic condition of the fiber during its processing. So, in this condition, the fiber was conditioned to withstand mechanical stresses in the plastic situation, forcing bending and deformation instead of breaking. Associated with the mechanical condition of the mill, the alkaline action favored the removal of soluble substances, as in the case of coconut fiber, wax, pectin and lignin [1].

Processing modified the natural fiber substantially. The color of the fibers changed from an orange tone to a lighter yellowish tone. Evidently, the removal of lignin, which is most responsible for the dark color, promoted the change in fiber color to a lighter tone. Figure 3 shows the fibers after each ball mill processing.

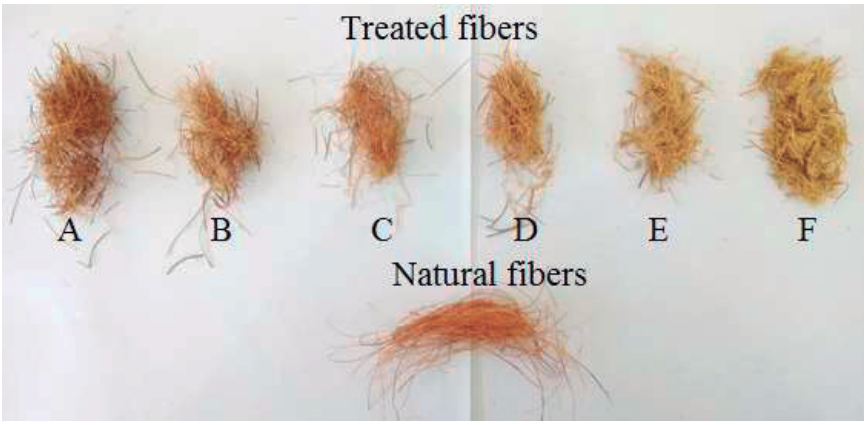

Figure 3 - Image of natural fibers and after processing in a ball mill

Conclusions

The combined processing of mechanical action with a planetary ball mill and the treatment in an aqueous alkaline solution demonstrated that the production of micronized fibers increases proportionally with the process time. After six hours of processing there was an increase of approximately 300% in the production of fines in relation to the one hour processing. In all process times, micronized fibers were obtained. As the processing time increased the color of the fibers changed from a dark orange to pale yellow.

Acknowledgements

The authors would like to thank the State University of Santa Cruz for the research conditions carried out at LAPOS, the Polymers and Systems laboratory.

References

1. C.C.M. Fornari Junior; Fibras vegetais para compósitos poliméricos, Editus, Ilhéus,2 017.
2. A.J.F. Carvalho; G. de Souza; M.C. Fares; Macromol. Symp 2019, 383, 1800068. https://doi.org/10.1002/masy.201800068.
3. S. Chhetri; H. Bougherara; Composites Part A: Applied Science and Manufacturing 2021, 140, 106146. https://doi.org/10.1016/j.compositesa.2020.106146.
4. H.G. Kotik; Matéria (Rio de Janeiro) 2019, 24. https://doi.org/10.1590/S1517-707620190003.0801
5. A.M. Weber; A. Matoski; L. Cechin; R.B. Tokarski; Engenharia Civil UM 2022, 61, 6-17. https://doi.org/10.21814/ecum.4149
6. R.Mukthan, S.K. Bhargava, S. Bankupalli, A.S.Ball. J. Sustain Bioenergy Syst.2016, 6: 72-92
7. S.S. Kumar; V.M. Raja; Composites Science and Technology 2021, 208, 108695. https://doi.org/10.1016/j.compscitech.2021.108695
8. D. Trayeb et al. Frontiers in Chemistry. 2020, 8, 392. https://doi.org/10.3389/fchem.2020.00392
9. P. Tayeb, H.A. Tayeb. Carbohydrate polymers. 2019, 224, 115149. https:// doi:10.1016/j.carbpol.2019.115149
10. J. Luo, Z. Fang, R.L. Smith. Prog. Energy Combust. Sci. 2014, 41, 56-93. https://doi.org/10.1016/j.pecs.2013.11.001
11. A. Ranjan, S. Singh, R.S. Malani, V.S. Moholkar. RSC Adv. 2016, 6, 65541-65562. **https://doi.org/10.1039/C6RA11580B**
12. S.M. Langari. IOSR J. Eng. 2014, 4, 14-28. ISSN (e): 2250-3021, ISSN (p): 2278-8719
13. Z. Jiang et al. Food Hydrocolloids. 2022, 127, 107515. https://doi.org/10.1016/j.foodhyd.2022.107515
14. J Zeng et al. BioResources. 2020, 15, 3809-3820. DOI: 10.15376/biores.15.2.3809-3820

INFLUENCE OF THE ADDITION OF MONTMORILLONITE CLAY NANOCHARGES ON THE PROPERTIES OF ACRYLIC RESIN COMPOSITES APPLIED TO THE DEVELOPMENT OF OCCLUSAL PLATES THROUGH ADDITIVE MANUFACTURING

Vanessa Bueno Pereira[1], Lílian Vanessa Rossa Beltrami[2], Diego Piazza[2], Thiago de Oliveira Gamba[1] and Ademir José Zattera[2*]

1 - Dentistry School, University of Caxias do Sul (UCS), R. Francisco Getúlio Vargas, 1130, Caxias do Sul/RS
2 -Postgraduate Program in Engineering of Processes and Technologies (PGEPROTEC), University of Caxias do Sul (UCS), R. Francisco Getúlio Vargas, 1130, Caxias do Sul/RS
(ademirjzattera@gmail.com)

Abstract - The creation of three-dimensional objects manufactured through digital models has been widely used in dentistry. Acrylic resins based on Poly Methylmethacrylate (PMMA), are the raw material of additive manufacturing, and can have their dynamic mechanical properties altered through the addition of nanoparticles, producing nanocomposites. Small amounts of nanocharges can be added to PMMA, creating a favorable interface between the resin matrix and the surface of the particles used. We sought to measure the properties of a specific resin for 3D printing, modified by the addition of 0.25% of Montmorillonite (MMT) clay nanocharges through sonification. The samples were characterized for their hardness (*Shore D*), abrasion, dynamic-mechanical, thermo-mechanical, thermogravimetric properties and contact angle. Considering the reported results, it is suggested that there was good dispersion of the MMT nanocharges in the PMMA matrix.

Keywords: *Three-Dimensional Printing, Polymethyl Methacrylate, Clay, Composites, Dentistry.*
Fundings: FINEP, FAPERGS

Introduction

Rapid prototyping, additive manufacturing or 3D printing, has the characteristics of sustainability, precision, speed, as well as the possibility of individualization and customization of parts, and is already the present when we refer to digital dentistry. Stereolithography (SLA) and Digital Light Processing (DLP) are the two main printing technologies present in the dental field, and a variety of light-curing polymers are available for this purpose [1]. Polymethyl methacrylate (PMMA)-based acrylic resin has unique characteristics such as low density, cost-effectiveness, aesthetics, ease of manipulation by the clinician and the capacity of its physico-mechanical properties to be adaptable, justifying its use and sovereignty. UV acrylic resin is offered to the clinician in liquid form, composed of a urethane dimethacrylate (UDMA) matrix, acrylic resin monomers, PMMA fillers and silica [2]. The aim of increasing PMMA hardness, impact and flexural strength, as well as modifying its sorption and solubility capacities, motivated this research. Deficiencies in these properties commonly lead to rapid wear and fracture of prosthetic parts [3]. The application of small amounts of nanocharges to PMMA has resulted in nanocomposites with improved properties due to the strong interactions between the nanoparticles and the polymer matrix. Several types of fillers

can be used in this process, silver nanoparticles, zinc oxide, graphene, silica and clay are some examples [4]. The montmorillonite (MMT) clay is the most used in the formation of nanocomposites [5]. MMT sheets have 1 μm diameter and 1 nm thickness and extensive surface area which favors their application in polymers [6]. In addition, MMT is marketed as a powder with a slightly yellowish white color, not aesthetically affecting the transparent appearance of PMMA at the time of incorporation [7]. Based on this, we sought to evaluate a PMMA-based photosensitive resin used for 3D printing of myorelaxant plates, modified by the addition of a pre-defined amount of Montmorillonite clay (MMT) nanocharges and evaluate their properties.

Experimental

Materials

Montmorillonite (MMT) type clays commercially identified as Cloisite (organically modified by quaternary ammonium salts), type 15A, 20A and 30B (Southern Clay Products Inc, division of Songhan Plastic Technology Co. Ltd.), UV liquid resin for printing occlusal plates on a 3D printer "Resina 3D Smart Print Bio Bite Splint Clear" (0.5 Pa.s and density 1.2 g/cm3) manufactured by the company Smart Dent®, of M.M. Tech Projetos Tecnologia Imp. e Exp. LTDA.

Methods

Photosensitive acrylic resin (100g) and MMT clays (0.25%) were weighed on a high precision balance (BEL Engineering, LW 303i with 0.001g resolution) and sonified for 30 minutes at 40% aplitude in a Sonics Vibra-Cell sonifier. A container with ice was used to dissipate the heat generated by the equipment and not overheat the resin. Visually, a nanocomposite of translucent and homogeneous appearance was obtained. For the design of the specimens, the 3D DLP FlashDLPrint software was used. The printing orientation of the parts was vertical. The standards recommended for the printing of the specimens were defined according to the fabricator and were not changed, not interfering in the final result of the prints. At the end of printing, the specimens were removed from the printer and immersed in isopropyl alcohol for 5 minutes to remove the surface resin from the samples, and then post-cured in a post-curing oven, remaining for the time recommended by the fabricator (15-20min). Afterwards, each group was packed, identified and sent for dynamic-mechanical (DMA), thermo-mechanical (TMA), thermo-gravimetric (TGA) tests and *Shore D* hardness, abrasion and compression analysis.

Results and Discussion

In ascending order of hardness results, we have that the RES-MMT 15A nanocomposite presented 75 hardness, showing to be inferior to RES, which presented 80 hardness. RES-MMT 20A presented 82 hardness, followed by the RES-MMT 30B nanocomposite with 85 hardness, these being the best results after the incorporation of the nanocharges, although they are not significant values. The increase in hardness of the specimens reduces surface wear when subjected to occlusal forces [8]. RES presented a percentage of 42% mass loss, equivalent to the RES-MMT 30B nanocomposite. The RES-MMT 20A nanocomposite showed 1% more weight loss compared to the pure resin. These results were not significant. The RES-MMT 15A composite presented the best result, where we observed 36% weight loss, 6% less than RES. We can observe a loss of weight close to the RES of the nanocomposites 20A and 30B that presented an increase in hardness in the Shore D test. In contrast, we have the improvement in wear resistance in the RES-MMT 15A nanocomposite. There are few records regarding the abrasive tribology of RES-MMT nanocomposites. Factors such as surface roughness, type and properties of the materials involved can affect the wear properties of a material. The particle size, the concentration used, the ratio of the filler to the matrix, and the type and amount of surfactants used should also be taken into

account, as they can affect the wear properties of the nanocomposite even after complete exfoliation of the nano-clays [9]. In the TMA analysis considering a temperature of 90ºC, RES presented approximately 0.95% expansion, while the RES-MMT 15A nanocomposite showed no significant difference compared to RES, with approximately 0.85% expansion. The RES-MMT 20A nanocomposite showed a expansion close to 0.45%, and the RES-MMT 30B nanocomposite showed around 0.55% expansion. The RES-MMT 20A nanocomposite obtained the lowest expansion rate compared to the others. All the nanocomposites prepared tended to expand less as a function of temperature compared to RES, as can be seen in Fig. 1.

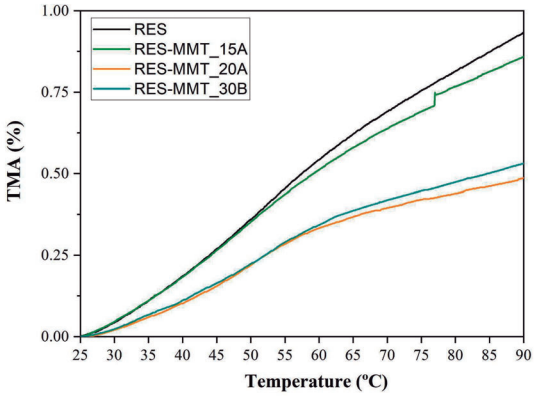

Figure 1- Thermo-Mechanical Analysis

In the TGA analysis, RES required a heating of approximately 265ºC to start degradation and the RES-MMT 20A nanocomposite 269ºC, showing similar behaviors between them. The RES-MMT 15A nanocomposite required 275ºC, being the nanocomposite with the best thermal stability among the materials, 10ºC more than that required for RES. The RES-MMT 30B nanocomposite was the first of the 4 groups to degrade, starting the process around 260ºC, as we can see in Fig. 2. It is suggested that the degradation of the nanocomposite starts with the breaking of weak chains in the matrix, followed by random breaks that require higher temperatures, this being the second phase of degradation.

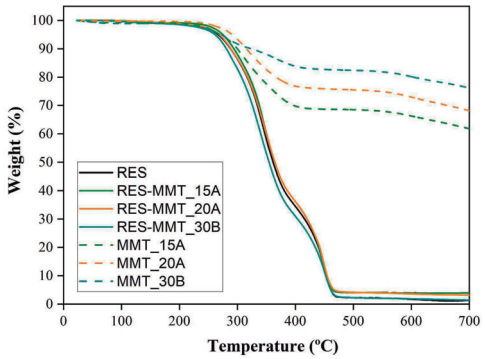

Figure 2- Thermogravimetric analysis

In the DMA analysis, as we can observe in Fig. 3 and 4, RES obtained a storage modulus of approximately 1500 MPa. The RES-MMT 15A nanocomposite showed a small decrease in storage modulus, around 1400 MPa. The RES-MMT 20A nanocomposite showed the best storage performance, with 12000 MPa, i.e. 10500 MPa higher than that found in RES, an extremely

significant result. The RES-MMT 30B nanocomposite also obtained excellent performance, with 9000 MPa, 7500 MPa more than RES. As with the storage modulus, RES and the RES-MMT 15A nanocomposite obtained close results, having a loss modulus of approximately 210 MPa. The RES-MMT 20A nanocomposite obtained the highest loss modulus, with 1300 MPa, and the RES-MMT 30B nanocomposite presented approximately 1000 MPa of loss. The loss modulus happens simultaneously with the storage modulus, where we have the "damping" of the material, that is, a amortization, which is the ability of the acrylic resin to absorb the mechanical energy applied on it and convert this energy into heat. The behavior of the polymer chains at temperatures and forces depends on the interactions created at the interface between the particles and the polymer matrix in the formation of nanocomposites. The exfoliation and effective linkage of the silica sheets with the PMMA matrix creates obstacles in the movement of the chains as well as the speed with which this happens. The opposite happens when there is the formation of weak linkages, due to poor dispersion, accelerating the process of relaxation and chain breaking [10].

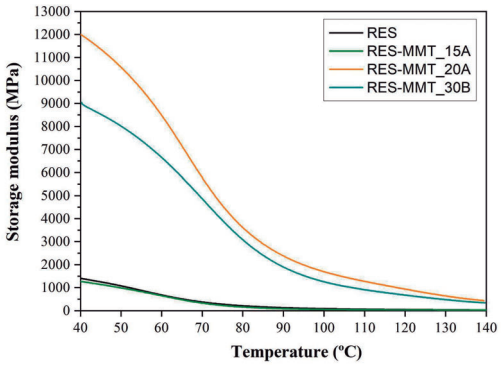

Figure 3- Storage Modulus by DMA

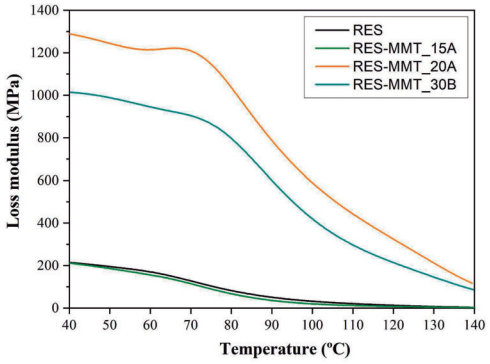

Figure 4- Loss Modulus by DMA

In the Tan Delta results, represented in Fig. 5, the RES presented a glass transition temperature of 86.1°C. The highest Tan Delta result was for the RES-MMT 20A nanocomposite, where the result found was 110.1 ºC, 24ºC more than that required for RES. The RES-MMT 30B nanocomposite showed 102.3 ºC. The RES-MMT 15A nanocomposite obtained a lower value compared to RES. The Tan Delta values, when elevated, indicate better energy absorption and better conversion in the form of heat, indicating better dissipation of the nanocharges in the matrix and better linkage of nanocharges with the polymer matrix.

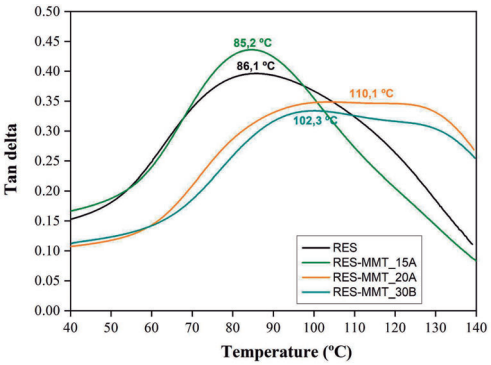

Figure 5- Tan Delta by DMA

As for the contact angle, RES presented a contact angle of 77º, followed by the nanocomposite RES-MMT 15A, with an angle of 78º. Both nanocomposites RES-MMT 20A and RES-MMT 30B presented 79º of contact angle. Young's equation considers that the surface where the contact angle test is performed must be plane, smooth and homogeneous. Experimental tests involving specimens often do not achieve all these requirements, and a rough surface with a high surface energy increases the wettability of liquids. The close results of the RES contact angle may indicate a higher presence of PMMA on the surface of the nanocomposites, or it may indicate the good distribution of the silica sheets on the specimen, so that as they were treated to have a more hydrophobic content, the wettability angle was increased minimally.

Conclusions

According to the results of the tests presented, we can indicate that the incorporation of 0.25% of clay nanocharges (MMT) in the PMMA matrix reduces the mobility of the polymer chains, and that a greater energy is required to initiate their movement, resulting in a more stable nanocomposite at elevated temperatures, more rigid and more resistant to wear. We can also observe a good behavior of the nanocomposite with respect to storage-dissipation, giving a better resilience to the material, impeding its deformation in the long term, and consequently its failure, essential properties for occlusal plates that are constantly receiving charges from Bruxism, suggesting an increase in the durability of occlusal plates printed by additive manufacturing through digital flow.

Acknowledgements

The authors would like to thank the Financier of Studies and Projects (FINEP) and Foundation for Research Support of the State of Rio Grande do Sul (FAPERGS) for the financial support. To the Polymer Laboratory University of Caxias do Sul (LPOL) for all the analysis reported in this work.

References

1. J. Jockusch; M. Özcan Dental Materials Journal 2020, 39 (3), 345–354. https://doi.org/10.4012/dmj.2019-123.
2. M. S. Zafar Polymers 2020, 12 (10). https://doi.org/10.3390/polym12102299.
3. C. Lourinho; H. Salgado; A. Correia; P. Fonseca Biomedicines 2022, 10, 2565. https://doi.org/10.3390/biomedicines10102565.
4. F. Shakeri; A. Nodehi; M. Atai Journal of the Mechanical Behavior of Biomedical Materials 2018. https://doi.org/10.1016/j.jmbbm.2018.09.033.
5. R. B. Valapa; S. Loganathan; G. Pugazhenthi; S. Thomas; T. O. Varghese Clay-Polymer Nanocomposites 2017, 29-81. https://doi.org/10.1016/B978-0-323-46153-5.00002-1.
6. K. S. Katti; H. Jasuja; S. V. Jaswandkar; S. Mohanty; D. R. Katti Materials Advances 2022, 3(20), 7484-7500. https://doi.org/10.1039/d2ma00528j.
7. S. Joseph; N. Mathew; A. T. Koshy; N. L. Jayalakshmi; V. Mathew Contemporary Clinical Dentistry 2019, 10(4), 658–663. https://doi.org/10.4103/ccd.ccd_737_17.
8. A. Grymak; J. N. Waddell; J. M. Aarts; S. Ma; J. J. E. Choi Journal of The Mechanical Behavior of Biomedical Materials 2022, 105053, 1751-6161. https://doi.org/10.1016/j.jmbbm.2021.105053.
9. A. Dasari; Z. Yu; Y. Mai; G. Hu; J. Varlet Composites Science and Technology 2005, 15–16. https://doi.org/10.1016/j.compscitech.2005.06.017.
10. E. Chehrazi; N. Taheri-Qazvini Langmuir: The ACS Journal of Surfaces and Colloids 2018, 34(47), 14358–14367. https://doi.org/10.1021/acs.langmuir.8b03160.

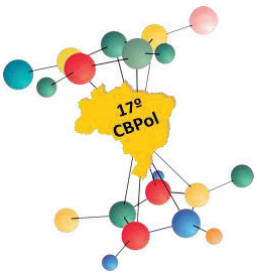

MAGNETICALLY ENHANCED ADSORPTION OF PHARMACEUTICALS FROM AQUEOUS MEDIUM USING MAGNETIC ALGINATE/POLYPYRROLE/$ZnFe_2O_4$ BEADS

Victória R. Soares[1*], Emilly Silva,[1] André Fajardo[1]

1 – Laboratório de Tecnologia e Desenvolvimento de Compósitos e Materiais Poliméricos (LaCoPol), Universidade Federal de Pelotas (UFPel), Campus Capão do Leão,, Pelotas-RS, Brazil.
(*) victoriarossoares@gmail.com

Abstract - The characteristics of the magnetic materials can be modulable due to exposition to a magnetic field, which allows to enhance its adsorption performance. This study describes the preparation of magnetic beads of alginate/polypyrrole/$ZnFe_2O_4$ (Alg/PPy/$ZnFe_2O_4$) and investigates the effect of an external magnetic field (EMF) on their adsorption performance of acetaminophen (ACT) and ibuprofen (IBU). Different from the pristine beads (Alg/PPy), the presence of an EMF altered the behavior of the magnetic beads, showing that these properties are affected by this external stimulus. Batch experiments revealed that the amount of ACT and IBU adsorbed by Alg/PPy/$ZnFe_2O_4$ is noticeably high 106 and 108 mg/g. The presence of an EMF increasing their adsorption capacity towards ACT and IBU by 14% and 12% compared to Alg/PPy. The results presented here suggest that magnetic-responsive materials like Alg/PPy/$ZnFe_2O_4$ are prominent for improving the treatment of wastewater containing these contaminants.

Keywords: *Magnetic materials; composites; ferrites; emergent contaminants; ibuprofen; acetaminophen.*

Fundings: The authors are thankful to Conselho Nacional de Desenvolvimento Científico e Tecnológico (CNPq, Brazil) for their financial support (Processes 404744/2018-4). The Coordenação de Aperfeiçoamento de Pessoal de Nível Superior, Brazil (CAPES/Proap) was financed in part this study (Finance Code 001).

Introduction

Population growth and global sanitary issues have contributed to the expansion of the pharmaceutical industries and drug consumption [1]. It is well-established that the large-scale production of pharmaceutical compounds requires the control of the processes from the production to their destination. In general lines, the incorrect disposal of these compounds represents a threat to diverse environments since their active principles are constantly found in insignificant amounts in potable water, wastewater, and surface water, interacting with biological systems, intoxicating animals, and hampering human health. Among the pharmaceuticals in the market, non-steroidal anti-inflammatories (AINEs) and analgesics are the two classes of drugs most prescribed and acquired without a prescription. The overconsumption of these drugs has a close relationship with their recurring presence in potable water sources [2]. Due to their high mobility, persistence, and resistance to degradation, the removal of these drugs from the aqueous environment is a challenge. To deal with this, researchers have been working on the development of various techniques and strategies to treat drug-contaminated water and wastewater. As noticed, adsorption is considered one of the most prominent processes to remove these drugs from water mainly because of its features (e.g., straightforward application, low cost, diversity of adsorbents, among others). Adsorbents with magnetic properties, for example, are attractive not only because they are readily recovered from the treating medium but also due to the possibility of modulating the physicochemical characteristics of the adsorbent when in the presence of an external magnetic field (EMF) [3]. An EMF can be applied

to enhance the adsorption performance, affecting the physical and chemical properties of solvents and the structure of the magnetic adsorbents. When dealing with polymeric materials filled with ferrites, which are oxides of ferrimagnetic origin, it is possible to assume a noticeable influence on the crosslinking process of these adsorbents, which will reflect in their physical, chemical, morphological properties, and adsorbent capacity [4]. To investigate the benefits associated with the use of an EMF on the adsorption of two worldwide consumed drugs from water in this study, we synthesized composite beads of alginate (Alg), polypyrrole (PPy), and zinc ferrites ($ZnFe_2O_4$) to the removal of acetaminophen (ACT) and ibuprofen (IBU).

Experimental

Synthesis of the beads: An acidic pyrrole solution (0.1 mol/L) was prepared using HCl (1 mol/L) and then, added dropwise to an Alg aqueous solution (3 wt%) up to achieve a volume ratio of 1:10. The resulting solution was stirred for 30 min at 80 °C. To proceed with the oxidative polymerization of pyrrole, a $FeCl_3$ solution (2 mol/L) was slowly added until the solution color changed to black. The reaction system was kept under stirring for another 5 h at 5 ºC. Afterward, the solution containing the polymers was dialyzed (MWCO 12,000–14,000 Da) against distilled water for 24 h. The purified solution of polypyrrole (PPy) and Alg was dropped (1 mL/min) into a $CaCl_2$ solution (3 wt%), which was kept under mild stirring. The beads, instantaneously formed due to the ionotropic gelation of the Alg chains, were recovered from the $CaCl_2$ solution after 60 min and washed in distilled water to eliminate the Ca^{2+} excess. Next, the purified beads were soaked in a glutaraldehyde solution (3 wt%) at pH 3 for 60 min to promote the chemical crosslinking. Finally, the dual crosslinked Alg/PPy beads were thoroughly washed in distilled water and oven-dried (50 ºC for 12 h). Magnetic Alg/PPy beads containing $ZnFe_2O_4$ (labelled as Alg/PPy/$ZnFe_2O_4$) were prepared using the same experimental protocol. However, 10 mg of $ZnFe_2O_4$ was dispersed in Alg/PPy solution (10 mL) before the crosslinking processes (with $CaCl_2$ and glutaraldehyde). The polymers: $ZnFe_2O_4$ mass ratio was fixed at 10:1 based on previous experiments. Fig. 1. summarizes the experimental steps to synthesize the materials studied in this work.

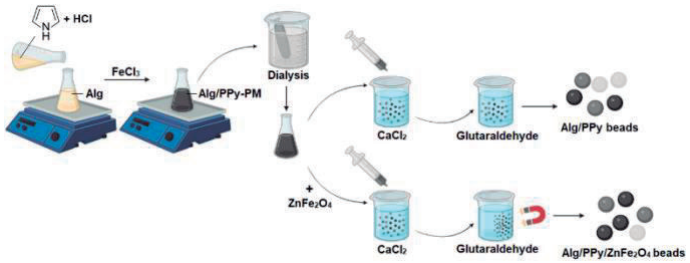

Fig. 1. Experimental protocol utilized to synthesize the magnetic and non-magnetic beads.

Adsorption experiments: Batch experiments were performed to investigate the ability of Alg/PPy and Alg/PPy/$ZnFe_2O_4$ beads to adsorb ACT and IBU. For these experiments, specific amounts of dry beads were put in Erlenmeyer flasks filled with ACT or IBU solutions (50 mL) at fixed initial concentrations (C_0), temperature, and pH. The flaks containing the solutions + beads were kept on an orbital shaker (150 rpm). At predetermined time intervals, a 500 µL aliquot was withdrawn from the drug solutions using a plastic syringe, filtered through a 0.45 µm syringe filter, and placed in a Quartz cuvette for analysis in a PerkinElmer Lambda35 UV-Vis spectrophotometer (Canada). Absorbance measurements were done at 429 nm and 220 nm for ACT and IBU. After each UV-Vis measurement, the aliquots were returned to the Erlenmeyer flasks. The effect of the following experimental parameters was also studied: Presence or not of an EMF; magnet distance from the adsorption flask (5–20 cm); beads dosage (10–50 mg), solution pH (5–7), and temperature (25–55 ºC).

Results and Discussion

FTIR analyses were used to characterize the chemical nature of Alg and the prepared materials, as shown in Fig. 2a. The FTIR spectrum of Alg showed a broad band in the range of 3700–3200 cm^{-1} due to the O–H stretching of hydroxyl groups and bands due to the C–H stretching at 2924 and 2858 cm^{-1}. Furthermore, the bands at around 943, 892, and 821 cm^{-1} are associated with different vibration modes of the guluronic and mannuronic units of the Alg. After the ionotropic crosslinking of Alg chains by Ca^{2+} ions, noticeable changes were observed for the bands associated with the carboxylic and hydroxyl groups of this polysaccharide. The FTIR spectrum of the Alg/PPy beads crosslinked by Ca^{2+} (denoted as Alg/PPy-Ca^{2+}) exhibited a broadening of the band ascribed to the O–H stretching, due to the interaction of the hydroxyl groups of Alg with the Ca^{2+} ions. As observed in the Alg/PPy spectrum, the bands in the range of 1100–980 cm^{-1} exhibited a higher intensity due to the contribution of C–O–C, C–C, and C–O stretching. The increase of these bonds can be associated with the crosslinking of GA with Alg, as explained by Huang et al. 2014. The reaction with GA should occur preferentially with the mannuronic units of Alg since its guluronic units are crosslinked by Ca^{2+} ions. Also, the FTIR analyses indicate the successful dual crosslinking of Alg chains, which allows inferring that the Alg/PPy beads are formed by a semi-interpenetrating network (semi-IPN). By comparison, the FTIR spectrum of Alg/PPy/$ZnFe_2O_4$ is quite similar to the spectrum of the bare beads. The characteristic bands of $ZnFe_2O_4$ were not observed because the bands proceeding from the polymer matrix overlap them. The small amount of $ZnFe_2O_4$ compared to the polymers also explain this result. However, the broadening of some bands associated with the functional groups of Alg is noticed. Also, the band ascribed to the asymmetric C=O stretching of the ionized carboxylic groups of Alg (at 1735 cm^{-1}) exhibited a lower intensity. It can be suggested from these data that the magnetic filler interacts with the polymeric matrix, which might be beneficial to their dispersion throughout the beads. The presence of ferrite in the polymeric material conferred the magnetic property to the adsorbent as it is possible to see in Fig. 2b.

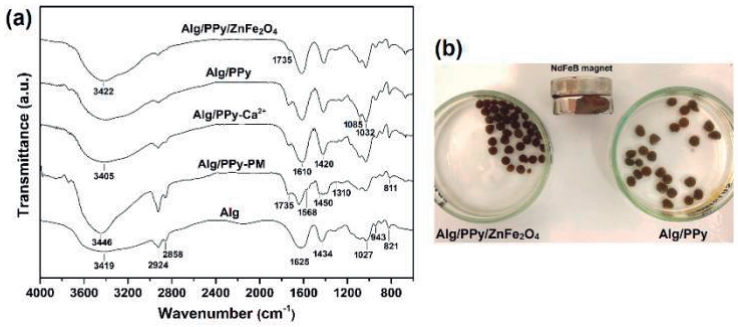

Fig. 2. (a) FTIR spectra of Alg, Alg/PPy-PM (physical mixture), Alg/PPy-Ca^{2+}, Alg/PPy, and Alg/PPy/$ZnFe_2O_4$ beads, (b) Photographic image of the prepared beads on the presence of a permanent magnet.

Fig. 3. shows the swelling data from the experiments performed in the presence of EMF. As observed, this external stimulus caused a minimal variation in the swelling behavior of Alg/PPy, whereas the magnetic beads exhibited a completely different behavior. Different from the experiment in the absence of EMF, Alg/PPy/$ZnFe_2O_4$ exhibited a fast initial swelling kinetics (up to 80 min), and the maximum swelling was increased to 158%. This value is around 1.8-fold higher than that calculated in the absence of EMF, which confirms that the swelling performance of Alg/PPy/$ZnFe_2O_4$ is tailorable. The responsiveness and efficiency of the magnetically enhanced swelling process occur because the magnetic beads have a more deformable macroporous structure due to the EMF. The action of the magnetic field alters the interaction between $ZnFe_2O_4$ particles and the hydrophilic groups of Alg/PPy/$ZnFe_2O_4$ enabling their interaction with water. Besides, the effect of the magnetic field will increase the number of H-bonds in the system and promote the formation of a network of hydrogen bonds, thus, increasing the interaction between the adsorbent and the swelling medium [3].

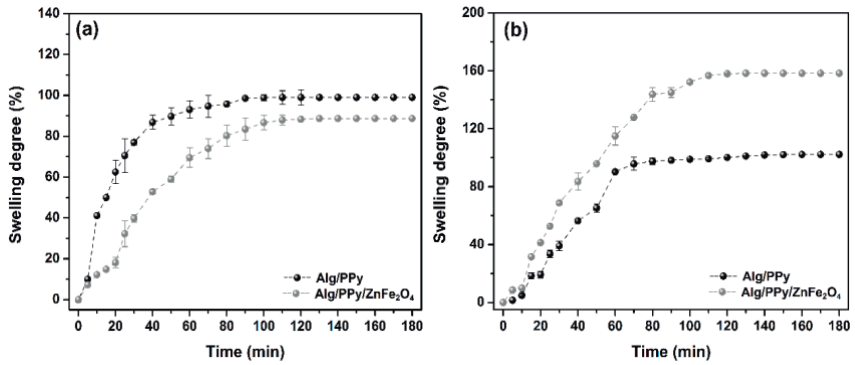

Fig. 3. Swelling curves for Alg/PPy and Alg/PPy/$ZnFe_2O_4$ in distilled water (a) in the absence and (b) in presence of an EMF.

The first was the effect of an EMF on the adsorption of ACT and IBU on the Alg/PPy and Alg/PPy/$ZnFe_2O_4$ beads. Overall, the magnetic beads showed higher adsorption capacity for both drugs compared to Alg/PPy independently of the EMF (Fig.4.), indicating that the composite formation by itself is already advantageous for this kind of application. The discrepancy regarding the adsorption capacity of the two beads is increased due to the presence of EMF, as observed. Indeed, the presence of the EMF increased the ACT adsorption by 14% and IBU adsorption by 12% on Alg/PPy/$ZnFe_2O_4$. On the other hand, no significant changes were observed in the q_e values calculated for Alg/PPy due to the presence of the EMF. The literature reports two main reasons to explain the enhancement of the adsorption process by using an EMF: (i) the Lorentz force generated by the field influences the orientation of adsorbate in solution and transfers them to the adsorbent [4]; and (ii) exposure to an EMF affects the adsorbent, through the phenomenon of magnetic memory, resulting in a more heterogeneous morphology that favors the adsorption process. This last phenomenon is easier observed in materials that have high magnetic susceptibility as Alg/PPy/$ZnFe_2O_4$ [3].

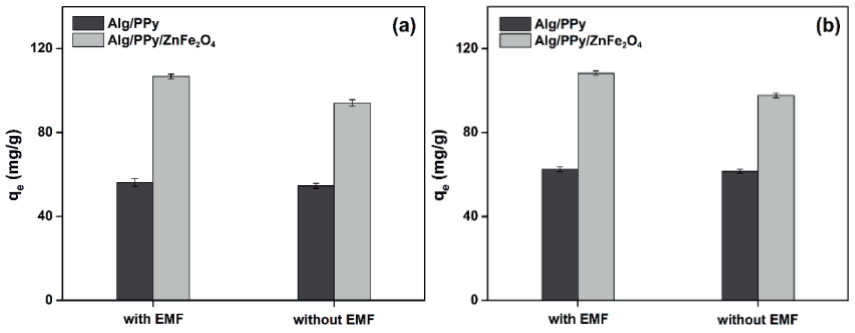

Fig. 4. Adsorption capacity of (a) ACT and (b) IBU on Alg/PPy and Alg/PPy/ZnFe2O4 in presence and absence of EMF (Conditions: Dosage 10 mg; C_0 350 mg/L; solution volume 50 mL; pH not adjusted; room temperature; orbital shaking 150 rpm; contact time 3 h).

To explain some properties of the beads, the processes of adsorption kinetics and isotherms were evaluated and the models that best suited the results obtained in this research were the pseudo-second order kinetics and the Freundlich adsorption model for the isotherms, these data usually assume that the adsorption process occurs due to a chemical bond between the adsorbent and the adsorbate. The high mechanical stability of these beads assured high removal rates (> 91%) even after ten consecutive reuse cycles. In short, this study indicated that the removal of ACT and IBU from the aqueous medium is enhanced by using the magnetic-responsive Alg/PPy/$ZnFe_2O_4$ beads. It is envisaged that the magnetic responsiveness presented by the original material be useful in the practical treatment of drug-contaminated water/wastewater.

Conclusions

Alginate/polypyrrole (Alg/PPy) beads were endowed with magnetic properties by entrapping zinc ferrites ($ZnFe_2O_4$) into their polymeric matrix. Characterization analyses indicated the interaction between the polymers and the magnetic nanoparticles. Moreover, the exposition of the magnetic beads (Alg/PPy/$ZnFe_2O_4$) to an EMF changed intrinsic properties such as swelling and pH_{PZC}. Adsorption experiments revealed that the presence of an EMF enhances the performance of the Alg/PPy/$ZnFe_2O_4$ for the removal of ACT and IBU from the aqueous medium. Indeed, the adsorption capacity of these drugs was increased by 14% and 12% due to the presence of an EMF. Conversely, the adsorption capacity of non-magnetic Alg/PPy beads did not change due to the EMF, confirming that the ferromagnetic nature of the Alg/PPy/$ZnFe_2O_4$ is crucial for this responsive behavior. The EMF also accelerated the drug adsorption on the magnetic beads by about 15%, especially in the initial stages of the adsorption process, which followed pseudo-second-order kinetics. Isotherm analysis indicated that the Freundlich model is adequate to explain the adsorption of both drugs on Alg/PPy/$ZnFe_2O_4$, and the mechanism involves electrostatic, H-bonds, and hydrophobic interaction forces. As determined, the drugs adsorbed on the magnetic beads can be desorbed, which allows their regeneration and reuse up to ten times. The high mechanical stability of these beads assured high removal rates (> 91%) even after ten consecutive reuse cycles. In short, this study indicated that the removal of ACT and IBU from the aqueous medium is enhanced by using the magnetic-responsive Alg/PPy/$ZnFe_2O_4$ beads.

References

[1] Ashuri, A., Miralinaghi, M., Moniri, E., 2022.Korean J. Chem. Eng. 39, 1880–1890. https://doi.org/10.1007/s11814-022-1104-5.

[2] Heybet, E.N., Ugraskan, V., Isik, B., Yazici, O., 2021. Int. J. Biol. Macromol. 193 (A), 88–99. https://doi.org/10.1016/j.ijbiomac.2021.10.084.

[3] Ren, Y., Yang J., Li, j., Lai, B., 2017. Chem, Eng. J. 330, 813 Journal of the mechanical behavior of biomedical materials 822. https://doi.org/10.1016/j.cej.2017.08.029

[4] Ma, J., Ma, Y., Yu, F., Dai, X.H., 2018. Environ. Sci. Tech. 52, 13925–13934. https://doi.org/10.1021/acs.est.8b05409.

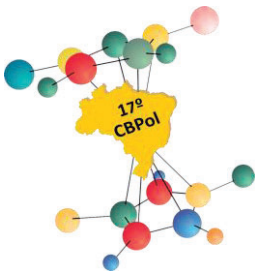

MAIN PROCESS PARAMETERS AND ANTIVIRAL PROPERTIES OF MELALEUCA OIL PICKERING EMULSION STABILIZED WITH NANOCELLULOSE

Greiciele da S. Ferreira[1], Daniel J. da Silva1 [2], Derval S. Rosa1

1- Federal University of ABC (UFABC), Santo André, SP, Brazil.
dervalrosa@ufabc.edu.br.

2 Center for Engineering, Modeling, and Applied Social Sciences (CECS), Federal University of ABC (UFABC), Av. dos Estados, 5001, CEP 09210-210, Santo André, SP, Brazil

Abstract

Essential oils are complex mixtures originating from lipophilic secondary plant metabolites with highly volatile compounds with antiviral properties. This work used cellulose nanofibers (CNF) to stabilize *Pickering* emulsions of MAEO (melaleuca essential oil). The main process parameters were analyzed by the design of the experiment, indicating that the amount of CNF and mixing time collaborated with stability, while oil concentration and homogenization rotation have little interference in the stability process. The viral assays against SARS-CoV-2 indicate damage to the Spike protein on the particle surface. The emulsions show good stability following these process parameters, good antiviral activity, and are environmentally friendly, causing less environmental damage.

Keywords: Oil essential, Melaleuca Alternifolia, Nanocellulose, SARS-CoV-2.

Introduction

Essential oils (EOs) are natural compounds with biological assets enabling excellent antimicrobial, antiviral, and antioxidant capacity. For this reason, they are considered a viable technological alternative to conventional chemical disinfectants. The antimicrobial capacity of the EOs is directly associated with the quantity of terpene chemical groups present in the EOs, for these components have an affinity for interaction with the biological structures of the microorganisms, leading to the formation of reactive oxygen species (ROS) that can cause irreversible damage to the microorganisms, compromising their metabolic activities, However, the OEs present limitations such as i) volatilization of actives ii) degradation iii) oxidation, iv) low solubility, these restrictions prevent the direct use in the manufacture of antiseptic, pharmaceutical, cosmetic and food products. [1, 2,3].

The Essentials oil of melaleuca alternifolia (MaEO) is extracted from the tea tree, a plant from Australia, by steam distillation of leaves and terminal branches. It has in its composition several functional groups of terpenes and terpenoids, among them, terpinenol-4-ol, γ-terpinene, α-terpinene, cymene, and α-terpineol that contribute synergistically to antimicrobial activity leading to inhibition of cellular respiration processes, rupture of the bacterial membrane inducing leakage of metabolites from microorganisms, consequently causing cell lysis or death [4,5,6].

Adding natural compounds is an alternative to protect the actives in essential oils and ensure their efficacy. Emulsification is a widely used technology to stabilize or control the release of active ingredients. Emulsions are dispersed systems formed by two immiscible liquid phases, the most common being oil-in-water and water-in-oil emulsions, stabilized by amphiphilic molecules or emulsifiers well established in the industry [7,8].

These auxiliary components ensure excellent emulsion stability over time to increase the shelf life of emulsion-based products, which is a crucial factor for industries. [9,2]. The replacement of synthetic surfactants with natural solid particles, such as cellulose, has been adopted in the market due to the environmental damage that those can cause. Cellulose presents advantages such as biodegradability, renewable biomass, and non-toxicity. Among the available cellulose structures, cellulose nanofibrils are considered a good option since they are fibrous nanostructures with high surface area and low production costs [1].

Cellulose nanofibrils (CNFs) are fibrous nanostructures with a diameter on the nanometer scale (less than 100 nm) that allow high surface area without high production energy and financial costs [10,11,12]. In this contribution, we evaluated various process parameters on the stability of *Pickering* emulsions of (O/W) using the designer of experiments (DoE) design of experiments. The instability phenomena (creaming, sedimentation), instability index and droplet size were analyzed and controlled over time. In addition, the antiviral activity of MaEO and the emulsions were investigated against SARS-CoV-2. From the DoE point of view, parameters on the preparation and stability of Pickering emulsions stabilized with CNF were revealed. The Pickering O/W emulsion inactivates the COVID-19 coronavirus, showing great potential for use in rapid sanitizing products and food packaging formulations capable of protecting food against SARS-CoV-2.

Experimental

The aqueous suspensions of CNF were homogenized in a high-intensity ultrasound (Sonics Vibra Cell, 400 W power and 24 kHz) for 10 min. The MaEO was mixed with a previously dispersed CNF suspension, and this mixture was homogenized in an Ultra-Turrax Blender, model IKA T25 (IKA Werke, Staufen, Germany). The following parameters were varied: CNF content in the aqueous suspension (0.5 and 1 % w/v), oil/water (O/W) ratio (20 and 30 % v/v), mixing speed (12,000 and 15,000 rpm) and mixing time (5 and 7 min). The emulsions were named XEO/YT/ZCNF/WRPM, where X corresponds to the MaEO content (% v/v), Y is the mixing time (min), Z is the CNF concentration (% w/v), and W is the mixing speed (rpm).

Results and Discussion

The stability of Pickering emulsions is related to the emulsifier's (CNF) content and the preparation process's parameters, such as (rotation time, CNF concentration, rotation in rpm, and oil and water concentration). According to the Design of Experiments tool, the stability index values are affected according to the process parameters. The emulsion stability index (ESI) increases with the amount of CNF due to the 3D network formations caused by the high interactions of CNF (Fig 1). [13,14,15].

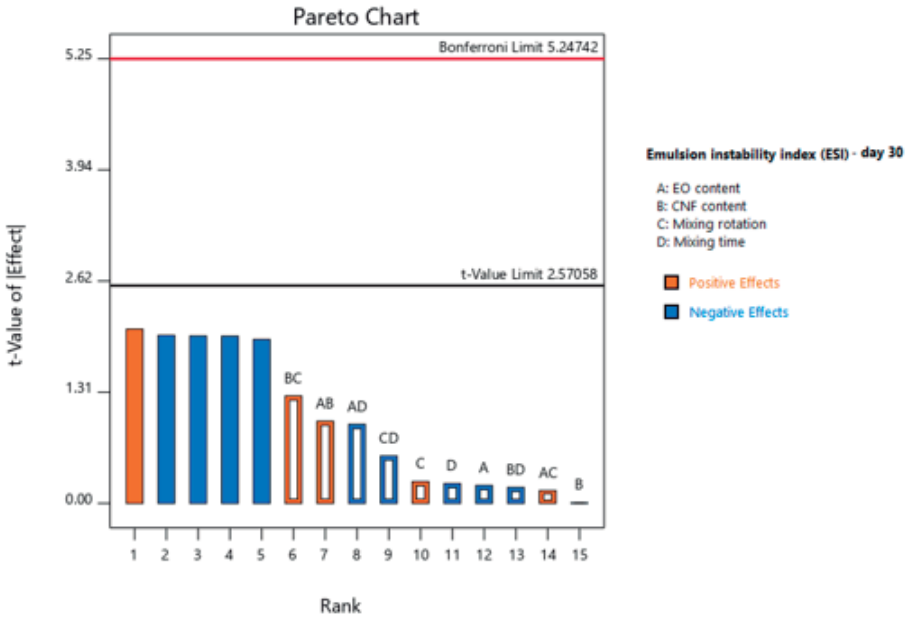

Figure 1: Gráficos de Pareto da análise factorial obtida pelo desenho de experiências (DoE) para o efeito dos factores utilizados para preparar as emulsões Pickering (teor de OE, teor de CNF, rotação da mistura e tempo de mistura) sobre o índice de instabilidade da emulsão (ESI) a 0 dias (a) e 30 dias (b) de armazenamento. A: Teor de EO. B: Teor de CNF. C: rotação da mistura. D: tempo de mistura. Duas letras: interacção simultânea dos factores. Efeito negativo: o factor reduz o ESI. Efeito positivo: o factor aumenta o ESI. Os factores acima do limiar de Bonferroni têm quase de certeza efeitos importantes sobre a propriedade. Os factores que ultrapassam o limiar do valor t têm efeitos potencialmente importantes sobre a propriedade.

MaOE concentrations negatively affect the stability of the emulsions. The rotation and homogenization time contribute to the system's stability over the storage time. An increase in the average diameter of MaEO droplets is observed with increasing oil concentration. Increasing the CNF content and mixing time prevents the coalescence of the oil droplets due to the Ostwald

ripening mechanism [9]. As can be observed in droplet morphologies, homogenization rotation and CNF content have synergistic significative effects on droplet stability (Fig 2).

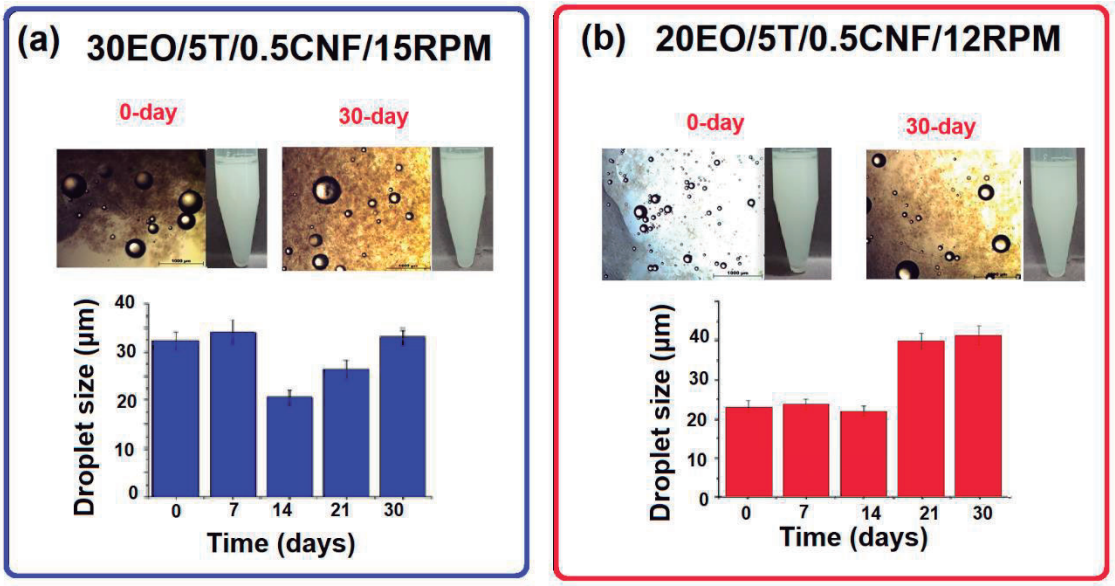

Figure 2: Fluorescence optical microscopy of the CNF-stabilized Melaleuca emulsion. Bar scale=100 µm

Pickering emulsions 30EO/5T/0.5CNF/15RPM and 20EO/5T/0.5CNF/12RPM are the most stable emulsions concerning the smallest droplet sizes and ESI values, including the smallest variations of these parameters over the 30-day storage period. These Pickering emulsions were subjected to antiviral testing against SARS-CoV-2.

The MaEO inactivated the viral load of SARS-CoV-2 in the viral inoculum medium at the same instant after contact with the essential oil. MaEO inactivated all SARS-CoV-2 virions in the viral inoculum medium immediately after contact with it, as indicated in Fig. 3a. The 30EO/5T/0.5CNF/15RPM emulsion was able to inactivate all SARS-CoV-2 virions within 15 minutes after direct contact, as all viral S proteins were damaged in the inoculum sample (Fig. 3b)

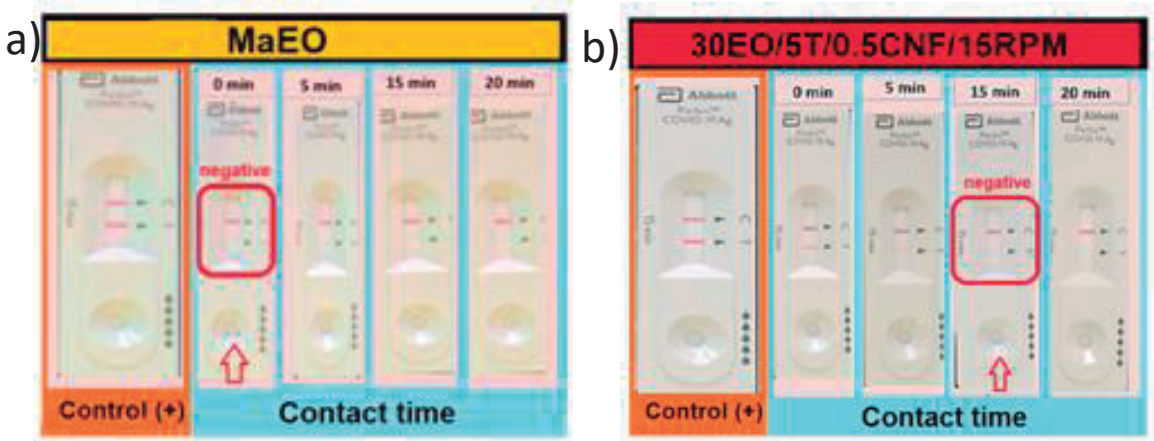

Figure 3: SARS-CoV-2 antiviral tests for the MaEO (a) and MaEO/water emulsions (b) after 0, 5, 15, and 20 min of direct contact. Negative results are highlighted in red squares.

Conclusions

Therefore, the *Pickering* emulsion of MaEO stabilized with CNF shows antiviral performance against SARS-CoV-2. Melaleuca alternifolia essential oil (MaEO) inactivates SARS-CoV-2 particles immediately by damaging its S proteins through capsid destruction, but its emulsions needed more time to inactivate, but it was possible to verify that *Pickering* emulsions have antiviral character.

Acknowledgment

The authors thank the CAPES (Code 001), CAPES-Pandemias (8881.504639/2020-01), MULTIUSER CENTRAL FACILITIES (UFABC), UFABC, and REVALORES Strategic Unit.

References

1. M. Angane; S. Swift; K. Huang; C.A. Butts, S.Y Quek; Foods. 11 2022. https://doi.org/10.3390/foods11030464.
2. Y. Cahyana; Y.S.E. Putri; D.S. Solihah; F.S. Lutfi; R.M. Alqurashi; H. Marta; Molecules. 27 (2022) 1–19. https://doi.org/10.3390/molecules27227872.
3. X. Bao; J. Wu; G. Ma; S. Int. 30 (2020) 669–676. https://doi.org/10.1016/j.pnsc.2020.08.001.
4. A. Romeo; F. Iacovelli; C. Scagnolari; M. Scordio; F. Frasca; R. Condò; S. Ammendola; R. Gaziano; M. Anselmi; M. Divizia; M. Falconi; Molecules. 27 (2022). https://doi.org/10.3390/molecules27123786.
5. A.M.S.-M; and F.A; Verdeguer Mercedes;. Inside. (2020) 159–173.
6. J. Voelker; R. Mauleon; M. Shepherd; Plant Syst. Evol. 309 (2023). https://doi.org/10.1007/s00606-023-01847-1.
7. B. Vörös-Horváth; S. Das; A. Salem; S. Nagy; A. Böszörményi; T. Kőszegi; S. Pál; Molecules. 25 (2020) 1–17. https://doi.org/10.3390/molecules25235544.
8. Y. Lu; J. Li; L. Ge; W. Xie; D. Wu; Carbohydr. Polym. 255 (2021) 117483. https://doi.org/10.1016/j.carbpol.2020.117483.
9. A.G. Souza; R.R. Ferreira; L.C. Paula; L.F.G. Setz; D.S. Rosa;, J. Mol. Liq. 320 (2020) 114458. https://doi.org/10.1016/j.molliq.2020.114458.
10. A.G. Souza; R.R. Ferreira; J.S. Marciano; E.R. Oliveira; M.M. Kato; E.D.C. Yudice; L.F. Setz; V.K. Rangari, D.S. Rosa; J. Polym. Environ. (2023). https://doi.org/10.1007/s10924-022-02750-5.
11. N. Bu; L. Huang; G. Cao; H. Lin; J. Pang, L; Wang, R; Mu, Konjac; glucomannan/Pullulan; A Physicochem. Eng. Asp. 650 (2022) 129553. https://doi.org/10.1016/j.colsurfa.2022.129553.
12. Y. Zhang; Y. Jiang; L. Han; B. Wang; H. Xu; Y. Zhong; L. Zhang; Z. Mao; X. Sui, Carbohydr. Polym. 179 (2018) 86–92. https://doi.org/10.1016/j.carbpol.2017.09.065.
13. P. Bertsch; M. Arcari; T. Geue; R. Mezzenga; G. Nyström; P. Fischer; Biomacromolecules. 20 (2019) 4574–4580. https://doi.org/10.1021/acs.biomac.9b01384.
14. G. da S. Ferreira; D.J. da Silva; D.S. Rosa; J. Mol. Liq. 372 (2023) 121183. https://doi.org/10.1016/j.molliq.2022.121183.
15. X. Liu; X. Qi; Y. Guan; Y. He; S. Li; H. Liu; L. Zhou; C. Wei; C. Yu; Y. Chen; Carbohydr. Polym. 224 (2019) 115202. https://doi.org/10.1016/j.carbpol.2019.115202.

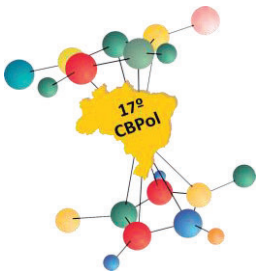

MONODISPERSE NANOPARTICLES PREPARED BY MICROEMULSION POLYMERIZATION

Tainara L. Souza, Sônia F. Zawadzki and Juliete S. Neves*

Department of Chemistry, Federal University of Paraná (UFPR), Curitiba, PR, Brazil julieteneves@ufpr.br

Abstract – Monodisperse nanoparticles have been successfully prepared through microemulsion polymerization of styrene and acrylated ester of canola oil. The acrylic ester was obtained in three stages: esterification, epoxidation and acrylic addition in triglycerides chains whose were derived from commercial canola oil. Influencing of the surfactant concentration on the particles diameter and size distribution was investigated. Stable polymer latices with 30 wt% of solids content were obtained with surfactant/monomer weight ratio up to 0.14, particle diameter less than 78 nm and Z_{ave} less than 0.2, showing latices with narrow particle size distribution (PSD).

Keywords: *Biopolymer, canola oil, styrene, polymer latex*

Introduction

Every year, sustainable practices have received an important place in the development of the industry, being reinforced by Agenda 21 that predicts a responsible action to meet the current and future needs.[1-3] In this context, petroleum derivatives are not welcome due to their low degradability rate, their contribution to global warming (greenhouse gas emissions) and the accentuation of environmental problems.[2-4] Therefore, the use of vegetable oils and their derivatives has become emerging to completely or partially replace fossil materials in polymerization reactions.[5] This is possible because vegetable oils show significant characteristics: high availability, low cost, renewable nature, low ecotoxicity, biodegradability, biocompatibility and potential to structural modification.[6-7]

Vegetable oils are triglycerides, whose fatty acid composition varies according to chain length and functionality.[6] The double bonds in these molecules allow for structural modification through thr insertion of reactive functional groups, with a subsequent use as monomers in polyaddition and/or polycondensation reactions.[8] Thus, the production of vegetable oils has increased significantly due to their application in new materials.[2]

Recent studies indicate the potential of tropical canola varieties in Brazil. Guiducci et al.[9] showed an average productivity of 3,000 kg/ha, emphasizing higher oil yield compared to soybean, besides resulting in lower production cost compared to corn. Canola oil, the material used in the present study, is rich in oleic acid (R = 18:1).[2] To be used as a base for polymer construction, this oil must undergo successive stages of modification: esterification, epoxidation and acrylation of methyl oleate.[4]

According to Moreno et al.[10] the olefinic functionality of the modified oleic acid allows the crosslinking and the formation of a network with improved mechanical properties. Thus, oleic acid is distinguished from others by its oxidative stability, high availability, ease of chemical modification, and low cost of extraction and commercialization. In addition, emulsion polymerizations using styrene and acrylated methyl oleate have shown high conversions, stable polymeric networks even

after longer storage and high molecular weight.[8] However, Meier et al.[2] indicate that although monomers based on acryl or methacryl of fatty alcohols are known in the industrial sphere, they are still poorly studied.
In this work, the microemulsion polymerization was used to prepare latices of styrene and acrylated esters of canola oil with monodisperse particles diameters less than 52 nm.

Experimental

Materials

Materials used: acrylic acid (AA) and styrene (Sty) monomers, canola oil, sodium hydroxide, methanol, hexane, acetic acid, toluene, hydrogen peroxide 30%, sodium bicarbonate, hydroquinone, sodium dodecyl sulfate, potassium persulphate and distilled water. The materials were used as received.

Methods

Preparation of functionalized fatty ester – The first step was the transesterification of the canola oil with methanol. In a 1000 mL round-bottom flask equipped with a reflux condenser, 225 g of canola oil, 200 mL (4.9 mol) of methanol and 2.3 g (5.6×10^{-2} mol) of NaOH were added and the mixture was heated to 65 ºC for 1h30 with moderate stirring. The mixture was then transferred to a separating funnel and the canola ester was washed three times with water to remove the residual methanol and NaOH. The second step was the epoxidation reaction of the double bond of the ester. In a 100 mL three-necked round-bottom flask, equipped with a reflux condenser, 5.4 mL (0.14 mol) of acetic acid, 20 g of fatty ester and 26.5 mL of toluene were added. The mixture was heated to 55 ºC and 96 mL (4.1 mol) of hydrogen peroxide was added dropwise while stirring. After complete addition of the hydrogen peroxide, the reaction system was kept at 55 °C with continuous stirring for 15 h. Then, the product was washed with saturated bicarbonate solution to remove the residual acetic acid. The last step was the reaction between acrylic acid and epoxidized fatty ester. In a 250 mL round-bottom flask, equipped with a reflux condenser, 7.7 g (0.11 mol) of acrylic acid, 15 g of epoxidized fatty ester and 0.13 g (1.2×10^{-3} mol) of hydroquinone were added. The reaction system was kept at 100 °C with continuous stirring of 6 h. Then, the functionalized fatty ester was washed with saturated bicarbonate solution to remove the residual acrylic acid.

Polymerization - In a 100 mL round-bottom flask, equipped with a reflux condenser, 3.84 g of styrene, 0.81 g of acrylic acid, 1.63 g of of functionalized fatty ester, 0.19 g of potassium persulphate, 38 g of distilled water and sodium dodecyl sulfate were added. Three different surfactant/monomer ratio, 0.03, 0.07 and 0.14, were evaluated. The reaction system was kept at 80 °C under continuous stirring for 2 h.

Nuclear Magnetic Resonance (NMR) analyzes were carried out using a Bruker AVANCE 400 NMR spectrometer operating at 9.4 T observing the ^{1}H nuclei at 400.13 MHz. Samples of approximately 200 µl were transferred into 5-mm NMR tubes and the volume was completed to 600 µl with deuterated chloroform containing tetramethylsilane (TMS) as the internal standard. The ^{1}H NMR spectra were recorded at 25 ° C. The analyzes were carried out at the Chemistry Department – UFPR.

Differential scanning calorimetry (DSC) analyzes were carried out using a NETZSCH DSC 200 F3 MAIA equipment. Samples were weighed in aluminum crucibles (approximately 8.0 mg) and the analyzes were programmed in heating/cooling cycles: 1) heating from 25 to 200 °C, isotherm for 5 min; 2) cooling from 200 to -40 °C; isotherm for 5 min; 3) heating from -40 to 200 °C. The heating and cooling rate was 10 ºC min^{-1} and the run was performed under N_2 atmosphere (40 mL min^{-1}). The data used refer to the second warm-up. The analyzes were carried out at the Chemistry Department – UFPR.

Dynamic Light Scattering *(DLS)* analyzes were carried out using a ZETASIZER NANO ZS at a Malvern Instruments and PANalytical (Egham, Surrey, United Kingdom) operating at 13° e 173°, scattered light detector with a 4 mV solid state and 632.8 nm laser wavelength. Data acquisition was performed using the software Zeta Sizer Nano v. 3.30. The analyzes were carried out at the BIOPOL Laboratory, at the Pharmacy Department – UFPR.

Results and Discussion

The functionalized fatty ester was evaluated by ^{1}H NMR spectroscopy and the results confirmed that the expected products were obtained at each step. In Figure 1a, the peak at δ = 3.67 ppm, which are related to three hydrogens of the methyl group of the ester, confirms the transesterification product obtained. In Figure 1b, the disappearance of the peak at δ = 5.35 ppm, which is related to the hydrogen associated with the unsaturated carbon and the appearance of peaks at δ = 2.88–3.12 ppm, associated with the hydrogens of the oxirane ring, confirm the epoxidation reaction. At last, in Figure 1c, the reaction between acrylic acid and epoxidized fatty ester was confirmed by the disappearance of the hydrogen peaks in the oxirane ring and the presence of peaks associated to the hydrogen of the unsaturated carbon in the acrylic group observed at δ = 5.83–6.41 ppm.

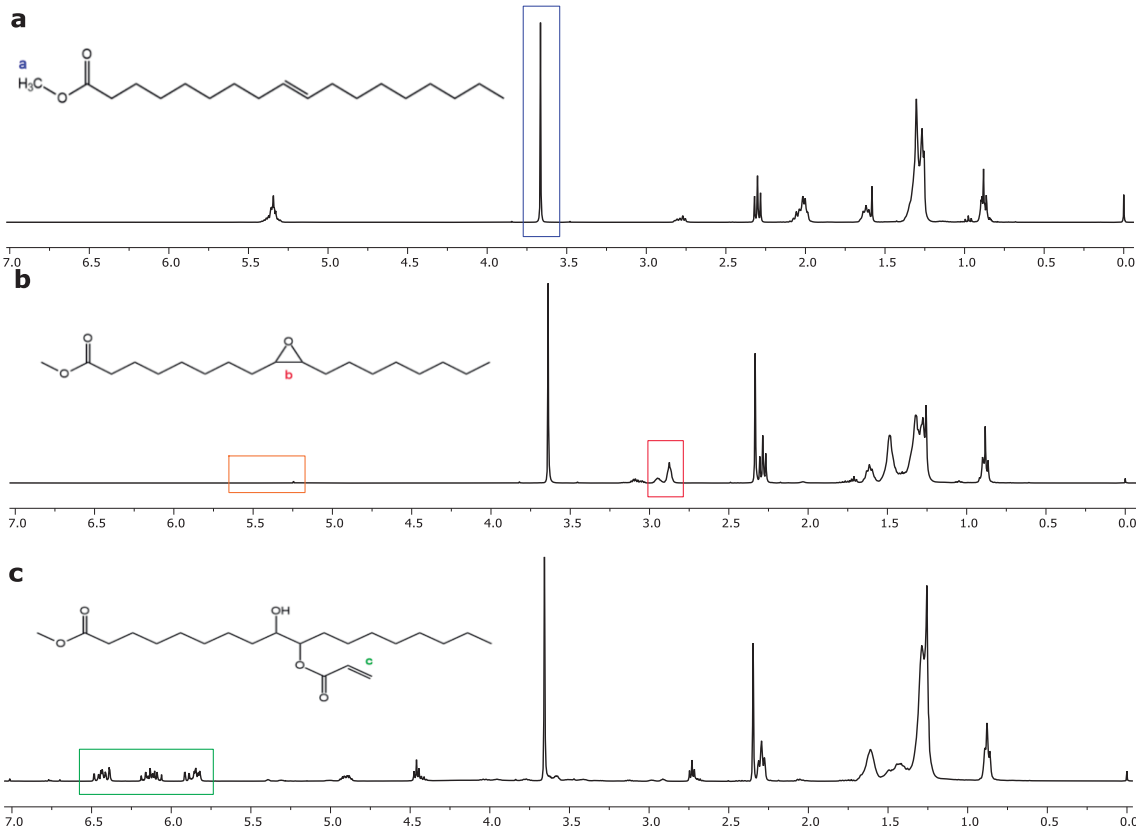

Figure 1 - ^{1} H NMR of functionalized fatty ester. a) ^{1} H NMR of product of transesterification reaction. b) ^{1} H NMR of product of epoxidation reaction. c) ^{1} H NMR of product of the reaction between epoxidized fatty ester and acrylic acid.

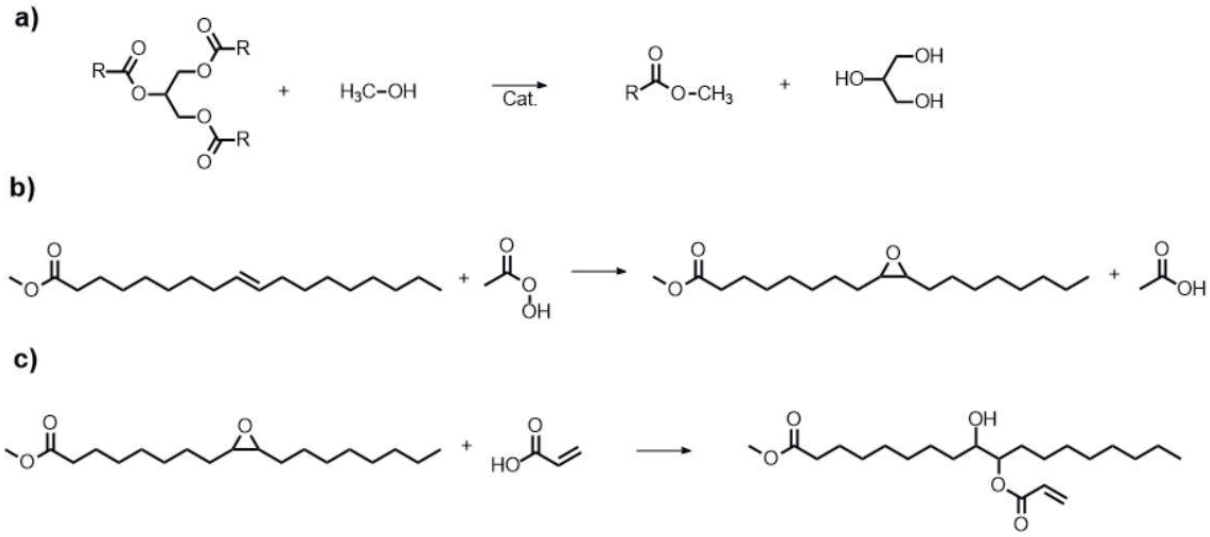

Figure 2 – a) Transesterification of triglyceride with methanol to methyl ester; b) Epoxidation reaction of the double bond of ester by a peroxy-carboxylic acid; c) Reaction between acrylic acid and epoxidized fatty ester.

In this work, polymeric nanoparticles were obtained by microemulsion polymerization and 5 wt% of acrylic acid was used as a co-stabilizer to reduce the styrene/water interfacial tension and improve latex stability by preventing clotting. The influence of surfactant content on particle diameter was evaluated and in Table 1 is possible to observe an inverse relation between surfactant/monomer ratio and particle size. By increasing the surfactant concentration, a decrease in particle diameter is observed. This is because increasing the concentration of anionic surfactant causes the nucleation of new particles. By comparing the number of particles per litre of latex, it was observed the higher number of particles when the surfactant concentration was higher. It was also observed that another factor can influence the particle diameter in microemulsion polymerization: the solubility of the monomer in the continuous phase.

An increase in solubility reduces the monomer/continuous phase interfacial tension and favors the dispersion of the monomer and the homogeneous nucleation, leading to the formation of smaller particles. When using monomers with low solubility in water, such as styrene and/or functionalized fatty esters, there is a greater difficulty in stabilizing the emulsion and forming monodisperse particles with reduced diameter. However, when comparing the results of the experiment 3 and 6 using the same concentration of surfactant, it was observed that by changing the monomer composition alone, no significant change in the particle diameter was found and the lattice sizes were homogeneously monodispersed.

Table 1 - 1Influence of the of anionic surfactant content in the particle diameter and Glass Transition Temperature.

Exp.	Composition[a]			Surfactant/monomer weight ratio	Particle diameter (nm)	PDI	C_p (L^{-1})[c]	T_g (°C)[d]
	AA	Sty	Ester[b]					
Exp.1	5	85	10	0.03	52	0.1	6.7×10^{18}	74
Exp.2	5	85	10	0.07	38	0.2	1.6×10^{19}	-
Exp.3	5	85	10	0.14	33	0.1	2.5×10^{19}	65
Exp.4	5	95	-	0.03	77	0.2	1.1×10^{18}	108
Exp. 5	5	95	-	0.07	46	0.2	3.1×10^{18}	-
Exp.6	5	95	-	0.14	36	0.1	2.0×10^{19}	75

[a]Monomer content in wt% of total monomers.
[b]Functionalized fatty ester.
[c] C_p = Particle number concentration – number of particles per volume of suspending medium.
[d] T_g = Glass Transition Temperature

The glass transition temperature of the polymers was determined by DSC. Comparing the data showed in Table 1, it can be observed that a variation of the T_g values with the surfactant concentration. The surfactant molecules can act as a plasticizer, decreasing the cohesive force between the polymer chains, decreasing T_g of the when surfactant concentration was increased. In experiments 1 and 4, the T_g of polymer also decreased with monomer composition changing.

Conclusions

In this work they were synthesized nanoparticles by microemulsion polymerization, with diameter between 33 and 78 nm, with PDI less than 0.2, indicating latices with narrow PSD. The canola vegetable oil was successfully modified and polymerized with styrene by radical polymerization mechanism. The results showed that the anionic surfactant concentration had more influence on particle diameter and T_g values than the monomer composition in this case.

Acknowledgements

The authors would like to thank Joslaine Jacumazo for the DLS analysis carried out at the Laboratory BIOPOL/UFPR and the NMR analysis performed at the Nuclear Magnetic Resonance Laboratory at the Federal University of Paraná (UFPR).

References

1. A. M. M. S. Medeiros, F. Machado, J. C. Rubim and T. F. L. McKenna, *Journal of Polymer Science Part A: Polymer Chemistry*, 2017, 55, 1422.https://doi.org/10.1002/pola.28511.
2. M. A. R. Meier, J. O. Metzger and U. S. Schubert, *Chemical Society Reviews*, 2007, 36, 1788.10.1039/B703294C.
3. MINISTÉRIO DO MEIO AMBIENTE, Agenda 21 global, https://antigo.mma.gov.br/responsabilidade-socioambiental/agenda-21/agenda-21-global.html#:~:text=A%20Agenda%2021%20pode%20ser,justi%C3%A7a%20social%20e%20efici%C3%AAncia%20econ%C3%B4mica.&text=Pre%C3%A2mbulo%20(Arquivos%20para%20Download%20Word%20ou%20PDF), (accessed May 2, 2023).
4. A. T. Jensen, C. Sayer, P. H. H. Araújo and F. Machado, *European Journal of Lipid Science and Technology*, 2014, 116, 37.https://doi.org/10.1002/ejlt.201300212.
5. A. T. Jensen, A. C. C. de Oliveira, S. B. Gonçalves, R. Gambetta and F. Machado, *Journal of Applied Polymer Science*, 2016, 133.https://doi.org/10.1002/app.44129.
6. J. S. Neves, L. F. Valadares and F. Machado, *Colloids and Interfaces*, 2018, 2, 46
7. L. Montero de Espinosa and M. A. R. Meier, *European Polymer Journal*, 2011, 47, 837.https://doi.org/10.1016/j.eurpolymj.2010.11.020.
8. S. P. Bunker and R. P. Wool, *Journal of Polymer Science Part A: Polymer Chemistry*, 2002, 40, 451.https://doi.org/10.1002/pola.10130.
9. R. d. C. N. Guiducci, P. S. Sabaini, A. N. Cardoso and B. G. Laviola, *Tropicalização da canola (Brassica napus L.) e inserção na cadeia produtiva de óleo vegetal: análise de cenário*, Embrapa Agroenergia, 2020.
10. M. Moreno, M. Goikoetxea and M. J. Barandiaran, *Journal of Polymer Science Part A: Polymer Chemistry*, 2012, 50, 4628.https://doi.org/10.1002/pola.26287.

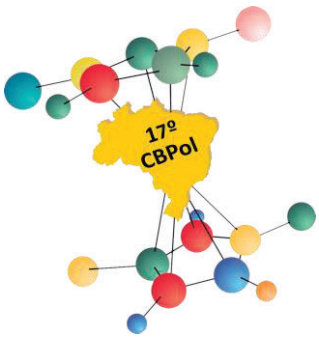

MORPHOLOGICAL INFLUENCE ON THE INCORPORATION OF NANOCELLULOSE INTO DE MEMBRANES POLYVINYLIDENE FLUORIDE (PVDF)

Tayse Circe Turossi[1], Ademir José Zattera[1], Camila Baldasso[1] and Jocelei Duarte[1].

1 – University of Caxias do Sul (UCS), Caxias do Sul, RS, Brazil

Abstract –
The addition of nanomaterials in polymer matrices has been highlighted in recent years, due to their advantageous characteristics compared to pure materials. The incorporation of natural fibers in polymers, such as nanocellulose, becomes a sustainable alternative, since they come from renewable resources. For polymeric membranes, the use of nanofibrillated cellulose (CNF) in the composition results in a greater specific surface area, thermal resistance, delay in the formation of encrustations (fouling), in addition to good mechanical properties and green properties, such as biodegradability and recyclability. The objective of this work was to produce and evaluate the morphology of polyvinylidene fluoride (PVDF) membranes incorporated with different proportions of CNF. For the production of membranes, the phase inversion method was used.by immersion-coagulationwith the solvente N,N-dimethylformamide (DMF) and distilled water being the non-solvent. The samples were identified as: PVDF, in the other words, 100% PVDF membrane, PVDF/0,5%CNF with addition of 0,5% nanocellulose in PVDF membrane and PVDF/1,0%CNF which means 1,0% nanocellulose added to the membrane of PVDF. Scanning electron microscopy (SEM) analysis showed an asymmetric morphology in the three membranes containing a thin dense layer on the surface, therefore, the selective layer and then a porous structure. Furthermore, the images indicated that the use of distilled water as a non-solvent resulted in an increase in the nominal pore size and in the porosity of the membranes with nanocellulose, due to the hydrophilic characteristics of the nanomaterial. According to the results obtained, the addition of CNF can be a viable alternative for application in membranes, maintaining and/or improving the filtration properties.

Keywords: Membrane, Nanocellulose, Nanocomposites, PVDF, Morphology.

Introduction

With the population increase and economic development, world organizations conjecture that from 2030, 17% of the world population will not have infrastructure for access to water [1]. Thus, it becomes necessary to search for new reuse processes. Therefore, because they have high treatment efficiency and do not generate hazardous solid waste, water treatment using polymeric membranes is an attractive alternative.

To improve the filtration efficiency and selective capacity of the membrane, in addition to partially replacing polymers, the incorporation of nanomaterials in polymeric membranes are being increasingly used. In order to provide different properties, reduce production costs and confer benefits to the functioning of the membranes, it is necessary to study the implantation of green nanomaterials, such as nanocellulose, since many are abundant on Earth and have biodegradability [2].

In the present work, PVDF membranes with the incorporation of nanocellulose were investigated, aiming at the morphological and porosity properties of the produced samples.

Experimental

Materiais

The polymer used to prepare the membranes was poly(vinylidene fluoride) (PVDF) in the form of pellets (SOLEF 1015/0078), and was supplied by Solvay Solexis Inc. Cellulose nanofibers were obtained through the defibrillation of bleached cellulose fibers from the genus Eucalyptus sp. The material was provided by Companhia de Celulose Riograndense.

The solvent used in preparing the membrane was N,N-dimethylformamide (DMF), supplied by Labsynth, with a purity of 99,8%. And the non-solvent was distilled water. For the solvent exchange step of the nanofibrillated cellulose pulp, ethanol (99,5% PA from the Anidrol brand) was used.

Métodos

Nanocellulose was prepared by defibrillating commercial cellulose in a high shear stone mill, model MKCA 6-2, MASUKO brand. Grinding was carried out for 5 hours at 2500 rpm to obtain fibers on a nanometric scale. The proportion used was 2,2% (w/v) cellulose/water.

Then, the solvent exchange of the nanofibrillated cellulose pulp was carried out in order to remove the water. Then, ethanol was added to the suspensions and centrifugation was carried out in triplicate at 4500 rpm for 10 minutes in a Novatécnica centrifuge, model NT 820.

The membranes were prepared using the phase inversion technique from a polymeric solution of 20% (w/v) of the total mass in DMF. Table 1 shows the proportions used in each sample.

Table 1– Nomenclature and proportions of membrane samples

Nomenclature	PVDF (g)	DMF (mL)	CNF (g)
PVDF	10	50	0
PVDF/0,5% CNF	9,95	50	0,05
PVDF/1,0% CNF	9,9	50	0,1

These solutions were maintained under constant agitation at a temperature of 70 ± 2 °C for 24 hours. After this period, the step of spreading the solution over a glass plate was carried out in order to form the polymeric film. To assist in this process, a stainless steel spreading knife with a controlled thickness of 200 μm was used. Then, the plate with the polymeric film was immersed in a coagulation bath with the non-solvent, distilled water, at a temperature of 23 ± 0,5 °C for 24 hours, enough time to ensure the precipitation of the polymer and the formation of membranes. solid. Finally, the membranes were dried at room temperature (23 ± 0,5 °C).

The morphology of the surface and the cross-section of the membranes were evaluated using a field emission scanning electron microscope (SEM) brand Tescan (Czech Republic) model MIRA-3. The samples were fractured in liquid nitrogen and covered with gold. Results of the nominal pore size of the samples were also obtained with the help of the Image Tools Software.

Membrane porosity was calculated based on the gravimetric method. The first step was to dry the membrane at 70 °C for 24 hours, after which it was weighed. Then, the sample was immersed in n-octanol (Merck, 97% purity) for 2 hours and weighed again. The porosity is calculated according to Eq. 1 [3].

$$\varepsilon = \frac{\left(\frac{M_f}{M_i}\right)}{\left(\frac{M_f}{\rho_m} + \frac{M_i}{\rho_o}\right)} \times 100 \quad (1)$$

Where, ε is the porosity of the membrane (%), M_f is the final mass after immersion in n-octanol (g), M_i is the initial mass (g), ρ_m is the membrane density (g/cm³) and ρ_o is the n-octanol density (0,82 g/cm³). To determine the density of the membrane, the gravimetric method is also used, following the ASTM-D792-13 standard [4]. The membrane is dried in an oven for 24 hours at 100°C and then weighed. Afterwards, it is immersed in ethanol (Merck, 99,9% purity) and the second weighing is carried out. Eq. 2 shows the density calculation

$$\rho_m = \left(\frac{M_1}{M_1 + M_2}\right) \times \rho_{et} \quad (2)$$

Where, ρ_m is the membrane density (g/cm³), M_1 is the initial sample mass (g), M_2 is the mass after immersion in ethanol (g) and ρ_{et} is the ethanol density (0,79 g/cm³).

Results and Discussion

The active surface and cross-section of the membranes are being compared in Fig 1 and Fig 2, respectively. As observed in the SEM, the membranes presented homogeneous morphology of granular formation with a spongy appearance and without significant alteration and precipitation with the addition of nanocellulose [5].

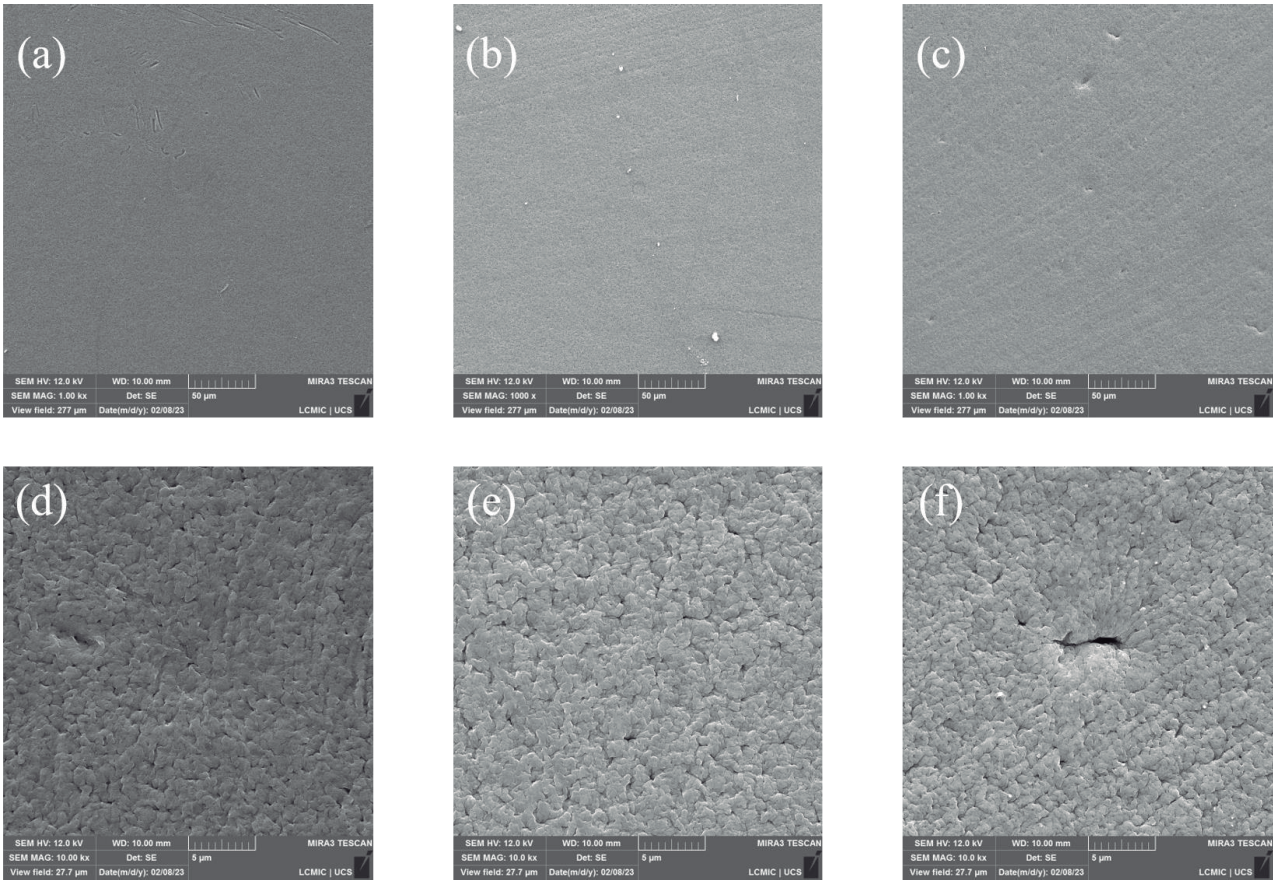

Figure 1–SEM of active surfaces with 1000x and 10000x magnification of samples (a, d) PVDF, (b, e) PVDF/0,5%CNF and (c, f) PVDF/1,0%CNF

The images obtained in Fig 2. show that all membranes presented asymmetrical morphologies formed by a fine dense surface structure, followed by a porous layer with the presence of macrovoids [5, 6]. This morphology is generated due to the high compatibility of the solvent (DMF) and non-solvent (distilled water) during phase inversion, providing a reduction in surface tension, thus a rapid precipitation of the polymer for the formation of membranes. These characteristics may favor a greater permeate flux, improving the filtration properties of the membrane [7].

Furthermore, it is evidenced that the incorporation of nanocellulose generate channels with more open pores, causing an increase in the size of macrovoids compared to the pure PVDF membrane. This is explained due to the hydrophilic nature of nanocellulose, which is favored by the use of non-solvent during phase inversion [5-7].

These results corroborate the values presented in Table 2, since the addition of nanomaterials, such as nanocellulose, increases the nominal pore size of the membranes. As observed, the membrane with 1,0% cellulose obtained larger pore sizes [8].

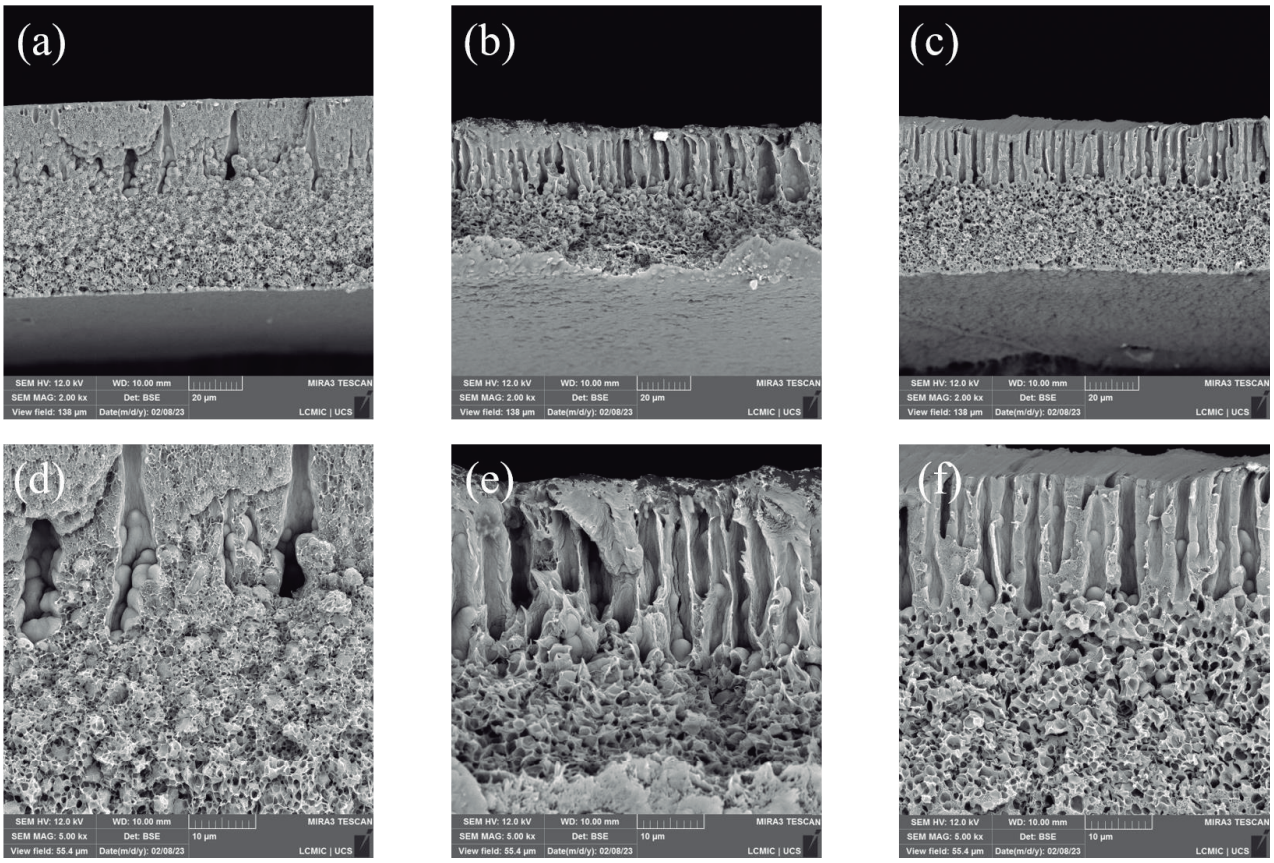

Figure 2–SEM of cross section with 2000x and 5000x magnification of samples (a, d) PVDF, (b, e) PVDF/0,5%CNF and (c, f) PVDF/1,0%CNF

Table 2– Nominal pore size and porosity of the membranes

Sample	Nominal pore size (µm)	Porosity (%)
PVDF	0,572	69,33
PVDF/0,5% CNF	0,694	70,44
PVDF/1,0% CNF	0,802	72,63

Conclusions

Given the above, it is concluded that the incorporation of nanocellulose is a viable alternative for the production of PVDF membranes using distilled water as a non-solvent. In the SEM analyses, it was noted that the nanocellulose provides an increase in the nominal size of the pores, thus increasing the macrovoids and porosity of the membranes. Future filtration analyzes will be necessary to evaluate this difference in pore structure and whether these will favorin a higher permeate flux.

Acknowledgements

Special thanks to professors and professionals at the University of Caxias do Sul and CNPq and CAPES for their financial support.

References

1. UNESCO. United Nations World Report on Water Resources Development. 2021.
2.Kargarzadeh, H. et al. Polymer 2017, 132, p. 368-393.https://doi.org/10.1016/j.polymer.2017.09.043.
3.SAFARPOUR, M.; KHATAEE, A.; VATANPOUR, V. Industrial & Engineering Chemistry. Research 2014, 53, p. 13370-13382. https://doi.org/10.1021/ie502407g.
4.ASTM – American Society for Testing Materials. ASTM D792-13, Standard Test Methods for Density and Specific Gravity (Relative Density) of Plastics by Displacement, ASTM International, West Conshohocken, PA, 2013.
5.Xu, Z. et al. Journal of Membrane Science 2016, 520, p. 281-293. https://doi.org/10.1016/j.memsci.2016.07.060.
6. Kuo, C. et al. Desalination 2008, 233, p. 40-47. https://doi.org/10.1016/j.desal.2007.09.025.
7. Lu, K.; Zuo, J.; Chung, T.Journal of Membrane Science 2017, 539, p. 34-42. https://doi.org/10.1016/j.memsci.2017.05.064.
8. Moyo, S. et al. Environmental Nanotechnology, Monitoring & Management 2022, 18, 100714. https://doi.org/10.1016/j.enmm.2022.100714.

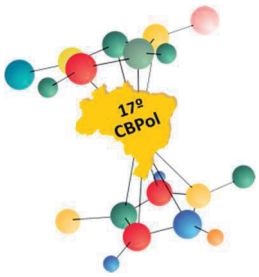

MORPHOLOGICAL STUDY OF COCONUT FIBERS MODIFIED BY MECHANICAL AGITATION IN AQUEOUS SOLUTION AND COMPARATION WITH ULTRASONIC AGITATION

Julio S. Souza, Celso C. M. Fornari Junior*

1 – Department of Engineering and Computer, State University of anta Cruz (UESC), Ilhéus, BA, Brazil
corresponding_celso@uesc.com.br

Abstract

Coconut fibers are promising materials for the construction of new composites because they have important mechanical properties, are produced in an integrated way with the environment and promote valorization in the agricultural field. However, for the formation of high-performance polymeric composites, for example, vegetable fibers must form a perfect interaction with natural or synthetic resins. In this way, to achieve better results in the properties of the new composite material, the surface of the vegetable fiber can be modified, changing its surface condition. In this sense, the study was dedicated to observing the morphological alteration of the fiber through action and processing by ultrasound and mechanical agitation in an aqueous medium. Five different cycles were evaluated and the results revealed that ultrasound agitation presented 0.89% and mechanical agitation 0.92% of weight loss.

Keywords: *Coconut fiber, Composite, Process.*

Introduction

The investigation and creation of new methodologies for the construction of materials with good chemical and mechanical properties, more ecologically correct, clean production and low cost is a goal to be pursued by today's society. The predicted population increase for the year 2050, which is between 9 and 10 billion inhabitants, is putting pressure on society as a whole towards greater sustainability and continuity of our existence [1,2]. Plant fibers are ecologically suitable materials to serve as raw material for the construction of polymeric composites and technological applications [3,4]. They have good mechanical and chemical properties, low abrasiveness in polymer processing equipment, low production and processing costs, clean and abundant production [5].
The interest in composite materials with plant fibers has drawn attention to research and has shown significant growth, due to the ease of obtaining associated with their properties [6,7]. However, in the construction of composite materials, it is the contact with the interfaces that is largely responsible for the union of the constituent materials. When two different materials are placed in contact, the interaction that occurs between them will be relative to the chemical and also physical conditions of each one. The chemical attraction is strongly influenced by polarity and will be greater the closer they are [8,9]. In addition to the chemical interaction between the constituents, the morphological factor also influences the final properties of the composite. In very pronounced reliefs of the fiber, significant grooves and depressions occur that can, in addition to accommodating other substances, such as moisture, oxygen, among others, hinder or prevent contact with the polymeric matrix [10]. Many works have been devoted to chemically modifying plant fibers, using specific chemical means. Many methods have been evaluated such as alkaline, silane, acetylation, maleic anhydride, stearic

acid, isocyanate, triazine, permanganate and fungal treatment. Physical treatments were also evaluated, such as ultraviolet, heating, corona effect, plasma. All treatments aim at modifying the surface of the plant fibers, seeking to achieve a better interaction between the fibers and the matrix [11-14].

The matrix-fiber interface is the responsible place where the union between the constituents will occur. A stronger attraction between them will be promoted due to the electrostatic attraction arising from the nature of their constituents. However, morphology also plays a unique and significant role in the interaction between materials. Fibers treated with an alkaline solution, for example, can remove the fatty coating and lignin exposing the cellulosic constituent more effectively. This modification, however, can be too pronounced, exposing the fibrous arrangement constituted by the microfiber bundle. Thus, the grooves and depressions on the surface will form the new fibrous morphology. This new constitution has its importance in the fiber-matrix interaction, being able to act as surface defects in the formation of the future composite. The final properties of the new material will be formed by the sum of constituents, interactions and defects that occur at the interface between different materials. This work was applied to investigate the influence of two types of treatments in aqueous alkaline solution for coconut fibers. Coconut fibers were subjected to equal treatment times by mechanical agitation and ultrasound. The results showed that the type of treatment alters the amount of fiber modification.

Experimental

The mechanically processed coconut fibers were hand selected and cut into 5 cm lengths. The fibers were dried in an oven at 130 ± 5 ºC before each processing. The fibers were weighed on an analytical scale Bioprecisa model FA2104N with four decimal places. Sodium bicarbonate solution was prepared in distilled water in the proportion of 8% w/w. An exact amount of 200 ml of solution and 5.00 g of fiber were used for each type of processing. For the mechanical agitation processing, a Sevitech agitator model CT-054 was used with a speed of 300 rpm. For the ultrasound processing, the Unic model Ultracleaner 14000 equipment was used. For both processes, a 500 ml beaker containing the fibers and the solution was used. The set was left to rest for one hour and then subjected to 30 minutes of agitation (ultrasonic or mechanical). Each cycle (rest and agitation) was performed and repeated being named as A (one cycle), B (two cycles) to E (five cycles). The coconut fiber was characterized by microscopic using Scanning microscopy electronic FEI model Quanta 250.

Results and Discussion

The studies carried out on coconut fibers revealed that the treatment by mechanical agitation and ultrasound modify the coconut fiber proportionally as a function of the process time. With each cycle performed on the fibers, a darker color appears in the solution. This change is related to the amount of solubles transferred to the solution. Lignin is mainly responsible for the color of the solution after processing. [15]. Fig. 1 presents the image of the solutions after each processing in mechanical agitation.

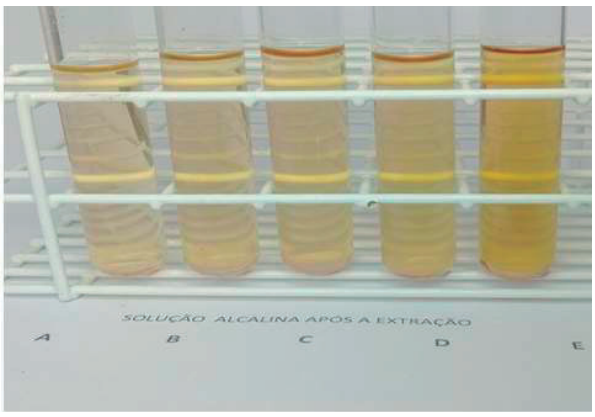

Fig. 1 – Solution after type of processing in mechanical agitation.

Fibers after treatment were investigated by scanning electron microscopy. Fig. 2 shows the image of the surface of natural coconut fiber, covered with the typical layer of wax, pectin and globular particles and the fiber treated by means of mechanical agitation after five processes.

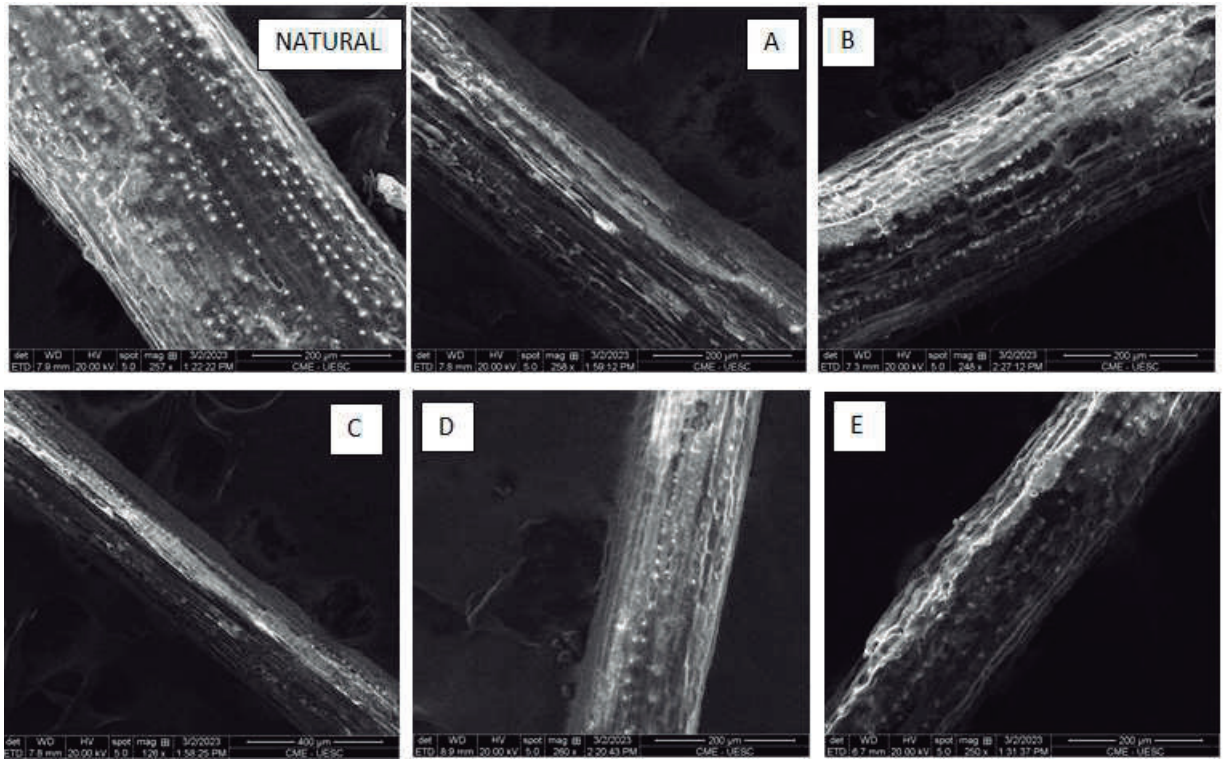

Fig. 2 – Morphology of natural coconut fiber after five processes of mechanical agitation. Magnification of approximately 250 times each image.

The treatment by mechanical agitation gradually modifies the original surface of the coconut fiber. In just one process (A), the globular particles are mostly removed, leaving a relatively small population even after the five processing steps (E). The same occurs with the fatty layer, which is removed in the first processing (A). After the fourth (D) and fifth processing (E) the depressions are pronounced with an irregular morphology. The studies evaluated the weight of the samples after each processing. Fig. 3 presents the results of gravimetry. Processing using mechanical agitation demonstrated a more significant decrease in fiber weight at all cycle numbers compared to the ultrasound process. The mechanical efficiency of agitation acts through the friction that occurs between the fibers and the solution. The impeller forcefully propels the fibers through the solution,

creating shear friction between the solution and the wall from beker. This flow profile proved to be sufficient to remove approximately 11% of the total fiber weight after five process cycles.

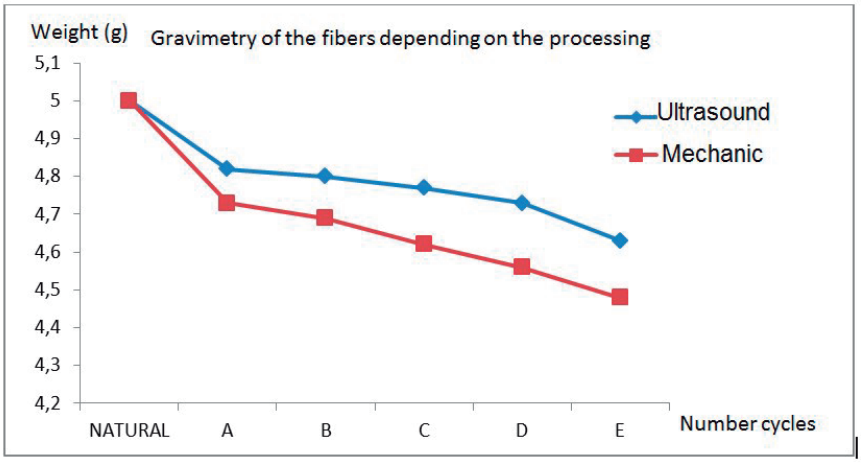

Fig. 3 – Gravimetry of natural coconut fiber after five processes of mechanical agitation.

The morphological modifications of the fiber after the processes (mechanical and ultrasound) were carried out using an aqueous solution of sodium bicarbonate, thus corroborating for a friendly and non-aggressive processing to the environment.

Conclusions

The study evaluated the modification of coconut fibers as a result of mechanical agitation processing, in addition to comparing the efficiency of mechanical agitation with ultrasound. For the time of mechanical agitation processing (60 minutes of rest and 30 minutes of agitation) the fiber presented significant modifications in relation to the external fat layer. After the fourth and fifth process, the fibers showed the cellulosic physical structure and respective grooves more clearly. The aqueous solution showed an increase in color tone, going darker as the number of processes increased. Both processes remove the fraction soluble in alkaline solution from the fiber, however, mechanical agitation is more efficient compared to ultrasound.

Acknowledgements

The authors would like to thank the State University of Santa Cruz for the research conditions carried out at LAPOS, the Polymers and Systems laboratory.

References

1. V.N. Amrutha; S.N. Geetha; Journal of Cleaner Production 2020, 247, 119131. https://doi.org/10.1016/j.jclepro.2019.119131.
2. D. Dorling; The Struggle for Social Sustainability 2021, 129- 154. https://doi.org/10.51952/9781447356127.ch007
3. N.M. Nurazzi; M.R.M. Asyraf; S. Fatimah Athiyah; S.S. Shazleen; S.A. Rafiqah; M.M. Harussani; S.H. Kamarudin; M.R. Razman; M. Rahmah; E.S. Zainudin; R.A. Ilyas; H.A. Aisyah; M.N.F. Norrrahim; N. Abdullah; S.M. Sapuan; A. Khalina; Polymers 2021, 13, 2170. https://doi.org/10.3390/polym13132170
4. S.S. Kumar; V.M. Raja; Composites Science and Technology 2021, 208, 108695. https://doi.org/10.1016/j.compscitech.2021.108695

5. A.J.F. Carvalho; G. de Souza; M.C. Fares; Macromol. Symp 2019, 383, 1800068. https://doi.org/10.1002/masy.201800068.
6. H.G. Kotik; Matéria (Rio de Janeiro) 2019, 24. https://doi.org/10.1590/S1517-707620190003.0801
7. A.M. Weber; A. Matoski; L. Cechin; R.B. Tokarski; Engenharia Civil UM 2022, 61, 6-17. https://doi.org/10.21814/ecum.4149
8. V. Mazzanti; R. Pariante; A. Bonanno; O.R. de Ballesteros; Composites science and technology 2019, 180, 51-59 https://doi.org/10.1080/09276440.2018.1549892
9. M.J.P. Macedo; A.L.A. Mattos; T.H.C. Costa; M.C. Feitor; E.N. Ito; J.D.D. Melo; Composite Interfaces 2019, 26, 871-886.
10. C.C.M. Fornari Junior; Fibras vegetais para compósitos poliméricos, Editus, Ilhéus, 2017.
11. N. Gama; S. Magina; A. Barros-Timmons; A. Ferreira; Progress in Additive Manufacturing 2021, 1-11. https://doi.org/10.1007/s40964-021-00226-x.
12. M. del Angel-Monroy; V. Escobar-Barrios; M.G. Peña-Juarez; L.E. Lugo-Uribe; J. Navarrete Damian; E Perez; JA Gonzalez-Calderon; Polymer Bulletin 2023, 1-28. https://doi.org/10.1007/s00289-023-04740-6
13. S. Chhetri; H. Bougherara; Composites Part A: Applied Science and Manufacturing 2021, 140, 106146. https://doi.org/10.1016/j.compositesa.2020.106146.
14. A. Gholampour; T. Ozbakkaloglu; Journal of Materials Science 2020, 55, 829-892. https://doi.org/10.1007/s10853-019-03990-y.
15. G. Lin; Q. Tang; H. Huang; J. Yu; Z. Li; B. Ding; Cellulose 2022, 29, n.7, 3689- 3701. https://doi.org/10.1007/s10570-022-04501-0

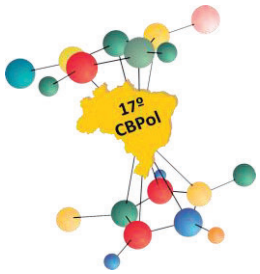

MULTIFUNCTIONAL MONTMORILLONITE CLAY/SILVER NANOPARTICLES COATINGS FOR MEDICAL TEXTILES

Fernanda C. S. Nobre[1], Andrielly C. Câmara[1], Brenno H. S. Felipe[3] Edson Noriyuki Ito[4], Iris Oliveira Silva[1,2]

1 – Graduate Program in Textile Engineering, Federal University of Rio Grande do Norte (UFRN), Natal, RN, Brazil
2 - Department of Textile Engineering, Federal University of Rio Grande do Norte (DET), Natal, RN, Brazil
iris.oliveira@ufrn.br

3 - Department of Textile Engineering, Federal University of Santa Catarina (UFSC), Blumenau, SC, Brazil
4 - Department of Materials Engineering (DEMat), Federal University of Rio Grande do Norte (UFRN), Rio Grande do Norte, RN, Brazil

Abstract - The objective of this study is to functionalize cotton fabrics by coating them with a mixture of AgNPs and organophilic montmorillonite clay to enhance their antimicrobial properties. This would allow the textile substrate to be used in various areas, including medicine. The results of this study, as observed through X-ray diffractogram and Fourier transform infrared spectroscopy analyses, demonstrated that the AgNPs adhered more effectively to the fabric when mixed with the clay compared to using the silver nanoparticles solution alone. Additionally, the fabric treated with the AgNPs solution did not show significant evidence of impregnation in the analyses. Therefore, incorporating AgNPs into the substrate mixed with clay yielded better results and offers potential applications in medical fields.
Keywords: *Synthesis, Silver, Clay, Coating.*

Introduction

In the textile industry, metallic nanoparticles have been used to enhance the functionality of fabrics, providing properties such as antimicrobial activity, UV protection, and super hydrophobicity, among others. This is possible because nanoparticles have an affinity for fabrics while preserving their breathability and tactile properties, ensuring durability [12]. Silver nanoparticles (AgNPs) were synthesized using the chemical reduction method, employing silver nitrate as the precursor and trisodium citrate as the reducing and stabilizing agent. The resulting AgNPs exhibited spherical morphologies with sizes ranging from 6 to 30 nm.[1,10]

However, due to the challenges in controlling the particle size, the full potential of nanoparticles is not always realized. To address this, researchers have explored the combination of nanoparticles with inert, stable, and environmentally friendly materials. This approach not only improves the performance of the nanoparticles but also enables the emergence of new properties [3,4].

Clays are one type of material that can be used for this purpose, offering advantages such as low cost and easy availability in the market. Among the clays employed, organically modified montmorillonite clay is commonly used. It belongs to the smectite family and its structure consists of a central octahedral layer of alumina sandwiched between two tetrahedral layers of silica. The intermediate layer contains cations and water molecules [3,4,7,11]. This clay material possesses a crystalline

arrangement that allows for expansion and compression of its interlayer while maintaining its two-dimensional crystallography [3,4].
In this study, the objective is to functionalize 100% cotton fabrics by coating them with a new mixture of AgNPs, montmorillonite clay, and chitosan. The aim is to impart multifunctional properties to the treated fabrics, including antimicrobial activity, UV protection, and more. By achieving this, the application of these textile substrates can be expanded to various fields, including medicine..

Experimental

Materials

Silver nitrate (AgNO3) and trisodium citrate (Na3C6H5O72H2O) were utilized to synthesize the nanoparticles using standard laboratory glassware and equipment. The montmorillonite clay employed in this study was Cloisite 30B®, which is organically modified with a quaternary ammonium salt (MT2ETOH: methyl, tallow, bis-2-hydroxyethyl, quaternary ammonium). The fabric utilized was 100% cotton with a weight of 177.77 g/m2. Additionally, chitosan from Selachii and the ALT-B TOUCH 35 equipment from Mathis were also used in the experiments.

Síntese de nanopartículas de prata, impregnação na argila montmorilonita e tingimento

Initially, a solution (1) was prepared by dissolving 0.102 g of silver nitrate in 600 ml of distilled water. Another solution (2) was prepared by dissolving 0.200 g of sodium citrate in 20 ml of distilled water. For the synthesis, solution 1 was heated while stirring at a speed of 1.5 rpm until it reached 90°C. Once the desired temperature was reached, 1.5 ml of solution 2 was added dropwise at a flow rate of 3 drops per minute. Subsequently, the clay was mixed with the nanoparticles. A concentration of 25 g of AgNPs solution per 500 ml (wt/V) was used, and the mixture was stirred for 10 minutes. The resulting mixture was then placed in an oven at 100°C until complete drying.
According to Table 1, eight coating processes were conducted on 100% cotton fabric. The coating process involved a duration of 30 minutes at a temperature of 70°C and a rotation speed of 40 revolutions per minute. Following impregnation and coating, the fabric samples were dried in an oven at 80°C.

Results and Discussion

In order to obtain results on the interaction between AgNPs and the fabric, various material characterizations were conducted. As a result, Table 1 was created to assign codes to the samples, thereby facilitating the information presented in the figure.

Table 1: Sample processing and coding.

Code	**Samples**
C	100% CO Fabric
CCh	100% CO Fabric + chitosan
CCl	100% CO Fabric + Cloisite clay
CChCl	100% CO Fabric + chitosan + Cloisite clay
CAgNPs	100% CO Fabric + AgNPs
CClAgNPs	100% CO Fabric + clay/ AgNPs
CChAgNPs	100% CO Fabric + chitosan + AgNPs
CChClAgNPs	100% CO Fabric + chitosan + clay/AgNPs

When analyzing Figure 1(a), which corresponds to the X-ray diffraction (XRD) pattern of the clay/AgNPs powder, characteristic peaks of silver (Ag) and clay are observed. The peaks at 36°, 62.3°, and 77° correspond to Ag, while the peak at 20.03° corresponds to the clay, indicating the presence

of both components in the powder. Additionally, the chitosan curve shows a peak at 20.05°, but it appears displaced and broad, indicating its amorphous nature.

It is important to analyze how this mixture interacts with the fabric using the same parameter. When observing Figure 1(b) and analyzing curve C, three peaks at 33°, 22.33°, and 15.14° can be observed, which are characteristic of the cellulose polymer present in the fabric. Comparing the other samples with the standard (C), it is noted that those with clay exhibit a peak at 22.3°. Similarly, the samples functionalized only with chitosan also exhibit this peak, while the peaks at 15.14° and 33° remain present in all samples.

Therefore, it can be concluded that the AgNPs adhere better to the fabric when combined with clay, as evidenced by the presence of clay peaks in the CClAgNPs and CChClAgNPs samples, indicating the incorporation of AgNPs into the clay structure.

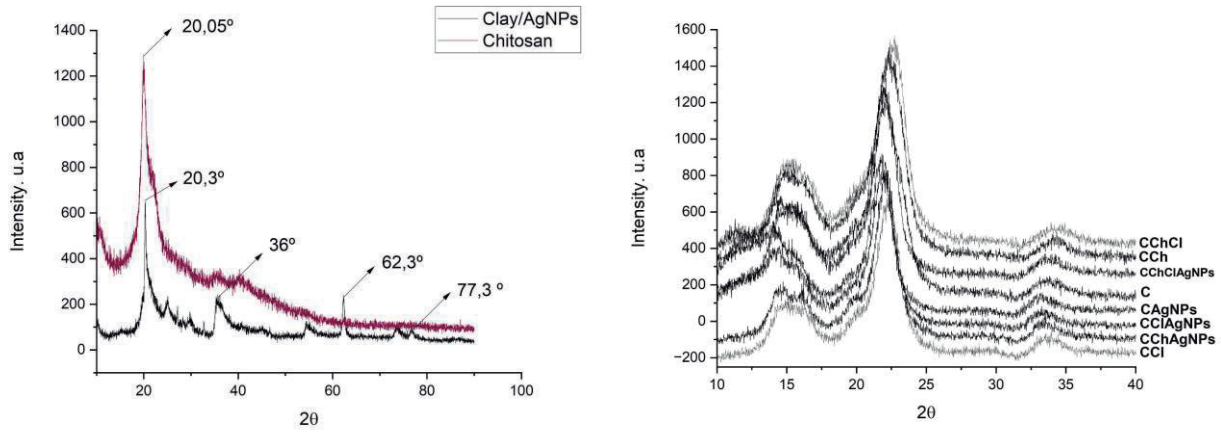

(a) (b)

Figura 1- (a) - Clay/AgNPs Diffraction Pattern and (b) - Fabric Sample Diffraction Pattern.

Regarding FTIR analysis, Figure 3(a) shows that the band at 1010.6 cm-1 corresponds to the Al-O-Si bending vibration in the octahedral sheets of the clay. The sharp band at 1,461.9 cm-1 indicates the asymmetric stretching modes of the Si-O bonds in the silica gallery structure and clay layers. Additionally, the band at 2,826.6 cm-1 suggests the presence of van der Waals interactions between the OH groups and AgNPs. This band can also be attributed to the silanol groups on the surface and adsorbed water molecules [13].

In Figure 3(b), similar trends are observed, indicating that the fabric's structure was not altered by the addition of AgNPs. However, it can be inferred that there was impregnation of AgNPs on the fabric's surface based on the FTIR analysis.

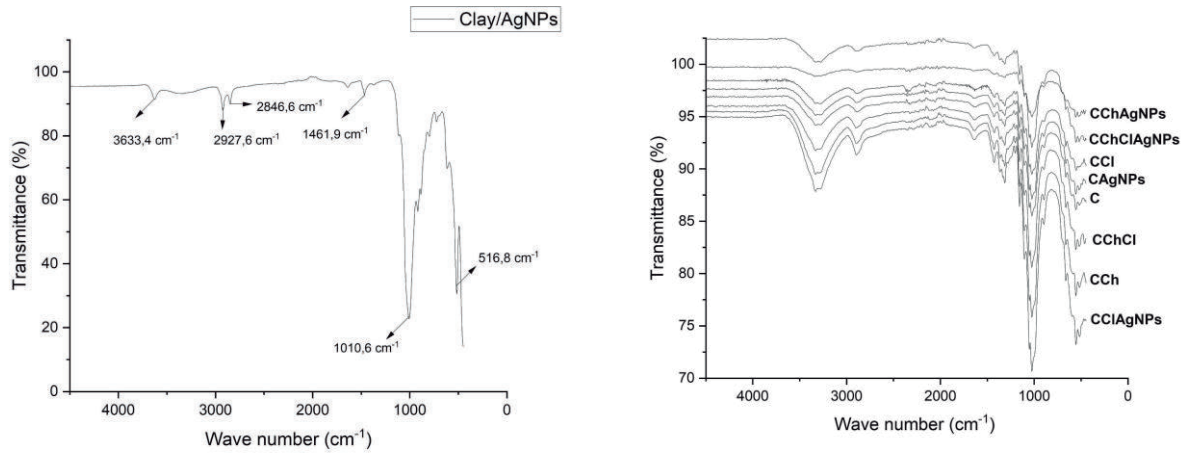

(a) (b)

Figure 3 - (a) Infrared Spectrum of Clay/AgNPs and **(b)** Infrared Spectrum of Fabric Samples.

Conclusions

Therefore, the functionalization of the fabrics through the deposition of AgNPs by coating has been demonstrated. The analyses confirm the presence of AgNPs and their effective interaction with the montmorillonite clay. However, further characterizations are required to fully understand how the nanoparticles interact with the fabrics.

Hence, this study opens up possibilities for creating multifunctional materials. The clay/AgNPs powder offers enhanced stability to the nanoparticles, making it suitable for the production of technical textiles with various applications in the medical field.

Acknowledgements

We would like to express our gratitude to the National Council for Scientific and Technological Development for providing the grant that supported this research.

References

1. M. Yusuf 2019, 97. https://doi.org/10.1007/978-3-319-68255-6_16.
2. R. Silveira; E. Agioletto; S. Arcaro; T. Gomes 2022, 19, 2638. http://dx.doi.org/10.4322/2176-1523.20222638.
3. A. F. M. Alves. Thesis, University of Rio Grande do Norte, 2022.
4. S. C. Motshekga; S. S. Raya; M. S. Onyango; M. Mombac 2013, 262. http://dx.doi.org/10.1016/j.jhazmat.2013.08.074.
5. S. M. Gamboa; E. R. Rojas; V. V. Martinez; J. V. Baudrit 2019, 5, 5. http://dx.doi.org/10.15406/ijbsbe.2019.05.00172.
6. C. V. Restrepo; C. C. Villa 2021, 15, 100428. https://doi.org/10.1016/j.enmm.2021.100428.
7. T.S. Wu; K.X. Wang; G.D. Li; S.Y. Sun; J. Sun; J.S. Chen 2010, 2. http://dx.doi.org/10.1021/am900743d.
8. X. Dong; X. Ji; H. Wu; L. Zhao; J. Li; W. Yang 2009, 113, 16. http://dx.doi.org/10.1021/jp900775b.
9. M. L. Budlayan 2020, 925, 012050. http://dx.org.doi/10.1088/1757-899X/925/1/012050.

10. N. M. Alandis; W. Mekhammer; O. Aldayel; J. A. Hefne; M. Alam 2019, 7129014. https://doi.org/10.1155/2019/7129014.
11. B. Khodashenas; H. R. Ghorbani 2015, 12. http://dx.doi.org/10.1016/j.arabjc.2014.12.014.
12. R. Khursheed, K. Dua et al. 2022, 25, 112951. https://doi.org/10.1016/j.biopha.2022.112951.
13. Z. M. H. Kheiralla; A. A. Rushdy; M. A. Betiha; N. A. N. Yakob 2014, 16. http://dx.org.doi/10.1007/s11051-014-2560-6.

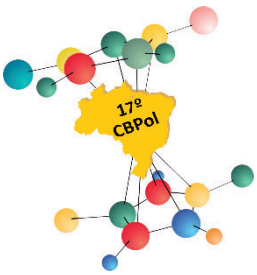

NANOCELLULOSE MODIFICATION USING MODIFIED-DTPA TO REMOVE METALLIC IONS INTO WATER

Paulo H. Camani[1], Rodrigo O. Lourenço[1], Talles B. da Costa[1], Derval S. Rosa[1]*

1 – Center for Engineering, Modeling, and Applied Social Sciences (CECS), Federal University of ABC (UFABC), Santo André, Brazil
derval.rosa@ufabc.edu.br

Abstract
This work aims to modify the cellulose nanostructures using a chelating agent derived from the diethylenetriaminepentaacetic acid molecule (DTPA) to remove Cr(VI), Cd(II), Zn(II), Mn(II), Ni(II), and Cu(II) from simulated water. The nanocellulose was modified in two different ways: The first was using a chelating agent derived from DTPA at concentrations of 1 and 3% by weight and implemented $NaPO_2H_2$ (SHP) on the reaction. The surface modification of the CNS was efficient, specifically for 3wt.% concentration, as evidenced by the presence of groups C=O stretching vibration and the bending vibration of N-H of DTPA chemical structure. This alteration in the FTIR spectra was confirmed by the decrease in the elemental hydrogen concentration, which can be linked to the surface modification of the nanocellulose. In addition, the nanoparticles had an average size increase, verified by the size distribution by DLS, as well as a change in their surface charges by Zeta potential, which improved the colloidal stability of CNSs modified with 3% without and with SHP.
Keywords: *nanocellulose; chelating agent; PS-DTPA.*
Fundings: FAPESP - 2019/16301-6, 2022/11133-0, and 2020/13703-3, CNPq - 308053/2021-4 and 403934/2021-4, and CAPES.

Introduction

Among the various chemical elements that may be present in water, heavy metals (currently called potentially toxic metals (PTMs) due to the ambiguity that the word heavy metals promotes [1] are a class of compounds with high toxicity and persistence (depending on their concentration), which result in several problems including precipitation, absorption, ion exchange, and biological threats, such as the accumulation of these elements in living organisms along the entire food chain. These effects put the lives of human beings at risk, as well as the fauna and flora present in contaminated ecosystems [2]. Nanocellulose can occur in nanofibrils, nanocrystals, and bacterial nanocellulose. It can be controlled from cellulose by mechanical, chemical, and biological methods. At the nanoscale, cellulose has unique properties, such as excellent mechanical properties, high stability, and high functionality. This biopolymer has a large specific surface area and abundant hydroxyl groups [3]. Despite all its advantages, nanocellulose can also be modified to improve its specific applications. In modification processes, functional groups are added to the surface structure of nanocellulose [4]. Several modification approaches can be applied. One of these approaches involves the optimization of nanocellulose for metal removal in an aqueous solution using anionization with methods such as anionization, cationization, or hydrophobization methods [2]. In this work, the functionalization of the nanocellulose was performed by surface modification using a commercial chelating agent (PS-DTPA) from the nanocellulose produced by eucalyptus residues for possible removal of divalent metal ions and hexavalent chromium.

Experimental

Nanocellulose isolation and its modification

Eucalyptus sawdust was pre-treated by mercerization with sodium hydroxide, followed by bleaching with hydrogen peroxide, assisted by microwaves to remove lignin and hemicellulose from the lignocellulosic fiber. After obtaining the pre-treated fibers, they were subjected to two subsequent mechanical methodologies for isolating cellulose nanostructures. Therefore, 2% (m/m) of the pre-treated fibers were dispersed in an aqueous solution and first subjected to homogenization at high shear rates (treatment 1) using Ultra-Turrax (Model T 25 digital, IKA) at 10,000 rpm for 20 min. The same solution was taken to ultrasonication (treatment 2), performed in a high-intensity ultrasound SONIC-750W, Vibracell, Sonics (MRC Ltd, Holon, Israel), using the power of 100 kJ, frequency of 70% at 60 °C, for 60 minutes. For surface modification using PS-DTPA (*PrimerSurf-DTPA*) chelating agent, an alkaline aqueous solution with pH 12 was initially prepared. Then, the previously calculated volume of DTPA 40% was added, considering 1% and 3% (by weight) of the compounds to be dispersed. The solutions were heated to approximately 70 °C and stirred for 24 hours. After 24 hours, the previously calculated nanocellulose weights were added considering 1% and 3% in solution, considering that nanocellulose and PS-DTPA were reacted in a 1:1 ratio. The samples remained under agitation at approximately 105 °C for 4 hours. Besides, following the methodology of Li and co-workers [5], in addition to adding the volume of DTPA 40% considering 1% and 3% of the compounds to be dispersed in this solution, sodium hypophosphite (SHP) $NaPO_2H_2$ was also added in the proportion of 5:1 of DTPA and SHP respectively. The solutions were heated to approximately 70 °C and stirred for 24 hours. After 24 hours, the 1% and 3% nanocellulose weights were added. The samples remained under agitation and heated at 105 °C for 4 hours.

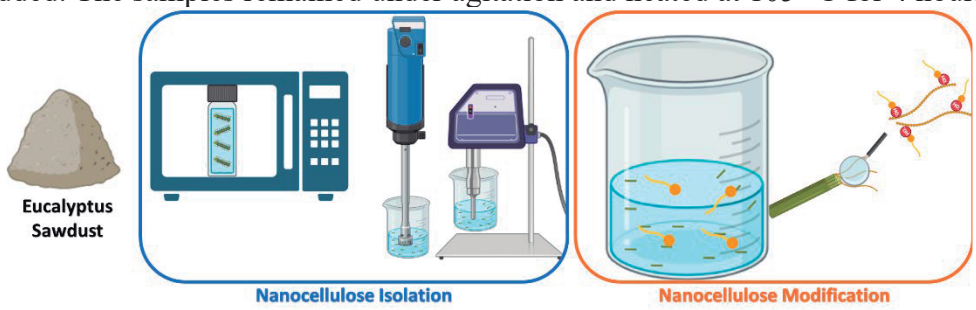

Fig. 1. Illustrative nanocellulose isolation scheme, followed by PS-DTPA modification.

Characterizations

The chemical groups present in nanocellulose and modified nanocelluloses were evaluated using Fourier transform infrared spectroscopy (FTIR), in a Frontier 94942 FTIR spectrophotometer equipment (PerkinElmer, USA), with the coupling of an attenuated total reflectance (ATR) accessory, using a spectral resolution of 4 cm^{-1}, 64 scans, with a spectral range of 4000-500 cm^{-1}. The particles' average size and the nanostructures' colloidal stability were evaluated using Zetasier NanoZS 3000 equipment (Malvern Instruments, UK). Measurements of both mean particle size and Zeta potential were performed in triplicate. Elemental analysis was performed to determine carbon, nitrogen, and hydrogen content before and after surface modification of the NECs using a Thermo Scientific FlashEA 1112 elemental analyzer. Metal ion sorption tests were conducted through a multielement evaluation of Cd(II), Zn(II), Ni(II), Mn(II), Cu(II), and Cr(VI) ions from a 0.3 $mMol.L^{-1}$ solution, containing all ions, at pH 4.0, at room temperature, under agitation at 135 rpm, for 24 hours, whose dosage of nanocellulose and modified nanocelluloses was $1g.L^{-1}$. The efficiency and sorption capacity was obtained from the aqueous solutions after testing, subjecting them to measurements in ion chromatography (940 Professional IC Vario, Metrohm, Switzerland) in duplicate.

Results and Discussion

After surface modification using PS-DTPA chelating agent, nanocellulose obtained from eucalyptus sawdust pre-treated fiber and isolated from combined mechanical isolation and modified nanocellulose using PS-DTPA and PS-DTPA plus sodium hypophosphite (SHP) were evaluated from

FTIR, whose spectra non- and modified nanocelluloses are presented in Fig.1.a. and Fig.1.b, respectively.

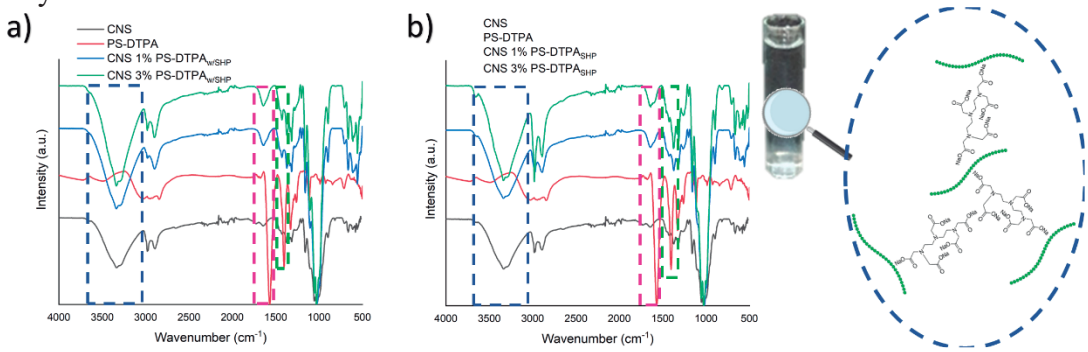

Fig. 2. *Illustrative nanocellulose isolation scheme, followed by PS-DTPA modification.*

Evaluating the FTIR spectra, it is noteworthy to observe that both in the case of nanocellulose modified with only PS-DTPA and PS-DTPA + SHP, in both cases, the nanocellulose obtained showed peaks and bands distinct from CNS. Comparing the CNS spectra with the modified nanocelluloses, even varying the percentage and the presence or absence of SHP with PS-DTPA, an increase in the band of 3428 cm^{-1} was verified, which is listed with the superposition of symmetric and asymmetric stretching vibrations from O-H or N-H, and the two peaks appearance at 1735 and 1645 cm^{-1}, that is attributed to the C=O double bond stretching vibration absorption peak in the ester group, that indicated the esterification reaction between CNS and DTPA, and the C=O stretching vibration and the bending vibration of N-H of DTPA chemical structure [5]. However, a notable difference observed for the modified nanocellulose without SHP compared to the modification containing PS-DTPA + SHP was the appearance of the peak at 1428 cm^{-1}, which is attributed to the C-N stretching vibration peak [6]. Table 1 presented particle size (nm), Zeta potential (mV), and elemental percentage of nitrogen, carbon, and hydrogen of CNS and modified CNSs, respectively.

Table 1. Particle size (nm), Zeta potential (mV), and elemental percentage of nitrogen, carbon, and hydrogen of CNS and modified CNSs, respectively

	First Peak - Particle Size (nm)	Second Peak - Particle Size (nm)	Zeta Potential (mV)	Nitrogen (%)	Carbon (%)	Hydrogen (%)
CNS	-	581 ± 173	-26.5 ± 2.7	0.2 ± 0,1	44.0 ± 2.7	6.3 ± 0.2
CNS 1% PS-DTPA$_{W/SHP}$	117.3 ± 8.5	508.0 ± 125.4	-28.0 ± 7.0	0.3 ± 0.0	34.5 ± 10.3	5.0 ± 1.4
CNS 3% PS-DTPA$_{W/SHP}$	109.2 ± 19.1	561.3 ± 103.3	-34.0 ± 5.0	0.4 ± 0.1	37.5 ± 3.2	5.2 ± 0.2
CNS 1% PS-DTPA$_{SHP}$	-	900.5 ± 212.0	-7.1 ± 3.0	0.6 ± 0.2	40.6 ± 1,0	6.0 ± 0,2
CNS 3% PS-DTPA$_{SHP}$	114.0 ± 37.0	702.5 ± 125.5	-33.6 ± 2.0	0.8 ± 0.1	36.0 ± 3.2	5.5 ± 0,7

After surface modification, the size distribution showed bimodal peaks compared to CNS, which showed a monomodal peak. Furthermore, an increase in particle size was verified by inserting the PS-DTPA molecule into the nanocellulose structure. Subsequently, the modification altered the surface charges obtained by the Zeta potential because as the modifier was inserted, especially at 3%, an increase in the potential value, in modulus, was verified. Camani and co-workers and Baggio, Camani, and Rosa showed that the increase in the average size of the nanocellulose, as well as Zeta potential values above 30 mV, are indications of an effective surface modification, especially for modification with 3wt% of the modifier [3,4].

This efficiency in the modification was attested by the decrease in the percentage of hydrogen present in the nanocellulose composition, especially for modification at 3% for samples without sodium hypophosphite, as observed by the FTIR spectra, at a concentration of 3%. De Souza and co-workers reported that a change in the elemental concentration of C, N, or H might indicate efficiency in the surface modification of nanocellulose [7]. Thus, the sorption efficiency of Cr(VI), Cd(II), Zn(II), Mn(II), Ni(II), and Cu(II) for samples of CNS and modified CNSs, respectively, is presented in Table 2.

Table 2. Sorption efficiency (%) of Cr(VI), Cd(II), Zn(II), Mn(II), Ni(II), and Cu(II) for samples of CNS and modified CNSs, respectively, measured after sorption.

	Cr(VI) (%)	Cd(II) (%)	Zn(II) (%)	Mn(II) (%)	Ni(II) (%)	Cu(II) (%)
CNS	100.0 ± 0.0	5.1 ± 1.1	6.3 ± 1.1	5.0 ± 1.4	7.5 ± 1.0	27.3 ± 3.1
CNS 1% PS-DTPA$_{W/SHP}$	12.4 ± 5.1	7.7 ± 0.2	9.0 ± 1.4	5.7 ± 0.4	13.5 ± 1.5	43.0 ± 6.0
CNS 3% PS-DTPA$_{W/SHP}$	18.3 ± 5.3	7.6 ± 0.2	7.4 ± 0.3	5.2 ± 1.5	10.5 ± 0.5	40,0 ± 3.3
CNS 1% PS-DTPA$_{SHP}$	11.1 ± 3.6	10.0 ± 6.2	8.0 ± 0.5	2.2 ± 2.6	10.5 ± 0.3	39.2 ± 1.6
CNS 3% PS-DTPA$_{SHP}$	4.6 ± 2.3	18.0 ± 5.3	18.0 ± 4.1	11.5 ± 5.0	55.0 ± 6.6	14.0 ± 6.5

Evaluating the percentage of removal of Cr(VI) and the bivalent ions [Cd(II), Zn(II), Mn(II), Ni(II), and Cu(II), it is notorious that the oxidation number of the ions had an impact on their removal results. Nanocellulose (CNS) obtained 100% removal of Cr(VI) but reduced removal when modified by PS-DTPA with and without the presence of SHP. This difference can be related to the presence of free hydroxyl groups in cellulose than modified nanocellulose, which could have promoted electrostatic interaction mechanisms and even the reduction of Cr(VI) to Cr(III), which resulted in high levels of removal of hexavalent chromium [8]. However, modified-nanocelluloses had better adsorption performance for divalent ions. It demonstrates the possible preference that modified-nanocellulose has for divalent ions than hexavalent chromium as CNS has better adsorption capacity performance to remove hexavalent chromium. This difference in adsorption capacity may have been regarded as heavy metal ionic size, ion radius, and ionic charge [9]. Besides, analyzing the concentration between the adsorption capacity of CNS 3% PS-DTPA$_{W/SHP}$ and CNS 3% PS-DTPA$_{SHP}$, modified-nanocellulose with 3% PS-DTPA+SHP improved Cu(II); however, there was a reduction of Ni(II) concentration for CNS 3% PS-DTPA$_{SHP}$, showing the specificity of two modified-nanocelluloses. Possibly, CN presented high Cr(VI) removal and low divalent ions removal due to hydroxyl groups. CNS-PSDTPA$_{W/SHP}$ removed divalent ions better than hexavalent chromium due to the PS-DTPA chemical structure's ester, carboxyl, and hydroxyl groups [10]. Thus, nanocellulose surface modification with PS-DTPA or PS-DTPA+SHP promoted high affinity for divalent metal ions than oxyanions such as Cr(VI), showing their specificity and preference.

Conclusions

The modified nanocellulose showed distinct groups from the PS-DTPA chelating agent molecule. Therefore, the modification could be proven by the decrease in the elemental hydrogen concentration compared to the CNS. It had a direct impact on the increase in particle size of the cellulose nanostructure, in which its average size was greater, with an increase in surface charges observed by the Zeta potential value, proving the change in surface charges of nanocellulose after modification with PS-DTPA, in 3% concentration by weight. As for the multielement removal of Cr(VI) and divalent metal ions, CNS showed a removal efficiency superior to divalent ions. However, a decrease in the removal of Cr(VI) was verified for nanostructures modified with PS-DTPA with and without sodium hypophosphite, still showing that the modification with 3% chelating agent was more satisfactory than 1%, having specificities in agreement with the presence of SHP. Without SHP, the modified nanocellulose had greater removal for Cu(II) and modified in the presence of SHP, greater removal of Ni(II) was verified. Therefore, an efficient modification was verified, whose modification with PS-DTPA and in the absence of SHP promoted better colloidal stability, particle size and a

tendency to remove all ions, highlighting Cu(II) and Cr(VII), unlike the than in the presence of SHP, which preferred to remove Ni(II) and Cr(VII), in greater removal efficiency.

Acknowledgments
This research was financed by Fundação de Amparo à Pesquisa do Estado de São Paulo (FAPESP) (2019/16301-6, 2022/11133-0, 2020/13703-3), Conselho Nacional de Desenvolvimento Científico e Tecnológico (CNPq) (308053/2021-4 and 403934/2021-4), and Coordenação de Aperfeiçoamento de Pessoal de Nível Superior (CAPES) (Finance Code 001). The authors thank the technical support of the Multiuser Experimental Center of UFABC (CEM-UFABC), CECS (UFABC), and REVALORES for assistance.

References

1. O. Pourret; A. Hursthouse International Journal of Environmental Research and Public Health, 2019, 16 (22), 4446. https://doi.org/10.3390/ijerph16224446.
2. A. Qiao; M. Cui; R. Huang; G. Ding; W. Qi; Z. He; J. J. Klemeš; R. Su Carbohydrate Polymers, 272, 118471. https://doi.org/10.1016/j.carbpol.2021.118471.
3. P. H. Camani; A. G. de Souza; D. S. Rosa Macromolecular Symposia, 2020, 394 (1), 2000110. https://doi.org/10.1002/masy.202000110.
4. G. M. Baggio; P. H. Camani; D. S. Rosa. Journal of Molecular Liquids, 2022, 346, 118231. https://doi.org/10.1016/j.molliq.2021.118231.
5. A. Li; D. Xu; M. Zhang; S. Wu; Y. Li; W. Sun; Y; Zhou; O. A. Madyan; M. Fan; J. Rao Cellulose, 2022, 1-16. https://doi.org/10.1007/s10570-021-04390-9.
6. Y. Shen; X. Li; Y. Lan; M. Zu; X. Liu; H. Huang; N. Zhou; R. Duan; L. Gan; J. Huang Cellulose, 2021, 28, 2905-2916. https://doi.org/10.1007/s10570-021-03693-1.
7. A. G. de Souza; G. F. de Lima; R. Colombo; D. S. Rosa Cellulose, 2020, 27, 5707-5728. https://doi.org/10.1007/s10570-020-03160-3.
8. X. Yuan; J. Li; L. Luo; Z. Zhong; X. Xie Polymers, 2023, 15(2), 388. https://doi.org/10.3390/polym15020388.
9. Y. Zheng; K. Sun; N. Wen; H; Rao; H. Ye; B. Yang Polymer Bulletin, 2023, 1-22. https://doi.org/10.1007/s00289-022-04665-6.
10. H. T. Kara; S. T. Anshebo; F. K. Sabir Journal of Nanotechnology, 2021, 1-15. https://doi.org/10.1155/2021/9966811.

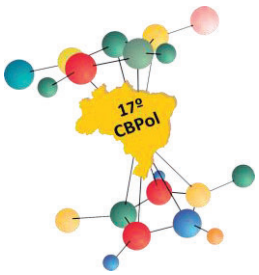

NANOPARTICLES FILLED WITH VETIVER ESSENTIAL OIL SYNTHESIZED BY NANOPRECIPITATION AND IONIC GELATION METHODS FOR DERMOCOSMETIC

Andressa Carvalho Câmara Januário[1], Gisele Cristina Valle Iulianelli[1]

1 – Instituto de Macromoléculas Eloísa Mano (IMA), Universidade Federal do Rio de Janeiro (UFRJ), Rio de Janeiro, RJ, Brazil
andressa@ima.ufrj.bt

Abstract
Bioactive compounds present in vetiver essential oil (*Chrysopogon zizanioides*) can benefit the skin due to their biological properties. However, due to its sensitivity to oxidation and degradation, protective methods are necessary. In this context, nanoencapsulation emerges as a promising alternative to preserve the functional properties of the essential oil, providing slow and controlled release and favoring the permeation of bioactive compounds into the dermis. Nanocapsules filled with vetiver essential oil were developed using the nanoprecipitation and ionic gelation methods to protect the oil properties and enhance the delivery of bioactives to the dermis, the innermost layer of the skin. Nanocapsules filled with vetiver essential oil were synthesized using poly-ε-caprolactone as the base polymer in nanoprecipitation, employing Tween®80, Span®60, and Pluronic® F-127 as surfactants, and distilled water and acetone as solvents. In the ionic gelation method, nanocapsules were prepared using sodium alginate as the polymer, Tween®80 as the surfactant, and calcium lactate as the cross-linking solution. The essential oil was analyzed by infrared spectroscopy (FT-IR) and nuclear magnetic resonance (NMR). The hydrodynamic diameter, polydispersity, and zeta potential of the polymeric nanoparticles were analyzed using dynamic light scattering (DLS) with a Zeta Potential Analyzer Nicomp Nano and also by FT-IR. The nanoparticles prepared using different techniques and surfactants exhibited variations in hydrodynamic volume, polydispersity, zeta potential, and pH, depending on the alterations in polymer concentrations, essential oil concentrations, and surfactant. Additional physical-chemical and biological characterization tests will be conducted to conclude the study.

Keywords: *Nanoencapsulation; Nanoprecipitation; Ionic gelation; Dermocosmetic; Essential oils.*

Fundings: CNPQ.

Introduction

Vetiver essential oil (*Chrysopogon zizanioides*, VEO) possesses several beneficial properties for the skin due to its high concentration of antioxidant bioactive compounds. One of its notable properties is its skin lightening ability, achieved by suppressing tyrosinase expression in melanogenesis [6, 10].

Nanoencapsulation of VEO provides significant advantages, such as the ability to deliver the active ingredient consistently to different layers of the skin. This controlled release allows for the use of lower doses of essential oil, increasing the effectiveness of cosmetics, while reducing toxicity and irritability, making it safe for topical use [7].

Nanometer-scale structures favor the permeation of nanoparticles into the skin, as they can penetrate the superficial layers of the stratum corneum. They can also accumulate in hair follicles, enabling the gradual release of bioactives into deeper layers of the skin. This permeation capability

of nanoparticles optimizes cosmetic treatments, allowing bioactives to reach target areas in a targeted and concentrated manner [9, 1].
Various techniques, such as nanoprecipitation and ionic gelation, can be employed to produce polymeric nanoparticles filled with VEO, resulting in materials with different properties, including size, surface charge, and drug-loading capacity [11].
Nanoprecipitation involves the formation of polymeric nanoparticles by controlled reduction of polymer solubility in a solvent partially miscible with distilled water. A polymer solution, in which the essential oil is dispersed, is poured into an aqueous medium containing a surfactant, which stabilizes the formed emulsion. Due to the rapid diffusion of the organic solvent in the aqueous medium, supersaturation occurs, leading to the precipitation of the polymer and the formation of nanoparticles. Ionic gelation, on the other hand, involves the dripping of a solution containing metal ions into an emulsion formed by the ionic polymer, essential oil, and surfactant. The ionic solution acts to cross-link the polymer, forming a gelatinous matrix [2, 4, 5].
By varying the techniques and their parameters such as polymer concentration, surfactant concentration, essential oil concentration, rate of polymer solution addition, rate of cross-linking solution addition, and solvent choice, it is possible to obtain nanoparticles with different characteristics and properties [2, 5].

Experimental
For the Fourier-transform infrared spectroscopy (FTIR) spectrum of Vetiver Essential Oil, a PERKIN-ELMER Frontier FT-IR/FIR spectrophotometer (version 10.4.2, serial number 98737) with an attenuated total reflectance (ATR) accessory was used, with 50 scans and a resolution of 4 cm^{-1}. The solvent-free Vetiver Essential Oil was directly placed on the ATR module.
The nuclear magnetic resonance (NMR) spectrum of Vetiver Essential Oil was obtained using a VARIAN Nuclear Magnetic Resonance Spectrometer - Model: Mercury 300MHz (IMA/UFRJ).
Two methods were employed to obtain the nanoparticle suspension: nanoprecipitation, according to Fessi (1988), and ionic gelation according to Hosseini (2013) [3, 8].
In both procedures, Vetiver Essential Oil from Phytoterápica® in São Paulo, Brazil, was used.
For nanoprecipitation, polycaprolactone (PCL) polymer (Mw = 80,000 g/mol) in pellet form was used. Two different procedures were applied, varying the types of stabilizers. The first procedure used Tween®80 (high HLB surfactant) and Span®60 (low HLB surfactant) as surfactants, while the second procedure used Pluronic® F-127 (high HLB surfactant). All reagents were purchased from Sigma-Aldrich® in São Paulo, Brazil. Acetone P.A. was used as the solvent.
In the first nanoprecipitation procedure, the organic phase consisted of PCL, Vetiver Essential Oil, Span®60, and acetone (Table 1). After preparation, the oily phase was poured into an aqueous solution containing Tween®80 under agitation. The suspension was kept under agitation to allow solvent evaporation.

Table 1 - Formulations of nanoprecipitation systems with Span®60 and Tween®80.

Sample	PCL (%w/v)	Span® 60 (%w/v)	Vetiver Essential Oil (%m/m)	Tween® 80 (%w/v)
PC0ST	0,75	0,75	-	0,1
PC3ST	0,25	0,75	5	0,1

- Not Contained.
Source: Compiled by the author.

In the second nanoprecipitation procedure, the organic phase contained PCL, Vetiver Essential Oil, and acetone (Table 2). After preparation, the oily phase was poured into an aqueous solution containing Pluronic® F-127 under agitation. The suspension was kept under agitation to allow solvent evaporation.

Table 2: Formulations of nanoprecipitation systems with Pluronic® F-127.

Sample	PCL (%w/v)	Pluronic® F-127 (%w/v)	Vetiver Essential Oil (%m/m)
PC0P	0,25	0,05	-
PC4P	0,25	0,1	10

- Not Contained.
Source: Compiled by the author.

For ionic gelation, sodium alginate and calcium lactate, both purchased from Alquimia® in São Paulo, Brazil, were used, along with Tween®80 (Table 3).
An adapted method from Hosseini et al. (2013) was employed, where the surfactant and dispersed oil were added to the alginate solution under agitation to form an emulsion. The cross-linking solution of calcium lactate was then dripped using a syringe pump and a 30 x 0.8 mm needle at a flow rate of 30 mL/h [8].

Table 3 – Formulations of systems prepared by ionic gelation.

Sample	Alginate (%w/v)	Tween® 80 (%w/v)	Vetiver Essential Oil (%m/m)	Calcium Lactate (%w/v)
ALG1T	0,06	1	800 µL*	0,06
ALG3T	0,06	1	5	0,06

- Not Contained.
Note: The amount of added oil is indicated in µL
Source: Compiled by the author.

After the preparation of the nanoparticles, values for average hydrodynamic diameter (MD), polydispersion index (PDI), and surface charge in terms of zeta potential (ZP) were obtained using dynamic light scattering (DLS) analyser with the Zeta Potential Analyzer Nicomp Nano (IMA/UFRJ). The analyses were conducted in three scans, each lasting 1 minute. pH was measured using a digital pH meter, Model B07G81TX93 – Homyl (IMA/UFRJ).
For a comprehensive and reliable characterization of the nanoparticulate systems for cosmetic purposes, the nanoparticles were freeze-dried. The samples were frozen in an ultra freezer (between -68 °C and -72 °C) for about 24 hours and then lyophilized for 72 hours (at -49 °C and 830 mmHg). Subsequently, FTIR spectroscopy was performed.

Results and Discussion

The OEV is a complex mixture of bioactives. The ^{1}H, ^{13}C, and APT NMR spectra indicated the presence of saturated hydrocarbons (aliphatic groups) and unsaturated (olefins and/or alkenes) as well as oxygenated compounds (aldehydes, ketones, esters, among others), indicating a significant amount of aromatic compounds (Fig.2).

Figure 2 - ^{1}H NMR spectrum at 299.9 MHz of VEO in CDCl3. (b) ^{13}C NMR spectrum at 75,4 MHz of VEO in CDCl3. (c) APT spectrum at 75,4 MHz of VEO in CDCl3.

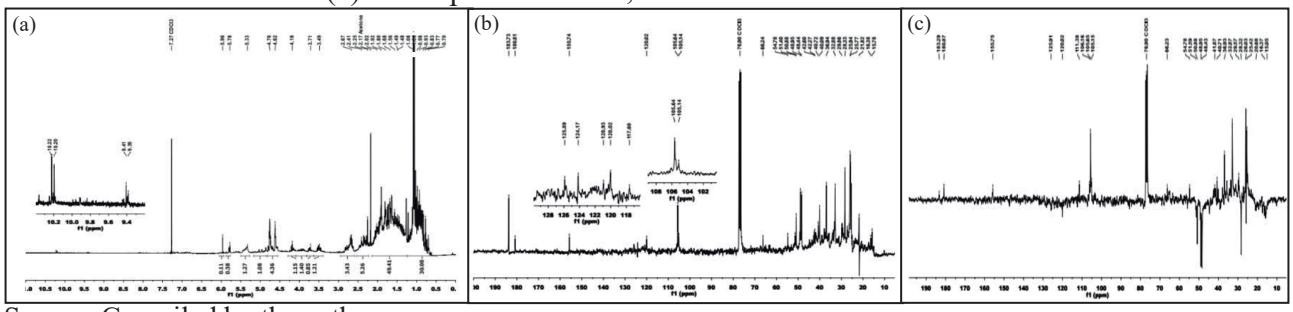

Source: Compiled by the author.

The FTIR spectrum (Fig 1) displayed bands of functional groups in accordance with the indications from NMR. The presented functional groups are consistent with the bioactives identified by Belhassena (2014) and Peng (2014), as determined through gas chromatography-mass spectrometry (GC-MS) and gas chromatography-olfactometry (GC-O) [3, 12].

Figure 1 - FTIR Spectrum of Vetiver Essential Oil, Samples Prepared by Nanoprecipitation with Pluronic® F-127, Span®60, and Tween® 80, and Ionic Gelation.

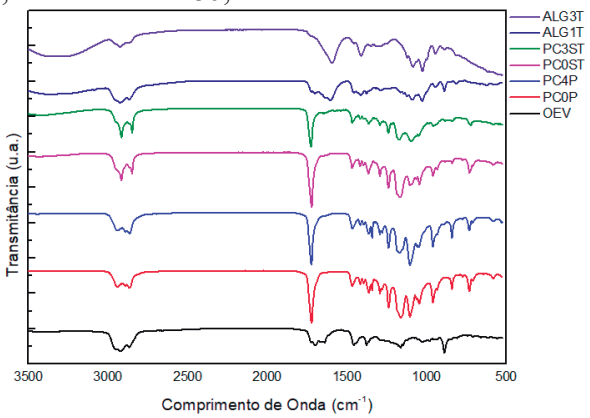

Source: Compiled by the author.

For the sample prepared with Pluronic® F-127, there is no differentiation in the spectrum between the empty sample and the loaded one, indicating that there were no new chemical bonds formed among the components of this nanosystem. The absence of oil signals strongly suggests that the oils were encapsulated within the polymer and surfactant layer, and due to the limitations of infrared penetration in solid bodies, their visualization in the spectrum would not be possible. For the nanocapsules prepared with Span® 60 and Tween® 80, there are slight shifts in the loaded sample compared to the empty nanoparticle in bands below 1417 cm-1, likely associated with the bioactive compound. This could indicate the presence of oils on the surface of the nanoparticles or free in the system. The ALG1T sample exhibited broadening and shifts in the positions of the bands, which might have occurred due to the excess oil present in the formulation.

Table 4 - Mean hydrodynamic diameter (MD), particle size distribution (PDI) in liquid form, pH, and zeta potential (ZP) of nanoparticles.

Sample	Nanopartículas recém preparadas			
	MD (nm)	PDI	pH	PZ (mV)
PC0ST	306,27 ± 1,89	0,33 ± 0,01	6,16 ± 0,1	-20,01 ± 1,62
PC3ST	187,97 ± 0,50	0,32 ± 0,01	5,34 ± 0,1	-13,75 ± 1,65
PC0P	304,00 ± 2,10	0,21 ± 0,01	6,73 ± 0,1	-31,02 ±0,01
PC4P	155,83 ± 0,74	0,24 ± 0,01	6,03 ± 0,1	-14,65 ± 3,54
ALG1T	453,4 ± 8,12	0,64 ± 0,01	5,91 ± 0,1	-420,49 ± 64,89
ALG3T	1294,3 ± 35,23	0,73 ±0,02	6,67 ± 0,1	-97,76 ± 26,14

Source: Compiled by the author.

The nanocapsules prepared by nanoprecipitation exhibited size, uniformity, and good stability in the form of a colloidal system [13]. For the samples prepared by nanoprecipitation with Pluronic® F-127, smaller values of MD and PDI were observed, along with higher absolute values of ZP, compared to the samples prepared with Tween® 80 and Span® 60. This demonstrates that Pluronic® F-127 was more efficient in generating particles with smaller sizes, thus providing a

larger surface area for contact, a narrower size distribution, and greater stability. These are desirable characteristics sought for the application of cosmeceuticals on the skin.

Conclusions

The utilization of polymeric nanoparticles loaded with Vetiver Essential Oil (Chrysopogon zizanioides) aiming to preserve and enhance the application of bioactive compounds contained in the oil, targeted for dermocosmetic treatments, represents a pioneering strategy in the production of high-performance products.

Each employed methodology produces nanoparticles with distinct characteristics, resulting from the selection of method, polymer, bioactive compounds, and stabilizers, as well as their interactions during the nanocapsule formation process. Further physicochemical and biological characterizations should be conducted for a more comprehensive comparison between the methods.

Acknowledgements

The authors would like to thank CNPq and the Instituto de Macromoléculas Eloísa Mano (IMA-UFRJ) for their support and financial assistance in conducting this work.

References

1. B. BEGINES, et al. Nanomaterials, 2020, 10, 1. https://doi.org/10.3390/nano10071403.
2. C. E. MORA-HUERTAS, et al. Journal of Pharmaceutics and Biopharmaceutics, 2012, 80, 1, 235. https://doi.org/10.1016/j.ejpb.2011.09.013.
3. E. BELHASSEN, et al. Chemistry & Biodiversity, 2014, 11, 11, 1821. https://doi.org/10.1002/cbdv.201400079.
4. H. Fessi et al. Patente Europeia 274961 A1, 1988.
5. J. A. B. VALLE, et al. Journal of Applied Polymer Science, 2021, 138, 21, 50482. https://doi.org/10.1002/app.50482.
6. N. Y. L. Aibibu; G. Zeng et al. Bioresource Technology, 2010, 101, 16, 6297. https://doi.org/10.1016/j.biortech.2010.03.028
7. S. J. D. P. DOS SANTOS et al. Research, Society and Development, 2021, 10, 12, e541101220308. https://doi.org/10.33448/rsd-v10i12.20308.
8. S. M., HOSSEINI et al. International journal of biological macromolecules, 2013, 62, 582. https://doi.org/10.1016/j.carbpol.2013.02.031.
9. S. S. GUTERRES, et al. Polymeric Nanoparticles. Nanocosmetics, p. 73-94, 2019. https://doi.org/10.1007/978-3-030-16573-4_5.
10. S.-T. Chou et al. Food Chemistry, 2012, 134, 1, 262. https://doi.org/10.1016/j.foodchem.2012.02.131.
11. T. P. W. BEZERRA, et al. Research, Society and Development, 2022, 11, 14, e99111436115. https://doi.org/10.33448/rsd-v11i14.36115.
12. X. PENG, et al. Chinese Journal of Ecology 2014, 33, 2, 335. http://www.cje.net.cn/EN/Y2014/V33/I2/335.
13. S. R., SCHAFFAZICK, et al. Química Nova, 2003, 26, 726. https://doi.org/ 10.1590/S0100-40422003000500017

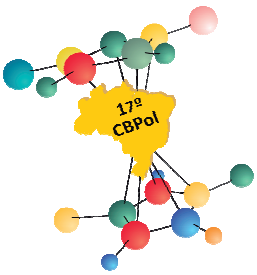

PHYSICAL AND RHEOLOGICAL CHARACTERIZATION OF RECYCLED PP NANOCOMPOSITE WITH MONTMORILLONITE CLAY

Alice da Costa Silva[1], Carlos H. R. Miltont[1], Adriano L.A. Mattos[2], Juciklécia S. Reinaldo[3], Carlos Alberto Paskocimas[4], Edson Noriyuki Ito[4]

1 – Graduate Program in Materials Science and Engineering (PPGCEM), Federal University of Rio Grande do Norte (UFRN), Rio Grande do Norte, RN, Brazil alice.silva.111@ufrn.edu.br; henrique.milfont@gmail.com
2 –Embrapa Tropical Agroindustry, Fortaleza, CE, Brazil adriano.mattos@embrapa.br
3 – Higher School of Technology, State University of Amazonas, Manaus, AM, Brazil jreinaldo@uea.edu.br
4 – Department of Materials Engineering (DEMat), Federal University of Rio Grande do Norte (UFRN), Rio Grande do Norte, RN, Brazil edson.ito@ufrn.br; carlos.alberto.paskocimas@ufrn.br

Abstract

The influence of the incorporation of organophilic montmorillonite clay (OMMT) and polypropylene grafted with maleic anhydride on the linear viscoelastic rheological behavior of recycled polypropylene (rPP) from mineral water bottles was investigated. The polymer nanocomposites were plasticized and homogenized in a twin screw co-rotational extruder with d = 16 mm and l/d = 40, varying in 1, 3 and 5 wt% of OMMT and using 3 wt% of PP-g-MA. After mixing, type I specimens were injection molded, according to ASTM D638. X-ray diffraction showed evidence of partial exfoliation of OMMT in the polymeric matrix. The rheological data obtained at low frequencies in the region of linear viscoelasticity, revealed significant changes in the rheological behavior of the polymer nanocomposites when compared to the rPP.

Keywords: *linear viscoelasticity, recycled polypropylene, montmorillonite clay, maleic anhydride.*

Introduction

Recycled polypropylene (rPP) can present a relevant combination due to its low cost and its versatility in terms of properties [1]. Aiming at its reuse, the production of polymer nanocomposites, through the incorporation of fillers to its matrix, has proved to be an attractive alternative. In research focused on this area, the study of the addition of nanolamellar silicates stands out, with a thickness of around 1 nm and a length of 100 to 1000 nm [2].

The polymer mixed with layered silicates, it can intercalate or exfoliate the layered silicates depending on the degree of attractive interactions between the matrix and the lamellae. However, when a polymeric matrix and a layered silicate do not have sufficient chemical affinity, with some alternatives arising, such as the modification of the layered silicate by treatment with surfactants and/or the use of compatibilization agents [3].

The incorporation of these fillers can change the viscoelastic behavior of the polymers, becoming dependent on the degree of dispersion of the organoclay aggregates, which in turn depends, among many factors, on the degree of attractive interactions between the polymeric matrix and the organoclay [3].

This study aimed to investigate the influence of the incorporation of montmorillonite organophilic clay (OMMT) and polypropylene grafted with maleic anhydride (PP-g-MA) on the linear viscoelastic rheological behavior of recycled polypropylene (rPP) from mineral water bottles.

Experimental

Materials

Recycled polypropylene (rPP) from 20L mineral water bottles (MFI= 8.85 g/10min), a natural and chemically modified organophilic montmorillonite clay with a quaternary ammonium salt (Cloisite® 30B), from Southern Clays, and a polypropylene grafted with maleic anhydride (Polybond® PB 3200), from Uniroyal was used.

The formulations of polymer nanocomposites vary by 1, 3 and 5 wt% of OMMT with and without 3 wt% of PP-g-MA, are shown in Table 1.

Table 1. Formulations of polymer nanocomposites used for physical and rheological characterization.

Materials	Formulation (pcr)
rPP	100
rPP /PP-*g*-MA	100/3
rPP /OMMT	100/1
rPP/OMMT/PP-*g*-MA	100/1/3
rPP /OMMT	100/3
rPP /OMMT/PP-*g*-MA	100/3/3
rPP/OMMT	100/5
rPP/OMMT/PP-*g*-MA	100/5/3

Extrusion and injection processing

The polymer nanocomposites were plasticized and homogenized in a co-rotational twin screw extruder model AX – DR16:40 from AX Plásticos Máquinas Técnicas, with d =16 mm and l/d = 40, using a temperature profile of 100/150/200/ 200/200/210/210/210/210 ºC from the feed to the die with a feed of 90 rpm and screw speed of 300 rpm.

The materials were granulated and dried for subsequent injecton molding of ASTM D638 tyoe-I tensile test specimens. Injection molding was carried out using an Arburg Allrounder 270S equipment with a temperature profile of 190/200/210/210/210ºC from the feed to the injection nozzle. The mold temperature was 40 °C with a cooling time of 40s.

X-Ray Diffraction (XRD)

The X-ray diffraction pattern of the formulations was performed using a Shimadzu diffractometer (model XRD-7000) with CuKα radiation (λ = 1.5418 Å) and step of 2º (2θ)/min. The test was performed in the 2θ range of 2.5 to 40º at room temperature.

Rheological characterization

Rheological analyses of the pure polymeric nanocomposites were analyzed in the linear viscoelastic region using an oscillatory shear rheometer (Thermo Scientific, model HAAKE

MARS). The samples were tested using a parallel-plate geometry (d = 25 mm) with a gap of 1 mm at 190ºC at an angular frequency from 50 to 0.015 rad/s.

Results and Discussion

X-Ray Diffraction (XRD)

Fig 1 presents the XRD patterns of the OMMT and the studied polymer nanocomposites. In Fig. 1a, the diffractograms for the incorporation of 1, 3 and 5 wt% of OMMT in the rPP are verified, observing the partial disappearance of the characteristic clay peak (d001=4.7º) in the polymer nanocomposites, showing signs of intercalation and partial exfoliation of the layered silicates in the polymeric matrix, caused by the penetration of the rPP molecules into the OMMT lamellae.

A similar result was observed for the incorporation of 3 wt% of PP-g-MA to polymer nanocomposites of rPP/OMMT, as can be seen in Fig. 1b. The formulations containing 1 wt% of clay showed signs of an exfoliated structure, implying a good dispersion of the same in the rPP matrix. Similar behavior was observed by Passador et al. [4].

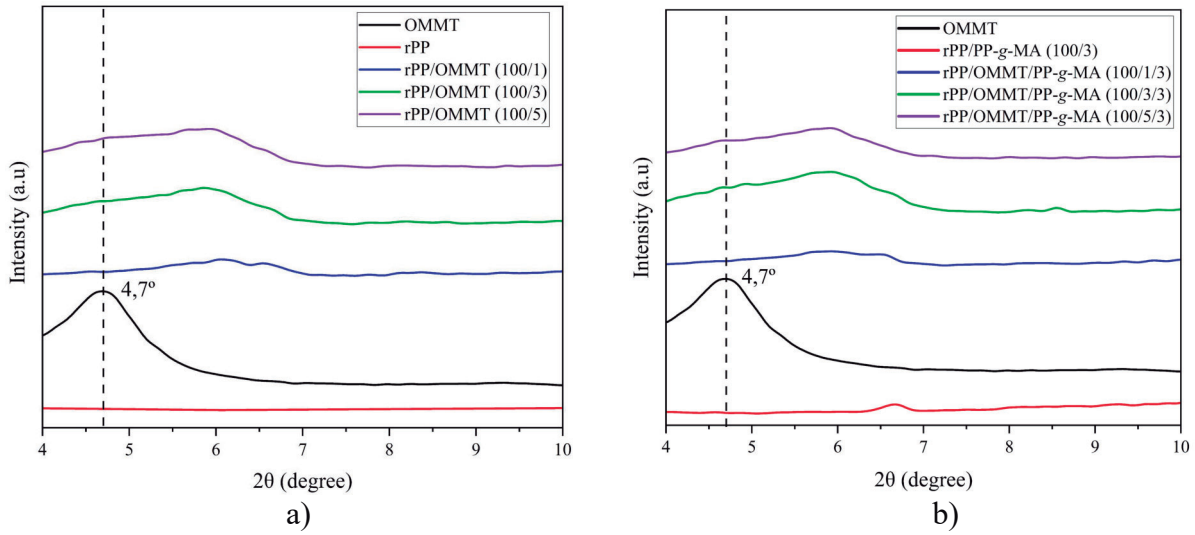

Figure 1. X-ray diffractogram in the angular range (2θ) from 4 to 10º of rPP with addition of 1, 3 and 5 wt% of OMMT. a) Without PP-g-MA. b) With 3 wt% of PP-g-MA.

Rheological characterization

Fig 2 presents the linear viscoelastic rheological behavior of rPP and polymer nanocomposites, revealing their storage modulus (G') and loss modulus (G"). By adding 3 wt% of PP-g-MA to rPP (Fig 2a), the composition showed a behavior partially different from that of rPP in its terminal zone, showing a reduction in the values of G' and G", which may be related to the difference in viscosity between rPP and PP-g-MA, showing evidence of its action as a plasticizer.

The incorporation of 1 wt% of OMMT to rPP and rPP/PP-g-MA (Fig.2b) caused an increase in the values of the storage modulus and loss modulus, observed in its terminal zone, giving indications that the clay may be influencing the rheological behavior of the rPP. The same trend is observed proportionally as the OMMT concentration increases to 3 and 5 wt% (Fig 2c and 2d). The incorporation of PP-g-MA contributed to the increase of G' and G", this can be attributed to the presence of attractive interactions, like hydrogen bonds, between the carbonyl groups and the

hydroxyl groups in the surfactant (MT2EtOH) of the clay used. A flow behavior was observed due to the existence of these attractive interactions between the polymeric matrix and the particulate surface. Similar behaviors were also observed by Zuh et al [5] and Lee et al. [6].

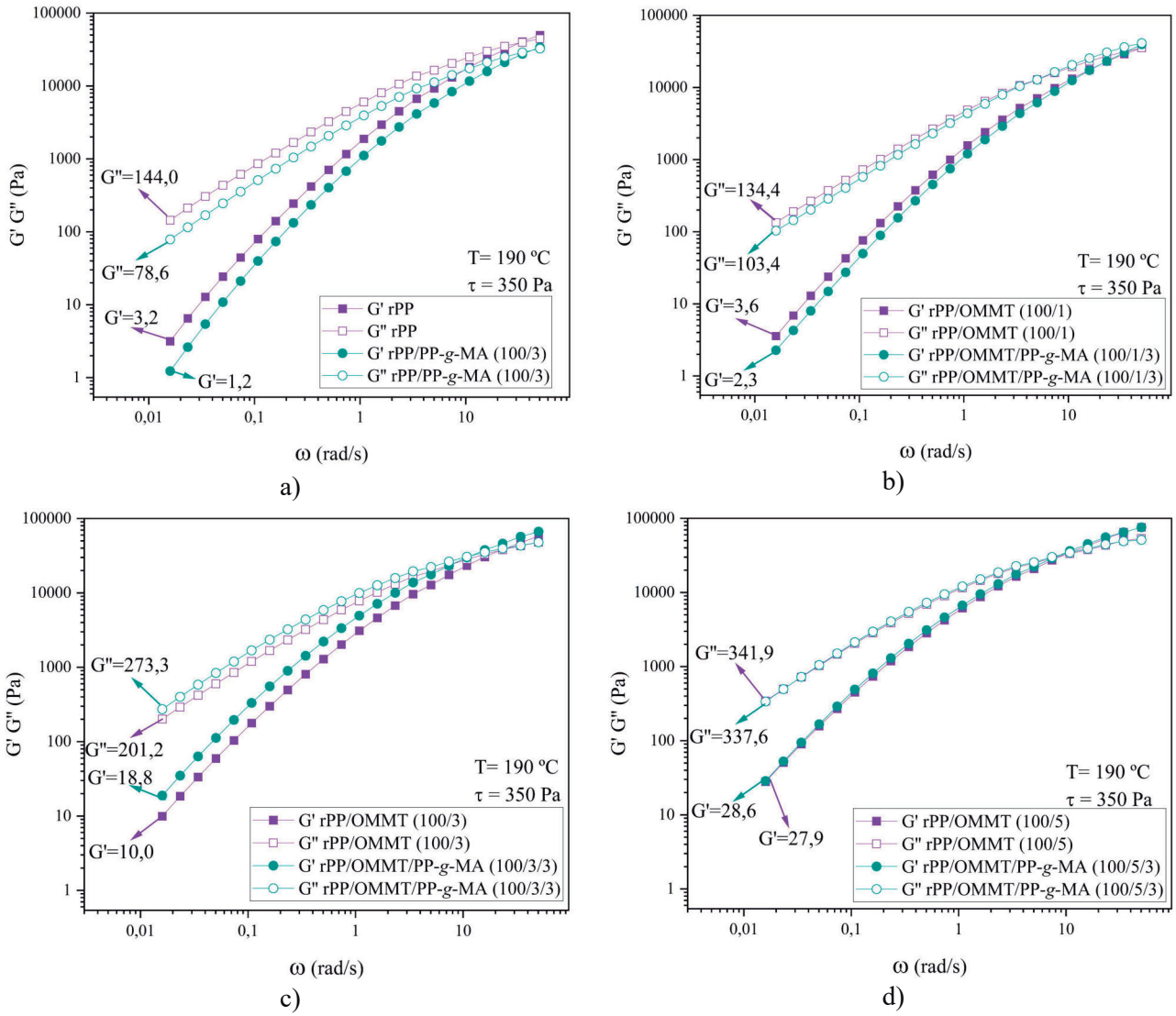

Figure 2. Log G' versus log G" for the rPP and the compositions with 3 wt% PE-g-MA. a) Without OMMT. b) With 1 wt% of OMMT. c) With 3 wt% of OMMT. d) With 5 wt% of OMMT.

Fig 3 shows complex viscosity curves as a function of angular frequency for rPP and for polymer nanocomposites. The compositions rPP/PP-g-MA (100/3 wt%), rPP/OMMT (100/1 wt%) and, rPP/OMMT/PP-g-MA (100/1/3 wt%) showed a lower complex viscosity when compared to rPP. The opposite occurred with the nanocomposites with and without PP-g-MA with 3 and 5 wt% of OMMT, showing the effect of clay incorporation in the rPP and the efficiency of the compatibilization with the PP-g-MA.

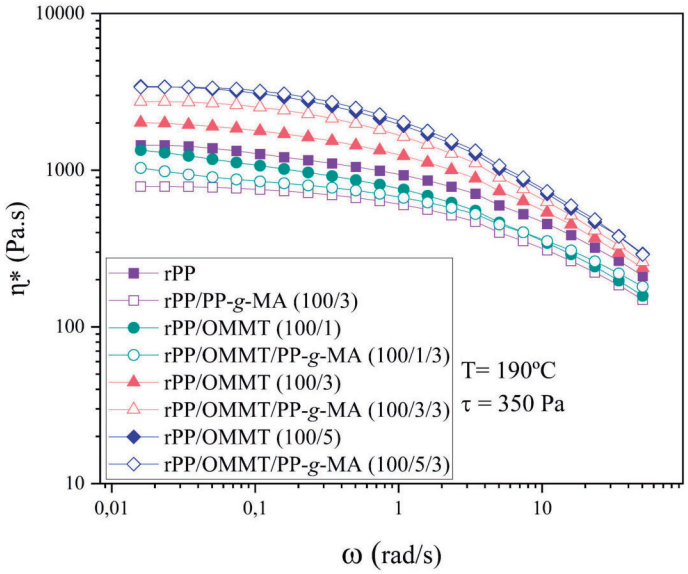

Figure 3. Complex viscosity versus angular frequency.

Conclusions

The physical behavior of the polymer nanocomposites showed evidence of intercalation and partial exfoliation of OMMT particles. The analysis in the linear viscoelasticity region showed evidence of the incorporation of rPP polymeric chains in the OMMT structures and the efficiency of the interfacial compatibilization agent PP-g-MA, through changes in the rheological behavior of rPP.

Acknowledgements

To the Água Cristalina company for supplying the rPP, to the development agency CAPES for the master's scholarship and to the Embrapa Tropical Agroindustry for the laboratory infrastructure.

References

[1] Chung MJ, Jang LW, Shim JH, Yoon JS. Preparation and characterization of maleic anhydride-g-polypropylene/diamine-modified clay nanocomposites. J Appl Polym Sci 2005;95:307–11. https://doi.org/10.1002/app.21224

[2] D.J. Carastan. PH.D Thesis, Polytechnic School of the University of São Paulo. 2007.

[3] Han, C. D. Rheology and processing of polymeric materials: Volume 1: Polymer Rheology (Vol. 1). Oxford University Press on Demand. 2007.

[4] Passador FR, Ruvolo-Filho AC, Pessan LA. Effects of different compatibilizers on the rheological, thermomechanical, and morphological properties of HDPE/LLDPE blend-based nanocomposites. J Appl Polym Sci 2013;130:1726–35. https://doi.org/10.1002/app.39265

[5] Zhu, S., Chen, J., Li, H., & Cao, Y. (2013). Effect of polymer matrix/montmorillonite compatibility on morphology and melt rheology of polypropylene nanocomposites. Journal of Applied Polymer Science, 128 (6), 3876-3884. https://doi.org/10.1002/app.38626

[6] Lee KM, Han CD (2003c). Macromolecules 36:7165. https://doi.org/10.1021/ma030302w

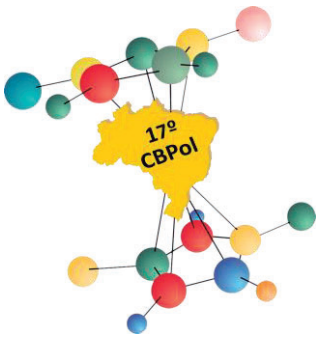

PLA/HNT NANOCOMPOSITES: INFLUENCE OF HNT CONTENT ON THERMAL, RHEOLOGICAL AND MECHANICAL PROPERTIES

Pedro H. S. Vieira and Juliano Marini *

Department of Materials Engineering (DEMa), Federal University of São Carlos (UFSCar), São Carlos, SP, Brazil
juliano.marini@ufscar.br

Abstract - Nanocomposites of poly(lactic acid), PLA, and halloysite nanotubes, HNT, have great potential for use in biomedical and packaging applications, combining biocompatibility with biodegradability. In this study, it was evaluated the influence of the HNT content (from 0 to 10 wt%) on the thermal (TGA, DSC), rheological and mechanical (uniaxial tensile test) properties of PLA nanocomposites obtained by melt mixing and compression molded into films. It was possible to observe that the presence and content of HNT did not significantly alter the decomposition behavior and the degree of crystallinity of the PLA and led to an increase in the elastic behavior in the molten state, greater mechanical rigidity, indicating the obtainment of nanocomposites with an adequate PLA-HNT interface, even without the use of compatibilizing agents or surface modification of the HNT.
Keywords: *Nanocomposites, poly(lactic acid), halloysite nanotubes, rheology, mechanical properties.*
Fundings: CNPq (processes # 120930/2017-0 and 427639/2016-6) and CNPq/FAPEMIG/CAPES (INCT/Midas, project # 465594/2014-0, subproject # 24998*26).

Introduction

In recent years, interest in biodegradable polymers obtained from natural renewable sources has been increasing, as sustainable development policies gain interest, whether due to a growing environmental awareness or even the reduction in the availability of fossil fuels. Another frontier area is materials for biomedical applications, highlighting the recent development of nanocomposites of polymeric matrices, which seek to optimize characteristics such as the mechanical performance of implants, acting as cell growth supports or even in obtaining smart devices, that react in a controlled manner to stimuli internal or external to the human body. Within this context, the use of poly(lactic acid), PLA, a biodegradable and biocompatible polymer obtained from renewable sources must be highlighted [1, 2]. The use of nanoparticles (NP) to improve specific properties of polymeric materials has been extensively studied in recent decades [3, 4]. In general, the reinforcement effect obtained depends mainly on the intrinsic characteristics of the NP (aspect ratio, geometry, surface area, stiffness, etc.), on obtaining a proper state of dispersion and distribution of the NP in the polymeric matrix and the compatibility/affinity between the two main components (polymer and NP). Recently, halloysite nanotubes (HNT) have been used as reinforcing fillers [5, 6] because they have very interesting characteristics such as a high aspect ratio and low percolation volumetric fraction, like carbon nanotubes, in addition to a chemical structure like montmorillonite, the most studied and used nanoparticle as a reinforcing agent in polymer matrices. In addition, HNT has a high level of biocompatibility and very low cytotoxicity [7] and, therefore, PLA/HNT nanocomposites have great potential for applications as functional materials in the

biomedical and packaging areas. The objective of this work was to evaluate the influence of the HNT content on the thermal, rheological, and mechanical properties of PLA nanocomposites obtained through melt mixing.

Experimental

Materials

- Poly(lactic acid), PLA, Ingeo Biopolymer 4043 D (NatureWorks), with MFI of 6 g/10min (210°C/2.16 kg, ASTM D792), and density of 1.24 g/cm^3.
- Halloysite nanotubes, HNT, Dragonite-XR (Applied Minerals Inc.), with surface area of 64.66 m^2/g, internal and external diameters of 15 and 50 nm, respectively, average length of 1.75 mm, and density of 2.52 g/cm^3.

Nanocomposites processing and molding

PLA nanocomposites with different HNT contents (0, 2.5, 5, 7.5, and 10 wt%) were obtained by melt mixing, using a HAAKE torque rheometer, model Rheomix 600p, roller-type rotors, at 180°C, 100 rpm and 5 min of mixing time. Films with average thickness of 200 μm were obtained by compression molding using a hot press from Marconi Equipamentos para Laboratórios, model MA098/A, at 180°C and 5 ton, using a four steps cycle: i) pre-heating of 2 min; ii) two cycles of pressing/venting; iii) final pressing for 2 min; iv) cooling under pressure for 10 min.

Characterization

The nanocomposites (prior to compression molding) were analyzed by thermogravimetry (TGA Q50, TA Instruments), from 30°C to 800°C, at 20°C/min in N_2 atmosphere. Storage (G') and loss (G'') moduli as function of oscillation frequency (ω) were measured in a stress-controlled rheometer (ARG2, TA Instruments), using parallel-plate geometry (plate diameter of 25 mm), gap of 1 mm, at 180°C, under N_2 atmosphere, applying a strain amplitude within the linear viscoelastic range.

Films were analyzed by DSC (Q2000, TA Instruments), at a heating rate of 10°C/min, from 30°C to 200°C, under N_2 atmosphere, and the degree of crystallinity (X_c) was calculated by:

$$X_C = \frac{\Delta H_m - \Delta H_{cc}}{(1-\varphi)\cdot \Delta H_m^0} \times 100\% \quad (1)$$

where ΔH_m is the enthalpy of fusion, ΔH_{cc} is the cold crystallization enthalpy, ΔH_m^0 is the enthalpy of fusion of 100% crystalline polymer (93 J/g for PLA), and φ is the mass fraction of HNT. Uniaxial tensile tests were performed according to ASTM D882, using a universal testing machine, model 5569 (Instron), at a strain rate of 12.5 mm/min.

Results and Discussion

The results of the TGA tests are shown in Fig. 1 and Table 1. It is possible to observe that the presence of halloysite accelerates the PLA decomposition process by about 10°C, due to the release of structural water present in the NP and due to the presence of Bronsted acid sites on its surface, that have a catalytic role in the pyrolysis of PLA [8]. However, this reduction is not significant to the point of disturbing the processability and applicability of the material.

The influence of the HNT content on the viscoelastic behavior of the PLA matrix was evaluated through rheological tests in oscillatory regime and the results are shown in Fig. 2(a). All compositions showed the typical behavior expected for molten thermoplastics, with G" > G' at the range of frequency analyzed. A gradual increase in G' is observed with increasing HNT content,

although no evidence of formation of a percolated network was observed even for high HNT contents, above the theoretical percolation threshold (~ 5 wt%). This increase, although significant, did not change the predominantly viscous behavior of PLA, possible due weak interactions between HNT and PLA (which can impact on the NP dispersion and distribution through the PLA matrix) or even a possible breakage of particles during processing.

Table 1 – Results of TGA (T_i, T_p, and T_f = initial, peak, and final temperatures of decomposition, respectively; residue = remaining mass at 800°C) and DSC (T_g, and T_m = glass transition and melting temperatures, respectively; X_c = degree of crystallinity) analyzes.

Sample	T_i (°C)	T_p (°C)	T_f (°C)	Residue (%)	T_g (°C)	T_m (°C)	X_c (%)
PLA	302	397	406	0.2	60.9	148.7	3.7
PLA/HNT 2.5	300	379	399	2.3	55.1	146.1	5.7
PLA/HNT 5	300	373	393	4.3	59.3	149.4	4.5
PLA/HNT 7.5	292	372	392	6.0	55.8	149.3	7.8
PLA/HNT 10	292	372	392	8.5	54.5	150.0	7.0

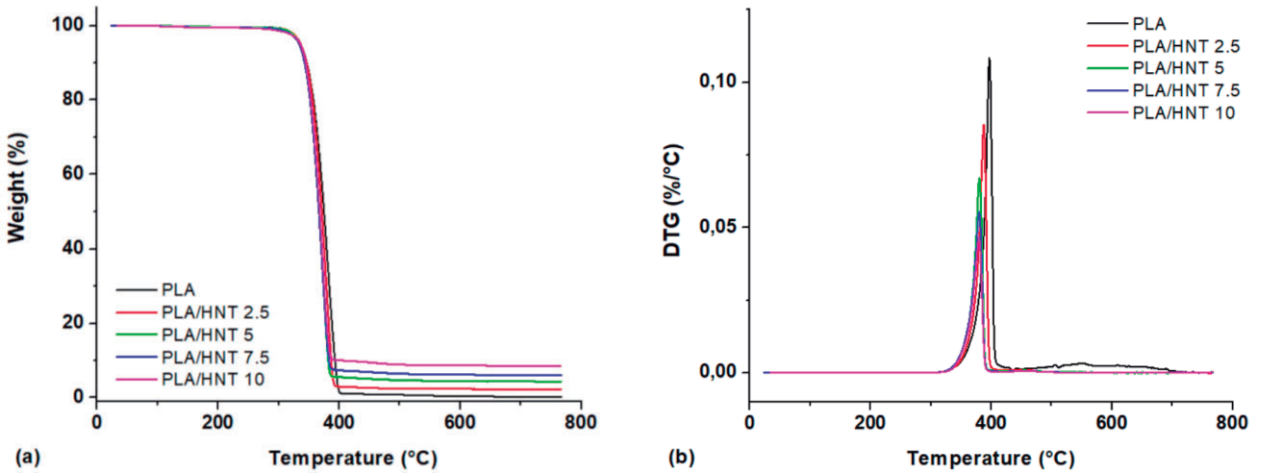

Figure 1 – TGA results: (a) weight loss and (b) derivative of weight loss as function of temperature for the PLA/HNT nanocomposites.

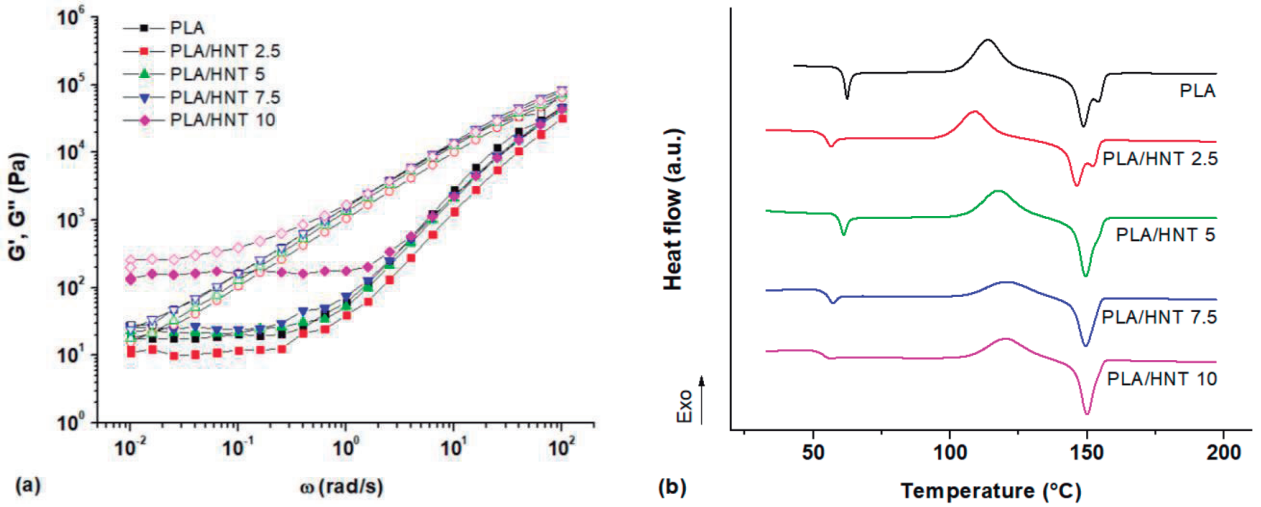

Figure 2 – (a) G' (solid symbols) and G'' (open symbols) as function of ω for the PLA/HNT nanocomposites. (b) DSC heating curves of the PLA/HNT films.

The compression molded films were evaluated by DSC and the results are shown in Fig. 2 (b) and Table 1. The presence and content of HNT did not significantly affect the transition temperatures (T_g, T_m) or the degree of crystallinity (X_c) of the films. There is a slight tendency towards a decrease in T_g and an increase in X_c with increasing HNT content.
PLA and PLA/HNT nanocomposites films with different HNT contents were characterized mechanically through tensile tests and the results are shown in Table 2. In general, all samples showed brittle behavior, typical of PLA, regardless of HNT concentration. The increase in HNT content increased the stiffness of the PLA films, without affecting the values of yield stress and yield strain, indicating that the PLA-HNT interface is not weak.

Table 2 – Results of tensile test. E = elastic modulus; σ_y = yield stress, ε_y = yield strain; σ_b = stress at break, ε_b = strain at break.

Sample	E (GPa)	σ_y (MPa)	ε_y (%)	σ_b (MPa)	ε_b (%)
PLA	2.76 ± 0.08	52.96 ± 3.65	2.44 ± 0.12	51.77 ± 3.84	2.57 ± 0.18
PLA/HNT 2.5	2.85 ± 0.12	52.06 ± 3.85	2.62 ± 0.19	49.33 ± 9.85	3.02 ± 0.37
PLA/HNT 5	2.84 ± 0.03	50.59 ± 4.27	2.31 ± 0.26	46.85 ± 2.66	2.72 ± 0.43
PLA/HNT 7.5	3.07 ± 0.15	49.93 ± 2.59	2.35 ± 0.15	48.64 ± 3.84	2.48 ± 0.11
PLA/HNT 10	3.23 ± 0.21	52.76 ± 2.41	2.34 ± 0.08	50.51 ± 2.63	2.52 ± 0.15

Conclusions

The feasibility of producing PLA/HNT nanocomposites by melt mixing was proven, obtaining materials with improvements in mechanical properties, without significant losses in processability and in the thermal behavior of the pure PLA matrix, even without the use of compatibilizing agents or surface modification of the HNT. The best results were observed for the PLA/HNT 10 nanocomposite, indicating an overall performance improvement with the increase in the HNT content.

Acknowledgements
The authors thank CNPq (processes # 120930/2017-0 and 427639/2016-6) and CNPq/FAPEMIG/CAPES (INCT/Midas, project # 465594/2014-0, subproject # 24998*26) for financial support.

References
1. V. DeStefano; S. Khan; A. Tabada Engineered Regeneration 2020, 1, 76-87. https://doi.org/10.1016/j.engreg.2020.08.002
2. M. S. Singhvi; S. S. Zinjarde; D. V. Gokhale Journal of Applied Microbiology 2019, 217, 1612-1626. https://doi.org/10.1111/jam.14290
3. S. C. Tjong Materials Science and Engineering: R: Reports 2006, 53, 73-197. https://doi.org/10.1016/j.mser.2006.06.001
4. J. Marini; R. E. S. Bretas Polymer Engineering and Science 2013, 53, 1512-1528. https://doi.org/10.1002/pen.23405
5. J. Marini; E. Pollet; L. Averous; R. E. S. Bretas Polymer 2014, 55, 5226-5234. https://doi.org/10.1016/j.polymer.2014.08.049
6. S. Therias; M. Murariu; P. Dubois Polymer Degradation and Stability 2017, 145, 60-69. https://doi.org/10.1016/j.polymdegradstab.2017.06.008
7. G. L. P. Silva; L. C. A. Morais; J. B. Olivato; J. Marini; P. C. Ferrari Journal of Biomaterials Applications 2021, 35, 1096-1108. https://doi.org/10.1177/0885328221995920

8. Y. H. Kim; S. H. Kwon; H. J. Choi; K. Choi; N. Kao; S. N. Battacharya Journal of Macromolecular Science 2016, 55, 680-692. https://doi.org/10.1080/00222348.2016.1187054

POLI(LACTIC ACID-CO-GLYCOLIC ACID)/POLY(VINYL ALCOHOL) CORE-SHELL ELECTROSPUN FIBERS

Thalles R. S. Rêgo[1], Anna L. M. M. Toledo[1] and Marcos L. Dias[1]*
1 – Institute of Macromolecules Professor Eloisa Mano, Federal University of Rio de Janeiro (UFRJ), Rio de Janeiro, RJ, Brazil thallesrafael@ima.ufrj.br

Abstract - The electrospinning technique can be used to create devices to aid in the regeneration of an injured tissue. This technique involves the formation of solid fibers from polymeric solutions through the application of a high-voltage electric field. Variations in the technique, such as the use of concentric integrated needles for producing fibers with a core-shell morphology, known as coaxial electrospinning, enable sustained release of bioactive agents in the biomedical field. This study discusses the effect of key parameters in electrospinning in order to obtain suitable core-shell fibers for the incorporation of a bioactive agent in the poly(vinyl alcohol) (PVA) core of the coaxial system, enveloped by a poli(lactic acid-co-glycolic acid) (PLGA). The study successfully demonstrated the successful production of defect-free core-shell PLGA/PVA fibers and evaluates the morphology as well as the electrospinning conditions to obtain these fibers. The study demonstrates that the polymers exhibited crystallinity in the core-shell fibers.
Keywords: *Coaxial electrospinning, Tissue engineering, Core-shell fibers.*

Introduction

Nanofiber production can be achieved through different processing techniques, including self-assembly, electrospinning, phase separation, molding, and vapor-induced polymerization [1,2]. Among these methods, electrospinning is recognized for its simplicity, versatility, and cost-effectiveness in producing nonwoven nanofibrous membranes from polymeric solutions or melts. While most studies have focused on polymeric solutions, electrospinning involves a setup comprising a syringe, needle, grounded collector, pump, and a voltage source connected to the needle [3,4]. The process begins by pushing the polymeric solution to the needle's tip, where it experiences an electric field. When the applied voltage surpasses the solution's surface tension threshold, a cone-shaped deformation known as the Taylor Cone forms in the polymer drop. The solution, under the electric field's influence, is ejected and undergoes elongation, forming a solid fiber as the electrified jet continuously stretches due to electrostatic repulsions. Solvent evaporation occurs until the jet reaches the collector [5-7].

Various parameters, including operational, polymeric solution, and environmental factors, can influence electrospinning [4,8]. Additionally, modifications to the apparatus, particularly the needle geometry, can impact the technique, such as the use of concentric needles in coaxial electrospinning to produce core-shell fibers [9]. Considering the possibilities offered by coaxial electrospinning, this study investigates the influence of voltage variation and the distance between the needle and collector on the formation of PLGA/PVA core-shell fibers.

Experimental

Materials

PLGA (LA:GA 85:15, M_w = 331,700, PuraSorb® PLG 8531) in pellet form was used in this study. PVA (M_w = 30,000 - 70,000, 87-90% hydrolyzed, Sigma-Aldrich) in powder form. The solvents used for the PLGA solution were chloroform PA purchased from Vetec Química Fina LTDA and *N,N*-Dimethylformamide ACS, ≥99.8% purchased from Sigma Aldrich. The PVA solution was prepared using distilled water.

Core-shell electrospun membranes of PLGA/PVA.

In this work, the electrospinning apparatus consisted of a high-voltage power supply, two infusion pumps, a coaxial needle with an inner diameter of 0.5 mm (25G) and an outer diameter of 0.8 mm (21G), and a grounded metal collector. The core solution was prepared by dissolving PVA in distilled water (15% w/v) at 80 °C for 3 hours, while a 3% w/v shell solution of PLGA was prepared by dissolving PLGA in a 4:1 v/v mixture of chloroform and dimethylformamide. The core and shell solutions were injected using 5 mL plastic syringes and independently pushed at flow rates of 0.16 mL/h and 0.5 mL/h, respectively. Previously, it was determined that the flow rate applied to obtain suitable PLGA fibers was 0.5 mL/h, and based on previous studies, it was found that the inner flow rate should be at least one third of the outer flow rate [10]. Therefore, a flow rate of of 0.16 mL/h and 0.5 mL/h was applied to the core and shell solutions, respectively. The voltage during the electrospinning process varied between 12.5 kV, 15.0 kV, 17.5 kV, and 20.0 kV, and the distance between the needle and collector varied between 12.5 cm, 15.0 cm, and 17.5 cm.

Characterizations

The samples obtained by electrospinning were characterized using scanning electron microscopy (SEM) technique, which allowed evaluating the morphology of the obtained fibers in terms of the presence of defects, average fiber diameter, and porosity. For sample preparation for SEM analysis, the membranes were coated with gold using a Sputter coater. The average fiber diameter was quantified using ImageJ software, by using 5 different 5000x pictures in order to obtain 30 clear fibers [11].

Fourier-transform infrared spectroscopy (FTIR) with an ATR accessory in the range of 4000 to 400 cm^{-1} was performed to observe the relative bands of functional groups of both polymers and the absence of solvents after electrospinning. X-ray diffraction analyses were performed on 2 cm x 2 cm sections taken from the electrospun membranes and porous membrane, using an Ultima IV X-rays Diffractomer with copper Kα radiation (λ=1.5418 Å) was used, with 2θ ranging from 2° to 60° and a scanning rate of 0.05 °/sec.

Thermogravimetric analysis (TGA) was used to characterize the thermal stability profile of the membranes, including the initial temperature and the temperature of maximum weight loss rate. The samples were heated from 25°C to 700°C at a rate of 10°C/min under a nitrogen flow of 60 mL/min. Differential scanning calorimetry (DSC) was used to determine the glass transition temperature (T_g), crystallization temperature (T_c), cold crystallization temperature (T_{cc}) and melting temperature (T_m), as well as the melting enthalpy (ΔH_m) of the polymer and sample crystallinity (X_c). Approximately 10 mg of the samples were subjected from 0°C to 200°C heating and cooling cycles under a nitrogen atmosphere at a rate of 50 mL/min. The determination of transition temperatures and enthalpy of fusion was performed using OriginPro® software.

Results and Discussion

The first parameter evaluated was the effect of the applied voltage on the size and regularity of the fibers. It can be observed that for sample A (Fig. 1A), PLGA/PVA fibers with uniform structures, free from beads or interdigitations, were obtained. The average fiber diameter and standard deviation of this sample were 584 ± 90 nm, indicating that a good balance between the parameters was obtained. During the electrospinning process, samples B, C, and D (Fig. 1B-D) exhibited difficulties, such as the formation of a dried cluster at the needle tip and dripping, which is reflected in the SEM results. Those samples present non-uniform fiber formation, clear differences in diameter, and discontinuities in the fibers (indicated by arrows), along with structural defects such as beads (indicated by circles) and interdigitations (indicated by asterisks). Therefore, it can be seen that the increase of the voltage was detrimental to the process, since the increased speed imposed by the higher voltages resulted in defective fibers and not enough time for them to dry before hitting the grounded collector [12].

As for the needle tip to collector distance, and using the same voltage, at 17.5 cm, sample E (Fig. 1E) showed a significant number of voluminous beads (indicated by circles), indicating the non-evaporation of the solvent, likely distilled water, which has low volatility and was used as the core solvent for PVA. Sample F (Fig. 1F) exhibited no defects in the fiber morphology, and the calculated average diameter and standard deviation were 776 ± 116 nm. For sample G (Fig. 1G), fiber discontinuity (indicated by arrow) and the presence of interdigitations (indicated by asterisk) were observed, suggesting the deposition of wet fibers on the collector. Lastly, sample H (Fig. 1H) also exhibited defect-free fibers, with an average diameter and standard deviation of 1127 ± 329 nm.

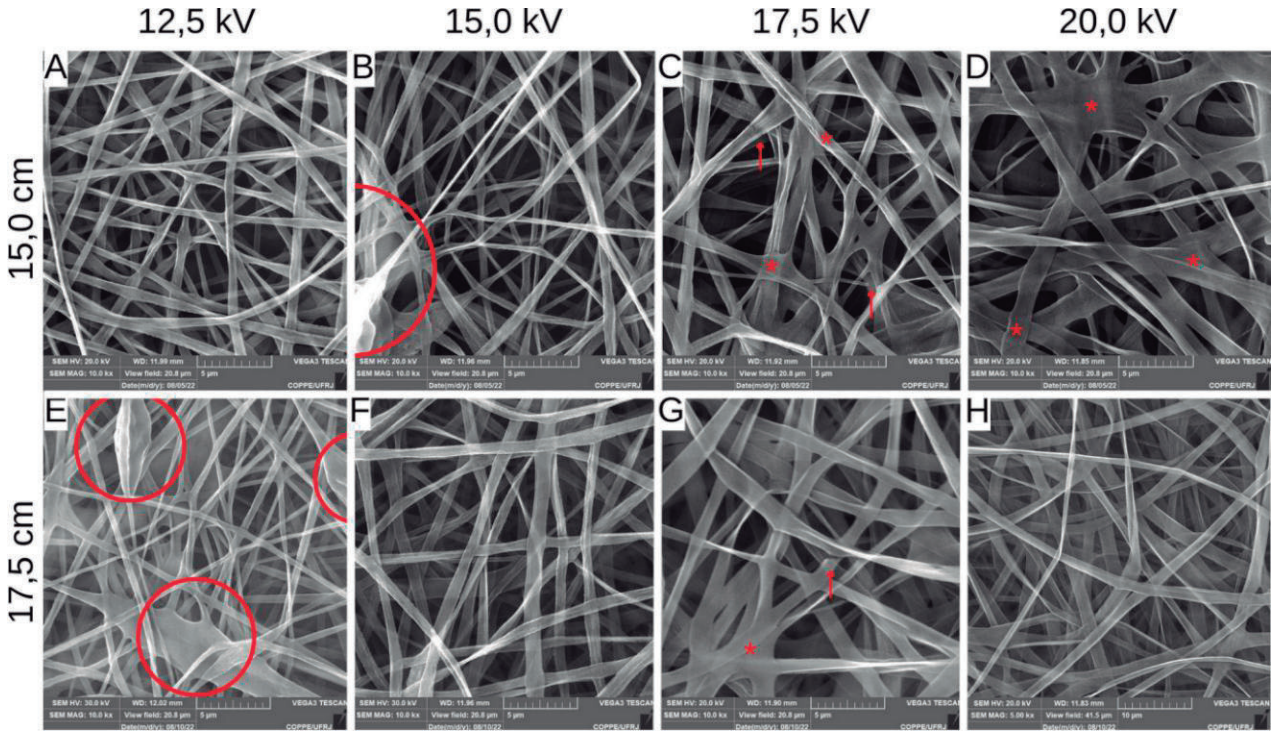

Figura 1 – SEM images of electrospun PLGA fibers obtained with needle-collector distance of 15.0 and 17.5 cm and voltages of 12.5, 15.0, 17.5 and 20.0 kV.

Due to its uniformity, absence of defects in fiber morphology, efficiency of the electrospinning process, and smaller average diameter and standard deviation, it was decided to proceed with this work using the electrospinning parameters of sample A. This means applying a voltage of 12.5 kV, a distance between the needle tip and collector of 15.0 cm, and an external flow rate of 0.5 mL/h and internal flow rate of 0.16 mL/h.

Aditionally, an electrospun membrane, loaded with fluorescein in the core solution was investigated with a Fluorescenct microscope and the core-shell structure was confirmed (Fig. 2A). To confirm the presence of a core-shell structure and the effective coating of the PVA core by the outer layer of PLGA, a study was conducted using Fourier-transform infrared spectroscopy (FTIR). The FTIR analysis of the core-shell fibers was compared to monolithic fibers of PLGA and PVA. The comparison of the surface composition of the fibers are presented in the infrared spectra of Fig. 2B, with a marked difference in the range of 600 cm^{-1} to 4000 cm^{-1} for PLGA, PVA, and the core-shell fibers composed of PLGA/PVA. Electrospun monolithic PVA fibers (PVAe) exhibit typical bands of hydroxyl groups at 3200 cm^{-1} to 3600 cm^{-1} [10]. These characteristic bands of PVA are not present in the spectrum of the PLGA/PVA fiber, which shows a profile similar to the curve of the monolithic PLGA fiber. Therefore, the absence of the characteristic hydroxyl groups of PVA indicates the absence of this polymer on the surface of the fibers. In the x-ray diffractogram of the electrospun membranes (Fig. 2C), the electrospun PVA sample exhibits a well-defined crystalline peaks at $2\theta = 19.7°$, as well as other peaks at $2\theta = 22.5°$ and $2\theta = 40.7°$. These peaks indicate the

presence of different types of crystals in the structure of the electrospun PVA, and the narrow base of these peaks indicates the high degree of crystallinity of the sample [13]. In the PLGA/PVA sample, a predominantly amorphous halo characteristic of PLGA is observed, but there is also a slight predisposition for the formation of a peak at 2θ = 19.7°, caused by the presence of PVA in the fiber formation (Fig. 2B).

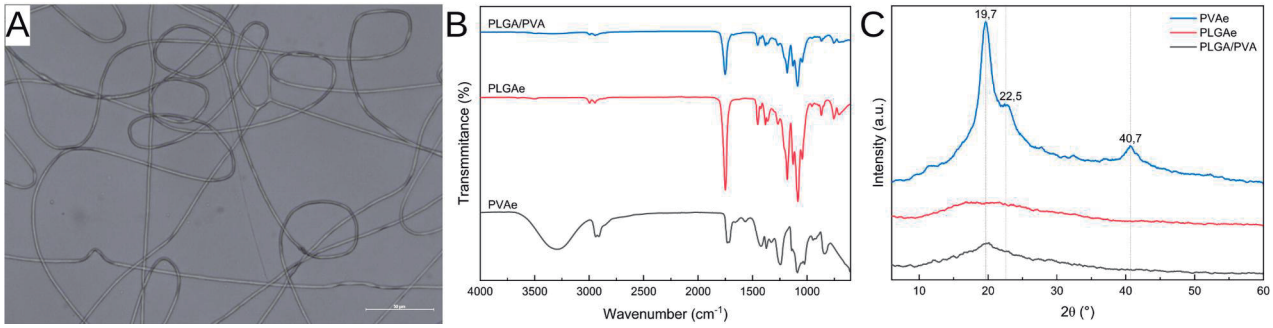

Figure 2 – Fluorescenct microscope (a) of PLGA/PVA core-shell fibers; FTIR spectra (b) and X-ray diffraction (XRD) curves (c) of monolithic PVA, PLGA and PLGA/PVA core-shell fibers.

Thermogravimetric analyses of the core-shell PLGA/PVA fibers revealed two degradation temperatures (T_{Onset}) at 254.05 °C and 415.43 °C, and maximum degradation rate temperatures at 279.82 °C and 432.14 °C, respectively (Fig. 3A). The first degradation event can be evaluated as an overlap of the degradation of the PLGA and PVA chains since the main degradation events of these polymers occur at similar temperatures. The second degradation event is likely a byproduct of the degradation of the PVA molecule present in the core of the core-shell fiber. Likewise, for the PLGA monolithic fibers, there is no indication of the presence of solvent, whereas both the PVAe and PLGA/PVA fibers present an event around 100°C that can be correlated to the water loss of the PVA phase in the fibers.

The DSC analysis of the core-shell PLGA/PVA membrane shows two glass transition temperatures at 43.2 °C and 52.8 °C. These two well-defined T_g values are shifted toward lower values when compared to the monolithic fibers of PLGA (PLGAe) and PVA. The temperature of 52.8 °C is most likely related to the T_g of PVA, which has its T_g shifted due to the presence of water in the polymer chain, acting as a plasticizer. A crystallization temperature (T_{cc}) and a melting temperature (T_m) are observed at 90.1 °C and 147.1 °C, respectively. The other thermal events are presented in Fig. 3B and Table 1.

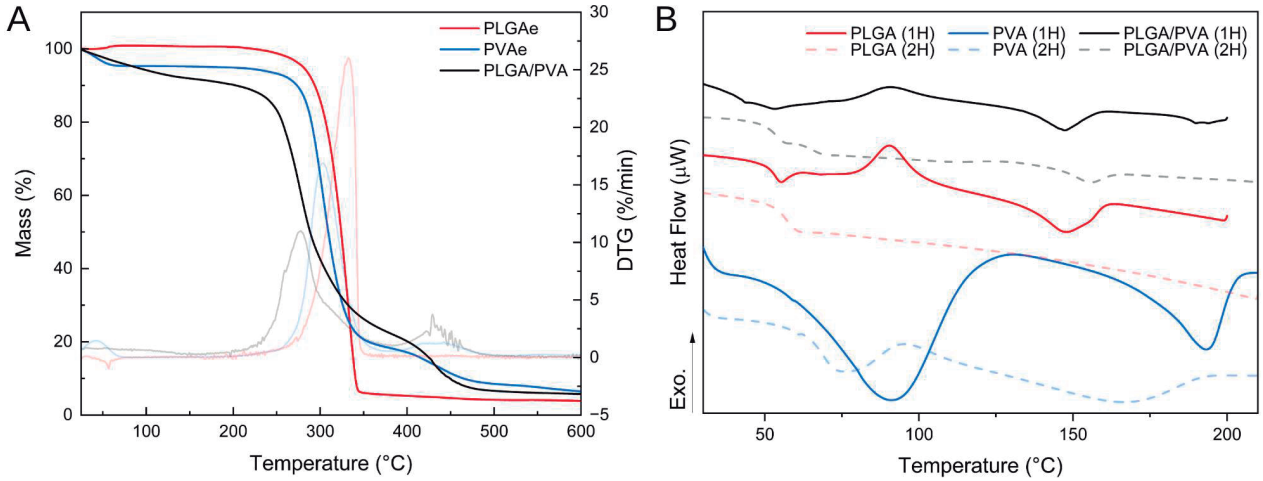

Figura 3 – TG and DTG curves (A) and DSC curves (B) of electrospun PLGA, PVA and PLGA/PVA core shell fibers.

Table 1 – Thermal transitions and crystallinity of electrospun PLGA, PVA and PLGA/PVA core shell fibers.

Sample	1st heating				2nd heating		
	Tg (ºC)	Tcc (°C)	Tm (°C)	Crystallinity (%)	Tg (ºC)	Tm (°C)	Crystallinity (%)
PLGAe	59.5	90.6	147.9	2.45	55.1	-	-
PVAe	91.0	-	193.3	21.21	73.6	158.8	7.86
PLGA/PVA	43.2 52.8	90.1	147.1	-	52.5 63.6	147.7	-

Conclusions

This work successfully achieved the fabrication of PLGA/PVA core shell fibers, as confirmed by the SEM analysis and Fluorescenct microscope. From SEM images, the morphological structure of the obtained fibers could be evaluated, comparing the parameters used during the electrospinning process. FTIR analyses served as a complementary technique indicating the successful encapsulation of the core solution inside the fiber by the coaxial electrospinning technique. Core-shell fibers were characterized for their crystalline profiles using XRD and DSC, revealing changes in the crystalline profile due to the electrospinning process. TGA analyses allowed to conclude that there was no residue of solvents in the electrospun membranes, which is a positive fact as the presence of toxic solvents such as chloroform could hinder their application.

Acknowledgements

The authors would like to express their gratitude to the Coordenação de Aperfeiçoamento de Pessoal de Nível Superior (CAPES) and the Fundação de Amparo à Pesquisa do Estado do Rio de Janeiro (FAPERJ) for the financial support provided through the Nota 10 scholarships during the completion of this work. Their contribution was fundamental to the development of this research.

References

1. R. J. Wade; J. A. Burdick, Nano Today 2015, 9(6), 722-742. https://doi.org/10.1016/j.nantod.2014.10.002.
2. S. Khorshidi; A. Solouk; H. Mirzadeh; S. Mazinani; J. M. Lagaron; S. Sharifi; S. Ramakrishna, Journal of Tissue Engineering and Regenerative Medicine 2015, 10(9), 715-738. https://doi.org/10.1002/term.1978.
3. B. Pant; M. Park; S. J. Park, Pharmaceutics 2019, 11(7), 305. https://doi.org/10.3390/pharmaceutics11070305.
4. N. Bhardwaj; S. C. Kundu, Biotechnology Advances 2010, 28(3), 325-347. https://doi.org/10.1016/j.biotechadv.2010.01.004.
5. J. Vonch; A. Yarin; C. M. Megaridis, Journal of Undergraduate Research 2007, 1(1), 1-6. http://dx.doi.org/10.5210/jur.v1i1.7444.
6. D. I. Braghirolli; D. Steffens; P. Pranke, Drug Discovery Today 2014, 19(6), 743-753. https://doi.org/10.1016/j.drudis.2014.03.024.
7. T. Sui; S. Ying; K. Titov; I. P. Dolbnya; J. C. Tan; A. M. Korsunsky, Materials & Design 2016, 110(15), 933-934. https://doi.org/10.1016/j.matdes.2016.08.097.
8. R. P. Gonçalves, Ph.D. Thesis, Federal University of Rio de Janeiro, 2015.
9. A. Haider; S. Haider; I. K. Kang, Arabian Journal of Chemistry 2018, 11(8), 1165-1188. https://doi.org/10.1016/j.arabjc.2015.11.015.
10. R. P. Gonçalves; F. F. F. Silva; P. H. S. Picciani; M. L. Dias, Materials Sciences And Applications 2015, 6(2), 189-199. http://dx.doi.org/10.4236/msa.2015.62022.
11. A. L. M. M. Toledo, Ph.D. Thesis, Federal University of Rio de Janeiro, 2020.
12. Y. Z. Long; X. Yan; X. X. Wang; J. Z; M. Yu, Electrospinning: Nanofabrication and Applications 2019, 21-52. https://doi.org/10.1016/B978-0-323-51270-1.00002-9.
13. M. Koosha; H. Mirzadeh, Journal of Biomedical Materials Research Part A 2015, 103(9), 3081-3093. http://dx.doi.org/10.1002/jbm.a.35443.

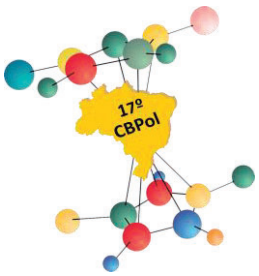

POLYETHERSULPHONE/ATTAPULGITE FLAT MEMBRANES AND THEIR PERMEATION PROPERTIES

Bruna A. Araujo[1], Rafael A. Dias[1], Renê A. da Paz [1], Vanessa N. Medeiros[1], Luiz A. Pessan[2] and Edcleide M. Araújo[1]

1 – Academic Unit of Materials Engineering (UAEMa), Federal University of Campina Grande (UFCG), Campina Grande, PB, Brazil
brunaaaraujo15@gmail.com
2 – Academic Unit of Materials Engineering (UFSCar), Federal University of São Carlos (UFSCar), São Paulo, SP, Brazil

Abstract

Flat membranes of Polyethersulfone (PES) and Attapulgite (ATP) were obtained by the solvent evaporation method to obtain dense membranes, aiming at their application in the gases separation. Through Fourier transform infrared spectroscopy analysis (FTIR), it is observed that the result of charged membranes is similar to that of pure PES; that is, they remain with the overlapping bands of PES and present similarities in the wavenumber ranges. The membranes microstructures morphology visualized by Scanning Electron Microscopy (SEM) presents a structure with a thin dense layer, spongy, and the pores presence. The membranes hydrophilicity was observed through the contact angle, and it was proven that the membranes containing PES as a matrix, when compared to the PES/ATP, present a higher contact angle due to the PES having low hydrophilicity. Atomic Force Microscopy (AFM) observed that they do not have a completely smooth surface, with some valley zones. Through water vapor permeation, it was observed that there is an increase in water vapor permeability for the membranes, which may be related to the increase in thickness and the presence of some voids. The Oxygen (O_2) permeability results showed a gradual increase in its permeability compared to that observed in the literature, as this reports that with the introduction of the load, it acts as a barrier, forming tortuous paths, resulting in a reduction in the permeability.

References

1. BAKER, R. W. Membrane technology and applications. 2004. **England: John Wiley and Sons**, 2007.
2.HABERT, A. C.; BORGES, C. P.; NOBREGA, R. **Processos de separação por membranas**. Editora e-papers, 2006. ISBN 857650085X.
3. Haider, B., Dilshad, M. R., ur Rehman, M. A., Akram, M. S., & Kaspereit, M. Haider, B., Dilshad, M. R., ur Rehman, M. A., Akram, M. S., & Kaspereit, M. (2020). *Journal of Natural Gas Science and Engineering*, *81*, 103406. https://doi.org/10.1016/j.jngse.2020.103406
4. Ismail, A. F., Norida, R., Rahman, W. A., Matsuura, T., & Hashemifard, S. A. *Desalination* (2011). *273*(1), 93-104. https://doi.org/10.1016/j.desal.2010.10.015

Fundings: The authors thank UFCG, CAPES, CNPq, and FAPESQ/PB for financial support.

Keywords: m*embrane, polyethersulfone, gas separation.*

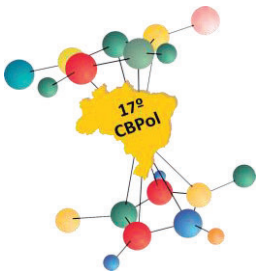

POLY(LATIC ACID) (PLA)/POE-G-GMA NANOCOMPOSITES REINFORCED WITH MWCNT FOR ANTISTATIC APPLICATION

Carlos B. B. Luna[1*], Eduardo S. B. Ferreira[1], Edson A. S. Filho[1], Renate M. R. Wellen[2] and Edcleide M. Araújo[1]

1 – Academic Unit of Materials Engineering, Federal University of Campina Grande (UFCG), Campina Grande, PB, Brazil, Av. Aprígio Veloso, 882 - Bodocongó, 58429-900
brunobarretodemaufcg@hotmail.com
2 – Department of Materials Engineering, Federal University of Paraíba, Cidade Universitária, 58051-900, João Pessoa, PB, Brazil.

Abstract

Polymeric products often accumulate surface static electrical charges, causing problems such as dust accumulation, electrical shock, electrostatic damage to computers and electronic components, electric spark, and film sticking [1]. Given this, to avoid these inconveniences, so-called antistatic materials have been designed, which alter the electrical properties of the product, reducing the electrical resistance to a value that allows the electrical charge dissipation [2]. Therefore, poly(lactic acid) (PLA) nanocomposites were prepared with carbon nanotubes (MWCNT), using poly(ethylene-octene) grafted with glycidyl methacrylate (POE-g-GMA) as an impact modifier. The effect of incorporating 1, 3, and 5 pcr (parts per hundred of resin) of MWCNT was investigated in PLA/POE-g-GMA systems. The nanocomposites were processed in a co-rotational twin-screw extruder and injection molded. Torque rheometry, impact strength, heat deflection temperature (HDT), electrical conductivity, and scanning electron microscopy (SEM) properties were evaluated. The torque of the PLA/POE-g-GMA nanocomposites increased with the addition of carbon nanotubes compared to pure PLA, suggesting an increase in viscosity. The impact strength of PLA was around 25.6 J/m, while the PLA/POE-g-GMA blend promoted a gain of 79.8%. Adding MWCNT in the PLA/POE-g-GMA system significantly increased impact strength with up to 1 pcr of MWCNT, with a value of 144.8 J/m. The impact strength decreased again above 1 pcr of MWCNT; however, the impact strength values were still higher than the PLA/POE-g-GMA system. This behavior was due to the more refined morphology of the nanocomposites, with the presence of carbon nanotubes, as verified in the SEM. Concerning HDT, the PLA/POE-g-GMA/MWCNT nanocomposites tended to suffer discrete increases, with the rise of the MWCNT content, compared with PLA and PLA/POE-g-GMA. Typical behavior of insulating material was found for PLA and the PLA/POE-g-GMA system, while the nanocomposites showed adequate electrical conductivity for antistatic packaging. The development of PLA/POE-g-GMA/MWCNT nanocomposites has technological potential, given their good mechanical and electrical properties, as well as the maintenance of the HDT of PLA, reinforcing the ability to apply electrostatic dissipation. In addition, PLA/POE-g-GMA/MWCNT nanocomposites can contribute to advancing green materials for advanced applications.

Keywords: PLA, impact modifier, nanocomposites, carbon nanotubes, antistatic application.

References

1. L. Vieira; E. Anjos; G. Verginio; I. Oyama; N. Braga; T. Silva; L. Montagna; M. Rezende; F. Passado. *Journal of Materials Science: Materials in Electronics* 2021, 32, 3929–3947. https://doi.org/10.1007/s10854-020-05178-6
2. M. Oviedo; O. Araújo; R. Faez; M. Rezende; M. Paoli. *Synthetic Metals* 2006, 156, 1249-1255. https://doi.org/10.1016/j.synthmet.2006.09.003

PREPARATION AND CHARACTERIZATION OF NANOSTRUCTURED HYDROGELS BASED ON KAPPA-CARRAGENAN AND CLOISITE-Na$^+$

Thamyres Graco Soares[1] (IC), Márcia Parente Melo da Costa[1], Ivana Lourenço de Mello Ferreira[1]*

1 – Instituto de Química, Universidade do Estado do Rio de Janeiro (UERJ), Rio de Janeiro, RJ, Brazil
ivanalmellof@gmail.com ; ivanamello@uerj.br

Abstract - In this work, hydrogels were prepared from a mixture of the polysaccharide *k*-carrageenan and Cloisite clay. Biohydrogels were prepared at room temperature. The concentration of *k*-carrageenan was 3% and the commercial montmorillonite (MMT) clay Cloisite Na$^+$ at 2% and 0.5%. The crosslinking time was kept constant at 24 h. The samples were characterized according to the swelling degree (SD) and by scanning electron microscopy (SEM). The main objective of this work was to study the morphology of the material and the swelling degree, which was greater than 100%, a result that classifies the materials as absorbent, with application as soil conditioners.

Keywords: *kappa-carrageenan, clay, morphology, swelling degree*

Introduction

Natural polymers from renewable sources are attracting increasing attention in a variety of fields as a way to achieve sustainable development [1]. Hydrogels are made up of one or more three-dimensional polymeric networks composed of interconnected macromolecular chains [2, 3]. Water-retentive polymers consisting of three-dimensional crosslinked and insoluble networks are able to retain and absorb large amounts of water [4]. This characteristic makes hydrogels applicable in many different areas [5]. The objective of this work was the characterization of nanostructured biohydrogels based on k-carrageenan and Cloisite Na+ and to analyze the hydrophilic and morphological properties.

The polysaccharide used for this study was k-carrageenan (Fig. 1), a sulfated polysaccharide, one of the main components of cell walls, extracted from red algae (Rhodophyta). It has gelling, stabilizing and thickening properties, in addition to being biodegradable with high water retention capacity and mechanical resistance in gels.

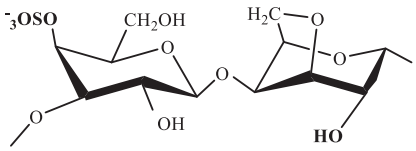

***k* - carragena**

Figure 1. Molecular structure of k-carrageenan.

Experimental

Preparation of the polysaccharide solution

An aqueous solution of k-carrageenan (Agargel) at a concentration of 3% (w/v) was prepared under magnetic stirring for 24 hours at room temperature. To prepare the clay-polysaccharide gels, the k-carrageenan solution was divided into two parts, each of which received 0.5% or 2.0% Cloisite Na^+. The samples remained under agitation for 24 hours. Then, a Cole-Parmer Masterflex 7554-90 peristaltic pump was used to drip the mixture (polysaccharide + clay) into a 0.3mol/L $CaCl_2$ solution to form microspheres. The microspheres were left in this solution for 24 hours at room temperature (25 °C). Then, the microspheres were separated and washed in deionized water and frozen and lyophilized for 48 hours.

Scanning electron microscopy (SEM)

To obtain the micrographs, the hydrogels were frozen, lyophilized and cut with a blade to obtain the smallest possible thickness, and were observed with a JOEL scanning electron microscope with the use of a tungsten filament.

Swelling degree

To determine the swelling degree, the dry hydrogels were weighed on an analytical balance. Then, a volume of deionized water sufficient to cover the entire sample was added. At each immersion time (1, 3, 6 or 24 hours) samples were removed and weighed on an analytical balance. The swelling degree (SD) was calculated according to Eq. 1.

$$SD = \frac{M_t - M_o}{M_o} \times 100\% \quad (1)$$

Where M_t is the mass of the swollen sample at time t and M_o is the initial mass of the sample before swelling.

Results and Discussion

Fig. 2 presents the swelling profile of the samples produced with the two clay concentrations.

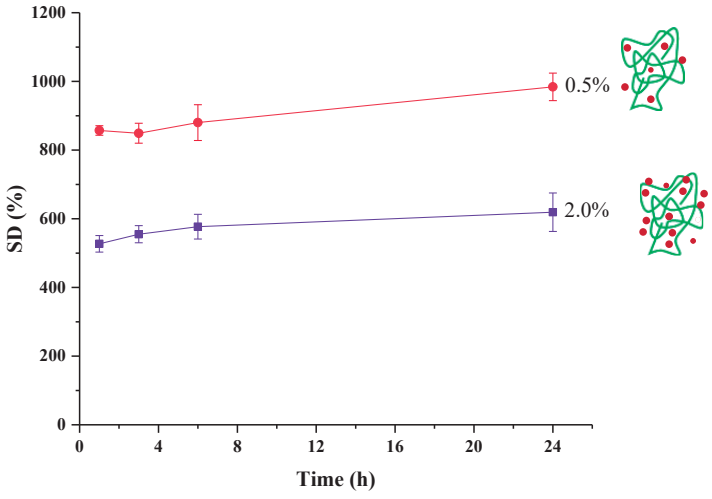

Figure 2. Swelling degree of the samples.

It can be noted that the biohydrogels had swelling degree greater than 100%, a result that classifies them as absorbent materials. In general, the increase in clay content tended to cause a decrease in the SD, probably because the higher concentration of clay in the biohydrogel prevented the entry of water, consequently decreasing the SD. Fig. 3 presents the micrographs of the biohydrogel mixtures of k-carrageenan and Cloisite Na^+ clay.

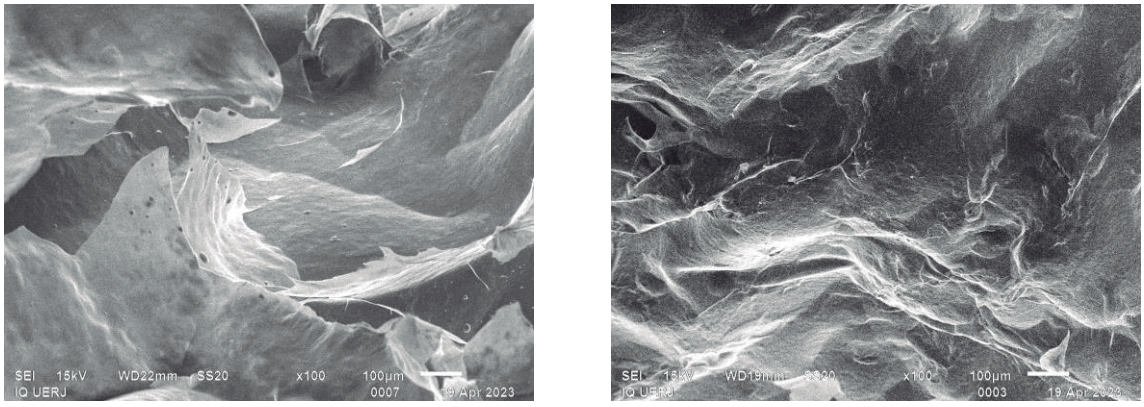

(a) **(b)**

Figure 3. SEM micrographs of samples: (a) 3% k-carrageenan + 0.5% clay and (b) 3% k-carrageenan + 2% clay.

Both compositions had morphology with certain rigidity and density. Fig. 3 (a) shows a more laminated surface, probably due to the 0.5% clay content, which promoted greater swelling. Fig. 3 (b) shows a surface with a more rigid and compact appearance. The apparent absence of pores corroborates the smaller SD.

Conclusions

The experimental results demonstrated that hydrogels based on k-carrageenan and Cloisite Na+ clay (0.5 or 2.0%) are absorbent materials with SD greater than 100%. The incorporation of clay produced morphology that varied from leafy in the samples with 0.5% clay to dense and compact morphology in the samples with 2.0% clay. The experiments presented in this work serve as preliminary studies for the development of composite biohydrogels prepared from polysaccharide and clay, for more environmentally sustainable materials applicable for soil conditioning.

Acknowledgment

We are grateful to Fundação Carlos Chagas Filho de Amparo à Pesquisa do Estado do Rio de Janeiro (FAPERJ) and Conselho Nacional de Desenvolvimento Científico e Tecnológico (CNPq) for financial support. This study was also partly financed by Coordenação de Aperfeiçoamento de Pessoal de Nível Superior (CAPES), Finance Code 001.

References

1. C. Alvarez-Lorenzo; B. Blanco-Fernandez; A.M. Puga; A. Advanced Drug Delivery Reviews, 2013, 65 (9), 1148-1171. https://doi.org/10.1016/j.addr.2013.04.016.

2. K. Baysal; A. Z. Aroguz; Z. Adiguzel; B. M. International Journal of Biological Macromolecules, 2013, 59, 342– 348. https//doi.org/ 10.1016/j.ijbiomac.2013.04.073.

3. F. A Aouada; M. R. Moura; E. A. Menezes; A. R. A. Nogueira; L. H. C. Mattoso Revista Brasileira de Ciência do Solo, 2008, 1643-1649. https://doi.org/10.1590/S0100-06832008000400029.

4. T. Savi; M. Marin; D, Boldrin; G. Incerti; S. Andri; A. Nardini Science of The Total Environment, 2014, 490, 467-476. https://doi.org/10.1016/j.scitotenv.2014.05.020.

5. T. R. Hoare; D.S. Kohane Hydrogels in drug delivery: Progress and challenges. Polymer, 2008, 49(8), 1993-2007. https://doi.org/10.1016/j.polymer.2008.01.027.

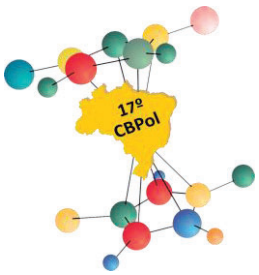

RHEOLOGICAL BEHAVIOR OF MELALEUCA OIL PICKERING EMULSIONS WITH CELLULOSE NANOFIBRILS

Greiciele da S. Ferreira[1], Daniel J. da Silva1 [2], Derval S. Rosa1*

1- Federal University of ABC (UFABC), Santo André, SP, Brazil.
dervalrosa@ufabc.edu.br.

2 Center for Engineering, Modeling, and Applied Social Sciences (CECS), Federal University of ABC (UFABC), Av. dos Estados, 5001, CEP 09210-210, Santo André, SP, Brazil

Abstract

Melaleuca alternifolia essential oil (MaEO) has many biological properties applicable in various technological sectors. A limitation of the direct use of melaleuca essential oil is oxidation, light and high temperature. This work used cellulose nanofibres (CNF) to stabilize Pickering emulsions of MAEO (tea tree essential oil) to preserve the active properties. The emulsions are prepared and kept at room temperature. This contribution evaluated the stability using the rheological behavior of the Pickering emulsions of MaEO. Small amplitude oscillatory shear analyses revealed the relationship between the strength of the internal microstructure and the relaxation processes, retardation processes and viscous flow behavior of the emulsions. The results show that the emulsions have good stability, and the droplet sizes and distributions were evaluated and contributed to a steady-state viscosity suitable for high stability, indicating longer shelf life.

Keywords: Oil essential, Melaleuca Alternifolia, Nanocellulose, Pickering emulsion rheology.

Introduction

Essential oils comprise a complex mixture (terpenes, terpenoids, aromatic and aliphatic constituents) obtained from raw vegetable materials. They are compounds with numerous properties such as therapeutic, antioxidant and biological applicable in various segments, pharmaceuticals, cosmetics, and food. The essential oil of Melaleuca (MaOE) has in its composition active ingredients such as terpinenol-4-ol, γ-terpinene, α-terpinene, cymene, and α-terpineol with favorable characteristics for biological application. A limitation of the direct use of this oil is that they are volatile substances and degradable with high sensitivity to light. Because of this, it is possible to use a mechanism to prevent the loss of these assets. In this sense, the Pickering emulsions preserve these volatile constituents with low molecular weight [1]

Emulsions are immiscible heterogeneous systems with one continuous phase and another dispersed phase, where these phases remain inside each other with the help of a surfactant, which decreases the interfacial energies, generating a system without instability phenomena. These stabilizing agents are essential in reducing the interfacial tension, favoring emulsion formation [2]. Conventional emulsions are made of synthetic substances with low biodegradability causing environmental impacts.

Cellulose nanofibrils (CNF) are natural polymers with a high potential to replace synthetic stabilizers. CNFs are cellulose nanostructures that are biodegradable, sustainable, renewable, and non-toxic [3, and present advantages for being obtained through low process steps with the use of reagents with less potential to cause environmental damage. In Pickering emulsions, stability occurs through solid cellulose particles leading to intermolecular interactions [4]

Pickering emulsions are mostly composed of oil and water and a stabilizing agent with natural characteristics because, in recent years, surfactants have raised serious environmental problems such as enzyme inhibition, water pollution, and difficulty in degradation, among others[5][6]. O nanocellulose de Fibras (CNF) Fibre nanocellulose (CNF) is a biopolymer with reactive hydroxyl groups in its structures and with characteristics of flexibility due to its aspect ratio length and width (L/D). CNF, when placed in an emulsion system, acts as an emulsifier, giving stability to the system by steric hindrance, making it difficult for droplets to coalesce, reference CNF)[[7].[8]

Cellulose nanofibrils (CNF) are natural polymers with a high potential to replace synthetic stabilizers. The CNFs are cellulose nanostructures that are biodegradable, sustainable, renewable, and non-toxic and can be obtained through low-process steps using reagents with less potential for environmental harm. Stability occurs through solid cellulose particles in Pickering emulsions, leading to intermolecular interactions. [5][7][9]

Pickering emulsions mostly consist of oil and water and a stabilizer with natural characteristics. In recent years, surfactants have raised serious environmental problems, such as enzyme inhibition, water pollution, and difficulty of degradation, among others. [8,9]. Nanocellulose Fibers (CNF) is a biopolymers with reactive Hydroxyl groups in their structures and with flexural characteristics due to its length to width (L/D) aspect ratio. CNF, when placed in an emulsion system, acts as an emulsifier, giving stability to the system by steric hindrance, making it difficult for droplets to coalesce (CNF reference)[7].

The rheological evaluations of Pickering's emulsions are useful to evaluate the final characteristics of the products because most of the procedures in the production of cosmetics depend on the flow of this material to define formulations, material packaging, storage, process parameters (pumping, mixing time, rotation). In this sense, the acceptance of cosmetics depends on rheology because it helps texture, skin feel, consistency, oiliness, and absorption. These factors interfere with the acceptability of the product in the market.

The work investigates the rheological behavior of Pickering emulsions of melaleuca oil that CNF stabilized. They were analyzed through oscillatory shear of small amplitude, the internal structure and the variations and distributions of the diameter in 30 days under static conditions.

Experimental

A CNF dispersion was prepared using high-intensity ultrasound (Sonics Vibra Cell, 400W power, 24 KHz) for 2 minutes. Then the MaEO oil was added to the CNF solution and homogenized with an Ultra-Turrax, model IKA T25 (IKA Werke, Staufen, Germany). The Pickering emulsion was made with the following parameters: CNF content (1% w/v) or (0.5% w/v), O/W ratio (30%v/v) and (20% v/v), homogenization speed (15,000 rpm and 12,000 rpm) and mixing time (5 or 7 min). The emulsion was designated XEO/YT/ZCNF/WRPM, where X corresponds to the MaEO content (% v/v), Y is the mixing time (min), Z is the CNF concentration (% wt/v), and W is the mixing speed (rpm).

The O/W emulsions were submitted to rheological measurements using a rheometer MCR-501 (Anton Paar, Austria), using a concentric cylinder geometry (specifications: body diameter=24.001 mm; body length=25.005 mm; inner cup diameter=40mm; active length=103.5 mm; positioning length=72.5 mm).

Results and Discussion

Emulsion systems are complex because they depend on numerous process variables. Two emulsions with process parameters with small differences between them have been analyzed emulsions (1) 30OE/5T/0.5CNF/15RPM and (2) 20EO / 5T / 0.5CNF / 12RPM. The steady-state shear viscosity (η) showed a shear-thinning fluid behavior. In this sense, the (η) decreases as the shear rate ($\dot{\gamma}$) increases because of the internal structure-breaking processes of the Pickering emulsion of MaEO/CNF. This behavior is based on the literature due to intermolecular interactions with low levels of energetic resistance [6].

The fragmentation of the internal structure of the emulsion includes the collapse of oil droplets, desorption of CNF, and phase aggregation accompanied by the orientation movement of oil droplets and CNF in the direction of the flow line (Fig. 1). The steady-state shear viscosity with a shear thinning behavior has a positive point on the cosmetic base in the sense of functional performance such as creams, gel, lotions, and foams, among others[10].

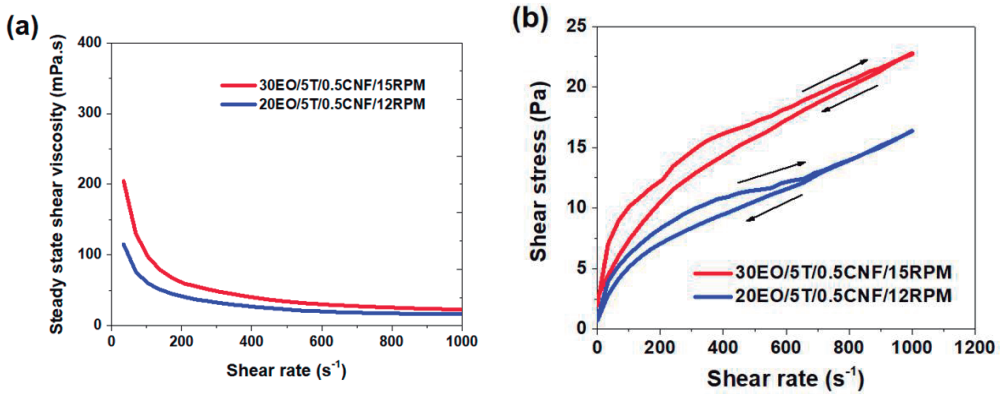

Figure 1: steady-state rheological curves of Pickering emulsions (30EO/5T/0.5CNF/15RPM and 20EO/5T/0.5CNF/12RPM): (a) steady-state viscosity (η) and (b) shear stress (σ) as a function of shear rate ($\dot{\gamma}$).

The linear viscoelastic domain of the oscillatory strain scanning tests exhibits the cohesive force of an internal multiphase structure. Multiphase systems exhibit a nonlinear viscoelastic response when their three-dimensional structure (network entanglement formed by the CNF) breaks down. (Fig 2). The cohesive energy density (E_c) was determined to investigate the energy resistance of the emulsions to rupture against mechanical shear stress. The critical storage modulus (G_c^') and the critical oscillation strain (γ_c) were extracted from the storage modulus versus strain curves as indicated in the inset of Fig. 2. It is possible to observe a difference in the internal structure according to the CNF content, in this sense, the network entanglements are undone leading to desorption of CNF at the droplet interface. However, a difference in the behavior of the two emulsions is noted when comparing the amount of CNF present in the systems [11].

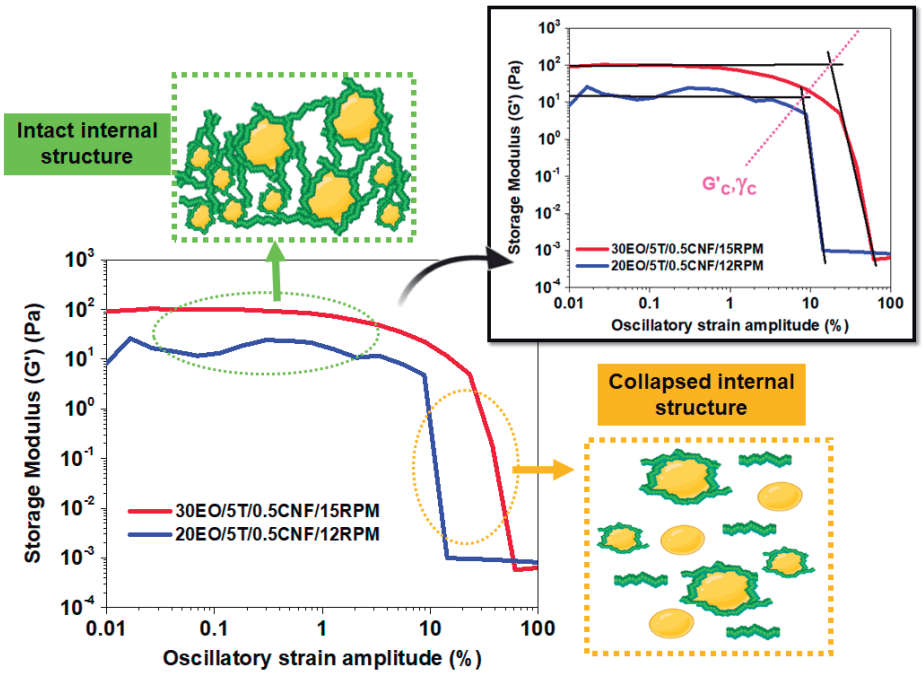

Figure. 2. rheological tests of Pickering emulsion tests (30EO/5T/0.5CNF/15RPM and 20EO/5T/0.5CNF/12RPM): strain sweep log-log curve

Conclusions

CNF was used to stabilize the Pickering emulsions with MaEO. It was observed that the amount of CNF used in the production of Pickering affects the internal structure of the emulsions. In this system, the smaller the amount of CNF used, the better it is for the system's stability. The rheologic tests indicate that the emulsions show a shear thickening behavior under oscillatory shear stress. However, the flow profiles of the emulsions do not obey the Cox-Merz rule since the emulsion shows a different flow behavior under steady state shear. Under mechanical shear stress, the relaxation processes are faster, and the elastic responses are slower in the emulsion due to the network entanglement.

Acknowledgment

The authors thank the CAPES (Code 001), CAPES-Pandemias (8881.504639/2020-01), MULTIUSER CENTRAL FACILITIES (UFABC), UFABC, and REVALORES Strategic Unit.

References

1. A. Masyita *et al*; Food Chem. X, vol. 13, no. January, p. 100217, 2022, https://doi: 10.1016/j.fochx.2022.100217.
2. Y. Cahyana, Y. S. E. Putri, D. S. Solihah, F. S. Lutfi, R. M. Alqurashi, and H. Marta, Molecules, vol. 27, no. 22, pp. 1–19, 2022, https://doi: 10.3390/molecules27227872.
3. A.G.Souza, R.R.Ferreira, E.R. Oliveira, M.M Kato, S. K. Mitra and D.S.Rosa Polysaccharides 2022,3(1),200-216 . https://doi.org/10.3390/polysaccharides3010010
4. G. da S. Ferreira, D. J. da Silva, L. Zanata, A. G. Souza, R. R. Ferreira, and D. S. Rosa, Carbohydr. Polym. Technol. Appl., vol. 3, p. 100208, 2022, https://doi: 10.1016/j.carpta.2022.100208.
5. L. Bai, S. Huan, W. Xiang, and O. J. Rojas, Green Chem., vol. 20, no. 7, pp. 1571–1582,2018, https:// doi 10.1039/c8gc00134k.
6. A. G. Souza, R. R. Ferreira, L. C. Paula, L. F. G. Setz, and D. S. Rosa, J. Mol. Liq., vol. 320,

p. 114458, 2020,https:// doi: 10.1016/j.molliq.2020.114458.
7. Y. Lu, J. Li, L. Ge, W. Xie, and D. Wu, Carbohydr. Polym., vol. 255, no. December 2020, p. 117483, Mar. 2021,https:// doi: 10.1016/j.carbpol.2020.117483.
8. G. da S. Ferreira, D. J. da Silva, L. Zanata, A. G. Souza, R. R. Ferreira, and D. S. Rosa, Carbohydr. Polym. Technol. Appl., vol. 3, no. April, p. 100208, 2022, https:// doi: 10.1016/j.carpta.2022.100208.
9. Y. Zhang *et al.*, Carbohydr. Polym., vol. 179, no. July 2017, pp. 86–92, Jan. 2018, https://doi: 10.1016/j.carbpol.2017.09.065.
10. T. Yi *et al.*, Materials (Basel)., vol. 13, no. 22, p. 5062, Nov. 2020, https://doi: 10.3390/ma13225062.
11. A. G. Souza, R. R. Ferreira, L. C. Paula, L. F. G. Setz, and D. S. Rosa, J. Mol. Liq., vol. 320, p. 114458, 2020, https://doi: 10.1016/j.molliq.2020.114458.

STUDY OF A SIPN APPLICABILITY AS A SOLID ELECTROLYTE FOR FUEL CELLS

Julia da Silva Menezes[1,2], Verônica Maria de A. Calado[1] and Ana Maria Rocco[2*]

1 – Laboratório de Termoanálises e de Reologia, Universidade Federal do Rio de Janeiro (UFRJ), EQ, RJ, Brazil

2 – Grupo de Materiais Condutores e Energia, Universidade Federal do Rio de Janeiro (UFRJ), EQ, RJ, Brazil

[*]amrocco@eq.ufrj.br

Abstract – In this work, membranes were synthesized for fuel cells based on a semi-interpenetrating polymeric network (SIPN) from the reaction of Diglycidyl ether of bisphenol A (DGEBA) and curing agent Triethylenetetramine (TETA) with Polyethyleneimine (PEI). The SIPNs comprised a constant mass ratio of 13% (m/m) TETA concerning DGEBA, with PEI concentrations of 41, 47, and 50% (m/m). Membranes obtained by casting were sulfonated ($SIPN_{TX}.SO_3H$) in two different molar ratios sulfonating agent:number of aromatic groups in the system (1:4 and 2:1). Fourier-transform infrared spectroscopy and 13CRMN proved the polymer sulfonation and atomic force microscopy (AFM) revealed a nanostructure based on the array of the hydrophilic-hydrophobic phases homogeneously distribute. Impedance electrochemical spectroscopy monitored the samples' conductivity and $SIPN_{T50}.SO_3H$ reached the higher conductivity of the samples series, 3.08×10^{-3} $\Omega^{-1}.cm^{-1}$, for a 2:1 degree of sulfonation. All membranes showed thermoactivated conductivity behavior. The study of conductivity data by Arrhenius indicated activation energies for proton conduction processes compatible with the Grotthuss mechanism, which is favored by higher temperatures and anhydrous conditions, indicating the excellent potential for use in PEMFC.

Keywords: SIPN, PEMFC, hydrophilic nanodomains, and conductivity

Introduction

The application of fuel cells based on proton conductive polymeric membranes (PEMFC) is a promising energy conversion alternative because of its low environmental impact. PEMFC is an electrochemical device that directly converts chemical energy into electrical energy [1]. In recent decades, there has been a growing need to develop and study new clean energy storage technologies, as public policies have increased the control of carbon emissions from burning fossil fuels. PEMFC is of interest because of its advantages of being efficient, easy to operate, low noise, safe, and low environmental impact. The polymeric solid electrolyte, polymeric membrane, from PEMFC is an essential component for the proper functioning of the cell, and the most used commercial membrane is still DuPont's Nafion®. Even so, the global community working on the theme considers it essential to replace it with membranes of lower cost and higher electrochemical stability at temperatures above 100 °C.

One of the least explored polymeric systems in these applications is the semi-interpenetrating polymeric network, SIPN. According to IUPAC, a SIPN is "*A polymer comprising one or more networks and one or more linear polymer(s) characterized by penetration, on a molecular scale, of at least one of the networks by at least some of the linear macromolecules*". A suitable solvent can usually extract the linear polymer [2].

The proton conduction membranes obtained must achieve desired properties, among which high ionic conductivity (~0.1 $S.cm^{-1}$ at 120°C), chemical and mechanical stability at elevated temperatures, in oxidizing and reducing environments, and low cost [3]

This work aimed at characterizing morphologically, spectroscopically, and electrochemically sulfonated SIPN polymeric membranes previously studied without chemical modification. The objective is to obtain improved membranes that can be operated under anhydrous conditions or in the presence of little water and minimize possible membrane damage during cell operation.

Experimental

Synthesis and Membrane Manufacturing

The synthesis of the SIPN used in the membrane started with diglycidyl ether of bisphenol A (DGEBA) and the curing agent triethylenetetramine (TETA) with Polyethyleneimine (PEI). SIPN was obtained by varying the PEI concentration at 47 and 50 % w/w concerning the total mass and for a constant mass ratio of 13%w/w TETA to DGEBA. The membranes were obtained by casting and after sulfonated. The procedure adopted for sulfonation is an adaptation from Elabd and Napadensky [4]. The reaction introduces a sulfonic group (SO_3H) into the aromatic ring of DGEBA.

Spectroscopy Studies

The infrared vibrational spectroscopic characterization, FTIR, of thin films was made in the region between 4000 and 400 cm^{-1}, using 4 cm^{-1} resolution and 32 scanning per spectrum. The analysis was performed in the horizontal attenuated reflectance mode, employing a zinc selection crystal (ZnSe).

A Solid State Nuclear Magnetic Resonance (13CRMN) AVANCE III (Brucker) spectrometer operating at 400 MHz at room temperature recorded the 13C NMR spectra of $SIPN_{TX}SO_3H$ (where X is the amount of PEI in the sample) membranes with 14 kHz frequency and acquisition time of 0.7 ms/d13s.

Morphological Studies, AFM

Atomic force microscopy (Digital Instruments, Dimension 3000) investigated the surface morphology of the prepared membranes by topographical and phase contrast methods with 1 cm^2 of the scanning size of the samples. A desiccator maintained the membranes before the measurements.

Electrochemical Impedance Spectroscopy, EIS

An AutoLab PGSTAT30/FRA device measured the electrochemical impedance spectra measurements in the frequency region between 10 mHz and 1 MHz. The membranes, previously hydrated for 24 h, were sandwiched between stainless steel blocking electrodes of 0.785 cm^2 in Teflon cells and studied between 20 and 80 ^oC, with temperature control, under 60 % relative humidity.

EIS was studied using the Nyquist diagram to determine the proton conductivity (σ), according to Eq. 1.

$$\sigma = L/(A.R_b) \quad (1)$$

where L and A are the thickness and area of the electrolyte membrane, respectively; R_b is the resistance. Arrhenius equation, Eq. (2) calculates the conductivity behavior with temperature.

$$\log(\sigma) = \log(A_0) - Ea/RT \quad (2)$$

where A_0, T, R, and E_a are the pre-exponential factor, the absolute temperature, the ideal gas constant, and the activation energy, respectively,

Results and Discussion

All SIPN samples originate membranes of good mechanical malleability and translucid after being immersed in water.

Spectroscopic Studies

Fig. 1 shows, illustratively, the FTIR spectra between 4000 and 900 cm^{-1} for the sulfonated sample $SIPN_{T41}SO_3H$ (2:1) and $SIPN_{T41}$. The band's appearance at 1057 cm^{-1} is due to $\nu_s(SO_3)$ of sulfonic acid linked to the membrane pending side chain. The FTIR spectrum shows a band attributed to $\nu_s(SO)$ at 1050 cm^{-1} [5]. The bands in the spectral regions between 1060 and 1100 cm^{-1} were due to vibrational modes of protonated sulfonic groups ($–SO_3H$) and ionized ($–SO_3–$), respectively. At 1400 cm^{-1}, the spectrum shows a band from the same group's methylene vibrations, rotation, flexion, shortening, and stretching [6].

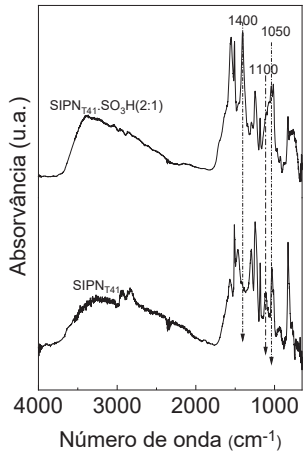

Figure 1: $SIPN_{T41}$ and $SIPN_{T41}.SO_3H$ (2:1) FTIR spectra between 4000 and 900 cm^{-1}.

RMN studies showed peaks below 50 ppm, related to sulfonic groups, between 40–80 ppm, relative to C-N (aliphatic carbon), and due to aliphatic carbon of alkyl chain (0 and 40 ppm). At 143 and 127 ppm a peak is attributed to aromatic carbon associated with sulfonic groups [7]. SIPN without sulfonation spectrum shows 114 and 156 ppm peaks related to aromatic carbon. The 13C NMR study corroborates the preliminary FTIR analysis.

Morphological Studies

Fig. 2 shows AFM images of $SIPN_{T47}$ (upper line) and $SIPN_{T47}.SO_3H$ samples (1:4) (lower line). To the left are topographic photos, and to the right, the phase contrast one. These images show the existence and the size of hydrophobic-hydrophilic domains, as well as changes in the phases that constitute the nanostructure of the membrane. Hiesgen *et al.* evaluated the correlation of hydrophilic nano dominium with waterproofing capacity [8]. In the figure, hydrophilic domains correspond to dark colors and hydrophobic ones to the lights. The images show, regardless of mode, greater homogeneity for $SIPN_{T47}.SO_3H$. Small hydrophilic phase clusters (PEI) are expected in the hydrophobic phase in $SIPN_{47}$. As the sulfonation of DGEBA occurs, hydrophilic sites are created in the DGEBA rings, which favors channel formation and gives more homogeneity to $SIPNx.SO_3H$ phase contrast images (x= % PEI on the membranes). The future study by MET of sulfonated membranes may better observe this behavior.

Electrochemical Impedance Spectroscopy Studies

Fig. 3(a) shows, illustratively, the Nyquist diagram for $SIPN_{T47}.SO_3H$ (1:4) at different temperatures, and 3(b) the conductivity behavior with the temperature for $SIPN_{T47}.SO_3H$ (1:4) and $SIPN_{T50}.SO_3H$ (1:4) sulfonated membranes. The spectra have the expected behavior for protonic driving polymeric electrolytes, where an almost semicircle-high frequency is associated with the

resistive behavior of charge transport through the membrane. Table 1 shows the average conductivity values (σ), calculated from spectra triplicates, and their deviation.

For $SIPN_{TX}.SO_3H$ (1:4), the conductivity observed was about 10^{-4} $\Omega^{-1}.cm^{-1}$, although the samples $SIPN_{T50}.SO_3H$ presented σ of 10^{-3} $\Omega^{-1}.cm^{-1}$. For the sulfonation degree 2:1, all compositions presented σ of 10^{-3} Ω^{-1} cm^{-1} with a maximum of $3{,}08x10^{-3}$ Ω^{-1} cm^{-1}, $SIPN_{T50}.SO_3H$ (2:1) at 80°C (Table 1). Samples $SIPN_{TX}.SO_3H$ (2:1) showed σ values in the order of 10^{-3} $\Omega^{-1}.cm^{-1}$, more significant than that got to the other sulfonations ratios.

Arrhenius's studies showed a thermo-activated behavior (Figure 3(b)) for the samples as more significant mobility of charge carriers with temperature is standard for similar systems. As the Ea presented values lower than 10 $kJ.mol^{-1}$, the charge transport mechanism in the system is of the Grottuss. This less water-dependent mechanism can maintain cell activity during humidification system failure.

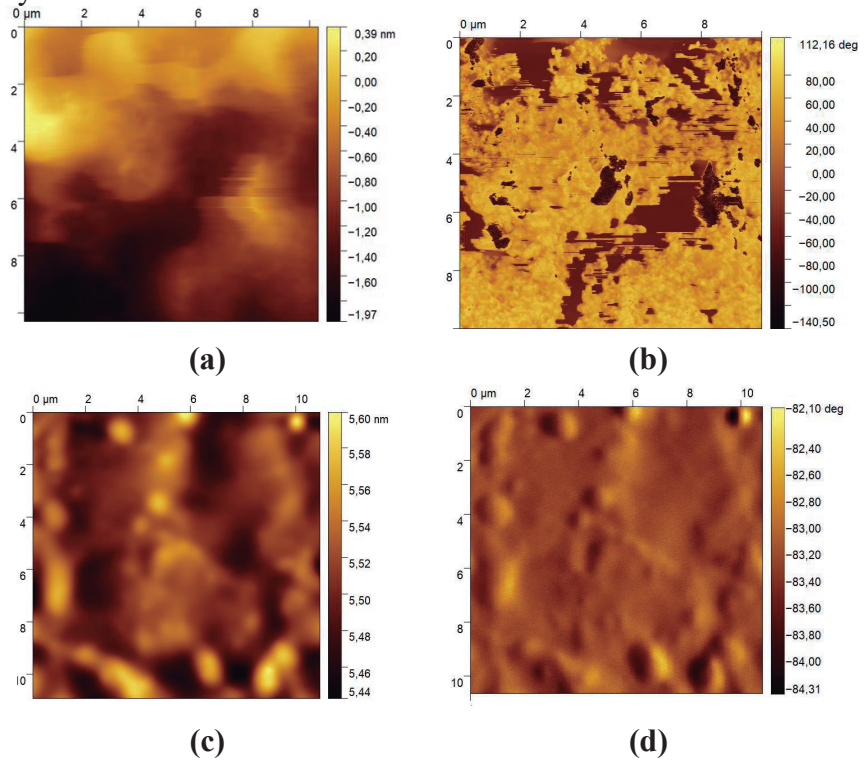

Figure 2. AFM images of $SIPN_{T47}$ (upper line) and $SIPN_{T47}.SO_3H$ (1:4) sample (lower line). To the left are topographic photos, and to the right, the phase contrast one .

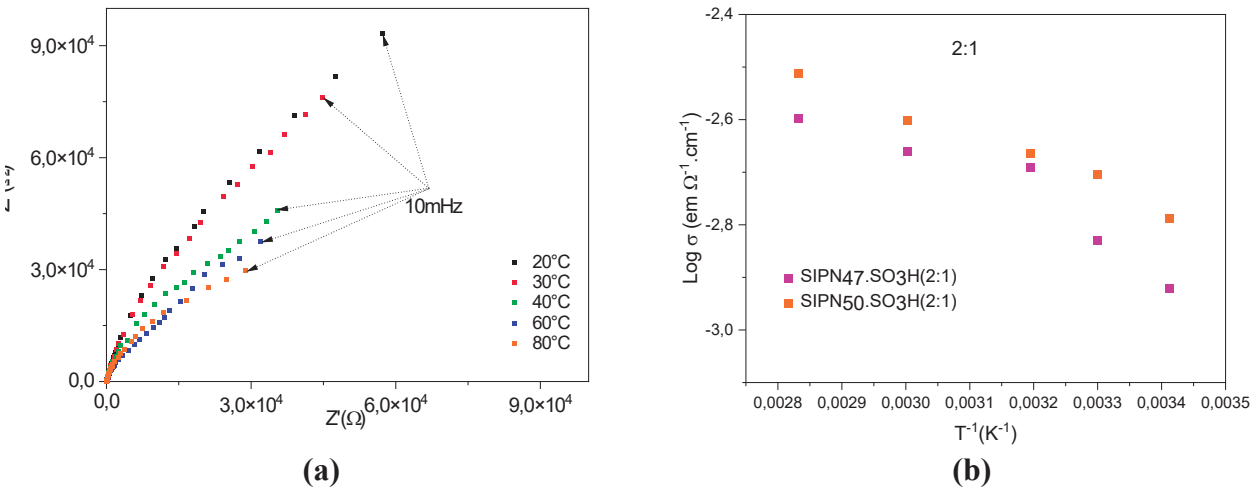

Figure 3. (a) EIS for $SIPN_{T47}.SO_3H$ (1:4) from 20 to 80 °C, and (b) log (σ) *vs* 1/T for de $SIPN_{TX}.SO_3H$ (2:1).

Table 1. Log(A_0), Ea, and σ, at 20º C and 80º C, for $SIPN_{T47}.SO_3H$ and $SIPN_{T50}.SO_3H$ at sulfonation ratios (1:4) and (2:1).

Amostra	Log (A_0)	Ea (kJ.mol^{-1})	σ (20 °C) (Ω^{-1}.cm^{-1})	σ (80 °C) (Ω^{-1}.cm^{-1})
$SIPN_{T47}.SO_3H$ (1:4)	1,96	2,349	(1,19±0,01)E^{-3}	(1,75±0,07)E^{-3}
$SIPN_{T50}.SO_3H$ (1:4)	1,21	4,118	(1,25±0,03)E^{-3}	(2,40±0,10)E^{-3}
$SIPN_{T47}.SO_3H$ (2:1)	1,06	4,430	(1,20±0,03)E^{-3}	(2,52±0,04)E^{-3}
$SIPN_{T50}.SO_3H$ (2:1)	1,25	3,698	(1,63±0,14)E^{-3}	(3,08±0,10)E^{-3}

Conclusions

FTIR and 13C NMR studies proved the chemical modification introducing the sulfonic group into the DGEBA ring. AFM analyses confirmed the nanostructure showing hydrophilic nanometric domains dispersed by the hydrophobic epoxy matrix already observed in the non-sulfonated sample. The lower degree of sulfonation analyzed (1: 4) displayed a homogeneous dispersion of these nano dominions. This membrane is promising for structure and conductivity correlations in future studies, as it had a conductivity (10^{-3} Ω^{-1}. cm^{-1}) of the same quantity order of higher sulfonation rations membranes. All samples presented a thermally activated σ behavior and a Grotthuss mechanism of protonic conduction (Ea < 10 KJ.mol^{-1}) favored under lower humidification conditions observed at high temperatures.

Acknowledgements

The authors thank FAPERJ for financial support (Grant No. E-26/010.000.982/2019).

References

1. R.G. Bodkhe; Shrivastava, Soni R.L.; R.B. Chadge International Journal of Electrochemical Science 2023, 100, 108. https://doi.org/10.1016/j.ijoes.2023.100108.
2. L. Chikh; V. Delhorbe; O. Fichet Journal of Membrane Science 2011, 368, 1. https://doi.org/10.1016/j.memsci.2010.11.020.
3. F.C. L.; M.S. Ismail; D.B. Ingham; K.J. Hughes; L. Ma; S.M. Lyth; M. Pourkashanian Renewable and Sustainable Energy Reviews 2022, 166, 112640. https://doi.org/10.1016/j.rser.2022112640.
4. Y.A. Elabd; E. Napadensky Polymer 2004, 45, 3037. https://doi.org/10.1016/j.polymer.2004.02.061.
5. R.K.Singh; K. Kunimatsu; K. Miyatake; T. Tsuneda Macromolecules 2016, 49, 6621. https://doi.org/10.1021/acs.macromol.6b00999.
6. R.M. Silverstein; G.C. Bassler Spectrometric Identification of Organic Compunds 7th ed, John Wiley & Sons, 2005.
7. Clark, 2022. Interpreting C-13 NMR Spectra. Acess in: 6 may 2023. https://chem.libretexts.org/Bookshelves/Physical_and_Theoretical_Chemistry_Textbook_Maps/Supplemental_Modules_(Physical_and_Theoretical_Chemistry)/Spectroscopy/Magnetic_Resonance_Spectroscopies/Nuclear_Magnetic_Resonance/NMR%3A_Experimental/Carbon-13_NMR/Interpreting_C-13_NMR_Spectra.
8. R. Hiesgen; E. Aleksandrova; G. Meichsner; I. Wehl; E. Roduner; K.A. Friedrich Electrochimica Acta 2009, 55, 423. https://doi.org/10.1016/j.electacta.2009.05.049.

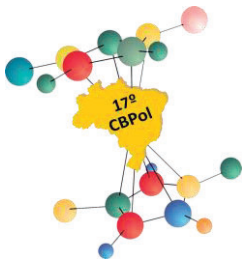

SURFACE-MODIFIED MICROFIBRILLATED CELLULOSE FROM EUCALYPTUS SAWDUST FOR POTENTIALLY TOXIC ELEMENTS REMOVAL FROM CONTAMINATED WATER

João G. Ribeiro[1], Rennan F. S. Barbosa[1] and Derval S. Rosa[1]*

1 – Center of Engineering and Social Science, Federal University of ABC (UFABC), Santo André, SP, Brazil
dervalrosa@yahoo.com.br

Abstract - Population growth and urbanization have led to global concerns regarding access to clean drinking water, as metal ions increasingly contaminate it. Metals such as cadmium, chromium, copper, manganese, zinc, and nickel are potentially toxic and pose risks to human health and the environment. Existing techniques to reduce contamination have limitations in terms of efficiency and cost. However, adsorption using microfibrillated cellulose (MFC) has emerged as a promising solution due to its high adsorption capacity, and the ability to modify its chemical groups (MFC-m) to enhance the removal of specific compounds and improve its effectiveness. This study focused on preparing MFC from eucalyptus sawdust and modifying it with carboxylic groups to adsorb cadmium, chromium, copper, manganese, zinc, and nickel. The results demonstrated that MFC-m effectively removed metals, particularly copper and nickel, making it a viable adsorbent for treating contaminated water.

Keywords: Cellulose, adsorption, water treatment, potentially toxic elements
Fundings: CAPES, FAPESP, CNPq

Introduction

With rapid population growth, urbanization, and increased human activities, ensuring access to safe drinking water has become a critical global concern. [1] One of the major challenges is water contamination caused by metal ions, which leads to a decline in water quality. This contamination poses significant health risks due to its high toxicity, non-biodegradability, and ability to bioaccumulate through the food chain. [2, 3] Metals such as cadmium (Cd(II)), chromium (Cr(VI)), copper (Cu(II)), manganese (Mn(II)), zinc (Zn(II)), and nickel (Ni(II)) are classified as potentially toxic elements (PTE) and have been linked to various diseases, including kidney and lung damage, bone disorders, autoimmune conditions, and various forms of cancer. [4]

Reducing heavy metal contamination in water is crucial for safeguarding population health. Although techniques like chemical precipitation, electrochemical treatment, and ion exchange [5] have been utilized, they suffer from efficiency and operational cost limitations. [3, 6] As an alternative, adsorption has emerged as a promising, cost-effective method that relies on the accumulation of molecules or ions on a solid adsorbent. Cellulose, particularly in the form of microfibrillated cellulose (MFC), a form of nanocellulose, has shown significant potential as an adsorbent due to its high adsorption capacity, attributed to its larger surface area and greater number of exposed hydroxyl groups. [6]

Notably, different forms of nanocellulose such as nanocrystalline cellulose (NC), microfibrillated cellulose (MFC), nanofibrillated cellulose (NFC), and bacterial cellulose (BC) have emerged as prominent options for various applications. MFC, derived from mechanical treatments or acid hydrolysis of macroscopic cellulose, exhibits a substantial surface area and an abundance of exposed hydroxyl groups, rendering it a highly efficient adsorbent. The hydroxyl groups on the surface of MFC play a pivotal role in the adsorption of heavy metals by forming complexes with

these ions. Moreover, these hydroxyl groups can be modified to introduce chemical groups, thereby further enhancing the adsorption capacity. Mechanically treating cellulose for MFC production is particularly efficient and cost-effective, making it ideal for industrial-scale processes. [7, 8, 9]

This study focuses on preparing MFC from eucalyptus sawdust residue and modifying its surface by introducing carboxylic groups through a reaction with succinic anhydride. The aim is to evaluate the adsorption capacity of the final MFC product against a solution containing cadmium (Cd(II)), chromium (Cr(VI)), copper (Cu(II)), manganese (Mn(II)), zinc (Zn(II)), and nickel (Ni(II)).

Experimental

MATERIALS

In this study, the lignocellulosic source chosen is eucalyptus sawdust residue (Eucalyptus citriodora) obtained from post-harvest and cutting activities in the state of Mato Grosso do Sul (MT, Brazil). The chemical reagents utilized include sodium chlorite ($NaClO_2$), sodium hydroxide (NaOH), potassium hydroxide (KOH), ethanol, nitric acid (HNO_3), succinic anhydride, dimethylformamide (DMF), propanone (acetone), and analytical standards of the target metal ions (Cd(II), Cr(VI), Cu(II), Mn(II), Zn(II), and Ni(II)). These reagents were purchased from Labsynth Produtos para Laboratórios (SP, Brazil).

METHODS

Before the MFC production, the eucalyptus fibers underwent a treatment process to eliminate lignin and extract the cellulose component. This method, inspired by the approach of Ferreira et al. [10], involved initial grinding of the fibers using a knife mill (model TE-625, Tecnal, SP, Brazil) followed by drying in an oven (model MA035/5, Marconi, SP, Brazil) at 70 ºC for 24 hours.

Subsequently, the fibers were treated with a $NaClO_2$ solution (3.8% w/v) at a ratio of 1 g of material to 20 mL of solution. The treatment was carried out for 2 hours at 50 ºC with continuous stirring. Following this step, the material was thoroughly washed until it reached a pH of 7 and then dried in an oven at 70 ºC for 12 hours [10].

Following the $NaClO_2$ treatment, the dried material was exposed to a solution comprising NaOH (10% w/v) and KOH (10% w/v) at a ratio of 1 g of material to 20 mL of solution. The mixture was allowed to react under stirring at room temperature for 2 hours. Subsequently, the fibers were thoroughly washed until reaching a neutral pH and dried in an oven at 70 ºC for 12 hours [10].

Following the pre-treatment, the fibers underwent a grinding process to produce microfibrillated cellulose (MFC). The material was moistened with an ethanol solution (80% v/v) in a 1:1 ratio and ground in a ball mill (model MA500, Marconi, SP, Brazil) for 3 hours. [61]

A modified procedure based on Hokkanen et al. [11] was employed to carboxylate the MFC. Initially, the MFC was reacted with 20% (w/v) NaOH under stirring at room temperature for 16 hours. Subsequently, the MFC was centrifuged, and a washing step was performed until reaching a pH of 7. Next, the MFC (1 g) was stirred for 24 hours in the presence of a succinic anhydride solution (1.75 g). To isolate the carboxylated MFC (MFC-m), a sequential washing process with various solvents was carried out: DMF, 95% ethanol, H_2O, HNO_3 solution (0.01 mol/L), H_2O, and acetone. Finally, the material was reacted with a Na_2CO_3 solution under stirring for 1 hour, forming the desired product, MFC-m.

CHARACTERIZATION

To gain insights into the structural and functional properties of the sawdust, MFC, and MFC-m, Fourier Transform Infrared Spectroscopy (FTIR) analysis was performed using a Frontier 94942 Spectrophotometer (PerkinElmer, USA). Additionally, the size of the cellulose microfibrils was determined using a BetterSize® ST Laser particle size analyzer (Lianing, China). These characterization techniques provided valuable information regarding the material's chemical composition and particle size distribution.

The thermal properties of the materials were investigated using Thermogravimetric Analysis (TGA) performed with the STA 6000 equipment (Perkin Elmer, USA). This technique allowed for the examination of the thermal stability and decomposition behavior of the samples.

To assess the sorption capabilities of the produced materials, the MFC and MFC-m were exposed to a multi-metal solution containing 1 ppm of Cd(II), Cr(VI), Cu(II), Mn(II), Zn(II), and Ni(II). The contact was established by stirring the mixture in a shaker at 150 rpm, with an adsorbent dosage of 1 g/L, while maintaining an initial pH of 4.5. Subsequently, an ion chromatograph coupled with a UV-Vis 940 Professional IC Vario spectrometer (Metrohm, Switzerland) was utilized to quantify the final concentration of ions in the solution after the sorption test. These analytical tools provided valuable insights into the thermal behavior and sorption capabilities of the materials under investigation.

Results and Discussion

FTIR

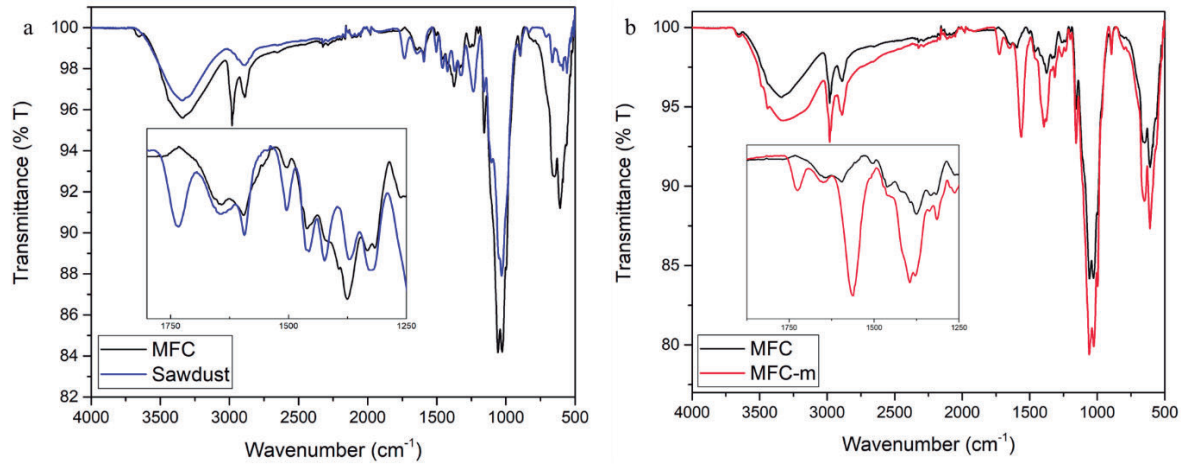

Figure 1 – Sawdust, MFC and MFC-m FTIR spectra.

In Fig 1a, the spectra of MFC and sawdust are depicted, revealing significant changes in the characteristic signals associated with hemicellulose and lignin. Notably, after the sawdust processing, the signals at 1734, 1594, 1504, 1457, and 1423 cm^{-1}, which are indicative of hemicellulose and lignin, vanish, indicating an effective removal of these components. [10] This observation suggests a successful purification process, leading to the isolation of cellulose-rich MFC.

Fig 1b illustrates the comparison of FTIR spectra between MFC and MFC-m, revealing distinct features. Both spectra exhibit characteristic cellulose-related signals, as summarized in Table 1. Notably, the MFC-m spectrum exhibits additional signals indicating successful chemical modification. Specifically, the presence of a peak at 1725 cm^{-1} corresponds to the C=O stretching of ester, while signals at 1562 and 1395 cm^{-1} correspond to the asymmetric and symmetric stretching of the carboxylate group ($-CO_2^-$), respectively. [10, 11]

Table 1 – Cellulose FTIR signals on MFC and MFC-m spectra.

Vibrational mode	MFC (cm^{-1})	MFC-m (cm^{-1})
OH stretching	3342	3334
C-H stretching	2890	2890
OH bending	1377	1379
C-O antisymmetric bridge stretching	1158	1158
C-O stretching	1058	1059
β-glycoside bonds elongation	896	895

LASER PARTICLE SIZE ANALYZER

The analysis of MFC and MFC-m involved fitting a Gaussian distribution to describe the cellulose microfibrils' hydrodynamic diameter size distribution. Both samples exhibited fibrils in the micrometer range. Specifically, MFC displayed an average diameter of 31.67 µm, with a D90 value (diameter of 90% of the particles) below 82.74 µm. On the other hand, MFC-m exhibited an average diameter of 18.67 µm, with a D90 of 54.63 µm.

THERMOGRAVIMETRIC ANALYSIS

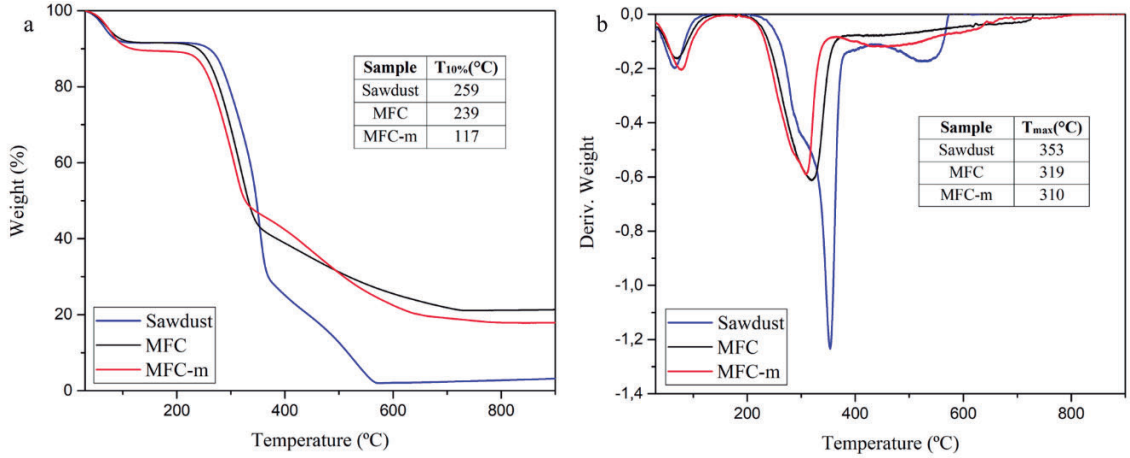

Figure 2 – Sawdust, MFC and MFC-m TGA and DTG curves.

The thermal properties of the samples were characterized using TGA (Thermogravimetric Analysis) and DTG (Derivative Thermogravimetry). The analysis revealed two main mass loss events in the samples. The first event corresponds to the loss of water, while the second event, indicated by T_{max}, represents the thermal degradation of cellulose. Notably, in the DTG of sawdust, a distinct thermal event is observed between 440 and 570 °C, corresponding to lignin's thermal degradation. However, this thermal event is absent in the MFC and MFC-m samples, confirming the successful removal of lignin. In Fig 2b, a trend is observed for T_{max}, where sawdust exhibits a higher T_{max} compared to MFC and MFC-m. This difference can be attributed to the smaller surface area of sawdust, which requires a higher temperature for cellulose degradation. The subtle variations in T_{max} and $T_{10\%}$ for MFC and MFC-m also indicate a successful modification, as observed in the FTIR analysis. [10, 12]

ADSORPTION

The multi-metal sorption tests conducted on sawdust, MFC, and MFC-m ion removal percentages are presented in Table 2. Analysis of the results reveals a significant increase in ion removal for most of the evaluated ions when comparing sawdust to MFC. This improvement can be attributed to the amplified surface area of MFC, facilitating enhanced interaction between hydroxyl groups and the metals in the solution. The expanded surface area of MFC enables a greater number of active sites for adsorption, leading to improved removal efficiency. [7]

Moreover, it was observed that introducing the carboxylate group by reacting cellulose microfibrils with succinic anhydride (MFC-m) resulted in increased removal of metal ions. This enhancement can be attributed to the carboxylate group's higher chelating power (bidentate) than the hydroxyl groups. Carboxylate groups in MFC-m provide stronger coordination sites for metal ions, leading to improved adsorption efficiency. Remarkably, MFC-m exhibited higher selectivity for copper and zinc adsorption than the other evaluated metals, demonstrating removal percentages exceeding 90%. [11]

Table 2 – Percent remotion of metallic ions by sawdust, MFC and MFC-m.

	% Remotion					
Sample	**Copper**	**Nickel**	**Zinc**	**Manganese**	**Cadmium**	**Chrome**
Sawdust	29,2±7,4	9,1±5,1	6,7±0,5	16,4±1,4	17,9±5,1	16,3±0,9
MFC	42,4±2,5	11,1±0,1	7,3±1,1	20,3±1,6	17,1±1,7	7,2±0,5

MFC-m	92,6±7,8	97,9±1,1	56,9±0,3	28,5±6,9	53,7±1,2	8,3±0,2

Conclusions

Microfibrillated celluloses without and with chemical modification were successfully prepared. FTIR and FTIR analyses confirmed the effective removal of lignin and hemicellulose from eucalyptus sawdust through chemical treatments ($NaClO_2$ and NaOH+KOH). The milling process achieved micrometer-scale particle sizes for MFC and MFC-m, measuring an average of 31.67 µm and 18.67 µm, respectively. The chemical modification of MFC using succinic anhydride was successful, as indicated by the presence of characteristic signals in the FTIR spectra of MFC-m, including ester carbonyl and carboxylate group signals. MFC-m demonstrated great potential as an adsorbent for treating waters contaminated with PTEs, exhibiting removal percentages exceeding 90% for copper and nickel and over 50% for zinc and cadmium in a multielemental assay. These results highlight that the MFC-m can be a low-cost alternative material with great potential to remove metal ions from contaminated water.

Fundings

This research was financed by FAPESP (2021/08296-2, and 2020/13703-3), CNPq (308053/2021-4 and 403934/2021-4), and (CAPES) (Finance Code 001).

Acknowledgements

The authors thank the technical support of the Multiuser Experimental Center of UFABC (CEM-UFABC), CECS (UFABC), and REVALORES for assistance.

References

1. K. de Mello et al.; Journal of Environmental Management 2020, 270, 110879. doi: 10.1016/j.jenvman.2020.110879.
2. S. Sharma; A. Bhattacharya; Applied Water Science 2017, 7, 3. doi: 10.1007/s13201-016-0455-7.
3. R. Barbosa et al.; Chemical Engineering Journal 2020, 395, 125055. doi: 10.1016/j.cej.2020.125055.
4. F. Haider et al., Ecotoxicology and Environmental Safety 2021, 211, 111887. doi: 10.1016/j.ecoenv.2020.111887.
5. A. Sharma et al; Journal of Polymers and the Environment 2022, 30, 1. doi: 10.1007/s10924-021-02185-4.
6. F. Fu; Q. Wang; Journal of Environmental Management 2011, 92, 3. doi: 10.1016/j.jenvman.2010.11.011.
7. R. Reshmy et al; Chemosphere 2021, 281, 130738. doi: 10.1016/j.chemosphere.2021.130738.
8. A. Qiao et al.; Carbohydrate Polymers 2021, 272, 118471. doi: 10.1016/j.carbpol.2021.118471.
9. K. Köse; M. Mavlan; J. Youngblood; Cellulose 2020, 27, 6. doi: 10.1007/s10570-020-03011-1.
10. R. Ferreira et al.; Materials Today Communications 2019, 100755. doi:10.1016/j.mtcomm.2019.100755
11. S. Hokkanen; E. Repo; M. Sillanpää; Chemical Engineering Journal 2013, 223. doi: 10.1016/j.cej.2013.02.054.
12. L. Burhenne et al.; Journal of Analytical and Applied Pyrolysis 2013, 101(), 177–184. doi:10.1016/j.jaap.2013.01.012

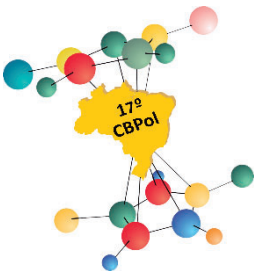

SYNTHESIS AND PHYSICOCHEMICAL CHARACTERIZATION OF NANOFIBERS FROM BIOCELLULOSE WASTE

Kely S. Bonfim[1*], Adhemar W. Filho[1, 2], Renan Da S. Fernandes[1], Fauze A. Aouada[1] and Márcia R. De Moura[1]

1 – Department of Physics and Chemistry, São Paulo State University (UNESP), School of Engineering, Ilha Solteira, SP, Brazil
kely.s.bonfim@gmail.com
2 – Federal Institute of São Paulo (IFSP), Ilha Solteira, SP, Brazil.

Abstract - Bacterial cellulose is a biopolymer free from impurities due to its biosynthesis that occurs through bacteria. Among the properties of this material, noteworthy are its high crystallinity, elevated Young's modulus, and excellent water absorption, which make it suitable for various applications such as food packaging, active release films, dressings, and cosmetics. This biopolymer can undergo oxidation processes for the extraction of bacterial cellulose nanofibers, enabling its chemical modification and functionalization with other molecules, thereby expanding its range of applications. Therefore, this study aims to extract bacterial cellulose nanofibers using the oxidation method mediated by 2,2,6,6-tetramethyl-1-piperidinyloxy. The results indicate that the oxidation occurred efficiently, the crystalline structure of the material remained unaltered, and the oxidation and sonication, contributed to the dispersion of these nanofibers.
Keywords: *Bacterial cellulose nanofibers; Biocellulose; Oxidation; Physical-chemical properties*

Introduction

Plant cellulose (PC) $(C_6H_{10}O_5)n$, a component of most plant fibers is considered the most abundant biopolymer on Earth [1, 2]. PC is formed by condensation polymerization of anhydroglucose units linked by β-1,4 glycosidic bonds [3]. The main properties of this homopolysaccharide include high chain rigidity, insolubility in water, and high hygroscopicity due to the presence of free hydroxyl groups and hydrogen bonds in the structure [4-6]. Although PC exhibits such properties, it contains impurities such as hemicellulose and lignin [7, 8].

However, bacterial cellulose (BC), or biocellulose, is free from these impurities as its biosynthesis occurs through bacteria, contributing to the reduction of environmental impacts and expenses with purification [9, 10]. BC, first identified in 1886 during vinegar fermentation [11], has the same chemical composition as PC, but the fiber dimensions and structural organization are different [12, 13], providing this biopolymer with distinct and unique properties such as nanoscale fibers, high crystallinity, high Young's modulus, and excellent water absorption [14]. Due to these properties, BC has applications in various fields, including food packaging, active release films, dressings, cosmetics, food, and electronics [15, 16].

In order to improve the properties of this material and expand its application field, research in these areas has focused on nanostructures, such as nanofibers, which are long and thin fibers with a high surface area, several μm in length, and a diameter ranging from 10-100 nm, depending on the source and aggregation state of the material [17, 18].

Mechanical methods were the first to be employed in the disintegration of BC for nanofiber production; however, the high energy demand required in this process rendered the method impractical. Chemical methods, such as 2,2,6,6-tetramethyl-1-piperidinyloxy (TEMPO)-mediated oxidation, have shown promise for obtaining bacterial cellulose nanofibers (BCNFs). Additionally, the addition of functional groups through oxidation can increase the reactivity of bacterial cellulose

with other materials, further expanding its properties and functionalities. This combination enables the production of advanced composites, with the potential to revolutionize the industry and the development of innovative technologies [19, 20].
Therefore, the purpose of this study is to produce BCNFs using the TEMPO-mediated oxidation method and to physicochemical characterize them in order to analyze the presence of chemical groups as well as the crystalline and morphological properties.

Experimental

TEMPO-Mediated Oxidation

10g of dried and ground BC waste (Nexfill®) were immersed in 1L of an aqueous solution containing: 0.16g of 2,2,6,6-tetramethyl-1-piperidinyloxy (Sigma-Aldrich); 1g of NaBr (Dinâmica), and 11% NaClO (Dinâmica). The pH of the system was maintained at 10.0 by adding a NaOH solution (mechanical stirring at 25 $\pm$ 2ºC for 2 hours). Then, the suspension was sonicated for 10 minutes (Unique Ultracleaner 1400), filtered, washed until reaching pH 7.0, and stored in a glass container under refrigeration for further analysis.

Yield (Y) and Water Content (WC)

The oxidation yield was calculated according to Eq. 1 [21] where mi = mass bacterial cellulose used on oxidation and mf = final mass after drying in an oven at 100°C until constant mass. The experiment was performed in triplicate. The water content present in the BCNFs were calculated according to Eq. 2 [22], where mi = initial mass and mf = final mass after drying in an oven at 100°C until constant mass. The experiment was performed in quadruplicate.

$$Y\ (\%) = \left(\frac{mf}{mi}\right) \times 100 \qquad (1)$$

$$WC\ (\%) = \left(\frac{mi-mf}{mi}\right) \times 100 \qquad (2)$$

Fourier Transform Infrared Spectroscopy (FTIR)

The samples in the form of films were analyzed using an Agilent Technologies Cary 630 FTIR spectrometer - ATR. Scan range: 4000 to 655 cm^{-1}, and resolution of 4 cm^{-1}.

X-Ray Diffraction

The samples were placed in glass sample holders in the diffractometer (Shimadzu - XRD-600). The analysis parameters used were: Cuα X-ray source; λ = 0.154 nm; voltage = 30 kV; current = 40 mA; angular range of 2θ from 4 to 60° and scanning speed of 2°/min. The crystallinity index of the samples was determined based on the literature [23] using the Segal equation [24] (Eq. 3):

$$CrI = \frac{(I_{200} - I_{am})}{I_{200}} \times 100 \qquad (3)$$

Scanning Electron Microscopy (SEM)

The analysis was performed using a ZEISS EVO/LS15 microscope operated at 10 kV.

Results and Discussion

Yield (Y) and Water Content (WC)

The yield of the oxidation process and total solids are presented in Table 1. It can be observed that the yield was satisfactory and close to that found in the literature [21]. Furthermore, the analysis of water content shows that the produced BCNFs have a high-water content in their structure.

Table 1 – Yield of synthesis and Total Solids of Bacterial Cellulose Nanofibers

Sample	Yield (%)	Water Content (%)
BCNF	82.68±2.40	98.84±0.07

Source: Author's own.

Fourier Transform Infrared Spectroscopy (FT-IR)

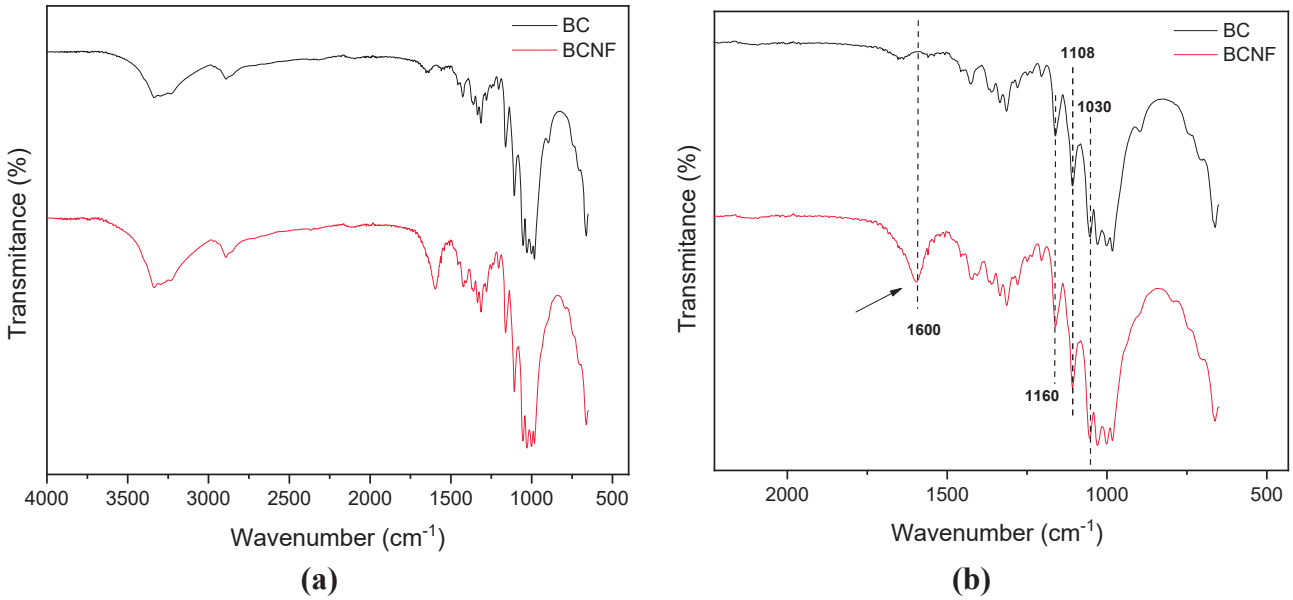

Figure 1 – Vibrational spectra in the infrared region for samples of BC and BCNF with scanning of: **(a)** 4000 - 655 cm^{-1} and **(b)** 2232-655 cm^{-1}. Source: Author's own.

The spectra of BC and BCNF are presented Fig. 1a and 1b. For both spectra, characteristic spectroscopic bands (peaks) of the cellulose structure are observed. For example, the band at 3324 cm^{-1} is attributed to the stretching of the O–H bond, while the bands at 1030 cm^{-1} and 1160 cm^{-1} correspond to the stretching of C–O and C–O–C bonds, respectively. The band at 2895 cm^{-1} corresponds to the stretching of aliphatic C–H bonds, and the bands at 1370 cm^{-1} and 1046 cm^{-1} are assigned to the angular deformation of C–CH_3 and the stretching of C–OH bonds, respectively [25, 26]. It is important to highlight that the oxidation process carried out on BC can be validated by this technique, particularly considering two factors:

I. The appearance of a new band at 1600 cm^{-1} corresponding to the carboxylate (COO-) group observed in the BCNF spectrum (Fig. 1a), which is not present in the BC spectrum (Fig. 1b).

II. The absence of aldehyde bands in the region of 1720 – 1740 cm^{-1}. This fact indicates that the oxidation process was efficient, meaning that the aldehyde groups (HC=O) were converted to carboxylate (-COO-), which is clearly observed at 1600 cm^{-1} [27].

X-Ray diffraction

The crystallographic analysis of BC and NFCB samples is presented in Figure 2.

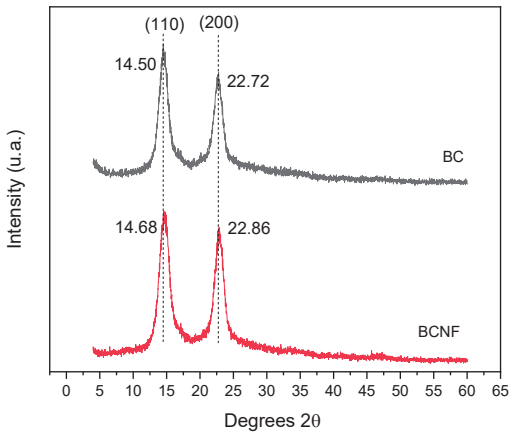

Figure 2 - X-Ray diffractograms to BC and BCNF samples. Source: Author's own.

It can be observed that both materials exhibit high crystallinity. The observed peaks were 14.50 and 22.72 for the BC sample, and 14.68 and 22.86 for the NFCB sample. The oxidation process maintained the crystallinity index of BC (Table 2). These results show that the carboxylate groups were introduced on the BC surface and in disordered regions [28].

Table 2 – Crystallinity Index of BC and BCNF

Samples	Crystallinity Index (%)
BC	89.52
BCNF	88.15

Source: Author's own.

Scanning Electron Microscopy (SEM)

The obtained micrographs for BC and NFCB samples are presented in figure 3a and 3b, respectively. By means of the SEM technique, it can be observed that BC exhibits a structure with long and tangled fibers, and the oxidation process followed by sonication contributed to a greater dispersion of the fibers.

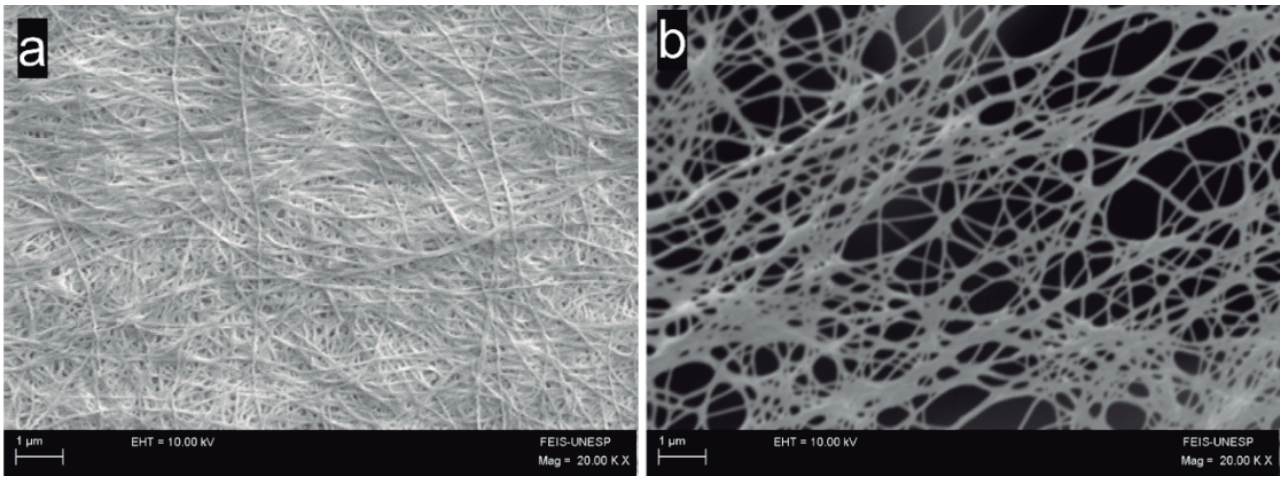

Figure 3 - Scanning Electron Micrographs at a magnification of 20,000x for the samples of: **(a)** Bacterial Cellulose Residue and **(b)** Bacterial Cellulose Nanofibers obtained via TEMPO-mediated oxidation. Source: Author's own.

Conclusions

The utilization of BC residue for TEMPO-mediated oxidation was efficiently performed. The FT-IR technique confirmed the insertion of carboxylic groups at the C6 position of BC. X-ray diffraction (XRD) was employed to demonstrate that the oxidation method employed in this study does not alter the crystalline structure of the material. Furthermore, scanning electron microscopy (SEM) revealed that oxidation and sonication contribute to the enhanced dispersion of these nanostructures. The obtained NFCBs hold potential for application in various fields that require such properties.

Acknowledgements

The authors thank the São Paulo Research Foundation (FAPESP) (Grants No. 2019/06170-1 and No. 2013/07296-2 CEPID) and CNPq (Grant No. 312530/2018-8). The Physics and Chemistry Department of the São Paulo State University (UNESP) and the PROPG are acknowledged for the financial support. This work was partially funded in by the Coordenação de Aperfeiçoamento de Pessoal de Nível Superior - Brazil (CAPES; Finance Code 001).

References

1. V. K. Gupta et al; Bioresource Technology 2016, 216. https://doi.org/10.1016/j.biortech.2016.05.106

2. A. Dufresne; Current Opinion in Colloid & Interface Science 2017, 29. https://doi.org/10.1016/j.cocis.2017.01.004
3. I. Göktürk et al; Journal of Chromatography B 2018, 1099. https://doi.org/10.1016/j.jchromb.2018.08.030
4. C. D. Zanon, Dissertação de Mestrado, Universidade Estadual de Campinas, 2016.
5. M. J. John; S. Thomas; Carbohydrate Polymers 2008, 71. https://doi.org/10.1016/j.carbpol.2007.05.040
6. M. R. Moreira, Dissertação de Mestrado, Universidade de São Paulo, 2009.
7. M. Islam et al; International Journal of Biological Macromolecules 2017, 102. https://doi.org/10.1016/j.ijbiomac.2017.04.110
8. C. Gao et al; Food Hydrocolloids; 2014, 36. https://doi.org/10.1016/j.foodhyd.2013.09.015
9. R. M. Viana et al; Carbohydrate Polymers 2018, 196. https://doi.org/10.1016/j.carbpol.2018.05.017
10. D. Zmejkoski et al; International Journal Biological Macromolecules 2018, 118. https://doi.org/10.1016/j.ijbiomac.2018.06.067
11. A. J. Brown Journal Chemical Society Transactions 1886, 49. https://doi.org/10.1039/CT8864900432
12. D. Renpeng et al.; Carbohydrate Polymers 2018, 194. https://doi.org/10.1016/j.carbpol.2018.04.041
13. N. F. Vasconcelos et al.; Carbohydrate Polymers 2017, 155. https://doi.org/10.1016/j.carbpol.2016.08.090
14. E. Pecoraro et al in Chapter 17. Bacterial Cellulose from Glucanacetobacter xylinus: Preparation, Properties and Applications. Elsevier Limited, 2008. https://doi.org/10.1016/B978-0-08-045316-3.00017-X
15. V. Revin et al Brazilian Journal of Microbiology 2018, 49. https://doi.org/10.1016/j.bjm.2017.12.012
16. A. F. Jozala et al Applied Microbiology Biotechnology 2016, 100. https://doi.org/10.1007/s00253-015-7243-4
17. H. Azeredo; M. Rosa; L. Mattoso; Industrial Crops and Production 2017, 97. https://doi.org/10.1016/j.indcrop.2016.03.013
18. K. Lee et al.; Macromolecular Bioscience 2014, 14.
19. https://doi.org/10.1002/mabi.201300298
20. Y. Wen et al.; Food Packaging and Shelf Life 2021, 29. https://doi.org/10.1016/j.fpsl.2021.100709
21. H. Luo et al.; Materials Chemistry and Physics 2013, 143(1). https://doi.org/10.1016/j.matchemphys.2013.09.012
22. M. Fischer et al.; Matéria 2018, 22. https://doi.or/10.1590/S1517-707620170005.0270
23. L. R. Lima et al.; Química Nova 2015, 38. https://doi.org/10.5935/0100-4042.20150131
24. L. Segal et al.; Textile Research Jornal 1959, 29(10). https://doi.org/10.1177/004051755902901003
25. Y. Yang et al.; Carbohydrate Polymers 2020, 228. https://doi.org/10.1016/j.carbpol.2019.115370
26. N. Zhang et al. Journal of Hazardous Materials 2016, 316. https://doi.org/10.1016/j.jhazmat.2016.05.018
27. E. S. Nascimento. Ph.D. Thesis, Universidade Federal do Ceará, 2018.
28. T. Saito and A. Isogai, Biomacromolecules 2004, 5(5). https://doi.org/10.1021/bm0497769

SYNTHESIS OF SBS/POLYPYRROLE FLEXIBLE FILMS: EVALUATION AS STRAIN SENSORS

Maurício F. de Aguiar[1], Andressa N. R. Leal[2], Mônica F. B. Rocha[1], Lúcio F. M. Cavalcanti[1], Celso P. de Melo[3], Kleber G. B. Alves[1,*].

1 – Department of Mechanical Engineering, Federal University of Pernambuco (UFPE), Recife, PE, Brazil
kleber.alves@ufpe.br
2 – Department of Chemical Engineering, Federal University of Pernambuco (UFPE), Recife, PE, Brazil
3 – Department of Physics, Federal University of Pernambuco (UFPE), Recife, PE, Brazil

Abstract – This work described the synthesis of flexible SBS films, its coating with polypyrrole (PPy), and the use of this SBS/PPy composite. While the SBS films were obtained through solution casting, the composite films were resulted from pyrrole in situ polymerization over SBS. The materials were characterized by scanning electron microscopy (SEM), Fourier-Transform infrared (FTIR), contact angle, and tensile testing. Based on the characterization, we verified that an homogeneous layer of PPy was deposited over the SBS films, and the composite maintained its elastomeric character, in which it presented an elongation of 819.6% ± 33.4%. In regards to the application at strain sensing, the composite proved to be very promising, since a ratio between the variation in electrical resistance and the electrical resistance of the film prior to deformation (ΔR/R0) was observed at approximately 8500 for an elongation of 100%.

Keywords: *SBS. Polypyrrole. Conductive composite. Strain sensor. Elastomeric.*

Introduction

Strain sensors are devices that convert mechanical strains into measurable signals. Depending on the type of this signal, the sensor can be classified such as resistive, capacitive, impedimetric, piezoelectric, and optical [1, 2]. These strain sensors are versatile. They can be found in several applications of our daily routine, such as monitoring the movement and health of humans, artificial muscles, soft robotics, and even in the entertainment industry [1-3].

In order to optimize the sensor properties and that it is functional, it is fundamentally important the definition of the materials used on the fabrication of this sensor. Therefore, it has been highlighted in the literature the use of composite films based on elastomeric and conductive particles, such as graphene, carbon nanotubes, and conductive polymers. Through the combination of these materials, it is possible to obtain a composite with both the mechanical properties of the elastomeric and the electrical properties of conductive materials [4-6].

This work aims to synthesize and characterize composite films of the copolymer SBS (styrene-butadiene-styrene) and polypyrrole (PPy), and the evaluation of this material as a resistive strain sensor. For this, flexible SBS films were obtained using the solution casting technique, and then the film was coated with PPy through in situ polymerization of pyrrole.

Experimental

The synthesis of SBS films were realized through solution casting using SBS D1155 E (Kraton, USA). For this, we prepared a 10% w/v solution of SBS using a tetrahydrofuran/dimethylformamide (THF/DMF) in a ratio of 70/30 v/v. This solution was kept

stirring for 2 hours to homogenize it. Then, we placed 5 mL on a 60 mm glass petri dish, and allowed it to evaporate the solvent at room temperature for 24 hours, followed by evaporation at 60C on an oven for 36 hours. Afterwards, the films were removed from the petri dish, and cut into 4 cm x 1 cm rectangles.

Before coating the films with PPy, we submitted them to an air plasma treatment during 5 minutes using a Plasma Cleaner PDC-002 (Harrick, USA). After turning the films hydrophilic, we coated them through in situ polymerization of pyrrole (Sigma-Aldrich, USA). For this, we added 48 mL of deionized water and the SBS-Plasma film on a 250 mL beaker, and allowed it to stir for 10 minutes on an orbital shaker SL-221 (Solab, Brazil). Then, we added 1 mmol of the monomer, and kept stirring for another 10 minutes. Afterwards, we added 2 mL of a 1 M solution of $FeCl_3$ (Neon, Brazil), and kept the solution stirring for 4 hours. The SBS/PPy composite obtained was removed from the beaker, cleaned with deionized water, and dried at room temperature. The polymerization took place under 120 rpm and temperature of 5 °C.

The synthesized materials were characterized using the techniques scanning electron microscopy (SEM), Fourier-Transform infrared (FTIR), contact angle, tensile testing, and two-probe measurements using a 2400 SourceMeter multimeter (Keithley, USA).

Results and Discussion

In order to evaluate the films' surface, before and after coating it with PPy, we present the SEM images in Fig. 1. As can be observed, SBS films have a smooth surface. On the other hand, after the coating, some nanoparticles can be observed on the composite films surface. Besides observing that these PPy presents a spherical morphology and are at the nanometric scale, it can be also seen that they cover the film evenly over its entire surface.

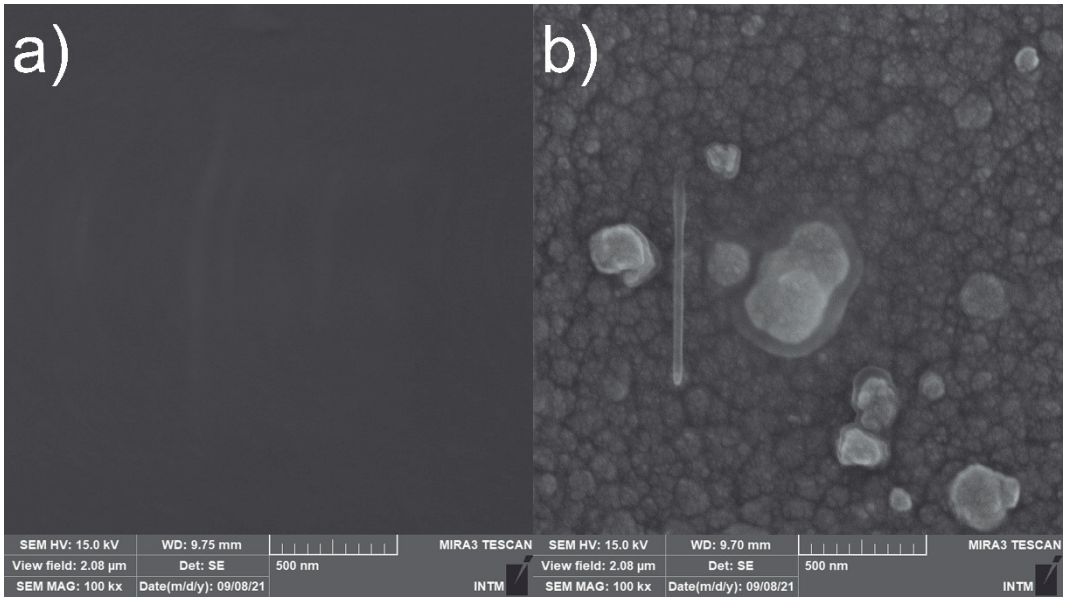

Figure 1 – SEM images of SBS (a) and SBS/PPy (b).

The materials' wettability analysis is a fundamental step at coating the film with PPy. For an efficient coating over all the surface, it is necessary for the film to have a hydrophilic character. Therefore, we present the materials' wettability in Fig. 2. As can be observed, SBS are hydrophobic, since its contact angle was 96° ± 1°, which can be also seen in other works at the literature [7, 8]. However, after surface treatment with air plasma, we have a contact angle value 33° ± 2° for the SBS-Plasma films, thus characterizing them as hydrophilic materials. This change are due to the introduction of functional polar groups on the films' surface [9]. Regarding the wettability of SBS/PPy, we have a contact angle of 75° ± 2°, which corresponds to a hydrophilic material.

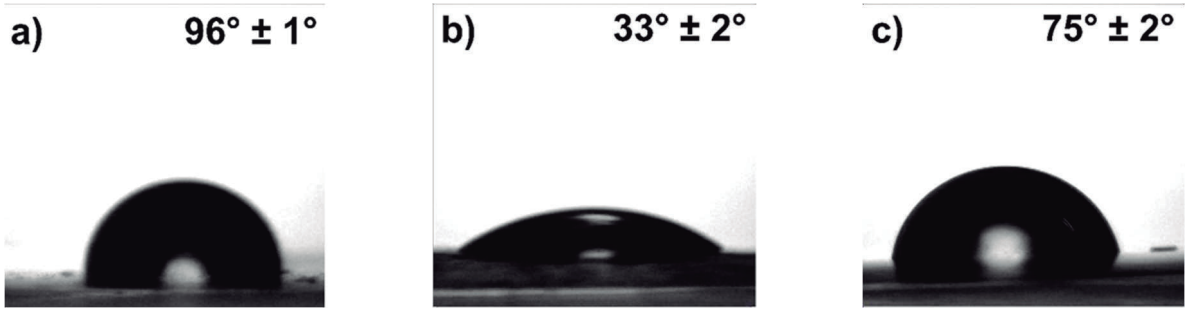

Figure 2 – Contact angle measurements of SBS (a), SBS-Plasma (b), and SBS/PPy (c).

The FTIR spectra of SBS, SBS-Plasma, PPy, and SBS/PPy are shown in Fig. 3. In regards to SBS, it can be observed both characteristic bands of polybutadiene and polystyrene, which corresponds to the copolymer. While for polybutadiene we observe an out-of-phase angular deformation of the trans-1,4 C=C at 964 cm^{-1} [10, 11], for the part related to polystyrene, we observe and stretching vibration of aromatic C=C at 1601 cm^{-1}, as well as the presence of monosubstituted benzene at 756 cm^{-1} and 697 cm^{-1} [11, 12]. As for the SBS-Plasma spectrum, we can observe the same bands of SBS. However, we can also see a band at 3300 cm^{-1} as well as the broadening of the 1651 cm^{-1}, which is related to the air plasma treatment. While the band at 3300 cm^{-1} is due to the stretching vibration of the O-H bonds, the other corresponds to the angular deformation vibration of the O-H bonds [9, 13]. Regarding the spectrum of PPy, the stretching vibration of the C=C and C-N of the aromatic rings are observed at 1537 cm^{-1} and 1450 cm^{-1}, respectively. At 1165 cm^{-1} we have the pyrrole breathing ring vibration. Finally, the 901 cm^{-1} and 783 cm^{-1} bands are related to out-of-plane angular deformation of the C-H bonds [14-16]. Finally, in the SBS/PPy spectrum, it is possible to observe characteristic bands of each material separately (SBS and PPy).

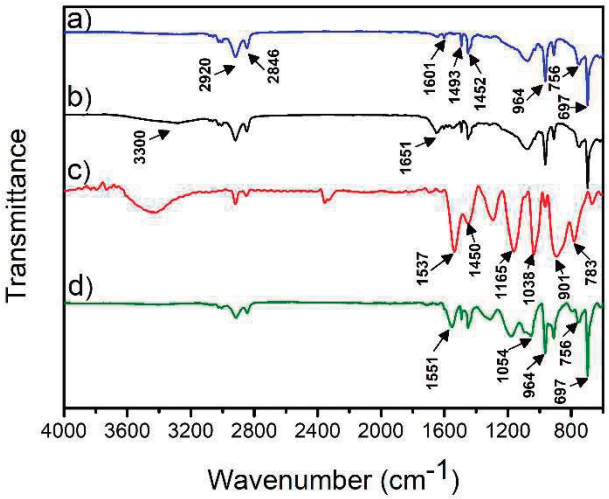

Figure 3 – FTIR spectra of (a), SBS-Plasma (b), PPy (c), and SBS/PPy (d)

The stress-strain curve of SBS/PPy can be seen in Fig. 4a. Through this result, it is seen that the composite film maintains the elastomeric behavior of SBS, since it presented an elongation of 819.6% ± 33.4%. In addition to this, the following properties are obtained: yield strength (2.42 ± 0.20 MPa), fracture stress (3.65 ± 0,21 MPa), and Young Modulus (63.7 ± 2.3 MPa). The preliminary results of SBS/PPy in strain sensing are presented in Fig. 4b. In both deformed (100%) and non-deformed (0%) films it is observed a linear behavior, which is characteristic of ohmic materials. Therefore, after doing a linear regression of the data, and thus obtaining their electrical resistance, we verified a variation in the electrical resistance (ΔR/R0) in the order of 8500. The justification for this increase is possibly related to the separation of the PPy chains on the SBS surface, and thus altering

the electrical conduction network, as well as the presence of breaks in the polymeric coating [2, 5, 17].

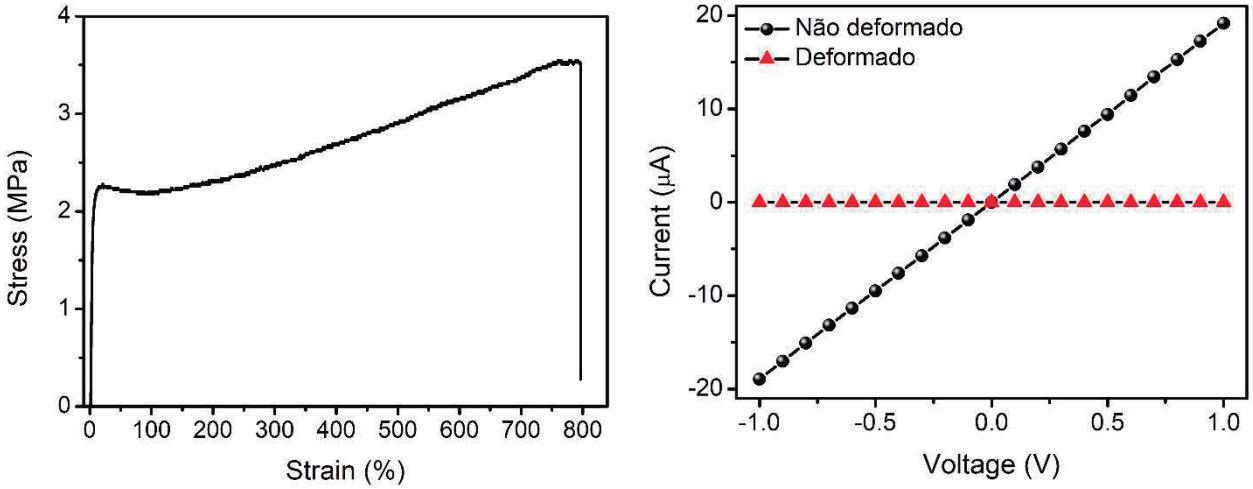

Figure 4 – Stress-strain curve of SBS/PPy (a), and two-probe measurements of SBS/PPy before and after deformation (b).

Conclusions

This work presents the synthesis and characterization of SBS and SBS/PPy films, and the evaluation of the composite films at strain sensing. Through the SEM images, we observed that the polymerization used were able to coat evenly all surface of SBS with PPy nanoparticles, which was also corroborated by FTIR results. In addition, it was verified that the SBS/PPy are elastomeric, and its elongation are 819.6% ± 33.4%. Finally, the preliminary analysis of SBS/PPy in strain sensing proved them to be a promising material.

References

1. M. A. U. Khalid; S. H. Chang. *Composite Structure, 2022, v. 284, p. 115214*. https://doi.org/10.1016/j.compstruct.2022.115214
2. S. Seyedin et al. *Materials Horizons, 2019, v. 6, n. 2, p. 219–249*. https://doi.org/10.1039/C8MH01062E
3. H. Liu et al. *Journal of Materials Chemistry C, 2018, v. 6, n. 45, p. 12121–12141*. https://doi.org/10.1039/C8TC04079F
4. H. Liu et al. *Journal of Materials Chemistry C, 2016, v. 4, n. 1, p. 157–166*. https://doi.org/10.1039/C5TC02751A
5. X. Xu et al. *Composites Part B: Engineering, 2021, v. 211, p. 108665*. https://doi.org/10.1016/j.compositesb.2021.108665
6. M. Amjadi et al. *ACS Nano, 2014, v. 8, n. 5, p. 5154–5163*. https://doi.org/10.1021/nn501204t
7. V. P. R. Remya et al. *Journal of Applied Polymer Science, 2021, v. 138, n. 10, p. 49985*. https://doi.org/10.1002/app.49985
8. H. C. Duong et al. *Journal of Membrane Science, 2018, v. 549, p. 420–427*. https://doi.org/10.1016/j.memsci.2017.12.024
9. S. Guruvenket et al. *Applied Surface Science, 2004, v. 236, n. 1–4, p. 278–284*. https://doi.org/10.1016/j.apsusc.2004.04.033
10. J. E. Kennedy; C. L. Higginbotham. *Materials Science and Engineering C, 2011, v. 31, n. 2, p. 246–251*.https://doi.org/10.1016/j.msec.2010.09.004
11. J. E. Kennedy et al. *Materials Science and Engineering C, 2009, v. 29, n. 5, p. 1655–1661*. https://doi.org/10.1016/j.msec.2009.01.015

12. D. P. Kepić et al. *Polymer International, 2018, v. 67, n. 8, p. 1118–1127*. https://doi.org/10.1002/pi.5620
13. R. Morent et al. *Surface and Interface Analysis, 2008, v. 40, n. 3–4, p. 597–600*. https://doi.org/10.1002/sia.2619
14. K. G. B. Alves et al. *Journal of Applied Polymer Science, 2013, v. 128, n. 5, p. 3170–3176*. https://doi.org/10.1002/app.38481
15. B. Chethan et al. *Sensors and Actuators B: Chemical, 2019, v. 296, p. 126639*. https://doi.org/10.1016/j.snb.2019.126639
16. I. M. Minisy et al. *Polymer, 2019, v. 174, p. 11–17*. https://doi.org/10.1016/j.polymer.2019.04.045
17. Y. Lu et al. *Biosensors and Bioelectronics, 2019, v. 123, p. 167–177*. https://doi.org/10.1016/j.bios.2018.08.037

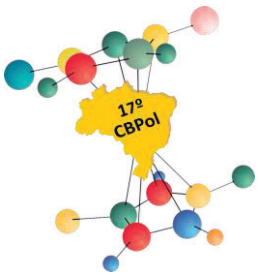

TENSILE PROPERTIES OF SELF-HEALING EPOXY COMPOSITES REINFORCED WITH GRAPHENE NANOPLATELETS

Ana Paula Nascimento [1]*, Cesar G. Ribeiro [1], Gustavo H. Zoschke[1], James Njuguna[2], Sergio H. Pezzin [1]

1 - Santa Catarina State University (UDESC), Center of Technological Sciences, Paulo Malschitzki Street #200, Zip Code 89219-710 Joinville, Santa Catarina, Brazil. anapaulanascimento0604@gmail.com
2 – Robert-Gordon University (RGU), School of Engineering, The Sir Ian Wood Building, Garthdee Road, Aberdeen, AB10 7GJ, United Kingdom.

Abstract – This work evaluated the tensile properties of self-healing composites of bisphenol-A diglycidyl ether (DGEBA) epoxy matrix containing poly(urea-formaldehyde) microcapsules filled with aminated polydimethylsiloxane (PDMS-a), reinforced with graphene nanoplatelets (GNP). The microcapsules were produced by interfacial polymerization, later infiltrated with the healing agent (PDMS-a) and further added to the epoxy matrix by mechanical stirring. A dispersion of GNP was then joined to the mixture together with the hardener to produce specimens for tensile tests by casting in soft molds. The results show that the presence of 1 wt% GNP changes the properties of the composites with an improvement in tensile strength and modulus in comparison with neat epoxy and specimens containing just microcapsules.
Keywords: *self-healing, epoxy, graphene, microcapsules, polydimethylsiloxane*
Fundings: Foundation for Research Support of Santa Catarina – FAPESC, National Council for Scientific and Technological Development (CNPq), Coordination for the Improvement of Higher Education Personnel (CAPES).

Introduction

The study of self-healing materials has been gradually growing, and this gives the possibility of increasing the useful life and improving the behavior of composites, reproducing the self-healing functionality observed in living organisms [1]. Common repair methods such as adhesives and resin sealing offer temporary healing solutions, as well as being time consuming, justifying the development of self-healing materials. The self-healing mechanisms are classified as intrinsic and extrinsic, and for the latter (extrinsic) the material does not have the latent self-repair function (intrinsic) and it is necessary to add a curing agent to the polymer matrix [2]. Extrinsic self-regeneration can take place by the use of microcapsules containing a healing agent, which can be ruptured by the growth of microcracks, releasing the healing agent and uniting the sides of the fissures, with no need for structural modifications in the polymer matrix. Poly(urea-formaldehyde) (PUF) is the most used material for the preparation of healing microcapsules, as it offers high mechanical and chemical resistance, low cost, and is fragile enough to break and release the healing agent [3]. Aminated polydimethylsiloxanes, which can be infiltrated in PUF microcapsules, proved to be a good healing agent, as it has high thermal stability (decomposition above 200 ºC) and an excellent interaction with epoxy matrices [4]. In the study by Weihermann [4] it was concluded that it would be desirable to use a catalyst to obtain a faster and more efficient crosslinking of PDMS-a in the epoxy matrix at room temperature, as well as the use of a reinforcement to compensate possible losses of mechanical properties by the addition of microcapsules. Graphene nanoplatelets (GNP) can be a good choice to address both issues, since graphene nanoparticles could reinforce the composite matrix, improving its mechanical performance, as well as have catalytic activity. There

are already studies of self-healing materials containing graphene nanoparticles that have improved properties compared to other conventional materials, such as improved mechanical properties, responsiveness to stimuli, high electrical and thermal conductivities, and greater healing efficiency [4,5].

Experimental

Synthesis of microcapsules and infiltration with PDMS-a

Hollow microcapsules were prepared following the procedures of Weihermann [4] and Da Costa [6]. After 4 hours of reaction, the microcapsules produced were washed with deionized water, vacuum filtered, and further dried at room temperature for 24 h. Hollow PUF microcapsules were then infiltrated with the healing agent (PDMS-a) following the procedure developed by Weihermann et al. [3], where PUF microcapsules is stirred with PDMS-a under vacuum for 5 h, filtered, and then washed with a solution of alcohol and chloroform (50/50) to eliminate the excess of non-encapsulated PDMS-a.

Preparation of tensile specimens

The specimens, prepared according to ASTM D368 standard, were divided into 4 types: neat epoxy matrix; epoxy matrix with graphene in different concentrations (0.5, 1 and 2 wt%) – Epoxy/GNP; epoxy matrix with PUF microcapsules (2 wt%) infiltrated with PDMS-a and graphene at 1 wt% – Epoxy/FPUF/GNP; and epoxy matrix with graphene (1 wt%) and hollow microcapsules (2 wt%) – Epoxy/HPUF/GNP. For the neat epoxy specimens, DGEBA (Araldite GY251) was mixed with its curing agent in the proportions indicated by the manufacturer and poured into soft silicone molds, where it was cured at room temperature for 24 h and post-cured for 1 h at 100 °C. For Epoxy/GNP specimens, the required amounts of GNP for each concentration were weighed in a glove box and mixed with DGEBA resin by sonication (3 min at 30% amplitude). The curing agent was then added to the mixture, which was poured into silicone molds. For the other two material types, the procedure was carried out in the same way, adding infiltrated (FPUF) or hollow PUF (HPUF) microcapsules to the mixture just before the curing agent.

Characterization of microcapsules and specimens

The microcapsules were characterized by optical microscopy to verify the morphology of the microcapsules and their average diameter. Optical microscopy was also used to examine whether PDMS-a infiltration was effective in the microcapsules. In characterizing the specimens, field emission scanning electron microscopy tests were carried out (SEM) in a JEOL field emission scanning electron microscope, model JSM-610JF with gold coating by sputtering, for morphological analysis. Tensile tests were carried out in an *Emic 23-100* universal testing machine, following ASTM D368.

Results and Discussion

Through optical microscopy, it was possible to verify that the formation of PUF microcapsules was efficient, with size distribution and morphology similar to those found by Da Costa [6].

The results of the tensile tests for Epoxy/GNP nanocomposites are shown in Fig. 1. The maximum stress supported by the specimen with neat epoxy is lower than those containing GNP. Among the specimens with GNP, the specimens with 1% GNP showed a maximum stress greater than the concentration of 0.5% by more than 24% - Fig. 1(a), as well as a higher Young's modulus - Fig. 1(b), but, on the other hand, at the 2% concentration, its maximum tension was significantly lower, probably due to the formation of agglomerates, as also reported by Da Costa [6].

In view of the results obtained, the use of 1% GNP was chosen to continue the study for the addition of hollow and PDMS-a-filled PUF microcapsules.

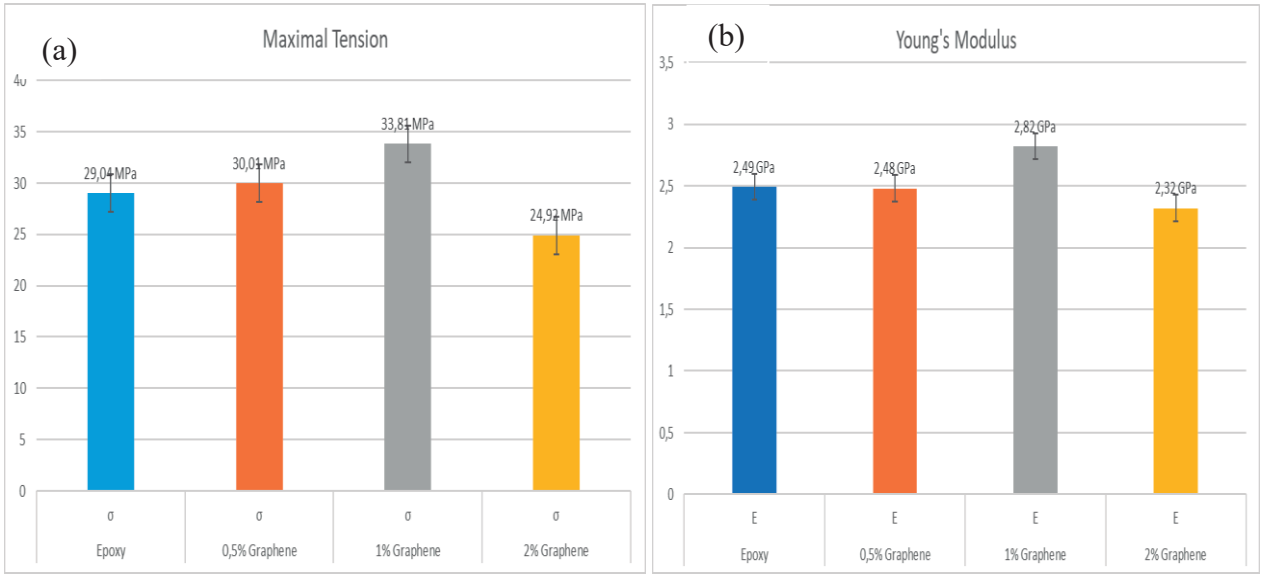

Fig.1 – Epoxy/GNP tensile test results. 1(a) - Maximum Stress and 1(b) - Young's Modulus

By SEM analysis - Fig. 2 -, it was possible to observe the fracture surface of Epoxy/GNP nanocomposites - Fig. 2(a), as well as the whole set of epoxy matrix, GNP and microcapsules (hollow and filled with PDMS-a) - Fig. 2(b,c,d).

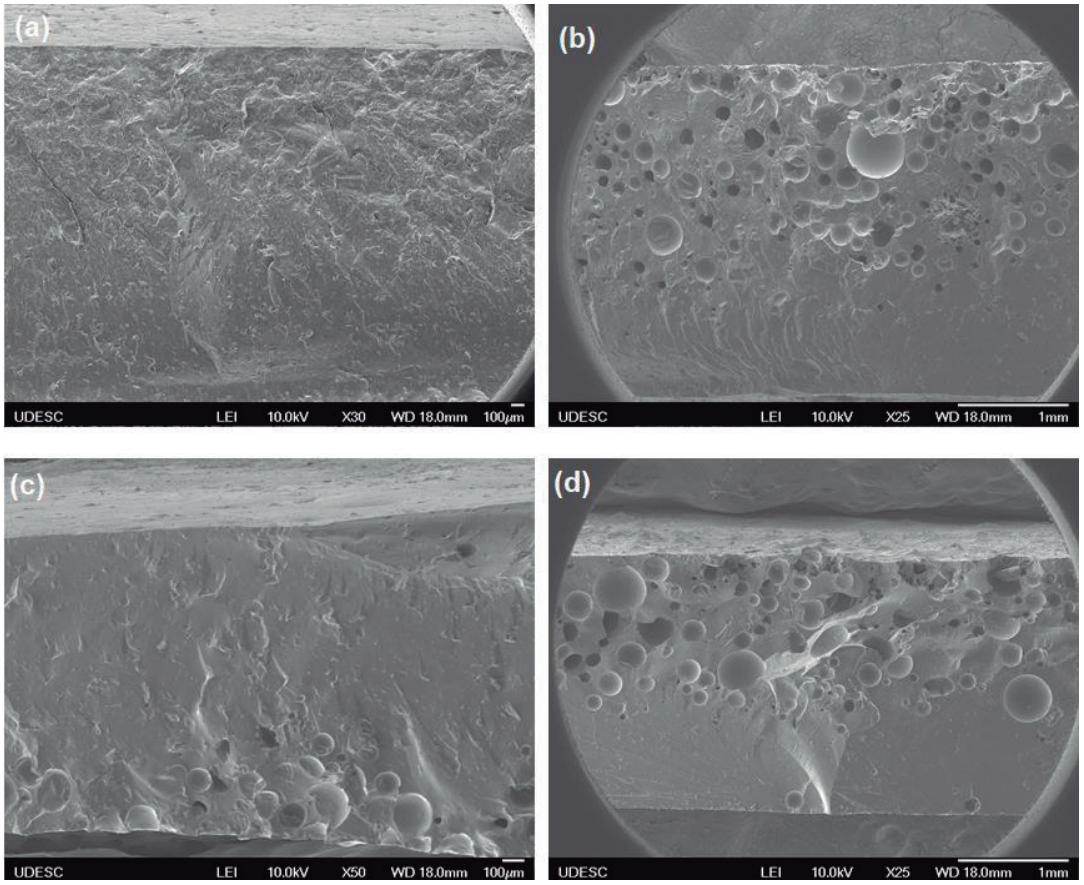

Fig. 2 – SEM analysis of the fracture surfaces of: (a) – 1% GNP; (b) – 1% GNP / 2% hollow microcapsules; (c) – 1% GNP / 2% microcapsules filled with PDMS-a; (d) – epoxy with 2% of hollow microcapsules.

Fig. 2(a) shows that GNP, at 1 wt% concentration, is well dispersed into the epoxy matrix. It is important to point out that in Fig. 2(c) there is a smaller number of microcapsules than in images (b) and (d) due to the higher masses of filled PUF microcapsules in comparison with hollow microcapsules (all were prepared at 2 wt%). It can be clearly observed that the microcapsules tend to concentrate on only one side of the specimen. The hollow ones in the upper side and the filled ones in the bottom side, as the former are lighter and the later are denser than the matrix. The presence of GNP does not seem to interfere with the distribution of the microcapsules.

The results of tensile test of specimens with the addition of HPUF and FPUF in Epoxy/GNP(1%) composites are shown in Table 2. It is possible to note that the presence of hollow microcapsules negatively interfered with the properties of the composite, with a maximum tension of only 17.6 MPa due to the presence of empty volumes, as they are filled with air. For the specimens with the addition of microcapsules filled with PDMS-a, the results were better than those with HPUF, but still lower than those found only with GNP reinforcement. The reason for this lower result may be due to their higher density, which causes the microcapsules to settle down and concentrate on only one surface of the specimen, i.e.., they and are not evenly distributed.

Table 2- Results of tensile tests of Epoxy/GNP composites with HPUF and FPUF

-	Epoxy	1% GNP	1% GNP 2% HPUF	1% GNP 2% FPUF
Max Tension - MPa	29.04	37.35	17.6	20.38
Max deformation – %	1.3	0.77	1.46	1.18
Young's Modulus - GPa	2.49	2.82	1.61	1.77

Conclusions

PUF microcapsules were successfully produced by interfacial polymerization, and through SEM it was concluded that the microcapsules disperse in the matrix in the presence of graphene nanoplatelets similarly to what happens without its presence, but that the density of the filled microcapsules interferes in the result of their dispersion. Tensile tests showed that the addition of 1% of the graphene reinforcement improved the mechanical properties of the composite and that the addition of 2% impaired these properties. It was also possible to conclude that the presence of hollow microcapsules negatively interfered in the tensile properties and that even though the addition of filled microcapsules improved the results in relation to the composites containing hollow ones, they were still inferior to those of composites with only GNP. These lower results are probably related to due to their high density, causing them to settle on only one surface of the specimen.

Acknowledgements

The authors are grateful to PIBIC-CNPq, FAPESC (2021TR928 and 2021TR778) and CAPES.

References

1. Thakur, Vijay K., Kessler, Michael R. Self-healing polymer nanocomposite materials: A review, Polymer, Volume 69, 2015, Pages 369-383, ISSN 0032-3861, https://doi.org/10.1016/j.polymer.2015.04.086
2. Ayeleru, Olusola O., Olubambi, Peter A. Concept of self-healing in polymeric materials, Materials Today: Proceedings, Volume 62, Supplement 1,2022, Pages S158-S162, ISSN 2214-7853, https://doi.org/10.1016/j.matpr.2022.04.811.

3. Weihermann, WRK, Meier, MM, Pezzin, SH (2019), Microencapsulated amino-functional polydimethylsiloxane as autonomous external self-healing agent for epoxy systems. J. Appl. Polym. Sci., 136, 47627. doi: https://doi.org/10.1002/app.47627.
4. Weihermann, Wanessa R. K, *et al*. Desenvolvimento de um sistema epoxídico autorregenerável utilizando polidimetiloxano amino funcional. Tese (Doutorado) - Universidade do Estado de Santa Catarina, Centro de Ciências Tecnológicas, Programa de Pós-Graduação em Ciência e Engenharia de Materiais, Joinville, 2015.
5. Li, G., Xiao, P., Hou, S., Huang, Y. Graphene based self-healing materials, Carbon, Volume 146, 2019.
6. Da Costa, S.F., Zuber, M., Zakharova, M., Mikhaylov, A., Baumbach, T., Kunka, D., Pezzin, S. H.. Nano Select. 2022, 3, 577. https://doi.org/10.1002/nano.202100091.

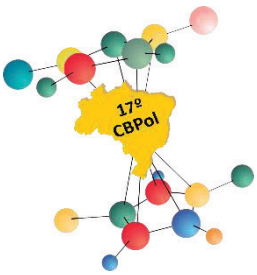

TITANIUM DIOXIDE NANOPARTICLES OBTAINED BY GREEN ROUTE AS AN UV-BLOCKER ADDITIVE IN POLYMERS

Laís Bomfim Borba[1*], Maria Elena Leyva González[1,2] and Estácio Tavares Wanderley Neto[2]

1 – Institute of Physics and Chemistry (IFQ), Federal University of Itajubá (UNIFEI), Itajubá, MG, Brazil
2 – High Voltage Laboratory (ISEE), Federal University of Itajubá (UNIFEI), Itajubá, MG, Brazil
*laisbb@unifei.edu.br

Abstract - Titanium dioxide nanoparticles (TiO_2NPs) are widely used in the plastic industry as an UV-blocker additive. In this work, TiO_2NPs were obtained through green synthesis using *Dillenia indica* L. leaf extract. TiO_2NPs were characterized using X-ray diffraction (XRD), scanning electron microscopy (SEM) and thermogravimetric analysis (TGA). The use of TiO_2NPs as an UV-blocker in a poly(propylene-co-ethylene) (EP) matrix was studied through artificial aging, exposing the samples to an UV fluorescent lamp in a chamber and measuring the degradation with the carbonyl index (CI) using Fourier-transform infrared (FTIR) spectroscopy. EP-TiO_2NPs compound was characterized by TGA and differential scanning calorimetry (DSC). The artificial aging revealed that TiO_2NPs and the commercial UV stabilizer show expected results to higher concentrations. Both showed UV stabilizing properties after longer exposure periods (four weeks).

Keywords: *Green synthesis*, *Dillenia indica L., titanium dioxide nanoparticles, poly(propylene-co-ethylene), UV-blocker additive*

Introduction

Polymeric materials acquired great importance to society in all fields of application, from general use plastics to high performance ones [1]. Under ultraviolet radiation, polymers go through oxidation reactions that may lead to premature failures. The reduction of the lifespan of a polymer is a huge problem that projectors, developers and the industry face and cause financial prejudices, physical damages, among other things [1, 2]. To improve the properties of a polymer and widen its applications, additives are purposefully added to it, and in the case of photodegradation, blockers, absorbers and stabilizers are examples of substances that minimize the effects of UV radiation, reducing failures and improving its resistance and durability in external areas. Titanium dioxide (TiO_2), like other inorganic pigments, block and disperse radiation, preventing it to reach chromophores under the polymer surface. The particle size is an important factor, as the titanium dioxide nanoparticles (TiO_2NPs) show greater UV absorption, letting the visible radiation pass and being able to be applied in transparent plastics [3].

Experimental

Materials

Titanium trichloride ($TiCl_3$) (15%) was purchased from Riedel-de Häen. *Dillenia indica* L. leaves were collected from the university *campus* and allowed to dry at room temperature for 48 h. Poly(propylene-co-ethylene) EP200K was purchased from Braskem and commercial UV stabilizer masterbatch was obtained from AMPACET.

Green synthesis of TiO_2NPs with Dillenia indica L. aqueous extract

The aqueous extract of *Dillenia indica L*. leaves was prepared by ultrasound assisted extraction. Firstly, the leaves were washed with distilled water and dried to 25°C during 24 h. Then for each gram of leaves it was added 20 mL of distilled water. Next, the system extraction was kept under ultrasonic bath (40 kHz) at 50°C for 60 min. Finally, aqueous extract of *Dillenia indica L*. leaves was obtained by gravity filtration. TiO_2NPs were synthesized by adding 6 mL of $TiCl_3$ (15%) to 35 mL of *Dillenia indica L*. extract at 50°C, keeping constantly stirring for 2 h. The solution was kept at 15°C for 24 h, then the precipitate of TiO_2/vegetal extract was gravity filtrated and dried for 24 h at 60°C. To characterization by SEM, X-ray diffraction and to preparation of EP-TiO_2NPs compound the powder of TiO_2NPs/vegetal extract of was calcinated to 500°C during 3h.

Physical-chemical characterization

FTIR measurements were taken with a Shimadzu IRTracer-100 spectrometer with ATR diamond/ZnSe accessory. The spectrum was obtained on transmittance mode, resolution of 4 cm^{-1}, from 4000 to 650 cm^{-1}. TGA measurements were carried out using TGA-50 (Shimadzu) under constant heating rate of 20°C.min^{-1} from room temperature to 1000°C (for TiO_2NPs); 800°C (for other samples) under N_2 atmosphere (50 mL.min^{-1}). The thermal properties were studied by melting temperature (Tm), melting heat (ΔHm) and the percentage of crystallinity (%C) from DSC. The analysis were performed using a differential scanning calorimeter DSC-60 Plus Shimadzu. Powder X-ray diffractograms were collected using X'Pert PRO (Malvern Panalytical), CuKα radiation (λ= 1,5406 Å), range between 5° and 90° (2θ) with step size of 0,02° and scanning speed of 5,0 sec.$step^{-1}$. SEM was conducted by EVO MA15 (Zeiss), operating at 20 kV, samples were previously metallized with Au in a Q150R ES (Quorum).

Preparation of EP polymer compounding and artificial aging study

The artificial aging study was realized using EP200K alone and polymer compounding of EP-TiO2NPs and EP-UV-stabilizer commercial. The EP polymers compounding was prepared using a combination of 99/1, 90/10 and 85/15 wt/wt of EP-TiO_2NPs and EP-UV-stabilizer. The polymers compounding was realized by manual physical mixed on Teflon for 15 seconds at 180°C. After manual processing, the samples were cooled down on room temperature. The artificial aging study was realized in a closed chamber with an UV ULTRA-VITALUX 300W OSRAM lamp. The measurements were taken by FTIR spectroscopy in different periods of UV exposure and the carbonyl index (CI) was calculated using Eq 1.

$$CI = \frac{area\ under\ absorption\ band\ from\ 1800\ to\ 1700\ cm^{-1}}{area\ under\ absorption\ band\ centered\ in\ 2720\ cm^{-1}} \qquad (1)$$

Results and Discussion

The SEM images show TiO_2NPs (Fig 2) with a morphology of nanoscale grains, aggregating and themselves forming bigger structures. Similar morphologies were reported for TiO_2NPs, obtained through other synthesis methods [3].

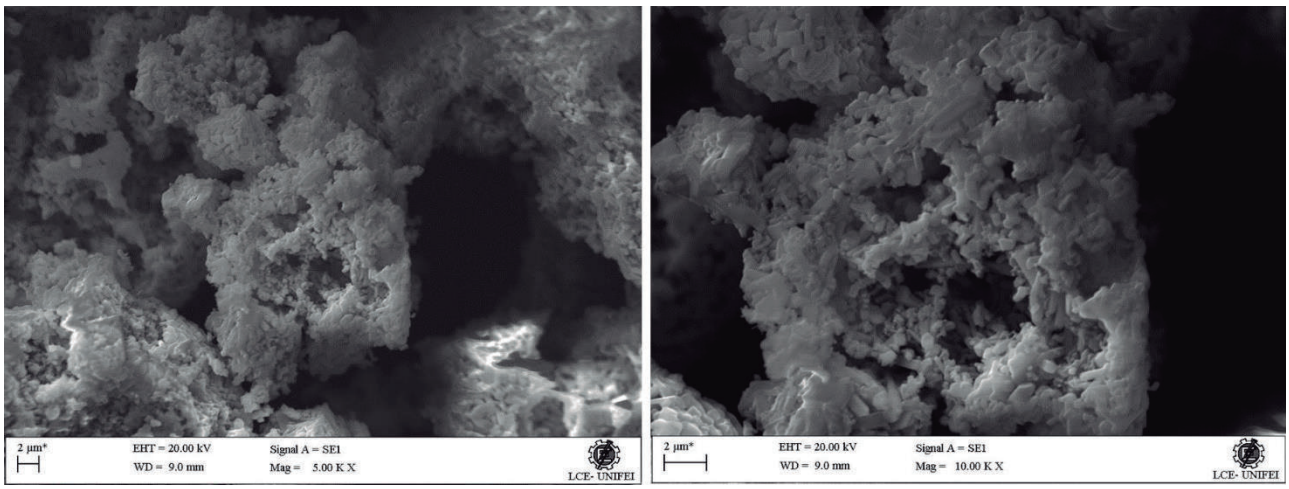

Figure 1 – SEM images of TiO_2NPs.

The obtained XRD pattern of TiO_2NPs (Fig 2 (a)) reveals that the product is highly crystalline and the crystallography planes are related to the anatase phase of TiO_2 [4]. The crystallite size was calculated from X-ray diffraction peaks by Scherrer equation [4], the average value found was 12.96±2.3 nm. TG/DTG curve of TiO_2/vegetal extract powder (Fig 2 (b)) show mass loss relative to humidity, low molecular weight compounds, polysaccharides, and secondary metabolites thermally stable. The 51,2% of remaining mass is related to the TiO_2NPs and other stable organic compounds that were not degraded until the temperature of 800°C.

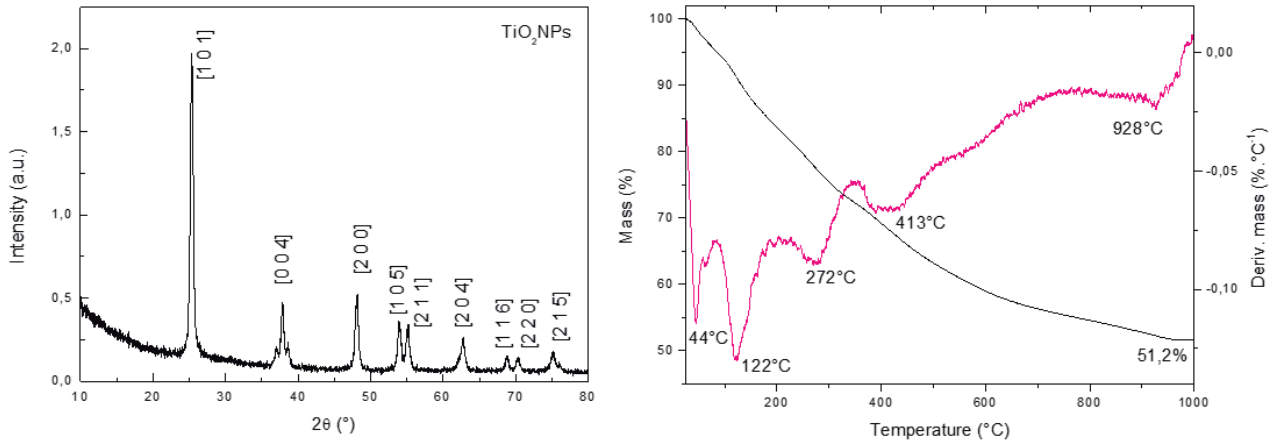

Figure 2 – XRD pattern of TiO_2NPs (a); TG/DTG curve of TiO_2NPs under N_2 atmosphere (b).

The carbonyl index was used to evaluate quantitatively the extend of polymer degradation. The CI was determinated by the ratio between specified area under the range of 1800 to 1700 cm^{-1} (related to carbonyl peaks) and a reference peak. The CI is useful not only to measure polyolefin oxidation, but also to predict the lifespan of polymeric materials in order to create stabilizers [5]. The CI of all samples was calculated using Eq 1. Fig 3 shows how the CI of every sample change over time during the exposure to UV radiation.

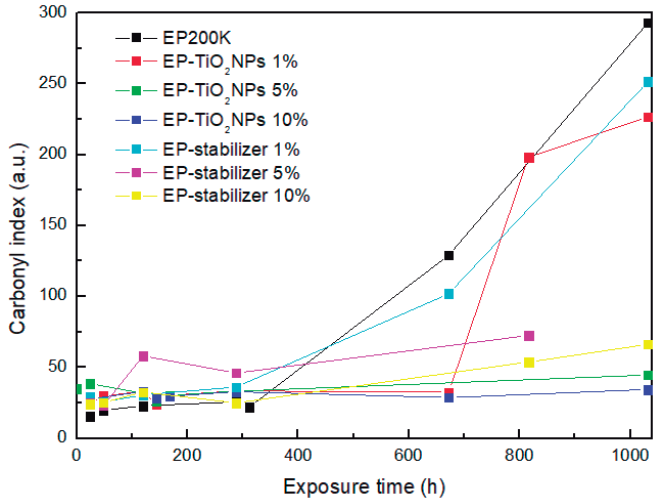

Figure 3 – Carbonyl index of all samples over total exposure time.

Table 1 shows that the crystallinity degree of EP copolymer is lightly affected by the presence of the TiO_2NPs.

Table 1. Characteristics of DSC curves and crystallinity degree.

Samples	**T_m (°C)**	**ΔH_m (J/g)**	**C (%)**
EP200K	164.7	23.1	11.1
EP-1% TiO_2NPs	160.4	10.5	9.6
EP-5% TiO_2NPs	161.3	22.2	10.2
EP-10% TiO_2NPs	161.5	28.1	9.7

Fig 4 compares DTG curves of samples before (a) and after (b) artificial aging. The Fig 4 (a) show that the presence of TiO_2NPs speed up the initiation of thermal degradation. But it does not have significant influence on maxima degradation temperature of the principal chain in EP copolymer.

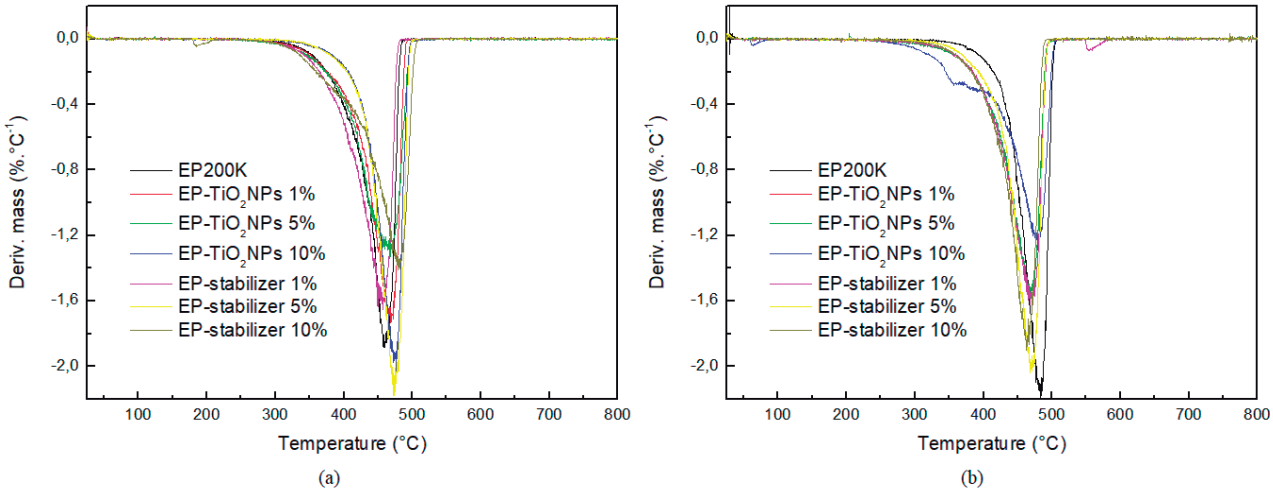

Figure 4 – DTG curves of prepared samples before artificial aging (a); after artificial aging (b).

The DTG curves (Fig. 4 (b)) shows that the oxidation degree present in the EP copolymer, after artificial aging, does not influence significantly on thermal degradation.

Conclusions

On this work, TiO_2NPs anatase phase were successfully obtained via green synthesis, confirmed by XRD. The artificial aging of EP-TiO_2NPs compound show UV stabilization to samples with higher concentration of additives (5 and 10%). The DSC analysis shows that the crystallinity degree of EP copolymer is not affected by the presence of the TiO_2NPs. DTG analysis of aged samples show that in the range studied the oxidation of the EP chains, it did not influence in the thermal degradation of EP copolymer. Therefore, we conclude that the TiO_2NPs synthesized by green route has potential to be used as an UV-blocker to polymers.

Acknowledgements

This research project to thank the Financial Support of Minas Gerais Research Funding Foundation (Fapemig) through the project APQ-02676-16.

.

References

1. M. Rabello, Ph.D. Thesis, University of Newcastle upon Tyne, 1996.
2. M. Rabello, Estruturas e Propriedades de Polímeros, e-guide, 2021.
3. M. Tolinski, *Additives for Polyolefins: Getting the Most Out of Polypropylene, Polyethylene and TPO*, William Andrew, USA, 2009.
4. S. Al-Taweel; H. Saud Journal of Chemical and Pharmaceutical Research 2016, 620. https://www.jocpr.com/articles/new-route-for-synthesis-of-pure-anatase-tio2-nanoparticles-via-utrasoundassisted-solgel-method.pdf
5. A. Kashale; K. Gattu; K. Ghule; V. Ingole; S. Dhanayat; R. Sharma; J. Chang; A. Ghule Composites Part B 99 2016, 297. https://doi.org/10.1016/j.compositesb.2016.06.015.
6. J. Almond; P. Sugumaar; M. Wenzel; G. Hill; C. Wallis e-Polymers 2020, 369. https://doi.org/10.1515/epoly-2020-0041.

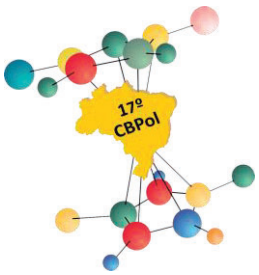

WATER ADSORPTION BEHAVIOR IN CARBON NANOTUBES PLASMA-FUNCTIONALIZED WITH MALEIC ANHYDRIDE AND UREA

Teresa T. Steffen[1]*, Luis C. Fontana[2], Peter Hammer[3], and Daniela Becker[4]

1 – Department of Production and Systems Engineering, University of Santa Catarina State (UDESC), Santa Catarina, SC, Brazil teresa.ts@udesc.br
2 – Department of Physics, University of Santa Catarina State (UDESC), Santa Catarina, SC, Brazil
3 – Department of Chemistry, São Paulo State University (Unesp), São Paulo, SP, Brazil
4 – Department of Mechanical Engineering, University of Santa Catarina State (UDESC), Santa Catarina, SC, Brazil

Abstract
Carbon nanotubes (CNT) were treated by inductively and capacitively coupled plasma, using radio frequency and asymmetric bipolar pulsed plasma sources, respectively. The source of functional groups to be attached to the CNT surface were the solid organic compounds maleic anhydride or urea. Oxygen and nitrogen groups were bonded to CNT, which was confirmed by XPS analysis. After treatment, CNT has become dry, meaning water content drops from 7.7 % (in pristine CNT) to zero, according to the fitting of O 1s high-resolution XPS spectra. After one year, samples were analyzed again. Although CNT treated with urea began to adsorb water, the nanoparticles treated with maleic anhydride remained dry even after being kept in a water solution for 24 hours. The results indicate the possibility of using the treated carbon nanotubes as adsorbing agents in water treatment applications.

Keywords: *carbon nanotube, plasma, functionalization, water adsorption*

Introduction

Carbon nanotubes (CNT) are very well-known nanoparticles by their excellent performance in electrical, thermal, and mechanical properties [1], and recently have drawn attention for being used as adsorbing agents in water treatment and desalination [2-4]. However, CNT needs to be surface functionalized to be applied in these uses to activate their surface and improve dispersion and adsorption capability [5]. Besides, the treatment of CNT can make them more effective in removing water pollutants, depending on the type of functional group inserted: oxygen groups facilitate dye removal, while nitrogen groups improve the adsorption of heavy metals [6,7]. Once the final use of the nanoparticles is related to an environmental problem, i.e., water resource, it is interesting also use an eco-friendly process to treat the CNT. Plasma treatment is an excellent technique to be used, replacing wet chemical routes that generate waste and second products [8]. Therefore, this work aims to use different plasma treatments and functionalizing agents to surface-modify CNT and evaluate their behavior related to water adsorption through XPS analysis.

Experimental

Materials

Multiwalled carbon nanotubes were purchased from Chengdu Organic Chemicals Co.Ltd., TNIM4 category, with purity > 95 %, external and internal diameter of 10-30 nm and 5-10 nm, respectively, and 10-30 µm length, according to the manufacturer. Maleic anhydride (purity > 98.5 %) was provided by Sigma-Aldrich, and urea (purity > 99 %) by Dinâmica Química

Contemporânea Ltda. Argon gas (ultrapure, purity > 99.999 %) was used in plasma treatment. Methanol (minimal dose 99,8 %) was purchased from Dinâmica Química Contemporânea Ltda and utilized to wash the samples before analysis.

Methods

CNT was manually mixed with the functionalizing agent (maleic anhydride or urea) in the solid state, according to previous work [9,10], before plasma treatment. The CNT mixed with MA was treated in an inductively coupled plasma (ICP) reactor, for 30 minutes, with 35 W powered by radio frequency [9]. The CNT mixed with urea was treated in a capacitively coupled plasma (CCP) reactor, for 30 minutes, with power supplied by an Asymmetric Bipolar Plasma Power Supply (ABiPPS) [10]. After treatment, samples were washed following the procedure described in another work [9]. Samples were kept closed in falcon tubes for one year, submerged in distilled water for 24 hours, centrifuged for 10 minutes, and dried at 70 °C for one hour. XPS analysis was conducted in three different periods throughout the samples' life: 1) after plasma treatment, 2) after one year, and 3) after water exposure for 24 hours. Samples were named according to it, as shown in Table 1.

Table 1

Sample name	Functionalizing agent	Plasma and source	Period throughout life
CNT	-	-	-
CNT.MA.P	Maleic anhydride	ICP, RF	After plasma
CNT.MA.Y	Maleic anhydride	ICP, RF	After one year
CNT.MA.W	Maleic anhydride	ICP, RF	After water exposure
CNT.U.P	Urea	CCP, ABiPPS	After plasma
CNT.U.Y	Urea	CCP, ABiPPS	After one year
CNT.U.W	Urea	CCP, ABiPPS	After water exposure

Summary of samples' names and respective characteristics

Characterization technique

Samples were chemically characterized by X-ray Photoelectron Spectroscopy (XPS) in a Thermo Scientific spectrometer (K-Alpha), operating at a base pressure below 10^{-7} m Bar. The X-ray Al-Kα (hν = 1486.6 eV) was used as the excitation source, and the pass energy was set to 200.000 eV for the survey and 50.000 eV for high-resolution scans. The number of scans, dwell time, and energy step size were set as 10, 10 ms, 1.000 eV for the survey, 5, 50 ms, and 0.100 eV for high-resolution scans. High-resolution spectra were fitted using the Voigtian function, a combination of Gaussian (70 %) and Lorentzian (30 %) profiles.

Results and Discussion

From XPS Survey, we obtained the samples' chemical composition (Table 2), which evidence the plasma functionalization of carbon nanotubes by the increase in oxygen content (for CNT.MA.P and CNT.U.P samples) and the appearance of nitrogen contribution (CNT.U.P sample). It is highlighted that for both samples (CNT.MA.P and CNT.U.P), water adsorption in carbon nanotubes drops from 7.7 % (from O 1s), in the CNT sample, to zero after treatment, which is a combination of plasma process along with methanol washed procedure, as explained in another work [10].

XPS data also provided the bonding type in each sample, obtained from fitting C 1s and O 1s spectra (Table 2). Interestingly, after one year, the sample treated by plasma with maleic anhydride (CNT.MA.Y) still had no water adsorbed. It indicates that CNT remains stable after air exposure and prolonged time. More than that should be highlighted the fact that even after suspension in water for 24 hours (CNT.MA.W), the nanoparticles did not recover their nature characteristic of keeping water in their inner, which is evidenced by O 1s fitting spectra that do not

show H_2O contribution (Fig 1). It could indicate that plasma modifications in carbon nanotubes were still on when the submission to water was tacked.

Table 2

Sample name	Atomic %			% related to area from C 1s or O 1s					
	C 1s	O 1s	N 1s	CC arom	C-H	C-O/ C-N	C=O	O-C=O/ $O=CN_2$	H_2O
	From Survey			From C 1s					From O1s
CNT	98.0	2.0	-	78.1	5.2	5.1	1.7	2.2	7.7
CNT.MA.P	96.5	3.5	-	77.5	6.1	4.5	1.9	3.2	-
CNT.MA.Y	97.0	3.0	-	79.3	4.4	4.5	1.9	2.4	-
CNT.MA.W	98.0	2.0	-	77.4	6.0	3.3	2.7	2.6	-
CNT.U.P	95.2	3.6	1.2	64.3	13.1	8.6	2.2	4.0	-
CNT.U.Y	96.2	3.0	0.8	59.8	17.1	9.1	2.7	3.1	5.1
CNT.U.W	95.7	3.4	0.9	61.2	16.1	9.0	2.8	3.6	8.7

XPS results obtained from Survey, C 1s, and O 1s spectra.

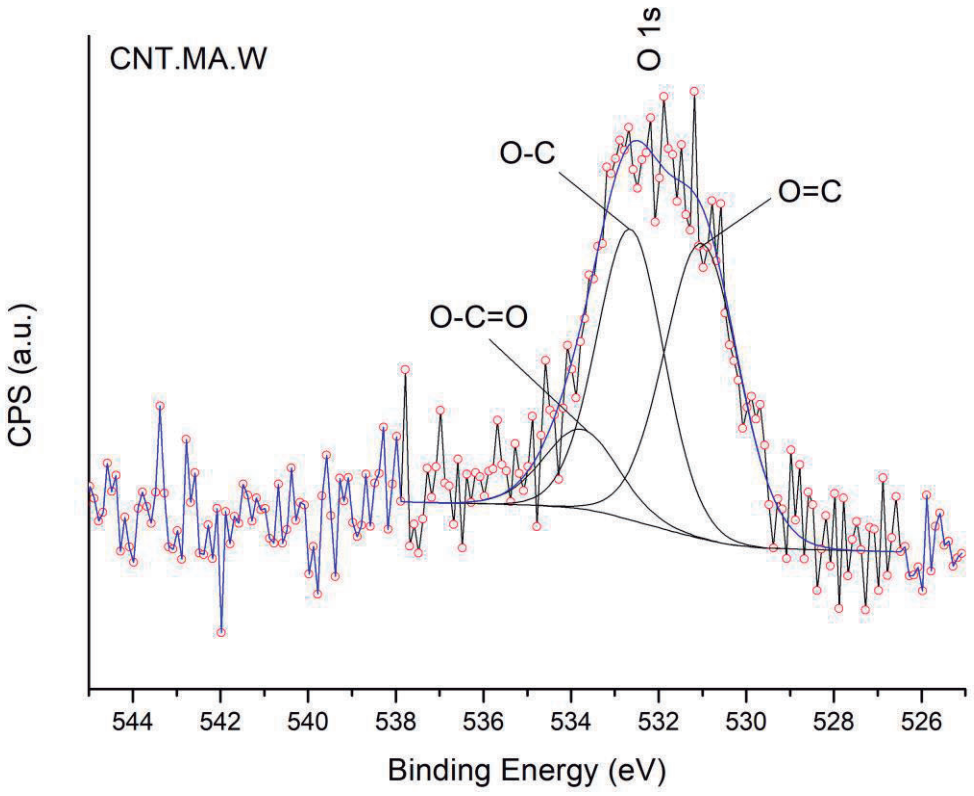

Figure 1 – XPS O 1s spectra fitted for CNT.MA.W sample, indicating no water molecules present.

Otherwise, for the sample treated with urea, despite the water elimination in the first analysis, just after plasma treatment (CNT.U.P), the adsorption returns to happen sometime within a year since the O 1s fitted spectra show a water component in the CNT.U.Y sample: 5.1 % (from O 1s). Besides, in this period, probably due to air exposure, there was a small hydrocarbon deposition in the CNT surface, observed by the increase in C-H bonds, which attenuated the oxygen and nitrogen signals. However, after water exposure for 24 hours, that effect is reverted, as can be seen by comparing the values of CNT.U.Y and CNT.U.W samples in Table 2. In previous work [10], it

was established that there seems to be a correlation between functional group content and the ability to CNT adsorb water: as the former increase, the latter decrease. So, as the functional groups were covered by hydrocarbons within a year, CNT would have recovered their ability to adsorb water.

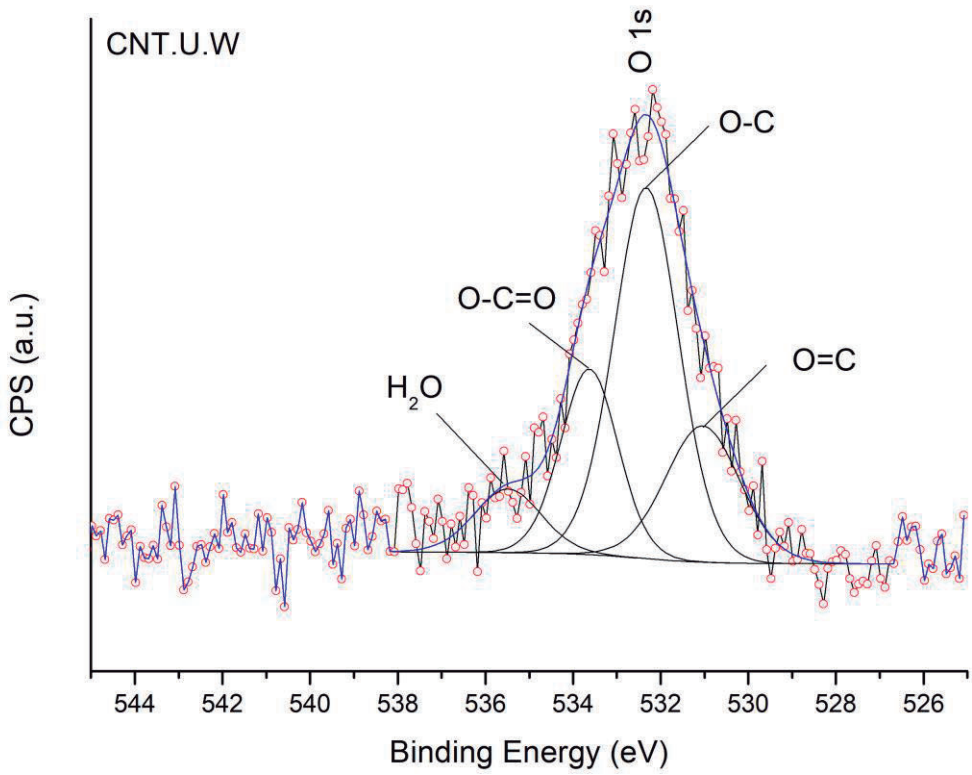

Figure 2 - XPS O 1s spectra fitted for CNT.U.W sample, evidencing water adsorbed in carbon nanotubes.

The different water absorption behavior between samples functionalized with maleic anhydride and urea could be related to functional groups formed in the CNT surface during the plasma treatment. Table 2 shows that C-O/C-N contributions for CNT.U.P are almost twice the values for CNT.MA.P, and C=O content in that one is also higher than in this one, which could favor the interaction with air and water in the long term. Besides, in the sample treated with urea, there are nitrogen atoms, which are not present in the CNT.MA.P sample. So, there is a clear difference in CNT behavior related to water adsorption depending on the plasma treatment to which they were submitted. Further analyses need to be done to establish the exact phenomenon that controls the recovery of CNT's ability to adsorb water.

Conclusions

Carbon nanotubes have been successfully functionalized by both RF-inductively and ABiPPS-capacitively coupled plasma, promoting attachment of oxygen and nitrogen groups by using maleic anhydride and urea as functionalizing agents. CNT.MA.P and CNT.U.P samples presented no water in their composition, meaning that surface functionalization resulting from plasma treatment alters CNT-water interaction. After one year, however, different behavior regarding water adsorption was observed for CNT treated with maleic anhydride or urea, the former the one who kept the ability to repeal water even after having been in an aqueous solution by 24 hours one year later. The nanoparticles' ability to repeal water, identified in this work, could indicate a possible application of

these modified CNT in water treatment once a selective particles' interaction is needed when CNT is used as adsorbing agent.

Acknowledgments
The authors would like to thank CAPES and PROMOP/UDESC for the financial support throughout the development of this project. The authors are also thankful for the Multi-User Facility infrastructure of Santa Catarina State University's Technological Sciences Center.

References

1. J. N. Coleman, et al. Carbon 2006, 44, 1624-1652. https://doi.org/10.1016/j.carbon.2006.02.038
2. B. Sarkar, et al. Science of the Total Environment 2018, 612, 561-581. https://doi.org/10.1016/j.scitotenv.2017.08.132
3. J. Xu, et al. Chemosphere 2018, 195, 351-364. https://doi.org/10.1016/j.chemosphere.2017.12.061
4. K. M. Lee, et al. Materials Science & Engineering B 2018, 236-237, 61-69. https://doi.org/10.1016/j.mseb.2018.12.004
5. M. U. Farid, et al. Chemical Engineering Journal 2017, 325, 239-248. https://doi.org/10.1016/j.cej.2017.05.020
6. R. K. Ibrahim, et al. Journal of Environmental Management 2019, 235, 521-534. https://doi.org/10.1016/j.jenvman.2019.01.070
7. D. Shao, et al. Chemical Engineering Journal 2012, 185-186, 144-150. https://doi.org/10.1016/j.cej.2012.01.06
8. B. Ouyang, et al, Materials Today Nano 2018, 3, 28-47. https://doi.org/10.1016/j.mtnano.2018.11.002
9. T. T. Steffen, et al. Applied Surface Science 2019, 491, 405-410. https://doi.org/10.1016/j.apsusc.2019.06.176
10. T. T. Steffen, et al. Applied Surface Science 2022, 583, 152493. https://doi.org/10.1016/j.apsusc.2022.152493

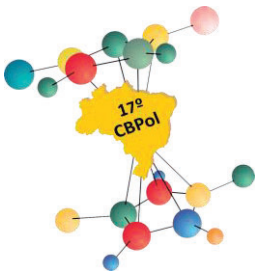

ALGINATE FILAMENTS REINFORCED WITH CELLULOSE NANOCRYSTALS FROM TEXTILE COTTON WASTE

Victor Kreutzfeld[1], Lucas S. Silva[1] and Andrea C. K. Bierhalz[1]*

1 – Department of Textile Engineering (DET), Federal University of Santa Catarina (UFSC) – Campus Blumenau, Blumenau, SC, Brazil andrea.krause@ufsc.br

Abstract - Cotton fiber is the most used natural fiber in the textile industry because of characteristics such as softness, breathability, and moisture absorption [1]. Along the cotton textile chain, a large amount of waste is generated, which represents environmental impacts. However, cotton has a high cellulose content and can be used to obtain cellulose nanocrystals (NCCs), which has attracted increasing attention for application as mechanical reinforcement in natural polymer matrices due to its high rigidity and crystallinity, low density, and biodegradability [2]. This study aimed to obtain NCCs from industrial textile cotton waste and to produce alginate filaments with different proportions of NCCs. The isolation of NCCs from cotton was performed by hydrolysis with an aqueous sulfuric acid solution at 60% (w/w) in reaction at 45°C and 45 minutes. The nanocomposite filaments were obtained by wet spinning of a 2% (w/v) sodium alginate solution containing different mass proportions of NCCs (1, 3, 5, 10, and 20 % (g NCC/g alginate) using an infusion pump at 80 mL/h. After extrusion, solidification took place in a 10% (w/v) $CaCl_2$ aqueous bath. NCCs with whisker shape, 11–19 nm diameter, crystallinity index of 87%, and reaction yield of 83% were obtained from hydrolysis. Mechanical results indicated that all NCCs concentrations significantly ($p < 0.05$) increase the tensile strength and reduced elongation at break of the nanocomposite filaments compared to the pure alginate filament. The greatest increase (> 200%) was observed for the 3% and 5% concentrations. In filaments with higher NCCs concentrations (10% and 20%), tensile strength was reduced, which can be attributed to the agglomeration of NCCs in the matrix. In general, it was concluded that it is possible to obtain NCCs from cotton waste and that concentrations of up to 5% can form nanocomposite alginate structures with promising mechanical properties.

References

1. C. Ling; L. Gui; Z. Wang *Industrial Crops and Products* 2023, *194*, 116264. https://doi.org/10.1016/j.indcrop.2023.116264.
2. J. Wang; X. Liu; T. Jin; H. He; L. Liu *Journal of Biomaterials Science, Polymer Edition* 2019, *30*, 919. https://doi.org/10.1080/09205063.2019.1612726.

Fundings: CNPq (Process 438821/2018-1).

Keywords: *Cellulose nanocrystals, cotton waste, alginate, nanocomposites.*

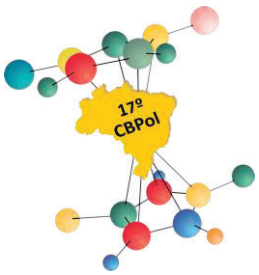

ANALYSIS OF NANOCOMPOSITES WITH PIEZOELECTRIC PROPERTIES COMPOUNDS OF POLY(VINYLIDENE FLUORIDE) AND GRAPHENE OXIDE

Anna L. Souza[1], Gabriel A. Caetano[1] and Wagner M. Pachekoski[1]

1 – Department of Mobility Engineering - Technological Center of Joinville, Federal University of Santa Catarina (UFSC), Joinville, SC, Brazil; annaluizagtba@gmail.com (A.S.); gabriel.alexandre.caetano@gmail.com (G.C.); wagner.pachekoski@ufsc.br (W.P).

Abstract - Poly(vinylidene fluoride) (PVDF) is a semicrystalline thermoplastic fluoropolymer, with crystallinity ranging between 40 and 60%, which can crystallize in four possible modifications, named alpha (α), beta (β), gamma (γ) and delta (δ). The β phase guarantees pyro and piezoelectric properties, that is, it converts mechanical energy into electrical energy and vice versa. One way to obtain the β phase is using a solution with dimethyl formamide (DMF) at a controlled temperature. The addition of graphene oxide (GO) to this solution can significantly increase the dielectric properties of PVDF, in addition to impacting changes in mechanical properties. Therefore, this work has the general objective of analyzing nanocomposites with piezoelectric properties, in addition to presenting the analysis of the GO dispersion in the polymeric solution and the thermal, morphological and electrical characterization of the resulting nanocomposites. The proposed methodologies were the generation of films and electrospinning, these requiring different realization processes. The best dispersion method found for the GO was direct dispersion in the solvent via cleaning ultrasound and the electrical characterization was performed using an oscilloscope. As a result, the nanocomposite film generated a maximum voltage value of 13 V and showed agglomeration of the GO in its morphology, while the electrospun blanket generated a voltage of 33 V for the material with the addition of oxide, in addition to providing better dispersion in the final nanocomposite.

References

1. N. An, et al. Polymer 2014, 132, 1.
2. C. Botas, et al. Elsevier 2011, 275.
3. M. G. Broadhurst; G. T. Davis. Ferroelectrics 1984, 60, 3.
4. G. Kang; Y. Cao. Journal Of Membrane Science 2014, 463, 145.
5. S. Nirmal. et al. In: Proceedings of society of photo-optical instrumentation engineers, preparation of reduced Graphene/PVDF nanocomposites using co-solvent approach, California 2012, 1.

Fundings: National Council for Scientific and Technological Development (CNPq).

Keywords: *Piezoelectricity. Nanocomposites. Poly(vinylidene fluoride). Graphene oxide. Electrospinning.*

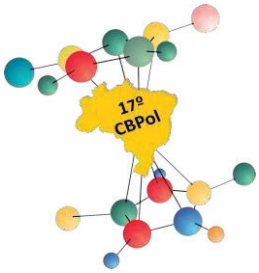

ANALYSIS OF THE MECHANICAL PROPERTIES OF NANO COMPOSITE OF PLA POLYMERIC MATRIX WITH VEGETABLE FIBER AND NANO PARTICLE SUBMITTED TO 3D PRINTING

Thais S. Silva[1]*; Joziane S. Cunha[1]; José C. M. Neto[2].

1 – Department of Materials Engineering, State University of Amazonas (UEA), Manaus, AM , Brazil
2 – Department of Materials Engineering, Universidade Estadual de Campinas (FEQ/UNICAMP), São Carlos, SP, Brazil
*Corresponding author: tss.emt18@uea.edu.br[1]**

Abstract - SARS-CoV-2 of zoonotic origin called corona virus, can result in severe acute respiratory syndrome (SARS). It was detected in Wuhan, Hubei Province, China, in early December 2019 (PAHO, 2018). Due to the rapid increase of infected people in the world, in March 2020, the COVID-19 pandemic was announced by the World Health Organization (WHO, 2020). Currently, to minimize contagion, the product most used during the pandemic by the population and health professionals is 70% alcohol, as it is low cost and easy to use. However, there has been an increase in the use of disposable packaging that harms the environment (ANVISA, 2020). Currently, there are works in the literature on bioplastics with vegetable fiber fillers, presenting good mechanical properties and using polymeric nanocomposites with nanoparticles of metallic oxides such as copper, where their incorporation can obtain optical, electronic, mechanical effects and antimicrobial improvements through the extrusion process of filaments that, in the latter case, the increase in biocidal capacity was associated with a synergistic effect of the two components present in the composite. Therefore, the matrix is not only a support for nanoparticles, but it can also improve the antibacterial performance and expand the possible applications of this material to meet different requirements in the biomedical area, water treatment and food industry (De Paoli, MA, 2017). Thus, the objective of this project is to produce by extrusion antimicrobial bioplastic filaments (PLA, Vegetal Fiber and Copper Nano Particle) to be submitted to 3D printing and to evaluate the mechanical and thermal properties.

References

1. PAN AMERICAN HEALTH ORGANIZATION. COVID-19 (disease caused by the new coronavirus). Brasília, DF, 2020.
2. National Health Surveillance Agency – ANVISA. Resolution of the collegiate board - RDC nº 222. Regulates Good Practices in the Management of Waste from Health Services and other measures. March 28, 2018.
3. De Paoli, M.A.; Degradation and Stabilization of Polymers, Chemkeis, 2nd ed, 2008. Available at http://www.chemkeys.com/blog/wpcontent/uploads/2008/09/polimeros.pdf. Accessed on December 23, 2017

Fundings: Research Support Foundation of the State of Amazonas - FAPEAM

Keywords: *PLA bioplastic, vegetable fiber, nanoparticle, antimicrobial, nanocomposites*

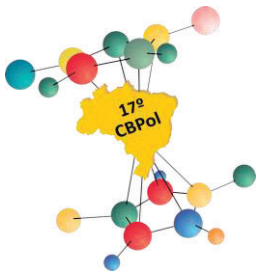

APPLICATION OF PANI/TITANIA HYBRIDS IN ELECTRORHEOLOGICAL FLUIDS

Vanessa Sobreiro Feitosa[1*] and Bluma Guenther Soares[1]

:

1 – Institute of Macromolecules Professora Eloisa Mano, Federal University of Rio de Janeiro (UFRJ), Rio de Janeiro, RJ, Brazil

vanessafeitosa@ima.ufrj.br

Abstract - Electrorheological (ER) fluids are intelligent materials that show reversible changes in their structure and in their rheological properties, exhibiting transitions from the lowest conducted state to the highest admitted state, when an external electric field is applied [1-2]. Normally, they are colloidal suspensions of polarizable solid particles, which may be organic or inorganic particles dispersed in a non-conducting liquid [3] such as silicone oil, paraffin, or vegetable oil. The ER effect is characterized by a dipole phenomenon, where the polarized particles are oriented parallel in the direction of the applied field, forming a columnar microstructure [4]. Some important ER fluids include liquids containing inorganic salts and oxides, conductive polymers, and other substances as dispersed phases [5]. A particularly promising family is polyaniline (PANI) and its derivatives, mainly due to its easy synthesis and low production cost [6]. The present work describes the synthesis of hybrids of PANI and organically modified titania, in different proportions (1:1, 1:2 and 2:1), and the formulation of the ER fluid in silicone oil, in a proportion of 15% w/v. The PANI/titania combination resulted in an improved electrorheological response when compared to the individual response of these particles. In addition, an increase in shear stress was observed with an increase in the shear rate, characteristic of ER fluids, and good electrical stability of the dispersion, thus indicating excellent electrorheological performance. Other characterizations were carried out, such as direct current (DC) and alternating current (AC) conductivity analysis, thermogrevimetry (TGA), Fourier-transform infrared spectroscopy (FTIR), differential scanning and calorimetry techniques (DSC), in order to confirm the synthesis of the proposed material and evaluate its properties.

References

1. A. Gozdalik.; H. Wycislik; J. Plocharski. Synthetic Metals, 109 (2000) 147-150. DOI:10.1016/S0379-6779(99)00216-7.
2. J.A Marins.; B.G. Soares.Coll. Surf. A – Physicochemical and Eng Asp 529 (2017) 311-319. DOI:10.1016/j.colsurfa.2017.05.091
3. A.V. Agafonov; A.G. Zakharov. Russian Journal of General Chemistry 80 (2010) 567-575. https://doi.org/10.1134/S1070363210030382
4. Y. Liang; D. Haung; X. Zhou; Z. Wang; Q. Shi; Y. Hong; H. Pu; M. Zhang; J. Wu; W. Wen. Journal Pre-proofs, 2022. https://doi.org/10.1016/j.eng.2022.01.014
5. H. Block.; J. P. Kelly. Journal of Physics D-Applied Physics 21 (1988) 1661-1677. DOI 10.1088/0022-3727/21/12/001
6. J.A. Marins; F. Giulieri.; B.G. Soares; G. Bossis. Synthetic Metals 185-186 (2013) 9-16. DOI:10.1016/j.synthmet.2013.09.037

Fundings: This study was financed in part by the Coordenação de Aperfeiçoamento de Pessoal de Nível Superior - Brasil (CAPES) - Finance Code 001

Keywords: *electrorheological fluids, polyaniline, titania.*

APPLICATION OF ZnO NANOPARTICLES IN THE DEVELOPMENT OF ACRYLIC RESIN-BASED PAINT WITH ANTIFOULING PROPERTIES

Leonardo R. da Maia[1], Dafne A. do Nascimento[1], Samanta Finsterbuch[2], Renato C. T. Porto[2] Patrícia Z. Uchôa[2], Jean C. Hoepfner[3], Wagner M. Pachekoski[1]

1 – Department of Mobility Engineering, Joinville Technological Center, Federal University of Santa Catarina (UFSC), Joinville, SC, Brazil
leonardo.ramthun@grad.ufsc.br
2 –Department of Chemistry, Center of Technological Sciences, Santa Catarina State University (UDESC), Joinville, SC, Brazil
3 – Center of Technological Sciences, Santa Catarina State University (UDSC), Joinville, SC, Brazil

Fouling is a phenomenon in which undesirable substances such as proteins, organisms and inorganic molecules accumulate on marine structures such as boats due to exposure to the environment. As these substances accumulate, they can cause several negative effects, such as reducing a ship's top speed and increasing fuel consumption. Thus arose the need to develop nontoxic antifouling coatings. The present research studied the incorporation of ZnO nanoparticles (NpZnO) into acrylic-based paint in the proportions 0,2%wt, 0,5%wt and 1%wt seeking it an anti-fouling characteristic through the antifungal and bactericidal properties that these nanoparticles have. The acrylic-based base paint used was provided by WEG Tintas company and the NpZnO were provided by the company Nório Nanotecnologia. The dispersion of the NpZnO in the matrix was carried out by sonication, and the resulting samples underwent characterizations, such as DSC, FTIR and TEM. To verify its bactericidal properties, samples of the NpZnO went through a microbiological analysis with *Escherichia coli*, *Bacillus subtillis,* and *Vibrio aestuarianus* following the adapted ASTM E2149 standard. Photos of the *Escherichia coli* analyses are showed in the Fig 1, with which was possible to confirm the reduce of the activities through 100%. In addition to these analyses, to verify its applicability, the samples were applied on steel plates and exposed to an environment that simulated marine conditions for a period of 30 days. This experiment has not yet been completed, however, so far, the three formulations have not shown signs of encrustation.

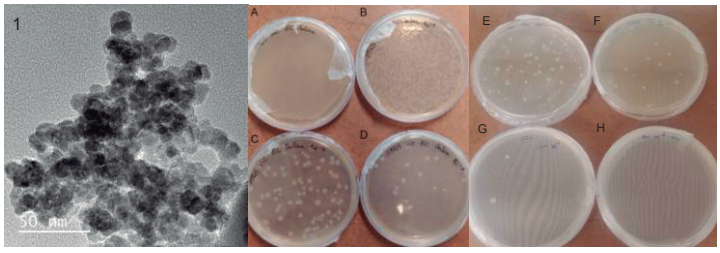

Figure 1 – NpZnO TEM image (1) and photos of the microbiological *Escherichia coli* analyses comparing the control dilutions (a, b, c, and d) with the NpZnO (e, f, g, and h) dilutions.

References

1. H. E. Yong; K. Krishnamoorthy; K. T. Hyun; S. J. Kim. Journal of Industrial and Engineering Chemistry 2015, 29, 39. http://dx.doi.org/10.1016/j.jiec.2015.04.020

Fundings: UFSC, NÓRIO - Nanotecnologia.
Keywords: *Antifouling, nanoparticles, coating, ZnO, marine.*

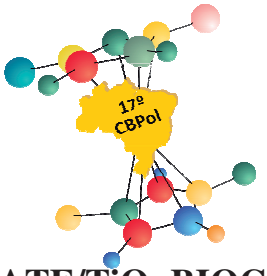

CELLULOSE ACETATE/TiO_2 BIOCOMPOSITES FOR WATER TREATMENT BY PHOTOCATALYSIS

Maria Eduarda de F. A. Telles*[1], Gonçalves J. Marrenjo[1], Marcos V. Ferreira[1], Osmando F. Lopes[1], Rosana M. N. Assunção[1,2] e Elaine Kikuti[1]

1 – Institute of Chemistry, Federal University of Uberlândia (UFU), Uberlândia, MG
elaine.kikuti@ufu.br
2 – Institute of Exact and Natural Sciences of Pontal, Federal University of Uberlândia (UFU), Ituiutaba, MG

Abstract - The development of biocomposites from renewable sources, such as cellulose acetate (CA), offers numerous advantages. CA exhibits excellent thermal, mechanical, morphological, and film formation properties, making it highly suitable for creating innovative materials designed for the removal of aqueous contaminants.[1] By combining a photocatalyst like TiO_2 with CA, a biocomposite (CA/TiO_2) can be formed, guaranteeing the removal and photodecomposition of effluent contaminants. This work aims to prepare biocomposites from a combination of CA and TiO_2 using the phase inversion method and pentanol as a porogenic agent for film preparation. The goal is to investigate their capacity to degrade methylene blue (MB), an organic compound commonly found in wastewater. A 10% weight ratio of TiO_2 and a 1:6 weight ratio of CA to pentanol were used to form the biocomposite CA/TiO_2. The MB degradation studies demonstrated that the CA/TiO_2 biocomposites exhibited remarkable efficiency in removing the organic dye through a combined process of adsorption and photodegradation. The photocatalytic properties of the biocomposite played a vital role in this process. When exposed to sunlight or artificial light, the TiO_2 component becomes activated, initiating a series of oxidation reactions. In our tests, a suspension of TiO_2 0,1mg in 50mL consumed almost 80% of MB in 30 minutes (Fig. 1). The addition of TiO_2 to the biocomposites guaranteed the degradation of the same amount of MB after 180 minutes. Therefore, the development of biocomposites utilizing cellulosic derivatives from renewable sources presented a promising approach to address the pressing issue of effluent treatment and contaminant removal. Despite the longer time to achieve the same amount of MB degradation, the use of the CA/TiO_2 biocomposites allowed for efficient removal and degrading of methylene blue. This demonstrates the benefits of combining the advantageous properties of cellulosic derivatives and photocatalytic materials for effective water effluent treatment.

References

1. Ligowski, E.; Santos, B. C.; Fujiwara, S. T. *Polímeros*, 2015, *25*, 70- 75. http://dx.doi.org/10.1590/0104-1428.1605

Fundings: The authors would like to thank PROPP, FINEP (INFR13 01.13.0371.00), Conselho Nacional de Desenvolvimento Científico e Tecnológico (CNPq).

Keywords*: Biocomposites, cellulose acetate*, e*ffluent treatment, titanium oxide.*

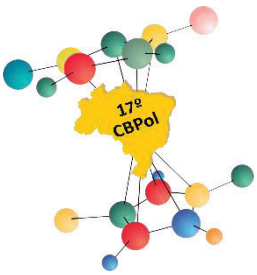

CONDUCTIVE FILMS BASED ON CARBON NANOTUBES AND CELLULOSE NANOFIBERS FOR SUPERCAPACITOR APPLICATION

Maycon J. Santos[2], Ane C. R. Pinto[1]*, Marcos V. Ferreira[1], Daniel Pasquini[1], Rosana M. N. Assunção[1,2], Elaine Kikuti[1]

1 – Institute of Chemistry, Federal University of Uberlândia, Uberlândia, MG, Brazil
anecristinerp@ufu.br
2 – Institute of Exact and Natural Sciences of Pontal, Federal University of Uberlandia, Ituiutaba, MG, Brazil

Abstract - The exponential growth in energy demand and the need for advances in the energy storage sector have driven the exploration of new materials that can be effectively used in electrical and electronic systems. In the present study, we evaluated the potential of nanocomposites composed of cellulose nanofibers (CNF), obtained by mechanical milling, and commercial carbon nanotubes (CNT) for application as supercapacitors. The preparation of these nanocomposites involved mechanically dispersing the CNT suspension in a 4.3% (w/v) CNF suspension using an ultra turrax. This was followed by vacuum filtration of the mixture and hot-pressing at 80°C for 20 minutes. We assessed the influence of the amount of added CNT on the nanocomposites by varying the CNT/CNF proportions to 50, 75, and 100% (w/w). Characterization of the nanocomposites included Fourier transform infrared spectroscopy (FTIR), Raman spectroscopy, X-ray diffraction (XRD), Thermogravimetry Analysis (TGA), cyclic voltammetry (CV) and galvanostatic charge/discharge (GCD). For the 50% (w/w) nanocomposite, the XRD spectrum exhibited two intense peaks at 2θ around 16° and 22°, characteristic of cellulose.[1] Additionally, a peak at 2θ near 26° was observed, attributed to the presence of CNT.[2] The nanocomposites displayed a capacitive and stable voltammetric profile, with increasing conductivity related to the increase in CNT content. Both CV and GCD analyses for the 50% (w/w) nanocomposite revealed a typical profile of supercapacitors with pseudocapacitance. The characterization results provided evidence of successful composite formation. Therefore, this study demonstrates the feasibility of employing CNF, a natural polymer derived from renewable sources, in combination with conductive materials like CNTs as a viable alternative for supercapacitor development.

References

1. SPINACÉ, M. A. S.; et. al. *Carbohydrate Polymers* 2009, *77*, 47-53. https://doi.org/10.1016/j.carbpol.2008.12.005.
2. KALINKE, A. H.; ZARBIN, A. J. G. *Química Nova* 2014, *37*, 1289-1296. https://doi.org/10.5935/0100-4042.20140202.

Fundings: We are grateful for the Universidade Federal de Uberlândia (UFU), PROPP, FINEP (INFR13 01.13.0371.00) and the financial support of the Conselho Nacional de Desenvolvimento Científico e Tecnológico (CNPq).

Keywords: *Supercapacitor, nanocomposite, carbon nanotubes, cellulose nanofibers.*

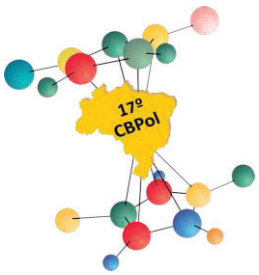

CONTROLLING IPMC ACTUATOR IN HIGH HUMIDITY ENVIRONMENT

Ariel G. Zuquello[1]*, Matheus C. Saccardo[2], Rafael Barbosa[2], Roger Gonçalves[3], Guilherme E. O. Blanco[3], Kaique A. Tozzi[4], and Carlos H. Scuracchio[2]

1 – Graraduate Program in Technology and Innovation Management, Community University of Chapeco Region, Chapeco, 89809-900, Brazi
ariel.zuquello@unochapeco.edu.br

2 – University of Sao Carlos (UFSCar), Graduate Program in Materials Science and Engineering, São Carlos, SP, Brazil
3 - Federal University of Sao Carlos (UFSCar), Graduate Program in Chemistry, São Carlos, SP, Brazil
4 - Univ. Grenoble Alpes, Univ. Savoie Mont Blanc, CNRS, Grenoble INP, LEPMI, UMR5279, 38000 Grenoble, France

Abstract – Ionomeric Polymer-Metal Composites (IPMC) are electromechanical devices that can change shape or format in response to electrical stimuli and vice versa. It's formed by a polymeric membrane covered on both sides by a noble metal electrode, usually platinum, silver or gold[1]. Also, they are light, flexible and present good mechanical/thermal resistance. So, they are promising materials for many technological applications. Since its operation mechanism consists of ionic migration, IPMCs can be electrically stimulated, promoting a displacement of the actuator, or mechanically stimulated, being used as a sensor, since the ionic migration promotes, in this case, an electrical response [2]. The environment's relative humidity strongly affects this ionic mobility, consequently affecting its mechanical and electrical responses. In other words, it will determine the device's performance. For these reasons, its mode of operation is, by default, non-linear, requiring strategies to overcome this condition. To mitigate this problem, studies have focused on using it in environments with controlled relative humidity [3]. When using it as a mechanical actuator, one of the biggest difficulties encountered is to keep the control of this actuator effective and as stable as possible with the actuation time. Thus, this work carried out the control of this actuator in an environment with high relative humidity (90%) for a certain period of time (1200 sec) under electrical stimulation of the step type and it was observed that it performed well in relation to the adjusted set point [4]. Subsequently, new tests with other relative humidities will be carried out.

References

1. W. Hong. *Mater. Science* 2016. Ames, 2016. doi.org/10.31274/etd-180810-5560
2. A. D. Drozdov. *Acta Mech*.2015, vol. 227. 437–465. doi.org/10.1007/s00707-015-1471-7
3. M. C. Saccardo et al. *Mater. Chem. Phys*. 2020, vol. 244. doi.org/10.1016/j.matchemphys.2020.122674
4. A. G. Zuquello et al. *Materials Research,* 2022, 25. doi.org/10.1590/1980-5373-MR-2021-0518

Keywords: *IPMC, Control system, relative humidities, performance.*

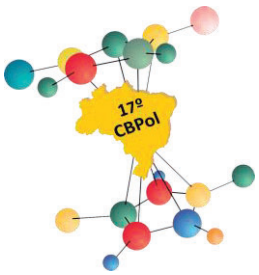

COTTON ANTIBACTERIAL ACTIVITY EVALUATION AFTER PLASMA FUNCTIONALIZED TiO_2 AND ZnO DEPOSITION

Maria E. P. Missner[1,2*], Luis C. Fontana[1], Daiani C. Savi[3], Teresa T. Steffen[1] and Daniela Becker[1]

1 – Laboratory of Plasmas, University Estadual of Santa Catarina (UDESC), Joinville, SC, Brazil
2 – Department of Textile Engineering, Federal University of Santa Catarina (UFSC), Blumenau, SC, Brazil
elisa.p.missner@ufsc.br
3 – Department of Biomedicine, Catholic University*, Joinville, SC, Brazil*

Abstract – Cotton material can provide a friendly environment for microbial growth when is in contact with the human body. This is certainly an undesirable effect, from the point of view of human health. In the way to mitigate it, nanoparticles can be attached to textiles using some binders that make a film on the fiber surface [1]. The present work investigates the fabric antibacterial behavior with deposition of the nanoparticles TiO_2 or ZnO, pristine and functionalized, on the cotton surface. Both nanoparticles were manually premixed with maleic anhydride, according to Steffen et al. [2], and then treated by radio frequency plasma, at 35 W, by 5 minutes, following the procedure established by Klok et al. [3]. Then, using the same parameters of Iwasaki et al. [4], the functionalized nanoparticles were deposited in the fabric through intermittent high voltage pulsed electrophoresis in an aqueous suspension composed by distilled water and the nanoparticles. After the deposition, fabric samples were washed with distilled water for 10 minutes and then dried in the oven with air circulation for 120 min. Before antibacterial test, the samples were exposed to UV light for 24 hours. A qualitative antibacterial activity was evaluated by using both a Gram-positive bacterium (*Staphylococcus aureus*) and a Gram-negative bacterium (*Escherichia coli*). Antibacterial activity of fabric for *E. coli* was much higher than for *S. aureus*. The results show the ability of the treated fabric to both prevent its growth and kill the bacteria. The mortality of *S. aureus* and *E. coli* in the fabric treated with functionalized TiO_2 after 24 hours of incubation was 75% and 98% respectively. Almost the same mortality was observed in the fabric in which was deposited functionalized ZnO: 72%, for *S. aureus*, and 98%, for *E. coli*. Note that it was not observed a significant difference in the antibacterial activity of the fabric by using nanoparticles pristine or functionalized by plasma. However different behaviors are expected in the antibacterial activity for fabric after washing, due to the better adhesion between nanoparticles and cotton provided by the functionalization.

References

1. V. F. Santos et al. *Cellulose 2023*. https://doi.org/10.1007/s10570-023-05211-x
2. T. T. Steffen et al. *Applied Surface Science* 2019, *491*, 405-410. https://doi.org/10.1016/j.apsusc.2019.06.176
3. L. A Klok et al. in Proceedings of 6th Brazilian Conference on Composite Materials, Tiradentes, 2022, Vol. 1, 544.
4. K. M. K. Iwasaki et al. *Applied Surface Science* 2023, *611*, 155548. https://doi.org/10.1016/j.apsusc.2022.155548

Fundings: This work was supported by the project PAP FAPESC-UDESC 2021TR874.

Keywords: *Titanium dioxide. Zinc oxide. Nanoparticles. Antimicrobial activity. Functional textiles.*

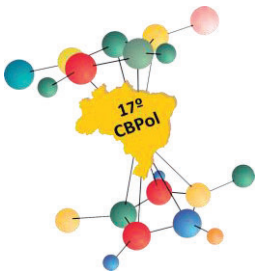

DEVELOPMENT OF CORE-SHELL PVC/PMMA/PANI MEMBRANES BY COAXIAL ELECTROSPINNING

Stephen Christina de Moraes [1*], Marcia Adriana Tomaz Duarte [2], Sérgio H. Pezzin [3],

1 – PPGEM, Federal University of Santa Catarina (UDESC). 89223-100 Joinville/SC, Brazil.
stephenmoraes7@gmail.com
2 – DBM Nano. Joinville/SC, Brazil. contato@dbmnano.com.br
3 – Center of Technological Sciences, Santa Catarina State University, 89223-100 Joinville/SC, Brazil.
sergio.pezzin@udesc.br

Abstract – Coaxial electrospinning is a modification of traditional electrospinning. This technique allows for the composition of more than one solution in the nanofiber, as it produces fibers with a core-shell structure. Due to its adaptability, it is widely used in the production of dressings, filters, sensors, biosensors, electrically conductive materials, among others. Electrospun membranes consist of randomly distributed nanofibers in a three-dimensional framework. Their structure, combined with electrical properties, is of interest in the field of electroelectronics. The objective of this study is to develop core-shell nanofibers using polyaniline (PANi), poly(methyl methacrylate) (PMMA), and polyvinyl chloride (PVC). Firstly, a coaxial device was developed in collaboration with DBM Nano Co. Subsequently, PMMA and PVC solutions were tested at different concentrations to study their effect and viscosity in the coaxial electrospinning process. The concentration of the PVC solution used was 15% and remained constant, while the concentration of the PMMA solution varied. It was observed that the difference in polymer concentrations between the solutions of PMMA and PVC resulted in poor wire formation. When a concentration of 5% PMMA was used, no nanofibers were formed as the solution only dripped. At 10% concentration, there was an improvement in wire formation, but dripping still occurred frequently, resulting in structural flaws. The formation of defect-free wires was observed when a concentration of 15% PMMA was used. This study also allowed for the determination of other process and environmental parameters.

References

1. Jiang, H., Wang, L., Zhu, K. Coaxial Electrospinning For Encapsulation And Controlled Release Of Fragile Water-Soluble Bioactive Agentes. Journal of Controlled Release, Elsevier, nov 2014.
2. Kaerkitcha, N., et al. Influence of the viscosity ratio of polyacrylonitrile/poly(methyl methacrylate) solutions on core–shell fibers prepared by coaxial electrospinning. Polym J 49, 497–502 (2017). https://doi.org/10.1038/pj.2017.8
3. Li, F., Zhao, Y., Song, Y. Core-Shell Nanofibers: Nano Channel and Capsule by Coaxial Electrospinning. Nanofibers, Ashok Kumar, Intech, 438p, fev. 2010.
4. Macdiarmid, A. G., et al. Polyaniline: a new concept in conducting polymers. Synth. Met., vol. 18, no 1–3, p. 285–290, fev. 1987.
5. Mastragostino, M., Arbizzani, C., Soavi, F. Polymer-based supercapacitors. J. Power Sources, vol. 97–98, p. 812–815, jul. 2001.

Keywords: *Polyaniline, Poly(methyl methacrylate), Polyvinyl chloride, Coaxial electrospinning.*

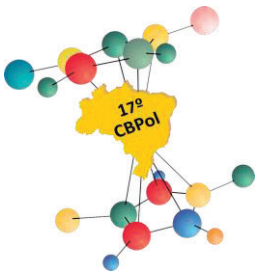

DEVELOPMENT OF ELECTROSPUN MEMBRANES OF PVDF/SILICA FUNCTIONALIZED WITH IONIC LIQUID FOR EFFLUENT TREATMENT

Nathalia O. A. dos Anjos[1*], Bluma G. Soares[1], Ruan Henriques[2], Jessica Pereira[2] and Julia G. G. de Souza[2]

*1 – Federal University of Rio de Janeiro, Alberto Luiz Coimbra Institute of Graduate Studies and Engineering Research, Metallurgical and Materials Engineering Program (PEMM/COPPE-UFRJ). *onathalia@coppe.ufrj.br*
2 – Federal University of Rio de Janeiro, Institute of Macromolecules, Laboratory of Polymeric Mixtures and Conducting Composites (IMA-LMPCC).

Abstract - Chromium compounds are widely used in industrial processes and are considered one of the most dangerous metal ions. With this, the removal of these potentially toxic elements from wastewater is very interesting. In this study, membranes composed of poly(vinylidene fluoride) (PVDF)/silica nanofibers functionalized with ionic liquid chlor-methylimidazole (IL-Cl) and zwitterionic (ZIL) were prepared using the electrospinning technique and characterized by Scanning electron microscopy (SEM), Thermal analysis by thermogravimetry (TGA) and Fourier transform infrared spectroscopy (FTIR). To prepare electrospun scaffolds, PVDF granules (20 w/v, weight/volume ratio) were dissolved in a mixture of DMF/acetone (3:1), along with 0.5% and 1% functionalized silica, then the fibers were spun under an electric field of 30 kV with a feed rate of 0.5 mL/h for 4 h. The use of electrospun nanofibers as an adsorbent is a relatively new approach and allows solving the difficulties of separating and recovering micro-sized adsorbents. PVDF maintains the mechanical stability and thermal resistance of the material, while the incorporation of functional groups allows it to strongly attract metal ions through chelation and electrostatic attraction. Finally, the preliminary evaluation of the membranes demonstrated efficiency as an adsorbent of Cr (VI) and Cr (III) of aqueous solution, through tests of adsorption in batch. The introduction of functionalized silica increased the adsorption capacity by 50% compared to the pure PVDF membrane, as well as improved the thermal stability and structure of the membranes. Furthermore, the characterizations proved that the processing conditions were satisfactory and balanced, forming randomly intercalated nanofibers and without distinct defects or agglomerations. Therefore, this study provides a potential approach for the preparation of membranes with good viability for application in environmental remediation by adsorption of metal ions.

References

1. A. P. A. Carvalho; B. G. Soares; S. Livi *European Polymer Journal* 2016, 83, 311322. https://doi.org/10.1016/j.eurpolymj.2016.08.030
2. L. C. Lins; F. Wianny; S. Livi; C. Dehay; J. Duchet-Rumeau; J. F. Gérard *Journal of Biomedical Materials Research Part B: Applied Biomaterials* 2017, 105(8), 23762393. https://doi.org/10.1002/jbm.b.33778
3. Y. A. Mohammed; et al. *Chemical Engineering Journal* 2023 461, 141972. https://doi.org/10.1016/j.cej.2023.141972

Fundings: This study was financed in part by the Coordenação de Aperfeiçoamento de Pessoal de Nível Superior – Brasil (CAPES) – Finance Code 001
Keywords: *Polymeric Membranes, Electrospinning, Functionalization, Adsorption, Chromium.*

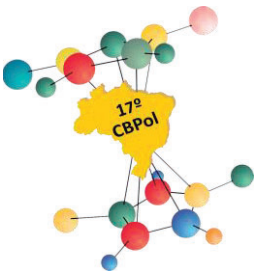

EFFECT OF CARBON NANOTUBE CONCENTRATION ON THE ELECTRICAL, THERMAL AND MECHANICAL PROPERTIES OF NANOCOMPOSITES WITH EPOXY MATRIX

Amanda C. Zanuso[1], Claudia Merlini[1]

1 – Graduate Program in Nanoscience, Processes and Advanced Materials (PPGNPMat), Federal University of Santa Catarina (UFSC), Blumenau, Sc, Brazil amandacallegarozanuso@hotmail.com

Abstract - Research and development of methodologies capable of creating new materials using carbon nanotubes in their structure represent a technological innovation capable of transforming low-cost products into advanced materials with high added value. Its remarkable properties, especially the high electrical conductivity and mechanical strength, make the carbon nanotubes promising in several applications. Allied to the variety of functions that polymers are able to perform, polymeric composites with carbon-based fillers receive considerable attention, both in academic and industrial research. The incorporation of carbon nanotubes (CNT) in polymer matrices makes it possible to improve the multifunctionality of polymers, providing them with better thermal, mechanical and electrical properties. In this work, carbon nanotubes were incorporated into liquid epoxy resin with the aid of a high-speed mechanical stirrer. After incorporating of the nanoparticles into the matrix, the nanocomposites were catalyzed with triethylenetetraamine and cured in an oven at 80°C for 180 minutes. The films were characterized in terms of glass transition temperature, storage modulus and electrical conductivity. With regard to electrical conductivity, 0.05 wt.% of the nanoparticle increases the conductivity of the matrix from $1.08x10^{-15}$ $S.cm^{-1}$ to $1.05x10^{-07}$ $S.cm^{-1}$. Larger fractions of the CNT in the matrix do not produce a significant increase, since the nanocomposite containing 1.00 wt.% of nanotube presented a conductivity of $7.80x10^{-06}$ $S.cm^{-1}$. Regarding the storage modulus, it is noticed that in smaller percentages, there is an increase in this property. While the epoxy resin has a modulus of 355.73 MPa, the nanocomposite with 0.05 wt.% load has a value of 529.81 MPa. The glass transition temperature obtained via Dynamic Mechanical Analysis (DMA) does not show significant change in its values. Thus, it is clear that carbon nanotubes are good electrical conductive additives, significantly increasing this property, as well as improving the mechanical properties of nanocomposites.

Keywords: *Carbon nanotubes; epoxy resin; nanocomposites; polymer matrix.*

References

1. Yadav, R., Tirumali, M., Wang, X., Naebe, M., & Kandasubramanian, B. *Defence Technology* 2020, 16, 107. https://doi.org/10.1016/j.dt.2019.04.008.
2. Spitalsky, Z., Tasis, D., Papagelis, K., & Galiotis, C. *Progress in Polymer Science* 2010, 35, 357. https://doi.org/10.1016/j.progpolymsci.2009.09.003.
3. Sinnott, S. B., & Andrews, R. *Critical Reviews in Solid State and Materials Sciences* 2001, 26, 145. https://doi.org/10.1080/20014091104189.

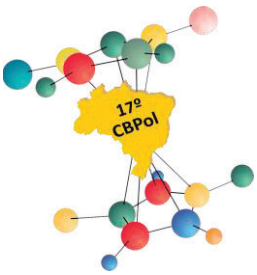

EFFECT OF CELLULOSE NANOCRYSTALS ON WATER ABSORPTION OF SULFONATED SBS BASED IONIC POLYMER METAL COMPOSITE

Vítor B. Salomão[1*], Paulo O. Gall[1], Guilherme E. de O. Blanco[1], Matheus C. Saccardo[1] and Carlos H. Scuracchio[1]

:

1 – Department of Materials Engineering (DEMa), Federal University of São Carlos (UFSCar), São Carlos, SP, Brazil
vitor.salomao@estudante.ufscar.br

Abstract – This research aims to evaluate the effect of cellulose nanocrystals (CNC) on the water absorption of sulfonated styrene-butadiene-styrene block copolymer (SSBS), therefore, improving the ionic conduction of SSBS-based ionic polymer-metal composite (IPMC). IPMCs are flexible materials, with an alternating metal/ionomer/metal structure, that shows a mechanical response to electrical stimuli and vice versa [1], thus resulting in a promising material in numerous applications, such as soft actuators, sensors, artificial muscles, and robotics. To supersede Nafion®, the most used polymer for IPMCs, which is expensive, environmentally problematic, and moisture sensitive [2], some alternatives have been developed, including the sulfonated styrene-butadiene-styrene block copolymer (SSBS) membranes. In this study, the ionomer was made by sulfonating the Kraton™ D-1155 E SBS with a mixture of acetic anhydride and sulfuric acid (1,75:1) for one hour in an inert atmosphere, leading to a sulfonation degree (SD) of 21%. The CNC was dispersed in the polymer in concentrations of 5, 10, or 15 wt% concerning the final nanocomposite weight by solubilizing both in THF and sonicating the solution for 2 hours. The membrane was fabricated by solvent casting. The water absorption of the membrane is crucial for the well-function of the IPMC, once not only the ion conduction is enabled by water but also the differential swelling of the material, responsible for its bending movement, is due to water movement inside of the membrane. As the main result, the CNC increased the water absorption by almost 50% mass-wise, promisingly improving the electrical-mechanic properties of the composite.

References

1. Y. Bahramzadeh and M. Shahinpoor. Soft Robotics 2014, 1, 1. https://doi.org/10.1089/soro.2013.0006.
2. Y. Tang; Z. Xue; X. Xie; X. Zhou. Sensors and Actuators A: Physical, 2016, 238, 167. https://doi.org10.1016/j.sna.2015.12.015.

Keywords: *IMPCs; Sulfonated SBS; Nanocomposite; CNC; Water absorption.*

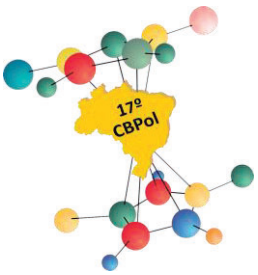

EFFECT OF CURING ON THE GLASS TRANSITION TEMPERATURE OF THE EPOXY/GNP SYSTEM

Lucas Carvalho[1], Joziel A. da Cruz[1], Patrik Fernberg[2], Sandro C. Amico[1], Otávio Bianchi[1*]

[1]Federal University of Rio Grande do Sul – Brazil

otavio.bianchi@ufrgs.br

[2]Luleå University of Technology – Sweden

Abstract: Epoxy systems are highly valued for their exceptional properties and find widespread use across various applications. A comprehensive understanding of the curing process is essential to achieve the desired material properties, particularly considering the influence of diffusion processes below the glass transition temperature. This study focuses on assessing the impact of graphene nanoplates (GNP) on the curing process by examining the degree of conversion at different glass transition temperatures (T_g). Interestingly, the addition of 1wt.% GNP does not significantly affect the cure and T_g of the epoxy. The observed behavior suggests a two-stage reaction, one occurring prior to gelation and another following. The findings indicate no substantial impact from treatment with GNP on the glass transition temperature (Tg) during the curing process.

Keywords: *Epoxy resin, Graphene nanoplatelets, glass transition temperature*.

Fundings: FAPERGS Inova Clusters Tecnológicos (Project 22/2551-0000839-9), STINT/CAPES (n. 88881.304743/2018-01) and Conselho Nacional de Desenvolvimento Científico e Tecnológico (n. 408193/2021-2 and 305814/2021-4).

Introduction

Epoxy resins are widely used in coatings, electrical insulation, adhesives, composites, and construction. Therefore, understanding the curing process is crucial to achieve the desired properties in these applications. The curing reaction involves the formation of complex crosslinked networks, which greatly influence the properties of epoxy systems. Factors such as resin and hardener chemistry, stoichiometric ratio, curing conditions, and adding additives and fillers contribute to the nature of these networks [1].

Nanoparticles can impact the viscosity and curing process of resins. This effect is typically attributed to the formation of a percolated network or the presence of oxygenated groups that accelerate the opening of the epoxide ring [1, 2]. For instance, graphene nanoparticles (GNP) and carbon nanotubes (CNT) can enhance the epoxy curing enthalpy. However, the effect on resin viscosity varies depending on their dispersion. For example, mechanical percolation is typically not observed in nanocomposites of GNP with epoxy (0-1 wt.%). On the other hand, systems containing 0-1 wt.% of CNT exhibit percolation at quantities exceeding 0.5 wt.% [3]. Notably, alterations in

viscosity will affect resin curing and consequently impact the final properties of the material, necessitating careful consideration of heat treatments after curing.

Changes in amorphous materials' mechanical and physical properties are inevitable when their molecular mobility undergoes alterations during the glass transition interval. To investigate the change in reaction rate during the vitrification process, the relationship between the glass transition temperature (T_g) and the conversion (α) of the partially cured reaction can be analyzed. This relationship helps determine the occurrence of vitrification during the curing process, where Tg equals the curing temperature (T_{cure}). If T_g is lower than T_{cure}, the reaction of a thermosetting material typically follows chemical kinetics. However, if T_g is higher than T_{cure}, the reaction rate becomes diffusion-controlled due to the rapid reduction in molecular mobility [4].

Considering the influence of graphene nanoparticles (GNP) on the epoxy system's curing process and its significance in designing, analyzing, and optimizing final materials, this study aims to compare the impact of GNP on epoxy resin curing. The study evaluates the performance of these particles in the curing process by measuring the degree of conversion at various glass transition temperatures (T_g).

Experimental

The epoxy resin used in this study is AR260, obtained from e-composites (Brazil), with an average molecular weight of 750 g/mol (measured via GPC using THF and polystyrene standards). The hardener employed is HY951, triethylenetetramine (TETA), purchased from Huntsman. A stoichiometric mixing ratio of 100 parts resin to 13 parts hardeners by weight is utilized, along with adding one part accelerator by weight. The hardener is added to the epoxy resin and mixed for two minutes. All these procedures are carried out at room temperature. The GNP was mixed by mechanical stringing and ultrasonicated (VCX 750 Sonics 20 kHz, 110 W, 60 min.) into the resin and hardener to prevent agglomeration.

DSC Q2000 differential scanning calorimeter was employed for calorimetric measurements. The analysis involved studying pure epoxy samples and epoxy samples containing 1 wt.% GNP. At each temperature, the isothermal analysis was conducted at 60, 80, 100, and 120 °C for various durations (5, 10, 20, 40, and 60 minutes). The sample size used was approximately 10 mg. During the analysis, the system temperature was maintained at the specified isotherm for the respective analysis time and then cooled to -90 °C to determine the glass transition temperature resulting from the curing conditions. Subsequently, the temperature was increased at a rate of 10 °C/min up to 250 °C to measure the residual heat of the reaction. To determine initial glass transition temperature, T_{g0} the samples were cooled to -90 °C and then heated at 10 °C/min. For infinite glass transition temperature, $T_{g\infty}$ determination, the samples underwent a complete curing cycle at 160 °C for one week. Subsequently, DSC measurements were performed at 10 °C/min from room temperature to 250 °C.

Results and Discussion

In the case of pure epoxy, the measured values for T_{g0} and $T_{g\infty}$ were -38.8°C and 103.4°C, respectively. When the epoxy was loaded with 1wt.% GNP, the corresponding values obtained were -37.2°C for T_{g0} and 104.7°C for $T_{g\infty}$. Fig. 1 illustrate the method employed to track the heat flux evolution over time during isothermal experiments, specifically comparing samples with equilibrium at 80°C and an isothermal duration of 5 minutes.

By integrating the heat flux curves and dividing the result by the sample mass, the integrated area in J/g is obtained. Next, the exothermic peaks of the respective sample are combined, and the percentage of reacted material is determined by comparing it with the total area. Finally, the conversion (α) of the reaction is calculated using Eq. 1,

$$\alpha(t) = \frac{\Delta H(t)}{\Delta H_{total}} \quad (1)$$

where $\Delta H(t)$ represents the enthalpy of the reaction at a specific isothermal time, which is characterized by being fast and exothermic. The term ΔH_{total} refers to the total enthalpy of the reaction.

By determining the conversions of neat epoxy and 1% GNP epoxy reactions, the study examines the vitrification transition during the curing process at temperatures 60, 80, 100, and 120 °C. This transition signifies the irreversible transformation from the epoxy to a glassy gel state, occurring when the system's glass transition temperature (T_g) matches the isothermal curing temperature. Once this transition is reached, the reaction kinetics are altered, impeding further reactions, although a slow diffusion process may persist within the glassy state [5].

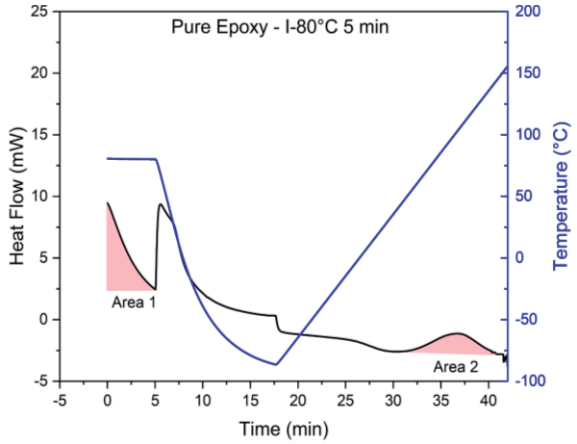

Figure 1 – Isothermal DSC scan of the pure epoxy sample at 80 °C for 5 minutes, followed by a cooling ramp to -90 °C and a heating ramp to 250 °C.

Fig. 2 provides a representative example of conversion curves obtained during a 60-minute timeframe at various isothermal temperatures. The results demonstrate that for both systems, temperatures of 100 and 120ºC yield a degree of conversion surpassing 0.8. At temperatures below 100ºC, the conversion level reaches approximately 0.6. In both cases, the curves display an initial rapid acceleration followed by a gradual reaction process, suggesting a diffusion-controlled mechanism. This behavior is typically observed when the system is near the glass transition temperature, indicating the influence of molecular mobility on the reaction kinetics [5].

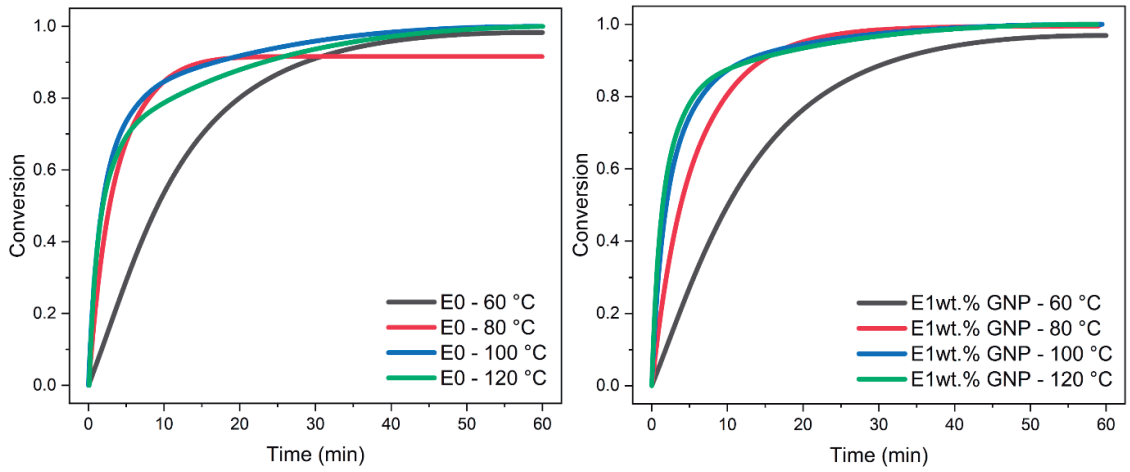

Figure 2 – Reaction conversion of epoxy systems as a function of isothermal cure time at 60, 80, 100 and 120 °C in 60 min., (a) pure epoxy and (b) 1wt.% GNP.

Based on the hypothesis that the molecular structure of a material is interconnected with its chemical conversion and that this molecular structure correlates with the glass transition temperature (T_g), we can deduce a direct association between T_g and the degree of conversion (α). The DiBenedetto equation is commonly employed as the constitutive equation to characterize this relationship within thermoset systems. This equation, expressed as Eq. 2, incorporates a parameter λ, which can be adjusted from 0 to 1 [5].

$$T_g = T_{g0} + \frac{(T_{g\infty} - T_{g0})\lambda\alpha}{1-(1-\lambda)\alpha} \quad (2)$$

The λ parameter of the DiBenedetto equation was adjusted according to Eq. 2, resulting in a value of 0.136 for the pure epoxy system and 0.096 for the epoxy with 1 wt.% GNP, as depicted in Fig. 3. These values align with previous findings in the literature [5]. No significant difference between the analyzed samples can be inferred since both fall within the same 95% prediction interval. This observation is expected because adding GNP does not significantly alter the T_g values. This outcome can be attributed to the absence of mechanical percolation, implying that the resin viscosity remains relatively unaffected, thus avoiding any hindrance in the reaction. Additionally, the presence of oxygenated groups, while increasing the enthalpy, may influence the initial stages of the reaction [1, 2].

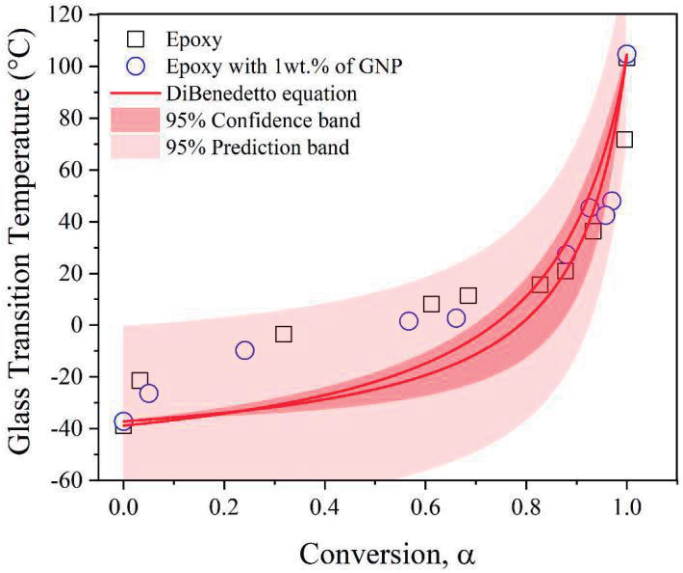

Figure 3 – T_g of epoxy system as a function of the degree of conversion with good correlation from experimental data using Eq. 2, for both systems R^2>0.81.

Considering the conversion value at the gel point of 0.58, it is evident that T_g points exhibit greater dispersion below this threshold as a function of the degree of conversion [5]. This phenomenon arises from the fact that at low conversion values, T_g is more reliant on the molecular mass of the resin. However, as the degree of conversion increases, T_g rises due to the formation of crosslinks. Consequently, these systems exhibit two distinct stages of T_g increase.

In the first stage ($T_{cure} < T_g$), the rate of T_g increase is rapid. However, as T_g approaches T_{cure}, the rate of growth diminishes significantly. The boundary between these two stages is called the point of vitrification. The rate of the chemical curing process primarily influences the curing reaction before vitrification. As the chemical reaction progresses and crosslink density rises, the discrepancy between the transient T_g value and the curing temperature decreases. The higher crosslink density creates a state that severely hampers the physical movement of molecules. In the second stage, the reaction becomes dominated by diffusion-controlled mechanisms, where the limited mobility of the active groups results in a substantial decrease in the overall rate of crosslinking conversion, often by several

orders of magnitude. This transition towards diffusion-type control is a consequence of the increasing crosslink density, which impedes the overall mobility of molecules and decreases the conversion rate.

Conclusions

The study investigated the impact of 1 wt.% graphene nanoparticles (GNP) on epoxy resin's curing and glass transition. The Dibenedetto equation established a correlation between the degree of conversion and the glass transition temperature of the systems. The findings indicate no substantial changes in the glass transition temperature (T_g) during the curing process.

Acknowledgments

The authors gratefully acknowledge the support received from various funding sources. The Brazilian Agency Coordenação de Aperfeiçoamento de Pessoal de Nível Superior (CAPES, Brazil), Finance Code 001, and project STINT/CAPES (n. 88881.304743/2018-01) are deeply appreciated. The Conselho Nacional de Desenvolvimento Científico e Tecnológico (CNPq, Brazil).

References

1. L. S. Cividanes; E. A. N. Simonetti; M. B. Moraes; F. W. Fernandes; G. P. Thim Polym Eng Sci 2014, 54, 2461. https://doi.org/10.1002/pen.23775.
2. R. Sheikh; A. Sufyan; K. Antonios; E. Ahmed; G. K. Panagiotis Thermochim Acta 2020, 694, 178785. https://doi.org/10.1016/j.tca.2020.178785.
3. J. A. Cruz; L. Paim; R. Joffe; P. Fernberg; S. Amico; O. Bianchi in 6th Brazilian Conference on Composite Materials, Minas Gerais, 2022.
4. M. Urbaniak, Polimery 2017, 62, 5. dx.doi.org/10.14314/polimery.2017.394.
5. H. Teil; S. A. Page; V. Michaud; J. A. E. Månson J Appl Polym Sci 2004, 93, 1774. https://doi.org/10.1002/app.20631.

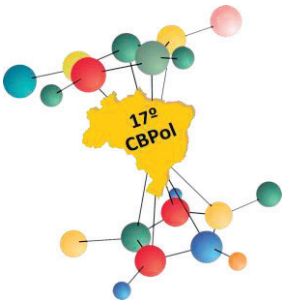

EFFECT OF GRAPHENE CONCENTRATION ON POLYCAPROLACTONE ELETROSPUN MEMBRANES

Sabrina dos S. Bento[1], Anna L. M. M. Toledo[2] and Marcos L. Dias[3]

1 –Institute of Macromolecules Professora Eloisa Mano, Federal University of Rio de Janeiro (UFRJ), Rio de Janeiro, Brazil

sabrina_bento@ima.ufrj.br

Production of membranes formed by polycaprolactone (PCL)/graphene nanofibers was performed by means of electrospinning. The membranes were made from a PCL solution (10% w/v) with varying graphene concentrations of 0.1%, 0.5%, 1.0%, 2.0 % and 5.0 wt% relative to the polymer. The solvents used were dichloromethane (DCM) and dimethylformamide (DMF) in a = 4:1 ratio, respectively. Prior to the electrospinning, for a better dispersion of the nanofiller in the polymeric solution, an ultrasonic sonicator with a tip was used for three minutes. From the determination of electrospinning parameters, membranes formed by PCL/graphene nanocomposite fibers were obtained, using a voltage of 17.5 kV, distance between the collector and the needle of 10 cm, and flow rate of 0.5 mL/h. The samples were analyzed by scanning electron microscopy (SEM) to evaluate the morphology of the nanofibers and a decrease in fiber diameter was observed after graphene insertion. Thermogravimetric analysis (TGA) was performed to evaluate the thermal stability of the nanofibers. No mass loss event related to solvent evaporation was observed, which means that the process solvent was evaporated during fiber formation. A decrease in the initial degradation temperature was also observed after graphene insertion. By means of X-ray Diffraction (XRD) it was possible to observe the degree of crystallinity of the electrospun mats. There was a decrease in the degree of crystallinity of the graphene-containing fibers compared to the PCL-only membranes, which may indicate that the graphene caused some physical impediment in the electrospun PCL polymer chain.

Key words: *electrospinning; polycaprolactone; graphene; nanotechnology, nanofibers.*

References

1. A. L. M. M. Toledo, B. S. Ramalho, P. H. S. Picciani, L.S. Baptista, A. M. B. Martinez and M. L. Dias. International Journal of Polymeric Materials and Polymeric Biomaterials 2020, 70:17, 1258-1270 https://doi.org/10.1080/00914037.2020.1785463.
2. C. L. S. Santos, M. L. Dias and M. H. P. Silva. Journal of Composite Materials, 2020, 55:11, 1485–1498 https://doi.org/10.1177/0021998320972179.
3. A. L. M. M. Toledo, Ph.D. Thesis, Federal University of Rio de Janeiro, 2020.
4. C. L. S. Santos, Ph.D. Thesis, Federal University of Rio de Janeiro, 2021.

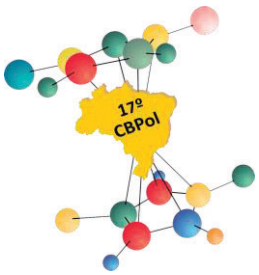

EFFECT OF GRAPHENE MORPHOLOGY ON THE PROPERTIES OF PBAT/GRAPHENE NANOCOMPOSITES FOR APPLICATION IN PACKAGING

Ivaneia B. B. Andrade[1*], Marcos L. Dias[1]

1 – Universidade Federal do Rio de Janeiro (UFRJ), Instituto de Macromoléculas Professora Eloisa Mano (IMA), Rio de Janeiro, RJ, ivibeltrao19@gmail.com.

Abstract-Poly (butylene adipate-co-terephthalate) (PBAT) is a synthetic, biodegradable copolymer, with relevant characteristics for versatile application, including packaging. Graphene is a derivative of graphite, carbon allotrope, that since discovered has emerged as an interesting reinforcement in nanocomposites for attributing significant improvements in the final properties of the composite, such as: mechanical properties, conductivity and barrier properties. The objective of this work is to study the formation of PBAT nanocomposites with graphenes of different morphologies and to investigate the properties that can provide an efficient material for use in packaging, with improved and sustainable final properties. As particles in the manufacture of composites, we are using two grades of graphene nanoplatelets (GNPs), grade 3 (GNP G3) and grade 4 (GNP G4). The nanocomposites were obtained by extrusion in equipment with a twin screw and fillers were added in the amounts of 0.5, 1 and 3% mass. In order to study the thermal behavior of pure materials and nanocomposites, SEM, TGA and DSC analyzes were carried out. FTIR and XRD analyzes are ongoing. The two graphenes have different morphological properties and, according to SEM analyses, GNP G3 showed different sizes of irregular particles, with aggregate formations and a wrinkled surface, indicating an amorphous character. GNP G4 presented a more uniform distribution of particles, featuring a more crystalline and defined appearance plaque formations. The TG curves showed, in the temperature range studied, greater mass loss for GNP G3 compared to GNP G4, indicating a greater number of defects and corroborating the SEM analyses. The morphological differences of the fillers imply differences in the properties that are being investigated in the composites for application in packaging. For the tensile tests, the samples were injected, according to the ASTM D638-14 standard, on ongoing analysis. Gas permeability analyzes are also in progress.

References

1. A. Ye; S. Wang; Q. Zhao; Y. Wang; C. Wang; C. Liu; C. Chen; *Materials letters* 2019, 253. https://doi.org/10.1016/j.matlet.2019.06.040
2. R. Geyer; J. R. Jambeck; K. L. Law; *Science Advances* 2018, *3*. Doi: 10.1126/sciadv.1700782.
3. L. T. Rao; H. Zhang; E. Billoti; K. Essa; L. Huang; Z. Feng; Y. Li; *Composites part A* 2019, 124. https://doi.org/10.1016/j.compositesa.2019.105483.
4. U. Hu; Y. Nu; G. Fu; P. Yue; M. Li; F. Peng; R. Sun; *International Journal of Polymer Science* 2018. https://doi.org/10.1155/2018/2097340.

Fundings: The authors are grateful for financial support from Capes.
Keywords: *Packaging; Graphene; PBAT; Nanocomposites; Extrusion.*

ELECTROSPINING IN THE MANUFACTURE OF ZnO AND PVB NANOCOMPOSITES TO CONTROL THE PROLIFERATION OF MICROORGANISMS

Renato C. T. Porto[1], Patrícia Z. Uchôa[1], Jean C. Hoepfner[2], SamantaFinsterbuch[2], Pâmela E. O. Emerich[3], Sérgio H. Pezzin[1]

1 – Chemistry Department, Center of Technological Sciences, Santa Catarina State University, Joinville, Brazil.
rctporto@gmail.com
2 – Center of Technological Sciences, Santa Catarina State University, Joinville, Brazil.
3 – Chemistry Department, Joinville Region University - Univille, Joinville, Brazil.

Abstract – The search for innovative materials is increasingly on the agenda in universities and industries around the world. In the control of diseases caused by viruses and bacteria, tissues that promote antibacterial activity by incorporating nanostructures such as zinc oxide are important allies of humanity. In the work in question, ZnO nanoparticles were incorporated into PVB structures through the electrospinning process. A proportion of 10% of ZnO nanoparticles supplied by the company Nório Nanotecnologia and synthesized by the green synthesis method was used, which provides better biocompatibility with the human body, the particles used had an average diameter of 50nm, values obtained through analysis of transmission electron microscopy. Antibacterial analyzes were carried out to validate the efficiency of the material in the control and proliferation of microorganisms, the results are shown in Figure 2, where when the control sample is compared with the sample containing the nanostructures in the conditions without dilution and dilutions of 10^{-1}, 10^{-2} and 10^{-3}, it is noted that values of up to 99.9% were obtained in the inhibition rate of the control of E. Coli proliferation by applying the method based on the AATCC 100 regulation.

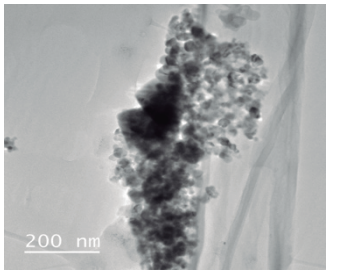

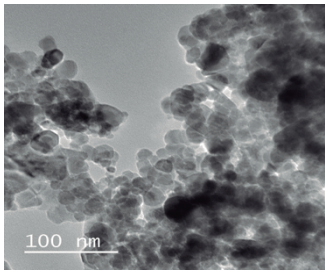

Figure 1 – TEM of ZnO samples with aproximation of 200nm and 100nm.

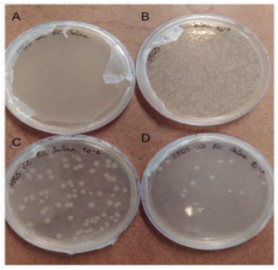

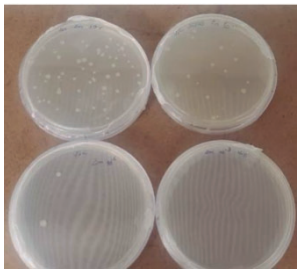

Control Sample ZnO Sample

Figure 2 - Antibacterial analysis of the synthesized nanostructures and the E. Coli Control under conditions (A) Without Dilution; (B) 10^{-1}; (C) 10^{-2}; (D) 10^{-3}.

References

1. F. YALCINKAYA; M. KOMAREK, M. International Journal of Molecular Science 2019, 20, 4317. https://doi.org/10.3390/ijms20174317
2. S. ANDRA; S. K. BALU; J. JEEVANANDAM; M. MUTHALAGU. Naunyn-Schmiedeberg's Archives of Pharmacology., 2021. https://doi.org/10.1007/s00210-021-02064-8

Fundings: FAPESC, CAPES and NÓRIO – Nanotechnology.
Keywords: *ZnO, PVB, Electrospinning, Antibacterial*

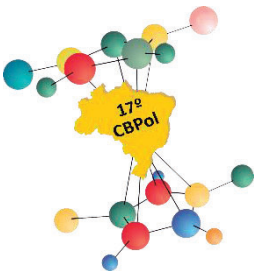

ELECTROSPUN MATS WITH ALIGNED FIBERS, BASED ON POLY(LACTIC ACID) CONTAINING CARBON NANOTUBES AND IONIC LIQUID

Amanda Olinek[1], Matheus Campos Hemkemaier [2], Sébastien Livi [3], Claudia Merlini[4]

1 Materials Engineering Special Coordination, Universidade Federal de Santa Catarinta (UFSC), Blumenau, SC, Brazil. amanda.olinek@grad.ufsc.br

2 – Graduate Program in Nanoscience, Processes and Advanced Materials (PPGNPMat), Universidade Federal de Santa Catarinta (UFSC), Blumenau, SC, Brazil. matheus.c.hemkemaier@gmail.com

3 - Université de Lyon, CNRS, Université Claude Bernard Lyon 1, INSA Lyon, Université Jean Monnet, UMR 5223, Ingénierie des Matériaux Polymères, CEDEX F-69621 Villeurbanne, France sebastien.livi@insa-lyon.fr

4 Graduate Program in Nanoscience, Processes and Advanced Materials (PPGNPMat), Universidade Federal de Santa Catarinta (UFSC), Blumenau, SC, Brazil. claudia.merlini@ufsc.br

Abstract

This work aims the development of electrospun mats with aligned fibers, based on poly(lactic acid) (PLA) containing multiwall carbon nanotubes (MWNTC) and ionic liquid (IL) to be used as nerves conduits in peripheral nerve regeneration. PLA was chosen because it is a biodegradable and biocompatible polymer [1]. The use of MWCNT can provide the necessary electrical stimulus in the application and the IL can improve the nanoparticles dispersion [1,2]. Polymeric nanofibers were developed based on PLA polymeric solutions, containing the IL. Then, carbon nanotubes (0.25; 0.5; 0.75 and 1.0 wt%) were incorporated into the solution and submitted to the ultrasonic processor to promote their dispersion. Therefore, the electrospinning process was conducted by using distance between needle and collector of 20 cm; applied electric voltage of 15 kV; feed flow rate of 1.02 mL/h and spin of 1025-1065 rpm. After electrospinning, the polymeric nanofibers were characterized to observe the microstructure and performanceIt was noted that the polymeric nanofibers showed good morphology and tendency to unidirectional alignment. With the increase of the MWCNT mass fractions there is an improvement in the fibers orientation due to the greater stretching of the polymeric solution. Furthermore, MWCNT agglomeration was not observed in the nanofibers. PLA fibers display a diameter of 0.99 ± 0.22 µm and for the mats with 1 wt% of MWCNT the fibers diameter was of 1.22 ± 0.40 µm, due to the increase in the solution viscosity. Regarding the tensile strength, the mats display a anisotropic behavior due to the alignment of fibers. PLA display tensile strength of 13.26 MPa in fibers direction (0°) and 3.35 MPa in the transversal (90°). The incorporation of MWCNT reduced the tensile strength of the mats, possible due to the agglomeration of carbon nanotubes inside the fibers. For PLA with 0.25 wt% of MWCNT the tensile was 5.56 (0°) and 4.45 (90°) MPa.

References:

1. Merlini, C.; Oliveira Castro, V.; Perli, G.; el Omari, Y.; Livi, S. Nanomaterials, 2023, 13, 1476. https://doi.org/10.3390/nano13091476
2. TOKOBARO, P. E. A. et al. Desenvolvimento de Compósitos Híbridos de Epóxi/Nanotubos de Carbono/Cargas Minerais e Avaliação das Propriedades Elétricas e Termomecânicas: efeito da viscosidade e do solvente. 143 f. Dissertação. Universidade Federal de São Carlos, São Carlos, 2018.

Keywords*: Electrospinning.Polymeric nanofiber. PLA. IL. MWCNT. Conduits*

ENCAPSULATION AND SUSTAINED RELEASE OF NATURAL LARVICIDE FROM POLYURETHANE/PIPERINE NANOPARTICLES

Amanda S. Lima[1], Roberta S. Rocha[2], Eduarda M. Lemes[2], Jessica Chaves[2], Karine M. Zepon[1], Josiane Prophiro[1], Rachel F. Magnago[1, 2]*

1 – Postgraduate Program in Environmental Sciences (PPGCA), University of South Santa Catarina (UNISUL), Palhoça, SC, Brazil
rachelfaverzanimagnago@gmail.com
2 – Laboratory of Active Materials, University of South Santa Catarina (UNISUL), Palhoça, SC, Brazil
3- Postgraduate Program in Materials Technology and Industrial Processes (ICCT), Feevale University, Novo Hamburgo, RS, Brazil

Abstract - Polymeric nanocapsule with natural actives have emerged as promising materials for controlling vectors of pathogens that cause diseases such as dengue and chikungunya provoking thousands of deaths annually (1). Polyurethanes have received limited attention in this area, so a new Polyurethane was prepared from the polycondensation reaction between polycaprolactone-triol (PM 300) and 1,6-hexamethylene diisocyanate at 55 °C for 6 h. The preparation of the nanoparticles was carried out using the single emulsion method and pure nanocapsules (PU) were prepared and loaded with 45 mg (PUPI45), 67.5 mg (PUPI67) and 90 mg (PUPI90) of piperine, then the zeta potential, particle size and dispersion index were measured by DLS. To determine the encapsulation efficiency, 4 ml of nanoparticles (diluted at 1:50) were placed in a falcon tube and subjected to centrifugation at 4,000 rpm. The non-encapsulated piperine fraction was determined by UV-vis, using a wavelength of 339 nm. To determine the release, dialysis membranes containing 2 ml of nanoparticles with piperine were submerged in 50 ml of natural water (25°C) and the released piperine was analyzed in a UV-vis spectrophotometer. For FTIR and TGA characterization, samples were lyophilized at -50 °C for 48 h. The PU, PUPI45, PUPI67 and PUPI90 showed particle size values of 280.37, 1395.78, 1693.11 and 1237.11 nm; dispersion index of 0.430, 0.072, 0.177 and 0.208; zeta potential of 3.72, -27.11, 4.39 and -39.67 mV, respectively, and despite the increase in particle size, an improvement in system stability was observed, except for PUPI67. The encapsulation efficiency was 80.68±1.75%, 89.23±1.31% and 38.24±1.84% for PUPI45, PUPI67 and PUPI90, is found in the literature PCL-based nanoparticle loaded with β-carotene (2), with 78.23% of EE. Due to the low encapsulation efficiency of PUPI90, piperine release assays were performed for PUPI45 and PUPI67. PUPI45 had a peak piperine release of ~60% at 36 h, slowly decaying and reaching ~30% at 250 h. PUPI67 peaked at ~45% at 144 hours and ~40% at 250 hours. The thermal stability of microparticles decreased with increasing piperine concentration. In this way, it is proposed that the microstructures can sustain the release of piperine for at least 10 days at room temperature.

References

1. J. G. Oliveira; et al. *Acta Tropica* 2022, *230*, 106395. https://doi.org/10.1016/j.actatropica.2022.106395.
2. M. J. Galindo-Pérez et al. LWT: Food Science and Technology 2018, 87, 333-341. https://doi.org/10.1016/j.lwt.2017.09.008

Fundings: We are grateful to PPGCA of UNISUL for the support in the experiments and analysis. This research is financed by: Fundação de Amparo à Pesquisa do Estado de Santa Catarina (FAPESC)

Keywords: *Polycaprolactone-triol, Polyurethane, Sustained release.*

ENCAPSULATION OF ESSENTIAL OILS ON CHITOSAN NANOPARTICLES WITH ANTIMICROBIAL PROPERTIES FOR FUNCTIONALIZATION OF FABRICS

Pedro G. V. Silva[1], Fernanda C. da Rosa[1], Patrícia B. Brondani[2], Larissa N. Carli[1]

1 – Coordenadoria Especial de Engenharia de Materiais, Universidade Federal de Santa Catarina(UFSC), Blumenau, SC, Brasil
larissa.carli@ufsc.br
2 – Departamento de Ciências Exatas e Educação, Universidade Federal de Santa Catarina (UFSC), Blumenau, SC, Brasil

The main goal of this work is the encapsulation of eucalyptus and lavender essential oils on chitosan nanoparticles for application in the functionalization of cotton fabric with antimicrobial properties [1-2]. Firstly, a solution of the chitosan (1% w/v) in acetic acid (1% v/v) was prepared and mixed with Tween 80 as surfactant. The essential oils were dissolved in ethanol and this oil phase was added to the aqueous chitosan solution during homogenization using a Ultra-Turrax® IKA at 13,000 rpm for 10 min. Then, sodium tripolyphosphate (TPP) was added dropwise to this emulsion and stirred under the same conditions for 40 min in order to promote crosslinks formation by ionic gelation [3]. The material obtained was washed using deionized water and centrifuged, and the samples were dried by lyophilization process. The encapsulation efficiency was 61.8%. Fourier transform infrared spectroscopy (FTIR) exhibited the characteristic bands of the materials used in the formation of nanocapsules. Transmission electron microscopy (TEM) and dynamic light scattering (DLS) confirmed the nanometric size of nanocapsules (~20 nm) with spherical core-shell morphology. Antimicrobial activity tests are yet to be performed to confirm the activity of the essential oils encapsulated in order to guarantee the efficiency of this material before impregnation in different fabrics in order to produce functional and durable materials.

References

1. Javid, A. *et al*. Journal of Microencapsulation 2014, v. 31, n. 5, p. 461–468. https://doi.org/10.3109/02652048.2013.879927.
2. Saleh, S. N. *et al*. International Journal of Biological Macromolecules 2021, v. 183, p. 23–34. https://doi.org/10.1016/j.ijbiomac.2021.04.059.
3. Hosseini, S. F. *et al*. Carbohydrate Polymers 2013, v. 95, n. 1, p. 50–56. https://doi.org/10.1016/j.carbpol.2013.02.031.

Fundings: Conselho Nacional de Desenvolvimento Científico e Tecnológico (Cnpq).

Keywords: *Nanoencapsulation, essential oils, chitosan.*

ENHANCED SCALE INHIBITION PERFORMANCE BY POLYPHOSPHATE ENCAPSULATION IN POLYELECTROLYTE COMPLEXES

Stéphanie C. de Morais[1] and Rosangela de C. Balaban[1]

1 – Chemistry Institute, Federal University of Rio Grande do Norte (UFRN), Natal, RN, Brazil
stephaniex_x@hotmail.com

Abstract - The efficiency in the inorganic scale inhibition process is directly related to the inhibitor's residence time and its action at the adsorption site [1,2]. This can be improved by encapsulating the inhibitor in a polyelectrolyte complex (PEC), which will have the function of performing a controlled release of this material in the rock matrix, allowing a longer-lasting inhibition process. For this purpose, poly (epichlorohydrin-co-dimethylamine) (EPI-DMA) and poly (4-styrene-sulfonic acid-co-maleic acid) (PSSMA) polyelectrolytic complexes were developed to encapsulate the sodium hexametaphosphate (SHMP) scale inhibitor. For the synthesis of the complexes, the concentrations of polycation and polyanion were varied as shown in Table 1 and the SHMP concentration was the same in all formulations (10 g L^{-1}). The PECs were characterized based on their particle size, zeta potential (ζ) and encapsulation efficiency (EE) of SHMP (determined by measuring phosphorus concentration using an inductive coupling plasma emission spectrometer). The characterization results are shown in Fig. 1 and were evaluated to select the formulation with the most suitable results for application in an inhibition process. As can be seen in Fig 1, in a fixed concentration of EPI-DMA, particle size decrease and ζ increase as PSSMA concentration decrease. Aiming the application in reservoir conditions is ideal a smaller particle size and positive ζ. Based on the formulations that meet this criterion, the sample 2 is the most suitable, with the smallest particle size, highest ζ and acceptable EE.

Table 1. PECs formulations

Sample	EPI-DMA concentration (g L^{-1})	PSSMA concentration (g L^{-1})
1	10	5
2	10	1
3	5	5
4	5	1

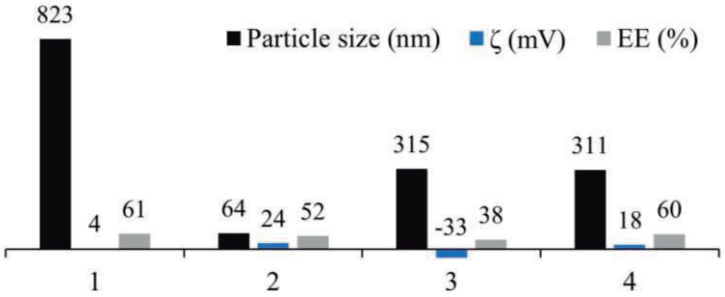

Figure 1. PECs characterization results

References

1. W. W. Frenier, M. Ziauddin, *Formation, Removal, and Inhibition of Inorganic Scale in the Oilfield Environment,* Society of Petroleum Engineers, Texas, 2008. https://doi.org/10.2118/9781555631406.
2. O. Vazquez, I. Fursov, E. Mackay. *J. Pet. Sci. Eng*. 2016, *147*, 302–307. https://doi.org/10.1016/j.petrol.2016.06.025.

Keywords: *Polyelectrolyte complex, scale inhibition, polyphosphate.*

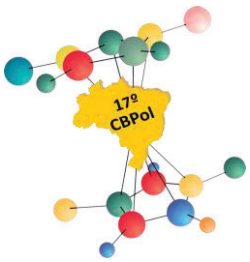

ENHANCING ELECTROSPINABILITY OF CHITOSAN: THE INFLUENCE OF PEO BLEND

Júlia Audrem Gomes de Oliveira[1*], Ricardo Martínez García[2] and Djalma Souza[1]

1 – Advanced Materials Laboratory (LAMAV), State University of the North Fluminense Darcy Ribeiro (UENF), Campos dos Goytacazes, RJ, Brazil

juliaaudrem@gmail.com

2 – National Council for Scientific and Technical Research, Institute of Engineering Technologies and Sciences (INTECIN), University of Buenos Aires (UBA), Buenos Aires, BUE, Argentina

Abstract – The development of water filtration membranes for environmental preservation has attracted considerable attention, given the prominence of electrospinning as the favored technique for their fabrication. In this context, polysaccharides have emerged as highly promising natural materials that can potentially replace synthetic polymers in various applications, including membranes, owing to their abundant availability in nature. Among these polysaccharides, Chitosan (Ch) distinguishes itself as an amino polysaccharide polymer with unique properties. However, the eletrospinability of chitosan is limited due to its polycationic nature and rigid chemical structure. The presence of strong hydrogen bonds restricts the mobility of polymer chain segments when exposed to an electric field, leading to jet breakage during the electrospinning process. To enhance the electrospinnability of chitosan, the utilization of blend systems incorporating other natural or synthetic polymers are currently being studied as a highly promising technique. This work aimed to investigate the influence of blending PEO into chitosan. Chitosan and polyethylene oxide (PEO) solutions were independently prepared with a concentration of 4 wt% in a solvent consisting of 50 wt% aqueous acetic acid. Subsequently, chitosan/PEO blend solutions were formulated by combining the individual solutions, maintaining an 80/20 ratio of chitosan to PEO. Nanofibers were produced through the electrospinning process considering some processing parameters. The nanofiber morphology was evaluated using scanning electron microscopy (SEM) and the results demonstrated that alterations in the processing parameters significantly influenced the characteristics of the nanofibers. The addition of PEO to chitosan had an impact on morphology, leading to the formation of more uniform fibers avoiding the electrospray effect when a pure chitosan solution was used. The electrospinning technique proved efficient in generating nanofibers from chitosan/PEO blends.

References

1. Pakravan, M.; Heuzey, M. C.; & Ajji, A. *Polymer 2011, 52(21), 4813-4824.* https://doi.org/10.1016/j.polymer.2011.08.034.
2. Xing, G.; Shao, L.; Du, Y.; Tao, H.; Qi, C. *Cellulose 2021, 28, 961-971.* https://doi.org/10.1007/s10570-020-03562-3.
3. Xing, G.; Shao, L.; Du, Y.; Tao, H.; Qi, C. *Cellulose 2021, 28, 961-971.* https://doi.org/10.1007/s10570-020-03562-3.

Fundings: The authors would like to thank Faperj and UENF for the resources provided for the development of this research.

Keywords: *electrospinning, chitosan, polyethylene oxide (PEO), membranes, nanofibers.*

EVALUATION OF AC AND DC ELECTRICAL PROPERTIES OF NATURAL RUBBER NANOCOMPOSITES WITH MWCNTs

Diego S. Melo[1], Carlos T. Hiranobe[2], Renivaldo J. dos Santos[2] and Michael J. Silva[1*]

1 Department of Physics, Ilha Solteira School of Engineering, São Paulo State University (UNESP), Ilha Solteira, SP, Brazil. michael.silva@unesp.br

2 Department of Engineering, School of Engineering and Sciences, São Paulo State University (UNESP), Rosana, SP, Brazil.

Abstract - The present work aims to prepare conductive polymeric nanocomposite based on vulcanized Natural Rubber (NR) as matrix and second phase multi-walled carbon nanotubes (MWCNT), aiming at application as piezoresistive sensor. The nanocomposite samples were produced in an open roller mixer, in which 100 phr of BN was used as reference, and the amount was kept fixed, as well as the vulcanizing agents (sulfur, zinc oxide, etc.) while varying the MWCNT concentrations (from 1 to 7 phr). To evaluate the properties of the NR/MWCNT nanocomposite conductive samples, electrical analyses were performed in dc and ac regime. Through the studies of electrical conductivity dc (σ_{dc}), it was possible to observe in which concentration of MWCNT occurred the insulating-conducting transition, that is, to determine the percolation threshold, whose value was equal to 2.7 phr. The impedance spectroscopy analysis was carried out between the frequency range of 0.01 Hz and 1 MHz. It was possible to observe that the samples presented electrical conductivity ac characteristic of disordered solids, that is, frequency dependent behavior. For the samples with MWCNT concentrations higher than the percolation threshold, it has been observed that the real part of the conductivity $\sigma'(f)$ demonstrated two well-defined regions, i.e., one independent of frequency and one dependent. On the other hand, the samples with MWCNT concentrations below the percolation threshold showed changes in the conductivity $\sigma'(f)$, and the analyses showed that frequency-dependent behavior for the entire frequency range studied. In summary, the results obtained in this study indicate that it is possible to obtain a conductive nanocomposite with a low percolation threshold, which makes it suitable for applications such as antistatic blankets, piezoresistive sensors, and electromagnetic radiation shielding device.

References

1. Matos, C. F.; Galembeck, F.; Zarbin, A. J. G. *Revista Virtual de Quimica*, 2017, n. 1, Vol. 9, 73– 96. DOI: 10.21577/1984-6835.20170008

2. Silva, M. J. et al. *Polymer Composites*, 2021,, n. 3, Vol. 42, 1519-1529. https://doi.org/10.1002/pc.25920

3. Moharana, S. et al. *Polymer Science - Series A*, 2017, n. 3, Vol. 59, 405–415. https://doi.org/10.1134/S0965545X17030130

Fundings: Coordenação de Aperfeiçoamento de Pessoal de Nível Superior – CAPES.

Keywords: *Natural Rubber, MWCNT, Conductive Nanocomposite, Piezoresistivity.*

EVALUATION OF AC AND DC ELECTRICAL PROPERTIES OF VULCANIZED NATURAL RUBBER NANOCOMPOSITES WITH MWCNTS: AN ANALYSIS BY MEANS OF THE ELECTRICAL MODULUS

Diego S. Melo[1], Carlos T. Hiranobe[2], Renivaldo J. dos Santos[2] and Michael J. Silva[1*]

1 Department of Physics, Ilha Solteira School of Engineering, São Paulo State University (UNESP), Ilha Solteira, SP, Brazil.
michael.silva@unesp.br
2 Department of Engineering, School of Engineering and Sciences, São Paulo State University (UNESP), Rosana, SP, Brazil.

Abstract - In this study, the preparation and characterization of a conductive polymer nanocomposite using vulcanized natural rubber (NR) as matrix and multi-walled carbon nanotubes (MWCNT) as second phase were carried out. The electrical properties of the NR/MWCNT nanocomposite samples were evaluated with variations from 1 to 5 phr MWCNT. The studies presented in this work include real and imaginary dielectric permittivity and real and imaginary electrical modulus. The dielectric properties of insulating materials are first described by analyzing the electrical modulus (M*), which is commonly used for this purpose. In addition, the electrical modulus also allows the evaluation of relaxation processes in conductive materials (ionic and electronic), which are obscured when analyzing the behavior of the real and imaginary dielectric constant (ε*) as a function of frequency. Due to the excellent electrical properties of the nanocomposite, even at low concentrations of MWCNT, the samples show potential applications as antistatic coatings and piezoresistive sensors.

References

1. Achour, M. E.; Brousseau, C.; Carmona, F. *Journal of Applied Physics*, 2008, n. 9, Vol. 103. https://doi.org/10.1063/1.2912985
2. Amoozegar, V.; Sherafat, Z.; Bagherzadeh, E. *Ceramics International*, 2021, n. 20, Vol. 47, 28260- 28267. https://doi.org/10.1016/j.ceramint.2021.06.241
3. Kanda, D. H. F.; Nagashima, H. N.; Malmonge, J. A.; Sakamoto, W.K.; Chierice, G. O. *Journal of Materials Science*, 2008, Vol. 43, 5436–5440. https://doi.org/10.1007/s10853-008-2843-3

Fundings: Coordenação de Aperfeiçoamento de Pessoal de Nível Superior – CAPES.

Keywords: *Natural Rubber, MWCNT, Conductive Nanocomposite, Electrical Module.*

EVALUATION OF ACID CONCENTRATION ON OBTAINING NANOCRYSTALS CELLULOSE AND SURFACE MODIFICATION BY SILANE

Katiusca Wessler Miranda[1,2*], Janaína L. L. Howarth[2], Sérgio H. Pezzin[1]

1 – PPGCEM, University of State of Santa Catarina (UDESC), Joinville, SC, Brazil katiusca.wessler@gmail.com
2 – Nanobiocell Nanotecnologia, Joinville, SC, Brasil

Abstract – In this study, the influence of H_2SO_4 concentration on the particle size distribution of cellulose nanocrystals (NCC) was evaluated, as well as, the surface modification of nanoparticles by silanization. Eucalyptus cellulose sheets kindly provided by CENIBRA were hydrolyzed with 20, 30 e 50 % (v/v) H_2SO_4 solutions for 40 minutes at 40 °C. The samples were named CV20, CV30 and CV50, respectively. Samples were centrifuged at 6,000 rpm at 10°C for 30 minutes until pH 6-7. Subsequently, it was lyophilized and characterized according to the size distribution by laser dispersion (DLS), zeta potencial (PZ), thermogravimetric analysis (TGA), field emission scanning electronic microscopy (FEG), transmission electronic (TEM) and infrared spectroscopy (FTIR). Samples were lyophilized and redispersed (1% w/v) in 100 mL of anhydrous ethanol by sonication at 30% amplitude for 30 minutes. Another solution was prepared with anhydrous ethanol and 5 mL of (3-Aminopropyl) triethoxysilane (APTES) under stirring for 30 minutes and acidified with acetic acid to pH 4 – 5. The solutions were stirred for two hours. After this time, the solution was centrifuged and washed with ethanol and centrifuged again (three cycles) to completely remove the residues. The DLS analyses showed that increasing the H_2SO_4 percentual influenced the particle size distribution. Only the CV50 sample showed hydrodynamic diameter of 256 nm and PZ equal to -26.0 mV. FEG and TEM microscopies confirmed the obtaining of nanocrystals when 50% (v/v) H_2SO_4 was used. TGA analyzes indicate that the reaction with APTES increased the thermal stability of the NCCs. However, FTIR spectra not evidenced the surface chemical modification of nanocrystals cellulose.

References

1. R. M. Neves; H. L. Ornaghi. Jr; A. J. Zattera; S. Amico. Carbohydrate Polymers 2020, 230, 115595. https://www.sciencedirect.com/science/article/pii/S0144861719312639
2. S. Ventura-Cruz; A. Tecante. Food Hydrocolloids 2021, 118, 106771. https://doi.org/10.1016/j.foodhyd.2021.106771

Fundings: The authors are grateful for the PDI-CNPq scholarship.

Keywords: nanocrystals cellulose, chemical modification, silanization

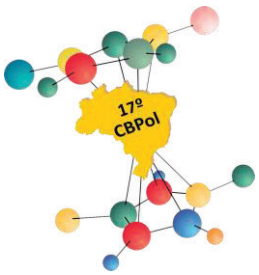

EVALUATION OF LDPE/GRAPHENE NANOCOMPOSITE IN ROTATIONAL MOULDING

Francisco P. Araújo Jr[1]*, Luis C. Mendes[1], Gerson A. V. Albitres[1].

1 – Institute of Macromolecules Professor Eloisa Mano, Federal University of Rio de Janeiro (UFRJ), Rio de Janeiro, RJ, Brazil
franciscoaraujo@ima.ufrj.br

Abstract

The development of new materials is a cornerstone to support the improvement of plastic part manufacturing processes. Nanocomposites can be used to facilitate the optimisation of process cycles, for rotation moulding it is extremely interesting as it has the high processing time. In order to promote better processability, a nanocomposite based on linear low density polyethylene (LDPE) loaded with graphene (n-GP) and processed under different rotomoulding conditions was developed. The effect of n-GP on LDPE properties was evaluated. Thermogravimetry indicated an increase in thermal stability when compared with the material without N-GP. Differential scanning calorimetry indicated a decrease in crystallinity in the rotomoulded part. The impact strength and tensile strength values were increased. By the nuclear magnetic resonance hydrogen technique in the time domain, a significant variation was observed in the domain curves and in the longitudinal relaxation times, indicating influence of the polymer/filler interaction on the material structure.

References

1. W. Mhike; W. W. Focke; J. K. Asante *Journal of Thermoplastic Composite Materials, 2018, 31*, *535* https://doi.org/10.1177/0892705717712634
2. M. Sabet; H. Soleimani *International Journal of Plastics Technology, 2018, 22,* 234. https://doi.org/10.1007/s12588-018-9225-8
3. E. Planes; J. Duchet; A. Maazouz; J. Gerard *Polymer Engineering & Science, 2018, 48,* 723. https://doi.org/10.1002/pen.21012
4. M. Sabet; H. Soleimani *Heliyon, 2019, 5*, 2053. https://doi.org/10.1016/j.heliyon.2019.e02053
5. P. N. Khanam; M.A. AlMaadeed; M. Ouederni; E. Harkin-Jones ; B. Mayoral; A. Hamilton; D. Sun *Vacuum, 2016, 130,* 63. https://doi.org/10.1016/j.vacuum.2016.04.022
6. Z. Li; B. Du; C. Han; H. Xu *Nature - Scientific Reports, 2017, 7,* 4015. https://doi.org/10.1038/s41598-017-04196-5

Keywords: *nanocomposite; LDPE ; graphene; mechanical and thermal properties; rotational moulding*.

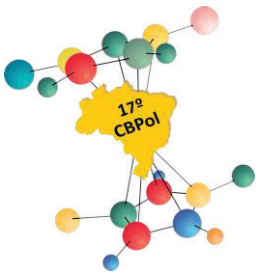

EVALUATION OF POLYDIMETHYLSILOXANE (PDMS) WITH ZINC OXIDE NANOSTRUCTURES AS AN ENCAPSULANT IN PHOTOVOLTAIC MODULES

Muriel R. Oliveira[1], Pedro L. Silva[2], Deuber L. S. Agostini[2], Clarissa A. Olivati[2], Leonardo L. Paim[1], Renivaldo J. Santos[1] and Flávio C. Cabrera[1].

1 - Faculdade de Engenharia e Ciências, Universidade Estadual Paulista (UNESP), Rosana, SP, Brazil
e-mail: muriel.r.oliveira@unesp.br
2 - Faculdade de Ciências e Tecnologia, Universidade Estadual Paulista (UNESP), Presidente Prudente, SP, Brazil

Photovoltaic modules carry layers of Ethylene Vinyl Acetate (EVA), with the objective of sealing (encapsulant) and protecting the cells against degradation by contact with the environment. However, due to the long lifespan of the modules (there is an estimation of at least 25 years with an efficiency of 85%) the EVA layer undergoes degradation (yellowing), reducing the degree of transmittance and consequently the efficiency of the modules. Thus, this work intends to replace the EVA layers by polydimethylsiloxane (PDMS) films with the incorporation of zinc oxide (ZnO) nanoparticles. PDMS is a fast curing, transparent and long-lasting material. ZnO nanoparticles have been used in the construction of sensors and solar cells, ultraviolet radiation blocking technology and even for their self-cleaning and bactericidal properties. Four PDMS films were prepared in the ratio of 3.0 g of polymer base to 0.3 g of curing agent. Three different volumes of suspension of zinc oxide nanoparticles (50µL, 100µL and 150µL) were then placed on their surface, with the purpose of comparing them to the PDMS film without nanoparticles. The films were deposited on photovoltaic cells by casting and taken to a stove at 70°C for 3 h. The electric currents (AC) generated by the photovoltaic cells were measured before and after the deposition of the films, using a 50W reflector. There was an increase in the generated current of 3.9% (50µL) and 11.59% (100µL) reaching the concentration limit at 150µL due to the opacity caused by the nanoparticles, without increasing the AC in the solar boards.

References

A. Becheri; M. Durr; P. L. Nostro; P. Baglioni Journal of Nanoparticle Research 2008, 10, 9318-3. https://doi.org/10.1007/s11051-007-9318-3.
F. J. Pern; A. W. Czanderna; K. A. Emery; R. G. Dhere The Conference Record of the Twenty-Second IEEE Photovoltaic Specialists Conference 1991, 1, 169275. https://doi.org/10.1109/PVSC.1991.169275.
L. Pislaru-Dănescu; E. Chitanu; Lucia-Andreea; El-Leathey; V. Marinescu; D. Marin; B. Sbarcea Electronic Materials Letters, 2018, 14, 0028-z. https://doi.org/10.1007/s13391-018-0028-z.
M. S. Ghamsari; S. Alamdari; W. Han; H. Park International Journal of Nanomedicine 2016, 2017:12, S118637. https://doi.org/10.2147/IJN.S118637.
N. Yu; X. Xiao; G. Pan Journal of Dispersion Science and Technology 2019, 40:11, 1484294. https://doi.org/10.1080/01932691.2018.1484294.
T. Wang; Z. Lu; X. Wang; Z. Zhang; Q. Zhang; B. Yan; Y. Wang Applied Surface Science 2021, 550, 149286. https://doi.org/10.1016/j.apsusc.2021.149286.

Keywords: *Solar cell; Photovoltaics; Energy efficiency; Nanomaterials; Zinc oxide;*

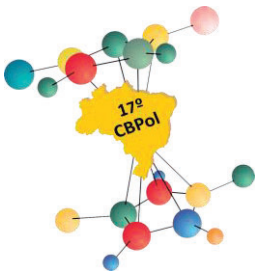

EVALUATION OF THE ANTIMICROBIAL EFFECT OF ZINC OXIDE MASTERBATCH ON HIGH DENSITY POLYETHYLENE

Fernando S. Lameiro[1], Andrea C. K. Bierhalz [2], Marília Miotto[3], Marcel Provenzi[3], Andrey M. P. Silva[1] and Claudia Merlini[4]

1 - Mechanical Engineering Department, Federal University of Santa Catarina, Florianopolis, SC, Brazil
fernandosl@outlook.com
2 - Textile Engineering Department, Federal University of Santa Catarina, Blumenau, SC, Brazil
3 - Food Science and Technology Department, Federal University of Santa Catarina, Florianopolis, SC, Brazil
4 - Materials Engineering Special Coordination, Federal University of Santa Catarina, Blumenau, SC, Brazil

Abstract

The impact of microorganisms on human health is a constant concern and an increasingly frequent theme in research, since they can cause diseases that are spread by different ways of propagation and contagion. Thus, antimicrobials are a fast and effective alternative to minimize the proliferation of various harmful agents, and Zinc Oxide (ZnO) is one of those that has gained momentum in recent decades. It stands out for the possibility of being presented in the form of micro or nano particles, for its broad spectrum of action, low cost of obtaining, and low toxicity when used in low amounts. ZnO can be easily incorporated into polymeric materials, widely used by the population in general. The objective of this study is to evaluate the antimicrobial effects of ZnO incorporation into High Density Polyethylene (HDPE), applied in the form of masterbatch at different concentrations, in relation to the properties of the polymer. Microbiological analyses were performed according to JIS Z 2801, with the *Escherichia coli* bacteria. Moreover, mechanical tests were also performed in order to evaluate the effect of different concentration if ZnO. Izod impact test were performed according to ASTM D 256 and tensile test according to ASTM D 638. The main results indicated that the higher the proportion of ZnO (1,0 %m) in HDPE, the greater the antimicrobial effect found, and that from 3% the desired effect is already reached in the composite. It was also noticed a little reduction in the mechanical properties as the incorporation of the inorganic particle increased. The addition of masterbatch (concentrated at 10%) allowed homogeneity and dispersion of the particles in the specimens of test, showing little change in polymer properties and greater antimicrobial effectiveness.

Table 1: Results antimicrobial and properties analysis

Concentration ZnO (%m)	Antimicrobial Activity R	Izod Impact (J/m)	Tensile Strength (Mpa)
PE	no action	130,34	23,50
0,05	-0,27	121,67	23,00
0,30	2,16	114,73	22,50
1,00	2,76	93,81	22,00

References

1. American Society for Test and Materials (ASTM). *Standard D 638, Standard Test Method for Tensile Properties of Plastics*, 2014.
2. American Society for Test and Materials (ASTM). *Standard D 256, Standard Test Methods for Determining the Izod Pendulum Impact Resistance of Plastics,* 2018.
3. JIS Z 2801: 2000. *Antimicrobial products: test for antimicrobial activity and efficacy*. 2000.

Keywords: *Masterbatch. Zinc oxide. High Density Polyethylene. Antimicrobial.*

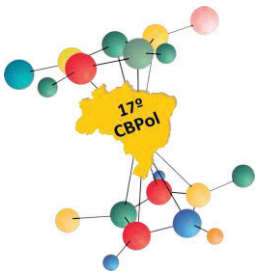

EVALUATION OF THE INCORPORATION OF BORON NITRIDE MICROPARTICLES AND NANOPARTICLES IN POLY(VINYL CHLORIDE) COMPOUND

Lana Taíse Peschel[1], Wagner Maurício Pachekoski[2]

1 – Department of Engineering and Mechanical Science, Federal University of Santa Catarina (UFSC), Joinville, SC, Brazil lana.peschel@hotmail.com
2 – Department of Engineering and Mechanical Science, Federal University of Santa Catarina (UFSC), Joinville, SC, Brazil

Abstract -Poly(vinyl chloride) or PVC is one of the most versatile polymers worldwide. For its processing, additives are incorporated to achieve the necessary properties for each application, stabilizers being among the indispensable ones, as PVC undergoes a degradation process when exposed to heat sources and ultraviolet radiation. Boron nitride (BN) is a material with excellent thermal and chemical properties, in addition to being mechanically robust and insulating. Its application to the PVC compound is promising and has the potential to improve the light stability of PVC, in addition to being able to positively influence the mechanical properties. The application of nanoscale materials in composites has been gaining prominence due to the high surface area of nanoparticles, which results in better interactions between materials. Therefore, the present work aimed to develop composites and nanocomposites of BN/PVC and evaluate the properties of the material. PVC compounds were produced, with a base formulation and application of 0.2%, 0.5% and 1.0% of BN in microparticle and nanoparticle. The TEM analysis showed that the BN particles have between 0.2-1.0 µm, while the nanoparticles have between 50-200 nm. The FTIR results showed that there was a bond between BN and PVC in the region of the 800 cm-1 band. In the evaluation of resistance to weathering, it was evident the protection that BN provided to PVC, in the sample in which there is no presence of this material, there was a significant change in color to yellow, indicating degradation. Comparing composites and nanocomposites, nanocomposites showed the best performance, especially the sample with 1% of BN nanoparticles. In the tensile test, it was identified that the application of BN resulted in increased tensile strength, where the nanocomposites showed superior results. Therefore, it was possible to confirm that the application of BN increased the resistance to weathering and improved the mechanical performance of PVC compounds, where the application of nanoparticles showed superior results.

References

1. A. Rodolfo Junior; C. T. Tsukamoto. Tecnologia do PVC. 3. Ed. São Paulo*: Instituto Brasileiro do PVC*, 2018.
2. J. Huang; J. Zhou; M. Liu. Interphase in polymer nanocomposites. *JACS Au*, v. 2, p. 280-291, 2022.
3. Z. Zheng; M. C. Cox; B. Li. Surface modification of hexagonal boron nitride nanomaterials: a review. *Journal of materials Science*, v. 53, n. 1, p.66-99, 2018.

Keywords: P*oly(vinyl chloride), Boron Nitride, Composite, Nanocomposite.*

EXTRACTION AND CHARACTERIZATION OF NANOCRYSTALS FROM PROCESS WASTES FOR APPLICATION IN TECHNOLOGICAL MATERIALS

Lara P. Tusek[1], Maria Alice Witt[1]

1 – Chemical Engineering Department, Pontifical Catholic University of Paraná (PUCPR), Curitiba, PR, Brazil
lara.tusek@pucpr.edu.br

Abstract - Biopolymers offer more significant benefits in terms of social, environmental, and financial sustainability when compared to synthetic polymers. Therefore, from a sustainability perspective, α-chitin derived from shrimp shell waste was chosen to obtain nanomaterials for subsequent application. The aim of this study is to evaluate the development and feasibility of nanoparticles obtained from waste, considering the most common naturally occurring waste. Accordingly, the chitin used in this study was obtained from a prior extraction process from shrimp shells and was submitted to different experimental conditions to obtain the respective nanocrystals. The acid hydrolysis method was selected for the extraction of nanocrystal, varying reflux conditions (no reflux or 6h) and the need of neutralization by washing the product. The Tyndall effect was observed for all extraction conditions, with the sample extracted under reflux and neutralization being the most stable. The best result represents the sample obtained using 0.5 g of chitin in 140 mL of 3 mol/L HCl aqueous solution, under reflux for 6 hours, filtered, and washed until reaching a neutral pH. The resulting powder was kept at 50 ºC for 2 days. The obtained material was subsequently characterized through Fourier Transform Infrared (FTIR) analysis and X-ray Diffraction (XRD), showing distinct absorption bands at 1649, 1621, 1554, 1009, 3429, 3259 and 1309 cm^{-1} and crystalline peaks of 19.0, 23.0, 26.0, 28.0, 32.0, 35.0, 39.0 and 48.0 degrees at 2θ, which were compared to the literature. The results confirm the success of obtaining nanocrystal structures from chitin waste. The following steps include extract the nanocrystals in a larger (lab) scale and test the adsorption capacity of nanochitin with respect to dyes.

References

1. D. Meng; J. Xie; G. Waterhouse; K. Zhang; Q. Zhao; S. Wang; S. Qiu; K. Chen; J. Li, C. Ma; Y. Pan; J. Xu *Journal of Applied Polymer Science* 2019, *137*, 48485. http://dx.doi.org/10.1002/app.48485.
2. K. Kishida; T. Mizuta; H. Izawa; S. Ifuku *Journal of composites Science* 2022, *6*, 6100280. https://doi.org/10.3390/jcs6100280.
3. N. Yang; W. Zhang; C. Ye; X. Chen; S. Ling *Biotechnology Journal* 2018, *14*, 201700754. https://doi.org/10.1002/biot.201700754.
4. X. Yang; J. Liu; Y. Pei; X. Zheng; K. Tang *Energy & Environmetal Materials* 2020, *3*, 12079. https://doi.org/10.1002/eem2.12079.

Keywords: *nanochitin; chitin; nanoparticles; biopolymers; adsorption.*

FABRICATION AND CHARACTERIZATION OF POLYPYRROLE NANOCOMPOSITES WITH CARBON QUANTUM DOTS

Gabriel S. Evangelho[1], Gustavo F. Galli[1], Lara F. dos Santos[1], Lucas N. Chavero[1]

1 – Laboratory of Optoelectronic Nanostructures (LabNanO), Department of Exact Sciences and Education (CEE), Technological Center for Exact Sciences and Education (CTE), Federal University of Santa Catarina (UFSC), Blumenau, SC, Brazil
ufscgabrielevangelho@gmail.com

Polypyrrole (PPy) is a redox-active aromatic heterocyclic conductive polymer having a pentagonal planar structure ($(C_4H_4NH)_n$). Its vast range of conductivities is due to its amazing ability to alternate between oxidized conductors and reduced insulators [1]. Carbon quantum dots (CQDs) are discrete nanoparticles with dimensions smaller than 10 nm, presenting high solubility in different media, the possibility of introducing functional groups and photoluminescence properties [2], which can be produced by electrochemical oxidation of ultrapure graphite rods. This work reports the fabrication and characterization of PPy/CQDs nanocomposites on silicon substrates. For the formation of the nanocomposite, the electrolytic cell is submerged in a aqueous solution of pyrrole monomer (Py), CQDs and dodecylbenzene sulfonic acid (DBSA). CQDs are simultaneously incorporated during the potentiostatic electropolymerization process of PPy using a fixed potential of 1.2 V and a deposited charge of 10-30 mC, with the electrochemical parameters strictly controlled. Optical microscopy images showed that the CQDs arranged themselves in the matrix in branched fractal structures, with higher density near the edges, where the electric field is more pronounced, suggesting that the intensity of the electric field along the sample influences the distribution of CQDs and formation of structures in the PPy matrix. From cyclic voltammetry measurements, it is verified that the current levels and the integral of the i(v) curve of the nanocomposite is greater than that of the pure PPy, indicating that the CQDs increased the electrical conductivity and the specific capacitance of the nanocomposite. Electrochemical impedance spectroscopy was used to study conductivity and charge transfer rates. Through the Nyquist diagrams and fits using the Randles circuit model, the charge transfer resistances were estimated, where the nanocomposite presented a lower value compared to the pure PPy, suggesting a faster electronic transfer rate. The addition of CQDs increases the polymeric films electrical and electrochemical properties.

References

1. L. X. Wang; X. G. Li; Y. L. Yang *Reactive and Functional Polymers* 2001, 47, 125. https://doi.org/10.1016/S1381-5148(00)00079-1.
2. R. Jelinek; in *Carbon Quantum Dots: Synthesis, Properties and Applications*, P. Araujo, Ed.; Springer, Tuscaloosa, 2016; Vol. 1, 1-14.

Fundings: CNPQ, FAPESC, INEO, LCME.

Keywords: *Conductive Polymers; Polypyrrole; Carbon Quantum Dots; Nanocomposites; Electrical Conductivity.*

FLUORESCENCE EMISSION FROM GELATIN CARBON DOT UNDER X-RAY FLUORESCENT IRRADIATION

Mayara Martins Caetano[1], Juliana Cristina Biazzotto[2], Roberto Santana da Silva[2], and Renata Galvão de Lima[1]*

1 – Instituto de Ciências Exatas e Naturais do Pontal-ICENP, Federal University of Uberlândia (UFU), Ituiutaba, MG, Brazil,
2 – Faculdade de Ciências Farmacêuticas de Ribeirão Preto, University of São Paulo (USP), Ribeirão Preto, SP, Brazil,
mayara.caetano@outlook.com.br

Abstract – Carbon dots (CDs) are nanoparticle which have characteristics of semiconductors and important photoluminescence properties[1]. CDs synthesis processes aim at sustainable methodologies and greener approach. CDs from natural polymers have been synthesized through a hydrothermal method[2]. In this work the gelatin carbon dots (CDg) were obtained from gelatin in aqueous suspension with different percentages of ethanol by hydrothermal method. The carbonized solid was dissolved in water, sonicated and centrifugated to separate the CDg as a yellow aqueous suspension and a solid agglomerated polymer. Both yellow aqueous suspension and the solid agglomerated polymer showed fluorescence emission under (Fig. 1a-b). The higher % of ethanol in the preparation provides appearance of a band in the visible region (~500 nm) under UV and x-ray fluorescence excitation.

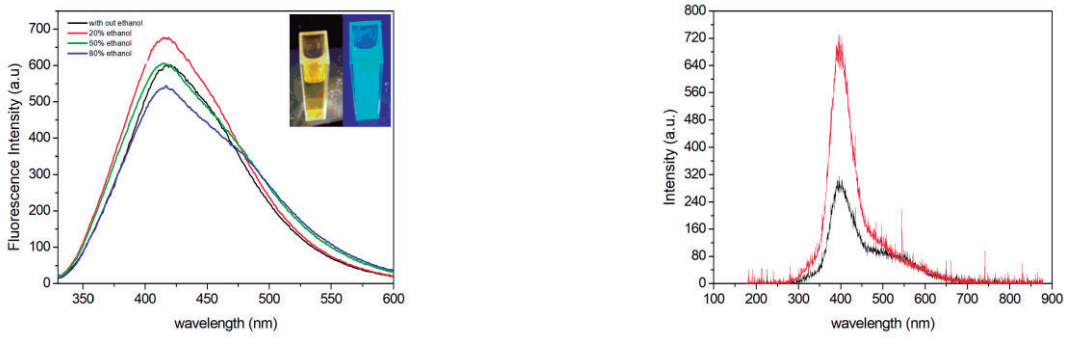

(a) (b)

Figure 1. Fluorescence emission spectra λ_{ex}=320 nm (a) for yellow aqueous suspension and x-ray fluorescence excitation (b) for solid carbonized (red line) and solid agglomerated polymer (black line).

References

1. B. D. Mansurya; Z. Altintas. A. *Nanomaterials 2021*, *11*, 2525. https://doi.org/10.3390/nano11102525.
2. Q. Liang; W. Ma; Y. Shi; Z. Li; X. Yang. *Carbon 2013, 60*, 421. http://dx.doi.org/10.1016/j.carbon.2013.04.055

Fundings: Capes for Mayara PhD scholarship. Acknowledgment for CIDRA (USP) by x-ray fluorescence emission.

Keywords: *natural polymer, carbon dot, hydrothermal method, fluorescence emission, x-ray fluorescence excitation*

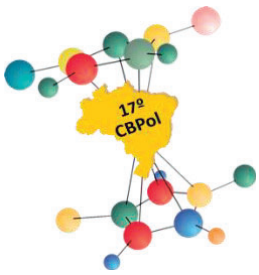

FORMULATION OF HIGH THERMAL PERFORMANCE XLPE NANOCOMPOSITE

Laura V. Carvalho[1], André B. Carvalho[1], Rafael Barbosa[1]* and Lidiane C. Cristina[1]

1 – Department of Materials Engineering (DEMa), Federal University of São Carlos (UFSCar), São Carlos, SP, Brazil
rbarbosa@ufscar.br

Abstract

In submarine electrical cables, low-density cross-linked polyethylene (XLPE) is one of the most widely used dielectric materials due to its mechanical, electrical, and thermal stability properties[1]. In this work, aiming to increase its thermal conductivity, without compromising the insulating capacity, a hybrid nanocomposite with hexagonal boron nitride (hBN) and multi-walled carbon nanotubes (MWCNT) was formulated[2,3]. The choice of fillers was conducted observing the high values of thermal conductivity associated with the electrically insulating nature of hBN, while the MWCNT was used carefully to improve the thermal transport without electrical resistivity loss[3]. The nanocomposite was obtained by melt mixing in a torque rheometer using hBN silanized with (3-aminopropyl) triethoxysilane (APTES) and MWCNTs. Differential exploratory calorimetry and gel content measurements (Table 01) showed no strong evidence of changes in matrix morphology. It is worth noting that without the presence of the nanotubes, which formed clusters dispersed throughout the network, almost twice as much hBN would be required, according to the Lewis-Nielsen model[4]. Therefore, based on the methodology employed, it was possible to build a thermally percolated hybrid network, with low filler fraction and without any loss in electrical conductivity.

Table 01

	XLPE	Hybrid
Gel content	46% ± 3%	48% ± 1%
Degree of crystallinity	32,8%	30,1%
Volumetric resistivity	$1{,}8.10^{16}$±$0{,}2.10^{16}$ Ω.cm	$2{,}4.\ 10^{16}$ ± $0{,}5.\ 10^{16}$ Ω.cm

References

1. M. Rafiq; et al. Nano Energy, 2022, 91, 106661. https://doi.org/10.1016/j.nanoen.2021.106661.
2. K. Sun; et al. Materials, 2019, 12, 746. https://doi.org/10.3390/ma12050746.
3. K. Kim; J. Kim Polymer, 2016, 101, 168. https://doi.org/10.1016/j.polymer.2016.08.0624.
4. F. Kargar; et al. ACS Applied Materials & Interfaces, 2018, 10, 43. https://pubs.acs.org/doi/10.1021/acsami.8b16616

Fundings: This study was financed in part by the Coordenação de Aperfeiçoamento de Pessoal de Nível Superior - Brasil (CAPES) - Finance Code 001. CAPES PROEX and PPGCEM-UFSCAR.

Keywords: Dielectric material, Boron nitride, Carbon nanotubes.

FRACTAL TYPE SELF ASSEMBLY FORMED BY CARBON QUANTUM DOTS INDUCED BY ELECTRIC FIELD IN POLYPYRROLE MATRIX

Gustavo F. Galli[1], Gabriel S. Evangelho[1], Lara F. dos Santos[1], Lucas N. Chavero[1]

1 – Laboratory of Optoelectronic Nanostructures (LabNanO), Department of Exact Sciences and Education (CEE), Technological Center for Exact Sciences and Education (CTE), Federal University of Santa Catarina (UFSC), Blumenau, SC, Brazil
gustavofg42@gmail.com

Fractals are infinitely complex patterns that are self-similar at different scales and sizes, which rise in situations far from thermodynamic equilibrium. In nature, common examples of fractal-type aggregations include snowflakes, plants and crystals [1]. Carbon quantum dots (CQDTs) are particles less than 10 nm in size that have interesting optical and electrical properties such as photostability, size-dependent emission and high conductivity [2], which, depending on the conditions, can form fractal-like structures. Polypyrrole (PPy) is an intrinsically conductive polymer that has a pentagonal planar structure ($(C_4H_4NH)_n$), and its wide range of conductivities is due to its amazing ability to alternate between oxidized conductors and reduced insulators [3]. The fabrication of fractal structures of PQCs on a PPy matrix can modify some of the optical, electrical, and electrochemical properties of these materials, making them candidates for applications in various devices, such as analytical sensors, biosensors, photocatalysts and optoelectronic. In this work, we report the formation of fractal structures induced by an electric field on a PPy matrix with PQCs. The PPy/PQCs matrix was formed by electropolymerizing pyrrole monomer (Py) on a silicon substrate at a constant potential of 1.2 V, with simultaneous incorporation of the PQCs in the polymeric structure and control of the deposited charge. The fractal aggregations are then generated by applying constant potentials to the polymeric matrix of PPy/PQCs using the chronoamperometry technique and a KCl solution as an electrolyte. Optical microscopy images revealed the formation of nanocomposites with a DLA-type fractal pattern along the entire length of the nanocomposite edge from applied potentials of 0.15 V. Chronoamperometry measurements using only pure water did not result in samples with fractal structures, thus indicating that the use of KCl as an electrolyte can play a catalytic role, stimulating the formation of these structures adjacent to the periphery of the nanocomposite film.

References

1. A. Crivoi; F. Duan *Physical Chemistry Chemical Physics* 2012, 14, 1449. https://doi.org/10.1039/C1CP22989C.
2. K. J. Mintz; Y. Zhou; R. M. Leblanc *Nanoscale* 2019, 11, 4634. http://dx.doi.org/10.1039/c8nr10059d.
3. L. X. Wang; X. G. Li; Y. L. Yang *Reactive and Functional Polymers* 2001, 47, 125. https://doi.org/10.1016/S1381-5148(00)00079-1.

Fundings: CNPQ, FAPESC, INEO, LCME.

Keywords: *Polypyrrole; Self Assembled; Fractal; Carbon Quantum Dots; Nanocomposite.*

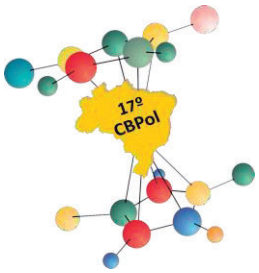

Functionalized leather for eliminating the SARS-CoV-2 virus

Ana Gabriele da Costa Sales[1], Gleison N. Marques[1], Roberta Y. N. Reis[1], Lara K. Ribeiro[1,2], Luis G. P. Simões[3], Daniel T. Minozzi[3], Juan Andrés[2], Marcelo Assis[2], Lucia H. Mascaro[1], and Elson Longo[1]

[1]CDMF, LIEC, Federal University of São Carlos - (UFSCar), São Carlos, SP, 13565-905 Brazil
[2] Department of Physical and Analytical Chemistry, University Jaume I (UJI), Castelló 12071
[3]Nanox Tecnologia S/A, 13562-400 São Carlos, SP, Brazil.
**Corresponding Author: gabicosta09@hotmail.com*

Abstract - The safe and efficient elimination of microbes such as bacteria, fungi, and viruses, including the SARS-CoV-2 virus, through biocidal surfaces remains a major technological challenge[1]. Currently, leather is used in different consumables in the industry and provides comfortable conditions for the growth of these infectious microorganisms [2]. This study explores the use of SiO_2-AgNPs composed of silica (SiO_2) and Ag nanoparticles (AgNPs) to functionalize leather with excellent virucidal and bactericidal capable of inactivating the SARS-CoV-2 virus and the *Staphylococcus aureus* (*S. aureus*) bacteria, respectively. The leather functionalized with SiO_2-AgNPs was characterized by SEM, EDS, AFM, FTIR, and XPS techniques. The immobilization of nanoparticles in the collagen fibers of leather results in a superficial modification, increasing the roughness of the material and the contact angle between the leather and the SiO_2-AgNPs. The treated leather reached an effectiveness of 99.93% against SARS-COV-2 and 99.99% against *S. aureus*. These results indicate that the functionalized leather with enhanced biocompatibility and biocidal activity is an efficient cleaning strategy with a low risk of degeneration that may be applied in various fields.

References

1. J.M. van Seventer, N.S. Hochberg, Principles of Infectious Diseases: Transmission, Diagnosis, Prevention, and Control, *International Encyclopedia of Public Health.* 2017 22. https://doi.org/10.1016/B978-0-12-803678-5.00516-6.
2. X. Wu, J. Wu, C. Mu, C. Wang, W. Lin, Advances in Antimicrobial Polymer Coatings in the Leather Industry: A Comprehensive Review, *Ind Eng Chem Res*. 60 2021 15004–15018. https://doi.org/10.1021/acs.iecr.1c02600.

Fundings: This work was partly funded by the São Paulo Research Foundation – FAPESP (FAPESP CEPID-finance code 2013/07296-2, FAPESP/BCO-2021/06128-5 and FAPESP/BCO-2021/11326-00), the Financier of Studies and Projects – FINEP, the National Council for Scientific and Technological Development – CNPq, and the Coordination of Improvement of Higher Education Personnel – CAPES (finance code 001). J.A. acknowledges Universitat Jaume I (project UJI-B2019-30), and the Ministerio de Ciencia, Innovación y Universidades (Spain) (project PGC2018094417-B-I00), AICO-GV nueva for financially supporting this research. M.A. was supported by the Margarita Salas postdoctoral contract MGS/2021/21 (UP2021-021) financed by the European Union-Next Generation EU.

Keywords: *Antimicrobial leather, coating, SiO2-Ag nanoparticles, SARS-CoV-2.*

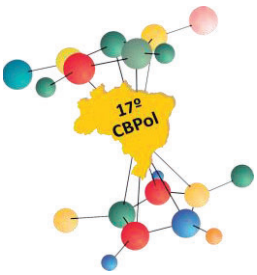

GALACTOMANNAN AS A CARRIER FOR α-BISABOLOL-LOADED NANOCAPSULES INTENDED FOR BIOMEDICAL APPLICATION

Jóice M. Scheibel[1*], Laiane S. da Silva[1], Leonardo F. Marques[1], Daniela L. T. Schmitt[2], Karina Paese[2] and Rosane M. D. Soares[1]

1 – Polymeric Biomaterials Research Group (Poli-BIO), Institute of Chemistry, Federal University of Rio Grande do Sul (UFRGS), Porto Alegre, RS, Brazil
joice.scheibel@ufrgs.br
2 – Faculty of Pharmaceutical Sciences, Federal University of Rio Grande do Sul (UFRGS), Porto Alegre, RS, Brazil

Abstract – Polymers are essential materials in modern society and have been improving the properties of commercial products applied in the biomedical area[1]. However, a higher level of sustainability still needs to be achieved. A possible alternative is the rational design of biomaterials and the replacement of synthetic polymers by natural polysaccharides. Our project aims to investigate the structural properties of galactomannan hydrogels and its ability as a carrier of nanocapsules containing α-bisabolol, an anti-inflammatory and non-allergenic molecule for biomedical purposes. The semisolid solution of nanocapsules was prepared by interfacial deposition of preformed polymer[2]. Five hydrogels' formulations were carried out by solubilizing 1.5 g of galactomannan in 10 mL of suspension of polymeric nanocapsules for 2 hours at 50 ºC. Then 20, 40 and 60% of crosslinking agent were added to the hydrogels. The presence of nanocapsules in the hydrogel matrix was evaluated by light scattering techniques (DLS) and nanoparticle tracking analysis (NTA). Swelling degree was performed at pH 4 and 7.4, for 24 and 48 h. DLS results demonstrated that the nanocapsules maintained their stability showing sizes of approximately 190 nm. NTA analysis corroborated to this result, since the NTA presented relative frequency values between 0 and 300 nm. The swelling degree of the modified galactomannan hydrogels was higher when compared to the unmodified gels, suggesting structural changes in the polysaccharide network. However, additional analysis for undertaking this behavior needs to be performed in order to investigate the effect of BTCA on polymer chains. Our preliminary results for galactomannan formulations shows an innovative and unprecedented combination that brings together the advantages of galactomannan in the formulation of hydrogels, combined with the recognized ability of polymeric nanocapsules in controlling the drug release rate and protecting the skin against irritability and allergies[3].

References

1. Z. Guo; A. A. Poot; D. W. Grijpma. *European Polymer Journal* 2021, *149*, 110388. https://doi.org/10.1016/j.eurpolymj.2021.110388
2. T. F. Terroso; K. B. Condotta; F. N. da Fonseca; et al. *Journal of Drug Delivery Science and Technology* 2016, *36*, 99-109. https://doi.org/10.1016/j.jddst.2016.10.002
3. C. G.Venturini; E. Jäger; C. P. Oliveira; et al. *Colloids and Surfaces A: Physicochemical and Engineering Aspects* 2011, *375,* 200–208. https://doi:10.1016/j.colsurfa.2010.12.011

Fundings: From CAPES and CNPq

Keywords: *Hydrogels, Galactomannan, α-bisabolol, Nanocapsules, Biomedical Application.*

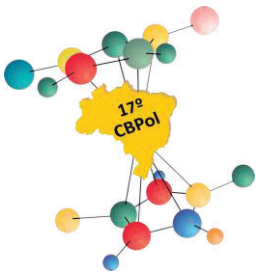

HYBRID MULTIFUNCTIONAL NANOCOMPOSITES BASED ON POLYAMIDE 10.10 AND TWO-DIMENSIONAL MATERIALS

Gabriel M. Pinto[1,2,3], Emna Helal[3], Hélio Ribeiro[1], Eric David[3], Nicole R. Demarquette[3], Guilhermino J. M. Fechine[1,2*]

1- School of Engineering, Mackenzie Presbyterian University, São Paulo, Brazil
2 - MackGraphe (Mackenzie Institute for Research in Graphene and Nanotechnologies), São Paulo SP, Brazil
3 - Department of Mechanical Engineering, Ecole de Technologie Supérieure, Montréal, Canada
**guilherminojmf@mackenzie.br*

Abstract - This work discusses the development of multifunctional hybrid polymer nanocomposites based on a bio-polyamide and different 2D materials, i.e., graphene oxide, hexagonal boron nitride, and molybdenum disulfide. We explore the potential for these materials to be used in emerging fields and investigate the degree of interaction between the nanomaterials and the polymer matrix. The methodology involved exfoliating the nanomaterials in liquid media and then processing them with the polymer matrix through melt compounding in a twin-screw extruder and further preparing samples through injection molding. The tensile properties, thermal conductivity, and dielectric relaxations of the composites were evaluated. It was observed that while thermal conductivity was not sensitive to the type or content of filler, the mechanical behavior of the polymer was significantly affected. The Young's modulus was reduced due to microstructural changes and lubricity effects of the nanosheets, but the overall energy absorbed by the material was improved depending on the nanofiller. The different levels of filler-polymer interactions, filler dimensions and dispersion, are supported by the investigation of molecular dynamics and microstructure, which show that the macromolecular mobility of the polymer chains was more strongly hindered by graphene oxide and hexagonal boron nitride than by molybdenum disulfide. In summary, this work introduces novel bio-based polyamide nanocomposites with adjustable properties based on the nanomaterials added, which have potential for use in various emerging fields.

Fundings: Fundação de Amparo à Pesquisa do Estado de São Paulo (Grant numbers: 2022/07054-8, 2020/11496-0, 2021/07858-7; CAPES-PrInt (Grant 88887.310339/2018–00)

Keywords: *Polymer nanocomposites, Polyamide 1010, Graphene oxide, Hexagonal boron nitride, Molybdenum disulfide.*

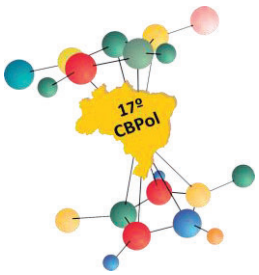

INFLUENCE OF MINERAL FILLERS IN CARBON BLACKS TRIMODAL MIXTURE ON THE COLORIMETRIC PROPERTIES AND MECHANICAL BEHAVIOR OF LOW-DENSITY POLYETHYLENE FILM: PART 3

Juliano M. Barbosa[1*], Hélio Ribeiro[1], Luiz Antônio Pessan[2]

1 – Engineering School, Materials Engineering, Mackenzie Presbyterian University, São Paulo, SP, Brazil
** barbosa_jm@yahoo.com.br*
2 – Department of Materials Engineering (DEMa), Federal University of São Carlos (UFSCar), São Carlos, SP, Brazil

Abstract

In this work, after the PART01[1], the best combination of Carbon Black (CB) trimodal mixture, with 3 different medium particle sizes was evaluated on LDPE colorimetric and rheological properties, through a Design of Experiments (DOE). It was determined that, the mixtures between small (S) and medium (M) particles developed greater Tinting Strength (TS) with lower viscosity, because of their synergistic blend. Already, in PART02[2], the blends (F18 and F13) had its dispersion improved by studying the twin-screw extrusion, evaluating the Specific Mechanical Energy (SME). It was also obtained higher TS with lower viscosity, determining that 600 rpm at 10 kg/h of feed rate (SME: 0.29 kWh/kg) called F18-P03, where it was developed the best results, mainly in TS. So, in this PART03, F18-P03 was filled[3] with $CaCO_3$, micro (D_{50}: 2.5 μm) or nanoparticulate (D_{50}: 40 nm) both at 10 or 20 wt%, to improving the economic aspect and mechanical properties[4,5], maintaining TS, TT, filter pressure value (FPV) and low viscosity[6], already obtained previously. Unfortunately, $CaCO_3$ has high refractive index and worked as low-performance white pigment, reducing TS, increasing FPV and interfering with viscosity of matrix, but to a lesser extent with nanoparticle at 10% (F18-P03-N10). In this way, it was possible to reduce the TT by almost 50%, in relation F18-P03, however, the TS reduced by 17% and the FPV increase from 1.5 to 50 bar, in addition, a considerable increase in the viscosity. As for the mechanical properties, the Young´s Modulus increased by 18% due to the growth in matrix stiffness, explained by the Law of Mixtures[7], but the toughness was reduced, since the tensile strength (F_{max}) and specific deformation (F_{max}), decreased by 8 % in relation to F18-P03. The properties balance must be associated with utilization of formulation, as extrusion or injection molding, which require specific concentrate characteristics.

References

1. J. M. Barbosa, C. A. G. Beatrice, L. A. Pessan; *Polímeros* 2022, 32. https://doi.org/10.1590/0104-1428.20220039
2. J. M. Barbosa, C. A. G. Beatrice, L. A. Pessan; *Polímeros* 2022, 32. https://doi.org/10.1590/0104-1428.20220053
3. G. Wypych; *Handbook of Fillers*, Plastics Design Library, New York, 1999.
4. J. B. Donnet; *Carbon Black: Science and Technology – Second Edition*; Marcel Dekker Editore, New York 1993
5. J. F. Zhang, X. S. Yi; *Journal of Applied Polymer Science* 2002, 86, 3527. https://doi.org/10.1002/app.11101
6. M. H. Aghajan, M. R. Kashani; *Polymer Testing* 2019, 78, 1 https://doi.org/10.1016/j.polymertesting.2019.106002
7. J. BRANDRUP, E. H. IMMERGUT; *Polymer Handbook*; 3ed, J. Wiley, New York, 1989.

Keywords: *Calcium Carbonate, Carbon black, Specific Mechanical Energy, Tinting Strength, Trimodal Particle Size Distribution*

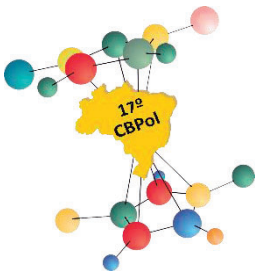

INFLUENCE OF NITROGEN DOPING ON THE CONDUCTIVE PHASE IN CONDUCTIVE HYDROGELS

Gabrieli Estefani Andriotti[1*], Jean Valdir Uchôa Teixeira[2], Bruno Mello de Freitas[2], Paulo Noronha Lisboa-Filho[1,2]

1 – Department of physics and meteorology, São Paulo State University (UNESP), Bauru, SP, Brazil
gabrieli.andriotti@unesp.br
2 – Materials Science and Technology program (POSMAT), São Paulo State University (UNESP), Bauru, SP

Abstract - A polymer is a macromolecule derived from the repetition of functional units (monomers) produced by a polymerization reaction and which have covalent bonds. Hydrogels are three-dimensional hydrophilic polymers that exhibit electrical conductivity by adding conductive charges, providing the material with greater electronic mobility. Graphene is a carbon-based material formed by a layer of independent sp^2 hybrid atoms, with a two-dimensional honeycomb crystalline structure, its oxide (OG) being a derivative of graphene and commonly synthesized by the well-known Hammers method. The reduction of graphene oxide (OGr) restores the structure and some of the properties of graphene, thus influencing different applications. This work plan aims to analyze the relationship between the electrical properties of the alginate hydrogel with the incorporation of OG, OGr, OG with nitrogen doping, and OGr with nitrogen doping, thus aiming to analyze the potential of each compound for the manufacture of conductive hydrogels. The materials used in this research were synthesized from the polymerization of sodium alginate with the incorporation of 1% in the mass of the particles. Its characterization was carried out using X-ray diffraction techniques, UV spectroscopy, cliclovoltametry, and charge and discharge tests, in acid, neutral and alkaline media. Based on these analyses, variations in the electrical resistivity of the hydrogels were observed, as well as in their charge storage capacity, thus indicating the possibility of this system in applications that require controlled conductivity and resistivity. It can be noticed that nitrogen doping in graphene oxide brings about changes regarding its hydrophilicity and surface tension shift.

References

Ji, D., Park, J. M., Oh, M. S., Nguyen, T. L., Shin, H., Kim, J. S., Kim, D., Park, H. S., & Kim, J. Nature Communications. 2022, 131. https://doi.org/10.1038/s41467-022-30691-z
2022
Yu, W., Sisi, L., Haiyan, Y., & Jie, L. RSC Advances. 2020, 2610, 15328. https://doi.org/10.1039/d0ra01068e

Fundings: Student Permanence Coordination (COPE) and Higher Education Personnel Improvement Coordination (CAPES).

Keywords: *Hydrogel, graphene oxide, reduction graphene oxide, conductive phase*

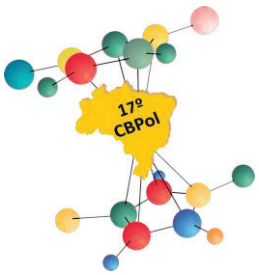

INFLUENCE OF OPERATIONAL PARAMETERS ON THE COLORING OF POLIAMIDE TEXTILES USING CURCUMIN/POLYMER NANOPARTICLES

Márcia G. Silva[1], Fernanda V. Leimann[2], Evandro Bona[2], Alexandre J. S. Ferreira[3], Nívea T. Vila[1], Odinei H. Gonçalves[2,3]*

1 - Department of Textile Engineering, State University of Maringá – UEM- Goioerê, PR, Brazil.
2 – Post-Graduation Program of Food Technology (PPGTA), Federal University of Technology – Paraná (UTFPR), Campo Mourão, PR, Brazil. odinei@gmail.com
3 – Department of Textile Engineering, Federal University of Santa Catarina (UFSC)- Blumenau, SC, Brazil.

Abstract – The dyeing of synthetic polymeric fabrics using natural dyes presents several challenges that hinder their large-scale use, such as low water affinity and low color fastness.[1] In this context, nanoencapsulation has proven to be a robust tool for improving the technological properties of natural compounds, and curcumin (derived from *Curcuma longa L.*) appears as a promising natural dye that can range in color from orange to yellow. The objective of this study was to evaluate the influence of pH (3 and 8), temperature (70 and 100°C), bath ratio (20 and 50), and encapsulating agent (PVP and Poloxamer 407) on the dyeing of polyamide using curcumin nanoparticles. A factorial design (2^{4-1}, significance level of 5%) was applied, and the color after dyeing, wash fastness, and staining on multifiber fabric (ISO 105-C06:2010) were evaluated. The nanoparticles obtained by the solid dispersion technique exhibited nanoscale sizes (Dynamic Light Scattering) and irregular morphology (Transmission Electron Microscopy). When comparing the colors of the fabric before and after dyeing, the results indicated lower coloration (ΔE), brightness (ΔL), and hue (Δh) at higher dyeing temperatures, and the use of Poloxamer 407 as an encapsulating agent favored dyeing. Only pH had an influence on color fastness, as increasing pH led to a reduction in the absolute value of Δh by 0.90. There was no significant change in total color difference (ΔE) when comparing the color of the fabric before and after the colorfastness test. The multifiber fabrics did not experience staining during washing, indicating good anchoring of the nanoparticles to the polyamide fibers. In conclusion, curcumin nanoparticles show promise for dyeing polyamide, encouraging further research for application in other synthetic fibers.

Keywords: *nanotechnology; PA; nanoencapsulation; Curcuma longa; Experimental Design.*

1. Elmaaty, T.A., Abouelenin, S., Elsisi, H. et al. Eco-friendly Approach for Dyeing Synthetic Fabrics with Natural Dyes Using Electron Beam Irradiation. Fibers Polym 23, 759–767 (2022) https://doi.org/10.1007/s12221-022-3144-1.

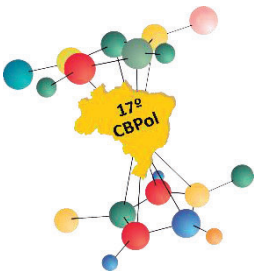

MANUFACTURE OF FIBROUS BANDAGES BY ELECTROSPINING WITH BACTERICIDAL EFFECT FOR PHOTODYNAMIC THERAPY

Alan Í. S. Morais[1], Idglan S. Lima[1], Leila S. S. M. Magalhães[1], Dih{ego Henrique Lima Damacena[1], Heurison S. Silva[1], Edson C. S. Filho[1], Anderson O. Lobo[1], Josy A. Osajima[1*]

1 – Interdisciplinary Laboratory of Advanced Materials - LIMAV, Graduate Program in Materials Science and Engineering - PPGCM, Federal University of Piauí - UFPI, Teresina, PI, CEP 64049-550, Brazil.
*e-mail: josyosajima@ufpi.edu.br

Abstract - Diabetes Mellitus (DM) is a global health problem that impairs the quality of life and brings high costs to public health [1]. Diabetic foot infection (DFI) is a severe complication of DM due to bacterial infection of lesions, which can cause lower limb amputations and even the patient's death [2]. In this study, polycaprolactone (PCL)/Pluronic nanofibers containing the methylene blue dye (MB) were developed to investigate the antimicrobial potential under visible light. The bandages were obtained using the electrospinning technique using different dye concentrations: 1mg/mL (MPCL-F-B1), 0.5 mg/mL (MPCL-F-B2), or 0.1 mg/mL (MPCL- F-B3). The micrographs by Scanning Electron Microscopy (SEM) demonstrated fiber formation. X-Ray Diffraction (XRD) and Fourier Transform Infrared Spectroscopy (FTIR) were realized, and it was possible to observe the characteristic peaks and infrared absorption bands, respectively. The presence of the dye in the bandage and the non-toxicity of the materials were proved. The photodynamic therapy test indicated the effectiveness of the bandages in antimicrobial terms under visible light (660 nm), and the membranes containing MB demonstrated remarkable antibacterial activities against the Gram-positive bacteria *Staphylococcus aureus* ATCC 25923, with about 99% of inhibition. These results suggested that the membrane is a promising material and could be used for the treatment of DFU and in other applications in areas resistant to bacterial infections.

References

1. International Diabetes Federation. IDF Diabetes Atlas, 9th edn. Brussels, Belgium: International Diabetes Federation, 2019.
2. M. Chang, Pharmacological Research. 2016. V. 107. P. 243–248. http://dx.doi.org/10.1016/j.phrs.2016.03.0081043-6618

Fundings: CNPQ, CAPES, FAPEPI e UFPI

Keywords: *Electrospinning, Diabetes mellitus, Photodynamic therapy, antibacterial.*

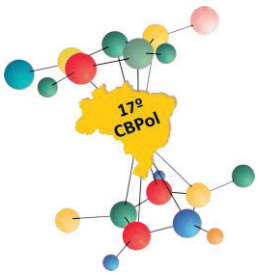

MECHANICAL PROPERTIES OF POLYPROPYLENE/CALCIUM CARBONATE MICRO AND NANOCOMPOSITES

Juliano M. Barbosa[1*], Caroline V. Pacheco[1], Gisele Szilagyi[1], Patrícia C. M. de Oliveira[1], Renato M. Peres[1], Hélio Ribeiro[1]

1 – Engineering School, Materials Engineering, Mackenzie Presbyterian University, São Paulo, SP, Brazil
**barbosa_jm@yahoo.com.br*

Abstract

The Principle of Combined Action (PCA) can be used to produce multiphase materials containing different constituents to obtain bests results regarding their combined properties when compared to with its constituents individually. In addition, the component phases must be chemically distinct and separated by an interface [1,2]. Several studies about polymeric composites[3,4] have demonstrated significant improvements in mechanical, as well as barrier properties, flame retardancy, thermal distortion resistance, mainly with nanoparticles, due to surface phenomena [5]. In this study, the mechanical properties of polymeric composites containing calcium carbonates ($CaCO_3$) microparticulate (D_{50} 1.7µm) and nanoparticulate (D_{50} 40nm) were determined and compared. The mineral fillers were characterized by XRD, SEM and BET, to determine its physical chemical properties[6]. After that, they were dispersed [7] at 20% in homopolymer polypropylene (PPh 10g/10min), with addition of 10% of compatibilizer maleic anhydride functionalized polypropylene [8] (PP-g-MAH), via twin screw extrusion (ZSK25 L/D40), varying the screw rotation speed (N: 250 and 500 rpm) and feed rate (Q: 10 and 15 kg/h), thus producing 8 $CaCO_3$ concentrates (*masterbatch*). Subsequently, each one was diluted in PPh by injection molding, generating composites with 0.5, 1.5, 5.0 and 10.0 wt% of $CaCO_3$. The final composites were characterized by XRD, SEM, Mechanical Tests, and Activation Volume (indirectly determined by Tensile Strength F_{max}, at different test speeds). Based on the results, the parameters that generated the best performance were 500rpm and 10kg/h, so, the nanocomposite Impact Strength increased by 7.8%, Young's Modulus by 9.3% and Tensile Strength (F_{max}) by 7.3%, in relation to microcomposite, besides, there was a significant increase in the degree of crystallinity with the nanoparticle. The Deformation (F_{max}) remained similar for both. It was observed that higher rotations provide greater energy to the system, improving the particles dispersion in the matrix, and this fact significantly reflected on these mentioned properties[9].

References

1. A. F. Padilha, *Materiais de Engenharia – Microestrutura e Propriedades,* Ed. Hemus, Curitiba, 2000.
2. W. D. Calister ; *Ciência e Engenharia dos Materiais: Uma Introdução*; Ed LTC, Rio de Janeiro 2002.
3. G. Wypych; *Handbook of Fillers*, Plastics Design Library, New York, 1999.
4. C. M. Chan; J. Wu; J. X. Li; *Polymer* 2012, 43, 2992. https://doi.org/10.1016/S0032-3861(02)00120-9
5. M. Rabelo; *Aditivação de Polímeros*; Artliber Editora, São Paulo, 2000.
6. K. Yang, Q. Yang, G. Li , Y. Sun; *Material Letters* 2006, 60, 805-809. https://doi.org/10.1016/j.matlet.2005.10.020
7. C. Lotti et al; *European Polymer Journal* 2008, 44, 1346. https://doi.org/10.1016/j.eurpolymj.2008.02.014
8. H. Fischer; *Materials science and Engineering C*, 2013, 763. https://doi.org/10.1016/j.msec.2003.09.148
9. R. N. Rothon; *Particulate-Filled Polymer Composites*; Rapra Technology Limited, Shawbury, 2013.

Keywords: *Activation Volume, Calcium Carbonate, Mineral filler, Nanocomposite, Polypropylene.*

MICROFIBRILLATED CELLULOSE DRYING TECHNIQUES AND MATERIAL PROPERTIES

Alexandre O. T. Cordeiro[1], Kaciane Andreola[2], Luciane F. G de Souza[2] and Cristiane R. Martins[1]*

1 – Institute of Environmental Chemical and Pharmaceutical Sciences, Federal University of São Paulo (UNIFESP), Diadema, SP, Brazil
cr.martins@unifesp.br
2 – Mauá Institute of Technology, São Caetano do Sul, SP, Brazil

Abstract – Since most nanofiber processes are carried out in the liquid phase, one of the most important factors to obtain individualized cellulose nanofibers is the drying technique (dehydration)[1]. The cellulose fibers can have a variety of morphologies and properties depending on the technology used for the water dehydration process[1,2,3,4]. This work aim to analyze different drying techniques applied to nanocellulose structures and the dried material properties. Microfibrillated cellulose (MFC) produced from bleached eucalyptus kraft pulp was provided by Suzano SA (Aracruz/ES, Brazil). MFC was dried by freeze drying at -20 °C[1], oven dried at 60 °C until a constant weight[4] and spray dried at 140 °C[2]. Dried materials morphology was examined using scanning electron microscopy (SEM) to verify the changes in the MFC structure due to the drying process (Fig 1). Viscosity was measured to compare rheological behavior after the drying process. The results showed that difference between viscosity measurements of never dried and redispersed MFC is due to the dimension of the MFC and its interaction with the system.

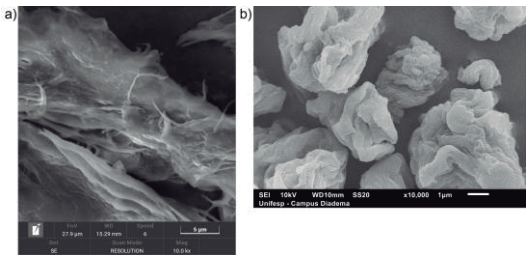

Figure 1 – SEM micrographs of never dried (a) and spray dried (b) MFC with magnification 10 kx.

References

1. M. VG. Zimmermann; C. Borsoi; A. Lavoratti; M. Zanini; A. J. Zattera, R. MC. Santana *Journal of Reinforced Plastics & Composites* 2016, 0(0), 1-16. https://doi.org/10.1177/0731684415626286.
2. R. Nardi; M. H. L. Silveira; G. Siqueira *Cellulose* 2020, 27. https://doi.org/10.1007/s10570-020-03392-3.
3. L. E. Silva; A. de A. dos Santos; L. Torres; Z. McCraffrey; A. Klamczynski; G. Glenn; A. R. de S. Neto; D. Wood; T. Williams; W. Orts; R. A. P. Damásio; G. H. D. *Tonoli Carbohydrate Polymers* 2021, 252, 117165. https://doi.org/10.1016/j.carbpol.2020.117165.
4. K. Li; D. Mcgrady; X. Zhao; D. Ker; H. Tekinalp; X. He; J. Qu; T. Aytug; E. Cakmak; J. Phipps; S. Ireland; V. Kunc; S. Ozcan *Carbohydrate Polymers* 2021, 256, 117525. https://doi.org/10.1016/j.carbpol.2020.117525.

Fundings: CNPq DAI with Suzano SA.

Keywords: *Nanocellulose*, *Microfibrillated cellulose, drying techniques.*

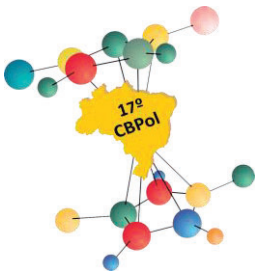

MIXED LIPOSOMES INCORPORATED WITH CURCUMIN AND SILVER NANOPARTICLES FOR PHOTODYNAMIC THERAPY

Yara S. Ricken[1*], Rodrigo H. Saatkamp[1], Heloisa D. Doring[1], Alexandre L. Parize[1], Camila F. de Freitas[1]

1 – Department of Chemistry, Federal University of Santa Catarina (UFSC), Florianópolis, SC, Brazil
**yara.ricken@posgrad.ufsc.br*

Abstract- Cancer is one of the primary causes of death in industrialized countries. Conventional therapeutic methods are capable of destroying tumors, but they also damage healthy tissues. In this study, we utilized (1,2-dipalmitoyl-sn-glycero-3-phosphatidylcholine-DPPC) mixed with F127 Pluronic to obtain DDPC/F127 liposomes as a promising alternative in drug delivery systems (DDS) for cancer therapy.[1] Compared to traditional liposomes they exhibit surprising improvements in stability and blood circulation. In addition, Photodynamic Therapy (PDT) has been studied as a less invasive alternative for cancer treatment.[2] The liposomes obtained by solid dispersion were used for the transport and solubilization of curcumin (CUR), whose anticancer photoactivity has been reported.[3] Aiming to increase its singlet oxygen generation through Metal Enhanced Singlet Oxygen Generation, CUR was combined with silver nanoparticles (AgNPs).[4] To obtain DPPC/F127/AgNPs, silver nitrate ($AgNO_3$) was reduced *in situ* by photoinduction with UV-Light[5] using sodium citrate ($Na_3C_6H_5O_7$), as a reductant and stabilizer agent, the passive incorporation was employed to include CUR and obtain DPPC/F127/AgNPs/CUR. The liposomes prepared were characterized by dynamic light scattering (DLS) and its hydrodynamic diameter (DH), polydispersity index (PI), and zeta potential (ZP, ζ) were determined. Transmission Electron Microscopy (TEM) was utilized to evaluate the morphology of the liposomes. AgNPs and CUR incorporated in liposomes were analyzed by UV-Vis and Fluorescence spectroscopy. In general, liposomes of DPPC/F127 (uncharged) presented DH of 70.34±0.24 nm, PI<0.25 and ζ close to zero. *In situ* synthesis of AgNPs followed by incorporation of CUR raised the DH to 125.9±1.84 nm for DPPC-F127/AgNPs/CUR keeping the PI<0.25 and ζ close to zero, confirming drug incorporation. Furthermore, TEM micrographs agree with the scattering technique. As desired, the plasmonic absorption spectra of the AgNPs overlapped the absorption spectrum of the CUR. Thus, the samples obtained so far are promising in the development of DDS for the loading of active drugs in PDT.

References:

1. C. F. De Freitas; I. R. Calori; A. L. Tessaro; W. Caetano; N. Hioka; *Colloids and Surfaces B: Biointerfaces 2019,* 181, 837-844. https://doi.org/10.1016/j.colsurfb.2019.06.027.
2. P. Babilas; S. Schreml; M. Landthaler; R. M. Szeimies *Photodermatology Photoimmunology and Photomedicine 2010*, 26-2, 118-132. https://doi.org/10.1111/j.1600-0781.2010.00507.x.
3. L. D. Dias; K. C. Blanco; Mfouo-Tynga I. S.; N. M. Inada; V. S. Bagnato *Journal of Photochemistry and Photobiology C: Photochemistry Reviews 2020*, 45, 100384. https://doi.org/10.1016/j.jphotochemrev.2020.100384.
4. Y. Zhang; K. Aslan; M. J. R. Previte; C. D. Geddes *Journal of fluorescence 2007*, 17, 345-349. https://doi.org/10.1007/s10895-007-0196-y.
5. P. S. Yerragopu; S. Hiregoudar; U. Nidoni; K. T. Ramappa; A. G. Sreenivas; S. R. Doddagoudar *International Research Journal of Pure and Applied Chemistry 2020*, 21-3, 37-50. https://doi.org/10.9734/irjpac/2020/v21i330159.

Fundings: CAPES/CNPQ.
Keywords: *Cancer, Pluronic, Phospholipids, Drug Delivery, Singlet Oxygen.*

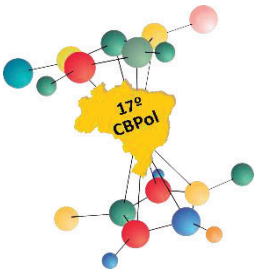

NANOCOMPOSITES OF *meso*-PORPHYRINS DERIVED FROM CARDANOL AND VANILLIN FOR APPLICATION IN ANTICORROSIVE ORGANIC COATINGS.

Malena G. Martins[1]; Lucas R. R. da Silva[2]; Paulo V. M. da Silva[3]; Rafaelly N. Araújo[3]; Vitória de P. Santos[3]; Leonardo M. de Menezes[3]; Sara J. Marciano[2]; Claudenilson da S. Clemente[3]; Diego Lomonaco[3]; Selma E. Mazzetto[3].

1-Department of Organic and Inorganic, Federal University of Ceará (UFC), Fortaleza, CE, Brazil
malenamartins@alu.ufc.br
2-Department of Engineering and Materials Science, UFC, Fortaleza, CE, Brazil.
3-Department of Organic and Inorganic, UFC, Fortaleza, CE, Brazil.

Abstract - Several strategies have been proposed to protect metals against corrosion triggered by environmental factors, among them the use of organic coatings, especially alkyd resins, which have good heat resistance, excellent brightness, and low cost. However, these coatings have some limitations, such as high permeability and low adhesion, hindering their application. Some researchers have sought to increase the efficiency of alkyd resins against corrosion by adding nanocomposites of organic and inorganic particles to the formulation. An example of this strategy is the addition of nanomaterials of the porphyrin type, which can decrease corrosion rates through adsorption on the surface of the metal, forming a protective film capable of reducing water absorption, in addition to having an extended π electronic system, allowing them to act as chelating agents with strong binding capacity and interaction with metal surfaces. The porphyrin macromolecules used in this work were of natural origin, derived from cardanol, a major constituent of cashew nutshell liquid (CNSL), whose double-bond positions allow numerous functionalizations, and vanillin, an aromatic compound containing two functions (aldehyde and phenol) that can be chemically modified to obtain new derivatives. We synthesized and characterized (by UV-Vis, FT-IR, ^{1}H NMR, TGA) a *meso*-porphyrin and its *meso*-metalloporphyrin derivative of zinc from cardanol and vanillin, and incorporated these nanocomposites in alkyd resins to ascertain their potential as anticorrosive agents through analysis of electrochemical properties, adhesion, hardness and chemical resistance. The results showed the efficiency of the porphyrin nanocomposites in alkyd resins to act as a physical barrier, preventing oxygen, water, and ions from acting on metal structures, providing greater adhesion and extending the life of coatings.

References

1. A. M. Deyab; G. Mele; A. M. Al-Sabagha; E. Bloise; D. Lomonaco; S. E. Mazzetto; C. Clemente. Progress in Organic Coatings. 2017, 105, 286-290. http://dx.doi.org/10.1016/j.porgcoat.2017.01.008.
2. N. M. A. Lima; T. T. Bezerra; M. O. Almeida; N. L. C. Rodrigues; C. H. C. Braga; J. I. S. Miranda; V. G. P. Ribeiro; G. F. Guimarães; J. M. Teixeira; D. Lomonaco; G. Mele; S. E. Mazzetto. Photodiagnosis and Photodynamic Therapy. 2020. 1. 102083-1. https://doi.org/10.1016/j.pdpdt.2020.102083.

Keywords: *Nanocomposites, Porphyrins, Coatings, Corrosion, Agroindustrial waste.*

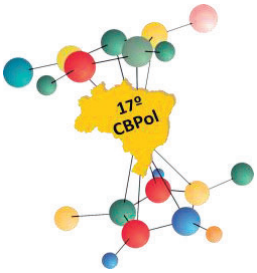

NANOCOMPOSITES OF POLYSTYRENE/PSEUDOBOEHMITE TREATED WITH OCTADECYLAMINE

Renan Barreto Santos[1], Joe Müller Barbosa Silveira[1], Ayrton Andre Bernussi[2], Isabella Tereza Ferro Barbosa[3], Juliano Martins Barbosa[1], Renato Meneghetti Peres[1], Antonio Hortencio Munhoz Jr.[1]*

1 – Department of Materials Engineering, Mackenzie presbyterian University (UPM), São Paulo, SP, Brazil
**ahmunhoz@yahoo.com*
2 – Texas Tech University (TTU), Lubbock, Texas, EUA
3 – Senac (SENAC), São Paulo, SP, Brazil

Abstract - Pseudoboehmite is a synthetic aluminium oxyhydroxide made up of nanoparticles and is generally obtained by the sol-gel[1] process. Its use is extensive, being used in drug-controlled release due to the high specific surface area[2,3] and obtaining nanocomposites[4]. In addition, some ceramic nanoparticles are recognized in the literature for improving mechanical and thermal properties, among others[4,5]. This study was performed to determine how high-impact polystyrene composite containing pseudoboehmite nanoparticles behaves when the pseudoboehmite is treated with octadecylamine to improve the compatibility of the ceramic with the polymer. Several techniques characterized Pseudoboehmite, and it was observed from the X-ray diffraction results that the only crystalline phase present was pseudoboehmite. High-impact polystyrene (HIPS) was donated by the company UNIGEL. The impact resistance and tensile strength tests show that the composites in which pseudoboehmite treated with octadecylamine were used showed higher values than the composites containing only pseudoboehmite and HIPS. It was also observed that adding treated pseudoboehmite to HIPS considerably reduced the Heat Deflection Temperature (HDT) and the Vicat softening temperature.

References

1. E.M. Moroz; K.I. Shefer; D.A. Zyuzin; A.S. Ivanova; E.V. Kulko; V.A. Goidin; V.V. Molchanov *React Kinet Catal. Lett.* 2006, 87, no. 2, 367 DOI:10.1007/s11144-006-0045-z
2. R.M. Peres; J.M.L. Sousa; M.O. Oliveira; M.V. Rossi; R.R. Oliveira; N.B. Lima; A. Bernussi; J. Warzywoda; B. Sarmento; A.H. Munhoz *Scientific Reports* 2021, 11, 15448. https://doi.org/10.1038/s41598-021-94325-y
3. C. Yan; A. Kelong; L. Yanlan; L. Lehui *Applied Materials & Interfaces* 2014, 8;6(1):655 DOI:10.1021/am404761h
4. A.H. Munhoz Jr.; R.M. Peres; L.H. Silveira; L.G.A. Silva; L.F. Miranda *Advances in Science and Technology* 2010. https://doi.org/10.4028/www.scientific.net/AST.71.28
5. T. Felix. Dissertação - Universidade Federal de Santa Catarina, 2010.

Fundings: PIBITI CNPq, and MackPesquisa.

Keywords: *nanocomposites, high-impact polystyrene, octadecylamine.*

NANOENCAPSULATION OF THE OILY EXTRACT OF *CHENOPODIUM AMBROSIOIDES L.* IN LIGNIN USING AN ANTISOLVENT METHOD

Samanta Finsterbuch[1], Patrícia Z. Uchôa[1], Renato C. T. Porto[1], Giovanna P. Kricheldorf[3], Jean C. Hoepfner[2], Sergio H. Pezzin[1]

1 – Chemistry Department, Center of Technological Sciences, Santa Catarina State University, Joinville, Brazil.
samantaafinsterbuch@gmail.com
2 – Center of Technological Sciences, Santa Catarina State University, Joinville, Brazil.
3 – Chemical Engineering Department, Univille, Joinville, Brazil.

The present work aims to study the encapsulation of the oily extract of *Chenopodium ambrosioides L.* (erva-de-santa-maria in Brazil) inside lignin nanocapsules. Due to the biodegradability and biocompatibility that lignin offers, along with the medicinal and repellent properties of *Chenopodium ambrosioides L.*, this study is aimed at potential applications in the medical, veterinary, and agricultural areas. The objective of performing the encapsulation of this active is to control its delivery to the chosen environment and extend its effect for a longer period. In this study, it was analyzed the 'one-pot' synthesis of the nanocapsules by using an antisolvent technique. The samples were submitted to thermal, chemical, and morphological characterization analyses, as well as loading analyses, encapsulation efficiency and degradation stability. Trough the SEM images of the obtained nanocapsules, with 0 and 1 month of shelflife presents in the Fig. 1, it was observed that the method was effective in entrapping the oily extract. Presenting a loading efficiency of 64% and an average diameter of 258 ± 110 nm.

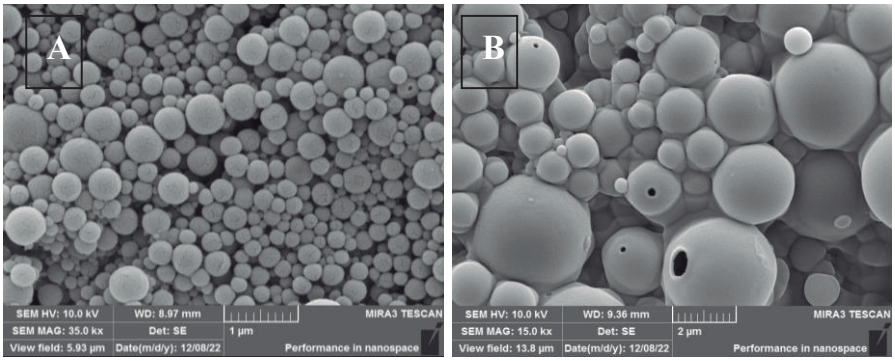

Figure 1 – SEM images of the nanocapsules with 0 and 1 month of shelflife (A and B respectively).

References

1. YEARLA, S. R.; PADMASREE, K. Exploitation of subabul stem lignin as a matrix in controlled release agrochemical nanoformulations: a case study with herbicide diuron. **Environ. Sci. Pollut. Res.**, v.23, p.18085 – 18098, 2016.
2. LI, H.; DENG, Y.; LIANG, J.; DAI, Y.; LI, B.; REN, Y.; QIU, X.; LI, C. Direct preparation of hollow nanospheres with kraft lignin: A facile strategy for effective utilization of biomass waste. **BioResources.**, v. 11, p. 3073–3083, 2016.

Fundings: FAPESC, CAPES and NÓRIO – Nanotechnology.

Keywords: *nanocapsules, lignin, encapsulation, antisolvent, Chenopodium ambrosioides L.*

NATURAL GUM FILMS AND SILVER NANOPARTICLES FOR EVALUATION OF ANTIBACTERIAL PROPERTIES

Francisco E. P. Santos[1,2], Albert S. Silva[1], Tânia P. Silva-Silva[1], Idglan S. Lima[1], Josy A. O. Furtini[1,2], Edson C. Silva-Filho[1,3]*

1 - Postgraduate Program in Materials Science and Engineering - PPGCM, Federal University of Piaui (UFPI), Teresina, PI, Brazil

2 - Postgraduate Program in physics- PPGF, Federal University of Piaui (UFPI), Teresina, PI, Brazil

3 - Postgraduate Program in chemistry- PPGQ, Federal University of Piaui (UFPI), Teresina, PI, Brazil

franciscoeroni@gmail.com

The use of natural gums for the synthesis of nanoparticles has been gaining momentum due to their multiple and lucrative applications in the industry, as well as their widespread availability[1]. Utilizing these gums facilitates the formation of polymeric films and enables antibacterial applications[1]. This study aims to produce films containing gum from the cashew tree (*Anacardium occidentale*) and silver nanoparticles in order to evaluate their antibacterial properties. The films were characterized by ultraviolet visible (UV-Vis) spectroscopy, dynamic light scattering (DLS), and zeta potential, in addition to the *Artemia salina* bioassay and antibacterial evaluation. The UV-Vis spectra of silver nanoparticles (AgNPs) revealed a characteristic peak in the 400 nm range, indicating surface plasmonic resonance[2]. DLS reveals a mean dimension of 4.94 nm and a Zeta potential with a charge of -9.94 mV. Against *Artemia salina*, no toxicity was detected. The antibacterial test revealed that nanoparticle-containing films inhibited bacterial growth. In conclusion, coatings containing silver nanoparticles demonstrated an antibacterial inhibiting effect and a lack of toxicity towards Artemia salina. Furthermore, the nanoparticles in the polymeric matrix exhibited stability and narrow size distribution.

References

1. BAR, Harekrishna et al. Green synthesis of silver nanoparticles using latex of Jatropha curcas. Colloids and surfaces A: Physicochemical and engineering aspects, v. 339, n. 1-3, p. 134-139, 2009. doi:10.1016/j.colsurfa.2009.02.008
2. MELO JR, Maurício Alves et al. Preparação de nanopartículas de prata e ouro: um método simples para a introdução da nanociência em laboratório de ensino. Química nova, v. 35, p. 1872-1878, 2012. doi:10.1590/s0100-40422012000900030

Fynding: CNPq, CAPES and FAPEPI

Keywords: *films, polysaccharide, silver nanoparticles.*

PHOTOSTABILIZATION OF HYBRID NANOCOMPOSITES BASED ON EPDM RUBBER, CARBON BLACK AND GRAPHENE OXIDE

Lucas P. de Lima[1,2], Patrícia M. S. Souza[1,2*], and Guilhermino J. M. Fechine[1,2]

1- School of Engineering, Mackenzie Presbyterian University, São Paulo, Brazil
2 - MackGraphe (Mackenzie Institute for Research in Graphene and Nanotechnologies), Mackenzie Presbyterian Institute, São Paulo, Brazil
** patriciasinohara@gmail.com*

EPDM rubber is a synthetic elastomer that when exposed to sunlight can be degraded over time, which requires the use of photostabilizers to slow this process. Some studies show that there is no effectiveness in the use of certain photostabilizers in EPDMs due to possible chemical reactions between them and the elastomeric matrix [1]. This work aims to produce and characterize nanocomposites based on EPDM, carbon black - CB (90 phr) and graphene oxide (GO) in order to evaluate the effect of GO as photostabilizer [2]. Two compositions were made using GO in the EPDM matrix (0.2 phr and 0.5 phr) in a Haake internal mixer and then molded and exposed to UV radiation incessantly for up to 672 hours (60°C). A composition containing 0.3 phr of the photostabilizer Tinuvin P was also prepared and exposed to UV radiation. Prior to accelerated aging, tensile test, hardness and swelling tests show that GO can act as an accelerating vulcanization agent. After exposure to UV radiation, the composition that had the lowest percentage change in its mechanical properties was that of 0.5 phr of GO, indicating that this nanomaterial may have acted as a filter, blocking the passage of UV radiation. The infrared spectra indicate the production of hydroxyl and carbonyl groups in all samples after irradiation, however, more intense for the base material (EPDM + CB). Tinuvin P was not effective for photostabilization of the material (when compared to GO) as it was consumed during vulcanization. These results show that GO may have acted both as an accelerating vulcanization agent before degradation and as a protective filter against UV radiation.

References

1. E. DUEK and M. DE PAOLI, "The Photo-oxidation of Epdm Rubber .3. Mechanistic Aspects and Stabilization," Web Sci., vol. 30, pp. 283–292, 1990.
2. S. Karimi et al., "A review on graphene's light stabilizing effects for reduced photodegradation of polymers," Crystals, vol. 11, no. 1, pp. 1–22, 2021.

Fundings: CNPq (314093/2021-4 and 130099/2021-0); FAPESP (2022/06541-2) and Ford Motor Company Brasil Ltda

Keywords: *EPDM, Polymer nanocomposites, Graphene, Photostabilization.*

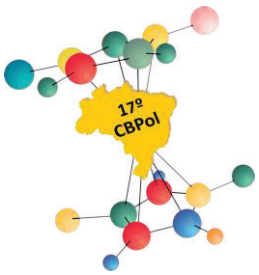

POLYCAPROLACTONE/AMINO-MODIFIED SODIUM ALGINATE ELECTROSPUN CORE-SHELL FIBERS

Anna L.M. M. Toledo[1*], Carolina S. Silva[1], Thalles R.S. Rêgo[1] and Marcos L. Dias[1]

1- Instituto de Macromoléculas Professora Eloisa Mano, Federal University of Rio de Janeiro (UFRJ), Rio de Janeiro, RJ, Brazil
annatoledo@ima.ufrj.br

Abstract - Electrospinning of alginate proposes several challenges due to its polyelectrolytic characteristics, tendency for high gelation at low concentration, high electrical conductivity, high surface tension and its own rigid and extended molecular structure [1]. This work sought to chemically modify sodium alginate by adding a 2,2'-(Ethylenedioxy)bis(ethylamine) (EDEA) to its carboxylic groups in order to obtain single fibers and later core-shell fibers of polycaprolactone (PCL) and modified sodium alginate (ALG-NH_3). The addition of EDEA to the alginate backbone was confirmed through H^1 NMR and FTIR with the appearance of typical absorption vibrations at 2890 cm^{-1}, 1700 cm^{-1} and 1243 cm^{-1}. TGA analysis show that the ALG-NH_3 presents a two-stage degradation with onsets at 48°C and 237°C. XRD analysis showed that the ALG-NH_3 presents an amorphous halo. For the electrospinning of ALG-NH_3, PVA was added in three different ratios (PVA:ALG-NH_3 = 4:1, 3:2 and 1:1) in order to obtain better fibers. A voltage of 14 kV at the needle and -1 kV at the static collector and flow rates of 0.05, 0.03 and 0.02 mL/h were used. The ratio of 4:1 presented fibers with defects, whereas the fibers obtained with the 3:2 ratio presented a few beads and the 1:1 presented several defects, in comparison the unmodified alginate fibers did not yield fibers with as much regularity of the fibers. Finally, in order to obtain core-shell fibers, a 10% (w/v) solution of PCL in 2,2,2-trifluoroethanol as the shell and a 4:1 mixture of 10% (w/v) PVA and 2% (w/v) ALG-NH_3 as the core were used. The same voltage was used to produce fibers whereas the shell flow rate was varied between 0.5-0.1 mL/h and the core between 0.05-0.02 mL/h. Several Janus nanofibrous structures were obtained as well as core shell fibers in different conditions, as observed via Fluorescence microscopy.

References:

1. N. Angel; S. Li; F. Yan; L. Kong *Trends in Food Science & Technology* 2022 , *120*, 308-324. https://doi.org/10.1016/j.tifs.2022.01.003

Fundings: The authors thank FAPERJ (grant number 204.558/2021 and 204.559/2021) for the financial support.

Keywords: *electrospinning, alginate, polycaprolactone, nanofibers, core-shell fibers*

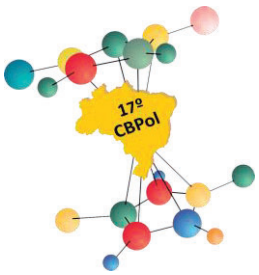

POLYMER NANOCOMPOSITES BASED ON ACRYLONITRILE BUTADIENE STYRENE (ABS) COPOLYMER, GRAPHENE NANOPLATELETS AND HEXAGONAL BORON NITRIDE

Natália F. Braga[1,2*] and Guilhermino J. M. Fechine[1,2]

1- School of Engineering, Mackenzie Presbyterian University, São Paulo, Brazil
2 - MackGraphe (Mackenzie Institute for Research in Graphene and Nanotechnologies), Mackenzie Presbyterian Institute, São Paulo, Brazil
natyfbraga@hotmail.com

Acrylonitrile Butadiene Styrene (ABS) is a terpolymer known by rigidity and strain resistance. The addition of two-dimensional fillers (2DF) is an approach to improve physical properties of polymers due to their exceptional intrinsic properties. Graphene nanoplatelets (GNP) and hexagonal boron nitride (h-BN) were employed to create ABS/GNP and ABS/h-BN nanocomposites. The 2DF were exfoliated in water and isopropyl alcohol. The masterbatch was produced by solid-solid deposition [1], followed by extrusion, then, it was prepared nanocomposites with 0.25, 0.5, 1.0 and 2.0 wt.%. It was produced specimens for tensile test, dynamical mechanical analysis (DMA) and thermal conductivity, by injection. The thermal conductivity of ABS is 0.20 W/mK and increased 13% with 0.25 wt% of h-BN, indicating the thermally conductive pathway. The storage modulus increased with 1 wt% of 2DF. The tan delta shifted to higher temperatures with lower filler content, indicating increasing in glass transition, associated to the restriction of chain mobility. Also, low 2DF contents influenced on tan delta peak, rinsing it from 1.6 to 2 in nanocomposites with 0.5 wt%, indicating compatibility and uniform dispersion between filler and matrix. The effectiveness coefficient is lower in the nanocomposites with 0.25 wt% of GNP and with 0.5 wt% of h-BN, indicating good effectiveness of these samples or a proficient distribution of the filler in the matrix. The ABS/h-BN presented higher Young´s Modulus and stress them ABS/GNP. The toughness increased in the ABS/h-BN with 0.25% of filler. The high specific area of 2DF could provide an excellent contact to the matrix, improving the properties of the nanocomposite. However, higher filler loads can conduct to an opposite response. Moreover, the exfoliation process may decrease the specific area due to the break of the flakes. The results showed that the 2DF can produce a material with improving mechanical and thermal properties to apply in materials for heat dissipation.

References

1. P. A. R. Muñoz; et. al. *eXPRESS Polymer Letters* 2018, 12, 930. https://doi.org/10.3144/expresspolymlett.2018.79

Fundings: The authors thanks FAPESP (2020/14302-2) for the financial support.

Keywords: *ABS. Polymer nanocomposites. Graphene. Hexagonal Boron nitride.*

POLYURETHANE WASTE AS A REDUCING AGENT OF SILVER NANOPARTICLES

Laís B. Borba[1*], Matheus S. Pimentel[1], Maria Elena L. González[2], Marilia Sonego[1], Mirian L. N. M. Melo[1]

1 – Institute of Mechanical Engineering (IEM), Federal University of Itajubá (UNIFEI), Itajubá, MG, Brazil
2 – Institute of Physics and Chemistry (IFQ), Federal University of Itajubá (UNIFEI), Itajubá, MG, Brazil
*laisbb@unifei.edu.br

Nowadays, it is very important to find new uses or add value for polymer wastes to be sold on as a new revenue stream. The present study focuses on the synthesis of silver nanoparticles (AgNPs) using silver nitrate ($AgNO_3$) as a precursor and polyurethane (PU) waste as a reducing agent. The PU waste is from mechanical recycling of refrigerators. Various proportions of AgNPs were synthesized, ranging from 10% to 60% Ag based on the weight of PU. Characterization of the PU waste was performed using thermogravimetric analysis (TG) and scanning electron microscopy (SEM). In addition to these techniques, the AgNPs were further characterized using energy dispersive X-ray spectroscopy (EDS) and X-ray diffraction (XRD). TG analysis revealed that the thermal decomposition of the PU waste occurred by a complex mechanism, comprising methylene diphenyl diisocyanate (MDI) and an unidentified polyol. The incorporation of AgNPs into the PU waste did not significantly affect its thermal stability. XRD results confirmed the presence of AgNPs in the PU waste. Residual peaks originating from the contaminants presents in the PU waste were also detected. Utilizing Scherrer's equation, the average size of the AgNPs was 10.82 nm. SEM images exhibited a morphology characterized by particles sprinkled with AgNPs and contaminants, which were further confirmed by EDS analysis.

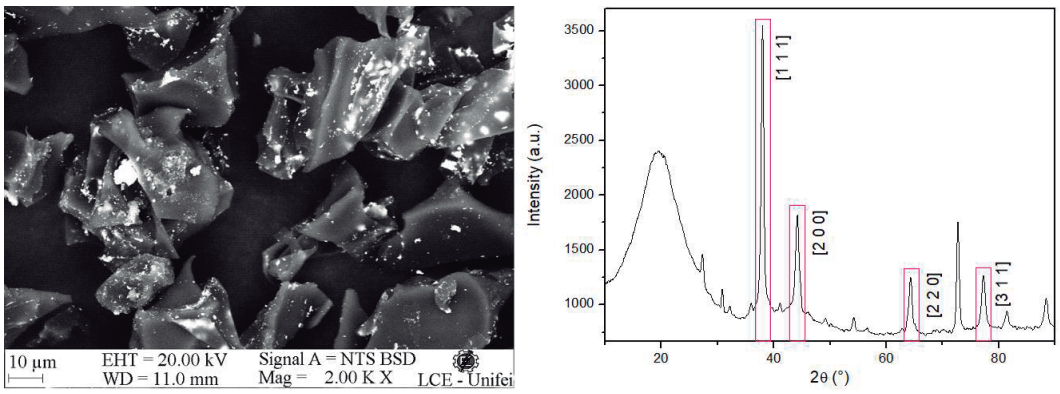

Figure 1 – SEM image of PU/AgNPs (a); XRD pattern of synthesized AgNPs (b).

References

1. Y. Nishiyama *et al Journal of Analytical and Applied Pyrolysis* 2020, 145, 104754. https://doi.org/10.1016/j.jaap.2019.104754.
2. B. Mehta *et al J. Phys.: Conf. Ser.* 2017, 836, 012050. https://doi.org/10.1088/1742-6596/836/1/012050.
3. R. Dias *et al Materials Research* 2010, 13(2), 211. https://doi.org/10.1590/S1516-14392010000200015.
4. O. Gazil *et al J. Mater. Chem. A* 2023. https://doi.org/10.1039/d2ta09405c.

Keywords: *Polyurethane waste, silver nanoparticles, reducing agent, thermal stability, XRD*

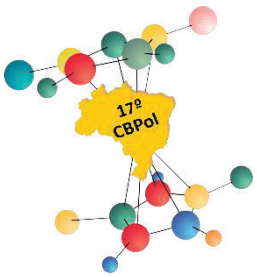

PREPARATION AND CHARACTERIZATION OF NANOPARTICLES FOR POTENTIAL APPLICATION IN TREATMENT OF CONTAMINATED WATER

Luiz H. T. Dubiginski[1], Maria Alice Witt[1]

1 – Chemical Engineering Department, Pontifical Catholic University Of Paraná (PUCPR), Curitiba, PR, Brazil
luiz.dubiginski@pucpr.edu.br

Abstract - The increasing complexity and challenges in efficiently treating effluents have led to the search for new methods and procedures for water decontamination. Among these methods, advanced oxidation processes (AOPs) have stood out, with heterogeneous photocatalysis being one of the most effective techniques. Zinc oxide (ZnO) nanoparticles have been studied for treating contaminated water due to their high electron mobility and photostability. ZnO has also demonstrated higher photocatalytic performance compared to titanium dioxide, another commonly used material for effluent treatment. In this project, ZnO nanoparticles were synthesized using reagents such as zinc acetate, sodium hydroxide, and ethanol. Photocatalysis tests were conducted under UV light excitation using methylene blue, phenol, and ibuprofen as model contaminants. The degradation of these contaminants was measured in intervals of 30 min with a spectrophotometer at 273 cm^{-1}. Successful acquisition of ZnO nanoparticles was confirmed as demonstrated by the Tyndall Effect test and SEM microscopy image. While promising results were achieved in the degradation of methylene blue and ibuprofen, the degradation of phenol did not reach the expected levels when compared to the literature. These differences might be related to the crystalline purity of the obtained ZnO, particle morphology, and the catalyst production process. In fact, the use of different production methods can impact photocatalysis effectiveness. The results suggest that the initial contaminant concentration and the amount of catalyst used had an influence on the degradation efficiency. One of the future steps includes incorporating these nanoparticles at cellulose-based material's surface such as filters.

References

1. J. Bohdziewicz; E. Kudlek; M. Dudziak. Desalination and Water Treatment 2016, 1552, https://doi.org/10.1080/19443994.2014.988411
2. H. Dewidar; S.A. Nosier; A.H. El-Shazly. Journal of Chemical Health & Safety 2018, 2, https://doi.org/10.1016/j.jchas.2017.06.001
3. B. Manikandan; T. Endo; S. Kaneko *et al*. J Mater Sci: Mater Electron 2018, 9474, https://doi.org/10.1007/s10854-018-8981-8
4. M. Tokumoto; V. Briois; C. Santilli *et al*. Journal of Sol-Gel Science and Technology 2003, 547, https://doi.org/10.1023/A:1020711702332
5. Y. Wang, Y. Liu, L. Zhang, M. Zhang, G. He, Z. Sun. Applied Surface Science 2019, 143743, https://doi.org/10.1016/j.apsusc.2019.143743

Keywords: *ZnO; nanoparticles; pollution; effluent treatment; photocatalysis.*

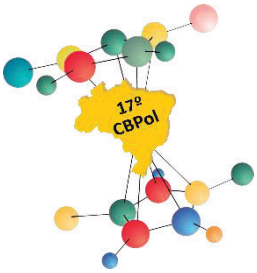

PREPARATION AND CHARACTERIZATION OF NANOSTRUCTURED HYDROGELS BASED ON CALCIUM ALGINATE AND MONTMORILLONITE

Maria Andreia G. da S. A. Sardinha[1] (IC), Márcia Parente Melo da Costa[1], Ivana Lourenço de Mello Ferreira[1*]

1 – Instituto de Química, Universidade do Estado do Rio de Janeiro (UERJ), Rio de Janeiro, RJ, Brazil
**ivanalmellof@gmail.com ; ivanamello@uerj.br*

Abstract: This work investigated the preparation and characterization of hydrogels based on sodium alginate and montmorillonite clay (Cloisite Na+), in order to form a polymeric network with good thermal stability and a high swelling degree. The polysaccharide concentration was 3% w/v and the clay content was 0.5% or 2%. The samples were characterized by thermogravimetry (TGA) and degree of swelling (Q). The results presented are valuable for understanding how the biodegradation of the polyelectrolyte complex occurs, aiming at planning future strategies to increase the time of action of the material in the soil.

Keywords: *sodium alginate; clay; calcium chloride; measurement of swelling degree; thermal stability.*

Introduction

Hydrogels are crosslinked hydroretentive polymers that are capable of absorbing and retaining a large amount of water [1]. They consist of one or more three-dimensionally structured polymer networks formed by macromolecular chains connected by crosslinks or physical interactions [2]. In this work, the crosslinking agent chosen was calcium chloride (CaCl2), because it is an easily accessible, inexpensive, and potent crosslinker of polysaccharides. Alginate is a polysaccharide produced mainly from brown algae and is composed of 1000-3000 building units linked together in an alternately rigid and flexible chain [3]. The binding of alginate with Ca^{2+} ions forms strong, insoluble spots. The clay used in this work was the commercial montmorillonite Cloiste Na^{+}, which is organophilic, i.e., contains organic molecules intercalated between the structural layers [4]. The objective of this work was to prepare a composite material based on sodium alginate with concentration of 3% w/v and montmorillonite clay (MMT) at different concentrations (0.5 and 2.0%), using $CaCl_2$ as a crosslinking agent, and thus produce a high-performance end product, i.e., with good thermal stability, high solvent resistance and high swelling degree (SD).

Experimental

Preparation of the sodium alginate solution
The aqueous solution of sodium alginate was prepared at a concentration of 3% (w/v) under magnetic stirring at room temperature until complete solubilization, which took 24 h.

Preparation of the hydrogels
To prepare the hydrogels, the two clay concentrations were achieved by weighing 1 g for the preparation at 0.5% concentration and 4 g for the preparation at 2.0% concentration. The clay was solubilized in a small amount of deionized water for complete delamination and kept under stirring for 1 h. After that, 200 mL of the aqueous sodium alginate solution (3% w/v) was mixed with 1 g of solubilized clay, and the same amount of sodium alginate solution with the 4 g of solubilized clay. The two mixtures were left under magnetic stirring for 24 h at room temperature until the mixtures were completely solubilized. The mixtures were poured over the 0.3 mol/L calcium chloride crosslinking solution under stirring, and were left in contact with this solution for 24 h. After this time, the samples were washed with deionized water, frozen (-4 °C), and freeze-dried for 48 hours.

Characterization
The thermal degradation behavior of the hydrogels was analyzed using a TA Instruments thermogravimetric analyzer (TGA), model TGA Q50, Series 0050-0390. The analysis was performed in the range of 50 to 800 °C with a heating rate of 20 °C/min.

Swelling degree
For determination of the swelling degree, the dried hydrogels were weighed to determine the dry mass. Then a volume of deionized water sufficient to cover the entire sample was added. After 1, 3, 6 or 24 hours, the water was removed and the swollen samples were weighed on an analytical balance.

Results and Discussion

Figure 1 shows the swelling profile of the produced samples. The swelling time (1, 3, 6 or 24 hours) of the hydrogels was evaluated for the two clay concentrations.

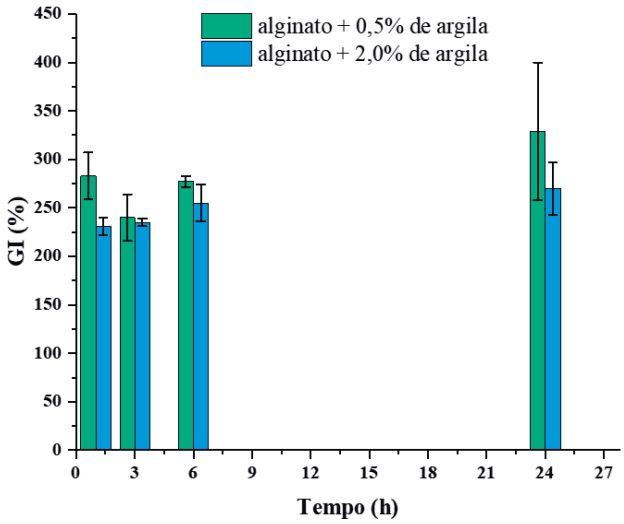

Figure 1. Swelling degree of the hydrogel samples

Based on the graph presented above, it is possible to note that regardless of the clay concentration, all hydrogels produced had a swelling degree higher than 100%, which characterizes them as superabsorbent materials. However, the hydrogel containing the lower clay content achieved a higher degree of swelling. This could be attributed to a greater flexibility of the alginate chains with water, while with higher clay content, this swelling was lower.

Figure 2 shows the TG and DTG curves of the samples of calcium alginate with clay at the two concentrations studied.

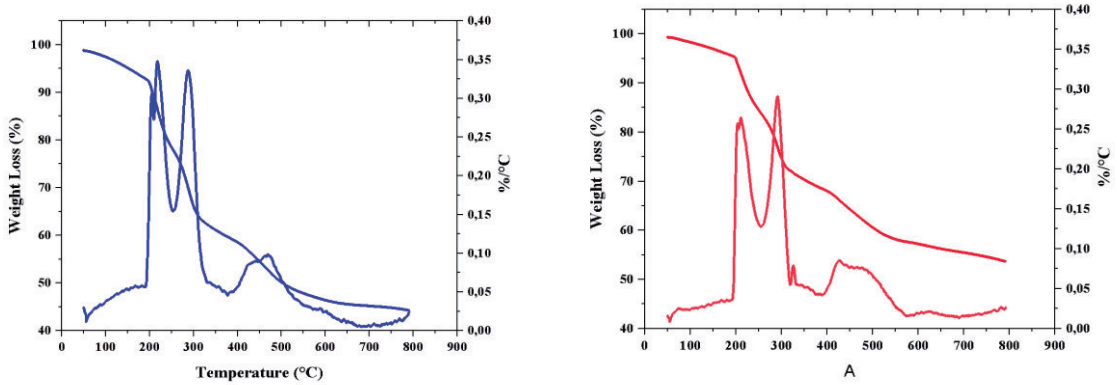

(a) (b)

Figure 2. TG and DTG curves: calcium alginate 3% + clay 0.5% (a) and calcium alginate 3% + clay 2.0% (b).

The graphs of the thermogravimetric analysis presented in Fig. 2 show that the material produced with higher MMT clay content (2%) had greater thermal stability, presenting a higher residue (Fig.2 b).

Conclusion

The experimental results demonstrated that hydrogels based on calcium alginate and MMT were absorbent materials, since they presented SD greater than 100%. The clay concentration in the composition of the hydrogels influenced the properties of the final product. The hydrogel with the highest clay concentration (2.0%) had the greatest thermal stability. However, the hydrogel with a lower clay concentration (0.5%) had higher absorbent capacity. We can conclude that these nanostructured hydrogels would have good performance as soil conditioners, since the clay helps to increase the thermal stability of the material.

Acknowledgments

We are grateful to Fundação Carlos Chagas Filho de Amparo à Pesquisa do Estado do Rio de Janeiro (FAPERJ) and Conselho Nacional de Desenvolvimento Científico e Tecnológico (CNPq) for financial support. This study was also partly financed by Coordenação de Aperfeiçoamento de Pessoal de Nível Superior (CAPES), Finance Code 001.

Bibliographic References

1. I. R. Oviedo; M. P. G. Gomez; H. C. Rodriguez; A. R. Martinez Polym. Int. Mater. 2008 (1)
2. ARAÚJO, Luciana Santos de. Preparation and evaluation of nanocomposite hydrogels based on alginate for the removal of Cu (Il) and Zn (Il) from aqueous solutions. 2014. 119 f. Dissertação (Mestrado em Química) - Instituto de Química, Universidade do Estado do Rio de Janeiro, Rio de Janeiro, 2014
3. Vidal Urquiza, Turner K., et al. "Effect of the Cross-Linking with Calcium Ions on the Structural and Thermo-Mechanical Properties of Alginate Films." MRS Proceedings, vol. 1355, 2011, https://doi.org/10.1557/opl.2011.1136.
4. Arndt, Aline, et al. "Avaliação Das Propriedades Físico-Químicas de Nanocompósitos de Polietileno Linear de Baixa Densidade E Montmorilonita Organofílica Obtidos Por Extrusão." *Matéria (Rio de Janeiro)*, vol. 22, no. suppl 1, 8 Jan. 2018, https://doi.org/10.1590/s1517-707620170005.0279.

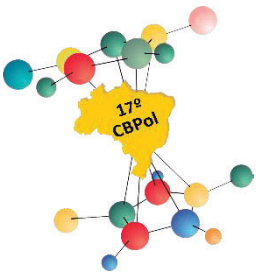

PREPARATION AND CHARACTERIZATION OF SOLUTION BLOWN PVA/CNCS NANOBIOCOMPOSITE FIBERS

Claudinei J. P. F. da Silva[1], Michelle S. Meruvia[2]

1 – Department of Chemical Engineering, Pontifical Catholic University of Paraná (PUC-PR), Curitiba, PR, Brazil
claudinei.pires@pucpr.edu.br
2 – Department of Mechanical Engineering, Pontifical Catholic University of Paraná (PUC-PR), Curitiba, PR, Brazil
michelle.meruvia@pucpr.br

Abstract – Poly(vinyl alcohol) (PVA) nanofibers have been widely utilized in various applications, predominantly in biomedical and food packaging fields, on account of this polymer's exceptional chemical and mechanical properties, ease of processability, biocompatibility and cost-effectiveness. Despite its benefits, however, PVA-only nanofibers are known to be fragile and vulnerable to aqueous environments. To overcome these limitations, the development of PVA composites has been pursued. Through solution blow spinning (SBS) method, composite nanofibers can be obtained at high efficiency and low cost, allowing potential scalability for commercial production. Within this framework, the present work targeted to prepare and characterize PVA/Cellulose nanocrystals (CNCs) nanobiocomposite fibers – as the incorporation of this nanofiller reportedly enhances the mechanical strength, improve water resistance and provide greater stability to its matrices – using a self-made SBS apparatus. To achieve this, 7 distinct solutions of PVA/CNCs were produced by mixing and dispersing, *via* ultrasonic treatment, different percentages of diluted CNCs suspensions in 10 – 16% w/v aqueous PVA solutions. The resultant solutions were composed of 0%, 1%, 2%, 3%, 4%, 5%, 6% w/v CNCs. They were solution blown and SBS solution parameters (concentration and viscosity) and process parameters (air pressure, work distance and nozzle diameter) were determined and adjusted, when needed, for each solution, ensuring alignment with their respective ideal spinnability ranges. Acquired fiber samples were analyzed according to morphology, crystalline structures, chemical interactions, thermal properties and wettability using scanning electron microscope (SEM), X-ray diffraction (XRD), Fourier transform infrared spectroscopy (FTIR), differential thermal analysis (DTA) and water-surface contact angle, respectively. Obtained results validate the successful integration of CNCs into the PVA matrix. To assess the effects of this reinforcement incorporation, comparative analyses were performed, examining characterization results of PVA/CNCs nanofibers in relation to PVA-only nanofibers and relevant literature outcomes.

References

1. K. Ashish; S. Sumit *Fibers* 2018, *6*, *3*, 45. https://doi.org/10.3390/fib6030045
2. L. D. John; M. B. Adam; D. S. Anthony; K. Peter *ACS Appl. Mater. Interfaces* 2016, *8*, *51*, 34951–34963. https://doi.org/10.1021/acsami.6b12994
3. S. P. Maria; H. Youssef; O. Z. Justin; J. P. Joel; J. R. Orlando *Biomacromolecules* 2010, *11*, *3*, 674-681. https://doi.org/10.1021/bm901254n

Keywords: *nanobiocomposite; poly(vinyl alcohol); cellulose nanocrystals; solution blow spinning; fibers.*

PROCESSING AND MECHANICAL PROPERTIES OF MICROFIBRILLATED CELLULOSE REINFORCED POLYPROPYLENE COMPOSITES

Alexandre O. T. Cordeiro[1] and Cristiane R. Martins[1]*

1 – Institute of Environmental Chemical and Pharmaceutical Sciences, Federal University of São Paulo (UNIFESP), Diadema, SP, Brazil
cr.martins@unifesp.br

Abstract – The study of cellulose nanomaterials has grown quickly in response to the rising need for environmentally friendly substitutes for fossil-derived products[1]. Because of its high elastic modulus and strength, microfibrillated cellulose (MFC), a mechanically fribrillated pulp primarily made up of nanofibrils, is a very desirable material[2]. Challenges associated with using MFC in such composites extend beyond polarity and include the need to create a homogeneous blend of the components as well as the low temperature stability of cellulose, which may present processing problems[2,3,4]. The goal of this study is to verify MFC loading content as well as the potential effects of MFCs low moisture content on the morphological, mechanical, thermal, and processing aspects of the composite. Never dried MFC cellulose (wet fiber web 4 wt % solid content) and MFC dried using the spouted bed drying method was used as reinforcement and PP composites were prepared in an internal mixer. SEM micrographs (Figure 1) revealed pronounced MFC agglomeration with never dried MFC (Fig 1b) that occurred during the mixture processing. Large MFC agglomerates can act as defects/stress concentrations points that can decrease the composite properties.

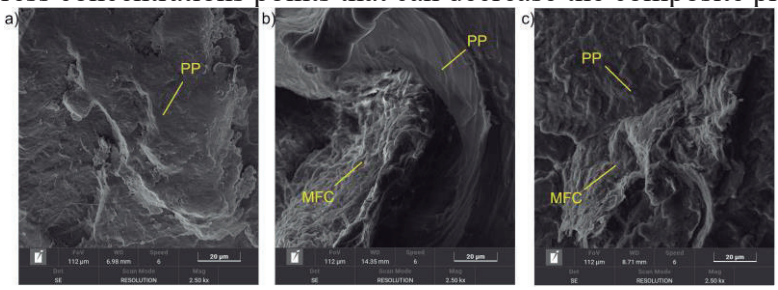

Figure 1 – SEM micrographs of PP (a) and composites with (b) never dried and (c) spouted bed dried MFC.

References

1. R. Trovagunta; T. Zou; M. Österberg; S. S. Kelley Carbohydrate Polymers 2021, 254, 117480. https://doi.org/10.1016/j.carbpol.2020.117480
2. K. Suzuki; H. Okumura; K. Kitagawa; S. Sato; A. N. Nakagaito; H. Yano Cellulose 2013, 20, 201-210. https://doi.org/10.1007/s10570-012-9843-9
3. H. S. Yang; D. J. Gardner; J. W. Nader Journal of Applied Polymer Science 2012, 128, 5. https://doi.org/10.1002/app.38513
4. K. Miyazaki; M. Hamadate; M. Terano; H. Nakatani Journal of Applied Polymer Science, 128. https://doi.org/10.1002/app.38284

Fundings: CNPq DAI with Suzano SA.

Keywords: *Nanocellulose*, *Microfibrillated cellulose, polypropylene,composites.*

PVDF NANOFIBERS WITH ZnO NANOSTRUCTURES FOR APPLICATION IN GAS SENSORS

Jéssica M. B. Corrêa[1], Lizandra M. Zimmermann[2] Lucas D. L. França[2] Beatriz M. Carvalho[1] and Deuber L. da S. Agostini[1]

1 – Department of Physics, Faculty of Science and Technology, São Paulo State University (FCT/UNESP), Presidente Prudente, SP, Brazil

2 – Department of Chemistry, Blumenau Regional University Foundation (FURB), Blumenau, SP, Brazil

jessica.mantelato@unesp.br

Abstract - The current world reality, driven by global challenges such as global warming, has promoted developing and improving sensors and nanosensors. Nanoscience has enabled the production of increasingly smaller nanostructures with unique characteristics, facilitating the miniaturization of technology. The change in property from bulk material to nanomaterial is due to the confinement of its carriers, either in one, two, or three spatial dimensions. Nanofibers developed through the electrospinning technique have gained space in their application in nanosensors due to obtaining different diameters, morphologies, and compositions, which have consolidated the technique. In addition to polymeric fibers, other classes of materials have been used as sensors, such as oxides, particularly zinc oxide (ZnO). A composite material can be advantageous compared to the materials that compose it individually. In this work, the main focus is the development of a composite formed by ZnO nanoparticles and poly(vinylidene fluoride), PVDF, for application in gas sensors. PVDF and PVDF/ZnO samples were produced by varying the stress parameter, and the composite was prepared by varying the proportion of nanoparticles. The morphological analysis includes scanning electron microscopy (SEM), and spectroscopy analysis includes Fourier transform infrared (FT-IR) and ultraviolet-visible (UV-Vis), in addition DC electrical conductivity measurements.

References

1. P. Recher; B.Trauzettel *Nanotechnology* 2010, *21*, 302001. https://doi.org/10.1088/0957-4484/21/30/302001

2. T. Wu; Z. Wang; M. Tian; J. Miao; J. Sun *Sensors and Actuators B: Chemical* 2018, *259*, 526-531. https://doi.org/10.1016/j.snb.2017.12.101

3. L. A. Mercante; R.S André; J. B. Macedo; A. Pavinatto; D. S. Correa *Química Nova*, 2021,*44*, 717-736. https://doi.org/10.21577/0100-4042.20170721

Fundings: FCT/UNESP, CAPES, CNPq, INEO and FAPESP

Keywords: PVDF; ZnO; gas sensors

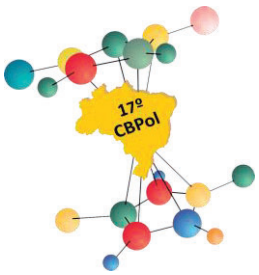

DEVELOPMENT OF SILOXANE-PMMA AND SILOXANE-PEO-PMMA HYBRID MATERIALS FOR FUTURE APPLICATIONS OF PROLONGED RELEASE OF PENICILLIN G

Andressa Rebecca Brito de Andrade[1], Thaís Drolhe Comparoni[1], Alexandre Carneiro Silvino[2], Kattya Gyselle de Holanda e Silva[3], Viviane de Oliveira Freitas Lione[3] e Karim Dahmouche[1]

1 - Campus de Duque de Caxias, Universidade Federal do Rio de Janeiro (UFRJ), Rio de Janeiro, RJ, Brasil
andressarebecca@ufrj.br
2 - Instituto de Macromoléculas (IMA), Universidade Federal do Rio de Janeiro (UFRJ), Rio de Janeiro, RJ, Brasil
3- Faculdade de Farmácia, Universidade Federal do Rio de Janeiro (UFRJ), Rio de Janeiro, RJ, Brasil

Abstract - - Prolonged drug release aiming for less toxic administration and providing a higher quality of life is a current topic. The need for prolonged release matrices is evident for the correct treatment of rheumatic fever, a pediatric heart disease treated with monthly intramuscular administration of penicillin G benzathine [1] until 21 years of age. Organic-inorganic hybrids [2], including Siloxane-polymer hybrids, are particularly interesting for drug release applications [3]. In this study, we prepared Siloxane-PMMA (poly (methyl methacrylate)) hybrid materials via the sol-gel process, presenting covalent bonds between the polymer chains and siloxane nanoparticles. Samples without Penicillin and containing 30% by mass of Penicillin G were prepared and characterized. In both families, infrared spectroscopy (FTIR) indicates the absence of the carbon-carbon double bond (C=C) between 1580 e 1680 cm^{-1}, suggesting that nearly all monomers were polymerized. In the samples with Penicillin G, the presence of the carbon-carbon double bond derived from the β-lactam ring of the drug at 1588 cm^{-1}, along with the detection of the characteristic hydroxyl group band at 3308 cm^{-1}, indicates that the hybrid matrix preserves the chemical integrity of the drug and illustrates the hydrophilic nature of the active compound and its water-retaining capacity in the material. The absence of peaks in the X-ray diffraction (XRD) pattern of the samples with Penicillin reveals that the drug has lost its crystalline structure and is, therefore, dispersed on a molecular scale in the matrix. The results of thermogravimetric analysis (TGA) show that the drug's degradation starts only around 200°C and does not significantly affect the PMMA degradation steps. Ongoing studies aim to develop Siloxane-PEO-PMMA hybrids to monitor drug release in a biological environment by changing the ratio between hydrophobic PMMA and hydrophilic PEO (polyethylene oxide), as well as reducing the moderate toxicity associated with PMMA.

References

1. K.G.H Silva; G. Barrat; A.G Oliveira and E. Egito. Quím. Nova 35 (9), 2012. https://doi.org/10.1590/S0100-40422012000900023.
2. M.Faustini; L. Nicole; E. Ruiz-Hitzky and C.Sanchez. Eur. J. Inorg. Chem., 5097–5105, 2012. https://doi.org/10.1002/adfm.201704158
3. J.A Oshiro Junior; M.Paiva-Abuçafy; E. Berbel Manaia; L.A Chiavacci, et al. Polymers, 8 (91), 2016. https://doi.org/10.3390/polym8040091

Fundings: We thank FAPERJ for their support through the ARC and Nanotechnology Research Networks programs in the State of Rio de Janeiro, as well as for the scholarship awarded to Andressa Rebecca Brito de Andrade.

Keywords: *Hybrid Materials, Siloxane-PEO-PMMA, Prolonged Drug Release, Penicillin G, Sol-Gel Method.*

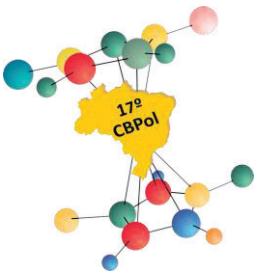

RECOVERY OF THE MECHANICAL PROPERTIES OF POST-CONSUMER ABS COPOLYMER BY INCORPORATION OF GRAPHENE OXIDE (GO) AND GRAPHENE

Lucas P. de Lima[1,2], Natália F. Braga[1,2*] and Guilhermino J. M. Fechine[1,2]

2- School of Engineering, Mackenzie Presbyterian University, São Paulo, Brazil
2 – MackGraphe (Mackenzie Institute for Research in Graphene and Nanotechnologies), Mackenzie Presbyterian Institute, São Paulo, Brazil

*natyfbraga@hotmail.com

Graphene has been studied in several areas due to its unique properties. One of the research fields of such material is on its insertion as nanofiller in polymeric matrices [1]. Acrylonitrile Butadiene Styrene (ABS) is one of the most widely used engineering polymers in various applications, especially in electronic equipment and automotive industry due to its good mechanical properties and low-cost processing. Several strategies have been used by the industry for the recycling of ABS to reduce the environmental impact of these materials. This project aims to develop a strategy using graphene (Gr) and graphene oxide (GO) in post-consumer ABS, recovering its mechanical (tensile and impact) properties. The nanocomposites were obtained by the mixture in the molten state, where the insertion of the filler in the polymer is made in a twin-screw extruder. Three compositions of the ABS/GO system were made (0.05, 0.1 and 0.3 wt.%) while for Gr systems the compositions were 0.5, 1 and 2 wt.%. Tensile and impact tests for all compositions and neat polymer were performed. The results showed an increase in tenacity (area under the stress x strain curve) for the nanocomposites, especially for 0.1 wt.% of GO with more than 200% when compared to the neat polymer. This may be due to the phenomenon of over lubrication of the stacked sheets of GO in the polymer [2]. The impact test showed an improvement, mainly with 0.5 wt.% of Gr content, reaching 160% more resistance when compared to the neat polymer. The results showed that there is a good interaction between the ABS matrix and both fillers (GO and Gr) leading to the mechanical properties recuperation of the polymer matrix after its processing.

References

1. P. A. R. Muñoz; et. Al. *eXPRESS Polymer Letters* 2018, 12, 930. https://doi.org/10.3144/expresspolymlett.2018.79
2. Ferreira, E. H. C., Andrade, R. J. E., & Fechine, G. J. M. Macromolecules, 52(24), 9620–9631. doi:10.1021/acs.macromol.9b01746 (2019).

Fundings: CNPq (314093/2021-4) and FAPESP (2020/14302-2)

Keywords: *ABS, graphene, graphene oxide, recycling, mechanical properties.*

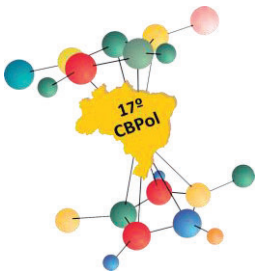

REPLACEMENT OF ETHYLENE VINYL ACETATE (EVA) LAYER BY POLYDIMETHYLSILOXANE COMPOSITES (PDMS) WITH GRAPHENE NANOSTRUCTURES IN PHOTOVOLTAIC MODULES

José Manuel Mejía Armijo,[1] Muriel R. de Oliveira,[1] Pedro L. Silva[2], Deuber L. da Silva Agostini,[2] Clarissa A. Olivati,[2] Leonardo L. Paim,[1] Renivaldo J. dos Santos,[1] Flávio C. Cabrera.[1]

1 - Department of Renewable Energy, São Paulo State University (UNESP), Rosana Campus, SP, Brazil
e-mail: j.armijo@unesp.br
2 - São Paulo State University (UNESP), Presidente Prudente Campus, SP, Brazil

Abstract – Due to aging process or delamination of the ethylene vinyl acetate (EVA) layers that protect (encapsulate) the solar cells the performance and useful life of photovoltaic modules is compromised, reducing the efficiency of photovoltaic cells. Here, we propose to replace the EVA layers by a composite of polydimethylsiloxane (PDMS) with the incorporation of graphene oxide nanoparticles. PDMS (silicone) can be deposited directly on the surface of the solar cells by casting, presenting fast curing, transparence in the region of interest and chemical inert. PDMS (Sylgard® 184, Sigma-Aldrich) in a 1:10 curing agent ratio (3 g: 0.3g) can be used to disperse the nanostructures throughout the polymer volume prior to the drying process. Different samples with quantities of graphene nanoparticles were tested, 50, 100, 150 and 500 microliters by sample, cured at 40°C during 3 h. Comparing the current generated before and after the deposition of composite films over the photovoltaic cell, as increased the amount of graphene oxide in the composite increases the current, reaching 3.4% for 500 microliters. In the next step high concentration of graphene oxide suspensions will be tested and the response of cells in solar simulator.

References

1. M. Oliveira; L. Soares; M. Viana; et al. *International Journal of Adhesion and Adhesives 2020, 100, 10259.* https://doi.org/10.1016/j.ijadhadh.2020.102595.
2. D. Kumi; S. Khan; S. Cho; et al. *Physica B: Condensed Matter, 2020, 576, 411711.* https://doi.org/10.1016/j.physb.2019.411711.

Keywords: *Solar cell; Photovoltaics; Energy efficiency; Nanomaterials.*

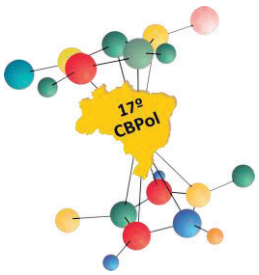

SINGLE WALL CARBON NANOTUBES AND ITS INFLUENCE ON PROPERTIES OF POLYMER NANOCOMPOSITES

Ricardo R. S. Barnasky[1]*, Pietro Rafael Ferreira[1], Felipe Bertola de Souza[1], Rafael Rank Storm[1], Kássia P. Vieira[2] and Claudemir Gracino[3]

1 – SENAI Innovation Institute for Structural Engineering, Maringá, PR, Brazil ricardo.barnasky@sistemafiep.org.br
2 – SENAI Innovation Institute for Electrochemistry, Curitiba, PR, Brazil
1 – Skintech Tecnologia, Maringá, PR, Brazil

Abstract - Nanocomposites are materials which can present modified properties due to several factors [1]. Among them, the nanoparticle and the amounts added in polymeric matrices may be considered the main factors. Using theses variables, unique properties may be reached and can be handled to specific applications. The commercial introduction of materials using carbon nanotubes is a competitive differential to new products and industries, bringing direct advantages, because the manipulation of materials in a nanoscale might be difficulted due to the nanoparticles and matrices characteristics [2]. This work aims to incorporate and evaluate the influence of single wall carbon nanotubes (SWCNTs) in thermoplastic materials. To do so, SWCNTs were applied in linear low-density polyethylene (LLDPE) and polypropylene (PP). The nanoparticles TUBALL™ MATRIX beta 809 were applied in the amount of 1% w/w for each matrix. The mixtures were extruded according to supplier recommendations. The materials were analyzed in a simultaneous thermal analysis (STA), for differential scanning calorimetry and thermogravimetric analysis, and the electrical behavior was analyzed with a surface resistance meter. The results indicated that the nanoparticles did not present a significant influence on the thermal properties of nanocomposites when compared to the pure matrix (LLDPE T_m123,38ºC and PP T_m167,24ºC). The electrical investigation indicated a dissipative characteristic for the materials (near 10^5 OHMS). This behavior represents a technological advantage to the industry use PP and PE as dissipative materials for health and security applications, for example [3]. This project is ongoing research and will investigate statistically if this behavior remains.

References

1. L. S. Schadler Nanocomposite Science and Technology 2003, 77-153. http://dx.doi.org/10.1002/3527602127.ch2.
2. S. Aszkiewicz; A. Szymczyk; A. Zubkiewicz; J. Subocz; R. Stanik; J. Szczepaniak Polymers 2020, 12, 6, 1356. http://dx.doi.org/10.3390/polym12061356.
3. S. M. Thompson; M. Talò; B. Krause; A. Janke; M. Lanzerotti; J. Capps; G. Lanzara; W. Lacarbonara Composite Structures, 2022, 295,115794. http://dx.doi.org/10.1016/j.compstruct.2022.115794.

Keywords: *Carbon nanotubes, Dissipative properties, Polymer nanocomposites.*

Study of electrospun mats of Poly(Acid Lactic) with Graphene nanoplatelets and Choline Bitartrate for use in nerve tissue engineering

Eric T Yida [1] , Matheus Campos Hemkemaier [1] , Sébastien Livi [2], Claudia Merlini [1]

1 – Materials Engineering Special Coordination, Universidade Federal de Santa Catarina(UFSC), Blumenau, SC, Brazil

ericyidajugger@gmail.com

2- Université de Lyon, CNRS, Université Claude Bernard Lyon 1, INSA Lyon, Université Jean Monnet, UMR 5223, Ingénierie des Matériaux Polymères, CEDEX F-69621 Villeurbanne, France

The main objective of this work is to study the properties of electrospun mats of Poli(Láctic Acid)(PLA) with Graphene Nanoplatelets(GN) and Ionic Liquid (IL) as nerve conduits. The focus is to achieve desirable properties for a neuroregenerative conduit, as for example, biocompatible mats, with porous structure and electrical conductivity [1]. It were used biocompatible materials, conductive nanoparticles (GN) and IL were used to increase the particle dispersion. Moreover, electrospinning was used to produce a 3D porous structure. To manufacture the membranes, the process starts by preparing the electrospinning solution, where PLA is solubilized using Dichloromethane(DCM) and Dimethylformamide (DMF), followed by adding IL that will assist in dispersing GN[2]. Then the solution was sonicated through the ultrasonic, right after the solution was transferred to a syringe so that it can be sent to the electrospinning system where the membrane will be formed using a fixed collector [3]. As for experimental results it obtained images from Scanning Transmission Electron Microscopy (SEM) of all membranes, control (PLA, PLA+IL) and the remaining increasing in GN mass 0.5%, 1%, 2%, 4%. It was observable that the electrospun mats had a 3D structure with continuous fibers randomly oriented. IL did not influence the morphology and led to a decrease of fibers diameter. Adding GN introduced small punctual flaws on the fibers, from agglomeration of graphene, however fibers stayed uniform, there also was an increase in diameter proportional to the amount of GN added. From Infrared spectroscopy it was observed that only the addition of IL resulted in the emergence of new bands at 3300 and 1750, possibly by the higher affinity with water.

References:

1. Castro, V. O. *Conduítes eletrofiados constituídos de fibras alinhadas de poli (ácido láctico-co-ácido glicólico) com nanopartículas condutoras para a regeneração de nervos periféricos,* Universidade Federal de Santa Catarina, Florianópolis, 2022
2. S-H. Tan, R. Inai, M. Kotaki, S. Ramakrishna, Polymer, 2005, 6128-6134. https://doi.org/10.1016/j.polymer.2005.05.068
3. COSTA, Rodrigo G. F. et al. *Eletrofiação de Polímeros em Solução: Parte I. Polímeros*,[S.L.], v. 22, n. 2, p. 170-177,2012. FapUNIFESP (SciELO).http://dx.doi.org/10.1590/s0104-14282012005000026.

Fundings: Cnpq

Keywords: *Poli(acid lactic), Graphene nanoplatelets, Choline bitartrate, Electrospinning, Nanocomposite.*

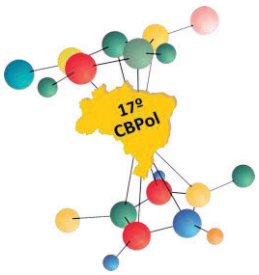

STUDY OF THE INCORPORATION OF CARBON NANOTUBES ON WATER BASED EPOXY INK

Dafne Aparecida do Nascimento[1], Victtor Henrique Queiroz Silva[2], Wagner Maurício Pachekoski [3]

Federal University of Santa Catarina

1 – Material Characterization Laboratory, Federal University of Santa Catarina (USFC), Joinville, SC, Brazil
dafne.nascimento66@gmail.com
2 – Material Characterization Laboratory, Federal University of Santa Catarina (USFC), Joinville, SC, Brazil
victtorqueirozs@gmail.com
1 – Material Characterization Laboratory, Federal University of Santa Catarina (USFC), Joinville, SC, Brazil
wagner.pachekoski@ufsc.br

Abstract - Water based ink has become a relevant area to research since the news regulations requirements have asked from industry alternatives with low quantity volatile organic compounds (VOC) in their formulation. These news resins produce translucent and transparent films with low environmental impact and diverse appliances at industrial uses. It is known that for a material to be considered as a nanocomposite it is needed to have nanometric dimensions, their use has been shown a new trend, once they modify the final properties of the material. In this class of materials, the carbon nanotubes (NTC) have been studied and developed on applications of materials reinforcements, because their insertion brings benefits at the final compound properties, such as the mechanical increasement and electric properties. The formulated ink has a composition of 100 grams of resin to 28 grams of hardener (100/28), with a 0.5% inclusion of NTCs. The modified ink was subjected to dispersion ultrasound for one hour. As a way to validate the experiment, the impact test was conducted using steel spheres launched onto a painted substrate to determine the potential energy the ink could absorb without rupturing. The adhesion test followed the standard established by ABNT NBR 11003:2023, and the viscosity test followed the standard ABNT NBR 5849:2015. The results suggest that the manufactured ink exhibited good potential energy absorption properties in the impact test, as it did not fracture at any point. However, the presence of heterogeneity between the ink and NTCs significantly decreased the adhesion between the film and the substrate. Regarding the viscosity test, an average flow time of 22.97 seconds was obtained, characterizing the ink as fluid.

References.
1. A.J.G. Zarbon; *New Chemistry* 2007, *1469*, 19081. https://doi.org/10.1590/S0100-40422007000600016.
2. C. S. Horikawa, Ph.D. Thesis, University of São Carlos, 2003.
3. R.V. Salvatierra, M.Sc. Thesis, Federal University of Paraná, 2010.

Keywords: *water-based ink, nanocomposite, carbon nanotubes (NTC) and formulation.*

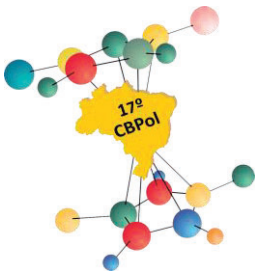

STUDY OF THE INFLUENCE OF THE SHAPE OF CARBON BLACK NANOPARTICLE AGGREGATES ON THE PROPERTIES OF NANOCOMPOSITES WITH AND WITHOUT BLOCK COPOLYMER

Anelise Fraga de Jesus[1*], Bruna Louise da Silva[1] and Luiz Antonio Ferreira Coelho[1]

1 – Department of Materials Science and Engineering, State University of Santa Catarina (UDESC), Joinville, SC. Rua Paulo Malschitzki, 200 – Campus Universitário, CEP 89.219-710
anelise.fdj@edu.udesc.br

Abstract - The aim of this study is to evaluate the effect dispersion of carbon black (CB) aggregates with the thermomechanical properties of the epoxy. For the dispersion of CB (mass fractions 1,5, 3 e 5%) in the epoxy, the block copolymer was used poly (ethylene glycol)/poly (propylene glycol)/poly (ethylene glycol) (PEG-b-PPG-b-PEG) with a molecular weight of 14,600 g/mol in the mass fraction of 10%. The characterizations performed included scanning electron microscopy (MEV-FEG) and transmission electron microscopy (MET) analyses. It was observed that the block copolymer contributed to the dispersion of CB. The morphological analyses showed that increasing the percentage of carbon black led to increased nanoparticle aggregates in the nanocomposites with and without the block copolymer. The nanocomposites with 1.5%, 3%, and 6% CB exhibited linear or branched aggregate structures, both in the presence and absence of the copolymer. Except for the 6% CB sample without the block copolymer, which presented a spheroidal and ellipsoidal cluster shape. This suggests that the block copolymer played a role in dispersing these nanoparticles in the epoxy matrix. It is believed that the potential contribution of the block copolymer in the dispersion of nanoparticles in the matrix may result in an increase in the values of the thermo-mechanical properties of the nanocomposites compared to the nanocomposites without block copolymer, given that the aggregates of this material were larger, therefore, dynamic mechanical analysis (DMA) wiil be performed.

Keywords: *epoxy, PEG-b-PPG-b-PEG, carbon black, mechanical properties*

References

1. B.L. SILVA. Universidade do Estado de Santa Catarina, 2018.
2. M Larrañaga; MD Martín; N Gabilondo; G Kortaberria; MA Corcuera; CC Riccardi; I Mondragon. *Polymer* international 2004, 1495, 1574. https://doi.org/10.1002/pi.1574
3. M. Wissler. Journal of Power Sources, 2006, 142, 064. https://doi.org/10.1016/j.jpowsour.2006.02.064
4. S. Kuester. - Universidade Federal de Santa Catarina, 2013.
5. P. C. Vargas.Universidade Federal de Santa Catarina, 2020.

STUDY ON THE INFLUENCE OF MATERIAL PARAMETERS IN ELECTROSPUN NANOMEMBRANES FROM AQUEOUS PVA SOLUTIONS

André Luiz dos Santos[1], Sergio Henrique Pezzin[2]
1 – Department of Materials Engineering, University of the State of Santa Catarina – (UDESC), Joinville-SC, Brazil
santandre@outlook.com
2 – Department of Chemistry, University of the State of Santa Catarina – (UDESC), Joinville-SC, Brazil

Abstract – Due to their unique characteristics, such as the formation of small pores, nanofibers have a variety of interesting applications [1] including the biomedical field, such as drug release, tissue engineering, and wound dressings [2]. However, for in situ applications such as wound dressings, miniaturized and more affordable portable electrospinning devices have been studied [3]. In this study, membranes composed of polymeric nanofibers were produced by electrospinning from an aqueous solution of poly (vinyl alcohol) (PVA), aiming to evaluate the influence of material parameters on the produced nanomembranes. A full factorial experimental design 3^2 was employed, and nine samples were produced in triplicate, using nine different solutions, which were combinations of three types of PVA with different molecular weight (Mn) ranges (low, medium, and high) at three different concentrations (8%, 9%, and 10%), dissolved in deionized water. A commercial electrospinning apparatus was used, and the selected and fixed process parameters were electrical voltage of 8 kV, collector/capillary distance of 6 cm, flow rate of 1.2 mL/h, and a static flat metal collector surface. These parameters were chosen to resemble those of a possible *in situ*, portable electrospinning system. The produced samples were evaluated using scanning electron microscopy (SEM). Among the nine different types of polymeric solutions employed, only four allowed the formation of nanomembranes under the specified conditions, with the smallest average fiber diameter being obtained with medium Mn PVA (average molecular weight range of 85,000 to 124,000 g/mol) at 8 wt% solution concentration. It exhibited an average fiber diameter of 95 nm and porosity of 49.6% (both measured through digital image processing software ImageJ).

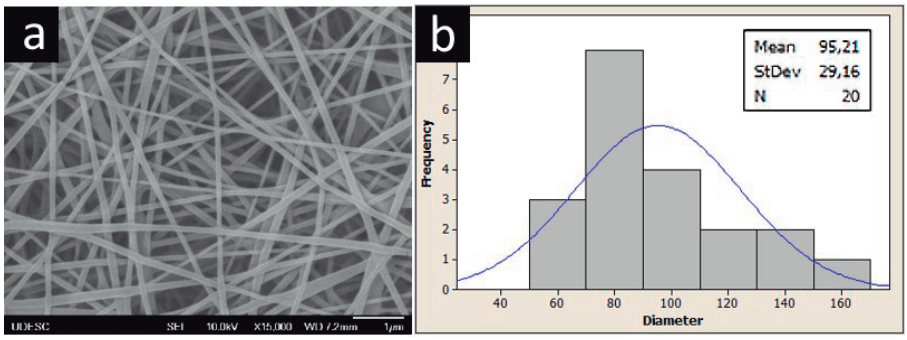

Figure 1 – a) SEM image of a sample with the smallest average diameter, b) diameter distribution histogram.

References
1. M.J. Divvela et al. Journal of Non-Newtonian Fluid Mechanics 2017, 247, 62–77. DOI 10.1016/j.jnnfm.2017.06.005
2. Z.M. Huang et al. Composites Science and Technology 2003, 63, 2223–2253. DOI 10.1016/S0266-3538(03)00178-7
3. B. Ding; X. Wang; J. Yu Electrospinning: nanofabrication and applications. [S.l.]: Elsevier, 2019.

Fundings: FAPESCand CAPES.

Keywords: *Nanofibers, Electrospinning, PVA, Material parameters, Design of Experiment.*

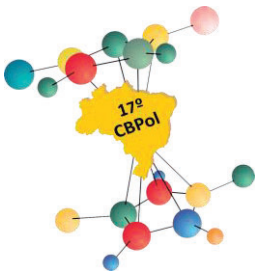

SUPERHYDROPHOBIC COATINGS BASED ON EPOXY RESIN CONTAINING ORGANICLY MODIFIED SILICA (ORMOSIL)

Msc. Jéssica Thaline Alves de Sousa[1], D.Sc. Bluma Guenther Soares[1], D.Sc. Adriana dos Anjos Silva [2]

1 – Universidade Federal do Rio de Janeiro, PEMM-COPPE, 21941-972 Rio de Janeiro, Brazil
jessica.thaline@coppe.ufrj.br
2 – Universidade Federal do Rio de Janeiro, Escola de Química, Centro de Tecnologia, Bl. E, 21941-909, Rio de Janeiro, RJ, Brazil

Abstract - The steel pipes used in the oil and gas sector are exposed to severe environmental conditions[1], so the metallic surfaces must have superhydrophobic characteristics. The coating with an epoxy resin matrix (ER) added with silica particles is the focus of this work. To prepare the coatings, commercial silica (AEROSIL® 200) was initially functionalized in situ using the Stober[2] method with organosilane modifiers containing fluorine and glycidyl groups with epoxy resin. Additionally, silica was also synthesized through hydrolysis and condensation of TEOS, functionalized with organosilanes in the epoxy matrix. Subsequently, the coating was applied by spray under a pressure of 20Pa, on a metallic substrate positioned at a 30º angle parallel to the compressed air gun, with a distance of 30 cm. The qualitative evaluation of the anticorrosive capacity of the coatings was made through measurements of the contact angle (AC) of water droplets (5 µL). The coating prepared from commercial silica with a fluorine-based modifying agent JTIS (ER/silica-modifier: 60/40 – 0.5g fluorsilane – 0.1g glyme), presented an AC of 154º. The coating from silica-TEOS, evolved in lower AC, the JTEOSIS sample (ER/silica-modifier: 60/40 - 1g fluorsilane – 0.2g glyme) presented AC of 141º. The superhydrophobic coating (JTIS) has a 10º sliding angle, self-cleaning power and greater abrasion resistance. This result can be explained because the Stöber method is associated with the addition of water[3], which impaired the hydrophobic characteristic of ORMOSIL, due to an inefficient removal of water injection that interact by hydrogen bonding with the hydroxyls on the surface of the particle of silica.

1. L. Popoola, A. Grema, G. Latinwo, B. Gutti, A. Balogun. *International Journal of Industrial Chemistry 2013, 4, 35.* https://doi.org/10.1186/2228-5547-4-35
2. W. Stöber, A. Fink, E. Bohn, *Journal of Colloid and Interface Science, 26, 1968*. https://doi.org/10.1016/0021-9797(68)90272-5.
3. T. Metroke, O. Kachurina, E. Knobbe, *Progress in Organic Coatings, 2002, 4*. https://doi.org/10.1016/S0300-9440(02)00063-2.

Fundings: CAPES

Keywords: *superhydrophobicity; organosilanes; epoxy resin; stober method; in situ method.*

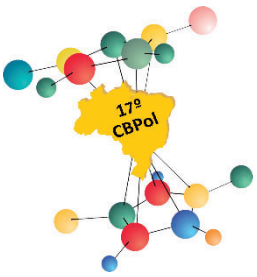

SYNERGISTIC COMBINATION OF NATURAL RUBBER LATEX AND LIGNIN FOR SUSTAINABLE WATER-BASED ADHESIVES

Juliana M. Silva[1, 2], Pedro I. C. Claro[2], Marcos V. Lorevice[2] and Rubia F. Gouveia[1, 2]*

1 – Center of Natural and Human Sciences, Federal University of ABC (UFABC), Santo André, SP, Brazil
2 – Brazilian Nanotechnology National Laboratory (LNNano), Brazilian Center for Research in Energy and Materials (CNPEM), Campinas, SP, Brazil
rubia.gouveia@lnnano.cnpem.br

Abstract - Natural rubber latex (NRL) and lignin are promising renewable materials with unique characteristics, demonstrating remarkable adhesion properties[1]. However, the potential synergy resulting from the combination of both biopolymers is poorly explored. Herein, we investigated the incorporation of NRL with lignin extracted by different pretreatments (organosolv, alkali, and Kraft) to develop a water-based adhesive. The nanoscale interaction between NRL and lignin was investigated by atomic force microscopy (AFM), revealing an intrinsic interaction with NRL according to the lignin extraction route. The mechanical properties of NRL-lignin films corroborated with the observed nanoscale interaction, indicating an ideal lignin pretreatment method for NRL-based adhesive formulation. The colloidal characterization demonstrated the solubilization of lignin in NRL, evidencing the chemical compatibility between these components, with colloidal stability reaching 50 days. As a proof-of-concept, various substrates were successfully adhered using the selected lignin in NRL water-based adhesive formulation. Shear mechanical tests of the bonded substrates exhibited superior performance of dried and underwater NRL-lignin joints in comparison to neat NRL. Notably, the adhesion strength was enhanced by 200%, 74%, 71% and 27% on glass, aluminum, polypropylene (PP) and wood substrates, respectively, in dry conditions. Furthermore, the adhesive demonstrated outstanding performance compared to certain commercial adhesives. These findings demonstrate the notable potential of NRL-lignin adhesive in bonding substrates with varying levels of hydrophobicity and porosity. The strategic selection of a lignin extraction route and the facile mixing of the components resulted in a sustainable adhesive with exceptional properties and a high potential for commercial applications.

References

1. R. F. Gouveia, N. M. Orra, Patent WO2019213730A1, 2019.

Fundings: This study was financed in part by the Coordenação de Aperfeiçoamento de Pessoal de Nível Superior – Brasil (CAPES) - Finance Code 001 and by the National Council for Scientific and Technological Development (CNPq) - Grants 380312/2020-4 and 380173/2022-0.

Keywords: *Renewable materials; underwater adhesion; nanocharacterization; mechanical mixture; shear mechanical tests.*

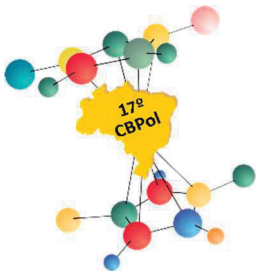

SYNERGISTIC EFFECT OF ADDING GRAPHENE NANOPLATES AND CARBON NANOTUBES IN PLA/PHBV BLENDS

Erick G. R. dos Anjos[1], Guilherme F. M. Morgado[1], Tayra R. Brazil[1], Francys K. V. Moreira[2], Juliano Marini[2] and Fabio R. Passador[1*]

1 – Polymer and Biopolymer Technology Laboratory (TecPBio), Federal University of São Paulo (UNIFESP), São José dos Campos, SP, Brazil
2 – Department of Materials Engineering (DEMa), Federal University of São Carlos (UFSCar), São Carlos, SP, Brazil.
fabio.passador@unifesp.br

Abstract – The addition of carbon materials such as graphene nanoplates (GNP) and carbon nanotubes (CNT) in polymeric blends enables application as functional electromagnetic packaging [1]. In this work, poly (lactic acid) (PLA) and poly (3-hydroxybutyrate-co-3-hydroxyvalerate) (PHBV) was chosen as the biodegradable polymeric matrix and the synergistic effect of the addition of GNP and CNT on the mechanical and electromagnetic properties was evaluated. PLA/PHBV blends (80/20) with the addition of 1 wt% CNT and/or 3 wt% GNP were processed using a double-screw extruder (AX Plásticos, model AX16:40DR). Tensile samples were inject-molded and the mechanical (tensile test) and electromagnetic properties were obtained. Regarding the mechanical properties, the synergistic effect was significant, the hybrid nanocomposite (with the addition of 1wt% CNT and 3 wt% GNP) present high ultimate tensile strength and elastic modulus compared to the nanocomposites with individual fillers. Analyzing the electromagnetic properties in the X band, it was observed that the hybrid nanocomposite presented a total attenuation (SE_T) of 7.5 dB at 10 GHz, a higher value than the individual nanocomposites (PLA/PHBV/CNT with SE_T of 6 dB and PLA/PHBV/GNP SE_T of 2 dB). These results drive the search and study of new contents of these carbon materials in the PLA/PHBV blend to reach the values of commercial applications.

References

1. Anjos, E.G.R.; Marini, J.; Gomes, N.A.S.; Rezende, M.C.; Passador, F.R. (2022). Synergistic effect of adding graphene nanoplates and carbon nanotubes in polycarbonate/acrylonitrile-styrene-butadiene copolymer blend. Journal of Applied Polymer Science, 139(37), e52873. https://doi.org/10.1002/app.52873

Fundings: The authors thank FAPESP (Process 2020/12501-8) and CNPq (Process 407288/2021-0) for financial support.

Keywords: *PLA, PHBV, graphene nanoplates, carbon nanotubes, electromagnetic properties.*

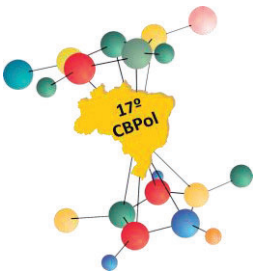

SYNTHESE OF NANOPARTICLES BY ELECTROSPINNING

Luana Priscila de Souza[1]*, Otavio Rodrigues Diniz[1], Beatriz Luci Fernandes[2] and Clayton Fernandes de Souza[1,2]

1 – School of Education and Humanities, Chemistry Undergraduate Course, Pontifícia Universidade Católica do Paraná (PUCPR), Curitiba, Paraná, Brazil
luana.priscila@pucpr.edu.br
2 – Health Technology Graduate Program, Pontifícia Universidade Católica do Paraná (PUCPR), Curitiba, Paraná, Brazil

The electrospinning is used to produce nanofibers from hydrogel solutions resulting in materials, such as membranes, that in presence of bioactive substances are explored in medical devices. Normally, the biopolymers with high viscous or emulsification properties are used in this technique, generating biomaterials with high surface area, roughness or porosity, resulting in an interesting functionality, capable to accelerate the healing process in occlusive dressing. However, recently new procedures based in electrospinning demonstrated the possibility to obtain nanoparticles, promoting an environment media to encapsulate bioactive substances with some adhesion on specific surface. Think in this situation, this work aimed to develop hydrogels systems, analyzing some conditions in the electrospinning process to obtain nanoparticles. The hydrogel aqueous solutions were prepared at concentrations of 1.5%wt. Considering this concentration, blends with other hydrocolloids (gellan gum-GL, gelatin-GLT and collagen-COL) was produced at different proportions (%), being 80/20% and 60/40% with fucogel®-FCG polymer in higher percentage. The rheological characteristics (pseudoplasticity), surface tension, electrospinning and scanning electron microscopy (SEM) were evaluated. The 1.5wt% hydrogel solutions showed pseudoplasticity ($n<1$), with viscoelastic characteristics, with the highest resistance to flow being the mixtures of FCG with GL and GLT, with surface tension values between 45 and 65 mN/m, indicating a surfactant character of the adopted hydrocolloids. In the electrospinning tests, only solutions with 100% FCG (1.5 wt%) showed flow and taylor cone formation, with a voltage of 10KV and a needle tip with a gauge of 24 and 25. Through the SEM analyses, it was observed that in the spinning process conditions was able to produce spherical particles with dimensions in the range of 50 to 550 nm of the FCG solution. The results indicate the viability and versatility of the electrospinning process, giving us a new field to explore this technique for biomedical applications.

References

1. k. Peranidze; T. V. Safronova; N. R. Kildeeva *Polymers*, 2022, *14*, 96. https://doi.org/10.3390/polym14010096.
2. A. D. J. Bombin; N. J. Dunne; H. O. Mccarty *Materials science & engineering c*, 2020, 114, 110994. https://doi.org/10.1016/j.msec.2020.110994
3. A. R. Alharbi; I. M. Alarifi; W. S. Khan; R. Asmatulu *Journal of Membrane and Separation Technology*, 2016, *05*, 38. http://dx.doi.org/10.6000/1929-6037.2016.05.02.1

Keywords: *Electrospinning, biopolymer, nanoparticles, hydrogels.*

SYNTHESIS AND DEPOSITION BY SLOT DIE COATING OF WATER BASED P3HT AND P3HT:PCBM NANOPARTICLES

Júlia Ketzer Majewski[1]*, Maiara Bassi Gobara[1] , Lucimara Stolz Roman[1]
1- Department of physics, Federal University of Paraná (UFPR), Curitiba, PR, Brazil
julia.kezer@ufpr.br

Abstract - The fabrication of nanostructured devices by traditional deposition methods such as spin coating and drop casting, limits the possible active area of these devices. With the slot die deposition technique, it is possible to make much larger active areas than other coating techniques, in many different substrates, allowing printing polymer nanoparticles in a similar way to a roll-to-roll printer inside the laboratory, facilitating the industry scalability of these nanostructures devices. The main goal of this study was the production of donor and acceptor nanoparticles in a stable suspension in water, which is a non-toxic and not harmful to the environment solvent, synthesized by miniemulsion technique, obtaining an adequate dispersion for film depositions. Slot-die films both in glass and acetate substrates with superficial treatments were made for comparing the possibilities of transferring the technique to other types of flexible substrates in the future. The morphological study of the films showed that the slot die coating printing methodology successfully produced an homogeneous film of the smaller nanoparticles with diameters of approximately 30 nm both in acetate and glass substrates. The characterization of the P3HT and P3HT:PCBM nanoparticles were also made for confirming the nanostructure and charge transfer of these materials for further applications, such as in organic photovoltaics.

References -
1. M. J. Bassi, PhD. Thesis, Universidade Federal do Paraná, 2021
2. M. J. Bassi; L. Wouk; W. Renzi; C.K. Oliveira; J.L. Duarte; I.A. Heisler; L.S. Roman, *synthetic metals 2021, 275*, 116740, https://doi.org/10.1016/j.synthmet.2021.116740.

Keywords: *Polymer Nanoparticles, Slot die coating, Thin films*

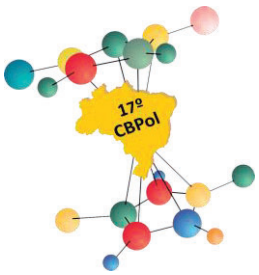

SYNTHESIS AND STABILIZATION OF SILVER NANOPARTICLES IN COPOLYMERIC MICELLES COMBINED WITH ROSE BENGAL COMBINED FOR PHOTODYNAMIC THERAPY

Heloisa D. Doring[1*], Yara S. Ricken[1], Camila F. de Freitas[1]

1 – Department of Chemistry, Federal University of Santa Catarina (UFSC), Florianópolis, SC, Brazil
**heloisa.diehl@grad.ufsc.br*

Abstract- Every year cancer statistics get even worse, being one of the main public health problems worldwide. In the face of this alarming situation, the development of new therapeutic modalities such as Photodynamic Therapy (PDT) has stood out in recent years as a promising alternative in the treatment of these malignant neoplasms[1]. In this study, Rose Bengal (RB) was used as a photosensitizer associated with silver nanoparticles (AgNPs) synthesized in the presence of the triblock copolymer Pluronic® F-127[2,3]. To obtain the nanostructured systems of F-127/AgNPs/RB, it is necessary to combine the solution of the silver nitrate precursor in the presence of a reducing/stabilizing agent, in this case, the F-127, which through the photoinduction process using a UV-LED (5 W of potency, λ_{max} of 370 nm) lead to the production of AgNPs. Finally, the photosensitizing drug, RB, was incorporated into the sample by the passive addition method. The samples were characterized by electronic absorption, fluorescence emission, and dynamic light scattering (DLS) spectroscopy. In general, the samples showed absorption bands and hydrodynamic diameter consistent with literature data, evidencing the formation of micelles incorporated with AgNPs and RB. Regarding the properties of the photosensitizer used, studies to determine the pKa were carried out to elucidate its protolytic equilibrium in micellar midea. The electronic absorption spectra were obtained in 40 solutions with different pH values and then a computational set (MASDA was used for the multivariate treatment of these data. Two pKa values were defined, 2.7 and 4.7, in addition to the protolytic and tautomeric equilibria of the RB. Thus, it was found that in the tests carried out, the predominant proteolytic species is the dianion, precisely the one that presents the highest molar absorptivity and, therefore, the best photophysical parameters. In this scenario, the results obtained so far demonstrate the project's promising character and its potential application in PDT.

References:

1. Correia, J.H.; Rodrigues, J.A.; Pimenta, S.; Dong, T.; Yang, Z. *Photodynamic Therapy Review: Principles, Photosensitizers, Applications, and Future Directions*. Pharmaceutics, v. 13, n. 3, 2021.
2. Sepulveda-Beltran, P.A.;Levine, H.; Altamirano, D.S et al.*Rose Bengal Photodynamic Antimicrobial Therapy: A Review of the Intermediate-Term Clinical and Surgical Outcomes*.American Journal of Ophthalmology, v. 243, p. 125-134, 2022.
3. Gomes,H.I.O.; Martins,C.S.M.; Prior,J.A.V. *Silver Nanoparticles as Carriers of Anticancer Drugs for Efficient Target Treatment of Cancer Cells*. Nanomaterials, v. 11, n. 4, p. 964, 2021.
4. De Freitas, Camila Fabiano et al. *Multivariate Analysis of Protolytic and Tautomeric Equilibria of Erythrosine B and its Ester Derivates in Ionic and Non-Ionic Micelles*. Journal of Molecular Liquids, v. 313, 2020.

Fundings: CAPES/CNPQ.
Keywords: *Cancer, Pluronic, Photodynamic Therapy, Drug Delivery, Singlet Oxygen*.

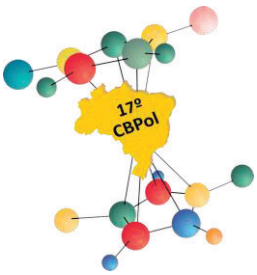

SYNTHESIS OF ALGINAT BEADS WITH FUNCTIONALIZED CLAYMINERAL APPLIED TO CHROMIUM REMOVAL

Julia G. Gomes de Souza[1*], Bluma G. Soares[2], Nathália Oliveira A. dos Anjos[2]

*1 – Federal University of Rio de Janeiro, Institute of Macromolecules, Laboratory of Polymeric Mixtures and Conducting Composites (IMA-LMPCC). *ju.gracielle@yahoo.com.br*
2 –Federal University of Rio de Janeiro, Alberto Luiz Coimbra Institute of Graduate Studies and Engineering Research, Metallurgical and Materials Engineering Program (PEMM/COPPE-UFRJ).

Abstract - Water contaminated with potentially toxic elements has highly damaging impacts on the ecosystem. Currently, chromium compounds have been identified as one of the most toxic pollutants to human health. In this work, alginate granules incorporated with clay mineral functionalized with ionic liquids were developed aiming at a promising application in the decontamination of water through the adsorption of Cr (III) and Cr (VI). The adsorbents were prepared based on sodium alginate (2%) and montmorillonite functionalized with chloro-methylimidazole (IL-CL) and zwitterionic (ZIL) ionic liquid (5%) or pure ionic liquids (30%), to improve their compatibility with metal ions. Despite the excellent adsorptive capacity, the direct application of clay minerals is complex, as the fine granulometry of the mineral is a limiting factor. Hence, the production of hydrogel granules as support generated with lyophilization is interesting for the formation of porous structures. The beads were characterized by Scanning electron microscopy (SEM) and Fourier transform infrared spectroscopy (FTIR). Preliminary adsorption tests were carried out in batches, evaluating the influence of effects such as temperature, pH of the medium and the amount of adsorbent on the removal of contaminants. The supernatant was analyzed by Atomic Absorption Spectrometry (AAS) to quantify the metal ion in solution. The characterizations could confirm the presence of pores in the samples and the incorporation of ionic liquids and montmorillonite in the produced beads. The adsorptive tests demonstrated that this material has potential for application in the removal of chromium, reaching an adsorption capacity of approximately 12 mg/g of active material, 25 times greater when compared to the use of pure alginate. The evaluation of the coadsorption of both substances are ongoing studies in this work, as well as the optimization of the adsorption process of a single substance seeking a better response in the adsorptive capacity of the materials.

References

1. J. A. Marins; B. G. Soares *Colloids and Surfaces* 2017, 529, 311319. https://doi.org/10.1016/j.colsurfa.2017.05.091
2. V. Gopalakannan; N. Viswanathan *International Journal of Biological Macromolecules* 2015, 72, 862867. https://doi.org/10.1016/j.ijbiomac.2014.09.024

Fundings: This study was financed in part by the Fundação Carlos Chagas Filho de Amparo à Pesquisa do Estado do Rio de Janeiro – Brasil (FAPERJ)
Keywords: *Alginate beads, Funcionalized claymineral, Ionic liquid, Adsorption, Chromium.*

SYNTHESIS OF POLYANILINE IN BACTERIAL CELLULOSE OBTAINED FROM KOMBUCHA TEA FERMENTATION

Karoline Gwiazdecki[1*], Ermerlinda Junkes[1], Marcia M. Meier[1], Andrea L. S. Schneider[2] and Carla Dalmolin[1]

1 – Department of Chemistry, Santa Catarina State University (UDESC), Joinville, SC, Brazil
karolgwiazdecki@gmail.com
2 – Universidade da Região de Joinville (Univille)

Abstract - Bacterial Cellulose (BC) has been getting much attention since last decade due to its numerous applications in polymer science, including as substrates for deposition of conducting polymers in order to improve their mechanical properties. Polyaniline (Pani) is one of the most popular conductive polymers with an easy synthesis and properties suitable for many electronic applications. However, its major disadvantages are the poor solubility and the infusible quality, which results in difficult processability and limits its practical applications. Composites with cellulosic materials and polyaniline (Pani) into the BC matrix have been studied as Pani electrodes in many applications, but the presence of an insulating network causes reduction in the conductivity values and the evaluation of electrochemical properties of the composites are difficult to explore. The main cause is that polyaniline synthesis occurs on the surface of the BC membrane and do not penetrate through all the membrane thickness, causing the formation of a 3D electrode with an inner insulating material that is resistive to current flow. In this work, we propose an easier synthesis of BC-Pani composites, using the well-known interfacial polymerization of aniline methodology, that promotes the polymer formation through all the high superficial area of BC by forcing monomer and oxidant to penetrate into the BC matrix by vacuum filtration. Infrared Spectroscopy (FT-IR) proved Pani formation and Scan Electron Microscopy showed it was deposited even in the inner surface of BC. This simple methodology produced a conductive membrane combining the mechanical properties of BC with the redox properties of polyaniline, which were observed by Cyclic Voltammetry and Electrochemical Impedance Spectroscospy.

Fundings: FAPESC.

Keywords: *polyaniline; bacterial cellulose; membranes; biopolymers*

THERMAL PROPERTIES CHARACTERIZATION OF PBAT NANOCOMPOSITES WITH GRAPHENE OXIDE AND CARBON BLACK

Patrícia M. S. Souza[1,2*], Karina L. F. Cardoso[1], Guilhermino J. M. Fechine[1,2]

1- School of Engineering, Mackenzie Presbyterian University, São Paulo, Brazil
2 - MackGraphe (Mackenzie Institute for Research in Graphene and Nanotechnologies), Mackenzie Presbyterian Institute, São Paulo, Brazil
** patriciasinohara@gmail.com*

Abstract –Nanocomposites of poly(butylene adipate-co-terephthalate)-PBAT and graphene oxide (GO) (0.05%, 0.1%, 0.25% and 0.50% in mass), aiming food packaging application, and nanocomposites based on PBAT, graphene oxide and carbon black (CB) (0.25% or 0.50% in mass of GO, with 1.5% of CB in mass), aiming mulch films application, were prepared by melt mixing using a extruder. The GO was obtained from exfoliation of graphite oxide (GrO) by an adapted Hummers method [1]. Raman analysis was conducted for GrO and for GO suspension. XRD GrO results indicated a peak of (002) plane at 2Θ = 10º (d spacing of 0.89 nm) due to the increase in planar spacing from graphite oxidation. TGA GrO results showed three mass loss stages: water elimination until 100ºC; removal of oxygen functional groups among 100 and 350 ºC; and oxidative pyrolysis of carbon framework [2], with mass loss of 14%, 42% and 29.5%, respectively. Raman analysis resulted in ratio I_D/I_G of 0.973 and 0.998 for GrO and GO, respectively, showing the presence of defects in their structure due to occurrence of oxidation [1]. The TGA results indicated that $T_{5\%}$ (temperature of 5% of mass loss) was at least 10ºC higher for most of the nanocomposites, in relation to the neat PBAT. The formulation with higher contents of GO and CB, presented $T_{5\%}$ of 356ºC, similar to neat PBAT (355ºC). The crystallization temperature (Tc) increased in the presence of CB, around 15ºC related to neat PBAT, indicating its influence as nucleating agent. In the second heating the melting temperature presented a small variation (121 to 126.6 ºC), and the crystallinity degree also varied in a small range (5.5 to 7.7%). In general, the results indicated improvement of thermal stability of nanocomposites with GO and CB related to neat PBAT, indicating its great potential for packaging and mulch films.

References

1. C.S. Andrade, A.P.S. Godoy, M.A.G. Benega, R.J.E. Andrade, R.C. Andrade, W.M. Silva, J.M. de O. Cremonezzi, W.A. de A. Macedo, P.L. Gastelois, H. Ribeiro, J. Taha-Tijerina *Nanomaterials* 2022, *261*, 1975. https://doi.org/10.3390/nano11081975.
2. P.L. Yap, S. Kabiri, S., D.N.H. Tran, D. Losic *ACS Applied materials & interfaces* 2019, 6, 6350. https://doi.org/10.1021/acsami.8b17131.

Fundings: FAPESP (grants 2022/06541-2 and 2022/07054-8)

Keywords: *PBAT, graphene oxide, carbon black, thermal properties*

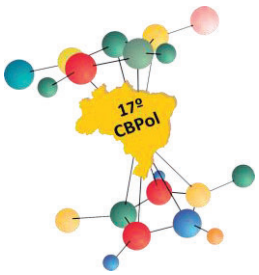

TITANIUM NANOPARTICLES ENCAPSULATED WITH ZWITTERION AND USE IN ELECTRORHEOLOGICAL FLUIDS

Keven Pimentel Delgiudice Gomes[1*], Jéssica Pereira S. da Silva[1] and Bluma Guenther Soares[1,2],

1 –Department of Materials Engineering Metallurgical and Materials (PEMM-COPPE)-Federal University of Rio de Janeiro, Rio de Janeiro, RJ, Brazil
pimenteldelgiudice@gmail.com
2- Institute of Macromolecules Professora Eloisa Mano (IMA), Federal University of Rio de Janeiro, Rio de Janeiro, RJ, Brazil

Abstract - Electrorheological (ER) fluids consists of a two-phase suspension, where phase-polarized particles are dispersed in an insulating medium such as silicone oil. When an external electric field is applied causing a rapid liquid−solid state transition and rapid increase of viscosity in the ER fluid [1-2]. After removing the electric field, the ER fluids return to their original liquid state. A variety of organic and inorganic materials have been used in ER fluids, such as silica, titanium dioxide (TiO_2) [3-4]. However, the performance of ER fluids depends on several factors, including the dielectric properties and polarizability of the particle. TiO_2 are promising for ER materials because they have high dielectric property and polarizability. However, the ER properties are poor and the polarizability limited due to the scarcity of active groups on its surface [4]. The objective of this work is to increase the polarizability of TiO_2 nanoparticles and thereby improve the ER effect. In this work, particles of titania encapsulated with imidazole sulfonate ionic liquid were prepared. The synthesis was performed using the sol gel method, using 1g of IL and 12g of titania tetrabutoxide. The ER fluids were prepared at 40% w/v, using silicone oil and with the aid of a sonicator for 20 min. The Electrorheological properties were evaluated as a function of the electric field, and a shear stress of 8.6Pa was observed for the sample with pure titania particle. The particle modified with zwitterion presented a shear stress of 645Pa. This result shows that the presence of ztwitterion imidazole sulfonate promoted an increase in polarity in the TiO_2 particle and consequently increased the ER response. Furthermore, the thermal properties were investigated through thermogravimetric analysis (TGA). The dielectric properties were also evaluated in order to investigate how this property influences the ER response. As well as Fourier transform infrared spectroscopy (FTIR) with the objective of showing the presence of functional groups that prove the encapsulation of the ztwitterion, the electrical conductivity and particle density were also evaluated.

References

1. **S. M.** Saabome; Y.S. Park; Y.G. Ko. Powder Technology, 2021, *394*, 986. https://doi.org/10.1016/j.powtec.2021.08.096
2. W. Sun , Y.Chen, H. Zheng , C. Li , B. Zhang , B. Wang , C. Hao, Z. Xing . Materials Chemistry and Physics, 2022, *282,* 125941 https://doi.org/10.1016/j.matchemphys.2022.125941
3. J.A. Marins, B. G. Soares, Colloids and Surfaces A, 2017, *529, 311.* http://dx.doi.org/10.1016/j.colsurfa.2017.05.091
4. Z. Zhao, Y.Yin, X. Jin, G. Zhang, L. Wang, Y.D. Liu, H. J. Choi. ACS Applied Nano Materials, 2021, *4,* 12382. https://doi.org/10.1021/acsanm.1c02835

Fundings: Faperj
Keywords: electrorheological fluids; titania particles; ionic liquid

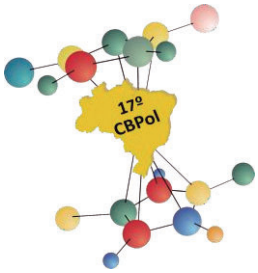

USE OF POLYSTYRENE/POLYPYROLE/ORGANOPHILIC MONTMORILLONITE MEMBRANE AS A HUMIDITY SENSOR

Eryca F. de Moura e Silva[1], Maurício F. de Aguiar[1], Mônica F. B. Rocha[1], Dáfenes B. R S. Silva[1], Andressa N. R. Leal[2],Celso P. de Melo[3] and Kleber G. B. Alves[1]*

1 – Department of Mechanical Engineering, Federal University of Pernambuco (UFPE), Recife, PE, Brazil
kleber.gbalves@ufpe.br
2 – Department of Chemical Engineering, Federal University of Pernambuco (UFPE), Recife, PE, Brazil
3 – Department of Physics, Federal University of Pernambuco (UFPE), Recife, PE, Brazil

Abstract – Conductive polymers have been the subject of research due to their highly attractive electronic, electrochemical, and optical properties. These polymers are used in different areas, such as energy conversion, energy storage, sensors, and adsorbents. Regarding the montmorillonite clays, they have a high capacity of exfoliation when placed in contact with water, which allows its modification by cation exchange, causing the change on its nature from hydrophilic to hydrophobic. In addition, quaternary ammonium salts are commonly used to change the polarity of clay, thereby increasing its affinity for organic components. In particular, polymer/clay nanocomposites have been extensively investigated in an attempt to establish how the clay can influence the polymers' properties. In addition, through the incorporation of conductive polymer, some of the clay's properties are improved, such as thermal, optical, solvent resistance, and flammability. In this sense, this work presents the synthesis and characterization of electrospun polystyrene (PS) membranes and their coating with polypyrrole (PPy) and organophilic montmorillonite (MMTO). Then, the PS/PPy/MMTO composite membrane was evaluated as a moisture sensor. O the characterization of the materials was carried out using X-ray diffraction (XRD) techniques, Fourier transform infrared (FTIR), ultraviolet-visible (UV-vis) absorption spectroscopy, contact angle and scanning electron microscopy (SEM). These techniques confirmed the montmorillonite organophilization process and its presence along the PPy in the composite membrane. Regarding the use of PS/PPy/MMTO as a humidity sensor, the analysis of changes in the electrical resistance of materials involves measurements with two probes. Therefore, the preliminary study showed that its detection properties increase with the addition of MMTO. Compost sensitivity increases from 105% to 497% after clay incorporation.

References

1. X. Guo; A. Facchetti. *Nature material*, 2020, 19, 922–928. https://doi.org/10.1038/s41563-020-0778-5.
2. Y. Zhu; J.O. Iroh; R. Rajagopolan; A. Aykanat; R. Vaia. *Energies*, 2022, 15, 1291. https://doi.org/10.3390/en15041291.
3. Y. Kang; C. Wang; C. Chen. *Journal of Applied Polymer Science*, 2022. 139, 23, 52323. https://doi.org/10.1002/app.52323.
4. G. M. Shabeeb; R. M. Abdullah, S. Nazar. *Journal of Nanostructures*, 2022, 12(4): 1086-1096. 10.22052/JNS.2022.04.029.

Keywords: *Nanocomposite. Montmorillonite clay. Conductive polymers. Gas sensor. Humidity sensor.*

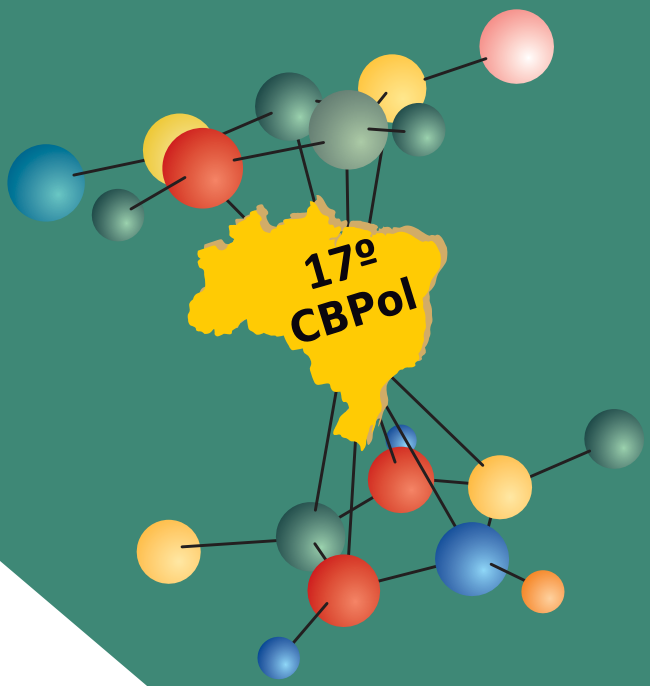

Blends, composites and polymer networks

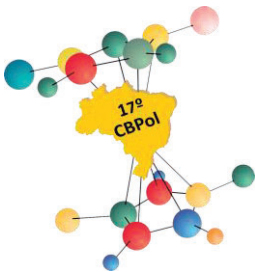

ALL-POLYSACCHARIDE *IN SITU* FORMING HYDROGEL OF CARBOXYMETHYL CHITOSAN AND ALDEHYDE-FUNCTIONALIZED HYDROXYETHYL CELLULOSE

Rafael F. N. Quadrado[1]*, Zhenghao Zhai[2], Kevin J. Edgar[2], André R. Fajardo[1]

1 – Laboratório de Compósitos e Materiais Poliméricos (LaCoPol), UFPel, Campus Capão do Leão, Pelotas, RS, Brazil
2 – Macromolecules Innovation Institute, Virginia Tech, Blacksburg, VA, USA.
(*) rafaelnq33@gmail.com

Abstract
In situ forming hydrogels have promise for many biomedical applications, especially for drug delivery. The hydrogel precursor solution can be injected at the target site, where it undergoes a sol-gel transition to afford a hydrogel. In this sense, the most important characteristic of these hydrogels is a fast gelation after application. We described herein an all-polysaccharide fast *in situ* forming hydrogel of carboxymethyl chitosan and a hydroxyethyl cellulose functionalized with aldehyde groups, which were appended by an acetal functionalization, followed by acid deprotection, thus, avoiding the breaking of the pyranose ring, as it would occur in periodate oxidation, the most common method to add aldehyde groups in polysaccharides. Through the simple mixing of the polysaccharide solutions, a fast gelation occurred, and an all-polysaccharide hydrogel was obtained after 1 min, indicating the potential use of this system as an *in situ* forming hydrogel.

Keywords: *In situ* forming hydrogel, fast gelation, polysaccharides.

Introduction

In situ forming hydrogels have promise for many biomedical applications, including tissue engineering, cell culture, wound healing, and drug delivery. For this type of hydrogel, the precursor solution can be injected at the target site, where it undergoes a sol-gel transition to afford a crosslinked hydrogel [1]. This feature allows the precise application of the hydrogel at the interest region, resulting in the local release of encapsulated bioactive compounds, and also permit the filling of irregular-shaped and deep lesion sites, as well as a better mouldability of the hydrogel to those sites, which improves its biocompatibility with the surrounding tissue [1]. On the other hand, the use of polysaccharides to prepare *in situ* forming hydrogels is very attractive due to their general non-toxicity, biocompatibility, biodegradability, and renewability [2]. In this context, hydroxyethyl cellulose (HEC) is an interesting polysaccharide derivative for the preparation of hydrogels due to its favorable mechanical and thermal properties, and water solubility [3]. Other interesting polysaccharide is carboxymethyl chitosan (CMCHT), obtained through the carboxymethylation of chitosan, since it has well-known bacteriostatic, hemostatic, and bioadhesive properties [2]. Herein, we selected these two polysaccharides to prepare an all-polysaccharide in situ forming hydrogel. To enable gelation, the HEC was functionalized with aldehyde groups, which reacted with the amine groups from CMCHT, forming imine bond crosslinks, and resulting in a hydrogel network. In this work, however, the aldehyde groups were not inserted into the HEC structure by common periodate oxidation, which would result in a significant DP loss, and a drop in the chemical stability of this polysaccharide derivative [2]. Instead, the aldehyde groups were appended in the HEC structure by

a two steps procedure. First, acetal moieties were introduced in the HEC, followed by an acid hydrolysis reaction to deprotect the aldehyde groups. Through this procedure, reactive aldehyde groups were appended in HEC without destroying its saccharide structure. We hypothesize that the aldehyde-functionalized HEC can be employed as a polysaccharide partner of CMCHT to prepare an all-polysaccharide hydrogel. We also hypothesize that the HEC-Ald and CMCHT solutions will quickly gel upon mixing, enabling *in situ* gelation of the resultant hydrogel.

Experimental

General procedure for the synthesis of the aldehyde-functionalized HEC

The synthesis of the aldehyde-functionalized HEC was executed in two steps, firstly appending acetal groups, which were deprotected by acid hydrolysis to afford the aldehyde groups. The **Scheme 1** summarized the experimental procedure employed. Briefly, to the HEC containing the acetal groups (labeled as HEC-Acetal), HEC (0.5 g) was dissolved in DMF (20 mL) for 2h at 60 ºC. After cooling, NaOH (1.95 g) was added into the system, which remained under vigorous stirring for 30 min. Afterwards, 2-chloroacetaldehyde dimethyl acetal (8 mL) was added drop-wise into the reaction flask. Finally, NaI (9 g) was added in the reaction flask, which remained under vigorous stirring for 48 h at 70 ºC under $N_{2(g)}$ atmosphere. The HEC-Acetal was recovered by extensive dialysis in water for 2 days, and subsequent freeze-drying. To convert the acetal groups to aldehydes, the HEC-Acetal (0.5 g) was dissolved in diluted HCl (0.2 M, 20 mL), and the resultant solution was stirred for 8 h at 80 ºC. Then, the solution was neutralized to pH 7 by adding some drops of a $NaHCO_3$ solution (5%-m/v). The neutralized was dialyzed against water for 2 days, and the aldehyde-functionalized HEC (denoted as HEC-Ald) was recovered by freeze-drying.

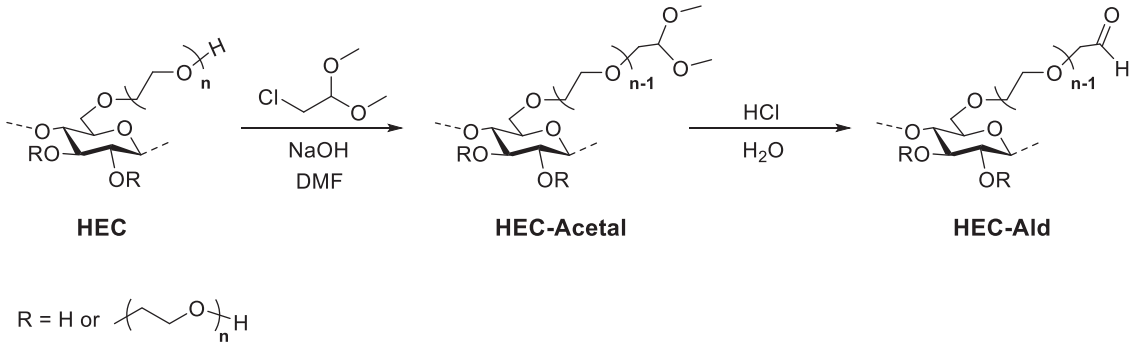

Scheme 1. Illustrative scheme for the synthesis of HEC-Ald. The structures drew were not meant to shown regioselectivity; they are depicted that way for clarity.

General procedure for the synthesis of carboxymethyl chitosan

The carboxymethyl chitosan (CMCHT) was prepared by reacting chitosan (deacetylation degree of 76%) with monocholoroacetic acid in the presence of NaOH. Briefly, chitosan (4 g) was dispersed in a mixture of isopropanol (32 mL) and distilled water (8 mL) under stirring for 2h at 50 ºC. Afterwards, monochloroacetic acid (6g) was dissolved in isopropanol (8 mL), and this solution was added in the reaction flask, which was stirred for 4 h at 50 ºC. The CMCHT was recovered precipitation after adding ethanol (200 mL) in the reaction flak. The precipitated CMCHT was separated by filtration, dialyzed against distilled water for 3 days, and freeze-dried. The DS(carboxymethyl) was estimated as 1.14, according to ^{1}H-NMR analysis (data not shown).

General procedure for the preparation of the HEC-Ald/CMCHT hydrogel

To prepare the hydrogel, certain amounts of HEC-Ald and CMCHT were dissolved in PBS (pH 7.4), and the resultant solutions was incubated at 37 ºC until gelation. Here, the total solid content of the hydrogels (5%, 10%, and 15%), and the HEC-Ald:CMCHT weight ratio (1:1, 5:1, and 1:5) were

varied to investigate the best conditions for the hydrogel preparation, which were defined as those conditions that resulted in a shorter gelation time.

Results and discussion

Synthesis of the aldehyde-functionalized HEC (HEC-Ald)

First, the HEC was functionalized with acetal moieties by reacting it with 2-chloroacetaldehyde dimethyl acetal through a simple etherification reaction (**Scheme 1**). In the presence of a base, the hydroxyl groups of HEC are deprotonated, being converted to the nucleophilic alkoxide groups, which displace the chloro atom from the 2-chloroacetaldehyde dimethyl acetal reagent following a nucleophilic substitution (SN2) mechanism. As a result, acetal moieties are introduced in the HEC structure. A summary of the experimental conditions tested for this reaction is shown in **Table 1**. Unfortunately, the reaction did not occur by simply reacting HEC with 2-chloroacetaldehyde dimethyl acetal in the presence of sodium hydroxide (NaOH) as base (**Table 1**, entry 1). Probably, under these conditions, a competing elimination reaction is favored instead of the nucleophilic substitution [4]. Considering that iodide (I^-) is a better leaving group than chloride (Cl^-), sodium iodide (NaI) was added into the reaction medium to generate in situ the 2-iodoacetaldehyde dimethyl acetal product in hopes of its capture by the alkoxide groups of HEC [5]. Upon addition of NaI (**Table 1**, entry 2) the reaction occurred, and the formed HEC-Acetal had a modest DS of 0.12, which was not increased by the addition of a higher amount of NaI (**Table 1**, entry 3). Replacing NaOH for sodium hydride (NaH), a stronger base with a higher potential to deprotonate the hydroxyl groups of HEC, decreased the DS of the obtained HEC-Acetal (Table 1, **entry 4**). This find indicates that the competing elimination reaction was favored in the presence of NaH. Increasing the quantity of 2-chloroacetaldehyde dimethyl acetal also reduced the DS of the obtained product (Table 1, **entry 5**), which suggest the feasibility of this reactant to the elimination pathway (i.e. the competing elimination of Cl^- is favored instead of its substitution by the alkoxide groups from HEC). Indeed, the reaction did not occur using a low amount of the acetal reagent (**Table 1**, entry 6). Likewise, when the amount of NaOH was reduced, in an attempt to reduce the alkalinity of the medium, and, thus, disfavor the elimination reaction, the reaction also did not occur (**Table 1**, entry 7). Performing the reaction for a longer time (96 h) also did not result in a higher DS (**Table 1**, entry 8).

Table 1. Experimental conditions employed in the synthesis of the HEC-Acetal.

Entry	Acetal reagent (equiv to –OH)	Base (equiv to –OH)	NaI (equiv to Acetal)	DS(Acetal)
1	15	10	–	–
2	15	10	1	0.12
3	15	10	2	0.12
4[a]	15	10	1	0.09
5	20	10	1	0.06
6	10	10	1	–
7	15	5	1	–
8[b]	15	10	1	0.12

[a]NaH was used as base.
[b]The reaction was performed for 96 h.

Therefore, after defining the best conditions for the synthesis of the HEC-Acetal (those described in the entry 1 of **Table 1**), the acid deprotection reaction of this derivative was optimized. All reactions were conducted in diluted HCl (0.2 M), however, time and temperature were varied, and the conversion efficiency was estimated from the reduction of the intensity of the acetal moiety signal in the respective ^{1}H-NMR spectrum of the obtained products. The deprotection was first

conducted at room temperature (~25 ºC) for 48 h, and only a conversion of 53% was achieved. Thus, the temperature was increased to 50 ºC, while reducing the reaction time to 24 h in order to avoid a significant drop in the DP and molecular weight of the product due to the acid hydrolysis of the glycosidic bonds. Again, only a low conversion efficiency of 50% was obtained in these conditions. However, when the temperature of the reaction was raised to 80 ºC, and the reaction time reduced to 8 h, a conversion efficiency of 100% was achieved. The complete conversion of the acetal groups to aldehydes in this conditions is evident from the analysis of the ^{1}H-NMR spectrum of the obtained product, which is shown in **Fig. 1**. As assessed, in the spectrum of the obtained HEC-Ald product, it is not possible to observe the signal from the methyl protons of the acetal moieties (at 3.50 ppm), while the signal from the hydrated form of the aldehyde groups is clearly observable (at 4.90 ppm) [1]. The molecular weight of this derivative was estimated by size exclusion chromatography (SEC). Expectedly, the molecular weight of the HEC-Ald was reduced in comparison to the starting HEC (from 105 kDa to 30.5 kDa). However, it is important to mention that the monosaccharide structure was not destroyed by this reaction, as it occurs in the common periodate oxidation, which also would induce a certain chemical instability to the polysaccharide derivative [2]. Moreover, a high conversion of the acetal groups to aldehyde is important for the further use of the HEC-Ald in the preparation of a hydrogel with CMCHT.

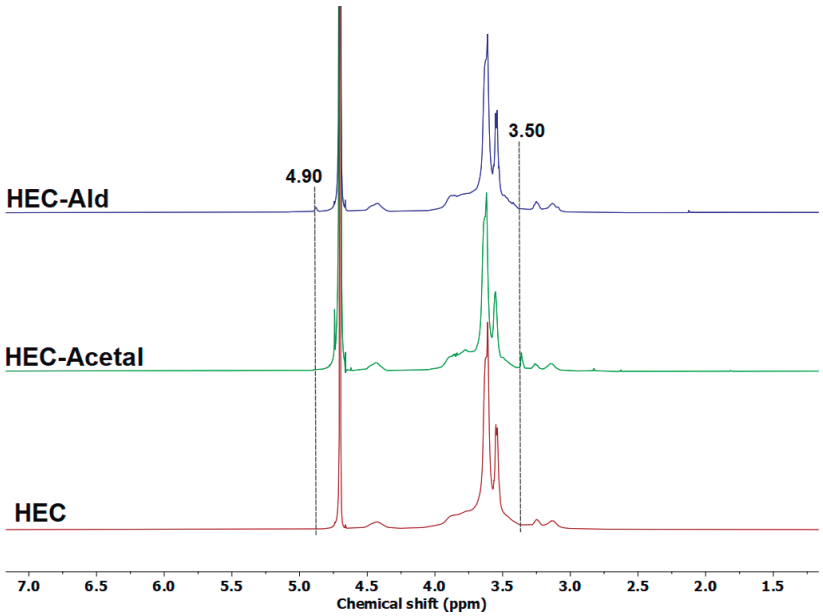

Figure 1. ^{1}H-NMR spectrum of HEC, HEC-Acetal, and HEC-Ald. D_2O was used as solvent.

Preparation of the HEC-Ald/CMCHT hydrogel

Supposedly, upon mixing, the HEC-Ald and CMCHT solutions undergo a sol-gel transition due to the reaction of the aldehyde groups with the amine groups, and the formation of imine bonds (C=N) between the polysaccharide chains. The formed imine bonds act as crosslinks of the hydrogel network. Typically, the formation of such bonds is a fast process, being attractive for the preparation of *in situ* forming hydrogels. Thus, to investigate the potential of HEC-Ald and CMCHT solutions as precursors of this type of hydrogel, the total solid content of the precursor solution, and the HEC-Ald:CMCHT weight ratio were varied. The results of these experiments are shown in the **Fig. 2**. The first important find is that the hydrogel was only formed in the presence of both HEC-Ald and CMCHT. A second relevant find is that the gelation process is faster as the amount of CMCHT increased. It is important to mention that a higher amount of CMCHT also means a higher quantity of amine groups (bottom of **Fig. 2**). Typically, the formation of imine bonds is boosted by an excess of amine [2]. Besides, considering that the amine groups from CMCHT have a limited nucleophilicity due to steric hindrance, an even higher amount of amine is

expected to be necessary for the imine bonds formation, which was the trend observed in the experiments. The gelation was also faster as the total solid content of the hydrogel precursor solution increased from 5% to 15% (w:w), likely due to additional hydrogen bonding and entanglements between the polysaccharides [3]. These additional interactions seemed to favor the imine bond formation, and boost the gelation process. Consequently, the hydrogel formulation with a total solid content of 15% (w:w), and a HEC-Ald/CMCHT weight ratio of 1:5 was able to form a hydrogel within 1 min. The gelation time range of this formulation is very attractive to prepare *in situ* forming hydrogels because the low-viscosity solution can be easily injected without needle-clogging, and gelling only at the target site. According to the results, by tailoring the solid content and weight ratio between the polysaccharides, an *in situ* forming hydrogel can be prepared by simple mixing of the HEC-Ald and CMCHT solutions.

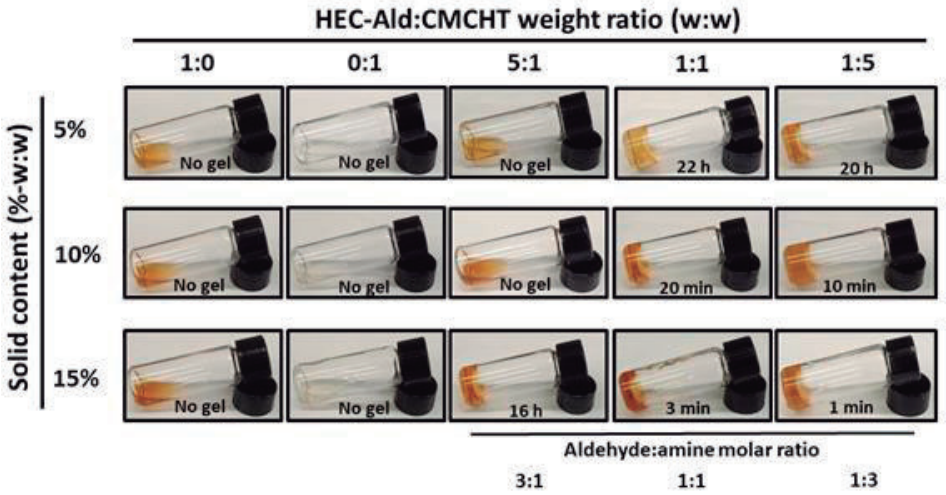

Figure 2. Summary of the experimental conditions tested for the hydrogel preparation.

Conclusion

In this study, we have successfully demonstrated the preparation of a potential all-polysaccharide *in situ* forming hydrogel of carboxymethyl chitosan (CMCHT) and an aldehyde-functionalized hydroxyethyl cellulose (HEC-Ald). The HEC-Ald derivative was prepared by appending acetal moieties into the HEC structure, followed by an acid deprotection reaction, affording the reactive aldehyde groups. Through this process, the destruction of the pyranose ring (i.e. monosaccharide structure) of HEC was avoided. Then, by simple mixing of the CMCHT and HEC-Ald solutions, a fast gelation occurred, and the hydrogel was obtained after 1 min, indicating its potential as an *in situ* forming hydrogel. The prepared hydrogel will be fully characterized in the future, where its spectroscopic and rheological properties, swelling and degradation behaviors, and potential use as drug carrier will be evaluated.

Acknowledgments

The authors thanks Braddy Hall (Virginia Tech) for the SEC analyses. R.F.N. Quadrado thanks CAPES (Brazil) for the PhD Sandwich Fellowship (PDSE, Process No. 88887.683320/2022-00).

References

1. R. Dimatteo, N. J. Darling, T. Segura, *Adv. Drug Deliv. Rev.* **127**, 167–184 (2018).
2. Y. Zhou *et al.*, *Carbohydr. Polym.* **300**, 120213 (2023).
3. H. Yin *et al.*, *Biomacromolecules*. **23**, 253–264 (2022).
4. M. Lachia, S. Iriart, M. Baalouch, A. De Mesmaeker, R. Beaudegnies, *Tetrahedron Lett.* **52**, 3219–3222 (2011).
5. C. Gao, S. Liu, K. J. Edgar, *Carbohydr. Polym.* **193**, 108–118 (2018).

ANTIMICROBIAL ACTIVE BIOCOMPOSITE USING PBAT, CACTUS FIBER AND CLOVE ESSENTIAL OIL

Gabrielly T. S. Vasconcelos[1], Michelle F. de Andrade[1], Ivo D. L. Silva[1], Viviane F. Caetano[1] Glória M. Vinhas[1], Yêda M. B. de Almeida*[1]

1 – Department of Chemical Engineering, University Federal of Pernambuco (UFPE), Recife, PE, Brazil
yeda.oliveira@ufpe.br

Abstract - The objective of this work was to produce and characterize active polymeric biocomposites using PBAT as a matrix, cactus fibers (CF) as a reinforcement material, and clove essential oil (CEO) as an active antimicrobial agent. 10 and 20% of fibers and 10% of CEO were used and the morphological, chemical, thermal, mechanical and antimicrobial properties were analyzed. By SEM, good adhesion was observed between the matrix and the fiber, by FTIR there was no chemical change due to the presence of the fiber and the appearance of a characteristic band of eugenol, indicating its incorporation in the composite. By TGA, a decrease in Tonset was observed with the addition of the CEO. The melting temperature remained close to that of pure PBAT. Stress at break decreased for all samples, with a significant increase in elastic modulus and a marked reduction in strain. Finally, the antimicrobial activity of CEO against E. coli and S. aureus bacteria was proven, and the antimicrobial potential of active films against E.coli bacteria was also verified. Thus, the composites have the potential for application in the food packaging industry, with the possibility of reducing the volume of PBAT by 20%.

Keywords: PBAT, cactus fiber, clove essential oil, antimicrobial composite.

Fundings: Capes - Coordenação de Aperfeiçoamento de Pessoal de Nível Superior. Facepe - Fundação de Amparo a Ciência e Tecnologia de PE

Introduction

A biocomposite consists of a composite material in which at least one of the constituents is a natural derivative, so its composition is quite diverse. The applicability of vegetable fibers in biocomposites has been studied, aiming to evaluate their influence on the material characteristics and viability for several applications, as well as mechanisms to improve their properties [1].

A high-value fiber can be extracted from the cactus, a species of the Cactaceae family and is characterized as a succulent plant abundant in arid and semi-arid regions of many countries, such as Brazil, Mexico, Bolivia, Argentina, the United States, Italy, Israel, and South Africa [2]. Its fibrous material, present in various parts of the plant, has the potential to act, for example, in composite materials [3].

Poly (butylene adipate co-terephthalate) (PBAT) is a versatile polymer that can be used with cactus fiber to produce biocomposites. PBAT was developed by the German company BASF in 1998 and is commercially known as ECOFLEX®, consists of a copolyester formed by monomeric units of 1,4-butanediol, terephthalic acid, and adipic acid is a biodegradable thermoplastic polymer that has excellent properties for packaging preparation, whose mechanical characteristics are similar to low-density polyethylene, in addition to being approved by Food and Drug Administration (FDA) [4].

An active biocomposite can be formed by inserting an antimicrobial agent such as clove essential oil. It is scientifically known as Syzigium aromatic, which is a vegetable with several medicinal properties, presenting a very specific aroma. The essential oil extracted from its leaves, flower buds and other parts of the plant has several constituents in its composition, which give it numerous properties, such as antimicrobial, anti-inflammatory, and antioxidant [5].
Thus, this work aimed to produce and characterize antimicrobial active biocomposites of PBAT reinforced with cactus fiber and added with clove essential oil as the active agent.

Experimental

Scanning Electron Microscopy (SEM)
The samples were fractured using liquid nitrogen and metalized with gold, at 5mA and 20 nm thick, for 2 minutes, in a Sanyu Electron equipment, model SC-701 Quick coater. Analyzed in a TESCAN MIRA3 microscope, with a high brightness FEG source and high vacuum at 10 V.

Fourier transform infrared spectroscopy (FTIR)
Samples were analyzed with Total Attenuated Reflectance (ATR) accessory in the region from 4000 cm^{-1} to 650 cm^{-1}, with 16 scans and 4 cm^{-1} resolution, on a Spectrum 400 spectrometer (Perkin Elmer)**.**

Thermogravimetric Analysis (TGA)
Performed in Mettler Toledo equipment, model 1STAR, and System, under nitrogen flow with a flow rate of 50 $mL.min^{-1}$. Measurements were recorded in the temperature range of 35 to 600 °C, at a heating rate of 20 °C.min-1, in alumina crucibles, with sample mass weighing between 3 and 10 mg.

Differential Scanning Calorimetry (DSC)
The DSC curves were obtained in the temperature range from 0 to 200 °C with a heating rate of 30 °C/min in the first heating stage and 10 °C/min for the second and third stages. Mettler Toledo equipment, model 1STAR, and System were used under a nitrogen atmosphere (50 $mL.min^{-1}$).

Tensile properties
*T*he elastic modulus, maximum tension at the break, and elongation at break were analyzed in an Emic Static Test Equipment, Trd 22 cell, a load of 500 N, and traction speed of 50 mm/min., at room temperature and without humidity control. The test was performed on 5 specimens (CP), for each composition, and their production was based on ASTM D638: 2014 CP type V.

Antimicrobial activity of CEO and composites
The antimicrobial activity of the essential oil was evaluated by the disk-diffusion technique in agar according to the methodology described by Silva et al., (2019) [6] using the microorganisms S. aureus and E. coli.
The antimicrobial activity of the composites was based on the methodology proposed by Dobre et al. (2012) [7].

Results and Discussion

The images obtained by SEM can be seen in Fig 1.

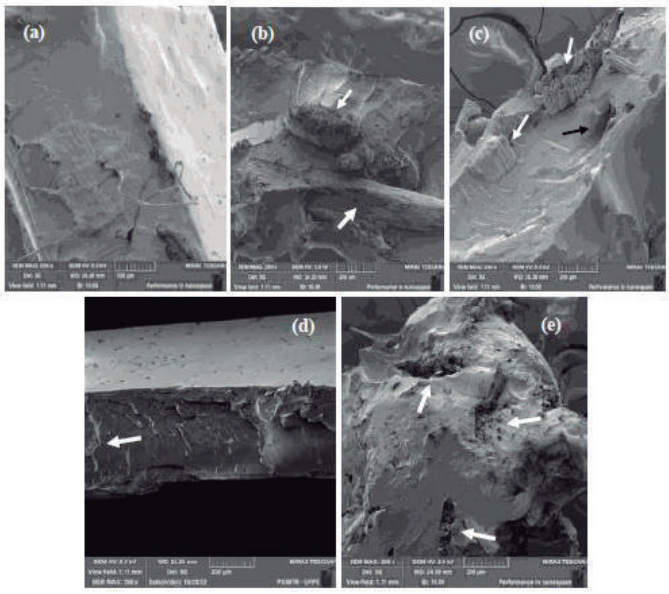

Fig 1. Cross-section morphology of PBAT and biocomposites.

For the PBAT, Fig 1 (a), a smooth and uniform surface can be observed, with the addition of 10% (Fig 6 (b)) and 20% of fibers (Fig 6 (c)) there is the appearance of a fiber agglomerate with the presence of porosities. This aspect may be indicative of a low chemical affinity between PBAT and fibers.

Similarities to the pure PBAT spectrum were observed in the infrared spectrum for composites with 10% and 20% cactus fibers. The appearance of broadband referring to the hydroxyl group at around 3340 cm^{-1}, which is found in abundance in vegetable fibers, becomes more visible, presenting itself as an indication of the presence of fibers in the samples [8]. Some peaks were also more intense, highlighting the regions at 1710 cm^{-1}, referring to the non-conjugated -C=O- stretching, and 726 cm^{-1}, referring to the rotation of the methylene group -CH_2.
For composites with CEO, a faint band appears at around 1509 to 1520 cm^{-1}, which may be indicative of the presence of CEO in the composites due to the presence of eugenol [9].

Tab. 1 shows the degradation temperatures of the samples.

Tab 1. Degradation temperatures obtained by TGA and DTG and results obtained by DSC

Samples	TGA		DSC		
	T_{onset} (°C)	$T_{max.deg}$ (°C)	T_c (°C)	T_m (°C)	X_c (%)
PBAT	376	416	76.69	120.83	16.29
PBAT/CF10	376	414	77.50	121.47	16.79
PBAT/CF20	374	415	79.00	122.09	17.47
PBAT/CF10/CEO	369	416	72.94	118.28	16.95
PBAT/CF20/CEO	367	414	75.56	118.70	17.20

Based on the values shown in Table 1, it can be seen that the degradation temperatures of the PBAT/CF10 and PBAT/CF120 composites remained close to the temperature of the PBAT since the temperature range for degradation of cactus fibers is around 350 °C [8].
For the composites incorporated with clove essential oil, a reduction in the values of T_{onset} can be seen, while T_{endset} and $T_{deg.max}$ remained constant. Indicating that the oil favored a reduction in the degradability of the composites, but did not change the final thermal stability.

By differential exploratory calorimetry (DSC) it is observed in Tab. 1 that the addition of fibers to PBAT favored an increase in T_m and T_c, while with the addition of CEO the opposite occurs, a reduction in these values. However, the Tm is still within the PBAT melting range. Regarding the degree of crystallinity, there is a slight increase for all composites, when compared to the pure polymer [10].

In the mechanical tensile test, stress at break, modulus of elasticity, and elongation at break were measured, whose values with their respective standard deviations are shown in Tab 2.

Tab 2. Tensile mechanical properties of PBAT and composite samples.

Samples	Stress at break (Mpa)	Modulus of elasticity (MPa)	Elongation at break (%)
PBAT	$12.43^{a} \pm 0.51$	$34.40^{a} \pm 0.56$	$774.47^{a} \pm 71.81$
PBAT/CF10	$9.41^{c} \pm 0.47$	$60.68^{b} \pm 3.45$	$243.55^{b} \pm 127.68$
PBAT/CF20	$8.55^{d} \pm 0.56$	$53.64^{c} \pm 4.36$	$421.03^{c} \pm 76.19$
PBAT/CF10/CEO	$9.30^{b,c} \pm 0.12$	$98.35^{d} \pm 5.92$	$104.21^{d} \pm 25.07$
PBAT/CF20/CEO	$8.74^{b,d} \pm 0.14$	$89.24^{e} \pm 4.34$	$72.80^{d} \pm 15.06$

It can be seen, from Tab 2, that the values for all properties studied varied significantly ($p<0.05$) with the increase in fiber concentration and with the incorporation of oil. It is estimated that the fiber reinforcement promoted a decrease in the tensile strength of the samples, gradually reducing the stress at rupture with the increase in fiber content, by up to 25%. Elongation at break also decreased significantly.
Regarding the CEO incorporation, there was an increase of up to 200% in PBAT, indicating that the presence of oil and fiber promoted an increase in the rigidity of the PBAT matrix.
Vegetable fibers, for example, are generally rigid materials, and therefore, their incorporation into the polymeric matrix should result in samples with a higher modulus of elasticity [11].
The addition of essential oils such as CEO has the characteristic of reducing the tensile strength and modulus of elasticity of the polymer [4].

The halo obtained by the disk-diffusion test can be seen in Fig. 2.

(a) (b)

Fig. 2 - Inhibition halos: (a) E. coli and (b) S. aureus

From the halo test (Fig. 2), it was possible to confirm the antimicrobial potential of the CEO. For E. coli bacteria, a halo of 6.50 ± 0.25 was obtained and for S. Aureus the halo was 6.25 ± 0.25. Clove oil showed inhibitory potential, but with resistance according to the National Committee for Clinical Laboratory Standards [12].
For the microbial analysis of the samples by measuring the absorbances, it was found that the medium containing only E. Coli showed a higher microbial growth when compared to the other samples. After 48 hours of incubation, the PBAT/CF10/CEO sample showed the lowest microbial

growth. The samples containing the fibers showed high microbial growth, higher than that observed for the PBAT. Indicating that the fibers can be a source of food for the analyzed bacteria. Thus, the antimicrobial potential was proven for the added samples.

Conclusions

It can be concluded that the addition of fibers did not change the thermal properties of PBAT, while the addition of CEO reduced the initial degradation temperature of PBAT, and increased Tm and Tc. There was a reduction in tensile strength and elongation, however, there was an increase in the stiffness of the samples with the addition of fibers. These characteristics were more accentuated by the presence of oil. In general, it is concluded that the development of a biocomposite using PBAT, cactus fiber, and clove essential oil is possible, but a better optimization of the number of fibers is necessary to improve the characteristics of the PBAT.

Acknowledgments

Capes - Coordenação de Aperfeiçoamento de Pessoal de Nível Superior. Facepe - Fundação de Amparo a Ciência e Tecnologia de PE

References

1. C. C. M. Fornari Junior, Fibras Vegetais Para Compósitos Poliméricos, Editus, Ilhéus, 2017.
2. Y. Mohamed-Yasseen; S. A. Barringer; W. E. Splittstoesser. Journal of Arid Environment, 1996, 32, 347–353. https://doi.org/10.1016/j.carbpol.2020.116178.
3. C. Sáenz; E. Sepúlveda; B. Matsuhiro. Journal of Arid Environments, 2004, 57. 275–290. https://doi.org/10.1016/S0140-1963(03)00106-X.
4. M. F. Andrade; I. D. L. Silva; G. A. Silva; P. V. D. Cavalcante, P. V. D.; T. F. Silva; Y. M. B. Almeida; G. M. Vinhas; L. H. Carvalho. LWT - Food Science and Technology, 2020, 125, 109148. https://doi.org/10.1016/j.lwt.2020.109148.
5. R.S. Affonso; M. N. Rennó; G. B. C. A. Slana; T.C.C. Franca. Revista Virtual de Química, 2012, 4, 146-161. https://doi: 10.5935/1984-6835.20120012.
6. A. J. Silva; L. P. Oliveira; J. C. P. Rezende; I. S. Saraiva. Sinapse Múltipla, 2019, 8, 33-40. http://periodicos.pucminas.br/index.php/sinapsemultipla.
7. L. Dobre; A. Stoica-Guzun; M. Stroescu; I. Jipa; T. Dobre; M. Ferdeş; Ş. Ciumpiliac. Chemical Papers, 2012, 66, 2, 144-151. https://doi.org/10.2478/s11696-011-0086-2
8. A.N. Balaji; K. J. Nagarajan. Carbohydrate Polymers, 2017, 174, 200-208. https://doi.org/10.1016/j.carbpol.2017.06.065.
9. J. C. C. Lima; J. C. N. Pereira; M. F. Andrade; G. S. Góis; I. T. A. Simões; M. A. A. D. Silva; Y. M. B. Almeida; G.M. VINHAS. Research, Society and Development, 2021, 10, 4, 1-14. DOI: http://dx.doi.org/10.33448/rsd-v10i4.14340.
10. K. Fukushima; W. Meng-Hsiu; S. Bocchini; A. Rasyida; M. Yang. Materials Science and Engineering: C, 2012, 32, 6, 1331‑1351. https://doi.org/10.1016/j.msec.2012.04.005
11. F. V. Ferreira; I. F. Pinheiro; M. Mariano; L. S. Cividane; J. C. M. Costa; N. R. Nascimento; S. P. R. Kimura; NETO, J. C. M.; L. M. F. Lona. Polymer Composites, 2019, 40, 3351-3360. https://doi.org/10.1002/pc.25196.
12. CLSI. 2018. *M02 Performance Standards for Antimicrobial Disk Susceptibility Tests***.** Clinical and Laboratory Standards Institute, 13th Edition.

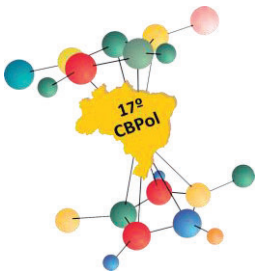

INFLUENCE OF COMPATIBILIZER AGENT ON THE PROPERTIES OF GREEN POLYETHYLENE COMPOSITES REINFORCED WITH BAMBOO FIBER

Mariane W. Bosenbecker[1], Eduarda V. Silva[1], Juliano Marini[2], Amanda D. de Oliveira[1]*

1 – Postgraduate Program in Materials Science and Engineering – PPGCEM/UFPEL - Rua Gomes Carneiro, Pelotas, RS, Brazil
2 – Department of Materials Engineering (DEMa), Federal University of São Carlos (UFSCar), São Carlos, SP, Brazil

Corresponding author: amandaoliveira82@gmail.com

Abstract

For polymer composites, a weak interfacial bond can cause problems during processing and affect the thermal properties of the resulting composites. A compatibilizing agent was used to address this limitation. To improve the interfacial bonding between bamboo fiber (BF) and low-density green polyethylene (LDBPE) matrix, polyethylene grafted with maleic anhydride (PE-g-MA) was employed. The composites were produced by the melt mixing method. Mass concentrations of 5 and 10% bamboo fiber and 3% maleic anhydride (AN) were applied. The composites were used in the form of pellets for the characterization of the material obtained. Through the results of the differential scanning calorimetry analysis it was possible to observe that the compatibilizing agent has a great influence on the thermal properties of the LDBPE composites.

Keywords: bamboo fiber, compatibilizing agent, composites, polyethylene grafted with maleic anhydride.

Introduction

Agroindustrial residues (coconut, rice husk, and sugarcane bagasse, among others), along with natural fibers, such as flax, jute, hemp, and sisal, are widely used as reinforcement in thermoplastic composites. In addition, other lignocellulosic fibers, such as bamboo, are being explored for this purpose. These fibers belong to an extensive botanical family, with several applications and uses [1,2].

Bamboo is known for its rapid renewal and growth can be used at an age of 3 to 4 years, compared to wood, bamboo can renew itself faster. It mainly consists of cellulose, lignin, and hemicellulose. Other constituents are protein, fat, pectin, tannins, pigments and ash [3]. The structural properties of bamboo based on the strength/specific mass and stiffness/specific mass ratios surpass those of wood and concrete and are even comparable to those of steel [4]. Bamboo has several applications in different sectors, including the manufacture of laminates, flooring, beams, plywood panels and other industrial products. However, bamboo processing results in a large amount of waste that could be recycled and reused, bringing additional economic and social benefits [5].

To improve the matrix-reinforcement interaction, compatibilizing agents that provide greater adhesion between the phases can be used. Polymers such as polyethylene have been modified with

maleic anhydride [6]. The use of maleic anhydride is a common method employed to address the lack of compatibility between the polymer matrix and plant fiber reinforced composites and chemically alter the resin by adding polar groups to the chain through grafting reaction with acrylic acid or AN. The effect on the incorporation of the reinforcement to the maleated polyethylene matrix can be understood by the esterification reaction, where hydrogen bridges of the cellulose interact with the AN to reduce the susceptibility of the material to moisture [7, 8].

In this context, this work aims to develop composites of low-density green polyethylene and bamboo fiber as reinforcement, initially evaluating different proportions of fiber addition in the composite and then using compatibilizer to evaluate the best interaction between fiber and polymer matrix.

Experimental

Materials

The collection of the raw material to obtain the bamboo fiber happened in a bamboo grove located in the countryside of Morro Redondo/RS. The polymer used was the low-density green polyethylene, known commercially as SLD4004 resin, which has a minimum content of 96% renewable source, determined according to ASTM D6866. Polyethylene grafted with maleic anhydride was used as a compatibilizing agent.

Preparation of the composites

To obtain the composite, the melt mixing method was used. For this, a single screw extruder was used, with a temperature profile of 140°, 145° and 150°C, corresponding to zones 1, 2 and 3, respectively. The composite materials were prepared with 5 and 10% by mass of bamboo fiber and 3% by mass of PE-g-MA.

Differential Scanning Calorimetry (DSC)

The differential scanning calorimetry (DSC) analysis was performed to investigate the melting temperature (T_m), crystallization temperature (T_c), and degree of crystallinity of the materials studied. An equipment from TA Instruments, model Q-1000, was used, with nitrogen as carrier gas, at a constant flow of 50 ml/min. The samples were initially heated from room temperature to 200 °C at a heating rate of 10 ºC/min, remaining at this temperature for 3 minutes. Afterwards were cooled down to 30 ºC at a rate of 10 ºC/min for the determination of the crystallization temperature (T_c) and again heated up to 200 °C at a rate of 10 ºC/min. The samples obtained after the extrusion process were analyzed. Crystallization and melting thermograms were recorded from the first cooling and second heating cycles. The crystallinity degree (X_c) of the studied materials was determined using Equation 1 [9]:

$$X_c = \frac{\Delta Hm}{\Delta H_m^0 (1-W)} * 100\% \quad \text{Eq. (1)}$$

Where ΔH_m is the experimentally obtained melting enthalpy, ΔH_0 the melting enthalpy of the hypothetical 100% crystalline LDPE (277.1 J/g) and Ø is the mass fraction of the reinforcement [9].

Results and Discussion

Differential Scanning Calorimetry (DSC)

Fig 1 shows the DSC thermograms of the cooling and second heating, respectively, of LDPE and composites. The corresponding values of melting temperature (T_m), melting enthalpy (ΔH_m), crystallization temperature (T_c), crystallization enthalpy (ΔH_c) are shown in Table 1.

Table 1 - Thermal parameters obtained from the DSC analysis.

Samples	T_m (°C)	T_c (°C)	ΔH_m (J/g)	ΔH_c (J/g)	X_c (%)
LDBPE	111.9	97.7	69.4	63.4	23.7
LDBPE/5%BF	112.1	97.3	63.6	61.0	22.8
LDBF/10%BF	112.2	97.3	61.4	57.8	23.3
LDBPE/5%BF/3%AN	112.5	96.8	63.4	59.3	22.7
LDBPE/10%BF/3%AN	111.3	97.6	64.3	66.5	24.4

The DSC thermograms showed only one endothermic and one exothermic transition and were also very similar to each other, which is a predominant characteristic of semicrystalline materials. An endothermic peak can be observed for the pure polymer at 111.9°C, which characterizes the melting temperature of LDBPE [10]. Overall, all samples showed T_c around 96-97°C and T_m of approximately 111-112°C regardless of the concentration of reinforcement used or whether it was modified by the addition of compatibilizer, indicating that the size distribution of the LDBPE crystallites was not considerably affected [11].

Referring to ΔH_m, a significant decrease in the enthalpy of the composites was observed when compared to the polymeric matrix pure. Besides, the ΔH_c also showed an decrease for the LDBPE/5%BF, LDBPE/10%BF and LDBPE/5%BF/3%AN composites compared to the polymeric matrix. When added different concentrations of fiber and 3%AN, it was found different behaviors in enthalpy values in relation to the matrix: while the use of 5%BF (LDBPE/5%BF/3%AN) was responsible for decreasing the enthalpy of crystallization, 10%BF (LDBPE/10%BF/3%AN) caused an increase in this value. In addition, the composites had a progressive decrease of Xc when compared with the LDBPE, with exception of the sample LDBPE/10%BF/3%AN.

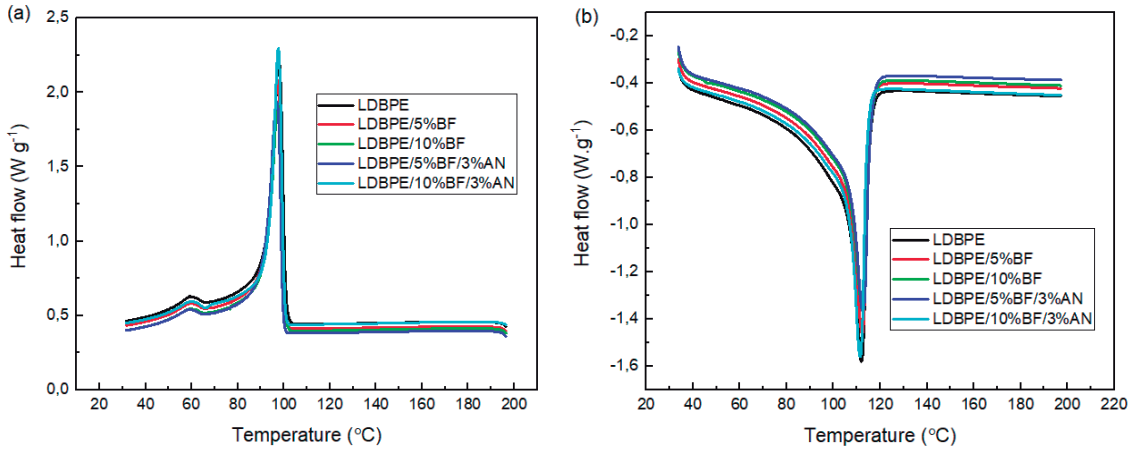

Figure 1 - DSC thermograms of LDBPE and composites: (a) cooling and (b) second heating.

Conclusions

Green polyethylene composites reinforced with bamboo fibers are a promising and sustainable material for various applications. Green polyethylene, produced from renewable sources, has a smaller carbon footprint than traditional polyethylene, making it an environmentally friendly choice. Apparently, the bamboo fiber does not alter the melting and crystallization temperatures of the composites in relation to the matrix, but reduces the degree of crystallinity. For the compatible samples, it can be concluded that the LDBPE/10%BF/3%AN composition presented a higher value in the degree of crystallinity, in relation to the pure polymer and in relation to the other composites.

References

[1] S. M, Rangappa et al. 2022. Lignocellulosic fiber reinforced composites: Progress, performance, properties, applications, and future perspectives. *Polymer Composites*, *43*(2), 645-691. https://doi.org/10.1002/pc.26413

[2] M. R. M Asyraf et al. 2022. Mechanical properties of oil palm fibre-reinforced polymer composites: A review. *Journal of Materials Research and Technology*, *17*, 33-65.https://doi.org/10.1016/j.jmrt.2021.12.122

[3] H. A, Khalil et al. 2012. Bamboo fibre reinforced biocomposites: A review. *Materials & Design*, *42*, 353-368. https://doi.org/10.1016/j.matdes.2012.06.015

[4] M. A dos Reis Pereira and T. Q. F Barata. 2015. Bamboo as sustainable material used in design and civil construction: species, management, characterization and applications. In *Key Engineering Materials* (Vol. 634, pp. 339-350). Trans Tech Publications Ltd. https://doi.org/10.4028/www.scientific.net/KEM.634.339

[5] C. H, Yeh and T. C, Yang. 2020. Utilization of waste bamboo fibers in thermoplastic composites: Influence of the chemical composition and thermal decomposition behavior. *Polymers*, *12*(3), 636.https://doi.org/10.3390/polym12030636

[6] O, Faruk, et al. 2014. Progress report on natural fiber reinforced composites. *Macromolecular Materials and Engineering*, *299*(1), 9-26.https://doi.org/10.1002/mame.201300008

[7] R, Maziero et al. 2019. Maleated polypropylene as coupling agent for polypropylene composites reinforced with eucalyptus and Pinus particles. *BioResources*, *14*(2), 4774-4791.http://ncsu.edu/bioresources

[8] L. D. P, Fajardo Cabrera de Lima et al. 2021. Use of organic acids in bamboo fiber-reinforced polypropylene composites: mechanical properties and interfacial morphology. *Polymers*, *13*(12), 2007. https://doi.org/10.3390/polym13122007

[9] S. V, Canevarolo Jr. 2006. Ciência dos Polímeros 2ª Edição. *Editora Artliber*.

[10] D, Oliveira de Castro et al. 2015. "Green polyethylene" and curauá cellulose nanocrystal based nanocomposites: effect of vegetable oils as coupling agent and processing technique. *Journal of Polymer Science Part B: Polymer Physics*, *53*(14), 1010-1019.https://doi.org/10.1002/polb.23729

[11] M, Guzman, M., and E. A, Murillo. 2015. The properties of blends of maleic-anhydride-grafted polyethylene and thermoplastic starch using hyperbranched polyester polyol as a plasticizer. *Polymer Engineering & Science*, *55*(11), 2526-2533.https://doi.org/10.1002/pen.24143

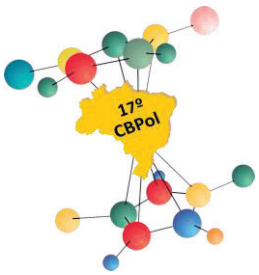

INVESTIGATION OF AGING IN EPOXY-MATRIX COMPOSITES

Ana Paula Cysne Barbosa[1]*

1 – Department of Materials Engineering, Federal University of Rio Grande do Norte, Natal-RN, Brazil
ana.cysne@ufrn.br

Abstract –
Epoxy matrix composites are widely used in applications in industry, including oil and gas, automotive, aeronautic and aerospace. Service conditions are various and environmental factors such as temperature, humidity, UV radiation or aggressive fluids may lead to the formation of microcracks and degradation of the polymeric matrix, which affect the properties of the composite. This work shows aging studies of epoxy-matrix composites, including observed chemical alterations and variations in mechanical properties of the composite material. The influence of different environmental agents on alterations of the epoxy matrix are discussed, along with changes in mechanical properties of the composite material. Investigations related to healing of composite materials with the addition of self-healing agents, which may potentially heal microcracks and extend service life of composite materials, are presented. Results show that the epoxy matrix is altered by environmental aging, with changes in mechanical properties of the composite. Planning of future studies related to aging of epoxy matrix composites are presented.

References (Times New Roman 10, bold) – Follow the examples in Times New Roman 10, single space line, justified paragraph, 1 column.

1. CYSNE BARBOSA, ANA P.; P. FULCO, ANA PAULA; S.S. GUERRA, ERICK ; K. ARAKAKI, FRANSCISCO ; TOSATTO, MÁRCIO ; B. COSTA, MARIA CAROLINA ; D. MELO, JOSÉ DANIEL . Accelerated aging effects on carbon fiber/epoxy composites. COMPOSITES PART B-ENGINEERING, v. 110, p. 298-306, 2017.
2. L. DA ROCHA, MIRELLA ; DE O. LEITE, MARAISA C. ; P. DA C. FERREIRA, EVANS ; D. MELO, JOSÉ D. ; C. BARBOSA, ANA PAULA . Accelerated aging effects in composites used as repair for pipes in oil industry. POLYMER COMPOSITES, v. 42, p. 5918-5929, 2021.
3. AZEVEDO DO NASCIMENTO, ALLANA ; TRAPPE, VOLKER ; DINIZ MELO, JOSÉ DANIEL ; CYSNE BARBOSA, ANA PAULA . Fatigue behavior of self-healing glass fiber/epoxy composites with addition of poly (ethylene-co-methacrylic acid) (EMAA). POLYMER TESTING, v. 117, p. 107863, 2023.
4. GUERRA, ÉRICK S.S. ; SILVA, BRUNA L. ; MELO, JOSÉ D.D. ; KALINKA, GERHARD ; BARBOSA, ANA P.C. . Microscale evaluation of epoxy matrix composites containing thermoplastic healing agent. COMPOSITES SCIENCE AND TECHNOLOGY, v. 232, p. 109843, 2023.
5. AZEVEDO DO NASCIMENTO, ALLANA ; FERNANDEZ, FERNANDO ; S. DA SILVA, FÁBIO ; P.C. FERREIRA, EVANS ; D. MELO, JOSÉ DANIEL ; CYSNE BARBOSA, ANA P. . Addition of poly (ethylene-co-methacrylic acid) (EMAA) as self-healing agent to carbon-epoxy composites. COMPOSITES PART A-APPLIED SCIENCE AND MANUFACTURING, v. 137, p. 106016, 2020.

Fundings: Financial support from Capes and CNPq is acknowledged.

Keywords: *epoxy, polymer matrix composites, aging, degradation, self-healing*

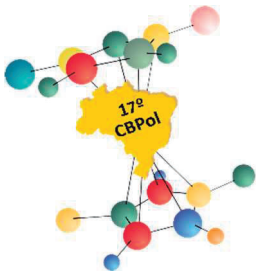

SYNERGISTIC EFFECT OF ADDING GRAPHENE NANOPLATES AND CARBON NANOTUBES IN PLA/PHBV BLENDS

Larissa Batista, Guilherme F. M. Morgado[1], Mirabel C. Rezende and Fabio R. Passador[1*]

1 – Polymer and Biopolymer Technology Laboratory (TecPBio), Federal University of São Paulo (UNIFESP), São José dos Campos, SP, Brazil
fabio.passador@unifesp.br

Abstract – The need to manufacture lighter vehicles, primarily targeting the new fleet of hybrid vehicles to be launched by 2030, has further motivated the automotive sector to invest in the development of composite materials [1]. The great world demand for composites in several sectors of the industry has resulted in the concern with sustainable routes for the return of the product to the production cycle, becoming an essential factor to make the use of this material feasible [2]. The main objective of this work is to study different techniques for recycling thermoset composite materials (carbon fiber/epoxy) from the production process of parts in the automotive sector. The composites were recycled using three routes: mechanical recycling (grinding), thermal recycling, and chemical recycling. Mechanical recycling resulted in a ground residue with the presence of particle agglomerates, with a mass loss of 3.4%, and the average size of the particles distributed between 3.5 and 4.5 mm. Thermal recycling was performed by pyrolysis in a tubular oven and it was carried out in times of 20, 45, and 60 min and resulted in clean carbon fibers in 60 min. Chemical recycling was performed with hydrogen peroxide (H_2O_2) and tartaric acid (TA) reagents in a 2:1 ratio (H_2O_2/TA) and resulted in fibers released after 180 min. The three routes studied are promising for the recovery of carbon fibers, which can be reused for the development of new composite materials.

References

1. Das, S., Warren, J., West, D., & Schexnayder, S. M. (2016). Global Carbon Fiber Composites Supply Chain Competitiveness Analysis. In Oak Ridge National Laboratory (Issue May). <https://www.nrel.gov/docs/fy16osti/66071.pdf%0Ahttp://www.osti.gov/servlets/purl/1333049/>.
2. Post, W., Susa, A., Blaauw, R., Molenveld, K., & Knoop, R. J. I. (2020). A Review on the Potential and Limitations of Recyclable Thermosets for Structural Applications. Polymer Reviews, 60(2), 359–388. https://doi.org/10.1080/15583724.2019.1673406.

Fundings: Federal Government Program 'Rota 2030', n° 27194.03.03/2020.01-00 for the financial support; the LEL/IPT for the coordination, and also FIPT, FUNDEP for the administrative support.

Keywords: *Recycling, carbon fiber, epoxy resin, thermoset composites, automotive sector.*

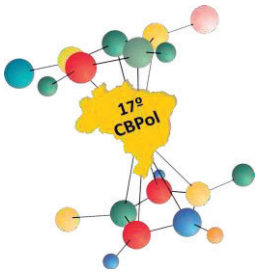

WOOD PLASTICS COMPOSITES BASED ON PVC REINFOCED WITH NATURAL FIBERS: COMMERCIAL APPLICATION S FOR PROFILES

Alcides Lopes Leao[1]*, Ivana Cesarino[1], Luis Guilherme L. Fernandes[1], Guilherme de Oliveira Martins[1]

1 – Department of Bioprocess and Biotechnology, São Paulo State University of (UNESP), Botucatu, SP, Brazil
alcides.leao@unesp.br

Abstract – The new paradigm in industry is preserving the environment and at the same time to be competitive and answer to emerging challenges for new materials. Natural fibers contributes to the development of natural products as those referred on this work. Thermoplastics composites, WPC, reinforced with several natural fibers and agro wastes were developed for structural applications, and with their properties depending mainly of the resin, additives, fillers and processing conditions. Troducts were fabricated at commercial scale in the company **Eko-Tech**, Botucatu, SP, using a conical extruder line. All the fibers were micronized and blended with PVC, additives and $CaCO_3$. WPC versus decking of natural wood proved to completely viable and even cheaper for the consumer, as it does not demand constant maintenance. Its durability and appearance over time collaborate to be a competitive product in the market. Its plea for non-deforestation (illegal wood), it also makes WPC a material with an environmental advantage. The waste utilization in its production also makes it a standard product of the circular economy model and biomass cascade use.

Fundings: This work is partially funded by FAPESP and by the company Eko-Tech Ltda.

Keywords: *circular economy, PVC, profiles, natural fibers, composites*

Introduction

As the name suggests, wood plastic composite (WPC) is a material created from a unique mixture of reforested wood (eucalyptus), various natural fibers (coir, pineapple, banana, sisal, bamboo, rice husk, etc.), additives and plastic resins (PVC, HDPE, PP or ABS). Worldwide, sawdust, cellulose, bamboo, peanut shells, various natural fibers and unused woodworking materials such as bark, shavings, are combined with plastic powder to form WPC, and this can even be recycled to create a new WPC, making WPC the best recyclable commodity.

WPC is an exciting material due to the fact that is created from a substance that starts out as a paste, it can be molded into virtually any shape and size, including arched or bent shapes. This innate flexibility also extends to color - WPC can be dyed or colored to suit virtually any design scheme. From a functional point of view, the natural fiber and plastic composite is moisture and rot resistant, which means it will aesthetically and fully last longer than regular wood. WPC is more heat resistant than regular wood, creating a product that can be used in places where regular wood can bend or warp. Also, can be used for a variety of construction projects in the same way as natural wood. Drilling, planning, sanding; everything is done as easily with WPC as with wood. Construction professionals may even find that wood fasteners such as nails and screws hold WPC better than regular wood. WPC is less likely to split or break when screws are used near the end of the planks, which can be a common problem when using real wood. WPC. It is a mixture of natural fibers, calcium carbonate and thermoplastic resins (PVC). Among its properties WPC profiles are

produced to resist weathering and exposure to UV rays, and also have the characteristic of being self-extinguishing in case of fire. It is a strong, high-quality flooring option, and can also be used for decks, railings, fences, pergolas, truck floors, pallets (PBR), landscaping, baseboards, skirting boards, frames, jambs, windows, doors, external or internal cladding, facades, to make door and window frames, furniture, etc.

Experimental

The products are prepared by the process of continuous extrusion, mixing the grounded fiber elements (rice husk or wood, inorganic fillers (calcium carbonate), plastic additives (flowing, stabilizers, etc., and heated thermoplastic resins, which are molded into the desired shape. Even recyclable thermoplastics can be used to prepare solid WPC. The option for PVC was due to several factors, including flammability, low carbon footprint, environment stability and cost.

The profiles were produced in a conical twin screw extruder, JWELL brand (126/60 mm), using a compounder. The tests follows the ASTM D7031-11 (ASTM, 2011) standard for WPC-based products. The resin used was from the company Braskem, SP 765 RA resin, with density 0.54 ±0.02 and particle size granulometry ≥250μm≤2% and ≥63μm≤95%. The natural fibers tested were micronized rice husk and sandpaper powder from Eucatex Company (Botucatu, SP). In all blends calcium carbonate is used. The blends tested are listed in **Table 1**. The additives are from the company Baerlocher.

Table 1. Blends compositions tested.

ITENS	**Treatment 1**		**Treatment 2**	
	PCR	**Mass %**	**PCR**	**Mass %**
PVC	100	50	100	50
Calcium carbonate	36.70	14.25	36.70	14.25
Rice husk	63.80	30	-	-
Wood powder (from MDF waste)	-	-	63.80	30
Baerlocher 1856	2.12	1	2.12	1
Baerlocher R531	4.24	2	4.24	2
Lubvin	0.64	0.3	0.64	0.3
Lubstab	4.24	2.0	4.24	2.0
Soyflex	0.32	0.15	0.32	0.15
Pigment (red and black)	0.64	0.3	0.64	0.3

The ductile properties of the composites were measured by a universal testing machine, brand Emic, model DL 3000. The blends produced were evaluated for their fluidity, in a flow index meter (MFI), brand Electra, according to the ASTM F1238 standard. Samples for flexural strength followed the ASTM D638-14 protocol, with a test speed of 50mm/min at room temperature and 50% relative humidity. Flexural properties were measured according to the ASTM D790-15Bprocedure, with a speed of 14mm/min, length of 52mm. The impact strength of the sample was measured in accordance with ASTM D256-10. Surface hardness was measured using a Zwick hardness tester, following the Shore D scale (ASTM D2240). All samples were packaged and labeled 48 hours before testing. For impact resistance, the tests were carried out in a Tinius Olsen impact analyzer, model 892, with a 6,779 J (5 ft.lb) pendulum at room temperature, following the standards for the Izod test (ASTM D-256- 97).

Results and Discussion

The testes for determination of physical-mechanical properties were carried out following ASTM (American Standard for Testing Materials) standards:

1. *Impact Resistance* - Izod impact resistance determination test carried out based on ASTM D256-

10 standard - Method A. Hammer used in the test with a capacity of 1J. Specimens obtained by

machining and conditioned 24 h after notching at 23±2ºC and 50±5% relative humidity. Test carried out on specimens without notch. The result obtained was reported when there was completebreakage with a mean of triplicates of 33.5 J/m, with a standard deviation of 4.21 J/m.
2. *Determination of Bending Properties* - Test carried out based on ASTM D 790-10 standard – Method A. Test specimens obtained by machining. Test speed 2.0 mm/min. Specimens conditioned at 23±2°C and 50±5 % relative humidity. Universal Testing Machine EMIC DL3000 with Class 1 load cell.
- Maximum Stress in Flexural, MPa 49.9
- Modulus of Elasticity, MPa 2128
3. *Determination of Water Absorption* - Test performed based on ASTM D570-98 standard. The specimens were immersed in distilled water for a period of 24 hours at room temperature. Test specimens in the form of plates obtained through a hot press (MH Equipments). Determination of Water Absorption, 1.2%
4. *Density Determination* - Test carried out following the ASTM D2395:2002 standard: 1.5 g/cm^3.
5. *Determination of water absorption and air humidity behavior* – Test carried out according to ASTM D1037:2006[a]. Result showing no effect or no or very low damage (just wets the surface).
6. *Weather and UV resistance UV chamber test*: the product surfaces treated with SayerlackPolisten deck varnish, formula designated for WPC, showed extremely high resistance.
7. *Skid resistance*: DIN 51097 standard - classification C (highest)
8. *Durability* (resistance to fungi that affect wood: The product was exposed at humid conditions (shower box) and showed no fungi attack or warping.
9. *Material weight*: The hollow decks weighed 2.533 kg/m (145 mm x 25 mm), which corresponds to 17.73 kg/m^2. The wainscoting was 1.17 kg/m linear. The rod was 2.15 kg/m linear. The benzene ring was 5.57 kg/m linear.

In **Figure 1, Figure 2 and Figure 3,** it is possible to observe the final products using the blends of PVC, calcium carbonate and rice husk**.**

Figure 1 – Dimensions: rod – 40 x 30 mm; beam – 90 x 40 mm; massive deck – 100 x 20 mm.

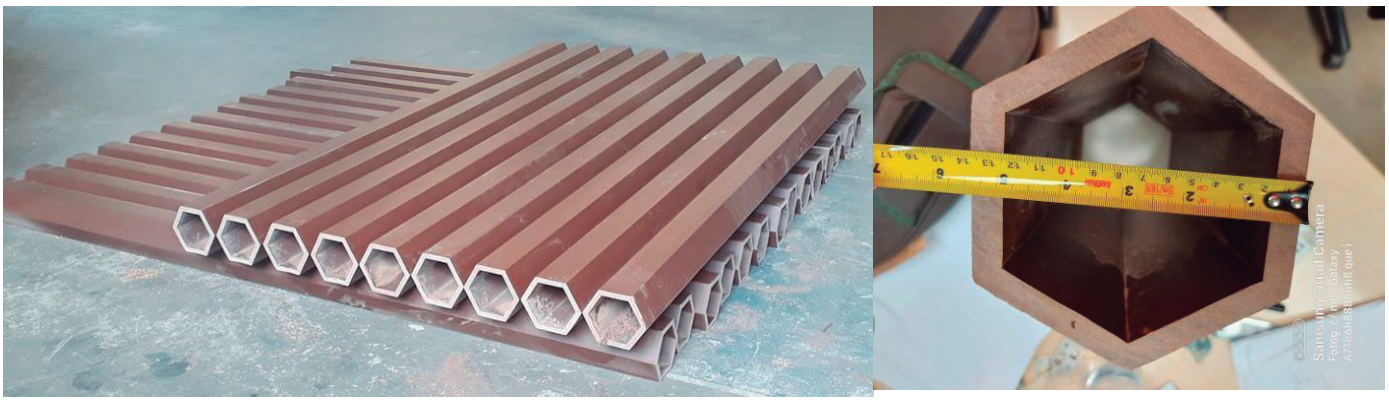

Figure 2 – Profiles for pergolas and fences (dimension: 140 mm external distance from each side).

Figure 3 – Use of WPC wainscoting with a typical composition.

Conclusions

The products developed showed in the present publication represents a category with many existing and emerging applications, varying from civil construction (structural and non-structural), automotive, airplanes, boats, etc. Although most of the WPCs are used for exterior decking and

other exterior board applications. It is a fast growing market in Europe, steady growth in USA and Canada, and an exponential growth in China and Southeast Asia. In our case, we consider not only the use of wood residues as reinforcement agent, but a whole set of natural fibers, such as coir, sisal, bamboo, rice husk, etc. The circular economy will pose an important role for the WPC market, since will reduce the pressure over the hardwood products, reduce the cost and weight and one of the most important one, to improve material properties such as strength and durability. Under the current pressure to reduce the fossil carbon footprint of the materials, natural fibers can offset the amount of non-renewable materials used in a product.

New developments will focus on improving material qualities, durability, low maintenance, cost and weight reduction, improve the perceptions amongst consumers. The incorporation of nanocellulose and biochar are the two goals for the present list of products available.

Acknowledgements

We are thankful to FAPESP (Process 2022/05306-0 for partially funding the project and the Eko-Tech Company Ltd., Botucatu, SP, for the commercial development of the product.

References

1. Carnietto, M. B. Dissertation. Análise de mercado de wood-plastic composite (WPC) no Brasil. UNESP. 2020.
2. Pickering, K. L. et al. A review of recent developments in natural fibre composites and their mechanical performance. Composites: Part A (2015), http://dx.doi.org/10.1016/j.compositesa.2015.08.038
3. Leao; A. L.; I, Cesarino; S. Narine; M. Sain. *Innovation Under the Bioeconomy Context in Brazil.* In: *Knowledge-Driven Developments in the Bioeconomy*. Andreas Pyka, Ed. Springer,pp. 97-116. 2017.
4. Mokhena, T. C. et al. Mechanical properties of fire retardant wood-plastic composites: Areview. Express Polymer Letters, vol. 15 Issue 8, pp. 744-780, 2021.
5. Minugu, O. P. et al. Effect of biomass derived biochar materials on mechanical properties of biochar epoxy composites. Journal of Mechanical Engineering Science, vol. 235(21), pp. 5626-5638, 2021.
6. Ogunsona, E. O.; Misra, M.; Mohanty, A. K. Impact of interfacial adhesion on the microstructure and property variations of biocarbons reinforced nylon 6 biocomposites. Composites Part A: Applied Science and Manufacturing, vol. 98:32- 44, 2017.
7. Qingfa, Z. et al. Mechanical properties of rice husk biochar reinforced high density polyethylene composites. Polymers, vol. 10, 286, 2018.
8. Quosai, P. et al. Characterization of biocarbon generated by high- and low-temperature pyrolysis of soy hulls and coffee chaff: for polymer composite applications. Royal. Society Open Science, vol. 5(8):171970, 2018.
9. Tadele, D. et al. A comparative life-cycle assessment of talc-and biochar-reinforced composites for lightweight automotive parts. Clean Technologies and Environmental Policy, 1-11, 2020.
10. Valavanidis, A. Concept and Practice of the Circular Economy Concept and Practice of the Circular Economy; Research Gate GmbH: Berlin, Germany, 2018.
11. Wang, X.; Yu, Z.; McDonald, A. G. Effect of different reinforcing fillers on properties, interfacial compatibility and weatherability of wood-plastic composites. J. Bionic Eng., vol. 16,pp. 337, 2019.
12. Schwarzkopf, M. J. & Burnard, M. D. Wood-Plastic Composites—Performance and Environmental Impacts. In: A. Kutnar and S. S. Muthu (eds.), Environmental Impacts of Traditional and Innovative Forest-based Bioproducts, Environmental Footprints and Eco-design of Products and Processes. Springer Science Media Singapore 2016.

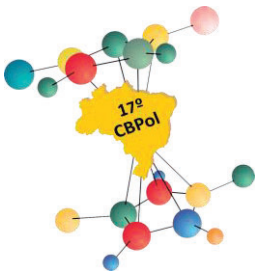

ARTESANAL HYBRID TECHNICAL TEXTILES REINFORCED POLYESTER COMPOSITES

Viviane M. Fonseca[1*]; Pedro T. Lima[2]; Ana L. Medeiros[1]; Erick J.P.A.Oliveira[1]; Laura H.Carvalho[3]; Alan J.L.Melo[4]

[1]Departamento de Engenharia têxtil – UFRN -Natal, RN, Brasil
[2] PPGET – UFRN - -Natal, RN, Brasil
[3]PGCEMAT- UFCG – Campina Grande, PB, Brasil
[4]IFRN – Caicó, RN, Brasil

viviane.muniz@ufrn.br

Abstract - This work developed technical fabrics for reinforcement in polyester matrix composites. The composites were tested under tensile stress and it was observed that the test direction influenced the mechanical performance of the composites. The use of hybrid fabrics kevlar/glass demonstrated to be a good alternative for the composites, particularly for the THA fabric.
Keywords: Kevlar; composites; hybrid fabric

Introduction

Composite material can be defined as the assembly of two or more materials, the resulting combination having properties superior to the properties of each of the constituent materials [1]. Fiber, yarn and fabric are some of the forms of reinforcement that are commonly applied to fiber reinforced composites and these forms have been widely applied, although when high performance technical textiles are used these materials exhibit high properties [2-]. Composite materials are a type of technical textile that is made by combining two or more materials to create a stronger, more durable product. The materials used in composite manufacturing can vary, but they typically include a combination of fibers, resins, and additives. This material can be customized to meet specific strength, weight, and performance requirements [6,7]. They are commonly used in aerospace, automotive, and marine applications, as well as in structural and architectural building designs [8-10].

A hybrid composite is a type of technical textile that is made from a combination of different materials, such as fibers, polymers, and metals. By combining multiple materials, hybrid composites can offer a unique combination of properties, such as high strength, durability, and thermal resistance. They are applied in a wide range of industries, including aerospace, defense, automotive, and marine applications and commonly used in structural engineering and building design, where they can provide increased strength and stability to structures [11;14].

Kevlar is a type of technical textile that is known for its exceptional strength and durability. It is made from a synthetic polymer called poly-paraphenylene terephthalamide (PPTA). The fibers are five times stronger than steel, making them ideal for use in a wide range of applications, including body armor, bulletproof vests, helmets, and various types of industrial equipment. These materials are lightweight and flexible, yet incredibly strong. Its unique properties are due to the way

the fibers are spun and woven together, creating a material that is resistant to cuts, abrasion, and impact. Kevlar is also resistant to heat, making it suitable for use in high-temperature environments. Kevlar reinforced composites are composite materials that use Kevlar fibers as reinforcement. Kevlar is a high-strength synthetic fiber that is commonly used in body armor, vehicle armor, and other applications where strength and durability are essential. When used as reinforcement in composites, Kevlar fibers provide added strength and stiffness to the material, making it more resistant to damage and deformation [1;3;5;9;10].

Hybrid fabric-based Kevlar is a type of Kevlar reinforced composite that uses a combination of Kevlar and other types of fibers to create a material with specific properties. By combining different types of fibers in this way, it is possible to create composites with a wide range of properties, making them suitable for many different applications [5].

Hybrid structures are made up of different materials that are combined in such a way as to take advantage of the individual properties of each of the components. In this way, it is possible to obtain materials with unique characteristics that are not present in pure materials. Another advantage of using hybrid structures is the possibility of reducing the costs of the production process, since less of the expensive noble metals are used to produce a particular material for a specific purpose. Therefore, the careful combination of these different components can lead to the development of new materials with better characteristics than their predecessors. This makes the use of these materials suitable in many advanced industrial applications where superior performance is required without dramatically increasing the cost of the final product [10-14].

Hybrid composites can show specific properties, depending on their composition and the structure of the reinforcement. Hybrid fabric reinforced composites exhibit high strength due to the combination of different reinforcing fibers. Because there are several types of fabrics available with varying fiber types or weaves that can be combined into hybrid laminates tailored towards specific requirements or environments [12-15].

Experimental

In this study, three composites were produced: Kevlar fabric reinforced isophthalic polyester resin (TA); hybrid kevlar fabrics reinforced isophthalic polyester resin (THV) and hybrid kevlar fabrics reinforced isophthalic polyester resin (THA). The composition of the fabrics was described in Table 1.

Table 1 – Technical sheet of fabrics.

Sample	Composition	Grammature (g/m^2)
TA	100% aramid	109
THV	65% aramid/ 35% glass fiber	80
THA	85% aramid/ 15% glass fiber	96

The composite was produced using compression molding. Laminate made of layers of biaxial fabrics produced using aramid fiber and development in laboratorial scale using handloom machine. The structure of the fabrics is plain weave. 6 Layers of fabrics are cutup with the mold dimensions (200x150 mm) and disposed in the mold. The isophthalic polyester resin RESAPOL LP 8847 is catalyzed using SUPERBUTANOX M50 0.05% v/v, octoate at 6% metal at a concentration of 0.02% v/v and DMA at a concentration of 0.01% v/v. The mold closed and the system pressed less than 5 ton for 12h at room temperature. The fiber content of the composites as around 24% (6 layers)

Tensile testing was carried using SHIMADZU AG-X 300 KN, at room temperature and 1 mm/min test speed and pre-tensile 1 Kgf, along the warp and weft direction out according to ASTM

D 3039 standards The fracture surfaces are evaluated using SEM SHIMADZU model VEGA3 LMU operating at 15 kV.

Results and Discussion

Based on the results of table 1, it is observed that despite the low reinforcement content of the composites, the use of the developed technical fabrics acted as a reinforcement element in the composites.

Comparing the results of the TA composites with the hybrid composites, THV and THA, it is observed that when tested in the warp direction the modulus is similar. This behavior is associated with the presence of aramid in the warp. However, for the THA composite tested in the warp direction when compared to the THV, the modulus was higher. This fact can be explained by the presence of aramid and glass in the weft of the THA fabric.

Table 2 – Tensile properties of the composites

COMPOSITE	s (MPa)	E(Mpa)	e (%)
Bare Resin	25±5	670±75	3,5±0,8
TA	221±10	4931±191	7±0,4
THV (weft direction)	207±14	4780±208	6,5±0,4
THV (warp direction)	69,4±4	2479±207	4,1±0,3
THA (weft direction)	214±20	4456±319	7,2±0,5
THA (warp direction)	112,7±12	3042±242	5,4±0,6

Figure 1 – SEM images of the fracture surface of isophthalic polyester resin A)500x B)800x

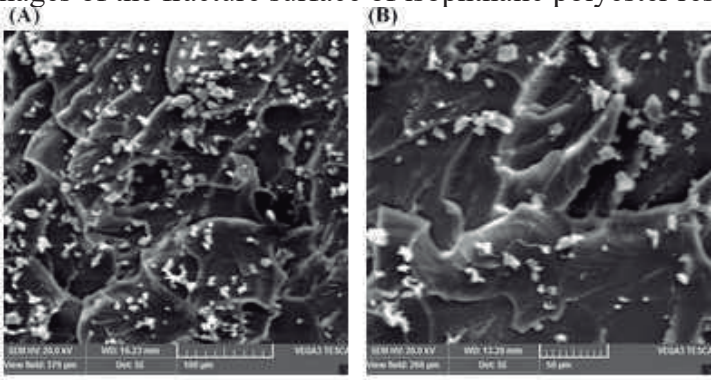

Figure 2 – SEM images of the fracture surface of TA composite (A) 500x; (B) 1250x

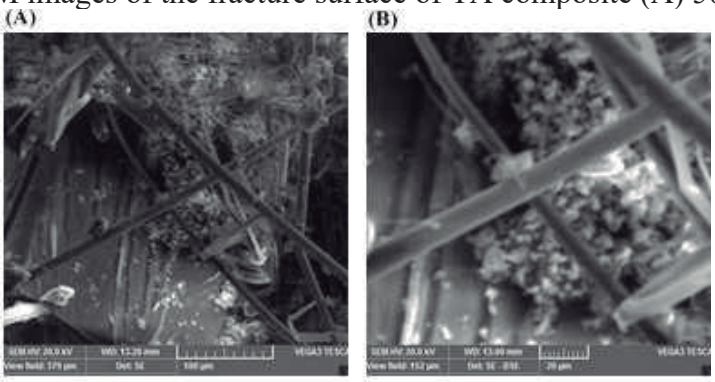

Figure 3 – SEM images of the fracture surface of THV composite tested in warp direction (A) 500x; (B) 700x

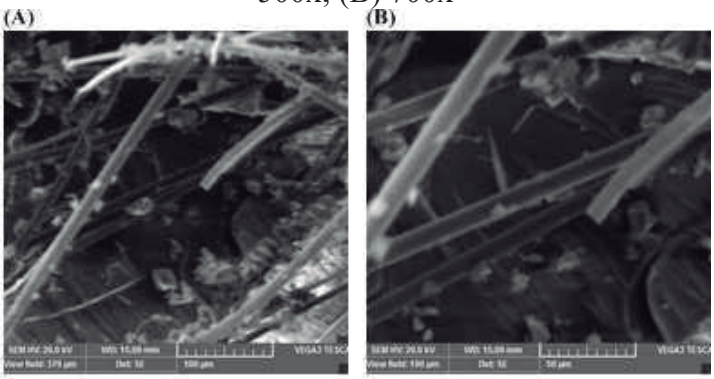

Figure 4 – SEM images of the fracture surface of THV composite tested in weft direction (A) 500x; (B) 700x

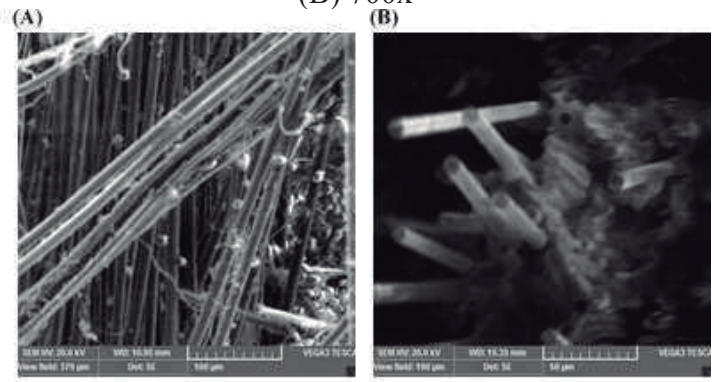

Figure 5 – SEM images of the fracture surface of THA composite tested in warp direction (A) 500x; (B) 700x

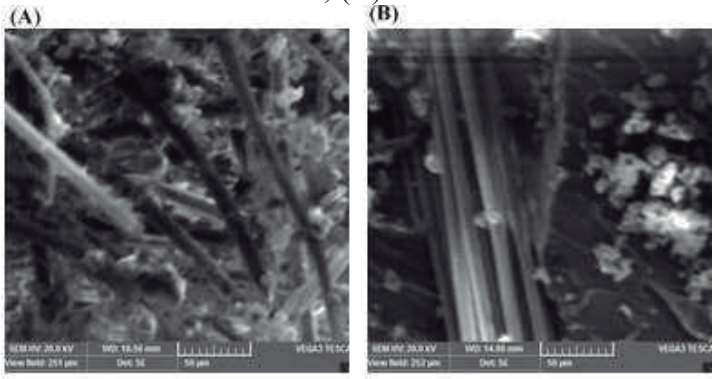

Figure 6 – SEM images of the fracture surface of THA composite tested in weft direction (A) 500x; (B) 700x

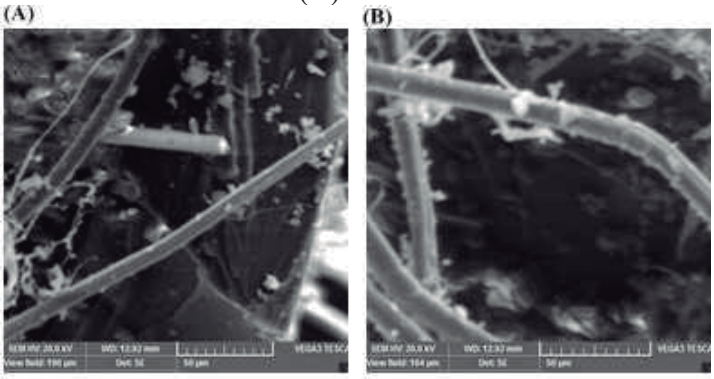

Conclusions

The technical fabrics produced were efficient as a reinforcement element.

The hybridization of the reinforcement structure becomes an alternative for composites in view of the stress request. Considering the use of glass fibers in the weft of the fabrics and combining with the aramid fiber, there is the possibility to produce soft composites with excellent mechanical performance.

References

1. R. Hsissou et al.; Polymer composite materials: A comprehensive review; *Composite Structures* 262; 113640; 2021
2. Holme; Adhesion to textile fibres and fabrics *International Journal of Adhesion & Adhesives* 19; 455 – 463; 1999
3. Manohar G. Kollegal and Srinivasan Sridharan; Strength Prediction of Plain Woven Fabrics; *Journal of Composite Materials*, 34(3), 2000, 240-257
4. M.I. Misnon et al.; Potentiality of utilising natural textile materials for engineering composites applications; *Materials and Design* 59; 359–368; 2014
5. S. Naik et al; A review on various aspects of Kevlar composites used in ballistic applications; *Materials Today: Proceedings* 21 1366–1374; 2020
6. Horrocks, A.R and Anand, S.C – *Handbook of Technical Textiles*; CRC Press 2000.
7. Reinhart,T.J.; "Introduction to Composites, in *Engineered Materials Handbook, Composites*", vol.1 - ASM International, Metals Park, EUA, 1987
8. Hufenbach, W.; Böhm, R.; Kroll, L.; Langkamp, A- "Theoretical and experimental investigation of anisotropic damage in textile reinforced composite structures*"*. *Mechanics of Composites* . 40 (6), 519-532; 2004.
9. H.L.Gower; D.S.Cronin; A.Plumtree - Ballistic impact response of laminated composite panels; International Journal of Impact Engineering; V35, Issue 9, 1000-1008; 2008,
10. R. Yahaya, S.M. Sapuan, M. Jawaid, Z. Leman, E.S. Zainudin; Mechanical performance of woven kenaf-Kevlar hybrid composites; J Reinforc Plast Compos, 33 (24), 2242-2254; 2014
11. N. Venkateshwaran, A. Elayaperumal, G.K. Sathiya; Prediction of tensile properties of hybrid-natural fiber composites; Composites Part B: Engineering, 43(2), 793-796, 2012
12. Harikrishna, M.; Ajeeth, K.; Ranganatha, S.; Thiagarajan, C. Fabrication and Mechanical Properties of Hybrid Natural Fiber Composites (Jute/Banana/Glass). Int. J. Pure Appl. Math., 119, 685–696; 2018.
13. CZP Júnior, LH De Carvalho, VM Fonseca, SN Monteiro, JRM d'Almeida, Analysis of the tensile strength of polyester/hybrid ramie–cotton fabric composites, Polymer Testing 23; 131–135; 2004
14. Amuthakkannan, P.; Manikandan, V.; Jappes, J.T.W.; Uthayakumar, M. Influence of stacking sequence on mechanical properties of basalt-jute fiber-reinforced polymer hybrid composites. J. Polym. Eng., 32, 547–554; 2012
15. Jang-Kyo Kim; Man LungSham; Impact and delamination failure of woven-fabric composites; Composites Science and Technology; 60 (5), 745-761; 2000

COMPARATIVE STUDY OF METHODS FOR PRODUCING STARCH/PVA BLEND FILMS BY CASTING

Helen Kotekewis[1]*, Ruth Marlene Campomanes Santana[1]

1 – Department of Materials Engineering, Federal University of Rio Grande do Sul (UFRGS), Porto Alegre, RS, Brazil
helen.kotekewis@gmail.com

Abstract - Thermoplastic starch is a natural biodegradable polymer with a capability to substitute petroleum based polymers in some applications. However, its high hydrophilicity results in limitations. The production of a blend with corn starch (CS) and polyvinyl alcohol (PVA), a synthetic polymer, could decrease the limitations of CS. Three methods were used to produce blend films (B) of CS/PVA with a 75/25 weight proportion. The first method started by mixing both polymers before the plasticizing of the CS. In the second method the PVA was added after the plasticizing. In the third method, the solubilization of the PVA and the plasticizing of CS were performed separately. Moisture absorption (MA) and contact angle (CA) characterizations had great results. MA was lowered in all of the blends compared to the CS film. The CA of the third blend film compared to the CS film was increased by 17%. All of the results showed that there are benefits to adding PVA to CS, especially with the third method.

Keywords: *biodegradable, starch, polyvinyl alcohol, blend, film.*

Introduction

The global impact of plastic waste has increased the search for alternatives in the industry. According to European Bioplastics, the biodegradable plastic market is expected to grow 12.6% in 2023 [1]. Many substitutions for biobased and biodegradable materials have been successful, but not all applications have suitable options of materials to reduce the pollution. The most common biodegradable polymers still have restrictions or disadvantages relating to properties, cost and large scale production.

Thermoplastic starch is a biodegradable and biobased source for polymeric material that has been largely studied to use as flexible packaging. Starch contains amylose and amylopectin that can be plasticized into a transparent film. It represents 29% of the studies on biodegradable films on Science Direct website (data found researching: “polymeric biodegradable films” and “polymeric biodegradable films starch”) [2]. The advantages of using starch are the low cost, multiple sources and easy processing into films. However, its high hydrophilicity results in poor mechanical properties of films produced with this material. It is necessary to use additives, nanofillers or to produce blends using synthetic polymers to improve those properties [3].

Polyvinyl alcohol (PVA) is a synthetic polymer which is also biodegradable and biobased. It is water soluble, which facilitates the production of miscible blends with starch by casting. The production of a blend with starch and PVA, could lower the water interaction properties of both polymers.

This study aims to produce and characterize starch/PVA blend films. The films will be produced by casting using 3 different methods. The goal is to improve properties and select an optimum method to produce such films to be used as flexible packaging.

Experimental

Materials

Corn starch (CS) was received from donation. Polyvinyl alcohol (PVA) was obtained from Dinâmica Química Contemporânea Ltda. The plasticizer, glycerol, was obtained from Vetec Química Fina Ltda.

Production of Films

The films were produced by casting method altering some of the process variables, resulting in 3 blends: B1, B2 and B3. All of the blends were made with CS (75%), PVA (25%), glycerol (33% w/w of CS) and distilled water.

The first method (B1) started by mixing corn CS and PVA with glycerol in distilled water. The solution was heated under stirring for 1 hour for the complete plasticizing of the starch. The second method (B2) consisted in the plasticizing of the starch for 30 minutes, with posterior addition of the PVA. The solution was stirred for another 30 minutes, maintaining the heat, until the total solubilization of the PVA. In the third method (B3), the plasticizing of the starch and the solubilization of the PVA were performed separately, during 30 minutes. Next, the PVA solution was added to the starch solution, then mixed with heat for 10 minutes.

In this study, all of the filmogenic solutions contained a volume of about 75-100 ml distributed in a 330 cm² silicone mold. The amount of polymeric materials (either CS, PVA or both) per film was 4 g. All of the methods used were followed by the evaporation of the solvent in an air circulating oven for 24 hours. After that, the films were peeled from de molds and placed in a silica desiccator until characterization tests. Similar methods were performed to the production of 100% CS and 100% PVA films.

Colorimetry

The optical and colorimetric analysis of the films was made by using a portable spectrophotometer (BYK), following the ASTM D2244-22 norm. The dimensionless parameters obtained were: luminosity (L*), color (a* and b*) and gloss (g). L* varies from white (100) to black (0). The color parameters vary from red (+a*) to green (-a*), and from yellow (+b*) to blue (-b*). And the gloss indicated whether there is more or less reflection of light on the surface of the film. Three measurements were made on each film composition against a white background.

Moisture Absorption

The moisture absorption of the films was measured through the ASTM D5229 method. The film samples were left in closed recipients with sodium chloride saturated saline solution, kept in an oven at 30°C with a relative humidity of 75%, according to the ASTM E104 - 02 norm. Each composition of film was tested with 5 samples.

Thickness

The thickness measurement of the films was done using a micrometer (Mainard, M-73010). Five measurements on 5 samples of each film composition were made.

Contact Angle and Surface Energy

The contact angle of the films was measured by Surftens 3.0 software using photos taken by a digital microscope with a magnification of 1,600 times. The photos were taken 1 second and 1 minute of residency on the films. The angles were measured of 10 drops of water and 10 drops of diiodomethane for every film composition. The surface energy was calculated by the Surftens 3.0 software.

Results and Discussion

The results of the characterization of the films will be used to compare the 3 methods for producing the blends, and to evaluate the effect of the PVA addition to CS. Fig 1 shows a comparison of the visual aspects of the 5 film compositions on different backgrounds. None of the samples seem to have any colors. PVA film is the most transparent film. B2 and B3 films are more translucent than the other films, especially B2. Fig 1 also shows that the blends have good miscibility, due to the fact that they have an homogeneous surface. The low standard deviation values of colorimetry and contact angle also confirm that.

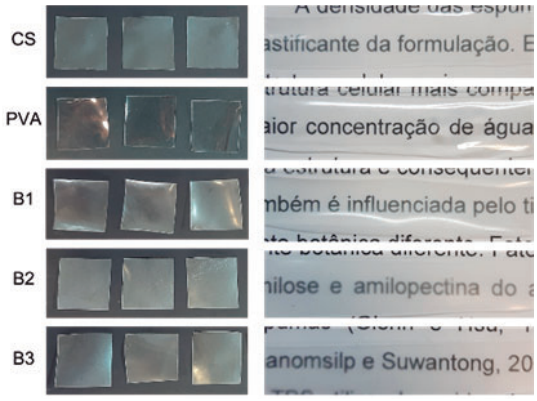

Figure 1 – Samples of the films on black background (left) and on written background (right).

The colorimetry parameters, at Table 1, confirm results previously discussed. The luminosity of the films decreased less than 1% in all of the blends compared to both CS and PVA films. An average of 89% means that the films are very close to the white background used in this test. The color parameters (a* and b*) revealed that the films have an inclination to shades of red and blue. The gloss has decreased on all of the blends, which can be observed as the translucency in Fig 1. The decreases were 2% for B1, 34% for B2 and 12% for B3, compared to the CS film. PVA film had double the gloss of CS film. The lowered gloss on the blend films indicates that a complex of PVA and starch was formed by hydrogen bonding, which reduces the transmittance of light, resulting in more translucent films compared to the transparent PVA film [4].

Table 1 – Colorimetry parameters of the films.

Film	L*	a*	b*	g
CS	89.65 ± 0.04	0.26 ± 0.02	-1.30 ± 0.05	60.87 ± 14.29
PVA	89.40 ± 0.25	0.45 ± 0.03	-1.52 ± 0.11	120.19 ± 7.42
B1	88.89 ± 0.22	0.29 ± 0.02	-1.21 ± 0.10	58.55 ± 4.17
B2	89.00 ± 0.09	0.21 ± 0.00	-1.09 ± 0.09	27.16 ± 1.14
B3	89.26 ± 0.03	0.31 ± 0.01	-1.31 ± 0.06	48.48 ± 4.63

Moisture absorption comparison is shown in Fig 2. All of the blends showed lower absorption, compared to the CS films (50.50%), especially the third blend, which had a 10% reduction. However, PVA film had the lowest absorption of moisture (25.87%), being the most hydrophobic composition. The explanation for the decrease of moisture absorption of the blends is that methyl groups substitute the hydroxyl groups of the amylose and amylopectin structures [5]. It is important to consider that the moisture and the water absorption of the films impact directly on

their biodegradation. The water is important because it allows the microorganism to grow. On the other hand, films with higher moisture content have lower mechanical properties, caused by an impact on the film's physical aspect, which can preclude the use as packaging material.

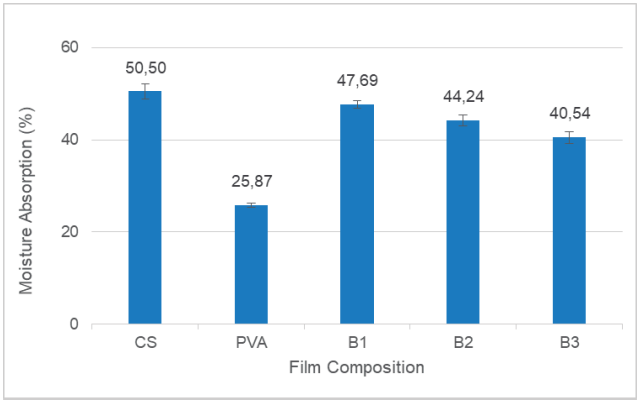

Figure 2 – Percentages of weight gained by moisture absorption of the films with 75% of relative humidity in 24 hours.

After 24 hours, the moisture absorption increased less than 5% for each film. This means that the highest absorption rate occurred within the first 24 hours.

The thickness of the blends were: 183 µm (B1), 164 µm (B2) and 129 µm (B3). The CS film had the lowest thickness (91 µm) and the PVA film had the highest (275 µm). B1 and PVA had the highest standard deviations. The moisture absorption can be related to the thickness of the films. Higher weight results in higher absorption. Amongst the blends, B1 had both the highest absorption and the highest thickness, followed by B2 and B3. The CS and PVA films showed opposite results. CS had the highest absorption with the lowest thickness, and PVA had the lowest absorption with the highest thickness. All of the films contained the same amount of polymeric materials (CS, PVA or both), however the volume of filmogenic solution per cm² can easily be controlled to manipulate the thickness of these films to decrease their moisture absorption.

The contact angle of the 3 blends compared to the CS film had increased, according to results in Fig 3. B1 increased 5%, B2 increased 4% and B3 increased 17% 1 second after the drop. B3 also had less than 2% difference of contact angle from the PVA film. Which means that the hydrophilicity of the third blend greatly increased with only 25% addition of PVA. The blends also had increases between 25 and 35% on the contact angle after 1 min of residency.

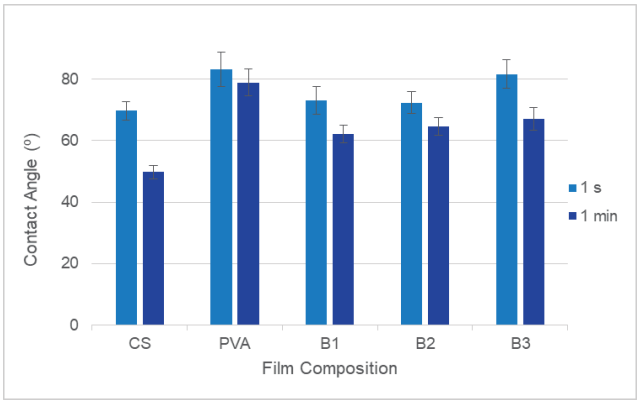

Figure 3 – Contact angles of the films with distilled water with one second and one minute of residency of the drops.

The number of polar groups directly affects the contact angle, because they create hydrogen bonds with water and increase the wettability of the surface [6]. It is noticeable that there are fewer hydroxyl groups on the blends than on the CS film.

To estimate the compatibility of the blends, the surface energy and the interfacial tension were calculated. Table 2 shows the surface energy data obtained by Surftens 3.0. Antonoff's method indicates that the interfacial tension is a subtraction of the surface energy of both polymeric films (CS and PVA) [7]. The results vary from 0.46 mJ/m² (1 s) to 10.82 mJ/m² (1 min), which concludes that the compatibility of the polymers is very high, resulting in highly miscible blends.

Table 2 – Polar (P), dispersive (D) and total (T) surface energy of the films in mJ/m² calculated with one second and one minute or residency of water and diiodomethane drops on the films.

Film	1 s			1 min		
	P	D	T	P	D	T
CS	9.79 ± 0.87	30.64 ± 1.10	40.43 ± 1.31	25.81 ± 1.56	25.62 ± 1.03	51.44 ± 1.60
PVA	3.65 ± 0.62	37.24 ± 1.71	40.89 ± 2,20	4.39 ± 1.01	36.23 ± 2.05	40.62 ± 1.87
B1	8.01 ± 1.82	31.45 ± 1.51	39.47 ± 2.17	16.01 ± 1.39	29.22 ± 1.42	45.22 ± 1.77
B2	7.21 ± 0.64	34.13 ± 0.50	41.34 ± 0.71	12.30 ± 1.10	31.14 ± 0.73	43.44 ± 0.67
B3	3.70 ± 0.97	34.51 ± 1.24	38.21 ± 1.24	11.13 ± 0.94	30.94 ± 1.26	42.08 ± 1.04

Conclusions

The process of producing starch/PVA blends by casting is very simple and shows remarkable results. The general aspect of the films were good, except for the gloss loss. Moisture absorption and water contact angle results showed a lower hydrophilicity of the blend films, compared to the CS film. Those results indicate an advantage of producing starch/PVA blends, especially because it only takes an addition of 25% of PVA to make such an improvement on the hygroscopicity of starch. The characterization results indicate that the blends are apparently miscible. The plasticizing and solubilization processes, when performed separately (B3), improved the properties of the blends.

Acknowledgements

To the Academic Excellence Program of the Higher Education Personnel Improvement Coordination (CAPES/PROEX) and to the Laboratory of Polymeric Materials at the Federal University of *Rio Grande do Sul* (LAPOL/UFRGS).

References

1. European Bioplastics, nova-Institute, 2022. https://www.european-bioplastics.org/market/
2. Science Direct. https://www.sciencedirect.com/. Access in: May, 3rd, 2023.
3. G. P. Singh et al. Polymers 2022, 14, 1987. https://doi.org/10.3390/polym14101987.
4. S. Masood et al. Journal of Polymer Research, 2022, 29, 528. https://doi.org/10.1007/s10965-022-03332-8.
5. Z. Guohua et al. Polymer Degradation and Stability, 2006, 91, 703-711. https://doi.org/10.1016/j.polymdegradstab.2005.06.008.
6. S. Patil et al. Food Bioscience, 2021, 44, 101352. https://doi.org/10.1016/j.fbio.2021.101352.
7. G. Biresaw; C. J. Carriere. Journal of Polymer Science, 2002, 40, 2248-2258. https://doi.org/10.1002/polb.10290.

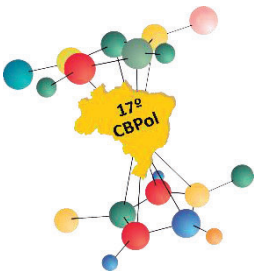

DIFFERENT MOLAR MASS OF PEG-B-PPG-B-PEG TRIBLOCK COPOLYMER: EFFECT ON THERMOSETTING SYSTEMS

Lohana V. Bataglini[1*], Rafaela F. Cossul[1], Luana Bettanin [1], Marlene Bampi[1], Marcia B. Schuster[1] and, Bruna L. Silva[2].

1 – Department of Food Engineering and Chemical Engineering, University of the State of Santa Catarina (UDESC), Pinhalzinho, SC, Brazil
lobataglini@gmail.com
2 – Multi-User Center, College of Technological Science, State University of Santa Catarina (UDESC), Joinville, SC, Brazil

Abstract – Copolymers have been presented as an alternative to increase the fracture toughness (K_{Ic}) of thermoset systems. In this work, epoxy matrix systems incorporated with Poly (ethylene glycol)-block-poly (propylene glycol)-block-poly (ethylene glycol) triblock copolymer (PEG-b-PPG-b-PEG) in different molar mass $\bar{M}n$ 4400 g/mol (BC44) or with 5800 g/mol - (BC58), both content 30% of PEG group in their structure, at concentrations 10, 20 and 30 wt. % were studied. At microscopy analysis, the samples with lower $\bar{M}n$ copolymer presented in fracture surface composed of self-assembled spherical/ellipsoidal domains, indicating phase separation. The glass transition temperature (Tg) reduced with increase of amount of block copolymer related to the epoxy matrix. The most evident reduction for the system with the highest $\bar{M}n$ copolymer and 30wt%. In the toughness test, the samples BC 44 showed the lowest values, and only with 10 wt.% of BC58 the K_{Ic} was higher than pure epoxy.
Keywords: *Triblock Copolymer; Toughness; Thermosets.*
Fundings: The authors would like to thank the financial resources provided by CNPq and FAPESC/PAP. (PROAP/AUXPE).

Introduction

High-performance thermosetting resins, such as epoxy resin based on bisphenol A diglycidyl ether (DEGEBA), are related to applications in science and several industrial sectors, mainly those related to engineering [1]. However, due to its brittle nature, this material has low fracture toughness compared to other engineering polymers, such as thermoplastics, since the crosslinked structure restricts molecular movement [2]. Based on this, incorporating triblock copolymers in epoxy systems has been presented as an alternative to improve fracture toughness [3,4]. On the other hand, studies have shown that adding block copolymers increased the system's mobility and decreased the glass transition of epoxy [5].

A large number of investigations have been carried out in the last two decades to obtain a better understanding of the behavior of thermoset systems modified by the addition of block copolymers [6-12]. Block copolymers are the focus of many research activities motivated by their intrinsic abilities to form micro or nanostructures [13].

Among the most investigated epoxy/copolymer systems are mixtures of epoxy with poly(ethylene oxide)-block-poly(propylene oxide) diblock copolymer (PEO-PPO) [14-16].The PEO block is mainly responsible for the physical interactions with epoxy-crosslinked aromatic amine [10, 16-18].The popularity of PEO and PPO block copolymers is due to their commercial availability, including

different proportions of each block, as well as the simplicity of the experimental procedure and the absence of any synthesis or chemical reaction with the system epoxy [12].
Silva et al (2018), studied the influence of adding triblock copolymer (PPG-PEG-PPG) to the epoxy. One of the copolymers contained 10% PEG while the other contained 50% PEG, the molar mass of both copolymers was similar. A miscible blend was obtained for 50% PEG and an immiscible blend for 10% PEG. The authors concluded that regardless of the position of the copolymer blocks, what influenced the miscibility of the systems was the fraction of PEG in the copolymer. Therefore, the objective of this work is to verify the influence of the molar mass of two PEG-b-PPG-b-PEG triblock copolymers on the thermal and mechanical properties of epoxy matrix systems.

Experimental Section
G*eneral Information*: For the matrix phase of the blends, the epoxy resin Bisphenol A diglycidyl ether (DEGEBA) was used, and the triblock copolymer Poly (ethylene glycol)-block-poly(propyleneglycol)-block-poly(ethylene glycol) (PEG-b-PPG-b-PEG $\bar{M}n$ 4400 g/mol (BC-44) and PEG -b-PPG-b-PEG, $\bar{M}n$ ~5800 g/mol (BC-58), both composed of 30% PEG block. Based on the company's Data Sheet, the copolymer with $\bar{M}n$ 4400 g/mol has a dynamic viscosity of 1,200 cP at 25°C and is in liquid form at room temperature [19]. Conversely, the copolymer with $\bar{M}n$ ~5800 g/mol is in a solid state at room temperature and has a dynamic viscosity of 350 cP at 60°C [20].
The hardening agent used for crosslinking the system was 4,4'- Diaminodiphenylmethane (MDA) ≥97.0% (GC)—All materials were obtained commercially from the company SIGMA – ALDRICH. Initially, resin and copolymers (10, 20 or 30 wt.%) were mixed for 10 min at 75 (± 5) °C in a digital magnetic stirrer for melt of resin, so as to the copolymer with higher molar mass. Then, the hardener (28.5 wt.% about the amount of epoxy) was added and mixed for 7 min. Subsequently, the mixture was poured into silicone molds, which were cured in an oven at 100 °C for 24 hours. A post-cure step was carried out in an oven for 1 h at 140 °C. The identification of the developed systems is represented in Table 1.

Table 1– Identification of the systems

	Copolymer					
Sample	PEG-b-PPG-b-PEG 4400 g/mol (BC44)			PEG-b-PPG-b-PEG 5800 g/mol (BC58)		
wt.%	10	20	30	10	20	30
BC44-10	x					
BC44-20		x				
BC44-30			x			
BC58-10				x		
BC58-20					x	
BC58-30						x

Characterization: The toughness test was carried out with SEBN (single-edge-notch bending) specimens, a 5 kN load cell, speed of 10 mm/min according to ASTM D5045. After the toughness test, the fractured region of the specimen was covered with gold and the scanning electron microscopy test (SEM-FEG) was performed. Differential scanning calorimetry (DSC) test was carried out under nitrogen atmosphere, with two heating cycles and one cooling cycle. The first heating was from 25 °C to 250 °C at a rate of 15 °C/min, followed by cooling from 250 °C to -75 °C at a rate of 10 °C/min. The second heating cycle was performed from -75 °C up to 250 °C, also at a rate of 10 °C/min.

Results and Discussion
Figure 1 (A) shows SEBN toughness samples, and (B, C and D) are FEG images of the fractured region. Through FESEM microscopy of the fracture surface, Fig 1B, C and D, the visual observations made on the samples in Fig. 1A can be confirmed. On the fracture surface, phase separation can be

observed in the samples with the lowest molar mass copolymer (BC44), where the sample containing 30 wt.% triblock copolymer with $\bar{M}n$ 4400 g/mol (BC44-30) presents BC self-assembled in spherical/ellipsoidal domains in the epoxy matrix, Fig.1C. In contrast, the sample containing 30 wt.% BC $\bar{M}n$ ~5800 g/mol (BC58-30) shows a homogeneous surface (Fig. 1D), with no visible phase separation, similar to the standard epoxy sample (Fig.1B).

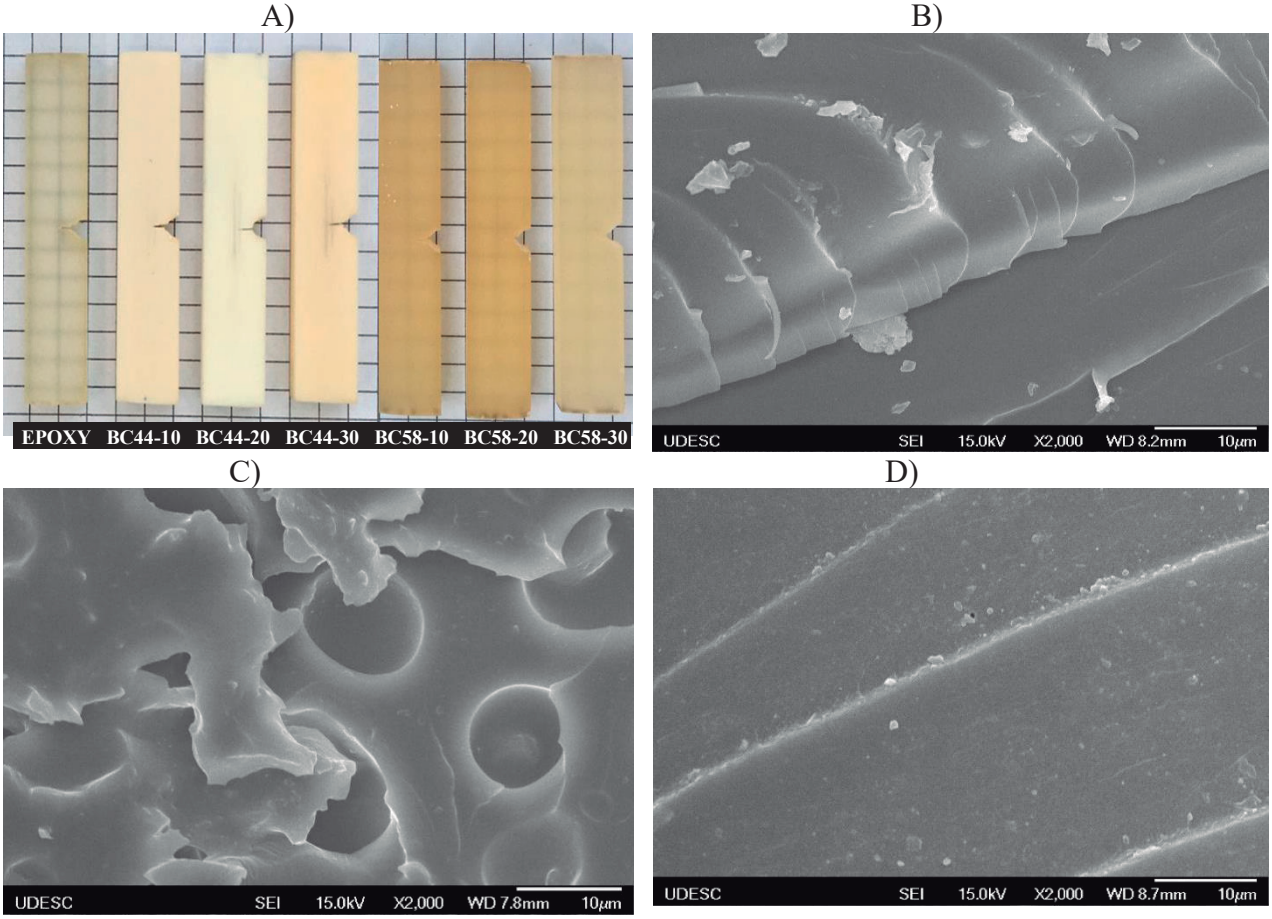

Figure 1 – Phase morphology A) cured samples; FESEM of B) EPOXY, C) BC44-30, D) BC58-30.

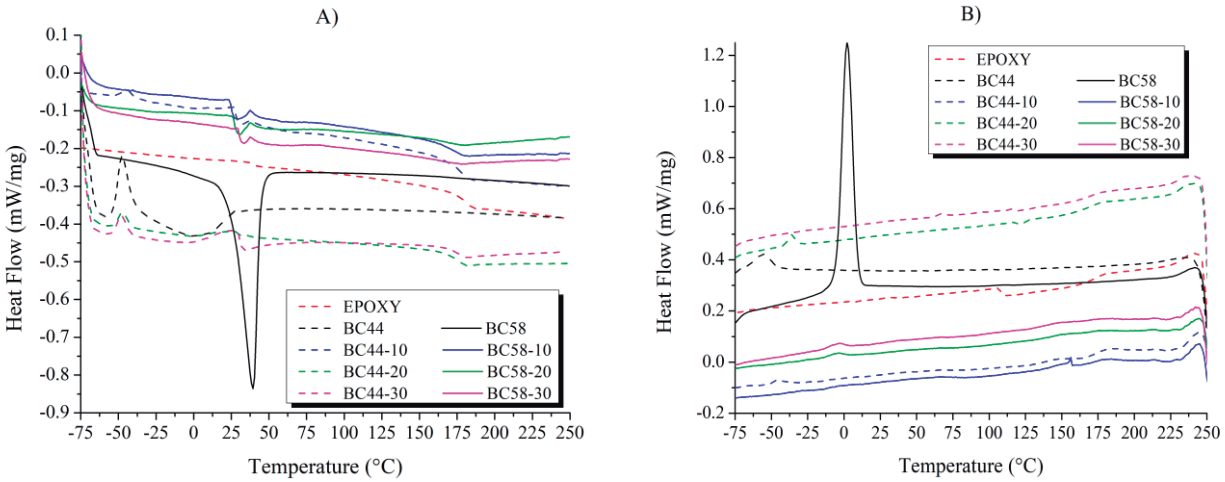

Figure 2 – DSC curves for A) Second Heating, B) First Cooling

From differential scanning calorimetry (DSC) (Fig. 2), it was observed that all samples containing wt.% of BC showed a decrease in the glass transition temperature (T_g) when compared to the sample containing only epoxy (Fig. 2A), which showed a T_g of 181 °C. This reduction can be associated with

repulsive interfacial interactions in systems with a change in mobility and systems with phase separation [21]. Increasing the amount of copolymer in the samples, the melting temperature (T_m) approached the value of the pure copolymer (Fig.2A). Though samples with BC58 did not show visible phase separation under microscopy, thermal events related to the copolymers in the system were observed, which indicates the possible formation of nanophases undetectable by FESEM [22]. Similar behavior was observed in the crystallization temperature (T_c) of the samples with BC58 (Fig.2B), except for the sample with 10 wt.%, which did not present the exothermic peak corresponding to the crystallization. This could be due to the low amount of BC in the matrix or partial miscibility of the copolymer in the matrix [5,23].

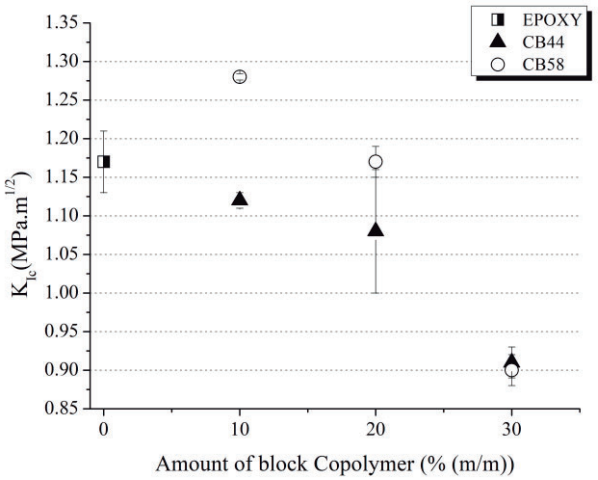

Figure 3 – Fracture Toughness.

From the toughness test (Fig.3), it was noted that all samples with BC44 showed a decrease in fracture toughness (K_{Ic}) about the standard epoxy sample, with the most significant reduction (23%) attributed to the sample with 30 wt.% BC. On the other hand, the sample with 10 wt.% BC58 showed an increase in K_{Ic} of 9%, which was expected considering that adding copolymers in thermosetting systems tends to increase the fracture toughness, because they can trigger mechanisms that absorb more energy [22, 24]. However, for the samples with 20 and 30 wt.% of BC58, this did not happen, with the sample with 20 wt. % BC presenting similar toughness to the system with pure epoxy, while for the sample with 30 wt.% BC, there was a reduction of 22%.

In addition, as both copolymers have a similar PEG-PPG structure, the increase in the amount of copolymers in the system may have led to saturation of the system, causing the PPG block to decrease the PEG/matrix interaction, causing an accumulation of internal stresses that favor early fracture of the system [5,25], which was more evident in the samples with lower molar mass copolymer.

Conclusions

In this work, two copolymers were presented, with identical block position and PEG fraction, differing only in molar mass and viscosity. Two distinct morphologies were obtained, one miscible and the other immiscible and/or partially miscible. As the difference in $\bar{M}n$ is small between the copolymers, the results suggest that the viscosity of the system interfered with the miscibility between the epoxy and the copolymer, where the copolymer with the lowest viscosity, CB58, at a mass fraction of 10% obtained increases of up to 9% in K_{Ic}.

Acknowledgements
Authors are grateful for the funding support from FAPESC – Brazil (PAP 2021TR854), CAPES - Brazil (PROAP/AUXPE) and Multi-User Facility infrastructure from Santa Catarina State University's Technological Sciences Center.

References

1. Q. Liu; X. Bao; S. Deng; X. Cai, Journal of Thermal Analysis and Calorimetry 2014, 118. https://doi.org/10.1007/s10973-014-4017-7.
2. L. Wang et al. Reactive and Functional Polymers 2022, 176, 105299. https://doi.org/10.1016/j.reactfunctpolym.2022.105299
3. D. B. Dwyer et al. Journal of Analytical and Applied Pyrolysis 2021,153,104978. https://doi.org/10.1016/j.jaap.2020.104978.
4. R. Pandita et al. Materialstoday: Proceedings 2020, 4. https://doi.org/10.1016/j.matpr.2020.05.398.
5. B. L. Silva; R. H. Bello; L. A. F. Coelho. Polymer International 2018, 67. https://doi.org/10.1002/pi.5633.
6. Q. Guo et al. Journal of Polymer Science Part B: Polymer Physics 2006, 44. https://doi.org/10.1002/polb.20747.
7. M. Larrañaga et al. Polymer 2005, 46. https://doi.org/10.1016/j.polymer.2005.05.102
8. J. M. Dean et al. Journal of Polymer Science Part B: Polymer Physics 2001, 39. https://doi.org/10.1002/polb.10062.
9. S. Ritzenthaler et al. Macromolecules 2002, 35. https://doi.org/10.1021/ma0121868.
10. E. Serrano et al. Macromolecular Rapid Communications 2005, 26. https://doi.org/10.1002/marc.200500131.
11. Q. Guo et al. Macromolecules 2003, 36. https://doi.org/10.1021/ma0340154.
12. M. Martin-Gallego et al. Composit Part A 2015, 71. https://doi.org/10.1016/j.compositesa.2015.01.010
13. A. V. Ruzette; L. Leibler. Nature Materials 2005, 4. https://doi.org/10.1038/nmat1295.
14. S. M. George at al. Industrial Engineering Chemistry Research 2013, 52. https://doi.org/10.1021/ie400813v.
15. R. Pandit et al. Nepal Journal of Science and Technology *2012, 13.* https://doi.org/10.3126/njst.v13i1.7445.
16. J. P. Pascault; R. J. J. Williams. Epoxy polymers: new materials and innovatiom. 1 Ed. Weinheim: Wiley-VCH, 2010. 1-12.
17. T. Wang et al. High Performance Polymers 2014, 27. https://doi.org/10.1177/0954008314542473.
18. M. Larrañaga et al. Polymer International, 2007, 56. https://doi.org/10.1002/pi.2289.
19. SIGMA-ALDRICH. "*Material Safety Data sheet",* available at: https://www.sigmaaldrich.com/BR/pt/product/aldrich/435457.
20. SIGMA-ALDRICH. "*Material Safety Data sheet",* available at: https://www.sigmaaldrich.com/BR/pt/product/aldrich/435465.
21. K. W. Putz et al. Macromolecules 2008, 41. https://doi.org/10.1021/ma800830p.
22. B. J. Cardwell; A. F. Yee. Journal of Materials Science 1998, 33. https://doi.org/10.1023/A:1004427123388.
23. X. L. Jiang; Y. Fan. Journal of Applied Polymer Science, 2011. 124. https://doi.org/10.1002/app.35307.
24. S. Balakrishnan; P. R. Start; D. Raghavan; S. D. Hudson. Polymer 2006,46. https://doi.org/10.1016/j.polímero.2005.10.053.
25. M. Larrañaga et al. Polymer International, 2004, 53. https://doi.org/10.1002/pi.1574.

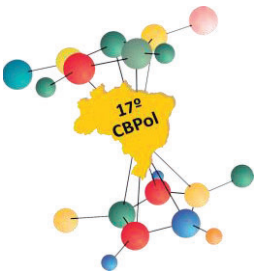

EFFECT OF pH ON THE ADSORPTION OF METHYLENE BLUE IN PECTIN/MONTMOROLINITE COMPOSITE HYDROGEL

Wilson B. F. Filho[1], Mirlene P. Vitorino[1,*], Karine P. Naidek[1,2], Alexandre T. Paulino[1,2,†]

1 – Postgraduation Program in Applied Chemistry, Santa Catarina State University (UDESC), Joinville, SC, Brazil
2 – Department of Chemistry, Santa Catarina State University (UDESC), Joinville, SC, Brazil
*Email: *mirlene.vitorino19@gmail.com; †alexandre.paulino@udesc.br*

Abstract

Water is one of the most widely used sources around the world as it is useful for the sanitation, human life, agriculture, livestock, and so forth. It is worth mentioning that the use of water has economic and social aspects that contribute to the world population. Many aqueous wastes generated by textile industries are harmful to the society due to their toxicity. Some residues are widely known as emerging pollutants, and when inappropriately disposed in the environment cause environmental impacts to the biome. Adsorption techniques are eco-friendly, low-cost, efficient strategies for the removal of emerging pollutants from water. Adsorption processes are affected by pH, temperature, ionic strength, pollutant concentration, and so forth. As pH is one of the most important parameters to study adsorption of pollutants in solid matrices due to electrostatic interactions between adsorbent and adsorbate, we have evaluated the effects of pH on the adsorption of methylene blue in pectin/montmorillonite composite hydrogels. In view of this, the point of zero charge on the hydrogel structure was determined to comprehend the adsorption phenomena. Overall, it was noticed that the point of zero charge significantly affects the adsorption due to changes of charges on the adsorbent structure by varying the solution pH.

Keywords: *pH. Pectin. Montmorillonite. Methylene Blue. Hydrogel*

Introduction

The industrial sectors are responsible by generations of high amounts of chemical residues that have to be adequately treated before disposing [1]. The disposal of wastes without proper treatment and management causes negative impacts on the environment due to their toxicity. It is important to monitor the impacts caused in the environment due to disposal of chemical substances as the emerging pollutants with the aim of proposing specific environmental legislations to control the pollution from textile industries. The effective degradation of various emerging organic pollutants present in the environment has become a technological challenge as the conventional treatment methods are not capable of purifying waters and wastewaters with high efficiency.

Advanced oxidation, membrane-filtration, electrochemical, adsorption are widely employed water and wastewater treatment techniques for the solution purification. Adsorption is considered a promising technology due to high efficiency, low-cost and easy operation [2]. Moreover, this technique contributes to the green chemistry [3]. In this sense, biodegradable adsorbent biopolymers as hydrogels and membranes based on polysaccharides are interesting and economically viable adsorbents for adsorption studies of emerging pollutants in water. Then, the aim of this work was to propose strategies to reduce the environmental pollution of waters contaminated by methylene blue

via adsorption studies under effects of pH, using pectin/montmorillonite hydrogels as adsorbent matrix.

Experimental

Synthesis of composite hydrogel

The pectin/montmorillonite hydrogel was synthesized in two steps: i) modifying pectin with glycidyl methacrylate, and ii) subsequent hydrogel synthesis by using acrylamide and potassium persulfate as described by research group [4, 5]. For the synthesis of the composite hydrogel containing montmorillonite (MMT), different masses of clay mineral (1, 5 and 10 wt-%) were added during the hydrogel crosslinking.

Point of zero charge

To determine the point of zero charge, it was analyzed the final pH after the equilibrium of each of them. In a specific range for each material the pH value was constant or with small variations, and from these values, taking an arithmetic mean, it was possible to determine the point of zero charge for each hydrogel.

Effect of pH on the adsorption of methylene blue in hydrogel

The effect of pH of methylene blue on the adsorption in hydrogels was evaluated by placing 100 mL of buffer solutions and pH values varying from 3 to 9, in 125-mL erlenmeyer flasks. For pH 3.0 and 4.5 was used 0.01 mol L^{-1} acetic acid buffer solution, whereas for pH 5.5 and 6.5 was used 0.01 mol L^{-1} potassium phosphate buffer solution, and for pH 7.5 and 9.0 was used 0.01 mol L^{-1} ammonium hydroxide buffer solution. All the experiments were performed in duplicate, collecting aliquots of methylene blue in solutions after adsorption processes at specific time.

Results and Discussion

Point of zero charge

Figure 1 shows the point of zero charge values for different pectin hydrogels.

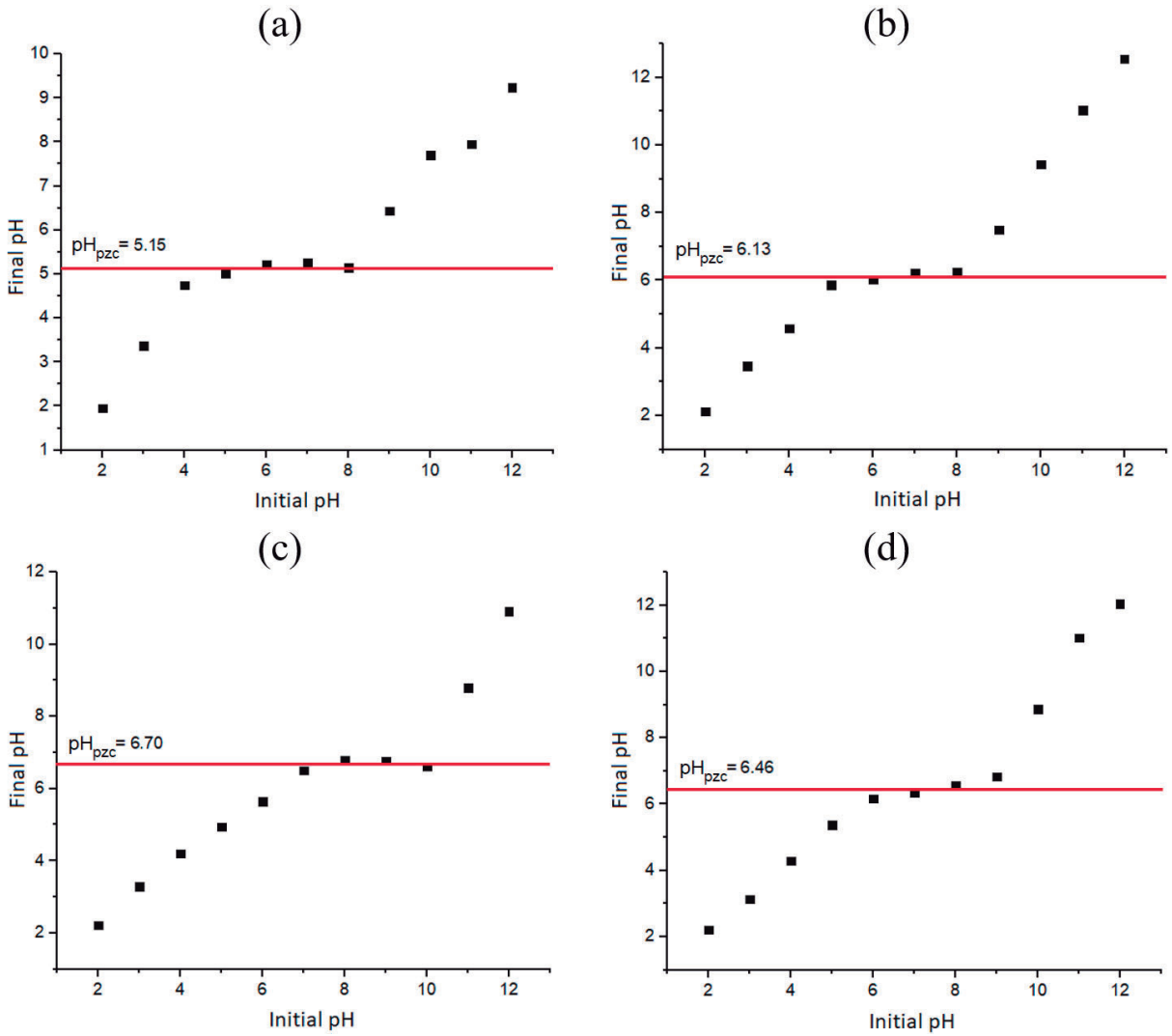

Figure 1 – Point of zero charge (pH_{PZC}) for pectin hydrogel (a) and composite hydrogels containing 1 (b), 5 (c) and 10% (d) montmorillonite.

The point of zero charge values calculated for the four hydrogels in (a), (b), (c), and (d) were 5.15, 6.13, 6.70, and 6.46, respectively. This indicates that the hydrogel structures are affected by the solution pH. In this case, their surfaces will be negatively charged at pH higher than the pH_{PZC}, with adsorption preferential of cationic pollutants, and positively charged at pH lower than the point of zero charge, with adsorption preferential of anionic pollutants. Depending on the pH, these types of hydrogels could be useful for the removal and selective separation of cations and anions in aqueous solutions.

Effect of pH on the adsorption studies

Figure 2 shows effects of pH on the adsorption of methylene blue in pectin hydrogels.

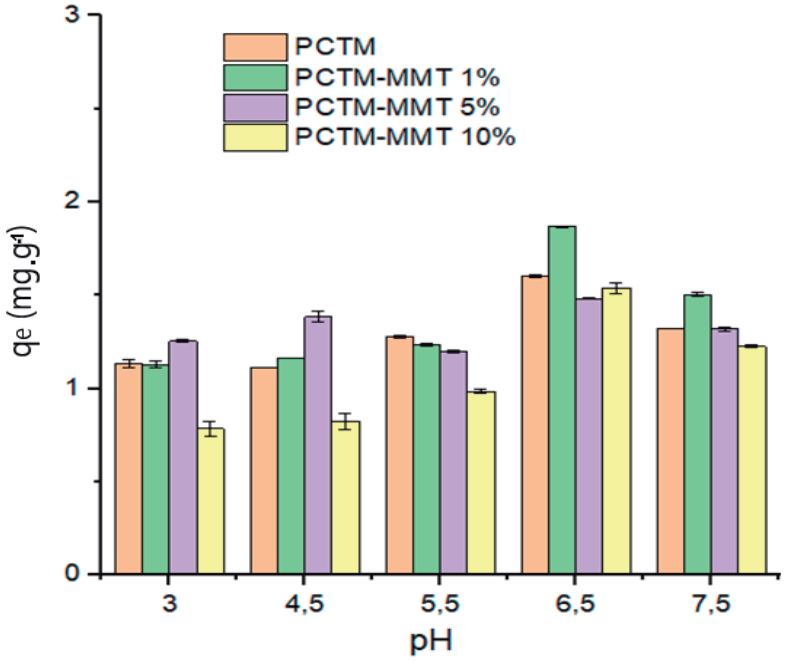

Figure 2 - Adsorption capacity (qe) of the pectin hydrogel (PCTM), pectin composite hydrogel containing 1 (PCTM-MMT 1%), 5 (PCTM-MMT 5%) and 10 % (PCTM-MMT 10%) of montmorillonite at different pH values.

As example, the adsorption capacity of PCTM, PCTM-MMT 1%, PCTM-MMT 5%, and PCTM-MMT 10% for methylene blue were, respectively, 1.702, 1.866, 1.720 and 1.737 mg of dye per g of dry hydrogel, at pH 6.5. Similar results were noticed for other pH values due to presence of ionized carboxyl groups on the polymeric networks of the hydrogels. When the pH is higher than the pKa of this group, which is ~4.0, stronger intermolecular interactions take place between hydrogel negatively charged and cationic dye (in this case, methylene blue). At this pH, the carboxyl groups are dissociated to form COO^-, increasing the number of ionized groups and the pollutant adsorption capacity. Moreover, electrostatic repulsion forces inside the hydrogel networks will also be increased, expanding the polymer chains, and favoring the intrapore diffusions. It also increases the adsorption capacity of cationic dyes such as methylene blue [5].

Conclusions

Pectin hydrogels demonstrated to be interesting biomaterials for the removal and selective separation of cationic and anionic pollutants in water and wastewater. However, high amounts of clay minerals in the hydrogel networks can significantly affect the adsorption capacity due to competition of cations and anions of the clay minerals with pollutants by the active adsorption sites of the hydrogels. The adsorption studies were also significantly affected by the solution pH. The best experimental conditions for the adsorption studies indicated percentages of pollutant removal ranging from ~59% to ~75%. As a conclusion, pectin hydrogels could be used as alternative

adsorbents for the adsorption, removal, and selective separation of cationic and anionic dyes in aqueous solutions.

Acknowledgements

CNPq, FAPESC, CAPES and UDESC

References

[1] M. Kuster; D. A. Azevedo; M. J. L. D. Alda; F.R.N. Aquino; D. Barceló. Environ. Int. 2009, 997-1003. DOI: https://doi.org/10.1016/j.envint.2009.04.006.

[2] A. T. Paulino, Dr. Tese, Universidade Estadual de Maringá, 2008.

[3] L. C. A. Oliveira; J. D. Fabris; , M. C. Pereira. Quím. Nova, São Paulo, 2013; v. 36, n. 1, p. 123-130. DOI: https://doi.org/10.1590/S0100-40422013000100022

[4] A. T. Paulino; L. A. Belfior; L. T. Kubota; E. C. Muniz; E. B. Tambourgi. Chemical Engineering Journal, 2006, 168, 68–76, 12037. DOI: https://doi.org/10.1016/j.cej.2010.12.037.

[5] A. Dalalibera; P. B. Vilela; T. Vieira; V. A. Becegato; A. T. Paulino. J. Environ. Chem. Eng. V 2020, Vol. 8, n. 5, p. 104465.

EFFECT OF THE INCORPORATION OF LIGNIN ON STARCH/PVA BLEND FILMS PRODUCED BY CASTING

Helen Kotekewis[1]*, Ruth Marlene Campomanes Santana[1]

1 – Department of Materials Engineering, Federal University of Rio Grande do Sul (UFRGS), Porto Alegre, RS, Brazil
helen.kotekewis@gmail.com

Abstract - Environmental issues caused by polymeric materials residue is an emerging problem. Biodegradable and biobased materials are great alternatives that need improvement on their properties. This study aims to produce and characterize starch/PVA blend films with lignin. The goal is to improve properties of the starch/PVA blend film and select an optimum amount of lignin. Flexible films were produced by casting using 75% of starch, 25% of polyvinyl alcohol and varying quantities of lignin (0, 0.5, 1 and 2%). Optical and water interaction properties were evaluated. The addition of lignin made the films more translucent and with an orange color. Moisture absorption dropped 34% with the incorporation of the additive. The film with 0.5% of lignin had a significant improvement of all the properties tested, showing a potential to be applied as flexible and biodegradable packaging material.

Keywords: *biodegradable, starch, polyvinyl alcohol, lignin, film.*

Introduction

The global impact of plastic waste has increased the search for alternatives in the industry. According to European Bioplastics, the biodegradable plastic market is expected to grow 12.6% in 2023 [1]. Many substitutions for biobased and biodegradable materials have been successful, but not all applications have suitable options of materials to reduce the pollution. According to data obtained by *ABRELPE,* almost 71 tons of plastic packaging residue was collected and directed to recycling in the year of 2022 in Brazil [2]. Biodegradable polymers are still a better option than recycling. But the most common biodegradable polymers, such as starch, still have restrictions or disadvantages relating to properties, cost and large scale production.

Thermoplastic starch/Polyvinyl alcohol (PVA) blends are made using two biobased biodegradable polymers, a natural one (starch) and a synthetic one (PVA). Starch represents 29% of the studies on biodegradable films on Science Direct website (data found researching: "polymeric biodegradable films" and "polymeric biodegradable films starch") [3]. The advantages of using starch are the low cost, multiple sources and easy processing into films. However, its high hydrophilicity results in poor mechanical properties of films produced with this material. The PVA addition to starch shows lower water interaction properties, improved mechanical and barrier properties, and also has excellent compatibility [4]. This blend has potential to be used as flexible packaging, but since both polymers are hydrophilic, the use of additives, such as lignin, can have an even greater impact on the water interaction properties of the film.

Lignin is an aromatic natural and renewable polymer which is extracted from plants. It represents one of the largests residues in the paper industry [5]. When used as an additive to starch films, lignin can increase the elasticity modulus and lower the hydrophilicity. Different properties

can also be introduced to the films by adding lignin, such as: antioxidant, antimicrobial, flame retardant and ultraviolet radiation blocking [6].

This study aims to produce and characterize starch/PVA blend films with lignin. The films will be produced by casting using 3 proportions of the additive, to evaluate its effects on the films. The goal is to improve properties of the starch/PVA blend film and select an optimum amount of lignin to produce films and use them as an biodegradable substitute to flexible packaging.

Experimental

Materials

Corn starch (CS) and lignin were received from donation. Polyvinyl alcohol (PVA) was obtained from Dinâmica Química Contemporânea Ltda. The plasticizer, glycerol, was obtained from Vetec Química Fina Ltda.

Production of Films

The films were produced by casting method. The composition of the blends was: CS (75%), PVA (25%), lignin (0, 0.5, 1 and 2% w/w of polymers), glycerol as plasticizer (33% w/w of CS) and distilled water as solvent.

The first step of the production of the films was the removal of the lignin insoluble particles. Distilled water was added to lignin (0.4% w/v), and then filtered using a tulle fabric. Different volumes of the solution were used for each film composition: B (0% lignin), BL05 (0.5% lignin), BL1 (1% lignin), BL2 (2% lignin).

Next, a mixture of starch, water, glycerol and lignin solution was stirred for 30 minutes, with the temperature starting as 40ºC and increasing slowly until 90ºC. After that, the PVA was added to the solution, and stirred for another 30 minutes, maintaining the heat. The filmogenic solution was distributed in a silicone mold, followed by the evaporation of the solvent in an air circulating oven for 24 hours. The films were peeled from de molds and placed in a silica desiccator until characterization tests.

Characterization Tests

Colorimetry

The optical and colorimetric analysis of the films was made by using a portable spectrophotometer (BYK), following the ASTM D2244-22 norm. The dimensionless parameters obtained were: luminosity (L*), color (a* and b*) and gloss (g). L* varies from white (100) to black (0). The color parameters vary from red (+a*) to green (-a*), and from yellow (+b*) to blue (-b*). And the gloss indicated whether there is more or less reflection of light on the surface of the film. Three measurements were made on each film composition against a white background.

Moisture Absorption

The moisture absorption of the films was measured through the ASTM D5229 method. The film samples were left in closed recipients with sodium chloride saturated saline solution, kept in an oven at 30°C with a relative humidity of 75%, according to the ASTM E104 - 02 norm. Each composition of film was tested with 5 samples.

Thickness

The thickness measurement of the films was done using a micrometer (Mainard, M-73010). Five measurements on 5 samples of each film composition were made.

Contact Angle

The contact angle of the films was measured by Surftens 3.0 software using photos taken by a digital microscope with a magnification of 1,600 times. The photos were taken 1 second and 1

minute of residency on the films. The angles were measured of 10 drops of water for every film composition. The surface energy was calculated by the Surftens 3.0 software. All of the films were tested using the smoother surface, the one which was in contact with the silicon mold.

Results and Discussion

The results of the characterization of the films will be used to evaluate the effect on the lignin on the blends and to compare the different proportions of lignin. The thickness of the films were (in µm): 164 (B), 141 (BL05), 171 (BL1) and 178 (BL2). The difference of thickness was up to 26%, with an increase of thickness with the increase of lignin, except for the B film.

Fig 1 shows a comparison of the visual aspects of the 4 film compositions on different backgrounds. All of the films have good transparency. The color of the films gets darker with the increase of lignin proportion. Some insoluble particles can be visible, with quantity increasing with the increase of lignin content.

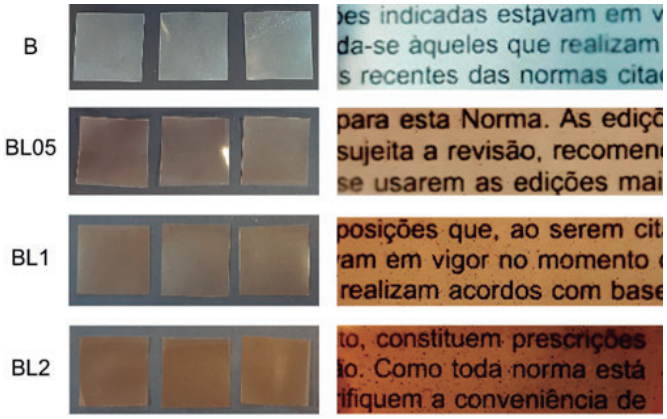

Figure 1 – Samples of the films on black background (left) and on written background (right).

The colorimetry parameters, at Table 1, confirm results previously discussed. The luminosity of the films decreased 10%, 15% and 29% with the addition of 0.5%, 1% and 2% of lignin, respectively. The color parameters (a* and b*) revealed that the lignin films have yellow and red colors, forming a shade of orange. Both color parameters increased with the raise of lignin content. The B film is the film with the lowest gloss. The increase of lignin reduced the gloss of the films. The transparency of the films is related to the size of the particles, if they are about the size of the wavelength of the visible spectrum, they will be more opaque. Also, the ultraviolet radiation blocking, which is important in food packaging applications, can be observed in films with lignin [7]. Further testing should be done to evaluate this property.

Table 1 – Colorimetry parameters of the films.

Film	L*	a*	b*	g
B	89,00 ± 0,09	0,21 ± 0,00	-1,09 ± 0,09	27,16 ± 1,14
BL05	80,10 ± 0,62	2,11 ± 0,22	10,34 ± 0,68	69,91 ± 5,76
BL1	75,70 ± 0,46	3,26 ± 0,14	15,67 ± 0,38	54,64 ± 0,24
BL2	63,25 ± 0,70	8,13 ± 0,41	26,08 ± 0,88	45,18 ± 2,72

Moisture absorption comparison is shown in Fig 2. The absorption decreased an average of 34% with the addition of lignin. BL2 showed the lowest humidity absorption. Those results were

similar to many researches using lignin in starch films. The explanation for the decrease of moisture absorption is that lignin, PVA and starch created a strong interaction that reduced the mobility and the diffusivity of the matrix material [8].

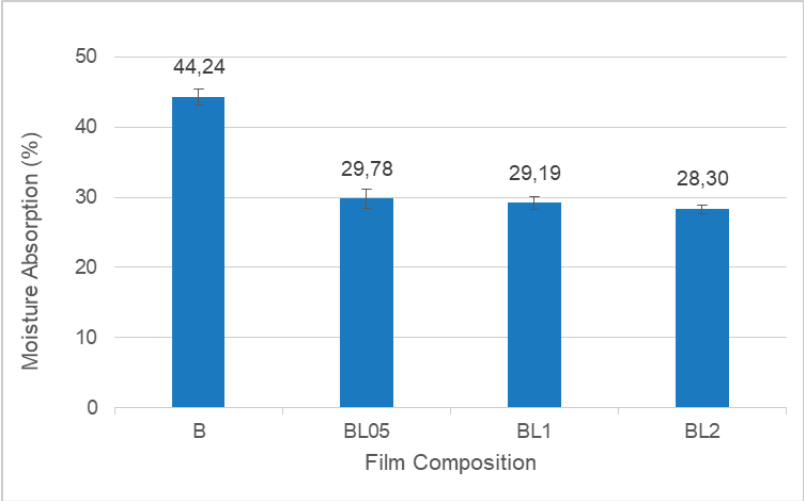

Figure 2 – Percentages of weight gained by moisture absorption of the films with 75% of relative humidity in 24 hours.

After 24 hours, the moisture absorption of the film without lignin increased 4.1% and the films with lignin lowered their mass between 2 and 6%. This means that the highest absorption rate occurred within the first 24 hours for all of the films.

The water contact angle of the films is shown in Fig 3. The only film with an increase of contact angle was the one with the least amount of lignin (BL05). BL1 and BL2 presented with a decrease of contact angle of 13 and 15%, respectively. However, the film without the additive had the highest contact angle after 1 minute of residency of the water drop.

Those results do not prove that the hydrophilicity of the films decreased with lignin, they actually go against the moisture absorption results, but the moisture absorption is not only related to the surface. A reason for this could be because more hydroxyl groups are present on the surface of the film, causing the water contact angle to reduce.

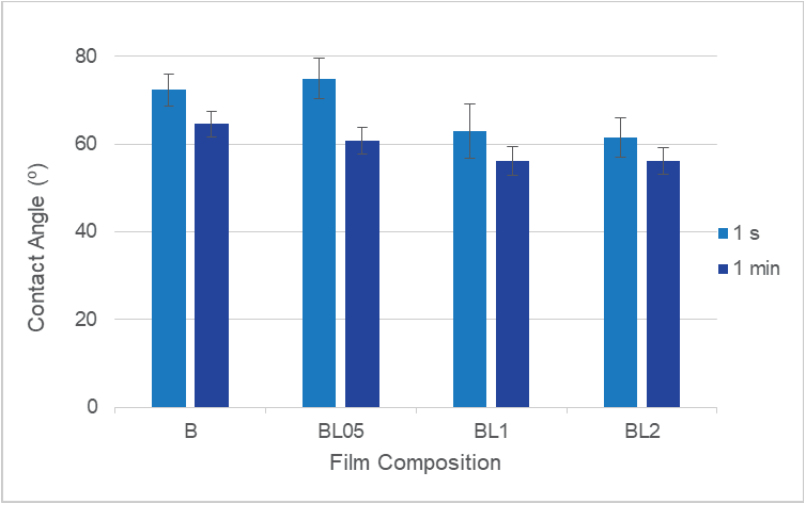

Figure 3 – Contact angles of the films with distilled water with one second and one minute of residency of the drops.

Conclusions

The process of producing starch/PVA blends with lignin is very simple and shows remarkable results. The general aspect of the films were good, except for the presence of some insoluble particles. A different approach on lignin filtering is being considered for the continuation of this research. The films were translucent with an orange color, and have potential to block ultraviolet radiation. Moisture absorption results were excellent even with the smallest amount of lignin. BL05 had the highest contact angle. The difference between the BL05 and the film with the lowest moisture absorption was less than 2%. Also, BL05 was thinner and had the best optical properties. It is noticeable that an addition of 0.5% of lignin resulted in a film with superior properties than 0, 1 or 2%.

Acknowledgements

To the Academic Excellence Program of the Higher Education Personnel Improvement Coordination (CAPES/PROEX) and to the Laboratory of Polymeric Materials at the Federal University of *Rio Grande do Sul* (LAPOL/UFRGS).

References

1. European Bioplastics, nova-Institute, 2022. https://www.european-bioplastics.org/market/
2. Panorama dos Resíduos Sólidos no Brasil 2022, Abrelpe, 2022.
3. Science Direct. https://www.sciencedirect.com/. Access in: May, 3rd, 2023.
4. S. Patil et al. Food Bioscience, 2021, 44, 101352. https://doi.org/10.1016/j.fbio.2021.101352.
5. E. A. Agustiany et al. Polymer Composites, 2022, 43, 8. https://doi.org/10.1002/pc.26824.
6. M. Mariana et al. Journal of Materials Research and Technology, 2021, 15, 2287-2316. https://doi.org/10.1016/j.jmrt.2021.08.139
7. I. Spiridon; C. Teaca; R. Bodirlau. Journal of Materials Science, 2010, 46, 3241–3251. https://doi.org/10.1007/s10853-010-5210-0.
8. T. AbdulRasheed-Adeleke et al. Molecules, 2022, 27 (22) 7708. https://doi.org/10.3390/molecules27227708.

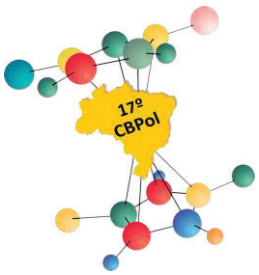

ELECTROSPRUN NANOFIBERS BLENDS PREPARED FROM POLYVINYL ALCOHOL /LIGNIN MIXTURES

Gabriela C. S. Pompêu[1]*, Luís Carlos de Morais[2] and Daniel Pasquini [1]

1 – Department of Chemical, Federal University of Uberlandia (UFU), Uberlandia, MG, Brazil
gabriela_csp@hotmail.com
2 – Institute of Exact, Natural and Educational Sciences, Federal University of Triangulo Mineiro (UFTM), Uberaba, MG, Brazil

Abstract - Lignin is a renewable material, cheap, and available in large amounts, thus the interest in its valorization is growing both in industry and in academic research areas. One possible approach is the formation of polymeric nanofibers blends by electrospinning. However, mixing lignin with polymers in aqueous solution is not so simple due to the low solubility of lignin molecules, so one solution is to chemically modify the lignins and make them soluble in water, thus allowing the production of mixtures in aqueous media. In this context, the nanofibers blends obtained from this solution by the electrospinning technique are highly attractive due to the unique combination of high surface/volume ratio, porosity, flexibility, mechanical performance, simple processing, and relatively low cost. Thus, this study proposed the production of electrospinning nanofibers blends from modified lignin and PVAl aqueous mixtures in the perspective of new products with high added value.

Keywords: *Blends. Nanofibers. Electrospinning. Lignin. PVAl.*

Introduction

The modification of polymers through the formation of blends is a consolidated technology that was developed in 1960. This technique stands out for presenting advantages such as modification of the glass transition temperature, increased fracture resistance, flexibility, improvement of optical properties, effectiveness, and improvement of the pure polymer at low cost. One of the main objectives of the use of blends is to gather the maximum performance of the agreed polymers, without drastically changing the properties of their components [1,2].

The polymeric blends obtained through the physical mixture of two or more polymers are made without the need to use intentional chemical reactions between the substances. Mixtures can be molded by solution and by mechanical mixing in the molten state [3]. According to Zarrintaj et al. (2020), miscibility is one of the extremely important factors in the mixture of polymers. When you have immiscible polymers, they become prone to phase separation and affect the surface topology of the blends. Thus, the materials used must be biocompatible and/or non-toxic, and in this profile, the polymers derived from nature, also known as biopolymers, are included [4].

The use of lignin biopolymers has grown due to the improvements that new technologies provide, in addition to the various properties that this material presents: high thermal stability, antioxidant, biodegradable, antimicrobial actions, and performance in several industrial and chemical areas. Thus, these materials are considered environmentally safe alternatives for the development of new polymeric mixtures and new applications, such as the production of nanofibers [5].

Nanofibers are nano-scale materials that have small pores connected to randomly deposited fiber layers. They are part of a new class of raw materials used in various applications with high-added value, like filtration [6], catalysis [7], energy conversion and storage systems [8], sensors [9], semiconductors [10], adsorbers [11] and so on. Above all, these nanofibers, with different aspects and specific diameters, are obtained from polymeric solutions through an electrospinning process. It is an electrohydrodynamic technique that results in the movement of a fluid through the application of an electrostatic field [12].

In this context, electrospun nanofibers blends were produced from polymeric aqueous mixtures, using polymer polyvinyl alcohol (PVAl) and different concentrations of carboxymethylated kraft lignin (CML-Na). They were characterized by morphological (SEM), structural (FTIR), and thermal (TGA) analysis, and correlated for the application of new materials.

Experimental

Preparation of PVAl/CML-Na solution mixtures

The isolated lignin was supplied by the Suzano Pulp and Paper industry. It was subjected to a carboxymethylation reaction using ethanol, sodium hydroxide, and monochloroacetic acid. After obtaining the modified lignin (CML-Na), the polymeric aqueous solution mixture were prepared using PVAl at 6 % (w/v) and CML-Na at 5, 10, and 15% (v/v). Each solution was homogenized in a magnetic stirrer for 30 minutes at 100 rpm.

Electrospinning

The electrospun nanofibers blends were produced following the experimental conditions proposed by Gois (2020), with some adaptations [13]. The system used was developed at the Polymer Recycling Laboratory (LABREPOL), with the assembly of the basic components of the process: high voltage source (with a capacity of up to 30 kV); flow controller; metallic fixed collector; isolation chamber. The polymer/lignin solution mixtures (PVAl/CML-Na) were subjected to the electrospinning process with a flow rate of 0.5 mL h^{-1}, a high voltage direct current source of 15 kV and a distance established between the tip of the needle to the collector of 10 cm.

Characterization of electrospun nanofibers blends

For the characterization of the formed product, morphological, structural, and thermal analyzes were carried out. Scanning Electron Microscopy (SEM) was performed using a Shimadzu SSX-550 model equipment for morphological evaluation and dimensioning of the produced nanofibers, with magnification of 2000 times and voltage acceleration of 5 kV. In the structural evaluation of the nanofibers, Absorption Spectroscopy in the Infrared Region by Fourier Transform (FTIR) was performed with KBr wafers in the region of 400 to 4500 cm^{-1}, resolution 4 cm^{-1}, 32 scans, with a Shimadzu IR Prestige-21 equipment. Finally, the thermal part was observed by Thermogravimetric Analysis (TGA), using 7 mg of the sample that was heated, in alumina crucibles, up to 850 ºC, at a heating speed of 10 ºC min^{-1}, under an oxidative atmosphere at 50 cm^3 min^{-1}.

Results and Discussion

The surface micrographs of electrospun PVAl/CML-Na nanofibers blends are shown in Fig. 1. We can observe that there was the formation of threads, with diameters smaller than 600 nm, even in different concentrations of lignin. It can also be observed, that with the increase in the concentration of lignin in the solution, the spacing between the formed threads decreases. In addition, another observation is related to the presence of polymeric agglomerations in the fibers (beads) formed by spraying jets during electrospinning of the lowest concentration of lignin present in the solution, as can be seen in Fig. 1a. As the concentration of CML-Na increased, fibers were more homogeneous,

spaced, and with a lower frequency of beads. That is, at higher concentrations there is no formation of beads because with the increase in viscosity, the viscoelastic force increases, which prevents the partial breaking of the charged jet, allowing the electric force to stretch it much more uniformly, occurring during the path to solvent evaporation more efficiently [13].

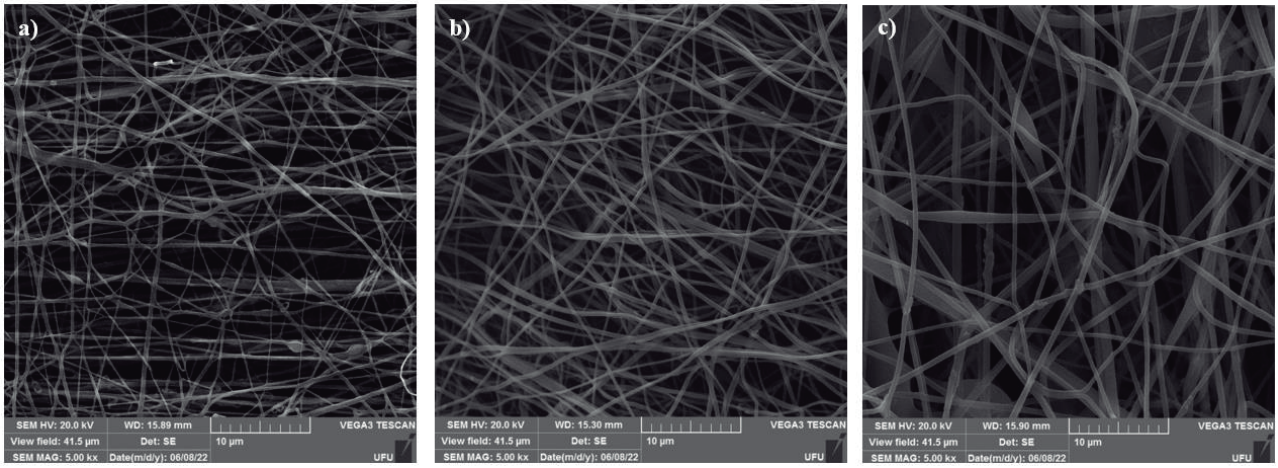

Figure 1 – SEM of electrospun PVAl/CML-Na nanofibers blends in concentrations of a) 5 %; b) 10 %; c) 15 % (w/v) of CML-Na.

From the FTIR curves presented in Fig. 2, the molecular structure and the identity of the functional groups present in the fibers can be elucidated. In the case of polymeric blends, we verified the presence of the functional groups of the two materials used, which constitute the nanofibers: PVAl and CML-Na, and the increase in the modified lignin content intensifies the peaks related to it [14].

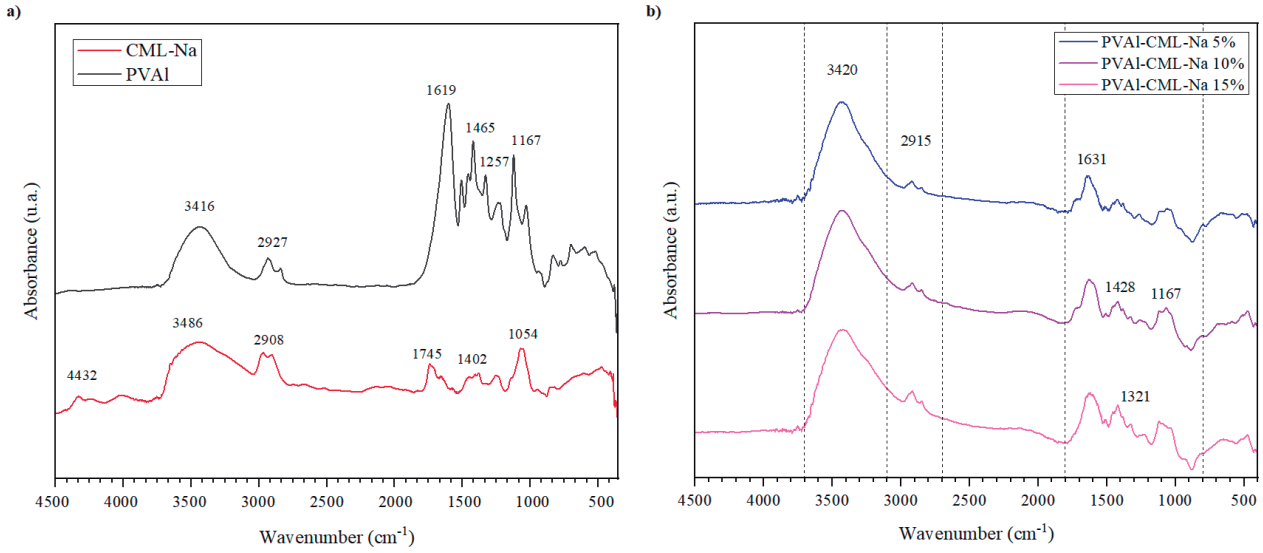

Figure 2 – FTIR graphs of a) PVAl and CML-Na, and b) PVAl/CML-Na electrospun nanofibers blends.

The main evidenced points, characteristic of both PVAl and CML-Na, were the bands in the region of 3420 and 1631 cm^{-1}, related to OH elongation and asymmetric carboxylate elongation respectively, and around 2915 cm^{-1}, whose characteristic is asymmetric CH_2 and symmetric carboxylate elongation. The peaks at 1619, 1257 and 1167 cm^{-1}, which indicate, respectively, vibration C=C aromatic ring, deformation of the guaiacyl ring and stretching of C-C and C-O sensitive to substitution of the aromatic ring, and typical character of HGS lignin (p-hydroxyphenyl,

guaiacyl, syringyl), are specific only for CML-Na [15,16]. Thus, as the concentration of carboxymethylated lignin in the blends increases, the behavior of the presented spectra becomes like that of CML-Na, which shows the presence of the main characteristic groups of lignin and that the mixture occurred effectively [17].

As for the thermal study, we can observe in Fig.3 the comparison of the thermal behavior between the individual materials before electrospinning (PVAl and CML-Na) and for the electrospinning nanofiber blends samples. It was possible to verify a decrease in the thermal stability of the PVAl when CML-Na was added in all concentrations of 5, 10 and 15%. Considering that CML-Na also has greater thermal stability, we can therefore conclude that the synergistic action of the mixture between CML-Na and PVAl leads to the production of a material with lower thermal stability. An increase in thermal stability was to be expected because of a possible increase in intermolecular interactions, mainly by hydrogen bonds, but what was observed was the opposite, that is, a reduction in thermal stability, which may then indicate that the mixing between these two compounds leads to a decrease in intermolecular interactions and consequently a reduction in thermal stability.

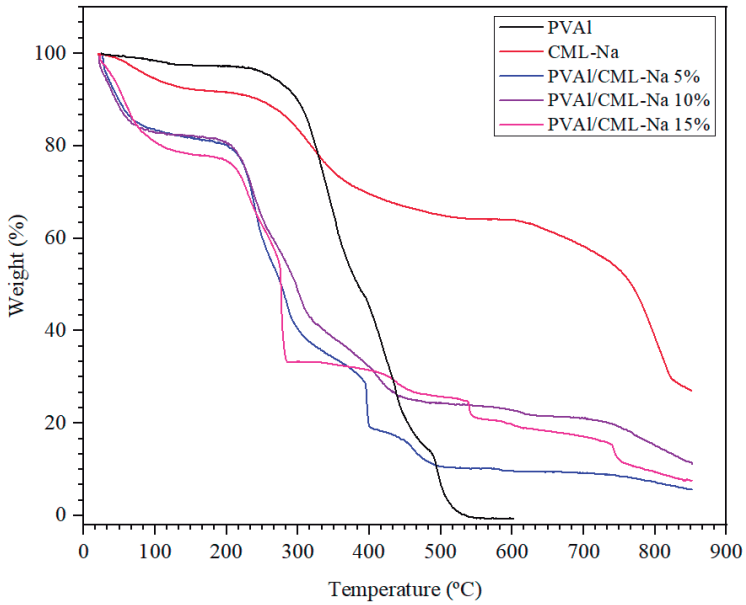

Figure 3 – TGA curves PVAl, CML-Na, and PVAl/CML-Na electrospun nanofibers blends.

Conclusions

▪ The use of polymeric aqueous solution mixtures showed excellent viability since it allows the production of electrospun fibers in regular sizes of up to 600 nm. Electrospinning using water as a solvent was not an obstacle to the formation of wires it even proved to be efficient in the evaporation process.

▪ The nanofibers blends formed by the combinations of PVAl and CML-Na were successfully obtained, in which the morphology of the materials was verified by the SEM. Increasing the concentration of modified lignin decreases the spacing between the formed nanofibers, making them more uniform, with emphasis on CML-Na 15 % (v/v), which in mass percentage (in grams) corresponds to 71.4 % of CML-Na present in the blend.

▪ In FTIR was verified functional groups of PVAl and CML-Na in the electrospun nanofibers which demonstrates that the formation of the blends was efficient. The similarities between the spectra are related to the concentration each the added materials.

▪ As for thermal properties, it is observed that the mixture of PVAl/CML-Na decreased thermal stability, probably due the reduction in the intermolecular interaction in the resulting blends.

Acknowledgements
The authors would like to acknowledge the funding support from CNPq, CAPES, FAPEMIG and FINEP.

References

1. B. Imre; K. Renner; B. Pukánszky. Express Polymer Letters 2014, 8, 1. https://doi.org/10.3144/expresspolymlett.2014.2.
2. D. A. D'Amico; M. L. I. Montes; L. B. Manfredi; V. P. Cyras. Polymer Testing 2016, 49, 22-28, 2016. https://doi.org/10.1016/j.polymertesting.2015.11.004.
3. T. Gao; Y. Li; R. Bao; Z. Liu; B. Xie; M. Yang; W. Yang. Composites Science and Technology 2017, 152, 111-119. https://doi.org/10.1016/j.compscitech.2017.09.014.
4. P. Zarrintaj; M. R. Saeb; S. H. Jafari; M. Mozafari. Compatibilization of Polymer Blends 2020, 511-537. https://doi.org/10.1016/B978-0-12-816006-0.00018-9.
5. A. Naseem; S. Tabasum; K. M. Zia; M. Zuber; M. Ali; A Noreen. International Journal of Biological Macromolecules 2016, 93, 296–313. https://doi.org/10.1016/j.ijbiomac.2016.08.030
6. X. Yin; J. Yu; B. Ding. Wiley 2020, 175–206. https://doi.org/10.1002/9783527342587.ch7.
7. V. Joshi; C. M. Srivastava; A. P. Gupta; M. Vats. Springer 2020, 213–248, Cham. https://doi.org/10.1007/978-3-030-29207-2.
8. L. Chen; J. Lv; L. Ding; G. Yang; Z. Mao; B. Wang; X. Feng; S. Zapotoczny; X. Sui. A Chemical Engineering Journal 2020, 400, 125950. https://doi.org/10.1016/j.cej.2020.125950.
9. N. Hui; X. Sun; S. Niu; X. Luo. ACS Applied Materials and Interfaces 2017, 9, 2914-2923. https://doi.org/10.1021/acsami.6b11682.
10. R. A. Wu; C. W. Lin; W. J. Tseng. Ceramics International 2017, 43, S535–S540. https://doi.org/10.1016/j.ceramint.2017.05.285.
11. J. D. A. B. Barbosa; C. A. de França; J. J. D. S. Gouveia; G. V. Gouveia; M. M. da Costa; H. P. de Oliveira. Journal of Applied Polymer Science 2019, 136. https://doi.org/10.1002/app.47479.
12. M. P. Cavalcante; H. P. Oliveira. Research, Society and Development 2021, 10, 5. https://doi.org/10.33448/rsd-v10i5.14953.
13. B. H. S. Gois, Ph.D. Thesis, State University Paulista, 2020.
14. R. G. F. Costa; J. E. Oliveira; G. F. Paula; P. H. S. Picciani; E. S. Medeiros; L. H. C. Mattoso; C. Ribeiro. Polímeros 2012, 22, 178-185. https://doi.org/10.1590/S0104-14282012005000018.
15. A. Kharazmi; N. Faraji; R. M. Hussin; E. Saion; M. M. Yunus; K. Behzad. Beilstein Journal of Nanotechnology 2015, 6, 529-536. https://doi.org/10.3762/bjnano.6.55.
16. M. K. Konduri; F. Kong; P. Fatehi. European Polymer Journal 2015, 70, 371-383. https://doi.org/10.1016/j.eurpolymj.2015.07.028.
17. H. M. Ibrahim; M. M. Reda; A. Klingner. International Journal of Biological Macromolecules 2020, 151, 821-829. https://doi.org/10.1016/j.ijbiomac.2020.02.174.

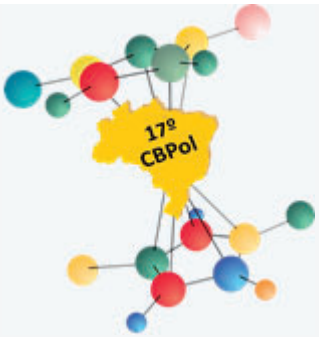

EVALUATION OF GRAPHENE INCORPORATION FOR MECHANICAL PROPERTIES OF POLYPROPYLENE COMPOSITES

Júlio Harada[1*], Claudio A. Marcondes[2], Maria da Conceição C. Pereira[1] and Leonardo G. A. Silva[1]
[1]*Instituto de Pesquisas Energéticas e Nucleares (IPEN-CNEN), São Paulo, SP, Brasil*
[2] *Universidade Estadual de Campinas (UNICAMP), Campinas, SP, Brasil*
**h.julio729@gmail.com*

Abstract - Graphene nanoparticles (GnP) was selected as an alternative reinforcement, nanofillers, to enhance the mechanical properties of polypropylene (PP-homo and PP-copolymer) and using compatibilizer, maleic anhydride graphitized with polypropylene (PP-*g*-MA) in a twin-screw extruder. The effect of GnP loading and the use of the PP-*g*-MA compatibilizer were studied. The influence on the mechanical properties of tensile strength, elongation, IZOD impact strength, and melting temperature in PP-homo and PP-copolymer were investigated and compared. Their improvement was observed up to a certain amount, depending on whether it is a homopolymer or copolymer. The PP copolymer has a greater affinity with graphene and the compatibilizer due to the elastomeric comonomer present in the copolymer.

Keywords*: graphene nanoparticles, polypropylene, homopolymer, copolymer.*

Funding*: CNPq, CAPES, FAPESP (nº 2019/01231-2) Foundations.*

Introduction

A graphene nanoparticle (GnP) is a single layer of carbon atoms packed into a honeycomb structure [1]. Following the independent discovery of graphene in 2004, a revolutionary amount of research was conducted to fully exploit graphene's exceptional properties. GnPs are graphene nanocrystals layered in the structure of platelets stacked by Van der Waal forces. The incorporation of GnPs in conventional polyolefins has promising potential in a wide range of applications due to their excellent thermal, mechanical, and electrical properties. Such composites can be employed in the fields of electronics, automotive, aerospace, sensors, and much more. Among many polymers, polypropylene (PP) is one of the most widely used thermoplastics due to its excellent physical and mechanical properties, chemical resistance, recyclability, high processability, and low cost [2]. The PP application field includes packaging, textiles (ropes and mats), automotive components, etc.

Due to the high potential of PP composites incorporated with GnPs, researchers extensively study the various properties of these materials, the performance of the composites is highly dependent on the physical characteristics of the GnPs. For example, Liang et al. [3] showed that the tensile modulus of pure PP (1.25 GPa) was 100% improved and reached up to 2.5 GPa with the use of GnPs with diameters smaller than 10 microns and thickness smaller than 5 nm. Chunhui et al. [4] also revealed that flexural strength is inversely proportional to graphite size. The crystallization behavior of the polymer matrix is also influenced when GnPs are present. Therefore, the size of GnPs must be chosen carefully to maximize performance. However, few studies systematically investigate the

influences of a wide range of GnPs sizes, ranging from a few to hundreds of microns, on the various properties of composites. Several physical properties, such as the number of particles per unit volume and surface area, vary with the size of the GnPs and therefore will also have to be considered when discussing various properties of composites.

In the work of the authors, Wang et al. [5] observed that the tensile properties of PP-GnP as the graphene concentration increased, the tensile strength and modulus increased, and the elongation at break decreased. The mechanical properties of the composites decreased at higher temperatures, 165 °C and 170 °C, due to more intense melting. Therefore, the melting temperature of 160°C was chosen as the ideal temperature. Furthermore, the compaction time is also a significant factor in the preparation of PP-GnP. For thermal properties, the single melting temperature analyzed decreased with 0.3% GnP loss of 6°C and 0.5% GnP loss of 4 °C, and the other thermal properties will be analyzed in another work. It was observed that both the use of GnP and the compatibilizer significantly influence the melting temperature of pure PP. The melting temperatures and crystallinity of PP-GnP increased as the amount of graphene increased, indicating that graphene also acts as a nucleating agent. The mechanical properties of the PP-GnP composites also increased with increasing graphene content, which indicates an effective charge transfer between the PP and GnP matrix (graphene). The melting composition can affect the dispersion of the composite PP-GnP and the interfacial interaction between graphene and PP chains, S. Natarajan et al. [6]. The melting temperature can lead to the orientation of molecular chains and graphene to hot stretching. Graphene agglomeration can interfere with the interfacial adhesion between PP composites, worsen the interfacial interaction between Graphene and the PP matrix and induce molecular orientation of the composite.

Experimental

Materials and processes±

PP homopolymer and copolymer (Braskem), GnP (Pro Cene), and PP-*g*-MA.

Extrusion of homopolymer and copolymer PP composites, with amounts of 0.3% *GnP* and 0.015% *PP-g-MA and* 0.5% *GnP* and 0.015% PP-*g-MA in* mass. The PP samples – homo and copolymer, the selected graphene and compatibilizer were extruded in a twin-screw extruder in composite grains.

Injection of test specimens - The granulated composite material was injected, for the following test specimens: tensile strength, Izod impact, hardness, and melting temperature, according to the ASTM/ISO.

Characterization of composites

The characterized mechanical properties and the corresponding ASTM/ISO standards:

- Tensile strength and elongation (ASTM D638), carried out at CETER-IPEN, São Paulo;
- Impact resistance - IZOD (ASTM D256), carried out at UNIGEL - São José dos Campos/SP;
- Surface hardness (ASTM D785), performed at Thermoblend - Santana de Parnaiba/SP;
- Melting temperature (ISO 11357), carried out at Thermoblend - Santana de Parnaiba/SP.
- Statistically significance: - reference of 10 samples.

Results and Discussion

The influence of the compatibilizer (PP-*g*-MA) and graphene (GnP) on the mechanical properties of **homopolymer PP composites** with amounts of 0.3% and 0.5% of GnP +*PP-g-MA* mass were analyzed.

Table 1, it is shown the results of the characterization of the PP-homopolymer, PP-homopolymer + GnP (0.3% and 0.5%).

Table 1: Results of the characterization of the PP-homopolymer, PP-homopolymer + GnP (0.3% and 0.5%)

MATERIAL	Graphene %	Melt Temp (°C)	Tensile Mpa	Elongation (%)	Hardness Shore D	IZOD			
						w notch (J/m)	WO notch (J/m)	w notch (kJ/m)	WO notch (kJ/m)
PP HOMO PURE	0	$180^{\pm 1.0}$	$34.7^{\pm 3.6}$	$86.7^{\pm 3.6}$	$71^{\pm 1.0}$	$60.4^{\pm 7.7}$	NB*	$5.3^{\pm 0.8}$	NB*
PP HOMO + GRAPHENE	0.3	$174^{\pm 1.0}$	$34.9^{\pm 1.0}$	$77.1^{\pm 14.3}$	$71^{\pm 1.0}$	$86.5^{\pm 3.9}$	NB*	$7.3^{\pm 0.4}$	NB*
PP HOMO + GRAPHENE	0.5	$176^{\pm 1.0}$	$34.4^{\pm 4.0}$	$73.^{\pm 8.2}$	$72^{\pm 1.0}$	$71.9^{\pm 3.2}$	NB*	$6.3^{\pm 0.3}$	NB*

NB* - no break

The curves of the mechanical properties of the PP-homopolymer, PP-homopolymer + GnP (0.3% and 0.5%) are shown in Figure 1.

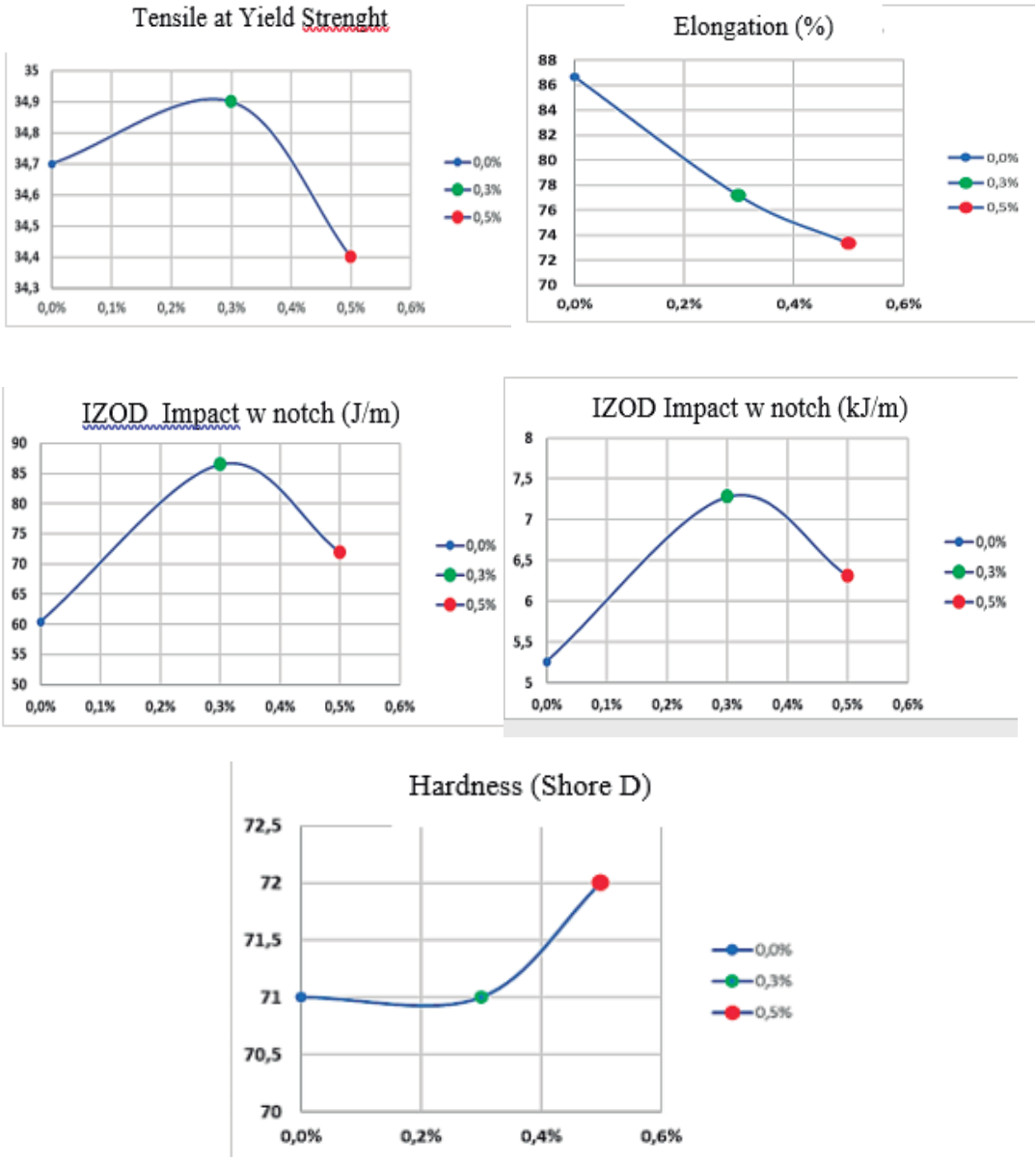

Figure 1: Results of the mechanical properties of the PP-homopolymer, PP-homopolymer + GnP (0.3% and 0.5%)

Tensile strength, with the incorporation of 0.3% GnP, increased by 0.2 MPa, and with a 5% GnP decrease of 0.3 MPa. **Elongation** with the incorporation of a 0.3% GnP decrease of 9.5% and with a 5% GnP decrease of 13.3%. **IZOD impact** with 0.3% GnP an increase of 26 J/m and with 0.5% GnP increase of 11 J/m. (NB*- no break). **Thermal properties**, melting temperature, the only analyzed, the addition of 0.3% GnP decrease of 6 °C (180 ºC-174 °C), the addition of 0.5% GnP decrease of 4 °C (180 ºC-176 °C), and the other thermal properties are still being evaluated. It was observed that both amounts of graphene and compatibilizer significantly influence the melting temperature compared with homo PP pure.

The influence of the compatibilizer (PP-*g*-MA) and graphene (GnP) on the mechanical properties of **PP-copolymer composites** with amounts of 0.3% and 0.5% of GnP in mass was analyzed.

Table 2, it is shown the results of the characterization of the PP-copolymer, PP-copolymer + GnP (0.3% and 0.5%).

Table 2: Results of the mechanical properties of the PP-copolymer, PP-copolymer + GnP (0.3% and 0.5%)

MATERIAL	Graphene %	Melt Temp (ºC)	Tensile Mpa (+-)	Elongation (%)	Hardness Shore D	IZOD			
						w notch (J/m)	WO notch (J/m)	w notch (kJ/m)	WO notch (kJ/m)
PP COPO PURE	0	168 $^{\pm 1.0}$	26 $^{\pm 0.9}$	42.1$^{\pm 2.2}$	52	69.3 $^{\pm 3,2}$	NB*	6.6 $^{\pm 0.,3}$	NB*
PP COPO + GRAPHENE	0.3	171 $^{\pm 1.0}$	28 $^{\pm 0.8}$	53.3$^{\pm 2.9}$	67	176.0$^{\pm 5,1}$	NB*	15.9 $^{\pm 0.5}$	NB*
PP COPO + GRAPHENE	0.5	172 $^{\pm 1.0}$	28.4$^{\pm 0.7}$	42.9$^{\pm 2.9}$	67	166.7$^{\pm 5,3}$	NB*	14.6 $^{\pm 0.5}$	NB*

NB* - no break

The curves of the mechanical properties of the PP-copolymer, PP-copolymer + GnP (0.3% and 0.5%) are shown in Figure 2.

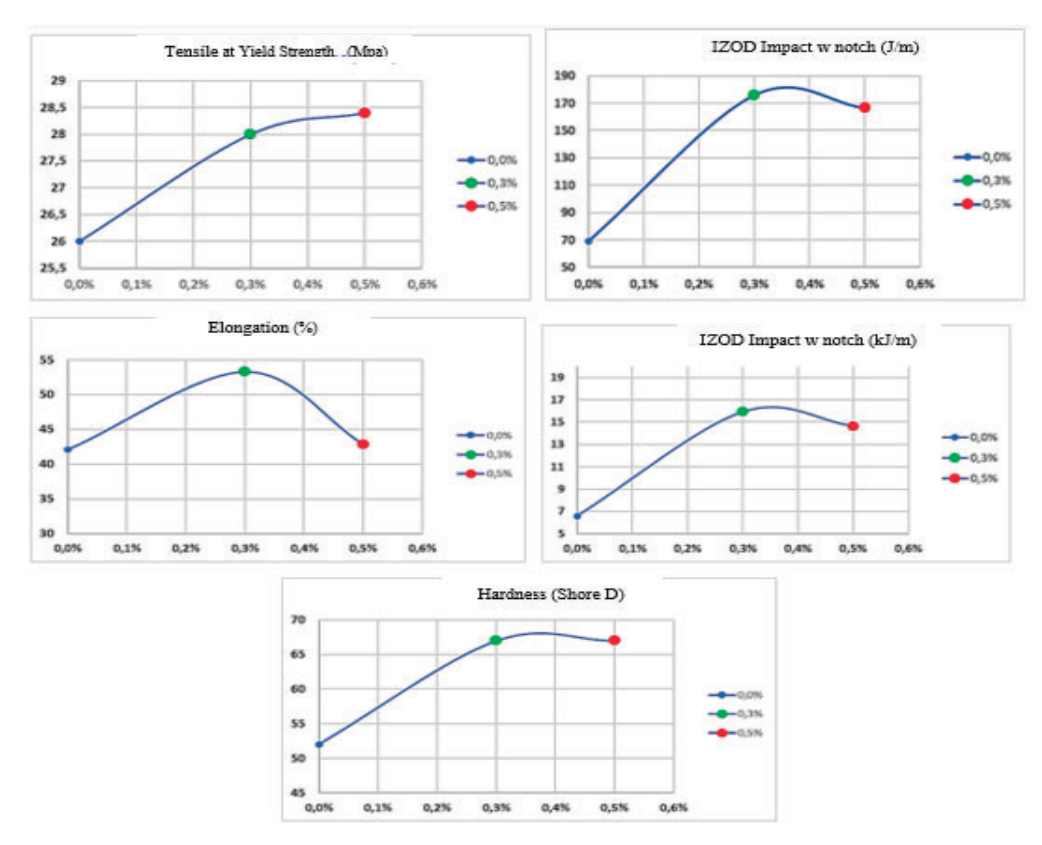

Figure 2: Results of the mechanical properties of the PP-copolymer, PP-copolymer + GnP (0.3% and 0.5%)

The **tensile strength**, incorporation of 0.3% GnP, increased by 2.0 MPa and with a 5% GnP increase of 2.4 MPa. The **resistance to elongation** with the incorporation of a 0.3% GnP increase of 11.2% and with a 5% GnP increase of 0.8%. The **IZOD impact** strength with a 0.3% GnP increase of 106.7 J/m; and with 0.5% GnP increase of 97.4 J/m. There is an ideal amount for addition of up to 0.3% GnP because beyond this amount there will not be a significant increase in the mechanical properties. The slipping effect of the GnP has a great influence on the results and an increase in the cost of the PP composite with GnP with quantities above. For **thermal properties**, melting temperature, GnP with 0.3% increased 3°C (168 ºC-171 °C), GnP with 0.5% increased 4 °C (168 ºC-172 °C), and the other thermal properties will be analyzed in future work complement. It was observed that both the GnP load and the compatibilizer significantly influence the melting temperature of pure PP copolymer.

Conclusions

PP-homopolymer composites with GnP and PP-*g*-MA**:** There is an ideal amount for adding up until 0.3% GnP because beyond this amount there was a drop in the mechanical properties, due to the agglomeration effect and the slipping effect of the GnP and an increase in the cost of the PP composite with GnP with amounts above.

PP-copolymer composites with GnP and PP-*g*-MA: It was observed that both the GnP loading and the compatibilizer have a significant positive influence on the mechanical properties and melting temperature of pure PP copolymer. The PP copolymer has a higher affinity with graphene and compatibilizer due to the elastomeric comonomer ethene, present in PP copolymer, which facilitated the interaction with graphene.

This work can provide an effective strategy to produce PP-GnP composites. Graphene additions with high intrinsic mechanical characteristics can improve the mechanical properties of the polymers and, simultaneously, improve the interfacial properties of PP-GnP.

Acknowledgments

The authors thank UNIGEL, and Thermoblend for their support in this work and CNPq, CAPES, and FAPESP for financial support.

References

1. C. N. R. Rao; A. K. Sood; K. S. Subrahmanyam; A. Govindaraj Graphene: The new two-dimensional nanomaterial. Angewandte Chemie International Edition, 48, 2009. doi.org/10.1002/anie.200901678
2. K. Kalaitzidou; H. Fukushima; L. T. Drzal Mechanical properties and morphological characterization of exfoliated graphite–polypropylene nanocomposites. Composites Part A: Applied Science and Manufacturing, 2007, 38, 1675–1682. doi.org/ 10.1016/j.compositesa.2007.02.003
3. J. Z. Liang; Q. Du; G. C. Tsui; C. Tang Tensile properties of graphene nano-platelets reinforced polypropylene composites. Composites Part B: Engineering, 2016, 95, 166–171. doi.org/10.1016/j.compositesb.2016.04.011
4. S. Chunhui; P. Mu; Y. Runzhang The effect of particle size gradation of conductive fillers on the conductivity and the flexural strength of composite bipolar plate**.** International Journal of Hydrogen Energy, 2008, 33, 1035–1039. doi.org/ 10.1016/j.ijhydene.2007.11.013
5. J. Wang; F. Song; Y. Ding; M. Shao The incorporation of graphene enhances the mechanical properties of polypropylene self-reinforced polymer composites. Materials and Design, Elsevier, journal homepage: www.elsevier.com/locate/matdes, 2020. doi.org/10.1016/j.matdes.2020.109073
6. S. Natarajan; R. Rathanasamy; S. K. Palaniappan; S. Velayudham; H. B. Subburamamurthy; K. Pal. Comparison of MA-g-PP effectiveness through mechanical performance of functionalized graphene reinforced polypropylene. Polímeros: Ciência e Tecnologia, 2020, 30, 2020035. doi.org/10.1590/0104-1428.05620

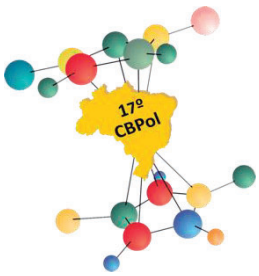

EVALUATION OF THE PHYSICAL AND MECHANICAL PROPERTIES OF POLYMERIC BLENDS WITH RESIDUES OF POLYPROPYLENE MASKS

Anderson R. Santos[1], Tiago V. da Silva[1], Ítalo R. Coura[2], Alexandro A. Silva[2], Patrícia S. O. Patrício[2], Wanna C. Fontes[1]

1 – Federal University of Ouro Preto (UFOP), Ouro Preto, MG, Brazil
anderson.ravik@aluno.ufop.edu.br
2 –Federal Center for Technological Education of Minas Gerais (CEFET), Belo Horizonte, MG, Brazil

Abstract - The Covid-19 pandemic has expanded the use of Non-Woven Fabric (NW), as seen in the manufacture of disposable masks on a large scale. As a consequence, environmental problems related to its disposal have intensified. In this context, the objective of this work was the reuse of polypropylene (PP) from post-consumer non-woven masks in the production of a virgin (vPP) and recycled (rPP) polypropylene blends. The influence of rPP on the physical-chemical and mechanical properties of the blends was evaluated. The post-consumer masks underwent cleaning and size reduction steps. The specimens were produced with different rPP contents by extrusion, pelletizing, and hot compression molding. The results showed that the higher the concentration of rPP in the blend, the lower its mechanical strength as its stiffness increases. However, blends with 50% rPP achieved properties equivalent to vPP, mainly concerning tensile strength.
Keywords: Blend, Polypropylene, Non-Woven Fabric, Waste Reuse, Covid-19 Pandemic.

Introduction

As the contamination of Covid-19 advanced, a growing demand for Personal Protective Equipment (PPE) could be observed, especially procedure gowns and surgical masks, whose mostly raw material is NW [1, 2]. NW is a PP-based polymeric material, convenient and low-cost. However, the indiscriminate use of it and improper disposal represent serious environmental risks since its decomposition can take hundreds of years [4]. The recommendation is to use disposable masks only once, for a maximum of 8 hours of activity [3], which favors waste generation. A possible strategy to reuse NW is to apply it in producing polymeric blends [5]. Generally, recycled polymer costs 40% less than virgin polymer; thus, replacing virgin polymer with recycled polymer provides cost reduction and increased competitiveness, in addition to helping to preserve the environment [6].

PP is one of the most commercialized thermoplastic polymers in the world, including in the composition of polymeric blends [7, 8, 9, 10], presenting advantages such as low cost, recyclability, and high thermal stability [11]. However, the recycling results in the loss of the mechanical and thermal properties of the polymers because they are submitted to high temperatures and high shear rates [12]. Some studies show the gradual loss of PP properties from sequential processing cycles, indicating the number of cycles supported by the PP related to the evaluated properties [10]. Even so, studies specifying blends with recycled NW are less frequent in the literature. Therefore, this work aimed to produce and evaluate the effects of adding rPP from the recycling of NW masks on polymeric blends' physical and mechanical properties. The masks were selected because of their ease of collection.

Methodology

Raw Materials and Molding Procedures to produce polymeric blends, vPP supplied by Piramidal, produced by Braskem, with a fluidity index equal to 3.5 g/10 minutes and density of 0.905 g/cm³ and NW residue from the controlled disposal of surgical masks were used. The masks were washed with water and detergent in a Colormaq LCB washing machine, soaked in water with 0.1% v/v chlorine for one minute, rinsed, and dried in the open air. Then, the parts not composed of PP (elastic bands, wires, etc.) were removed and discarded. The remaining material was fragmented in a Marconi knife mill, model MA 580, with a 1.75 mm sieve attached. rPP and vPP were processed by varying the rPP content by 0, 25, 50, 75, and 100% m/m in a Thermo Scientific single screw extruder, model HaakE Polylab, with a temperature of 175 ºC in the three heating zones and 45 rpm. After being extruded, the material was pelletized in an AxPlástico Pelletizer, Model AX Gran, in grains of approximately 3.70 mm in length. The samples were molded from pelleted grains by hot compression in a hydraulic press with heating, SOLAB brand, model SL11, at a temperature of 180 ºC and 25 MPa of closure for 5 minutes samples were withdrawn after resting for 30 minutes under pressure equal to the molding pressure. Figure 1 presents a flowchart with the raw materials and processes of producing samples from blends and control samples (composed entirely of vPP or rPP).

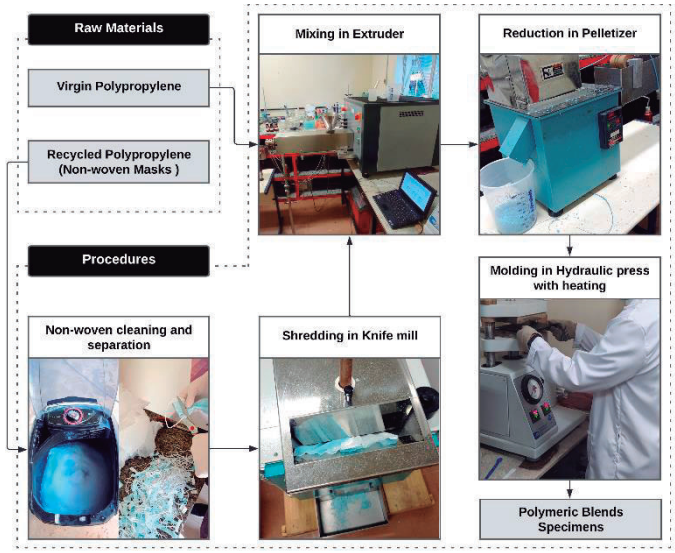

Figure 1 – Photograph of raw materials, the cleaning processes, separation of NW, and production of samples.

Tensile and flexural strength tests were carried out using an Instron Universal Testing Machine, model EMIC 23-20, following Standards D638 [13] and D790 [14], respectively. After 24 hours of immersion, the water absorption test was performed following the conditions and formula of Standard NBR 9486 [15]. Masses were determined using a METTLER TOLEDO precision scale, model PG203-S. The results were obtained from the arithmetic mean of 6 samples tested, with a precision of 0.1%.

Results and discussion

Photographs of the samples of the pure polymers, virgin and recycled, 100vPP and 100rPP, respectively, and the blends are shown in Figure 2. The visual appearance is due to the blue pigment used in some of the layers of NW that make up the masks. The specimens of the blends showed heterogeneities, which became more visible with the higher rPP content. Heterogeneities may have occurred due to contaminants in the PP, such as pigments, which are present in some fabric fibers. Heterogeneity can be improved by processing in extruders with higher mixing power or shear.

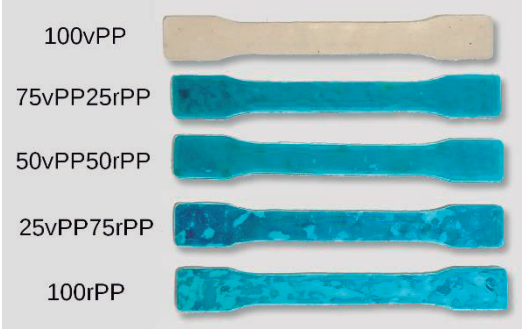

Figure 2 – samples photographs of pure polymers and blends with some contents of the vPP and rPP.

The tensile test results for the materials are shown in Figure 03. Compared to vPP, rPP showed a 25% decrease in tensile strength and a 75% reduction in elongation at break. Young's modulus (Figure 03 b) for rPP is 20% higher than for rPP. There is an increase in the stiffness of the polymer. Barbosa et al. [10] studied blends of recycled PP and virgin PP produced by extrusion processing, then molding the specimens by pressing. The authors obtained values of mechanical properties similar to those obtained for the rPP/vPP blends.

The 75vPP25rPP and 50vPP50rPP blends showed tensile strength, stiffness, and deformation values until failure intermediate to those of the pure materials: vPP and rPP. In addition, the values are similar to each other, considering the standard deviation. The variations were attributed to the heterogeneities observed in the test specimens, as seen in Figure 2. The 25vPP75rPP blend presented the evaluated mechanical properties, tensile strength, deformation until failure, and stiffness more like the rPP.

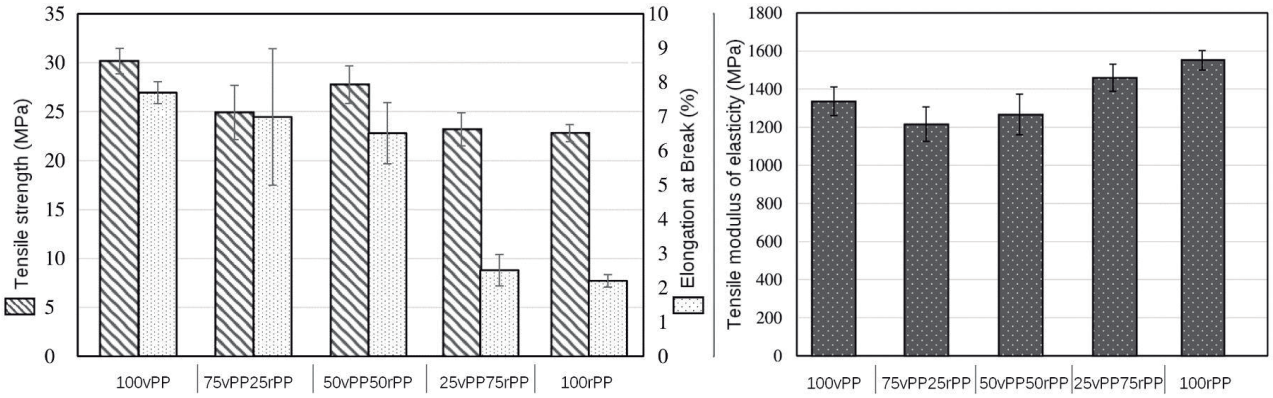

Figure 3 – Graphs of (a) Tensile strength and Elongation at Break and (b) Tensile modulus of elasticity for PPV and rPP and vPP/rPP blends.

Figure 4 presents the results of tension and deformation at maximum force for the flexion test. Comparing the pure materials, vPP and rPP, it was verified that there was a loss of 39% in flexural strength, changing from 53.6 MPa to 32.9 MPa. As observed in the tensile test, the bending deformation drastically reduced for the rPP concerning the vPP.

The values of flexural strength and maximum flexural deformation obtained for the blends with higher vPP contents, 75 and 50 %m/m, are similar to those obtained for pure vPP, considering the standard deviation. As for the 25vPP75rPP blend, the values obtained are intermediate to those of the pure materials.

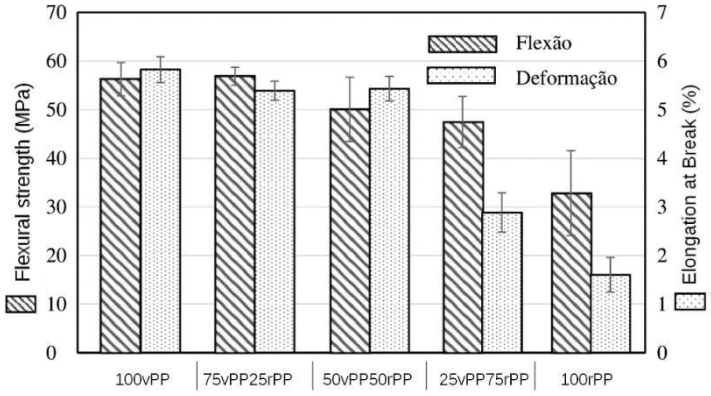

Figure 4 – Graph of (a) Resistance to flexion and deformation

Table 1 presents the average water absorption values of pure materials and blends after immersion in water for 24 hours. All materials showed low water absorption. Only rPP showed higher water absorption than the others, which can be associated with additives at low levels. The blend samples generally did not show pores capable of contributing to water absorption.

Table 1 – Water absorption values (%) for materials based on vPP and PPR.

Sample	Water absorption (%)	Sample	Water absorption (%)
100vPP	0.013 ±0.009	25vPP75rPP	0.014±0.017
75vPP25rPP	0.012±0.020	100rPP	0.037±0.026
50vPP50rPP	0.014±0.012		

Conclusion

The vPP and vPP blends, with contents varying between 25 and 75% by mass of the polymers, were successfully obtained and characterized. The results obtained from the mechanical tests of traction and flexion and water absorption were compared to materials containing pure polymers, vPP and rPP. The PP from NWs (rPP) showed worse mechanical properties than virgin PP since it was previously processed. Generally, the blends with contents of up to 50% of rPP presented the mechanical properties evaluated in the tensile test intermediate to those of the pure materials. The properties determined in the bending test for the same blends are similar to those of pure vPP, considering the standard deviation. The blends containing 75% NW by mass showed lower mechanical properties than the others. In addition, it was verified that the hydrophobicity of the blends did not show significant variation, evaluated by the absorbed water content.

Notably, the number of disposable masks used during the pandemic was very high, and, despite the reduction, they continue to be used, especially in hospital environments. Other non-woven items are also used in different sectors. With this, the work showed a promising path for the environmentally more appropriate destination of pandemic waste, such as NW from disposable masks, compared to disposal in landfills or incineration processes. If there is an interest in producing colored materials, the pigment used is also used according to the device used.

Acknowledgment

To the CAPES, CNPq, and FAPEMIG for financial support. To DEURB, DECIV, PROPEC, PROPPI, and UFOP for their help in carrying out and presenting this research.

References

1. SOUZA, Diego de Oliveira. *A saúde dos trabalhadores e a pandemia de COVID-19:* da revisão à crítica. Vigilância Sanitária em Debate: Sociedade, Ciência & Tecnologia, v. 8, n. 3, p. 125-131, 2020. DOI: 10.22239/2317-269x.01627.
2. HOELZEL, Carlos G. M.; RIBEIRO, Luana C. M. *Manual do projeto EPI* - UFG [Internet]. 2020. Goiânia: Cegraf UFG. 74 p.
3. RAURELL-TORREDÀ, Marta *et al.* Reflections arising from the COVID-19 pandemic. *Enfermería Intensiva* (English ed.), v. 31, n. 2, p. 90-93, 2020.
4. SCHEEREN, Denise; MÄHLMANN, Cláudia Mendes; MÜLLER, Franciélli. Avaliação das propriedades de um compósito de matriz polimérica de polipropileno reciclado reforçado com resíduo de madeira. *Tecno-Lógica*, v. 24, n. 2, p. 132-141, 2020.
5. SANTOS, Cayane Genro *et al.* Uso de blendas poliméricas em nano e microencapsulação. Disciplinarum Scientia| Naturais e Tecnológicas, v. 16, n. 2, p. 311-323, 2015.
6. FERNANDES, Beatriz L.; DOMINGUES, Antonio J. Caracterização mecânica de polipropileno reciclado para a indústria automotiva. *Polímeros*, v. 17, p. 85-87, 2007. DOI: 10x1590:S0104-14282007000200005.
7. SANTOS, Luciene da S. *et al.* Estudo do efeito da adição de PP reciclado nas propriedades mecânicas e de escoamento de misturas de PP/EPDM. Polímeros, v. 23, p. 389-394, 2013.
8. MATIAS, Áurea A. *et al.* Use of recycled polypropylene/poly (ethylene terephthalate) blends to manufacture water pipes: An industrial scale study. Waste Management, v. 101, p. 250-258, 2020.
9. STOIAN, Sergiu Alexandru et al. Recycled polypropylene with improved thermal stability and melt processability. *Journal of Thermal Analysis and Calorimetry*, v. 138, n. 4, p. 2469-2480, 2019.
10. BARBOSA, L. Gustavo; PIAIA, Matheus; CENI, G. Henrique. Analysis of impact and tensile properties of recycled polypropylene. *International Journal of Materials Engineering*, v. 7, n. 6, p. 117-120, 2017.
11. QIU, Wulin *et al.* Preparação e características de compósitos de celulose altamente cristalina com polipropileno: Efeitos do polipropileno maleado e do conteúdo de celulose. *Journal of Applied Polymer Science*, v. 87, n. 2, pág. 337-345, 2003.
12. KIM, Hee-Soo *et al.* The effect of types of maleic anhydride-grafted polypropylene (MAPP) on the interfacial adhesion properties of bio-flour-filled polypropylene composites. *Composites Part A: Applied Science and Manufacturing*, v. 38, n. 6, p. 1473-1482, 2007.
13. AMERICAN SOCIETY FOR TESTING AND MATERIALS (ASTM). *D638 – 14*: Standard test method for Tensile properties of plastics. West Conshohocken, PA, 2014.
14. AMERICAN SOCIETY FOR TESTING AND MATERIALS (ASTM). *D790-07:* Standard Test Methods for Flexural Properties of Unreinforced and Reinforced Plastics and Electrical Insulating Materials. West Conshohocken, PA: Astm, 2007.
15. ASSOCIAÇÃO BRASILEIRA DE NORMAS TÉCNICAS (ABNT). *NBR 9486*: Compensado – Determinação da absorção de água. Rio de Janeiro, 2011.

IMPACT EVALUATION OF GLASS FIBER / POLYESTER WATERPROOF COMPOSITE SUBJECTED TO TEMPERATURA AND ACID ENVIRONMENT

Bruno C. Gary[1*], Gerson Marinucci[1] and Leonardo G. A. Silva[1]

1 – Instituto de Pesquisas Energéticas e Nucleares, (IPEN-CNEN), São Paulo, SP, Brazil
bruno.caravelas@usp.br

Abstract - Polymer composites have a wide range of chemical applications, with strong performance in the paper and cellulose and sugar-alcohol industry due to the chemical resistance such materials offer because of the presence of the polymer matrix. The literature shows that vinyl ester resins offer chemical resistance for these applications, however at a higher price than commercial resins, such as unsaturated polyesters. The aim of this research was to evaluate the chemical resistance of glass fiber reinforced waterproof polyester resin composites (GFPO). Composite was manufactured by hand lay-up and the waterproof polyester specimens were kept immersed in a buffer solution with pH 3 at 70 °C for 150 days. To evaluate the behavior of waterproof polyester composites, IZOD impact tests were performed and compared with properties of the vinyl ester composites. After the chemical resistance test, the GFPO composite presented an Impact resistance of 1683 J/m with a absorbed energy of 5.3 J. In conclusion, a waterproof polyester resin composite can be a good option for applications in corrosive environments where a vinyl ester resin composite would be applied.

Keywords: *composite, vinyl ester, polyester, sealing, acid environment.*

Introduction

Composite materials offer numerous benefits covering a wide range of applications, with emphasis on the automobile industry, civil construction, aeronautics, sugar and alcohol, pulp and paper, wind energy, laser equipment and chemical industries, being an excellent choice for manufacturing components subjected to static and dynamic stresses [1] because of its high specific mechanical strength and fatigue resistance. Boeing 787 and Airbus A350 airplanes show the benefits of using composite materials, which, according to the respective manufacturers, present 50% and 53% in mass, providing a reduction of 11% and 14% in mass compared to conventional airplanes of the same class. Therefore, it allows a significant reduction in fuel consumption and contributing to the reduction of CO_2 emissions, thus definitively paving the way for using composites in all aeronautical segments.

However, polymeric composite structures can be compromised when used in aplications where polymer matrix can be damaged by environment condition. There are numerous structural components made of composite materials that constituent materials can fail when subjected to the condition of an aggressive environment, if they are not properly designed for this specific use.

For applications in aggressive media, vinyl ester resins have experienced a large number of applications in acidic or alkaline media, for example in storage tanks for organic raw materials,

such as aqueous polymeric emulsions, lubricants and surfactants. However, some resins, such as polyester, for example, which have a high demand and offer an attractive price, can seriously compromise a composite in aggressive environments [2] if used inappropriately and even affect the production of a company.

In general, the degradation of materials represents a high expense for the industry, either due to an early stop for maintenance or even by reducing the lifespan of the component or structure [3]. Studies that propose the evaluation of materials in aggressive media are particularly important in marine environments, oil and gas production, sugar and alcohol industries, chemical plants, pulp and paper and energy conversion and generation systems, including fossil and nuclear.

Some authors [4, 5] have developed new methodologies to perform accelerated physical degradation tests on pultruded profiles of glass fiber reinforced vinyl ester matrix composites [6], others have studied, in a short period of time, the durability of a reinforced vinyl ester matrix composite with fiberglass exposed to six different environmental conditions [7]. It is also found in the literature that applications of composite materials that interact with corrosive fluids work with a temperature of 70 °C [8].

The aim of this research was to evaluate the chemical resistance of glass fiber reinforced waterproof polyester composites (W-GFPO) and compare with the behavior of glass fiber reinforced polyester composites (GFPO). Both composites were manufactured by hand lay-up polyester specimens and waterproofed with epoxy resin were kept immersed in a buffer solution with pH 3 at 70 °C for 150 days.

Experimental

Materials

The GFPO panels were manufactured by Afinko Polímeros with a plain weave fabric of 330 gm^{-2}, both in a hand lay-up process, and a fiber ratio of 55% in volume. The resins used in this study were unsaturated polyester (PO).

To waterproof the GFPO, now called W-GFPO, a bisphenol-F epoxy resin-based coating was used, which was supplied by Masterpol Adhesives, under the trade name of M-CR500. Fig. 1 shows the GFPO and W-GFPO samples.

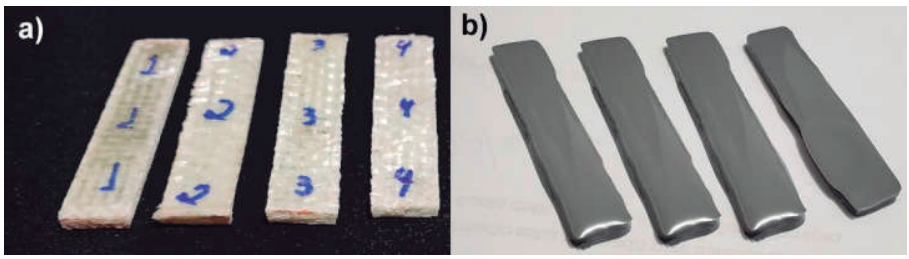

Figure 1: Composite samples: a) GFPO, b) W-GFPO

The waterproofing membrane is composed by an epoxy resin and a cycloaliphatic amine. Compared to aliphatic amines, cycloaliphatic amines offer less volatility, greater light stability, less reactivity, less toxicity and better color retention. In pure state, they find great difficulty in curing at room temperature, due to their low reactivity [9].

A pH 3 buffer solution was used to evaluate the chemical resistance of W-GFPO composites. Buffered solutions are solutions that resist changes in pH when small amounts of strong acid or strong base are added to them. The pH variations that occur in the buffered solutions are insignificant when compared to the variations in the unbuffered solutions; therefore, these solutions are used to keep the pH constant to prepare solutions of defined pH.

Temperature and acid environment

The samples were immersed in a buffer solution and kept in a temperature-controlled oven at 70 ºC, as shown in Fig. 2, and isolated to avoid evaporation of the solution. Thickness and mass measurements were performed daily for 150 days and no significant changes were identified compared to samples before the test, indicating that the waterproofing agent preserved the chemical attack.

Figure 2: Oven with controlled temperature for samples storage

Characterization methods

In order to characterize the GFPO samples were kept under temperature and acid environment and IZOD impact tests were performed.

The IZOD impact properties of the composites were determined by testing guided by ASTM D1822, with geometry of 3.2 x 12.7 x 127 mm. The IZOD impact test was carried out in the NZ Phipolymer equipment, model XRL-400, with a pendulum of 22 J and calibrated in 2022.

A glass mold with rubber seals was used to manufacture the composite plates and a Macrotop saw, model SFM-750, a Manrod milling machine model ZX-40HC/PC (MR-205-B) and a mask with the oriented geometries for machining the samples.

Results and Discussions

Table 1 shows the results of the composite impact tests. A small drop around 0.4% in the absorbed energy property can be seen, when comparing GFPO and W-GFPO specimens, which should be associated with the post-curing effects. With longer chemical test times, 12 and 24 months, the literature shows [11] that this property tends to increase after an initial decrease. The specimen for chemical testing had the waterproofing agent; however, the authors [11] do not offer any reinforcing properties to the composite.

Table 1: IZOD impact test results of GFPO and W-GFPO composites before and after chemical testing

Composite	GFBO	W-GFBO
Impact resistance (J/m)	5.3	5.2
Absorbed energy (J)	1683	1676

Conclusions

A waterproof polyester resin composite can be a good choice for applications in corrosive environments where a vinyl ester resin composite would be applied, providing cost savings where a more expensive option would be used to obtain similar results. The study with a temperature of 70 °C proved to be effective in use in important fields, such as sugar and alcohol industries, chemical plants, pulp and paper.

Acknowledgements

The authors are grateful for financial support from FAPESP, CNPq and CAPES. The authors are also grateful for the supply of waterproofing products by Masterpol.

References

[1] G. Mansour, K. Tsongas, D. Tzetzis. Composites Part B: Engineering, v. 94, 2016, 152–159.

[2] J. M. Margolis. Advanced Thermoset Composite Industrial and Commercial Applications, 1986, 74-107.

[3] K. J. Kurzydlowski, M. Lewandowska, W. Swieszkowski. Faculty of Materials Science and Engineering. 2007, 43.

[4] B. Benmokrane, A. H. Mohamed, A. Elsafty. Compos. B Eng. v. 114, 2017, 163–174.

[5] G. Carra, V. Carvelli. Compos. Struct. v. 108, 2013, 1019–1026.

[6] Y. Miyano, M. Nakada, N. Sekine. Composites: Part B. v. 35, 2004, 497-502.

[7] H. Y. Kim, H. Park, Y. J. You, C. K. Moon. Structural Engineering, 2016, 291- 295.

[8] G. Nhels. Tecniplas extends useful life of composites equipment used in paper mill by 50%. Disponível em: <https://www.compositesworld.com// > fev. 2021. Acesso em: 10 junho. 2021.

[9] MASTERPOL. Datasheet. Impermeabilizante MASTERPOX CR500, out. 2019.

[10] G. Marinucci in *Polymeric Composite Materials - Fundamentals and Technology*, Ed.; Artliber, São Paulo, 2011, 15-39.

[11] F. S. Cabral, J. R. Correia, M. P. Rodrigues, F. A. Strain, An International Journal for Experimental Mechanics, 2012, 162-173.

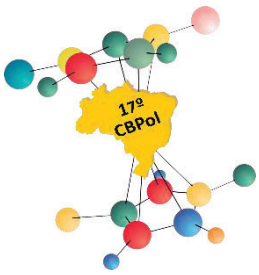

INFLUENCE OF CURE CONDITIONS ON CROSSLINKG AND DYNAMIC MECHANICAL BEHAVIOR OF EPOXY

Linconl A. Teixeira *, Michaella S. B. Fialho and Sandra M. da Luz

Mechanical Sciences Graduate Program, University of Brasília (UnB), Brasília, DF, Brazil
*linconl_araujo@hotmail.com**

Abstract - The experimental determination of cure-dependent viscoelastic properties is of utmost importance for the processing and use of materials based on epoxy resin for structural application. Although this complex topic is frequently addressed in the literature, there are different standards of the curing process and few general guidelines to obtain the best curing cycles. Hence, three different cure conditions applied to epoxy were conducted in this work, including their preparation and evaluation. Dynamic mechanical analysis (DMA) is commonly used to characterize epoxy resin at temperatures ranging from room temperature above their glass transition temperatures. The viscoelastic behavior of epoxy resin and properties such as storage modulus, loss modulus, and damping were experimentally evaluated. The analysis was conducted from 35 to 220 °C in an equipment operating in its three-point bending mode at 1 Additionally, the cure degree was evaluated by Fourier transformer infrared (FTIR). Hz. The epoxy resin samples were submitted to three curing conditions: First - the epoxy resin (1st cycle) was cured at room temperature for 24 h with a post-cure at 120 °C for 1h; Second, the epoxy resin (2nd cycle) was cured in an oven at 100 °C for 4 h; and the Third - the sample was prepared by mixing epoxy resin, hardener, and accelerator in a proportion 100:38:1, cured at room temperature without post-cure, named epoxy resin (accelerator). The FTIR analysis shows the cure degree was achieved for the three curing conditions studied, with a confirmation of the decrease/disappearance of bands at 858 and 917 cm^{-1}. Also, DMA results showed the epoxy resin (2nd cycle) exhibited an improvement in E' (2300 MPa) and E" (137 MPa) compared to other cure experiments. Further, the epoxy resin (1st cycle) showed a higher T_g (135ºC) in relation to other cycles. To conclude, the mobility of the epoxy chains was affected by different curing cycles. Also, the accelerator without post cure is not capable to give the fully cure.

Keywords: *Dynamic mechanical analysis, DMA, epoxy resin, curing cycle.*

Introduction

Epoxy resin is one of the main thermosetting polymers and is versatile in advanced engineering materials applications. Thus, the curing process involving these materials is one of the most important and complex steps in manufacturing polymeric composites, as it uses a certain level of energy that promotes the polymerization of the matrix. In addition, the curing process obeys the mixture in stoichiometric quantities and homogenization to guarantee the material's expected properties [1].

The curing reaction of epoxy resins is carried out through the hardener, which initiates the formation of three-dimensional crosslinks. Depending on the mechanism, external energy is necessary. The thermal profile applied to cure the system resin/ hardener is called the curing cycle and consists of heating phases, temperature levels, and controlled cooling. The change in density, viscosity, and shrinkage phenomena can affect the cured material. Moreover, the curing process can be accompanied by a post-curing cycle, where the aim is to achieve the final properties of the polymeric matrix, such as the highest cure degree [2]. Furthermore, it is convenient to define a minimum glass transition temperature where the thermal and mechanical stability of the epoxy resin can be achieved.

However, for the curing process to occur, these matrices depend on curing agents that catalyze the formation of crosslinks, which directly affects the mechanical properties of the material [3]. Trying to understand the curing process of an epoxy resin more effectively can also contribute to selecting a resin that meets needs related to processability and performance.
Hence, measuring and understanding the cure-dependent viscoelastic properties is of significant interest for epoxy matrices processing for structural application. This study's main objective is to study the effect of different curing cycles or conditions on dynamic mechanical epoxy resin properties. Moreover, this study is expected to determine the best curing cycle for the analyzed material, thus choosing the cycle that makes the epoxy matrix more resistant to the stresses applied to the material.
Additionally, DMA is a technique typically capable of measuring subtle transitions in thermosetting polymers, thus through this analysis, phenomena such as T_g (glass transition temperature) and the impact of crosslinking on the curing cycle of highly crosslinked resins are usually only measurable by DMA because methods such as DSC can't be sensitive enough [4]. Furthermore, DMA has become an essential technique for determining the viscoelastic properties of fiber-reinforced composites and analyzing the influence of fibers on the curing process and their impact on their properties.

Experimental

Materials

All experimental tests were performed with a commercially available Araldite LY 5052 epoxy resin and Aradur 5052 hardener from HUNTSMAN, USA.

Specimen manufacturing

All the specimens were prepared by mixing proper quantities of epoxy resin and hardener in a proportion of 100:38. The epoxy resin was submitted to three curing conditions: First - the epoxy resin (1st cycle) was cured at room temperature for 24 h with a post-cure at 120 °C for 1h; Second, the epoxy resin (2nd cycle) was cured in an oven at 100 °C for 4 h; and the Third - the sample was prepared by mixing epoxy resin, hardener, and accelerator in a proportion 100:38:1, cured at room temperature without post-cure, named epoxy resin (accelerator).

Methods

FTIR spectra were collected using a Fourier transform infrared spectrometer (NICOLET IS10 from Thermo Scientific). Each spectrum was recorded in the 400 – 4000 cm^{-1} with a resolution of 4 cm^{-1} and 128 scans.
The Dynamic Mechanical Analyzer used to characterize the epoxy specimens was a NERZSCH, model 242 E Artemis. The test was conducted over flat rectangular specimens with 50 × 10 × 2.5 mm dimensions using a three-point bending fixture with a free length of 20 mm. Then, the analysis was performed with a constant heating rate of 2 °C/min, 1 Hz frequency at 35 to 220 °C range.

Results and Discussion

An investigation of its chemical behavior was carried out using the FTIR technique to better understand the epoxy resin curing process and the effect that the different curing cycles and conditions can have on the material properties. Fig. 1 shows the spectra of the epoxy resin at the end of its curing process for each condition, and in the detail, the highlighted bands at approximately 845 and 914 cm^{-1}, correspondent to the stretching of the C-O bond related to the epoxy ring's vibrations. Note that the intensity of bands 845 and 914 cm^{-1} at the end of epoxy resin (1st cycle) and resin epoxy (accelerator) decreased and practically disappeared in cycle 2nd, suggesting that the epoxy rings reacted during curing and became part of the epoxy network. Moreover, the decrease or disappearance of these bands corresponds to the curing of the epoxy resin [6].

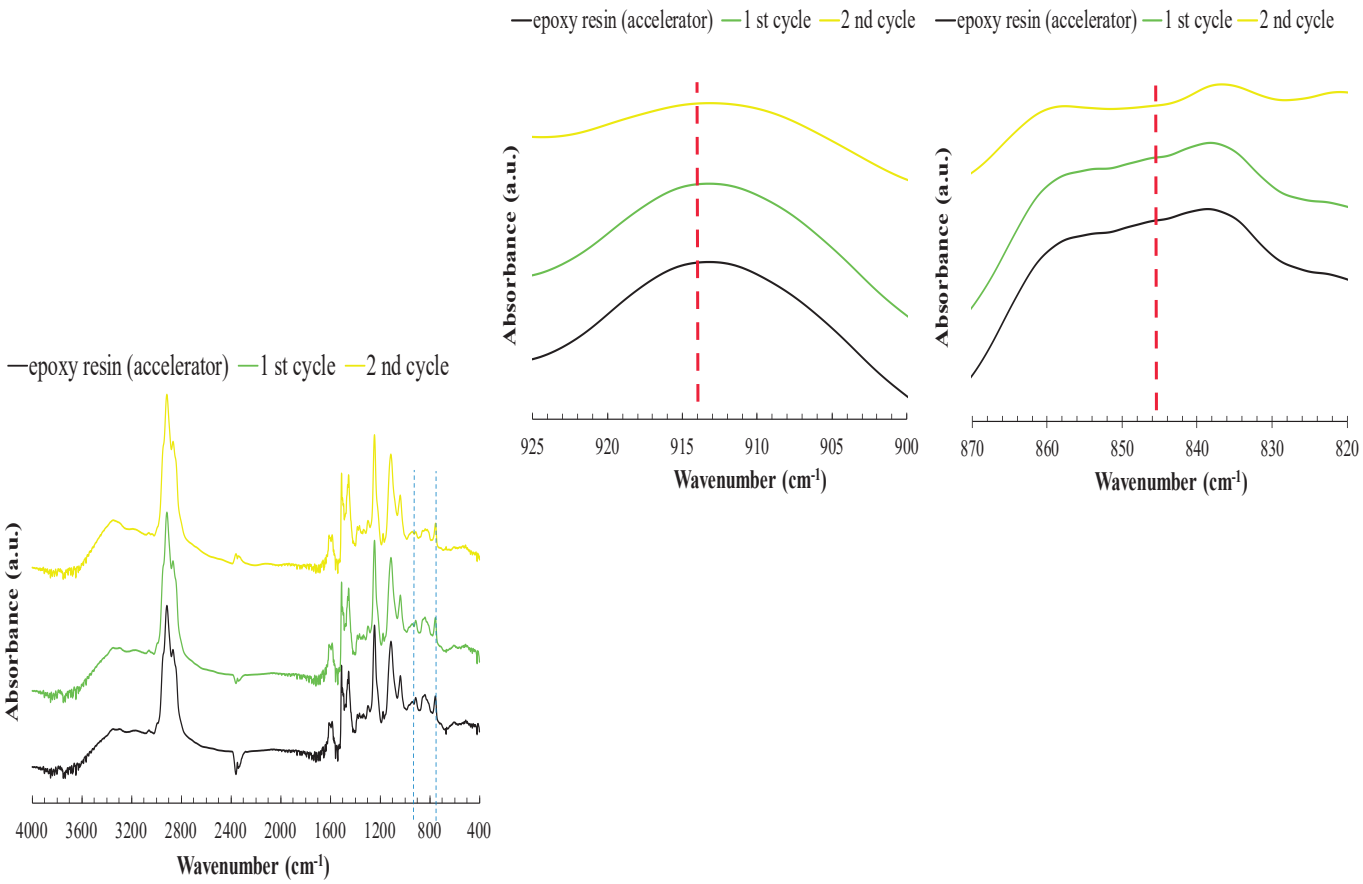

Figure 1. FTIR spectra of the epoxy resin with different cure conditions. The inset shows the subtraction spectra the highlighted bands at approximately 845 and 914 cm^{-1}.

Fig. 2 shows the dynamic properties vs. temperature for all specimens. Also, Tanδ (damping ratio), storage modulus (E'), and loss modulus (E") curves for all specimens as a function of temperature can be found. It is observed that the different curing conditions were able to cause differences in the dynamic properties of the epoxy resin. From this Fig.2 we can determine the gel time (crosslinks have progressed to forming an "infinitely" extended network across the specimen) of the specimens studied by crossover the curves E', E". As we can observe (see Fig. 2), the gel time changed according to the different curing conditions.

The corresponding values from Fig. 2 have been provided in Table 1. It is evident from Table 1 that 2nd cycle has the highest peak of Tanδ (0.57). This is attributed to strong molecular mobility provoked by curing at higher temperatures. Furthermore, this higher Tanδ indicates that the capacity energy absorption by the material is higher [7]. Also, Tanδ peak values for the 1st cycle and accelerator samples decreased 33% and 27%, respectively, in respect to the 2nd cycle, which means the post-cure process and the insertion of the accelerator in the curing cycles reduced the ability of the material to dissipate more energy. The 1st cycle allows a higher T_g occasioned by the post-cured process. However, the post-cured on the epoxy resin decreases the material's stiffness due to reduced chain mobility caused by additional cross-linking in the post-cured samples [4].

Table 1 shows a variation of the E' of the epoxy resin with different cures. The 2nd cycle exhibited a storage modulus of 2300 GPa, an increase of 155% compared with the 1st and epoxy resin (accelerator), which revealed a similar storage modulus of 900 GPa. This means that the 2nd cycle increased the epoxy matrix capacity to support mechanical constraints with recoverable viscoelastic deformation. In particular, the stiffness is substantially increased within this cycle. Regarding the

reduction of E′ to 1st and epoxy resin (accelerator), the lower molecular mobility of the polymer chain for these specimens implies the loss of stiffness [8].
Also, in Table 1, the epoxy resin epoxy resin (accelerator) exhibits the lowest loss modulus value, 28 MPa, because of the increasing molecular mobility of the polymer chain caused by the accelerator. Around 380% improvement in the E″ is observed for epoxy resin 2nd cycle compared to epoxy resin 1st cycle. This may be attributed to the strong resistance to molecular mobility offered by crosslink networks [9].

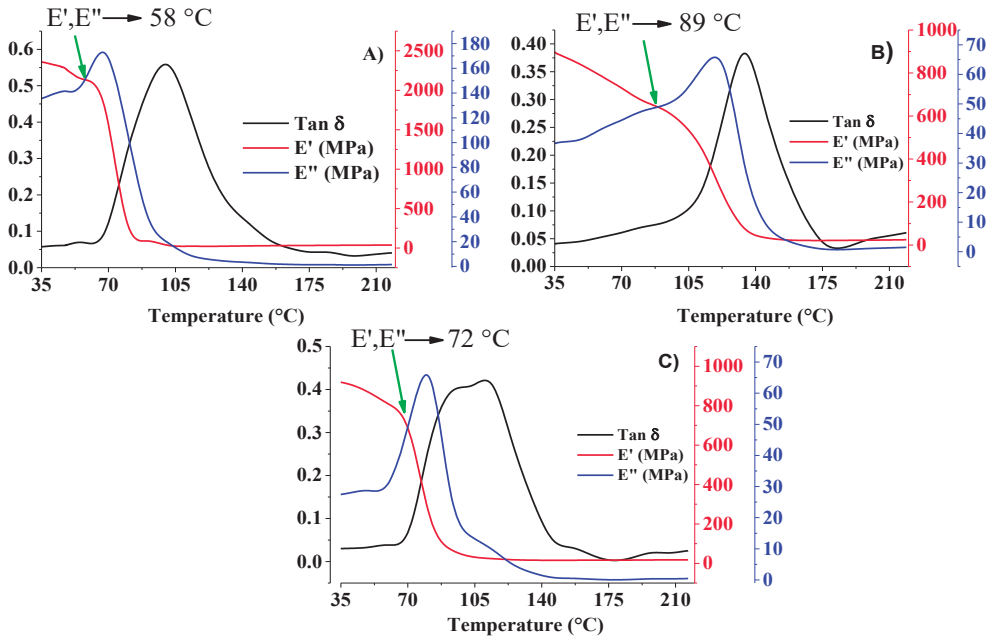

Figure 2. The dynamic properties vs. temperature of the epoxy resin with different cures. A) Specimen cured in an oven at 100 °C for 4 h. B) At room temperature for 24 h with a post-cure at 120 °C for 1h. C) Specimens cured with the accelerator at room temperature for 24 h. At frequency level 1 Hz.

Table 1. Dynamic mechanical analysis of epoxy resin with different cures.

Specimen	T_g from Tanδ_{max} [°C]	Peak height of Tanδ curve	Storage Modulus (E'$_{max}$) [MPa]	Loss Modulus (E"$_{max}$) [MPa]
Epoxy resin (1st cycle)	135	0.38	900	38
Epoxy resin (2nd cycle)	100	0.57	2300	137
Epoxy resin (accelerator)	100	0.43	900	28

Conclusions

The FTIR analysis confirmed that the different epoxy resin cures could cure the materials analyzed with the decreased/disappearance of the 858 and 917 cm^{-1} bands. DMA results showed a considerable effect of curing cycles on the viscoelastic properties of the epoxy resin. Amongst the specimen's analyses, 2nd cycle exhibited an impressive improvement in E' (2300 MPa) compared to other specimens. Further, the storage modulus was higher when the specimens were cured at higher

temperatures, contributing to the epoxy matrix achieving a greater crosslink. This made o epoxy resin more resistant to support mechanical stress.
Moreover, the 2nd cycle has the highest peak of Tanδ (0.57). This higher Tanδ indicates that the capacity energy absorption by the material is higher. It is very worth mentioning that loss modulus also follows an improvement for the 2nd cycle. This may be attributed to the strong resistance to molecular mobility offered by the crosslink networks formed in higher temperatures. Furthermore, the different temperatures used to cure the epoxy resin were able to modify the properties of the thermosetting matrix, in addition, the use of the accelerator did not contribute to the gain of properties.

Acknowledgments

The authors would like to thank CAPES for providing a scholarship to the first author. The authors also thank DPG/UnB, FAPDF, and CNPq for their financial support of this project.

References

[1] Tziamtzi CK, Chrissafis K. Optimization of a commercial epoxy curing cycle via DSC data kinetics modelling and TTT plot construction. Polymer (Guildf) 2021;230:124091. https://doi.org/10.1016/j.polymer.2021.124091.
[2] Campana C, Leger R, Sonnier R, Ferry L, Ienny P. Effect of post curing temperature on mechanical properties of a flax fiber reinforced epoxy composite. Compos Part A Appl Sci Manuf 2018;107:171–9. https://doi.org/10.1016/j.compositesa.2017.12.029.
[3] Deringer T, Gröschel C, Drummer Di. Influence of mold temperature and process time on the degree of cure of epoxy-based materials for thermoset injection molding and prepreg compression molding. J Polym Eng 2018;38:73–81. https://doi.org/10.1515/polyeng-2016-0409.
[4] Goertzen WK, Kessler MR. Dynamic mechanical analysis of carbon/epoxy composites for structural pipeline repair. Compos Part B Eng 2007;38:1–9. https://doi.org/10.1016/j.compositesb.2006.06.002.
[5] Gupta MK, Srivastava RK. Mechanical , thermal and dynamic mechanical analysis of jute fibre reinforced epoxy composite 2015.
[6] Pereira Barros JJ, Dayane dos Santos Silva I, Jaques NG, Lia Fook MV, Ramos Wellen RM. Influence of PCL on the epoxy workability, insights from thermal and spectroscopic analyses. Polym Test 2020;89:106679. https://doi.org/10.1016/j.polymertesting.2020.106679.
[7] Menard KP. Dynamic Mechanical Analysis : A Practical Introduction. vol. 2. New York: 2008.
[8] Vinu Kumar SM, Senthil Kumar KL, Siddhi Jailani H, Rajamurugan G. Mechanical, DMA and Sound Acoustic behaviour of Flax woven fabric reinforced Epoxy composites. Mater Res Express 2020;7:085302. https://doi.org/10.1088/2053-1591/abaea5.
[9] Murugan R, Ramesh R, Padmanabhan K. Investigation on Static and Dynamic Mechanical Properties of Epoxy Based Woven Fabric Glass/Carbon Hybrid Composite Laminates. Procedia Eng 2014;97:459–68. https://doi.org/10.1016/j.proeng.2014.12.270.

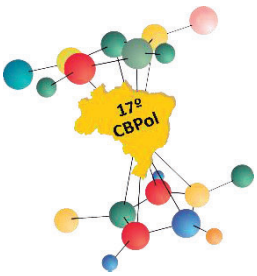

MODIFICATION AND CHARACTERIZATION OF *LUFFA CYLINDRICA* FIBERS WITH ZINC NANOFERRITE

Eduardo Gavazzoni[1]*, Fernando G. S. Júnior [2], Paulo R. S. Bittencourt[3] and Juliana R. Kloss[1]

1 – Academic Department of Chemistry and Biology, Federal University of Technology – Paraná (UTFPR), Curitiba, PR, Brazil dugava19@gmail.com
2 – Institute of Macromolecules Eloísa Mano (IMA), Federal University of Rio de Janeiro (UFRJ), Rio de Janeiro, RJ, Brazil
3 – Academic department of chemistry (DAQ), Federal University of Technology – Paraná (UTFPR), Medianeira, PR, Brazil

Abstract – *Luffa cylindrica* fibers, better known as vegetable sponges or loofahs, already possess various characteristics for technological applications. With the intention of obtaining superior properties, modification and incorporation of a metallic nanoparticle were performed. The vegetable sponge was initially treated with sodium hydroxide to decrease the lignin percentage of the material. Zinc ferrite nanoparticles were synthesized through the co-precipitation method in a solution to anchor them onto the fiber surface. The Luffa cylindrica/$ZnFe_2O_4$ material was characterized by FTIR, SEM, XRD, and TEM. The results demonstrated a reduction in the lignin percentage after alkaline treatment and the attachment of zinc ferrite nanoparticles onto the fiber surface, resulting in a material with potential for technological applications.

Keywords: *Natural fibers, metallic nanoparticles, composites, alkaline treatment.*

Introduction

To improve the properties of the vegetable sponge, one alternative could be the incorporation of metallic nanoparticles. For instance, zinc ferrite nanoparticles have a wide range of applications due to their physical and chemical properties, as well as their high surface area, which results in increased reactivity. Moreover, they exhibit high thermal and chemical stability, making them attractive for use in composite materials and in water treatment and environmental pollutant processes [1].

Vegetable sponge fibers have already been used as a support for metallic nanoparticles. For instance, a combination of nickel and zinc ferrites with calculated proportions was used to evaluate the electrical properties of the material [2]. In another study, ferrites were prepared using the combustion method for the degradation of organic dyes [3]. A different combination of zinc and aluminum oxides was investigated for water decontamination purposes [4]. Considering the advantages offered by ferrites, zinc ferrite stands out due to its reliance on easily accessible and low-cost reagents.

The structure of the zinc ferrite nanoparticles, represented in Figure 1, is classified as spinel structure, characterized by a three-dimensional crystal lattice composed of zinc and iron atoms. The spinel structure is one of the most common crystal structures in inorganic materials and is known for its high thermal, chemical, and mechanical stability [3,4].

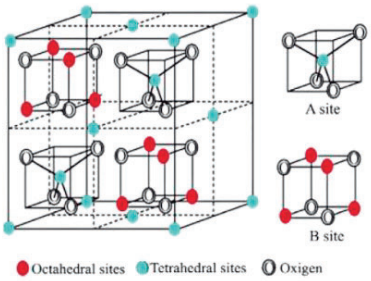

Figure 1 - Chemical structure of zinc ferrite ($ZnFe_2O_4$)

Based on the information presented, the objective of this study was to modify and characterize Luffa cylindrica fibers with zinc ferrite nanoparticles, aiming for future applications in geopolymers matrices and the field of contaminant removal in aqueous solutions.

Experimental

In order to obtain the vegetable sponge (VS) with specific characteristics for modification with nanoparticles, an alkaline treatment was performed using sodium hydroxide (NaOH) through two methods. The first method involved weighing 5.0 g of powdered vegetable sponge and adding 0.5 $mol.L^{-1}$ sodium hydroxide solution under constant stirring for 1 hour at room temperature. The mixture was then filtered, washed with distilled water, and dried in an 80°C oven until a constant mass was achieved. The second method utilized a 0.1 $mol.L^{-1}$ sodium hydroxide solution and involved heating the mixture at 100°C, followed by the subsequent steps as previously mentioned.

Both methodologies were applied to powdered vegetable sponge and natural fiber vegetable sponge. All samples, before and after treatment, were analyzed using Fourier-transform infrared spectroscopy (FTIR), X-ray diffraction (XRD), and scanning electron microscopy (SEM) to evaluate possible changes in morphology and assess the effectiveness of the alkaline treatment in lignin removal or reduction.

For the synthesis of Luffa cylindrica/$ZnFe_2O_4$, a solution of zinc chloride ($ZnCl_2$) and iron chloride ($FeCl_3$) was initially prepared in the stoichiometric ratio of 1:2, respectively. The vegetable sponge, previously treated by the two methods mentioned, was added to the solution along with sodium hydroxide (NaOH) to adjust the pH and induce precipitation. The system was maintained under constant stirring and heated at 60°C for 1 hour, followed by drying in an oven at 75°C for 24 hours. For treatment method 1, the material was identified as BVFe1, while for treatment method 2, it was labeled as BVFe2. The same procedure was repeated with the fibers of the vegetable sponge treated by the two alkaline methods, resulting in BVFe3 for method 1 and BVFe4 for method 2.

The characterization of the modified vegetable sponge with zinc ferrite nanoparticles was carried out using techniques such as Fourier-transform infrared spectroscopy (FTIR), scanning electron microscopy (SEM), X-ray diffraction (XRD), and transmission electron microscopy (TEM).

Results and Discussion

Initially, the results obtained from the FTIR analysis of the pure vegetable sponge and Luffa cylindrica/$ZnFe_2O_4$ are presented (Figure 2).

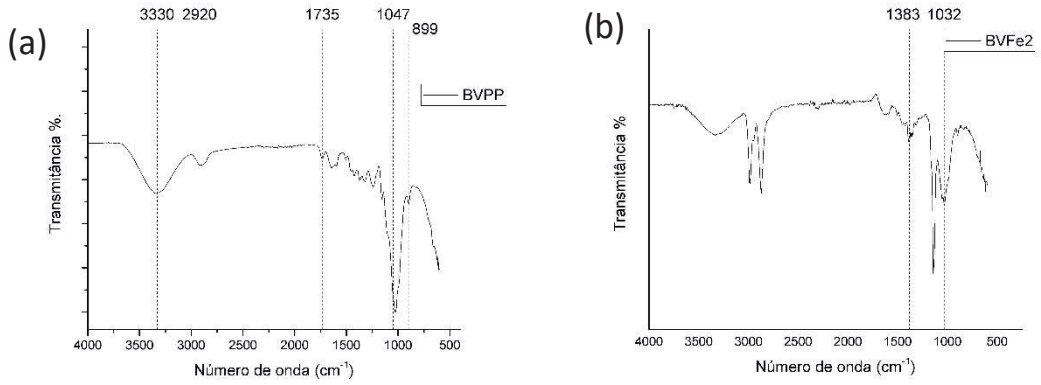

Figure 2 - FTIR of the pure vegetable sponge (a) and the *Luffa cylindrica*/$ZnFe_2O_4$ material (b).

In the spectrum (Fig. 2a), several characteristic bands of lignocellulosic materials were observed. These include a band at a wavelength of 3330 cm^{-1}, corresponding to the stretching vibration of the -OH bond present in the cellulose structure, and a band at 2920 cm^{-1} representing symmetric (-CH_3) and asymmetric (-CH_2) stretching vibrations, which can be attributed to the methyl and methylene groups present in cellulose, hemicelluloses, and lignin. These results are in accordance with the findings of Martinez-Pavetti et al. [5].

In the spectrum (Fig. 2b), two prominent bands at wavelengths of 1032 and 1383 cm^{-1} were observed, corresponding to the Zn-O bonds present in the zinc ferrite nanoparticles, as also reported in the study by Kesraoui, Bouzaabia, and Seffen [4].

The Figure 3 shows the X-ray diffraction (XRD) diffractogram of the pure vegetable sponge (VS) and *Luffa cylindrica*/$ZnFe_2O_4$ (powdered) samples.

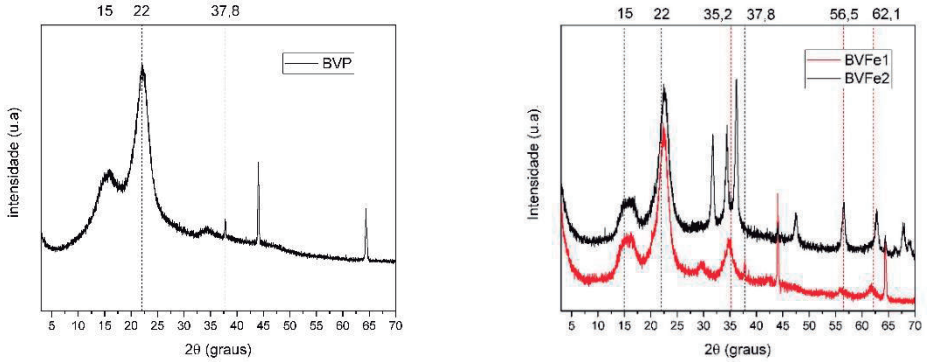

Figure 3 - Diffractogram of the pure vegetable sponge sample (a) and the BVFe1 and BVFe2 materials (b).

The data demonstrated peaks at 2θ values of 15, 22, and 37.8 for the pure vegetable sponge, which correspond to the crystalline portion of cellulose. These values are consistent with the findings of Martinez-Pavetti et al. [5]. The calculation of the crystalline portion of the material was performed by determining the area of the peaks in the diffractogram, following Eq. 1, where l_crystalline is the area of the crystalline portion and l_amorphous is the area of the amorphous portion. The calculation resulted in a crystalline content of 34.79% for the pure vegetable sponge.

$$[\%\ \text{crystallinity} = \frac{l\ crystalline}{l\ crystalline + l\ amorphous} \text{ x } 100] \quad (1)$$

For the *Luffa cylindrica*/$ZnFe_2O_4$ compositions, crystallinity values of 51.98% were observed for BVFe1 and 53.68% for BVFe2. These values are higher compared to the pure vegetable

sponge due to the addition of an inorganic material with a crystalline structure. These findings are consistent with those reported in the literature by other authors [1,2].

After the addition of zinc ferrite nanoparticles, the appearance of peaks corresponding to the spinel structure of the ferrite nanoparticles was observed at 2θ values of 35.2°, 56.5°, and 62.1° [5].

Regarding the SEM analysis, the obtained images for the powdered *Luffa cylindrica*/$ZnFe_2O_4$ (a) and (b) and the fiber samples (c) and (d), as shown in Figure 4, it was observed that in the BVFe2 sample, the nanoparticles were fixed on the surface, possibly due to the high surface area of the powdered sponge. In contrast, in the images (c) and (d) of the vegetable sponge fiber, a more pronounced uniformity in the distribution of the nanoparticles was observed.

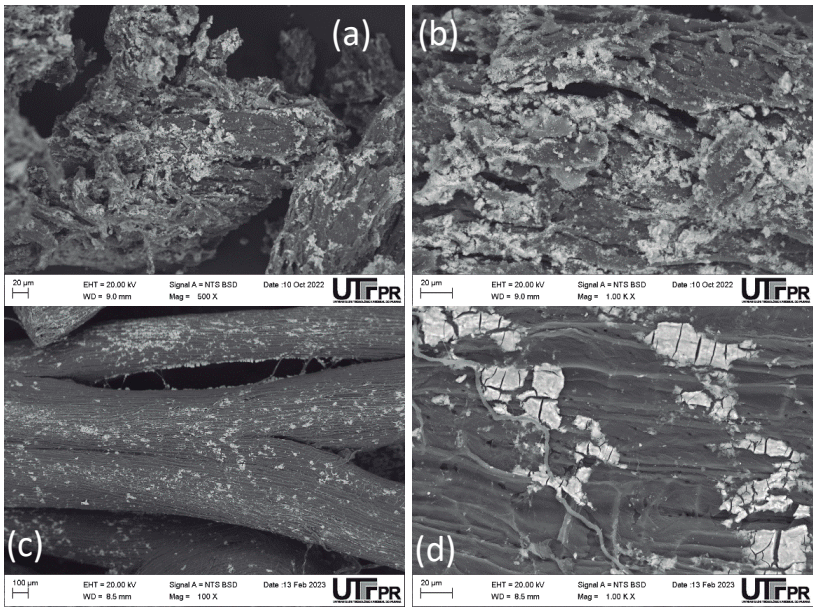

Figure 4 – SEM images of the powdered *Luffa cylindrica*/$ZnFe_2O_4$ samples (a) and (b) and the fiber samples (c) and (d).

A study conducted by Kesraoui, Bouzaabia, and Seffen [4] with vegetable sponge fibers also observed a greater uniformity in the distribution of metallic nanoparticles along the fibers compared to the powder form. This characteristic is advantageous for applications such as water decontamination using the fiber and metal oxides.

The TEM analysis was also performed for the samples, and the results are shown in Figure 5.

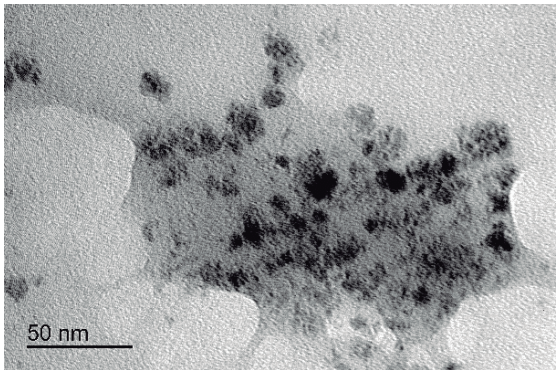

Figure 5 - The TEM image of the synthesized material with vegetable sponge fiber at a zoom of 100,000x

The TEM image of *Luffa cylindrica* fiber showed the presence of deposited ferrite nanoparticles on the vegetable sponge. The light gray regions indicate that the fiber is serving as a

support for the ferrite nanoparticles, which has been previously studied by Ahmad et al. and Yang et al. [2,3]. Additionally, an agglomeration region can be observed, which may be attributed to the preparation method of the suspensions and the magnetic interaction between the ions, as explained by the authors [2,7,8].

The diameter of the ferrite nanoparticles ranged from 7 nm to 22 nm, and it was directly measured by the analysis equipment. This particle size is consistent with authors who synthesized ferrite nanoparticles using the co-precipitation method [1,7,8].

Through the performed analyses, it was possible to evaluate the compositions obtained by incorporating coprecipitated ferrite nanoparticles into Luffa cylindrica fibers.

Conclusions

The conducted analyses revealed a modification in the crystallinity of the material after the addition of ferrite nanoparticles, with metallic nanoparticles being fixed at the nanoscale on the surface of the *Luffa cylindrica* fibers, as observed in the SEM and TEM images. These findings indicate the formation of a material with organic properties from *Luffa cylindrica* and inorganic properties from zinc ferrites. Further studies will be conducted in the future to explore the potential of this material in various applications.

Acknowledgements

The Coordination for the Improvement of Higher Education Personnel (CAPES), the Federal University of Technology - Paraná (UTFPR), the Graduate Program in Chemistry (PPGQ), the Laboratory of Polymeric Materials (LaMaPo), the Multiuser Center for Materials Characterization (CMCM), and the Electron Microscopy Center at the Federal University of Paraná (CME-UFPR).

References

1. S. Hazra; N. N. Ghosh. Journal of Nanoscience and Nanotechnology 2014, 14, 1983–2000. https://doi.org/10.1166/jnn.2014.8745
2. A.F. Ahmad, et al. Polymer 2017, 9, 1-15. https://doi.org/10.1166/jnn.2014.8745
3. Q. YANG, et al. Materials Research Bulletin 2018, 106, 409-417. https://doi.org/10.1016/j.materresbull.2018.06.029
4. A. Kesraoui; S. Bouzaabia; M. Seffen Water 2019, 26, 11524–11534. https://doi.org/10.3390/w11071326
5. B. M. Martinez-Pavetti, et al. Journal of Materials Research and Technology 2021, 14, 2420-2427. https://doi.org/10.1016/j.jmrt.2021.07.141
6. M. Kumar, et al. Environmental Science: Water Research & Technology 2020, 6, 491–514. https://doi.org/10.1039/C9EW00858F
7. S. R. Patade Nanomaterials and Energy 2020, 9, 8-13. https://doi.org/10.1680/jnaen.19.00006
8. S. Li, et al. Journal of Materials Science: Materials in Electronics 2021, 32, 13511–13526. https://doi.org/10.1007/s10854-021-05928-0

STATISTICAL EVALUATION OF ELECTROMAGNETIC ABSORPTIVITY OF PDMS/CNT/GNP COMPOSITES

Alessandra de A. P. Gabino[1,2]*, Bluma Guenther Soares[1,2]

1- Laboratory of polymeric blends and conductive composites - IMA/UFRJ, Centro de Technologic, CP 68525, 21941-909, Rio de Janeiro, RJ
2- Metallurgical and Materials Engineering Program – COPPE/UFRJ, CP 68505, 21941-972, Rio de Janeiro, RJ
Corresponding author ale.gabino@metalmat.ufrj.br

Abstract – Using the Simplex Axial design of experiments technique, polymeric composites of polydimethylsiloxane (PDMS), filled with hybrid fillers of carbon nanotubes (CNT) and graphene nanoplatelets (GNP) were analyzed concerning their electromagnetic absorptivity in the Ku frequency band (12.4 to 18 GHz). For a confidence level of 95% ($\alpha = 0.05$), linear, quadratic and special cubic models were adjusted to the experimental data. Special cubic model provided statistical significance (p-value = 0.0192) and high prediction capacity ($R^2 = 0.9639$), confirmed by the adjusted coefficient of determination (adjusted $R^2 = 0.8918$). The resulting equation and the Pareto chart of standardized effects revealed that, for this property, CNT was the most influential component because of its morphology, which facilitates the structuration of the conductive network. Despite that, the synergistic effect of CNT and GNP was evident, both in electromagnetic absorptivity and electric conductivity.
Keywords: *PDMS, hybrid fillers, electromagnetic shielding, absorptivity, design of experiments.*

Introduction

In modern routine, we live surrounded by electroeletronic equipment, which continuously emits electromagnetic waves (EMW). These random emissions produce invisible pollution in the environment, manifesting as electromagnetic interference (EMI) in other equipment [1] and is potentially harmful to human health, causing headaches, fatigue, nervousness, insomnia and ever cancer [2]. In order to mitigate the effects of such pollution, the concept of EMI shielding emerged, consisting of a barrier that stops the propagation of EMW from a medium to another. Classicaly, metals are the chosen material for such application, however, their shielding mechanism is mainly based on wave reflection. In this sense, only the environment beyond the shield is protected against unwanted EM radiation, which does not contribute to solve the EM pollution problem. Researchers turned their attention to materials with EM absorbing properties [3,4], with special attention to conductive polymeric composites (CPC) [5].

CPCs are produced by incorporing conductive fillers into insulating polymeric matrices. Carbonaceous fillers, such as carbon nanotubes (CNT), graphene nanoplatelets (GNP), graphite (G) and carbon black (CB) are the most popular conductive fillers, for their relatively good interaction with the carbonic chains of polymers. Beyond a specific amount of filler mixed in the polymer, called electric percolation threshold, the conductive particles are too close or in contact with each other, structuring a conductive network inside the matrix [6], tunning the electrical condutctivity of the originally insulating composite. The percolation threshold must be reduced to avoid processing problems and damage to mechanical properties of the material, and a commonly used strategy to reduce it is combining two different fillers, to obtain a synergistic effect on the material's properties

[7]. CNT, for exemple, presents high conductivity and high aspect ratio, which favors the formation of the conductive network; GNP, on the other hand, besides high conductivity, has a plate-like morphology, improving the chances of interaction with EMW [8], making the two particles good candidates for combination in hybrid fillers.
PDMS is an elastomeric polymer of the silicone family. It is the most simple silicone with amazing properties such as high flexibility, thermal and chemical stability, hidrophobicity, optical transparency and lubricating effect, also being comercialy cheap and available [9,10,11]. Most important, it is a non-toxic material, biocompatible and environmentally friendly, being widely used in medical supplies [12].
Design of experiments (DOE) consists of a group of statistical concepts used to optimize useful data gathering, with the least number of experiments possible. Mixture design is used when the material's properties are function of the components' relative quantities, and not their absolute amount. Axial simplex centroid is a mixture design technique in which, for a system of 3 components, 10 experiments are needed: 3 pure samples, 3 binary samples and 4 ternary samples. This method is distinguished from the classic simplex centroid because it presents 3 additional points in the ternary mixture region, axial to the centroid point, making it a better predictor of the ternary region of the experimental space [10]. The result of the statistical treatment is a mathematical model adjusted to the experimental data, relating the desired property to the ratio of each component in the mixture. Linear, quadratic and special cubic models are commonly used for mixture designs and, as the complexity of the model increases, the number of parameters increases as well. The result of the mathematical modeling is a response surface, which predicts the property value for any mixture composition within the experimental space and determines the composition that maximizes its value [8,13].
The objective of this work was to statistically evaluate the synergistic effect of CNT and GNP in the electromagnetic absorptivity of PDMS composites, using the axial simplex centroid technique to adjust three different complexity models to the experimental data.

Experimental
PDMS kit Sylgard^{TM} 184 Silicone Elastomer, provided by Dow Chemical Company; Carbon nanotubes NC7000, produced by Nanocyl S.A.; Graphene nanoplatelets xGnP Grade M (average diameter 25 μm) provided by XG Sciences Inc.
Fillers were dispersed in the polymer base using an ultrasound mixer Fisherbrand^{TM} Q500 (500 W, 20 kHz) for 30 min. The curing agent was added and the mixture was degassed in vaccum for 15 min. Curing was conducted at 100 °C for 35 min.
Electromagnetic absorptivity (RL) was determined from the S-parameter (S_{11}), mesured in the Ku-band (12.4 to 18 GHz), using a vector network analyzer (VNA) PNA-L from Agilent Technologies, coupled with a wave guide and using metal-backed configuration, with a metal plate fixed to the sample holder. Samples had 2 mm thickness.
Alternate current electric conductivity (σ_{AC}) was measured in a dielectric interface Solartron SI 1260, from Agilent Technologies. Measurements were conducted in 0.1 V, from 10 mHz to 100 kHz, with samples of 1 mm thickness and 25 mm diameter. The surface of the samples was previously covered with a thin layer of gold, to improve the contact with the electrodes.
Composition of the samples prepared is presented in Table 1. Mass content of fillers (CNT and GNP) was fixed from 0% to 2%. The models adjusted to the experimental data was the linear, quadratic and special cubic, presented in Eq. 1, 2 and 3, respectively. Statistical treatment of data was conducted in Statistica V14.0 software, considering a confidence level of 95% (α=0.05).

$$\hat{y} = Ax_1 + Bx_2 + Cx_3 \quad (1)$$

$$\hat{y} = Ax_1 + Bx_2 + Cx_3 + ABx_1x_2 + ACx_1x_3 + BCx_2x_3 \quad (2)$$

$$\hat{y} = Ax_1 + Bx_2 + Cx_3 + ABx_1x_2 + ACx_1x_3 + BCx_2x_3 + ABCx_1x_2x_3 \quad (3)$$

$\hat{y}$ = Desired property = RL (dB).

x_i = ratio of component i. i = 1 for PDMS; 2 for CNT; 3 for GNP.

A, B, C, AB, AC, BC, ABC = parameters of the models.

Results and Discussion

Electromagnetic absortivity, or reflection loss (RL), is a parameter that allows the evaluation of the electromagnetic absorption capacity of absorbing materials. The experimental data adjusted to the models was the average RL values for each sample in the Ku-band frequency range, according to Table 1. The statistical results for the three evaluated models are presented in Table 2.

Table 1 – Absorptivity and electric conductivity (0.01 Hz) of the DOE samples

Real components (wt%)			**Pseudo-components (wt%)**			**RL (dB)**	**σ_{AC} (S/m)**
PDMS	**CNT**	**GNP**	PDMS	CNT	GNP		
100	0	0	1	0	0	5.27	3.45×10^{-13}
98	2	0	0	1	0	15.95	1.75×10^{-4}
98	0	2	0	0	1	6.49	4.38×10^{-12}
99	1	0	0.5	0.5	0	5.02	1.38×10^{-5}
99	0	1	0.5	0	0.5	5.84	2.30×10^{-12}
98	1	1	0	0.5	0.5	12.15	2.65×10^{-5}
98.67	0.67	0.67	1/3	1/3	1/3	15.57	3.53×10^{-3}
99.33	0.33	0.33	2/3	1/6	1/6	8.22	2.47×10^{-4}
98.33	1.33	0.33	1/6	2/3	1/6	12.08	9.31×10^{-5}
98.33	0.33	1.33	1/6	1/6	2/3	10.48	1.19×10^{-4}

Table 2 – Statistics of three different complexity models adjusted to RL

Model	**R^2**	**Adjusted R^2**	**p-value**
Linear	0.5466	0.4170	0.0628
Quadratic	0.7085	0.3442	0.5807
Special cubic	0.9639	0.8918	0.0192

Among the three evaluated models, only special cubic presented statistical significance, since its p-value is inferior to the significance level of 0.05. The coefficient of determination (R^2) revealed that it also has the strongest prediction capacity, since its coefficient is very close to unity, which was confirmed by the adjusted R^2. In addition, adjusted R^2 values show that the increase in the model's complexity, with the addition of the ternary parameter (ABC), was beneficial for the predicition capacity of the special cubic model, compared to the quadratic model, since there was a considerate increase in this parameter. In short, the special cubic model can explain 89% of the variance in RL caused by the ratio of components in the mixture, which is a satisfactory result.

The values for the special cubic model parameters are presented in Table 3. Numeric analysis allows to identify the most relevant components and interactions that contribute to the property of the material. Among the unitary paramenters, that refer to the individual contribution of the components, parameter B, referent to CNT, is of greatest influence in absorptivity, followed by parameter C, referent to GNP. Concerning the binary parameters, BC, which refers to the interaction between CNT and GNP, is 3 orders of magnitude higher than AB and 5 orders of magnitude higher than AC. Naturally, parameter A, referent to pure PDMS, and the binary parameters that involve the polymer (AB and BC) have inferior contribution to absorptivity

compared to the parameters referent to the fillers, since PDMS has negligible electromagnetic properties.

Table 3 – Parameters of the adjusted special cubic model

Parameter	Value
A	5
B	57036
C	480
AB	-57674
AC	-429
BC	-24695673
ABC	25206618

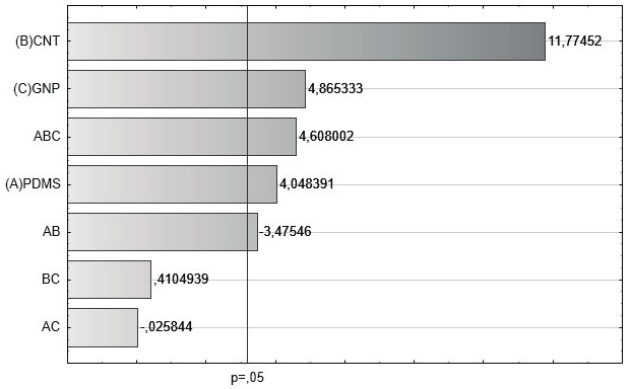

Figure 1 – Pareto chart of standardized effects

The statistical analysis of the parameters of the model, using the Pareto chart of standardized effects (Figure 1), confirms the greatest contribution and statistical relevance of parameter B, referent to the individual contribution of CNT, followed by parameters C and ABC.

The highlighted performance of CNT in the electromagnetic absorptivity in PDMS composites is justified by the electric condutcivity of the composites, presented in Table 1. Composites filled with CNT presented conductivity 6 and 7 orders of magnitude higher than those with the same amount of GNP, and such behavior has already been observed in literature [14,15,16]. The main difference between CNT and GNP is the morphology of particles, which is of paramount importance for the structuration of a conductive network of filler particles. Due to its high aspect ratio [17], CNT presents nearly 1D particles, which easily connect with each other. GNP, on the other hand, has plate-like particles, presenting limited mobility and possibility of interconnection. A properly structured network produces intense polarization, charge dissipation and ohmic losses [18,19], contributing to the dissipation (absorption) of EM radiation in the interior of the composite.

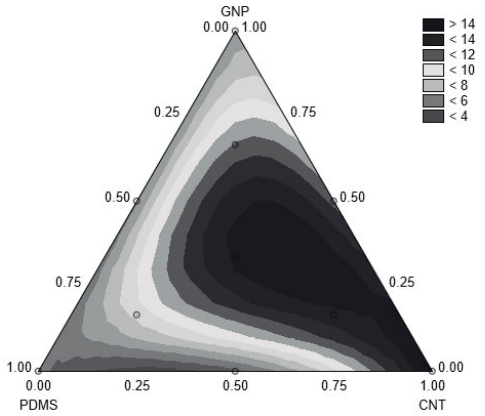

Figure 2 – Response surface for the special cubic model adjustment to the absorptivity data in the Ku band

The response surface for the adjusted special cubic model (Figure 2) shows that the best results for electromagnetic absorptivity is in the ternary mixture region, between the centroid point and the CNT vertex. Despite CNT presenting more relevant contribution to absorptivity (numerical and statistically), the synergistic effect of fillers is evident for this property. Synergy can also be observed in the conductivity results, since all of the ternary composites presented better results than binary composites with only GNP. The best performance was achieved by centroid point CNT/GNP

0.67:0.67%, which presented higher conductivity than CNT 2%, even with smaller amount of filler added.

Conclusions

Three different complexity mathematical models were adjusted to the electromagnetic absorptivity experimental data of PDMS composites filled with hybrid filler of CNT and GNP. Special cubic was the only model to present statistical significance, also presenting the strongest prediction capacity. In addition, the synergistic effect of the hybrid filler in the absorptivity of PDMS composites was statistically verified, and similar behavior was also observed in electric conductivity of the prepared materials.

References

1. S. Sankaran; K. Deshmukh; M. B. Ahamed; S. K. K. Pasha; Composites, Part A 2018, 114, 49. https://doi.org/10.1016/j.compositesa.2018.08.006.
2. R. B. J. Chandra; B. Shivamurthy; S. D. Kulkarni; M. S. Kumar, Mater. Res. Express 2019, 6, 1. https://doi.org/10.1088/2053-1591/aaff00.
3. J. M. Thomassin; C. Jérôme; T. Pardoen; C. Bailly; I. Huynen; C. Detrembleur, Mater. Sci. Eng., R 2013 74, 211. https://doi.org/10.1016/j.mser.2013.06.001.
4. P. Kumar; U. N. Maiti; A. Sikdar; T. K. Das; A. Kumar; V. Sudarsan, Polym. Rev. 2019, 59, 687. https://doi.org/10.1080/15583724.2019.1625058.
5. D. Jiang; V. Murugadoss; Y. Wang; J. Lin; T. Ding; Z. Wang; Q. Shao; C. Wang; H. Liu; N. Lu; R. Wei; A. Subramania; Z. Guo, Polym. Rev. 2019, 59, 280. https://doi.org/10.1080/15583724.2018.1546737.
6. A. A. P. Gabino; B.G. Soares; A. A. Silva; J. Appl. Polym. Sci. 2021, 138, 49857. https://doi.org/10.1002/app.49857.
7. H. Zhang; G. Zhang; M. Tang; L. Zhou; J. Li; X. Fan; X. Shi; J. Qin, Chem. Eng. J. 2018, 353, 381. https://doi.org/10.1016/j.cej.2018.07.144.
8. B. B. Neto; I. S. Scarminio; R. E. Bruns, Como Fazer Experimentos, Unicamp, Campinas, 2001.
9. U. Eduok; O. Faye; J. Szpunar, Prog. Org. Coat. 107, 111, 124. https://doi.org/10.1016/j.pnsc.2018.05.004.
10. M. P. Wolf; G. B. S. Beugelaar; P. Hunziker, Prog. Polym. Sci. 2018, 83, 97. https://doi.org/10.1016/j.progpolymsci.2018.06.001.
11. G. G. Morbioli; N. C. Speller; A. M. Stockton, Anal. Chim. Acta 2020, 1135, 150. https://doi.org/10.1016/j.aca.2020.09.013.
12. J. Stieghorst; T. Doll, Addit. Manuf. 2018, 24, 217. https://doi.org/10.1016/j.addma.2018.10.004.
13. R. O. Costa; J. P. Coutinho; R. L. S. R. Santos, J. Appl. Polym. Sci. 2021, 139, 51504. https://doi.org/10.1002/app.51504.
14. S. E. Zakiyan; H. Azizi; I. Ghasemi, Compos. Sci. Technol. 2017, 142, 10. https://doi.org/10.1016/j.compscitech.2017.01.025.
15. G. Wang; Q. Yu; Y. Hu; G. Zhao; J. Chen; H. Li; N. Jiang; D. Hu; Y. Xu; Y. Zhu; A. G. Nasibulin, Compos. Commun. 2020, 21, 100417. https://doi.org/10.1016/j.coco.2020.100417.
16. Y. Wang; P. Wang; Z. Du; C. Liu; C. Shen; Y. Wang, Adv. Compos. Hybrid Mater. 2022, 5, 209. https://doi.org/10.1007/s42114-021-00320-2.
17. D. Lu; Z. Mo; B. Liang; L. Yang; Z. He; H. Zhu; Z. Tang; X. Gui, Carbon, 2018, 133, 457. https://doi.org/10.1016/j.carbon.2018.03.061.
18. O. Navas; M. Arjmand; U. Sundararaj, Polymer 2017, 114, 122. https://doi.org/10.3390/polym13020230.
19. Y. Wu; Z. Wang; X. Liu; X. Shen; Q. Zheng; Q. Xie; J. K. Kim, ACS Appl. Mater. Interfaces 2017, 9, 9059. https://doi.org/10.1021/acsami.7b01017.

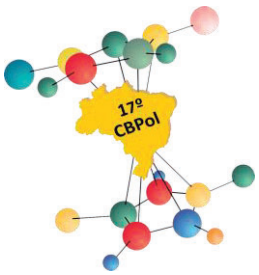

STRUCTURAL PERFORMANCE OF HYBRID FIBER-METAL LAMINATES WITH NATURAL AND SYNTHETIC FIBERS

Vilson D. Libera Junior[1,2*], Linconl A. Teixeira[1], Carla T. M. Anflor[3,], Divino E. Teixeira[4] and Sandra M. Luz[1]

1 – Mechanical Sciences Graduate Program, University of Brasília (UnB), Brasília, DF, Brazil.
2 – Federal Institute of Education, Science and Technology of Goiás (IFG), Uruaçu, GO, Brazil.
[*]vilson.dalla@ifg.edu.br
3 – Integrity of Engineering Materials Graduate Program, Group of Experimental and Computational Mechanics, University of Brasília (UnB), Gama, DF, Brazil.
4 – Brazilian Forest Service (SFB), Forest Products Laboratory (LPF). Brasília, DF, Brazil.

Abstract - This work aims to investigate the influence of the hybridization effect on the mechanical behavior and failure mechanism of fiber-metal laminates (FML) produced with hybrid reinforcement of natural and synthetic fibers. Fiber-metal laminates were obtained using metallic layers of 2024-T3 aluminum sheets and carbon, glass, and sisal fibers prepregs. Hybrid FMLs were fabricated using a hot-pressing process. Data related to strength, modulus and strain were obtained through tensile tests coupled to the Digital Image Correlation (DIC) technique, then the results were interpreted using analysis of variance (ANOVA). Analysis of stress-strain curves indicated that the difference in elastic properties between metallic and FRP layers largely affected the FML delamination process, and directly influenced the tensile load and deformation behavior of the laminates. The mechanical results indicated that the interface between the sisal composite and the metallic layer strongly depends on the nature of the fiber, which also controls the intensity of residual stresses.

Keywords: *Fiber-metal laminates. Hybrid composites. Mechanical properties. DIC. Residual stresses.*

Introduction

Fiber metal laminates (FMLs) are hybrid structural materials composed of thin layers of metal alloy sheets and fiber-reinforced polymer composites. Fiber-to-metal composite technology combines the advantages of metallic materials and fiber-reinforced polymer matrix systems [1]. FMLs are an excellent example of obtaining a material with improved behavior through the combination of the mechanical properties of its constituents. A more recognized classification for FMLs is based on the organization and composition of their constituent materials. In general, FMLs can be classified mainly by base metals in their composition and polymer composites, consisting of a fiber-reinforced matrix [2].

The composite layers commonly used in FMLs are of the Fiber Reinforced Polymer (FRP) type and can be classified according to the reinforcing fibers and constituent polymer matrices. Carbon and glass fibers are the most commonly investigated and used fibers in FMLs [3]. Despite that, composites based on renewable sources or biocomposites have emerged as ecologically friendly alternatives to traditional composite materials due to recent environmental and sustainability concerns [4]. Biocomposites reinforced with natural fibers have been used in many applications and highlighted because they have low cost and non-abrasive properties during processing [5].

Due to the wide application of FMLs in engineering structures, their mechanical properties have been extensively investigated in terms of experimental methods, numerical techniques, analytical models, flexural performance, impact resistance, and fatigue performance, among others. The study

of these properties, coupled with other analysis techniques, such as Digital Image Correlation (DIC) has constantly been increasing. This method can be applied to measure full-field deformation of the hybrid composite specimen. Studies on the tensile behavior of FMLs using the DIC technique have been conducted by many researchers [6,7], and they concluded that the strain rate of FML is dependent of the materials layers. The degree of strength increase depends on the stacking sequence of FRP layers. From this point of view, this work aims to evaluate the structural performance of hybrid fiber-metal laminates with natural and synthetic fibers through tensile test DIC-monitoring.

Experimental

Preparation of prepregs

Sisal fibers (Sisalsul, Ltd.) were used, available *in natura,* and with an approximate length of 80 cm, unidirectional carbon fiber (UC300), and glass fiber E (VEW130) fabrics, were from the Barracuda Advanced Composites. An Araldite® LY 1564 epoxy resin was used as a polymer matrix with the curing agent Aradur® 22962, both from Huntsman Advanced Materials.

Initially, the sisal fibers were subjected to a chemical treatment based on a solution of 5% (w/v) sodium hydroxide (NaOH) tested and validated through previous studies [8]. The matrix solution was prepared at room temperature by mixing the DGEBA epoxy monomer with the curing agent. The unidirectional fabrics of sisal, carbon, and glass (50 v%) were impregnated with the matrix solution through manual lamination. The prepregs were packed, protected from the weather with a polyethylene film covering each face of the material and stored in a refrigerator at -18 °C for the subsequent production of fiber-metal laminates.

Manufacturing of FMLs

The aluminum alloy used for lamination of the FMLs was the aircraft aluminum 2024-T3 in the form of 0.5 mm thick sheet. Aiming better adhesion to the polymer composite, the sheets were subjected to an anodizing process. The unidirectional prepregs used are sisal/epoxy, carbon/epoxy, and glass/epoxy with a fiber fraction by volume of about 50 v%.

The material distributions in different FMLs were [AL/0/AL], and organized the 0_{6C} nomenclature, which represents in sequence: the unidirectional direction (0°), the number of layers of composite (6, 4, 2, or 1), and the type of prepreg used (C - carbon, G - glass, or S - sisal). The FMLs were manufactured using the hot compression molding technique in a hydraulic press with 300 x 300 mm heated plates (WABASH, 10000 psi). Before the pressing process, the prepregs were maintained at room temperature for 1 h and then stacked on the aluminum layers with seven different combinations. The set of layers was deposited on a peel ply film followed by a release film layer, as shown in the diagram in Fig. 1. Then, the material was inserted into the press, where a pressure of 5 MPa was applied to the set. The plates were then heated at a heating rate of 5 °C/min from room temperature to 80 °C. Then, the set was kept in isotherm for 30 min. The heating was stopped after the curing time, and the composites were removed from the press. In the end, the laminates presented excellent dimensional stability.

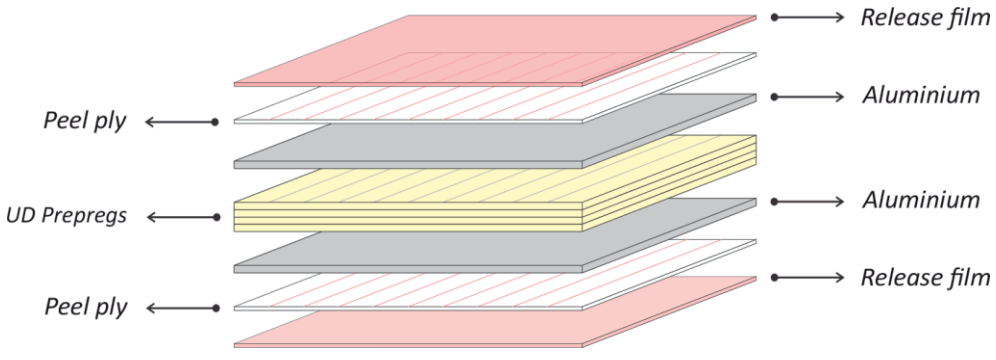

Fig. 1. Layer stacking scheme for pressing the FMLs with unidirectional (UD) polymer composites.

Mechanical characterization coupled to DIC

The specimens for the Tensile Test with DIC were prepared according to ASTM D3039 [9] recommendations with dimensions of 200 x 25 x 3 mm. Tensile tests were performed according to ASTM D3039 [9] on a universal mechanical testing machine INSTRON 8801 with a 100 kN load cell. 5 CPs were tested for each group, and the test speed was 2 mm/min.

Data related to the deformation of the specimens during the tensile test was collected using the DIC technique with the Q-400 system from Dantec Dynamics. In this procedure, two cameras were installed in front of the mechanical testing machine with a focus adjusted to the position of the specimen analyzed, where the sample surface was uniformly illuminated by a red lamp between the cameras (Fig. 2). During the test, images were captured at 1 s intervals. The recording started with the beginning of the tensile test in such a way that the data obtained in both methods could be synchronized later. The images' analysis and the deformations in the X and Y axes were performed using the ISTRA 4D software (Dantec Dynamics).

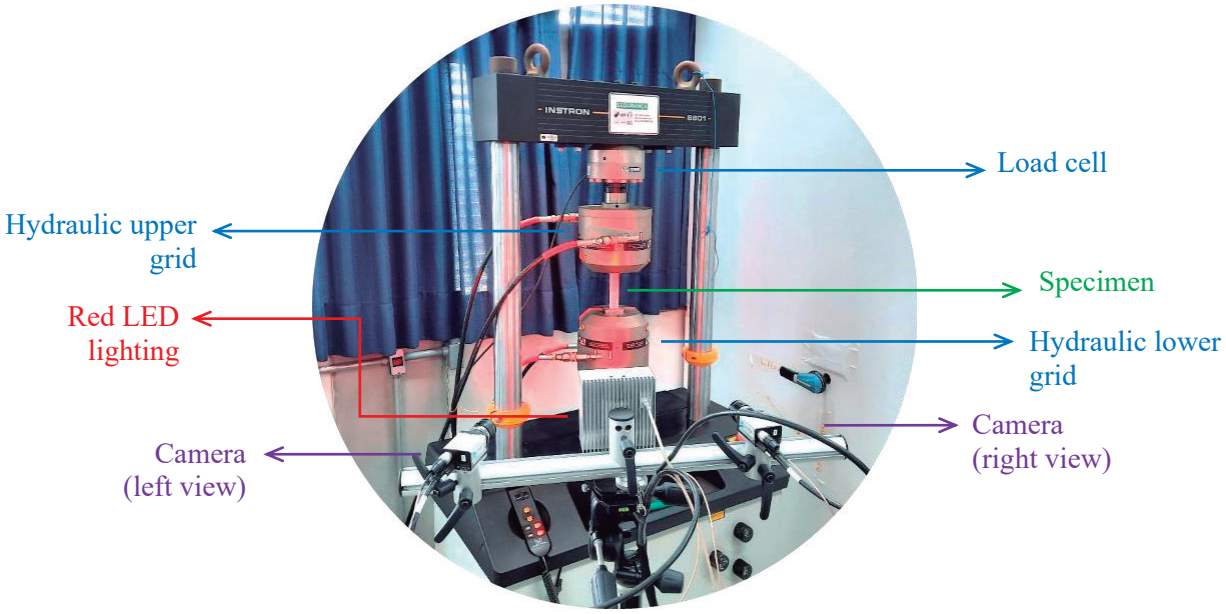

Fig. 2. Experimental configuration of the tensile test with DIC-monitored.

After the tensile test, photographs were taken of each specimen to analyze the failure mechanism. The observed failure modes were associated and identified according to ASTM D3039 [9]. In addition, failures were correlated with the composition of constituent layers, failure stresses, and the occurrence of delamination in each group of FMLs.

Results and Discussion

In the tensile tests, the stress-strain curves (σ - ε) of the FMLs with single reinforcement (carbon, glass, and sisal), as well as hybrid FMLs (sisal/carbon and sisal/glass) were obtained. The strain presented in the curves of Fig. 3 represents the y-axis strain obtained by the DIC technique. Structure failure mechanisms for each set of specimens were captured and analyzed.

The maximum stresses and strains were recorded at failure, describing a typical tensile failure of a ductile material. In general, the samples failed at the specimen center in the maximum shear plane of stress. Thus, the stress hardening effect is negligible from the stress-strain curve presented.

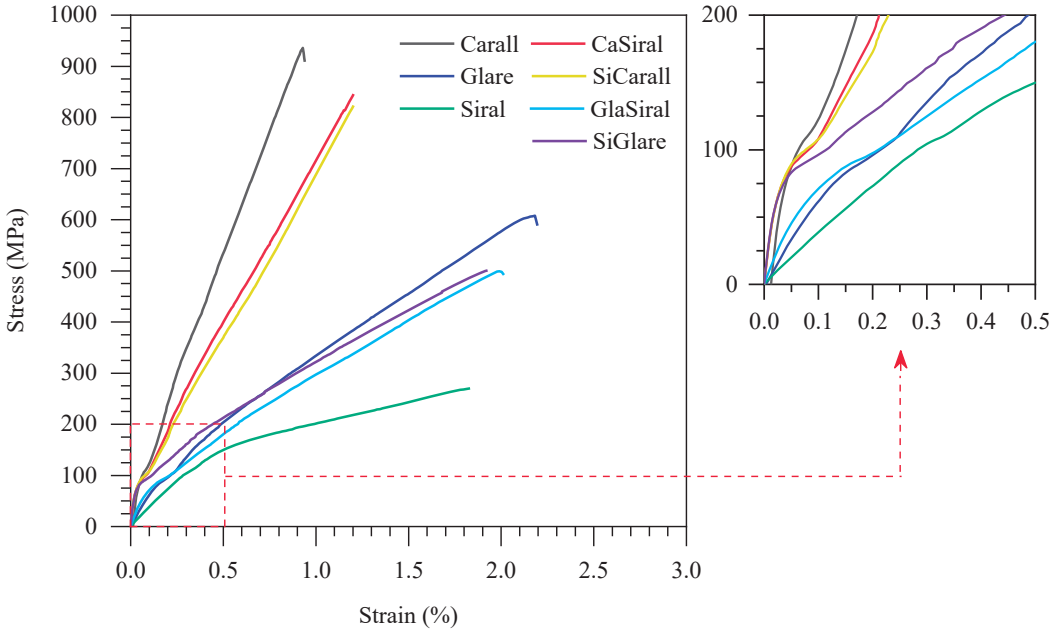

Fig. 3. Stress-strain curve of FMLs.

The mean values of the tensile properties tested, including Young's modulus (E), failure stresses (σ_y), failure strains (ε_f), and Poisson's ratio (n) are summarized in Tab 1. The standard deviation values are also provided.

Tab 1. Summary of tensile properties of FMLs.

FML	FRP Prepregs sequence	Young's modulus E (GPa)	Failure stress σ_y (MPa)	Failure strain ε_f (%)	Poisson's ratio ν
Carall	Carbon	36.2 ± 0.64	948.8 ± 38.59	1.11 ± 0.06	0.34 ± 0.02
Glare	Glass	22.3 ± 0.28	604.5 ± 19.89	2.10 ± 0.54	0.36 ± 0.09
Siral	Sisal	22.2 ± 1.27	262.6 ± 9.23	1.86 ± 0.08	0.33 ± 0.01
CaSiral	Carbon/ Sisal/ Carbon	34.6 ± 1.13	880.3 ± 39.75	1.30 ± 0.10	0.33 ± 0.03
SiCarall	Sisal/ Carbon/ Sisal	33.6 ± 1.63	828.6 ± 16.76	1.31 ± 0.08	0.33 ± 0.09
GlaSiral	Glass/ Sisal/ Glass	21.4 ± 1.64	492.0 ± 27.39	2.12 ± 0.16	0.35 ± 0.08
SiGlare	Sisal/ Glass/ Sisal	21.4 ± 0.43	507.2 ± 17.49	2.07 ± 0.12	0.36 ± 0.09

The data shows that Carall FML presented the highest tensile strength, which was expected since this material has only carbon fiber composite reinforcement. It can be noted that the FML hybridization did not significantly affect its mechanical properties since the CaSiral and SiCarall groups obtained a reduced strength of 7.2% and 12.7%, respectively. The same behavior was observed for the hybrid FMLs with sisal and glass fibers. As expected, Young's modulus of FMLs with carbon fiber was higher than that of the other groups. According to Hu et al. [10], carbon fibers have a higher modulus of elasticity than aluminum. Thus, during the tensile test, the fibers sustained the stresses distributed along with the composite length to guarantee a higher resistance.

To compare the different tensile and failure response mechanisms of FMLs, Fig. 4 displays the digital images correlated to the tensile test. Unlike the strain results presented in the stress-strain curves, the images show the displacements at the y-axis from the specimen's front surface during the tensile test. The images presented were taken at the last moment before the failure of each specimen. It is noted that once the 0° fiber layers break, the deformation of the entire FML specimen occurs only in the metallic layers. More importantly, the deformation is located around the fiber break point (due to the lack of fiber -bridge effect [6]).

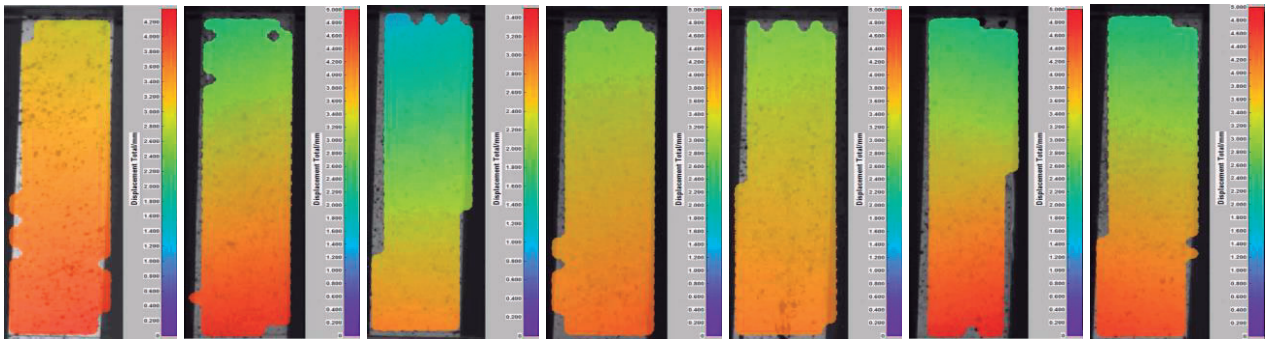

(a) (b) (c) (d) (e) (f) (g)

Fig. 4. Experimental configuration of the tensile test DIC-monitored. Carall (a), Glare (b), Siral (c), CaSiral (d), SiCarall (e), GlaSiral (f), SiGlare (g). Red color indicates larger displacement.

In general, it is possible to observe in Fig. 4 that the hybrid composites (d, e and f and g) present, on average, a smaller displacement at rupture when compared to the non-hybrid FML. This phenomenon can be confirmed by analyzing the DIC image of the Siral FML. Since it contains low modulus natural fibers, it consequently presents a smaller displacement until rupture because the properties of this material were transferred to the hybrid composite [8].

Conclusion

Sisal fibers FMLs and sisal/ synthetic fibers FMLs were obtained successfully. According to the stress-strain curves of the hybrid materials produced, the most efficient distribution of layers occurs when sisal fibers are concentrated in the core of the FML since these fibers present a certain amount of moisture, affecting the adhesion region between the FRP and the metal layer. In general, the hybrid composites offer a smaller displacement at rupture when compared to the non-hybrid FML. It was found that the FML hybridization did not significantly affect its mechanical properties, and it can provide an eco-friendlier and sustainable when compared to the traditional FML materials.

Acknowledgements

This work was supported by Capes, CNPq and DPG-UnB, and FAP-DF.

References

1. T. Sinmazçelik, E. Avcu, M.Ö. Bora, O. Çoban. Mater. Des. 32 (2011) 3671–3685. https://doi.org/10.1016/j.matdes.2011.03.011.
2. T. de Boer. Next Generation Fibre Metal Laminates, Fibre Met. Laminates. (2001) 39–51. https://doi.org/https://doi.org/10.1007/978-94-010-0995-9_3.
3. L. Hamill, D.C. Hofmann, S. Nutt. Adv. Eng. Mater. 20 (2018) 1–8. https://doi.org/10.1002/adem.201700711.
4. M. Fan, F. Fu, Advanced High Strength Natural Fibre Composites in Construction, Elsevier, 2017.
5. R.M. Leão, S.M. Luz, J.A. Araujo, K. Novack. J. Nat. Fibers. 12 (2015) 574–586. https://doi.org/10.1080/15440478.2014.984048.
6. J. Sun, A. Daliri, G. Lu, D. Ruan, Y. Lv. Mater. Des. 183 (2019) 108139. https://doi.org/10.1016/j.matdes.2019.108139.
7. M. Sasso, E. Mancini, G.S. Dhaliwal, G.M. Newaz, D. Amodio. Compos. Struct. 222 (2019) 110922. https://doi.org/10.1016/j.compstruct.2019.110922.
8. V.D. Libera Junior, L.A. Teixeira, S.C. Amico, S. Maria da Luz. Polym. Polym. Compos. 30 (2022). https://doi.org/10.1177/09673911221087591.
9. ASTM International, ASTM D3039 - Standard Test Method for Tensile Properties of Polymer Matrix Composite Materials, Annu. B. ASTM Stand. (2017). https://doi.org/10.1520/D3039.
10. Y. Hu, J. Zhou, F. Ji, Y. Zhang, Y. Duan, Z. Guan, J. Tao. Int. J. Light. Mater. Manuf. 3 (2020) 317–327. https://doi.org/10.1016/j.ijlmm.2020.05.001.

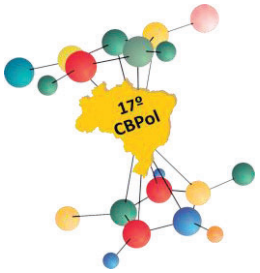

THERMAL, MECHANICAL, RHEOLOGICAL, AND MORPHOLOGICAL CHARACTERIZATION OF THE EXTRUDED PLA/PE-G-MA/CNC SYSTEM WITH AND WITHOUT CONTROLLED ELONGATIONAL FLOW DEVICE.

Bruno A. B Cordova[1], Milena M. Nogueira[1], Eduarda Kowalsky[1], Fábio C. Nunes and Benjamim de M. Carvalho[1]

1 – Department of Materials Engineering (DEMA), State University of Ponta Grossa (UEPG), Ponta Grossa, PR, Brazil

bruno.cordova2013@gmail.com

Abstract

The use of biodegradable polymers has grown every year, due to environmental concerns, being used in several applications, such as packaging and 3D printing. It is common the use of composites due to your combination of properties. In this work, has tried the compatibilization of Poly (Lactic Acid), or PLA, with Crystalline Nanocellulose using a Polyethylene grafted with Maleic Anhydride (PE-g-AM), combined with the use of an Elongational Flow Device couple in a monoscrew extruder to improve the dispersion of NCC in polymeric matrix. The results appoint that the compatibilization it wasn't possible, necessitating a new approach, such as using a different compatibilizer or modify the process conditions. In other side, the elongational flow improved the dispersion of PE-g-AM particles and of NCC in the composites.

Keywords: *PLA, Compatibilitzion, elongational flow, Nanocellulose*

Introduction

Biodegradable polymers, also known as "biopolymers", are gaining attention as an alternative to overcome the issues related to nonbiodegradable polymeric waste, as it shows excellent stability and high durability and tends to accumulate in the environment [1–4]. Biopolymers are prone to degrade naturally due to the effect of microorganisms or enzymes depending on environmental conditions [1], like cellulose, lignin, and starch. Another class is the natural-based or bio-based synthetic polymers derived from renewable resources, such as poly (lactic acid), or polylactide (PLA), which have been applied in food packaging, compost bags or agriculture [2].

PLA is a high molar mass aliphatic thermoplastic polymer (>100,000 g mol-1) with excellent combination of properties outstanding properties, such as low toxicity, easy processability, and biodegradability. This polymer is obtained from renewable sources and stands out due to its good mechanical properties and moderate thermal stability [3]. PLA is usually used in 3D printing and packaging, but has limitations such as brittleness, slow rate of crystallization, and hydrolysis.

In the last years, numerous studies have proposed the reinforcements of biodegradable polymers with cellulose nanocrystals (CNC) as an alternative to improve the mechanical and thermal properties while maintaining biodegradability [4]. CNC offers high rigidity and good thermal stability. Furthermore, they are biodegradable, biocompatible, non-abrasive, and have a non-toxic character [3]. CNCs are obtained by removing the amorphous region of the crystalline cellulose, isolating the veins (also called whiskers or rods), typically by acid hydrolysis.

To improve the CNC adhesion between the polymer blend components, coupling agents can be used [2]. The PE-g-MA (polyethylene grafted maleic anhydride) aims to increase the adherence between the polymeric phases to obtain a blend by a series of consecutive reactions due to the load exchange mechanism between phases. Depending on the monomer added, the chain polarity can

change, allowing secondary physicochemical interactions between the components of the mixture [2]. Overall, compatibilization using agent coupling may increase phase adhesion and decrease the size of the dispersed particles.

To enhance the dispersion of CNC particles, an elongation flow device was used. In general, common devices of processing of melt polymers, like extrusion and mixers [5], make use of shear flow to promote and enhance the dispersion of second phase. But also known that elongational flow is more effective to dispersion when compared with shear flow, due the ability of break agglomerates and redistribution in polymer matrix [6].

Composite processing typically is based on conventional methods such as pultrusion, injection molding, and extrusion, and their final properties depend on the mixture homogenization and processing conditions, such as dispersion and temperature, among others [3]. Therefore, the use of an elongation flow in addiction of shear flow of conventional processing enhances the dispersion of second phase particles in the polymeric matrix, what would improve the properties of processed material.

The compatibilization of PLA with other reinforcements combined with the utilization of elongational flow can create a wide range of new composites, with enhanced properties and, consequently, new applications. This study aims to investigate the effects of CNC and PE-g-MA in PLA obtained by the extrusion process. Moreover, it aims to evaluate the impact of controlled extensional flow, using the device developed by GOES et al. [7]. Furthermore, the study aims to investigate how the compatibilization process can influence act on the polymer interface and modify the properties of PLA filaments.

Experimental

Materials

PLA (grade: 4042D, 92% L-lactive units, Nature Works) was used as the polymeric matrix. Cellulose nanocrystals (CNC 9005-22-5, Celluforce) were used as the reinforcement phase, and polyethylene grafted with 1% maleic anhydride (PE-g-MA, Polybond® 3039, Chemtura) content, and MFI of 4 g/10 min^{-1} (ASTM D1238, 190°C, 2,16 kg^{-1}) was used as a coupling agent.

Processing of compositions

PLA, CNC and PE-g-MA were dried for 24 h at 60 °C. The compositions are presented in Table 1. In this process, the biocomposite precursors were initially pre-mixed and then processed by a mini single screw extruder homemade, of three zones, in temperatures of 170-170-200°C and 20 rpm. The filaments were extruded through a ring-shaped matrix with and without elongation flow device (EFD), which consist in 5 pairs of rings of brass, with opening 2-4 and 2-8 mm alternating. The obtained filaments were cooled using a water bath system (25°C) and finally collected by a filament winder.

Table 1 – Composition of filaments

Sample code	PLA (% wt)	PE-g-MA (% wt)	CNC (% wt)
PLA	100	0	0
PLA/PE-g-MA	95	5	0
PLA/CNC	99	0	1
PLA/PE-g-MA/CNC	94	5	1

Characterization of filaments

The mechanical behavior of filaments was realized in a universal testing machine Shimadzu AG-1, with force cell of 10 kN and strain rate of 5 mm min^{-1}, where was obtained the tensile strength of material.

The rheological behavior of the composites was evaluated in the TA Instruments DHR-2 parallel plate oscillatory rheometer. The interval between the plates used was 1 mm. All measurements were performed at 200 ºC under the nitrogen atmosphere and 0.1 to 700 rad s-1 angular frequency range.

DSC analysis was performed using Shimadzu's DSC 60 equipment following the ASTM D3418-15 guidelines. Samples went through a heating cycle at 10º C min-1 rate and cooling at 5 ºC min-1 rate. Two heating ramp ranging from 30 to 200 ºC was performed, followed by colling from 200 to 30 ºC. PLA and PE-g-MA crystallinity degree (Xc) was calculated using Eq. 1:

$$XC\ (\%) = \frac{\Delta H_m - \Delta H_{cc}}{\Delta H_m{}^o} \quad (1)$$

where Xc is the crystallinity percentage, ΔHm is the crystalline melting enthalpy of the sample obtained by DSC [14], ΔHc_C is the crystallization enthalpy occurring during heating, and, in case of PE-g-MA, the value is zero. ΔHm^o is the equilibrium fusion enthalpy for the theoretically 100% crystalline material, in this case, 93,6 J g^{-1} of PLA [3] and 293 J g^{-1} PE-g-MA.

Results and Discussion

Mechanical Properties

In this mechanical test the filament produced through extrusion were subjected to testing and the corresponding values of Tensile Strength are presented in Table 2.

Table 2 Tensile Strength of Filaments.

Sample	w/o EFD (MPa)	EFD 2-4 (MPa)	EFD 2-8 (MPa)
PLA	55,9 ± 4,2	56,3 ± 4,3	58,3 ± 5,1
PLA/PE-g-MA	51,0 ± 4,4	52,6 ± 3,3	40,9 ± 7,1
PLA/CNC	55,0 ± 1,6	56,8 ± 3,2	42,1 ± 10,1
PLA/PE-g-MA/CNC	46,7 ± 6,8	53,9 ± 2,1	50,9 ± 5,0

There was not a significant variation in tensile strength of the compositions, although some compositions (highlighted in red) exhibited a significant reduction. In the three compositions, the quality of the extruded filament was poor, with low dimensional control and some defects such as agglomerates and excessive fragility. The statistical tests did not reveal significative difference among the remaining compositions.

Still, the values are compatible with the properties of PLA commonly use in polymer processing process. The composition that showed low properties also show low quality of filament when are processed, like superficial defects, presence of agglomerates and low dimensional control.

The next steps will involve testing 3D printing of filaments, observing the quality and proprieties of printed pieces.

Rheological Analysis

The parallel plates rheometry assay was performed for all compositions. Fig. 1 shows an overall reduction in the complex viscosity values when the angular frequency increased, confirming the shear thinning behavior of biocomposites. Minimal differences were in modulus and rheological behavior among of composites. However two formulations exhibited very low viscosity (PLA/CNC EFD 2-8 and PLA/PE-g-MA EFD 2-8). These compositions also exhibited low mechanical strength as indicated in Table 1.

Figure 1 Complex viscosity (η) of the biocomposites as a function of the angular frequency (ω).*

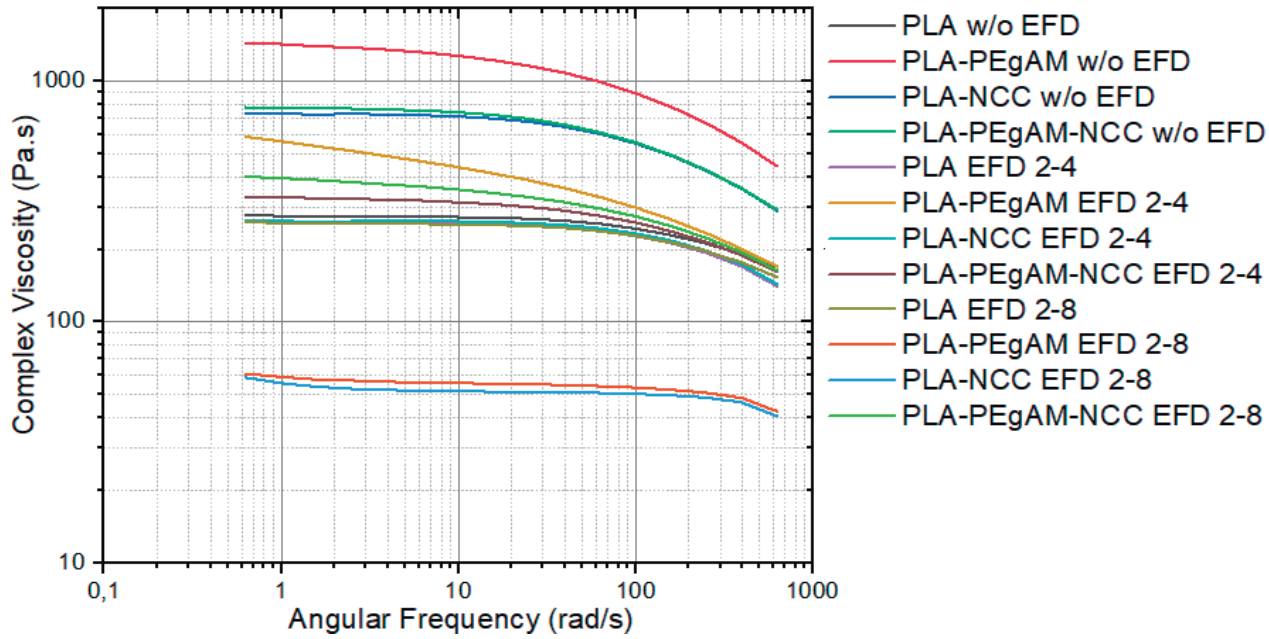

Morphological Analysis

SEM analysis was used to evaluate the obtained biocomposites, and the result are showed in Fig 2. The analysis revealed the presence the two phases with distinct morphologies. The continuous phase correspond to PLA while "spheres" are the PE-g-MA

Figure 2 SEM of PLA/PE-g-MA with EFD 2-8

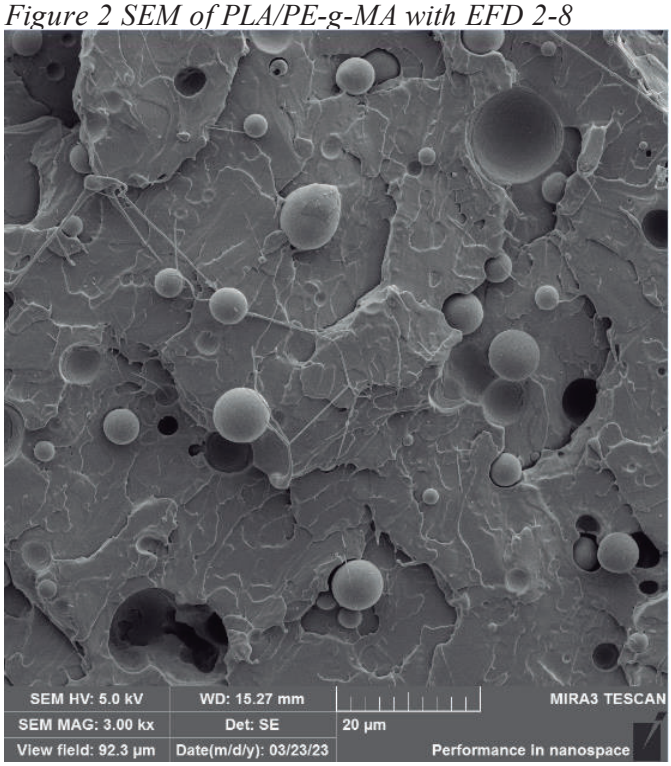

The particles of PE-g-MA had a diameter size of 250 µm before the extrusion processing. However, after the production of filament, they showed a size variation ranging from 2-25 µm at most. The presence of interface between the PLA and the PE-g-MA, what's is a indicative of a low level of compatibilization between materials. This can possibly be attributed to chemical differences between the PLA and the PE, combined with presence of an rigid polymeric matrix. The results in

the work of NUNES et al, what used the PLA/PBAT with PE-g-MA [3], demonstrated effective compatibilization with a continuous polymeric matrix.

Differential Scanning Calorimetry - DSC

Table 2 shows the thermal transitions of composites, as well the crystallinity of material.

Table 2 Thermal Transition of Composites after extrusion

Composition	T_G PLA (°C)	T_{CC} PLA (°C)	T_M PE (°C)	T_M PLA (°C)	ΔH (J g^{-1})	X_C (%)
PLA w/o DFE	62,8	99,7	---	179,9	23,8	24,7
PLA/PE-g-MA w/o DFE	63,3	96,7	127,8	178,8	25,9	28,3
PLA/CNC w/o DFE	62,9	99,5	---	179,2	27,5	28,9
PLA/PE-g-MA/CNC w/o DFE	63,4	96,3	127,4	178,9	24,1	26,6
PLA DFE 2-4	61,9	98,9	---	179,1	31,2	32,4
PLA/PE-g-MA DFE 2-4	62,9	95,2	126,2	178,2	26,9	29,4
PLA/CNC DFE 2-4	62,5	99,0	---	178,9	25,9	27,1
PLA/PE-g-MA/CNC DFE 2-4	61,9	94,7	127,9	178,1	28,3	31,2
PLA DFE 2-8	62,5	99,0	---	179,4	29,7	30,8
PLA/PE-g-MA DFE 2-8	64,6	94,7	127,3	178,6	28,7	29,8
PLA/CNC DFE 2-8	62,5	97,4	---	178,3	32,0	33,6
PLA/PE-g-MA/CNC DFE 2-8	62,6	96,2	127,5	178,6	33,2	36,7

Differences in thermal transitions between PLA and PE-g-MA are hardly noticeable, however the use of Elongation Flow Device (EFD) led to an improvement of crystallinity of composites. This improvement can be attributed to the enhanced dispersion of particles in matrix polymeric, as related by GOES et al. [7]. Moreover, using rings with larger difference of diameter also contributed the improved dispersion.

Conclusions

The compatibilization of PLA and CNC using PE-g-MA was not effective, requiring adjustments, such as changing the compatibilizer and/or processing conditions for futures studies. On the other hand, the use of elongational flow improve the dispersion of particles in matrix polymer, resulting in better properties of the composites and filaments produced by extrusion.

Acknowledgements

The authors are grateful to Coordination for the Improvement of Higher Education Personnel (CAPES) and Araucaria Foundation for the financial support and the Multi-User Laboratory Complex (CLABMU) for the structure and technical support.

References (Times New Roman 12, bold)

1. H. Moustafa, A. Youssef, N. Darwish, A. Abou-Kandil, Composites Part B Eng. 2019, 172, 16. https://doi.org/10.1016/j.compositesb.2019.05.048

2. B. Imre, B. Pukánszky Eur. Polym. J. 2013, 49, 1215. https://doi.org/10.1016/j.eurpolymj.2013.01.019

3. F. C. Nunes, K. C. Ribeiro, F.A. Martini, B. R. Barrioni, J. P. F. Santos, B. M. Carvalho J. Appl. Polym. Sci. 2021, 145 (32), 51342. https://doi.org/10.1002/app.51342

4. C. Miao, W. Y. Hamad Curr. Opin. Solid State Mater. Sci. 2019, 23, 100761. https://doi.org/10.1016/j.cossms.2019.06.005

5. A. Graf, Y. Zakharko, S. P Schießl, C. Backes, M. Pfohl, B. S. Flavel, J. Zaumseil Carbon 2016, 105, 593. https://doi.org/10.1016/j.carbon.2016.05.002

6. O. Faruk, A. K. Bledzki, H. P. Fink, M. Sain, Prog. Polym. Sci.2012, 37, 1552. http://dx.doi.org/10.1016/j.progpolymsci.2012.04.003

7. M. A. Goes, J. P. F. Santos, B. M. Carvalho Polímeros: Ciência e Tecnologia 2022, 32(2). https://doi.org/10.1590/0104-1428.20210116

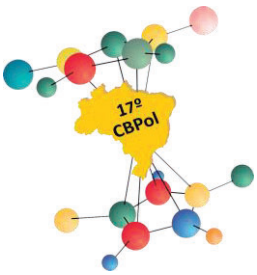

THERMOPLASTIC CORN STARCH/VISCOSE YARN WASTE BIOCOMPOSITES PROCESSED BY EXTRUSION-COMPRESSION MOLDING

Renan F. Menegassi de Souza[1]* and Márcia A. S. Spinacé[1]

1 – Natural and Human Sciences Center - CCNH, Federal University of ABC
renan.menegassi@ufabc.edu.br

Abstract -
The development of biodegradable materials has been increased due to petroleum-based material waste. In this work, thermoplastic corn starch (TPS) was reinforced with viscose yarn waste (VW) to produce TPS/VW biocomposites, prepared by mechanical stirring and processed by extrusion-compression molding technique. Corn starch (CS), TPS and VW were characterized, as well as, TPS/VW biocomposites. CS showed different shapes and 46.4 % of index crystallinity. TPS matrix presented 40.6 % of crystallinity index, a homogeneous surface without rough regions. VW showed smooth surface composed by a mixture of cellulose I and II. The results of the tensile tests of TPS/VW biocomposite containing 40 wt. % of VW contents achieved the greatest increase in tensile strength (336 %) and Young's modulus (862 %), indicating a good interaction of fiber/matrix due to their chemical. TPS/VW biocomposites processed by extrusion-compression molding technique present potential application in engineering area.
Keywords: *Biopolymers. Mechanical stirring, Mechanical testing. Microstructural analysis.*
Fundings: UFABC, CAPES and FAPESP.

Introduction

Polymers materials have been used as an alternative for metal and ceramic materials applications. They present low weight and cost, and good design for several products and areas. Thus, conventional polymer waste is causing some social and environmental problems. Aiming the reduction of using polymeric petroleum-based materials, researchers are developing biodegradable materials from biopolymers like starch [1-2].

Starch is a polysaccharide consisted of amylose and amylopectin chains accountable of amorphous and crystalline regions, respectively. Starch is organized in granules with semi-crystalline structure. Amylose chain is linear and flexible with helical segment composed of α-D-glucose units joined by α-1-4-glycosidic bonds. Amylopectin is a large and highly branched chain by α-1-6-glycosidic bonds of the α-1-4-D-glucose backbones. It is more packed and denser than amylose due to its double helix conformation [3, 4]. Starch is widely studied due to its low cost and high production, highlighting its potential in research above other biopolymers. Unlike thermoplastics behavior, native starch presents melting temperature above its thermal degradation and is brittle. In addition, it is difficult to handle and has a limited range of applications. Some alternatives processes may overcome these drawbacks [5, 6]. Thermoplastic starch (TPS) can be produced by destructuring and modifying native starch granules under heat and shear in the presence of plasticizers, such as water and glycerol. TPS can be used in applications for no long time of use [5]. Furthermore, TPS properties and processing conditions are similar to those used for polyolefins. Thus, the most conventional method used in the preparation of TPS is extrusion. Also, TPS can be prepared in classical plastic processing technologies, such as film casting and compression molding. However,

the research on TPS biocomposites has been increased due to the drawbacks of TPS, such as poor mechanical strength and water-sensitivity. The reinforcements in the polymeric matrix to produce TPS biocomposites are bio-based materials like lignocellulosic or natural fibers [2, 7].
The natural fiber present similar chemical composition with the starch chains and is an interesting alternative to incorporate in the starch matrix for obtaining better performance. The renewability and biodegradability properties of the natural fibers provide good environmental benefits and potentialize their application [2, 7]. Whereas lignocellulosic fibers are made up of cellulose and some non-cellulosic compounds, the regenerated cellulosic fibers are composed only by cellulose structure, which impacts the physical and mechanical properties, and also the chemicals interactions. Both fibers present low cost and easy processability, which are interesting properties for a reinforcing phase [2]. Viscose fiber is a regenerated cellulosic fiber produced by the classical viscose process. The regeneration, extrusion and xanthogenation of cellulose occur in the presence of acids compounds. The fabric is composed by viscose fiber yarn and a certain amount of viscose yarn waste (VW) is a subproduct generated during the fabric weaving process [8, 9]. An alternative to recycle these VWs is the application as reinforcement in TPS biocomposites.
In this work, TPS/VW biocomposites were prepared by a two-step method, including mechanical stirring followed by extrusion-compression molding (EX) technique. CS, TPS, VW and TPS/VW biocomposites were characterized by X-ray diffraction (XRD), scanning electron microscopy (SEM) and tensile test.

Experimental

Materials

Native corn starch (CS) was obtained from the local market. Viscose yarn waste was supplied by Cs Franco Ind. Com. Textil Ltd., Cabreúva-SP, Brazil. Glycerol (Dinâmica®, 99,5 %), citric acid (Sigma-Aldrich®, 99,5 %) and deionized water (Spencer®) were used as received.

Preparation of TPS and TPS/VW biocomposites

Mechanical stirring at 80 ºC was performed to prepare TPS and TPS/VW biocomposites. Deionized water (87.0 wt.% of dry base), glycerol (26.0 wt.% of dry base) and citric acid (0.9 wt.% of dry base) were used as plasticizers for the TPS process. The corn starch aqueous suspension was mixed and heated at 80 (± 5) ºC under magnetic stirring (from 800 to 1200 rpm) until the viscosity significantly increased forming the starch gelatinized. Thus, a granular morphology was obtained formed the material obtained was cooled at room conditions for 5-7 days. For TPS/VW biocomposite, granules materials were prepared containing VW contents of 10, 20, 30 and 40 wt%, called TPS/VW10, TPS/VW20, TPS/VW30 and TPS/VW40, respectively.

Extrusion-compression molding technique

A single screw extruder with a 420 mm screw operating at 40 rpm was used to carried out the extrusion of granules materials. 90, 100 and 110 °C were the temperatures from feed to die zone, respectively. Finally, a ~15 cm length extruded strand was compression-molded in a hydraulic press for 3 min at 105 (± 1) °C under a load of 3 tons into metal plates. The extrusion-compression molding (EX) technique was performed to obtain TPS-EX and TPS/VW-EX biocomposites films, which were air-cooled for 24 h.

X-ray diffraction (XRD) characterization

The diffraction patterns were measured on an X-ray diffractometer (Bruker AXS®, model D8 Focus) with a CuKα radiation (λ = 0.1541 nm) at 40 kV and 40 mA. Scattered radiation was detected in the range of 2θ = 5º-70º, with data acquisition taken at intervals of 2 º.min^{-1}.
The crystallinity index (χc) of CS sample was calculated using the diffraction halo height intensity method (Eq. 1), where H_a (a.u.) and H_c (a.u.) are the maximum intensity of the halo related to the amorphous region and crystalline region, respectively [10].

$$\chi_c(\%) = \left(\frac{H_c}{H_c - H_a}\right) x\ 100 \qquad (1)$$

The χc of VW sample was calculated using the classical and most described method in literature for cellulose that is the diffraction peak height intensity method (Eq. 2), where I_{020} (arbitrary units, a.u.) is the maximum intensity of the (020) peak for cellulose II at around 22º 2θ and I_{am} (a.u.) is the intensity at 16º 2θ, related to the amorphous scattering [11].

$$\chi_{c\,(VW)}(\%) = \left(\frac{I_c - I_{am}}{I_a}\right) x\ 100 \qquad (2)$$

Scanning electron microscopy (SEM) characterization

Samples morphologies were characterized by SEM measurements performed on a JEOL-JSM-6010LA microscope instrument with an accelerating voltage of 10 kV. A gold layer (~ 30 nm) was coated on the surface of each sample using a Sputtering Leica ACE200 to avoid charging. TPS/VW biocomposites morphology was characterized by SEM measurements on cryogenically fractured samples.

Tensile test characterization

Tensile tests of TPS and TPS/VW biocomposites were performed according to ASTM D882-10 in a universal testing machine (EMIC®, model DL-10000) using a 0.5 kN load cell at a rate of strain of 4 mm/min and a gauge length of 50 mm.

Results and Discussion

The SEM micrographs of CS and cryogenic fracture surface of TPS-EX are presented in Fig 1. CS showed different granule shapes and sizes ranging from 8 to 53 µm, as previous reported in the literature [4, 12]. TPS-EX sample showed a homogeneous surface without rough regions due to the shear provided by the screw. The extrusion process breaks the granules and increases the gelatinization efficiency of the starch [13]. Fig 1 also shows the morphology of VW and is observed smooth surfaces of fibers composed of microfibrils with average width of 6 (± 3) µm. This kind of morphology depends on the steps of the classical viscose process that removes non-cellulosic compounds [14, 15].

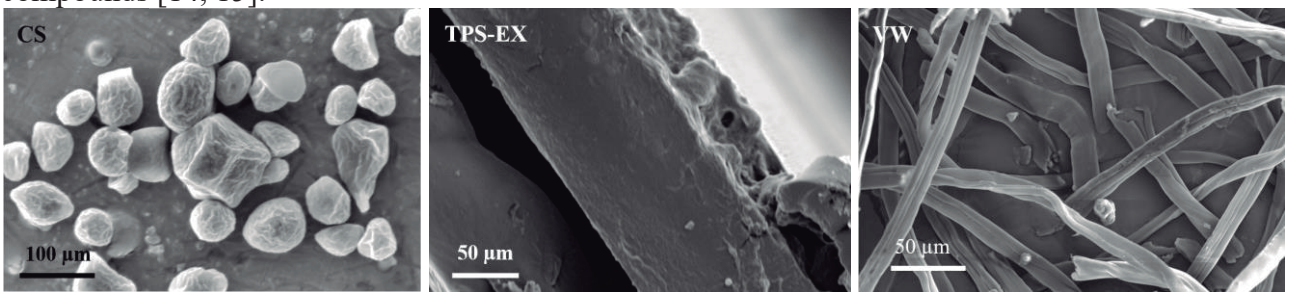

Figure 1 – Scanning electron micrographs of CS, cryogenic fracture surface of TPS-EX, and VW.

X-ray diffractogram of CS is shown in Fig 2 and the peaks at 2θ = 15.1°, 17.2° and 22.9º are related to its A-type crystalline structure, rich in amylopectin chains. The A-type crystalline structure is consisted of amylopectin chains with 23–29 glucose units length that carry no branches themselves and arrange as densely packed double helices in a staggered monoclinic lattice [3]. In TPS-EX diffractogram, Fig 2, peaks at 2θ = 17.1° and 22.2° related to the A and B-type crystalline structures, respectively, are observed. This B-type crystalline structure found can be attributed to amylose crystallization or even to amylopectin recrystallization [13]. In addition, the peak at 2θ = 19.8° is related to processing-induced V_H-type crystalline structure formed by the crystallization of amylose in single helices involving glycerol or lipids [4]. Depending on storage conditions and starch sources, the crystalline index (χc) can range from 20 % to 45 % [12]. The χc value for CS was 46.4 % and for TPS-EX was 40.6 %, as expected [4, 5]. Starch granules are destructed during gelatinization and preparation of TPS, and an amorphous material is obtained [5]. Fig 2 also shows the VW diffractogram and peaks at 2θ =12.5º and 21.4º related to the $(1\bar{1}0)$ and (020) planes of cellulose II, respectively, are observed [15]. A first subtle peak was observed at 2θ =16.1º, related to the (110) crystallographic plane of cellulose I phase, indicating the presence of an unchanged phase after the viscose production [15]. Overlapping the peaks around at 20.5º due to the presence of

amorphous content, it is the peak related to the (110) crystallographic plane of cellulose II phase [8, 9]. The χc value of viscose fiber can range from 41 % to 78 % and the obtained for VW was 73.3 %, highlighting its potential to reinforce polymeric composites [8, 15].

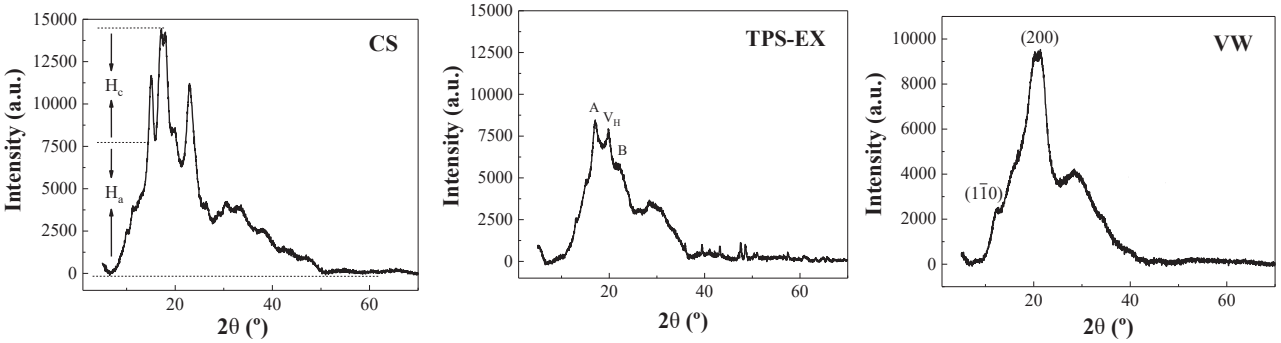

Figure 2 – X-ray diffractograms of CS, TPS-EX and VW.

The cross-section morphology of the TPS/VW-EX biocomposites performed by SEM is presented in Fig 3. The SEM micrographs of the TPS/VW-EX biocomposites reveal decreasing void content as the VW content increases, suggesting the strong fiber/matrix bond due to their chemical similarity by intermolecular hydrogen bonds and Van der Waals forces [6]. The absence of cracks on the TPS/FV40-EX biocomposites matrix indicates it as the potential candidates for achieving the better mechanical properties.

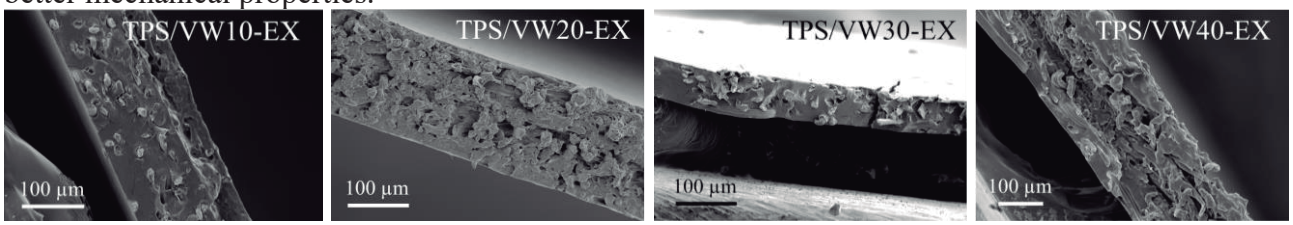

Figure 3 – SEM micrographs of TPS/VW-EX biocomposites after cryogenic fracture.

Mechanical properties, as tensile strength, Young's modulus and elongation at break, of the TPS-EX and TPS/VW-EX biocomposites films were obtained by tensile test, Fig 4. Increasing VW content, the average tensile strength values of the TPS/VW-EX biocomposites were all increased. The film of TPS/VW40-EX biocomposite shows average value of tensile strength of 4.94 MPa, which corresponds to a 336 % increase compared to TPS-EX film (1.47 MPa). This result supports the SEM micrographs, indicating the improvement in the mechanical properties due to the even mixing of starch and fiber that enhances the interface binding force and suggests the good interaction of fiber/matrix in the biocomposites. The film of TPS/VW40-EX shows average Young's modulus value of 124.41 MPa that corresponds to 862 % increase in stiffness compared to TPS-EX film (14.43 MPa). This result can be attributed to the high χc value of VW performed by XRD analysis, showing the influence of VW on the TPS mechanical properties and the importance of reusing VW for new applications, as composites reinforcement.

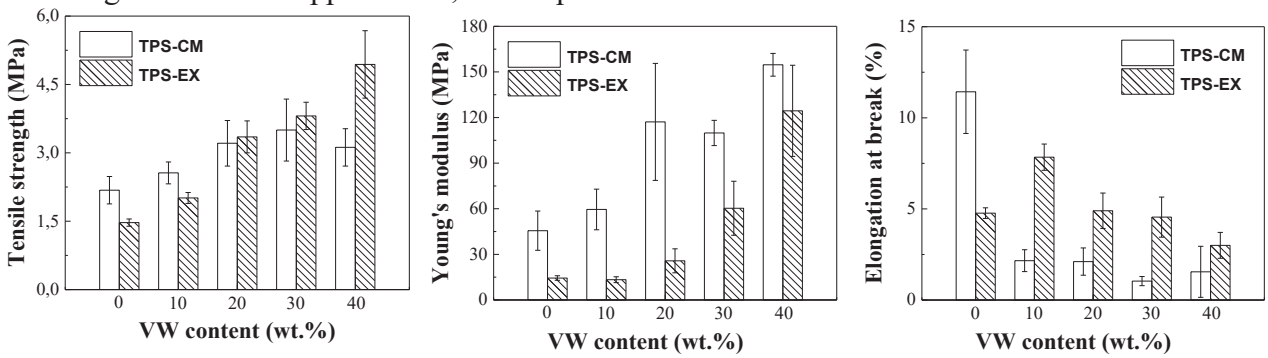

Figure 4 – Mechanical properties of TPS/VW biocomposites: error bars represent standard deviations.

The average elongation at break values of the TPS/VW10-EX biocomposite (7.84 %) shows an increase of 164 % compared to TPS-EX film (4.77 %), indicating a significant variation in ductility.

However, TPS/VW40-EX biocomposite achieved the better mechanical result and showed average value of elongation at break of 3.00 % that is 37 % less than elongation at break value of TPS-EX film (4.77 %). A biocomposite better than TPS in mechanical properties was produced.

Conclusions

TPS/VW-EX biocomposites with VW content (10-40 wt.%) were successfully processed by two-step method, including mechanical stirring followed by extrusion-compression molding technique. TPS/VW40-EX biocomposite showed tensile strength average value of 4.94 MPa, increasing 336 % on TPS-EX film property (1.47 MPa). The screw shearing provided breaking CS granules for achieving better mechanical properties. In addition, the recycling importance of VW was showed in its interesting properties as reinforcement to be used in biocomposites of TPS matrix.

Acknowledgements

Authors acknowledge financial support received from Federal University of ABC (UFABC) and Higher Education Improvement Coordination (CAPES, 23038.009634/2016-71), as well as to São Paulo State Research Foundation (FAPESP, 10/17804-7) by the support of Prof. Spinacé's laboratory. The authors are also grateful for the experimental support provided by the Multiuser Central Facilities of the UFABC and the Technological Research Institute (IPT) for tensile test.

References

1. A. Khan et al. Journal of Food Process Engineering 2016, 40, 3. https://doi.org/10.1111/jfpe.12447.
2. C. S. Miranda et al. Materials Today: Proceedings 2015, 2, 1. https://doi.org/10.1016/j.matpr.2015.04.009.
3. K. Bashir; M. Aggarwal. Journal of Food Science and Technology 2019, 56, 2. https://doi.org/10.1007/s13197-018-3530-2.
4. M. A. Villar et al., *Starch-Based Materials in Food Packaging: Processing, Characterization and Applications*, Elsevier, London, 2017.
5. A. Ghanbari et al. International Journal of Biological Macromolecules 2018, 112, https://doi.org/10.1016/j.ijbiomac.2018.02.007.
6. S. Karimi et al. International Journal of Biological Macromolecules 2016, 91, http://dx.doi.org/doi:10.1016/j.ijbiomac.2016.06.061.
7. J. Ahmed et al. *Starch-Based Polymeric Materials and Nanocomposites: Chemistry, Processing, and Applications*, Taylor & Francis Group, Florida, 2012.
8. X. Colom; F. Carrillo. European Polymer Journal 2002, 38, 11, https://doi.org/10.1016/S0014-3057(02)00132-5.
9. K. S. Prado; D. Gonzales; M. A. S. Spinacé. International Journal of Biological Macromolecules 2019, 136, https://doi.org/10.1016/j.ijbiomac.2019.06.124.
10. S. H. D. Hulleman; J. M. van Hazendonk; J. E. G. van Dam. Carbohydrate Polymers 1994, 261, https://doi.org/10.1016/0008-6215 (94)80015-4.
11. L. Segal et al. Textile Research Journal 1959, 29, 10, https://doi.org/10.1177/004051755902901003.
12. R. Thakur et al. International Journal of Biological Macromolecules 2019, 132, 1, https://doi.org/10.1016/j.ijbiomac.2019.03.190.
13. L. J. D. Amaral et al. Polímeros 2016, 26, http://dx.doi.org/10.1590/0104-1428.2001.
14. G. Vanitjinda; T. Nimchua; P. Sukyai. International Journal of Biological Macromolecules 2019, 122, https://doi.org/10.1016/j.ijbiomac.2018.10.191.
15. K. S. Prado; M. A. S. Spinacé. Materials Research 2015, 18, 3, http://dx.doi.org/10.1590/1516-1439.311514.

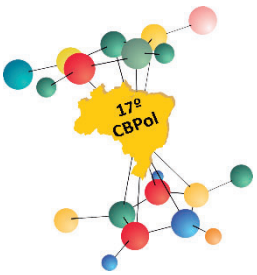

TRANSMITTANCE AND THERMAL STABILITY OF REGENERATED CELLULOSE FILMS WITH SILVER NANOPARTICLES AND PLASTICIZERS

Lays F. de M. S. Kataoka[1]*, Marial del P. H. Falla[2] and Sandra M. Luz[1]

1 – Mechanical Sciences Program, Brazil University of Brasília, Brasília, DF, Brazil
*lays.furtado94@gmail.com
2 – Engineering Materials Integrity Program, University of Brasília, Brasília, DF, Brazil

Abstract - The nanocomposite films from jute fibers can be promising for application in electronic devices. Silver nanoparticles (AgNPs) can be added to these films to provide their conductivity. Additionally, plasticizing these films can improve the physical or chemical properties, allowing more application options for these conductive films. This work studied the transmittance and thermal stability of regenerated cellulose films (RCF) by adding AgNPs and plasticizers. Carboxymethylcellulose (CMC), Sorbitol, and Glycerol plasticizers were incorporated at 15 wt.% to produce the nanocomposite films containing 0.5 wt.% of AgNPs. Further, the films were characterized by Ultraviolet-visible Spectroscopy (U–Vis), thermogravimetry and its derivative thermogravimetry (TGA/DTG), and Fourier Transform Infrared (FTIR) Spectroscopy analyses. An average size of 9 nm for AgNPs was verified. Incorporating AgNP in the films decreased the transmittance in relation to pure RCF and reduced the thermal stability temperature. The thermal stability of the studied samples ranged from around 197 °C to 230 °C. In addition, sorbitol exhibited better responses from higher transmittance and thermal stability than CMC and glycerol in RCF and nanocomposite films.

Keywords: *jute fiber; regenerated cellulose films; silver nanoparticles; transmittance; thermal stability.*

Introduction

Plant-derived fibers composed of lignocellulose and possessing a significant proportion of cellulose have garnered considerable interest due to their plentiful, renewable, and naturally occurring polymers. Jute (*Corchorus capsularis*) is among the natural fibers which stand out as one of the most abundant and cheapest sources of cellulose, having several applications on a world scale and being surpassed by cotton [1]. Cellulose can be applied in various forms, such as fibers, films, and composite materials, for several industrial uses [2]. Among these forms, conductive cellulose films are studied primarily for their applications in high-value electronic devices such as sensors, transistors, solar cells, supercapacitors, electromagnetic shielding, and other elements [3]. The regeneration of cellulose can carry out the manufacturing of these films. For this, cellulose's fibrous and semi-crystalline structure must be broken down in a dissolution process and then undergo a subsequent coagulation step [3]. Systems that use alkaline solutions such as sodium hydroxide (NaOH) for cellulose dissolution are considered more cost-effective, and toxic substances are not used or produced throughout the process. As a result, water becomes a potential coagulant in the NaOH aqueous dissolution system because it is easily accessible and presents controlled results, such as porosity [4].

Conductive materials such as metals, inorganic oxides, conductive polymers, and carbon materials can be physically or chemically introduced into their structure. Metals exhibit high conductivity and low transmittance. Inorganic oxides exhibit high conductivity and transmittance without flexibility, conductive polymers exhibit excellent flexibility, although relatively low

conductivity and transmittance, and carbon materials exhibit relatively moderate conductivity and transmittance [3]. Due to their excellent conductivity, metal nanoparticles such as silver can be applied in regenerated cellulose films. These conductive films can be promising candidates for the manufacture of electronic components, as seen in previous works [5]. A homogeneous morphology was also observed, without agglomerates, indicating an increase in the degree of molecular orientation of the films obtained by the regenerated process of the samples, probably due to the plasticizing effect of carboxymethylcellulose (CMC), used to stabilize the silver nanoparticle solution. This effect can improve the physical and chemical properties of the films, allowing for more application options for these conductive films.

Plasticizers derived from renewable sources such as glycerol and sorbitol are polyols compatible with RCF films that can improve the mechanical flexibility of films and modify other physicochemical properties, as thermal stability improvement [6]. In addition to conductivity, factors such as transmittance, chemical composition, and application temperature range should be studied. Then, in this work, we evaluated the transmittance and thermal stability of the regenerated cellulose film of jute fibers by adding silver nanoparticles (AgNPs) and plasticizers. CMC, Sorbitol, and Glycerol were used as plasticizing agents.

Experimental

Synthesis of silver nanoparticles and Characterization

To obtain the nanoparticle solution, 450 mL of an 18.0 x 10^{-6} mol/L sodium borohydride ($NaBH_4$, 98%, Dynamic) solution was kept below 3 °C in an ice bath and added to an Erlenmeyer flask under vigorous magnetic stirring. Through a burette, 150 mL of a 9.0 x 10^{-6} mol/L solution of silver nitrate ($AgNO_3$, 99.9%, Neon) was added at an additional rate of 1 drop/s. The chemical reaction between $NaBH_4$ and $AgNO_3$ in those concentrations resulted in a AgNPs at 250 ppm. To avoid silver nanoparticle aggregation, the solution was stabilized with 0.6 g of CMC (Sigma–Aldrich), which it has the function to coat the nanoparticles. The silver nanoparticle solution, prepared by drying a small drop on a copper grid, was characterized by Transmission Electronic Microscopy (TEM) in the JEOL JEM 1011 equipment, with a voltage of 40 kV. Size measurements and statistical analysis of silver nanoparticles dimensions were taken from TEM images using the ImageJ software.

Obtaining Regenerated Cellulose Films with Silver Nanoparticles

The bleached jute cellulose was obtained in previous work [5]. Then, it was ground in an automatic analytical mill Quimis Q298A for 30 seconds. Depending on the sample, as showed in the Table 1, each solution was prepared as followed: To obtain the RCF film, 2.2 g of cellulose was dissolved in 100 mL of a pre-cooled solution (-12°C for 18 h) containing 8% (w/v) NaOH solution. To achieve the cooling conditions, the solution was kept in a freezer for at least 18h to reach around -12ºC equilibrium. Also, to obtain the RCF with the AgNPs, 26 mL of nanoparticles solution at 250 ppm was added to achieve 0.5 wt.% of silver nanoparticle content, before the pre-cooling. To prepare the RCF films with the plasticizers, the CMC, sorbitol (98%, Dynamic), and glycerol (98%, Synth) in an amount corresponding to 15 wt.% with respect to cellulose were added to the pure RCF solution. Also, the same process was performed for the nanocomposites, which resulted in nanocomposites containing 15 wt.% of plasticizer and 0.5 wt.% of silver nanoparticle. To dissolve the solution, all samples were submitted under vigorous stirring at 3000 rpm and room temperature every 7 min.

Table 1 – Composition of regenerated cellulose films.

Sample	Plasticizer (wt.%)	AgNP (wt.%)	Sample	Plasticizer (wt.%)	AgNP (wt.%)
RCF	-	-	RCF - Sorbitol	15% Sorbitol	-
RCF - AgNP	-	0.5%	RCF - Sorbitol - AgNP	15% Sorbitol	0.5%
RCF - CMC	15% CMC	-	RCF - Glycerol	15% Glycerol	-
RCF - CMC - AgNP	15% CMC	0.5%	RCF - Glycerol - AgNP	15% Glycerol	0.5%

To mold the films and regenerate the cellulose, the mixture containing cellulose, and nanoparticles was subjected to centrifugation at 4000 rpm for 10 min to exclude the undissolved part and perform degassing. Then, 7 mL of the resulting solution was poured onto a polypropylene Petri dish with a diameter of 85 mm. The RCF and nanocomposite films were pre-dried at room temperature for 18 h until gelation. Afterward, the sample was immersed in a water bath (distilled water) at room temperature for 15 min to coagulate and regenerate the cellulose. Finally, the films were dried at room temperature for 48 h before the characterization.

Ultraviolet-visible Spectroscopy (UV–Vis)

The RCF and nanocomposite films were assessed with the Evolution 220 Thermo Scientific equipment to determine the transmittance. The transmittance spectra of the films were analyzed across wavelengths ranging from 200 to 800 nm.

Thermogravimetric Analysis (TGA)

The jute fibers and the fibers from each treatment step until cellulose was bleached and the RCF film was characterized via thermogravimetry analysis (TGA: SDT Q600 TA Instruments). Approximately 10 mg of each sample was analyzed in alumina pans. The analysis was conducted under a nitrogen atmosphere (flow rate 50 mL/min) and a heating rate of 10 °C min^{-1} from 30 to 600 °C.

Fourier Transform Infrared (FTIR) Spectroscopy

FTIR spectra of RCF and nanocomposite films were obtained using a Fourier-transform infrared spectrometer (NICOLET IS10, Thermo Scientific) by transmittance accessory from 500 to 4000 cm^{-1} with 64 scans collected at an interval of 4 cm^{-1}.

Results and Discussion

Figure 1a shows the transmission micrograph of the silver nanoparticle solution synthesized in this work. Through the micrograph, it is seen that the nanoparticles have a homogeneous size. The average size found for the nanoparticles was 9.0 ± 2.0 nm, with spherical characteristics within the range normally obtained in the literature using the synthesis method from silver nitrate and sodium borohydride solutions [7].

The UV-Vis results are presented in Figure 1b and the transmittance values for the films at 550 and 800 nm. The transmittance curve for all RCF films was observed throughout the wavelength range between 200 and 800 nm [5]. Figure 1b reveals low transmittance of the RCF - CMC - AgNP, RCF – Glycerol and RCF - Glycerol - AgNP films in the UV region, suggesting that these samples have anti-UV properties. In the visible region of the spectra, there was an increase in transmittance in all films. In addition, the transmittance of silver nanocomposites decreased with the incorporation of plasticizers due to these components providing increased absorption in accordance with seen in the literature [6].

The RCF sample obtained a high transmittance value, as reported in some studies with similar applications for regenerated cellulose films [3]. Incorporating sorbitol into RCF - Sorbitol increased the transmittance value to greater than pure RCF. However, containing plasticizers in RCF-CMC and RCF- Glycerol samples decreased the transmittance in relation to RCF, with the latter experiencing a significant decrease upon adding glycerol.

The presence of a transmittance band near 300-400 nm for the nanocomposite films containing AgNPs, indicates the existence of this component in the samples. The bands in this wavelength range are related to these spherical metal nanoparticles. As observed in the spectra, AgNPs with smaller sizes exhibit an absorption peak at shorter wavelengths [7]. Regarding the nanocomposite films, the RCF - Sorbitol - AgNP sample had lower transmittance than the RCF – AgNP. However, it was the plasticizer with the best result compared to the other plasticizers, with the RCF - CMC - AgNP sample having the highest loss of transmittance.

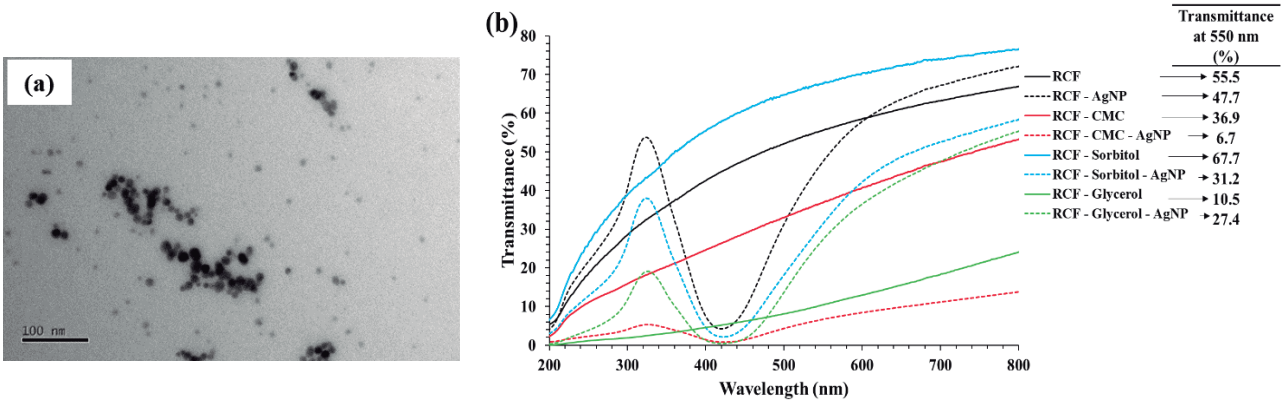

Figure 1 – (a) Transmission micrograph of the AgNP solution, (b) UV-Vis spectra of RCF and nanocomposite films.

The TG and DTG curves of RCF and nanocomposite films are shown in Figure 2a. A thermal event occurs at temperatures below 100°C for all samples due to moisture loss [5]. Also, there are information regarding the thermal stability temperatures of the samples and the temperature of the main degradation peak corresponding to cellulose, which ranged from approximately 253°C to 334°C. The least thermally stable samples with cellulose degradation peaks shifted to lower temperatures were those with glycerol, probably due to this component degrading at lower temperatures [6]. The most thermally stable sample is the RCF, where the incorporation of both plasticizer and AgNP influenced to decrease in the stability of the samples.

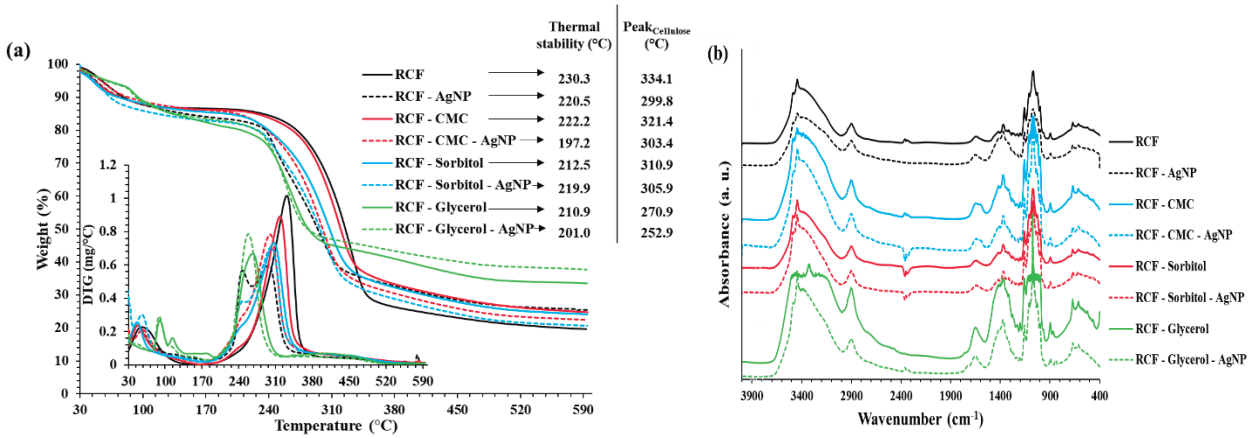

Figure 2 – a) Curves TGA, DTG, and thermal stability temperatures for RCF and nanocomposite films. (b) Fourier-transform infrared spectroscopy (FTIR) spectra for the same samples.

The FTIR spectra of the controlled regenerated cellulose and nanocomposite films are shown in Figure 2b. The absorption bands around 3440 cm^{-1} indicate the presence of cellulose due to the stretching of the hydrogen-bonded O-H, and around 2900 cm^{-1} corresponds to the stretching of the C-H functional group [6]. For nanocomposite films, a shift was observed in the C=O stretching from 1636 cm^{-1} to 1642 cm^{-1}, possibly due to the interaction between silver nanoparticles and the carbonyl group, suggesting coordination between them [5,8]. The absorption band around 1410 cm^{-1} is associated with the symmetrical bending of CH_2 in cellulose, indicating correspondence with the cellulose II polymorph. A doublet at 1333-1311 cm^{-1} and a band at 1365 cm^{-1} were observed, corresponding to the angular bending of the COH and HCC bonds, ordinarily present in crystalline cellulose [9]. The peaks between 997 and 1200 cm^{-1} are also characteristic of cellulose. The peaks at 1170 cm^{-1}, 1040-1070 cm^{-1}, and 894 cm^{-1} are related to the stretching of the C-O vibrations and C-H deformation of the skeletal pyranose ring of cellulose [5]. At 997 cm^{-1}, there is a CO stretching peak.

No chemical bond between cellulose and NaOH was identified from the FTIR. A peak relative to glycosidic bonds is around 894 cm^{-1} [10]. In the films with glycerol, the appearance of a peak around 850 cm^{-1} is observed, corresponding to the vibrations of the O-O groups [11].

Conclusions

Incorporating AgNPs and plasticizers in nanocomposite films decreased the transmittance in relation to RCF films due to these factors causing an increase in sample absorption, making it difficult for light to pass through. AgNPs nanocomposite films were less thermally stable than RCF without nanoparticles. Incorporating plasticizers also contributed to a drop in thermal stability, with RCF being the most stable sample. Sorbitol was the plasticizer that exhibited better transmittance and thermal stability compared with CMC and glycerol in RCF and nanocomposite films. The FTIR spectra made it possible to visualize the film's functional groups, characteristic of cellulose and plasticizers used. Furthermore, it also showed band shift, possibly the interaction between AgNPs and the carbonyl group in films.

Acknowledgments

The authors thank FAPDF, CNPq, CAPES and DPG/UnB for the financial support.

References

1. U.H. Erdoğan; Y. Seki; G. Aydoğdu; B. Kutlu; A. Akşit Journal of Natural Fibers 2016, *13*, 158. https://doi.org/10.1080/15440478.2014.1002149.
2. H.P.S. Abdul Khalil; A.H. Bhat; A.F. Ireana Yusra Carbohydrate Polymers 2012, 87, 963. https://doi.org/10.1016/j.carbpol.2011.08.078
3. X. Liu; W. Xiao; X. Ma; L. Huang; Y. Ni; L. Chen; X. Ouyang; J. Li Carbohydrate Polymers 2020, *250*, 1. https://doi.org/10.1016/j.carbpol.2020.116969.
4. T. Budtova; P. Navard Cellulose 2016, *23*, 5. https://doi.org/10.1007/s10570-015-0779-8.
5. L. F. de M. S. Kataoka; R. M. Leão; A. B. Gontijo; M. del P.H. Falla; S. M. Luz Materials Today Communications 2022, *33*, 1. https://doi.org/10.1016/j.mtcomm.2022.104645.
6. J. Pang; X. Liu; X. Zhang; Y. Wu; R. Sun Materials 2013, *6*, 1270. https://doi.org/10.3390/ma6041270.
7. N. Leopold; B. Lendl The Journal of Physical Chemistry B 2003, 107, 5723. https://doi.org/10.1021/jp027460u.
8. Q. Yang; F. Wang; K. Tang; C. Wang; Z. Chen; Y. Qian Materials Chemistry and Physics 2003, *78*, 495. https://doi.org/10.1016/S0254-0584(02)00379-6.
9. L. N. Ludueña; A. Vecchio; P. M. Stefani; V. A. Alvarez Fibers and Polymers *2013*, *14*, 1118. https://doi.org/10.1007/s12221-013-1118-z.
10. E.V.R. Almeida; E. Frollini; A. Castellan; V. Coma Carbohydrate Polymers 2010, 80, 655. https://doi.org/10.1016/j.carbpol.2009.10.039.
11. G. Ayala; A. C. Agudelo; R. Vargas DYNA 2012, *79*, 138.

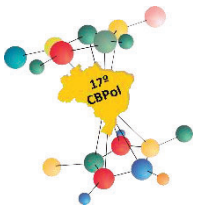

ANTIOXIDANT PROPERTIES OF BIOPOLYMERIC ONION (*ALLIUM CEPA* L.) FILMS MODIFIED WITH LAPONITE CLAY

Maciel L. Barbosa[1], Leticia M. de Oliveira[2], Robert da S. Paiva[1], Alessandra C. Dametto[3], Diogenes dos S. Dias[3], Clovis A. Ribeiro[3], Magdalena Wrona[4], Cristina Nerín[4], Hernane da S. Barud[5], Sandra A. Cruz[1,*].

1 - Department of Chemistry, Federal University of São Carlos (UFSCar), Rod. Washington Luiz, s/n - Monjolinho, São Carlos, São Paulo, Brazil.
maciel96lb@gmail.com
2 - Federal University of the São Francisco Valley (Univasf), Av. Antônio C. Magalhães, 510, Country Club, Juazeiro, Bahia, Brazil.
3 - São Paulo State University (UNESP), Institute of Chemistry, R. Prof. Francisco Degni, s/n – CP 355, Araraquara, São Paulo, Brazil.
4- Universidad de Zaragoza, Instituto de Investigación en Ingeniería de Aragón (I3A), María de Luna 3, 50018, Zaragoza, Spain
5 - University of Araraquara (Uniara), Laboratory of Biopolymers and Biomaterials (BIOPOLMAT), R. Carlos Gomes, 1338 - Centro, Araraquara, São Paulo, Brazil

Materials considered biodegradable and originating from agro-industrial waste have been gaining increasing prominence in the industrial axis. Besides coming from renewable resources, they have unique characteristics, such as non-toxicity, biocompatibility and, biodegradability. Recently, our research group prepared onion-based bioplastics, with promising results regarding their thermal, mechanical and, barrier properties. It is therefore a promising material to be employed in the packaging area. In the present work, the effect of Laponite clay concentration on the antioxidant properties of onion-based films was investigated. The films were prepared via hydrothermal, a methodology protected by BioSmart Nano. The material were investigated by X-ray diffraction (XRD), field emission scanning electron microscopy (FE-SEM), contact angle, Fourier transform infrared spectroscopy (FTIR-ATR), water vapor barrier properties (WVP) and antioxidant activity. The XRD data indicate an increase in the crystallinity in the laponite-containing materials FTIR analyses indicated a band at approximately438 cm^{-1}, characteristic of the deformation of the Mg-O and S-O groups of the clay, confirming the modification. SEM results indicated a relatively irregular surface that decreased with increasing clay content. Data of transmittance in the UV region indicate a value equal to zero, suggesting that the analyzed materials can act as blockers of the passage of this type of radiation, which can allow for a longer shelf life of foods.These results are supported by the data obtained in the antioxidant test, in which the modification of the films with 5 and 10% of Laponita increases the antioxidant potential of the films and reduces the hydrophilic characteristic. Thus, the results suggest that the formation of Laponite and onion composites can be an important strategy for the development of natural polymers in the area of packaging for food contact.

1. S. Abbasi; S. A. Haeri *Microchemical Journal* 2021, 171, 106831. https://doi.org/10.1016/j.microc.2021.106831
2. D. dos Santos Dias; C. G. Otoni; R. R. da Silva; A. B. Meneguin; L. H. C. Mattoso; H. S. Barud; C. A. Ribeiro *Industrial crops and products* 2020, 145, 111847. https://doi.org/10.1016/j.indcrop.2019.111847
3. J. M. Silva; H. S. Barud; A. B. Meneguin; V. R. Constantino; S. J. Ribeiro *Applied Clay Science* 2019, *168*, 428-435. https://doi.org/10.1016/j.clay.2018.12.003
4. J. S. Sidhu; M Ali; A. Al-Rashdan; N. Ahmed *Journal of food science and technology* 2019, *56*, 1811-1819. doi.org/10.1007/s13197-019-03625-9

Keywords: *Biopolymer, Onion films, Composite, Laponite, Antioxidant*

A STUDY OF MIXED-MATRIX POLYSULFONE-RECAM® FILTRATION MEMBRANE MORPHOLOGY

Priscila Anadão, Fabio J. Esper, Hélio Wiebeck

1 – Department of Materials Engineering, University of São Paulo (USP), São Paulo, SP, Brazil
priscila.anadao@gmail.com

Abstract - Polysulfone is commonly used to prepare filtration membrane due to its availability, low cost, ease of processing and high thermal, mechanical and chemical resistance. However, it presents low hydrophilicity, resulting in fouling onto membrane surface. Generally, chemical modifications are employed but thermal, chemical and mechanical resistance are decreased. Aiming to reduce hydrophobicity and to maintain the original resistances, composite technology is employed, by adding a ceramic material into polymer matrix. Hence, preparation and characterization of mixed-matrix polysulfone-Recam® and polysulfone-Recam®-silver nanoparticles filtration membranes is presented in this work [1]. Recam® is a carbonous material composed by lightly tilted graphene plans and carbon nanotubes. Membranes were prepared by a combination of solution dispersion and wet-phase inversion method. These solutions were characterized by coagulation time and rheology measurements and membrane morphology was visualized by SEM. Recam® membrane surface is dense due to the solvent hydrophilicity and also due to polysulfone chain adsorption onto Recam® structure. Inversely, silver nanoparticle membranes have nanopores on their surfaces since diffusion is delayed due to high viscosity dispersion. Therefore, in both membranes, two are the factors that guide their formation, which are: thermodynamical favoring and rheological hindrance.

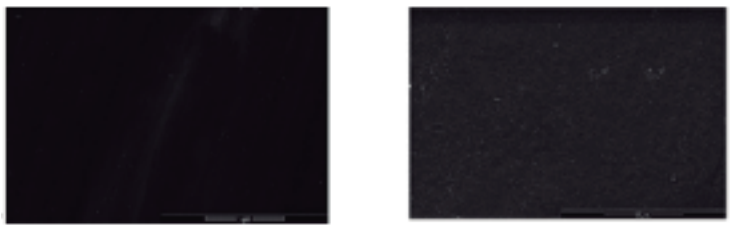

Figure 1 - SEM images of polysulfone-Recam® and polysulfone-Recam®-silver nanoparticles surfaces. .LH

References
1. P. Anadão, *Ciência e Tecnologia de Membranas,* Artliber, São Paulo, 2010.

Fundings: Capes is acknowledged.

Keywords: *membrane morphology, filtration membrane, composite membrane, polysulfone.*

DEVELOPMENT AND CHARACTERIZATION OF UPCONVERSION COMPOSITE FILMS OF CELLULOSE ACETATE-BUTYRATE/$NaYF_4$:Yb^{3+}, Er^{3+} FOR LUMINESCENT THERMOMETRY APPLICATIONS

Matheus V. B. Silva[1], Lucas H. Pereira[2], York E. Serge-Correales[2], Fábio J. Caixeta[2], Sidney J. L. Ribeiro[2], Rosana M. N. Assunção[3] and Harumi Otaguro[4*]

1 – Institute of Chemistry (IQ), Federal University of Uberlândia (UFU), Uberlândia, MG, Brazil
mvicente.quim@gmail.com
2 – Institute of Chemistry (IQ), São Paulo State University "Júlio de Mesquita Filho" (Unesp), Araraquara, SP, Brazil
3 - Faculty of Integrated Sciences Pontal (FACIP), Federal University of Uberlândia (UFU), Ituiutaba, MG, Brazil
4 – Center for Marine Studies (CEM), Federal University of Paraná (UFPR), Pontal do Paraná, PR, Brazil

Abstract – The development of thermometers based on upconverison photoluminescence of lanthanide ions has attracted attention as a potential method to measure the temperature of moving objects, liquid or gaseous flows and physiological media. These materials exhibit high thermal sensitivity and high spatial resolution in short acquisition times[1]. The hexagonal-phase $NaYF_4$:Yb^{3+}, Er^{3+} luminophore (β-$NaYF_4$:Yb^{3+}, Er^{3+}) is one of the best for this, due to its high intensity of visible light emission using near-infrared (NIR) radiation as an excitation source[2]. To combine these crystals with transparent polymer matrices is needed to keep it stable without losing its functionality. In this work, composite films of cellulose acetate butyrate (CAB) and particles of β-$NaYF_4$:Yb^{3+}, Er^{3+} were produced aiming at potential application in nanothermometers. The particles were synthesized by hydrothermal route with oleic acid (RE/OA) and stabilized with nitrosonium tetrafluoroborate ($NOBF_4$) in *N*,*N*-dimethylformamide (DMF). The composite films were prepared with different concentrations of CAB, particles (1 – 10 %w/w) and plasticizer (Tween 80®) (2.5 – 20 %w/w) using the 2^k factorial design. They were characterized with photoluminescence spectroscopy (PL), UV-Vis spectroscopy, scanning electron microscopy (SEM), energy-dispersive X-ray spectroscopy (EDX) and, X-ray diffraction (XRD). PL spectra showed an increase in luminescence with higher concentrations of particles, however, the transmittance percentual was lower. In addition, high concentrations turned the films more brittle. The thermal and mechanical properties will be analyzed by differential exploratory calorimetry (DSC) and thermodynamical mechanical analysis (DMTA). The thermal sensitivity will be analyzed by PL spectroscopy varying the temperature.

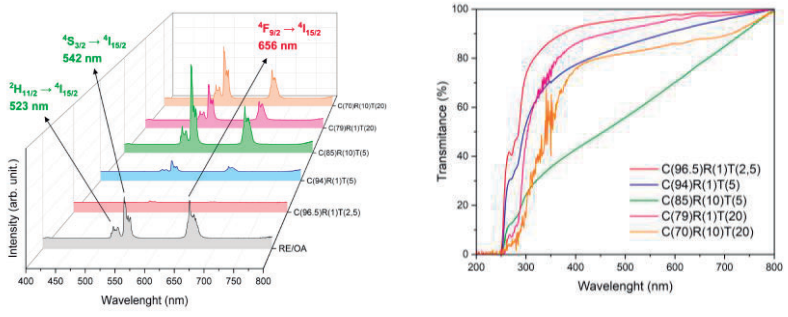

Figure 1 – (a) PL spectra and (b) UV-Vis spectra of composite films.

References

1. A. G. Bispo Júnior; P. C. Sousa Filho; F. A. Sigoli in *Lantanídeos: Química, Luminescência e Aplicações*, F. A. Sigoli, A. G. Bispo Júnior, P. C. Sousa Filho, Ed.: Átomo, Campinas, 2022; 285-299.
2. A. Kavand *et al*., *ACS Appl. Nano Mater*, 2021, 4, 5319-5329. https://doi.org/10.1021/acsanm.1c00664.

Fundings: CNPq, CAPES, FAPEMIG, FAPESP, Finep.
Keywords: *Upconversion luminescene, Composite films, Luminescent thermometry.*

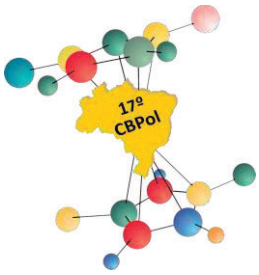

EFFECT OF NATURAL-BASED PLASTICIZERS ON PROPERTIES OF POLYHYDROXYBUTYRATE FILMS

Pedro C. Rosendo[1], Armando F. de Jesus[1], Irina M. Factori[2], Neuma M. Pereira[2], Gustavo S. G de Almeida[2], Anderson Maia[2], Rondes F. S. Torin[1,2]*

1 – Department of Polymers, Faculty of Technology of Mauá (FATEC), Paula Souza State Center for Technological Education of the São Paulo State Government - CEETEPS, São Paulo, SP, Brazil
rondes.torin@fatec.sp.gov.br; rondes.torin@gmail.com
2 – SENAI Institute of Innovation in Advanced Materials and Nanocomposite, SENAI Mario Amato unit in São Bernardo do Campo, São Paulo, SP, Brazil.

Abstract – Polyhydroxybutyrate (PHB) is a biodegradable alternative to conventional plastics derived from fossil sources. It is known for its impressive thermal and mechanical properties, as well as its compatibility with conventional processing machines[1,2]. PHB has significant potential for applications in the medical field and tissue engineering, owing to its biocompatibility with the human body and its ability to support cellular therapies. Due to its unique properties3, PHB holds promise for developing new materials. This study aims to investigate the thermal and mechanical properties of PHB films using the casting methodology. Additionally, we examine the impact of different plasticizers on the film's composition to enhance its characteristics. The experimental approach involves obtaining films through the solvent evaporation method, where a filmogenic solution is prepared using a suitable solvent. The solution is evenly poured into a Petri dish, allowing the solvent to evaporate and form a thin polymer layer. To evaluate the effect of plasticizers, they are added at various concentrations to the polymeric solution. Subsequently, the obtained samples undergo Fourier-transform Infrared spectroscopy (FTIR), Differential Scanning Calorimetry (DSC), and mechanical analysis for a comparative study of the results. Three bio-based plasticizers, PM1, PM2, and PM3, were tested at concentrations ranging from 1% to 3%. While no significant variations were observed in the FTIR and DSC spectra, the PM3 plasticizer exhibited improved mechanical performance at a 3% concentration. These results indicate the optimal conditions for obtaining PHB films with enhanced performance, showing promising potential for various applications, such as coatings, membranes, scaffolds, and wound healing.

References

1. L.S. Nair; C.T. Laurencin *Progress in Polymer Science* 2007, 32, 8-9. http://doi.org/10.1016/.progpolymsci.2007.05.017
2. J.C. de Andrade Alves; G.S. da Silva; K. C. de Souza; I. D. de L. Silva; C. F. da Silva; V. F. Caetano; G. M. Vinhas *Research, Society and Development* 2021, 10, 2. https://doi.org/10.33448/rsd-v10i2.12547
3. L. Savenkova; Z. Gercberga; V. J. P. B Nikolaeva; A. Dzene; I. Bibers; M. Kalnin *Process Biochemistry* 2000, 35, 6. https://doi.org/10.1016/S0032-9592(99)00107-7

Fundings: The authors thank FAPESP (grant no. 2023/07677-8) for the financial support.

Keywords: polyhydroxybutyrate*; films; plasticizers; casting; properties.*

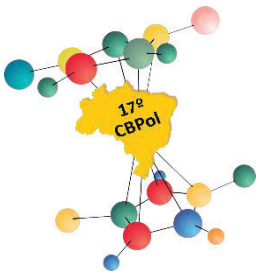

EFFECTS OF ELECTROPHORETIC DEPOSITION OF CARBON NANOTUBES ON JUTE FIBERS

Amanda Valcanaia[1], Kelvin Masakazu[1], Ricardo de Medeiros[2], Luis C. Fontana[1], Daniela Becker[2]

1 – Laboratory of Plasma -Films and Surfaces, Center for Technological Science, UDESC, Joinville, SC, Brazil
amanda.valcania@edu.udesc.br
2 – Mechanical Engineering Department, Center for Technological Science, UDESC, Joinville, SC, Brazil

Abstract – Natural fibers (NF) as reinforcement in polymeric composites represent an emerging alternative in the mechanical, automotive, and aerospace industries, stemming from the growing demand for sustainable materials and cost reduction. NF are derived from renewable resources and are biodegradable. However, in addition to their ecological characteristics, they are also low-density materials, enabling lightweight compositions, which makes these fibers highly attractive. Among NF, jute fiber (JF) is a promising material due to its strength, lightweight nature, and reduced cost. Therefore, the present study aims to investigate the utilization of JF as a substrate for the deposition of carbon nanotubes (CNT) through the electrophoretic deposition (EPD) technique. For the deposition method, a solution containing 0.5% (by mass) of CNT in deionized water (H2O) was used, and the surfactant Sodium Dodecyl Sulfate (SDS) was added in a 1:520 ratio to the solution mass to ensure its stability. The characterization of the samples was performed using thermogravimetric analysis (TGA) and electrochemical impedance spectroscopy (EIS). The TGA results showed effective deposition of CNT on the fibers, resulting in a residue mass exceeding 15%. The impedance analysis indicated that the CNT deposition increased electrical conductivity by four orders of magnitude. Thus, the acquired results demonstrate the potential of utilizing JFs as reinforcement for polymeric composites.

References

1. BEGUM K; ISLAM MA. Natural Fiber as a substitute to Synthetic Fiber in Polymer Composites: A Review. Research Journal of Engineering Sciences, v. 2, n. 3, p. 46–53, 2013.
2. IWASAKI, K. M. K. et al. Carbon nanotube deposition through intermittent high voltage pulsed electrophoresis on jute fibre. Applied Surface Science, v. 611, p. 155548, fev. 2023.
3. RASTOGI, R. et al. Comparative study of carbon nanotube dispersion using surfactants. Journal of Colloid and Interface Science, v. 328, n. 2, p. 421–428, 15 dez. 2008.

Fundings: The authors acknowledge the financial support of the Santa Catarina State Research and Innovation Funding Agency (FAPESC grant: 2020TR1450 and 2021TR1283). As well as the financial support of the National Council for Scientific and Technological Development (CNPq).

Keywords: *Natural fibers, jute fibers, polymer composites, electrophoretic deposition, carbon nanotubes.*

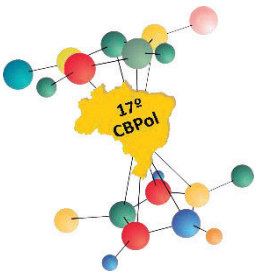

ESTIMATION OF CREEP AND FATIGUE LONG TERM BEHAVIOR OF A GLASS-FIBER/POLYPROPYLENE COMPOSITE USING SHORT TERM DATA

Marco A. F. Gobbi[1,2*], Cristiano Richter[1], Renato T. de Vargas[2], Cristiano Krug[3], Tales S. Daitx[1] and Maximiliano Segala[1]

1 – Institute of Chemistry, Federal University of Rio Grande do Sul (UFRGS), Porto Alegre, RS, Brazil
2 – Braskem S/A, São Paulo, SP, Brazil
3 – Institute of Physics, Federal University of Rio Grande do Sul (UFRGS), Porto Alegre, RS, Brazil
marco.gobbi@braskem.com.br

Abstract – The present work has the purpose to evaluate the viscoelastic properties of a glass-fiber/polypropylene composite (GFPP) and to estimate its creep and fatigue life. Both creep and fatigue experiments were carried on a dynamical-mechanical analysis equipment (DMA) with dual cantilever clamp. Creep life was evaluated through time-temperature superposition principle (TTSP) as proposed by Tajvidi *et al*. [1] using 12 min creep experiments with 2 MPa stress at different temperatures. The shift-factors used to build the creep master curve were obtained by frequency scans on the same temperatures as the creep experiments. The resulting creep master curve was adjusted using a power law model with good agreement to the experimental data. Another model, proposed by Findley [2] was used, with improvements on the agreement between adjusted and experimental data on initial creep times. The proposed models can be used to estimate the creep deformation at a given time, being a useful tool to estimate the material creep life, given an acceptable deformation. Fatigue tests were carried at 23 °C for 1 million cycles at 4 Hz and the oscillation displacement was controlled at 250 µm (0.45% strain), while the required stress was recorded. For the estimation of fatigue life, the Fatigue Modulus concept, as proposed by Hwang and Han [3] was used. The method yielded good agreement between experimental data and the model. The resulting fatigue life of the composite is estimated above 10^9 cycles. Both of the creep models and the Fatigue Modulus concept showed good agreement with experimental data meaning that they are a useful tool for material selection and comparison. The information yielded with the short-term experiments can be used to model longer term behaviors and, thus, be used as a decision-making tool when selecting a material for a specific and desired application.

References

1. M. Tajvidi; R. H. Falk; J. C. Hermanson *J Appl Polym Sci* 2005, *97*, 1995-2004. https://doi.org/10.1002/app.21648.
2. W. N. Findley *Polym Eng Sci* 1987, 27, 582-585. http://doi.org/10.1002/pen.760270809.
3. W. Hwang; K. S. Han *J. Compos. Mater*. 1986, 20(2), 154-165. https://doi.org/10.1177/002199838602000203.

Fundings: The authors are grateful to Braskem S/A, Conselho Nacional de Desenvolvimento Científico e Tecnológico (CNPq), Coordenação de Aperfeiçoamento de Pessoal de Nível Superior (CAPES) and Fundação de Amparo à Pesquisa do estado do Rio Grande do Sul (PRONEX/FAPERGS - Finance Code 16/2551-0000470-6) for financial support.

Keywords: *Creep and fatigue life, dynamical-mechanical analysis, Glass-fiber/polypropylene composite, Life cycle, Mathematical model.*

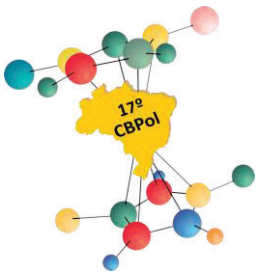

EXTRUSION SEQUENCE FOR ENHANCED DISPERSION OF MICROFIBRILLATED CELLULOSE IN PLA/PCL BLENDS: IMPACT ON MORPHOLOGY AND MECHANICAL PROPERTIES

Paula do P. Dias[1] and Marcelo A. Chinelatto[1]*

1 – Department of Materials Engineering, University of São Paulo (USP), São Paulo, SP, Brazil

mchinelatto@sc.usp.br

Abstract – The dispersion of microfibrillated cellulose (MFC) within a polymer blend is significantly influenced by the order of its introduction and processing during extrusion [1]. Proper extrusion order enhances dispersion efficiency, ensuring uniform distribution of MFC throughout the matrix and influencing interfacial adhesion with the polymer [2,3]. Improved dispersion promotes the dispersion of MFC as individual fibrils, minimizing agglomeration and clustering and resulting in enhanced mechanical properties, thermal stability, barrier properties, and biodegradability [4]. This study aims to assess the influence of extrusion sequence on the morphology and properties of compatibilized PLA/PCL blends reinforced with MFC. The blend composition remained consistent for all samples, with variations limited to the order of component extrusion. Four extrusion protocols were used: EXT – all components extruded together in one step; EXPLA - MFC extruded with PLA first, followed by PCL and compatibilizer in a second extrusion process; EXPCL – MFC extruded with PCL first, followed by PLA and compatibilizer in a second extrusion process; EXCOMPAT – PLA, PCL, and compatibilizer mixed in a first extrusion process, with MFC added to the blend in a second extrusion. A compatibilized PLA/PCL blend without MFC addition served as the control sample to evaluate the influence of MFC dispersion on PCL droplet size within the PLA matrix. In the case of an immiscible blend like PLA/PCL, compatibilization is essential to promote interaction between the phases and to impart mechanical properties that draw contributions from both components. In this study, the compatibility of the blend was assessed through two key factors: the size of the dispersed PCL phase and the resulting mechanical properties exhibited by the final blend. Morphological and mechanical characterizations were conducted using Scanning Electron Microscopy (SEM) and tensile tests following ASTM D638. Analysis of 300 PCL particles in each sample revealed that the EXT protocol promoted a smaller PCL droplet size, resulting in improved mechanical properties, particularly tensile strain, which reached 80% for the EXT sample compared to an average of approximately 20% for the other samples. These findings have significant implications for the design and development of polymer blends with enhanced properties in various practical applications, foremost considering that all blends produced in this work are biodegradable and biocompatible.

References

1. A. Taguet; P. Cassagnau; J. M. Lopez-Cuesta. *Progress in Polymer Science*, 2014, *39*, 1526. Doi: 10.1016/j.progpolymsci.2014.04.002.
2. J. R. Tao; D. Yang; Y. Yang; Q. M. He; B. Fei; M. Wang. *Polymer* 2022, *252*, 124963. Doi: 10.1016/J.POLYMER.2022.124963.
3. C. B. B. Luna; D. F. da Silva; E. M. Araujo; T. J. A. de Melo; E. O. T. Bezerra; D. D. Siqueira; A. D. de Oliveira. *Macromolecular Symposia* 2019, *383*, 1800046. Doi: 10.1002/masy.201800046.
4. X. Wu; F. G. Torres; F. Vilaseca; T. Peijs. *Journal of Biobased Materials and Bioenergy*, 2008, *1*, 341. Doi: 10.1166/jbmb.2007.008.

Fundings: Coordenação de Aperfeiçoamento de Pessoal de Nível Superior – Brasil (CAPES) – Finance Code 001 and Fundação de Amparo à Pesquisa do Estado de São Paulo (FAPESP), Processo n° 2018/23542-7.

Keywords: *Polymer processing; Extrusion sequence; Biodegradable polymers; Microfibrillated cellulose*.

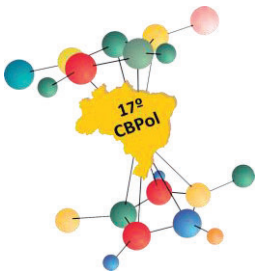

INTERFACIAL IMPROVEMENT OF JUTE FIBRE EPOXY COMPOSITE USING INTERMITTENT HIGH VOLTAGE PULSED ELECTROPHORESIS DEPOSITION

K. M. K. Iwasaki[1], A. Valcanaia[1], G. Zucco[1], R. De Medeiros[1], L. C. Fontana and[2] D. Becker[1]

1 – Department of Mechanical Engineering, Santa Catarina State University (UDESC), Joinville, SC, Brazil
kelvin.iwasaki@edu.udesc.br
2 – Department of Physics, Santa Catarina State University (UDESC), Joinville, SC, Brazil

Abstract – In recent decades, there has been significant interest in utilizing natural fibre-reinforced composites (NFC) for industrial applications. Natural fibres (NF) are a biodegradable resource, are found in abundance in nature and have low density, which results in composites with attractive specific mechanical properties. On the other hand, NC has some limitations, including low thermal stability and poor adhesion between the fibre and matrix. A weak fibre-matrix bonding implies poor load transfer onto the NF due to their hydrophilic character of them, affecting the mechanical performance of the NFC. However, several surface modifications promote an enhancement of the interfacial adhesion of the phases, such as coupling agents, polymer treatment and deposition of nanostructure carbon materials (NCP) on the fibre surface. Recently, studies have shown that introducing carbon nanotubes (CNT) into conventional fibre-reinforced polymer composite improves the mechanical and functional properties, including inter-laminar shear strength (ILSS). Among the techniques used to introduce CNT on the fibre surface, the electrophoresis deposition (EDP), which is a colloidal processing technique based on the movement of charged particles suspended in a solution. Commonly, the conventional EDP process applies direct current and low voltages. Therefore, this study aims to analyse the effects of CNT deposition through intermittent high-voltage electrophoresis deposition (EDP) in the adhesion between epoxy and jute fibre (JF). To evaluate the interfacial adhesion of the composite, the apparent ILSS, short beam shear (SBS) test, based on ASTM D2344M, is performed using a universal testing machine (Instron). According to this norm, the samples (3 samples) must show the relation between the span and thickness around 4:1, aiming to minimize bending stress and maximize shear stress induced. vacuum-assisted resin transfer moulding (VARTM) was used to manufacture the jute fibre epoxy composite (JFEC). According to the results of the apparent ILSS evaluated, the incorporation of the CNT on the JF surface showed a positive effect on the interlaminar performance of JFEC, resulting in an increase of the interfacial adhesion around 10% about composite reinforced with JF as received (without the CNT deposition). This enhancement of the mechanical property of the JFEC can be ascribed to the nanoscale roughness promoted by the CNT deposition, which can act as mechanical interlocking.

Fundings: The authors acknowledge the financial support of the Santa Catarina State Research and Innovation Funding Agency (FAPESC grant: 2017TR1747, 2020TR1450, 2020TR1450 and 2021TR843). As well as the financial support of the CNPq (process number 304795/2022-4), CAPES and UNIEDU/FUMDES.

Keywords: *Natural fibres. Composites materials. Inter-laminar shear strength. Interfacial adhesion.*

ON THE PEG-*B*-PCL MULTIBLOCK COPOLYMER LOCALIZATION IN PLA/PCL BLENDS *VIA* AFM-IR

Lucas H. Staffa[1,2], Sílvia H. P. Bettini[1] and Marcelo A. Chinelatto[2]*

1 – Department of Materials Engineering, Federal University of São Carlos (UFSCar), São Carlos, SP, Brazil
2 – Department of Materials Engineering,University of São Paulo (USP), São Carlos ,SP,Brazil mchinelatto@sc.usp.br

Abstract – In physical compatibilization, not all compatibilizer molecules diffuse towards the interface, either because they are trapped in a polymeric phase or due to the interface saturation that occurs after the critical micellar concentration[1]. Since interfacial saturation limits the effective compatibilizer content at the interface, the investigation of selective localization of compatibilizers is essential to defining mixing protocols and optimal content of compatibilizers in a mixture[2]. The aim of this study was to use hybrid AFM tip-enhanced nanoscale IR spectroscopy (AFM-IR) to map specific chemical groups of two different multiblock copolymers based on poly(ethylene glycol) and poly(ε-caprolactone) (PEG-*b*-PCL) of different block lengths, but same total molar mass, in order to estimate its location in a poly(acid lactic) and poly(ε-caprolactone) (PLA/PCL) blend. It was observed that adding 1 wt% of the smaller block size copolymer there is a majority presence in the interface (**Fig 1**). However, when adding 5 wt%, regardless of the molecular structure, the compatibilizers diffused towards the PLA matrix, evidencing interface saturation and a greater preference for the PLA phase. Also, the larger block size compatibilizers showed a better compatibilizing effect, saturating the interface with lower content, however, segregating more easily as a micelle in the matrix.

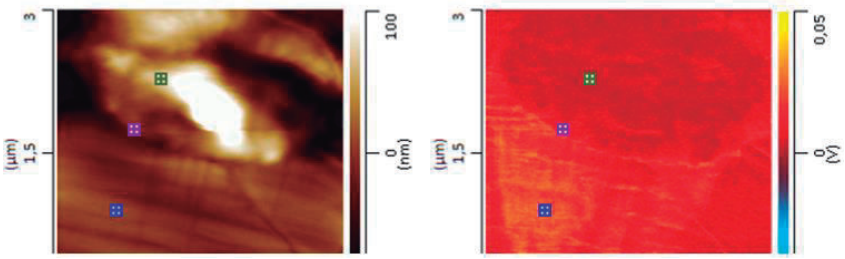

Figure 1 (a) Surface AFM image and (b) chemical mapping at 1660 cm^{-1} for PLA/PCL with 1 wt% of smaller block size copolymer.

References

1. I. Fortelný; J. Jůza *Materials* 2021, *14(24)*, 7786. https://doi.org/10.3390/ma14247786.
2. C. Harrats, S. Thomas, G. Groeninckx in *Micro- and nanostructured multiphase polymer blend systems: phase morphology and interfaces*; CRC Press, New York, 2006; 1st ed.

Fundings: CAPES – Finance Code 001 and FAPESP – Finance Code 2018/23542-7. This research used facilities of the Brazilian Nanotechnology National Laboratory, part of the Brazilian Centre for Research in Energy and Materials, a private non-profit organization under the supervision of the Brazilian Ministry for Science, Technology, and Innovations. The AFM staff is acknowledged for the assistance during the experiments AFM-25553 and 27461.

Keywords: *PLA/PCL, AFM-IR, Multiblock copolymer, Compatibilizers localization.*

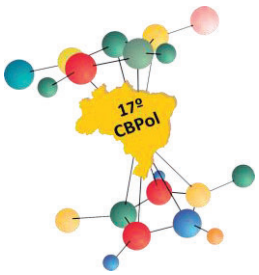

PLASMA FUNCIONALIZATION OF ZINC OXIDE THROUGH ORGANIC COMPOUNDS

Larissa A. Klok[1], Henrique R. Sabedra[1], Teresa T. Steffen[1], Luis C. Fontana[1], Peter Hammer[2], Felippe Magliato Marega[3], Lidiane Cristina Costa[3], Luiz Antonio Pessan[3] and Daniela Becker[1]*

1 – Department of Materials Engineering, Center for Technological Sciences, UDESC, Joinville, SC, Brazil
2 – Department of Quemistry, São Paulo State University, UNESP, São Paulo, SP, Brazil
3 – Department of Materials Engineering, São Carlos Federal University, UFSCar, São Carlos, SP, Brazil
daniela.becker@udesc.br

Abstract - Poly (lactic acid)/zinc oxide (PLA/ZnO) composite is a promising material to produce scaffolds, used in bone regeneration. However, ZnO severely degrades the polymeric matrix. In the way to prevent PLA degradation by ZnO, this particle can be surface modified. This work proposes ZnO surface treatment by plasma, using two functionalization agents: lactic acid (LA) and maleic anhydride (MA). The mixtures of ZnO with LA and MA were performed manually in a mass proportion of 30:70 (ZnO:LA) and 90:10 (ZnO:MA). The samples were treated by Radio Frequency Capacitively Coupled Plasma in times of 5 and 15 minutes with a power supply at 35 W, using argon as working gas (36,5 sccm) in a pressure of $6{,}9x10^{-1}$ Torr. Samples treated were washed with methanol (for MA) and distilled water (for LA) to remove unreacted molecules, and characterized by XPS (X-Ray Photoelectron Spectroscopy) and FTIR (Fourier Transform Infrared Spectroscopy) to analyze the influence of the functionalizing agents in the functional groups formed on the surface of ZnO, and Thermogravimetric Analysis (TG) to verify the thermal behavior of the treated particles and non-treated. The analysis of the results indicated that ZnO was functionalized by plasma, in different ways with LA and MA. The functionalization of ZnO with LA preferably occurs through the formation of a complex between the Zn^{2+} ion and the carboxylate salt (COO^-) arising from the dehydration reaction of lactic acid, showing better results for 5 minutes of treatment. With MA, functionalization occurs preferably through the formation of C-Zn bonds, with 15 minutes being the time that most favors changes in ZnO. Both functionalizations are possible due to the formation of oxygen vacancies caused in the oxide through the plasma discharge. Thus, it is concluded that the plasma is an efficient tool to functionalize ZnO, using organic compounds in the solid phase.

References

1. I. Armentano et al. Biodegradable polymer matrix nanocomposites for tissue engineering: A review. Polymer Degradation and Stability, 95, 2010. (http://dx.doi.org/10.1016/j.polymdegradstab.2010.06.007).
2. M. Qu et al. Zinc oxide nanoparticles catalyze rapid hydrolysis of poly(lactic acid) at low temperatures. Journal Of Applied Polymer Science, 131, 2013. (http://dx.doi.org/10.1002/app.40287).

Fundings: This work was supported in part by FAPESC [project 2020TR1450].

Keywords: *Functionalization; zinc oxide; Plasma; Lactic Acid; Maleic Anhydride.*

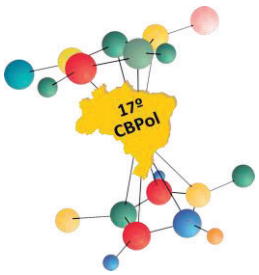

PRODUCTION OF POLYSULPHONE/ALUMINE HOLLOW FIBER MEMBRANES FOR WASTEWATER TREATMENT

Vanessa da N. Medeiros[1*], Andréa D. P. da Silva[1], Edcleide M. Araújo[1] Renê A. da Paz[1], Pamela T. V. da Silva[1] and Sandriely S. L. Oliveira[1]

1 – Academic Unit of Materials Engineering (UAEMa), Federal University of Campina Grande (UFCG), Campina Grande, PB, Brazil
vanismedeiros@gmail.com

Abstract - The membrane separation process (PSM) has stood out significantly in the treatment of water and effluents, aiming at its reuse and improvement of its quality, in a scenario characterized by the scarcity of water resources. The use of this process separates suspended chemical components from the effluent, improving the color, turbidity and pH of the treated water. Due to the increase in competitiveness in the industrial sector, which started to demand an increasing productivity of processes, it led to the development of some configurations of membranes, such as hollow fiber type membranes. These membranes can be produced by different techniques, and the most used method is the phase inversion using the immersion-precipitation technique. In this work, polysulfone and polysulfone/alumina hollow fiber polymeric membranes were developed using the phase inversion method. The samples were characterized by Scanning Electron Microscopy, Apparent Porosity and Contact Angle. In addition, the membranes were evaluated through flow measurements with distilled water and with synthetic effluent and the turbidity of the permeate was analyzed. A change in the morphology in the cross-section of the membranes was verified, as well as a correlation between the amount of alumina and the hydrophilicity of the membrane. As the alumine concentration increases, the membranes show greater porosity. Thus, this greater number of pores can be correlated with the increase in flux inside the membrane. Therefore, the addition of alumine to the membranes significantly improved the flux and also resulted in a decrease in permeate turbidity.

Fundings: The authors thank UFCG, CAPES, CNPq (Proc. 151375/2022-4), and FAPESQ/PB for financial support..

Keywords: *Hollow fiber membrane, polysulfone, alumina.*

SPECTROSCOPIC, ELETRICAL AND MORPHOLOGICAL CHARACTERIZATIONS OF CONDUCTIVE POLYMER HYDROGELS FOR APPLICATION IN HYBRID SUPERCAPACITORS

Denis W. S. Nascimento, Márcia R. Moura, José A. Malmonge and Fauze A. Aouada*

Physics and Chemical Department, São Paulo State University (Unesp), School of Engineering, Ilha Solteira, Brazil
**** fauze.aouada@unesp.br***

Due to current energy demand, new energy storage and accumulation devices are extensively studied. One possible alternative to conventional batteries are the supercapacitors (SCs) due to their inherent performance and advantages [1]. In this sense, a new class of materials, called conductive polymer hydrogels (CPHs), that combine the benefits of organic conductors like polyaniline (PAni) and hydrogels emerges as a possibility to form new SCs. They exhibit remarkable synergistic properties that associate the expansion and flexibility behavior of hydrogels with the electroactivity of the conductive polymers [2]. A synthesis method used to obtain CPHs can be done using renewable polysaccharides (biopolymers) such as interlaced or copolymerized cellulose in hybrid hydrogel networks. This strategy can modify the hydrophilic and mechanical properties of chains of hydrogels, and the sorption or desorption of solutes by these systems. An example of a polysaccharide obtained through chemical modification of cellulose is the carboxymethylcellulose (CMC). CMC is a water-soluble polymer that has been used in a wide range of technological applications such as in hybrid hydrogels. The objective of this work was to perform spectroscopic and morphological characterization of CPHs composed of PAAm/CMC/PAni. The results demonstrated that the CPHs obtained from free radical polymerization [3], followed by interfacial polymerization of PAni using ammonium persulfate as initiator, presented good reproducibility and conductivity values in the order of 10^{-2} S/cm. The spectroscopic characterization showed characteristic bands of CMC and doped PAni, and also confirmed the formation of dendritic microcrystals attributed to the fractal growth of Pani, showing their incorporation into the composites. Finally, we can highlight that the composites presented good stability, reproducibility and electrical performance with potential for the development of new SCs.

References

1. K. Kyunghwa; et al. *Applied Sciences* 2019, *8*, 1547. http://dx.doi.org/10.3390/app9081547.
2. H. Xinting et al *Journal of Materials Chemistry A* 2020, *44*, 23059. http://dx.doi.org/10.1039/d0ta07468c.
3. F. C. Tanaka et al *Journal of Polymer and the Environment* 2021, *29*, 3389. https://doi.org/10.1007/s10924-021-02126-1

Fundings: São Paulo Research Foundation (FAPESP) (2018/18697-1; 2013/07296-2), National Council for Scientific and Technological Development (CNPq) (MCTIC Grant #406973/2022-9 through INCT/Polysaccharides – National Technology-Science Institute for Polysaccharides; MRM 315513/2021-7; FAA 312414/2018-8; 316174/2021-1). This study was financed in part by the Coordenação de Aperfeiçoamento de Pessoal de Nível Superior – Brasil (CAPES) – "Finance Code 001".

Keywords: *Conductive polymer hydrogels, Carboxymethylcellulose, Polyaniline, Supercapacitors.*

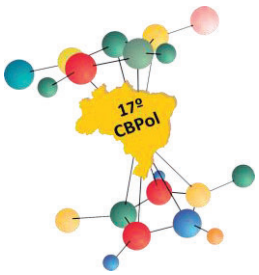

SYNTHESIS AND CHARACTERIZATION OF FLAT MEMBRANES FROM POLYMERIC BLENDS

Rafael A. Dias[1*], Pamela T. V. da Silva[1], Rodholfo, S. B. Ferreira[2], Vanessa N. Medeiros[1], Bruna A. Araujo[1], Edcleide M. Araújo[1] and Hélio L. Lira[1].

1 – Academic Unit of Materials Engineering (UAEMa), Federal University of Campina Grande (UFCG), Campina Grande, PB, Brazil
rafaelagradias96@gmail.com
2 – National Institute of the Semi-Arid (INSA), Campina Grande-PB, Brazil

Abstract

Polymeric membranes have stood out in the industry as efficient tools for treating effluents. In this study, polymeric solutions of pure polymers Polysulfone (PSU) and Polyethersulfone (PES) were prepared, as well as their blends, adding Polyvinylpyrrolidone (PVP) as a viscosifying agent. These solutions were used to produce flat membranes through the phase inversion method. The main objective of this work was the development, characterization, and application of these membranes in the effluents treatment. Fourier transform infrared spectroscopy (FTIR) analysis demonstrated strong interactions among the polymers, indicating the miscibility and compatibility of the PSU/PES blend. Contact angle measurements determined that PES matrix membranes had lower contact angles than those with PSU matrix, due to the superior hydrophilicity of PES. Scanning electron microscopy (SEM) investigations revealed alterations in pore quantity, size, and uniformity, as well as the presence of "fingers," in membranes with varying polymer compositions. Water flow tests and treatment of a synthetic effluent containing red dye confirmed the superior performance of PSU matrix membranes with regard to permeate flux and turbidity removal.

Fundings: The authors thank UFCG, CAPES, CNPq, and FAPESQ/PB for financial support.

Keywords: *flat membranes, polymer blends, polyethersulfone, polysulfone.*

ACCELERATED WEATHERING ENVIRONMENT: INFLUENCE ON MECHANICAL AND THERMAL PROPERTIES OF CF/PA6 COMPOSITES

Larissa S. Montagna[1]*, Guilherme F. M. Morgado[1], Fabio R. Passador[1] and Mirabel C. Rezende[1]

1 – Polymer and Biopolymer Technology Laboratory (TecPBio), Federal University of São Paulo (UNIFESP), São José dos Campos, SP, Brazil
larissa.s.montagna@gmail.com

Abstract – During their useful life, carbon fiber reinforced thermoplastic polymers (CFRTP) are exposed to aggressive environmental factors, which can affect and degrade their properties, including thermal and mechanical properties, resulting in a decrease in their useful life in service. Polyamide 6 (PA6) has been standing out, as it requires lower processing temperatures and the same equipment used for the processing of conventional polymers [1]. However, PA6 is a highly hygroscopic polymer, meaning that the presence of moisture can result in degradation by hydrolysis of the amide group, which high temperatures can accelerate. The influence of ultraviolet (UV) radiation combined with oxygen and temperature results in photo-oxidative, and thermo-oxidative degradation, respectively, causing scission of polymeric chains, and micro-cracking [2]. This work evaluated the effect of accelerated aging using a weathermeter machine (after 400 h, 800 h, and 1200 h), on the mechanical (tensile test) and thermal (differential scanning calorimetry, DSC) properties. Mechanical properties results showed that the weathering conditions did not cause a significant effect on the ultimate tensile strength (UTS) values, but promoted, initially, an increase in this property, due to the increase in the stiffness of the material. Furthermore, as the exposure time increased, there was an increase in the degree of crystallinity (Xc) of PA6. This fact may be related to the breaking of intramolecular bonds and the reorganization of the polymeric chain that is associated with the crystalline regions, resulting in an increase in the crystalline phase and consequently greater stiffness and tensile strength.

References

1. Kondo, M.Y., Montagna, L.S., Morgado, G.F.M., Castilho, A.L.G., Batista, L.A.P.S., Botelho, E.C., Costa, M.L., Passador, F.R., Rezende, M.C., Ribeiro, M.V. Polímeros 2022, 32(2), e2022023. https://doi.org/10.1590/0104-1428.20220042
2. Ranby, B., Rabek, J.F. Journal of Molecular Structure, 1976, 33, 1, 152-153. https://doi.org/10.1016/0022-2860(76)80158-5

Fundings: Federal Government Program 'Rota 2030', n° 27194.03.03/2020.01-00 for the financial support; the LEL/IPT for the coordination, and also FIPT, FUNDEP for the administrative support.

Keywords: *Polyamide 6, Carbon Fiber, Composites, Ultraviolet radiation, Accelerated weathering, Mechanical and thermal properties.*

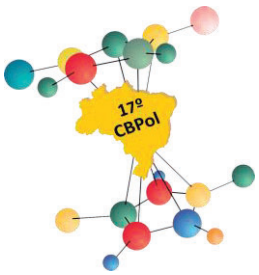

ANALYSIS OF THE PROJECT OF AN AUTOMOTIVE CRANKCASE USING THE PC/ABS BLEND

Cauê P. de Carvalho[1], Daniel Q. R. de Freitas[1], Rogério G. da Silva[1], Talita A. dos Santos[1*]

1 - Plastic Product Development Department, Technology College (FATEC East Zone), São Paulo, SP, Brazil
talita.santos51@fatec.sp.gov.br

Abstract –The use of polymers in the automotive sector is advantageous due to the reduction in vehicle weight, resulting in greater efficiency with lower fuel consumption and consequent reduction in the emission of gases. This study aimed to evaluate the possibility of to use PC/ABS blend in an automotive crankcase through computer simulation and mechanical tests before and after the degradation test in automotive oil for 135 days at 85°C. The values of maximum stress, Young's modulus and flexural modulus did not change significantly between tests performed before and after degradation in automotive oil, whereas elongation at break and impact strength decreased significantly, which is caused by degradation through cross-linking reactions of butadiene in ABS. Computer simulation showed that although there are points of stress concentration in the PC/ABS crankcase design, it can be a cost-effective alternative and also offers a 58% weight reduction over the aluminum crankcase.
Keywords: *Aluminum; Automotive; Crankcase; Blend; PC/ABS.*

Introduction

In the automotive market, there is a constant search for the partial replacement of metallic materials by polymers, blends or compounds aiming at better performance, lower cost and lighter weight, which results in lower gas emissions due to lower fuel consumption [1]. For example, for every 100 kg of polymeric parts used in a car that weighs about 1 ton, it is estimated a 7.5% saving in fuel consumption and a reduction of 2 to 3 times in the consumption of other materials [2].

Due to a constant need to improve and raise the performance level of engines, it is essential that there are alternative alternatives to replace metallic materials with polymeric materials. Among the various metal parts that make up the vehicle, the crankcase stands out, which is generally made of aluminum alloy and has the main function of storing the car's oil, being indispensable for the operation of the car, as well as ensuring the lubrication of the vehicle. Engine, avoiding overheating and decanting the impurities that passed through the oil filters [3]. The temperature of the oil that is stored inside the crankcase, under normal vehicle conditions, is between 40 and 70°C, but if there is any type of deregulation in the engine, this temperature can reach between 90 and 100°C [4]. It should be noted that, associated with the card, a card protector made of steel is generally used to protect the vehicle card from impacts suffered by vehicle circulation. Despite the non-mandatory use of the card protector, its use is acceptable to increase the useful life of the vehicle [5].

An alternative for replacing automotive aluminum crankcases is the use of blends that are able to provide the ideal balance of properties between the polymers that compose them. The PC/ABS (polycarbonate/acrylonitrile-butadiene-styrene) blend stands out [6, 7]. Both PC and ABS have been used in the automotive sector for years, however, with the use of a PC/ABS blend we achieved a material with good mechanical resistance, good resistance to degradation and good processability, which is advantageous for applications of high service life, as is the case in the automotive sector [6].

Therefore, this work aimed to study, by means of mechanical tests and computational simulation, the viability of replacing the automotive aluminum crankcase with a crankcase manufactured with a PC/ABS blend (PULSETM 2000EZ). Comparison of properties between the crankcase manufactured in aluminum and the crankcase manufactured using the PC/ABS blend was used for the computational simulation.

Experimental

Obtaining the test specimens

The blend PULSETM 2000EZ (Trinseo) with PC/ABS composition and fluidity index (260°C/5kg) 15 - 20g/10min and density 1.14g/cm³ was used. Initially, the PC/ABS blend pellets with 6% (m/m) black masterbatch (Engeflex) were dried for 1 hour at 100 (±5) °C in an oven (Marconi, MA035). Standard ISO I79/1eA and ISO 527 specimens were injected in a Battenfeld injection molding machine (SB 1450/400), with 4 temperature zones at 210, 230, 235 and 240 °C.

Conditioning and dimensions of test specimens

Prior to performing the mechanical tests, the specimens were conditioned in accordance with ASTM D-618, for 40 h at 23 (± 2) °C and relative humidity of 50 (± 10) %. The thickness of the specimens were obtained using a Mitutoyo digital specimeter.

Tensile tests

The tensile test was performed on an Instron (5566) equipment in accordance with ISO 527(2019), using 5 specimens with dimensions of (115 x 10 x 4) mm, with 110 mm of separation between the grips, speed of 50 mm/min and a load cell of 30 kN. The parameters analyzed were maximum stress, elongation at break and Young's modulus.

Flexion modulus test

The flexion modulus test was performed on an Instron universal machine (5566), following the requirements of the ISO 178 standard, on 5 specimens with dimensions (80 x 10 x 4) mm.

To carry out the test, the base was gauged so that the supports were 64 mm apart it needs to be positioned 16 times the thickness of the specimen. The test was interrupted when the deformation of the specimen reached 3.5% of the initial dimensions.

Impact Resistance

The charpy impact resistance test was carried out in accordance with ISO 179/1eA on 5 specimens with dimensions (80 x 10 x 4) mm that were previously notched in a motorized carving machine (Ceast) at an angle of 46°. The test was performed on a Resil Impactor (6967 - Ceast), the base was used with a distance between the supports of 62 mm and a pendulum of 4 J.

Computational simulation of an automotive crankcase using PC/ABS blend and alumínio

The software used to create the mathematical geometry was NX (version 12.0, 2017), a product of Siemens Digital Industries Software. No software NX foi usada a análise Pre/Post simulation com a função sol 101 Linear statics – Global Constrainsts, que consegue simular deslocamento, tensão e reação nos pontos de apoio. For this work, a crankcase project for large vehicles was elaborated, aiming at the bus and truck market, where a large volume of oil is needed for each vehicle. The oil capacity that a large vehicle crankcase must hold is between 10 and 18 L.

Automotive oil degradation test

The bodies and traction, impact and bending tests were submitted to the degradation test, where they were submerged in automotive oil 5W30 (Mobil Super) inside a transparent glass container, for 135 days at a temperature of 80 (± 5) °C in a greenhouse (De Leo). The bodies and evidence were removed from the oil and washed manually 5 consecutive times with neutral detergent and then dried in an oven at 80°C for 5 hours. Traction, impact and flexion tests were carried out on the degraded specimens following the parameters described above.

Results and Discussion

Visual appearance of the samples before and after the degradation test in automotive oil

Fig. 1 a shows the photograph of the degradation test that the samples of PC/ABS were submitted, it is observed that the test specimens remained completely submerged in the oil at a temperature of 80 (± 5) °C, which is within the temperature range that the oil in the automotive crankcase can reach [4]. During the degradation test, the samples were not subjected to mechanical stress and were kept in a closed oven, away from ultraviolet radiation. Both PC and ABS are susceptible to photodegradation [8] effect of chemodegradation caused by oil and thermodegradation due to crankcase working temperature.

Fig. 1 b shows the photograph of the specimens before and after the degradation test in oils, where it is observed that there was a loss of brightness after the degradation. This result is in line with what was expected for the occurrence of degradative processes in the blend, since the degradation of ABS causes loss of brightness and the degradation of PC causes yellowing, however, due to the black masterbath used in the formulation, it was possible to identify only the change brightness [8,9]. The loss of brightness in polymers, mainly in the automotive industry, is a very important market factor, however, the automotive crankcase is located at the bottom of the vehicle, which makes the loss of brightness irrelevant in this case.

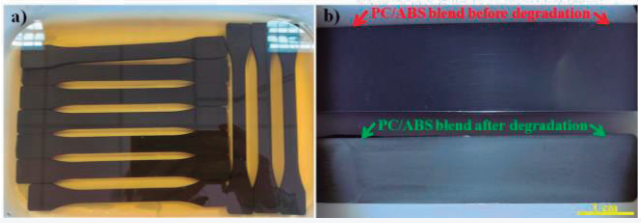

Figure 1: Photographs **a)** Traction specimens submerged in automotive oil during the degradation test; **b)** PC/ABS specimens before and after the degradation test in automotive oil.

Mechanical properties (tensile test, impact test and flexion test)

The results for the mechanical and tensile, bending and impact tests before and after breaking in oil are shown in Fig. 2. Observing the results of the tensile tests shown in Fig. 2 (a, b and c), it is noted that for the maximum stress and Young's modulus supported by the blend before and after the deficiency test, no significant change in the properties was observed, however, for the elongation value had a drastic decrease after the degradation test. For the flexural modulus test, note that the values were similar before and after degradation. And for the impact resistance test, it is observed that there was about 38% in impact resistance.

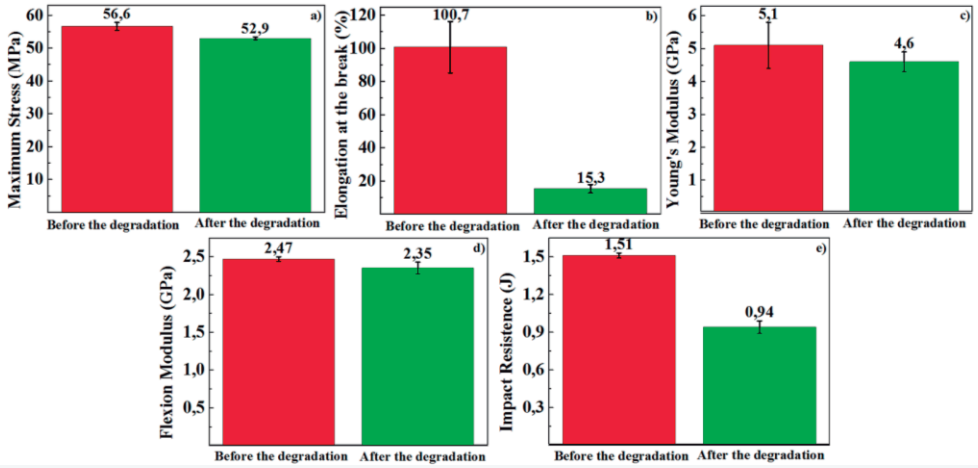

Figure 2: Results of mechanical properties before and after degradation for **a)** maximum (MPa) stress obtained from the tensile test; **b)** elongation at the break (%) obtained from the tensile test; **c)** Young's modulus (GPa) obtained from the tensile test; **d)** Flexion modulus (GPa) and e) Impact Resistance (J).

The mechanical tests, especially the elongation at break and impact resistance, showed a significant change in properties, which is mainly caused by the presence of butadiene in ABS. Butadiene has two double bonds in the main chain which makes the two carbons adjacent to the double bonds more susceptible to degradation by auto-oxidation. The degradation mechanism of butadiene is the formation of crosslinks that makes the butadiene rubbery domain rigid and causes a decrease in impact strength. Likewise, the decrease in elongation is explained, due to the greater rigidity generated in the degradative process. An alternative to improve resistance to butadiene chemodegradation is the use of ABS, which is a copolymer of acrylonitrile, ethylene and styrene, because with the replacement of butadiene by ethylene, the effect of chemodegradation is reduced [9].

Computacional simulation

Fig. 2 a shows the three-dimensional mesh used to create the simulations in the NX software. Fig. 2 b and c show the density comparison between the crankcase made of aluminum and made with the PC/ABS blend. The aluminum density used for the simulation was 2.7 g/cm^3 [10] and the density of the PC/ABS blend is 1.14 g/cm^3 (provided by the manufacturer).

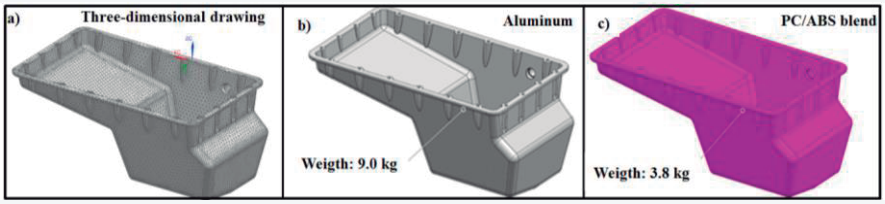

Figure 3: a) Three-dimensional drawing of an crankcase using **b)** an aluminum alloy; **c)** PC/ABS blend.

It can be seen that the crankcase made of aluminum weighs 9 kg, if it were manufactured with the PC/ABS blend it would weigh 3.8 kg, which is equivalent to a decrease of approximately 58% in the weight of the crankcase. Vehicle weight reduction is extremely advantageous for better vehicle performance, reduced fuel consumption, as well as implying a reduction in gases generated by combustion such as carbon dioxide and carbon monoxide) [2]. In addition to the decrease in density, with the manufacture of a PC/ABS crankcase there is a decrease in production costs.

After making the mesh, the tension applied to the x, y and z axes was evaluated with the crankcase made of aluminum and with the PC/ABS blend (Fig. 4).

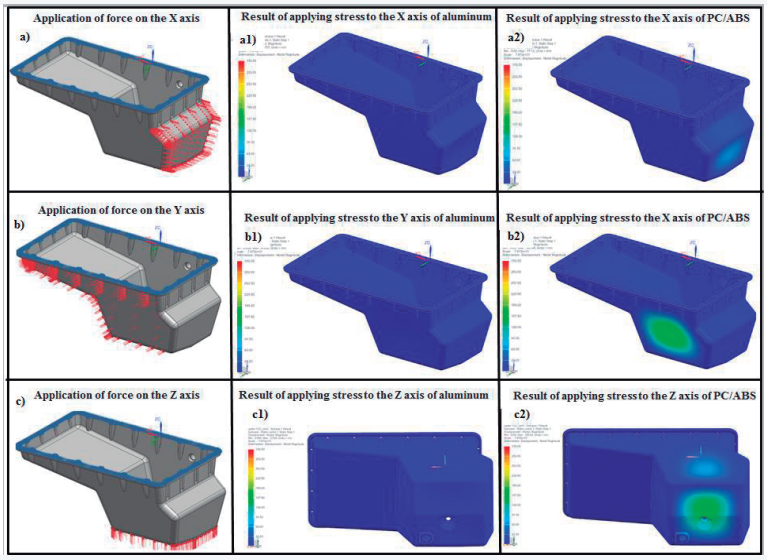

Fig. 4: Computer simulation analysis on the X axis (a, a1 and a2), Y axis (b, b1 and b2) and Z axis (c, c1 and c2) for aluminum and for the PC/ABS blend.

For the simulation, a force of 1000N was applied (obtained from experimental values of automakers in São Bernardo do Campo - SP). The tensile mechanical property values used in the simulation of the PC/ABS blend were those obtained experimentally before the oil degradation test, and the values used for aluminum are those provided by Mezzomo and Moraes, 2020 for aluminum 1200H14.

Analyzing the Figures, it is observed that there is a small concentration of tension (greenish tone) in the X and Z axis in the PC/ABS crankcase, which indicates a point with less resistance. The applied force simulation for aluminum did not show any visible signs of stress (completely blue coloration). Therefore, it is noted that the simulation properties of the aluminum crankcase are greater compared to PC/ABS, however, they meet the minimum standards required, since they do not present a red color, which would indicate rupture of the material with the applied force. The points of stress concentration in the crankcase made of PC/ABS can be minimized by studying the geometry of the crankcase, which was not evaluated in this work [3].

Conclusions

Through computer simulation, it was possible to observe that the crankcase made of PC/ABS is lighter and cheaper than the crankcase made of aluminum, which would result in better vehicle performance and lower fuel consumption, however, with the simulation of force application on the X, Y and Z axes, it was observed that the crankcase showed some points of stress accumulation that can be minimized through a more in-depth study of the crankcase geometry. Degradation tests in automotive oil showed that there was a decrease in the elongation at break (tensile test) and in the impact resistance, which is caused by the presence of the Butadiene monomer in the ABS and which causes crosslinking reactions by auto-oxidation, making the structure more rigid. Through the analysis of the results obtained in this work, we have an indication that it would be economically and environmentally advantageous to manufacture an automotive crankcase using the PC/ABS blend, however, for the actual application of the PC/ABS blend in a crankcase, it would be necessary to carry out tests of degradation in order to analyze degradation by stress cracking and by metallic contaminants present in automotive oil, as well as the evaluation of the best design and formulation to avoid stress concentration and minimize degradation in the part.

Acknowledgements

Fatec Zona Leste, CPE - Compostos Plásticos de Engenharia and UFABC.

References

1. Deshmukh, K. et al. Polymer Adv. Tech. 2022, 3023-3047, 10991581. https://onlinelibrary.wiley.com/doi/10.1002/pat.5771
2. Hemais, A. C. Polymers: Science and Tech. 2003, 107-114. http://dx.doi.org/10.1590/S0104-14282003000200008
3. Manuel Ignacio Ayala Chauvin, Miguel Botto-Tobar. Sustainability, Energyand City, Springer, Switzerland, 2021.
4. Dyson, C. J; Priest, M; Lee, P. M. Tribology Letters, 2023, 2-16. https://doi.org/10.1007/s11249-022-01686-0
5. Soriano, A.; Antonio, J. Publicaciones Didacticas, 2016, 78.
6. Saeed, F. et al. *Journal of Chem. Tech., 2020, 64-69, 10.247.* https://doi.org/10.2478/pjct-2020-0029
7. Canevarolo, J. S. Ciência dos Polímeros, 3ª ed., Artliber, São Paulo, 2010.
8. Ermi. B. D et al. Polymer Deg. and Stab., 2020, 11, 109330. https://doi.org/10.1016/j.polymdegradstab.2020.109330
9. De Paoli, M. A. Degradation and stabilization of polymers. Chemkeys. São Paulo, 2008.
10. Callister, W. D., Science and materials engineering. John Wiley & Sons, Inc., 2002.

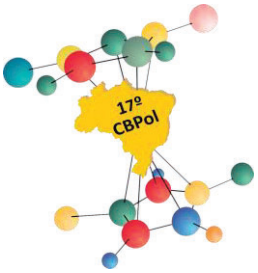

ANALYSIS OF THERMAL AND MORPHOLOGICAL PROPERTIES OF PVA/CHITOSAN BLENDS INCORPORATED WITH PITAYA EXTRACT

Erica dos S. Ribeiro[1], Elaine N. Aquino[1], Artemis. M. Ceschin[2], Nizamara. S. Pereira[1*]

1 – Instituto Federal de Brasília, Departamento de Química, Brasília-DF, Brazil
e-mail: nizamara.pereira@ifb.edu.br
2 – Universidade de Brasília, Departamento de Engenharia Elétrica, Brasília-DF, Brazil

Abstract - Films of a mixture of polyvinyl alcohol (PVA) and chitosan (Ch) modified by the presence of pitaya extract (ExPy) in their composition were prepared by solution casting of the PVA/Ch. The properties of the new materials were analyzed by thermogravimetric analysis (TGA) and scanning electron microscopy (SEM). The results observed show that the pitaya extract caused a slight reduction in the thermal stability of the PVA/Ch blend and modified its morphological structure, both on the surface and in the inner part of the polymeric matrix.

Keywords: *PVA, chitosan, pitaya, TGA, MEV*

Introduction

The packaging of food is produced with substances like glass, polymers and nanocomposites. The properties of these materials should not affect the quality of products and their production have been raised due to low cost, protection from moisture, oxigen, heat, odor, microorganisms and still possess good tensile strength. However, the packaging prepared from the petrochemical-rooted plastics had a crucial effect on the environment [1]. The development of packaging degradable materials has become the center of attention, because it is possible to reduce the production of waste which is in line with the trends of a sustainable economy [2]. There are many possibilities on how to prepare the active packaging considering that there are a lot of different compositions utilized [2]. The latest research into active packaging has included the incorporation of natural active substances into polymeric matrices. These natural active substances have antioxidant and antimicrobial activities, such as essential oils [3,4], extracts of green tea [4], blueberry, red grapes, parsley extract[1], dyes, flavors, probiotics and prebiotics [5]. In addition to the antioxidant properties, these natural substances improve the stability and increase the shelf life of the product [4]. With that in mind, this work aims to incorporate pitaya extract into a polymeric matrix composed of a mixture of two known biodegradable polymers: polyvinyl alcohol (PVA) and chitosan (Ch) and its thermal, optical, morphological and antioxidant properties were analyzed.

Experimental

Preparation of the extract of pitaya (ExPy)

The fruit pulp was crushed using a mixer, the infusion was carried out with 400 mL of water at 90°C for 10 minutes. Subsequently, the sample was centrifuged at 5000 rpm for 30 minutes. After centrifugation, the extract was vacuum filtered. All extracts were stored and frozen in order to remain preserved.

Preparation of polymeric blends (PVA/Ch) with pitaya extract incorporated in the polymeric matrix

The polymeric blends were prepared according to the literature (with adaptations). Initially, 0.35 g of chitosan was weighed. The weighed chitosan mass was dissolved in 50 mL of a 1% acetic acid solution. The chitosan (Ch) solution was taken to a sonicator for 2h. Subsequently, the solution was maintained under magnetic stirring for 15 h at a temperature of 40 ºC. Separately, 5g of PVA was weighed and dissolved in 50 mL of distilled water. Then 2 mL of glycerol was added and the solution remained under magnetic stirring for 1 h at an average temperature of 50°C. After this period of time, the PVA solution, kept under constant agitation, was cooled to room temperature. To obtain the PVA/Ch polymeric blend, the Ch and PVA solutions were mixed under magnetic stirring for one hour at room temperature. Then, this polymeric solution was sonicated for 15 minutes in order to completely homogenize the solution. After this process of preparing the PVA/Ch blend, the ExPy was added to the solution and mixed to obtain PVA/Chitosan/ExPy polymeric blends with 9 and 16% (v/v) proportion for extract of pitaya. Then, the solution remained under stirring for 10 min at 25°C. After sample homogenization, the PVA/Ch/ExPy blends with its extract was poured onto a non-stick surface and placed in an oven at an average temperature of 50ºC for 19h. The samples were analyzed by the Shimadzu Model TGA/DTG-60H thermogravimetric system. The sample pan was placed in the balance system equipment and the temperature was raised from 22 to 650 °C at a heating rate of 10°C per minute in synthetic air. The micrographs were obtained using the JEOL JSM-7000F microscope, under tension of 15 and 5 kV, allocated in the Microscopy and Microanalysis laboratory of the Instituto de Biology at UnB.

Results and Discussion

The thermal property of films was evaluated by means of TGA. It can be seen in Fig. 1 that the ExPy demonstrated one thermal degradation stages within a temperature range from 24 to 189°C. The mass loss between 80°C and 115°C (T_d 112°C) was likely due to the decomposition of betacyanins and loss of water. This means that the addition of pitaya extract reduced the thermal stability of the polymeric chain. The first stage occurred from 25 to 125°C and was associated with the loss of moisture.

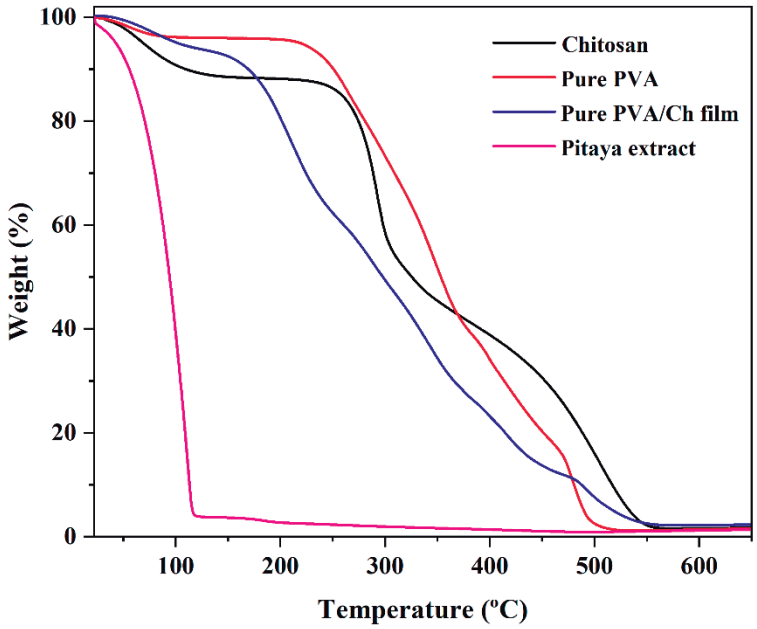

Figure 1- TGA curves of the (a) chitosan pure film; (b) PVA pure film; (c) PVA/Ch blend pure and (d) pitaya extract

The chitosan presented three degradation stages in the range temperature from 30 to 600°C (Fig. 1). The first stage occurred from 51 to 105°C (T_d 67ºC) and was associated with the loss of moisture. The second stage was associated with the thermal degradation of the polymer and occurred from 273 to 304°C (T_d 293ºC). The degradation of chitosan start with the rupture of the β-glycosidic linkages between the N-glucosamine and N-acetyl glucosamine moieties and ends with the release of a complex gaseous mixture mainly composed of H_2O, NH_3, CO, CO_2, CH_3COOH, and CH_4. Third stage of degradation is attributed to the further combustion of the residual organic compounds (T_d 506°C) [6]. TG curve for the PVA pure reveals four stages of degradation (Fig.1). The first occurs at 54,5°C with an equivalent mass loss 3,9%. This first weight loss may be associated with loss of volatiles and moisture (water) from the polymeric matrix. In the second thermal event, the moment of more expressive degradation takes effect at 265°C with loss of mass equivalent to 74,3 %. The third stage of degradation happens at 348°C and shows 20,3% mass loss and the last stage revealed mass loss of 0.6% at 477ºC. Thermal analysis of the PVA/Ch pure film revealed four stages of degradation within some range of temperature. The first stage of degradation occurs at 75°C corresponding to the loss of moisture; the second stage at 210°C that can be associated with the loss of amine units from the chitosan polymeric chain [7]; the third stage of degradation takes place at 346ºC and can be attributed to thermal degradation of the PVA polymeric chain, since pure PVA presents a greater mass loss stage close to this temperature. The last stage of degradation occurs at 490°C and it is probably equivalent to the combustion of polymer chain residues.

TGA curves of the PVA/Ch/ExP films with 9 and 16% (v/v) of pitaya extract showed four thermal degradation stages within a temperature range from 30 to 600°C (Fig. 2).

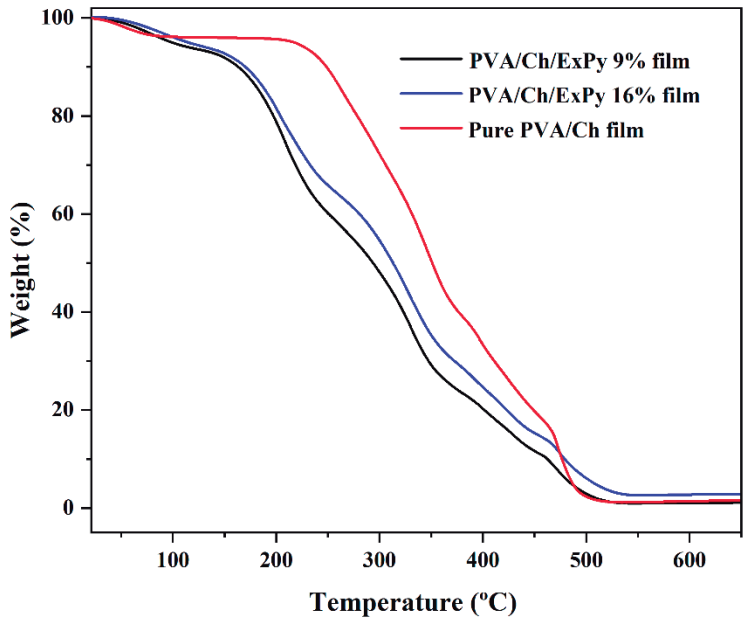

Figure 2- TGA curves of the PVA/Ch/ExPy 9 and 16% films and pure PVA/Ch film.

The second and third stages can be associated with the thermal degradation of the betacyanins and of the polymer, while last stages degradation can be attributed to waste burning of the organic compounds. The PVA/Chitosan/ExPy blends presented a thermal behavior similar to pure PVA/chitosan. The pitaya extract caused a slight T_{onset} of the PVA/Ch blend.

In the first stage of degradation, the pitaya extract promoted a slight improvement in the thermal stability of the films, however, in the third stage occurs a reduction in T_d3 and an increase in mass loss can be observed indicating a reduction of the thermal stability. Data can be analyzed through Table 1.

Table 1 - Values of the Tonset, maximum decomposition temperature and weight loss (%) to each stage of degradation of the materials.

Samples	T_{onset} (°C)	T_d1 (°C)	Weight loss (%)	T_d2 (°C)	Weight loss (%)	T_d3 (°C)	Weight loss (%)	T_d4 (°C)	Weight loss (%)
PVA pure	40.0	54.5	3.9	265.0	74.3	348.0	20.3	477.0	0.6
Chitosan	51.2	66.0	11.6	292.0	50.6	506.0	36.0	-	-
PVA/Ch blend film	44.2	75.6	6.6	210	33.5	348.0	57.9	492	0.6
PVA/Ch/ExPy 9% (v/v)	45.2	76.0	6.4	206.0	37.6	331.0	54.9	471.0	0.4
PVA/Ch/ExPy 16% (v/v)	50.8	87.0	6.1	200.0	29.3	326.0	61.4	474.0	0.6
Pitaya extract	80.1	112.0	95.9	-	-	-	-	-	-

The SEM micrographs of the surface of PVA/Ch blended films, pure and pitaya extract incorporated, are presented in Fig. 3. The surface morphology of PVA/Ch pure film shows a compact and smooth surface, which means PVA and Ch mixture has good compatibility due to the existence of hydrogen bonding interactions between Ch and PVA. The presence of pitaya extract in the polymeric film promoted the emergence of holes in the morphology of the materials, indicating the incorporation of the extract in the polymeric matrix of blend (Fig.3).

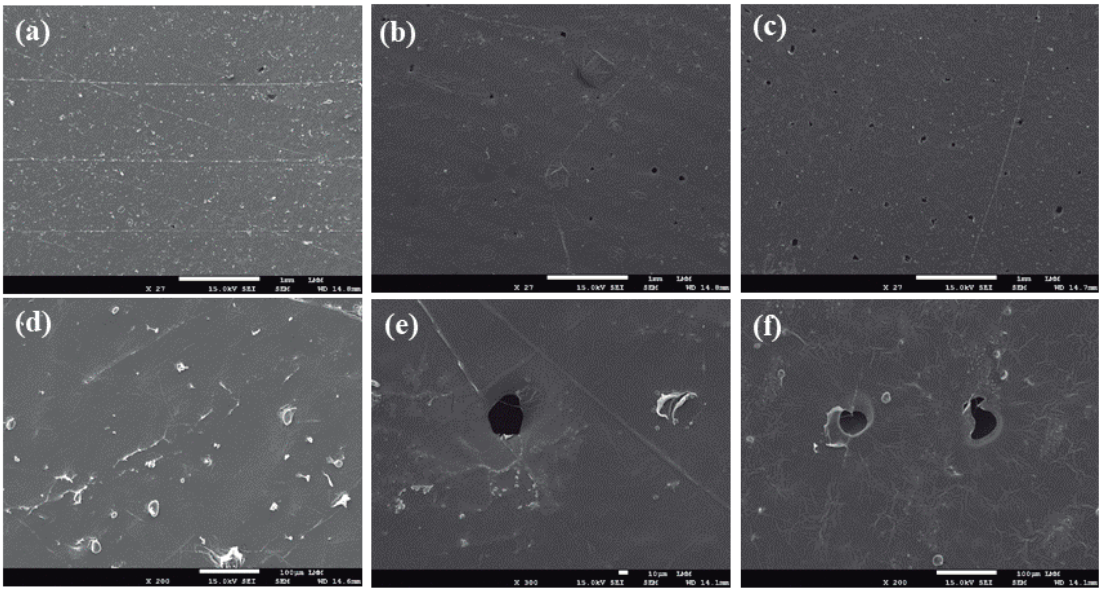

Fgure 3 - SEM images of the surface of polymer films prepared by casting solution of (a) PVA/Ch; (b) PVA/Ch/ExPy 9% (v/v), (c) PVA/Ch/ExPy 16% (v/v) at 27x magnification and (d) PVA/Ch; (e) PVA/Ch/ExPy 9% (v/v), (f) PVA/Ch/ExPy 16% (v/v) at 200x magnification

These same holes caused by the presence of pitaya extract can be seen inside the material considering an increase of 200 and 500x in the image of the materials.

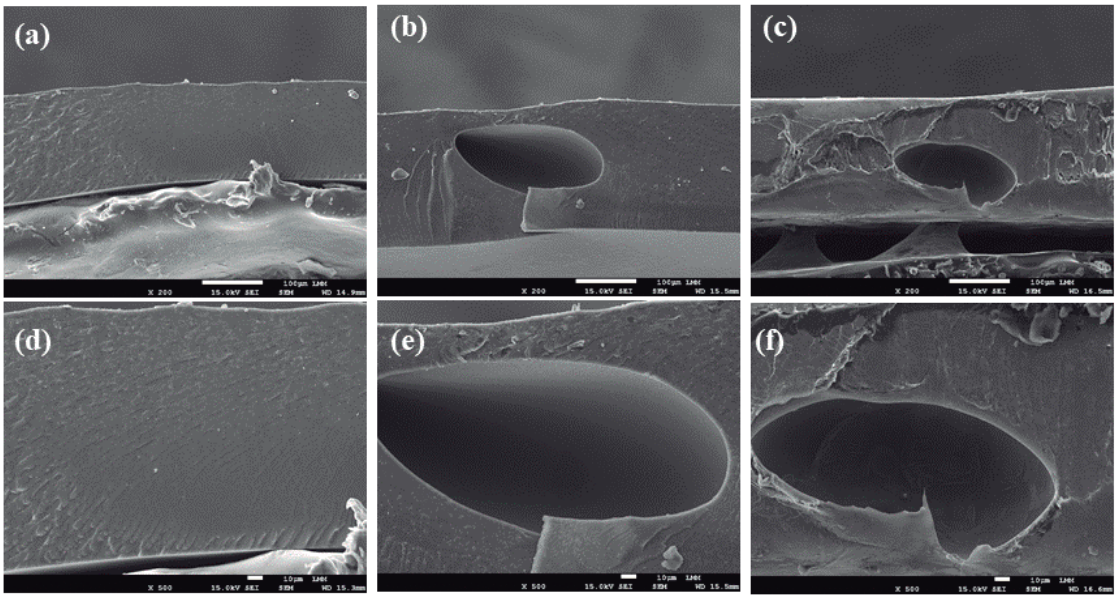

Figure 4 - SEM micrographs of the inside of the polymer films prepared by casting solution of (a) PVA/Ch; (b) PVA/Ch/ExPy 9% (v/v), (c) PVA/Ch/ExPy 16% (v/v) at 200x magnification and (d) PVA/Ch; (e) PVA/Ch/ExPy 9% (v/v), (f) PVA/Ch/ExPy 16% (v/v) at 500x magnification

Conclusions

The PVA/Ch films with pitaya extract incorporated in the matrix polymeric blends were prepared using solution casting of PVA mixed with amounts of Ch 50% v/v. Effects of the presence of the pitaya extract on the structures and properties were studied. The good blend compatibility between the PVA and Ch has been confirmed as expected. However, the presence of pitaya extract in two different concentrations promoted a slight reduction in the thermal stability of the blend, as well as changes in the morphology of the surface and the inner part of the polymeric material.

Acknowledgements

The authors would like to thank the Federal Institute of Brasilia (IFB) and FAPDF for financial support.

References

1. A. Thulasisingh; K. Kumar; B. Yamunadev; N. Poojitha, S. SuhailMadharHanif; S. Kannaiyan Polymer Bulletin, 2022, 79, 4467. https://doi.org/10.1007/s00289-021-03767-x.

2. S. Dordevic; D. Dordevic; P. Sedlacek; M. Kalina; K. Tesikova; B. Antonic; B. Tremlova; J. Treml; M. Nejezchlebova; L. Vapenka; A. Rajchl; M. Bulakova Polymers 2021, 13, 3388. https://doi.org/10.3390/polym13193388.

3. R. Ribeiro-Santos, M. Andrade; N. RMelo.; A. Sanches-Silva, Trends in Food Science & Technology 2017, 61, 2017, 132..

4. J. C. Nunes; P. T. S. Melo; M. V. Lorevice; F. A. Aouada; M. R. Moura Journal of Food Science and Technology, 2021, 58, 1.

5. S. Shankar.; D. Khodaei; M. Lacroix, Food Hydrocolloids 2021, 117, 106750. https://doi.org/10.1016/j.foodhyd.2021.106750.

6. R. Rodríguez-Rodríguez; Z. Y. García-Carvajal; I. Jiménez-Palomar; J. A. Jiménez-Avalos; H. Espinosa-Andrews; Journal Applied Polymer Science 2019, 47149. DOI: 10.1002/app.47149.

7. E. A. C. Filho; M. M. Paiva; B. G. b. Santos; K. O. Santos; W. J. b. Sousa; P. C. A. Júnior, M. J. B. Cardoso; Research, Society and Development, 2021, 10, 119101522665. DOI: http://dx.doi.org/10.33448/rsd-v10i15.22665.

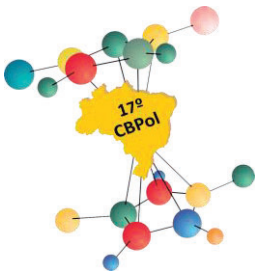

BIODEGRADABLE COMPOSITES OF SUGARCANE BAGASSE AND POLYURETHANE

Carla M. Saitirio[1], Karina O. F. da Silva[1], Maria V. C de Paula[1], Natália F. de Paula[1], Talita A. dos Santos[1*]
1 - Plastic Product Development Department, Technology College (FATEC East Zone), São Paulo, SP, Brazil
talita.santos51@fatec.sp.gov.br

Abstract – Due to the environmental problems caused by improper disposal of polymers, alternatives are being sought to partially replace non-biodegradable polymers. Among these alternatives, biodegradable polymers are found, and in this work, the production and characterization of a biodegradable composite composed of sugarcane bagasse with biodegradable polyurethane derived from castor oil were carried out. Composites were successfully obtained using treated fibers, as alkaline treatment reduces fiber water absorption and allows for the formation of a regular composite. The addition of fibers to the polyurethane resulted in increased impact resistance and decreased hardness, showing that the fibers act as a reinforcing agent. Biodegradation tests showed that the composite degrades over a period of more than 60 days. The study and characterization of biodegradable polyurethane composites with sugarcane bagasse fibers prove to be a promising alternative for replacing conventional polyurethane.
Keywords: *biodegradable composites, poliuretane, sugarcane bagasse.*

Introduction

Due to the high rate of improper disposal of polymeric materials, efforts are being made to find alternatives that are less harmful to the environment [1]. Biodegradable materials are considered as a viable option for partially replacing non-biodegradable polymers since they have a shorter degradation period, thereby preventing unwanted accumulation in the environment [2]. Notably, lignocellulosic fibers and biodegradable polyurethane are prominent among the biodegradable polymers. Biodegradable polyurethane is a thermosetting polymer comprising a pre-polymer (a mixture containing diisocyanate) and a polyol derived from renewable sources like castor oil, commonly known as ricin oil [3]. Despite being a thermosetting polymer, polyurethane becomes biodegradable due to the use of a polyol derived from vegetable oil, making it consumable by microorganisms within a short period and non-toxic in both usage and handling [3]. On the other hand, lignocellulosic fibers, which are renewable, consist of three main components: hemicellulose, cellulose, and lignin. Among various lignocellulosic fibers, sugarcane bagasse stands out as an agro-industrial residue with low added value and high production in Brazil [4]. To utilize sugarcane bagasse fiber (BC), pretreatment methods such as water washing to remove sugars or chemical treatments can be employed. The commonly used chemical treatment is alkaline treatment with sodium hydroxide, known as mercerization, which can partially remove hemicellulose and lignin from the fiber composition [4]. A composite material comprising sugarcane bagasse fiber and biodegradable polyurethane would offer advantages due to its biodegradability and non-toxic nature, making it suitable for diverse applications, including medical purposes. Hence, this study aimed to investigate biodegradable composites made of short fibers of sugarcane bagasse and biodegradable polyurethane.

Experimental

Preparation of sugarcane bagasse

The sugarcane bagasse was collected at a local market in the municipality of São Paulo. The washing process was carried out following the procedures described by Santos and Spinacé, 2017. Initially, the sugarcane bagasse was immersed in room temperature water (23 °C) for a period of 72 hours in a sealed glass container. It was then rinsed with running water to remove impurities. Subsequently, it was air-dried for 48 hours at room temperature. After drying, the fibers were ground using a food processor (PHILCO) and sieved. After drying, the fibers were sieved and designated as BCN (none treated sugarcane bagasse fiber).

Alkaline treatment of sugarcane bagasse

The alkaline treatment was carried out using an 8% (w/v) sodium hydroxide solution at 80°C on a heating plate (Logen) for one hour with manual agitation every 5 minutes. The ratio used was 1 L of NaOH solution to 200 g of BC fiber. Subsequently, the fibers were rinsed with running water until the washing water reached pH 7 (measured using a pH strip). The drying process was conducted in a polypropylene tray in an oven (De Léo) at 70°C for 48 hours. After drying, the fibers were sieved and designated as BCT (treated sugarcane bagasse fiber).

Composite preparation

The composites were prepared using a biodegradable polyurethane resin IMPERVEG (AGT 1315) with a ratio of 1:1.2 (w/w) of Component A (pre-polymer) and Component B (polyol derived from castor oil). Components A and B of the resin were weighed in a polypropylene container and manually mixed for 2 minutes. After complete mixing of Components A and B, 10% (w/w) of dried BCN or BCT fibers, previously dried for 12 hours in an oven (DE LEO), were added and homogenized. The resin was cured in polycarbonate molds using soybean oil as a mold release agent. The total curing period for the resin was 7 days. The composite prepared with PU and BCT were referred to as PU/BCT and the composite prepared with PU and BCN were referred to as PU/BCN.

Shore A hardness test

The Shore A hardness test was performed using a durometer (HOMIS, HT - 6510OA), and the average hardness value was obtained by measuring the hardness at 10 points on the specimen, according to ASTM-D-2240.

Impact Resistance

The charpy impact resistance test was carried out in accordance with ISO 179/1eA on 5 specimens with dimensions (80 x 10 x 4) mm. The test was performed on a Resil Impactor (6967 - Ceast), the base was used with a distance between the supports of 62 mm and a pendulum of 4 J.

Biodegradation test

For the biodegradation test, the fertilized soil (West Garden) was manually sieved, and then 10g of soil was diluted in 50 ml of water and homogenized on a magnetic stirrer (Logen) for 10 minutes. The pH was measured using a pH strip, and the obtained value was 7. Next, 2 kg of sieved soil was added to a refractory container with dimensions of 30x20x7 cm, and 40% (w/w) water was added. Then, 5 samples of pure PU, PU with treated fiber, and PU with untreated fiber were inserted into the soil. The container with soil and samples was kept at 36°C in a bacteriological incubator for 60 days, and the samples were removed from the soil and photographed after 7, 45, and 60 days.

Results and Discussion

Uniform composites were successfully obtained using BCT fiber, as shown in the PU/BCT composite photo (Fig. 1a). However, for the PU/BCN composite, which utilized BCN fiber, the

formation of composites was not possible due to swelling during the curing period, resulting in an irregular surface with numerous bubbles (Fig. 1b and c), rendering it unsuitable for testing. The successful production of the PU/BCT composite was attributed to the alkaline treatment, which partially replaced the hydroxyl groups in the fiber chains and removed amorphous regions. This treatment led to reduced moisture absorption from the environment and improved adhesion between the fiber and the matrix, enabling the successful fabrication of the composites [5, 7]. On the other hand, when using untreated fiber, water absorption occurs during the hardening period (removal from the mold after a minimum of 8 hours of curing and full hardness achieved after 1 week), resulting in composite swelling, irregularities, and the formation of bubbles. Therefore, despite generating waste, the alkaline treatment in this case allowed for the production of high-quality composites.

Figure 1: Photographs of (a) PU/BCT composite and (b) and (c) PU/BCN composite.

The results of the Shore A hardness and impact resistance tests conducted on the PU samples and PU/BCT composite are presented in Table 1. The hardness of the PU is consistent with values reported in the literature for conventional PU (derived from the mixture of a polyol and diisocyanate), indicating that the biodegradable PU used in this study possesses similar properties [6]. It is noteworthy that the hardness of the PU is slightly higher than that of the PU/BCT composite, which can be attributed to the fibers used, as they contribute to a decrease in hardness due to their predominant composition of cellulose, hemicellulose, and lignin.

The impact resistance results demonstrate that the PU/BCT sample exhibits approximately 2.8 times higher impact resistance compared to PU, indicating that the fibers act as reinforcement agents and contribute to a reduction in stiffness in the composite. This finding aligns with previous studies on alkali-treated short sugarcane bagasse fibers [7]. Alkali treatment not only reduces the hygroscopic nature of the fiber but also decreases the content of hemicellulose and lignin, thereby enhancing the reinforcement effect on PU and resulting in a significant increase in impact resistance [7].

Table 1: Results of Shore A hardness and impact resistance tests for PU and PU/BCT.

Sample	Shore A hardness (A)	Impact resistance (J)
PU	93,6 (± 3,6)	0,22 (± 0,01)
PU/BCT	84,9 (± 4,8)	0,62 (± 0,15)

The photos of the biodegradation test (Fig. 2) showed that the initial signs of material degradation began after 45 days of biodegradation testing. By the 60th day of the test, degradation was evident through the appearance of erosions, color changes, and soil strongly adhered to the specimens. It is also noticeable that the degradation starts with the fibers, which is expected due to their higher hygroscopic nature compared to PU [2]. Therefore, the degradation period of the PU/BCT biocomposite exceeds 60 days, but visual indications of its degradation can be observed from the 45th day of composted soil biodegradation testing.

Figure 2: Photographs of PU/BCT and PU samples after 7, 45, and 60 days of biodegradation testing in composted soil.

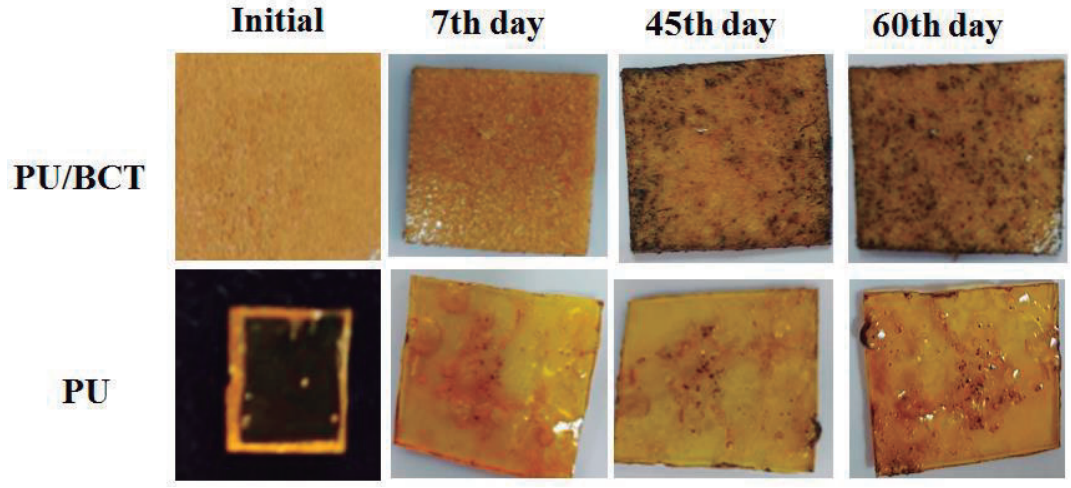

Conclusions

A biodegradable polyurethane composite was successfully obtained using only the treated sugarcane bagasse fibers. The composite with untreated fibers experienced swelling during the curing process, rendering it unusable. The alkaline treatment of the sugarcane bagasse fibers reduces the amorphous phase and water absorption, enabling the production of the polyurethane composite. The addition of fibers to the polyurethane increased impact resistance and decreased hardness, indicating that the fibers acted as reinforcing agents. Biodegradation tests in composted soil showed that the composite degrades over a period exceeding 60 days. The use of the biodegradable polyurethane composite with treated sugarcane bagasse fibers as a replacement for conventional polyurethane shows promise. However, further tests are necessary to facilitate its application.

Acknowledgements

Fatec East Zone and Federal University of ABC.

References

1. R. Geyer, J. R. Jambeck, L. Law. Science Advances, 2017, 7, 290485. https://doi.org/10.1126/sciadv.1700782
2. S.K. Kale et al. J Biochem Tech, 2015, 6, 0974-2328.
3. M. D. Burkart et al. J Appl Polym Sci. 2022;139:e53062. https://doi.org/10.1002/app.53062
4. M. A. S. Spinacé et al. J. Renew. Mater., 2018, 6. ttps://doi.org/10.7569/JRM.2018.634101
5. A. Oushabi. Composites Part B: Engineering, 2019, 174, 107059. http://dx.doi.org/10.1016/j.compositesb.2019.107059.
6. D. S. Rosa, C. G. F. Guedes. Polymers, 2003, 13, 64-71. http://dx.doi.org/10.1590/S0104-14282003000100012.
7. S. P. S. Tita, J. M. F. de Paiva, E. Frollini. Polymers: Science and Technology, 2002, 12, 228-239.

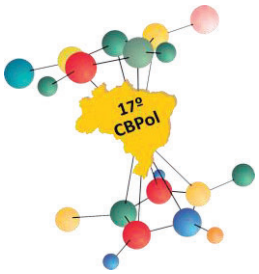

BRAZIL NUT BUR PARTICLES REINFORCED POLYPROPYLENE COMPOSITE

Bruno M. Freitas[1,2*], Jamisdean S. Santos[2], José C. M. Neto[2], Gabrieli E. Andriotti[1], Jean V. U. Teixeira[1] and Paulo N. L. Filho[1]

1 – Department of Physics, School of Sciences, Avenida Luiz Edmundo Carrijo Coube, 14-01, Vargem Limpa, CEP 17033-360, Bauru, São Paulo, Brazil. - bm.freitas@unesp.br
2 – Department of Materials Engineering, School of Engineering, Amazonas State University, Avenida Darcy Vargas, 1200, Parque Dez de Novembro, CEP: 69065-020, Manaus, Amazonas, Brazil.

Abstract - Natural fibers have been shown to have great potential for use in polymer composites. This study made composites with Polypropylene (PP), reinforcing their mass with a proportion of 20 wt% from the Brazil nut bur particles. The composite was processed in a single thread extruder machine, and samples were produced in an injection molding machine. Thus, the composite and particulate samples were analyzed using Differential Scanning Calorimetry (DSC), Thermogravimetric Analysis (TGA), Derivative Thermogravimetry (DTG) and Scanning Electron Microscopy (SEM). The polymer composites have presented a starting point for degradation around 226 ºC, slightly reduced if compared to the PP, with 232 ºC, which is also observed too in DSC analysis, showing a reduction in the heat flux values, lower than PP. The exploitation of Brazil nuts bur as a composite would be an alternative to using this material since the tests have indicated that the raw material has good thermal properties.

Keywords: *Brazil nut bur, Polypropylene, Composite, Amazon rainforest.*

Fundings: Fundação de Amparo à Pesquisa do Estado do Amazonas - FAPEAM. Universidade Estadual Paulista "Júlio de Mesquita Filho" - UNESP. Universidade do Estado do Amazonas - UEA.

Introduction

The search for a technology directed to preserving the environment and raw materials from renewable sources has motivated worldwide research centers to study the use of natural resources and agroindustry by-products [1-2] and research focused on its low-cost applications in the manufacture of composites in different regions of the world showed satisfactory results in the last decade [3]. The use of natural lignocellulosic fibers has become popular all over the world, as they are abundant and low-cost materials that facilitate a number of technical properties [4], have high strength, high fracture toughness and elasticity, and have proven to be useful for their diversity, versatility, renewability and sustainability [5], abundant, cheap, light in weight, strong and non-abrasive, and can be excellent reinforcements for plastics, replacing or reducing the use of synthetic fibers in several applications [6].

Some European countries with high environmental awareness have established the application of Lignocellulosic Fiber Embedded Polymer Composites in automotive applications [7-9], and studies carried out in Germany and in the EU predicted great market potential for composites with natural fibers [8]. The consistent implementation of improvements and optimization in the production process has also advanced using methods to reduce waste, improve inputs, reuse, recycling, conservation, and increase energy efficiency. In the Amazon Forest, thousands of families live directly from the forest extractivism. A considerable part of the income comes from the extraction process of the eatable Brazil nut (Betholletia excelsa). For the commercial extraction of this activity, usually only almonds are used and all the rest of the fruit is waste, between 80 % and 90 %. In Brazil the use wood-plastic composites is still not very significant. Thus, this work will develop a

chemical and mechanical analysis of a composite material by adding a proportion of 20 % of mass from the Brazil nut fibers to a polymer of the Polypropylene (PP) type.

Experimental

The PP (PP-H06) was provided Braskem with a melt flow index of 2.1 g/10 min, density 905 kg/m³, bendind stress of $15x10^8$ Pa, traction resistance $35x10^6$ Pa, stretching to traction with 10 %, Rockwell Hardness R of 102, impact force with IZOD fit at 23 ºC of $3.1x10^3$ J/m, deflection point under load of $455x10^3$ Pa at 107 ºC, and $182x10^7$ Pa at 57 ºC and vicat softening point at 10 N and 154 ºC.

The company ECONUT provided the Brazil nut burs, at Aruanã's farm in Itacoatiara, an Amazon's inland city, Brazil. Were broken into irregular pieces with a bench vice, and then it was made a basic washing with running water to remove impurities, such as earth. After washing, the nut burs were dried in a Quimis greenhouse (model Q-317M-72) at 60 ºC / 6 hours to remove the moisture. The Brazil nut burs were grounded in a knife mill for size reduction. Then, the fibers were classified by granulometry with the aid of sieves, and the particles retained in the 0.35 mm mesh were used to produce the composite material. These particles were treated with an aqueous solution of sodium hydroxide (NaOH) at a 5 % concentration of mass per volume of water under constant agitation for one hour. After, the fiber was washed with deionized water until its pH neutralization and then dried at 60 ºC / 48h. Drying the particles before the composite's preparation is an essential factor, once the water present in it complicates the interaction between particles and matrix.

In the single thread extruder machine (model ZGH 28950), the composites were produced in the form of pellets, with a proportion of 20 wt% Brazil nut bur particles (~ of 0.35 mm) compared with the amount of the PP, with temperatures from 190 to 205 ºC among the stages of extrusion.

To perform the morphology of the composite in SEM, the rupture test was performed (ASTM D638) after the injection of the extruded material in an injection machine (model HAITIAN HTF60W-II) with a capacity of 35 ton. and injection temperature between 190 to 205 ºC.

For analysis of PP and composites, the equipment used for DSC was SDT TA Instrument Q600. Samples were measured about 10 mg. and the heating rate was 10 ºC/min to a final temperature of 500 ºC with 5.0 Nitrogen gas flow of 30 ml/min. The crucible used in the tests was the coverles 90 µl aluminum oxide. The analysis TGA of the composite and the particles was conducted under temperature conditions ranging from 10 to 500 ºC in an atmosphere of nitrogen, with a heating rate of 10 ºC/min on a Thermal Analyzer STA 449 F3 Jupiter (Netzsch).

Results and Discussion

Differential Scanning Calorimetry (DSC)

In Fig 1, it's possible to observe that reductions in the enthalpy values have been identified at the characteristic peaks of the composite compared to the PP. Even if it's not complete due to initial test temperature, the first peak indicates the glass transition temperature (TG) of the material.

The composite presented a TG equal to 17.9 ºC, while the PP resulted in a lower transition temperature equal to 3 ºC. The interaction between fiber and PP may result from this "increase in transition temperature". These temperatures are very similar to the study carried out by [10], where a thermoplastic starch biocomposite reinforced with 16 % w/w of bleached cellulosic fibers from Eucalyptus urograndis presented a TG of 17 ºC, and for the thermoplastic the result was 2 ºC.

The second endothermic peak is characterized by the melting transition (T_m) and the first fragment of degradation in the PP and the composite. They have presented 5.35 and 3.93 mW values, respectively, and a very similar temperature value of about 164 ºC for the composite and 165.4 ºC for the polymer. In the third peak, representing an exothermic event is typically associated with the degradation of the polymer matrix by the heat release. A reduction in the central enthalpy value of the composite has been observed to 13.9 mW, while PP showed 24.7 mW at a temperature of about 300 ºC, and the composite was approximately 282 ºC. However, it has been noticed peaks after the final degradation of the composite, which refers to the chemical components of the particulate, mentioned in TGA/DTG, as the degradation of cellulose and lignin, resulting in material ashes.

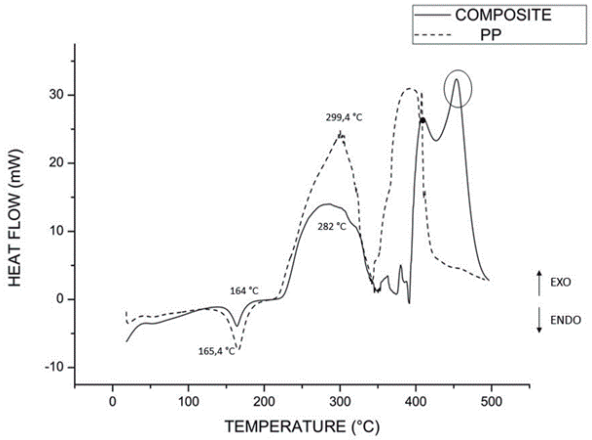

Figure 1 - DSC comparison between the composite with 20 wt% of particles and the PP.

Thermogravimetry (TGA / DTG)

The TGA was performed on the composite to determine the degradation in comparison to the PP. In Fig 2 (a), the first variation reduced the composite mass by about 3 to 4 % in a temperature of 164.5 ºC, where it's located the first evident degradation, withdrawing the water waste still existing. In a study developed by [11], the first activation peak was observed at 107-108 °C using injection-molded composites of cellulose, starch and 5, 10 and 15 wt% by weight of sisal fibers, concluding that yes, temperature isn't affected by the addition of fibers at this stage.

The degradation of the own composite has started at a temperature of 224.4 ºC. From 229 to 375.2 ºC there was an exponential degradation rate, resulting in a loss in mass of 4 to 69 %. In the study [11], the second peak appeared at 180, 176 and 172 ºC for composites with fiber content of 5, 10 and 15 wt% by weight, respectively. Another phenomenon described by DTG occurred during the degradation leap, indicating cellulose degradation, a natural and crystalline element more common in rigid fibers [12]. The final degradation temperature of the composite was about 400 °C, in the other hand, another distinct peak was noticed in the remaining 13 wt%. This was attributed to the lignin degradation, which occurs between 280 to 500 ºC, resulting in about 6 wt% of final.

In PP, Fig 2 (b), the initial degradation temperature was approximately 232 ºC, which was higher than the 1 % composite, and the loss in mass at this point was equal to 1 %. The final degradation temperature was 397 ºC, resulting in a mass of 17 % that, at the end of the test, has represented only 1.88 %. Comparing the composite with the PP, there was a slight reduction in the initial and final degradation temperature of the composite and both samples there was a great mass degradation in the temperature range between 220 and 400 ºC, approximately (Fig 2). For an amide polyester biocomposite with jute fiber, by DTG, the fiber's highest decomposition related to thermal stability was at 307 ºC (63.4 % of mass loss) and for the polymer was at 385 ºC (88.88 % of mass loss). The thermal stability of the composite between these temperatures was 339 ºC (64.24 % of mass loss).

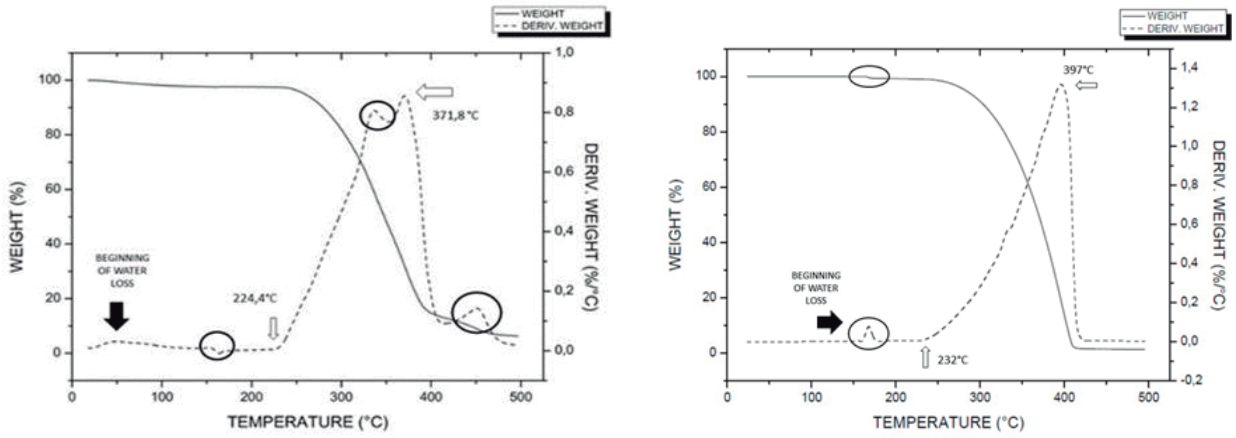

Figure 2 - TGA and DTG (a) composite (b) PP.

Scanning electron microscopy (SEM)

In Fig 3(a), before the mercerization treatment in Brazil nut bur particles, parenchyma cells are observed, with an isodiametric circular shape and measuring approximately 40µm, belonging to a primary region called exocarp [13]. In addition, waxes, oils and particulate matter are also present on the surface of the fiber [14].

Fig 3(b), after the mercerization treatment, still shows the presence of parenchyma cells, but with a change in their surface structure. The presence of this fibrillar format formed by elongated cells, with thick secondary lignified cell walls [13], is called mesocarp. This microfibrillar structural shape presents greater roughness than the circular shape, improving adhesion to the polymer during use as fillers and which, due to its morphology, tend to increase the tensile strength of the material [13]. This exposure to the most central layer also led to the elimination of possible contaminating agents, which would compromise the properties of the composite, such as waxes, oils and particulate matter that was identified in Fig 3(a), resulting in an effective cleaning and structural modification by the process of mercerization.

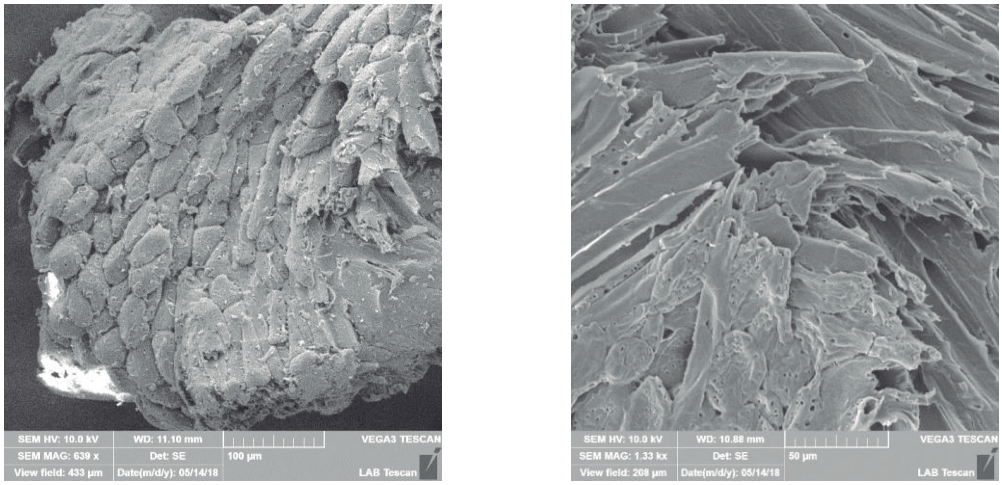

Figure 3 - Brazil nut bur particles (a) before mercerization treatment; (b) after mercerization treatment.

The analysis of the composite was carried out after failure by traction and interrupted areas were found, but this was expected due to fractures in the specimen (Fig 4). In terms of the inserted reinforcement, there is a distinct interaction between the particles and the matrix, which remain fitted and attached to their own polymeric matrix even after the mechanical tests. It's also important to highlight minor surface defects in the fibers and air bubbles, which could be worse if the fibers are not treated. The surface treatment of the fiber aims to improve the adhesion between the fiber and the matrix, playing an important role in improving the properties of composites [15].

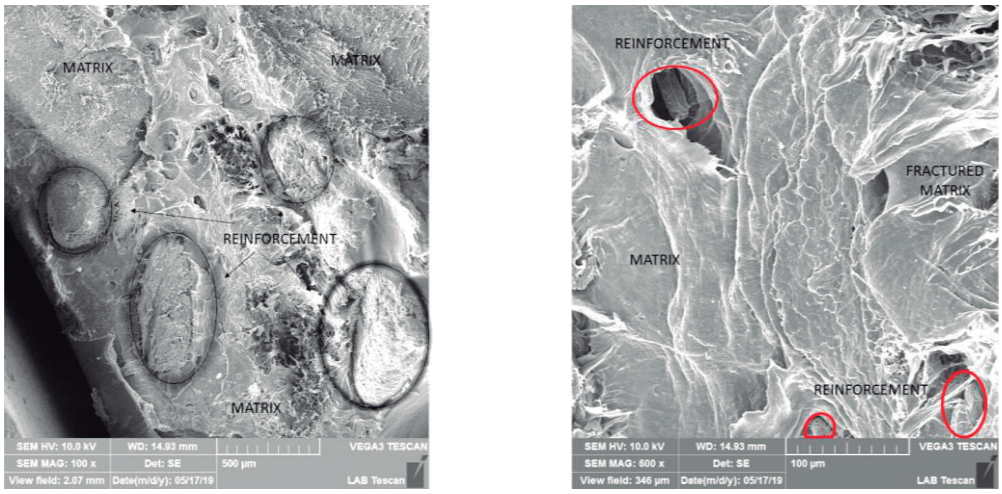

Figure 4 - SEM held in the ruptured area of the composite specimens with 20 % particles.

Conclusion

In the composite there was a decrease in their energies in each characteristic peak, indicating that the heat flux is more constant and the energy dissipation is more homogeneous, causing superior thermal stability compared to PP. The value of the heat flux in the fusion zone (T_m) decreased by more than 26 % in the composite in relation to PP and in the degradation zone there was also a decrease of almost 44 % for the composite. The reduction in the initial degradation temperature of the composite in relation to PP was almost 3.3 %, but it didn't cause considerable changes in its applications and properties. SEM revealed good compatibility and adhesion between the matrix and the inserted particles, even without the use of a compatibilizing agent.

With these results, it's possible to indicate applications for PP reinforced with particulates from the Brazil nut hedgehog in furniture sectors that can use the composite material to manufacture chairs, tables, doors, cabinets, and other objects that do not suffer such temperature stress.

Acknowledgements

FAPEAM / UNESP / UEA / LabMatPro / GFAMN.

References

1. A. Javadi; Y. Srithep; J. Lee; S. Pilla; C. Clemons; S. Gong; L.-S. Turng. Composites Part A: Applied Science and Manufacturing, 2010, 41, 982. https://doi.org/10.1016/j.compositesa.2010.04.002.
2. D. Piñeros-Hernandez; C. Medina-Jaramillo; A. López-Córdoba; S. Goyanes. Food Hydrocolloids, 2017, 63, 488. https://doi.org/10.1016/j.foodhyd.2016.09.034.
3. J. Fiorelli; D. D. Curtolo; N. G. Barrero; H. S. Júnior; E. M. J. A. Pallone; R. Johnson. Industrials crops and products, 2012, 40, 69. https://doi.org/10.1016/j.indcrop.2012.02.033.
4. D. L. Rocha; L. U. D. T. Júnior; M. T. Marvila; E. C. Pereira; D. Souza; A. R. G. Azevedo. Polymers, 2022, 14, 2043. https://doi.org/10.3390/polym14102043.
5. L. Zamora-Mendoza; F. Gushque; S. Yanez; N. Jara; J. F. Álvarez-Barreto; C. Zamora-Ledezma; S. A. Dahoumane; F. Alexis. Bioengineering, 2023, 10, 804. https://doi.org/10.3390/bioengineering10070804.
6. A. Hadjadj; O. Jbara; A. Tara; M. Gilliot; F. Malek; E. M. Maafi; L. Tighzert. Composite Structures, 2016, 135, 217. https://doi.org/10.1016/j.compstruct.2015.09.043.
7. J. Yang; Y. C. Ching; C. H. Chuah. Polymers, 2019, 11, 751. https://doi.org/10.3390/polym11050751.
8. M. Karus; M. Kaup. Journal of Industrial Hemp, 2008, 7, 119. https://doi.org/10.1300/J237v07n01_10.
9. K. Shaker; Y. Nawab in *Lignocellulosic Fibers: Sustainable Biomaterials for Green Composites*. SpringerBriefs in Materials, Switzerland, 2022; Vol. 1, 1-65.
10. A. A. S Curvelo; A. J. F de Carvalho; J. A. M Agnelli. Carbohydrate Polymers, 2001, 45, 183. https://doi.org/10.1016/S0144-8617(00)00314-3.
11. V.A. Alvarez; R.A. Ruseckaite; A. Vázquez. Polymer Degradation and Stability, 2006, 91, 3156. https://doi.org/10.1016/j.polymdegradstab.2006.07.011.
12. H. Yang; R. Yan; H. Chen; D. H. Lee; C. Zheng. Fuel, 2007, 86, 1781. https://doi.org/10.1016/j.fuel.2006.12.013.
13. G. P. Petrechen, M.Sc. Dissertation, Federal University of São Carlos, 2017.
14. R. D. Campos, Dr. Thesis, University of São Paulo, 2015.
15. J. Y. Boey; C. K. Lee; G. S. Tay. Polymers, 2022, 14, 3737. https://doi.org/10.3390/polym14183737.

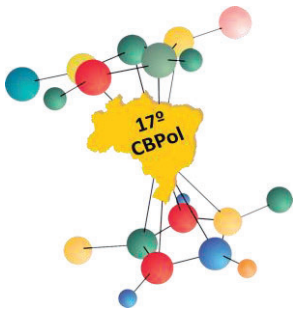

CHEMICAL AND THERMAL EVALUATION OF A COMPOSITE FOAM BASED ON CASSAVA STARCH, CLAY AND RAMIE FIBERS

Nayara T. Bohnenberger[1], Gabriela Pozzebon[1], Mara Z. de Andrade[2], Ana P. Bilck[2], Édson L. Francisquetti[2] and Daiane Romanzini[1]

1 – Postgraduate Program in Materials Technology and Engineering (PPGTEM), IFRS, Campus Feliz, Feliz, RS, Brazil ;daiane.romanzini@feliz.ifrs.edu.br

2 – Postgraduate Program in Materials Technology and Engineering (PPGTEM), IFRS, Campus Farroupilha, Farroupiha, RS, Brazil

Abstract - Starch foams can be an alternative to the use of expanded polystyrene, as they come from an abundant, renewable and biodegradable source. However, for a starch-based foam to acquire good properties, it is necessary to incorporate other additives/substances into the system. Therefore, this study aimed to evaluate the influence of Cloisite® 30B clay and ramie fibers on the chemical and thermal properties of starch foams. Stirring was done followed by a thermoforming step. The samples were evaluated using Fourier Transform Infrared Spectroscopy and Thermogravimetric Analysis. Infrared spectra indicated increased water absorption by samples containing ramie fibers. The thermal analysis indicated a increase by 5 to 6 ºC in the thermal stability of the foams with the addition of these materials. It was concluded that the addition of fibers and clay influenced thermal stability and the fiber is responsible for more pronounced water incorporation at the final material.

Keywords: Starch Composite Foam. Ramie Fiber. Clay. Thermal Properties.

Introduction

Plastics is mainly originated from the petrochemical industry, and their worldwide production is estimated at 300 million tons per year, leading to increased pollution and depletion of a non-renewable resource. In addition, food packaging is considered a major source of marine pollution [1]. A study involving two Catalan rivers found that they carry about 6 tons of plastic per year to the sea [2], contributing to the high content of microplastics that has been detected both in seafood for human consumption, and in the soil [3-4]. In Switzerland, around 90% of floodplain soils contain microplastics [5].

Expanded polystyrene (EPS), a material widely used in packaging and as an insulator, contributes significantly to the socio-environmental impacts of microplastics. Although there are techniques to promote the recycling of this polymer, these tend to be costly and cause environmental damage, with destinations for EPS being sent to landfills or treatment by incineration, chemical recycling and mechanical processes [6].

For this reason, starch is a good alternative to replace EPS, due to its abundance, low cost and because it comes from a renewable source [7]. However, for this material to acquire certain characteristics of mechanical and structural resistance and water absorption, it is necessary to incorporate other additives/substances to the system. Previous studies used grape stalks [8], pineapple peel fibers [9] and eggshell, shrimp peel or with calcium carbonate as reinforcement [10]. In order to understand the influence of these materials on the composite properties, the chemical interactions with the starch matrix and the thermal stability were investigated [11]. The authors incorporated cotton microfibers and natural rubber in a starch matrix, and it was verified through TGA that the ideal temperature to process the composites is in the range of 220°C. They also

verified that the addition of higher levels of microfibers led to a small reduction in the thermal stability of the composites [11]. Given the above, the present study aimed to evaluate the influence of Cloisite® 30B clay and ramie fibers on the chemical and thermal properties of the starch composite foam.

Experimental

Materials: Cassava starch from Pilão Amidos Ltda. (Guaíra – PR) was used. According to the technical bulletin, the maximum moisture content is 14% and pH between 4.5 – 6.5. As plasticizing agents, glycerol from the brand Anidrol (Diadema - SP) and distilled water were used, which also acted as a physical expansion agent [10]. In addition, the following additives were added: guar gum from the brand Zona Cerealista (Guarulhos – SP), to prevent sedimentation, and magnesium stearate from the brand Bianquímica Comercial (Franca – SP), as a release agent. Ramie fibers were supplied by Sisalsul (São Paulo – SP). In addition, organically modified montmorillonite trade name Cloisite ® 30B, a natural montmorillonite modified with quaternary ammonium salt, was purchased from the Southern Clay Products (USA), and it has a particle size of less than 6μm (d50) and basal spacing of 18.5 Å (d001).

Methods: The ramie fibers were previously cut, shredded and washed with distilled water for 10 min. Then, the fibers were oven dried for 1 h at 105 °C, as reported by [12] and ground through 2 mm sieve in a knife mill (SL-31, Solab). Starch foams were produced from different contents of fiber, starch and water (Table 1), and the limit of the fiber content used was less than 20 g of fiber/100 g of solids, according with the study reported by [13].

Table 1. Content of constituents for sample preparation

Sample denomination	Starch (g)	Ramie Fiber (g)	MMT (g)	Water (mL / 100 g of solids)	Glycerol (g /100g of solids)
Control	100	0	0	100	5
MMT5	95	0	5	110	10
F10	90	10	0	200	10
F15	85	15	0	200	10
F10MMT5	85	10	5	250	10
F15MMT5	80	15	5	275	10

The constituents were stirred with the mixer (Philco PMX700, Brazil) until homogenization. In all samples, 2% (w/w) magnesium stearate and 1% (w/w) guar gum were added. The material was poured onto a flat grill plates (Black & Decker Plus, Brazil) with dimensions of 20.5 x 20.5 cm and coated with Teflon. Then, the mixture was submitted to the molding technique, between 180 and 220 °C for 5 min.

Material Characterization: Fourier Transform Infrared Spectroscopy (FT-IR) was carried out by the Analysis Center - UTFPR campus Pato Branco, in a spectrophotometer FT-MIR (Spectrum Frontier PerkinElmer, USA), using the attenuated total reflectance (ATR) accessory. The spectra were recorded in the region range between 4000 and 500 cm^{-1} with a resolution of 4 cm^{-1} and 16 scans. Thermogravimetric analysis (TGA) was carried out by the Federal Institute of Education, Science and Technology of Rio Grande do Sul – Campus Farroupilha. A thermal analyzer (Perkin Elmer TGA, USA) was used at a rate of 10 ºC.min^{-1} in nitrogen atmosphere (50 mL.min^{-1}), in the range of 25 − 800 °C.

Results and Discussion

Fig. 1 shows the spectra of starch foams, as well as Cloisite® 30B and ramie fiber. In the spectrum of Cloisite® 30B, the characteristic stretching band of free hydroxyl groups (OH^-) from the clay surface was observed at 3628 cm^{-1}. At 2922 and 2854 cm^{-1}, bands related to the symmetric and asymmetric vibration of the CH_2 group were observed [14]. The band present at 1464 cm^{-1} are

associated to the vibrations of the CH_3 and CH_2 groups and at 915, 795 and 517 cm^{-1}, bands are characteristic of the octahedral layers of the aluminosilicate. The band at 1003 cm^{-1} is related to Si—O—Si bonds [8].

Figure 1. Spectra of (a) Cloisite®30B clay, ramie fiber (b) and starch foams: control, MMT5, F10, F15, F10MMT5 and F15MMT5

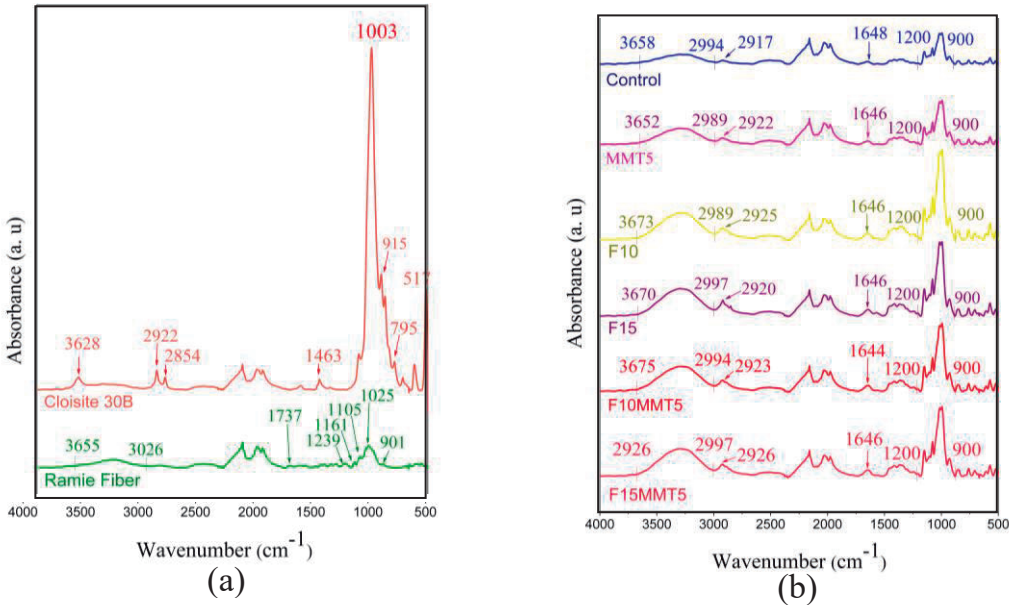

As for the ramie fibers, the characteristic bands of the OH^- groups, present in the structure of cellulose, water and lignin, occurred at 3335 cm^{-1}. The band related to the vibration of C—H, present in cellulose and hemicellulose, was observed at 2891 cm^{-1} and the band at 1737 cm^{-1} is related to the vibrational stretching of C=O of the carbonyl and acetyl groups, present in hemicellulose [15]. The band at 1239 cm^{-1} corresponds to the C—O vibration of esters, ether and phenolic groups, which are related to the waxy layer present on the surface of the ramie fibers. The low intensity bands at 1161 and 1105 cm^{-1} are characteristic of hemicellulose and cellulose, due to C—O—C deformation or stretching vibrations, and at 1025 cm^{-1} is related to the stretching vibrations (C—O) and (O—H) of cellulose. Finally, the band at 901 cm^{-1} corresponds to the CH deformation, being related to the intensity of the amorphous region [15].

In the foam spectra, the bands between 2997 and 3675 cm^{-1} are associated with both the acetal groups (C—O—C) and the OH^- groups of starch [8,16]. These bands may be evidence of hydrogen bonds between the foam constituents during the thermoforming process, due to the stretching of the vibrational complexes that are associated with the OH^- groups [8, 17]. The most intense bands were observed in samples containing fibers and this may also indicate an increase in the hydrophilicity of the foams [18].

The bands showed between 2917 - 2025 cm^{-1} were more intense in the samples containing fibers and may be associated with the stretching of the C-H group [16]. The low intensity bands, which were observed in the region of 1646 cm^{-1}, are related to the angular bending of the hydroxyl groups of water molecules, suggesting interaction between water and other constituents of the foam [16, 17]. Those bands between 1200 and 900 cm^{-1} are related to the C—O—C vibrations, which are characteristic of starch and other types of polysaccharides. The highest intensity bands were observed in samples containing fibers.

In general, the bands indicate that there was interaction between the constituents of the foam. However, it is also possible to observe the high affinity with water, which limited the use of starch-based materials for dry food storage. According to the data presented, the use of natural fiber contributes to an increase in water absorption.

From the results of the thermogravimetric analysis (TGA) and the first derivative (DTG), the thermal stability and the degradation temperature of the starch, fiber and clay foams were analyzed. Figure 2 shows the TGA and DTG curves for these materials. For all samples, initial mass losses were observed, associated with volatilization of adsorbed and surface water (Fig. 2 b) [11,14].
For ramie fiber, a second stage of mass loss was observed (Fig. 2 c), which occurred from 246 to 309 °C and is associated with the decomposition of hemicellulose and pectins [19]. It was also verified that the maximum degradation rate of this reinforcement occurred at 384 °C and is associated with cellulose decomposition (Table 2) [19]. In the foam curves (Fig. 2 c), the peaks corresponding to the maximum degradation rates can be observed, which occurred due to the degradation of the anhydroglucose units of the matrix. Starch, as it is present in higher concentrations in the formulation, is the constituent that most affects the thermal stability of foams [16]. The addition of fibers and Cloisite® 30B led to a small increase in thermal stability and degradation temperature, which can be seen in Figure 2 and Table 2.

Figure 2. Thermograms: (a) TG, (b) magnification of the highlighted area and (c) DTG curve

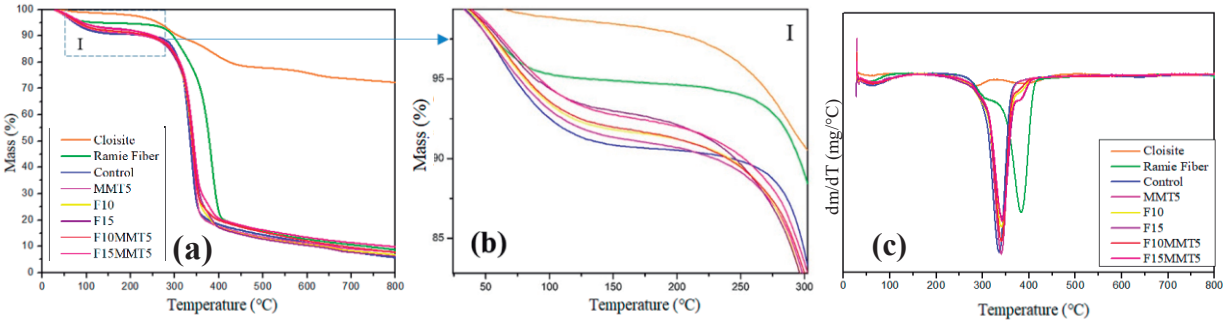

Table 2. Summary of TGA results: maximum degradation temperature and shoulder temperature.

Sample denomination	T_{pico} (°C)	T_{ombro} (°C)	Residual mass (%)
Cloisite® 30B	285	-	72,25
Ramie Fiber	384	-	8,60
Control	335	-	5,74
MMT5	340	-	7,81
F10	340	373	6,79
F15	341	373	6,15
F10MMT5	340	373	7,76
F15MMT5	341	371	9,77

In samples F10, F15, F10MMT5 and F15MMT5, the formation of a shoulder can be observed (Fig. 2 c) at temperatures close to the temperature of maximum degradation of ramie fibers, which is more accentuated for samples with higher reinforcement content. This behavior is according with Sanhawong et al. [11], who evaluated the effect of latex on cassava starch biofoams reinforced with cotton fibers. At the end of the experiment, the starch foams presented residual mass in the range of 5 to 10% (Table 2). The samples containing Cloisite® 30B (MMT5, F10MMT and F15MMT5) showed the highest values of residual mass, due to the predominantly inorganic composition of the clays, followed by the samples containing only fiber (F10 and F15). By TGA results, it was verified that all the constituents of the foam composite were not affected by the temperature process.

Conclusions

In this work, preliminary studies were carried out, in order to evaluate the influence of the ramie fiber content and the addition of Cloisite® 30B on the chemical and thermal properties of the foams. The thermal properties of the foams were not affected by the addition of clays and fibers.

Based on the FTIR results, foams containing fiber interact strongly with water, which may limit the use of this material for storing low-water foods. The next step of the present study is to produce composite foams with reduced wather absorption, by the incorporation of essential oil or silicones. For this reason, the FTIR results will be correlate with the water absorption tests. The essential oil starts to lose mass at low temperature, near the process temperature, for this reason, understand the TGA analysis results is important in order to define the process temperature and to control the thermal stability of the foams.

Acknowlodgments
The present work was carried out with the support of the Federal Institute of Education, Science and Technology of Rio Grande do Sul (IFRS), and FAPERGS 10/2021 edict, process 22/2551-0000612-4 - auxílio recém-doutor (ARD)). The authors are also grateful to the Multi-user Laboratory Analysis Center at the UTFPR (UTFPR), Campus Pato Branco, for the FTIR performed analysis.

References
1. R. E. J. Schnurr; V. Alboiu; M. Chaudhary; R. A. Corbett; M. E. Quanz; K. Sankar; H. S. Srain; V. Thavarajah; D. Xanthos; T. R. Walker. Mar. Pollut. Bull. 2018, 137, 157, http://dx.doi.org/10.1016/j.marpolbul.2018.10.001.
2. G. F. Schirinzi; M. Köck-Schulmeyer; M. C. D. González-Fernández; G. Hanke; M. Farré; D. Barceló. Sci. Total Environ. 2020, 714, 136807, http://dx.doi.org/10.1016/j.scitotenv.2020.136807.
3. L. G. A. Barboza; A. D. Vethaak; B. R. B. O. Lavorante; A. K. Lundebye; L. Guilhermino. Mar. Pollut. Bull. 2018, 133, 336, http://dx.doi.org/10.1016/j.marpolbul.2018.05.047.
4. Y. Chae; Y. J. An. Environ. Pollut 2018, 240, 387, http://dx.doi.org/10.1016/j.envpol.2018.05.008.
5. M. Scheurer; M. Bigalke. Environ. Sci. Technol 2018, 52, 3591, http://dx.doi.org/10.1021/acs.est.7b06003.
6. N. D. Gil-Jasso; E. A. Giles-Mazón; G. Soriano-Giles; E. W. Reinheimer; V. Varela-Guerrero; M. F. Ballesteros-Rivas. 2022, 307, 121835, http://dx.doi.org/10.1016/j.fuel.2021.121835.
7. S. Tabasum; M. Younas; M. A. Zaeem; I. Majeed; M. Majeed; A. Noreen; M. N. Iqbal; K. M. Zia. Int. J. Biol. Macromol. 2019, 122, 969, http://dx.doi.org/10.1016/j.ijbiomac.2018.10.092.
8. J. B. Engel; A. Ambrosi; I. C. Tessaro. Carbohydr. Polym. 2019, 225, 115234, http://dx.doi.org/10.1016/j.carbpol.2019.115234.
9. A. Cabanillas; J. Nuñez; J. P. Cruz-Tirado; R. Vejarano; D. R. Tapia-Blácido; H. Arteaga; R. Siche. Polym. Compos. 2019, 27, 496, http://dx.doi.org/10.1177/0967391119848187.
10. K. Kaewtatip; C. Chiarathanakrit; S. Riyajan. Powder Technol. 2018, 335, 354, http://dx.doi.org/10.1016/j.powtec.2018.05.030.
11. W. Sanhawong; P. Banhalee; S. Boonsang; S. Kaewpirom. Ind. Crops Prod. 2017, 108, 756, http://dx.doi.org/10.1016/j.indcrop.2017.07.046.
12. D. Romanzini**,** Universidade de Caxias do Sul, Caxias do Sul, 2012.
13. Vercelheze, A. E..; Fakhouri, F. M.; Dall'antônia, L. H.; Urbano, A.; Youssef, E. Y.; Yamashita, F.; Mali, S. Carbohydr. Polym. 2012, 87, 1302, http://dx.doi.org/10.1016/j.carbpol.2011.09.016.
14. I. F. Leite; C. M. O. Raposo; S. M. L. Silva. Cerâm. 2008, 54, 303.
15. G. P. Otto; M. P. Moisés; G. Carvalho; A. W. Rinaldi; J. C. Garcia; E. Radovanovic; S. L. Fávaro. Compos. B. Eng. 2017, 110, 459, http://dx.doi.org/10.1016/j.compositesb.2016.11.035.
16. C. M. Machado; P. Benelli; I. C. J. Tessaro. Biol. Macromol. 2020, 165, 1706, http://dx.doi.org/10.1016/j.ijbiomac.2020.10.048.
17. D. K. M. Matsuda; A. E. Verceheze; G. M. Carvalho; F. Yamashita; S. Mali. Ind. Crops Prod. 2013, 44, 705, http://dx.doi.org/10.1016/j.indcrop.2012.08.032.
18. H. Abral; A. Hartono; F. Hafizulhaq; D. Handayani; E. Sugiarti; O. Pradipta. Carbohydr. Polym. 2019, 206, 593, http://dx.doi.org/10.1016/j.carbpol.2018.11.054.
19. L. Ding; X. Han; L. Cao; Y. Chen; Z. Ling; J. Han; S. He; S. Jiang. J. Bioresour. Bioprod 2022, 7, 190, http://dx.doi.org/10.1016/j.jobab.2021.11.002.

CHITOSAN-BASED MULTILAYER FILM INCORPORATED WITH BIOACTIVE COMPOUNDS FROM JABOTICABA PEEL

Marcelle L. Gomes[1], Elis Regina C. Barreto[2], Luisa B. Avila[3] and Gabriela S. da Rosa[1,2]*

1 – Chemical Engineering, Federal University of Pampa (UNIPAMPA), Bagé, RS, Brazil
marcellegomes.aluno@unipampa.edu.br
2 – Graduate Program in Science and Materials Engineering, Federal University of Pampa (UNIPAMPA), Bagé, RS, Brazil
3- Graduate Program in Chemical Engineering, Federal University of Santa Maria (UFSM), Santa Maria, RS, Brazil

Abstract - The use of packaging plays a fundamental role in the food industry, ensuring protection, conservation and safety of products throughout the entire supply chain. However, the increased consumption of packaging has raised environmental concerns with its disposal, as many of these polymers are resistant to biodegradation. Regarding this situation, biodegradable packaging based on biopolymers and natural extracts rich in bioactive compounds appears, representing an important alternative. Thus, the present work aimed to produce a multilayer biopolymeric film based on chitosan, incorporated with bioactive compounds from jaboticaba peel, aiming to enhance the performance of important properties for use in the food industry. The jaboticaba peel extract was obtained using ultrasound assisted extraction technique under the conditions of 1 min and 88 °C, showing 89.83±0.05% of antioxidant activity, 159.43±3.71 mg GAE.g^{-1} (b.s.) of total phenolic compounds and 2235.37±34.21 mg.$100g^{-1}$ (b.s.) of total anthocyanin. The obtained extracts were added to the filmogenic solution containing chitosan, for the preparation of multilayer films, using the casting method. Thus, by the characterization of the control multilayer film (CMF) and active multilayer film (EMF), it was possible to observe a 63.5% change in the film color, as well as an increase in thickness after the incorporation of the extract. When analyzing the mechanical properties, it was found that the addition of the extract decreased the tensile strength and increased the elongation rate, followed by a reduction of approximately 20% in the film swelling index. By the study, it was possible to verify that the material showed potential for use in active food packaging.
Keywords: *Packaging; Biopolymer, Bioactive compounds, Ultrasound assisted extraction.*

Introduction

World's population growth has been affecting the rise of the production of solid residues such as food packaging, because of high demand for food, as they have in their composition polymers derived from non-renewable sources that lead to environmental and socioeconomic crises. Therefore, the development of new materials and technologies to minimize this problem have gained prominence in the food industry, such as the development of biopolymeric materials [1, 2].

Biopolymeric materials can be obtained based on proteins, lipids and polysaccharides as base, presenting a wide range of applications, including food packaging. These aim to protect the physical and biological properties of a certain product. Due to the low mechanical and barrier properties, it is necessary to seek strategies to improve them, the addition of plasticizers and the formulation of multilayer films [2, 3].

The multilayer biopolymeric structure formulation allows the combination of different compositions, thus promoting greater efficiency in food protection, reducing environmental impact and material waste. In this sense, chitosan is an important biopolymer, obtained by the deacetylation of chitin originating from crustaceans, having antimicrobial properties, flexibility, high permeability to water vapor and biocompatibility, becoming an important constituent in the production of biopolymeric packaging for food or biological products [4, 5].

Therefore, bioactive compounds become interesting for incorporation in biopolymeric matrix, due to their functional properties, such as antioxidant, antimicrobial and anti-inflammatory properties that can contribute to improvements to the determined application [6].

In this perspective, the addition of a natural bioactive compound to the production of a multilayer film, such as jaboticaba peel extract, has potential for incorporation in material for food packaging using biopolymeric matrix. Therefore, the present work aims to analyze and evaluate the properties of multilayer films based on chitosan incorporated with bioactive compounds from jaboticaba peels (*Plinia cauliflora*) as pontential for food packaging.

Experimental

The jaboticaba used was obtained in Santa Maria (-29.88926, -53.87125), Rio Grande do Sul. For the preparation of the jaboticaba peel sample the following operations were used: manual separation, previous washing with running water and sodium hypochlorite solution (3% v/v), frozen of peels and lyophilized for 48 h at -50 °C, grinding in an analytical mill and sieving to standardize the granulometry of the particles in 0.250 mm, obtaining the jaboticaba peel powder (JPP).

To the extraction of bioactive compounds contained in the jaboticaba peel, 0.5 g of the JPP was used in 50 mL of acidified water with pH 1 (adjusted using hydrochloric acid solution at 0.1 M), used as a solvent, then the extraction carried out in the ultrasonic sonicator (ECOSONICS ULTRONIC QR, Brazil) during 1 min at 88 °C.

Subsequently, the obtained extract was characterized according to the phenolic contents (TPC) according to the methodology described by Singleton and Rossi [7], antioxidant activity using the methodology proposed by Brand-Williams, Cuvelier, and Berset [8] and total anthocyanins from Avila *et al.* [9].

To obtain the chitosan films, the casting technique was used, according to the methodology described by Wang *et al*. [10]. The film-forming solution was prepared by dissolving 1 g of chitosan powder in 75 mL of 1% (v/v) acetic acid solution, along with 0.3 g of glycerol at room temperature (± 25 °C). The solution was stirred (100 rpm) for 3 h until it became a homogeneous mixture, after the mixture was placed in *Petri* dishes, followed by drying in an oven during 7 h at 40 °C, first layer. The second layer was added to the filmogenic solution and 25 mL of jaboticaba extract, added on the first layer and subjected to drying in the oven under the same conditions from the previous film. For the development of the control multilayer film (CMF) the same process mentioned above was used, however the two layers contained the same formulation as the first layer.

Finally, the multilayer film obtained was evaluated according to the color, using a spectrophotometer, thickness, using a digital micrometer (Insize-IP65, China), mechanical properties according to the ASTM Standard D882-18 [11], where the tensile strength and elongation at break of the films were evaluated using a texturometer, swelling index, analyzed according methodology proposed by Bunhak *et al*. [12] and morphological through scanning electron microscopy (SEM).

Results and Discussion

According to the analysis of the extraction of bioactive compounds present in the jaboticaba peel, the values obtained were the (159.43±3.71) mg.GAE.g^{-1} (b.s.) for the total phenolic compounds, (89.83±0.05) % for antioxidant activity and (2235.37±34.21) mg.100g^{-1} (b.s.) of total anthocyanins. The antioxidant activity is comparable to the result presented by Avila *et al.* [13], which obtained an antioxidant activity of 78.61 % for the jaboticaba peel extract using the maceration method for 1 h. However, we can identify that the extraction method used in the present study was more efficient since was obtained showed a higher antioxidant percetage than obtained by maceration teechnique and in short time. The total phenolic compounds found was higher than reported by Carvalho [14], who obtained 131 mg GAE g^{-1}(b.s) for jaboticaba peel using water as

solvent and the maceration technique. Total anthocyanin content reported was also higher than that reported by Neves *et al.* [15] who, using the ultrasound assisted extraction technique and ethanol as solvent at 40 °C for 1 h, obtained 672.34 mg.100g^{-1}(b.s). Through the results obtained, it can be infer that the use of a acid solvent, as well as a high temperature, favored the extraction process of the bioactive compounds. According to Barros [16], acidic solutions can rupture the cell wall of the plant matrix and consequently increase the extraction efficiency of bioactive compounds.

The multilayer films were analyzed, and the results of the color analysis are shown in Table 1, followed by the parameters L^*, a^*, b^* e ΔE.

Table 1– Results obtained by analysis of film color.

Film	L^*	a^*	b^*	ΔE
CMF	89.23 ± 0.72	-2.59 ± 0.31	12.5 ± 2.72	-
EMF	45.60 ± 2.36	20.96 ± 2.16	52.15 ± 1.02	63.5

From the obtained results, it is possible to observe that the addition of extract to the multilayer film (EMF) caused a darker color compared to the control multilayer film (CMF), as demonstrated by th L^* patameter that indicates luminosity. The a^* and b^* parameters, responsible for the chromatic coordinates, were positive, the first indicating a predominance of the red color and the following with a predominance of yellow. The results found by Avila *et al.* [13] when developing a monolayer film based on carrageenan and incorporated with the jaboticaba peel extract were positive for the a^* and b^* parameters, also demonstrating a darker color with the addition of the extract, with a color variation of 96.5% compared to the control film.

The results of the mechanical analysis of the multilayer films and the swelling index are shown in Table 2.

Table 2- Results obtained for the mechanical properties of the material.

Film	Thickness (mm)	σ (MPa)	E (%)	Swelling index (%)
CMF	0.136 ± 0.020	11.02 ± 3.95	19.0 ± 4.22	62.02 ± 3.16
EMF	0.166 ± 0.008	4.41 ± 0.57	33.21 ± 4.07	43.68 ± 4.36

According to the results obtained for the analysis of the tensile strength, a similar behavior was observed compared to the study reported by Avila *et al.* [13], who developed carrageenan monolayer films and obtained a decrease in the maximum stress from 10.69±1.61 MPa for the control film to 6.08±0.33 MPa for the film incorporated with extract. Besides that, it was verified that the addition of extract increased the elongation at the break of the film. This observation corroborates the study carried out by Martiny *et al.* [17], that observed that when incorporation of olive leaf extract into carrageenan films resulted in a plasticizing effect to the material. Thus, it was possible to observe that in the present study, the development of a multilayer film incorporated with natural extract increased the tension necessary for the rupture of the material and was also for increasing its elongation. Regarding the swelling index, it was possible to observed that the multilayer film incorporated with extract showed a lower swelling index when compared to the control film. This fact may be due to the addition of the extract that increased its thickness, making it a more compact structure and more resistant to moisture. The values found in this study are close to those reported by other studies with chitosan films and other biopolymers. Riaz *et al.* [18] observed a reduction in the degree of swelling, from 57.38% to 40.49%, due to the presence of hydrophilic groups in the chitosan molecule when analyzing chitosan monolayer films with Chinese chive root extract. According to Rosina *et al.* [19], the decrease in the swelling index is essential for packaging, to avoid the film from absorbing moisture from the environment.

The multilayer film were also evaluated for their structure by SEM analysis and are showed in Figure 1.

Figure 1- Images from SEM of the multilayer films (A) CMF (B) EMF.

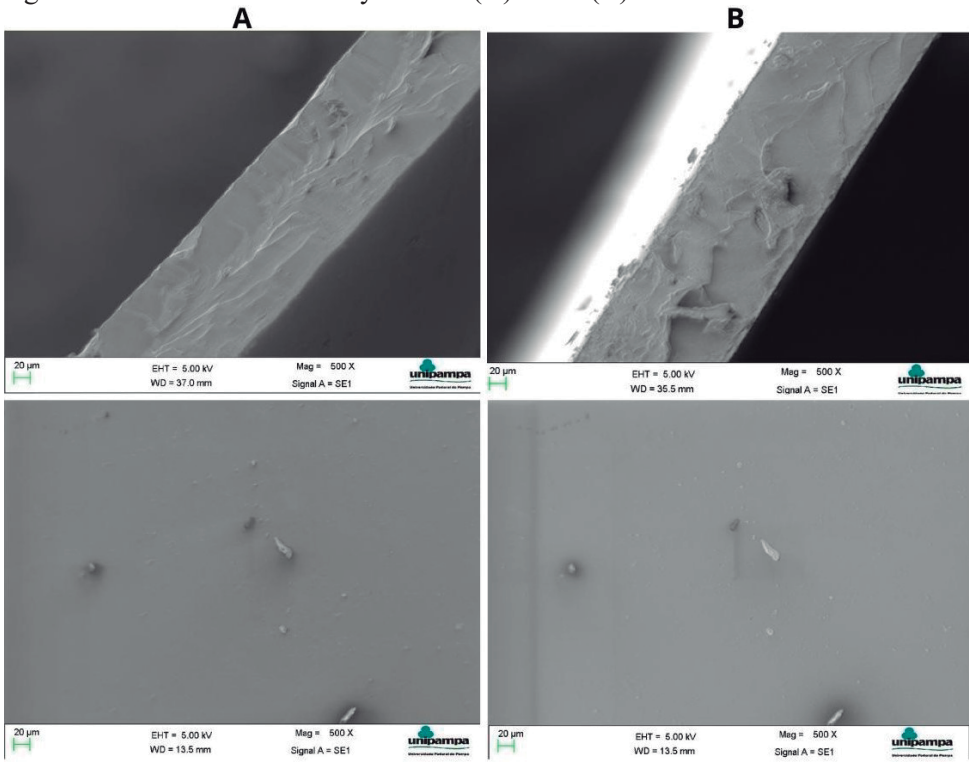

The analysis of the micrograph of the surface of the films showed that all of them present a homogeneous surface, indicating a good miscibility between the components. However, clumps were observed on the surface of the films, which can be attributed to bubbles due to the chitosan solubilization process. Furthermore, during the casting process of the two layers, it is not possible to visually distinguish the separation between them, as the layers are composed of the same biopolymer. However, in a study conducted by Neto *et al.* [20], they developed a multilayer film using chitosan and konjac glucomannan. A clearly defined interface between the layers with phases separation was observed, indicating that the structure of each biopolymers was preserved. This difference in results suggests that the choice of materials and the manufacturing process can play an important role in the quality and uniformity of the obtained films.

Conclusions

The extraction of bioactive compounds by ultrasound using acidified water as solvent showed satisfactory results in terms of antioxidant activity, total phenolic compounds and total anthocyanin. Characterization of the films containing extract showed an increase in film thickness compared to the control films. It was possible to identify a reduction in the swelling index from 62.02% of the CMF to 43.68% of EMF a decrease in the tensile strength of 11.02 MPa for 4.41 MPa of the EMF, while the percentage of elongation increased from 19% of CMF to 33.21% of the EMF.

The casting technique used to elaborate the multilayer films proved eficiente. Thus, homogeneous films with easy plates removal were obtained, presenting uniformity. However, it was possible to identify the undesirable presence of bubbles, requiring alternative methodologies to the removal, as a step before forming films in the oven.

Therefore, the multilayer films elaborated in this study exhibited promising characteristics as food packaging materials, with good active, mechanical properties and ability to package water-rich foods. This result highlights the potential of these films and bioactive compound of jaboticaba peel

as a viable option for applications in the food industry. In future stages, it is interesting to study methodologies for reducing bubbles after the chitosan dissolution process, as well as improving their characteristics and evaluating the antioxidant and antimicrobial action of the films when applied to active food packaging.

Acknowledgements
Research group process engineering in particulate systems, FAPERGS, CAPES, CNPq and UNIPAMPA.

References

1. Landim, Ana Paula Miguel et al. Polímeros. 2016, v. 26 https://doi.org/10.1590/0104-1428.1897.
2. Henrique, C. M., Cereda, M. P. e Sarmento, S. B. S. P. Food Science and Technology. 2008, v. 28, n. https://doi.org/10.1590/S0101-20612008000100033.
3. LAVORGNA, M. *et al*. Carbohydrate Polymers, Barking, v. 82, n. 2, p. 291-298, 2010. https://doi.org/10.1016/j.carbpol.2010.04.054.
4. OLIVEIRA, V. R. L. de. Dissertação (Mestrado em Ciência e Engenharia de Materiais) - Universidade Federal Rural do Semi-Árido, Mossoró, 2017.
5. Laranjeira, M. C. M. and Fávere, Valfredo T. Química Nova. 2009, v. 32, n. 3. https://doi.org/10.1590/S0100-40422009000300001.
6. Verruck, S. et ai. (2022). Revista CSBEA, v.4 n.1. https://doi.org/10.5965/24473650412018111.
7. SINGLETON, V. L., ROSSI, J. A. American Journal of Enology and Viticulture, California, v. 16, p. 144–158, 1965. https://doi.org/10.5344/ajev.1965.16.3.144.
8. BRAND-WILLIAMS, W., CUVELIER, M. E., BERSET, C. LWT - Food Science and Technology, Amsterdam, v. 28, p. 25–30, 1995. https://doi.org/10.1016/S0023-6438(95)80008-5
9. AVILA, L. B. et al. In Proceedings of XXXIX Congresso Brasileiro de Sistemas Particulados ENEMP 2019, Belém. Anais eletrônicos. Campinas, Galoá, 2019. Vol. 2, 2019.-116438
10. WANG, H. et al. Food Chemistry, Amsterdam, v. 283, p. 397-403, 2019. https://doi.org/10.1016/j.foodchem.2019.01.022.
11. ASTM - American Society for Testing and Materials. D882-18: Standard test method for tensile properties of thin plastic sheeting, 2018.
12. BUNHAK, E. J. et al. Química Nova, São Paulo, v. 30, n. 2, p. 312-317, 2007. https://doi.org/10.1590/S0100-40422007000200014
13. AVILA, L. B. et al. Molecules, New Jersey, v.25, n. 23, p. 55-63. https://doi.org/10.3390/molecules25235563.
14. CARVALHO, G. G. Dissertação (Mestrado em Alimentos e Nutrição)- Universidade Estadual de Campinas, 2013.
15. NEVES, L. S. S. e SANTOS, R. P. Trabalho de Conclusão de Curso (Graduação em Ciência e Tecnologia de Alimentos) - Instituto Federal de Educação, Ciência e Tecnologia, Campus Inhumas, Goiás, 2019.
16. BARROS, H. D. F. Q. et al. Food Research International, 2019. Vol. 124. p.16-26. https://doi.org/10.1016/j.foodres.2019.01.010.
17. MARTINY, T. R. et al. Food Science and Nutrition, Nova Jérsia, v. 8, n. 7, p. 3147– 3156, 2020. https://doi.org/10.1002/fsn3.1554.
18. RIAZ, A. *et al*. International Journal of Biological Macromolecules, Amsterdam, v. 114, p. 547-555, 2018. https://doi.org/10.1016/j.ijbiomac.2018.03.126.
19. ROSINA, Claudia Renata *et al*. Revista Brasileira de Ciências Farmacêuticas, v. 40, p. 425-431, 2004. https://doi.org/10.1590/S1516-93322004000300020.
20. NETO, R. J. G. *et al*. Carbohydrate Polymers, Amsterdam, v. 212, p. 59-66, 2019. https://doi.org/10.1016/j.carbpol.2019.02.017.

COMPARISON BETWEEN LLDPE COMPOSITES CONTAINING RESIDUES OF BACURI MESOCARP (BM) AND BACURI SEED (BS)

Cléverson F. S. Gabriel[1]*, Gabriela M. dos Santos[1] and Marcia G. de Oliveira[1]

1 – Polymeric Materials Technology Laboratory (LAMAP), Materials Division (DIMAT), Materials Technology Coordination (COTEM), National Institute of Technology (INT), Rio de Janeiro, RJ, Brazil
cleverson.fernandes@int.gov.br

Abstract – This work aimed to develop composites of LLDPE with residues from the pulp (BM) and seed (BS) of Bacuri, containing 5, 10 and 15% filler. Analyzing the mixture process, the BS acted as a processing auxiliary, decreasing the value of the torque and the specific energy, whereas the BM compounds values were closer to the pure LLDPE. The composites viscosity results corroborated the processability, effectively demonstrating that BS increased the fluidity of the material. The elongation at break of the composites with BS showed higher results than the BM composites, probably due to this greater fluidity of the BS composites. Tensile strength results of all composites containing filler were lower than pure LLDPE, with composites with BM showing lower values than composites with BS. The morphological analysis indicated that BM produced specimens with more grooves, which explained this lower mechanical performance. Despite not demonstrating effective reinforcement, BS and BM could still be used as filler in LLDPE, depending on the desired properties of the final product.

Keywords: *LLDPE, Bacuri, Viscosity, Mechanical Properties, Fracture Morphology.*

Introduction

Brazil is a favorable country for the development of various agricultural and forestry crops, due to factors related to climate and soil quality, in addition to having large tracts of land available for different crops. With regard to agricultural products typical of the northern region and neighboring states of the Amazon region, there are several species that stand out for their biodiversity and their unique characteristics, presenting great potential in the food industry and in the cosmetics industry. Natural waste generated due to various economic activities involving species such as cupuaçu, açaí, Brazil nuts, ucuuba, bacuri, among others, contribute to the contamination of the environment, especially water and soil resources [1].

The use of these residues in the preparation of polymeric composites can be a viable approach to reduce the environmental impact caused by them. However, the use of Bacuri as filler in polymeric compositions has not yet been explored, especially in the segment of polymeric films. The Bacuri, scientific name Platonia insignis is typically found in the eastern Amazon region, in addition, it can also be found in transition areas from the forest biome to the cerrado. Bacuri contains a sweet and sour pulp (Bacuri Mesocarp - BM) rich in potassium, phosphorus and calcium, which is consumed directly or used in the production of sweets, ice cream, juices, jellies, liqueurs and other delicacies. Furthermore, the oil extracted from its seeds is used as an anti-inflammatory and healing agent in the cosmetics industry [2-4].

The polymeric film industry is always looking for solutions that offer cost reduction without significantly altering its productivity and processability. These solutions must keep the product competitive in the market, taking into account its minimum requirements, such as mechanical resistance, processability, among others, according to the final application of the film. It is possible

to lower the overall cost of a polymeric compound by adding filler. ASTM D1566 defines filler as a solid material, generally of low particle size, that can be added in relatively large proportions to a polymer for technical or economic reasons.
Linear low density polyethylene (LLDPE) is one of the most used polymers in film production, due to its numerous structural advantages, it is an ethylene copolymer obtained from the polymerization of ethylene and α-olefins. LLDPE is a thermoplastic that is widely used in packaging, providing products to be used in bubble wrap, disposable diapers, sanitary napkins, canvas, bags in general, among other applications [5-7]. Therefore, the goal of this work was to develop composites containing both dry Bacuri pulp residues, called Bacuri mesocarp (BM), and ground bacuri seed residues (BS) in compositions containing LLDPE as a matrix and thus evaluate its mechanical and processability properties.

Experimental

The LLDPE and composites were prepared by melt intercalation in an internal mixing chamber coupled to a torque rheometer Haake Polylab OS. The rotor used was of the Roller type, at 150°C, with a speed of 60 rpm for 10 minutes. The formulations, in weight content (%), used in this work are presented in Table 1.

Table 1 – Composites formulation in weight content (%)

Composition	LLDPE (%)	Bacuri Seed (%)	Bacuri Mesocarp (%)
LLDPE	100	0	0
LLDPE + 5% BS	95	5	0
LLDPE + 10% BS	90	10	0
LLDPE + 15% BS	85	15	0
LLDPE + 5% BM	95	0	5
LLDPE + 10% BM	90	0	10
LLDPE + 15% BM	85	0	15

The specimens for the mechanical tests and the rheological analysis were molded by compression, according to their respective standards, in a hydraulic press MA 098/A400 with a pressure of up to 55 MPa at 150°C, for 10 minutes in the hot press and then cooled using the same pressure and time in the cold press. Rheological analysis was carried out on a Haake Mars II oscillatory disk rheometer as an accessory with 20 mm parallel plate geometry. All tests were carried out at 150°C. Complex viscosity (η*) was measured through a strain variation test from 0.01% to 500%, at a constant frequency of 1 Hz. The tensile strength test was carried out in a mechanical testing machine EMIC DL3000 with a 1000 N load cell and a speed of 100 mm/min, according to ASTM D638 standard, type V specimen. The morphology of the composites fractured in liquid nitrogen was evaluated by scanning electron microscope FEI Company, model INSPECT S50 with 20 kV voltage.

Results and Discussion

Mixture Processability analysis

The first stage of the analysis consisted of the incorporation of Bacuri residues in the LLDPE matrix. Fig 1 shows the evolution of the equipment torque as a function of time (Fig 1A) and the specific energy of the mixture as a function of time (Fig 1B). The first peak in Fig 1A refers to the addition of LLDPE and, over time, the polymer passes into the molten state, therefore, its fluidity increases and the torque decreases drastically. In approximately 3 minutes, the filler was added. The total mixing time was 10 minutes.

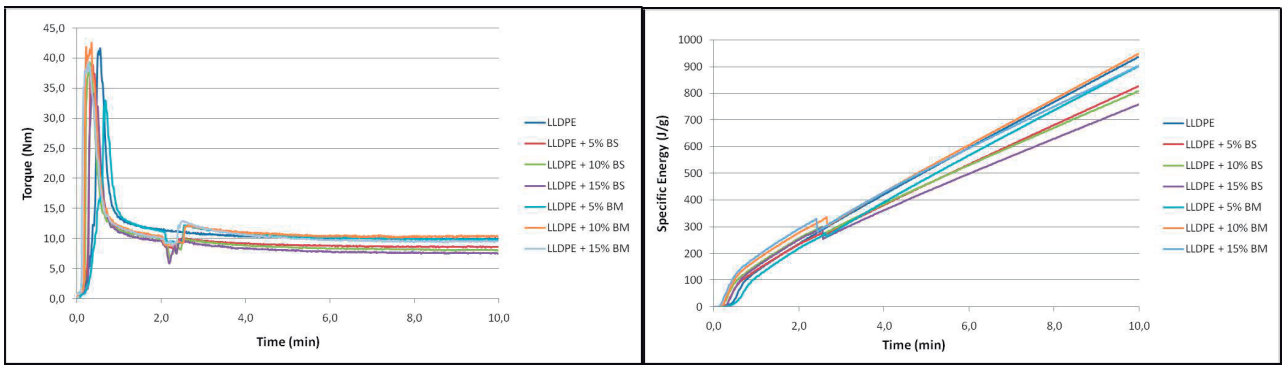

Figure 1 - A: Torque (Nm) over mixing time and B: Specific energy (J/g) over mixing time.

The torque required to perform mixing was lower for samples containing BS when compared to BM, which emphasizes that BS can be a better processing auxiliary than BM. This fact becomes more pronounced when analyzing the specific energy values (Fig 1B). In Table 2, this effect can be better observed when evaluating the final torque and maximum specific energy of the mixtures.

Table 2 - Final torque and specific energy of the mixtures.

Composition	Final Torque (Nm)	Maximum Specific Energy (J/g)
LLDPE	10,0	938
LLDPE + 5% BS	8,6	828
LLDPE + 10% BS	8,1	810
LLDPE + 15% BS	7,6	760
LLDPE + 5% BM	9,9	903
LLDPE + 10% BM	10,3	949
LLDPE + 15% BM	9,5	905

It can be highlighted that the BM mixtures presented values of torque and specific energy much closer to the pure LLDPE values when compared to the BS samples, which presented lower values. This fact can be explained by the presence of a vegetable oil visually present in greater quantity in the seed part compared to the pulp (mesocarp). To prove that the fluidity of the material with BS increased in relation to the others, it was necessary to evaluate the viscosity of the material in an oscillatory viscometer.

Viscosity analysis

With the analysis of the complex viscosity of the material as a function of deformation (Fig 2) it was evident that both BM and BS acted as a material flow facilitator by presenting lower viscosity values compared to pure LLDPE. This processing auxiliary action is more pronounced in the BS, corroborating the processability analysis. Looking only the BM results, it is possible to notice that the LLDPE + 5% BM and LLDPE + 10% BM formulations had very similar results, meanwhile, the LLDPE + 15% BM formulation had lower viscosity. This formulation with a higher BM content made the material more brittle, proven in the tensile strength test, with this there was greater ease of movement (flow) of the material, reducing the viscosity. The opposite effect to BM was observed for BS in an LLDPE matrix. The greater amount of BS, causes an increase in viscosity. Probably, a smaller amount of BS brings about the sliding effect of the oil present in the seed, facilitating the flow. As the BS was added, a greater interaction between the filler and the polymer may have occurred, this interaction may have provided the material with greater resistance to flow, resulting in higher viscosities.

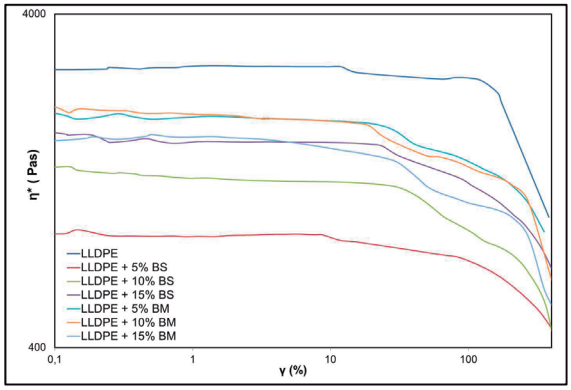

Figure 2 - Complex viscosity versus deformation.

Mechanical Results

Through the analysis of the mechanical results presented at Fig 3, it was possible to verify that the BM filler had a bigger damage effect than the BS filler in terms of loss of elongation at break (Fig 3A) and tensile strength (Fig 3B). The lower BM values can be explained by a lack of compatibility between the matrix and the filler. The BM made the material more brittle, decreasing its mechanical strength, a fact that was confirmed in the fracture morphology analysis. Among the compounds with filler, LLDPE + 5% BS was the one that presented the highest elongation value at break, this result is compatible with the viscosity, being the compound containing filler the one that managed to flow better and elongate. Of all compounds, the one with the lowest mechanical values was LLDPE + 15% BM. In fact, the BM increased the fragility of the material, in the analysis of the fracture morphology it became more evident that this filler had little compatibility with the polymer and as its content in the compounds increased, this fragility became more evident with the decrease in mechanical resistance.

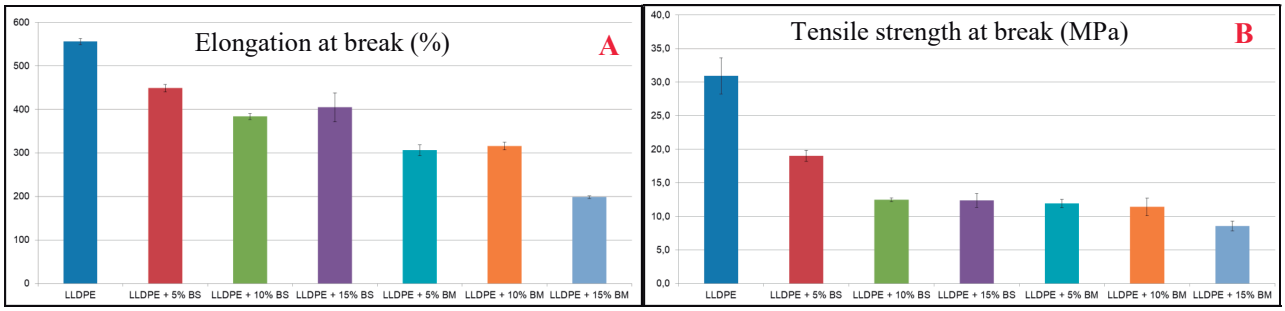

Figure 3 - A: Elongation at break (%); B: Tensile strength at break of LLDPE and BS/BM composites.

Fracture Morphology

In Fig 4A it is possible to analyze the fractured surface of pure LLDPE, observing the appearance of some "grooves" consistent with the elasticity of the material, which is widely used for making films. Fig 4E, Fig 4F and Fig 4G show the fracture morphologies of LLDPE compounds containing 5, 10 and 15% BM. The appearance of valleys and galleries was evident, consistent with a lower polymer charge interaction, this lack of compatibility may have been responsible for the lower mechanical results of these BM compounds. Fig 4B, Fig 4C and Fig 4D show the fracture morphologies of LLDPE compounds containing 5, 10 and 15% BS, respectively. The morphology of the composites with BS showed less holes than those of the BM, which suggests that the BS presented greater compatibility with the polymeric matrix, justifying the mechanical results.

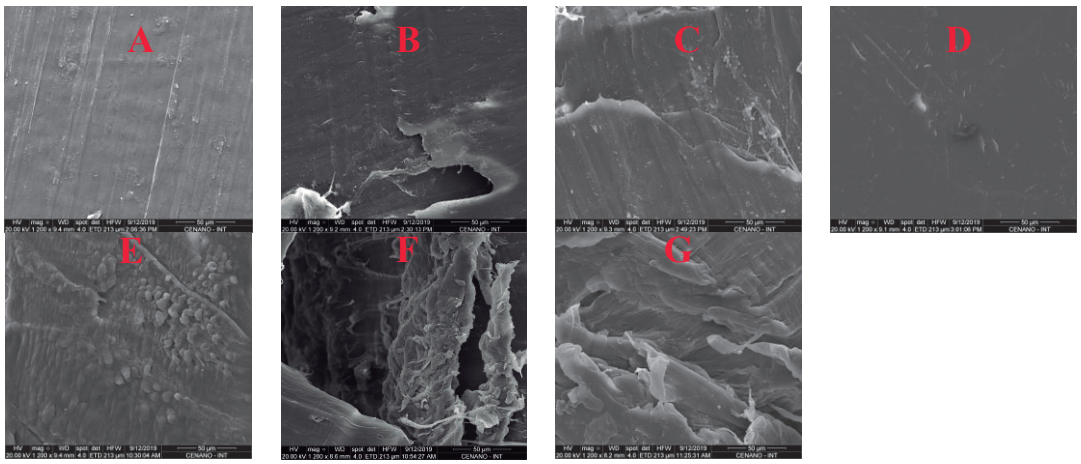

Figure 4 - SEM of the fractured material in liquid nitrogen, being: A: Pure LLDPE (1200x); B: LLDPE + 5%BS (1200x); C: LLDPE + 10%BS (1200x); D: LLDPE + 15%BS (1200x); E: LLDPE + 5%BM (1200x); F: LLDPE + 10%BM (1200x) G: LLDPE + 15%BM (1200x)

Conclusions

The BM residue showed a lower compatibility with the LLDPE when compared to the BS, this was evident in the fracture morphology results. According to the viscosity and processing results, the BS could be used as a processing auxiliary and reduce the energy demand needed to perform the mixing of the polymeric matrix with the filler, this effect was much smaller for the BM. The formulation with the lowest amount of bacuri seed (LLDPE + 5% BS) was the one that most improved chain movement, indicating that this formulation could be used in situations where low viscosity was required. Despite the mechanical results for both BS and BM, being lower than pure LLDPE, this would not inhibit the commercial use of these formulations, especially in smaller amounts of filler, mainly in the case of a waste that, if disposed of in the wrong way, could harm the environment. Therefore, the commercial use of these formulations will depend on the minimum required properties of the final product.

Acknowledgements

The authors would like to thank INT and CNPq for logistical and financial assistance. Valdir Florêncio of the Military Engineering Institute (IME), for the Bacuri donation. To Cenano-INT for the scanning electron micrographs.

References

1. R. M. L. Novaes; R. A. A. Pazianotto; M. Brandão; B. J. R. Alves; A. May; M. I. S. Folegatti-Matsuura. Global Change Biology 2017, 23, 3716. https://doi.org/10.1111/gcb.13708
2. A. K. O. Homma; J. E. U. De Carvalho; A. J. E. A. De Menezes. Ciência Hoje 2010, 46, 39. https://ainfo.cnptia.embrapa.br/digital/bitstream/item/25022/1/homma-bacuri.pdf
3. T. W. Bispo; C. L. Braga; C. C. Lima; S. F. Rocha. Revista Grifos 2021, 31, 01. https://doi.org/10.29327/soberebpc2021.342291
4. L. P. Aguiar; R. W. Figueiredo; R. E. Alves; G. A. Maia; V. A. B. Souza. Food Science and Technology 2008, 28, 423. https://doi.org/10.1590/S0101-20612008000200024
5. P. Schouterden; G. Groeninckx; B. Van der Heijden; F. Jansen. Polymer 1987, 28, 2099. https://doi.org/10.1016/0032-3861(87)90048-6
6. A. J. Peacock in *Handbook of Polyethylene: structures, properties and applications*, Taylor & Francis Inc, London, 2000.
7. M. A. Spalding; A. M. Chatterjee in *Handbook of Industrial Polyethylene and Technology*, John Wiley & Sons, Hoboken, 2017.

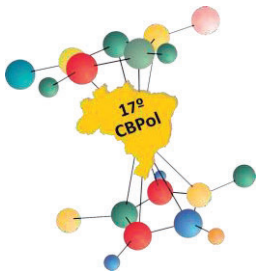

COMPATIBILITY BETWEEN PBAT AND SWEET POTATO STARCH: INFLUENCE OF THE COMPATIBILIZING AGENT

Michelle F. de Andrade[1], Cecilãne R. D. S. R. de Assis[2]*, Grazielle R. Cerqueira[2], Viviane F. Caetano[1], Djalma A. de Oliveira[2], Carolina L. Morelli[3], Yêda M. B. de Almeida[1].

1 – Department of Chemical Engineering, Federal University of Pernambuco (UFPE), Recife, PB, Brazil
mifelixsilva@hotmail.com
2 - Center for Exact and Natural Sciences (CCEN), Federal University of Pernambuco (UFPE), Recife, PB, Brazil
3 – Department of Mechanical Engineering (DEMEC), Federal University of Pernambuco (UFPE), Recife, PB, Brazil

Abstract – Blends of poly (butylene adipate co-terephthalate) (PBAT) and sweet potato starch (SPS) can be an alternative for the production of biodegradable packaging. However, the hydrophobic matrix of PBAT and the hydrophilic matrix of starch reduce important properties, so the addition of compatibilizing agents can improve adhesion between the matrices. Therefore, the study aimed to analyze the insertion of different concentrationsof citric acid (CA) and maleic anhydride (MA) in the chemical, physical and mechanical properties of PBAT/SPS blends. In the results, no chemical alterations were observed by FTIR. There was an increase in crystallinity, obtained by XRD, for samples containing compatibilizing agents. By TGA and mechanical tensile tests, the incompatibility of PBAT and SPS was confirmed by the appearance of characteristic starch bands, indicating that it may be a stress concentrator. Finally, it was observed that the addition of CA and MA did not favor improvements.

Keywords: *PBAT, sweet potato starch, citric acid, maleic anhydride, compatibilization.*

Fundings: Facepe - Fundação de Amparo a Ciência e Tecnologia de Pernambuco.

Introduction

Plastics are the most used materials in the production of packaging in general, this is due to their numerous properties, including lightness, flexibility, and cost, among others [1]. The development of biodegradable materials, mainly polymeric blends, which have properties equivalent to conventional plastics, could be a significant alternative for the reduction/replacement of certain classes of packaging.

Poly (butylene adipate-co-terephthalate) (PBAT), also known under the trade name Ecoflex®, has attracted great interest as a potential replacement for high-density polyethylene (HDPE). It is a biodegradable polymer, with high flexibility, high strength, and good tear resistance, and is approved for food contact applications. What hinders the high applicability of the PBAT is its high cost. Therefore, one way to reduce its production cost is to mix it with a more economically viable material, starch [2].

Starch is the second most abundant natural polymer and can be extracted from several renewable resources, such as plant tubers, and grain seeds, among others [1]. It is low-cost, renewable, and biodegradable. However, starch films have low mechanical properties and low water vapor barriers, making their applications limited to use as food packaging [3].

These two polymers have important characteristics; however, they are incompatible with each other. Therefore, to improve this characteristic, the object of this study was to analyze the properties of PBAT/sweet potato starch (SPS) films with different concentrations of coupling agents - citric acid and maleic anhydride.

Experimental

Materials

PBAT, trade name Ecoflex® F Blend C1200, manufactured by BASF; Sweet potato starch purchased at the local market; Glycerol PA. brand VETEC as a plasticizer for sweet potato starch and coupling agents Citric Acid (CA) PA – PM:192.12 brand NEON; and Maleic Anhydride (MA) P.S. – PM: 98.06 from the DINÂMICA brand.

Sample preparation

Samples of PBAT, PBAT/SPS (sweet potato starch) and PBAT/SPS/citric acid (CA), and PBAT/SPS/maleic anhydride (MA) were produced. The SPS concentration varied from 10% (90.10), 30% (70.30), and 50% (50.50) by adding 1.5% (CA1 and MA1) and 0.75% (CA2 and MA2) of coupling agents. Initially, the samples of sweet potato starch, 30% glycerol, 20% water, and the concentrations of CA and MA about the weight of the starch used were prepared, later the PBAT and the starch were conditioned in an oven at 70 ºC for 24 hours to remove moisture and then placed in a desiccator. All formulations were prepared in a Thermo Scientific twin-screw co-rotational extruder, model Haake MibiLab II. The mixing temperature was 130 °C, rotation speed 70 rpm, and residence time 3 min. The films and specimens were prepared in a Thermo Scientific injector, model Haake MiniJet II. The melt temperature remained at 135 ºC, mold temperature at 45 ºC, holding time of 10 seconds, and pressing pressure of 650 Pa.

Fourier Transform Infrared Spectroscopy (FTIR)

FTIR was used to visualize the characteristic vibrational bands of PBAT/Starch blends. The test was carried out in SHIMADZU IR TRACER 100 equipment. The films will be analyzed under the following conditions: mid-infrared region in the range of 4000 to 400 cm^{-1}, resolution of 4 cm^{-1}, and 45 scans.

X-Ray Diffraction (XRD)

The XRD was performed in Bruker equipment, model D2 PHASER. The analysis conditions were: applied voltage of 30 kV and current of 10 mA (radiation CuKα= 1.5418 Å), in the range of 2θ = 5-45° and a velocity of 2°. min^{-1}. Using the OriginPro 8.5 software, the crystallinity index (CI) was obtained through Eq. 1.

$$CI(\%) = \frac{A_c}{A_c + A_a} \times 100 \quad (1)$$

Where Ac is the crystalline region's area and Aa is the amorphous region's area.

Thermogravimetric analysis (TGA)

The samples were subjected to heating from 30 to 600 ºC at a rate of 10 ºC.min^{-1}, in an N_2 atmosphere and a flow rate of 50 mL.min^{-1} using the METTLER TOLEDO TGA 2 Star System equipment. Furthermore, the activation energy (A_e) of the degradation reaction was calculated according to Broido's method [4].

Mechanical tensile test

From the mechanical tensile test, the values of elastic modulus, maximum stress, and specific deformation were obtained for all formulations. The production of the specimens followed the D638 CP type V standard and the test was carried out in MTS – ExceedTM equipment, model E42, load of 500 N and pulling speed of 50 mm.$min.^{-1}$, at room temperature and without humidity control. Six specimens per formulation were used.

Results and Discussion

The infrared spectra and X-ray diffractograms of PBAT, sweet potato starch, and samples with different starch concentrations and with 1.5% CA and MA can be seen in Fig 1.

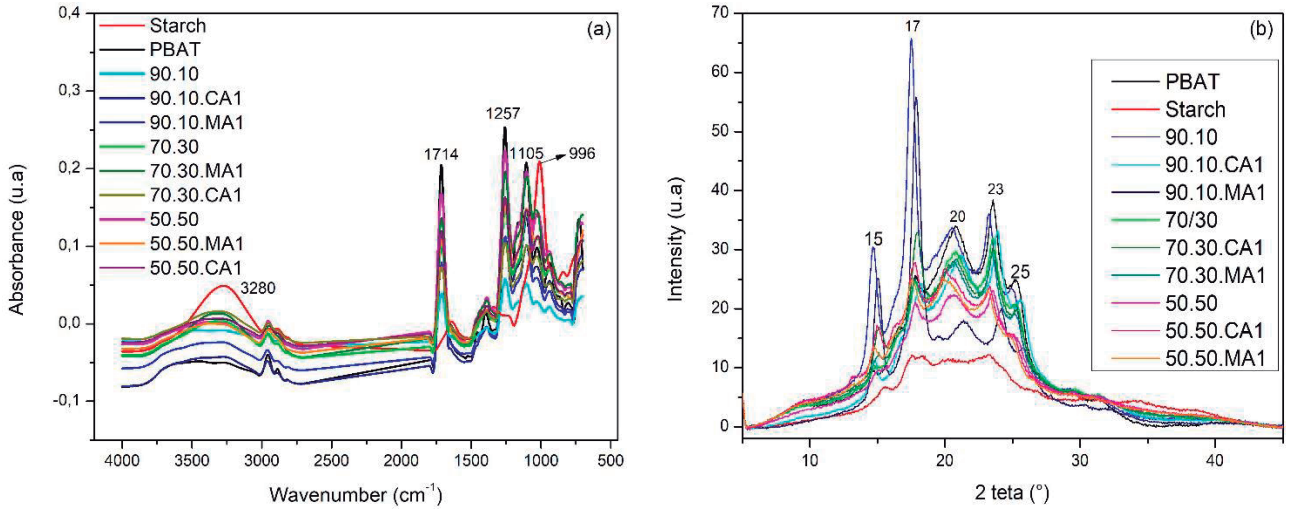

Figure 1. (a) Infrared spectra and (b) X-ray diffractograms of PBAT, sweet potato starch, samples with different starch concentrations and 1.5% CA and MA.

From the infrared spectra shown in Fig 1 (a), it is possible to verify the absence of bands in the regions around 1714 cm^{-1}, 1257 cm^{-1}, and 1105 cm^{-1}, which are not present in the starch spectrum and are characteristics of the PBAT. There was a reduction in the intensity of the peak at 996 cm^{-1}, characteristic of starch, and an enlargement in the region around 3280 cm^{-1}, for all samples, being more accentuated for those with higher starch contents. In general, the insertion of starch altered some characteristic regions of the PBAT, intensifying, mainly the region of the OH group. The addition of CA and MA did not change the chemical pattern of the samples.

Therefore, it is seen that the vibrational modes of PBAT were not altered with the presence of starch and compatibilizing agents. This behavior may be related to a weak interaction between PBAT, starch, CA, and MA, not forming new chemical interactions capable of altering some vibrational mode. The hydrophobic matrix of PBAT and hydrophilic starch make these two materials incompatibles, making their chemical interaction difficult.

The X-ray pattern of starch shows a practically amorphous characteristic, with a crystallinity index (I_c) of 2.68%, it has an A-type crystalline structure, with the characteristic 2θ peaks at approximately position 15.1º, 17.2º, 18.0º and 23.1º.

The PBAT showed a crystallinity index of 13.4%, and the characteristic diffraction peaks are at 2θ = 16.3º, 17.6º, 20.3º, 23.1º, and 25.0º which correspond to the crystal planes (011), (010), (110), (100), and (111) [5].

The addition of starch reduced the intensity of the peaks, which causes a decrease in the crystallinity index of the samples. However, both 1.5% and 0.75% CA and MA improved the crystallinity of samples 90.10, 70.30, and 50.50.

From the thermogravimetric analysis, the influence of starch and coupling agents on the thermal stability of PBAT can be observed, and thus, the influence of these different concentrations can be verified. The thermogravimetric curves, TGA and DTG, can be seen in Fig 2.

It can be seen that PBAT degradation occurs in a single stage, while starch has three stages of degradation. As the starch concentration increases in the samples, new stages of degradation occur. Furthermore, it is noted that the coupling agents did not interfere with the degradation temperatures.

Note that as the starch content in the samples increased, there was a decrease in T_{onset}, but $T_{deg.max}$

practically did not change. Furthermore, there was the emergence of new degradation temperatures for the 70.30 and 50.50 groups, characteristic of starch.

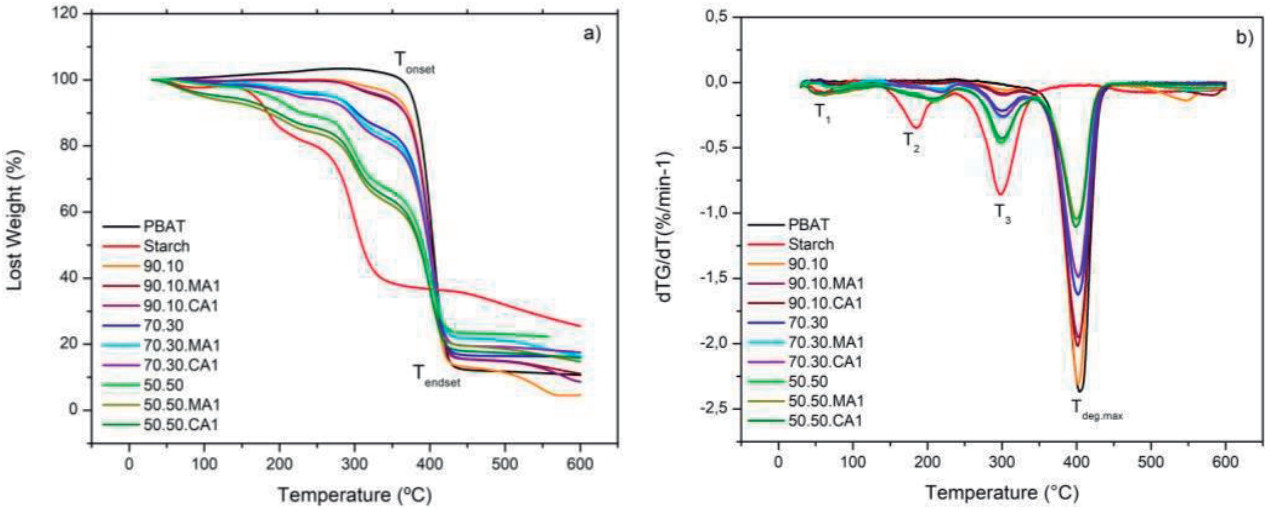

Figure 2. Thermogravimetric analysis a) TGA and b) DTG for samples containing 1.5% MA and CA.

PBAT starts its degradation process around 381 ºC and maximum degradation around 404 ºC. On the other hand, starch starts its degradation process at around 60 ºC due to water evaporation, and maximum degradation is around 298 ºC. The T_{onset} of samples 90.10 (379 ºC), 70.30 (376 ºC), and 50.50 (351 ºC) decreased with the starch concentration but maintained the final degradation values (T_{endset}) close to those obtained for pure PBAT.

Finally, it appears that the compatibility between starch and PBAT was not efficient, given the appearance of regions of degradation resulting from the two materials together. The different starch concentrations did not modify the $T_{deg.max}$ of the PBAT but reduced the T_{onset} of the degradation process.

From the value obtained from Tonset, the temperature at which mass loss begins, we can see that the increase in starch concentration reduced the thermal stability of PBAT. Thus, samples containing higher starch contents degrade at lower temperatures. Therefore, it is necessary to submit the samples to processing temperatures lower than the Tonset to avoid the initiation of the degradation process.The values obtained for the activation energy can be seen in Tab 1. Regarding activation energy, there was a reduction with increasing starch concentration. This behavior indicates that less energy is needed to start the degradation process. This reduction may be a consequence of the interaction of starch in the PBAT polymeric chain, reducing inter and/or intramolecular interactions, and facilitating the initiation of the degradation process.

The results obtained from the mechanical traction test and activation energy (A_e) can be seen in Tab 1.

Table 1. Values of maximum stress, elastic modulus, specific deformation, and activation energy (Ae).

Samples	Maximum tension (MPa)	Elastic modulus (MPa)	Specific deformation (%)	A_e (kJ/mol)
PBAT	13.90 ± 2.43	140.96 ± 8.91	183.27 ± 46.50	278.71
Starch	-	-	-	65.77
90.10	10.85 ± 0.61	147.47 ± 7.24	122.46 ±19.38	236.52
90.10.CA1	9.70 ± 0.42	128.24 ± 10.56	89.69 ± 11.54	210.34
90.10.CA2	9.35 ± 0.43	134.09 ± 14.77	85.91 ±19.56	210.88
90.10.MA1	10.05 ± 0.79	137.38 ± 8.31	107.48 ± 4.38	205.81
90.10.MA2	9.62 ± 0.32	131.27 ± 4.6	97.00 ± 5.75	207.28

70.30	7.25 ± 0.20	109.46 ± 2.17	13.08 ± 1.99	150.65
70.30.CA1	6.95 ± 0.16	99.39 ± 9.33	12.88 ± 2.09	176.99
70.30.CA2	6.75 ± 0.20	103.37 ± 6.12	10.55 ± 0.51	165.91
70.30.MA1	6.85 ± 0.26	99.82 ± 5.17	12.11 ± 1.42	179.11
70.30.MA2	5.90 ± 0.58	89.57 ± 1.29	9.41 ± 1.21	165.91
50.50	4.55 ± 0.10	75.69 ± 1.97	8.50 ± 0.39	91.52
50.50.CA1	4.90 ± 0.18	76.87 ± 4.07	8.96 ± 0.63	91.09
50.50.CA2	4.82 ± 0.25	69.58 ± 1.58	7.98 ± 1.08	84.78
50.50.MA1	4.00 ± 0.20	65.28 ± 2.43	8.63 ± 0.80	79.15
50.50.MA2	4.78 ± 0.17	66.37 ± 3.02	8.73 ± 2.05	79.16

For the tensile mechanical test, the PBAT samples and the 90.10 sample showed a ductile behavior with high deformation. The 70.30 sample still showed a ductile behavior, however, its deformation was significantly smaller compared to the PBAT and 90.10 samples. The sample with 50% starch, however, presented a brittle behavior with insignificant deformation. Therefore, it can be confirmed that the increase in starch concentration decreases the ductile characteristic of PBAT, which may have acted as a stress concentrator, facilitating its rupture.
Concentrations 90.10 and 70.30, even with lower values than pure PBAT, still have a maximum stress value greater than 3.5 MPa, which is the stress required to use polymeric materials in packaging [6]. The addition of coupling agents did not improve the mechanical properties of the samples.

Conclusions

The results obtained confirmed the incompatibility between the PBAT and sweet potato starch matrix. Citric acid and maleic anhydride coupling agents did not alter the properties of the analyzed samples. Furthermore, it was observed that the increase in starch concentration considerably reduced the mechanical properties of the films, however, the 90/10 and 70/30 samples showed appropriate mechanical strength for use as packaging. Finally, studies using higher concentrations of CA and MA should be carried out to indicate the efficiency of these agents as compatibilizers for the analyzed polymeric matrices.

Acknowledgments
FACEPE, INTM and UFPE.

References

1. R. Muthuraj; M. Misra; A.K. Mohanty. Journal of Applied Polymer Science 2018, 135. https://doi.org/10.1002/app.45726.
2. M. Dammak; Y. Fourati; Q. Tarrés; M. Delgado-Aguilar; P. Mutjé, S. Boufi. Ind. CropsProd. 2020, 144. https://doi.org/10.1016/j.indcrop.2019.112061.
3. X. Zhai; W. Wang; H. Zhang; Y. Dai; H. Dong; H. Hou. Carbohydr. Polym. 2020, 239,116231. https://doi.org/10.1016/j.carbpol.2020.116231.
4. A. Broido. J Polym Sci Part A-2. 7 (1969) 1761–1773. https://doi.org/10.1002/pol.1969.16007101.
5. X. Zhai; M. Li; R. Zhang; W. Wang; H. Hou. Int. J. Biol. Macromol. 2023, 227. https://doi.org/10.1016/j.ijbiomac.2022.12.194.
6. Y.J. Kim; H.M. Lee; O.O. Park. Polym. Eng. Sci. 35 (1995) 1652–1657. https://doi.org/https://doi.org/10.1002/pen.760352012.

COMPOSITE AEROGELS CONTAINING NANOCELLULOSE: NANOCELLULOSE ON CROSSLINKING AND CADMIUM REMOVAL

Paulo H. Camani[1], Carolina Paschoalini[1], Karina M. Sato[1], Derval S. Rosa[1*]

1 – Center for Engineering, Modeling, and Applied Social Sciences (CECS), Federal University of ABC (UFABC), Santo André, Brazil
derval.rosa@ufabc.edu.br

Abstract - This work aims to study the influence of nanocellulose on the crosslinking process of starch matrix composite aerogels containing nanocellulose (NC) and evaluate the removal of Cd(II). An increase of 591%, 617%, and 255% was verified for FTIR deconvolution's crosslinking ratio on the aerogel structure. Concomitantly, the high crystallinity of composite aerogels was confirmed due to the high degree of crosslinking caused by the addition of NCs in the aerogel structure. Nanocellulose caused the densification of the aerogel and the increase of crystalline domains in the aerogel, changing chain conformation. In addition, the presence of nanocellulose and its high density of hydroxyl groups, seen in the FTIR spectra, significantly impacted the removal of Cd(II), which promoted a growth from 30% to 99 to 100% of reduction of Cd(II) ions, also increasing the adsorption capacity of composite aerogels compared to NC-free aerogels.
Keywords: *aerogel; nanocellulose; composite.*
Fundings: FAPESP - 2019/16301-6 and 2020/13703-3, CNPq - 308053/2021-4 and 403934/2021-4, and CAPES.

Introduction

Potentially toxic elements (PTEs) are "elements that occur naturally throughout the Earth's crust and play important biochemical and physiological roles in plants and animals and biological, thus fulfilling various oxidation-reduction reactions in the human body". In high concentrations, PTEs are considered environmental contaminants, causing many human diseases through exposure [1]. Aerogels have interesting adsorptive properties and high surface area and promote the possibility of adsorbent recyclability depending on the structure and the removed contaminant [2]. The so-called composite aerogels arise to improve properties and synergistic effects, based on the same theory of matrix phase and dispersed phase, to improve the final material's properties, which is given the science and technology widely studied for composite materials [3]. Nanocellulose helps control the chemical interface, which is essential in the selectivity of adsorbents, improves properties, and generates a high specific surface area due to its anisotropic structure. The addition of nanostructures in starch aerogels aims to intensify their adsorbent effect and optimize properties to improve compatibility and complexation with contaminants [4]. Therefore, this work aims to evaluate the influence of nanocellulose on the crosslinking of starch composite aerogels containing nanocellulose, as well as the removal of Cd(II) ions from simulated waters.

Experimental

Composite aerogel preparation

The methodology for preparing the nanocellulose solution was adapted from [5,6]. A sodium hydroxide and urea solution were used to disperse the nanocellulose to promote better dispersion of the cellulose nanostructures in the corn starch matrix. For this, the dispersed nanocellulose solution was added in the sodium hydroxide addition step so that it could be easily homogenized, as shown

in Fig. 1. The concentrations of nanocellulose that were added for the development of composite aerogels were 1, 3, and 5% by weight [7].

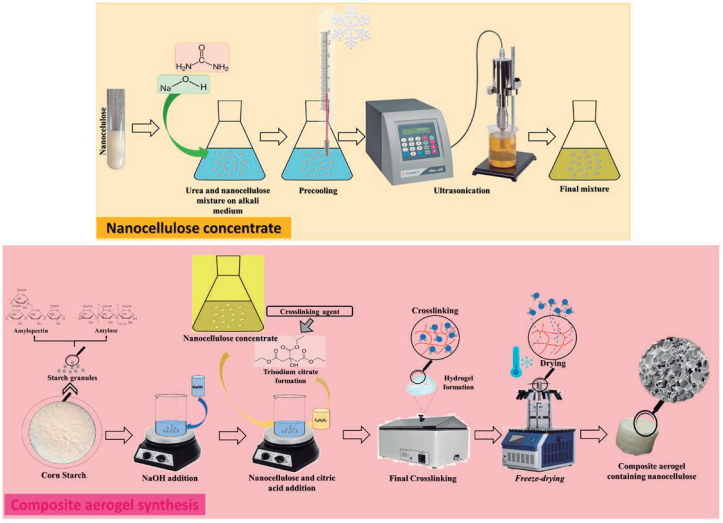

Fig. 1. Illustrative scheme of composite aerogel preparation containing nanocellulose.

Characterizations

The chemical groups present in nanocellulose and modified nanocelluloses were evaluated using Fourier transform infrared spectroscopy (FTIR), in a Frontier 94942 FTIR spectrophotometer equipment (PerkinElmer, USA), with the coupling of an attenuated total reflectance (ATR) accessory, using a spectral resolution of 2 cm^{-1}, 64 scans, with a spectral range of 4000-500 cm^{-1}. The crystallinity of nanocellulose and composite aerogels was evaluated by X-Ray Diffraction (XRD) using a STOE-STADI P diffractometer, varying the range in 2θ, from 10 to 80.735 °, with a step of 0.015 °, using a curved Germanium (111) monochromator and CuKα1 radiation, with a wavelength of 1.54060 nm and an integration time of 60 s for each 1.05 °. Metal ion sorption tests were conducted through a mono element evaluation of Cd(II) ions from a 100 ppm solution, at pH 4.0, at room temperature, under agitation at 120 rpm, for 12 hours, whose dosage of nanocellulose and modified nanocelluloses was 30 $g.L^{-1}$. The aqueous solutions' efficiency and sorption capacity was obtained after testing, subjecting them to measurements in inductively coupled plasma mass spectrometry (ICP-MS), using Agilent Technologies equipment, model 7900 (Hachioji, Japan), in triplicate.

Results and Discussion

Fig. 2 presents the FTIR spectra of nanocellulose (NC) and composite aerogels containing different concentrations of 0, 1, 3, and 5% cellulose nanostructures.

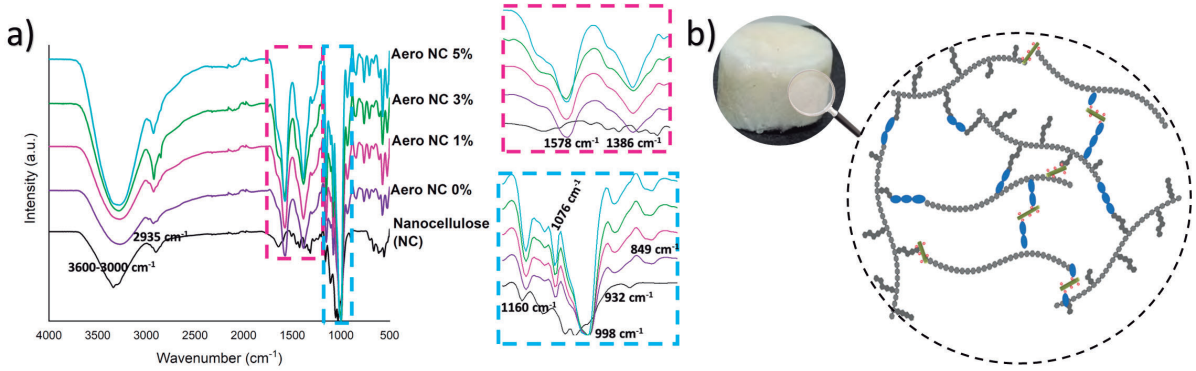

Fig. 2.a) FTIR spectra for aerogels containing different concentrations of nanocellulose, highlighting nanocellulose (NC), and aerogels containing 0%, 1%, 3%, and 5%, respectively, and b) illustrative scheme of crosslinking.

With the addition of NCs in concentrations of 3 and 5% in the corn starch aerogel, an increase in the band's intensity located at 3600-3000 cm^{-1} was observed, which is associated with stretching the –OH hydroxyls. It may indicate more hydroxyls due to hydrogen bonds between starch and nanocellulose [5]. Furthermore, the peak at 2935 cm^{-1}, which refers to the symmetric and asymmetric stretching of –CH bonds, becomes more pronounced at a concentration of 3%. In addition, an increase is also seen for the band associated with carbon-hydrogen bonds and angular deformations, shearing, and twisting of functional group bonds, as well as peaks at 1386 cm^{-1}, 1160 cm^{-1}, 1076 cm^{-1}, and 930 cm^{-1}. According to Perumal and Wang and co-workers, the increase in some of these peaks may be related to the presence of cellulose nanofibrils in the composite aerogel, proving the change in the composite structure compared to the aerogel without nanocellulose [8,9].

Table 1. Crystallinity, the ratio between the areas of the crosslinking agent peaks (at 1582 cm^{-1}) to the starch groups (at 995 cm^{-1}), adsorption capacity ($mg.g^{-1}$), and adsorption Efficiency (%) of NC, starch-based aerogels, and composite aerogels containing NCs.

Samples	Crystallinity (%)	The ratio between the areas of the crosslinking agent peaks (at 1582 cm^{-1}) to the starch groups (at 995 cm^{-1})	Adsorption Capacity ($mg.g^{-1}$)	Adsorption Efficiency (%)
NC	77.0	-	-	-
Aero NC 0%	15.3	1.5	1.0 ± 0.2	30.0 ± 0.5
Aero NC 1%	74.3	2.1	2.2 ± 0.2	99.4 ± 0.0
Aero NC 3%	76.0	2.4	2.5 ± 0.2	99.9 ± 0.0
Aero NC 5%	94.0	1.8	2.5 ± 0.2	100.0 ± 0.0

Evaluating the ratio between the 1582 cm^{-1} and 995 cm^{-1} peaks described in Table 1, we obtained ratio values of 1.5, 2.1, 2.4, and 1.8 for Aero NC 0% samples, 1%, 3%, and 5%, respectively. Therefore, a 40%, 60%, and 20% increase was verified for the ratio that defines how much the aerogel structure is crosslinked. Thus, the composite aerogel samples containing 1 and 3% had this increase in value, followed by the concentration of 5% NC. Yue and co-workers synthesized polyacrylamide and sodium alginate aerogels containing nanocellulose. They observed that nanocellulose provides new hydrogen bonds between the chains of the polyacrylamide and alginate matrix, helping to increase the degree of hydrogel crosslinking, characterized as a multifunctional crosslinking agent. It promotes structure densification and alteration of intrinsic properties, such as increasing the mechanical strength of hydrogels [10].

From the crystallinity results presented in Table 1, a higher relative crystallinity of 74.3, 76.0, and 94.0% were observed for the composite aerogels containing 1, 3, and 5% of NCs than the aerogel without NC (Aero NC 0%). Salim and co-workers observed increased crystallinity due to cellulose and crosslinked starch in the porous structures of cellulose/polyvinyl alcohol/crosslinked starch paper foams. These structures promote nucleation centers, promoting the greater organization of the crystalline arrangements of the polymeric system [11], thus causing an increase in the relative crystallinity value. On the other hand, when we consider the nanocellulose, there was a small decrease in the crystallinity value for the Aero NC 1% and Aero NC 3% samples and an increase for the Aero NC 5% sample. De Morais Zanata, Battirola, and Gonçalves also observed this decline in crystallinity by comparing polysilsesquioxane aerogels containing cellulose nanocrystals [12]. However, the relative crystallinity increase of the aerogels was achieved.

From the adsorption capacity results shown in Table 1, it is observed that there was 2.15 times increase in adsorption capacity for the aerogels containing cellulose nanostructures compared to the aerogel without nanocellulose (Aero NC 0%). If compared for each composite aerogel versus the composite aerogel, this increase is 2.15 for the aerogel containing 1% NC and 2.5 times growth for

the 3 and 5% NC aerogels. The adsorption efficiency reached 99 to 100% removal of cadmium (II) ions, that is, removing all the contaminant from the medium, with 3.3 times increase in adsorption efficiency compared to the aerogel without nanocellulose. Nguyen and co-workers removed 99% methylene blue using cellulose nanofibrils and graphene oxide aerogels as adsorbents. They mention that the synergistic effect between the structures promotes an increase in removing this contaminant [13]. Thus, the increase in adsorption capacity using composite aerogels may be associated with some hypotheses. First, because cellulose nanostructures have a high density of hydroxyl groups and the presence of carboxyl groups, these groups promote interaction with cadmium ions, thus generating interaction and their capture from the aqueous medium by chelation effects or electrostatic interaction [14].

Conclusions

The addition of nanocellulose in the starch aerogel matrix generated an increase in the crosslinking of the aerogel, which was verified by the deconvolution of the FTIR spectra and controlled by the increase in the crystallinity of the aerogel, which is generated by the conformational change of the chains due to the high formation of crosslinks, increasing crystalline domains. In addition to the impact on aerogel crosslinking, nanocellulose resulted in a higher density of available hydroxyl groups, which generated an increase from 30% to 99-100% in adsorption efficiency, and a slight increase in adsorption capacity.

Acknowledgments

Fundação de Amparo à Pesquisa financed this research do Estado de São Paulo (FAPESP) (2019/16301-6 and 2020/13703-3), Conselho Nacional de Desenvolvimento Científico e Tecnológico (CNPq) (308053/2021-4 and 403934/2021-4), and Coordenação de Aperfeiçoamento de Pessoal de Nível Superior (CAPES) (Finance Code 001). The authors thank the technical support of the Multiuser Experimental Center of UFABC (CEM-UFABC), CECS (UFABC), and REVALORES for assistance.

References

1. E. S. Omutange; J. O. Manyala; A. N. Wekesa; O. Osano; T. Munyao; A. A. Otieno; L. Etiégni, *Environmental Impact and Remediation of Heavy Metals*, InTechOpen, 2022.
2. M. Yan; W. Huang; Z. Li International Journal of Biological Macromolecules, 2019, 136, 927–935. https://doi.org/10.1016/j.ijbiomac.2019.06.144.
3. S. Groult; S. Buwalda; T. Budtova. Biomaterials Advances, 2022, 135, 212732. https://doi.org/10.1016/j.bioadv.2022.212732.
4. B. Yuan; L. Li; V. Murugadoss; S. Vupputuri; J. Wang; N. Alikhani; Z. Guo. ES Food & Agroforestry, 2020, 1(7), 41-52. https://doi.org/10.30919/esfaf0004.
5. J. Chen; Z. Long; J. Wang; M. Wu; F. Wang; B. Wang; W. Lv. Cellulose, 2017, 24, 4449-4459. https://doi.org/10.1007/s10570-017-1423-6.
6. Y. Jiang; X. Xie; Y. Chen; Y. Liu; R. Yang; G. Sui. Journal of Materials Chemistry C, 2018, 6(32), 8679-8687. https://doi.org/10.1039/C8TC02900H.
7. K. Zuo; J. Wu; S. Chen; X. Ji; W. Wu. Cellulose, 2019, 26, 9661-9671. https://doi.org/10.1007/s10570-019-02774-6.
8. C. Wang; H. Cao; L. Jia; W. Liu; P. Liu. Carbohydrate Polymers, 2022, 291, 119568. https://doi.org/10.1016/j.carbpol.2022.119568.
9. S. Perumal; H. Lee; S. Jeon; D. H. Yoon, I. W. Cheong. Journal of Polymer Research, 2021, 28, 1-9. https://doi.org/10.1007/s10965-021-02693-w.
10. Y. Yue; X. Wang; J. Han; L. Yu; J. Chen; Q. Wu; J. Jiang. Carbohydrate polymers, 2019, 206, 289-301. https://doi.org/10.1016/j.carbpol.2018.10.105.
11. M. H. Salim; Z. Kassab; E. H. Ablouh; F. Z. S. A. Hassani, M. El Achaby. Industrial Crops and Products, 2023, 192, 116074. https://doi.org/10.1016/j.indcrop.2022.116074.

12. D. de Morais Zanata; L. C. Battirola; M. D. C. Gonçalves. Cellulose, 2018, 25, 7225-7238. https://doi.org/10.1007/s10570-018-2090-y.
13. V. T. Nguyen; L. Q. Ha; T. D. Nguyen; P. H. Ly; D. M. Nguyen; D. Hoang. ACS omega, 2021, 7(1), 1003-1013. https://doi.org/10.1021/acsomega.1c05586.
14. Y. Wang; Y. Li; Y. Zhang; Z. Zhang; Y. Li; W. Li. Carbohydrate Polymers, 2021, 267, 118233. https://doi.org/10.1016/j.carbpol.2021.118233.

COMPOSITES OF POLYESTER RESIN WITH DIFFERENT COMBINATIONS OF FIBERGLASS REINFORCEMENTS OBTAINED BY PULTRUSION

Laura G. Moscone[1], Rodrigo Bernardi[2], Rosmary N. Brandalise[1]*
1 – Graduate Program in Process and Technology Engineering-(PGEPROTEC), University of Caxias do Sul (UCS), Caxias do Sul, RS, Brazil
2 –Randon Implementos, Caxias do Sul, RS, Brazil
3 –Pultrusão do Brasil/Passo de Torres, SC, Brazil
* rnbranda@ucs.br

Abstract - The use of composites can be considered an excellent alternative for the replacement of metals and ceramics, precisely because of their properties such as lightness, dimensional stability and mechanical strength, which offer a wide range of applications in industry. With this concept in mind, in the present study, composites were developed using polyester resin (UP) and different glass fiber combinations of filaments, fabrics (WF) and mats (MAT) produced by pultrusion process. The morphological and mechanical properties were evaluated. As for the morphological properties, a homogeneous distribution was observed with few voids in the matrix, the UP/MAT sample standing out. The fabric-reinforced sample exhibited the highest tensile and impact strength among the composites studied.

Keywords: *Composites; Glass fiber; Pultrusion; Polyester resin.*

Introduction

Composite materials have great potential for use in industry due to their different properties compared to metals [1,2]. A composite material consists of a matrix, called the continuous phase, in which polyester resin is commonly used, and a discontinuous phase, which can serve as reinforcement and can be composed of different types of fibers, natural and synthetic [3,4]. The reinforcement can be made in different ways, such as filaments, i.e., single fibers, nonwovens, i.e., an association of short fibers arranged randomly, and woven fabrics, i.e., long fibers arranged in a pattern with different orientations [4]. There are several methods for producing composites, and their application depends on the matrix and reinforcement used and the type of product desired [5].

Processing of composites by pultrusion is applied in cases where it is a continuous process, maintaining the cross-section along the web [6]. The process starts with the use of the matrix, which can be done by injection or by an impregnation tank. In the case of the impregnation tank, the reinforcements are passed through the tank and impregnated with the resin, which flows through the mold and is pulled by a system at the end of the process [7]. This proposal aims to develop composites by the pultrusion process with isophthalic polyester resin and different combinations of glass fibers, namely filaments, mats and fabrics, validated by the results of morphological and mechanical properties.

Experimental

Materials and manufacturing

The isophthalic polyester resin used is from Embrapol, OMEGA 1017 (Brazil), with viscosity between 2800 and 3300 cP. The glass fibers are from Owens Corning, in the form of

direct roving yarn SE1200, in the form of Unifilo continuous glass fiber fabric (300 $g.m^{-2}$) and in the form of TDS glass fiber fabric, LT0350, with an orientation of 0º and 90º (500 $g.m^{-2}$). For the production of the composites, the pultrusion process was used in collaboration with the company Pultrusão do Brazil (Brazil). It was carried out with a pultrusion machine that has three zones: the alignment and impregnation zone, the heating zone (180°C) and the drawing zone. In the composition of the composites, a total of 55% by weight of glass fiber reinforcement was used in the different forms proposed.

Test methods

The composite materials were characterized by morphological and mechanical properties. Morphology was studied with a scanning electron microscope (SEM) (MIRA3, Czech Republic), the sample was analyzed after a manual fracture and also through a polished surface exposing the cross section, being later exposed to gold deposit. For the mechanical properties, in the case of tensile strength, a Universal Testing Machine (DL 20000, EMIC, Brazil) was used according to ASTM-D638, type I, with a force of 2000 kgf, a base length of 300 mm and a speed of 5 $mm.min^{-1}$, where the test piece has dimensions of 165 x 19 mm, and 10 tests were performed. The impact resistance was tested by the Izod method with a notch (45º) following the ASTM-D256-06 standard. It was performed with a load of 7.5 J provided by a pendulum, which strikes the sample positioned vertically, the test was carried out on 10 specimens.

The mechanical properties tests were carried out considering the orientation of the process, being the x axis, the entrance of the reinforcements in the pultrusion line, passage through the resin bath and other components and entry into the matrix, and the y axis, is the direction perpendicular to the matrix entry.

The coding of the composites used in this work was according to the composition of the sample, being then polyester resin with filaments and fiberglass blanket (UP/MAT), and, polyester resin with filaments and fiberglass fabric (UP/ WF).

Results and Discussion

Figure 1 shows the microscopic images of the developed composites at SEM.

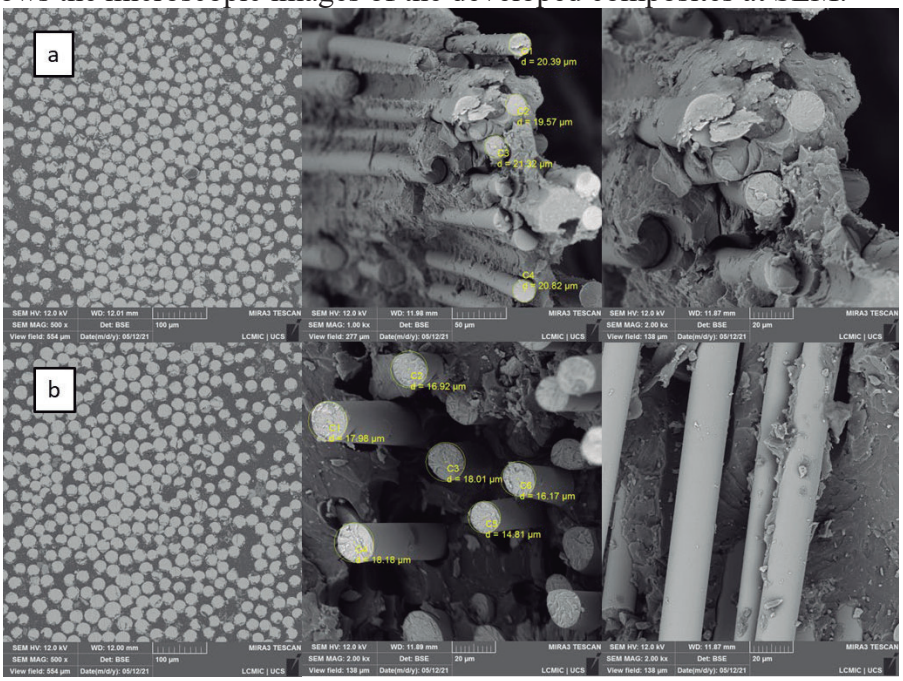

Figure 1 – Photomicrographs of pultruded composites (SEM), (a) UP/MAT and (b) UP/WF.

The morphology of the specimens allowed observation of the interaction of the reinforcements with the matrix. In Fig. 1, dark areas (polyester resin) and light areas (glass fiber) can be seen, as well as the presence of agglomerates, which can be explained by the high viscosity of the resin used (viscosity between 2800 and 3300 cP compared to an epoxy viscosity of 520 and 620 cP), which hinders the wettability of the system and promotes the agglomeration of the reinforcements. Comparing the types of reinforcements studied, the composites with the cover showed a greater interaction between the matrix and the reinforcement. This can be confirmed by the presence of resin in the fibers according to the micrographs, and in the samples with the blanket, it is possible to notice a more evident interaction between the fiber and the matrix, due to the greater presence of resin in the fiber after fracture.

Table 1 shows the results of the analysis of the tensile strength and impact resistance of composites developed with different types of reinforcement, analyzing two directions, parallel to the reinforcement and perpendicular to the reinforcement.

Table 1 - Tensile and impact strength in X and Y directions of specimens UP/MAT and UP/WF

Sample	Test specimen orientation	Tensile strength (MPa)	Deformation (%)	Tensile modulus (MPa)	Impact strength (kJ/m^2)
UP/MAT	X Axle	280 ± 30	13.0 ± 0.1	3479 ± 10	145 ± 5
	Y Axle	31 ± 3.0	4.0 ± 0.3	1498 ± 12	*
UP/WF	X Axle	311 ± 25	13.0 ± 1.1	3174 ± 65	151 ± 12
	Y Axle	87 ± 6.0	7.0 ± 0.6	742 ± 59	*

*Only specimens in the X-direction were evaluated.

In the evaluation of the types of reinforcement used, the fabric showed better properties, with higher values for tensile strength than the blanket, and showed similar values for modulus of elasticity and elongation at break, maintaining the variations. This behavior was also observed in a study by Rudoy et al. [5], who also analyzed composites made of polyester resin reinforced with a mat and reinforced with glass fiber fabric, and the results were 38.5% higher for the fabric specimens. This is due to the fact that the fabric is more efficient as reinforcement for mechanical forces due to its arrangement, which guarantees greater resistance. As for the direction of the sample, the samples taken in the X direction had a higher tensile strength than those taken in the Y direction, proving that the resistance is more efficient in the direction parallel to the reinforcement. The values obtained for the modulus of elasticity in the tensile direction were higher for the specimens taken in the X direction, starting from the filaments and the entry of the set into the die. This is mainly due to the resistance that the orientation of the filaments imparts to the composite. For impact strength, the specimen with the fabric reinforcement performed better, confirming the tensile strength results. Thus, the composite with filaments and fabric exhibited better mechanical performance due to the ordering of the fabric, which acts as a more effective barrier against external agents (tensile), while the composite with filaments and fabric exhibited better performance. Morphologically, due to the randomness of the fabric, it allows a better impregnation of the resin in the system, making more difficult the occurrence of voids.

Conclusions

The present work aimed to evaluate the morphological and mechanical properties of polyester resin composites with glass fiber reinforcement, distinguishing between filaments with cover and filaments with fabric. With respect to the type of reinforcement, the composites made of filaments with fabric showed the best mechanical performance and the composites made of filaments with fabric showed the best morphological performance. When comparing the direction of

the sample, the machine drawing direction, i.e., parallel to the filaments, was found to be more effective. It can be concluded that the performance of composites obtained by the pultrusion process varies according to the type of reinforcement used, with better mechanical strength when fiberglass fabric is used.

Acknowledgements

The authors thank CAPES-PROSUP and the National Council for Scientific and Technological Development (CNPQ) for the Productivity Research PQ2 grant and the companies Randon Implementos/Brazil and Pultrusão do Brasil/Brazil.

References

1. L. Bank, *Composites for construction: structural design with FRP materials,* John Wiley & Sons, New York, 2006.
2. Y. Choi; R. Yuan *Journal of Composites for Construction* 2003, 7, 356-362. https://doi.org/10.1061/(ASCE)1090-0268(2003)7:4(356)
3. D. Srinivasagupta; S. Potaraju; J. Kardos; et al. *Composites Part A: Applied Science and Manufacturing* 2003; 34, 835-846. https://doi.org/10.1016/S1359-835X(03)00182-9
4. I. Baran; I. Straumit; O. Shishkina; et al Composite Structures 2018, 195, 74-82. https://doi.org/10.1016/j.compstruct.2018.04.030
5. I. Baran; K. Cinar; N. Ersoy; R. Akkerman; J. Hattel *Archives of computacional methods in engineering* 2017, 24, 365-395. https://doi.org/10.1007/s11831-016-9167-2
6. Z. Awad; T. Aravinthan; Y. Zhuge; et al *Materials & Design* 2012; 33, 534-544. https://doi.org/10.1016/j.matdes.2011.04.061
7. S. Rahatekar; J. Roux *Journal of Composite Materials* 2016; 37, 1067-1082. https://doi.org/10.1177/0021998303037012005

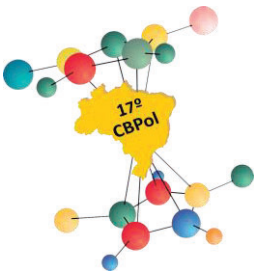

DEVELOPMENT OF CHITOSAN HYDROGELS FOR METAL REMOVAL IN CONTAMINATED WATER

Rennan F. S. Barbosa[1] and Derval S. Rosa[1*]

1 – Center of Engineering and Social Science, Federal University of ABC (UFABC), Santo André, SP, Brazil
dervalrosa@yahoo.com.br

Abstract

The presence of metal ions in contaminated water from industrial processes with toxic potential has led to great concern regarding their effects on human health. Conventional treatment processes are inadequate for their removal, so new technologies must be investigated. The use of three-dimensional porous systems, such as hydrogels, is a potential material for removing these contaminants. The present work aims to investigate the influence of production parameters of chitosan hydrogels, using the design of experiments methodology, to evaluate the effect of chitosan and crosslinker molar ratio. Different formulations were submitted to the water absorption and metal adsorption tests, and it was possible to evaluate that the concentration of chitosan and the chitosan/glutaraldehyde ratio are relevant factors to optimize the concentrations of the reagents and the water absorption and metal contaminant adsorption capacities.

Keywords: *Chitosan hydrogel, metal ion, water decontamination.*

Fundings: This research was financed by FAPESP (2021/08296-2 and 2020/13703-3) and CNPq (308053/2021-4 and 403934/2021-4).

Introduction

According to the World Health Organization (WHO), at least 2 billion people use a contaminated drinking water source, and by 2025 half of the world's population could live in a water-scarce area. Among the main contaminants that raise concern today are microorganisms, emerging organic contaminants and metal ions [1]. Among these, the frequency of metal ions in water is apprehensive because they present several harmful effects to human health reported, also due to their toxic and carcinogenic nature. In addition, they are non-biodegradable, and their toxicity, observed even at low concentrations, can be aggravated by bioaccumulation and biomagnification phenomena, which increase the degree of exposure along the food chain [2].

Given this scenario, several technologies have been applied to treat effluents to minimize the impact caused by these metals on health and the environment. Different conventional techniques can be used to remove metal ions, such as solvent extraction, ion exchange, chemical precipitation, and reverse osmosis [3]. However, these processes are limited because of high cost, generation of toxic by-products or long treatment times [4]. Based on the limitations associated with conventional processes, new alternatives have been researched, and one process that has shown the potential to meet the demands of metal contaminant removal is based on the adsorption process. The adsorption is based on the presence of binding sites on the surface of the adsorbent material, which makes it a process highly influenced by the surface area of the material. This process is competitive because it has low cost, smooth and flexible operating parameters, low energy consumption and high efficiency [5].

Hydrogels are three-dimensional polymeric structures produced by crosslinking, which exhibit high hydrophilicity and the ability to absorb large volumes of water. The water absorption capacity derives from surface groups, such as hydroxyl groups (OH), amines (NH_2), carboxylic (COOH), amide ($CONH_2$) and sulfone (SO_3H) [6]. The high porosity of these materials guarantees them a

high surface area that can be used to adsorb different contaminants. In addition, the surface characteristics can be modified to control the diffusion process and the adsorption kinetics.

Polysaccharides have attracted much attention in developing hydrogels due to their biodegradability, biocompatibility, non-toxicity and low cost. Na and collaborators highlight using chitin, chitosan, cellulose, starch, alginate, and their blends, copolymers, and composites for metal removal in aqueous systems [7]. Chitosan has drawn attention among these materials due to its high natural abundance. Moreover, its chemical structure presents amine groups, and as reported by Upadhyay and collaborators, these groups guarantee the chitosan hydrogel's capacity to remove metal ions [8].

Hydrogels have been studied as potential adsorbent materials in the literature, and the mechanism associated with this process is quite complex and depends on the materials used and the target contaminant. This adsorption process can involve several simultaneous interactions, including electrostatic interactions, ion exchange, hydrophobic interactions, coordination interactions (chelation), and π-π [9]. Understanding the influence of each mechanism present is fundamental for formulating an optimized and robust system that can be applied for metal ion removal in different systems.

Based on that, the present work aims to investigate the influence of production parameters of chitosan hydrogels, using the methodology of design of experiments. The developed systems were evaluated concerning the effect of the proportion of chitosan and crosslinking agent on water absorption and metal ion removal properties.

Experimental

Materials

In this study, chitosan was provided by Polymar (Fortaleza – Ce). Glutaraldehyde was used as a reticulation agent, and analytical standards of the target metal ions (Cd(II), Cr(VI), Cu(II), Mn(II), Zn(II), and Ni(II)) were employed for the sorption essays. All reagents were purchased from Labsynth Produtos para Laboratórios (SP, Brazil).

Methods

For the development of chitosan hydrogels, an experimental planning study was carried out in order to select the optimal condition for hydrogel production. For hydrogel production, the chitosan was previously solubilized in a solution of acetic acid (2% v v^{-1}) in different concentrations (1, 2 and 3% w v^{-1}). For hydrogel formation, glutaraldehyde was used as a crosslinking agent at different concentrations (between 1 and 10% v m^{-1}). Response surface planning was employed to evaluate the effect of the proportion of chitosan and crosslinking agent, and 18 formulations were generated. As variáveis de resposta foram as propriedades de absorção de água e remoção de íons metálicos dos hidrogéis desenvolvidos.

Characterization

The water absorption capacity of the hydrogels will be evaluated through the degree of swelling, considering mass variation as a function of the time of a sample kept in an aqueous medium, according to Equation 1, where Mt is the swelling mass, and Ms is the dry mass.

$$Q = \frac{Mt}{Ms} \qquad (1)$$

A modular ion chromatograph 940 Professional IC Vario (Metrohm, Switzerland) with detection limits of μg L^{-1} will be used for the adsorption studies. To evaluate the potential of the hydrogels, a selectivity study was performed using an equimolar solution of copper, nickel, zinc, manganese, cadmium and chromium where each metal was at a concentration of 0.17 mmol L^{-1} so that the solution had a total concentration of 1.02 mmol L^{-1}. The solution was prepared at pH 4 to avoid precipitation effects that could affect the analysis of the results. For comparison purposes, the

samples before the modification were also evaluated. The samples were in contact with the solution for 48 h under stirring, and after this period, the aliquots were evaluated using the Ion Chromatograph to evaluate the concentration of ions in the solution.

Results and Discussion

Response surface planning was employed to evaluate the effect of the proportion of chitosan and crosslinking agent, generating 18 formulations. The response variables were the developed hydrogels' water absorption and metal ion removal properties. Table 1 presents the composition variation performed through the experimental planning. After preparation, the samples were washed in 3 cycles to remove non-crosslinked glutaraldehyde and then stored for characterization.

Table 1 - Formulations and nomenclature of the samples according to the experimental planning.

Sample	Chitosan concentration % (m v^{-1})	Glutaraldehyde concentration (v m^{-1})	Sample	Chitosan concentration % (m v^{-1})	Glutaraldehyde concentration (v m^{-1})
QH1	2,0	10,0	QH10	2,5	3,2
QH2	2,0	4,0	QH11	2,0	10,0
QH3	3,0	3,2	QH12	2,0	1,0
QH4	2,5	5,5	QH13	3,0	10,0
QH5	3,0	1,0	QH14	2,5	1,0
QH6	3,0	1,0	QH15	2,5	7,7
QH7	2,5	10,0	QH16	3,0	10,0
QH8	2,0	7,0	QH17	3,0	7,7
QH9	3,0	5,5	QH18	2,0	1,0

Note: the colors in the table indicate the concentration of chitosan, red for 2%, blue for 2.5%, and green for 3%.

To evaluate the swelling capacity of the hydrogels, the water absorption test was performed for 1, 2 and 7 days, and the result is shown in Table 2.

Table 2 - Water absorption of chitosan hydrogels.

	Absorption (%)				Absorption (%)		
Sample	1 day	2 days	7 days	Sample	1 day	2 days	7 days
QH1	158 ± 1	157 ± 4	168 ± 3	QH10	190 ± 9	210 ± 7	200 ± 14
QH2	201± 3	207 ± 1	210 ± 1	QH11	158 ± 1	159 ± 4	150 ± 10
QH3	230 ± 5	228 ± 14	241 ± 1	QH12	325 ± 7	343 ± 4	360 ± 16
QH4	204 ± 33	199 ± 18	199 ± 18	QH13	157 ± 3	154 ± 2	156 ± 1
QH5	271 ± 4	284 ± 6	305 ± 2	QH14	271 ± 12	281 ± 4	312 ± 6
QH6	275 ± 2	280 ± 6	295 ± 4	QH15	174 ± 1	160 ± 5	172 ± 2
QH7	166 ± 1	153 ± 1	157 ± 2	QH16	167 ± 11	165 ± 18	169 ± 23
QH8	177 ± 9	171 ± 14	170 ± 8	QH17	161 ± 2	159 ± 4,6	165 ± 4
QH9	178 ± 22	202 ± 7	198 ± 11	QH18	303 ± 3	317 ± 5	357 ± 14

All hydrogels showed a high degree of water absorption, greater than 100%, after 1 day of testing, this being a typical behavior of hydrogels, as reported by Liu and collaborators [10]. Furthermore, it is observed that some samples stood out with absorption of more than 200%, such as samples QH2 to QH6, QH12, QH14 and QH18, with samples QH12 and QH18 exceeding 300% water absorption. It is worth noting that QH12 and QH18 represent duplicates of the preparation conditions of the hydrogels, so this indicates that the hydrogel using 2% chitosan and 1% glutaraldehyde has a high-water absorption capacity. It is observed that the samples with higher

water absorption presented the use of a lower content of glutaraldehyde, which may indicate a lower crosslinking of the hydrogel structure and allow the availability of functional groups capable of absorbing water [11].

The metal ion removal performance of the developed hydrogels was evaluated through the metal ion selectivity assay, and the result is presented in Table 3.

Table 3 - Percent removal of metal ions from the developed hydrogels.

	Removal (%)					
Sample	Copper	Nickel	Zinc	Manganese	Cadmium	Chromium
QH1	75,1 ± 0,3	0,9 ± 4,7	3,70 ± 5,1	11,8 ± 5,4	7,4 ± 0,4	99,8 ± 0,3
QH2	61,7 ± 0,1	9,3 ± 0,7	4,80 ± 0,4	15,7 ± 0,6	8,5 ± 0,3	100,0 ± 0,0
QH3	57,0 ± 0,6	6,2 ± 0,3	2,70 ± 0,6	13,3 ± 0,7	7,3 ± 0,2	100,0 ± 0,0
QH4	64,8 ± 1,5	4,2 ± 1,3	3,60 ± 2,9	10,4 ± 2,9	13,4 ± 4,7	100,0 ± 0,0
QH5	74,0 ± 6,8	1,5 ± 0,8	1,30 ± 1,8	6,8 ± 10,6	1,9 ± 12,9	100,0 ± 0,0
QH6	54,5 ± 0,7	0,8 ± 1,1	1,80 ± 1,5	12,3 ± 1,8	8,2 ± 3,1	96,0 ± 0,6
QH7	44,5 ± 2,6	5,5 ± 0,7	4,0 ± 1,3	14,9 ± 0,1	8,6 ± 3,9	99,7 ± 0,4
QH8	42,8 ± 4,8	6,9 ± 4,1	3,8 ± 2,0	14,2 ± 1,4	6,0 ± 0,6	100,0 ± 0,0
QH9	41,5 ± 0,7	6,3 ± 0,2	3,9 ± 0,2	13,6 ± 0,2	11,1 ± 0,1	100,0 ± 0,0
QH10	45,0 ± 0,4	10,7 ± 0,4	4,8 ± 0,4	18,2 ± 0,3	15,4 ± 0,4	99,3 ± 0,9
QH11	49,3 ± 0,6	6,3 ± 0,2	0,3 ± 0,2	11,2 ± 0,4	6,0 ± 0,2	100,0 ± 0,0
QH12	74,0 ± 4,6	5,6 ± 0,3	4,3 ± 1,8	13,6 ± 2,8	10,1 ± 4,0	98,6 ± 1,9
QH13	58,5 ± 8,8	5,9 ± 1,1	4,6 ± 0,2	15,1 ± 0,9	9,0 ± 5,6	100,0 ± 0,0
QH14	44,7 ± 4,3	3,2 ± 3,6	2,9 ± 1,5	13,1 ± 0,1	5,6 ± 0,9	97,6 ± 0,4
QH15	57,3 ± 0,1	9,3 ± 6,6	5,9 ± 0,6	15,9 ± 1,1	11,5 ± 3,4	100,0 ± 0,0
QH16	34,9 ± 7,4	10,6 ± 2,6	2,7 ± 0,2	14,7 ± 0,6	8,0 ± 2,2	100,0 ± 0,0
QH17	39,5 ± 5,9	7,0 ± 1,1	3,8 ± 0,5	13,5 ± 2,1	8,9 ± 1,8	100,0 ± 0,0
QH18	56,0 ± 0,2	5,2 ± 3,0	5,8 ± 0,4	15,5 ± 1,3	12,9 ± 0,8	98,8 ± 1,7

Evaluating the hydrogels, it is observed that there was a low removal rate for 4 of the 6 ions evaluated. This result shows a low affinity of the chitosan matrix for removing these ions. The interaction of chitosan with metallic ions can occur through functional groups that include hydroxyls and amines. However, the crosslinking process promotes the formation of covalent bonds, reducing the availability of these groups and possibly impacting the sorption capacity of the hydrogels developed. Even so, it is worth noting that the hydrogels presented a significant removal potential for copper and chromium.

In the case of copper removal, a great variation of removal was observed depending on the composition employed, which indicates that the degree of crosslinking of the sample should directly influence the groups available for interaction and removal of the metal ion. In this sense, the samples QH1, QH5, and QH12 stood out, reaching a removal degree of around 70%. Mallik and collaborators also highlighted the potential of chitosan for copper removal using chitosan-based adsorbents [12].

Regarding chromium removal, a total removal was observed under the test conditions, considering the deviation between the samples, indicating that the chitosan matrix presents a high affinity for chromium removal. The literature corroborates this result and is associated with interaction with hydroxyls, protonated amines, and amide groups (SETHI et al., 2022).

The results of water absorption and removal of metal ions were used as a response to the experimental planning developed to select the conditions of preparation of hydrogels that enhance the properties obtained. The analysis of the results was performed using the software *Design Expert*,

defining as a condition that the concentration of chitosan was in the range used in the formulations and that the concentration of glutaraldehyde was minimized. Based on this condition, the software highlighted the samples QH12 and QH18, which replicate the same formulation. Thus, this condition was selected as the optimal condition for producing hydrogels with optimum properties for metal removal. Furthermore, future work will explore the optimization of the properties of the hydrogels obtained by inserting agents with a higher chemical affinity to the other metal ions investigated.

Conclusions

In this work, the design of experiments methodology was used to produce chitosan hydrogels and evaluate the relationship between the concentration of chitosan and crosslinking agent with the properties of hydrogels. Eighteen different formulations were produced, and it was possible to note that the increase in the concentration of crosslinking agent reduces the water absorption properties, and the samples with 2% crosslinking agent stood out with absorption higher than 300%. In addition, the metal ion removal properties are also impacted in this process due to the lower availability of active groups. The hydrogels developed stood out for chromium and copper removal, reaching removals of 100% and 75%, respectively, for the conditions studied. The sample using 2% chitosan and 1% glutaraldehyde was selected through the response surface analysis as the best formulation for preparing the hydrogels. The results demonstrate the success of producing hydrogels, aiming to understand the optimal formulation conditions, which can serve as a basis for new materials to remove and recover metals in contaminated water.

Acknowledgements

The authors thank the technical support of the Multiuser Experimental Center of UFABC (CEM-UFABC), CECS (UFABC), and REVALORES for assistance.

References

1. Masindi V, Muedi KL in Heavy Metals, Hosam El-Din M Saleh and Refaat F, Ed; Intechopen Limited, London, 2018, 215-233.
2. Barbosa RFS, Souza AG, Maltez HF, Rosa DS. . Chemical Engineering Journal 2020; 395, 125055. https://doi.org/10.1016/j.cej.2020.125055.
3. Wang R, Guan S, Sato A, Wang X, Wang Z, Yang R, et al. Journal of Membrane Science 2013, 446, 376–382. https://doi.org/10.1016/j.memsci.2013.06.020.
4. Fu F, Wang Q. Journal of Environmental Management 2011, 92, 407-418. https://doi.org/10.1016/j.jenvman.2010.11.011.
5. Joseph L, Jun BM, Flora JRV, Park CM, Yoon Y. Chemosphere. 2019, 229, 142–159. https://doi.org/10.1016/j.chemosphere.2019.04.198.
6. Weerasundara L, Gabriele B, Figoli A, Ok YS, Bundschuh J. Hydrogels: Critical Reviews in Environmental Science and Technology 2020, 51, 1970-2014. https://doi.org/10.1080/10643389.2020.1776055.
7. Na Y, Lee J, Lee SH, Kumar P, Kim JH, Patel R. Polymer-Plastics Technology and Materials 2020; 59, 1770–1790. https://doi.org/10.1080/25740881.2020.1768545.
8. Upadhyay U, Sreedhar I, Singh SA, Patel CM, Anitha KL. Carbohydrate Polymers 2021; 251, 117000. https://doi.org/10.1016/j.carbpol.2020.117000.
9. Sinha V, Chakma S. Journal of Environmental Chemical Engineering 2019; 7, 103295. https://doi.org/10.1016/j.jece.2019.103295.
10. Liu, Y., Wang, R., Wang, D., Sun, Z., Liu, F., Zhang, D., & Wang, D. Food Hydrocolloids 2022, 127, 107546. https://doi.org/10.1016/j.foodhyd.2022.107546.
11. Machado, T. S., Crestani, L., Marchezi, G., Melara, F., de Mello, J. R., Dotto, G. L., & Piccin, J. S. Carbohydrate Polymers 2022, 277, v. 277, 118868. https://doi.org/10.1016/j.carbpol.2021.118868.
12. Mallik, A. K., Kabir, S. F., Rahman, F. B. A., Sakib, M. N., Efty, S. S., & Rahman, M. M. Journal of Environmental Chemical Engineering 2022, 10, 108048. https://doi.org/10.1016/j.jece.2022.108048.

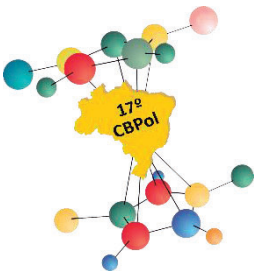

DEVELOPMENT OF CORN STARCH HYDROGELS FOR SORPTION OF POTENTIALLY TOXIC METALS

Eduarda L. da Silva[1], Livia T. D'Alcantara[1], Talles B. da Costa[1] and Derval dos S. Rosa[1]*

1 – Center for Engineering, Modeling, and Applied Social Sciences (CECS), Federal University of ABC (UFABC), Santo André, derval.rosa@ufabc.edu.br

Abstract - This study evaluated the process conditions (crosslinking time and drying temperature) in the development of biodegradable starch-based hydrogels for the uptake of potentially heavy metals (copper (Cu^{2+}), zinc (Zn^{2+}), nickel (Ni^{2+}), manganese (Mn^{2+}), cadmium (Cd^{2+}), and hexavalent chromium (Cr^{6+})) by sorption technique. The Amidex 3001 hydrogel produced with crosslinking time of 1 h and drying temperature of 90 °C favored the process, reaching a maximum water uptake of about 210%. The starch-based hydrogels presented the following metallic affinity order: $Cr^{6+} > Cd^{2+} > Ni^{2+} > Cu^{2+} > Zn^{2+} > Mn^{2+}$. Cr^{6+} sorption capacity was close to 90%, while for the other divalent cations (Zn^{2+}, Cd^{2+}, Ni^{2+}, Mn^{2+}, and Cu^{2+}), it was less than 20% regardless of the process conditions (crosslinking time and drying temperature). Thus, starch-based hydrogels are efficient alternative for wastewater treatment.

Keywords: *Hydrogels; Corn starch; crosslinking; Sorption; Toxic metals.*

Fundings: This research was financed by Fundação de Amparo à Pesquisa do Estado de São Paulo (FAPESP) (2020/13703-3, 2022/11133-0), Conselho Nacional de Desenvolvimento Científico e Tecnológico (CNPq) (308053/2021-4, 403934/2021-4), and Coordenação de Aperfeiçoamento de Pessoal de Nível Superior (CAPES) (Finance Code 001).

Introduction

Hydrogels are characterized by being highly porous cross-linked polymer networks, which have as their main advantage the ability to retain large amounts of water without generating changes in their chemical structure. These networks are formed through the cross-linking of polymer chains. Hydrogels are commonly used in various applications, such as in drug delivery systems, hygiene products, agriculture, pharmaceuticals, and the medical industry [1].

These materials are known to be the new biomaterials of this era for their unique properties such as biodegradation capacity, stability in chemicals and biofluids, stable structure, biocompatibility and ecofriendly character, as well as wide absorption capacity of metabolites and nutrients that are in soluble water [2]. By absorbing metabolites and water-soluble nutrients, hydrogels will be able, for example, to retain heavy metals that contaminate humans, bringing various effects to the body, such as problems in the nervous system, carcinogenic effects, gene mutations and even effects on the reproductive system [3].

This contamination is essentially due to the improper disposal of industrial effluents that cause the contamination of the extremely important natural resource for the planet: water. The seriousness of this situation is evidenced by the conclusion generated by the UNESCO World Water Development Report 2017 (WWAP, 2017), which states that 80% of the industrial and urban wastewater consumed returns to the environment without adequate pre-treatment. This has caused negative impacts to the ecosystem and generated accumulation in the trophic chains that ends up contaminating humans. Among the elements that make up industrial effluents, we can highlight heavy metals like cadmium (Cd), lead (Pb), nickel (Ni), chromium (Cr), arsenic (As), copper (Cu), iron (Fe), among others [4].

Currently, the use of hydrogels in water treatment is advantageous due to its reusable character, attracting greater relevance. In this work, we synthesize hydrogels based on corn starch crosslinked with trisodium citrate, which also has the benefit of being a material from renewable sources, low cost, non-toxic, abundantly, economically suitable, biocompatible, hydrophilic, and biodegradable material. Thus, the aim of this study is to evaluate the process conditions (crosslinking time and drying temperature) in the synthesis of biodegradable hydrogels based on corn starch to investigate the water absorption capacity and removal of potentially heavy metals (Cu^{2+}, Mn^{3+}, Ni^{2+}, Zn^{2+}, Cd^{2+}, Cr^{6+}) from an aqueous medium.

Experimental

Materials

For the experiments, three starches were used: Amisol 3408, Amidex 3001, and Hylon VII. All starches were obtained from corn, but they differ in their amylose and amylopectin contents, with Amisol 3408 containing 28 wt% amylose and 72 wt% amylopectin, Amidex 3001 containing 27 wt% amylose and 73 wt% of amylopectin, and Hylon VII containing 70 wt% amylose and 30 wt% amylopectin.

Starch-based hydrogels synthesis

Starch-based hydrogels were prepared according to the methodologies proposed by Camani et al. [5]. The different corn starches (Amisol 3408, Amidex 3001, and Hylon VII) were suspended in ultrapure water, in distinct lots. After starches dissolution, sodium hydroxide (13 g/L) was added, and the mixtures were mechanically stirred. Then, citric acid (19.4 g/L) was added to form the crosslinking agent by reaction with sodium hydroxide. The crosslinking process occurred with the system under mechanical stirring for 1 or 2 h, in distinct lots. After that, the system was heated at 90 °C for 1 h in a water bath. Finally, the hydrogels obtained were dried in an oven at 90 °C for 24 h or 60 °C for 48 h, in distinct lots.

Water absorption

The experiments to evaluate the water absorption by starch-based hydrogels were performed in triplicate. Absorption assays were caried out by immersing 0.1 g of dry hydrogel pieces in 50 mL of ultrapure water. The samples were taken out ultrapure water at pre-determined intervals, pat-dried and the specimens weighted and immersed again. The degree of swelling (*DS*) can be defined by Equation (1).

$$DS = \frac{(m_t - m_i)}{m_i} \cdot 100 \quad (1)$$

wherein, m_i is the initial dry mass of hydrogels (g) and m_t is the swollen mass of hydrogels at time *t* (g).

Sorption assays

Synthetic solutions of potentially toxic metals (PTMs) were prepared by dissolving the salts of zinc nitrate ($Zn(NO_3)_2 \cdot 6H_2O$), cadmium ($Cd(NO_3)_2 \cdot 4H_2O$), copper ($Cu(NO_3)_2 \cdot 3H_2O$), manganese ($Mn(NO_3)_2 \cdot 4H_2O$), nickel ($Ni(NO_3)_2 \cdot 6H_2O$), and potassium dichromate ($K_2Cr_2O_7$) in ultrapure water. The affinity of starch-based hydrogels for Cu^{2+}, Zn^{2+}, Ni^{2+}, Cd^{2+}, Mn^{2+}, Cr^{6+} (0.05 mmol/L each) were performed using 5g/L of hydrogel in water. The sorption affinity assays were conducted in a

shaker incubator at room temperature (~ 25 °C) and pH between 4.0 – 4.5 using HNO_3 solution (0.2 to 1.0 mol/L). After 24 h, PTMs concentrations were determined by ion chromatography, IC (940 Professional IC Vario, Metrohm, Switzerland). Removal efficiencies ($\%R$) were determined by Equation (2).

$$\%R = \frac{(C_0 - C_e)}{C_0} \cdot 100 \quad (2)$$

wherein, C_0 is the PTMs initial concentration (mmol/L) and C_e is the PTMs concentration at equilibrium (mmol/L).

Results and Discussion

Water absorption

Water absorption is an important property to define the end-use applications of hydrogels. Figure 1 presents the degree of swelling of the starch hydrogels in relation to the variation of process conditions (crosslinking time and drying temperature), as well as the crosslinking process.

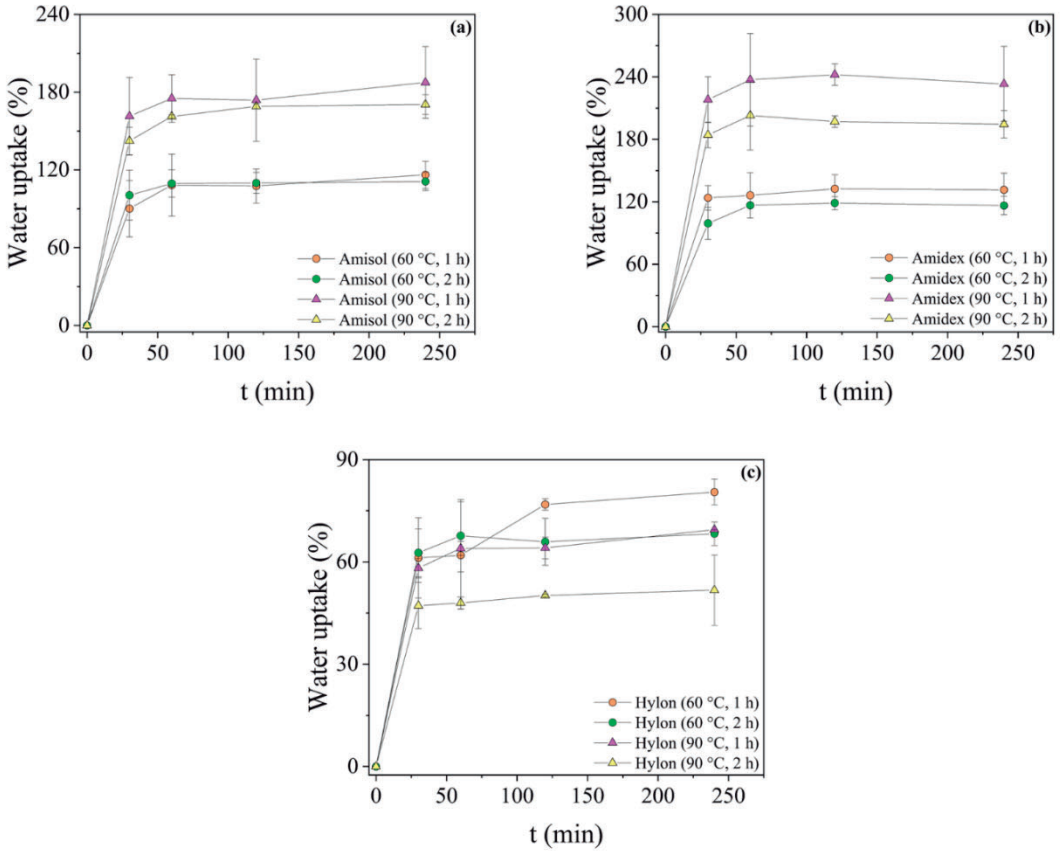

Figure 1 – Water uptake (%) of corn starch hydrogels with different contents of amylose/amylopectin and crosslinking time/drying temperature.

From the water absorption results, all hydrogels showed considerable water uptake during the first hour of immersion. After reaching the equilibrium time (~1 h), it was verified that starch hydrogels with medium amylose content (Amisol 3408 and Amidex 3001) showed similar behavior in terms of water absorption capacity. The highest uptake water capacities were achieved with crosslinking time and drying temperature of 1 h and 90 °C, respectively. Under these conditions, the

maximum water absorption achieved were around 180 and 210% for Amisol 3408 and Amidex 3001 hydrogels, respectively. With increasing crosslinking time to 2 h, there was a slight reduction in water absorption to about 150 and 180% for Amisol 3408 and Amidex 3001 hydrogels, respectively. Additionally, there was a reduction in water uptake (around 90%) by the hydrogels with the reduction in the drying temperature to 60 °C in both crosslinking times investigated (1 and 2 h).

On the other hand, regarding the hydrogel with high amylose content (Hylon VII), there was an increase of water absorption from about 45 to 90% with decreasing drying temperature from 90 to 60 °C and crosslinking time from 2 to 1 h. This indicates that the higher amylose content probably increased the rigidity conformation of the hydrogel. This behavior resulted in less molecular chain mobility, diffusivity, water retention within the pores, and hydrogel volume.

Sorption affinity

In effluent samples, heavy metals are found with other potentially toxic contaminants at varying concentrations, affecting their sorption efficiency due to competition for binding sites [6]. Thus, the performance of starch-based hydrogels was also investigated in synthetic wastewater with six coexisting ions (Cr^{6+}, Zn^{2+}, Cd^{2+}, Ni^{2+}, Mn^{2+}, and Cu^{2+}) (Figure 2).

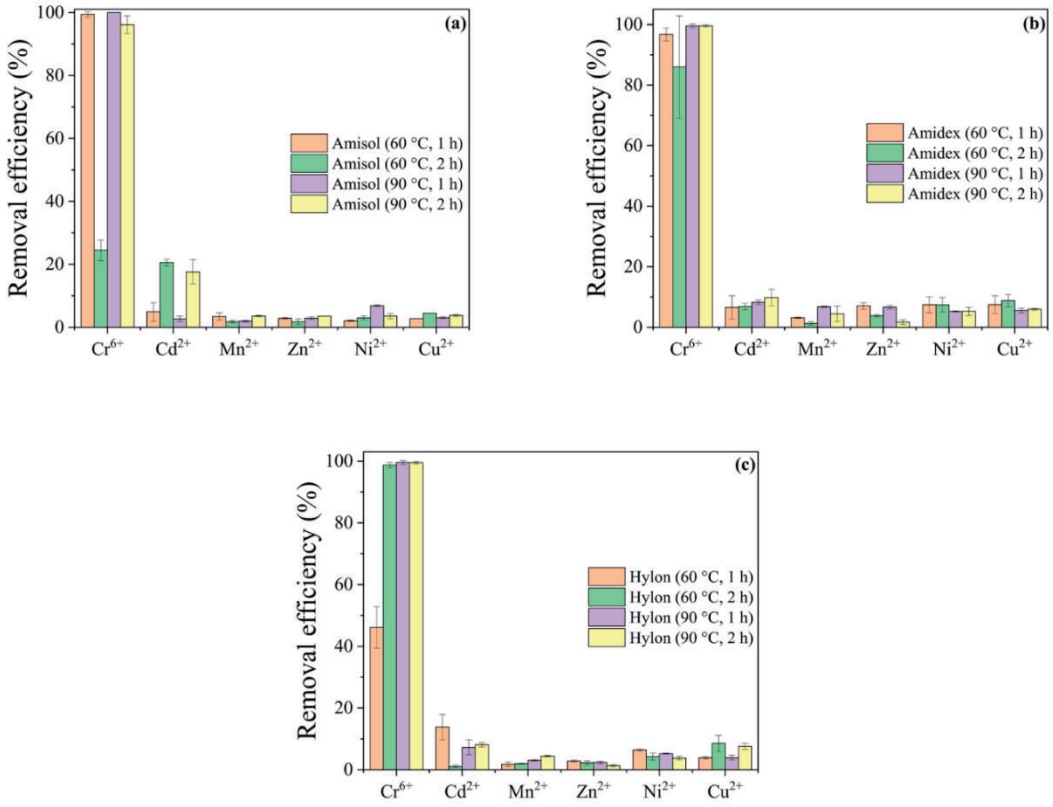

Figure 2 – Sorption affinity of PTMs ions (Cu^{2+}, Cd^{2+}, Mn^{2+}, Zn^{2+}, Ni^{2+} and Cr^{6+}) by corn starch-based hydrogels.

From Figure 2, the following order of sorption selectivity was found: $Cr^{6+} > Cd^{2+} > Ni^{2+} > Cu^{2+} > Zn^{2+} > Mn^{2+}$. Cr^{6+} removal by Amisol 3408 hydrogel showed values greater than 90%, however, this value was reduced to about 20% under the conditions of crosslinking time of 2 h and drying temperature of 60 °C. For the Amidex 3001 hydrogel, Cr^{6+} sorption rate was close to 90%

regardless of the process conditions (crosslinking time and drying temperature). The Hylon VII hydrogel also showed high Cr^{6+} removal efficiencies (> 90%), although the preparation with a drying temperature of 60 °C and crosslinking time of 1 h achieved a lower Cr^{6+} sorption rate of around 50%. Noticeably, the removal rates of coexisting ions were very low at all process conditions (crosslinking time and drying temperature) evaluated, which demonstrated impressive selectivity of starch-based hydrogels toward Cr^{6+} over divalent cations. This is because Cr^{6+} in the aqueous medium exists in the form of oxyanions ($[CrO_4]^{2-}$, $[Cr_2O_7]^{2-}$, $[H_2CrO_4]$, and $[HCrO_4]^-$) depending on the pH, and there is no competitive adsorption relationship between oxyanions and divalent cations [7]. This indicates that the electrostatic interaction of positively charged divalent ions (e.g., Zn^{2+}, Cd^{2+}, Ni^{2+}, Mn^{2+}, and Cu^{2+}) with corn starch hydrogels competes slightly with the electrostatic interaction of corn starch hydrogels hydrogels with negatively charged oxyanions [8].

Conclusions

The present study showed that starch-based hydrogels is a promising adsorbent for use in the uptake of heavy metals, such as oxyanions of Cr^{6+} in aqueous media. The results showed a direct effect of the process conditions (crosslinking time and drying temperature) of the starch-based hydrogels synthesis on the water uptake adsorptive process efficiency. The Amidex 3001 hydrogel produced with crosslinking time of 1 h and drying temperature of 90 °C favored the process, reaching a maximum water uptake and Cr^{6+} removal of about 210% and 98%, respectively. Therefore, to deeply understand the sorption process, additional studies will be carried out, including thermal, morphological, and chemical analyses.

Acknowledgements

The authors thank the technical support of the Multiuser Experimental Center of UFABC (CEM-UFABC), CECS (UFABC), and REVALORES for assistance. The authors also thank Ingredion Company for donation of the corn starches.

References

1. Y. Guo; B. Jiwoong; F. Zhiwei; L. Panpan; Z. Fei; Y. Guihua Chemical Reviews 2020, 120, 7642-707. https://doi.org/ 10.1021/acs.chemrev.0c00345
2. M. Qamruzzaman; F. Ahmed; M.I.H. Mondal Journal of Polymers and the Environment 2022, 30, 19-50. https://doi.org/10.1007/s10924-021-02180-9
3. O. Pulgarín; D. Larrea-Wachtendorff; G. Ferrari Gels 2023, 9, 87. https://doi.org/10.3390/gels9020087
4. M.A. Hossain; H.H. Ngo; W.S. Guo; T.V. Nguyen International Journal of Geomate 2012, 2, 227-234. ISSN:2186-2982(P), 2186-2990(O)
5. P.H. Camani; M.G.M. Gonçalo; R.F.S. Barbosa; D.S. Rosa Journal of Applied Polymer Science 2021, 138, 50863. https://doi.org/10.1002/app.50863
6. H.M. Marwani; H.M. Albishri; E.M. Soliman; T.A. Jalal Journal of Dispersion Science and Technology 2012, 33, 549-555. https://doi.org/10.1080/01932691.2011.574941
7. C. Xu; Y. Xu; D. Zhong; H. Chang; J. Mou; H. Wang; H. Shen Carbohydrate Polymers 2022, 296, 119872. https://doi.org/10.1016/j.carbpol.2022.119872
8. C. Xu; Y. Xu; D. Zhong; H. Chang; J. Mou; H. Wang; H. Shen International Journal of Biological Macromolecules 2023, 239, 124266. https://doi.org/10.1016/j.ijbiomac.2023.124266

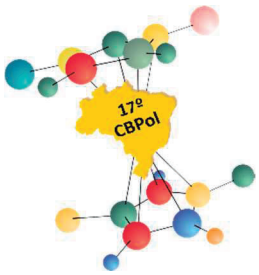

DEVELOPMENT OF HIGH-DENSITY POLYETHYLENE COMPOSITES WITH MACAIBA BARK

Renê A. da Paz[1*], Stephanne Kelly F. Silva[1], Vanessa da N. Medeiros[1], Danilo D. Siqueira[1], Pamela T. V. da Silva[1], Edcleide M. Araújo[1],

1 – Academic Unit of Materials Engineering (UAEMa), Federal University of Campina Grande (UFCG), Campina Grande, PB, Brazil
reneanisio@gmail.com

Abstract - The use of natural raw materials in the manufacture of polymeric composites has been extensively studied, as it tends to improve mechanical and thermal properties, in addition to being more environmentally viable. High-Density Polyethylene (HDPE) composites reinforced with macaíba bark powder were developed. After being processed, they underwent tensile and Izod impact resistance tests, contact angle measurements, and optical microscopy. The material loaded with larger granulometry (#25) showed better performance in optical microscopy, contact angle, and also in the tensile test. In the impact test, the composites absorbed less energy compared to Pure HDPE, and this can be explained by the poor adhesion among the phases. From the analysis, it was evidenced that a good dispersion of the polymer in the macaíba bark powder.

Keywords: *Composites, Polyethylene, Macaíba.*

Introduction

The use of materials from renewable sources has been extensively studied due to the environmental and economic advantages they offer when compared to synthetic materials [1-3]. The macaíba palm (*Acrocomia Aculeata*) is a species native to tropical forests and can be found in several regions of the country [4]. The fruit is divided into four parts: epicarp, mesocarp, endocarp, and almond [4-6].

Composites are multiphase materials formed by elements (matrix and reinforcement) that aim to exhibit superior properties, in many aspects, than each individual component. The addition of correct fillers in adequate concentrations results in a new material with better characteristics than the pure constituents [7]. In the combination of materials, the geometry and orientation of the reinforcing material significantly influence strength, toughness, dimensional and thermal stability. Taking into account the composites formed by particulate elements, these can structurally be spherical, cubic, tetragonal, or in other ways (regular or irregular). However, most are equiaxed[8].

Polyethylene is obtained during the polymerization of ethylene and can be considered as a partially crystalline, flexible material, with properties that are influenced by the proportions of the amorphous and crystalline phases. Linear high-density polyethylene (HDPE) is highly crystalline with a low branching content. HDPE can be used in making crates for drinks, bottles of alcohol and chemical products, buckets, drums, pipes for liquids and gas, fuel tanks, packaging for milk, juice, lubricating oil, pesticides, etc. [9,10].

The fillers do not have a good chemical affinity with the polymeric matrix since the polymers are predominantly nonpolar in nature, and the fillers are polar. Therefore, it is necessary to add a compatibilizing agent to avoid agglutination of fillers and facilitate their dispersion in the polymeric matrix [11].

There are not many studies in the literature related to the use of bark from *Acrocomia aculeata* in polymeric composites. The interest arose in studying the insertion of the bark of *Acrocomia Aculeata* in composites with linear high-density polyethylene, aiming at improving the mechanical properties.

Experimental

Materials

The polymer matrix used was High-Density Polyethylene (HDPE), commercial code (IH57), supplied by BRASKEM (Brazil). As compatibilized, polyethylene grafted with maleic anhydride (PE-g-MA), supplied by Polybond, was used. The reinforcement material was Macaíba Bark - *Acrocomia Aculeata* (CM), purchased in local markets in Campina Grande-PB.

Methodology

All compounds were dried in a vacuum oven (80 °C) before the process. The HDPE/CM concentrates were prepared by melting intercalation using a Thermo Cientific Haake Polylab QC torque Rheometer. The procedure for mixing HDPE/CM (1:1) was as follows: 130 °C, 60 rpm, 10 min and 50 g of material, 25 g of CM and 25 g of HDPE were mixed and placed in the rheometer chamber. Subsequently, the material was removed from the chamber and crushed in a knife mill.

The HDPE L and concentrates were processed using a Werner-Pfleiderer extruder, L/D = 40, ZSK 18 mm model, Coperion—Germany, configured to operate with a temperature of 180 °C in all zones, speed of 250 rpm and feeding rate of 3kg/h.

Specimens were injected using an Arburg Injector, Model Allrounder 207C Golden Edition—German. The temperature profile of 180°C was used in all zones with the mold at 20°C. Specimens for tensile, impact, flexion and HDT were injected according to the standards ASTM D638 (Type I), D256, D790 and D648, respectively.

Characterization of Materials:

For the optical microscopy analysis, cross-sections of the composite samples were performed in a trinocular petrographic optical microscope - OPTON brand.

Tensile tests were carried out by ASTM D638 on an EMIC universal equipment model DL10000 using a 50 kN load cell at a strain rate of 50mm/min, operating at room temperature. The results were determined from an average of 5 specimens for each composition.

The IZOD impact resistance was performed on notched specimens using a CEAST Resil 5.5 type equipment and a 2.75 J pendulum, by ASTM D 256, at room temperature.

The surface's wettability degree was evaluated by the portable contact angle, Phoenix-I model from Surface Electro Optics - SEO, and the measurements were repeated in triplicate with the drop volume of 20 µl of distilled water.

Results and Discussion

Morphological analysis

Optical microscopy evaluated the surfaces of materials fractured during the impact test to determine their interface properties. Fig. 1 shows the microscopic structure of pure polymer and composites at two magnifications (40 and 250) at 25 and 50 mesh.

Fig. 1 shows that the composite layers need to be better compacted, with no good percolation of the matrix in the reinforcement. This suggests that there was probably not good adhesion between the phases (matrix and filler), a necessary condition to obtain good mechanical properties [12]. There are also (#50) some regions rich in macaíba bark powder (brown), indicated by arrows, a significant amount of voids, and agglomerates. Thus, the identified structural defects contributed to the mechanical performance presented by the material [13]. The presence of these regions could be more interesting, as they can concentrate tensions and reduce the material's mechanical and viscoelastic strength, leading to the composite's catastrophic failure.

In general, it is observed that the composites present in some regions have a more significant number of polymer pockets. These regions are probably related to the parameters used in the injection molding process and/or to the rheological characteristics of the polymer. During the solidification of the material, a possible variation of injection molding may have occurred, hindering the flow of the polymer in the reinforcement, thus impairing the distribution of the matrix in the load [14].

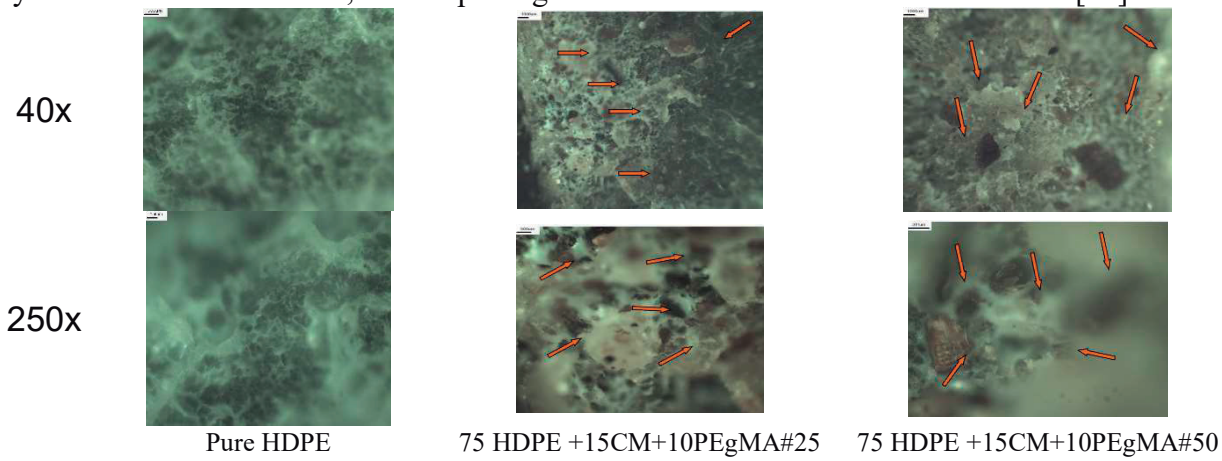

Figure 1 – Optical microscopy of the cross section of pure HDPE and its composites.

Tensile Test

Tab. 1 contains data on the tensile test for HDPE and its composites. The insertion of reinforcing fillers tends to increase the polymers' strength and modulus of elasticity. Usually, the granulometry, concentration, and distribution of the particles influence the interaction between the phases (continuous and dispersed) of the composite [16]. It is observed that the shell tends to have a behavior more compatible with a filling load than with a reinforcing load [16, 17]. In the material reinforced with particles of smaller granulometry, there was a reduction of 8.98% of the maximum strength and 13.42% of the tensile strength about Pure HDPE; in addition, it was verified that the addition of macaíba bark powder promoted a slight increase in the stiffness of the composites by 17.54% and 10.63%, (75HDPE+15CM+10PEgMA#25) and (75HDPE+15CM+10PEgMA#50) respectively, for the larger and smaller grain sizes. This behavior can be explained by weak interfacial adhesion, which decreases tensile strength. The presence of the compatibilizing agent was not enough to promote an improvement in the adhesion of the filler in the matrix [17].

Table 1 - Mechanical Tensile Test: HDPE; 75HDPE+15CM+10PEgMA#25 and 75HDPE+15CM+10PEgMA#50.

Samples	Maximum force (kgf)	Maximum Tension (MPa)	Tensile strength at break (MPa)	Elongation (%)	Elastic Modulus (MPa)
Pure HDPE	88,66±5,59	20,27±0,89	5,70±0,0	567,16±0,0	327,61±10,08
75 HDPE +15CM+10PEgMA #25	87,60±2,11	20,51±0,51	4,97±2,34	37,16±10,30	385,08±13,36
75 HDPE +15CM+10PEgMA #50	80,7±3,76	17,55±0,27	7,26±4,27	129,66±11,35	362,43±20,91

The material reinforced with an enormous granulometry load performed better in the tensile test, as the maximum force and maximum tension remained close to pure HDPE. At the same time, the modulus of elasticity increased considerably, making it more rigid and causing loss of ductility.

Fig. 2 illustrates Pure HDPE's stress versus strain graph and composites reinforced with macaíba bark powder. Samples that approached the averages of maximum force and elastic modulus were used. The presence of elastic deformation region followed by flow to a plastic region is observed, which is characteristic of thermoplastic polymers and their composites [18]. The insertion of load promoted a reduction in the tenacity of the materials, evidenced by the smaller area under the curve until failure.

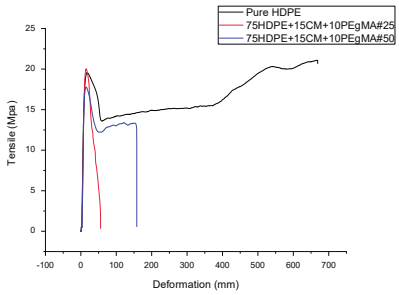

Figure 2 – Stress x strain curves: HDPE; 75HDPE+15CM+10PEgMA#25 and 75HDPE+15CM+10PEgMA#50

Izod Impact Strength

Thermoplastic composites generally show high strain rates in the impact test, as there is not enough time for the chains to slip and plastically deform [6]. In tab. 2, it appears that the composites absorbed less energy compared to HDPE; this happens because the insertion of the load increases the heterogeneity of the material, reducing the weight and elasticity of the molecular chain making it more fragile.

Table 2 – Impact strength: HDPE; 75HDPE+15CM+10PEgMA#25 and 75HDPE+15CM+10PEgMA#50.

Samples	(J/m)
HDPE	492,98±10,86
75 HDPE +15CM+10PEgMA#25	64,77±2,87
75 HDPE +15CM+10PEgMA#50	85,94±3,68

The particle size of the reinforcement particles is one factor that influences the mechanical properties because, as the load becomes finer, the specific surface area increases, promoting a better interface between the phases that constitute the material [12]. The composite reinforced with particles of smaller granulometry showed better results. However, the interaction between the phases was still insufficient to increase the energy absorption related to Pure HDPE. The load concentration, geometry, and interfacial adhesion contribute to this property's reduction [18].

Wettability Test - Contact Angle

Wettability is the ability of a liquid to maintain contact with a solid surface, resulting from intermolecular interactions when the two are brought together. A balance of adhesive and cohesive forces determines the degree of wetting (wetting). It can be determined from the angle that the liquid forms on the surface in contact with the solid, called the contact angle[19]. In polymeric surfaces, in addition to surface tensions, other factors such as roughness, chemical heterogeneity, molecular orientation, and partial solubility of the polymer influence the contact angle measurements. Tab. 3 presents the average values of the contact angles obtained, with their respective standard deviations relative to the measurements carried out on the surface of the pure polymer and composites reinforced with macaíba bark powder. The measurements indicate that the composite produced with larger granulometry had lower surface tension. The more excellent wettability is related to the capacity of the macaíba powder to be involved in the polymeric matrix. From these results, it can be seen that the incorporation of the compatibilizer had little influence on the wettability of the composites.

Table 3 – Average contact angles: Pure HDPE, 75HDPE+15CM+10PEgMA#25 and 75HDPE+15CM+10PEgMA#50.

Materials	Contact Angle
PEAD	69,32 ± 0,48
75 HDPE +15CM+10PEgMA#25	96,86 ± 0,80
75 HDPE +15CM+10PEgMA#50	87,64 ± 0,26

Conclusions

The analysis of the HDPE+CM compounds showed that it would be more advantageous to process the materials with 15% of the CM bark powder, varying only their granulometry (#25 and #50). The reinforced composite with an enormous granulometry load (#25) performed better in the optical microscopy, contact angle, and tensile test since the strength and the maximum tension remained close to the Pure HDPE. At the same time, the elastic modulus increased considerably, making it more rigid and generating a loss of ductility. In the impact strength, the composites absorbed less energy than pure HDPE, which the poor adhesion among the phases can explain. Consequently, more than the compatibilizing agent was needed to improve this characteristic. From the analysis, it was evidenced that there was a good dispersion of the polymer in the macaíba bark powder.

Acknowledgements

The authors are grateful to UFCG (Federal University of Campina Grande), FAPESQ (Research Support Foundation of the State of Paraíba), CAPES (The Higher Education Personnel Improvement Coordination) and CNPq (National Council for Scientific and Technological Development, Brasilia/DF, Brazil) for financial support.

References

1. F. Z. Arrakhiz; M..el achaby; M. Malha; M. O. Bensalah,; O. Fassi-Fehri; R Bouhfid; K. Benmoussa; A. Qaiss. Materials & Design 2013, 43. https://doi.org/10.1016/j.matdes.2012.06.056
2. W. Nuthong; P. Uawongsuwan,; W. Pivsa-Art; H. Hamada, .Energy Procedia 2013, 34, https://doi.org/10.47385/cadunifoa.v1.n1.236.
3. M. Ramesh; K. Palanikumar; K. H. Reddy. Composites Part B: Engineering 2013, 48,. https://doi.org/10.1016/j.compositesb.2012.12.004.
5. GRAY, M; KUNZE, H. *Acrocomia Aculeate*. Brisbane: Palm and Cycad Societies of Australia. Disponível em: http://www.pacsoa.org.au/w/index.php?title=*Acrocomia_aculeata*. Acesso em: 29/03/2023.
6. G. M. A. C. Lorenzi. Ph.D. Thesis. Federal University of Paraná, 2006.
7. J. C. Silva. *Macaúba: fonte de matéria-prima para os setores alimentício, energético e industrial*. Viçosa: Departamento de Engenharia Florestal, UFV, 2007. 63 p.
8. É. G, Maich, Master's Thesis, La Salle University Center, 2010.
9. G. Marinucci. *Materiais compósitos poliméricos, fundamentos e tecnologias*. Editora Altiber, Brazil, 2011.
10. M. L. C. Machado; N. C. Pereira; L. F. Miranda; M. C. Terence Polímeros: Ciência e Tecnologia 2010, 20, https://doi.org/10.1590/S0104-14282010005000011
11. L. M. Candian. Master's Thesis, Sao Carlos School of Engineering at the University of Sao Paulo , 2007.
12. M. A Paoli, *Degradação e Estabilização de Polímeros*., Editora Altiber, Brazil, 2009.
13. A, E Santos, Master's Thesis, Federal University of Rio Grande do Norte, 2007.
14. R, P. Nadolny, Master's Thesis. Federal University of Paraná, 2013.
15. R. L Mazur. Ph.D. Thesis, Paulista State University 2010.
16. H. M. Costa; V. D. Ramos; M. C. Andrade; P. S. R. Q Nunes. Polímeros 2016, 26, p.75-81.
17. M. S, Rabello. Aditivação de Polímeros, Editora Altiber, Brazil, 2000.
18. O, A. Souza, Master's Thesis, University Center of Volta Redonda, 2018.
19. L. Pinasu, Ph.D. Thesis. Federal University of Bahia, 2018.

DEVELOPMENT OF MAGNETIC COMPOSITES OF POLYPROPYLENE (PP) AND MAGNETITE MICROPARTICLES (FE_3O_4)

Patrícia R. Miranda[1], Palova S. Balzer[2*] and Ana P. T. Pezzin[2]

1 – Department of Process Engineering and Cristal Master, Joinville Region University (UNIVILLE) and Master Cristal, Joinville, SC, Brazil
2 – Department of Process Engineering and Cristal Master, Joinville Region University (UNIVILLE), Joinville, SC, Brazil palovabalzer@univille.com.br

Abstract - *This work describes the development and magnetic (FE_3O_4) characterization of magnetic composites based on the extrusion of polypropylene (PP) with the incorporation of magnetite microparticles, propylene-ethylene copolymer elastomer (PBE) and compatibilizer (PE-g-MAH). Magnetite-reinforced polymeric matrices have been studied in recent years in order to develop materials with technological applications aimed at engineering and biomedicine. In order to optimize the use of magnetic composites and their applications, this work intends to promote the improvement of the ductility of composites with PP matrix, as well as contribute to a better understanding of their properties. The incorporation of magnetite microparticles into the composite was carried out through a twin screw extruder with eleven heating zones. The samples were characterized by X-ray diffraction (XRD), and vibrating sample magnetometry (VSM). The XRD analysis showed the occurrence of intercalation and exfoliation of magnetite microparticles in the composites. The magnetic characterization shows how the saturation magnetization increases with the amount of magnetite added to the material. The production and characterization of the magnetic composites allowed determining the variation of their properties, according to the magnetite concentration and the presence or absence of propylene-ethylene copolymer elastomer and compatibilizer incorporated in the polymeric matrix. These properties make this material a promising raw material for the development of products and engineering applications based on magnetic polymeric composites. These applications may include, for example, the production of materials with an electromagnetic interference shielding function.*

Keywords: *Magnetic composite. Magnetite (FE_3O_4). Polypropylene. Propylene-ethylene copolymer. Compatibilizer (PE-g-MAH). Flexibility*

Introduction

The nature of the magnetoresistance change in magnetic polymeric composites has not yet been fully understood (RAMAZANOV et al., 2019). Thus, polymeric compositions with magnetic charges and other functional charges are of great interest, both from the theoretical point of view of their structure and in relation to their properties and practical application.

Polypropylene is appreciated for its remarkable and diverse qualities such as low density, excellent chemical and corrosive resistance, dimensional stability, recyclability, flexibility, good processability and low cost, which have contributed to make it ideal for a wide range of applications (MADDAH, 2016).

Magnetite can be used in technological applications such as heat sinks or packaging for electronic devices with shielding against disturbing radio frequencies and microwaves (WEIDENFELLER; HÖFER; SCHILLING, 2002). It can also be used in biomedicine due to its low cytotoxicity (HAMOUDEH et al., 2007), in computing devices for data storage and in the

design of parts for biomedical use that change shape when exposed to the presence of magnetic fields (ZHENG et al. al., 2009).

The incorporation of magnetite particles in considerable concentrations (above 5%) causes an increase in the rigidity of the polymers due to the high modulus of elasticity of its crystals (150 GPa), leading to a reduction in the resistance to impact (KHANDAN; et al., 2020). Thus, this work aimed to develop composites with magnetic property, ductility, balanced tensile strength and processing fluidity, through the incorporation of magnetite microparticles, propylene-ethylene copolymer (PBE) elastomer and PE-g-MAH compatibilizer in the matrix of the PP.

Experimental

The mixtures of PP, PPMOD, PP10%MAG, PPMOD10%MAG without LLDPE-g-MAH, PPMOD10%MAG, PP20%MAG and PPMOD20%MAG were made in a Henchel mixer, with a mixing capacity of 5 kg. Each mixture was under cold stirring for 10 min. Sample formulas are listed in tables 1 and 2.

Table 1 - Sample formulas without addition of magnetite microparticles

Materials	MAG (%)	PP (%)	PPMOD (%)
PP	-	100	88
Magnetite	100	-	-
PBE	-	-	8
PEBDL-g-MAH	-	-	3

Table 2 - Sample formulas with the addition of magnetite microparticles

Materials	PP10% MAG (%)	PPMOD10%MAG without PEBDL-g-MAH (%)	PPMOD10 %MAG (%)	PP20% MAG (%)	PPMOD20 %MAG (%)
PP	90	82	78	80	68
Magnetita	10	10	10	20	20
PBE	-	8	8	-	8
PEBDL-g-MAH	-	-	3	-	3

The equipment used to prepare the pelletized samples was a twin-screw extruder with an L/D ratio of 56, model EME-20, manufactured by the metallurgical company Scarpa.

1 X-Ray Diffraction (XRD)

The X-ray diffraction analysis was carried out in the Shimadzu XRD 6000 equipment, using Kα copper radiation, wavelength (λ) of 1.54056 nm, voltage of 40.0 kV, current of 30.0 mA and angles 2θ ranged from 5° to 70°.

2 Magnetism Measurements - Vibrating Sample Magnetometry (VSM)

The magnetic properties of magnetite powder (MAG) and samples were verified using the EZ9MicroSense vibrating sample magnetometer (VSM).

Results and Discussion

Figure 01 shows the diffractogram of magnetite, polypropylene with and without modification and magnetic composites. The α crystalline phase of polypropylene is evidenced in samples PP, PPMOD, PP10%MAG, PPMOD10%MAG without LLDPE-g-MAH, PPMOD10%MAG, PP20%MAG and PPMOD20%MAG through the peaks at angles of 13.9º; 16.8°; 18.3°; 21.2°; and 21.9°; which correspond, respectively, to planes (110), (040), (130), (111), and (131). The characteristic diffraction peaks of the β phase correspond to angles (2θ) 16.1º; 25.2°; and 28.2º, which correspond, respectively, to the crystallographic planes (300), (310) and (130) (LIMA, 2014).

Figure 01 - X-ray diffractogram of samples MAG, PP, PPMOD, PP10%MAG, PPMOD10%MAG without LLDPE-g-MAH, PPMOD10%MAG, PP20%MAG and PPMOD20%MAG.

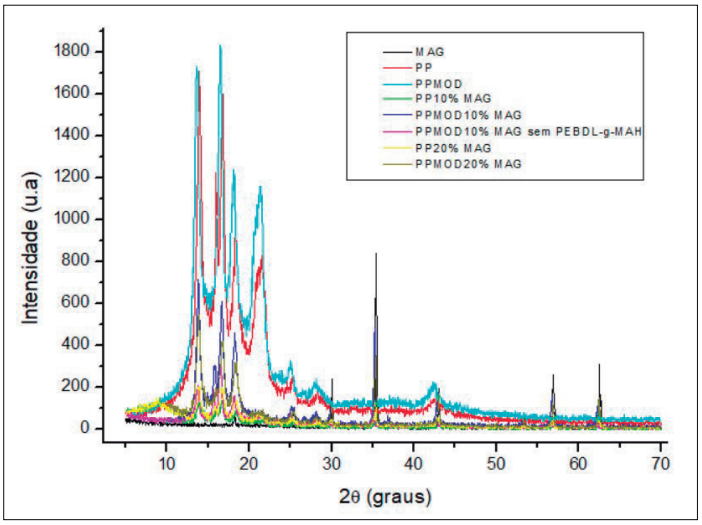

In the composites (PP10%MAG, PP10%MAG without LLDPE-g-MAH, PPMOD10%MAG, PP20%MAG and PPMOD20%MAG) the presence of polypropylene was verified in the region from 13 to 28°, which characterize the α and α phases. β of the PP. However, a reduction in the characteristic peaks of the α and β crystalline phases of polypropylene is evidenced, which indicates a possible synergistic interaction between the phases and, probably, the polypropylene is involving the magnetite particles. Similar results were presented by Garzon, et al. (2017) and Boery (2019).

The analysis of the regions of diffraction peaks characteristic of magnetite in the diffraction patterns of the magnetic composites (PP10%MAG, PPMOD10%MAG without LLDPE-g-MAH, PPMOD10%MAG, PP20%MAG and PPMOD20%MAG) allows identifying the occurrence of intercalation and exfoliation of microparticles in composites. This fact is evidenced due to the increase in the interplanar distance perceived in the X-ray diffractogram through the displacement of the diffraction peaks (angular position) to slightly smaller angles, as can be seen in Figure 01, which focuses on the region of 33 and 40° of the diffractogram.

The analysis of Figure 2 demonstrates that the samples of magnetic composites modified with the LLDPE-g-MAH compatibilizer (PPMOD10%MAG and PPMOD20%MAG), showed peaks of greater intensity in the characteristic regions of magnetite diffraction, which may infer a lower degree of exfoliation of microparticles. These results may suggest that the type of compatibilizer used in this study affected the morphology of the composites, that is, it originated predominantly intercalated magnetic composites or even that the extrusion process of polypropylene and magnetite composites modified with PBE and LLDPE-g-MAH need to be adapted in terms of process parameters in order to provide a greater degree of exfoliation of the microparticles.

Figure 2 - X-ray diffractogram of samples MAG, PP, PPMOD, PP10%MAG, PPMOD10%MAG without LLDPE-g-MAH, PPMOD10%MAG, PP20%MAG and PPMOD20%MAG.

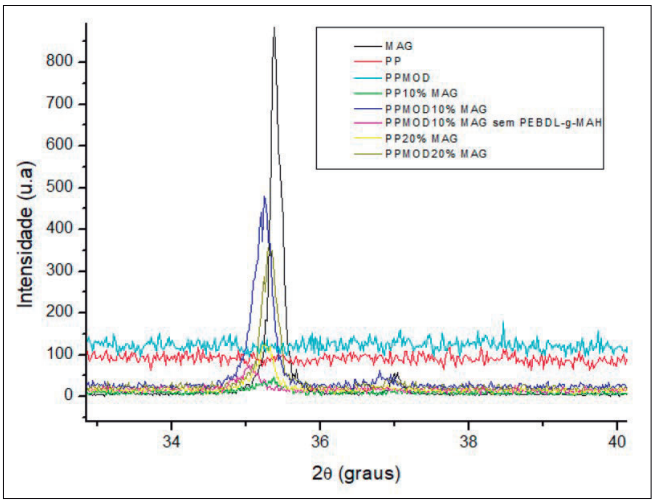

Magnetism Measurements - Vibrating Sample Magnetometry (VSM)

From the hysteresis curves, it was possible to determine the values of coercivity (Hc), saturation magnetization (Ms) and remanent magnetization (Mr) of the studied samples, which are presented in table 3.

Table 3 - Values of coercivity (Hc), saturation magnetization (Ms) and remanent magnetization (Mr) of the MAG, PP, PPMOD, PP10%MAG, PP10%MAG without LLDPE-g-MAH, PPMOD10%MAG, PP20% values MAG and PPMOD20%MAG

Sample	Hc (Oe)	Ms (emu/g)	Mr (emu/g)
MAG	67,9	90,2	5,5
PP	0	0	0
PPMOD	0	0	0
PP10%MAG	72,9	8,0	0,6
PPMOD10%MAG sem PEBDL-g-MAH	79,2	4,2	0,3
PPMOD10%MAG	72,0	13,9	1,2
PP20%MAG	74,0	15,9	1,3
PPMOD20%MAG	75,8	15,2	1,1

In general, it can be observed that the samples with magnetite incorporation showed very narrow hysteresis curves with low values of remanent magnetization (Mr) and coercive field (Hc), characteristic behavior of a ferrimagnetic soft magnetic material, that is , of non-permanent magnets, which magnetize and demagnetize very easily (DINIZ; et al, 2015).

It is also verified that the coercivity (Hc) of the composites does not depend on the concentration of magnetite incorporated in the polymer, this fact can be attributed to the distribution of the microparticles and the random orientation of the magnetic moments. Similar results were presented by Ramajo, et al., 2009, Guo, et al., 2007 and Garzon, et al. (2017).

The saturation magnetization obtained in the MAG sample, composed only of magnetite microparticles, presented a value of 90.2 emu/g, similar results were found in the works of Posada (2015) and Lara-Gonzales (2019) which indicated values of 81.22 emu/g and 84 emu/g, respectively.

The concentration of magnetite microparticles in the magnetic composite directly influences the saturation magnetization. In this study, the highest Ms value obtained in the composites with 10% magnetite was 13.9 emu/g, whereas in the composite with 20% magnetite an Ms of 15.9 emu/g

was obtained. In studies, such as the one by Lara-Gonzalez (2019), Ms values at room temperature of high-density polyethylene (HDPE) magnetic composites with the addition of 10 and 20% magnetite microparticles, with an average particle size of 14 .6 microns were 5.49 and 5.97 emu/g, respectively. Posada (2015), obtained Ms values of 17.21 and 25.72 emu/g for HDPE composites with the addition of 10 and 20% magnetite microparticles, respectively. The magnetite used in the study by Posada (2015) had particles with sizes ranging from 0.8 to 57 microns. With the analysis of the Ms values of the magnetic composites in this study and similar studies, with the incorporation of 10 and 20% of magnetite microparticles, it is believed that one of the factors that directly impacts the Ms value is the dispersion of the microparticles in the composite, which would justify the same class of material (magnetite microparticles) presenting such variation in saturation magnetization.

Conclusions

The analysis of the regions of diffraction peaks characteristic of magnetite in the diffractograms of the magnetic composites proved the occurrence of intercalation and exfoliation of the microparticles in the composites. The FTIR analysis revealed that the introduction of magnetite in the polypropylene matrix does not promote chemical changes in the polymer structure.

It was also found that magnetite increases the thermal stability of PP and that its impact on the fluidity index of the polymeric matrix is insignificant. The values of saturation magnetization (Ms) and coercivity (Hc), measured by VSM, prove the magnetic properties of the composites.

Acknowledgements

Center for Technological Sciences at the State University of Santa Catarina (UDESC) in Joinville, Cristal Master Company, Magnetism Laboratory of the Physics Institute of the Federal University of Rio Grande do Sul (UFRGS) and Joinville Region University (Univille).

References

1. M. N. O. Boery, Ph.D. Thesis, Campinas State University – UNICAMP. Campinas, 2019.
2. V. C. S. Diniz, et al. Ceramic, 2015, 61, 10.1590. https://doi.org/10.1590/0366-69132015613591909.
3. A. O. Garzon et al. Revista de la Academia Colombiana de Ciencias Exactas, Físicas y Naturales, 2017, 41, 0.18257. https://doi.org/10.18257/raccefyn.422.
4. Z. GUO, et al. Journal of applied physics, 2007, 101, 10.1063. https://doi.org/10.1063/1.2711074.
5. A. Khandan, et al. Dental Hypotheses, 2020, 11, 10.4103. https://doi.org/10.4103/denthyp.denthyp_11_20.
6. L. Á. Lara-Gonzalez.Ph.D. Thesis, Universidad Pedagógica y Tecnológica de Colombia (UPTC), Tunja, 2019.
7. H.A. Maddah. American Journal of Polymer Science, 2016, 6, 10.5923. http://doi.org/10.5923/j.ajps.20160601.01.
8. POSADA, A. O. G. Posada. MSc. Universidad Nacional de Colombia, Bogotá, 2015.
9. RAMAJO, L. A. et al. Composites Part A: Applied Science and Manufacturing, 2009, 40, 10.1016. https://doi.org/10.1016/j.compositesa.2008.12.017.
10. M. Ramazanov, et al. Journal of Elastomers & Plastics, 51, 2019, 10.1177. https://doi.org/10.1177/0095244318768652.
11. WEIDENFELLER, B.; HÖFER, M.; SCHILLING, F. Thermal and electrical properties of magnetite filled polymers. Composites Part A: Applied Science and Manufacturing, vol. 33, agosto 2002. p. 1041–1053.
12. X. Zheng, et al. Colloids and Surfaces Part B Biointerfaces, 71, 2009, 10.1016. http\\doi: 10.1016/j.colsurfb.2009.01.009.

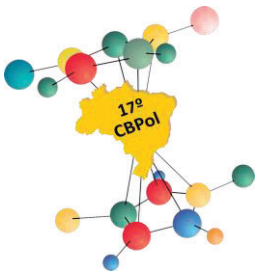

DEVELOPMENT OF SYNTHETIC COMPOSITE WITH RECYCLED HIGH DENSITY POLYETHYLENE (HDPE) MATRIX AND FIBERGLASS REINFORCEMENT

Kelson S. G. Vilhena[1*], Milenna A. B. Rodrigues[1] and Thais S. Santos[1]

1 – Superior School of Technology, State University of Amazonas, Av. Darcy Vargas, 1200, 69050-020, Manaus, Amazonas Brazil.

*ksgv.emt17@uea.edu.br**

Abstract - In the last decade, the thermoplastic composites industry has shifted its focus from the development of advanced high-performance composites to the development of low-cost engineering composites. In this context, compounds consisting of polymer matrices, such as high-density polyethylene, loaded with inorganic particulate fillers and reinforced with glass fibers, are inserted (Khanam, P.N.; Al Maadedd, M.A.A, 2015). In order to expand the field of applications of high density polyethylene, some properties such as: high coefficient of thermal expansion, narrow temperature range, low values of mechanical properties in traction and flexion for applications that require greater strength and resistance, low electrical and thermal conductivity for certain applications, among others, can reach desirable values through the development of compounds formulated with this polymer as a matrix (Zhang, S. et al, 2011). Glass fibers stand out as the synthetic fibers most used as a reinforcing element in composites, as they have the following properties: low coefficient of thermal expansion, ease of processing and low cost (Alam, A.K.M.M, 2011). Therefore, the objective of this project is to collect and sanitize recyclable and reusable polymeric materials such as HDPE to be a matrix and produce composite materials with fiberglass reinforcement through extrusion and plastic injection, observing, in accordance with ASTM D-1238, evaluating the properties mechanical, optical and thermal in order to emphasize the reduction of synthetic polymeric materials in the environment.

References:

1. Khanam, P.N.; Al Maadedd, M.A.A. Processing and characterization of polyethylene-based composites. Advanced manufacturing: Polymer & Composites Science, v.1, n.2, p.63-79, 2015.
2. Zhang, S; Cao, X.Y.; Ma. Y.M.; Ke, Y.C.; Zhang, J.K.; Wang, F.S. The effects of particle size and content on the thermal conductivity and mechanical properties of Al2O3/high density polyethylene (HDPE) composites. Express Polymer Letters, v.5, n.7, p.581-590, 2011
3. Alam, A.K.M.M.; Shubhra, Q.T.H.; Al-Imran, G.; Barai, S.; Islam, R.; Rahman, M. Preparation and characterization of natural silk-fiber reinforced polypropylene and synthetic E-glass fiber-reinforced polypropylene composites: a comparative study. Journal of Composite Materials, v. 45, n. 22, p. 2301–2308, 2011.

Fundings: pro dean of extension - PROEX.

Keywords: *HDPE, Fiberglass, composites, reuse, recycling*

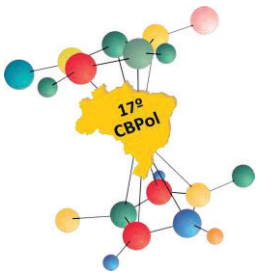

EFFECT OF BACURI SEED (BS) NATURAL FILLER ON PBAT

Gabriela M. dos Santos[1*], Cléverson F. S. Gabriel[1] and Marcia G. de Oliveira[1]

1 – Polymeric Materials Technology Laboratory (LAMAP), Materials Division (DIMAT), Materials Technology Coordination (COTEM), National Institute of Technology (INT), Rio de Janeiro, RJ, Brazil
gabriela.moura@int.gov.br

Abstract
The goal of this work was to develop PBAT biocomposites with agroforestry residue, evaluating the effects of adding different proportions of residue on the mechanical and rheological properties of the material. The residue used was Bacuri seed (BS) classified with particle size between 0.84 mm and 0.59 mm and its morphology and thermal stability were evaluated. Regarding the processing of the mixture, both the torque and the specific energy decreased according to the addition of the filler, showing that the BS acts as a processing auxiliary, increasing the fluidity of the mixture, a fact that is also proven by the rheological analysis. For the mechanical properties, the addition of BS caused a drop in the tensile strength compared to pure PBAT and an increase in the level of elongation, indicating that for the BS contents analyzed, this filler presents a potential use as a processing auxiliary and as a filler.

Keywords: *PBAT, Bacuri Seed, Biodegradable Polymer, Agroforestry Waste, Organic Filler.*

Introduction

Bacuri, found in the eastern Amazon region and in transition areas from the forest biome to the cerrado, is a fruit with the scientific name Platonia insignis. The fruit contains a bittersweet pulp rich in potassium, phosphorus and calcium, which is consumed directly or used in the production of sweets, ice cream, juices, jellies, liqueurs and other delicacies. Its bark is also used in regional cuisine and the oil extracted from its seeds is used as an anti-inflammatory and healing agent in popular medicine and in the cosmetics industry [1-3]. Much of the residue of this fruit corresponds to the part of the seed that, after extracting the oil, is completely discarded. To date, there are still no articles published in international journals on the use of Bacuri seed (BS) as filler in polymeric compositions, in particular, in biodegradable polymers such as PBAT.

The PBAT is a synthetic and biodegradable random copolymer of butylene adipate and terephthalate that has high thermal stability, elongation at break (as high as 700%), wear, and fracture resistance. Its characteristics are similar to low-density polyethylene (LDPE) and linear low-density polyethylene (LLDPE), being indicated mainly for the manufacture of packaging films, agricultural films (mulch) and compostable garbage bags [4]. Its main advantage compared to LDPE and LLDPE is its biodegradation, being a more environmentally friendly polymer, especially in a country like Brazil that disposes about 40% of the garbage collected improperly [5]. And the main disadvantage of PBAT is its high price compared to other polymers in the same segment on the market.

The use of biodegradable polymers in combination with low-price organic fillers has proven to be a good approach to produce cost-effective composites in order to address pollution issues and develop products with superior mechanical properties. Therefore, the goal of this work was to develop a biocomposite containing Bacuri seed residues (BS), and to evaluate the use of 5, 10 and 15 phr of this agroforestry residue as filler in biodegradable composites containing PBAT as matrix.

Experimental

The BS was received dried and ground. Therefore, the first stage of the work was its granulometric classification in a sieve of different opening sizes. The material was used with a granulometry from Mesh tyler 28 (0.59 mm) to Mesh tyler 20 (0.84 mm). The BS and the cryo-fractured composites morphology was analyzed using a scanning electron microscope (SEM) FEI Company, model INSPECT S50, a voltage of 15kV, low vacuum mode, using a backscatter detector (BEI), and the samples were covered with gold. Thermogravimetric analysis (TGA) was performed on the Q500 Thermoanalyser from TA Instruments in a flow stream from room temperature to 800°C, with a heating rate of 10°C/min. The PBAT and composites were prepared by melt intercalation in an internal mixing chamber coupled to a torque rheometer Haake Polylab OS. The rotor used was the Roller type, at 140°C, with a speed of 80 rpm for 15 minutes. The formulations were 0, 5, 10 and 15 phr (parts per hundred resin) of Bacuri Mesocarp per 100 phr of PBAT, and were named PBAT, PBAT5BS, PBAT10BS and PBAT15BS respectively. The specimens for the mechanical tests and the rheological analysis were molded by compression, according to their respective standards, in a hydraulic press MA 098/A400 with a pressure of up to 55 MPa at 140°C, for 10 minutes in the hot press and then cooled using the same pressure and time in the cold press. Rheological analysis was carried out on an Anton Paar MCR301 rheometer using a model CTD450 furnace as an accessory with 25 mm parallel plate geometry. All tests were carried out at 140°C. Complex viscosity (η*) was measured through a strain variation test from 0.01% to 500%, at a constant frequency of 1Hz. The storage modulus (G') and the Loss modulus (G”), were measured through an angular frequency variation test from 0.1 to 100 rad/s, in the linear viscosity region (10% constant strain). The tensile strength test was carried out in a mechanical testing machine EMIC DL3000 with a 1000 N load cell and a speed of 100 mm/min, according to ASTM D638 standard, type V specimen.

Results and Discussion

Bacuri Seed Analysis

Regarding the granulometric classification, for this project it was decided to use the particle size between 0.84 mm and 0.59 mm. The BS morphology is presented in Fig 1 (A; B; C) shows irregular particles, with low porosity and high roughness.

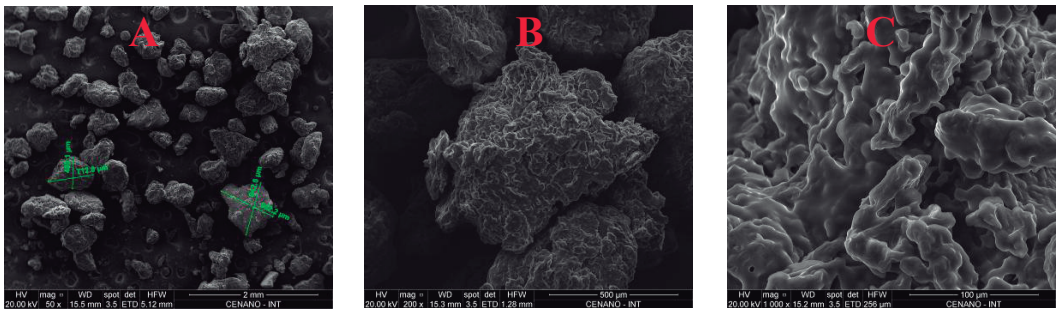

Figure 1 - Scanning electron microscopy of the Bacuri Seed A: 50x; B: 200x and C: 1000x.

The thermogravimetric analysis of the filler is shown in Fig 2. Note that the BS has excellent thermal stability, showing only a small loss of weight related to water loss up to 200ºC and a maximum degradation at 391ºC, a value close to the degradation temperature of the PBAT, which indicates that the filler should not impair the thermal resistance of the biocomposite. The BS left a residue of 8.33%.

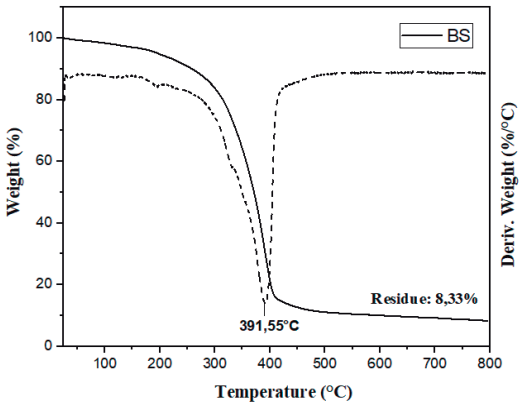

Figure 2 – Termogravimetric analysis of Bacuri Seed.

Mixture Processability Analysis

Fig 3 shows the evolution of the equipment torque as a function of time (Fig 3A) and the evolution of the specific energy of the mixture as a function of time (Fig 3B). The first peak in the torque evolution graph (Fig 3A) refers to the addition of the PBAT and the inflection in the curve at approximately 3 minutes refers to the addition of the filler (BS). As the material passes into the molten state, its fluidity increases and the torque drastically decreases until it remains constant, a sign that the mixture has been homogenized. It was evident that when adding larger amounts of BS, the torque needed to keep the mixture at constant speed decreased, indicating that the filler is acting as a processing auxiliary, increasing the fluidity of the mixture. This effect is mainly pronounced when observing the variation of the slope of the straight line in the evolution graph of the specific energy of the mixture as a function of time (Fig 3B). As BS is an oily material, as the mixing time elapses, this oil adheres to the polymeric matrix, facilitating the non-linear mixing. With this, it is possible to indicate that the BS acted as a processing auxiliary, increasing the fluidity of the mixture. In Table 1, this effect can be better observed when evaluating the final torque of the mixture and the final specific energy.

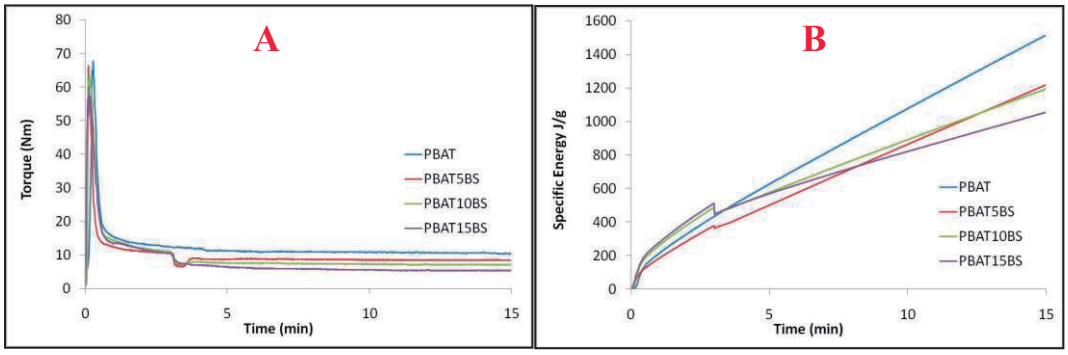

Figure 3 - A: Torque (Nm) over mixing time and B: Specific energy (J/g) over mixing time.

Table 1 - Final torque and specific energy of the mixtures.

Experiment	Final Torque (Nm)	Final Specific energy (J/g)
PBAT	9.9	1452
PBAT5BS	8.4	1217
PBAT10BS	7.1	1193
PBAT15BS	5.3	1054

Rheological analysis

Fig. 4 shows the variation of the complex viscosity of the material as a function of deformation. The viscosities of PBAT and composites were very similar, but as BS was added, the complex viscosity

of the composite decreased, that is, the fluidity of the material increased, corroborating the processing results.

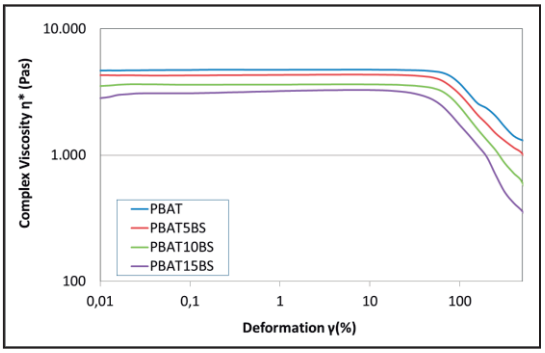

Figure 4 - Complex viscosity versus deformation.

The variation of G' and G" with increasing angular frequency are shown in Fig 5A and Fig 5B, respectively. The values of G' were very close, which means that the addition of BS had little influence on the elasticity of the material, as evidenced by the result of tensile strength. Very close G" values were also observed, following the material viscosity results. These results indicate few changes in the viscoelastic behavior of the material as filler is added, therefore, few changes would be necessary to manufacture a PBAT product with BS compared to pure PBAT.

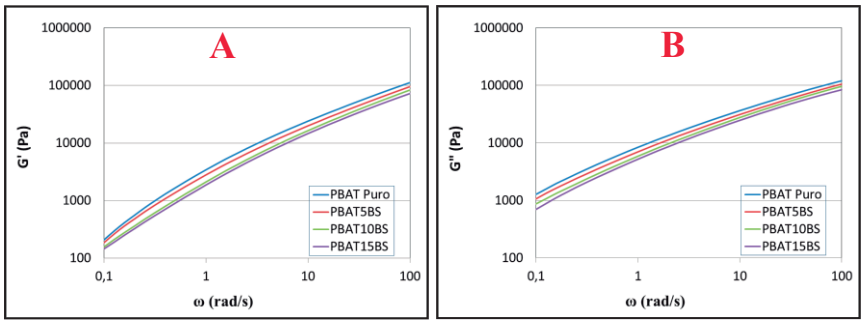

Figure 5 - Variation of the storage modulus (G') (A) end Loss modulus variation (G") versus angular frequency (B).

Mechanical Results

In Fig 6A and Fig 6B the elongation and the tensile strength at break of the material are shown.

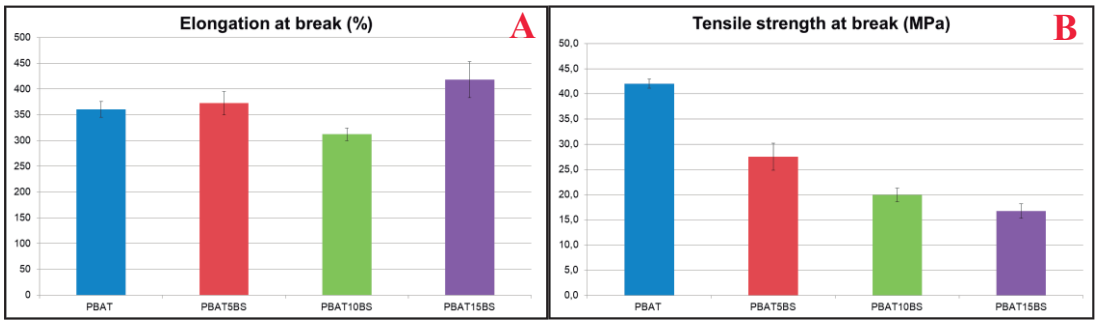

Figure 6 - A: Elongation at break (%); B: Stress at break of PBAT and composites with Bacuri Seeds.

Analyzing the results from elongation at break, for the BS composites, a linearity of the results within the experimental error was observed, corroborating the results of G". This result is an indication that when the most important property analyzed is elongation, more BS residues can be added as a way to make the final product cheaper. Regarding the tensile strength at break, it was evident the decrease of this property as BS was added.

Fracture Morphology

The fractured surface of pure PBAT is observed in Fig 7A and Fig 7B, and it is possible to notice the appearance of some "scales" consistent with the elasticity of the material. Fig 7(C-H) are presented the morphologies of the composites of PBAT with BS, in these micrographs it is possible to verify the presence of holes resulting from the detachment of BS from the polymeric matrix (PBAT). The chemical difference between polymers and natural fillers in composites could cause low compatibility between both materials generating voids or gaps at the interface, which lead to reduction in some mechanical properties, especially tensile strength.

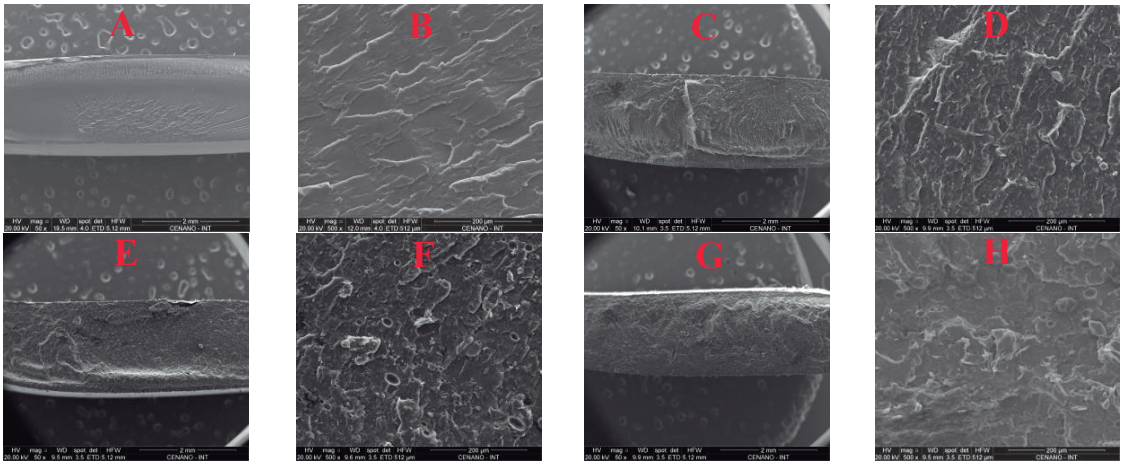

Figure 7 - SEM of the fractured material in liquid nitrogen, being: A: PBAT (50x); B: PBAT (500x); C: PBAT5BS (50x); D: PBAT5BS (500x); E: PBAT10BS (50x); F: PBAT10BS (500x); G: PBAT15BS (50x); H: PBAT15BS (500x).

Conclusions

Bacuri Seed is low-cost filler and PBAT/BS composites are biodegradable, environmental friendly, and cost effective. For the analyzed BS contents, the filler proved to be able to be used as a processing auxiliary or as filler, but not as reinforcement, as it did not effectively improve the mechanical results. Products based on these compounds have great potential since their mechanical Properties are still suitable for several applications.

Acknowledgements

The authors would like to thank INT and CNPq for logistical and financial assistance. Valdir Florêncio of IME, for the Bacuri donation. Ana Maria Furtado of UERJ and Regina Célia Reis of UFRJ for complementary analysis. To Cenano-INT for the scanning electron micrographs.

References

1. A. K. O. Homma; J. E. U. De Carvalho; A. J. E. A. De Menezes. Ciência Hoje 2010, 46, 39. https://ainfo.cnptia.embrapa.br/digital/bitstream/item/25022/1/homma-bacuri.pdf
2. T. W. Bispo; C. L. Braga; C. C. Lima; S. F. Rocha. Revista Grifos 2021, 31, 01. https://doi.org/10.29327/soberebpc2021.342291
3. E. de C. F. R. Rodrigues; A. K. O. Homma; O. R. Kato; A. J. E. A. De Menezes. Boletim de Pesquisa e Desenvolvimento (CPATU) 2021, 147, 01. https://www.infoteca.cnptia.embrapa.br/infoteca/handle/doc/1131637
4. A. M. Zamora *et al.* in *Atlas do Plástico: Fatos e números sobre o mundo dos polímeros sintéticos*, K. Schächtele, Ed.; Fundação Heinrich Boll, Rio de Janeiro, 2020, Vol. 1, 1-64.
5. ABRELPE. Panorama dos resíduos sólidos no brasil 2021. https://abrelpe.org.br/panorama-2021/

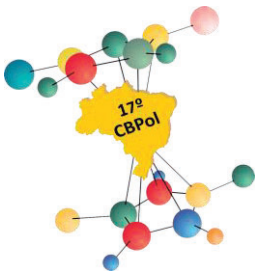

EFFECT OF INCORPORATING RECYCLED FLEXOGRAPHIC PHOTOPOLYMER PLATE PARTICLES INTO AN EPOXY MATRIX

Marina Kauling de Almeida[1], Lara Vasconcellos Ponsoni[1], Matheus Vinícius Gregory Zimmermann[1]

1 – Universidade do Extremo Sul Catarinense (UNESC), Av. Universitária, 1105, CEP 88806-000, Criciúma, SC, Brazil.
marinakauling.a@gmail.com

Abstract – A thermosetting epoxy polymer composed of diglycidyl ether of bisphenol A and triethylenetetramine was modified by incorporating flexographic photopolymer plate residues. The residues were processed in two ways: a) by grinding and performing particle size classification (PP) and b) by polyester layer separation and grinding the elastomeric fraction by cryogenic grinding (ER). Both residual particles were incorporated into the epoxy at concentrations of 2.5, 5 and 7.5 wt%. The main results indicate that PP was not efficient as a modifier of the epoxy system, was observed a reduction in mechanical properties (maximum tensile strength and deformation) in the samples with PP. When the ER is incorporated, an increase in tensile property, deformation capacity and impact resistance was observed in samples. Scanning electron microscopy analysis showed a greater presence of voids in formulations produced with PP, which corroborates the decrease in the tensile strength of these samples.

Keywords: *Epoxy, residues, elastomer residue, mechanical properties.*

Introduction

The use of residues as reinforcement or fillers in polymeric compositions is a practice that has gained great prominence in recent years and continues to grow, since it contributes to the valorization and reuse of discarded materials. In addition, these materials also promote specific changes in the polymeric material, such as increasing stiffness, improving toughness or even reducing product costs. The recycling and valorization of residues produced in processes reduces costs and provides new opportunities for limiting the use of natural resources; as a direct consequence, there is a reduction in environmental impact and production costs [1].

One of the fastest growing sectors in recent years is polymer packaging. Among all polymeric materials, flexible films are becoming increasingly popular, mainly due to their versatility, light weight, strength and printability, among other properties [2,3]. However, as a result of this activity, one of the main residues generated from the production of flexible packaging is photopolymer plates used in the flexography step of polymeric film production. Photopolymer plate residues are essentially formed by two distinct materials: (I) a base polyester, which has the goals of supporting the photopolymer plate and guaranteeing its dimensional stability, and (II) a photopolymer elastomer. Photopolymers are light-sensitive materials (photosensitive) responsible for the formation of graphics and counter graphics. During exposure to UV radiation, photopolymer monomers polymerize (crosslinking the plate material), leaving these areas resistant to chemical action during the development process. No exposure areas are removed during this process [4]. These materials have a relatively short lifespan, and after that, they are usually sent to landfills.

Despite the large industrial consumption of these materials in the plastic packaging sector, there are few solutions or applications for their reuse or even relevant publications about the recycling or reuse of these plates used in flexographic printing. However, it is known that the use of

recycled elastomers, when incorporated into other resins in small amounts, can modify the properties of the polymer matrix, such as toughness and impact resistance.

For thermoset materials, one of the polymers that has been investigated with combinations of elastomer residues is epoxy. Epoxy-based resins are thermosetting polymers that are relatively easy to process and relatively inexpensive. This material is often used as a matrix in high-performance composites. However, although most epoxy-based resins have high stiffness and specific strength, they are fragile due to their highly crosslinked network structure [5,6]. Thus, an undesirable property of epoxy is its low resistance to crack propagation, which makes it a fragile material. Several methods have been proposed to increase the strength of epoxy resins, one of the most successful methods is the use of composite materials based on "epoxy-rubber" due to their low cost and easy fabrication, and their use is increasing due to their performance and wide range of functional properties [5,7,8]. Among the different epoxy modifiers, rubber particles have good performance as a hard and tough modifier of polymer matrices [9-11]. Epoxy resins can be modified by incorporating a particulate elastomer, which will lead to the formation of a second phase in the material, altering the material's morphology. The incorporation of an elastomeric phase in a thermoset matrix is a common means of increasing fracture toughness, as reported by Almeida et al. (1998) [12], and according to Kaynak et al. (2003) [13], the main advantage of this method is the control of particle size and volume fraction. According to Tang et al. (2012) [14], the major toughening mechanisms involving rubber particles are debonding/cavitation, localized shear banding of matrix, as well as rubber particle bridging. However, with the improvement in fracture toughness and/or tensile strength, other desirable properties of rubber-epoxy resins, such as the elastic modulus and failure strength may decrease significantly [14-16].

Thus, this study aims to evaluate the influence of the use of the residue of photopolymer plates discarded from the plastic packaging industry as a modifying agent of mechanical properties in an epoxy system composed of diglycidyl ether of bisphenol A and triethylenetetramine (DGEBA/TETA).

Experimental

Materials

The residue of useless photopolymer plates originating from the flexography process of polymeric packaging was kindly provided by Canguru Plásticos Ltd. located in Criciúma/SC, Brazil. Bisphenol A diglycidyl ether epoxy resin (DGEBA), with the trade name Araldite F, and cold curing agent triethylenetetramine (TETA), with the trade name Aradur 951, were purchased from Maxepoxi Industrial e Comercial Ltd. The toluene used to separate the components of the photopolymer plates was obtained from Dinâmica Química Contemporânea Ltd.

Methods

In this study, the photopolymer flexographic plates were recycled and evaluated in the form of two residues used as epoxy resin modifiers: (I) residues in their natural form, by which only mechanical processes of grinding and granulometric classification were applied, called photopolymer plates (PPs), and (II) residues after phase separation (constituents), preferably achieved using the elastomeric fraction of the material, called elastomer residues (ERs). In condition II, first, the components of the useless photopolymer plate were separated, in which a Soxhlet extractor was used by adopting the methodology described by Cordeiro et al. (2010) [4]. Subsequently, the PPs and ERs were processed by mechanical grinding using a Mecanofar MF160 knife mill with a Ø 10 mm sieve. After this step, the natural plates were micronized by a mechanical process using a knife mill and particle size classification, while the ER was again micronized by a cryogenic process using a Netzsch Attritor highenergy mill operated at 1400 rpm for a grinding time of 3 h in a cryogenic atmosphere with liquid nitrogen. In the end, particles with particle sizes smaller than 24 mesh (0.5 mm) were obtained in both processes.

In the preparing of the sample PP or ER/epoxy, was used a stoichiometric ratio between the epoxy resin (DGEBA) and the curing agent TETA of 0.67; the resulting sample was denoted 13 PHR (13 grams per 100 parts of resin). Both residues (PP and ER) were added at percentages of 0 (no modifier), 2.5, 5 and 7.5 wt% to the epoxy/DGEBA system. First, the resin was weighed and manually mixed with the curing agent (TETA), PPs and ERs in a beaker (50 mL) for approximately 1 minute in the proportions described with the aid of a glass rod. The mixtures were placed under vacuum for 15 minutes to remove the bubbles and then poured into a stainless-steel cast previously coated with aluminum film and release agent to facilitate extraction. The specimens were cured at room temperature and characterized after 10 days of production.

Morphological analysis of the ER, PP residue and epoxy was performed by scanning electron microscopy (SEM) using a JEOL JSM-6390 instrument. Due to the need to obtain a conductive surface, the samples were covered with a thin film of gold applied by sputtering a Denton Desck IV vacuum metallizer. The mechanical properties of epoxy with and without modifiers were determined by measuring tensile strength with Emic DL10000 equipment using a 10 kN load cell and speed of 1 mm·min-1 according to the ASTM D638 standard. All tests were conducted at 25 ± 2°C. Five specimens were used to determine the tensile strength property of each sample.

Results and Discussion

Fig 1 shows the micrographs obtained by performing SEM on the PPs and ER after processing. The milling method interfered with the morphology of the particles. The plate milled by a mechanical process only (and particle size classification) resulted in more irregular particles with great variation in particle size and morphology. In the rubber particles ground by a high-energy cryogenic process, the size and morphology of this material were uniform. The mean size observed in the ER particles was 250 ± 53 μm.

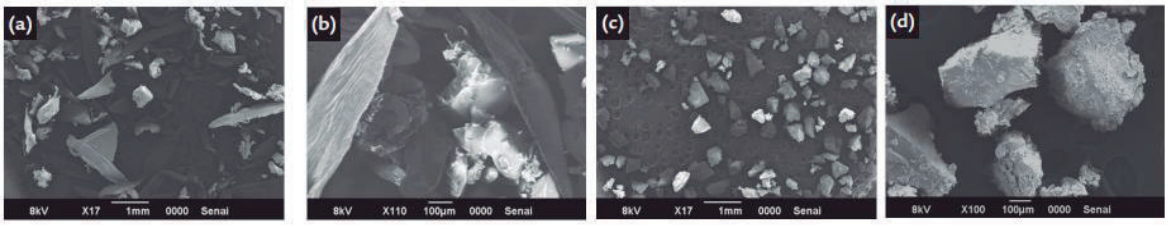

Figure 1 – SEM micrographs of the PPs (a and b) and ER (c and d) after processing.

Table 1 shows the tensile strength and impact strength results obtained from the mechanical tests performed on the epoxy and epoxy modified with PPs and ER. It was observed that the PP particles did not bring significant variation in the impact strength of the epoxy. The ER particle increased the impact strength by up to 21.3% (Epoxy/ER5 sample) when compared to unfilled epoxy. Although and within experimental errors, 5 wt% of ER seems to be sufficient to bring a significant change in impact property compared to neat epoxy resin. The presence of the PP modifier, when compared to unfilled epoxy, tends to reduce the tensile strength of the epoxy and considerably reduce the deformation capacity of these samples with the 3 evaluated contents. The ER modifier, on the other hand, increases the tensile strength at contents of 2.5 and 5 wt% and does not significantly change the deformation of materials modified with ER compared to pure epoxy, except for the epoxy/ER 2.5 sample, which showed a significant improvement in deformation capacity. This fact may be associated with the shape of the ER being more regular than that of the PP, as well as the removal of impurities from the photopolymer plate and the presence of voids in the epoxy matrix, as will be shown below. A similar ultimate tensile strength reduction behavior of epoxy with rubber particles was also reported by Manjunatha et al. (2010) [17].

Table 1 – Tensile properties of epoxy with and without PP and ER modifiers.

Sample	Tensile strength (MPa)	Strain at Break (mm/mm)	Elastic Modulus (GPa)	Izod Impact strength (kJ/m²)
Epoxy	22.93 ± 1.69	0.10 ± 0.01	3.18 ± 0.34	16.4 ± 1.1
Epoxy/PP2.5	13.88 ± 1.41	0.04 ± 0.01	5.02 ± 1.53	16.7 ± 1.2
Epoxy/PP5	20.08 ± 2.62	0.02 ± 0.01	4.34 ± 1.15	14.5 ± 3.7
Epoxy/PP7.5	15.28 ± 2.28	0.02 ± 0.01	7.13 ± 0.46	15.2 ± 2.6
Epoxy/ER2.5	29.12 ± 2.22	0.20 ± 0.02	3.99 ± 1.63	16.1 ± 3.2
Epoxy/ER5	29.07 ± 2.92	0.14 ± 0.09	5.48 ± 1.49	22.8 ± 1.1
Epoxy/ER7.5	21.66 ± 1.81	0.10 ± 0.05	4.66 ± 1.28	19.9 ± 3.5

Many authors attribute the decrease in the elastic modulus and increase in the deformation capacity of the epoxy system to the incorporation of rubber particles [5,10,17,18], a fact not observed in the samples with ER and PP particles, which suggests that these particles presented a reinforcing and non-toughening character. Interestingly, the sample reinforced with PP showed a decrease in tensile strength, but an increase in the elastic modulus, which is possibly associated with a decrease in the deformation capacity of the sample. Samples reinforced with ER particles showed an increase in tensile strength and an increase in modulus, when compared to pure epoxy, but lower when compared to samples reinforced with PP. This fact may be associated with the greater deformation capacity of these samples. PP particles probably cannot transmit the same characteristics observed using conventional rubbers, which suggests that PPs are more rigid than ER or conventional rubbers.

To understand the failure mechanism associated with the inclusion of PP and ER particles, the failure surfaces of the specimens were examined using SEM. Fig 2 shows the SEM micrographs obtained for the fracture region of the samples after the tensile strength test. The absence of holes and voids in pure epoxy was observed, and all samples modified with PPs and ER showed voids. Comparatively, the epoxy samples with the PP residue seem to have more bubbles than the samples with ER. This may be because PPs contain residue of paints and solvents, which during processing can volatilize and generate these bubbles. When ER undergoes the phase separation, cryogenic grinding and drying process, this component is reduced by the extraction of the solvents used in the process.

According to Irez et al. 2020 [5], in a study on epoxy modification using EPDM residues as the elastomeric phase, a reduction in the tensile strength was also observed with the addition of the elastomer. The authors credit this reduction to the low interfacial adhesion between the elastomer and the epoxy causing the formation of voids. Crosslinked elastomers provide few active sites on the surface of rubber particles, which makes it difficult to form chemical bonds with epoxy. Additionally, due to this low compatibility, voids can form in the epoxy matrix, which gives rise to low tension transfer from the matrix to the rubber particles, reducing the overall stiffness of the compounds. During solidification, different concentrations of rubber and epoxy can bring some inequalities in the balance of internal tensions, which leads to void formation at the existing interfaces. Furthermore, with the increase in the content of recycled rubber particles, the possibility of observing agglomerations increases. Therefore, these agglomerations could create weak parts (weak points) in the composite. Consequently, when the composites are subjected to loading, these voids and agglomerates mentioned above constitute the weak points of the composite where cracks can start/occur. This state results in premature failure. This mechanism may be associated with the low tensile strength response of samples reinforced with PP. Fig 3 shows SEM micrographs of the epoxy/ER5 sample, with emphasis on the particle-fiber interface region. The particles show moderate interaction with epoxy, with regions with good wettability and interaction (Fig 3a) and regions of voids (Fig 3b) caused both by the presence of agglomerates, by the volatilization of particle components such as moisture or residues of paints or by changing the viscosity of the resin.

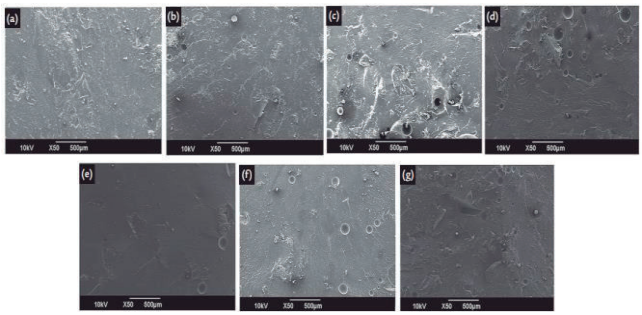

Figure 2 – SEM micrograph of (a)pure epoxy, (b)EP/PP 2.5; (c)EP/PP 5; (d)EP/PP 7.5; (e)EP/ER 2.5; (f)EP/ER 5; and (g)EP/ER 7.5.

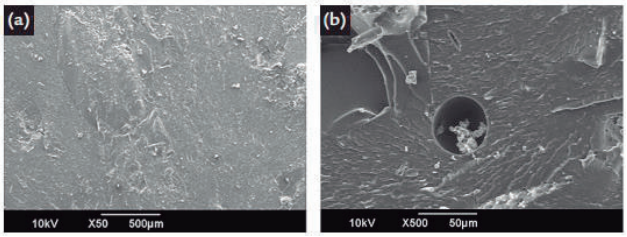

Figure 3 – SEM micrograph showing the interface region in the epoxy/ER composite with (a) good interaction and (b) weak interaction in the interface region.

Conclusions

The DGEBA/TETA epoxy system was modified by two different residues from flexographic photopolymer plates in different mass fractions, and the impact of incorporating these two types of particles from photopolymer plate residues on the mechanical properties of epoxy was analyzed. The processing and separation of the polyester fraction contributes to the production of an epoxy system with superior mechanical properties (tensile and impact strength). The incorporation of PP particles was not effective in improving the deformation/elongation capacity of the epoxy when subjected to mechanical tensile action, which suggests that the incorporation of this material brings a reinforcing and non-toughening characteristic to the epoxy. However, after beneficiation and phase separation, the epoxy samples modified with ER particles showed an improvement in their maximum stress and deformation properties. By morphological analysis of the fracture region, voids were observed in all samples containing PPs and ER, a fact not observed in pure epoxy. The processing of the residue of photopolymer plates, with the separation of the polyester fraction, contributes to the production of more homogeneous particles, which makes this material more applicable for epoxy modification.

References

1. BEAUSON, J.; LILHOLT, H.; BRONDSTED P. Journal of Reinforced Plastics and Composites, v. 33, n. 16, p. 1-15, 2014.
2. HOU, P.; XU, Y.; TAIEBAT, M.; LASTOSKIE, C. M.; MILLER, S. A.; XU, M. Journal of Cleaner Production, 201, p. 1052-1060, 2018.
3. MORRIS, B.Elsevier, 2016.
4. CORDEIRO, C. C.; BERNARDIN, A. M.; DA SILVA, L. et al. Journal of Applied Polymer Science, 118, p. 1436-1441, 2010.
5. IREZ, A. B.; BAYRAKTAR, E.; MISKIOGLU, I. Polymers, 12, p. 448, 2020.
6. ZAVARECH, S.; VAHDAT, G. Journal of Reinforced Plastics and Composites, v. 31, n. 4, p. 247-258, 2012.
7. RAMOS, V. D.; COSTA, H. M.; SOARES, V. L. P.; NASCIMENTO, R. S. V. Polymer Testing, v. 24, n. 3, p. 387-394, 2005.
8. KIM, D. S.; CHO, K.; KIM, J. K.; PARK, C. E. Polymer Engineering and Science, v. 36, n. 6, p. 755-768, 1996.
9. QUAN, D.; IVANKOVIC, A. Polymer, 66, p. 16-28, 2015.
10. TSAI, J. L.; HUANG, B. H.; CHENG, Y. L. Journal of Composite Materials, v. 43, n. 25, ´p. 3107-3123, 2009.
11. DADFAR, M. R.; GHADAMI, F. Materials & Design, 47, p. 16-20, 2013.
12. ALMEIDA, J. R. M.; MONTEIRO, S. N. Polymers for Advanced Technologies, 9, p. 216-221, 1998.
13. KAYNAK, C.; CELIKBILEK, C.; AKOVALI, G. European Polymer Journal, 39, p. 1125-1132, 2003.
14. TANG, L. C.; ZHANG, H.; SPRENGER, S.; YE, L.; ZHANG, Z. Composites Science and Technology, 72, p. 558-565, 2012.
15. TANG, L. C.; WANG, X.; WAN, Y. J.; WU, L. B.; JIANG, J. X.; LAI, G. Q. Materials Chemistry and Physics, 141, p. 333-342, 2013.
16. SANKAR, H. R.; KRISHNA, P. V.; RAO, V. B.; BABU, P. B. Proceedings of the Institution of Mechanical Engineers, Part L: Journal of Materials: Design and Applications, v. 224, n. 2, p. 63-70, 2010.
17. MANJUNATHA, C. M.; TAYLOR, A. C.; KINLOCH, A. J. Journal of Reinforced Plastics and Composites, v. 29, n. 14, p. 2170-2183, 2010.
18. ABADYAN, M.; BAGHERI, R.; KOUCHAKZADEH. M. A. Journal of Applied Polymer Science, 125, p. 2467-2475, 2012.

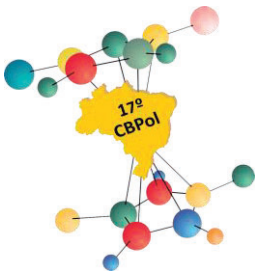

EFFECT OF NON-HALOGENATED FLAME RETARDANT ON ABS/PC BLEND PROPERTIES

Cindy S.T. Barduchi[1] and Baltus C. Bonse[1]*

1 – Department of Materials Engineering, Centro Universitário FEI, São Bernardo do Campo, SP, Brazil
prebbonse@fei.edu.br

Abstract - A blend commonly used in the automotive and electronics industries is ABS/PC, a mixture of two engineering thermoplastics that combines polycarbonate's toughness and thermal resistance with the excellent processability of acrylonitrile-butadiene-styrene. The fire resistance of ABS/PC can be improved using flame retardants. However, these additives may alter mechanical and thermal properties. In this study, different ABS/PC blend formulations were produced with varying proportions of non-halogenated flame retardant, with and without impact modifier. The changes caused by the combination of additives were assessed regarding mechanical strength, processability, and flame retardancy. The flame retardant reduced mechanical and thermal properties such as elongation, impact resistance, and heat deflection temperature while increasing tensile modulus. When the impact modifier was added, tensile modulus and impact strength were partially recovered, with no significant interference with elongation, tensile strength, heat deflection temperature, and flammability.
Keywords: *Polymer blend. Polycarbonate. ABS. Flame retardant.*

Introduction

One of the strategies used to develop new materials is the creation of polymer blends. These blends allow for cost reduction without compromising desired properties, enable the control and adjustment of properties without creating entirely new polymers, facilitate the formation of high-performance mixtures by combining synergistic polymers, and promote the reuse of industrial and post-consumer waste [1].

The Acrilonitrile-Butadiene-Styrene/Polycarbonate (ABS/PC) blend is a commercially important blend with enhanced properties and cost reduction. It offers increased impact strength and heat deflection temperature (HDT) compared to neat ABS and improved processability, low-temperature toughness, and cost efficiency compared to PC. This blend finds extensive use in automotive and electro electronic components [2].

In applications such as household appliances, lighting, and electrical components, it is crucial to enhance the fire resistance of polymers, which can be achieved by incorporating flame retardants that reduce the material's flammability. However, due to their persistence, bioaccumulation, and toxicity, conventional flame retardants containing halogenated components with bromine pose risks to human health and the environment. As a result, there is a growing need to explore non-halogenated flame retardants to ensure their effectiveness and minimize their negative impact on engineering properties. This shift is driven by socio-environmental legislative measures like REACH (Registration, Evaluation, Authorisation, and Restriction of Chemicals) and RoHS (Restriction of Hazardous Substances), as well as the Stockholm Convention [3].

Therefore, this study aims to compare the effects of using a non-halogenated phosphorus-based flame retardant in an ABS/PC blend. Not only the fire resistance will be analyzed but also the

engineering properties of the compound, considering variations in proportions, additives, and processing conditions.

Experimental

Proprietary PC and ABS were used. The non-halogenated flame retardant (FR) used was a low melting point (101-107°C) polymeric phosphate ester, containing 10.7% phosphorus, with a density of 1.3 g/cm^3. This FR is widely used in the industry and recommended for application in ABS/PC blends, in addition to offering processing advantages compared to other non-halogenated additives currently available for the same purpose.

To recover the impact strength affected by the addition of FR, a random copolymer of ethylene and methyl acrylate was used, as impact modifier, containing between 27 and 31% methyl acrylate, with a melting point of 61 °C, and a density of 0.95 g/cm^3. Modified anhydrous citric acid was used as stabilizer, with a melting point of 153 °C and density of 1.66 g/cm^3.

To delay the thermooxidative degradation of the compound in the presence of heat two antioxidants were used: (1) based on phosphite ester containing up to 0.2% 2,4-di-tert-butylphenyl and a melting point between 183 and 187 °C. (2) a thioether with a melting point between 50 and 55 °C.

All the materials were donated by a company from the thermoplastic manufacturing sector in the state of São Paulo, Brazil.

PC, ABS, and additives were tumble-mixed and melt-blended in a Thermo Scientific HAAKE PolyLab OS RheoDrive corotating twin-screw extruder (16 mm, L/D =25). Test specimens were injection molded in a Battenfeld HM 60/350 injection molding machine. Prior to extrusion and injection molding, PC and ABS were oven dried in a vacuum oven for 4 h at 120°C and 80 °C, respectively.

Injection molding was carried out at a temperature profile between 185 °C and 200 °C, and a mold temperature of 60 °C. The injection molded specimens were subjected to the following tests: tensile at 50 mm/min according to ASTM D638, Izod notched impact according to ASTM D256, using a 5.3J pendulum, three-point bending at 1,3 mm/min (span = 50 mm) according to ASTM D790, heat distortion temperature (1,82 MPa) according to ASTM D648. It should be mentioned that tensile strength and strain at break were obtained using a crosshead speed of 50 mm/min, distance between grips of 50 mm and an extensometer with 500% maximum strain. To determine tensile modulus a 50 mm extensometer with a 10% strain capacity and a speed of 5 mm/min up to 2% strain were used. The modulus was then obtained from the slope of the straight line formed in the range between 0 and 0.3% strain. Except for HDT testing, in which 3 specimens were used, for all other tests 5 to 10 specimens were used.

Results and Discussion

The mechanical test results are depicted in Figure 1 and Table 1. To assess potential statistical differences in the means among different formulations, all results underwent analysis of variance (ANOVA).

Figure 1 shows the variation in mechanical properties with varying contents of flame retardant and impact modifier. When FR is incorporated into the blend, the impact strength (Fig. 1a) decreases substantially (compare 30/70/0/0 with 30/70/12/0). When 3 phr of impact modifier is added, the impact strength is partially recovered (30/70/12/3). A significant drop in the strain at break can also be seen after the incorporation of FR. However, contrary to impact strength, the impact modifier does not result in partial recovery of the property. As shown in Fig 1b, incorporating the FR in the blend increases tensile modulus, indicating that FR is a relatively rigid filler. Rigid particulate fillers tend to reduce the ductility, toughness, and impact strength of ductile matrices, as is the case of PC and ABS, and this reduction is more significant when there is a lack of compatibility between the filler and the matrix [4].

Regarding the reference sample, 30/70/0/3, formulations 30/70/10/3, 30/70/12/3, and 30/70/15/3 showed a reduction in strain at break of 64%, 89% and 87%, respectively.
In the study by Hou et al. [5], the strain at break values decreased when adding FRs compared to neat PC/ABS (up to 10% reduction with 14% TPP). They attributed this to decreased PC content when higher amounts of FRs were used.
Furthermore, according to Pogorelcnik et al. [6], excessive amounts of FRs can also lead to poor dispersion in PC/ABS, causing adverse effects on tensile properties.

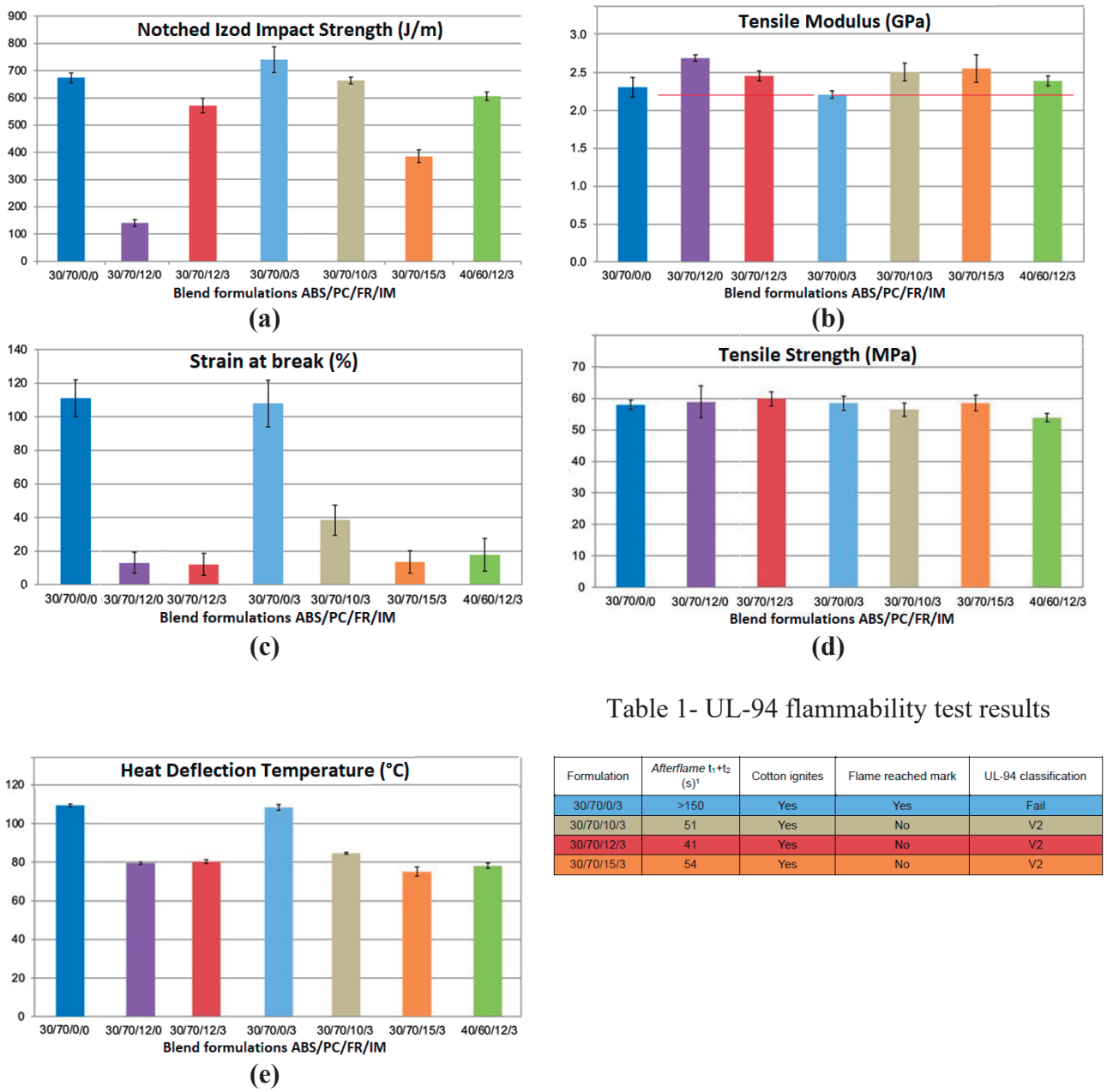

Table 1- UL-94 flammability test results

Formulation	*Afterflame* t_1+t_2 (s)[1]	Cotton ignites	Flame reached mark	UL-94 classification
30/70/0/3	>150	Yes	Yes	Fail
30/70/10/3	51	Yes	No	V2
30/70/12/3	41	Yes	No	V2
30/70/15/3	54	Yes	No	V2

Figure 1 - Variation in blend properties after incorporation of flame retardant and impact modifier.

Previous studies have shown that the lack of compatibility between non-halogenated flame retardants and polymer matrices reduces specific mechanical properties, such as impact and tensile strength. However, when a compatibilizer is used, the mechanical properties can be partially or fully recovered [7].
According to Fig 1e, the HDT for different concentrations of FR also exhibits a trend of decreasing values with increasing FR content. Several studies report the adverse effects of incorporating FR on

mechanical properties, chemical resistance, and HDT. They also mention that certain FRs can interfere with the action of other additives, especially photo stabilizers [5,8].
Table 1 presents the flammability test results, classifying the 30/70/10/3 formulation as a failure in flame retardancy, according to the UL-94 standard, as this blend could not extinguish the flame applied to the test specimens. In this sample, no FR was added, and the ABS incorporated into the blend inhibits the intrinsic flame propagation characteristic of PC, contributing to the observed dripping and high flames. On the other hand, the other formulations that used FR exhibited fire resistance; however, they did not show significant changes among the different concentrations of FR used.

Conclusions

The findings obtained by incorporating a non-halogenated flame retardant demonstrate notable effects on various mechanical properties of ABS/PC compounds. Specifically, the results indicate an enhancement in fire resistance and tensile modulus, along with a substantial reduction in strain at break. However, a slight decrease in tensile strength, as well as a decline in impact strength and thermal deflection temperatures, were observed with increasing concentrations of the additive. It is worth noting that all tested concentrations of the flame retardant adhered to the V2 classification as per the UL94 standard, which establishes criteria for assessing the flammability levels of plastic materials.
In conclusion, using flame retardants exhibits potential as a feasible solution in ABS/PC composites. Despite the positive effects on fire resistance and tensile elastic modulus, incorporating these additives entails some mechanical drawbacks. Nevertheless, these drawbacks can be partially mitigated by applying impact modifiers.

Acknowledgements

The authors acknowledge Aditive Plásticos (São Paulo, Brazil) for allowing the use of their laboratory for the flammability tests.

References

1. A. I. Isayev; S. Palsule *Polymer Blends and Composites: Chemistry and Technology*, John Wiley & Sons, New York, 2017
2. S. V. Levchik; E.D. Weil. Journal of Fire Sciences 2006, 24. doi: 10.1177/0734904106055997
3. N. Amarnath; D. Appavoo; Lochab. ACS Sustainable Chem. Eng. 2018, 6, 1, 389–402 https://doi.org/10.1021/acssuschemeng.
4. M. Rabello and M-A. de Paoli, Aditivação de Termoplásticos, Artliber Editora Ltda, São Paulo, 2013.
5. S. Hou; Z. Li, Y. Zhang, P. Jiang. Polymer Degradation and Stability, 2020.
6. B. Pogorelcnik, I. Pulko, T. Wilhelm, M. Zigon. Journal of Applied Polymer Science, 2019.
7. R. G. Bringel, Master Thesis, Centro Universitário FEI, 2018.
8. G. Pritchard, Plastic Additives. Shawbury, Shrewsbury, Shropshire SY4 4NR, UK: Rapra Technology, 2005.

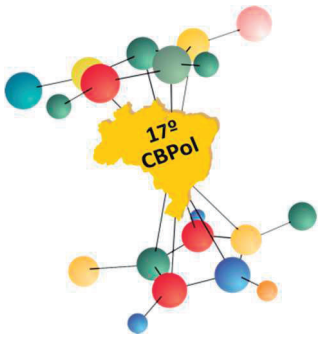

EFFECTS OF LONG-TERM HYGROTHERMAL AGING ON THE MECHANICAL BEHAVIOR OF CARBON FIBER/EPOXY COMPOSITE

Andréa K. Silva[1,3], Tanila P. De Faria G. Leal[1,3], Silvana Navarro Cassu[1,2]

1 – Aeronautics Institute of Technology (ITA), São José dos Campos, SP, Brazil
2 –Institute of Aeronautics and Space (IAE), São José dos Campos, SP, Brazil
3 –EMBRAER, São José dos Campos, SP, Brazil
kaarolinesiilva@gmail.com.br

Abstract –Polymeric composites have gained attention in the aerospace sector and have been used in parts of aerospace vehicles such as aircraft. These vehicle types are continuously exposed to environmental conditions, which can cause irreversible damage in the long term. This study evaluated the long-term hygrothermal effects on carbon fiber/epoxy-based composite through 21 months and the effect of drying the aged polymeric composite (APC) on recovering mechanical properties. APC dynamic mechanical results showed a reduction of the glass transition temperature (Tg) of the epoxy network by approximately 10 ºC from 5 months of aging due to the plasticizing moisture effect. The Tg of the dried APC increased by approximately 30 ºC, and the storage modulus enhanced by about 20 %, both attributed to the post-curing reaction. The APC interlaminar properties, measured by the interlaminar shear strength test, were reduced compared to the unexposed material. The initial interlaminar shear strength was not recovered even after APC drying. The results showed that the longer the exposure time, the worse the recovery of the properties due to the irreversible degradation of the composite.
Keywords*: polymeric composite, degradation, DMA, ILSS,*

Introduction

Composite materials are composed of two or more components. The combination of the properties of each constituent results in the final material properties, providing numerous advantages and applications. Due to the technological advancement in polymeric composites, these materials have been widely used in the aerospace industry. Nevertheless, these materials are sensitive to long-term environmental exposure, such as the ones an aircraft is exposed to during its life cycle. The main environmental conditions that cause material aging are temperature and humidity, which can severely degrade the polymeric composite [11]. The presence of moisture can promote swelling and plasticizing effects of the polymer matrix, or degrade the fiber-matrix interface, reducing mechanical properties of the composite [7]. The environmental effects caused by hygrothermal aging can be reversible for a short exposure period. However, when exposure occurs in the long term, the effects may be irreversible due to the water molecules bonding with the polymeric networkand its penetration into the composite structure. Moreover, regulatory agencies require knowledge of composite behavior under environmental conditions for aerospace applications.

The acceleration of the composite aging can be reached using a climatic chamber, in which the moisture and temperature conditions are controlled [1]. The accelerated aging test has the advantage of being faster than the natural exposure of the composite. This study investigates the performance of cured carbon fiber/epoxy composite after long-term hygrothermal aging. In addition, the recovery effect in mechanical performance after drying the aged composite was also evaluated.

Experimental

The composite material, a unidirectional carbon fiber pre-impregnated with epoxy resin (DGEBA), was manufactured by Toray Industries, INC. The material was cured in an autoclave at (177±5)°C, at a heating rate of (1.7±1.1)°C.min^{-1},under the pressure of (85+15) psi. The curing temperature was maintained for 180minutes. Before releasing pressure, the vessel was cooled to 60 °C using a cooling rate of (2.78±1.1) °C.min^{-1}.

All samples were dried according to ASTM D5229 (procedure D) at a temperature of (60°C±5)°C until they reached the effective moisture equilibrium. This parameter is used for both samples after hygrothermal conditioning or oven drying. The effective moisture is reached when the mass of the material changes by less than 0.020% after the employed procedure.

For the aging process the specimens were submitted to additional conditioning periods of 10, 16, and 21 months. After each aging period, the specimens were dried at (60°C±5)°C in an oven until they reached the equilibrium at dry conditioning. Reference specimens were not exposed to hygrothermal aging. The average absorbed moisture content was defined as the ratio between the mass of the conditioned specimen and the mass of the oven-dried specimen. The specimen weightings were performed weekly, according to Procedures A [1].

Interlaminar shear strength tests, ILSS, were performed using testing equipment MTS Criterion Series 40, in flexion mode at a 3-point clamp, applying a transverse load speedof1.27mm/min until failure according to ASTM D2344.

The viscoelastic properties of the specimens were obtained using the equipment DMA 8000, PerkinElmer, with dual-cantilever clamp, and a heating rate of 3°C.min^{-1} from -100°C to 300°C, frequency of 1HZ, the amplitude of 20μm, according to the standard ASTM D7028.

Results and Discussion

The laminates were analyzed when exposed to the effective moisture (85±5)% and temperature (70±5)ºC. Fig 1 shows the variation of absorbed moisture by carbon fiber/epoxy composite specimens with two different thicknesses during long-term exposure to a hygrothermal environment. It is possible to notice how quickly the mass of the composite increases when conditioned for 140 (121/2) days. After this period, there was a slight progressive increase in absorbed moisture until approximately 320 (181/2) days. After that, the moisture absorption remained almost constant until 780 (281/2) days. The specimens with different thicknesses showed similar absorbed moisture curves. It is worth noting that the moisture absorption increased even after achieving the moisture equilibrium defined by ASTM D5229, which is reached by a material when there is no additional change in its average moisture content over a specified time period. The time period used in this work was XX weeks. The diffusion process governs the moisture penetration into the composite, which involves the absorption of water molecules by the polymeric matrix and their transporting through the composite pre-existing microvoids. Several diffusion models describe the moisture transport into polymers, and the most well-known is the Fick model [2]. The Fick model behavior for a moisture absorption curve is represented by a growing trend followed by a saturation plateau [2]. However, in the present study as shown in Fig 1, a two-stage diffusion model (non-Fickian) can better explain the moisture absorption behavior by the studied polymeric composite. Berens and Hopfenberg [4] studied and described the first moisture absorption stage as diffusion-controlled and the second, dependent on molecular relaxation and degradation of the polyvinyl chloride material. The second stage of moistures absorption can occur through different mechanisms such as by the interaction of part of the absorbed moisture with the polar groups of the epoxy phase, interrupting a possible additional cross-linking of the polymeric network. It is worth mentioning that most of the composite prepregs reach around 93% of curing degree, meaning that some polymer chains are kept unreacted and available for the additional curing reaction [12]. Other mechanisms that can occur in the second stage are the induction of damages in the fiber/matrix interface, such as debonding and cracking [5]; and the polymer relaxation, which occurs when the penetrant molecule enters the polymer chain and

generates an osmotic stress large enough to lead to molecular relaxation [4,2].DMA and ILSS tests were performed to understand better the effect of aging on the composite and are presented as follows.

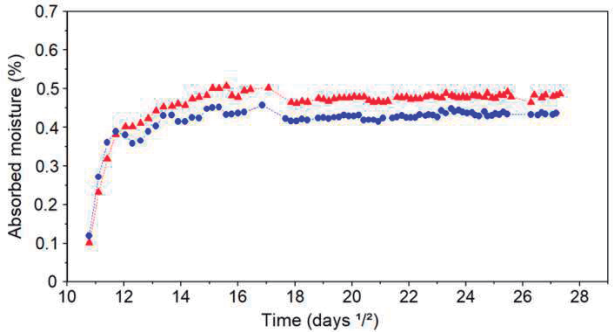

Figure 1-Variation of absorbed moisture by the carbon fiber/epoxy composite under the hygrothermal aging. Specimens of composite with different thickness:(-▲-)3.06 mm and(-●-) 1.91mm.

Literature [5,6] reports that the effects caused by moisture are reversible, and some properties can be recovered, suggesting that the drying process effectively removes the water absorbed by the polymeric composite. Moisture absorption can cause the plasticization of the epoxy network. Other effects, such as hydrolysis, saponification, and leaching, can occur after increasing hygrothermal aging time, increasing molecular mobility, and reducing the Tg values [7].

The results in this study showed that removing the most absorbed water from composites was possible after the short-term exposure (5 months) and non-exposed specimens by drying them at 60°C until reach equilibrium (approximately 4 months). On the other hand, for the composite under long-term hygrothermal exposure (10,16 and 21 months) it is possible to observe most water molecules remaining in the composite molecular structure.

Dynamic mechanical (DMA) analysis was used to evaluate the aging effects on the viscoelastic properties of the composite after hygrothermal aging (APC) and after drying. The behavior of the Tg of the composite was monitored. In **Fig 2-a**, the variation of the Tg values, obtained by the maximum peak of the tanδ curves of APC and dried APC, are shown as a function of the aging time. The Tg of the APC decreased by about 10 ºC, from 195 ºC down to 185 ºC, after being conditioned for 5 months, and this value remained practically constant throughout the 21 months of aging. This behavior indicates a possible post-curing reaction of the epoxy network occurring during long-term aging, which should mask the effect caused by plasticization. Drying the aged composites caused an increase in Tg values by approximately 30 ºC compared to the non-exposed composite. This result can be attributed to post-curing effects [6], which according to Adamson [6] can occur during aging, even keeping the aging temperature as low as 70 ºC. The Tg behavior of the APC and dried APC showed that even though moisture removal is possible by drying the specimens at 60ºC, the irreversible post-curing reaction occurred during the aging and the drying process, causing a changing of the polymeric phase molecular structure, which affect the polymeric composite performance.

The variation of the storage modulus (E') at 100ºC is shown in **Fig 2-b**. The E' value slightly reduces for carbon fiber/epoxy composite after 5 months of conditioning. The E' increases from 10 months of aging and stabilizes until 21 months, and it was similar to the E' value observed for unexposed composite. The reduction in E' at 5 months of conditioning is probably due to the plasticizing effect of the polymer matrix, while its increase with aging time should be associated with the post-curing effect. Aged composite drying caused an increase in E' values. Above 16 months of aging, the dried APC showed E' values approximately 20% superior to the unexposed reference composite. The DMA results show that the E' and Tg of the fiber carbon/epoxy composite are predominantly affected by post-curing reactions during the aging and drying process.

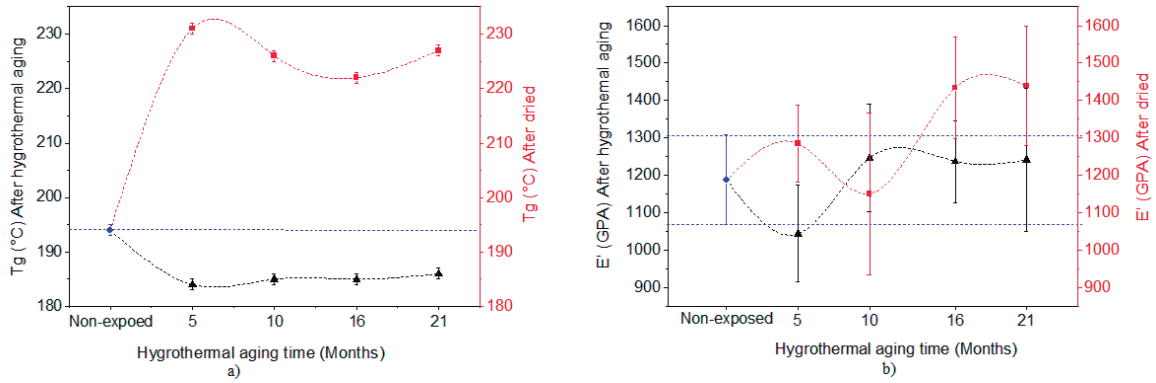

Figure 2: Variation of DMA parameters obtained for the carbon fiber/epoxy composite submitted to the hygrothermal aging, and after the drying the aged composite. (a) Glass transition temperature (Tg) and (b) Storage modulus (E') at 100ºC.

The interlaminar shear strength (ILSS) results are shown in **Fig 3**. As expected, all epoxy-carbon composites aged before drying presented a reduction in interlaminar shear strength properties compared to the non-exposed sample. This response is due to the presence of water molecules in the laminate, which results in the collapse of Van der Waals interactions, weakening the adhesion between carbon fiber and epoxy network interface [9]. In addition, the moisture diffusion mechanism contributed to the reduction of mechanical properties due to the loss of interfacial adhesion, inducing microcracks.

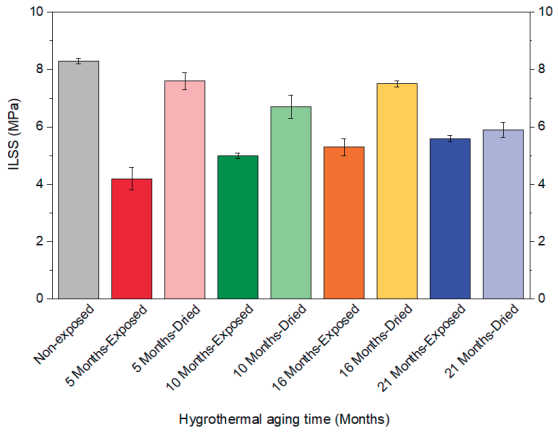

Figure 3: Interlaminar shear strength of carbon fiber/epoxy composite submitted to the hygrothemal aging.

This behavior was also found in the literature [9] for a composite of carbon fibers and epoxy resin conditioned at 60°C and 100% relative humidity. However, different from the literature, in the present study the carbon fiber/epoxy composites gradually increased the interlaminar shear strength after the hygrothermal exposure period. A similar result was found in the literature [10], observing a slight improvement in mechanical properties caused by aging, which was attributed to post-curing reactions of the polymeric matrix. The interlaminar shear strength was also evaluated after drying the aged specimens, which presented a partial recovery of this property compared to the unexposed composite. According to the literature [4], the water absorbed by the laminates usually results in reversible plasticization of the matrix, reducing the Tg. However, the association of humidity and temperature can cause significant changes in the composite stiffness due to degradations during aging, as seen in this study.

Conclusions

The study aimed to evaluate how long-term hygrothermal aging affects epoxy-based composite and the effectiveness of drying to recover its mechanical properties. The non-Fickian model better explained the water absorption of the polymeric composite and its diffusion behavior, which occurred

in two stages, the initial stage controlled by Fick's diffusion. The second stage of water absorption seemed to be controlled by interfacial debonding and possible relaxation of the polymeric phase that allowed slight increases in water absorption. The hygrothermal exposure led mainly to irreversible degradation of the composite, causing a decrease in its Tg associated with the plasticizing effect. Additionally, drying the aged composite caused an increase in Tg, which was attributed to post-curing reactions. ILSS test showed that the interlaminar properties decreased compared to the unexposed material, and even after composite drying, it can not recover the initial interlaminar shear strength. In addition, it was evident that the longer the exposure time, the worse the recovery of the properties of the polymeric composite, which can be attributed to irreversible material degradation.

Acknowledgements
This study was financed in part by the Coordenação de Aperfeiçoamento de Pessoal de Nível Superior - Brasil (CAPES) - Finance Code 001.

References

1. ASTM D5229 - Moisture Absorption Properties and Equilibrium Conditioning of Polymer Matrix Composite Materials.
2. J. Crank. Journal of Polymer Science 1953,11,151-168. https://doi.org/10.1002/pol.1953.120110206.
3. Bond DA. Journal of Composite Materials, 2005, 39(23), 2113-2141. doi:10.1177/0021998305052030.
4. A.R Berens, H.B.Hopfenberg, Polymer 1978, 19(5), 489-496. https://doi.org/10.1016/0032-3861(78)90269-0.
5. Bond, D. A., and Smith, P. A. ASME. Applied Mechanics Reviews. 2006; 59(5), 249-268. https://doi.org/10.1115/1.2202873.
6. Adamson, M. J. J. Mater. Sci., 1980, 15, 1736–1745.https://doi.org/10.1007/BF00550593.
7. Vistasp M. Karbhari. Composites Part A: Applied Science and Manufacturing, 2022, 153, 106705. https://doi.org/10.1016/j.compositesa.2021.106705.
8. Mascia L, Kouparitsas Y, Nocita D, Bao X. Polymers, 2020, 12(4), 769. https://doi.org/10.3390/polym12040769.
9. RuiGuo, Chenggao Li, Guijun Xian. Engineering Structures, 2023, 274,115176. https://doi.org/10.1016/j.engstruct.2022.115176.
10. Xian G, Li H, Su X. Journal of Composite Materials. 2013, 47(18), 2275-2285. doi:10.1177/0021998312457099.
11. S. Aessi, G. Pitarresi, G. Spadaro.Composites Part B: Engineering, 2014, 67, 145-153.https://doi.org/10.1016/j.compositesb.2014.06.006.
12. K.M.B. Jansen, M.F. Zhang, L.J. Ernst, D.-K. Vu, L. Weiss. Microelectronics Reliability, 2020, 107, 113596. https://doi.org/10.1016/j.microrel.2020.113596.
13. ASTM D2344 - Standard Test Method for Short-Beam Strength of Polymer Matrix Composite Materials and Their Laminates.
14. ASTM D7028 - Standard Test Method for Glass Transition Temperature (DMA Tg) of Polymer Matrix Composites by Dynamic Mechanical Analysis (DMA).

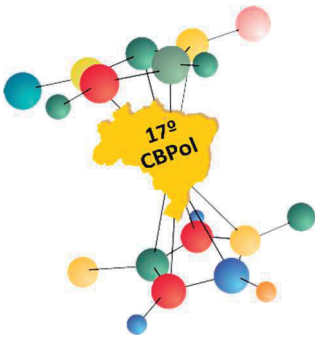

EVALUATION OF BARRIER THE WATER VAPOR PROPERTIES AND COMPATIBILITY OF EVA/THERMOPLASTIC STARCH BLENDS

Wagner guadagnin[1] , Daiane Romanzini[2], Maurício Cardoso Kade[1], Mara Zeni de Andrade[1], Fernando Reis[1], Clair José Frighetto[1], Gerson Frighetto[1], Diego Guerra[1], Danieli Mutzenberg[1] , Ana Paula Bilck[1], and Edson Luiz Francisquetti[1*],

1, 1 Department of Science and Materials Engineering, Instituto Federal de Educação, Ciência e Tecnologia do Rio Grande do Sul (IFRS), Farroupilha, RS, Brazil*
2 Department of Science and Materials Engineering, Instituto Federal de Educação, Ciência e Tecnologia do Rio Grande do Sul (IFRS), Feliz, RS, Brazil
edson.francisquetti@farroupilha.ifrs.edu.br

Abstract
The objective of this work was to manufacture films based on ethylene-vinyl acetate copolymer (EVA) with 28 wt % of vinyl acetate and thermoplastic starch (TPS)plasticized with 30 wt% glycerol. The blends (70, 60, and 50 wt% of EVA) were characterized according to microstructure and barrier properties. The combination of TPS-EVA resulted in films with homogeneous surfaces. The introduction of EVA into the starch matrix led to the formation of films with lower water vapor permeability (WVP), resulting in greater stability for relative humidity and lower WVP.

Keywords: *microstructure, starch, ethylene-vinyl acetate, water vapor permeability*

Introduction

Starch in its native form is widely used as a filler, but its melt-processing by conventional methods, in the presence of plasticizers such as glycerol, leads to a thermoplastic matrix (thermoplastic starch, TPS) useful for many applications such as in packaging, food packaging and biomedical applications [1,2]. The plasticized starch can be industrially processed with traditional melt-processing methods such as extrusion, injection molding, and film blowing. The overexploitation of natural resources and accelerated climate change has led industries to incorporate more environmentally friendly materials and technologies into their processes. Despite the aforementioned advantages, the mass application of TPS is limited by its poor mechanical properties and high moisture adsorption, coupled with the structural instability resulting from changes in these properties as a function of time and the relative humidity to which they are exposed.

An interesting approach to improve the properties and the stability during the application of thermoplastic starch is by blending with other hydrophobic polymers such as polyethylene (PE), polycaprolactone (PCL) and ethylene-vinyl acetate (EVA) [3,4,5]. Copolymers of ethylene-vinyl acetate (EVA) are a class of widely used polymers, with a wide range of industrial applications such as flexible packaging, membranes, cable and wire, hose and tube, photovoltaic encapsulants, footwear and biomedical applications. Da Róz et al. [7] reported the processing of compatible EVA/TPS blends. The study showed the addition of 2.5 wt % of hydrolyzed EVA improves the mechanical, thermal and water absorption characteristics of TPS. Sessini et al. [5] observed that blending biodegradable polymers such as TPS with non-biodegradable polymers like EVA leads to the increase of compostable polymer percentage in partially-degradable materials, giving possible solution for the

end-life of these materials after their use, also observed that EVA/TPS (19 wt% vinyl acetate (VA) and native pea starch) and their nanocomposite blends are immiscible in the spherical TPS microdomains with an inhomogeneous size distribution are dispersed in the EVA matrix. Furthermore, phase detachment was observed indicating poor adhesion between the EVA and TPS phases. However, in the case of nanocomposites, a more homogeneous size distribution of the spherical microdomains of the TPS was observed compared to the pure blends, as well as a strong decrease in phase disconnection, indicating better compatibility between the different polymeric phases probably due to the addition of nanoclays. Thus, the objective of this study was to prepare blends of TPS and EVA, using corn starch and EVA with 28% acetate, where there was a variation in the incorporated EVA content (70, 60 and 50% by weight). In order to obtain a better understanding of the microstructure and barrier properties, the mixtures were characterized by scanning electron microscopy (SEM) and water vapor permeability (WVP).

Experimental

The blends were produced with native cornstarch (Cargill, USA), ethylene-vinyl acetate copolymer with 28 wt % of vinyl acetate (Brasken Brazil) and glycerol (Dinâmica, Brazil). Blends of 30, 40, and 50 wt% TPS (70:30 w/w starch/ glycerol) were manually mixed with 70, 60, and 50 wt% EVA and extruded to produce pellets. The extrusion was carried out in a pilot single-screw extruder (SEIBT extruder, model ES-35-FR BGM, EL-25 model, Brazil). After this time, the pellets were extruded to produce films in a two-rolls calender mixer MH-300 (MH Equipamentos, Brazil).

Microstructure Properties

The samples were fractured in liquid nitrogen and analyzed using a Scanning Electron Microscope (SEM TM3000, Hitachi), operating at an accelerating voltage of 5 kW.The samples were deposited on a 70 mm diameter and 50 mm high support, prepared with a carbon tape. The images were collected at 300 x magnification.

Water Vapor Permeability (WVP)

The trays water vapor permeability (WVP) was determined gravimetrically according to the ASTM E-96-00 [8] under a relative humidity gradient of 33-64 %. The tests were conducted in duplicate.

Results and Discussion

The WVP of the blends ranged from 1.7×10^{-6} to 2.8×10^{-6} g.(m.Pa.day)$^{-1}$ (Tab.1), are similar when compared to the neat EVA (2.3×10^{-6} g/m.Pa.day). The addition of starch in the EVA blends did not change the permeability of the films, indicating good interaction between the two matrices.

The permeability results are in accordance with films produced with Ecoflex® F Blend C1200 [9]. For this reason, the studied blends could be used in future applications such as packaging. Furthermore, the WVP of the biodegradable polymer poly (butylene adipate-co-terephthalate) (PBAT) is around $3.3x\ 10^{-6}$ g/m.Pa.day under a 0-85 RH gradient and PBAT/TPS blends (50:50 w/w) are around $3.0x10^{-6}$ g/m.Pa.day [10]. Olivato et al. [11] evaluated the WVP in films of TPS/PBAT (50:50) using 0-75% as RH gradient and reported values of 5.4×10^{-6} g /m.Pa.day.

Table 1. Water Vapor Permeability (WVP) of the films.

Sample	Water Vapor Permeability (VWP) g.(m.Pa.day)$^{-1}$
Neat EVA	2.354E-06
30 TPS	2.492E-06
40 TPS	1.715E-06
50 TPS	2.841E-06

The surface scanning electron microscopy (SEM) results of the films are shown in Fig 1. The structure was compact, smooth, and shows the presence of small starch granules in images with 50% TPS (a) and 40% TPS (b). when mixing two polymers through the extrusion process, one must ensure that there is a good distribution associated with a good dispersion of the dispersed phase over the matrix, as observed in Figure 1. If poor dispersion occurs, it may result in polymeric agglomerates, possibly due to entanglement of the polymeric chains that can cause an impediment to the transmission of stresses, in Figure 1o, are starch granules (TPS) dispersed in the EVA matrix and with uniform sizes indicating a good dispersion and distribution.

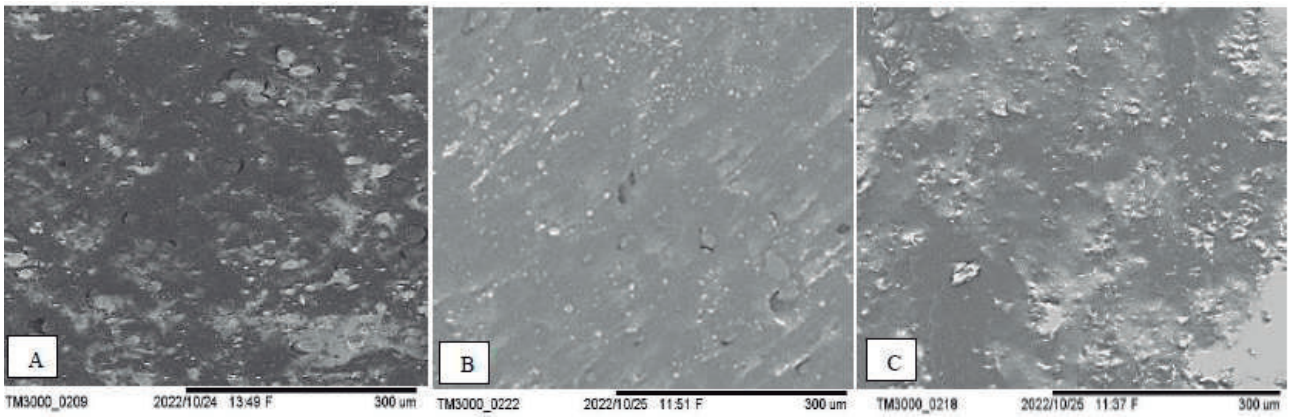

Figure 1. SEM micrographs of surfaces samples: (a) 50 TPS, (b) 40 TPS, and (c) EVA pure

Conclusions

In this work, a good interaction of blends of EVA with 28% acetate and corn starch (EVA/TPS,) was observed, in which both polymeric phases showed partial miscibility (compatibility) with the homogeneous distribution of TPS in the polymeric matrix. The mixture of biodegradable and renewable polymers, such as TPS, with non-biodegradable polymers, such as EVA, is an alternative to increase the percentage of compostable polymers in partially degradable materials.

Acknowledgments

The authors would like to thank Instituto Federal de Educação, Ciência e Tecnologia do Rio Grande do Sul (IFRS), and Fundação de Amparo à Pesquisa do Estado do Rio Grande do Sul (Fapergs) for their support in the characterization analyses and financial support.

References

1. A. P. Bilck; Jiang; F. Yamashita; L. A. Marzano-Barreda. Carbohydrate Polymer Technologies and Applications 2021,2, 25,100088. http://dx.doi.org/10.1016/j.carpta.2021.100088.
2. A. J. Felix de Carvalho, E. Trovatti in Biomedical Applications for Thermoplastic Starch; Wiley Online Library, 2016. https://doi.org/10.1002/9781119117360.ch1.
3. Y. Hammache; A. Serier; S. Chaoui. Mater. Res. Express 2020, 7, 025308. https://doi.org/10.1088/2053-1591/ab7270.
4. H. Sadeghi; G. H. Nazockdastb. Polymers 2022, 245, 124729. https://doi.org/10.1016/j.polymer.2022.124729.
5. V. Sessini, M. P. Arrieta, J. M. Raquez, P. Dubois, J. M. Kenny, L. P. Polymer Degradation and Stability 2019, 159, 184-198. https://doi.org/10.1016/j.polymdegradstab.2018.11.025.
6. S. Giri, C. Wan, Flexible and Stretchable Electronic Composites, 2016, 61-85. https://doi.org/10.1007/978-3-319-23663-6_3
7. A. L. DaRóz; A. M. Ferreira; F. M. Yamaji; A. J.F .Carvalho. Carbohydrate Polymers, 2012, 90, 34-40. http://dx.doi.org/10.1016/j.carbpol.2012.04.055.
8. American Society for Testing and Materials (ASTM), 2000. Standard Test Methods for Water Transmission of Material. ASTM, Philadelphia (E-96-00).
9. BASF Chemical Performance Polymer. 2023, ecoflex+F+Blend+C1200_000000000030516354_SDS_GEN_BR_pt_7-0.pdf
10. A.P. Bilck; C. M. O. Müller; J. B. O; S. M; M.V. E. Grossmann; F. Yamashita. Polímeros, 2015, 25 (4), 331-335. http://dx.doi.org/10.1590/0104-1428.1803.
11. J.B. Olivato; M.V.E. Grossmann; F. Yamashita, F; M.M. Nobrega; M.R.S. Scapin; L. Pessan. International Journal of Food Science & Technology, 2011, 46(9), 1934-1939. https://ifst.onlinelibrary.wiley.com/doi/10.1111/j.1365-2621.2011.02704.x

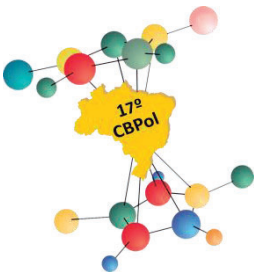

EVALUATION OF BENDING PROPERTIES OF POLYESTER COMPOSITES AND PLANT FIBERS COATED WITH INVERTED SUCROSE

Julio S. Souza, Celso C. M. Fornari Junior*

1 – Department of Engineering and Computer, State University of anta Cruz (UESC), Ilhéus, BA, Brazil
corresponding_celso@uesc.com.br

Abstract

The production of alternative materials from renewable sources and more environmentally friendly is a goal that many researchers have been pursuing around the world. The formation of polymeric composites with plant fibers is a promising path, due to the intrinsic properties that plant fibers have. In addition to considerable mechanical properties, natural production in harmony with the environment and biodegradability are important factors for the continuity of life. This work seeks to understand, even partially, the mechanism of interaction that occurs between the coconut vegetable fiber and the polymeric polyester matrix. Morphology is one of the most important aspects for the fiber-polymer interaction and this work modified the fiber surface with the application of an inverted sucrose layer. The composites were evaluated using a three-point bending test and demonstrated that fibers treated with inverted sucrose were bether in mechanical strength.
Keywords: *Fiber, Composite, Polymer.*

Introduction

Society is facing several challenges, facing the population growth of our era. The increase in consumption due to the increase in population requires a solution to the demand and production of goods from the productive sector. Until now, our society has been based and sustained itself on finite energy sources, such as oil. In the case of materials, many types used by industry also come from non-renewable sources, such as metals for example [1-3]. However, this extractive system is causing concerns about the future discontinuity of supply. On the other hand, the plant kingdom offers renewable resources and correct and environmentally friendly production. Vegetable fibers are an example of this, where they constitute a natural polymer with high abundance and relatively low cost. These materials are biodegradable and do not harm the carbon cycle, being naturally incorporated by decomposition and reused in the construction of new cellulosic chains. Due to this, many researchers have been interested in making composites with plant fibers. The addition of fibers to synthetic and natural polymers forces the displacement of the polymeric matrix by the presence of fibers, thus decreasing proportionally their amount. In the same way, the fibers can add greater properties to the new material, increasing its application capacity. Composite materials are materials that can express the properties of the constituent materials, thus seeking to explore the potential of each material that is present. This would be a huge gain for engineering, as the sum of the properties would increase the composites' capacity in relation to their properties [4-7]. And in fact this can happen if there is a perfect union between the constituents of the composite. The strong union between the two materials will link the properties of both and form a new material with the sum of the two properties. But, in the real case of forming polymeric composites with vegetable

fibers, this union depends on many factors. The first and perhaps not the main one is the polar nature of fibers and polymers. In sum, there is the fiber morphology, aspect ratio, physical surface, chemical composition that needs to adjust and be compatible with the polymeric network. For this reason, many studies have explored the surface modification of plant fibers, using numerous artifices and possible reactions [8-10].
The alteration of the coconut fiber surface was evaluated in this work. Coir fiber coating with an inverted sucrose solution was studied. The aim is to reduce the morphological characteristic that appears in an accidental and irregular way in the coconut fiber. Inverted sucrose is a material from a renewable source, biodegradable and which has affinity with cellulosic chains. This process presents low aggressiveness to the environment and low cost of use and application. Preliminary results showed a gain in relation to the same composite built with untreated natural fibers.

Experimental

Coir fibers were visually selected and cut into regular lengths of 20 mm. The so-called natural fibers were not treated and the so-called coated fibers were treated as follows: The fibers were placed in an alkaline solution bath consisting of sodium bicarbonate at a concentration of 8% w/w. The bath time was 60 minutes at rest and 30 minutes in ultrasound. A Unique model Ultra Clear 1400 device was used. Afterwards, the fibers were removed from the solution and washed in water three times and, using a paper filter, placed in an oven for 120 minutes at 115 ± 5 ºC. Afterwards, the fibers were cooled to room temperature for 60 minutes and placed in an inverted sucrose solution at a concentration of 50 g of sucrose, 1 g of citric acid and 100 g of distilled water. The solution was heated to 100 °C for one minute and allowed to cool to room temperature. The fibers after processing in ultrasound were weighed using an analytical scale with two decimal places, Marte model M2K. The coated fibers were placed in an oven for 120 minutes at 115 ± 5 ºC before composite formation. The composites were made with unsaturated polyester and methyl ethyl ketone initiator in the proportion of 2% w/w. The composites were post-cured at 80°C for 60 minutes. Flexion tests were performed according to ASTM D790 procedure B.

Results and Discussion

The morphology of vegetable fibers is peculiar to each species. Coconut fibers have a fatty layer covered by scales made of wax and pectin. This natural condition may favor the impact resistance of the fruit, but it does not favor the physical and chemical coupling and interaction with most polymeric matrices. The fatty layer prevents physical contact with the fibrous bundles, preventing any chemical interaction with the polymeric matrix. Fig 1 shows the image of the surface of the natural coconut fiber (A) and the fiber after treatment in alkaline sodium bicarbonate solution and ultrasound (B).

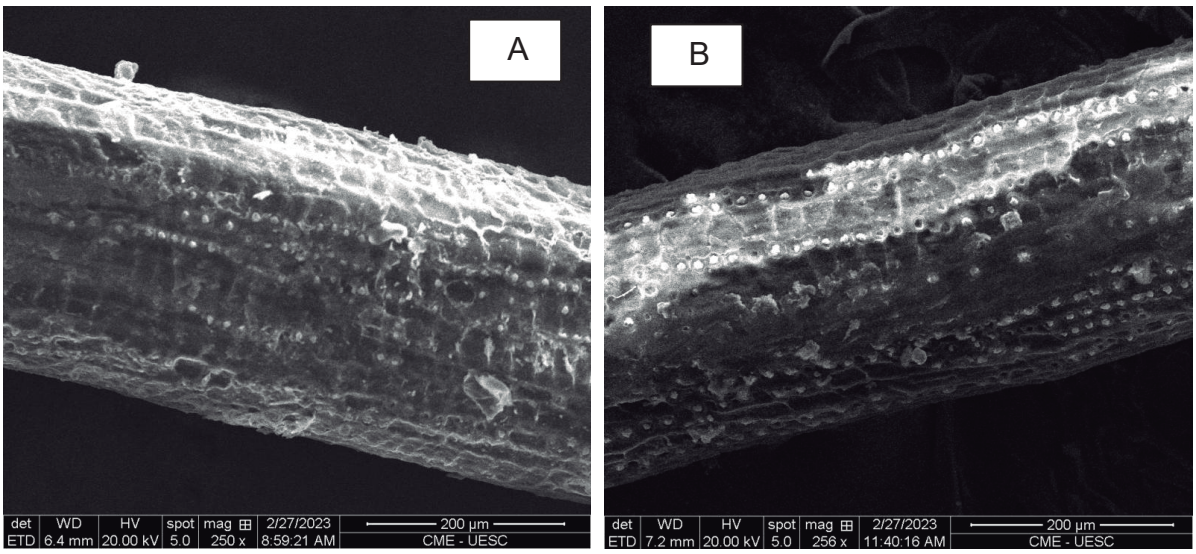

Figure 1 – Image of the surface of natural coconut fiber (A) and after treatment in alkaline solution (B)

The alkaline solution treatment is able to remove a large part of the superficial fatty layer of the coconut fiber. Fig 2B, shows the surface of the coconut fiber after treatment with alkaline solution and demonstrates that the original scales of the fiber were changed to a more uniform and less bumpy layer. At the same time, the globular particles were removed from the natural fiber. Fig 2 shows the globular particles on the surface of the coconut fiber (A) and the accommodation of the particles after removal (B).

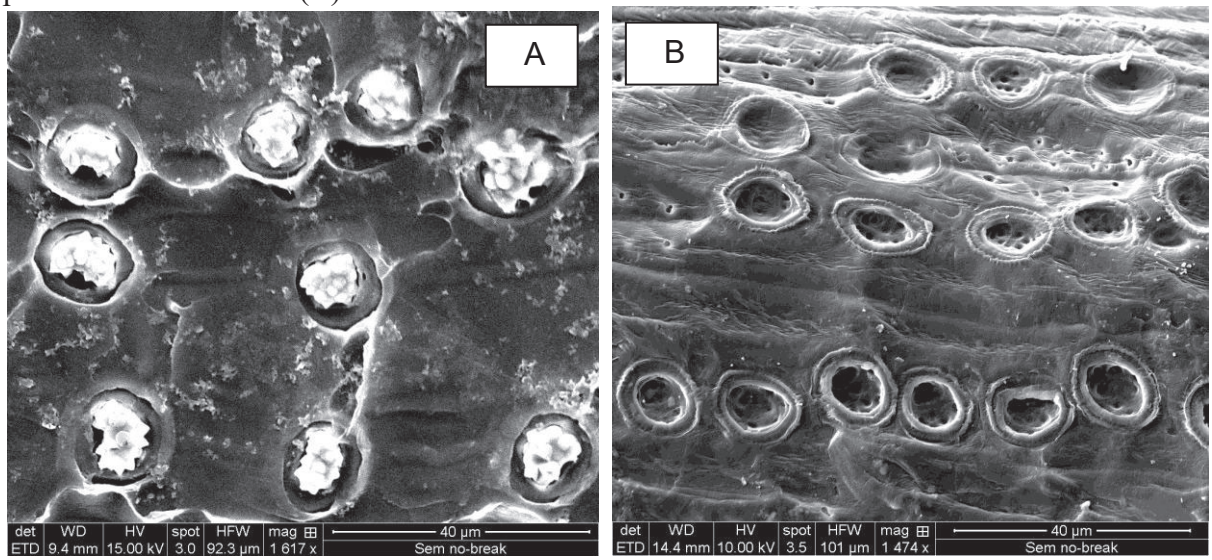

Figure 2 – Image of globular particles on the surface of coconut fiber (A) and housing without globular particles (B).

The globular particles present on the surface of the coconut fiber are globules with a shape tending to spheres, but with great irregularity and star-shaped points. This condition could favor the mechanical anchoring and the coupling of the polymeric matrix, promoting a physical interweaving between the fiber and the resin. On the other hand, the irregularity of the particles and the pointed star-shaped appearance can act as irregular points of interaction with the polymeric matrix. In this way, the relevance of the particles would be weak points of interaction and that can nucleate the population of cracks that will lead to the rupture of the composite body. The treatment applied to coconut fibers significantly reduced surface irregularities and minimized fiber morphology. This can be a positive point in the sense of equalizing the morphological conditions of the fiber. From

this condition, the fibers were immersed in an inverted sucrose solution and placed in an oven, in order to form a cover on the surface. The specimens were evaluated according to the three-point bending test. The results presented in Fig 3 demonstrate that the fibers treated with inverted sucrose presented superior results in relation to the natural fibers. The morphological conditions of the treated fibers were the main factor for the increase of the mechanical resistance of the composite. Smoothing the surface reduces the amount of imperfections and favors contact with the polymeric matrix. The flatter and more regular surface disfavors the accommodation of gases or moisture that could settle in the recesses or micro reliefs, thus allowing greater physical contact with the macromolecular chains.

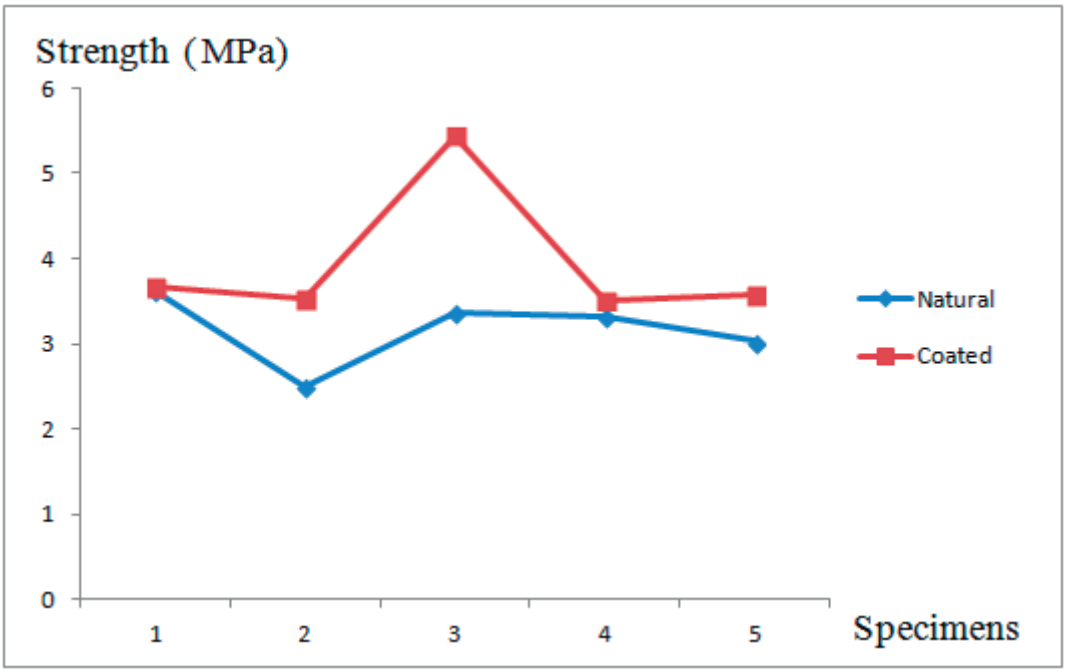

Figure 3 - Flexural strength in three points of composites with polyester and natural coconut fiber and coated with inverted sucrose.

The tests of the bending test carried out with the composites, presented variable results when analyzed individually. The polyester resin has a high viscosity, which makes it difficult to homogenize the initiator, which is the precursor of the cross-linking reaction. As a result, dispersion requires agitation of the resin and at the same time has a tendency to incorporate gaseous particles from the atmosphere. The final result of the composite is the combination of process conditions and the interaction and properties of the fibers. For this reason, there was dispersion in the results of flexural strength of the samples. Table 1 presents the flexural strength results.

Table 1 – Three-point flexural strength values of composites made with polyester and natural fibers and fibers covered with inverted sucrose.

Specimens	Natural (MPa)	Coated (MPa)
1	3,62	3,66
2	2,5	3,52
3	3,37	5,44
4	3,32	3,5
5	3,03	3,58

Conclusions

The results showed that the treatment of coconut fiber with an alkaline solution of sodium bicarbonate was enough to modify the surface of the coconut fiber, reducing the amount of globular particles and promoting an increase in the number of cavities. Three-point bending tests recorded an increase in bending strength in all composites made with fiber covered with inverted sucrose compared to composites made with natural fiber.

Acknowledgements

The authors would like to thank the State University of Santa Cruz for the research conditions carried out at LAPOS, the Polymers and Systems laboratory.

References

1. D. Fróna; J. Szenderák; M. Harangi-Rákos Sustentability 2019, 11, 5816. https://doi.org/10.3390/su11205816.
2. A. D. Tripathi; R. Mishra; K. K. Maurya; R. B. Singh; D. W. Wilson The role of functional food security in global health 2019, 3-24. https://doi.org/10.1016/B978-0-12-813148-0.00001-3
3. M. M. Maja; S. F. Ayano Earth Systems and Environment 2021, 5, 217-283. https://doi.org/10.1007/s41748-021-00209-6.
4. S. Gómez-Suarez; E. Córdoba-Tuta Revista UIS Ingenierías 2022, 21, 163-178. https://doi.org/10.18273/revuin.v21n1-2022013.
5. HG Kotik Matéria (Rio de Janeiro) 2019, 24. https://doi.org/10.1590/S1517-707620190003.0801.
6. C. C. M. F. Junior; J. H. de Oliveira Sales; C. S. S. BRANDÃO The Journal of Engineering and Exact Sciences 2022, 8, 1 – 13. https://doi.org/10.18540/jcecvl8iss10pp15047-01i.
7. Y. N. Wearn; L. S. Montagna; F. R. Passador Matéria (Rio de Janeiro) 2020, 25. https://doi.org/10.1590/S1517-707620200001.0873.
8. M. H. Hamidon; M. T. H. Sultan; A. H. Ariffin; A. U. M. Shah Journal of Materials Research and Technology 2019, 8, 3327-3337. https://doi.org/10.1016/j.jmrt.2019.04.012.
9. K. Senthilkumar; N. Rajini; N. Saba; M. Chandrasekar; M. Jawaid; S. Siengchin Journal os Polymers and the Environment 2019, 27, 1191-1201. https://doi.org/10.1007/s10924-019-01418-x.
10. M. Asim; M. Jawaid; H. Fouad; O. Y. Alothman Composite Structures 2021**,** 267, 113913. https://doi.org/10.1016/j.compstruct.2021.113913.

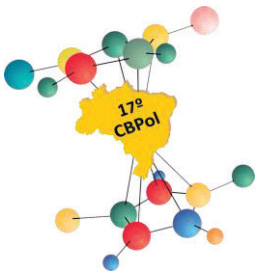

EVALUATION OF RECYCLED POLYPROPYLENE PROPERTIES WITH BANKNOTE-REINFORCED

Ingrid A. dos S. Matusinho[1*], Ítalo R. Coura[1] and Patrícia S. de O. Patricio[1]

1 – Department of Chemistry, Centro Federal de Educação Tecnológica de Minas Gerais (CEFET-MG), Minas Gerais, MG, Brazil.
ingrid.asm26@gmail.com

Abstract
Annually, the Central Bank of Brazil issues millions of banknotes. In addition to issuing banknotes, the institution is responsible for maintaining the quality of the circulating medium by collecting and removing inadequate banknotes from circulation. The consequence of their short useful life and withdrawal of a large number of banknotes from circulation due to poor conservation is the generation of a large amount of waste. Consequently, the elimination of banknote waste without effective direction has led to a significant accumulation of this residue. According to the proposed law, the Central Bank is responsible for properly managing its waste. In these circumstances, studies and improvements are necessary to develop processes that are efficient in the recovery or reuse of banknote waste.
The banknotes are made from cotton fiber paper coated with a polymeric resin. A possible destination for this waste is its use as a filler or reinforcement for polymers. Furthermore, in view of the amount of polypropylene waste generated and its loss of mechanical and thermal properties when recycled, the banknotes can be used to maintain or improve the properties of recycled polymers. In view of this perspective, the present work aims to propose a reduction in the accumulation of waste banknotes and polypropylene in the environment, to develop and evaluate the properties of the use of notes as reinforcement in recycled polypropylene.Polymeric composites were developed by using recycled polypropylene (PPR) as the polymeric matrix and the banknote residues (BK) as filler. The composites PPR-BK were elaborated by homogenizing the matrix and filler, using a laboratory homogenizing machine, in concentrations of 10, 20, and 30% in mass of the banknote residues. The assessment of the properties was carried out through the characterization by Infrared Spectroscopy (FTIR), Contact angle, Tensile Test, and Accelerated Weathering Test.According to the results, the incorporation of banknote residues as filler contents to recycled polypropylene provided an increase in the hydrophilicity of the composites compared to pure PPR, and the polymer exhibited better mechanical properties against weathering. The composites at a concentration of 10% w/w provided an increase in the Young's modulus values and maximum resistance against traction when compared to those not exposed to weathering. Furthermore, the incorporation of filler contents at a concentration of 10% w/w provided an increase in the Young's modulus in relation to the matrix exposed and non-exposed to weathering.

Keywords: *Polypropylene, recycled, banknotes,* filler*, composites.*

Introduction

The banknotes have a short useful life, with a period of use until they become unsuitable for circulation due to their dire conditions. In addition to issuing and monitoring, the issuing institutions are responsible for the activity of sanitation of the circulating medium, aiming to keep the money in circulation with good conditions of use, thus assuming responsibility for the waste generated. This activity, in general, is regulated by law, providing principles and guidelines related to solid waste management.[1] In Brazil, the banking network collects millions of banknotes each year, and those not in good circulation conditions are destroyed. Incineration is used to destroy banknotes, but this technique has become increasingly inadequate as it allows for releasing toxic waste into the environment. [2]

Currently, banknotes are crushed and compacted, consequently, there is a large accumulation of waste without specific direction.[3] In this context, due to the growing concern with solid waste management and the enormous environmental impact they generate, studies and improvements of processes that are efficient in recovering or reusing waste banknotes are encouraged. Among the reported destinations, there is everything from composting to the use of banknote waste as fuel in cement kilns (co-processing), in the manufacture of ecological bricks, production of recycled paper, furniture items, among others. [4];[5]

Considering that banknotes are made from cotton fiber paper coated with a polymeric resin, a possible destination for this waste is its use as filler or reinforcement for polymer. [6]

The addition of fillers can be used to maintain or improve the properties of polymers being useful when it comes to the polymer recycling process.[2]; [7]; [8] The recycling has been used as an alternative to reduce the amount of plastic waste discarded in the environment, [9]; [10] although some properties of polymers are compromised when they are subjected to processing conditions, high temperatures and shear (mechanical recycling). The mechanical recycling is a generally more environmentally friendly method for reusing polymers. Furthermore, the recycled material offers savings in terms of market prices, when compared to virgin products, since it has a 40% lower cost than that of virgin resin. [11]

Chibani et al. (2016) [12] developed polypropylene (PP) reinforced with up to 20% m/m of the cardboard waste. The results obtained showed that the increase in the fiber content increases the modulus of elasticity of the polymer. However, elongation at break and tensile strength decreased with this increase in fiber content. Leon et al. (2016) [13] evaluated polypropylene reinforced with residual bamboo particles through extrusion and compression molding. Residues were classified according to size and added in different proportions to the PP. It was found that the increase of bamboo particles in the composite material causes increases in moisture, density and water absorption properties. Filho et al. (2017) [10] conducted studies on the effect of thermal and mechanical properties on recycled and pure PP and cellulose fibers in proportions of up to 40 %wt. It was found that the recycled polypropylene (PPR) composites, with 30 %wt in fibers, and the virgin PP composites, with a percentage of 20% in fibers better mechanical strength.

In view of this perspective, to reduce the accumulation of waste banknotes and polypropylene in the environment, the present work aims to develop materials using recycled polypropylene as a polymer matrix and waste banknotes as filler. The composites PPR-BK were characterized using Infrared Spectroscopy (FTIR), Contact angle, Tensile Test, and Accelerated Weathering Test.

Experimental

Recycled polypropylene (PPR) was supplied in granular form by RCA Plásticos Company. The banknotes (BK) were provided by the Central Bank of Brazil's Department of Circulation and had particle sizes ranging from 2.0-3.0 mm. The PPR and the BK residues were placed in the mixing chamber of a Homogenizer (Drais) model MH-100 from the brand MH Equipment. The banknote contents were used at 10%, 20%, and 30% wt of the mixture. After the polymer melted, homogenization was maintained for approximately 5 seconds. Then, the equipment was turned off, and the mixture obtained was removed. The same procedure was performed with the pure matrix (PPR). The materials obtained through homogenization were ground in a knife mill, Marconi model MA 580.The infrared spectroscopy was performed with the Shimadzu IRPrestige-21 Spectrophotometer with an ATR accessory. Thirty scans were performed in the region between 4000 and 400 cm^{-1} at room temperature.

The measurements of the sample contact angle (θ) were carried out in triplicate on different regions of the samples. It used a wettability test apparatus at an ambient temperature of 24 °C. The samples were placed on the support, and then deionized water of standardized volume (10.00 μL) was dripped onto the sample's surface. The images were obtained by filming the test using the

AMCap program, and the contact angle (θ) was calculated using the ImageJ program. The contact angle (θ) was given by measuring at least twice three drops deposited on each film. Later, the arithmetic mean of the measurements and the standard deviation were calculated.

The tensile tests were carried out in the Instron universal testing machine, model EMIC 23-20, operated at room temperature (~23°C). The materials were submitted to the test using clamps for tensile testing at a test speed of 50 mm.min^{-1}. The results were obtained from an average of 6 specimens tested for each composition of exposed materials and not exposed to weathering.

Results and Discussion

In the FTIR spectrum of the recycled polypropylene and PPR-banknotes (Fig. 1), it was possible to identify the typical bands of the polymer groups at 2950, 2866, and 2840 cm^{-1}, which refer to the asymmetric stretching of methylene (ν_{asym}.C-H$_3$), the symmetrical stretches (ν_{sym}.CH$_3$) and (ν_{sym}.CH$_2$), respectively. Two bands associated with the deformations of the methyl group (-CH$_3$) in the region of 1376 cm^{-1} (ν_{sym}.CH$_3$) and 1453 cm^{-1} (ν_{asym}.CH$_3$) can be observed. There are also low-intensity bands at 842 and 725 cm^{-1} corresponding to the angular deformations of the C-H bonds (δC-H), and at 1170 cm^{-1} for carbon-carbon stretching (νC-C) of the polymer chain. [12];[14];[15];[16] The bands in the 500-400 cm^{-1} range can be attributed to the stretching of the iron-oxygen bond (νFe-O), corresponding to the pigments in recycled polypropylene. Black inorganic pigments applied to plastics are made up of iron oxides (Fe_3O_4, $(FeCO)Fe_2O_4$). [17] Furthermore, the contamination of recycled polypropylene by low-density polyethylene was identified in the FTIR spectrum of the PPR due to the appearance of the characteristic low-density PE bands. The main bands that characterize polyethylene appear in the range of 2918 and 2840 cm^{-1}, and 1463 cm^{-1} corresponding to the C-H stretching vibrations and the vibration deformation band of the CH$_2$ group, respectively. Bands associated with the amorphous/crystal form of PE are also noted at 720-730 cm^{-1}. [18];[19] The material analyzed (commercial recycled PP) may have another polymer in its composition in addition to polypropylene as recycled.

The banknotes spectrum (Fig. 1) shows typical cellulose bands, associated with the cellulosic O-H stretching and asymmetric stretching C-H in the range of 3500 and 3200 cm^{-1} and at a wavenumber of 2900 cm^{-1}, respectively. The band at 1312 cm^{-1} is associated with the C-O-H (δC-O-H) bending vibrations, and at 1052 and 1000 cm^{-1}, they correspond to the stretches of the C-O-C bonds.[16]; [20];[21];[22] It was also possible to detect the presence of bands attributed to the metal-oxygen bonds, corresponding to the pigments present in the banknote, pearl effect pigments. Among the numerous pigments used, these have a metallic appearance resulting from different thicknesses and combinations of titanium and iron oxides on mica, providing the effect of iridescence.[23] The bands in the region between 600 and 420 cm^{-1} correspond mainly to the stretching of the metal-oxygen bonds (νTi-O, νFe-O) of the titanium (TiO2) and iron (Fe2O3) oxides present

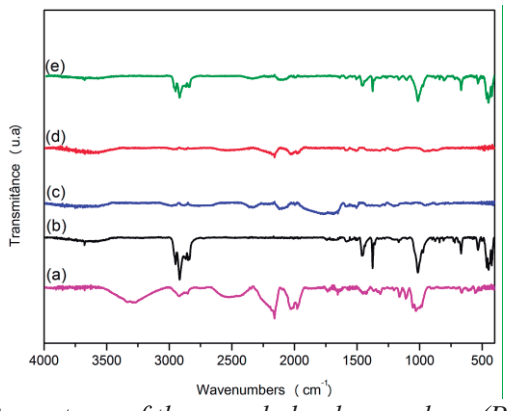

Figure 01- *FTIR spectrum of the recycled polypropylene (PPR) and PPR-banknotes. (a)Banknotes; (b) PPR; (c) PPR-10BK; (d) PPR-20BK; (e) PPR-30BK.*

Fig 2. shows the contact angle measured between the drops of water on the surface materials at the top and the average values of the contact angles. It was observed that all samples presented a mean contact angle characteristic of hydrophilic materials. In the case of recycled polypropylene, the high hydrophilicity, when compared to non-recycled PP, is justified due to pores on the surface of the polymeric films and the presence of metallic oxides, as shown in the FTIR spectra. For composites, the hydrophilicity is higher compared to pure PPR, which is justified by adding banknotes composed of cotton fibers. The hydroxyl groups (–OH) present in the chemical structure of the fibers promote hydrogen bonds between the cellulose of the cotton fiber and the water molecules. [24] The hydrophilicity did not vary significantly with the banknote content added.

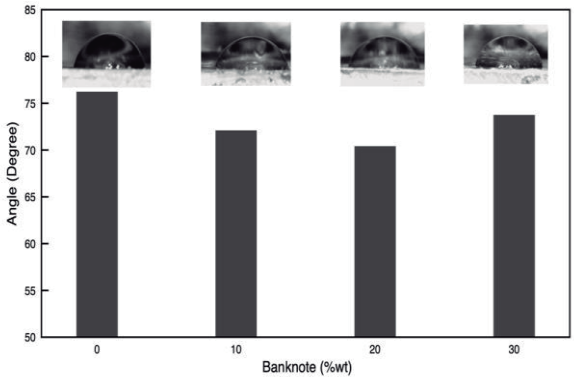

Figure 02- *Contact angle*.

The tensile tests of the composites (PPR-BK) and recycled polypropylene (PPR) were conducted to evaluate the influence of fillers on the mechanical properties of the materials before and after exposure to weathering. The results of the tensile tests of the materials exposed to accelerated weathering (PPR) and those not exposed to weathering (PPRS) are presented in Fig.3.

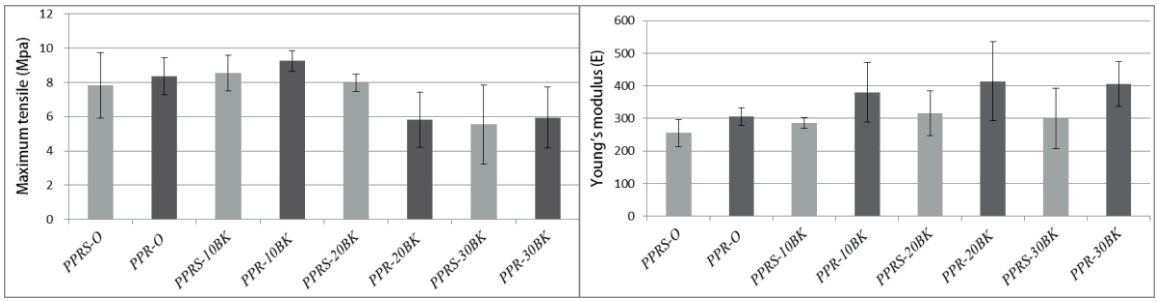

Figure 03- *Maximum tensile e Young's modulus.*

According to the results obtained from the tensile tests, the incorporation of banknote waste as filler content in recycled polypropylene led to changes in its mechanical strength properties. The incorporation of filler content promoted an increase in its stability against degradation when exposed to weathering. The composites at a concentration of 10% w/w (PPR-10BK) showed an increase in Young's modulus values and maximum resistance against traction when compared to non-exposed materials (PPR-10BK).

The incorporation of composite filler increased Young's modulus in relation to the matrix, particularly for composites that were exposed to weathering. Furthermore, the incorporation of filler contents at a concentration of 10% w/w provided an increase in composite Young's modulus in relation to the matrix, for both exposed and non-exposed materials. This better result is due to the fact that higher filler contents can compromise its dispersion in the matrix, and consequently, the dispersed phase starts to act as a defect, which leads to early matrix rupture and a compromise of its mechanical properties.

Conclusions

It was concluded that the incorporation of waste money bills as filler into recycled polypropylene provided materials with better mechanical properties against weathering. The results showed that the incorporation of banknote waste at a concentration of 10% w/w improved the strength of the composites, producing materials with higher values of Young's modulus and tensile strength in relation to the pure matrix when exposed to weathering. Therefore, the banknote residues acted as reinforcement fillers for the recycled polypropylene when exposed to weathering.

References

1. BRASIL. Lei nº 12.305, de 2 de agosto de 2010. Institui a Política Nacional de Resíduos Sólidos; altera a Lei no 9.605, de 12 de fevereiro de 1998; e dá outras providências. Brasília, DF: Diário Oficial da República Federativa do Brasil, Cap. I. Art, 1° p.1. [2010].

2. F. Gu; P. Hall; N. J. Miles. Journal of Cleaner Production 2016, 115. https://doi.org/10.1016/j.jclepro.2015.12.062.

3. BANCO CENTRAL DO BRASIL (Brasil). Cédulas inadequadas à circulação, 2022.

4. E. Franco. Dinheiro limpo: As cédulas de real fora de circulação, que eram incineradas, agora são trituradas e viram matéria-prima para a confecção de cadernos, blocos, brindes, objetos de decoração e até adubo. ISTOÉ, Tecnologia & meio ambiente. 2012.

5. BANCO CENTRAL DO BRASIL (Brasil). Relatório de Gestão do exercício de 2018:Sustentabilidade Ambiental. Brasília, DF, 2019, 103-105.

6. C. S. B. Gil, et al. Journal of applied polymer science 2019, 1, 2019 https://doi.org/10.1002/app.48232.

7. P. F. Sommerhuber; T. Wang; A. Krause. Journal of Cleaner Production 2016, 121. https://doi.org/10.1016/j.jclepro. 2016.02.036.

8. Narinder, S. Composites Part B: Engineering 2017, 115, https://doi.org/10.1016/j.compositesb.2016.09.013

9. W. D. Calister; D. G. Rethwisch. *Ciências e Engenharias de Materiais: Uma Introdução.* Ed.; LTC, Rio de Janeiro, 2012.

10. C. Spadetti; Polímeros: Ciência e Tecnologia 2017, 27. https://doi.org/10.1590/0104-1428.2320.

11. C. H. Pereira, et al. Revista Eletrônica de Materiais e Processos 2018, 13, 1. ISSN 1809-8797

12. N. Chibani, et al. Journal of Vinyl & additive Technology 2016, 22,3https://doi.org/10.1002/vnl.21437

13. L. Léon, et al. Revista Mexicana de Ciencias Forestales 2016, 7, 38. https://doi.org/10.29298/rmcf.v7i38.6.

14. J. R.Silva; L.S. Nunes, M. S. Rabello.Revista Eletrônica de Materiais e Processos 2016, 11, 2. I SSN 1809-8797.

15. Z. T. Yaoa, et al. Journal of Hazardous Materials 2013, 262, https://doi.org/10.1016/j.jhazmat.2013.08.062.

16. D, L. Pavia, et al. Introdução à Espectroscopia. Introdução à Espectroscopia. Cengage Learning Ed.; São Paulo, 2016; Vol.2, 16-59.

17. F. D. Jafelicci. B.Sc. University of Uberlândia, 2019.

18. I. Borovanska, et al. Journal of Elastomers & Plastics 2012, 44, 6. https://doi.org/10.1177/0095244312441731

19. Z. McCaffrey. Industrial Crops and Products 2018, 125. https://doi.org/10.1016/j.indcrop.2018.09.012 .

20. L. P. R. Cruz. Ph.D. Thesis, University of Rio Grande do Norte, 2017.

21. E. Império. Vibrational Spectroscopy 2015, 79. https://doi.org/10.1016/j.vibspec.2015.05.004

22. O. G. Paniz, et al., Revista Matéria 2018, 23, 4. https://doi.org/10.1590/S1517-707620180004.0578

23. J. M. R. Fazenda, Tintas – ciência e tecnologia, Blucher Ed.; São Paulo, 2009; Vol. 4, 394- 397.

24. M. V. S. Pinto. Ph.D. Thesis, University of Campina Grande, 2018.

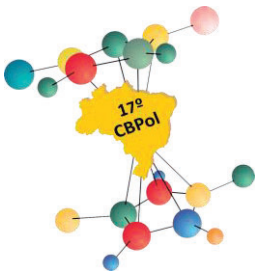

EVALUATION OF SODIUM ALGINATE MEMBRANES INCORPORATED WITH RED ARAÇÁ (*PSIDIUM CATTLEYANUM* SABINE) EPICARP EXTRACT

Marcio L. D. Carvalho[1], Douglas H. Lacorte[2], Luísa B. Avila[3], Caroline C. Moraes[2] and Gabriela S. da Rosa[123]
1 –Chemical Engineering, Federal University of Pampa (UNIPAMPA), Bage, RS, Brazil
marciocarvalho.aluno@unipampa.edu.br
2 – Graduate Program in Science and Materials Engineering, Federal University of Pampa (UNIPAMPA), Bage, RS, Brazil
3 –Graduate Program in Chemical Engineering, Federal University Santa Maria (UFSM)), Santa Maria, RS, Brazil

Abstract - Due to the increasing demand for sustainable materials, the use of plant extracts and natural polymers has become attractive. In this study, sodium alginate membranes with the addition of red araçá extract were developed and evaluated for potential applications in topical dressing. The addition of the extract resulted in a significant reduction in water vapor permeability (WVP), indicating a more efficient mass diffusion barrier. Water solubility increased from 50.18% (MC) to 41.43% (ME), demonstrating improved membrane stability. The mechanical properties for MC and ME showed a tensile strength of 8.468 and 6.676 MPa, respectively, and an elongation at break of 6.676 and 8.190%, respectively. It can be concluded that sodium alginate membranes with the addition of red araçá extract exhibit promising characteristics for use in wound dressings, offering mechanical strength, appropriate permeability, and physical stability. These results suggest that these membranes could be an interesting alternative to synthetic polymers for medical applications.
Keywords: *Biopolymers, Bioactive, Phenolic Compounds, Topical Dressings*

Introduction

Due to the growing demand for sustainable and renewable materials, the use of plant extracts and natural polymers has become attractive. These options can be an alternative to synthetic products, obtained from finite sources and are polluting and harmful to the environment. Among the different types of biopolymers, sodium alginate stands out as a polysaccharide synthesized by brown algae, which possesses wound healing properties and non-toxicity, making it useful in biomedicine. It is even possible to add new characteristics and enhance its functions [1]. A sustainable way to improve this material is through the application of natural extracts obtained from plant matrices with bioactive properties, which can confer antioxidant action to the product.

In this regard, araçá, *Psidium cattleyanum* Sabine, a typical fruit from Rio Grande do Sul, emerges as a potential source of bioactive compounds and can be found in two morphotypes: yellow and red. Both contain phenolic compounds in their composition, with the red araçá standing out for its high content of anthocyanins in its epicarp, compounds responsible for its coloration. These compounds can be used to add bioactive properties to sodium alginate, making it even more useful in the field of biomedicine [2].

Therefore, the present study aims to produce sodium alginate membranes activated with red araçá extract and characterize them in terms of thickness, water vapor permeability (WVP), water solubility, and mechanical properties.

Experimental

Maceration was apllied for the extraction of bioactive compounds from the epicarp of red araçá, similar to the one used by Avila et al. [3] for extracting jabuticaba peel. The samples were obtained in the city of Candiota, RS. For this purpose, the samples were previously sanitized with 2% sodium hypochlorite, lyophilized at -50°C for 24 h, ground, and sieved through a 60 *mesh* sieve to standardize their particle size (dp < 0.272 mm). The extraction was performed by maceration using a ratio of 1 g of sample and 50 mL of 40% (v/v) ethanolic solvent in a *Dubnoff* bath at a temperature of 70°C for 2 h under constant agitation at 80% of the equipment's capacity.

The sodium alginate membranes were prepared using an alginate with a viscosity between 300-400 CPs at 20°C (Êxodo Científica). A 2% (w/v) solution of the biopolymer was prepared [4]. using a mechanical stirrer at 600 rpm. Then, 2 % (w/v) of glycerol were added to the mixture as a plasticizer. The solution was stirred until the plasticizer was completely dissolved, and then transferred to an ultrasonic bath for 30 min to remove any remaining air bubbles. Subsequently, the solution was distributed onto a Petri dish and dried in a forced convection oven at 40°C for 24 h. After removing the membranes from the oven, they underwent a crosslinking process by immersion in a 0.1% (w/v) CaCl2 solution and 1% (w/v) glycerol for 1 h, followed by another drying step at 30°C for 12 h. To obtain the active membranes, with plant extract present in their formulation, the same procedure was followed, but with the addition of 1% (w/v) of previously lyophilized extract.

Membranes were characterized Thickness of the membranes was measured using a digital micrometer (Insize, model IP65), with 10 random measurements. The water vapor permeability (WVP) test was conducted following the standards ASTM E96/96 by [5]. 30 g of anhydrous calcium chloride (CaCl2) were weighed and sealed with the membranes in Falcon tubes. The tubes were placed in desiccators, where the relative humidity was maintained at 50%. After staying in the desiccator for 10 days, the samples were weighed to check the mass gain of CaCl2.

The water solubility of the membranes was determined using the method proposed by [6] with modifications. The analysis was performed in triplicate, with samples measuring 2x2 cm. Initially, the samples were dried in a forced circulation oven at 60°C for 24 h and weighed. Then, the samples were immersed in water under agitation at 50 rpm for 24 h at room temperature. The suspension was filtered, and the residue was dried at 60°C for 24 h and subsequently weighed.

The membranes were also evaluated for their mechanical properties, tensile strength, and elongation. The standard ASTM D822 by [7] was used for this purpose, and the tests were conducted using a texture analyzer (Stable Micro Systems, model TA.TX). Through these tests, the tensile strength and percentage of elongation at break were quantified.

Finally, a statistical analysis was conducted using the Tukey test, through statistical software (STATISTICA 7), to determine if there were significant differences in thickness, WVP (Water Vapor Permeability), water solubility and mechanical properties between the control membranes and the membranes incorporated with red araçá extract.

Results and Discussion

The results obtained for the analysis of thickness, water vapor permeability (WVP), water solubility, tensile strength, and elongation at break are presented in Table 1.

Table 1. Characterization of membranes

	MC	**ME**
Thickness (mm)	0,135 ± 0,022 [a]	0,1172 ± 0,016 [a]
WVP (g/msPa)	$2.479.10^{-09} \pm 5.940.10^{-11}$ [a]	$1.906.10^{-09'} \pm 2.244.10^{-10}$ [b]
Water solubility (%)	50.18 ± 1.86 [a]	41.43 ± 0.67 [b]

Tensile strength (MPa)	8.468 ± 1.248 [a]	6.676 ± 0.360 [a]
Elongation at break (%)	15.372 ± 2.575 [a]	8.190 ± 1.468 [b]

.

The results obtained for thickness are consistent with those reported in the literature, which [8] also reported similar thickness values of 0.131 ± 0.020 mm and 0.144 ± 0.016 mm for the sodium alginate control film and sodium alginate films with green propolis extract, respectively. Additionally, the thickness of the membranes showed no significant difference with the addition of the natural extract.

Regarding the WVP values, there was a significant difference, indicating a reduction in this parameter with the addition of red araçá extract. The water vapor permeability (WVP) values for the MC and ME membranes were $2.479.10^{-09}$ ± $5.940.^{10-11}$ g/m.s.Pa and $1.906.10^{-09}$ ± $2.244.10^{-10}$ g/m.s.Pa, respectively. Previous studies have reported similar values for sodium alginate membranes cross-linked with Ca2+. Rhim et al. [9] obtained a value of $1.0870.10^{-09}$ ± $0.09.10^{-09}$ g/m.s.Pa using a 1% (w/v) CaCl2 solution. The cross-linking of the membranes had a positive impact on their barrier properties, reducing the segmental mobility of the polymer and limiting the exchange of moisture between the environment and the anhydrous calcium chloride inside the tubes.

The water solubility obtained is consistent with the value reported by Chen et al. [10], which is 49.7 ± 0.2%. The same pattern was also observed when adding sodium alginate membranes, with a constant decrease in this parameter with increasing thymol content. Therefore, the results obtained in this study are favorable for application in topical dressings, since wounds on the skin release exudate, which the material will come into contact with.

The tensile strength values obtained were 8.468 ± 1.248 MPa for the control membrane and 6.676 ± 0.360 MPa for the membrane with the extract. These results are higher than those reported by Bakar et al. [11], who described a value of 4.0 ± 1.0 MPa for control sodium alginate membranes and values ranging from 4.0 ± 0.4 to 5.1 ± 0.8 MPa for sodium alginate membranes with different concentrations of Ageratum conyzoides extract. According to [12], this may be due to particles present in the red araçá extract that interact with the polymeric matrix, forming defect points or stress concentration points in the membranes. Thus, [13, 14] suggest that tensile strength values around 11.5 MPa are favorable for application as topical dressings

The crosslinked sodium alginate membranes with and without the addition of extract showed good mechanical strength, flexibility, and favorable thickness for use as dressings. In the crosslinking process, it was possible to decrease the water solubility of the material, with a mass loss due to solubility of approximately 50% and 41% for MC and ME, respectively. It was also observed that the material is permeable to water vapor, contributing to a moist environment. Therefore, the use of alginate membranes with the addition of red araçá epicarp extract presents itself as an interesting alternative to synthetic polymers for various applications, such as dressings.

Finally, the results for elongation at break were consistent with the literature. Rhim et al. [9], who developed crosslinked membranes using two methods (film blending and film immersion), obtained values ranging from 8.2 ± 2.2 to 3.4 ± 1.4 % for crosslinked sodium alginate membranes at different concentrations of CaCl2 solutions. It is also possible to observe a significant decrease in this parameter due to the addition of red araçá extract.

Conclusions

The crosslinked sodium alginate membranes, both with and without the addition of the extract, exhibited good mechanical strength, flexibility, and suitable thickness for use as dressings. In the crosslinking process, it was possible to reduce the water solubility of the material, resulting in a mass loss of approximately 50% for MC and 41% for ME. Additionally, it was observed that the material is permeable to water vapor, contributing to its application in a moist environment.

Therefore, the use of alginate membranes with the addition of red araçá epicarp extract presents itself as an interesting alternative to synthetic polymers in various applications, especially in the field of topical dressings. The combination of good mechanical properties, flexibility, reduced water solubility, and water vapor permeability makes these membranes suitable for promoting wound healing and maintaining a favorable environment for tissue regeneration. In future steps, it would be interesting to study the release of bioactive compounds present in the membranes with the extract and their wettability.

Acknowledgements

Acknowledgment to the Research Group in Engineering of Particulate Systems Processes (GPEPSP), FAPERGS, CAPES, CNPq and the Federal University of Pampa (UNIPAMPA).

References

1. [1] BRITO, G. F. et al. Revista Eletrônica de Materiais e Processos, 2011, v. 6, n. 2, p. 127-139http://www2.ufcg.edu.br/revista-remap/index.php/REMAP/article/view/222. Acesso em: 03 mar. 2021.
2. [2] PEREIRA, E. S. et al. Food Bioscence, 2020, v. 37, n. 12, p. 1-9 https://doi.org/10.1016/j.fbio.2020.100665. Acesso em: 07 fev. 2022.
3. [3] AVILA, L. B. et al. Polymers, 2020, v. 12, n. 12, p. 2916 https://doi.org/10.3390/polym12122916.
4. [4] PACHECO, M. S. et al. International Journal of Biological Macromolecules, 2020, v. 152, p. 803–811 https://doi.org/10.1016/j.ijbiomac.2020.02.140.
5. [5] ASTM. Método: E96/96. Philadelphia: Americam Society for Testing Materials, 2016.
6. [6] GONTARD, N. et al. Food Science and Technology, 1994, v. 29, n. 1, p. 39–50 https://doi.org/10.1111/j.1365-2621.1994.tb02045.x.
7. [7] ASTM. D 882. Philadelphia: Americam Society for Testing Materials, 2018
8. [8] MARANGONI, Food Hydrocolloids for Health, 2022. v 2, p 1-8 https://doi.org/10.1016/j.fhfh.2022.100094
9. [10] RHIM et al. Colloids and Surfaces B: Biointerfaces, 2021, v 207 https://doi.org/10.1016/j.colsurfb.2021.111999.
10. [11] CHEN et al. Journal of Advanced Research. Química Nova, 2009, v. 8, n. 3, p. 217-233 https://doi.org/10.1016/j.jare.2017.01.005.
11. [12] BAKAR et al. IOP Conference Series: Materials Science and Engineering, 2018, v 374, p 17 -18 https://doi.org/10.1088/1757-899X/374/1/012087.
12. [13] CHI et al. Journal of Cleaner Production, 2020, v 244 https://doi.org/10.1016/j.jclepro.2019.118862.
13. [14] HASSAN et al. Journal of Polymers and the Environment, 2018, v 26, p 235-243 https://doi.org/10.1007/s10924-017-0944-2.
14. [15] ABASSI et al. International Journal of Biological Macromolecules, 2020, v 155, p 751 – 765 https://doi.org/10.1016/j.ijbiomac.2020.03.248.

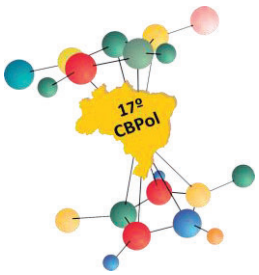

EVALUATION OF THE EFFECT OF DIFFERENT LEVELS OF CITRIC ACID ON THE PHYSICOCHEMICAL PROPERTIES OF CASSAVA STARCH/POLY(BUTYLENE SUCCINATE) BLENDS

Raul F. A. Santos[1]*, Gustavo A. D. Urena[1], Patrícia S. O. Patricio[2] and Alessandra A. Lucas[1]

1 – Graduate Program in Materials Science and Engineering (PPGCEM), Federal University of São Carlos (UFSCar), São Carlos, SP, Brazil
rfasantos@estudante.ufscar.br
2 – Department of Materials Engineering (DEMAT), Federal Center for Technological Education of Minas Gerais (CEFET-MG), Belo Horizonte, MG, Brazil

Abstract – In this study blends of cassava starch with poly(butylene succinate) (PBS) were developed, containing citric acid. The materials were processed in a Haake torque rheometer and samples were obtained for characterization by thermal pressing. The concentration of citric acid in the compositions ranged from 0 to 5%. The samples were characterized by water absorption and water weight loss tests. The absorption results indicated possible reduction of the hydrophilic character of the starch blends, as a consequence of the presence and effect of the citric acid concentration. However, the weight loss results showed that there was a greater loss of material in water for the samples containing the acid. Thus, the water absorption results were influenced by the loss of material, causing the impression that the water absorption of the samples was lower.

Keywords: *Starch, Poly(butylene succinate), Citric acid, Blends.*

Introduction

Conventional petrochemical-based polymers such as polyethylene and polypropylene are often used in the production of plastic packaging because of their properties such as flexibility, strength, transparency, etc. [1]. However, most synthetic polymers have a difficult degradability, causing their accumulation when disposed of in the environment [2]. Starch is a polymer with advantageous characteristics, which makes it a very interesting material in replacing some polymers of petrochemical origin [3], because it is biodegradable, has high availability and low cost [3-4].

From its native state, starch undergoes a process defined as gelatinization, whose product is called thermoplastic starch (TPS) [5-6]. Thermoplastic starch is a biodegradable, renewable, low-cost raw material polymer [7], but its high sensitivity to water and low mechanical properties make its application limited [7-8]. However, some alternatives have been proposed to circumvent these limitations, such as blending between TPS and another biodegradable polymer [8-9].

Poly(butylene succinate) (PBS) is a biodegradable aliphatic polyester, which can be an environmentally friendly alternative to be blended with starch [8], another possibility involves the chemical modification of starch [10], through the use of crosslinking agents such as carboxylic acids [11]. Therefore, this work was developed with the objective of investigating the influence of

varying the concentration of citric acid, on the physicochemical properties of starch-based blends with PBS.

Experimental

Materials

The commercial cassava starch was purchased in the city of São Carlos-SP and produced by Amafil Indústria e Comércio de Alimento Ltda. The poly(butylene succinate) (PBS) with code TH803S, was produced by Xinjiang Blueridge Tunhe Chemical Industry Co., Ltd., with flow index of FI = 18±2 g/10min and melting temperature of 114°C. The reagents used was glycerol from Exodus Scientific and citric acid from Synth.

Preparation of the compositions

The materials were dried in an oven with hot air circulation from TECNAL, model TE-394/2, at 100°C for 30 min. After drying, with the exception of PBS, the starch, glycerol, and citric acid were premixed. The materials were processed in a Haake torque rheometer, model Rheomix 600p and with "roller" type rotors, at 120°C and a speed of 80 rpm for 10 min and then were pressed in a thermal press at 120°C for 2 min to obtain the specimens. Cassava starch 70 wt.%, PBS 30 wt.%, and glycerol 25 wt.% were used. The citric acid was varied in 0, 1, 3 and 5 wt.%. The glycerol and citric acid content was based on the dry starch content.

Characterization tests

Water absorption

The test was performed following the ASTM D570-98. The samples were previously dried in an oven with hot air circulation, of the TECNAL model TE-394/2, at 50°C for 24 hours. Then, the samples were weighed to obtain the value of the initial dry weight (w_1) and after weighing, they were immersed in 100 mL of distilled water remaining for 1, 3, 5, 7, 9 and 11 hours in immersion. For each immersion time reached, the samples were removed and weighed again to obtain the value of wet weight (w_2). The percentage of absorbed water was calculated using Eq. 1. The measurements were performed in triplicate.

$$WA(\%) = \frac{w_2 - w_1}{w_1} x100 \qquad (1)$$

Weight loss in water

After finishing the water absorption test, the wet samples that were immersed in distilled water were again dried in an oven at 50°C for 24 hours. Then they were weighed, obtaining the value of the final dry weight (w_3). The weight loss test was performed according to ASTM D570-98. The measurements were performed using Eq. 2 and in triplicate. w_1 is the initial dry weight of the samples before the absorption test.

$$WL(\%) = \frac{w_1 - w_3}{w_1} x100 \qquad (2)$$

Results and Discussion

One of the main limitations of thermoplastic starch is associated with its sensitivity to water, due to its hydrophilic character [12]. Therefore, physicochemical analyses of the starch blends were performed, through water absorption and weight loss in water tests.

Water absorption

Fig.1 illustrates the results of the percentage of absorbed water of the pure starch blends and with citric acid (1-5%).

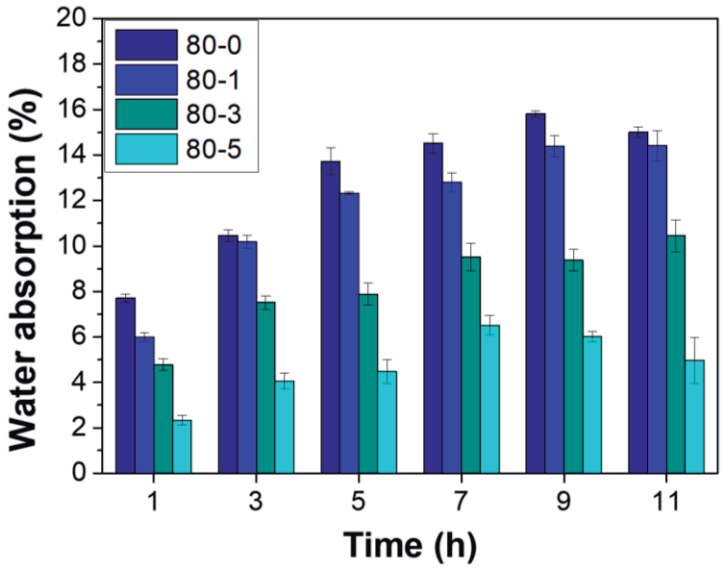

Figure 1 – Percent water absorption of TPS/PBS blends without and with citric acid (0-5%).

The results showed that regardless of the immersion time, the samples without acid were those that exhibited the highest percentage of absorbed water. This behavior was already expected, as a consequence of the hydrophilic character of starch, resulting from the presence of hydroxyl groups present in its structure [13]. Possibly, the samples did not absorb a higher percentage of water due to the hydrophobic nature of the incorporated PBS [14].

For the samples containing citric acid, the absorption decreased as the concentration of the acid increased. This may have occurred, due to the replacement of hydroxyl groups naturally present in starch, by hydrophobic ester groups [15], resulting from the esterification reaction between the hydroxyl group of starch and carboxyl of citric acid [16]. Another possible condition observed in the work of Prachayawarakorn and Tamseekhram [17], which contributes to reduced water absorption, is crosslinking reactions. However, only the results of water absorption are not sufficient to state that there was cross-linking of the samples, because it may occur only esterification reactions, which also contribute to a lower absorption.

Regarding the effect of immersion time, as the time increased the greater was the amount of water absorbed for all samples, regardless of composition. However, it was expected that the percentage of absorption of the samples would reach a constant value in longer times, but it was observed that for some samples, the absorption reduced after 9 hours. This result may have occurred due to the starch granules in their native state, which were not completely gelatinized during processing, dissolving the samples in water.

Weight loss

The weight loss results of the pure blends and the blends with different citric acid contents are illustrated in Fig. 2. The results were obtained after the water absorption test.

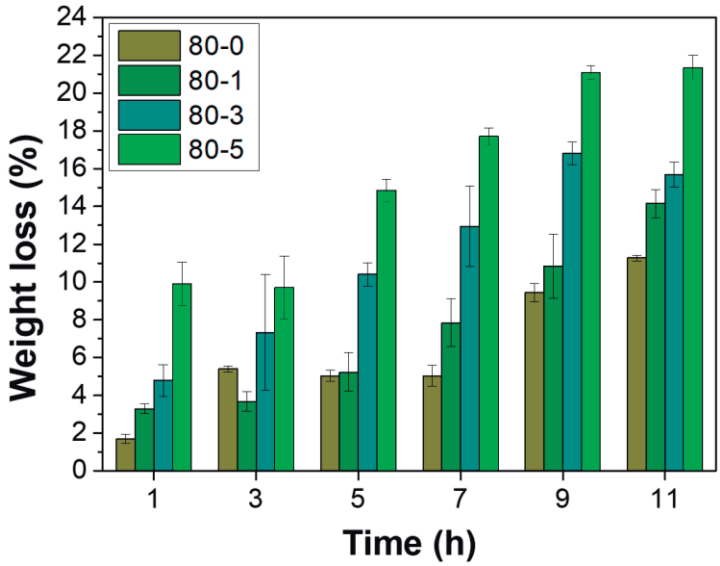

Figure 2 – Percent weight loss of starch blends as a function of immersion time.

For each exposure time, the results showed that the weight loss of the samples became increasingly greater along with the increase in citric acid content, especially for the sample containing 5% of the acid. Furthermore, regardless of composition, weight loss increased with the time the samples were immersed in water. However, it was expected that the samples without acid would present a higher value of weight loss, in relation to the samples containing the acid.

As mentioned in the previous result, if there were esterification and/or cross-linking reactions of the starch promoted by the presence of citric acid, there would be fewer hydrophilic groups available to react with water molecules, so less weight loss would occur. Therefore, this greater loss may have occurred due to the acid hydrolysis of the starch chains during processing, which made the samples more soluble in water [18] or as a result of the dissolution of starch granules that were not completely gelatinized.

From these results, it was observed that the lower water absorption of the samples with citric acid demonstrated in the previous result, occurred due to the loss of material solubilized in water and not through esterification and/or cross-linking reactions, as was proposed. If these reactions were to occur, not only would the absorption be lower, but also the weight loss for the samples containing the acid would decrease. Thus, the calculation of the percent absorption will contain an error, because the values of the wet weight measurements will be lower than the actual value, due to the loss of material during immersion. These results also confirm, because at longer immersion times there was a reduction in absorption, due to the loss of material in the water.

Conclusions

The physicochemical analysis of the starch blends demonstrated, that although the samples containing citric acid presented a lower absorption in function of the citric acid content, differently it was observed in the results of weight loss a greater loss for the samples containing acid, influencing the absorption results. Thus, possibly the processing conditions were not so effective to

provoke the necessary reactions or interactions between the citric acid and the starch, so as to hinder the absorption and the loss of material in water.

Acknowledgements

This study was financed in part by the Coordenação de Aperfeiçoamento de Pessoal de Nível Superior - Brasil (CAPES) - Finance Code 001. The authors thank the Graduate Program in Materials Science and Engineering (PPGCEM) and the CNPq – Conselho Nacional de Desenvolvimento Científico e Tecnológico for the financial support for this work with scholarship, process 132347/2020-2.

References

1. J. Muller; C. González-Martínez; A. Chiralt, Materials, 2017, 10, 952. https://doi.org/10.3390/ma10080952
2. X. Wang; K. Yang; Y. Wang, Journal of Macromolecular Science, Part C: Polymer Reviews, 2007, C43, 3. https://doi.org/10.1081/MC-120023911
3. A. L. Chaudhary; M. Miler; P. J. Torley; P. A. Sopade; P. J. Halley, Carbohydrate Polymers, 2008, 74. https://doi.org/10.1016/j.carbpol.2008.05.017
4. P. G. Seligra; L. E. Moura; L. Famá; J. I. Druzian; S. Goyanes, Polymer International, 2016, 15. https://doi.org/10.1002/pi.5127
5. R. A. Shanks; L. M. W. K. Gunaratne, Journal of Thermal Analysis and Calorimetry, 2011, 106, 93. https://doi.org/10.1007/s10973-011-1620-8
6. G. Li; P. Sarazin; B. D. Favis, Macromolecular Chemistry and Physics, 2008, 209. https://doi.org/10.1002/macp.200700637
7. L. Avérous; C. Fringant, Polymer Engineering and Science, 2001, 41. https://doi.org/10.1002/pen.10768
8. Q. Yin; F. Chen; H. Zhang; C. Liu, Advanced Materials Research, 2015, 1119. https://doi.org/10.4028/www.scientific.net/AMR.1119.306
9. V. O. Bulatović; V. Mandić; D. K. Grgić; A. Ivančić, Journal of Polymers and the Environment, 2021, 29. https://doi.org/10.1007/s10924-020-01874-w
10. A. H. M. Zaina; A. W. M. Kahara; N. Z. Noriman, Procedia Chemistry, 2016, 19. https://doi.org/10.1016/j.proche.2016.03.064
11. J. Y. Kim; Y. Lee; Y. H. Chang, International Journal of Food Properties, 2017, 20. https://doi.org/10.1080/10942912.2017.1368551
12. E. Olsson; M. S. Hedenqvist; C. Johansson; L. Järnström, Carbohydrate Polymers, 2013, 94. https://doi.org/10.1016/j.carbpol.2013.02.006
13. M. Kaseem; K. Hamad; F. Deri, Polymer Science, 2012, 54. https://doi.org/10.1134/S0965545X1202006X
14. D. Liu; Z. Qi; Y. Zhang; J. Xu; B. Guo, Starch/Stärke, 2015, 67. https://doi.org/10.1002/star.201500060
15. M. R. Amin; F. R. Anannya; M. A. Mahmud; S. Raian, Journal of Polymer Research, 2020, 27. https://doi.org/10.1007/s10965-019-1983-2
16. E. Chabrat; H. Abdillahi; A. Rouilly; L. Rigal, Industrial Crops and Products, 2012, 37. https://doi.org/10.1016/j.indcrop.2011.11.034
17. J. Prachayawarakorn; J. Tamseekhram, J. Sci. Technol, Songklanakarin Journal of Science and Technology, 2019, 41. https://doi.org/10.14456/sjst-psu.2019.45
18. J. B. Olivato; M. V. E. Grossmann; A. P. Bilck; F. Yamashita, Carbohydrate Polymers, 2012, 90. http://dx.doi.org/10.1016/j.carbpol.2012.05.009

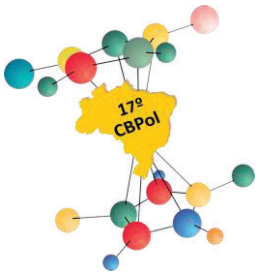

EVALUATION OF WEAR RESISTANCE OF LLDPE/UHMWPE BLENDS

Cardoso M Pollyana[1,3], Azevedo B Joyce[1,2]*, Barbosa D V Josiane[1], Ueki M Marcelo [3]

1 – Pós-graduate Program PPGGETEC, University Center Senai Cimatec, Salvador, Bahia, Brazil
2- Institute of Science, Technology and Innovation, Federal University of Bahia, Camaçari, BA, Brazil
joyce.azevedo@ufba.br
3- Graduate Program in Materials Science and Engineering—P2CEM, Federal University of Sergipe, Aracaju, SE, Brazil

Abstract – UHMWPE is widely used for manufacturing total hip arthroplasty components. However, during its useful life, the interaction of UHMWPE with metallic or ceramic parts can lead to loosening of the implant and/or loss of properties. Therefore, modifications of this polymer in the form of blends have been widely used as an alternative to obtain materials with specific properties. In this work, the wear resistance of LLDPE/UHMWPE blends with different component proportions was evaluated using the Slurry abrasion method. Toughness and hardness properties were also determined as well as the wear surface morphology. The results indicated that with the increase of UHMWPE in the blend there is a decrease in the volumetric loss, which characterizes a greater to wear resistance and greater hardness.

Keywords: Blends; LLDPE; UHMWPE; Wear Resistance.

Introduction

The formation of blends from the mixture of two polyethylenes is being increasingly evaluated for several applications. The use of UHMWPE is increasing mainly due to the search for the modification of its characteristics and, consequently, the expansion of the applicability of this material, or in some cases, just to facilitate its processing [1].

One of the possibilities for forming UHMWPE blends for applications in orthopedic prostheses is HDPE. They are similar in terms of molecular structure, crystalline melting temperature, permeability and chemical inertness, but UHMWPE exhibits exceptional low temperature impact strength, high abrasion resistance, excellent resistance to stress cracking development, low coefficient of friction, and high resistance to fatigue [2]. Despite these properties, with UHMWPE, total hip prosthesis loosening still occurs due to wear of the acetabulum and research aims to minimize this deficiency [3].

Currently, the wear caused by the polymer-metal tribological system is the main reason for failure in total hip and knee prostheses, due to the release of particles and, consequently, formation of the inflammatory process and subsequent loosening of the prosthesis.

Lucas et al. 2011 [4] evaluated the abrasion resistance of the HDPE/UHMWPE system, where they identified an increase in wear resistance with the increase in the percentage of UHMWPE. The wear mechanism observed for blends of this type (HDPE/UHMWPE) is characterized by the formation of fibrils, and this process is stronger and contains higher levels of fibrils in samples containing a higher amount of UHMWPE. In this context, this work obtained blends of LLDPE with different concentrations of UHMWPE and carried out the evaluation of wear resistance through the Slurry abrasion method.

Experimental

Materials

In this work, linear low-density polyethylene (LLDPE) of commercial grade ML 3601 – U with hexene comonomer, fluidity index of 3.3 g/10 min and density of 0.939 g/cm² was used as matrix. UTEC 6540 commercial grade ultra-high molecular weight polyethylene (UHMWPE) was added to the LLDPE in powder form, with a density of 0.925 g/cm². The polyethylene used is produced and sold by Braskem.

Methods

Advanced brand press was used, with a plateau heated by electrical resistances, pressure of 60 kgf/cm2 and opening speed of 200 mm/second. For stress relief from the forming process, the specimens were immersed in water for 1 hour, at a controlled temperature of 90 °C. The time and temperature parameters used in the process of conformation of the plates were established according to the thermal properties of the LLDPE, therefore, the samples were heated to 160°C for 30 min and presented adequate conditions of conformation.

The wear resistance was determined using the Slurry abrasion method, according to ISO 15527 standard. average diameter of 80μm and a concentration of 3g. The specimens, in the form of plates, with dimensions of 10x10x3cm were obtained from all formulations.

To determine the tenacity, a tensile test was carried out in an EMIC equipment, model DL 200, following the ISO 527 type 5A standard without the use of an extensometer and displacement rate of 50mm/min.

The Vickers microhardness test was carried out with a model HMV Shimadzu microhardness tester with a point in the shape of a pyramid at 136°, a load of 1.961N for 15 seconds at 10 different points. The assay was performed at room temperature on a flat, scratch-free plate. After removing the drilling load, the length of the indentation diagonals was measured with a resolution of 1μm.

The morphology of the mixtures was investigated by scanning electron microscopy using a JEOL Scanning Electron Microscope (SEM), model Carry Scopy JSM-6510LV from JEOL, with an accelerating voltage of 20kV.

Results and Discussion

The type of wear occurring in the blends was evaluated using the Ratner-Lancaster correlation (Fig. 1). Through this correlation, Lancaster in 1968 showed that the wear resistance of polymers is associated with the ability of these materials to plastically deform without fracture, that is, their toughness [5]. It is observed that a linearity in the correlation was not identified, which may characterize that the wear mechanism was not purely abrasive. Briscoe 1981 [6] recommends that it is difficult to identify only one wear mechanism in polymers, due to interfacial connections.

With the increase of UHMWPE in the mixture, a decrease in tenacity is identified (Fig 2). The amorphous and crystalline phases govern the tensile and abrasive performance of polyethylenes [6]. Some studies show that the amorphous phase strongly contributes to the increase in wear resistance, the crystalline phase does not have a significant influence on this property. Thus, the addition of UHMWPE reduces toughness, which predicts a reduction in wear resistance in blends with higher concentrations of this polymer [5;7].

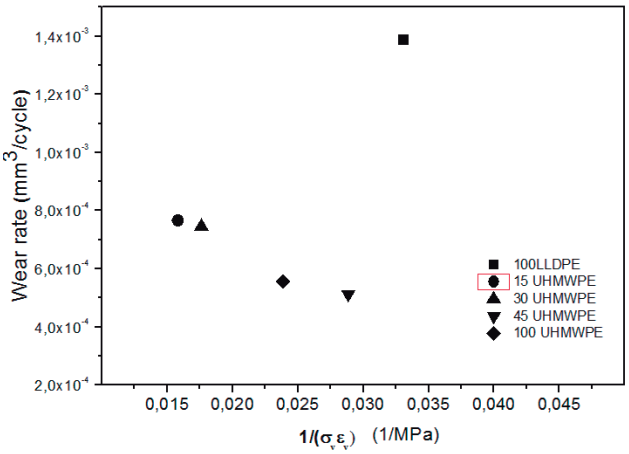

Figure 1 - Ratner-Lancaster correlation for abrasive wear:σ_y e ε_y

Some authors report the correlation of wear resistance with energy absorption capacity. Good abrasion resistance is related to the ability to absorb energy by its own deformation and low coefficient of friction [8]. The property that characterizes the absorption of energy for a material is its tenacity, therefore, the greater the tenacity of the material, the greater the resistance to abrasion [9]. With the increase of UHMWPE in the mixture, a decrease in tenacity is identified (Fig. 2), which can be related to its immiscibility in the melting state and the liquid-solid phase separation due to the different crystallization rates between LLDPE and UHMWPE [10].

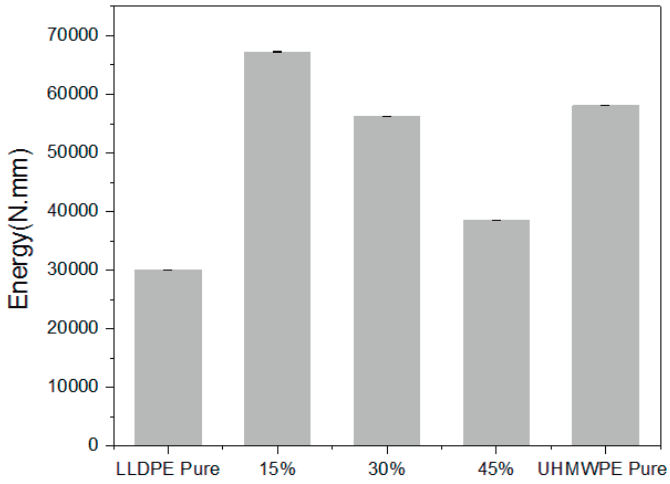

Figure 2 - Variation of absorbed energy for LLDPE/UHMWPE blends

Fig. 3 shows the variation of Vickers micro hardness of the blends. It is observed that the greater the percentage of UHMWPE in the blend, the greater the hardness. Studies involving PE have observed a relationship between hardness and crystallinity, although direct proportionality between them is not observed over a wide range of crystallinity. Molinari and Tuckart 2016 [11] evaluated the variation of micro hardness with crystallinity, where they identified that hardness shows an increasing tendency with increasing crystallinity level.

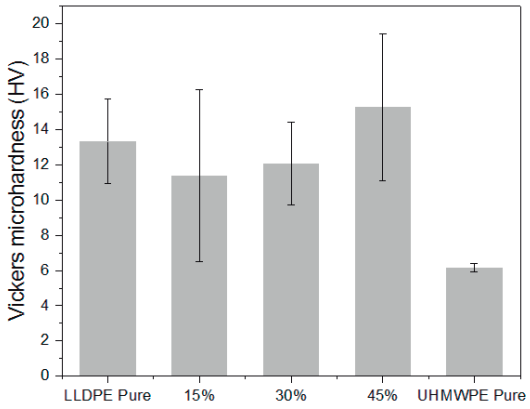

Figure 3 – Vickers micro hardness variation with LLDPE/UHMWPE blend.

The wear surface morphology for the blends (Fig. 4) demonstrated a typical feature of the adhesion wear mechanism, where a small piece of material is removed from one surface and becomes attached to the adjacent surface [12-13].

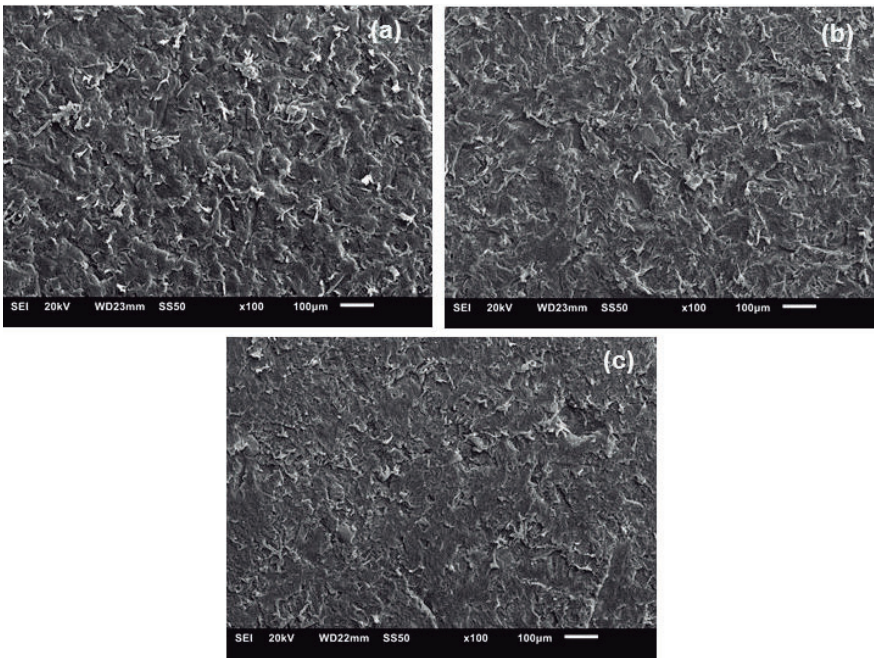

Figure 4 - Micrograph of the wear surface for the blends: (a) 85/15; (b) 70/30 and (c) 55/45.

Conclusions

The presence of abrasive wear was identified in blends of LLDPE and UHMWPE in images obtained by SEM. However, the evaluation through Ratner-Lancaster correlation indicated that the wear mechanism is not purely abrasive. The addition of UHMWPE reduces the tenacity of the blends by changing the morphology by increasing the presence of crystalline phase which in turn influences the increase in hardness.

References

1. Cardoso, Pollyana Melo et al. Development and Characterization of LLDPE Blends with Different UHMWPE Concentrations Obtained by Hot Pressing. Polymers, 2022, v. 14, n. 18, p. 3723.
2. Thomas, Sabu and P. M. Visakh. 2011. Handbook of Engineering and Specialty Thermoplastics. edited by S. Thomas and P. M. Visakh. Hoboken, NJ, USA: John Wiley & Sons, Inc. Retrieved.
3. Schwartsmann, Carlos Roberto, Leonardo Carbonera Boschin, Ramiro Zilles Gonçalves, Anthony Kerbes Yépez, and Leandro De Freitas Spinelli. 2012. "New Bearing Surfaces in Total Hip Replacement." Revista Brasileira de Ortopedia 47(2):154–59.
4. Lucas, Alessandra De A., José D. Ambrósio, Harumi Otaguro, Lidiane C. Costa, and José A. M. Agnelli. 2011. "Abrasive Wear of HDPE / UHMWPE Blends." Wear 270(9-10):576–83.
5. Ferreira, Eder HC, and Guilhermino JM Fechine, 2021. "High abrasive wear resistance polyethylene blends: an adapted Ratner–Lancaster correlation." Polymer Bulletin: 1-18.
6. Briscoe, B. 1981. "Wear of Polymers: An Essay on Fundamental Aspects." Tribology International 14(4):231–43.
7. Kurtz SM. 2004. The UHMWPE handbook: ultra-high molecular weight polyethylene in total joint replacement. Elsevier, Amsterdam.
8. Budinski, Kenneth G. 1997. "Resistance to Particle Abrasion of Selected Plastics." Wear 203-204:302–9.
9. Cenna, A. A., S. Allen, N. W. Page, and P. Dastoor. 2003. "Modelling the Three-Body Abrasive Wear of UHMWPE Particle Reinforced Composites." Wear 254(5-6):581–88.
10. González, Jeanette et al. 2017b. "Rheological and Mechanical Properties of Blends of LDPE with High Contents of UHMWPE Wastes." Journal of Applied Polymer Science 134(26):1–13.
11. Molinari, E. C. and M. D. Failla W. R. Tuckart. 2016. "The Effect of Crosslinks on the Sliding Wear of High-Density Polyethylene." Tribology Letters 64(2):1–12. Retrieved ("http://dx.doi.org/10.1007/s11249-016-0763-y).
12. Nevelos, J. 2004. "Surface Engineering of Prosthetic Knee Components." Knee 11(3):163–67.
13. Burger, N. D. L., P. L. de Vaal, and J. P. Meyer. 2007. "Failure Analysis on Retrieved Ultra High Molecular Weight Polyethylene (UHMWPE) Acetabular Cups." Engineering Failure Analysis 14(7):1329–45.

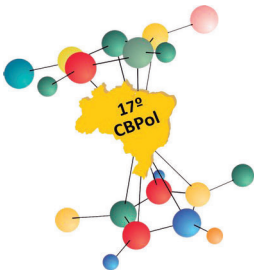

EXPANDED GRAPHITE AS REINFORCEMENT OF POLYPROPYLENE

Arthur Biagiotti[1], Cassiano M. N. Romagnolli[1]*, Dielly C. O. Araujo[1], Luis F. Costa[1], Grazielle R. de Cerqueira[2], Carolina L. Morelli[1,2]

[1] *Materials Engineering Department, Federal University of Itajubá – Campus Itabira– UNIFEI, Itabira, MG, Brazil*

*cassiromagnolli@gmail.com

[2] *Materials Science Program, Federal University of Pernambuco – UFPE, Recife, PE, Brazil*

Abstract - Polypropylene is widely used in several applications because of its versatile properties. However, reinforcements should be necessary for specific applications, such as in sectors with fire risk and where high mechanical resistance is required. Expanded graphite is a potential reinforcement, especially because of its nanosize, good corrosion resistance, good electrical conductivity and high thermal conductivity. The present work analyzed the mechanical, morphological and thermal properties of a polypropylene composite filled with 3 %wt. of expanded graphite. The graphite was successfully expanded by the electrochemical intercalation method and exfoliated by ultrasonic bath. The composite was prepared through melt extrusion and thermopressing and presented an increase of 50% in the modulus of elasticity regarding the pure matrix. The expanded graphite also acted as a nucleating agent, increasing the temperature of crystallization and the crystallinity.

Keywords: *Electrochemical intercalation, expanded graphite, polypropylene, composites, extrusion.*

Introduction

Polypropylene (PP) is a widely used polymer because of its properties such as low density, low cost and easy processing, as well as good mechanical properties such as flexural and tensile strength [1]. Several authors studied the addition of reinforcements in polypropylene aiming to increase its modulus of elasticity, electrical conductivity, thermal conductivity, among others [2-4].

Among the reinforcements used, graphite has interesting characteristics such as good corrosion resistance, good electrical conductivity and high thermal conductivity. In materials with high thermal conductivity, heat can be well distributed throughout the material, leading to a slowdown in the increase in the temperature at the surface. When these particles of high thermal conductivity are introduced to polymers, this effect tends to delay the decomposition of the polymer and the consequent release of flammable volatile material, delaying the ignition of the material [5,6].

Structurally, graphite consists of carbon atoms with the hexagonal arrangement, which interact among other carbons in the same plane by relatively weak secondary Van der Waals forces [3]. Graphite intercalation happens when intercalating agents can place themselves between graphite lamellae, increasing the interlamellar space [7].

There are several routes through which the production of intercalated graphite can be made such as liquid intercalation, electrochemical, vapor-phase transport and co-intercalation [3]. The electrochemical intercalation method is performed by placing graphite flakes in a solution of sulphuric acid and nitric acid, resulting in a positive charge of graphite sheets and the appearance of repulsion forces between them. This

generates the separation between the layers and allows the insertion of the intercalating agents.
After graphite intercalation, it can be expanded, which consists in giving a thermal shock at high temperatures, causing a rapid volatilization of the acids and the expansion in the graphite c-axis of up to 300 times, pushing their lamellae and increasing interlamellar spacing, what results in the achievement of graphite nanometric sizes [8].. Expanded graphite has good mechanical, electrical and thermal properties, besides anti-flame behaviour, being a multifunctional reinforcement to be applied in several areas [3].
In the present work, a composite of polypropylene reinforced with expanded graphite was developed and characterized through mechanical, morphological and thermal analysis.

Experimental

Polypropylene (PP) was acquired from Petroken (Brazil) and graphite flakes were kindly donated by Grafite do Brasil (Brazil).
Graphite expansion was performed based on the procedure of Chen et al. [9] with some modifications. It was divided into three stages, as commented in the sequence: intercalation of graphite; expansion of graphite; exfoliation of the expanded graphite.
For the step of graphite intercalation, 120g of graphite flakes were submerged in a 9:1 sulfuric acid / nitric acid solution, during 8 hours, at room temperature. After the intercalation, the graphite underwent dialysis in distilled water, for acid neutralization, until it reached pH 6. In the sequence, graphite was recovered under vacuum filtration and dried at 100°C in the oven during 12 hours.
For graphite expansion, the intercalated graphite was added to an alumina crucible and placed inside an oven at 1000°C for 30 seconds. A total amount of 40g of expanded graphite was obtained.
The exfoliation of the expanded graphite was done in an ultrasound bath, in which the expanded graphite (EG) was immersed in pure ethanol for 6 hours. After this, it was vacuum filtered and dried at 100°C in an oven for 12 hours.
The extrusion of PP with 3 %wt. of EG was done in a SEIBT ES25 single screw extruder. The temperature profile was: 160°C (feeding zone); 190°C (compression zone); 200°C (metering zone) and 210°C (die). After extrusion, the components were dried in an oven at 80ºC for 5 hours and submitted to thermopressing in a Solab SL11 press for sheet molding. The pressing was done at 210°C, with a pressure of 6 tons for 18 minutes, using a metallic mold with dimensions of 100 mm x 100 mm x 1 mm. From the molded sheets, specimens of dimensions 1 cm x10 cm x 1 mm were cut to perform tensile tests.
Scanning Electron Microscopy (SEM) was done with a microscope from Tescan, model Vegan 3, operated at a voltage of 5.0 kV, aiming to confirm the graphite expansion.
Thermogravimetric analysis (TGA) was performed in a DTG-60 from Shimadzu with synthetic air, from room temperature to 700ºC and a temperature rating of 10°C.min^{-1}.
The differential scanning calorimetry (DSC) was performed in a nitrogen atmosphere, in three steps: heating from 0°C to 200°C, cooling from 200ºC to 0 °C, and heating again from 0ºC to 200°C, at a rate of a 10°C.min^{-1}. The crystallinity (X_c) was obtained according to Eq. 1, using the value of 209 J.g^{-1} as the heat of fusion of the 100% crystalline polypropylene ($H_{100\%}$), and considering the real PP content (97%) in the case of composites. ΔH_m represents the heat of fusion obtained through the area of the melting peak from the first DSC heating.

$$X_C = \frac{\Delta H_m}{\Delta H_{100\%}} .100 \qquad [1]$$

For tensile tests, specimens were cut from the thermopressed sheets following the standard ASTM D 6287. Tests were performed in an Instron/Emic, model 23-100, based on standard ASTM D 882-02.

Results and Discussions

The morphological differences in graphite before and after the expansion can be observed in Fig. 1. In Fig. 1-D it can be noticed an expanded lamella with the folding or wormlike structure, different from the graphite flakes aspect observed in the C image. In the A and B images it can be observed the compact aspect of the natural graphite (A) and the separation and disorderly aspect of the lamellae in the expanded graphite (B). Moreover, the nanoscale of the expanded graphite lamellae can be noticed, confirming that the objective of graphite expansion was achieved.

The results of TGA are presented in Table 1 and the curves are exhibited in Fig. 2. It can be observed a significant mass loss of expanded graphite only after 650 ºC, being associated with oxidation in synthetic air atmosphere. The thermal degradation of pure polypropylene and of the composite started about 300ºC (T_{onset}) and there was a small difference between their temperatures of maximum degradation rate ($T_{max_degradation}$), obtained from the derivative of the TGA curve (DTG). This value was 20ºC higher for the composite than the one observed for the pure PP. The increase in PP thermal stability with graphite addition was also observed in the works of Bensalah et al. [10], and Ren et al. [11]. According to these authors, graphite act as a barrier restricting the evolution of volatile product during degradation**,** resulting in the effect of a thermal stabilizer. As commented before, this delay in polymer decomposition arising from graphite addition contributes positively to applications of insulating threads with risk of fire, since the release of flammable volatiles resulting from the decomposition of the organic polymer is also delayed, delaying the ignition of the material.

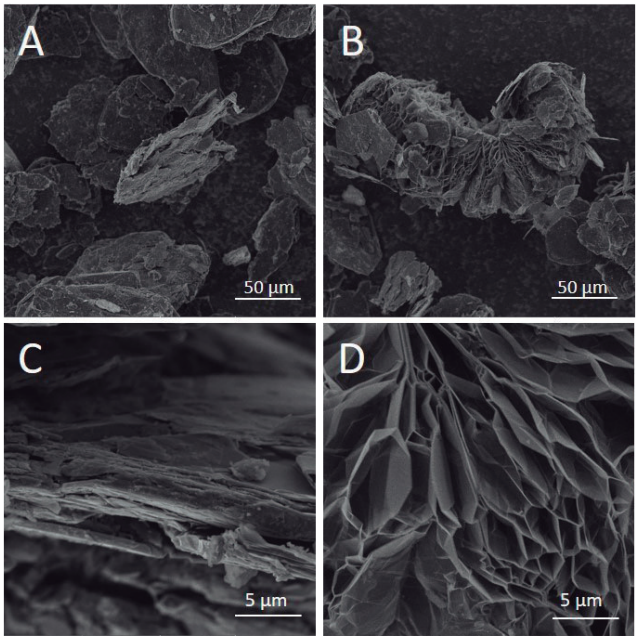

Figure 1 SEM micrographs of natural graphite (A and C); and expanded graphite (B and D).

Table 1 Temperatures of degradation onset (T_{onset}), from TGA curves, and temperatures of maximum degradation rate ($T_{max_degradation}$), from DTG peaks.

	T_{onset}(°C)	$T_{max_degradation}$(°C)
Polypropylene (PP)	300	350
Expanded Graphite (EG)	650	750
Composite (PP + EG)	300	370

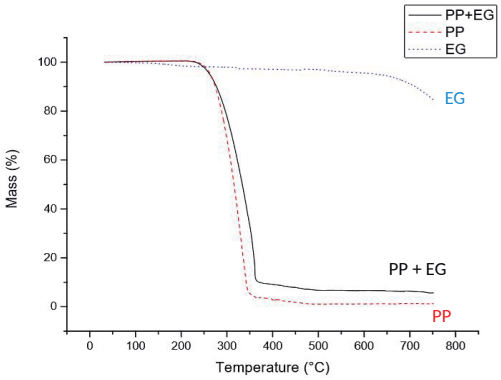

Figure 3 TGA curves of polypropylene (PP), expanded graphite (EG) and the composite (PP+EG).

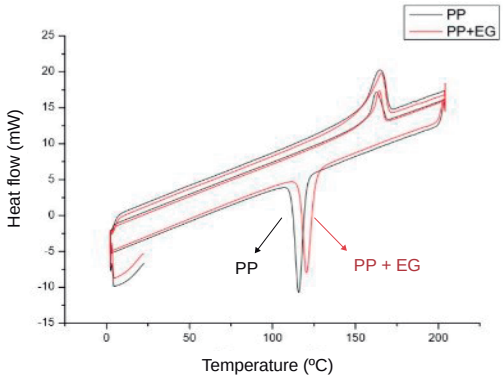

Figure 4 DSC curves of PP and PP+EG. The exothermic sense is down.

The results obtained from DSC analysis are presented in Table 2 and Fig.4. From the first heating curve it was observed that the melting temperature of the composite and the pure PP were really close, around 160ºC, without significant differences. In the other hand, there was a difference observed in the crystallinities obtained from these melting peaks, which were 88% and 81% for the composite and PP, respectively. Nonetheless, this increase in crystallinity (X_c) was not observed in the second heating, after removal of the thermal history associated with processing. This means that in the conditions applied during the thermopressing process, the presence of graphite was able to affect PP crystallinity (obtained from the first heating). But this effect was not evident and significant in conditions of very slow cooling rates, such as those applied in DSC analysis that resulted in the crystallinities measured from the second heating.
However, the graphite action as a PP nucleant agent was confirmed through the crystallization temperature of the composite (125ºC), measured from the cooling curve, that was significantly higher than the one observed for the pure PP (110ºC), as can be clearly observed in Fig. 4. The graphite nucleation effect was also observed by Bensalah et al. with graphite contents up to 5 %wt [10].

Table 2 Melting temperatures obtained from the first heating (T_{m1}) and from the second heating curves (T_{m2}), with the respective crystallinities calculated from these peaks (X_c); and the crystallization peak temperature (T_c) obtained from the cooling curve.

	T_{m1} (°C)	T_{m2} (°C)	Tc (°C)	X_{c1} (%)	X_{c2} (%)
Polypropylene (PP)	159	164	110	81	96
Composite (PP + EG)	162	165	125	88	91

As can be seen in Table 3, the addition of EG increased in 50% the PP modulus of elasticity, confirming the potential of graphite as a reinforcement of PP matrix. On the other hand, the breaking strength of the composite was 40% lower than the value of the pure PP.

Table 3 PP: polypropylene; EG: expanded graphite; PP+EG: composite; E: modulus of elasticity; σ_b: breaking strength; ε_b: elongation at break.

	E (MPa)	$\sigma\sigma_b$ (MPa)	ε_b (%)
Polypropylene (PP)	667 ± 39	24 ± 2	14 ± 1
Composite (PP + EG)	987 ± 167	14 ± 3	3 ± 1

Conclusions

The expansion of graphite through the electrochemical intercalation technique was successfully performed and confirmed by scanning electron microscopy. The expanded graphite acted as a PP nucleating agent increasing 15°C the crystallization temperature and the crystallinity of the thermopressed composite. The addition of expanded graphite increased the temperature of maximum degradation rate of PP, indicating that graphite acted as a barrier restricting the evolution of volatile product during degradation**,** resulting in the effect of a thermal stabilizer. The addition of expanded graphite to polypropylene by melt extrusion increased in 50% the elastic modulus of the pure matrix.

References

1. S. Zhang S, A.R. Horrocks Progress in Polymer Science 2003, 28, 1517. https://doi.org/10.1016/j.progpolymsci.2003.09.001.

2. T. Iman; Y. Seld; M. Sarikanat Polymer Composites 2018, 1. https://doi.org/10.1002/pc.24643.

3. D.D.L. Chung Journal of Materials Science 2002, 37, 1475. http://dx.doi.org/10.1023/A:1014915307738.

4. A. Kaushal; V. Singh Journal of Applied Polymer Science 2021, 139(1), 51444. https://doi.org/10.1002/app.51444.

5. B. Dittrich; K.A. Wartig; D. Hofmann; R. Mülhaupt; B. Schartel Polymer Degradation and Stability 2013, 98 (8), 1495. http://dx.doi.org/10.1016/j.polymdegradstab.2013.04.009.

6. H. Cirmad; S. Tirkes; U. Tayfun Journal of Thermal Analysis and Calorimetry 2022, 147, 2229. https://doi.org/10.1007/s10973-021-10656-y.

7. Y. Zongrong; L. Xuemei; Q. Yu; L. Jie Materials Research Bulletin 2008, 43, 2677. https://doi.org/10.1016/j.materresbull.2007.10.027.

8. A. Yasmin; J. Luo; I.M. Daniel Composites science and technology 2006, 66, 1182. https://doi.org/10.1016/j.compscitech.2005.10.014.

9. G. Chen; W. Dajin; W. Weng; W. Cuilling Carbon 2002, 1. http://dx.doi.org/10.1016/S0008-6223(02)00409-8.

10. H. Bensalah; K. Gueraoui; H. Essabir; D. Rodrigue; R. Bouhfid; Q. A. el Kacem. Journal of Composite Materials 2017, 51(25), 3563. https://doi.org/10.1177/0021998317690597.

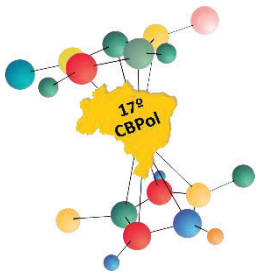

FLOW BEHAVIOR AND DEGRADATION OF HIGH DENSITY POLYETHYLENE (HDPE) AND ULTRA HIGH MOLAR MASS POLYETHYLENE (UHMWPE) BLENDS

Jullyani M. D. da Silva[1], Gabriel C. G. Duarte[2], Mariana de O. Silva[2], Ryan F. dos Santos[2], Luziany G. da Nóbrega[2], Fabiana de C. Fim[1,2], Lucineide B. da Silva[1,2*]

1 - Graduate Program in Materials Science and Engineering (PPCEM), Federal University of Paraiba (UFPB), João Pessoa, PB, Brazil

2 – Department of Materials Engineering (DEMAT), Federal University of Paraiba (UFPB), João Pessoa, PB, Brazil

fabianafim@ct.ufpb.br

Abstract - The objective of this work was the preparation of blends (High Density Polyethylene (HDPE)/Ultra High Molecular Mass Polyethylene (UHMWPE), using a Haake internal mixer with subsequent compression molding. The blends were prepared by melting the mixture of 0, 10, 20 and 30% (w/w) of UHMWPE in HDPE. The processability of the blends was evaluated by Torque Rheometry. From the percentage of 20% (w/w) of UHMWPE, there was an increase in the torque with the mixing time, not being observed its stabilization. There was an increase in temperature and mixing energy due to the increase in HDPE viscosity. Furthermore, higher levels of UHMWPE made its dispersion in HDPE more difficult, impairing the processing of these blends. Blends with 10 and 20% (w/w) of UHMWPE were more thermally stable than HDPE.

Keywords: B*lends, processability, torque rheometry, thermogravimetry.*

Introduction

High density polyethylene (HDPE) has good flow properties, can be processed by traditional processes such as injection molding, extrusion and so on. Its chemical structure is one of the simplest, being able to be constituted by only hydrogen and carbon and it has a high chemical resistance. In addition, it is durable and resistant, so it can be converted into pipes, fuel tanks and even hoses [1,2]. On the other hand, in UHMWPE, the polymeric chains are much superior to those of HDPE. This ensures that certain properties of the material (UHMWPE) are preferable in relation to other types of PE, such as high abrasion resistance, high chemical resistance, good mechanical properties and flexibility [3]. This allows the UHMWPE to be used in several fields, as well as in prostheses and other surgical instruments, due to its good biocompatibility and chemical resistance [4]. The expectation is that by mixing HDPE with UHMWPE, the properties of the blends will be even more interesting than those of neat HDPE, expanding its applicability in more attractive markets.

The objective of this work was to prepare HDPE blends with contents of 10, 20 and 30% by weight of UHMWPE in order to verify its effect on the processability of HDPE and thermal stability.

Experimental

Materials

Ultra-high molecular weight polyethylene (UHMWPE) commercial powder (UTEC batch 3041) and High Density Polyethylene (HDPE) IA58 (Braskem/Brazil) and Irganox antioxidant (Sigma-Aldrich/Brazil).

Preparation of (HDPE/UHMWPE) Blends

For the preparation of the blends, the process of blending by melting was used. Blends of 0, 10, 20 and 30% (w/w) of UHMWPE were made and named: HDPE, UH10, UH20 and UH30, respectively, with the addition of 1% of irganox, an antioxidant. Before processing, the materials were dried in an oven at 70 °C for 24 hours. First, the melting takes place in a Haake Mixer (PolyLab model RHEOMIX OS), then the material was chopped and molded by compression in a hot press (MARCONI model MA 700).

In the Haake melting process, a temperature of 190 °C was used for a time of 15 minutes and a speed of 50 rpm. In the press a temperature of 190 °C was used for 5 minutes with a pressure of 12 tons, resulting in a film.

Processability of Blends by Torque Rheometry

Using the torque rheometer, the unit of mixing energy consumed (Wu) to disperse the UH particles within the HDPE matrix can be investigated, as other authors have also studied for other polymeric materials [5-7]. According to [8], Wt [J] is total mixing energy, being determined from the area under the curve of torque versus time during the test, according to Equation 1.

$$\mathrm{Wt} = 2\pi \mathrm{N} \int_{t2}^{t1} M \, \mathrm{dt} \qquad (1)$$

Where N is the rotor speed [rpm], t1 and t2 are the initial and final times [min], respectively, and M is the mixing torque [N.m].

In addition, the mixing energy unit (Wu) measures the total energy consumed to disperse the UH in the HDPE matrix at a certain level, according to the determination made for other polymeric materials [6,7], through Equation 2.

$$\mathrm{Wu} = \frac{\mathrm{Wt}}{\mathrm{Vb}} \qquad (2)$$

Where Wu [J] is the total mixing energy and Vb is the volume [m^3] of the rheometer's mixing chamber.

Thermogravimetry (TG)

Thermogravimetric curves were obtained from a Shimadzu DTG model 60H thermal analyzer. The samples were placed in a platinum crucible with weights ranging from 10 to 13 mg and heated from room temperature to 800 °C with a heating rate of 20 °C/min under a nitrogen flow of 20 ml/°C.

Results and Discussion

Blend mixtures in the torque rheometer provided information on flow behavior during processing, reflecting changes in the material being processed [9]. Therefore, the torque value when the polymer is molten is associated with the viscosity of the melt, as well as with the processability of the blends [10,11]. The torque curves in Fig. 1a show that in terms of the initial mixture in the first minutes, the blends melted with behavior similar to HDPE, resulting in a gradual decrease in the torque value. With the passage of mixing time the blend with 10% UH reached a stable torque as well as the HDPE. However, blends with 20 and 30% UH showed an increase in torque with time, possibly indicating molecular orientation caused by the addition of UH. Since the occurrence of thermal degradation can be ruled out due to the addition of blends with 1% antioxidant. In Fig. 1b it is observed that the temperatures in the stability region between the samples were increased as the UH was added, indicating that thermal modification occurred in the blends. Fig. 1c shows the energy expended during the mixing of pure HDPE and blends. The presence of UH in HDPE caused an increase in energy

consumption during mixing. As UHMWPE has a very high molecular mass, more work was required to carry out the mixtures and, consequently, a greater expenditure of energy as a function of time. The processability of blends compared to neat HDPE can become more costly with this increase in energy consumption.

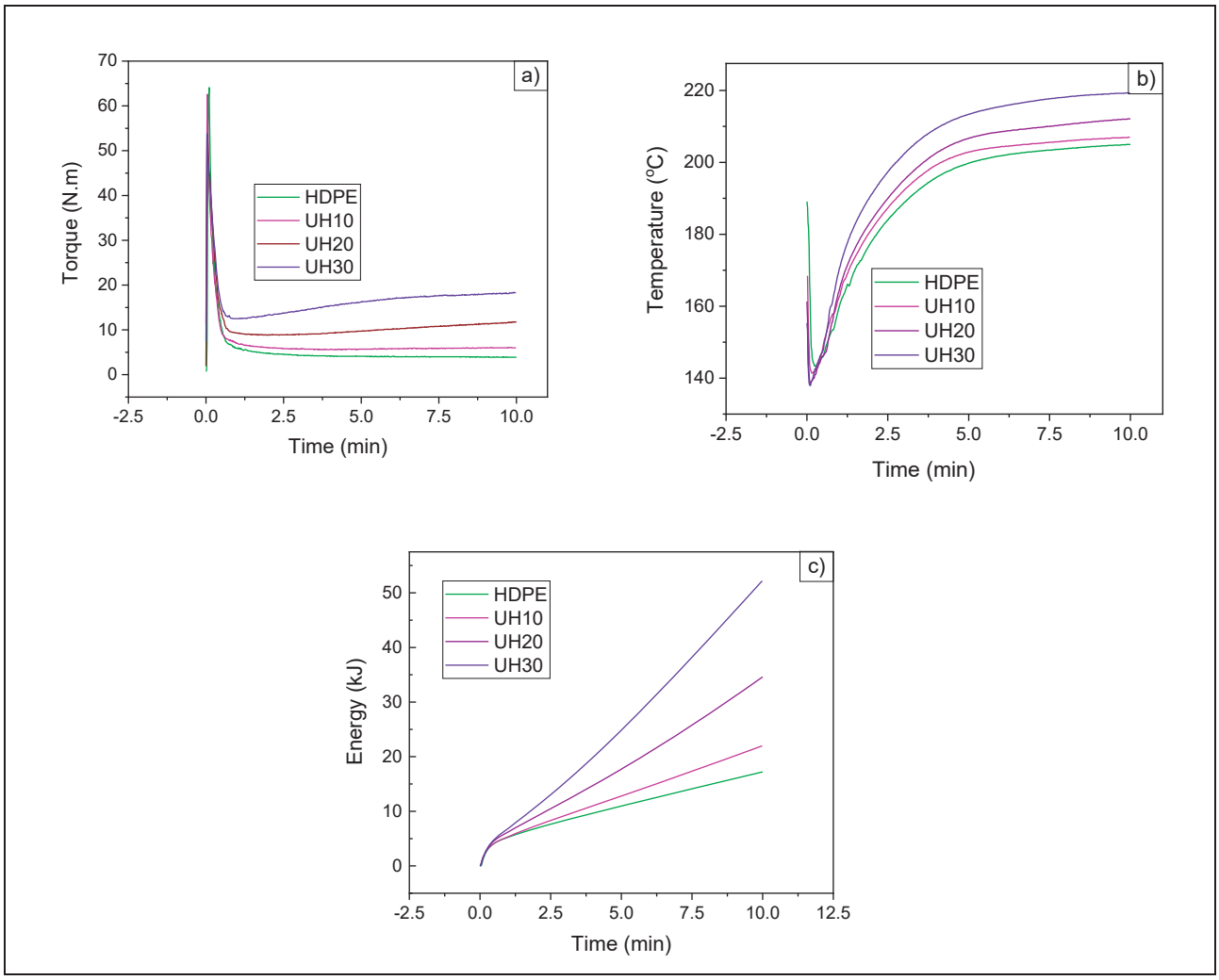

Figure 1: a) curves of torque versus time; b) curves of mixing temperature versus torque; c) curves of mixing energy versus time.

Table 1 presents process parameters obtained from the curves of torque versus time, obtained at 50 rpm for 10 min to better clarify the effect of UH on the flow behavior of HDPE. The total mixing energy (Wt) of the blends and the required energy (Wu) to disperse UH in HDPE were calculated using equations 1 and 2, respectively. The addition of UH increased Wt, indicating more energy expenditure in processing the blends, a similar result observed in Figure 1c. This same trend was verified in the width at mid-height of the torque peak (dx). In addition, Wu indicates greater difficulty in dispersing higher amounts of UH in HDPE. Regarding the interval (ΔT) between the temperature obtained in steady-state torque (Tstb) and the test temperature, it is observed that the addition of UH increased ΔT, suggesting that greater friction occurred between HDPE and UH macromolecules, according to [8] in styrene butadiene rubber (SBR) composites with carbon black. On the other hand, [12] observed an increase in ΔT in blends of polystyrene and recycled styrene butadiene rubber and attributed it to an increase in the mechanical work of mixing due to the strong interfacial interaction between the constituents of the blend.

Fig. 2 the TG and DTG curves of neat polymers and blends with 10, 20 and 30% (w/w) of UHMWPE. The data obtained through the TG and DTG curves are available in Table 1.

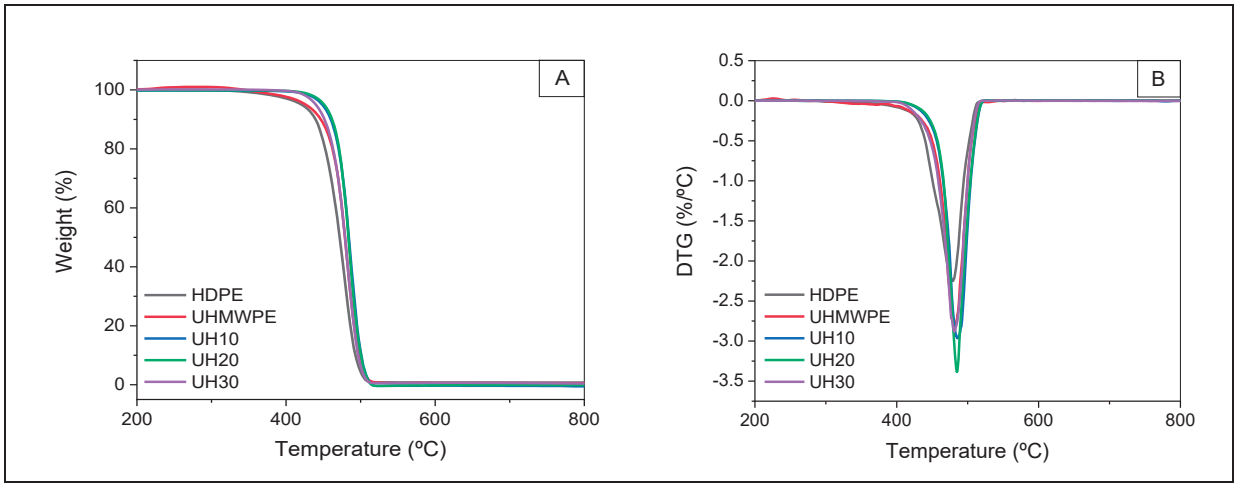

Figure 2: a) TG curves and b) DTG curves for the neat polymers and blends.

Table 1: Moisture of mixing energy (Wu), total mixing energy (Wt) obtained in the torque rheometer and data from thermogravimetry.

Sample	Wt (J)	Wu (J/m^3)	dx	Tstab (N.m)	ΔT	Ti (°C)	Tp (°C)
HDPE	54.84	$7.9x10^{-7}$	0.183144	203.6 °C	13.74	422	478
UH10	65.19	$9.4x10^{-7}$	0.303776	205.7 °C	15.63	430	489
UH20	100.74	$1.5x10^{-6}$	0.282546	209.1 °C	19.63	431	485
UH30	174.15	$2.5x10^{-6}$	0.255846	219.5 °C	27.34	425	480
UHMWPE	-	-	-	-	-	422	478

Where dx: peak torque width at half height; ΔT: temperature during the experiment; Tstab: torque stabilization temperature; Ti: initial degradation temperature and Tp: DTG peak temperature (maximum degradation rate).

It is possible to verify an increase in the degradation temperatures of the blends compared to the neat HDPE. This indicates that the presence of UHMWPE in the matrix causes the material to have a gain in thermal stability due to shifting the degradation temperatures to higher values. Blends of 10 and 20% UHMWPE in HDPE are the most thermally stable as the values of (Ti) increased from 422 ºC to 430 ºC and 431 ºC respectively.

Conclusions

The mixture of HDPE with UHMWPE can represent gains in HDPE properties due to the excellent properties of UHMWPE. Therefore, it was of interest in this work to investigate the processability of the blends at a rotation rate of 50 rpm. From 20% of UHMWPE, there was an increase in torque with time, indicating molecular orientation, as well as the mixing energy, the torque stabilization temperature were increased, suggesting difficulty in dispersing the ultra high molecular weight polymer in HDPE and consequent greater energy expenditure for the production of blends with higher levels. The UHMWPE provided gains in thermal stability in the blends.

Acknowledgements
The authors gratefully Federal University of Paraiba (UFPB) for scientific initiation (PIBIC and PIVIC). This work was funded by the Public Call n. 03 Produtividade em Pesquisa PROPESQ/PRPG/UFPB PIF13399-2020.

References

1. Freitas, S. R. Freitas Ph.D. Thesis, Federal University of ABC, 2017.
2. H. S. Jaggi.; B. K. Satapathy.; A. R. Ray J. Polym. Res. 2014, 21, 482.
3. A. B. Boscoletto; R. Franco; M. Scapin; M. Tavan Eur. Polym. J. 1997, 33, 97.
4. B. Aldousiri; A. Shalwan; C.W. Chin Adv. Mater. Sci. Eng. 2013, 2013, 1
5. T. Weber; M.G. Oliveira; M. Zeni; et. al. Polym. Bull. 2008, 61, 217.
6. P. T. Dolezal; P. S. Johnson Rubber Chem. Technol. 1980, 53, 252.
7. B. Y. Li Press. Chem. Ind. China 2000, 237, 335.
8. A. Zhang; L. Wang; Y. Zhou Polym. Test. 2003, 22, 133.
9. K. L. K. Lim; Z. A. Mohd Ishak; U. S. Ishiaku; A. M. Y. Fuad; A. H. Yusof; T. Czigany; B. Pukanszky; D. S. J. Appl. Polym. Sci. 2005, 97, 413.
10. J. Jiao; S. J. Wang; M. Xiao; Y. Xu; Y. Z. Meng Polym. Eng. Sci. 2007, 47, 174.
11. M. Gahleitner Prog. Polym. Sci. 2001, 26, 895.
12. C. B. B. Luna; E. M. Arauújo; D. D. Siqueira; D. D. S. Morais; E. A. S. Filho; M. V. L. Fook Journal of Elastomers & Plastics 2020, 52, 3.

FOAM COMPOSITES REINFORCED WITH MDF POWDER: EFFECTS ON MECHANICAL PROPERTIES AND SUSTAINABILITY

Tiago Fachini [1*] , Flavia Costa [2] Lizandro Manzato [2], Mara Zeni de Andrade[1]and Edson Luiz Francisquetti [1]

1 Instituto Federal de Ciência e Tecnologia do Rio Grande do Sul IFRS-Farroupilha-Rs-Brasil
2- Instituto Federal do Amazonas- Campus Manaus Distrito Industrial Polo de inovação de Manaus
**tiago.fachini@hotmail.com*

Abstract – Foam composites reinforced with vegetable fibers offer an attractive combination of excellent mechanical properties and reduced density, providing a sustainable alternative for manufacturing thermal and acoustic insulation panels when compared to polymer composites. This study explores the effects of incorporating medium-density fiberboard (MDF) powder to create a foamed composite of poly(ethylene-co-vinyl acetate) (EVA)/MDF. The composites were foamed using azodicarbonamide as a thermal expansion agent. Remarkably, the presence of MDF powder with varying particle sizes in the cellular composite did not significantly impact the density, hardness, resistance to continuous cycles of bending, and resilience of the resulting panels. These findings demonstrate the potential of using MDF as a filler material in EVA foam composites without compromising their desirable properties, offering promising opportunities for sustainable waste management and eco-friendly construction materials.

Keywords: *composite, MDF, foams, EVA.*

Introduction

In Brazil, a large part of the raw material used in furniture manufacturing comes from agglomerated wood panels, mainly medium-density fibers (MDF), sets of particles or wood fibers, joined by a thermosetting polymer such as urea formaldehyde and paraffin under appropriate pressure and temperature [1]. The use of MDF produces waste in the form of scraps that are often used as a source of heat for boilers, but if instead of being reused as a heat source, the waste scraps were reconstituted, these scraps would generate around 630000 new panels [2]. The use of MDF waste, when compared to the use of solid wood waste, is a topic that is little explored and has limited publications in Brazil [3]. Composites using wood waste can be divided into two groups: wood-polymer composites (WPC), which contain sawdust and natural fiber composites (NFC) reinforced with wood fibers or particles [4].

On the other hand, polyolefin foams are used in different applications, due to their interesting properties, such as surface-volume ratio, empty volume, low pressure loss, resistance, and toughness. Depending on the polymer used in the foam formation, there may be variations in the physical, mechanical, and electrical properties. In the case of polyolefin foams, the properties will depend on the processing parameters and type of formulation, with compression molding being the most common technique for the production of polyolefin foams. Among the different polyolefins to produce foams with different properties, there are polyethylenes, polypropylene, and ethylene-vinyl acetate (EVA). EVA foams are used in various applications, such as shoe soles and midsoles, sports equipment, and panels for insulation. [5]

The present study aims to obtain expanded WPC, with an EVA matrix, with different contents of MDF powder (0, 10, 20, 30, 40, and 50 PHR). The behavior regarding resilience, density, hardness, and deformation after 100000 cycles of bending, compression deformation, and abrasion wear will be evaluated.

Experimental

Materials

The composites formulation used EVA (HM 728 Braskem). The calcium carbonate $CaCO_3$ (Natural C-Carbomil), zinc oxide ZnO (Brasóxidos Br-500), stearic acid (AES) (Baerocid SP-1 V Baerlocher), dicumyl peroxide (DCP 40 SPA Retilox), azodicarbonamide (ADCM Sinochem) and zinc stearate ($(C_{18}H_{35}O_2)_2$ (Minerios Ouro Branco) were also used. MDF was obtained from the sawdust of furniture companies in Bento Gonçalves-RS. Different formulations with the variation of MDF mass were produced and are shown in Table-1

Table 1 : EVA/MDF composite formulations

Sample	EVA (PHR)	Sawdust MDF (PHR)	$CaCO_3$ (PHR)	ZnO (PHR)	Stearic acid (PHR)	DCP (PHR)	ADCM	zinc stearate (PHR)
MS 0	100	0	5	9	2	1	15	1
MS 10	90	10	5	9	2	1	15	1
MS 20	80	20	5	9	2	1	15	1
MS 30	70	30	5	9	2	1	15	1
MS 40	60	40	5	9	2	1	15	1
MS 50	50	50	5	9	2	1	15	1

The materials were mixed in an intensive H&M mixer, and passed through a double roll calender to form the sheets that were expanded in a hydraulic press at 180°C, at a pressure of 3kgf. They were kept in the press for 6 minutes before being opened.

Characterization Methods

The particle size was determined according to ASTM D6913-04(2009). The density of the sheets was obtained according to ASTM D 3575. The percent deformation was determined through adaptation of ASTM D3575 compression deformation. Resilience was determined according to DIN 53512 and the Ascer C type hardness according to ASTM 2240.

Results and Discussion

Particle size of MDF

In Table 2, the particle sizes present in the MDF powder are shown. The majority of particles are retained in sizes 48 (0.354 mm), 65 (0.230 mm), and 100 (0.149 mm) mesh, corresponding to 74% of the sample. Particle size can influence the size of foam cells, since particles distributed in the polymer matrix can facilitate the migration of gas generated by the expansion agent to the region of the fiber/matrix interface, influencing the rheological and mechanical properties of the composites. Finer particles produce composites with higher density and thicker cell walls at the edges of the cells, providing composites with higher cell density and more homogeneous cell size. [09]

Table 2: Particle size distribution of MDF powder.

strainer	Volume (g)	%	Accumulate (%)
Mesch 10	0.5	0.5	0.5
Mesch 20	1.0	1.0	1.5
Mesch 28	1.84	1.84	3.34
Mesch 35	11.88	11.88	15.22
Mesch 48	20.21	20.21	35.43
Mesch 65	28.05	28.05	63.48
Mesch 100	26.33	26.33	89.81
Mesch 150	5.62	5.62	95.43
Mesch 200	4.57	4.57	100.00
Mesch 270	0.00	0.00	0.00

-10+ 200

Density of expanded panels

The differences in densities observed in Table 3 were not significant among the composites, possibly due to the higher concentration of particle size between 80-100 mesh. According to Zimmermann and colleagues, this particle size influences the formation of more uniform cells and good cell density, promoting the formation of high-quality panels with little density variation, even at different load levels. [9]

Table 3: Density of different composites

Sample	Density ($Kg.m^{-3}$)	Standard Deviation
MS0	0.445	0.0017
MS10	0.385	0.0030
MS20	0.424	0.0439
MS30	0.414	0.0416
MS40	0.414	0.041
MS50	0.396	0.039

Deformation after 100000 cycles, Resilience %, and Hardness

In Table 4, it is observed that even with the addition of MDF powder at different concentrations, there is no deformation after 100000 cycles, probably due to the fact that the formed cells did not collapse with the addition of MDF. Paiva and colleagues obtained similar results when adding crosslinked, ground EVA waste with diverse particle size distributions and at different percentages [11]. The resilience of the 10, 20, 30, and 40 PHR samples showed similar behavior, around 40%, while the sample without MDF powder showed a resilience of 50%. This behavior was expected since wood has a higher elastic modulus than EVA, and its introduction into the matrix causes a loss of elastic property of the matrix, but there was no variation observed among the different compositions, possibly due to the EVA enveloping all MDF particles, absorbing the energy. In the sample with 50 PHR, the resilience dropped by 60% compared to pure EVA, possibly indicating the saturation level of the EVA matrix, causing MDF agglomeration and compromising the elasticity of the composite and reducing its energy absorption capacity. Hardness depends on the foam

formulation and also on the type of cell and its density. In this study, a hardness of 75 Asker C was observed for pure EVA, while the hardness of the composites varied from 70 to 85.

Table 4: Results of deformation after100.000 cycles, resilience, and hardness of EVA foams with the addition of MDF power.

Sample	deformation after100.000 cycles (%)	Resilience (%)	Hardness Asker C
MS0	0.00	50	75
MS10	0.00	40	70
MS20	0.00	40	80
MS30	0.00	40	85
MS40	0.00	40	85
MS50	0.00	30	80

Conclusions

Therefore, the obtained results demonstrate that the addition of MDF powder has the potential to be used as a filler in expanded EVA sheets. This is because no significant losses have been observed compared to pure EVA. The proposed WPC (Wood-Plastic Composite) could be beneficial in reducing improper disposal in the environment, either through landfill deposition or incineration of MDF waste. This could significantly contribute to more sustainable waste management practices. However, it is important to emphasize that further analyses should be conducted to confirm the feasibility of using these EVA panels, following the ASTM D 3575 standard, which establishes the standard test methods for flexible cellular materials made from olefin polymers.

Acknowledgements

The authors would like to thank IFRS for the laboratory support provided for the experiments, and IFAM for the contribution of the performed analyses.

References

1. 1- DE FREITAS, Angelo; LENZ, Denise Maria. Produção de painéis de madeira com resíduos de MDF e MDP da indústria moveleira e resina à base de tanino de Acácia Negra. Engevista, v. 21, n. 1, doi https://doi.org/10.22409/engevista.v21i1.22658
2. 2- Centro Nacional de Tecnologias Limpas, Instituto Senai de Tecnologia em Madeira e Mobiliário, SENAI 2014.
3. 3- WEBER, Cristiane; IWAKIRI, Setsuo. Utilização de resíduos de compensados, MDF e MDP para produção de painéis aglomerados. Ciência Florestal, v. 25, https://doi.org/10.5902/1980509818460
4. 4- THUMM, Armin et al. Processing and properties of MDF fibre-reinforced biopolyesters with chain extender additives. International Journal of Polymer Science, v. 2018, https://doi.org/10.1155/2018/9601753
5. 5- SIPAUT, Coswald S.; HALIM, Husna A.; JAFARZADEH, Mohammad. Processing and properties of an ethylene–vinyl acetate blend foam incorporating ethylene–vinyl acetate and polyurethane waste foams. Journal of Applied Polymer Science, v. 134, n. 16, doi:10.1002/app.44708.
6. 6- JUNIOR, Cristiano Zenaide Paiva et al. Performance of ethylene vinyl acetate waste (EVA-w) when incorporated into expanded EVA foam for footwear. Journal of Cleaner Production, v. 317, p. 128352, 2021. https://doi.org/10.1016/j.jclepro.2021.128352

7. 7- KWON, Min Ji et al. Preparation and properties of ethylene-vinyl acetate copolymer-based blend foams. Journal of Elastomers & Plastics, v. 53, n. 1, p. 68-82, 2021. https://doi.org/10.1177/00952443199003 75
8. 8- HU, Xiaohong et al. Weathering characteristics of wood-plastic composites compatibilized with ethylene vinyl acetate. BioResources, v. 15, n. 2, p. 3930-3944, 2020. DOI:10.15376/biores.15.2.3930-3944
9. 9- ZIMMERMANN, Matheus VG et al. The influence of wood flour particle size and content on the rheological, physical, mechanical and morphological properties of EVA/wood cellular composites. Materials & Design, v. 57, p. 660-666, 2014. doi.org/10.1016/j.matdes.2014.01.010
10. 10- SIPAUT, Coswald S.; HALIM, Husna A.; JAFARZADEH, Mohammad. Processing and properties of an ethylene–vinyl acetate blend foam incorporating ethylene–vinyl acetate and polyurethane waste foams. Journal of Applied Polymer Science, v. 134, n. 16, 2017. DOI: 10.1002/APP.44708
11. 11- JUNIOR, Cristiano Zenaide Paiva et al. Performance of ethylene vinyl acetate waste (EVA-w) when incorporated into expanded EVA foam for footwear. Journal of Cleaner Production, v. 317, p. 128352, 2021. doi.org/10.1016/j.jclepro.2021.128352
12. 12- ALONZO, Rebecca et al. Effects of basketball shoe midsole hardness on lower extremity biomechanics and perception during drop jumping from different heights. Applied Sciences, v. 10, n. 10, p. 3594, 2020. https://doi.org/ 10.3390/app10103594.For articles: Q. Jiang; T. Horozov; A. Bismarck Polymer 2022, 261, 125406. https://doi.org/10.1016/j.polymer.2022.125406.
13. For thesis: F. H. Dutra, Ph.D. Thesis, University of Southampton, 1995.
14. For books without editor: E. Haslam, *Shikimic Acid Metabolism and Metabolites,* John Wiley & Sons, New York, 1993.
15. For books with editor: J. G. Buchanan; H. Z. Sable in *Selective Organic Transformations,* B. S. Thyagarajan, Ed.; Wiley-Interscience, New York, 1972; Vol. 2, 1-95.
16. For patents: F. R. Lyle, U.S. Patent 5 973 257, 1985; *Chem. Abstr.* 1985, *65*, 2870.
17. For proceedings: O. Barbosa in Proceedings of 10th Brazilian Catalysis Conference, Salvador, 1999, Vol. 1, 343.

FRACTOGRAPHIC ANALYSIS OF RECYCLED CF/PPS COMPOSITES

Larissa S. Montagna[1]*, Guilherme F. M. Morgado[1], Fabio R. Passador[1] and Mirabel C. Rezende[1]

1 – Polymer and Biopolymer Technology Laboratory (TecPBio), Federal University of São Paulo (UNIFESP), São José dos Campos, SP, Brazil
larissa.s.montagna@gmail.com

Abstract – The growing demand for carbon fiber reinforced thermoplastic (CFRTP) is due to easy processing, combined with good mechanical properties, especially lightness, which results in a reduction in fossil fuel consumption. Additionally, CFRTP is 100% recyclable and is being increasingly used in the aerospace and automotive industries [1]. Along with this growing demand, comes the need to understand the performance of components during their service life, and consequently the modes of failure or premature and unexpected damage that can occur during service [2,3]. In this way, the application of fractographic studies has been growing, as it is an extremely important means of aiding the interpretation of fracture aspects of composite materials applied in the most diverse sectors. The objective of this work was to analyze the morphology of the tensile fracture using scanning electron microscopy, SEM, and optical microscope, MO, of laminates developed from the mechanical recycling of semipreg scraps of carbon fiber (CF) reinforced poly(phenylene sulfide) (PPS) composites from the manufacturing of the aerospace industry, aiming to contribute to more sustainable waste management and the reduction of the use of natural resources, and that presents the desired quality to be reinserted in the industrial production process for non-structural components. Through the morphological analysis of the fracture surfaces, it was possible to identify the failure modes and the main fractographic aspects present on the fracture surface. Furthermore, from the images obtained, it was possible to increase knowledge of the behavior of the recycled composite in service or even to have information for preventive corrections in the processing and the feasibility of using thermoplastic composite scraps, in addition to contributing to the understanding of the way of failure of this class of materials. As a result, it was possible to observe in the micrographs of the fracture surface, the layers of the semipreg CF/PPS scraps ordered, and the absence of visible defects, as well as the identification of the direction of crack propagation through the DAFFs (Directly Attributable Fiber Failures).

References

1. Montagna, L.S., Morgado, G.F.M., Lemes, A.P., Passador, F.R., Rezende, M.C. Journal of Thermoplastic Composite Materials, 2022, 0(0) 1–26. https://doi.org/10.1177/08927057221108912
2. D. Purslow. Matrix fractography of fiber-reinforced thermoplastics, Part 1. Peel failures. Composites. 18, 5, 365-374, 1987. https://doi.org/10.1016/0010-4361(87)90360-0
3. Greenhalgh, E.S. Failure analysis and fractography of polymer composites. ISBN 978-1-84569-217-9 (book), 2009.

Fundings: Federal Government Program 'Rota 2030', n° 27194.03.03/2020.01-00 for the financial support; the LEL/IPT for the coordination, and also FIPT, FUNDEP for the administrative support.

Keywords: *Poly(phenylene sulfide), Carbon Fiber, Composites, Recycling and Reuse, Morphology.*

HYBRID BIOCOMPOSITE BASED ON BACTERIAL CELLULOSE WITH HYDROXYAPATITE PARTIALLY SUBSTITUTED BY Mg/Zn AND Mg/Sr FOR GUIDED BONE REGENERATION

Elouise Gaulke[1], Michele C. F. Garcia[2,3], Andréa L.D.S. Schneider[1,3], Ana P. T. Pezzin[1]*

1 – Postgraduate Program in Process Engineering, University of the Joinville Region (UNIVILLE), Joinville, SC, Brazil
anapezzin@yahoo.com.br
2 – Postgraduate Program in Chemical Engineering, Federal University of Santa Catarina (UFSC), Florianópolis, SC, Brazil
3 – Department of Chemical Engineering, University of the Joinville Region (UNIVILLE), Joinville, SC, Brazil

Abstract - In tissue engineering, guided bone regeneration (ROG) emerges as a form of treatment for bone defects. It can use bacterial cellulose (CB) as a scaffold, as it has a porous nanostructure in 3D with good mechanical properties, is biocompatible and has high water retention capacity. This study aimed to synthesize CB hybrid biocomposites containing hydroxyapatite (HAP) partially replaced by mg/zn and mg/sr. The samples were characterized by porosity analysis, FTIR, TGA, MEV/EDS and DRX; The antimicrobial properties test was also performed. The results demonstrated HAP crystals incorporated into the CB; The samples produced had pure CB thermal stability, and the studied concentrations and biocomposites did not have antimicrobial activity. However, EDS analysis confirmed the incorporation of Mg, Zn and Sr elements, which may benefit the scaffold, promoting bone regeneration.
Keywords: *Bone regeneration; Bacterial cellulose; Hydroxyapatite; Biocomposites.*
Fundings: The authors acknowledge the financial support of CAPES and UNIVILLE for the project.

Introduction

Bone defects are deformities that affect bone tissue, originating in trauma or disease. About 20 million surgeries are performed annually to treat such defects, and they usually need some graft to repair the injury [1]. Guided bone regeneration (ROG) emerged as an alternative to treat these bone defects and induce tissue repair. This technique aims to form an isolated space using scaffolds, which are surgically implanted barriers to guide bone regeneration and not allow the passage of fibrous tissues or other soft tissues to the injured area [2]. The scaffolds used in Rog need to be suitable biological substitutes, similar to the extracellular matrix of bone tissue [3-4]. Thus, bacterial cellulose (CB) membranes can be an excellent barrier option, as they are considered a natural, biocompatible biomaterial [5] and have a surface that allows the adsorption of other substances, forming biocomposites and further enhancing its use [3]. Thus, incorporating calcium phosphate sources, called Hydroxyapatites (HAP) in CB, would provide bone connection properties, and this biocomposite could act as scaffolds [1,3]. The partial replacement of HAP calcium (CA) with other metal ions found in the man's body has had benefits, as it enhances the physicochemical properties of the material and, consequently, improves the biological response of bone implants [6]. Magnesium (Mg) plays an essential role in bone growth, as it stimulates the propagation of osteoblasts, and their absence can cause bone fragility [7]. Zinc (Zn) is fundamental to bone metabolism and may promote apoptosis of osteoclastic cells, inhibiting bone resorption and, consequently, the mineralization of the bone matrix [8]. Strontium (Sr) can stimulate bone formation by proliferating osteoblasts and inhibiting osteoclastic cells, reducing bone resorption [9:

4]. Thus, based on this context, this work studied the partial replacement of hydroxyapatite with the hybrid composed of Mg/Zn and Mg/Sr in the bacterial cellulose membranes, aiming to produce a biocomposite for the application in guided bone regeneration.

Experimental

CB Synthesis and Biocomposites Production

The CB was synthesized by *Komagataeibacter hansenii* and cultivated in mannitol at 30 ° C in static conditions for 9 days. The membranes were purified with 0.1 m to 80 ° C NaOH for 60 min, washed with distilled water to pH 7, and sterilized.

For the preparation of the control sample, CB was immersed in a vial containing 40 mL of the 1st immersion solution ($CaCl_2$ 0,1 M, pH 6.58, 24 h, 80 rpm) aiming at the production of a material containing only hydroxyapatite (HAp). The membranes were washed with distilled water and immersed in 40 ml of the 2nd immersion solution (Na_2HPO_4 0,06 M, pH 8, 24 h, 80 rpm) [10].

In order to partially replace the calcium of the HAP with another metal ion, hybrid samples were prepared. The 1st immersion solution contained: $CaCl_2$, $MgCl_2$ e $ZnCl_2$ (0,1 M, pH 6); or $CaCl_2$, $MgCl_2$ and $SrCl_2$ (0.1 M, pH 6.2) in the proportions described in Table 1. The membranes were in these hybrid solutions at 24 h and 80 rpm. After this period, they were washed with distilled water and placed in the 2nd immersion solution (Na_2HPO_4 0.06 m, pH 8, 24 h, 80 rpm). The concentrations of the solutions were determined based on the 1.67 ratios between the metal and the phosphorus of the apatites [11].

Table 1 - Concentration and nomenclature of samples

Sample		Concentration HAp % (V/V)			
		Ca^{+2}	Mg^{+2}	Zn^{+2}	Sr^{+2}
C	CB/ HAp - Control	100	-	-	-
M_1	CB/ 1% Mg – 4% ZnHAp	95	1	4	-
M_2	CB/ 2,5% Mg – 2,5% ZnHAp	95	2.5	2.5	-
M_3	CB/ 4% Mg - 1% ZnHAp	95	4	1	-
M_4	CB/ 1% Mg – 4% SrHAp	95	1	-	4
M_5	CB/ 2,5% Mg – 2,5% SrHAp	95	2.5	-	2.5
M_6	CB/ 4% Mg - 1% SrHAp	95	4	-	1

Characterization of Biocomposites

CB membranes and formed biomaterials were lyophilized and then characterized by porosity techniques, FTIR/ATR, MEV/EDS, TGA and DR-X. The antimicrobial properties of the samples were analyzed by the Bauer disk diffusion technique [12].

Results and Discussion

The porosity of the biomaterials was determined according to Zeng and Ruckenstein [13], where the results obtained indicated that after the incorporation of the HAp partially replaced by Mg-Zn and Mg-Sr, the biocomposites had an average porosity of 64%. However, there was a 34% decrease in its percentages compared to pure CB, as the inorganic material was deposited on the surface. Suggesting that the deposition of the HAP occurred on the surface and inside the CB [2]. In the fir spectra analyzed (Fig 1), it was possible to observe a slight band curvature in the region between 3500-3200 cm^{-1}, indicating the presence of the CB hydroxyl group. This milder presence of hydroxyls may indicate a broad HAP cover on the CB matrix, suggesting its mineralization. There was also a reduction in band intensities between 1160 and 1110 cm^{-1}, indicating a good connection between CB and HAp, improving biocomposite stability [2]. In all spectra, it was possible to observe the presence of intense bands in 1030 and 962 cm^{-1}, indicating the presence of the phosphate group in the biomaterials produced. Another band that presented relevance in the samples analyzed is located at 880 cm^{-1}, which corresponds to the carbonate ion (CO_3^{-2}), suggesting the

absorption of carbon dioxide in the air [2]. An apatite containing carbonate in CB fibers produces a material similar to bone tissue apatite [10].

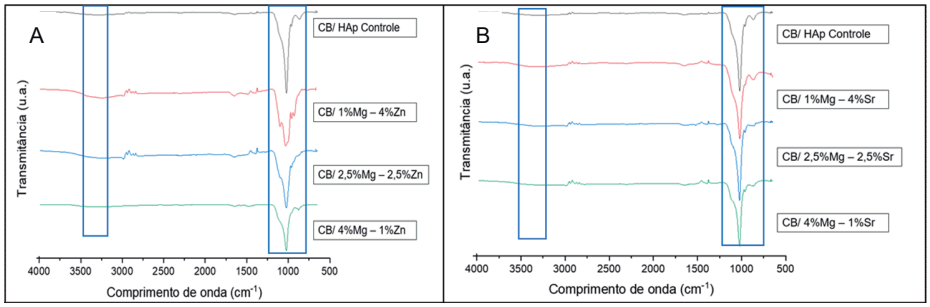

Figure 1 – FT-IR/ATR analysis of biocomposites: A) CB/HAp Mg/Zn; and B) CB/HAp Mg/Sr.

The thermal degradation profile of the biocomposites (Fig 2) indicated the presence of 5 stages of mass loss for most samples. The 3rd stage of degradation is the most prominent and occurs at temperatures between 340 - 386 °C. This thermal event is characteristic of CB's degradation, causing its depolymerization and dehydration, resulting in carbonaceous waste [2, 10]. Pure CB degradation occurs at around 300 °C [5, 2]. The analyzed biocomposites presented this stage at a higher temperature, suggesting higher thermal stability than pure CB. Notably, all samples had a high percentage of waste (55.56% - 80,30%), confirming the presence of an inorganic phase in biocomposites due to the deposition of HAP in CB fibers.

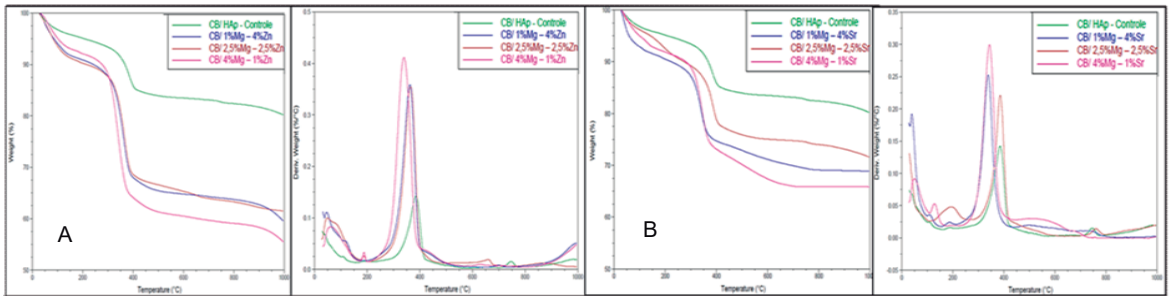

Figure 2 – TG and DTG curves of biocomposites: A) CB/HAp Mg-Zn; B) CB/HAp Mg-Sr.

Partially replaced biocomposites diffractograms (Fig 3) have a decrease in the grade of crystallinity when compared to the CB/HAP control sample, indicating that partial replacement of Ca ion by Mg/Zn or Mg/Sr caused a reduction of 30 % on average, in their crystallinity degree [8]. The characteristic peaks of CB ($2\theta \approx 14.5$ and 22.6º) were observed in the analyzed samples. Already the HAp has diffraction peaks at $2\theta \approx 26º$ and 32º. Other lower peaks are typical of HAp, found at $2\theta \approx 33º$, 40º, 46º and 54º [2]. All biocomposites produced demonstrated these characteristic peaks of the HAp, confirming the incorporation of phosphate sources into the CB fibers, which was also observed in the FTIR analyses.

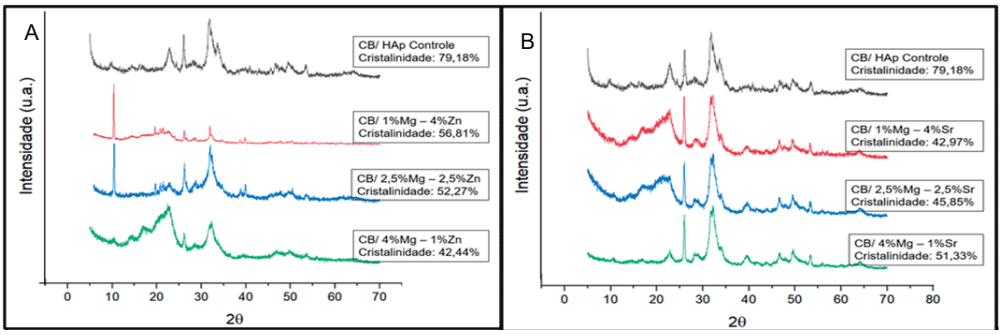

Figure 3 – Ray diffractograms - X of biocomposites: A) CB/HAp Mg-Zn; B) CB/HAp Mg-Sr

The micrographs obtained (Fig 4) show a dense layer of HAp crystals on the CB/HAp-control surface compared to pure CB. These crystals are in a relatively globular or rosetta form and rosetta format and blades, indicating that biocomposite mineralization was adequate. EDS analysis for the control biocomposite confirmed the presence of the Ca and P elements [2]. Partial replacement of Ca ions with Mg-Zn hybrid lightly altered crystal morphology compared to the control sample, as they were in lamellar and needle format. It was observed that the higher the concentration of Zn in the samples, the greater the presence of needle crystals, and the more acidic pH favors this condition [14]. The samples partially doped by the Mg-Sr hybrid showed a high density of lightly globular blades shaped crystals, and the formation of crystals in CB fibers occurred evenly and homogeneously. EDS's analysis confirmed the presence of the CA, P, MG, Zn or Sr elements for each sample.

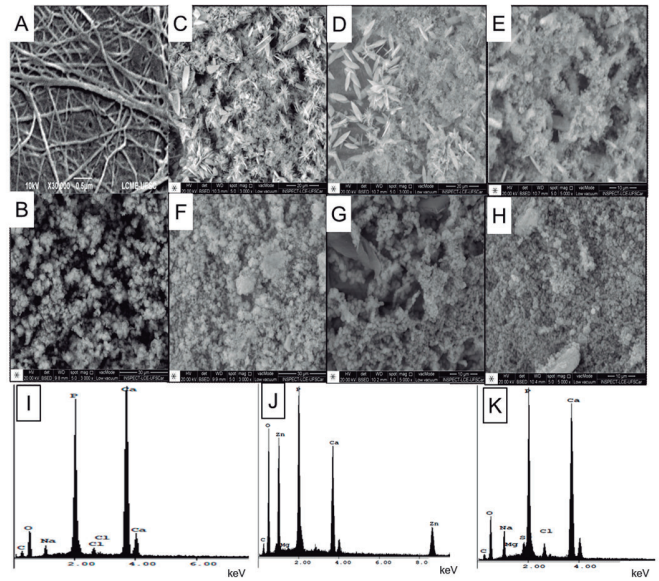

Figure 4 – Surface micrographs A) CB pura; B) CB/HAp - Controle; C) CB/1%Mg - 4%Zn; D) CB/2.5%Mg – 2.5%Zn; E) CB/4%Mg - 1%Zn; F) CB/1%Mg - 4%Sr; G) CB/2.5%Mg – 2.5%Sr; H) CB/4%Mg - 1%Sr; I) EDS CB/HAp – Control; J) EDS CB/HAp Mg-Zn; K) EDS CB/HAp Mg-Sr.

No biocomposite had antibacterial action for E. coli and S. aureus microorganisms, ie, no bacteria growth inhibition halo was observed. This fact can be justified by the low concentration of the used Mg, Zn and Sr elements [15]. However, incorporating these metal ions enables the promotion of other characteristics to biocomposites produced; thus, they can be used as scaffolds.

Conclusions

The bacterial cellulose membranes presented themself as a suitable matrix for inserting metal apatites. The results show that partially replaced HAp biocomposites have maintained a good percentage of porosity and hydroxyls available to make calls. The FTIR test showed that phosphate groups were incorporated into the CB. Carbonated apatite was also observed, which makes the biomaterial closer to the bone tissue apatite. TGA's analysis indicated the presence of the inorganic phase in CB, suggesting the formation of metal apatites; In addition, the biocomposites produced had higher thermal stability than pure CB. The results obtained by the DRX analysis confirmed the presence of HAp crystals and peaks, indicating the incorporation of the Mg, Zn and Sr. MEV analyses confirmed the mineralization of the CB matrix with HAp crystals. In the concentrations studied, biocomposites did not have antimicrobial activity. However, EDS analysis confirmed the incorporation of Mg, Zn and Sr elements into biocomposites, which may benefit scaffold, promoting bone regeneration.

Acknowledgements

The authors would like to thank the UNIVILLE and UFSCar laboratories for the analyses.

References

1. M.T. Maia; É.P.C.G. Luz; F.K. Andrade; M. de F. Rosa; M. de F. Borges; M.R.A. Arcanjo; R. S. Vieira. Polymer Reviews 2021, 61, 4. https://doi.org/10.1080/15583724.2021.1896543.
2. M.C.F. Garcia, Dr. Thesis, Federal University of Santa Catarina, 2022.
3. S. Pina; R.F. Canadas; G. Jiménez; M. Perán; J.A. Marchal; R.L. Reis; J.M. Oliveira. *Cells Tissues Organs*. 2017, *204*, 150. doi: 10.1159/000469703
4. E.P.C.G. Luz; B.S. Das Chagas; N.T. De Almeida; M. De F. Borges; F.K. Andrade; C.R. Muniz; I. I. Castro-Silva; E.H. Teixeira; K. Popat; M. De F. Rosa; R. S. Vieira. Materials Science and Engineering C 2020, 116, 111175. https://doi.org/10.1016/j.msec.2020.111175.
5. S.J. An; S.H. Lee; S.I. Jeong; J.S. Park; H.J. Gwon; E.S. Kang; C.M. Jeong; Y.M. Lim. *International Journal of Molecular Sciences*. 2017, 18, 2236. https://doi.org/10.3390/ijms18112236
6. G.G. Santos; V.L.C. Nunes; S.M.O. C. Marinho; S.R.A. Santos; A.M. Rossi; F.B. Miguel. Brazilian Journal of Biology, 2021, 81, 1. https://doi.org/10.1590/1519-6984.217769.
7. S. K. Padmanabhan; P. Nitti; E. Stanca; A. Rochira; L. Siculella; M. G. Raucci; M. Madaghiele; A. Licciulli; C. Demitri. Materials 2021, 14, 22. https://doi.org/10.3390/ma14226942.
8. A. Dias, Dr. Thesis, Federal University of Minas Gerais, 2020.
9. M. Hassan; M. Sulaiman; P. D. Yuvaraju; E. Galiwango; I. U. Rehman; A. H. Al-Marzouqi; A. Khaleel; S. Mohsin. Journal of Functional Biomaterials, 2022, 13, 1. https://doi.org/10.3390/jfb13010013.
10. S. Saska; H.S. Barud; A.M.M. Gaspar; R. Marchetto; S.J.L. Ribeiro; Y. Messaddeq. *International Journal of Biomaterials*. 2011, 2011,1. doi:10.1155/2011/175362
11. S. Nath; B. Basu; A. Sinha. *Trends Biomater*. 2006, 19. 2, 93.
12. A.W. Bauer; W.M.M. Kirby; J.C. Sherris; M. Turck. The American Journal of Clinical Pathology, 1966, 45, 3.
13. X. Zeng; E. Ruckenstein. Industrial & Engineering Chemistry Research, 1996, 35, 11. https://doi.org/10.1021/ie960270j.
14. J. da S.R. Neto, Dr. Thesis, Federal University of Santa Catarina, 2015.
15. F. Ai; L. Chen; J. Yan; K. Yang; S. Li; H. Duan; C. Cao; W. Li; K. Zhou. Journal of Sol-Gel Science and Technology, 2020, 95, 1 http://dx.doi.org/10.1007/s10971-020-05285-0.

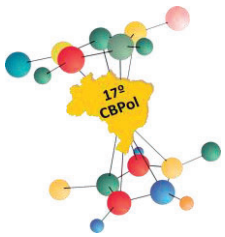

HYDROPHOBIC AND FLEXIBLE POLYURETHANE FOAMS REINFORCED WITH MICROCRYSTALLINE CELLULOSE FIBERS FOR OIL SPILL CLEAN UP

Lara Vasconcellos Ponsoni[1*], Matheus Vinícius Gregory Zimmermann[1], Marina Kauling de Almeida[1], Ademir José Zattera[2], Ruth Marlene Campomanes Santana[3].

1 – Universidade do Extremo Sul Catarinense (UNESC), Av. Universitária, 1105, CEP 88806-000, Criciúma, SC, Brazil.
2 – Universidade Federal do Rio Grande do Sul (UFRGS), Av. Bento Gonçalves, 9500, CEP 91501-970, Porto Alegre – Brazil.
3 – Universidade de Caxias do Sul (UCS), R. Francisco Getúlio Vargas, 1130, CEP 95070-560, Caxias do Sul – Brazil.
** E-mail address: ponsonilara@gmail.com*

Abstract – In this study, open cell polyurethane (PU) foams with the addition of microcrystalline cellulose (MCC) were formulated and chemically modified with organosilane to be used as an absorbent system for oil spill cleanup in water. The influence of MCC concentration on mechanical properties and chemical treatment with organosilane were evaluated. In addition, the sorbents were characterized based on their surface modification and sorption capacity. The main results indicated that the surface treatment on the solid fraction of the foams was effective, pointed out by the contact angle, thus increasing the hydrophobicity of the samples. As the MCC content increases in the composition, the compressive strength tends to be higher and the thickness of the organosilane layer increases, due to the increased roughness of the PU higher the density, which negatively affects the sorption capacity of the samples. However, the results obtained in the samples showed hydrophobic and oleophilic character.
Keywords: Polyurethane foams. Nanocellulose. Oil spill.

Introduction

Oil contamination has been an environmental problem since the beginning of its large-scale extraction and use. The total global volume of tanker oil spill in the year of 2022 was approximately 15,000 tonnes, according to ITOPF (International Tanker Owners Pollution Federation) [1]. Oil spills usually occur during the extraction and transportation process, causing economic, environmental, and social impacts. Oil spilled into water is spread immediately. Its volatile components can undergo evaporation and contaminate the air. Simultaneously, the oil can be emulsified in oil-water, making it difficult to extract and remove [2].

To minimize the impacts caused by oil spills, some techniques for water-oil separation have been studied, such as: flotation, centrifugation, adsorption, gravimetric separation, electrochemical, and biodegradation. The sorption process has been highlighted as a technique for treating industrial effluents and an efficient and economical alternative for remediating areas affected by oil spills. In this process, there are simultaneous involvement of absorption, adsorption, and desorption processes, where in absorption the oil is accumulated within the system and in adsorption the oil is retained on the surface of the solid part of the sorbent.[3]

Polyurethane (PU) foams are formed by a polymerization reaction between a di-isocyanate or tri-isocyanate and a hydroxylated (polyol), generating a polyurethane chain. The PU's application can include upholstery to reinforced materials with sorption capacity. Among the properties of the foams, when produced with high open cell concentrations, viscoelastic properties allow sorption and desorption of oils. The development of the oleophilic and hydrophobic properties are related to sorption and desorption, by the use of certain reagents as organosilanes for modifications during the preparation of the foams [4].

Microcrystalline cellulose (MCC) is generated from purified and partially depolymerized cellulose. MCC can be produced from a lot of cellulosic sources, but cotton and wood are usually the main sources for the fabrication. The most common applications of MCC include a binder and filler in

food, medical tablets, and especially as a reinforcement agent in the development of polymer composites. MCC is considered as a potential reinforcement to turn the composites into a biodegradable material and to reduce the costs, meanwhile keeping the desired properties [5].
In view of the difficulty involved to clean up oil spills in the water sources around the planet, urge the need to create alternative options that are capable of sorption the oil. With the knowledge that polyurethane foams can acquire hydrophobic and oleophilic properties based on the addition of organosilane chemical treatment [6]. Also, when microcrystalline cellulose is added to obtain the composite, there is the goal to improve the mechanical properties.

Experimental

Materials

For the development of PU foams, Voranol WL 4010 polyol and Voranate™ T-80 TDI toluene diisocyanate (TDI), supplied by Dow Brasil Sudeste Industrial Ltda., were used. The amine catalyst (Dabco® 2033 Catalyst) was supplied by Air Products, and the organometallic tin octanoate catalyst (Kosmos® 29) was supplied by Evonik Industries. The surfactant, commercially known as Niax silicone L-595, was supplied by Momentive Performance Materials Inc. Methylene chloride, a deionizing agent supplied by Brasil Sudeste Industrial Ltda, and deionized water were used. Microcrystalline cellulose (MCC), Sigmacell Type 20 grade, particle size approximately 20 μm, code S3504, was supplied by Sigma-Aldrich S.A. For the hydrophobic coating of PU foams, triethoxyvinylsilane (TEVS) (supplier code: 175560) and tetraethoxysilane (TEOS) (supplier code: 13190) were used, both supplied by Sigma-Aldrich.The oils used for the sorption tests were as follows: Ipiranga SAE 5W30 oil (lubricating motor oil) with a density of 0.86 $g.cm^{-3}$ at 20 ºC and a kinematic viscosity of 70 cSt at 40 ºC, soybean oil (vegetable oil–cooking oil) with a density of 0.91 $g.cm^{-3}$ at 20°C and a kinematic viscosity of 32 cSt at 40 °C, kerosene (fuel oil) with a density of 0.78 $g.cm^{-3}$ at 20 °C and kinematic viscosity of 2.2 (max) cSt at 40°C.

Methods

The PU foams formulated with MCC concentration, expressed in parts per hundred polyols (pphp). Four levels of MCC were used in a standard composition of flexible PU foams, considering a theoretical density of 10 $kg.m^{-3}$. The formula consisted in 100 pphp of methylene, 80 pphp of diisocyanate, 6 pphp of water, 0.3 of amine, 3.3 of silicone, 0.5 of octoate, and 22 of chloride. The amounts of MCC varied according to the sample, being for PU 1 without the addition of MCC, PU.C10 with 10 pphp, PU.C20 with 20 pphp, PU.C30 with 30 pphp, and PU.C40 with 40 pphp.
PU foams were produced by the batch method using a Fisaton 715 propeller mixer with a rotational speed of 2500 rpm. Initially, water, amine, silicone, and different concentrations of MCC were added to the polyol and stirred for 80 s. Then, tin octanoate was added and mixed for 40 to 50 s. Thereafter, TDI and chloride were added to the blend with vigorous stirring for approximately 10 to 15 s and then the mixture was poured into a mold for free expansion, to form the foam. Expansion time was approximately 1 min. The foam was cured for 48 h in a controlled temperature of 23 °C. The treatment for PU foam hydrophobization was carried out using an organosilane-based coating. At first, organosilane hydrolysis was carried out by a solution of water:alcohol (70:30) with 1% (mass) of organosilane TEVS and 1% (mass) of TEOS. Acetic acid (approximately 10 mL for each liter of solution) was added dropwise to stabilize the pH of the solution to 4.5. The solution was stirred for 2 h. After this, foam samples (25 x 25 x 25 mm^3) were immersed in the solution and stirred slowly with a magnetic bar stirrer for 4 h. Later, the foams were removed from the solution, the excess liquid was drained, and the samples were dried (with the occurrence of concomitant organosilane curing) at 120 °C for 4 h.

Characterization

To perform the analysis of the density of the samples, five specimens, each sized 25 x 25 x 25 mm³, were used per sample, and the densities of the foams were calculated using Eq. 1 as described in ASTM D3574-11.

$$\rho_f = \frac{m_f}{v_f} \times 10^6 \quad (1)$$

Where ρf is the foam density (kg.m^{-3}), mf is the mass (g) and vf is the volume (mm^3) of the specimen, which was calculated from the measurement with a caliper. Sample morphology was evaluated by field emission scanning electron microscopy (FEG-SEM) using a Shimadzu device (Superscan SS-550 model) and a Tescan microscope (model Mira3). The test was performed on five specimens, all samples were precoated with gold (Au) and 15 kV voltage was used. The foam area was observed vertically, in the direction of expansion of the samples. The compressive strength tests of the PU foams were carried out in a universal testing equipment EMIC model DL 2000 with specimens measuring 50 x 50 x 25 mm³ and compression speed of 50 mm.min^{-1}. The tension required to reduce the thickness of the specimen by up to 80% of its initial thickness was evaluated, according to ASTM D3574-11. The hydrophobicity of a material can be evaluated by the contact angle of a drop of water deposited on its surface [7]. When this contact angle is greater than 90° it is convenient to define it as hydrophobic

Results and Discussion

Fig. 2 shows the results of bulk density of PU foams with different content of MCC and after treatment with organosilane, where the samples containing organosilane represented by PU.S. Increasing the content of MCC causes an increase in the bulk density of the samples, a result already expected, since cellulose is an additional composition. It is also necessary to consider that, with the addition of cellulose to polyol, there is a proportional increase in the viscosity of this phase, which impacts the restriction of the expansion capacity of the foam, coupled with the fact that cellulose fibers occupy the empty spaces within the polyurethane molecules and can promote an increase in foam density [8].

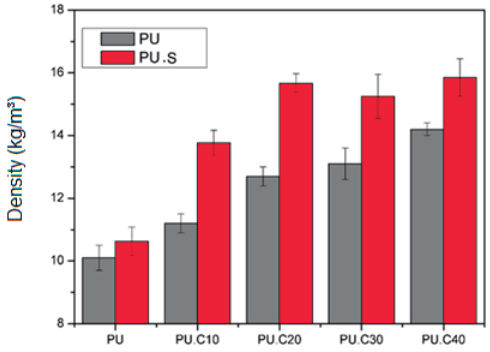

Figure 2: Density of PU samples with different MC contents and with (PU. S) and without (PU) organosilane-based hydrophobic treatment.

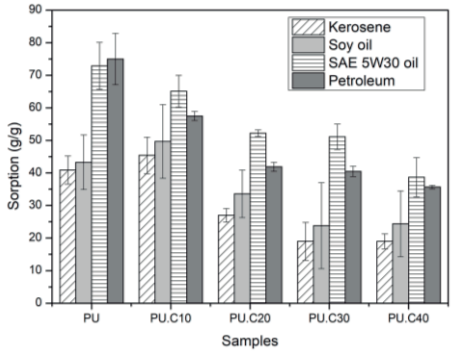

Figure 3: Static sorption capacity of PU foams with different cellulose contents.

It is also observed that after the hydrophobic chemical treatment, all samples showed higher density values in relation to their analogues without the treatment, a fact associated with the incorporation of organosilane layers on the surface of the solid fraction of the foam. It is noteworthy that, compared to the pure PU sample (that had approximate increase of 7%), and the samples containing MCC, after chemical treatment, showed a more expressive increase in density, with an increase of 27% for PU.C10, 29% for PU.C20, 20% for PU.C30 and 14% for PU.C40. The increase in density of the foams with MCC may be associated with the higher surface roughness of the solid fraction, which may have caused the formation of thicker layers of organosilane on the surface of the foam solid fraction.

Fig. 4 presents the micrographs obtained by SEM of the PU samples with different levels of MC and with and without hydrophobic treatment. It is possible to observe that, after the treatment with

organosilane (a), the samples presented a rigid coating layer, in which during the cutting of the samples, it was fragmented, exposing more evident the organosilane coating layer, as seen in the images (b) and (c). The pure PU (a), before chemical treatment presents a smoother surface, which may contribute negatively to the adhesion of the organosilane on the surface, and under mechanical stress, deteriorate and can be removed more easily. The presence of MCC at figure (d) and (e), thicker layers of organosilane were observed, and no significant tricks and detachments were found, camparatively to the PU and as observed in the micrographs.

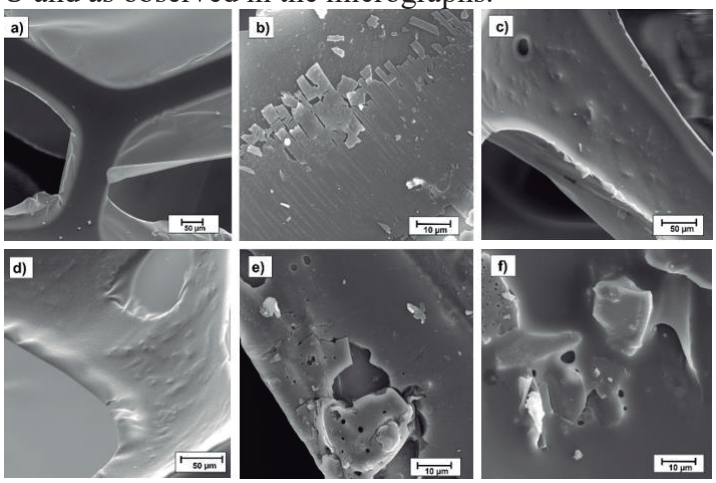

Figure 4: SEM microscopy of (a) untreated pure PU, (b) pure PU with organosilane, (c) and (d) untreated PU.C40 and (e) and (f) PU.C40 with organosilane.

The hydrophobic character of the PU foams was determined by measuring the contact angle of their previously pressed foam obtained by a mechanical press surface, with water (polar liquid), which is defined as the angle between the solid surface and the tangent line of the liquid phase at the solid phase interface. The contact angle obtained in all samples silanized with the liquid of maximum surface tension was greater than 110º at time t=0, indicating a surface with hydrophobic characteristics. The cellulose-reinforced foams showed a slight increase in the angle, due to the greater interaction of the foam surface with the organosilane and the stability that the addition of cellulose brings to the foam. The contact angle of the water with the substrate surface is related to the functional groups present on the solid surfaces of the PU foam. After 5 min of the test, the water droplet measurements on the silanized PU foam showed a slight decrease in the contact angle compared to t=0, probably due to the migration of water into the compensated porous structure [9]. The foam without the chemical treatment showed higher water migration into the foam after 5 minutes.

According to the results all the samples treated with the organosilane showed hydrophobic character. The larger the contact angle, considering water as the fluid, the greater the selectivity and the interaction of the foam with the oil, enabling greater efficiency in oil removal, as well as playing an important step in the beginning of the oil sorption process [10]. Fig. 4 presents the static sorption capacity of PU foams with different cellulose contents, coated with organosilane and evaluating the influence of different types of oils. Firstly, a higher sorption capacity is observed for PU foams with more viscous oils. This phenomenon is mainly attributed to oil desorption after removal from the system. More viscous oils have greater difficulty in flowing out of the foam and require longer desorption times, thus a greater amount of oil is retained inside the foam. As the adopted desorption time was 30 s for all samples, it was expected that the foams would have a higher sorption capacity for more viscous oils. The sorption process is directly influenced by the viscosity of the oil, and oils with high viscosity have an easier anchorage and retention in porous polymer systems compared to less viscous oils [11]

In a comparative analysis between the samples studied, with increasing cellulose content in the PU foams there is a tendency for the sorption capacity of all the oils to decrease. This reduction is

directly associated with the raise in density of the foams with increasing MCC content since the morphology of the cell structure of the foams was similar. Duong & Burford [12] studied the effect of sorption capacity of PU foams by evaluating the density of PU foams, the viscosities of oils and temperature on the sorption behavior of oils in different PU foams. They reported that the sorption capacity increases significantly with decreasing density of the foams, due to the raise in the number of open cells, cell morphology and, that this behavior also depends on the oil viscosity as well as the oil temperature (test temperature). The data presented in Fig. 3 show the sorption capacity in grams of oil per gram of sorbent, i.e., as the foam density increases, there is a tendency for the sorption capacity to decrease, because the increase in sample mass (constant volume) is directly related to the sorption capacity of the foam.

Conclusions

The development of the polyurethane foams reinforced with microcrystalline cellulose chemically modified with organosilane was succeed as an absorbent system, as it is possible to visualize in the results of the contact angle test and in the sorption capacity of the samples. Creating a mechanism that meets part of the need for oil-in-water removal. It was also observed that the content of MCC increases the compressive strength, and the thickness of the foams. Although, the use of MCC in the composition is responsible for a higher density which negatively affects the sorption capacity of the samples, that was seen during the characterization stage. Nevertheless, the samples obtained showed hydrophobic and oleophilic character designed for the research conducted. Turning the use of microcrystalline in polymeric foams attractive, especially attached to the relatively low-cost and lower density when compared to the inorganic fillers conventionally used.

References

1. ITOPF - International Tanker Owners Pollution Federation. “Oil tanker spill statistics 2022” (ITOPF, 2022), https://www.itopf.org/knowledge-resources/data-statistics/statistics/. Accessed 25 April 2023.
2. L. Zhang, J. Xie, X. Luo, X. Gong, and M. Zhu. *Chem. Eng. Sci.,* v. 273, p. 118663, (2023). http://dx.doi.org/10.1016/j.ces.2023.118663.
3. M. V. G. Zimmermann, A. J. Zattera, B.R. Fenner, and R.M.C. Santana. *Polym. Bull.,* v. 78,142 (2020). http://dx.doi.org/10.1007/s00289-020-03169-5.
4. Y. Liu, J. Ma, Wu T, X.Wang , G. Huang, Y. Liu, H. Qiu, Y. Li, W. Wang, J. Gao. *ACS Appl Mater Interfaces* V. 5, 10018 (2013).
5. A., Bayat, S.F. Aghamiri, A. Moheb, G.R. Vakili-Nezhadd. *Chem Eng Technol*, V., 281525 (2005)
6. S. Chung, MT. Suidan, A. D. Venosa *Chem Eng Technol* V.34:1989–1996 (2011).
7. Wu, Z.; Li, C.; Liang, H.; CHEN, J.; YU, S. *Angewandte*, 2997–3001, 2013.
8. J. Andersons, M. Kirpluks, and U. Cabulis, *Materials,* v.13(12), 2725 (2020). doi:10.3390/ma13122725
9. S. Hussain. PhD thesis. Department of Chemical Engineering and Applied Chemistry, University of Toronto, Toronto, 2014.
10. Cunha, A. G.; Freire, C.; Silvestre, A; Neto, C.P.; Gandini, A.; Belgacem M. N.; Chaussy, D.; Beneventi, D. *Journal of Colloid and Interface Science*, v. 344, p 588–595, 2010.
11. Tanobe, V.O.A.Tese (Doutorado em Engenharia e Ciência dos materiais) – Universidade Federal do Paraná, Curitiba, 2007.
12. Duong, H.T.T.; Burford, R.P. Journal of Applied Polymer Science, v. 99, p. 360, 2006.

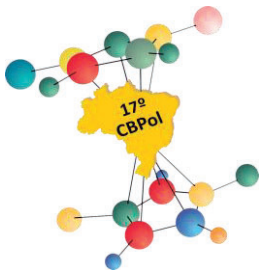

INFLUENCE OF DIFFERENT ORGANIC ACIDS AS COUPLING AGENTS ON THE THERMAL PROPERTIES OF HDPEpc/CURAUA FIBER COMPOSITE

Vanessa Z. Kieffer[1*], Edson L. Francisquetti[2] and Ruth M. C. Santana[1]

1 – Department of Materials Engineering, Federal University of Rio Grande do Sul (UFRGS), Porto Alegre, RS, Brazil.
2 – Federal Institute of Education, Science and Technology of Rio Grande do Sul (IFRS), Farroupilha, RS, Brazil.
*vanessa.kieffer@ufrgs.br

Abstract - The search for sustainable materials has led to the increased use of thermoplastic composites reinforced with fibers from renewable sources, mainly vegetable fibers. However, chemical treatments and coupling agents are often necessary to improve interfacial fiber-matrix adhesion due to these fibers' hydrophilic nature. Thus, one of the current challenges is to find a method to improve this adherence efficiently and sustainably. As an alternative, the present study aims to analyze the influence of different organic acids as a coupling agent in composites with post-consumer high-density polyethylene (HDPEpc) matrix reinforced with curaua fiber (FC). The samples were characterized using thermogravimetric (TGA) and differential scanning calorimetry (DSC) techniques. The results showed that, like the effect observed with maleic anhydride grafted polyethylene (PEgAM), using organic acids improves the thermal stability of the HDPEpc/30FC composites. Suggesting that using organic acids can be a viable alternative to chemical treatments and coupling agents of synthetic origin.
Keywords: *coupling agent, high-density polyethylene, curaua fiber, injection molding, thermoplastic composite.*

Introduction

The use of recycled materials and natural fibers in the production of composites has become increasingly common in recent years, aiming at environmental sustainability and cost reduction [1–3]. However, due to these fibers' hydrophilic nature, chemical and physical treatments and coupling agents are often necessary to improve adhesion between the natural fibers and the recycled polymeric matrix [4]. Thus, one of the current challenges of this process is to find a method to improve fiber-matrix adhesion efficiently and, at the same time, sustainably. Coupling agents of organic origin are being researched for their use as coupling agents in composites reinforced with vegetable fibers as an alternative to synthetic coupling agents to solve this problem [5–7]. Castro *et al.* used canola and castor oil as coupling agents in high-density biopolyethylene (HDBPE) composites reinforced with curaua fiber (FC). The authors reported that incorporating vegetable oils could be used to modify the properties of the fiber-matrix interfaces for materials prepared from hydrophilic fibers, such as lignocellulosic fibers, and hydrophobic matrices, such as HDBPE [5]. Poletto, Zattera, and Santana, in addition to maleic anhydride grafted polypropylene (PPgAM), used hexanoic (C6), octanoic (C8), decanoic (C10), and dodecanoic (C12) acids as coupling agents in recycled polypropylene (PPr) composites reinforced with wood flour. The authors observed that using organic acids improved interfacial adhesion and, consequently, improved the mechanical and thermal properties of the materials [6]. Lima used citric acid, lauric acid, palmitic acid, and PPgAM as coupling agents in PP/Bamboo Fiber composites. The author reported that among the organic acids, citric and palmitic acids showed similar behavior to PPgAM regarding the composite materials' mechanical, physical, and thermal properties [7].

Based on the positive results observed with the use of oils and organic acids, it is certainly justifiable to carry out new studies that explore the use of different types of organic acids as coupling agents, highlighting citric acid ($C_6H_8O_7$), found naturally in many citrus fruits such as lemons, oranges, and tangerines; the malic acid ($C_4H_6O_5$), found naturally in various fruits, such as apples, pears, and grapes, and is also present in some plants and animals; the tartaric acid ($C_4H_6O_6$), who can be found naturally in many fruits, such as grapes, dates, and bananas, as well as some plants, such as tamarind; and the myristic acid ($C_{14}H_{28}O_2$), a saturated fatty acid, found naturally in many plants and animals, including nuts, seeds and vegetable oils [8, 9].
In short, organic acids are natural chemical compounds that can be found in various organic sources such as plants, fruits, flowers, and other living organisms [10]. These compounds can have a wide range of properties, including the ability to bind to other components, which makes them potential coupling agents in polymer matrix composites reinforced with plant fibers. Therefore, to replace the synthetic coupling agent, PEgAM, with an organic coupling agent, the present study aims to analyze the influence of different organic acids on compatibilized reinforced post-consumer high-density polyethylene (HDPEpc) composite materials with curaua fiber (FC).

Experimental

Materials

For the formulation of composites, was selected the post-consumer high-density polyethylene (HDPEpc) as a polymeric matrix, coming from jars/packaging of manipulated products; curaua fiber (FC) as reinforcement; maleic anhydride grafted polyethylene (PEgAM) as synthetic coupling agent. And to find an alternative for PEgAM were used as organic acids, citric acid (AC), malic acid (AMá), myristic acid (AMi), and tartaric acid (AT) from Êxodo Científica. The compositions, in percentage of mass, of the evaluated samples are specified in Table 1.

Table 1 – Samples' Formulation.

Sample	HDPEpc (%)	FC (%)	Coupling Agent (%)
HDPEpc	100	-	-
s/AA	70	30	-
PEgAM	67	30	3
AC	67	30	3
AMá	67	30	3
AMi	67	30	3
AT	67	30	3

Then, the materials were mixed and homogenized in the *HAAKE Rheomix OS Polylab* mixing chamber to obtain the composite material. This mixture underwent a process of granulometry reduction, and later, the specimens were made by the injection molding process in a *Mini-Jet II* piston injector.

Characterization Methods

The thermal characterization of the samples was conducted using the techniques of thermogravimetric analysis (TGA) and differential scanning calorimetry (DSC). To perform the analysis related to the mass variation as a function of temperature was used TGA equipment, *Q50 - TA Instruments*, programmed in the temperature range of 25 to 1000 °C with a heating rate of 20 °C/min, under an N_2 atmosphere (10 mL/min), as established in the ASTM E-1131 standard. And to obtain the melting temperatures and enthalpies of the samples, it was used DSC equipment, *Q20 - TA Instruments*, programmed in the temperature range of 25 to 200 °C with a heating/cooling ramp of 10 °C/min, under an N_2 atmosphere (50 mL/min), according to the ASTM D-3418 standard.

Results and Discussion

Thermogravimetric Analysis (TGA)

The TGA/DTG thermogravimetric analysis evaluated the samples' thermal stability and degradation. In Fig. 1 are presented the thermogravimetric curves (TGA) and the derived from thermogravimetric curves (DTG) of the samples analyzed.

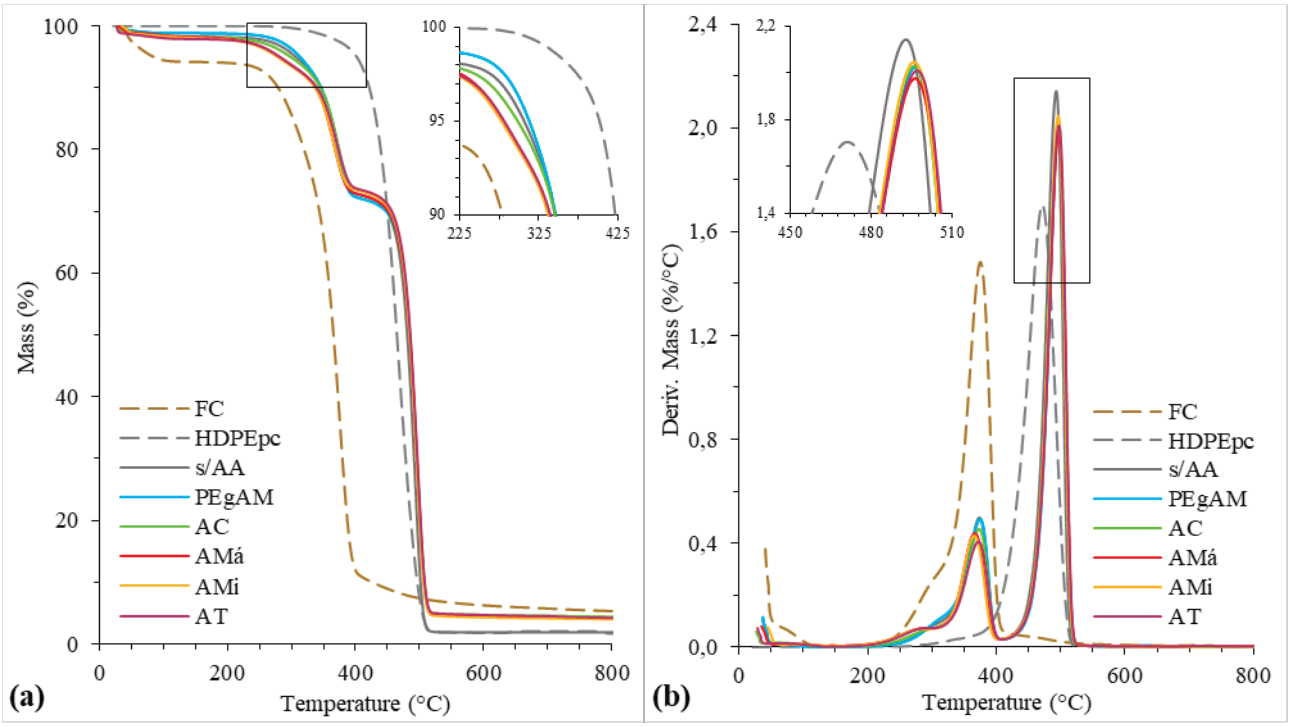

Figure 1 – Curves of the analyzed samples: (a) TGA and (b) DTG.

In Fig. 1-a, it is observed that the FC has three stages of mass loss, the first corresponds to moisture and some low molecular weight extractives present in plant fibers, the second to hemicellulose and to cellulose (in a more significant proportion of mass) and the third to lignin. In counterpart, for the injected HDPEpc sample, only one stage of decomposition is observed, corresponding to the polymeric matrix. In turn, two principal decomposition stages can be observed for samples of composite materials. The first stage, between 250 and 400 ºC, where a shoulder and a maximum peak occur, corresponds to fiber degradation (hemicellulose and cellulose, respectively). In the second stage, between 425 and 525 ºC, the most significant loss of mass occurs, corresponding to the decomposition of the polymer. Moreover, lastly, it follows a slow degradation, which may correspond to lignin and residues/ashes present in the samples.

In Fig. 1-b, the DTG curves complement and confirm the information obtained from the TGA curves. In the composites, one shoulder and two peaks can be observed, with the shoulder and the peak having the lowest intensity (between 250 and 400 ºC) corresponding to the components of the curaua fiber and the highest intensity peak (between 425 and 525 ºC), corresponding to the polymeric matrix, HDPEpc.

As shown in the approximation of Fig. 1-a, initially, the PEgAM and s/AA samples showed greater thermal resistance, which may be due to the influence of impurities and other extractives more resistant to decomposition present in these samples. However, after a 10% mass loss, the AC composite acquired a thermal resistance analogous to the PEgAM sample. Other authors observed similar behavior, suggesting that the composites coupled with citric acid have a more significant interfacial interaction due to the reaction of the functional groups of citric acid and the hydrophilic groups on the surface of the curaua fiber [7]. The results obtained through the analysis of the TGA/DTG curves of the samples are shown in Table 2.

Table 2 – Results of the analyzed samples' thermal properties (TGA/DTG).

Sample	TGA					DTG	
	T (°C) 5%wt	T (°C) 10%wt	HDPEpc (%)	FC* (%)	Ash (%)	1st T_p (°C)	2st T_p (°C)
FC	84.47	279.14	-	95.03	4.97	375.30	-
HDPEpc	401.63	421.42	98.12	-	1.88	-	471.35
s/AA	306.52	345.30	70.94	27.16	1.90	373.85	493.01
PEgAM	313.05	345.94	68.50	27.69	3.81	374.81	496.48
AC	298.43	345.43	69.66	26.35	3.99	373.18	496.03
AMá	280.39	337.60	69.09	27.08	3.83	366.61	496.54
AMi	278.02	336.94	69.72	26.50	3.78	365.80	496.08
AT	281.31	339.54	69.77	26.27	3.96	372.04	497.26

* Included the loss of moisture mass and fiber extractives.

Differential Scanning Calorimetry (DSC)

To evaluate the thermal behavior and the effect of different coupling agents us the composite materials (HDPEpc/30FC), a thermal analysis by DSC was conducted through three scans. Fig. 2 shows the curves obtained through the second heating of the DSC technique.

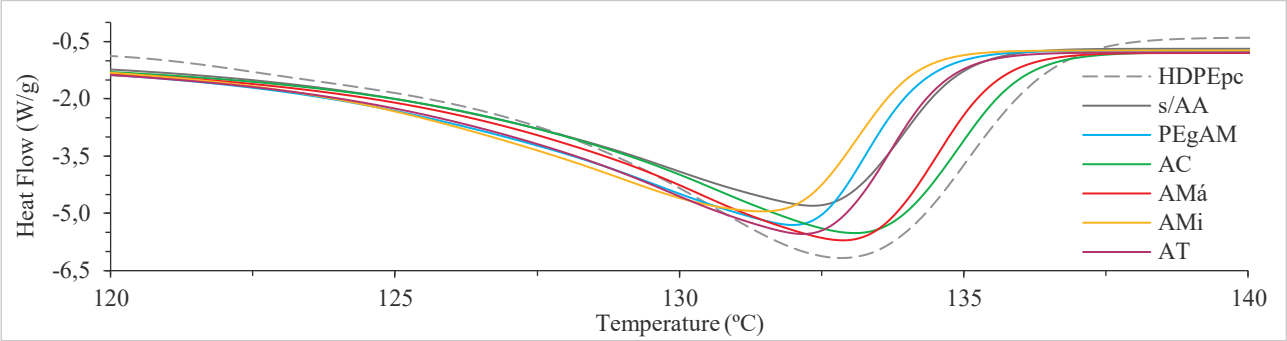

Figure 2 – Second heating curves of the samples analyzed using the DSC technique.

In Fig. 2, it can be observed that the composites' melting peaks are less intense than the peak of HDPEpc, suggesting that the fiber may be affecting the crystallization of the composite material. This could be due to several factors, including the size, shape, and orientation of the fibers, as well as their interaction with the polymeric matrix. These results corroborate previous studies, which indicated that the presence of FC can hinder the crystallization of the composite material, reducing the mobility of the polymeric chains in the region close to the fibers [11]. Data obtained through the DSC curves were used to calculate the degree of crystallinity of the samples with Eq. 1.

$$Xc = \frac{\Delta H_m}{(\Delta H^{\circ}_m \times W)} \times 100\% \quad (1)$$

Where (Xc) is the crystallinity index; (ΔH_m) is the melting enthalpy of the sample; (ΔH°_m) is the melting enthalpy of the PEAD, hypothetically, 100% crystalline. In literature [12], the most frequent value found for the melting enthalpy of HDPE is 293 J/g; and (W) is the mass fraction of the polymers in each sample.

As shown in Table 3, the s/AA sample has a low degree of crystallinity, 67.33%, when compared to the other analyzed composites. However, it is noted that there was an increase in the degree of crystallinity of the AC and AMá samples, indicating an improvement in the fiber-matrix interaction, where the composites were compatibilized with organic acids that also can act as a flow agent [7]. Furthermore, when compared to the s/AA composite, the addition of coupling agents in the

HDPEpc/30FC composites caused an increase in the enthalpy of fusion, highlighting AMá. This higher energy required for melting to occur suggests that the addition of organic acids provides better adhesion between the phase fiber-matrix of the composite material. This is because when a material melts, it is necessary to provide energy for the molecules to separate and for the material to change phase. If there is a strong interaction between the phases because of using a coupling agent, this required energy may be greater [13].

Table 3 – Melting temperature (T_m), melting enthalpy (ΔH_m), and degree of crystallinity (Xc) of the samples.

Sample	T_m (°C)	ΔH_m (J/g)	Xc (%)
HDPEpc	132.87	241.40	87.55
s/AA	132.39	138.10	67.33
PEgAM	132.00	152.00	77.43
AC	133.09	162.60	82.83
AMá	132.88	167.80	85.48
AMi	131.46	148.40	75.59
AT	132.16	159.10	81.05

Conclusions

Based on the results obtained in the present study, it can be concluded that incorporating organic acids into the composite materials was beneficial for the thermal stability and the degree of crystallinity of the materials, as well as the addition of the synthetic coupling agent, PEgAM. Thus, it is evident that using organic acids can be a viable and sustainable alternative to chemical treatments and coupling agents of synthetic origin. Furthermore, using a recycled polymeric matrix combined with reinforcement and compatibilizer of natural origin appears as an excellent option to produce environmentally sustainable materials.

Acknowledgements

We are grateful to the Laboratory of Polymeric Materials (LaPol) of UFRGS, CAPES, and CAPES PROEX for all the support for elaborating this research.

References

1. A. L. Marinelli; M. R. Monteiro; J. D. Ambrósio; M. C. Branciforti; M. Kobayashi; A. D. Nobre. Polímeros 2008, 18(2). doi.org/10.1590/S0104
2. I. Bressiani Jr.; A. C. Keinert; A. Ellenberger; U. L. Belini. Mix Sustentável 2020, 6(4). doi.org/10.29183
3. E. P. Calegari; B. F. de Oliveira. Sustentabilidade em Debate 2016, 7(1). doi.org/10.18472
4. S. R. Albinante; E. B. A. V. Pacheco; L. L. Y. Visconte. Quím Nova 2013, 36(1). doi.org/10.1590/S0100
5. D. O. Castro; F. Passador; A. Ruvolo-Filho; E. Frollini. Compos A: Appl Sci Manuf 2017, 95. doi.org/10.1016
6. M. Poletto; A. J. Zattera; R. M. C. Santana. Polymer Compos 2014, 35(10). doi.org/10.1002
7. L. P. F. C. Lima; Thesis, Federal University of Rio Grande do Sul (UFRGS), 2020.
8. L. A. Ríos Vásquez, *La química orgánica aplicada a nuestro diario vivir*, Colômbia, 2019.
9. T. M. Devlin, *Bioquímica con aplicaciones clínicas*, Reverté, Espanha, 2015.
10. R. J. Pereira; G. N. L. Nascimento, *Compostos Bioativos Vegetais,* Palmas, 2014.
11. V. Z. Kieffer; R. M. C. Santana in Proceedings of 24th Brazilian Congress of Materials Engineering and Science, Águas de Lindóia, 2022.
12. S. V. Canevarolo Jr., *Técnicas de Caracterização de Polímeros*, Artliber, São Paulo, 2004.
13. A. K. Lau; A. P-Y. Hung, *Natural Fiber-Reinforced Biodegradable and Bioresorbable Polymer Composites*, Elsevier, 2017.

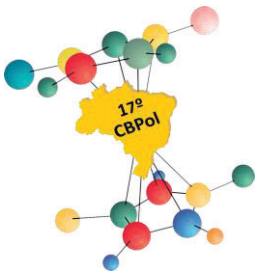

INFLUENCE OF NATURAL EXPOSURE ON CASTOR OIL BASED POLYURETHANE REINFORCED WITH MACADAMIA RESIDUES

Bianca A. R. Silva[1], Lorena C S. Balieiro[2], Daniella R. Mulinari[2],
1 – Department of Chemistry and Environmental, State University of Rio de Janeiro (UERJ), Resende, RJ, Brazil
biancaandraderangel@gmail.com
2 – Department of Mechanical and Energy, State University of Rio de Janeiro (UERJ), Resende, RJ, Brazil

Abstract - The agro-industrial sector has been expanding more and more and with its high demand, the agro-industrial residues generated do not have an environmentally correct destination. In order to minimize the use of residues that do not damage the environment and contribute to a better circular economy, the use of macadamia residues (RM 5-20% by weight) in polyurethane foams based on castor oil under aging was analyzed. Physical, morphological, and mechanical properties were determined before and after outdoor exposure to observe the impact after weathering. RM contributes to increasing the compressive behavior in non-exposed samples and after exposure, the results suggest that the degradation can act by increasing the reticulation density even with the structural alterations presented as yellowing and voids. These results suggest a promising material for the circular economy.

Keywords: *Macadamia residues, Castor oil based Polyurethane; Composites, Natural exposure*

Introduction

Currently, the agricultural industry is experiencing exponential growth, which favors the global economy, however, there is also a high volume of organic waste being generated. This fact causes damage to the environment if not discarded or reused correctly Tavares et al. [1]. An alternative so that these residues do not cause negative impacts on society is the reuse to produce new material since agro-industrial residues have a low cost, good biodegradability, and high mechanical resistance. Among the industrial residues, the production of whole Macadamia nut stands out. Global macadamia production in 2021 was 241,420 tons with shells, which is equivalent to 65,835 tons in the form of grains and 175,585 tons of waste INC et al. [2]. The disposal of macadamia nuts is a problem due to the high costs associated with landfills, so reuse ends up being more viable since it can have applicability in several sectors such as energy generation through incineration, hydro chars processing, and polymer matrix reinforcement. Researchers have sought methods of reuse so that waste is not discarded in the environment. Silva et al. studied the reuse of PP-based composite macadamia and obtained satisfactory results in improving the properties analyzed Silva et al. [3]. Another attractive to reuse this waste could be using a filler in polyurethane foams (PU) Costa et al. [4]. Polyurethane foams (PU) are a versatile family of materials mainly obtained by combinations of polyols and polyisocyanates. Due to the multiplicity of their structures, PUs can be used in various forms and applications. Cellular materials are the largest part of this market (more than 60 %) with segments including the furniture, automotive, bedding, insulation, building, or construction markets Gandara et al. [5].
In this work, the macadamia residues in castor oil-based polyurethane foams were studied to evaluate the physical, morphological, and mechanical properties before and after natural exposure.

Experimental

Preparation of the composites and neat PU

Composites were manufactured using the situ foaming method Costa and Gandara et al. [4, 5]. First, the pristine PU manual mixing of castor oil-based polyol and prepolymer was made respecting the proportion of 1:1 for 50 s at room temperature (27 °C) in molds. After 24 h, foams were removed from the molds to guarantee their complete expansion, and then the samples were cut for the characterization tests. The composite foams were synthesized from the macadamia nutshell residues (MR) mixture with the castor oil-based polyol, and after that, the prepolymer was added to the mixture. The sequential steps for the foam were analog to the neat PU foam. Samples were named PU/MRX%, where X represents the percentage of macadamia nutshell residues (5, 10, 15, and 20 wt%) inserted in the PU.

Characterization of the composites and neat PU

Stereomicroscopy (optical microscopy) of the samples was realized using the ZEISS DISCOVERY V12 stereomicroscope to inquire about the surface pores' morphological aspect, shape, and distribution. The average density of the neat PU and their composites were determined in triplicate by cutting the foams into cubic shapes (10x10x10 mm^3). The specimens were weighed, and their mass was divided by the calculated volume.

Neat PU and its composites were subjected to compression tests by an EMIC testing machine (model DL2000) with pneumatic grippers with a 5 kN load cell, following the ASTM D 695-15 standard, with 5 $mm.min^{-1}$ at 20% deformation. The dimensions of the samples of the specimens were 50×50×25 mm and positioned between the two parallel plates for compression.

Neat PU and its composites underwent natural environmental aging for 12 months (November 2021 to November 2022) following ASTM G-7 and ASTM G-147 standards. The test was performed in quintuplicate for each type of sample. The samples were evaluated and weighed during the first week, after ten days, and once a month for 12 months. The mass loss of the samples after environmental aging was determined by the difference between the sample mass after exposure to the open air (m_f) and the sample mass before exposure (m) as described by Eq. (1).

$$Weight\ loss\ (\%) = \frac{m - m_0}{m_0} \times 100 \qquad \text{Eq. (1)}$$

Results and Discussion

Morphological analysis of pure PU foam showed a porous surface with a high content of closed cells and pore distribution with an average size of 1485 ± 531 μm, as observed in Fig. 1. However, the insertion of macadamia residues altered these characteristics. Analyzing the morphology of the composites was observed that the pore sizes gradually decreased according to the insertion of macadamia residues (MR), highlighting the PU/MR20% samples, which showed a reduction of 40 and 44%. A similar trend was obtained by Gandara et al. when developed a new composite material based on sugarcane bagasse fibers reinforced in polyurethane for the sorption of vegetal oil Gandara et al. [5]. According to Tiuc et al. the natural fiber acts as a nucleating agent for the formation of pores Tituc et al. [6]. With the nucleation of a greater number of cells occurring at the same time, the availability of gas decreases for cell growth, causing the formation of smaller pores Czlonka et al. [7]. In addition, PU composites presented open and interconnected pores with different sizes/shapes Costa et al. [4]. The foam density of pure PU and its composites directly influences the type of PU foam structure and its mechanical performance Silva et al. [8]. The densities presented by the composites reinforced with MR corroborate their morphologies (Fig. 1). Composites with the lowest MR contents showed lower density due to open pores and lower amounts. On the other hand, composites with higher MR content had higher density due to more closed pores and greater quantity. After environmental aging was observed a yellowing, voids, and

a slight increase in pore size, which caused a decrease in the density. This fact can be occurred due to a combined effect of temperature, humidity, and UV radiation. Also, this change after environmental aging interfered in the mechanical Properties and mass loss.

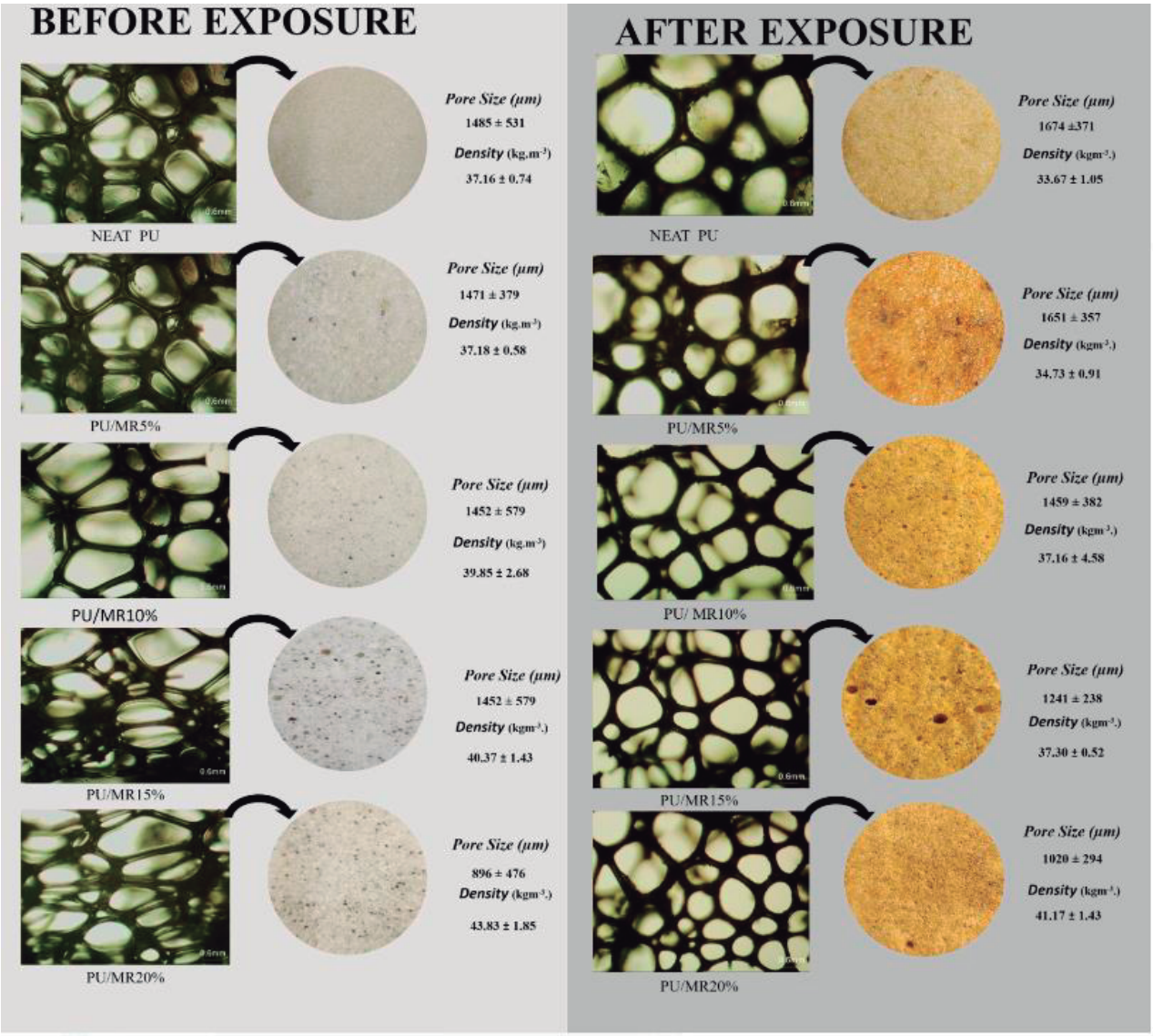

Figure 1- Optical microscopy (40x) and photographs of composites reinforced with macadamia residues before and after natural aging (both in the rise direction).

Analyzing the data obtained, it is noted that neat PU has a compressive strength of 0.24 ± 0.01 MPa. In the literature, a similar result was reported Nguyen et al. [9]. When incorporating MR in the PU matrix, the particle size exerted some influence on the compressive strength values. The PU/MR20% composite obtained a compressive strength increase of 12.5% compared to the pristine PU foam. When studying polyurethane composites and palm sheath residues, Moghim et al. [10] reported a trend toward this increase in strength, which can be attributed to the interaction of the isocyanate groups of the PU matrix and the O-H groups of the cellulosic fibers. An unexpected increase in the compressive strength of the exposed samples after environmental aging was also observed, which resulted in resistant and less brittle foams. This fact must be related to humidity, thermal effects, and wind. The humidity affected in the mass loss, as can be observed in Fig. 2. The results obtained in the first week of weight loss for pure PU and its composites showed a significant weight gain for all samples on the 50th day (11/Nov/2021) compared to the other days of the aging

period. A possible hypothesis for this behavior is the absorption of water due to the rainy day and also the chemical degradation such as the cleavage of the urethane group present in the polymeric chain Gandara et al. [5]. Thus, the formulation of new foams containing MR may be a viable way to manage this waste.

Table 1: Data of the compressive strength of foams before and after natural aging.

Samples	Before environmental aging Compressive strength (MPa)	After environmental aging Compressive strength (MPa)
Neat PU	0.24 ± 0.01	0.44 ± 0.05
PU/MR5%	0.23 ± 0.03	0.38 ± 0.03
PU/MR10%	0.21 ± 0.02	0.44 ± 0.10
PU/MR15%	0.21 ± 0.05	0.37 ± 0.03
PU/MR20%	0.27 ± 0.02	0.38 ± 0.07

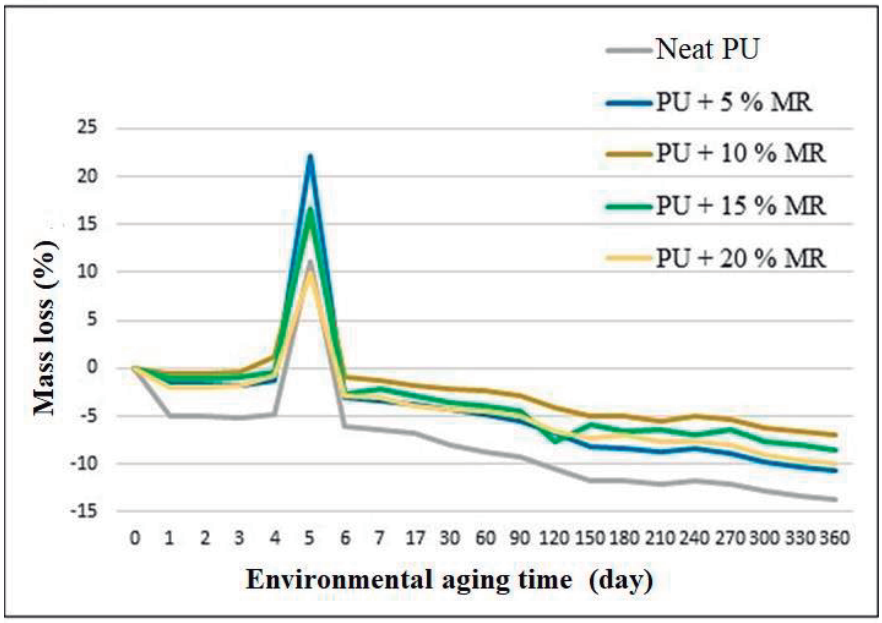

Figure 2- Graphic of the mass loss x environmental aging time (day).

Conclusions

The effect of macadamia residue (MR) used as reinforcement in polyurethane (PU) foams based on castor oil was evaluated under environmental aging. Optical microscopy showed that the addition of MR in PU foams caused a nucleating effect producing foams with higher density and smaller cell sizes than neat PU. In the exposed samples, a slight increase in pore size was observed. However, environmental aging caused yellowing, voids, and roughness gain of the materials compared to non-aging samples. The compressive strength of the composites increased according to the addition of macadamia residues. An unexpected increase in the compressive strength of the exposed samples after natural aging was also observed, which resulted in resistant and less brittle foams. All changes in PU/MR after environmental aging occurred due to a combined effect of temperature, humidity, and UV radiation. Thus, after the studies presented, there was evidence of a reduction in pores after the addition of fiber, a decrease in density, and an increase in mechanical resistance. Therefore, it is concluded that these PU/MR composites in different amounts of 5, 10, 15, and 20% are an environmentally correct way to dispose of MR waste and promising for various applications, thus contributing to the circular economy.

Acknowledgments
This research was funded by Fundação Carlos Chagas de Amparo à Pesquisa do Estado do Rio de Janeiro - FAPERJ (E-26/200.636/2023 and E-26/210.450/2021).

References

1. J. Tavares, L. Lucena, G. Henriques, R. Ferreira and M. Dos Anjos Construction and Building Materials 2022, 346, 128467. https://doi.org/10.1016/j.conbuildmat.2022.128467
2. INC, Conselho Internacional de Nozes e frutos secos, 2022. https://www.nutfruit.org/industry/news/detail/global-statistical-review-macadamia
3. N. Silva, L. Cortat, and D. R. Mulinari. Journal of Polymers and the Environment 2021, 29(10), 3271–3287. https://doi.org/10.1007/s10924-021-02112-7
4. M. Costa, L. Martins, L. Maia and D. Mulinari Journal Mater Cycles Waste Management 2021, 23, 1431–1444. https://doi.org/10.1007/s10163-021-01224 -5
5. M. Gandara, D. Mulinari., L. Monticelli and M. Capri Journal of Natural Fibers, 2020, 8:12, 1983-1994. https://doi.org/10.1080/15440478.2019.1710653
6. A. Tituc, O. Nemes, H.Vermesan and A. Toma Composites Part B: Engineering, 2019, 165, 120-130. https://doi.org/10.1016/j.compositesb.2018.11.103.
7. S. Czlonka, N. Sienkiewicz, A. Kairyté and S.Vaitkus Polymer Testing 2019, 78, 105986. https://doi.org/10.1016/j.polymertesting.2019.105986
8. N. Silva, L. Cortat; E. Texeira, L. Baptista, D. Orlando, D. Mulinari Waste Management 2023, 155, 220-229. https://doi.org/10.1016/j.wasman.2022.11.004.
9. T. Nguyen; P. Dao, C. Decker and P. Nguyen-tri Progress in Organic Coatings 2018, 124, 137-146. https://doi:10.1016/j.porgcoat.2018.08.013
10. M. Moghim, M. Keshavarz and M. Zebarjad Polymer Bulletin 2019, 76, 227–239. https://doi.org/10.1007/s00289-018-2384-0.

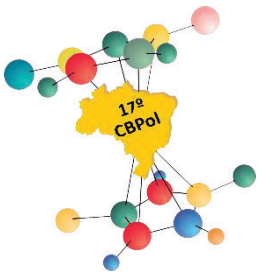

INFLUENCE OF SODIUM BENTONITE CLAY CONCENTRATION ON THE PROPERTIES OF BIOCOMPOSITES BASED ON BABASSU COCONUT MESOCARP STARCH AND ALGINATE

Pablo D. S. Silva[1*], Casi S. dos Santos[2], Louryval C. Paixão[3], Allan Kardec D.B. Filho[4] and Audirene A. Santana[1]
1 – Department of Chemical Engineering, Federal University of Maranhão (UFMA), Ma, Brazil*
pablo.daniel@discente.ufma.br
2 – RENORBIO Graduate Program, Federal University of Maranhão (UFMA), Ma, Brazil
3 - Coordination of the Interdisciplinary Bachelor of Science and Technology, Federal University of Maranhão (UFMA), Ma, Brazil
4 - Department of Electrical Engineering, Federal University of Maranhão (UFMA), Ma, Brazil

Abstract - This study was carried out to investigate the impact of incorporating bentonite clay in different concentrations (0.25%, 0.75% and 1.25%) in biocomposites consisting of alginate and starch obtained from mesocarp babassu coconut. The main objective was to analyze the physical and mechanical properties of these materials. The results showed that as the clay concentration increased, the moisture content and solubility of the composite also exhibited a corresponding increase. Additionally, it was observed that the water vapor permeability and thickness of the biocomposites increased proportionally with the addition of clay. Regarding the mechanical properties, the tensile strength and Young's modulus exhibited a linear correlation with the concentration of bentonite, whereas elongation demonstrated a proportionate decrease. The Fourier Transform Infrared (FTIR) spectra showed interactions among these components that contributed to the stabilization and properties of the formed biocomposites.
Keywords: *Biocomposite, Bentonite, Alginate, Babassu, starch*

Introduction

The consumption of synthetic polymers, known as plastics, has expanded by approximately 36% since 2010, becoming the most widely used polymers in our contemporary society. It is evident that these compounds are employed in various sectors such as packaging, automotive, pharmaceutical, information technology, among others, providing invaluable benefits to human needs. However, considering environmental principles, the concern becomes urgent in the face of the current scenario, as the exploitation of non-renewable degradable sources leads to serious consequences for the environment, in addition to the excessive amount of time it takes for such material to decompose. In view of this panorama, one of the alternatives adopted to mitigate these challenges is the use of biopolymers, which are biodegradable materials and, being from natural sources, are more environmentally friendly in terms of producing fewer greenhouse gases [1-3].

The babassu coconut mesocarp starch (BCMS), which is a natural polymer, presents advantages in terms of environmental protection, cost-effectiveness, absence of toxicity, ease of degradation, abundance in the state of Maranhão - Brazil, among others, which makes it one of the critical points of green materials research. Although it has relatively good biocomposite formation properties, its mechanical properties are insufficient. Therefore, aiming to enhance the mechanical capabilities of starch-based materials, many researchers add various substances, such as plasticizers and crosslinking agents.

The use of bentonite clay as a reinforcing agent presents itself as an efficient alternative to significantly enhance mechanical, thermal, and water vapor permeability (WVP) properties. This clay is predominantly composed of montmorillonite ($Al_2O_3.4(SiO_2).H_2O$), a phyllosilicate mineral with a sheet-like structure, belonging to the 2:1 clay mineral family. This family is characterized by the

presence of tetrahedral and octahedral sheets that interconnect to form layers. The tetrahedral sheets consist of silica-oxygen tetrahedra, while the octahedral sheet is composed of aluminum, iron, or magnesium, coordinated to tetrahedral sheets through six oxygen molecules. These layers are linked together by interlayer cations, hydrogen bonds, or van der Waals forces [4-5].

Sodium alginate, obtained from marine algae, is a linear polysaccharide composed of β-D-mannuronate and α-L-guluronate, linked by 1-4 glycosidic bonds. It is a material with characteristics such as biodegradability, biocompatibility, and absence of toxicity, which make alginate an attractive material for numerous applications in the food, pharmaceutical, textile, biomedical, paper industries, and industrial waste treatment [6-7].

Therefore, this study aimed to evaluate the biocomposites composed of BCMS, alginate, and bentonite clay through characterizations of moisture content, water solubility, WVP, mechanical properties, and Fourier Transform Infrared Spectroscopy (FTIR).

Experimental

Materials

Sodium bentonite clay (BrasilMinas Indústria e Comércio Ltda, Brazil), sodium alginate (Isofar, Brazil), Mesocarp of Babassu Coconut obtained on the campus of the Federal University of Maranhão (UFMA, Brazil), glycerol, calcium chloride dihydrate, sodium hydroxide (NaOH), sodium metabisulfite, and ethyl alcohol (Synth, Brazil) were used.

Purification of Babassu Coconut Mesocarp

For starch extraction, the mesocarp powder underwent a successive sieving process using a fine mesh with an aperture size of 0.053 mm. Subsequently, the obtained material was washed in a solution containing sodium metabisulfite (1:2 w/v) to prevent starch browning. After agitation for 10 minutes, the solution was vacuum-filtered. Then, several washes were performed using a 0.05 mol/L NaOH solution, followed by washes with absolute ethanol to remove organic residues present in the extracted starch. Finally, the material was filtered again and placed in a controlled-temperature oven at 40°C for 24 hours.

Development of Biocomposites

Three compositions were prepared with different clay concentrations (0.25%, 0.75% and 1.25%) by adding 400 ml of distilled water to a 600 ml beaker, stirred using a "turrax" (10000 rpm) and maintained at a temperature of 80ºC. Then, 3g of BCMS (obtained in the previous step) was added and stirred for 15 minutes. The solution was cooled at 70ºC, and 8g of sodium alginate was gradually incorporated. Next, the in natura sodium bentonite clay was added to the solution (at the defined concentrations), maintaining at a constant temperature of 70ºC. To increase its plasticity, 5 ml of glycerol were added in the solution, which was then cooled to a temperature of 40ºC. Finally, 30 ml of 1% $CaCl_2$ (crosslinking agent) were added. Due to rapid crosslinking, the solution was added to the mixture at a maximum flow rate of 1 ml/min and stirred for a period of 20 minutes to obtain a homogeneous solution. The resulting biocomposites were carefully placed on acrylic plates and subjected to a drying process in an air-circulating oven, maintaining a constant temperature of 40ºC for a period of 18 to 20 hours. After the drying process was completed, the biocomposites were removed from the plates and stored in desiccators with a relative humidity of approximately 43%.

Characterization

The biocomposites were characterized as follows: 1) Moisture content (ω) - determined by the gravimetric technique using the AOAC methodology (Association of Official Analytical Chemists) [8]; 2) Water solubility (S) - determined according to the methodology proposed by Irissin-Mandata with modifications [9]; 3) Thickness (δ) - determined using a digital micrometer (resolution of 0.01 mm), with nine measurements taken at random points on the biocomposites; 4) Water vapor permeability (WVP) - using the ASTM E96/E96M-16 method [10]. 5) Mechanical properties - evaluated through tensile tests using a universal testing machine (BIOPID, Brazil). The elongation at break (e), tensile strength (TS), and Young's modulus (E) were determined according to ASTM D882 standards [11]; 6) Fourier Transform Infrared Spectroscopy (FTIR) - analyses of the in natura

bentonite clay, BCMS, sodium alginate, and biocomposites were conducted using an IRPrestige-21 spectrometer, Shimadzu. The spectral scan was performed in the range of 4000 to 400 cm^{-1}, employing the Attenuated Total Reflection (ATR) mode; 7) Statistical Analysis - quantitative data were expressed as mean values ± standard deviation. Analysis of variance and Tukey's test were used to determine statistically significant differences ($p<0.05$) between the data using Statistica V.9.

Results and Discussion

Figure 1 shows the Fourier Transform Infrared Spectroscopy (FTIR) spectra of BCMS (a), sodium alginate (b), sodium bentonite (c), and the biocomposites (d).

The BCMS (Fig. 1a) exhibits absorption bands at 3291 cm^{-1} (O-H stretching vibrations), 2911 cm^{-1} (symmetric stretching of CH_2), 1627 cm^{-1} (adsorbed H_2O vibrations and C=O stretching), 1322 cm^{-1} (N-H stretching and C-H bending), as well as absorptions in the region between 1200 and 600 cm^{-1} (carbohydrate vibrations). Sodium alginate (Fig. 1b) shows absorptions at 3448 cm^{-1} (-OH), 1637 cm^{-1} (asymmetric stretching vibration of COO groups), 1419 cm^{-1} (symmetric stretching vibration of COO groups), and 1099 cm^{-1} (C-O stretching). Sodium bentonite (Fig. 1c) exhibits absorptions at 3695 cm^{-1} (OH stretching vibration), 796 cm^{-1} (Al-Mg-OH stretching), 938 cm^{-1} (carboxylic acid group OH bending), 1421 cm^{-1} (alkane H bending), 698 cm^{-1} (Si-O stretching), 539 cm^{-1} (Si-O-Al stretching), and 470 cm^{-1} (Si-O-Si stretching). However, analyzing the FTIR of the biocomposites (Fig. 1d), the spectra reveals several characteristic absorptions suggesting interactions between these components. The absorption at 3841 cm^{-1} indicates the possibility of hydrogen bonding between the hydroxyl (OH) groups present in BCMS and sodium alginate and/or bentonite. The absorption at 2336 cm^{-1} suggests an interaction between BCMS and (C=O) groups present in bentonite and/or sodium alginate. The absorption at 2125 cm^{-1} indicates a possible ionic or electrostatic interaction between BCMS and the (COO-) groups of sodium alginate. Finally, the absorption at 1873 cm^{-1} suggests physical interactions between BCMS and bentonite through (Si-O) or (Si-O-Al) bonds. These interactions can contribute to the stabilization and properties of the biocomposites [12-15].

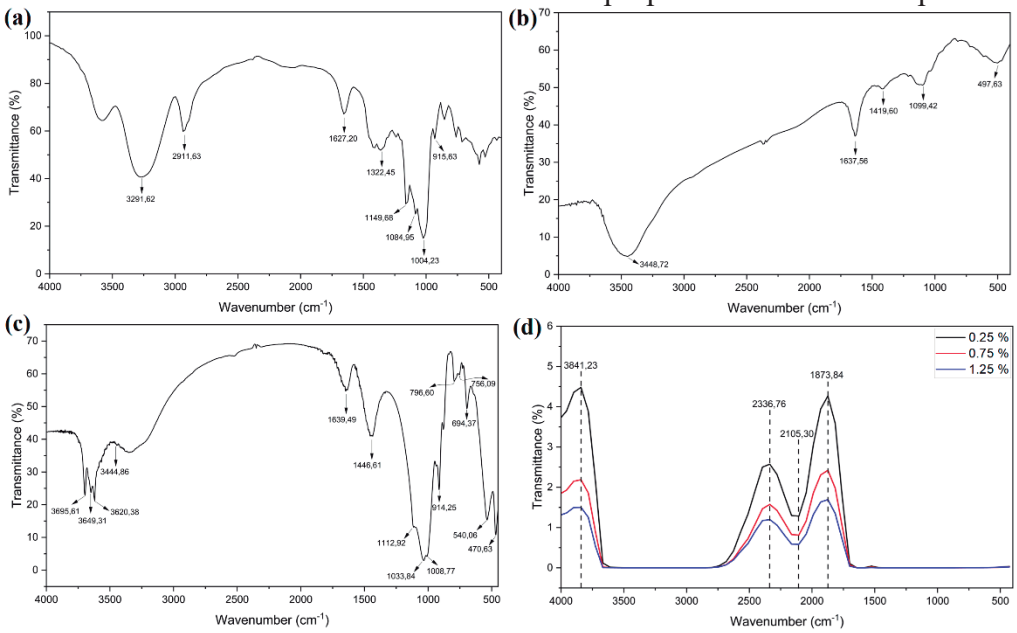

Fig. 1 – FTIR: (a) BCMS, (b) Sodium alginate, (c) Sodium bentonite, and (d) Biocomposites.

Table 1 presents the characterization data of biocomposites based on BCMS, sodium alginate, and different concentrations of sodium bentonite clay.

Due to its highly porous layered structure, clay is recognized for its water retention capacity within its layers, which becomes more evident with increasing clay concentration. This phenomenon is clearly observed in the present study, as shown in Table 1. It was found that as the clay concentration increased, the corresponding moisture content was recorded as 14.25%, 16.70%, and 19.49% for the concentrations 0.25%, 0.75% and 1.25% of clay, respectively. Simultaneously, the

material solubility also increased proportionally with the addition of bentonite, presenting values of 18.64%, 32.59%, and 47.95%. This trend can be attributed to the absence of attractive forces between the molecules present in bentonite, which favored water absorption and resulted in higher moisture content and solubility of the biocomposite. Previous research documents that biocomposites composed of alginate crosslinked with calcium exhibit high moisture content and solubility close to 100%. However, the incorporation of BCMS and clay in the biocomposite resulted in a slight reduction in hydrophobicity, indicating that these components provided a structure that stabilized the biopolymers, reducing such properties [16-17].

Table 1: Moisture content (ω), water solubility (S), thickness (δ), water vapor permeability (WVP), tensile strength (TS), elongation (e), and Young's modulus (E).

Clay concentration (%)	0.25	0.75	1.25
ω (%)	14.250±0.002^{a}	16.700±0.002^{b}	19.49±0.002^{c}
S (%)	18.640±0.220^{a}	32.590±0.310^{b}	47.95±0.370^{c}
δ (mm)	0.147±0.001^{a}	0.165±0.004^{b}	0.214±0.001^{c}
WVP[(g.mm)/(m^2.dia.k]	3.840±0.040^{a}	5.832±0.071^{b}	8.625±0.051^{b}
e (%)	2.538±0.055^{c}	2.001±0114^{b}	1.494±0.045^{a}
TS (MPa)	1.055±0.024^{a}	1.211±0.084^{b}	1.389±0.031^{c}
E (MPa)	42.142±1.103^{a}	53.217±2.986^{b}	93.064±3.371^{c}

Mean ± standard deviation of repetitions. Means with lowercase letter in each column indicate no significant difference at ($p<0.05$) according to Tukey's test.

It is also possible to observe an increase in WVP with values of 3.84, 5.83, and 8.62 (g.mm)/(m^2.day.kPa), as well as an increase in thickness to 0.14, 0.16, and 0.21 mm of the biocomposites with the addition of clay. It was expected that the presence of clay would reduce permeability; however, a weak electrostatic interaction effect resulted in higher porosity and the emergence of cavities in the polymeric structure of the materials. These cavities, by increasing the available empty spaces, facilitate the movement of water vapor through the material. This property becomes even more evident as the biocomposites become thicker [18].

The addition of bentonite to the biocomposites has shown a significant linear effect on the improvement of mechanical properties such as TS and E, while a decrease in elongation occurs. The results obtained in this study revealed a progressive increase in TS of the biocomposites as the bentonite content was gradually increased. The recorded values were 1.06 MPa, 1.21 MPa, and 1.39 MPa. This increase in tensile strength can be attributed to the presence of bentonite, which acts as a reinforcing agent in the biocomposite matrix. Additionally, a linear increase in the Young's modulus was also observed. The recorded values were 42.14 MPa, 53.22 MPa, and 93.06 MPa for increasing concentrations of bentonite. The observed increase in Young's modulus indicates a higher stiffness and resistance of the biocomposite to deformation, which is consistent with the results obtained for TS. On the other hand, there was a decrease in the elongation of the biocomposites. The recorded values were 2.53%, 2.00%, and 1.49%. This reduction in elongation can be attributed to the increased stiffness of the biocomposite due to the presence of bentonite. The higher stiffness may limit the material's deformation capacity before rupture occurs, resulting in lower elongation. Additionally, both glycerol and cross-linking agent present in the biocomposite influenced its mechanical properties. Therefore, the increase in bentonite concentration resulted in an increase in tensile strength and Young's modulus [19-21].

Conclusions

In this study, it became evident that bentonite clay at different concentrations significantly impacted various properties, such as water retention, solubility, WVP, and mechanical properties, indicating that higher clay concentrations contributed to higher moisture content and solubility of the material. Additionally, the weak electrostatic interaction resulted in increased porosity, which influenced WVP and allowed for more efficient movement in the biocomposites. Regarding the mechanical properties, bentonite acted as a reinforcing agent, increasing TS (tensile strength) and

Young's modulus, while reducing elongation. These findings highlight the potential of bentonite clay as a promising component in the formulation of biocomposites with enhanced properties for various applications, such as in the biodegradable materials industry. Future investigations can focus on optimizing concentrations and combinations of components to further explore the properties and applications of these improved biocomposites.

Acknowledgements

FAPEMA (Maranhão Scientific and Technological Research and Development Support Foundation); Analytical Center of UFMA; BrasilMinas for supplying the clay.

References

1. K. Jyoteshna; S. Ritu: Materials Today: Proceedings. 2022, 12109, https://doi.org/10.1016/j.matpr.2022.12.109

2. L. Kaiulani; S. Gabriela; L. Jeane; H. Juliana: Journal of Management & Environmental Sustainability. 2020, https://doi.org/10.19177/rgsa.v9e02020570-587

3. R. Ana; P. Louryval; R. Adones; L. Ilmar; S. Gustavo; R. Geyse; M. Alan; F. Allan; S. Audirene: Journal of Polymers and the Environment. 2021, 1212-1226, https://doi.org/10.1007/s10924-020-01952-z

4. B. Khadija; Q. Abou; B. Rachid: International Journal of Biological Macromolecules. 2022, 210, 663-668, https://doi.org/10.1016/j.ijbiomac.2022.04.222

5. S. Mrithula; M. Monalisha; T. A: Carbohydrate Polymer Technologies and Applications. 2021, 2, 100173, https://doi.org/10.1016/j.carpta.2021.100173

6. Z. Minghui; C. Hongyan; International Journal of Biological Macromolecules. 2023, 233, 123462, https://doi.org/10.1016/j.ijbiomac.2023.123462

7. K. Priya; U. G; R. Arpita; P. Sagar: Journal of Industrial and Engineering Chemistry. 2023, 122, 303-325, https://doi.org/10.1016/j.jiec.2023.02.031

8. AOAC International. Official Methods of Analysis of AOAC International. 2007, 17

9. M. Irissin; B. Gérard; B. Bernard; G. Nathalie: European Polymer Journal. 2001, 37, 1533-1541, https://doi.org/10.1016/S0014-3057(01)00039-8

10. ASTM International. ASTM E96/E96M-16. Standard Test Methods for Water Vapor Transmission of Materials. 2016

11. ASTM International. ASTM D882. Test Method for Tensile Properties of Thin Plastic Sheeting, 2018

12. B. C. Maniglia, Ph.D. Thesis, University of São Paulo, 2017

13. P. Rúben; T. Ana; C. Daniela; M. Ausenda; B. Paulo: International Journal of Polymer Analysis and Characterization. 2011, 16, 449-464, https://doi.org/10.1080/1023666X.2011.599923

14. K. Awinash; L. Pradip: Materials Today: Proceedings. 2020, 22, 737–742, https://doi.org/10.1016/j.matpr.2019.10.037

15. C. John: Encyclopedia of Analytical Chemistry. 2006, 1–22, https://doi.org/10.1002/9780470027318.a5606

16. B. Lopamudra; M. Monalisha; T. Arunachalam: Environmental Technology & Innovation. 2022, 25, 102180, https://doi.org/10.1016/j.eti.2021.102180

17. P. Louryval; L. Ilmar; K. Allan; S. Audirene: Journal of Applied Polymer Science. 2019, 136, 48263, https://doi.org/10.1002/app.48263

18. B. Tan; N. Thomas: Journal of Membrane Science. 2016, 514, 595–612, https://doi.org/10.1016/j.memsci.2016.05.026

19. S. N. Darrel; J. J. Maya: Polymers. 2020, 12, 2279, https://doi.org/10.3390/polym12102279

20. S. Hanna; G. Karolina; M. P. Edyta; K. Ilona: Starch. 2017, 69, 1500325, https://doi.org/10.1002/star.201500325

21. S. Mrithula; M. Monalisha; T. A: Carbohydrate Polymer Technologies and Applications. 2021, 2, 100173, https://doi.org/10.1016/j.carpta.2021.100173

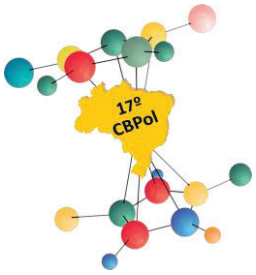

INFLUENCE OF THE ADDITION OF PEG-B-PPG-B-PEG AND PPG-B-PEG-B-PPG TRIBLOCK COPOLYMERS IN THERMOSETTING SYSTEMS

Lohana V. Bataglini[1*], Rafaela F. Cossul[1], Maria L. P. Maia [1], Luana Bettanin[1], Marlene Bamp[1], Marcia B. Schuster[1*] and, Bruna L. Silva[2].

1 – Department of Food Engineering and Chemical Engineering, University of the State of Santa Catarina (UDESC), Pinhalzinho, SC, Brazil
lobataglini@gmail.com
2 – Multi-User Center, College of Technological Science, State University of Santa Catarina (UDESC), Joinville, SC, Brazil

Abstract – In this work, the phase separation by microscopy and the mechanical performance under tensile test and fracture toughness of systems with triblock copolymer (PEG-PPG-PEG; $\bar{M}n$ ~ 1100 g/mol - EPE) or with (PPG-PEG-PPG; $\bar{M}n$ ~ 3300 g/mol – PEP), in concentrations of 10 and 20 wt.% in the epoxy matrix, were evaluated. Microscopic analysis showed that, only the pure matrix and the system with 10 wt.% EPE did not present visible phase separation and maintained the mechanical resistance of the pure matrix. In the other systems, self-assembled spherical domains of triblock copolymers were visualized and resulted in lower tensile strength than the pure epoxy. On the other hand, the system with 20 wt.% of PEP obtained a 10% increase in toughness in relation to the matrix. In this way, we see that the increase in the molar mass of the copolymer decreased the miscibility of the copolymer in the matrix and benefited the toughness of the epoxy.

Keywords: *Triblock copolymer; Toughness; Strength*.
Fundings: The authors would like to thank the financial resources provided by CNPq and FAPESC/PAP. (PROAP/AUXPE).

Introduction

Epoxy resins represent a group of prepolymers widely known for their ease of adhesion to other materials and their thermosetting three-dimensional structure when cured. These resins are commonly cured using hardeners with an amine functional group. However, the crosslinking reaction reduces the system's mobility and gives it the nature of brittle fracture [1,2]. Incorporating block copolymers (BC) in epoxy systems has emerged as an alternative to improve their mechanical properties, especially fracture toughness [1,3].

These epoxy/block copolymer systems have attracted the attention of researchers due to the self-assembled and nanophase-separated structure presented by some BCs that can generate nanostructured thermosets with different properties [1,3,4]. Recent studies have shown that the incorporation of block copolymer in nanocomposites also helped in the stabilization of carbon nanoparticles and increased the fracture toughness. The addition of different block copolymers (PPG-b-PEG-b-PPG) resulted in an increase in the mobility of the matrix and a decrease in the glass

transition temperature, except for copolymers that presented phase separation. That could be caused by the unfavorable physical interaction between the epoxy and the PPG group [5,6].
Thus, this work aims to study the influence of the addition of triblock copolymers on the mechanical properties of the epoxy matrix and its correlation with the phase morphology of the systems.

Experimental Section

General Information: As the matrix phase was used bisphenol A diglycidyl ether (DEGEBA) epoxy resin and 4,4'-diaminodiphenylmethane hardener. For the blends systems, triblock copolymer was added, being poly(ethylene glycol)-block-poly(propylene glycol)-block-poly (ethylene glycol) (PEG-PPG-PEG) $\bar{M}n$ ~ 1100 g/mol or poly(propylene glycol)-block-poly(ethylene glycol)-block-poly(propylene glycol) (PPG-PEG-PPG), $\bar{M}n$ ~3300 g/mol, referred to in this work as EPE and PEP, respectively. Both copolymers are composed of 10% PEG blocks. All materials were obtained from the Sigma-Aldrich.

Preparation of blends: Resin and copolymers (10 and 20 wt.% about the amount of the matrix) were mixed for 10 min at 75±5 °C in a digital magnetic stirrer. Then, the hardener (28.5 wt.% about the amount of resin) was added, and the mixing was continued for another 7 min. Subsequently, the mixture was poured into silicone molds, and cured in an oven at 100 °C for 24 hours and post-cured for 1 h at 140 °C.

All systems were evaluated by field emission microscopy (FESEM), photography, tensile test according to DIN53504 and fracture toughness according to SENB specimens and ASTM D5045. The identification of the developed systems is represented in Table 1.

Table 1– Identification of the systems

Components	Identification		
	Pure	Amount of block copolymer (%(m/m)	
		10 wt.%	20 wt.%
PEG-b-PPG-b-PEG 1100g/mol	-	EPE-10	EPE-20
PPG-b-PEG-b-PPG 3300g/mol	-	PEP-10	PEP-20
Resin (DEGEBA)	EPOXY	-	-

Results and Discussion

Fig.1A shows SENB samples of all prepared systems. It can be observed that the only translucent samples are the pure epoxy and the EPE-10 system, 10% PEG-b-PPG-b-PEG in the epoxy matrix, and the other systems were opaque. This difference may be associated with the phase separation of the systems and may indicate that the copolymer with a lower molar mass and the PEG component at the tips form a miscible and/or partially miscible system with the addition of 10 wt.% in the matrix. From the fracture microscopy of the samples (Fig.1B, 1C, 1D, 1E and 1F), it can be observed that the samples with pure epoxy (Fig.1B) and EPE-10 (Fig.1C) present homogeneous phase fracture surface. In contrast, 20wt.% PEG-b-PPG-b-PEG (Fig.1D) as well as both composition (10 and 20wt.%) of PPG-b-PEG-b-PPG (Fig. 1E and Fig.1F, respectively), presented a fracture surface composed of self-assembled spherical/ellipsoidal domains resulting from the spinodal decomposition of the copolymer during the cure process, indicating phase separation. This result corroborates what was observed in Fig.1A about the translucency of the samples, where sample EPE-

10 was similar to the matrix, meaning, it did not form microscopic phases as observed in the other samples.

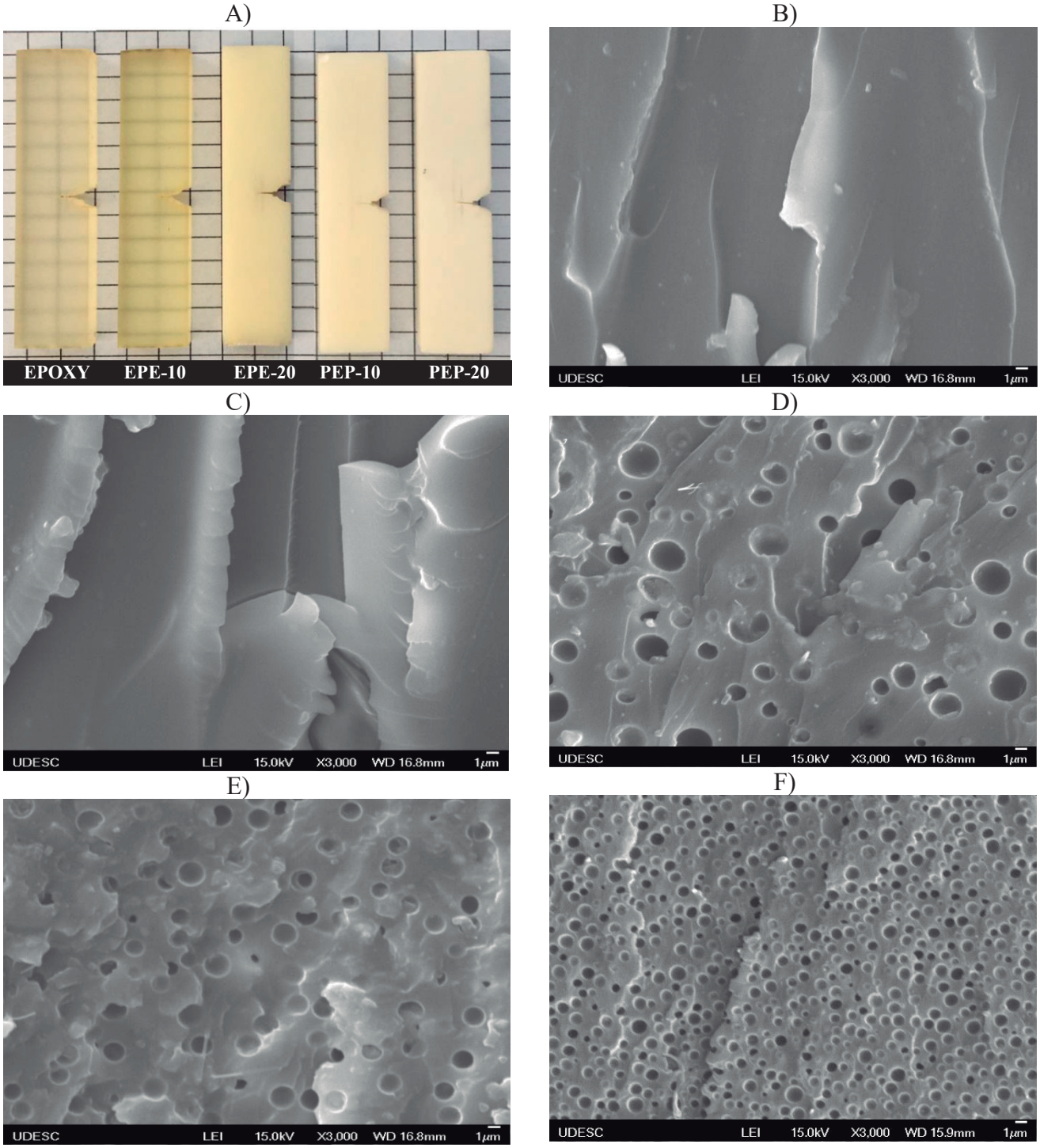

Figure 1 – Phase morphology A) Cured samples, B) Epoxy, C) EPE-10, D) EPE-20, E) PEP-10. F) PEP-20

Considering that the PPG group presents low dispersion in the matrix phase, a phase separation was observed in the samples in which the amount of copolymer was increased by 10wt. % to 20wt.%

(EPE-10) and in those with copolymer with the biggest molar mass and the PPG group at the ends of the chain (PEP-10 and PEP-20). The phase separation can be associated with the low affinity between the epoxy resin and the PPG block of the copolymer, which indicates that the favorable interaction between the PEG and the matrix was not enough to stabilize the microphases formed during curing, which resulted in a system composed of circular micelles [6,7]. Furthermore, regardless of the PEG position, if there is sufficient fraction for the PPG to form the nucleus and the PEG stays at the ends, immiscibility occurs with the epoxy phase [8].

The addition of 20 wt.% of PPG-b-PEG-b-PEG (PEP-20) in the epoxy resulted in systems with the highest fracture toughness (K_{Ic}) (Fig. 2A), increase about 10% in relation to the pure matrix. On the other hand, EPE-20 sample, which also formed copolymer micelles, decreases 8% the fracture toughness in relation to the matrix. This result is very interesting, and contradicts the literature, which states that the position of the PPG block at the end is unfavorable to toughening. [6].

Both systems with 10 wt.% triblock copolymer have similar fracture toughness as the matrix, and the K_{Ic} value of the sample without phase separation (EPE-10) is subtly lower than the sample with self-assembled spherical/ellipsoidal domains (PEP-10). Furthermore, in the samples with 20 wt.% of copolymer, the difference is much greater, with an increase of 10% of PEP-20 in relation to the EPE-20 system. Thus, probably the size of the PEG block of the PEP copolymer with a molar mass of 3300 g/mol influenced the interaction between the self-assembled micelles and the epoxy matrix, causing an improvement in the interfacial adhesion and thus resulting in more tenacious systems.

The increase in K_{Ic} for systems with copolymer with higher molar mass, separated by macrophases, was also observed by Larrañaga et al. (2007), who suggested that the presence of self-assembled spherical/ellipsoidal domains in the matrix hinders crack propagation and results in higher values of fracture toughness when compared to miscible or microphase-separated systems.

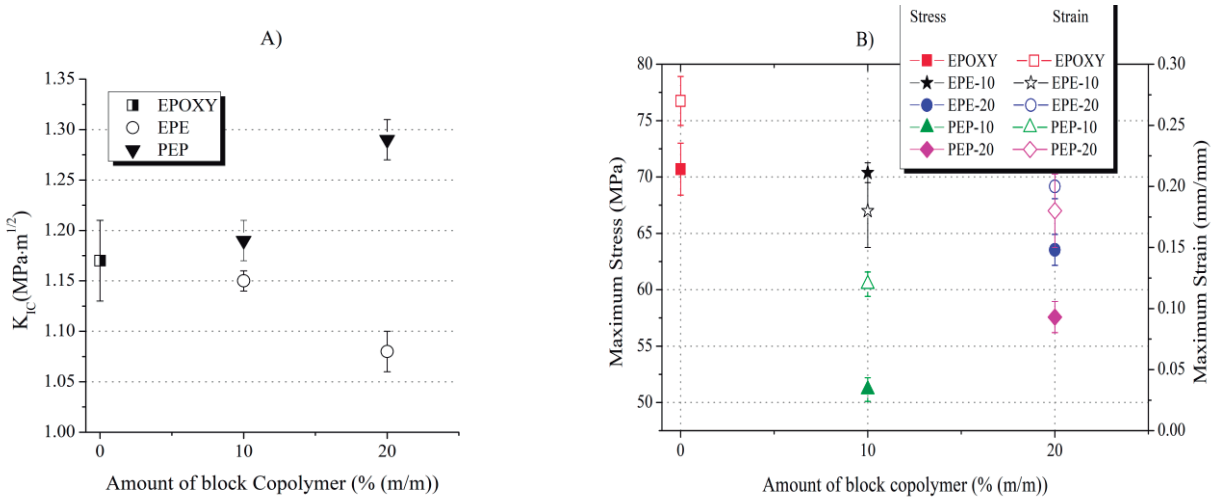

Figure 2 – Mechanical tests A) Fracture toughness and B) Tensile

For the tensile test, the samples with phase separation showed the lowest values of ultimate stress. Samples containing 10 wt.% and 20 wt.% of the PPG-b-PEG-b-PEG copolymer were reduced by 28% and 19%, respectively, compared to the epoxy. Similarly, the sample containing 20 wt.% of PEG-b-PPG-b-PEG exhibited a reduction of 10%. On the other hand, the system that did not present the copolymer self-assembled spherical/ellipsoidal domains in the microscopies obtained similar resistance to the pure matrix. A decrease in maximum supported stress is expected in systems with soft phases, as with chain mobility increases, lower is the hardness and tensile strength supported by

the specimen [9,10]. Furthermore, phase separation, could lead to internal stresses accumulation, resulting in sample early fracture [11].

Conclusions

In this work it was possible to verify the influence of the position of the PEG block and the molar mass of the triblock copolymer in the phase separation and mechanical properties of the epoxy. The samples with the higher molar mass copolymer resulted in toughness system highest than the pure epoxy. The system with the higher molar mass copolymer (3300 g/mol), and thus the longer PEG block, resulted in a tougher system than the pure matrix or the systems with the 1100 g/mol molar mass copolymer. In this way, the size of the PEG block positively influenced the fracture performance of the systems, and in systems with a longer block, even in the center of the structure (PEP-33), the adhesion of self-assembled spherical/ellipsoidal copolymer domains the matrix was more efficient, increasing the energy expended in the fracture.

Acknowledgements

Authors are grateful for the funding support from FAPESC – Brazil (PAP 2021TR854), CAPES - Brazil (PROAP/AUXPE) and Multi-User Facility infrastructure from Santa Catarina State University's Technological Sciences Center.

References

1. D. B. Dwyer et al. Journal of Analytical and Applied Pyrolysis 2021,153,104978. https://doi.org/10.1016/j.jaap.2020.104978.
2. L. R. Souza et al. Materialstoday Communications 2022, 30, 102988. https://doi.org/10.1016/j.mtcomm.2021.102988.
3. R. Pandita et al. Materialstoday: Proceedings 2020, 4. https://doi.org/10.1016/j.matpr.2020.05.398.
4. L. Wang et al. Reactive and Functional Polymers 2022, 176, 105299. https://doi.org/10.1016/j.reactfunctpolym.2022.105299.
5. M. B. Schuster; C. V. Opelt; D. Becker; L. A. F. Coelho. Polymer Composites, 2017. 39. https://doi.org/10.1002/pc.24599.
6. B. L. Silva; R. H. Bello; L. A. F. Coelho. Polymer International 2018,67. https://doi.org/10.1002/pi.5633.
7. M. Larrañaga et al. Polymer International 2007, 56. https://doi.org/10.1002/pi.2289.
8. B. L. Silva; M. B. Schuster; D. Becker. L.A.F Coelho. Materials Research, 2022. 25.20210522. https://doi.org/10.1590/1980-5373-MR-2021-0522.
9. **S.** Balakrishnan; P. R. Start; D. Raghavan; S. D. Hudson. Polymer 2006,46. https://doi.org/10.1016/j.polymer.2005.10.053.
10. B. J. Cardwell; A. F. Yee. Journal of Materials Science 1998, 33. https://doi.org/10.1023/A:1004427123388.
11. B. L. Silva, Ph. D. Thesis, University of the State of Santa Catarina (Udesc), 2018.

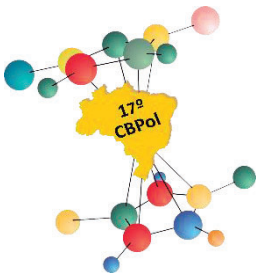

INFLUENCE OF THE INCORPORATION OF *AGAVE ANGUSTIFOLIA FIBERS VAR. MARGINATA* (FAAM) IN THE MECHANICAL AND THERMAL PROPERTIES OF THE COMPOSITE UNSATURATED POLYESTER/FAAM

Roseméri B. dos Santos da Silva[1*], Michel Picanço Oliveira[1], Jordão Cabral Moulin[1], Verônica Scarpini Candido[2]

*1 – Department of Sciences Forest and Wood, Federal University of Espírito Santo (UFES), Jerônimo Monteiro 29550-000, ES, Brazil; * rosemeribarbosadossantos@hotmail.com*

2 – Amazon Natural Resources Engineering Program, Federal University of Pará – UFPA, Belém 66075-110, Brazil

Abstract – This study focuses on the development of composites using unsaturated polyester reinforced with different weight percentages (10%, 20%, and 30%) of fibers derived from the leaf of Agave angustifolia var. marginata (FAAM). The mechanical properties of the composites were evaluated through tensile testing, while their thermal properties were analyzed using thermogravimetry (TG) and derived thermogravimetric (DTG) techniques. The results revealed that the inclusion of FAAM led to notable improvements in the modulus of elasticity, tensile strength, tenacity, and maximum strain at break of the composites. However, the incorporation of FAAM did not significantly impact the thermal properties of the composite materials. These findings contribute to the understanding of the potential applications of FAAM based composites in various engineering fields, where enhanced mechanical performance is desired without compromising thermal stability.

Keywords: *lignocellulosic fiber, agave fiber, mechanical proprieties, biocomposites.*

Introduction

Environmental concerns regarding the generation of plastic waste and the implementation of regulations have motivated the development of environmentally friendly materials with characteristics capable of meeting the new demands of modern industry [1,2]. In this context, plant fibers, known as lignocellulosic fibers (LFs), have been used as substitutes for different synthetic fibers (glass, carbon, aramid) in the production of composite materials [1,3,4]. Research indicates that FLs have several advantages over synthetic fibers such as low cost, low density, biodegradability, recyclability, non-toxic and easily available. These factors triggered the insertion of a wide variety of FLs as a reinforcing agent in polymeric composites [5-7].

The *A. angustifolia var. marginata* is a succulent plant of the botanical genus Agave, belonging to the Agavaceae family, so that the fibers extracted from its leaves present a great potential for application in the production of green composites [8]. A recent study [9] showed that with different fiber volume fractions and fiber lengths, the bending and tensile behavior of the polyester/FAAM composite was significantly improved. The maximum tensile strength was found for a fiber volume of 25% and fiber length of 20 mm. However, the thermal properties of these materials were not evaluated. From then on, this study sought to investigate in more detail the influence of the incorporation of long FAAM in polyester composites. Considering that, the research focuses on the application of in nature fibers, of long size and oriented in the polyester matrix. This study is based on the investigation for further information on the tensile and thermal properties of reinforced

composites with contents of 10%, 20% and 30% by weight of FAAM in the unsaturated polyester matrix.

Experimental

Obtaining the composites

The leaves of A. angustifolia var. marginata were collected in the southern region of the state of Espírito Santo (Alegre-ES), from plants found in garden beds. After collection, the thorns from the margins and tips of the leaves were removed and then washed with water to remove impurities from the leaf surface. For fiber extraction, the sheets were subjected to a pressing process using a two-roll manual mill. After being macerated, they were immersed in water for a period of 18 hours to facilitate the removal of unwanted parts present in the leaves. To extract the fibers, the leaves were scraped, and small bundles were manually removed and washed in running water to completely remove the mucilage. The fibers were dried in an oven with air circulation at 60°C for 3 hours, and then cut for the manufacturing step of the composites. For the preparation of the polymer composites, polyester resin (UC 2120 AC PLUS) and butanox catalyst (M-50) supplied by Redelease (Brazil) were used in the proportion of 2% of catalyst in relation to resin, as recommended by the manufacturer.
The composite samples were made in silicone molds with the addition of 10, 20 and 30% by weight of FAAM, with long and aligned fibers with about 112 mm in length, occupying the total length of the mold. The mixture of resin and catalyst was poured into the mold containing the fibers and homogenized in them, ensuring soaking and wettability. This mixture was inserted until completing the mold volume.
The specimens were prepared according to the pre-established dimensions for specimens for tensile tests according to ASTM D638 standard [10]. Then, the molds were placed in a pressure reactor at 90 Psi (Isostatic) at room temperature for at least 24 hours until the polymerization process was completed, with the reach of the specimens.

Characterization

For maximum stress analysis, the five composite samples were produced according to the standard for each fiber composition, based on ASTM 638 [10]. The samples were submitted to traction tests in a universal machine of the model DL 10,000 EMIC at room temperature, with a crossover speed of 1mm/min and load cell of 5000 N until the rupture of the specimen. The powder samples of the composites passed in the mesh sieve #40 and retained in the mesh #60 were thermally analyzed using a Setaran Thermogravimetric Analyzer, model LabSys Evo, with heating conditions from room temperature up to 800 °C and heating rate of 10 °C/min in nitrogen atmosphere.
Analysis of variance (ANOVA) was used to find distinctions between the samples with Tukey's test was applied with 5% significance.

Results and Discussion

The Fig. 1 presents the representative graphs for the properties of maximum stress strength, strain, modulus of elasticity and toughness of the composites. The Fig. 1-a indicates that with the increase of the fiber content in the composite higher values of maximum stress are obtained, which are associated with the strength of the composites when reinforced by fibers [9]. It is observed that the average strength of composites with 20% by weight of FAAM had a percentage increase of 180±9%, while composites reinforced with 30% by weight of FAAM had an increase of 293±2% compared to the pure matrix, with associated deviation (percentage variation) compared to neat polyester. It was observed that there was no significant difference between the tensile strength values of the composite

of 10% by weight of FAAM with the polymer without fiber addition. In observation to Fig. 1-b, it is noted that pure polyester exhibited higher strain values, which is related to its higher elastic deformation capacity compared to the fiber-reinforced matrix. This fact is notorious when analyzing the graph in Fig. 1-b, where, for composites, strain increased from 3.2% to 5.6% with increasing reinforcement, however, the pure matrix strained 12.0%.

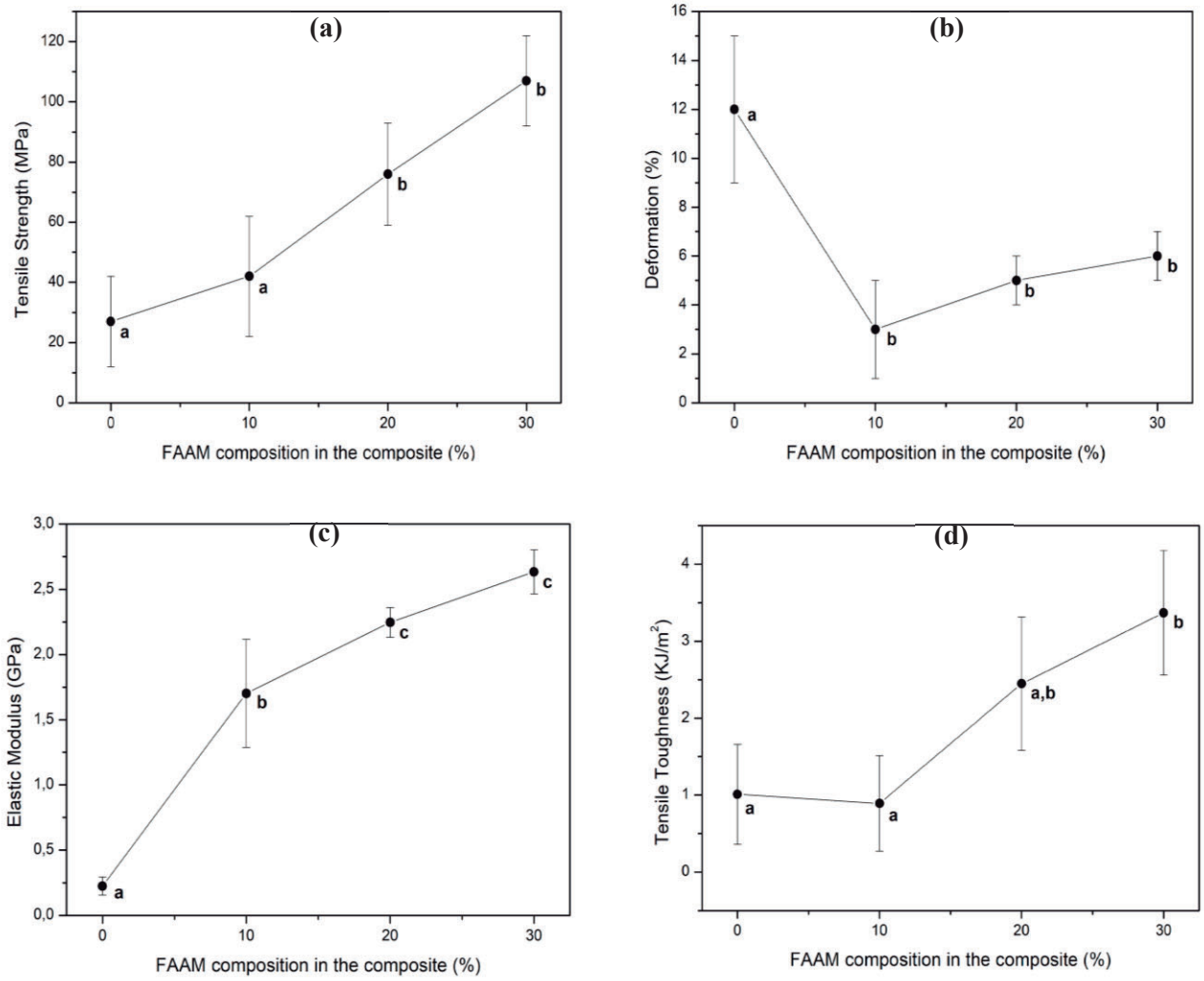

Figure 1- Variation with the percentage of FAAM (% by weight) for medium values of: (a) resistance to maximum stress, (b) deformation, (c) modulus of elasticity and (d) toughness of composites with 10, 20 and 30% fiber. The letters "a", "b" and "c" in the graphs highlight the perceptible distinctions between the analyzed groups found in the statistical analysis.
*Values followed by at least one letter between dots indicate non-significant distinctions in a 95% confidence condition ($p<0.05$).

From Fig. 1-c, it is seen that with the increase of the concentration of FAAM in the polyester matrix the greater the resistance to elastic deformation, that is, the greater the stiffness of the composite materials [11]. Statistical comparisons indicate that there was a significant difference between FAAM reinforced composites and neat polyester.
This behavior is also observed for toughness (Fig. 1-d), in which the average values of toughness increase as fiber is added, due to the increased strength of the material, but this occurs when fiber contents above 10% by weight are incorporated. It observed a percentage increase of 142±33% and 234±24% for the composition of 20 and 30% of FAAM, respectively, in relation to the polyester matrix, evidencing an increase in energy absorption until the rupture in traction of composite

materials, which is in line with other works such as Shahzad (2017) and Sathiamurthi et al. (2021) [12, 6].

The thermogravimetric analysis was performed in order to investigate the thermal stability and degradation properties of FAAM-reinforced composites with 10, 20 and 30% by weight of fiber. The Fig. 2 shows the behavior of thermal degradation for the polyester and the developed composites.

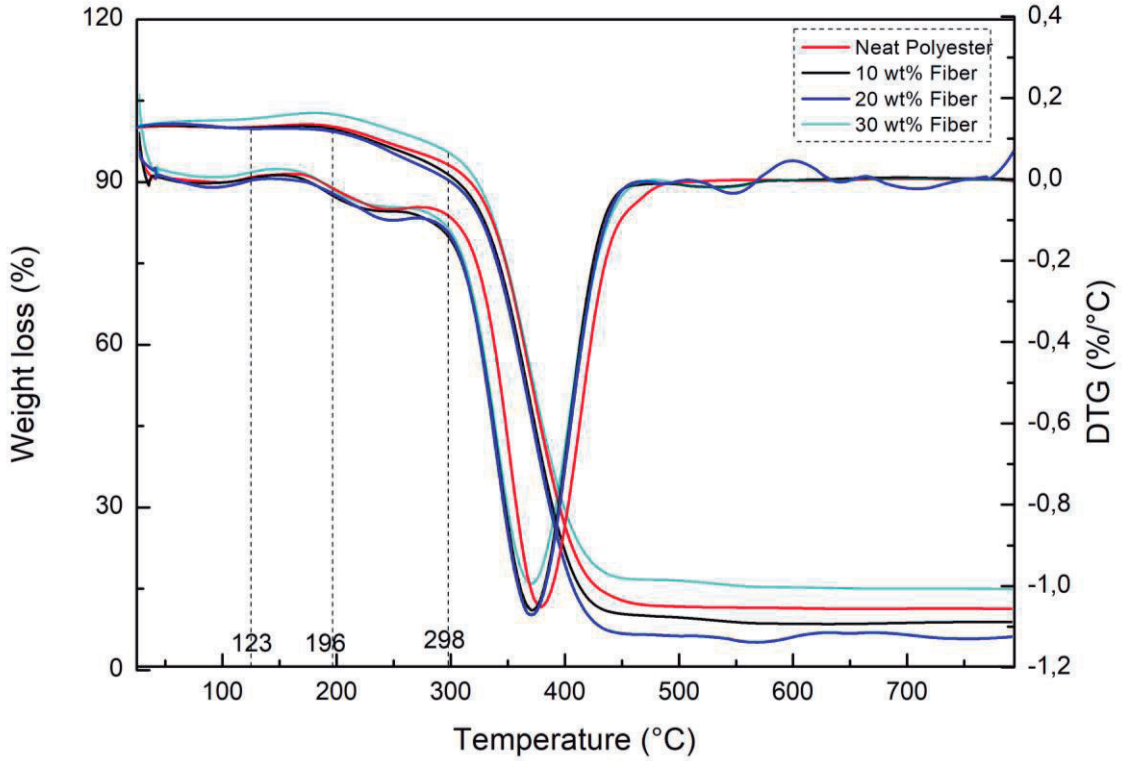

Figure 2 - TGA and DTG thermogram for polyester and composites with 10, 20 and 30% FAAM.

From the thermogravimetric curves, it is initially observed an almost imperceptible stage between 25°C to 123°C that is associated with moisture loss by evaporation [13] due to the influence of the hydrophilic character of plant fibers. The beginning of an accentuation corresponds to the thermal degradation of the polyester and composites that started at a temperature close to 196°C, becoming intense from approximately 298°C. Between 200°C and 300°C, polyester had 7.18% of loss of its mass, while composites reinforced with 10%, 20% and 30% of FAAM presented, respectively, 8.57%, 9.13% and 7.22% of initial mass loss. Thus, both polyester and composites showed good thermal stability up to approximately 200°C.

In general, the insertion of FAAM provided less thermal stability to the polymeric composites compared to the pure matrix. This behavior can be better verified by the TGA curve, in which the intense degradation of the materials was identified, at about 298°C for polyester and 295°C, 293°C and 292°C for composites reinforced with 10, 20 and 30% fiber, respectively. It is evident that the thermal property of the fiber-reinforced composite was influenced by the addition of FAAM fibers in the polyester matrix, where the peaks of maximum degradation for the composites were shifted to slightly lower temperatures [14].

Conclusions

The addition of FAAM in the unsaturated polyester matrix influenced significant improvements in the mechanical tensile strength of the composites, so that the insertion of 30% by weight of FAAM

demonstrated greater efficiency in the mechanical strength of the composites, with an increase in the percentage variation in relation to the pure matrix of 293%, resulting from the efficiency in the load transfer between the fibers and the polyester matrix. As for the thermal properties, the FAAM provided little significant variations in the stability of the composites, so that both the polyester and the composites showed a good thermal stability up to approximately 200°C. The results show that FAAM have reinforcing properties and can be applied in the manufacture of polymeric composite materials.

Acknowledgements

To FAPES and CNPQ for the financial support during the development of this research.

References

1. L. Stelea, et al. Characterisation of hemp fibres reinforced composites using thermoplastic polymers as matrices. Polymers, v. 14, ed. 3, 2022. https://doi.org/10.3390/polym14030481
2. M. V. F. Ferreira, et al. Thermogravimetric characterization of polyester matrix composites reinforced with eucalyptus fibers. Journal of Materials Research and Technology, v. 6, ed. 4, p. 396-400, 2017. https://doi.org/10.1016/j.jmrt.2017.09.002
3. M. Y. Khalid, et al. Natural fiber reinforced composites: Sustainable materials for emerging applications. Results in En-gineering, v.11, n.100263, 2021.
4. B. M. M. Gonçalves, et al. Surface Treatments of Coffee Husk Fiber Waste for Effective Incorporation into Polymer Bio-composites. Polymers, v. 13, ed. 19, 2021.
5. H. M. Nascimento, et al. Obtention and characterization of polypropylene composites reinforced with new natural fibers from Yucca aloifolia L. Composites Part B: Engineering, v. 227, n. 109414, 2021.
6. P. Sathiamurthi, et al. Fiber extraction and mechanical properties of Agave Americana/Kenaf fiber reinforced hybrid epoxy composite. Materials Today: Proceedings, v. 46(17), p. 8594-8601, 2021.
7. B. A. Praveena, et al. Study on characterization of mechanical, thermal properties, machinability and biodegradability of natural fiber reinforced polymer composites and its Applications, recent developments and future potentials: A compre-hensive review. Materials Today: Proceedings, v. xxx, 2021.
8. T. Ramakrishnan; P. S. Sampath. Investigation of Physico-Mechanical and Moisture Absorption Characteristics of Raw and Alkali Treated New Agave Angustifolia Marginata (AAM) Fiber. Materials Science (Medziagotyra), v. 24, n. 1, 2018.
9. T. Ramakrishnan, et al. Effect of Moisture Content on Mechanical Properties of AAM Natural Fiber-Reinforced Isophthalic Polyester Composites. Advances in Materials Science and Engineering, v. 2022, ID: 3533143, p.10, 2022.
10. ASTM International. Standard Test Method for Tensile Properties of Plastics Designation: D638-10. ASTM Standards, 2010.
11. J. S. Binoj; J. S. Bibin. Failure analysis of discarded Agave tequilana fiber polymer Composites. Engineering Failure Analysis, v. 95, p. 379-391, 2019.
12. A. Shahzad. 11- Mechanical properties of lignocellulosic fiber composites. Lignocellulosic Fibre and Biomass-Based Composite Materials: Processing, Properties and Applications - Woodhead Publishing Series in Composites Science and Engineering, p. 193-223, 2017.
13. M. A. O. Medeiros, et al. Síntese e caracterização de poliésteres insaturados a partir da reação do glycerol com ácido fumárico. Congresso brasileiro de Polímeros, 2009.
14. Q. Zuo, et al. Prediction and analysis of properties of ramie fiber staple yarn reinforced unsaturated polyester composite based on fiber packing density. Composites Part B: Engineering, v. 237, n. 109869, 2022. DOI: https://doi.org/10.1016/j.compositesb.2022.109869.

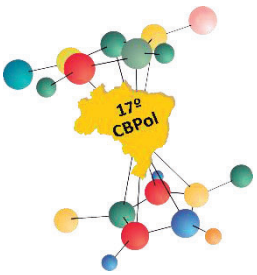

INFLUENCE OF THE MODIFICATION OF BREWER'S SPENT GRAIN FIBERS ON CONTACT ANGLE MEASUREMENTS OF THERMOPLASTIC STARCH COMPOSITES

Maria N. Castanho[1*], Karen S. do Prado[1], Jane M. F. de Paiva[1,2]

1 – Materials Science Program (PPGCM-So), Federal University of São Carlos (UFSCar), Sorocaba, SP, Brazil
**nataliacastanho92@gmail.com*
2 – Department of Production Engineering (DEP-So), Federal University of São Carlos (UFSCar), Sorocaba, SP, Brazil

Abstract - The use of starch to obtain biodegradable films of thermoplastic starch (TPS) has several advantages, such as being natural, renewable, abundant and low cost. However, generally, TPS has low values of mechanical properties and high hydrophilicity. The addition of natural fibers to TPS is an effective method to improve its performance. In this context, this work used barley bagasse fibers (BSG), industrial residue of beer production, as reinforcement in composites based on TPS, in order to obtain composites with better mechanical properties and lower hydrophilicity. Composites of TPS were developed, with incorporation of barley bagasse fibers without modification and modified by alkaline treatment and carbonization. The films were produced using a microwave appliance for heating and molded by tape casting. Contact angle measurements were then performed in the developed films. The addition of modified fibers reduced the hydrophilicity of the films.
Keywords: *Thermoplastic starch, composite, brewer's spent grain, natural fibers, wettability.*

Introduction

Starch is one of the important natural polymer materials, which has the advantages of abundant resource, low pollution-free cost, biodegradation and renewable [1]. To make it suitable for industrial applications such as packaging, starch needs to be processed in the presence of a plasticizer, with the application of heating and mechanical shear stresses, to obtain the product termed thermoplastic starch (TPS) [2]. However, TPSs have low mechanical strength and high-water sensitivity. Thus, to overcome these disadvantages, there is a need to incorporate reinforcing fillers, such as lignocellulosic fibers or nanofibers, to produce new low-cost starch biocomposites with improved properties [3]. Natural fibers are potential reinforcements that are currently in great demand due to their natural abundance and susceptibility to biodegradability, and when used as fillers or reinforcement in natural polymers, the resulting products are environmentally friendly and of improved physical properties [2].

In recent years, the use of vegetable fibers obtained from agricultural waste has received great attention due to the wide source, low price, abundant content of lignocellulose material and high added value [3]. Agricultural residues include straw, bagasse, rice husks, coffee beans and forest activity residues. Brewer's Spent Grain (BSG) is the main industrial by-product of beer production, and is generated in large quantities. Being composed basically of the insoluble solid fraction and not degraded of the barley grain [4]. The inclusion of BSG fibers in biodegradable materials based on thermoplastic starch represents a promising alternative to improve polymer performance, producing new value-added products [5].

Although natural fibers have good properties, it is common to make modifications such as alkaline treatment and fiber pyrolysis. The surface treatment by alkaline solution, alters the topology and

morphology of the fiber, by removing non-cellulosic surface compounds such as oils, waxes and impurities, allowing the best interaction with the polymer matrix [6]. And in pyrolysis, part of the organic matter is decomposed and volatilized, obtaining a porous and high carbon material [7].
Thus, the application of BSG fibers in thermoplastic starch matrix composites is an option in the development of sustainable composite materials, improving properties such as hydrophilicity of TPS.

Experimental

Preparation of BSG

The BSG supplied by Bamberg Brewery (Sorocaba-SP, Brazil) was dried, ground and sieved in sieves of 35 and 100 mesh.

Alkali treatment

The alkaline treatment in the fibers was performed based on the methodology used by [8], with adaptations. Approximately 10 grams of BSG fibers were placed in a beaker containing 200 ml of sodium hydroxide solution (5% NaOH) for 30 minutes. After this time, the fibers were washed with approximately 2 L of deionized water until reaching the pH close to that of water, and were then vacuum filtered and dried in an oven with air circulation at 50°C for 24 hours.

Biochar

The biochar was performed by the pyrolysis of the ground BSG, using muffle of the brand JUNG, model N1100, at 200, 300 and 400ºC, for 3 hours, in porcelain crucibles with lid. After reaching room temperature, it was passed through 100 mesh sieve.

Preparation of TPS/BSG composite films

Cornstarch Farmal CS3650 (Ingredion, Brazil) was used to prepare TPS films. The TPS was produced using 10 wt% cornstarch, 5 wt% glycerol (Alphatec, Brazil), and 85 wt% deionized water. For the composites, 1wt% of BSG was added.
The samples were named according to the size of the sieve used (35 and 100), treatment used to prepare the fibers: BSG (untreated fibers), BSG-T (alkaline treated fibers) and BSG-B (biochar) and fiber pyrolysis temperature (200, 300 and 400).
The method of film preparation used was defined according to our previously reported study [9]. Briefly, a microwave heating device was used, under 450 W power, with breaks for manual agitation. During the first minute, the breaks were every 20 seconds. In the sequence, the breaks were performed every 10 seconds until a gelatinized mixture with gel aspect was obtained. The films were cast by tape casting, with the device leveling blade opening at 1.2 mm. Then, the films were taken to the oven without air circulation, with a temperature of 30°C, until complete drying.

Contact Angle Measurements

Contact angle measurements were performed using a Ramé Hart goniometer, model 250 Standart, using distilled water as solvent. Measurements were performed immediately after the drop on the film surface, measurements were performed in triplicate for each sample.

Results and Discussion

In Fig 1 it is possible to observe the images and the mean values of contact angle for the TPS and the composites. The angles obtained for both the surface of the TPS films and the surfaces of the composites were less than 90°, indicating that the samples have hydrophilic characteristics.

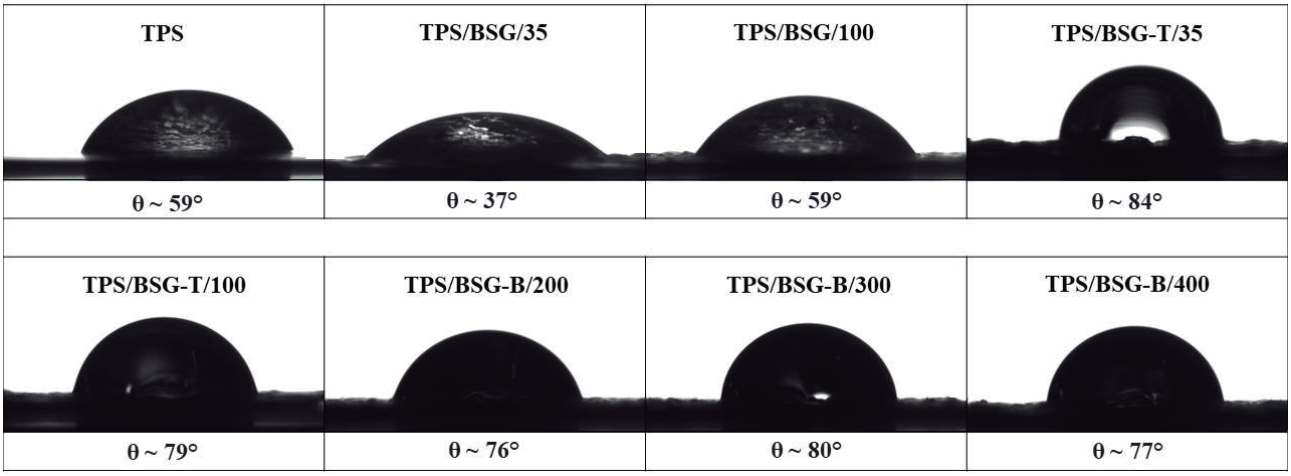

Figure 1 - Contact angle images and measurements for TPS and composites.

The TPS films presented angle value of 59°. This value is similar to those found in the literature, ranging from 30 to 59° [3, 10-12].
When untreated fibers (TPS/BSG35 and TPS/BSG100) were incorporated into the TPS, no improvement in the hydrophilic characteristics of the composites occurred. However, when treated or biochar fibers (TPS/BSG35-T, TPS/BSG100-T, TPS/BSG-B200, TPS/BSG-B300 and TPS/BSG-B400) were incorporated, there was an increase in contact angle values, as can be observed in figure 1. The addition in the values of contact angle indicate that the alkaline treatment and carbonization of the BSG fibers resulted in the reduction of wettability of the surface of the composites, making them less hydrophilic. This may be related mainly to the improvement of the chemical interaction between the fibers and the polymer matrix [12]. Therefore, the surface wettability of composites is mainly related to the degree of crosslinking between fibers and starch macromolecules [11]. These properties are also in accordance with the mechanical properties observed in a previous publication [13], where the BSG fibers treated in alkaline solution, or biochar, when added in TPS films, acted as reinforcement, increasing the values of tensile strength of the composites in relation to the TPS films without the incorporation of fibers.

Conclusions

The use of alkaline treated fibers and biochar significantly altered the contact angle values of the composites, for higher angle values, indicating that the composites became less hydrophilic. The reduction of hydrophilicity minimizes the absorption of water by the material, a characteristic that can interfere with mechanical properties in a negative way. One of the main limitations of TPS use is due to its high hydrophilicity, so the reduction of this characteristic provides greater applicability of this material.

Acknowledgements

This study was supported by the Coordination for the Improvement of Higher Education Personnel (CAPES) and CNPq (314814/2021-3). The authors acknowledge the Materials Science Program (PPGCM-So) and Bamberg Brewery for providing brewer's spent grain.

References

1. Y. Liu; R. Wu, Z. Liang; et al. Journal of Polymers and the Environment. 2023, 31, 1427. https://doi.org/10.1007/s10924-022-02709-6.
2. A. Rasheed-Adeleke; E. C. Egwim; E.R. Sadiku; et al. Molecules. 2022, 27, 7708. https://doi.org/10.3390/molecules27227708.

3. J. Zhang; F. Zou; H. Tao; et al. Industrial Crops and Products. 2023, 194, 116358. https://doi.org/10.1016/j.indcrop.2023.116358.
4. S. I. Mussatto; G. Dragone; I. C. Roberto. Journal of Cereal Science. 2006, 43, 1. https://doi.org/10.1016/j.jcs.2005.06.001.
5. A. C. Lopes; A. B. Klosowski; B. M. Carvalho; et al. International Journal of Food Science and Technology. 2022, 57, 5523. https://doi.org/10.1111/ijfs.15893.
6. A. Hasan; M. S. Rabbi; M. M. Billah. Cleaner materials. 2022, 41 100078. https://doi.org/10.1016/j.clema.2022.100078.
7. S. Li; X. Li; Q. Deng; et al. Materials and Design. 2015, 85, 54. https://doi.org/10.1016/j.matdes.2015.06.163.
8. A. De Campos; K. B. R. Teodoro; J. M. Marconcini; et al. Polímeros, 2011, 21, 217. https://doi.org/10.1590/S0104-14282011005000039.
9. M. N. Castanho; K. S. do Prado; J. M. F. de Paiva; Polymer Composites. 2022, 43, 811. https://doi.org/10.1002/pc.26412.
10. T. Chaiyaso; P. Rachtanapun; N. Thajai; et al. Scientific Reports. 2021, 11, 19945. https://doi.org/10.1038/s41598-021-99417-3.
11. P. Yin; X. Dong; W. Zhou; et al. RSC Advances. 2020, 10, 23632. https://doi.org/10.1039/d0ra04523c.
12. Q. Zhang; H. Xu; W. Lu; et al. Science of the Total Environment. 2020, 737, 139770. https://doi.org/10.1016/j.scitotenv.2020.139770.
13. M. N. Castanho; K. S. do Prado; J. M. F. de Paiva in IX Workshop de Pesquisa e Tecnologia em Ciência dos Materiais, Sorocaba, 2022, Vol. 1, 33.

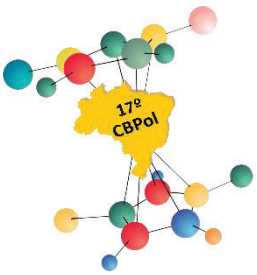

INFLUENCE OF THE MODIFICATION OF BREWER'S SPENT GRAIN FIBERS ON THE BIODEGRADABILITY OF THERMOPLASTIC STARCH COMPOSITES

Maria N. Castanho[1*], Karen S. do Prado[1], Jane M. F. de Paiva[1,2]

1 – Materials Science Program (PPGCM-So), Federal University of São Carlos (UFSCar), Sorocaba, SP, Brazil
**nataliacastanho92@gmail.com*
2 – Department of Production Engineering (DEP-So), Federal University of São Carlos (UFSCar), Sorocaba, SP, Brazil

Abstract - Environmental concerns are contributing to the growing interest in renewable materials. Among natural polymers, starch stands out due to its high biodegradability without producing toxic waste. Biodegradable polymers are those that at the end of their life cycle are degraded by the action of microorganisms. This study aimed to evaluate the biodegradability of thermoplastic starch (TPS) composite films, and brewer's spent grains (BSG) fibers modified by alkaline treatment in 5% NaOH solution and pyrolysis at 400 °C. The test was performed by mass loss analysis of film samples that were inserted into the soil and removed every 7 days, in a period of 7 weeks. The results showed that TPS composites with the addition of BSG fibers with or without alkaline treatment, had a higher biodegradation potential, making them more sensitive to attacks of microorganisms. While TPS composites with the addition of pyrolyzed BSG fibers, maintain biodegradability like TPS without fiber incorporation.
Keywords: *Thermoplastic starch, composite, brewer's spent grain, natural fibers, biodegradability.*

Introduction

Biodegradability is the term that defines the potential of organic molecules, including polymeric materials, to be broken down into smaller molecules by the action of microorganisms [1]. Biodegradable materials when released into the environment are colonized by microorganisms and decomposed into gases such as CO_2, CH_4 and N_2, water and biomass [2]. Bio-based and biodegradable materials represent an alternative to reduce the environmental impact of non-degradable polymers, with technical and economic feasibility, exhibiting a wide range of applications in various fields such as biomedical materials, cosmetics, packaging among others [3]. Thermoplastic starch is one of the biopolymers that stands out for its high biodegradability, in addition to low cost and abundance [4].

However, thermoplastic starch also has some disadvantages that restrict its applications, such as strong hydrophilic character and low mechanical properties, particularly in wet conditions [5]. To improve the physical and thermochemical properties, biopolymers are often improved for final product applications, through the development of composites, through the incorporation of natural fiber reinforcements [6]. Cellulose, hemicellulose, and lignin are the main components of natural fibers, which have properties such as high mechanical strength, low density, and toxicity, are biodegradable and low cost, and can act as reinforcement or load in TPS composites [7]. Natural fibers derived from industrial process residues can be used as reinforcement in TPS composites, such as barley bagasse (BSG).

BSG is the main industrial by-product of beer production, generated in large quantities [8], and it consists basically of the insoluble and undisturbed part of the barley grain, which are the husks and pericarp layers [9]. The inclusion of BSG fibers in TPS-based materials represents a promising

alternative to improve polymer performance and maintain its biodegradability [3]. Despite the good properties of natural fibers, it is common to use modifications such as alkali treatment and fiber pyrolysis.
The alkaline treatment of fibers is based on the surface treatment, by changing the topology and morphology of the fiber, due to the removal of superficial non-cellulosic compounds, such as oils, waxes and impurities, allowing improvement of the interaction with the polymer matrix [10]. And in pyrolysis, much of the organic matter is decomposed and volatilized, removing most of the functional groups, obtaining a porous and high carbon material [11].
Thus, this study aimed to study the influence of modifications in BSG fibers on the biodegradability of TPS composite films, through the analysis of mass loss of samples incubated in soil.

Experimental

Preparation of BSG

The BSG supplied by Bamberg Brewery (Sorocaba-SP, Brazil) was dried, ground and sieved in a 100 mesh sieve.

Alkali treatment

The alkaline treatment in the fibers was performed based on the methodology used by [12] with adaptations. Approximately 10 grams of BSG fibers were placed in a beaker containing 200 ml of sodium hydroxide solution (5% NaOH) for 30 minutes. After this time, the fibers were washed with approximately 2 L of deionized water until reaching the pH close to that of water and were then vacuum filtered and dried in an oven with air circulation at 50°C for 24 hours.

Biochar

The biochar was performed by the pyrolysis of the ground BSG, using muffle of the brand JUNG, model N1100, at 400ºC, for 3 hours, in porcelain crucibles with lid. After reaching room temperature, it was passed through 100 mesh sieve.

Preparation of TPS/BSG composite films

Cornstarch Farmal CS3650 (Ingredion, Brazil) was used to prepare TPS films. The TPS was produced using 10 wt% cornstarch, 5 wt% glycerol (Alphatec, Brazil), and 85 wt% deionized water. For the composites, 1wt% of BSG was added. The samples were named according to the treatment used to prepare the fibers: BSG (untreated fibers), BSG-T (alkaline treated fibers) and BSG-B (biochar).
The method of film preparation used was defined according to our previously reported study [13]. Briefly, a microwave heating device was used, under 450 W power, with breaks for manual agitation. During the first minute, the breaks were every 20 seconds. In the sequence, the breaks were performed every 10 seconds until a gelatinized mixture with gel aspect was obtained. The films were cast by tape casting, with the device leveling blade opening at 1.2 mm. Then, the films were taken to the oven without air circulation, with a temperature of 30°C, until complete drying.

Evaluation of biodegradability

Biodegradation tests were performed based on the method described by MARTUCCI and RUSECKAITE, 2009 [14]. Samples of films with known weight (Wi), previously dried in an oven at 105°C for 6 h. The samples were buried in moist soil. The evaluation of weight loss (WL) was performed in triplicate, removing the soil samples, and cleaning them with the aid of a brush to remove the excess soil from the sample. Subsequently, the samples were oven dried at 105ºC for 6 hours and weighed (Wf). Samples were taken from the soil every 7 days over a period of 7 weeks. The weight loss (WL) of the material was calculated using the equation 1:

$$\%WL = \frac{Wi-Wf}{Wi} \times 100 \quad (1)$$

The samples were photographed before being inserted into the soil and were also photographed every 7 days after being removed from the soil, during the period of 7 weeks, for later comparison.

Results and Discussion

At the initial stage of degradation of the films in the soil, the diffusion of water causes the effect of swelling in the films, which in turn increases the bacterial attack. According to the data, on the seventh day, the film samples showed mass loss values between 18 and 28% (Fig 1).

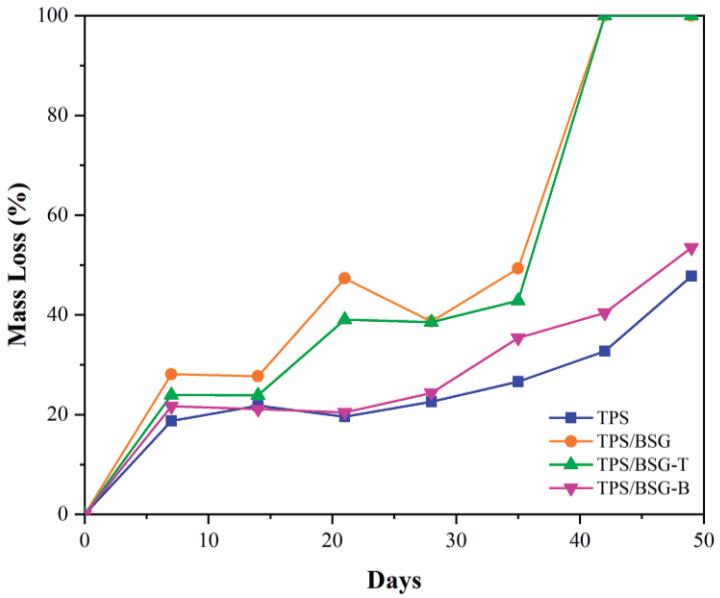

Figure 1 -Mass loss during the biodegradation test of TPS and composite films TPS, TPS/BSG, TPS/BSG-T and TPS/BSG-B.

During the test, the composites TPS/BSG and TPS/BSG-T showed similar behavior, as can be observed in Fig 1. After 21 days, the samples showed a mass loss greater than 40%, and on the 42nd day it was no longer possible to separate the fragments from the soil samples for weighing. This result is like the result obtained in a previous study [13], where TPS films were developed with 10% glycerol and untreated barley bagasse fibers with different grain sizes (35, 60 and 100 mesh) and the films also showed advanced degradation after the 21st day.

TPS and TPS/BSG-B composites also showed similar behavior. On the 28th day the samples presented mass loss between 22 and 24%. And at the end of the test the mass losses for the films TPS and TPS/BSG-B were 48 and 53%, respectively.

The accelerated degradation of the composites containing the fibers with or without alkaline treatment can be attributed to the affinity between the moisture in the fibers and the soil microbial activity. That is, composites that absorb more water increase microbial activity and, consequently, increase the rate of degradation. Studies suggest that TPS composites with higher fiber contents have greater biodegradation potential, making it more susceptible to microbial attack [15].

As for the composite TPS/BSG-B, which obtained the lowest biodegradability when compared to the composites TPS/BSG and TPS/BSG-T, may be related to the reaction at high temperature during the pyrolysis process, where much of the organic matter present in the fibers is decomposed and volatilized, removing most of the functional groups [16].

Figure 2 shows the photographs of the samples of films taken from the soil weekly.

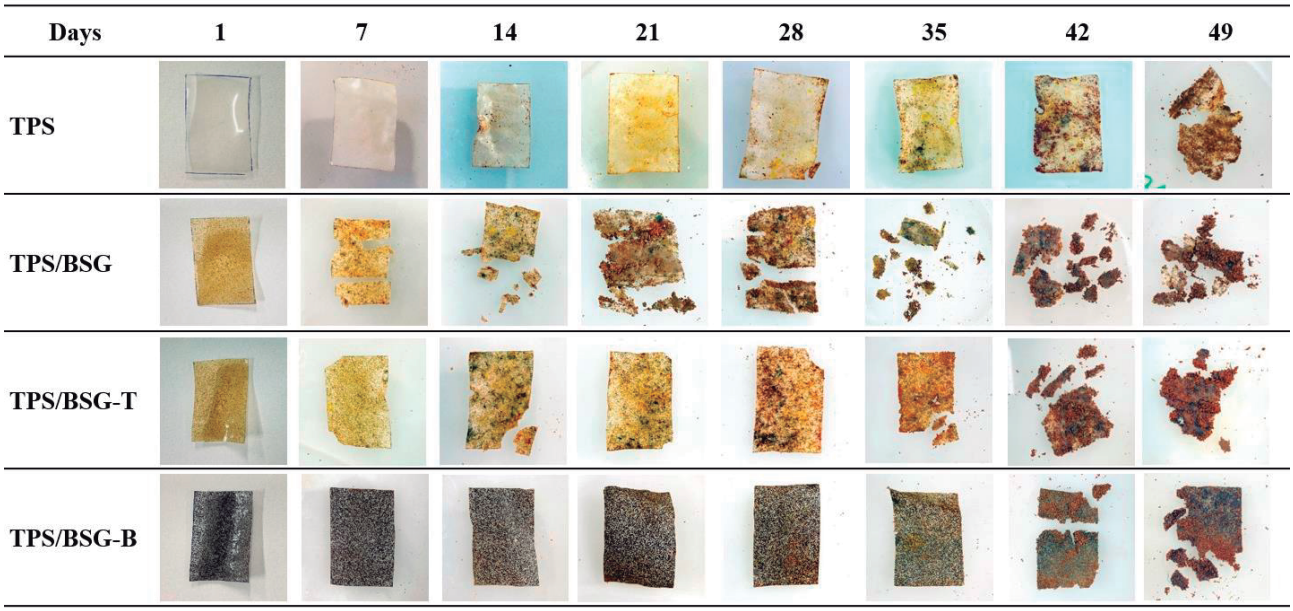

Figure 1 - Images of samples of TPS and composites TPS/BSG, TPS/BSG-T and TPS/BSG-B after removal from the soil.

Observing the TPS samples (Figure 2), only after 21 days it is possible to observe small yellowish spots, caused by the action of microorganisms and the color change of the samples, due to the formation of biofilm on the surface of the samples. After 35 days it is noted the intensification of the spots, now also present green spots, but still with the preserved shape, and without cracks. After 42 days, it is possible to observe the beginning of the degradation of the sample and the presence of cracks. And after 49 days, fragments of the samples were removed in an advanced state of degradation.

For the samples of the composites TPS/BSG and TPS/BSG-T, from the 7th day it is possible to observe the action of microorganisms, by means of yellowish and greenish stains, indicating the formation of microbial biofilm and the fracture of some samples. And after the 42nd day, it was not possible to weigh the remaining samples, because it was not possible to clean the material fragments, when trying to clean the fragments, they fragmented into smaller parts. The total degradation of the material was therefore considered.

For the TPS/BSG-B composite samples, it should be noted that there were no significant changes in the appearance of the samples until the 35th day. Only after 42 days was a significant visual change observed in the samples; at the end of the test the TPS/BSG-B samples showed mass loss of approximately 54%.

Conclusions

All the developed composites were biodegradable. The composites containing fibers with or without alkaline treatment presented higher biodegradation potential, due to higher affinity of the fibers with the soil microbiota, making them more susceptible to attacks of microorganisms. While TPS composites with addition of biochar, maintain biodegradability similar to TPS without fiber incorporation.

Acknowledgements

This study was supported by the Coordination for the Improvement of Higher Education Personnel (CAPES) and CNPq (314814/2021-3). The authors acknowledge the Materials Science Program (PPGCM-So) and Bamberg Brewery for providing brewer's spent grain.

References

1. F. Degli-Innocenti; M. Barbale; S. Chinaglia; et al. Polymer Degradation and Stability. 2022, 199, 109934. https://doi.org/10.1016/j.polymdegradstab.2022.109934.
2. H. A. Ajwa; M. A. Tabatabai. In Biol Fertil Soils 1994, 18, 175. https://doi.org/10.1007/BF00647664.
3. A. C. Lopes; A. B. Klosowski; B. M. Carvalho; et al. International Journal of Food Science and Technology. 2022, 57, 5523. https://doi.org/10.1111/ijfs.15893.
4. V. O. Bulatović; V. Mandić; D. Kučić Grgić; et al. Journal of Polymers and the Environment. 2021, 29, 492. https://doi.org/10.1007/s10924-020-01874-w.
5. L. Yu; K. Dean; L. Li. Progress in Polymer Science. 2006, 31, 576. https://doi.org/10.1016/j.progpolymsci.2006.03.002.
6. S. Baidurah. In Polymers. 2022, 14, 4928. https://doi.org/10.3390/polym14224928.
7. M. Combrzyński; A. Wójtowicz; A. Oniszczuk; et al. Materials. 2022, 15, 5061. https://doi.org/10.3390/ma15145061.
8. A. Hejna; M. Marć; D. Kowalkowska-Zedler; et al. Polymers. 2021, 13, 879. https://doi.org/10.3390/POLYM13060879.
9. M. del M. Contreras; A. Lama-Muñoz; J. M. Romero-García; et al. In Waste Biorefinery. 2021, 1, 305. https://doi.org/10.1016/B978-0-12-821879-2.00011-9.
10. A. Hasan; M. S. Rabbi; M. M. Billah. Cleaner materials. 2022, 41 100078. https://doi.org/10.1016/j.clema.2022.100078.
11. S. Li; X. Li; Q. Deng; et al. Materials and Design. 2015, 85, 54. https://doi.org/10.1016/j.matdes.2015.06.163.
12. A. De Campos; K. B. R. Teodoro; J. M. Marconcini; et al. Polímeros, 2011, 21, 217. https://doi.org/10.1590/S0104-14282011005000039.
13. M. N. Castanho; K. S. do Prado; de Paiva, J. M. F. Polymer Composites. 2022, 43, 811. https://doi.org/10.1002/pc.26412.
14. J. F. Martucci; R. A. Ruseckaite. Journal of Applied Polymer Science. 2009, 112, 2166. https://doi.org/10.1002/app.29695.
15. A. Edhirej; S. M. Sapuan; M. Jawaid; et al. Polymer Composites. 2018, 39, 1704. https://doi.org/10.1002/pc.24121.
16. Y. D. Hernandez-Charpak; T. A. Trabold; C. L. Lewis; et al. Biomass Conversion and Biorefinery, 2022, 12, 4349. https://doi.org/10.1007/s13399-022-02340-4.

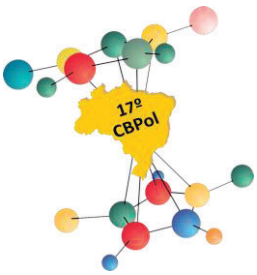

INFLUENCE OF UV SENSITIVITY ON STAB RESISTANCE OF KEVLAR® FABRICS IMPREGNATED WITH SHEAR THICKENING FLUIDS (STFs)

Thiago F. Santos[1], Caroliny M. Santos[1], Eriadna G. S. Martins[1], Marcos S. Aquino[1], Sanjay M R[2]*, Suchart Siengchin[2], J. H. O. Nascimento[3] and Ivan Medeiros[1].

1 – Textile Engineering Post Graduation Program (PPGET), Federal University of Rio Grande do Norte, Natal, Rio Grande do Norte, Brazil.

2 – Natural Composites Research Group Lab, Department of Materials and Production Engineering, The Sirindhorn International Thai-German Graduate School of Engineering (TGGS), King Mongkut's University of Technology North Bangkok (KMUTNB), Bangkok, Thailand.

3 – Postgraduate Program in Chemical Engineering, Technology Center, Federal University of Rio Grande do Norte, Av. Prof. Sen. Salgado Filho, 3000, Natal, Rio Grande do Norte, 59072-970, Brazil.

Abstract

The use of Kevlar in the field of ballistic and stabbing protection has been studied by researchers in polymeric composites for this purpose. This study presents additional knowledge on energy absorption and dissipation in Kevlar fabric structures impregnated with non-Newtonian fluid, especially targeting the improvement under impact protection that is deeply associated with STFs, as well as color change, accelerated ageing (QUV) and penetration depth (drop tower test). In addition, Fourier transforms infrared spectroscopy (FTIR), Scanning Electron Microcopy (SEM) were performed. The research shows that there was a good distribution of STF particles on the surface of the Kevlar fabric, promoting increased friction between the yarns and the interfilament, further increasing performance and, consequently, improving the mechanism of energy absorption and dissipation and, also, the effectiveness of penetration in relation to non-impregnated Kevlar® fabric. Regarding the protection efficiency against UV exposure (250–400 nm region), there was a significantly decreased compared to those non-impregnated Kevlar® woven with STFs. The FTIR analysis showed that the ageing conditions, after UV exposure, did not produce new functional groups, that is, there was no chemical modification. Finally, Kevlar fabric impregnated with STFs improved penetration depth performance with the blades independent of the blade type with up to 81% increase in resistance. This result was improved due to interactions between the STFs nanoparticles, yarns and even high-performance woven impregnated with non-Newtonian fluid.

Keywords: *Ageing process, Woven, Silane, Stab resistance, Photodegradation.*

Introduction

Kevlar® is a popular synthetic fiber widely used in the production of high-performance protective clothing, including body armor, due to its excellent strength and abrasion resistance properties. However, it is known that Kevlar® fibers are susceptible to degradation when exposed to ultraviolet (UV) radiation, which can compromise the material's overall stability and effectiveness in protecting against external threats. To address this issue, researchers have explored the use of shear thickening fluids (STFs) to enhance the stab resistance of Kevlar® fabrics. STFs are non-Newtonian fluids that exhibit a sudden increase in viscosity in response to external stress or impact, thus reducing the likelihood of penetration by sharp objects. This paper aims to investigate the influence of UV sensitivity on the stab resistance of Kevlar® fabrics impregnated with STFs, with the goal of developing more durable and reliable protective clothing for various applications [1].

Santos, Thiago, et al. 2018 studied the influence of silane coupling agent in non-Newtonian fluid, in the impact resistance and flexibility results [2]. The stab performance for Kevlar impregnated with silane agent showed results significantly higher than others fabrics non-impregnated, authors associated this results with the formation of siloxane bonds due to the coupling agent. Santos, Thiago Félix dos, et al. 2019 studied the influence of silane agent on shear thickening fluid (STF) under mechanical properties of the composite for ballistic protection. the silane compound is a type of coupling agent that can act on this adhesion because it increases the friction between the particles [3]. Santos, Santos, Thiago F, et al. 2020 studied through experimental design of 2^3 with 2 replicates and 3 central points in order to verify the penetration (drop tower) and friction force among the yarns (yarn pull out tests) in the Kevlar® woven fabrics

impregnated with NNFs to support new possibilities of development and production of new high efficiency impact protection panels [4]. Currently, it is known that fabrics impregnated with STFs seem to have excellent durability, however, the conditions of use can influence the useful life of the material. In their study Tsinas, Zois, et al. 2022, investigated some of these factors that favor the aging of STFs, as well as fabrics for impact protection applications. For, the effects of aging strongly limit the useful life cycle of these protective armor. Up to the present moment, Żurowski, Radosław, et al. 2022 studied comprehensive analyzes of STF aging products to demonstrate the limitations of the wide usage of innovative materials. Exposure to UV light gives an overview of the stability of the STFs and their shelf life, especially when the accelerated aging process was used and the aged STFs were obtained.

This work aims to analyze the influence of UV radiation in fabrics impregnated with STFs. For this, proposes to study photodegradation phenomena action in high-performance materials used for stabbing protection, consisting of Kevlar® woven impregnated with STFs. Were performed color change analysis (ΔE), accelerated ageing (QUV), penetration depth (drop tower test), Fourier transforms infrared spectroscopy (FTIR) and Scanning Electron Microcopy (SEM).

Experimental

Manufacture and Characterization of Kevlar® Woven Impregnated with STFs.

This paper shows the coupling agent silane aminopropyltrimethoxysilane (APTES), polyethylene glycol with molecular weight 400g/mol (PEG 400), ethyl alcohol (99% ethanol), and silica nanoparticles (7nm). High-performance Kevlar® woven composed of Aramid (poly ρ-phenylene terephthalamide) was used in all experiments. Kevlar® woven structure (1x1) with a density of 7 weft/cm and warp/cm, respectively, count number 3750 ± 16 dTex in both directions (weft and warp) and a grammage of 497 ± 25g/m².

Preparation of shear thickening fluids.

The preparation was carried out with 86% ethanol and 2% aqueous solution by weight, while APTES was added (3% by weight) then mixed via ultrasonication so 5 min was allowed for hydrolysis and silanol formation; then, silica nanoparticles (4% by weight) were added and mixed for 15 min (ultrasonication). Finally, polyethylene glycol (5% by weight) was added to the mixture, and the solution was mixed again for 3 min to complete the preparation of Shear Thickening Fluids.

Impregnation of Shear Thickening Fluids in Kevlar woven.

The impregnation process used was denominated as 'foularding', in which, Kevlar® woven was cut with dimensions of 8cm in length and 8cm in width. After that, Kevlar® woven was immersed in STFs for 5 min. Then, Kevlar® woven passed through two compressing rollers of foulard with the speed of 3m / min, under the pressure of 0.5 bar, to extract the STFs excess in Kevlar® woven. Finally, ethanol was subsequently removed through stinted evaporation process in the laboratory under 75 ºC for 90s condition, as well as, the final pick-up (%) of impregnated Kevlar® fabric was calculated and exhibited 25%. Thus, 3 overlapping layers were prepared for each target.

Results and Discussion

Analysis of SEM in impregnated and non-impregnated Kevlar® woven with STFs.

The SEM results showed the non-impregnated Kevlar® woven and the nanoparticles presence distribution in impregnated Kevlar® woven with STFs as shown in **FIG. 1**.

There is no presence of the STFs or distribution of nanoparticles over the surface of the non-impregnated Kevlar® woven and in the filaments of the fabric as in **FIG. 1(a)**. However, **FIG. 1(b)** displays the STFs presence and nanoparticles distribution under and between the filaments as well as still: few nanoparticles are dispersed over the surface of the fabric filaments, and there is also a higher concentration of the nanoparticles in the inter-filaments space acting mainly to increase the friction at low shear rates, favoring the performance of the impregnated Kevlar® woven.

Finally, the analysis concludes that the distribution of the nanoparticles and interaction between the nanoparticles of the STFs and filaments (Kevlar® woven) has a fundamental role in the impact strength characteristics improvement of the impregnated Kevlar® woven.

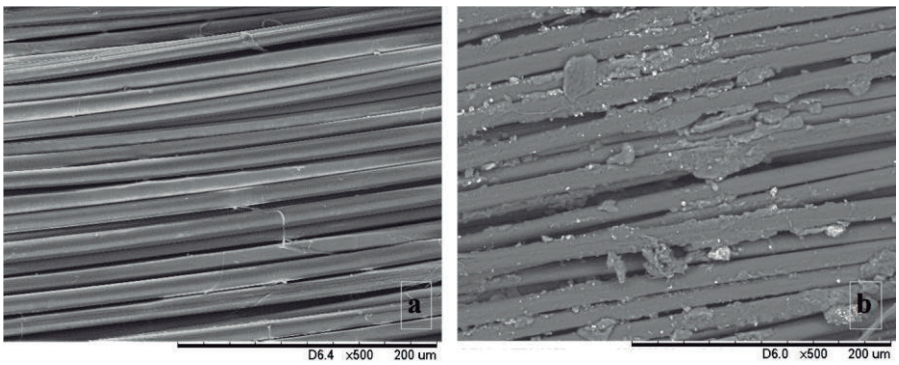

FIGURE 4. SEM of the (a) non-impregnated and (b) impregnated Kevlar woven with STFs.

Analysis of reflectance spectrophotometer in impregnated and non-impregnated Kevlar® woven with STFs.

The diffuse-reflected spectrophotometry was used for measuring the color change, in which the light reflected on the Kevlar® woven (impregnated and non-impregnated with STFs) was collected in an integration sphere and calibrated with the measurement of a pure white standard (100% reflection) and a pure black standard (zero reflection) over the entire wavelength spectrum of visible light near-ultraviolet (250–400 nm) and near-infrared (700–850 nm).
The impregnated Kevlar® woven effectively increased color change (ΔE), as observed in **FIG. 2a**; i.e. the protection efficiency against UV exposure decreased significantly compared to those non-impregnated Kevlar® woven with STFs.
The non-impregnated Kevlar® woven exhibited smaller color change (3.4) compared to the impregnated Kevlar® woven with STFs (20), that is, the impregnated Kevlar® woven showed color change about 6 times larger than the non-impregnated Kevlar® woven as shown in **FIG. 2b.** and **FIG. 1(b)**. Thus, impregnated Kevlar® woven showed larger color change about 592.9% compared to non-impregnated Kevlar® woven, meaning the impregnated Kevlar® woven with Shear Thickening Fluids were more sensitive to UV exposure corresponding to the wavelength of 340 nm (UVA). It was understood then that the impregnation of Shear Thickening Fluids in Kevlar® woven did not promote the improvement of UV protection (when increased sensitivity to UV) since the silica nanoparticles present in the Shear Thickening Fluids absorb the visible UV region 250–400 nm).

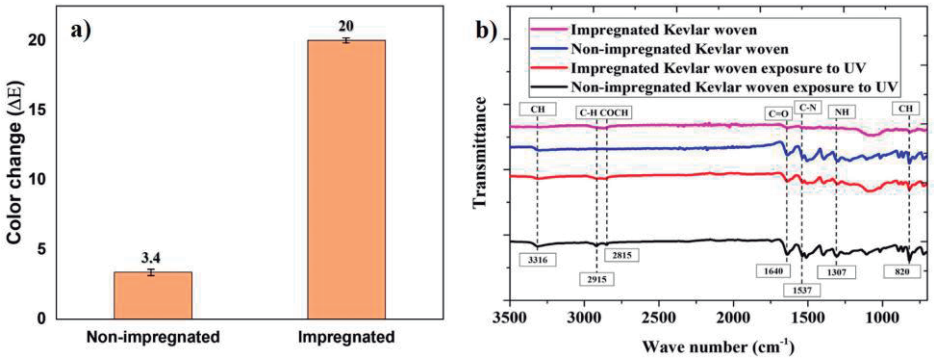

FIGURE 2. (a) Color change and (b) FTIR in impregnated and non-impregnated Kevlar woven with STFs.

Analysis of FTIR in impregnated and non-impregnated Kevlar® woven with STFs.

The changes produced by the exposure to UV were evaluated by comparing the FTIR spectra of the impregnated and non-impregnated Kevlar® woven before and after exposure to the photodegradation in QUV (during the 180 hours), as shown in **Fig. 2a**.
Surface degradation reactions can be observed in the FTIR spectra of Kevlar® woven (impregnated and non-impregnated) before and after UV exposure. Even though no evolution of a new peak is observed after UV exposure, the intensity of the amide-related peaks changes significantly (as exhibited in peak at about 1100 cm^{-1}). In this case the biggest change after accelerated photo-aging occurs at the peak of amide I. Then, the increase in the intensity of the C=O stretch peak (1100 cm^{-1}) as a consequence of the oxidation of the amide groups. The transmitting characteristics of each wave number on impregnated and non-impregnated Kevlar® woven of the FTIR spectra were related to the amide group and the aromatic ring; at 1307 cm^{-1} and 1539 cm^{-1}, a combination occurs in the flexing and stretching of N-H and C-N groups (amide III and II), respectively. As to the wavenumber at 1639 cm^{-1}, which corresponds to the stretching of the C O group (amide I), and the vibrations in the wavenumber at 2819 cm^{-1} and 2916 cm^{-1}, such measures were attributed to the stretching of the C-H groups as well as of aldehydes groups, and still; the wave number at 3317 cm^{-1}

corresponds to the N-H stretch, which occurs when the carbonyl and amine were in trans configuration. The FTIR spectrum showed that the ageing conditions, after UV exposition, did not produce new functional groups. However, the intensity of the main wave number varies after ageing (1307 cm^{-1}, 1539 cm^{-1}, 1639 cm^{-1}, 2819 cm^{-1}, 2916 cm^{-1}, 3317 cm^{-1}).

As exhibited on **TABLE 1**, the intensity of the wavenumber at 1307 cm^{-1} (amide III) increased after exposure to UV for both impregnated and non-impregnated Kevlar® woven with STFs. This indicates a partial chain scission, generating amide (N-H groups). However, the intensity of the wavenumber at 1537 cm^{-1} (amide II) decreases only for the non-impregnated Kevlar® woven with STFs, which indicates the scission in the main chain. The normalized wave number intensity attributed to 1640 cm^{-1} (amide I), decreased after exposure to UV for the non-impregnated Kevlar® woven with STFs and increased the impregnated Kevlar® woven with STFs.

The ageing promoted by UV caused scission of the C-N bonds of the macromolecule main chain, forming oxidized species. On the other hand, after the exposure to UV, it was observed an increase in the intensity of wave number at 2815 cm^{-1} for the non-impregnated Kevlar® woven and intensity decrease in this same wave number of impregnated Kevlar® woven with STFs, while the intensity of wave number at 2915 cm^{-1} – the non-impregnated Kevlar® woven with STFs – does not significantly vary and impregnated Kevlar® woven with STFs increasing the intensity of wave number after the exposed. Finally, the normalized intensity of the band corresponding to 3316 cm^{-1} (amide) does not significantly vary after the exposed ageing for non-impregnated Kevlar® woven with STFs, but there was an increase (13.6%) of wave number intensity at 3316 cm^{-1} in impregnated Kevlar® woven with STFs.

TABLE 1. The intensity of the FTIR characteristic bands of the impregnated and non-impregnated Kevlar® woven, normalized by the 820 cm^{-1} wave number, before and after exposure to UV.

Wavenumber (cm^{-1})	Normalized Intensity			
	Non-impregnated Kevlar woven		Impregnated Kevlar woven	
	Non-exposure to UV	Exposure to UV	Non-exposure to UV	Exposure to UV
1307	1.07	1.10	1.06	1.13
1537	1.14	1.10	1.08	1.15
1640	1.20	1.14	1.07	1.18
2815	1.36	1.44	1.10	1.00
2915	1.37	1.36	1.08	1.24
3316	1.34	1.35	1.08	1.25

Observations suggest that exposure of Kevlar® woven impregnated with Shear Thickening Fluids promotes larger sensitivity to UV, producing scission in the macromolecule main chain by photolysis and/or photodegradation and subsequently photo-oxidation.

Analysis of drop tower test in impregnated and non-impregnated Kevlar® woven with STFs.

the results of the (Drop Tower) test impact using 2 types of stabbings (S1 and P1) for the impregnated and non-impregnated Kevlar® woven with STFs revealing the penetration depth of each blade (P1 and S1) about impregnated and non-impregnated Kevlar® woven with STFs. It was observed that the impregnated Kevlar® woven with STFs compared to the non-impregnated Kevlar® woven with STFs exhibited significant performance in the penetration depth (independent of the blade type) as shown on **FIG. 4**. However, the geometry type of the blade's stabbings (as shown on **FIG. 3c** and **FIG. 3d**) influence the effectiveness of the penetration, once the sharpness of the cutting blade and angle of the blade stabbing tip favors the impact.

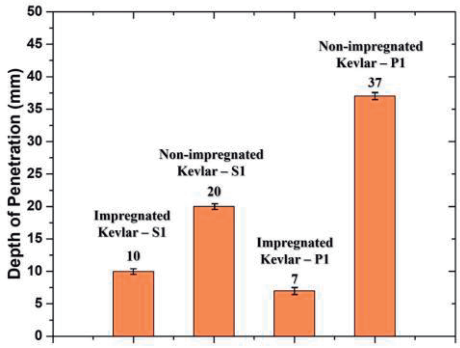

Figure. 4. Penetration depth with the blades ''S1 and P1'' in impregnated and non-impregnated Kevlar with STFs.

In addition to the impregnated Kevlar® woven with STFs exhibiting a significant reduction in penetration depth, absorption behavior, and in dissipation of residual kinetic energy of impact as shown on **FIG. 4**; it promotes a significant increase in the penetration resistance (50% for blade S1 and 81,7% for P1) when compared to the non-impregnated Kevlar® woven with STFs as listed on **FIG. 4**. Finally, the impregnated Kevlar® woven with STFs exhibited the best impact protection performance, independently of the blade types (S1 and P1), once they presented lower values of penetrations depth and consequently good absorption behavior and dissipation of residual kinetic energy from impact. This result was attributed to the increase in friction associated with the Shear Thickening Fluids because the latter ones promoted an increase in the friction between the yarns eventually resulting in the best mechanism of resistance absorption and dissipation to the impact, as well as the larger performance of impact resistance as shown on **FIG. 4.**

Conclusions

The research shows the increase in friction between the yarns and inter-filament further the performance of the STFs (Kevlar woven impregnated) and consequently improvement of the mechanism of absorption and dissipation of energy and still, the efficacy of penetration compared to non-impregnated Kevlar® woven. The aging time of STF samples corresponds to approximately three months of natural aging indoors, and the aging causes visible changes in their appearance. From the above results it is clear that these Kevlar woven impregnated with non-Newtonian fluid undergo severe degradation and accelerated photo-ageing upon exposure to UV, due to high UV Sensitivity. It has been observed that the effective effectiveness of innovative materials based on shear thickening fluids may be compromised due to the marked increase in UV sensitivity and photo-aging. The aging time of causes visible changes in appearance of Kevlar woven impregnated with STFs. Our results reveal the necessity of development of new STFs that under during exposure to UV conditions it has stability to photo-aging, deterioration, low UV sensitivity, and significantly reduce the deterioration of their properties (photo-aging stability).

Acknowledgements

This study was supported by our Lord and financed in part by Coordenação de Aperfeiçoamento de Pessoal de Nível Superior - Brazil (CAPES) - Finance Code 001. We thank our colleagues at the Textile Quality Control Laboratory – LABCTEX and Textile Engineering Post Graduate Program - PPgET at the Federal University of Rio Grande do Norte.

References

[1] T. Santos, C. Santos, M. Aquino, S. Mavinkere Rangappa, S. Siengchin, J.H.O. Nascimento, I. Medeiros, Effects of UV sensitivity and accelerated photo-aging on stab resistance of ρ-aramid fabrics impregnated with shear thickening fluids (STFs), Heliyon. 9 (2023) e15020. https://doi.org/10.1016/J.HELIYON.2023.E15020.

[2] T.F. Santos, C.M. Santos, R.T. Fonseca, K.M. Melo, M.S. Aquino, F.R. Oliveira, J.I. Medeiros, Experimental analysis of the impact protection properties for Kevlar® fabrics under different orientation layers and non-Newtonian fluid compositions, J. Compos. Mater. (2020). https://doi.org/10.1177/0021998320916231.

[3] T.F. Santos, C.M.S. Santos, M.S. Aquino, D. Ionesi, J.I. Medeiros, Influence of silane coupling agent on shear thickening fluids (STF) for personal protection, J. Mater. Res. Technol. (2019). https://doi.org/10.1016/j.jmrt.2019.07.013.

[4] T.F. Santos, C.M. Santos, M.S. Aquino, F.R. Oliveira, J.I. Medeiros, Statistical study of performance properties to impact of Kevlar® woven impregnated with Non-Newtonian Fluid (NNF), J. Mater. Res. Technol. 9 (2020) 3330–3339. https://doi.org/10.1016/j.jmrt.2020.01.027.

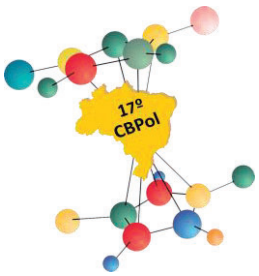

LUFFA CYLINDRICA GRAFTED WITH POLYETHYLENEIMINE: A POTENTIAL ADSORBENT TO TREAT POST-COVID-19 WASTEWATER

Juliê S. da Costa[1]*, Débora R. S. dos Santos[1] and André R. Fajardo[1]

1 – Laboratório de Tecnologia e Desenvolvimento de Compósitos e Materiais Poliméricos (LaCoPol), Centro de Ciências Químicas, Farmacêuticas e de Alimentos, Universidade Federal de Pelotas (UFPel), Pelotas, RS, Brazil
ju_scosta@yahoo.com

Abstract – The use of natural adsorbents to remove emerging contaminants from water has grown in scientific and non-scientific areas; however, depending on the characteristics of these contaminants, the efficiency of these materials is limited. In the present work, polyethyleneimine (PEI), a synthetic polymer, was grafted onto the fibers of *Luffa Cylindrica* (LF), a natural sponge, as a strategy to increase its capacity to adsorb drugs used during the Covid-19 pandemic, such as ampicillin (AMP) and nitazoxanide (NIT). Characterization analyses demonstrated that the physical-chemical and morphological properties of LF changed after PEI grafting (LF-g-PEI). Experimentally, it was observed that the grafted LF allows enhancing the AMP adsorption by 30% and NIT by 36% compared to raw LF. Based on these finds, LF grafted with PEI can be ranked as a prominent adsorbent capable of treating water contaminated by drugs used during Covid-19.

Keywords: *Adsorption, sponge gourd, emerging contaminants, pharmaceuticals, water treatment.*

Introduction

In March 2020, the World Health Organization (WHO) declared a global pandemic due to the potentially lethal effects caused by the new coronavirus (Covid-19) [1]. Since then, there has been an increase in the production and consumption of drugs to deal with the consequences caused by the virus, diagnosing the virus, and even mitigating or preventing contamination [2]. Higher drug consumption resulted in a higher volume of discarded pharmaceutical waste [3]. Among the many drugs used during the Covid-19 pandemic, there is ampicillin (AMP), which is an antibiotic widely used to treat bacterial infections that affect humans and animals, such as bacteria that can reach the respiratory system, the main organ affected by the Covid-19 virus [2]. Drugs with antiparasitic properties, such as nitazoxanide (NIT), have also been used. This drug has high antiviral activity and is used in the treatment of protozoa and various types of helminths, and various viral infections too [4]. The hydrophobic nature of some drugs limits their removal by conventional treatment plants. To solve this issue, the adsorption technique has been widely applied to remove this class of contaminants. Among the various adsorbent materials used, those developed from agricultural biomass products are a great adsorbent alternative because they are bioavailable and renewable [5]. Luffa Cylindrica (LF) is an example of this type of biomass. LF is a subtropical plant that due to its ecological, structural, and morphological characteristics, has attracted attention for applications in adsorption. However, it has a hydrophilic nature, which limits its ability to adsorb contaminants with a hydrophobic nature [6].

Aiming at the development of a potentially applicable adsorbent in the removal of AMP and NIT drugs from post-Covid-19 wastewater, the present work proposed combining the structural and functional characteristics of LF with polyethyleneimine (PEI). PEI is a synthetic polymer that has

several primary, secondary, and tertiary amine groups in its structure [7]. This polymer was grafted onto LF using Glutaraldehyde (Glut) as a crosslinking agent. It is expected that the amine groups from PEI make it possible to increase the adsorbent properties of LF concerning AMP and NIT drugs [8]. To evaluate this hypothesis, a series of batch adsorption studies were carried out.

Experimental

Grafting of PEI onto LF: Firstly, the raw LF sponge was cut into small pieces (cubic shape, 1 cm^3), thoroughly washed with an ethanol/H_2O solution (70:30 v/v) three times, and oven-dried at 50 °C for 24 h. The clean LF (1.30 g) was added to a beaker filled with distilled water (200 mL) and kept under vigorous stirring. A second solution was prepared, where 0.65 g of PEI was solubilized in 65 mL of water. The PEI solution was added by drop to the LF dispersed solution. The reaction mixture was stirred at 50 °C for 5 h. Then, 306 µL of glutaraldehyde (Glut) was added to the reaction mixture and kept under stirring at room temperature (~20 ºC) for 2 h. Afterward, the PEI grafted sponge (LF-g-PEI) was recovered, washed with distilled, and oven-dried at 50 °C for 24 h.
Characterization: The samples LF and LF-g-PEI samples were characterized by Fourier transform infrared spectroscopy (FTIR), thermogravimetric analysis (TGA), and scanning electron microscopy (SEM).
Adsorption studies: Batch experiments were performed to evaluate the ability of the prepared sponges to adsorb AMP or NIT from the aqueous medium. Specific amounts of LF or LF-g-PEI were added to Erlenmeyer flasks filled with AMP or NIT aqueous solutions (30 mL) at fixed initial concentrations (C_0) and pH values. After 3 h, the concentration of these solutions was analyzed again by UV-Vis spectroscopy.

Results and Discussion

FTIR analysis was used to characterize the chemical composition of LF and LF-g-PEI sponges and confirm the grafting of PEI onto LF. As seen in Fig. 1, the spectrum obtained for LF exhibited characteristic bands ascribed to its major components (i.e., cellulose and lignin). The broadband centered at 3447 cm^{-1} is attributed to the O–H stretching (–OH groups) of cellulose and lignin, while bands at 2925 and 2855 cm^{-1} are attributed to the C–H stretching of CH_x groups of cellulose [6]. Bands in the range 1650–1550 cm^{-1} are due to the combination of C=O stretching and C=C aromatic stretching of the lignin moiety [9]. The lignocellulosic nature of LF is also denoted by the presence of two bands at 1419 and 1254 cm^{-1}, attributable to the C–H stretching of $–CH_3$ groups and C–O stretching of $–OCH_3$ groups present in the lignin structure. The band at 1050 cm^{-1} is due to C–O–C stretching of pyranose rings, typically observed for polysaccharides like cellulose [10]. In the branched PEI spectrum, broadband related to the overlapping of N–H bond stretches of secondary and primary amines was observed between 3559 and 3104 cm^{-1}. The bands observed at 1655 and 1601 cm^{-1} are characteristic of the bending of N–H bonds of primary and secondary amines, respectively [11].

The spectrum obtained for LF-g-PEI showed the characteristic bands of their precursor materials and some new bands, which confirm PEI grafting on the LF backbone. A band at 3385 cm^{-1} is due to the overlapping stretching of O–H bonds from LF and N–H bonds from PEI [8]. Also, there is an increase in the intensity of the bands referring to the stretching of the C–H bonds of the CH_x groups (2925 and 2855 cm^{-1}) and the appearance of a new band around 800 cm^{-1} referring to the bending of the C–H bonds [12]. The Schiff base structure, denoted by the C=N bond, was confirmed by the observance of a new band at 1642 cm^{-1}. The appearance of this bond is due to the grafting of the amino group of PEI with the aldehyde group of Glut. The flexion band of the N–H bond of PEI was shifted to a lower wavelength (1567 cm^{-1}) after grafting it onto the cellulose skeleton of the LF, and the band at 1163 cm-1 referring to the stretching of the C–N bond of PEI [11]. Therefore, the FTIR analysis indicates the grafting of the PEI onto the LF using Glut as a grafting agent.

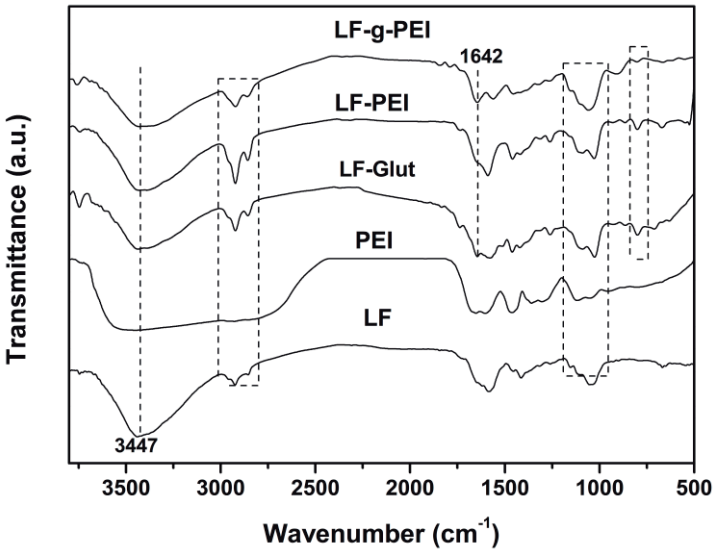

Figure 1: FTIR spectra of LF, PEI, LF-Glut, LF-PEI, and LF-g-PEI.

The TGA/DTGA curves for the LF and LF-g-PEI samples are shown in Fig. 2a and 2b. As can be seen, LF and LF-g-PEI samples exhibited three weight-loss stages within the temperature range of 30–500 °C. All samples showed a weight loss of 5% in the first stage (30 to 100 °C) due to the evaporation of free water molecules. The second stage of LF (from 230 to 300 °C) was attributed to the thermal depolymerization of its hemicellulose moieties. The third stage (from 320 to 400 °C) of LF is related to the depolymerization of cellulose [6]. The LF-g-PEI sponge showed TGA/DTGA curves similar to those obtained for LF; however, PEI grafting on the LF backbone increased the temperature ranges associated with the thermal degradation of the LF structure. These data indicate that PEI grafting onto the LF skeleton occurred and resulted in fibers with higher thermal stability. The increase in the thermal stability of the fibers is related to the new chemical bonds that were formed during the grafting process with Glut, which is a crosslinker known to increase thermal stability [11].

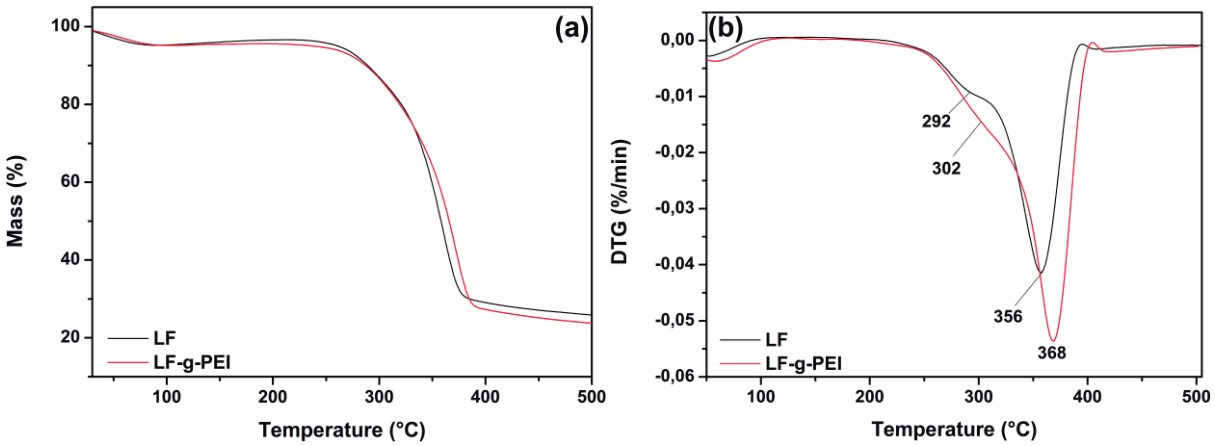

Figure 2: (a) TGA and (b) DTG curves of LF and LF-g-PEI.

Images obtained by SEM for LF (Figs. 3a-b) show the surface of fibers is rough and dense without porosity [6]. After the grafting reaction (Figs. 3c-d) the surface of LF-g-PEI fibers shows dendritic wrinkles; however, this surface remains dense and without porosity [12]. Furthermore, it can be said that the PEI grafting process on the LF skeleton occurred uniformly, as the morphology described above can be observed in the entire length of the analyzed fibers [11].

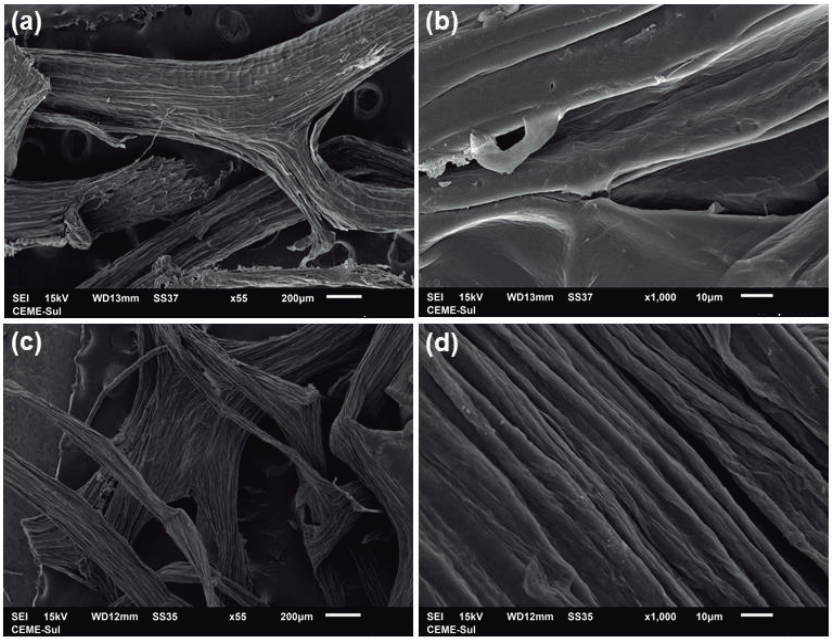

Figure 3: Images obtained by SEM from LF (a) x55 and (b) x1000 and LF-g-PEI (c) x55 and (d) x1000.

In Fig. 4 it is observed that the adsorption kinetic behavior for AMP and NIT is similar. Overall, the adsorption capacity (q_t) values computed for the adsorption of both drugs on LF and LF-g-PEI increased as the contact time goes on. Until 10 min of contact, the adsorption process runs fast due to the excess of adsorption sites available on the adsorbents. These sites are occupied over time, and the adsorption kinetics slowed down until reaching the equilibrium condition. Herein, adsorption equilibrium was reached after 60 min of contact between the drug solutions and the modified material (LF-g-PEI). The maximum adsorption capacity of LF-g-PEI was 11.46 mg/g for AMP removal and 29.59 mg/g for NIT removal. The grafting of PEI resulted in a material, LF-g-PEI, with an adsorption capacity 30% higher in AMP removal and 36% higher in NIT removal, when compared to the adsorption capacity of LF. Therefore, it can be said that the insertion of PEI in the LF structure played a crucial role in improving the adsorption performance of the material, considering that LF-g-PEI has a greater number of active sites.

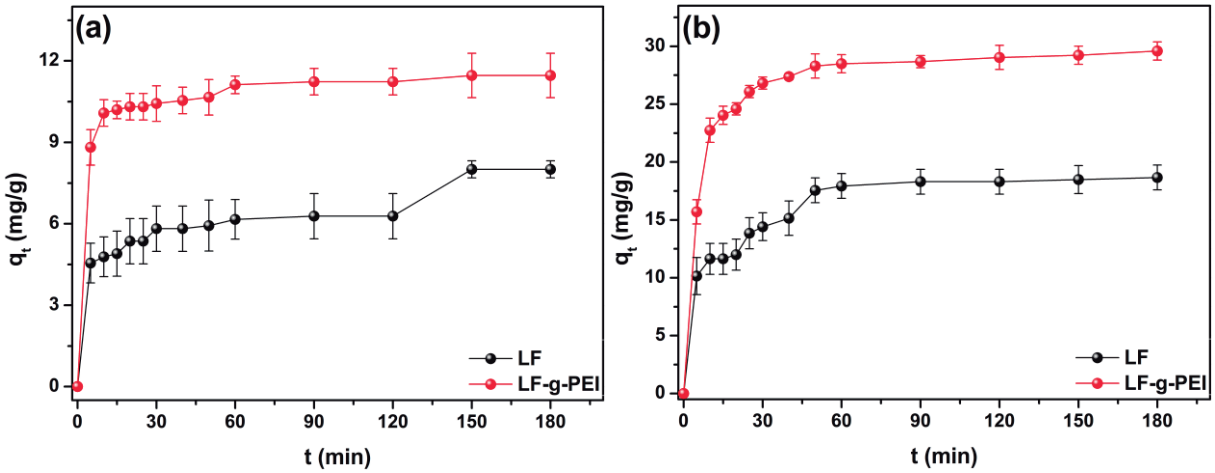

Figure 4: Adsorption capacity for (a) AMP and (b) NIT on LF and LF-g-PEI as a function of the contact time.

Conclusions

In the present work, it was possible to conclude that a simple and effective modification of the LF with PEI was performed, aiming to improve the adsorption capacity of two emerging contaminants (AMP and NIT). The modification of the LF was carried out by a grafting reaction with PEI using Glut as a cross-linking agent. Until now, grafting has been confirmed by FTIR, TGA, and SEM techniques. The characterization of LF-g-PEI revealed that grafting, which changed its chemical composition also changed its thermal stability and morphology. Furthermore, the adsorption experiments demonstrated that PEI grafting significantly increased the adsorption capacity of LF-g-PEI compared to LF and that it can adsorb AMP and NIT. Together, these results indicated that high adsorption capacities are achieved using minimum dosages of the modified adsorbent (30 mg) and mild experimental conditions.

References

1. Kumari, M., Kumar, A., 2021. Sci. Total Environ. 778, 146303. https://doi.org/10.1016/j.scitotenv.2021.146303
2. Al-Musawi, T.J., Mengelizadeh, N., Taghavi, M., Mohebi, S., Balarak, D., 2021. Biomass Convers. Biorefinery. https://doi.org/10.1007/s13399-021-01962-4
3. Pashaei, R., Dzingelevičienė, R., Bradauskaitė, A., Lajevardipour, A., Mlynska-Szultka, M., Dzingelevičius, N., Raugelė, S., Razbadauskas, A., Abbasi, S., Rees, R.M., Buszewski, B., 2022. Water 14, 3082. https://doi.org/10.3390/w14193082
4. Al-kuraishy, H.M., Al-Gareeb, A.I., Elekhnawy, E., Batiha, G.E.-S., 2022. Mol. Biol. Rep. 49, 11169–11176. https://doi.org/10.1007/s11033-022-07822-2
5. de Gisi, S., Lofrano, G., Grassi, M., Notarnicola, M., 2016 Sustainable Materials and Technologies, 9, 10–40. https://doi.org/10.1016/j.susmat.2016.06.002
6. Khadir, A., Negarestani, M., Mollahosseini, A., 2020. J. Environ. Chem. Eng. 8, 103734. https://doi.org/10.1016/j.jece.2020.103734
7. Maher, S., Smith, L.A., El-Khoury, C.A., Kalil, H., Sossey-Alaoui, K., Bayachou, M., 2023. Molecules 28, 1612. https://doi.org/10.3390/molecules28041612
8. Guo, D.-M., An, Q.-D., Xiao, Z.-Y., Zhai, S.-R., Shi, Z., 2017. RSC Adv. 7, 54039–54052. https://doi.org/10.1039/C7RA09940A
9. Ighalo, J.O., Adeniyi, A.G., Eletta, O.A.A., Ojetimi, N.I., Ajala, O.J., 2020. Sustain. Water Resour. Manag. 6, 1–11. https://doi.org/10.1007/s40899-020-00485-6
10. Mohana Krishnudu, D., Sreeramulu, D., Venkateshwar Reddy, P., 2019. Int. J. Integr. Eng. 11, 290–298. https://doi.org/10.30880/ijie.2019.11.01.029
11. Zhang, J., Li, Y., Dai, Y., Lin, T., Shao, H., Liu, Y., Liu, X., 2023. Chem. Eng. J. 456, 140995. https://doi.org/10.1016/j.cej.2022.140995
12. Chen, X., Liu, L., Luo, Z., Shen, J., Ni, Q., Yao, J., 2018. React. Funct. Polym. 125, 77–83. https://doi.org/10.1016/j.reactfunctpolym.2018.02.009

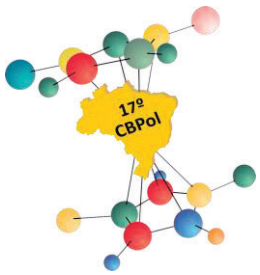

MAGNESIUM POWDER REINFORCED CASTOR OIL FOAMS: PHYSICAL AND MORPHOLOGY ANALYSES

Guilherme R. Santana[1], Daniella R. Mulinari[1] and Monique O. T. da Conceição[1]*

1 – Department of Mechanical and Energy, Resende-RJ, State University of Rio de Janeiro (UERJ), Resende, RJ, Brazil

guilherme.rodrigues@discentes.fat.uerj.br; monique.osorio@fat.uerj.br.

Abstract - Currently, studies on composites have significantly increased, which is justified by the combinations that can be made between a polymer and a reinforcement. Polyurethane (PU) foam has been used for various applications such as medical science, automobiles, coatings, adhesives, sealants, paints, textiles, marine industries, wood composites, and apparel [1]. The addition of materials such as fibers, metals, and waste, among others, to pure PU often provides an improvement in properties, enabling the PU foam to be used in different applications. In this study, polyurethane (PU) foams were synthesized from castor oil-based polyol and methylene diphenyl diisocyanate (MDI) with a ratio of 1:1, reinforced with the 5 and 10 wt.% magnesium (Mg) as the metallic reinforcement coming from a machining process waste. The effect of Mg on PU/Mg foam composites was evaluated on morphology, density, and wettability. As a result, the hydrophobicity of the composite increased compared to pure PU, and the density varied due to the low density of magnesium. The results showed that the composite content of 10 wt.% of Mg has a lower density and higher contact angle, compared to the other samples.

Keywords: *Magnesium residue, Castor oil based Polyurethane, Composite, Morphology*

Introduction

PU has been highlighted as a very versatile material compared to other polymers, with properties altered by the amount of isocyanate and polyol added to the mixture. Characteristics such as flexibility and hardness come from the isocyanate due to its short chains that promote more compact segments. In contrast, polyol has the particularity of generating long segments that consequently present more flexible chains [1].

Reinforced polyurethane has been widely used to construct, repair, reinforce, and protect civil engineering infrastructures [2]. With these applications comes the need to study these composite materials, to verify the properties arising from the added reinforcement and thus determine the feasibility of use in these areas. An example of studies already carried out was particulate aluminum, in which increased density and thermal stability compared to pure polyurethane foam were observed [3].

Among reinforcements, magnesium can be highlighted, because it is the eighth most present element in the Earth's crust, representing 2.5% of the material available on the entire surface [4]. Properties such as low density (1.74 g/cm^3) and corrosion resistance are characteristic features of this element compared to aluminum, for example [5]. Also, it presents a market value lower than other materials and significant characteristics for various applications. An example of these properties is its ability to remain stable due to the formation of an oxide layer produced at normal temperatures [6].

An application of PU reinforced with Mg is in the area of bone tissue engineering [6]. Classified as a biomaterial, magnesium presents biocompatibility, and its degradation is non-toxic to the human body. The idea of the study was to develop a coating composed of magnesium and polyurethane to mitigate the wear process of the titanium surface through corrosion and to increase the adhesive strength between the surface of the orthopedic prosthesis and the substrate [7]. It can be affirmed that the study of the physical and morphological properties of the composite with magnesium reinforcement is of great value to promote further studies on magnesium. In this context, the aim of this work was to study the addition of Mg as reinforcement on PU foam.

Experimental

Materials

Magnesium powder (Mg) was obtained as waste from a machining process. Polyurethane company (Minas Gerais, Brazil) supplied the polyol (Biopol L40ACX, 796 mg KOH g^{-1}), derivative from castor oil, and isocyanate (Biopol p-MDI, 4,4-diphenylmethane diisocyanate, solvent-free, and average %NCO equal to 30–32).

Polyurethane foams and composites

Samples of neat PU, PU+5%Mg, and PU+10%Mg were produced. The polyurethane foams were manufactured by mixing polyol and isocyanate (prepolymer) in a mass ratio of 1:1. The mixture of the reagents was done manually at room temperature for 50s, the temperature reached in the polymerization process was around 55 °C because it was an exothermic reaction. To produce the composites, the waste magnesium powder (5 and 10 wt.%) was mixed to the polyol for 2 min and then added to the isocyanate, by following the procedure above. After 24 h, the foam was removed from the molds.

Characterization

Density

The materials specimen's dimensions (10 × 10 × 10 mm^3) were cut and weighed to analyze the apparent density. Densities were determined, by dividing the weight of the specimens by the calculated volume. The values presented correspond to the average density determined for five samples of each material.

Morphology

The PU and its composites foams morphology was examined by Optical microscopy (OM) and scanning electron microscopy (SEM). A BTK B100 (DIGILAB) metallographic microscope was used to observe the foam's surface. The analysis of foam's morphology and distribution of cell sizes was conducted by examining cellular structure images captured with Hitachi TM3000 scanning electron microscopy. The observations were carried out under high-vacuum conditions and at an accelerating voltage of 5 kV.

Contact angle

A contact angle goniometer Ramé-Hart (300-F1) measured the surface hydrophobicity of PU foams and their composites, using the DROP image-standard software. Therefore, 5 µl droplets of the water

solution were deposited on the surface of each composite and PU. The average of five measurements was evaluated.

Results and Discussion

Fig. 1 shows the representation of the samples in 3D and the images collected from the optical microscope and contact angle. The addition of Mg in the PU matrix significantly reduced the pore size compared to the neat PU and, consequently, increased the number of pores per area, as shown in the OM column (Fig. 1). The particles of Mg can act as a nucleating agent for the formation of pores, and with the nucleation of a greater number of cells occurring at the same time, the availability of gas decreases for cell growth, causing the formation of smaller pores [8]. In Figure 1.c., the results of the contact angle for all samples are shown. The Pu+10%Mg exhibited an 18% increase in the contact angle when compared to neat PU. This result shows that addition of Mg increases hydrophobicity of composite.

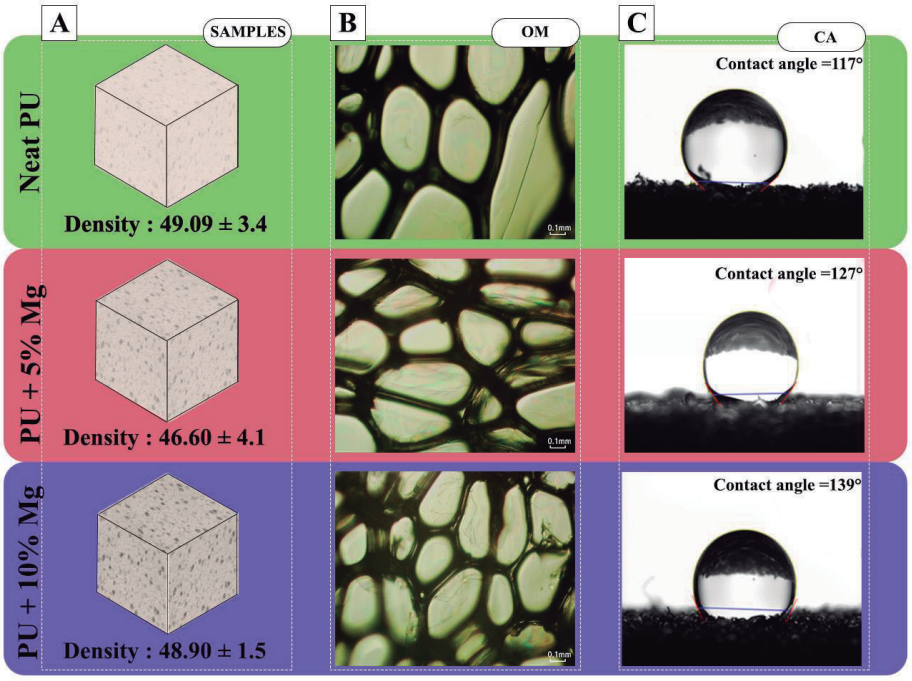

Figure 1. Schematic representation of pure PU and composites: (a) 3-D samples representation, (b) OM images at 40x magnification, (c) contact angle (CA) images.

Figure 2 shows the SEM images of the PU+5%Mg and PU+10%Mg samples, revealing both open and closed cells. As the amount of Mg added to the foam increased, the cell size decreased, leading to a reduction in density [8]. In Figure 2c, the cell size of the Pu+10%Mg sample is highlighted, indicating a decrease compared to the PU+5%Mg sample. This observation is consistent with the results obtained from the contact angle measurements, which showed a higher contact angle for the PU+10%Mg sample compared to the PU+5%Mg sample. The decrease in hydrophobicity can be attributed to the tendency of pore size reduction caused by the interaction between the polymeric chains and the magnesium reinforcement [8], resulting in smaller pore sizes as the amount of pores increases

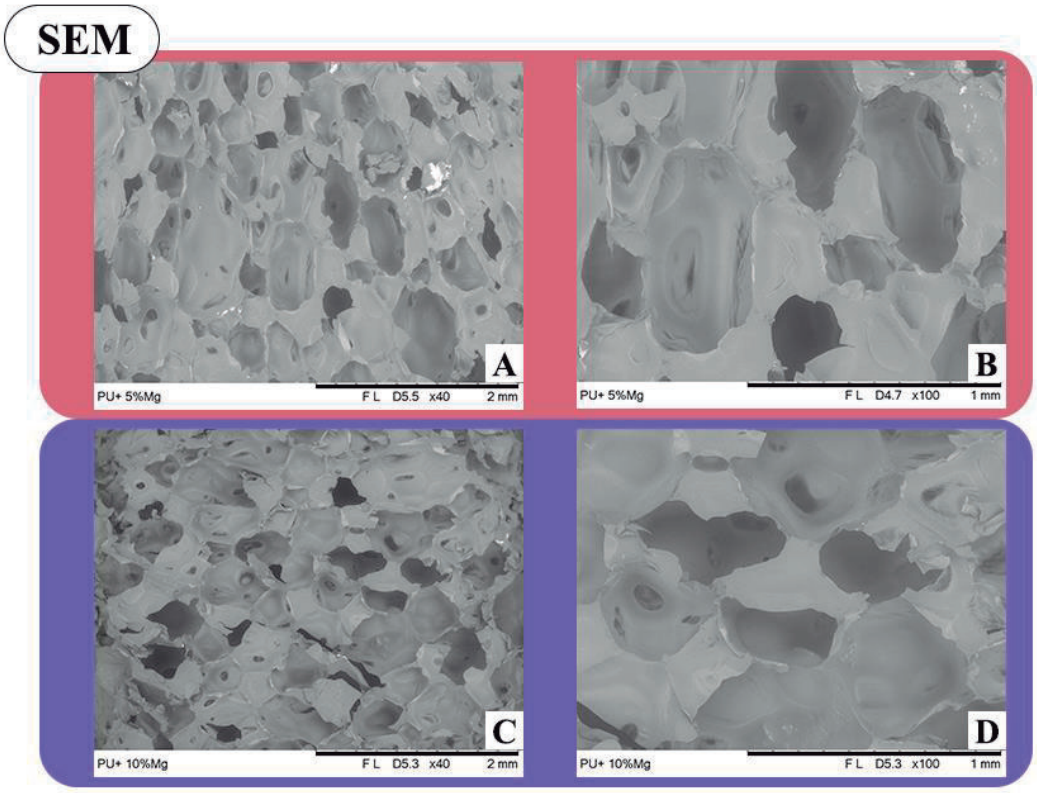

Figure 2: SEM images of PU + Mg composites with the respective percentages and magnifications: (a) PU+5%Mg 40x, (b) PU+5%Mg 100x, (c) PU+10% Mg 40x, (d) PU+10% Mg 100x.

Conclusions

In this study, a composite using magnesium residue (Mg) as a reinforcement (5 and 10 wt%) on castor oil-based polyurethane (PU) foam was developed for new studies and applications. The Mg addition in PU materials reduced the porous size, promoting increased hydrophobicity and reduction in density. Results also indicated that the adding the Mg to PU foam influenced the morphological and physical properties. For this reason, the addition of magnesium contributes to the development of a unique composite, presenting a more porous material, hydrophobicity and being less dense than pure PU.

Acknowledgments

This research was funded by Fundação de Amparo à Pesquisa do Estado do Rio de Janeiro - FAPERJ (E-26/211.435/2019 and E-26/210.450/2021).

References

[1] A. Das; P. Mahanwar Advanced Industrial and Engineering Polymer Research 2020, *3*(3), 93–101. https://doi.org/10.1016/j.aiepr.2020.07.002.

[2] X. Li; J. Li; J. Wang; J. Yuang; F. Jiang; X. Yu; F. Xiao Construction and Building Materials 2021, *304*, 124639. https://doi.org/10.1016/j.conbuildmat.2021.124639.

[3] M. Oliveira; D. Orlando; D. Mulinari Journal of Inorganic and Organometallic Polymers and Materials 2020, *30*, 5157–5167. https://doi.org/10.1007/s10904-020-01645-z.

[4]W. Jahnen-Dechent; M. Ketteler Clinical Kidney Journal 2012, *5*(Suppl 1), i3. https://doi.org/10.1093/ndtplus/sfr163.

[5] M. O. T. Da Conceição, Ph.D. Thesis, Federal University of Rio de Janeiro, 2014.

[6] B. Xu; K. Miao; J. Yang; B. Lou Advanced Materials Research 2011, *152–153*, 1262–1266. https://doi.org/10.4028/www.scientific.net/amr.152-153.1262.

[7] A. Abdal-hay; M. Agour; Y. Kim; M. Lee; M. Hassan; H. El-Ainin; A. Hamdy; S. Ivanovski European Polymer Journal 2019, *112*, 555–568. https://doi.org/10.1016/j.eurpolymj.2018.10.012.

[8] S. Adnan; N. Zaidi; Y. Daud; F. Zainuddin AIP Conference Proceedings 2018, *2030*. https://doi.org/10.1063/1.5066691.

Mechanical behavior and gel content of poly(vinylidene fluoride)/ thermoplastic polyurethane blends dynamically cross-linked with amine.

João Victor Mesquita Salustiano[1] Johnny De Nardi Martins[2], Arthur Braun[3]

1 – Post Graduation Program in Nanosciences, Processes and Advanced Materials(PPGNPMat), Federal University of Santa Catarina(UFSC), Campus Blumenau, Blumenau, SC.
joaomesqs20@gmail.com

2 – Post Graduation Program in Nanosciences, Processes and Advanced Materials(PPGNPMat), Federal University of Santa Catarina(UFSC), Campus Blumenau, Blumenau, SC.

3 – Federal University of Santa Catarina(UFSC), Campus Blumenau, Blumenau, SC.

Abstract - Polyvinylidene Fluoride (PVDF)/Thermoplastic Polyurethane (TPU) blend crosslinked with Hexamethylene Diamine were prepared through melt blending in an internal mixer. The study investigated the mechanical behavior and gel content as a function of crosslinking agents in the polymer blend. The results showed that the addition of amine improved the mechanical properties of the blend, and as the higher the amount of amine, the greater the increase in the material's gel content could be observed.
Keywords: *Polymer blend; Polyvinylidene Fluoride; Thermoplastic Polyurethane; Amine.*

Introduction

Polymer blends are widely studied due to their unique properties, which combine the characteristics of two or more distinct polymers. This procedure enables the production of new polymeric materials in a shorter period of time and sometimes at a lower cost [1]. The blend produced and in this work combined polyvinylidene fluoride (PVDF) and thermoplastic polyurethane (TPU). This combination allows the production of materials with good mechanical, chemical, and thermal properties [2].

It is mentioned that PVDF is a polymer with high chemical and thermal resistance, and has several applications in industry, from the production of pipes to the manufacture of medical devices[3]. On the other hand, TPU has interesting properties such as flexibility and resistance to abrasion, which makes it possible to use it in several areas, such as the production of footwear and coatings. However, obtaining homogeneous blends between these polymers is a challenge, due to their different chemical and physical characteristics.

In addition, TPU can be dynamically crosslinked with amine, which has been used to improve the mechanical properties of thermoplastic polymers such as polypropylene (PP) where dynamic crosslinking with amine can improve the mechanical properties of PP, such as impact resistance and the rigidity[4].This technique consists of adding an amine to the TPU, during melt blending , which reacts with the isocyanate groups present in the polymer chain, promoting the formation of

crosslinks. This process increases the rigidity of the TPU, which improves its mechanical properties [5].
It is noted that the study of the mechanical behavior and gel content of these blends is important to assess the feasibility of their use in practical applications. This foundation is important to justify the relevance of the study and to indicate the direction that will be followed in the research, making it possible to develop new materials with better performance and lower cost, which can boost the polymer industry.
In this work polyvinylidene fluoride (PVDF)/thermoplastic polyurethane (TPU) blend crosslinked with Hexamethylene Diamine were prepared through melt blending in an internal mixer. The study investigated the mechanical behavior and gel content as a function of crosslinking agents in the polymer blend.

Experimental

Materials
Poly(vinylidene fluoride)(PVDF) (Kynar®, density 1.78 g/cm³, melt index 1.90 cm³/10 min), Elastomer thermoplastic polyurethane (TPU) (density 1.20 g/cm3, index fluidity 5.04 g/10 min), kindly donated by the company Matoflex Ltda.
Hexamethylenediamine 98% (MM 116.20 g/mol, density 0.89 cm3, Surface tension 71.5 mN/m in 1g/L at 20 °C) and Dimethylformamide (DMF) were commercially acquired

Preparation of Blends
The melt blending of PVDF, TPU and amine was done in a Haake torque rheometer (Rheomix-600P) equipped with two counter-rotating roller blades, at 190°C and 100 rpm for 10 min. At that moment, materials were prepared in the following proportions: 60/40 wt/wt of PVDF/TPU with concentration of 0, 1, 2 and 4 phr of amine as crosslinking agent.

Mechanical properties
The test specimens of the tie type were prepared in accordance with the ASTM D 638 standard by means of hot pressing with approximately 1.5 MPa of pressure at a temperature of 180°C for 10 min. Tensile strength tests were done in accordance with ASTM D638-14 using an Instron 2300 Series 23 equipment, with a 5 kN cell and a displacement speed of 5 mm/min at room temperature.

Gel Content
The tests were done based on the ASTN D2765 - 11 Standard. Samples were weighing approximately 0.3 g on an analytical balance. Then, the samples were placed in 120-mesh metallic cages. These were previously weighed, and fixed with metallic wire being coupled to a condensation system formed by a round-bottom flask containing dimethylformamide (DMF). This apparatus were heated by a blanket and coupled to a ball condenser, which in turn was connected to a cooling flow. The samples remained for 6 hours under flow. At the end, the samples were dried in an oven for 12 hr and weighed in order to determine the gel content of the samples based on the following Equation 1:

$$\text{Gel Content} = \left[1 - \frac{(W3 - W4)}{(W2 - W1)} \right] \text{x } 100 \quad (1)$$

At where,

W1 = cage weight (sealed on three sides, one side open).
W2 = weight of sample and cage (sealed on three sides, one side open).

W3 = weight of polymer sample and cage, after being clamped, closed.
W4 = sample and cage weight after extraction and drying.

Results and Discussion

Gel Content
The results are displayed in Tab.1.

Table 1: Gel content of materials

Material	Gel content (%)
PVDF	0,6
TPU	9
PVDF/TPU 0 Amine	9
PVDF/TPU - 1 phr Amine	25
PVDF/TPU - 2 phr Amine	30
PVDF/TPU - 4 phr Amine	51

Table 1 shows the rising in gel content as a function of amine concentration in the blend. It was demonstrated that there was formation of crosslinked chains due to the reaction of an amine group with the isocyanate. This reactive group was formed in higher temperature, during melt processing, due to the dissociation equilibrium of the TPU [5].

Tensile Test
The mechanical properties are shown in Tab. 2 and Figure 1. We observed that the blend had an increase in the tensile strength as compared to the neat polymers. This trend indicated a possible synergistic effect in the blend. The blends with 1 and 2 phr of amine had almost the same values for tensile at break. However the blend with 4 phr of amine had the lowest value. This behavior could be associated with a partial fragmentation of TPU crosslinked phase due to low shear during processing [6]. The elongations at break were lower for the blend with 2 phr of amine, mainly due to the higher crosslinking density which restricts the macromolecular movements. The same trend could not be observed in the other blends. This behavior needs to be further elucidated.

Table 2: Mechanical behavior of the PVDF,TPU and the 60/40 blend of pure polymers and with the addition of amine.

Material	Tensile Strenght at Break (MPa)	Elongation at Break (%)
PVDF	59	42
TPU	45	1388
PVDF/TPU 0 Amine	64	52
PVDF/TPU - 1 phr Amine	66	69
PVDF/TPU - 2 phr Amine	66	54
PVDF/TPU - 4 phr Amine	47	59

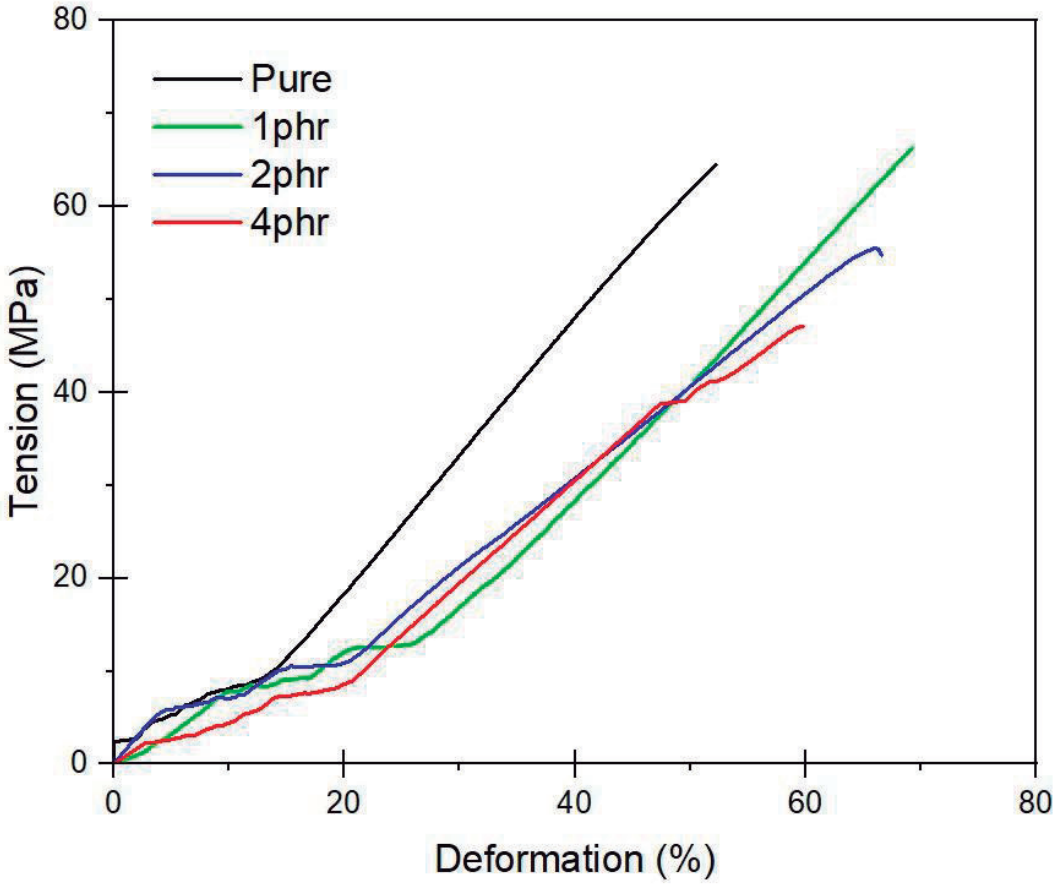

Figure 1 - Stress–strain curves of the PVDF/TPU blends (weight ratio: 60/40) with various contents of amine.

.

Conclusions

Tensile tests showed that the material had its mechanical behavior modified. The addition of amine promoted an increase in the degree of crosslinking of the material, causing to the blend an increasing in mechanical strength and reduced elongation at break in the blends with the addition of amine at 2 phr .The results obtained showed that there were improvements in the mechanical resistance of the PVDF/TPU blend, which became possible with the addition of the amine crosslinker, allowing future applications to be more effective in terms of material use.

Acknowledgements

The authors acknowledge the POLICOM - Laboratory of Polymers and Composites of the Department of Mechanical Engineering of the Federal University of Santa Catarina for the use of the infrastructure and to CAPES for supporting science with grants for researchers. We are also thankful for Mantoflex Company - Caxias do Sul -RS for kindly supplying the polymers used in this study.

References

1. OLIVEIRA, C. F. P. Production and characterization of thermoplastic starch and its mixtures with polypropylene. 2015, Thesis (Doctorate in Engineering) University of São Paulo, São Paulo, 2015
2. DIAS, P. D. P. Biodegradable Blends Of Poly(Lactic Acid) And Poly(Ɛ-Caprolactone) Tenacified By Non-Reactive Compatibilization – Influence Of Compatibilizer Content. 2016, Dissertation (Master in Science), University of São Paulo, São Carlos, 2016.
3. Y. Wu, XB Yu, YM Yang, BY Li, YC Han, Polymer 46 (2005) 2365
4. Yamada, T., & Otsuka, H. (2005). Reticulation of polypropylene with dynamic cross-linking agents. Journal of Applied Polymer Science, 96(2), 349-356.
5. Rodrigues, P.C., Ackelrud, L. Networks and Blends of Polyaniline And Polyurethane: Correlations Between Composition and Thermal, Dynamic Mechanical and Electrical Properties. Polymer. v.44, p. 6891 - 6899, 2003.
6. Zhao, Y., Song, M., Zhou, S., Liu, C., & Zhang, J. (2019). Improvement of mechanical properties of ethylene-vinyl acetate copolymer by dynamic cross-linking with multifunctional amines. Journal of Applied Polymer Science, 136(6), 47185.

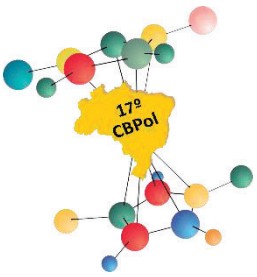

MIXED MATRIX FILMS BASED ON PEBAX® FILLED WITH LAYERED DOUBLE HYDROXIDES

Djeison P. R. Moreth[1], Fátima M.Z. Zotin[1], Luz A. P. Santos[1] and Rodrigo A. dos Reis[1]*

1 – Institute of Chemistry, State University of Rio de Janeiro (UERJ), Rio de Janeiro, RJ, Brazil
rdosreis@uerj.br

Abstract – Mixed matrix polymeric materials filled with inorganic particles have been studied in order to take advantage of the synergy between the flexible, versatile and moldable characteristics of polymers and the superior strength, the chemical resistance, and the thermal stability of inorganic additives. In this study, the effect of incorporating lamellar double hydroxide nanoparticles containing different molar ratios of metals on the thermal, mechanical, and gas permeation properties of films based on PEBAX® was evaluated. PEBAX® is the trade name of thermoplastic elastomers made of poly(ether-block-amide) with distinct properties in terms of lightness and ease of processing, good resistance to most chemicals, flexibility and high mechanical strength. The particles in the matrix changed the thermal resistances of films based on PEBAX® and improved their mechanical properties and CO_2/CH_4 separation performance. Hydrotalcite-like with more anions favors the transport of CO_2.
Keywords: *Mixed matrix films; gas permeation; PEBAX®; hydrotalcite-like compounds;* CO_2/CH_4 separation.

Introduction

Mixed matrix polymeric films containing inorganic fillers present superior characteristics as compared to the pristine materials, mainly when the particles are nanodispersed and well embedded among the polymer chains [1,2]. Lamellar double hydroxide (LDH) nanoparticles, a 2D material, can be synthesized with different combinations of metal ions and types of compensation anions, which gives it different interplanar distances, and hydration water contents. Thus, they can be tailored to fit well in a specific polymer in order to produce a promising material for a given application. LDH nanofillers have been incorporated into polymeric matrices to improve the mechanical properties, resistance to flammability, and general physical properties of polymers [2].
Thermoplastic elastomers made of poly(ether-block-amide) under the trade name PEBAX® are lightness and ease of processing, presenting good resistance to most chemicals, flexibility and high strength. Mixed matrix films based on PEBAX® copolymers developed for a wide spectrum of applications (e.g., biomedical, olefin separation, gas separation, fuel cells and sensors) [3,4]. Recently, mixed matrix films produced by the LDH nanodisperse into PEBAX® 1657 presented simultaneous enhancements in CO_2 permeability and CO_2/CH_4 selectivity [5,6] when compared with the pristine polymer. Despite PEBAX® 2533 presents the highest CO_2 permeability among copolymers from PEBAX® series [4,7], it was not found in any gas permeation tests involving films produced with LDH nanodisperse in this material. Further, the influence of the LDHs metallic structure on gas permeation in mixed matrix membranes has not still been reported.
Thus, this work aims to evaluate the influence of the Mg/Al ratio in LDH and solid content on mechanical and thermal properties of mixed matrix films produced by the dispersion of LDH fillers

into PEBAX® 1657 or PEBAX® 2533. In addition, it is also intended to evaluate the effect of such variables on the permeability of CO_2 and CH_4.

Experimental

The hydrotalcite-type materials were synthesized by the co-precipitation method at constant pH, as described elsewhere [8], using molar *x*-ratios (*x*=Al/(Mg+Al)) equal to 0.20, 0.25 and 0.33. The mixed matrix films were produced by a method adapted as proposed elsewhere [9,10]. Firstly, a solution with 10 wt% of one PEBAX® was prepared by dissolving the polymers in the appropriate solvent: ethanol/water (70/30) for PEBAX® 1657 and isopropanol/n-butanol (50/50) for PEBAX® 2533.
The Thermogravimetric Analysis (TGA) was performed in a SDT Q600 TA Instruments-under N_2. Fourier transform infrared spectroscopy (FTIR) spectra were obtained using a Frontier MIR/FIR spectrometer Perkin Elmer. X-ray diffraction (XRD) measurements were carried out on a Rigaku Miniflex. After coating the samples with gold, images of scanning electron microscopy (SEM - acronym for Scanning Electron Microscopy) were obtained with a JEOL microscope, model JSM-IT200, with an electron beam by field emission. The mechanical tests were carried out in an EMIC universal testing machine, DL-2000. Modulus of elasticity and stress at break were determined according to ASTM D882-12.
The permeability tests were performed in a system which was designed to measure the permeability of a single gas through the constant volume/variable pressure method [11–13]. All reported results for permeability tests have uncertainties less than 10% of the mean within a 95% confidence interval, between 3 and 5 samples were analyzed.

Results and Discussion

Characterizations of LDH are shown in Fig.1. The wideband at 3427-3480 cm^{-1} can be attributed to the stretching of OH groups connected to Al^{3+} and Mg^{2+} in the layers [14]. The characteristic peaks of LDHs in the planes *(003), (006)* and *(009)* observed in XRD confirm the formation of a hydrotalcite structure [8]. Smooth changes are observed in crystalline structures of hydrotalcite-type compounds when they are synthesized with different *x* ratios, for example, the intensity of the ν_3 antisymmetric vibration FTIR band of CO_3^{-2} around 1362-1655 cm^{-1} (Fig 1a), decrease as lower *x* ratios, because of the lower content of compensation anions in the interlayer of the LDH. This effect is due to the decline in the force of attraction between the positively charged layer, confirmed by the shift of the XRD characteristic peaks of *(003)* plane to smaller angles as *x*-ratio is reduced (Fig 1b). As a result of wider interlayer spaces and lower anion content, it is observed an increase of the interlayer water content, confirmed by an intensified FTIR bands for water bending vibration (1616-1642 cm^{-1}), shifted to higher wavenumber as *x* ratio decreases. Because the electrostatic attraction of the layer decreases, water removal becomes easier to the HT-0,20 (Fig 1c). The decomposition profiles (Fig 1c) are in accordance with those reported in the literature for hydrotalcite compounds, with a total weight mass loss of ~43% by mass up to 750 °C [15].

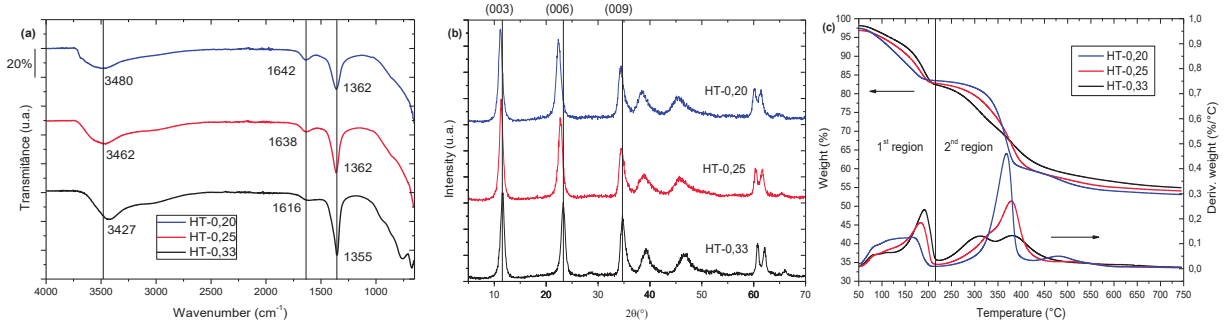

Figure 1 – Characterization of LDHs: (a) FTIR spectra; (b) X-ray diffractograms; (c) TG/DTG curves.

Comparing cross-section morphology of the films produced with pristine PEBAX® 1657 (Fig. 2) and of those carrying 5 wt% of LDH with *x* equal to 0.33 (denoted by 1657 0.33 5%), it is reasonable to say that the LDH particles were well dispersed and embedded in PEBAX® matrix without interface defects. These nanodisperse morphology was also confirmed by the EDS mapping of Mg and Al in the cross-sectional of 1657 0.33 5% film, although no extra interaction strength was identified among the LDH nanoparticles and the PEBAX® chains. Thus, all characteristic bands of FTIR of the matrix remained unchanged after the addition of LDH (Fig 3a and 3b), as also observed elsewhere [5]. Both FTIR spectra of pristine PEBAX® 1657 and PEBAX® 2533 are in accordance with the literature [10,13]. It is worth noting an increase in the broadband intensity around 3500 cm^{-1} as LDH content grows up to 5 wt%. Besides, the first peak of the LDHs around 2θ equal to 11° were observed in the diffractogram for all mixed matrix films (Fig 3c). Similar results were obtained with the other mixed matrix films produced in this work. Further, all films reached peaks around 2θ equal to 24°, in the crystalline region of the polyamide segments. The amorphous segments of the material were confirmed by the halo around 2θ equal to 20° related to the PEO segment [16]. Note that the intensity of these peaks decreased when the LDH content grows up to 5% (Fig 3c). At this composition, LDHs seem to interfere on the crystalline domains of PA-6 in PEBAX® 1657 and improve the thermal resistance of the PEBAX® 2533 (Fig 3d). Comparing the mixed matrix films based on PEBAX® 1657, it is noted that the mass loss of those filled with LDH with *x* equal to 0.33 starts at higher temperatures, followed by those filled with LDH with *x* equal to 0.25 and 0.20 (Fig.3e), which follow the same trend presented by the pristine LDHs.

No significant changes were observed in the transport of gases through films with 2 wt% of LDH. The pristine PEBAX® 2533, due to its longer PEO segment, produces films with elastic modulus 10 timers lower than those observed for films based on PEBAX® 1657, but similar stress at break (Figs 4a and 4b). The introduction of LDH promotes, on average, an increase of 35% in elastic modulus regardless of filler content or *x*-ratio adopted. Due to these noted elastomeric feature of PEBAX® 2533 (Fig 4b), which is little affected by the presence of different types of LDH at levels of up to 5 wt%, no significant gain was observed in CO_2 permeability, nor in its selectivity related to CH_4 (Fig 4c). Even though the fillers add some other diffusion mechanism to the films, the introduction of the different LDHs do not contribute any extra freedom degree to the gas permeation through the original polymeric matrix. Operating pressure has a subtle effect on CO_2 permeability, but no gain in selectivity, probably due to the compaction of the flexible PEBAX® 2533 matrix, which reduces the free volume available for gas diffusion.

On the other hand, there is a significant improvement in the CO_2 transport properties through PEBAX® 1657 films with 5 wt% LDH with *x*-ratio of 0.25 and 0.33 to 0.5 bar (Fig. 4c). Such improvements at lower pressure suggest an activated diffusion mechanism to the CO_2, since the simultaneous increase in permeability and selectivity data cannot be attributed only to the slight changes in mechanical properties (Fig 4a and Fig 4b). Compensation anions and hydration water in LDH interlamellar galleries participate in the facilitated transport of CO_2 [6]. Such facilitated transport seems to be dominated by the anion content, since the best performance is achieved by fillers with *x*-ratio equal to 0.33. Furthermore, the increase in selectivity suggests that the creation of tortuous pathways caused by the presence of LDHs leads to restriction of CH_4 diffusion. Facilitated CO_2 transport is less noticeable at 4 bar, as this diffusion mechanism is negatively affected as transport agents approach saturation.

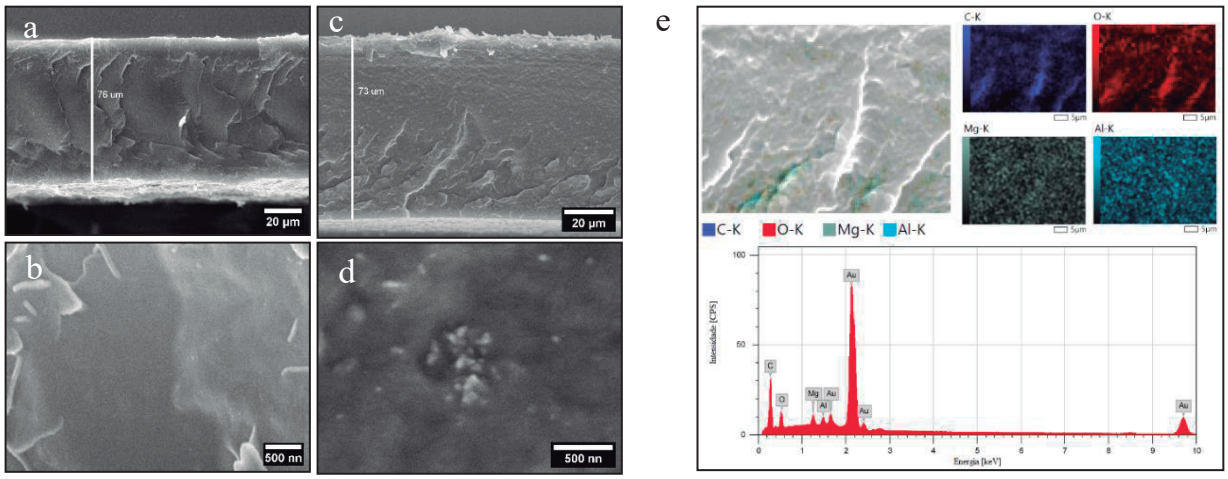

Figure 2 – Cross-section SEM images of pristine PEBAX® 1657 (SED 25.0 kV) (a, x800), (b, x30.000), and 1657 0.33 5% (SED 20.0 kV) (c, x1000), (d, x50,000). (e) EDS map of the cross-section of 1657 0.33 5%.

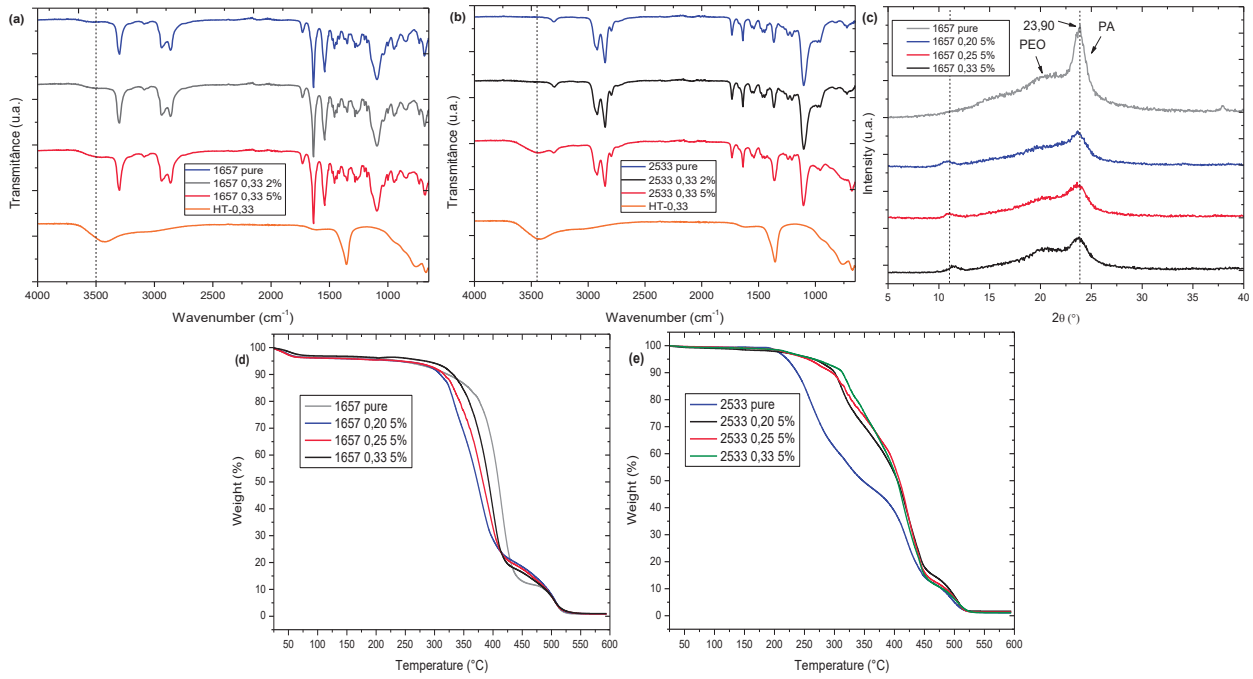

Figure 3 – FTIR spectra for films based on (a) PEBAX® 1657 and (b) PEBAX® 2533; (c) X-ray diffractograms for pristine PEBAX® and composite films (5 wt%); TGA for films based on (d) PEBAX® 2533 and (e) PEBAX® 1657.

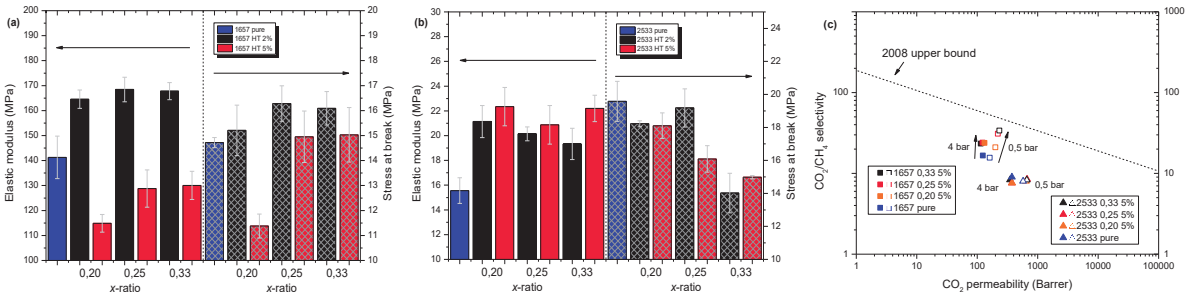

Figure 4 – (a) Mechanical properties of pure PEBAX® 1657 and composite materials; (b) mechanical properties of pure PEBAX® 2533 and composite materials; (c) CO_2/CH_4 separation performances of pure polymers and composites.

Conclusions

The dense films were successfully prepared by the solution-casting method. The conducted studies show that the presence of the particles in the matrix can change the thermal resistances, improve the mechanical properties and CO_2/CH_4 separation performance. Incorporation of 2% LDH in PEBAX® 1657 resulted in a 20% increase in elastic modulus and 10% increase in tension at break. In PEBAX® 2533, on the other hand, the addition of 2 or 5 % resulted in a 30 % increase in elastic modulus. The introduction of LDHs has improved the permeability and selectivity of the PEBAX® 1657 matrix. The presence of LDHs in these films favored the permeability to CO_2, while it hindered the diffusion of methane. The best result shows a selectivity increase of 110% in 1657 0.33 5% at 0.5 bar compared to the neat material. This indicates that hydrotalcite-like material with more anions favors the transport of CO_2.

Acknowledgements
Djeison Moreth thanks CAPES for the master's scholarship.

References

1. Huang SC, Deng C, Wang SX, Wei WC, Chen H, Wang YZ. Polym Degrad Stab 2019;165:126–36. https://doi.org/10.1016/j.polymdegradstab.2019.05.006.
2. Mochane MJ, Magagula SI, Sefadi JS, Sadiku ER, Mokhena TC. Crystals 2020;10:1–26. https://doi.org/10.3390/cryst10070612.
3. Clarizia G, Bernardo P. Membranes (Basel) 2022;12. https://doi.org/10.3390/membranes12111096.
4. Armstrong S, Freeman B, Hiltner A, Baer E. Polymer (Guildf) 2012;53:1383–92. https://doi.org/10.1016/j.polymer.2012.01.037.
5. Wang Y, Zhang N, Wu H, Ren Y, Yang L, Wang X, et al. J Memb Sci 2021;618:118691. https://doi.org/10.1016/j.memsci.2020.118691.
6. Liao J, Wang Z, Gao C, Li S, Qiao Z, Wang M, et al. Chem Sci 2014;5:2843–9. https://doi.org/10.1039/c3sc53334d.
7. Bondar VI, Freeman BD, Pinnau I. J Polym Sci Part B Polym Phys 2000;38:2051–62. https://doi.org/10.1002/1099-0488(20000801)38:15<2051::AID-POLB100>3.0.CO;2-D.
8. Cavani F, Trifirò F, Vaccari A. Catal Today 1991;11:173–301. https://doi.org/10.1016/0920-5861(91)80068-K.
9. Kardani R, Asghari M, Hamedani NF, Afsari M. J Ind Eng Chem 2020;83:100–10. https://doi.org/10.1016/j.jiec.2019.11.018.
10. Meshkat S, Kaliaguine S, Rodrigue D. Sep Purif Technol 2018;200:177–90. https://doi.org/10.1016/j.seppur.2018.02.038.
11. Bernardo P, Jansen JC, Bazzarelli F, Tasselli F, Fuoco A, Friess K, et al. Sep Purif Technol 2012;97:73–82. https://doi.org/10.1016/j.seppur.2012.02.041.
12. Casadei R, Baschetti MG, Yoo MJ, Park HB, Giorgini L. Membranes (Basel) 2020;10:1–20. https://doi.org/10.3390/membranes10080188.
13. Sanaeepur H, Mashhadikhan S, Mardassi G, Ebadi Amooghin A, Van der Bruggen B, Moghadassi A. Korean J Chem Eng 2019;36:1339–49. https://doi.org/10.1007/s11814-019-0323-x.
14. Lin Y-J, Li D-Q, Evans DG, Duan X. Polym Degrad Stab 2005;88:286–93. https://doi.org/10.1016/j.polymdegradstab.2004.11.007.
15. Arhzaf S, Naciri Bennani M, Abouarnadasse S, Ziyat H, Qabaqous O. Mediterr J Chem 2020;10:625. https://doi.org/10.13171/mjc10602007021464sa.
16. Ebadi R, Maghsoudi H, Babaluo AA. J Nat Gas Sci Eng 2021;90. https://doi.org/10.1016/j.jngse.2021.103947.

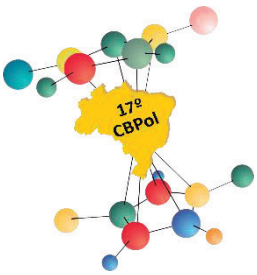

MODIFICATION OF *LUFFA CYLINDRICA* WITH β-CYCLODEXTRIN FOR THE ADSORPTION OF EMERGING CONTAMINANTS IN AQUEOUS MEDIUM

Débora R. S. dos Santos*, Juliê S. da Costa and André R. Fajardo

Laboratório de Tecnologia e Desenvolvimento de Compósitos e Materiais Poliméricos (LaCoPol), Universidade Federal de Pelotas (UFPel), Campus Capão do Leão, Pelotas, RS, Brazil
(*) deborarosane15@gmail.com

Abstract: The high consumption of compounds classified as emerging contaminants (ECs) has accelerated the deterioration of the environment, particularly the hydric resources. As a strategy to abate this scenery, this study aims to develop adsorbent materials based on Luffa cylindrica (LF) modified with β-cyclodextrin (β-CD) via grafting reaction. It is envisaged that this modification enhances the capacity of LF to adsorb ECs from water. Characterization analyses confirmed the modification, which imparted thermal and morphological changes in the LF fibers. A spectrophotometric assay determined that the amount of β-CD per gram of modified material is around 530 mg. Currently, adsorption experiments are in progress to evaluate the effect of the β-CD grafting on the adsorption efficiency of the modified LF.
Keywords: Adsorption, sponge gourd, water treatment.

Funding: Débora R. S. dos Santos thanks the CNPq/Brazil for her PIBIC fellowship.

Introduction

As well reported, population growth has generated a high amount of a new group of pollutants compounds known as emerging contaminants (ECs). The release of these compounds into the aqueous environment impacts human health and aquatic organisms. Overall, ECs encompass a variety of substances (such as pharmaceuticals, cosmetics, steroid hormones, and agrochemicals) [1,2]. Although the sale of this drug has been banned in several countries (USA, Spain, Finland, etc), some countries, such as Brazil, continue to sell it in the form of pills or gel formulations. Nimesulide, when compared to other anti-inflammatory drugs (diclofenac, ibuprofen, and piroxicam), is more effective. Therefore, it has a high consumption, which is directly related to its appearance in water and wastewater. In view of the lack of knowledge about its safety profile and the necessity to protect human health and biodiversity, the removal of this contaminant from water/wastewater is crucial to maintain the ecosystem and sustainable development [3]. So, different methods have been developed (including filtration, precipitation, coagulation, centrifugation, flotation, etc.) and utilized for this task. Amongst them, adsorption processes using agricultural biomass products as adsorbent materials have gained attention because they offer advantages such as high removal efficiency, absence of toxic secondary contaminants, natural availability, and biodegradability [1,2]. In this sense, the natural Luffa cylindrica (LF) is a good candidate for adsorption due to its structural and morphological properties (e.g., high macro porosity, tenacity, resistance, and rigidity) [4]. Despite this, LF has a few numbers of active sites on the surface of its fibers to interact with EC molecules [5]. To overcome this limitation, a new strategy using cyclodextrin (CDs), such as β-cyclodextrin (β-CD), is proposed to modify the cellulosic matrix of LF. Cyclodextrins are a group of cyclic oligosaccharides constituted

by six (α-CD), seven (β-CD), and eight (γ-CD) glucopyranoside units. The β-CD have a structure that looks like a cup or a cone (toroidal shape), its primary hydroxyl groups are positioned outside at the edges of its structure, and their secondary hydroxyl groups are responsible for intramolecular H-bonds and cannot rotate. This arrangement configuration results in rigid chains and the external cavity of β-CD shows a hydrophilic surface combined with a hydrophobic nature of the internal cavity, allowing the formation of inclusion complexes with EC molecules, for example [6]. The combination of cellulose/cyclodextrin is generally focused on controlled drug delivery, adsorption, and separation of various compounds. Based on this, the modification of the LF fibers with β-CD using citric acid as a crosslinker is proposed in this study as a strategy to increase the ability of LF to adsorb EC, like nimesulide, from the aqueous medium.

Experimental

Grafting of β-CD on LF: Firstly, raw LF was cut into cubic pieces (1 cm^3), washed with an EtOH/H_2O (70:30 v/v) solution three times, and oven-dried at 50 °C for 24 h. The purified LF (2 g) was added to a NaOH solution (5 w/v-%, 200 mL), which was stirred for 2 h at 50 °C. The sample, labeled as LF(NaOH), was recovered, washed with distilled water until neutral pH (pH ~7), and then oven-dried at 50 °C for 48 h. For the grafting reaction, an aqueous solution was prepared by dissolving 5 w/v-% of β-CD, 2 w/v-% of citric acid, and 2 w/v/-% of sodium hypophosphite in 10 mL of H_2O. Approximately 1 g of LF(NaOH) was immersed in this solution for 30 minutes, allowing the sponge fibers to absorb the solution. After 30 min, the sample was removed from the solution and oven-dried at 80 °C for 5 min. A curing process was made on the sponge (where the β-CD grafting with citric acid occurred), which consisted of exposing the sponge to a temperature of 150 °C for 15 min. After this time, the sponge was washed with distilled water at 50 °C for 5 min. Finally, the LF(NaOH)-g-β-CD sample was washed again with distilled water at room temperature, oven-dried (50 °C for 24 h), and stored for later characterization and use.

Characterization techniques: The samples of modified sponges were characterized by morphological, surface, and thermal decomposition properties, through chemical and analytic techniques such as FTIR, TGA, SEM, and phenolphthalein method.

Results and Discussion

The FTIR technique was used to characterize the chemical structure of LF, LF(NaOH), LF(NaOH)-g-β-CD sponges, and β-CD. In Fig. 1a, the spectrum of LF after alkaline treatment (LF(NaOH)) is observed, where a band around 3447 cm^{-1} associated with stretching of O–H bonds of the hydroxyl groups present in cellulose and lignin is present. The bands observed at 2925 and 2855 cm^{-1}, which are attributed to the stretching of C–H bonds of CHx groups in cellulose, show that after the alkaline treatment, cellulose became more available on the surface of the material, as can also be observed in the range of 1650–1550 cm^{-1} corresponding to the combination of stretching of C=O and C=C bonds of the aromatic ring of the lignin fraction [7]. After treatment with NaOH, the band around 1050 cm^{-1} referring to the stretching of the C–O–C bond of the pyranose rings becomes more intense due to the alkaline treatment that increases the cellulose fraction on the surface of the fibers [8].

For the LF(NaOH)-g-β-CD spectrum, Fig. 1b, the presence of characteristic bands of its precursor materials was observed with some changes. A decrease in the intensity of the band related to the stretching of the O–H bond of the hydroxyl groups (3444 cm^{-1}) of the sponge and β-CD, which were being consumed due to the grafting mediated by the citric acid. Moreover, it was observed that the bands related to the stretching of the C–H bond of the $–CH_x$ groups of cellulose were shifted to 2196 and 2847 cm^{-1}, respectively, due to the overlap of the vibration of the CH_2 groups of β-CD. The grafting of β-CD onto the sponge structure using citric acid as a crosslinker was confirmed by the emergence of new bands between 1600 and 1740 cm^{-1}, corresponding to the stretching of the C=O bond of the ester groups formed during the grafting process [9]. Considering the results observed with

the FTIR analysis, it is believed that the grafting of β-CD onto LF(NaOH) using citric acid as a crosslinking agent has occurred.

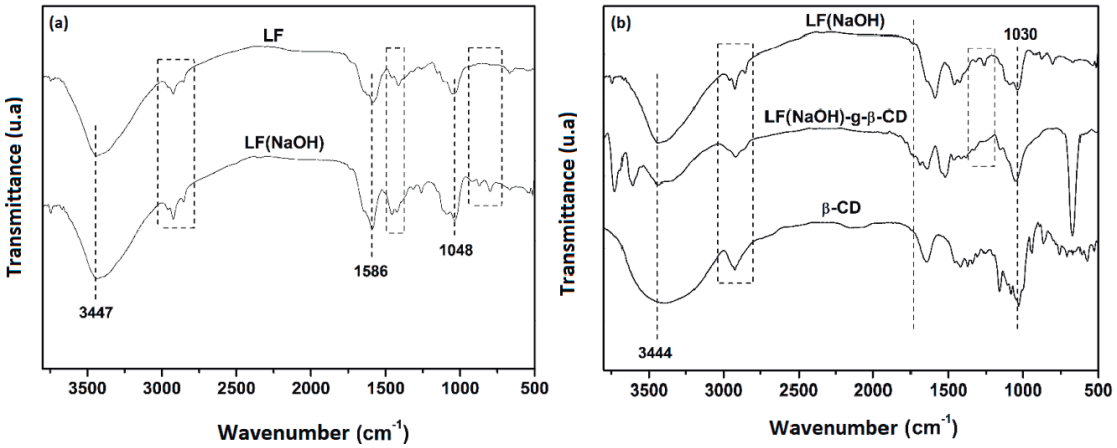

Figure 1: (a) FTIR spectra of LF and LF(NaOH) and (b) FTIR spectra of LF(NaOH), LF(NaOH)-g-β-CD and β-CD.

TGA analysis was performed for LF, LF(NaOH), and LF(NaOH)-g-β-CD samples, as shown in Fig. 2. The TGA curves exhibited an initial weight loss (~6%) for all samples, corresponding to the evaporation of free water molecules that are adsorbed in the sponge fibers. After the alkaline treatment, no weight loss stage related to hemicellulose depolymerization in LF(NaOH) was observed. For the LF(NaOH), the last stage occurred between 260 and 380 °C, where 61% of its weight was lost. The LF(NaOH)-g-β-CD presented the second weight loss with a maximum of 248 °C due to the citric acid decomposition. Also, as in the other samples, the last stage (from 290 to 380 °C) resulted in 54% of the weight loss, related to the depolymerization of cellulose and degradation of β-CD. The increase in temperature in this last stage occurs because more energy is required to decompose the material after the grafting process [10]. This temperature increment to the decomposition of LF(NaOH)-g-β-CD is associated with the grafting reaction, corroborating the FTIR data [11].

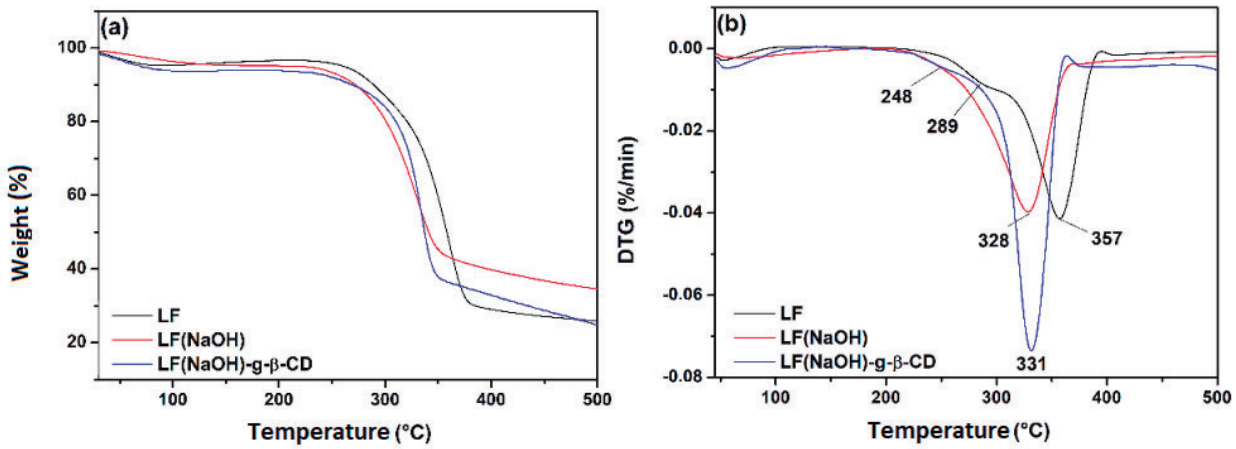

Figure 2: (a) TGA and (b) DTG curves of LF, LF(NaOH) and LF(NaOH)-g-β-CD.

Images obtained by SEM were analyzed to investigate the morphology of the LF(NaOH) and LF(NaOH)-g-β-CD samples (Fig. 3). It can be observed that after the alkaline treatment, LF(NaOH) fibers have a smoother surface morphology with fewer striations and irregularities. Additionally, the sample surface appears to be a group of coalesced fibers. Despite the severity of the alkaline treatment, the fibers maintained their integrity [4]. On the other hand, the morphology of the sponge after the β-CD grafting process is completely different from that of the LF(NaOH) sample. It was

observed that the LF(NaOH)-g-β-CD sample presents a more rugged morphology but without porosity [8].

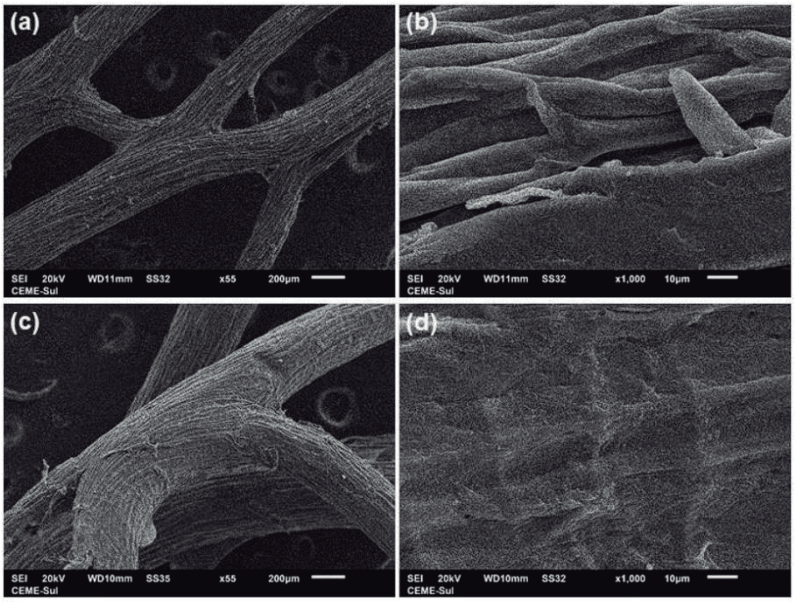

Figure 4: Images obtained by SEM from LF(NaOH) [(a) x55; (b) x1000] e LF(NaOH)-g-β-CD [(c) x55; (d) x1000].

The quantification of β-CD was performed by a spectrophotometric method, measuring changes in the UV-Vis absorption of phenolphthalein. In short, changes in the absorption of the phenolphthalein peak (552 nm) in basic pH occurs due to the formation of a complex between the β-CD cavities and phenolphthalein, reducing the concentration of free dye in solution [12]. In Fig. 4, it can be observed that as the sponge mass increases, the absorption band of phenolphthalein decreases. Therefore, by using the constructed calibration curve, it was estimated that there is approximately 15,9 mg of β-CD in a sample of 30 mg of LF(NaOH)-g-β-CD. This confirms the presence of β-CD in this sample and corroborates the changes observed in the FTIR, TG/DTG, and MEV analyses.

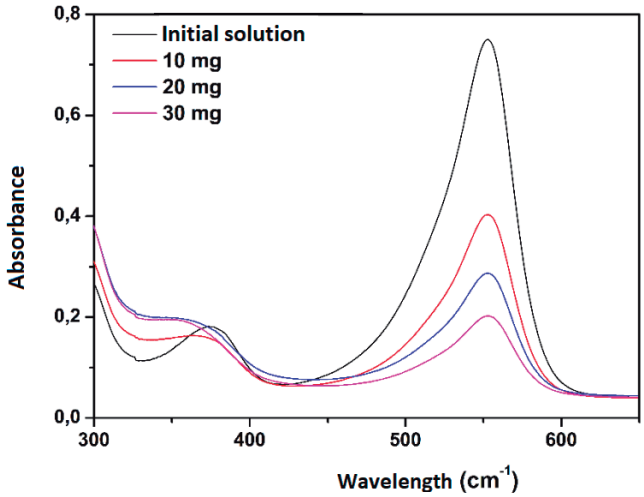

Figure 4: Scanning curves of phenolphthalein solution with different mass of LF(NaOH)-g-β-CD.

Conclusions

In this study, an alkaline treatment was performed on the LF sponge to make it more reactive for chemical modifications. The post-alkaline treatment sponge (LF(NaOH)) was modified with β-CD through a grafting reaction using citric acid as a crosslinking agent. So far, the material has been characterized by FTIR, TGA, and SEM techniques. The characterization of LF(NaOH)-g-β-CD

revealed that grafting resulted in changes in the material's chemical composition, increased thermal stability, and a change in fiber surface. Also, the presence of β-CD in the samples was confirmed by the analysis of the phenolphthalein adsorption, using different masses of LF(NaOH)-g-β-CD. So far, the next step for this study is to test the modified sponge to adsorb nimesulide from the aqueous medium.

References

1. Basheer, A.A., 2018. J. Mol. Liq. 261, 583–593. https://doi.org/10.1016/j.molliq.2018.04.021
2. Sophia A., C., Lima, E.C., 2018. Ecotoxicol. Environ. Saf. 150, 1–17. https://doi.org/10.1016/j.ecoenv.2017.12.026
3. Caldas, S.S., Arias, J.L.O., Rombaldi, C., Mello, L.L., Cerqueira, M.B.R., Martins, A.F., Primel, E.G. 2019. J. Braz. Chem. Soc., 30. https://doi.org/10.21577/0103-5053.20180154
4. Khadir, A., Motamedi, M., Pakzad, E., Sillanpää, M., Mahajan, S., 2021. J. Environ. Chem. Eng. 9. https://doi.org/10.1016/j.jece.2020.104691
5. Akay, O., Altinkok, C., Acik, G., Yuce, H., Ege, G.K., 2021. Eur. Polym. J. 161, 110856. https://doi.org/10.1016/j.eurpolymj.2021.110856
6. Cova, T.F., Murtinho, D., Pais, A.A.C.C., Valente, A.J.M., 2018. Front. Chem. 6. https://doi.org/10.3389/fchem.2018.00271
7. Ye, C., Hu, N., Wang, Z., 2013. J. Taiwan Inst. Chem. Eng. 44, 74–80. https://doi.org/10.1016/j.jtice.2012.08.006
8. Noone, S., Purushothaman, K., Pradhan, R., 2020. Mater. Today Proc. 33, 1026– 1031. https://doi.org/10.1016/j.matpr.2020.07.051
9. Rehan, M., Mahmoud, S.A., Mashaly, H.M., Youssef, B.M., 2020. React. Funct. Polym. 151, 104573. https://doi.org/10.1016/j.reactfunctpolym.2020.104573
10. Abdul Manas, N.H., Kumar, N.K.M.F., Mohd Shah, N.A., Ling, G.Y., Azelee, N.I.W., Fuzi, S.F.Z.M., Masngut, N., Bunyamin, M.A.H., Illias, R.M., El Enshasy, H.A., 2023. Sustainability 15, 1559. https://doi.org/10.3390/su15021559
11. Sadaquat, H., Akhtar, M., 2020. J. Incl. Phenom. Macrocycl. Chem. 96, 333–351. https://doi.org/10.1007/s10847-020-00977-0
12. Mihailiasa, M., Caldera, F., Li, J., Peila, R., Ferri, A., Trotta, F., 2016. Carbohydr. Polym. 142, 24–30. https://doi.org/10.1016/j.carbpol.2016.01.024

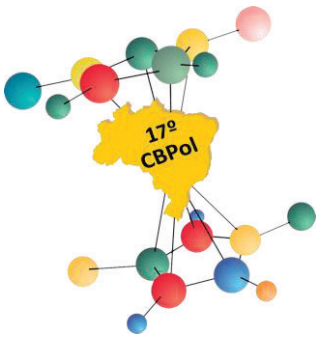

MORPHOLOGY AND MECHANICAL PROPERTIES OF A COMPOSITE FOAM BASED ON CASSAVA STARCH, CLAY AND RAMIE FIBERS

Nayara T. Bohnenberger[1], Gabriela Pozzebon[1], Mara Z. de Andrade[2], Ana P. Bilck[2], Édson L. Francisquetti[2] and Daiane Romanzini[1]

1 – Postgraduate Program in Materials Technology and Engineering (PPGTEM), IFRS, Campus Feliz, Feliz, RS, Brazil

nayara.bohnenberger@aluno.feliz.ifrs.edu.br; gabrielapozzebon2@gmail.com; daiane.romanzini@feliz.ifrs.edu.br

2 – Postgraduate Program in Materials Technology and Engineering (PPGTEM), IFRS, Campus Farroupilha, Farroupiha, RS, Brazil

edson.francisquetti@farroupilha.ifrs.edu.br

Abstract - The inadequate destination and final disposal of expanded polystyrene has been causing numerous environmental problems, being fundamental the development of alternative materials, such as starch foams. However, it is necessary to improve structural and mechanical characteristics of these materials. In this context, this study aimed to evaluate the influence on the morphology and mechanical properties of starch foams containing Cloisite® 30B clay and ramie fibers. Stirring was done followed by a thermoforming step. Good expansion of the material and a reduction in density were observed with higher fiber contents. There was an increase from 17.5 to 75.71% in impact resistance with the addition of fibers and/or clay, in relation to the control sample. Likewise, there was an increase in modulus (3.67 – 17.43%) and flexural strength (3.90 – 7.14%) with the addition of ramie fibers. In general, an improvement in the mechanical properties and density of starch foams were observed.

Keywords: Starch Composite Foam. Ramie Fiber. Clay. Mechanical Properties.

Introduction

Plastics have brought advantages to society, due to their mechanical strength and durability, but their inadequate disposal have been causing serious environmental problems. Coming mainly from the petrochemical industry, their worldwide production is estimated at 300 million tons per year, leading to increased pollution and depletion of a non-renewable resource [1-2]. Expanded polystyrene (EPS), a material widely used in the manufacture of packaging and in insulation applications, contributes significantly to the socio-environmental impacts of microplastics. Therefore, it is essential to develop biodegradable materials from renewable sources, such as starch, which has been investigated for the production of food packaging [3-4].

Unlike EPS, for a starch-based foam to achieve adequate structural and mechanical resistance characteristics, it is necessary to incorporate other additives/substances into the system. The presence of the plasticizer increases the mobility of amylose and amylopectin macromolecules, by weakening intermolecular hydrogen bonds. The increase in the mechanical properties of starch foam, in general, can be achieved by incorporating natural fibers and agro-industry residues, which are abundant and biodegradable. Cassava starch foams have already been reinforced with grape stems [5], pineapple peel fibers [6], eggshells, shrimp shells or with calcium carbonate [7] and coconut waste fibers [8].

Ramie fiber, which is found in Paraná, for many years was an important source of income for small producers, as it was used in the production of flax. [9]. However, there was a 91% drop in its

production between the 1970s and 1990s. with the arrival of Chinese synthetic linen [9]. Therefore, the use of ramie fibers can encourage its production, leading to job creation. These fibers are extracted from the stem of a plant belonging to the *Urticaceae* family and the *Boehmeria genus*. Given the above, the present study aimed to evaluate the influence of Cloisite® 30B clay and ramie fiber on the morphology and mechanical properties of cassava starch composite foams.

Experimental

Materials

Cassava starch from Pilão Amidos Ltda. (Guaíra – PR) was used. According to the technical bulletin, the maximum moisture content is 14% and pH between 4.5 – 6.5. As plasticizing agents, glycerol from the brand Anidrol (Diadema - SP) and distilled water were used, which also acted as a physical expansion agent [10]. In addition, the following additives were added: guar gum from the brand Zona Cerealista (Guarulhos – SP), to prevent sedimentation, and magnesium stearate from the brand Bianquímica Comercial (Franca – SP), as a release agent. Ramie fibers were supplied by Sisalsul (São Paulo – SP) and Cloisite ® 30B, a natural montmorillonite modified with quaternary ammonium salt, was purchased from the Southern Clay Products (USA), with a particle size of less than 6µm (d50) and basal spacing of 18.5 Å (d001).

Fiber treatment

The ramie fibers were previously cut, shredded and washed with distilled water for 10 min. Then, the fibers were oven dried for 1 h at 105 °C, as reported by Romanzini (2012), and ground through 2 mm sieve in a knife mill (SL-31, Solab).

Starch Foam Production

Starch foams were produced from different fiber contents, starch and water (Table 1), and the limit of the fiber content used was less than 20 g of fiber/100 g of solids, according with the study reported by Vercelheze et al. (2012).

Table 1. Content of constituents for sample preparation

Sample denomination	Starch (g)	Ramie Fiber (g)	MMT (g)	Water (mL / 100 g of solids)	Glycerol (g /100g of solids)
Control	100	0	0	100	5
MMT5	95	0	5	110	10
F10	90	10	0	200	10
F15	85	15	0	200	10
F10MMT5	85	10	5	250	10
F15MMT5	80	15	5	275	10

The constituents were stirred with the mixer (Philco PMX700, Brazil) until homogenization. In all samples, 2% (w/w) magnesium stearate and 1% (w/w) guar gum were added. The material was poured onto a flat grill plates (Black & Decker Plus, Brazil) with dimensions of 20.5 x 20.5 cm and coated with Teflon. Then, the mixture was submitted to the molding technique, between 180 and 220 °C for 5 min.

Material Characterization

The density was determined according to the ASTM D 3575 (2001) standard. Five specimens with dimensions of 2 cm x 2 cm were used. The mass was determined on an analytical scale and the dimensions were measured with a manual micrometer. To determine the density, Eq. 1 was used and the arithmetic mean of the 5 samples was calculated.

$$d\left(\frac{g}{cm^3}\right) = \frac{m}{v} \qquad (1)$$

The morphology of the material was analyzed by Scanning Electron Microscopy, using a Field Emission Scanning Electron Microscope (FEG-SEM) (Tescan Orsay Holding MIRA 3 - LMU, Czech Republic). For this, fractured impact test samples were used. Images of the surface and the cross-section of the formulations were obtained. The samples were dried in an oven at 105 °C for 24 h, cut and stored in a desiccator for one week. Then they were covered with a thin layer of gold. Acceleration of 10 kV was adopted.The impact test followed the ASTM D256-10 (2018) standard. The analysis was conducted using a 0.5 J pendulum. The specimens without notching were cut with dimensions of 63.5 x 12.5 mm with varying thicknesses. The flexural strength and modulus of elasticity were performed according with ASTM D790:17 standard, using a universal testing machine (INSTRON 5969R, Brazil), operating with a load cell of 500 N. The test was performed with a strain rate of 0.01 mm/mm/min. Five specimens were analyzed, with dimensions of 125 x 25 mm. The samples were previously stored for 48 h at 23 ± 2 °C and 50 ± 5% relative humidity.
The density and the mechanical tests results were submitted to the analysis of variance (ANOVA), with a significance of 95%, and the Tukey Test. Data that do not show significant difference between them were identified with the same superscript.

Results and Discussion
Fig. 1 shows cross-sectional micrographs of the samples. In all formulations, voids were observed, resulting from the water evaporation stage, showing that the material expanded.

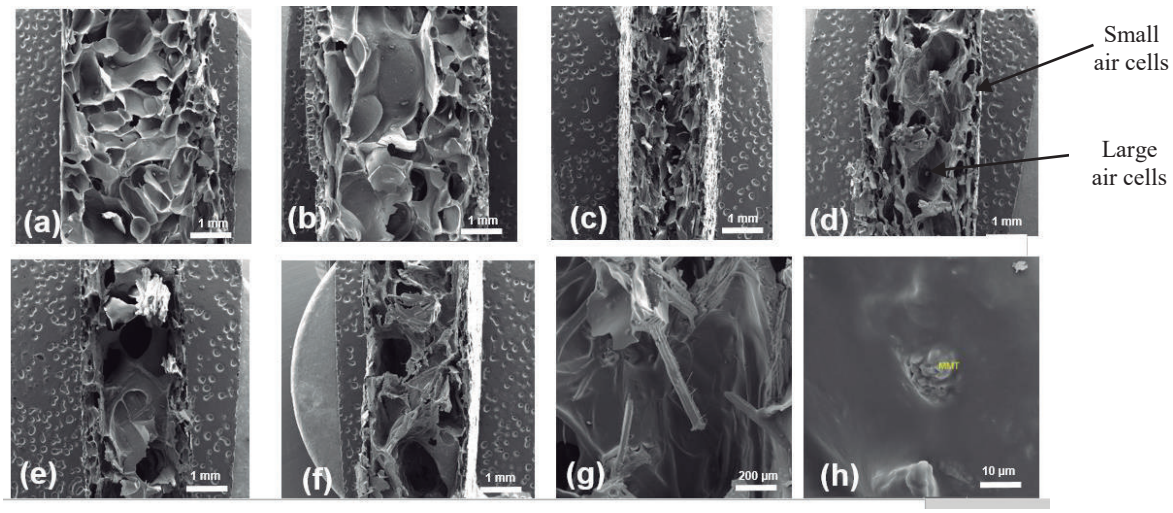

Figure 1. Scanning electron microscopy of the cross-section of the samples at 50x magnification: (a) control; (b) MMT5; (c) F10; (d) F15; (e) F10MMT5; (f) F15MMT5; (g) ramie fiber in the F15 foam; (h) clay in the F15MMT foam.

In samples containing Cloisite® 30B and fiber (Fig. 1 b; c; d; e; f), it was observed a denser outer layer with small air cells, with average diameter of 0,2 mm, while the inner layer is formed by large cells, with diameter between 0,6 and 0,9 mm. This structure, called sandwich, is characteristic of starch foams obtained through thermoforming, has been previously observed in the literature [13,12] and could be explanined by the surface contact with the heated mold, that dries quickly and does not expand a lot [14]. The internal air cells, which are larger and open, are formed with the water vapor liberation, which leads to the rupture of the structure [5, 14].
For the internal structure, the F10 sample presented smaller open cells than the F15 sample. The samples produced with fibers and clays showed large and irregular air cells, which justifies the low density of these foams.
The results of the thickness and density analysis are shown in Tab. 2. The thickness of the samples ranged from 2.46 to 3.80 mm, with a significant difference between the formulations, possibly to

the equipment used in the thermoforming, which did not allow the use of uniform processing conditions. Authors who used a hydraulic press obtained foams with no significant difference in thickness [12].
The starch foam densities ranged between 0.1209 and 0.3211 g/cm^3, in accordance with values reported in the literature [12]. The smallest values for density were presented by samples F15 and F15MMT5, which contain 15% of fibers. Vercelheze *et al.* (2012), who produced starch foams with sodium montmorillonite and sugarcane bagasse fibers, observed the same behavior. The authors attributed this reduction in density to the improvement in expansion capacity with the incorporation of fibers and nanoclays. The F10 sample is denser than the F15. This may be related to the structure (Fig. 1 c; d), in which it is observed that the former has smaller air cells.

Table 2. Thickness, density, impact resistance, modulus of elasticity and flexural strength of starch foams

Sample denomination	Thickness (mm)	Density (g/cm^3)	Impact resistance (J/m^2)	Modulus of elasticity (MPa)	Flexural strength (MPa)
Control	3,82^{a}	0,2286^{b}	177^{c}	109^{a}	1,54^{abc}
MMT5	2,94^{b}	0,3211^{a}	208^{bc}	67^{b}	1,23^{bc}
F10	2,22^{d}	0,2729^{b}	275^{ab}	128^{a}	1,65^{ab}
F15	2,72^{bc}	0,1579^{c}	293^{a}	113^{a}	1,60^{ab}
F10MMT5	2,43^{cd}	0,2290^{b}	311^{a}	62^{b}	0,88^{c}
F15MMT5	2,60^{c}	0,1208^{c}	262^{ab}	54^{b}	0,40^{d}

Tab. 2 also shows the impact resistance results of the starch foams. It was observed that the addition of ramie fibers significantly improved the impact resistance of the foams, as samples F10 and F15 showed an increase of 55.37 and 65.53%, respectively, in relation to the control sample. This behavior may be associated with good dispersion of the fiber in the matrix, as can be seen in Fig. 1 1g. . An increase of 17.5%1 was also verified in the impact resistance of the MMT5 sample in relation to the control sample, possibly associated with the addition of Cloisite® 30B. The same behavior was observed for F10MMT5 sample, which showed resistance 36% higher than F10. In the case of F15MMT5, the opposite occurred, as there was a 31% decrease in relation to F15. This may have occurred because the samples produced with this formulation had large open cells close to the surface and because of the clay agglomeration, observed in Fig.1 .f;h.
Samples F10 and F15 showed the highest values of modulus of elasticity and flexural strength. While the modulus was 3.67 and 17.43%, respectively, higher than the modulus of the control sample, the flexural strength was 3.90 and 7.14% higher. According to Sanhawong *et al.* (2017) this is due to the satisfactory transfer of stresses between the matrix and reinforcement, which occurred due to the good adhesion via hydrogen bonds between the ramie fibers and the starch, and the good dispersion of the reinforcement in the matrix.
The MMT5 sample, which is the densest, showed modulus of elasticity and impact resistance of 38.53 and 20.12%, respectively, lower than the control sample. According to Machado, Benelli and Tessaro (2020), foams with higher densities end up being more rigid and less flexible. This decrease may also be associated with the clusters that were observed in the micrographs (Fig. 1), which may have led to the decrease in these properties.
Despite having low density, samples F10MMT5 and F15MMT5 showed the lowest values of modulus of elasticity and flexural strength. According to Vercelheze *et al.* (2012) the addition of combined fibers to clays may have reduced starch-starch interactions. In the case of the F15MMT5 sample, it could also be related to the large voids close to the surface (Fig. 1). This is because in flexural results, the surface ends up being subjected to the highest stress values [16].

Conclusions

In this work, preliminary studies were carried out on the properties presented by starch foams, with the intention of evaluating the influence of the ramie fiber content and the addition of

Cloisite® 30B on the morphological and mechanical properties of the foams. The foams presented a good visual appearance, with no cracks. The micrographs also indicated the formation of a sandwich-like structure, according with information related in the literature.
The addition of 15% fibers led to a large reduction in density, but the same did not occur for samples containing 10% of this reinforcement. The mechanical properties were greatly influenced by these constituents, as they led to increased impact resistance. The addition of fibers also led to an increase in modulus and flexural strength, while the addition of clays may have led to a reduction in these properties.

Acknowlodgments
The present work was carried out with the support of the Federal Institute of Education, Science and Technology of Rio Grande do Sul (IFRS), and of the Foundation for Research Support of the State of Rio Grande do Sul (FAPERGS) 10/2021 edict, process 22/2551-0000612-4 - AUXÍLIO RECEM-DOUTOR (ARD)).

References

1. H. Cheng.; L Chen; D. J. Mcclements; T. Yang.; Z. Zhang; F. Ren; M. Miao; Y. Tian; Z. Jin. Trends Food Sci. Technol. 2021, 114, 70, http://dx.doi.org/10.1016/j.tifs.2021.05.017.
2. L. Pan; D. Yu; Y. Zhang; C. Zhu; Q. Yin; Y. Hu; X. Zhang; R. Yue; X. Xiong. Sci. Total Environ. 2021, 781, 146753, http://dx.doi.org/10.1016/j.scitotenv.2021.146753.
3. Y. Zhao; J. S. Teixeira; M. Gänzle; M. Saldaña. J Supercrit Fluids 2018, 137, 101, http://dx.doi.org/10.1016/j.supflu.2018.03.010
4. S. Tabasum; M. Younas; M. A. Zaeem; I. Majeed; M. Majeed; A. Noreen; M. N. Iqbal; K. M. Zia. Int. J. Biol. Macromol. 2019, 122, 969, http://dx.doi.org/10.1016/j.ijbiomac.2018.10.092.
5. J. B. ENGEL; A. AMBROSI; I. C. TESSARO. Carbohydr. Polym. 2019, 225, 115234, http://dx.doi.org/10.1016/j.carbpol.2019.115234.
6. A. Cabanillas; J. Nuñez; J. P. Cruz-Tirado; R. Vejarano; D. R. Tapia-Blácido; H. Arteaga; R. Siche. Polym. Compos. 2019, 27, 496, http://dx.doi.org/10.1177/0967391119848187.
7. K. Kaewtatip; C. Chiarathanakrit; S. Riyajan. Powder Technol. 2018, 335, 354, http://dx.doi.org/10.1016/j.powtec.2018.05.030.
8. W. Nansu; S. Ross; G. Ross; S. Mahasaranon. Mater. Today: Proc. 2021, 47, 3594, http://dx.doi.org/10.1016/j.matpr.2021.03.623.
9. BNDES, 1996, http://repositorio.ufu.br/bitstream/123456789/14159/1/d.pdf.
10. C. S. Figueiró, Universidade Federal do Rio Grande do Sul, Porto Alegre, 2021.
11. D. Romanzini**,** Universidade de Caxias do Sul, Caxias do Sul, 2012.
12. Vercelheze, A. E..; Fakhouri, F. M.; Dall'antônia, L. H.; Urbano, A.; Youssef, E. Y.; Yamashita, F.; Mali, S. Carbohydr. Polym. 2012, 87, 1302, http://dx.doi.org/10.1016/j.carbpol.2011.09.016.
13. D. K. M. Matsuda; A. E. Verceheze; G. M. Carvalho; F. Yamashita; S. Mali. Ind. Crops Prod. 2013, 44, 705, http://dx.doi.org/10.1016/j.indcrop.2012.08.032.
14. R. L. Shogren; J. W. Lawton; W. M. Doane; K. F. Tiefenbacher. Polym. 1998, 39, 6649.
15. B. F. Bergel; L. L. Araujo; Santana, R. M. Carbohydr. Polym. Technol. Appl. 2021, 2, 100167, http://dx.doi.org/10.1016/j.carpta.2021.100167.
16. W. Sanhawong; P. Banhalee; S. Boonsang; S. Kaewpirom. Ind. Crops Prod. 2017, 108, 756, http://dx.doi.org/10.1016/j.indcrop.2017.07.046.
17. C. M. Machado; P. Benelli; I. C. J. Tessaro. Biol. Macromol. 2020, 165, 1706, http://dx.doi.org/10.1016/j.ijbiomac.2020.10.048.

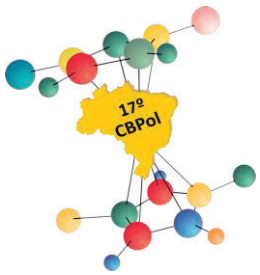

NANOCELLULOSE AEROGELS FROM EUCALYPTUS WASTES: MECHANICAL PERFORMANCE AND CADMIUM REMOVAL

Gabriel D. Lemes[1], Rafaela R. Ferreira[1], Paulo Henrique Camani[1], Derval S. Rosa[1*]

1 – Center for Engineering, Modeling, and Applied Social Sciences (CECS), Federal University of ABC (UFABC), Santo André, Brazil
derval.rosa@ufabc.edu.br

Abstract – Nanocellulose-based aerogels are promising adsorbent materials due to their high mechanical properties and the high removal capacity of pollutants in this water. Therefore, a nanocellulose-based aerogel using biomass-based nanocellulose was obtained by NaOH/urea dissolution, followed by freeze-drying, washing, and freeze-drying, and this aerogel was evaluated from mechanical performance and cadmium removal. The obtained aerogels were structurally stable, with a shrinking rate of 19.2 ± 2.2%, density of 0.1 ± 0.0 $g.cm^{-3,}$ and 95 ± 2% porosity. The material reached a compressive modulus of 26.2 ± 7.4 kPa, compressive strength at a break of 1012.5 ± 12.0 kPa, and 85.5 ± 2.3% compressive strain. A 100% cadmium (II) adsorption rate was achieved for higher adsorbent dosages (0.5 g) and concentrations of contaminants (100 ppm). A possible adsorption mechanism may be linked to the high density of available hydroxyl groups, showing nanocellulose-based aerogels as a possible robust green alternative adsorbent for cadmium (II) contaminated waters.
Keywords: a*erogel; nanocellulose; adsorption.*
Fundings: *FAPESP - 2019/16301-6, 2022/01382-3, and 2020/13703-3, CNPq - 308053/2021-4 and 403934/2021-4, and CAPES.*

Introduction

One of the most intriguing properties of aerogels is their high surface area. It provides many applications, such as thermal and acoustic insulation, gas adsorption, remediation of contaminated areas, sorption and desorption of metal ions and drugs in the body, energy storage, and catalysis [1]. It can also be easily separated from an aqueous solution and has a low processing cost, making it an ideal adsorbent solution widely used for removing organic and inorganic pollutants from contaminated water. Aerogels are versatile materials, where several factors such as precursor materials and their proportion, processing techniques, drying methods, additives, and crosslinkers, among others, can change their intrinsic characteristics, highlighting the pore size, surface area, and consequently, its final properties such as density, shrinkage rate, mechanical performance, and removal of PTEs [3,4]. Therefore, the objective of this work is the applicability of a nanocellulose aerogel from eucalyptus residues for mechanical performance in compression and removal of bivalent cadmium from simulated water.

Experimental

Cellulose nanostructures isolation and nanocellulose-based aerogel synthesis

For the isolation of cellulose nanostructures, the eucalyptus sawdust residue was first subjected to microwave-assisted pre-treatments, in which mercerization with sodium hydroxide was applied, followed by bleaching with hydrogen peroxide [4]. After obtaining the pre-treated fibers, they were subjected to two subsequent mechanical methodologies for isolating cellulose nanostructures. 2% (m/m) of the pre-treated fibers were dispersed in an aqueous solution and first subjected to homogenization at high shear rates using an Ultra-Turrax (Model T 25 digital, IKA) at 10,000 rpm for 20 minutes [5]. The same solution was taken to ultrasonication, performed in a high-intensity

ultrasound SONIC-750W, Vibracell, Sonics (MRC Ltd, Holon, Israel), using the power of 100 KJ, frequency of 70% at 60 °C, during 30 and 60 minutes [6]. Nanocellulose was prepared in duplicate. Therefore, for the synthesis of nanocellulose aerogels (Fig. 1), 6 g of nanocellulose were homogenized in 40 mL of an alkaline solution of NaOH (3.4 g) and urea (6.0 g) pre-cooled at -12 °C using a water ice bath. The solution was maintained at low temperatures (between 0 and -12 °C) until complete homogenization of the cellulose, which then received volumes of 1 mL of pure epichlorohydrin, being homogenized again. The mixtures were ultrasonicated using a high-intensity ultrasound (Sonics 750 W, Vibracell, Sonics) for 10 and 20 min, at a power of 100 kJ, with an amplitude of 40%, and then subjected to mechanical stirring for 1 h. The homogenized dispersion rested for 3 h. The resulting dispersions were neutralized with an acid HCl solution (10 mol.L^{-1}), adjusting the pH of the samples. The resulting colloidal solutions were frozen in molds at -6°C for 24 h and taken to freeze-drying at -98°C for 48 h, using a lyophilizer (Lyophilizer Liotop K105) to obtain nanocellulose aerogels. After freeze-drying the nanocellulose hydrogels, the samples were immersed in distilled water three times to remove the excess crosslinking agent [7].

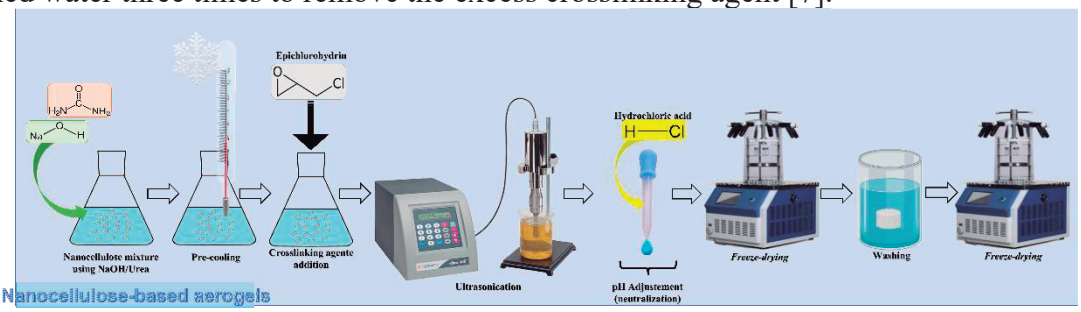

Fig. 1. Illustrative scheme of nanocellulose aerogel preparation using eucalyptus-based wastes.

Results and Discussion

The nanocellulose aerogel obtained a stable, dense, and continuous interconnected structure [8], as found by Dilamian and Nozoori. In addition to the stable and dense structure obtained, an acceptable shrinkage rate for aerogel is 25% [9], so the aerogel developed in this work had a shrinkage rate of 19.2 ± 2.2%, that is, 5.8% lower than the acceptable shrinkage rate, showing less impact of the freeze-drying process, as well as the stability of the crosslinked structure of the aerogel. The aerogel also obtained apparent density and porosity of 0.1 ± 0.0 g.cm^{-3} and 95 ± 2%, respectively. Besides, Fig. 2 shows the stress versus deformation curves for the nanocellulose aerogel to evaluate the mechanical performance of nanocellulose aerogels.

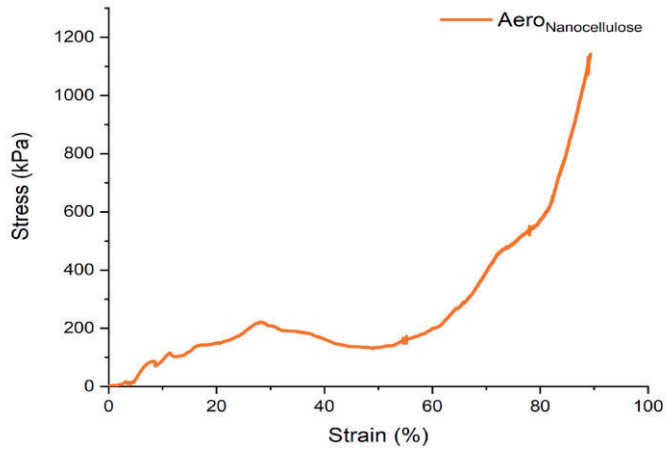

Fig. 2. Stress (KPa) versus strain (%) for nanocellulose aerogel.

Evaluating the aspect of the stress versus strain curve shown in Fig. 2, three distinct regions are verified, with emphasis on linear elasticity, flow, pore densification, and collapse [10]. As for the mechanical performance values, Table 1 elucidates the values of compressive modulus, maximum strength at break, and compressive strain, respectively.

Table 1. Mechanical compressive performance values for nanocellulose aerogel.

Mechanical Performance Values	**Aero$_{Nanocellulose}$**
Compressive Modulus (kPa)	26.2 ± 7.4
Compressive Strength at Break (kPa)	1012.5 ± 12.0
Compressive Strain (%)	85.5 ± 2.3

The compressive modulus reached 26.2 ± 7.4 kPa, consistent with the literature that reached values close to 44 kPa, attributing this lower result to the highly porous structure and higher pore volume [11]. Therefore, one hypothesis that explains the low modulus is the high porosity and pore density [12], which generates a higher concentration of compressive stress in the pore structure, decreasing its rigidity, that is, making the material more fragile.

In addition to changing the compressive modulus, the compressive strength at break reached values of 1012.5 ± 12.0 kPa and compressive strain of 85.5 ± 2.3 %, respectively. A hypothesis observed by the modulus is the high porosity, as well as the average pore size, which allows the aerogels to have greater deformation. In addition, as a higher proportion of nanocellulose by weight was used to develop the aerogel, there is a greater densification of the structure [13], and together with the increase in relative crystallinity, this leads to a better mechanical performance of this aerogel.

From the adsorption systems of the bivalent cadmium ion [Cd(II)], the nanocellulose aerogel was tested as an adsorbent. After the respective adsorption times, the evaluation of the adsorption capacity and adsorption/removal efficiency were performed by Inductively Coupled Plasma Mass Spectroscopy (ICP-MS).

First, for the system that contained only TNT (without the presence of the nanocellulose aerogel), it showed imprecision and a large analytical deviation after 48 h of testing and at an initial concentration of 20 ppm, reaching an adsorption capacity of 0.03 ± 0.05 mg.g^{-1} and efficiency of 0.2 ± 0.3%. For an initial concentration of 100 ppm, after 48 h of testing, an adsorption capacity of 1.2 ± 1.0 mg.g^{-1} and an efficiency of 10.0 ± 6.1 % were achieved. Possibly the TNT (non-woven fabric), which is made of PP, only absorbed the content on its surface (in some cases), due to the wettability of its fibers by water. Wei and co-workers stated that TNT made from PP has characteristics such as disordered fiber structure, high specific surface, low cost, and degradable nature, but due to its hydrophobicity and inert chemical structure, these result in low affinity with water and adsorption of metals [14]. Table 2 and 3 shows values of adsorption capacity and efficiency for the systems containing the bivalent cadmium ion at the initial concentration of 20 ppm and 100 ppm, varying the dosage, related to the measured times, respectively.

Table 2. Results of adsorption capacity (mg.g^{-1}) for the systems containing the bivalent cadmium ion at the initial concentration of 20 ppm and 100 ppm, varying the dosage, related to the measured times, respectively.

Adsorption Capacity (mg.g^{-1})		
Systems with an Initial Concentration of 20 ppm	**t = 12 h**	**t = 48 h**
Aero$_{Nanocellulose\ W0.5\ g}$	1.1 ± 0.1	1.1 ± 0.1
Aero$_{Nanocellulose\ W3.0\ g}$	0.7 ± 0.4	0.7 ± 0.4
Systems with an Initial Concentration of 100 ppm	**t = 12 h**	**t = 48 h**
Aero$_{Nanocellulose\ W0.5\ g}$	5.4 ± 0.8	5.4 ± 0.8
Aero$_{Nanocellulose\ W3.0\ g}$	2.6 ± 0.1	3.1 ± 0.9

Table 3. Results of adsorption efficiency (%) for the systems containing the bivalent cadmium ion at the initial concentration of 20 ppm and 100 ppm, varying the dosage, related to the measured times, respectively.

Adsorption Efficiency (%)		
Systems with an Initial Concentration of 20 ppm	**t = 12 h**	**t = 48 h**
$Aero_{Nanocellulose\ W0.5\ g}$	100.0 ± 0.0	100.0 ± 0.0
$Aero_{Nanocellulose\ W3.0\ g}$	100.0 ± 0.0	100.0 ± 0.0
Systems with an Initial Concentration of 100 ppm	**t = 12 h**	**t = 48 h**
$Aero_{Nanocellulose\ W0.5\ g}$	100.0 ± 0.3	100.0 ± 0.1
$Aero_{Nanocellulose\ W3.0\ g}$	100.0 ± 0.0	100.0 ± 0.0

Evaluating the adsorption capacity (Table 2) of the nanocellulose aerogel, regarding the adsorption time, no difference was noticed between 12 and 48 h of contact between the aerogel and the aqueous solution containing the bivalent cadmium. It is due to the adsorption saturation process of the nanocellulose aerogel in 12 h of contact. Mo and co-workers observed the same adsorption equilibrium phenomenon in 10 h of contact of cellulose nanofibrils aerogels obtained by oxidation with TEMPO [15]. As for the adsorbent weight used, the aerogel containing less weight (0.5 g) had better adsorption capacity than the aerogel containing 3.0 g of dosage. According to Shanmugarajah and co-workers, increasing the dosage of nanocellulose can increase the active sites available for dye molecules to interact, improving the removal efficiency. However, if it has a high dosage, there is the possibility of aggregation and agglomeration of cellulose nanostructures, resulting in a decrease in removal, occurring mainly in the length of the diffusion path of molecules into the adsorbent [16].
Comparing the initial concentration of divalent cadmium ion, an increase of 4.9 and 3.5 times in the adsorption capacity was verified for comparing the adsorbent weight of 0.5 g and 3.0 g, in a time of 12 h. Wang and co-workers observed the same trend, in which as the concentration of hexavalent uranium contaminant increased, an increase in the adsorption capacity was verified due to the greater amount of ions available for interaction with the free hydroxyls present in the nanocellulose aerogel [17].
Considering the adsorption efficiency (%) of the nanocellulose aerogel, highlighted in Table 3, no difference was verified in any of the cases, that is, in all conditions, even with variations in adsorbent weight, adsorption time and concentration initial contaminant, in all cases the efficiency was 100% of adsorption. This result of 100% adsorption efficiency is due to the high removal of cadmium ions from the contaminating aqueous solution. Geng and co-workers achieved excellent removal of cadmium ions by using nanocellulose aerogels modified by amino radicals and silanes [18]. However, excellent removal was achieved without modification of the nanocellulose. Comparing the nanocellulose aerogel developed in this work with other adsorbents, the composite aerogel of reduced graphene oxide and montmorillonite achieved the removal of 93% of cadmium ions, which is lower than what was achieved by the nanocellulose aerogel. It is possibly due to the presence of a high density of hydroxyl groups in the nanocellulose structure, which interacted with cadmium ions, effectively removing it from aqueous environments.

Conclusions

As a green alternative, nanocellulose aerogels had lower density, higher porosity, and a shrinkage rate of less than 25%, characterizing it as an efficient aerogel. Evaluating the mechanical performance, capacity, and removal efficiency, the nanocellulose aerogel generated excellent mechanical properties, whose maximum resistance to compression reached an increase of 31 times compared to aerogels described in the literature. Furthermore, an efficiency of 100% of cadmium (II) adsorption was achieved, exceptionally for higher adsorbent dosages (0.5 g) and higher concentrations of contaminants (100 ppm). Therefore, its possible adsorption mechanism consists of the high density of available hydroxyl groups of nanocellulose, which have a better affinity with

divalent cadmium. These results show that nanocellulose aerogel is an excellent candidate to be applied as an adsorbent for water contaminated with divalent cadmium ions, as well as having excellent mechanical strength, and still has a sustainable appeal due to the lignocellulosic waste raw material that nanocellulose was isolated.

Acknowledgements
This research was financed by Fundação de Amparo à Pesquisa do Estado de São Paulo (FAPESP) (2019/16301-6, 2022/01382-3, 2020/13703-3), Conselho Nacional de Desenvolvimento Científico e Tecnológico (CNPq) (308053/2021-4 and 403934/2021-4), and Coordenação de Aperfeiçoamento de Pessoal de Nível Superior (CAPES) (Finance Code 001). The authors thank the technical support of the Multiuser Experimental Center of UFABC (CEM-UFABC), CECS (UFABC), and REVALORES for assistance.

References
1. P. H. Camani; M. G. Gonçalo; R. F. Barbosa; D. S. Rosa. Journal of Applied Polymer Science 2021, 138(34), 50863. https://doi.org/10.1002/app.50863.
2. H. Liu; B. Geng; Y. Chen; H. Wang. ACS Sustainable Chemistry & Engineering 2017, 5(1), 49-66.https://doi.org/10.1021/acssuschemeng.6b02301.
3. M. Mariana; A. K. HPS; E. B. Yahya; N. G. Olaiya; T. Alfatah; A. B. Suriani; A. Mohamed. Journal of Water Process Engineering 2022, 45, 102481. https://doi.org/10.1016/j.jwpe.2021.102481
4. P. H. Camani; B. F. Anholon; R. R. Toder; D. S. Rosa. Cellulose 2020, 27, 3591-3609. https://doi.org/10.1007/s10570-020-03019-7.
5. M. Mahardika; H. Abral; A. Kasim; S. Arief; M. Asrofi. Fibers 2018, 6(2), 28. https://doi.org/10.3390/fib6020028.
6. I. Filipova; V. Fridrihsone; U. Cabulis; A. Berzins. Nanomaterials 2018, 8(9), 640. https://doi.org/10.3390/nano8090640.
7. D. Ciolacu; F. Doroftei; G. Cazacu; M. Cazacu. Cell. Chem. Technol 2013, 47, 377-386.
8. M. Dilamian; B. Noroozi. Carbohydrate Polymers 2021, 251, 117016. https://doi.org/10.1016/j.carbpol.2020.117016.
9. J. P. Vareda; A. Lamy-Mendes; L. Durães. Microporous and Mesoporous Materials 2018, 258, 211-216. https://doi.org/10.1016/j.micromeso.2017.09.016.
10. W. Sakuma; S. Yamasaki; S. Fujisawa; T. Kodama; J. Shiomi; K. Kanamori; T. Saito. ACS Nano 2021, 15(1), 1436-1444. https://doi.org/10.1021/acsnano.0c08769.
11. F. Jiang; Y. L. Hsieh. ACS Applied Materials & Interfaces 2017, 9(3), 2825-2834. https://doi.org/10.1021/acsami.6b13577.
12. R. Ghafari; M. Jonoobi; L. M. Amirabad; K. Oksman; A. R. Taheri. International Journal of Biological Macromolecules 2019, 136, 796-803. https://doi.org/10.1016/j.ijbiomac.2019.06.104.
13. A. E. Donius; A. Liu; L. A. Berglund; U. G. Wegst. Journal of the Mechanical Behavior of Biomedical Materials 2014, 37, 88-99. https://doi.org/10.1016/j.jmbbm.2014.05.012.
14. P. Wei; H. Lou; X. Xu; W. Xu; H. Yang; W. Zhang; Y. Zhang. Applied Surface Science 2021, 539, 148195. https://doi.org/10.1016/j.apsusc.2020.148195.
15. L. Mo; H. Pang; Y. Tan; S. Zhang; J. Li. Chemical Engineering Journal 2019, 378, 122157. https://doi.org/10.1016/j.cej.2019.122157.
16. B. Shanmugarajah; I. M. Chew; N. M. Mubarak; T. S. Choong; C. Yoo; K. Tan. Journal of Cleaner Production 2019, 210, 697-709. https://doi.org/10.1016/j.jclepro.2018.10.342.
17. Y. Wang; Y. Li; Y. Zhang; Z. Zhang; Y. Li; W. Li. Carbohydrate Polymers 2021, 267, 118233. https://doi.org/10.1016/j.carbpol.2021.118233.
18. B. Geng; Z. Xu; P. Liang; J. Zhang; P. Christie; H. Liu; S. Wu; X. Liu. International Journal of Biological Macromolecules 2021, 190, 170-177. https://doi.org/10.1016/j.ijbiomac.2021.08.186.

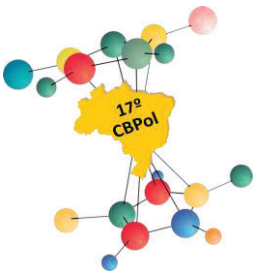

PAAM/RHA HYDROGELS AS AN INTERNAL CURING AGENT IN MORTARS AND CONCRETES

Edson A. de Almeida[1*], Fábio R. Krunger[2], Regiane da S. Gonzalez[3] and Edvani C. Muniz[1,4]

1 – Department of Chemistry, State University Maringá (UEM), Maringá, PR, Brazil
edsonalmeida2009@gmail.com
2 – Department of Civil Construction, Federal Technological University of Paraná (UTFPR-CM), Campo Mourão, PR, Brazil
3 – Department of Chemistry, Federal Technological University of Paraná (UTFPR-CM), Campo Mourão, PR, Brazil
4 – Department of Chemistry, Federal University of Piaui (UFPI), Teresina, PI, Brazil

Abstract

Internal curing is a process that consists of adding a material to the cement mixture that is capable of releasing water during the process of hardening the mixture, having as function to reduce effects of water lost through evaporation and self-desiccation. Hydrogels are polymeric materials able to absorb and release water, becoming a good material to promote internal healing at cement mixture. In this work, the use of a polyacrylamide hydrogel with rice husk ash as an internal curing agent for mortars and concrete was studied, with the aim of studying whether this material can contribute to the hydration process of the cementitious medium, as well as its influence on the final product. The analysis of the results showed that the hydrogel contributes to the mortar hydration process, thus providing an increase in mechanical strength and reduction of shrinkage, while for concrete a reduction in mechanical strength was obtained.

Keywords: *Hydrogel, Mortar, Concrete, Polyacrylamide, Resistance.*

Introduction

Internal curing is a process that consists of supplying water to the cementitious medium using some material present in the mixture of the cementitious formulation [1]. This material works as a water reservoir, capable of releasing water contributing to the medium hydration, thus supplying the water lost by evaporation or self-desiccation [2].

Different materials can be used as an internal curing agent, but hydrogels have been gaining prominence in this application [2]. Hydrogels are polymeric materials that have a three-dimensional structure and can quickly absorb water and releasing the absorbed water in a controlled way [3]. The ability from hydrogel to retain water and/or aqueous liquid causes it to acquire a size and weight greater than its own weight and dry size [4]. This property is quantified through the swelling ratio (Q), or water uptake (WU), that can achieve more than 3,000 fold.

Thus, hydrogels are potential candidates to be used as an internal curing agent. This work aims to use rice husk ash-containing polyacrylamide hydrogel (PAam/RHA) to be applied as an internal curing agent for mortars and concrete, maintaining the same water/cement ratio (w/c) and to study its influence on mechanical properties and shrinkage.

Experimental

Materials

The materials used: Portland cement CP II-Z type, Brazilian standard sand, commercial sand, crushed stone, water and hydrogel containing rice husk ash. The hydrogel synthesized from the polymerization acrylamide monomer (AAm), the crosslinking agent N,N'-methylenebisacrylamide (MBAAm, at 1 wt-%), and addition of 10 wt-% rice husk ash (obtained at a temperature of 600 °C). After synthesis, the hydrogels were dried and ground to sizes of less than 250 mesh. The degree of swelling value of the hydrogels was about 13.5 g/g.

Methods

Mortar and concrete Production

Table 1 shows the mass ratio of the materials used to prepare the cementitious media. The cement pastes were prepared by mixing cement, water and hydrogel. To prepare mortars and concrete, the procedures follow the scheme shown in Fig. 1.

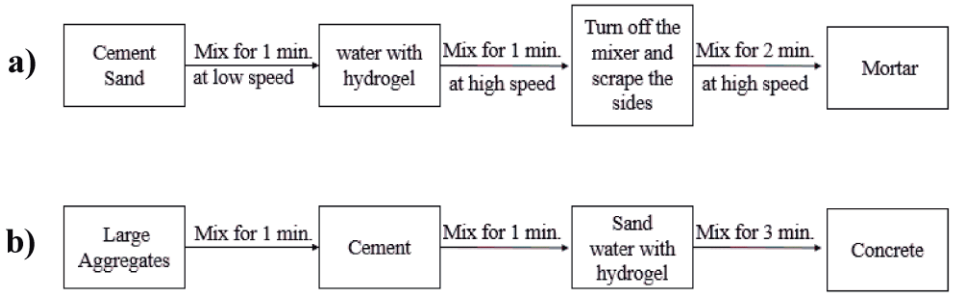

Figure 1. Procedure for preparing: a) mortar; b) concrete.

The hydrogel was swollen in water until it reached equilibrium (20 hours), before preparing the cementitious medium. After carrying out the molding process, the specimens were properly identified and stored in the same place, under the same environmental conditions, with room temperature between 14 and 23 °C, and relative humidity ranging from 65 to 79 %.

Compression test

The procedures for the mortar compression test followed the NBR 7219/1996 [5] standard and the compression tests for the concrete followed the NBR 5739/1994 [6] standard. For this test, cylindrical specimens were used (with dimensions of 100 mm in height and 50 mm in diameter for mortars, and 200 mm in height and 100 mm in diameter for concrete).

The compressive strength was determined using an EMIC test machine model Pc 100. The analyzes were carried out in quadruplicate at ages 7, 28 and 45 days for mortar and 7 and 28 days for concrete. The strength was calculated considering the breaking load as a function of the cross-sectional area of the specimen.

Retraction test

The retraction tests for the mortar followed the procedures described in the NBR 15261/2005[7] standard, and prismatic specimens were used. The amount of shrinkage (or expansion) was determined from the average of triplicates for ages 7 and 28 days. The retraction or expansion was obtained by equation 1

$$\varepsilon_i = (L_i - L_0) / 0.25 \qquad (1)$$

where ε_i is the dimensional measurement that can indicate retraction (negative values) or expansion (positive values), measured at age "$_i$", Li is the measurement performed at age "$_i$" and L_0 and the measurement performed after the body is removed-test (age 0).

Table 1: Mass and volume proportions among the components for the production of mortar and concrete.

Cement medium		w/c ratio	Trace			Hydrogel %
			Cement	Sand	Crushed stone	
Mortar (w/w)	Mort-Ref	0.48	1	3	-	0
	Mort-001	0.48	1	3	-	0.01
	Mort-003	0.48	1	3	-	0.03
	Mort-01	0.48	1	3	-	0.1
Concrete (v/v)	Conc-Ref	0.48	1	2	3	0
	Conc-003	0.48	1	2	3	0.03

Results and Discussion

Compression Test

Fig. 2a shows the result for the the mortar compression test at 7, 28 and 45 days. The addition of PAAm/RHA hydrogel was able to change the mechanical strength of the mortar. It was observed that the addition of 0.1% hydrogel at the age of 7 days leads to a not harmful but a small mechanical resistance reduction, once that resistance after completed healing (28 days) was higher than the reference mortar.

Through the results obtained, it can be said that the addition of hydrogel in the mortar is able to eliminate the effects caused by the loss of water by evaporation, thus acting in the hydration process of the mortar, thus guaranteeing an improvement in the mechanical resistance [8].

It is important to point out that the results obtained refer to mortars with the same w/c ratio, that is, the same amount of water was used for all prepared mortars and the hydrogels were swollen in the water used to prepare the mixtures to really guarantee that no extra water was added. This fact becomes important to evaluate the influence of the hydrogel on the mechanical properties of mortars [9].

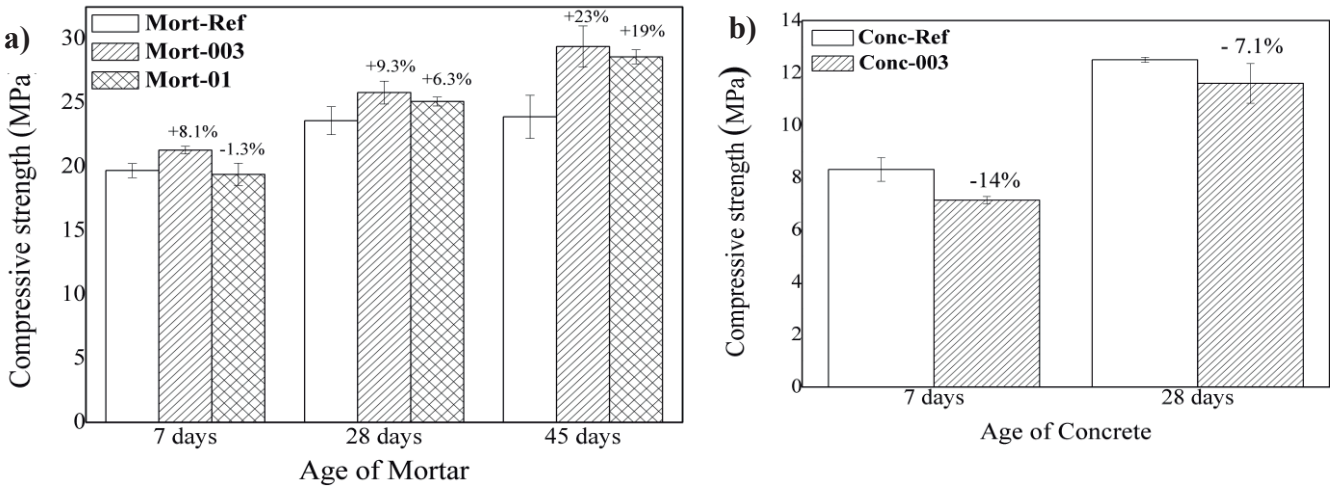

Figure 2. Compressive strength: a) for mortars with addition of PAAm/RHA b) for the reference concrete and for the concrete added with 0.03 % with addition of PAAm/RHA hydrogel, at the ages of 7 and 28 days.

One aspect that is little considered, in literature, is the chemical structure of the hydrogel used as an internal healing agent [4]. The chemical structure can influence the ability to absorb and release water from the hydrogel. Consequently, the matrix shrinks, after water being released, will form larger voids, thus impairing the mechanical strength of the materials. The PAAm/RHA hydrogel has a low degree of swelling and provides hydration of the environment without the formation of large pores/voids in the mortar matrix.

Fig. 2b showing the results for the concrete pressure test at 7 and 28 days unlike mortars, there was no increase in resistance, but a reduction, this may be linked to the inherent microcracks of the material, which can be enhanced by the formation of voids close to these micro-cracks, thus causing a reduction in resistance. It can still be observed that the resistance of the concrete was lower than that of the mortar, this difference may be linked to the quality of the materials used in the preparation of the concrete [10].

Retraction test

The shrinkage test was carried out for the mortars with the addition of two levels (0.03% and 0.1%) of hydrogel for the ages of 7 and 28 days. The test result is shown in Table 2. The shrinkage data for the mortar with hydrogel addition and without hydrogel are close, however, it can be noted that the addition of 0.03% caused a slight reduction in shrinkage, indicating that the hydrogel can be used to reduce shrinkage in cementitious medium.

Table 3. Results of the retraction test.

Mortar	**7 days (mm)**	**28 days (mm)**
Mort-Ref*	-0.42 ± 0.15	-0.44 ± 0.20
Mort003	-0.34 ± 0.15	-0.38 ± 0.15
Mort-Ref**	-0.27 ± 0.05	-0.41 ± 0.06
Mort01	-0.24 ± 0.06	-0.40 ± 0.04

(*) tests carried out with the same climatic condition as Mort003;
(**) tests carried out with the same climatic condition as Mort01;

The small reduction in shrinkage for the 0.03% content is yet another indication that the hydrogel improves the hydration of the cement medium, since the shrinkage process is linked to

self-drying. Still through the data presented in Table 2, it can be noted that the studied contents were not capable of delaying the retraction of the mortars. However, existing data from other studies demonstrating that the addition of contents superior to 0.1% of hydrogel can eliminate completely the retraction process [11-12].

Conclusions

The addition of small amounts of PAAm/RHA hydrogel in mortars containing the same w/c ratio promoted an increase in mechanical strength and a potential to be used to prevent shrinkage, thus indicating that the PAAm/RHA hydrogel was able to act with internal curing agent. As for concrete, the addition of hydrogel was not efficient, causing a reduction in strength. However, this does not indicate a failure of the material with an internal curing agent, but that it can potentiate an inherent failure of the material itself.

Acknowledgements

The authors are grateful to Capes (for the Master fellowships of EAA). ECM is grateful to CNPq for the financial supporting, Grant #408767/2021-9, #402030/2022-2, and #307429/2018-0. EAA is grateful to UTFPR-CM for laboratory facilities for material preparation and some characterizations.

References

1. P. F. Silva Junior. Ph.D. Thesis, University of Brasilia, 2017.
2. A. Danish; M. A. S. Mosaberpanah; M. U. Salin Journal of Materials Science, 2020, 56(1), 136-172. https://doi.org/10.1007/s10853-020-05131-2.
3. M. R. Guilherme; F. A. Aouda; A. R. Farjado; A. F. Martins; A. T. Paulino; M. F. T. Davi; A. F. Rubira; E. C. Muniz European Polymer Journal, 2015, 72(11), 365-385. https://doi.org/10.1016/j.eurpolymj.2015.04.017
4. C. Spagnol; F. H. A. Rodrigues; A. G. V. C. Neto; A. G. B. Pereira; A. R. Farjado; E. Radovanovic; A. F. Rubira; E. C. Muniz European Polymer Journal, 2012, 48(3), 454-463. https://doi.org/10.1016/j.eurpolymj.2011.12.005
5. L. B. Agostinho; F. G. Borges; E. F. Silva; D. V. M. R Cupertino Revista Matéria, 2020, 25(4), 1-12. https://doi.org/10.1590/S1517-707620200004.1160
6. M. A. Calesco; A. Watanuki Filho; M. R. Moura; F. A. Aouada Cerâmica, 68(385), 97-107 https://doi.org/10.1590/0366-69132022683853161.
7. A Koppe; M. Mancio; T. L. A. C. Rocha; F. Brehm in Proceedings of 9th National Meeting, 7th Latin American Meeting, 2nd Latin American Meeting and European on Buildings and Sustainable Communities, São Leopoldo, 1403-1413.
8. X. Ma; J. Liu; Z. Wu; C. Shi Construction and Building Materials, 2017, *131*(2), 476-484. https://doi.org/10.1016/j.conbuildmat.2016.11.090
9. B. L. Agostinho. M.Sc. Dissertation. University of Brasilia, 2017.
10. V. Mechtcherine; M. George; C. Schroef; A. Assmann; W. Brameshuber; A. B. Ribeiro; D. Cusson; J. Custódio; E. F. Silva; K. Ichimiya; S. Klemm; K. Klover; A. N. M. Lopes; P. Lura; V. T. Nguyen; H. W. Reinhardt; R. D. Toledo-Filho, J. Weiss; M. Wyrzykowski; G. Ye; S. Zhutovsky Materials and Structures, 2013. 42(3), 541-562. https://doi.org/10.1617/s11527-013-0078-5
11. J. Liu; Z. Ou; J. Mo; Y. Wang; H. Wu Construction and Building Materials, 155(26), 239-249. https://doi.org/10.1016/j.conbuildmat.2017.08.061
12. J. Justs; M. Wyrzykowski; D. Bajare; P. Lura Cement and Concrete Research, 76(10), 82-90 https://doi.org/10.1016/j.cemconres.2015.05.005

PBAT BIOCOMPOSITES WITH BRAZIL NUT SHELL FIBERS (CP)

Gabriela M. dos Santos[1*], Paula A. M. Alves[1], Cléverson F. S. Gabriel[1] and Marcia G. de Oliveira[1]

1 – Polymeric Materials Technology Laboratory (LAMAP), Materials Division (DIMAT), Materials Technology Coordination (COTEM), National Institute of Technology (INT), Rio de Janeiro, RJ, Brazil
gabriela.moura@int.gov.br

Abstract
The constant search for materials with a set of improved properties has increased research on fiber reinforcement composites. In this work, composites with different fillers contents (5, 10 and 15%) were produced with poly(butylene adipate-co-terephthalate) (PBAT) and Brazil nut shell fibers (CP). The effects of adding different grades of residue on the mechanical and rheological properties of the material were analyzed. The filler was classified with particle size under 75 µm and its chemical structure and thermal stability were evaluated. Regarding the mixture processability analysis, all evaluated composites presented very close torque curves, indicating that possibly the polymeric matrix would have the capacity to incorporate a greater amount of filler without a considerable disturbance of the system. For the mechanical properties, the addition of CP caused a decreased in the tensile strength and elongation valor compared to pure PBAT. Despite these lower results, the Brazil nut can be an economic and sustainable alternative as commercial filler depending on the minimum properties required by the final product.

Keywords: *Brazil Nut, PBAT, Biodegradable Polymer, Mechanical Properties, Natural Fiber Composites.*

Introduction

To meet the market's need to have different properties gathered in the same material, composites are gaining prominence in the development of research and increasingly space in the input market for industries. Blending of biodegradable polymers as well as using low-price organic fillers aiming to produce cost-effective composites, besides being an alternative to solve pollution issues, might be a method of developing products with superior mechanical properties [1].

The use of natural resources for the production of polymeric composites is an alternative of great technological importance, for being a renewable, recyclable, biodegradable and low-cost source. The Brazil nut is widely used as food and in cosmetic industries. The seeds are rich in lipids and protein, and also present a considerable amount of selenium. The production of Brazil nut is a result of extractive activities and has become one of the main commercial products from the northern region of Brazil [1, 2]. To date, there are very few research on the use of Brazil nut (CP) as filler in polymeric compositions, in particular, in biodegradable polymers such as PBAT.

The poly(butylene adipate-*co*-terephthalate) (PBAT) is a synthetic and biodegradable aliphatic aromatic copolyester consisting of two types of comonomer, a rigid butylene terephthalate segment consisting of 1,4-butanediol and terephthalic acid monomers and the flexible butylene adipate section consisting of 1,4-butanediol and adipic acid monomers. This material has properties similar to nonbiodegradable polymers like polyethylene with high ductility and low modulus of elasticity. However, the low heat resistance, inferior rigidity and its high price compared to other polymers in the same segment on the market are the major shortcomings of PBAT to extend its applications [3].

In order to address pollution issues and develop products with superior mechanical properties, the use of biodegradable polymers in combination with low-price organic fillers is an alternative to

produce cost-effective composites. Therefore, the goal of this work was to develop a biocomposite of PBAT and Brazil Nut Shell Fibers (CP), and to evaluate the influence of different proportions of this agroforestry residue (5, 10 and 15%) on the mechanical and rheological properties of this material.

Experimental

The CP was received in natura, and the first step was the manual separation of the nut and shell. Then the shell was processed in a RETSCH MM400 mill and its granulometry classification was carried out, being used in this work the fraction below 75 μm. The filler was characterized by Fourier transform infrared spectroscopy (FTIR) on the THERMO NICOLET Nexus 470 equipment, using the KBr matrix pressed disk method, at the sample:matrix ratio of 1:100, in transmittance mode, range reading from 4000 to 400 cm^{-1} and 32 scans; and thermogravimetric analysis (TGA), which was performed on the NETZSCH STA409 PC in a flow stream from room temperature to 560°C, with a heating rate of 10°C/min and N_2 atmosphere. The PBAT and composites were prepared by melt intercalation in an internal mixing chamber coupled to a torque rheometer Haake Polylab OS. The rotor used was the Roller type, at 140°C, with a speed of 80 rpm for 15 minutes. The formulations were 0, 5, 10 and 15 phr (parts per hundred resin) of Brazil nut shell fibers per 100 phr of PBAT, and were named PBAT, PBAT5CP, PBAT10CP and PBAT15CP respectively. The specimens for the mechanical tests and the rheological analysis were molded by compression, according to their respective standards, in a hydraulic press MA 098/A400 with a pressure of up to 55 MPa at 140°C, for 10 minutes in the hot press and then cooled using the same pressure and time in the cold press. For the rheological analysis, was used an Anton Paar MCR301 rheometer with a model CTD450 furnace as an accessory with 25 mm parallel plate geometry. All tests were carried out at 140°C. Complex viscosity (η*) was measured through a strain variation test from 0.01% to 500%, at a constant frequency of 1Hz. The storage modulus (G') and the Loss modulus (G”), were measured through an angular frequency variation test from 0.1 to 100 rad/s, in the linear viscosity region (10% constant strain). The tensile strength test was carried out according to ASTM D638 standard using the type V specimen, in a mechanical testing machine EMIC DL3000 with a 1000 N load cell and a speed of 100 mm/min.

Results and Discussion

Brazil Nut Shell Fibers Analysis

The CP infrared spectrum is shown in Fig 1A and the thermogravimetric analysis in Fig 1B. Regarding the infrared analysis, it is possible to observe absorption bands at 3300 cm^{-1} referring to hydroxyl groups of cellulose, hemicellulose and lignin; at 2950 cm^{-1} referring to C-H bondings; at 1550 cm^{-1} C=C bonds of lignin aromatic groups; and at 990 cm^{-1} C-O-C bonds associated with lignin and hemicellulose [4].

Regarding the thermal analysis, the fiber shows a degradation in three phases; the first referring to water loss up to 150ºC, the second referring to hemicellulose degradation (from 150 to ≈380ºC) and the third referring to lignin degradation and total cellulose degradation (from 380 to 560ºC). The material presented a residue of 5.8% [4].

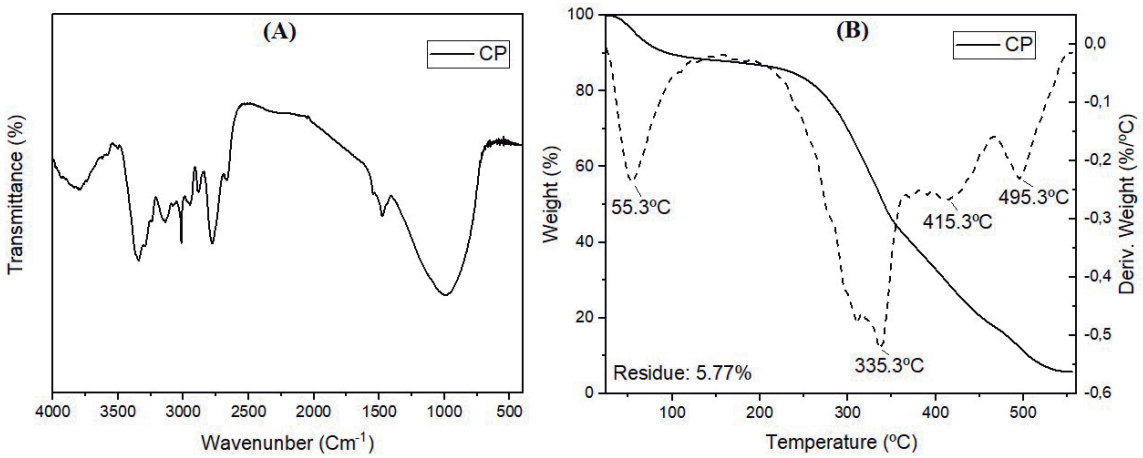

Figure 1 – A: FTIR; B: TGA of Brazil nut shell fibers.

Mixture Processability Analysis

The analysis of the processability of the mixture consists of evaluating the variation in torque required to keep the equipment rotation constant (Fig 2A) and the specific energy associated with this torque (Fig 2B).

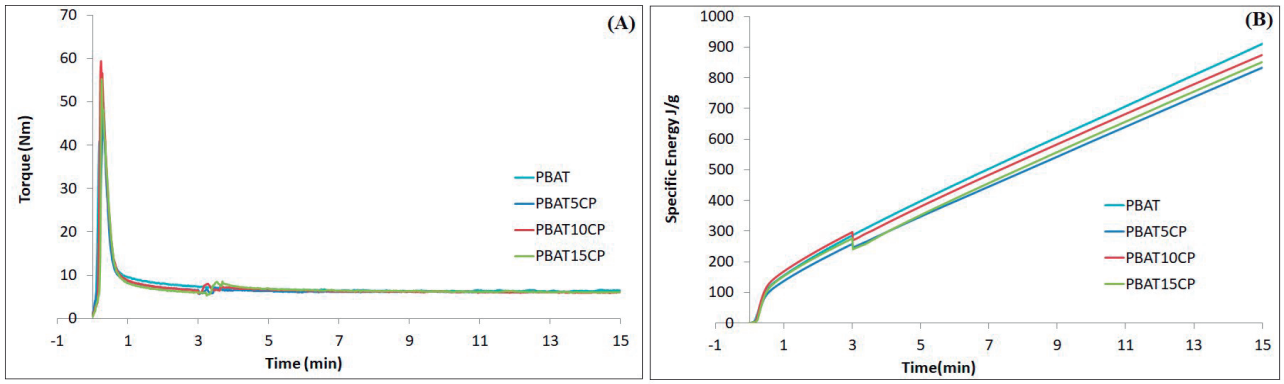

Figure 2 - A: Torque (Nm) over mixing time; B: Specific energy (J/g) over mixing time.

The first peak in the torque graph (Fig 2A) refers to the addition of pure PBAT. In approximately 3 minutes, the small variation in the graph refers to the addition of filler. All evaluated composites presented very close torque curves, indicating that possibly the polymeric matrix would have the capacity to incorporate a greater amount of filler without a considerable disturbance of the system. In Table 1 it is possible to notice this proximity of values more clearly. With the addition of filler, there was a small drop in the final torque values, but all composites showed very similar values. The same effect is observed for the specific energy, very close curves among the compositions with filler and values always below the pure PBAT. These results indicate that the fluency of the material was very little changed with the addition of filler, a fact that was confirmed by the rheological analysis of the compositions.

Table 1 - Final torque and specific energy of the mixtures.

Experiment	Final Torque (Nm)	Final Specific Energy (J/g)
PBAT	6.6	910
PBAT5CP	6.0	832
PBAT10CP	6.1	876
PBAT15CP	6.1	851

Rheological analysis

Fig 3 shows the variation of the complex viscosity of the material as a function of deformation. Viscosity represents the resistance to the flow of the material. The pure PBAT and composite PBAT5CP viscosities were very similar, as well as the viscosities of PBAT10CP compared to PBAT15CP (mainly at greater deformations) were also very close, but below pure PBAT. Thus, it is possible to state that smaller amounts of filler could be added to the PBAT without significantly altering its flow characteristics. In addition, larger amounts of CP tend to slightly decrease the viscosity of the material. It may be necessary to add larger amounts of filler and assess whether this effect is pronounced.

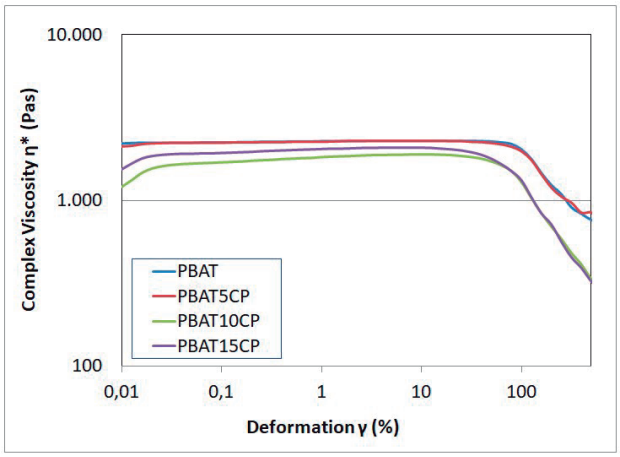

Figure 3 - Complex viscosity versus deformation.

This very similar viscoelastic behavior between composites and pure PBAT is more pronounced when analyzing G' (Fig 4A) and G" (Fig 4B) as a function of angular frequency. The storage modulus (G') is related to the elastic part of the material, while the loss modulus (G") is related to the viscous part of the material and the dissipation of elastic energy. The values of G' were very close, which means that the addition of Brazil nut shell had little influence on the elasticity of the material. The same behavior was observed for G", in accordance with the results of the material viscosity. These results indicate few changes in the viscoelastic behavior of the material as filler is added and corroborate the results of the processability analysis.

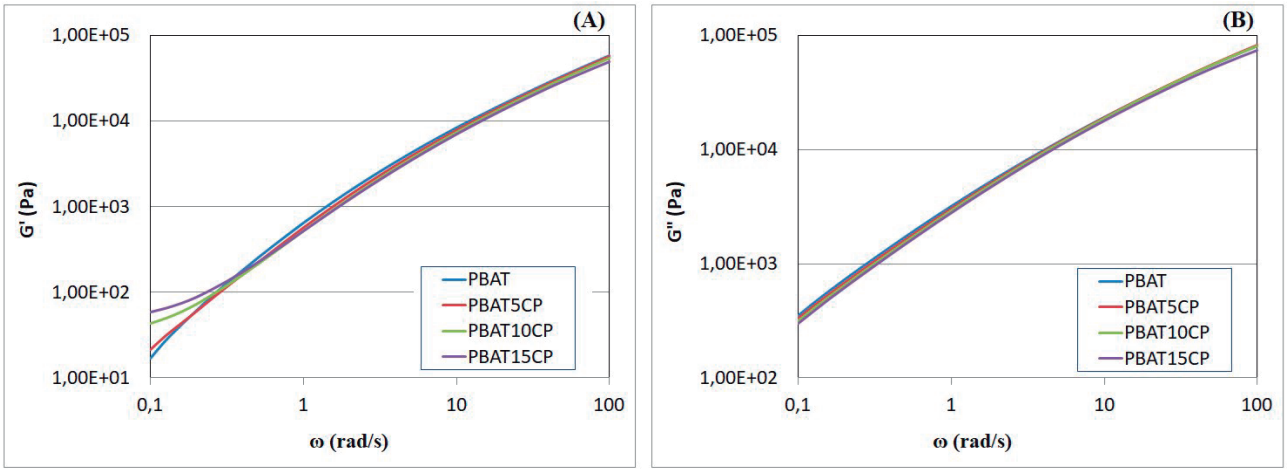

Figure 4 - A: Variation of the storage modulus (G') versus angular frequency; B: Loss modulus variation (G”) versus angular frequency.

Mechanical Results

Analyzing the results of elongation at break (Fig 5A) and stress at break (Fig 5B) it's possible to observe a slight tendency for these values to reduce as filler was added. Based on the results presented, it's evident that the filler did not significantly favor movements of the polymeric chains, thus the elongation value at break did not improve. In fact, the presence of filler disturbed the system, generating pressure accumulation points that did not help to disperse the fracture energy, thus facilitating the material's fracture, decreasing the stress values at rupture. With this, it can be concluded that the filler, in the amounts evaluated, did not reinforce the polymeric matrix, however its use can still be explored depending on the minimum properties required by the final product.

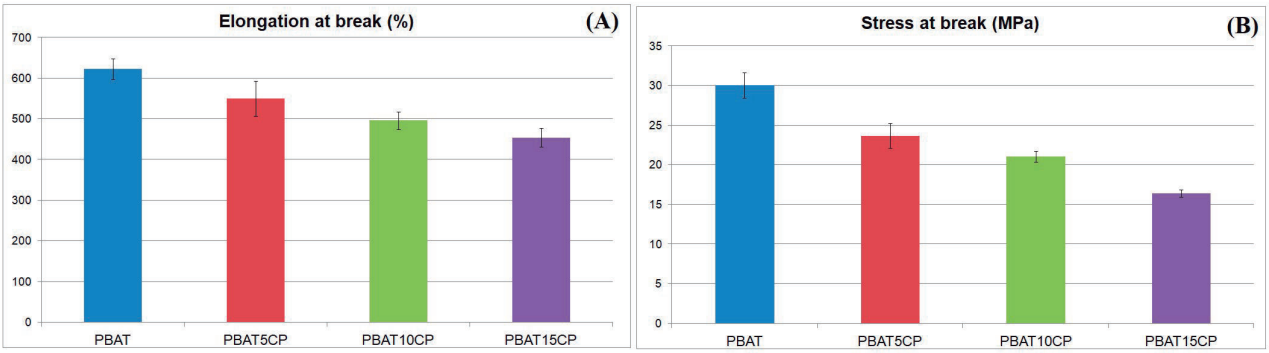

Figure 5 - A: Elongation at break (%); B: Stress at break of PBAT and composites with CP.

Conclusions

The use of Brazil nut shell fibers as filler in polymeric matrices is an economic and sustainable alternative for the use of an agroforestry residue. Its application in PBAT allows the conservation of its biodegradability, possibly even favoring it, and reduces the final cost of the product, making it more competitive in the market. The results of this work showed with the processing of the mixture, that all the evaluated composites presented very close torque curves, indicating that possibly the polymeric matrix would have the capacity to incorporate a greater amount of filler without a considerable disturbance of the system. The rheological analysis indicated few changes in the viscoelastic behavior of the material as the filler are added, corroborating the results of the processability analysis. For the mechanical properties, the addition of CP caused a decrease in tensile strength and elongation compared to pure PBAT, indicating that for the CP contents analyzed, this material did not act as a reinforcement. Besides that, the Brazil nut can be an economical and sustainable alternative as filler in PBAT, if the main goal is reducing the price of the product, always meeting the minimum requirements of mechanical properties of the final product.

Acknowledgements

The authors would like to thank INT and CNPq for logistical and financial assistance; and professor Ana Maria Furtado of the State University of Rio de Janeiro (UERJ) for complementary analysis.

References

1. V. C. Beber e*t al*. Materials, 2018, 11, 820. https://doi.org/10.3390/ma11050820
2. R. M. Nogueira *et al*. Associação Brasileira de Engenharia Agrícola 2014, 34, 963. https://doi.org/10.1590/S0100-69162014000500015
3. H. Zhao; H. Liu; Y. Liu; Y. Yang. RSC Advances, 2020, 10, 10482. https://doi.org/10.1039/c9ra10827k
4. L. O. Aprelini, MSc. Master, Universidade Fedral de Ouro Preto, 2016.

PBAT BIOCOMPOSITE WITH BACURI MESOCARP (BM) RESIDUE

Cléverson F. S. Gabriel[1]*, Gabriela M. dos Santos[1], Alene D. Nascimento[1,2] and Marcia G. de Oliveira[1]

1 – Polymeric Materials Technology Laboratory (LAMAP), Materials Division (DIMAT), Materials Technology Coordination (COTEM), National Institute of Technology (INT), Rio de Janeiro, RJ, Brazil
cleverson.fernandes@int.gov.br
2 – Laboratory of Bioinorganic and Coordination Compounds, Department of Inorganic Chemistry, State University of Rio de Janeiro (UERJ), Rio de Janeiro, RJ, Brazil

Abstract - This work aimed to develop PBAT biocomposites with agroforestry residues from Bacuri Mesocarp (BM). The BM was sieved and classified with particle sizes between 0.84 mm and 0.59 mm, and the morphology was evaluated. In the analysis of the mixture processing, both the torque and the specific energy decreased as the filler was added, indicating that the BM acted as a processing auxiliary, increasing the fluidity of the mixture, a fact confirmed by the rheological analysis, in particular the complex viscosity that decreased with adding the filler. Evaluating the meeting point of the storage modulus curve (G') with the Loss modulus (G"), at higher frequencies as BM is added, there is an indication that the molar mass of the polymer has decreased, impairing the mechanical results. Despite the results of the evaluated composites showing lower values than pure PBAT, this does not inhibit its commercial use as filler, depending mainly on the properties and minimum costs required of the final product.

Keywords: *PBAT, Biodegradable Polymer, Bacuri, Rheology, Mechanical Properties.*

Introduction

The Bacuri scientific name *Platonia insignis* is the fruit of the Bacuri tree, which can reach more than 30 meters in height and 2 meters in diameter. It is typically found in the eastern Amazon region, but it is also present in areas of transition from the forest to the Cerrado biome. This fruit comes almost entirely from family extractive activity and has significant economic importance in the states of Maranhão, Pará, Piauí and Tocantins, especially in the state of Pará, which is the main producer and consumer of the Bacuri [1, 2].

Poly(butylene adipate-co-terephthalate), also known as PBAT, is a biodegradable polymer produced by fossil sources from the results of associations of 1,4-butanediol with adipic acid and 1,4-butanediol with terephthalate acid [3, 4]. According to the ASTM D883 standard, biodegradable polymers are the ones in which degradation is the result of the action of microorganisms such as bacteria, fungi and algae, under certain conditions of heat, humidity, light, oxygen, organic nutrients and adequate minerals.

The use of PBAT on a large scale still comes up against its main disadvantage, which is its high price, on average, 3 to 4 times more expensive than LDPE and LLDPE. One way of trying to lower the price of PBAT final products and make them competitive in the plastics market would be to add fillers to these matrices. ASTM D1566 defines filler as a solid material, generally of low particle size, that can be added in relatively large proportions to a polymer for technical or economic reasons. Therefore, the goal of this work was to develop a biocomposite containing milled and dry Bacuri pulp, called Bacuri Mesocarpo (BM) and from that, to evaluate the technical viability of using 5, 10 and 15 phr of this agroforestry residue as a filler in biodegradable composites containing PBAT as a matrix.

Experimental

The first stage of the work was the granulometric classification of BM in a sieve with different opening sizes. The material was received dry and subsequently ground in a ball milling machine. The BM and the cryofractured composites morphology was analyzed using a scanning electron microscope (SEM) FEI Company, model INSPECT S50, a voltage of 15kV, low vacuum mode, using a backscatter detector (BEI), and the samples were covered with gold. Energy dispersive spectroscopy (EDS) is associated with scanning electron microscopy equipment (SEM) and was used for qualitative and semi-quantitative microanalysis of the chemical elements present in the BM sample. The PBAT and composites were prepared by melt intercalation in an internal mixing chamber coupled to a torque rheometer Haake Polylab OS. The rotor used was the Roller type, at 140°C, with a speed of 80 rpm for 15 minutes. The formulations were 0, 5, 10 and 15 phr (parts per hundred resin) of Bacuri Mesocarp per 100 phr of PBAT, the formulations were named PBAT, PBAT5BM, PBAT10BM and PBAT15BM respectively.

The specimens for the mechanical tests and the rheological analysis were molded by compression, according to their respective standards, in a hydraulic press MA 098/A400 with a pressure of up to 55 MPa at 140°C, for 10 minutes in the hot press and then cooled using the same pressure and time in the cold press. Rheological analysis was carried out on an Anton Paar MCR301 rheometer using a model CTD450 furnace as an accessory with a 25 mm parallel plate geometry. All tests were carried out at 140°C. Complex viscosity (η*) was measured through a strain variation test from 0.01% to 500%, at a constant frequency of 1Hz. The storage modulus (G') and the Loss modulus (G") were measured through an angular frequency variation test from 0.1 to 100 rad/s, in the linear viscosity region (10% constant strain). The tensile strength test was carried out in a mechanical testing machine EMIC DL3000 with a 1000 N load cell and a speed of 100 mm/min, according to ASTM D638 standard, type V specimen.

Results and Discussion

Bacuri Mesocarp Analysis

In this study, BM with particle sizes ranging from 0.84 to 0.59 mm was used. Figure 1 (A, B, and C) depicts the BM morphology, which shows irregular particles with low porosity and high roughness.

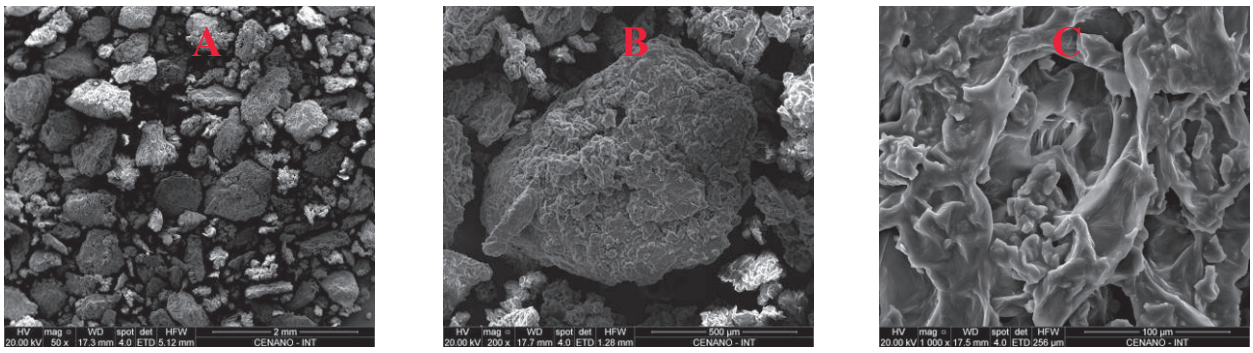

Figure 1 - Scanning electron microscopy of the Bacuri Mesocarp particle A: 50x; B: 200x and C: 1000x.

Table 1 - Energy Dispersive Spectroscopy of Bacuri Mesocarpo.

Element	Quantity in Quantity of Matter (%)	Bulk Quantity (%)
Carbon (C)	87,4	76,5
Oxygen (O)	6,7	7,8
Potassium (K)	4,6	13,1
Sodium (Na)	0,5	0,8
Magnesium (Mg)	0,4	0,7
Chlorine (Cl)	0,4	1,0

Energy dispersive spectroscopy (EDS), presented in Table 1, demonstrated that most of the elements present in the sample are carbon and oxygen, referring to the organic molecules of the BM, in addition, the BM is rich in calcium, potassium and other elements.

Mixture Processability Analysis

Fig 2 shows the evolution of the equipment torque as a function of time (Fig 2A) and the specific energy of the mixture as a function of time (Fig 2B).

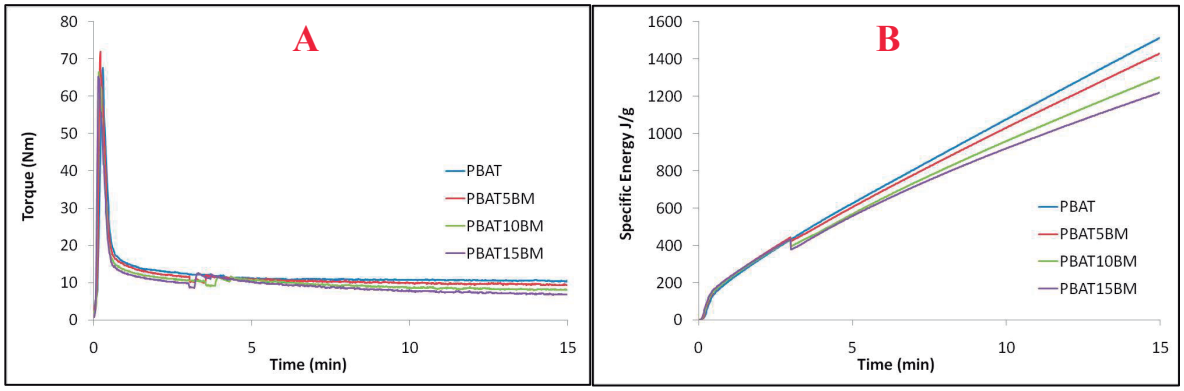

Figure 2 - A: Torque (Nm) over mixing time and B: Specific energy (MJ/g) over mixing time.

Analyzing Fig 2A, the first peak refers to the addition of PBAT and as the material passes into the molten state, its fluidity increases and the torque decreases drastically. In approximately 3 minutes, the filler was added. In Fig 2B it is evident that when adding larger amounts of BM, the torque necessary to keep the mixture at constant speed decreases and, consequently, the specific energy also decreases. With this, it is possible to indicate that the BM acted as a processing auxiliary, increasing the fluidity of the mixture. In Table 2, this effect can be better observed when evaluating the final torque and specific energy of the mixtures.

Table 2 - Final torque and specific energy of the mixtures.

Experiment	Final Torque (Nm)	Final Specific energy (J/g)
PBAT	9,9	1452
PBAT5BM	9,0	1393
PBAT10BM	8,1	1308
PBAT15BM	6,9	1227

Rheological analysis

Viscosity represents the resistance to the flow of the material. The lower the viscosity of a material the greater its flowability. Fig. 3 shows the variation of the complex viscosity of the material as a function of deformation.

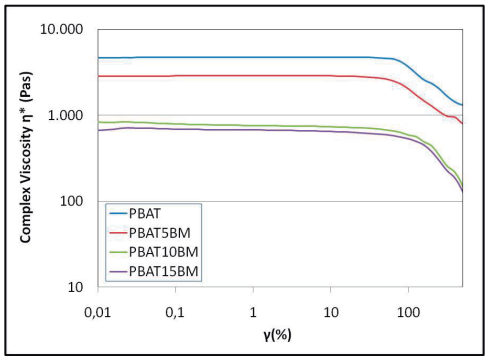

Figure 3 - Complex viscosity versus deformation.

For composites with BM, as the filler was added, there was a decrease in the viscosity of the mixture with PBAT, corroborating the processing results. The viscosities of PBAT10BM and PBAT15BM were very close, indicating saturation of this processing auxiliary effect.
The storage modulus (G') is related to the elastic part of the material, while the loss modulus (G") is related to the viscous part of the material and the dissipation of elastic energy. The variation of G' and G" with increasing angular frequency are shown in Fig 4A and Fig 4B, respectively. As BM was added, there was a decrease in G', which means a decrease in the elasticity of the material, which is directly related to the tensile strength test. The same occurred for G", following the results of the material's viscosity, which indicates an increase in its fluidity.

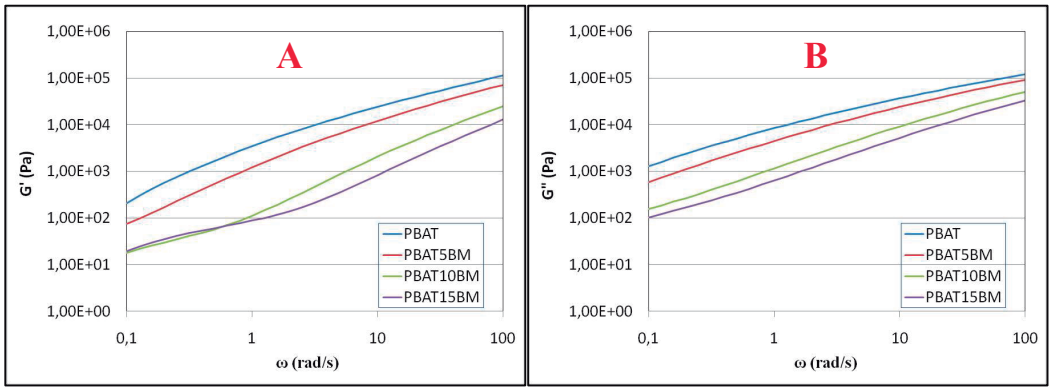

Figure 4 - Variation of the storage modulus (G') (4A) end Loss modulus variation (G") versus angular frequency (4B).

Mechanical Results

The possible lack of compatibility between the BM and the polymeric matrix (PBAT) and the indications that this filler is making the material less toughness, impaired the mechanical results of these composites, both for Elongation at Break (Fig 5A) and Stress at Rupture (Fig 5B).

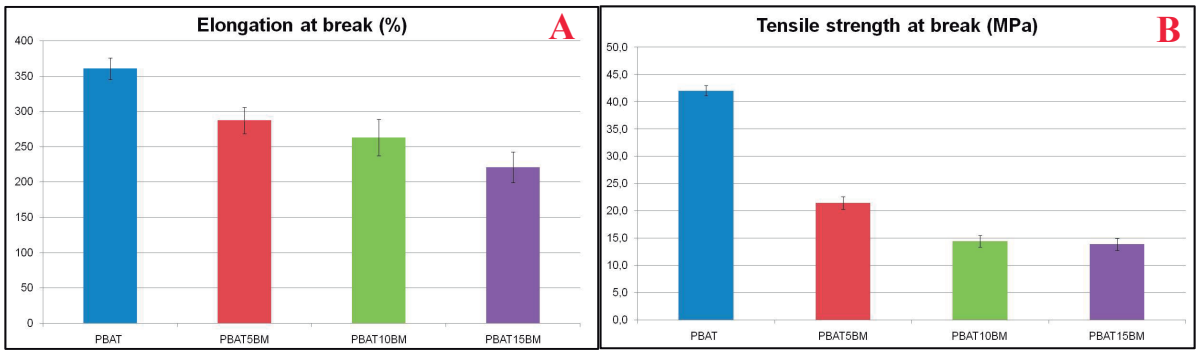

Figure 5 - A: Elongation at break (%); B: Stress at break of PBAT and composites with Bacuri Mesocarp.

Analyzing the elongation at break results, for the BM composites there was a decrease as the filler was added. With this, the impairment in the movement and accommodation of the polymer chains in the filler was evident, the filler may be decreasing the molar mass of the composite formed, making it more brittle and decreasing its stress at break, these hypotheses were confirmed by evaluating the fracture morphology.

Fracture Morphology

In Fig 6A and Fig 6B it is possible to analyze the fractured surface of pure PBAT, observing the appearance of some "scales" consistent with the elasticity of the material. Fig 6 (C-H) the morphologies of the composites of PBAT with BM are presented. In these micrographs, the appearance of holes resulting from the detachment of the BM from the polymeric matrix (PBAT) is

evident, in addition to rough regions that reinforce the idea that the BM is decreasing the molar mass of the polymeric compound. It is also possible to note that all these holes presented have a smooth surface, strong evidence of the lack of compatibility of the BM with the PBAT.

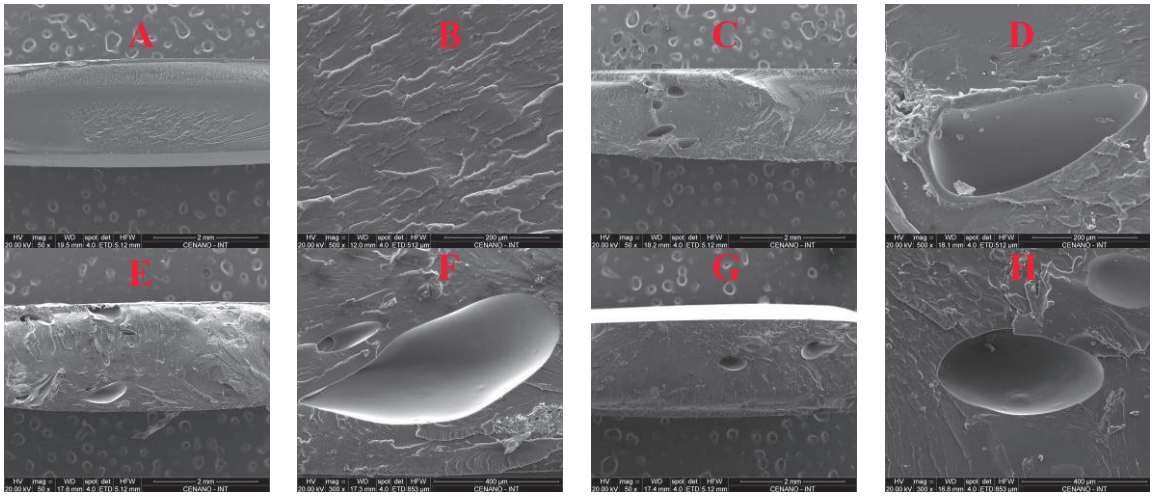

Figure 6 - SEM of the fractured material in liquid nitrogen, being: A: Pure PBAT (50x); B: Pure PBAT (500x); C: PBAT5BM (50x); D: PBAT5BM (500x); E: PBAT10BM (50x); F: PBAT10BM (300x); G: PBAT15BM (50x); H: PBAT15BM (300x).

Conclusions

The Bacuri mesocarp residue did not show good compatibility with the evaluated polymer, this was evident in the results of rheology and fracture morphology, however, from the processability, viscosity and G" data, it was evident that BM can be used as a medium for decrease the viscosity of the PBAT, increasing its fluidity and thereby decreasing the torque and consequently the mechanical energy required to carry out the mixing process. Despite the mechanical results, where both elongation and stress at break of the composites are smaller than pure PBAT, don't inhibit the commercial use of this mixture, mainly in smaller quantities of the filler. This will depend on the minimum required properties of the final product.

Acknowledgements

The authors would like to thank INT and CNPq for logistical and financial assistance. Valdir Florêncio of the Military Engineering Institute (IME), for the Bacuri donation. Ana Maria Furtado of the State University of Rio de Janeiro (UERJ) and Regina Célia Reis of the Federal University of Rio de Janeiro (UFRJ) for complementary analyses. To Cenano-INT for the scanning electron micrographs.

References

1. A. K. O. Homma; J. E. U. De Carvalho; A. J. E. A. De Menezes. Ciência Hoje 2010, 46, 39. https://ainfo.cnptia.embrapa.br/digital/bitstream/item/25022/1/homma-bacuri.pdf
2. T. W. Bispo; C. L. Braga; C. C. Lima; S. F. Rocha. Revista Grifos 2021, 31, 01. https://doi.org/10.29327/soberebpc2021.342291
3. J. C. De Sousa, MSc. Master, Federal University of Pernambuco, 2016.
4. A. M. Zamora *et al.* in Atlas do Plástico: Fatos e números sobre o mundo dos polímeros sintéticos, K. Schächtele, Ed.; Fundação Heinrich Boll, Rio de Janeiro, 2020, Vol. 1, 1-64.

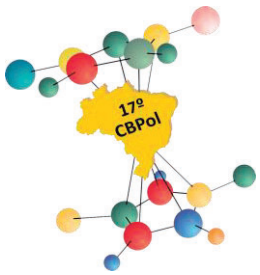

POLY(BUTYLENE-ADIPATE-CO-TEREFTALATE) BIOCOMPOSITES WITH CORN STRAW FOR FOOD PACKAGING

Fernanda V. Amorim[1], Márcia R. Luiz[2], Carolina L. Morelli[3], Mariana A. Henrique[1], Glória M. Vinhas[1] and Yêda M. B. de Almeida[1]

1 – Department of Materials Science, University of Pernambuco (UFPE), Recife, PE, Brazil
amorimfernandaamorim20@gmail.com
2 – Department of Sanitary and Environmental Engineering (DESA), State University of Paraíba (UEPB), Campina Grande, PB, Brazil
3- Deartment of Mechanical Engineering (DEMEC), Federal University of Pernambuco (UFPE), Recife, PE, Brazil

Abstract - The pollution caused by the incorrect disposal of polymers is responsible for major environmental impacts, because the degradation of these polymers from non-renewable sources is very slow. An alternative to minimize this impact on the environment is the use of biodegradable polymers, such as Poly(butylene-adipate-co-terephthalate) (PBAT) with vegetable fiber insertion, which has good mechanical properties, high biodegradability in the environment and good processability, especially for films, a property that produces a biocomposite suitable for packaging production. Thus, in this study, biodegradable matrix biocomposites (PBAT) were developed with corn straw (PM) fibers with and without chemical treatment.The fibers that underwent chemical treatment were submitted to alkaline treatment of 2 and 4% in an autoclave, at 121°C and 1 atm, for 10 min. Subsequently, the biocomposites were processed, containing a 15% fiber load, in natura and treated, in a mini-extruder and characterized by Infrared Spectroscopy (FTIR), X-Ray Diffraction (XRD), Scanning Electron Microscopy (SEM) and thermogravimetric analysis (TGA). The alkaline treatment of the fibers was efficient in removing the hemicellulose and lignin present. It was also verified that the fibers, in natura and treated, inserted in the PBAT had a reasonable adherence to the matrix, which was verified after the cryogenic fracture process, thus favoring a better mechanical performance of the biocomposites. Another relevant result concerns the thermal stability of the PBAT matrix during processing, which may be attributed to the insertion of the fibers.

Keywords: *PBAT, corn straw, fibers, biocomposites.*

Introduction

Several alternatives have been sought to minimize the environmental impact caused by conventional polymers. An important alternative is the use of biodegradable polymers. An example of a biodegradable polymer that emerged due to these new demands is Poly(butylene-adipate-co-terephthalate) (PBAT) with the trade name Ecoflex®, being an alternative to conventional plastics, where its properties were designed to meet the requirements of a biodegradable plastic: good mechanical and thermal properties (aromatic terephthalate part) associated with processability and biodegradability (aliphatic part) [1].

The development of biocomposites made with biodegradable polymer matrices and natural fiber reinforcements has evolved a lot in recent times [2], where the inclusion of natural fibers in polymeric matrices is one of the ways to obtain materials with better quality, increasing their biodegradability, where cellulosic materials are used as reinforcement because they have properties such as tensile strength and appropriate elastic modulus, characteristics necessary for some composites and even these fibers are not abrasive, have low densities and have lower costs compared to synthetic fibers [3].

However, the hydrophilic nature of agro-industrial waste affects adhesion to a hydrophobic polymeric matrix. So these fibers need to be treated to remove lignin before use; To this end, several

types of treatments have been proposed, which can be classified as chemical methods that use strong acids or alkaline compounds (H_2SO_4, NaOH and H_2O_2) and as physical treatments by steam explosion or depressurization, among others [4]. In this context, the characterization and development of new technologies to explore other potential applications are necessary as alkaline treatments aided by autoclaves at temperatures and pressure not so high may emerge as alternatives to reduce reaction times [5].

Thus, in view of the innovation and need for investigation of this new material, this work aims to prepare biocomposites of poly(butylene adipate-co-terephthalate) (PBAT) and corn straw (PM) by extrusion, for the possible production of plastic packaging as a final product.

Experimental

To carry out this research, the PBAT matrix, trade name Ecoflex® F Blend C 1200 produced by BASF, Corn Straw purchased in local trade and NaOH P.A. was used.

For the first pre-treatment phase, corn straw was ground in a knife mill and separated according to its granulometry using a set of sieves (ABNT sieves) with meshes between 80 and 200 mesh, with openings of 0.177 and 0.075 mm, for the use of alkaline treatment, where after granulometric selection [6], the second phase consisted of the alkaline treatment (Mercerization), where the corn straw fibers were immersed in an alkaline solution of NaOH at 2 and 4% (w/v), and subsequently subjected to thermal treatment in an autoclave at a temperature of 121 °C for different time intervals of 10 minutes [5]. Biocomposites of poly(butylene-adipate-co-terephthalate) (PBAT) and corn straw (PM) were produced in the composition of 15% (by mass) of the fibers. All compounds were prepared and mixed by extrusion in a 15 mL DSM Xplore co-rotational conical twin screw mini-extruder, with temperature of 150°C, screw speed of 100 rpm and residence time of 10 min [7].With the objective of characterizing the fibers and biocomposites, FTIR spectroscopy analyzes were carried out using a scan from 4000 to 400 cm^{-1} with 16 scans per sample and a spectral resolution of 4 cm^{-1} using the Horizontal Attenuated Total Reflection accessory (Horizontal Attenuated Total Reflectance - HATR), X-ray diffraction performed in a Bruker D2 Phase equipment, with parameters of radiation CuKα (λ = 1.54 Å) with voltage of 30 kV and current of 10 mA, angular sweep from 5° to 45 ° (Bragg angle - 2θ) and angular step of 0.05° per second, morphology of the fracture surface of the biocomposites (vitreous fracture using the technique with N_2 and metallized with gold) characterized by scanning electron microscopy, analyzed in the equipment model MIRA-3 by Tescan Mira, equipped with a high-brightness FEG source, using a voltage of 3 kV at different magnifications.

The TGA analysis was carried out in the Mettler Toledo TGA-Star System equipment, with a heating rate of 10°C/min, nitrogen atmosphere with a gas flow rate of 50 mL/min, in an alumina crucible with 5 - 10 mg of material for each analysis.

Results and Discussion

After the milling process, the PM fibers were standardized in two granulometries a of 0.250 mm (PM1) and 0.150 mm (PM2) to evaluate the power of the alkaline treatment in relation to its granulometry as well as its better adherence in the matrix/reinforcement interface during the manufacturing process of biocomposites due to the greater uniformity of their grains [8], thus, after being subjected to alkaline treatment (2 and 4% NaOH), FTIR analysis were performed (Figure 1a) in order to investigate an indication of whether there was a change in the functional groups of the components during the treatment in relation to the two granulometries of the residues.

Thus, comparing the two granulometries, exposed to the same alkaline treatment, it is possible to visualize the absorption bands of 1739 cm^{-1} referring to C=O lignin bonds, 1645 cm^{-1} referring to C-H bonds of lignin aromatic groups and 1251 cm^{-1} referring to C-O-C groups present in hemicellulose, where it shows that the alkaline treatment is efficient in the fibers due to the disappearance and reduction in the intensity of the peaks, where the modification of the absorption bands suggests the effect of the alkaline treatments on the residues, possibly showing the degradation

of lignin structures and thus the availability of cellulose surface area would be increased for enzymatic hydrolysis, as observed by studies such as MUTHUVELU K.S. and collaborators [9].

Figure 1 – a) FTIR graphics and b)X-ray diffractograms of PM1, PM2 fibers treated with 2 and 4% NaOH

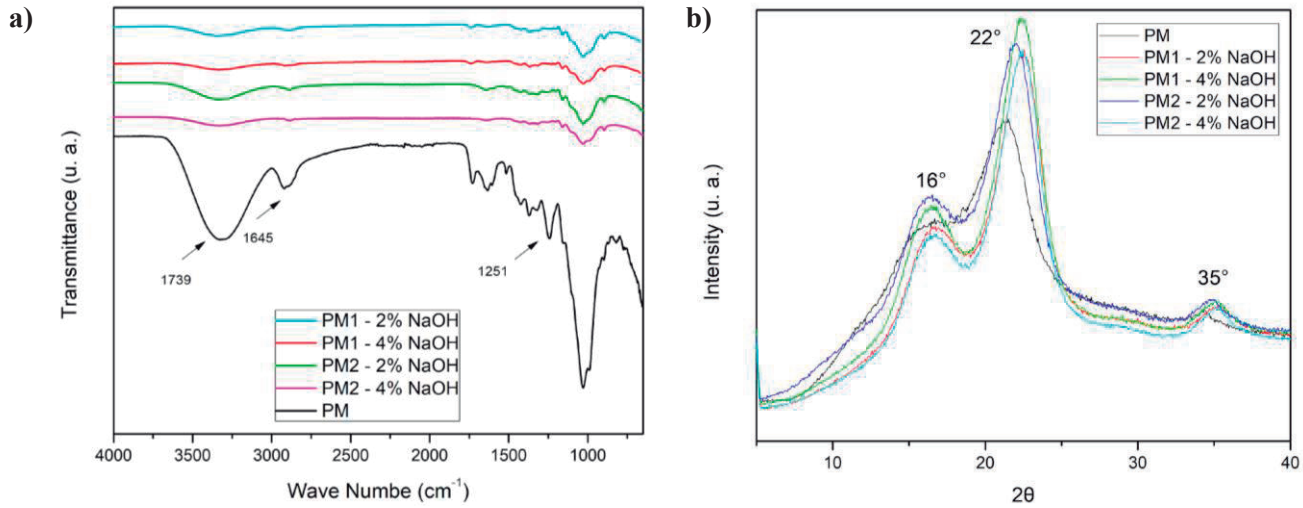

Regarding the crystallinity of the fibers as a function of the studied granulometries, the X-ray diffractogram (Figure 1b) obtained for all fibers without and with treatment, presents peaks related to cellulose I around 22°, which correspond to plane 002 of lattice planes of glycosidic rings as the main peak of native cellulose and planes 101 and 040 located at 16 and 35°, respectively,evaluating the effect of treatment intensity in relation to granulometry, the diffractograms of the samples show a more evident increase in intensity and narrowing of the reflection peaks in plane 101 and 002 around 16 and 22°, respectively, for the treatment performed on both residues with granulometry of 0.150 mm, indicating the removal of the amorphous parts of the hemicellulose and lignin microfibrils, as well as an increase in the Crystallinity Index from 28.6% of the PM to 45.1% of the PM1 - 2% NaOH and 52.7% of the PM2 – 2% NaOH as well as 55.6% of PM1 – 4% NaOH and 55.8% of PM2 – 4% NaOH, which can be attributed, among other factors, to the fact that the change in crystallinity is primarily associated with removal amorphous lignin and hemicellulose [10]. To evaluate the changes in the spectra related to PBAT, the insertion of PM fibers, PM1 – 4% NaOH and PM2 – 4% NaOH, was chosen, according to the fibers inserted with and without treatment in a proportion of 15%, it was possible to identify the characteristic bands of the components in the biocomposites. Figure 2a, referring to the spectra and according to the manufacturer Basf, the pure PBAT Ecoflex® matrix presents bands at 2950 cm^{-1} in relation to aliphatic and aromatic C-H; at 1710 cm^{-1} of the C=O ester group and 1267 cm^{-1} of C-O; in 1017 cm^{-1} of the substituted benzene ring and in 727 cm^{-1} of the methylene groups also found in [4], where the spectra of pure PBAT and PBAT with corn straw fibers with/without treatment, were presented practically identical, indicating that the presence of straw did not alter the matrix. Avaliando a inserção das fibras de PM, PM1 e PM2 ao PBAT, Figure 2b, initially observing the evaluated final temperature rates (Tf), the values of all biocomposites were higher than pure PBAT [11], with Tf = 453.05 °C for PBAT, Tf = 459.47 °C for PBAT+ PM, Tf = 457.93 °C for PBAT+PM1 – 4% NaOH and Tf = 463.04 °C, however the thermal stability of the biocomposites was not significantly altered by the addition of fibers, which may indicate that the fibers promote protection thermal to PBAT.

According to the SEM images, Figure 3, it can be observed that the images of the biocomposites during the cryogenic fracture process, presented fractured by fragile mechanism, where the residues are randomly dispersed, which can also be observed the presence of empty spaces of rounded shape, characterizing microcavities (dimples) that may be evidence of a weak chemical

interaction that is related to the hydrophilic character of the residues and the hydrophobic matrix, these empty spaces are more present in the matrix of PBAT with PM [12].

Figura 2 - a) FTIR spectrum and b) Sample thermograms; Pure PBAT, PBAT +PM, PBAT+PM1 – 4% NaOH and PBAT+PM2 – 4% NaOH.

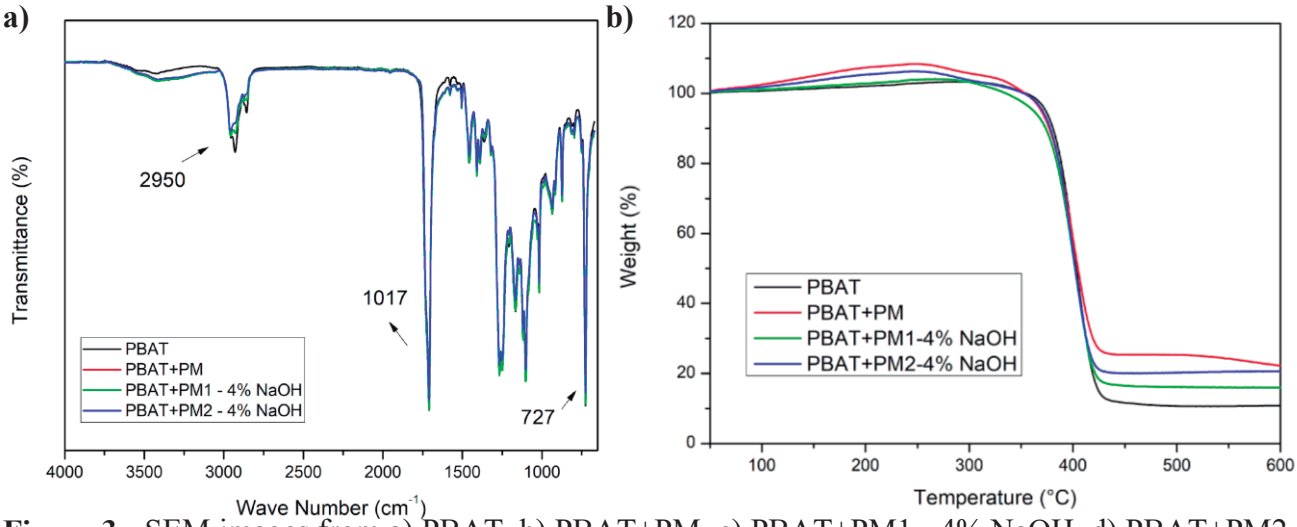

Figure 3 - SEM images from a) PBAT. b) PBAT+PM. c) PBAT+PM1 - 4% NaOH. d) PBAT+PM2 - 4% NaOH.

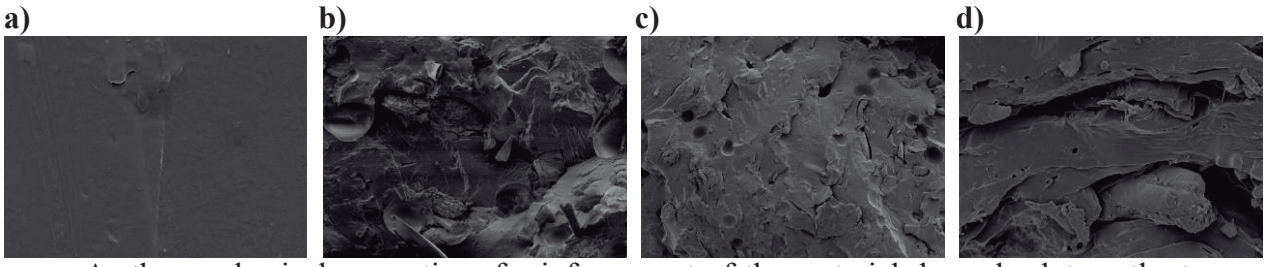

As the mechanical properties of reinforcement of the material depend a lot on the type of physical and chemical interaction between its components, studying interfacial adhesion is an important factor in the behavior of biocomposites, since the improvement of properties, mainly mechanical ones, tends to increase if necessary. adhesion between the two phases (reinforcement/matrix)[13].

Conclusions

The results obtained showed that the alkaline treatment on the fibers was more efficient in the removal of hemicellulose and lignin, which caused a reasonable adherence to the matrix, which was verified after the cryogenic fracture process, thus favoring a better mechanical performance of the biocomposites.

As well as the infrared results indicate that the insertion of fibers in the PBAT did not change the chemical properties, even increasing the thermal stability of the PBAT matrix during processing. Therefore, preliminary results confirm the potential use of these systems in packaging.

Acknowledgements

The authors would like to thank the National Council for Scientific and Technological Development, CNPq, for financial support. In addition, we would also like to thank the Laboratories of the State University of Paraíba-UEPB and the Integrated Petroleum Technology Laboratory-LITPEG.

References

1. COSTA, A. R. de M. **Blendas de poli (ß-hidroxibutirato) e poli (butileno-adipato-tereftalato) e seus compósitos com babaçu: efeito da composição e das condições de processamento**. Tese (Doutorado), Centro de Ciências Exatas e da Terra (CCET), Programa de Pós-Graduação em Ciência e Engenharia de Materiais, Universidade Federal do Rio Grande do Norte Natal, 2019.

2. AMORIM, G. E. P. **Desenvolvimento e caracterização do filme antimicrobiano de polibutileno adipato-co-tereftalato (pbat) com óleo essencial de cravo da índia para utilização em embalagem.** Monografia (Trabalho de conclusão de curso) - Unidade Acadêmica de Serra Talhada, Universidade Federal Rural de Pernambuco, Serra Talhada, 2019.

3. ALVES, C.; FERRÃO, P. M. C.; SILVA, A. J.; REIS, L. G.; FREITAS, M.; RODRIGUES, L. B.; ALVES, D. E. **Ecodesign of automotive components making use of natural jute fiber composites.** Journal of Cleaner Production, v.18, p. 313-327, 2010.

4. ARNI, S. AL. **Extraction and isolation methods for lignin separation from sugarcane bagasse: a review.** Ind. Crops Prod. 115, 330–339, 2018.

5. CABRAL, M. M. S., ABUD, A. K. DE S., ROCHA, ALMEIDA, M. S. R. DOS S., GOMES, R. M. R. G., M. A. **Composição da fibra da casca de coco verde in natura e após pré-tratamentos químicos.** Engevista, v. 19, n. 1, p. 99-108, 2017.

6. AZEVEDO, J. B. VIANA, J. D., CARVALHO, L. H. DE, CANEDO, E. L. **Avaliação da Biodegradação em Compósitos com Fibras Naturais através de Perda de Massa e Produção de CO_2.** Rev. Virtual Quim. V. 8, n. 4, pg. 1115 1129, 2016.

7. MORELLI, C. L. **Processamento e estudo das propriedades de filmes e peças injetadas de nanobiocompósitos de nanocristais de celulose e matrizes biodegradáveis.** Tese (Doutorado) - Centro de Ciências Exatas e de Tecnologia, Programa de Pós-Graduação em Ciência e Engenharia de Materiais, Universidade Federal de São Carlos, São Carlos, 2014.

8. CASTANHO, M. N. **Desenvolvimento e caracterização de filmes poliméricos de amido de milho com incorporação de fibras de bagaço de cevada.** Dissertação (Mestrado) -Universidade Federal de São Carlos, Campus Sorocaba, Sorocaba, 2020.

9. MUTHUVELU K.S., RAJARATHINAM, R., KANAGARAJ, L. P., RANGANATHAN, R. V., DHANASEKARAN, K., MANICKAM, N. K. **Evaluation and characterization of novel sources of sustainable lignocellulosic residues for bioethanol production using ultrasound-assisted alkaline pre-treatment**. Waste Management. n. 87, pg. 368–374, 2019.

10. BRAGA, D. G. **Tratamentos químicos das fibras do mesocarpo de açaí para a produção de filmes de nanocelulose e nanocompósitos de quitosana.** Dissertação (Mestrado) - Programa de Pós-Graduação em Ciências Florestais (PPGCF), Campus Universitário de Belém, Universidade Federal Rural da Amazônia, Belém, 2019.

11. SANTOS, E. B. C. **Efeitos dos tratamentos superficiais dos resíduos industriais de fibra de piaçava nas propriedades térmicas e termodinâmico - mecânica de compósitos à base de polihidroxibutirato (phb).** Tese (Doutorado) - Centro de Tecnologia, Programa de Pós-Graduação em Ciência e Engenharia de Materiais, Universidade Federal da Paraíba, João Pessoa, 2019.

12. PINHEIRO, I. F. **Biocompósitos poliméricos de poli(butileno adipato-co-tereftalato) - PBAT e fibra natural de Munguba, nativa da Amazônia (Pseudobombax munguba).** Dissertação (Mestrado) - Universidade Estadual de Campinas, Faculdade de Engenharia Química, Campinas, 2012.

13. MACIEL, C. C. **Moldagem e comparação de propriedades de compósitos de poli(butileno adipato-co-tereftalato) reforçados com tecidos de fibras vegetais.** Dissertação (Mestrado) - Campus Sorocaba, Programa de Pós-Graduação em Ciência dos Materiais, Universidade Federal de São Carlos, Sorocaba, 2019.

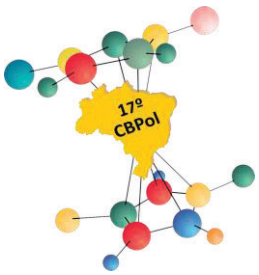

PRODUCTION OF BIODEGRADABLE PACKAGING FROM RENEWABLE SOURCES

Paulo R. C. C.[2]; Michele D. M. M.[2]; Ana P. B. G.[2]; Ingrid L. L.[2]; Luciano P.[1]; Tatiana B. R. N.[2]

1 - Materials Area - ISI for Union and Conformation of Materials at SENAI CIMATEC; Salvador-BA
2 - Food and Beverage Technology Area at - SENAI CIMATEC; Salvador-BA
paulo.correia@fbter.org.br

Abstract

Bioplastics have been gaining prominence in the development of sustainable packaging and are advantageous as they are derived from renewable sources and capable of meeting a variety of industrial applications. Continuous improvement of these materials is necessary to further drive their utilization and contribute to sustainability. This study aimed to produce biodegradable films through flat extrusion using PLA, starch, glycerol, and citric acid, and characterize them in terms of mechanical properties. The addition of thermoplastic starch (TPS) to the PLA film resulted in a lower modulus of elasticity, a significant increase in elongation at break, as well as a reduction in maximum stress and stiffness. These results indicate that thermoplastic starch can be a promising filler in polymeric matrices, with potential for cost reduction.

Keywords: *materials, eco-friendly, extrusion, compostable.*

Introduction

The significant increase in the use of petroleum-derived polymers in various applications over the past decades has raised environmental concerns, as these materials are quickly discarded and take a long time to degrade, causing a negative impact on the environment. In response to this issue, new commercial polymers are being developed, utilizing renewable resources and exhibiting biodegradable characteristics [1].

These sustainable polymers aim to minimize the environmental damage resulting from large-scale disposal in nature. By opting for biodegradable polymers, it is possible to reduce the accumulation of long-lasting plastic waste and promote a more sustainable life cycle for materials used in various industrial applications. Additionally, the development of these renewable polymers contributes to decreasing dependence on non-renewable resources, such as petroleum, and promotes a transition to a more circular and sustainable economy [2].

Among naturally biodegradable polymers derived from renewable resources, starch stands out as one of the most promising materials due to its abundance and low cost. Starch is compatible with widely used extrusion processes in the manufacturing of conventional films, and when combined with plasticizers, it can acquire thermoplastic characteristics, forming what is known as thermoplastic starch (TPS). However, the application of starch as a material for films intended for food packaging has been limited due to its relatively low mechanical and barrier properties. To overcome these limitations, various research studies have explored the addition of starch to other materials, such as synthetic biodegradable polymers. These polymer blends or combinations can

result in films with improved mechanical and barrier properties, making them more suitable for the protection and preservation of food. These improvements are of utmost importance in ensuring the quality and safety of packaged products, as well as expanding the possibilities for the application of starch-added films in different sectors of the food and packaging industry. [3].

Research has explored the use of synthetic biodegradable polymers, such as PBAT and PLA, for film production. These synthetic polymers have favorable mechanical and thermal properties, making them suitable for use in combination with thermoplastic starch. However, a significant challenge is the high production cost of these polymers, which hinders their widespread application. The search for more economically accessible alternatives is essential to promote the sustainable use of these materials in different industrial sectors [3,4].

By exploring the combination of starch with synthetic biodegradable polymers, it is possible to obtain films with improved mechanical properties while reducing production costs. This is crucial in making these materials more commercially viable and expanding their use in applications that require biodegradable packaging and films. [5]. In this context, the present study aimed to produce films through the flat extrusion process using PLA and thermoplastic starch, and to characterize them in terms of their mechanical properties.

Flat extrusion is a widely used technique in the industry for the production of plastic films, providing an efficient and cost-effective process. The incorporation of thermoplastic starch into PLA aims to leverage the beneficial properties of starch, such as its biodegradability and renewable origin, while also seeking to improve the processability and mechanical characteristics of PLA. The characterization of the mechanical properties of the films is essential to assess the suitability of these materials for various applications, such as packaging and agricultural films. By understanding the mechanical properties, it is possible to identify potential improvements in the production process and formulation of the films, aiming to achieve more sustainable, economically viable materials with good performance in use.

Experimental

The spaghetti strands and films of each formulation mentioned in Table 1 were produced using a twin-screw flat extruder with an L/D ratio of 40 mm. The equipment used was an AX-Plásticos extruder, model DR1640, manufactured in Brazil. The thickness of each film specimen was determined at three different points using a micrometer. This precise and repetitive measurement allowed for obtaining information about the uniformity of the film thickness produced, which is important to ensure product quality and consistency.

Table 1 - Developed formulations**.**

	Concentration of components (%)			
Formulation	PLA	Starch	Glycerol	Citric Acid
Pure PLA	100	-	-	-
70/30	70	21	8,55	0,45
60/40	60	28	14,4	0,60

The produced films were characterized through tensile tests using an Emic universal testing machine, model DL 2000, with a distance of 100 mm between the grips of the equipment. The test was performed using a 500 N load cell at a deformation rate of 25 mm/min, according to ASTM D-882-91 [6]. Rectangular specimens with a width of 25 mm and a length of 190 mm were prepared for this purpose. This testing method allowed for evaluating the mechanical properties of the films, such as tensile strength, elongation at break, and modulus of elasticity. It provided valuable

information about the performance of biodegradable films in terms of strength and flexibility, offering important data to assess their suitability as packaging materials.

Results and Discussion

The flat extrusion method proved to be efficient in producing films with thin thickness, both with pure PLA and the addition of thermoplastic starch (TPS). The concentrations used were 60% PLA/40% TPS and 70% PLA/30% TPS. The measured thickness values were approximately 20 µm for pure PLA, 23 µm for the 60/40 formulation, and 24 µm for the 70/30 formulation. These thicknesses are suitable for flexible packaging applications, providing a lightweight and versatile material. The ability to produce thin films is an advantage of the flat extrusion method, allowing for the manufacturing of more efficient packaging in terms of material and resource usage. This contributes to waste reduction and a more sustainable approach in the development of biodegradable packaging.

One observed advantage was that the addition of TPS to PLA did not hinder the processing of the blends. Furthermore, the films produced with the incorporation of TPS exhibited greater flexibility compared to the pure PLA film, which has a rigid characteristic that may limit its application in certain types of packaging. Another positive aspect is that the addition of TPS enabled a 30 °C reduction in the processing temperature compared to the temperature required for processing pure PLA. This temperature reduction can have beneficial implications for energy efficiency and production costs, as well as facilitating the manufacturing of biodegradable films. These results indicate that the inclusion of TPS in the blends offers advantages both in terms of processability and final film properties, making them more suitable for various packaging applications.

Figure 1 shows the films developed on a flat die. The samples were guided to the winder by the puller rolls.

PLA 60/40 70/30

Figure 1 - Flat die extrusion of PLA and TPS films at 60/40 and 70/30 concentrations.

Figure 2 presents the data obtained for the tensile test of PLA and PLA with TPS films. The results obtained for the stress at maximum force parameters indicated a reduction in values compared to the pure PLA film. The 60/40 and 70/30 TPS formulations showed decreases of 35.57% and 52.28%, respectively. These results demonstrate that the addition of TPS resulted in a reduction in the stiffness of the films, making them more flexible. This change in stiffness is desirable in packaging as it provides greater malleability and impact resistance, contributing to the

protection of packaged products. Therefore, the addition of TPS offered an advantage in the development of more flexible and adaptable packaging, providing greater efficiency and safety in the storage and transportation of food and other products.

The addition of thermoplastic starch (TPS) to PLA also resulted in a decrease in the elastic modulus, with reductions of 25.34% and 44.13% for the 60/40 and 70/30 formulations, respectively. These results are consistent with a study conducted by Kim et al. [7], which showed that the addition of corn starch to PBAT reduced the tensile strength as the percentage of corn starch increased (10, 20, 30, and 40%). This effect is attributed to the lack of interaction between the hydrophobic interfaces of PBAT and the hydrophilic interfaces of starch, which can result in lower cohesion and mechanical strength in the films. These studies emphasize the importance of balancing the addition of fillers, such as starch, to ensure the attainment of suitable mechanical properties in biodegradable films.

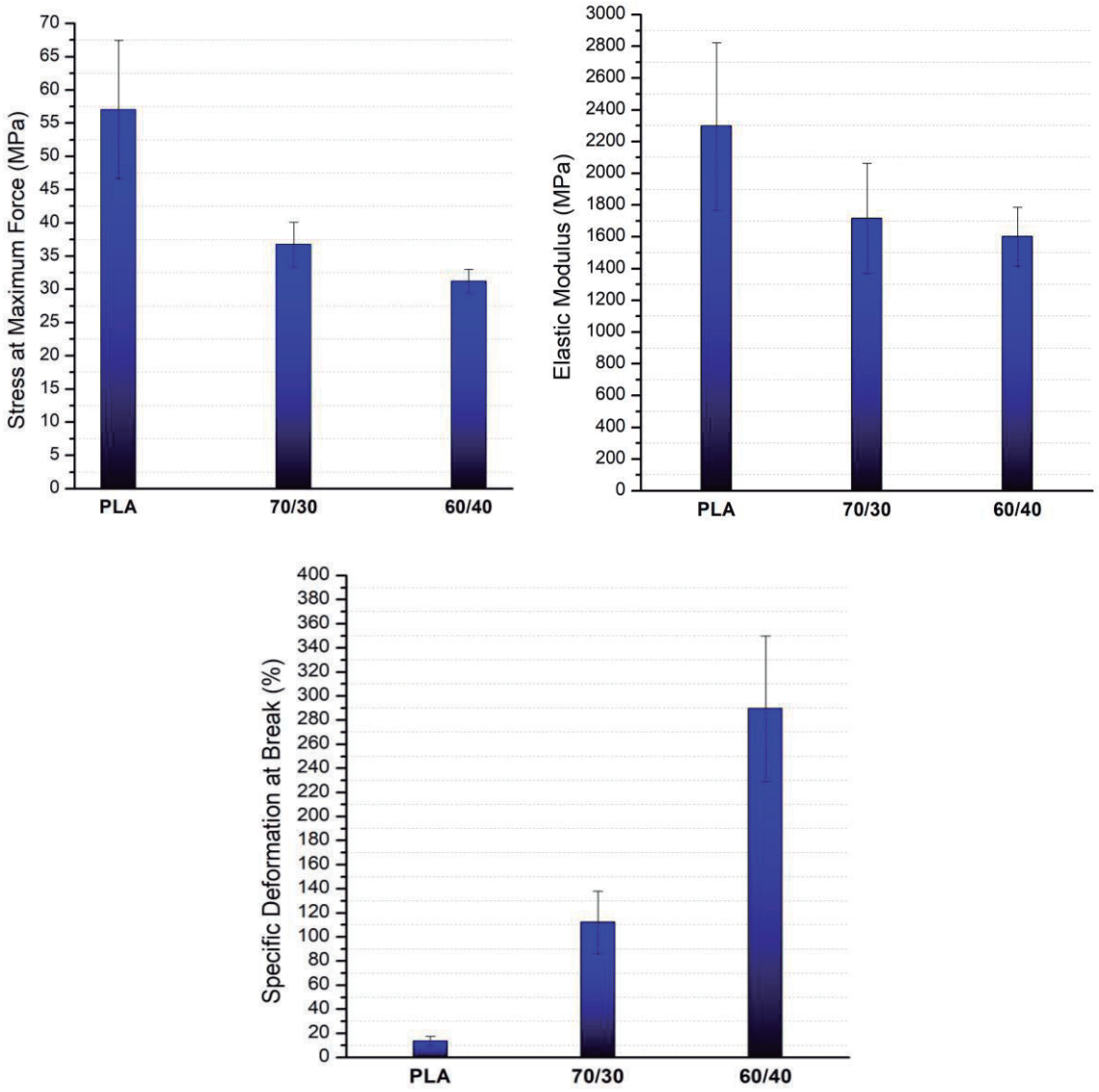

Figure 2 - Values of maximum force stress (MPa), elastic modulus (MPa), and specific elongation at break (%) for PLA, 60/40, and 70/30 films.

The addition of TPS resulted in a significant increase in the specific elongation at break parameter compared to pure PLA film. Films with a 70% TPS proportion showed an 837.86% increase in this property, while films with a 60% TPS proportion showed a 2,163,03% increase. This enhancement can be attributed to the presence of glycerol, which acted as a plasticizer during the formation of thermoplastic starch. The addition of glycerol helps improve the flexibility and deformability of the films, making them more suitable for applications such as flexible packaging. These results emphasize the importance of proper formulation and the use of additives such as glycerol to optimize the mechanical properties of biodegradable films.

Conclusions

The results of this study demonstrated the feasibility of producing biodegradable films with potential applications in food packaging and other areas at a reduced cost. The addition of thermoplastic starch (TPS) improved the mechanical properties of the films compared to pure PLA when processed by flat extrusion. The developed biodegradable films showed great potential as sustainable alternatives to replace conventional packaging, contributing to the reduction of environmental impact. Future studies could focus on further optimizing the film properties and exploring different industrial applications to drive the widespread adoption of these environmentally friendly materials.

Acknowledgements

To Centro Universitário SENAI CIMATEC and EMBRAPII, for granting the scholarship and support for carrying out the project.

References

1. M. Niaounakis, (2019). *Recycling of flexible plastic packaging*. William Andrew.
2. V. M. et al. Azevedo (2017). Effect of replacement of corn starch by whey protein isolate in biodegradable film blends obtained by extrusion. Carbohydrate Polymers, 157, 971-980.
3. Azeredo, H. M. C., Waldron, K. W (2016). Crosslinking in polysaccharide and protein films and coatings for food contact - A review. Trends in Food Science and Technology, v. 52, p. 109-122,
4. A. R. S. Rossin, et al. (2023). Biodegradable Polymers in Drug Delivery. *Handbook of Bioplastics and Biocomposites Engineering Applications*, 211-228., 211-228.
5. Murariu, M., & Dubois, P. (2016). PLA composites: From production to properties. Advanced drug delivery reviews, 107, 17-46.
6. ASTM. Standard Test Methods for Tensile Properties of Thin Plastic Sheeting. In: Annual Book of American Society for Testing and Material, Designation D882- 91. Philadelphia, USA, 1996.
7. Kim, J. H., Lee, J. C., & Kim, G. H. (2015). Study on poly (butylene adipate-co-terephthalate)/starch composites with polymeric methylenediphenyl diisocyanate. *Journal of Applied Polymer Science*, *132*(16).

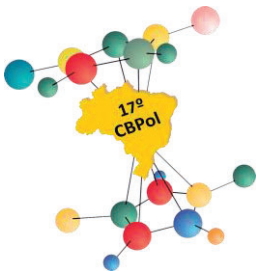

PROTON CONDUCTING MEMBRANES BASED ON SODIUM ALGINATE AND PROTIC IONIC LIQUIDS

Alene D. Nascimento[1], Lilian F. Senna[1], Silvana Mattedi[2], and Rodrigo A. dos Reis[1]*

1 – Institute of Chemistry, State University of Rio de Janeiro (UERJ), Rio de Janeiro, RJ, Brazil rdosreis@uerj.br
2 – Department of Chemical Engineering, Federal University of Bahia (UFBa), Salvador, Ba, Brazil

Abstract - Nafion® is the most used commercial polymer in polymeric electrolyte fuel cells (PEMFC). However, as it depends on water as an electrolyte, its performance drops sharply at temperatures above 80ºC. Thus, operations at temperatures above 100ºC would require new materials involving non-volatile electrolytes dispersed in compatible polymeric matrices forming films with promising chemical, thermal, mechanical, and electrochemical properties. In this work, the influence of the PIL chemical structure on the chemical, morphological, thermal, mechanical, and electrochemical properties of sodium alginate (NaAlg)-based mixed matrix films was analyzed. The formation of interconnected channels and a stronger network of hydrogen bonds involving the hydroxyl groups of NaAlg and PILs resulted in more conductive films, but with less promising thermal and mechanical properties. NaAlg-based films formed with [BHEA][Ac] or [m-2HEA][Ac] are promising for applications in PEMFC at temperatures above 100°C.
Keywords: *Proton-exchange film, sodium alginate, protic ionic liquids, mixed matrix films, electrochemical properties*

Introduction

Industrial growth, urbanization, and modernization has imposed an increase in global demand for electric power [1]. Polymer electrolyte membrane fuel cells (PEMFCs), devices that exhibit high energy density, high efficiency, and fast startups, are emerging as a promising alternative for more efficient, sustainable, and flexible electricity generation [2]. Nafion® is the most widely used commercial polymer in PEMFCs. However, its application is limited due to its dependence on water as an electrolyte, which leads to the following limitations: (i) low tolerance to carbon monoxide, requiring high-purity hydrogen; (ii) low heat transfer rates; (iii) slow kinetics at the cathode; and (iv) complex water management. Some of these limitations are mitigated when PEMFCs are operated at higher temperatures (100 - 200 °C) [3], but water management becomes even more complex at temperatures above 80°C [4].

An alternative membrane to the use of Nafion® should incorporate a polymer with suitable thermal and mechanical properties for its application in PEMFC, along with a good distribution of an electrolyte with low vapor pressure at temperatures between 100 and 150°C [3; 5-7]. Ionic liquids (ILs), besides having low vapor pressure, also include many charge carriers and high conductivity values under anhydrous conditions [8-9]. Sodium alginate (NaAlg) consists of units of β-D-mannuronic acid and α-L-guluronic acid linked at positions (1,4), conferring hydrophilic, water-soluble, biocompatible, biodegradable, inexpensive [10], and stability at temperatures above 100°C. Its chemical structure, rich in hydroxyls, carbonyls, and ether-type segments, favors the formation of a strong network of hydrogen bonds with protic ionic liquids (PILs) containing hydroxyls, ensuring a good distribution of this electrolyte for the formation of films with good electrochemical properties at temperatures above 100°C [11].

The present paper analyzes the influence of the chemical structure of PILs on the chemical, morphological, thermal, mechanical, and electrochemical properties of mixed matrix films based on NaAlg. The analyzed PILs were 2-methylhydroxyethylammonium acetate ([m-2HEA][Ac]), 2-

methylhydroxyethylammonium propanoate ([m-2HEA][Pr]), 2-methylhydroxyethylammonium butanoate ([m-2HEA][Bu]), 2-hydroxyethylammonium acetate ([2HEA][Ac]), and bis-hydroxyethyl ammonium acetate ([BHEA][Ac]), allowing the evaluation of the influence of the alkyl arm size of the cation or the anion, and the number of hydroxyl groups.

Methodology

Preparation of the NaAlg-based matrix films

The PILs were synthesized, characterized, and kindly provided by UFBa [12]. The sodium alginate (NaAlg) used has a molecular weight of 4.7 x 10^4 Daltons and an M/G ratio of 1.69 (Sigma-Aldrich). NaAlg-based films containing 40 wt% of one of the analyzed PILs were prepared as follows: (i) in separate containers, NaAlg and the PIL were dissolved in deionized water under stirring for 24 h at room temperature to form 2 wt% solutions; (ii) the solutions were then mixed and stirred for 4 hours at 60°C in proportions that ensure a content of 40 wt% of PIL in the polymer matrix; (iii) after 12 hours at rest, the solution was poured onto leveled Teflon plates; and (iv) drying was carried out in a natural convection oven at 40°C for periods ranging from 72 to 96 h.

Characterization of the NaAlg-based natrix films

The proton conductivity of the films was obtained by electrochemical impedance spectroscopy using a Metrohm AutoLab potentiostat, model PGSTAT 220N, and a two-probe method with calibrated copper electrodes validated with a 0.01 mol.L^{-1} KCl standard solution. The electrode-conductor medium system was placed inside a Faraday cage with temperature control. The frequency and temperature ranges used were from 0.1 Hz to 1 MHz at open circuit potential (after 30 min of stabilization) and with an amplitude of 30 mV, and from 25°C to 120°C, respectively. The analysis was evaluated in triplicate, and the uncertainty was calculated at a 95% confidence interval. The experimental curves were used for conductivity calculations [13].

The Thermogravimetric Analysis (TGA) was performed in a Q50 Thermogravimetric Analyzer (TA Instruments). The samples were placed in an alumina crucible under a flow of 50 mL.min^{-1} of N_2 and a rate of 10°C.min^{-1}, at room temperature and 900ºC. The initial degradation temperature (T_{onset}) was obtained from the derivative thermogravimetry curve (TGD) (ASTM E2550-11, 2011). Fourier Transform Infrared (FTIR) spectra were obtained using a Frontier MIR/FIR spectrometer (Perkin Elmer) with an attenuated total reflectance (ATR) accessory. All spectra were collected in the range of 4000-600 cm^{-1} with a resolution of 4 cm^{-1} and 16 scans. After coating the samples with carbon, images of a field emission gun scanning electron microscopy (FEGSEM) were obtained using a JEOL microscope, model JSM-7100F, with secondary electron detector, electron beam acceleration from 3 to 5 kV and variable boost for cross section. The mechanical tests were carried out in an EMIC universal testing machine, DL-2000, with an operational load of 20 kN, initial spacing between the claws of 40 mm and speed of spacing of the claws of 12.5 mm.min^{-1}. For each formulation, between three and five samples with a width of 10 mm were analyzed according to ASTM D882-12.

Results and Discussion

The films with different PILs exhibited a dense, yellowish, and opaque appearance (Fig 1a-b). The cross-section of the pure NaAlg film showed a granular morphology with rarely disconnected defects, likely formed during fracture (see red arrows in Fig 1c). On the other hand, the presence of the PIL resulted in significant heterogeneity, typical of mixed matrix membranes. The morphology observed in the films containing [m-2HEA][Ac] or [BHEA][Ac] showed interconnected channels throughout their structure (Fig 1d), while films formed with the addition of [m-2HEA][Pr], [m-2HEA][Bu], or [2HEA][Ac] exhibited porous, sponge-like structures (Fig 1e). The film formation process led to a separation between an PIL-rich phase, generating channels or pores, and a NaAlg-rich phase, delimiting the morphological structure [14].

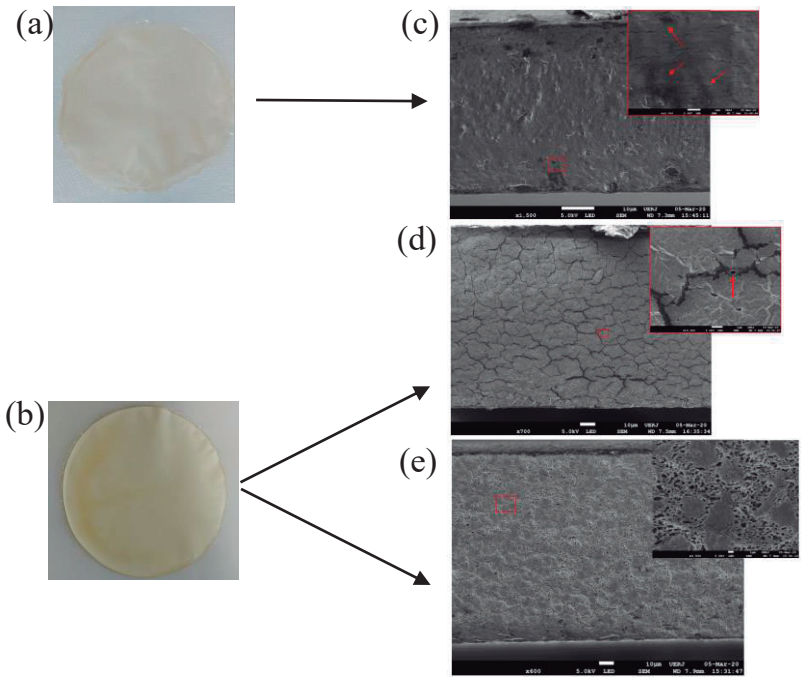

Figure 1 – General appearance of (a) pure NaAlg films and b) mixes matrix films; and SEM images of c) pure NaAlg film, d) film with 40 wt% of [m-2HEA][Ac], and e) film with 40 wt% of [2HEA][Ac].

In the FTIR spectra (Fig 2a), shifts to lower wavenumber values are observed in the bands related to the O-H stretching of the films containing PIL. Such displacement suggests an intensification of the H bonding network in the presence of PIL [15]. The [BHEA][Ac] produced the greatest displacement of this band (38 cm^{-1}), likely due to its two hydroxyl groups. Comparing the PILs with $[Ac]^-$ anion, [2HEA][Ac] produced a smaller displacement of this band (15 cm^{-1}) than that observed in films containing [m-2HEA][Ac] (29 cm^{-1}). The shifts caused by the increase in the anion alkyl chain in the $[m\text{-}2HEA]^+$ series followed the order: $[Ac]^-$ (29 cm^{-1}) < $[Pr]^-$ (32 cm^{-1}) < $[Bu]^-$ (35 cm^{-1}). In summary, the compatibility of the PIL and NaAlg is mainly governed by the H bonding network involving the hydroxyl groups of both materials, which becomes slightly intensified as the alkyl arm size of both the cation and the anion of the PIL increases.

The observed differences in morphologies (Fig 1) are therefore a consequence not only of the cross-interactions between the material constituents but also of the PIL chain length. Relatively weaker interactions or larger chains PIL with lower mobility during drying seem to favor a spongy structure. On the other hand, the intensification of interactions among PIL molecules during film drying and water removal favors the formation of channels. This behavior follows the trend observed in SPEK membranes with imidazole-type ionic liquids [16].

The influence of the PIL structure on the thermal resistance of the films (T_{onset}) and their mechanical properties (Fig 2b) also helps to explain the plasticizing effects produced by these polymer/PIL interactions. The films formed with the [m-2HEA]+ cation series exhibit similar T_{onset} values (166 °C, 167 °C, and 160 °C for the anions $[Ac]^-$, $[Pr]^-$, and $[Bu]^-$, respectively), elastic modulus, and stress at break (Fig 2b), confirming that the alkyl arm length of the anion has little effect on the H bonding network, as suggested by the FTIR spectra.

Confirming that [BHEA][Ac] showed the most plasticizing effect, the films involving this PIL exhibited the greatest drop in T_{onset} (from 201°C to 154°C), and the poorest mechanical properties (Fig 2b). There is no statistical evidence to differentiate the mechanical properties of the film containing [2HEA][Ac] from those observed in films involving the $[m\text{-}2HEA]^+$ cation series, although significant variations were verified for their thermal resistances. [2HEA][Ac] was the least plasticizing PIL, leading to the lowest T_{onset} drop (from 201°C to 175°C). The heterogeneity observed in the micrographs of the mixed matrix films (Fig 1d-g) justifies the large variability in the

mechanical property data. It should be noted that the mechanical properties of NaAlg films doped with [BHEA][Ac] are consistent with those found elsewhere [17].

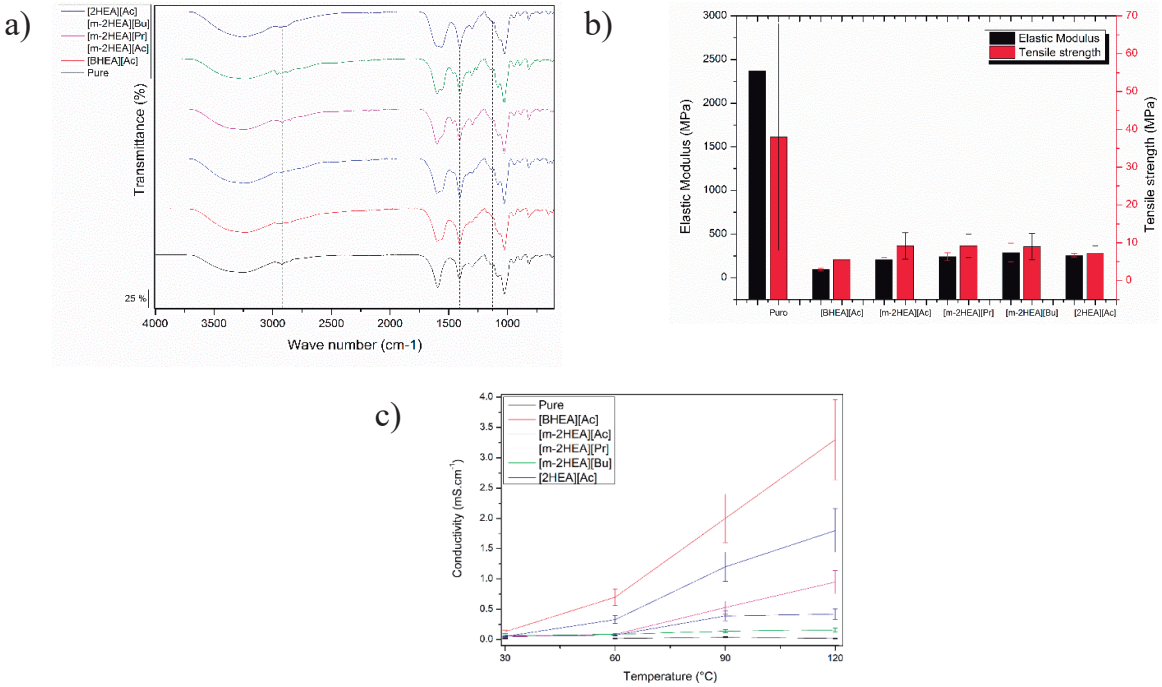

Figure 2 – a) Full FTIR with lines orienting to the main bands, b) Mechanical properties of membranes, c) Variation of conductivity with temperature of pure and mixed matrix films with different PILs.

Although the conductivity of pure NaAlg was not influenced by temperature, the values obtained for all mixed matrix films escalated with increasing temperature (Fig 2c). Both the conductivity values of the films and their variation with temperature presented the following order: [BHEA][Ac] > [m-2HEA][Ac] > [m-2HEA][Pr] > [2HEA][Ac] > [m-2HEA][Bu]. This sequence reflects that the film conductivity depends on the that of the PIL, the interaction between the PIL and the polymeric matrix, and the cross-sectional morphology. Although [2HEA][Ac] is one of the PILs with the highest conductivity among those analyzed, its interaction with NaAlg was the weakest, resulting in the second-lowest conductivity film, surpassed only by the film containing [m-2HEA][Bu], the PIL that exhibited the poorest conductivity values when pure. This also explains why the film containing [m-2HEA][Pr] has higher conductivity than the one containing [m-2HEA][Bu], even though the latter interacts slightly better with NaAlg. The films with a morphology marked by interconnected channels ([BHEA][Ac] and [m-2HEA][Ac]) exhibited more promising electrochemical properties, even though pure [BHEA][Ac] had the lowest conductivity among those selected for this study.

Pure [m-2HEA][Ac] exhibits a conductivity 1.7 times higher than pure [BHEA][Ac] at 120°C. However, the film formed with this PIL presented half the conductivity of the film formed with [BHEA][Ac] at the same temperature. As discussed by Malik et al. [16], the interactions between the polymer and the IL significantly influence the electrochemical properties of mixed matrix films with similar morphology. This result reinforces the possibility that ionic conductivity also occurs through the nanostructure of the polymer swollen with the PIL, and not just through the channels produced by phase separation.

The films produced exhibited conductivities of the same order of magnitude as the values observed for the SPEEK film with an alkylimidazolium phosphate-type PIL (3.16 $mS.cm^{-1}$ at 145°C without humidification). For this film, the authors reported a maximum power density of 203 $mW.cm^{-2}$ [10], which is higher than that observed for fully humidified 100% remodeled Nafion® at

60°C (193.78 mW.cm^{-2}) [11]. This comparison suggests that the films studied in this work are promising for applications in PEMFCs above 100 °C.

Conclusions

The different PILs produced differences in the morphological, chemical, thermal, mechanical, and electrochemical properties in NaAlg-based films. The films exhibited a typical mixed matrix morphology, but PILs that simultaneously exhibited stronger interactions with NaAlg and easier mobility within the polymer matrix tended to form interconnected channels throughout the cross-section, while the others tended to form a spongier structure. The formation of interconnected channels and a stronger network of hydrogen bonds involving the hydroxyl groups of NaAlg and PILs resulted in more conductive films, but with less promising thermal and mechanical properties. Among the mixed matrix films produced in this work, those produced with [m-2HEA][Ac] exhibited conductivity in the same order of magnitude as those with [BHEA][Ac], but with slightly higher mechanical strength and considerably better mechanical properties.

Finally, it may be said that NaAlg-based films formed with 40 wt% of [BHEA][Ac] or [m-2HEA][Ac] are promising for applications in PEMFC at temperatures above 100°C, although further studies should be proposed to improve their thermal and mechanical properties.

Acknowledgements

The authors thank FAPERJ for the master's scholarship for Alene D. N. and financial support provided to the project E-26/211.925/2021.

References

[1]F. R. Pazheri, M. F. Othman, and N. H. Malik, Renewable and Sustainable Energy Reviews, vol. 31, pp. 835–845, 2014, doi: 10.1016/j.rser.2013.12.020.
[2]O. Z. Sharaf and M. F. Orhan, Renewable and Sustainable Energy Reviews, vol. 32, pp. 810–853, 2014, doi: 10.1016/j.rser.2014.01.012.
[3]A. Chandan et al., J Power Sources, vol. 231, pp. 264–278, 2013, doi: 10.1016/j.jpowsour.2012.11.126.
[4]J. Zhang et al., J Power Sources, vol. 160, no. 2, pp. 872–891, 2006, doi: 10.1016/j.jpowsour.2006.05.034.
[5]H. Chen et al., , J Memb Sci, vol. 596, no. August 2019, p. 117722, 2020, doi: 10.1016/j.memsci.2019.117722.
[6]S. S. Araya et al., Int J Hydrogen Energy, vol. 41, no. 46, pp. 21310–21344, 2016, doi: 10.1016/j.ijhydene.2016.09.024.
[7]P. R. Jothi and S. Dharmalingam, , J Memb Sci, vol. 450, pp. 389–396, 2014, doi: 10.1016/j.memsci.2013.09.034.
[8]R. Prado and C. C. Weber, Applications of Ionic Liquids. Elsevier B.V., 2016. doi: 10.1016/B978-0-444-63713-0.00001-8.
[9]D. Zappi et al., Talanta, vol. 194, pp. 26–31, 2019, doi: 10.1016/j.talanta.2018.10.001.
[10] Z. Yaqun, W. Zhi, Z. Chenxin, W. Jixiao, and W. Shichang, Chin J Chem Eng, vol. 21, no. 10, pp. 1098–1105, 2013, doi: 10.1016/S1004-9541(13)60574-1.
[11] N. Shaari and S. K. Kamarudin, J Power Sources, vol. 289, pp. 71–80, 2015, doi: 10.1016/j.jpowsour.2015.04.027.
[12] D. Santos et al., J Mol Liq, vol. 222, pp. 867–872, 2016, doi: 10.1016/j.molliq.2016.07.048.
[13] A. D. Nascimento, R. A. Reis, J. P. S. Santos, S. Mattedi, and L. F. Senna, J Chem Thermodyn, vol. 145, p. 106093, 2020, doi: 10.1016/j.jct.2020.106093.
[14] J. C. Jansen, K. Friess, G. Clarizia, J. Schauer, and P. Iz, , Macromolecules, vol. 44, pp. 39–45, 2011, doi: 10.1021/ma102438k.
[15] B. Cong et al., Mater Des, vol. 142, pp. 221–228, 2018, doi: 10.1016/j.matdes.2018.01.039.
[16] R. S. Malik, S. N. Tripathi, D. Gupta, and V. Choudhary, Int J Hydrogen Energy, vol. 39, no. 24, pp. 12826–12834, 2014, doi: 10.1016/j.ijhydene.2014.06.060.
[17] Q. F. Li et al., J Memb Sci, vol. 347, no. 1–2, pp. 260–270, 2010, doi: 10.1016/j.memsci.2009.10.032.

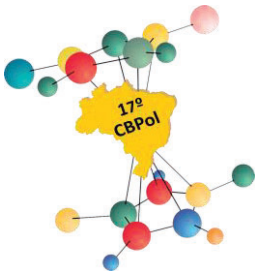

REMOVAL OF METHYLENE BLUE DYE BY PVDF/RGO MICRO/NANOSTRUCTURAL MEMBRANES PRODUCED BY AIRBRUSHING

Luiz F. Malmonge[1*], Thuany G. Maraschin[2], Nara R. S. Basso[2], Mirian C. Santos[3], Gabriel C. Dias[1].

1 - Department of Physics and Chemistry (DFQ), São Paulo State University (UNESP), Ilha Solteira, SP, Brazil, luiz.malmonge@unesp.br
2 – Polytechnic School, Pontifical Catholic University (PUC), Rio Grande do Sul, RS, Brazil
3 - Department of Analytical, Physical-Chemistry and Inorganic Chemistry (DQAFQI), Institute of Chemistry, São Paulo State University (UNESP), Araraquara, SP, Brazil.

Abstract: Micro and nanofibrous poly(vinylidene fluoride)(PVDF) membranes with graphene oxide were obtained by the solution blow spinning technique from a commercial airbrush, concentrations of 1, 3 and 5% by mass were incorporated. They were characterized and used in the adsorption of the dye Methylene Blue (MA) in aqueous medium. Scanning electron microscopy analyzes SEM/FEG, showed the presence of smooth fibers with an average diameter of less than 100 nm, in addition to some imperfections due to increased content. FTIR results indicated the presence of the characteristic bands of the α and β phase of PVDF, in addition to the presence of RGO, confirming their presence in the membranes. The adsorption tests revealed that the membranes with the highest content and in the time of 120 hours have the configuration for removal of the AM dye in the aqueous medium.
Keywords: PVDF, RGO, Airbrushing, Membranes, Adsorption.

Introduction

Annually, tons of toxic materials harmful to living organisms are emitted by chimneys and sewage systems of industries, agricultural activities, and mining, which has been affecting the hydrosphere and polluting water bodies worldwide. In this perspective, the impacts triggered by the textile industry and the excessive water consumption in other processes along the textile production chain, particularly in dyeing, cause soil contamination with a range of toxic contaminants, including dyes. These compounds are difficult to decompose and can cause contamination and degradation of the environment. Given these issues in textile production, the purification of water contaminated with dyes before it is discharged into the environment is necessary, and adsorption technology, combined with micro and nanostructure [1-5] membrane fabrication technology, is a promising and cost-effective method for water purification, as it also offers high efficiency. In this context, carbon-based materials, similar to Reduced Graphene Oxide (RGO), have been widely explored for adsorption applications due to their good chemical stability, structural diversity, low density, and suitability for large-scale production.

In this study, PVDF/RGO membranes were produced using the Sequential Blending and Stretching (SBS) adaptation through the aerography technique, applied for the adsorption of Methylene Blue (MB) dye in an aqueous medium.

Experimental

Materials

The polymer used was poly(vinylidene fluoride) - PVDF, purchased from Atofina do Brasil - Solef 1.008, in powder form. The solvent used was N,N-Dimethylformamide (DMF),

manufactured by Synth Produtos para Laboratório Ltda., both used as received. The Reduced Graphene Oxide (RGO) was obtained from the Laboratory of Organometallics and Resins (LOR)/Escola Politécnica/PUCRS, through the Graduate Program in Engineering and Materials Technology (PGETEMA)[6]. The precursor graphite, Grafine 99200 (particle size <75 μm), was obtained from Nacional de Grafite Ltda.

Obtaining the membranes

Initially, the PVDF solution was prepared by dissolving the polymer in DMF at a concentration of 40% (w/v) at a temperature of 70°C under magnetic stirring for approximately 20 minutes, followed by cooling to room temperature. Simultaneously, RGO/DMF solutions were prepared at room temperature by dispersing RGO in quantities of 1, 3, and 5mg in 10mL of DMF. These dispersions were sonicated for 20 minutes with intermittent intervals of 5 minutes. After this process, the RGO dispersion solution was added to the PVDF/DMF solution. The final concentration of the PVDF-RGO/DMF solution was fixed at 20% (w/v). This solution was kept under magnetic stirring at room temperature until homogeneous and then added to the airbrush for membrane formation. Pure PVDF membranes were obtained from the PVDF/DMF solution without the addition of RGO.

Characterization

The FTIR-ATR spectra were obtained using a Bruker Vertex-70 V spectrophotometer. The samples were analyzed using the attenuated total reflectance technique with a total of 128 accumulations and a resolution of 4 cm^{-1}. The measurements were performed in the range of 4,000 to 500 cm^{-1}. The SEM/FEG analyses were conducted using a JEOL JSM-7500F instrument equipped with PC-SEM operating software. The concentration of the unadsorbed AM contaminant in the membrane was determined and quantified using UV-visible spectroscopy at a temperature of 25ºC.

Results and Discussion

For the incorporation of 1mg of RGO particles, the formation of dispersed micro and nanofibers throughout the sample region was observed, as well as clusters of material (Fig. 1a). For the micrographs of nanofibers with 3mg of RGO (Fig. 1b), a similar morphology to the sample with 1mg of RGO was observed, but with improved sample homogeneity, showing fewer defects and an increase in the quantity of more well-defined micro and nanofibers. For 5mg of incorporated RGO (Fig. 1c), a similar morphology to the previous samples was observed, but the formed micro and nanofibers appeared thicker. The defects in the samples were likely due to the lack of a constant jet of solution at the airbrush nozzle. This inconsistency could be attributed to factors such as the non-homogeneity of the solution due to RGO dispersion, which could cause frequent nozzle clogging, and the viscosity of the solution, which can affect the flow from the reservoir to the nozzle as the process is gravity-driven.

Furthermore, the incorporation suggests that RGO particles are ejected more rapidly towards the collector, leaving behind quantities of material that are lost during the formation process. Despite regions showing well-defined and delineated nanofibers, the material, in general, did not exhibit overall homogeneity [7-9].

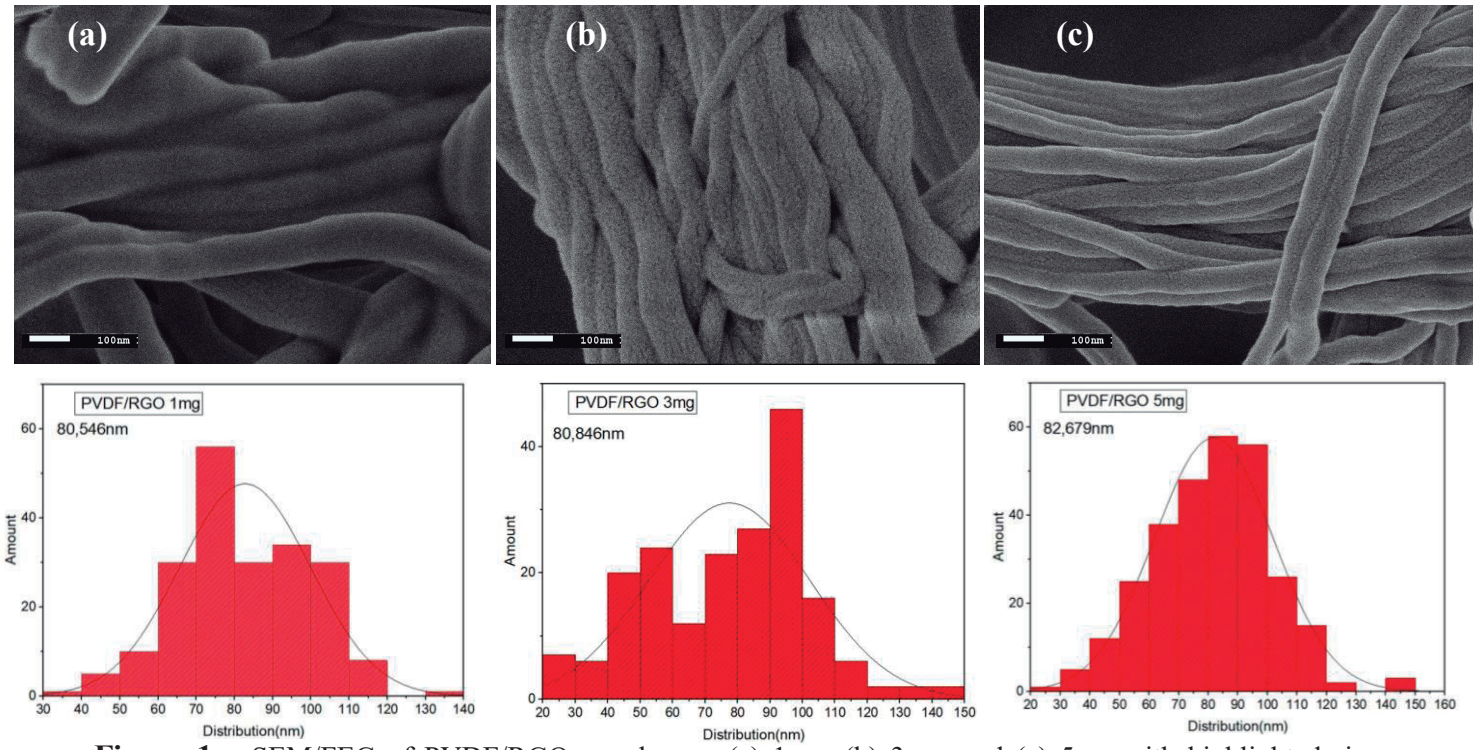

Figure 1 – SEM/FEG of PVDF/RGO membranes (a) 1mg; (b) 3mg, and (c) 5mg with highlighted size distribution**.**

In the results of FESEM, which provide more details about the morphology of micro and nanofibers, a generally smooth material with well-defined fibers and mostly interconnected structures was observed (Figs. 1d, 1e, and 1f). With an increase in the amount of RGO, a slight increase in thickness was observed. This fact is related to the increased viscosity of the solution, imperfections, and agglomerates, as. The average diameters ranged from 80.55 nm for the sample with 1mg of RGO to 82.68 nm for the sample with 5mg.

The results of FTIR analysis of the PVDF/RGO membranes are presented in Fig. 2. The FTIR spectra confirmed the presence of characteristic bands at 1,275 cm^{-1}, 1,400 cm^{-1}, 1,169 cm^{-1}, 1,072 cm^{-1}, 840 cm^{-1}, 880 cm^{-1}, 764 cm^{-1}, and 745 cm^{-1}, corresponding to the characteristics of PVDF [7].

In the RGO spectrum, a band at 3,452 cm^{-1} was observed, corresponding to the stretching vibration of the (-OH) bond in (C-OH) groups, with possible contributions from carboxylic acids and water. The band at 2,380 cm^{-1} is associated with stretching vibrations in the sp2 plane of the C=C bond. The bands at 1,641 cm^{-1} are related to the in-plane stretching vibration of the C=C bond, while the peaks at 1,475/1,373 cm^{-1} correspond to the bending vibrations of hydroxyl groups (C–OH), and the peak at 1,238 cm^{-1} corresponds to the bending vibrations of epoxy groups (C–O–C). All the above peaks are characteristic of GO; however, in the case of RGO, their intensity decreases due to the decomposition of these groups during the thermal reduction process [10,11].

At 2,935 cm^{-1}, a band attributed to the asymmetric and symmetric stretching vibrations of OG (graphene oxide) was observed. The band at 1,726 cm^{-1} is attributed to the presence of (C=O) bonds and is associated with the presence of RGO. An increase in the intensity of this band was observed for higher amounts of RGO present in the membranes [11].

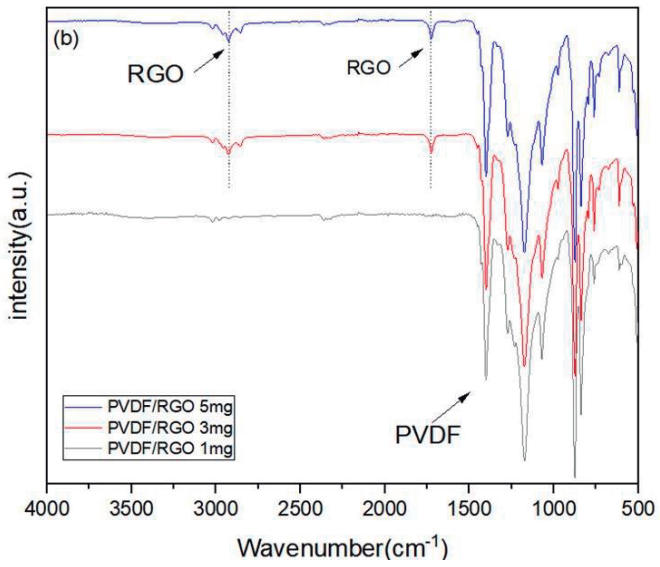

Figure 2 - FTIR of PVDF/RGO membranes

The concentration of RGO adsorbent incorporated in PVDF membranes has a strong influence on the adsorption process. Measurements were conducted at room temperature using PVDF/RGO samples containing 1mg, 3mg, and 5mg of RGO. The concentration and pH of the aqueous solutions containing the contaminant were kept constant at 5.0mg/L and 7.0, respectively. It was observed, except for pure PVDF, that the adsorption process behavior was proportional to the increase in RGO content. The adsorption of the AM dye increased as more adsorbent was used, with the 5mg membranes showing the best results. A considerable decrease in concentration (ppm) was observed. This is because a higher amount of material provides the membranes with a greater number of sites that can accommodate the dye molecules, in addition to the micro-nanofibers within their walls. The loading results obtained for the membranes as a function of contact time with the AM adsorbate solution are presented in Fig. 3 and Table 1.

It was found that water may face more difficulty in penetrating the pores and spaces between the nanofibers due to the characteristics of the PVDF matrix, which would, to some extent, hinder and limit the approach of molecules to the adsorption sites, despite the hydrophilic nature of RGO. This may have resulted in a faster saturation of the adsorption sites, justifying the long periods for the stabilization of the curve and the achievement of the maximum adsorption capacity [12-15].

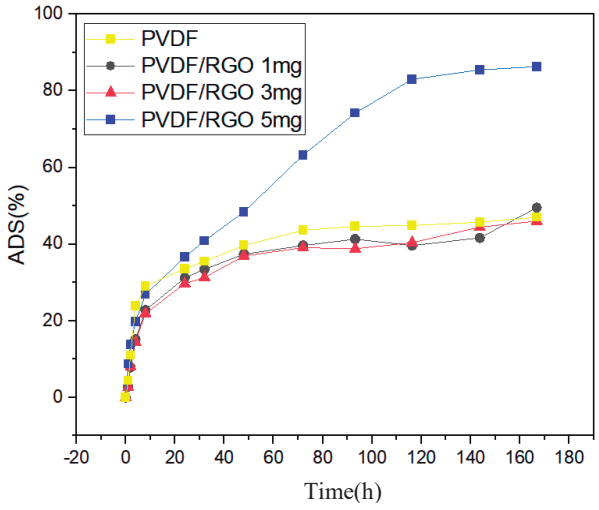

Figure 3 – Kinetic curve of PVDF/RGO in relation to the percentage of adsorption of total mass of AM in aqueous medium as a function of time

Table 1 - Kinetic results of PVDF/RGO membranes in aqueous medium, for concentration, mass adsorbed per gram, and percentage of adsorption, both at a time of 120 hours

Sample*	Contact Time	Methylene Blue		
		Concentration (ppm)	q_{eq} (mg/g)	Adsorption (%)
PVDF	**120h**	2,790	0,500	44,87
PVDF/RGO 1mg		3,075	0,518	39,65
PVDF/RGO 3mg		3,190	0,483	40,42
PVDF/RGO 5mg		0,968	1,161	83,04

*(V=25mL)- (puro) C_0 = 5,069ppm; m = 0.091mg; (1mg) C_0=5,097ppm; m=0,0897mg/ (3mg) C_0 = 5,176ppm; m=0.0886mg)/ (5mg) C_0 = 5,713ppm; m = 0.0817mg.

The values can be directly associated with the morphological and hydrophobic characteristics of the matrix. Additionally, this behavior can be explained by the amount of particles within the material, encapsulated, and due to the membrane formation and obtaining process itself, its dimensions, irregular shape, as well as the difficulty in overcoming the surface tension barrier of the polymeric matrix in an aqueous environment [16-19].

Conclusions

Micro and nanostructured membranes of PVDF/RGO were obtained by the SBS technique through the adaptation of a commercial airbrush. The incorporation of RGO enhanced the adsorptive properties of the new material, with a concentration of 5mg and a time of 120 hours being the optimal parameters for dye removal in an aqueous medium.

Acknowledgments

The authors are grateful for the financial support provided by the CAPES (88887136426/2017/00), CNPq (465571/2014-0) and FAPESP (2014/50945-4) and National Institute for Alternative Technologies of Detection, Toxicological Evaluation and Removal of Micropollutants and Radioactives (INCT-DATREM).

References

1. T. K. Waluyo, M. Lempang Journal of Hunan University Natural Sciences 2022, 49 (12), 23. https://doi.org/10.55463/issn.1674-2974.49.12.3
2. A M. V. Martin, D. C Flores, F. D.C. Siacor, E. B. Taboada, N. P. B. Tan, Nanotechnology 2022, 33(49), 495602. https://doi.org/10.1088/1361-6528/ac8b8b
3. F. T. G. Dias, S. P. Rempel, L. D. Agnol, O. Bianchi. Journal of polymer research 2020, 27, 205. https://doi.org/10.1007/s10965-020-02173-7
4. G. C. Dias, T. S. P. Cellet, M. C. Santos, A. O. Sanches, L. F. Malmonge, Journal of Polymer Research 2019. 26, 87. https://doi.org/10.1007/s10965-019-1731-7
5. G. Pavoski, T. Maraschin, F. C. Fim, N. M. Balzaretti, G. B. Galland, C. S. Moura, N. R. S. Basso, Materials Research 2017, 20 (1), 53. https://doi.org/10.1590/1980-5373-MR-2015-0528

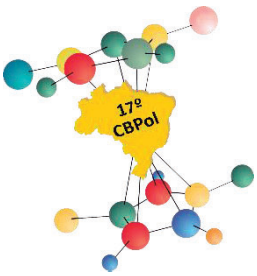

REVALORIZATION PINECONE RESIDUES REINFORCED ACRYLONITRILE BUTADIENE STYRENE (ABS) COMPOSITE FILAMENTS FOR 3D-PRINTING BY FDM

Thalita da Silva Neto[1], João Vitor Gomes[2], Paulo H, F. Pereira[2], and Daniella R, Mulinari[1]*

1 – State University of Rio de Janeiro (UERJ), Department of Chemistry and Environmental, Resende-RJ, Brazil
2 – State University of Rio de Janeiro (UERJ), Department of Mechanic and Energy, Resende-RJ, Brazil

thalita.neto@discentes.fat.uerj.br; daniella.mulinari@fat.uerj.br.

Abstract – This study presents an alternative for the revalorization of solid waste from pinecone residues for use as reinforcement in acrylonitrile butadiene styrene (ABS) composite filaments as a potential for 3D printing by FDM. Filaments were prepared with the insertion of a percentage of 2% wt pinecone fiber in ABS matrix, in two different ways: *in natura* and bleached fibers. A thermokinetic mixer processed the ABS/pinecone fibers (2% wt.) composites. After, the filaments were prepared by a mini extruder and printing 3D by FDM. Filaments were characterized by Scanning Electron Microscopy (SEM), and thermal analysis was evaluated by Differential Scanning Calorimetry (DSC). The use of bleached fiber in composite filaments increases composites' thermal stability compared to *in natura* fiber in composite filaments. On the other hand, the filament with *in natura* fiber presented a better printability. So, the insertion of pinecone fiber in the ABS matrix can be a low-cost feedstock for 3D printing.

Keywords: *ABS, pinecone fiber, 3D printing, FDM technology, composite filaments.*

Introduction

Additive manufacturing (AM) technology has been applied in several areas since the 1980s, mainly in the automobile and aeronautical industries [1]. One of the most relatively recent techniques used in AM is three-dimensional printing (3D- printing), which has been a trend in research, due to its ability to model quickly, allowing the integration into computer-aided design (CAD) software packages [2]. Among 3D-printing methods, the FDM (Fused Modelling Deposition) technology stands out for its reliability, simple fabrication process, producing objects with good resolution, and vast material customization [3]. However, commercially available FDM machine presents a limitation of heating element/chamber temperature of 300°C, which restricts the processing of higher melting temperature materials [4].

Because of this, the development of composite materials, such as natural fiber-reinforced has been a subject of recent research, mainly with an alternative to non-biodegradable. Besides, they are highlighted for their low cost, low density, and abundance with a potential to improve polymer mechanical properties.

Among natural fibers, pinecone stands out for its abundance, and it is one of the most common residues in North America, which makes it a promisor reinforcement [5]. For those reasons, this study purposes an alternative for pinecone (*Pinus elliottii*) fibers residues as a reinforcement in acrylonitrile-butadiene-styrene (ABS), with an objective to obtain composite filaments for FDM 3D-

printing usage, aiming the advantages of offered by natural fibers in composites, developing new potential properties.

Experimental

Materials

The pinecone residues were donated by a farm producer and ABS was provided by Ineos Styrolution of Brazil (GP-35). The fiber was oven-dried at 80°C for 24h, posteriorly crushed, and sieved (35 mesh) in a mill Willye, model TE-650 (Tecnal Equipamentos Científicos Ltda., Piracicaba, Brazil).

Obtaining treated fibers of pinecone

The pre-treatment was realized with NaOH solution (4% w/v) for 1h under constant stirring at room temperature. Then, the solution was filtered by a vacuum filter, and the remained fibers were washed in distilled water.

Obtaining bleached fibers from pinecone

To obtain bleached fibers, firstly the fibers were pretreated with NaOH solution (4% w/v) for 1h under constant stirring at room temperature. Then, the solution was filtered by a vacuum filter, and the remained fibers were washed in distilled water.

Treated fibers were previously dried at 80°C for 24h. After that, they were bleached with a 1:1 solution of NaOH (1 mol. L^{-1}) and H_2O_2 30% (v/v) at 70 °C for 1 h. The fibers were filtered to remove the excess reagents, repeating all processes one more time. After, the fibers were washed with distilled water until obtain a neutral pH and posteriorly dried at 60°C for 24 h, obtaining bleaching fibers.

Characterization of the fibers

The morphology of the fibers was analyzed by Scanning electron microscopy (SEM) through a microscope (model TR-3000, HITACHI Ltd., Tokyo, Japan) with tungsten filament, secondary electron detector, 5kV, and low-vacuum. A double face 3M tape fixed the foam samples on brass support.

Preparation of composite filaments

A thermokinect mixer model MH-50H (MH Equipamentos Ltda., Guarulhos, SP, Brazil) at a high-speed rate rotation (5250 rpm) for 55 s was used to mix ABS with the raw, and bleached fibers of the pinecone with a percentage of 2% wt. Then, they were milled in a knife mill (Plastimax Indústria e Comércio Ltda, Barueri, Brazil) and dried at 50 ºC for 2 h.

The filaments were obtained using a mini extruder (brand Weellzoom, model B Desktop, Guangdong Prov, China), with a temperature range of 190-195°C. Then, the diameter measurements were realized on each test specimen at the interval of 50 mm using a caliper rule for ten samples. The density was calculated as the ratio of mass per unit volume. Composites filaments were tested in a 3D printer model Sethi3D S3X.

Characterization of ABS/fibers from pinecone filaments composites

The microstructural analysis of the filament's surface and cross-section was executed by scanning electron microscopy technique, using a microscope HITACHI with tungsten filament operating at 5kV, employing a low-vacuum technique and secondary electron detector at different magnifications (i.e.50×, 200×).

Thermal analyses were performed to evaluate the stability of the fibers, ABS, and composite filaments. Thermogravimetric analysis was conducted using a simultaneous TGA/DSC thermal

analyzer, Model SDT Q600 (TA Instruments). Experiments were carried out using a specimen weight of 5 mg under nitrogen as purging gas, utilizing a heating rate of 10 ºC.min^{-1}, from 30 ºC to 600 ºC.

Design and printing of 3D samples
Cylindrical shapes with dimensions 3.20 x 23.5 mm (height x diameter) with an orthogonal-projection structure were projected in CAD 3D Inventor software.

Mechanical Properties
To evaluate the mechanical properties of the printed specimens, a Shore D type digital manual hardness tester was used, in ambient temperature, according to the ASTM D2240 standard, available at the Department of Materials and Technologies of UNESP, Guaratinguetá-SP, Brazil.
3D printed specimens of pure ABS, ABS + 2% FN (*in natura* fiber), and ABS + 2% BF (bleached fiber) properties were measured in Shore D scale hardness, based on the average of ten measurements with their standard deviation.

Results and Discussion
The treatment realized in the fibers caused changes in their morphology. Figure 1-a evidenced the tubular morphology with a circular section of the pinecone raw fiber. After, the treatment the increased amount of exposed cellulose on the fiber surface, increased the reaction sites [6], [7]. Furthermore, in the bleached fiber there was a significant increment of roughness (Figure 1-d), the apparent changes in the bleached fiber surfaces are associated with the removal of impurities, lignin, and hemicellulose [8].

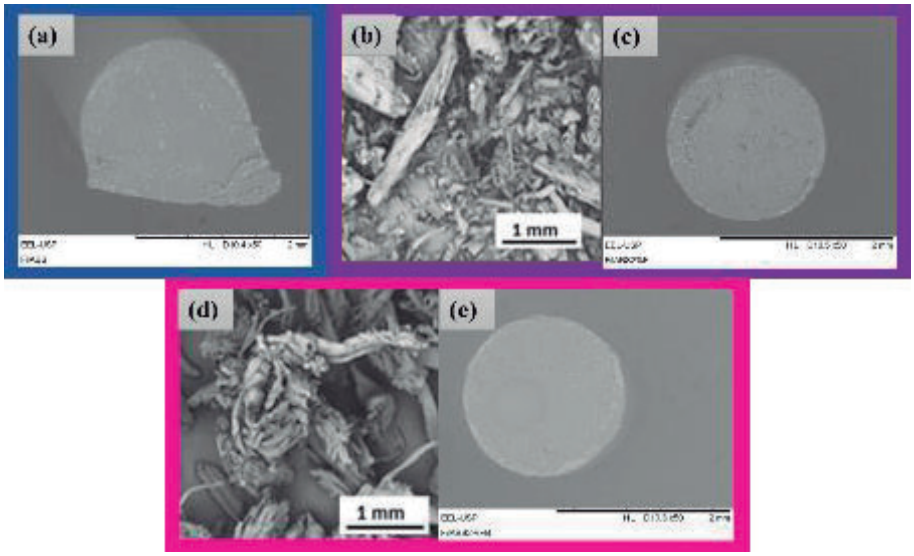

Figure 1: SEM images of (a) pure ABS filament; (b) raw pinecone fiber; (c) ABS + 2% FN; (d) bleached pinecone fiber; (e) ABS + 2% BF.

Regarding the thermal properties, Figure 2 shows the DSC curves of each filament, which all demonstrate the same profile. The glass transition temperature (Tg) is indicated in the range of 90-120°C [9]. The endothermic peak around 420°C is related to ABS decomposition. The similar DSC behavior demonstrates that the insertion of the pinecone fiber did not interfere with the processability and printability of ABS polymer.
The composite filaments evidenced a slight variation in the filament diameters, as well as a processing temperature.

Observing the cross-section SEM images of filaments in Figure 1, the pure ABS (Figure 1-a) filament shows a solid cross-section without visible voids. In contrast, the addition of the fiber leads to visible porosities in the filament. It was also noted in Figure 1-e, the bleached fiber presented a good interfacial bonding with the ABS matrix, once it was uniformly distributed and embedded throughout the wire cross-section when compared to *in natura* fiber added.

Figure 3 presents the samples printed by the 3D printing FDM process. As can be seen, the obtained samples revealed some irregularities in their visual aspect, which can be related to printer issues, such as low bed adhesion and polymer flow. The ABS + 2% FN exhibited better printability, due to the effective interaction between fiber and polymer matrix with an appropriate viscosity [10]. While the ABS + 2% BF filament presented difficulties in printing, with constant flow failures.

The Shore D was used to evaluate the mechanical prosperities of each printed specimen, showing that with the addition of the fiber, the hardness decreased. Besides, the filament with the bleached fiber presented a lower value of hardness.

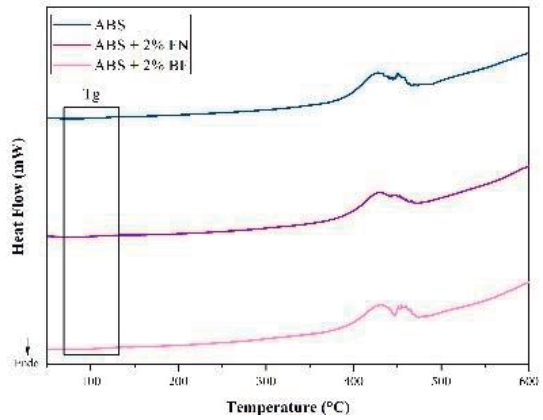

Figure 2: DSC curves of composite filaments: pure ABS; (b) ABS + 2% FN; (c) ABS + 2% BF.

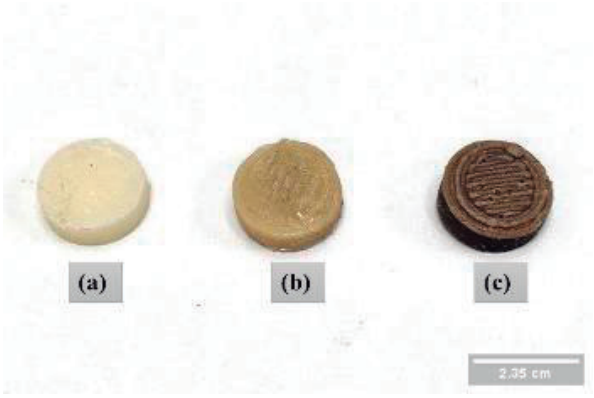

Figure 3: Design print of composite filaments: (a) pure ABS; (b) ABS + 2% FN; (c) ABS + 2% BF.

Table 1 presents the diameter, printer parameters, and Shore D measurements for each composite sample.

Table 1: Parameters of filaments and printed samples.

Parameters	Pure ABS	ABS + 2% FN	ABS + 2% BF
Nozzle Temperature (ºC)	230	250	250
Bed Temperature (ºC)	110	115	115
Cooling (%)	100	100	100
1st printed layer speed ($mm.s^{-1}$)	20	20	20
Print speed ($mm.s^{-1}$)	40	40	40
Height of subsequent layers (mm)	0.06	0.06	0.06
Shore D	40.5 ± 4.7	39.3 ± 3.7	36.6 ± 5.5
Diammeter of filament (mm)	1.70 ± 0.1	1.72 ± 0.5	1.71 ± 0.2
Density ($g.cm^{-3}$)	1.05 ± 0.02	1.13 ± 0.04	1.10 ± 0.02
Processing Temperature (°C)	190	195	195

Conclusions

In this research, the effect of *in natura* and bleached pinecone fiber in ABS matrix was evaluated. Analyzing the results, it was noted that despite the influence of thermal stability and morphological

differences, these facts did not interfere with the diameter and density of filaments. The bleached fiber percentage increases composites' thermal stability compared to ABS + 2% FN, at the same time, the filament with *in natura* fiber presented a better printability. For this reason, the insertion of pinecone fiber in the ABS matrix, in addition to contributing to better thermal stability, can be a low-cost feedstock for 3D printing applications.

Acknowledgments
This research was funded by FAPERJ (E-26/010.101232/2018 and E-26/010.001800/2015).

References

[1] E. Åkerlund, A. Diez-Escudero, A. Grzeszczak, and C. Persson, "The Effect of PCL Addition on 3D-Printable PLA/HA Composite Filaments for the Treatment of Bone Defects," *Polymers (Basel)*, vol. 14, no. 16, Aug. 2022, doi: 10.3390/polym14163305.

[2] R. Hashemi Sanatgar, C. Campagne, and V. Nierstrasz, "Investigation of the adhesion properties of direct 3D printing of polymers and nanocomposites on textiles: Effect of FDM printing process parameters," *Appl Surf Sci*, vol. 403, pp. 551–563, May 2017, doi: 10.1016/j.apsusc.2017.01.112.

[3] R. T. L. Ferreira, I. C. Amatte, T. A. Dutra, and D. Bürger, "Experimental characterization and micrography of 3D printed PLA and PLA reinforced with short carbon fibers," *Compos B Eng*, vol. 124, pp. 88–100, Sep. 2017, doi: 10.1016/j.compositesb.2017.05.013.

[4] N. Mohan, P. Senthil, S. Vinodh, and N. Jayanth, "A review on composite materials and process parameters optimisation for the fused deposition modelling process," *Virtual Phys Prototyp*, vol. 12, no. 1, pp. 47–59, Jan. 2017, doi: 10.1080/17452759.2016.1274490.

[5] N. Rambabu, S. Panthapulakkal, M. Sain, and A. K. Dalai, "Production of nanocellulose fibers from pinecone biomass: Evaluation and optimization of chemical and mechanical treatment conditions on mechanical properties of nanocellulose films," *Ind Crops Prod*, vol. 83, pp. 746–754, May 2016, doi: 10.1016/j.indcrop.2015.11.083.

[6] D. Ray, B. K. Sarkar, A. K. Rana, and N. R. Bose, "Effect of alkali treated jute fibres on composite properties," *Bulletin of Materials Science*, vol. 24, no. 2, pp. 129–135, Apr. 2001, doi: 10.1007/BF02710089.

[7] A. Valadez-Gonzalez, J. M. Cervantes-Uc, R. Olayo, and P. J. Herrera-Franco, "Effect of fiber surface treatment on the fiber–matrix bond strength of natural fiber reinforced composites," *Compos B Eng*, vol. 30, no. 3, pp. 309–320, Apr. 1999, doi: 10.1016/S1359-8368(98)00054-7.

[8] G. Basu, L. Mishra, and A. K. Samanta, "Appropriate bleaching technique for coconut fiber," *Journal of Natural Fibers*, vol. 16, no. 3, pp. 442–452, Apr. 2019, doi: 10.1080/15440478.2017.1423263.

[9] C. A. Correia, L. M. de Oliveira, and T. S. Valera, "The Influence of Bleached Jute Fiber Filler on the Properties of Vulcanized Natural Rubber," *Materials Research*, vol. 20, no. suppl 2, pp. 466–471, Oct. 2017, doi: 10.1590/1980-5373-mr-2017-0126.

[10] L. S. Martins *et al.*, "A versatile filler in polyhydroxyalcanoates filaments for FDM: A diverse panorama for pullulan application," *Mater Today Commun*, vol. 28, Sep. 2021, doi: 10.1016/j.mtcomm.2021.102690.

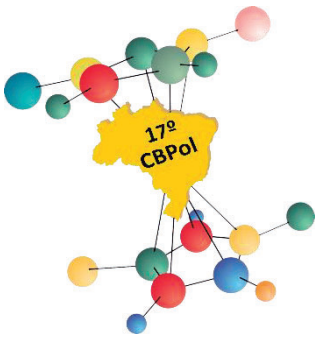

RICE HUSK FILLED PLA/PBAT COMPOSITES FOR FOOD CONTAINERS: PROCESSABILITY, RHEOLOGICAL AND THERMAL PROPERTIES

Nicole B. Agostini[1]*, Vanessa Z. Kieffer[1], Edson L. Francisquetti[2] and Ruth M. C. Santana[1]

1 – Department of Materials Engineering, PPGE3M, Federal University of Rio Grande do Sul (UFRGS), Porto Alegre, RS, Brazil
2 – Federal Institute of Education, Science and Technology of Rio Grande do Sul (IFRS), Farroupilha, RS, Brazil.
*nicole.agostini@ufrgs.br

Abstract - This study investigated the potential of using polylactic acid (PLA), polybutylene adipate-co-terephthalate (PBAT), and rice husk (RH) composite as alternative materials for food containers. The composite was prepared using an internal mixer and characterized by torque vs. time mixing curves, melt flow index (MFI), thermogravimetric analysis (TGA), and differential scanning calorimetry (DSC). The results showed that adding PBAT and rice husks improved the thermal stability of the composite and decreased the melting temperature and crystallinity degree. The MFI decreased with the incorporation of rice husks, indicating good filler dispersion in the matrix. Since it is a byproduct of rice production, rice husk-filled composites can reduce the cost of material production and minimize environmental impact during the packaging life cycle. These findings suggest that the PLA/PBAT/RH composite shows potential as a sustainable alternative to traditional food packaging materials.
Keywords: *PLA, PBAT, rice husk, biodegradable, food packaging.*

Introduction

The widespread use of non-biodegradable materials for packaging applications has led to growing concerns about environmental pollution [1]. The accumulation of plastic waste in the natural ecosystem poses a threat to the environment and has implications for human health and well-being. To address these concerns, it is crucial to explore sustainable alternatives and adopt eco-friendly practices that can help reduce the negative impact of packaging waste on our planet [2].

Biodegradable and compostable materials have emerged as potential alternatives to conventional plastics to address these concerns [1,3]. Polylactic acid (PLA) and polybutylene adipate terephthalate (PBAT) are two biodegradable polymers extensively studied for food packaging applications [1]. However, these materials often have limitations in terms of their mechanical and barrier properties, which can affect their suitability for specific food packaging applications. Also, PLA/PBAT blends can be more expensive than traditional petroleum-based plastics, which may limit their widespread adoption in the food packaging industry [1]. Modifying the composition of the polymer blend, such as incorporating different types of polymers or adding natural fillers, can improve the properties and minimize production costs [3].

A rice husk is a natural sheath formed around rice grains during growth [4]. Rice husks have gained attention as a natural filler in polymer composites due to their abundance, low cost, and desirable properties. As a byproduct of rice production, their use in composites provides a sustainable and

environmentally friendly solution [4, 5]. Incorporating rice husks in polymer matrices can modify their mechanical properties, final weight, and resistance to weathering and also make the final product more economically competitive [4]. Overall, using rice husks in polymer composites shows great promise in providing sustainable and high-performance materials for various applications.

In recent years, researchers have explored blending natural fillers with biodegradable material to overcome the costs of polymer processing and improve the properties of biodegradable polymers for food packaging applications [1]. In this study, we investigate using rice husk as a natural filler in a PLA/PBAT composite for food containers. We evaluate how thermal and rheological are affected by the composition of the composite material and assess its potential as a sustainable and biodegradable food packaging material. The results of this study are significant for developing environmentally friendly food packaging materials that can tackle the environmental impact of conventional plastic packaging in the food industry.

Experimental

Materials

The materials used in this study were PLA (Ingeo™ Biopolymer 4043D), PBAT (Ecoflex® F Blend C1200), and rice husk (RH) provided by local producers. The PLA/PBAT blends and composites with rice husk were prepared using a mixing chamber (Thermo Scientific HAAKE™ Rheomix OS) at a temperature of 170°C, 60 rpm and a mixing time of 8 minutes. Therefore, the samples were pressed at 170°C under 6 ton to form the sheets used in the compression molding processing. All the specimens were able to be molded in food trays. The formulations studied were named BL1, BL2, CO1, CO2, CO3, and CO4. The compositions of these samples are presented in Table 1.

Table 1 – Composition of PLA/PBAT/rice husks blends.

Sample	PLA (%)	PBAT (%)	RH (%)
BL1	90	10	0
BL2	80	20	0
CO1	80	10	10
CO2	70	10	20
CO3	70	20	10
CO4	60	20	20

Characterization

Thermogravimetric analysis (TGA) was carried out using a TA Instruments TGA Q50 thermogravimetric analyzer. The samples were heated from room temperature to 930°C at a heating rate of 20°C/min under a nitrogen atmosphere with a 10 mL/min flow rate. Each test consumed samples of about 15 mg.

Differential scanning calorimetry (DSC) was conducted using a TA Instruments DSC Q20 calorimeter. The samples were heated from 25°C to 200°C at a heating rate of 10°C/min, then cooled to 25°C at a cooling rate of 10°C/min, and finally reheated to 200°C at a heating rate of 10°C/min under a nitrogen atmosphere with a 50 mL/min flow rate. About 5 mg of the sample was used for each test. The degree of crystallinity (X_c) of PLA was calculated using Eq. 1[6].

$$X_c = \left(\frac{\Delta H_m - \Delta H_{cc}}{\Delta H_{m_{100}}(w_{PLA})}\right) \times 100 \quad (1)$$

Where ΔH_m the melting enthalpy of the tested sample, ΔH_{cc} is the cold-crystallization enthalpy of the tested sample, $\Delta H_{m_{100}}$ is the theoretical melting enthalpy of the 100% crystalline (93 J/g) [6] and w_{PLA} is the weight fraction of the PLA in the sample.

The melt flow index (MFI) was measured according to ASTM D1238-13 standard on a Ceast Modular Melt Flow Tester with a 2.16 kg load and at temperatures of 170, 190, and 210°C. The melt flow index was calculated as the mass of the polymer flowing through a capillary of a specified length and diameter over a specified time.

Results and Discussion

The torque vs. mixing time curves obtained during the preparation of the PLA/PBAT/RH composites are shown in Fig.1. The total torque corresponds to the area under the curve. The mixing torque suffered no alteration as PBAT content in the blends increased, indicating an equal viscosity of the melt for the blends. Overall, the composites filled with rice husk presented higher stabilized torque – measured around 5 min of mixing - compared to the blends with equal PBAT content, which indicates that RH can increase the viscosity of the melt. Thus, the final torque observed in composite CO4 may be due to the higher contents of PBAT (20%) and rice husk (20%).

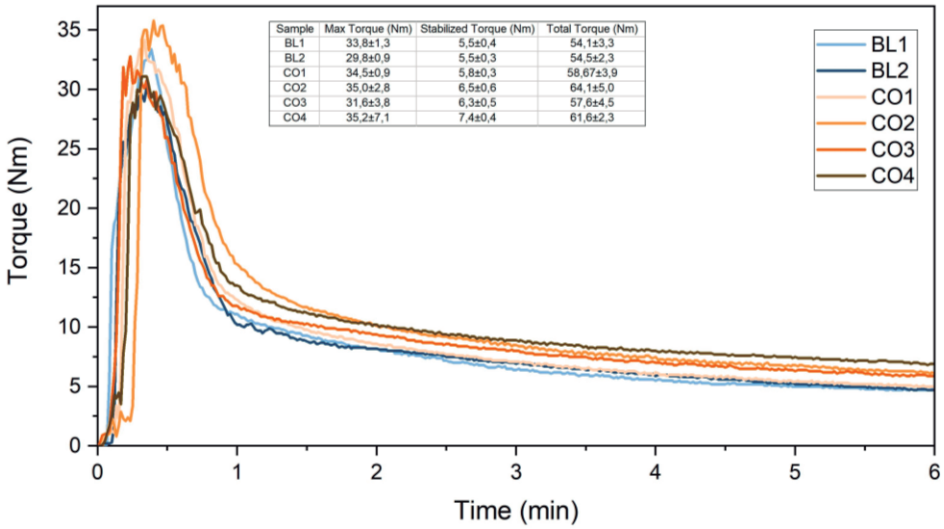

Figure 1 – Torque vs. mixing time of PLA/PBAT blends and RH filled composites.

The MFI of the pure materials, PLA/PBAT blends, and RH filled composites is shown in Fig. 2. The MFI is an indirect indication of the viscosity of the melt; the higher the MFI, the lower the viscosity. All the samples reported lower viscosity in the higher testing temperature (210°C) due to increased molecule kinetic energy. Compered to neat blends, the addition of rice husks led to a decrease in the MFI, indicating an increase in the viscosity of the melt, as already observed during the mixing of samples. This decrease in the MFI may be attributed to the high aspect ratio and low surface energy of the rice husks, which hinder the movement of the polymer chains and reduce the flowability of the melt.

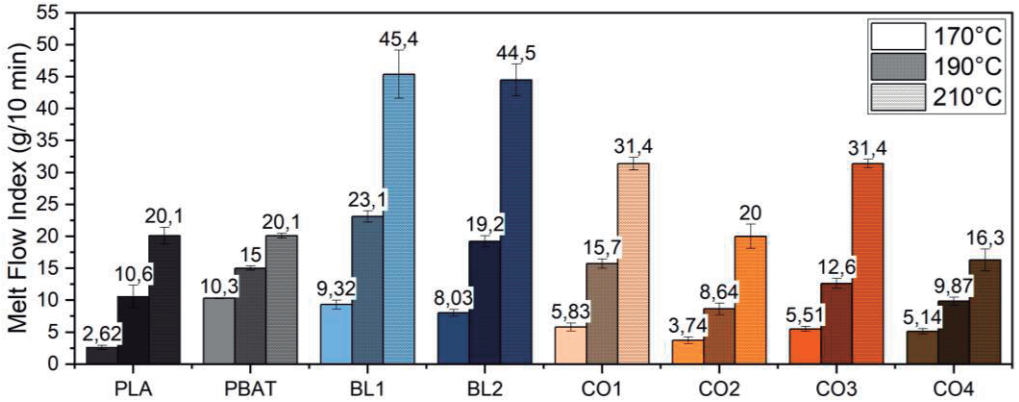

Figure 2 – MFI in three temperatures of pure polymers, PLA/PBAT blends and RH filled composites.

The TGA thermograms of the samples in the study are shown in Fig. 3. It was noticed that PBAT has a higher onset temperature than PLA; thus, the blends and composites with 20%PBAT presented higher thermal stability. PBAT also confers higher residues at 600°C (3.59 wt%), indicating that carbonization occurs more severely for PBAT than for PLA [7]. Albeit CO2 and CO4 showed higher residues, 9.41 wt% and 7.83 wt%, respectively, possibly due to char formation during RH degradation process. The decomposition processes of all the blends and composites could not be distinguished obviously from the TG curves. Two processes of thermal decomposition signaling to PLA and PBAT phases can be observed via DTG curves, where the intensity of degradation each event is related to the weight fraction of the component [7].

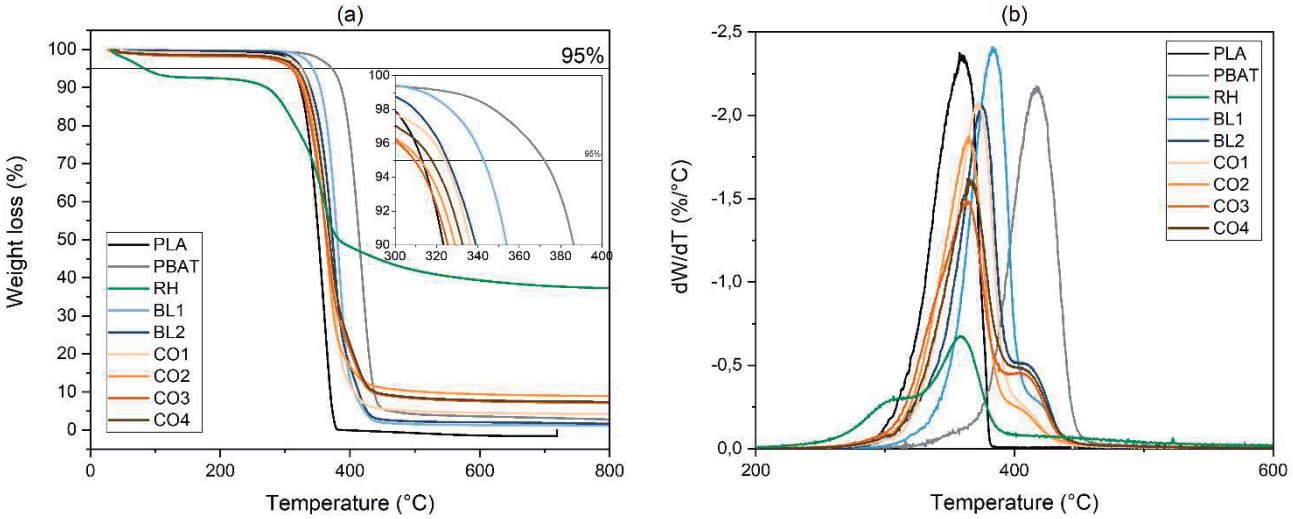

Figure 3 – (a) TG and (b) DTG curves of pure polymers, PLA/PBAT blends and RH filled composites.

Fig. 4 presents the second heating DSC thermograms for the blends and composites. The glass transition, cold crystallization, and melting are distinctly observed in the curves. It is noted that PLA glass transition temperature (Tg) remains constant through the compositions (~ 60 °C), indicating that the other components do not affect the amorphous phase. PBAT has a negative Tg (-30 °C) [6]; thus, the analyses do not observe the event. The addition of rice husk affects the crystallinity phase, where the samples with a higher amount of rice husk (20%) modify the reorganization phenomena of the crystals during the heating run due to the nucleation effect promoted by the presence of the particles. The relative amplitude of cold crystallization and melting peaks determined from DSC measurement showed that these blends were mostly amorphous, with the lower and higher crystallinity degree reported for blend BL1 (1.43%) and composite CO4 (2.42%), respectively.

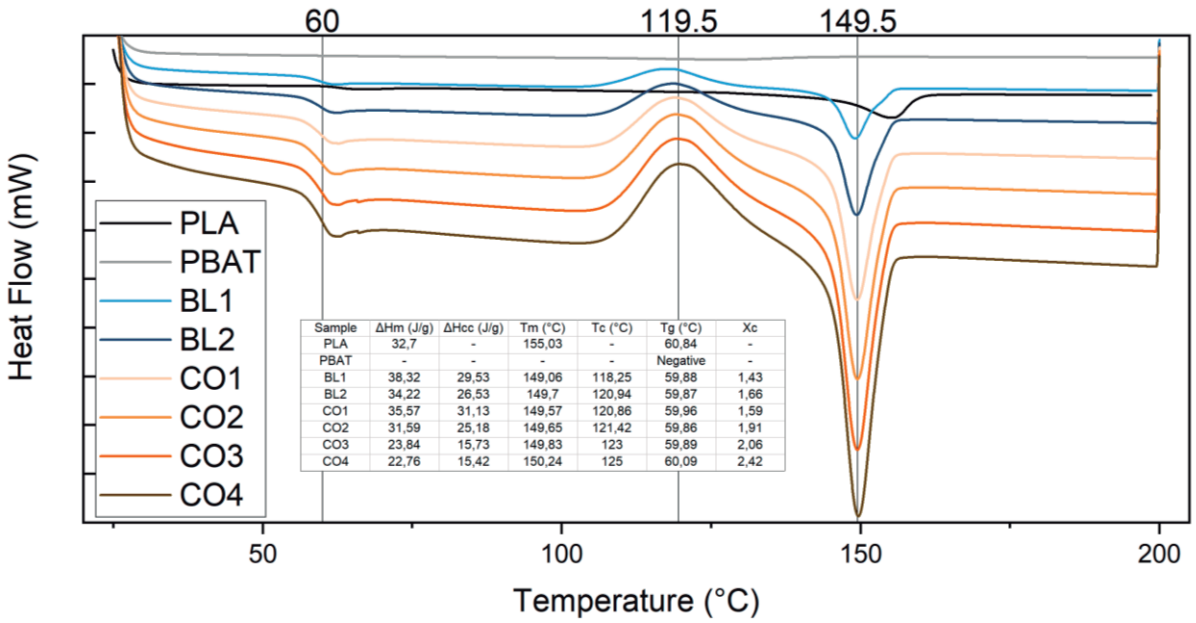

Sample	ΔHm (J/g)	ΔHcc (J/g)	Tm (°C)	Tc (°C)	Tg (°C)	Xc
PLA	32,7	-	155,03	-	60,84	-
PBAT	-	-	-	-	Negative	-
BL1	38,32	29,53	149,06	118,25	59,88	1,43
BL2	34,22	26,53	149,7	120,94	59,87	1,66
CO1	35,57	31,13	149,57	120,86	59,96	1,59
CO2	31,59	25,18	149,65	121,42	59,86	1,91
CO3	23,84	15,73	149,83	123	59,89	2,06
CO4	22,76	15,42	150,24	125	60,09	2,42

Figure 4 – DSC thermograms of pure polymers, PLA/PBAT blends and RH filled composites obtained from second heating scan.

Conclusions

In conclusion, this study investigated the potential of using PLA/PBAT/RH composites as an alternative material for food containers. The results indicate that adding rice husk to the composites modifies their rheological properties, increasing viscosity and reducing flowability. The composites' thermal properties were also improved, with higher thermal stability related to the amount of PBAT phase. Therefore, the PLA/PBAT/RH composites could be a promising solution for developing sustainable food packaging materials, as they can withstand high temperatures. Further studies are necessary to investigate the mechanical and barrier properties of the composites, as well as their composition for specific applications.

Acknowledgements

The authors thank the Laboratory of Polymeric Materials at UFRGS for supporting the research and CAPES, CAPES-PROEX and CNPq for the aid granted.

References

1. L. Ncube; A. Ude; E. Ogunmuyiwa; R. Zulkifli; I. Beas, Materials 2020, 13(21), 1–24. doi.org/10.3390/MA13214994
2. R. Geyer; J. Jambeck; K. Law, Science Advances 2017, 3(7). doi.org/10.1126/SCIADV.1700782.
3. D. Nakayama; F. Wu; A. Mohanty; S. Hirai; M. Misra, ACS Omega 2018, 3(10), 12412–12421. https://doi.org/10.1021/ACSOMEGA.8B00823.
4. R. Arjmandi; A. Hassan; K. Majeed; Z. Zakaria, Journal of Polymer Science 2015, 2015, 32. doi.org/10.1155/2015/501471.
5. S. Yap; S. Sreekantan; M. Hassan; K. Sudesh; M. Ong, Polymers 2020, 13(1), 104. doi.org/10.3390/POLYM13010104.
6. P. Chaiwutthinan; S. Chuayjuljit; S. Srasomsub; A. Boonmahitthisud, Journal of Applied Polymer Science 2019, 136 (21). doi.org/10.1002/APP.47543.
7. S. Xiang; L. Feng; X. Bian; G. Li; X. Chen, Polymer Testing 2020, 81. doi.org/10.1016/j.polymertesting.2019.106211.

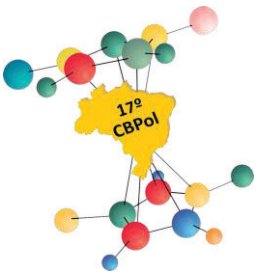

SELF-HEALABLE MULTI-NETWORK HYDROGELS OF POLY(ACRYLIC ACID)/POLY(VINYL ALCOHOL) AND FE^{3+} IONS: DESIGN, CHARACTERIZATION AND SELECTIVE ADSORPTION OF CATIONIC DYE

Henrique P. Mota*, Rafael F. N. Quadrado and André R. Fajardo

Laboratory of Technology and Development of Composites and Polymeric Materials (LaCoPol), Federal University of Pelotas (UFPel), Pelotas, RS. (*) henriquecomprs@gmail.com

Abstract: The pollution of aquatic environments by organic contaminants, mainly dyes, is a worrying reality. As a result, the demand for robust and innovative systems increased over the last few years. The development and application of a hydrogel based on multiple polymeric networks with self-healing properties are reported in this study. For this, poly(acrylic acid) (PAAc), poly(vinyl alcohol) (PVA), and Fe^{3+} ions were utilized. The multi-network configuration allowed the PAAc/PVA@Fe^{3+} hydrogel to reach a high self-healing percentage (> 88.0%) in only 8 h. Batch adsorption studies using methylene blue (MB) and methyl orange (MO) was performed to investigate the best conditions for using these hydrogels as adsorbents. Overall, the adsorption of MB is preferred over MO due to the electrostatic interactions between the cationic dye and the hydrogel. Also, the PAAc/PVA@Fe^{3+} hydrogel exhibited high recycling and reusing potential and long-term performance, which are additional benefits considering the practical application of these adsorbents.

Keywords: *hybrid materials; self-healing; methylene blue; multi-network; adsorption.*

Fundings: The authors thank the CNPq/Brazil for financial support. This study was financed in part by the Coordenação de Aperfeiçoamento de Pessoal de Nível Superior, Brazil (CAPES/Proap), Finance Code 001.

Introduction

Currently, the demand for colored plastics, paper, textiles, and cosmetics has increased considerably. Hence, problems related to the improper disposal of dye-colored materials and inadequate treatments increased too. This has become a serious environmental issue as organic dyes cause adverse effects on aquatic life and human health, even at low concentrations [1]. Methylene blue (MB) and methyl orange (MO) are representative examples of cationic and anionic dyes, respectively, and are responsible for a significant portion of dye pollution [1]. Therefore, their removal from water bodies is essential. Among the treatments already applied, adsorption stands out and has been proven to be a cost-effective, simple, and efficient method for dye removal [2]. The selection of the adsorbent is critical to the adsorption process, and materials such as biochar [1], metal-organic framework (MOF) [2], polymeric hydrogels [3], and others have been developed to treat dye-contaminated water. Polymeric hydrogels, which possess attractive physicochemical and structural properties, are among the most popular adsorbent materials utilized for dye removal. In contrast, some types of hydrogels, usually those chemically crosslinked and with a single polymeric network, exhibit poor mechanical properties, which restricts their reusability and application in large-scale processes [4]. To overcome this limitation, the development of hydrogels with self-healing properties and multi-networks has been investigated. Such hydrogels can spontaneously

form new crosslinking points within their network when broken, resulting in excellent mechanical durability and longevity [5]. Recently, Cao et al. developed dual-network self-healable hydrogel using hydroxypropyl chitosan, poly(acrylamide), and poly(vinyl alcohol) (PVA) for Cr(VI) adsorption. The prepared hydrogels showed superior mechanical and adsorption performance because of the reversible dynamic crosslinking process [6]. In this study, self-healable multiple-network hydrogels were prepared by combining poly(acrylic acid) (PAAc), PVA, and Fe^{3+} ions, and characterized for their adsorption capacity of MB and MO. PAAc and PVA were chosen due to their hydrophilicity and non-toxicity, which have stimulated their use for the preparation of physically and chemically crosslinked hydrogels for adsorption uses [5]. The multiple-network structure of the hydrogel enhances its mechanical properties, while the self-healing property ensures longevity and reusability. It is hypothesized that this hydrogel can exhibit selective adsorption towards cationic dyes like MB, ranking it as a promising candidate to treat MB-polluted waters.

Experimental

Synthesis and characterization of the PAAc/PVA and PAAc/PVA@Fe^{3+} hydrogels

For the hydrogel synthesis, 600 mg of PVA was added to a two-round flask containing 6 mL of distilled water and solubilized under stirring for 1 h at 90 °C. The PVA solution was cooled to 30 °C and then, 11 mg of Fe^{3+}, 2 mL of AAc, and 2 mg of MBA were added to the reaction system, which was stirred for 15 min for homogenization. Next, KPS (20 mg previously dissolved in 1 mL of distilled water) was added. The homogeneous solution was transferred to a cylindrical mold (15 mm diameter), which was placed in a vacuum oven at room temperature to remove air bubbles (around 30 min). After that, the oven temperature was increased to 60 ºC to promote the polymerization and simultaneous crosslinking of the AAc monomers by MBA. This process lasted 3 h. Following this step, the mold containing the hydrogel was frozen at -20 °C overnight and subjected to 3 cycles of freeze-thaw (1 h of freezing and 30 min of thawing). Finally, the obtained PAAc/PVA@Fe^{3+} hydrogel was dried by lyophilization (-50 ºC, 24 h). The hydrogels named PAAc/PVA were synthesized in the same way, however, without the addition of metallic ions, for comparison purposes. The synthesized hydrogels were characterized by Fourier Transform Infrared (FTIR), Scanning Electron Microscopy (SEM) and mechanical properties. Batch adsorption experiments were conducted in 250 mL Erlenmeyer flasks filled with individual stock solutions of MB or/and MO (50 mL) placed on an orbital stirrer (100 rpm). Typically, dry hydrogel samples were put into the flasks and at defined time intervals, aliquots (about 4 mL) were withdrawn and analyzed by using a UV-Visible (UV-Vis).

Results and Discussion

Characterization of the PAAc/PVA and PAAc/PVA@Fe^{3+} hydrogels

Fig 1. shows the FTIR spectra recorded for PVA, PAAc, PAAc/PVA hydrogel, and PAAc/PVA@Fe^{3+} hydrogel. The spectrum of PVA and PAAc showed bands at 3420 and 1417 cm^{-1} assigned the stretching and bending vibration of the O–H bond (hydroxyl groups). Bands at 2934, 1090, and 810 cm^{-1} are attributed to asymmetric stretching of the C–H bond (CH_2 groups) and stretching of C–O and C–C bonds [4]. In the spectrum of PAAc, bands at 1746 and 1643 cm^{-1} are due to the asymmetric and symmetric stretching of the C=O bond (carboxylic groups). Also, the broad band centered at 3408 cm^{-1} is assigned to the stretching of the O–H bond (carboxylic groups), while the bands around 2900 cm^{-1} are due to the stretching of the C–H bond [7]. Bands at 1238 and 1165 cm^{-1} are assigned to stretching of the C–O bond coupled with the bending of the O–H bond and stretching of the C–C bond, respectively [7]. After hydrogel formation, the spectrum of PAAc/PVA exhibited some bands referring to the precursor materials; however, some modifications were observed. The band assigned to the stretching of the O–H bond (around 3420 cm^{-1}) increased in intensity and exhibited a sharpening, which suggests the reduction of intramolecular H-bonds concomitantly to the increase of hydroxyl groups proceeding from PVA and PAAc. During the

polymerization and chemical crosslinking of PAAc with MBA, hydroxyl groups are partially consumed and the interpenetration of the PAAc network through the PVA chains decreases their intermolecular interactions. However, the shoulder-type band around 3250 cm^{-1} indicates the formation of H-bonds due to the interaction of the hydroxyl groups of PVA caused by the freeze-thaw processes [5]. According to the literature, the alternate freeze-thaw cycles promote the alignment of the PVA chains allowing the physical interaction of its hydroxyl groups via H-bonds. PVA crystallites are formed due to these interactions, acting as crosslinking points of the second network. Xu et al. [8] observed that the hydrophilic PVA chains also physically interact and form H-bonds with the PAAc network, which confer additional stability and strength to the hydrogel. This is confirmed by analyzing the bands assigned to the asymmetrical and symmetrical stretching of C=O bonds, which were shifted from lower wavenumber compared to the PAAc spectrum [9]. Changes in the bands observed in the 1250–1000 cm^{-1} region compared to the PVA and PAAc spectrum also suggests the participation of C–O bonds in the physical crosslinking process [9]. Lastly, the shoulder-like band around 1680 cm^{-1} is attributable to the stretching vibration of a secondary amide group, confirming the chemical crosslinking of PAAc with MBA [9]. From these data, it is corroborated that two crosslinked networks are combined to form the PAAc/PVA hydrogel. The incorporation of Fe^{3+} ions into the hydrogel matrix triggered changes in the spectrum of PAAc/PVA@Fe^{3+} compared to PAAc/PVA. For example, the band at 1725 cm^{-1} appears due to the C=O bonds of non-ionized carboxylic groups of PAAc, indicating the reduction of H-bonds with PVA [5]. The presence of Fe^{3+} weakens these interactions. In contrast, the broadening of the band in the range of 1700–1500 cm^{-1} suggests that part of the carboxylic groups in the hydrogel matrix interacts electrostatically with the Fe^{3+} ions [5]. The decrease in intensity and broadening of the band assigned to the O-H bond also indicates the hydroxyl groups (of PVA and PAAc) interactions with the metallic ions. Indeed, the coordination of these electronegative groups to Fe^{3+} ions aids in stabilizing them into the hydrogel matrix, as explained elsewhere [9].

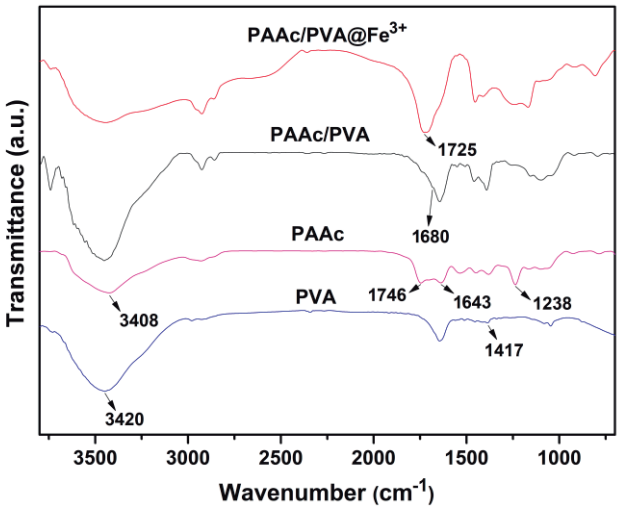

Figure 1 – FTIR spectra of PVA, PAAc, PAAc/PVA hydrogel and PAAc/PVA@Fe^{3+} hydrogel.

The self-healing properties of the PAAc/PVA@Fe^{3+} hydrogel was characterized by applying a mechanical compression test compression protocol (strain ~ 65–70%). When the two halves of this hydrogel were put together after the cutting process, the mechanisms to make self-healing possible are explained as follows: the Fe^{3+} ions in the polymeric matrix migrate to the interface by diffusion and consequently act on the healing of the broken PAAc chains forming new dynamic ionic bonds with that fractured region. The hydrogen bonds between the PVA-PVA and PVA-PAAc chains also positively influence the self-healing process, as already mentioned by Edwards et al. [10]. The self-healing process at the PAAc/PVA@Fe^{3+} hydrogel interface occurred at room temperature, in

absence of any external aid and compressive forces, only with the action of time (8 h). Subsequently, the self-healing ability was evaluated at different time intervals after fracture (1 h and 2 h), named PAAc/PVA@Fe^{3+} SH1 and SH2, respectively. Once the polymeric chains are repaired with this mechanism of dynamic ionic bonds and hydrogen bonds, the hydrogel samples present a mechanical resistance close to the virgin hydrogel. As shown in Fig 2., the self-healed (SH) hydrogel can be compressed to the same strain as the virgin sample, and the measured mechanical properties are slightly similar. Both the compressive strength calculated for the self-healed (SH and SH1) hydrogels were slightly lower compared to the values determined for the virgin hydrogel. However, the PAAc/PVA@Fe^{3+} SH2 hydrogel showed lower compressive strength, thus being able to infer that after 2 hours of fracture of the material, its self-healing process is somewhat impaired. Confirming the results of self-healing, SEM analyses were carried out, which made it possible to observe the healed and unhealed portion on the surface of the hydrogel.

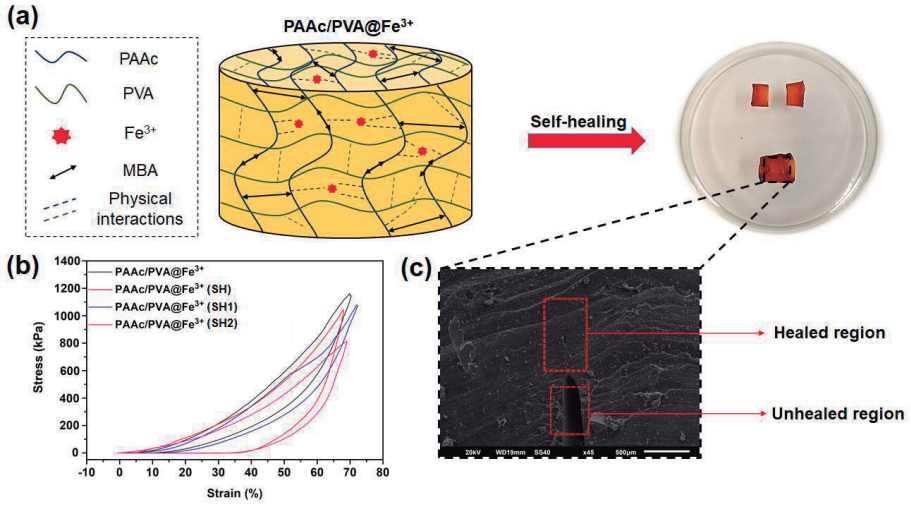

Figure 2 – Illustrative representation of the bonds and interactions in the hydrogel and the self-healing process (a), stress-strain curves for PAAc/PVA@Fe^{3+} virgin and self-healed (SH, SH1 and SH2) hydrogel (b) and SEM analysis of fracture region (c).

Adsorption experiments

After optimization parameters of adsorption such as hydrogel mass, pH, and initial dye concentration. We found that the best adsorption capacity for both MB and MO was obtained using 0.1 g of hydrogel, adsorption conducted without pH adjustment (6–7), and an initial dye concentration of 100 ppm. In addition, the hydrogel showed a greater adsorption capacity for MB (26.9 mg/g) compared to MO (16.1 mg/g), being directly related to the surface charge of the hydrogel being mostly negative in this pH range (pHpzc ~4), which favors the adsorption of cationic dyes by electrostatic interactions. In addition, it was also evaluated the adsorption capacity against a mixture of dyes (1:1 MB:MO) evaluated using the concentration of both at 30 ppm. In Fig 3., it is possible to notice that we again have a higher adsorption affinity for the cationic dye (MB), an interesting result, since one of the limiting factors of large-scale adsorptive processes is the low selectivity [2].

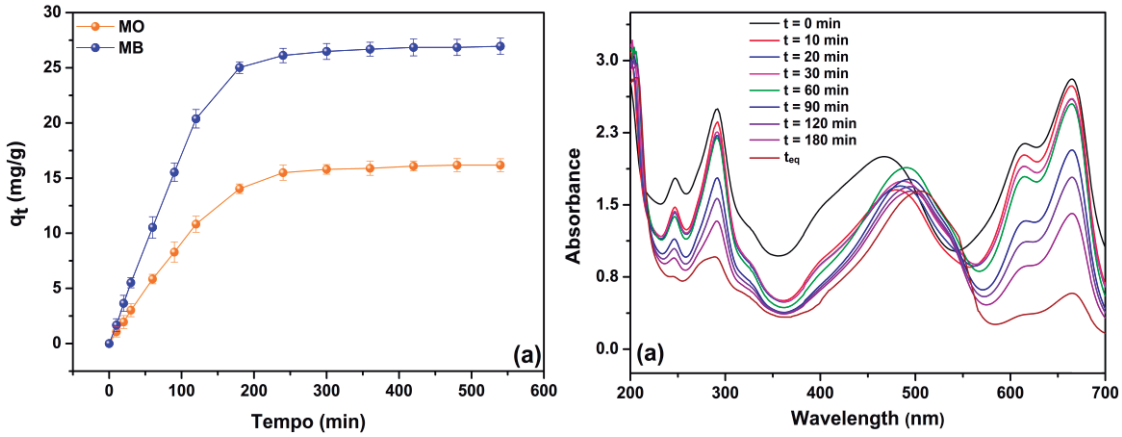

Figure 3 – Adsorption capacity (q_t) of MB and MO in single solution under optimized conditions (a) and UV-Vis spectra for the adsorption process of dyes in a binary mixture (MB:MO) (b).

Conclusions

In this study, a self-healing multiple-network hydrogel was developed using PAAc, PVA, and Fe^{3+} ions. This hydrogel was characterized by FTIR, SEM, and mechanical analysis, which proved its good mechanical resistance and self-healing capacity. The multiple-network structure of the hydrogel enhances its mechanical properties, while the self-healing property ensures longevity and reusability. The PAAc/PVA@Fe^{3+} hydrogel was successfully tested in the adsorption of cationic and anionic dyes. As observed, it exhibited selective adsorption for MB, which makes this hydrogel a promising candidate for the selective removal of dye pollutants from water bodies.

Acknowledgments

The authors would like to thank the organizing committee of the 17th CBPol.

References

[1] T. Wu, G. Yang, J. Cao, Z. Xu, and X. Jiang., Chem. Eng. Res. Des. 2022, *188*, 330–341.

[2] J. Li et al., J. Environ. Chem. Eng. 2022, *10*, 107880.

[3] Y. Işikver., Fibers Polym. 2017, *18*, 2070–2078.

[4] Z. Zhuang, L. Wu, X. Ma, W. Diao, and Y. Fang., J. Appl. Polym. Sci. 2018, *135*, 46847.

[5] Z. Jing, Q. Zhang, Y. Q. Liang, Z. Zhang, P. Hong, and Y. Li., Polym. Int. 2019, *68*, 1710-1721.

[6] J. Cao *et al.*, Int. J. Biol. Macromol. 2021, *174*, 89-100.

[7] M. M. Basuni and M. Mohammedy., Research Journal of Pharmaceutical , Biological and Chemical Sciences. 2019, *10*, 135-146.

[8] H. Xu, F. K. Shi, X. Y. Liu, M. Zhong, and X. M. Xie., Soft Matter. 2020, *16*, 4407-4413.

[9] Y. H. F. Al-qudah, G. A. Mahmoud, and M. A. Abdel Khalek., J. Radiat. Res. Appl. Sci. 2014, *7*, 135-145.

[10] J. V. Edwards., *Modified fibers with medical and specialty applications*. Ed.; Springer, *1*, 2006.

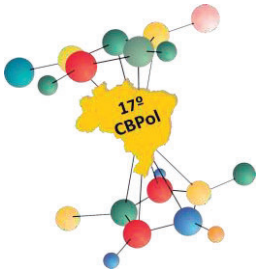

SORPTION KINETICS OF CATIONIC DYES IN PECTIN-CLAY MINERAL COMPOSITE HYDROGELS

Wilson B. F. Filho[1], Mirlene P. Vitorino[1,*], Priscila K. Naidek[1,2], Alexandre T. Paulino[1,2,†]

1 – Postgraduation Program in Applied Chemistry, Santa Catarina State University (UDESC), Joinville, SC, Brazil
2 – Department of Chemistry, Santa Catarina State University (UDESC), Joinville, SC, Brazil
*Email: *mirlene.vitorino19@gmail.com; †alexandre.paulino@udesc.br*

Abstract

The water contamination has become a major concern due to improper disposal of contaminants in the environment without efficient treatment. In view of this, water and wastewater treatment methods have been studied with the aim of reducing environmental impacts to the biome. An alternative to solve this problem is using pectin-clay mineral (using montmorillonite as clay mineral model) hydrogels for the sorption and removal of pollutants (using methylene blue as pollutant model) from water. However, it is important to study sorption kinetic models to comprehend the types of interactions among polymer matrices and pollutants and propose strategies for the environmental remediation. In this work, three kinetic models (nonlinear pseudo-first order, nonlinear pseudo-second order, and Elovich) were employed to evaluate the capacity of sorption of methylene blue in pectin-clay mineral hydrogels. The kinetic data assisted in the definition of real-world application strategies for the removal of cationic textile dyes, in addition to selective separation of cationic and anionic species in water and wastewater.

Keywords: *Sorption. Kinetic. Pectin. Montmorillonite. Methylene Blue. Hydrogel*

Introduction

As the chemical industries have increased the quantity of compounds used for numerous applications, there is a consequent generation of wastes that need to be adequately treated [1]. Commonly, domestic, and industrial wastewaters are discarded without treatment or adequate prior management, causing serious environmental impacts [2]. Besides the impacts on the environment, several chemical substances found in urban and industrial wastewaters are considered problematic due to the lack of effective legislation for their regulation in terms of environmental safety and public health [3].

Technologies that could be useful in the development of novel wastewater treatment methods include photocatalysis, membrane filtration, electrochemistry, and sorption. Photocatalysis and sorption are quite promising, as these methods involve the use of inexpensive natural materials and sunlight [4]. Specifically, sorption involves the removal of pollutants from an aqueous solution using a solid sorbent, such as activated charcoal, zeolites, carbon nanotubes, polysaccharides, spinning industry discards, hydrogels, and membranes [1-4]. Hydrogels prepared by using natural polysaccharides are inexpensive, have high water absorption capacity and are non-toxic, biodegradable, hydrophilic and insoluble [5].

The aim of this study was to perform the removal of emerging pollutants from water and wastewater using methylene blue (MB) as pollutant model and pectin-based hydrogel modified with

montmorillonite (MMT) as the sorbent. The focus for the Brazilian Polymer Conference, 2023 (CBPOL, 2023) was to evaluate nonlinear pseudo-first order, nonlinear pseudo-second order and Elovich kinetic models to comprehend some parameters that could help in the sorption processes in real-world situations.

Experimental

Synthesis of pectin-clay mineral composite hydrogel

Known amounts of pectin were dissolved in flasks containing ultrapure water at pH 3.5, and glycidyl methacrylate. After modification of the polysaccharide, new amounts of this product were employed for the hydrogel synthesis as follows: Masses of polysaccharide modified with glycidyl methacrylate were dissolved in ultrapure water, followed by the addition of acrylamide and potassium persulfate. After homogenization of this solution and crosslinking in an oven, the formed solid hydrogel was applied in the sorption and kinetic studies of methylene blue as pollutant model. Modified hydrogels were synthesized with the addition of 1, 5 and 10% (m/m) montmorillonite during the final synthesis step.

Sorption Kinetic

Sorption kinetics were estimated using the non-liner pseudo-first order (Equation 1), pseudo-second order (Equation 2) and Elovich (Equation 3) kinetic models:

$$qt = qe(1 - e^{-kt}) \qquad (1)$$

$$qt = \frac{kq_e^2 t}{1 + kq_e^2 t} \qquad (2)$$

$$q_t = \frac{1}{\beta}\ln(1 + \alpha\beta t) \qquad (3)$$

in which k is the sorption rate (min^{-1}), t is sorption time (min), qt is sorption capacity (mg g^{-1}) at a specific time, α is the initial sorption rate (mg g^{-1} min^{-1}) at each time t (min) and β is the desorption constant (mg g^{-1}) related to the covering of the surface of the sorbent and the activation energy for the occurrence of chemisorption.

Results and Discussion

Sorption Kinetic

The sorption kinetics of methylene blue (MB) in the pectin hydrogel (PCTM) and composite hydrogels containing 1 (PCTM 1%), 5 (PCTM 5%) and 10% (PCTM 10%) montmorillonite are presented in Table 1.

Table 1 – Results of pseudo-first-order, pseudo-second order and Elovich kinetic models in sorption of methylene blue in pectin hydrogel (PCTM) and composite hydrogels containing 1 (PCTM 1%), 5 (PCTM 5%) and 10% (PCTM 10%) montmorillonite.

Kinetic Model	Paremeters	PCTM	PCTM 1%	PCTM 5%	PCTM 10%
		AM	AM	AM	AM
Pseudo first order	R^2	0.8353	0.9898	0.9984	0.9603
	K_1 (min^{-1})	0.0012	0.0177	0.0043	0.0024
	q_e (mg g^{-1})	1.4780	1.4460	1.3489	0.7666
	q_t (mg g^{-1})	1.5785	1.5786	1.3872	0.7834
	χ^2	329.56	35.873	21.171	218.74
Pseudo second order	R^2	0.8775	0.9976	0.9943	0.9728
	K_2 (min^{-1})	0.0028	0.0165	0.0054	0.0035
	q_e (mg g^{-1})	1.3417	1.5214	1.4116	0.8510
	q_t (mg g^{-1})	1.3943	1.5951	1.4221	0.9374
	χ^2	245.03	8.1836	75.478	150.14
Elovich	R^2	0.9398	0.9864	0.9760	0.9795
	α (mg min g^{-1})	0.0089	0.0824	0.0217	0.0046
	β (g mg^{-1})	3.4353	3.9416	4.1590	5.7590
	χ^2	120.50	46.219	318.93	113.21

The most appropriate kinetic model for explaining the sorption of MB in PCTM and PCTM 10% was the nonlinear Elovich model. This conclusion was based on the hither larger R^2 values and lower χ^2 values. With the Elovich model, the solid surfaces of sorbents are assumed to be heterogeneous, as occurs with three-dimensional hydrogel networks. The high β values indicate that the desorption rate is high and physisorption is occurring between the hydrogel and pollutant [6]. Physisorption is useful for studying hydrogel and dye recovery processes in the treatment of wastewater from the textile industry, enabling the recovery of water and dye for reapplication in a sustainable process. For the sorption of MB in PCTM 5%, the nonlinear pseudo-first-order model was the most appropriate for explaining the sorption kinetics. In this case, there are no intramolecular interactions between the hydrogel and pollutant, which is a characteristic of physisorption. For the sorption of MB in PCTM 1%, however, the nonlinear pseudo-second-order model was the most appropriate. In this case, high R^2 values, low χ^2 values and similarity between the *qe* (experimental) and *qt* (theoretical) values were found, confirming that limiting step of the process is chemisorption. When chemisorption occurs, intramolecular interactions between the sorbate and sorbent are assumed [7]. Changes in the kinetic mechanisms show that the sorption process can be adjusted to specific of polymeric materials and composites during wastewater treatment processes.

Conclusions

Based on the sorption studies with methylene blue in water, the biomaterials synthesized in this study are potential polymeric matrices for the treatment of wastewater. The best removal rates of methylene blue were achieved with the composite hydrogel modified with 1% montmorillonite. The change in the hydrogel network with the incorporation of montmorillonite is of interest due to the creation of active sites in the interlamellar spaces of the clay, which increases cationic and anionic pollutant sorption capacity. These hydrogels could be useful for studies involving the preconcentration of anionic species for subsequent separation and quantitative determination.

Acknowledgements

CNPq, FAPESC, CAPES and UDESC

References

[1] A.G.B. Pereira; F.H.A. Rodrigues; A.T. Paulino; A.F. Martins; A.R. Fajardo. A review, J Clean Prod 2021, 284, 124703. DOI: https://doi.org/10.1016/j.jclepro.2020.124703

[2] S. Martin; W. Griswold. Human Health Effects of Heavy Metals: Briefs for Citizens, Environ Sci Technol. 2009, Vol.8, nº 11.

[3] G. Genchi; A. Carocci; G. Lauria; M.S. Sinicropi; A. Catalano. Nickel: Int J Environ Res Public Health 2020, 679–700, 17030679. DOI: https://doi.org/10.3390/ijerph17030679

[4] M.J. Paz; T. Vieira; H. Enzweiler; A.T. Paulino. J Environ Chem Eng. 2022, 106967. DOI: http://dx.doi.org/10.1016/j.jece.2021.106967.

[5] J. Li; W.R.K. Illeperuma; Z. Suo; J. J. Vlassak. ACS Macro Lett 2014 3, 520–523.

[6] V.J. Inglezakis; S.G. Poulopoulos; H. Kazemian. Microporous and Mesoporous Materials 2018, 166–176, 272. DOI: https://doi.org/10.1016/j.micromeso.2018.06.026

[7] B.K. Martini; T.G. Daniel; M.Z. Corazza; A.E. D. Carvalho. J Environ Chem Eng 2018, 6669-6679. DOI: http://dx.doi.org/10.1016/j.jece.2018.10.013.

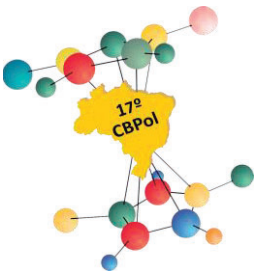

STARCH-BASED COMPOSITE HYDROGEL ENHANCED BY ACTIVATED CARBON FROM THE BANANA PEEL: MORPHOLOGICAL, CHEMICAL AND THERMAL PROPERTIES

Lana S. Maia[1], Paulo Henrique F. Pereira[2], Talles B. Costa[3], Deval S. Rosa[3], and Daniella R. Mulinari[2*]

1 – Department of Chemistry and Environmental, State University of Rio de Janeiro (UERJ), Resende, RJ, Brazil
2 – Department of Mechanical and Energy, State University of Rio de Janeiro (UERJ), Resende, RJ, Brazil
3 – Center for Engineering, Modeling, and Applied Social Sciences (CECS), Federal University of ABC (UFABC), Santo André-SP, Brazil
lanasiqueiram@gmail.com, dmulinari@hotmail.com

Abstract - Composite hydrogels are highly porous structures with a significant adsorption capacity, making them promising materials for wastewater treatment. Recognizing the potential of these materials, an eco-friendly hydrogel composite was developed using starch and reinforced with activated carbon derived from banana peels (BPAC). The hydrogels underwent characterization through SEM, FTIR, TGA/DTG, and water absorption tests. The results indicated that the addition of 5% BPAC to the hydrogel caused alterations in the chemical structure, resulting in a more porous surface. The FTIR spectra indicated a successful crosslinking process within the structure, showing that the addition of BPAC improved thermal stability. Furthermore, water absorption analysis demonstrated that all materials exhibited substantial water uptake within the first hour with the incorporation of BPAC.

Keywords: *Hydrogel composites, Starch, Activated carbon, Banana peel, cross-linking*

Introduction

The global management of water pollution has been a focus of the scientific community, involving innovative technologies that can effectively remove pollutants from wastewater [1]. Wastewater has become increasingly hazardous since pollutants can accumulate in living organisms and the environment, causing significant environmental imbalances [2]. Therefore, the development of technologies for the removal of contaminants is necessary.

In this scenario, hydrogels have been employed for being a 3D-structured polymeric network, usually composed of hydrophilic chains [3]. The increasing interest in hydrogels is justified by their great potential in several areas of medical research (drug delivery systems, scaffold materials for cell and tissue engineering) and environmental research (absorbent materials) [4, 5]. The most common physicochemical characteristics of hydrogels are high hydrophilicity, mechanical and environmental stabilities, and an interesting porous surface area. Additionally, the material offers benefits such as biocompatibility and biodegradability [6]. Such properties are strongly influenced by the cross-linking type, chemical structure, composition, and morphology [4].

In the design and development of these materials, the incorporation of fillers into the structure has been investigated, since reinforcement can lead to improved performance in the intended application, as well as reduced operational costs. The use of activated carbon from agro-industrial residues has shown promise due to advantages such as lower cost and more readily available natural

sources [7]. Thus, the present work aims to develop a natural polymer-based hydrogel, specifically starch reinforced with activated carbon from banana peels (BPAC).

Experimental

Materials

To prepare the hydrogels, corn starch Amidex 3001 was used, which was purchased from Ingredion Incorporated (São Paulo, Brazil). Sodium hydroxide (NaOH), and Citric acid ($C_6H_8O_7$) were purchased from Dinâmica, Química Contemporânea Ltda. Activated carbon obtained from the banana peel (BPAC) was prepared from methodology development by the present authors.

Hydrogels processing

To obtain hydrogels, firstly, an adequate amount of corn starch and distilled water were mixed under constant agitation (280 rpm) at 40 °C. Subsequently, Sodium hydroxide (NaOH) was added to the solution. After a reaction time of 3 h, citric acid was added. The reaction time after acid addition is 17 h. Then, the hydrogels were submitted to a water bath at 90 °C for 1 h. Finally, the prepared material was poured into a plastic mold and dried in an oven at 70 °C for 48 h.

To investigate the effect of activated carbon on the hydrogel structure, a similar procedure was performed and activated carbon obtained from the banana peel (BPAC) was responsible for the composition of 5% of the total weight. Fig. 1 shows the adopted methodology.

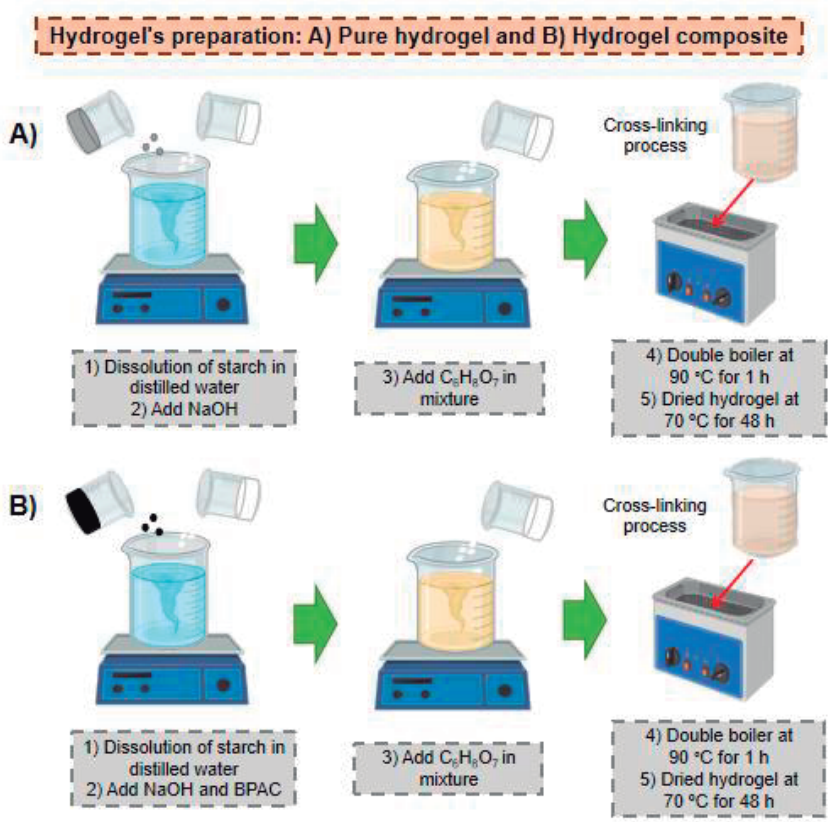

Figure 1 - Schematic representation of the adopted methodology obtaining pure hydrogel (A) and hydrogel+5%BPAC (B).

Characterization

Scanning electron microscopy (SEM) was used to investigate the porous structure of pure hydrogel and hydrogel+5%BPAC in a microscope (model TR-3000, HITACHI Ldta., Tokyo, Japan) with tungsten filament, secondary electron detector, 5kV, and low-vacuum. Fourier-transform infrared spectroscopy (FTIR) analysis was employed to study the functional groups and specific bands of the

samples by a spectroscope (Frontier 94942, PerkinElmer Inc., Massachusetts, USA) with attenuated total reflectance (ATR) diamond accessory, with 64 scans, 4cm^{-1} of spectral resolution, in the range of 4000-500 cm^{-1}. Thermogravimetric analysis (TGA) was realized to detect the thermal stability and decomposition temperature of the samples, using an SDT Q600 thermogravimetric analyzer from TA Instruments. The temperature range was 25-600 °C, under N_2 atmosphere (10 mL min^{-1}) at a heating rate of 10 °C min^{-1}.

Degree of swelling

Specimens (pure hydrogel and its hydrogel+5%BPAC) were immersed in distilled water at room temperature to conduct adsorption experiments. The experiments were carried out at pre-determined times of 5 min, 10 min, 15 min, 30 min, 45 min, 1 h, 2 h, 4 h, 6 h, 24 h, and 48 h. At each defined time, the samples were removed from the distilled water, and any water present on the surface was removed using paper tissue. The specimens were then weighed and re-immersed. The degree of swelling (DS) was calculated using Eq. 1, where mf is the mass of the swollen hydrogel at a specific time t in grams, and mi is the mass of the dried hydrogel at time t=0 in grams.

$$DS = \frac{m_f - m_i}{m_i}.100 \qquad (1)$$

Results and Discussion

Fig. 2a and 2b evidenced the good dispersion of BPAC in the hydrogel structure, which provided the development of the hydrogel+5%BPAC with a rough and porous structure.

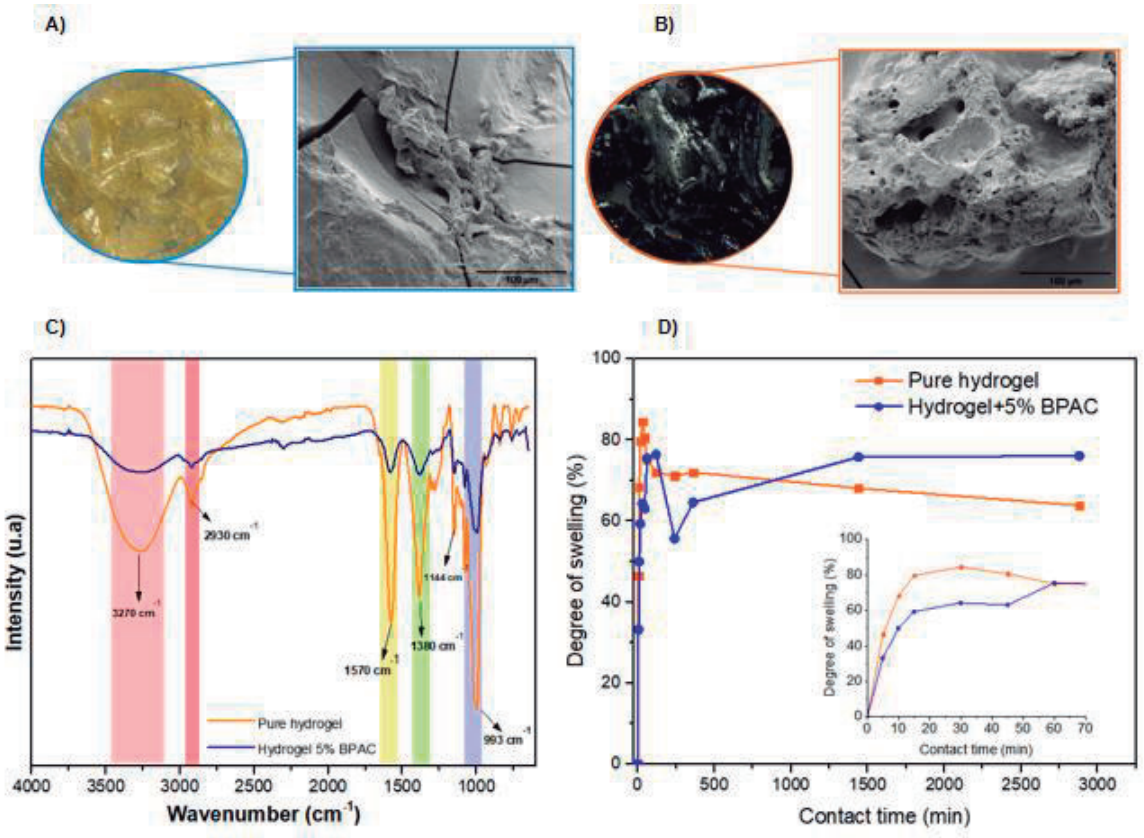

Figure 2 - Illustrative representation of pure hydrogel and composite hydrogel+5%BPAC: (a) SEM of the pure hydrogel; (b) SEM of the hydrogel+5%BPAC, (c) FTIR of the samples; and (d) water absorption of the samples.

This feature could favor the mechanical and absorption properties [1,4, 8]. Based on the FTIR spectra (Fig. 2c), the characteristic peaks of the pure hydrogel at 3270 cm^{-1} and 2930 cm^{-1} can be explained as the O-H, and C-H stretching vibrations, respectively. The peak at 1570 cm^{-1} was the C=O bend in the -COOH groups. The bands at 1380 cm^{-1} and 1144 cm^{-1} were associated with the $–CH_2$ shear vibration and C–O induced vibration in starch, respectively. The hydrogel+5%BPAC showed a reduction in the intensity of mentioned bands compared to the pure hydrogel [4]. This could be due to the reduction of free hydroxyl groups in starch and the establishment of new crosslinking interactions with the functional groups present on the AC surface [3,8]. Also, it was possible to observe that the insertion of BPAC favored the increased water transport efficiency (Fig. 2d). This behavior is the result of the highly formatted/connected void portion on the surface [1,8]. Regarding the TGA/DTG graphics (Fig. 3), the incorporation of BPAC in the hydrogel structure was able to drastically change the thermal stability, resulting in improved thermal stability [4].

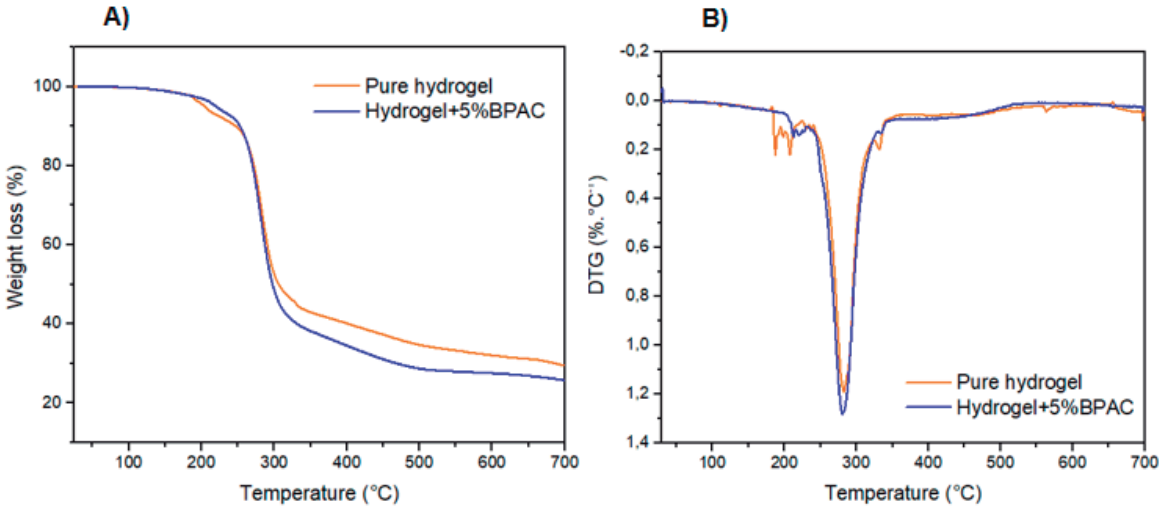

Figure 3 - Illustrative representation of pure hydrogel and composite hydrogel 5%BPAC: (a) TG; and (b) DTG.

Conclusions

Composite hydrogels reinforced with activated carbon (Hydrogel+5% BPAC) were prepared and their morphology, chemical and thermal properties, and swelling behavior were evaluated. Based on the results, it can be concluded that the developed hydrogels exhibited a good dispersion of BPAC within the hydrogel structure, promoting the formation of surface pores with a macroporous structure. The FTIR spectra indicated a reduction in band intensity, suggesting the formation of crosslinking bonds between BPAC and the hydrogel structure. The hydrogel with 5% BPAC also impacted proportionally in water absorption and thermal stability compared to the pure hydrogel. Thus, the hydrogel+5% BPAC composite emerges as a potential renewable material application.

Acknowledgments

The authors gratefully acknowledge the funding by FAPESP, Brazil, under grants 2020/13703-3, and FAPERJ, Brazil, under grants E-26/203.905/2022.

References

1. B. Salahuddin; S. Aziz; S. Gao; Md. Hossain; M. Billah; Z. Zhu; N. Amiralin Polymer, 2022, 14, 5074. https://doi.org/10.3390/ polym14235074.

2. A. Elgarahy; H. Mostafa; E. Zaki; S. El Saeed; K. Elwakeel; A. Akhdhar; E. Guibal International Journal of Biological Macromolecules, 2023, 232, 123355. https://doi.org/10.1016/j.ijbiomac.2023.123355.
3. W. Ding; H. Liang; H. Zhang; H. Sun; Z. Geng; C. Xu Journal of Water Process Engineering, 2023, 51, 103414. https://doi.org/10.1016/j.jwpe.2022.103414.
4. L. Cao and N. Li International Journal of Biological Macromolecules, 2021, 177, 383-391. https://doi.org/10.1016/j.ijbiomac.2021.02.097.
5. H. Garcia; A. S. Barros; C. Gonçalves; F. M. Gama; A. M. Gil European Polymer Journal, 2008, 44, 2318-2329. https://10.1016/j.eurpolymj.2008.05.013.
6. M. Ahmadian and M. Jaymand Coordination Chemistry Reviews, 2023, 486, 215152. https://doi.org/10.1016/j.ccr.2023.215152 0010-8545.
7. I. Demiral; C. Samdan Chemical Papers 2022, 76, 2193-2207 https://doi.org/10.1007/s11696-021-02011-0.
8. Y. Deng; J. Chen; J. Huang; X. Yang; X. Zhang; S. Yuan; W. Liao Cellulose 2020, 27, 397-3988 https://doi.org/10.1007/s10570-020-03055-3.

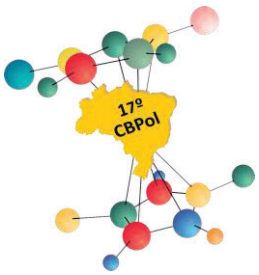

STUDY, CHARACTERIZATION AND ANALYSIS OF HDPE COMPOSITES REINFORCED BY FIBERS FROM THE BABASSU PALM (ARECACEAE)

Maria Gabriela de Freitas Rodrigues[1], Adalberto Gomes de Miranda[1], Renato Moreira Teixeira Junior [1], Antônio Estanislau Sanches [2], João D'Anuzio Lima de Azevedo [2] and Renata de Oliveira Teixeira[3] *

1 – Department of Materials Engineering, University of the State of Amazonas (UEA), Manaus – AM, Brazil; mgfr@uea.edu.br;agmiranda@uea.edu.br; rmtj.mec@uea.edu.br

2 – Mechanical Engineering Department, University of the State of Amazonas (UEA), Manaus – AM, Brazil; asanches@uea.edu.br, jdlazevedo@uea.edu.br

3 – Department of Production Engineering, Federal University of Amazon (UFAM), Manaus, AM, Brazil; renatadoliveirat@hotmail.com

ABSTRACT. Study, characterization and analysis of polyethylene polymeric composites (HDPE) with babassu palm fibers (Arecaceae). Through the technological development of industries, new polymeric composites based on materials with low environmental impact have stimulated several researchers from different areas of knowledge. Thus, this work aimed to evaluate the mechanical properties of composites reinforced with babassu powder (Arecacea) in high-density polyethylene (HDPE) matrix, with the objective of analyzing the effect of babassu powder, as a reinforcement in the mechanical properties of HDPE. The fiber obtained was used for the preparation of polymeric composites at concentrations of 5 wt.%, 10 wt.% and 20 wt.% in relation to HDPE. Tensile-strength tests were carried out according to ASTM D638 in order to analyze the main mechanical properties: elastic modulus, ultimate strength and ductility. As expected, it was observed that the values of the modulus of elasticity increased with the increment of the fiber concentration, while the values of tensile strength remained unchanged and those of ductility reduced. The best results were found for the concentration of 5 wt.% with babassu powder. Increases of 40% and 0.6% for the modulus of elasticity and ultimate strength, respectively were observed in relation to the neat matrix. In view of the good incorporation of babassu fiber and HDPE this study became promising in the production of these composites, as there was no previous surface chemical treatment in the fiber.

Keywords: *HDPE, polymercomposites, babassu.*

Introduction

The use of composite materials has developed greatly in recent years, composites reinforced with natural fibers, including synthetic fibers. In this context, research for the replacement of synthetic fibers with natural fibers as reinforcement of polymer matrices is growing every year.

The emergence of composites as a separate class occurred in the mid-20th century, when multi-phase composites were deliberately designed and manufactured as polymers reinforced with glass fiber. These multi-phase composite concepts offer the opportunity to create a wide variety of materials with a combination of properties that cannot be met by traditional metal alloys, ceramics or monolithic polymeric materials [1].

The arrival of these new materials brings with it a positive aspect of the use of raw materials from renewable sources, minimizing environmental problems, thus developing environmentally sound materials with the highest possible process compatibility. As a source of renewable natural

resources, natural fibers are cheap, biodegradable, recyclable, non-toxic and can be incinerated. They are used as reinforcements in polymers and partially replace synthetic fibers such as asbestos, carbon, nylon and glass which, despite their excellent mechanical properties, have some disadvantages, such as, abrasive to processing equipment, dense, non-biodegradable and expensive. They produce products with very high recycling costs and some of these synthetic fibers are harmful to human health [2].

In this regard, we have as an option the use of the natural fibers existing in Brazil, mainly those located in the Amazon. And for this purpose, the present work brings the palm of babassu that belongs to the botanical family Arecacease present in much of Latin America. In Brazil, it is scattered in the Amazon, the Atlantic Forest, the Cerrado and the Caatinga where it occurs naturally in several states.

The babassu has great incursion power from disturbed areas and can reach between 10-30 meters in height, and can have between 20-50 cm in diameter. It has fruits that are very appreciated, both by man and wildlife, where they are found. Each crop can have between 3 and 5 curls, and each curl can produce 300 to 500 cocos. The peak of fruiting occurs from the eighth year and reaches full production after 15 years [3].

The fiber of the Arecacea palm tree is found in the stems of the tree, known as strawberry and can bring various benefits because it is a palm native to the region. It is found abundantly and continuously throughout the year, making it of great importance for the use, as well as the study of the physico-chemical properties of this biomass [4].

In the context of this work, composites were produced using high density polyethylene (HDPE) and babassu fiber. The choice of the polymer matrix was due to the extensive use of HDPE in the manufacture of composites reinforced with fibers and the good results derived from this research medium.

All this is only possible because HDPE is a highly linear polymer with a compact and dense structure, offering chemical resistance, excellent mechanical properties and low cost, allowing it to be used as a substrate. polymer reinforced with babassu powder. However, since composites must meet the requirements of ownership, it is imperative to study the properties of the composites resulting in determining their properties and in the selection process to apply them.5

For purposes of study and characterization, this work proposes the use of high-density polyethylene (HDPE) as a polymeric matrix for the formation of composites with fibers from the stems of the Babassu palm tree, in proportions of 5%, 10% and 20% in mass of fibers.

Materials and Methods

The materials used in this research were BRASKEM's high-density polyethylene (HDPE) polymeric matrix and babassu fiber.

The fiber was extracted manually from the stem of the Babassu palm tree in the municipality of Iranduba-AM. HDPE has been provided by the UEA/EST P&D laboratory. Fig.1 illustrates the fibers of babassu and the stems of the babassu palm.

Figure 1. The fibers of Babassu and the palm tree.

Grind

The samples of Babassu fibers were dried in a drying oven for 2 hours at 50 °C, and subsequently milled in a Willey TE-680 knife mill, subsequently used granulometry 30 and reprocessed with 20 mesh. Secondary grinding was carried out to obtain an appropriate granulometry for the processing of the composite, as shown in Fig.2.

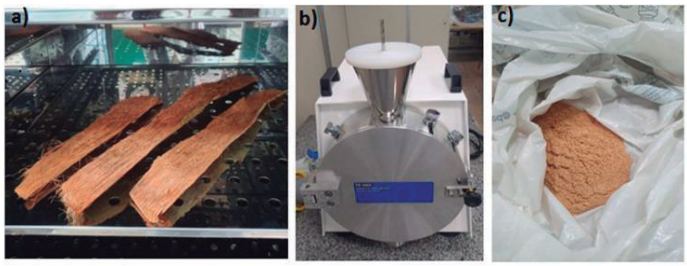

Figure 2. Fibers of Babassu in the greenhouse (a), Willey Knife Mill TE-680 (b) and ground fiber (c).

Extrusion

Ground Babassu fibers at concentrations of 5%, 10% and 20% were added to the HDPE matrix. The mixture was previously homogenized and then extruded at a temperature of 185°C with a rotation of 45 rpm in the single screw extruder (AX Plastic, AX 1626). The extruded filaments were dried for 2 hours so that all moisture was removed. Subsequently they were granulated in the mini-granulator (AX Plastic, 00316) and then stored for the production of the test bodies.

Injection

After the extrusion process, a production of the test bodies was carried out. Thus, five Type IV tensile test bodies according to ASTM D638 were produced for each concentration studied. The test bodies were molded by injection (AX Plastics, 00318). The mold was at room temperature of 25 °C with injection temperature of 185 °C and pressure of 0.8 MPa.

Figure 3. Injection device(a) and (b) traction mold containing a test body.

Mechanical Testing: Traction

Tensile tests were carried out on the Universal Traction Testing Machine (Instron) in the R&D laboratory. The 5 type IV tensile test bodies were tested by traction in accordance with ASTM D638. The test was conducted on a universal test machine with a load cell of 150 kN and a test speed of 5 mm/min.

Results and Discussion

Tensile tests were carried out for all the samples studied. Thus, Graphic 1, illustrates the tension vs. deformation charts only for the compounds containing 5% in mass (black), 10% (red) and 20% (azul). The results obtained from the average of the five test bodies for the mechanical properties of module elasticity, tensile strenght and ductility are illustrated in Table 1. The observed results for the properties of Table 1 were 350±0,04 MPa for the elasticity module, approximately 15±0,95 MPa to the tensile strenght and 5,07±3,80 to the ductility relative to pure HDPE. The results are consistent with those presented in the literature for the HDPE polymer.

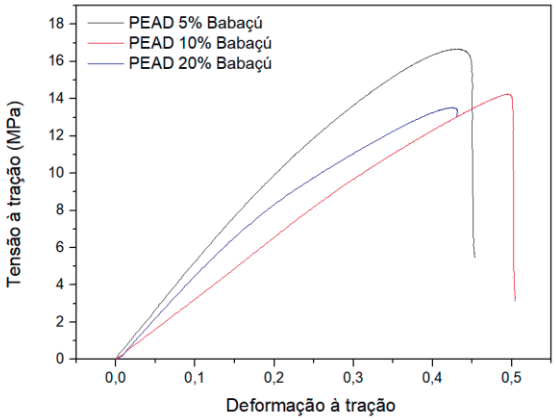

Figure 4 - Tension vs deformation chart for HDPE compounds with 5%, 10% and 20 % mass of babassu fiber.

Table 1 - Summary of the mechanical properties of pure HDPE polymer and its composite.

Módulo de elasticidade (MY)			
PEAD	**5 %**	**10 %**	**20 %**
0,35±0,04	0,49±0,06	0,56±0,02	0,81±0,03
Limite de resistência à tração (LRT)			
15,03±0,46	15,12±0,95	14,00±1,80	14,30±0,75
Ductilidade			
5,10±3,80	0,15±0,05	0,11±0,01	0,10±0,02

After adding the powder load at concentrations of 5, 10 and 20%, variations in the mechanical properties of the produced compounds were observed. In relation to the elasticity module, a significant increase was observed. Increases of 40, 60 and 130% compared to pure HDPE. While the tensile strenght values remained constant within the error margin for all samples, with a slight increase of 0.60% for the concentration of 5% in mass. However, the ductility values were lower compared to pure polymer. For the three concentrations, reductions of almost 100% of the values were observed. The results found in this work are consistent with those in the literature. Furtado et al. (2020) studied the degradation of compounds with fibers obtained from babassu stems at concentrations of 5, 10 and 20 % by mass. The authors carried out the surface chemical treatment of the fibers, however, found values similar to those obtained in this work without any surface Chemical treatment.

Conclusions

By being a renewable source, Babassu fiber is a material that has great advantages, with a high availability in our country, mainly north and northeast, low cost, and above all biodegradable.

Although there was no surface treatment in the fiber, it was possible to obtain satisfactory results from the produced compounds. Thus, the bio-compound containing 5 % by mass of powder fibers proved to be the formulation chosen due to the increased mechanical strength and rigidity properties. By possessing this characteristic / property, the compound could be used in applications that require higher rigidity and strength than pure polymer. It is completely disqualified for use where ductility is required.

References

1. CALLISTER, W. D., Ciência e Engenharia de Materiais: Uma Introdução. John Wiley & Sons, Inc., 2021.

2. MOTHÉ, C. G.; DE ARAÚJO, C. R. Caracterização Térmica e Mecânica de Compósitos de Poliuretano com Fibras de Curauá. Polímeros: Ciência e Tecnologia, v. 14, n. 4, p. 274-278, 2004.

3. CARRAZZA, L. R.;CRUZ E ÁVILA, J. C.;SILVA, M. L. Manual Tecnológico de Aproveitamento Integral do Babaçu (Attalea spp.). Manual Tecnológico, 68 (2012).

4. FURTADO, J. B.; Filho, P. A.;OLIVEIRA, T. P.;CAETANO, M. R.;ARAÚJO, I. M.;FIGUEIREDO, F. C.;SANTOS, J. R. Caracterização química da fibra do caule da palmeira de babaçu natural e após tratamento. Revista de Engenharia e Pesquisa Aplicada, v.9, 2020.

5. DE ARAUJO, C. R.; SAMPAIO, M. S. Obtenção e caracterização de compósitos de polietileno de alta densidade (PEAD) com fibra de coco. The Journal of Engineering and Exact Sciences, v. 06, n.5, 2020.

6. FURTADO, J. B. M; FILHO, P. A. F; OLIVEIRA, T. P; CAETANO, M. R. S; ARAÚJO, I. M. S; FIGUEIREDO, F. C; JÚNIOR, J. B. S. Caracterização química da fibra do caule da palmeira de babaçu natural e após tratamento. Revista de Engenharia e Pesquisa Aplicada, v.5, n. 3, p. 56-64, 2020.

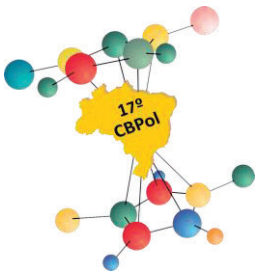

STUDY OF THE PLASTICIZER EFFECT OF CASTOR OIL DERIVATIVES IN THE PREPARATION OF FLEXIBLE PHBV FILMS

Duanne Maciel Scremin Miyazyaki, Stephannye Batista Ribeiro, Caio Bruno Livero, Juliete Silva Neves and Sônia Faria Zawadzki

Laboratório de Materiais Poliméricos/LAMAP – Programa de Pós-graduação em Química/PPGQ
Universidade Federal do Paraná/UFPR
livero@ufpr.br; zawadzki@ufpr.br

Abstract – Poly(hydroxybutyrate-co-hydroxyvalerate) (PHBV) is a polyester that, due to its high crystallinity, produces rigid films. This paper aimed to produce flexible PHBV films from the plasticizers addition, as ricinoleic acid esters, in 5, 10, 15, 30 and 50% (w/w) content. The films were prepared by casting and analyzed by differential scanning calorimetry (DSC), X-ray diffraction, eletronic microscopy, Fourier-transform infrared spectroscopy, and tensile mechanical testing (ASTM D882-02). The DSC results showed a decrease in the Tg value with the plasticizer addition and a reduction in crystallinity degree. Tensile tests showed a decrease in tensile strength, elastic modulus, and elongation properties. After evaluating the results, it can be suggested that there is an effective interaction between plasticizer and PHBV by the amorphous phase, but the elongation decreasing can be considered as a consequence of the remaining crystallinity of the PHBV. Therefore, it can be affirmed that the use of ricinoleic oil derivatives led to the obtaining of more flexible PHBV films.
Keywords: *PHBV, ricinoleic acid, plastificant, oligoester*

Introduction

The class of biodegradable polyester polymers is important as they can serve as a source of carbon and nutrients for microorganisms of the soil. Among these polyesters, it can be cited polyhydroxyalkanoates (PHAs), which are obtained from the bacterial fermentation process, and are mainly characterized by poly-3-hydroxybutyrate (PHB) and poly(3-hydroxybutyrate-co-3-hydroxyvalerate) (PHBV) [1]. PHB and PHBV polymers, as well as the others among the PHAs, are non-toxic, biocompatible, and biodegradable materials [2].

However, these polymers have poor mechanical properties, such as low tensile strength, low elongation, and low impact strength [1]. These characteristics make them difficult to process, in addition to producing weak and very fragile films.

PHBV compared to PHB, has superior mechanical properties, however, they are not good enough to be used in applications that require greater processability [1]. For this, it is necessary to add other components to the PHBV polymeric matrix that can provide changes and improvements in the characteristics of the films.

Plasticizers constitute an option for improving the properties of PHBV, considering that they are substances that, when added to a polymeric material, modify important properties, such as flexibility, processability, softness and smoothness [3]. The plasticizer is added in varied amount and acts to reduce macromolecular interactions, making the material more flexible. In addition, the plasticizer may be able to increase the tensile strength of the polymer in the mechanical testing and enable the modification of other properties [4]. Materials with low molecular weight such as monomers and oligomers have been studied as possible plasticizers.

Seeking to reduce the crystallinity and increase the resistance of the polymer, the improvement in the mechanical properties makes the practical application of PHBV to be expanded. Therefore, the present article aims to produce PHBV films using polyesters (oligomers) derived from castor oil derivatives, such as ricinoleic acid, for application as plasticizers and to analyze the films produced by techniques, such as Fourier transform infrared spectroscopy (FTIR), differential scanning calorimetry (DSC), X-ray diffraction (XRD), scanning electron microscopy (SEM) and mechanical tensile test.

Experimental

Materials

Poly(hydroxybutyrate-co-hydroxyvalerate) (Mn = 130,000 g mol-1, Biocycle® L 110, industrial PHBV, Serrana, Brazil). Chloroform, Synth. Polyesters from the castor oil derivative, ricinoleic acid, were used as plasticizers, namely: a) DMS17, polyester based on RADEG (ricinoleic acid and diethylene glycol) and succinic acid (SA), b) DMS18, based on diethylene glycol and SA, c) DMS19, polyester based on RADEG and phthalic acid (PA) and d) DMS20, composed by diethylene glycol and PA. The diol to anhydride ratio for the polyester's synthesis were 2:1. The materials were used as received [5].

Films Preparation

To obtain the films, a solution of 3.25% PHBV in chloroform was prepared [6]. Next, the amounts of oligoesters, DMS17, DMS18, DMS19 and DMS20, calculated as a function of the initial weight (2g) of PHBV in chloroform, were added to each composition, in order to prepare films containing 5, 10, 15, 30 and 50% (w/w) plasticizer. After solubilization, the solution was poured into glass molds (100x100 mm), which were partially covered and placed in a closed environment with a saturated atmosphere of chloroform for the slow evaporation of the solvent, favoring the preparation of uniform films. The solvent was slowly evaporated at room temperature for over about four days.

Fourier Transform Infrared Spectroscopy (FTIR)

FTIR analyzes were carried out using the attenuated total reflectance (ATR) technique, in the Bruker Alpha II equipment, between the 500 and 4000 cm^{-1} regions, with 19 min^{-1} scans and 4 cm^{-1} resolution. This technique allows the direct use of the film under the crystal of the equipment, and through the reflectance of the film, the spectrum is recorded. The analyzes were run at the CEB Laboratory, at the Pharmacy Department – UFPR.

Differential Scanning Calorimetry (DSC)

Differential scanning calorimetry (DSC) analyzes were carried out using a NETZSCH DSC 200 F3 MAIA equipment. Samples of PHBV films with and without plasticizers were weighed in aluminum crucibles (approximately 10.0 mg) and the analyzes were programmed in heating/cooling cycles: 1) heating from 20 to 200 °C, isotherm for 5 min; 2) cooling from 200 to -100 °C; isotherm for 5 min; 3) heating from -100 to 200 °C. The heating and cooling rate was 10 ºC min^{-1} and the run was performed under N_2 atmosphere (40 mL min^{-1}). The data used refer to the second warm-up. The analyzes were carried out at the Chemistry Department – of the Federal University of Paraná (UFPR).

X-Ray Diffraction (XRD)

The PHBV polymer films were examined in an X-ray diffractometer Shimadzu XRD-6000, scan of 2º min^{-1} and 2θ from 5 to 50º, copper Kα radiation (λ = 1.5418Å), current of 40 mA and voltage of 40 KV, for the observation of peaks indicative of crystallinity and amorphous regions of PHBV. [7-8]. These analyzes were carried out at the Chemistry Department of the Federal University of Paraná (UFPR).

Mechanical tensile test (ASTM D 884-02)

The films were produced in 100x100 mm plates. The specimens were cut in rectangular shape (10x85 mm). The average thickness of the films was 0.180 mm. The specimens (eight pieces per composition) were submitted to the mechanical testing in an INSTRON 5566 universal testing machine. The space between the claws was 25 mm, with an applied force of 1 KN at a speed of 10 mm min^{-1} until the specimens fractured. These analyzes were carried out at the Chemistry Department of the Federal University of Paraná (UFPR).

Results and Discussion

The polymeric films were obtained by casting, with an additive percentage of 5 to 50%, using oligoesters DMS17 to 20 as plasticizers. All polyesters have terminal hydroxyl (–OH) groups and this characteristic is important for PHBV, as these groups can help in the incorporation of the material due to the favorable intermolecular interaction. Most of the films showed homogeneous characteristics, without exudation of the plasticizer and, even, a higher opacity compared to pure PHBV film.

Fourier Transform Infrared Spectroscopy (FTIR)

The spectrum of the pure PHBV film, as well as the spectra of compositions with plasticizers, showed the same characteristic bands, such as axial strain of –C-H at 2987 cm^{-1}, axial strain of saturated aliphatic esters at 1732 cm^{-1}, angular strain asymmetric of the -C-H bond at 1454 cm^{-1}, angular deformation of the -C-H bond referring to CH_3 groups at 1389 cm^{-1}, the deformation corresponding to the C-O- of saturated esters was observed between 1200 and 1100 cm^{-1} and the angular deformation at C-H plane was at 1059 cm^{-1} [9]. By FTIR technique it is not possible to analyze the incorporation of the plasticizer, because, in oligoesters plascticisers, the characteristic bands of CH, CH_2, C=O bonds are also in the pure PHBV, which ends up leading to an overlapping of bands and the impossibility to verify the presence or not of the additive in the polymer. The spectra containing 15% of each additive can be analyzed in Fig 1.

Figure 1 – Comparison between the FTIR spectra of pure PHBV and compositions with 15% (w/w) plasticizers content.

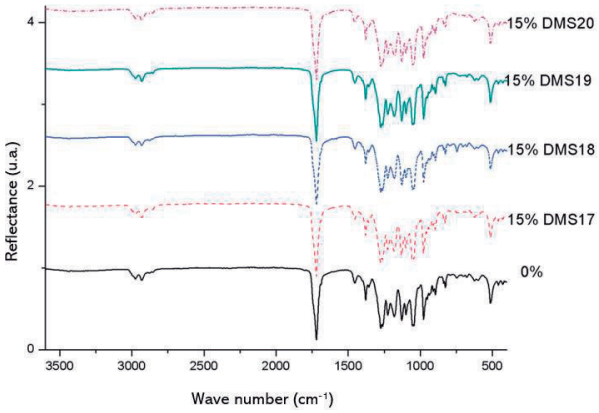

Figure 2 – XRD diffractograms revealing the profiles of PHBV films with DMS17 polyester.

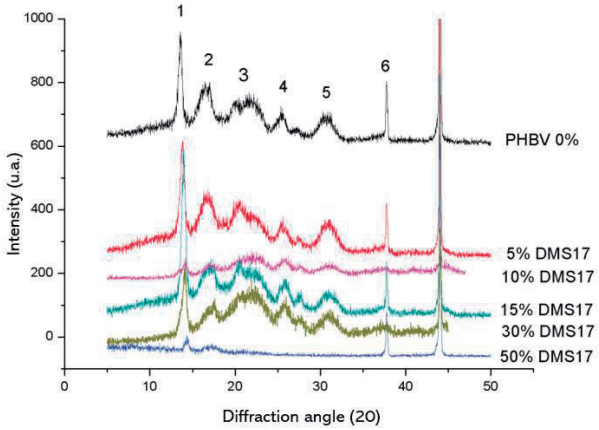

Source: Scremin (2020)

X-Ray Diffraction (XRD)

For pure PHBV, the following 2θ values were observed which corresponding to the respective crystal planes: 13.5° (020), 16.9° (110), 20.0° (101), 21.6° (111), 25.5° (121) and 30.8° (200) (SENHORINI, 2010). By analyzing the angles of the crystalline peaks, it was determined that, in all compositions, the 2θ angle values remained equal to those of pure PHBV, indicating that the

addition of plasticizer does not change the crystalline peaks. However, a difference was observed between the areas of the crystalline peaks and the respective fraction of the amorphous region: as the plasticizer is added, this difference is altered. The smaller the area of the observed crystalline peaks, less rigid the material will be. Consequently, the amorphous area of the material will be larger. Fig 2 shows the XRD graph of the films based on PHBV and oligoester DMS17 (RADEG + succinic anhydride, SA).
In general, all films showed a similar profile according to the increasing additive addition. There was a decrease in the crystalline segments of each one, which favored the alteration of the properties of PHBV, however, the additive does not lead to obtaining an amorphous material, that is, the plasticizer alters the crystallinity, but does not reduce it by 100%.

Differential Scanning Calorimetry (DSC)
According to the analyses, particularly for PHBV, some interesting observations can be pointed out: the polymer exhibited one glass transition temperature (Tg) and two melting temperatures (Tm). The crystallization event (Tc), normally apparent in the sample cooling step, appeared in the heating, between Tg and the first Tm. This last aspect has already been observed previously for PHBV and it was reported in the literature by Senhorini (2010).
In compositions with oligoesters (DMS17 to DMS20), a decrease in the glass transition temperature (Tg) value was observed with the increasing addition of plasticizer, which indicates an increase in mobility in the amorphous region of the polymer, suggesting the plasticizer effect. In addition, there was an increase in the crystallization temperature (Tc) and the melting temperature (Tm) was not altered, indicating that, in a way, the additive interacts, in some degree, with the crystalline fraction. Fig 3 it is possible to observe the Tg decrease profile of each of the films produced.

Figure 3 –Effect of plasticizer in the amorphous phase: variation of Tgs in PHBV films.

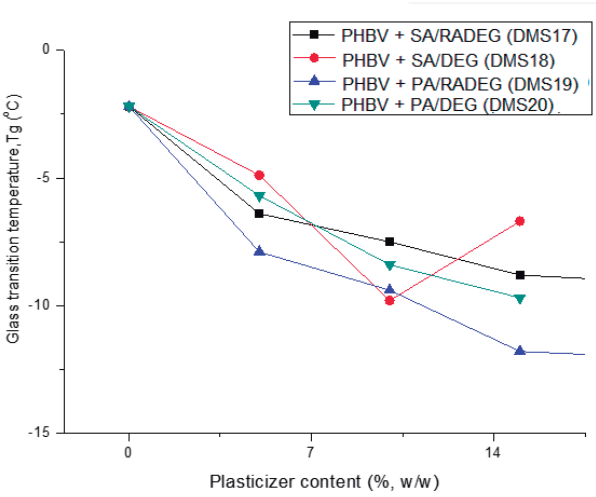

Source: Scremin (2020)

Mechanical tensile test – Standard ASTM D 884-02
The results indicated that, in all compositions, as the proportion of additive was increased, the tensile strength decreased. Young's modulus increased with the lowest proportion of plasticizer (5%) and then decreased. Elongation was also affected, suffering a decrease. From these results, it can be observed that the plasticizer can affect crystallinity, but not enough to promote greater elongation. The mechanical properties profiles suggest that the polymer absorbs the additive, withstands the imposed force, but break easily. The graphs shows the profile of the mechanical properties for each composition (Fig 4).

Figure 4 – Effect of plasticizer addition on the mechanical behavior of the films. a) tensile strength b) Young's modulus. c) elongation

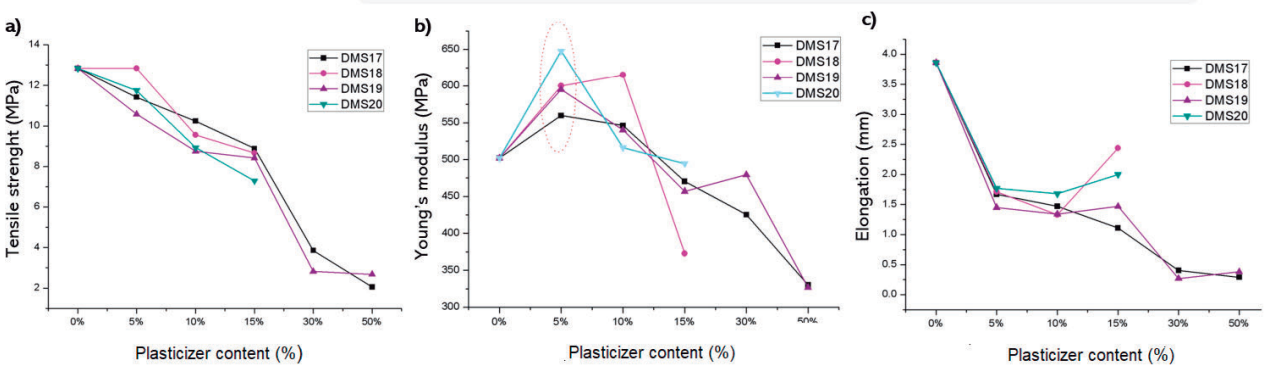

Source: Scremin (2020)

The mechanical behavior of the films may be influenced by three factors: presence of plasticizer, presence of cavities and remaining crystallinity of PHBV. Given these results, it is possible to suggest that the additive interacts more easily with the amorphous fraction of PHBV. The interaction with the crystalline fraction occurs, but it is hindered by the greater intensity of the intermolecular forces between the PHBV chains, that is, the additive cannot completely reduce the polymer-polymer interactions in the crystalline phase.

Conclusions

All applied oligomers (DMS17 to 20) were able to the proposal of this project to increase the flexibility of PHBV, improving the physical properties and, consequently, increasing the possibility of applications of this polymer with versatile characteristics. In this respect, oligomeric polyesters based on vegetable oils can be used in other polymeric matrices, to change the mechanical properties, as observed in this paper.

Acknowledgements

The authors thank to the Department of Chemistry and the Federal University of Paraná (UFPR) and they are also grateful to CAPES foundation for providing the financial support for this work.

References

1. A. Rodriguez-Uribe et al. Composites Part C: Open Access, 2021, 6, 100201. https://doi.org/10.1016/j.jcomc.2021.100201.
2. M. L. Tebaldi et al. Journal of Drug Delivery Science and Technology, 2019, 51, 115-116. https://doi.org/10.1016/j.jddst.2019.02.007.
3. S. F. Zawadzki. Dissertation, Federal University of Rio de Janeiro, 1989.
4. R. Avolio et al. European Polymer Journal, 2015, 66, 533-542. https://doi.org/10.1016/j.eurpolymj.2015.02.040.
5. D. M. Scremin. Dissertation, Federal University of Paraná, 2020.
6. H. D. M. Follmann. Dissertação, Universidade Federal do Paraná, 2009.
7. S. V. Canevarolo Jr, *Ciência dos polirneros:* um testo básico para tecnólogos e engenheiros, Artliber, São Paulo, 2002.
8. S. R. Schaffazick et al. Química Nova, 2003, 26, 5. https://doi.org/10.1590/S0100-40422003000500017.
9. G. A. Senhorini. Dissertation, Federal University of Paraná, 2010.

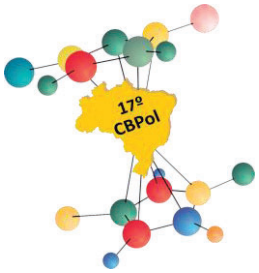

SUSTAINABLE ALTERNATIVES FOR PACKAGING: EXPLORING THE HIGROSPICITY OF BIODEGRADABLE MATERIALS BASED ON PLA, PBAT, AND RICE HUSK

Vanessa Z. Kieffer[1]*, Nicole B. Agostini[1], Edson L. Francisquetti[2] and Ruth M. C. Santana[1]

1 – Department of Materials Engineering, Federal University of Rio Grande do Sul (UFRGS), Porto Alegre, RS, Brazil.
2 – Federal Institute of Education, Science and Technology of Rio Grande do Sul (IFRS), Farroupilha, RS, Brazil.
*vanessa.kieffer@ufrgs.br

Abstract - The present study aims to develop a sustainable material using biodegradable polymers combined with agroindustry residues, to find more sustainable options to reduce the negative environmental impact of single-use food packaging. Different formulations containing polylactic acid (PLA), polybutylene adipate-co-terephthalate (PBAT) in the form of blends (BL), and composites (CO) reinforced with 10 and 20% of rice husk (RH) were prepared to identify the most appropriate formulation to produce a material biodegradable with the specific properties required for its application in packaging. The samples were characterized using moisture absorption, water absorption, and contact angle measurements. The results showed that PLA, PBAT, BL1, and BL2 behave similarly. Furthermore, it was observed that samples containing lower RH content (10%wt) showed lower hygroscopicity and hydrophilicity compared to the other composites. Concluding, as well as the PLA/PBAT blends, the composite materials containing rice husk are potential substitutes for single-use food packaging.
Keywords: *PLA, PBAT, Rice Husk, Biodegradable Packaging, Sustainability.*

Introduction

The growing concern about environmental pollution caused by the accumulation of plastic waste has driven the search for sustainable alternatives for single-use food packaging. Faced with these concerns, it is essential to seek sustainable solutions and adopt ecologically responsible practices to minimize the negative impact caused by single-use packaging waste on our planet [1]. Therefore, the development of biodegradable materials for packaging has gained prominence as a promising solution to replace non-biodegradable conventional polymers [2, 3].

One of the alternatives is using biodegradable polymers, such as polylactic acid (PLA) and polybutylene adipate-co-terephthalate (PBAT), which come from renewable sources and have characteristics suitable for packaging applications [4, 5]. PLA is a polymer obtained from renewable sources, such as corn starch, and is biodegradable in industrial composting [3]. Conversely, PBAT is a copolymer combining polybutadiene and adipate terephthalate properties, being flexible and biodegradable in composting [4].

These biodegradable materials have shown promise as alternatives to conventional polymers in packaging, since they have physical and mechanical properties suitable for various applications, such as food transport and storage, protective packaging, and packaging for electronic products, among others [5]. In addition, these materials are biodegradable; they can decompose naturally in the environment, reducing the accumulation of plastic waste and minimizing the environmental impact.

However, in addition to the biodegradable polymer options already available on the market, it is essential to emphasize that the selection of materials to develop new formulations depends on the specific properties, availability, and cost of the raw materials used. In this context, developing new

formulations of sustainable materials by combining biodegradable polymers with residues, such as rice husks (RH) is interesting. Rice husk is rich in cellulose, lignin, and other organic components, which makes it a residue with a solid potential to produce sustainable materials for food packaging. In addition, the use of agroindustry residues contributes to the reduction of the environmental impact, since the use of a certain percentage by mass of rice husk in the formulation of the biodegradable material will help to reduce the amount of agricultural waste improperly discarded, promoting a more sustainable approach [6].

Therefore, the purpose of the present study is to develop a sustainable material using PLA/PBAT combined with rice husks (RH), aiming to replace single-use food packaging. The mixture of biodegradable polymers with agroindustry residues can be an exciting strategy for developing eco-friendly packaging, considering the availability, properties, and costs of the raw materials, as well as the compatibility and desired performance for the specific application.

Experimental

Materials

For the formulation of the samples, two biodegradable polymers were selected, PLA (Ingeo™ Biopolymer 4043D) and PBAT (Ecoflex® F Blend C1200); and as filler, rice husks (RH) provided by local producers. Different formulations were produced to determine the most suitable formulation for getting the most cost-effective biodegradable material, as specified in Table 1.

Table 1 – Formulation of samples.

Samples	PLA (%)	PBAT (%)	RH (%)
PLA	100	-	-
PBAT	-	100	-
BL1	90	10	-
BL2	80	20	-
CO1	80	10	10
CO2	70	10	20
CO3	70	20	10
CO4	60	20	20

The materials were mixed and homogenized in a HAAKE Rheomix OS Polylab mixing chamber, to obtain blends (BL1 and BL2) and composite materials (CO1, CO2, CO3, and CO4). Then, the mixtures were compressed in a hydraulic press at 170 ºC and, subsequently, the trays were made by thermoforming.

Characterization Methods

To compare the hygroscopicity of the thermoformed polymeric plates, according to the ASTM D5229 standard, a moisture absorption test was carried out in controlled relative humidity chambers at a constant temperature of 30 ºC, using 75% relative humidity saturated saline solution. The water absorption content was evaluated through the immersion test in distilled water, according to ASTM D570, to determine the degree of hydrophilicity of the samples. And a wettability test was performed based on the ASTM D7334 standard to complement the barrier study of biodegradable materials. In this test, the images were acquired through a contact angle measurement system with a digital optical microscope, and the contact angle calculations were performed using the Surftens software. The statistical analysis of the variance (ANOVA) of obtained results has been carried out using the software Origin. A one-way ANOVA and a Tukey's test were used to check for statistical differences among groups ($p \leq 0.05$).

Results and Discussion

Moisture Absorption

The humidity test was carried out in a controlled environment to analyze the behavior of the samples in the long term, where measurements were carried out every seven days until the increase in mass was considered substantially saturated, totaling 35 days, as shown in Fig. 1.

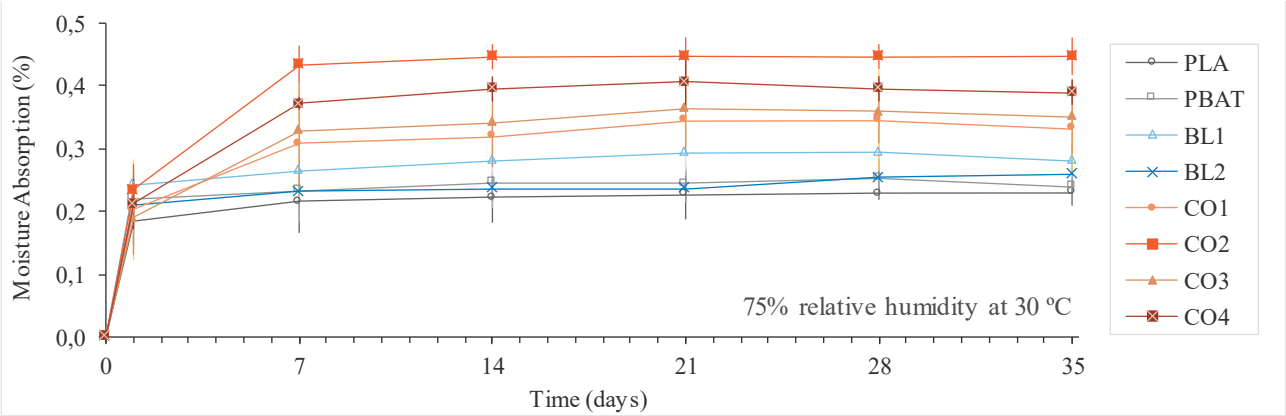

Figure 1 – Result of the average moisture absorption content of the analyzed samples in the long term.

In Fig. 1 it is possible to observe that, in the first seven days, moisture absorption was faster. According to Ighalo *et al.*, this is because the driving force of mass transfer is initially very high [7]. However, all samples achieved stability in moisture absorption after 14 days of testing, with values below 0.5%. An analysis of variance (ANOVA) was performed to evaluate the measurements found for the samples after 35 days of testing. Thus, statistically, it was verified that there are no significant differences between the PLA, PBAT, BL1, and BL2 samples. Regarding the PLA/PBAT/RH composites, it was found that CO2 (70|10|20) absorbed more moisture, with a value of 0.45%, followed by CO4 (0.39%), CO3 (0. 35%) and CO1 (0.33%). The greater amount of absorbent material present in the CO2 and CO4 composite formulation can explain this. However, it is important to point out that even with this higher moisture absorption, the value remained below 0.5%, which is considered satisfactory for application in packaging according to ISO 187.

Water Absorption

The hydrophilic nature of rice husk makes water absorption a critical aspect of producing materials for use in packaging [8, 9]. To analyze the behavior of the samples in the long term, immersion tests were carried out, where measurements were carried out every seven days until the increase in mass was considered substantially saturated, totaling 42 days, as shown in Fig. 2.

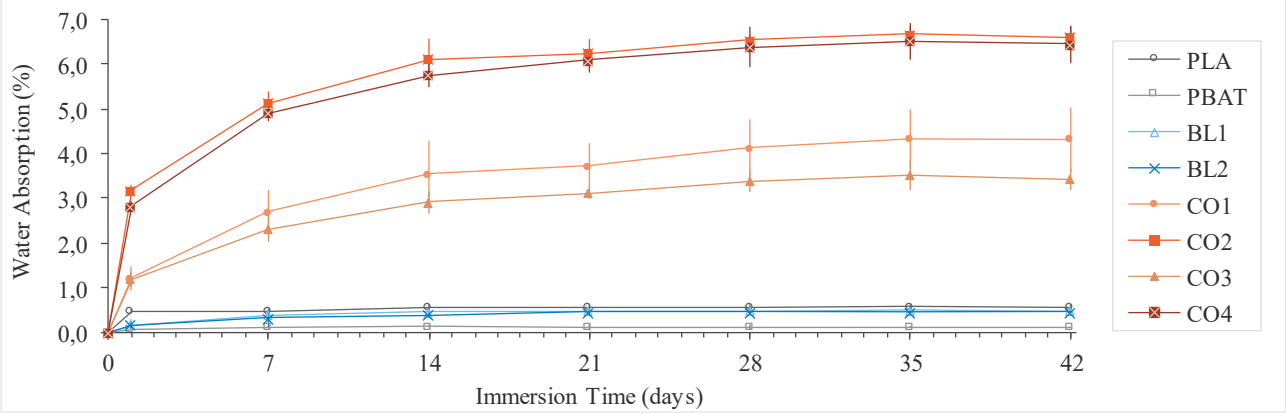

Figure 2 – Result of the average water absorption content of the analyzed samples in the long term.

As predicted, the result showed that the PLA/PBAT/RH samples had a higher water absorption content. Because, the rice husk is composed of different types of components, with cellulose being one of the main constituents. In addition to cellulose, rice husk contains lignin, hemicellulose, silica, proteins, and lipids in varying amounts [8]. Although its composition varies, rice husk has strong hydrogen bonds due to its basic cellulose constitution, being highly hydrophilic [9]. Therefore, when incorporated into a polymeric matrix, rice husk can act as a water retention agent and, in addition, increase the porosity of the composite material. This can allow for greater penetration and retention of water in the matrix, resulting in greater water absorption [10].

From the analysis of variance (ANOVA), it can be concluded that there are no significant differences between the samples PLA, BL1, and BL2. In the case of PLA/PBAT/RH composites, the results showed that CO2 and CO4 are statistically equal, as well as CO1 and CO3, which means that these composites have similar behavior in terms of water absorption.

However, it is important to emphasize that the CO1 and CO3 samples showed minor water absorption compared to the other composites, suggesting more significant interfacial interaction and homogeneity of the samples. Suggesting that these samples are more suitable for applications where water resistance is an important property.

Contact Angle

The contact angle test was carried out to study the effect of incorporating fibers into the polymeric matrix, specifically on the surface's hydrophobicity changes. For such, after the deposition of the drop of water on the surface, images were captured at 3 and 180 seconds to analyze the surface wettability of the composite material. Figure 3 shows the deposited water droplet pictures on the analyzed samples, and Fig. 4 shows the results of contact angles.

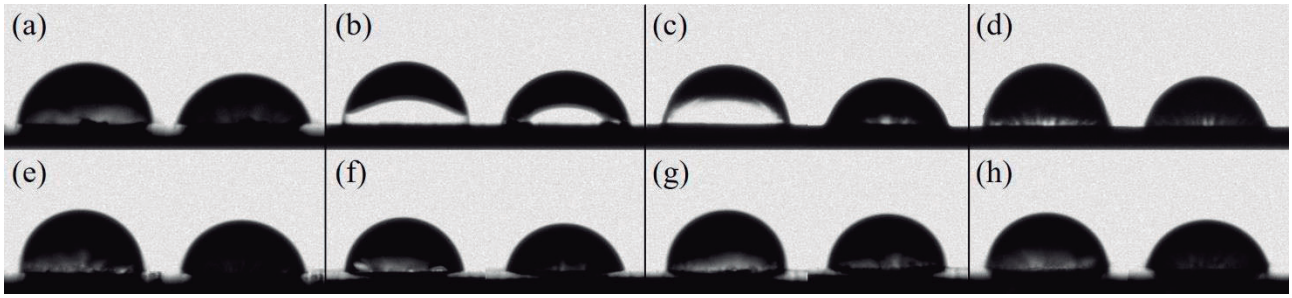

Figure 3 – Images of water droplets on the surface of the samples in 3 and 180s, respectively: (a) PLA; (b) PBAT; (c) BL1; (d) BL2; (e) CO1; (f) CO2; (g) CO3 e (h) CO4.

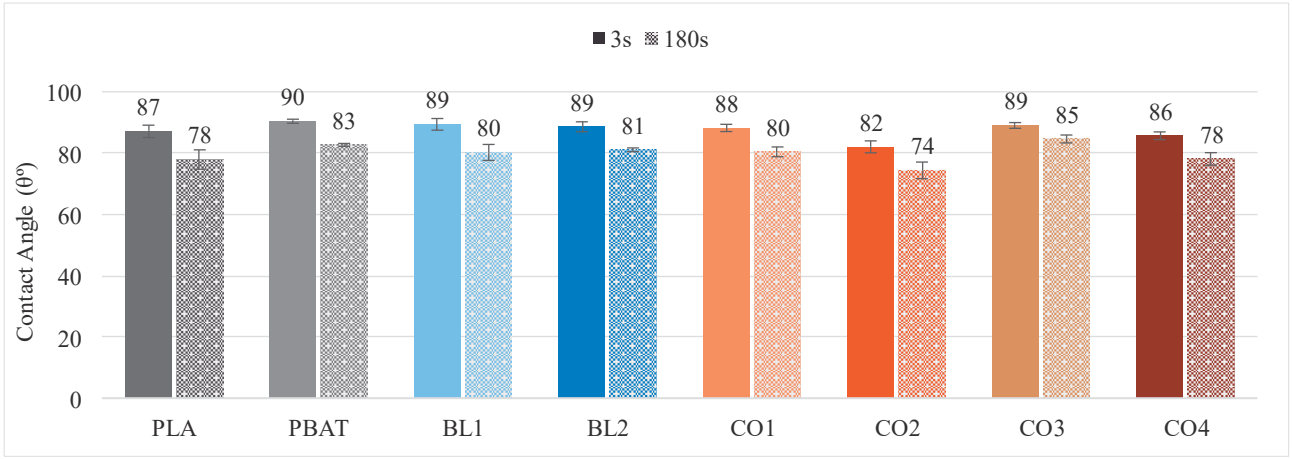

Figure 4 – Comparative result of the contact angle of the analyzed samples.

In Fig. 3, comparing the behavior of water droplets under the surface of the samples, it is possible to suggest that the PBAT is more hydrophobic than the other samples, as less water droplet scattering is seen.

Regarding the composite materials, the results indicate that the CO2 and CO4 composites have greater hydrophilicity, which may be due to a higher rice husk content (20%wt) and, consequently, a lower homogeneity in the sample than the other analyzed composites. On the other hand, the CO1 and CO3 composites showed lower hydrophilicity, highlighting CO3.

It is noteworthy that despite the addition of rice husk, the composites showed good contact angles. This feat can be explained by the Cassie-Baxter phenomenon; when a textured surface comes into contact with a liquid, the liquid does not completely wet the surface, forming small air pockets trapped between surface irregularities. In this case, textured surfaces appear more hydrophobic than smooth surfaces [11].

Conclusions

The results obtained showed that the PLA, PBAT, BL1, and BL2 samples showed similar behavior. Furthermore, the CO1 and CO3 composites showed lower hygroscopicity and hydrophilicity when compared to the other composites. Concluding that, as well as biodegradable polymer mixtures, composite materials with a biodegradable polymeric matrix combined with rice husk are potential substitutes for single-use food packaging due to their barrier properties. However, further studies are necessary to investigate the mechanical properties, biodegradability, and potential for industrial-scale production.

Acknowledgements

The authors would like to thank the Laboratory of Polymeric Materials (LaPol) of the Federal University of Rio Grande do Sul (UFRGS), CAPES, CAPES PROEX, and CNPq, for all the support for the development of this research.

References

1. R. Geyer; J. Jambeck; K. Law, Science Advances 2017, 3(7). doi.org/10.1126
2. D. Ferreira; P. Silva; T. F. Madeira. Am J Entrep Innov 2019, 1(2). doi.org/10.33871/26747170
3. A. C. S. Oliveira; S. V. Borges. Rev Eletr de Mat e Proc 2020, 15(1). repositorio.ufla.br
4. R. S. Silva, MSc. Thesis, University Presbiteriana Mackenzie, 2016.
5. D. Myalenko; O. Fedotova. Polymers (Basel) 2023, 15(7). doi.org/10.3390/polym15071619
6. L. R. Souza; L. M. Souza; D. P. S. Bernardi; P. C. L. Santos; M. Hávila; O. C. Neto. *Embalagem produzida a partir da Casca de Arroz,* Publicar Editora, 2021.
7. J. O. Ighalo; A. G. Adeniyi; O. O. Owolabi; S. A. Abdulkareem. Int J Sustain Eng 2021, 14(5). doi.org/10.1080/19397038
8. E. R. Lopes; A. L. Medina; A. S. Ribeiro; J. N. Brandalise; A. M. Nunes. Quím Nova 2017, 40(9). doi.org/10.21577/0100-4042.
9. O. P. Fleig, MSc. Thesis, Federal University of Rio Grande do Sul (UFRGS), 2020.
10. S. A. Abdulkareem; A. G. Adeniyi. J Eng Res Dev 2018, 1(2). hdl.handle/123456789/3515
11. 12. M. Nosonovsky; B. Bhushan. Curr Opin Colloid Interface Sci 2009, 14(4). doi.org/10.1016

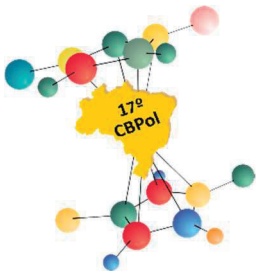

SUSTAINABLE POLYURETHANE FOAM WITH RICE HUSK ASH RESIDUES WITH POTENTIAL APPLICATION IN THE ADSORPTION OF PESTICIDES IN WATER FOR HUMAN CONSUMPTION

Verenna S. Guedes [1]*, Bruna N. Morato [1], Eliane Ayres [2], Ricardo O. Correia [3], Rodrigo Lambert Oréfice [3], Marcelo Libânio [4], and Marys L. B. Almeida [1]

1 - Department of Materials Engineering and Construction, Federal University of Minas Gerais (UFMG), Belo Horizonte, MG, Brazil

verenna.guedes@gmail.com

2- Department of Production Systems at the University of the State of Minas Gerais, Belo Horizonte, MG, Brazil

3 - Department of Metallurgical and Materials Engineering, Federal University of Minas Gerais (UFMG), Belo Horizonte, MG, Brazil

4 - Department of Sanitary and Environmental Engineering, Federal University of Minas Gerais (UFMG), Belo Horizonte, MG, Brazil

Abstract

The high cost of activated carbon as an adsorbent used in the treatment of water for human consumption opens up the possibility of using alternative materials for removing contaminants. The objective of this ongoing research is to develop sustainable polyurethane foams from the incorporation of different amounts of rice husk ash residues to investigate the removal of mancozeb, glyphosate and 2,4D pesticides in aqueous solutions. Scanning electron microscopy images showed high porosity and interconnectivity between pores, favoring the adsorption process. Fourier transform infrared spectroscopy spectra and assignments confirmed the main characteristic bands of the foams. The Thermogravimetry evidenced the decomposition of the foams in three stages, about 280ºC, 390ºC and 450ºC, attributed to the urethane and urea connections, and to the polyether and polyester, respectively. For the residue there was no mass loss up to 800°C. The adsorption experiments are ongoing and soon the findings will be reported. This approach meets potential scientific, technological and economic benefits.

Keywords: *sustainable polyurethane foam, adsorption, rice husk ash wastes, pesticide removal, water treatment.*

Fundings: Minas Gerais State Research Support Foundation (FAPEMIG).

Introduction

The global production of pesticides has been growing exponentially over the years, reaching 4 million tons in 2022 with an annual increase close to 12% [1,2]. However, studies have shown that only 1% of the agrochemicals used in crops are actually directed to pest control, thus damaging the surrounding ecosystem and natural resources [2]. In Brazil, the amount of pesticides consumed has increased from 241.000 in 2010 to over 720.000 tons in 2021 [3].

According to the Brazilian Institute for the Environment and Renewable Natural Resources, glyphosate, 2,4-D and mancozeb accounted for 56% of the 510.000 tons of active ingredients sold in Brazil in 2018 and are found in varying concentrations in water sources [3]. This assertion can be corroborated by the drastic reduction in the maximum permissible value for mancozeb, from 180 ug/L to 8.0 ug/L, in the current potability standard published in May 2021 [4]. The European Union prohibits the use of Mancozeb, while Brazilian legislation allows its use [4,5]. Mancozeb is associated with chronic health problems, organ toxicity, thyroid problems, and effects on the neurological and respiratory systems [6,7].

There is evidence that the conventional treatment of water that supplies close to 75% of the Brazilian population, involving coagulation, flocculation, sedimentation and filtration, is not significantly efficient in removing pesticides. Activated carbon of vegetable, mineral or animal origin stands out as the most used adsorbent in water treatment, predominantly in powdered form. However, the high cost often makes its use unviable, especially for small supply systems. Especially for charcoal produced in Brazil based on coconut shell, the applied dose of around 10 mg/L would represent a cost of approximately US$3.2/100 m^3, something like 70% of the total cost of chemical products used in potabilization. The frequent presence of pesticides in water bodies, the low removal rate in treatment plants and the high cost of activated carbon have encouraged the study of alternative adsorbents.
Polyurethane foams have chemical and physical properties suitable for the adsorption of organic contaminants, with high removal efficiency, chemical and thermal resistance, low cost, easy obtaining and handling. Waste materials (agricultural and industrial) have been used as adsorbents or incorporated into polymer matrices to capture organic contaminants [8,9]. Agricultural residues are an abundant source of porous materials rich in active functional groups. Rice husk constitutes about 20% of the 650 million tons of rice produced annually in the world [10]. The calcination of rice husk produces rice husk ash (RHA), a network of silica particles that, once incorporated into a polymeric matrix, results in composites with improved properties for the adsorption process.
In this context, the present research aims at the improvement of sustainable polyurethane foams, from different amounts of rice husk ash residues for potential use in the adsorption of the pesticides glyphosate, 2,4-D and mancozeb in natural waters. Satisfactory results from the application of developed polyurethane foams in the removal of the three pesticides under study and widely used in Brazil, will open perspectives for a wide range of research given the significant spectrum of these microcontaminants being present in the supply sources.

Experimental

Materials

The RHA was kindly provided by the commercial Silcca Nobre®, Indiana Distribuição-Brasil, after gasification process in fluidized bed. Biopol® 411 was obtained from PoluUrethane (Ibirité, Brazil); polypropylene glycol (PPG 2000) from Sigma-Aldrich (St. Louis, USA); 80:20 mixture of 2,4-toluene diisocyanate and 2,6-toluene diisocyanate from Sigma-Aldrich; Tin (II) 2-ethylhexanoate (TIN II Liocat® 29, Miracema-Nuodex - Campinas, Brazil); silicone (Tegostab® B 8135, Evonik - Essen, Germany). Maconzeb, glyphosate and 2,4-D herbicides were obtained from Sigma-Aldrich.

Foam Production

The production of polyurethane foam followed the methodology developed and consolidated by [9] in which RHA was incorporated into the mixture of polypropylene glycol and Biopol® 411 with percentages of 20% and 50% of the mass of polyols, being denominated of PUI-RHA20 and PUI-RHA50, respectively. These were mechanically mixed at 1000 rpm for 5 minutes and then the TIN(II) catalyst, silicone surfactant and deionized water (DI water) were added, again subjecting them to stirring at 1000 rpm for 2 min more. Then, 2,4-toluene diisocyanate and 2,6-toluene diisocyanate in a ratio of 80:20 was added (TDI) to the mixture and stirred for another 30s. Finally, the mixtures were left curing for 72 hours at environment temperature. In Table 1, the denominations and compositions for the synthesized foams are represented, being PU the foam without the incorporation of RHA.

Table 1 – Denominations and compositions for the developed foams.

Espumas	Biopol411 (g)	PPG2000 (g)	Silicone (g)	TIN II (g)	Água DI (mL)	TDI (g)	RHA (g)
PU	11,25	1,25	0,10	0,025	0,40	11,65	0,00
PUI-RHA20							2,50
PUI-RHA50							6,25

Characterizations

Thermogravimetry was performed in an Exstar 7200 equipment (Seiko-SII Nanotechnology, Inc.) in a nitrogen atmosphere and heated from 25 to 800ºC at a rate of 10ºC min^{-1}. FTIR spectra were recorded using a Thermo Scientific Nicolet 6700 spectrophotometer in ATR mode, scanning in the range 450-4500 cm^{-1}, with an average of 32 scans and a resolution of 4 cm^{-1}.

Determination of Pesticides Concentration and Adsorption Capacity

A UV-vis spectrometer (UV-2600, Shimadzu Corporation, Japan) with spectra in the range of 185-450 nm and a quartz cuvette (Kasvi, Brazil) will be used to identify the concentration of pesticides whose specific absorbances are referenced: 279 nm, 193 and 229, mancozeb, glyphosate and 2,4D, respectively [11, 15, 16]. The adsorption capacities will be investigated by immersing 120 mg of each adsorbent sample in an aqueous solution with a concentration of 500 ppm of each pesticide at natural pH. The experiments will be conducted at room temperature (25 ± 3 °C), in 100 mL amber glass vials (Pyrex), which will be shaken in a Fisaton shaker (model 786) for 24 hours, following the methodology of [9]. Subsequently, small aliquots will be collected from the solution in each vial with a 20 mL syringe will be filtered with a 33 mm Millex-HV filter and analyzed. The adsorption capacities will be determined as differences between the initial and post-adsorption concentrations of pesticides [9,12].

Results and Discussion

Fig.1 shows scanning electron microscopy images of PU (a), RHA (b), PUI-RHA20 (c) and PUI-RHA50 (d) materials. It can be observed that the foams produced showed high porosity and interconnectivity between the pores, evidencing satisfactory conditions for the adsorption process. The RHA is distributed with considerable homogeneity in the polymeric matrix, Fig 1(c), (d), and may increase the pesticides removal efficiency.

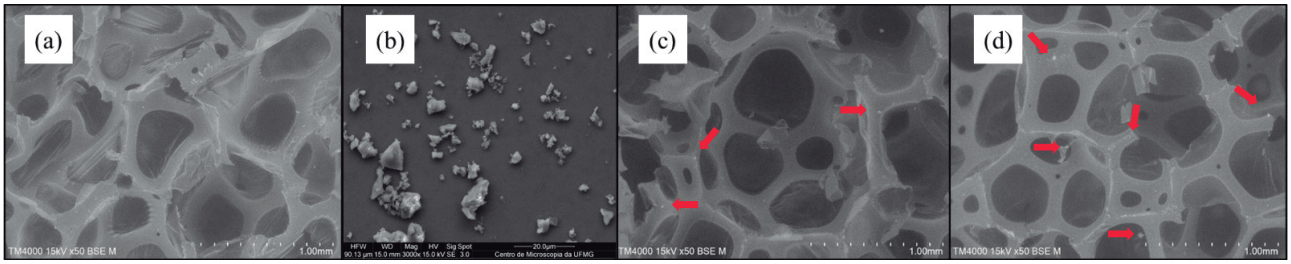

Figure 1 – SEM of PU foam (a), RHA residue (b), PUI-RHA20 (c) and PUI-RHA50 (d) foams.

Fig. 2 shows the FTIR spectra of the RHA, PU and their composites. The band at ~3300 cm^{-1} was assigned to the stretching vibrations of N-H groups, while the peaks at ~ 2900 and 2800 cm^{-1} were assigned to asymmetric and symmetric C-H stretching vibrations, respectively [9,11]. Between 2300 and 2230 cm^{-1}, the band of PU and composites is characteristic of the stretching vibration of residual NCO groups. An absorption band ranging from ~ 1700 cm^{-1} to ~ 1600 cm^{-1} corresponds to the carbonyl of the polyester of Biopoly 411 used in the synthesis of the samples and the stretching vibration of the carbonyl of urethane and urea (C=O). In the region of ~ 1520 cm^{-1}, the band corresponding to C-N stretching and N-H deformation can be observed. The characteristic C-N stretch of the tertiary amide and the N-H strain were observed near 1200 cm^{-1}, and the band corresponding to the C-O-C stretch of the aliphatic polyether PPG 2000 was detected around 1040 cm^{-1} [9,11,14]. The FTIR obtained for the RHA is shown in more detail and one can perceive, in the regions below 1100 cm^{-1}, the vibrations associated with the structures of the silicates and aluminosilicates of the residue [13,14].

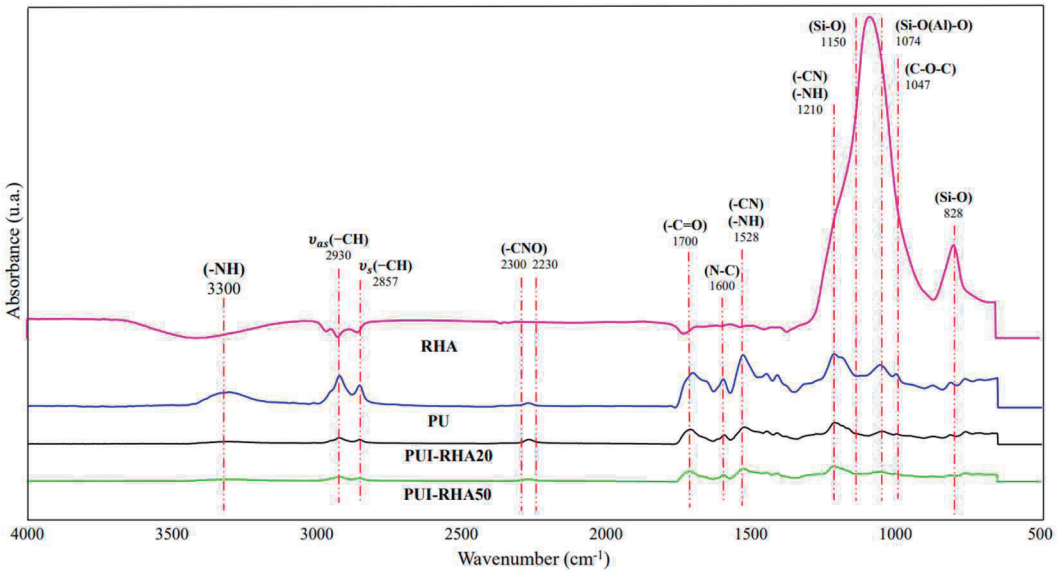

Figure 2 – FTIR from RHA, PU, PUI-RHA20 and PUI-RHA50.

Fig. 3 shows the characterization TGA curves of PU and its composites evidenced the decomposition of the foams in three stages, about 280ºC, 390ºC and 450ºC, attributed to the urethane and urea connections, and to the polyether and polyester, respectively [14]. As expected, for a given temperature, the greater the amount of residue incorporated in the foam, PUI-RHA50, Fig. 3(b), the lower the mass loss. For the residue, Fig. 3(a) there was no mass loss up to 800°C.

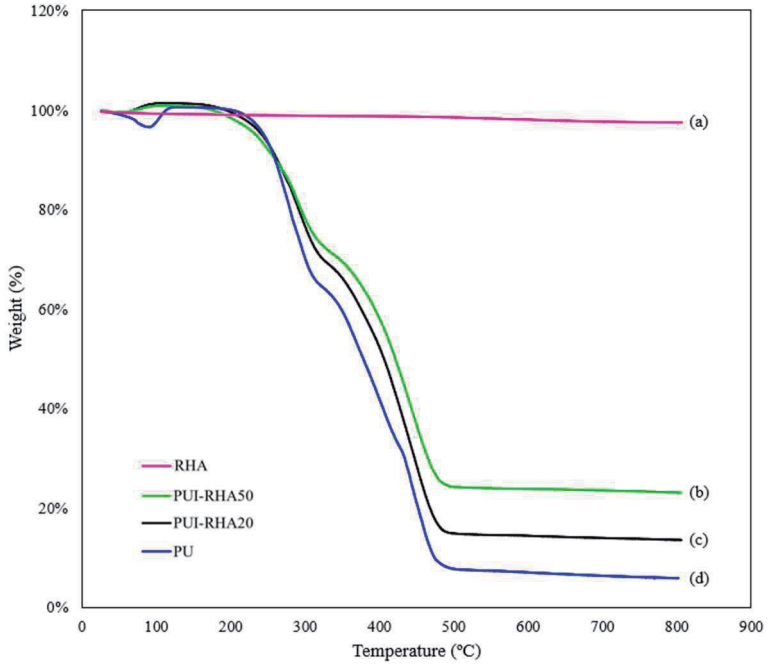

Figure 3 – TGA curves of RHA, (a), PUI-RHA50 (b), PUI-RHA20 (c) and PU (d).

Conclusions

The adsorbents being developed in this work in progress, polyurethane foams of plant origin with rice husk ash residue, showed dimensional stability, high porosity and interconnectivity between the pores. A preliminary adsorption test showed that the removal efficiency of the pesticide mancozeb in aqueous solution was significantly higher for the adsorbent synthesized with a high percentage of

RHA. The produced composites, low cost and easily obtainable, may constitute as sustainably viable alternatives, in the removal of contaminants, to water treatment plants for human consumption.

Acknowledgements
The authors thank Minas Gerais State Research Support Foundation (FAPEMIG), for funding research.

References

1. F. P. Carvalho, *Food and Energy Security* 2017, 6, 48-60. https://doi.org/10.1002/fes3.108.
2. Heinrich-Böll-Stiftung; Friends of the Earth Europe; Bund Fur Umwelt; Natursxhutz in The Pesticide Atlas 2022, Heinrich-Böll-Stiftung, Ed.; Heinrich-Böll-Stiftung, Berlin, 2022.
3. Instituto Brasileiro do Meio Ambiente e dos Recursos Naturais Renováveis. Boletim 2021 - Série com a Produção, Importação, Exportação e Vendas por ingredientes ativos: Histórico de comercialização 2000- 2021 dados BI. Available in: https://www.gov.br/ibama/pt-br/assuntos/quimicos-e- biologicos/agrotoxicos/relatorios-de-comercializacao-de-agrotoxicos/relatorios-de- comercializacao-de-agrotoxicos, may. 2023.
4. Ministério da Saúde. Portaria GM/MS n.º 888, de 4 de maio de 2021. Available in: https://www.in.gov.br/, fev. 2023.
5. U.S. Department of Agriculture. European Union: Mancozeb Non-Renewal and MRL Review. Available in: https://www.fas.usda.gov/, dec. 2020.
6. J. A. Buledi; A. Mallah; A. R. Solangi; I. M. Palabiyik; N. Qambrani; F. Karimi; Y. Vasseghian; H. Karimi-Maleh Food and Chemical Toxicology 2022, 161, 112843. https://doi.org/10.1016/j.fct.2022.112843.
7. J. C. Dall'Agnol; M. F. Pezzini; N. S. Uribe; D. Jovelevith, *European Review for Medical and Pharmacological Sciences* 2021, 25: 4113-4120. https://doi.org/10.26355/eurrev_202106_26054.
8. H. D. da Rocha; E.S. Reis; G.P. Ratkovski; R. J. da Silva, F. D.S. Gorza, G. C. Pedro, C. P. de Melo *Journal of the Taiwan Institute of Chemical Engineers* 2020 110, 8-20. https://doi.org/10.1016/j.jtice.2020.03.003.
9. M. L. B. Almeida; E. Ayres; M. Libânio; D. S. Gamarano; C. C. Ribeiro; R. L. Oréfice Journal of Polymers and the Environment 2020, 28, 2511–2522. https://doi.org/10.1007/s10924-020-01794-9.
10. A. D. N'Diaye; C. Boudokhane; M. Kankou; H. Dhaouadi. Chemistry and Ecology 2019, 35, 678-692. https://doi.org/10.1080/02757540.2019.1604692.
11. R. Zamora-Sequeira; F. Alvarado-Hidalgo; D. Robles-Chaves; G. Sáenz-Arce; E. D. Avendano-Soto; A. Sánchez-Kopper; R. Starbird-Perez Polymers 2019, 11, 1449. https://doi.org/10.3390/polym11091449.
12. L. M. S. Barbosa; B. E. L. Baêta; A. L. C. Barros; M. L. B. Almeida; M. Libânio Water Practice & Technology 2022, 18, 231. https://doi.org/10.2166/wpt.2022.174.
13. V. Volli; A. R. K. Gollakota; C. Shu. Science of the Total Environment 2021, 792, 148392. https://doi.org/10.1016/j.scitotenv.2021.148392.
14. M. L. B. Almeida, E. Ayres, F. C. C. Moura, R. L. Oréfice Journal of Hazardous Materials 2018, 346, 285-295. https://doi.org/10.1016/j.jhazmat.2017.12.033.
15. M. R. Páez, Y. Ochoa-Munoz, J. E. Rodriguez-Paez. Efficient removal of a glyphosate-based herbicide from water using ZnO nanoparticles (ZnO-NPs). Biocatalysis and Agricultural Biotechnology 2019, 22, 101434. https://doi.org/10.1016/j.bcab.2019.101434.
16. H. Chawla, S. Garg, J. Rohilla, A. Szamosvölgyi, A. Efremova, I. Szenti, P. P. Ingole, A. Sápi, Z. Kónya, A. Chandra, Visible LED-light driven photocatalytic degradation of organochlorine pesticides (2,4-D & 2,4-DP) by Curcuma longa mediated bismuth vanadate. Journal of Cleaner Production 2022, 367, 132923.

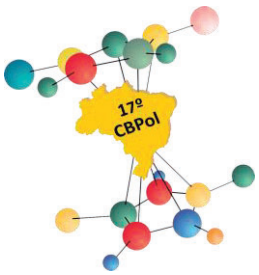

SYNTHESIS AND CHARACTERIZATION OF BACTERIAL CELLULOSE MEMBRANES INCORPORATED WITH ZINC OR SILVER NANOPARTICLES

Bruna Segat[1*], Izabel Cristina Nóvak[1,2], Geasi Lucas Martins[1,2], Michele Cristina Formolo Garcia[1], Karina Cesca[3], Denise Abatti Kasper Silva[1], Andrea Lima dos Santos Schneider[1,2], and Ana Paula Testa Pezzin[2]

1 - Department of Chemical Engineering, University of the Joinville Region (UNIVILLE), Joinville, SC, Brazil.
2 - Master's Program in Process Engineering, University of the Joinville Region (UNIVILLE), Joinville, SC, Brazil.
3 - Postgraduate Program in Chemical Engineering, Federal University of Santa Catarina (UFSC), Florianopolis, SC, Brazil
**brusegat@gmail.com*

Abstract - Bacterial cellulose (BC) has great potential to be used in several applications due to its excellent biocompatibility, high water retention capacity and structure that allows modifications. Thus, incorporating metallic nanoparticles (Nps) into BC can potentiate its characteristics, attributing antimicrobial properties to it. Silver (AgNp) and zinc (ZnNp) Nps are efficient antimicrobial agents. In this context, this work aimed to incorporate BC membranes with ZnNp or AgNp and characterize their properties. For this, membranes were synthesized and incorporated with zinc (BC/ZnNp) and silver (BC/AgNp) and then characterized by thermogravimetric analysis (TGA), x-ray diffraction analysis (XRD) and antimicrobial assay. The TGA showed a high residue content for the incorporated membranes, suggesting the incorporation of Nps, which XRD also confirmed. However, the membranes did not show antimicrobial activity due to the low concentrations incorporated.
Keywords: *Bacterial Cellulose. Antimicrobial Agents. Metallic Nanoparticles.*
Fundings: The authors are grateful for the financial support of UNIVILLE for the project.

Introduction

Many biomaterials are currently being studied, emphasizing biopolymers that, due to their characteristics, become suitable for various applications, such as industrial, biomedical, cosmetic, and food. Among the biopolymers there is bacterial cellulose (BC), a natural biomaterial that stands out for having superior properties and a nature that allows desired modifications [1]. Despite having the same chemical structure as plant cellulose, it isn't associated with hemicellulose and lignin, discarding an additional purification step and making it more industrially attractive [2]. In addition, BC membranes have good mechanical properties, high levels of crystallinity, high water retention capacity and excellent biocompatibility [3].

Even though BC is a biomaterial with several characteristics, it does not have antimicrobial properties. Still, its surface is rich in hydroxyl groups that allow the adsorption of metallic ions or metallic nanoparticles (Nps) [4-5]. In this context, metal particles and Nps associated with the BC membrane stand out as they show good antibacterial properties due to the significant contact area allowing more interactions with molecules [6]. There are many metal ions and Nps with antimicrobial activity that can be used, such as silver (Ag) and zinc oxide (ZnO) [7].

Silver and its compounds are well known to have efficient antimicrobial properties due to their large surface area, providing better contact with microorganisms [8]. In most studies, AgNp is considered non-toxic; however, a greater surface area can promote a more significant release of Ag^{+} ions, which are related to nanoparticle toxicity and antimicrobial action [9].

Zinc compounds have also been shown to be efficient antimicrobial agents, standing out for their nontoxicity at high concentrations, being exceptionally thermally stable and with a mechanism of action through the release of zinc ions (Zn^{2+}), interacting with the bacterial cell wall destroying the cellular integrity [7].
Thus, the present study aimed to evaluate the potential for incorporating silver and zinc Nps into BC membranes and to characterize them in terms of their properties. Different concentrations of suspensions were tested. BC membranes incorporated with Nps have potential applications in the medical field, such as dressings with antimicrobial properties. This work is an initial study of the development of these biomaterials to use them in such applications and to the state of the art.

Experimental

Preparation of BC Membranes

The bacterium *Komagataeibacter hansenii* ATCC 23769 was used to produce bacterial cellulose membranes. The Mannitol culture medium was used in the cell activation phase and membrane production phase, consisting of mannitol (20 g/L), peptone (5 g/L), yeast extract (5 g/L), phosphate disodium (2.7 g/L) and citric acid (1.15 g/L), being autoclaved at 121 ºC for 20 min. Cells were activated in an Erlenmeyer flask (125 mL) containing 50 mL of medium, incubated at 30 °C under static conditions for two days. Afterward, the inoculum was transferred to the culture medium at a rate of 20% (v/v) and kept at 30 ºC in static condition for nine days. The formed membranes were washed with distilled water and treated in 0.1 M sodium hydroxide (NaOH) for 1 h at 80 °C in a thermostatic bath. The membranes were submerged in distilled water, which was changed daily until the pH of the water reached neutrality. Subsequently, the membranes were autoclaved and stored in a refrigerator for the other procedures.

Incorporation of zinc nanoparticles and silver nanoparticles into the membrane

Suspensions of ZnNp or AgNp in distilled water at concentrations of 0.1% or 0.2% (w/v) were prepared in a beaker. Then, the suspensions were kept under magnetic stirring for 15 min and placed in an ultrasonic bath for 30 min for homogenization. To incorporate the Nps into BC, the BC membranes were previously manually pressed with absorbent paper to remove excess water and favor the absorption of the suspensions. The amount of water removed from the BC was quantified, then the membranes were soaked in a Nps suspension corresponding to the volume removed. The membranes were rotated every 6 h to ensure more homogeneous absorption of the suspensions, and after 48 h, the membranes had already absorbed the entire volume of the suspension. This test was conducted at room temperature.

Thermogravimetric Analysis (TGA)

The TGA was carried out in TA Instruments equipment, model TGA-Q50, to know the thermal stability of the biomaterials and the effects of the incorporations in the membranes. The samples were placed in a platinum sample holder and heated from 25 to 1000 °C at 10 °C/min under an inert atmosphere (N_2) to determine the mass loss.

X-ray Diffractometry (XRD)

The XRD was performed in MiniFlex600 equipment (SmartLab, Rigaku) using CuKα radiation, voltage 40 kV, 1.5 mA. The 2θ scatter angle ranges from 5° to 50° at 0.05°/s. This analysis was carried out to characterize the phases present in the incorporated membranes.

Antimicrobial Assay

To evaluate the antimicrobial activity of BC/ZnNp and BC/AgNp membranes were used Gram-negative bacteria *Escherichia coli* (ATCC 8735) and yeast *Candida albicans* (ATCC 6539), using the disk diffusion technique. The test microorganisms were pre-cultured for 24 h at 35 ºC in Brain

Heart Infusion (BHI) medium. Afterward, the microorganisms were diluted in a sterile 0.85% (w/v) saline solution until reaching the turbidity standard of 0.5 on the McFarland scale. Then, the microorganisms were uniformly plated in Petri dishes with Mueller-Hinton (MH) medium. Then, discs of BC, BC/ZnNp and BC/AgNp with 6 mm in diameter were distributed over the plates, and these were stored in an oven at 37 ºC for 24 h. After this period, the inhibition halos were analyzed.

Results and Discussion

Synthesis and Incorporation of Bacterial Cellulose Membranes

After nine days of culture, the formation of membranes at the liquid-air interface was observed. The formed membranes had a gelatinous, moldable and homogeneous appearance, in addition to a structure that was quite resistant to rupture by manual traction. BC membranes initially showed a slightly yellowish color due to residual compounds of the culture medium. After the purification step, they became colorless or opaque white, depending on the thickness of the membrane obtained. After ZnNp incorporation, the membrane acquired a whitish color compared to pure BC, a characteristic color of the ZnNp solution. While for incorporation with AgNp, a change in the color of the BC from translucent to yellowish was observed, indicating the incorporation of AgNp into the membrane.

Thermogravimetric Analysis (TGA)

Fig 1 shows the TG and DTG curves for membranes incorporated with ZnNp and AgNp. All membranes exhibited a slight loss of mass below 200 °C. This first stage corresponds to the loss of water adsorbed by the BC membrane [10].

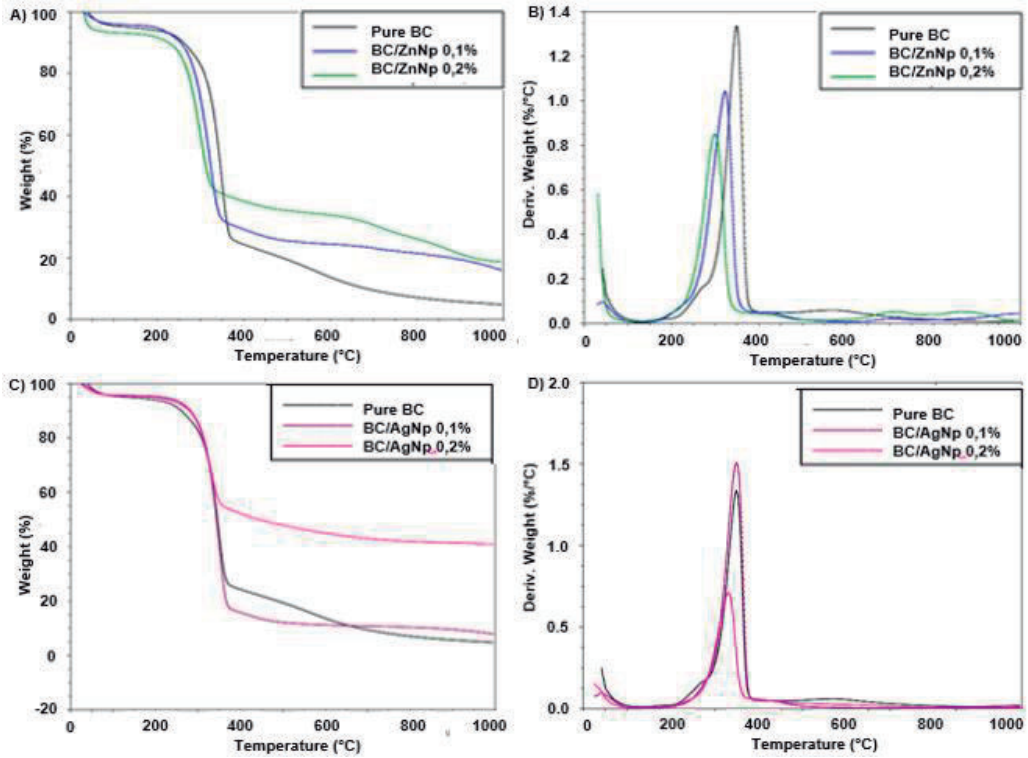

Figure 1 - A) TG and B) DTG curves for membranes incorporated with ZnNp and C) TG e D) DTG curves for membranes incorporated with AgNp.

A more accentuated second stage occurred around 300 ºC, also observed for all membranes. This stage is associated with cellulose degradation, including dehydration, depolymerization and decomposition of glucose units [11]. A third stage, referring to carbonaceous residues, was

identified only for the pure BC membrane, which occurred with a T_{peak} of 577 ºC and a mass loss of approximately 8%.
The incorporated membranes, except for the BC/AgNp 0.1%, demonstrated a temperature of maximum degradation (T_{peak}) of the second stage lower than the pure BC, as well as the percentage of mass loss, thus reporting a reduction in the thermal stability of the BC membranes when incorporated with AgNp [12].
The BC/ZnNp 0.1% and 0.2% membranes presented a fourth stage with a T_{peak} of 706 ºC, with a loss of 1% and 6% in mass, respectively. The degradation of carbonaceous residues (about 20%) extends to around 800 ºC; thus, it is believed that this fourth stage, observed only for BC/ZnNp, is about the degradation of carbonaceous residues since the temperature is within the suggested range as well as the percentage of mass loss [13].
It was found that the pure BC membrane had the lowest percentage of residue, approximately 4.79%. After a temperature of 1000 ºC, the residue can be composed of inorganic particles that have not degraded and organic material that has not been calcined by the inert atmosphere [14].

X-ray Diffractometry (XRD)
XRD was used to characterize the phases of the materials incorporated with ZnNp and AgNp (Fig 2). it is observed that the three characteristic peaks of cellulose are observed for all membranes at 2Θ = 14.4º, 16.7º and 22.5º [15]. Thus, there was the preservation of the diffraction pattern of BC in all membranes; however, it is observed the appearance of tenuous peaks for membranes BC/ZnNp 0.1 and 0.2%, BC/AgNp 0.1 and 0.2 %.

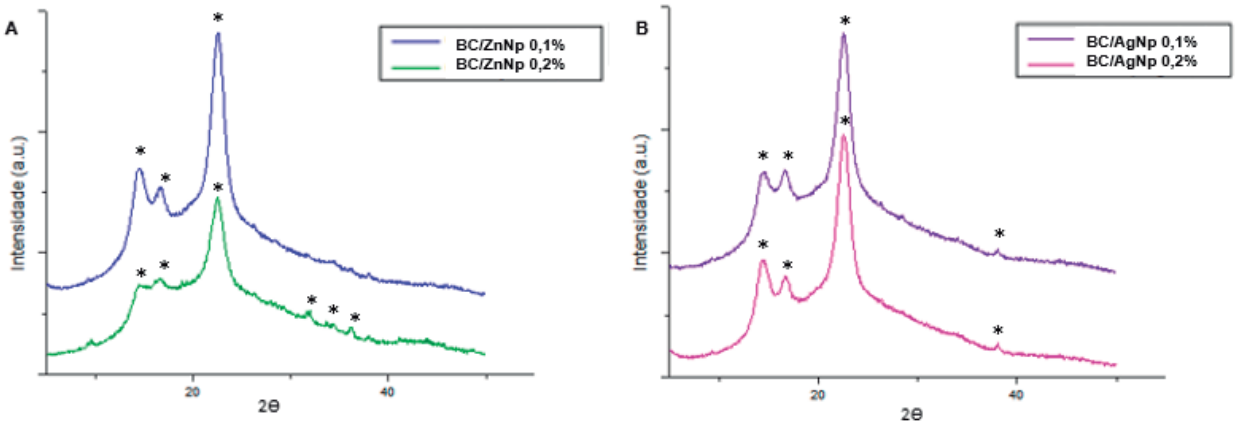

Figure 2 - X-ray diffraction of membranes A) BC/ZnNp and B) BC/AgNp

The BC/ZnNp 0.1% and 0.2% (Fig 2A) showed mild peaks at 2Θ = 32º, 34.3º and 36.1º, characteristic for zinc and consistent with the literature [16]. A peak appeared for membranes incorporated with AgNp, less intense at 2Θ = 38.4º [17]. Furthermore, the low intensity of these peaks suggests a low concentration of AgNp in the membrane.

Antimicrobial Assay
It wasn't possible to observe antimicrobial effect in the functionalized membranes. The pure BC membrane corresponded to expectations, not showing a halo of inhibition, as it does not have antimicrobial activity, justifying the need to incorporate metallic ions to prevent wound infections. [18]. This way, antimicrobial activity was expected for the BC/AgNp and BC/ZnNp membranes since the Nps are proven antimicrobial agents. Still, the absence of inhibition halos may be linked to the low concentration of Nps or possible agglomerations during the incorporation [16-17]. In addition, although the initial concentration of solutions with antimicrobial agents is known, it is not

known the exact amount that was absorbed by the membrane nor if the agents diffused into the culture medium.

Conclusions

The characterization analyses carried out showed the incorporation of Nps. The TGA showed a higher residue content for the incorporated membranes and XRD confirmed the presence of Nps in the membranes. However, the analyzes showed that the Nps were in low concentrations, mainly due to the low-intensity peaks in the XRD and the behavior similar to that of pure BC in the TGA, justifying the absence of an inhibition halo in the antimicrobial activity assay. New studies should be carried out with higher concentrations of Nps aiming at a better application of BC membranes.

References

1. Z. Hussain; W. Sajjad; T. Khan; F. Wahid. Cellulose 2019, 26, 2895–2911. https://doi.org/10.1007/s10570-019-02307-1
2. Y. Lee; S. An; E. Bae; H. Gwon; J. Park; S. Jeong; Y. Jeon; S. Lee; Y. Lim; J. Huh. Materials 2017, 10(3), 320; https://doi.org/10.3390/ma10030320
3. S. An; S. Lee; J. Huh; S. Jeong; J. Park; H. Gwon; E. Kang; C. Jeong; Y. Lim. Int. J. Mol. Sci. 2017, 18(11), 2236; https://doi.org/10.3390/ijms18112236
4. I.M.S. Araújo; R.R. Silva; G. Pacheco; W.R. Lustri; A. Tercjak; J. Gutierrez; J.R.S. Júnior; F.H.C. Azevedo; G.S. Figuêredo; M.L. Vega; S.J.L. Ribeiro; H.S. Barud. Carbohydrate Polymers 2018, 179; 341-349. doi: 10.1016/j.carbpol.2017.09.081
5. G.M. Olyveira; J.E.R. Chanfrau,; L.M.M. Costa; P. Basmaji; B. Ambrozini; E. Pizoni; A.C. Guastaldi. J. Bionanoscience, 2017, 11, 573-577. https://doi.org/10.1166/jbns.2017.1477
6. C.P. Gong; S.C. Li; R.Y. Wan. J Photochem Photobiol B, 2018,183, 137-141, doi: 10.1016/j.jphotobiol.2018.04.030.
7. A.P. Capelezzo; L.C. Mohr; F. Dalcanton; C.R.D.M. Barreta; M.A.P.M. Martins; M.A. Fiori; J.M.M. de Mello. Quím. Nova, 2018, 41(4), https://doi.org/10.21577/0100-4042.20170187
8. P. Mathur; S. Jha; S. Ramteke; N.K. Jain. Artif Cells Nanomed Biotechnol, 2018, 46(1), 115-126, doi: 10.1080/21691401.2017.1414825.
9. N. Durán; W.R. Rolim; M. Durán; W.J. Fávaro; A.B. Seabra. Quím. Nova 2019, 42(2), https://doi.org/10.21577/0100-4042.20170318
10. J.P.B. Souza, Bel. Monography, Federal University of Ceará, 2019.
11. A.F.S. Costa; F.C.G. Almeida; G.M. Vinhas; L.A. Sarubbo. Front. Microbiol. 2017, 8, https://doi.org/10.3389/fmiBC.2017.02027
12. M.R. Fischer; M.C.F. Garcia; A.L. Nogueira; L.M. Porto; A.L.S. Schneider; A.P.T. Pezzin. Matéria 2017, 22(1), https://doi.org/10.1590/S1517-707620170005.0270
13. R.T.A. Machado; A.B. Meneguin; R.M. Sábio; D.F. Franco; S.G. Antonio; J. Gutierrez; A. Tercjak; A.A. Berretta; S.J.L. Ribeiro; S.C. Lazarini; W.R. Lustri; H.S. Barud. Industrial Crops and Products 2018, 122, 637-646, https://doi.org/10.1016/j.indcrop.2018.06.048
14. A. Mocanu; G. Isopencu; C. Busuioc; O. Popa; P. Dietrich; L. Socaciu-Siebert. Scientific Reports 2019, 9, 17687. https://doi.org/10.1038/s41598-019-54118-w
15. L.R. Lima; D.B. Santos; M.V. Santos; H.S. Barud; M.A. Henrique; D. Pasquini. E. Pecoraro; S.J. L. Ribeiro. Quím. Nova 2015, 38 (9), https://doi.org/10.5935/0100-4042.20150131
16. A. Khalid; R. Khan; M. Ul-Islam; T. Khan; F. Wahid. Carbohydr Polym 2017, 164, 214-221; doi: 10.1016/j.carbpol.2017.01.061.
17. T. Maneerung; S. Tokura; R. Rujiravanit. Carbohydrate Polymers 2008, 72(1), 43-51, https://doi.org/10.1016/j.carbpol.2007.07.025
18. H.S. Barud; T. Regiani; R.F.C. Marques; W.R. Lustri; Y. Messaddeq; S.J.L. Ribeiro. Journal of Nanomaterials 2011, 721631, https://doi.org/10.1155/2011/721631

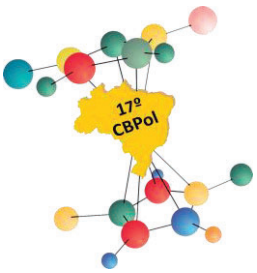

SYNTHESIS OF HYDROGEL BASED ON MODIFIED PECTIN AND POLY (VINYL ALCOHOL) FOR IMMOBILIZATION OF METALLIC NICKEL FOR CATALYTIC APPLICATIONS

Pâmela Macchion (IC)[1]*, Jaqueline F. de Souza (PG)[2], Henrique P. Mota (PG)[1] and André R. Fajardo (PQ)[1]

1 – Laboratório de Tecnologia e Desenvolvimento de Compósitos e Materiais Poliméricos (LaCoPol), Universidade Federal de Pelotas (UFPel), Campus Capão do Leão, Pelotas-RS, Brazil
(*) pamelamacchion10@gmail.com
2 – Laboratório de Bioinorgânica e Materiais Porfirínicos (LBMP), Universidade Federal de Santa Maria (UFSM), Santa Maria-RS, Brazil.

Abstract: Reactions catalyzed by nickel (Ni) supported on three-dimensional materials have been growing in the industrial and academic environment due to their inherent reactivity and recycling/reuse potential. In this research work, a hydrogel of pectin modified with amino groups (Pec-NH_2) and poly(vinyl alcohol) (PVA) was synthesized for supporting metallic Ni. The modification of pectin was confirmed by FTIR and thermal analyses, which also confirmed the hydrogel formation. Preliminary studies demonstrated that the Pec-NH_2/PVA hydrogels adsorb and stabilize Ni^{2+} ions, which can be reduced to Ni^0 in the presence of $NaBH_4$. It is envisaged that the heterogenization of Ni could be helpful to increase its catalytic performance, for instance, in cross-coupling reactions.

Keywords: *Heterogeneous catalysis; transition metal; nickel; hydrogel; organic synthesis.*

Introduction

Over the years, catalysts gained notoriety in the academic and industrial fields due to their interesting characteristics. In short, the catalysts increase the speed of chemical reactions without being consumed. Besides, they reduce the generation of secondary and undesirable products [1,2]. Reactions mediated by the catalysts (i.e., catalysis) are classified into homogeneous and heterogeneous. Homogeneous catalysts are those that have the same phase as the reaction mixture. As they have a large contact area to interact with the reagents, the reactivity of these catalysts is advantageous. However, homogeneous catalysts are difficult to separate from the reaction medium. As the procedure requires several steps for complete purification/regeneration, the separation becomes time-consuming and often unfeasible [2]. That way, heterogeneous catalysts have a different phase of the reaction mixture and, therefore, they present easier separation and the cheapest treatments for regeneration. These features endow heterogeneous catalysis with a greener character. Researchers involving transition metals as homogeneous and heterogeneous catalysts have become increasingly relevant in the academic field. The fact that such metals have incomplete d orbitals makes it easier to add or remove electrons from these regions during the reaction [2,3].

Among the metals usable in catalysis, nickel (Ni^{2+}) has proved to be an excellent catalyst in organic reactions with low-cost compared to noble metals [4]. Despite numerous studies using transition metals as homogeneous catalysts, the idea of using them supported on solid materials has become more advantageous, since, as mentioned earlier, heterogeneous catalysts can be recovered and reused more easily. Currently, there are several types of support for these metals, such as zeolites, ceramics, polymers, and others [5]. Among these supports, hydrogels have become promising, as

these three-dimensional solids consist of hydrophilic polymer chains that stabilize the metals, avoiding their agglomeration. This feature facilitates the support of the metal in the hydrogel structure [2,6]. Analyzing the polysaccharides currently used as the basis of these hydrogels, pectin (Pec) provided remarkable and advantageous characteristics. Due to its numerous carboxyl (–COOH) and hydroxyl (–OH) groups, Pec can increase reactivity by derivatization. According to Surjyakanta et al., 2017. [7] by modifying Pec with amino groups (–NH_2), there is, in fact, an improvement in reactivity, which benefits both the immobilization of transition metals and the crosslinking of the material [7,8]. The association of Pec with synthetic polymers like poly(vinyl alcohol) (PVA) allows for obtaining hydrogels with superior properties. PVA chains can form physically crosslinked networks due to hydrogen bonds (intra and intermolecular), enabling additional reinforcement without using external chemical crosslinkers [9].

Based on this information, this work aims to develop a hydrogel based on PVA and Pec modified with amino groups (Pec-NH_2) to act as a solid support for metallic Ni. It is expected that the heterogeneous catalyst prepared in this work be useful in organic reactions (e.g., Suzuki cross-coupling reaction) [10].

Experimental

Synthesis of Pec-NH_2 derivative: At first, raw Pec was de-esterified following the methodology proposed by Xiao et al. [11]. The product was labeled as Pec-des. Next, for the modification with amino groups, Pec-des (1.0 g) was added to a beaker containing distilled water (15 mL) at 60 °C and stirred until complete solubilization. Afterward, *N*-hydroxy succinimide (NHS) (0.288 g) and 1-ethyl-3-[3-dimethylami-nopropyl]-carbodiimide (EDC) (0.5 g) were added to the reaction mixture, which stirred at 25 °C for 0.5 h. Then, ethylenediamine anhydrous (EN) (2.0 mL) was added to the system and left under stirring for 8 h at 25 °C. Finally, the solution was dialyzed for 12 h against water, frozen (-20 °C, 12 h), and lyophilized (-50 °C, 24 h).

Preparation of Pec-NH_2/PVA hydrogel: Pec-NH_2 (0.833 g) was added to a beaker containing distilled water (25 mL) at 60 °C and solubilized. In parallel, PVA (0.833 g) was solubilized in distilled water (25 mL) at 90 °C. Then, both solutions were mixed (0.5 h) at room temperature, and the pH of the resulting mixture was adjusted (pH ~ 4). Under previously specified conditions, glutaraldehyde (80 µL) was added to the mixture under stirring (0.5 h) to promote the chemical crosslinking. Afterward, the Pec-NH_2/PVA mixture was subjected to 6 cycles of freezing and thawing (1 h thawing and 2 h freezing), and finally, the obtained hydrogel was lyophilized (-50 °C, 48 h).

Immobilization and in situ reduction of Ni: Standard solutions of $NiCl_2$ (8 g/L) in distilled water were prepared. The Pec-NH_2/PVA hydrogel (50 mg) was added to an Erlenmeyer flask containing the Ni^{2+} solution (50 mL) and left on an orbital shaking (100 rpm) for 12 h. The Ni^{2+} loaded hydrogels (Pec-NH_2/PVA@Ni^{2+}) were washed with distilled water and dried in an oven (40 °C, 24 h). Finally, Pec-NH_2/PVA@Ni^{2+} hydrogels were soaked in a $NaBH_4$ solution (0.05 mol/L) for 4 h to reduce the Ni^{2+} ions. The Pec-NH_2/PVA@Ni hydrogel was washed with distilled water and oven-dried (40 °C, 24 h).

Results and Discussion

The characterization of the precursor materials used for the synthesis of hydrogels and their modifications were carried out using the FTIR technique. In Fig 1a, there are the spectra of Pec, Pec-des, and Pec-NH_2. Firstly, characteristic bands were observed in the Pec spectrum, such as at 3388, 2938, 1742, and 1645 cm^{-1} referring to the stretching of the bonds O–H, C–H, C=O of ester, and C=O of free carboxylic groups, respectively [12]. After the de-esterification process, the Pec-des spectrum showed some modifications, such as shifting the O–H stretch band to a higher wavenumber (3388 to 3434 cm^{-1}). Also, there were reductions in the intensity of the C–H stretch band at 2938 cm^{-1} and the C=O ester stretch at 1742 cm^{-1}. Such modifications may be inferring that the methodology used for de-esterification was efficient [13]. After functionalization with EN, the Pec-NH_2 spectrum again

showed characteristic bands of Pec with some changes. The band at 3434 cm^{-1} was sharpened and shifted to a lower wavenumber (3388 cm^{-1}), suggesting a decrease in the –OH groups (hydroxyl and carboxyl). The band at 1645 cm^{-1} showed greater intensity when compared to the band at 3388 cm^{-1}, characterizing the contribution of the C=O amide stretching. Furthermore, the appearance of the band at 1564 cm^{-1} refers to the N–H bending. These findings highlighted here so far confirm the functionalization of Pec-des [7]. The degree of functionalization was also calculated using a titration technique described by Ren et al., 2019. [14], which is based on free –COOH groups. A functionalization degree of ~67% was determined, which means that more than half of the free –COOH groups of Pec-des were functionalized, forming a $–COONH(CH_2)_2NH_2$ moiety. In Fig 1b. there are the spectra recorded for the precursor polymers and the Pec-NH_2/PVA hydrogel. First, in the PVA spectrum, it is possible to observe the bands in the regions of 3420 and 1417 cm^{-1}, referring to the stretching and bending of the O–H bond, respectively. The bands at 2934, 1090, and 810 cm^{-1} are attributed to the C–H, C–O, and C–C stretching, necessarily in that order [9]. After synthesis of the hydrogel, some bands reappear; however, with some modifications. The band at 3388 cm^{-1} observed in the previous spectrum was shifted to a higher wavenumber (3445 cm^{-1}). Besides, the band referring to the O–H bending bond was shifted to a higher wavenumber (from 1410 to 1450 cm^{-1}). These modifications may represent intramolecular (PVA–PVA) and intermolecular (Pec-NH_2–PVA) interactions via hydrogen bonds formed during the freeze-thaw process [15]. The band around 2938 cm^{-1} referring to the C–H stretching showed an enhancement in its intensity compared to the band at 3445 cm^{-1}. This change in the spectrum may be related to the presence of additional CH_2 groups due to the crosslinking with glutaraldehyde. At 1564 cm^{-1} it is possible to observe the band referring to the N–H bending, which was less intense. Finally, the shoulder-like band at 1700 cm^{-1} corresponds to the C=N bond, these points confirming chemical crosslinking [16]. Together, the FTIR data confirm the formation of a dual-crosslinked network in the Pec-NH_2/PVA hydrogel.

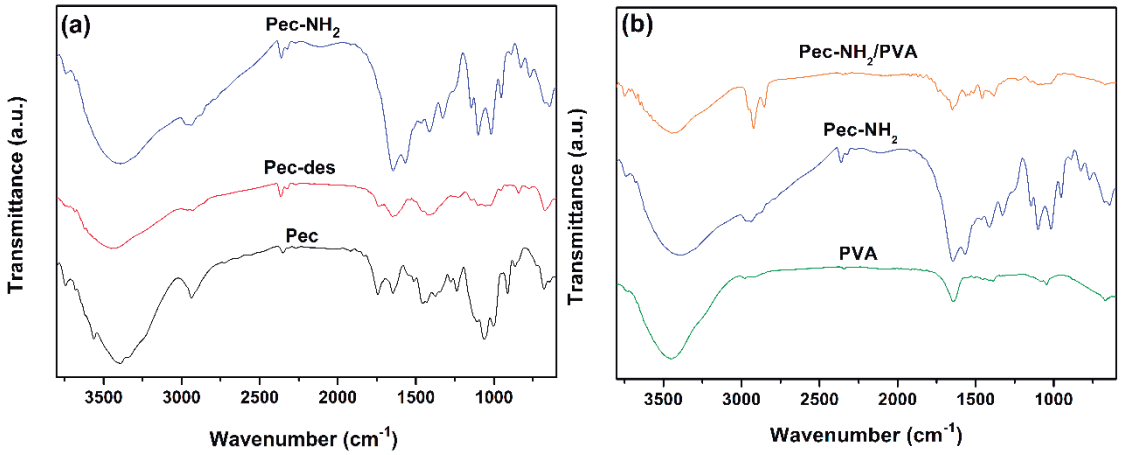

Figure 1. (a) FTIR spectra of Pec, Pec-des and Pec-NH_2; (b) spectra of PVA, Pec-NH_2 and Pec-NH_2/PVA.

The modification of Pec with the amino groups and obtaining of the Pec-NH_2/PVA hydrogels were characterized by the thermogravimetric technique (TGA) and its first derivative (DTG), shown in Figs. 2a-d. First, the TGA curve of Pec exhibited three main stages of weight loss. The first stage shows a weight loss of 7%, which occurred in the range of 50 to 100 °C. This stage is related to the elimination of water present in the sample. Together, the second and third stages imparted a weight loss of approximately 70% at maximum temperatures of 240 and 315 °C, respectively [12]. The Pec-des thermogram also showed three defined weight loss stages. The first stage shows a loss of 10% and occurred in the temperature range of 50–110 °C, referring to the removal of water from the sample. The second stage showed a maximum temperature of 140 °C (weight loss of 8%), and it is associated with the decarboxylation of pectin. The last stage occurred with a maximum of 230 °C, representing a mass loss of approximately 30%. In this range, there was thermal decomposition of

pectin [17]. There is a difference in the thermal regions where mass losses occur when Pec and Pec-des are compared, and this fact can be attributed to the elimination of most of the ester groups [11]. For the Pec-NH_2 thermograms, the stage due to the weight loss of the –COOH groups was attenuated, and an additional stage of observed. This stage may be associated with thermal degradation of the functionalized amino portions of Pec-NH_2, centered at a temperature of 186 °C. As discussed in other works, the insertion of amino groups reduces intramolecular and intermolecular hydrogen bonds, which explains a smaller residue at the end of the heating process [17]. The TGA curve of PVA exhibited four weight stages. The first represents a weight loss of 5%, occurring in the temperature range of 100 to 189 °C due to the elimination of water. The second stage imparted a weight loss of 62%, with the maximum occurring at the temperature of 265 °C. At this stage, the elimination of hydroxyl groups occurs, which leads to the formation of polyenes [9]. The third stage represented a weight loss of 17%, occurring at a maximum temperature of 430 °C due to the degradation of polyene by Diels-Alder cyclization and radical reactions. The last stage occurs above 480 °C causing a 10% weight loss. In this stage, the decomposition of carbonaceous fractions of the PVA takes place [9]. When evaluating the influence of the heating process on the Pec-NH_2/PVA hydrogel, three stages of weight loss are observed in different temperature regions regarding its precursor materials. In the first stage, there is the elimination of free water entrapped in the hydrogel matrix. This weight loss is 8% and occurs in a temperature range of 60–120 °C. In the second stage, 55% weight loss occurred due to the elimination of the PVA hydroxyl groups, degradation of the functionalized amino groups of Pec-NH_2, and part of the polysaccharide chains. This stage occurs at a maximum of 276 °C [18]. Finally, the last stage occurred with a maximum of 421 °C and 9% of weight loss. Such loss is due to the thermal decomposition of carbonaceous fractions of both PVA and modified pectin [18].

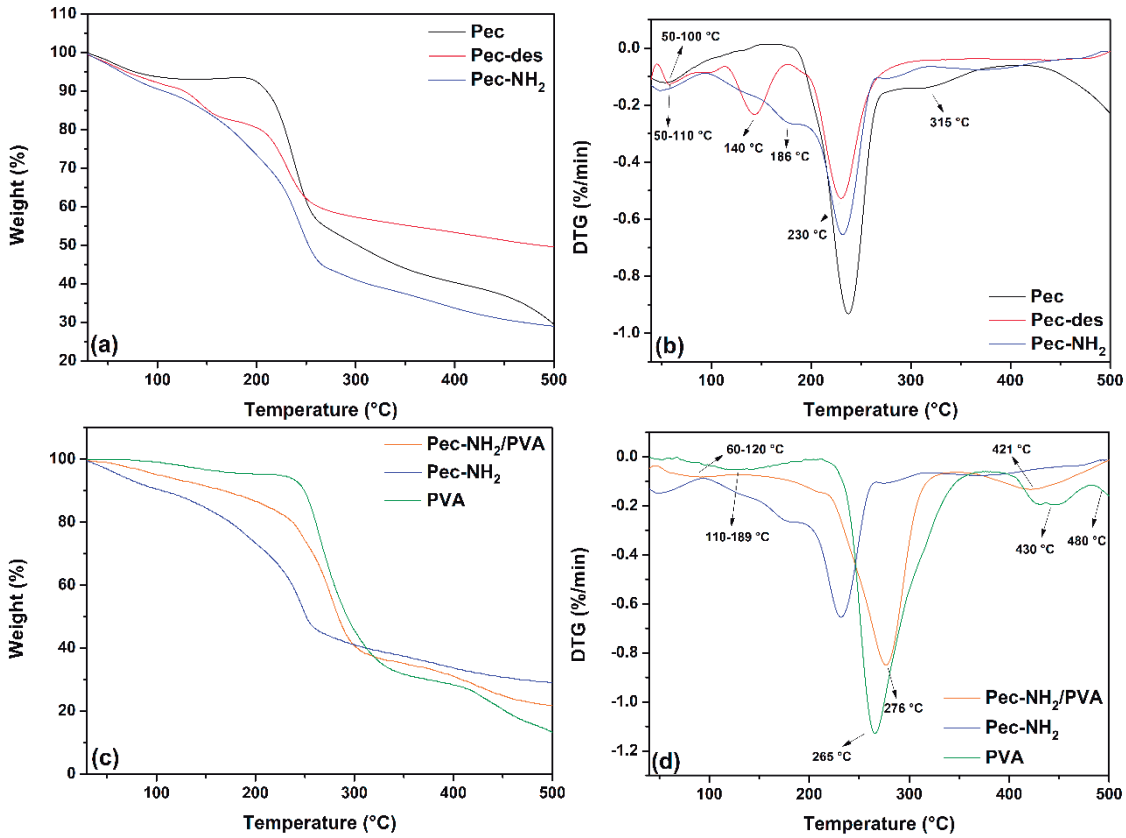

Figure 2. (a) TGA and (b) DTG curves of Pec, Pec-des and Pec-NH_2. (c) TGA and (d) DTG curves of PVA, Pec-NH_2 and Pec-NH_2/PVA; (d) DTG of PVA, Pec-NH_2 and Pec-NH_2/PVA.

Conclusions

In this present study, to improve the reactivity of Pec and assist in the immobilization of metallic Ni in the material, the modification of this polymer with amino groups was done. Also, PVA was used to enhance the hydrogel reinforcement without the use of external crosslinkers. It is worth mentioning that, according to the FTIR and TGA/DTG results, it was possible to observe that crosslinking of the hydrogel was made successfully. From future perspectives, the obtained hydrogel will be characterized to present other relevant properties, such as analysis of the amount of nickel adsorbed, crosslinking density, stability through mechanical analysis, and catalytic activity in Suzuki coupling reactions. Finally, it is extremely important to emphasize that reuse tests should be performed to complement the efficiency of the heterogeneous catalyst.

References

[1] M. Ashraf, M. S. Ahmad, et al. Coordination Chem. Rev. 2023, 478, 214928. https://doi.org/10.1016/j.ccr.2022.214928.

[2] GI. Dzhardimalieva, AK. Zharmagambetova, et al. Kinectis and Catalysis 2020, 61, 198-223. https://doi.org/10.1134/S0023158420020044.

[3] X. Liu, F. Liu. Carbohydr. Polym. 2023, 310, 120726. https://doi.org/10.1016/j.carbpol.2023.120726.

[4] JH. Park, E. Hong, et al. Korean J. Chem. Eng. 2017, 34, 2610–2618. https://doi.org/10.1007/s11814-017-0164-4.

[5] L. Li, Z. Xu, et al. Ceram. Int. 2022, 48, 11, 15236-15242. https://doi.org/10.1016/j.ceramint.2022.02.054.

[6] J. Xu, X. Liu, et al. Eur. J. 2018, 100, 86-95. https://doi.org/10.1016/j.eurpolymj.2018.01.020.

[7] S. Rana, S. B. Jonnalagadda. Catal. Commun. 2017, 92, 31-34. https://doi.org/10.1016/j.catcom.2016.12.023.

[8] S. E. Rafiea, H. Ibrahimb, et al. Egypt. J. Chem. 2021, 64, 581-591. http://doi.org/10.21608/ejchem.2020.43996.2892.

[9] C. Y. Wong, W. Y. Wong, et al. React Funct Polym. 2022, 171, 105-160. https://doi.org/10.1016/j.reactfunctpolym.2022.105160.

[10] B. A. Baviskar, P. V. Ajmire, et al. Sustain. Chem. Pharm. 2023, 32, 100953. https://doi.org/10.1016/j.scp.2022.100953.

[11] X. Hua, H. Yang, et al. Food Biosci. 2018, 23, 91-99. https://doi.org/10.1016/j.fbio.2018.03.011.

[12] E. F. Lessa, M. S. Gularte, et al. Carbohydr. Polym. 2017, 157, 660-668. https://doi.org/10.1016/j.carbpol.2016.10.019.

[13] J. Wu, M. Yin, et al. J. Mater. Sci. 2020, 55, 12607-12620. https://doi.org/10.1007/s10853-020-04898-8.

[14] H. Ren, E. Cunha, et al. Nanoscale Adv. 2019, 1, 1432-1441. https://doi.org/10.1039/C8NA00280K.

[15] S. Rehmani, M. Ahmad, et al. Polym. Bull. 2017, 74, 737–761. https://doi.org/10.1007/s00289-016-1743-y.

[16] O. Akakuru, B. Isiuku. J. Phys. Chem. Biophys. 2017, 7, 1-7. https://doi.org/10.4172/2161-0398.1000256.

[17] A. R. Fajardo, L. C. Lopes, et al. Carbohydr. Polym. 2012, 87, 1950-1955. https://doi.org/10.1016/j.carbpol.2011.09.096.

[18] M. Sari, J. Kaban, et al. Adv. Mater. Lett. 2020, 2267, 1. https://doi.org/10.1063/5.0016521.

SYNTHESIS, SPECTROSCOPIC AND THERMAL STUDY OF NETWORKS CONTAINING POLY(STYRENE-CO-MALEIC ANHYDRIDE)

Ana M. Rocco*, Anna D.F.F. Monsores, Beatriz D.A. Ribeiro and Luis H.C. Lacerda

Federal University of Rio de Janeiro (UFRJ), School of Chemistry,
Conducting Materials and Energy Group, Rio de Janeiro – RJ, Brazil
amrocco@eq.ufrj.br

Abstract - Through the reaction of Bisphenol A diglycidyl ether with the curing agent 4.4'diaminodiphenyl-sulphone in the presence of the Poly(styrene-co-maleic anhydride) was obtained a polymeric network system. FTIR indicates the DGEBA/DDS reticulation by the disappearance of the characteristic absorption of the epoxy ring at 912 cm^{-1}. It also suggests the opening of the PSCAM anhydride molecular structure ring in all SIPN samples, indicated by the disappearance of the two characteristic absorptions at 1774 cm^{-1} and 1850 cm^{-1}, assigned as the symmetric and asymmetric stretching vibrations of the anhydride carbonyl group. The TGA and DTG analyses showed the samples' thermal stability with the onset of decomposition above 280 ºC and the presence of water up to approximately the same temperature, serving the polymeric system for medium-temperature electrolyte applications. DSC observed the absence of thermal processes at the temperature of using membranes in PEMFC. This work suggests that the system obtained might be promising for future applications in studying electrolytes for PEMFC.
Keywords: *Poli(styrene-co-anhydride maleic, Bisphenol A diglycidyl ether, network, membrane, fuel cell.*
Fundings: FAPERJ: E-26/010.000.982/2019

Introduction

Currently, the research and development of sustainable, efficient, and renewable means of energy have become constant, and among the proposals for replacing an energy source from the combustion of fossil fuels are fuel cells (FC). Proton exchange membrane fuel cells (PEMFC) are electrochemical conversion devices dependent on the constant and external supply of oxidizing (O_2) and reducing (H_2) agents for their performance [1]. PEMFC performance is directly related to its component membrane, which is a solid electrolyte responsible for ionic transport and also serves as a barrier to prevent the crossover of methanol or H_2 to the cathode reducing FC activity [2]. DuPont's Nafion®, since the initial studies, is the most widely used polymeric membrane in PEMFC; its proton conductivity can achieve around 10^{-2} Ω cm^{-1} [3] in a hydrated condition at high temperatures. A hydrophobic polytetrafluoroethylene backbone chain can characterize the molecule, which is regularly spaced nearby the perfluorovinyl ether side chains and has a copolymer molecular architecture. At higher temperatures, the membranes undergo substantial dehydration; their ionic conductivity decreases, and the performance characteristics of PEMFCs fall. Platinum catalyst poisoning by carbon monoxide decreases at temperatures higher than 100 °C [4, 5], so operating de FC at higher temperatures is desirable. Semi-interpenetrating polymeric network systems (SIPN) are still statistically understudied today. SIPNs have structural advantages, improving the electrochemical stability of the membrane and facilitating the exchange of the linear component with suitable commercial polymers for ionic conductivity improvement. Depending on the used polymers and crosslinking agent, it is possible to proceed with the sulfonation of the SIPN to simulate the nanostructure of Nafion®, with a hydrophobic-hydrophilic molecular arrangement,

plus the sulfonic groups that can form tubular structures to ionic conduction. These molecular modifications can become the system prone to the crossover of the gas/or ethanol. It is necessary to have the right balance between hydrophilic-hydrophobic sites, water absorption capacity, and polymeric porosity.

Our group has worked with the synthesis of the semi-interpenetrating polymer network (SIPN) for use on membranes, starting with Bisphenol A diglycidyl ether (DGEBA) and the curing agent triethylenetetramine (TETA) or 4.4'diaminodiphenyl-sulphone (DDS) and highly hydrophilic commercial linear polymers. The present work aims to synthesize a series of DGEBA/DDS/ Poly(styrene-co-maleic anhydride) networks with an expectation to achieve systems like semi-interpenetrating or interpenetrating polymer networks for future study of a conductive protonic membrane.

Experimental

SIPN synthesis

The synthesis methodology and obtaining polymeric membranes by casting were based on the group's previous work [1]. It was necessary to adjust the solvent, replacing ethanol with acetone, due to the poor solubility of PSCAM in an alcoholic medium. Synthesis used 30 mL of acetone, and the molar ratio of DGEBA and DDS was maintained at 1:1, with a constant mass of 0.5000 g and 0.3646 g, respectively, varying mass amounts of PSCAM (33, 38, 41, 47, and 50 mass %). Fig. 1 shows the structures.

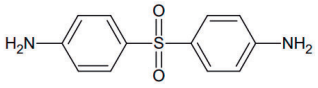

4.4'diaminodiphenyl-sulphone (DDS)

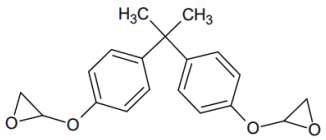

Bisphenol A diglycidyl ether (DGBA)

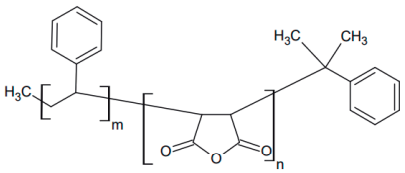

Poly(styrene-co-maleic anhydride) - (**PSCAM**)

Figure 1 - Structural formulas of DGEBA, DDS e PSCAM

Infrared Vibrational Spectroscopy

The vibrational infrared spectroscopy (FTIR) characterized the synthesized SIPN membranes to monitor the crosslinking reaction. A Nicolet Magna-IR760 analyzed the spectral region from 400 to 4000 cm^{-1} with 128 scans and 1 cm^{-1} resolution on transmittance mode.

Simultaneous thermal analysis (TGA/DSC)

Thermogravimetric analysis (TGA) and differential scanning calorimetry (DSC) studied the thermal behavior and stability of the synthesized membranes. Measurements were performed simultaneously on SDTQ600 equipment (TA Instruments) with a complementary DSC heat flux sensor. About 5 mg of sample in alumina crucibles were employed, using a heating rate of 10 ^{o}C/min from room temperature to 1000 °C under nitrogen flow (100 mL/min). The samples were previously dried and kept in a desiccator.

Results and Discussion

Infrared Vibrational Spectroscopy

The PSCAM-based membrane formed films with dimensional stability without visual roughness (Fig 2a). Fig. 2 shows SIPNx's spectra (x= 33, 38, 41, 47, and 50 PSCAM mass %). The results confirmed the DGEBA crosslinking through the disappearance of the band at 912 cm^{-1} - characteristic of the epoxy ring - and the emergence of a band at 1186 cm^{-1}, associated with the formation of ether groups during the reaction of curing and a low-intensity band at 1635 cm^{-1} attributed to OH stretching. Bands referring to the symmetric and asymmetric stretching of the sulfone group ((O=S=O)) of the DDS were identified in the regions between 1200-1070 and 1350-1250 cm^{-1}, respectively, evidencing the formation of crosslinked polymer for all synthesized SIPN. The spectra indicated the anhydride conversion concerning the PSCAM molecular structure in SIPN. The disappearance of anhydride signals at 1860 and 1776 cm^{-1} indicates anhydride conversion. The additional band at 1708 cm^{-1} was assigned to the formed carbonyl vibration of a carboxylic acid, as observed by Brusch and coworkers [6].

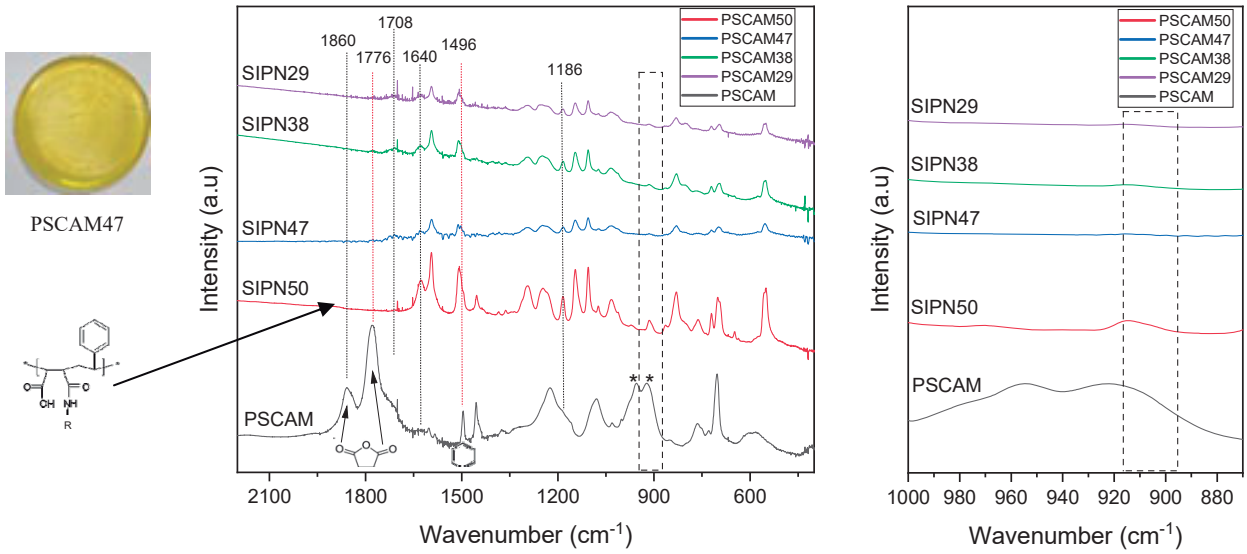

Figure 2 - (a) Macrograph image of the SIPN47 (PSCAM 47%) membrane and detail of the anhydride ring opening, (b) SIPNx's FTIR spectra from 400 to 2100 cm^{-1} and (b) magnification of spectral region between 860 and 1000 cm^{-1}

Thermal analysis

Fig. 3 shows for SIPNx membranes (a) TGA and (b) DTG curves from 100 to 1000 °C, and Fig. 4 shows the DSC curves in the temperature ranges (a) 15 a 1000 °C e (b) 15 a 500 °C.

The membranes showed thermal stability greater than 280°C, and all samples showed water retention at temperatures between 90 and 250°C, according to the TGA/DTG analyses in the first stage of mass loss. The TGA/DTG analysis indicated the onset of polymeric degradation at 290°C, which extended to approximately 500°C, depending on the sample composition. TGA curves, additionally, show a displacement of the onset of thermal decomposition of the synthesized SIPN samples, compared to their precursors, which becomes more evident in the DTG curves (Fig. 3b). In the work carried out by Chen and coworkers [7], where the authors investigated the PSCAM reticulation with N-phenylamino methyl POSS, authors associate this behavior with network formation, which increased thermal stability. The lost water mass, verified as more significant than expected, can be due to water from the hydrolysis of PSCAM anhydride groups, resulting from the probable reaction [8]. Future 13C NMR analysis would be necessary to confirm these observations.

DSC analysis revealed two exothermic peaks in the PSCAM curve, at 380°C and 710°C, referring to the exit of volatile groups and the phase transition of polymer melting. Membranes with 38, 47, and 50% PSCAM showed exothermic peaks at 400 and 750°C, the first associated with the fusion of the DGBA/DDS polymeric network and the second referring to the fusion of PSCAM or its reaction product. In membranes 33, 41, and 44% PSCAM, a single peak is observed, associated with the fusion of the network, mainly the PSCAM volatile grouping. DSC curves did not indicate thermal events up to 290 ^{o}C or in the membrane application range (up to 150 ^{o}C). The chemical structure of the polymeric system needs to be confirmed by additional spectroscopic analyses.

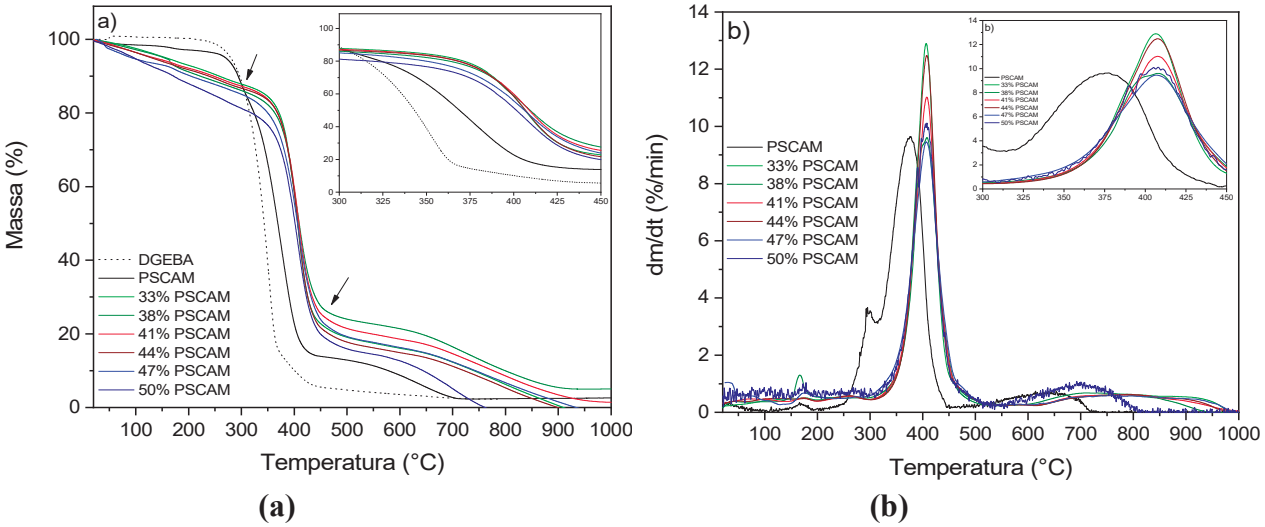

Figure 3 - TGA (a) and DTG (b) curves for SIPNx membranes from 100 to 1000 ^{o}C

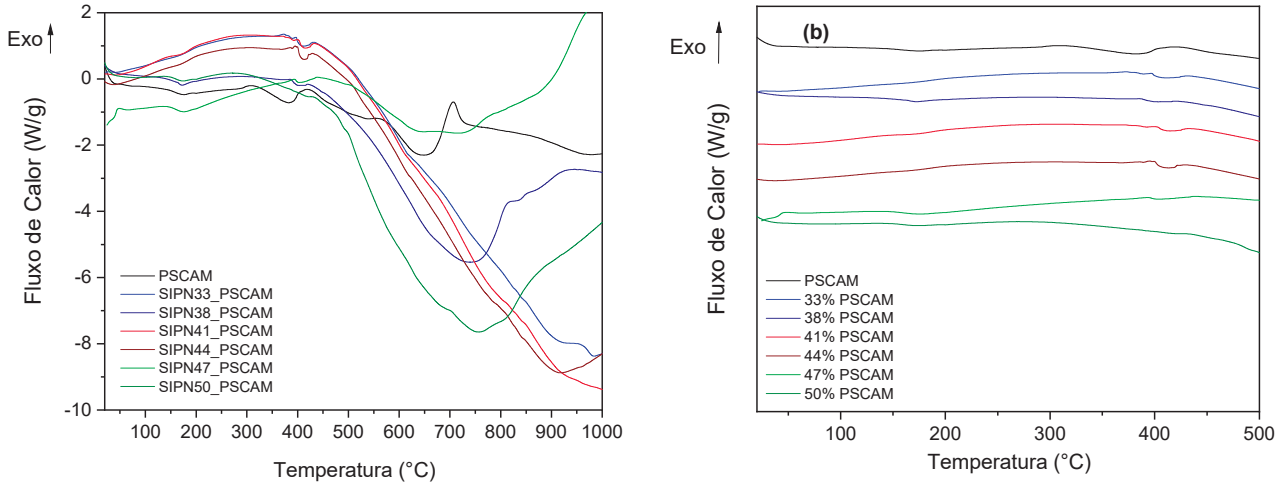

Figure 4 - DSC curves for SIPNx membranes in the temperature ranges (a) 15 a 1000 ^{o}C e (b) 15 a 500 ^{o}C.

Conclusions

SIPN samples based on DGEBA/DDS and PSCAM were synthesized, and membranes with dimensional stability were obtained. FTIR indicates the DGEBA/DDS reticulation, as expected. It also suggests the opening of the PSCAM anhydride molecular structure ring in all SIPN samples, indicated by the disappearance of the two characteristic absorptions at 1774 cm-1 and 1850 cm-1, assigned as the symmetric and asymmetric stretching vibrations of the anhydride carbonyl group. Solid 13C NMR studies are necessary to elucidate the fundamental nature of the system as a SIPN or IPN.

The TGA and DTG analyses showed the samples' thermal stability with the onset of decomposition above 280 ºC and the presence of water up to approximately the same temperature, serving the polymeric system for medium-temperature electrolyte applications. DSC observed the absence of thermal processes at the temperature of using membranes in PEMFC. The present work indicated that the system studied might be promising for future applications in studying electrolytes for PEMFC.

Acknowledgments
FAPERJ: E-26/010.000.982/2019

References

1. J.S. Menezes; F.A. Loureiro; V.M.A. Calado; A.M. Rocco Journal of Thermal Analysis and Calorimetry 2022, 147, 9469. https://doi.org/10.1007/s10973-022-11211-z.
2. F.A. Zakil; S.K. Kamarudin; S. Basri Renew Sust Energ Rev. 2016; 65, 841. https://doi.org/ 10.1016/j.rser.2016.07.040. D.
3. G. Alberti, M. Casciola; L. Massinelli; B. Bauer J Membrane Sci. 2001, 185, 73. https:// doi. org/ 10. 1016/ S0376- 7388(00) 00635-9.
4. P.J. Pérez-Díaz; A. Medina-Ramírez; I.G. Esquivel; G.G. Ruiz; B. Ruiz-Camacho Ionics 2021, 27, 1813. https:// doi. org/ 10. 1007/ s11581- 021- 03922-4.
5. A.M. Rocco AM; K.V. Melo; C.J.A. Mota; M.V. David; I.N. Souza Ionics 2019, 25, 253. https:// doi. org/ 10. 1007/s11581- 018- 2572-9.
6. M. Bruch; D. Mader; F. Bauers; T. Loontjens; R. Mulhaupt Journal of Polymer Science Part A: Polymer Chemistry 2000, 38, 1222. https://doi.org/10.1002/(SICI)1099-0518(20000415)38:8<1222::AID-POLA5>3.0.CO;2-Z.
7. P.C. Chen; X. Huang; Q. Zhang; K. Xi; X. Jia Polymer 2013, 54, 1091. http://dx.doi.org/10.1016/j.polymer.2012.12.047
8. G.D. Guerra; N. Barbani; M.L.Coluccio; C. Cristallini J Appl Biomater Biomech 2006, 4, 97. https://doi.org/10.1177/228080000600400204.

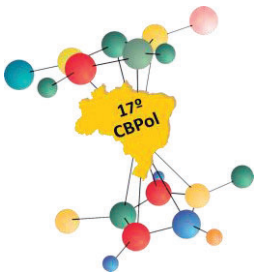

THE CO-COMPATIBILIZATION EFFECT OF NANOFILLERS IN IMMISCIBLE SYSTEMS BASED ON POLYETHYLENE AND POLYESTER FROM OFFSHORE PLATFORMS

Ian dos S. Costa[1], Ana Lúcia N. da Silva[1], Renan H. G. Almeida[1], Bianca R. Mandarino[1], Laiza M. Racca[2].
1 – Instituto de Macromoléculas Professora Eloisa Mano – Universidade Federal do Rio de Janeiro (IMA/UFRJ), Rio de Janeiro, RJ, Brazil.), São Paulo, SP, Brazil ianscosta@ima.ufrj.br
2 – Centro de Tecnologia da Indústria Química e Têxtil (SENAI CETIQT), Rio de Janeiro, RJ, Brazil

Abstract – Polymers blends are a class of materials that arouse the interest of several industrial sectors due to the possibility of balancing properties that are not found in pure polymers. Most polymeric systems are immiscible and need compatibilization to present attractive characteristics to the market. In face of this, the work has as motivation to generate new functional composites to the packaging market through the compatibilization of the immiscible system between high-density polyethylene (HDPE) and PET coming from anchorage cables waste. The work evaluated the compatibilizing effect of HDPE grafted with maleic anhydride and calcium nanocarbonate between the phases of the blends, as well as the co-compatibilizing effect. Such evaluation was carried out through thermogravimetric analysis (TGA), differential scanning calorimetry (DSC) and Melt Flow Index (MFI). The morphology of the samples was observed through scanning electron microscope (SEM).

Keywords: *Polymer blends, polyethylene, polyester, nanofillers.*

Introduction

Polymer blends are versatile, chemically stable, lightweight, and cost-effective materials. However, their poor miscibility often leads to non-homogeneous distribution and weak adhesion, resulting in low mechanical properties. This study focuses on producing packaging materials using an immiscible system of high-density polyethylene (HDPE) and recycled polyester (PET) from offshore platform anchoring cables. Different compatibilization processes, including co-compatibilization, are evaluated to enhance material properties. The research aims to develop functional materials with improved mechanical properties, economically attractive as an alternative to developing entirely new matrices. The study also addresses environmental concerns by utilizing recycled resins and evaluating the role of compatibilizers in enhancing the properties of these blends. By emphasizing the importance of compatibilization and the utilization of recycled plastics, the research contributes to a more sustainable approach to polymer production.

Experimental

This study employed high-density polyethylene (HDPE) as the matrix and polyester (PET) derived from scrapped mooring rope fibers as the dispersed phase. The potential compatibilizers used were: calcium carbonate nanoparticles ($nCaCO_3$) with modified surface through myristic acid coating, obtained by the carbonation process, and commercial malleated polyethylene (HDPE-g-MA) were used.

Synthesis of $CaCO_3$-AM Nanoparticles

The synthesis of $CaCO_3$ nanoparticles followed a study by Racca [6] to optimize the conditions for obtaining particles with a narrow size distribution and smaller sizes. Myristic acid was chosen as the

surface modifier due to its higher thermal stability and smaller particle size compared to other commercial modifiers. The synthesis process included the reaction of a solution of tripolyphosphate anhydride (Na_3PO_4) with calcium oxide (CaO) in water, where a gas mixture of CO_2 and N_2 was introduced. The reaction was monitored until the pH reached 7-7.5, followed by the addition of a myristic acid solution. This method allowed for the controlled synthesis of $CaCO_3$ nanoparticles with tailored particle size and surface modification [6]. The nanoparticle size was determined by Dynamic Light Scattering – DLS analysis. The $CaCO_3$ nanoparticle size had an average size of 90 nanometers.

Design of Experiments and preparation of the blends

In this study, Analysis of Variance (ANOVA) based on a 2^k simple factorial design was adopted, where "k" corresponds to the number of process variables to be evaluated in the preparation of the nanocomposites. For this study, we considered k=3. The factors and levels adopted in the study can be observed in Table 1:

Table 1: Factors and levels established in the 2^k design:

		LEVELS		
VARIÁVEIS	**CODE**	**HIGH (+)**	**INTERMEDIATE (0)**	**LOW (-)**
SCREW SPEED (RPM)	X1	300	200	100
COMPATIBILIZER (wt. %)	X2	3	1,5	0
FILLER (wt. %)	X3	3	1,5	0

In this way, the statistical design encompasses 2 levels plus a central point, in duplicate, observing the most relevant variables of the system and optimizing the analysis of the results. Table 2 shows the experimental design.

Table 2: planning matrix

	CODED VARIABLES			UNCODED VARIABLES		
EXP	X1	X2	X3	SPEED. (RPM)	COMP (wt. %)	FILLER (wt.%)
1	-	-	-	100	0	0
2	-	+	-	100	3	0
3	-	-	+	100	0	3
4	-	+	+	100	3	3
5	+	-	-	300	0	0
6	+	+	-	300	3	0
7	+	-	+	300	0	3
8	+	+	+	300	3	3
9	0	0	0	200	1.5	1.5
10	0	0	0	200	1.5	1.5
11	0	0	0	200	1.5	1.5

It should be noted that, for all experiments conducted, the content of HDPE and PET was fixed at 90/10 (wt.%), respectively.

Processing and determination of residence time.

The nanocomposites were processed using a Twin Screw Extruder at temperatures ranging from 90 to 270°C. Systems based on HDPE/PET (90/10, wt.%) were produced. To determine the residence time of the systems during processing, an optical system comprising a webcam connected to a Linux computer with a Python program was employed during processing. A tracer, consisting of dark blue pigmented HDPE pellets, was used to track the residence time of the samples under high temperature and shear rate. The program started capturing continuous images once the processing reached a steady and uniform state. The tracer was added to the main feeder, and the exact moment of addition was recorded by the system operator. By analysing the average RGB color of the extruded area and converting it to the HSV color system, the program determined the saturation of the tracer color, thus indicating the processing time of the material.[7]

Characterization of the nanocomposites

The mechanical properties (elastic modulus and toughness properties) of the nanocomposite were analyzed through tensile testing, were carried out in the EMIC equipment, model DL300 (ASTM D638). The thermal stability of the systems was analyzed by thermogravimetric analysis (TGA), was performed using approximately 20 mg of sample. The material was heated up to 900 ºC at a heating rate of 10 ºC/min, under a nitrogen atmosphere with a flow rate of 90 ml/min. The TGA measurements were conducted using a Q 500 thermogravimetric analyzer from TA Instruments. The flow behavior of the materials was evaluated by melt flow index (MFI) analysis (ASTM D1238), in DYNISCO equipment, model LMI 4000.

Results and Discussion

Mechanical and flow behaviors.

The study investigated the effects of process variables on the mechanical and flow properties of HDPE/HDPE-g-MA/PET nanocomposites (Table 3).

Table 3: Mechanical properties of the systems

EXP	X1	X2	X3	Elastic Modulus (MPa)	Toughness (MPa)	MFI ($g.10\ min^{-1}$)
1	-	-	-	1232 ± 17	527 ± 41	1,9 ± 0,1
2	-	+	-	1181 ± 20	653 ± 38	1,2 ± 0,1
3	-	-	+	959 ± 25	492 ± 18	2,4 ± 0,2
4	-	+	+	943 ± 20	437 ± 12	2,6 ± 0,1
5	+	-	-	1058 ± 24	567 ± 26	2,6 ± 0,1
6	+	+	-	889 ± 15	884 ± 27	1,6 ± 0,6
7	+	-	+	952 ± 9	423 ± 15	2,3 ± 0,1
8	+	+	+	901 ± 7	457 ± 27	2,9 ± 0,1
9	0	0	0	957 ± 21	546 ± 41	2,5 ± 0,1
10	0	0	0	935 ± 20	521 ± 41	2,7 ± 0,2

Surprisingly, increasing the content of $nCaCO_3$ nanoparticles resulted in a decrease in the Elastic Modulus, indicating a loss of material stiffness. On the other hand, for the Toughness property, increasing the compatibilizer content and decreasing the nanofiller content led to higher values. Incorporating the traditional compatibilizing agent (HDPE-g-MA) into the HDPE/PET matrix significantly increased toughness, while the addition of $nCaCO_3$ nanofiller decreased the property, suggesting a reduced interaction between HDPE and PET phases. These findings deviated from the expected enhancement of properties with the addition of modified nanofillers. Figures 1 show the Interaction graphics of mechanical.

Figure 1: Interaction graphics: (a) Elastic modulus and (b) Toughness of the HDPE/PET systems

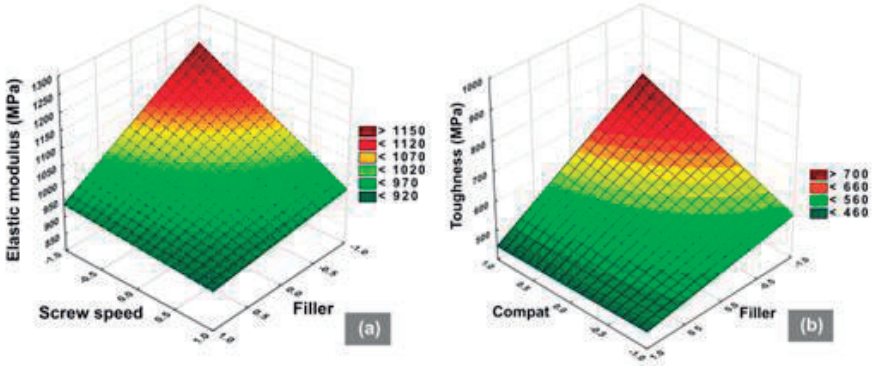

Scanning electron microscopy

SEM micrographs (Figure 2) revealed important insights regarding the interaction between phases in the HDPE/HDPE-g-MA/PET system. The addition of $CaCO_3$ nanoparticles led to larger domain sizes, suggesting a deterioration in the phase interaction. This effect was more pronounced at a screw speed of 100 rpm. Interestingly, at a rotation of 300 rpm, smaller sizes of the dispersed PET phase were observed even without the compatibilizer, possibly due to the higher shear rate breaking the domains. The micrographs also showed "bridging points" between phases in the presence of HDPE-g-MA, which were absent when CaCO3 nanoparticles were added. These observations provide an explanation for the observed decrease in mechanical properties.

Figure 2: Scanning Electron Micrographs of composites: (a) and (D) HDPE/PET; (B) and (E) HDPE/HDPE-g-MA/PET and (C) and (F) HDPE/HDPE-g-MA/PET/CaCO3

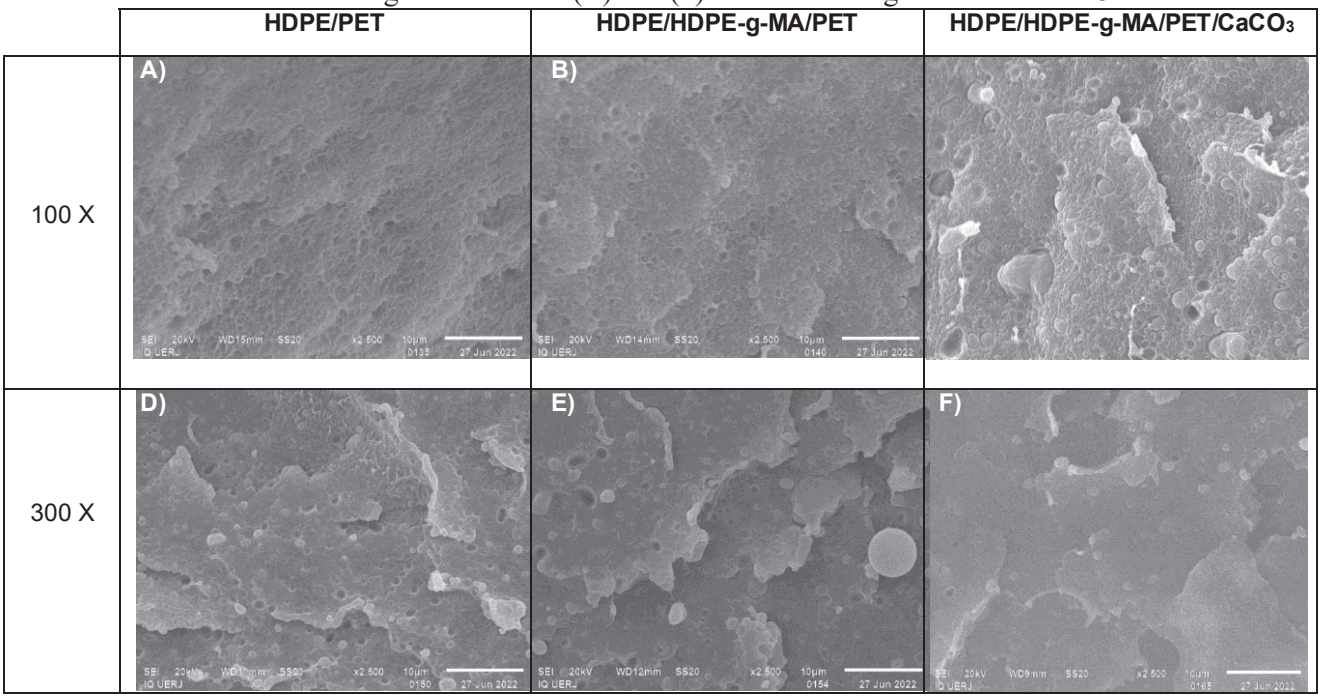

Thermal Properties

Regarding the thermal stability of the analysed systems, evaluated in terms of the maximum degradation temperature (TMAX), it was observed that, according to the experimental design, higher filler contents led to an increase in the thermal stability of the blends. According to Wang et al. (2007), this increase in thermal stability observed in systems with the nanofiller can be attributed to the fact that during the degradation process in the analysis equipment (TGA), the nanofiller leads to the formation of a protective physical barrier layer of $CaCO_3$ particles on the surface of the melt, thus reducing the degradation rate of polymeric matrix.

Residence Time Determination

The statistical analysis also shows that the process variable Mixing Speed was the most relevant for the parameter Residence Time, meaning that the lower the screw speed, the longer the residence time of the melt within the extruder, which was expected. Therefore, the profile of the Residence Time Distribution (RTD) curve of the system processed at higher screw speed (300 rpm) tends to produce slightly narrower RTD curves, as shown in Figure 3.

Figure 3: Residence time saturation curves as a function of time for different systems.

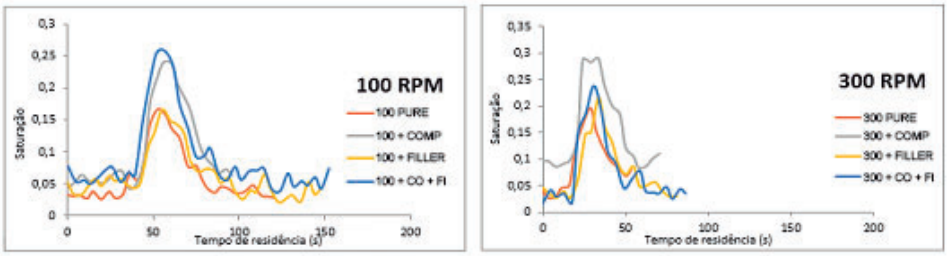

The curves of the HDPE/HDPE-g-MA/PET systems show broader profiles compared to other systems, possibly due to a decrease in the melt flow index. Higher screw speeds resulted in faster material flow towards the extruder matrix but also causing greater disorder in the output flow. Additionally, the HDPE/HDPE-g-MA/PET systems exhibit smaller tails in the curves, indicating a potential increase in phase interaction within the molten mass, potentially influenced by the presence of the compatibilizing agent. However, the systems with $CaCO_3$ nanoparticles exhibited elongated tails caused by "dead zones" within the extruder.

Conclusions

The statistical analysis demonstrates that the addition of a compatibilizer into the HDPE/PET system increases the toughness property by up to 56%, while increasing the $nCaCO_3$ content decreases this property. The $nCaCO_3$ nanofiller addition to the HDPE/HDPE-g-MA/PET also decreased the elastic modulus, indicating reduced interaction between the HDPE/PET phases. Additionally, higher filler contents improve the thermal stability of the blends, reducing the degradation rate of HDPE. SEM analysis and residence time are influenced by screw speed. Higher speeds lead to smaller dispersed phase domains and slightly narrower curves.

Acknowledgements

To FAPERJ for financial support through the process 201.726/2021, CNPq and UERJ for the partnership.

References

1. DORIGATO, A. v. 4, n. 2, p. 53–69, 2021. https://doi.org/10.1016/J.AIEPR.2021.02.005
2. ZHANG, F. et al. v. 282, p. 124523, 2021. https://doi.org/10.1016/J.JCLEPRO.2020.124523
3. TAGUET, A.; CASSAGNAU, P.; LOPEZ-CUESTA, J. M. v. 39, n. 8, p. 1526–1563, 2014. https://doi.org/10.1016/j.progpolymsci.2014.04.002
4. RACCA, L. M. et al. v. 21, n. 11, 2019. https://doi.org/10.1007/s11051-019-4693-0
5. MANDARINO, Bianca da R.; SILVA, Ana Lúcia N. da; MICHEL, Ricardo C.. v. 394, n. 1, p. 2000065, dez. 2020. Wiley. http://dx.doi.org/10.1002/masy.202000065.
6. WANG, W., Zeng, X., Wang, G., Chen, J. vol 106, pag 1932 – 1938. 2007. DOI: 10.1002/app.26833
7. E. P. SOARES in proceedings 21º CBECIMAT− Congresso Brasileiro de Engenharia e Ciência dos Materiais, Cuiabá, 2014. p. 403-018

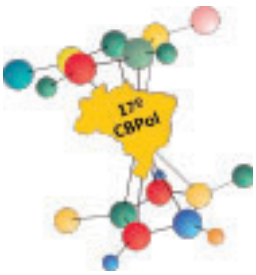

THE EFFECTS OF AGING ON GLASS FIBER-EPOXY COMPOSITES WITH IMPACT DAMAGE.

Maria A. P. Damasceno[1], João F. B. Pontes[2], Ana P. C. Barbosa[3]

1 – Department of Materials Engineering, Federal University of Rio Grande do Norte (UFRN), Natal, RN, Brazil
maria_pdamasceno@hotmail.com

Abstract - Composite materials cover applications in several areas such as aerospace and naval, uniting the attractive mechanical properties and the low density of the constituent components, becoming a possibility to replace more traditional materials such as metallic materials. However, composite materials can undergo degradation through exposure to environmental agents, with consequent change of properties. Thus, it becomes important to know the extent of effects of aging on the material. This present work seeks to evaluate alterations presented by glass fiber-epoxy composites after environmental aging, subjected to impact tests to compare the results with non-aged samples. The specimens were produced with prepreg glass fiber-epoxy in a hot press and were cut with water jet according to the size prescribed in the ASTM D7136 standard for impact tests. Half of the samples were subjected to aging for 30 days and the other half reserved in the desiccator. All samples were submitted to the impact test for comparison of results, analyzed in scanning electron microscope (SEM) and Fourier Transform Infrared Spectroscopy (FTIR). A visual evaluation was carried out on the samples after the impact test, in order to analyze the influence of aging related to the impact energy and the affected area. Spectroscopy allowed the evaluation of chemical changes in the epoxy matrix with glass fiber reinforcement. Morphological alterations, including defects accentuated by aging, were investigated based on SEM analyses. It was observed that environmental aging can affect the performance of composite materials, especially when it comes to applications that suffer impact damage.

References:

1. K. K. Chawla, *Composite Materials*. New York, NY: Springer New York, 1998.
2. W. D. Callister Jr; D. G. Rethwisch, *Materials science and engineering – an introduction*, *9. ed*. Rio de Janeiro: LTC, 2016.
3. J. F. B. Pontes, Master 's Thesis, Federal University of Rio Grande do Norte, 2022.
4. A. P. B. Cysne; A. P. P. Fulco; E. S. S. Guerra; F. K. Arakaki; M. Tosatto; M. C. B. Costa.; J. D. D Melo *Accelerated aging ef ects on carbon fiber/epoxy composites*. Composites Part B: Engineering, [S.L.], v. 110, p. 298-306, fev. 2017. Elsevier BV. http://dx.doi.org/10.1016/j.compositesb.2016.11.004.
5. A. D7136, "Standard Test Method for Measuring the Damage Resistance of a Fiber-Reinforced Polymer Matrix Composite to a Drop-Weight Impact Event," ASTM Int.Des. D, vol. i, no. C, pp. 1–16, 2005.

Fundings: The authors acknowledge CNPq for financial support.

Keywords: *Composites; Impact; Aging.*

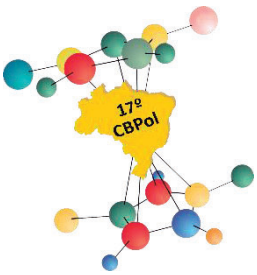

THE EFFECTS OF COPPER POWDER ON THE PROPERTIES OF ABS

Vicente F. Moritz[1,2]*, Harald Prévost[3], Declan M. Devine[2], Carlos A. Ferreira[1]

1 – Postgraduate Programme in Mining, Metallurgical and Materials Engineering (PPGE3M), Federal University of Rio Grande do Sul (UFRGS), Porto Alegre, RS, Brazil vicente.moritz@ufrgs.br
2 – PRISM Research Institute, Technological University of the Shannon (TUS), Athlone, Ireland
3 – ENSIACET, Institut National Polytechnique de Toulouse, Toulouse, France

Abstract - In industry, several materials applications require bespoke characteristics such as mechanical strength, light weight and improved thermal conductivity, which cannot be simultaneously achieved by metals or ceramics alone. Polymer-metal composites are an engineering solution with potential to fill that gap. This study describes the development of an ABS/copper composite material compounded through extrusion and then injection-moulded. The maximum content of copper (60%w/w) yielded the greatest Young's modulus, hardness and thermal conductivity, and a higher impact strength compared to the 30%w/w-copper composite.
Keywords: *ABS composites, 3D Printing, Additive manufacturing, Polymer/metal composites*
Funding: This publication has results from research conducted with the financial support of Enterprise Ireland under the Technology Gateway Programme, Grant Number TG-2017-0114 (APT Ireland), and Science Foundation Ireland (SFI), Grant Number SFI 16/RC/3918, co-funded by the European Regional Development Fund.

Introduction

Polymer-metal composites are of particular interest for applications in which either thermal or electrical conductivity is required, since polymers are not intrinsically conductive [1]. For instance, concern has arisen due to warpage and distortion caused by thermal expansion on polymer-based 3D-printed parts, while inserts for injection hybrid moulds or electromagnetic structures such as antennas would benefit from properties that usual polymer materials lack [1–4]. Within this frame of reference, metal-reinforced polymers have become an alternative material to overcome those issues.

Masood and Song (2004) developed a new composite of nylon reinforced with iron particles [5]. They extruded the composite and produced filaments for fused deposition modelling (FDM), and then used that additive manufacturing (AM) technique to print inserts for hybrid moulds; the researchers also injection-moulded LDPE and ABS using the printed insert. Nikzad et al. (2011) and Sa'ude et al. (2013) investigated ABS composites filled with copper having metal contents of up to 40%V/V, observing a significant improvement of ABS thermomechanical properties which could potentially lead to high performance, functional prototypes for a wide range of applications manufactured by FDM process [6,7]. Carbon fibre-reinforced ABS filaments were analysed by Ning et al. (2015), reporting that increasing carbon fibre content increases tensile strength and Young's modulus despite, however, contrastingly reducing toughness, yield strength, and ductility [8]. Kumar et al. (2019) investigated the behaviour of melt flow index (MFI) rates of ABS/aluminium composites for extrusion-based AM processes, noticing that the flow index increases with extrusion load and temperature, and that the filler loading has distinct effects depending on the content [9].

In this context, this study arises as an initial trial that aims to evaluate the influence of presence and content of copper on the mechanical properties and thermal conductivity of ABS. ABS-matrix copper-reinforced composites were prepared by extrusion with two filler ratios for compounding and then injection-moulded. The feasibility of the composite obtained as a potential candidate for thermally-conductive polymer composite was assessed through material characterisation techniques including tensile, impact and hardness testing, thermal conductivity and melt flow index analyses.

Experimental

Materials

Commercial-grade ABS was supplied by LG Chemical under trade name TR-557I as a transparent, impact resistant material. Copper powder 325 mesh (>99.0%, particle size <45 μm) was supplied by East Coast Fibre Glass.

Composites extrusion and injection moulding

ABS and copper powder were mixed and extruded in a co-rotating twin-screw Leistritz Macromatex II (ϕ 27 mm, 36:1 L/D ratio), with a 200-230 °C temperature profile at 30 rpm. Prior to compounding, ABS and copper powder were dried at 80 and 110 °C respectively, both for 2 h. Following extrusion, obtained composites were pelletised. Composite formulations were designed with one variable factor at three levels; the polymer/metal ratios are presented in Table 1.

An Arburg 370E Allrounder injection moulding machine (ϕ 30 mm screw) was utilised with a 195-220 °C temperature profile. Specimens for tensile (ASTM D638 type I) and impact tests (unnotched ASTM D6110 Charpy) and ϕ 25 mm discs were moulded. Allowing for higher filler contents, injection pressure was optimised, in order to prevent both short shots and flash (Table 1). Holding time and pressure were 7 s and 500 bar, and mould temperature was 55 °C, with cooling time of 30 s and total cycle time of 42.4 s.

Table 1 - ABS and copper powder contents for the composite formulations prepared.

	ABS-vir	ABS-30%Cu	ABS-60%Cu
ABS [%w/w]	100	70	40
Copper [%w/w]	0	30	60
Inj. Pressure [bar]	800	900	1070

Characterisation

Stress-strain tensile tests were performed in a Zwick Roell universal testing machine with a 10 kN loadcell, based on ASDM D638-14. Test speed was 5 mm·min^{-1} and gauge length was 50 mm. Charpy impact test was carried out with mechanically-notched specimens based on ASTM D6110-10 in a Ceast Resil 6844 digital machine with a 4 J hammer. Hardness tests were carried out on a CV Instruments Ltd. Shore Durometer digital machine, with test load of 5.0 kg.

The thermal conductivity, k, of the specimens was measured using a H111A Heat Transfer unit (P.A.Hilton Ltd.). A disc specimen (ϕ 25 mm, thickness 2.0 mm) was fitted between two parallel-plate copper blocks. Voltage and current of 80 V and 0.109 A were applied. Finally, the surface temperatures were estimated according to the manufacturer's instructions, and k for the materials was calculated based on Fourier's Unidirectional Heat Transfer Law.

Melt flow index (MFI)

The melt flow studies were carried out using a Zwick Roell Cflow plastometer with a 2 mm die and were based on ASTM D1238-13. Testing was performed under a load of 2.16 kg at 230, 245 and 260 °C. It is well known that a molten polymer's shear viscosity — and, hence, its MFI — depends

upon the temperature, enabling the flow process mechanism to be associated to a flow activation energy, E_a, which can be estimated through a modified Arrhenius-Eyring equation:

$$MFI = B \times \exp(E_a / RT) \qquad (1)$$

where E_a can be calculated from the slope of ln(*MFI*) as a function of $1/T$, B is a constant, R is the gas constant — approximated to 8.3143 $J \cdot mol^{-1} \cdot K^{-1}$ —, and T is the temperature in K [10]. MFI values for each sample were calculated at each temperature as the average of the material extruded within each of ten spans of 30 s, with the respective standard deviations.

Results and Discussion

Tensile testing results indicate that the copper content has a significant effect on all the mechanical properties evaluated (Table 1), as indicated by the analyses of variance (ANOVA) performed, with $p < \alpha = 0.01$. The copper powder raised the Young's modulus E to values ca. 50% greater for ABS-60%Cu in comparison to ABS-vir. Contrastingly, all copper-loaded specimens had brittle fracture during the tensile test. ABS-vir exhibited a mean yield point at $\sigma_Y = 43.3$ MPa and $\varepsilon_Y = 3.3\%$. This reveals a major embrittling effect of the copper filler on the matrix, representing a considerable loss in terms of toughness. Overall, the mechanical behaviour under tensile loading follows the same trend observed by previous studies [2,3]. Significant differences were found for all the three formulations regarding E and σ_{max}. The reasons for this behaviour may lie in the nonhomogeneous dispersion of voids and particles, possibly leading agglomerations to cause stress concentrations [11]. As the metal-polymer interface plays a fundamental role on the mechanical properties, another factor affecting the metal-polymer bonding integrity is the metal's oxide morphology and stability. Since the formulations contain no coupling agent to promote enhanced interface interactions, there may be insufficient bonding between the metal particle and the polymer matrix [6].

Table 2 - Tensile properties of ABS and copper composites.

Property	ABS-vir	ABS-30%Cu	ABS-60%Cu
Young's Modulus E [MPa]	1885.0 *(±18.97)*	2329.4 *(±16.52)*	2853.1 *(±18.52)*
Tensile Strength σ_{max} [MPa]	43.4 *(±0.36)*	33.7 *(±1.71)*	38.1 *(±1.56)*
Stress at Break σ_B [MPa]	31.9 *(±3.64)*	33.7 *(±1.71)*	38.1 *(±1.56)*
Strain at Break ε_B [%]	5.2 *(±1.44)*	1.6 *(±0.11)*	1.5 *(±0.09)*

$n = 16$

Resulting brittleness is endorsed by the decrease in impact strength, with values for ABS-30%Cu and ABS-60%Cu as low as 28% and 39% of that of ABS-vir (Figure 1). It suggests a poor adhesion between matrix and reinforcement as a low-energy cleavage path leads to reduced energy dissipation through the matrix [4]. Conversely, increasing the copper content to 60% actually enhanced the mechanical behaviour as it raised both tensile and impact strengths by 13% and 39%, respectively, in comparison to 30% copper content. The cross-section fracture surfaces resulting from the Charpy test can be observed in Figure 2. ABS-vir specimens present clear evidence of deformation as the impact rupture took place, while these signals are absent in the composites. Additionally, voids can be noticed on the composites cross-section. Shore D testing results indicate that the copper content has significant effect also on the surface hardness characteristics (ANOVA, $p < 0.01$) as significant differences were found for all the three materials. The values obtained showed an increasing trend alike to those of tensile and impact strengths between ABS-30%Cu and ABS-60%Cu, which are similar to results previously reported by Singh et al. (2018) and Moritz et al. (2021) [3,12]. Adding metallic particles changes the polymer matrix's microstructure, and the introduction of more grain boundaries due to increasing the copper content causes the composite to reach greater hardness values [13]. Reinforcement ratio also has significant effects on k (ANOVA, $p < 0.01$), although ABS-vir and

ABS-30%Cu are statistically equal. ABS-60%Cu exhibited the highest thermal conductivity, ca. 16% greater than that of the neat ABS. Other studies have suggested that, beyond a minimum filling threshold, particles agglomerates in the interfacial surface would create a conductive path, enhancing thermal conduction properties [4,6,13].

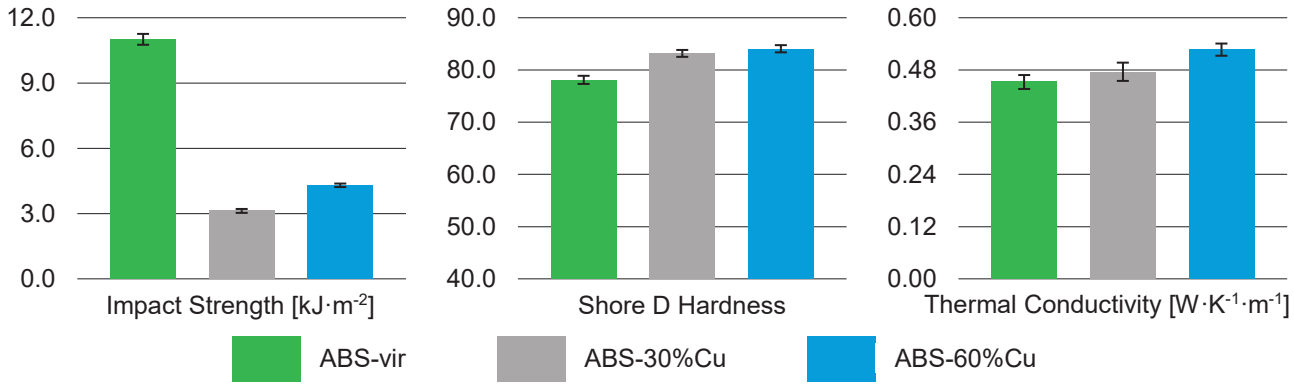

Figure 1 - Properties of ABS and copper composites: impact strength (left), Shore D hardness (centre) and thermal conductivity (right).

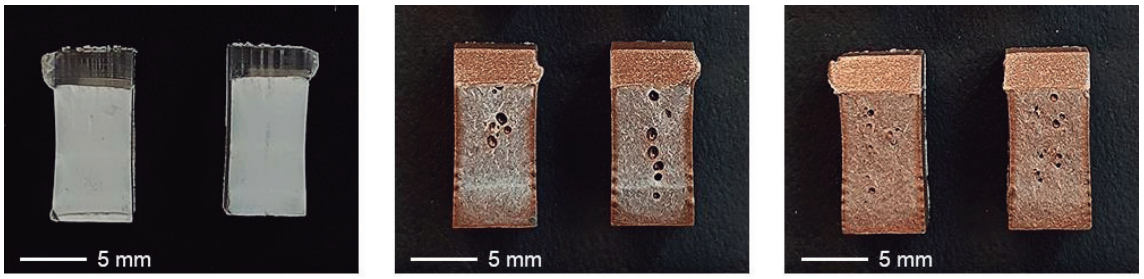

Figure 2 - Examples of cross-section fracture surface obtained from the Charpy impact test for ABS-vir (left), ABS-30%Cu (centre) and ABS-60%Cu (right).

Copper powder is observed to increase the MFI relative to neat ABS (Table 3 and Figure 3), despite of the need to adjust the injection pressures in order to achieve suitable moulding conditions. Usually a thermoplastic's MFI decreases with increasing filler content due to more intense filler-filler interactions. [3,9]. However, Kumar et al. (2019) reported that small amounts of filler could raise the MFI [9]. In this case, filler-filler agglomerates would be weak and break under the shear force that orientates the flow direction. ABS presents a main degradation step that starts from 300 °C, with onset point at ca. 365 °C, therefore no thermal degradation events are expected to take place within the temperature range utilised in the test [14,15]. Moreover, Singh et al. (2018) attribute increased MFIs of heavily-loaded composites to excess density effects [12]. E_a of ABS-60%Cu is ca. 20% greater than those of ABS-vir and ABS-30%Cu, which suggests that, despite being higher in density, the copper powder restricts the molten material flow so that more energy is required for the metal particles to flow through the matrix [10].

Table 3 - Melt flow index and flow activation energy E_a for ABS and copper composites.

Material	MFI [g·10 min^{-1}]			E_a	R^2
	230 °C	245 °C	260 °C	[kJ·mol^{-1}]	
ABS-vir	2.69 (±*0.10*)	5.73 (±*0.20*)	10.24 (±*1.11*)	99.44	0.9966
ABS-30%Cu	4.51 (±*0.36*)	9.11 (±*0.52*)	16.80 (±*1.41*)	97.74	0.9995
ABS-60%Cu	3.88 (±*0.07*)	7.75 (±*0.24*)	19.71 (±*0.67*)	120.70	0.9897

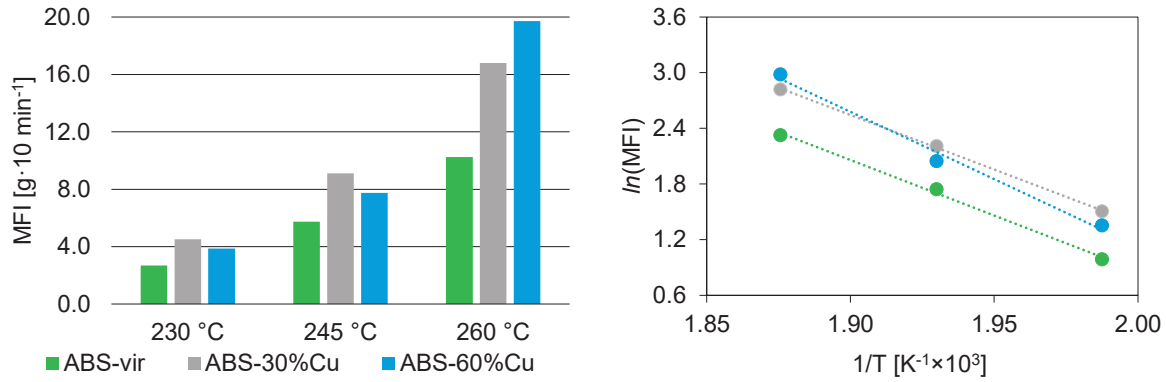

Figure 3 - Melt flow index for ABS and copper composites at the tested temperatures (left); plot of *ln*(MFI) as a function of 1/*T* (right).

Conclusions

Copper powder-reinforced ABS composites have been studied. The metallic filler promoted an expressive increase in Young's modulus and Shore D hardness, but caused the composites to become brittle with reduced tensile strength and elongation at break. Brittleness was also noticed during the Charpy testing, as the impact strength decreased with inferior energy dissipation due to poor adhesion on the polymer-filler interface. On the other hand, the composite with the highest content of copper powder (60%w/w) exhibited improved thermal conductivity. Furthermore, the copper particles played a flow-promoter role, raising the MFI at all temperatures tested relative to neat ABS.

References

1. K.A. Hamzah *et al*. J. Thermoplast. Compos. Mater. 35 (2022) 3–16. DOI: 10.1177/0892705719869405.
2. S. Hwang *et al*. J. Electron. Mater. 44 (2015) 771–777. DOI: 10.1007/s11664-014-3425-6.
3. V.F. Moritz, C.A. Ferreira, D.M. Devine, in: Proc. IMC37, Irish Manufacturing Council, Dublin, IRL, 2021.
4. T.J. Quill *et al*. Appl. Compos. Mater. 25 (2018) 1205–1217. DOI: 10.1007/s10443-017-9661-1.
5. S.H. Masood, W.Q. Song. Mater. Des. 25 (2004) 587–594. DOI: 10.1016/j.matdes.2004.02.009.
6. M. Nikzad, S.H. Masood, I. Sbarski. Mater. Des. 32 (2011) 3448–3456. DOI: 10.1016/j.matdes.2011.01.056.
7. N. Sa'ude *et al*. Int J Eng Res Appl. 3 (2013) 1257–1263.
8. F. Ning *et al*. Compos. Part B Eng. 80 (2015) 369–378. DOI: 10.1016/j.compositesb.2015.06.013.
9. N. Kumar *et al*. Int. J. Mater. Prod. Technol. 59 (2019) 194. DOI: 10.1504/IJMPT.2019.102931.
10. M. Poletto. Maderas: Cienc. y Tecnol. (2018) 0–0. DOI: 10.4067/S0718-221X2018005004401.
11. A.M. Alghadi, S. Tirkes, U. Tayfun. Mater. Res. Express. 7 (2019) 015301. DOI: 10.1088/2053-1591/ab551b.
12. R. Singh, R. Kumar, I. Ahuja. Rapid Prototyp. J. 24 (2018) 1455–1468. DOI: 10.1108/RPJ-05-2017-0094.
13. G. Hu *et al*. Procedia Manuf. 38 (2019) 1236–1243. DOI: 10.1016/j.promfg.2020.01.215.
14. A.T. Roussi, E.C. Vouvoudi, D.S. Achilias. Thermochim. Acta. 690 (2020). DOI: 10.1016/j.tca.2020.178705.
15. P. Kumar *et al*. Polym. Compos. 43 (2022) 4569–4587. DOI: 10.1002/pc.26713.

THERMAL AND MECHANICAL PROPERTIES OF ARAMID FIBER REINFORCED POLYPROPYLENE

Andressa Antunes Carneiro[1], Daiane Romanzini[2], Vagner Grison[1], Rafael R. Dias[3], Iaci M. Pereira[3] e Ademir Zattera[1]

1 – Postgraduate Program in Engineering of Processes and Technologies (PGEPROTEC), Universidade de Caxias do Sul (UCS), R. Francisco Getúlio Vargas, 1130, Caxias do Sul/RS)
acarneiro971@gmail.com
2 - Postgraduate Program in Materials Technology and Engineering (PPGTEM), Federal Institute of Rio Grande do Sul (IFRS), Feliz, RS, Brazil
3 - Laboratório de Materiais, Centro Tecnológico do Exército (CTEx), Rio de Janeiro, RJ.

Abstract – The aim of this study was to investigate thermal and mechanical properties of polypropylene composites reinforced with aramid fiber (AF), by varying the length (25 and 50 mm) and the fiber content (5, 10 and 20 wt.%). Differential Scanning Calorimetry (DSC), thermogravimetry (TGA), viscosity, tensile and flexural tests were performed to obtain the data. The results indicated that the polypropylene composite with 10% AF showed a significant increase in the degree of crystallinity (χc), compared to samples with 5% and 20% of fiber content, and higher flexural strength results. No major changes in the melting (Tm) and crystallization (Tc) temperatures of the produced composites were observed.

Keywords: *Polypropylene, aramid fiber and fiber length.*

Introduction

The use of fibers in a polymeric matrix (composites) is very common in various industrial applications. Composites are a multiphase combination material of two or more components with different properties and different forms, and it not only maintains the main characteristics, but also shows new character which are not possessed by any of the original components. These materials are formed by a phase called “matrix” or “continuous phase” and another “dispersed phase”, that is embedded in the matrix [1].

Polypropylene (PP) is the most commonly used polymer as a matrix in fiber composites. It is capable of competing with higher-cost plastics in the market and being used in various applications due to its low processing temperature, adequate mechanical properties, crystallinity, relatively high melting point, crystalline phase that maintains mechanical strength at high temperatures, availability and cost, low density, and high rigidity [1].

Aramid fiber (AF), or Kevlar, is widely used in the manufacture of ballistic vests, usually employed in the multilayer format, and may contain intermediate layers of polymeric films. It is widely used in high-performance composite applications due to its excellent mechanical, thermal, and chemical properties. Kevlar shows high specific strength and modulus, as well as high thermal resistance and chemical inertia, making it an attractive option to replace metallic and carbon or glass fibers in some applications [2].

This work aims to develop a single-layer material for use in ballistic vests. Thus, the effect of different fiber length (25 and 50 mm) and content (5, 10 and 20 wt.%) in polypropylene (PP) was investigated.

Experimental

Materials
The homopolymer H301 polypropylene was obtained from Braskem. The fiber used was para-aramid A314 KV K129, supplied by Barrday Advanced Material Solutions (Cambridge, USA).

Methods
The aramid fabrics were manually cut into two different lengths, 25 mm and 50 mm, and then defibrated. The material mixture was processed in a closed Brabender mixer, model Mixer 50 EHT, for 10 min at 180 °C. The processed material was pressed into plates (14 cm × 16 cm) in two different stages: a hot press temperature of 200 °C for 5 min with 10 tons and then cold-pressed for 7 min with 8.5 tons. The plates were cut with a water jet cutter (dimensions of xx × xx) and subsequently dried in an oven at 80 °C for 24 h.

Characterizations
Thermogravimetric Analysis (TGA, Shimadzu, TGA 50 equipment) was performed using a temperature range of 25 °C to 800 °C and a heating rate of 10 ºC.min^{-1}, using nitrogen in a flow rate of 50 ml.min^{-1}. Differential Scanning Calorimetry (DSC) analysis (Shimadzu, DSC 60 equipment) was performed under nitrogen gas flow (50 ml.min^{-1}), from room temperature to 200 °C, and two thermal cycles were carried out, using a heating rate of 10 °C.min^{-1}. The crystallinity of the samples was calculated based on the enthalpy values obtained in the DSC curves. Crystallinity was calculated based on Eq. 1 and the enthalpy values for the first heating curve of the composites. In Eq. 1, ΔH is the composite melting heat (enthalpy), ΔH_0 is the melting heat for 100% crystalline PP (209 J/g) [3 and 4], and w_{PP} is the weight fraction of the polymer matrix.

$$Xc = \frac{\Delta H}{\Delta H_0 w_{pp}} . 100 \quad (1)$$

To evaluate viscosity at different shear rates, capillary rheology analysis was performed using a Ceast SR 20 equipment with a size capillary of 20/1 mm at a temperature of 190 °C. Shear rates of 10, 30, 50, 100, 200, 300 and 500 s^{-1} were used. The tensile and flexural tests were carried out on a universal testing machine (EMIC, model DL 2000), according to ASTM D790 and ASTM D638 standards, speed of 50 mm.min^{-1} and 1.5 mm.min^{-1}, respectively, on 5 specimens, with a load cell of 200 kgf.

Results and Discussion

The tensile strength and modulus of elasticity results are presented in Figure 1 for different aramid fibers contents and lengths. A decrease in tensile strength (Figure 1a) was observed with an increase in fiber content for all the composites, if compared with neat polypropylene (AF 0%). This behavior suggests weak interaction between the fiber and the matrix, possibly due to the fiber agglomeration and energy dispersion reduction, which generates stress concentration and favors fiber displacement in the polymeric matrix [3]. The average tensile strength of the fiber samples ranged from 22.99 MPa to 36.15 MPa, while the matrix showed a value of 35.62 MPa. The modulus of elasticity (Figure 1b) increased with higher fiber contents, with the 50 mm fiber length samples being slightly stiffer than the neat polypropylene matrix (AF 0%), while the others remained below this value. The average values of the modulus of elasticity varied from 508.58 MPa to 648.62 MPa, with 585.38 MPa for PP 100%. According to the literature, an increase in tensile strength and modulus of elasticity was expected with an increase in fiber content [5]. However, the fiber agglomerates in the matrix during processing, especially for longer fibers (50 mm), and may have contributed to

decreased modulus, also influencing the standard deviation of the samples, due to the lack of fiber homogeneity in the test specimens.

The flexural strength and flexural modulus results are presented in Figure 2, for different aramid fibers lengths and contents. In general, samples with shorter fiber length (25 mm) showed an increased flexural strength, if compared to the matrix (PP 100%). The AF 10% (25 mm) sample achieved the highest average values (39.26 MPa), being 21.85% greater than the matrix (PP 100%, 32.22 MPa). On the other hand, samples with longer fiber length (50 mm) may have been affected by the processing, showing a greater tendency for fiber agglomeration. The flexural modulus showed increased values as the fiber content increases, for both lengths (25 mm and 50 mm), with emphasis on the samples with 25 mm fiber length. The sample with the highest rigidity was AF 20% long fiber (50 mm), with an average value of 1201.56 MPa. However, this sample also showed greater material irregularity, with a standard deviation of ± 449.31 MPa. Meanwhile, the AF 10% (25 mm) sample resulted in 1167.96 ± 216.35 MPa.

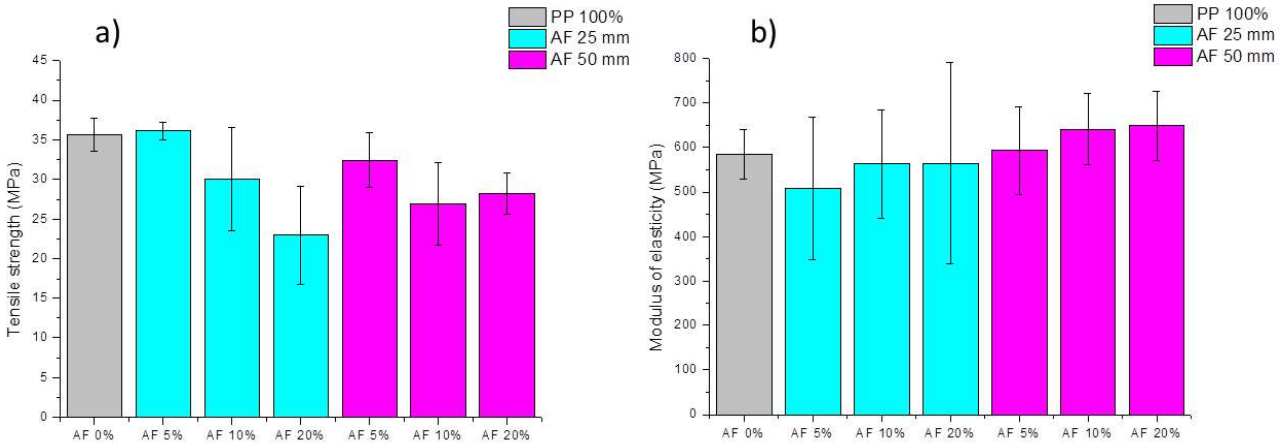

Figure 1 – Influence of para-aramid fibers content and length on the tensile strength in a) and elastic modulus in b).

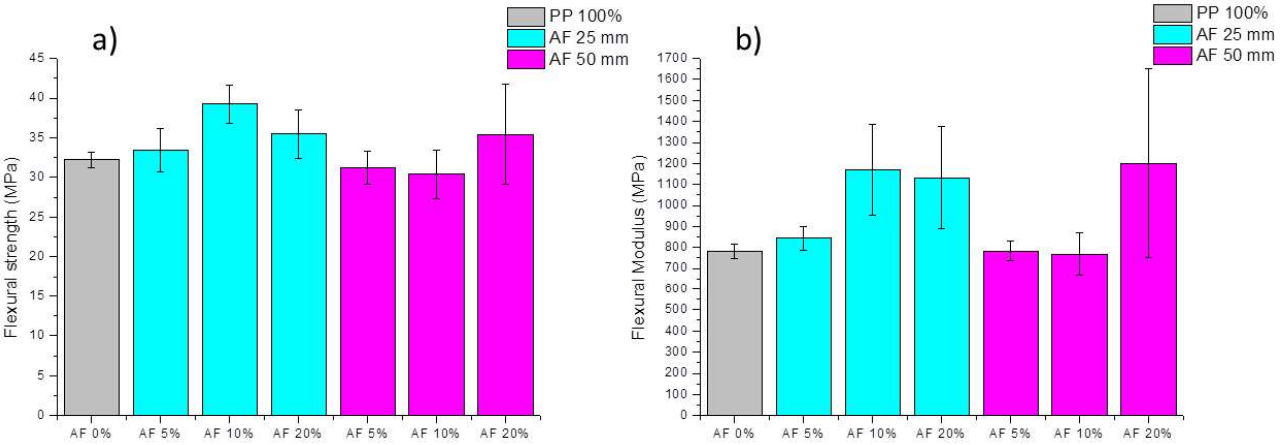

Figure 2 – Influence of para-aramid fibers content and length on the flexural strength in a) and flexural modulus in b).

The rheological analysis of the composites is shown in Figure 3, and an increase in viscosity of the composites is observed with the addition of fibers [6], if compared to the matrix (PP 100%). Among the composites, the AF 5% samples showed lower viscosity if compared with the others (AF 10% and AF 20%). This behavior is related to the lower effort required for fiber orientation in the capillary [7] due to the lower fiber content. The change in the final part of the curve, with the increase in the load level (10% and 20% of fiber), is related to the softening of deformation caused

by the breaking of interactions between load/matrix [8]. The similarity of the curves between the concentrations of 10% and 20% of fiber may be related to the saturation of the influence of fiber on the behavior of the polymeric matrix.

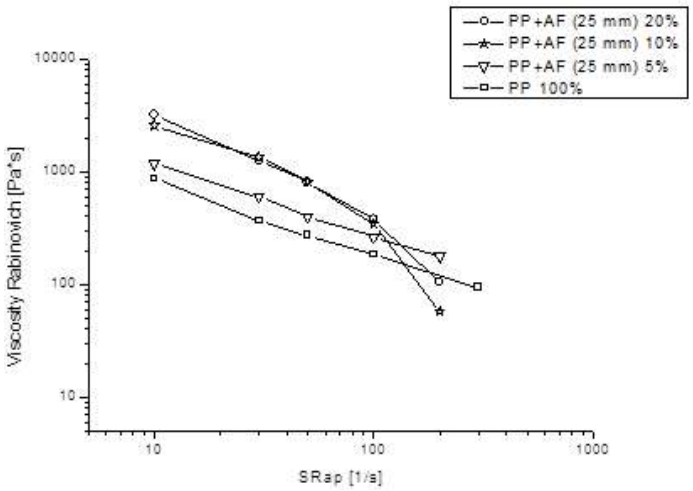

Figure 3 – Rheological analysis carried out at 190 °C of the pure matrix (PP 100%) and composites with different aramid fiber content (5%, 10%, and 20%).

The TGA curves are illustrated in Table 1. It is important to observe the influence of aramid fiber in the composite thermal stability. The sample with the most promising result in the flexural test (PP + AF (25 mm) 10%) was selected, and the thermal behavior was compared with the matrix (PP 100%) and the fiber (AF 100%). A shift in the composite curve is observed when the reinforcing fiber is added compared to the matrix [2], evidencing an increase in thermal stability for the composite ($T_{máx}$ = 451,48°C) in comparison with the neat polypropylene (Tmax = 438.32°C). The sample with PP + AF (25mm) 10% presented two peaks of thermal decomposition related to the two materials used (PP and AF).

Table 1 – Thermal stability of the neat PP, PP+AF(25mm)10% and AF 100% sample.

Sample	$T_{10\%}$ (°C)	$T_{50\%}$ (°C)	T_{i1} (°C)	$T_{máx1}$ (°C)	T_f degradatio1 (°C)	T_{i2} (°C)	$T_{máx2}$ (°C)	T_f degradatio2 (°C)
PP 100%	383,7	427,3	289,23	438,32	456,88	-	-	-
PP+AF (25mm)10%	397,1	442,7	303,41	451,48	476,95	566,16	588,49	601,90
AF 100%	566,6	707,3	485,65	575,86	601,45	-	-	-

The values obtained in Table 1, which present the temperatures for mass loss in the ranges of 10% and 50%, corroborate with this result due to the increase in the onset degradation temperature for the mixture (PP + AF (25 mm) 10%) in relation to the matrix. According to [3], this may be due to two possible effects. The first is related to the delay in heat propagation in the composite, caused by the formation of a protective layer of fibers around the PP chains at temperatures below the fiber decomposition temperature. The second effect concerns the formation of a protective layer of carbon covering the surface of PP, preventing heat and oxygen propagation at a temperature higher than the critical decomposition temperature of the fiber. Furthermore, for aramid fiber, the T50% was reached after the degradation peak. The final temperature (T_f) of the degradation peak corresponds to 32% weight loss.

In the DSC analysis (Table 2), the melting temperature of the composites showed a maximum variation of ± 2 °C compared to the PP matrix, whose T_m obtained was equal to 167.25°C. The crystalline peak temperature (T_c) showed a slightly gradual increase with the fiber content increased, compared to neat PP (T_c = 118.61°C), however, it remained around 123°C. The literature

[4] suggests that fibers would act as nucleating agents in the polymer matrix and consequently increase the values of T_m, T_c, but this behavior was not so pronounced in the obtained data. When analyzing the results of the enthalpy variation (ΔH) and crystallinity (Xc) of the samples, according to the variation in the aramid fiber content, an increase in crystallinity is observed for the concentration of 10% aramid fiber, and it can be concluded that this fiber content favors nucleation. On the other hand, the 5% and 20% fiber contents do not act as nucleating agents due to the low amount of fiber and excess fiber, respectively [3]. The composites with 10% fiber content show a considerable increase in crystallinity, with the fibers acting as nucleating agents, increasing crystallinity and favoring the results showed in mechanical properties [3 and 4]. The flexural properties of the (PP + AF (25mm) 10%) sample corroborate this statement.

Table 2 – Melting temperature (T_m), crystallization temperature (T_c) and degree of crystallinity (X_c) in relation to the percentage of fiber.

Sample	PP 100%	PP + AF (25mm) 5%	PP + AF (25mm) 10%	PP + AF (25mm) 20%
T_m (°C)	167,25	168,03	166,44	169,03
T_c (°C)	118,61	122,91	123,04	123,06
ΔH (J/g)	85,42	79,65	89,64	53,49
Xc (%)	40,87	40,12	47,66	31,99

Conclusions

Analyzing the performance of polypropylene composites by varying length (25 mm and 50 mm) and aramid fiber content (5, 10 e 20%) was evaluated. The rheological analysis indicated small variation between the percentages of 10% and 20% fiber, due to the possible fiber saturation, for the sample with 20%. From the flexural strength tested samples, those with a fiber length of 25 mm obtained better results, with emphasis on the sample with 10% fiber (PP+AF (25 mm) 10%). Through TGA analysis, an increase in thermal stability was observed with the addition of fiber. The degree of crystallinity analysis indicated a higher value for the sample with 10% fiber that corroborate with the flexural results.

Acknowledgements

The authors would like to thank CNPq and CAPES for the financial support. The authors are also grateful to the Laboratório de Polímeros Universidade de Caxias do Sul (LPOL) for all the analysis reported in this work and to the support of the IFRS.

References

1. C. Spadetti et al. Polímeros 2017, 27, 84–90.
2. M. Mukherjee, C.K. Das; A.P. Kharitonov Polymer Composites 2006, 27, 2, 205–212.
3. X. Chen; S. Zhang; G. Xu; X. Zhu;W. Liu; Journal of Applied Polymer Science 2012, 125, 1166–1175.
4. S. Houshyar; R. A. Shanks; A. Hodzic; Applied Polymer Science 2005, 96, 2260–2272.
5. S. Fu; et al. Composites Science and Technology 2018, 163, 141–150.
6. F. Asoodeh; et al. Journal of Industrial Textiles 2021, 51, 8452S–8471S.
7. J. K. Kim; J. H. Song Journal of Rheology 1997, 41, 5, 1061–1085.
8. L. Zhao, et al. Journal of Materials Science 2010, 46, 8, 2495–2502.

THE STUDY OF THE BEHAVIOR OF TE PP/PS BLEND UNDER STRESS CRACKING

Milenna A. B. Rodrigues[1*], Kelson de S. G. Vilhena[1]

1 – Superior School of Technology, State University of Amazonas, Av. Darcy Vargas, 1200, 69050-020, Manaus, Amazonas Brazil.

*mabr.emt@uea.edu.br**

Abstract - Due to the technological advancements achieved in recent years and the demand for high-performance materials, polymeric materials have become prominent in replacing conventional materials due to their characteristics. Given this high demand for polymeric materials, it becomes necessary to acquire knowledge about the polymer's service life because, like other materials, they are also subject to radiation, humidity, heat, and contact with various fluids, factors that alter their rheological and mechanical properties, thereby affecting the material's service life (Corazza, 1995). Consequently, it is necessary to obtain knowledge about failure types through various polymer-fluid combinations (Turnbull et al., 2000) in order to prevent failures. One way to obtain new polymeric materials is through the processing of polymeric blends, which is a versatile technological solution usually cheaper and faster than synthesizing new polymers (Paoli, 2008). Stress cracking is a phenomenon that limits and compromises the application of polymeric materials and is the most common type of fracture in polymers, representing approximately 25% of failures in service. For this reason, stress cracking is considered a silent killer. The general objective of this study is to evaluate the resistance of the PP/PS blend to stress cracking in different active fluids. For this purpose, test specimens will be obtained and analyzed under tension/deformation conditions in the presence of ethanol and octanol. The PP/PS blends will be used with weight concentrations of 70/30, 50/50, and 30/70 percent.

References:

1. CORAZZA, E. C. R. F. Termoplásticos: os materiais e suas transformações. 4. ed. São Paulo, 1995.
2. DE PAOLI, M. A. Degradação e Estabilização de Polímeros. 1ª ed. São Paulo: Artliber Editora, 2009.
3. TURNBULL, A.; MAXWELL, A. S.; PILLAI, S. Comparative assessment of slow strain rate, 4-pt bend and constantload test methods for measuring environment stress cracking of polymers. Polymer Testing, v. 19, p.117-129, 2000.

Fundings: pro dean of extension - PROEX.

Keywords: Polymeric Materials, Stress Cracking, Blends, Active Fluids

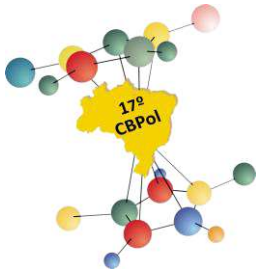

UV-VIS, PHOTOLUMINESCENCE AND ANTIOXIDANT PROPERTIES OF OF PVA/CHITOSAN BLENDS MODIFIED WITH PITAYA EXTRACT

Erica dos S. Ribeiro[1], Artemis. M. Ceschin[2], Nizamara. S. Pereira[1*]

1 – Instituto Federal de Brasília, Departamento de Química, Brasília-DF, Brazil
e-mail: nizamara.pereira@ifb.edu.br
2 – Universidade de Brasília, Departamento de Engenharia Elétrica, Brasília-DF, Brazil

Abstract - Polyvinyl alcohol (PVA) has been widely applied in industries due to its low cost, non-toxicity and biodegradability. PVA together with polymers from renewable sources can form materials with new optical and antioxidant properties through the blending process. It is possible to insert natural substances that can act as antioxidants within the polymeric matrix of the mixture. In this work, the PVA/Ch blends were altered with pitaya extract, which caused changes in the optical activities and increased the antioxidant properties of the polymer blend.

Keywords: *blends, chitosan, pitaya, antioxidants, UV-VIS, PL*

Introduction

Nowadays, most packages are produced from synthetic polymers derived from petroleum, producing a lot of waste. Considering environmental issues and the world's demand for biodegradable packaging, natural polymers have received much attention from researchers to form active films. Among the biopolymers or polymers from renewable sources studied for the development of active packaging, we can mention chitosan [1], gelatin [2] and starch [3]. Among the biodegradable synthetic polymers, there is poly(vinyl alcohol) (PVA), a water-soluble and biodegradable polymer which is nontoxic and has application in different fields such as resins, medical, building industry and packaging materials [4,5]. Polymers from renewable sources possess high solubility in water, but possess poor barrier and mechanical properties. To improve these characteristics, the method of preparing blends and/or composites, with or without the addition of additives is used [6]. Polymer blends involve combining two or more polymers to give rise to a new material without drastically changing the attributes of the original polymers. Additives such as plasticisers, crosslinking, antimicrobial and antioxidants can be incorporated into polymeric matrix to enhance the properties of the films [6]. Antioxidants are widely used in the plastic industry, aiming at protecting polymers during their oxidation process. Polymer oxidation occurs when there is exposure of the material to an aggressive environment under heating in the presence of oxygen. In these conditions, free radicals are generated, leading to chain scission reactions, cross-linking or to the auto-catalysis of oxidation reactions [7]. The antioxidants derived from plants act similarly and are commonly used for different materials, protecting from oxygen action and its reactive forms [8]. Natural antioxidants prevent the formation of free radicals, intercept the oxidizing agents created, inhibit chain reactions and prevent the initiation stage of the emission process of metals such as cadmium, mercury, copper and lead, maintained in this way as natural stabilizers. Moreover, some antioxidants are capable, not only of counteracting the reactive forms of oxygen, but also absorbing UV radiation projecting

photodegradation compounds [8]. In addition, additives extracted from plants have natural dyes that can change the optical properties of the polymeric blend, expanding its application beyond active packaging. In this way, this work prepared polymer blends from PVA and chitosan (Ch) with pitaya extract incorporated into a polymeric matrix of the blend and its optical and antioxidant properties were analyzed.

Experimental

Preparation of the extract of pitaya (ExPy)

The fruit pulp was crushed using a mixer, the infusion was carried out with 400 mL of water at 90°C for 10 minutes. Subsequently, the sample was centrifuged at 5000 rpm for 30 minutes. After centrifugation, the extract was vacuum filtered. All extracts were stored and frozen in order to remain preserved.

Preparation of polymer blends (PVA/Ch) with pitaya extract incorporated in the polymeric matrix

The polymer blends were prepared according to the literature (with adaptations). Initially, 0.35g of chitosan was weighed. The weighed chitosan mass was dissolved in 50 mL of a 1% acetic acid solution. The chitosan (Ch) solution was taken to a sonicator for 2h. Subsequently, the solution was maintained under magnetic stirring for 15 h at a temperature of 40 ºC. Separately, 5g of PVA was weighed and dissolved in 50 mL of distilled water. Then 2 mL of glycerol was added, and the solution remained under magnetic stirring for 1 h at an average temperature of 50°C. After this period, the PVA solution, under constant agitation, was cooled to room temperature. To obtain the PVA/Ch polymeric blend, the Ch and PVA solutions were mixed under magnetic stirring for one hour at room temperature. Then, this polymeric solution was sonicated for 15 minutes in order to completely homogenize the solution. After this process of preparing the PVA/Ch blend, the ExP were mixed in the solution to obtain PVA/Chitosan/ExPy polymer blends with 9 and 16% (v/v) proportion for extract of pitaya. Then, the solution remained under stirring for 10 min at 25°C. After sample homogenization, the PVA/Ch/ExPy blends with its extract were poured onto a non-stick surface and placed in an oven at an average temperature of 50ºC for 19h. UV-VIS spectra of the films were obtained on a Perkin Elmer spectrophotometer (model Lambda 35), operating in the range of 800-190 nm. The Fluorescence spectra of the solution films were recorded on an LS-55 fluorescence spectrometer (Perkin Elmer). The photoluminescence (PL) study was obtained at excitation wavelength 240 nm. The antioxidant activity of the samples was evaluated by the modified methods according to Dordevic et al [9]. Approximately 100 mg of the film sample was weighted and 20 mL of ethanol was added. The samples were sonicated for 30 min and kept for 24h in ethanol. After 24h, the extracts were filtrated, 3 mL of extract and 1 mL of 0.1 mM DPPH solution in ethanol were mixed. The samples were incubated at laboratory temperature in the dark for 30 min and the absorbance was measured at 517 nm by spectrophotometer Perkin Elmer Lambda 35. Each sample was measured in triplicate and the antioxidant property of the films was expressed as percent inhibition of the DPPH radical (DPPH inhibition %), calculated according to Eq. 1:

$$DPPH\ inhibition\ (\%) = \left(\frac{A_0 - A_1}{A_0}\right) x\ 100,$$

where A_0 is the absorbance of the DPPH radical and A_1 is the absorbance of the sample.

Results and Discussion

The UV-VIS spectrum for pitaya extract showed an absorption band in the range of 450 to 620 nm with a maximum at 536 nm (Fig.1). This absorption range resulted from the existence of betalains pigments belonging to pitaya extract. Betalains have antioxidant properties which favor light absorbing because these pigments exist in nature in association with various copigments [10].

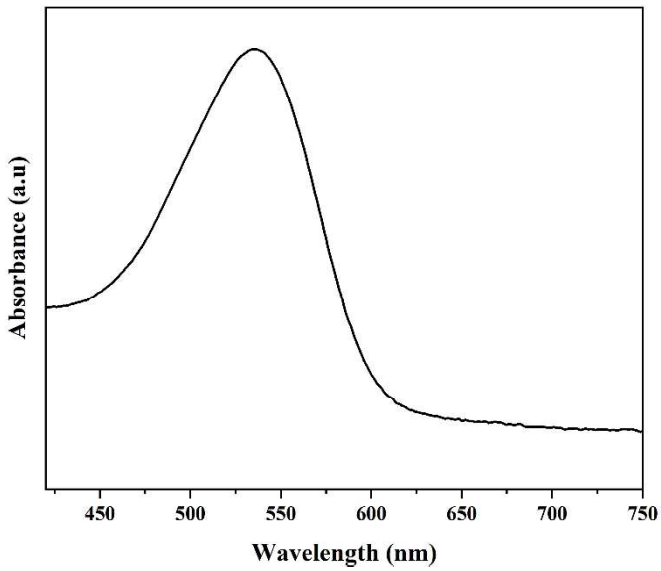

Figure 1 - Spectrum of UV-VIS of pitaya extract.

When ExP was incorporated into the PVA/Ch film to produce PVA/Ch/ExPy with 9 and 16% (v/v), it altered the absorption properties of the polymeric blend, producing a new absorption band in the range of 250 to 450 nm with a maximum at 305 nm (Fig. 2). The sample with the highest extract content showed absorption intensity as expected. The shift in the absorption maximum to shorter wavelengths can be attributed to the intermolecular interactions of the pitaya extract with the polymeric chains of the blend. The results confirm the incorporation of pitaya extract to the PVA/chitosan film since the pure blend film does not show absorption in this region of the spectrum (Fig. 2b).

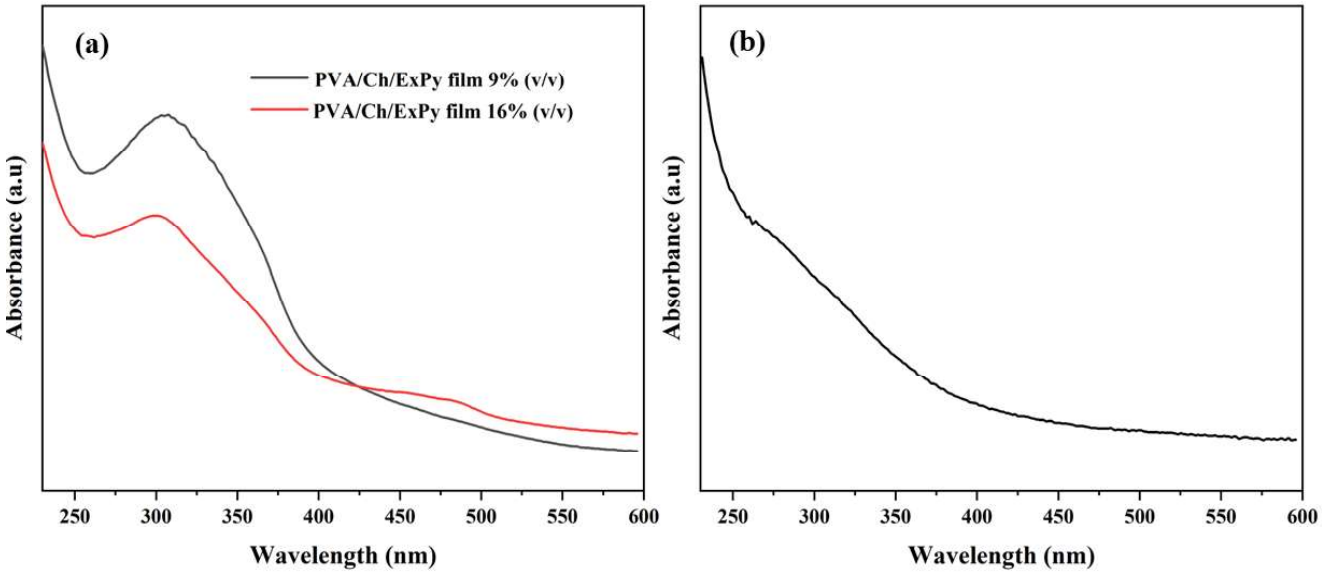

Figure 2 - Spectra of UV-VIS of (a) PVA/Ch/ExPy 9 and 16% (v/v) film and (b) pure PVA/Ch blend film.

The photoluminescence emission spectra (PL intensity *vs* wavelength) of the PVA/Ch, PVA/Ch/ExPy 9 and 16% are depicted in Fig. 3. For the study of photoluminescence properties, several spectra were taken at an excitation wavelength of 240 nm. The photoluminescence spectra of PVA/Ch presented two emission bands with maximum at 384 nm and 725 nm. PVA/Ch has photoluminescence at 384 nm that can be attributed to the amine group present in Ch which is protonated, and it has a lone pair of electrons in an aqueous acid [11]. The PL spectrum of pitaya

extract showed two emission bands with a maximum at 380 nm and 725 nm. The PVA/Ch/ExP blends and pure PVA/Ch blend revealed a PL spectrum similar to pitaya extract with emission maximum at 382 nm to principal band and to second emission in the range 725-742 nm. This means that the polymeric chain of the blend allowed the pitaya extract to manifest its light-emitting property without changes or suppression.

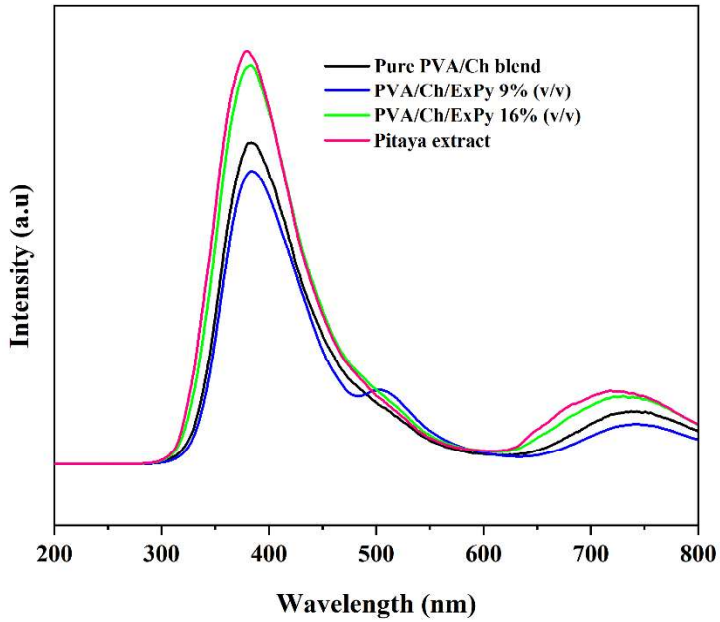

Figure 3 - Spectra of photoluminescence of the PVA/Ch blend pure and PVA/Ch/ExPy 9 and 16% (v/v)

In Figure 4, the pure PVA/Ch film presented the DPPH inhibition of 77,2%, indicating that there was a good antioxidant property in pure PVA/Ch film. The PVA/Ch/ExPy 9 and 16% films presented a slightly higher DPPH inhibition with 82.5 and 82%, respectively.

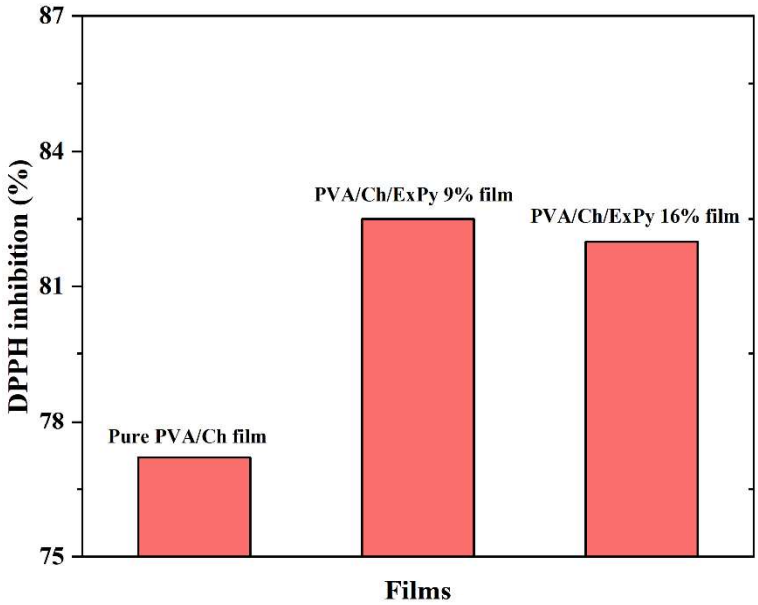

Figure 4 - DPPH inhibition (%) of the polymeric materials.

Previous studies [12] have shown that pure PVA film has no antioxidant properties. However, the presence of chitosan in the blend formulation considerably increased DPPH inhibition. The incorporation of pitaya extract contributed to the polymeric material having an inhibition of more

than 80% of DPPH. DPPH absorbance decreased because DPPH was eliminated by chitosan and pitaya extract through hydrogen donation and pitaya extract through the donation of hydrogen to the DPPH radical to form a stable molecule, resulting in the change of color of the solution. In general, the presence of pitaya extract increased the inhibition power of the DPPH radical in PVA/Ch films.

Conclusions

The polymer blends of PVA/Ch incorporated with pitaya extract were prepared, and their opticals and antioxidants properties were evaluated. The addition of pitaya extract altered the absorption property of the blend. All solutions of polymer blends, when excited at a wavelength of 240 nm, showed an emission spectrum similar to the pitaya extract. The presence of the extract provided a slight increase in the antioxidant property of pure PVA/Ch film.

Acknowledgements

The authors would like to thank the Federal Institute of Brasilia (IFB) and FAPDF for financial support.

References

1. Y. Xu,.; Development and properties of bacterial cellulose, curcumin, and chitosan composite biodegradable films for active packaging materials, Carbohydrate Polymers, 260, 2021, 117778 - 117788.
2. J. C. Nunes;.*Journal of Food Science and Technology*, 2021, 58, 1.
3. M. Dammak, . Y. Fourati, Q. Tarrés, M.Delgado-Aguilar; P. Mutjé, S.Boufi, *Industrial Crops & Products*, 2020. 144, 2020, 112061.
4. J. A. da Cruz, A. B. da Silva, B. B.S. Ramin, P.R. Souza, K.C. Popat, R.S. Zola, M. J. Kipperd, A. F. Martins, Materials Science & Engineering C 2020, 107, 110357.
5. J. Naman; S. V. Kumar; C. Sakshi. Journal of the Mechanical Behavior of Materials, 2017, 26, 213. DOI: https://doi.org/10.1515/jmbm-2017-0027.
6. I. S. V. Silva, R. M. F.Sousa, A. Oliveira, W. J. Oliveira, L. A. C. M., D. Pasquini, H. Otaguro, Carbohydrate Polymers 2018 , 202, 203.
7. A. Rigoussen; P. Verge, J. M. Raquez, P. Dubois, ACS Sustainable Chem. Eng. 2018, 6, 10, 13349.
8. O. Olejnik, A. Masek, A. Kiersnowski Polymers 2020, 12, 74.
9. S. Dordevic, D.Dordevic, P. Sedlacek, M. Kalina, K. Tesikova, B. Antonic, B. Tremlova, J. Trem, M. Nejezchlebova, L. Vapenka, A. Rajchl, M. Bulakova, Polymers 2021, 13, 3388. https://doi.org/10.3390/polym13193388
10. R. Syafinar, N. Gomesh, M. Irwanto, M. Fareq, Y. M. Irwan Journal of Engineering and Applied Sciences 2015, 10, 6354.
11. S. Kumara, B. Krishnakumar, A.J.F.N. Sobral, J. Koh Carbohydrate Polymers, 2019, 205, 559.
12. R.Tan,F. Li, Y. Zhang,Z. Yuan, X. Feng, W. Zhang, T. Liang, J. Cao, C. F. De Hoop, X. Peng, X. Huang Journal of Nanomaterials, 2021, 1. https://doi.org/10.1155/2021/4821717

ACTIVE COMPOSITE FILMS – CARBOXYMETHYLCELLULOSE/ CURCUMIN AND EGG-SHELL POWDER COMPLEX

Lara M. M. Oliveira[1*], Felipe P. C. Gomes[1] and Yeda M. B. de Almeida[1]

1 – Department of Chemical Engineering, Federal University of Pernambuco (UFPE), Recife, PE, Brazil
lara.melooliveira@ufpe.br[*], felipe.pcgomes@ufpe.br, yeda.oliveira@ufpe.br

Abstract – Developing sustainable alternatives for current single-use packaging is an important technological transformation to increase biological nutrient cycles in a circular economy framework. Carboxymethylcellulose (CMC), a biodegradable polymer, was used as the polymeric matrix of composite films using egg-shell waste particles as a support for an active compound. Egg-shell waste was milled to reach a fine powder, then it was taken into a muffle furnace and calcinated at 900°C for 4 h. [1] After that, the powder was hydrated with distilled water (10:3 w/v), and then mixed with curcumin ethanolic solution (2,71 mM), thus forming the curcumin and egg-shell powder complex (CCO). Active films were obtained by casting method, incorporating the dried active complex to the CMC solution (20% w/w). The composite film was analyzed in contact with a fatty food simulant (50 mL of soybean oil) after 10 minutes and after 10 days. The results in Fig. 1 show the main FTIR-ATR spectra: it is noticeable that some bands related to CMC groups could have been influenced by the contact with the oil. The active films also exhibit characteristic peaks at 871, 1589 and 1795 cm^{-1}, corresponding to carbonate groups, indicating the presence of the CCO in the films, i.e., the active properties of the composite were maintained even after the contact with the oil, corroborating for its potential application as active food packaging.

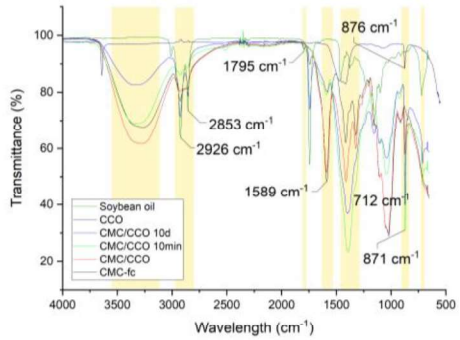

Figure 1 – FTIR-ATR spectra of CCO, soybean oil, CMC control film (CMC-cf) and the active films before (CMC/CCO), after 10 min (CMC/CCO 10min) and after 10 days (CMC/CCO 10d) immersed in soybean oil.

References

1. I. M. El-Nahhal; J. K. Salem; H. Z. L. Okal; F. S. Kodeh; A. A. Elmanama. *Journal of Sol-Gel Science and Technology* 2022, *101*. https://doi.org/10.1007/s10971-021-05709-5.

Fundings: The authors would like to acknowledge the financial support of CAPES.

Keywords: *Active composite; carboxymethylcellulose films; curcumin; egg-shell powder.*

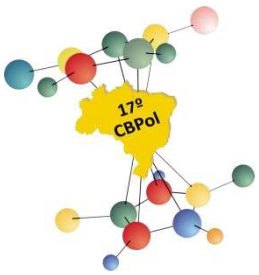

BIOCOMPOSITES BASED ON PBAT AND SPENT COFFEE GROUNDS: EVALUATION OF BIODEGRADATION IN SOIL AND SIMULATED MARINE ENVIRONMENT

Debora C. da S. Santos[1,2], Carolina Q. Passos[1,2], Simone M. de Rezende[1,2], Fernanda C. F. Braga[1], Marcelo F. L de Oliveira[1] and Marcia G. de Oliveira[1]*

1 – Instituto Nacional de Tecnologia (INT), Divisão de Materiais (DIMAT), Laboratório de Tecnologia de Materiais Poliméricos (LAMAP), Rio de Janeiro, Brazil
2 – Faculdade de Filosofia, Ciências e Letras Souza Marques, Rio de Janeiro, Brazil
debora.cristina@int.gov.br

Abstract – The use of spent coffee grounds (SCG) from domestic disposal carried out by households in dumps and that consist of lignocellulosic natural fibers can be a renewable reinforcement agent and low-cost alternative in the production of biodegradable polymers composites for the developing friendly artifacts. In this work, composites were prepared by mixtures poly(butylene adipate-co-terephthalate) (PBAT) with 50 wt. % of spent coffee grounds, untreated (PBAT/SCG) and treated via sodium hydroxide (PBAT/SCGT), on an internal chamber mixer equipped with ROLLER type rotors, followed by compressed molding. The SCG and composites were characterized by infrared spectroscopy (FTIR), thermogravimetric analysis (TGA) and scanning electron microscopy (MEV). Tensile mechanical tests of samples were performed for evaluate the mechanical properties The biodegradation was evaluated using simulated soil method (ASTM G 160) and simulated marine environment (ASTM D1141/6691), monitoring the weight loss, visual inspection and morphological of surface biodegraded analysis. FTIR spectra of SCG treated show low absorption bands at 2924 cm^{-1} and 1740 cm^{-1} regions when compared SCG untreated. It may be assigned -CH, CH_2 and C=O stretching and bending vibration, indicating the removal of part of the hemicellulose and lignin from the natural fiber structure. The results of Young modulus of the PBAT/SCGT presented increased values than biocomposite untreated and PBAT pure due a great interfacial area between components after alkali treatment. The thermal resistance of all composites showed a similar weight loss curve profile as a function of temperature, but was noted a slight reduction in the initial degradation temperature (T_{onset}), when compared to the curve profile of the PBAT. The results of biodegradation tests showed that composites with spent coffee grounds treated presented higher weight loss than PBAT pure for both methods. It was noted this, the composites in marine environment absorbed water before starting the decomposition process.

References

1. SANTOS, DEBORA CRISTINA da SILVA. Use of spent coffee grounds as reinforcement for the production of biodegradable composite with pbat. Trabalho de Conclusão de Curso (Graduação em bacharelado em Química) - Faculdade de Filosofia, Ciências e Letras Souza Marques. Rio de Janeiro. 2022.
2. LEOW , Y.; YEW, P.Y.M.; CHEE, P.Y.; LOH, X.J.; KAI, D. Recycling of spent coffee grounds for useful extracts and green composites. RSC Adv., v.11, p. 2682-2692, 2021.
3. CRUZ, MONICK ALVES. Evaluation of biodegradability of commercial polymers by simulated marine environment method. Dissertação (Mestrado em Química) – Instituto de Química. Universidade do Estado do Rio de Janeiro. Rio de Janeiro. 2016.

Keywords: *Coffee grounds, PBAT, Residue, Copolyester. Biodegradation.*

BIOPOLYMER-BASED HYDROGELS FOR Cd^{2+} ION REMOVAL IN AQUEOUS MEDIUM

Paula P. Silva[1*], Vinicius A. M. Gomes[1]; Juliano Brisola[1]; Gizilene Maria de Carvalho[1]

1 – Chemistry graduate program, State University of Londrina (UEL), Londrina, PR, Brazil
paula.paulino94@uel.br

In recent decades several studies have been carried out aiming at the development of polysaccharide hydrogels for the removal of dyes and polluting metals in wastewater. Cellulose hydrogels are a sustainable alternative and have several advantages when it comes to the sorption process, including high swelling capacity, low toxicity, and easy preparation, make them a promising sorbent material. [1]. In this sense, this study sought to use water-soluble polysaccharide, alginate (AL) and carboxymethylcellulose (CMC) to enhance adsorption capacity cellulose (CEL) for removal of Cd^{2+} in aqueous medium.The CEL/AG and CMC/ALG hydrogels were produced from solutions (3% m/v) of CEL and AL, (1% m/v) of CMC, with a 50/50 proportion of polymers and gelled in a chloride solution of calcium (1% w/v). Scanning electron microscopy (SEM) analysis showed that the CEL/AL 50/50 hydrogel has an irregular spherical external morphology, while the CMC/AL 50/50 has a more compact surface. The result of the kinetic study shows that the removal efficiency of 83% of the Cd^{2+} ion in the first 60 min for the CEL/AL 50/50 hydrogel and of 56% in the first 120 min for CMC/AL 50/50. The Langmuir, Freundlich and SIPs adsorption isotherms were used to analyze the adsorption equilibrium over the entire concentration range from 5 to 50 mg. L^{-1}. The adsorption of Cd^{2+} onto CEL/AL 50/50 was multi-layer and controlled, which could be well illustrated by Freundlich with a n values between 1 to 10 and a correlation coefficient (R^2) of 0.903, indicating that the surface of the adsorbent is heterogeneous and it has adsorption sites in different layers. For the CMC/AL 50/50 hydrogel, the Sips model presented the best fit, with values of R^2 0.970 and value of n = 2.39, indicating that there may be simultaneous contribution of adsorption in monolayer and at multiple sites [2].

References

1. F. P. VIANA, K. R. A. SANTOS, A. M. A. AMORIM, V. A. OLIVEIRA, A. C. M. O. MONTEIRO, AND E. C. LIMA. International Journal of Biological Macromolecules.v.191: 222–232, 2021.
2. REDLICH, O.; PETERSON, D. L. Journal of Physical Chemistry.v.63.1024–1024,1958.

Acknowledgments: This work was carried out with the support of the Coordination for the Improvement of Higher Education Personnel-Brazil (CAPES) and Fundação Araucária/Brazil. LMEM-Laboratorio de Microscopy et Microanalyse.

Keywords: Biopolymers; Adsorption; polluting metals.

CATALYSTS IN POLYHIDROXYESTER BASED VITRIMERS

Marcos L. Dias[1*], Marcio Nele[2] and Rodrigo H. Cunha[1]

1 - Universidade Federal do Rio de Janeiro, Instituto de Macromoléculas Professora Eloisa Mano, Av. Horácio Macedo, 2030, 21941-598, Rio de Janeiro, RJ, Brazil.
mldias@ima.ufrj.br

2 - Escola de Química, Av. Athos da Silveira Ramos, Universidade Federal do Rio de Janeiro, Av. Athos da Silveira Ramos, 149, 21941-909, Rio de Janeiro, Brazil

Abstract – Conventional crosslinked polymers (thermosets) are polymer networks with strong permanent crosslinks that are not reprocessable and cannot be physically recycled for high value applications. Differently from thermosets, vitrimers are polymer networks with dynamic or reversible crosslinks in which covalently linked chains can have its topology reorganized by bond exchange reactions without compromise the material integrity [1,2]. One interesting class of vitrimers are those based on catalyst containing polyhidroxyesters in which reversible bonds are related with transesterification reactions. In this context, this contribution presents results of the study on polyhydroxyesters synthesis based in diepoxy monomers such as diglycidyl polyethylene glycol (PEGDGE) and di and tricarboxylic acids (ex. sebacic acid (SA) and citric acid (CA)) in presence of different metal catalysts (zinc, tin and antimony) used to promote network curing and reprocessing by thermal-induced transesterification reactions. The effect of catalyst concentration on curing kinetics, and the dynamics of the bond exchange reaction in the polymer network. The vitrimer freezing topology transition temperature (Tv) was evaluated by thermal expansion and dynamic mechanical analyses. All these catalysts showed to effectively promote the fast curing and network formation and to modify the network Tv.

References

1. D. Montarnal, M. Capelot, F. Tournilhac, L. Leibler *Science* 2011, 334, 965. https://doi.org/10.1126/science.1212648
2. A. Jurowska, K. Jurowski *Chemik* 2015, 69, 392.

Fundings: The authors thank the Brazilian agencies CNPq (Grant 307364/2018-6) and FAPERJ (E-26/202.538/2019) for financial support.

Keywords: *Vitrimer, polyethyleneglycol diglycidyl ether, sebacic acids, citric acid, polyhydroxyester, catalyst*

CHARACTERIZATION OF NATURAL RUBBER-BASED FIBROUS BIOCOMPOSITE REINFORCED WITH BIOACTIVE GLASS-CERAMIC PARTICLES FOR BIOMEDICAL APPLICATIONS

Luiz R. M. Lima[1], Guilherme F. Caetano[2,3], Viviane O. Soares[4], José A. Malmonge[1], Michael J. Silva[5,*]

[1] São Paulo State University (UNESP), Faculty of Engineering, Department of Physics and Chemistry, Ilha Solteira, São Paulo, 15385-000, Brazil.
[2] Graduate Program in Biomedical Sciences, University Center of Hermínio Ometto Foundation, FHO, Araras 13607-339, SP, Brazil.
[3] Division of Dermatology, Department of Internal Medicine, Ribeirao Preto Medical School, University of Sao Paulo, Ribeirao Preto, 14049-900, Sao Paulo, Brazil.
[4] Universidade Estadual de Maringá (UEM), Câmpus Regional de Goioerê, Rua Reitor Zeferino Vaz, s/n - Jardim Universitário, 87360-000, Goioerê, Paraná, Brazil.
[5] São Paulo State University (UNESP), Faculty of Engineering and Science, Department of Energy Engineering, Rosana, São Paulo, 19274-000, Brazil. e-mail: michael.silva@unesp.br

Abstract - In this study, a new fibrous mat biocomposites formed with natural rubber (NR) and containing BL0 or BioS particles was developed using solution blow spinning technique. In order to assess fiber formation and BG dispersion in fibrous specimens, SEM morphological analyses were conducted. It was observed that average fiber diameter (d_m) increased with the incorporation of BG in NR fibers, i.e., for pure NR, the d_m value was 74.47 ± 24.54 µm, while for NR/BioS and NR/BL0 the values were 78.96 ± 30.54 µm and 84.75 ± 25.69 µm, respectively. The TG/DTG tests indicate that NR/BioS and NR/BL0 fibrous biocomposites display similar thermal profiles to neat NR, whose main events occur between 290°C and 450°C, indicative of structural degradation of NR chains. According to the mechanical tensile test, adding BioS or BL0 to the NR-based biocomposite enhanced the tensile strength at break and elastic modulus, as compared to neat NR. As a result of dynamic mechanical analysis (DMA), the stored modulus and loss factor of the fibrous specimens of NR/BioS (70/30) and NR/BL0 (70/30) displayed higher values than those of the NR fibrous sample, since the specimens became more rigid as BG quantity was increased. The indirect cytotoxicity tests showed that NR, NR/BL0, and NR/BioS fibrous biocomposite promoted MSC attachment, i.e., greater than 70% viability. In addition to improving tensile properties and biological properties of NR-based fibrous biocomposite, BioS and BL0 particles have been shown to have potential applications in biomedicine.

Fundings: 21/10512-5 – FAPESP

Keywords: *Natural Rubber, Bioactive glass-ceramic, Fibrous mast biocomposite*

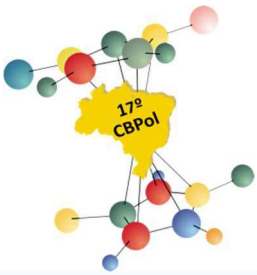

COCONUT FIBER TREATED AS A FUNCTION OF TIME WITH METAKAOLIN AND INDUSTRIAL ASH SOLUTION

Renato R. Monteiro, Celso C. M. Fornari Junior*

1 – Department of Engineering and Computer, State University of anta Cruz (UESC), Ilhéus, BA, Brazil
corresponding_rrmonteiro@uesc.br

Abstract
The promotion of a strong interaction between plant fibers and polymer matrices promises the formation of materials with higher mechanical performance. The search for materials with better properties offers the goods production sector the opportunity to replace conventional materials with more sustainable, friendly and ecologically correct composites. However, the chemical natures of plant fibers and polymers need to approach in order to increase the mutual attraction in order to promote a greater electrostatic interaction and/or mechanical anchoring. In this work, coconut fiber was modified in order to promote nucleation and the growth of embedded crystals on the surface of the fiber. This condition alters the morphology and chemical condition of the fiber, and may promote better interactions with polymeric matrices. The fibers were in contact with pozzolanic solutions at temperature and environmental conditions for different time intervals. The images revealed a considerable population of crystals in the fibers that were subjected to these conditions.

Keywords: *Coconut fiber, Composite, Metakaolin.*

Introduction

World population growth has marked an upward march, and statistics point to a world population between 9 and 10 billion inhabitants in the year 2050 [1]. Given these perspectives, the productive sector must be organized to maintain and supply society's consumption demand, in order to preserve the best well-being of the entire population. Adjustments and conditions must be favorable to maintain society's comfort in terms of energy, services, food and materials [2,3]. The productive sector has the duty to adjust itself to the challenge of supplying the products necessary for the better well-being of society. In this forecast, the manufacturing sector needs to find alternatives in relation to new materials that present significant properties and that may replace materials from non-renewable sources. The productive sector is moving in the direction of finding materials with considerable mechanical properties and, above all, sustainability and respect for the environment. Since the last decade, the industrial sector has replaced conventional materials with polymers in numerous applications, such as metals and glass [4]. Cellulose is an important constituent of plant fibers and is the most abundant natural polymer on earth. In addition to renewable, pollution-free production with carbon sequestration, biodegradability, low production cost, low abrasiveness and considerable mechanical properties [5-7].

The agricultural production of coconut in Brazil in 2019, according to data from the Brazilian Institute of Geography and Statistics, surpassed the number of 1,500,000,000 fruits, placing the country among the five largest world producers of the fruit. The inner shell of the coconut (mesocarp) is composed of a fibrous cellulosic structure interspersed with a soft, low-density structure, consisting of 90% water and mineral salts and 10% fiber by weight. The fibers have a density between 1.1 and 1.4 g/cm3 and between 95 and 230 MPa of tensile strength [8]. Dry coconut fibers consist of approximately 40% cellulose, 45% lignin and 15% hemicellulose.

Numerous researchers have been dedicated to the investigation of composites and plant fibers. Although vegetable fibers present promising applications in substitution of other materials, they have specific peculiarities that need to be better understood in order to guarantee greater properties of future composite materials. Cellulosic fibers have a hydrophilic nature, mainly due to hydroxyl groups positioned along the chain. This characteristic or property goes in the opposite direction to a large number of hydrophobic polymers, generating an incompatibility between them, which does not allow achieving greater or better properties in the future material. In this sense, many works have been carried out to modify the surface of plant fibers or polymers, and have shown satisfactory results [9-12]. The union that occurs between the vegetable fiber and the polymer matrix plays a fundamental role in the cohesion of the composite and will be reflected in the final properties of the material. The binding forces that act in the fiber-polymer interfacial region can occur in different ways, isolated or together. Electrostatic chemical interaction is usually present between these materials, especially if there are compatible polar natures. Interdiffusion and mechanical anchoring or interlocking can also favor a better union between the fiber and the matrix. Chemical reactions, in turn, can also occur depending on energetic conditions [13]. In this study, coconut fibers were modified in order to possibly promote better anchoring or interlocking strength with polymeric matrices. The fibers were brought into contact with pozzolanic solutions at ambient conditions. In this way, there was spontaneous nucleation of crystals on the surface of the fiber, promoting a population of these crystals. The work evaluated two types of mineral solution and different times of contact between the fiber and the solution. The images revealed that a considerable number of crystals nucleate and develop on the surface of the coconut fiber in relatively short times.

Experimental

The coconut fibers used in this work come from the region of Una, state of Bahia, by means of defibrillation in industrial equipment. The fibers were then manually cut into 25 mm lengths. The fibers were submitted to pre-treatment with a 20% w/w NaOH solution for 20 minutes and at rest. In sequence, the fibers were washed in running water for 5 minutes, repeating this procedure three times and neutralized in a 10% acetic acid solution. The fibers were then placed in a 10% w/w acetic acid solution for 5 minutes. Then the fibers were dried with a paper towel and placed in a metallic plate and taken to an oven at 120 ± 5 ºC for a period of 60 minutes. The pozzolanic solutions of industrial ash and metakaolin were made just before use. For this, distilled water were used. The solutions were made at concentrations of 10 and 30% by weight of solute and solvent (w/w). After the time elapsed for each contact process of the coconut fiber with the solution, the fibers were dried at room temperature. Metakaolin was kindly donated by Metacaulim do Brasil.

Results and Discussion

Coconut fruit fibers are made up of a sequence of nanocellulose bundles specially distributed and structured by the presence of hemicellulose, thus initially constituting a physical and rigid microstructure which is packaged and protected by a layer of lignin. The union and compaction of these microstructures will originate larger and bulky fibrous bundles, which in turn will culminate in the cellulosic macrofiber [8]. The outer surface of the coconut fiber has a peculiar structure and is covered by a layer of fatty substances, with the presence of salts and pectin [14-17]. These conditions that the fiber presents can be modified through specific treatments. Many methods were used to modify the physicochemical conditions of coconut fiber, using heated water, solvents, alkaline solutions, peroxides, silanes. Among chemical methods, the use of alkaline NaOH solution has been evaluated by several researchers [18-20]

These treatments have been used with the aim of modifying the external structure of the fiber, mainly eliminating impurities, fatty substances, lignin and hemicellulose. Longer alkaline treatments, in turn, can destroy the cellulosic fiber structure, breaking down the hemicellulose and

exposing cellulose filaments. These modifications with alkaline solution may favor a better interaction/adhesion between the fiber and the composite matrix compared to fibers without modifications or treatments. Figure 1 shows the surface of untreated and treated coconut fiber, where the layer of fatty substance covers the surface in the form of scales and coexists with rounded globular particles.

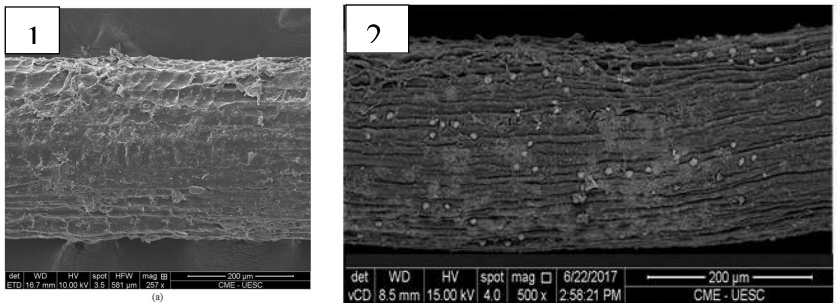

Figure 1 – Micrograph of coconut natural fiber (1) and after treatment with metakaolin (2)

Synthetic fibers such as glass fibers are also used industrially in the manufacture of polymer composite parts, mainly due to their mechanical resistance properties. However, to increase the properties of composites, some treatments are applied to these fibers using, for example, silane, hydrofluoric acid, phosphoric acid, among others. Depending on the type of application, a specific treatment can be performed, aiming to achieve a certain result. These treatments promote the surface modification of the glass fiber, promoting chemical bonds or roughness, improving chemical interaction and anchoring with the polymeric matrix [21-23]

In the case of composites with vegetable fibers, chemical treatments can modify the chemical structure of the fibrous surface by removing components or by grafting binding agents to the polymeric matrix. These modifications can promote greater electrostatic approximation between hydrophilic fibers and hydrophobic polymers and, consequently, greater interaction between the constituents. Many binding agents have been evaluated in studies, such as: maleic anhydride [24], silanes [25], epoxy [26] and have been shown to promote positive improvements in composite properties.

Science has shown that altering the fibrous structure, as well as modifying the polymeric matrix, can promote a more concise fiber/polymer interaction, benefiting the energetic bonds between both materials. Thus, the present study seeks to evaluate the formation of crystals on the surfaces of coconut fibers, in order to promote mechanical and possibly chemical anchorage points between this and the polymeric matrix. The crystals spontaneously deposited onto the fiber surface and show significant adhesion.

From the contact of the vegetable fiber with mineral aqueous solution, the formation of solids on the fibrous surface was quantitatively evaluated by means of scanning electron microscopy. The process took place at room temperature and was observed as a function of time. The deposition and growth of crystals occurred spontaneously and under thermodynamically natural conditions. The process proved to be of low environmental risk and low operational cost.

Metakaolin is a pozzolamic mineral consisting mainly of silica and alumina called siliceous or alumino-siliceous materials and found in silica fume, ashes and calcined clays (where metakaolin is found). These finely divided structures can react in the presence of water and calcium at room temperature to form calcium silicates or aluminates [27].

The coconut fibers previously treated with an alkaline solution proved to be without the original fatty layer. The conditions applied in this study were sufficient to remove most or all of the region that covered the outermost part of the fiber. The fibers were exposed in relation to their microstructure and presented long and parallel grooves in the direction of the fibers. The furrows are the result of the approximation of two cylindrical microbundles of fibers, which tend to reduce

the space between them as they gain depth. The fibrous microbundles have an average diameter of 8 microns.

The studies evaluated the influence of the industrial ash solution concentration with different concentrations and contact time. The evaluations used images taken by scanning electronic microscopy and with magnification of 2000 times. This allows for a better quantitative comparison between images to assess crystal growth. Figure 2 shows the fibers that remained in a 10% w/w solution of industrial ash and different times. For 10 minutes, some crystals grew on the surface of the pre-treated coconut fiber. As the contact time with the solution increases, the crystal population tends to increase, even if very discreetly. Probably the condition of 10% w/w of the solution, because it offers a poor and low concentration of ions, favors very slowly the nucleation and growth of crystals on the surface of the fiber. However, the contact of the fiber with the solution was favorable to the formation of crystals.

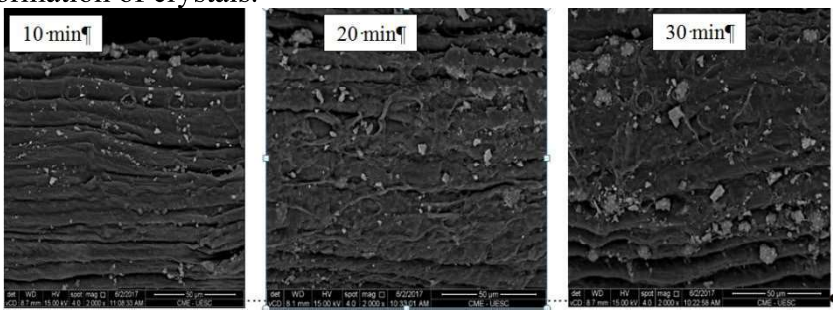

Figure 2: Pre-treated coconut fiber in contact with a 10% w/w industrial ash solution and varying times.

The contact of the pre-treated coconut fiber with the solution of 30% w/w of industrial ash demonstrated the nucleation of crystals on the fiber. As the length of time the fiber remains in the solution increases, the crystal population increases. For the time of 30 minutes there was a significant nucleation of crystals, covering approximately 50% of the coconut fiber surface. In this condition, crystal growth appears to occur in preferred locations. There are regions of the fiber surface with an accentuated population of crystals and other regions that are free. Figure 3 shows the fibers that remained in a solution of 30% w/w of industrial ash and different times.

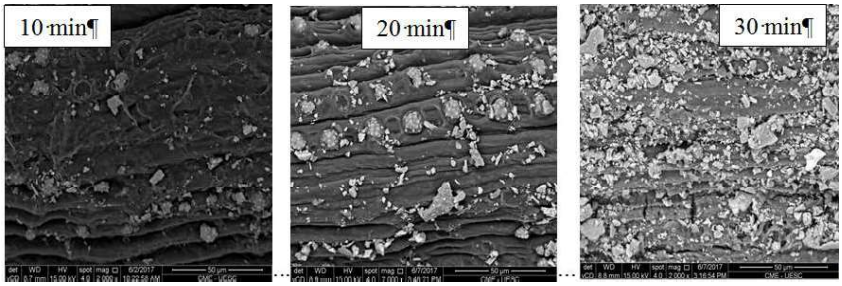

Figure 3: Pre-treated coconut fiber in contact with a 30% w/w industrial ash solution and varying times.

Preliminary tests with isophthalic polyester composites and vegetable fiber in the natural state and treated with metakaolin, demonstrated that the resistance of the composite to flexion was around 30% higher with treated fiber compared with natural fiber.

Conclusions

The nucleation of crystals from pozzolanic aqueous solutions of ash and metakaolin at concentrations of 10 and 30% by weight are able to promote the nucleation and growth of crystals on coconut fiber treated with NaOH solution, after 10 minutes of contact. Increasing the contact time promotes a greater population of crystals on the fiber surface. The natural conditions for nucleation and growth of crystals on coconut fiber are low energy consumption and simple to operate, promoting processes that are friendlier to the environment.

Acknowledgements

The authors would like to thank the State University of Santa Cruz for the research conditions carried out at LAPOS, the Polymers and Systems laboratory.

References

1- K. C. O. Saath, A. L. Fachinello.. Rev. Econ. Sociol. Rural, Brasília 2018, 56.

2- C. Brancaleone. Política & Sociedade. 2020, 19, 301-336

3- S. S. Franco;, P. R. Santanna. UNIFESO-Humanas e Sociais, 2021, 6, 24-37.,

4- T.G.Y. Gowda, M.R. Sanjay, K. S. Bhat, P. Madhu, P. Senthamaraikannan, B. Yogesha. Polymer matrix-natural fiber composites: An overview. Cogent Engineering 2018, 5, 1-13..

5- S. Dixit, GOEL, R. Goel, A. Dubey, P. R. Shivhare, T. Bhalavi. Polymers from Renewable Resources, 2017, 8

6- A. Kumre, R.S. Rana, R. Purohit. Materials Today Proceedings, 2017, 4, 3466-3476

7- P, P. Manimaran, K. Senthamaraikannan, M. M. R. Sanjay. Journal of Natural Fibers 2018, 15, 29-38.

8- C. C. M. FORNARI JUNIOR,. Fibras Vegetais para Compósitos Poliméricos, Editus, 1 Ed., Universidade Estadual de Santa Cruz. Ilhéus 2017. http://www.uesc.br/editora/livrosdigitais2018/fibras_vegetais.pdf

9- V. Mazzanti, R. Pariante, A. Bonanno, O.R. Ballesteros, F. Mollica, G. Filippone. Composites Science and Technology 2019, 180, 51-59.

10- M. L. Silva, W. J. S. Silva A. K. L. S. Pereira. Brazilian Journal of Development. 2020, 6, 86238-86250.

11- K. S. L. Barbosa, W.S. T Santos, MENDES B. H. A. Mendes, W. R. Banna, D. S. Costa, J. A. S. Souza, D. S. Costa. Brazilian Applied Science Review 2020, 4, 1474-1481

12- S. S. Chattopadhayay, R. K. KHANDAL, R Uppaluri, A. K. Ghoshal. Journal of Applied Polymer Science, 2011, 121, 2226-2232.

13- H. Mohit, V. A. M. Selvan. Composite Interfaces 2018, 25, 629-667.

14- A. S. Moura, R. Demorib, R. M. leão, C. L C. Frankenbergd, R. C. M. Santana. Materials Today Communication 2019, 18, 191-198.

15- M. Arsyad, I. N, G, Wardana, Y.S. Pratikto. Revista Matéria 2015, 20, 169-177.

16- S. A. Hussain, V. Pandurangadu, K. Palanikuamr.. International Journal of Engineering Science and Technology (IJEST). 2011, 3.

17- D. M. Oliveira, , M. O. H. Cioffia, K. Beninia, C. C. C. Voorwalda. H. J. Cornelis. Procedia Engineering 2017, 200, 357-364.

18- A. I. S. Brigida, V. M. A. Calado, L.R.B. Gonçalves, M. A. Z. Coelho Carbohydrate Polymers 2010, 79, 832-838.

19- R. M. Leão, S. M. Luz, J. A. Araujo, K. Novack. Journal Natural Fibers, 2015, 12, 574-586

20- A. May-pat, V. A. Gonzales, P. J. Herrera-Franco. Polymer Testing. 2013, 32, 1114-1122.

21- R. R. Dittrich. Tese apresentada ao Programa de Pos Graduação, Setor de Tecnologia, Universidade Federal do Paraná,2006.

22- A. D. C. M. Valdivia, V. R. Novais, M. S. Menezes, , M. Roscoe. C. E. Giomarâes, C. J. Soares,. Brazilian dental Journal 2014, 25.

23- O. Laban E. Mahdi. International Journal of Adhesion and Adhesives. 2017, 78, 234-239.

24- M. E. G. Lopez, R. R. Ortiz, , R. M. Gonzalez, J. A. S. Guzman, A. A. Fonseca PComposite Interfaces, , 2018, 25, 515-538.

25- Y. Nishitani, T. Kajiyama, T. Yamanaka Materiais, 2017, 10, 1-21.

26- D. Battegazzore, A. Frache, M. L. Maspoch. Com Part B: Engineering. 2018, 148, 188-197.

27- F. C. Mattos; M. R. F. Gonçalves. Matéria Rio de Janeiro, 2019, 24.

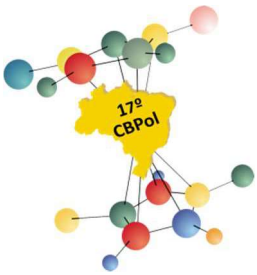

COMPARATIVE STUDY OF THE EXTRACTION OF SOLUBLES FROM COCONUT FIBER IN AQUEOUS ALKALINE SOLUTION UNDER SHAKING AND REST

Jhonatas M. Riqueza, Renato R. Monteiro, Celso C. M. Fornari Junior*

1 – Department of Engineering and Computer, State University of anta Cruz (UESC), Ilhéus, BA, Brazil
corresponding_celso@uesc.com.br

Abstract - The exploration in the construction of polymeric composites with vegetable fibers is a more ecologically correct alternative for the supply of materials and raw materials to the productive sector. Due to numerous factors, vegetable fibers present great opportunities for the construction of new materials that can supply the industrial demand. However, one of the main factors responsible for achieving excellent properties in composites is undoubtedly the interaction that occurs between their constituents. The morphology of the vegetable fiber is of great importance in the construction of materials with high mechanical performance, since it is responsible for the union with the polymeric matrix. This work was dedicated to investigate the response of coconut fiber when in alkaline aqueous solution. Different process times were evaluated and under conditions of agitation and rest. The results showed that the soluble extraction rate varies with time.

Keywords: *Coconut fiber, Composite, Process.*

Introduction

The search for more ecologically correct alternatives is a worldwide goal to be achieved. However, the production and consumption of goods and products involves the transformation of raw materials, many of which are non-renewable. In current times, it is necessary to find alternatives for the production of goods where the raw materials can come from renewable sources. Efforts to understand and deepen knowledge in composite materials with plant fibers is undoubtedly an alternative path, both in terms of developing more ecological alternatives and in the use of renewable and environmentally friendly raw materials [1, 2],

However, despite the construction of polymeric composites with vegetable fibers being an ecologically correct and promising path for the near future, the understanding of the science that involves the union of these materials does not seem to reach the needs of the industry. Many polymeric composites with vegetable fiber have relative mechanical properties and are already part of the cartel in the industrial production sector [3-5]. On the other hand, exploring the properties of plant fibers, associated with polymeric matrices, involves greater interaction between the fiber and the matrix itself. In this sense, many researchers have promoted the chemical modification of the fiber, using coupling agents or binding agents [6-8]. The results showed to be promising and improve the final properties of the composites in most cases.

Fiber morphology is the an important factor to achieve good properties in the composite. It is who will be responsible for the physical-chemical union between both materials, fiber and polymeric matrix. In this way, it is essential to evaluate and understand the study of the modification of vegetable fiber, in order to know which conditions can possibly be achieved and how this occurs.

This work was dedicated to understanding the comportament of coconut vegetable fiber in relation to contact with alkaline aqueous solution. Different times of fiber contact with the solution were evaluated and the results showed that the soluble extraction rate varies as a function of time.

Experimental

The work used a digital scale with four decimal places, Bioprecisa, model FA 2104N. Servitech mechanical stirrer, model CT 054 with rotation of 300 rpm and four blades of 40 x 20 mm. A 500 ml beaker was used for soluble extractions. An oven was used for drying the fibers at a temperature of 130 ± 5 ºC. Filter paper was used for filtering the solutions. Distilled water was used to wash the fibers after each test time. The fibers were filtered through filter paper and then washed three times with 200 ml of distilled water for each washing process. Four types of tests were performed with different times of 24 hours each. The test conditions were at rest (RE) and under agitation (AG). The tests took place at an ambient temperature of 26 ºC. Alkaline sodium bicarbonate aqueous solution was used in the proportion of 8% w/w.

Results and Discussion

The results revealed that as the contact time increases with the alkaline solution and the fiber, more solubles are extracted from the fiber into the solution. However, the extraction rate proved to be variable throughout all processes. The studies revealed that after the time of contact with the solution at rest (RE) and under agitation (AG) the extraction was quantitatively different and increasing with the increase of the contact time. Initially the rate was low and increased with the number of extractions. For the tests conducted in 24 hours of rest, the fiber decreased by 4.5% in weight. The modification that the solution causes is initially in the most external part of the fiber. This process removes the covering layer of coconut fiber, which is composed of wax, fat and pectin. The wax layer is a protective barrier that initially covers the fibrous structure, isolating it from external agents, preventing the solution from coming into direct contact with the structure fiber physics. Figure 1 shows the image of natural coconut fiber (A), with the structure representing scale and the fiber treated in 1M NaOH alkaline solution for one hour (B). After the alkaline treatment, the fatty layer was removed, thus exposing the cellulose fiber microbundles [9,10]

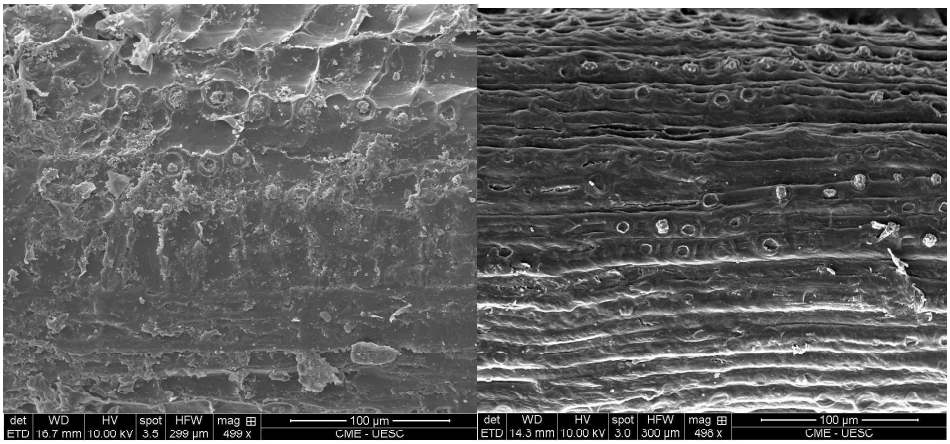

Figure 1: Natural coconut fiber (A) and coconut fiber treated in NaOH solution.

For the assay and 24 hours approximately 5.4% of soluble were extracted. The percentage difference between the rest and agitation condition was less than 1%, indicating that there were no significant differences in these conditions. The soluble extraction rate is 0.00939 g/h for RE and 0.01131 g/h for AG.

During the contact time, the outermost layer of the fiber is removed by the main action of the alkaline solution, showing little influence of agitation or resting modes. After the contact time of 48 hours, there was approximately twice the absolute extraction of soluble from the fiber, compared to the time of 24 hours. The difference between the RE and AG conditions was approximately 1% and the amount of mass extracted was approximately equal to twice that of the 24-hour assay. The extraction rate of soluble is 0.01114 g/h for RE and 0.01203 g/h for AG.

The mass extraction rate is relatively constant up to a total time of 48 hours, corroborating the dissolution of the outermost wax layer still remaining. The results indicate that in this first extraction step, the dissolution of the wax layer is the predominant step in the extraction rate of soluble. The results indicate that there is no significant difference between the conditions of rest and agitation, practically repeating the results of the 24-hour test. Under these conditions, the extraction of lignin contained inside the fibers has possibly not started yet due to the probable impossibility of contacting the solution with the inside of the fiber. However, for times equal to 72 hours, there is a significant difference in relation to the process in RE and AG. The difference for the two conditions increases approximately 3.5%, indicating that the agitation conditions at that moment are more favorable for the extraction of soluble. The extraction rate of soluble is 0.007775 g/h for RE and 0.010169 g/h for AG. The removal of soluble in the RE condition decreased the rate in relation to shorter extraction times, indicating that only the contact of the fiber with the solution does not seem to increase with the removal of soluble from the fiber

Possibly, the removal of the wax covering allowed the exposure of the fibrous bundles, which now suffer the action of chemical and mechanical leaching. It is interesting to observe the influence of agitation compared to extraction in the resting condition. The forced contact of the fiber with the solution under agitation seems to favor and promote the continuous action of the solution in the extraction of soluble.

For the extreme condition of the test, equal to 96 hours, mass extractions increased in relation to other extraction times. However, the extraction difference in relation to the RE and AG extraction modes was approximately 4.5%. This difference is the largest for all process times, indicating that time directly influences the removal of soluble. However, the results revealed that the mechanical action that promoted the agitation of the solution is significantly important to assist in the removal of soluble. The extraction rate of soluble is 0.00633 g/h for RE and 0.00868 g/h for AG. The extraction rate decreased with processing time which may have been due to the decrease in solution strength as it approached the saturation point. Table 1 presents the mass values and the differences for each extraction process.

Table 1 - Mass of fibers to dry before and after the extraction process

Sample	Time (h)	Initial mass (g)	Final mass (g)	Mass difference (g)	Loss percentage (%)
1 RE	24	5,0042	4,77867	0,22553	4,5068
2 AG		5,0043	4,73283	0,27147	5,4247
3 RE	48	5,0075	4,47239	0,53511	10,6861
4 AG		5,0078	4,43002	0,57778	11,5376
5 RE	72	5,0090	4,44920	0,55980	11,1758
6 AG		5,0050	4,27280	0,73220	14,6293
7 RE	96	5,0023	4,39460	0,60770	12,1484
8 AG		5,0077	4,17441	0,83329	16,6401

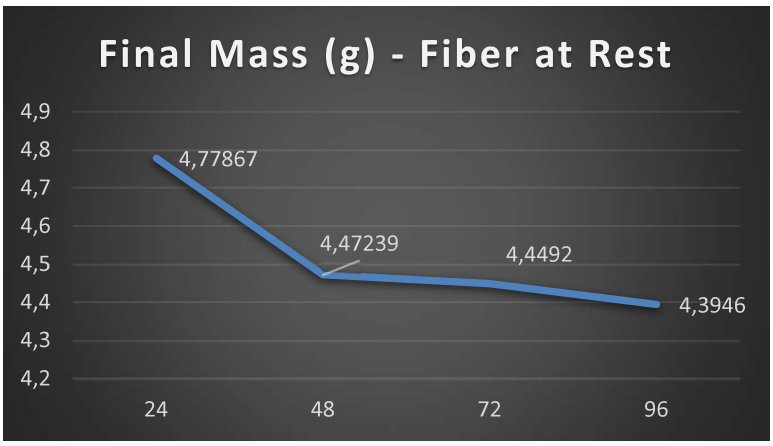

Figure 2 - Results of fiber mass fractions after each extraction process

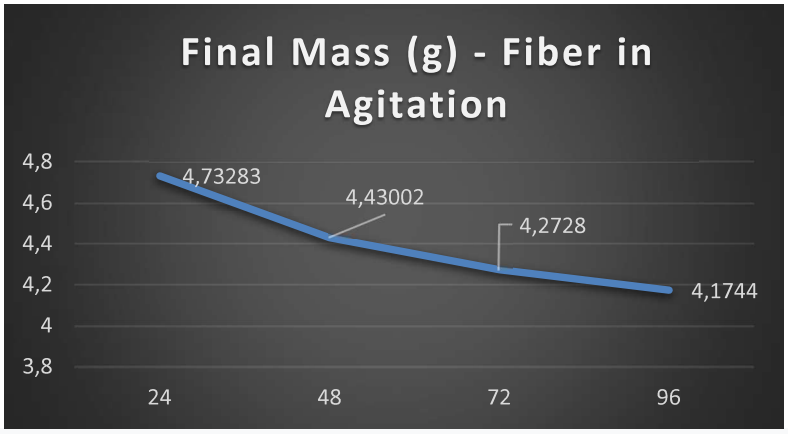

Figure 3 - Results of fiber mass fractions after each extraction process

In the extraction tests, the residues of the solution of each process time were collected. From right to left are the solutions resulting from increasing times (24, 48...) in both test conditions. For the RE condition, the solutions demonstrate more transparency and for the AG condition, the color of the solution is more accentuated. The presence of soluble, mainly lignin, is responsible for the orange color.

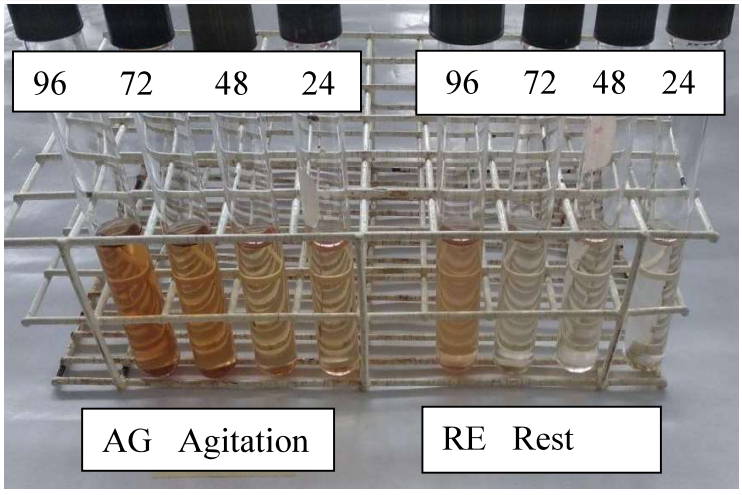

Figure 4 – Aqueous alkaline solutions after each process and type of extraction:

Acknowledgement: The authors thanks for the State University of Santa Cruz for the support for this work.

Conclusions

The works demonstrated that the coconut fiber in alkaline solution varies the condition of extraction of solubles in function of the time of contact and the condition of rest or agitation. For the first 48 hours of processing, the difference in weight of soluble fiber extraction was approximately 1% and the extraction rates were approximately 0.01 g/h for the extraction and resting processes. After 72 hours, the difference in solubles extracted in both conditions was approximately 3.5% and the extraction rate for the resting condition decreased and the agitation rate remained approximately constant. However for the time of 96 hours, the difference in weight extraction for both conditions was approximately 4.5% and the extraction rates decreased for both process conditions. Coconut fibers in alkaline solution at rest and under agitation have different behavior as a function of time.

References

1. S. Y NAYAK. M. T. H. Sultan, S. B. Shenoy, C. R. Kini, R. Samant, A. U. M. Shah, P. Amuthakkannan. **Journal of Natural Fibers**, v. 19, n. 5, p. 1648-1658, 2022.
2. G. Y. G. THYAVIHALLI. **Frontiers in Materials**, v. 6, p. 226, 2019.
3. .A. GHOLAMPOUR, T. OZBAKKALOGLU. **Journal of Materials Science**, v. 55, n. 3, p. 829-892, 2020.
4. M. Y. KHALID, A. Rashid, Z. U. Arif, W. Ahshad, H. Arshad, A. A. Zaidi. **Results in Engineering**, v. 11, p. 100263, 2021.
5. M. ZWAWI, M**olecules**, v. 26, n. 2, p. 404, 2021.
6. P. JAGADEESH. M. Puttegowda, S. R. Mavinkere, S. Siengchin. **Polymer Composites**, v. 42, n. 12, p. 6239-6264, 2021.
7. D. P. FERREIRA; J. CRUZ, R. FANGUEIRO. **Green composites for automotive applications**. Woodhead Publishing, 2019. p. 3-41.
8. R. LATIF, S. Wakeel, K. N. Zaman, S. S. Noor, S. L. Verna, Z. K. **Journal of Reinforced Plastics and Composites**, v. 38, n. 1, p. 15-30, 2019.
9. C. C. M. FORNARI JUNIOR Fibras Vegetais para Compósitos Poliméricos. Ed. Editus, Universidade estadual de Santa Cruz, Ilhéus, 2017.
10. S. P. SIMELANE, D. M. MADYIRA. **Smart, Sustainable Manufacturing in an Ever-Changing World: Proceedings of International Conference on Competitive Manufacturing (COMA'22)**. Cham: Springer International Publishing, 2023. p. 701-713
11. M. ASIM, M. T.Paridah, M. Chandrasekar, R. M. Shahroze, M. Jawaid, M. Nasir, R. Siakeng. **Iranian Polymer Journal**, v. 29, p. 625-648, 2020.

COMPOSITES BASED ON BACTERIAL CELLULOSE/Ag_3PO_4 WITH POTENTIAL ANTIMICROBIAL ACTION

Amanda L. Generoso[1*], Lais R. de Lima[1], Marcelo de Assis[2], Hernane S. Barud[3], Sandra A. Cruz[1]

1 – Departament of Chemistry, Federal University of São Carlos (UFSCar), São Carlos, SP, Brazil
2 – Department of Analytical and Physical Chemistry, University Jaume I (UJI), Castelló 12071, Spain
3 – Laboratory of Biopolymers and Biomaterials, University of Araraquara (UNIARA), Araraquara, SP, Brazil
**Corresponding Author E-mail: amandalyane@estudante.ufscar.br*

Abstract - The recent spread of the coronavirus pandemic (COVID-19), as well as other emerging microbial infections, are complex and often difficult to control and treat, which making them one of the main obstacles to public health. In this context, there is a demand for the development of advanced materials that inactivate microorganisms aiming at the protection of the human population. Bacterial Cellulose (BC) is an extremely pure multifunctional biopolymer, biocompatible and biodegradable. The BC architecture composed of nanofibers with high porosity, that contribute to modifications and incorporation of substances in your matrix to improve or add properties and expanding your applicability. This work proposes a more efficient methodology to synthesize composite BC films with silver particles, a vacuum filtration was used to force the formation of silver phosphate (Ag_3PO_4) crystals on the bulk of BC films and create a gradiente of particle content. Therefore, the objective was to develop of a composite containing properties from silver particles, and properties from bacterial cellulose, ensuring a biocompatible and non-toxic material with potential antimicrobial activity. The influence of the incorporation of different concentrations of Ag_3PO_4 on the properties of the biopolymer was investigated using spectroscopic, thermal and morphological techniques. The antimicrobial effect of composite membranes was evaluated using microbiological assays with pathogenic species of gram-positive and gram-negative bacteria (*S. aureus* and *E. coli*) and fungi (*C. albicans*). It is proposed that the composite film developed has potential for use in the food industry, for applications in antimicrobial active packaging.

References

1. A. J. Jawad *Global Journal of Materials Science and Engineering* 2020. https://doi.org/10.36266/GJMSE/108.
2. L. R. Lima; D. B. Santos; M. V. Santos; H. S. Barud; M. A. Henrique; D. Pasquini; E. Pecoraro; S. J. L. Ribeiro *Química Nova* 2015, 38, 9, 1140-1147. https://doi.org/10.5935/0100-4042.20150131.
3. N. Pogorelova; E. Rogachev; I. Digel; S. Chernigova; D. Nardin *Materials*, 2020, 13(12), 2849. https://10.3390/ma13122849

Keywords: *composites, bacterial cellulose, silver phosphate, antimicrobial effect.*

CONSOLIDATION AND CHARACTERIZATION OF CARBON FIBER/SNAP CURE EPOXY RESIN LAMINATES PRODUCED BY PREPREG HOT PRESSING

Guilherme Ferreira de Melo Morgado[1], Larissa Stieven Montagna[1], Fabio Roberto Passador*[1], Mirabel Cerqueira Rezende[1]

1 – Polymer and Biopolymer Technology Laboratory (TecPBio), Federal University of São Paulo (UNIFESP), 330 Talim St., São José dos Campos 12231-280, Brazil.

morgado@unifesp.br

Abstract - Carbon fiber reinforced polymer (CFRP) composites have gained a significant amount of attention in recent years due to their superior mechanical properties, such as high strength-to-weight ratio and stiffness, compared to traditional engineering materials. These properties make them suitable for use in a variety of applications, including aerospace, automotive, and sports equipment [1]. The matrix material in CFRP plays an important role in determining the final mechanical properties of the composite. In this study, a snap cure epoxy resin was used as the matrix material in the CFRP composite. The snap cure process is a relatively new technology in the manufacturing of CFRP composites, which allows for faster curing times and thus reduces production costs [2]. The goal of this study was to consolidate the CFRP composite using the prepreg hot pressing technique and evaluate its properties through ultrasound, acid digestion, and tensile strength testing. Different hot-pressing cycles were tested, resulting in optimal parameters, such as temperature and pressure. The results of the ultrasonic inspection and acid digestion revealed that the optimal samples did not have significant defects. The tensile tests showed that the laminates had high strength and stiffness, with an average tensile strength of 700 MPa and an elastic modulus of 60 GPa. In conclusion, the prepreg hot-pressing technique was effective in consolidating the carbon fiber/epoxy resin laminates, resulting in high-quality specimens with no significant defects. Tensile strength tests demonstrated that the laminates had high strength and stiffness, making them suitable for use in a variety of structural applications. Overall, the results of this study demonstrate the effectiveness of the hot-pressing technique for producing high-quality carbon fiber/epoxy resin laminates from snap cure prepreg.

References

1. Kondo, M.Y., Montagna, L.S., Morgado, G.F.M., Castilho, A.L.G., Batista, L.A.P.S., Botelho, E.C., Costa, M.L., Passador, F.R., Rezende, M.C., Ribeiro, M.V. Polímeros 2022, 32(2), e2022023. https://doi.org/10.1590/0104-1428.20220042.
2. Costa M. L., Rezende M. C., Paiva J.N. F., Botelho E. C. Polymer-Plastics Technology and Engineering 2006, 45(10). https://doi.org/10.1080/03602550600887251

Fundings: Federal Government Program 'Rota 2030', n° 27194.03.03/2020.01-00 for the financial support; the LEL/IPT for the coordination, and FIPT, FUNDEP for the administrative support.

Keywords: *Carbon fiber; Snap cure epoxy resin; Composite material; Ultrasound inspection; Tensile testing*

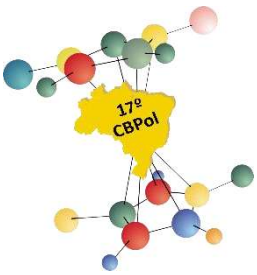

DEVELOPMENT OF FILTERING SYSTEMS BASED ON POLYSACCHARIDES BY ELECTROSPINING

Luana Priscila de Souza[1*], Beatriz Luci Fernandes[2] and Clayton Fernandes de Souza[1,2].

1 – School of Education and Humanities, Chemistry Undergraduate Course, Pontifícia Universidade Católica do Paraná, Curitiba, Paraná, Curitiba, Brazil
luana.priscila@pucpr.edu.br
2 – Health Technology Graduate Program, Pontifícia Universidade Católica do Paraná (PUCPR), Curitiba, Paraná, Brazil

Currently several types of adsorbents are developed for the treatment and purification of liquids and gases and due to a growing environmental crisis, there is an urgent need to improve water and air quality and to develop antiviral and bactericidal filtering systems. In this way, biopolymers, such as cashew tree gum-CTG and *Kappa*-carrageenan-*K*C, are an attractive alternative for the development of these systems due to chemical structures and viscous properties using water as solvent, that able to explore in electrospinning process. The CTG is a complex heteropolysaccharide exuded from the stem of the *Anacardium occidentale* tree and by its structural similarity and physical-chemical properties with a commercial gum arabic, and *K*C is a linear sulfated polysaccharide extracted from seaweeds, which has the ability to form strong gels and the viscosity can be modulated depending on the concentration or in the presence of other molecules or ions. Based on the characteristic of these polymers, the aim of this work was to evaluate the potential application of CTG and *K*C solutions in electro- and blow- spinning techniques to produce nanofibers for filters systems. In this way, several concentrations (6% m/m, 10% m/m, 15% m/m and 20% m/m) were prepared with purified polysaccharides and was submitted to electrospinning (voltage = 6 kV, flying distance = 6 cm and flow rate 30 microliters/min) and blowing spinning systems (pressure of 2 bar, a flight distance of 50 and flow rate 30 microliters/min). The previous results indicated the viscous dependence to obtain taylor cone, in range of 100-200 mPa or fiber formation in blowing conditions. As conclusion, there are able to produce membranes with high surface area and porosity based on CTG and KC systems.

References

1. K. C. S. Andrade; C. W. P de Carvalho; C. Y. Takeiti; H. M. C. de Azeredo; J. da S. Corrêa; C. M. Caldas *Polímeros* 2013, 23 (5), 667-671. https://doi.org/10.4322/polimeros.2013.004
2. H. T. Ha; D. X. Cuong; L. H. Thuy; P. T. Thuan; D. T. Tuyen; V. T. Mo et al. *Molecules* 2022, 27 (4), 1268. https://doi.org/10.3390/molecules27041268
3. Y. Lei; X. Zhao; D. Li; L. Wang; Y. Wang *Foods* 2022, 11(5), 734. http://dx.doi.org/10.3390/foods11050734
4. L. Tong; X. Kang; Q. Fang; W. Yang; S. Cen; Q. Lou et al. *J Texture Stud* 2022, 53(1), 122–32. https://doi.org/10.1111/jtxs.12624

Keywords: *electrospinning techniques, Cashew Tree Gum, Kappa carrageenan, filtration systems, polysaccharides.*

DEVELOPMENT OF SULFONATED PEEK IONIC POLYMER METAL COMPOSITES: ELECTROMECHANICAL CHARACTERIZATIONS

Guilherme E. de O. Blanco[1]*, Renan L. Valerio[1], Rafael Barbosa[1], Matheus C. Saccardo[1], Kaique A. Tozzi[2] and Carlos H. Scuracchio[1]

1 – Department of Materials Engineering (DEMa), Federal University of São Carlos (UFSCar), São Carlos, SP, Brazil
guilhermeedublanco@gmail.com
2 - Univ. Grenoble Alpes, Univ. Savoie Mont Blanc, CNRS, Grenoble INP, LEPMI, UMR5279, 38000 Grenoble, France

Abstract - Ionic polymer-metal composites (IPMCs) are smart and bio-inspired materials with a metal/polymer/metal structure that can deform in response to electrical stimuli and vice versa [1]. Usually, they are flexible, biocompatible, have low density, and low actuation voltage, making them promising materials in various applications such as soft actuators, artificial muscles, sensors, and robotics. The most widely used polymer for these purposes is Nafion®, however, it is expensive, not environmental friendly, moisture sensitive, and has poor performance at high temperatures [2]. In this sense, several efforts have been conducted to develop alternative membranes, including the sulfonated poly(ether-ether-ketone) (SPEEK). Therefore, the aim of this study is to evaluate the effect of different sulfonation degrees (SD) on its electromechanical performance, using the post-sulfonation of VICTREX™ PEEK 450G™. SPEEK membranes were fabricated by the post-sulfonation method, and named SPEEK-X (X = sulfonation time in hours). SPEEK-1, SPEEK-6, and SPEEK-12 presented SD of 44, 72, and 91% respectively. The membranes were fabricated by solution casting, and the IPMCs were manufactured by an electroless plating method, and then incorporated with H^+ counter ions. Comparative studies with Nafion® 117 were conducted. Electromechanical tests were conducted under different relative humidity (RH) (30, 60, and 90%) under DC voltage (1-5 V). Increasing SD shows higher values of bending strain actuation. Fig 1 compares both bending strains of Nafion and SPEEK-12, after 60 seconds of electrical stimulus. This result shows that SPEEK is a promising candidate to substitute Nafion as an intelligent and bio-inspired device with relatively reduced cost.

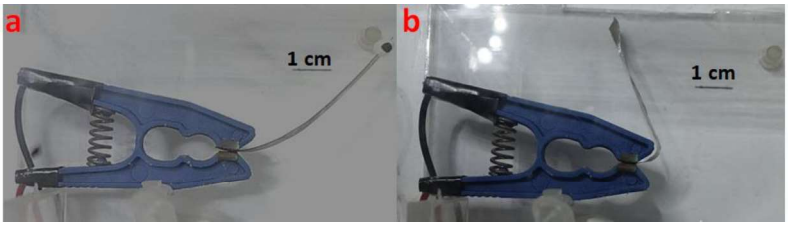

Figure 1 – Bending strain actuation of Nafion (a) and SPEEK-12 (b) under 90% RH and 5 V.

References

1. Y. Bahramzadeh and M. Shahinpoor. *Soft Robotics 2014, 1, 1.* https://doi.org/10.1089/soro.2013.0006.
2. Y. Tang; Z. Xue; X. Xie; X. Zhou. *Sensors and Actuators A: Physical*, 2016, 238, 167. https://doi.org10.1016/j.sna.2015.12.015.

Fundings: CNPq (process 161101/2021-6), Fapesp (process 2022/10033-2) and CAPES - Funding Code 001.

Keywords: *IPMCs; Sulfonated PEEK; Sulfonation Degree; Electromechanical Performance*

DYNAMICAL-MECHANICAL PROPERTIES OF RECYCLED POLYMER FROM MULTILAYER FILMS AFTER STRUCTURAL CHANGE BY HIGH SHEAR RATE

Antonio J. A. Junior*, Emerson F. Silva, Clodoaldo Saron

Department of Materials Engineering, Engineering School of Lorena (EEL), University of São Paulo (USP), São Paulo, SP, Brazil, aajosejunior@usp.br

Abstract – The recycling of polymer waste from multilayer films used as packaging presents some barriers due to the complex composition of the material, leading to the formation of immiscible polymer blend when it is mechanically recycled by conventional processing. The aims of this study was to evaluate the dynamical-mechanical behavior as function of temperature of recycled polymer from packaging film waste after mechanical processing in internal mixer under high shear rates at different processing times. Samples of polymer waste (Film-waste) based on polyethylene and reference of virgin low-density polyethylene (LDPE) were processed in internal mixer MH-600 under atmosphere of nitrogen, maintaining a rotation at 4500 rpm by 30, 60 and 90 s after polymer melting. Afterward, the materials were processed by injection molding for preparation specimens. The dimensions of the specimens were adjusted for 50 x 10 x 3,2 mm to subsequent dynamical-mechanical analysis (DMA) in a NETZSCH DMA 242 E Artemis in flexion mode, using a dual cantilever device from -150 to 150 ºC, at a heating rate at 2 $K.min^{-1}$ and frequency of 1 Hz. The DMA analysis of the Film-waste has showed characteristic dynamic-mechanical relaxations of LDPE as well as relaxation of others polymers. The mechanical processing at high shear rate produces changes in the DMA curves, depending of the processing time. Thus, structural changes can be caused by shear rate, which can lead to the polymer mixture compatibilization.

Keywords: Recycling, Multilayer films, LDPE, Shear Rate, DMA.

Fundings: National Council for Scientific and Technological Development - CNPq (Proc. 309583/2020-9) and FAPESP (Proc. 2020/14318-6).

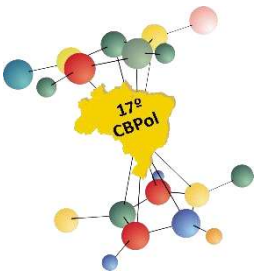

EFFECT OF ALGINATE ADDITION ON THE PHYSICOCHEMICAL PROPERTIES OF CHITOSAN FILMS

Andressa E. Sobczyk[1*], Júlia M.F. Pavoni[1], Cláudia L. Luchese[1], Débora J. L. Faccin[1], Nilo S. M. Cardozo[1], Isabel C. Tessaro[1]

1 – Department of Chemical Engineering, Federal University of Rio Grande do Sul (UFRGS), Porto Alegre, RS, Brazil
*andressa.enq@gmail.com

Abstract - Biodegradable polymers from renewable sources are gaining prominence in the biomedical area, mainly for application as dressings, since they can act as partial substitutes for some non-biodegradable synthetic materials used in this area. Chitosan is a biodegradable biopolymer with various applications due to its functional properties, such as antibacterial activity and non-toxicity. However, it has high hydrophilicity, and the films produced from this macromolecule present a high degree of swelling when in contact with water, hindering its use in some applications. There are alternatives to overcome these limitations, including its combination with biopolymers of different characteristics to achieve the desired properties in the final material. This work aimed to evaluate the influence of alginate incorporation on the physicochemical properties of chitosan films prepared by casting. The polymeric solutions were made separately, with chitosan solubilized in an acid medium (lactic acid solution, 1% v/v) and alginate in water. The two solutions were mixed to obtain composite chitosan-alginate (1:1) films (CA). Pure chitosan films (C) were also prepared as a reference. The produced films were characterized by thickness measurements, the visual aspect and morphology, water absorption capacity (WAC), water vapor permeability (WVP), and chemical structure analysis. Macroscopically, all films were homogeneous, transparent, and easy to handle. Compared to C films, CA films showed larger apparent surface roughness, perceptible to the touch, higher thickness (71 %), and higher WVP values (1667 %). The chitosan films were completely soluble in water. However, the combination with alginate prevented dissolution and CA films showed greater stability in the presence of water, presenting only moderate swelling. The improvements observed in the properties of CA films indicate that the combination of these compounds is promising since some limitations of films containing only chitosan can be overcome.

Fundings: Coordenação de Aperfeiçoamento de Pessoal de Nível Superior (CAPES), Conselho Nacional de Desenvolvimento Científico e Tecnológico (CNPq).

Keywords: *biodegradable polymers, casting, films, stability in water*

Effect of Carboxymethyl Cellulose (CMC) Concentration and Glycerol Plasticizer Variation on the Production of Plastic Films via Casting Method

Ana Gabriele da Costa Sales[1], Gleison N. Marques[1], Maria Inês B. Bernardi[2], and Lucia H. Mascaro[1]

[1]CDMF, LIEC, Federal University of São Carlos - (UFSCar), São Carlos, SP, 13565-905 Brazil

[2] Instituto de Física de São Carlos, Universidade de São Paulo (IFSC-USP), São Carlos, SP, 13560-970, Brazil

**Corresponding Author: gabicosta09@hotmail.com*

Abstract - The use of natural polymers has attracted attention due to the reduction of environmental impacts related to their disposal[1]. In this sense, cellulose and its derivatives are often considered for applications in the field of food packaging due to their properties, such as bioavailability and the possibility of forming blends with other biopolymers[2]. Carboxymethylcellulose (CMC) is one such derivative that shows good solubility in water and is therefore also widely used in the pharmaceutical sector, drug delivery applications, and producing films for use as food packaging[2]. Thus, the objective of this work was to investigate the effect of CMC concentration and the use of glycerol on the thermal, mechanical, and barrier properties of films formed by the casting method. The films produced were characterized by TG-DTA, DSC, SEM, AFM, and contact angle techniques. SEM images revealed homogeneity in the formation of films without the presence of regions with agglomerated particles. This conformity on the surface was confirmed through AFM measurements, which demonstrated a significant decrease in the roughness of the films from 4.89 nm to 0.33 nm, indicating that the increase in CMC helps to standardize the surface of the sample. Thermal analysis performed using TG/DTA did not indicate a significant difference in the thermal behavior of the films. On the other hand, the contact angle measurements indicated an increase in the hydrophobicity of the films in which the plasticizer was incorporated. These results indicate that the investigated and optimized concentrations of CMC/Glycerol can be used for food packaging production.

References

1. Bridson, J. H.; Gaugler, E. C.; Smith, D. A.; Northcott, G. L.; Gaw, S. Leaching and Extraction of Additives from Plastic Pollution to Inform Environmental Risk: A Multidisciplinary Review of Analytical Approaches. J Hazard Mater 2021, 414, 125571.
2. Liu, Y.; Ahmed, S.; Sameen, D. E.; Wang, Y.; Lu, R.; Dai, J.; Li, S.; Qin, W. A Review of Cellulose and Its Derivatives in Biopolymer-Based for Food Packaging Application. Trends Food Sci Technol 2021, 112, 532–546.

Fundings: This work was partly funded by the São Paulo Research Foundation – FAPESP (FAPESP CEPID-finance code 2013/07296-2, FAPESP/BCO-2021/06128-5) and Coordination of Improvement of Higher Education Personnel – CAPES (finance code 001).

Keywords: *Carboxymethylcellulose, biopolymers, glycerol, food packing.*

EFFECTS OF ACCELERATED AGING ON A GLASS FIBER - EPOXY COMPOSITE WITH SELF-HEALING AGENT FOR PIPELINE REPAIR IN THE OIL INDUSTRY

Taynnara M. Veloso[1*], Ana P. C. Barbosa[2]

1 – Department of Materials Engineering (DEMAT), Federal University of Rio Grande do Norte (UFRN), Natal, RN, Brazil,
tavelosoo@gmail.com

Abstract - The global oil industry employs in all process sectors, from the exploration phase of the reserve to the distribution of the refined product, metallic pipelines to transport fluids, which, due to their corrosive nature, cause internal damage to the metallic structure. Likewise, the environment in which the oil and gas pipelines are subjected damages them externally. As a resource for prolonging service life by means of exposed defects, composite materials have been used as a repair for oil and natural gas pipelines since the 1990s, due to their high chemical resistance, thermal and mechanical performance. However, studies about the aging effects of these repairs are scarce, once fundamental for their development. Furthermore, the use of materials capable of self-healing is another promising alternative in the pursuit for increased service life, along with reduced costs associated with the maintenance of these repairs during service. Therefore, the objective of this work was to evaluate the effects of accelerated aging on a glass fiber composite with epoxy polymer matrix, applied as pipeline's repair, with and without potential self-healing agents, subjected to cycles of saline water immersion and air exposure. The self-healing agent inserted in the composite of this work was the poly(ethylene-co-methacrylic acid) (EMAA). The tests conducted to study the aging effects and the addition of the potential self-healing agent were: mass variation, scanning electron microscopy (SEM), Fourier transform infrared spectroscopy (FTIR), and permeability test.

References

1. W. D. Callister; J. D. G. Rethwisch, *Materials Science and Engineering, an Introduction*, Wiley, 2018.
2. K.K. Chawla, *Composite Materials,* Springer, New York, 2012.
3. G. Marinucci, *Polymeric Composites Materials: Fundamentals and Technology*, Artliber, São Paulo, 2011.
4. A.P.C. Barbosa; A.P.P. Fulco; E.S.S. Guerra; F.K. Arakaki; M. Tosatto; M.C.B. Costa; J.D.D. Melo; *Accelerated aging effects on carbon fiber/epoxy composites*, Composites Part B: Engineering. 2017, v.110, p. 298–306. https://doi.org/10.1016/j.compositesb.2016.11.004.
5. M. L. da Rocha; M. C. de O. Leite; E. P. da C. Ferreira; J. D. D. Melo; A. P. C. Barbosa; *Accelerated Aging Effects In Composites Used As Repair For Pipes In Oil Industry; Polymer Composites*, 2021, 1. https://doi.org/ 10.1002/pc.26271.
6. A.A. do Nascimento; F. Fernandez; F. S. da Silva; E. P. C. Ferreira; J. D. D. Melo; A. P. C. Barbosa; *Addition of Poly(ethylene-co-methacrylic acid)(EMAA) as Self-Healing Agent to Carbon-Epoxyy; Composites* Part A. 2020, v. 137. https://doi.org/10.1016/j.compositesa.2020.106016.

Fundings: The authors would like to acknowledge the Brazilian funding agencies PRH32.1, ANP and Finep.

Keywords: *Pipelines, composites, glass-epoxy, aging, self-healing.*

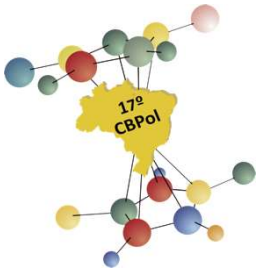

EFFECTS OF DIFFERENT CURING AGENT TYPES AND STOICHIOMETRY RATIO ON THE CROSSLINKING GRADE AND ITS CORRELATION WITH THE YELLOWING RATE OF WATER-BASED EPOXY CLEAR COATINGS

Mauro S. Da Silva[1] and Hélio Wiebeck[2]

1 – Department of Materials Engineering, University of São Paulo (USP), São Paulo, SP, Brazil
corresponding: maurodasilva@usp.br
2 – Department of Materials Engineering, University of São Paulo (USP), São Paulo, SP, Brazil

Abstract - Two components epoxy systems play an important role on protective coatings due to their unique properties such as corrosion resistance, mechanical and chemical resistances. Systems based on amine curing agents and liquid epoxy Bisphenol A resins are the most used not only due to their excellent properties but also for their competitive cost, however, one of the main side effects of epoxy systems is the poor yellowing resistance when exposed to UV radiation. Water-based systems were introduced to comply with increasingly strict requirements in terms of atmospheric emissions of volatile organic compounds. This work has the objective to study the effects of different types of curing agents and the stoichiometry ratio plays on the yellowing process to understand how this degradation process occurs trying to indicate ways to control in some way this phenomenon.

Keywords: *Epoxy, Water-based, Coatings, Yellowing, UV radiation*

Introduction

Epoxy resins play an important role as protective coatings due to their chemical inertness that allows good corrosion protection, besides their chemical resistance, electrical insulation properties, and adhesion to heterogeneous substrates. Two-component epoxy/amine systems are widely used in civil construction and industrial maintenance. However, the currently used systems generally contain high levels of volatile organic compounds (VOCs) that are harmful to human health and the environment. Thus, to improve the environmentally friendly character of this class of materials, there is a movement to shift the solvent-borne system to water-borne ones [1,2].

Waterborne coatings are widely used as an effective method of protecting against corrosion on metallic substrates, and several works have reported the importance and effectiveness of these materials. Wang et al. (2019) prepared waterborne epoxy coatings with graphene modified with lignin for anticorrosive applications and reported that nanocomposite coatings showed an anti-corrosion effect due to the labyrinth effect caused by the fillers. Sheng et al. (2021) prepared waterborne polyurethane composites containing MXene nanosheets and reported low corrosion current and UV-blocking properties [3,4].

Despite the excellent applicability and economic interest, epoxy systems are sensitive to exposure to UV radiation, not only as a function of the incidence of sunlight but also of the visible light spectrum. The polymeric structure undergoes photochemical damage on the surface of the applied paint film, resulting in its degradation. The use of additives that block and absorb UV radiation is common to delay this effect but results in high costs and relatively low effectiveness for long periods of exposure during the working time of the painted substrate. As a result of the degradation process, the coatings are subjected to chalking, gloss loss, and yellowing, decreasing the coating capacity to shield the substrate, and implying a complete loss of function. Liu et al. (2021) prepared waterborne epoxy resin containing emulsified asphalt to improve mechanical properties and reported waterproof performance, aging, and wear resistance. Li et al. (2020) prepared epoxy coating with polyether amine-functionalized graphene oxide and reported that the filler was important to avoid the yellowing of the coating, quantified by color parameters [5-7].

Substantial work has been done to improve the waterborne epoxy coatings weathering resistance to guarantee long shelf-life for these materials without properties loss, such as color, mechanical resistance, and others. Among the main properties, several additives are usually incorporated, such as nanoparticles, graphene, etc. [8-10].

The aim of this work is the development of waterborne epoxy coatings using aminic-curable substances to reduce color deterioration and property loss.

Experimental

Materials

Westlake Epoxy (Texas, USA) kindly donate the water-based epoxy resin dispersion and the five different types of curing agents (Table 1). The epoxy resin dispersion has solids content of 55-59%, equivalent epoxy weight of 480-600 g/eq, and viscosity at 25°C of 600-6000 cP. Momentive Performance Materials (New York, USA), donate the leveling agent additive and the deionized water. The co-solvent was acquired by The Dow Company (Michigan, USA). The chemical structures of the curing agents are confidential.

Table 1. Raw materials used in the work.

Raw material	Description	Abreviation	Characteristics
Epoxy Resin	Waterborne Epoxy Dispersion Resin	WEDR	Film-forming agent
Curing Agent 1	Water-Reducible Polyamine Curing Agent	WRCA	Reaction catalyst for epoxy systems
Curing Agent 2	Waterborne Dispersion Polyamine Curing Agent	WDCA	Reaction catalyst for epoxy systems
Curing Agent 3	Water-Reducible Unmodified Aliphatic Amine Curing Agent DT	WRDT	Reaction catalyst for epoxy systems
Curing Agent 4	Water-Reducible Unmodified Aliphatic Amine Curing Agent TT	WRTT	Reaction catalyst for epoxy systems
Curing Agent 5	Water-Reducible Modified Polyamine Curing Agent	WMCA	Reaction catalyst for epoxy systems
Deionized Water	Waterbased Solvent	WBS	Diluent for waterborne systems
Co-Solvent	Glycol-based Solvent	GBS	Diluent for waterborne systems
Leveling Additive	Silicon-based Solvent	SBA	Levelling additive for coatings

Methods

The formulations were done based on the stoichiometry of the system considering the amine hydrogen proportion elated to the epoxy content (Table 2). Due to the high isotherm experiments from 5 to 8 were excluded of this work because there was immediate polymerization and the curing agent hardened at the time of mixing between parts A and B of these tests. Usually the stoichiometry ratio is 1:1 to maximize the crosslinking density, as reported in previous works. Stel panels were sprayed using conventional spray gun at the thickness of 75 micrometers. The sprayed panels were cured during 30 minutes at 60°C and after were cured at room temperature (25°C) during seven days [11,12].

Table 2. Developed formulas used in the work.

Part A_Resin	Experiment 1	Experiment 2	Experiment 3	Experiment 4	Experiment 5	Experiment 6	Experiment 7	Experiment 8
Epoxy Resin	99,50	89,55	99,50	89,55	99,50	89,55	99,50	89,55
Leveling Additive	0,50	0,45	0,50	0,45	0,50	0,45	0,50	0,45

Part B_Hardener	Experiment 1	Experiment 2	Experiment 3	Experiment 4	Experiment 5	Experiment 6	Experiment 7	Experiment 8
Curing Agent 1	24,50	24,50	*	*	*	*	*	*
Curing Agent 2	*	*	47,00	47,00	*	*	*	*
Curing Agent 3	*	*	*	*	4,00	4,00		*
Curing Agent 4	*	*	*	*	*	*	5,00	5,00
Curing Agent 5	*	*	*	*	*	*	*	*
Co-Solvent	9,80	9,80	18,80	18,80	1,60	1,60	2,00	2,00
Deionized Water	14,70	14,70	28,20	28,20	2,40	2,40	3,00	3,00

Part A_Resin	Experiment 9	Experiment 10	Experiment 11	Experiment 12	Experiment 13	Experiment 14	Experiment 15	Experiment 16
Epoxy Resin	99,50	89,55	99,50	89,55	99,50	89,55	99,50	89,55
Leveling Additive	0,50	0,45	0,50	0,45	0,50	0,45	0,50	0,45

Part B_Hardener	Experiment 9	Experiment 10	Experiment 11	Experiment 12	Experiment 13	Experiment 14	Experiment 15	Experiment 16
Curing Agent 1	*	*	12,20	12,20	12,20	12,20	12,20	12,20
Curing Agent 2	*	*	*	*	*	*	*	*
Curing Agent 3	*	*	2,15	2,15	*	*	*	*
Curing Agent 4	*	*	*	*	2,50	2,50	*	*
Curing Agent 5	46,00	46,00	*	*	*	*	22,90	22,90
Co-Solvent	18,40	18,40	5,74	5,74	5,88	5,88	7,04	7,04
Deionized Water	27,60	27,60	8,61	8,61	8,82	8,82	10,56	10,56

After this period the panels were placed in the QUV/A chamber for 500 hours. Periodically the color changes and gloss changes were measured using BYK Garner equipment, as schematically illustrated in the figure 1. The DSC analysis were already made with the objective to identify the Tg of each experiment [13].

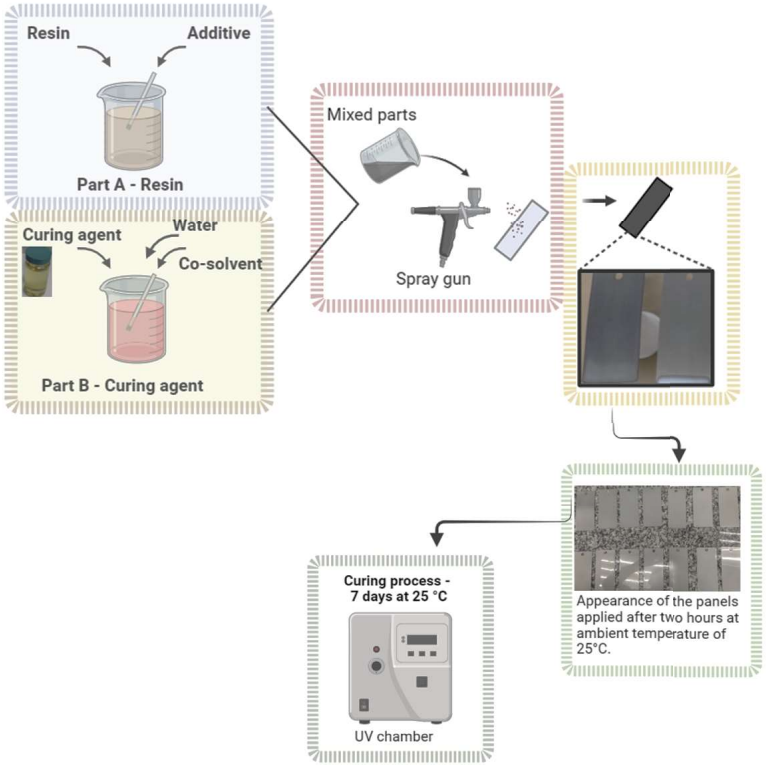

Figure 1. Schematic illustration of the coatings' fabrication technique to produce UV-resistant materials. Created with Biorender.com

Results and discussion

The developed formulas were identified as Test Panels (TP) from 1 to 16 and the Figure 1 and Figure 2 shows the appearance of the panels before the exposure and after 500 hours of QUVA exposure. After exposure were observed loss of gloss and color change.

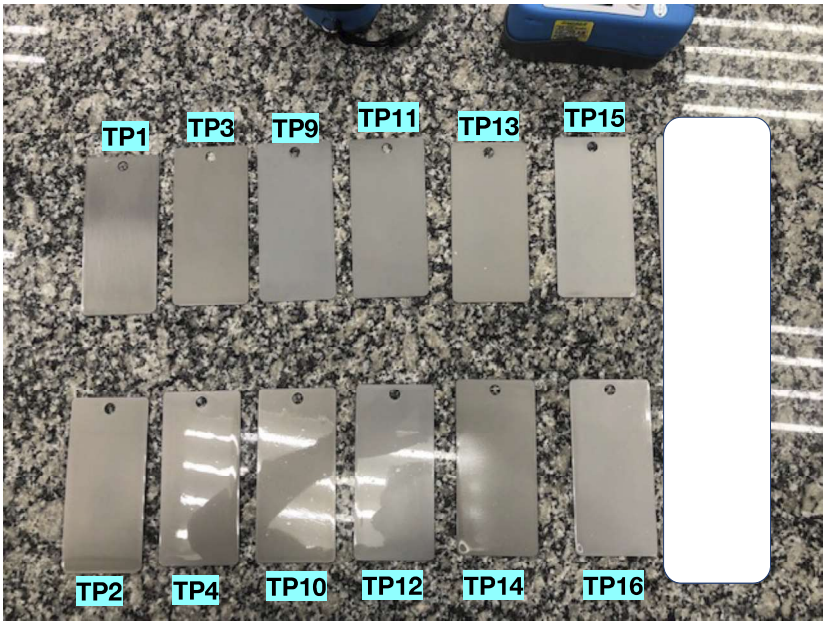

Figure 2. Test panels before the QUVA exposure

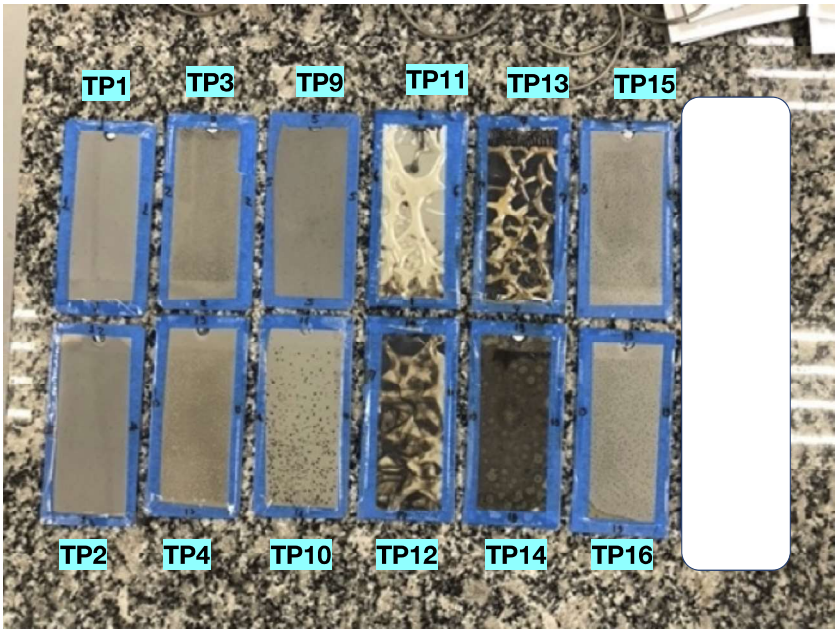

Figure 3. Test panels after 500 hours of QUVA exposure

The figure 2 and figure 3 shows how the color and gloss evolves during the measurements made from time to time until the completion of the 500 hours of exposure.

The experiments from 9 to 16 showed the greatest variation in brightness and color, that can be associated to the loss of crosslinking density.

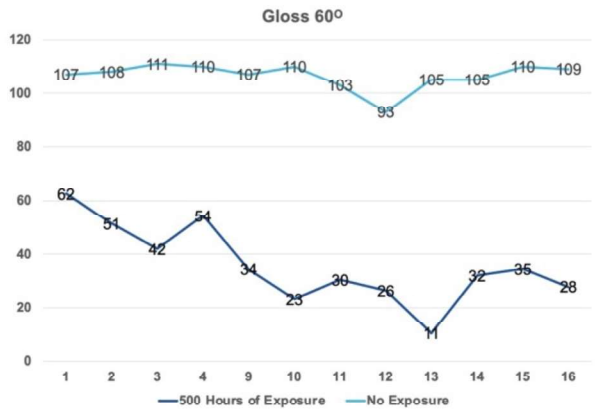

Figure 3. Gloss variation

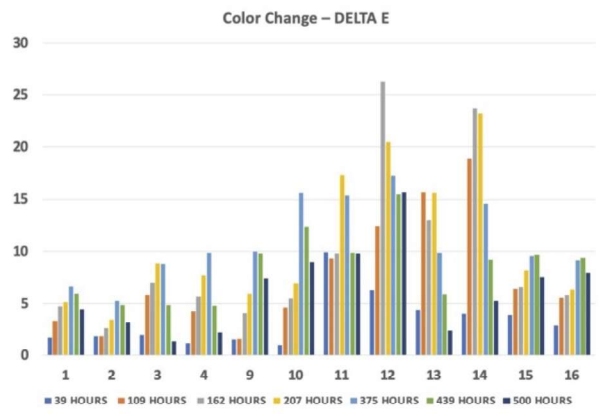

Figure 4. Color change

References

1. MAY, C. A. Epoxy Resins, Chemistry and Technology. Marcel Dekker, Inc., 2. ed. New York, 1988.
2. NICHOLSON, J. W. The Chemistry of Polymers. The Royal Society of Chemistry, 3. ed. Cambridge, 2006.
3. S. Wang; Z. Hu; J. Shi; G. Chen; Q. Zhang; Z. Weng; K. Wu; M. Lu; Applied Surface Science 484, 2019, 759-770, https://doi.org/10.1016/j.apsusc.2019.03.229.
4. X. Sheng; S. Li; H. Huang; Y. Zhao; Y. Chen; L. Zhang; D. Xie; Journal of Materials Science 56, 2021, 4212-4224, https://doi.org/10.1007/s10853-020-05525-2.
5. F. Liu; M. Zheng; X. Fan; H. Li; F. Wang; X. Lin; Construction and Building Materials, 274, 2021, https://doi.org/10.1016/j.conbuildmat.2020.122059.
6. J. Li; W. Shan; J. Cui; H. Qiu. G. Yang; S. Zheng; J. Yang; Journal of Coatings, Technology and Research, 17, 2020, 171-180, https://doi.org/10.1007/s11998-019-00252-z.
7. DAN, A. Preparation of Waterborne Epoxy Dispersion and its Application in 2K Waterborne Epoxy Coatings. Progress in Organic Coatings, Vol. 136, 2019.
8. JIN. F. L. Synthesis and Application of Epoxy Resins: A Review. Journal of Industrial and Engineering Chemistry, Vol. 29, 2015.
9. ALMEIDA, E. Corrosion Performance of Waterborne Coatings for Structural Steel. Progress in Organic Coatings, Vol. 37, 1999.
10. THE COUNCIL OF THE EUROPEAN JOURNAL. The Limitation of Emissions of Volatile Organic Compounds Due to the Use of Organic. 1999.
11. FAZENDA, J. M. R. Tintas: Ciência e Tecnologia. Blucher, 4. ed. São Paulo, 2009.
12. TRACTON, A. A. Coatings Technology: Fundamentals, Testing and Processing Techniques. CRC Press, 3. ed. New York, 2006.
13. WEGMANN. A. Chemical resistance of waterborne epoxy/amine coatings. Progress in Organic Coatings, Vol. 32, 1997.

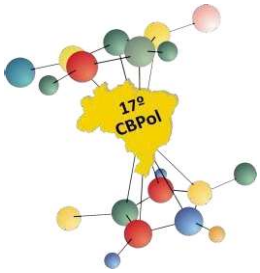

EVALUATION OF COMPATIBILIZATION IN RECYCLABLE BLENDS AND COMPOSITES FROM THE AMAZON

Thais S. Santos[1]*; Bianca M. Silva[1]; Eduardo S. Coelho[1]; Isaac A. T. Monteiro[1]; Raiane. C. Silva[1]; José C. M. Neto[2].

1 – Department of Materials Engineering, State University of Amazonas (UEA), Manaus, AM , Brazil
2 – Department of Materials Engineering, Universidade Estadual de Campinas (FEQ/UNICAMP), São Carlos, SP, Brazil
*Corresponding author: tss.emt18@uea.edu.br[1]**

Abstract - The world production of synthetic polymers exceeded 100 million tons per year, plastic represents 20% of this volume and is the main recyclable product buried instead of being properly destined for recycling, worth, on average, R$ 5.08 billion generated per year (ABIPLAST, 2014). PP is recycled by a larger number of companies, but it does not reach the 100 t/month range. Its applications are in domestic use, it is low cost and easy to process, which makes it excellent for industrial use in packaging (Papadopoulou, C. P. et al., 2000). PET and HDPE are among the most consumed plastics in the market, due to their increasinguse, in the disposable packaging sector, ranking first and second, respectively (ZHANG, J. P.et al., 2018). PET has excellent property with good mechanical strength, it can increase the rigidity of PP at higher temperatures, while polyolefin can facilitate the crystallization of PET by heterogeneous nucleations, further increasing the strength of the mixture (Papadopoulou,
C. P. et al., 2000). Composite materials with the addition of fillers with natural fibers are motivated by a greater environmental awareness, due to waste disposal problems and the depletion of petrochemical resources (DITTENBER et al., 2012). There are in the literature mixtures of PP, PET and HDPE polymers with different functionalization strategies, as well as different compatibilization and processing methods. Thus, the objective of this work is toevaluate the behavior of the properties of recyclable materials.

References

1. Associação Brasileira da Indústria do PET – ABIPET. (2013). 9º CENSO da Reciclagem de PET no Brasil, 2013. Retrieved 2015 April 9, from http://www.abipet.org.br.
2. Papadopoulou, C. P., & Kalfoglou, N. K. (2000). Comparison of compatibilizer effectiveness for PET/PP blends: their mechanical, thermal and morphology characterization. Polymer, 41(7), 2543-2555. http://dx.doi.org/10.1016/S0032-3861(99)00442-5.
3. ZHANG, J. P.; ZHANG, F. S. Recycling waste polyethylene film for amphoteric superabsorbent resin synthesis. Chemical Engineering Journal, v. 331, p. 169-176, 2018.

Fundings: Dean of Extension – PROEX.

Keywords: *recycling, PET, composites, polypropylene, products*

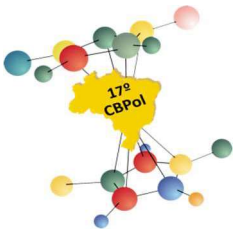

EVALUATION OF THE EFFECTS OF USING COMPATIBILIZERS IN HDPE COMPOSITES WITH TREATED COCONUT FIBER

Andressa de Carvalho Amorim[1], Elaine Meireles Senra[3], Renan Henriques G. de Almeida[3], Ana Lúcia N. da Silva[2, 3]

1 – Chemistry, Federal Institute of Educantion, Science and Technology of Rio de Janeiro (IFRJ), Rio de Janeiro, RJ,Brazil - andressaamorim2509@gmail.com

2 – Environmental Engineering Program (PEA), Federal University Of Rio de Janeiro (UFRJ), Rio de Janeiro, RJ, Brazil

3- Institute of Macromolecules Professor Eloisa Mano (IMA), Federal University of Rio de Janeiro (UFRJ), Rio de Janeiro, RJ, Brazil

Abstract

Polymeric composites of natural fibers have a lower environmental impact with regard to the abusive use of plastics in society. However, the hydrophilic nature of the fibers, that is, high water absorption capacity, make them incompatible with hydrophobic thermoplastic polymers, such as high density polyethylene (HDPE) [1]. In order to improve this compatibility of the fiber with the polymeric matrix, in the present study, a process of chemical treatment of the fiber was carried out, in addition to the use of compatibilizing agents [2]. The treatment on the surface of the fiber consists of three stages, washing, mercerization and bleaching, where the lignin and the other components no fiber cellulose will be removed [1]. The compatibilizing agent actuate at the interface of immiscible polymeric mixtures, reducing the interfacial tension of the materials and increasing the compatibility between the phases. In this work, the effects of adding a compatibilizer (HDPE-g-MA) to a HDPE composite with in natura and treated coconut fiber were evaluated. The fiber content used in the composite was 15%, varying only the compatibilizer content by 1% and 2%, m/m. A Corrotational Double Screw TecTril Extruder was used to obtain the composites and then the materials were processed in an Arburg injector to obtain the tensile and impact resistance specimens. Tests were then carried out on the flow index (MFI), thermogravimetry (TGA), tensile strength and impact strength of the composites obtained. The results showed that the composites that contain the treated fiber, have greater resistance to impact, however with the addition of compatibilizer in this matrix with treated fiber, there is a decrease of this property, in both analyzed concentrations (1% and 2% HDPE-g-MA). In the tensile strength test, the incorporation of the fiber generated an increase in the stiffness of the material, however, as for the addition of compatibilizer, no significant variations were observed.

Keywords: *Polymer, high density polyethylene, composite, coconut fiber, compatibilizer*

References

1. FURTADO, Josélia Borges de Moura; FILHO, Paulo Afonso Furtado; OLIVEIRA, Thalyta Pereira; CAETANO, A Marlo Rodrigues de Sousa; FIGUEIREDO, Francisco Cardoso; JÚNIOR, José Ribeiro dos Santos. Compósitos de Polietileno/Fibra - Caracterização e Degradação. Revista Virtual de Química, [S. l.], v. 12, n. 1, 2 mar. 2020.

2. ZHANG, C.L., FENG, L.F., GU, X.P., et al., "Efficiency of graft copolymers as compatibilizers for immiscible polymer blends", Polymer, v. 48, 2007

EVALUATION OF THE MECHANICAL PROPERTIES OF POLYMERIC BLENDS PRODUCED FROM EXPANDED POLYSTYRENE (EPS) AND WASTE TIRE RUBBER (WTR)

Antonio J. Andrade Junior*, Silma S. Barros, Emerson F. Silva and Clodoaldo Saron

Department of Materials Engineering (DEMAR), Engineering School of Lorena (EEL), University of São Paulo (USP), Lorena, SP, Brazil aajosejunior@usp.br

Abstract - There is a growing concern with the disposal of polymeric waste, mainly from packaging and disposable products, as these wastes produce environmental impacts. New studies for the development of techniques and new types of recycled materials are important to contribute to the circular economy, increasing the benefit of the material and allowing its competitive insertion in the market[1]. The expanded polystyrene (EPS) is a widely used product, mainly due to its thermal, acoustic and electrical insulation properties, other use is in packaging due to its impact resistance property. However, most of its applications are disposable and this material presents difficulties in its recycling, mainly due to its low density[2]. When densifying the polystyrene, the product becomes rigid and fragile, however after the incorporation of a ductile phase like rubber, the material toughens[3]. In this context, blends of recycled polystyrene (PS) with waste tire rubber (WTR) were produced, in the presence and absence of the compatibilizing agent styrene-butadiene-styrene (SBS). Mechanical tensile and impact strength tests of the blends were carried out according to the standards ASTM D638 and ASTM D256 respectively, in order to observe the effect of the WTR content and the effect of the presence of the compatibilizing agent SBS. The PS showed tensile strength around 16 MPa, the PS/WTR presented values around 20 MPa and PS/SBS/WTR presented maximum value at 28 MPa for the blend containing 10 wt% of WTR. The elongation at break increases as a function of the rubber content, arriving up to 8% for PS/SBS/TRW30, which is double of the PS. Young modulus for recycled PS is around 800 MPa while the presence of 30wt% WTR produce significant changes, 700 MPa for non-compatilibized blend (PS/TRW) and 600 MPa for compatibilized blend (PS/SBS/TRW)[4,5]. The PS/SBS/TRW showed the impact resistance arrives 5 kJ/m2 against PS/WTR around 3kJ/m2 and PS around 2kJ/m2. It can be concluded that the method used together with the rubber and the compatibilizer resulted in the improvement of the mechanical properties.

References

1. I. Tsuchimoto; Y. Kajikawa *Sustainability* 2022, 14, 16340. https://doi.org/10.3390/su142416340.
2. S. C. Ugwu; C. M. Obele *World Journal of Advanced Engineering Technology and Sciences* 2023, 8, 315-329. https://doi.org/10.30574/wjaets.2023.8.1.0057.
3. D. F. Silva; C. B. B. Luna; G. Silva; E. M. Araujo; T. J. A. Melo *Revista Eletrônica de Materiais e Processos* 2014, 9, 92-97. http://www2.ufcg.edu.br/revista-remap/index.php/REMAP/article/viewFile/423/313.
4. K. Bedjaoui; R. Krache; A. M. Fernández; M. Guessoum *Materials Research Express* 2019, 6, 105334. http://dx.doi.org/10.1088/2053-1591/ab38e7
5. C. B. B. Luna; D. F. Silva; S. K. T. Basílio; E. M. Araújo *Semina: Ciências Exatas e Tecnológicas* 2014, 35, 149-158. https://doi.org/10.5433/1679-0375.2014v35n2p149.

Fundings: National Council for Scientific and Technological Development - CNPq (Proc. 309583/2020-9) and FAPESP (Proc. 2020/14318-6).

Keywords: *Toughened Blends. Expanded polystyrene. Waste Tire Rubber. Recycling. Mechanical resistance.*

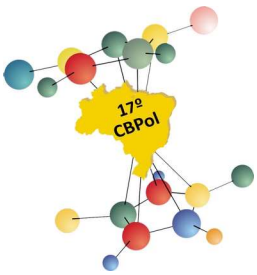

EXPLORING THE USE OF A THERMOMECHANICAL ANALYZER TO ASSESS THE AGING OF PROPELLANTS

Juan Peixoto Barroco Magalhães[1], Maurício Ferrapontoff Lemos[1], Ana Paula da Silva[1], Priscila Simões Teixeira Amaral[1] and Fernanda Santos da Luz[1]*

1 - Materials Technology Group, Navy Research Institute (IPqM), Rio de Janeiro, RJ, Brazil
** fernanda.luz@marinha.mil.br*

Abstract - The present work aims to explore the potential of a thermomechanical analyzer to evaluate the physical and mechanical properties of solid rocket propellants AP/Al/HTPB-based. Exploratory studies were carried out on cylindrical specimens from the same lot under different conditions. Following the Van't Hoff rule (1), two years of artificial aging was applied in an oven at 60°C for 29 days. The Young modulus and relaxation modulus of ten samples were evaluated. In addition, the coefficient of thermal linear expansion for the samples in both condition, with and without aging, were measured. By using a range of deformation from 0 to 0.2% and a deformation rate of 0.5 mm/min, it was possible to calculate the Young modulus through linear regression of the results (2). In the relaxation modulus tests, the same deformation rate was adopted, up to limit deformation of 0.18% to 0.2%, in which the force required to keep this deformation was measured over time. The standard relaxation modulus was defined as the value of the modulus after ten times the time to reach the limit deformation (3). In the thermal linear expansion test, a heating rate of 5°C/min was used, with an initial temperature of 30°C and a maximum of 82°C. It was found that the average Young modulus of the aged specimens was higher than that of the non-aged specimens. However, there was a reduction of the coefficients of thermal-linear expansion, as well as those of the average standard relaxation modulus in comparison to the values of the initial lot.

1. W. M. Adel; G. Liang. *Chinese Journal of Aeronautics* 2018, *32(2)*: 361-368. https://doi.org/10.1016/j.cja.2018.08.003.
2. ASTM. ASTM E111 – 17: Standard Test Method for Young's Modulus, Tangent Modulus, and Chord Modulus. West Conshohocken: ASTM International, 2017.
3. P. R. Ferreira. Master Thesis. Military Institute of Engineering, 2022.

Fundings: CNPQ

Keywords: *Thermomechanical analyzer; solid propellant; aging; Young modulus.*

FRACTOGRAPHIC ANALYSIS OF FATIGUE FAILURE IN CFRP COMPOSITE WITH PA6 MATRIX

Guilherme Ferreira de Melo Morgado[1], Larissa Stieven Montagna[1], Fabio Roberto Passador*[1], Mirabel Cerqueira Rezende[1]

1 – Polymer and Biopolymer Technology Laboratory (TecPBio), Federal University of São Paulo (UNIFESP), 330 Talim St., São José dos Campos 12231-280, Brazil.

morgado@unifesp.br

Abstract - Carbon fiber reinforced polymer (CFRP) composites are widely used in different industries due to their high strength-to-weight ratio and excellent mechanical properties [1]. The matrix material plays a critical role in determining the overall mechanical properties of CFRP composites. In this study, polyamide 6 (PA6) was used as the matrix material for CFRP composites, and its effect on the composite's mechanical properties was investigated through fractography analysis. Fatigue strength tests were conducted on the specimens, and the fractured surfaces were examined using scanning electron microscopy (SEM) to study the fracture mechanisms. The results showed that the CFRP composites with PA6 as the matrix exhibited a mixed fracture mode consisting of fiber pull-out, matrix cracking, and delamination. The fracture surfaces of the specimens showed a rough and irregular texture, indicating the presence of a significant amount of matrix material on the fractured surface. These aspects resulted in a mixed fracture mode, with the fiber pull-out being the predominant mode. Fractographic analysis of the fractured surfaces provided about the fracture mechanisms in the CFRP composites. The presence of matrix cracking and delamination also contributed to the overall fracture mechanism of the composite [2]. In conclusion, the results of this study showed that PA6 can be used as a matrix material in CFRP composites, but its use may result in lower mechanical properties compared to other matrix materials, such as epoxy. The fractographic analysis provided valuable insights into the fracture mechanisms of the composite, which can aid in the development of improved CFRP composites with PA6 as the matrix material.

References

1. Kondo, M.Y., Montagna, L.S., Morgado, G.F.M., Castilho, A.L.G., Batista, L.A.P.S., Botelho, E.C., Costa, M.L., Passador, F.R., Rezende, M.C., Ribeiro, M.V. Polímeros 2022, 32(2), e2022023. https://doi.org/10.1590/0104-1428.20220042.
2. Greenhalgh, E., *Failure analysis and fractography of polymer composites*, Woodhead Publishing in Materials, Cambridge, 2009.

Fundings: Federal Government Program 'Rota 2030', n° 27194.03.03/2020.01-00 for the financial support; the LEL/IPT for the coordination, and FIPT, FUNDEP for the administrative support.

Keywords: *Carbon fiber; PA6 matrix; Fractography; Fatigue; Composite materials*

GREEN COCONUT (COCOS NUCIFERA) LONG FIBER POLYMERIC BIOCOMPOSITE WITH NATURAL BIOACTIVE COMPOUNDS

Jurandi T. S. Muniz[1] and Felipe P. C. Gomes[2]*

1 – Undergraduate Program in Industrial Chemistry, Federal University of Pernambuco (UFPE), Recife, Brazil.
jurandi.tiago@ufpe.br
2–Chemical Engineering Department, Federal University of Pernambuco (UFPE), Recife, Brazil.
*felipe.pcgomes@ufpe.br**

Abstract – Natural fiber biocomposites are important alternatives to traditional polymeric materials that are non-biodegradable. This work evaluated the formulation of a polymeric composite using minimal processed green coconut fibers. Solutions with 6%wt. of corn starch and 2%wt. of carboxymethylcellulose (CMC) in water were gelatinized before incorporation of 2,5 g of sanitized coconut fibers. Glycerol was used as a plastifier and the effects of citric acid and tannic acid were studied using a factorial experimental design. Finally, the mixture was dried using a convection oven and molded using a hot press. Combination of citric acid with thermoplastic starch allows better mechanical properties and may improve the interface between the matrix and the cellulosic fibers, acting as a reticulation agent. While the tannic acid, naturally present in the fibers or added during the preparation of the composite, can act as a bioactive compound with antioxidant properties. The proposed design aims to achieve a composite that is less brittle, more resistant to fungal development and to moisture absorption with good mechanical properties.

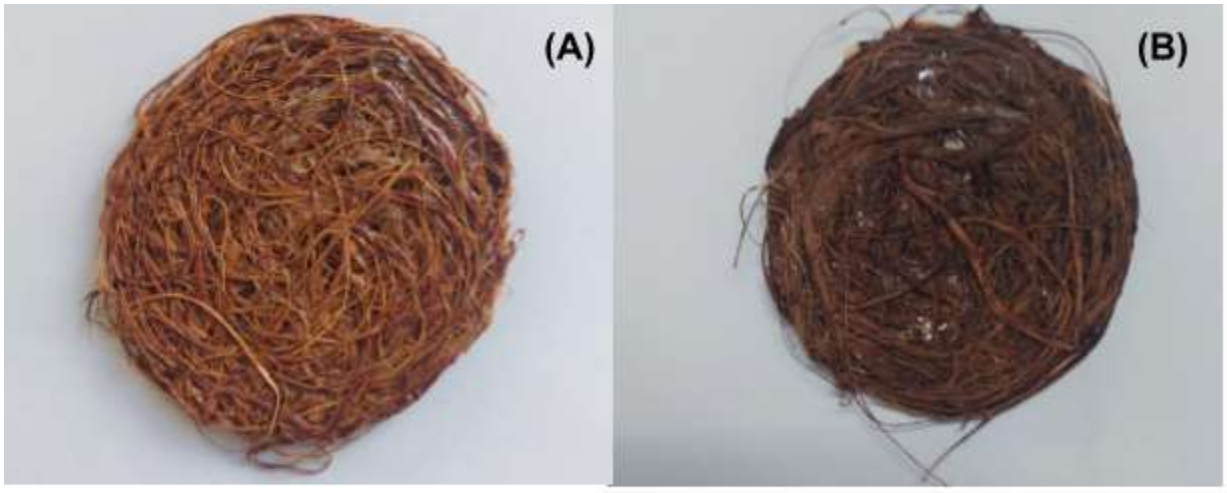

Fig. 1 – Green coconut fibers biocomposite with (A) thermoplastic starch and (B) CMC matrix.

Fundings: The authors would like to acknowledge the financial support of CNPq-Brazil through PIBIC scholarship.

Keywords: *Bioactive compounds; Crosslinking agent; Green coconut; Long fibers composite.*

GREEN TPV BASED ON PE RECICLABLE AND WASTE TYRE

Flavia Gonçalves[1], Monica C. C. dos Santos[1], Alex [1] and Alex S. Sirqueira[1]*

1 – Laboratório de Estatística e Matemática Aplicada (LEMA), Universidade do Estado do Rio de Janeiro (UERJ), Rio de Janeiro, RJ, Brasil alex.sirqueira@uerj.br

Abstract - Thermoplastic Vulcanized (TPV) are a class of materials capable of combining the elastic properties of vulcanized rubbers and the recyclability of thermoplastics. However, their production involves the use of synthetic polymers that are highly resistant to degradation, making these materials environmentally polluting. In this study, TPVs were developed using polymer waste as raw material (tire powder and LDPE). The processing was carried out in an open mill mixer, and the vulcanization system used was sulfur-based, with the addition of compatibilizers: EVA and SBR. The addition of compatibilizers was necessary because the polymers involved in TPV production are highly incompatible. The formulation used was 70:30 (LDPE/tire powder). After processing, the samples were pressed using a hot hydraulic press to obtain test specimens. The mechanical properties of the TPVs were determined, including tensile deformation, hardness, density, and MFI. The TPVs compatibilized with EVA showed higher deformation, MFI, and resilience. However, the TPVs compatibilized with SBR exhibited higher elastic modulus and rupture strength. The samples were subjected to accelerated aging in an oven for 70 hours. The EVA-compatibilized samples showed better retention of the original properties.

References

1. COSTA, L. B.; OLIVEIRA, R. N.; **Sirqueira, A. S.**. Green thermoplastic vulcanized based on recycled polyethylene and waste tire powder. RESEARCH, SOCIETY AND DEVELOPMENT, v. 11, p. e50011427421, 2022.
2. ERREIRA, I. P. ; SIRQUEIRA, A. S ; SANTOS, T. A. ; NACCACHE, M. F ; Soares, Bluma G. . Rheological Studies of SBS/EVA Blends modified with bio-based Cashew Nut Shell Liquid. Journal of Elastomers and Plastics, v. 03, p. 1-16, 2021.

Fundings: FAPERJ.

Keywords: *Elastomers, Thermplastic Vulcanized, Waste Tyre, Vulcanization, mechanical proerties*

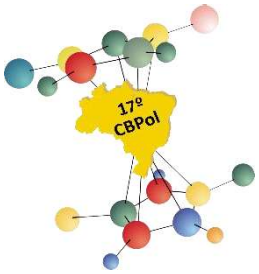

IMPREGNATION OF POLYCARBONATE/POLY(L-LACTIC ACID) BLENDS WITH CLOVE EXTRACT ASSISTED BY SUPERCRITICAL CO_2

Jorge A. P. Monteiro[1]*, Suel E. Vidotti, Mathilde Champeau[1]

1 – Center for Engineering, Modeling and Applied Social Sciences, Universidade Federal do ABC (UFABC), Santo André, SP, Brazil

jorge.monteiro@ufabc.edu.br

Abstract – Polymers able to release natural extracts are relevant systems in many fields such as food packaging, wound care, cosmetics, and agriculture. A promising alternative in comparison to wet impregnation processes to load natural extracts into polymeric matrixes is CO_2 supercritical ($scCO_2$) impregnation (SCI) since it enables to reach higher extract loadings and is a more sustainable process. When in its supercritical state (above 31.1 °C and 7.4 MPa), CO_2 can dissolve the extract's compounds and carry them in the polymer. While the SCI of a single molecule in a polymer is well understood, working with natural extracts is challenging due to their complex composition and strategies to control both the total extract loading (EL) and their release are essential. In a previous project, we investigated the SCI of clove extract in polycarbonate (PC) and poly(L-lactic acid) (PLLA). PC and PLLA were selected for having different chemical structure and thermal properties, and their CO_2 sorption and swelling is reported in the literature [1]. Clove extract is selected as a model of extract since it contains a rather simple composition *i.e.* four compounds: two oxygenated compounds (eugenol (70.1 %) and eugenyl acetate (17.1 %)) and two hydrocarbons (β-caryophyllene (10.67 %) and α-humulene (2.20 %) [2]. In this project, we aimed at obtaining immiscible blends of polycarbonate/poly(L-lactic acid) with different PC/PLLA ratio, and impregnating them with clove extract at 35 °C and 20 MPa. First, the blends microstructure was characterized by Scanning Electron Microscopy and confirmed the presence of two phases. In this impregnation condition, a discrepant EL was obtained in PC and PLLA (8.2 vs 42 %). The EL decreased with the PC/PLLA ratio and a drop was observed between 50/50 and 75/25. For the first time, we prove the possibility to tune the EL by controlling the composition of a blend. The interactions between the clove extract and the polymers were evaluated by Fourier transform infrared spectrometry. According to Differential Scanning Calorimetry curves, clove extract acts as a plasticizer for both PC and PLLA, but the T_g and T_m shifts are more pronounced in the case of PLLA.

References

1. JORDÃO, A. M. et al. Supercritical CO_2 Impregnation of Clove Extract in Polycarbonate: Effects of Operational Conditions on the Loading and Composition. **Processes**, v. 10, n. 12, p. 2661, dez. 2022. https://doi.org/10.3390/pr10122661.

2. MEDEIROS, G. R.; FERREIRA, S. R. S.; CARCIOFI, B. A. M. High pressure carbon dioxide for impregnation of clove essential oil in LLDPE films. **Innovative Food Science & Emerging Technologies**, v. 41, p. 206–215, 1 jun. 2017. https://doi.org/10.1016/j.ifset.2017.03.008.

Keywords: *supercritical CO_2, PC/PLLA, polymeric blends, clove extract.*

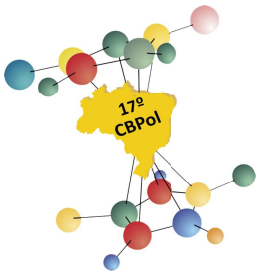

IMPRESSIVE MECHANICAL AND BIOLOGICAL PROPERTIES OF FILMS OF QUATERNIZED CHITOSAN

Danielle Bitencourt Faria[1], Patrícia Santos Lopes[2], Classius Ferreira da Silva[1], Mariana Agostini de Moraes[1*]

1 – Department of Chemical Engineering, Federal University of São Paulo (UNIFESP), Diadema, SP, Brazil
danielle.bitencourt@unifes.br. mamoraes@unifesp.br
2 – Department of Pharmaceutical Sciences, Federal University of São Paulo (UNIFESP), Diadema, SP, Brazil

Abstract – Chitosan is one of the most abundant biopolymers in the world, it has several biological properties, and is highly used for applications in this area[1]. However, due to its limited solubility only in acidic pH, some derivations called quaternizations appear to enable chitosan to be soluble in any pH range[2].The quaternization method consists of exchanging the available amines in the chitosan molecule for quaternary complex through a chemical process[3,4]. Due to scarcity of studies on films of quaternized chitosan, arise the necessity to explore the relation between quaternization process and molar mass in films of chitosan. Thus, the aim of this study was to prepare films of quaternized quitosan with different molar masses and characterize the films in terms of chemical, mechanical and biological properties. By FTIR, it was possible to observed in the films of quaternized chitosan the presence of the quaternary group and a high presence of hydrogens bounds interacting directly with the chitosan polysaccharide chain, which does not occur when common films of chitosan are analyzed. Also, the films of quaternized chitosan exhibited an impressive elasticity (95% to 130% of deformation), comparable to elastomeric films, being possible to perform fatigue tests, which is not common to films of chitosan. Moreover, the films of quaternized chitosan showed excellent antimicrobial properties against *Staphylococcus aureus* (ATCC 6538) and *Escherichia coli* (ATCC 8539), demonstrating that films of quaternized chitosan have excellent properties for applications in medical field, especially in controlling infections. It is possible to conclude that films of quaternized chitosan present important mechanical and biological properties which are not found in common films of chitosan, showing an important relevance in materials research.

References

1. Zhang, X.; Ismail, B. B.; Cheng, H.; Jin, T. Z.; Qian, M.; Arabi, S. A.; Liu, D.; Guo, M. Carbohydr Polym 2021, 273, 118616.
2. Fiamingo, A.; Oliveira, O. N.; Campana-Filho, S. P. ChemRxiv 2020, 1–10.
3. Pathak, K.; Misra, S. K.; Sehgal, A.; Singh, S.; Bungau, S.; Najda, A.; Gruszecki, R.; Behl, T. Polymers (Basel) 2021, 13 (15), 1–31.
4. Freitas, E. D.; Moura, C. F.; Kerwald, J.; Beppu, M. M. Polymers (Basel) 2020, 12, 1–41.

Fundings: This work was supported by CAPES.

Keywords: Quaternized chitosan, mechanical properties, and biological applications.

INACTIVATION OF SARS-CoV-2 IN POLYELECTROLYTE FILM BASED ON PECTIN/POLY(DIALLYLDIMETHYLAMMONIUM CHLORIDE)

Guilherme Ribeiro de Carvalho* and Liliane Maria Ferrareso Lona

Department of Bioprocesses and Materials Engineering, School of Chemical Engineering, University of Campinas (UNICAMP), Campinas, SP, Brazil.

gr.carvalho@yahoo.com.br

Abstract – Sars-CoV-2, a virus that causes serious respiratory infections, can remain active on the surface for up to three days and thus contaminates the individual who touches it. Therefore, the objective of this work was to develop a new antiviral polyelectrolyte film based on pectin (P) and poly(diallyldimethylammonium chloride) (PDADMAC) using the solvent casting technique. Control film (P) and film with P and PDADMAC (P/PDADMAC) were systematically investigated regarding morphology, mechanical properties, and activity against the SARS-CoV-2 virus. The films presented a cohesive surface without separation of phases and cracks. Adding PDADMAC significantly affected the mechanical properties of the films ($p<0.05$), increasing the maximum tensile strength (TS) (from 7.28 ± 0.68 MPa to 15.8 ± 0.94 MPa), with TS value compared to low-density polyethylene (LDPE). In addition, the polyelectrolyte film (P/PDADMAC) was able to inactivate 99.9% of SARS-CoV-2 after one minute of direct contact with the virus. The PDADMAC action against the SARS-CoV-2 virus derives from the quaternary ammonium groups present in the structure of this polymer. These functional groups interact with the cell membrane of the pathogen, which causes its dissolution and, consequently, inactivates the virus. Therefore, this study demonstrated the efficacy of PDADMAC in preparing pectin-based film with improvements in mechanical properties and antiviral activity against SARS-CoV-2.

Fundings: The authors would like to acknowledge the Coordination for the Improvement of Higher Education Personnel – CAPES and São Paulo Research Foundation – FAPESP (Grant 2021/ 09341-1).

Keywords: Polyelectrolyte film; Antiviral film; Pectin; PDADMAC.

INFLUENCE OF MIXING SEQUENCE ON THE SELECTIVE LOCALIZATION OF CELLULOSE NANOCRYSTALS IN POLY(LACTIC ACID)/POLY(Ɛ-CAPROLACTONE) BLENDS

Felipe H. O. Silva[1] and Marcelo A. Chinelatto[1]

1 – Department of Materials Engineering, University of São Paulo (USP), São Paulo, SP, Brazil
mchinelatto@sc.usp.br

Abstract – This work aims to investigate the influence of the mixing sequence on the selective localization of the cellulose nanocrystals (CNC) in immiscible polymer blends of poly(lactic acid) (PLA) and poly(ε-caprolactone) (PCL). The mixtures were prepared from the molten state, in a corrotacional intermeshing twin-screw extruder. Three different mixing sequences were used: all components were extruded together in a single step (SEQ1); initially, CNC was extruded with PLA and later the CNC+PLA mixture was extruded with PCL (SEQ2) and, CNC was initially mixed with PCL and then extruded with PLA (SEQ3). The PLA/PCL ratio used was 80/20% (% wt) and the CNC concentration was fixed constant at 3% (% wt). In polymer systems like those that the one used in this study, kinetic factors, such as mixing order, are decisive in the localization of the CNC [1-3]. The micrographs of morphology obtained in SEQ3 (Fig 1) revealed a smaller droplet size of the dispersed phase, indicating suppression of coalescence and better interfacial adhesion.

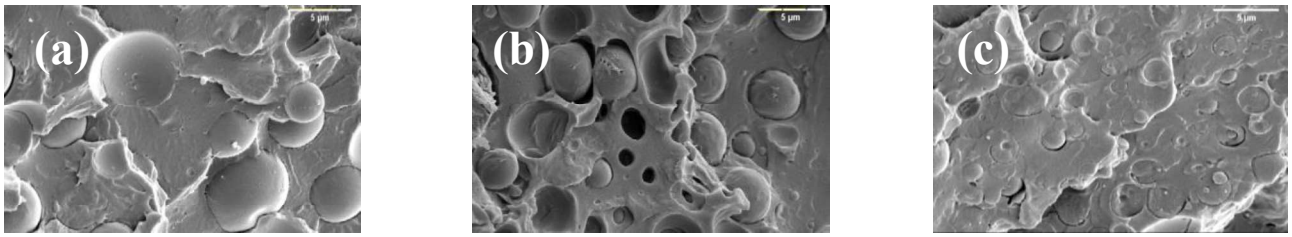

Figure 1 – SEM micrographs of the cryogenically fractured surfaces of the PLA/PCL/CNC mixtures (a) SEQ1, (b) SEQ2 and (c) SEQ3.

References

1. J. Aguiar; M. Decol; W. Pachekoski; D. Becker. *Polymer Engineering and Science*, 2018, 59. https://doi.org/10.1002/pen.24908.
2. A. Ostafinska; I. Fortelny; M. Nevoralova; J. Hodan; J. Kredatusova; M. Slouf. *Royal Society of Chemistry*, 2015, (5), 12. https://doi.org/10.1039/C5RA21178F.
3. G. Siqueira; J. Bras; A. Dufresne. *Polymers* 2010, 2(4), 728-765. https://doi.org/10.3390/polym2040728.

Fundings: Coordenação de Aperfeiçoamento de Pessoal de Nível Superior (CAPES), Brasil, Finance Code 001 and Fundação de Amparo à Pesquisa do Estado de São Paulo (FAPESP), Brasil, process nº 2018/23542-7.

Keywords: PLA/PCL blends, cellulose nanocrystal, CNC, compatibilization, selective localization.

INFLUENCE OF THE WASHING PROCESS ON THE PROPERTIES OF CHITOSAN-ALGINATE COMPOSITE FILMS

Andressa E. Sobczyk[1*], Débora J. L. Faccin[1], Nilo S. M. Cardozo[1], Isabel C. Tessaro[1]

1 – Department of Chemical Engineering, Federal University of Rio Grande do Sul (UFRGS), Porto Alegre, RS, Brazil
*andressa.enq@gmail.com

Abstract - The combination of chitosan (cationic polysaccharide) with alginate (anionic polysaccharide) leads to the formation of polyelectrolyte complexes (PEC), which have been used mainly for applications as dressings in biomedical areas. The complexation of these macromolecules by strong amino-carboxylic electrostatic interactions and hydrogen bonds results in better final product performance when compared to that obtained with films prepared by only one single polymer. However, the processing conditions can affect the resulting complex structure, influencing the final material properties. In this work, chitosan-alginate films were prepared by casting and a water-washing step was introduced as a post-casting treatment. The preparation of the films was performed according to the following steps: (i) chitosan was solubilized in an acid medium (acetic acid solution, 1% v/v) and alginate in water; (ii) mixing of the chitosan and alginate solutions to obtain the film-forming suspension and correction of its pH to 7, using NaOH 1 M; (iii) casting; and (iv) washing with distilled water followed by a second drying step. Thickness, visual appearance, liquid absorption capacity (LAC), water vapor permeability (WVP), and mechanical properties were evaluated before and after washing. The unwashed composite films showed great heterogeneity in appearance and properties when in contact with air humidity, probably due to excess base. The washing treatment allowed the homogenization of the films and reduced the variability in the evaluated properties. Besides, the washed films showed lower thickness (47% lower), greater stiffness, and greater LAC (87% higher for distilled water) than the unwashed ones. The reduction of variability promoted by the washing treatment was particularly important for WVP data, whose standard deviation for the unwashed films was of the same order as the obtained mean values. Therefore, the additional washing treatment significantly affected the chitosan-alginate PEC films and improved the reproducibility of the evaluated properties.

Fundings: Coordenação de Aperfeiçoamento de Pessoal de Nível Superior (CAPES), Conselho Nacional de Desenvolvimento Científico e Tecnológico (CNPq).

Keywords: *polyelectrolyte complexes, chitosan, alginate, films*

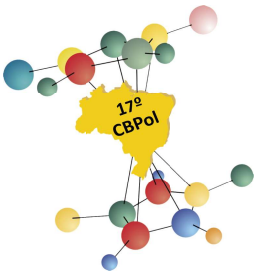

INFLUENCE OF UNTREATED AND ALKALI-TREATED BARLEY BAGASSE ON MECHANICAL PROPERTIES OF POLYESTER RESIN COMPOSITES

Gabriel Luiz Corrêa[1], Claudia Merlini[1,2]

1 - Materials Engineering Special Coordination, Federal University of Santa Catarina (UFSC), Blumenau, SC, Brazil
gabriel.l.correa@grad.ufsc.br
2 - Graduate Program in Nanoscience, Processes and Advanced Materials (PPGNPMat) Federal University of Santa Catarina (UFSC), Blumenau, SC, Brazil
claudia.merlini@ufsc.br

Abstract

Research on composites made from natural fibers and waste is very popular due to advantages such as lower costs and environmental impact. This project aims to manufacture, characterize, and compare polyester resin composites made with barley bagasse, a waste from the beer production process. Washed and alkaline treated barley bagasse samples were used to analyze their influence on composite properties. The first step is to wash the bagasse with water to remove residues from previous processes. Afterwards the material is heated upon 70 ºC inside a hothouse for 48 hours until complete drying. The samples selected for chemical treatment were inserted in aqueous solutions containing 1 %, 3 %, 5 % and 10 % of NaOH for 1 hour, then washed and dried again. All composites were manufactured with polyester resin and a volumetric fraction 35 % of barley bagasse through mechanical mixing of about 200 rpm at room temperature compression molding (approximately 20 ºC) loaded with 1 ton for 24 hours. The characterization includes tensile strength test and Fourier transform infrared spectroscopy (FTIR) of composites. The tensile strength test demonstrated that there is a tendency to increase the maximum strength of the composites by increasing the NaOH concentration in the solution used for chemical treatment, when comparing only washed and washed treated samples. It was not observed any pattern change on maximum strain and Young's modulus. Infrared spectroscopy of composites did not reveal any shifting or emergence of new bands, resulting in the same spectrum for all composites, which can indicate the absence of chemical interaction between matrix and residue. It was concluded that the alkaline treatment contributes to increase the composites mechanical strength and that the composites with fibers treated with 5 % of NaOH demonstrated the best results.

Keywords: Alkaline treatment; Barley bagasse; Composites; Polyester.

LECITHIN MODIFIED KAPOK FIBER/HYDROXYPROPYL METHYLCELLULOSE/GRAPHITE COMPOSITES: THERMAL AND ACOUSTIC PROPERTIES

Daiana M. F. Sandrini[1,*], Balaji Krishnasamy[2], Marina F. Pillis[3] and Denise F. S. Petri[1]
1 – Institute of Chemistry, University of São Paulo (USP), São Paulo, SP, Brazil daiana_dmf@hotmail.com
2 – Polymer Engineering Laboratory, PSG Institute of Technology and Applied Research, Neelambur, India
3 – Nuclear Energy Research Institute (IPEN), São Paulo, SP, Brazil

Abstract - Natural fibrous materials are interesting for sustainable building construction materials[1]. In this work, kapok fibers (KF) were modified with soy lecithin (SL) to enable the compatibilization with hydroxypropyl methylcellulose (HPMC). KF, which are hollow hydrophobic fibers (Fig. 1a), turned hydrophilic after the modification with SL (Fig. 1b), which contains two hydrophobic chains and a zwitterionic (PO_4^{3-} and NH_4^+) head group. Elemental analysis (CHN) and FTIR-ATR spectra evidenced the presence of SL on the surface of KF. Composites of KF-LS (72 wt%) and HPMC (28%) presented mean apparent density (ρ) of 0.051 ± 0.005 g/cm³. When the amount of HPMC was kept constant, but KF/LS was partially substituted by graphite (G), the composites HPMC/KF-LS/G0.2 (28 wt% /59.4 wt% /12.6 wt%) and HPMC/KF-LS/G0.3 (28 wt% /56 wt% /16 wt%) (Fig. 1c) presented ρ values of 0.059 ± 0.002 g/cm³ and 0.058 ± 0.009 g/cm³, respectively. The thermogravimetric analysis (TGA) showed that the temperature of degradation increased from 306 ºC (HPMC/KF-LS) to 312 ºC (HPMC/KF-LS/G0.3), and the ash content increased from 10% (HPMC/KF-LS) to 22% (HPMC/KF-LS/G0.3). The sound absorbance coefficient of HPMC/KF-LS increased as the frequency increased, achieving a maximum value of 0.45 at 1500 Hz, which is like other natural fibers[1]. These findings indicted that the novel HPMC/KF-LS/G composites could be applied as green building materials.

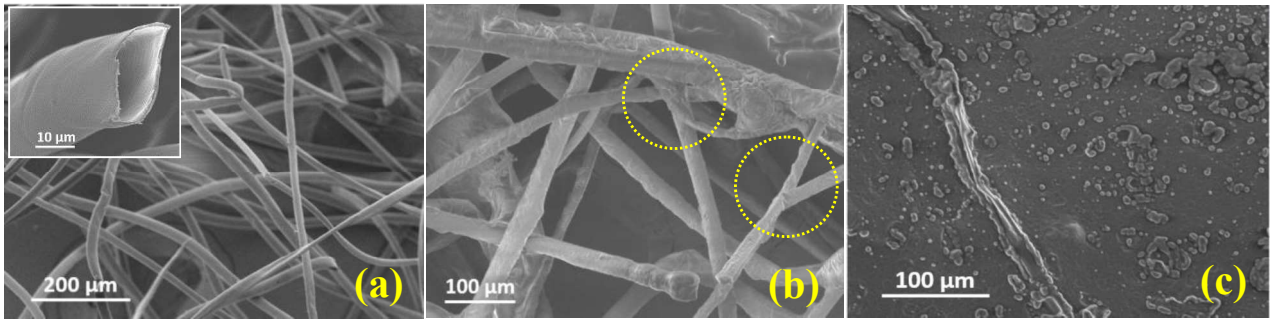

Figure 1 – SEM images of (a) KF, (b) KF-LS and (c) HPMC/KF-LS/G0.3.

References.
1. U. Berardi; G. Iannace *Building and Environment* 2015, *94*, 840. http://dx.doi.org/10.1016/j.buildenv.2015.05.029

Keywords: *kapok fiber, soy lecithin, hydroxypropyl methylcellulose, graphite, composites*

MECHANICAL AND THERMAL PROPERTIES ANALYSIS OF GLASS FIBER-REINFORCED POLYAMIDE 9T COMPOSITES FOR ENGINEERING

Maurício Baesso[1], Matheus Hromatka[2] Diego Salvaro[2] Vanessa Castro[3] Claudia Merlini[3] and Cristiano Binder[3]

1 – Department of Mechanical Engineering (EMC), Federal University of Santa Catarina (UFSC), Florianópolis, SC, Brazil.

mauricio.baesso@labmat.ufsc.br
matheus.h@labmat.ufsc.br
diego.salvaro@labmat.ufsc.br
vanolivicastro@gmail.com
claudia.merlini@ufsc.br
cristiano.binder@labmat.ufsc.br

Abstract - Research and development of new polymeric composites play a crucial role in enhancing both quality and performance of engineering components, while also addressing sustainability and energy efficiency requirements. In this study, the mechanical and thermal properties of glass fiber-reinforced Polyamide 9T composites were investigated with varying fiber contents (30, 35, and 50 wt%) for application in engineering components. The composites were fabricated using injection molding and subjected to tensile tests to evaluate their tensile strength and modulus of elasticity. Thermogravimetric analysis (TGA) was conducted to investigate the thermal behavior of the composites, while the morphology was evaluated through scanning electron microscopy (SEM). The results showed a significant increase in tensile strength and stiffness with the addition of glass fibers to the Polyamide 9T composites. Furthermore, an improvement in thermal stability was observed with increasing fiber content. SEM analysis revealed a homogeneous distribution of glass fibers within the Polyamide 9T matrix, indicating good interfacial adhesion between the components. Glass fiber-reinforced Polyamide 9T composites demonstrate promising potential as lightweight and high-performance materials for engineering components. The substitution of conventional materials with these composites can lead to lighter components with increased strength and improved energy efficiency, contributing to sustainable solutions in the engineering industry and resource consumption reduction.

References.

1. **Recent developments in the manufacturing technologies of composite components and their cost-effectiveness in the automotive industry A review study. Composite Structures. 2021**
2. **S. Das, "the Cost of Automotive Polymer Composites:a Review and Assessment of Doe'S Lightweight materials Composites Research," Oak Ridge Natl. Lab., p. 1, 2001.**
3. **R. Autay, S. Missaoui, J. Mars, and F. Dammak, Mechanical and tribological study of short glass fiber-reinforced PA 66, Polymers and Polymer Composites, vol. 27, no. 9. pp. 587–596, 2019, doi: 10.1177/0967391119853956.**
4. **M. Y. Lyu and T. G. Choi, Research trends in polymer materials for use in lightweight vehicles, Int. J. Precis. Eng. Manuf., vol. 16, no. 1, pp. 213–220, 2015, doi: 10.1007/s12541-015-0029-x.**

Keywords: *Polymeric composites, Polyamide 9T, Glass fiber, Mechanical properties.*

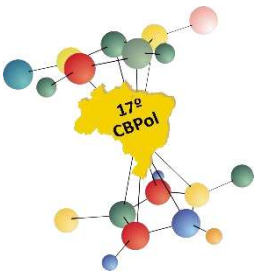

MORPHOLOGICAL, MECHANICAL AND THERMAL CHARACTERIZATION OF CARBON FIBER REINFORCED PETG AND PLA AFTER MANUFACTURING PROCESS WITH THE FFF TECHNIQUE

Clécia S. Borges[1], Maria E. A. C. Alves[1], Reinaldo S. J. Júnior[1], Erica C. Almeida[1], Werviles D. B. Santos[1], Vaneide Gomes[1], Celso C. M. F. Junior[1].

1 – Department of engineering and computing (DEC), State University of Santa Cruz (UESC), Ilhéus, BA, Brazil
csborges.egm@uesc.br

Recently, additive manufacturing (AM) techniques, such as FFF (fused filament fabrication), became popular due to the ability to produce complex parts with fewer manufacturing steps involved and with possibilities to change product properties. Aiming to expand the opportunities of using this technology, this study intends to morphologically, mechanically and thermally characterize 3D printed parts using poly(lactic acid) (PLA) and poly(ethylene terephthalate glycol) (PETG) reinforced with carbon fibers (CF) by varying printing parameters. The samples followed the ASTM D638-14 standard, Type I, manufactured by FFF. In the impression parameters the infill percentage was varied by 20%, 40% and 80% and the layer height by 0.15 mm and 0.30 mm. The mechanical characterization was performed with tensile test, revealing that the increase of the infill percentage and layer height induces directly in the increase of the modulus of elasticity and tensile strength limit in both materials. PLA/CF demonstrated superior mechanical performance, higher maximum stress and higher stiffness, indicating more intense adhesive bonding forces between carbon fibers and PLA, compared to PETG. For morphological characterization, Scanning Electron Microscopy (SEM) was applied to observe the arrangement and orientation of the carbon fibers, and the interface between the fibers and the matrix. In both filaments, the fibers were aligned in the longitudinal section and after printing presented a small level of disorder in some areas, in addition to adhesion failures between the fibers and the matrix. Thermal characterization was performed by means of Thermogravimetry (TGA) and Differential Scanning Calorimetry (DSC) in order to evaluate whether the incorporation of the fibers altered the thermal properties of the composites and to verify the thermal stability, phase transitions and melting temperature.

Keywords: *PLA with carbon fiber, PETG with carbon fiber, morphological and thermal characterization, 3D printing, tensile testing.*

MORPHOLOGY AND MECHANICAL PROPERTIES OF PBAT/PLA BIOCOMPOSITES WITH CELLULOSE IMPROVED BY DISC REFINING

Thiago R. Correia[1]*, Beatriz Girão[1], Marcos V. C. Gonçalves[2], Ana M. F. de Sousa[1]

1 – Instituto de Química, Rio de Janeiro State University (UERJ), Rio de Janeiro, RJ, Brazil

**thiagocorreia87@gmail.com*

2 – Instituto de Física, Rio de Janeiro State University (UERJ), Rio de Janeiro, RJ, Brazil

Abstract - Biocomposites reinforced by natural fibers are relevant in research for new materials, enabling the replacement of traditional polymers by improving mechanical properties and reducing raw material costs.[1,2] Cellulose refining is a mechanical process widely applied to this material in the Pulp & Paper industry with the objective of improving the mechanical properties of the fiber.[3] This process generates physical effects in this material that increase the surface area of the fibers, favoring applications such as filler in composites.[4] The poly(butylene adipate terephthalate) (PBAT) and poly(lactic acid) (PLA) are two biodegradable polymers and the mixture of both has excellent mechanical properties, often equaled to traditional polymers.[2] Biocomposites based on PBAT/PLA are of industrial and scientific interest and the use of natural fibers as reinforcement for this mixture has been encouraged.[1,2] In this work, the influence of the presence of different levels of refined fiber from pine cellulose on the mechanical, morphological and thermal properties of a commercial mixture of PBAT/PLA was studied. Pine cellulose fibers were submitted to the refining process and subsequently applied as filler in PBAT/PLA-based composites. Mechanical and morphological properties of the obtained materials were studied. The characterization of the fibers FIG.1 showed that the refining was efficient in the morphological and chemical modification of both materials (cellulose and loofah), evidenced by scanning electronic microscopy. In addition, the composites with 10% of refined cellulose fibers content shows significant improvements in the elastic modulus value and impact resistance.

Figure 1 – SEM images to cellulose fibers and PBAT/PLA/cellulose composite and mechanical test results.

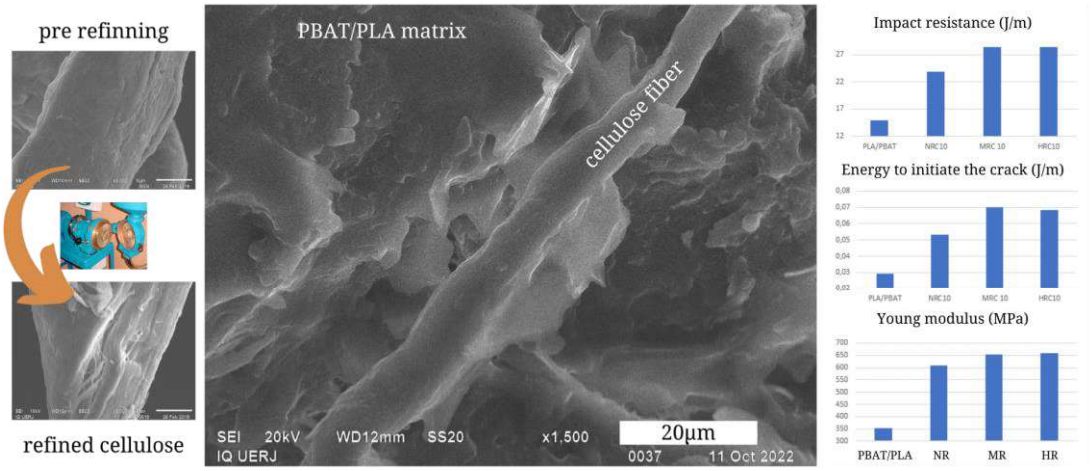

References:

1. Gharehkhani, S.; Sadeghinezhad, E. *Carbohydrate Polymer*, 115, 785-803, 2015 https://doi.org/10.1016/j.carbpol.2014.08.047
2. Sousa, S., Costa, A. P., & Simões, R. *Composites Part A*: 121, 273-282. 2019. https://doi.org/10.1016/j.compositesa.2019.03.024
3. Saibuatrong, W.; Cheroennet, N.; Suwanmanee, U. *Journal of Cleaner Production*, 158, 319–334, 2017. https://doi.org/10.1016/j.jclepro.2017.05.006
4. Jones, B. W., Venditti, R., Park, S., Jameel, H. *BioResources,* 12 (3), 4567-4593. 2017. https://doi.org10.15376/biores.12.3.4567-4593

Fundings: CAPES.

Keywords: *Natural fibers, microscopy, sustainability*

MORPHOLOGY CHARACTERIZATION OF SULFONATED POLY(STYRENE-*B*-BUTADIENE-*B*-STYRENE)

Paulo O. Gall[1]*, Vítor B. Salomão[1], Carlos H. Scuracchio[1]

1 – Department of Materials Engineering (DEMa), Federal University of São Carlos (UFSCar), São Carlos, SP, Brazil
paulo.o.gall@gmail.com

Abstract - Ionomeric polymer-metal composites (IPMCs) are smart materials made of an ionomeric polymer stacked between two metal electrodes that deform in response to electrical stimuli and vice-versa. Their flexible nature, low actuation voltage, high durability and chemical stability makes them attractive candidates for applications in soft actuators, robotics and sensors. Nafion® is widely used in the fabrication of said materials, despite its high cost, low recyclability and biodegradability [1]. Its actuation mechanism is based on the dislocation of solvated ions inside the polymer layer towards the negative electrode through channels formed by thermodynamic interactions between the polymer's constituents [2]. Block copolymers are known to display very distinct morphologies and can be chemically modified to introduce ionic conductivity by chain sulphonation. Poly(styrene-*b*-butadiene-*b*-styrene) (SBS) is an interesting starting material due to its availability, recyclability, and elastomer characteristics that could improve on an IPMC's mechanical properties. It readily phase separates, and depending on composition could develop cylindrical or gyroid morphologies, ideal when we consider the actuation mechanism of IPMCs [3]. Therefore, the goal of this study is to evaluate the morphology of thin films made of sulphonated SBS (s-SBS), with different levels of sulfonation to identify the relation between sulfonic group concentration and self-assembly properties. Sulphonated SBS is made by post-sulfonation of styrene blocks, with sulfonation degree (SD) controlled by reaction time. Films of s-SBS are then produced by solvent casting and subjected to scanning electron microscopy (SEM), along with atomic force microscopy (AFM) for identification of microdomains.

References

1. L. A. Hirano; M. T. Escote; L. S. Martins-Filho; G. L. Mantovani; C. H. Scuracchio, Artificial Organs, 2011, 35(5), 478–483. https://doi.org/10.1111/j.1525-1594.2011.01259.x
2. T. D. Gierke; G. E. Munn; F. C. Wilson Journal of Polymer Science: Polymer Physics Edition, 1981, 19(11), 1687–1704. https://doi.org/10.1002/pol.1981.180191103
3. X. Wang; M. Goswami; R. Kumar; B. G. Sumpter; J. Mays Soft Matter, 2012, 8(11), 3036. https://doi.org/10.1039/C2SM07223H

Fundings: CAPES (process 88887.704455/2022-00), FAPESP (process 2022/14231-3), and CAPES – Funding Code 001.

Keywords: *IPMCs, sulfonated SBS, morphology*

NANOCELLULOSE HYDROGELS DERIVED FROM PALM SHEATHS: SYNTHESIS AND CHARACTERIZATION

Alícia C. Ribeiro[1], Arthur de C. Bento[2], Guilherme do Nascimento[3], Atilano A. Vegini[4] and Vinicyus R. Wiggers [5]

1 – Department of Chemical Engineering, University of Blumenau (FURB), Blumenau, SC, Brazil
aliciar@furb.br
2 – Department of Chemical Engineering, Regional University of Blumenau (FURB), Blumenau, SC, Brazil
arthurcarvalho@furb.br
3 – Department of Chemical Engineering, Regional University of Blumenau (FURB), Blumenau, SC, Brazil
gdnascimento@furb.br
4 – Department of Chemical Engineering, Regional University of Blumenau (FURB), Blumenau, SC, Brazil
avegini@furb.br
5 – Department of Chemical Engineering, Regional University of Blumenau (FURB), Blumenau, SC, Brazil
vwiggers@furb.br

Abstract – The use of lignocellulosic fibers in nanotechnological products is being studied more due to their low cost of production and multifunctionality[1]. Organic residues, such as palm heart sheath, are rich in fibers and are commonly discarded in the agroindustry[2]. The most applied techniques for extracting cellulose from organic waste are alkaline, acid, or enzymatic hydrolysis reactions[3]. In this study, micro and nanocellulose fibers were extracted from mechanical pulp of palm heart sheath using hydrogen peroxide (H_2O_2) solution in an alkaline as proposed by Nascimento (2022), to synthesize nanocellulose hydrogels under different conditions. The methodology consists of the sonication of suspensions containing treated biomass and deionized water (H_2O) at different concentrations and sonication periods. The samples were then left to rest for at least 24 hours for the formation of hydrogel. Qualitative and quantitative analysis were performed to assess the chemical and physical properties of the samples. Scanning electron microscopy (SEM) was used to confirm the formation of nanostructures. Sample densities were determined using pycnometry. The water release content was obtained from the difference in mass.

References

1. Carvalho JPF, Silva ACQ, Silvestre AJD, Freire CSR, Vilela C. Spherical cellulose micro and nanoparticles: A review of recent developments and applications. *Nanomaterials*. 2021;11(10):1-35. doi:10.3390/nano11102744
2. Camargos C. Compósitos de Nanocristais e Nanofibrilas de Celulose: Preparação, Caracterização e Potenciais Aplicações em Processos de Restauração de Documentos e Obras de Arte sobre Papel. Published online 2016.
3. Higa F, Tambourgi E, Giannetti A. Aplicação do peróxido de hidrogênio como reforço da deslignificação do bagaço de cana-de-açucar. *Exacta*. 2012;10(2):281-288. doi:10.5585/exacta.v10n2.3557

Nascimento G. Produção de nanofibras de celulose a partir da pasta mecânica de bainha de palmito. Universidade Regional de Blumenau, 2022.

Fundings: CNPq, Biopasta and Estrada

Keywords: *biomass; hydrogel; cellulose; nanocellulose*

OBTAINING AND CHARACTERIZING PVDF-HFP/PVA/CLAY COMPOSITES FOR THE REMOVAL OF ORGANIC CONTAMINANTS IN AQUEOUS MEDIUM

Mirian C. Santos[2*], Felipe R. Oliveira[1], Luiz F. Malmonge[1]

[1]Department of Physics and Chemistry (DFQ), São Paulo State University (UNESP), Ilha Solteira, SP, Brazil,
[2] Department of Analytical, Physical-Chemistry and Inorganic Chemistry (DQAFQI), Institute of Chemistry, São Paulo State University (UNESP), Araraquara, SP, Brazil.
mirian.cristina@unesp.br

Abstract - The accumulation of untreated dyes in water sources can adversely affect human health and the environment due to the complex molecular structure of these dyes with toxic and carcinogenic properties[1]. The development of new materials capable of adsorbing these contaminants is undoubtedly essential. In this way, the research has as objective the production of spheres (by the drip method) of composite of the poly(vinylidene fluoride-hexafluoropropylene) - PVDF-HFP and Poly(vinyl Alcohol) – PVA (PVDF-HFP/PVA) with the incorporation of clay Montmorillonite K-10. The evaluation of their efficiency in adsorption was done through kinetic studies[2], in aqueous medium, of the organic contaminant, methylene blue. The concentration of the methylene blue contaminant not adsorbed by the samples was determined using UV visible. The adsorption tests showed that the composite is potentially effective for removing organic dyes, according to the isotherm parameters (Table). The Langmuir diagram (Fig. 1 and 2) fits the experimental data, since the R^2 values were closest to 1, so it can be assumed that adsorption occurs in a monolayer.

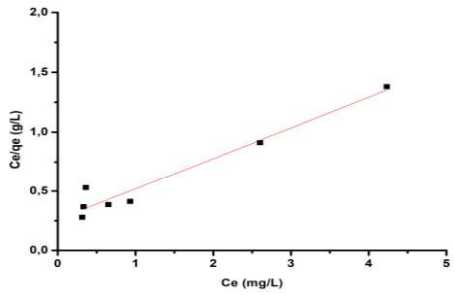

Figure 1 - Fit to the Langmuir isotherm model.

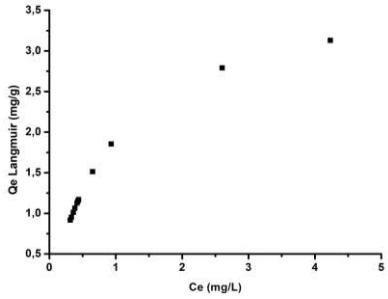

Figure 2 - Langmuir isotherm.

Table - Langmuir model parameters in aqueous media

Langmuir	
$q_{máx}$	3,89
K_L	0,980
R^2	0,9418
R_L	0,15
Ads (%)	90,70

1. M. A. Islan; S. Sabar S.; A. Benhouria; W.A. Khanday; M. Asif; B.H. Hameed. *Journal of the Taiwan Institute of Chemical Engineers* 2017, 74, 96–104. https://doi.org/10.1016/j.jtice.2017.01.016
2. R. F. Nascimento; A. C. A. Lima; C. B. Vidal; D. Q. Melo; G. S. C. Raulino *Adsorção: aspectos teóricos e aplicações ambientais*. 1. Ed. Fortaleza: Imprensa universitária, 2014. 258p

Funding: The authors are grateful for the financial support provided by the CAPES (grant #88887136426/2017/00), CNPq (grant #465571/2014-0 and 1306822017-9) and FAPESP (grants #2014/50945-4**). Acknowledgments:** National Institute for Alternative Technologies of Detection, Toxicological Evaluation and Removal of Micropollutants and Radioactives (INCT-DATREM)

Key-words*: PVDF-HFP, adsorptive, composite, organic contaminants***.**

OXYALKYLATED LIGNIN POLYOL FOR POLYURETHANE SYSTEMS: RHEOLOGY AND CURE KINECTICS

Thiago do Carmo Rufino[1], Lara Tavares dos Santos[2], Rogerio Ramos de Sousa Junior[3], Demetrio Jackson dos Santos[3,4]*

1 – Polyurethanes, The Dow Chemical Company, Jundiaí, SP, Brazil[1]
2 – Entropic Solutions: biomass based technologies, São Caetano, SP, Brazil[2]
3 - Nanoscience and Advanced Materials Graduate Program (PPG-Nano), Federal University of ABC (UFABC), Santo Andre 09210-580, Brazil[3]
4- Center of Engineering, Modeling and Applied Social Sciences, Federal University of ABC (UFABC), Santo Andre 09210-580, Brazil[4] demetrio.santos@ufabc.edu.br

Abstract – Polyurethanes (PU) are versatile polymers applied in several industrial areas, reaching an annual global consumption of approximately 25 million tons. As widely reported, renewable resources are essential to support PU developments, which promote sustainability and continuous improvement for the environment. In this line, Kraft lignin (KL) has brought attention for being the second most available polymer in the nature, obtained in large scale with constant and reproducible properties[1]. Due to abundance of functional groups in its structure, technical KL can be used in PU formulations as neat and modified raw material. The later comprises an important strategy to improve lignin reactivity and to enable KL usage in mixture with different polymers[1], specially KL modified by oxyalkylation[2]. Although extensively investigated, there is still a lack of information regarding to rheological behavior, dispersion stability and polymerization kinetics for these lignin-containing materials. Moreover, there are additional challenges to isolate these variables when formulating PU[3]. Thus, the aim of the present work was to formulate lignin-based PU comprised by polyethers of similar molar mass (polyethylene glycol (PEG) and polypropylene glycol (PPG), $M_n \approx 400$ g/mol) in combination with polymeric methylene diphenyl di-isocyanate (PMDI), resulting in PU based on PEG/PMDI and PPG/PMDI with different levels of modified KL (MKL). Lignin oxyalkylation was investigated by FTIR-ATR and DSC. Rheology and dispersion stability of polyols with different ratios of PEG/PPG and MKL contents were studied by oscillatory rheometry and visual analysis. At last, the curing of the PU were monitored by TMOR, a recent technique based on temperature modulation optical refractometry, to indicate the progress of the chemical reaction. The results allowed to elucidate the behavior of the system as a function of type of polyether, MKL content, and temperature and their effect over polyol viscosity and polymerization rate, all critical parameters for the PU industry.

Fundings – The authors acknowledge FAPESP (process #2017/22936-9 and #2019/05460-6) and The Dow Chemical Company for the financial support.

Keywords – *lignin, polyurethane, polyethylene glycol, polypropylene glycol.*

References

1. A. Grossman, W. Vermerris, *Curr Opin Biotechnol*, 2019, 56, 112-120, http://doi.org/10.1016/j.copbio.2018.10.009.
2. J.R. Gouveia, C.L. da Costa, L.B. Tavares, D.J. dos Santos, *Mini-Reviews in Organic Chemistry*, 2019, 16, 345-352, http://doi.org/10.2174/1570193x15666180514125817.
3. X. Ma, J. Chen, J. Zhu, N. Yan, *Macromol Rapid Commun*, 2021, 42, e2000492, http://doi.org/10.1002/marc.202000492.

PHOTOCATALYST IMMOBILIZATION ON ELECTROSPUN FIBERS FOR THE DEGRADATION OF THE DRUG PARACETAMOL

Fabiana S. Lima[1] , Alessandra R. Medeiros [1*], Douglas C. Dragunski [1] and Josiane Caetano [2] .

1 – Department of Chemistry, State University of Maringá (UEM), 87020-900 Maringá-PR, Brazil
corresponding_ale.ruuyz@gmail.com
2 – State University of Western Paraná - UNIOESTE, 85903-00, Toledo-PR, Brazil.

This work used the electrospinning technique to obtain polymeric fibers of poly(butylene adipate-co-terephthalate) (PBAT) and cellulose acetate (AC) created with TiO_2/g-C_3N_4 in order to promote the photocatalytic reduction of the drug paracetamol (PCT). The polymeric fibers were cross-linked with citric acid in order to increase their stability in water. TiO_2/g-C_3N_4 was synthesized from the chemical modification of TiO_2 with g-C_3N_4. This material was incorporated into the polymeric solution of PBAT/AC in the proportions of 1%, 5% and 10% (m/m). Subsequently electrospun, cross-linked and subjected to photocatalytic degradation tests, in the proportion of 5% (m/m) being chosen for the study because it presents higher percentage of drug degradation. The synthesized material TiO_2/g-C_3N_4 showed a higher photocatalytic potential compared to pure TiO_2 and pure g-C_3N_4, these being 50.5%, 13.1% and 26.1%, respectively. The study of photocatalytic degradation of PCT was carried out by varying the pH of the medium at 5.0, 7.0 and 9.0, with pH 9.0 being the most efficient, degrading approximately 86.0%. Three cycles of degradation were performed with the polymeric fibers, which showed that they can be reused without having to promote their exchange in a system. Finally, the fibers were characterized by Scanning Electron Microscopy (SEM), Fourier Transform Infrared (FTIR), Mechanical Analysis and Contact Angle techniques. Through these analyses, it was possible to identify the incorporation of TiO_2/gC_3N_4 into polymeric fibers, as well as their flexibility with polymers, demonstrating changes in thermal stability and improvement in mechanical properties and wettability of the same after crosslinking with citric acid[1,2,3] .

References

1. He T, Zhou Z, Xu W, Cao Y, Shi Z, Pan WP. Compos Sci Technol. 2010, 70(10):1469–75. https://doi.org/10.1016/j.compscitech.2010.05.001
2. Zhu J, Xiao P, Li H, Carabineiro SAC. ACS Appl Mater Interfaces; 2014, 6(19):16449–65. https://doi.org/10.1021/am502925j
3. Liao W, Murugananthan M, Zhang Y. Phys Chem Chem Phys, 2015 ;17(14):8877–84. https://doi.org/10.1039/C5CP00639B

Keywords: *Electrospinning, Photocatalysis, Paracetamol*

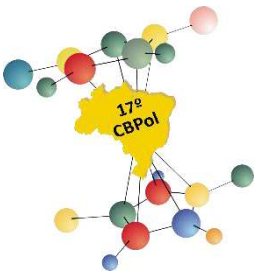

POLYURETHANE-TYPE MATRICES SYNTHESIZED FROM LIGNOSULFONATE AS POLYOL: FORMATION OF COMPOSITES REINFORCED BY LIGNOCELLULOSIC FIBERS SIMULTANEOUSLY WITH SYNTHESIS

Nilson de O. Brait Neto[1], Lidiane. P. Gonçalves[1], Leonardo B. Canto[2], Luiz A. Ramos[1] , Elisabete Frollini[1]*

1 – São Carlos Institute of Chemistry, University of São Paulo (USP), São Paulo, SP, Brazil
nilsonneto@usp..br
2 – Department of Materials Engineering (DEMa), Federal University of São Carlos (UFSCar), São Carlos, SP, Brazil

Abstract - The present study investigated the formation of hybridly plant fiber-reinforced composites simultaneously with the synthesis of bio-based polyurethane (PU) matrices. Sodium Lignosulfonate (NaLS) and castor oil (CO) were used as a polyol, with the latter aiding in the dispersion of solid reagents. No solvents or catalysts were utilized during the reaction, and the polymeric diphenylmethane diisocyanate was the chosen isocyanate. The reinforcements were sisal mats and/or short curauá fibers (3 cm long, randomly distributed), with the presence or not of MCC as an additional reinforcement. The process used was molding under pressure and temperature cycles. The materials were characterized by thermogravimetric (TGA) and dynamic mechanical (DMA) analyses, flexural and impact tests, infrared spectroscopy, and scanning electron microscopy (SEM). The infrared spectra didn't show a vibrational band at 2250 cm^{-1}, indicating that all isocyanate was consumed during the reaction. The TGA analysis revealed the thermal stability of all materials up to 240 ºC. The DMA tan delta curves showed glass transition (T_g) of approximately 42 ºC and 18 ºC for the -unreinforced PU and composites, respectively. The flexural tests at room temperature (about 25 ºC) showed that composites reinforced with curauá and microcrystalline cellulose fractured, and those with sisal mat didn't fracture and were evaluated for up to 5% deformation. During the impact test, the matrix composite reinforced solely by sisal mat did not fracture. In addition, the composite reinforced by sisal mat, curauá fibers, and MCC exhibited superior impact resistance compared to the other fractured materials during the test. The SEM images showed good adhesion at the interface matrix-fibers and homogeneous dispersity of the MCC used as reinforcement. The materials were prepared from a highly renewable content using a derivate of lignin, i.e., lignosulfonate. This raw material has not yet been widely explored in the production of polymeric materials, and the results of our research show promising applications in industries such as automotive, aeronautical, and nautical.

References -

1. F. Oliveira, L. Gonçalves, M. Belgacem, E. Frollini, *Ind Crops Prod 2020*, 155, 112821. https://doi.org/10.1016/j.indcrop.2020.112821.
2. L. Wang, W. Ma, L. Deng, S. Liu, T. Yang, *Marine Structures 2023*, 89, 103396. https://doi.org/10.1016/j.marstruc.2023.103396
3. A. Aguilar, T. Twardowski, *EFB Bioeconomy Journal 2022*, 2, 100041. https://doi.org/10.1016/j.bioeco.2022.100041.

Keywords: *Composite, Lignosulfonate, Polyurethane*

PREPARATION AND CHARACTERIZATION OF POLYETHERIMIDE/CLAY MEMBRANES

Renê A. da Paz[1], João Pedro B. G. de Araújo[1], Vanessa N. Medeiros[1], Pamela T. V. da Silva[1*], Bruna A. Araújo[1], Edcleide M. Araújo[1].

1 – Academic Unit of Materials Engineering (UAEMa), Federal University of Campina Grande (UFCG), Campina Grande, PB, Brazil
*reneanisio@gmail.com

Abstract - Water treatments are ways to minimize impacts on the environment. Worldwide, processes have been developed that efficiently use inputs, reuse water, and minimize energy expenditure and effluent emissions. Membrane technology is sustainable development, being increasingly evident and accepted at industrial levels. Membrane separation processes are frequently used in the food, chemical, pharmaceutical, and biochemical industries. Where they are used to purify, fractionate and concentrate solutions, especially aqueous ones. Based on this, interest arose in producing membranes from polyetherimide and montmorillonite clay (MMT) using the phase inversion technique, aiming to evaluate the influence of clay on membranes for treating liquid effluents. By XRD, it was observed that the MMT peak appears more evident in the compositions with more than 17% of polymer and higher clay content. From the SEM, it was observed that the surface of the pure PEI membrane presented a poreless structure compared to the others. By TG, two decomposition steps were visualized. The Tg of the polymer registered in the second heating in the DSC presents a standardized thermal history. Contact angle measurements indicated that the inclusion of clay altered the wetting capacity of the membranes. The flow, both in distilled water and in water with dye, in the PEI/clay membranes started high and, over time, reached its stabilization around 10 minutes of testing. The membrane with the highest clay content showed the most significant flow and the greatest reduction in turbidity. It was concluded that the presence and content of clay altered the morphology of the membrane, contributing to an increase in the flow and that they are efficient for treating aqueous effluents from the textile industry.

Fundings: The authors thank UFCG, CAPES, CNPq, and FAPESQ/PB for financial support.

Keywords: *Polyetherimide, montmorillonite clay, flat membrane.*

PROCESSING PARAMETERS AS POTENTIAL VARIABLES TO TPS/PVOH BLENDS SENTIVITY TO WATER

Marcos V. B. Nicolino[1] and Lidiane C. Costa[1,2,3]*

1 – Federal University of Sao Carlos, Graduate Program in Materials Science and Engineering, Rodovia Washington Luiz, km 235 SP-310, 13565-905, São Carlos, São Paulo, Brazil
2 – Federal University of São Carlos, Department of Materials Engineering, Rodovia Washington Luiz, km 235 SP-310, 13565-905, São Carlos, São Paulo, Brazil
3 – Center of Characterization and Development of Materials (CCDM), Federal University of São Carlos, Rod. Washington Luiz, Km 235, São Carlos, CEP: 13.565-905, Brazil
lidiane@ufscar.br

Thermoplastic starch (TPS) is a biodegradable polymer with hydrophilic characteristics derived from renewable sources. It finds applications in agriculture, hygiene, catering, and packaging, but processing difficulties and limited water sensitivity hinder its use. An effective solution is blending TPS with a second hydrophilic and biodegradable polymer, like polyvinyl alcohol (PVOH) [1]. In this study, PVOH and cornstarch were hydrated with 30% glycerol and then fed into a twin-screw extruder. TPS and PVOH were mixed in varying proportions (TPS/ PVOH) with the addition of 1%wt. citric acid (CA). The samples underwent torque rheometry, thermogravimetric analysis (TGA), and Soxhlet extraction with water. Torque rheometry revealed increased torque for PVOH +1% CA, 80/20, and 70/30 blends after 5 minutes, while 90/10 and pure TPS showed a downward trend. TGA of the blends exhibited four phases of thermal decomposition that can be associated with the pure materials. The first phase, from 160 to 250 °C, represents the thermal decomposition of glycerol, with an average mass loss of 28%, indicating that the blends did not experience significant plasticizer loss during processing and rheometry [2]. This suggests that torque increase is likely due to PVOH cross-linking rather than plasticizer evaporation [3]. In Soxhlet extraction, PVOH +1% CA that underwent extrusion and rheometry (EH) showed 45% mass loss, while PVOH (EH) without CA lost approximately 90%. Similarly, extruded only PVOH samples with and without CA experienced around 90% mass loss, suggesting CA and rheometry time, shear and temperature facilitated possible PVOH cross-linking. The 90/10 blend exhibited the highest mass loss (75%) among the blends, while 80/20 and 70/30 blends had average losses of 65% and 60%, respectively. Therefore, incorporating PVOH and suitable blending processes offer potential for enhancing TPS properties and achieving desired water sensitivity for specific applications.

1. X Tang; S. Alavi; Carbohydrate Polymers 2011, 85, 7-16. https://doi.org/10.1016/j.carbpol.2011.01.030
2. J. Zanela; J. B. Olivato; A. P. Dias; M. V. E. Grossmann; F. Yamashita; Journal of Applied Polymer Science 2015, 42697. DOI: 10.1002/app.42697
3. F. C. Nascimento; L. C. V. Aguiar; L. A. T. Costa; M. T. Fernandes; R. J. Marassi; A. S. Gomes; J. A. Castro; Polymer Bulletin 2021, 78, 917-929. https://doi.org/10.1007/s00289-020-03142-2

Fundings: This study was financed in part by the Coordenação de Aperfeiçoamento de Pessoal de Nível Superior - Brasil (CAPES) - Finance Code 001. The authors acknowledge CAPES Scholarship grant 88887.371837/2019-00.

Keywords: *Thermoplastic Starch blend. PVOH crosslinking. TPS PVOH blend. Citric acid. Processing conditions.*

PRODUCTION AND CHARACTERIZATION OF A SIMPLE AND LOW-COST BACTERIAL CELLULOSE/SILICA GEL COMPOSITE.

Rafael G. C. da Silva[1], Karina C. de Souza[2], Sara H. de Oliveira[1], Magda R.S. Vieira[3], Severino L.U. Filho[3] and Glória M. Vinhas[1]*

1- Chemical Engineering Department, Federal University of Pernambuco (UFPE), Recife, PE, Brazil;
2- Center for Exact and Natural Sciences, Federal University of Pernambuco (UFPE), Recife, PE, Brazil;
3- Mechanical Engineering Department, Federal University of Pernambuco (UFPE), Recife, PE, Brazil
**gloria.vinhas@ufpe.br*

Abstract - Polysaccharides/silica gel (SG) composites were reported as a new class of functional materials with desired properties for various applications, such as water purification treatment. In the field of adsorption, crosslinked polysaccharides/SG composites have high adsorption capacities compared to individual polysaccharides or silica gel [1]. In this sense, the present work sought to develop a sustainable and low-cost composite of Bacterial Cellulose (BC)/SG with potential application to pollutant remediation. SG particles were synthesized according to Wang *et al.* [2]. Two BC/SG composite materials were prepared from 30 ml of two different concentrations of SG (0.6% and 5.6%) mixed with 20 g of a BC paste. The BC paste was prepared by adding 109.569 g of wet BC in 50 mL of H_2O under mechanical stirring. The drying of the material was carried out in an oven at 50°C for 24 hours. The characterization of the BC/SG composite was carried out by Scanning Electron Microscopy (SEM), X-ray Dispersive Spectroscopy (EDS) and roughness analysis (Taylor Hobson Intra). The SEM images (Fig. 1) showed uniform incorporation of the SG particles in the BC matrix for both studied conditions. The EDS showed peaks of Si, O and C, characteristic of the elemental composition of SG (Si and O) and BC (C and O). The increase in surface roughness can lead to a potential application of the composite as a bioadsorbent for heavy metals [1].

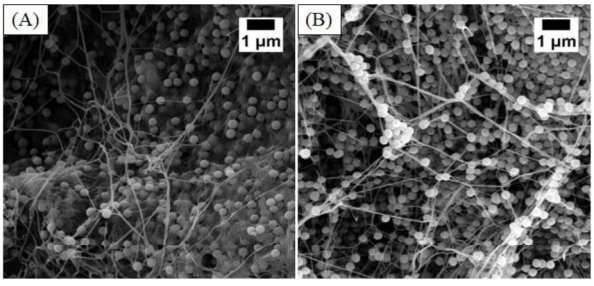

Figure 1 – SEM images of the BC/SG composite obtained for the different SG concentrations of (A) 0,6% and (B) 5,6%.

References:
1. K. Baskaran, M. Ali, K. Gingrich, D. L. Porter, S. Chong, B.J. Riley, C.W. Peak, S.E. Naleway, I. Zharov, K. Carlson. *Microporous and Mesoporous Materials* 2022, 336, 111874. https://doi.org/10.1016/j.micromeso.2022.111874.
2. S. Wang, C. Liu, G. Liu, M. Zhang, J. Li, C. Wang. Applied Surface Science 2011, 258, 258, 806-810. https://doi.org/10.1016/j.apsusc.2011.08.100.

Keywords: *Bacterial Cellulose, Silica Gel, Composite, Characterization.*

PRODUCTION OF BIOCIDAL POLYMERIC COATINGS BASED ON ALKYLATED POLYETHYLENEIMINE AND PMMA BLENDS

Rafael A. Netto[1], Marta C. T. Duarte[2], Camila Delarmelina[2], Liliane M. F. Lona[1*]

1 – Laboratory of Analysis, Simulation and Synthesis of Chemical Processes (LASSPQ), Department of Materials Engineering and Bioprocesses (DEMBio), State University of Campinas (UNICAMP), Campinas, SP, Brazil
netto.affonso@gmail.com
2 – Division of microbiology (DMB), Pluridisciplinary Center for Chemical, Biological and Agricultural Research (CPQBA), State University of Campinas (UNICAMP), Campinas, SP, Brazil

New and efficient solutions are needed to inactivate a broad spectrum of pathogenic microorganisms upon direct contact, especially on surfaces prone to recurring contaminations, such as healthcare environments and touchscreen electronic devices [1,2]. Quaternary ammonium compounds are efficient in inactivating these microorganisms due to electrostatic interactions between the positive charges of the quaternary nitrogen atoms and negative charges present on microorganisms' cell walls or lipoprotein envelopes, which makes them cleave and release the genetic material to the extracellular environment, thus inactivating their ability to inoculate into host cells [3,4]. That makes alkylated polyethylenimine (QA-PEI) promising to inactivate a broad spectrum of microorganisms due to its high density of quaternary nitrogen atoms. This work aimed to produce films of blends of QA-PEI and polymethyl methacrylate (PMMA) by solubilization followed by drop-casting method producing PMMA/QA-PEI samples with proportions of 0%, 1%, 2%, 5%, and 10% in weight of QA-PEI into the PMMA matrix. The sample's capacities to inactivate microorganisms were assessed by performing inhibition halo tests against the gram-positive bacteria *S. Aureus* and the gram-negative bacteria *E. Coli*, which results showed that even though inhibition haloes were not fully formed, QA-PEI was effective in inhibiting both bacteria, as it was clear that biofilm was not formed over the samples films and on their surroundings. Inhibition halos were not formed is because the PMMA matrix did not solubilize into the bacterial culture media, so QA-PEI did not diffuse on the culture media, which would have formed the inhibition halos. In addition, the mechanical and thermal resistance characterization showed no significant differences between pure PMMA and the samples of PMMA/QA-PEI blends, indicating that the presence of QA-PEI did not significantly alter these properties.

References

1. C. P. Gerba, A. L. Wuollet, P. Raisanen, G. U. Lopez, Amer. J. of Infection Control, 2016, 44, 3, 358-360, https://doi.org/10.1016/j.ajic.2015.10.013.,
2. A. Klibanov, *J. Mater. Chem.*, 2007, 17, 2479–2482, https://doi.org/10.1039/B702079A
3. S. Farah, O. Aviv, N. Laout, S. Ratner, N. Beyth and A. J. Domb, *Colloids and Surfaces B: Biointerfaces*, 2015, 128, 614–619, 10.1016/j.colsurfb.2015.03.006
4. D. Park, J. Wang, A. Klibanov, *Biotechnol. Prog*., 2006, 22, 584−589, https://doi.org/10.1021/bp0503383

Fundings: CNPq, Grant number: 140443/2020-7 and FAPESP, Grant number: 2021/09341-1.

Keywords: *quaternary ammonium compounds*, *alkylated polyethyleneimine, biocidal surfaces, biocidal films, bacteria*

PRODUCTION OF CELLULOSE-POLYACRILICACID HYDROGELS

Gabriela de Paula Souza[1]*, Paula Paulino Silva[1] and Gizilene Maria de Carvalho[1]

1 – Department of Chemistry, State University of Londrina, Londrina (UEL), PR, Brazil
gabriela.de.paula@uel.br

Abstract – Cellulose hydrogels (HGs) are biocompatible and have low toxicity, coming from a renewable source. They can be formulated as films, membranes, gels and microparticles, combined or not with other materials. This versatility allows the adaptation of cellulose HGs to suit specific requirements for a variety of applications [1,2]. The aim of this work was the synthesis and characterization of HGs from cellulose and polyacrylic acid (PAA), with the compositions: (100/0; 75/25; 60/40; 50/50). The HGs were prepared by radical polymerization of acrylic acid (AA) in cellulose solution (NaOH/urea, 7/12%m/m) using potassium persulfate (KPS) as initiator. Typically, a solution of cellulose (3%) in NaOH/urea was prepared [3] and AA, KPS (3%) and N,N-methylenebisacrylamide (15%) was added, under stirring, at 25 ºC. After 30 minutes epichlorohydrin (8%) was added. The mixture was heated to 50°C, poured into a Petri dish, regenerated with 5% H_2SO_4 (v/v). The HGs were immersed in distilled water until reached ~pH 5 and dried at 100°C for 12 hours. Swelling (%S), infrared (FTIR) and nitrogen physisorption (BET) analyzes were performed. All HGs presented microporous structure. The %S decreased with increasing amount of AA which can be explained by the increase in crosslink density. By the FTIR spectra it was verified a decrease in the intensity of the band at 3344 cm^{-1} and the appearance of a band at 1712 cm^{-1}, attributed to the formation of ester bonds from cellulose and PAA, increasing the density of crosslinks of these HGs, forming more compact networks, confirming what was observed in the %S analyses. HGs with lower amounts of AA are brittle and fracture during the washing procedure. Increasing the amount of AA in the formulation decreases the %S of the material. However, it is possible to adapt the formulation to obtain HGs with suitable properties for the required applications.

References

1. S. H. Zainal; N. H. Mohad; N. Suhaili; F. H. Anuar; A. M. Lazim; R. Othaman. Journal of Materials Research and Technology 2021, 10, 935. https://doi.org/10.1016/j.jmrt.2020.12.012.
2. N. Nasution; H. Harahap; N. F. Dalimunthe; M. H. S. Ginting; M. Jaafar; O. O. H. Tan; H. K. Aruan; A. L. Herfananda. Gels 2022, 8, 568. https:// doi.org/10.3390/gels8090568.
3. J. Zhou; L. Zhang. *Polymer Journal, Nature Publishing Group 2000, 32*, 866. https://doi.org/10.1295/polymj.32.866.

Acknowledgments: This work was carried out with the support of the Coordination for the Improvement of Higher Education Personnel-Brazil (CAPES), CNPq and Fundação Araucária/Brazil. Prebiotic Chemistry Laboratory (LQP)

Keywords: B*iomaterial; crosslinking; swelling.*

PRODUCTION OF CELLULOSE/PVOH/CHONDROITIN SULFATE MEMBRANES AND POTENTIAL APPLICATIONS AS A TRANSDERMAL MEMBRANE

Juliano Brisola[1], Paula Paulino Silva[1], Vinicius A. M. Gomes[1*] and Gizilene Maria de Carvalho[1*]

1 – Department of Chemistry, University of state of Londrina (UEL), Londrina, PR, Brazil
*vinicius.23051999@uel.br

Abstract - Transdermal membranes have the ability to perform dual functions, aiding healing and as a drug carrier. In this work, membranes based on cel/PVOH/SC were developed with different compositions of SC incorporated with paracetamol and cross-linked with epichlorohydrin. The membranes were produced by the casting technique from mixtures of aqueous solutions (3% w/v) of PVOH and SC and alkaline solution (NaOH/urea) of cel. The membranes were characterized by moisture content (%TU), water vapor permeability (WVP), fluid-handling capability (FHC). The kinetic behavior of paracetamol release was investigated by using the models of Korsmeyer Peppas, Peppas Sahlin, and Weibull to fit the experimental data obtained using a Franz cell. The physical-chemical results (Table 1) showed that the addition of SC resulted in a reduction in FHC %TU and WVP values. However, the values obtained were still acceptable for use as a transdermal membrane. Paracetamol release was fast within the first 2 h (4-11%). The greater the amount of SC present in the membrane, the smaller the amount of SC released. Furthermore, the release kinetics data fit the empirical Weibull model, showing b values between $0.35<b<0.75$ indicating a mechanism of paracetamol release controlled by Fickian diffusion. It is concluded that the casting technique was a simple and efficient method to produce cellulose/PVOH/SC membranes, with promising physicochemical characteristics to use as wound dressing.

Table 1 – Moisture content data (%TU); fluid handling capacity (FHC); water vapor permeability (WVP) of the blends.

Samples	%TU*	*FHC(g.10cm^{-2}.24h^{-1})	*WVP(g.Pa^{-1}.s^{-1}.m^{-1})
CEL	22,15^{a}	9,41^{a}	5,73^{a}
PVOH	-	-	2,71^{cd}
CP	10,00^{b}	3,63^{b}	4,41^{ab}
CPS1	13,12^{b}	3,48^{b}	3,09^{bc}
CPS2	11,00^{b}	3,47^{b}	2,01^{cde}
CPS3	9,74^{b}	4,26^{b}	1,24^{de}
CPS5	10,31^{b}	5,15^{b}	0,78^{e}

(*) Means with different letters are statistically different from each other by Tukey's test ($p < 0.05$)

References

M. Miotke; J. Strankowska. *Polymer Bulletin 2020*. https://doi.org/10.1007/s00289-019-02755-6

Keywords: *Kinetics. Biopolymers. Biomaterial. Blends.*

PROPERTIES OF ALGINATE CAPSULES: A COMPARATIVE STUDY USING DIFFERENT CROSSLINKERS

Maximiliano Alvarez*[1,2], Letícia F. Balcewicz[2], Renata P. Sanches[2], Bruno C. da Silva[3], Izabel C. Riegel-Vidotti[2]

Insert here the author(s) affiliation(s). Write the e-mail of the author to whom correspondence should be addressed. Example:
1 – Department of Chemical Engineering, Federal University of Paraná (UFPR), Curitiba, PR, Brazil
alvarezmaximiliano@ufpr.br
2 – Department of Chemistry, Federal University of Paraná (UFPR), Curitiba, PR, Brazil
3 - Nova Pesquisa Química LTDA, Curitiba, PR, Brazil

Abstract - The objective of this study was to encapsulate bergamot essential oil (BEO) in alginate beads prepared with calcium (Ca^{2+}) or iron III (Fe^{3+}) and to investigate the properties of these capsules under gastrointestinal conditions[1,2]. Additionally, chitosan was applied as coating material to the alginate beads using two different methods: one-stage and two-stage methods. In the one-stage method, an emulsion containing alginate and BEO was dropped into a solution containing chitosan and the crosslinking agent, using a peristaltic pump. The resulting capsules crosslinked with Ca^{2+} were named ACQ1 and with Fe^{3+}, AFQ1. In the two-stage method, the alginate beads were first prepared and then immersed in a solution containing chitosan. The corresponding capsules were named ACQ2 and AFQ2. Alginate beads without chitosan were named AC and AF. The characterization of the capsules was performed by scanning electron microscopy, Fourier transform infrared spectroscopy (FTIR), encapsulation efficiency (EE%) and release analysis in PBS buffer (pH 7.4) for 3 hours and hydrochloric acid with sodium chloride (pH 2.0)[3] for 2 hours. The results indicated that the capsules displayed distinct release profiles depending on the crosslinking agent, chitosan coating, and pH conditions. Additionally, the encapsulation efficiency varied across the different types of beads, with Fe^{3+} beads exhibiting higher encapsulation efficiency than Ca^{2+} beads, except for AC. However, it was observed that the Fe^{3+} beads also showed faster release rates when compared to the Ca^{2+} beads.

References:

1. B.C. da Silva; A.C. Bastos; J. Tedim; M.G.S. Ferreira, C.E.B. Marino, I.C. Riegel-Vidotti, *J. Braz. Chem. Soc. 2022*, 33(8):987–996. https://doi.org/10.21577/0103-5053.20220065.
2. R. P. Sanches, Msc. Master's Thesis, University of Paraná, 2022.
3. ANVISA. Farmacopeia Brasileira Agência Nacional de Vigilância Sanitária [Internet]. 2010. Available from: www.anvisa.gov.br

Fundings: UFPR, CAPES, CNPq and CME-UFPR.

Keywords: *alginate; chitosan; oil; ionotropic gelation*

REACTIVE COMPATIBILIZATION OF PEBD/PP BLENDS USING NATURAL CLAY

Silma de S. Barros, Antonio J. A. Junior, Emerson F. Silva, Clodoaldo Saron*
Department of Materials Engineering, Lorena Engineering School - EEL-USP, Lorena, SP, Brazil
saron@usp.br

Abstract – Bentonites clays have been widely used as fillers in polymers such as in polyolefins due to the low cost and formation of nanofillers, leading to significant changes in performance of mechanical properties of the material. Polyolefins (polyethylene and polypropylene) represent above 50% of global consume of thermoplastics, generating large amounts of waste, which is a challenge for recycling. Although the use of bentonite clays as filler is consolidated, studies have showed the action of bentonite clays on induction or catalysis of structural changes in polyolefin when the clay is incorporated to polymer on high shear rate[1]. Thus, the aim of study has been to evaluate the action of a natural bentonite clay on the polymer low-density polyethylene (LDPE), polypropylene (PP) and LDPE/PP blend after thermomechanical processing under high shear rate and inert gas nitrogen. An internal mixer MH 600 was used for thermomechanical processing. Afterward, the materials processed by injection molding in a Diplomat Spazio Dw-130 for confection of tensile and impact specimens, which were used to characterization of mechanical, thermal, rheological, chemical and morphological properties with the purpose of the identification the structural changes in materials and related consequences on properties of these materials. Bentonite clay showed significant action on structural modification in polymeric chain of LDPE and PP. However, these changes have been more intense in PP. The molecular recombination, mainly for LDPE/PP blend, may also have occurred with probable formation of copolymers LDPE-PP. The study led to a better understanding on the interaction between bentonite clay and polyolefin matrix as well as the structural and properties changes in the polymers, which can be important for development of new polymer materials and improvement of practices for mechanical recycling of polyolefins.

Keywords: *Polyolefin, natural clay, bentonite, recycling*

Fundings: National Council for Scientific and Technological Development - CNPq (Proc. 309583/2020-9) and FAPESP (Proc. 2020/14318-6).

References

D. S. Luiz; C.; Saron, C. *J. Mater. Cycles Waste Manag.* 2022, 24, 2445. https://doi.org/10.1007/s10163-022-01502-w

REDOX-RESPONSIVE HYDROGELS OF THIOLATED PECTIN: POTENTIAL VEHICLES FOR DRUG RELEASE

Rafael F.N. Quadrado*, André R. Fajardo

Laboratório de Tecnologia e Desenvolvimento de Materiais Poliméricos (LacoPol), UFPel, Brazil.
(*) rafaelfnq@hotmail.com

Hydrogels are one the utmost polymeric materials employed in drug delivery, especially those constituted with polysaccharides due to their biocompatibility, and non-toxicity[1]. These hydrogels can be prepared by physical or chemical crosslinking of the polysaccharide chains, where the latter have been gained special attention since the crosslinking process is easily controlled[1]. To improve the efficiency of this type of hydrogel towards drug release, the chemical crosslinks should have a responsive nature, allowing their breaking in the presence of a trigger, such as pH or temperature[1]. A scarcely explored type of chemical crosslinks are those with a redox-responsive nature, which is intriguing since many redox molecules are present in different wounds (from burn to scratch wounds)[1]. In the presence of physiological redox agents, the redox-responsive crosslinks are broken, facilitating the controlled and local release of drugs from the hydrogel. Within this framework, we have developed a redox-responsive hydrogel of thiolated pectin crosslinked by disulfide bonds, which are broken in the presence of physiological redox molecules, such as cysteine or glutathione[1]. The crosslinking of the thiolated pectin chains was induced by the addition of potassium persulfate (KPS), which reacts with the thiol groups, and promotes the formation of the disulfide bonds. Through several characterization analyses (FTIR, rheology, swelling, weight loss), we have demonstrated the redox-responsiveness of the prepared hydrogels. Nonetheless, the hydrogels were able to control the release of acetaminophen, a model drug, accordingly to the redox condition of the medium.

References

1. Y. Cao, Y. Yao, Y. Li, X. Yang, Z. Cao, G. Yang *J. Colloid Interface Sci.* 2019, *544*, 121–129. https://doi.org/10.1016/j.jcis.2019.02.049.

Keywords: *Hydrogel, redox-responsiveness, thiolated pectin, drug release.*

RESPONSE SURFACE METHODOLOGY TO MAXIMISE THE SWELLING OF STARCH AND ACRYLIC ACID BASED HYDROGELS

Isabel R. Maurate-Fernandez[1], Diego D. Pinzon-Moreno[1], Maria V. Carranza-Oropeza[1]

1- Faculty of Chemistry and Chemical Engineering, National University of San Marcos, Lima, Peru
mcarranzao@unmsm.edu.pe

Abstract

The present study proposes the synthesis and maximization of swelling of hydrogels based on starch and acrylic acid. The synthesis of hydrogels was based on the methodology proposed by Zhang, et al 2016 using a central composite experimental design. The study region comprised an N, N'-metilenbisacrilamida (MBA) concentration range of 0.0156 to 1.6844% and a polymer ratio of 4.17 to 9.83 g acrylic acid/gstarch. The synthesized hydrogels were immersed in distilled water until equilibrium swelling was reached. Then the equilibrium swelling values were entered into Minitab software and using response surface methodology the swelling of the hydrogels was maximized as a function of polymer ratio (g acrylic acid/g starch) and MBA concentration. The results were fitted to a quadratic model (95% confidence), with the optimum swelling value being 622.31 g/g for a concentration of 0.016% MBA and 7 g acrylic acid/g starch. Therefore, the study demonstrated that the swelling of starch-acrylic acid-based hydrogels can be maximized by adjusting the polymer ratio and MBA concentration using the equation described in the present study.

Figure

Fig 1. Swelling response surface

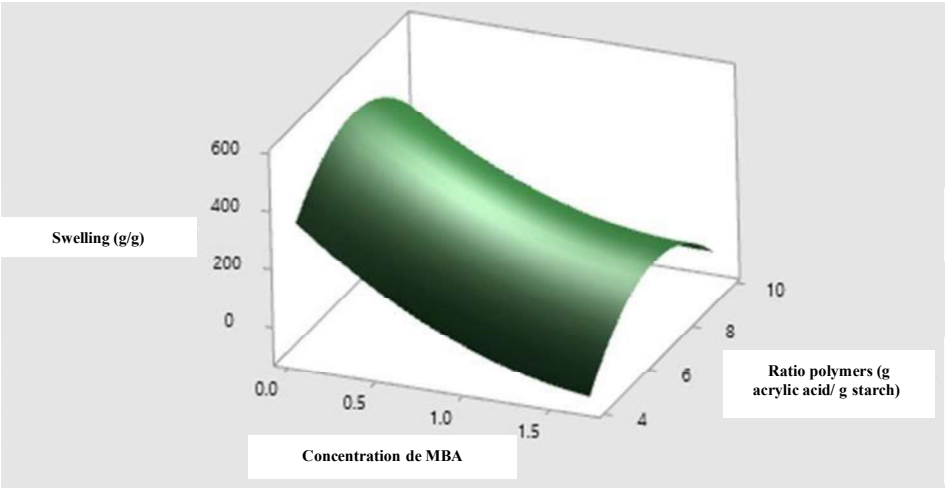

References

1. Zhang, Y.; Gao, P.; Zhao, L.; Chen, Y. 2016. *Frontiers of Chemical Science and Engineering* 2016, *10, 147–16.* https://doi.org/10.1007/s11705-015-1546-
2. Zhang, Y.; Zhao, L.; & Chen, Y. 2016. *Journal of Macromolecular Science* 2016, *55, 662–679.* https://doi.org/10.1080/00222348.2016.1187051
3. H. Gutiérrez-Pulido; R. de la Vara-Salazar. *Análisis y diseño de experimentos*, McGraw Hill Interamericana, México, 2008; 384-42.

Keywords: *Hydrogel, starch, swelling, composite center design, response surface methodology*

RHEOLOGICAL CHARACTERIZATION AND STUDY OF MECHANICAL AND THERMAL PROPERTIES OF NATURAL RUBBER AND POLYBUTADIENE BLENDS WITH ADDITION OF POLYURETHANE RESIDUE

Carlos T. Hiranobe[1], Marco A. G. Cruz[1], Samara S. Araújo[1], Diego S. Melo[2], Eduardo R. Budemberg[1], Flávio C. Cabrera[1], Leonardo L. Paim[1] and Renivaldo J. dos Santos[1]*

1 – Department of Engineering, School of Engineering and Sciences, São Paulo State University (UNESP), Rosana, SP, Brazil

renivaldo.santos@unesp.br

2 – Department of Physics, Ilha Solteira School of Engineering, São Paulo State University (UNESP), Ilha Solteira, SP, Brazil

Abstract - Polyurethane (PU) is a versatile material widely used as thermal insulation in refrigerators and in the construction industry. Additionally, it can be employed in equipment and glassware packaging, as well as in footwear, clothing, and surgical materials. The diverse use of polyurethane also generates a significant amount of waste and residue material. In this study, micronized polyurethane residue was incorporated as a reinforcing filler in natural rubber, polybutadiene rubber, and a blend of natural and polybutadiene rubbers (50/50) using an open roll mill mixer at a friction ratio of 1:1.25, according to ASTM D3182 standard. The vulcanized composites with 15 phr (per hundred rubber) of PU were characterized through rheometric testing (ASTM D2084), density, hardness (Shore A), abrasion resistance, Fourier-transform infrared spectroscopy (FTIR), and thermogravimetric analysis. The results showed that the vulcanization time of the polybutadiene rubber composite is longer, but in the rubber blend, this time is reduced and practically equal to that of the natural rubber composite. In abrasion resistance tests, there is greater wear for the polybutadiene composite, but this resistance is increased when compared to the polymeric blend. The FTIR spectra showed that the blend presents the chemical structures of natural rubber, polybutadiene, and PU residue. Thermogravimetric analysis demonstrated that the polybutadiene composite is more resistant to thermal degradation than the natural rubber composite, whereas the blend exhibited two well-defined degradation temperatures. Therefore, it can be inferred that the polybutadiene composite is recommended for applications requiring thermal resistance, while the rubber blend can be used in works that demand mechanical strength, thus contributing to the value enhancement of rubber products and the reduction of environmental impact.

Keywords: *Composite, polybutadiene rubber, polyurethane residue, thermogravimetric analysis, rheometry.*

STUDY OF POLYMERIC COMPOSITES FROM LDPE/NATURAL FIBERS FROM THE AMAZON

Silma de S. Barros[1]*, Antonio J. A. Junior [1], Flávio A. de Freitas[2], Clodoaldo Saron[1]
1 – Department of Materials Engineering, Lorena Engineering School - EEL-USP, Lorena, SP, Brazil
2 – Amazon Biotechnology Center – CBA, Industrial District, 69075-351, Manaus, Amazonas, Brazil.
engenharia.silma@usp.br

Abstract - Since 1950, about 6.33 billion tons of polymers have been produced worldwide; 9 and 12% of these wastes have been recycled or incinerated, and about 4.9 billion tons have been discarded in landfills or the environment, threatening ecosystems across the planet. On the other hand, agro-industrial production, especially the oil palm culture, has a high output; its production is even greater than that of rapeseed and six times greater than soybeans. For example, Brazil produced 2,867,986 tons only in 2020. Moreover, the northern region is Latin America's largest oil palm producer, generating countless wastes. Therefore, this research seeks alternatives for using and applying these materials in the form of polymeric composites. To make the composites, firstly, a study was carried out on the fibers, such as knowing their lignocellulosic content and extracting the cellulose, using $NaClO_2$ and glacial acetic acid at a temperature of 70 °C for 5 hours, and drying until constant weight. After that, the cellulose was washed with a sodium hydroxide (NaOH) solution diluted at 17.5% m/v, washed for 2 min with distilled water, and dried to constant weight. Subsequently, for the manufacture of the composites, the materials (LDPEr/cellulose) at concentrations of 0, 3, 5 and 7% of cellulose together with 2.5% PE-g-AM as a compatibilizer were added in a thermokinetic mixer homogenizer MH at 4,050 rpm, to create a homogeneous mixture between LDPE/fiber/compatibilizer. After that, the material was ground and then subjected to injection molding using a SPAZIO DW-130 brand injector, with a temperature profile of 170, 180, 190, and 200 °C for feeding to the nozzle and holding pressures of 80 and 110. Then, the specimens were submitted for mechanical tests and thermal analyses. The samples with the addition of cellulose fiber tended to decrease the tensile strength increasing fiber percentual Fig. 2 (17.16 to 13.5MPa) and the TGA analysis occurred in 2 stages of degradation, since cellulose starts its degradation around 230°C.Therefore, it can be understood that the cellulose extracted from the residues of the palm bunches can be easily applied in the polymeric matrix of LDPEr.

Keywords: *Polymers, natural fibers, composites*

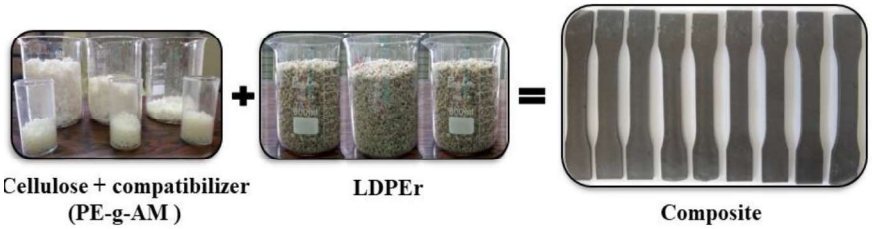

Figure 1: Materials and composites developed.

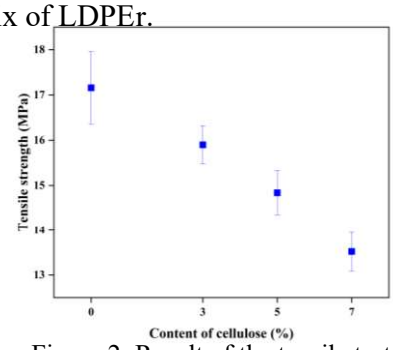

Figure 2: Result of the tensile test

Fundings: Coordenação de Aperfeiçoamento de Pessoal de Nível Superior – CAPES; Nacional de Metrologia, Qualidade e Tecnologia (INMETRO-PRONAMETRO); National Council for Scientific and Technological Development - CNPq (Proc. 309583/2020-9), FAPESP (Proc. 2020/14318-6) and To company Brasil Bio Fuels for the donation of palm oil residues.

References

KEDZIERSKI, Mikaël; FRÈRE, Dominique; LE MAGUER, Gwénaël; BRUZAUD, Stéphane., 2020. DOI: 10.1016/j.scitotenv.2020.139985.

JEON, Jong Min; PARK, So Jin; CHOI, Tae Rim; PARK, Jeong Hoon; YANG, Yung Hun; YOON, Polymer Degradation and Stability, *[S. l.]*, 2021. DOI: 10.1016/j.polymdegradstab.2021.109662.

ALBUQUERQUE, Tânia Gonçalves; COSTA, Helena S.; SILVA, Mafalda Alexandra; OLIVEIRA, M. Beatriz P. P. Trends in Food Science and Technology, *[S. l.]*, 2019. DOI: 10.1016/j.tifs.2019.01.005.

STUDY OF THR TRIBOLOGICAL PROPERTIES OF PARTS OBTAINED BY 3D PRINTING USING PET FOLAMENT WITH CARBON FIBER

Maria Eduarda A. C. Alves,[*1] Vaneide Gomes, [*2] Érica C. Almeida [*3] Erickson F. M. S. Silva. [*4]

1 – Graduação em Engenharia Mecânica, Universidade Estadual de Santa Cruz (UESC), Ilhéus, BA
2 - Departamento de Engenharias e Computação, Universidade Estadual de Santa Cruz (UESC), lhéus, BA
vgomes@uesc.br
3 - Departamento de Engenharias e Computação, Universidade Estadual de Santa Cruz (UESC), Ilhéus, BA
4- Departamento de Engenharias e Computação, Universidade Estadual de Santa Cruz (UESC), Ilhéus, BA

Abstract: Additive Manufacturing (AM) has been presenting itself as an interesting technology due to the insertion of a new manufacturing model. In order to expand the application opportunities of this technology, this research aims to analyze the tribological properties of parts manufactured by the process using PET and PLA filaments with carbon fiber. Tribological knowledge helps to improve the safety, service life, as well as the reliability of the components obtained. The specimens were printed on a Delta 3D printer. Tribological analyzes were carried out from the reciprocal test, to determine the coefficient of friction of the manufactured specimens and evaluate their behavior. The influence of surface hardness on the results of loss of mass and depth in Z was verified, with a reduction in adhesive wear.

Keywords: Additive manufacturing, melt and deposition modeling, PET and PLA/Carbon fiber filaments, tribology

Reference

1. Song, R,; Telenko, C. Journal of Cleaner Production, 2017 v. 148, p. 895-904..
2. . L.M. Bollig, M.V. Patton, G.S. Mowry, B.B. Nelson-Cheeseman, IEEE Trans. Magn. 53 (2017) 1–6.
3. Neres, K.S.V; Almeida, E.C; Barquete, D.M; Camargo,J.C; Silva, E.F.M.S. Anais do 15º Congresso Brasileiro de Polímeros (15 CBPOL) – Bento Gonçalves, RS – 27 a 31 de outubro de 2019

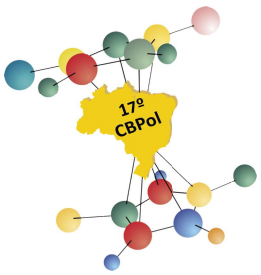

SYNTHESIS OF COMPOSITES MEMBRANES BASED ON SPEEK/SGO FOR APPLICATION IN PEMFC

Luanda S. de Moraes[1]*, Marcela Carrera de Castro[1], Sérgio Pinheiro de Oliveira[2], Jorge Trota Filho[1,2]

1 –Materials Department, UERJ, RJ, Brazil, luandasmoraes@gmail.com
2 – Force Metrology Laboratory, INMETRO, Xerém, RJ, Brazil

Abstract –Polymeric composites are propelling materials of new properties and applications. Graphene and derivatives are fillers with special chemical and transport properties. The present investigation aimed to synthesize Sulfonated Graphene Oxide (SGO) in order to add special properties to composites membrane with Poly(ether-ether-ketone) sulfonated (SPEEK), with ion exchange potential. Recently, it was discovered at Maricá city in Rio de Janeiro there is natural hydrogen production, a fact that represents important potential for the use on Fuel Cells (FC) in the promising expansion of the hydrogen economy (1). Sulfonated GO was performed according to literature methodology (2). The Sulfonated PEEK (SPEEK) was conducted by dissolution in concentrated H_2SO_4, N_2, at 60°C, for 9h. The SPEEK was precipitated in cold distilled water. The composite membranes were prepared by dissolving SPEEK in NMP (1-methyl-2-pyrrolidone), stirring, at 60°C and N_2 atmosphere (3). The SGO in the proportions 0.25%, 0.5%, 1% w/w were poured into the SPEEK polymeric solutions, under stirring, by 24 hours. The composite membranes SPEEK/SGO were shaped by casting in Petri plates, dried under vacuum for 24 h at 70 °C. The properties of SPEEK-SGO membranes and their PEMFC (Proton-exchange membrane fuel cells) application potential were investigated. The Raman spectroscopy results confirmed the incorporation of sulfonic groups in the SGO, with ratio I_D/I_G (3, 4). The FTIR (Fourier-transform infrared spectroscopy) showed the presence of new peaks between 1185 to 1330 cm^{-1}, 990 to 1130 cm^{-1} and 1036 cm^{-1}), confirming the success of GO sulfonation process (4, 5). The ion exchange capacity and the degree of sulfonation of the SPEEK membranes were determined by titration and confirmed by the FRX (X-Ray Fluorescence) technique (6) which determined the sulfur content in the SGO (~60%) and in the SPEEK-SGO membranes (~70%). The DSC (Differential Scanning Calorimetry) and TGA (Thermal gravimetric analysis) results confirmed that SGO acted as a reinforcement in the SPEEK polymeric matrix, increasing the thermal stability of the membranes.

References:

1. Fontes de hidrogênio natural são encontradas em Maricá. https://www.marica.rj.gov.br/noticia/fontes-de-hidrogenio-natural-sao-encontradas-em-marica/
2. CHANGKHAMCHOM, S., SIRIVAT, A. Polymer-Plastics Technology and Materials, 1900-1913. 2019. Disponível em: https://doi.org/10.1080/25740881.2019.1587770
3. MARRERO, J. C. *et. al*. Polímeros, 27 (3), 189-194,2017. http://dx.doi.org/10.1590/0104-1428.07216
4. GAO, S. *et al*. Journal of Applied Polymer Science, 2018. https://doi.org/10.1002/app.46547
5. ZHANG, J., JIANG, D. Carbon 67, 784-791. 2014. https://doi.org/10.1016/j.carbon.2013.10.078

Fundings: Fundação de Amparo à Pesquisa do Estado do Rio de Janeiro – FAPERJ
Keywords: *Graphene Oxide;Sulfonated Graphene oxide; SPEEK;Composite, Sulphonated Degree; PEMFC.*

SYNTHESIS OF KRAFT LIGNIN-IRON NANOPARTICLES AND ITS APPLICATION ON POLYSULPHONE MEMBRANES FOR BIOGAS PURIFICATION

Jardel M. de Lima[1] and Daniel Eiras[1]
1 – Graduate Program in Chemical Engineering, Federal University of Paraná (UFPR), Curitiba, PR, Brazil
jardel_ml@ufpr.br

Abstract - This research has the objective to study the synthesis of iron-lignin nanoparticles for application in dense polysulfone membranes, for N_2, CO_2 and CH_4 permeation. A nanoprecipitation method by Chen *et al*. (2022) was applied resulting into iron-lignin particles with different morphologies. FTIR-ATR analysis showed peaks around 3400 and 1652 cm^{-1} that indicate the formation of iron hydroxyl and iron nitrate complexes, respectively (Wang, Cui e Jiang, 2011). MEV and TEM (Fig 1. left) inspections made possible to observe circular particles formed when THF was used as solvent whereas the use of DMF resulted in elongated shapeless particles. Temperature influenced the particles diameters: 40 ºC, THF as solvent resulted into 166.87 ± 69.70 nm (softwood) and 158.75 ± 64.61 nm (hardwood), and 25 ºC, THF as solvent resulted into 118.39 ± 42.11 nm (softwood) and 115.86 ± 33.92 nm (hardwood). These four particles were analyzed with ANOVA and it was concluded with 5% level of significance that the respective diameters of the particles are different. Afterwards, permeation tests (constant pressure/variable volume) were carried out with the application of pure lignin and iron-lignin into PSU membranes. MEV showed interfacial defects between particles and PSU membranes (Fig 1. right). The best result obtained for selectivity was the softwood lignin particle precipitated at 0 ºC and THF as solvent, showing the selectivity of 26.54 for CO_2/N_2, a better result when compared to 12.39 for a pure PSU membrane found by Tavasoli *et al*. (2018). However, this good result does not change the fact that the most of the membranes in this study presented worse selectivities when compared to pure PSU membranes.

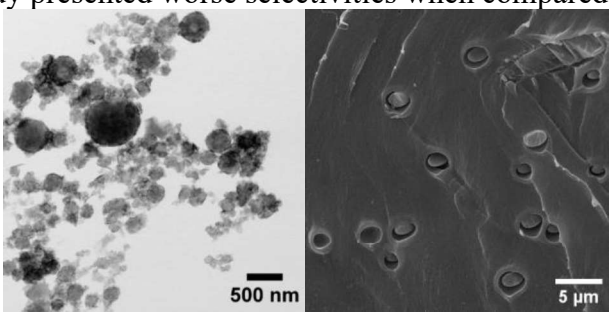

Fig 1. Softwood-iron particle (left); Hardwood PSU Membrane (right)

References:
1. L. Chen; S. Luo; C. Huo; Y. Shi; J. Feng; J. Zhu; W. Xue; X. Oiu. Green Chemistry, v. 24, n. 1, p. 285–294, 2022. https://doi.org/10.1039/D1GC03651C.
2. E. Tavasoli; M. SADEGHI; H. Riazi; A. Shamsabadi; M. Soroush. Fibers and Polymers, v. 19, n. 10, p. 2049-2055,2018. https://doi.org/10.1007/s12221-018-8424-4.
3. WANG, H.-L.; CUI, J.-Y.; JIANG, W.-F. Synthesis, characterization and flocculation activity of novel Fe(OH)3–polyacrylamide hybrid polymer. **Materials Chemistry and Physics**, v. 130, n. 3, p. 993–999, nov. 2011.

Keywords: *Iron-lignin nanoparticle, nanoprecipitation, Lignin, gas permeation, and biogas.*

SYNTHESIS OF POLYURETHANES FROM THERMALLY DEGRADED VEGETABLE OIL POLIOS DOPED WITH LIGNIN FROM MALTE BASCASSE

Cristiane M. Finzi-Quintão[1*], Katia M. Novack[1,2] Kevin S. Amaral[1], Lavínia M. G. Coimbra[2]

1 – Post Graduation Program of Materials Engineering, University of Ouro Preto (UFOP), Ouro Preto, MG, Brazil, finzi@ufsj.edu.br
2 – Department of Industrial Chemistry, University of Ouro Preto, Ouro Preto (UFOP), MG, Brazil
3 – Department of Chemistry, Biotechnology and Bioprocess Engineering, University of São João del Rei (UFSJ), Ouro Branco, MG, Brazil

Abstract - Polyurethanes are widely used polymers due to their diverse properties. They are formed by chemical reactions between compounds containing isocyanate groups and compounds containing hydroxyl groups (mainly polyols), resulting in a three-dimensional polymeric structure. Polyurethanes have a wide range of physical and chemical properties that can be adjusted by changing the chemical composition or using additives. Initially, such polymers were synthesized from petroleum derivatives, but the high value of the primary raw material made it necessary to search for materials from renewable sources. As a result, vegetable oils are prominently used in the synthesis of polyurethanes, together with lignin, a natural biopolymer obtained from plants and which gives the final product mechanical and thermal properties similar to those of mineral origin, making it a more sustainable alternative. The aim of this study is to synthesize polyurethanes from thermally degraded vegetable oils doped with malt bagasse lignin using a *one-shot* method using *in situ* polyols synthesized by the performic acid method. The oil used in this process is extracted in a period of 48 hours and the malt bagasse used in the operation comes from the brewing industry. The lignin extraction is based on the methodology used in the patent "Lignin-Based Polyols from Black Liquor and Glycerol" (US Patent 2012/0202907.2012, August 9). Tests carried out on the extracted oil revealed a hydroxyl value of 30.79 mgKOH/g, indicating its potential for polyurethane synthesis.
Keywords: polyurethanes, lignin, biopolymer**,** synthesis

References

1. V. de Macedo, M,V, Zimmermmann, L.S. Koester, L.C. Scienza, A.J. Zattera, Obtenção de espumas flexíveis de poliuretano com celulose de pinus elliottii, UFRGS, 2017.
2. V.B. Veronese, Relação estrutura propriedade de espumas rígidas de poliuretano à base de óleos vegetais, (2009) 121.
3. K. Kurple, N. Kurple U.S Patent 2012/0202907.2012
4. A.F.F. de Vasconcelos, O.E.S. Godinho, Uso de métodos analíticos convencionados no estudo da autenticidade do óleo de copaíba, Química Nova. 25 (2002) 1057–1060. https://doi.org/10.1590/s0100-40422002000700002.
5. A. D1957-86(2001)-, Standard Test Method for Hydroxyl Value of Fatty Oils and Acids (Withdrawn 2007).

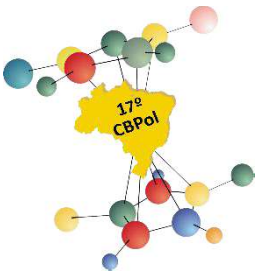

TANNIN COMPATIBILIZING ACTION IN BAMBOO FIBER REINFORCED GREEN LOW DENSITY POLYETHYLENE COMPOSITES

Eduarda V. Silva[1], Mariane W. Bosenbecker[2], Tiago T. M. Zanon[3], Juliano Marini[3], Amanda D. de Oliveira[2]

1 – Technological Development Center (CDTec), Materials Engineering – Federal University of Pelotas (UFPEL), Pelotas, RS, Brazil
2 – Technological Development Center (CDTec), Postgraduate Program in Materials Science and Engineering – PPGCEM/UFPEL – Federal University of Pelotas (UFPEL), Pelotas, RS, Brazil
3- Department of Materials Engineering – DEMa, Federal University of São Carlos (UFSCar), São Carlos, SP, Brazil
corresponding author: amandaoliveira82@gmail.com

Abstract – The development of composites from polymeric raw materials reinforced with natural fibers grows every day, mainly because these materials have good mechanical properties, low cost and reduce the environmental impact that the dependence on fossil resources provides. In order for the composites to have good properties, it is necessary to use compatibilizing agents that act by filling the interfaces between the matrix and the reinforcement. The tannins are a natural alternative to act in the compatibilization of these composites because have a chemical structure similar to the synthetic compatibilizers. Through this concept, the present work developed composites materials of low density green polyethylene (LDGPE) reinforced with bamboo fiber using tannin as compatibilizer in order to evaluate the effect of tannin variation in the properties of the composite. First, the bamboos were crushed to obtain the fibers. Four samples were prepared: 1- pure LDGPE; 2- LDGPE with 5% bamboo fiber (LDGPE/5BF); 3- LDGPE with 5% bamboo fiber and 1% tannin (LDGPE/5BF/1T); 4- LDGPE with 5% bamboo fiber and 3% tannin (LDGPE/5BF/3T). The composites were processed in a single screw extruder, and injected in a bench injection molder to make the specimens. Composites and pure LDGPE were characterized by mechanical tests and water absorption. In the mechanical tests performed it was shown that the addition of the reinforcement in the polymeric matrix was efficient, increasing its elastic modulus. In the water absorption test, sample LDGPE/5BF/3T had a decrease in water absorption compared to the other samples.

References (Times New Roman 10, bold) –

1. T. Boronat; V. Fombuena; D. Garcia-Sanoguera; L. Sanchez-Nacher; R. Balart. Materials & Design 2015, https://doi.org/10.1016/j.matdes.2014.12.027.
2. S. V. Canevarolo in Ciência dos Polímeros. Um curso básico para tecnólogos e engenheiros. 2. Ed. Artiliber, São Paulo, 2006; Vol. 1, 289.
3. S. Luo; J. Cao; W. Sun. Polymer Composites 2017, https://doi.org/10.1002/pc.23821.
4. A. L. Missio, et al. *Polymer Composites 2017*, https://doi.org/10.1002/pc.24498.
5. A. Pizzi. *Monomers, Polymers and Composites from Renewable Resources 2008*, https://doi.org/10.1016/B978-0-08-045316-3.00008-9.

Keywords: *Composite; Raw materials, polymer; Compatibilizer; Natural fibers; Tannin.*

TENSILE PROPERTIES OF RECYCLED ABS/RECYCLED CARBON FIBER FABRIC/JUTE FABRIC COMPOSITES

Meire N. Hosokawa[1], Maria N. Castanho[1], Jane M. F. de Paiva[1,2]*

1 – Program in Materials Science (PPGCM), Federal University of São Carlos (UFSCar), São Carlos, SP, Brazil
*jane@ufscar.br
2 – Department of Production Engineering, Federal University of São Carlos (UFSCar), São Carlos, SP, Brazil

Abstract - Over the years the combination of fibers (vegetable and synthetic) offers opportunities to produce new materials[1]. The aim of this work was to carry out a study on the tensile properties of hybrid composites. A recycled polymer, acrylonitrile butadiene styrene (rABS) was used as a matrix. Recycled carbon fiber (rFC) fabrics were obtained from the thermal treatment of carbon fiber reinforced composites at 500°C for 2 hours to recover the carbon fibers[2]. Three bidirectional jute fibers fabric were also used. A plain weave fabric composed of jute (T1 - weight 365 $g.m^{-2}$); a basket weave fabric composed of jute (T2 - weight 445 $g.m^{-2}$); and hybrid fabric composed by jute (weft) and cotton (warp) (T3 - weight 360 $g.m^{-2}$). Hot compression molding was the process used to manufacture the composites: rABS/1rFC (98/2% by weight, respectively); rABS/2rFC (95/5, w/w); rABS/1rFC/1T1 (90/1.5/8.5, w/w); rABS/1rFC/1T2 (88/2.5/9.5, w/w) and rABS/1rFC/1T3 (90/2/8, w/w), which were submitted to 200°C for 30 minutes and 6 tons. For the tensile tests (ASTM D3039) a load cell of 2000kgf and a speed of 2.0 $mm.min^{-1}$ were used. The results showed that by incorporating a layer of recycled carbon fiber fabric (rABS/1rFC) there was a 20% increase in the tensile strength compared to rABS, whose values were 39.12±6.16MPa and 32.56±1.14MPa, respectively. Considering the hybrid composites, the combination of a layer of carbon fiber fabric and a layer of jute fiber did not promote a significant increase in the tensile strength of the hybrid composites compared to rABS, whose values were 28.00±7.41MPa, 34.47±4.74MPa, and 30.86±5.76MPa. In addition, the composite rABS/1rFC/1T1 showed the lowest value of tensile strength, indicating that the tensile strength is influenced by the weight of the jute fiber fabric. The mechanical anchoring is the main fiber/matrix adhesion mechanism in composites reinforced with lignocellulosic fibers. All composites showed higher values of modulus of elasticity, reaching a percentage increase of up to 71% compared to rABS. Thus, the results of the tensile tests showed that the incorporation of recycled carbon fiber fabrics and jute and cotton fiber fabrics promotes an increase in the stiffness of the composites and, also, there is a decrease in the strain values when compared to the rABS. In this way, the process of remanufacturing these materials is an alternative to reusing high-added value waste and inserting them in the production chain.

References

1. M.Y. Khalid, et al. Int J Mater Form 2021, 14, 1085–1095. https://doi.org/10.1007/s12289-021-01624-w
2. M. M. Hosokawa, J. M. F. Paiva in Proceedings of the 16º CBPol, Ouro Preto, October, 2021, Vol. 1, 1038.

Fundings: CAPES (Financing Code 001) and CNPq (314814/2021-3).

Keywords: *Hybrid composites, recycled carbon fibers, lignocellulosic fibers, tensile properties.*

THE EFFECT OF CONDUCTIVE MIXTURES OF EVA/PP/CNT ON ELECTROMAGNETIC PROPERTIES

Sena, A. Silva[1] and Soares, B. Guenther[2]

1. Instituto de macromoléculas Professora Eloisa Mano, Universidade Federal do Rio de Janeiro (IMA-UFRJ) - Rio de Janeiro-RJ, Brasil.
2. Instituto de macromoléculas Professora Eloisa Mano, Universidade Federal do Rio de Janeiro (IMA-UFRJ) - Rio de Janeiro-RJ, Brasil.

In recent years, combustion has increased significantly with the manufacture of new miniaturized devices that have led to increased health damage and failures in electrical systems and devices, among others (ZHANG, et al, 2020). Thus, it is necessary to develop new materials that absorb electromagnetic radiation (MARE) (YUAN et al., 2020). The processing of electrically conductive polymeric mixtures has been gaining space, due to their quick and easy processability, excellent electrical conductivity, low cost, in addition to better thermal and mechanical properties. Conductive polymer blends of poly (ethylene-co-vinyl acetate) (EVA), polypropylene (PP) with the addition of carbon nanotube (CNT) may be promising materials in applications that minimize rail flow (ZAO et al., 2022; ZHANG et al, 2020). EVA/PP mixtures varying the concentration of CNT (0.3; 0.5; 0.7; 1.0 and 1.5%) were prepared by the melting method under the processing conditions used was 80 rpm, 200 °C and 10 minutes. Two different types of specimens were prepared, pressure and injection, in order to evaluate their effect on reflection loss (RL) properties. Both forms of preparation showed good RL results, between -25 and -35 dB. But, as Exemplary with 0.7 and 1% of remaining CNT had higher values of RL in the Ku band with 99.90% pregnant energy. It was concluded that the EVA/PP/CNT mixtures have excellent electromagnetic absorption characteristics.

References

ZHAO, B.; LI, Y.; JI, H.; BAI, P.; WANG, S.; FAN, B.; GUO, X.; ZHANG, R.. *Carbon* v. 176, p. 411–420, 2021.https://doi.org/10.1016/j.carbon.2021.01.136

ZHANG, Q.Y.; LI, H.S.; GUO, B.H.; GUO, Z.X.; YU, J. *Chinese Journal of Polymer Science*, v. 38, n. 6, p. 593–598, 2020. https://link.springer.com/article/10.1007/s10118-020-2370-5 https://doi.org/10.1007/s10118-020-2370-5.

YUAN, B.; TAO, H.; WANG, S.; CHEN, G.; ZHAN, Y.; WANG, Y. & ZHOU, J. *Composites Communications,* v. 27, p. 100-858, 2021. https://doi.org/10.1016/j.coco.2021.100858.

Keywords: *Polymeric blends, absorbent material, EVA/PP, carbon nanotube*

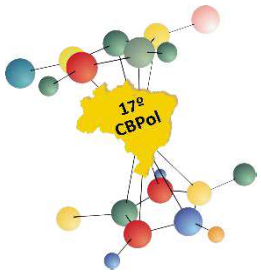

THE INFLUENCE OF MAGHEMITE ON CALCIUM ALGINATE-BASED BIOHYDROGEL FORMATION

Caroline C. de Amorim[1] (IC), Márcia P. M. Costa[1], Ivana L. M. Ferreira[1*]

1 – Instituto de Química, Universidade do Estado do Rio de Janeiro (UERJ), Rio de Janeiro, RJ, Brazil
**ivanalmellof@gmail.com ; ivanamello@uerj.br*

Abstract: In this work, particles of magnetic material (maghemite) were incorporated in different (1 and 3%) in sodium alginate-based hydrogels. The concentration of polysaccharides was 3% solubilized for 24h at room temperature (25°C) and crosslinked with 0.3 mol/L of calcium chloride for 30 minutes. Those samples were characterized by its morphology by scanning electron microscopy (SEM), thermal stability by thermogravimetry (TGA) and X-ray diffraction (XRD). The present work has as main objective to investigate the influence of magnetic material in different concentration (1 and 3%), the thermal stability and the possible interactions in calcium alginate's matrix.
Keywords: *sodium alginate; crosslinked; magnetic material; thermal stability; morphology.*

Introduction

Hydrogels are three-dimensional (3D) and generally non-crystalline materials with the ability to absorb large amounts of water while maintaining their dimensional stability [1]. The three-dimensional network of hydrogels in their swollen state can be maintained by crosslinking. Chemically, hydrogels have linear polymer chains covalently linked through crosslinks. On the other hand, physically crosslinked hydrogels have physical domains associated with chain entanglement: hydrophobic interaction, hydrogen bonding, crystallinity, and/or ionic complexation [2]. Hydrogels can be formed by both natural and synthetic polymers [2]. They are classified as neutral or ionic, depending on the nature of the groups directly attached to the polymer chains [3]. The advantages of using natural polymers are their nontoxic and hydrophilic nature, biodegradability, biocompatibility and possibility of solubilization without organic solvents [5, 4]. Hydrogels can respond differently when the characteristics of the external environment are altered, such as pH, ionic strength, or the presence of some specific chemical substances, e.g., dyes, pesticides, and/or crosslinking agents. [3] In this work, biohydrogels were produced by mixing sodium alginate (ALG), a polysaccharide extracted from brown seaweed; a linear copolymer composed of mannuronic acid and guluronic acid arranged in block structure, which was capable of forming gels at room temperature that remained stable at high heat by means of reaction with divalent cations; and calcium chloride ($CaCl_2$), forming thermostable gels by exchanging the sodium ions of alginate with calcium ions, forming a three-dimensional crosslinked structure of polymer chains. This crosslinking increased the mechanical strength and barrier properties of alginate, causing the gel to be insoluble in water (DONG et al., 2006). The

synthesis of maghemite was accomplished by the coprecipitation technique (TSENG et al., 2007), in which the maghemite was modified with oleic acid (C18H34O2). The present study also aimed to analyze the influence of the addition of iron oxide in different concentrations (1 and 3%) on the hydrogels based on calcium alginate. To achieve this goal, the morphology and thermal stability of the hydrogels were analyzed.

Experimental

For the synthesis of the biohydrogel, a 3% sodium alginate (Sigma-Aldrich) solution was prepared, and then calcium chloride ($CaCl_2$) (Sigma-Aldrich) 0.3 mol/L was added to the sodium alginate solution, under stirring. For the synthesis of maghemite, 14.07g of ferrous sulfate ($FeSO_4$) and 27 g of ferric chloride ($FeCl_3$) were solubilized in 50 mL of water. Both solutions were produced under magnetic stirring. Then the solutions were mixed in a 500 mL round-bottom flask containing ammonium hydroxide (NH_4OH) and 10 mL of oleic acid ($C_{18}H_{34}O_2$). The flask was kept in a thermostated water bath at 80 ºC for 30-40 minutes, then left at rest at room temperature (~ 25 °C). After preparation of the material, the pH was adjusted by constant washing with an ethanol and water solution until the pH reached the desired value, pH = 7. The final product was stored in glass jars protected from light at room temperature. After the synthesis of the maghemite, either 1 or 3% was added in the sodium alginate solution, under mechanical stirring for 20 minutes. Then the crosslinker ($CaCl_2$) was added. The hydrogels formed were washed in deionized water, frozen and freeze-dried for 48 hours. Finally, the morphology was analyzed, in which the samples were coated with a thin layer of gold to increase their conductivity and protect against localized heating. For image capture, secondary electron detectors and X-ray energy dispersive spectra were used. Thermogravimetric analyses (TG/DTA) of samples were performed using Q500 V20. Build39, in the 20–900◦C temperature range, at a heating rate of 20◦C/min^{-1} under nitrogen atmosphere. The initial temperature of degradation was determined by the intersection between the tangent line at the inflection point of the TG curve after onset of degradation and the tangent in the zero line. The crystalline/amorphous structures of the biohydrogels were analyzed in a Bruker D8 X-ray diffractometer (XRD) with CuKα, radiation source, at 40 kV and operating at a wavelength of 1.542Å.

Results and Discussions

Figure 1 shows the X-ray diffractogram of the polysaccharide (alginate), with and without $CaCl_2$ (a), the maghemite (MM) (b) and the compositions (c). While odium alginate presented a peak at 2θ ~ 14, indicative of crystallinity, another peak was observed at 2θ ~ 21, related to the amorphous portion of the polysaccharide. Calcium alginate presented a totally different diffractogram from sodium alginate (Figure 1a) due to the presence of the crosslinker ($CaCl_2$). The loss of crystallinity and the increased rigidity of the alginate polymer chain were evident when the biopolymer was crosslinked with Ca^{2+} ions. The diffractogram (Fig. 1b) confirmed the chemical nature of the maghemite (γ-Fe_2O_3) synthesized, by peaks at 2 q = 30.1, 35.6, 43.2, 53.5 and 57.0°. The diffractogram (Fig 1c) referring to the compounds of ALG-Ca + MM had the same profile, where amorphous behavior of both compounds and the presence of maghemite were observed.

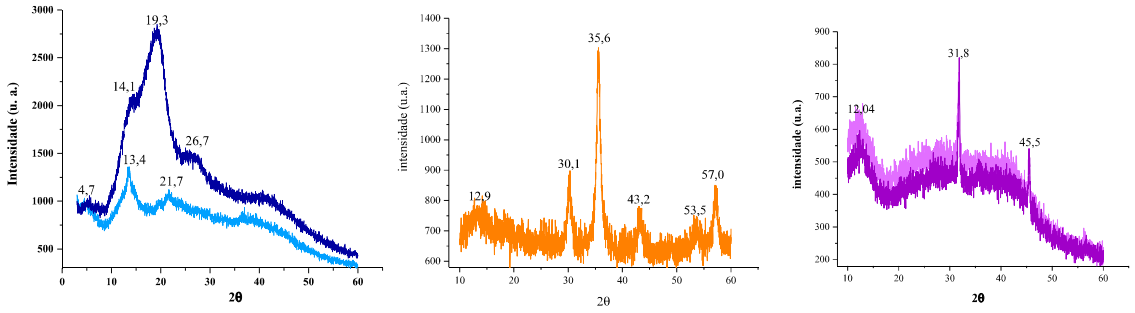

(a) (b) (c)

Fig. 1. XRD spectra: Na-ALG; Ca-ALG; maghemite; Ca-ALG+ 1% maghemite; Ca-ALG + 3% maghemite.

Figure 2 presents the TG-DTG curves of pure polysaccharide (Na-ALG), the biohydrogel without maghemite (Ca-ALG) and of the compounds.

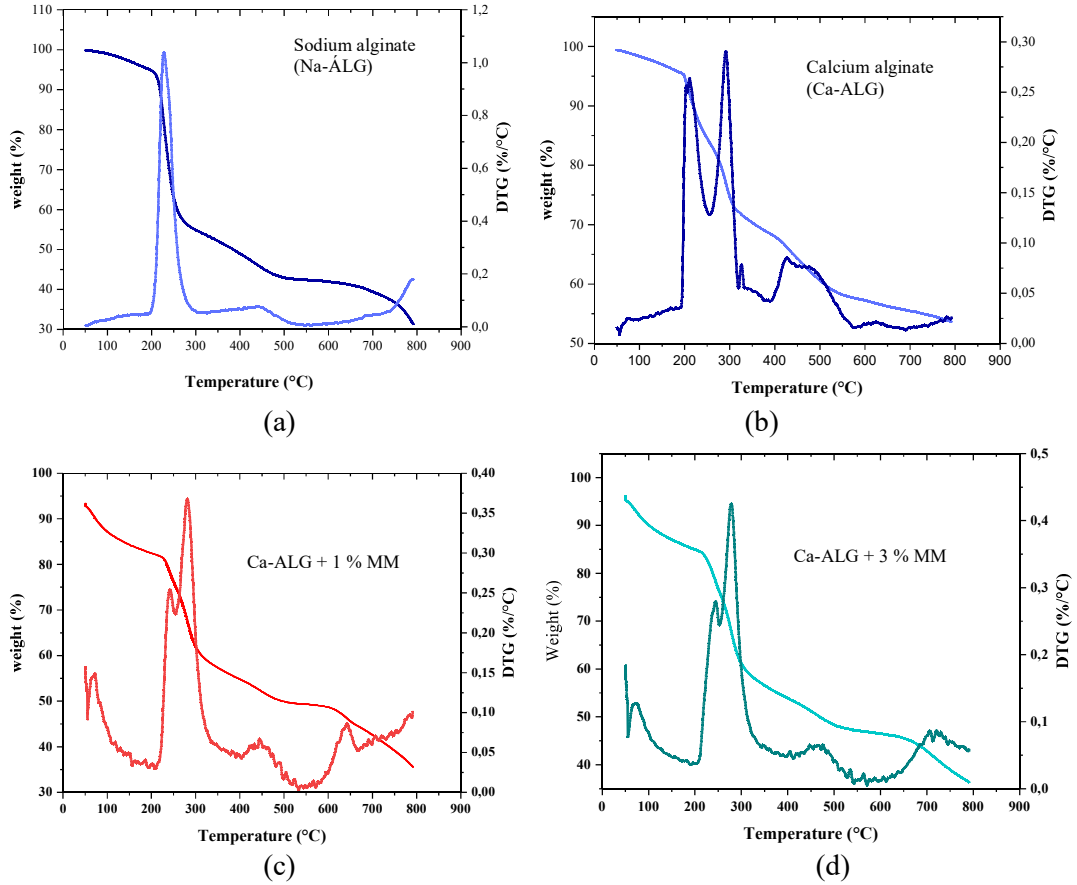

Fig.2. TG and DTG curves of the samples.

Table 1 shows the weight loss, initial degradation temperature (T_{onset}) and the temperature of maximum degradation of the polysaccharide (T_{max}) with and without the crosslinking agent and the compounds (biohydrogels with maghemite).

Table 1. Temperature of thermal decomposition of pure polysaccharide and biohydrogel with and without maghemite.

Samples	Decomposition temperature			
	T_{onset} (°C)		T_{max}(°C)	
	T_1	T_2	T_1	T_2
Sodium alginate	243		448	
Calcium alginate	209	290	415	512
Ca-ALG +1.0 % MM	227	279	436	618
Ca-ALG +3.0 % MM	218	274	442	638

Comparison of the samples of pure polysaccharide (Fig. 2a) and those after incorporation of the crosslinker (Fig. 2b) revealed that the presence of the crosslinker ($CaCl_2$) tended to increase the biohydrogel's thermal resistance. The compounds with 1 and 3% MM had higher T_{onset} than in pure calcium alginate (Figures 2 (a) and (b)), indicating higher thermal resistance of the compounds. In addition to that, the initial weight loss was due to water loss.

Figure 3 shows the samples' surfaces by scanning electron microscopy (SEM): sodium alginate with 1% maghemite (a) and calcium alginate with 3% maghemite (b).

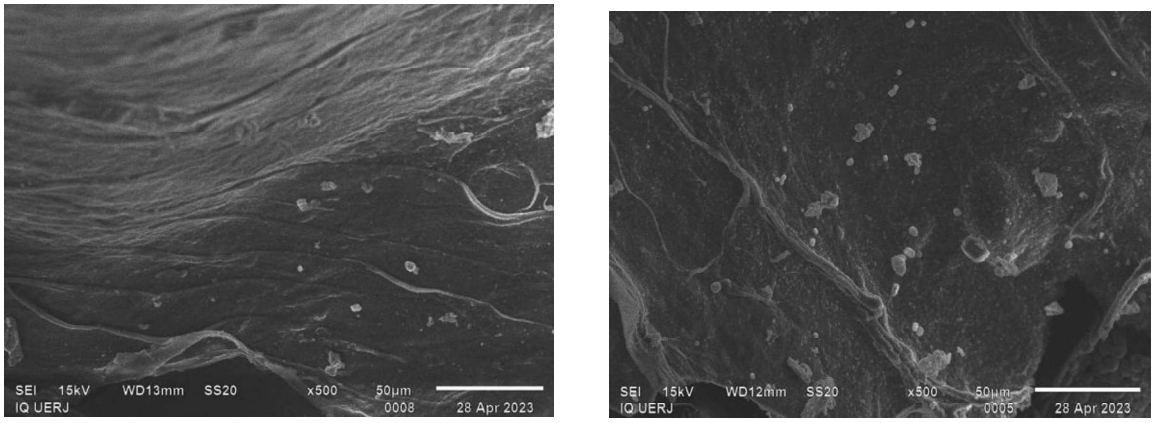

(a) (b)

Fig. 3. SEM micrographs of the biohydrogels samples with MM.

The micrographs presented above (Fig.3) show rough surface morphology and some rigidity, probably due to the crosslinker. The presence of MM at the two concentrations in the biohydrogel matrix is also indicated in Fig. 3(b).

Figure 4 shows the magnetization of the biohydrogel when stimulated by a magnet. At the highest MM concentration, 3% (b), the response was faster than at the lowest with concentration (1%).

(a) (b)

Fig.4. Biohydrogel with 1% maghemite (a) and 3% maghemite (b).

Conclusion

The experimental results showed that maghemite affected the biohydrogel due to the interaction between calcium alginate and iron, presenting a response to the stimulus of a magnet. Scanning electron microscopy showed rough surface morphology, increasing with rising iron content. The XRD presented the same profile in both compounds with incorporation of maghemite in the biohydrogel based on calcium alginate.

Acknowledgment

We are grateful to Fundação Carlos Chagas Filho de Amparo à Pesquisa do Estado do Rio de Janeiro (FAPERJ) and Conselho Nacional de Desenvolvimento Científico e Tecnológico (CNPq) for financial support. This study was also partly financed by Coordenação de Aperfeiçoamento de Pessoal de Nível Superior (CAPES), Finance Code 001.

References

1. A. Patel; K. Mequanint. In: Biomedical Engineering – Frontiers and Challenges. Cap. 14, p. 275.
2. M. R. Moura; A. F. Rubira; E. C. Muniz. Polímeros: Ciência e Tecnologia 2008, 18, (2), 132.
3. J. Berger; M. Reist; J. M. Mayer; O. Felt; R. Gurny. European Journal of Pharmaceutics and Biopharmaceutics 2004, 57, 19.
4. M. R. Guilherme; F. A. Aouada; A. R. Fajardo; A. F. Martins; A. T. Paulino; M. F.T. Davi; A. F. Rubira; E. C. Muniz. European Polymer Journal 2015, 72, 365.
5. T. R. Hoare; D. S. Kohane. Polymer 2008,49, (8), 1993.
6. O. B. G. Assis; V. L. Silva. Polímeros: Ciência e Tecnologia 2003, 13, (4), 223.
7. M. Borgogna; B. Bellich; A. Cesàro. Marine Drugs 2011, 9, 2572.
8. M. C. Koetting; J.T. Peters; S. D. Steichen; N. A. Peppas. Materials Science and Engineering R 2015, 93,

THERMO-OXIDATIVE DEGRADATION ANALYSIS OF A POLYMER BLEND COMPOSED OF HDPE, EVOH AND PA-G-MA APPLIED IN THE AUTOMOTIVE

Jardel J. O. SIlva[1,2], Grazielle R. Cerqueira[1], Djalma Alves de Oliveira[3], Carolina L. Morelli[1,3] and Kleber B. G. Alves[1]

1 - Department of Mechanical Engineering, Federal University of Pernambuco, 50670- 901, Recife, PE, Brazil
2 - Department of Process Engineering and Development, Stellantis South America, 55900-000, Goiana, PE.
3 - Materials Science Program, Federal University of Pernambuco, 50670-901, Recife, PE, Brazil
jardel.silva@ufpe.br

Abstract - In the current automotive market, the high demands and increasing vehicle qualification requirements stand out, with a focus on reducing emission rates and enhancing vehicle safety. These elements are becoming increasingly common in the automotive industry. To meet these demands, the market has been constantly seeking new material solutions. A 10% increase in vehicle mass results in a 4.6% decrease in fuel efficiency, which, in turn, increases pollutant gas emissions. In this context, polymeric materials have become a widely used option in vehicle construction, thanks to the remarkable technological advancements in plastics in recent years. However, degradation and durability remain the main limitations in the application of polymers in the automotive industry. This study aims to further investigate the thermo-oxidative degradation process of the HDPE + EVOH + PE-g-MA blend. This blend is a result of reusing the scraps from the fuel tank manufacturing process and is commonly used as one of the tank layers. For this study, six experimental conditions were conducted, which were analyzed using the following techniques: Differential Scanning Calorimetry (DSC), Melt Flow Index (MFI), Scanning Electron Microscopy (SEM), Fourier Transform Infrared Spectroscopy (FTIR), carbonyl index, and tensile testing. From the analyses, it was observed that the residence time inside the extruder is the primary factor contributing to the blend degradation, followed by the percentage of EVOH in the samples. In other words, the longer the residence time and the higher the percentage of EVOH, the greater the kinetic rate of thermo-oxidative degradation reaction. These findings are supported by the increase in carbonyl index, as well as the rise in melt flow index and specific degradation peaks observed in the FTIR curves.

References

1. Zhang, J. et al. A Review on Application of Plastics in Automobile. Polymers, v. 13, n. 7, p. 1134, 2021.
2. Lakshmi, P. P. et al. Studies on the degradation of high-density polyethylene in automotive applications. Polymer Degradation and Stability, v. 113, p. 79-89, 2015.
3. Li, C. et al. Synthesis and characterization of polyethylene-graft-maleic anhydride compatibilizer for polyethylene/polyamide 6 blends. Polymer Engineering & Science, v. 58, n. 2, n. 198-205, 2018.
4. Mittal, V. Performance of bio-based materials in fuel storage applications. In V. Mittal (Ed.), Performance of bio-based building materials (pp. 215-228). Springer, 2008.
5. Tokoro, R. et al. Investigation of degradation mechanisms of EVOH in the presence of oxygen by ATR-IR and FT-IR spectroscopy. Journal of Applied Polymer Science, v. 123, n. 3, p. 1469-1477, 2012.
6. Wang, Q.; Zhang, Y.; Han, X.; Zhou, Y.; Xue, l. Enhancing the compatibility and mechanical properties of HDPE/EVOH blends by utilizing reactive compatibilizers based on HDPE-g-AMH and EVOH-g-GMA. Polymer Engineering & Science, v. 56, n. 9, p. 1036-1044, 2016.

Keywords: *PEHD, EVOH, Blends, Degradation, Fuel Tank*

THERORICAL PREDICTION OF h-BN AND SI_3N_4 NANOPARTICLES FINAL LOCALIZATION IN PP/EOC POLYMER BLEND NANOCOMPOSITES AND ITS IMPACT IN THERMAL CONDUCTIVITY

André B. de Carvalho[1*], Rafael Barbosa[2] and Lidiane C. Costa[1,2,3]

1 – Post-Graduate Program in Materials Science and Engineering (PPGCEM), Federal University of São Carlos (UFSCar), São Carlos, SP, Brazil
2 – Department of Materials Engineering (DEMa), Federal University of São Carlos (UFSCar), São Carlos, SP, Brazil
3 – Materials Development and Characterization Center (CCDM), Federal University of São Carlos (UFSCar), São Carlos, SP, Brazil.

*andre.balogh@estudante.ufscar.br

Abstract

The increasing demand for energy necessitates the development of novel insulating materials. Polymers are extensively employed in such applications, serving as electrical insulators. However, these materials possess low thermal stability. High electrical current flowing through high voltage cables leeds a substantial temperature rise caused by the Joule Effect, which limits the maximum operating temperature and accelerates cable degradation. This issue can be addressed by enhancing the thermal performance of polymers through the incorporation of thermally conductive fillers. The final localization of nanoparticles primarily depends on thermodynamic factors, melt processing, and rheological behavior [1]. In this study, immiscible polymer blends of Polypropylene/Ethylene-Octene copolymer (60%PP/40% EOC %wt) were prepared, both unfilled and filled with 0,25wt% of hexagonal boron nitride (h-BN) and 0,75 wt% of silicon nitride (Si_3N_4) nanoparticles, using a twin co-rotating extruder. The theorical prediction of the final localization of the nanoparticles was calculated by estimating the wetting coefficient. The materials were analyzed using rheological, contact angle, thermal conductivity and SEM. The results confirmed the immiscibility of PP and EOC, leading to the development of a co-continuous morphology. Interfacial tension measurements, employing Guggenheim's equation, revealed the nanoparticles preference for interacting with the EOC phase at room temperature, with a tendency to migrate towards the PP phase as the temperature reached 200°C. The rheological analysis suggests that the nanoparticles were trapped by the EOC phase. Thermal conductivity results exhibited improvements upon the addition of nanoparticles.

References

1. L. B. Canto, Polymer Testing 2019, 135-142. https://doi.org/10.1016/j.polymertesting.2018.11.012.

Keywords: *Polymer blends*, *nanoparticles*, *interfacial tension*, *final localization, thermal conductivity.*

Acknowledgments: This study was financed in part by the Coordenação de Aperfeiçoamento de Pessoal de Nível Superior - Brasil (CAPES) - Finance Code 001. CAPES process 88887.704650/2022-00 and PPGCEM UFSCar.

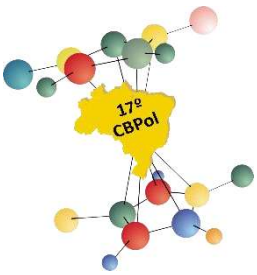

USE OF CELLULOSE AND ALGINATE BEADS WITH MAGNETITE NANOPARTICLES FOR ADSORPTION OF CADMIUM IONS

Vinicius A. M. Gomes[1*], Paula P. Silva[1], Juliano Brisola[1] and Gizilene M. de Carvalho[1]

1 – Department of Chemistry, State University of Londrina (UEL), Londrina, PR, Brazil
*vinicius.23051999@uel.br

Abstract - The release of toxic metals into water bodies is a current and recurring environmental problem caused by industrial and urban growth [1]. Biodegradable adsorbent materials are a relevant alternative because they are low cost, sustainable and ecological for the removal of metal ions in aqueous medium. This work aims to produce bioadsorbents using cellulose (CEL) and alginate (ALG) with magnetite nanoparticles (MAG) and evaluate their efficiency in the removal of cadmium ions (Cd^{2+}). The CEL/ALG and CEL/ALG/MAG beads were produced by ionic gelation in $CaCl_2$ 3% (w/v) from polymeric solutions (3% (w/v) in the proportion of 50/50% (v/v) and 30% of the MAG (synthesized by coprecipitation). The surface area (SA) and pore size (PS) of the beads were determined by nitrogen physisorption and the Cd^{2+} adsorption tests were performed with variation of the adsorbent mass (0.1 - 0.5 g) and time of contact (0 - 480 min). To explain the kinetic behavior of the adsorption, pseudo-first order (PFO) and pseudo-second order (PSO) non-linear models were verified. The CEL/ALG/MAG beads have higher values of SA 0.6196 $m^2 . g^{-1}$ and PS 6.961 nm, compared to CEL/ALG of 0.1776 $m^2 . g^{-1}$ and 2.483 nm, respectively. The SA increase may be a result of the incorporation of MAG in the beads. The CEL/ALG/MAG and CEL/ALG beads showed efficiency in removing Cd^{2+} between 97.65% and 98.66%. After 240 min of adsorption, the CEL/ALG and CEL/ALG/MAG beads reached equilibrium, indicating that the active sites were saturated [2]. The data better fit the PSO kinetic model with R^2 greater than 0.99 and adsorption capacity more consistent with the experimental results for CEL/ALG and CEL/ALG/MAG beads, suggesting chemisorption as the controlling step of the adsorption rate [3].

References

1. D. J. Babu; P. King; Y. P. Kumar. International Journal of Environmental Science and Technology 2019, 16, 1885. https://doi.org/10.1007/s13762-018-1747-2.
2. A. S. A. Rahman; A. N. A. Yahaya; N. A. Khalil; A. N. S. Fizal; M. A. S. A'zim; M. S. Hossain; M. Zulkifli. IOP Conference Series: Materials Science and Engineering 2021, 1195, 012052. doi:10.1088/1757-899X/1195/1/012052.
3. N. Maaloul; P. Oulego; M. Rendueles; A. Ghorbal; M. Díaz. Environmental Science and Pollution Research 2021, 28, 46523. https://doi.org/10.1007/s11356-020-10158-8

Fundings: This work was carried out with the support of the Coordination of Improvement of Higher Education Personnel-Brazil (CAPES), Fundação Araucária-Brazil and CNPQ.

Keywords: *biopolymers; polysaccharides; blends; composites*.

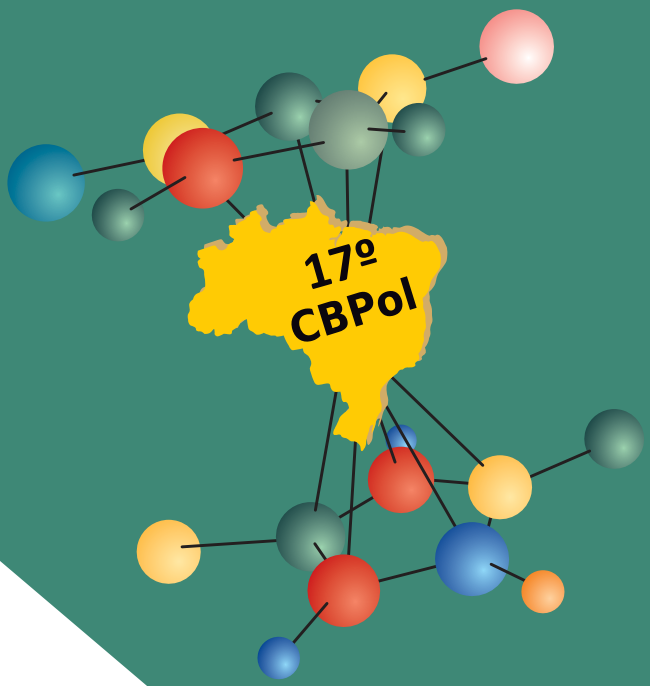

Processing and materials design

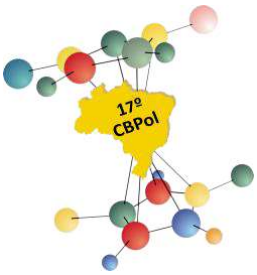

ADDITIVE MANUFACTURING OF BIOACTIVE COMPOSITES

Lidiane C. Costa[1,2]*, Eduardo H. Backes[1], Samarah V. Harb[1], Juliano Marini[1,2], Felippe M. Marega[2], Thiago de A. Augusto[2], Daniel Ap. Cunha[2], Daniela Becker[3], Larissa Klok[3], Teresa T. Steffen[3], Luiz A. Pessan[1,2]

1 – Department of Materials Engineering (DEMa), Federal University of São Carlos (UFSCar), São Carlos, SP, Brazil
lidiane@ufscar.br
2 – Federal University of Sao Carlos, Graduate Program in Materials Science and Engineering, Sao Carlos, SP, Brazil.
3 – Department of Mechanical Engineering, State University of Santa Catarina (UDESC), Joinville, SC, Brazil

Abstract - The increase in life expectancy and trauma caused by accidents has led to a growth in the number of interventions for bone repairs and motivated the development of new materials for application in bone tissue engineering, with emphasis on the development of *scaffolds* capable to mimic the natural extracellular matrix of bone to enable the connection, proliferation and differentiation of cells. One way to obtain bioactive scaffolds is the production of biocompatible and bioabsorbable polymer-based composites (such as poly(lactic acid), PLA) with bioactive fillers. Conventional composite production techniques usually employ high temperatures and shear rates, and a severe degradation of the polymer matrix can be triggered when ions released by the bioburden interact during the mixing process. The control of the molar mass of the polyester matrix can be carried out through surface treatment of the fillers or the use of a chain extender. The addition of this compound modifies the viscoelastic behavior of the matrix, making it feasible to process the composite by extrusion-based methods, such as additive manufacturing. Another way to control matrix degradation is by reducing the surface area of charge/matrix contact and the exposure time of the molten polymer to the bioactive fillers, using the filler in the form of continuous fibers. Our research group has been developed bioactive materials for tissue engineering and scaffolds of polymer matrix/bioactive fiber has been obtained by additive manufacturing. Since length, filler concentration and fiber orientation influence composites characteristics, modulations of mechanical properties can be obtained in order to simulate the behavior of bones that have spongy and compact regions, through 3D printing of structures containing continuous and particulate fibers (in the matrix composite), being the printing of filaments with continuous fibers and the modulation of the properties the main development challenges.

Fundings: This study was financed in part by the Coordenação de Aperfeiçoamento de Pessoal de Nível Superior - Brasil (CAPES) - Finance Code 001; CNPq 405008/2021-0; CNPq 307742/2022-9; FAPESP 2017/09609-9; FAPESP 2019/27415-2 and FAPESP 2022/03157-7.

Keywords: *PLA; continuous fibers; bioactive particles; scaffolds; additive manufacturing.*

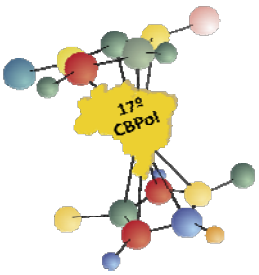

NEW TOOLS FOR PROCESSING BIOBASED MATERIALS

Antonio J. F. Carvalho[1]*

1 – Department of Materials Engineering, São Carlos School of Engineering, University of São Paulo (USP), São Paulo, SP, Brazil corresponding_toni@sc.usp.br

Abstract In recent years, there has been an increasing interest in biobased materials such as starch, chitosan and cellulose as substitute for petroleum non-biodegradable synthetic plastics. However, due to its particular characteristics, in particular polar and water affinity character, the processing of these materials is a challenge. As a consequence, great efforts have been made to develop new ways to process these materials. Reactive extrusion has been used to tune starch in thermoplastic starch compositions, new blend methods have been used to produce thermoplastic chitosan and new processing methods have been used to produce wood pulp fiber and nanofibrilated cellule composites. Here we discuss some of these new processing methods. In particular, the use of charges to produce very homogeneous nanocellulose composites in non-polar vinyl polymers [1], thermoformable panels of nanocellulose and vinyl polymers [2] and continuous fibers from interfacial complexation of anionic surface charged nanocellulose and cationic natural polyelectrolytes [3]. Blends of thermoplastic chitosan processed by melting are also discussed as a very promising way to improves the use of this functional material. Another processing tool using charges is interfacial complexation of chitosan and carbohymethylcellulose to produce filaments of high resistance. The development of new processing tools if of fundamental importance for improves the use of biobased material. We thank CNPq and CAPES for financial support.

References

1. Carvalho, A.J.F.; Trovatti, E.; Casale, C.A., J. Mol. Liq., 272, 387-394 (2018).
2. Chiromito, E.M.S.; Trovatti, E.; Carvalho, A.J.F., J. Renew. Mater., 7(5), 403-413, (2019).
3. Grande, R., Trovatti, E., Carvalho, AJF and Gandini, A., J. of Mater. Chem. A, 5, 13089 – 13103 (2017).

Funding: This study was financed in part by Conselho Nacional de Desenvolvimento Científico e Tecnológico (CNPq) proc. 303847/2019-0 and by CAPES due to the work of several students in the research group.

Keywords: *Biobased polymers; cellulose; starch; chitosan; polymer processing.*

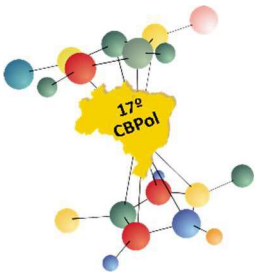

EXPLORING MECHANICAL PROPERTIES OF 3D PRINTING FILAMENTS: A COMPREHENSIVE STUDY OF BRAZILIAN MARKET PRODUCTS

Leonardo C. Freitas[1], Katielly V. Polkowski[1], Marina R. de Andrade[1] and Rodrigo D. O. Polkowski[1]

1 – TRL9 LAB TESTES E ANÁLISES TÉCNICAS LTDA, Salvador, BA, Brazil
e-mail: contato@trl9.tech

Abstract – Additive manufacturing or 3D printing is a field that has grown remarkably and is likely to continue that growth in the years to come. The 3D printing market in Brazil is experiencing similar behavior with a growth trend, on the other hand, not many studies or technical data are being produced focusing on the feedstock materials available on the Brazilian market, and this lack of information can lead to many uncertainties and doubts for the final client. This study aims to focus on that gap, performing tensile studies for the 3 most used materials (PLA, ABS and PETG) in 3D printing globally, extracting valuable data for the Ultimate Tensile Stress (UTS) and Yield Limit for some of the most representative Brazilian filament manufacturers.

Keywords: *3D printing, additive manufacturing, mechanical properties, filament testing.*

Introduction

The field of additive manufacturing has seen significant growth in recent years, with 3D printing and is still in projected growth with a CAGR (Compound Annual Growth Rate) higher than 12% (globally) according to the report from Mordor Intelligence [1], emerging as a prominent method for fabricating complex geometries and functional parts according to Tay *et al*. [2]. North America gets the spot for the largest filament market, with Asia Pacific being the fastest-growing market and Brazil being highlighted as the main South American market for 3D printing filaments. According to a study published by Markets and Markets [3], the expectation is for growth in terms of revenue moved by 3D printing from US$ 15 billion to US$ 34.5 billion from 2023 to 2028 globally and, although there are no reference numbers on the Brazilian market, professionals working on that area estimate that the 3D printing market in Brazil is indeed growing, but not as steep as the global market.

Despite the wide availability of filaments for 3D printing in the Brazilian market, a comprehensive analysis of their mechanical properties is currently missing, and it is noted that not all 3D filament manufacturers provide data sheets for their products, which limits users' ability to take tough decisions on the mechanical properties of the printed filament. This knowledge gap hinders the development of optimized printing parameters and limits the potential applications of 3D-printed parts.

As with any other manufacturing process, the mechanical properties of 3D printed objects largely depend on the feedstock's characteristics, as shown by the report made by Mordor Intelligence [1]. With the wide variety of filament materials available in the market, understanding their mechanical properties is crucial for developing optimized printing parameters and selecting suitable materials for various applications. As pointed out by Bittencourt [4], the most commonly used thermoplastic filaments for Fused Deposition Modelling (FDM) process are Polylactic Acid (PLA), Acrylonitrile Butadiene Styrene (ABS) and Glycol-modified Polyethylene Terephthalate (PETG), each one of them with its intended purpose and usage. PLA stands out for its easy printability and sustainability but also presents low-temperature resistance and while ABS can outperform PLA for temperature resistance, but its difficulty to print takes the highlight. PETG is a good middle ground, with good

mechanical and thermal resistances and easy printability, but Bittencourt [4] advises that it's not good for printing small parts.
The company's 3D Fila, 3D Lab and GT3Max are some of the largest Brazilian filament producers, being strong competitors in the market and all of them have PLA, ABS and PETG filament options. This study will provide a thorough analysis of the mechanical properties of these filaments and will assist in selecting materials suitable for various applications and contributing to the development of optimized printing parameters for reliable, high-quality 3D printed parts. Tensile properties were analyzed and compared with expected reference values and, although some issues have been raised, the results of filaments from Brazilian producers show relevant values when compared with literature references.

Materials and methods

For this study, the most commonly used materials for 3D FDM printing were selected to be evaluated, which are: PLA, ABS and PETG [4]. Three of the most relevant competitors in the Brazilian filament market were selected: 3D Fila, 3D Lab and GT3Max. Table 1 presents the list of all filament materials with the recommended 3D printing set-up configuration provided by the filament manufacturers. From this point onwards, codes from 1 to 3 will be assigned to the selected manufacturers but do not represent the order previously presented. A Prusa Research MK3S+ printer was used to produce the specimens, using the 3D print parameters shown in Table 1 and a layer height of 0.3 mm.

Table 1 – Filament Materials and 3D Printing Parameters

Filament Material	Nozzle temperature (°C)	Bed temperature (°C)
PLA	X(*)	60
ABS	245	110
PETG	255	115

(*) The common recommended printing temperature for PLA was 215°C, but for Manufacturers #1 and #2 the temperature of the nozzle had to be changed to185°C due to stringing issues on higher temperatures. The Manufacturer #3 had no problem using the recommended temperature (215°C) to print the test specimens.

The tensile strength of each material was tested using EMIC equipment model DL 200. Each test specimen was clamped into the machine and pulled at a constant rate of 5 mm/min until failure. Results for Yield Strength, UTS and Young's Module are presented in Table 2. Figure 1 shows the specimen dimensions and geometry according to ASTM D638 standard, type IV [5].

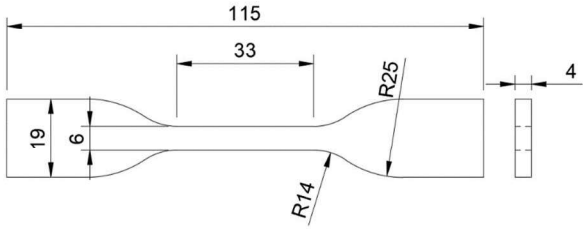

Figure 1 - Tensile specimen's dimension and geometry

For each material and filament manufacturer, five test specimens were printed in two different printing orientations: flat on the build plate (0-degree orientation) and vertical (90-degree orientation). This was done to evaluate the material's maximum strength (0-degree) and layer adhesion (90-degree), representing the best- and worst-case scenarios for an object printed using FDM. Specimen for both printing orientation: vertical and horizontal, both with 100% infill and with the one printed on the horizontal plane, having the infill aligned with the expected force.

Results and Discussion

All the data related to the yield strength and ultimate tensile strength (UTS) collected from the tensile tests were compiled in Table 2, organized by the filament manufacturer, filament material and specimens printing orientations. The average number and the respective standard deviation for the five test specimens are presented in Table 2. The expected and observed behavior of the failure on the 90-degree specimens occurs between layers, below the yield limit, and without plastic deformation. Therefore, only the UTS was described for the 90-degree specimen.

Table 2 – Tensile Tests Results

Filament Manufacturer	Filament Material	Print orientation	Yield Strength [MPa] (σ)	UTS [MPa] (σ)	Young's Module [MPa] (σ)
1	PLA	0°	46.23 ±1.24	50.30 ±1.38	2559 ±64.5
		90°	-	14.39 ±0.93	1753 ±25.7
	ABS	0°	29.42 ±0.46	29.66 ±0.43	1658 ±23.0
		90°	-	10.81 ±1.37	1193 ±36.6
	PETG	0°	25.86 ±1.17	34.09 ±2.32	1713 ±53.2
		90°	-	16.07 ±3.15	1237 ±146.8
2	PLA	0°	50.32 ±3.15	51.36 ±3.06	3004 ±41.5
		90°	-	14.77 ±1.84	2486 ±44.2
	ABS	0°	33.94 ±1.68	34.54 ±1.68	1516 ±69.1
		90°	-	9.77 ±0.72	1414 ±21.9
	PETG	0°	24.02 ±1.63	35.88 ±2.13	1516 ±69.1
		90°	-	7.64 ±4.21	936 ±61.6
3	PLA	0°	53.63 ±0.93	55.93 ±1.84	3097 ±126.1
		90°	-	37.87 ±3.15	2869 ±53.3
	ABS	0°	29.11 ±1.13	31.70 ±0.97	1921 ±62.6
		90°	-	16.30 ±0.85	1587 ±3.5
	PETG	0°	33.82 ±1.42	43.17 ±1.64	1900 ±26.3
		90°	-	22.24 ±5.58	1605 ±20.0

From the data in Table 2, PLA showed superior results compared to ABS and PETG, being more rigid material and less flexible than ABS and PETG. On the other hand, ABS and PTEG obtained lower mechanical property results, which gives them a higher degree of flexibility and less brittle compared to PLA. The data provided in Table 2 has been distributed in the next 3 figures to have a more visual comparison of the tensile test results. In these figures, an additional reference value from the literature was also included as a baseline for extra comparison.

Figure 2 - Results for Yield Strenght and UTS for PLA

The Figure 2 shows the results for PLA where it can be observed that, regarding the 0-degree configuration, the material from the Brazilian manufacturers is in agreement with the reference value [6,7], but with a slight improvement in all results for Manufacturer #3. Considering the 90-degree specimens, the reference value obtained is significantly higher than the values achieved by Manufacturers #1 and #2, being UTS of 35.65 MPa against to 14.3 and 14.7 MPa, respectively. Several factors can affect the layer adhesion of the material and, in this case, the main reason for this

discrepancy is likely due to the printing temperature required for PLA filament material [8, 8]. Most references, including the manufacturers themselves, recommend a temperature of around 215°C. However, when printing at this temperature, material leakage and excessive stringing between printed parts occurred on the filament from Manufacturers #1 and #2, resulting in a rough surface finish and irregularities in the parts. Those problems can lead to stress concentration and premature failure. Therefore, the nozzle temperature was reduced to 185°C in order to avoid these issues on the 3D-printed specimens. In order to investigate the stringing issue, the melt flow index (MFI) was measured for all the feedstocks herein studied, and, as expected, it was observed the PLA from Manufacturer #3 had the lowest MFI among them (4.9 g/min), which would explain the stringing issues found on Manufacturers #1 (5.6 g/min) and #2 (6.8 g/min). With all data herein presented, PLA from Manufacturer #3 would win the overall results, as it has performed on pair or better with the reference values, and outperformed Manufacturers #1 and #2 in all the results while not having stringing issues.

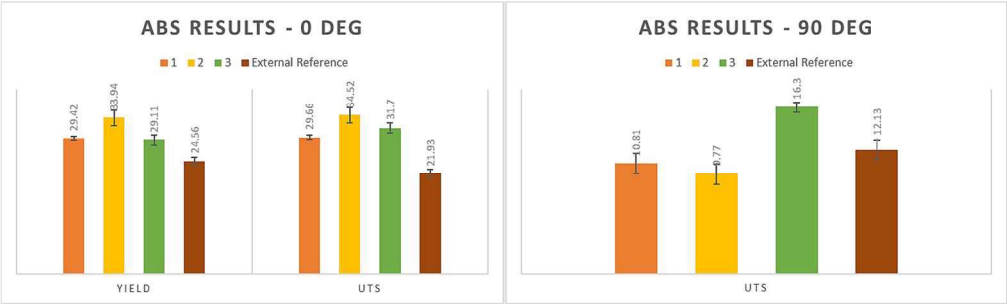

Figure 3 - Results for Yield Strenght and UTS for ABS

The Figure 3 presents the data for ABS specimens. Observing the results is possible to see a very correlation among the overall result for the Brazilian market and the results achieved by the reference [10]. The 0-degree specimens achieved higher levels in comparison to the reference results and the 90-degree specimens reaching values on pair with the reference as well. The Manufacturer #2 was the best performance on 0-degree orientation while Manufacturer #3 took the spotlight when referring to layer adhesion (90-degree orientation). From those results, it is possible to observe that the recommended ABS Manufacturer will highly depend on the printed object application, meaning that for parts that can be designed with the expected load aligned with the printing direction, Manufacturer #2 should be the best choice, but if this cannot be achieved, Manufacturer 3 would be better because it achieved close results to Manufacturer #2 but with better performance regarding layer adhesion.

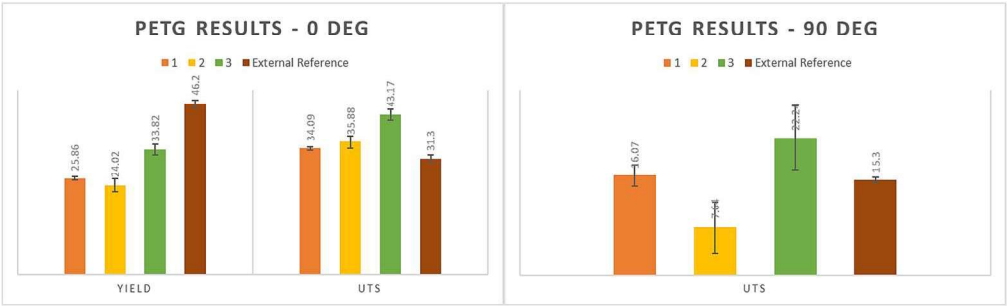

Figure 4 - Results for Yield Strenght and UTS for PETG

Regarding PETG specimens, the Figure 4**Figure 3** presents the tensile test results. It was possible to observe a high standard deviation in the 90-degree specimens must probably due to the instability of the object during printing, with a more intensity with the filament of the Manufacturer #2, which also presented the lowest UTS values. All other 3D-printed samples herein presented were made on Prusa's texturized print bed, a steel sheet which is powder coated PEI surface, which gives a rougher surface finish, allowing for the first layer to be more adhered on the printer bed, as reported by Prusa Research [11]. However, the Manufacturer #2 of PETG did not adhere to this surface during printing, even with the recommended temperature for the bed and material. To complete the print, the bed was

changed to the original flat steel sheet, adhesive was applied on the bed and the print speed was reduced to as low as 10 mm/s. Due to that, it is recommended to perform a contact angle measurement on all materials to further investigate this issue (surface compatibility issue). For PETG, Manufacturer #3 wins again, with better performance and outperforming the reference values [12] for material's strength and layer adhesion.

Conclusions

In this study, three different filament materials (PLA, ABS and PETG) from three different Brazilian manufactures (3DLab, GT3Max and 3DFila) were evaluated for mechanical properties. The data indicate that PLA material produced by the Brazilian manufacturers performed similarly to the expected values when tested in the 0-degree setting. Likewise, when examining ABS samples, the 0-degree samples exceeded the reference level and the 90-degree samples achieved values comparable to the reference. As discussed throughout the article, some further studies need to be concluded in order to verify some of the open points presented in this study. The surface compatibility (contact angle) of both Prusa's printer beds and for all the materials herein presented needs to be measured in order to understand the issues regarding 3D printing stability. Observing the overall results, one it is possible to observe that Manufacturer #3 was the most consistent and could outperform the competition in most of the materials tested, thanks to its better results on layer adhesion (90-degree).

Acknowledgments

The authors are grateful to the TRL9 LAB company and to the Brazilian Research Agency-CNPq for all the technical and financial support. We are also grateful for 3D Fila and GT3Max which provided the filament samples used for their 3D-printed specimens.

References

1. Mordor Intelligence, 3D Printing Filament Market Report: Size, Share, Growth and Trends, 2021. Available at (Jun12th, 2023): https://www.mordorintelligence.com/pt/industry-reports/3d-printing-filament-market
2. Tay, Y. W. D., Panda, B., Paul, S. C., Noor Mohamed, N. A., Tan, M. J., & Leong, K. F. 3D Printing Trends in Building and Construction Industry: A Review. Virtual and Physical Prototyping. 2017, 12(3), 261-276. https://doi.org/10.1080/17452759.2017.1326724
3. Markets and Markets, 3D Printing Market Size, Share & Industry Growth Analysis Report. 2023. Available at (Jun12th, 2023): https://www.marketsandmarkets.com/Market-Reports/3d-printing-market-1276.html
4. Bittencourt, M.R. 3D Printer Filaments. Technical Book Nr.1, IFC, Camboriú, 2021
5. ASTM D638 Standard. Available at (Jun12th, 2023): https://www.astm.org/d0638-14.html
6. Hanon, M. M., Marczis, R., & Zsidai, L. Influence of the 3D Printing Process Settings on Tensile Strength of PLA and HT-PLA. 2020, 65(1), 38-46. https://doi.org/10.3311/ppme.13683
7. Anderson, I. Mechanical Properties of Specimens 3D Printed with Virgin and Recycled Polylactic Acid. 2017, 4(2), 110–115. https://doi.org/10.1089/3dp.2016.0054
8. Thumsorn, S., Prasong, W., Kurose, T., Ishigami, A., Kobayashi, Y., & Ito, H. Rheological Behavior and Dynamic Mechanical Properties for Interpretation of Layer Adhesion in FDM 3D Printing. 2022, 14(13), 2721. https://doi.org/10.3390/polym14132721
9. Torabi, H., McGreal, H., Zarrin, H., & Behzadfar, E. Effects of Rheological Properties on 3D Printing of PLA and PHA Hybrid Materials. 2023. https://doi.org/10.1021/acsapm.3c00271
10. Markiz, N., Horváth, E. M., & Ficzere, P. (2020). Influence of printing direction on 3D printed ABS specimens. 2020, 26(3), 127-130. https://doi.org/10.30657/pea.2020.26.24
11. Prusa Research, Double-sided textured PEI powder-coated spring steel sheet. Available at (Jun12th, 2023): https://www.prusa3d.com/product/double-sided-textured-pei-powder-coated-spring-steel-sheet
12. Amza, C. G., Zapciu, A., Constantin, G., Baciu, F., & Vasile, M. Enhancing mechanical properties of polymer 3D printed parts. 2021, 13(4), 562. https://doi.org/10.3390/polym13040562

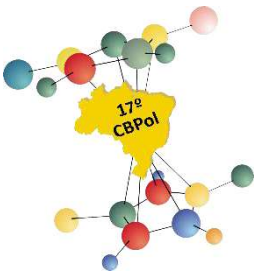

STUDY OF 3D PRINTED BILAYERD PLA HONEYCOMB COMPONENTS FOR MICROWAVE ABSORBING APPLICATIONS

Debora P. Schmitz[1]*, Leonardo Santana[3], Guilherme M. O. Barra[3], Bluma G. Soares[1,2]

1- Instituto de Macromoléculas (IMA), Universidade Federal do Rio de Janeiro (UFRJ), Rio de Janeiro, RJ.
dehschmitz@gmail.com
2- Departamento de Engenharia Metalúrgica e de Materiais, Universidade Federal do Rio de Janeiro (UFRJ), Rio de Janeiro, RJ.
3- Universidade Federal de Santa Catarina (UFSC), Florianópolis, SC.

Abstract – In this work we investigate the influence of thickness ratio between a PLA/CNT conductive (PLAc) and a PLA non-conductive layer of a bilayer honeycomb structure on the component's electromagnetic wave absorbing efficiency. Two cell sizes were analyzed, the components overall thicknesses were fixed at 4 mm, and the bilayer components were measure first with the non-conductive layer as top layer, then with the conductive layer as top layer. When the neat PLA was kept as the first layer, the samples with 1 mm PLA and 3 mm PLAc configuration showed the best RL value, of around -25 dB. On the other hand, when the component was measured with the conductive layer at the top, the sample with 1 mm PLAc and 3 mm PLA exhibited the best result with RL reaching -27 dB. For both cases the samples with the larger cell size showed better results throughout.
Keywords: B*ilayer electromagnetic wave absorber, honeycomb structure, Fused Filament Fabrication, multi-material.*
Fundings: Fundação de Amparo à Pesquisa do Estado do Rio de Janeiro - FAPERJ.

Introduction

The need to mitigate the electromagnetic pollution cause by the large amount of electronic devices used in a daily basis, has led to a large amount of effort put into find better and easier ways to create materials that can help decrease this pollution. In order to obtain a component that has high absorption properties, works on a broad range of frequencies and is light weight, recent researches have pivot to the application of multi-materials structural components, based on polymer composites. A great advantage of these components is that they can be made hollow, which would result in a less dense product that has the added benefit of increasing its effectiveness by promoting scattering and multiple reflection of the electromagnetic wave inside the absorber [1,2]. Honeycomb structures are good candidates for developing microwave absorbing components due to their high strength-to-weight ratio, and the ability to achieve the desired electromagnetic response by changing its geometry [1,3].

There are several methods to produce functional materials, with additive manufacturing being the one which has shown important growth in the last two decades. Additive manufacturing, or 3D printing, differently from traditional manufacturing, produces components by adding material layer by layer, according to a pre-defined program, decreasing waste and increasing the freedom of form. Among the many types of 3D printing, filament fusion fabrication (FFF) is a good option when working with thermoplastic polymers, due to its low cost and easy application [4].

The microwave absorption efficiency of multi-layer components are showed to be enhance by the combination between a matching layer, that works to improve the impedance matching, and an absorbing layer, that reduces the energy of the incident electromagnetic wave. Generally, the

matching layer is made out of a material with low electromagnetic properties, while the absorbing layer presents higher conductivity [2,5,6].
Therefore, the main goal of this study is to find the best thickness ratio between conductive and non-conductive layer of a honeycomb structure that yields the most desirable outcome for microwave absorbing applications, with the highest possible electromagnetic radiation absorbing properties with the least amount of the conductive PLA.

Experimental

Materials

The 3D printed honeycombs were manufactured using commercial polylactic acid (PLA) filaments, supplied by 3D Lab™ (Brazil). Two different types of PLA were used: (i) *PLA transparente*, a 1.75 mm diameter neat PLA filament, and (ii) *PLA condutivo*, a 1.75 mm diameter filament made from a PLA and carbon nanotubes (CNT) composite.

Manufacturing of 3D printed honeycombs

The honeycombs were printed via fused filament fabrications (FFF) on a Creality™ Ender3 3D printer, equipped with a BMG dual gear extrusion system, using the open-source PrusaSlicer (version 2.3.3) software to control the 3D printing process. The printer parameter setup was: nozzle diameter of 0.4 mm; layer thickness of 0.1 mm (first layer 0.3 mm); print speed of 20 mm/s (first layer 15 mm/s); extrusion temperature of 220 °C; heated bed temperature of 60 °C; 3 perimeters, honeycomb fill pattern and fill density of 10% (cell size of 7.5 mm) and 20% (cell size of 3.5 mm). Fig. 1 displays the printed honeycombs, with the two materials and two cell sizes, where the cell size corresponds to the internal diagonal of the hexagonal shape.

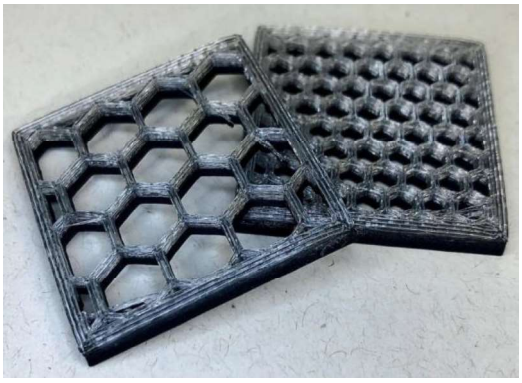

Figure 1 – Printed PLA honeycomb, with neat and conductive PLA, and the two cell sizes.

Preparation of the bilayer components

The honeycombs were printed with thicknesses of 1, 2 and 3 mm, for both materials. They were them assembled in a way that kept the overall thickness of the sample at 4 mm, but varied the ratio between neat and conductive PLA. Single material samples, with 4 mm thickness, were also measured. The components configuration is described in Table 1.

Table 1. Bilayer components configuration

Sample	*Neat PLA thickness*	*Conductive PLA thickness*	*Fill density*
PLA10[4mm]	4 mm	-	10%
PLA20[4mm]			20%
PLA10[1mm]PLAc10[3mm]	1 mm	3 mm	10%
PLA20[1mm]PLAc20[3mm]			20%
PLA10[2mm]PLAc10[2mm]	2 mm	2 mm	10%
PLA20[2mm]PLAc20[2mm]			20%

PLA10[3mm]PLAc10[1mm] PLA20[3mm]PLAc20[1mm]	3 mm	1 mm	10% 20%
PLAc10[4mm] PLAc20[4mm]	-	4 mm	10% 20%

Electromagnetic Properties

The reflection loss (RL) analysis was executed on an ENA vector network analyzer, model E5080B, from Keysight Technologies, with a rectangular waveguide in the X-band (8.2-12.4 GHz) and Ku-band (12.4-18 GHz) frequency range.

Results and Discussion

The bilayer samples described in the "Preparation of the bilayer components" section were measured in two different ways: first the neat PLA honeycomb layer was maintained as top part of the sample, as the matching layer, afterwards the components were turn to place the conductive layer (PLAc) as the top layer. Besides the bilayer components, single material samples were also measured. The RL curves, for the samples with the neat PLA as top layer, are shown in Fig. 2.

Since the samples thicknesses were kept at 4 mm, the analyzed changes between the samples were the thickness layer ratio between neat and conductive PLA and the cell size. For both cell sizes the combination that showed best result was the samples with a 1 mm neat PLA layer combined with a conductive layer of 3 mm (green curves), with values of RL bellow -10 dB (90% of attenuation) for a large frequency range. At the same, time the cell size that showed the highest RL results was the 7.5 mm (fill density of 10%), with values of around -25 dB. Besides that, the sample PLA20[2mm]PLAc20[2mm] showed similar behavior to PLA20[1mm]PLAc20[3mm], but with slightly inferior values and on a smaller frequency range, starting at 11 GHz instead of 9.6 GHz. It is important to point out that the PLAc10[4mm], i.e., single material sample made out of conductive PLA, also reached values lower than -10 dB, however the attenuation remains at -15 dB with a larger amount of conductive filler, which would result in bigger costs.

The mechanism for the increase in microwave absorption for the bilayer samples, compared with the single materials ones, could be attributed to the combination of a matching layer that allows the incident wave to penetrate the material, with the conductive layer that interacts with the wave resulting in multiple reflections between those two layers. Furthermore, the increase in the conductive layer thickness raises the dipole polarization improving the absorption [2].

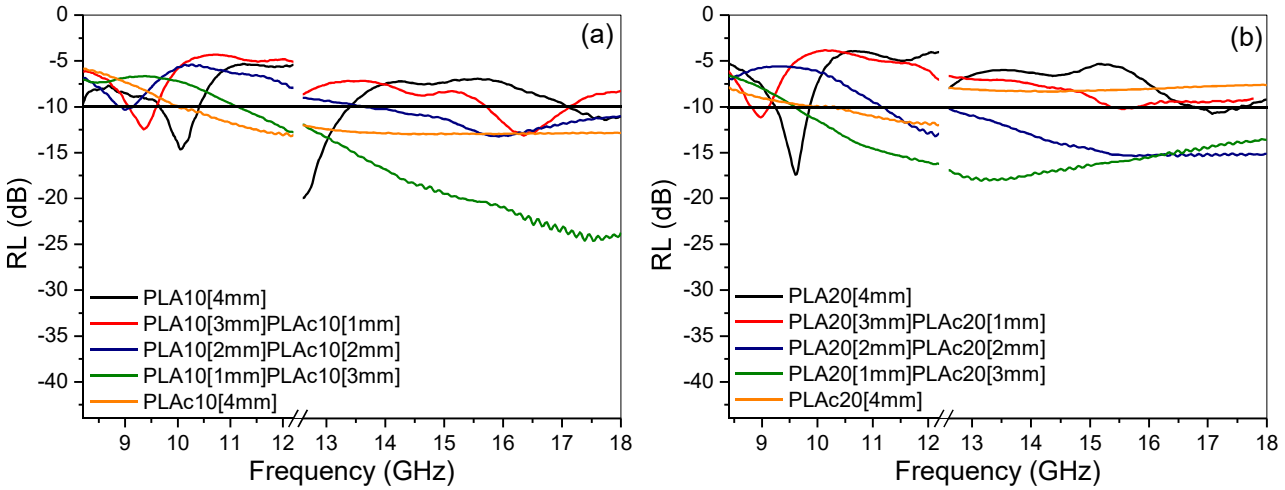

Figure 2 – Bilayer PLA honeycomb with the conductive honeycomb as the bottom layer, with (a) cell size of 7.5 mm (fill density of 10%) and (b) 3.5 mm (fill density of 20%).

To better understand how this bilayer material reacts to the incident electromagnetic wave, measurements with the PLAc as top layer were also performed (Fig. 3). Opposed to how the first experiment went, this time the samples with 1 mm of conductive layer were the ones that showed better results, with the PLAc10[1mm]PLA10[3mm] sample reaching RL values of around -27 dB and the sample PLAc20[1mm]PLA20[3mm] values of -29 dB. The component with larger cell (fill density of 10%) presented RL bellow -10 dB from 11 to 18 GHz, while the one with smaller cell ranged from 10 to 18 GHz. The other samples with the larger cell also showed promising results, with desirable values of RL for a large bandwidth.

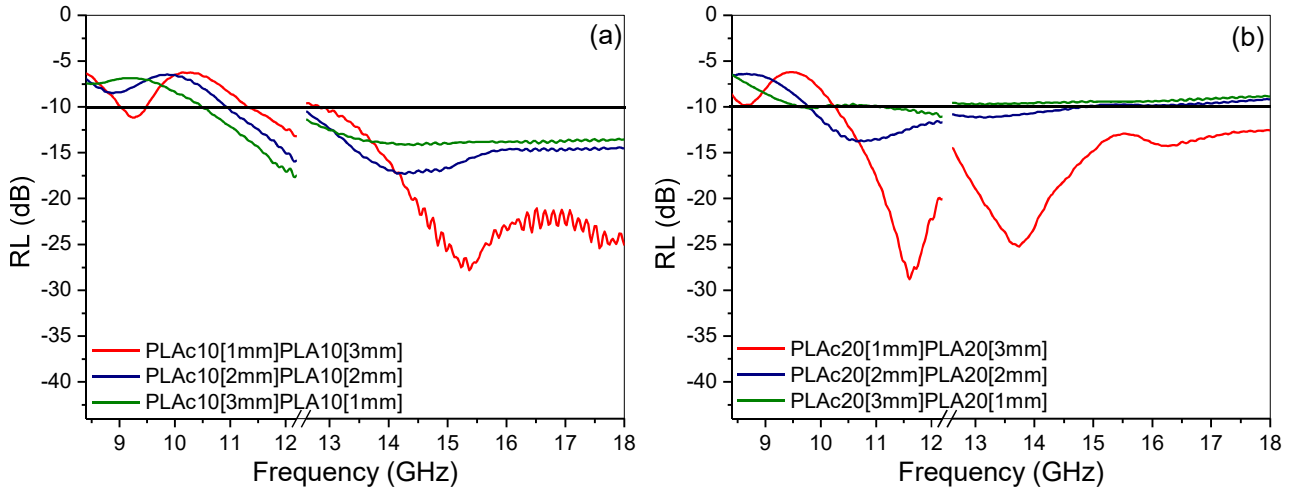

Figure 3 – Bilayer PLA honeycomb with the conductive honeycomb as the top layer, with (a) cell size of 7.5 mm (fill of 10%) and (b) 3.5 mm (fill of 20%).

The obtained results were interesting and unexpected, since the highest values correspond to the samples with the least amount of conductive material. One reason that could be attributed to this behavior is that by distancing the conductive layer from the reflective plate, by adding the neat PLA, the electromagnetic waves that were able to penetrate the first conductive layer would remain trapped between them. However, when the first layer is too thick, the incident wave has a harder time passing through it and is more easily reflected, which results in poorer RL values. This explanation would also account for the higher values of RL obtained by the honeycomb with larger cell size, since it would be easier for the wave to breach the first layer.

Conclusions

In this work, bilayer honeycomb components comprised of a non-conductive neat PLA layer and a conductive PLA/CNT layer were analyzed. The influence of cell size and ratio between the layers in the electromagnetic wave absorbing properties of the components was studied. The measurements were first carried out with the neat PLA as the top layer, then with the conductive PLA (PLAc) as top layer. The best microwave absorbing results were obtained by the PLA10[1mm]PLAc10[3mm], the PLAc10[1mm]PLA10[3mm] and the PLAc20[1mm]PLA20[3mm] samples, with RL reaching values of -25 dB, -25 dB, and -29 dB, respectively. Most of the studied samples also displayed large effective absorption frequency bandwidth, with RL below -10 dB (90% of attenuation), especially for the Ku band, with the larger cell components (fill of 10%) showing better results overall.

The interesting fact that should be highlighted is that for the samples with the PLAc as top layer, very good electromagnetic radiation absorbing properties were achieved with a conductive layer of only a 1 mm thickness and larger cell sizes (fill density of 10% - 7.5 mm), which means that the amount of filler used would be small, relatively to the total component thickness, and that the final total cost of the component wouldn't be too expensive. Finally, this work emphasizes the capability

of 3D printed honeycomb structures to be applied as microwave absorbing components, which are lightweight and structured sound materials.

Acknowledgements
This work was sponsored in part by Conselho Nacional de Desenvolvimento Científico e Tecnológico - CNPq (Grant number 305206/2020-6 and 309125/2020-0), and Fundação de Amparo à Pesquisa do Estado do Rio de Janeiro - FAPERJ (Grant number E-26/010.000.982/2019 and E-26/204.380/2021).

References

1. D.P. Schmitz, B.G. Soares, G.M.O. Barra, L. Santana. Polymer Composites. 2023, 44, 2250. https://doi.org/10.1002/pc.27240
2. P. Gong, Y. Li, C. Xin, Q. Chen, L. Hao, Q. Sun, Z. Li. Ceramics Int. 2022, 48, 9873. https://doi.org/10.1016/j.ceramint.2021.12.190
3. H. Pang, Y. Duan,X. Dai, L. Huang, X. Yang, T. Zhang, X. Liu. J. Mater. Sci. Technol. 2021, 88, 203. https://doi.org/10.1016/j.jmst.2021.01.072.
4. V. Shanmugam, M.V. Pavan, K. Babu, B. Karnan. Polym. Compos. 2021, 42, 5656. https://doi.org/10.1002/pc.26275.
5. A. Rinaldi, A. Proietti, A. Tamburrano, M.S. Sarto. IEEE Trans Electromagn Compat. 2018, 60, 1454. https://doi.org/10.1109/TEMC.2017.2775660
6. B.S. Kwak, W.H. Choi, Y.H. Noh, G.W. Jeong, J.G. Yook, J.H. Kweon, Y.W. Nam. Composites Part B: Eng, 2020, 191, 107952. https://doi.org/10.1016/j.compositesb.2020.107952

THE USE OF NATURAL CLAY AS A FILLER IN POLYPROPYLENE COMPOSITES FOR 3D PRINTING PURPOSES

Marcelo Strassburger[1], Aline Zanchet[2], Eveline Bischoff[1], Douglas Alexandre Simon[1]*

1 – Instituto Federal do Rio Grande do Sul (IFRS), Farroupilha, RS, Brazil
**douglas.simon@farroupilha.ifrs.edu.br*
2 – Universidade de Caxias do Sul - UCSgraphene, Caxias do Sul, RS, Brazil

Abstract The use of clays as reinforcements in polymers has been employed for many years in both academic and industrial settings. Currently, there is an interest in exploring new clay deposits to increase availability. The clays found in the Horizontina/RS region have not yet been characterized or studied for their potential in polymer composites. Therefore, the objective of this research is to evaluate the tensile strength, impact strength, and printability (warpage and surface quality) of 3D printed parts. Composites were prepared with clays from this region, polypropylene (Maxio RP347 Braskem S.A) and maleic anhydride-grafted polypropylene compatibilizer. Two clays from different sources were tested at concentrations of 5%. The clays resulted in a slight increase in the elastic modulus of about 10% and improved impact resistance, but a great improvement in printability was achieved. These findings demonstrate the feasibility of additive manufacturing of polymer-clay composites, leading to new applications and improved properties.

Keywords: *Clay, PP copolymer, 3d printing, characterization.*

Introduction

To improve the properties of PP, researchers have explored the development of composites with the addition of inorganic fillers, particularly nanoparticles [1]. Several methods have been developed to obtain composites, such as in-situ polymerization, solution incorporation, and melt intercalation. Melt intercalation has gained popularity due to its cost-effectiveness, high processing rates, and compatibility with existing industrial polymer processing equipment, such as extruders and injection molders [2].

Furthermore, the choice of an appropriate clay source is vital to obtain superior properties, as different sources may have distinct chemical characteristics. In the region of Horizontina, Rio Grande do Sul, there are underexplored clay deposits currently used for low-value brick production. Characterizing clay samples from these deposits could lead to their application in higher-value uses, such as incorporation into PP to enhance mechanical and thermal properties.

One promising processing technique in materials engineering is additive manufacturing (AM), commonly known as 3D printing. Over the past few decades, AM has gained significant scientific and industrial attention, primarily due to the expiration of its initial patents, coupled with a decrease in printer and consumable costs [3]. This research introduces a technical innovation by cataloging two previously unreported clay sources.

Our main goal is understanding the effect of adding in natura clay from a deposit in the city of Horizontina (state of Rio Grande do Sul) to the formation of a composite with polypropylene and compatibilizer for the production of filament for 3D printing, used in the Fused Deposition Modeling (FDM) technique.

Experimental

Materials

The PP RP 347 (manufactured by Braskem S.A.) used is a random copolymer of propylene and ethylene, with a melt flow index of 10.0 g/10 min, density of 0.902 g/cm³, and a melting temperature of 165 °C. Gray clay (GC) and yellow clay (YC) from Hélio A. Strassburger Mine - ME were employed. PPgMA, a maleic anhydride modified polypropylene, was used as a compatibilizer. It has a melting point of 157 °C, density of 0.91 g/cm³, and a melt flow index of 115 g/10 min. Mineral water from Ametista Spring in Lajeado, Rio Grande do Sul, was used for washing.

Method

Initially, 250 ml of clay were dispersed in 10 liters of washing water and homogenized using an electric mixer. The mixture was left to settle for 7 days, and 5 liters of the suspension were replaced with fresh washing water four times. The clays were then sieved using a 635 mesh sieve and dried at 80 °C for 24 hours. The final yield was 23.0 g of GC and 21.0 g of YC.

Samples of PP with different proportions of clays and compatibilizer were prepared according to the concentrations specified in Table 1. Each sample was extruded to produce 250 g of filament with a diameter of 1.75 ± 0.5 mm. A single-screw extruder (Seibt, ES-18) with a heating ramp ranging from 105 °C to 155 °C was used, with the die temperature set at 155 °C.

Table 1 – Samples concentrations

Samples	PP (g)	PPgMA (g)	GC (g)	YC (g)
PP+2%PPgMA	147,0	3,0	-	-
PP+2%PPgMA+5%GC	139,5	3,0	7,5	-
PP+2%PPgMA+5%YC	139,5	3,0	-	7,5

The test specimens were modeled using CAD software (Fusion 360) following the ASTM D638 and ASTM D256 standards. They were then exported to Ultimaker Cura software, version 5.0.1, in "stl" format. A printer specifically developed for this study was used to print the test specimens. Printing parameters are present in Table 2.

Table 2 – Printing Parameters

Layer Height (mm)	0,2
Printing Temperature (º C)	185
Nozzle Diameter (mm)	0,4
Table Temperature (º C)	150
Perimeter Layers	5
Infill Percentage (%)	100
Printing Speed (mm/s)	60
Cooling Fan	Not Present
First Layer Speed (mm/s)	20

Characterization

For the mechanical tests, tensile strength test was conducted. Five specimens were printed for each sample, and a universal testing machine (EMIC, model DL200) with a 5000 N load cell

was used. The specimens were tested at a crosshead speed of 5 mm/min according to the ASTM D638 standard. They were stretched until a 50 mm limit was reached.

The Izod impact strength was evaluated at room temperature (23 °C) using a Zwick equipment (model D-7900) with a 1 J hammer, following the ASTM D256 standard. The notches in the specimens were created during the printing process.

Also, composite printability will be evaluated as warpage and surface quality, as a qualitative measurement of roughness.

Results and Discussion

Tensile Strength

The Young's modulus of PP+2%PPgMA and the composites with 5% GC and YC from the samples prepared by MA are presented in Figure 1. It was not possible to analyze the pure PP sample due to its lack of adhesion to the print bed. Among the various parameters obtained from the mechanical tests, the elastic modulus is the best indicator of the degree of clay layer exfoliation [4].

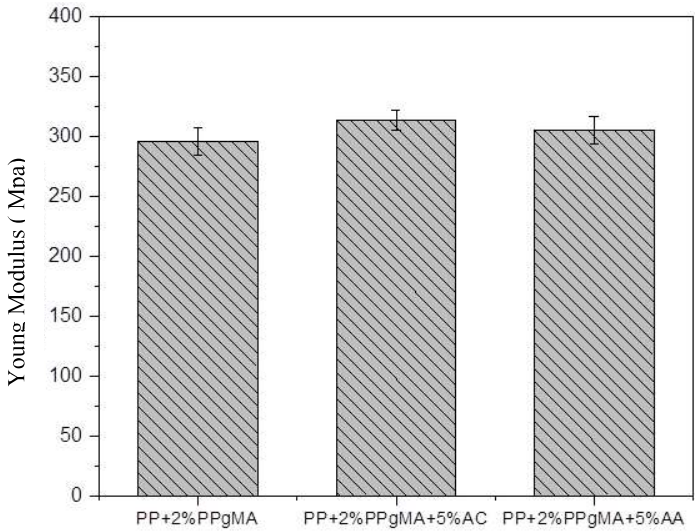

Figure 1 - Elastic Modulus of the compositions

A slight increase in the elastic modulus was observed with the addition of clays compared to the PP+2%PPgMA sample, within the normal range of standard deviation. The maintenance of this property indicates that both clays are suitable as fillers for FDM printing filaments, provided that improvements in printability and dimensional stability are indicated, as presented below.

The Izod impact strength results for the FDM-printed specimens are shown in Figure 16. A positive influence of the addition of 5% clay can be observed, regardless of the clay type used. The combination of maintained rigidity and a slight increase in toughness due to the presence of clay is an interesting result for most applications [4].

The clay seems to contribute to the dispersion of impact energy, typically associated with tortuous crack propagation caused by clay dispersion [4]. This result may also be associated with a decrease in the crystallinity of the samples.

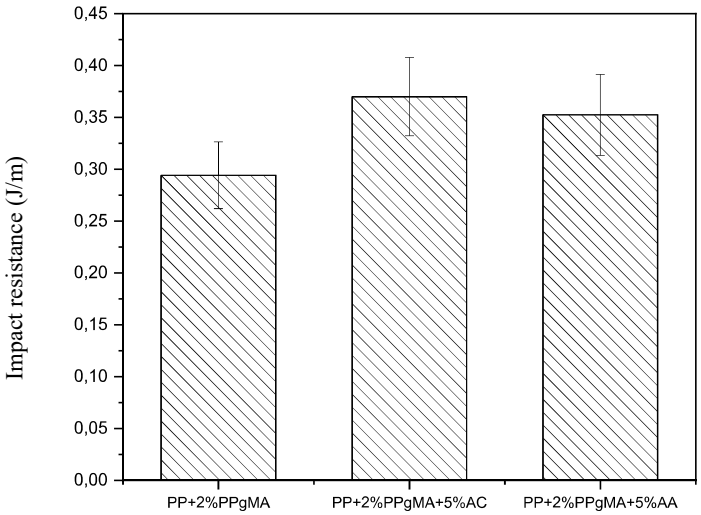

Figure 2 - Impact Resistance of Compositions

The ability to print a material and maintain its geometry depends on several factors. Firstly, the temperature of the print bed is directly related to material adhesion and, therefore, to part deformation and warping [5]. Secondly, the difference in material flowability to be extruded should be considered in the printing parameters, as it may require the application of a correction factor called the "extrusion multiplier". Additionally, higher crystallinity content leads to greater contraction of the printed object, resulting in shape variation and separation between printing layers [5].

The ends of the test specimens are most affected by warping due to faster cooling of the inner parts and temperature gradient during cooling [3]. Figure 3 presents the cross-sectional profile, which should be rectangular but shows a semi-elliptical shape against paralleled metallic plates.

Figure 3 - Cross-sectional profile of the printed sample.

It is important to note that the pure PP filament did not adhere properly to the print bed, except at temperatures above Tc, resulting in the production of a non-uniform molten mass that solidified only after turning off the bed heating. In Figure 4, we can observe the surface quality/roughness of the printed parts. The figure shows the test specimens printed with yellow clay. The test specimens were similar for both clays.

Figure 4 - Image of the surface of the printed PP+2%PPgMA+5%YC specimens. Left: top view. Right: side view from a 45º angle.

Conclusions

From the collection and washing of the clay, filament production for 3D printing was carried out through melt intercalation, obtaining material for FDM application. Changes in complex viscosity were expected due to reduced chain mobility of the polymer with the addition of clay. This condition mildly affected the mechanical properties, with stiffness maintained for samples with clay compared to pure PP, and an increase in toughness. This indicates that both clays are suitable as fillers for FDM printing filaments.

Based on the experimental results and subjective assessment of printability, it can be concluded that Yellow Clay is more suitable for the in-situ incorporation into polypropylene composites, providing an interesting alternative for industrial applications.

To broaden the scope of the results, further research on homopolymer polypropylenes can enhance the understanding of the effect of clay in printing. The optimization of printing parameters also significantly impacts the mechanical properties, enabling improved outcomes.

Acknowledgements

This study was supported by the Instituto Federal de Educação, Ciência e Tecnologia do Rio Grande do Sul (IFRS).

References

1. T. Derbe; S. Temesgen; M. Bitew. A Short Review on Synthesis, Characterization, and Applications of Zeolites. Advances in Materials Science and Engineering, 2021.

2. E. Bischoff; T. Daitx; D. Simon; H. Schrekker; S. Liberman; R. Mauler. Organosilane-functionalized halloysite for high performance halloysite/heterophasic ethylene–propylene copolymer nanocomposites. Applied Clay Science 2015, 112, pp.68-74;.

3. J. Lee; A. Jia ; C. Chua. "Fundamentals and applications of 3D printing for novel materials." Applied materials today 7 (2017): 120-133.

4. E. Bischoff, D. Simon; S. Liberman; R. Mauler, Influence of the dispersing agents to obtain polymer–clay nanocomposites processed in two-steps using thermokinetic mixer. Journal of Materials Science 2020, 55, pp.6537-6550.

5. PACZEK, D. in Proceedings of 9th International Conference on Manufacturing Science and Education, Sibiu, Romania, 2019.

INFLUENCE OF PRINT ORIENTATION ON THE MECHANICAL PROPERTIES OF 3D-PRINTED PLA AND PETG MATERIALS

Lucas L. B. Ramos[1], Rafael Beck[1], K. K. Iwasaki[1], Luis G. S. Rosa[1], Daniela Becker[1] and Ricardo De Medeiros[1]*

1 – Department of Mechanical Engineering, Santa Catarina State University (UDESC), Joinville, SC, Brazil
ricardo.medeiros@udesc.br

Abstract – Over the past decade, there has been significant interest in utilizing thermoplastics for industrial applications, construction, and various automobile components. On the other hand, 3D printing is an evolving manufacturing technology that shows promise in reducing production costs and shortening product development cycle times when compared to traditional manufacturing methods. The rapid advancements in 3D printing technology have opened up new opportunities for researchers to enhance processes, optimize parameters, and improve the properties of printed products. This study aims to compare the mechanical properties of specimens manufactured using 3D printing technology, focusing on two specific materials: PLA and PETG. The specimens were printed in three different orientations: 0º, +/-45º, and 90º. Printing parameters included a speed of 60 mm/s, 100% infill density, and the lines pattern without walls. Five specimens were produced for each combination of material and print orientation. For PLA, the printing and bed temperatures were set at 195 ºC and 60 ºC, respectively, while for PETG, the corresponding temperatures were 230 ºC and 80 ºC. Tensile tests were conducted following the ASTM D638 standard on the flat orientations of the specimens. Digital Image Correlation (DIC) was used to analyse the differences observed in the strain characteristics of these materials under uniaxial tensile load for the investigated print orientations. After the specimens ruptured, an optical microscope was utilized to examine not only the adhesion but also the possible failure modes. The traction test results revealed that PLA exhibited a 21.1% higher maximum tensile strength than PETG in the 0º print orientation. However, for both the 90º and +/- 45º print orientations, PETG demonstrated superior performance with a 13.7% and 12.3% higher maximum tensile strength than PLA, respectively. Finally, this research contributes to the ongoing efforts in advancing 3D printing technology and optimizing material selection for diverse industrial and engineering applications.

Fundings: The authors acknowledge the financial support of the Santa Catarina State Research and Innovation Funding Agency (FAPESC grant: 2017TR1747, and 2021TR843). As well as, Coordination for the Improvement of the Higher-Level Personnel (CAPES Finance Code 001). Ricardo De Medeiros acknowledges the financial support of the National Council for Scientific and Technological Development (CNPq process number: 304795/2022-4).

Keywords: *3D printing. PLA. PETG. Mechanical properties. Orientation.*

INJECTION OVERMOLDED POLYMER-METAL HYBRID STRUCTURES

Gean H. M. Oliveira, Rayana L. Vasconcelos, Mário A. Morozo, Renan Adauto, Giuliana M. Luiz and Leonardo B. Canto*

Department of Materials Engineering (DEMa), Graduate Program in Materials Science and Engineering (PPGCEM), Federal University of São Carlos (UFSCar), São Carlos, SP, Brazil
leonardo@ufscar.br

Abstract – Polymer-metal hybrid (PMH) structures are specifically designed and manufactured to merge the relevant characteristics of each material into a single structure.[1] In this regard, metal insert injection overmolding is a widely used polymer-metal assembly technology. It is based on the injection molding of polymers, an automated, fast, cost effective and accurate method of manufacturing parts with the most varied and complex shapes and sizes, with the difference that the metal part is positioned in the mold cavity and then overmolded with polymer. In direct-adhesion injection overmolding the joining between polymer and metal components is attained by physical and/or chemical adhesion forces, which are achieved by surface preparation of the metal part through micro/nanoscale structuring or through the application of adhesion promoters.[1,2] In this study, we address the injection overmolding joining of polycarbonate (PC), thermoplastic polyurethane (TPU) and nanocomposite of polyamide 6 and graphene oxide with AA6061 aluminum alloy, and of composites of high-density polyethylene (HDPE) and poly(lactic acid) (PLA) filled with hydroxyapatite with Ti6Al4V titanium alloy. The preparation of the polymer composites, surface structuring of the metals, injection overmolding process, interface microstructure and mechanical performance of hybrid polymer-metal joints are detailed. Fine-tuning of injection overmolding conditions and metal surface microstructure led to strong joints with cohesive failure in the polymer and/or metal.

References

1. S. T. Amancio-Filho; J. F. dos Santos *Polymer Engineering and Science* 2009, *49*, 1461. https://doi.org/10.1002/pen.21424.
2. R. L. Vasconcelos; G. H. M. Oliveira; S. T. Amancio-Filho; L. B. Canto *Polymer Engineering and Science* 2023, *63*, 691. https://doi.org/10.1002/pen.26244.
3. M. Grujicic; V. Sellappan; M. A. Omar; N. Seyr; A. Obieglo; M. Erdmann; J. Holzleitner *Journal of Materials Processing Technololgy* 2008, *197*, 363. https://doi.org/10.1016/j.jmatprotec.2007.06.058.

Fundings: This work was supported by FAPESP – São Paulo Research Foundation, Brazil (grant number 2018/24296-0), CNPq – National Council for Scientific and Technological Development, Brazil (grant numbers 309258/2020-0, 164791/2018-3 and 132355/2020-5), CAPES – Coordenação de Aperfeiçoamento de Pessoal de Nível Superior – Brazil (grant numbers 88887.334837/2019-00, 88887.569948/2020-00 and 88887.511885/2020-00). This study was financed in part by the Coordenação de Aperfeiçoamento de Pessoal de Nível Superior - Brasil (CAPES) - Finance Code 001.

Keywords: *polymer-metal hybrids, joining, composite, injection molding.*

POLYPROPYLENE MEMBRANE COATED WITH POLY (1-VINYLPYRROLIDONE-CO-VINYL-ACETATE) ELECTROSPUN FOR RESPIRATORY FACE MASKS

Ariane R. S. Rossin[1,2]*, Fabiana S. L. Cardoso[1,2], Josiane Caetano[2], Mônica Lopes Aguiar[3], Gabriela Brunosi Medeiros[3], Eduardo Radovanovic[1], Wilker Caetano[1] and Douglas C. Dragunski[1,2]

1 – Department of Chemistry, State University of Maringá (UEM), Maringá, PR, Brazil, ariane.rossin@gmail.com
2 – Center of Engineering and Exact Sciences, State University of West Paraná (Unioeste), Toledo, PR, Brazil
3 – Department of Chemical Engineering), Federal University of São Carlos (UFSCar), São Carlos, SP, Brazil

Abstract – The pandemic caused by SARS-CoV-2 has demonstrated that health personal protective equipment still needs more advanced research for its improvement. In this regard, electrospinning can be used as an alternative extra protective barrier for airborne pathogens [1]. In this work, we propose the electrospinning of poly (1-vinylpyrrolidone-co-vinyl-acetate) (P(VP-co-VAc)) as a coating to polypropylene (PP) membranes used in commercial masks for improved particle retention. As a characterization method, scanning electron microscopy (SEM), permeability test (Per) and filtration efficiency of sodium chloride (NaCl) aerosol particles (diameters from 9 to 300 nm) using Scanning Mobility Particle Sizers (SMPS) were used. SEM demonstrates the deposition of nanofibers on PP pores. Per results show that PP/(P(VP-co-VAc)) purchased from PP shows a decrease (Figure 1a), indicating a resistance passage of the particles and their retention more easily. For PP/(P(VP-co-VAc)) the efficiency (Figure 1b) is improved, reaching a maximum of 60%. For suitable filters two important characteristics are required, high collection efficiency and low-pressure drop, therefore, improvements to the electrospinning process under the PP should be evaluated.

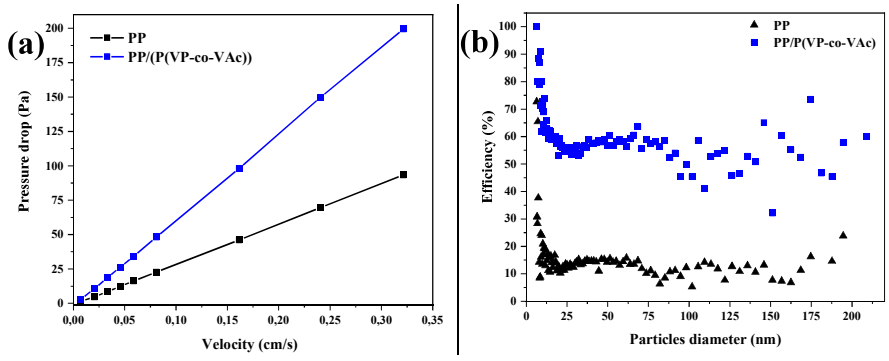

Figure 1. Filtration test (a)Pressure drop versus velocity and (b)collection efficiency.

Keywords: e*lectrospinning, air filtration, personal protective equipment, material development, polymer.*

References

[1] Rossin, A. R. S., Spessato, L., Cardoso, F. D. S. L., Caetano, J., Caetano, W., Radovanovic, E., & Dragunski, D. C. Polymer Bulletin, 2023, 1-24.

A NEW COATING METHOD FOR PRODUCING CONDUCTIVE POLYMER COMPOSITES FILLED WITH NANO-EXPANDED GRAPHITE

Wallyson S. Ramos[1], Daniel E. S. de Sousa[1], Jéssica C. Pereira[1], Talabi S. Isaac[2], Alessandra de A. Lucas[1]*

1 – Graduate Program in Materials Science and Engineering, Federal University of São Carlos (UFSCar), São Carlos, SP, Brazil alucas@ufscar.br
2 – Department of Materials and Metallurgical Engineering, [2]University of Ilorin, Ilorin, Kwara State, Nigeria

Abstract - Conductive polymer composites (CPCs) can be compounded by different coating methods. However, they show some disadvantages as non-solvent recovery and scalability. Thus, this study investigated a new coating method to produce CPCs filled with nano-expanded graphite (nEG). The surfaces of polyethylene terephthalate/polyethylene/aluminum (PET/PE/Al) and polylactic acid/polybutylene succinate (PLA/PBS) powders were coated with up to 10 wt% of nEG and 5 wt% of nEG using a thermokinetic mixer, respectively. The electrical resistivity and morphology of the nanocomposites were evaluated using an HP resistivity meter and polarized light optical microscope, respectively. The results showed a sharp decrease in the resistivity of PLA/PBS and PET/PE/Al filled with 1wt% nEG due to easy formation of conductive paths in a segregated structure. PLA/PBS/nEG and PET/PE/Al/nEG presented electrical resistivity values which are ideal for being tested as sensors or electromagnetic shielding materials.

Keywords: *Segregated Structure, Electrical Properties, Polymer Composites, Coatings, Nanomaterials*

Fundings: This study was financed in part by the Coordenação de Aperfeiçoamento de Pessoal de Nível Superior - Brasil (CAPES) - Finance Code 001 and the Conselho Nacional de Desenvolvimento Científico e Tecnológico – Brasil (CNPQ).

Introduction

Nano-expanded graphite (nEG) is a lamellar material with several layers of stacked graphene sheets, and it is characterized by excellent electrical and mechanical properties [1]. However, several factors such as spacing, orientation and dispersion of the nanofillers within the polymer matrix can impact the performance of electrically conductive composites [2]. In this way, compound methods have a critical effect on the creation of electrical conductive path in such composite. Coating is a method used to decrease the electrical resistivity and percolation threshold of composites. Currently, sonication in presence of isopropyl alcohol and ball milling are two ways of coating polymers powders with carbon nanofiller.

The coating method by sonication in the presence of isopropyl alcohol is a procedure developed by Prof. Drzal's group for coating polypropylene powder with nEG [3]. The incorporation of this technique in the fabrication of polypropylene nanocomposites led to a decrease in the composites percolation threshold and promoted increased electrical conductivity that is up to 10^{-3} S/cm. Nevertheless, this method requires non-solvent recovery and additional production steps, which can increase the cost of fabricating electrically conductive composites. Another way of building conductive paths in polymers with nanofillers is by coating the polymer using ball milling technique [4]–[7]. This method, which is based on the application of compressive/shear forces does not require the use of solvent [8]. However, ball milling can reduce the aspect ratio of nanofillers,

which can impair electrical and mechanical properties of the CPCs [3], [6]. Scalability is another problem of this method.
An alternative to the above-mentioned methods can involve the use of a thermokinetic mixer. A thermokinetic mixer, also called a high-intensity dispersive mixer, is a device that transfers kinetic energy to a solid through high-speed rotating blades [9]. Thus, the system temperature will increases without the application of external heating during mixing [9], [10]. Although there are different configurations (Brabender, Haake and Drais), the operating mechanism of thermokinetic mixers follows the same principle and involved three main processes: breakage of nanofiller agglomerates, mixing and homogenization [9], [11]. Moreover, this equipment can be employed to coat polymer powder with nEG due to high lubricating capacity of the nanofiller does not allow the coated polymer to melt. The adoption of this coating technique in the production of CPCs can offer advantages such as scalability, simplicity and non-use of solvents, which could mitigate the drawbacks associated with previous preparation methods.
Consequently, this work studied the use of a thermokinetic mixer to delaminate and coat the surface of PLA/PBS and PET/PE/Al powders with nano-expanded graphite. The produced composites were characterized by polarized light optical microscopy (PLOM) and their electrical resistivity in direct current was also determined. Based on the literature considered in this study, the utilization of this coating technique for creating conducting paths in CPCs is novel and has not been previously investigated. The first set of promising results based on this novel production route is presented in this article. Given these results, PLA/PBS and PET/PE/Al reinforced with nEG are promising candidates for use as sensors and electromagnetic shielding materials.

Experimental

2.1. Materials

Two different matrices were used in powder form for the preparation of the CPCs: polylactic acid/polybutylene succinate (PLA/PBS) and polyethylene terephthalate/polyethylene/aluminum (PET/PE/Al). The PLA/PBS blend (C 301), which has a 70/30 weight proportion of PLA and PBS respectively, was provided by Biomater, São Paulo, SP, Brazil. The PET/PE/Al (with 18 wt% PET, 54 wt% PE and 28 wt% Al) composite was obtained from discarded packaging material and supplied by Natura, Cajamar, SP, Brazil. Finally, ground nano-expanded graphite was supplied by Nacional de Grafite and has a diameter of 11 micrometers and a mean thickness of 30 nanometers. The nanocomposites with different concentrations of nEG were evaluated as shown in Table 1.

Table 1. Composites composition.

Matrix	nEG Filler (wt%)
PLA/PBS	1 wt%, 3 wt% and 5 wt%
PET/PE/Al	1 wt%, 3 wt%, 5 wt%, 7.5 wt% and 10 wt%

2.2. Preparation of composites

PLA/PBS and PET/PE/Al composites with different concentrations of nEG were prepared using a thermokinetic mixer (MH Industrial). Each of the composite formulations was blended at the pre-mixer velocity for 10 seconds followed by the maximum velocity of 2600 rpm for 30 seconds.

2.3. Compression Molding

The composite powders containing various quantities of nEG were molded in a hydraulic press model MA 098/AR15. The materials were molded for 2 minutes at 190 °C with an initial pressure of 3 tons for 60 s and 5 tons for another 60 s. The system was cooled using circulating water and 165 mm x 165 mm x 2 mm plate specimens were obtained.

2.4. Characterizations

Circular specimens with a diameter of 4 cm and a thickness of 0.2 cm were produced from the hot-pressed samples and used to determine volumetric electrical resistivity. The electrical resistivity of each composite was measured according to ASTM D257 at 23 °C and 50% relative humidity. An HP resistivity meter (High Resistance Meter) model 4339B with an HP resistivity cell sample holder (model 16008B) was used for the measurement. The composites morphology was studied by observing about 20 µm microtomed thin films through a polarized light optical microscope (Leica, DMRXP) with an attached camera (ZEISS, AxioCam ERc5s). The obtained images were analyzed using AxioVision Rel. 4.8 software.

Results and Discussion

The electrical resistivity values of the PLA/PBS/nEG and PET/PE/Al/nEG composites are shown in Table 2.

Table 2. Electrical resistivity of the conductive polymer composites

Composition	Electrical Resistivity (Ω.cm)
PET/PE/AL	6.80×10^{14}
PET/PE/AL/1wt%nEG	2.31×10^{4}
PET/PE/AL/3wt%nEG	2.12×10^{4}
PET/PE/AL/5wt%nEG	3.34×10^{4}
PET/PE/AL/7.5wt%nEG	6.57×10^{4}
PET/PE/AL/10wt%nEG	2.14×10^{4}
PLA/PBS	1.08×10^{12}
PLA/PBS/1wt%nEG	$<10^{4}$
PLA/PBS/3wt%nEG	$<10^{4}$
PLA/PBS/5wt%nEG	$<10^{4}$

As seen in Table 2, the electrical resistivity of PET/PE/Al (6.80×10^{14} Ω.cm) was lower than pure PET (10^{17} Ω.cm) and pure PE (10^{17} Ω.cm) [12], [13]. This can be attributed to the presence of aluminum particles in the composite. PLA/PBS blend also presented a coherent value of resistivity (1.08×10^{12} Ω.cm) in line with information available in the literature [14]. PLA/PBS and PET/PE/Al resistivities are high, and they can be defined as insulators [15]. Generally, materials are characterized based on electrical resistivity as electrostatic dissipative (between 10^{6} and 10^{11} Ω.cm), conductive (from 10^{5} to 10 Ω.cm) and highly conductive (below 10 Ω.cm) [15]. Figure 1 shows electrical resistivity as a function of nEG content for both PLA/PBS and PET/PE/Al nanocomposites. As seen in Figure 1, the addition of 1wt% nEG led to a sharp fall in the resistivity of PET/PE/Al and PLA/PBS. PLA/PBS/1wt%nEG showed a reduction higher than 8 orders of magnitude in its electrical resistivity, while PET/PE/Al/1wt%nEG showed a decrease by 10 orders of magnitude. The decrease of the samples' volume resistivity can be attributed to the presence of conductive paths in a segregated structure. According to Pang (2014), a segregated structure is observed when conductive fillers are localized at the interface of polymeric granules of conductive polymer composites [15]. Thus, such material will show better electrical properties than composites with randomly distributed filler [15]. This was reported by several authors that studied polymer composites reinforced with conductive carbonaceous nanofillers [16]–[21]. The segregated structure was verified through morphological evaluation of PLA/PBS/3wt%nEG by polarized light optical microscopy as shown in Figure 2.

As seen in Figure 2, PLA/PBS/3%nEG showed a segregated structure where two zones are observed: dark and light zones. The dark zones are nEG-rich regions, while the light zones are formed by PLA/PBS blend. This image shows the presence of conductive paths built by accumulation of nEG at interfaces of the PLA/PBS granules. The sample morphology showed that the use of a thermokinectic mixer for coating the polymer particles is a viable method for producing CPCs, even at a low concentration of nEG (1 wt%). The results presented in this study are similar to

those obtained in previous related works. For example, Al-Saleh (2016) observed the formation of a segregated structure in Ultra High Molecular Weight Polyethylene (UHMWPE) powder coated with graphene nanoplatelets (GNP) via dry-mixing [21]. A decrease of 11 orders of magnitude in the electrical resistivity, which corresponds to 3 x 10^3 Ωcm, was observed when 3 wt% of the nanofiller was added [21]. Yiqun Wang (2017) also observed the same behavior for UHMWPE/GNP composites prepared using ethanol-assisted dispersion [22]. Regarding the composite with 3.8 wt% of GNP, the presence of interconnecting conductive channels resulted in a resistivity of 10^3 Ωcm [22]. The resistivity values (≤10^4 Ω.cm) obtained in this present study showed that PLA/PBS/nEG and PET/PE/Al/nEG are conductors and can be tested as sensors or electromagnetic shielding materials. The expected morphology for PET/PE/Al/nEG composites will be similar to the one presemted in Figure 2.

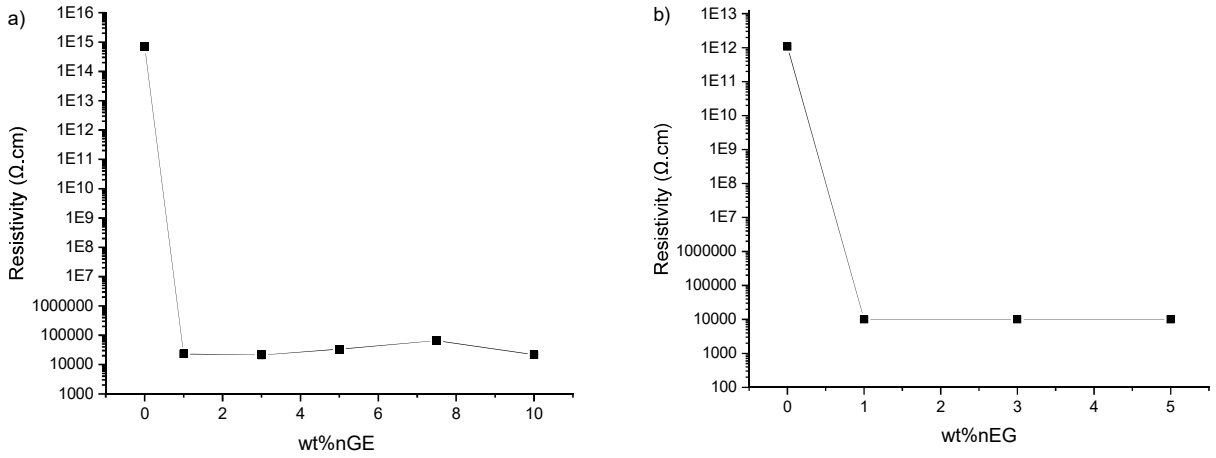

Fig. 1: Electrical resistivity of (a) PET/PE/Al/nEG and (b) PLA/PBS/nEG nanocomposites.

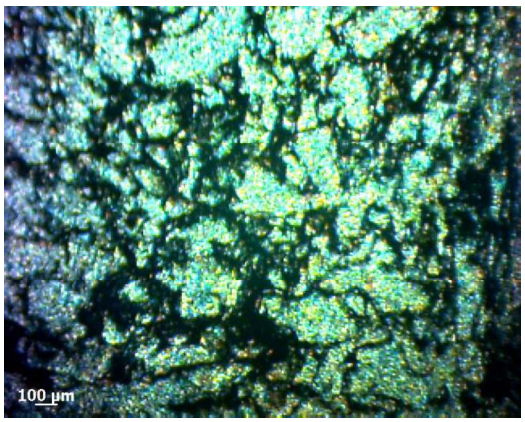

Fig. 2. Conductive paths in a segregated structure of PLA/PBS/3wt%nEG.

Conclusions

In this work, a unique coating method involving the use of a thermokinetic mixer was used to produce conductive polymer composites reinforced with nano-expanded graphite. This method was efficient for creating well-distributed conductive paths, which reduces the electrical resistivity of PLA/PBS and PET/PE/Al. In the case of PLA/PBS/nEG composite, the electrical resistivity corresponds to a decrease higher than 8 orders of magnitude. Regarding PET/PE/Al/nEG, the electrical resistivity was reduced by 10 orders of magnitude. The excellent results were attributed

to the formation of conductive paths in a segregated structure. Both composites (PLA/PBS/nEG and PET/PE/Al/nEG) are ideal for use as sensors and can be further tested as electromagnetic shielding materials. Finally, this work showed that coating by a thermokinetic mixer is a very promising method for the production of conductive composites in a large scale and the technique is suitable for coating polymer powders.

References

[1]Friedrich K., Breuer U.Multifunctionality of Polymer Composites: Challenges and New Solutions. Elsevier Inc., New York, 245–261 (2015).

[2]Jiang X., Drzal L.: Polymer Composites (2012), 636–642.https://doi.org/10.1002/pc.22187

[3]Kalaitzidou K., Fukushima H., Drzal L. T., Composites Science Technology (2007). 2045–2051. https://doi.org/10.1016/j.compscitech.2006.11.014

[4]Dweiri R., Jordan Journal of Mechanical and Industrial Engineering (2015). 1–8.

[5]Jiang X., Drzal L. T. Journal of Applied Polymer Science (2011). 525–535. https://doi.org/10.1002/app.34891

[6]Dweiri R., Suherman H., Sulong A. B., Al-Sharab J. F.Science and Engineering of Composites Materials (2018). 1177–1186.https://doi.org/10.1515/secm-2017-0122

[7]Guo Y., Zhang Y., Wu H., Guo S. Composites Science and Technology (2021). 1-9.https://doi.org/10.1016/j.compscitech.2021.109010

[8]Pielichowski K., Majka T. Polymer omposites with Functionalized Nanoparticles. Elsevier Inc., New York, 47-83 (2018).

[9]Harris. R. Coloring Technology for Plastics Plastics Design Library, New York, 189–197 (1998).

[10] Costa I. L. M., Zanini N. C., Mulinari D. R. Journal of Inorganic and Organometalic Polymers and Materials (2021). 220–228. https://doi.org/10.1007/s10904-020-01709-0

[11]Silva T. F., Menezes F., Montagna L. S., Lemes A. P., Passador F. R.Journal of Applied Polymer Science (2019).1–8. https://doi.org/10.1002/app.47273

[12]McCrossan K. Polymer-Carbon Nanotube Composites: Preparation, Properties and Applications. Woodhead Publishing Limited, New York ,545–586 (2011).

[13]Xiang D., Wang L., Tang Y., Hill C. J., Chen B., Harkin-Jones E. International Journal of Materials Research (2017). 322–334. https://doi.org/10.3139/146.111482

[14]Sivanjineyulu V., Behera K., Chang Y. H., Chiu F. C.. Composites Part A Applied Science and Manufacturing (2018). 30–39. https://doi.org/10.1016/j.compositesa.2018.08.009

[15]Pang H., Xu L., Yan D. X., Li Z. M. Progress in Polymer Science (2014). 1908–1933 https://doi.org/10.1016/j.progpolymsci.2014.07.007

[16]Wang P., Zhang J., Dong L., Sun C., Zhao X., Ruan Y., Lu H. Chemistry of Materials (2017). 3412–3422 https://doi.org/10.1021/acs.chemmater.6b04734

[17]Chen L., Jia W., Lan Z., Tang X., Zhu F., Xiong Z. Organic Electronics (2018), 165–169 https://doi.org/10.1016/j.orgel.2018.01.015

[18]Lebedev O. V., Ozerin A., Kechek'yan A., Shevchenko V. Polymer Composites (2017), 1–10. https://doi.org/10.1002/pc.24532

[19]Vovchenko L., Matzui L., Oliynyk V., Launets V., Mamunya Y., Maruzhenko O. Molecular Crystals and Liquid Crystals (2018). 186–198 https://doi.org/10.1080/15421406.2018.1555349

[20]Rehman A. U., Ikram M., Kan K., Zhao Y., Zhang W. J., Zhang J., Liu Y., Wang Y., Du L., Shi K. Sensors Actuators B: Chemical (2018). 285–295. https://doi.org/10.1016/j.snb.2018.08.004

[21]Al-Saleh M. H. Journal Physics D: Applied. Physics (2016)1–8.10.1088/0022-3727/49/19/195302

[22]Wang Y., Yang J., Zhou S., Zhang W., Chuan R. Journal of Materials Science: Materials in Electronics (2017). 91–96 https://doi.org/10.1007/s10854-017-7892-4

CHEMICAL AND MECHANICAL EVALUATION OF COMPOSITE FILAMENTS FOR 3D PRINTING

Iago R. de Abreu[1], Renato de S. N. Junior[1], Allef G. da S. Fortes[1], Rudy Folkersma[2], Luigi V. Leitão[3], Fábio D. P. Marques[3], Arthur A. S. Sampaio[3], Layara L. R. L. de Castro[1], Daniella S. C. Andrade[4] Tatianny S. Alves[1,3], Renata Barbosa[1,3]

1 – Postgraduate in Materials Science and Engineering (PPGCM), University Federal of Piauí (UFPI), Teresina, PI, Brazil
2 – NHL Stenden University of Applied Sciences, Emmen, Netherlands
3 – Materials Engineering Course/CT, Federal University of Piauí (UFPI), Teresina, PI, Brazil
4 – Materials Science Program, Federal University of Pernambuco (UFPE), Recife, PE, Brazil
rrenatabarbosa@yahoo.com

Abstract - The addition of fillers in raw materials used in additive techniques has provided improvement to the process and has also enabled new applications. The objective of this study was to evaluate the chemical and mechanical properties of filaments composed of polymer blend based on poly (lactic acid) - PLA and poly (butylene adipate-co-terephthalate) - PBAT with zinc oxide, a biocide and carnauba wax, future use in filter membranes. The compounds and filaments were produced by means of a monoscrew extruder, with 3% zinc oxide, 1% biocide and 1% carnauba wax. The filaments were evaluated by infrared spectroscopy (FTIR) and mechanical behavior via tensile strength tests. The results showed that the loads of zinc oxide, carnauba wax and biocide did not cause chemical changes in the composite, as observed in the FTIR spectra. The tensile strength was reduced with the addition of zinc and had a slight increase in the presence of carnauba wax and biocide in relation to the pure polymer.
Keywords: *Filament, 3D printing, FDM, Composites.*

Introduction

Additive manufacturing, or popularly 3D printing, is a manufacturing process that uses the addition of successive layers of material for the formation of a part. It is widely used in various fields such as robotics, automotive industry, medicine and has numerous advantages such as ease of process and economy in industrial prototyping. In addition, it also highlights the freedom and possibility of manufacturing complex geometries [1-3].

The most widespread method of 3D printing is molten deposition modeling (FDM) using thermoplastic filaments produced from various materials such as polyurethane (PU), acrylonitrile butadiene styrene (ABS) and polylactic acid (PLA) being the most widespread and used [4]. Thus, the study by other environmentally friendly materials, in addition to PLA, and distant from petroleum products, has gained space in the field of research as new alternatives for biodegradable materials [1,2].

Associated with these factors, the addition of loads has provided the stability of resources in terms of workability or printability of the material during the printing process [1,4,5]as well as the effect of these additives in a specific application such as the manufacture of filter membranes for water oil separation by prototyping has been investigated [6,7].

The literature reports extensive exploration and great capacity of some materials in the application highlighted earlier. Zinc oxide, for example, receives a lot of attention and is applied

due to its efficient catalytic capacity, low cost and non-toxicity, in addition, it has antibacterial capacity that expand its applicability [3,8]. Allied to this, carnauba wax, composed of a mixture of hydrophobic compounds, has no impact on the environment because it is biodegradable, and is widely used commercially as a water repellent [8,9]. This demonstrates potential in employment and potential for new approaches such as the use in filaments for 3D printing.

This study aimed to develop and evaluate the chemical and mechanical properties of composite filaments formed from a biodegradable polymer matrix based on PLA/ PBAT (Poly (acid) lactic / (Polybutylene adipate-co-terephthalate)) incorporating zinc oxide, a commercial biocide and carnauba wax as polymeric additives in order to enable the prototyping of filter membranes for application in oil/water separation.

Experimental

Materials

It was used as polymeric matrix the commercial blend Ecovio® (EC), produced by BASF SA, and formed by Poly (lactic acid) - PLA and Poly (butylene adipate-co-terephthalate) - PBAT. For the formation of the composites, the following additives were used: Commercial Biocide Sanitized MB E 22-70 (BC), Zinc oxide (ZnO) and Carnauba wax (CW).

Preparation of the composites

The materials were previously mixed using the concentrations of 3% for zinc oxide and 1% for the biocide and carnauba wax, respectively, in relation to the polymer blend. Subsequently, the compositions were processed in a single screw extruder model AX-16 of the brand AX plastics (L/D = 26) under the temperature profile of 170, 175 and 180 C and screw speed of 40 rpm. The composite obtained was cooled in water and granulated in pelletizer.

Filament preparation

The pelletized composites obtained in the previous stage were dried in an oven at 80 C for 4h and soon after the filaments were prepared using extruder of the same brand under the same temperature and screw speed conditions. The cooling was carried out by bathing in water at room temperature, with the aid of a chiller equipped with coolers of the brand Filmaq3D. The dimensions of the filaments were controlled by means of a winder, same brand, acting in the process of pulling the filaments, allowing diameter adjustment during the process. The traction parameters were adjusted in the rotation speed of the winding roller, allowing the reach of the required filament pattern, corresponding to 1.75 ± 0.10 mm.

Characterizations

Fourier Transform Infrared Spectroscopy - FTIR

The FTIR spectra were obtained in Nicolet Summit FTIR spectrometer equipment operating in total attenuated reflectance (ATR) mode. The scan was used in the range of 4000 to 500 cm^{-1} totalizing 16 scans in the analysis. The analyses were performed in the laboratory GREENPAC (Polymer Application Center - NHL Stenden), Netherlands.

Tensile Strength

The tensile strength test was performed on the filaments according to ASTM D3379. Five samples of each composition were selected and the test was conducted under the speed if 5 mm/min, with a load cell of 5 kN in a universal machine EMIC, model DL 30000, belonging to the Materials Engineering Course of the Federal University of Piauí.

Results and Discussion

Fourier Transform Infrared Spectroscopy – FTIR

The Fig 1 shows the FTIR spectra of the composite filaments (EC/3ZnO; EC/3ZnO/BC and EC/3ZnO/BC/CW) and the polymer matrix (EC) so that it is possible to analyze the chemical interactions between the PLA/PBAT blend, zinc oxide, biocide and carnauba wax.

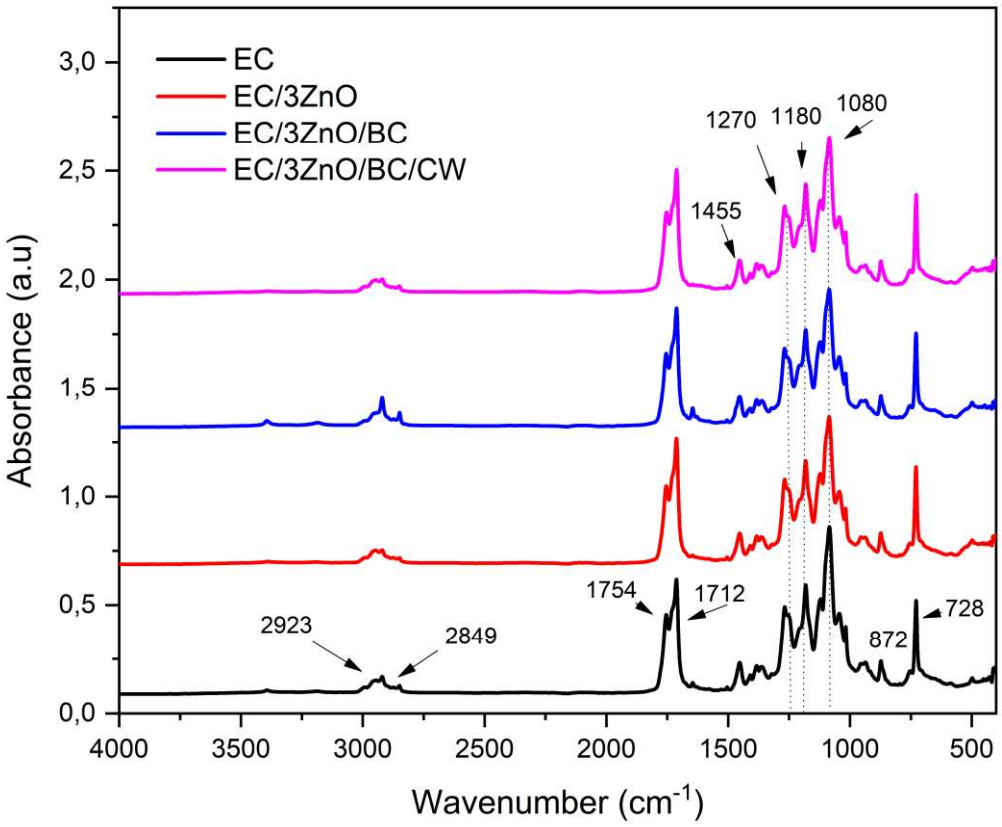

Fig 1. Infrared spectrum for EC, EC/3ZnO, EC/3ZnO/BC, EC/3ZnO/BC/CW compositions.

The FTIR of the polymer blend filament as well as all composites presented bands at 1712 cm^{-1} and 1754 cm^{-1}, referring to the C=O elongation vibrations (ester group) present in PLA and PBAT [1]. The bands observed in the region of 2923 cm^{-1} and 2849 cm^{-1} are associated with symmetric and asymmetric stretching vibrations of the methyl group (CH_3) [5]. The peaks observed in 1455 cm^{-1} and 1270 cm^{-1} refer respectively to the antisymmetric bending vibration of the CH_3 group of the PLA phase and the symmetric elongation vibration of the PBAT phase CO [10].

At 1180 and 1080 cm^{-1}, the bands are characteristic of the C=O stretch vibration [1]. The amorphous and crystalline phases of the PLA are represented by peaks at 872 and 757 cm^{-1} respectively. The bending vibration band of the CH plane of the PBAT benzene ring is represented in 728 cm^{-1}[1,10].

It is also possible to observe that there were no changes due to the incorporation of the biocide and the carnauba wax. The literature reports peaks referring to C-H, C=O, C≡C, C-N, N-H bonds in 1848, 1468, 1515, 1161 and 722 cm^{-1}, respectively [9]. Similarly, the biocide compound encapsulated with EVA, did not induce change in the composites. This behavior possibly refers to

the chemical groups being from the same region with characteristic peaks in 1736, 1370, 1238, 1020 and 608 cm^{-1} [11].

In relation to zinc oxide, load in greater percentage in the composite, similarly, it was not possible to identify the peaks and the formation of new peaks due to the insertion of this load. The literature reports elongation Zn-O in the regions of 906 - 644 cm^{-1} and in 1507 - 1378 cm^{-1} attributed to asymmetric stretching of oxygen present in the composition [2,12]. Given this discussion, the absence of new bands in composites compared to polymer blend, it is concluded that there was no interaction with the incorporation of additives.

Tensile Strength

The tensile strength of the filaments is an important property aiming the applicability in the extrusion process as well as its accommodation and storage in reels. In order to be able to transport the material to the extrusion head the filament must have sufficient resistance in the transport by pulleys [4].

In Fig. 2, the mechanical behavior of the blends filaments (EC) and their composites (EC/3ZnO; EC/3ZnO/BC; EC/3ZnO/BC) is illustrated.

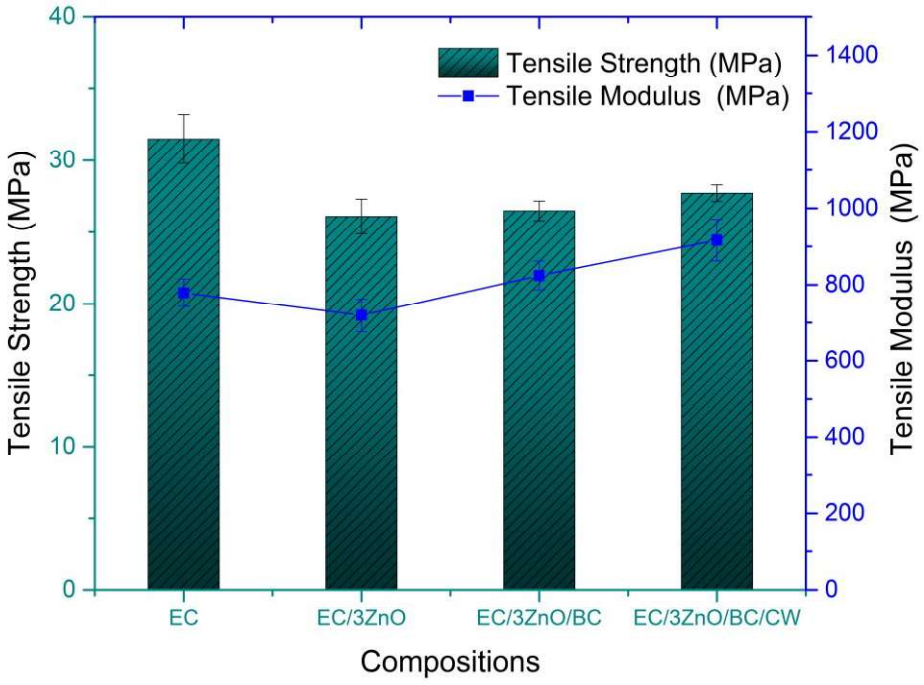

Fig. 2. Tensile strength and modulus of elasticity for compositions EC, EC/3ZnO, EC/3ZnO/BC, EC/3ZnO/BC/CW

According to the results, the filament composition of the pure polymer presented the highest values of mechanical properties among the other compositions. The results with slight decrease in the values can be attributed to the non-distribution of the load in the filament extrusion process, resulting in weak interfacial adhesion of particles and polymer matrix [2,4].

It was also observed that when compared the values of the modulus of elasticity of the filament of the pure polymer with the composition EC/3ZnO note material reduction became less rigid, however, with incorporation of the biocide and especially the carnauba wax the values became higher than reported in previous compositions. Therefore, the incorporation of biocide and carnauba wax increased the stiffness of the filament. Mathew, Das, TP & Kumar, 2022 [1] evaluated the tensile strength properties of filaments composed of the PLA/PBAT blend in varied

percentages and observed a reduction in tensile strength, flexion, and modulus of elasticity with increased percentage of PBAT, however, with 40 % it was noted the reduction in elongation attributed to the increase of the dispersed phase.

Conclusions

Filaments for additive manufacturing FDM were produced and evaluated when their chemical and mechanical properties. The FTIR spectra showed the absence in the formation of new bands with the insertion of fillers in the polymer blend, showing no chemical changes in the composites. The evaluation of the tensile strength properties indicated reductions with the incorporation of zinc oxide and slight increase with the addition of carnauba wax and biocide in relation to the blend filament. The filaments produced presented characteristics to be applied in functionalized membranes for water/oil treatment, however further studies and characterizations on the viability of the product, as an innovative character of the work, will be necessary new prospects are open for membrane production without the need for extra surface treatment.

Acknowledgements

The authors would like to thank Universidade Federal do Piauí; the Laboratory of Polymers and Conjugated Materials (LAPCON); NHL Stenden University of Applied Science; GREENPAC Laboratory (Polymer Application Center); Piauí State Research Support Foundation (FAPEPI); National Council for Scientific and Technological Development (CNPq) and Funding: This work was supported by the CNPq [process number: 308446/2018-6] and [process number: 308309/2022-7].

References

1. Mathew, J., Das, J. P., Tp, M., & Kumar, S. Journal of Polymer Research 2022, 29(11), 474. https://doi.org/10.1007/s10965-022-03320-y.
2. Jamnongkan, T., Jaroensuk, O., Khankhuean, A., Laobuthee, A., Srisawat, N., Pangon, A., ... & Huang, C. F. Polymers 2022, 14(3), 600. https://doi.org/10.3390/polym14030600.
3. Kumbhakar, P., Ambekar, R. S., Mahapatra, P. L., & Tiwary, C. S. Journal of Hazardous Materials 2021, 418, 126383. https://doi.org/10.1016/j.jhazmat.2021.126383.
4. Spoerk, M., Sapkota, J., Weingrill, G., Fischinger, T., Arbeiter, F., & Holzer, C. Macromolecular materials and engineering 2017, 302(10), 1700143. https://doi.org/10.1002/mame.201700143.
5. Yang, J., Li, W., Mu, B., Xu, H., Hou, X., & Yang, Y. International Journal of Biological Macromolecules 2022, 202, 482-493. https://doi.org/10.1016/j.ijbiomac.2022.01.090.
6. Han, L., Chen, C., Shen, L., Lin, H., Li, B., Huang, Z., ... & Hong, H. Journal of Materials Chemistry A 2022, 10(22), 12055-12061. https://doi.org/10.1039/d2ta01971j
7. Koh, J. J., Lim, G. J., Zhou, X., Zhang, X., Ding, J., & He, C. ACS applied materials & interfaces 2019, 11(14), 13787-13795. https://doi.org/10.1021/acsami.9b01753.
8. Lozhechnikova, A., Bellanger, H., Michen, B., Burgert, I., & Österberg, M. Applied Surface Science 2017, 396, 1273-1281. http://dx.doi.org/10.1016/j.apsusc.2016.11.132.
9. Ge, C., Xu, X., Ma, F., Zhou, J., & Du, C. International Journal of Molecular Sciences 2022, 23(13), 7422. https://doi.org/10.3390/ijms23137422.
10. Shankar, S., & Rhim, J. W. Food Packaging and Shelf Life 2019, 21, 100327. https://doi.org/10.1016/j.fpsl.2019.100327.
11. Park, K., Sadeghi, K., Panda, P. K., Seo, J., & Seo, J. Journal of the Taiwan Institute of Chemical Engineers 2022, 134, 104301. https://doi.org/10.1016/j.jtice.2022.104301.
12. Valerio, T. L., Maia, G. A. R., Gonçalves, L. F., Viomar, A., Banczek, E. D. P., & Rodrigues, P. R. P. Materials Research 2019, 22. https://doi.org/10.1590/1980-5373-MR-2018-0864.

COMPARATIVE ANALYSIS OF ROTOMOLDING AND INJECTION PROCESSES FOR THE MANUFACTURE OF HDPE PRODUCTS

Henrique R. Mença[1*], Camila Figueiró[2], Cristiane M. Becker[2], Frederico Eggers[2], Otávio Bianchi[1], Sandro C. Amico[1]

1 – Federal University of Rio Grande do Sul – UFRGS, Pos-Graduate Program in Mining, Metallurgical and Materials Engineering – PPGE3M, Porto Alegre, RS, Brazil – (*) corresponding author: henriquemenca@gmail.com
2 – SENAI Institute of Innovation in Polymer Engineering – ISI Polímeros, São Leopoldo, RS, Brazil

Abstract – HDPE is widely used and can be shaped using various techniques. Rotational molding offers complex geometries and hollow profiles, while injection molding provides high speed and dimensional stability. This study compares the effects of these processes on HDPE in its properties. Results show that rotomolded samples had higher crystallinity (59.76%) and elastic modulus (647.87 MPa), while injected samples performed better in the impact test (55 kJ/m²). The choice of molding process should consider specific product requirements.
Keywords: *HDPE, rotomolding, injection, physical and mechanical analysis*
Funding: FAPERGS (Inova Clusters Tecnológicos n. 22/2551-0000839-9)

Introduction

High-density polyethylene (HDPE) is a widely used thermoplastic due to its excellent combination of properties, such as chemical resistance, high mechanical strength compared to other commodity polymers, rigidity and ease of processing (low melting temperature), among others [1]. For this reason, HDPE can be found in various industrial sectors, including pipelines, cable coatings, automotive components, storage tanks, a standard household products like bottles, toys and packaging. Its versatility and range of properties make it the top choice for applications requiring mechanical and chemical resistance, low cost, impermeability and non-toxicity [2].

HDPE can be molded using different manufacturing processes, with the leading techniques being rotational molding and injection molding. Rotational molding involves heating a filled hollow mold and rotating it to distribute the material uniformly along the walls. After cooling, the mold is opened and the final piece is extracted [3, 4]. This process offers advantages like unique pieces with complex geometries. However, this technique tends to be slower than other shaping processes, like injection molding, and its parts can experience significant shrinkage [3, 4, 5].

Injection molding is a modern and versatile process for molding thermoplastics. It involves melting the polymer material in an injection chamber and then pouring it into a closed mold to cool and solidify the product [6]. The process offers high production speed and excellent dimensional stability for mass production. It allows for the incorporation of complex details like reinforcements and holes. However, it comes with a high initial cost, long setup times, and can result in residual stresses in the final material [5, 6].

Both processes have their advantages and disadvantages, but it is essential to understand the significant differences between each technique in order to choose the best option according to the specific needs of each desired product. This article will address the comparison between rotational molding and injection molding processes for high-density polyethylene, aiming to elucidate the influence of these techniques on its properties and characteristics resulting from each one.

Experimental

Material

In this work, high-density polyethylene HD4601U from Brasken was used. The polymer was acquired in micronized form (60 µm), specifically designed for the rotational molding. The HDPE has a melt flow index of 2.0 g/10 min, a density of 0.942 g/cm³ and a melting temperature of 129 °C.

Material Processing

Since the material was in micronized form (Fig 1), a preliminary extrusion step was required to form pellets, which were later used in the injection process. The extruder (Fig 1–a.1) used in this step was a Brabender Twin Screw Multipurpose extruder, where the material was extruded at a screw rotation speed of 180 rpm, average torque of 53 Nm, initial polymer mass temperature of 198 °C, feeding rate of 2 kg/h and pelletizer speed of 8600 rpm. The temperatures used in the six heating zones of the equipment were between 175 and 190 °C. The resulting material in pellet form can be seen in Fig 1–a.2.

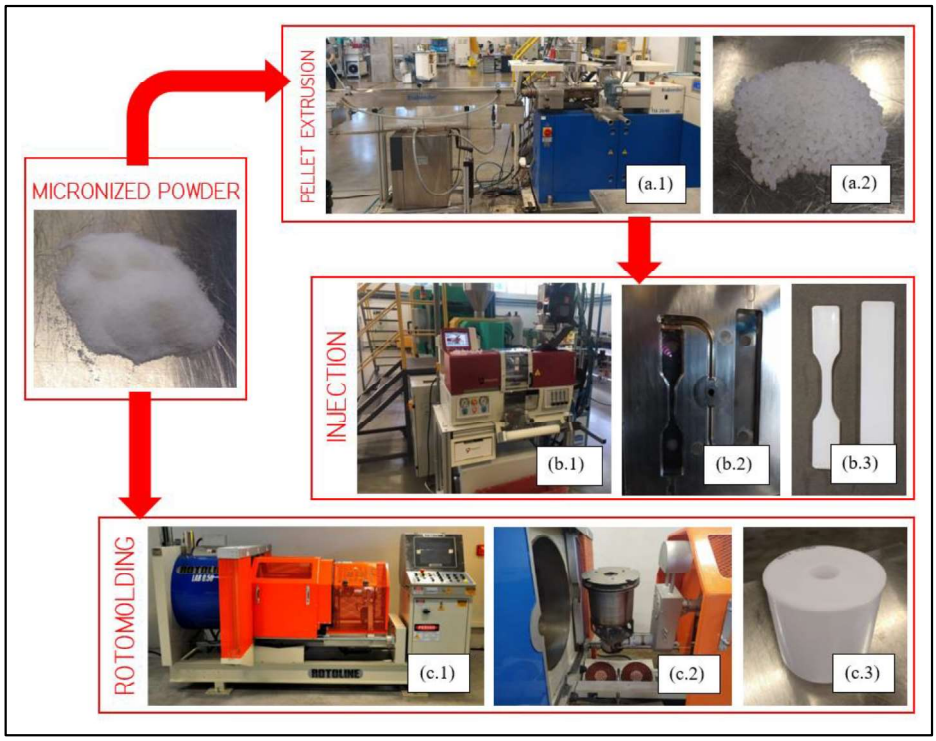

Figure 1 – Production process of HDPE samples

The injection of the test specimens was carried out using a horizontal Babyplast 10/12 injection molding machine (Fig 1–b.1). The test specimens (Fig 1–b.3) were produced in the required dimensions for subsequent testing using specific molds for each test (Fig 1–b.2). The processing conditions are presented in Table 1.

Table 1 – Injection parameters for HDPE samples

Parameters	Impact samples	Tensile samples
Temperatures (°C)		
H1 – Plasticization	190	
H2 – Nozzle	185	
H3 – Nozzle Tip	180	
Metering		
Plasticization speed (%)	60	
Metering volume (mm³)	19	14
Decompression stroke	5	

Injection and pos-injection	
Actual injection pressure (bar)	105
Injection speed (%)	20
Pos-injection pressure (bar)	80
Switch-over volume (mm³)	5
Injection time (s)	4.1
Pos-injection time (s)	6
Times	
Cooling time (s)	18
Cycle time (s)	34.1

For the production of rotomolded samples, a Rotoline LAB 0.50 rotational molding machine (Fig 1–c.1) and a circular mold with dimensions of Ø202 × 200 mm (as shown in Fig 1–c.2) were used. The heating parameters in the rotational molding process, including an oven temperature of 250 °C for 18 min, arm speeds of 4 rpm and 1 rpm, and a reversal time of 5 min. The cooling parameters consisted of an oven time of 16 min and arm speeds of 4 rpm and 1 rpm. After cooling, the vessel-shaped part was removed from the mold (Fig 1–c.3) and machined to extract the test specimens.

Physical and Thermal Characterization of Rotomolded and Injected HDPE

To evaluate the physical and thermal properties, DSC analysis was performed on HDPE samples in pellet, injected, and rotomolded forms. The samples weighing 12 ± 2.65 mg were analyzed using a TA Instruments Q200 instrument under a nitrogen atmosphere. The analysis followed a temperature program consisting of an isothermal hold at 30 °C for 2 min, a heating ramp from 30 °C to 200 °C at a rate of 10 °C/min, and an isothermal hold at 200 °C for 2 min [7].

The obtained data were plotted using the free software TA Universe Analyses, and values for the peak melting temperature (T_{peak}) and melting enthalpy (ΔH_f) were extracted from the resulting graph. The crystallinity index (X_c) was calculated using Eq. 1, where ΔH_f^0 represents the heat of fusion for a hypothetical 100% crystalline polymer (assumed to be 293 J/g) [7].

$$\boldsymbol{X_c}(\%) = \frac{\Delta \boldsymbol{H_f}}{\Delta \boldsymbol{H_f^0}} \boldsymbol{.100} \qquad (1)$$

Scanning electron microscopy (SEM) characterization was performed using a Joel JSM-6010LA microscope to assess the morphology of the processed polymer. Samples taken from the fracture region of the impact test were gold-coated and examined at an approximate magnification of X30, with a working distance (WD) of 12 mm and a voltage of 15 kV.

Mechanical Characterization of Rotomolded and Injected

To assess the mechanical properties, the injected and rotomolded specimens were tested for tensile and impact properties. The tensile test was performed by ASTM D638 standard using Type I specimens. The samples were tested on an Instron universal testing machine using 500 mm/min as displacement rate and a 5 kN load cell. The Izod impact test was conducted in accordance with ASTM D256-10. The test was performed on a Resil Impactor CEAST equipment, using a 4 J hammer for the injected samples and a 2 J hammer for the rotomolded samples. All samples in both testes were conditioned at a temperature of 23 °C and a humidity of 50% for 40 h prior to testing.

Results and Discussion

The DSC analysis results are presented in heat flow versus temperature graphs (Fig 2). It can be observed that the material processing had a slight influence on the material's melting temperature. Although, significant differences were observed in the melting enthalpy values of the rotomolded (an increase of ~20% compared to the HDPE pellets). This probably occurs due to the difference in processing temperatures of each forming method, which enables a better arrangement of the polymer chains as the processing energy increases. This also reflects in the crystallinity indices of the material,

where values of 59.76%, 49.52% and 49.28% were obtained for rotomolded, injected and pellet, respectively. This is a factor of great importance, since the HDPE applications in products probably will be limited since higher levels of crystallinity improve density, stiffness, and temperature-related properties, but reduce impact resistance and transparency [1, 5, 7].

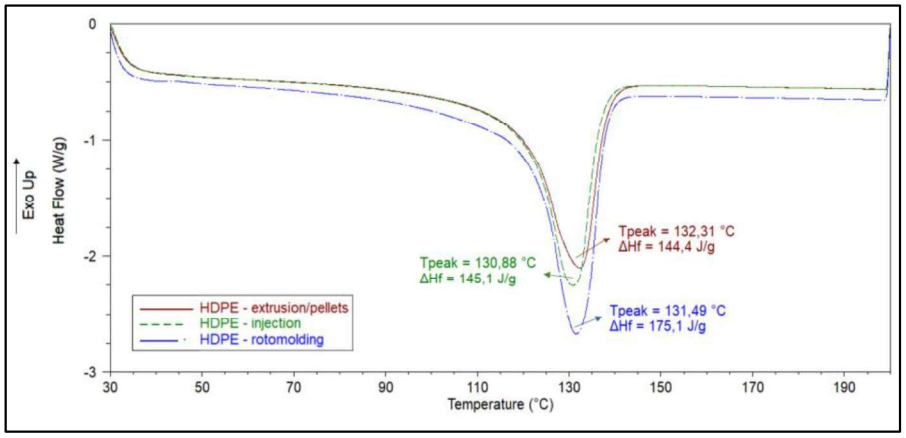

Figura 2 – DSC curves for PEAD pellet (extrusion), PEAD injection and PEAD rotomolding

The tensile test results are presented in Table 2, showcasing notable differences between the rotomolded and injected HDPE samples. The rotomolded HDPE exhibited superior modulus results compared to the injected samples, with an increase of approximately 29%. This finding aligns with the differential scanning calorimetry (DSC) analysis outcomes. Notably, no statistically significant differences were observed in terms of maximum yield stresses and yield deformation. However, the injected polymer displayed higher deformation values at rupture, reaching approximately 550% compared to the rotomolded counterpart. This disparity could be attributed to more void defects in the rotomolded HDPE, primarily due to the absence of pressure application for conformation during the process [5].

Table 2 – Results from Tensile test of HDPE samples

Sample	*Yield stress (MPa)*	*Yield strain (%)*	*Rupture stress (MPa)*	*Rupture strain (%)*	*Young's modulus (MPa)*
Rotomolding	17.97 ± 2.01	9.87 ± 0.72	10.01 ± 1.68	30.61 ± 10.71	647.87 ± 55.21
Injection	16.96 ± 1.08	10.63 ± 0.32	12.23 ± 0.51	196.48 ± 60.38	503.64 ± 41.26

In Fig 3 we can see the results for the Izod impact test (Fig 3a) and post test samples (Fig 3b). Injected samples obtained better results than rotomolded samples (about 62%). That was already expected due to the higher stiffness contents of the rotomolded samples. However, it is worth mentioning that the samples had different behaviors in their rupture. The rotomolded samples showed partial breakage (+ 90% of the total section), while injected samples showed non-breakage (less than 90%). These results can also be related to the possibility of voids in rotomolded samples.

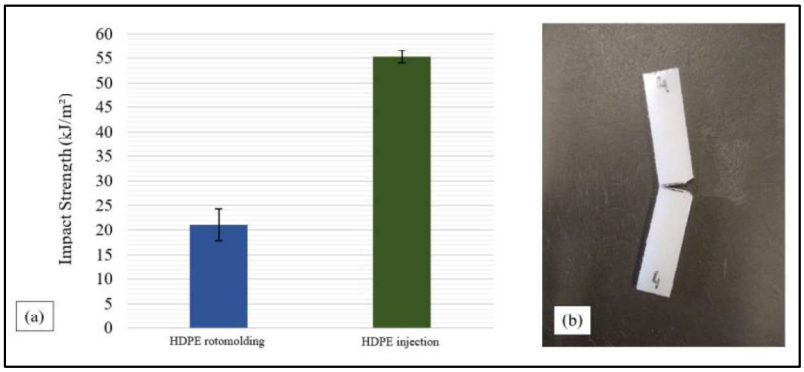

Figure 3 – Graphics from Impact test (a) and samples after test (b)

The impact-fractured samples were subjected to SEM testing, and the corresponding images are displayed in Figure 4. Fig 4a reveals the region's deformation marks (striations), indicating the impact-induced deformation, but no voids are observed. In contrast, the rotomolded sample (Fig 4b) exhibits visible void regions resulting from the processing, which might contribute to the premature fracture of the specimens. The morphology depicted in these images appears to be the primary factor responsible for the lower mechanical properties observed in the rotomolded HDPE samples.

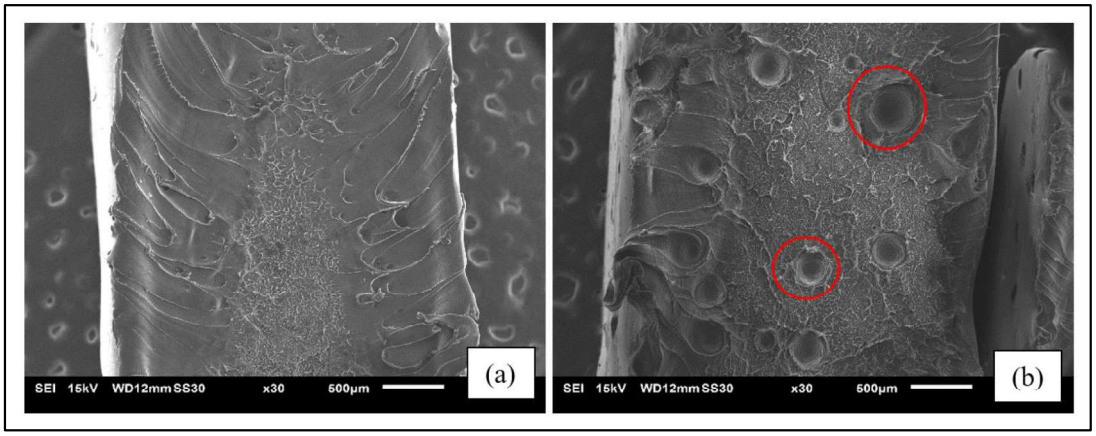

Figure 4 – SEM images from fractured impact samples: (a) injected and (b) rotomolded

Conclusion

This study compared HDPE properties obtained through rotomolding and injection molding. Both techniques had a noticeable impact on the material. Rotomolded HDPE showed higher crystallinity and melting enthalpy, while injected HDPE and pellets differed. Tensile tests indicated that rotomolded HDPE had a higher elasticity modulus, indicating increased stiffness, while injected samples were more ductile. Impact tests showed superior performance in impact resistance for injected HDPE, but void defects were observed in rotomolded samples, potentially affecting their impact performance. These findings emphasize the significant influence of the processing technique on the mechanical properties and morphology of HDPE. They provide valuable insights for selecting the appropriate molding process based on the specific requirements of the desired product.

Acknowledgments

The authors thank FAPERGS (Inova Clusters Tecnológicos n. 22/2551-0000839-9) for financial support.

References

1. F. M. B. Coutinho; I. L. Mello; L. C. de Santa Maria. Polímeros 2003, 13(1), 1 – 13. https://doi.org/10.1590/S0104-14282003000100005.
2. T. Wani; S. A. Q. Pasha; S. Poddar; H. V. Balaji. Internacional Journal of Engineering Research & Tecnology 2020, 9(5), 861 – 864. https://doi.org/ 10.17577/IJERTV9IS050569.
3. Y. Dou; D. Rodrigue. Journal of Cellular Plastics 2022, 58(2), 305 – 323. https://doi.org/10.1177/0021955X211013793.
4. P. L. Ramkumar; D. M. Kulkarni; V. V. Chaudhari. Sãdhanã 2014, 39(3), 625 – 635. http://doi.org/10.1007/s12046-013-0223-4.
5. J. E. A. Posser; M. R. Policena. Revista Liberato 2022, 23(40), 113 – 222. https://doi.org/10.31514/rliberato.2022v23n40.p149.
6. P. K. Kennedy, PhD Thesis, Eindohoven University of Technology, 2008. https://doi.org/10.6100/IR634914.
7. A. V. C. de Araujo; L. C. Scienza; A. L. A. Soares; V. Martins in *Meio Ambiente, Sustentabilidade e Agroecologia*, T. A. Rodrigues; J. Leandro Neto; D. O. Galvão; Atena Editora, 2019, Vol. 6, 43 – 52. https://doi.org/10.22533/at.ed.347191604

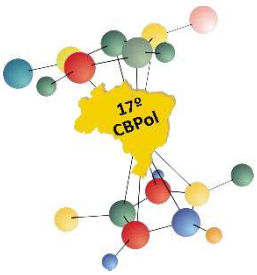

DEPOSITION OF STAINLESS-STEEL FILMS ON EPOXY FIBERGLASS REINFORCED COMPOSITE BY MAGNETRON SPUTTERING

Bruno J. Storgatto[1], Abel A. C. Reeco[2], Daniela Becker[1]

1 – Graduate in Materials Science and Engineering Program, Santa Catarina State University (UDESC), Joinville, SC, Brazil, brunojornada@gmail.com
2 – Physics Department, Santa Catarina State University, UDESC, Joinville, SC, Brazil;

Abstract - With the increasing need for renewable energy sources, Brazil's wind generation has shown significant growth. A wind turbine converts the wind's kinetic energy into torque, converted into electrical energy. This type of generation is susceptible to the effects of weather, such as rain, which generates some damage to the components of the wind turbine. One of these damages is the erosion of the blades; they are manufactured based on epoxy resin reinforced with fiberglass to have high mechanical resistance and low weight. This erosion causes surface defects, increasing drag and reducing generation efficiency and the cost of energy produced. One way to avoid the formation of these defects is to apply a coating that protects the blade material and reduces aerodynamic losses. Therefore, this work will study the application of thin metallic films deposited by the Magnetron Sputtering process on a substrate of polymeric composites based on epoxy resin reinforced with fiberglass taken from a wind turbine blade. This process has already been studied in aeronautical applications, obtaining an increase in the material's application life and reducing maintenance.
Keywords: Magnetron Sputtering, Epoxy composites, thin metallic films

Introduction

The wind turbine generator converts the wind energy by the blade into the rotation, which rotates the rotor of the electric generator, which will convert it into electrical energy. One of the main components of the wind generator is the blade, which corresponds to 15 to 20% of the cost of each generator and is made of polymer composite materials reinforced with fiberglass and/or carbon [1]. Due to its importance, defects can reflect severe damage that may impact the safety of the machine or the efficiency of energy generation is the reason for routine inspections for quality control. Even for a wind generator under normal operating conditions (without ice/snow impact or sand abrasion), it may suffer the effect of erosion by rain [2]. This effect is representative and occurs mainly at the leading edge, as each blade receives the impact of several drops during a rain event amplified by the blade tip's high speed during operating conditions; this effect is known as Leading Edge Erosion (LDE). In this way, it is normal for blades in regular service to suffer a loss of efficiency due to increased roughness generated by wear or erosion by rain [2]. The impact generated by the defect reflects an increase in blade drag and a reduction of aerodynamic efficiency; in a comparison carried out in a wind tunnel, it was possible to measure a reduction of up to 6% in the lifting force and an increase of up to 86% in drag as erosion is more significant in the area and deeper [3]. When simulating erosion level variations in a wind tunnel, it is possible to observe an increase in drag from 6% to 500%, which results in a loss of up to approximately 23% of energy production [4]. It has been studied that increasing surface hardness might be an option for increasing erosion resistance in low-angle impacts and abrasion [5].

An alternative for increasing the surface hardness, and with good adhesion capacity, are the coatings of metallic thin films by the Magnetron Sputtering process. This process can be summarized as a chamber where a vacuum is applied and filled with a gas atmosphere (argon is

generally used), a direct current voltage is applied, one of the poles being on the target (target – material that will be used in the deposition) and the substrate (material to be coated). The applied voltage can ionize the argon into positive ions that bombard the target, pulling electrons from its surface that deposit on the substrate. This methodology has been studied and shown satisfactory results for increasing wear resistance and reducing friction of steel components [6]. In these studies, it is possible to observe that after application, it is possible to increase more than 400% in hardness compared to the initial substrate, maintaining good adhesion and decreasing surface friction [6]. By applying the Magnetron Sputtering, it is possible to control the coating parameters (thickness, number of layers, crystalline structure, and resistance) that increase durability and better adhesion to the substrate [7]. Additionally, by employing pulsed voltage techniques [8] or varying the atmospheric flow rate [9], it is possible to control the crystalline structure and the surface hardness of the coating, showing the versatility of this solution. These results, as previously mentioned, show how promising this technique can be if applied to the leading edges of wind turbine blades to increase the resistance to erosion caused by rain. However, more studies need to be on this technique using substrates made of epoxy resin composites reinforced with fiberglass. So the main objective of this work is to study the application of thin metallic films deposited by the Magnetron Sputtering process on a substrate of polymeric composites based on epoxy resin reinforced with fiberglass taken from a wind turbine blade.

Experimental

Epoxy Composite Fiberglass Reinforced

For this work, samples were taken from the lamination of a wind generator blade produced in Brazil on the cover region and will serve as a reference for thin film application tests. This sample is made of Epikote Resin MGS RIMR035 resin from the manufacturer Hexion, applied by the vacuum infusion method reinforced with fiberglass of the Biax 800 and Biax 450 types.

Magnetron Sputtering Target material

AISI 316L steel was used for the thin film material, this material has in its alloy the element Ni (12%) that stabilizes the steel in the austenite phase even at room temperature, in addition to C (max 0.03%, the denomination L indicates less amount of carbon to facilitate the welding process), Cr (17%) and Mo (2.5%) [10].

Magnetron Sputtering Process

For the application of thin film was applied the Magnetron Sputtering technique is the most indicated given the objective of the work and based on the substrate material studied. Experimental equipment from the Laboratory of Plasma, Films, and Surfaces of the Department of Physics at UDESC will be used. Process parameters will be similar to those applied in work by [11], where the deposition of stainless-steel films on polymeric substrates was studied. The samples were taken from a segment of the wind blade where the materials present consisted only of resin and fiberglass. The samples were sanded using 80, 120, 400, and 600-grit sandpaper for surface standardization. Three different conditions for deposition analysis were configurated, as shown in Tab.1. The process exposure time was defined to obtain the same layer thickness for each process condition and to avoid the sample overheating to avoid polymer degradation.

Table 1 Magnetron Sputtering Conditions applied in this study.

Deposition	Power (W)	Time (minutes)	Sample name
01	100	150	100W_150m
02	200	72	200W_72m
03	300	52	300w_52m

Characterizations Technics: SEM

The coating surface layer morphology were analyzed by Field Emission Scanning Electron Microscopy (FE-SEM), Jeol JSM 6701F model. For the measure the layer thickness, silicon samples were placed next to the epoxy samples during the deposition process. They were broken (exposing the film thickness), and the measurement was performed from the image obtained via SEM and subsequent analysis in the ImageJ software. For the grain size measurement, an analysis of 80 grains of each process was performed and measured using ImageJ software and SEM images.

Results and Discussion

SEM Analysis

The thicknesses were measured at ten points of each sample using ImageJ software and the details of the measures found are in Tab.2. It is observed that the deposition conditions (definition of time and power of the process) were successful since the thicknesses found were very close for the three conditions.

Table 2 Layer Thickness

Sample	Average Thickness µm	Std Deviation µm	Deposition Rate µm/s
100W_150m	1,802	0,017	0,200
200W_72m	1,654	0,018	0,383
300W_52m	1,631	0,008	0,523

Fig.1 shows the SEM image of the 100W_150m sample, in which, in detail A, it is possible to evaluate the region deposited on the epoxy resin and on the fiberglass; the deposition was uniform in the area of the material without the presence of excessive or most evident cracks. This difference in the surface appearance is better observed in Fig.1, detail B. On the polymeric matrix, it is possible to observe a regular surface with a flat formation (highlight 1 of Fig.1B); since there was the exposure of the fiberglass after the preparation of the samples, it is noted that the layer followed the "wavy" form due to the fiber. According to [11] the behavior of most Sputtering coatings copy the surface characteristics (in this case, the form) of the deposited substrate. The study corroborates this effect [12], where the deposition was made on a complex epoxy matrix, and the layer thickness shows that the coating copied the shape of the substrate. In some regions of the interface between the fiber and resin phase, disordered grain growth occurred, possibly due to the surface presented irregularities (highlight 3 of Fig.1B). As observed in the study of [11] and [13], the appearance of cracks occurred both in the application of the film on polymers and metals. It was also noted that the higher the deposition rate, the greater the number of cracks. The lowest deposition rate studied in this paper is 81% higher than that studied by [13], where he observed the beginning of crack formation. Possibly due to this behavior, cracks in the film are also observed, as shown in highlight 4 of Fig.1 B. The appearance of cracks and surface finish is more evident in samples 200W_72m and 300W_52m, where the deposition rate was considerably higher and repeats similar behavior in the work of [11] and [13]. The deposition rate applied on the 200W_72m and 300W_52m samples is 91.5% and 161.5%, respectively, higher than the applied on the 100W_150m sample. Detail of the surface finishing of samples 200W_72m and 300W_52m are shown in Fig.2.

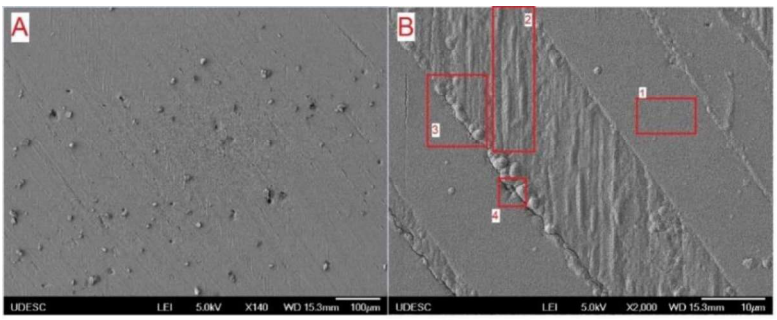

Figure 1 SEM image of 100W_150m sample

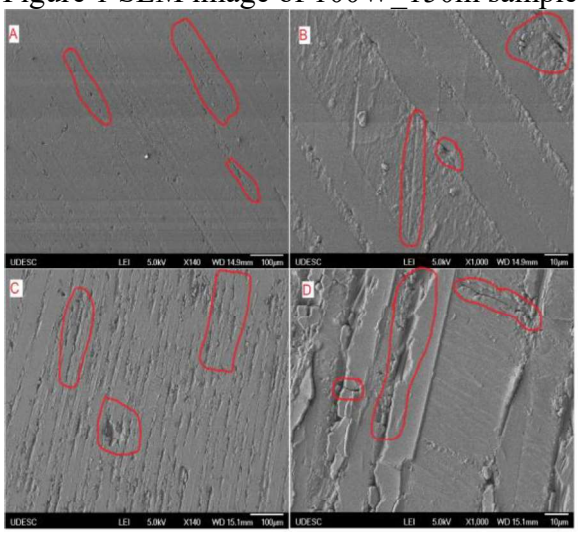

Figure 2 SEM analysis of samples 200W_72m (A & B) and 300W-52m (C & D) samples

The general appearance (separating a region without defects) for the three coatings can be seen in Fig.3. It is possible to observe the formation of columnar grains. For grain size analysis, 80 grains were randomly measured, and the result, as shown in Tab.3. As observed in work by [12], even with the increase in the deposition rate, there was no significant change in grain size.

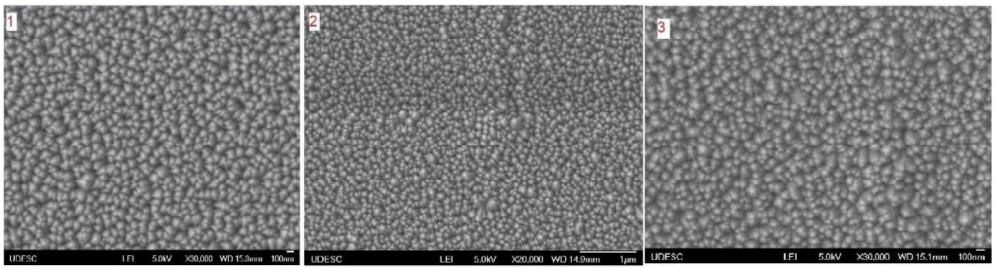

Figure 3 General aspect of the layer deposited using the coating 100W_150m (1), 200W_72m (2) and 300W_52m (3).

Table 3 Grain size of each sample

Sample	Average Size µm	Std Deviation µm
100W_152m	121,52	31,70
200W_72m	129,83	37,10
300W_52m	126,95	35,65

The surface irregularities in the region of the exposed fiber prevented the formation of a thin film in some parts (valleys), as can be seen in Fig.4 . This effect was also studied by [12], where the SEM

images were observed irregularities in the coating of complex shapes due to the position of the target and the substrate.

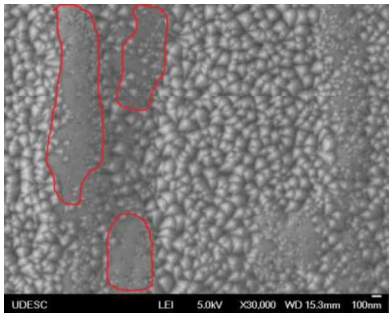

Figure 4 Sample with 100W_150m coating with demarcation of areas where there was no film deposition (region highlighted in red).

Conclusions

In this study, it was possible to show through the analyzes carried out in the SEM that the deposition of thin metallic films can be carried out on a composite substrate made of fiberglass-reinforced polymer (epoxy polymer base). This coating had similar characteristics to other studies with other substrates. It was also evident that factors such as power and speed of deposition are important in controlling surface characteristics. For higher deposition rates (higher power), more significant crack formation and lack of uniformity in the film were observed. Additionally, the variation of these factors did not interfere with forming grains.

References

1. R. Yang; Y. He; H. Zhang Renewable and Sustainable Energy Reviews 2016, 60, http://dx.doi.org/10.1016/j.rser.2016.02.026.
2. J. Chen; J. Wang; A. Ni J. Coat. Technol. Res. 2019, 16, https://doi.org/10.1007/s11998-018-0134-8.
3. N. Gaudern Journal of Physics: Conference Series 2014, 524, 012031, doi:10.1088/1742-6596/524/1/012031.
4. A. Sareen; C. A. Sapre; M. S. Seling Wind Energy 2014, 17, DOI: 10.1002/we.1649.
5. L. M. Jr; Wind Energy 2019, 22, DOI: 10.1002/we.2378.
6. C. L. P. España; A. A. C. Recco; J. J. Olaya Coatings 2018, 8, 381, doi:10.3390/coatings8110381.
7. B. Coto; P. Hallander; L. Mendizabal; F. Pagano; H. Kling; R. Ortiz; J. Barriga; L. Selegard Wear 2021, https://doi.org/10.1016/j.wear.2020.203575.
8. M. V. F. Schroeder; A. A. C. Recco Matéria 2019, 24, 10.1590/S1517-707620190001.0611.
9. C. M. Garzón; G. A. Vergara; A. A. C. Recco Materials Research 2020, 23, e20190453, https://doi.org/10.1590/1980-5373-MR-2019-0453.
10. A. L. V. Silva; P. R. Mei *Aços e Ligas Especiais*, Edgar Blücher, São Paulo, 2006.
11. Rodrigues C. D. Master degree Dissertation, Universidade do Estado de Santa Catarina, 2022.
12. A. R. G. Taormina; C. M. Kurpies; R. Schwaiger; A. M. Hodge Advanced Engineering Materials 2022, 24, 2101264, DOI: 10.1002/adem.202101264.
13. H. Köçkar; N. Kaplan; A. Karpuz; H. Kuru; B. Kaya Journal Of Superconductivity and Novel Magnetism 2019, 32, https://doi.org/10.1007/s10948-018-4968-1.

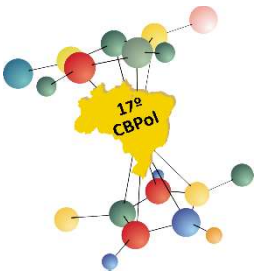

DEVELOPMENT AND IMPROVEMENT OF THE QUALITY OF PULTRUDED COMPONENTS AND INSPECTION REQUIREMENTS

Juliana B. Oliveira[1]*, João V. P. N. Gomes[1], Ricardo Francisco Gouveia[1], Michelle L. Costa[1,2]

1 – Lightweight Structures Laboratory (LEL), Advanced Materials, Instituto de Pesquisas Tecnológicas (IPT), São José dos Campos, SP, Brazil
2- Departamento de Materiais e Tecnologia, Universidade Estadual Paulista (UNESP), Guaratinguetá, SP
julianabovi@ipt.br

Abstract - This work presents the analysis related to the virtual models of pultrusion processing of composites made of fiberglass and phenolic resin. In this process, a comparison was established between the estimated results in the computational modeling with the process in full scale, using data collection, through the use of thermocouples positioned inside the mold, next to the profile in production, with the aid of monitoring equipment during the manufacture of pultruded composites. Then, the quality of the materials produced was evaluated from thermal characterizations by differential scanning calorimetry (DSC) and by thermogravimetric analysis (TGA), non-destructive analysis by ultrasound and mechanical tests of tensile, bending and SBS (short beam strength). These results suggest a promising perspective for the potential contribution of the computational simulation methodology in the quality of manufactured pultruded composites.

Keywords: *composites; pultrusion; fiberglass; phenolic resin; computational modeling; mechanical tests.*

Introduction

Composites are widely used in the aerospace, automobile, maritime, military and power generation industries, mainly due to their high energy absorption capacity, effective acoustic insulation, fire resistance and construction flexibility [1]. The field of application of composites expands as more accessible methods for synthesizing raw materials are discovered. Currently, composite materials are found largely in industrial sectors, covering a large percentage of manufactured materials, that is, unlike a few decades ago, when its application was limited to small artifacts, such as bonnets and front cones of rockets, in the current decade the fuselage and wings of aircraft are completely produced from composites reinforced with high-performance fibers [2,3]. In this way, the inherent high specific mechanical strength, low density, as well as chemical and corrosion resistance make them ideal for future applications [3]. However, to obtain the properties mentioned above, it is important to know the parameters that influence the manufacturing process of these materials, which can affect their performance. Such parameters include defects such as microcracks, voids, low adherence of the interface between reinforcement and matrix, among others, which may promote premature failure of the components. Therefore, through the use of numerical models, it is possible to evaluate similar influences in the production of composites and try to avoid them [4-6].

Composite materials can be manufactured in different ways, however, the focus in this work will be on the manufacture of composites via the pultrusion process. The pultrusion process is a continuous and automated manufacturing method for uniform section products, in composite materials, polyester, phenolic, vinyl ester resins among others, reinforced with fiberglass, aramid or carbon fiber. Fiberglass is the most common reinforcement, the most commonly used formats being thread, blanket and fabric. For a better understanding of the process, a comparison can be made with the extrusion of thermoplastic materials. While in the extrusion process the materials are heated and

"pushed" through a mold and the profile is cooled down to its final solid form, in pultrusion the materials are "pulled" through the mold and their cooling occurs in this same process. [7].

According to results presented by [5], which analyzed the pultrusion process by computer simulation, the presence of residual stresses and distortions, negatively affect the structural and geometric properties of the components. According to the author, residual stresses can, depending on their magnitude, produce cracks and microcracks during curing in polymeric composites. As considered by [8], several studies carried out by [4,5], also consider the thermochemical properties of composites for the development of experimental studies and numerical modeling of the curing process, in addition to variables such as the temperature along the profile section, the process speed and the component's degree of curing.

Experimental

Production of pultruded composites

To carry out the pultrusion process, as a starting material for the production of composites, TEX 4400 rovings and blanket made of chopped fiber with a grammage of 300 g/m^2, both made fiberglass, were used. The resin used was Resafen® P3394L/I2012L phenolic resin. As recommended by the supplier in its technical bulletin, the resin formulation for the composite was carried out considering the composition of 62% Resafen P 3394 L, 15% Resafen I 2012 L, 1.5% calcium stearate, 8% alumina, 12% industrial talc and 1.5% release agent. The materials previously shown were incorporated into the bicomponent resin with the aid of a rod associated with a "cowles" type disperser, coupled to the shaft of a rotational electric motor, both adapted in LEL/IPT (Lightweight Structures Laboratory). The CSI40-PE S-LI polyester veil was also used in the profile produced.

Pultruded composites were produced with dimensions of 200 mm width and 4 mm thickness (Fig 1), with operating speed of 140 mm/min, monitored by a rotational sensor present in the equipment, in contact with the surface of the pultreded during its advance. The temperatures of the thermal zones, present in the mold used, were maintained symmetrically, respectively from the beginning to the end of the mold, at 70 °C, 100 °C and 180 °C.

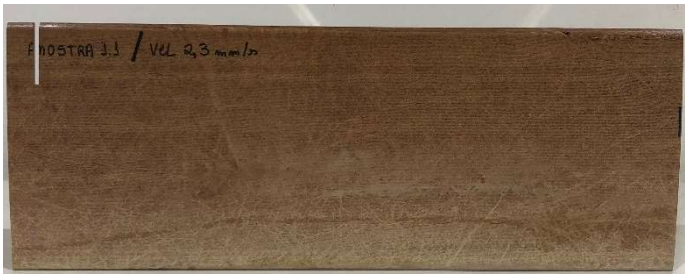

Figure 1 – Pultruded composite, manufactured at LEL/IPT.

Virtual planning of experiments and correlation with the production environment

Based on the data on the properties of the phenolic resin used, the fiberglass and the manufactured composites, such as: density, specific heat and thermal conductivity, in addition to the results of thermal analysis by DSC of the polymer (to verify the curing temperature of the phenolic resin), refinement of the virtual modeling of the pultrusion process was performed.

The comparison between the estimated results in a virtual environment and the real process was carried out through the evaluation of the temperature pultruded estimated in the computational modeling and the data collected experimentally, introducing thermocouples next to the material inside the mold, in the central region of the pultruded, with the aid of monitoring equipment during the processing of the composite.

Thermal analysis, ultrasonic non-destructive testing and mechanical characterizations

To verify and establish process operating temperature limits, TGA analyzes were performed to determine the degradation temperature of the phenolic resin used. The parameters used were: sample weight of 10mg; heating rate 10°C/min, N_2 atmosphere at 100 mL/min in platinum sample holder. DSC analyzes were carried out to observe the presence or not of residual curing in the produced composites. The parameters used were: sample mass 10mg; aluminum hermetic sample holder; heating rate of 10°C/min in N_2 at 50 mL/min.

To evaluate the quality of the processed composites, acoustic inspection tests by ultrasound, SBS [11], tensile [12] and bending [13] were carried out. With 5 samples being tested in each mechanical test.

Results and Discussion

The results evaluation of the virtual model and its comparison with the temperature data obtained during the processing of the material via pultrusion are shown in Fig 2, where the dotted line, in blue, refers to the temperature curve obtained virtually and the curves in red and green correspond to data acquired experimentally.

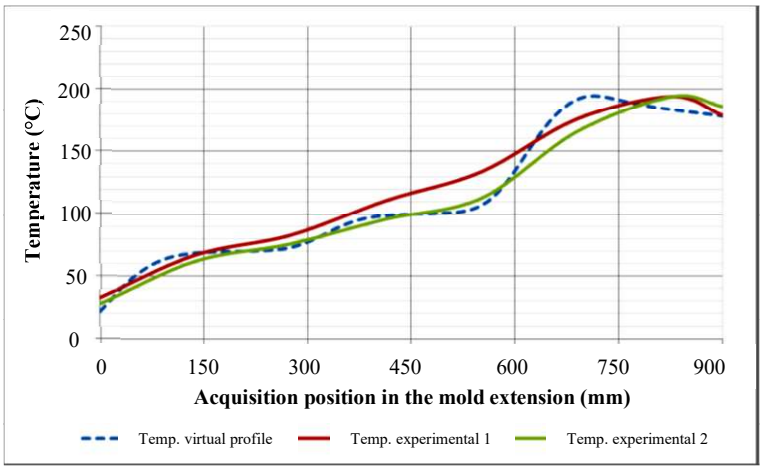

Figure 2 – Comparative result of the temperature pultruded evaluated in a numerical model and in two temperature acquisitions inside the tool.

Due to the proximity observed in the results of the analysis above, between the experimental data and that obtained by the virtual method, this can be considered a promising result that could, with the evolution of the method, safely support the companies in the sector, in the search for optimization of their production parameters to contribute to the final quality of their products.

From the TGA analyzes of both the phenolic resin and the pultruded composite, it can be concluded that during the processing via pultrusion of the materials, temperatures of up to 240 °C did not cause profile degradation problems, which, if it did, would compromise the quality of the manufactured pultruded.

The DSC curve of the manufactured pultruded did not show exothermic peaks, indicating that there is no residual cure in the fiberglass/phenolic resin composite sample, as expected by the results of the virtual model. At least two endothermic peaks are observed from 250 °C, superimposed on an exothermic peak, indicating thermal decomposition of the polymeric matrix (which can be confirmed by the result presented in the TGA analysis).

In Fig 3, the result obtained by ultrasound analysis is shown, this image being representative of the quality standard of the pultruded produced. In the analysis of the results below, the tonality uniformity of the material was evaluated, seeking to reach higher attenuation percentages (in red in the color scale). This scale uniformity can be considered as an indication of material uniformity, since regions with polymer consolidation variations, for example, would return signals of distinct attenuations varying between the blue and red scales throughout the analysis.

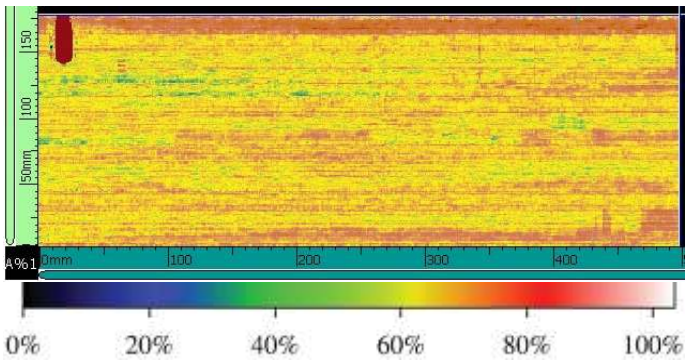

Figure 3 – C-scan ultrasound map for the pultruded composite.

In Fig 3, it was possible to verify that the processed material presented homogeneity throughout its extension, since in the analysis carried out, the yellowish color observed above, remained constant throughout the material, possibly indicating a high impregnation of the reinforcement in the matrix and a reduced presence of voids.

Table 1 shows the results of the mechanical characterizations performed. Just as a reference, the values of the mechanical properties present in the ABNT 15708-5 and ACMA (2010) [9,10] standards were also included in this table. It should be noted that the property limits established by the standards mentioned above, are for informational purposes only, not being the objective of this work the fulfillment of these requirements, as these are achieved through specific design of structural pultruded.

Table 1 – Results of mechanical characterizations by SBS, tensile and bending of pultruded

	*A (MPa)	*B (MPa)	*C (GPa)	*D (MPa)	*E (GPa)	*F (MPa)	*G (GPa)	*H (MPa)	*I (GPa)
Results	34.04	399.92	30.22	15.74	4.25	474.06	21.31	47.50	6.21
Standard deviation	0.54	12.54	1.17	0.29	0.17	24.93	0.59	4.62	0.32
Coefficient of variation	2%	3%	4%	2%	4%	5%	3	10%	5
ABNT 15708 E17 [9]	15	170	17	30	5	170	-	70	-
ABNT 15708 E23 [9]	25	240	23	50	7	240	-	100	-
Ref ACMA [10]	24.13	137.90	12.40	48.30	4.8	206.85	11.03	89.60	6.20

***Notes:** A is the interlaminar shear strength; B and D are the maximum tensile strength, in the axial and transverse fiber directions, respectively; C and E are the tensile elastic modulus, in the axial and transverse fiber directions, respectively; F and H are the maximum bending strength, in the axial and transversal fiber directions, respectively; G and I are the elastic modulus to bending, in the axial and transversal fiber directions, respectively.

The results of the mechanical characterizations demonstrated the ability of the processed material to meet the mechanical properties established within the limits of ABNT 15708-5 and ACMA [9,10]. Although the pultruded evaluated in the work was not constituted in order to achieve these goals, aiming to safeguard the process comparison factor established in this study, most of the samples bordered or exceeded the limits required by the standards.

Conclusions

The results of the non-destructive ultrasound inspection analyze showed good correlation with the low standard deviation values presented in Table 1, for most samples, after the mechanical characterizations made in the fiberglass and phenolic resin composites, indicating that the

manufactured material showed good homogeneity throughout its length (which can be verified by the result presented in the ultrasound analysis).

Already the virtual model pultrusion processing, associated with thermal characterizations of differential scanning calorimetry (DSC) and thermogravimetry (TGA), proved to be a valuable tool to address adequate processing parameters of pultruded composites, depending on the raw material used, allowing a better understanding of safe operating temperatures, the curing kinetics of the material employed, and the specific characteristics of each production line used for the manufacture of pultruded materials.

Acknowledgements

The authors are grateful for Petrobras and National Council for Scientific and Technological Development (CNPq) (304876/2020-8).

References

1. S. Sikdar; W. Ostachowicz. Polymer Testing, 2019, v. 73, p. 31-38. https://doi.org/10.1016/j.polymertesting.2018.11.011.
2. P. Taynton *et al*. Polymer Chemistry, 2016, v. 7, p. 7052-7056. https://doi.org/10.1039/c6py01395c.
3. P. S. Owuor *et al*. Reinforced Plastics, 2018, v. 62, p. 263-265. https://doi.org/10.1016/j.repl.2017.07.005.
4. I. Baran; J. Hattel; R. Akkerman; C. Tutum. Composite Materials, 2015, v. 22, p. 99-118 https://doi.org/10.1007/s10443-014-9394-3.
5. I. Baran; K. Cinar; N. Ersoy; R. Akkerman; J. Hattel Architecture Computational Methods Eng, 2017, v. 24, p. 365-395. https://doi.org/10.1007/s11831-016-9167-2.
6. L. S. Santos, Mater's Degree. Dissertation, Federal University of Rio de Janeiro, 2009.
7. M. B. Hennemann; C. R. Silva; E. L. Schneider. Revista Tecnologia e Tendências, 2019, a. 10, n. 1, p 132-149. https://doi.org/10.25112/rt&t.v10i1.1501.
8. A. Safanov; P. Carlone; I. Akhatov. Composite Structures, 2018, v. 184, p. 153-177.
9. ABNT 15708-5: Indústrias do petróleo e gás natural - Perfis pultrudados - Parte 5: Perfis estruturais, 2011.
10. AMERICAN COMPOSITES MANUFACTURERS ASSOCIATION (ACMA), PreStandard for Load & Resistance Factor Design (LRFD) of Pultruded Fiber Reinforced Polymer (FRP) Structures (Final), 2010.
11. AMERICAN SOCIETY FOR TESTING AND MATERIALS (ASTM). ASTM D2344/D 2344M-00: Standard Test Method for Short-Beam Strength of Polymer Matrix Composite Materials and Their Laminates. West Conshohocken, p. 8, 2016.
12. AMERICAN SOCIETY FOR TESTING AND MATERIALS (ASTM), ASTM D3039/D 3039M–00: Standard Test Method for Tensile Properties of Polymer Matrix Composite Materials. West Conshohocken, p. 13, 2014.
13. INTERNATIONAL STANDARDS ORGANIZATION (ISO), ISO 14125: Fibre-reinforced plastic composites — Determination of flexural properties. p. 19, 1998.

EFFECT OF FILLING PERCENTAGE ON THE TENSILE STRENGTH OF PARTS PRINTED BY FDM

Luana B. Concatto[1], MSc Eliane N. Mota[2], Dra Carmen I. W. Calcagno[3]

1 – Products and Materials Integrated Development Laboratory (DIMP), Federal Institute Sul-Riograndense (IFSUL), Sapucaia do Sul, RS, Brazil carmencalcagno@ifsul.edu.br

Abstract - Nowadays, it is necessary to understand new technologies that meet consumer demand for personalized products, considering that the development of rapid prototyping for companies as well as the use of 3D printers is gaining more space. In this context, this work aimed to study the influence of filling percentage on the tensile strength of parts obtained by FDM. Parts designed in CAD were printed in PLA, with different filling percentages (25%, 50%, 75%). The results of the stress test were analyzed and compared. The concentric-style parts showed superior tensile strength against the line styles, with a 20.4% increase in maximum stress when the filling was 75%. Despite the observed influence on tensile strength, the maximum strain was the same in all tested conditions. It was concluded that the parts manufactured with the concentric filling presented better performance, resulting in greater tensile strength in a shorter production time.
Keywords: *Fused Deposition Modeling, Tensile Strength, Filling, 3D Printing.*

Introduction

The growing demand for new products, along with the need for customization, has led companies to develop new technologies that meet customer demand, meeting quickness and quality requirements in the manufacture of products. To meet the needs of the market, additive manufacturing, known as 3D printing, has been gaining more and more space, being one of the technologies of Industry 4.0.

The FDM (Fused Deposition Modeling) technique is one of the additive manufacturing techniques where the molten material is deposited layer by layer, being a low-cost alternative that brings accuracy to the prototyping of complex geometries [1,2].

Additive manufacturing using the FDM technique uses different process parameters to produce parts, such as extrusion temperature, layer orientation, and filling percentage [3]. Material properties can change according to the parameters used at the time of printing, and studies suggest that the way layers get deposited influences the strength of the material, and with "smart deposition" strength and toughness can be improved [4,5]. Thus, for example, a study showed that the selected parameters could influence the resistance of the material, such as printing orientation, extruder nozzle diameter, and filling density, and with 100% filling parts resisted traction of 60.29MPa and the change to 80% filling caused a low decrease in resistance, going down to 58.44MPa, which represents good mechanical performance, associated with a shorter printing time and lower consumption of material [6].

The style of filament used also influences the resistance of the part and, for example, a comparative study showed that parts produced with a 30% filling of the grid style in Poly (lactic acid) - PLA were more resistant to traction than the parts of Polycaprolactone (PCL), whose average tensions were 41.20MPa and 9.68MPa, respectively [7].

With the modernization of 3D printers, it is possible to choose between different styles of filling, and studies have shown that the tensile strength changes depending on the style of filling [8, 9]. A theoretical study indicates that concentric, zigzag, and line fill styles tend to be more resistant to tensile stresses [10].

In this context, this work aimed to study the effect of the influence of filling percentage on the tensile strength of parts obtained by FDM from two styles of fillings: line and concentric.

Experimental

The parts were designed in SolidWorks, in the dimensions of the specimen type I of ASTM D638-14. To analyze and configure the possibilities of FDM printing, it was used the Ultimaker's Cura slicing software. The printing parameters used are presented in Table 1. The parts were produced in PLA (1.75mm diameter, 3DLAB) with two styles of fillings, line and concentric, using different percentages of filling, 25%, 50% and 75%. The printer used was an Ender model 5.

Table 1. Parameters for printing specimens

Printing Parameters	
Extrusion temperature	200°C
Bed temperature	50°C
Printing speed	80 mm/s
Extruder nozzle diameter	0,4 mm
Wall thickness	0,8 mm

The mass, width, and thickness of the printed parts were individually measured, whose averages were compared to each other and the one designed. The tensile tests were carried out following ASTM D638-14, using 8 specimens, in an Instron Universal Testing Machine, from the Quality Control and Characterization Laboratory of the IFSUL campus Sapucaia do Sul. Test speed is set as 2 mm/min with a 30kN load cell. The resulting maximum tension and maximum elongation results were compared by ANOVA, with a confidence level of 95%.

Results and Discussion

This study tested the tensile strength of parts manufactured with line and concentric filling styles using three different filling percentages (25%, 50%, and 75%). Fill styles were selected from another study, where line, concentric, and zigzag style fills had the largest cross-sectional areas, so line and concentric style was chosen for the study, taking into account the shortest printing times [7]. The parts were printed separately, with an average time of 42 minutes and 39 minutes for the line and concentric styles, respectively. Table 2 presents the data of the printed parts.

Table 2. Dimensional results of printings and tensile strength test.

	Lines			Concentric		
	75%	**50%**	**25%**	**75%**	**50%**	**25%**
Time (min)	46	43	39	42	39	36
Mass 1 (g) *	9^{a}	8^{b}	7^{c}	9^{a}	8^{b}	7^{c}
Mass 2 (g)**	8,4 +/- $0,1^{d,f}$	7,2 +/- $0,3^{e,g}$	6,7 +/- $0,6^{e,h}$	8,3 +/- $0,2^{d,f}$	7,3 +/- $0,1^{e,g}$	6,1 +/- $0,2^{e,h}$
Width (mm)	13,1 +/- $0,1^{i}$	13,0 +/- $0,0^{j,l}$	13,0 +/- $0,1^{j,m}$	12,9 +/- $0,0^{k}$	12,9 +/- $0,0^{l,k}$	13,0 +/- $0,1^{m,k}$
Thickness (mm)	3,3 +/- $0,1^{n}$	3,4 +/- $0,1^{o,q}$	3,4 +/- $0,1^{o,r}$	3,4 +/- $0,1^{p}$	3,4 +/- $0,1^{p,q}$	3,4 +/- $0,1^{p,r}$
Tension (Mpa)	25,0 +/- $2,2^{s}$	18,6 +/- $2,1^{t,w}$	17,9 +/- $1,5^{t}$	30,1 +/- $1,1^{u}$	24,6 +/- $2,4^{v}$	18,6 +/- $2,2^{x,w}$
Strain (%)	7,9 +/- $0,9^{y}$	8,1 +/- $1,2^{y}$	7,2 +/- $1,4^{y}$	8,4 +/- $1,5^{y}$	9,0 +/- $1,1^{y}$	9,1 +/- $2,0^{y}$

* Mass 1 represents the masses estimated by the slicing software, and mass 2 represents the masses of the printed parts.
** Different superscripts represent significantly different results (ANOVA Factor, $p < 0.05$).

Table 2 presents the printing time in each tested condition and the average mass, width and thickness values. Parts printed with the line style took, on average, 4 minutes longer to print than the concentric style parts, which represents an increase of at least 8% in printing time. Line-style parts, with filling less than or equal to 50%, statistically had the same width and thickness, with averages of 13.0 ± 0.08 mm and 3.4 ± 0.08 mm, respectively. On the other hand, the widths and thicknesses of the concentric style parts are statistically equal, regardless of the filling percentage.

Line-style printed parts with filling of 50% and 25% obtained statistically the same mass, being 6.9 ± 0.5g, while those with filling of 75% obtained 16.6% more mass. The concentric parts differed in the three percentages of filling tested, the parts with filling of 75% had an average of 8.3 ± 0.2g, and those with filling of 25% filling had 36% less mass in the printed parts. When the comparisons were made between the same percentages of filling (for example, 75% line versus 75% concentric), the parts had statistically the same mass. And even when compared with the masses estimated by the slicing software, the actual masses were, on average, 0.6g smaller for the line style and 0.8g smaller for the concentric style. Figure 1 presents the graphs of stress versus strain that best represent the observed averages.

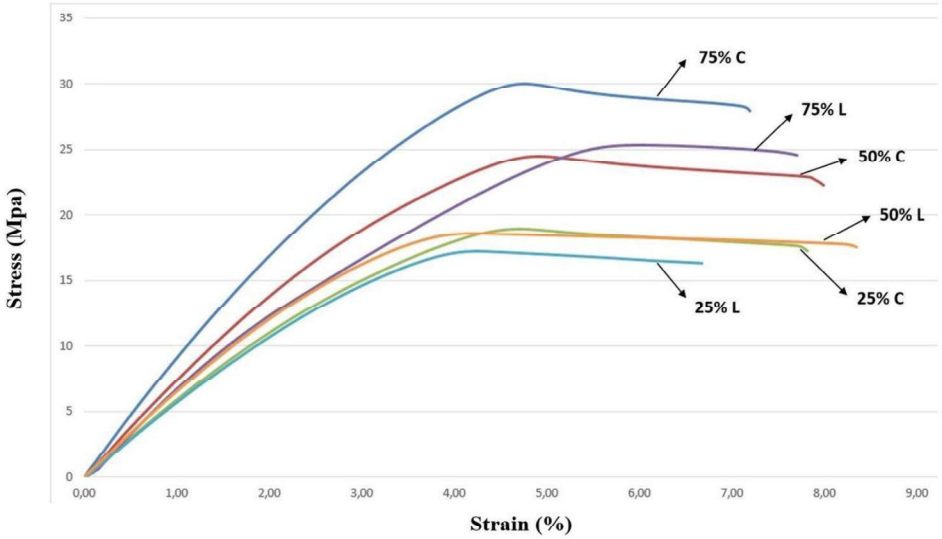

Figure 1: Stress versus strain graph, where C represents concentric, and L represents lines.

In the parts manufactured with line-style filling, it was identified that the samples with a percentage lower than or equal to 50% resulted in the same maximum stress, with an average of 18.3 ± 0.5 MPa. When the fill factor was 75%, the observed strength was 25.0 ± 2.2 MPa, representing a 38.8% increase in maximum stress.

In the parts manufactured with concentric filling, the maximum stress values were different for the three evaluated percentages of the fillings, being 30.1 ± 1.1MPa for filling of 75%, 24.6 ± 2.4 MPa for 50%, and 18.6 ± 2.2 MPa for parts manufactured with the filling of 25%.

When comparing the parts produced with filling of 75%, both lines and the concentric styles had the same mass (8.3 ± 0.2g per piece) and, in both situations, a higher density resulted in greater resistance, considering that for the concentric style an increase of 61.8% was identified in relation to the parts with lower density (25%), while for the lines style it was an increase of 36.6% in comparison with the ones with lower density (25%). For all manufacturing conditions tested, elongation was statistically equal and remained at 8.3 ± 1.5%.

Comparing the results of the two styles of filling, the concentric presented superior resistance compared to the lines, with a 20.4% increase in the maximum stress in the parts with filling of 75% compared to those with the same filling of the line style.

Comparing the parts manufactured with concentric and line fillings (filling of 50%) it was observed that the first style presented a maximum stress 34.4% higher, showing a better performance in the parts manufactured with this filling style. Also, the tensile strength of the pieces with filling of 25% of the concentric style is statistically equal to the resistance of the parts with filling of 50% of the line style.

Conclusions

After analyzed carried out, it was possible to conclude that the parts printed by FDM, with concentric filling obtained better results compared to the parts of the line-style. Since, the concentric-style parts with 25% filling obtained tensile strength results equal to the line-style parts with 50% filling.

Even when analyzing the masses of each filling percentage, statistically, the concentric-style parts with 75% filling obtained the same mass as the line-style parts with the same filling percentage, but with superior tensile strength, being 20.4% more resistant.

It is concluded that concentric-style parts, in addition to being more resistant and having the same mass as the line-style parts, are faster to print and with less material, reach higher resistance values, thus generating savings throughout the process.

Acknowledgements

PROPESP – IFSUL and FAPERGS.

References

1. B. J. B. Martínez; et. al. Enfoque UTE 2019, V.10. N.3, p. 13-29. http://ingenieria.ute.edu.ec/enfoqueute/e-ISSN: 1390-6542 / p-ISSN: 1390-9363.
2. R. B. Kristiawan; et. al. Open Engineering 2021; 11: 639–649.
3. S. Maidin; et. Al. Jurnal Teknologi (Sciences & Engineering) 2022, p. 133–141. https://doi.org/10.11113/jurnalteknologi.v84.17802.
4. P. Lanzillotti et al. IFAC Papers OnLine 2018, p. 1353–1358.
5. S. Wang; et. al. Polymer Testing 2020, 106483. https://doi.org/10.1016/j.polymertesting.2020.106483.
6. M. Hikmat; S. Rostam; Y. M. Ahmed. Results in Engineering 2021, 11, 100264. https://doi.org/10.1016/j.rineng.2021.100264.
7. J. Z. P. Agudelo; C. N. Tovar. Iteckne 2019, V. 16, N. 2, P. 117-117. https://doi.org/10.15332/iteckne.v16i2.2354
8. J. Giri; et al. Materials Today: Proceedings 2021, V.47, P. 5856-5861. https://doi.org/10.1016/j.matpr.2021.04.2838
9. V. Cabreira. Dissertation. Federal University of Rio Grande do Sul 2018.
10. M. A. T. Mattos. Monography. Federal Institute Sul-Riograndense (IFSUL) 2021.

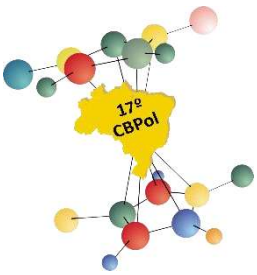

EFFECT OF ULTRA HIGH MOLAR MASS POLYETHYLENE (UHMWPE) ON HIGH DENSITY POLYETHYLENE (HDPE) PROCESS PARAMETERS

Ryan F. dos Santos[1], Luziany G. da Nóbrega[1], Gabriel C. G. Duarte[2], Maria Edvania de A. Lima[2], Fabiana de C. Fim[1,2], Lucineide B. da Silva[1,2*]

1 - Graduate Program in Materials Science and Engineering (PPCEM), Federal University of Paraiba (UFPB), João Pessoa, PB, Brazil

2 – Department of Materials Engineering (DEMAT), Federal University of Paraiba (UFPB), João Pessoa, PB, Brazil

lucineide@ct.ufpb.br

Abstract - High density polyethylene (HDPE) and ultra high molecular mass polyethylene (UHMWPE) blends were mixed at concentrations of 100/0, 90/10, 70/30, all containing 1% Irganox Antioxidant. In this study, it was possible to evaluate torque and torque stabilization temperature as a function of time during mixing in the Torque Rheometer, with speed varying from 20 to 40 RPM. It was found that for the highest speed, the initial torque as a function of time of the 70/30 blend was lower than that of the 90/10 blend, but also increased with time. The molecular orientation of the polymer chains may have had some effect on this result. Furthermore, the higher content of UHMWPE in the blends made the processability of HDPE more difficult due to the increase in torque during the homogenization phase of the melt, requiring a higher temperature.

Keywords: *Torque rheometer; UHMWPE; HDPE.*

Introduction

In several industrial applications, high density polyethylene (HDPE) has been used due to its good mechanical properties, characteristics of easy manufacture, being considered one of the most important and durable polyethylenes. This is due to its physical and chemical resistance. The advantages over other polyethylenes are in terms of more uses and applications. Its molecular structure, different from others, consists of molecules with little branching, with few flaws, and this determines its linearity [1,2].

On the other hand, ultra-high molecular weight polyethylene (UHMWPE) is considered an engineering polymer. This is due to its excellent mechanical properties, such as toughness. It is a general-purpose tough material, and its interest in the industry is growing. The molecular structure of UHMWPE differs from that of HDPE, whose polymer chains are much longer than those of other types of polyethylene (PE). As a consequence, certain properties of UHMWPE are better than other types of PE, such as high abrasion resistance, high chemical resistance, good mechanical properties and flexibility, and it is sometimes considered as engineering plastic [3].

Regarding the equipment used in this research, the Haake torque rheometer has the function of mixing the polymers, providing relevant data for the process [4-6]. It consists of a heated chamber in the shape of a figure eight, with two internal rotors in the shape of semi-threads, leaving a free volume of 50g of material for mixing. For this purpose, elements are needed that conduct precise speed measurement and torque monitoring (precise torque sensor). All this information is required to process the material properly. Data from this equipment can be used in process modeling [7]. Process parameters, including rheological properties, can be inferred from changes in torque over time, reflecting changes in material viscosity during the mixing process [5,6].

The general objective of this article is to determine the process parameters of HDPE/UHMWPE blends with two concentrations using the torque rheometer, varying rotation speeds to verify the effect of UHMWPE on HDPE process parameters.

Experimental

Materials

Ultra-high molecular weight polyethylene (UHMWPE) commercial powder (UTEC batch 3041) and High Density Polyethylene (HDPE) IA58 (Braskem/Brazil) and Irganox antioxidant (Sigma-Aldrich/Brazil).

Processing of blends in a Torque Rheometer

It was carried out in a PolyLab OS - Thermo Scientific torque rheometer, with the operation of roller-type rotors and with a rotation speed of 20, 30 and 40 rpm, under a temperature of 190 °C, all lasting 10 minutes and with air atmosphere. The mixing chamber mass was held constant at 50g for all samples in this work. For each rotation, triplicates were made to verify the parameters accurately. The compositions of the blends were calculated in percentage by weight, being 100/0, 90/10, 70/30, named by HDPE, UH10 and UH30, respectively. All samples containing 1% Irganox Antioxidant. Before mixing, the samples were dried in an oven at 70°C for 24 hours.

Fluidity Index Measurement (FIM)

According to the ASTM D 1238 standard, it was possible to obtain the fluidity index. In this analysis, five grams of each sample were used. The parameters used were: temperature of 190 °C and load of 2.16 kg. The plastometer used was Melt Flow MODULAS LINE from CEAST.

Results and Discussion

Torque Analysis

The torque is said to be directly proportional to the viscosity of the polymer under analysis in the torque rheometer [8]. Table 1 shows that when evaluating the HDPE at different rotations, the initial torque to melt the polymer increased with the rotation up to 30 RPM, while it decreased at the rotation of 40 RPM, certainly the higher shear rate for this rotation may have contributed to this reduction. With the course of the test time up to 10 min, practically for all the rotations studied, no changes were observed in the torques at steady state. The blend with 10% UH from the rotation of 30 RPM showed values of initial torques close to each other. For all investigated rotations, the initial torques for the blend with 30% UH were lower than the values for pure HDPE and the blend with 10%. However, specifically for the 30% UH content, over time, the torque increased, not reaching steady state in the time established in the experiment. According to Lim et al. [9], the HDPE blend with 50% UHMWPE content only reached melting and stabilization in a time of 20 min. The effect of reducing the initial torque of the blends can be suggested as a possible slippage of the UH powder between the HDPE chains, reducing its viscosity due to the physical effect, since this polymer does not melt at the HDPE processing temperature. The steady state torque increased over time for the 30% blend, being greater with increasing rotation, which could be due to the possible molecular orientation of the polymeric chains of the UH embedded in the HDPE, implying in more difficult processability with the increase in viscosity.

Table 1: Values of initial and steady state torques for HDPE and blends.

	Initial torque (N.m)			Steady state torque (N.m)		
Sample	20 RPM	30 RPM	40 RPM	20 RPM	30 RPM	40 RPM
HDPE	57,90± 2,01	63,54 ± 4,74	58,84 ± 2,13	7,1± 0,20	7,52 ±0,42	8,74±0,35
UH10	52,42± 3,35	56,42 ±4,31	56,43 ±1,87	4,87± 0,52	5,39 ± 0,52	6,89 ±0,57
UH30	47,81± 7,29	55,39 ± 0,38	55,38 ± 6,38	8,21±0,56	9,11 ± 0,63	12,41± 0,61

Melt Homogenization Temperature Analysis

Table 2 shows the temperature values at the stationary torque of the samples for the different speeds. HDPE and blend temperatures increased with rotation and blend composition. For the speed of 20 RPM, it can be seen in Table 2 that there was a slight variation in temperature between the blends. However, at the rotation of 40 RPM, this temperature variation increased when comparing the HDPE and the UH10 blend with the UH30 blend. The greater temperature variation, with the greater rotation is reflected in a greater mechanical work to homogenize the blends.

Table 2: Torque stabilization temperature of the blends.

	20 RPM	**30 RPM**	**40 RPM**
HDPE	199,98±0,922	201,81±0,044	203,34±2,08
UH10	200,51±0,044	202,47±0,044	204,43±0,031
UH30	203,67±0,054	208,46±0,063	214,24±0,031

Fluidity Index Analysis (FI)

Table 3 presents the results of the fluidity index measurements of the analyzed samples. Analysis of the fluidity of the samples showed that the addition of UHMWPE to the HDPE impacted its fluidity, making it impossible to flow into the blend composition with a higher content of ultra high molecular weight polymer. This result suggests that a lubricant can act by separating the chains, improving the sliding and flow of macromolecules over each other. Therefore, for these samples, the most appropriate type of processing would be compression molding according to Silva, J. M. D., et al. [10].

Table 3: Fluidity Index Measurement for HDPE and blends.

Samples	FIM
HDPE	6,96±0,33
UH10	3,93±0,11
UH30	-

Conclusions

Blends of pure HDPE and UHMWPE, with 2 different percentages, were evaluated through process parameters using a torque rheometer. The rotation and the UHMWPE content had an effect on the processability of the HDPE. An increase in torque with mixing time of the 30% blend revealed the possibility of molecular orientation of HDPE caused by the presence of UHMWPE. Energy consumption was higher with increasing rotation and concentration, reflected in the increase in temperature for melt homogenization. The processability of the pure polymer became more difficult with the addition of UHMWPE and the melt index measurement showed that UHMWPE reduced the flowability of HDPE, with no appreciable flow to the blend with higher UHMWPE content.

Acknowledgements

The authors gratefully Federal University of Paraiba (UFPB) for scientific initiation (PIBIC and PIVIC). This work was funded by the Public Call n. 03 Produtividade em Pesquisa PROPESQ/PRPG/UFPB PIF13399-2020.

References

1. Freitas, S. R. Freitas Ph.D. Thesis, Federal University of ABC, 2017.
2. H. S. Jaggi.; B. K. Satapathy.; A. R. Ray J. Polym. Res. 2014, 21, 482.
3. A. B. Boscoletto; R. Franco; M. Scapin; M. Tavan Eur. Polym. J. 1997, 33, 97.
4. R. E. S. Bretas; M. Zanin; M. Farah; S. A. Cruz Revista Polímeros Ciência e Tecnologia 2008, 18, 144.
5. T. Tincer; M. Coskun Polym. Eng. Sci. 1993, 33, 1243.
6. L. Zhu; H. N. Fan; Z. Q. Yang; X. H. Xu Polym. Plast. Technol. Eng. 2010, 49, 208.
7. A. R. M. Costa; T. G. Almeida; S. M. L. Silva; L. H. Carvalho; E. L. Canedo Polym Testing 2015, 42, 115.
8. C. B. B. Luna; W. A. da Silva; E. M. Araújo; D. D. Siqueira; D. B. O. Akidauana Revista Matéria 2020, 25, 3.
9. K. L. K. Lim; Z. A. Mohd Ishak; U. S. Ishiaku; A. M. Y. Fuad; A. H. Yusof; T. Czigany; B. Pukanszky; D. S. J. Appl. Polym. Sci. 2005, 97, 413.
10. J. M. D. Silva; S. V. C. R. Coutinho; R. K. M. Diniz; A. N. F. Almeida; M. E. A. Lima; F. C. Fim Macromol. Symp. 2019, 383, 1800017.

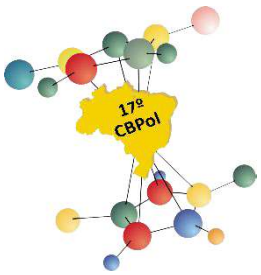

EFFECTS OF 3D FDM PRINTING PARAMETERS ON MECHANICAL PROPERTIES OF POLY(LACTIC ACID) FOR UPPER LIMB ORTHOSES

Ana C. C. Abrão[1], Baltus C. Bonse[2], Sandro L. Vatanabe[1], Marko Ackermann[1]
[1]Department of Mechanical Engineering, Centro Universitário FEI, São Bernardo do Campo, SP, Brazil
[2]Department of Materials Engineering, Centro Universitário FEI, São Bernardo do Campo, SP, Brazil
mackermann@fei.edu.br

Abstract - Additive manufacturing, also known as 3D printing, is a versatile technology that allows for customization and the production of complex geometries. One application of 3D printing is in the production of orthoses for patients undergoing rehabilitation or as an assistive technology for daily activities. Fused Deposition Modeling (FDM) is commonly used due to its low cost and ability to adapt to specific user characteristics. PLA is a popular polymer for these applications due to its biocompatibility, rigidity, flowability, and strength. Tests were conducted to investigate the effects of infill density and the number of contours on the mechanical properties of printed parts. Results showed that increasing infill density from 50% to 100% increased elastic modulus and tensile, flexural, and impact strengths. An increase in contours from one to three increased flexural modulus and tensile and flexural strengths, with little effect on tensile modulus and impact strength.
Keywords: *Additive manufacturing. Upper limb orthoses. PLA. Mechanical properties*

Introduction

In health applications, 3D printing is already being used to manufacture advanced and specialized prototypes, including orthoses, prostheses, and specific organs [1-3]. As the use of additive manufacturing in critical applications such as healthcare continues to grow, studies on the printing process and its effect on mechanical properties are becoming increasingly important to fulfil specific requirements and clinical needs [3].

In the manufacture of upper limb orthoses [4], the most used materials are relatively high-temperature thermoplastics, with an emphasis on ABS and PLA, which have moderately low cost, thermal, and impact resistance [5]. PLA is a biodegradable, non-toxic, and biocompatible material [6], making it suitable for use as a rehabilitation product [7]. It offers good mechanical properties, such as stiffness, and mechanical strength, in addition to excellent flowability during the extrusion process. The modeling characteristics, materials, and type of orthosis are evaluated by a responsible professional and vary according to the patient's needs.

Relevant parameters in FDM additive manufacturing include the number of contours, the distance between filaments, contour thickness, extrusion nozzle geometry, infill density and pattern, displacement speed, extrusion speed and temperature, and the material to be extruded [8]. Particularly, the number of contours and infill density have been shown to directly influence the mechanical properties of the final part in 3D printing by FDM [9]. Previous studies have performed flexural and tensile tests on extruded PLA specimens to analyze the influence of infill density and pattern, extrusion temperatures, contour thickness, printing direction, and extrusion temperature on the mechanical properties of the printed material [10,11].

Within this context, the main objectives of this study were to determine the effect of infill density and the number of contours on mechanical properties of specimens representative of the structure of upper limb orthoses made of PLA by FDM additive manufacturing.

Experimental

The test specimens were printed using Cliever PLA - Cobalt Blue filament and a Sethi S4X FDM 3D printer. The fixed printing parameters were: filament diameter of 1.75 mm; nozzle diameter and temperature of 0.5 mm and 210 °C, respectively; bed temperature of 65 °C; printing speed of 80 mm/s; contour thickness of 0.25 mm; linear infill geometry; and flat-wise build orientation.

For the tensile tests, 10 formulations were printed, with infill densities of 50, 60, 70, 80, 90, and 100%, and 1, 2, 3, and 4 contours. For the flexural and notched Izod impact tests, 4 formulations were printed, with infill densities of 50 and 100% and 1 and 3 contours. For each formulation (number of contours/% infill density), 5 specimens were tested.

The tensile test followed the ASTM D638-08 standard, using a 1 mm/min test speed and an extensometer with a maximum strain of 5%. The bending test was carried out according to the ASTM D790-07 standard, using a test speed of 1.4 mm/min with a 50 mm span. Both tests were performed in an Instron 5567 universal testing machine. The Izod impact test was carried out in an Instron Ceast 9050 impact tester following ASTM D256-10, using a 1 J pendulum.

Results and Discussion

The results of the mechanical tests are illustrated in Figures 1 and 2. All results were subjected to analysis of variance (ANOVA) to check whether averages among formulations were statistically different or not.

Fig 1 shows the variation of tensile and flexural load and modulus with increasing infill density and contours.

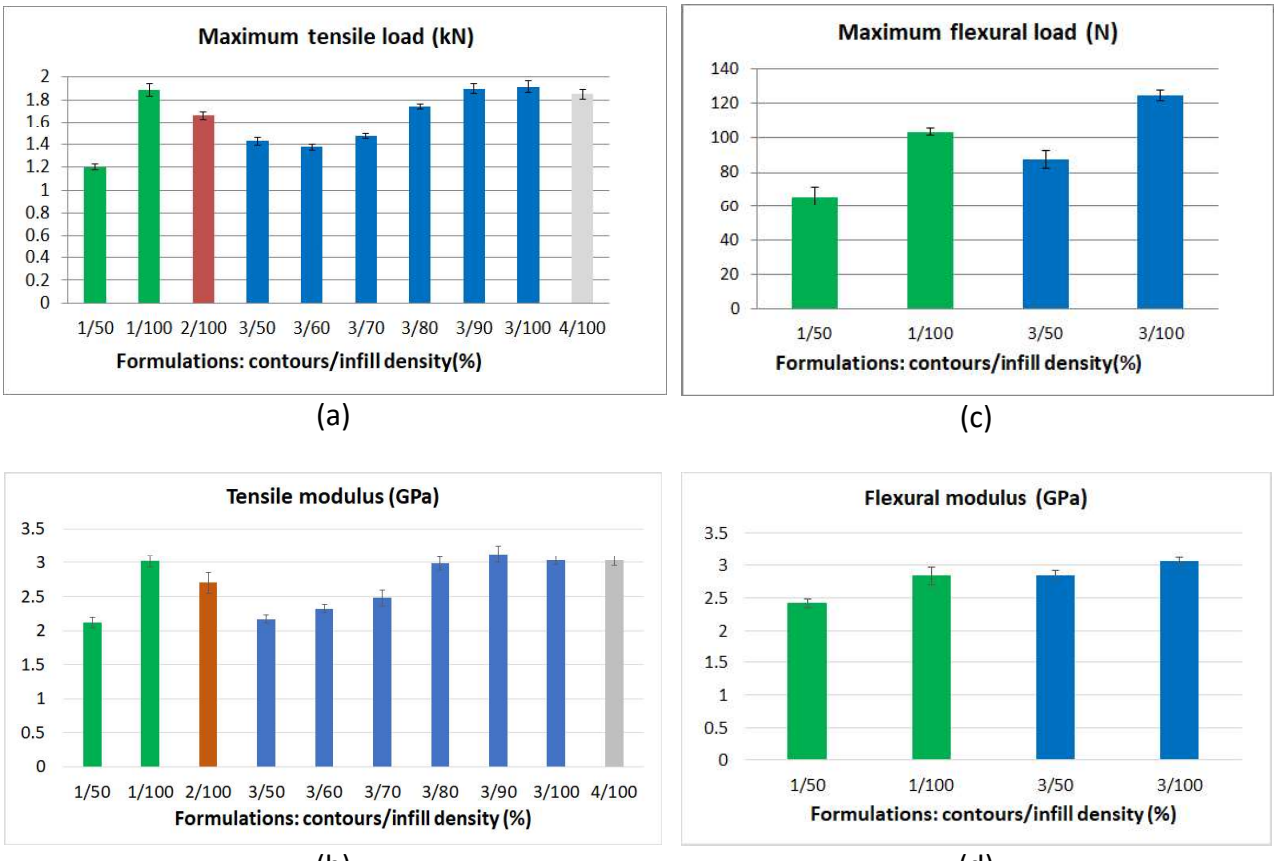

Figure 1 –Tensile and flexural load and modulus as a function of contours and infill density

The effect of infill density on the mechanical properties can be assessed by comparing formulations 1/50 and 1/100 (1 contour) and formulations 3/50, 3/60, 3/70, 3/80, 3/90, and 3/100 (3 contours). Note that, both for 1 contour and 3 contours, an increase in infill density leads to higher values of maximum tensile load (Fig 1a) and modulus (Fig 1b), indicating an increase in the strength and stiffness of the test specimen. This can be attributed to the larger amount of material used when increasing the infill density. The additional material enhances the strength and stiffness of the resulting part. A part with 50% infill density contains more pores than one with 100% infill density. Since pores can be considered defects in the part, an increase in pores (lower infill density) weakens the part. Consequently, a part with a lower infill density is expected to be less rigid and less resistant than one with a higher infill density. This finding was also observed by Cwikla et al. [12].

Another significant observation pertains to the test specimens printed with 3 contours. It is worth noting that infill densities ranging from 80% to 100% yield similar tensile modulus values, while an infill density of 90% or 100% results in comparable maximum tensile loads. In other words, less material can achieve the same stiffness and maximum tensile load, leading to time and cost savings. For maximum flexural load (Fig 1c) and flexural modulus (Fig 1d), similar trends to tensile load and modulus are observed with increasing infill density, comparing formulations 1/50 vs. 1/100 and 3/50 vs. 3/100, which can also be attributed to the decrease in pore density.

The effect of contours on the tensile properties can be assessed by comparing formulations 1/50 to 3/50 and 1/100 to 2/100, 3/100, and 4/100. As shown in Fig 1a, only at 50% infill density an increase in the contour affects maximum tensile load, increasing this property. At 100% infill density, increasing the contours from 1 to 4 does not affect the maximum tensile load, if the 2/100 formulation is not considered. A possible explanation for the more substantial influence of the number of contours on the 50% infill compared to the 100% infill is that the contours correspond to regions with a higher concentration of material. Therefore, any increase in material would have a more significant effect on specimens with lower infill (50%) than on those with higher infill (100%), as the latter already have a higher overall material density.

If the 2/100 formulation is also disregarded in Fig 1b, increasing the number of contours also shows no effect on tensile modulus, either at 50% or 100% infill.

Regarding the effect of contours on the flexural properties, in contrast to the tensile properties, the number of contours directly affects the flexural properties of the test specimens, both for 50% and 100% infill. The influence of the number of contours is observed on all assessed flexural properties (Fig 1c, Fig 1d, and Fig 2a). The more substantial effect of the number of contours on the flexural properties can be attributed to the nature of the mechanical load on the test specimens during bending, which is more localized in regions far from the neutral axis, precisely the region most affected by the increase in contours.

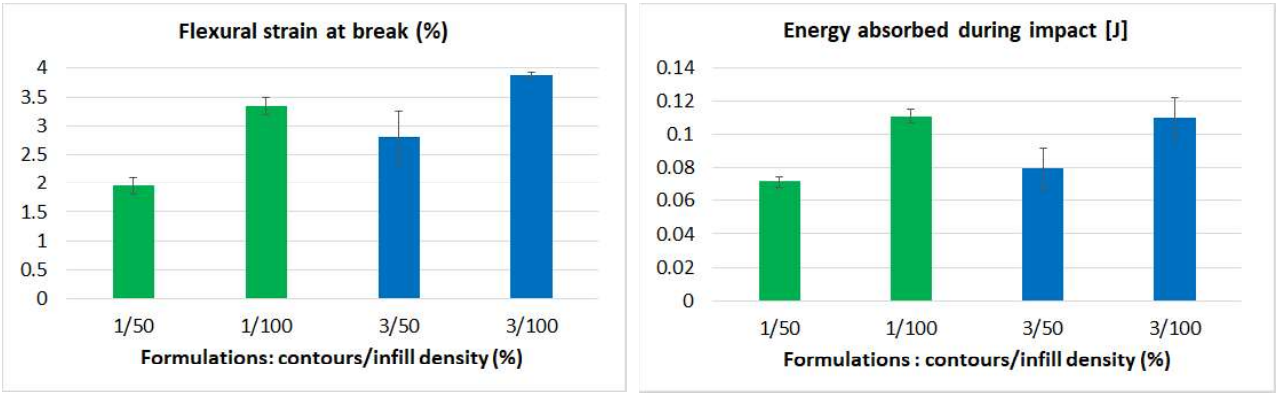

(a) (b)

Figure 2 –Flexural strain at break and impact energy as a function of the number of contours and infill density

The results of the energy absorbed during notched Izod impact testing are depicted in Fig 2b. It is evident that for both 1 contour and 3 contours, increasing infill density (1/50 vs. 1/100 and 3/50 vs. 3/100) increases the amount of energy that can be absorbed to break the specimen, which makes sense as pore density decreases, i.e., fewer flaws in the specimens to weaken the specimen. However, increasing contours from 1 to 3 at the same infill density (1/50 vs. 3/50 and 1/100 vs. 3/100) does not affect the absorbed impact load. This might be because the contours were sectioned on one side of the specimen by the notch used in this specific Izod test.

Conclusions

Tests were conducted to investigate the effects of infill density and the number of contours of 3D FDM printed parts on the mechanical properties: maximal tensile load, tensile modulus, maximal flexural load, flexural modulus, flexural strain at break, and energy absorbed during impact.

As for the influence of infill density, the results show that an increase from 50% to 100% incremented the values of all the mechanical properties investigated, leading to parts that are more rigid and resistant against tensile, bending, and impact loads. The tensile tests for intermediate infill density values, however, show similar tensile moduli for 80%, 90%, and 100%, and tensile loads for 90% and 100%, indicating less material can be used in the design of orthoses with the same stiffness and maximum tensile load, leading to time and cost savings.

The results reveal that increasing the number of contours increases the values of the flexural properties. Conversely, additional contours have little effect on impact and tensile properties, except for the maximal tensile load at an infill density of 50%. This indicates that the choice of the number of contours should take the predominant loading mode of the orthosis part (bending or tensile) into account.

Acknowledgements

We thank the HealthTech company Fix It for manufacturing and supplying the test specimens for this study.

References

1. B. A. Maia, Master's Dissertation, Universidade Federal de Goiás, 2016.
2. T. L. Gerstle; M. S. Ahmed; S. K. Peter; T. L. Bernard; J. L. Samuel, Plastic and Reconstructive Surgery, 2014, 133 (2). 10.1097/01.prs.0000436844.92623.d3.
3. G. Baronio; S. Harran; A. Signoni, Applied Bionics and Biomechanics, 8347478, 2016. https://doi.org/10.1155/2016/8347478.
4. R. C. Lima, *Órteses de Membros Superiores*, https://www.increasing.com.br/2022/10/orteses-de-membros-superiores.html. (website accessed on 05.27.2023)
5. A. L. M. Ferrari; A. D. P. dos Santos; T. M. C. G. P. de Souza; F. O. Medola, Florianópolis, Human Factors in Design, 2019, 8 (16). https://doi.org/10.5965/2316796308162019051
6. C. G. Silva; P. A. L. Campini; D.B. Rocha; D. S. Rosa, Composites Science and Technology, 2019, 179. http://dx.doi.org/10.1016/j.compscitech.2019.04.010.
7. C. N. C. Lam, Advances in Colloid and Interface Science, 2002, 96. https://doi.org/10.1016/S0001-8686(01)00080-X.
8. M. W. M. Cunico, *Impressoras 3D: O Novo Meio Produtivo***,** Concep3d Pesquisas Científicas Ltda, Curitiba, 2015.
9. T. Alves; A. V. S. de Jesus; G. V. S. Pinto; R. R. M. Ribeiro; L.K. O. Rodrigues, Desafios, 2021, 8 (1). https://doi.org/10.20873/uftv8-9605.
10. I. C. C. Rosa, Trabalho de Conclusão de Curso, Universidade Federal de Uberlândia, 2019.
11. A. P. R. Croucillo; J. D. Arruda; L. J. V. Franco; J. F. Leite; M. R. Carvalho, Tecnologia em Metalurgia, Materiais e Mineração. Avaliação das características mecânicas do PLA, impressa

em 3D, para aplicação em próteses em animais de pequeno e médio porte, 2018, 15 (3). http://dx.doi.org/10.4322/2176-1523.1593.
12. G. Cwikla; C. Grabowik; K. Kalinowski; I. Paprocka; P. Ociepka, IOP Conference Series: Materials Science and Engineering, 2017, 227, 012033. http://dx.doi.org/10.1088/1757-899X/227/1/012033.

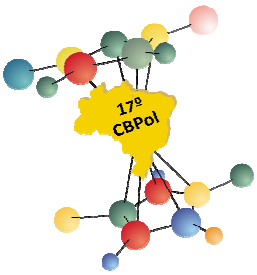

EVALUATION OF MECHANICAL PROPERTIES OBTAINED BY ADDITIVE MANUFACTURING CORRELATED WITH INJECTION MOLDING

Isaac S. Bezerra[1], Carlos H. R. Milfont[2], Felipe P.C. Gomes[2], Adriano L. A. Mattos[3], Caroline D. Vilar[4] and Edson N. Ito[5]*

1 – Graduate Program in Materials Science and Engineering (PPGCEM), Federal University of Rio Grande do Norte, Natal, RN, Brazil isaacsb.mec@gmail.com, henrique.milfont@gmail.com
2 – Chemical Engineering Department, Federal University of Pernambuco, Recife, PE, Brazil felipe.pcgomes@ufpe.br
3 – Embrapa Tropical Agroindustry, Fortaleza, CE, Brazil, Brazil adriano.mattos@embrapa.br
4 – Biomedical Engineering Department, Federal University of Rio Grande do Norte, Natal, RN, Brazil caroline.vilar@ufrn.br
5 – Materials Engineering Department, Federal University of Rio Grande do Norte, Natal, RN, Brazil
**edson.ito@ufrn.br*

Abstract – The demand for plastic objects has grown exponentially, promoting the search for efficient and sustainable production techniques. A great attention has been dedicated to additive manufacturing (AM) performed by fusion and deposition modeling (FDM) of thermoplastic filaments. This work produced specimens of different materials through FDM using printing nozzles with diameters from 0.3 to 0.6 mm and through a traditional processing technique, namely injection molding. Samples were subjected to morphological and mechanical characterization by tensile test, which indicated improvements in the mechanical properties of specimens printed using nozzles with smaller diameters, possibly due to the reduction of internal voids revealed by scanning electron microscopy (SEM). In addition, results indicated that FDM may be causing orientation of polymer chains.

Keywords: *Additive manufacturing, Injection molding, Printing nozzles.*

Introduction

Injection molding can manufacture highly complex three-dimensional polymeric artifacts, but it has been associated with a large capital and operating costs, plus additional costs for each new project developed [1]. In contrast, additive manufacturing, also known as 3D printing (3DP), can perform fusion and deposition modeling (FDM) using thermoplastic filaments, thus allowing to manufacture complex artifacts through a layer-by-layer addition of material. As a result, it can achieve similar with low capital cost equipment, that are easy to operate, with low percentage of material disposal and possibility of change the model digitally without additional costs. Another important aspect is the diversity of polymeric filaments available in the market [2-6].

The most commercialized thermoplastic filaments for 3DP are poly(acrylonitrile-co-butadiene-co-styrene) (ABS), glycol-modified poly(ethylene terephthalate) (PETG), also known as bottle grade PETG, and poly(lactic acid) PLA, which all demonstrate good processability properties [7]. ABS has high rigidity and impact resistance, while PETG is mostly used in packaging applications due to its good mechanical and chemical resistance, associated with barrier to gases and odors, brightness and translucency. On the other hand, PLA shows good mechanical properties, coupled with thermal stability, biocompatibility and minimal environmental impact due to its biodegradability [8-10].

This work aimed to measure and compare the mechanical properties of specimens produced by injection molding and 3DP with different diameters of printing nozzles.

Experimental

Materials

PLA, ABS and PETG filaments were obtained from 3DFILA. All materials were oven-dried before processing and characterization to eliminate moisture at 60°C for 6 hours in a vacuum oven.

Methods

Manufacturing of test specimens

ASTM D638 standard type 1 specimens were produced by injection molding in an Arburg model Allrounder 270 S, under the conditions indicated in Table 1. Specimens with same dimensions were produced by 3DP by FDM using printing nozzles of 0.3, 0.4, 0.5 and 0.6 mm, with 100% infill density, 45° raster angle and nozzle temperature of 200°C, 220°C and 240°C for PLA, PETG and ABS respectively.

Table 1 – Injection molding parameters

Materials	Temperature profile (°C)	Mold temperature (°C)	Cooling time (s)
ABS	210/220/230/240/240	40	40
PETG	200/210/220/230/230	40	40
PLA	180/190/200/200/210	40	40

Mechanical characterization

Tensile tests were carried out in a universal testing machine, EMIC model DL-3000, with a 30 kN load cell. The test speed used for ABS and PLA was 1mm/min until 0.5% strain, and then increased to 5 mm/min until rupture. For PETG the initial speed was set to 1 mm/min up to 0.5% strain, and increased to 50 mm/min until failure, following ASTM D638 standards.

Morphological characterization

Specimens were cryofractured and subjected to surface analysis using a benchtop scanning electron microscope (SEM), HITACHI model TM 3000, operated at 5 kV with a tungsten filament.

Results and Discussion

In Figure 1(a) were presented the results for elongation at break, which demonstrates a plateau of properties between the printed samples, even using different diameters of nozzles. While the specimens produced via injection molding presented up to three times more deformation before failure in comparison with 3DP samples. This difference can indicate that in the injection molding process there is less chain orientation, as it is expected that the high strain rate experienced by the polymer melt in the printing nozzle during deposition can lead to chain unraveling and orientation. As a result of this conformation, with less entangled chains the elongation at break is reduced, while specimens produced by injection molding presented highly entangled polymeric chains that allow greater elongation at break.

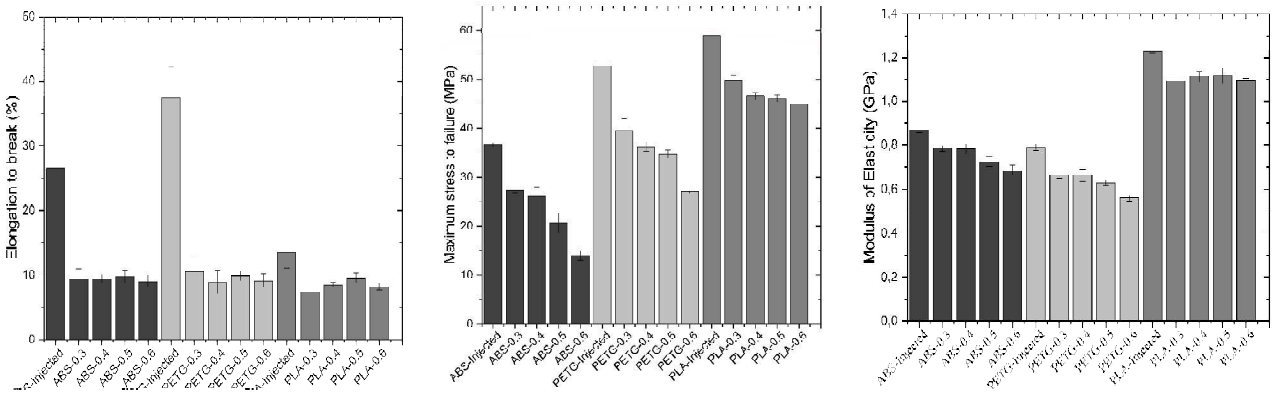

(a) (b) (c)

Figure 1 – Mechanical characterization tensile test specimens of ABS, PETG and PLA produced by injection molding and 3DP with different printing nozzle diameters: a) Elongation at break; b) Maximum tensile stress; c) Modulus of elasticity.

Figures 1(b-c) show results of maximum stress to failure and elastic modulus presented by different production methods and materials tested. The results for 3DP samples indicated that smaller printing nozzles provide higher mechanical resistance, probably due to a decrease in external and internal voids, attenuating their interactions as stress concentrators, as visualized by morphologies shown in Figure 2. Among the tested materials, PLA showed the best stress-strain relationship, in addition to being more stable considering the influence of different fabrication methods and printing nozzles used.

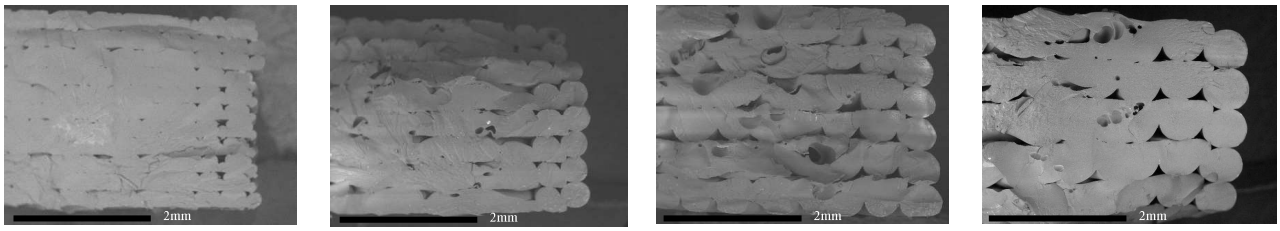

(a) (b) (c) (d)

Figure 2 – Scanning electron microscopy of printed samples with different nozzle diameters: a) 0.3mm; b) 0.4mm; c) 0.5mm; d) 0.6mm

Conclusions

This work revealed that the specimens manufactured by 3DP may failure with smaller deformation when compared to injection molded samples with similar geometry. This result is being associated with the chain alignment caused when passing through the extruder nozzle during FDM. The change in the diameters of printing nozzles impacted the mechanical properties of tested samples, indicating that smaller diameters can provide smaller voids and consequently better properties. However, it is important to notice that evidence show that printing with larger diameters provide a greater area of weld lines, which, due to their orientation towards the direction of tensile forces, confer greater resistance.

Acknowledgements

The authors are grateful to CAPES for granting financial support.

References

1. Fakhar Manesh M, Pellegrini MM, Marzi G, Dabic M. Knowledge Management in the Fourth Industrial Revolution: Mapping the Literature and Scoping Future Avenues. IEEE Trans Eng Manag. 2021;68(1):289–300.
2. Laguna OH, Lietor PF, Godino FJI, Corpas-Iglesias FA. A review on additive manufacturing and materials for catalytic applications: Milestones, key concepts, advances and perspectives. Mater Des [Internet]. 2021;208:109927. Available from: https://doi.org/10.1016/j.matdes.2021.109927
3. Carrell J, Gruss G, Gomez E. Four-dimensional printing using fused-deposition modeling: a review. Rapid Prototyp J. 2020;26(5):855–69.
4. Han T, Xu Y. Mechanical Automation Design and Manufacturing Based on Artificial Intelligence Technology. J Phys Conf Ser. 2021;1852(2).
5. Garzon-Hernandez S, Garcia-Gonzalez D, Jérusalem A, Arias A. Design of FDM 3D printed polymers: An experimental-modelling methodology for the prediction of mechanical properties. Mater Des [Internet]. 2020;188:108414. Available from: https://doi.org/10.1016/j.matdes.2019.108414
6. Ngo TD, Kashani A, Imbalzano G, Nguyen KTQ, Hui D. Additive manufacturing (3D printing): A review of materials, methods, applications and challenges. Compos Part B Eng [Internet]. 2018;143(December 2017):172–96. Available from: https://doi.org/10.1016/j.compositesb.2018.02.012
7. Amza CG, Zapciu A, Baciu F, Vasile MI, Nicoara AI. Accelerated aging effect on mechanical properties of common 3d-printing polymers. Polymers (Basel). 2021;13(23):1–13.
8. Popescu D, Zapciu A, Amza C, Baciu F, Marinescu R. FDM process parameters influence over the mechanical properties of polymer specimens: A review. Polym Test. 2018;69(May):157–66.
9. Shkundalova O, Rimkus A, Gribniak V. Structural Application of 3D Printing Technologies: Mechanical Properties of Printed Polymeric Materials / Konstrukcinis 3D Spausdinimo Technologijų Taikymas: Spausdintų Polimerinių Medžiagų Mechaninės Savybės. Moksl - Liet ateitis. 2018;10(0):1–8.
10. Santana L, Alves JL, Sabino Netto A da C, Merlini C. A comparative study between PETG and PLA for 3D printing through thermal, chemical and mechanical characterization. Rev Mater. 2018;23(4).

EVALUATION OF THE FEASIBILITY OF RECONDITIONING ABS SAMPLES MANUFACTURED BY 3D PRINTING

Luana A. Patrocínio [1], Gisele DC Antolin [1], Mauricio Q. Antolin [2], Juliane C. Marin [1], Mônica CC dos Santos [3]

1 – Department of Metallurgical Engineering (DEPMET), State University of Rio de Janeiro (UERJ), Rio de Janeiro, RJ, Brasil, 2114422049@uezo.edu.br
2 – Department of Computing (DEPCOMP), State University of Rio de Janeiro (UERJ), Rio de Janeiro, RJ, Brasil
3 – Department of Materials Engineering (DEPMAT), State University of Rio de Janeiro (UERJ), Rio de Janeiro, RJ, Brasil

Abstract – ABS is one of the most used materials for 3D printing. This material has the problem of being a petroleum derivative. Thus, for environmental and economic reasons, the recycling of this material in other applications would be extremely important for the sector. Therefore, this work discusses the possibility of using reused ABS, from the comparison of the mechanical properties of specimens manufactured by 3D printing. For this, specimens were made with crushed and pressed ABS from unused parts. The results show that the tensile and impact strength of these parts were significantly reduced, probably due to the parameters used during the reconditioning of the material, which caused the occurrence of voids. However, recycling this material is feasible in projects involving less mechanical resistance.

Keywords: Recycling, 3D printing, ABS

Introduction

Rapid Prototyping, popularly known as 3D printing, is a technology that has revolutionized the way of producing objects, with the possibility of creating parts from a digital model in three dimensions. This process is based on adding flat layers of material such as plastic, metal or polymer to build a physical object [1].

One of the great advantages of 3D printing is the possibility of manufacturing complex parts from the model information generated in CAD, which is used for process planning [1-2]. This allows the creation of objects with complex shapes and sizes that would be expensive to produce using other techniques such as machining or injection molding. In addition, 3D printing also enables the production of customized parts, tailored for specific use and for mechanical resistance tests [1].

Another advantage of 3D printing is its efficiency in the prototyping process, since before printing it is possible to test different ideas and adjust details of the digital model to arrive at the best version of the object, delivering greater mechanical resistance to the final project. This means that it is possible to save time and resources in the product development stage, avoiding failures that could only be found in the final manufacturing [3].

Despite still being a constantly evolving technology, 3D printing has already been used in several sectors, such as medicine and architecture. In the health area, for example, it is possible to print pre-surgical models of organs in full size, which enables better planning for the medical team, and an infinity of surgical plans to be tested, thus reducing surgery time and patient exposure to infections [4].

Recycling is one of the alternatives to reduce the use of oil, carbon dioxide emissions and the amount of polymeric waste and its negative impacts of disposal. One of the great benefits is given by the possibility of substituting in certain applications, such as the automotive area, virgin material for recycled polymer, without losing great properties and even reducing the use of oil. However, one of the great challenges of recycling materials is to maintain their properties in this process [5,6].

In addition, there are other challenges that need to be overcome, especially when the objective is to implement a product with a commercial purpose, such as the need for high quality materials, surface finish and the feasibility of large-scale production.

Polymers are materials that have in their structure repetition of units linked by covalent bonding, which can occur naturally or synthetically. Commonly, the filaments used in 3D printing are composed of thermoplastic polymers (plastics that reach a pasty state when heated), this makes these materials likely to be used after reuse. [7]

Acrylonitrile butadiene styrene (ABS) is one of the most used materials in 3D printing due to its strength and ease of printing. However, thermoplastic ABS is a non-biodegradable type of plastic, which can have a negative environmental impact if not disposed of properly [8-9]. An alternative to reduce this impact is the recycling of ABS. This can be done by reprocessing ABS printed objects that are no longer used.

Thinking about it, this work intends to compare the differences in the mechanical properties of parts manufactured with virgin ABS and parts manufactured with reused ABS, where for the thermopressing the test specimens made in the 3D printer with virgin ABS that have already passed the tests will be used as raw material. mechanics. In this way, this work will compare ABS parts subjected to two different processing routes: 3D printed parts with different amounts of wall (route 1) and ABS parts manufactured from ABS parts that were unusable and that were subjected to thermopressing to originate new parts that we will call reused ABS (route 2).

Experimental

The parts were manufactured in ABS via 3D printing, using the fused deposition modeling (FDM) method. This method occurs from the extrusion of the heated filament, which progressively deposits this material layer by layer on a heated table, thus forming the part [1]. In this work, specimens were made for Charpy (ASTM D6110) and tensile (ASTM D638) tests with 20% filling, varying the number of walls between 3 and 6 (route 1).

To find out if the mechanical properties of ABS are affected by reprocessing, unused ABS parts, manufactured with the same parameters as the parts from route 1, underwent a reuse process (route 2). First, these pieces had their sizes manually reduced with the aid of a hammer, to reach the ideal size to pass through the knife mill. Soon after grinding, the powdered material was placed under a hollow mold, until it was filled and taken to a hydraulic press at a temperature of 225ºC (the same temperature used in the 3D printing process). After that, the pieces went through two degassing processes and then were pressed at 5ton for five minutes. After this time, the mold was taken to a cold hydraulic press and pressed at 3ton to solidify the parts for another five minutes. After this manufacturing process, the specimens were submitted to Charpy (ASTM D6110) and tensile (ASTM D638) tests at TECPOL. The mechanical tensile tests were carried out according to the ASTM D638 standard, at a speed of 5 mm/min, in the universal test equipment Schimadzu model AG-X PLUS, while the impact tests were carried out in the instron impact testing machine. Fig. 1 shows specimens for tensile testing manufactured by route 2.

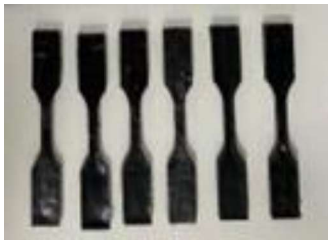

Figure 1: Specimens (route 2) manufactured with reconditioned ABS. Source: Author (2023).

Results and Discussion

After making the specimens, they were submitted to tensile and Charpy tests. Table 1 presents the results of the mechanical tests of the specimens from Route 1 (for different amounts of walls) and route 2, which involved the manufacture of specimens using reused ABS in the form of solid bodies, due to the pressing process.

TABLE 1: RESULTS OBTAINED FOR THE MECHANICAL TESTS.

Parts	σ_m (MPa)	σ_r (MPa)	E (GPa)	σ_e (MPa)	Average Impact Resistance (J/m)
3 Walls (route 1)	16,23±0,39	14,83±0,72	0,45±0,042	15,61±0,51	113,84±20,29
4 Walls (route 1)	18,71±0,14	17,49±0,23	0,45±0,037	17,57±0,46	147,32±6,38
5 Walls (route 1)	21,15±0,33	18,54±0,57	0,46±0,035	20,42±0,18	177,19±2,58
6 Walls (route 1)	23,30±0,35	21,00 ± 0,88	0,49±0,054	22,46±0,24	178,08±3,11
Reused ABS (route 2)	7,83±0,35	5,66±0,12	0,40±0,059	7,52±0,51	133,04±23,07

σ_m – Avarege stress; σ_r – Rupture stress; E – Young Modulus e σ_e – Yield stress

Source: Author (2023).

Analyzing the results of the test specimens made with the change in the number of walls and keeping the filling at 20%, it is noted that the values of yield stress, rupture stress, and maximum stress increased as the wall thickness increased, being the maximum value of the yield stress found equal to 22.46 MPa. Therefore, evaluating the question of resistance, the pieces with 6 walls showed better mechanical properties in relation to the pieces with a smaller number of walls. The specimens made with reconditioned material from route 2 had a yield stress value much lower than all specimens manufactured in route 1, despite the specimens from route 2 being massive.

Regarding the Young modulus, we can highlight that there was no appreciable variation in this property due to the change in the number of walls or in comparison to refurbished ABS.

Regarding impact resistance, from Table 1, it is possible to observe that the value increased with the increase in the number of walls. Specimens made with 3 walls using route 1 averaged 113.84 J/m, while specimens made with ABS repurposed from route 2 averaged 133.04 J/m. In this way, we can observe that the impact strength of the test specimens from route 2 is located between the values

of the test specimens with walls equal to 3 and 4 from route 1. Both results of tensile strength and impact strength demonstrate that reprocessing significantly affected the mechanical properties of the materials. The specimens using 6 walls (route 1) have higher values in all results, unlike specimens made with reconditioned ABS. (route 2).

The low values found for the mechanical properties of the route 2 test specimens may be associated with several factors directly linked to the material and the way it was processed. Assuming that ABS is a copolymer composed of a combination of acrylonitrile, butadiene and styrene, where acrylonitrile provides thermal resistance, butadiene provides resistance to impact and styrene provides brightness, rigidity and ease of processing, the steps that involve the reconditioning of the material for route 2 (breaking, grinding, heating and pressing), may have reduced the strength of these specimens by changing the properties of the butadiene that is present in this copolymer. In this way, we can conclude that it is possible to use the repurposed ABS from route 2, however, its resistance will be reduced.

Another issue to be discussed in relation to the difference in results of parts made with Reused ABS from route 2 and parts with ABS from route 1, may have been caused at the time of manufacturing the test specimens, as the parts after their manufacture had voids in its internal structure, arising from failures in the pressing process (fig. 2).

It is worth mentioning here that in the manufacturing process of the parts of route 2, during pressing the material was placed under a mold, taken to the hydraulic press at a temperature of 225ºC and subjected to two degassing processes, which is fundamental to allow the removal of gases volatiles released by the material when heated. Thus, the existence of voids may have caused the reduction of the mechanical properties of these specimens.

FIGURE 2: Internal part of the part after the tensile test. Source: Author (2023).

It is assumed that these voids could be related to several causes, such as: The insufficient temperature of the mold and the degassing process carried out quickly, which could have meant that the air did not have time to escape. As it is a reused material, the contamination of the raw material by other plastics, due to the use of the same molds, can also be pointed out as one of the reasons.

Conclusions

ABS recycling can be a viable alternative to reduce the environmental impact of 3D printing. In addition to being a sustainable practice, recycling ABS can also represent savings for the user, who can reuse the material in new prints. However, as observed in this work, the mechanical properties of reused materials are inferior to those obtained by virgin material. This fact may be due to the existence of voids that were observed in the material and that may have originated due to failures in the pressing process. It is suggested changes in reuse parameters in future works and an investigation of the reuse

of the material from the manufacture of a filament with reconditioned material, and submitted to the same printing parameters of parts made with virgin ABS.

References

[1] Fredrick R. Ishengoma. Adam B. Mtaho. 3D Printing: Developing Countries Perspectives. International Journal of Computer Applications (0975 – 8887) Volume 104 – No 11, October 2014

[2] Chamil Abeykoon, Pimpisut Sri-Amphorn, Anura Fernando. Optimization of fused deposition modeling parameters for improved PLA and ABS 3D printed structures. International Journal of Lightweight Materials and Manufacture
Volume 3, Issue 3, September 2020, Pages 284-297

[3] TRISCIUZZI, Leonardo. APLICAÇÃO DA IMPRESSÃO 3D NO SETOR NAVAL. Trabalho de Conclusão de Curso. Curso de Engenharia Naval e Oceânica. 2018.

[4] Custódio Leopoldina De Brito Guerra Neto, Danilo Alvez Pinto Nagem, Hélio Roberto Hékis Karilany Dantas Coutinho, Ricardo Aleysandro De Medeiros Valentim. Tecnologia 3D na saúde. Editora: UFRN. 2018.

[5] Luís Gustavo de Mello Paracêncio. Jonathan Henkemeier Pereira. Kaique de Camargo. Paulo Sergio dos Santos. Pedro Henrique Gavioli. Ruan Vitor De Souza Soares Da Silva. PROJETO E ESTUDO DE UM DISPOSITIVO DE VALORIZAÇÃO DE RESÍDUO DO POLÍMERO ABS. Revista de Engenharia e Tecnologia. V. 11 No. 2, Ago/2019.

[6] Mazher Iqbal Mohammed, Daniel Wilson, Eli Gomez-Kervin, Callum Vidler, Lucas Rosson and Johannes Long. The recycling of E-Waste ABS plastics by melt extrusion and 3D printing using solar powered devices as a transformative tool for humanitarian aid. Solid Freeform Fabrication 2018: Proceedings of the 29th Annual International Solid Freeform Fabrication Symposium – An Additive Manufacturing Conference Reviewed Paper

[7] Márcia Aparecida da Silva Spinacé e Marco Aurelio De Paoli. A TECNOLOGIA DA RECICLAGEM DE POLÍMEROS. Quim. Nova, Vol. 28, No. 1, 65-72, 2005.

[8] Mazher Iqbal Mohammed, Anirudra Das, Eli Gomez-Kervin, Daniel Wilson, Ian Gibson. EcoPrinting: Investigating the use of 100% recycled Acrylonitrile Butadiene Styrene (ABS) for Additive Manufacturing. Solid Freeform Fabrication 2017: Proceedings of the 28th Annual International Solid Freeform Fabrication Symposium – An Additive Manufacturing Conference.

[9] Ritesh Kumar, Kambiz Sadeghi, Jaeyoung Jang, Jongchul Seo. Mechanical, chemical, and bio-recycling of biodegradable plastics: A review. Science of The Total Environment
Volume 882, 15 July 2023, 163446

INJECTION OVERMOLDED POLYMER-WOOD HYBRID STRUCTURE

Gean H. O. Marcatto[1,2,3], Gabriel V. Silva[1], Leonardo B. Canto[1,2]*

1 – Department of Materials Engineering (DEMa), Federal University of Sao Carlos (UFSCar), São Carlos, SP, Brazil.
leonardo@ufscar.br
2 – Graduate Program in Materials Science and Engineering (PPGCEM), Federal University of Sao Carlos (UFSCar), São Carlos, SP, Brazil.
3 – IMAT Institute of Materials Science, Joining and Forming, Graz University of Technology, Graz, Austria.

Abstract – A hybrid joint of polyamide 6 (PA6) and *Aspidosperma polyneuron* ("peroba rosa") wood was obtained by direct-adhesion injection overmolding. A machined piece of wood was manually positioned into the mold cavity and then overmolded with molten polymer to produce a half-lap splice joint. The joint was subjected to lap-shear testing and an outstanding shear strength of 5.2 MPa ± 1 MPa was obtained with failure in the polymer component by transverse crack propagation. Cross-section images of the joints showed good micro-anchoring of the polymer into the wood surface.

Keywords: *PA6, wood, joining, injection molding.*

Introduction

There is a growing industrial interest in the use of polymers for the manufacture of products and parts used in various commercial and social sectors [1]. Parallel to this, the use of wood has been growing in several areas thanks to its good mechanical properties allied to its natural and renewable origin [2]. In the search for lightweight structures, polymer-wood hybrid joints are excellent candidates, although they have been little explored in the literature in view of the great technological potential they offer. The proper hybridization of a polymer with wood in the form of a hybrid structure could combine in a single piece the desirable properties of both materials, while minimizing their shortcomings. The variety of characteristics and properties of polymers and wood could enable the development of remarkable properties suited to a wide variety of applications [3, 4]. In the automotive industry, for instance, polymer-wood hybrid structures may be used for interior components such as instrument panel, center compartment, glove box, and door panel. Injection overmolding is extremely advantageous, since it is a highly widespread, automated, scalable process that allows the obtaining of parts with complex geometries and with high dimensional accuracy, combined with fast molding cycles. Moreover, injection overmolding allows control of the variables that are known to influence the interfacial adhesion of hybrid structures with polymers, such as viscosity, pressure and contact time of the molten polymer with the substrate to be hybridized [5].

This work aims at develop a hybrid joint of polyamide (PA6) and *Aspidosperma polyneuron* wood through injection overmolding. The mechanical strength of the joint was evaluated by single lap shear testing on half-lap splice joints and the joint interface was investigated by scanning electron microscopy (SEM). This contributed to a better understanding of polymer-wood hybrid structures, aiming at a larger scale utilization from the improvement in the manufacturing process and the structure design and performance.

Experimental

Materials

The polymer component was polyamide (PA6), grade Ultramid C 200 Natural supplied by BASF SA company. It is a semicrystalline engineering thermoplastic widely used in automotive parts that combines high stiffness, strength and chemical resistance.

The wood component was *Aspidosperma polyneuron* ("peroba rosa"). It is Brazilian hardwood widely used for structural building applications.

Methods

Figure 1 shows all the steps to produce the polymer-wood hybrid joint via injection overmolding. First, a timber was kept in an air-circulating oven at 45 °C until constant weight. Afterwards, the dried timber was machined with the wood fibers in the longitudinal axis direction. The dimensions of the wood piece were 56.5 mm x 24.8 mm x 3.2 mm (length x width x thickness) and a 12.7 mm x 24.8 mm x 1.6 mm recess was machined at one end of the wood piece. Then, the wood piece was manually positioned inside the cavity and overmoded with molten polymer to produce a half-lap splice polymer-wood joint. Specimens were produced using an Arburg Allrounder 270V injection molding machine operating under the following conditions: barrel temperature of 240 °C, mold temperature of 80 °C, flow rate of 40 $cm^3\ s^{-1}$, holding pressure of 400 bar for 15 seconds, and cooling time of 45 s. Four replicates were produced and tested.

The mechanical strength of the PA6/wood joints was evaluated by lap-shear tensile testing based on ASTM 1002-D standard using an Instron 5569 universal testing machine, with a distance between grips of 60 mm and crosshead speed of 1.3 mm min^{-1}.

PA6/wood joints were cut along the longitudinal and transverse axes, polished with 1200 grit sandpaper and diecasting paste, cleaned in a solution of distilled water and detergent with ultrasonic bath and then dried with compressed air. The polymer-wood interface was analyzed by scanning electron microscopy (SEM) using a Philip XL-30 FEG instrument with BSE detector operated at an acceleration voltage of 25 kV. Prior to SEM analysis, the samples were sputter coated with gold.

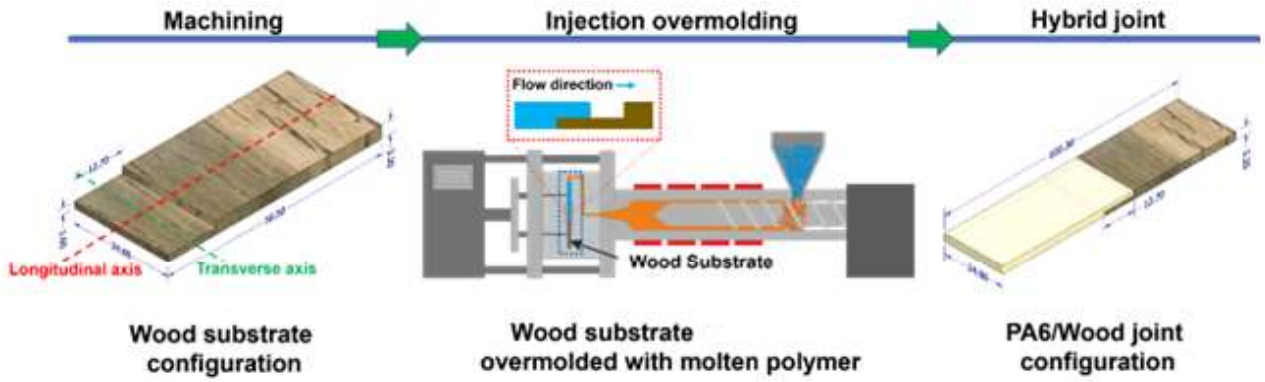

Figure 1: Steps for manufacturing a hybrid polymer-wood joint via injection overmolding. First, the wood is dried and machined. This is followed by positioning the wood substrate inside the mold cavity and overmolding with molten polymer. A half-lap splice polymer-wood hybrid joint is then obtained.

Results and Discussion

The lap-shear force by displacement curves of the PA6/wood joints are shown in Figure 2. The average ultimate lap-shear force (ULSF) was 1643 N ± 272 N and the average displacement at break was 0.9 mm ± 0.2 mm. Considering an overlap area of 12.7 mm x 24.8 mm a lap-shear strength of 5.2 MPa ± 1 MPa is achieved, which is comparable to those of other related joints reported in the literature [4].

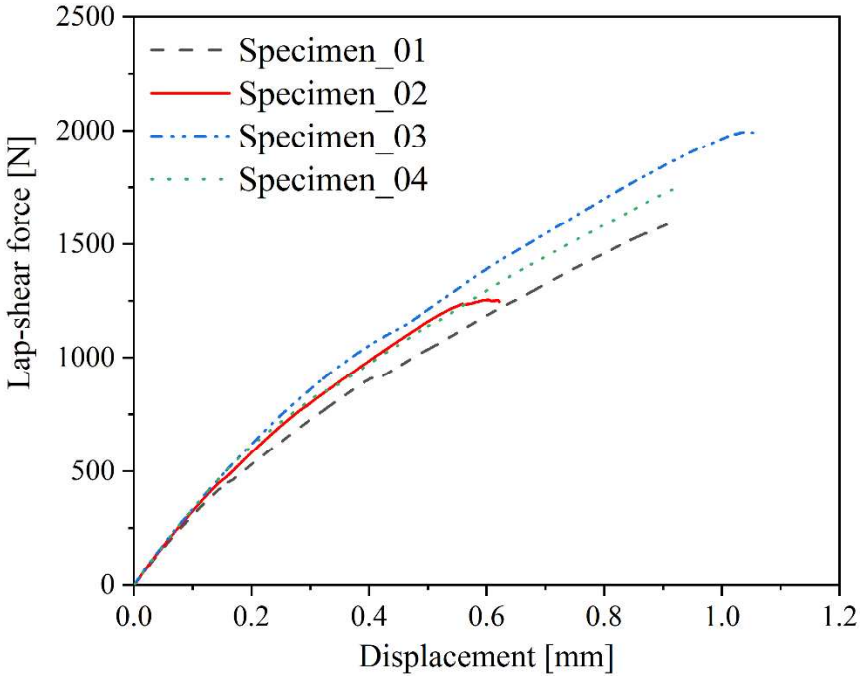

Figure 2: Lap-shear force-per-displacement curves for injection overmolded PA6/wood joint specimens.

Figure 3 shows images of injection overmolded PA6/wood joint specimens subjected to single-lap shear testing. All specimens failed on the polymer side near the tip of the wood piece through the propagation of a transverse crack. This shows that the polymer-wood interface is stronger than the polymer component and future studies with a smaller overlap area are needed to determine the polymer-wood interfacial strength. Due to the different stiffness of PA6 and wood, the mechanical loading in the overlap area is a combination of shear and bending stresses. In the fracture region, the polymer is subjected to a combination of tensile and bending stresses, which resulted in brittle failure during the lap-shear testing.

The cross-sections of the PA6/wood joint in the longitudinal and transverse directions are shown in Figure 4a-b. The polymer was able to fill the irregularities of the wood surface providing mechanical interlocking between the joint components. PA6 is polar and has low viscosity in the molten state, which should have provided good wettability on the wood substrate during injection molding. In addition, it is speculated that hydrogen bonds may occur between the amide groups of PA6 chains and the hydroxyl groups of wood cellulose, which would provide an additional adhesive mechanism to the joint interface.

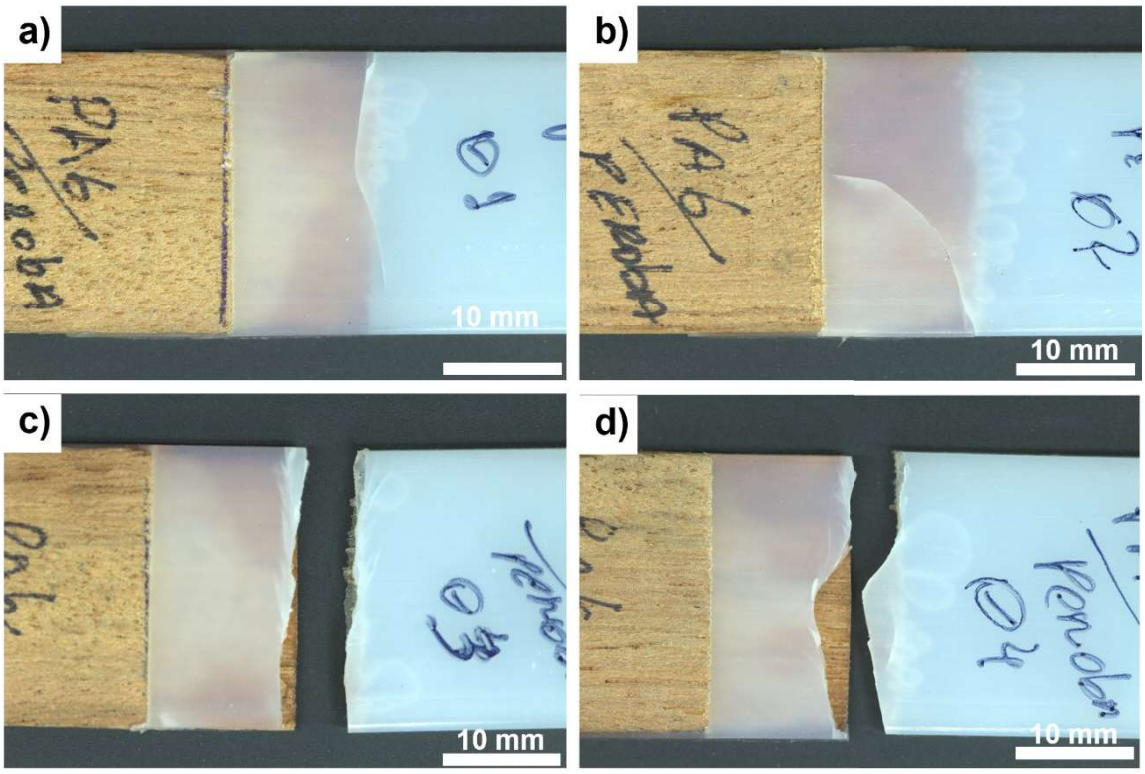

Figure 3: Images of injection overmolded PA6/wood joint specimens subjected to single-lap shear testing. Transverse fracture occurred in the polymer component. a) Specimen_01; b) Specimen_02; c) Specimens_03; and d) Specimen_04.

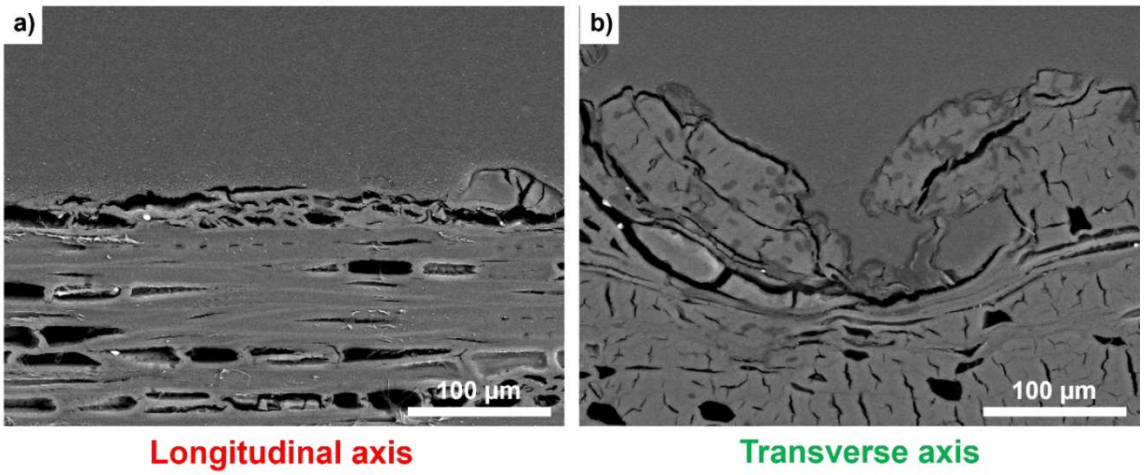

Figure 4: Cross-section SEM images (longitudinal (a) and transverse (b) axes) of the PA6/wood joint produced via injection overmolding. Polymer on the top side and wood on the bottom.

Conclusions

An injection overmolded hybrid joint of polyamide 6 (PA6) with *Aspidosperma polyneuron* wood substrate with outstanding average shear strength of 5.2 MPa ± 1 MPa was obtained. Cross-section SEM images show good filling of the polymer into wood surface irregularities, which led to a strong polymer-wood interface and failure on the polymer component by transverse crack propagation. This outcome is promising for the development of polymer-wood hybrid structures with potential applications in the furniture, transportation and household sectors.

Acknowledgments

This study was supported by FAPESP – São Paulo Research Foundation, Brazil (grant number 2018/24296-0) and CNPq – National Council for Scientific and Technological Development, Brazil (grant numbers 309258/2020-0 and 164791/2018-3). This study was financed in part by the Coordenação de Aperfeiçoamento de Pessoal de Nível Superior - Brasil (CAPES) - Finance Code 001. The authors are grateful to the Laboratory of Structural Characterization (LCE/DEMa/UFSCar) for use of the general facilities.

References

1. M. Y. Lyu; T. G. Choi International Journal of Precision Engineering and Manufacturing 2015, 16, 213. https://doi.org/10.1007/S12541-015-0029-X.
2. Y. Ding; Z. Pang; K. Lan; Y. Yao; G. Panzarasa; L. Xu; M. Lo Ricco; D. R. Rammer; J. Y. Zhu; M. Hu; X. Pan; T. Li; I. Burgert; L. Hu Chemical Reviews 2023, 123, 1843. https://doi.org/10.1021/acs.chemrev.2c00450.
3. D. Kohl; P. Link; S. Böhm Procedia CIRP 2016, 40, 557. https://doi.org/10.1016/j.procir.2016.01.133.
4. A. Stadlmann; A. Mautner; M. Pramreiter; A. Bismarck; U. Müller Polymers 2021, 13, 2849. https://doi.org/10.3390/polym13172849.
5. R. L. Vasconcelos; G. H. M. Oliveira; S. T. Amancio-Filho; L. B. Canto Polymer Engineering and Science 2023, 63, 691. https://doi.org/10.1002/pen.26244.

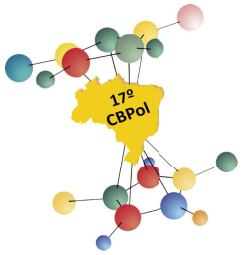

POROUS DEVICES FOR WATER DECONTAMINATION MANUFACTURED BY 3D PRINTING AND RICE HUSK SILICA

Daniel de S. Gamarano[1]*; Caroline S. Pagnan[1]; Mercês Coelho da Silva[2]; Marys Lene B. Almeida[3]; Eliane Ayres[1]

1 – Post Graduation Program in Design (PPGD), State University of Minas Gerais (UEMG), Belo Horizonte, MG, Brazil
dgdanielgamarano@gmail.com
2 – Federal University of Itajubá (UNIFEI), Itajubá, MG, Brazil
3 – Federal University of Minas Gerais (UFMG), Belo Horizonte, MG, Brazil

Abstract - Water contamination can occur for several reasons and triggers several environmental problems, related not only to the beds of rivers, seas, lakes, and groundwater but also to the air and soil, contributing to an increase in the number of diseases in the population and degradation of the environment. There are several actions in the world in search of processes, solutions, and the use of new technologies in favor of improving and controlling water quality offered to the population. This article brings a previous analysis of the doctoral research that analyzes the use of 3D printing to create devices that can be used in processes of absorbing contaminants. For this, rice husk silica was used for the absorption analysis. The previous results show promise for the construction of cleaning systems.

Keywords: *Polylactic acid; Rice husk silica; 3D printing.*

Introduction

Different strategies have been developed for the treatment of polluted water [1, 2]. Many studies bring manufacturing support from 3D printing and, later, perform a surface functionalization with adsorbents, known as adsorbent devices [3], like silica. As a product of the combustion of rice husk to generate energy, rice husk ash is formed by silica and carbon, apart from small amounts of other constituents [4]. This project brings from the analysis of the development of a 3D printing structure and the use of silica for the analysis of water decontamination. For this, blue methylene was considered as the reference substance for the analysis.

Experimental

Materials

Natural PLA filament (1.75mm) is from the Cliever (MG, Brazil). Rice husk silica is from Silcca Nobre (SP, Brazil).

3D impression

The research used the Voolt 3D brand 3D printer, which operates by the FDM method, with a 0.30 mm ejector nozzle, using a 1.75 mm filament. The printer has a maximum resolution of 0.05 mm of layer height, with heating of 195°C of the ejector nozzle. For the modeling of the devices, the SolidWorks program was used, and for the slicing of the device for printing, Ultimaker Cura was used. In the development of the devices, two main characteristics were considered: the creation of filled spaces that would allow the creation of circulation passages for the water. The analysis of the filling was done through the study of the proposals pre-established by the software. The gyroid

structure was chosen for filling the geometric shapes were identified, and filling proposals were evaluated.

Characterizations

Scanning Electron Microscopy (SEM)

The PLA surface morphology with the rice ashes was analyzed using a Hitachi 4000 Plus electronic benchtop model with an electron beam operating at 5kV, from 50 to 300x magnification.

Absorption of Blue Methylene

The release behavior of rice husk silica in water, 5.0g was immersed in 50mL of deionized water in a glass beaker with 5ppm concentration. The solutions were stirred using a magnetic stirrer for 24h.

Results and Discussion

Scanning Electron Microscopy (SEM)

Silica husks consist mainly of cellulose (25-35%), hemicellulose (18-21%), lignin (26-31%), silica (15-17%), and ash (2-5%). As it is a material of natural origin, its composition varies according to the climate, area of cultivation, and species [5]. The silica obtained from rice husk has been investigated for several applications [5]. Note that the particles have angular shapes with the presence of pores. Fig. 1 shows the characteristics of the silica powder.

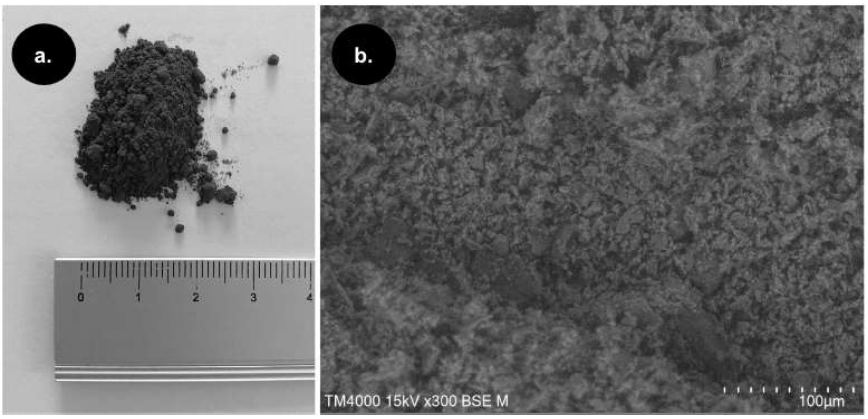

Figure 1: Morphology of the silica powder used 300x magnification.

3D impression

This research of a practical nature sought the formal geometric study bioinspired in organic structures for water filtration processes. For this, research was carried out on the Biomole platform [6], and since then, previous research has been carried out using the phylum Porifera as a reference, belonging to the kingdom Metazoa, which includes sponges, sessile animals that have a body perforated by pores, allowing the entry of water in the animal's body. In their geometry, they present body asymmetry and are segmented, with the body looking like a vessel, with an internal cavity called the atrium. It has an opening in the upper region, called osculum. They have no real tissues or organs. Its formal structure is pertinent for water filtration analysis, considering due to the following points: symmetrical structure; structure composed of pores; and structure with channels that direct the flow of water. 3D printing allows for good and controllable porosity, which is beneficial for adsorption, as the greater the roughness, the greater the surface area available for contact [7], which can contribute to the deposit of adsorbent material, such as silica (Fig 2).

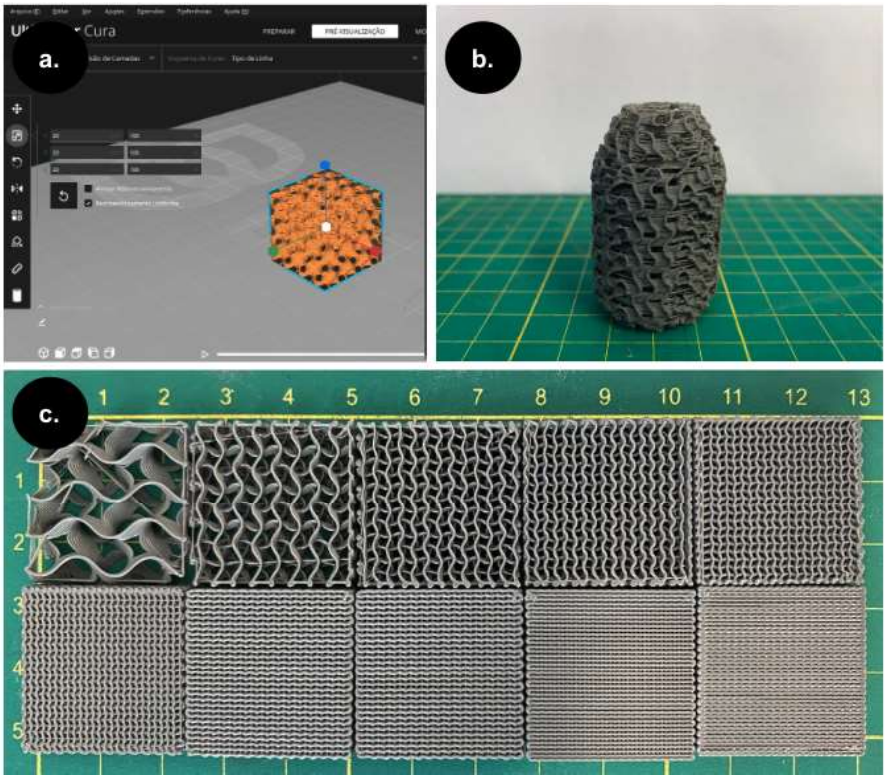

Figure 2: 3D printing development process. (a) use of the Cura software (b) creation of biomimetic forms of the support (c) analysis of the gyroid filling from 10% to 100%.

The devices were produced in PLA, and the adhesion of the silica was carried out as shown in del Rio *et al.* experiment [8], with a water-resistant adhesive, in the form of a spray, applied to the surface. Before the adhesive dries, the forms were sprayed with pre-treated RHA and left to dry at room temperature.

Adsorption of Blue Methylene

Methylene blue is a slightly toxic dye, belonging to the class of phenothiazides and absorbs intensely in the UV-visible region (λmax=664 nm in water). Solutions of this substance are blue when in an oxidizing environment. After 24h, the substance precipitated to the bottom of the beaker (Fig 3), showing the adsorption capacity of silica [9].

Figure 3: Action of silica after 24 hours of contact.

Conclusions

In conclusion, the structure produced by 3D printing, using the material obtained from rice husk, has great potential to be used for the desorption of contaminants in water. Rice husk silica has adsorbent power, which makes it possible to interact with contaminants, and as carried out in this previous research with the use of blue methylene, it showed promise for use in decontamination processes. In this stage of the research, the analysis of adsorption with silica powder was carried out, however, the next steps of the research will be carried out through the analysis of the evaluation of dye adsorption performance using RHA-coated 3D printed structures. Also, new studies need to evaluate the behavior of models produced in 3D and their interaction in water, in addition to the complete characterization of the PLA device with rice husk silica.

Acknowledgments

The authors thank Minas Gerais State Research Support Foundation (FAPEMIG), Coordination for the Improvement of Higher Education Personnel (CAPES), and the National Council for Scientific and Technological Development (CNPq) for funding research.

References

1. I. J. Fernandes; D. C. Felipe; A. L. Sánchez; A. L. D Camacho; T. L. A. C. Rocha; C. A. M. Moraes; V. C. Souza Mat. Res. 20 (Suppl 2) 2017 https://doi.org/10.1590/1980-5373-MR-2016-1043
2. M. Rioa; M. Villar; S. Quesadaa; G. T. Palominoa; L. Ferrer; C. P. Cabelloa. Applied Materials Today 24 (2021) 101130. https://doi.org/10.1016/j.apmt.2021.101130.
3. A. Fagundes; J. Lira, N. Padoin; C. Soares; H. Riella. Journal of Environmental Chemical Engineering 10 (2022) 108049. https://doi.org/10.1016/j.jece.2022.108049
4. H. S. Far; M. Najafi; M.Hasanzadeh; M. Rabbani ACS Appl. Mater. Interfaces 2022, 14, 44488−44497, https://doi.org/10.1021/acsami.2c13830
5. L. C. G. S. Santos, Ph.D. Thesis, Universidade do Estado de Minas Gerais, 2021.
6. C. Moraes; I. J. Fernandes, J. Iara; D. Calheiro; A. G. Kieling; F. A. Brehm; M. R. Rigon; J. A. B. Filho; I. A. Schineider; E. Osorio. The Journal for a Sustainable Circular Economy, v. 32, n.11. http://dx.doi.org/10.1177/0734242x14557379
7. Biomole http://biomole.asknature.org/
8. M. Rio; M. Villar; S. Quesadaa; G. T. Palominoa; L. Ferrer; C. P. Cabelloa. Applied Materials Today 24 (2021) 101130. https://doi.org/10.1016/j.apmt.2021.101130
9. M. P. Campos, Master dissertation, Universidade do Estado de Minas Gerais, 2018.

STUDIES ON PLA STRUCTURES USING 3D PRINTING FOR RADAR ABSORBING PROPERTIES

Tamara Indrusiak[1*], Iaci M. Pereira[1], Luis D. P. Farias[1], Matheus S. Domingos [1], Debora P. Schmitz[2], Leonardo Santana[4], Guilherme M. O. Barra[4], Bluma G. Soares[2,3]

1- Centro Tecnológico do Exército, Rio de Janeiro, RJ

tammy.indrusiak@gmail.com

2- Departamento de Engenharia Metalúrgica e de Materiais, Universidade Federal do Rio de Janeiro (UFRJ), Rio de Janeiro, RJ

3- Instituto de Macromoléculas, Universidade Federal do Rio de Janeiro (UFRJ), Rio de Janeiro, RJ

4- Universidade Federal de Santa Catarina (UFSC), Florianópolis, SC

Abstract- The aim of this study is to compare the efficacy of honeycomb structures and 3D printed periodic cellular structures made of PLA in absorbing electromagnetic radiation. Additionally, the study investigates the impact of material thickness and comparing honeycomb structures to fully filled structures. The results indicate that all 3D printed PLA structures had na reflectivety(RL) with peaks around -15dB and a bandwidth of 0.5GHz. Furthermore, the study found that the auxetic honeycomb and the combination of the auxetic honeycomb had better RL results than the honeycomb due to their greater surface area for interaction with electromagnetic radiation. All structures outperformed a fully solid structure, highlighting the importance of geometric effects on electromagnetic properties. The study also compared the RL results from 4 and 8mm honeycomb structure emphasizing the significant impact of the thickness on absorb electromagnetic radiation.

Keywords: *honeycomb, periodic celllular, 3D printing, absorbing property, thicknesss influence*

Introduction

In the 21st century, there has been a great demand for the development of functional materials in the manufacturing and production field. Unlike traditional manufacturing processes such as drilling, milling, and sawing, additive manufacturing, also known as 3D printing, can produce three-dimensional parts through the sequential stacking of material layers, allowing for the possibility of infinite possibilities for rapid prototyping with customized and precise properties [1]. It offers many advantages such as design freedom, flexibility, project complexity, and high sustainability. Almost any type of material such as metal, ceramics, and polymers can be used as raw materials in 3D printing to manufacture a variety of complex structures. Thus, 3D printing covers a wide range of applications such as Biomedicine, Mechanical Engineering, Aeronautics and Astronautics, Electronics, and Integrated Circuits [2].

Currently, the major focus in electromagnetic radiation absorber research is on composition design methods for three-dimensional absorber structures [3]. The most commonly absorber structures studied inlcude honeycomb, pyramidal structure and multilayer structure [4]. Among these, the honeycomb structures is widely used in the radar absorption field due to their periodic cellular structure, which allows wave absorption in a wide frequency range [3,5], as well as their high strength-to-weight ratio, which provides a low-density material with mechanical strength [6]. However, the limitation of thickness in 3D structures has been observed [7]. As a result, some studies have explored alternative approaches by modifying the periodic structures to achieve optimal performance [8]. For example, printing a 2 mm honeycomb structure with high quality and desirable mechanical properties would have challenges.

The objective of this study is to compare the electromagnetic radiation absorbing properties of honeycomb structures and 3D printed periodic cellular structures. Additionally, a comparative study will be conducted between the thickness of the honeycomb.

Experimental

Materials

For printing the parts, commercial Polylactic Acid (PLA) from 3DFila was used, the 1.75mm Prime Gray PLA Filament.

Electromagnetic Properties

The reflectivity (RL) analyses were performed on a vector network analyzer (VNA) model PNA-L model N5231A, 300 kHz - 13.5 GHz, from Agilent Technologies, with a waveguide in the X-Band with a cross-sectional area of 23 x 10 mm.

3D structures production

The structures were 3D printed using fused filament fabrication (FFF) on a GTMax3D Core A3 printer, with printing parameters presented in Table 1. Fig. 1 illustrates the filament deposition.

Table 1- 3D Printing Parameters

Parameters	**Values**
Layer thickness	0.2 mm
Printing Orientation	In plane
Extrusion temperature	215°C
Bed temperature	60°C
Extrusion multiplier	1.1
Printing speed	40 mm/s for infill and 20 mm/s for perimeters

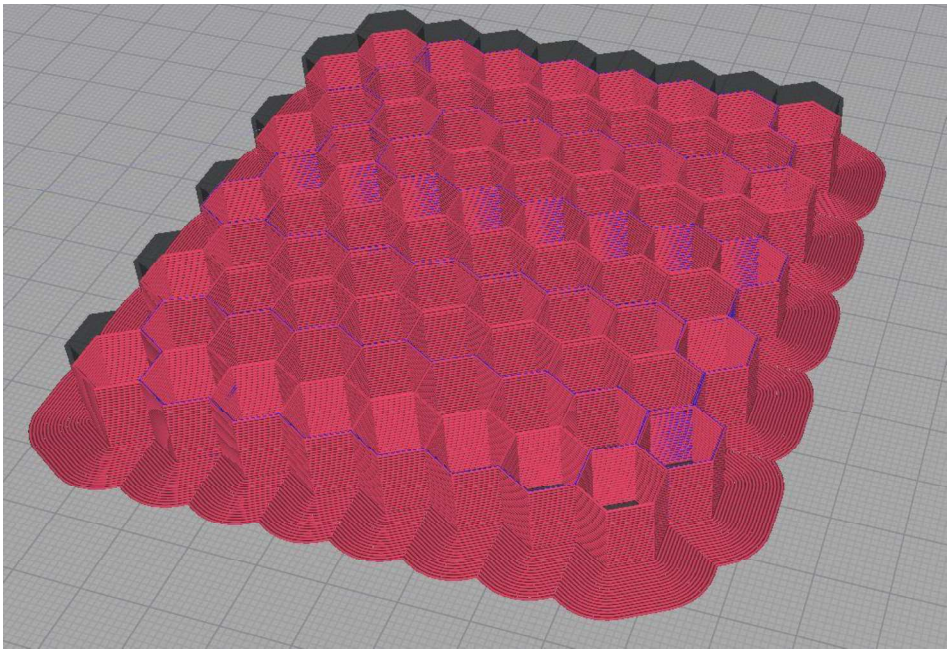

Figure 1- The filament deposition.

Fig 2 shows the design and printed structures: honeycomb, honeycomb reentry, auxetic structure, and two combined honeycomb-auxetic structures. The strucutre design is based on Birman et al study [9].

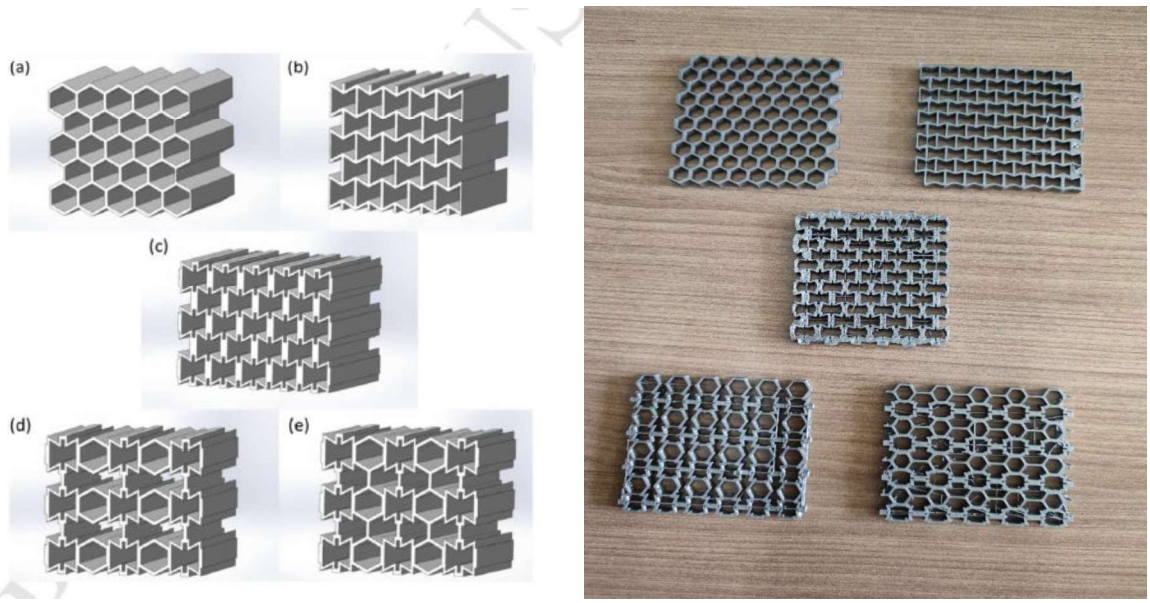

Figure 2 - Cell and printed structure designs: (a) Honeycomb, (b) Honeycomb reentry, (c) Auxetic structure, (d) and (e) Honeycomb auxetic structure [9].

Results and Discussion

Fig 3 shows the RL result of these prints from Fig 2.

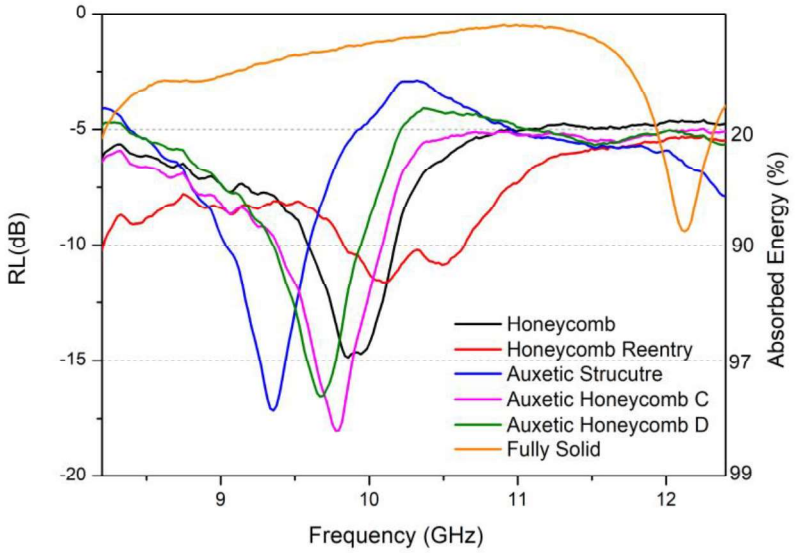

Figure 3- The RL results of the 3D printed

It can be observed that all 3D printed structures exhibit a RL < -5dB, with peaks around -15dB and bandwidth of 0,5GHz that correspond to 97% of absorb energy. The Reentry Honeycomb structure display a RL around -10dB up to approximately 11GHz. Notably, all samples were printed using only unloaded PLA, indicating that the print shape aids in absorption through multiple internal reflections, and the geometrical effect plays a vital role in wave absorption. The RL result for the auxetic and the combination of the auxetic honeycomb was higher than the honeycomb structure, probably due to these structures provide a greater surface area for interaction with electromagnetic radiation. It is important to emphasize that all structures produce better results than a fully solid structure, demonstrating the significance of geometric effects on electromagnetic

properties. Consequently, other periodic strucutre can be explored as radar absorbing material and used instead of honeycomb. Comparing the present results with those found in the literature for periodic structures, Liu et al. [7] investigated the reflection performance of a hierarchical grid structure with a thickness of 22 mm. They achieved an average reflectivity of -17.4 dB across the X-band frequency range, with all values below -10 dB. In another study, Schimitz et al. [8] examined the influence of honeycomb design parameters, such as cell size, thickness, and infill density levels, on the RL. They reported the best X-band results for a honeycomb with 5 mm thickness, achieving an RL< -10 dB over a 3.4 GHz bandwidth with a 10% infill. Notably, the Auxetic Honeycomb C exhibited a reflectivity of -18 dB, showing promising results. To further enhance this performance, optimizing certain parameters and exploring combinations with other conductive additives could position this structure as a highly effective microwave-absorbing material. The present work emphasizes the significant impact of the geometric characteristics on the RL performance.

The thickness of honeycomb structures was also evaluated, with structures printed at 4 and 8 mm thickness, based on previous studies. Fig 4 shows the 3D printing strutcutes.

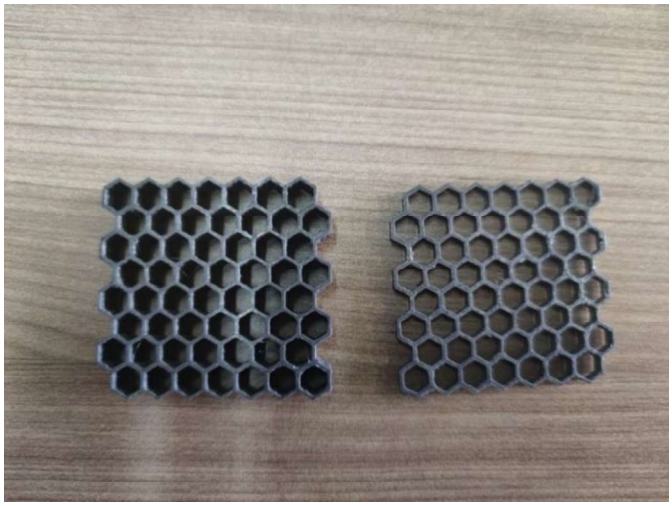

Figure 4 - Honeycomb structures with thicknesses of 8 and 4 mm.

Figure 5 shows the RL results for comparing thickness.

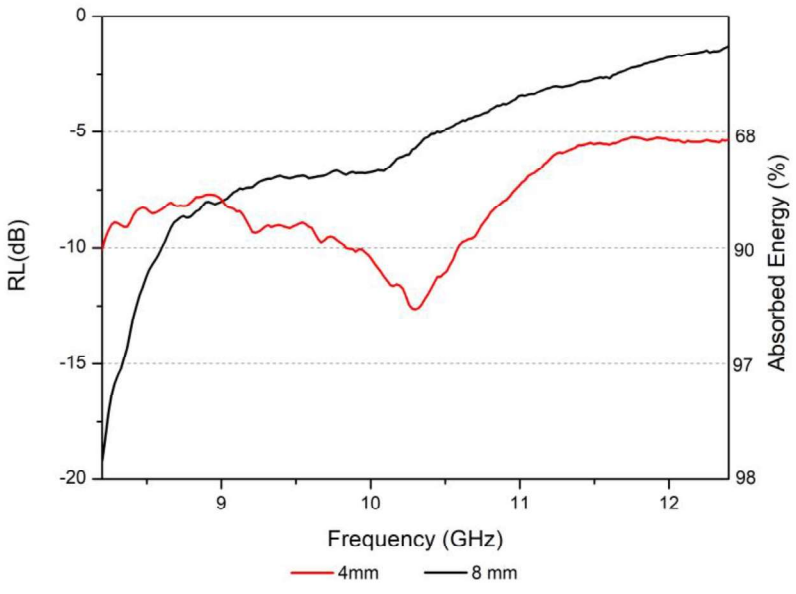

Figure 5 - RL of honeycomb with thicknesses of 4 and 8 mm.

Fig. 5 shows that the 8mm Honeycomb structure delivers good performance at lower frequencies up to 9GHz, followed by a gradual decrease as frequency increases. At 9GHz and beyond, the 4mm structure exhibits the best RL. This outcome can be explained by the fact that, at lower frequencies, the 8mm structure benefits from multiple reflections, whereas, as frequency increases, this effect may decrease, reducing phase cancellation across the thickness. In contrast, the 4mm structure appears to benefit from this cancellation effect, and as the material does not have any load to aid absorption, this thickness was considered optimal for this study.

Conclusions

The present study aimed to compare the electromagnetic radiation absorbing properties of honeycomb structures and 3D printed periodic cellular structures. The results indicate that all 3D printed structures exhibit a RL < -5dB, with peaks around -15dB (97% absorbed energy) and bandwidth of 0.5GHz, while the Reentry Honeycomb structure displays a RL around -10dB (90% absorbed energy) up to approximately 11GHz. It was observed that the print shape aids in absorption through multiple internal reflections, and the geometrical effect plays a vital role in wave absorption. The auxetic and the combination of the auxetic honeycomb produced better results than the honeycomb structure, probably due to their greater surface area for interaction with electromagnetic radiation. Furthermore, all structures perform better than a fully solid structure, demonstrating the significance of geometric effects on electromagnetic properties. Finally, the thickness of these materials significantly impacts their ability to absorb electromagnetic radiation. The 8mm Honeycomb structure delivers good performance at lower frequencies up to 9GHz, followed by a gradual decrease as frequency increases, while the 4mm structure exhibits the best RL at 9GHz and beyond, benefitting from phase cancellation across the thickness. Consequently, other periodic strucutre can be explored as radar absorbing material and used instead of honeycomb.

References

1. Y. Arboui; P. Agaicak; A. Chevalier *et al.* Journal of Material Science, 2017, 52, 4988-4996. https://doi.org/10.1007/s10853-016-0737-3
2. H. Guo; R. Lv 2019; S. Lai. Nano Materials Science, 2019, 1, 101-115. https://doi.org/10.1016/j.nanoms.2019.03
3. S. M. Baek; W. J. Lee; S. Y. Kim *et al.* Composite Strutures, 2022, 289, 115471. https://doi.org/10.1016/j.compstruct.2022.115471
4. P. Gong; Y. Li; C. Xin *et al.* Ceramics International, 2022, 48, 9873-9881. https://doi.org/10.1016/j.ceramint.2021.12.190
5. Z. Pei; Y. Xu; F. Wei *et al.* Journal of Magnetism and Magnetic Materials, 2020, 493, 165742. https://doi.org/10.1016/j.jmmm.2019.165742
6. P. Gong; L. Hao; Y. Li *et al.* Carbon, 2021,185, 272-281. https://doi.org/10.1016/j.carbon.2021.09.014
7. Z. Liu; S. Wang; J. Shao *et al.* Composites Part B, 2022, 247, 110316. https://doi.org/10.1016/j.compositesb.2022.110316
8. D. P. Schmitz; B.G. Soares; G. M. O. Barra *et al*. Polymer Composites, 2023, 44, 2250-221. https://doi.org/10.1002/pc.27240.
9. V. Birman; G. A. Kardomateas. Composites Part B: Engineering, 2018, 142, 221-240. https://doi.org/10.1016/j.compositesb.2018.01.027

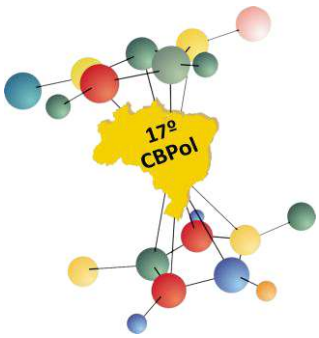

THE INFLUENCE OF PRESSURE IN ELECTRICAL RESISTANCE WELDING OF CARBON FIBER/POLY(ARYL ETHER KETONE) THERMOPLASTIC COMPOSITE

João Victor P. N. Gomes[1]*, Rodrigo Bueno de Souza[2], Juliana Bovi Oliveira[1], Luís Felipe de Paula Santos[1,2], Michelle Leali Costa[1,2], Edson Cocchieri Botelho[2]

1 – Lightweight Structures Laboratory (LEL), Advanced Materials, Instituto de Pesquisas Tecnológicas (IPT), São José dos Campos, SP, Brazil
joaogomes@ipt.br
2 –Departamento de Materiais e Tecnologia, Universidade Estadual Paulista (UNESP), Guaratinguetá, SP, Brazil

Abstract – Thermoplastic composites are versatile and have been widely studied due to many factors as being recyclable, having simple storage and being able to pass through different types of processing in short time cycles. These characteristics turn welding a good way to join these materials with a relatively simple and fast process. So, resistance welding has been a noteworthy topic for these classes of materials there are gaining importance in different areas of industry. The main contribution of this work relies on evaluating the influence of pressure on the resistance welding of thermoplastic composites. A resistance element composed of a glass fiber semipreg and a stainless-steel metallic mesh was made by hot compression molding process. The element was used to weld the composite laminates varying the welding pressure. Electric current and time were fixed for all samples except the last one that used a different welding time. Welded joint strength was studied using lap-shear strength tests, and fractographic analysis using an optical microscope. The highest lap-shear strength result was found using pressure of 1.5 MPa and the lowest with pressure of 3.5 MPa. All samples present an adhesive failure. In addition, it was observed the presence of voids in the welded area.
Keywords: *Resistance welding; Thermoplastic composites; Lap-shear strength; Fracture analysis; Failure analysis*

Introduction

Composite materials, especially carbon fiber reinforced polymer (CFRP) have been increasingly used in different areas of industries including aerospace. Thermoplastic materials have gained more visibility due to its properties of recyclability and also maintaining high mechanical e chemical properties when compared to thermoset composites. PAEK (poly(aryl ether ketone)), PEEK (poly(ether ether ketone), PEI (poly(ether imide), PPS (poly(phenylene sulfide), and others are considered high-performance thermoplastics [1].

Two important topics are that these materials are able to pass through fast processing cycles when compared to thermosets and also have the ability to join them using welding techniques. In this scenario, the use of thermoplastic composites has gained attention, especially from the aerospace industry. One of the ways of joining is resistance welding [1]. There are also different types of welding however, the cited one had some advantages like low manufacturing cost and simplicity [1-2].

The resistance welding process consists of the heating of a resistive element caused by the Joule effect as a result of electric current passing through it. Due to the heating, the melting or glass transition temperature of a thermoplastic matrix is reached and with the aid of pressure, the composite laminates are welded. Resistance welded joints are usually composed of a heating

element and extra pure polymer [2]. There are at least three principal processing parameters that directly influence the quality of weld: welding pressure, welding time and power input (electric current) [2-4].

Experimental

The materials used for this work were carbon fiber (CF) 5HS/poly (aryl ether ketone) (PAEK) (CW 0312 Cetex TC1225) laminates approximately 2.5 mm thick. The laminates were welded using a resistance welding element composed of a metallic mesh of stainless steel AISI 304 MESH 300 and a semipreg of glass fiber (GF) 4HS/PAEK (GW0120 TC1225).

First, the resistance element was consolidated using a hot press machine with the metallic mesh in the middle of 2 semipreg of GF/PAEK, (used to isolate the stainless steel from the carbon fiber of the laminates). Strips of approximately 25.4mm width were cut to be used in the welding process. The CF/PAEK laminates were also cute in 25.4mm width and 127mm length according to ASTMD5868.

Aiming the evaluation of the pressure influence during the resistance welding process. Four sample groups with different parameters were performed as Table 1 shows. It is worth mentioning that the D samples were performed just to evaluate the influence of welding time using 1.5 MPa pressure.

Table 1. Samples with respective welding parameters.

Sample Group	Pressure (MPa)	Time (s)	Electric current (A)
A	0.3	60	35
B	1.5	60	35
C	3.5	60	35
D	1.5	90	35

Source: Author.

To perform the lap-shear strength test (LSS – ASTM D5868) was used a universal mechanical analysis (Instron 5982) and to evaluate the fracture surface was used an Olympus DSX 500 (HRSU) microscope with a 5X lens.

Results and Discussion

2.1 Lap-shear strength results:

Table 2 shows the results with the respective standard deviation for each sample group. It could be noticed that sample B (1.5 MPa pressure) presents the highest mean value (15.48 MPa), which means that this pressure induced a stronger weld/adhesion between the materials. On the other hand, sample C (3.5 MPa pressure) presents the lowest mean value (13.14 MPa). These results are in accordance with the literature, as it shows the best pressure in thermoplastic materials are approximately 0.8 MPa [5]. It is also known that an ideal pressure depends on some factors as material properties and samples dimensions, but usually, the pressure values do not present such differences.

Another interesting point is that adding more 30 seconds in the welding time using the pressure that presents the best LSS result did not influence significantly the average result, reaching 0.41 MPa of difference. However, this difference could indicate that sample D was influenced by a higher temperature in the edge of the welding area, usually called the “edge effect” by the literature [1] that occurs by reason of poor conduction between metal mesh and air (convection) compared to metal mesh and laminates (conduction), weakening, this way, the interface due to reach temperatures close to the degradation of polymer matrix or causing current leakage. Probably producing wider specimens and reducing the clamping distance of the electrodes this effect could be diminished.

Even though it was compared the results, the values obtained in this work were not close to the highest found in the literature, a good weld would induce LSS results close to 30-40 MPa, but

52 MPa was already reached [3, 6]. There are some possibilities to justify these results that will be presented in next section.

Table 2. Lap-shear strength results.

Sample Group	Lap-shear Strength (MPa)
A	14.24 ± 1.98
B	15.48 ± 0.30
C	13.14 ± 1.85
D	15.07 ± 0.96

Source: Author.

2.2 Fracture and failure analysis:

Fig 1 shows a general overview of the failure surfaces of each sample group analyzed. It could be noticed that the pressure influenced the heat transfer in the welding area, this could conclude due to a significant not melted area presented in C samples, indicated by the red circles. Samples A, B, and D did not present such a different welding area failure.

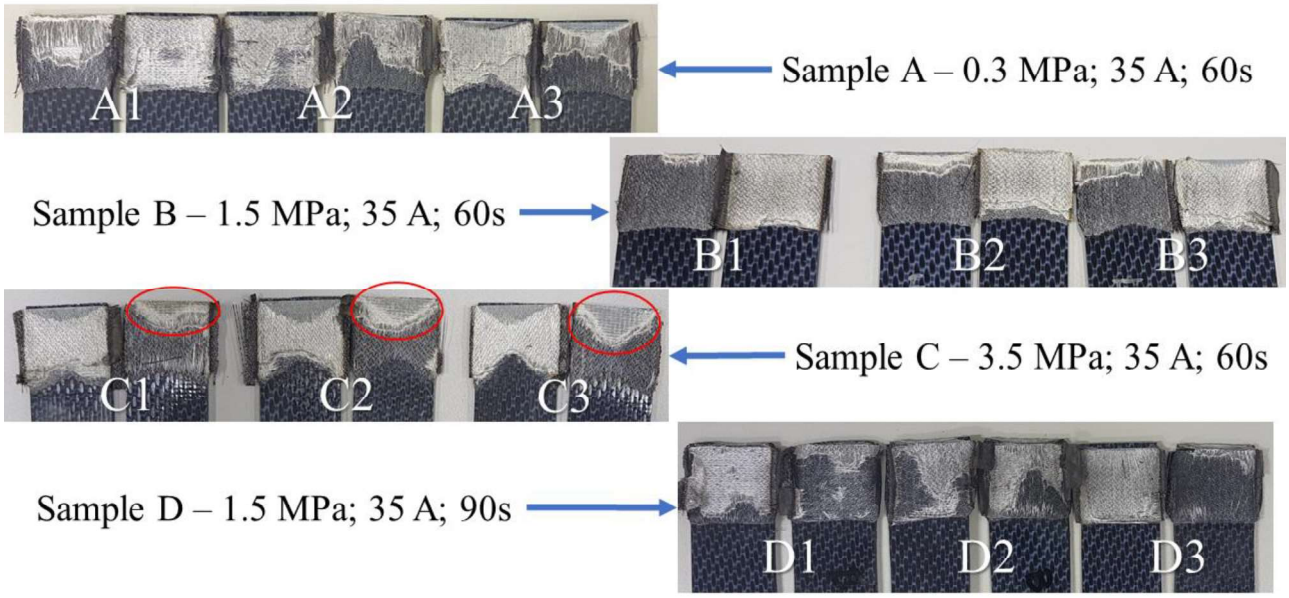

Figure 1 – General overview of samples' failure surface. Source: Author

Using a microscope to amplify welded area and evaluate more aspects. It could be noticed that all the samples had an adhesive failure, also called interfacial failure, between CF/PAEK laminates and GF/PAEK that composed the resistance welding element [1,7]. In addition, an interlaminar failure occurs in the resistance welding element passing through GF/PAEK, metallic mesh, and GF/PAEK from the other side. All this information could be seen in Fig 2.

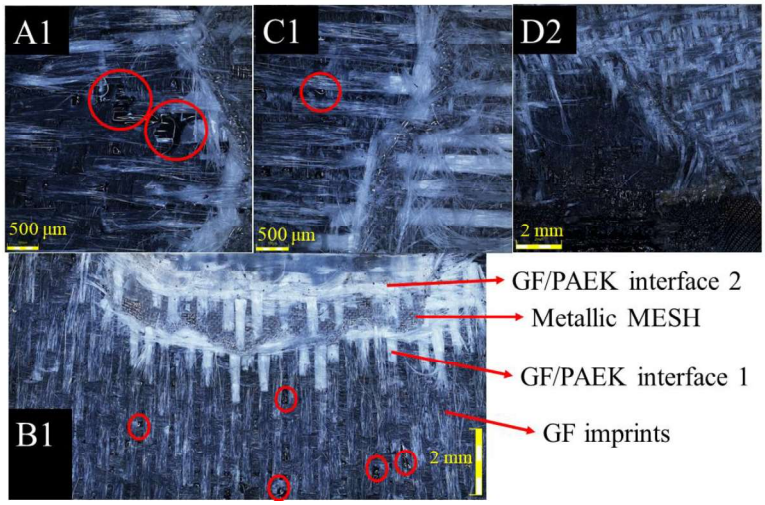

Figure 2 – Microscope images of samples failure surfaces 5X. Source: Author.

Other additional information is that some voids are noticed, indicated by the red circles in Fig 2, usually more expressive in lower pressures, in this case, delamination is induced because it is not capable to consolidate the laminate. A microcopy in the transverse area could be performed to certify this behavior and the formation of voids in the welded area.

According to the literature [6], high pressure in resistance welding processes can reach low values of LSS due to two main reasons. First, it could flatten the fabric causing a reduction of mechanical anchorage favoring less interaction between the polymer matrix and the woven surface, turning the weld weaker. Second it could result in a thinner layer of polymer in the welded area resulting a poor adhesion between fiber and matrix in the interface.

Relating the results from lap-shear and microscope images the small values of LSS could be justified through the failure type showing that there is a weak adhesion between glass fiber and CF/PAEK laminates.

It is worth mentioning that there are several parameters that could affect the resistance welding performance that was not evaluated in this brief work. For example, the metallic mesh surface area contact (mesh number and wire diameter), welding time, electric current, composite laminates properties as heat conduction of fiber and matrix, and glass fiber fabric used in resistance element to isolate. In addition, some process issues as the edge effect influenced by clamping distance as well as metallic mesh isolation could be present in our welding set-up as limitations.

In order to achieve better results, it could be suggested the change of other parameters already mentioned as metallic mesh, minimize the edge effect during the welding process and improve the welding set-up experiment to monitor the temperature and heat distribution inside the weld area.

Conclusions

The resistance welding of CF/PAEK laminates using 60 seconds of welding time, 35 amperes of DC electric current, and pressure of 1.5 MPa present the highest LSS value (15.48 MPa), this could be considered small according to the literature. The lowest was shown with 3.5 MPa (highest pressure analyzed) indicating that high pressure induced a weaker interface interaction due to harming the heat distribution, turning the polymer layer in the interface thin and making the mechanical anchoring difficult in the fabric. The added time in sample D did not influence significantly the LSS results. All the samples present an adhesive failure between the glass fiber/PAEK layer and carbon fiber/PAEK laminate and also an interlaminar failure inside the resistance element.

Acknowledgements
The authors would like to thank Toray Advanced Composites for supplying the thermoplastic laminates, and students and technicians who helped in the analysis and sample preparation. The authors are grateful for National Council for Scientific and Technological Development (CNPq) (304876/2020-8 and 306576/2020-1).

References

1. D. Stavrov; H. E. N. Bersee. Composites Part A: Applied Science and Manufacturing. 2004, 36, 39-54. https://doi.org/10.1016/j.compositesa.2004.06.030.
2. H. Shi; I. F. Villegas; H. E. N. Bersee. Composites Part A: Applied Science and Manufacturing. 2013, 55, 1-10. https://doi.org/10.1016/j.compositesa.2013.08.00.
3. C. Ageorges; L. Ye; YW. Mais; M. Hou. Composites Part A: Applied Science and Manufacturing. 1998, 29(8), 899-909. https://doi.org/10.1016/S1359-835X(98)00022-0.
4. C. Ageorges; L. Ye; YW. Mais; M. Hou. Composites Part A: Applied Science and Manufacturing. 1998, 29(8), 911-919. https://doi.org/10.1016/S1359-835X(98)00023-2.
5. H. Shi, Ph.D. Thesis, Delft University of Technology, 2014.
6. M. Dubé; P. Hubert; J. N. Gallet; D. Stavrov; H. E. Bersee; A. Yousefpour. Journal of composit materials. 2012, 46(8), 911-919. https://doi.org/10.1177/0021998311412986.
7. L. C. M. Barbosa; S. D. B. Souza; E. C. Botelho; G. M. Cândido; M. C. Rezende. Engineering Failure Analysis. 2019, 102, 60-68. https://doi.org/10.1016/j.engfailanal.2019.04.032.

3D-PRINTED ELECTRODES: THE CASE OF IMMUNOSENSOR FOR THE EARLY DIAGNOSIS OF PARKINSON'S DISEASE

Cristiane Kalinke[1], Paulo R. de Oliveira[2], Craig E. Banks[3], Bruno C. Janegitz[2] and Juliano A. Bonacin[1]*

1 – Institute of Chemistry, University of Campinas (UNICAMP), 13083-859, Campinas, São Paulo, Brazil
**jbonacin@unicamp.br*
2 – Department of Nature Science, Mathematics and Education, Federal University of São Carlos (UFSCar), 13600-970, Araras, São Paulo, Brazil
3- Faculty of Science and Engineering, Manchester Metropolitan University, Manchester M1 5GD, United Kingdom

Abstract - In this abstract[1] we would like to demonstrate the versatility of 3D printing technology as a strategic platform for the immobilization of biomolecules, aiming for the fabrication of biosensors. For this, 3D-printed electrodes produced from the conductive filament of PLA (polylactic acid) and graphene[2,3] were modified and used for the detection and quantification of PARK7/DJ-1 protein. The changes in the level of this protein are related to Parkinson's disease. The analytical performance was achieved for the detection of the protein by using both voltammetric and impedimetric techniques with precision and accuracy. The 3D-printed immunosensor produced was successfully applied for the detection of the protein (PARK7/DJ-1) in human blood serum and artificial cerebrospinal fluid samples. This approach can allow the early diagnosis of Parkinson's disease and/or the routine monitoring of the biomarker in different stages of the disease. This method allows us to conclude that 3D printing can be combined with electrochemical methods in the development of versatile, reliable, and feasible biosensors.

References

1. Cristiane Kalinke, Paulo R. de Oliveira, Craig E. Banks, Bruno C. Janegitz and Juliano A. Bonacin; *Sensors and Actuators B: Chemical* 2023, *381,* 133353 - https://doi.org/10.1016/j.snb.2023.133353
2. Pãmyla L dos Santos, Vera Katic, Hugo C. Loureiro, Matheus F. dos Santos, Diego P. dos Santos, André LB Formiga, Juliano A Bonacin; Sensors and Actuators B: Chemical *Chemical* 2019, *281,* 837 - https://doi.org/10.1016/j.snb.2018.11.013
3. Cristiane Kalinke, Naile V. Neumsteir, Gabriel O. Aparecido, Thiago V. B. Ferraz, P. L. Dos Santos, Bruno C. Janegitz, Juliano A. Bonacin; Analyst, 2020, *145(4)*, 1207 - https://doi.org/10.1039/C9AN01926J

Fundings: Coordenação de Aperfeiçoamento de Pessoal de Nível Superior, CAPES (Finance Code 001, Pandemias 88887.504861/2020-00 and 88887.712315/2022-00), São Paulo Research Foundation, FAPESP (grants #2021/07989-4, 2019/00473-2, 2019/01844-4, 2017/21097-3, and 2013/22127-2, Conselho Nacional de Desenvolvimento Científico e Tecnológico, CNPq (303338/2019-9 and 308203/2021-6).

Keywords: *3D-Printed Electrodes, 3D-Printing, Immunosensor, Early diagnosis Parkinson's disease*

ASSESSMENT OF SHAPE MEMORY PROPERTIES IN COMPOSITE 4D PRINTING FILAMENTS OF PLA/TPU

Ana P. Knopik[1], Cristian de O. Romera[2], Antônio I. Magalhães[2], Emanuel Martins[2] and Juliana R. Kloss[1]

1 – Academic Department of Chemistry and Biology, Federal University of Technology – Paraná (UTFPR), Curitiba, PR, Brazil aknopik@ertbio.com
2 – Earth Renewable Technologies (ERT), Curitiba, PR, Brazil

Abstract - Additive manufacturing has garnered significant attention over the past decade as a rapidly growing sector within complex manufacturing[1]. Suitable materials and proper variation in the printing settings may result in the production of parts with time-dependent shapes that can be tuned through environmental stimuli[2,3]. Given that these parts can either change their shape over time to a pre-programmed three-dimensional shape or revert to an initial design, this process has become referred to as four-dimensional (4D) printing[2]. This study had the objective of evaluating compositions based on poly(lactic acid) (ERT1, ERT2) and thermoplastic polyurethane (TPU, Mirathane E270) to 4D printing filaments. The ERT1, ERT2, ERT1/TPU and ERT2/TPU (80/20), were processed in twin-screw extruder at 50/200/200/200/200/200/210 °C. Analyzed the tensile strength, elongation at break, melt flow index, thermal deflection temperature and toughness of the injected samples were carried out. Besides, the shape memory test (Fig.1) was performed with the compositions by heating the fine filament, initial length of 50 mm and diameter 1.5-2.0 mm, for 240 s at 80 °C. While the filament was heated, it has been molded into a helical intermediate shape using a metal tube and got cold for 80 s in a beaker with water at 7.5 °C. Then, heated the sample for 85 s at 80 °C and was obtained final shape. ERT1 presented a final length of 47.7±0.6 mm comparing with ERT1/TPU which showed to 49.7±0.6 mm, property observed to studies which showed to PLA exhibited flexible nature and shape memory by the addition of TPU. The ERT2/TPU induced poor shape memory than ERT1/TPU and ERT1, however higher extrusion stability. The next step will be printing a cubic structure to repeat the shape memory test. According to the results, the PLA/TPU compositions have been potential properties of 4D printing filaments to application biomedical, robotic and aerospace.

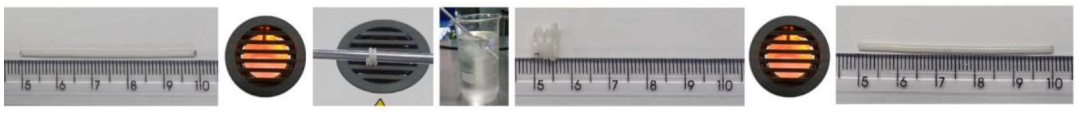

Figure 1. ERT1/TPU shape memory test. (a) initial shape. (b) first heating sample. (c) molded to a helical shape. d) cooling sample. (e) intermediate shape. (f) final heating sample. (g) final shape.

References

1. H. Liu; F. Wang; W. W; X. Dong; L. Sang. *Composites Part B*, 2023, *248*, 110382. https://doi.org/10.1016/j.compositesb.2022.110382.
2. S. Boyacioglu; M. Kodal; G. Ozkoc. *European Polymer Journal*, 2020, *122*, 109372. https://doi.org/10.1016/j.eurpolymj.2019.109372.
3. G. F. M. Morgado; N. K. de Moura; E. F. Martins; C. A. Escanio; E. H. Backes; J. Marini; F. R. Passador. *Journal of Polymer Research,* 2022, *29*, 533. https://doi.org/10.1433/7851/02/4112-2035.

Keywords: *four-dimensional printing; smart materials, biobased; poly(lactic acid); polyurethane.*

CORRELATION BETWEEN UV-CURING INKJET ADHESION AND AIR PLASMA TREATMENT IN POLYURETHANE COATING

Maria Augusta S. Yokomishi [1], Rogério S. Scotton[1], Mauricio P. Oliveira[1], Lilia M Guerrini [1*]

1 - Laboratory of Polymer Synthesis and Process, Institute of Science and Technology, Federal University of São Paulo (UNIFESP), São José dos Campos, SP, Brazil

guerrini@unifesp.br

Abstract – The digital printing process allows to print photos and drawings directly on different substrates and/or coatings. However, the implementation of digital printing still needs studies, mainly due to the type of substrate used, the physical-chemical properties of the inks, the chemical characteristic of the surface coating and the variables of the printing [1,2]. This work aims to evaluate the influence of the atmospheric plasma jet treatment on polyurethane (PU) coating surface to improve the adhesion of printing inks. The study of the surface treatment of the PU coating by air atmospheric plasma jet was carried out before inks printing with different distances, speeds of plasma jet application and the treatment time (days) as shown in Table 1. The PU coating surfaces before and after treatment were evaluated for contact angle (Table1). Printed PU coating were evaluated for adhesion, gloss, hardness and image quality. Figure 1 shows the printed sample and results of the adhesion test. The treatment via atmospheric plasma jet can efficiently reduce the contact angle of the PU coating. A promising result related with the anchoring of the ink on the PU coating was found in the sample treated with plasma at 4 mm and 17 mm/s. This study brings pertinent information about the influence of the plasma treatment on the PU coatings and the adhesion of the ink after printing.

Table 1. Plasma treatment conditions and duration of the treatment. Plasma power at 850W.

Conditions	Sample	d (mm)	v (mm/s)	Contact angle (°)			
				0 day	1 day	2 days	4 days
1	1-1 – 1-2	2	34	24.6	37.1	37.0	37.8
2	2-1 – 2-2	4	34	26.0	43,2	46.4	48.7
3	3-1 – 3-2	8	34	34.0	41.2	38.8	46.8
4	4-1 – 4-2	2	17	22.0	31.7	32.8	36.7
5	5-1 – 5-2	4	17	27.2	37.7	35.0	39.4
6	6-1 – 6-2	8	17	30.8	40.3	40.4	48.6

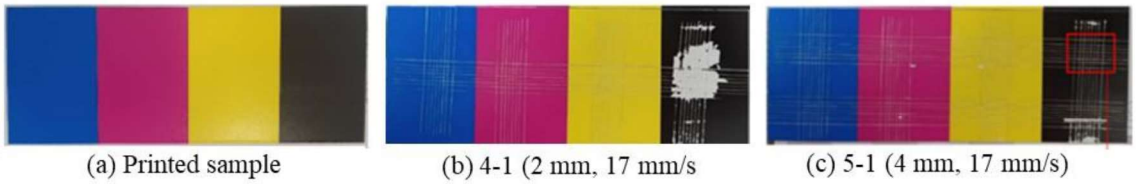

(a) Printed sample (b) 4-1 (2 mm, 17 mm/s (c) 5-1 (4 mm, 17 mm/s)

Figure 1. (a) Printed inkjet sample; samples after adhesion test (b) 4-1 and (c) 5-1.

References

1. R. S. Scotton; M. P. Oliveira; L. M Guerrini. *Progress in Organic Coatings* 2021, *158*, 106389. https://doi.org/10.1016/j.porgcoat.2021.106389
2. T . S. M. Mui, L.L.G. Silva, V. Prysiazhnyia, K.G. Kostova. *Journal of Adhesion Science and Technology,* 2015, vol. 30, 2. http://dx.doi.org/10.1080/01694243.2015.1099863

Fundings: Fundação de Amparo à Pesquisa (FAPESP) proc.2021/079470-1

Keywords: polyurethane coating, inkjet, plasma, treatment.

DEGRADATION UNDER PROCESSING OF A PLA/EGGSHELL

Daniella S. C. Andrade[1]*, Lara M. M. Oliveira[2], Renata Barbosa[3], Tatianny S. Alves[3] and Yêda M. B. de Almeida[1]

1 – Materials Science Program, Federal University of Pernambuco (UFPE), Recife, PE, Brazil
daniella.andrade@ufpe.br
2 – Department of Chemical Engineering, Federal University of Pernambuco (UFPE), Recife, PE, Brazil
3 – Graduate Program in Materials Science and Engineering, Federal University of Piauí (UFPI), Teresina, PI, Brazil

Most polymers degrade under processing, mostly by thermally stimulated processes. While thermogravimetric methods could be used to estimate the ultimate thermal stability, incipient degradation (loss of molar mass), which may significantly affect material properties, are better studied by rheological techniques. During the last stage of processing (melt processing) in an internal mixer at constant rotor speed, torque is proportional to viscosity, which a very sensitive measure of the molar mass of the polymer. Since viscosity also depends on temperature, torque is adjusted to a reference temperature taking into consideration a temperature coefficient experimentally determined. Measuring the average adjusted torque and its rate of change in a brief time interval, and considering the "universal" 3.4-power law dependence of the viscosity with the mass-average molar mass, it is possible to estimate the relative rate of change of the molar mass, which may be taken as a measure of the rate of incipient degradation during processing. This procedure has been applied to the study of polymers, blends and compounds.[1-5] In the present work, polylactic acid (PLA) and chicken eggshell (3, 5 and 7%w) measuring up to 100µm were mixed and processed in an internal laboratory mixer with rotor speed varying from 30 to 150 rpm, keeping the temperature constant of the mixer chamber walls at 180°C. The results showed that the higher rotation speed is associated with a lower rate of degradation in compositions containing eggshell, indicating a better distribution and dispersion of solid particles that also provided greater thermal stability to the melt. Highlighting that high rotor speed is a better processing operating parameter for composites.

1. T. S. Alves; J. E. Silva Neto; L. H. Carvalho; E. L. Canedo. *Polymer Testing* 2015, 50.
2. V. A. D. Marinho; C. A. B. Pereira; M. B. C. Vitorino; A. S. Silva; L. H. Carvalho; E. L. Canedo. *Polymer Testing* 2017, 58.
3. L. T. A. Reul; C. A. B. Pereira; M. F. Sousa; R. M. Santos; L. H. Carvalho; E. L. Canedo. *Polymer Composites* 2019, 40.
4. D. S. C. Andrade; E. L. Canedo; L. H. Carvalho; R. Barbosa; T. S. Alves. *Materials Research* 2021, 24.
5. E. S. B. Ferreira; C. B. B. Luna; D. D. Siqueira; E. A. Santos Filho; E. M. Araujo; R. Wellen. *Sustainability*, 2021, 13.

Fundings: The authors are grateful to CAPES (Coordination for the improvement of Higher Education Personnel) and FACEPE (Foundation for the Support of Science and Technology of the State of Pernambuco) for the financial support.

Keywords: *PLA, eggshell, degradation, rheology, processing*.

DEVELOPMENT OF BIODEGRADABLE COMPOSITES FOR ADDITIVE MANUFACTURING USING POLY(BUTYLENE SUCCINATE) AND COCOA RESIDUES

Robson P. Araújo[1]*, Cesar A. G. Beatrice[2] and Lidiane C. Costa[1,2,3]

1 – Department of Materials Engineering (DEMa), Graduate Program in Materials Science and Engineering (PPGCEM), Federal University of Sao Carlos (UFSCar), São Carlos, SP, Brazil. araujorobson07@gmail.com
2- Department of Materials Engineering (DEMa), Federal University of São Carlos (UFSCar), São Carlos, SP, Brazil
3- Center for Characterization and Development of Materials (CCDM), Federal University of São Carlos (UFSCar), São Carlos, SP, Brazil

Abstract - In this work, biodegradable composite filaments were produced from Poly(Butylene Succinate) (PBS) and cocoa bean shell waste (CBS). The extrusion process was utilized to produce the composite filaments, incorporating up to 20 %wt of the natural filler into the PBS matrix. The filaments were characterized for their dynamic rheological properties and assessed for process and print quality. Following the 3D printing, the morphological, mechanical, thermal and soil disintegration (composting) properties were evaluated. The rheological characterization of the filaments showed changes in the viscoelastic behavior of the composites compared to the pure PBS matrix [1]. The results suggest that the incorporation of CBS can facilitate the application in Fused Deposition Modeling (FDM) [2]. The printability of the developed biodegradable composite filaments was considered satisfactory. Furthermore, the composites exhibited thermal stability during the printing process and the DSC analysis indicated a minor variation in their crystallinity post-printing [3]. Regarding the mechanical properties, the composite showed a 21.8% increase in the elastic modulus value, while the tensile strength and elongation at break showed a reduction with the incorporation of the filler. The disintegration rate in soil, which indicates a biodegradation process, was increased, showing a value of 48% after 156 days of composting, while a disintegration rate of only 4.7% was observed for the pure PBS matrix [4]. The results indicate that CBS can be used to increase and modulate the rate of biodegradation of the PBS matrix used for the production of filaments for application in FDM.

References

1. V. Mazzanti; F. Mollica; *Polymer 2020,* 12, 2304. https://doi.org/10.3390/polym12102304.
2. Zhou, Y; Xia, X; Liu, X; Huang, B; Xiao, L; Qian, Q; Chen, Q; *Macromolecular Materials and Engineering 2019*, *304*, 1900021. https://doi.org/10.1002/mame.201900021.
3. M. V. Candal; I. Calafel; N. Aranburu; M. Fernández; G. Gerrica-Echevarria; A. Santamaria; e A. J. Müller; *Additive Manufacturing 2020,* 36, 101408. https://doi.org/10.1016/j.addma.2020.101408.
4. M. I. Peñas; R. A. Pérez-Camargo; R. Hernández; e A. J. Müller; *Polymers 2022,* 14, 1025. https://doi.org/10.3390/polym14051025.

Keywords: *additive manufacturing, poly(butylene succinate), biodegradable, composites, cocoa bean shell.*

ELECTROSTATIC CHARGED FUNCTIONAL 3D PRINTED POLYMERS

Ezequiel Lorenzett[1], Yan A. S. da Campo[2], Kelly S. Moreira[1], Pedro R. Lorenzoni[2] and Thiago A. L. Burgo[1,2,3]*

1 – Department of Chemistry, Federal University of Santa Maria (UFSM), Santa Maria, RS, Brazil
ezequiel.lorenzett@acad.ufsm. br
2 – Department of Physics, Federal University of Santa Maria (UFSM), Santa Maria, RS, Brazil
3 – Department of Chemistry and Environmental Sciences, São Paulo State University (UNESP), São José do Rio Preto, SP, Brazil

Thermoplastic polymers belong to a class of synthetic polymers and are widely used due to their versatile properties. When these polymers are heated close to their melting temperature, they exhibit a highly viscous liquid state. This high viscosity makes them easily moldable, rendering them ideal for use in additive manufacturing technology, specifically in fused deposition modeling 3D printing [1]. In the 3D printing process, the polymers are arranged as filaments, which are melted and extruded through a metal nozzle, and then deposited onto a substrate. During this process, various effects of polymer electrification can be observed, including extrusion, friction, phase change, strain gradients, contact surfaces between different materials (polymer/substrate) or identical materials, and solid-liquid interfaces under temperature gradients [2][3][4][5]. Consequently, this generates an accumulation of charges in printed objects, with the magnitude varying according to the type of polymer, substrate, and selected printing parameters. In this study, we conducted an extensive investigation using a non-contact Kelvin probe [6] to demonstrate the spontaneous formation of charges in five polymers (ABS, PETG, PLA, TPU, and Nylon) during and after printing. These five polymers were printed on three different substrates (glass, steel, and PTFE). Subsequently, the glass substrate was selected as the standard, and the influence of printing parameters on electrification was evaluated. Furthermore, experiments were conducted to investigate the effect of contact between identical polymers. Additionally, the half-life times of the charges were determined. This approach paves the way for numerous advancements, including the in-situ fabrication of electrets, the production of parts with controlled electrical charge, the use of pre-electrified molds in energy harvesting devices or wearable electronics. Surprisingly, this is the first report of such behavior.

References

[1] Zhang. *SusMat.* 2021, 1, 1, 127-147. https://doi.org/10.1002/sus2.11
[2] Krusenbaum, A., Grätz. *Chem. Soc. Rev* 2022 ,51, 2873–2905. https://doi.org/10.1039/D1CS01093J
[3] K.S. Moreira. *JAP.* 2021, 129, 23 234502. https://doi.org/10.1063/5.0048989
[4] T. A. L. Burgo and F. Galembeck. *Lagmuir* 2012, 28 n.19, 7404-7416. https://doi.org/10.1021/la301228j
[5] Gross, B.. *Phys*. Rev. 1954, 94, 1545–1551. https://doi.org/10.1103/PhysRev.94.1545
[6] E. Lorenzett et al, *Journal of Applied Physics* 2021 129, 204502. https://doi.org/10.1063/5.0049008

Fundings: CAPES, CNPq, INOMAT.

Keywords: *3D printed*, *electrification, extrusion, contact, charge build up.*

MELT MIXING PROCESS PARAMETER ANALYSIS OF PVDF/EVA FILLED WITH GNP TO INSURE BEST PROPERTIES

Beatriz S. Cunha[1]*, Débora P. Schmitz[2], Bluma G. Soares[1,2]

1 – Departamento de Engenharia Metalúrgica e de Materiais, Universidade Federal do Rio de Janeiro (UFRJ), Rio de Janeiro, RJ, Brasil
beatriz.cunha@outlook.com
2 – Instituto de Macromoléculas Professora Eloisa Mano, Universidade Federal do Rio de Janeiro (UFRJ), Rio de Janeiro, RJ, Brasil

Abstract - The understanding of process parameters and how they influence the material's properties is very important to achieve the desired result. This work aims to establish the best melting mixing conditions to obtain a high conductive composite, base on recycled Poly(vinylidene fluoride) (PVDF) and Ethyl Vinyl Acetate (EVA) (65:35 wt%) blend, filled with graphene nanoplatelets (GnP). The study was carried out using a composite with 10 wt% of GnP added to the PVDF/EVA blend matrix, and the analyzed parameters were speed, temperature and time of mixture in a micro compounder MC 15 HT (by Xplore). At the end, a master batch approach was employed, with the best acquired parameters, to compare with the one step method. Electrical conductivity, rheological properties, and morphology were investigated. The samples processed at a the highest speed (200 rpm), highest temperature (210 °C) and mixing time of 3 min showed the best conductive value, of around 10^{-5} $S.m^{-1}$. From the rheological study, we could conclude that the sample with the highest conductivity have better distribution of GnP in the matrix. Regarding the master batch versus one step approach, the best result was achieved by adding all the components at the same time.

Keywords: *Poly(vinylidene fluoride), Ethyl Vinyl Acetate, graphene nanoplatelets, processes parameters, conductivity.*

NIOBIUM OXIDE (Nb_2O_5) AS A FILLER FOR PLA FILAMENTS: 3D PRINTING IN BIOMEDICAL APPLICATIONS

Anderson A. Horta[1], Caroline S. Pagnan[1] and Eliane Ayres[1]*

1 – Postgraduate program in Design (PPGD), State University of Minas Gerais (UEMG), Belo Horizonte 30140-092, Brazil

eliane.ayres.pu@gmail.com.br

Abstract - Brazil has international leadership in reserves and ore production such as iron and niobium [1]. In this context the use of niobium pentoxide (Nb_2O_5), abundant oxide in the Brazilian territory, was chosen to be studied to expand their applications in order to add value. The present project aims to develop a myoelectric transradial upper limb prosthesis, with national components, through low-cost digital fabrication, using high-performance composite material, composed of poly(lactic acid) (PLA) and different contents of Nb_2O_5. The research methodology, which brings together the development of assistive technologies and 3D printing, was divided into two stages: (i) production of PLA/Nb_2O_5 filaments for 3D printing and (ii) digital fabrication of the myoelectric prosthesis prototype. Herein, the masterbatch technique was used to incorporate Nb_2O_5 (Sigma-Aldrich SKU 208515) into PLA [2]. Briefly, PEG 6000 was manually mixed with Nb_2O_5 in a ratio of 1:1 at 60 °C. After cooling, the mixture was grounded and passed through a 100-mesh sieve. The amount of powder (MB), corresponding to 0.1, 0.25 and 0.50% over PLA, was blended with PLA pellets before extrusion to give rise to the filaments. Fig. 1 shows SEM image of MB and the effect of MB addition on the mechanical properties of PLA.

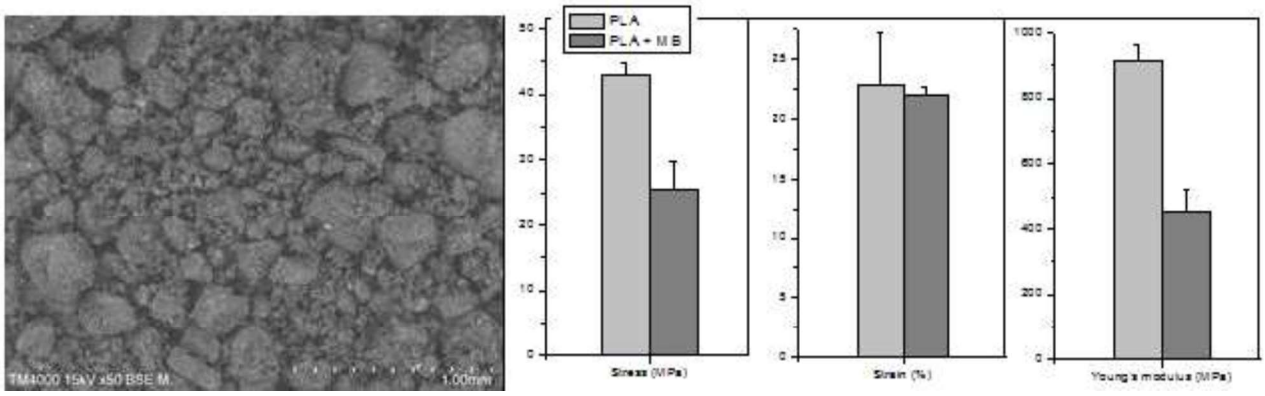

Figure 1 – SEM image of MB and mechanical properties in traction of PLA and PLA/MB (0.5%).

Tensile test results of PCL/Nb_2O_5 composites also showed a moderate decrease in tensile properties [3]. Here, the presence of the PEG used to prepare the MB might have accentuated the decrease of properties.

References

1. https://www.inova.rs.gov.br/upload/arquivos/202006/16181825-plano-de-ciencia-tecnologia-e-inovacao-para-minerais-estrategicos.pdf. Accessed 30 may 2023
2. C. S. Pagnan; A. C. Mottin; R. L.Oréfice; E. Ayres; J. J. D. Câmara Journal of Polymers and the Environment 2018, 26, 1169-1178. https://doi.org/10.1007/s10924-017-1026-1
3. J. C. Sousa; A. R. M. Costa; J. C. Lima; S. A. Arruda; Y. M. Almeida; E. L. Canedo Polymer Composites 2020, 41(4), 1265-1276. https://doi.org/10.1002/pc.25452

Fundings: Financiadora de Estudos e Projetos (FINEP) ref. Finep nº 0166/21, Grant/Award Number: 01.22.0275.00. Referring to Chamada Pública MCTI/FINEP/AÇÃO TRANSVERSAL Materiais Avançados e Minerais Estratégicos 2020.

Keywords: *Niobium oxide-PLA composite filaments, Nb_2O_5-PEG masterbatch, 3D Printed myoelectric prosthesis*

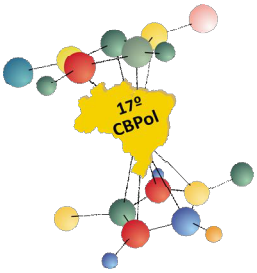

SUSTAINABLE DEVELOPMENT OF PLA/COFFEE GROUNDS FILAMENTS AT DIFFERENT CONTENTS: EVALUATION OF MECHANICAL STRENGTH

Carolina Q. Passos [1,2], Débora C. da S. Santos[1], Simone M. de Rezende [1,2], Marcelo F. L. de Oliveira [1], Fernanda C. F. Braga[1] and Marcia G. de Oliveira[1*]

1 – Instituto Nacional de Tecnologia, Rio de Janeiro, Rio de Janeiro, RJ, Brazil

fernanda.braga@int.gov.br / carolina.quaresma@int.gov.br

2 – Faculdade de Filosofia Ciências e Letras Souza Marques (FFCLSM), Rio de Janeiro, RJ, Brazil

Abstract - Vegetable residues emerge as an alternative to traditional reinforcement fillers, commonly used in polymeric composites, playing an important role when reintroduced in the process as a raw material and ceasing to be an environmental liability [1]. With the same sustainable bias, 3D printing is currently seen as a green process, since it creates high-quality three-dimensional objects without high energy cost, in addition to minimizing the generation of common burrs in traditional processes such as molding by injection and compression [2]. The PLA filaments and their composites with different incorporated of contents of coffee grounds - BC (0; 2.5; 5; and 7.5 wt. %) were processed in a co-rotating single screw extruder and characterized according to the melt index flow. Specimens for tensile strength and flexural strength, hardness, morphology by scanning electron microscopy and water absorption were obtained by 3D printing and the parameters used during fabrication were 210 °C with filling geometry and density of octet and 75% respectively [3], by the melt deposition modeling (FDM) method. The results obtained indicated that the increase in the BC content favored the reduction of the viscosity of the composites, when compared to the pure PLA matrix and, consequently, lower hardness. This behavior was possibly caused by the lipid content that constitutes the coffee grounds [4], thus acting as a processing aid facilitating its incorporation into the matrix, as visualized by the SEM. However, a significant reduction in tensile and flexural strength was verified according to the increase in the amount of BC residue. On the other hand, it was found that the increase in the amount of residue incorporated into the matrix was proportional to the water absorption, due to the hydrophilicity of the filler. Such results indicate that BC can favor the biodegradation of composites, not making them an environmental liability after disposal.

Acknowledgments: For the CNPq financial support and the assistance of SENAI CETIQT in the process of the extrusion filaments.

References

1. Rozi, Nasrullah Mat; Hamid, Hamidah Abdul; Hossain, Md. Sohrab; Khalil, Nor Afifah; Yahaya, Ahmad Naim Ahmad; Fizal, Ahmad Noor Syimir;Haris, Mohd Yusoff; Ahmad, Norkhairi; and Zulkifli, Muzafar. Enhanced mechanical and thermal properties of modified oil palm fiber-reinforced polypropylene composite via multi-objective optimization of in situ silica sol-gel synthesis. Polymers, v. 13, p. 3338, 2021.
2. Mota, Carlos Augusto; et al. Influence of Processing Parameters on the Mechanical Strength of PLA Parts Manufactured by FDM Additive Manufacturing. Brazilian Journal of Manufacturing Engineering, São Paulo, v. 5, n. 1, p. 76-83, Jan./Mar. 2021.
3. C. Q. Passos; S. M. De Rezende; M. F. L. De Oliveira; F. C. F. Braga; M. G. De Oliveira. Circular economy and 3D printing: impact of angle and printing speed on flexural strength. XVII Regional Meeting of the Brazilian Society of Chemistry - SBQ-RJ, Rio de Janeiro, 2022.
4. De Bomfim, Anne Shayene Campos; De Oliveira, Daniel Magalhães; Voorwald, Herman Jacobus Cornelis; Benini, Kelly Cristina Coelho de Carvalho; Dumont, Marie-Josée; and Rodrigues,Denis. Valorization of spent coffee grounds as precursors for biopolymers and composite production. Polymers, v. 14, p. 437, 2022.

Keywords: *3D printing, PLA, coffee grounds, biodegradable polymers and sustainable.*

SUSTAINABLE GRAPHENE OXIDE-CHITOSAN FILTER ELEMENTS

Áquila Oliveira de Alencar*, Gláucia Regina Medeiros Burin, Helton José Alves

Laboratory of Materials and Renewable Energy (LABMATER), Federal University of Paraná (UFPR), Palotina-PR, Brazil - aquila.alencar@ufpr.br

Abstract

Innovations in the field of nanotechnology provide opportunities and applications in different segments, including the mobility sector. Chitosan foams can be used as filter elements for the automotive sector due to their adsorptive characteristics, but they have limited mechanical strength and flexibility. Graphene oxide (GO) nanoparticles can be incorporated into polymer matrices to enhance filtration properties and mechanical resistance. This work incorporated GO into chitosan-based polymer matrices structured in the form of low-density foams. The foams were produced according to patent number BR1020150292597 [1]. Chitosan was obtained from shrimp shells processed at the Federal University of Parana (UFPR) and presented a deacetylation degree of 94% and molar mass of 27 kDa. Different percentages of GO relative to chitosan mass (0 to 5% m/m) were incorporated in acetic acid solution and sonicated for 5 minutes (2s/2s pulse). For foam preparation, chitosan was dissolved in the acetic acid solution containing GO until complete homogenization. Commercial neutral emulsifier was added to the chitosan solution (with or without GO) followed by mechanical incorporation of air with a household mixer. The foam was uniformly spread on 1 cm thick and dried at 70 °C [1,2]. The samples were characterized by Scanning Electron Microscopy (SEM)/Energy Dispersive Spectroscopy (EDS) and bulk density by mass/volume ratio. Irregular pores with diameters of 40-200 μm were observed on the bottom surface and circular pores with diameters of 2-140 μm were observed in the top layer. The elements C, O and N were detected in the chemical composition of foams. The bulk density of samples ranged from 6.3 to 8.3 x 10^{-2} g.cm^{-3}. The incorporation of GO in chitosan foams represents an innovation considering the multifunctional character of the developed material.

References

1. Muniz, G. I. B.; Masson, M. L.; Ellendersen, L. S. N.; Alves, H.J. Patente BR1020150292597, INPI -Instituto Nacional da Propriedade Industrial, 2015.
2. Ellendersen, L. D. S. N.; Milinsk, M. C.; Feroldi, M.; Zadinelo, I. V.; dos Santos, L. D.; de Muniz, G. I. B.; Gasparrini, L. J.; Alves, H. J. *Journal of Environmental Chemical Engineering* 2018, *6*, 5. https://doi.org/10.1016/j.jece.2018.09.019.

Keywords: *Composite materials, Biopolymer, Foams.*

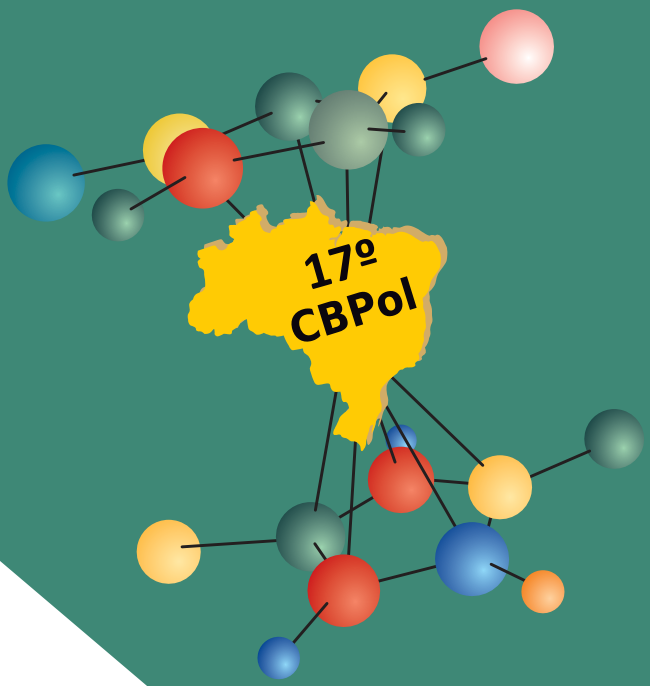

Rubber and Elastomers

USE OF ELASTOMERS IN THE MANUFACTURE OF MECHANICAL SENSORS AND ACTUATORS : FLEXIBLE ELECTRODES AND BEYOND

Carlos H. Scuracchio [1*], Matheus C. Saccardo[1], Roger Goncalves [2], Ariel G. Zuquello[3], Sandra A. Cruz[2], Rafael Barbosa[4]

1 – Programa de Pós Graduação em Ciência e Engenharia de Materiais (PPGCEM), Federal University of São Carlos (UFSCar), São Carlos, SP, Brazil; 2 – Department of Chemistry (DQ), Federal University of São Carlos (UFSCar), São Carlos, SP, Brazil; 3 - Community University of the Chapecó Region, Chapecó, SC, Brazil
4 – Department of Materials Engineering (DEMa), Federal University of São Carlos. SP. Brazil
*carlos.scu@ufscar.br

Abstract – Mechanical sensors and actuators based on ionic electroactive polymers, iEAP's presents several advantages over their traditional analogues: lightness, relatively easy construction, miniaturization capability, reduced cost, etc. Among these materials, we can also highlight the use of elastomers, which add high flexibility and a wide range of mechanical properties that can be exploited in order to adapt to specific applications. In this work will be addressed two main types of elastomers and their use in sensors and actuators based on iEAP's: vulcanized elastomers, VE's, and thermoplastic elastomers, TPE's. EV's are mainly used in the manufacture of flexible electrodes, opening a very promising field in the area of device construction, due to their robustness. On the other hand, TPE's of the block copolymer type can be synthesized so that they present sensitive behavior to deformation, combining the possibility of adjusting their mechanical and viscoelastic properties (by choosing the types and the arrangement of the blocks in the copolymer). In this presentation will be shown some proposals that are being developed in the Smart Materials Research Team, SMaRT, of the Department of Materials Engineering, DEMa, of the Federal University of São Carlos, UFSCar. The goal is to show how elastomers can be used as smart materials in the area of electronics and soft robots, taking advantage of their unique characteristics. To this end, SMaRT has set up a structure of aracterization and application of these devices that allows their characterization in various types of situations.

References

1. R. Barbosa ; R. Gonçalves; K. A. Tozzi; M. C. Saccardo; A. G. Zuquelo ; C. H. Scuracchio. *Journal of Applied Polymer Science*, 2022, 52325. https://doi.org/10.1590/1980-5373-MR-2022-0609
2. K. A. Tozzi, R. Gonçalves, M. C. Saccardo, A. G. Zuquelo, E. Sgreccia, R. Narducci, C. H. Scuracchio M. L. Divona, *Journal of Applied Electrochemistry*, 2022, s10800-022-0177, doi: 10.1007/s10800-022-01776-w
3. R. Barbosa ; R. Goncalves; G. E. O. Blanco, K. A. Tozzi; M. C. Saccardo; A. G. Zuquelo; C. H. Scuracchio, Electrochemica Acta, 2022, 435, 141341, https://doi.org/10.1016/j.electacta.2022.141341

Fundings: The authors would like to thank FAPESP (processes 2023/05676-4, 2022/14231-3, 2022/04348-0, 2020/02696-6, 2018/09761-8, 2018/07001-6), CAPES, CNPQ (process 314006/2020-6) and INCT – MIDAS (process 24998*26)
Keywords: *sensors, actuators, electroactive polymers, IPMC, functional materials*

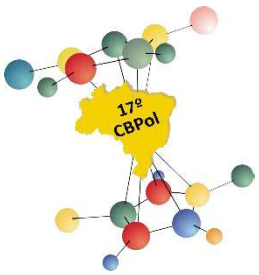

EFFECT OF THE USE OF RICE HUSK ASH (RHA) AS A NON-CONVENTIONAL FILLER IN NITRILE RUBBER (NBR) COMPOSITIONS

Thiago C. Lopes[1], Leila L. Y. Visconte [1], Ana Lúcia N. da Silva[1]
1 – Institute of Macromolecules Professor Eloísa Mano (IMA), Federal University of Rio de Janeiro (UFRJ), Rio de Janeiro, RJ, Brazil
thiagocastro@ima.ufrj.br

Abstract: In elastomeric compounds and composites, different types of non-conventional fillers have been evaluated due to the need to develop new materials aligned with the use of natural raw materials or with less environmental impact. In this scenario, this work intends to evaluate the effect of incorporating a non-conventional filler, rice husk ash (RHA), in nitrile rubber compositions. To do this, important parameters of curing, mechanical properties (tensile and tear strengths and hardness) and density of cross-links were evaluated. Preliminary results indicated a good reinforcing action of RHA in the compositions considering the increase in the values of maximum torque, tensile strength and elongation at break, as a function of the increase in the incorporated filler content. Furthermore, the increasing density of cross-links with increasing filler content suggests that RHA may be acting as a co-curing agent in the vulcanization process.

Keywords: *elastomers; rice husk ash; mechanical properties; rheometric properties; crosslinking density.*

Introduction

In the last decades, the constant need to produce different materials which meet the environmental issues has demanded and boosted the development friendly ecologically products, impacting towards a pollution free and ecological healthier industrial production [1,2]. Among material types, elastomeric ones are characterized by being multicomponent systems, whose types, processing parameters, crosslinks formation and the effects of reinforcing fillers as carbon black and silica (said conventional ones), have crucial role on the final properties and applicability.

In this scenario, the development of elastomeric materials has increased due to the possibility of using different components, in balanced proportions, to obtain adequate properties for a wide range of applications [1,5]. As a result, materials from natural sources, industrial and urban waste, have been the subject of several studies to assess their potential action as an unconventional filler in elastomeric compositions, such as, for example, carbonized coconut fibers [6], rubber residue from tires [7], EVA residue from shoes [8] and rice husk ash [9].

The objective of this work was to evaluate the rheometric and mechanical behavior of nitrile rubber (NBR) compositions with different contents of rice husk ash (RHA).

Experimental

In this work, NBR (N-615B; Mooney Viscosity 33 ML_{1+4} 100°C, 33% acrylonitrile) from Nitriflex S/A Indústria e Comércio was used as the elastomeric matrix for the compositions. The

formulation used for preparing the compositions was based on ASTM D-3187, shown in Table 1, with the addition of three other components (di(2-ethylhexyl) phthalate (DOP), Irganox and RHA).

Table 1: Formulation for the different compositions based on NBR.

Component	Amount (phr)
NBR-N615	100
Estearic Acid	1.0
Zinc Oxide	3.0
Sulfur	1.5
TBBS*	0.7
Irganox	1.5
DOP	1.0
RHA	0.0 // 10.0 // 20.0 // 40.0

*n-tert-butyl-benzothiazole sulfonamide

The compositions were prepared in an open cylinder mixer (LRMR-SC 150/0 Lab Tech Engineering Company LTD.) based on ASTM D-3182 standard with roller speed of 24/34 rpm (1: 1.44) and temperature of 50°C (+/- 10°C). Four compositions were prepared and coded as follows:

- GP-DOP1 - Pure gum without filler addition and with 1 phr of DOP;
- RHA10-DOP1 - NBR with the addition of 10 phr of RHA and 1 phr of DOP;
- RHA20-DOP1 - NBR with addition of 20 phr of RHA, and 1 phr of DOP;
- RHA40-DOP1 - NBR with addition of 40 phr of RHA, and 1 phr of DOP.

For the evaluation of the rheometric properties, the ASTM D-2084 standard was followed, using a temperature of 150 ºC on a Rubber Processing Analyzer (RPA2000, Alpha Technologies). The evaluated mechanical properties followed their respective standards: tensile strength (DIN-53504) and tear strength (ASTM D-624B) analyzed on a universal testing machine (EMIC DL-3000) and hardness (ASTM D-2240) on a shore tester (A-2, The Shore Instrumental MFG Co. Inc.).

The cross-link density was estimated concerning the rheological aspect with on a RPA. This method is based on the relationship between the elastic modulus values (G') before and after vulcanization, as an association of the contribution resulting from the physical contributions (X_{PHY}), coming from the physical entanglements existing in the sample before curing, and the total contributions (X_{TOT}), sum of the physical, from physical entanglements, and chemical (X_{CHE}) contributions, coming from the crosslinks formed during vulcanization. From these relationships, it is possible to estimate the chemical contributions directly associated with cross-linking of vulcanized materials through the relationships observed in Equations 1, 2, 3 and 4. This method is described in previous works [10-12].

- $X_{TOT} = X_{PHY} + X_{CHE}$ **Equation (1)**
- $X_{TOT} = (G'_{0,5Hz})/(2*RT)$ **Equation (2)**
- $X_{PHY} = (G'_{5Hz})/(2*RT)$ **Equation (3)**
- $X_{CHE} = G'_{0,5Hz}/(2*RT) - G'_{5Hz}/(2*RT)$ **Equation (4)**

Results and Discussion

Rheometry

From rheometry it is observed that, comparing GP-DOP1 with the compositions with RHA, the pre-vulcanization time (t_{s1}) and optimal cure time (t_{90}) reduced with the increase of the incorporated RHA content, characterizing shorter times required for induction and completion of the

vulcanization process. Consequently, the curing rate index (CRI) increased in all compositions with RHA, indicating an improvement in the vulcanization rate when compared to the pure gum, as quantified in Table 2. This can be explained by some factors such as a possible action of the RHA as a co-agent in the vulcanization process, helping to form a reticulated network.

Torque values showed an increasing trend as a function of the increase in the incorporated RHA content. The minimum torque (M_L) is associated with the viscosity of the material while the maximum torque (M_H) is associated with the final structural stiffness of the vulcanized material, with the torque variation (ΔM) being the difference between this initial pre-vulcanization state and the final state after vulcanization, and is therefore associated with cross-link density. This suggests an increase in viscosity in the mixtures, a gain in stiffness of the vulcanized material, in addition to a higher density of crosslinks resulting from the addition of RHA. With this, there is an indication of good interaction between the RHA and the NBR matrix, reinforcing action of the RHA, in addition to an action as a co-agent of vulcanization, optimizing the density of cross-links formed.

Table 2: Rheometric parameters at 150°C.

Composition - NBR	t_{s1} (min)	t_{90} (min)	CRI (1/min)	M_L (dN*m)	M_H (dN*m)	ΔM (dN*m)
GP-DOP1	10.93	31.94	4.76	1.00	12.20	11.20
RHA10-DOP1	7.69	27.80	4.97	1.17	14.41	13.24
RHA20-DOP1	7.03	25.19	5.51	1.33	15.86	14.53
RHA40-DOP1	5.43	26.07	4.84	1.55	19.00	17.45

Mechanical Properties: Tensile Strength, Tear Strength and Hardness

Comparing results of tensile test of RHA filled compositions with the unfilled compound, GP-DOP1, Table 3 shows an increase of approximately 12.5% for modulus at 100%, when adding 20 phr of RHA, while the addition of 10 and 40 phr did not imply an increase or decrease in this value. In tensile strength, an increase of approximately 14.65, 29.94 and 30.57% was noted when adding, respectively, 10, 20 and 40 phr of RHA. When adding particles more rigid than the matrix, once the matrix-load interaction is minimally satisfactory, there is a gradual gain in this material rigidity, being observed from increasing values of modulus and tensile strength. Another outstanding parameter was the increase of approximately 12.05, 16.54 and 16.52% for the elongation at break, when adding, respectively, 10, 20 and 40 phr of RHA. This result suggests a good matrix-load interaction, allowing not only an increase in tensile strength, but also the maximum deformation capacity of the matrix under the applied tension during stretch.

Table 3: Mechanical Properties: tests of stress strain, tear resistance and hardness

Composition	Modulus at 100% (MPa)	Stress at Break (MPa)	Elongation at break (%)	Tear Strength (N/mm)	Hardness (Shore A)
GP-DOP1	0.80 (±0.01)	1.57 (±0.43)	465.71 (±98.33)	16.69 (±2.08)	44.00 (±0.67)
RHAA10-DOP1	0.80 (±0.02)	1.8 (±0.08)	521.82 (±14.52)	12.18 (±1.26)	47,00 (±0.67)
RHA20-DOP1	0.90 (±0.03)	2.04 (±0.20)	542.73 (±52.19)	12.66 (±0.60)	49.00 (±0.44)
RHA40-DOP1	0.80 (±0.03)	2.05 (±0.06)	542.64 (±43.76)	14.24 (±0.34)	54.00 (±0.67)

In the tear strength test, Table 3 shows a decrease in this property with the addition of CCA for all compositions as compared to the pure gum composition. However, when comparing the compositions with added filler, a trend towards an increase in resistance was noted as a function of the incorporated RHA content. Hardness, as well as properties such as maximum torque, modulus at 100% and tensile strength, is directly associated with the structural stiffness of the material, although measured differently. An increase in hardness values was observed as the incorporated RHA content also increased, as occurred in the values of maximum torque and tensile strength, which corroborates this increase in the stiffness of the vulcanized material.

Crosslink Density

A clear increase in the density of cross-links was observed along with the increase in the amount of incorporated RHA, in Fig 1. This behavior denotes an action of RHA as a co-agent in the vulcanization process, causing an increase in the cross-links formed, favoring the increase in the density of the reticulated network formed. Such behavior can be corroborated by the torque variation previously observed with the same trend, since it is related to the variation between the initial and final moment of the vulcanization process.

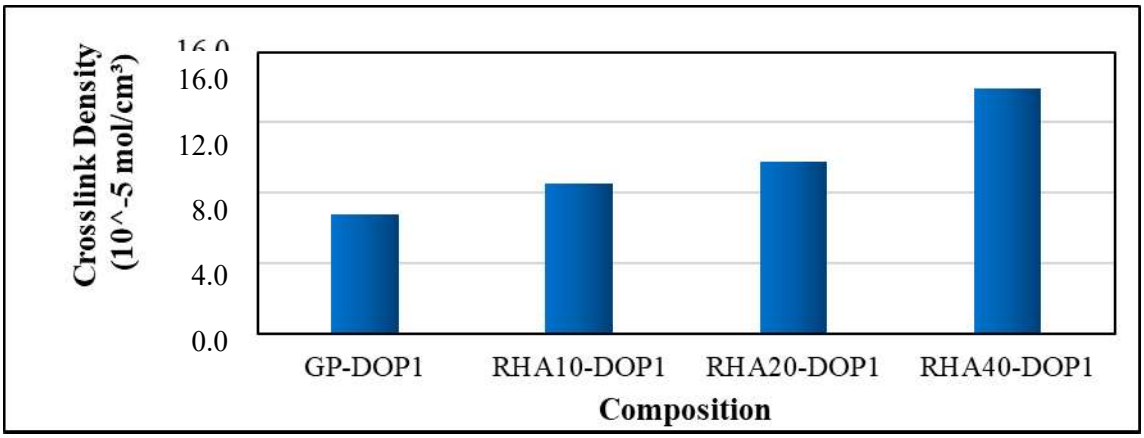

Figura 1: Crosslink density by RPA.

Conclusions

The results obtained allowed observing a good capacity to reinforce of CCA filler for NBR compositions, given by the increase in the torque values together with the increase in the main parameters of the tensile strength tests. It is worth highlighting the increase in tensile strength capacity without compromising the elastomeric deformation capacity, also guaranteeing a gain in this property, which may be indicative of factors such as good matrix-filler interaction, due to a good dispersion capacity during the processing. In addition, the crosslink density increased for all compositions as a function of the increase in filler content.

Higher filler contents will still be evaluated under the same optics presented in this work. It is also possible, and recommended, to carry out other tests and complementary analyzes in order to confirm the considerations about the properties evaluated and discussed in this work.

Acknowlegments

The authors thank CNPq (307889/2022) and CAPES for financial support and Nitriflex S/A Indústria e Comércio for providing the NBR rubber.

Bibliography

1. L. Natrayan; S. Kaliappan, S.; Baskara S.S.; S. Sekar; Pravin P.P.; G. Velmurugan; Tewedaj O.T. International Journal of Chemical Engineering, 2022, 5086365. https://doi.org/10.1155/2022/5086365
2. Nikolay D.; Mihail M. Elastomer-based composite materials: mechanical, dynamic and microwave properties, and engineering applications. Academic Press, Oakville, 2018.
3. Ming Z.; Hui C.; Jiaxin Y.; Yibo W.; Shuxin L. Ruofan L. Journal of Applied Polymer Science, 139 (25), e52048, 2022. https://doi.org/10.1002/app.52048
4. MENTE et al., 2016; Mente P.; Motaung T.E.; Hlangothi S.P. Polymer Science 2016, 2, 1. https://doi.org/10.4172/2471-9935.100015
5. Manjunathan K.; M. Meikandan; S. Kaliappan; M. Karthick; S. Sekar; Pravin P.P.; S. Raja; L. Natrayan; Prabhu P. International Journal of Chemical Engineering 2022, 1864446. https://doi.org/10.1155/2022/1864446.
6. F.O. Aguele; C.I. Madufor, American Journal of Polymer Science 2012, 2, 3. http://dx.doi.org/10.5923/j.ajps.20120203.02
7. Nicolas C.; Oguzhan O.; Carlos E.F.; Gregory S.; Jean-François T.; Maria L. M. Polymer Testing 2021, 107313.https://doi.org/10.1016/j.polymertesting.2021.107313
8. Diana L.; Maria J.F.; Rui R.; Joana M. D. Journal of Cleaner Production 2015, 92. https://doi.org/10.1016/j.jclepro.2014.12.063.
9. V.C. Sthuramalingam; S. Prabagaran; K. Ganesan. Materials Today Proceedings 2021, 37, parte 2. https://doi.org/10.1016/j.matpr.2020.07.654.
10. Shirley L.; Henry P.; A.Y. Coran. Rubber Chemistry and Technology 1994, 67, 5. https://doi.org/10.5254/1.3538716
11. P.P. Chattaraj; R. Mukhopadhyay; D.K. Tripathy. Rubber Chemistry and Technology 1997, 70, 1. https://doi.org/10.5254/1.3538421.
12. Worawan P.; Kannika S.; Charoen N. Journal of Applied Polymer Science 2009, 113, 2. https://doi.org/10.1002/app.30036.

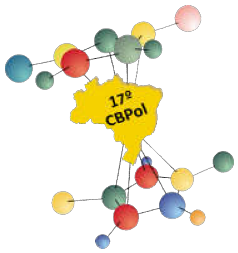

STUDY OF THE DEGRADATION BY HYDROLYSIS OF POLYMERS USED AS DAMPING PARTS

Cátia D.F. Klein[1], Francieli Albani[1], Carlos L. P. Carone[1], Fernando D.P.Morisso [1], e Vanusca D. Jahno[1,2*]

1-Universidade Feevale, PPG profissional em Tecnologia de Materiais e Processos Industriais, Novo Hamburgo, RS

2- Universidade Feevale, PPG em Qualidade Ambiental, Novo Hamburgo, RS

catiaklein06@gmail.com, vanusca@feevale.br*

Abstract

In this work, a comparison between two commercial polymers was made, a polyether polyurethane and a copolyester based on polybutylene terephthalate (PBT), which, accordingly to the literature, are indicated for use as damping parts in a transport system. These polymers were exposed to aging by hydrolysis at 70°C and analyzed after 30, 60 and 90 days by tensile strength and follow-up by IFTR to check for possible degradations. The results obtained demonstrated that the polyurethane did not change the bands in the IFTR and presents an increase in the results of rupture force, % of elongation and tension of rupture with the time exposed. The copolyester, on the other hand, showed a gradual loss in the mechanical properties and the FTIR showed significant changes, indicating deterioration. The loss in mechanical properties due to degradation with heat and humidity caused a reduction in the molar mass of the polymers, which resulted in the decrease of the useful life of the parts and the damping capacity.

Keywords: *polyurethane, COPE, Hydrolysis, mechanical properties, damping parts*

Introduction

The railpads play a fundamental role in transport fastening systems, as they reduce noise and vibration caused by impact on the ground and perform a better distribution of loads, increasing the useful life of the parts. The types of polymeric materials used in the composition of the shock absorbing insoles are important to obtain good efficiency and durability of the fixation system [1, 2].

The mechanical properties of polymeric materials can change accordingly to Variations in the environmental conditions to which they are exposed during their use. Aging by hydrolysis is a process of deterioration of the chemical and physical integrity of polymeric materials, when there is a reduction in molar mass due to chain breakage due to the combined effect of heat and humidity [3,4,5].

Among the accelerated degradation tests, the authors Boubakri et al (2019) [3] studied the hygrothermal aging in a thermoplastic polyurethane based on polycaprolactone. The study addressed the effect of polyurethane aging on thermal, mechanical and tribological properties. Dorna (2016) [6] and Bernaducci (2016) [7] studied the effects of aging by hydrolysis on polyamides 11 and polyamide 6,6 respectively and evaluated the thermal and mechanical properties. Loyer et al (2020) [5]

studied the thermal aging of PBT and carried out follow-ups by GPC and crystallinity percentages by DSC.

The objective of this work is the evaluation of aging by hydrolysis of polyether-based polyurethane and a PBT-based thermoplastic copolyester (COPE).

Experimental

Two commercial polymers were used, one of which is polyether polyurethane and the other a PBT-based copolyester (COPE) to carry out the study. These materials were cut as test specimens in the shape of ties, as shown in Figure 1.

(a) (b)

Figure 1. Image of the specimens for the aging test (a) PU and (b) COPE
Source: Feevale University, 2023

Results and discussion

The Table 1 presents the tensile strength results obtained on the polyurethane specimens before accelerated aging by hydrolysis and after collections at 30, 60 and 90 days of exposure.

Table 1. PU tensile strength after aging by hydrolysis.

	PU exposure time in hydrolysis 70°C			
	Inicial	**30 days**	**60 days**	**90 days**
Rupture force (N)	**784,60**	**904,50**	**1031,00**	**1131,00**
Peak/large(N/mm)	**78,40**	**90,55**	**100,31**	**113,10**
Elongation (%)	**509,00**	**580,00**	**629,60**	**762,00**
Rupture tension (MPa)	**13,10**	**15,10**	**17,19**	**18,85**

Accordingly to the results shown in Table 1, the rupture force, the elongation, and the rupture tension showed an increase in values accordingly to the time they were exposed in the condition of humidity and temperature of 70°C. In the period of 90 days, the breaking strength increased by 44.15%, the elongation by 49.70% and the breaking stress by 43.89%. This behavior may be attributed to the synthesis process of this PU, the increase in flexible segments and the consequent reduction in the content of rigid segments leads to a composition of greater elasticity [8].

The infrared spectra of the PU polymer before the hydrolysis test and the 30, 60 and 90 days collections are presented in Figure 2.

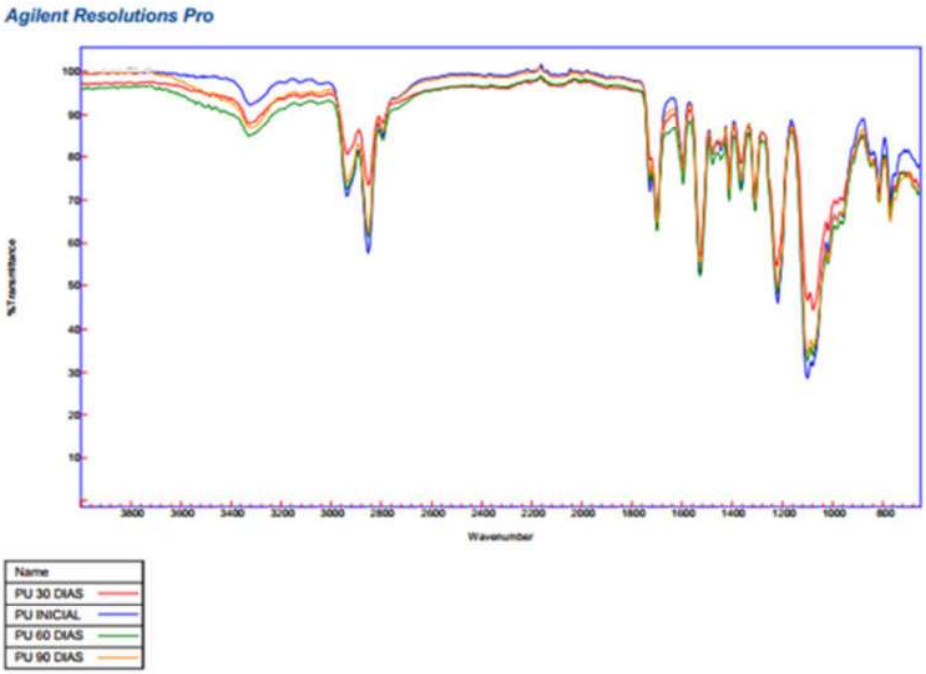

Figure 2 – Infrared spectra of polyurethane samples after hydrolysis at 70°C

Accordingly to the spectra presented in Figure 2, the absorptions showed small changes in intensity and no degradation was observed in the period of 30, 60 and 90 days of exposure to hydrolysis at 70°C of the polyurethane.

Table 2 presents the tensile results obtained on the COPE specimens before accelerated aging by hydrolysis and after collections at 30, 60 and 90 days of exposure.

Table 2. COPE tensile results after aging by hydrolysis.

	COPE exposure time in hydrolysis 70°C			
	Inicial	**30 days**	**60 days**	**90 days**
Rupture force (N)	**1371,44**	**1200,75**	**844,15**	**992,44**
Peak/large(N/mm)	**228,57**	**200,13**	**140,69**	**165,41**
Elongation (%)	**679,00**	**623,44**	**443,67**	**616,21**
Rupture tension (MPa)	**4,04**	**3,85**	**3,80**	**3,17**

As for the tensile results of the COPE specimens shown in Table 2, a reduction in rupture forces, elongation and rupture tension was observed with the passage of time of exposure to hydrolysis at 70°C. In 90 days there were a loss of 38.19% in breaking strength, 10% in elongation and 27.44% in breaking tension. This behavior is justified by the loss of molar mass and consequent increase in the percentage of crystallinity that increases the fragility of the polymer [5,9].

The overlapping of COPE spectra after hydrolysis showed significant differences between collections, as shown in Figure 3.

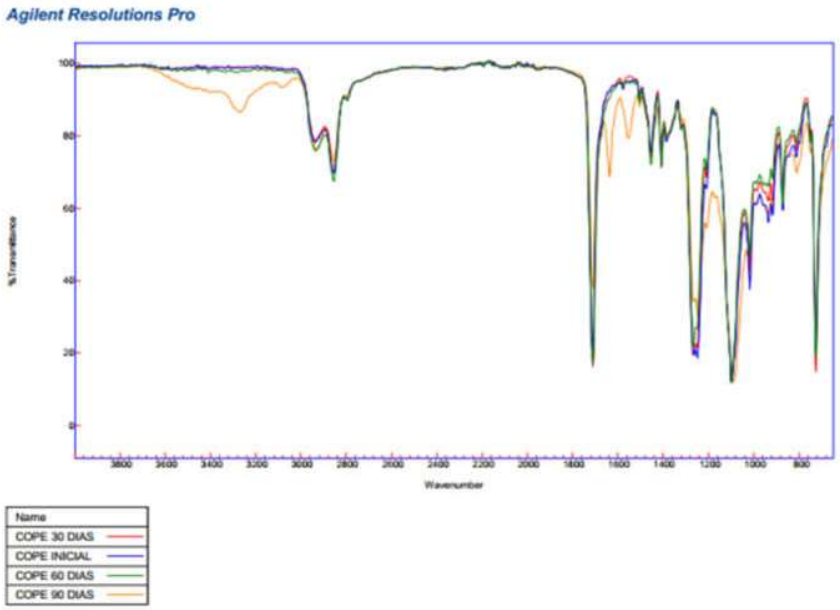

Figure 3. Infrared spectra of COPE samples after hydrolysis at 70°C

The absorptions 2935 cm^{-1} and 2851cm^{-1}, 1700cm^{-1}, 1280cm^{-1} and 1100 cm^{-1}, referring to the deformations of methylene, carbonyl, C-O-C of aromatics and C-O of aliphatics, respectively, had small changes over time. After 90 days, a more abrupt change in the spectrum was noticed with absorptions at 3270 cm^{-1}, 1640 cm^{-1} and 1540 cm^{-1}, referring to N-H deformations of amides. As it is a commercial polymer, there is a great possibility that blends with other polymers or even flow agents with amidic structures has been used in the composition.

Conclusions

The polymer samples studied showed very different results, the polyether polyurethane did not undergo degradation in aging by hydrolysis at 70°C in mechanical tests or by IFTR in the investigated period of 90 days. COPE, on the other hand, showed significant changes in mechanical properties in 90 days, with a loss of 38.19% in breaking strength, 10% in elongation and 27.44% in breaking strength. The follow-up of the IFTR also showed significant changes in several regions of the spectrum over time, indicating polymer degradation. In this way, it is concluded that polyether polyurethane presents a better resistance to aging by hydrolysis at 70°C and a better service life when compared to COPE, being a good alternative for cushioning insole.

References

1. A. Oregui et al. Obtaining railpad properties via dynamic mechanical analysis. Journal of Sound and Vibration, v.363, p 460-472, 2016
2. L.Cong et al. Microstructure development of thermoplastic polyurethanes under compression: The influence from first-order structure to aggregation structure and a structural optimization. Polymer, v.53, 2012
3. A.Boukabri et al. Investigations on hygrothermal aging of thermoplastic polyurethane material. Materials and Design, v.30, 2009
4. M.Pinto. Estudo higrotérmico de compósitos poliméricos reforçados por fibras vegetais juta/algodão manufaturado por RTM: Caracterização mecânica e sorção de água. Tese de Doutorado, Programa de Pós-Graduação em Engenharia de Processos, da Universidade Federal de Campina Grande. Campina Grande, 2018
5. C.Loyer et al. PBT plasticity loss induced by oxidative and hydrolysis ageing. Polymer Degradation and Stability, v .181, 2020
6. M.Dorna et al. Estudo da Degradação da Poliamida 11 pela Técnica de Índice de Fluidez (MFI). Monografia - UFRJ, Rio de Janeiro, RJ, Brasil. Abril, 2016
7. D.Benaducci et al. Estudo da estabilidade térmica e propriedades mecânicas de nanocompósitos de poliamida 6,6 com nanofibras de celulose. Revista Matéria, v.21, 2016
8. F.Aquino. Estudo do Envelhecimento de Poliuretanos Aplicados na Indústria de Petróleo. Dissertação, Programa de Pós-Graduação em Química, da Universidade do Estado do Rio de Janeiro, 2009
9. M.Pyda. Melting and Crystallization of Poly(butylene terephthalate) by Temperature-Modulated and Superfast Calorimetry. Journal of Polymer Science: Part B: Polymer Physics, v. 44(9),1364 – 1377,2006

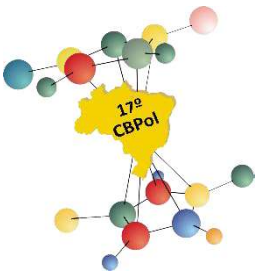

EVALUATION OF THE THERMOMECHANICAL AND WEAR PROPERTIES OF RUBBER PADS USED IN HEAVY MILITARY VEHICLES

Moisés Xavier Guimarães Valentim[1,2a], William Lemos Bevilaqua[3], Inácio da Fontoura Limberger[1], Clarissa Piccinin Frizzo [4], Vania Denise Schwade[4], Natália de Freitas Daudt[1]

1 – Department of Mechanical Engineering, Federal University of Santa Maria (UFSM), Santa Maria, RS, Brazil

2 – Parque Regional de Manutenção3 - Pq R Mnt/3 - Exército Brasileiro, Santa Maria, RS, Brazil

3 – Industrial Technical College, Federal University of Santa Maria (UFSM), Av. Roraima, 1000, Santa Maria, 97105900, Brazil

4 – Department of Chemistry, Federal University of Santa Maria (UFSM), Santa Maria, RS, Brazil

Abstract – Some heavy military vehicles have shown that rubbers pads from different manufactures perform very differently regarding durability. According to that issue, in this study two types of rubber pads used in heavy vehicles were evaluated in terms of mechanical properties, wear, etc., to determine the characteristic required to improve rubber pads durability. One of the pads was the original produced for the vehicle (named P1) and the other was produced in Brazil (named P2). The rubber pads were characterized by wear test, uniaxial tensile test, Shore A Hardness, thermal gravimetric analysis (TGA) and Fourier transform infrared spectroscopy (FTIR). As the main results, the shore A hardness of P1 and P2 were very similar: 80 shore A hardness for P1 and 75 for P2; However, tensile strength and wear rate were very different: 15,5 MPa and 0,129 g/h for P1 and 10,7 MPa and 0,312 g/h for P2. Therefore, shore A hardness it is not a good parameter to evaluate the properties of wear of these types of rubber.

References

P., David Zoltan; B., Tamas; P., Kornél. Hybrid reinforcement of styrene-butadiene rubber nanocomposites with carbon black, silica, and graphene. *Journal of Applied Polymer Science*, v. 139, n. 32, p. e52766, 2022. https://doi.org/10.1002/app.52766.

P., Pramuko Ilmu; D., Agung Setyo; F., Bambang Waluyo. Effect of Black Carbon Composition on Hardness, Strength, Wear Resistance and Grip Coefficient of Tire Compound. In: *Journal of Physics: Conference Series*. IOP Publishing, 2021. p. 012090. 10.1088/1742-6596/1858/1/012090

H., R. et al. Effect of silicon nitride on physical properties of SBR. *Materials Today: Proceedings*, v. 43, p. 3833-3836, 2021. https://doi.org/10.1016/j.matpr.2020.11.421.

W., Y. P. et al. A comparative study on wear behavior and mechanism of styrene butadiene rubber under dry and wet conditions. *Wear*, v. 356, p. 1-8, 2016. https://doi.org/10.1016/j.wear.2016.01.025.

Keywords: *Rubber pad, Heavy military vehicles, Wear.*

NATURAL RUBBER NANOCOMPOSITES FOR SENSING APPLICATIONS

Rafael Barbosa [1]*, Roger Gonçalves[2], Guilherme E. de O. Blanco[1], Matheus C. Saccardo[1], Kaique A. Tozzi[3], Ariel G. Zuquello[4] and Carlos H. Scuracchio[1]

1 – Federal University of Sao Carlos (UFSCar), Graduate Program in Materials Science and Engineering, São Carlos, SP, Brazil
rbarbosa@ufscar.br
2 – Federal University of Sao Carlos (UFSCar), Graduate Program in Chemistr), São Carlos, SP, Brazil
3 - Univ. Grenoble Alpes, Univ. Savoie Mont Blanc, CNRS, Grenoble INP, LEPMI, UMR5279, 38000 Grenoble, France
4- Community University of Chapecó Region, Polytechnic School, Chapecó, Santa Catarina, Brazil

Abstract – Conductive elastomeric composites (CECs) have been evaluated as flexible materials for soft electronics. In this work, natural rubber nanocomposites were prepared to achieve tailored electrical conductivity and sensing properties with diverse processing methods via latex mixing and incorporation of conductive fillers like carbon nanotubes and carbon black. Pursuing high filler dispersibility, the latex method was chosen as the main processing step, enabling the possibility to apply high sonication energy and wet functionalization with surfactants in the fillers. The nanocomposites were tested using electrical impedance spectroscopy in the stationary state, when stretched in several strains until 300%, and when stretched in 5000 cycles of uniaxial tensile deformation. In addition, the nanocomposites were stacked with an ionomeric polymer (Nafion®) in a sandwich-like form, acting as flexible electrode to strain and displacement sensor. The test apparatus is presented in Fig. 1. The results were satisfactory when compared with the conventional ionic polymer-metal composite (IPMC) sensor based on platinum electrodes, with lower sensing amplitude but good capability of sensing different types of displacement velocity (linear, quadratic, cubic).

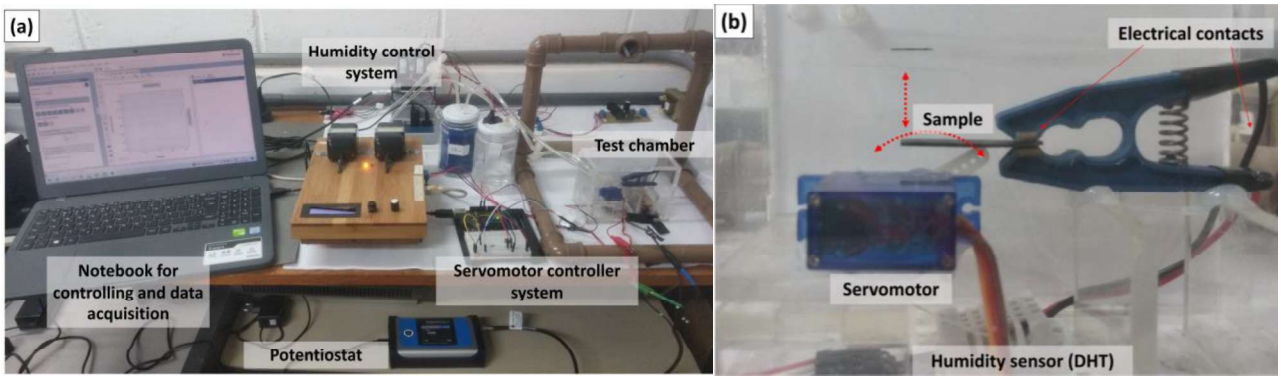

Figure 1 – (a) Apparatus for the deformation and displacement sensing test. (b) Test chamber zoom.

Fundings: This study was financed in part by the Coordenação de Aperfeiçoamento de Pessoal de Nível Superior - Brasil (CAPES) - Finance Code 001. Financial grant by FAPESP, process #2018/07001-6.

Keywords: *Rubber nanocomposite, rubber processing, sensors, latex mixing*

PAYNE EFFECT IN NR COMPOUNDS WITH SUSTAINABLE FILLERS USING DYNAMIC MECHANICAL CHARACTERIZATION

Abel C. G. Neto[1]*, Sandra R. Scagliusi[1], Hélio Wiebeck[1], Patricia Calvão[1], Ticiane S. Valera[1]

1 – Department of Metallurgical and Materials Engineering, University of São Paulo (USP), São Paulo, SP, Brazil
abell_neto@usp.br

Abstract – In this work, Dynamic Mechanical Analysis (DMA) tests were carried out to evaluate the viscoelastic properties of vulcanized natural rubber (NR) with addition of silica and different sustainable fillers, like rice husk silica, rice husk ash, and a vegetable organic filler. The dynamic mechanical analyzes of elastomeric composites were performed in a DMA 3200 (TA Instruments), at room temperature. All experiments were conducted in compression mode, at a frequency of 1 Hz, using specimens with 6 mm thick and 15 mm wide. To observe the effect of strain amplitude on the viscoelastic properties, strain sweeps, from 0.2 to 5% strain, were performed. In elastomeric composites, it is well known, from Payne's work[1], that when the filler-filler distance increases, the stiffness caused by van der Waals forces decreases. The rupture of the filler-filler structure releases the elastomer molecules trapped between the fillers, what causes the decrease. Consequently, a reduction in the values of the dynamic storage modulus, and maximum points in the dynamic loss modulus and damping factor curves, can be observed [2-5]. In this work, it was observed that the storage modulus of the composites decreased when the strain amplitude increased, the dynamic loss modulus and damping factor curves increased, whereas the unfilled compounds exhibited no changes. This effect was more pronounced for silica and rice husk silica fillers.

References

1. A.R. Payne, J. Appl. Polym. Sci. 1962, 6, 368–372. https://doi.org/10.1002/app.1962.070062115.
2. A.H. Muhr, Rubber Chem. Technol. 2005, 78, 391–425. https://doi.org/10.5254/1.3547890.
3. T. Nickel, S. Reddy, S. Behdad, T. Rauschmann, in: 194th Tech. Meet. Rubber Div., 2018.
4. R. Li, L.Z. Sun, Interact. Multiscale Mech.2011, 4, 239–245. https://doi.org/10.12989/imm.2011.4.3.239.
5. G. Hou, W. Tao, J. Liu, X. Zhang, M. Dong, L. Zhang, J. Appl. Polym. Sci. 2018, 135 1–9. https://doi.org/10.1002/app.45749.

Fundings: Conselho Nacional de Desenvolvimento Científico e Tecnológico (CNPq), Fundação para o Desenvolvimento Tecnológico da Engenharia – FDTE (projetos números 1842 e 1485)

Keywords: *Rubber, Sustainable filler, Payne effect, Dynamic Mechanical Analysis, Rheology.*

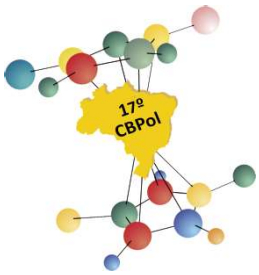

EFFECT OF PEPTIZER ON NATURAL RUBBER AND CHLOROBUTYL RUBBER

Amanda Faria Baruel[1,2*], Sandra Aparecida Coelho de Mello[1], Flávio Henrique de Oliveira Felipe[2] and Silvana Navarro Cassu[1,2]

1 –Institute of Aeronautics and Space (IAE), São José dos Campos, SP, Brazil

2 – Aeronautics Institute of Technology (ITA), São José dos Campos, SP, Brazil

amandabaruel@ita.br

Abstract – During manufacture, rubbers go through the mastication process, aiming to improve the processability and the incorporation of fillers and additives. This study evaluated the effect of physical or chemical peptizers on the properties of natural rubber (NR) and chlorobutyl rubber (CIIR). The mastication process decreased the number-average molecular weight (Mn) and increased polydispersity (PDI) of NR, while peptizers addition had little effect on the molecular weight of CIIR. Chemical peptizer accentuated the mastication effect in the NR, presenting lower Mn and lower weight-average molecular weight (Mw). The peptizer addition accelerated the vulcanization, showing lower scorch time (ts_1) and lower vulcanization temperature. The rubbers with peptizer showed a lower vulcanization degree, presenting lower maximum torque (M_H) and lower enthalpy of vulcanization.

Keywords: *Mastication, Crosslink-density, Enthalpy of vulcanization, Molecular weight*

Fundings: Coordenação de Aperfeiçoamento de Pessoal de Nível Superior - Brasil (CAPES) - Finance Code 001 and Conselho Nacional de Desenvolvimento Científico e Tecnológico (CNPq) project number 422016/2017-9.

Introduction

Natural rubber (NR) has a very wide molecular distribution, with molecular weight ranging from 30,000 $g.mol^{-1}$ to 10 million $g.mol^{-1}$ [1]. Furthermore, its polydispersity (PDI), which is the ratio between the weight-average molecular weight (Mw) and the number-average molecular weight (Mn), can reach 9.0 depending on the clone used to obtain the latex [2]. This polydispersity and molecular distribution give the rubber unique properties, which are not achieved in synthetic rubbers [2].

During processing, especially of high-viscosity rubbers such as NR, the mastication step is crucial in order to reduce viscosity by lowering the molecular weight, thus improving processing and facilitating the incorporation of additives. Peptizing agents can be used at this step to help and accelerate the mastication process [2–4].

There are two types of peptizers, chemical and physical. Chemical peptizers act through chain scission, capturing the free radicals formed during mastication, acting as chain terminators, preventing polymer recombination, and thus allowing a reduction in the molecular weight of the elastomer and, therefore, the reduction of the viscosity [2]. On the other hand, physical peptizers act as internal lubricants, reducing viscosity without breaking the polymeric chain [2,3].

CIIR/NR blends have been used due to improved properties, such as damping, gas permeability, aging resistance, and metal adhesion [5–7]. Aiming to study NR/CIIR in the future, the action of a chemical and a physical peptizer in both rubbers was evaluated. Their influence on the molecular weight and on the vulcanization process of both rubbers was the focus of this study.

Experimental

Materials

Chlorobutyl Rubber CIIR-1301 was purchased from Zhejiang Cenway Materials Co, Ltda, Natural Rubber GEB01 and physical peptizer, a stearate, was provided from Orion, and chemical peptizer, a bis(2- benzamido phenyl) disulfide, was provided from New Bor.

Methods

Samples were prepared using a two-roll mixing mill LUXDOR operated at 30 °C. First, the NR and CIIR elastomers were processed with two types of peptizer without adding other fillers, according to **Table 1**, to evaluate the molecular weight change. For other analyses, rubbers were prepared with and without peptizer, using the same amounts of fillers (Carbon Black N330, ZnO, Aromatic Oil, Stearin) TMTM, Sulfur, and CBS were added at the end of the process.

The samples molecular weight was measured by gel permeation chromatography (GPC), on an Agilent Technologies instrument, model 1100, with three columns, using as eluent (1mL/min) tetrahydrofuran (THF) with 1% of Trifluoroacetic acid, and Refractive Index Detector. Polystyrene with Mp between 580 $g.mol^{-1}$ to 6.7 x 10^6 $g.mol^{-1}$ was used as a standard for calibration.

Rheometric analysis was carried out in a moving die rheometer (MDR) from ALPHA Technologies, model PREMIER MDR, at 145°C with a frequency of 100 cpm (1.67 Hz) and 1° rotation angle, according to ASTM D5289.

DSC analyses were carried out on a TA Instruments DSC Q-100. Samples were sealed in aluminum pans, and the analyses were carried out under a nitrogen gas flow of 100 mL/min, temperature range from -90 °C to 250 °C at a scanning rate of 10°C/min.

Table 1. Chemical composition of the NR and CIIR rubbers.

Materials	NR	CIIR	Physical peptizer	Chemical peptizer	Mastication time (min)
NR-R	100	0	0	0	0
NR-M	100	0	0	0	5
NR-P	100	0	3	0	5
NR-C	100	0	0	3	5
CIIR-R	0	100	0	0	0
CIIR-M	0	100	0	0	5
CIIR-P	0	100	3	0	5
CIIR-C	0	100	0	3	5

R – Raw; M-Masticated; P – Physical peptizer; C- Chemical peptizer

Results and Discussion

Firstly, rubbers without other fillers were analyzed by GPC to evaluate the peptizer and mastication effect on the molecular weight of the rubbers (**Fig 1**). The mastication process reduced the Mn of NR by approximately 40% due to breaking the polymer chain by mechanical shear, rupturing the primary bonds of the isoprene macromolecules [6,8,9], and increasing the polydispersity (PDI). The literature explains that this mechanical rupture of the NR is limited, and to increase and intensify this effect, a chemical peptizer is needed [4]. The chemical peptizer decreased the Mn of NR even more than the mastication process, approximately 50%, and decreased Mw, showing an increase in the amount of shorter chains and the break of the longest chains. Furthermore, when adding the physical peptizer, the NR showed an increase in Mw and PDI.

On the other hand, CIIR presented an increase of approximately 20% in Mn and decreased PDI in the mastication process and with physical or chemical peptizer addition.

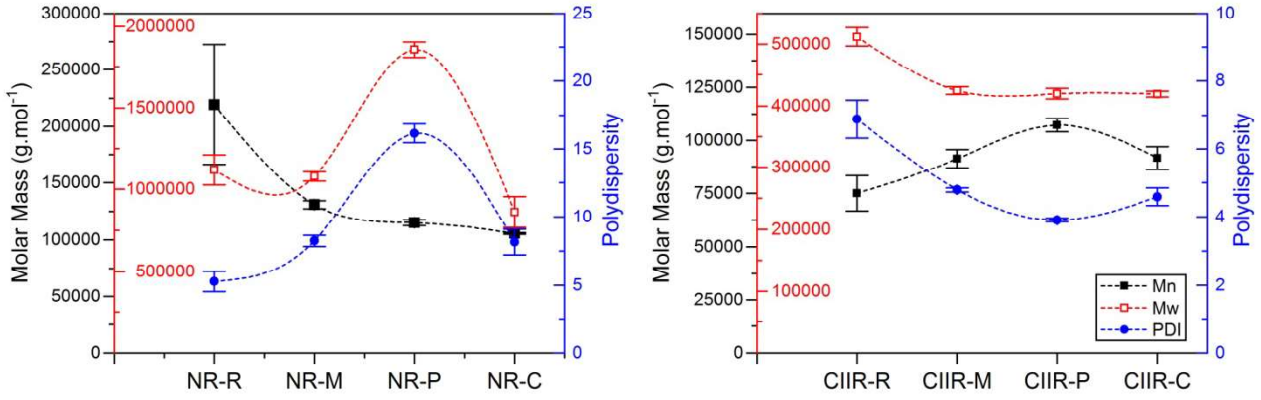

Figure 1. GPC results of CIIR and NR.

The influence of the peptizer in the vulcanization of the NR and CIIR rubbers was also evaluated. For this purpose, rubbers were prepared with other fillers and additives, such as carbon black, sulfur, stearin, and others, as described in the methods section. The results obtained by rheometric analysis are shown in **Fig. 2**, and the parameters are summarized in **Table 2**. It can be seen that in the NR matrix, the physical peptizer had little effect on the vulcanization process. However, it decreased the scorch time (ts_1), indicating that the peptizer accelerated the onset of the vulcanization. The chemical peptizer had a more prominent effect, accelerating the vulcanization, decreasing ts_1 and the optimum vulcanization time (t_{90}), also decreasing the minimum torque (M_L), which can be attributed to the decrease of the initial viscosity of the rubber. The difference between maximum torque (M_H) and minimum torque (M_L) is often used to characterize the crosslink density, which was slightly lower when adding the peptizer to the NR matrix, indicating a lower crosslink degree when compared with the NR without peptizer. The NR with the chemical peptizer showed the lowest value of torque, which can be attributed to a lower degree of unsaturation of the rubber due to the chemical break of these bonds in the presence of the chemical peptizer. On the CIIR matrix, the physical peptizer showed a similar behavior compared to the effect on the NR matrix, accelerating the vulcanization and a slightly lower degree of crosslink. CIIR-P also showed a smaller M_L, indicating a slight reduction of the CIIR viscosity. However, the chemical peptizer showed a retardant effect, increasing the ts_1, and decreasing the difference between M_H and M_L, indicating a reduction in the crosslinking density.

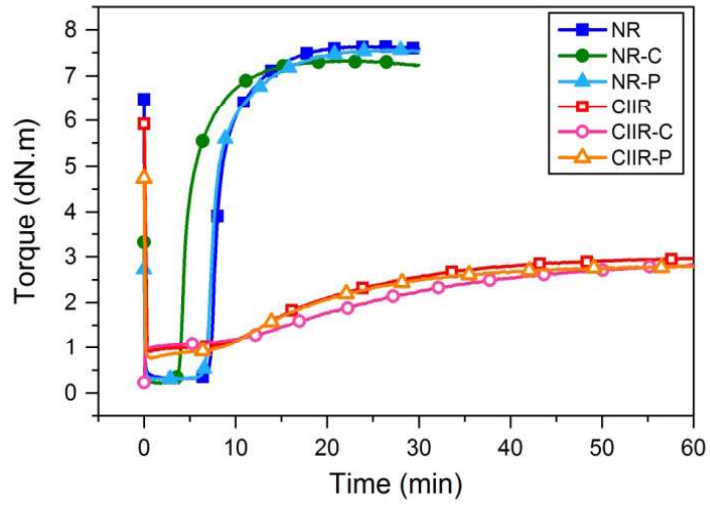

Figure 2. Rheometric curves obtained at 145 °C of the rubbers with and without peptizers.

Table 2. Rheometric parameters obtained at 145 °C of the rubbers with and without peptizers.

	M_L (dN.m)	M_H (dN.m)	ts_1 (min)	t_{90} (min)	$M_H - M_L$
NR	0.31	7.65	7.44	12.79	7.34
NR-C	0.20	7.33	4.10	9.51	7.13
NR-P	0.29	7.57	7.00	13.09	7.28
CIIR	0.92	3.13	19.20	48.84	2.21
CIIR-C	0.97	2.84	26.40	45.29	1.86
CIIR-P	0.76	2.80	17.28	34.50	2,04

The vulcanization of rubbers was followed by DSC (**Fig. 3),** and the parameters are shown in **Table 3**. The rubbers containing peptizer presented slightly higher Tg than the rubbers without peptizer. For all NR samples, the Tg in the second heating shifted to a higher temperature, which can be related to the vulcanization process. CIIR samples showed a similar Tg in the first and the second heat. An exothermic peak related to the vulcanization of the rubbers can be observed for both rubbers. The enthalpy of the reaction can be associated with the degree of crosslinking. The lower the enthalpy, the lower the crosslinking considering the same rubber. For the NR samples, the addition of peptizer decreased the enthalpy of vulcanization and shifted the peak to lower temperatures, indicating a lower degree of crosslink as seen by rheometric analysis.

CIIR rubbers present an endothermic peak around 95 °C due to the melting process of calcium stearate present in the CIIR elastomer [10]. CIIR rubber also presented the exothermic peak related to the vulcanization, showing first a double peak between 125° C and 200 °C and a third peak between 200 °C and 250°C. The exothermic double peak is influenced by a simultaneous endothermic event due to the evaporation of volatiles, such as H_2S and HCl [10]. The third peak can be attributed to the vulcanization process of CIIR. The addition of the chemical peptizer changed the DSC profile of CIIR, reducing the intensity of the last peak at approximately 225ºC and increasing the enthalpy.

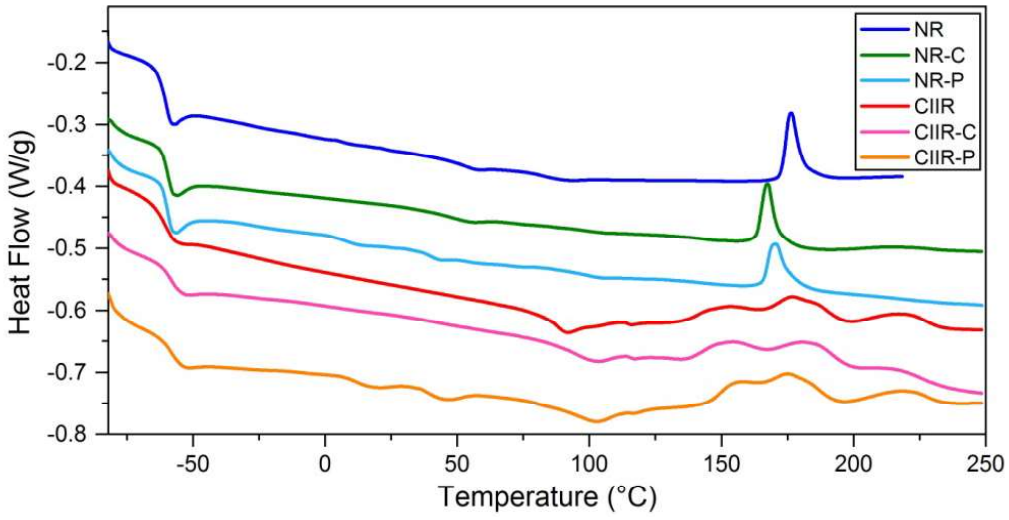

Figure 3. DSC curves of the rubbers with and without peptizer.

Table 3. DSC parameters of the rubbers with and without peptizer.

	Tg 1st heat (°C)	Tg 2nd heat (°C)	ΔH_{EXO} (J/g)	T_{EXO} (°C)
NR	-60.3 ± 0.1	-58.3 ± 0.2	4.26 ± 0.03	176.3 ± 0.1
NR-C	-59.6 ± 0.1	-57.5 ± 0.1	3.56 ± 0.03	169.6 ± 1.0
NR-P	-59.6 ± 0.2	-57.6 ± 0.1	3.64 ± 0.07	167.8 ± 0.3
CIIR	-60.1 ± 0.5	-60.0 ± 0.1	12.53 ± 1.38	177.1 ± 0.1
CIIR-C	-58.5 ± 0.8	-58.0 ± 0.1	15.69 ± 0.67	181.5 ± 0.3
CIIR-P	-58.5 ± 0.2	-58.3 ± 0.1	14.05 ± 0.25	174.9 ± 0.1

Conclusions

The mastication process caused a reduction in Mn due to the mechanical broken of the rubber chain, increasing the PDI. Chemical peptizer accentuated the mastication effect in the NR matrix. Although in the CIIR matrix, peptizers showed little effect. The addition of peptizer, mainly the chemical peptizer, in both rubbers accelerated the vulcanization, reducing the ts_1, and a lower temperature of vulcanization was also observed by DSC. Rubbers containing peptizer also presented lower crosslink density, as observed by rheometric analysis with lower M_H, in DSC analysis with reduced enthalpy.

Acknowledgements

This study was financed in part by the Coordenação de Aperfeiçoamento de Pessoal de Nível Superior - Brasil (CAPES) - Finance Code 001. The authors gratefully acknowledge the financial support given by Conselho Nacional de Desenvolvimento Científico e Tecnológico (CNPq) project number 422016/2017-9 and by Agência Espacial Brasileira (AEB),

References

1. N. M. Mathew in *Rubber Technologist's Handbook*. S. K. De; J. R. White, Eds.; Smithers Rapra Publishing, 2001, 11-18.
2. *Rubber Compounding: Chemistry and Applications*, B. Rodgers, Ed.; New York: Marcel Dekker, 2004.
3. H. L. Stephens in *Rubber Technology,* M. Morton, Ed.; Springer Science, Business Media Dordrecht, 1999, 20-58.
4. R. F. Ohm in *The mixing of rubber*, R. F. Grossman, Ed.; Springer Science & Business Media, 1997, 91-102.
5. G. Hermenegildo; E. Bischoff; R. S. Mauler; M. Giovanela; L. N. Carli; J. S. Crespo, J. *Elastomers Plast.*, 2017, 49, 47–61, https://doi.org/10.1177/0095244315627855.
6. J. K. Paduvilan; P. Velayudhan; A. Amanulla; H. J. Maria; A. Saiter-fourcin; S. Thomas, *Nanomaterials*, 2021, 11, 1098-1112. https://doi.org/10.3390/nano11051098.
7. X. Shi; X. Yuan; X. Guo; F. Zeng; G. Liu *Polym. Adv. Technol.*, 2022, 33, 3522–3531. https://doi.org/10.1002/pat.5805.
8. N. Sombatsompop; P. Rungrattawachai; N. Bouvaree; K. Eaksrisakul *Polym. Test.*, 2001, 20, 317–320. https://doi.org/10.1016/S0142-9418(00)00038-6.
9. M. Pike; W. F. Watson *J. Polym. Sci.*, 1952, 3, 229–251. https://doi.org/10.1002/pol.1952.120090305.
10. K. G. Hendrikse; W. J. McGill *J. Appl. Polym. Sci.*, 2011, 79,1309–1316. https://doi.org/10.1002/1097-4628(20010214)79:7<1309::AID-APP190>3.0.CO;2-3

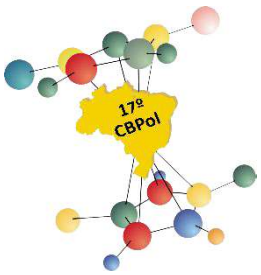

EFFECT OF SOYBEAN POLYOL CONTENT ON PHASE SEPARATION OF THERMOPLASTIC POLYURETHANE OBTAINED BY REACTIVE EXTRUSION

Juliano R. Ernzen[1,2], Angel Marcos-Fernández[3] and Otávio Bianchi[4,2*]

1 – Mantoflex poliuretanos, Caxias do Sul, RS, Brazil
2 – Programa de Pós-Graduação em Engenharia e Ciência dos Materiais (PGMAT), Universidade de Caxias do Sul (UCS), Caxias do Sul, RS, Brazil
3 – Institute of Polymer Science and Technology (ICTP-CSIC), Elastomers Group, Madrid, Spain
4 – Department of Materials Engineering (DEMAT), Federal University of Rio Grande do Sul (UFRGS), Porto Alegre, RS, Brazil

Abstract – This study aimed to investigate the effect of the partial replacement of polyol polyester with polyol from soybean oil on the structure and properties of thermoplastic polyurethanes (TPUs) produced by reactive extrusion. The results showed that when the amount of soy polyol exceeded 5wt.%, there was an increase in molecular mass and gel formation in TPUs. However, this increase was accompanied by the formation of non-regular structures, which reduced the hydrogen bonding density without affecting the amount of ringed segments dispersed in the flexible ones. Additionally, an increase in the glass transition temperature and a smaller phase separation were observed. These findings can be helpful in the development of PUs with tunable structures.

Keywords: Thermoplastics polyurethane, renewable polyol, reactive extrusion.

Fundings: OB (grant number 308567/2018-8 and 305814/2021-4). AMF (project PID2020-119047RB-I00).

Introduction

Segmented thermoplastic polyurethanes (TPUs) are an important class of polyurethanes (PUs) composed of thermodynamically incompatible soft segments (SS), derived from macrodiols, and hard segments (HS), formed by a diisocyanate and a low molecular weight diol (chain extender) [1]. The polarity, solubility parameters (δ_i), and the number of chemical groups capable of hydrogen bonding plays a fundamental role in the microphase separation between the HS and SS segments, affecting the morphology and physicochemical and mechanical properties of the copolymer.

While using renewable sources for PU monomers is not new, the synthesis of TPUs using renewable source polyols remains challenging due to the conversion of soybean oil-based polyols obtained by the epoxidation of double bonds into polyfunctional monomers [2-4]. However, alternative approaches, such as using diacids produced by the Diels–Alder reaction or acids like ricinoleic acid to obtain suitable polyols for TPUs synthesis and partial substitution of petrochemical polyols as adjustments in the reaction process, are being explored [5]. Such approaches produce TPUs with exciting properties, including more excellent hydrolysis resistance than conventional polyesters. In this work, we investigate the synthesis and phase separation of TPUs using reactive extrusion, partially replacing the polyol with a renewable source polyol obtained by the epoxidation of soybean oil.

Experimental

Materials

The TPUs were synthesized using 4,4'-diphenylmethane diisocyanate (MDI) purchased from Dow Chemical, Brazil (ISONATE 125M, NCO content = 33.5 wt.%, ρ = 1.23 $g.cm^{-3}$) as the isocyanate, and 1,4 butanediol (BDO, ρ = 1.02 $g.cm^{-3}$) purchased from Dow Chemical, Brazil as the chain extender. Polyester polyols (Coating YA7220, ρ = 1.15 $g.cm^{-3}$, the molecular weight of 2000 $g.mol^{-1}$, hydroxyl index of 55-60 $mgKOH.g^{-1}$) were procured from Coating, China. A renewable source polyol was also used, which was obtained by epoxidizing soybean oil and had a hydroxyl index of 90 mgKOH.g-1, ρ = 0.97 $g.cm^{-3}$, and molecular weight of 2000 $g.mol^{-1}$[2].

Reactive extrusion

The blends of the renewable polyol with a polyester polyol, ranging from 1 to 50 wt.%, were prepared via mechanical stirring at 80°C for 15 minutes. The pre-polymer was formed in a 5L stainless steel vessel by adding MDI and incorporating the polyol blends. This mixture was maintained at 80°C and stirred during the reactive extrusion process. All TPUs were synthesized with ~50 wt.% HS and a functional groups ratio of 1.05/1 NCO/OH. The pre-polymer and chain extenders were added to maintain a constant production rate of around 2 $kg.h^{-1}$ of TPU in an LTE 16-48 co-rotating twin-screw extruder (LabTech Engineering Company Ltd., Thailand) with a length-to-diameter ratio (L/D) of 48. The processing temperature range was between 160 to 220°C, and the screw speed was set to 250 rpm. The screw had two mixing sections with kneading elements staggered at 30, 60, and 90°, separated by conveying elements. These processing conditions resulted in an average residence time of roughly 300 seconds. After extrusion, the polymers were cooled in water (25°C) and pelletized for subsequent characterization.

Size exclusion chromatography (SEC)

The molecular weight of the TPUs was measured through size exclusion chromatography (SEC) using dimethylformamide with 1% of BrLi as an eluent in a Perkin-Elmer series 200 chromatograph equipped with a refraction index detector. The samples were prepared at a concentration of 10 $mg.mL^{-1}$, and a flow rate of 1 mL.min-1 was maintained during analysis. The injected volume was 10 μL, and the columns temperature was set at 35°C. Calibration curves were established using polystyrene standards.

Fourier transform infrared spectroscopy (FTIR)

The chemical structure of the TPUs and the impact of the renewable polyol on phase separation were analyzed using Fourier transform infrared spectroscopy (FTIR, Perkin-Elmer Spectrum 400 spectrometer) in attenuated total reflection mode (ATR) with a diamond crystal positioned at 45°. The samples were scanned 32 times across the range of 4000–450 cm^{-1}, with a resolution of 2 cm^{-1}. Additionally, the extent of hydrogen bonding and the dispersion of hard segments within the soft phase were determined via mathematical deconvolution [3, 6].

Differential scanning calorimetry (DSC)

Differential scanning calorimetry (Mettler Toledo, DSC 822e) was employed to determine the thermal transitions of the polyols and TPUs under a nitrogen atmosphere (50 $mL.min^{-1}$). Samples weighing 9-10 mg were analyzed from -70 to 240°C, with a heating rate of 10 $°C.min^{-1}$. The T_g value is reported at the onset point, and the variation of heat capacity (ΔC_p) is calculated at the midpoint (ΔT_g). In addition, model reactions were conducted with MDI-BDO at 80ºC, under mechanical stirring, for 1 hour to identify the specific transition temperatures of the rigid phase.

Results and Discussion

Gel formation was observed in samples containing over 5wt.% soybean oil polyol, rendering it impossible to solubilize the entire sample. Therefore, for samples containing 10wt.% and 20wt.%,

the molecular mass values only apply to the non-gelled fractions. Measurements were not possible for samples containing 50wt.% renewable polyol. For TPU, an Mn value of 70 kg/mol and M_w/M_n of 1.74 were observed. When 1wt.% renewable polyol was added, the values remained almost unchanged at 115 kg/mol and 1.76, respectively. However, with 5wt.% renewable polyol, the molar mass increased to 136 kg/mol, and the polydispersity was 2.68. For the soluble fractions of samples containing 10wt.% and 20wt.%, molar masses of 98 kg/mol and M_w/M_n of 2.2-2.7 were observed. Furthermore, adding 1wt.% soybean oil polyol significantly increased the mass with minimal variation in polydispersity. The increase in M_w/M_n values directly impacts the flow stability during the reaction, thus making this TPU a promising candidate for extrusion-forming processes [6].

The impact of renewable polyol content was evaluated by analyzing six specific bands in the 1500-1800 cm^{-1} region, as previously established by studies exploring the relative abundance of hydrogen bonds. Gaussian functions were employed to make mathematical adjustments for each spectrum. These six bands were identified as: (I) 1675 cm^{-1} for H-bonded urethane carbonyl groups in the ordered phase of hard segments, (II) 1700 cm^{-1} for H-bonded urethane carbonyl groups in the disordered phase of hard segments, (III) 1710 cm^{-1} for H-bonded carbonyl groups in the soft-hard segment, (IV) 1728 cm^{-1} for free carbonyl from urethane groups in the hard segment, (V) 1740 cm^{-1} for carbonyl-carbonyl interactions in the soft segments, and (VI) 1745 cm^{-1} for free carbonyl in the soft segment. In addition, the weight fractions of hydrogen-bonded urethane groups (X_b), hard segment dispersed in the soft segment (W_h), mixed-phase weight fraction (MP), soft phase weight fraction (SP), and hard phase weight fraction (HP) were determined according to literatures [3, 6].

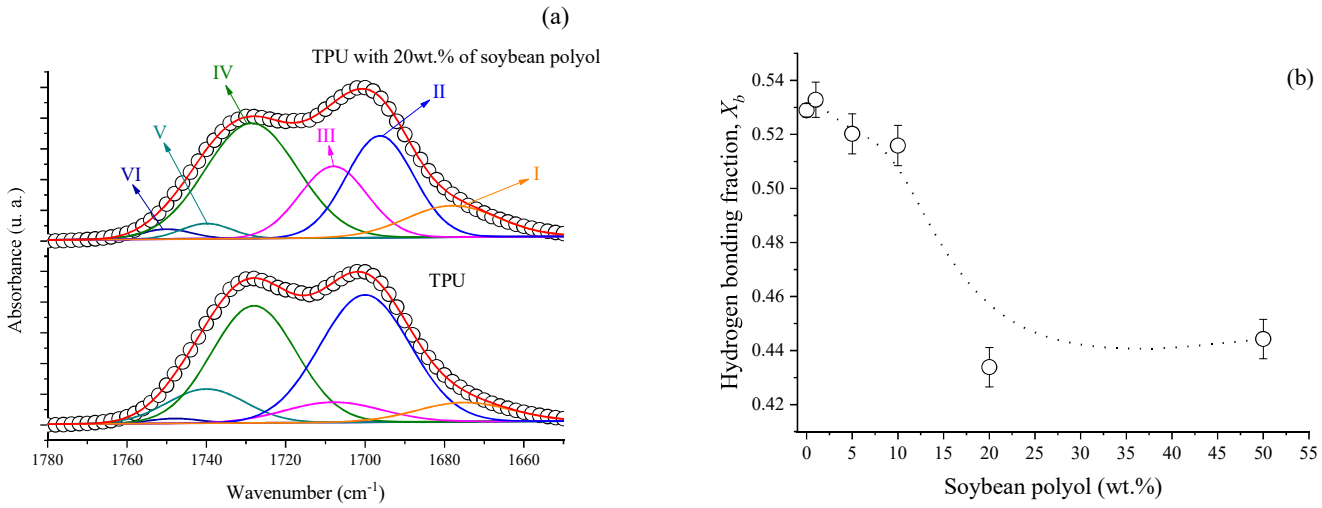

Fig 1. (a) Carbonyl region of the FTIR spectrum corresponding to the 1780-1660 cm^{-1} was deconvoluted to identify and separate the different molecular components contributing to the signal. (b) The fraction of hydrogen bonding present in the samples.

As anticipated, incorporating a renewable polyol source leads to a decrease in the hydrogen-bonding fraction, X_b, which reflects the higher concentration of polar groups in the flexible phase. However, it should be noted that there is a relative increase in the band associated with the hydrogen bonds occurring in the flexible phase when soy polyol is increased, as evidenced by the corresponding decrease in the band at 1728 cm^{-1}. Additionally, the proportion of rigid phase dispersed in the flexible phase remained relatively constant at ~0.29, as did the mixed phase fraction at about ~0.13. The SP values of all TPUs were around 0.68, as were the HP values, which were approximately 0.32.

Adding 5wt.% soy polyol to the TPUs initially caused a reduction in their T_g from -18ºC to -24ºC. This reduction was due to increased free volume and branching in the main chain. However, crosslinks would become evident if more than 5wt.% soy polyol were added due to the polyol's

polyfunctionality. As a result, the T_g would increase significantly to values up to 82ºC with 50 wt% of the polyol. The degree of phase separation (DS) was estimated based on the assumptions of Camberlin and Pascault [7], and the estimated values showed a linear trend ($DS = -0.72 * polyol\ (wt.\%) + 77.67$, R>0.98). This trend indicated a reduction in phase separation, which was a consequence of the smaller difference in solubility parameters, according to Cruz et al [8].

Conclusions

The structure of the polyol is a crucial factor that affects the properties and structure of polyurethanes. Generally, the addition of polyol can lead to a reduction in the density of hydrogen bonds, which may result in a decrease in mechanical properties. However, our results showed that adding 1wt.% of polyol increased the molecular weight of the polyurethanes, which resulted in improved rheological stability without forming gels or significant changes in T_g and phase separation. These findings provide valuable insights into the relationship between the structure and properties of polyurethanes and can guide the development of polyurethane-based materials with optimized properties.

Acknowledgements

The authors thank the financial support from the Brazilian Agency Coordenação de Aperfeiçoamento de Pessoal de Nível Superior (CAPES). OB thanks for National Council for Scientific and Technological Development (CNPq). AMF thanks the Spanish Ministerio de Economía e Innovación for partial finantial support.

References

1 . M. Asensio, V. Costa, A. Nohales, O. Bianchi, C.M. Gómez, Polymers, 2019, 11, 1910. https://doi.org/10.3390/polym11121910.
2 . D. Favero, V.R. Marcon, T. Barcellos, C.M. Gómez, M.J. Sanchis, M. Carsí, C.A. Figueroa, O. Bianchi, Journal of Molecular Liquids, 2019, 285, 136.
https://doi.org/10.1016/j.molliq.2019.04.078.
3 . D. Favero, V. Marcon, C.A. Figueroa, C.M. Gómez, A. Cros, N. Garro, M.J. Sanchis, M. Carsí, O. Bianchi, Journal of Applied Polymer Science, 2021, 138, 50709.
https://doi.org/10.1002/app.50709.
4 . L.N. Dang, S. Le Hoang, M. Malin, J. Weisser, T. Walter, M. Schnabelrauch, J. Seppälä, European Polymer Journal, 2016, 81, 129.
https://doi.org/10.1016/j.eurpolymj.2016.05.024.
5 . C. Bueno-Ferrer, E. Hablot, F. Perrin-Sarazin, M.C. Garrigós, A. Jiménez, L. Averous, Macromolecular Materials and Engineering, 2012, 297, 777.
https://doi.org/10.1002/mame.201100278.
6 . J.R. Ernzen, C.H. Romoaldo, C. Gommes, J.A. Covas, A. Marcos-Fernández, R. Fiorio, O. Bianchi, Polymers, 2022, 14, 3164.
https://doi.org/10.3390/polym14153164.
7 . Y. Camberlin, J.P. Pascault, Journal of Polymer Science: Polymer Chemistry Edition, 1983, 21, 415.
https://doi.org/10.1002/pol.1983.170210211.
8 . J.A. Cruz, S.C. Amico, O. Bianchi, Journal of Polymer Research, 2023, 30, 1.
https://doi.org/10.1007/s10965-022-03393-9.

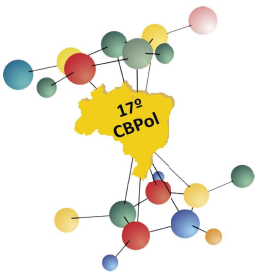

ELASTOMERS AND CHAOS: AN UNCONVENTIONAL PERSPECTIVE ON ELECTROMECHANICAL COUPLING AND ITS RELATIONSHIP WITH FAILURE FORECASTING

Yan A. S. Campo[1*], Ezequiel Lorenzett[2], Kelly S. Moreira[2], Pedro R. Lorenzoni[1], Thiago A. L. Burgo[3]

1 – Department of Physics, University of Santa Maria (UFSM), Santa Maria, RS, Brazil yanaraujosantos@gmail.com
2 – Department of Chemistry, University of Santa Maria (UFSM), Santa Maria, RS, Brazil
3 – Institute of Biosciences, Letters and Exact Sciences, Universidade Estadual Paulista, São José do Rio Preto, SP, Brazil

Abstract - Elastomers are widely used in various industries due to their mechanical properties: high deformation, wear resistance, and vibration isolation [1]. Recent discoveries reveal periodic surface electrification in rubbers, synchronized with stretching [2]. Applying chaos theory, we efficiently predict fatigue failure in rubbers [3]. Our study monitors electrostatic potential in rubber during different fatigue regimes, observing real-time phase portraits. Using Python-based software, we generate attractors to identify the fatigue process and intervene before rupture, enhancing reliability.
Keywords: *Chaos theory, Elastomers, Rubber, Electromechanical coupling.*

Introduction

Elastomeric materials are extensively utilized in various industrial sectors, primarily due to their remarkable mechanical properties, including wear resistance, high deformation capacity, and effective vibration isolation [4]. Despite their inherent deformability and ability to restore to their original shape, elastomers are not immune to wear and eventual failure under mechanical stress. Components made from rubber often experience failure due to the nucleation and growth of defects and fractures when subjected to varying mechanical loads [5]. Fatigue failure, which occurs when rubbers are exposed to cyclic mechanical stresses or deformations, poses significant risks to equipment and operators. Therefore, accurately predicting the fatigue life of elastomeric materials is crucial for preventive maintenance, timely replacement of rubber parts, and maximizing their operational lifespan [6].

Hence, the objective of this study is to explore potential correlations between the physicochemical properties of elastomeric materials and their mechanical-to-electrical transduction, aiming to develop real-time mechanisms for the detection and prevention of fatigue failures. By investigating these relationships, we aim to provide valuable insights that can contribute to the enhancement of maintenance practices and the extension of the operational lifespan of elastomeric components.

Experimental

The electrostatic potential of the natural rubber samples was continuously monitored using a Kelvin electrode (6000B-6, Trek Inc., USA) at a fixed point during stretching cycles with a frequency of 1Hz. Additionally, electrostatic potential profiles along the sample were obtained at various levels of stretching. The time series data of the electrostatic potential were utilized to generate attractors plotted in two dimensions, specifically $V(t + \Delta t)$ vs. $V(t)$, with a delay of $\Delta t = 10$ measured points

(equivalent to 0.08s). This delay was found to be optimal for the data obtained in this study and served as a convenient attractor representation.
To complement the electrostatic potential analysis, mechanical deformation analysis was conducted using digital image correlation (DIC). Sequential images captured during the stretching process were processed using a Python code incorporating the muDIC package. This approach enabled precise measurement of the mechanical deformations occurring along the sample.
By integrating these techniques, we gained comprehensive insights into the electrostatic potential and mechanical behavior of the natural rubber samples. This multifaceted analysis contributes to a deeper understanding of the material's properties and responses to external stimuli, paving the way for improved characterization and potential applications in various fields.

Results and Discussion

Figures 1a and 1c present the measured electrostatic potentials, while Figures 1b and 1d illustrate the corresponding phase portraits of the latex system. In general, these phase portraits exhibit regions of varying divergence. Notably, the orbits tend to converge as they approach $V(t + \Delta t) = 0$ kV and $V(t) = 0$ kV, indicating the presence of attractors. These attractors represent specific states towards which the chaotic system tends to evolve, effectively capturing the system's inherent tendencies. As the rubber material approaches the point of fracture, the phase portrait becomes increasingly divergent.

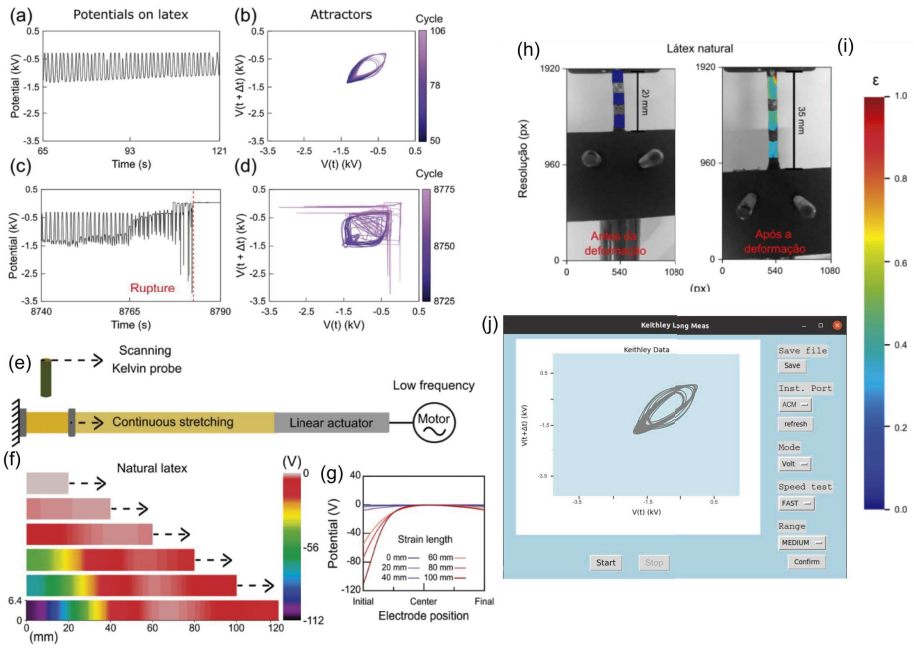

Figure 1: Electrostatic potential at the beginning of the test (a) and final (c), and their respective phase portraits (b, d), (e) scan setup scheme, (f) electrostatic maps at different degrees of stretching and (g) potential profiles. Images used in DIC, (h) with relaxedand(i) stretched sample, and (j) real-time phase portrait generation software.

Figure 1e displays the electrostatic potential maps obtained for both relaxed and stretched rubber samples, providing a schematic representation. Additionally, Figure 1f presents a representative potential map for natural latex, accompanied by profiles in Figure 1g. The relaxed latex demonstrates electrostatic potentials close to zero, while negative potentials emerge predominantly near the stationary holder after stretching. Some areas even reach values of up to 100 V, while the potentials remain low near the moving holder of the testing machine. To identify regions of greater deformation during the stretching process and investigate potential correlations between the

deformation gradient and electrostatic potential along the samples, the DIC method was employed. After a 15 mm stretch (Figure 1i), the natural latex sample exhibited significant deformation, particularly near the fixed holder, compared to the relaxed sample (Figure 1h). These findings align with the electrostatic potential maps, providing further support. In latex, the highest degree of deformation is observed near the fixed rod, coinciding with the lowest values of electrostatic potential.

Conclusions

The physicochemical properties of elastomers play a crucial role in the conversion of mechanical energy to electrical signals. In fact, the variations in chemical compositions and mechanochemical reactions occurring during fatigue tests result in notable distinctions in the electrostatic behavior [3]. The methods proposed in this study make significant contributions to the real-time prediction of fatigue failure in rubbers subjected to periodic stretching regimes. They also aid in identifying the regions most susceptible to potential fractures, providing valuable tools for accident prevention and preventive/predictive maintenance practices. Furthermore, through the interpretation of the real-time phase portrait (Figure 1j) generated using Python-based software, it becomes possible to track the onset of failure and gain insights into the underlying mechanisms.

Acknowledgements

This work was supported by MCTIC, INCT/INOMAT, CNPq, CAPES, FAPESP and UFSM.

References

[1] TOBAJAS, R. et al. A New Multiparameter Model for Multiaxial Fatigue Life Predictionof Rubber Materials. Polymers, v. 12, n. 5, may 2020. ISSN 2073-4360.

[2] SANTOS, L. et al. Rubber Surface Change and Static Charging under Periodic Stress. Colloids and Interfaces, v. 2, n. 4, nov 2018. ISSN 2504-5377.

[3] CAMPO, Y. A. S. et al. Electromechanical coupling in elastomers: a correlation between electrostatic potential and fatigue failure. Physical Chemistry Chemical Physics, v. 23, 2021.

[4] TOBAJAS, R. et al. A New Multiparameter Model for Multiaxial Fatigue Life Prediction of Rubber Materials. Polymers, v. 12, n. 5, may 2020. ISSN 2073-4360.

[5] MARS, W.; FATEMI, A. A literature survey on fatigue analysis approaches for rubber. International Journal of Fatigue, v. 24, n. 9, sep 2002. ISSN 01421123.

[6] ZHANG, J. et al. Strain energy-based rubber fatigue life prediction under the influenceoftemperature. Royal Society Open Science, v. 5, n. 10, oct 2018. ISSN 2054-5703.

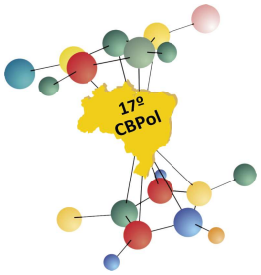

EVALUATION OF THE INTERACTION BETWEEN BIOCHAR AND ELASTOMERS OF DIFFERENT POLARITIES FOR APPLICATION OF BIOCHAR AS REINFORCEMENT FILLER

Willian B. Ribeiro[1], Giovani B. Bérti[1], Marcelo Godinho[1] and Rosmary N. Brandalise[1]*
1 – Graduate Program in Process and Technology Enginnering (PGEPROTEC), University of Caxias do Sul (UCS), Caxias do Sul, RS, Brazil rnbranda@ucs.br

Abstract – The present work aims to study the interaction of biochar with elastomers of different polarity, poly(cis-1,4-isoprene) (NR) and poly(butadiene-co-acrylonitrile) (NBR), based on their bound rubber, rheometry, chemical and mechanical properties. Additionally, it seeks to analyze the reinforcing properties of the filler (biochar) through contact angle measurements, X-ray diffraction (XRD), and specific surface area determination by N_2 adsorption. Biochar, despite exhibiting a smaller superficial area (3 $m^2 \cdot g^{-1}$) typical to inert fillers, interacted with all elastomers possessing semi-reinforcing properties, due to its turboestratic crystalline structure, making the mechanical properties of the biochar produced temperature (900 ºC) better than the biochar produced with a lower temperature (400 ºC). Finally, the production of biochar by pyrolysis and the mechanical and physical properties observed in elastomeric compounds with biochar provided these potential properties to replace carbon black in semi-reinforced applications.
Keywords: *Interaction, pyrolysis, biochar, carbon black, elastomeric compound.*

Introduction

European legislation restricts the marketing of products containing more than 1 ppm of polycyclic aromatic hydrocarbons (PAH), which makes it difficult to continue using traditional components of the rubber industry, such as carbon black [1]. To replace carbon black, the replacement filler must have suitable functional groups and morphology to allow interaction with the elastomer [2]. To achieve these properties, thermochemical processes such as pyrolysis allow the conversion of biomass into a possible reinforcing filler (biochar) with properties that favor interaction with elastomers, with the advantage of being derived from a renewable resource and having a lower concentration of PAH [3].

The study of the interaction biochar-elastomers offers several opportunities to control process to improve the performance of the filler. Current knowledge of the use of biochar as a reinforcing filler in elastomer compounds is similar to what researchers knew about carbon black in 1907. Considering the possibility of obtaining biochar from the pyrolysis of Pinus spp. biomass and the influence of temperature on the properties of biochar, the present work aims to study the interaction of biochar with elastomers of different polarity used as reinforcing material instead of carbon black, based on the properties resulting from the different temperatures during the pyrolysis of biomass.

Experimental

Pyrolysis process

The system consists of a Sanchis furnace with an internally coupled stainless steel reactor. The reactor was electrically heated with resistors of 1900 W each, with two type K thermocouples placed inside the reactor and operating in batch mode. The condensation of vapors in bio-oil was carried out according to the adaptation of the standard CEN/TS 15439. The experiments of pyrolysis of biomass were carried out at 400 ºC and 900 ºC for 30 minutes and an inert gas flow (N_2) of 200 $mL.min^{-1}$ until a mass of biochar for the production of elastomeric compounds was obtained. The coding of the biochar is: BIO400 for the biochar produced at 400 ºC and BIO900 for the biochar produced at 900ºC.

Characterization of the produced biochar

Biochar prepared at 400 °C and 900 °C was ground in a Retsch planetary ball mill, Emax (Germany), using 50 mL tungsten carbide vessels and stainless steel balls of 4.0 mm and 3.0 mm. The following parameters were used for the grinding process: Mass ratio (m/m) between biochar and spheres of 4.5, stirring speed of 575 rpm for 30 minutes. X-ray diffraction (XRD) analysis was performed in a Shimadzu XRD-6000 diffractometer (Japan) using CuKα radiation (λ = 0.15406 nm), 40 kV voltage and 30 mA current. The biochar samples were analyzed in the 2θ range from 10° to 90° with 0.05° resolution and 2 s integration time. The biochar specific surface area by N_2 adsorption was determined by the isothermal adsorption method using the Brunauer-Emmet-Teller method (BET) according to ASTM D6556-19. The biochar surface free energy test using the contact angle was performed using the sessile drop method [4]. The samples were shaped into a disk by compression molding. The liquids selected for the study were distilled water and toluene. To obtain information on the surface properties of the biochar, surface free energy analysis was performed using the dispersive London component and the specific polar component according to the Fowkes method [4]. The surface and droplet images were taken using a Panasonic digital camera. Surftens software was used to determine the contact angle.

Preparation of the elastomeric compounds

ASTM D3192-09 was adopted for the base formulation of NR, and the following amounts in phr were held constant for all samples: NR - 100.0, ZnO - 5.0, stearic acid - 3.0, filler - 50.0, sulfur - 2.5, MBTS - 0.6 and for the base formulation of NBR ASTM D3848-03 was adopted and the following amounts in phr were kept constant for all samples: NBR - 100.0, ZnO - 3.0, stearic acid - 1.0, filler - 50.0, sulfur - 1.5, TBBS - 0.7. The elastomer formulations were first processed in a hand-made torque rheometer similar to a Haake type with a useful volume of the mixing chamber of 65 cm^3. The compounds were prepared at 100ºC, 60 rpm, roller mixer and a processing time of 10 minutes, adding elastomer, activators and filler. After a resting period of 24 hours, the premix prepared in the torque rheometer was added in a two-roll mill (MH -600 - Brazil) at 60 ºC, adding the accelerator and sulfur to the premix. For the elastomeric compounds, the following coding was used: (NR) for the unfilled NR compound; (NR/CB) for the NR compound with carbon black; (NR/BIO400) for the NR compound with biochar made at 400 °C; (NR/BIO900) for the NR compound with biochar made at 900 °C. The same was adopted for NBR, changing only the rubber abbreviation (NBR, NBR/CB, NBR/BIO400, NBR/BIO900).

Characterization of elastomeric compounds

The elastomeric compounds were characterized after mixing in a torque mixer by quantifying the bound rubber content based on extraction of the elastomeric compound with the solvent toluene for NR and acetone for NBR. Samples of about 1 g were immersed in 200 mL of solvent at 25 °C for 45 h. They were then oven dried to constant mass [5]. The bound rubber content was calculated according to equation 1.

$$BR = \frac{W_{fg} - W_t \cdot \left[\frac{m_f}{(m_f + m_r)}\right]}{W_t \cdot \left[\frac{m_r}{(m_f + m_r)}\right]} \quad (1)$$

Where BR is the content of bound rubber (%); W_{fg} is the mass of gel filler (g); W_t is the mass of sample (g); m_f is the amount of filler on the mixture (phr); m_r is the amount of rubber in the mixture (phr). Characterization of the elastomeric compounds was based on rheometric properties determined using a Tech Pro Rheotech OD + (USA) oscillating disk rheometer in accordance with ASTM D5289-19a on an unvulcanized sample of approximately 5 g from the roller mixer compound at 160 ºC with an amplitude of 1º and a deformation frequency of 1.67 Hz for 30 minutes. The rubbers taken from the two-roll mill were vulcanized by compression molding in a Shultz hydraulic press, model PHS

15 T (Brazil), at 160 ºC for a period corresponding to the optimum vulcanization time (t_{90}) determined from the rheometric curve with plates of dimensions 150×150×2 mm prepared and cut for the mechanical tests according to ASTM D3182-16. The tensile strength was determined according to ASTM D412-16 in an Emic universal testing machine, model DL-3000 (Brazil), with a load cell of 20 kN and a crosshead speed of the claws of 500 mm·min^{-1} on five specimens.

Results and Discussion

X-ray diffraction (XRD) analysis of biochar samples

In Fig. 1(a), a peak at 15.87º, a narrow peak at 22.89º, and the peak at 43.5º could be observed, indicating the presence of the cellulose structure. The degradation of cellulose starts at 315 ºC and is not yet complete in the production of biochar at 400 ºC, indicating the presence of an amorphous structure in the biochar [6]. A low intensity peak was observed at 43.5ºC, which is indicated in the studies of Pusceddu et al. [6] as the beginning of the formation of the turbostratic phase of carbon in the biochar. For the BIO900 sample [Fig. 1(b)], a broader peak was observed at 23 ºC, relative to the biochar prepared at 400 ºC, indicating that part of the crystalline cellulose structure was degraded. The peak at about 43.6º and 79.84º signals the development of a graphitic structure, which occurs as the material becomes more carbonized and represents ideal active sites for filler-elastomer interaction, as reflected by the increase in tensile strength [7].

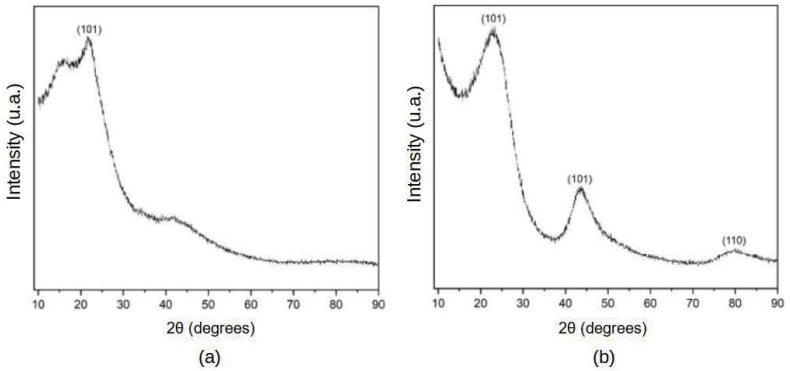

Figure 1. Diffractograms of the produced biochar samples at (a) 400 ºC e (b) 900 ºC.

Surface area analysis by N_2 adsorption of biochar samples

The specific surface area (S_{BET}), specific external surface area (S_{EXT}), specific micropore area (S_{MICRO}) and micropore volume (V_{MICRO}) results for the biochars are presented in Table 1.

Table 1. Textural properties of the biochars BIO400 e BIO900.

Samples	S_{EXT} ($m^2 \cdot g^{-1}$)	S_{MICRO} ($m^2 \cdot g^{-1}$)	S_{BET} ($m^2 \cdot g^{-1}$)	V_{MICRO} ($cm^3 \cdot g^{-1}$)
BIO400	2.01	0.86	2.87	0.007
BIO900	2.17	0.84	3.02	0.000

Surface analysis of BIO400 and BIO900 biochar showed that the biochar has a small microporous area after grinding. The increase in porosity makes the material ineffective for use as a filler reinforcement in elastomeric compounds, since the mechanical stability of the material is inverse to the porosity [8]. The biochar produced at these temperatures (400 ºC and 900 ºC) had a surface area of about 2 $m^2 \cdot g^{-1}$, which is due to the decomposition of the lignocellulosic material that eliminates volatile substances blocking the pores due to the effect of the pyrolysis temperature [9].

Surface free energy analysis by the contact angle method of biochar samples

The samples showed moderate values for the dispersive component, 28.5 mJ·m^{-2} for the two biochars, and low values for the polar component, 16.6 mJ·m^{-2} for BIO400 and 11.2 mJ·m^{-2} for BIO900 (high values are above 40 mJ·m^{-2}), indicating low agglomeration potential and producing a

simple structure that does not provide reinforcement compatible with carbon black [10]. The BIO900 sample exhibited greater hydrophobicity than the BIO400 sample, indicating less interaction with polar compounds observed by the larger contact angle, while the opposite was true for toluene, a nonpolar liquid, and the samples exhibited an angle of 0º.

Table 2. Surface free energy of the biochars.

Samples	θ_{WATER} (º)	$\theta_{TOLUENE}$ (º)	γ^{D}_{S} (mJ·m^{-2})	γ^{SP}_{S} (mJ·m^{-2})	γ_{S} (mJ·m^{-2})
BIO400	120.4 ± 0.3	0.0	28.5	16.6	45.1
BIO900	128.6 ± 0.3	0.0	28.5	11.2	39.7

Characterization of mixtures and elastomeric compounds – Bound rubber content

The data presented in Table 3 show that biochar has a better interaction with polar elastomers than carbon black, with a higher bound rubber content for NBR than for NR. The bound rubber content can increase with the unsaturation of the polymer due to the interaction of the oxygen-containing groups on the surface of the filler, usually at 100 °C. Furthermore, the polarity of the filler and the elastomer also exert influence over the bound rubber content [11].

Table 3. Bound rubber content for NR and NBR based elastomeric mixtures.

Compounds	Bound Rubber (%)	Compounds	Bound Rubber (%)
NR/CB	17.8	NBR/CB	26.5
NR/BIO400	11.6	NBR/BIO400	81.2
NR/BIO900	6.7	NBR/BIO900	45.4

Rheometric characterization of elastomeric mixtures

Elastomeric compounds with biochar showed the lowest values of minimum torque (M_L) (Table 4), indicating a less irregular final structure of the filler compared to compounds with carbon black, which causes less clogging of the rubber during filling, as indicated by the low viscosity [12]. NR/BIO900, NR/CB, NBR/BIO900 and NBR/CB compounds showed the lowest values for optimum vulcanization time (t_{90}), while NR/BIO400 and NBR/BIO400 showed the highest vulcanization time compared to the standard formulation. This difference was attributed to the pH of the filler, as fillers with an acidic pH increase the vulcanization time due to adsorption of basic accelerators and the pyrolysis temperature affects the pH of the biochar, increasing the pH as carbonization progresses [7].

Table 4. Rheometric properties of NR and NBR elastomeric mixtures.

Compounds	M_L (dN·m)	M_H (dN·m)	t_{S1} (min)	t_{90} (min)	CRI (min^{-1})
NR	2.8	15.5	3.4	8.2	20.8
NR/CB	7.4	30.5	1.4	6.5	19.4
NR/BIO400	1.1	20.2	3.8	10.1	15.9
NR/BIO900	2.2	16.6	2.8	5.4	38.9
NBR	2.6	15.0	4.4	9.2	20.9
NBR/CB	4.5	12.6	3.1	6.7	28.1
NBR/BIO400	3.8	14.8	4.4	11.9	13.5
NBR/BIO900	2.9	7.4	4.6	8.3	27.2

M_L – minimum torque; M_H – maximum torque, t_{S1} – scorch time, t_{90}– optimum cure time.

Mechanical characterization of elastomeric compounds

Fig. 2 shows that the blends with biochar have a reduction in tensile strength of about 69.2% for NR/BIO400 and about 6.8% for NR /BIO900 compared to the blend without filler. When comparing with NR/CB, NR/BIO900 presented a similar value, 12.7±0.9 MPa, compared to 15.8±1.7 MPa for NR/CB. This result is due to the interaction between filler and elastomer, because the presence of oxygen along the filler increases the polar component and weakens the interaction with nonpolar

elastomers. Samples with biochar were found to strengthen the NBR with an increase of 206.8% for NBR/BIO400 and 275.2% for NBR/BIO900 compared to samples without filler. Contrary to Leblanc [13], according to which fillers with a specific surface area of less than 10 $m^2 \cdot g^{-1}$ are considered inert fillers, both types of biochar showed an enhancing effect, even with a specific surface area of about 3 $m^2 \cdot g^{-1}$.

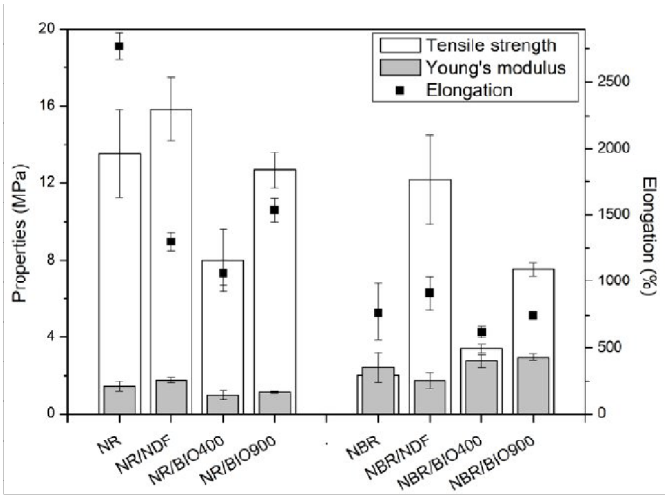

Figure 2. Tensile strength, Young's modulus and elongation at break for NR and NBR compounds.

Conclusion

The influence of temperature on the pyrolysis process of biomass shows that the higher temperature (900 ºC) causes an increase in pH and a decrease in the concentration of oxygen and polar components. At the lowest temperature (400 ºC), the concentration of oxygen and polar component increases, while pH decreases. These parameters affect the rheometric properties, especially t_{90}, and the mechanical properties when rubber reinforcement is involved. The temperature of 900 ºC is the most promising for the production of biochar as a filler in elastomers.

References

1. S. Hamm; T. Frey; R. Weinand; G. Moninot; N. Petiniot Rubber Chemistry and Technology 2009, 82, 2, 214-228. https://doi.org/10.5254/1.3548246.
2. C. O. Okoye; I. Jones; M. Zhu; Z. Zhang; D. Zhang Journal of Cleaner Production 2021, 279, 123336. https://doi.org/10.1016/j.jclepro.2020.123336.
3. F. Amalina; A. S. A. Razak; S. Krishnan; A. W. Zularisam; M. Nasrullah Cleaner Materials 2022, 3, 100045. https://doi.org/10.1016/j.clema.2022.100045.
4. S. Park; J. Kim Journal of Adhesion Science and Technology 2001, 15, 1443-1452. https://doi.org/10.1163/156856101753213295.
5. S. Qian; J. Huang; W Guo; C. Wu J Macromol Sci Part B Phys 2007, 46, 3, 453-66.https://doi.org/10.1080/00222340701257588.
6. E. Pusceddu; A. Montanaro; G. Fioravanti; S. F. Santilli; P. U. Foscolo; I. Criscuoli; A. Raschi; F.Miglietta International Journal of New Technology and Research 2017, 3, 3, 39-46.
7. K. Weber; P. Quicker Fuel 2018, 217, 240-261. https://doi.org/10.1016/j.fuel.2017.12.054.
8. A. Tomczyk; Z. Sokołowska; P. Boguta Reviews in Environmental Science and Biotechnology 2020, 19, 191-215. https://doi.org/10.1007/s11157-020-09523-3.
9. M-J. Kang; Y-J. Heo; F-L. Jin; S-J. Park Carbon letters 2016, 18, 1-10. https://doi.org/10.5714/CL.2016.18.001.
10. C. G. Robertson; N. J. Hardman Polymers 2021, 13, 538. https://doi.org/10.3390/polym13040538.
11. J. L. Leblanc, *Filled polymers: science and industrial applications,* CRC, Boca Ratón, 2010.

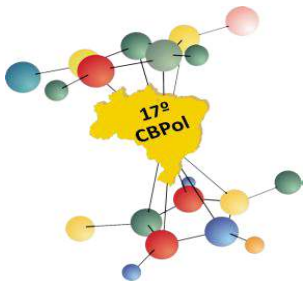

EVALUATION OF THE MECHANICAL PROPERTIES AND ADHESIVE STRENGTH OF POLYCHLOROPRENE-BASED ADHESIVES

Gabriel B. Rosa[1, 2*], Sandra A. C. Mello[2], Silvana N. Cassu[1, 2]

1 –Aeronautics Institute of Technology (ITA), São José dos Campos, SP, Brazil
gabrielgbr@ita.br
2 –Institute of Aeronautics and Space (IAE), São José dos Campos, SP, Brazil

Abstract
In the present study, polychloroprene (CR) compounds containing different vulcanization agents and fumed silica at varied content were evaluated for application as adhesives. The vulcanization systems were based on zinc oxide (ZnO) or ferric acetylacetonate (FeAc). The fumed silica content varied from 0.3 up to 2.0 phr only in CR-FeAc compounds. The rheometric results indicated that the CR compounds containing FeAc reached higher crosslink density, approximately 1.5 higher than that observed for the CR compound vulcanized with ZnO system. After vulcanization, the CR-ZnO compound showed the highest tensile strength and elongation at break. In the T-Peel tests, in which different solvents were tested in the unvulcanized CR compounds, the compositions containing ZnO in toluene/methyl ethyl ketone showed the highest adhesive strength. Among the CR-FeAc compounds, the addition of 2 phr of fumed silica results in the highest tensile strength and elongation at break, while the compound containing 1 phr of fumed silica showed the highest adhesive strength.
Keywords: *Neoprene; fumed silica; ZnO; FeAc.*

Introduction

Elastomeric adhesives are designed to provide a strong and flexible bond between two substrates. Adhesives work by forming a bond between two surfaces, which can be achieved through various mechanisms such as chemical bonds, intermolecular forces, and electrostatic attraction [1]. Polychloroprene (CR), also known as neoprene, is a type of synthetic rubber that is widely used as an adhesive. It has excellent adhesive properties and is commonly used in various applications, including bonding metal and polymeric materials. Polychloroprene rubber is naturally tacky, and different fillers can easily be incorporated, strongly influencing the final properties. Usually, the fillers used are in micrometric scales, such as precipitated silica, carbonates, and kaolins. However, applying nanometer-sized fillers can bring even greater gains to the material properties. Generally, very low nanofiller content can improve mechanical, thermal, and rheological properties. Moreover, the vulcanization system also should affect the final properties of the rubber compounds [1,2]. The vulcanization system most commonly used in the vulcanization of CR is ZnO-based. However, the disposal of these compounds has been described as harmful to nature, especially in aquatic environments, due to the release of metal oxides, mainly ZnO [3].

The system proposed in the present study uses a crosslinking system based on iron acetylacetonate (FeAc), a more environmentally friendly substitute. In this system, triethanolamine (TEOA) was used to keep the medium alkaline, providing a smooth and efficient crosslinking [3], and fumed silica was employed as filler.

Experimental

The CR compounds were prepared using a W-type neoprene (Denka); fumed silica (Cab-o-sil–M5, CABOT); triethanolamine (TEOA, NEON); methyl ethyl ketone (MEK, NEON); toluene (Química Moderna). Ferric acetylacetonate was synthesized from the dissolution of ferric chloride in water, followed by the addition of ammonium hydroxide. This solution was kept under stirring for 2 h. Then acetylacetone was added, and the solution was stirred for another 3 h. After that, the product was filtered, washed, and vacuum dried at 60°C for 24 h. CR compounds (CR-FeAc and CR-ZnO) were prepared in a Lab Mill 350 roller mill (COPE). Initially, the CR elastomer was processed through the roller and formed a paste, and then the additives were added in no particular order.

The CR-FeAc compounds contained 100phr of CR, 0.1phr of FeAc, and 4phr of TEOA. Furthermore, the CR-FeAc compounds were differentiated based on the amount in phr of fumed silica in their composition (0.3; 0.6; 1; 2). The naming of these compounds included the fumed silica amounts added in brackets after the acronym CR-FeAc(x). The CR-ZnO compound was used as a reference, and it contained about 53% inorganic filler, with approximately 10% of precipitated silica. This compound cannot have its composition detailed for reasons of confidentiality.

The adhesives preparation was carried out by the solubilization of the unvulcanized CR compounds in different solvents. The adhesives were named CR-ZnOY, and Y refers to the initial letter of the used solvent, T (toluene) or M (methyl ethyl ketone). All CR-FeAc adhesives were prepared only by solubilization in MEK (Table 1).

Table 1: Composition of the CR adhesives based on their respective CR compounds

Adhesive	Solvent	Vulcanization agent	Filler
CR-ZnOM	MEK	ZnO/MgO	Precipitated silica
CR-ZnOMT	MEK/Toluene	ZnO/MgO	Precipitated silica
CR-ZnOT	Toluene	ZnO/MgO	Precipitated silica
CR-FeAc(0.3)	MEK	FeAc	Fumed silica
CR-FeAc(0.6)	MEK	FeAc	Fumed silica
CR-FeAc(1)	MEK	FeAc	Fumed silica
CR-FeAc(2)	MEK	FeAc	Fumed silica

The vulcanization of the CR compounds was monitored by rheometry analyses performed in the Premier MDR equipment (Alpha Technologies), obtaining viscosity parameters such as Mooney Low (ML) and High (MH) and vulcanization. The test was conducted at a temperature of 145°C for 90 minutes for all specimens.

The tensile test was performed in the ZWICK 1474 equipment, with a speed of 256 mm/min and a 5 kN load cell (ASTM D412). This test aimed to evaluate the behavior of vulcanized CR compounds. The specimens were prepared soon after processing in press at 145°C according to the respective t90 obtained in the rheometry study. The hardness test was also performed for the specimens using the equipment INSTRON S1, following ASTM D2240, with a contact time of 1 second.

The T-peel test was conducted according to ASTM D1876-08 to evaluate the effectiveness of the CR adhesives. The test was performed using two laminate panels of unvulcanized (acrylonitrile-co-butadiene) rubber (NBR) substrate, with the respective adhesive spread on both surfaces and bonded together. After this, the specimens were vulcanized in an autoclave for 6 hours at 145°C and 5 kgf/cm^2, subsequently conducted to the T-Peel test, which was conducted in the ZWICK 1474 equipment, started in tensile mode with a speed of 256 mm/min and 5 kN load cell.

Results and Discussion

Initially, the rheometry test was performed, which is a widely used technique to investigate the vulcanization process of elastomers, aiding in the evaluation of the efficiency of the vulcanization process, as well as monitoring the changes arising from the interactions between the elastomer and crosslinking promoting agents and fillers [4]. In Fig 1 and Table 2, it is possible to see the rheometric profiles of each CR compound. Comparing CR compounds containing FeAc and ZnO, it is possible to see that the CR-ZnO presented the lowest torque values throughout the test. This behavior should be associated with the crosslinking density of the studied vulcanization systems. The (M_H-M_L) values can be used to indicate the crosslinking density [5]. The CR compound vulcanized with FeAc showed M_H-M_L values about 1.5 above that observed for CR-ZnO, indicating higher crosslinking density for the former. It is also worth mentioning the difference in the filler/CR contents used in the compounds containing the different crosslinking systems. While CR-FeAc contained a maximum of 2 wt% silica, CRZnO contained approximately 53 wt% filler. In the latter case, in the rheometric test, about 47 wt% of CR will be vulcanized compared to the 98 wt% or more of CR involved in vulcanization in CR-FeAc compounds, which can also be reflected in the torque values.

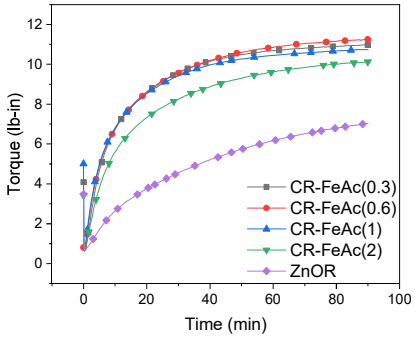

Figure 1: Rheometric curves obtained at 145°C for the CR compounds containing the vulcanization system based on FeAc or ZnO.

Table 2: Rheometric data obtained for CR compounds.

CR Compound (145°C)	M_L (±0,01 dN.m)	M_H (±0,01 dN.m)	t_{50} (min)	t_{90} (min)	M_H-M_L
CR-FeAc(0.3)	0.66	10.99	7.33	35.73	10.33
CR-FeAc(0.6)	0.73	11.25	7.43	40.15	10.52
CR-FeAc(1)	0.81	10.75	6.74	35.43	9.94
CR-FeAc(2)	0.74	9.99	9.76	48.97	9.25
CR-ZnO	0.63	7.31	21.62	67.56	6.68

M_L: Mooney low; M_H: Mooney high; t_{50}: time taken to 50% vulcanization; t_{90}: time taken to 90% vulcanization.

The tensile test was conducted on vulcanized CR compounds to verify their mechanical performance considering the different compositions. Vulcanized polychloroprene has tensile strength values among 7-17 MPa and elongation at break of 200%-600% [6]. In this study, the highest tensile strength (11 MPa) and elongation at break (~ 800%) were observed for CR-ZnO (Fig 2-a), which can be associated with the high amount of filler present in this compound. On the other hand, the CR-FeAc compounds showed much lower tensile strength and elongation values than the CR-ZnO compound. The magnification of the CR-FeAc curves is shown in Fig 2-b. Considering only the filler variation of the fumed silica in CR-FeAc compounds, although they do not follow a pattern, the CR-FeAc(2) reached the highest tensile strength (1,75 MPa) and elongation at break (400%) in comparison to the other CR-FeAc compounds containing up to 1phr of fumed silica. CR-FeAc compounds containing 0.6phr and 1phr of fumed silica show very similar results, and the CR-FeAc(0.3) shows an average result between then and CR-FeAc(2).

The hardness test was also performed for vulcanized compounds (Table 3). The behavior of the tensile and hardness tests suggests that the silica particles must be in the nanometer scale up to 1phr, which would justify the higher values of tensile strength and hardness found for the compounds containing 0.6 and 1phr of silica. The 0.3 phr content, even at the nanometer scale, should not be enough to cause the increase in tensile strength and hardness of the respective compound. The silica dispersion from 2phr should be on a micrometric scale, resulting in the observed change in mechanical behavior, with a lower value of elastic modulus and hardness and higher elongation.

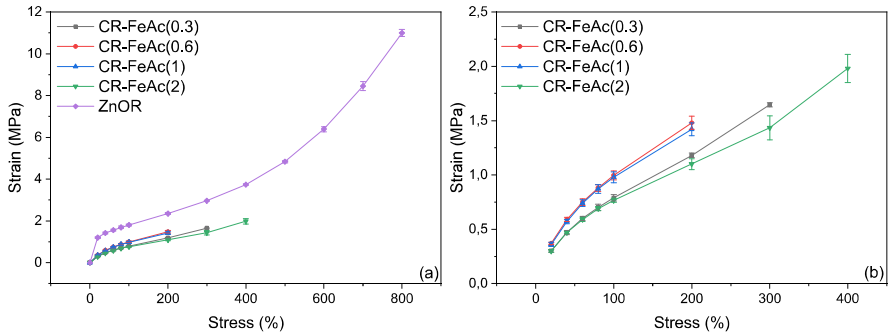

Figure 2: Tensile strength curves overall (a) and only formulations containing FeAc magnified (b).

Table 3: Hardness of the CR compound.

CR Compound	CR-ZnO	CR-FeAc			
		0.3	0.6	1	2
Hardness	64	39	42	43	38
Standard deviation	2	1	1	1	1

The quantification of the adhesive strength between the CR adhesives and the NBR substrate, previously bonded, after both go through the vulcanization process was obtained by the T-Peel test. In this test, peeling should be symmetrical, and failure should preferably propagate to the center of the adhesive bond line [7]. All analyzed adhesives showed cohesive visual failure in all specimens and reached the maximum course of the equipment without total rupture, except the NBR bonded with CR-ZnOM adhesive that broke before the maximum course of the equipment.

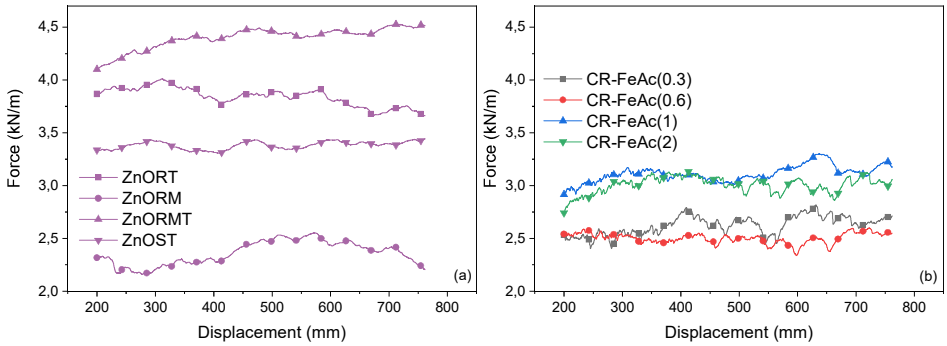

Figure 3: Strength curves obtained in the T-Peel test for NBR specimens containing CR-ZnO (a) and CR-FeAc(x) adhesives (b).

Comparing the force curves obtained by the T-Peel test for the NBR substrate jointed with the CR adhesives, it can be observed that the NBR bonded with CR-ZnOMT adhesive showed the best performance when compared to the others. The reason for this may be the mixture of the solvents MEK and toluene, which were able to help the CR chains to penetrate better into the NBR substrate, improving the co-vulcanization of the different rubbers. This result can be related to the optimal Hildebrand solubility parameter (∂)[8] of the solvent mixture relative to NBR and CR

rubbers, which at the present concentration of 80:20 has ∂ equal to 19.1 $MPa^{1/2}$, being very close to the values of NBR (19.0 $MPa^{1/2}$) and polychloroprene (16.6-19.2 $MPa^{1/2}$). On the other hand, the worst-performing adhesive was observed for NBR bonded with CR-ZnOM, the only one that broke entirely before the equipment limit (962 mm). The poor performance may be associated with the adhesive application, which may not have been homogeneous enough, or even the analysis conditions, considering that MEK has a high-speed evaporation rate (2,5~3,3)[8,9] compared to the evaporation rate of toluene, reducing the NBR swelling and consequently the penetration of the CR chains into NBR. Referring to Fig 3b, all had very similar performances, with a little highlight for the CR-FeAc(1), which presented the highest adhesive strength. Since the CR-FeAc adhesives were solubilized in MEK, the effect of the rapid evaporation rate of MEK may have interfered with specimen preparation, resulting in the poorer adhesive performance of these compounds.

Conclusions

The CR-FeAc compounds showed higher crosslinking density than those vulcanized by the ZnO-based system. The vulcanized CR-ZnO compound showed the highest tensile strength and elongation values at break, attributed to the high filler content present in this compound. The adhesive obtained by solubilization of CR-ZnO in toluene/MEK showed the highest adhesive strength in the T-peel test. Among the CR-FeAc adhesives, the highest tensile strength, elongation, and adhesive strength values were observed for the compounds containing 2 and 1 phr, respectively.

Acknowledgements

This study was financed in part by the Coordenação de Aperfeiçoamento de Pessoal de Nível Superior - Brasil (CAPES) - Finance Code 001. In addition, the authors gratefully acknowledge the financial support given by Conselho Nacional de Desenvolvimento Científico e Tecnológico (CNPq) project number 422016/2017-9 and by Agência Espacial Brasileira (AEB).

References

1. A. Guchait; A. Saxena; S. Chattopadhyay; T. Mondal. Influence of Nanofillers on Adhesion Properties of Polymeric Composites 2022, 7, 3844-3859. https://doi.org/10.1021/acsomega.1c05448
2. D. K. Meincke; A. O. Ogliari; F. A. Ogliari. Influence of different fillers on the properties of an experimental vinyl polysiloxane 2016, 30(1), 36. https://doi.org/10.1590/1807-3107BOR-2016.vol30.0036
3. A. Dziemidkiewicz; M. Pingot; M. Maciejewska. Metal complexes as new pro-ecological crosslinking agents for chloroprene rubber based on heck coupling reaction 2019, 92(3), 589-597. https://doi.org/10.5254/rct.19.81465
4. M. Khabiri; S.H. Jafari; M.R. Pourhossaini; H.A. Khonakdar. Investigations on matrix network characteristics in NBR/silica nanocomposites 2018, 135(16), 1-11. https://doi.org/10.1002/app.46170
5. A. Dziemidkiewicz; R. Aniszka; A. Blume; M. Maciejewska. Reaction mechanism of halogenated rubber crosslinking using a novel environmentally friendly curing system 2020, 84, 106354. https://doi.org/10.1016/j.polymertesting.2020.106354
6. C. Chandrasekaran. Raw Materials for Rubber Lining Compounds 2017, 77-86. http://dx.doi.org/10.1016/b978-0-323-44371-5.00011-6
7. A.V. Poncius. Adhesion and Adhesives Technology: An Introduction 2012, 3.
8. J. Brandrup; E.H. Immergut; E.A. Grulke. Polymer handbook 1999, 4, 2366.
9. M.J.L. Caetano. Velocidade de evaporação de solventes 2019. Available in: https://www.ctborracha.com/borracha-sintese-historica/materias-primas/solventes/velocidade-de-evaporacao-de-solventes/Accessed May 05, 2023

MAGNESIUM OXIDE AS ACTIVATOR FOR NITRILE RUBBER COMPOUNDS: VULCANIZATION KINETICS AND CROSSLINK DENSITY

Giovana R. B. Graça[1*], Arianne A. da Silva[1], Ana M. F. de Sousa[1], Nakédia M. F. Carvalho[1], Cristina R. G. Furtado[1]

[1]*Chemistry Institute, Rio de Janeiro State University (UERJ), Rio de Janeiro, RJ, Brazil*
giovanarbg@gmail.com.br

Abstract – During the vulcanization process, crosslinks are formed, which play an important role in the mechanical and thermal properties of the rubber product. Zinc oxide (ZnO) is currently the most commonly used activator in the vulcanization process of rubber, but it is considered toxic to the aquatic environment at certain concentrations. In this work, the possibility of replacing zinc oxide by magnesium oxide (MgO) in nitrile rubber (NBR) with 33% and 45% acrylonitrile (ACN) content was investigated based on rheometric data, vulcanization kinetics, and crosslink density measurements.

Keywords: *Cross-link density, acrylonitrile butadiene rubber, kinetics, rheology, rubber vulcanization.*
Fundings: The authors thank Nitriflex for donating the rubber compounds' raw materials. This study was supported by the CAPES) [: PhD Scholarship received by Arianne A. da Silva]; Conselho Nacional de Desenvolvimento Científico e Tecnológico (CNPQ) [P2-309461/2021-9 received by Ana Maria Furtado de Sousa and PQ-2/2018: 313831/2018-1 received by Nakédia M. Freitas de Carvalho] and Fundação Carlos Chagas Filho de Amparo à Pesquisa do Estado do Rio de Janeiro – FAPERJ [JCNE 2018: E-26/203.023/2018 and Grupos Emergentes 2019: E-26/010.002171/2019 received by Nakédia M. Freitas de Carvalho; APQ1 2019: E-26/010.001927/2019 received by Ana Maria Furtado de Sousa]

Introduction

In recent years, the interest in materials that do not harm the environment has rapidly increased, which is an obvious issue considering the vast usage of zinc oxide, especially in the rubber industry. Although zinc oxide is the most efficient and widely used cure activator for sulfur vulcanization of rubber, studies pointed out that it can become toxic when in excess, particularly in aquatic systems [1-2]. Even though it is known that magnesium oxide (MgO) does not perform similarly to zinc oxide, studies have been made in order to investigate and improve its use so as to replace the ZnO or be used as co-cure activator.

This study compared the activator performance of MgO and ZnO in the vulcanization of nitrile rubber compounds with 33% and 45% of acrylonitrile-containing. The crosslink density was determined through the swelling at equilibrium method and the Flory-Rehner [3] equation. This result makes it possible to analyze whether more or less sulfur bonds were formed between the polymeric chains when replacing ZnO with MgO. Such an analysis is important since these sulfur bonds have an impact on the material's stiffness. The empirical model proposed by Isayev [4] was used to determine the rate constant (k), the reaction order (n) and the apparent energy of vulcanization (E_a), parameters that make it possible to analyze the vulcanization kinetics of the samples. Values of rheometric data such as lowest (M_H) and highest torque (M_L), induction time (ts1), and optimum curing time (t90) were also determined and will be discussed.

Experimental

Two grades of nitrile rubber (NBR) with 33% and 45% of acrylonitrile, carbon black (40phr), sulfur (1.5phr), stearic acid (1.0 phr), TBBS (0.7phr) , ZnO (3.0phr), and MgO (3.0phr) were kindly donated by Nitriflex. The rubber compounds were made in a closed mixer according to ASTM D3187. The experimental code used is: XX%-YY, where XX% is the acrylonitrile content (33% or 45%) and YY is the type of activator (ZnO: 3 phr or MgO: 3phr).
Rheometric curves were obtained in an oscillating disc rheometer (ODR) according to the ASTM 2084 standard at temperatures of 155, 160, 165, and 170 °C. Samples were vulcanized at 160 °C and respective t90 on the ODR.
The initial energy of activation (E_i) was calculated through the following equation (Eq. 1):

$$ln\,(ti) = ln\,(t0) + \frac{E_i}{RT} \quad (1)$$

The kinetic parameters were determined by the empirical model proposed by Isayev [4] (Eq.2), which makes it possible to determine the rate constant (k) and reaction order (n) for each of the samples. The linearization of the Arrhenius equation (Eq. 3) and the values obtained for k and the inverse of the temperature were used to calculate the apparent energy of vulcanization.

$$\alpha = \frac{k \cdot t^n}{1 + k \cdot t^n} \quad (2)$$

$$k = k_0 \cdot e^{\frac{-E_a}{RT}} \quad (3)$$

To perform the swelling at equilibrium method, the samples were dipped in acetone and toluene for swelling. All samples were properly weighed before, during, and after the swelling process was done. With the values obtained during the swelling process, it is possible to calculate the crosslink density ([X]) through the Flory-Rehner equation (Eq. 4) [3]:

$$[X] = \frac{-[ln\,(1 - v_r) + v_r + \chi \cdot v_r^2]}{V_0 \cdot (v_r^{1/3} - v_r/2)} \quad (4)$$

Where v_r is the volume fraction of the swollen rubber, χ is the rubber-solvent interaction parameter and V_0 is the molar volume of the solvent.

Results and Discussion

Figure 1 and Table 1 shows the rheometric curves and parameters, respectively.

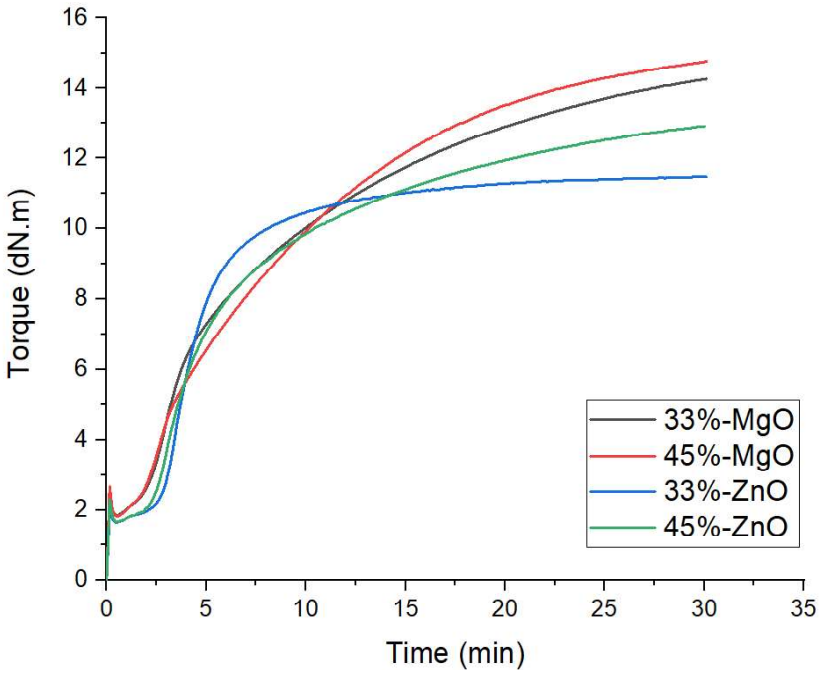

Fig 1. Rheometric curves torque versus time for all four NBR compounds.

Table 1. Rheometric values obtained through an oscillating disc rheometer.

	33%-MgO	**45%-MgO**	**33%-ZnO**	**45%-ZnO**
ts1 (min)	2.2	2.1	2.9	2.6
t90 (min)	20.8	19.9	10.2	19.0
M_L (dN.m)	1.9	1.87	1.69	1.71
M_H (dN.m)	10.47	11.04	8.09	9.5
$\Delta M = (M_{H-ML})$ (dN.m)	12.37	12.91	9.78	11.21

Through the oscillating disc rheometer, values for the lowest torque (M_L) and the highest torque (M_H) were obtained, thus making it possible to calculate ΔM. The highest ΔM were presented by the samples with MgO, while the lowest values obtained were from ZnO, indicating the higher rigidity caused by the crosslinks in the samples of magnesium oxide.

The induction time (ts1) and optimum curing time (t90) for each of the samples are shown in Table 1. Equal to what was already observed in previous works [6-7], the values obtained for ts1 are smaller for compounds with MgO, while the values for t90 showed a smaller time required for the compound with ZnO samples to achieve 90% of its maximum torque. A smaller ts1 implies a smaller scorch safety time, which is the time for torque to increase one unit above M_L. For t90, smaller values are preferred since a shorter curing time would minimize the energy consumed during the curing process.

In order to better understand the effect of the activator type on starting the vulcanization, the initial energy of activation (E_i) was determined using Eq. 1, with the results shown in Table 2. In general, the E_i for all compounds containing ZnO were lower than those containing MgO, though the difference was not significant.

Table 2. Kinetic parameters obtained through the empirical model proposed by Isayev.

	33%-MgO	**45%-MgO**	**33%-ZnO**	**45%-ZnO**
E_i (kJ/mol)	95 ± 0	109 ± 1	85 ± 0	90 ± 0

Figure 2 shows the curves of conversion versus time for all NBR compounds.

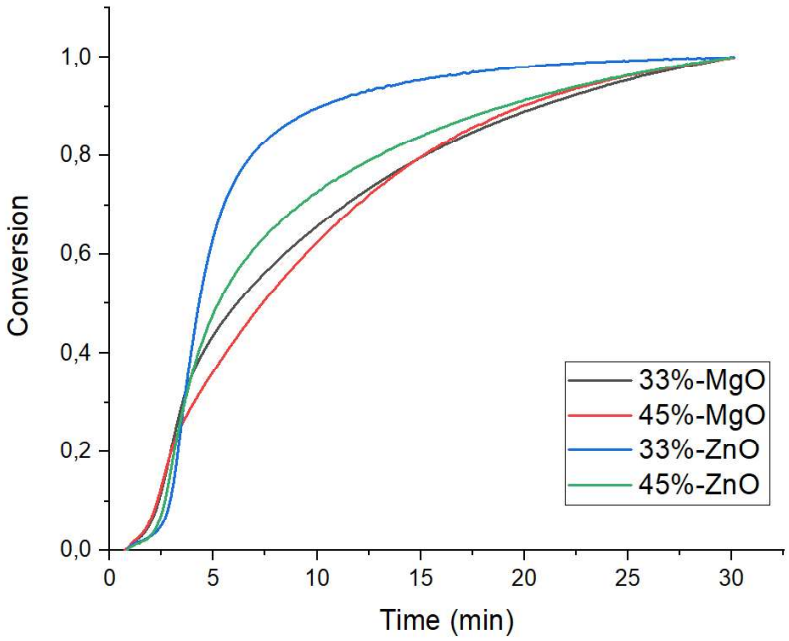

Fig 2. Conversion throughout the time for all four samples.

Higher conversions at smaller times are preferred; therefore, with the curve presented in Figure 2, the samples with ZnO would be superior to the ones with MgO since a smaller time would be required to reach higher percentages of conversion, while the samples with MgO appear to have smaller inclinations for both contents of acrylonitrile. Table 3 displays the apparent energy of vulcanization (E_a) calculated using the rate constant (k) from Isayev's [4] model (Eq.2).

Table 2. Kinetic parameters obtained through the empirical model proposed by Isayev.

	33%-MgO	**45%-MgO**	**33%-ZnO**	**45%-ZnO**
E_a (kJ/mol)	195 ± 6	122 ± 1	381 ± 11	350 ± 9

The E_a values obtained for MgO compounds were lower than those obtained for ZnO compounds. Smaller values for E_i and E_a are preferred since the reaction rate is not so temperature increase dependent. The increase in the percentage of acrylonitrile resulted in the increase of the values of E_i for both magnesium and zinc oxide, while a decrease was observed in E_a for both activators, and according to the results obtained, the impact of the acrylonitrile content is higher for the samples with MgO.

The values of crosslink densities determined using toluene and acetone as solvents are shown in Table 3. It is observed that the type of solvent influences the results of crosslink density, with higher values observed for acetone, as expected, given that acetone is a better solvent for NBR than toluene.

Table 3. Cross-ink density obtained through the swelling at equilibrium method with acetone and toluene.

Solvent used in the analysis	**33%-MgO**	**45%-MgO**	**33%-ZnO**	**45%-ZnO**
[X] in Acetone (mol/cm^3) *10^{-4}	5.95 ± 0.23	5.12 ± 0.28	5.77 ± 0.11	4.38 ± 0.48
[X] in Toluene (mol/cm^3) *10^{-4}	3.07 ± 0.01	2.85 ± 0.01	2.54 ± 0.01	2.37 ± 0.11

Although the differences in [X] values between the NBR samples are not significant, it appears that the NBR compounds containing MgO have higher [X] values, regardless of the acrylonitrile content.

In this study, the crosslink density can be associated with ΔM because the same type and amount of filler and system cure are used, except for the type of activator. Therefore, it is expected that if a sample has a higher cross-link density, it is bound to have a higher ΔM. Such a correlation is observed in this work, since the samples of MgO presented higher values for both cross-link density and ΔM.

Conclusions

Based on the results gathered and shown in this work, MgO works well as a ZnO substitute for the vulcanization of NBR, but it appears that MgO does not follow the same pattern as ZnO does, as shown by the difference in properties obtained throughout this study. The samples with MgO did present higher values for crosslink density than the ones with ZnO, which indicates more sulfur bonds are formed during the vulcanization process, making the rubber more rigid. The ΔM for samples with MgO was also higher, further proving the higher rigidity conferred to the material by substituting the activator. The apparent energy of vulcanization of the MgO samples was lower than the one obtained for the ZnO samples. Such results indicate MgO can be a promising replacement for ZnO as an activator in the NBR vulcanization process.

Acknowledgements

The authors would like to thank Nitriflex, CAPES, CNPQ, FAPERJ and UERJ for supporting the development of the research.

References

1. S. Mostoni; P. Milana; B. Di Credico; M. D'Arienzo; R. Scotti. Catalysts 2019, 9(8), 664. https://doi.org/10.3390/catal9080664
2. Bodar CWM, Pronk MEJ, Sijm DTHM (2005) The European Union Risk Assessment on Zinc and Zinc Compounds: The Process and the Facts. Integrated Environmental Assessment and Management 1:301-319.
3. P. Flory; J. Rehner. The Journal of Chemical Physics, 1943. 11, 512-520. https://doi.org/10.1063/1.1723791
4. A. Isayev; J. Deng. Rubber Chemistry and Technology, 1988. 61, 350-361. https://doi.org/10.5254/1.3536192
5. E. Leroy; A. Souid; A. Sarda; R. Deterre. Polymer Testing, 2013, 32, 1614. https://doi.org/10.1016/j.polymertesting.2012.08.012
6. M. Guzmán; B. Vega; N. Agulló; U. Giese; S. Borrós. Rubber Chemistry and Technology, 2012, 85, 38-55. https://doi.org/10.5254/1.3672428
7. A. Silva; E. Rocha; C. Furtado; A. Sousa; N. Carvalho. Polymer Bulletin, 2021, 78, 6205-6219. https://doi.org/10.1007/s00289-020-03430

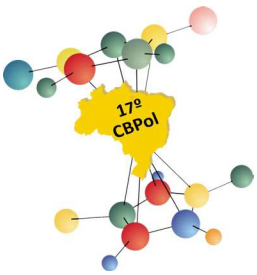

RHEOMETRIC, RHEOLOGICAL AND MECHANICAL PROPERTIES OF ELASTOMERIC COMPOUNDS CONTAINING SBR AND GRAPHENE NANOPLATELETS

Morgana D. Oliveira[1], Suélen Moresco[2], Rosmary N. Brandalise[1*]

1 – Graduate Program in Materials Science and Engineering*, (PPGMAT),*
University of Caxias do Sul (UCS),
Caxias do Sul, RS, Brazil,
**rnbranda@ucs.br;*
2 – Vipal Rubber Technology and Research Center, Nova Prata, RS, Brazil

Abstract – Elastomeric compounds consist of two or more materials that together form a new material with unique properties. There are countless applications for elastomeric artifacts, including automotive, footwear, construction, and biomaterials. The applications can be extended by using graphene nanoplatelets. Graphene can improve the physical, chemical, electrical, thermal and optical properties of elastomer materials. Therefore, in this work, the rheometric, rheological, and mechanical properties of blends of poly(butadiene-co-styrene) (SBR) according to ASTM D3848-03 standard and graphene nanoplatelets were investigated using masterbatch, with dispersion by conventional mixing methods. The results showed an improvement in rheometric properties consistent with the rheology of the blends and a 45% improvement in tear strength for the sample with the incorporation of 0.4% m/m graphene nanoplatelets.

Keywords: *elastomeric compounds, SBR, graphene nanoplatelets, mixing equipment.*

Introduction

SBR, together with natural rubber, accounts for more or less 60% of the world's rubber production. About 75% of SBR production is for the tire industry [1]. Some of the properties of SBR are: good abrasion and tear resistance and elasticity. Its disadvantages include lower resistance to ozone, solvents, and flame [2].

The addition of nanomaterials to elastomeric compounds is expected to improve its chemical and physical properties. In addition, nanomaterials promise savings in compounding, since their use for reinforcement requires smaller amounts of raw materials.

Graphene is composed of a monoatomic compound of carbon and is stronger and stiffer than steel due to its two-dimensional structure. It is also currently the lightest material with the largest surface area compared to graphite, a material from the same family [3]. It has unique properties such as high thermal conductivity, mechanical resistance, and high electronic mobility in the range of 200000 $cm^2.Vs^{-1}$. Therefore, graphene can be used in biomaterials, sensors, capacitors, coatings, and as a component of thermoplastics, thermosets, and elastomers [4].

In composites, graphene and its derivatives face the challenge of being incorporated into the polymeric matrix [5]. The main methods for dispersion of graphene in polymer matrices are solution methods, freeze drying, sonication and ultrasonication. The mechanical method has been shown to be less efficient for graphene dispersion. Closed mixing and open mixing are the conventional mixing methods used in the elastomer industry.

In view of this, this work aims to evaluate the rheometric, rheological and mechanical properties of SBR-based elastomer blends in which graphene nanoplatelets have been incorporated in the form of a masterbatch using conventional mixing methods in the elastomer industry, closed mixers and open mixers.

Experimental

The raw materials used in this work are: SBR, stearic acid, zinc oxide, N-tert-butyl-2-benzothiazole sulfenamide and sulfur, all of which were provided by Borrachas Vipal S.A (Nova Prata - RS). The masterbatch of graphene nanoplatelets (average 20 layers) was from Znano Grafeno (Caxias do Sul - RS). The development followed the ASTM D3848-03 formulation, adapted only for the incorporation of 0.2 and 0.4% (w/w) graphene nanoplatelets in the form of a masterbatch.

In an initial development, blends were made in which the accelerator activators and graphene nanoplatelet masterbatch were added to the SBR in a Copé brand Banbury type closed mixer, while the accelerator and vulcanizing agent were added to the compound in an open mixer, also Copé brand, model Lab Mill 350. The coding of these mixtures is: MF/SBR/NPG0.0%, MF/SBR/NPG0.2% and MF/SBR/NPG0.4%. Another development was carried out directly in the open mixer with the same previous composition, ASTM D3848-03, with the masterbatch of graphene nanoplatelets incorporated directly into the SBR. The blends of this second stage were coded as follows: MA/SBR/NPG0.2% and MA/SBR/NPG0.4%. Vulcanization was performed by compression molding in a Copé hydraulic press, model Lab. Press 215, at a temperature of 150°C for the optimum vulcanization time, which was determined using a rheometer with oscillating disk, model MDR 2000, from Alpha Technologies (ASTM D5289-12). From this test, in addition to the parameters of optimum vulcanization time (t_{90}), maximum torque (M_H), minimum contact (M_L) and process safety time (t_{s1}), the vulcanization index (CRI) was calculated using equation 1.

$$CRI = 100 / (t_{90} - t_{s1})$$

Mooney viscosity of the mixtures was evaluated in a Mooney MV 2000 instrument from Alpha Technologies. The standard selected for validation of the rheological test was ASTM D1646-07, and the INSTRON universal tester, model SN5206, was used for the tensile strength test in accordance with ASTM D624-00.

Results and Discussion

Table 1 shows the results for the rheometry and rheology of the elastomer compounds.

Table 1 - Vulcanization and rheological test parameters.

Samples	t_{90} (min)	M_H (dN.m)	M_L (dN.m)	t_{s1} (min)	CRI	Mooney viscosity [M_L 1+4 (100°C)]
MF/SBR/NPG0.0%	50.4	8.29	0.73	25.1	3.9	43.1
MF/SBR/NPG0.2%	43.0	8.71	0.73	22.5	4.9	43.1
MF/SBR/NPG0.4%	40.4	8.78	0.72	22.4	5.6	43.7
MA/SBR/NPG0.2%	47.3	8.62	0.75	24.2	4.3	43.3
MA/SBR/NPG0.4%	44.2	9.14	0.77	25.5	5.4	49.2

It was observed that the samples containing graphene nanoplatelets and processed in MF had lower values for t90 and ts1 compared to the standard without the addition of graphene nanoplatelets and relative to the samples processed in MA. This decrease in t_{90} and t_{s1} parameters means a reduction in processing and vulcanization time, resulting in processing savings [6]. The M_L, attributed to the viscosity of the polymer system, showed higher values when graphene nanoplatelets were added to the formulation when the compounds were prepared in MA. These values were confirmed by Mooney

viscosity, except for the sample with MA/SBR/NPG0.4%, which showed increased viscosity. For M_H, the indicator of crosslinks and modulus at 100 and 300%, the results showed an increase for all samples with graphene nanoplatelets, which was more pronounced for the sample MA/SBR/NPG0.4%. The rationale for this result is that graphene acts as a processing aid and promotes the formation of crosslinks through the polymer matrix, making the material more compact and bringing its chains closer together.

In terms of the CRI values found, the samples containing graphene nanoplatelets showed higher values compared to the standard samples, regardless of the type of mixing equipment. High CRI values indicate high vulcanization rates of the compound, a factor observed in the studied compounds containing graphene nanoplatelets.

Figure 1 shows the results of the mechanical tensile strength of the samples with and without the addition of graphene nanoplatelets at the different percentages and in the different mixing equipment.

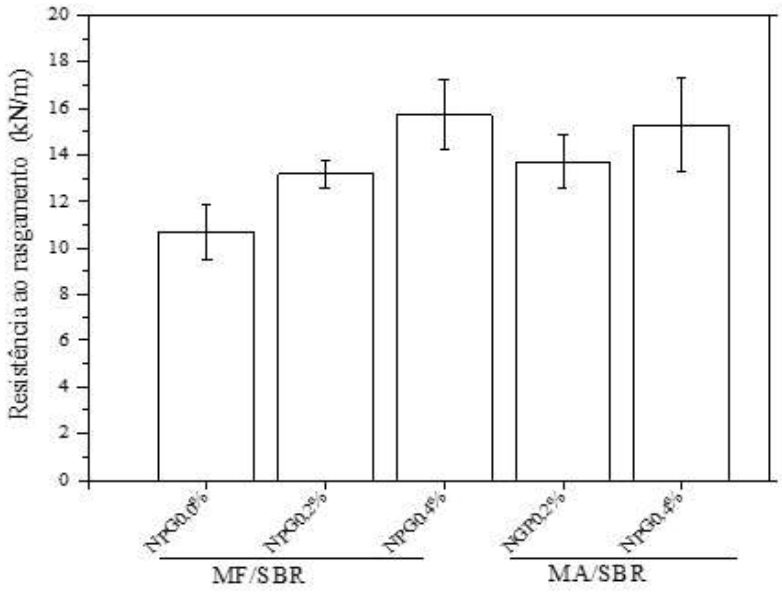

Figure 1– Tear strength of specimens with and without the addition of graphene nanoplatelets in different mixing devices.

Higher levels of graphene nanoplatelets (MF/SBR/NPG0.4% and MA/SBR/NPG0.4%) resulted in an increase in tensile strength of about 45 and 41%, respectively, compared to the standard without the addition of graphene nanoplatelets. graphene. For samples with a lower percentage of graphene nanoplatelets (MF/SBR/NPG0.2% and MA/SBR/NPG0.2%), the increase was 23 and 25%, respectively. In this way, the type of mixer used does not differ in the tear strength results, which is a positive aspect since the masterbatch can be incorporated into an open mixer.

Conclusions

As for the rheometric results, the reduction of the two times, the optimal vulcanization time and the safety time, allows a shorter vulcanization time, which is confirmed by the CRI values. The viscosity of the compounds (M_L and Mooney) does not show any obvious variations in terms of the content of incorporated graphene and the type of mixer, with the exception of the MA/SBR/NPG0.4% mixture. The addition of graphene nanoplatelets leads to an increase in tensile strength of 45 and 41% for MF/SBR/NPG0.4% and MA/SBR/NPG0.4%, respectively, compared to the sample without graphene nanoplatelets.

Acknowledgements

The authors thank CAPES-PROSUP and the National Council for Scientific and Technological Development (CNPQ) for the Productivity Research PQ2, the companies Borrachas Vipal S. A, Znano Grafeno and the University of Caxias do Sul.

References

1. A. Khan, *et* al. Preparation of Styrene-Butadiene Rubber (SBR) Composite Incorporated with Collagen-Functionalized Graphene Oxide for Green Tire Application 2022, 8, 161. https://doi.org/10.3390/gels8030161.
2. E. J. Mark; B. Erman; M. C. Roland. *The science and technology of rubber*, Elsevier, USA, 2013; 4ª ed.
3. V. D. E. J. Segundo; O. E. Vilar. Grafeno: Uma revisão sobre propriedades, mecanismos de produção e potenciais aplicações em sistemas energéticos 2016, 11, 54-57. Disponível em: http://www2.ufcg.edu.br/revista-remap/index.php/REMAP/article/viewArticle/493. Acesso em: 13 Out. 2022.
4. G. J. A. Zarbin; M. M. Oliveira. Nanoestrutura de carbono (nanotubos, grafeno): Quo Vadis? 2013, 36, 1533-1539. https://doi.org/10.1590/S0100-40422013001000009.
5. S. YARAGALLA, *et al*. Chemistry associated with natural rubber–graphene nanocomposites and its effect on physical and structural properties, 2015, 74, 792-802, 2015. https:// doi.org/10.1016/j.indcrop.2015.05.079.
6. D. TORANI; J. S. CRESPO; R. N. BRANDALISE. Influence of ZnO on the properties of elastomeric compositions and their leached extract, 2019, 29. https://doi.org/10.1590/0104-1428.07218.

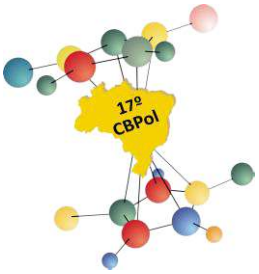

STUDY OF THERMO-OXIDATIVE AGING OF FLUORINATED GASKETS (FKM) USED IN PLATE HEAT EXCHANGERS

Elias L. de Souza[1], Gabriel B. Dutra[1], Mateus S. Zanzi[1], Rafael S. Ribeiro[1*]

Department of Mobility Engineering, Federal University of Santa Catarina (UFSC), Santa Catarina, Brazil.
s.rafael@grad.ufsc.br

Abstract – Gaskets are sealing elements used in plate heat exchangers, which are subjected to aggressive conditions during service. In particular, the compression state, together alongside temperatures, can cause a premature deterioration of properties. To monitor and prevent such a situation, this study uses the TTS (time-temperature superposition) method and Arrhenius to predict the lifetime of FKM gaskets. For this purpose, thermo-oxidative aging was conducted at different temperatures up to 6 months, monitoring Compression Set (CS) and Shore A hardness. The results indicate that the gasket can withstand periods up to almost 300 days in service for an operating temperature of 140 °C.
Keywords: Thermo-oxidative aging. FKM. Heat exchangers. Compression set. Lifetime prediction
Fundings: The authors wish to thank PETROBRAS for their financial support of this research.

Introduction

Heat exchangers are widely used in the petrochemical industry, serving sectors that require thermal exchange of process fluids. Therefore, research and work on preventing failures and predicting the lifetime of gaskets used in heat exchangers are welcome.

Among the works already conducted, Kömmling; *et al.* [1] studied the influence of aging on the sealing capacity of FKM, HNBR and EPDM rubber, where FKM rubber showed greater resistance to thermo-oxidative aging in air. Salehi; *et al*. [2] evaluated the behavior of different rubbers (NBR, EPDM, FKM, and PTFE) in saline water and corrosive vapors. As a result, FKM rubber showed the lowest degradation rate among the materials studied but had low resistance to decompression. Other studies present the prediction of the lifetime of rubbers based on accelerated thermo-oxidative aging in relation to the operating condition, Kömmling; *et al.* Souza; *et al.* [3,4].

Based on the literature and applications of gaskets in service, this work presents the monitoring of the thermo-oxidative properties of gaskets made with fluoroelastomers (FKM) subjected to accelerated aging for periods up to 180 days as a function of aging temperatures of 80, 110, 140 and 170 °C to estimate the time it will take for leakage to occur, considering a CS of 79%. Thus, it is possible to predict failure, avoiding the shutdown of thermal exchange systems in operation, which can cause loss of system productivity.

Experimental

In this study, commercial gaskets made of Viton A 401-C with an irregular shape were used, as illustrated in Fig 1. To obtain the test specimens, 10 mm segments were cut from the gaskets themselves.

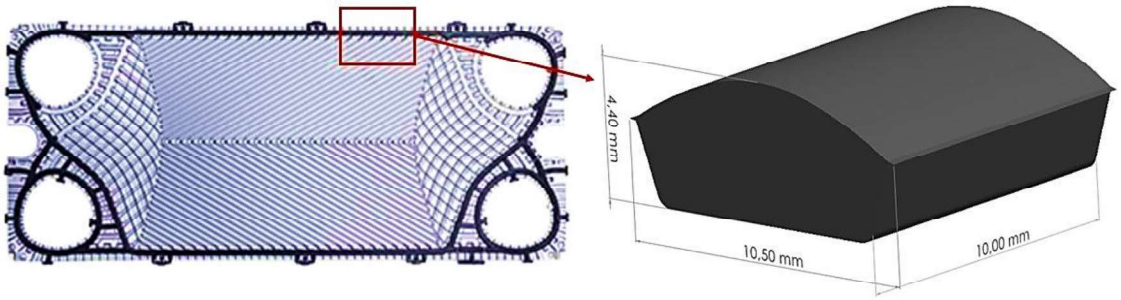

Figure 1: Representation of the extraction of test specimens from the entire gasket.

The tests were conducted in air-circulating and temperature-controlled ovens, adopting a compression of 25% of the initial height of the samples. The temperatures analyzed were 80, 110, 140 and 170 °C for periods of 3, 7, 15, 30, 45, 90 and 180 days. Stainless steel devices were used, each with eight specimens for analyzed condition, which were machined, grinded and polished to ensure measurement accuracy and correct alignment of the plates.

For hardness, measurements were taken using a Mitutoyo HH 336 Shore A type digital durometer, following ISO 7619-1:2010 for vulcanized or thermoplastic rubbers with adaptation for the measurement location, using the top of the test specimens to perform the measurements.

Compression set can be understood as the permanent deformation of the material. Data acquisition was based on ISO 815-1:2019 standard, for values ranging from 75 to 100 Shore A with adaptation in the viscoelastic recovery time after 24h sample decompression, which was based on preliminary experiments.

The indentation modulus profile was obtained along the cross section of the test specimens using a bidirectional displacement system in a (x,y) plane, coupled to an universal testing machine. The modulus value is obtained by the ratio of the force perceived by the load cell (Instron 100 N) and the displacement. For each of the 15 points evaluated along the section, in the region between 3 and 5 N (linear "force x displacement" relationship), the modulus profile is obtained by considering the average of two measurements obtained under the same condition. Thus, the results are expressed in the form of a color map generated by the "Statistica" software.

For the failure condition, as reported in the literature and similar studies, Zanzi; *et al.* [5], the failure criterion assumed for the gasket was a compression set (CS) of 79%.

The lifetime prediction was conducted using the TTS (Time Temperature Shift) method and the Arrhenius curve, using a reference temperature that reached the failure criterion to estimate the lifetime at other temperatures.

Results and Discussion

Based on the results presented in Fig 2, it is possible to observe that all temperatures showed an increase in CS over time, a behavior that occurs due to a combination of chain scission and crosslinking reactions. Crosslinking due to oxidative bonds in a compressed state prevents the rubber from returning to its initial height, causing this permanent deformation, as observed in other studies, Souza; *et al*. Kömmling *et al.* [6,7].

However, given the thermal-oxidative aging resistance of the material, only the samples aged at 170 °C reached the failure criterion while at the other temperatures, the samples did not exceed 60% in the CS value.

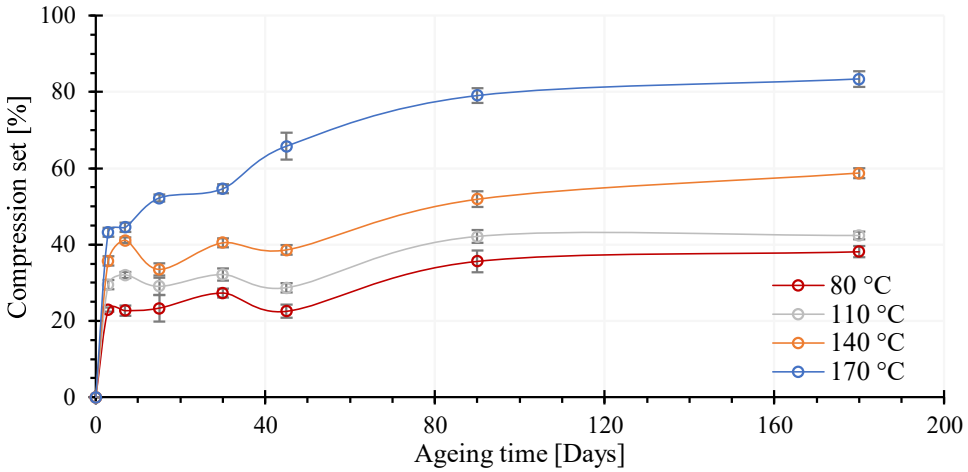

Figure 2 – Compression set evolution during the aging time.

According to the hardness curves illustrated in Fig 3, the hardness values remain close to the initial value throughout the period, except at the temperature of 170 °C. Unlike the CS, the hardness tends to decrease with chain scission and increase with crosslinking. Thus, a balance between its chemical reactions may have occurred at temperatures up to 140 °C. At 170 °C, crosslinking may have predominated after 30 days, resulting in an increase in hardness of around 3.5 Shore A.

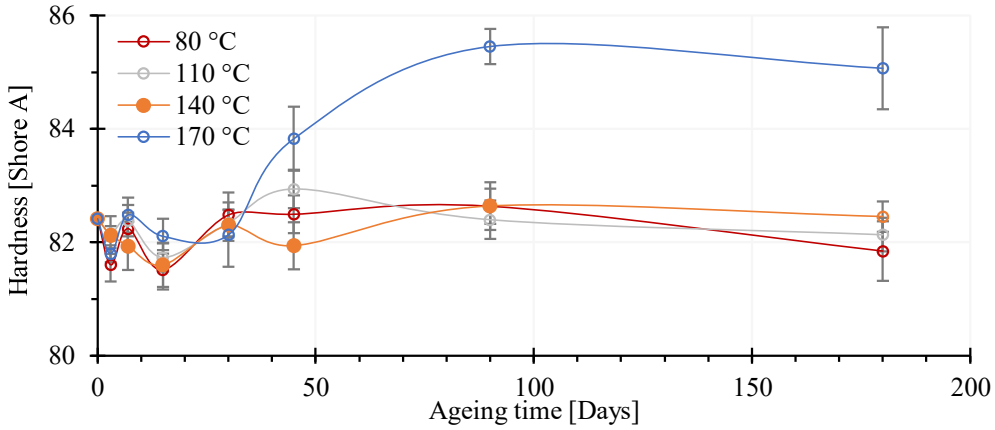

Figure 3 – Hardness evolution as a function of the aging time and temperature.

Fig 4 shows the indentation modulus profile of the samples through a color map, where lighter colors indicate higher stiffness and darker colors indicate lower stiffness.

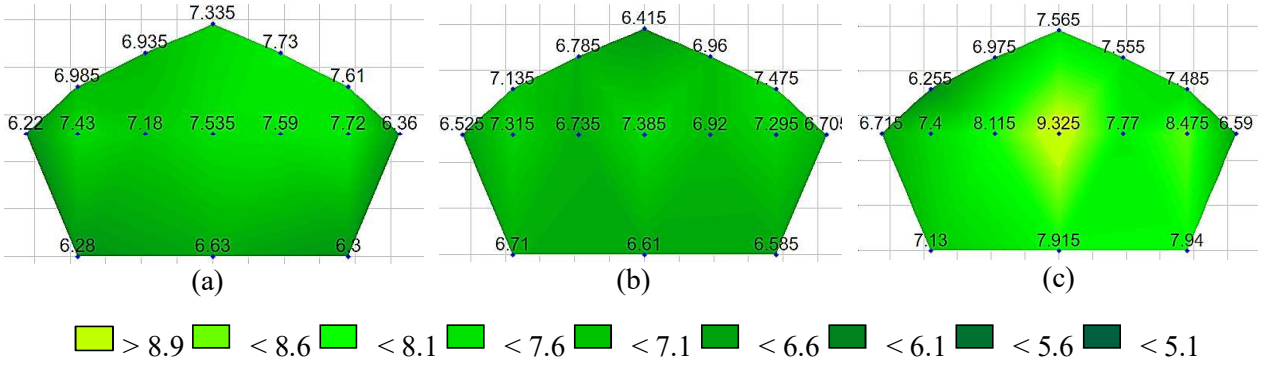

Figure 4 – Indentation modulus profile, (a) unaged; and aged at (b) 80 °C and (c) 170 °C for 180 days.

It is common in some types of rubber for a non-uniform oxidation profile to occur, where oxygen consumption is greater than its diffusion rate towards the center of the body, called the DLO effect (diffusion limited by oxidation), as demonstrated by similar studies, Linde; *et al*. [8]. In these cases, the stiffness in the center and outer layer of the rubber shows a significant difference. To verify such a situation, indentation modulus tests were performed, as presented in Fig 4.

Based on the indentation modulus profiles, an increase in stiffness is observed in the center of the sample at a temperature of 170 °C, as shown in figure (c). However, overall, the results show an almost uniform aging throughout the cross-section of the samples. Fig 5(a) represents the TTS (Time Temperature Shift) master curve plotted from the displacement of the CS curves to the reference temperature of 170 °C. (b) displays the Arrhenius curve generated from regressions based on the shift factor and the reference temperature. In addition, WLF method was applied to estimate C1 and C2 values. When employing a reference temperature of 170 °C, and auxiliary temperatures of 110 and 80 °C, the values -33.3947 and 2063.68 were obtained for C1 and C2, respectively.

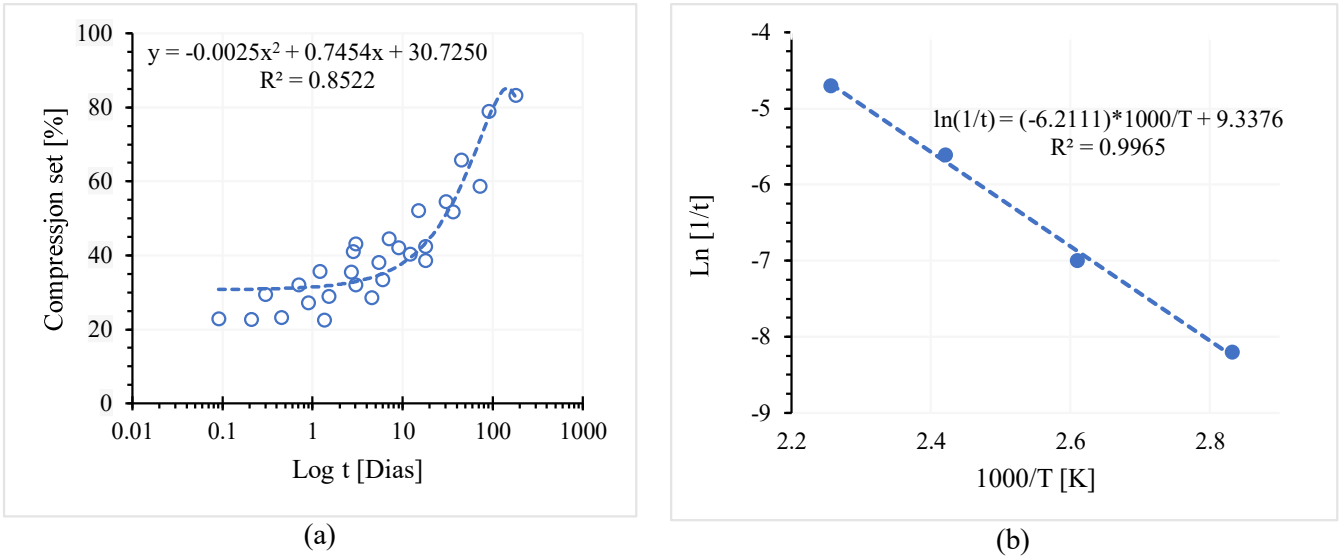

Figure 5 – (a) Application of the TTS method through shifted master curve and (b) Master curve of Arrhenius.

Table 1 compiles the predicted lifetime values according to the Arrhenius curves as a function of the reference time for different temperatures.

Table 1 – Lifetime prediction.

Temperature [°C]	80	100	120	140	170
Days	3856	1501	643	299	108
Years	11	4	2		

According to the results obtained, there is a noteworthy influence of temperature on the predicted time to failure. For gaskets used in service at 80 °C, the predicted lifetime was 11 years while for a temperature of 170 °C the lifetime dropped to 108 days.

Conclusions

- For the CS curves, only at 170 °C the failure criterion occurred. Such results demonstrate the high service temperatures and oxidative stability of the material.
- With the hardness graphs, it was possible to observe that the stiffness of the material remained almost unchanged for temperatures up to 140 °C. From this temperature, an increase in hardness can be noticed, an event that may be associated with the density of cross-links.
- The results of the indentation moduli profiles did not show any occurrence of the DLO effect during the entire analyzed period.
- Finally, with the table of predicted lifetime, it is possible to make a better selection when choosing gaskets for the operating condition of the heat exchanger.

Acknowledgements

The authors wish to thank PETROBRAS for their financial support of this research.

References

1. A. Kömmling; *et al*. Macromolecular Symposia 2017, 373, 1600157. https://doi.org/10.1002/masy.201600157
2. S. Salehi; *et al*. Polymer testing 2019, 75, pages 48-63. https://doi.org/10.1016/j.polymertesting.2019.01.015
3. A. Kömmling; M. Jaunich; D. Wolff Polymer Degradation and Stability 2020, 179, 109278. https://doi.org/10.1016/j.polymdegradstab.2020.109278
4. E. Souza; *et al*. Journal of Applied Polymer Science 2022, 140, e53419. https://doi.org/10.1002/app.53419
5. M. Zanzi; *et al*. Journal of Applied Polymer Science 2020, 139, e52523. https://doi.org/10.1002/app.52523
6. E. Souza; *et al*. Polymer Engineering and Science 2021, 61, pages 3001-30016. https://doi.org/10.1002/pen.25813
7. A. Kömmling; M. Jaunich; D. Wolff Polymer Degradation and Stability 2016, 126, pages 39-46. https://doi.org/10.1016/j.polymdegradstab.2016.01.012
8. E. Linde; *et al*. Polymer Degradation and Stability, 2021, 189, 109598. https://doi.org/10.1016/j.polymdegradstab.2021.109598.

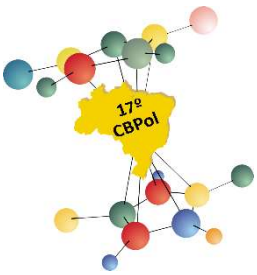

THERMAL BEHAVIOR OF NBR VULCANITES ACTIVATED WITH PLANT-EXTRACT-DERIVED MAGNESIUM OXIDE

Arianne A. da Silva*, Ana M. F. de Sousa, Cristina R. G. Furtado e Nakédia M. F. de Carvalho

Centro de Tecnologia e Ciências, Instituto de Química, Universidade de Estado do Rio de Janeiro (UERJ), Rio de Janeiro, RJ
(*) *ariannesilvado20201@ppgq.uerj.br*

Abstract - This work aims to study the thermal behavior and thermal degradation of nitrile rubber compounds with different vulcanization activators. The active activators used were zinc oxide (ZnO) the usual activator and magnesium oxide (MgO-green) synthesized by a green route used as a substitute for ZnO. In addition to the thermal degradation studied by the Flynn–Wall–Ozawa method and crosslink density by the equilibrium swelling method, the mechanical properties before and after thermal aging were observed for the thermal evaluation of these materials.

Keywords: *green magnesium oxide, vulcanization, thermal behavior, activator, NBR*

Fundings: The authors thank Nitriflex for donating the rubber compounds' raw materials. This study was supported by the CAPES) [: PhD Scholarship received by Arianne A. da Silva]; Conselho Nacional de Desenvolvimento Científico e Tecnológico (CNPQ) [P2-309461/2021-9 received by Ana Maria Furtado de Sousa and PQ-2/2018: 313831/2018-1 received by Nakédia M. Freitas de Carvalho] and Fundação Carlos Chagas Filho de Amparo à Pesquisa do Estado do Rio de Janeiro – FAPERJ [JCNE 2018: E-26/203.023/2018 and Grupos Emergentes 2019: E-26/010.002171/2019 received by Nakédia M. Freitas de Carvalho; APQ1 2019: E-26/010.001927/2019 received by Ana Maria Furtado de Sousa]

Introduction

Nitrile rubber (NBR) is a synthetic elastomer with exceptional resistance to oil and nonpolar solvents. As sealing elements, NBR is widely used in the chemical and petrochemical industries [1-2]. In order to produce technical materials, rubber must be vulcanized to form a three-dimensional network. In rubber formulation, several additives compose vulcanization systems, but it is well known that zinc oxide (ZnO) is the most commonly used activator [3]. However, the use of ZnO in rubber has been contested due to the fact that it can become toxic above a certain concentration, particularly in aquatic environments, thereby posing a significant environmental problem [4]. Therefore, studies that seek to replace ZnO with alternative oxides can help find a solution to this problem [5-7]. In our previous paper [7], magnesium oxide green-synthesized (MgO-green) with *Camellia sinensis* leaf extract appeared to be a viable substitute for zinc oxide (ZnO) [7]. However, additional characterizations are required to produce evidence supporting the replacement of ZnO with MgO-green. This study aims to compare the thermal behavior of nitrile rubber (NBR) composites filled with carbon black and vulcanized with zinc oxide and magnesium oxide-green.

Experimental

Materials

MgO green-synthesized as described in ref 7. NBR N-615 (33% acrylonitrile),carbon black N330, sulfur (S), ZnO, stearic acid, N-tert-butyl-2-benzothiazole-sulfenamide (TBBS) were donated by Nitriflex S.A. Indústria e Comércio

Preparation of NBR compounds

Table 1 shows the NBR formulations. The mixtures were prepared in a two-roll mixing mill (Luxor, model BML 150) according to the ASTM D3187 standard. The formulations used were: NBR: 100phr (per 100 parts of rubber), N330: 40phr, S: 1.5phr, ZnO or MgO-green: 3phr, AE: 1phr and TBBS: 0.7phr. Rubber sheets (150 x 150 x 2mm) were vulcanized in a hydraulic press at 18 MPa of pressure, 160°C of temperature, and t90 time.

Table 1 – NBR formulation, amount in part per hundred rubber (phr).

Component	ZnO	bio-MgO
NBR	100	100
ZnO	3	-
MgO-green (82.4% of purity)	-	3.6
Stearic acid	1	1
Sulphur	1.5	1.5
TBBS	0.7	0.7
Carbon black	40	40

Thermal degradation

Thermal degradation was investigated in a Q50 series thermogravimetric analyzer from TA Instruments with a scanning temperature of 25 to 600 °C and a heating rate of 5, 10, and 30 °C/min under a nitrogen atmosphere. The activation energy of vulcanizate decomposition was computed using Eq.1 based on the Flynn-Wall-Ozawa method [8] outlined in ASTM E1641.

$$E_a = \left(\frac{-R}{b}\right)\frac{dln\beta}{d\left(\frac{1}{T}\right)} \quad (1)$$

wherein E_a is the estimated activation energy, R is the universal gas constant, b is the constant assuming n = 1, β is the heating rate (°C/minute), and T is the temperature of weight loss (°C). The E_a can be determined using the slope between lnß and 1/T at a constant weight loss. In order to investigate the early stages of degradation, weight loss values of 0.5, 0.6, 0.7, 0.8, 0.9, 1.0, 5.0, and 20% were employed in this study.

Thermal aging

The relative deterioration resistance of composites was investigated by comparing crosslink density, Shore A hardness, and tensile properties before and after elevated temperature exposure in the presence of air. The test specimens were exposed in a forced-air oven at 100°C for 72 hours, according to ASTM D573.

The crosslink density was determined based on solvent swelling measurements using the Flory-Rehner equation [9] (Eq.2).

$$[X] = -\frac{[ln(1-v_r)+v_r+\chi v_r^2]}{V_0\left(v_r^{\frac{1}{3}}-\frac{v_r}{2}\right)} \quad (2)$$

wherein [X] is the density of cross-links; v_r is the volume fraction of rubber in a swollen vulcanized sample in equilibrium; V_0 is the molar volume of the solvent (acetone: 73.40 cm3 / gmol); χ is the interaction parameter between the solvent and the elastomer [10]. In this determination, the volume of carbon black and zinc and magnesium oxides was discounted in the value of v_r.

The Shore A hardness was measured using a Parabor hardness meter in accordance with ASTM D2240.Tensile tests were conducted on EMIC DL2000 according to ASTM D411.

Results and Discussion

Figure 1 shows the superposition of weight loss versus temperature curves for NBR composites with ZnO and MgO-green at heating rates of 5, 10, and 30°C/min. To investigate if replacing ZnO with MgO modifies the thermal behavior of the composite, ln (β) versus 1/T graphs were plotted for the early stages of degradation (Fig. 2), i.e., weight loss of 0.5, 0.6, 0.7, 0.8, 0.9, 1.0, 5.0, and 20%. It is important to say that those values of weight loss were considered after 300 °C of temperature in order to just consider the rubber degradation. Table 2 shows the E_a determined for the curve shown in Fig.2.

Figure 1 - TGA at different heating rates of (a) ZnO; (b) MgO-green

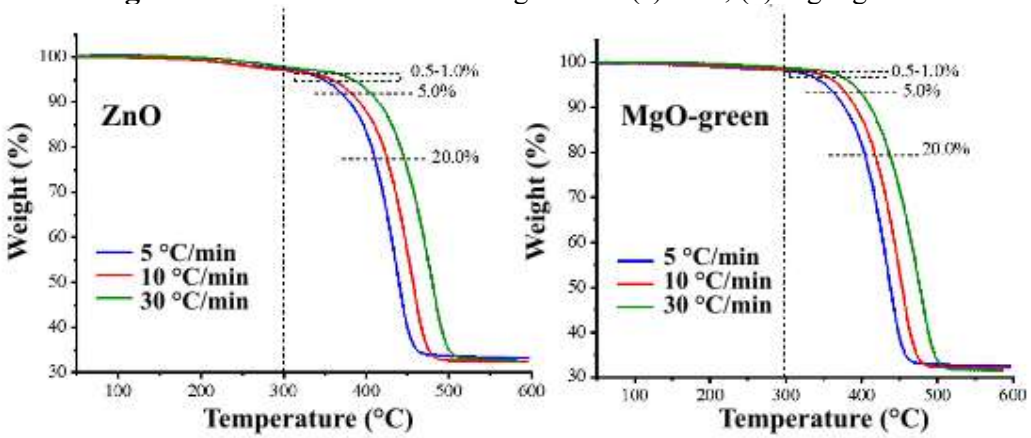

Figure 2 - Ln (β) variation as a function of 1/T for formations with: (a) ZnO and (b) MgO-green

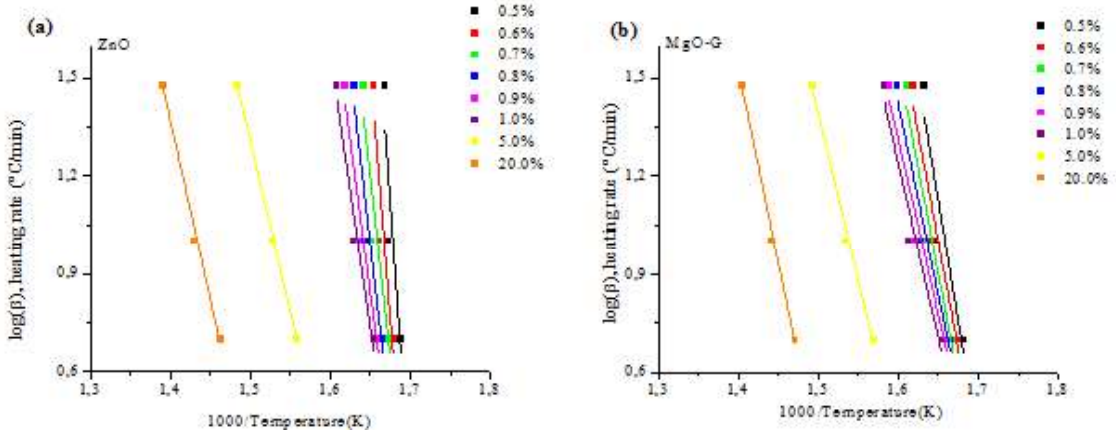

Table 2 - Activation energy (Ea) by Flynn–Wall–Ozawa method

Weight loss (%)	ZnO		MgO-green	
	E_a(kJ/mol)	R^2	E_a(kJ/mol)	R^2
0.5	700	0.8314	272	0.8910
0.6	614	0.8786	242	0.9404
0.7	427	0.8975	237	0.9463
0.8	411	0.9430	215	0.9647
0.9	352	0,9493	196	0.9660
1	309	0.9623	194	0.9551
5	194	0.9991	205	0.9997
20	211	0.9954	215	0.9969

The E_a values for NBR compounds with MgO are approximately 220 kJ/mol during the initial stages of degradation, whereas E_a values for NBR compounds with ZnO shows trend of reduction. In addition, for the 0.5-1% of weight loss, the E_a values of the NBR composite containing ZnO were greater than those containing MgO. This difference was attributed to the activator-induced variation in the crosslinking formation of NBR, as shown in Table 3 for the unaged samples.

Table 3 – Crosslink Density and Mechanical Properties before and after thermal aging

Property	ZnO (unaged)	ZnO (Aged)	MgO-green (unaged)	MgO-green (Aged)
Crosslink Density ($mol.cm^{-3}$)	3.8E-04	8.4E-04	5.9E-04	7.3E-04
Mechanical Properties				
Shore A Hardness	62 – 63	68 – 69	65 – 66	68 – 69
M100% (MPa)	2.08 – 2.15	3.53 – 3.62	2.32 – 2.40	3.08 –3.16
Tensile strength (MPa)	24.8 – 26.6	27.0 – 29.1	24.1 – 26.0	21.3 –23.2
Ultimate Elongation (%)	748 – 805	464 – 521	510 – 561	361 – 412

Table 3 shows the comparison of the properties of NBR composites with MgO and ZnO. The values of mechanical properties displayed are based on Fisher's least significant difference (LSD) procedure. They are constructed in such a way that if two means are the same, their intervals will overlap 95.0% of the time. In general, it appears that the NBR composite with MgO exhibited greater resistance to aging than the composite with ZnO, indicating that the formation of crosslinks is activator-dependent.

Conclusions

Synthesized by an ecologically more friendly route, MgO-green is a promising and valuable activator to replace ZnO because it contributes to producing a crosslink network that shows a potential improvement in the thermal stability of the material.

Acknowledgements

The authors would like to thank Nitriflex, CAPES, CNPQ, FAPERJ and UERJ for supporting the development of the research.

References

1. W.Low; W. Zhang; H.Wang; T. Jin; X.Liu.. Engineering Failure Analysis, 2018, 92, 1-11. https://doi.org/10.1016/j.engfailanal.2018.05.006
2. X. Wei; H. Wu; L. Zhang; S. Zhang; Y. Xiao; T. Luo Journal of Failure Analysis and Prevention, 2018, 18, 628–634. https://doi.org/10.1007/s11668-018-0451-3
3. Y. Zou et al. Compos Part A, 2016, 87, 297. https://doi.org/10.1016/j.compositesa.2016.05.006
4. S. Mostoni; P. Milana; B. Di Credico; M. D'arienzo; R. Scotti.. Catalysts, 2019, 9 n. (8), 664. https://doi.org/10.3390/catal9080664
5. K. Roy, et al. J. Appl. Polym. Sci, 2015, 42705,1 -7. https://doi.org/10.1002/app.42705
6. A. Zanchet; F.D.B. Sousa.; J. S. Crespo; C.H. Scuracchio, Journal of Cleaner Production, 2018, 174, 437- 446. https://doi.org/10.1016/j.jclepro.2018.09.203
7. A. A. Silva; E.B.D. Rocha; C. R. G Furtado et al. Polym. Bull. 2020. https://doi.org/10.1007/s00289-020-03430-x
8. C. Erbetta; R. Azevedo; K. S. Andrade; M. E. S. R. Silva; R. F. S. Freitas; R. G. Sousa; Materials Sciences and Applications, 2017, 8, 979-991. https://doi.org/10.4236/msa.2017.813072

9. W.G. Hwang; K.H. Wei; C.M. Wu, Polymer Engineering and Science, 2004, 44, 2117–212. https://doi.org/10.1002/pen.20217
10. I.T.D. Oliveira; E.B.V. Pacheco;L. L. Y. Visconde; M. R ,L. Oliveira; M. M. M. Rubinger Polímeros: Ciência e Tecnologia, 2010, 20, 366-370. http://dx.doi.org/10.1590/S0104-14282010005000059

VULCANIZATION AND MECHANICAL PROPERTIES OF NR/CIIR BLENDS

Amanda Faria Baruel[1,2*], Sandra Aparecida Coelho de Mello[1] and Silvana Navarro Cassu[1,2]
1 –Institute of Aeronautics and Space (IAE), São José dos Campos, SP, Brazil
2 – Aeronautics Institute of Technology (ITA), São José dos Campos, SP, Brazil
amandabaruel@ita.br

Abstract –Polymeric blends have been widely utilized in a variety of applications. Blending Natural Rubber (NR) with chlorobutyl rubber (CIIR) can lead to improved processability, a material with enhanced damping properties, and reduced material aging. In this study, NR and CIIR were blended with different contents of these elastomers, maintaining the amounts of fillers constant. Scorch time (t_{s1}) and optimum cure time (t_{90}) increased with increasing CIIR content, showing a higher processability safety of the blends with higher amounts of CIIR. All compositions showed a similar Tg by DSC analyses, and the vulcanization exothermic peak shifted to higher temperatures with increasing CIIR content. The addition of CIIR to the NR matrix decreased mechanical properties, such as tear strength, tensile strength at break, and elongation at break. Even though with on CIIR, the rubber presented the maximum elongation at break.
Keywords: *Rheometry, DSC, Reversion, Processability time*
Fundings: Coordenação de Aperfeiçoamento de Pessoal de Nível Superior - Brasil (CAPES) - Finance Code 001 and Conselho Nacional de Desenvolvimento Científico e Tecnológico (CNPq) project number 422016/2017-9.

Introduction

Natural rubber (NR) is an organic polyisoprene obtained mainly from *Hevea brasiliensis* [1]. This rubber has a wide molecular distribution and unique properties not achieved by synthetic rubbers. Its properties include abrasion resistance, good hysteresis properties, fast deformation and recovery, high tear strength, and high tensile strength. However, it presents low fatigue strength and generally has low resistance to degradation under heat [2].

Chlorinated Butyl Rubber (CIIR) is a copolymer of isobutylene with a small portion of isoprene (usually around 2 %) [3], which confers to this elastomer better resistance to aging compared to NR. This low degree of unsaturation provides a low degree of curing by conventional vulcanization systems. Due to the isoprene portion, sulfur or a sulfidic accelerator can be used in its vulcanization, while the active chlorine vulcanizes with the ZnO system [4]. Halogenated butyl rubbers have a significant advantage over butyl rubber, such as the increased compatibility with diene rubbers, thus allowing it to be mixed with NR [5].

In the present study, CIIR was added to NR to increase the processability time, enhance aging properties and evaluate mechanical properties, such as tension at break and tear strength. For the intended application, the NR is the main rubber, however, blends with higher CIIR contents were also evaluated for a better understanding of its effect on rheological properties.

Experimental

Materials

Chlorobutyl Rubber CIIR-1301 was purchased from Zhejiang Cenway Materials Co. Ltda, which contains a small quantity of calcium stearate used to improve stability. Natural Rubber

GEB01 and sulfur were purchased from Fragon Produtos para Indústria de Borracha Ltda.

Methods

Samples were prepared using a two-roll mixing mill LUXDOR operated at 30 °C. TMTM, Sulfur, and CBS were added at the end of the process. NR and CIIR blends were prepared using the same amounts of fillers, varying the proportion of elastomers. **Table 1** shows the chemical composition of the blends. Compounds were named according to the NR fraction, e.g., 80NR is the compound with 80 phr NR and 20 phr CIIR.

Table 1. Chemical composition of the blends.

Compounds (phr)*	**100NR**	**80NR**	**70NR**	**50NR**	**30NR**	**20NR**	**0NR**
NR	100	80	70	50	30	20	0
CIIR	0	20	30	50	70	80	100
ZnO	5	5	5	5	5	5	5
N330	12	12	12	12	12	12	12
Aromatic Oil	12	12	12	12	12	12	12
Stearin	1	1	1	1	1	1	1
Sulfur	1	1	1	1	1	1	1
TMTM	0.3	0.3	0.3	0.3	0.3	0.3	0.3
CBS	1.5	1.5	1.5	1.5	1.5	1.5	1.5

**phr: parts per hundred rubber*

Rheometric analysis was carried out in a moving die rheometer (MDR) from ALPHA Technologies, model PREMIER MDR, at 145°C with a frequency of 100 cpm (1.67 Hz) and 1° rotation angle, according to ASTM D5289.

DSC analyses were carried out on a TA Instruments DSC Q-100. Samples were sealed in aluminum pans, and the analyses were conducted in a nitrogen gas flow of 100 mL/min, temperature range from -90 °C to 250 °C at a heating rate of 10°C/min.

Mechanical properties were measured at 25ºC using the Zwick 1474 test machine at 500 mm/min speed. Tensile properties were measured according to the ASTM D412 [6] with a dumbbell sample shape type C(115 x 25 x 2) mm. Tear strength was determined according to the ASTM D624sample type C (102 x 19 x 2) mm [7].

Results and Discussion

The rheometric analysis is one of the most common analyses to measure the vulcanization profile of rubbers and to evaluate important parameters, such as minimum torque (M_L), maximum torque (M_H), scorch time (ts_1), defined as the time needed to increase the M_L by 1 unit, and optimum cure time (t_{90}), which is the time required to achieve 90% of the maximum vulcanization. The rheometric curves of rubbers and their blends are shown in **Fig 1**, and the parameters are summarized in **Table 2**. Scorch time (ts_1), which measures the processability time, was progressively increased by adding CIIR to the NR matrix, indicating a longer processability time with increasing CIIR content. The cure rate index (CRI), which measures how fast the vulcanization occurs, decreases with increasing CIIR content. This behavior can be attributed to a lower overall unsaturation of the blend compared to the pure NR and, therefore, lower efficiency to vulcanize with sulfur [8], delaying the vulcanization time.

A reversion on the blend with over 50phr of NR can also be observed. The percentage of reversion at any time is defined as **Eq. 1**, where M_t is the torque at any cure time [9]. In this study, the reversion was evaluated at 60 min. **Table 2** shows that the higher the amount of CIIR, the lower

the reversion, and over 50 phr of CIIR, the reversion cannot be observed. This process is associated with the degradation of the NR, and the break of the sulfidic chains formed in the vulcanization process, indicating a better thermal resistance in the presence of CIIR.

$$R=\frac{(M_H-M_t)}{(M_H-M_L)} \text{ X } 100 \qquad (1)$$

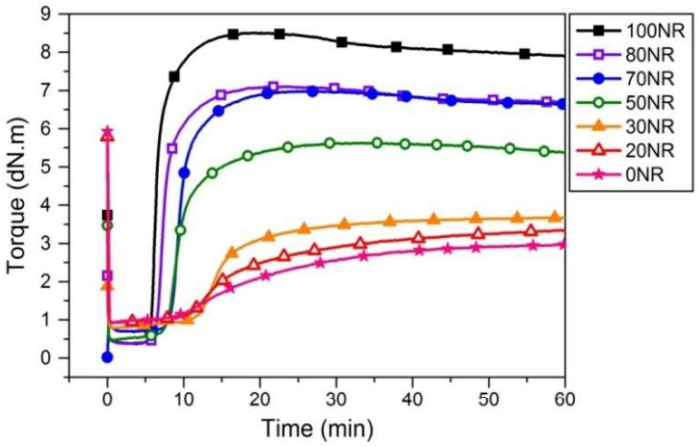

Figure 1. Rheometric curves obtained at 145ºC for NR/CIIR blends.

Table 2. Rheometric parameters obtained at 145ºC for NR/CIIR blends.

	M_L (dN.m)	M_H (dN.m)	M_{60} (dN.m)	R[a]	ts_1 (min)	t_{90} (min)	CRI[b]
100NR	0.37	8.51	7.90	7.50%	5.90	9.82	25.51
80NR	0.38	7.11	6.70	6.05%	6.76	11.35	21.79
70NR	0.68	6.98	6.63	5.56%	8.73	13.89	19.38
50NR	0.45	5.63	5.38	4.80%	8.43	16.04	13.14
30NR	0.78	3.68	3.68	0%	13.80	26.63	7.79
20NR	0.93	3.34	3.34	0%	15.27	40.00	4.04
0NR	0.92	2.96	2.96	0%	19.20	37.16	5.57

[a]R - Reversion percentage
[b]CRI – Cure rate index $100/(t_{90}-ts_1)$

Usually, the Tg can be used to study the miscibility in a blend. A single Tg or a well-separated Tg indicates a miscible or an immiscible system, respectively [10]. However, in this case, the Tg of NR and CIIR are similar and, therefore, cannot predict miscibility [11]. In **Fig. 2**, a single Tg can be observed for all blend compositions, presenting values very close to each other. The blends presented higher Tg when compared with CIIR or NR rubber; the higher the CIIR content on the blend, the higher the Tg. For all samples, the Tg in the second heating shifted to a higher temperature, which can be related to the vulcanization process (**Table 3**).
The rubbers 50NR, 30NR, 20NR, and 0NR, present an endothermic peak around 95 °C due to the melting process of calcium stearate present in the CIIR elastomer [4], the higher the CIIR content, the higher the intensity due to a higher amount of calcium stearate on the blend. An exothermic peak related to the vulcanization of the rubber can also be observed.With the increase of CIIR content, the vulcanization peak is broadened and shifted to a higher temperature ($T_{max-exo}$), which indicates a delay and a slower vulcanization rate, as seen by the rheometric analysis (**Table 3)**.The rubbers 30NR and 20 NR show the appearance of a second exothermic peak, and CIIR shows three exothermic peaks. Due to the Chlorine present in the CIIR, this rubber can also vulcanize with ZnO, which can explain different DSC peaks.

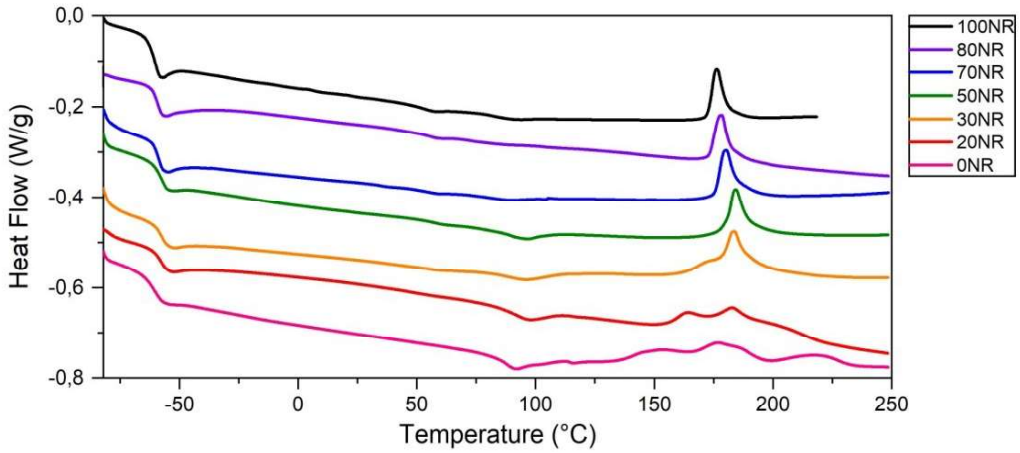

Figure 2. DSC curves of NR/CIIR blends.

Table 3. DSC parameters of NR/CIIR blends.

	Tg 1stheat (°C)	Tg 2ndheat (°C)	ΔH_{endo} (J/g)	ΔH_{exo} (J/g) (±1)	ΔT_{exo} (°C)	$T_{max\text{-}exo}$ (°C)
100NR	-60.3 ± 0.5	-58.3 ± 0.5		4 ± 0.5	5.2 ± 0.5	176.3
80NR	-59.7 ± 0.5	-57.2 ± 0.5		5 ± 0.5	5.8 ± 0.5	177.5
70NR	-58.7 ± 0.5	-56.5 ± 0.5		6 ± 0.5	6.4 ± 0.5	179.4
50NR	-58 ± 1	-56 ± 1	1.7 ± 0.5	7 ± 0.5	6.9 ± 0.5	183.7
30NR	-57.9 ± 0.5	-57.2 ± 0.5	1.7 ± 0.5	11 ± 1	11 ± 1	183.7
20NR	-57-5 ± 0.5	-57.5 ± 0.5	2.1 ± 0.5	13 ± 0.5	43.4 ± 0.5	182.9
0NR	-60.1 ± 0.5	-60 ± 0.5	2.8 ± 0.5	13 ± 1	45.1 ± 0.5	177.1

The neat rubbers and their blends were submitted to tensile and tear resistance tests. It was not possible to obtain specimens of NR20 and NR30 due to bubbles and failures during the vulcanization, probably due to a poor covulcanization between NR and CIIR. In Fig. 3, it is possible to notice that the addition of CIIR causes a progressive decrease of tensile strength at break, indicating a more fragile material. Adding CIIR up to 50 phr causes a slight decrease of the elongation at break. However, for the rubber with only CIIR in its composition, the elongation reached the maximum of the equipment without breaking, probably due to a smaller crosslink density than the other rubbers. The tear strength decreased with increasing CIIR content. The hardness of the blends, Shore A (**Table 4**), presented no considerable variations, except for the 0NR, which is softer than the others, probably due to lower vulcanization.

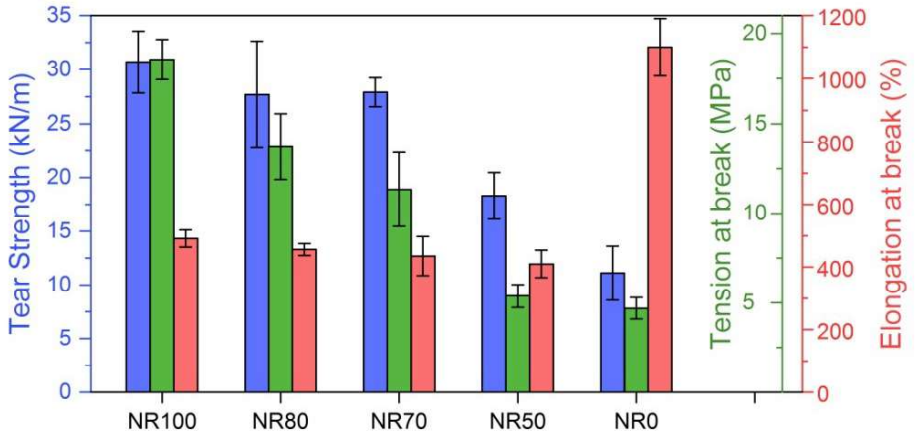

Figure 3. Mechanical properties of NR/CIIR blends.

Table 4. Values of mechanical properties of NR/CIIR blends.

	Tear strength (kN/m)	Elongation at break (%)	Tension at break (MPa)	Shore A
100NR	31 ± 3	491 ± 28	19 ± 1	41 ± 1
80NR	28 ± 5	459 ± 19	14 ± 2	38 ± 0
70NR	28 ± 1	435 ± 62	11 ± 2	38 ± 1
50NR	18 ± 2	410 ± 44	5 ± 1	41 ± 1
0NR	11 ± 2	1099 ± 91	5 ± 1	22 ± 1

Conclusions

The addition of CIIR rubber to the NR matrix increased the processing time of the rubber and also decreased the cure rate, prolonging the curing time in the processing condition studied. These results could be attributed to a lower unsaturation degree of the CIIR. With the increase of CIIR content, a decrease in reversion was observed. A single Tg was observed for the blends, but due to the similar Tg of raw NR and CIIR, miscibility could not be evaluated using this parameter. With CIIR addition, the vulcanization peak was broadened and shifted to a higher temperature. Mechanical properties decreased with CIIR addition, due probably to a lower unsaturation degree of the CIIR and the sulfur-based vulcanization system used.

Acknowledgements

This study was financed in part by the Coordenação de Aperfeiçoamento de Pessoal de Nível Superior - Brasil (CAPES) - Finance Code 001. The authors gratefully acknowledge the financial support given by Conselho Nacional de Desenvolvimento Científico e Tecnológico (CNPq) project number 422016/2017-9 and by Agência Espacial Brasileira (AEB).

References

[1] *Rubber Technology*, M. Morton, Ed.; Springer Science, Business Media Dordrecht, 1999.
[2] *Rubber Compounding: Chemistry and Applications*, B. Rodgers, Ed.; New York, Marcel Dekker, 2004.
[3] B. S. Solis; B. Rodgers; B. B. Sharma; N. Tambe; W. H. Waddell *Rubber Plast. News* 2007, 36, 13-15.
[4] K. G. Hendrikse; W. J. Mcgill; J. Reedijk; P. J. Nieuwenhuizen *J. Appl. Polym. Sci.* 2000, 78, 2290-2301. https://doi.org/10.1002/1097-4628(20001220)78:13<2290::AID-APP60>3.0.CO;2-P
[5] G. Hermenegildo; E. Bischoff; R. S. Mauler; M. Giovanela; L. N. Carli; J. S. Crespo *J. Elastomers Plast.* 2017, 49, 47-61. https://doi.org/10.1177/0095244315627855.
[6] ASTM, D412-16 *Standard Test Methods for Vulcanized Rubber and Thermoplastic Elastomers – Tension*, 2009.
[7] ASTM, D624 *Standard Test Method for Tear Strength of Conventional Vulcanized Rubber and Thermoplastic Elastomers*, 2020.
[8] S. H. Botros *Polym. Plast. Technol. Eng.* 2002, 41, 341-359. https://doi.org/10.1081/PPT-120002572.
[9] K. Boonkerd; C. Deeprasertkul; K. Boonsomwong *Rubber Chem. Technol.* 2016, 89, 450-464. https://doi.org/10.5254/rct.16.85963.
[10] J. Riba; M. Á. Mansilla; T. Canals; R. Cantero *Mater. Res.*2019, 22, e20180415. http://dx.doi.org/10.1590/1980-5373-MR-2018-0415.
[11] N. K. Dutta; D. K. Tripathy *J. Elastomers Plast.* 1993, 25, 158–179. https://doi.org/10.1177/009524439302500204.

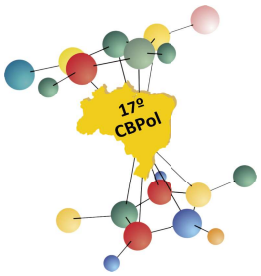

A STEP TOWARDS UNDERSTANDING THE INTERACTION BETWEEN RUBBER CARBOXYL GROUPS AND LIGNIN THROUGH ATR-FTIR AND DMA

Gustavo N. Campos*, Elisson B. D. da Rocha, Ana M. F. de Sousa, Marco A. G. de Figueiredo, and Cristina R.G. Furtado

Instituto de Química, Universidade do Estado do Rio de Janeiro, São Francisco Xavier Street, 524, Maracanã, 20550-900, Rio de Janeiro, RJ, Brasil.
(*) gustavo_ncampos@hotmail.com

The pursuit for renewable raw materials is leading the paper and pulp industry to treasure its byproducts, such as lignin, which is biobased, renewable, and biodegradable. Lignin could also be used as a rubber reinforcing filler. However, the polarity of lignin affects its compatibility with rubbers due to their nonpolar backbone. Carboxylated nitrile rubber (XNBR) has carboxyl groups in its backbone that form ionic bonds with zinc oxide, present with most formulations. These groups could increase the rubber/lignin interaction. In this study, hardwood Kraft lignin was mixed with commercial XNBR using a two-roll mill. The weight percentage of lignin was set between 0 and 28%, and the rubber carboxyl groups content was between 1 and 7% of the weight of rubber. Compounds with 28% lignin increased elastic modulus at 100% from 1.7 to 6.3 MPa in XNBR 7%, while in XNBR 1%, the increase was from 1.2 to 1.9 MPa. This difference shows that rubber carboxyl groups are key to rubber/lignin interaction. Using the second derivative from Attenuated total reflection Fourier Transform Infrared Spectroscopy (ATR-FTIR) it was observed that lignin decreased the band corresponding to the carboxylic acid/zinc oxide ionic bond (1590 cm^{-1}) and increased the non-bonded dimer carboxylic acid band (1698 cm^{-1}), indicating that lignin is interfering in the formation of these ionic bonds. The temperature sweep performed in dynamic mechanical analysis (DMA) revealed a thermal transition for unfilled compounds, attributed to carboxylic acid and zinc oxide ionic clusters. This thermal transition was not observed in compounds containing more than 10% lignin, supporting the ATR-FTIR results. In conclusion, the ATR-FTIR and DMA results indicate the interaction between XNBR and lignin is happening not through the carboxyl groups, but through the carboxylic acid/zinc oxide ionic bonds instead. This result is an important step towards creating more sustainable rubber materials.

Fundings: The authors thank Nitriflex for donating the rubber compounds' raw materials and Suzano for donating the lignin. This study was supported by the Fundação de Amparo à Pesquisa do Estado do Rio de Janeiro (FAPERJ) [E-26/200.289/2021: PhD Scholarship received by Gustavo N. Campos] and Conselho Nacional de Desenvolvimento Científico e Tecnológico (CNPQ) [P2-309461/2021-9 received by Ana Maria Furtado de Sousa].

Keywords: *Kraft Lignin; XNBR; bio-based filler; ATR-FTIR; DMA.*

CHARACTERIZATION OF NATURAL RUBBER COMPOUNDS WITH PRECIPITATED RICE HUSK SILICA

Sandra R. Scagliusi*, Carla A. Correia, Flavia L. Silva, Abel C. G. Neto, Patrícia S. Calvão, Samuel M. Toffoli, Ticiane S. Valera, Hélio Wiebeck

Department of Metallurgical and Materials Engineering, University of São Paulo (USP), São Paulo, SP, Brazil
*scagliusi@usp.br

Abstract – Silica (silicon dioxide) is a small particle size reinforcing filler for different types of rubber such as natural rubber (NR) and styrene butadiene rubber (SBR), due to its ability to increase abrasion resistance and stiffness of the polymeric matrix [1]. Brazil annually produces about 10 million tons of rice. From this production, rice husk is a residue, whose burning can generate about 25-wt% of ash [2]. Rice husk ash has good potential as a filler, since it is predominantly composed of silica, with the advantage of being originated from a renewable source [3]. Depending on the burning intensity, ash with higher or lower silica content can be generated: the white ash (the highest silica content) is obtained by burning the rice husk at temperatures between 700 and 1000 °C, while the dark ash is obtained at lower temperatures, ranging from 450 to 700 °C [4]. In this work a comparative study between rice husk ash commercial fillers, black (SVA) and white ash (Oryzasil) in natural rubber compounds, was performed. Precipitated silica (Zeosil-175) was also used as a filler in a NR reference compound, for comparison purposes. Mechanical properties such as tensile and tear strengths, and hardness were evaluated. Scanning electron microscopy images of the composites fracture surface after tensile tests were also analyzed. The compound with SVA showed the poorest mechanical properties, whereas the tensile and tear strengths of compounds with white ash (Oryzasil) and Zeosil-175 precipitated silica showed similar values. Therefore, the white rice husk ash may be considered as an alternative filler for the reinforcement of NR compounds.

1. O. Pereira, R.J. Macieski, D. E. Finkler, D. Petkowicz, R.M. Dal Lago, M. L. Mignoni, Research, Society and Development, v. 11, n. 6, DOI: http://dx.doi.org/10.33448/rsd-v11i6.28831, 2022.
2. G. C. Nascimento, L. Dominguini, J. M. M. Mello, J Dal Magro, H. G Riella, &Fiori, M. A., Brasil. Ciência e Natura, 37(3). https://doi.org/10.5902/2179460x15262,2015, 2015.
3. H. M. da Costa, L. L. Y. Visconte, R. C. R. Nunes, C. R. G. Furtado, Congresso Brasileiro de Engenharia e Ciência dos Materiais, 14., 2000, São Pedro - SP. Anais
4. H. E. Haxo, Jr.; P. K. Mehta, Rubber Chemistry and Technology 48 (2): 271–288, https://doi.org/10.5254/1.3547453, 1975.

Keywords: *Rice Husk, Natural Rubber, Silica, Reinforcement Filler*

DEVELOPMENT OF MATERIAL BASED ON NATURAL RUBBER LATEX FOR BIOMEDICAL APPLICATIONS

Danielle Restelatto[1*], Mariana Roesch-Ely[1], Marcelo Giovanela[1], Janaina da Silva Crespo[1]

1 – Area of Exact Sciences and Engineering, University of Caxias do Sul (UCS), Caxias do Sul, RS, Brazil
drestelatto1@ucs.br

Abstract – Natural rubber latex (NRL) have been widely used in the biomedical industry. However, for some applications, such as the production of surgical gloves and catheters, the mechanical properties of latex need to be improved. The cure of this elastomer is carried out from the vulcanization process in which from the addition of chemical agents and heat, many crosslinks occur between the poly(cis-1,4-isoprene) chains of the NRL. In this sense, this work aims to determine a formulation, based on NRL, to promote suitable mechanical and chemical properties for biomedical applications. The study of the mechanical properties was carried out through tests of tensile strength (ASTM D412) and tear strength (ASTM D624). Due to the desired application for the material, swelling index in commonly used solvents for hygiene, such as water with soap and alcohol 70% (v/v), was carried out based on adaptations of ASTM D3616. The results showed that a material with high mechanical (20.7 MPa) and tear (39.7 $N \cdot mm^{-1}$) resistance was produced. However, due to the lower amount of cross-links in the chains, the formulations that used lower levels of vulcanizing agents are inadequate for biomedical applications that demand greater mechanical resistance due to the handling to which they will be submitted. Swelling index in both evaluated solvents, after 40 h of immersion, was less than 5% (w/w) even for formulations with lower cross-linking levels. After selecting the best formulation among those evaluated, an additive based on silver nanoparticles was incorporated to promote antibacterial activities, which proved to be bactericidal for *Escherichia coli* bacteria and bacteriostatic for *Staphylococcus aureus*.

References

1. N. B. Guerra; J. Bortoluz; A. R. Bystronsk.; A. E. D. Maddalozzo; D. Restelatto; M. Roesch-Ely; D. M. Devine; M. Giovanela; J. S. Crespo. Compounds, 2023, 3, 310-333. http://dx.doi.org/10.3390/compounds3020023.
2. J. Supramaniam; D. Y. S. Low; S. K. Wong; B. F. Leo; B. H. Goh; S. Y. Tang. Chemical Engineering Journal, 2022, 437, 135440. http://dx.doi.org/10.1016/j.cej.2022.135440.
3. P. Rojruthai; N. Payungwong; J. T. Sakdapipanich. Progress In Rubber, Plastics And Recycling Technology, 2021, 38, 125-138. http://dx.doi.org/10.1177/14777606211062909.
4. T. Li; Y. Su; D. Wang; Y. Mao; W. Wang; L. Liu; S. Wen. International Journal of Biological Macromolecules, 2022, 195, 449-455. http://dx.doi.org/10.1016/j.ijbiomac.2021.12.029.

Keywords: *Natural rubber latex, Vulcanization, Biomedical applications, Mechanical properties, Antibacterial activities.*

EFFECT OF ACCELERATED AGEING ON THE PHYSICAL AND MECHANICAL PROPERTIES OF THE RUBBER COVER COMPOUND OF A CONVEYOR BELT

Carla A. Correia[1], Flavia L. S. Freitas. [1], Pedro G. Lins[1], Patrick A. Falqueto[2], José J. Penagos[3], Christiano G. Bastos Andrade[1], Hélio Wiebeck[1]; Samuel M. Toffoli[1], Ticiane S. Valera[1*]

1 – Department of Metallurgical and Materials Engineering - Polytechnic School - University of São Paulo
**tsvalera@usp.br*
2– Vale S/A, Vitória, ES, Brazil
3 – Instituto Tecnológico Vale, Ouro Preto, MG, Brazil

Abstract

Conveyor belts used in mining, for the transport of ores either in mining sites or in ports (to load the ships), exhibit a complex structure composed, in the outside, of a thick layer of a rubber compound, whose main function is to coat and protect the belt against the effects of abrasion, tearing, chemical attack, or other adverse conditions resulting from material transport [1-3]. However, it is known that rubber compounds are susceptible to aging caused by climatic conditions, such as UV rays, heat and humidity, that can affect their physical-mechanical properties leading to failures in the belts during the transport process [2, 4]. Thus, in this work, the rubber covering layer of a conveyor belt reinforced with steel cords, manufactured in Brazil, was submitted to an accelerated aging test performed in a weatherometer chamber for 1000 hours, in order to simulate the aggressive effects of the environment (exposure to artificial sunlight and humidity), based on ASTM G155. Specimens were submitted to tensile, abrasion, and hardness tests. The results showed that the tensile strength and maximum elongation reduced to 24% and 34%, respectively, in comparison to the non-aged composite. Abrasion resistance reduced to 59%, and the compound hardness increased 13% after the exposure. SEM images of rubber surface after 1000 hours of chamber exposure showed a network of microcracks, evidencing the degradation effect of the aging. Therefore, the results indicated that the conditions tested significantly affected the physical-mechanical performance of the rubber cover compound, which, in turn, can contribute to a decrease in the useful life of the conveyor belts.

Keywords: *Conveyor belts, rubber compound, aging, physical-mechanical properties.*

References

1. W. Molnar, M. Varga, P. Braun, K. Adam, E. Badisch. *Wear* 2014, 1-6, 320 (1). https://doi.org/10.1016/j.wear.2014.08.007.
2. K. B. Vaccioli, P.G. Lins, P.A. Falqueto, J.J. Penagos, C.G Bastos Andrade, M. Yee, H. Wiebeck, S. M. Toffoli, T. S. Valera, *Proceedings of the 24th Brazilian Congress of Engineering and Materials Science (CBECiMat)*, Águas de Lindóia, SP, 2022.
3. B. Nins, J. J.Penagos, L. Moreira, D. Münch, P. Falqueto, C. C. Viáfara, A. R. da Costa. *Wear* 2022, 506-507. https://doi.org/10.1016/j.wear.2022.204439
4. K. Hu, J. Yang. *Materials Research Express* 2022, Vol. 9(9). https://doi.org/10.1088/2053-1591/ac934f.

EFFECT OF MIXTURE OF ACCELERATORS AND ADDITION SEQUENCE OF ADDITIVES ON THE PROPERTIES OF NATURAL RUBBER (NR) AND STYRENE-BUTADIENE COPOLYMER (SBR) ELASTOMERIC MATRIX

Steffany S. G. Pacheco[1], Thiago C. Lopes[1] and Leila L. Y. Visconte[1]*

1 – Institute of Macromolecules Professor Eloisa Mano (IMA), Federal University of Rio de Janeiro (UFRJ), Rio de Janeiro, RJ, Brazil
steffanygomes@ima.ufrj.br

Abstract – Mixtures of elastomers are widely used to meet demands for properties, usually requiring, among other additives, a vulcanization system containing sulfur and accelerators [1,2]. When these additives have greater affinity for one of the phases of the mixture, they result in differences in the degree of crosslinking of each phase, affecting the properties [3]. To evaluate this effect in NR/SBR mixtures, a mixture of accelerators and different ways of incorporating the additives were tested. Therefore, the objective of this work is to determine the properties of an elastomeric matrix of NR/SBR when: 1) a mixture of accelerators is used containing a non-commercial accelerator bis(4-Methylphenyldithiocarbimate)Zincate(II) of Tetrabutylammonium – ZNIBU(Z) and the commercial accelerator N-t- butyl-benzothiazole sulfenamide – TBBS(T); 2) the effect of different sequences for incorporating the additives on the rheological and mechanical properties of the mixtures, and their dispersion in the phases. The formulations used (in phr) were: pure NR or SBR(100) – Mixtures NR(50) / SBR(50); other additives: zinc oxide (3.0); stearic acid (2.0); aminox(2.5); sulfur(1.5); TBBS(1.1) and ZNIBU(4.8); for mixing accelerators, only half of each was used; the compositions were made in a roller mixer and submitted to rheometric analysis in RPA and mechanical tests. The following pure mixtures were made: NR_Z; NR_T; $NR_{Z/T}$ / SBR_Z; SBR_T; $SBR_{Z/T}$. As for the mixtures: M1 – initially the rubbers are mixed with subsequent incorporation of additives; M2 – half of each additive is incorporated in eachrubber and later homogenized [4]. The rheometric analyzes and mechanical tests of pure samples showed that ZNIBU has a preference for NR while TBBS is better solubilized in the SBR phase, favoring the degree of crosslinking of the samples, with higher torque values, higher curing speed and better mechanical performance. As for the mixtures, the greatest influence observed was on the T_{90} (Optimum Cure Time) of the samples.

References:

1. J. Mark.; B. Erman; M. Roland. *The Science And Tecnology Of Rubber*, 4. Ed; Elsevier, 2013.
2. M. Entezam; I. Zarei.; H. A. Khonakdar. *Polymer Bulletin 2021*, 0123456789. https://doi.org/10.1007/s00289-021-03576-2.
3. Junkong, P.; Morimoto, R.; Miyaji, K.; Tohsan, A.; Sakaki, Y.; Ikeda, Y. 4772–4785, 2020. https://Doi.Org/10.1039/C9ra10358a.
4. L. L. Y. Visconte et al. *Journal Of Applied Polymer Science,2004,* V.93, N.2, P.483–489.

Fundings: The authors thank CNPq and CAPES for financial support of this work.

Keywords: *Mixtures of elastomers; mixture of accelerators; different ways of incorporating; ZNIBU.*

EVALUATION OF ANTIOXIDANT AND ANTIOZONANT PROTECTIVE AGENTS ON THE MECHANICAL PROPERTIES OF EPDM

Claudio F Maffra[1], Edson Francisquetti[2], Daiane Romanzini[3]

1 – Postgraduate Program in Materials Technology and Engineering (PPGTEM), IFRS, Campus Feliz, Feliz, RS, Brazil; claudiofmaffra@gmail.com
2 – Postgraduate Program in Materials Technology and Engineering (PPGTEM), IFRS, Campus Farroupilha, Farroupilha, RS, Brazil

Although ethylene-propylene-diene monomer (EPDM) has high resistance to thermo-oxidative aging, the polymers chains can undergo scission when exposed to temperatures above 140 ºC, limiting EPDM shelf life. In order to minimize thermal degradation, by creating a chemical barrier against ageing, protective agents, such as N(1,3-dimethyl-butyl)-N'-phenyl-p-phenylenediamine (6PPD) and 2,2,4-trimethyl-1,2-dihydroquinoline (TMQ) are commonly used. However, since EPDM has high resistance to oxygen and ozone, the inclusion of these additives is not common in these elastomers [1-4]. For this reason, the aim of this study was to evaluate the resistance to EPDM ageing with the incorporation of TMQ and 6PPD. EPDM samples were prepared with carbon black, plasticizers, rubber auxiliary agents and accelerators, in two different formulations, EPDM (without protective agents) and EPDM_PA (with 2 phr of TMQ and 2 phr of 6PPD protective agents). The samples were produced in a 1 L closed mixer, for 5 min, and transferred into a cylinder. The tensile test was performed at room temperature (ASTM D412) and at 96 h to 170 ºC (adapted from ASTM D473 and D412). The results showed (Table 1) that the addition of 6PPD and TMQ enhanced the EPDM ageing resistance, increasing the tensile strength from 7,58 (EPDM) to 10,78 MPa (EPDM_PA), in relation to those samples tested at room temperature. For this reason, the use of TMQ and 6PPD could improve mechanical properties of EPDM when exposed to temperatures around 170 ºC.

Tabel 1. Tensile test results for the studied samples.

Sample	Tensile test (at room temperature)		Tensile test (at 96 h to 170 ºC)	
	Tensile strength (MPa)	Elongation (%)	Tensile strength (MPa)	Elongation (%)
EPDM	7,77 ± 0,80	446,88 ± 21,05	7,58 ± 0,20	-24,38 ± 8,51
EPDM_PA	6,69 ± 0,59	628,13 ± 56,58	10,78 ± 0,56	31,38 ± 8,47

REFERENCES

1. M.V. Duin, C. HaBmann. *Handbook of Sinthetic Rubber*, Arlanxeo performance Elastomers, Dormagem, 2002.
2. N. Ning, Q. Ma, Y. Zhang, Polymer Degrad Stab 2014, 01037. https://doi.org/10.1016/j.polymdegradstab.2014.01.037
3. L. Qingkun, P. Wei, C. Cong, X. Meng, Q. Zhou, *Polymer Degradation and Stability*, https:/doi.org/10.1016/j.polymdegradstab.2022.110155
4. J. Li, C. Zhou, D. Cao, H, Liu H, *Material Science inc. Nanomaterials and Polymers*, 2020, https://doi.org/10.1002/sltc202001279

Keywords: *Rubber, EPDM, Antioxidant and antiozonant*

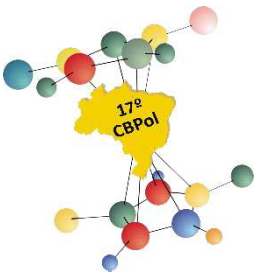

EVALUATION OF PHYSICAL-MECHANICAL PROPERTIES OF ELASTOMERIC MIXTURES

Daiane Omizzollo Negri [1,2] *, Suélen Moresco [2] and Janaína da Silva Crespo [1]

1 - Graduate Program in Engineering and Materials Science, University of Caxias Do Sul (UCS), Caxias do Sul, RS, Brazil
donegri@ucs.br
2 - Vipal Rubbers, Nova Prata, RS, Brazil

The development of polymeric blends aims to satisfy various industrial requirements such as the need to facilitate processing and broaden the range of properties, either by varying the type, relative amounts or morphology of each component. One of the advantages that polymeric blends have is the ease of adjusting the properties to the needs of use, being important to generate mechanical, chemical or barrier properties and improve the processability of the polymers [1]. Taking into account the importance of polymers in elastomeric formulations, the present study aims to evaluate the influence of the mixture of different polymers, such as natural rubber (NR), butadiene-styrene copolymer (SBR) and polybutadiene (BR), in the Mechanical and aging properties of elastomeric formulations. The formulations were characterized by rheometric and mechanical properties, glass transition temperature (T_g), solvent swelling and aging properties. The T_g results obtained indicated that the NR/SBR polymeric blend is immiscible and that the NR/BR and SBR/BR blends are miscible. The NR/SBR polymeric blend obtained better performance in tensile properties. While the SBR/BR polymeric blend showed a lower percentage of swelling, a greater amount of crosslinks and greater resistance to wear. The results obtained lead to the conclusion that both the miscibility and the immiscibility that were presented by the studied blends did not influence the results of the evaluated properties, since the blends presented intermediate results to their respective pure polymers.

1. VOSSEN, C. A, Doctoral Thesis, University of São Paulo, 2009.

Keywords: *polymers, polymer blends, formulations, miscibility, properties*

EXAMINING THE DISPERSION OF ACAI RESIDUE AS A FILLER IN NATURAL RUBBER MATRIX USING RHEOMETRY, SEM-EDX, AND TENSILE STRENGTH IN THE PRODUCTION OF ECO-FRIENDLY BIOCOMPOSITE

Samara S. Araúlo[1], Gleysson T. A. Santos[2], Gabrieli R. Tolosa[2], Eduardo R. Budemberg[1], Aldo E. Job[2], Carlos T. Hiranobe[1], Flávio C. Cabrera[1], Leonardo L. Paim[1] and Renivaldo J. Santos[1]*

1 – Department of Engineering, School of Engineering and Sciences, São Paulo State University (Unesp), Rosana, SP, Brazil renivaldo.santos@unesp.br

2 – Department of Physics, Faculty of Science and Technology, São Paulo State University (Unesp), Presidente Prudente, SP, Brazil

Abstract - The study employed the fibers found in the acai seed (*Euterpe Oleracea Mart.*) as reinforcement material in composites with a natural rubber (NR) matrix. Following the processing of the acai pulp, the seed is commonly discarded as waste. Within this research, the compounds were prepared in an open roll mill with a friction ratio of 1:1.25, following ASTM D3182 standard, in proportions of 0, 10, 20, 30, 40, and 50 phr (per hundred rubber) of acai residue. The acai seeds were exposed to the sun for a period of 12 hours to remove excess moisture. Then, they were ground into powder using a blade mill, sieved to a particle size of 30 mesh, and placed in an oven at 104 °C for 24 hours. In the first step, natural rubber, reaction activators (zinc oxide and stearic acid), plasticizers (polyethylene glycol 4000 and naphthenic oil), antioxidant (vulcanox), and micronized acai residue as a filler were added to the mixer. After homogenizing the mixture, it was left at room temperature (23 °C) for 24 hours. In the second step, the mixture was returned to the mixer to add the cross-linking agent (sulfur) and vulcanization accelerators (MBTS and TMTD). After homogenizing the mixture, it was left at room temperature for 4 hours. Upon completing these steps, the composite underwent rheometric tests (ASTM D2084) and was subjected to a thermopress for the preparation of test specimens. The degree of acai filler dispersion in natural rubber was determined based on the minimum and maximum torque results obtained from the rheometry. Additionally, scanning electron microscopy with energy-dispersive X-ray spectroscopy (SEM-EDX) analysis and tensile strength tests were performed on the specimens before and after accelerated aging. The results indicated that lower minimum torque values tend to correspond to lower viscosity, facilitating the mixing of reagents and fillers in the polymer matrix, thereby improving the degree of filler dispersion in the rubber. The SEM images also demonstrated good interaction between the filler and the matrix. In the tensile strength tests, proper filler-matrix adhesion increased the rigidity of the composite and resulted in higher tensile strength values. Therefore, this study demonstrated the feasibility of using acai residue as a filler in natural rubber matrix.

Keywords: *Acai, Natural rubber, Biocomposite, Filler, Rheometry.*

Table1. Results of the properties of natural rubber composites with acai waste.

Composites NR/Acai	Min. torque (dNm)	Max. torque (dNm)	Degree of dispersion	Stress (Mpa)	Strain (%)
0 phr	1.40 ± 0.06	20.43 ± 0.61	0	5,2 ± 0.7	1871 ± 28
10 ph	1.53 ± 0.07	24.01 ± 1.25	-0.1	5.4 ± 0.3	1691 ± 33
20 phr	1.95 ± 0.06	26.47 ± 1.27	0.1	5.8 ± 0.9	1615 ± 71
30 ph	1.98 ± 0.11	29.12 ± 1.38	0	6.2 ± 0.4	1553 ± 27
40 phr	2.03 ± 0.16	31.13 ± 0.94	0.1	7 ± 00.8	1321 ± 48
50 phr	2.37 ± 0.18	34.83 ± 1.27	0	8.6 ± 0.4	1117 ± 52

INFLUENCE OF ACCELERATED AGING IN WEATHEROMETER CHAMBER ON THE ADHESION OF A FABRIC-REINFORCED CONVEYOR BELT

Pedro G. Lins[1], Flavia L. S. Freitas[1], Carla A. Correia[1], Patrick A. Falqueto[2], José J. Penagos[3], Christiano G. Bastos Andrade[1], Hélio Wiebeck[1], Samuel M. Toffoli[1], Ticiane S. Valera[1*]

1 – Department of Metallurgical and Materials Engineering - Polytechnic School - University of São Paulo
tsvalera@usp.br
2 – Vale S/A, Vitória, ES, Brazil
3 – Instituto Tecnológico Vale, Ouro Preto, MG, Brazil

Abstract – Conveyor belts used by the mining industry, for ore transportation, have a highly resistant internal structure, due to the presence of a steel cord structure or polymer woven fabric reinforcement, as well as due to the thick outer layers of rubber coating. Failures in such conveyor belts happen because of a variety of causes, such as ore impact, trapped material, damage to belt edge, worn top cover, damage caused by cleaners, splicing failures, belt bending and belt delamination, wich is considered adhesion failure. The strong adhesion between the fabric and the rubber matrix is achieved through physical and chemical interactions [1], but aging can lead to reductions or even loss of these adhesive properties [2]. One of the most used tests to evaluate the adhesion between the constituents of conveyor belts, and widely used as a tool for controlling the quality of adhesion, is the one described in ISO 252 standard. In this study, a fabric-reinforced conveyor belt manufactured in Brazil, was subjected to accelerated aging testing in a weatherometer chamber, where the effects of weathering (exposure to sunlight and periodical water spray) are simulated. The test was based on the ASTM G155 standard, and the test specimens were prepared according to ISO 252:2008, method A. The specimens remained in the chamber for 1500 hours, after what were subjected to a peel test layer by layer since the top cover to the bottom according to the ISO 252 standard. The effect of aging was evident in all detachments when compared to the results obtained in the non-aged belt. The upper layers closest to the exposure were more affected than the lower layers. The results of the peel test showed a loss of 81% in the adhesion strength in the upper layer compared to an 24% decrease in the lower layer.

Keywords: Conveyor belting, Adhesion, Ageing

[1] Ooji, W.J.. Rubber Chemistry and Thechnology, 1984, 57, 3, 421-456. https://doi.org/10.5254/1.3536016
[2] Patil, P.P., Ooji, W.J.. Rubber Chemistry and Technology, 2005, 78, 1, 1255-173. https://doi.org/10.5254/1.3547868
x

INFLUENCE OF PROCESSING ON THE DISPERSION OF CARBON NANOTUBES IN RUBBER COMPOSITES

Priscila A. L. Campini[1]*, Felipe G. Ornaghi[2], Suel E. Vidotti[2]*

1 – Programa de Pós-graduação em Ciência e Engenharia de Materiais, Universidade Federal do ABC (UFABC), Santo André, SP, Brazil. priscila.lucio@ufabc.edu.br
2 – Centro de Engenharia, Modelagem e Ciências Sociais Aplicadas (CECS), Universidade Federal do ABC (UFABC), Santo André, SP, Brazil. suel.vidotti@ufabc.edu.br

Abstract - There's a current trend in the transport sector to improve the energy efficiency and performance of vehicles. In this scenario, an alternative is reducing the rolling resistance of tires, using precipitate silica as substitute for traditional fillers like carbon black (CB) [1,2,3]. However, this replacement requires the addition of conductive particles to dissipate electrostatic charges generated by tire friction [4]. In this work, multiwall carbon nanotubes (MWCNT) were added in natural rubber (NR)/butadiene rubber (BR) (ratio 1:1) compounds aiming to produce elastomers with antistatic properties. Based on the electrical percolation curve (Fig 1a), the concentration of MWCNT was determined to achieve adequate conductivity for antistatic rubber products (10^{-4} to 10^{-8} S/m) [5]. The percolation threshold was obtained with the addition of 13.5 phr (7 % wt.) of MWCNT, showing a conductivity of $8.3x10^{-5}$ S/m, compared to 2.43 x 10^{-6} S/m for 40 phr of CB. The influence of processing on the electrical conductivity of the samples was investigated using two different routes, r2S or r3S. The r2S route resulted in higher conductivity for the elastomeric compound 13.5phr_r2S (5.07 x 10^{-3} S/m) (Fig 1b). The greater efficiency of the r2S route allowed the reduction of MWCNT concentration to 10 phr, maintaining the antistatic properties (2.71 x 10^{-5} S/m) required for the application.

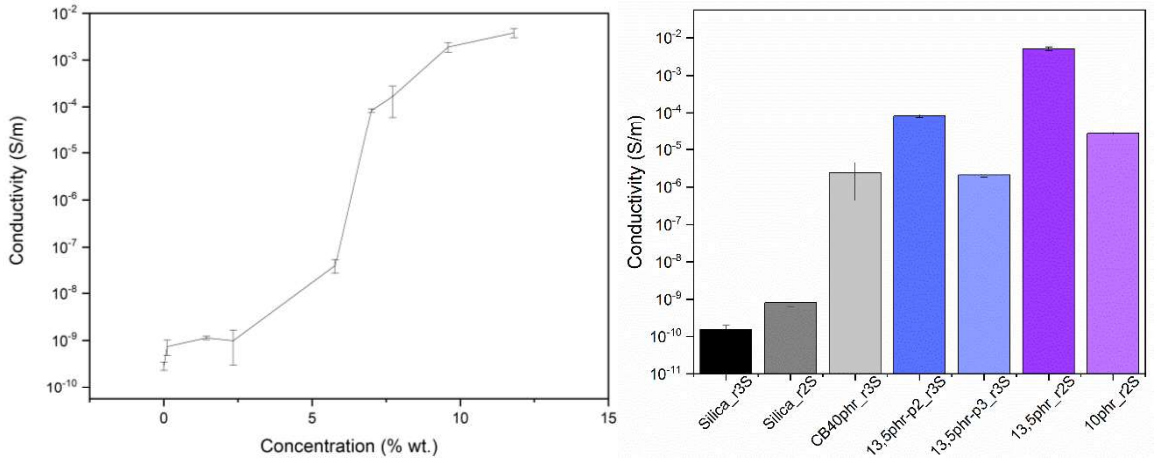

(a) (b)

Figure 1 – Electrical percolation for MWCNT (a); samples conductivity (b).

References

1. I.E. Agency, Energy efficiency, 2021.
2. Brasil, Relatório Anual do Programa Rota 2030-Mobilidade E Logística, 2021.
3. V. Bijina, P.J. Jandas, S. Joseph, J. Gopu, K. Abhitha, H. John, *Polymer Bulletin* 2022. https://doi.org/10.1007/s00289-022-04445-2.
4. K. C. Yong, A. K. Che Aziz, *Advanced Materials Research* 2013, *60-63*, 795. https://doi.org/10.4028/www.scientific.net/AMR.795.60
5. American Society for Testing and Materials. ASTM D991-89 (2020) - Standard Test Method for Rubber Property—Volume Resistivity of Electrically Conductive and Antistatic Products.

Funding: This study was supported by Prometeon Tyre Group, AutoScience Technologies, EMBRAPII and UFABC.

Keywords: *carbon nanotubes; natural rubber; butadiene rubber; electrical conductivity; antistatic properties.*

MORPHOLOGICAL AND MECHANICAL PROPERTIES OF HYBRID EPDM/GRAPHENE NANOCOMPOSITES

Luana Decheti Gaike[12]*, Douglas Alexandre Simon and Eveline Bischoff[1]
1 – Instituto Federal do Rio Grande do Sul (IFRS), Farroupilha, RS, Brazil
2 – Ciaflex Indústria de borrachas
luanadgaike@gmail.com

Abstract This paper investigates the effect of graphene oxide (GO) and reduced graphene oxide (rGO) on the morphology and mechanical properties of ethylene-propylene-diene (EPDM) rubber. The samples were compatibilized with an ethylene elastomer chemically modified with maleic anhydride (E-g-MA) and prepared with melt mixing method. Dispersion of rGO particles within rubber matrix were proven scanning electron microscopy (SEM) and the modified microstructure of samples showed that the fracture surfaces of the compatibilized nanocomposites were rougher than the samples prepared using just rGO. The mechanical analysis indicated that the incorporation of rGO resulted in greater improvements in tensile strength, elongation-at-break, and hardness compared to those samples prepared with GO.
Keywords: Graphene oxide, Reduced graphene oxide, ethylenepropylene-diene monomer (EPDM) and mechanical properties

Introduction

Ethylene-Propylene-Diene Monomer (EPDM) rubber is a synthetic rubber that has been employed in various applications such as seals and outdoor use due to its resistance to water, ozone, weathering, and aging [1]. EPDM is produced through the copolymerization of ethylene and propylene monomers, along with the diene unsaturated monomer, which provides greater flexibility and vulcanization capability [2].

However, EPDM has some limitations, such as low chemical resistance, thermal stability, and sensitivity to temperature increase, which promote molecular mobility and consequently reduce mechanical properties [3]. Therefore, an alternative to expand the range of EPDM applications is the development of elastomeric nanocomposites. Among the most researched nanoparticles in recent years, graphene stands out, consisting of a single layer of carbon atoms organized in a two-dimensional hexagonal crystal lattice [4]. The presence of a conjugated network of sp^2 hybridized carbons provides graphene excellent physicochemical properties [5], such as mechanical strength, elastic modulus, and flexibility when compared to other types of nanoparticles [6]. Originally, graphene was defined as being composed of a single layer or sheet, and later also referred to structures composed of small amounts of neatly stacked layers or sheets (few-layers) [5].

Currently, there are several methods to obtain graphene from graphite, with the main ones being mechanical and chemical exfoliation. It is worth noting that, regardless of the method, controlling the number of layers and defects in the structure is still challenging [6].

For many applications, such as the development of polymer nanocomposites, the use of graphene oxide (GO) and reduced graphene oxide (rGO) seems to be more interesting due to their better chemical interaction with polymer matrices [7]. This process involves the oxidation of graphite using strong oxidizing agents such as sulfuric acid, nitric acid, permanganates, and chlorates, resulting in the formation of functional groups between the graphite layers and structural

defects in its hexagonal structure. Subsequently, these layers can be sonicated to facilitate the dispersion process when incorporated into polar polymeric matrices [8]. When applied to nonpolar polymeric matrices such as EPDM, the use of rGO becomes more suitable, which is obtained as a subsequent step to graphene oxidation and involves the reduction of the number of functional groups using reducing agents such as hydrazine, dimethylhydrazine, and borohydride [6].

In the literature, several studies address the effects of graphene oxide in EPDM. Allahbakhsh et al. [9] reported a decrease in the curing time of EPDM with the incorporation of graphene oxide, which was justified by the reaction between zinc oxide and the oxidized surface of the nanoparticle. In the work of [10], the incorporation of 60 phr of graphene spheres into EPDM increased the thermal conductivity from 0.29 $W.m^{-1}K^{-1}$ to 18.43 $W.m^{-1}K^{-1}$ by 62 times. A significant increase in thermal conductivity in EPDM/silicone blends with graphene additives, as well as increases of 291% in tensile strength and 48% in elongation with the addition of 6% by weight of graphene, were reported by Aziz et al. [11] and [12], respectively.

However, in order to achieve enhanced properties, the incorporation of a compatibilizing agent, such as maleic anhydride, is necessary to increase the interfacial adhesion between the polymer and the nanoparticle leading to improved distribution and dispersion.

Thus, in this study, the effect of incorporating graphene oxide (GO) and reduced graphene oxide (rGO) nanofillers on the properties of EPDM will be investigated with the aim of expanding its range of applications.

Experimental

Materials and Methods

Ethylene propylene diene monomer rubber (EPDM) Nordel 4760 with Mooney viscosity ML (1 + 4) at 100 °C of 60, ethylene content of 67% and ENB of 4% was purchased from Dow Chemical. Compatibilizing agent Fusabond N416 (DuPont), ethylene elastomer chemically modified with maleic anhydride (E-g-MA). The curing system (Sulfur (S), Stearic Acid, Zinc Oxide (ZnO), TMTD and MBTS) were supplied by Minerais Pedra Branca. Graphene oxide (GO) and reduced graphene oxide powder was purchased from Boomatech

The rubber blends were prepared by using a two-roll mill (Luxor) for 20 min based on the formulation in Table 1. First EPDM was added followed by the nanoparticles and compatibilizing agent, and concluded with the addition of vulcanization accelerators.

Table 1

Samples	EPDM	ZnO	Stearic Acid	S	TMTD	MBTS	E-g-MA	GO	rGO
				EPDM					
EPDM	100	5	1,5	2	0,5	0,5	-	-	-
EPDM/0,5E-g-MA	100	5	1,5	2	0,5	0,5	0,5	-	-
EPDM/0,5GO	100	5	1,5	2	0,5	0,5	-	0,5	-
EPDM/0,5rGO	100	5	1,5	2	0,5	0,5	-	-	0,5
EPDM/0,5E-g-MA/0,5GO	100	5	1,5	2	0,5	0,5	0,5	0,5	-
EPDM/0,5E-g-MA/0,5rGO	100	5	1,5	2	0,5	0,5	0,5	-	0,5
EPDM/1E-g-MA/1rGO	100	5	1,5	2	0,5	0,5	1	1	-

Characterizations

The fractured surface of the specimens was analyzed by scanning electron microscopy (SEM) using a FEG (M/s Tescan-Mira3LMH) microscope operating at low vacuum mode, using a large field detector (LFD) and an acceleration voltage of 5–30 kV. The samples were previously sputter-coated with gold to increase their electric conductivity

For tensile strength, dumbbell-shaped samples (Die D) were cut from the molded sheets according to ASTM D 412-06a. The tests were performed at a crosshead speed of 500 mm/min using an Emic DL-3000 instrument, after conditioning the specimens at 23 ± 2 °C and at a relative humidity of 50 ± 5% for 40 h. Five specimens were analyzed, and the average and standard deviation were calculated.

The hardness measurement of the composites were carried out in Shore A durometer as per ASTM D2240.

Results and Discussion

Morphological characterization of EPDM nanocomposites

The SEM images of the fractured surfaces of the EPDM samples with rGO can be observed in Fig 1. A smoother surface can be seen in the image of pure EPDM (Fig 1a). As the rGO is added, a rougher appearance can be observed, characteristic of the presence of nanoparticles (Paran et al., 2020). The presence of small voids in the sample containing 0.5 phr of rGO (Fig 1b) indicates the presence of agglomerated particles that have been pulled out [7]. The use of the compatibilizing agent (Fig 1c), smaller voids and a more homogeneous distribution of rGO particles can be observed. Pasbakhsh et al. [13] also observed an increase in the roughness of EPDM when the compatibilizing agent was added, due to the enhanced interfacial interaction between the halloysite nanoparticle (HNT) and the EPDM matrix. This effect is maintained when the concentration of rGO and compatibilizing agent is doubled (Fig 1d), as a homogeneous distribution of rGO particles can be observed throughout the analyzed surface.

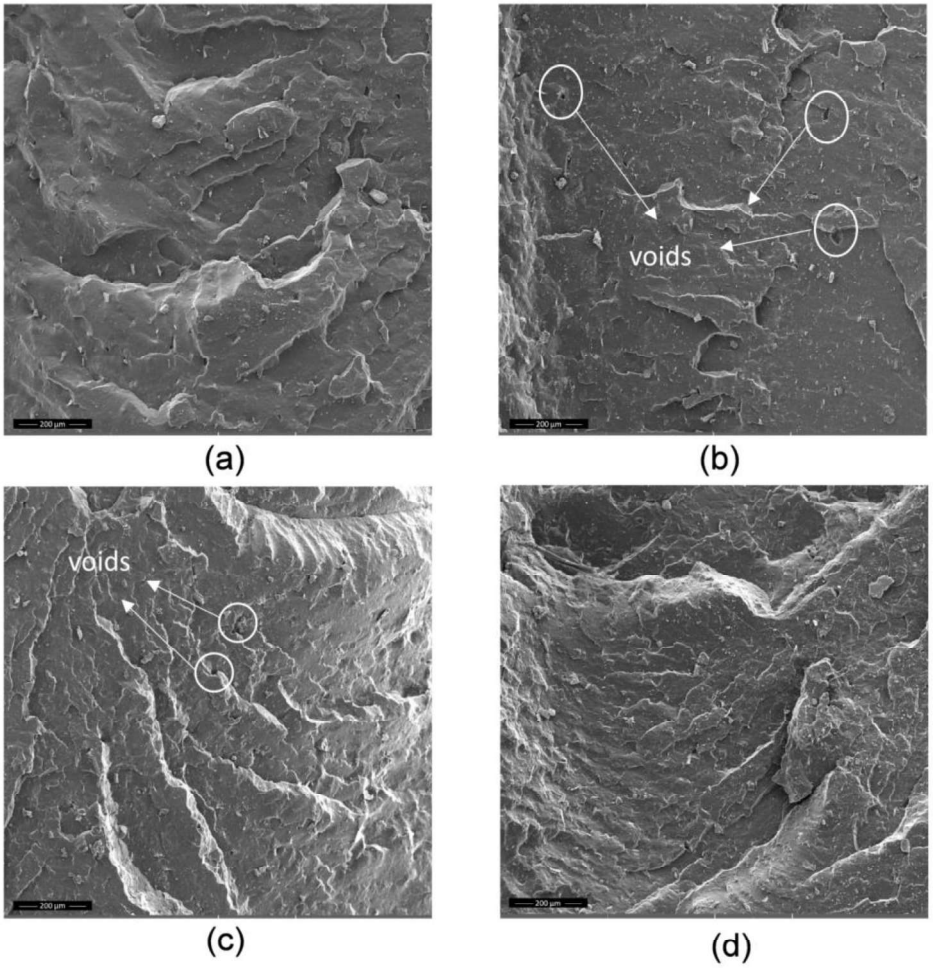

Figure 1: SEM micrographs of: (a) EPDM; (b) EPDM/0,5rGO; (c) EPDM/0,5E-g-MA/0,5rGO and (d) EPDM/1E-g-MA/1rGO

Mechanical Properties of EPDM nanocomposites

The addition of nanoparticles to polymeric matrices promotes improvements in their mechanical properties [14]. However, the reinforcing effect is directly related to the characteristics of the interface, as well as the nature of the specific interactions between the polymer and the reinforcing fillers [7].

Table 2 presents the results of tensile strength, elongation at break and hardness. The addition of 0.5 phr of rGO to the EPDM matrix led to higher increases in tensile strength (38%) compared to the sample containing 0.5 phr of GO (10%). Similarly, the use of the compatibilizing agent also resulted in a greater increase in the tensile strength of the nanocomposites, and this effect is more pronounced (55%) in the sample prepared with rGO (EPDM/0,5E-g-MA/0,5rGO). It can also be observed that doubling the concentration of rGO (1 phr), with the compatibilizing agent, (EPDM/1E-g-MA/1rGO) increased the tensile strength by 2.4 times.

Table 2 Results of tensile strength, elongation at break, and hardness tests.

Samples	Tensile Strength (Mpa)	(%)	Elongation at Break (%)	(%)	Hardness
EPDM					
EPDM	1,7±0,08	-	209±18	-	50
EPDM/0,5E-g-MA	1,6±0,12	-9	443±15	112	55
EPDM/0,5GO	1,9±0,10	10	218±18	4	52
EPDM/0,5rGO	2,4±0,12	38	231±14	10	52
EPDM/0,5E-g-MA/0,5GO	1,9±0,15	13	257±16	23	50
EPDM/0,5E-g-MA/0,5rGO	2,7±0,15	55	293±13	40	54
EPDM/1E-g-MA/1rGO	4,1±0,15	138	489±18	133	59

Conclusions

The influence of GO and rGO on the morphological and mechanical properties of EPDM was investigated. The incorporation of rGO, along with a compatibilizing agent, resulted in a more uniform distribution of particles. As a result, significant improvements were observed in the mechanical properties, attributed to the reinforcement effect of rGO particles.

Acknowledgements

This study was supported by the Instituto Federal de Educação, Ciência e Tecn.ologia do Rio Grande do Sul (IFRS).

References

1. M. A. Bashir, N. Iqbal, M. Shahid, Quratulain and R. Ahmed Journal of Applied Polymer Science 2014, 131, https://doi.org/10.1002/app.39423.

2. Q. Liu, J. Li, Y. Jiang, C. Cong, L. Xu, Y. Zhang, X. Meng and Q. Zhou Polymer Degradation and Stability 2021, 185, 109475. https://doi.org/10.1016/j.polymdegradstab.2020.109475.

3. A. Salimi, F. Abbassi-Sourki, M. Karrabi and M. H. R. Ghoreishy Polymer Testing 2021, 93, 106989. https://doi.org/10.1016/j.polymertesting.2020.106989.

4. A. Nihmath and M. Ramesan Polymer Testing 2020, 89, 106728. https://doi.org/10.1016/j.polymertesting.2020.106728.

5. R. Ghosh and H. Kalita Carbon Trends 2022, 9, 100198. https://doi.org/10.1016/j.cartre.2022.100198.

6. F. Zhang, K. Yang, G. Liu, Y. Chen, M. Wang, S. Li and R. Li Composites Part A: Applied Science and Manufacturing 2022, 107051. https://doi.org/10.1016/j.compositesa.2022.107051.
7. B. Mensah, S. I. Kang, W. Wang and C. Nah Mechanics of Advanced Materials and Modern Processes 2018, 4, 1-12. https://link.springer.com/article/10.1186/s40759-017-0034-0.
8. S. Jeong, S. Yang, B. G. Kim, H. J. Lee, J. J. Bae, J. H. Kim, J. M. Kim, W. Lee, J. Y. Hwang and S. Choi Carbon 2023, 203, 221-229. https://doi.org/10.1016/j.carbon.2022.11.041.
9. A. Allahbakhsh, S. Mazinani, M. R. Kalaee and F. Sharif Thermochimica acta 2013, 563, 22-32. https://doi.org/10.1016/j.tca.2013.04.010.
10. A. Ma, X. Wang, Y. Chen, J. Yu, W. Zheng and Y. Zhao Composites Communications 2019, 13, 119-124. https://doi.org/10.1016/j.coco.2019.04.005.
11. S. Azizi, G. Momen, C. Ouellet-Plamondon and E. David Polymer Testing 2020, 84, 106281. https://doi.org/10.1016/j.polymertesting.2019.106281.
12. Z. Yuan, W. Li, C. Li and L. Ye Composites Part A: Applied Science and Manufacturing 2019, 121, 254-264. https://doi.org/10.1016/j.compositesa.2019.03.039.
13. P. Pasbakhsh, H. Ismail, M. A. Fauzi and A. A. Bakar Polymer Testing 2009, 28, 548-559. https://doi.org/10.1016/j.polymertesting.2009.04.004.
14. S. M. R. Paran, G. Naderi, F. Javadi, R. Shemshadi and M. R. Saeb Materials Today Communications 2020, 22, 100763. https://doi.org/10.1016/j.mtcomm.2019.100763.

PREDICTION OF CURE CHARACTERISTICS OF RUBBER COMPOUNDS WITH RECOVERED CARBON BLACK USING ARTIFICIAL NEURAL NETWORKS

Marco A. G. Cruz[1], Eduardo R. Budemberg[1], Carlos. T. Hiranobe[1], Guilherme P. Cardim[1], Rogério E. Garcia[2]e Renivaldo J. dos Santos[1]

[1]*São Paulo State University (Unesp), School of Engineering and Sciences, Rosana,*

[2]*São Paulo State University (Unesp), School of Engineering and Sciences, Presidente Prudente,*

Avenida dos Barrageiros, 19274-000, Rosana, SP, Brasil.

Corresponding author: marco.galindo@unesp.br

Abstract - With the growing environmental degradation compromising the quality of life, the need for sustainable solutions to minimize environmental impacts becomes evident. In this context, the large quantity of unusable tires discarded worldwide further exacerbates this crisis. Several studies in the field of pyrolysis have been conducted for processing these tires with the objective of producing oil, gas, and recovered carbon black (rCB). All these generated byproducts are fuels, and rCB can also be reintroduced into the rubber processing area as a filler. Its use is considered a friendly alternative to commercial carbon black as it provides reductions in carbon dioxide (CO2) emissions, energy consumption, and can provide mechanical reinforcement in rubber compounds. In this study, composites of natural rubber with rCB from truck tires with a particle size of 120 mesh were produced, and their rheometric and mechanical properties were investigated. Based on the experimental results, we present a trained artificial neural network (ANN) model using Matlab software to predict the curing properties of mixtures with different rCB contents (0 to 50 phr). The input rheometric parameters used were optimal curing time, minimum and maximum torque, and the results of the mechanical tests, Shore A hardness (ASTM D 2240), and abrasion resistance (ASTM D 5963). To train the model, 90 experimental data points were used out of a total of 100, with the remaining 10 used for network validation. The predicted results from the model showed excellent agreement with the tested experimental data, with a maximum prediction error of less than 1%. It is concluded that ANNs are a powerful tool for intelligently modeling the curing process of rubber mixtures. Furthermore, this approach has the potential to be applied in a wide range of applications in the rubber industry.

Keywords: *Artificial Neural Networks, Recovered Carbon Black, Natural Rubber, Vulcanization.*

PRODUCTION OF COMPOSITES BASED ON NATURAL RUBBER/SYNTHETIC RUBBER: RHEOMETRICAL AND MECHANICAL PROPERTIES

Arthur P. Carvalho, Eduardo R. Budemberg, Carlos T. Hiranobe, Flavio C. Cabrera, Leonardo P. Paim, Renivaldo J. Santos*

São Paulo State University (Unesp), School of Engineering and Sciences, Rosana,
renivaldo.santos@unesp.br
Avenida dos Barrageiros, 1881, Centro, Primavera/Rosana-SP CEP 19.274-00

Abstract – In this work, natural rubber (NR) and styrene-butadiene synthetic rubber (SBR) composites were produced in a 50/50 ratio using micronized polyurethane (PU) waste from the refrigeration industry as filler. The vulcanization system used was the semi-efficient (SEV). The interaction of filler in the polymeric matrix and the mechanical properties of the composites were investigated. The composites were produced by varying the filler content between 0-40 phr in an open mixer, and the specimens were made employing thermopressing at a temperature of 160°C (ASTM D 3182), with dimensions of 15 x 15 cm and thickness of 2 mm. The characterization of the composites was carried out using the techniques of rheometry (ASTM D 5289), density (ASTM D 297), hardness (ASTM D 2240), tensile strength (ASTM D 412), the density of crosslinks by swelling in organic solvents using the Flory-Rehner equation. Furthermore, the composites were submitted to Lorentz-Park analysis to study the interaction effect between the filler and the polymeric matrix. The results showed a strong interaction between the filler and the matrix. Crosslink density values increased with increasing filler. The mechanical properties improved. The hardness rose from 50 (pure gum) to 75 Shore A (composite with 40 phr of PU), and the tensile strength value rose from 4.2 MPa (pure gum) to 7.3 MPa (composite with 40 phr of PU), evidencing the excellent dispersion and interaction filler-matrix. However, the deformation at break was reduced from 800% (pure gum) to 300% (composite with 40 phr of PU). The composites have mechanical properties for industrial applications, such as casual shoe soles.

Fundings: The authors are grateful for the financial support Process FAPESP 2020/05549-4.

Keywords: *Vulcanization, PU residue, Lorentz-Park, elastomers.*

PROPERTIES OF CONVEYOR BELT RUBBER COVERS USED IN MINING

Christiano G. Bastos Andrade[1], Flavia L. S. Freitas[1], Carla A. Correia[1], Pedro G. Lins[1], Patrick A. Falqueto[2], José J. Penagos[3], Hélio Wiebeck[1], Samuel M. Toffoli[1], Ticiane S. Valera[1]

1 – Department of Materials Engineering, Polytechnic School, University of São Paulo (USP), São Paulo, SP, Brazil
tsvalera@usp.br
2 – Vale S/A, Vitória, ES, Brazil
3 – Instituto Tecnológico Vale, Ouro Preto, MG, Brazil

Abstract - The conveyor belts for ore transportation are basically composed of a core that has high resistance encased in protective rubber covers. Two types of reinforcements or carcass are commonly used in the construction of ore conveyor belts: a single layer of uniformly tensioned steel cords with diameters and distribution design that provide the necessary resistance for the specific application or layers of polymeric woven fabrics. Two conveyor belts that are used for the same applications in mining, despite having very different maximum operating tension, caused by their different carcass materials (fabric or steel cord), have similar abrasion resistance during operations. Thus, this work analyzed the rubber covers of these two belts, to identify similarities and differences between the rubber compounds. The compounds were characterized by: X-ray fluorescence (XRF), X-ray diffraction (XRD), scanning electron microscope / energy dispersive spectroscopy (SEM/EDS), thermogravimetric analysis (TGA/DSC), Fourier-transform infrared spectroscopy (FTIR), neutron activation analysis (NNA), inductively coupled plasma optical emission spectroscopy (ICP-OES) and analysis of carbon and sulfur by combustion. The chemical analyzes showed the presence of the same elements in the two rubber compounds, some of which were attributed to vulcanization agents, such as sulfur and zinc, and others such as calcium, magnesium, and silicon, were attributed, also using XRD and SEM/EDS analysis, to minerals, such as talc and calcite, normally used as fillers in rubber compounds. The results of the thermal analyzes corroborated the previous results, confirming the similarity between the two cover rubber compounds.

Keywords: *Conveyor belts, Rubber, Fabrics, Steel Cord, Characterization.*

STEEL CORD CONVEYOR BELT ADHESION AFTER ACCELERATED AGING

Flavia L. S. Freitas[1], Carla A. Correia[1], Pedro G. Lins[1], Christiano G. Bastos Andrade[1], Patrick A. Falqueto[2], José J. Penagos[3], Hélio Wiebeck[1]; Samuel M. Toffoli[1], Ticiane S. Valera[1*]

1 – Department of Metallurgical and Materials Engineering - Polytechnic School - University of São Paulo
tsvalera@usp.br
2 – Vale S/A, Vitória, ES, Brazil
3 – Instituto Tecnológico Vale, Ouro Preto, MG, Brazil

Abstract – Steel cord conveyor belts represent an important system for the mining industry, once it transports ore over long distances. It comprises two elements: the reinforcements and the covers [1]. This transport system demands maintenance and replacement of worn-out components, which reflect in high financial costs and interruptions of the production [2]. The mechanical performance of the covering rubber decreases with time, due to aging caused by environmental factors, which are well known degradation precursors for polymeric materials. Moreover, the strong adhesions between polymer and metal reinforcement in conveyor belts are based on chemical interactions and aging can promote a reduction in the adhesion, allowing failure effects that may compromise their performance in use [3,4]. This study aimed to analyze the adhesion of the steel cords to the rubber compound, in steel cord reinforced conveyor belts, after exposure to accelerated aging. The conveyor belt specimens were subjected to different conditions, promoted by different equipment, such as weatherometer, oven with humidity, and QUV irradiation chambers, for a period of 1000 hours, in order to separate the effects of the weather, temperature with humidity, and ultraviolet radiation. The specimens extracted from a cross section of a conveyor belt were prepared in the 3-cord configuration and were tested and analyzed by pull-out tests based on SANS 1366:2013 and ISO 8094:2013 standards. The specimens showed unusual rupture when subjected to exposure in a weatherometer chamber and in a humid oven. In this latter situation, the specimens showed a decrease of around 39% in the adhesion strength, when compared to the specimens tested in the other chambers. The QUV irradiation chamber had the least influence on belt degradation and cord adhesion strength. Therefore, the results indicated that the aging factors analyzed can contribute to the possible origin of adhesion failures during the use of conveyor belts.

Keywords: *Conveyor belts, aging, adhesion, degradation*

References

1. M. Bajda in IOP Conference Series: Earth and Environmental Science, Czech Republic, 2018, Vol 221, 012098.
2. F. Hakamia; A. Pramanika, N. Ridgwaya; A.K. Basakb *Tribol. Int*. 2017, 111, 148-158, https://doi.org/10.1016/j.triboint.2017.03.010
3. Y. Ituoh; H. Gu; K. Satoh; Y. Jutsuna *Strutural Eng.* 2006, *23*, 176-190. https://doi.org/10.2208/jsceja.62.176.
4. D. Dobrotă *J Adhes Sci Technol.* 2013, 27, 125-135, https://doi.org/10.1080/01694243.2012.701511.

STUDY OF REINFORCMENT PROPERTIES OF *DRACAENA TRIFASCIATA* FIBERS IN NATURAL RUBBER COMPOSITES

Henrique P. Cardim[1], Flávio C. Cabrera[1], Altibano Ortenzi[2] and Renivaldo J. dos Santos[1]*

1 – Engineering Department, São Paulo State University (UNESP), Rosana, SP, Brazil
renivaldo.santos@unesp.br
2 – Department of Civil Engineering, State University o Londrina (UEL), Londrina, PR, Brazil

Abstract – The increase of researches about functional materials is leaded of ideas the represents quality in results for several industrial applications. Due environmental issues, materials coming from natural resources has increased the demand, according to the industrial concerns in eco-friendly materials. The objective of this work is the characterization of *Dracaena trifasciata* (snake plant) fibers to reinforcement application in the production of a composite material with natural rubber. Mechanical properties of *D. trifasciata* fibers has been proved promisors according to the results of a tensile strength test realized in 30 filaments, the summarized data is presented in table 1. Due to the conical shape of *D. trifasciata* filaments and the water dissolution method applied a Fourier Transform Infrared Spectroscopy (FTIR) analysis confirmed no variations in the chemical-biological composition. Were produced composites of natural rubber with *D. trifasciata* fibers (as reinforcement) in several proportion (0 to 40 phr). The composites were characterized by rheometric analysis ASTM D2084[1], density ASTM D297[2], toughness at Shore A scale ASTM D2240[3] and abrasion D5963[4]. The results shown that density and toughness values increased with the fibers insertion, the weight loss suffered a discreet reduction. The wild availability of this fibers enable the use as reinforcement in elastomeric materials.

Table 1 – Mechanical properties of *Dracaena trifasciata* fibers.

	Young's Modulus (GPa)	Tensile Strength (MPa)	Failure Strain (%)
Average	28.43	357.92	1.47
S.D.	9.95	112.63	0.33

References

1. ASTM D2084, "Standard Test Method for Rubber Property - Vulcanization Using Oscillating Disk Cure Meter". ASTM American Society for Testing Materials, 2019.
2. ASTM D297 "Standard Test Methods for Rubber Products – Chemical Analysis". ASTM American Society for Testing Materials, 2021.
3. ASTM D2240 "Standard Test Method for Rubber Property – Durometer Hardness" ASTM American Society for Testing Materials, 2010.
4. ASTM D5963, "Standard Test Method for Rubber Property – Abrasion Resistence (Rotary Drum Abrader)" ASTM American Society for Testing Materials, 2022.

Keywords: *Composites, Natural Rubber, Vulcanization, Dracaena trifasciata Fibers, Rheometric.*

THE EFFECT OF LIGNIN ON SELF-HEALING AND SHAPE MEMORY OF CARBOXYLATED NITRILE RUBBER WITH DIFFERENT CARBOXYL GROUP CONTENT

Beatriz Girão*, Gustavo N. Campos, Elisson B. D. da Rocha, Ana M. F. de Sousa, Marco A. G. de Figueiredo, and Cristina R.G. Furtado

Instituto de Química, Universidade do Estado do Rio de Janeiro, São Francisco Xavier Street, 524, Maracanã, 20550-900, Rio de Janeiro, RJ, Brasil.
(*) girobeatriz@gmail.com

In recent years, there has been significant research on smart elastomers, materials that can react to an external stimulus and still maintain an elastomeric behavior. Two important properties of smart materials are shape-memory and self-healing. Carboxylated nitrile rubber (XNBR) has carboxyl groups added to its backbone that can form ionic bonds with oxides of some metals, such as zinc. These ionic bonds are temperature-dynamic and can impart the elastomer with shape memory and self-healing properties. While this is known for unfilled compounds, most rubber formulations include fillers to improve the material's mechanical properties, and research concerning the impact of the filler on smart elastomers is invaluable. Lignin, a highly functional material belonging to a class of complex organic polymers, serves as a vital structural component in the support tissues of most plants. As a byproduct of the paper and pulp industry, lignin holds great potential as a biobased, renewable, and biodegradable material that can be utilized as a filler for reinforcing rubber. Understanding the impact of lignin on smart elastomers could further increase their applications. In this research, rubber compounds were made with hardwood kraft lignin, XNBR (with 1 and 7% carboxyl group content), and a sulfur vulcanization system. Their self-healing and shape-memory properties were evaluated using tensile tests and a dynamic mechanic analyzer (DMA), respectively. Our results show that lignin plays a significant role in improving the shape memory of XNBR compounds. The inclusion of lignin increased the shape fixation (to near 80%) and the shape recovery (to at least 40%) of both types of XNBR. However, lignin decreased the self-healing of both XNBR compounds. These findings suggest that lignin has a positive impact on the shape-memory characteristics of elastomers, further bolstering its potential as a multifunctional and relevant filler.

Fundings: The authors thank Nitriflex for donating the rubber compound's raw materials and Suzano for donating the lignin. This study was supported by the Universidade do Estado do Rio de Janeiro (UERJ) [PIBIC 2022 Scholarship received by Beatriz Girão], the Fundação de Amparo à Pesquisa do Estado do Rio de Janeiro (FAPERJ) [E-26/200.289/2021: PhD Scholarship received by Gustavo N. Campos], and Conselho Nacional de Desenvolvimento Científico e Tecnológico (CNPQ) [P2-309461/2021-9 received by Ana Maria Furtado de Sousa].

Keywords: *Lignin; Self-healing; Shape-memory; Rubber; XNBR.*

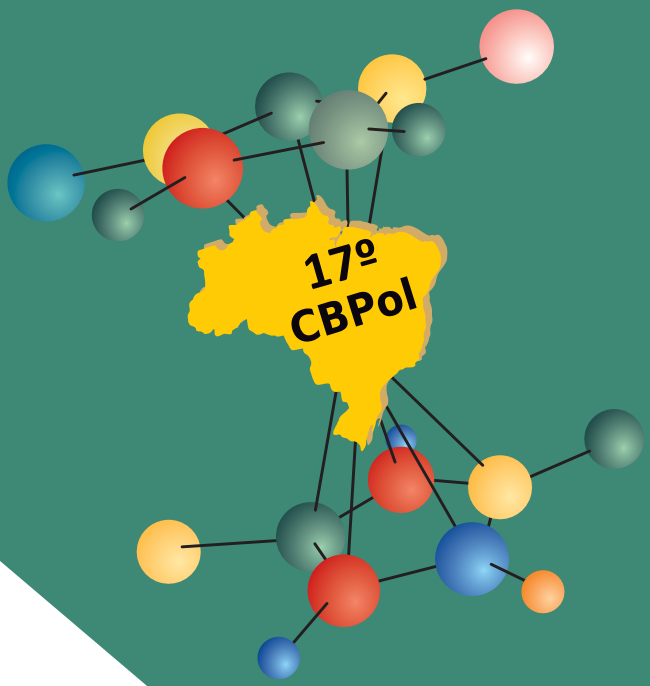

Recycling and environmental issues associated with polymers

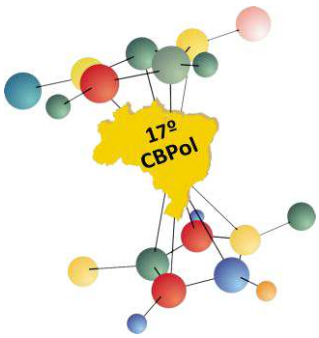

AN OVERVIEW OF THE GAPS IN MICROPLASTIC RESEARCH THAT POLYMER SCIENCE CAN HELP TO FILL

Walter Ruggeri Waldman[1]*

1 – Departamento de Física, Química e Matemática (DFQM), Universidade Federal de São Carlos, Sorocaba, Brazil
walter@ufscar.br

Abstract - Since their discovery, synthetic polymers have proven to be versatile materials, meeting a wide range of important demands in our society. Their low cost, physical properties, and ease of processing make plastics able to seize the market, and nowadays, it is a material we cannot live without. The widespread use of plastic gave rise to the issue of plastic pollution, which has proved difficult, perhaps even impossible, to manage effectively. Plastic pollution has several faces and impacts; the most pervasive, and subject of this talk, are the microplastics. Microplastics are small, air- and waterborne fragments detected in the most remote corners of Earth and inside the inner parts of our body (since we eat, drink, and breathe them). Plastic pollution is visible and perceived as a threat to the extent that a legally binding Global treaty on this issue is currently under discussion by the United Nations Environment Programme (UNEP). Despite the growing body of scientific literature and the ongoing actions of international organizations, we still lack a comprehensible understanding of the true impacts on human health and the environment, and more research on the topic must be developed to answer this question. This presentation aims to underscore the key role of polymer scientists to help create insights to fill some of the current gaps in the field, like 1) the production of environmentally relevant micro and nanoplastics to enable adequate toxicological experiments; 2) the lack of knowledge about the properties and presence of nanoplastics; 3) the development of cheaper and faster separation protocols for microplastics in water, air, and soil to address the lack of data in South America and Africa.

Keywords: *microplastics, nanoplastics, plastic pollution, separation protocols.*

PCR(PP AND PE) SOURCES CHARACTERISTICS AVAILABLE FOR PRODUCTS AND APLICATIONS DEVELOPMENTS: A CONCEPT CHALLENGE

Regina Funck Nonemacher[1], Priscila dos Santos[1],Fernando Silveira[2] and Marcelo Farah*

:

1 – Technology and Innovation Center Laboratory, Braskem, Triunfo-RS, Brazil

2 – Advanced Analytics, Braskem, Triunfo-RS, Brazil

3- Product Engineering -Circular Economy, Braskem, Triunfo-RS, Brasilmarcelo.farah@braskem.,com

Abstract - Working in a polyolefins business using plastic waste sources from various post-consumer sources (PCR) is a considerable challenge, given the diversity of materials that compose them. Formulation design for many applications is highly impacted by material characteristics, being a seasonal, selective "average" of all available grades of virgin polyolefin resins, plus processing and usage effects. Many sources of waste must be sent for chemical/advanced recycling and their composition is also relevant for the design of plants and treatment of their by-products. In this sense, the understanding of physical-chemical properties is essential for the final control of recipes and processes for maintaining the minimum characteristics to have applications with technical requirements. Rigid sources of PP and PE and flexible sources of PE are addressed in this work showing the variability and characteristics observed in different batches of materials. In some cases the variability is significant bringing complexity, evidenced by rheological, thermal and mechanical analyses. These data are in the process of statistical collection over time.

Keywords: *recycling, polymer properties, polymer characterization, PCR source*

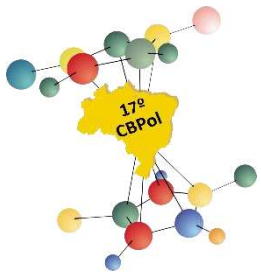

RECYCLING OF POLYMERIC WASTE AIMING EDUCATION FOR SUSTAINABLE DEVELOPMENT

Emanuelle Ruppel[1*], Anna L. M. S. Cavalcanti[2], Danilo C. Silva[2], Marli T. Everling[2], João E. C. Sobral[2], Carlos M. Sacchelli[3] and Noeli Sellin[1,2,4]

1 - Department of Chemical Engineering, University of Joinville Region (UNIVILLE), Joinville, SC, Brazil
emanuelle.ruppel@univille.br
2 – Graduate Program in Design, University of Joinville Region (UNIVILLE), Joinville, SC, Brazil
3 – Department of Mobility Engineering, Federal University of Santa Catarina (UFSC), Joinville, SC, Brazil
4 – Graduate Program in Process Engineering, University of Joinville Region (UNIVILLE), Joinville, SC, Brazil

Abstract - This article reports on activities of the project "Maker Space of Education for Sustainable Development Based on Design for Change", whose objective is based on the education for sustainability and maker culture, focused on the problem of polymeric waste, aiming to disseminate concepts and practice of sustainability among elementary and high school students. Bibliographical research was carried out to gather information about the current scenario related to the recycling of polymeric materials; preparation of didactic/instructional materials for training teachers and students for the theme involved; and promotion of three workshops: (1) Workshop of collection, identification, and separation of polymeric waste, (2) Workshop of creativity and (3) Workshop of polymeric waste recycling using a Mobile Laboratory. The activities were applied in a municipal school in Joinville/SC and to students from the 9th grade of elementary school. The whole experience promoted awareness and collaborated with training for action through education focused on sustainable development.
Keywords: *Polymeric waste, Sustainability, Environmental education*
Fundings: FAPESC.

Introduction

Despite the benefits promoted by polymeric materials, the accelerated growth in the production and consumption of products derived from these materials has generated major challenges for the environment and the human species itself [1]. Currently, almost 400 million tons (Mt) are produced per year [2]. Sanitary landfills, dumps, incineration, poor management, and non-reuse of polymeric waste are still very common today, causing environmental, economic, and social impacts [3].

In 2019, estimates indicated that 6.1 Mt of plastic waste ended up in aquatic environments and 1.7 Mt ended up in the oceans. It is believed that there is currently 30 Mt of plastic waste in the seas and oceans and another 109 Mt agglomerated in rivers, which could end up in the oceans [4]. More recent research shows a potential for fragmentation of plastic materials over time into micro and nanoparticles, which are found in different ecosystems around the world [5]. The ingestion of micro and nano plastics has been shown to be increasingly frequent by both animals and humans and their effects on health are not yet known [1].

The dissociation between raw materials and the environment worsens with the development of the consumer society and puts life at risk due to the depletion of natural resources and environmental pollution and brings ethical questions that encompass both social responsibility and sustainability. To change a posture culturally constructed over generations, it is necessary to encourage and guide younger people who are starting to build an understanding of cultural values. Among the possible

strategies is education for sustainable development. In view of this, this work aimed to contribute to education aimed at sustainable development, in a municipal school in the city of Joinville/SC, using mechanical recycling of polymeric waste and awareness of the adversities that they cause in nature when they are not used and are inappropriately allocated.

Experimental

Through bibliographical research, a survey of information was carried out on the scenarios of recycling of polymeric materials in the world, national and regional scopes, and on methods of identification and processes of mechanical recycling of polymeric residues. The information was used in the preparation of teaching and instructional materials, which were used to train teachers and applied in workshops to students from the participating school.
The activities of the project were applied at the Teacher Eladir Skibinski Municipal School. The 9th grade of elementary school and the "Tempo de Avançar" project (totaling 72 students) and the subjects of Arts and Sciences were defined to carry out the workshops.
Guidance was given for the campaign to collect polymeric waste for the workshops, which was organized and implemented by the school and involved students from all grades.
Three workshops were carried out with students from the defined groups: (1) Workshop on identification and separation of waste by recycling code (NBR 13230, 2008) [7] and density and combustion tests, based on procedures described by Manrich et al [8] and GEPEQ [9]; (2) Creativity workshop, in which students received information about polymer waste recycling processes and their transformation into products; (3) Recycling workshop, carried out using a Mobile Laboratory composed of an extruder, an injection machine and a compressor oven, based on Precious Plastics [10] projects and built by outsourced companies (Fig. 1).

Figure 1: Equipment of the Mobile Laboratory, (a) injection machine, (b) extruder and (c) compressor oven.

Results and Discussion

Scenarios for the production and recycling of polymeric materials
Bibliographic research regarding the world, national and regional panorama of polymeric waste and plastic recycling showed a worrying scenario. Worldwide, it is estimated that 9.2 billion tons of plastics were produced between 1950 and 2017 [3]. Data from the OECD (Organization for Economic Cooperation and Development) report indicate that, of all plastic waste generated in 2019, 22% were poorly managed and/or not collected, 49% were sent to landfills, 19% were incinerated and only 9% were recycled [4].
In more recent data, the world production of plastics in 2021 reached the mark of 390.7 million tons, 90.2% of which comes from fossil fuels, 8.3% from post-consumer recycled plastics and only 1.5% biologically based [11].
According to the 2021 Profile of Abiplast (Brazilian Plastic Industry Association), in 2020, 23.1% of plastics were recycled in Brazil, a percentage 0.9% lower than that verified in 2019, but still above the world average. The mechanical recycling of post-consumer plastics in Brazil was 884.4 thousand tons [12]. Analyzing a regional scenario, the Ambiental Limpeza Urbana e Saneamento company is

responsible for managing solid waste in the city of Joinville/SC. Waste from selective collection is sent to recycling associations and cooperatives, which are registered and accredited by the Urban Infrastructure Department. According to the company, only in the first month of 2022, around 542.52 tons of solid waste were collected in selective collection in Joinville [13]. According to the ASSECREJO cooperative, which receives most of the selective collection waste from the company Ambiental and waste that is delivered by other companies and voluntarily by the population, in the same period, 22.8% was plastic waste in general (high-density polyethylene and low-density polyethylene - HDPE and LDPE, polypropylene - PP, polyethylene terephthalate - PET, polyvinyl chloride - PVC, polystyrene - PS, among others). In the first quarter of 2023, 2.1 thousand tons of recyclable waste were registered, representing 6.76% of all waste collected in the municipality [14]. According to ABRELPE (Brazilian Association of Public Cleaning and Special Waste Companies), on the national average, plastics are responsible for 16.8% of dry recycled waste [15], a figure lower than that of the municipality of Joinville. This information and other complementary ones were used in the training of teachers and in the workshops carried aout at the school, aiming to present the scenario related to polymeric waste and will also be later fed into a virtual platform, which is being finalized, and which will serve as support material for replication of the experience at other schools.

Results of activities and workshops at school

The activities at Teacher Eladir Skibinski Municipal School started with meetings with the director and teachers to define which grades and subjects were most related to the proposal of the Maker Space Project, and Sciences and Arts subjects and the classes of the 9th grade of elementary school and of the "Tempos de Avançar" project were defined to the application of workshops for the identification and recycling of polymer waste. Teachers of these subjects were trained through presentations and workshops involving content on polymers (main types, chemical structures, applications, identification methods and recycling technologies). The school promoted a campaign to collect post-consumer plastics (preferably bottle caps), in which students from all grades at the school participated.

The teacher of Science subject carried out a dynamic with the students, in which they prepared posters with the main types of plastic consumed, their applications and the recycling code for each one, so that the students would learn to separate polymeric waste.

In the Identification Workshop, through density tests (in water, oil, saline and hydroethanolic solution) and combustion (material behavior and analysis of smoke pH) of the polymer residues, the students participated actively, performing the proposed tests with the guidance from the teacher, the scholarship holders of the Chemical Engineering and Environmental and Sanitary Engineering courses and the professor linked to the Maker Space Project. Several samples of polymeric waste were taken, including six types: PET, HDPE, PVC, LDPE, PP and PS. The workshop was applied at the school's Science Laboratory and the classes were separated into 6 groups of 5 students so that everyone could carry out the experiments. From the experiments and understanding of the physical and chemical principles involved in each one, the students were able to separate the samples according to their respective polymeric resins of origin and correlate them with the contents of the Sciences subject.

The Creativity Workshop was held in the Arts class, in which important points were explained to students about the problem of incorrect disposal of polymeric waste, the importance of recycling and the technologies used, mainly, in mechanical recycling. The Mobile Laboratory equipment that would be taken to school and used in the recycling workshop was presented to students. In addition, students were asked to make a representative and simple drawing associated with the theme of the Maker Space project (polymeric waste and sustainable development). The selected design was a sea turtle due to its relationship with marine pollution caused by polymeric waste in different ways. Based on this, a mold in the format of the drawing was designed and modeled in CAD (Computer-aided design) and machined in aluminum in a CNC (Computer Numerical Control) machining machine from

Univille. The gifts were made in the injection molding machine in the recycling workshops. For the gifts, caps of different colors collected and separated by the students were used, which were previously crushed in a knife mill belonging to the UDESC. The Mobile Laboratory will be contemplated by a mill, also based on the Precious Plastics project [10], which is still being built by the research group. More than 100 turtle-shaped keychains were produced to be given to students and teachers of the classes involved. In the recycling workshop, it was decided, for practical reasons, to use only the caps to demonstrate the recycling processes to the students. The Mobile Laboratory's equipment was previously tested to define the operating conditions and then taken to the school for the polymer waste recycling workshop. The workshop was held in the Science Laboratory and the classes were divided into groups of 10 students so that they could observe and participate in the demonstration of each equipment of the Mobile Laboratory. Two banners were taken, one explaining the Maker Space Project and the other about the recycling steps and the Mobile Laboratory equipment. First, the thermoforming process was demonstrated in the compressor oven, then the extrusion process and finally the injection process. More keychains were produced, and the students could visualize the transformation of the polymeric waste into a product designed by them.
The entire experience at the school was recorded through photos, recordings, and interviews (Fig. 2) and it will also serve to feed the virtual platform of the Maker Space Project, as described above.

Figure 2: Photos of the activities and workshops carried out at the school

Conclusions

From the workshops carried out at the school, the experience of the students and active learning, derived from the process of recycling polymer waste for the development of new products, promoted awareness of sustainable development in its social, environmental and economic dimensions. At the same time, the experience contributed to the training of human resources to act through education for sustainable development.

Acknowledgements

To FAPESC for financing the project, CNPq and UNIEDU for scientific initiation scholarships and to Teacher Eladir Skibinski Municipal School for the partnership in the development of activities.

References

1. WWF – Fundo Mundial para a Natureza. Solucionar a poluição plástica: transparência e responsabilização. Disponível em: https://promo.wwf.org.br/solucionar-a-poluicao-plastica-transparencia-e-responsabilizacao. Acesso em: mar. 2023.
2. Plastic Oceans. *Plastic Pollution Facts*. Disponível em: https://plasticoceans.org/the-facts/. Acesso em: mai. 2023.
3. UNEP - United Nations Environment Programme (2021). Drowning in Plastics – Marine Litter and Plastic Waste Vital Graphics. Disponível em: https://www.unep.org/resources/report/drowning-plastics-marine-litter-and-plastic-waste-vital-graphics. Acesso em: mar. 2023.
4. OECD - Plastic pollution is growing relentlessly as waste management and recycling fall short. Disponível em: https://www.oecd.org/newsroom/plastic-pollution-is-growing-relentlessly-as-waste-management-and-recycling-fall-short.htm. Acesso em: mar. 2023.
5. LEHNER, R. et al. Emergence of Nanoplastic in the Environment and Possible Impact on Human Health. Environ. Sci. Technol. 2019, 53, 4, 1748-1765. https://doi.org/10.1021/acs.est.8b05512.
6. FRAGA, S. C. L. *Reciclagem de Materiais Plásticos - Aspectos Técnicos, Econômicos, Ambientais e Sociais,* Saraiva Ed.; São Paulo, 2014.
7. ASSOCIAÇÃO BRASILEIRA DE NORMAS TÉCNICAS. ABNT NBR 13230:2008 – Embalagens e acondicionamento plásticos recicláveis – identificação e simbologia, Rio de Janeiro, ABNT, 2008.
8. MANRICH, S.; FRATTINI, G.; ROSALINI, A. C. Identificação de plásticos: uma ferramenta para reciclagem. São Carlos: EDUFSCar, 1997.
9. GEPEQ – Grupo de Pesquisa em Educação em Química (IQ-USP). Separação e Identificação de Plásticos - Experimentos de Química - Portal e-Aulas. Disponível em: https://www.youtube.com/watch?v=_yt18HwthGE. Acesso em: nov. 2022.
10. PRECIOUS PLASTICS. Machines. Disponível em: https://preciousplastic.com/solutions/machines/overview.html. Acesso em: mai. 2023.
11. PLASTICS EUROPE. Plastics – the Facts 2022. Disponível em: https://plasticseurope.org/knowledge-hub/plastics-the-facts-2022/. Acesso em: mar. 2023.
12. ABIPLAST – Associação Brasileira da Indústria do Plástico. Perfil 2021: As indústrias de transformação e reciclagem de plástico no Brasil. Disponível em: https://www.abiplast.org.br/publicacoes/perfil-2021/. Acesso em: mar. 2023.
13. PMJ - Prefeitura Municipal de Joinville. Joinville registra aumento da quantidade de material reciclável coletado. Disponível em: https://www.joinville.sc.gov.br/noticias/joinville-registra-aumento-da-quantidade-de-material-reciclavel-coletado/. Acesso em: abr. 2023.
14. EVERLING, M. T.; SELLIN, N.; SILVA, D. C.; SACCHELLI, C. M.; BOETTCHER, M. Espaço Maker: design e educação para a sustentabilidade em escolas públicas. Impact Projects, v. 1, n. 1, p. 139-154.
15. GANDRA, A. Índice de reciclagem no Brasil é de apenas 4%, diz Abrelpe. Agência Brasil. Rio de Janeiro, 5 jun. 2022. Disponível em: https://agenciabrasil.ebc.com.br/geral/noticia/2022-06/indice-de-reciclagem-no-brasil-e-de-4-diz-abrelpe. Acesso em: abr. 2023.

STRATEGIES, TECHNOLOGIES AND MATERIALS FOR REDUCING THE ENVIRONMENTAL IMPACT OF OCEAN PLASTIC WASTE

Rodrigo Lambert Oréfice*
Department of Metallurgical and Materials Engineering, Federal University of Minas Gerais (UFMG), Av. Antônio Carlos, 6627 - Campus da UFMG, Pampulha, Belo Horizonte, MG, Brazil.
*rorefice@demet.ufmg.br

Abstract - The presence of plastic waste has largely affected a series of ecosystems, including those associated with oceans, rivers and lakes, as it generates a large number of harmful consequences for the environment and other outcomes, such as the reduction of fauna biodiversity and alteration of the food chain, impairment of recreation, tourism and sports activities, in addition to damages to human health and to the development of dependent communities. In this work, strategies, technologies and materials developed by the research group will be presented with the general objective of reducing the environmental impact of plastic waste, for example, when present in oceans, rivers and lakes. In this context, results will be shown involving, among others: the incorporation of self-repair mechanisms and response to external stimuli to natural and biodegradable polymers; the manipulation of the interface of nanocomponents aiming to increase the recyclability of polymers; the insertion of nanocomponents in polymers and blends to enhance degradation and other properties; the use of natural polymers in advanced applications; the generation of superhydrophobic surfaces in natural polymers; the formulation of polymeric foams derived from natural resources useful in the purification of contaminated water.

References

1. Watt, E.; Picard, M.; Maldonado, B.; Abdelwahab, M. A.; Mielewski, D. F.; Drzal, L. T.; Misra, M.; Mohanty, A. K.: Ocean plastics: environmental implications and potential routes for mitigation–a perspective. *RSC advances*, 2021, 11(35), 21447-21462. http://doi.org/10.1039/D1RA00353D.
2. Jambeck, J. R.; Geyer, R., Wilcox, C.; Siegler, T. R.; Perryman, M.; Andrady, A.; Narayan, M.; Law, K. L: Plastic waste inputs from land into the ocean. *Science*, 2015, 347(6223), 768-771. http://doi.org/10.1126/science.1260352
3. Li, W. C.; Tse, H. F.; Fok, L.: Plastic waste in the marine environment: A review of sources, occurrence and effects. *Science of the Total Environment*, 2016, 566, 333-349. http://doi.org/10.1016/j.scitotenv.2016.05.084
4. Zheng, J.; Suh, S. Strategies to reduce the global carbon footprint of plastics. *Nature Climate Change*, 2019, 9(5), 374-378. https://doi.org/10.1038/s41558-019-0459-z

Fundings: CNPq

Keywords: *biopolymers, nanocomposites, ocean plastic waste*

ESTRATÉGIAS, TECNOLOGIAS E MATERIAIS PARA A REDUÇÃO DO IMPACTO AMBIENTAL DO LIXO PLÁSTICO OCEÂNICO

Rodrigo Lambert Oréfice*
Departamento de Engenharia Metalúrgica e de materiais, Universidade Federal de Minas Gerais (UFMG), Av. Antônio Carlos, 6627 - Campus da UFMG, Pampulha, Belo Horizonte, MG, Brasil.
*rorefice@demet.ufmg.br

Resumo - A presença do lixo plástico tem afetado amplamente uma série de ecossistemas, incluindo aqueles associados a oceanos, rios e lagoas, por gerar inúmeras consequências danosas ao meio ambiente e seus desdobramentos, como na redução da biodiversidade da fauna e alteração da cadeia alimentar, comprometimento de atividades de recreação, turismo e práticas esportivas, além de prejuízos à saúde humana e ao desenvolvimento das comunidades dependentes. Neste trabalho serão apresentados estratégias, tecnologias e materiais desenvolvidos pelo grupo de pesquisa com o objetivo geral de reduzir o impacto ambiental do lixo plástico, por exemplo, quando presente em oceanos, rios e lagoas. Neste contexto, serão mostrados resultados envolvendo, dentre outros: incorporação de mecanismos de autorreparo e resposta a estímulos externos a polímeros naturais e biodegradáveis; manipulação da interface de nanocomponentes visando aumento da reciclabilidade de polímeros; inserção de nanocomponentes em polímeros e blendas para acentuar degradação e outras propriedades; utilização de polímeros naturais em aplicações avançadas; geração de superfícies superhidrofóbicas em polímeros naturais; formulação de espumas poliméricas derivadas de fontes naturais úteis na purificação de águas contaminadas.

Referências

1. Watt, E.; Picard, M.; Maldonado, B.; Abdelwahab, M. A.; Mielewski, D. F.; Drzal, L. T.; Misra, M.; Mohanty, A. K.: Ocean plastics: environmental implications and potential routes for mitigation–a perspective. *RSC advances*, 2021, 11(35), 21447-21462. http://doi.org/10.1039/D1RA00353D.
2. Jambeck, J. R.; Geyer, R., Wilcox, C.; Siegler, T. R.; Perryman, M.; Andrady, A.; Narayan, M.; Law, K. L: Plastic waste inputs from land into the ocean. *Science*, 2015, 347(6223), 768-771. http://doi.org/10.1126/science.1260352
3. Li, W. C.; Tse, H. F.; Fok, L.: Plastic waste in the marine environment: A review of sources, occurrence and effects. *Science of the Total Environment*, 2016, 566, 333-349. http://doi.org/10.1016/j.scitotenv.2016.05.084
4. Zheng, J.; Suh, S. Strategies to reduce the global carbon footprint of plastics. *Nature Climate Change*, 2019, 9(5), 374-378. https://doi.org/10.1038/s41558-019-0459-z

Fundings: CNPq

Keywords: *biopolímeros, nanocompósitos, lixo plástico oceânico.*

WHEN NANOCELLULOSE MEETS MICROORGANISMS: TO KILL OR NOT TO KILL?

Caio G. Otoni[1]*, Bruno D. Mattos[2], Eduardo M. Daniél[3], Marco Beaumont[4], Orlando J. Rojas[5] and Watson Loh[6]

1 – Graduate Program in Materials Science and Engineering (PPGCEM) & Department of Materials Engineering (DEMa), Federal University of São Carlos (UFSCar), São Carlos, SP, Brazil – caio.otoni@ufscar.br
2 – Department of Bioproducts and Biosystems, Aalto University, Espoo, Finland
3 – Department of Physics, Federal University of São Carlos (UFSCar), São Carlos, SP, Brazil
4 – Institute of Chemistry of Renewable Resources, University of Natural Resources and Life Sciences (BOKU), Vienna, Austria
5 – BioProducts Institute (BPI), University of British Columbia (UBC), Vancouver, Canada
6 – Institute of Chemistry, University of Campinas (Unicamp), Campinas, SP, Brazil

Cellulose stands out for its potential as renewable resource for assembling robust materials finding use in numerous applications in the pursuit of the circular bioeconomy. Upon mechanical comminution of its native hierarchical, nanofibers (CNF) are obtained boasting unique properties arising from high aspect ratio and flexibility, while mirroring the mechanical strength, biodegradability, biocompatibility, and ability to undergo surface modification that are inherent to cellulose [1]. We herein aimed to harness these exceptional features of CNF as building blocks that enable unlocking novel avenues towards materials that interact in a tailored fashion with microbial cells. Specifically, the goals of this endeavor were to (A) inhibit spoilage/pathogenic microorganisms while (B) maintaining the viability of their technologically relevant counterparts by using CNF as materials-forming brick. We showcase these strategies by assembling (A) solid foams that inactivate *Escherichia coli* cells, taken as an undesirable bacterial model, and (B) supraparticles carrying live *Saccharomyces cerevisiae* cells, chosen as model yeast. To inactivate bacterial cells (A), CNF was surface-grafted with quaternary ammonium moieties either *via* sodium periodate oxidation into dialdehyde cellulose followed by treatment with Girard's reagent T [2] or covalent attachment of glycidyltrimethylammonium chloride (GTMAC) [3]. Surface charge density was varied from 0.07 to 0.34 mmol/g by different stoichiometries among the reagents. Freeze-cast cryogels removed *E. coli* cells from culture medium to different extents in a charge-dependent manner. On the other vein (B), uncharged CNF interlocked active *S. cerevisiae* cells into *quasi*-spherical supraparticles drop-cast onto a superhydrophobic PTFE substrate. The porous assembly allowed access to the nutrients required for fermentation and CO_2 production. In summary, CNF was demonstrated to interact differently with microbials cells depending on the surface chemistry: while the former strategy (A) is promising for biocidal surfaces, the latter (B) is applicable for maintaining cell viability in microswimmers. These systems are being continuously optimized towards actual practical application.

References

1. B.L. Tardy *et al. Chemical Reviews* 2021, *121*, 14088–14188. doi.org/10.1021/acs.chemrev.0c01333
2. C.G. Otoni *et al. ACS Applied Bio Materials* 2019, *2*, 1975–1986. doi.org/10.1021/acsabm.9b00034
3. C.E.P. Silva *et al. Journal of Colloid and Interface Science* 2020, *574*, 207-216. doi.org/10.1016/j.jcis.2020.04.001

Funding: São Paulo Research Foundation (FAPESP; grants no. 2017/07013-1 and 2022/08780-4).

Keywords: *cellulose nanofibers, antimicrobial surfaces, supraparticles, yeasts, microswimmers*.

==

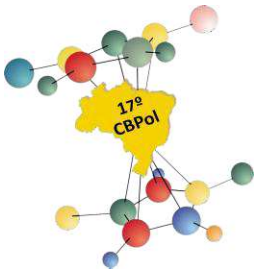

ASPECTS OF HIGLY MICROPLASTIC CONTAMINATION IN THE ATLANTIC FOREST ESTUARY

Duclerc F. Parra [1], Giovana Gimiliani[1], Jacinete L. dos Santos [1], Marycel E. B. Cotrim [1]
1 – Nuclear and Energy Research Institute, Sao Paulo, Brazil
dfparra@ipen.br

The Atlantic Forest is one of the richest regions in terms of biodiversity in the world. Originally the biome covered about 15% of the national territory. Currently, only about 12.4% (SOS MATA ATLÂNTICA, 2021) of well-preserved forest remnants remain in the country [1]. Regarding mangrove areas, in the state of São Paulo there are about 223 km², according to the Atlas of mangroves in Brazil, with about 120.5 km² of this total in Baixada Santista. Analyzes of sediments collected at Santos estuarine mangroves, in various points show a high concentration of microplastics generated from industrial processes or even anthropogenic activity. These solid particles based on (< 5 mm) are today one of the main environmental problems. The microplastics present in the sediment samples were quantified after drying and sieving amount limited of sediment. FTIR and micro-Raman spectroscopy identified filaments and fragments of microplastics (MPs) as commom polymer spectra. Also additives and herbicides were present in some MPs. All polymeric types identified (<5mm) have wide applications and demands by packaging, civil construction, automotive, electrical and electronics, and textile sectors.

Keywords : *microplastic, sediment, Santos estuary, micro-Raman, polymer*
Fundings: CAPES, FAPESP

Introduction

The SESS is located in the Santos basin in a sedimentary area that extends over approximately 352 thousand km², covering the northern portion of the coast of the state of Santa Catarina, the southern portion of the state of Rio de Janeiro, and the entire coast of Paraná and São Paulo [2]. In addition to the characteristic and dynamic conditions of the estuary, settlements of irregular dwellings lacking a basic sanitation system are present in that coastal region.

Nowadays the estuaries of the world are considered important for filtering microplastics from the coastal water avoiding the ocean integration of contamination.

In addition to the presence of the Port of Santos and the Petrochemical Complex of Cubatão, the estuarine channels and rivers of the SSES are directly influenced by the tidal regime, in addition to harboring an important mangrove ecosystem, considered a permanent preservation area strongly impacted by human activities. Irregular occupation [3] and the presence of sanitary landfills and municipal dumps weaken the environment [4-6]. Considering that one branch of Billings, the cleanest and least contaminated, goes to Santos. There is no way that the pollution comes from reservoirs of the plateau to the estuary of the SEES. However, hydrodynamic dispersion associated with high and low tides may well explain this high contamination of the Santos-São Vicente estuary

other the anthropogenic influence in the local of high population density, in the interior of the estuary.
The present study of microplastic contamination in the Santos estuary is focused on a detailed investigation given its importance for the conservation of human health and local biota.

Experimental

The sediment mangrove samples were collected in Van Veendrag at total of 8kg in each site. The total of eleven sites were collected and This procedure involves sediment collection, drying, sieving (2.0, 1.0, 0.5 and 0.25 mm mesh sizes), and examination of the samples retained in each sieve. The results of particles per gram of sediment was considered as the microplastic abundance. This method by Gimiliani et al.(2020) described at http ://dx.doi.org/10.1016/j.cscee.2020.100020 estimates the total microplastic abundance and distribution [6].

Results and Discussion

The Fig 1 shows the site of collected samples. The area of higher density of microplastic was the Rio dos Bugres were the abundancy of microplastics varied from 43000-93000 particles per kg of sediment.

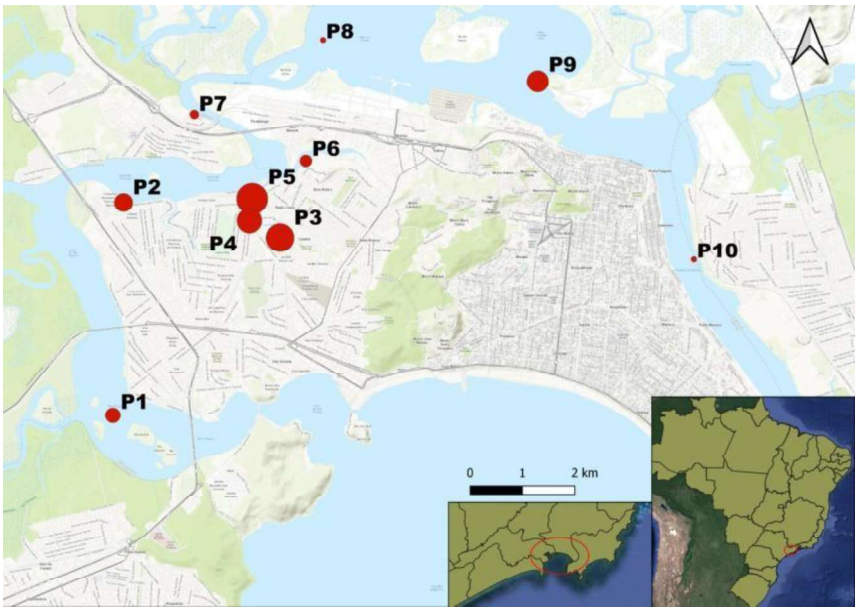

Figure 1- Illustration of microplastics abundancy in the estuary of Santos**.**

The higher density of microplastics, Fig 1, is shown in the Rio dos Bugres where the community of Duque grows. But it was clear that not only the anthropogenic effects defined the environmental pollution of that local. The transportation of microplastics depends greatly of the hydrodynamic of the estuary [8].
In terms of morphology of the particles, the abundancy of fragments and fibers or lines, as observed by microscopy, is represented in Fig 2.

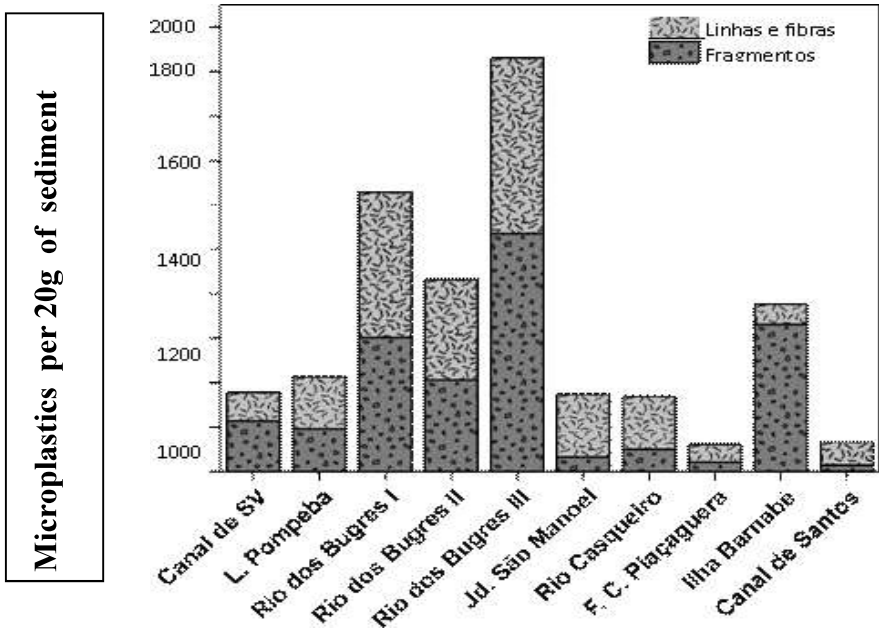

Figure 2- Ocorrence of fragments, and fibers/ lines per 20g of sediments for each site investigated.

Conclusions

This study verified the ubiquity of microplastics in the matrices evaluated and found microplastics to be present at levels that create potential risks for humans and the environment. The data on the composition, characteristics, and distribution ofmicroplastics presented herein may be used in future research or environmental monitoring and food safety assessment programs.

Acknowledgements

The authors thank to CNEN for project support and grants Edital 6: n° and for IPEN/CLA for micro-Raman analysis.

References

1. **SOS MATA ATLÂNTICA, 2021. https://www.sosma.org.br/conheca/mata-atlantica/. Acesso em: 10/03/2023.**
2. **M. A. Viana ; V. de O. Marum. *Cadernos Metrópole*, 2020. 22(48), 617–644.https://doi.org/10.1590/2236-9996.2020-4813.**
3. **F. A Moschetto; R. B. Ribeiro; D. M. de Freitas. *Ocean & Coastal Manag.* 2021, 200, 105418. https://doi.org/10.1016/j.ocecoaman.2020.105418**
4. **D. M. S. Abessa; E. C. P. M. Souza; B. R. F. Rachid; L. P. Zaroni . *Integrative ecotoxicological assessment of a complex tropical estuarine system*. In: HOFFER (ed.), Marine Pollution: New Research, Nova Science Publishers Inc., New York, p. 125-159, 2008.**
5. **CETESB2019. https://cetesb.sp.gov.br/aguas-interiores/wp-content/uploads/sites/12/2013/11/Ap%C3%AAndice-O-Perfis-Sedimentares.pdf**
6. **G. T. Gimiliani; G . Fornari; M. M. Redígolo; J. O. W. V. Bustillos; D. M. S Abessa; M. A. F. Pires. *Case Studies in Chemical and Environmental Engineering* 2020, 2, http://dx.doi.org/10.1016/j.cscee.2020.100020.**
7. **A. Turra; A. B. Manzano; R. J. S. Dias; M. M. Mahiques; L. Barbosa; D. Balthazar-Silva; F. T. Moreira. Three-dimensional distribution of plastic pellets in sandy beaches: shifting paradigms. *Scientific Reports* 2014, 4, 4435. http://doi.org/10.1038/srep04435.**

DEVELOPMENT OF POLYLACTIC ACID MEMBRANE BY PHASE INVERSION ROUTE WITH HIGH POROSITY AND HYDROPHOBICITY

Alessandro R. Paulazzi[1], Angelo O. Silva [1], Cintia Marangoni[1] *

1 – Federal University of Santa Catarina (UFSC) Technological Center (CTC), Post-graduation Program in Chemical Engineering (PósENQ), Florianópolis, SC, Brazil
cintia.marangoni@ufsc.br

Abstract - In this work, it has been developed polylactic acid (PLA) membranes using the phase inversion route (NIPS) with polyethylene glycol (PEG) as a pore-forming agent. The membranes were characterized in terms of thickness, contact angle, swelling degree, and porosity of the formed films. The membranes exhibited asymmetric formation, with an average thickness ranging from 0.20±0.02 to 0.24±0.02 mm. The contact angle test indicated hydrophilicity on the upper part and hydrophobicity on the lower part, attributed to the increased PEG concentration and membrane roughness. The average porosity increased with the pore-forming agent, reaching 86.46±0.63% for the M3 membrane, which showed a higher swelling degree (97.73%) after 48 hours. These membranes have the potential for applications in processes requiring hydrophobic porous membranes, such as membrane distillation.
Keywords: *Polylactic acid, Membrane, Biopolymer, Swelling degree*
Fundings: CNPq; CAPES

Introduction

Lactic acid has recently become a commercially interesting compound, mainly due to its use as a monomer to produce polylactic acid (PLA), a biocompatible and biodegradable biopolymer. Lactic acid is obtained from renewable sources, such as sugar or starch, through the biorefining process [1]. PLA has various potential applications and can be adapted into different resin grades and processed into a variety of products. The denomination term "polylactic acid" refers to a variety of polymers made from lactic acid, including poly-D-lactic acid (PDLA), poly-L-lactic acid (PLLA), and poly-D, L-lactic acid (PDLLA attracting attention as a sustainable key polymer, along with other notable characteristics such as gas barrier properties, elasticity, biocompatibility, thermoplasticity, UV barrier, hydrophobicity, stiffness, and high mechanical strength. All of these properties promote PLA application in membrane manufacturing [1], [2].

Due to their good thermal and mechanical stability, appropriate flexibility, and high permeability, biodegradable materials like PLA are highly useful for membrane manufacturing. Using PLA as membrane precursor in substitute for non-degradable traditional polymer is a step towards protecting the environment [3].

The miscibility of PLA in different nonpolar organic solvents holds great potential for membrane preparation, likewise as through the non-solvent-induced phase separation (NIPS) method. In this process, a controlled separation occurs in which the polymer solution is transformed from the liquid phase to the solid phase [4].

However, PLA membranes were found to be weakly hydrophobic and prone to fouling [5], [6]. This characteristic can be a disadvantage for their use in some membrane separation processes, such as

reverse osmosis and microfiltration. However, it opens up possibilities for application in other membrane-related fields, such as membrane distillation and pervaporation. Therefore, in this work, the formation of a PLA membrane with different concentrations of the pore-forming agent polyethylene glycol (PEG) using the NIPS method was studied to obtain hydrophobic PLA membranes and evaluate their influence according to the pore-forming agent added.

Experimental

Materials

The membrane synthesis used polylactic acid (PLA) (Sigma-aldrich) as the polymer, polyethylene glycol 400 (PEG) (Synth, P.A.) was used as the pore-forming agent, and dimethylformamide (DMF) (Anidrol, N,N P.A. ACS, 99.8% purity) was used as the solvent for the solution. Distilled water was used as the non-solvent and for contact angle evaluation end swelling degree. Absolute ethanol (Anidrol, P.A. 99.5% purity) was used in the porosity test.

Membrane synthesis

The membrane solution was prepared by adding 15% (w/w) of PLA at varying concentrations of 0, 1, 2.5, and 5% (w/w) of PEG to the DMF solvent, resulting in solutions named M0, M1, M2, and M3, respectively. The solution was gently heated (60 °C) and stirred for 4 h to ensure complete dissolution of the polymer in the solvent. After this period, the solutions were sonicated to a 30 min ultrasonic bath. The solution was spread using a glass rod on a rectangular glass plate measuring 15.0 cm x 25.0 cm, with the edges sealed with 0.36 mm thick insulating tape. Immediately after spreading, the glass plate with the solution was submerged in a coagulation bath of deionized water at room temperature. After 24 h, the plate with the membrane was removed from the coagulation bath and covered with another glass plate to prevent deformation during drying. After more 24 h, the top glass plate was removed to allow excess moisture to leave the membrane. The drying process occurred naturally at ambient conditions (20 °C).

Membrane characterizations

The thickness of the formed membranes was determined by taking ten random measurements using a digital caliper (MTX 316119). The hydrophobicity of the membranes was evaluated by measuring the contact angle, where triplicate measurements were performed using a Goniometer (Ramé-Hart, 250) in conjunction with DROPimage imaging software. The measurements were conducted using distilled water, and the volume of the droplet used for each measurement was 5 µL.

To determine the porosity (ε), square samples of the membranes measuring 1.0 cm x 1.0 cm were dried in an oven at 60 °C until their mass no longer varied significantly. The dried samples were then placed in a desiccator and weighed. The samples were submerged in 99.5% absolute ethanol for 24 h to allow the ethanol to occupy the pore volume. The wet samples were then weighed. The procedure was performed in triplicate, and the results were calculated using Eq. 1, where m_u is the mass of the wet sample in kg, m_s is the mass of the dry sample in kg, ρ_e is the density of the ethanol used in $kg.m^{-3}$ ($789\ kg.m^{-3}$), and ρ_m is the density of the dry sample in $kg.m^{-3}$. In the case of PLA membranes, ρ^m is the density of the polymer itself ($1240\ kg.m^{-3}$).

$$\varepsilon = \frac{\frac{mu-ms}{\rho e}}{\frac{mu-ms}{\rho e+\frac{ms}{\rho m}}} \quad (1)$$

The swelling index (SI) of the membrane in water was determined in samples of the membranes (1 x 1 mm) on immersion in distilled water. The wet weight (m_u) was measured after removing excess water from the surface of the membrane using absorbent material. The weight of the dry membrane

(Ps) was determined after drying in a vacuum oven at 60°C for 24 h. The degree of swelling was calculated according to Eq. 2, where m_u is the mass of the wet sample in kg, and m_s is the mass of the dry sample in kg.

$$Si = \frac{mu - ms}{ms} \; x \; 100 \qquad (2)$$

Results and Discussion

PLA membrane

By producing different membranes, it was possible to evaluate the morphological differences in the different faces of the formed membranes. The M0, M1, M2, and M3 membranes exhibited distinct characteristics between the upper and lower faces, indicating asymmetry in the pore structure of the membranes due to the tendencies of the NIPS methodology. Fig. 1. shows an image of the PLA membrane (M3) formed using the phase inversion (NIPS) methodology.

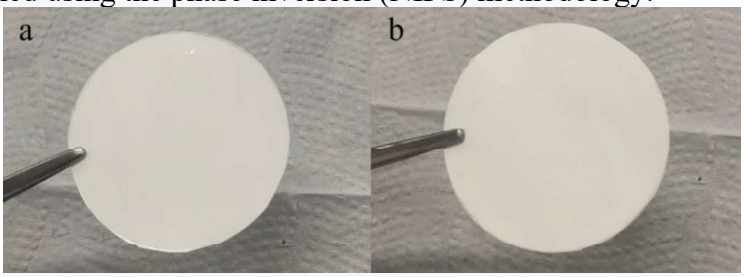

Figure 1- PLA membrane (M3) formed by the NIPS methodology. (a) Top surface; (b) Bottom surface.

This occurrence of different surfaces is due to the intrinsic NIPS process. The coagulation of PLA occurs when the polymer solution film is immersed in the water bath. During this process, the polymer solvent, DMF, is gradually removed, causing the gelation of PLA. Then, the top surface of the membrane is in direct contact with water, while the bottom surface is in contact with the glass plate, which can result in a difference in the speed at which the coagulation phenomenon occurs, with the top surface coagulating faster than the bottom surface. Tawil et al. (2018) observed this same tendency when using the NIPS methodology for PLA membrane production. The average thickness of the obtained membranes was 0.20 ± 0.02 mm, 0.22 ± 0.024 mm, 0.22 ± 0.01 mm, and 0.24 ± 0.02 mm for the M0, M1, M2, and M3 membranes, respectively [7].

Hydrophobicity

The hydrophobicity of the membranes is shown in Fig. 2. It is worth noting that all PEG containing membrane exhibits hydrophobicity on the bottom surface, which supports the indication of structural asymmetry in the PLA membrane formed by the NIPS methodology. The membrane M3 presents the most distinct hydrophobicity.

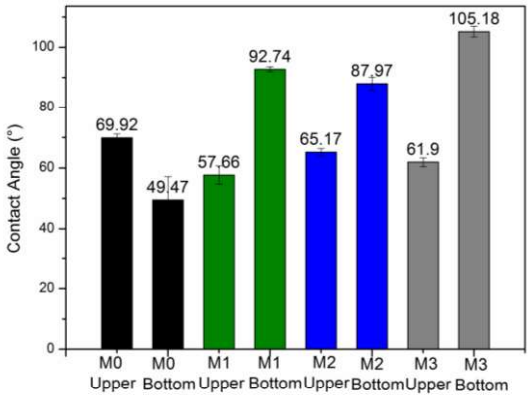

Figure 2- Results of contact angle tests on the top and bottom surfaces of the M0, M1, M2, and M3 membranes.

Nigiz et al. (2023) observed in the contact angle of PLA membranes was 99° [8]. On the other hand, Shokri et al. (2022) obtained a contact angle of 85° with pure PLA membranes [9]. The results in the literature demonstrate the intrinsic hydrophobic nature of PLA, and there is a tendency for an increase in membrane hydrophobicity with an increase in PEG concentration, which may be related to a possible increase in membrane porosity and roughness.

Porosity and swelling degree

The obtained results demonstrate that the membranes have high total porosity. The M3 membrane, with the highest PEG concentration (5%), reached the highest porosity of 86.46 ± 0.81 %, which represented a 7% increase compared to the M0 membrane. The M0, M1, and M2 membranes had total porosities of 79.44 ± 0.15 %, 80.94 ± 0.27 %, and 76.21 ± 0.74 %, respectively. When compared to the literature, it can be observed that the results are consistent with the formation of PLA membranes using the NIPS methodology. Table 1 provides a comparison of porosity with different authors.

Table 1- Comparison of porosities obtained by the author and reported in the literature.

Porosity (%)	Reference
86,50 ±0,87	M3
81,40	(LIU et al., 2022) [10]
78,00	(SHOKRI et al., 2022) [9]

The results also demonstrate that the use of PEG as a pore-forming agent has contributed to an increase in the porosity of PLA membranes using the NIPS methodology. The swelling degree profile of the membranes was evaluated until 48 h and is shown in Fig. 3.

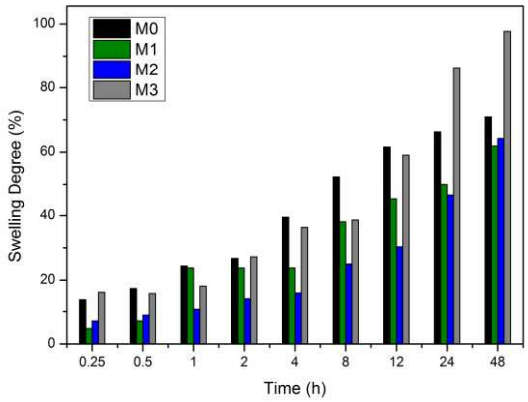

Figure 3- Swelling profile of membranes M0, M1, M2 and M3 during 48h.

The results demonstrate that the membrane increased porosity of the M3 membrane caused the membrane to swell a greater amount of water at the end of 48 h, a greater increase than that evaluated in the other membranes. The M0 membrane initially had greater water retention, which may be related to its hydrophobicity, superior to the other membranes on both sides.

Conclusion

In this study, PLA membranes were developed using polyethylene glycol as a porogen agent through the phase inversion method known as NIPS. Visual analysis revealed that the formed structures tended to exhibit asymmetry in pore size distribution between the different faces of the membrane. The M3 membrane, with a higher concentration of PEG during formation, exhibited distinct hydrophobicity between its faces, which supported the hypothesis of membrane asymmetry. The

membranes demonstrated high porosity, and the use of PEG facilitated increased porosity. Based on all the presented results, it can be concluded that the developed membrane has great potential for use in various membrane separation processes, such as pervaporation.

Acknowledgements
The authors are grateful to the Conselho Nacional de Desenvolvimento Científico e Tecnológico (CNPq, Brazil) and Coordenação de Aperfeiçoamento de Pessoal de Nível Superior (CAPES, Brazil) for financial support. Also, the authors are grateful to the Central Analysis of the Chemical Engineering Department at Federal University of Santa Catarina for the membrane characterization results.

References
1. T.A. Swetha; V. Ananthi; A. Bora; N. Sengottuvelan; K. Ponnuchamy; G. Muthusamy. International Journal of Biological Macromolecules, 2023, 234, 123703. https://doi.org/10.1016/j.ijbiomac.2023.123703
2. A. Mehmood; N. Raina; V. Phakeenuya; B. Wonganu; K. Cheenkachorn. Materials Today: Proceedings, 2023, 72, 3049–3055. https://doi.org/10.1016/j.matpr.2022.08.387
3. V. Vatanpour; A. Dehqan; S. Paziresh; S. Zinadini; A.A. Zinatizadeh; I. Koyuncu. Separation and Purification Technology, 2022, 296, 121433. https://doi.org/10.1016/j.seppur.2022.121433
4. N. More; M. Avhad; S. Utekar; A. More. Polymer Bulletin, 2022, 80, 1117–1153. https://doi.org/10.1007/s00289-022-04135-z
5 A. Moriya; P. Shen; Y. Ohmukai; T. Maruyama; H. Matsuyama. Journal of Membrane Science, 2012, 415–416, 712–717. https://doi.org/10.1016/j.memsci.2012.05.059
6. Z. Xiong; Y. Zhong; H. Lin; F. Liu; T. Li; J. Li. Journal of Membrane Science, 2017, 533, 103–111. https://doi.org/10.1016/j.memsci.2017.03.028
7. E. Al Tawil; A. Monnier; Q.T. Nguyen; B. Deschrevel. European Polymer Journal, 2018, 105, 370-388. https://doi.org/10.1016/j.eurpolymj.2018.06.012
8. F.U. Nigiz; B. Karakoca. Applied Clay Science, 2023231, 106721. https://doi.org/10.1016/j.clay.2022.106721
9. E. Shokri; B. Khanghahi; E. Esmizadeh; H. Etemadi. International Journal of Environmental Science and Technology, 2022, 19, 4167–4180. https://doi.org/10.1007/s13762-021-03592-9
10. F. Liu; B. Li; D. Sun; F. Li; X. Pei. Korean Journal of Chemical Engineering, 2022, 39, 1307–1315. https://doi.org/10.1007/s11814-021-0992-0

EVALUATION OF THE BACTERIAL CELLULOSE DEGRADATION OF MEMBRANES IN NATURAL ATMOSPHERE OF THE SERTÃO REGION

Amanda C. O. Diniz[1]*, José F. Q. Pereira[2], Jackson R. S. Silva[2], Gabriel B. L. Vitorino[2], Andréa M. S. S. Brito[2] and Glória M. Vinhas[3]

1 – Post Graduation Program in Materials Sciences (PGMTR), Federal University of Pernambuco (UFPE), Recife, PE, Brazil
amanda.odiniz@ufpe.br
2 – Rural Federal University of Pernambuco in the Academic Unit of Serra Talhada (UFRPE/UAST), Serra Talhada, PE, Brazil
3 – Department of Chemical Engineering, Federal University of Pernambuco (UFPE), Recife, PE, Brazil

Abstract - To reduce the pollution caused by conventional plastics, several new polymers using biodegradable raw materials have been proposed. Among them, bacterial cellulose (BC) biopolymer has been suggested for several applications. In this context, the objective of this work was to evaluate the atmospheric degradation of dry BC from the genus K. hansenii, produced in 2 media (an alternative medium without addition of free carbohydrate, non-fermentable glucose (P100) and the standard medium, Hestrin-Schramm (HS)). The samples evaluated are biodegradable, biocompatible and non-toxic. 7 HS and 14 P100 samples were exposed along 75 days to atmospheric conditions in Serra Talhada/PE. They were evaluated for mass loss, thickness, and physical/visual inspection over time. All samples were susceptible to environmental attack, and the HS membranes were more noticeable due to changes in coloration, higher percentage of mass loss and decreased thickness compared P100, thus P100 showed greater resistance.

Keywords: *Biodegradable, biopolymer, atmospheric degradation*

Introduction

Petrochemical polymers often have prolonged degradation cycles, which makes their waste a serious environmental problem. In this sense, there is a need to employ biopolymers, which stand out for being environmentally friendly, sustainable, and presenting physical-chemical properties compatible with fossil sources, but with the additional advantage of being biodegradable [1].
Cellulose $(C_6H_{10}O_5)_n$ is a linear syndiotactic homopolymer consisting of D-anhydroglucopyranose units linked by β-1,4 glycosidic bonds, with repeated units (glucose dimer or cellobiose). This macromolecule is found in plants, but can also be produced by microorganisms, such as bacteria, an exemplary genus being *Komagataeibacter hansenii*. Although the chemical composition of bacterial cellulose (BC) is identical to that of plant cellulose, its properties are superior due to the nanometric dimensions of its fibers, high purity (absence of hemicellulose, lignin, and pectin residues), biocompatibility, biodegradability, and non-toxicity. These characteristics confer advantages to BC regarding to mechanical strength and enable its wide application in industry [2-3]. Due to the chemical nature of bacterial cellulose (BC), the degradation process is irreversible, since changes occur in the chemical and physical structure of the material, affecting properties such as integrity, molecular weight, structure, mechanical strength, and fragmentation [4]. Degradation can be caused by abiotic factors such as sun, heat, and humidity, known as atmospheric degradation or natural weathering, and biotic factors such as bacteria, fungi, and algae [5].

Feel studies about atmospheric degradation of BC were reported, and they have shown that the deterioration of cellulose in animal and human tissues is a slow process due to the absence of the hydrolysis reaction that attacks the β-1,4 linkage. Therefore, although having a degradable material that can be used on an industrial scale, it is necessary to optimize and synchronize the degradation time and understand the influence on mechanical properties under different climatic conditions, to make it a viable commercial product [6].
Another relevant factor to be considered is the culture medium used for industrial scale production, since around 30% of costs are directed only to the fermentation medium, limiting the participation of bacterial cellulose (BC) in the market. This is because some standard media for BC production, such as the Hestrin-Schramm (HS) medium, have a high cost. Therefore, it is essential to develop new low-cost media, rich in nutrient sources, for BC production, to ensure its application in various fields [7-8].
Thus, in this study, bacterial cellulose membranes enriched with an alternative medium lacking fermentable carbohydrates (referred to in this study as P100) and Hestrin-Schramm (HS) membranes were used to evaluate the behavior of these materials under abiotic factors (exposure to the atmosphere of the Sertão do Pajeú) through the percentage of mass loss and physical/visual inspection.

Experimental

Materials

The *Komagataeibacter hansenii* bacterium deposited in the culture bank of the microbiology laboratory at UFPE was used as a BC producer for the preparation of culture media and inoculum. For the inoculum preparation, the saline medium [9] was used, and for the HS standard medium, the composition described by [10] and adapted by [11] was used. For the alternative P100 medium, non-fermentable carbohydrates were used.

Production of bacterial cellulose membranes

The inoculum was prepared using 200 mL of saline solution plus 2 mL of P.A. ethyl alcohol and three loops of Komagataeibacter hansenii bacteria in static culture. The inoculum was incubated for 72 hours. After this period, 5 mL of the inoculum was transferred to 50 mL culture media containing P100 (100% w/v) and the standard HS medium at the same concentration, with the addition of 0.5 mL of P.A. ethyl alcohol. The bacterial cellulose membranes were produced in situ under static conditions for 15 days at 28°C ± 2°C. After the fermentation period, the membranes were washed with distilled water and then submerged in distilled water in Erlenmeyer flasks and sterilized in an autoclave at 120ºC, 1 atm for 15 min. After cooling to room temperature, the membranes were dried in a freezer at -2°C until a constant weight was achieved by removing the water. Subsequently, they were exposed to the study of atmospheric degradation.

Atmospheric degradation and physical and visual inspection

The present study was conducted in the municipality of Serra Talhada - PE (altitude 429 m, latitude 07°59'7" South and longitude 38°17'34" West) with natural atmospheric exposure of the region. Seven samples of the standard HS medium and 14 samples of the P100 medium were used, with dimensions of (4.0 cm x 1.0 cm). They were then placed in a device with holes to avoid water accumulation and fastened to the surface with a copper wire to prevent them from being lost due to wind action. The samples were analyzed for mass, thickness (measured with a Mitutoyo micrometer), and visual aspect (color and flexibility) before exposure (day 0) and at intervals of 7, 15, 30, 45, 60, and 75 days. For each removal of a standard HS membrane, two P100 samples were

removed for comparative test. During the degradation study, meteorological data, such as temperature, rainfall, and relative humidity, were collected and recorded from the database of the National Institute of Meteorology portal [12].

Calculation of mass loss

The percent mass loss R (%) was calculated for the days (0, 7, 15, 30, 45, 60 and 75) according to Eq. 1, where Mo is the initial mass and Mt is the final mass [13].

$$R(\%) = \frac{Mo - Mt}{Mo}.100 \quad (1)$$

Results and Discussion

Fig. 1 illustrates the percent mass loss profile of the dried samples during monitoring of the HS and P100 membranes.

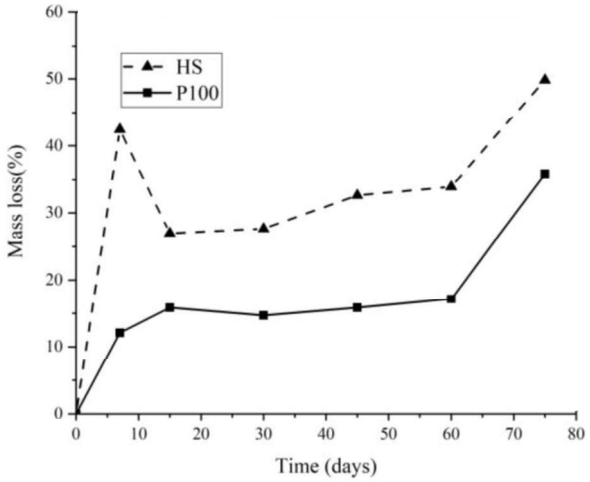

Figure 1 - Percent mass loss of HS and P100 membranes.

The results obtained for the thickness (mm) and visual appearance parameters of the bacterial cellulose membranes from HS and P100 media are presented in Table 1 for the samples analyzed at 0, 7, 15, 30, 45, 60, and 75 days.

Table 1 - Parameters for thickness and visual aspect.

Membranes	Thickness (mm)	Visual aspect
HS_1 - 0	$0.018 \pm 6x10^{-4}$	Porous and flexible orange color
$P100_{1.2}$ - 0	$0.011 \pm 6x10^{-4}$	Porous and flexible white color
HS_2 - 7	$0.010 \pm 6x10^{-4}$	Porous and rigid white color
$P100_{3.4}$ - 7	$0.010 \pm 6x10^{-4}$	Porous and rigid white color
HS_3 - 15	$0.009 \pm 6x10^{-4}$	Porous and rigid white color
$P100_{5.6}$ - 15	$0.010 \pm 6x10^{-4}$	Porous and rigid white color
HS_4 - 30	$0.010 \pm 6x10^{-4}$	Porous and rigid white color
$P100_{7.8}$ - 30	$0.010 \pm 6x10^{-4}$	Porous and rigid white color
HS_5 - 45	$0.009 \pm 6x10^{-4}$	Porous and rigid white color
$P100_{9.10}$ - 45	$0.010 \pm 6x10^{-4}$	Porous and rigid white color
HS_6 - 60	$0.010 \pm 6x10^{-4}$	Porous and rigid white color
$P100_{11.12}$ - 60	$0.007 \pm 6x10^{-4}$	Porous and rigid white color
HS_7 - 75	$0.008 \pm 6x10^{-4}$	Porous and rigid white color
$P100_{13.14}$ - 75	$0.008 \pm 6x10^{-4}$	Porous and rigid white color

*Mean ± Standard deviation. For each removal of a standard HS sample, two P100 samples were removed.

In the highlighted Fig. 2, one can observe the color change (orange - white) of the HS membranes after 7 days of exposure to the abiotic factors.

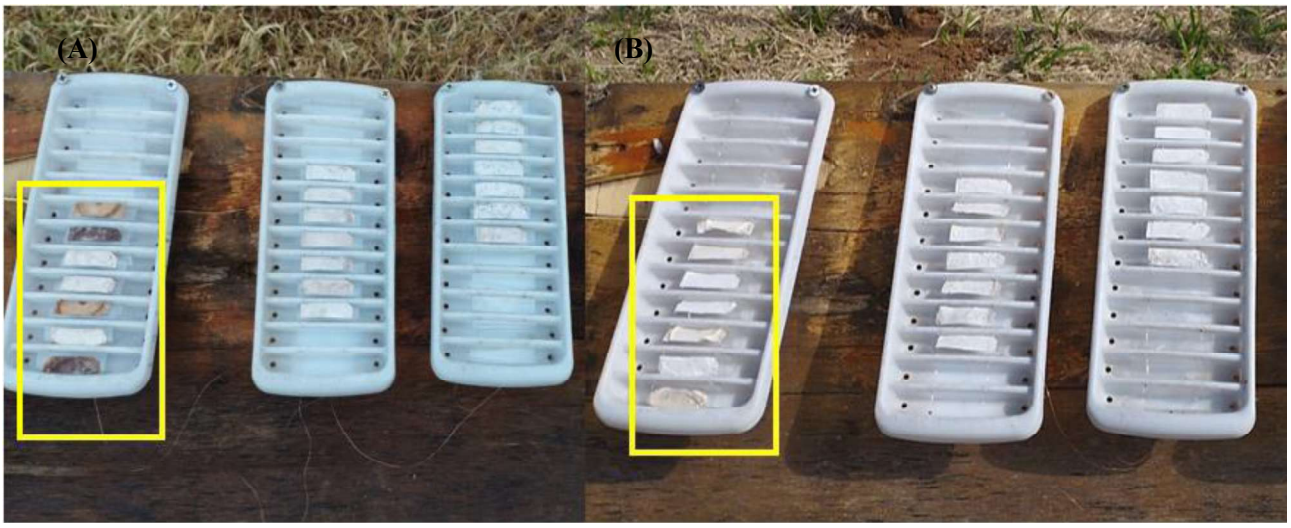

Figure 2 - (A): before exposure to abiotic factors and **(B):** after 7 days of exposure.

Analyzing Fig. 1 and Table 1, it can be understood that the highest peaks of percentage loss correspond to rainy days in the region at 7 and 75 days, with a rainfall index of 23.3 mm and 29.2 mm, respectively [14]. Additionally, membranes from the alternative P100 medium showed a tendency of lower percentage mass loss between days 7 to 75 when compared to HS samples, indicating that the material is more resistant to adverse conditions with exposure periods. This is consistent with the study conducted by Camargo (2020) [1], who used BC in its wet aspect in the HS medium under natural weathering conditions and observed significant mass loss at 75 days. During the exposure period, the temperature and average humidity of the environment were 27°C and 54.8%, respectively [12].

Conclusions

During the experiment, it was observed that the membranes from the alternative medium P100 had a lower tendency towards percentage of mass loss, did not change in coloration, and presented greater resistance, manually evaluated, compared to the membranes from medium HS. This suggests that P100 medium may have broad applications in industry, as it is a low-cost medium. Additionally, the BC from the HS medium underwent a change in its physical and visual appearance after 7 days of exposure to abiotic factors, changing color from orange to white, decreasing in thickness, and becoming rigid. However, to more detailed analysis, it is necessary to continue the study to identify the resistance time of each type of membrane to atmospheric conditions.

Acknowledgements

Laboratory of Microbiology (UFPE/DEQ), Chemical Analysis Group GAQ/UFRPE-UAST, National Council for Scientific and Technological Development (CNPQ) for the doctoral scholarship, Advanced Analytical Chemistry Center of Pernambuco (NUQAAPE/FACEPE/PRONEX - APQ-0346-1.06/14), PhD. Adriano do Nascimento Simões (UFRPE/UAST), PhD. Ivo Diego de Lima Silva (UFPE) for the support.

References

1. M. S. A. Camargo; A. P. Cercal; V. F. Silveira; K. C. B. Mancinelli; R. M. M. Gern; M. C. F. Garcia; G. P. Apati; A. L. dos Santos; A. P. T. Pezzin. Macromol Symp 2020, 394, 2000149. https://doi.org/10.1002/masy.202000149.

2. H. Shaghaleh; X. Xu; S. Wang. RSC Adv 2018, 8, 825-842. Doi: 10.1039/C7RA11157F.

3. M. Ghozali; Y. Meliana; M. Chalid. Materials Today: Proceedings 2021, 44, 2131-2134. https://doi.org/10.1016/j.matpr.2020.12.274.

4. S. Torgbo; P. Sukyai. Polymer Degradation and Stability 2020, 179, 109232. https://doi.org/10.1016/j.polymdegradstab.2020.109232.

5. L. H. I. Mei; P. D. S. C. Mariani. *Overview of environmentally degradable polymers or plastics (PADs)*, G. Flamboyant, Ed.; Campinas, 2005; Vol. 1, 41.

6. G. Helenius; H. Bäckdahl; A. Bodin; U. Nannmark; P. Gatenholm; B. Risberg. Journal of Biomedical Materials Research Part A 2005, 76, 431-438. https://doi.org/10.1002/jbm.a.30570.

7. M. Güzel; Ö. Akpinar. Int. J. Biol. Macromol. 2020, 162, 1597–1604. https://doi.org/10.1016/j.ijbiomac.2020.08.049.

8. H. Khan; V. Saroha; S. Raghuvanshi; A. K. Bharti; D. Dutt. Carbohydrate Polymers 2021, 260, 117807. https://doi.org/10.1016/j.carbpol.2021.117807.

9. K. C. Souza, et al. Patent BR 102014027203-8 A2, 2020.

10. B. S. Hungund; S. G. Gupta. Journal of Microbial & Biochemical Technology 2010, 2, 127-133. doi:10.4172/1948-5948.1000037.

11. F. P. Gomes; N. H. C. S. Silva; E. Trovatti; L. S. Serafim; M. F. Duarte; Armando J. D. Silvestre; C. P. Neto; C. S. R. Freire. Biomass and Bioenergy 2013, 55, 205-211. https://doi.org/10.1016/j.biombioe.2013.02.004.

12. National Institute of Meteorology of Brazil – INMET. Climatological Norms (1961/1990). Brasília - DF, 1992. Station A349.

13. P. K. Roy; S. Tito; P. Surekha; E. Tulsi; C. Deshmukh; C. Rajagopal. Polymer Degradation and Stability 2008, 93, 1917-1922. https://doi.org/10.1016/j.polymdegradstab.2008.07.016.

14. Agronomic Institute of Pernambuco (IPA). Index Session Pluviometric. Serra Talhada, 2022.

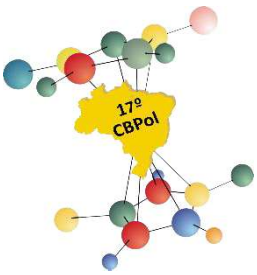

MECHANICAL BEHAVIOR OF CASSAVA STARCH BIOFILMS WITH WINE INDUSTRY BY-PRODUCTS PARTICLES.

Bruna P. Zanfonato[1]*, Nicole M. da Costa[1], Rafael S. K. Zacarão[1], Andréia Z. Dinon[1], Marcia B. Schuster[1]

1 – Department of Food Science and Technology, Santa Catarina State University (UDESC), Pinhalzinho, SC, Brazil.
**brunazanfonato159@gmail.com*

Abstract - The demand for environmentally friendly alternatives to polymeric materials, associated by the substantial waste produced by the wine industry, making active biodegradable films an enable area of study. This work aims to produce and characterize cassava starch biofilms with varying percentages of grape waste flour (0, 0.5, 2, and 4 wt.%) and 20 wt.% glycerol. The film structure was evaluated by transmission optical microscopy and the mechanical properties by tensile test. The films were produced by casting method with ultrasonic treatment. A uniform structure indicated good flour incorporation into the cassava starch. The addition of flour caused a significant decrease in tensile strength of the films containing 2 or 4% of flour, compared to the pure film. However, the total deformation is maintained. Density and thickness values gradually increased with the amount of flour added to the films. Thus, it is verified that the biofilms analyzed are promising for the packaging industry.

Keywords: *Biofilms; wine industry; casting method; microscopy; tensile test.*

Fundings: FAPESC – Brazil (PAP 2021TR854) and CAPES – Brazil (PROAP/AUXPE)

Introduction

Brazil generates approximately 79 million tons per year of solid waste, 13.5 % of which is plastic, thus occupying the fourth position of the countries with the world's most significant plastic waste production [1].

Due to the high demand for plastics today and their intermittent consumption, many lines of research have emerged to evaluate the production of this material from alternative resources. Biodegradable films are mainly composed of organic matter and biodegradable sources. They decompose into simple compounds in the biodegradation process under the influence of yeasts, bacteria, or fungi. It is a promising alternative to replace, at least partially, the conventional synthetic polymers of plastic packaging [2].

Starch is a material that stands out in the production of biofilms due to its characteristic biodegradability when released into the environment, renewable source, low cost, and excellent availability for use on an industrial scale. A plasticizer is incorporated to modify the adhesion, mechanical and thermal properties because starch-only films are normally brittle and not very flexible. For starch-based biofilms, the most used plasticizers are polyols such as glycerol. Due to its compatibility and interaction with starch chains, glycerol increases molecular mobility and, consequently, the flexibility of starch films [2,3,4,5].

To reduce the cost of producing biodegradable films and adding value to food by-products, fruit and vegetable processing residues are used to develop in films, edible coatings, and bioactive packaging. Food packaging systems aim not only to ensure food safety but also to prolong storage time and decrease the negative impact of synthetic polymers on the environment [6].

Among the diversity of fruits in nature, the grape reaches a prominent position due to the volume produced worldwide and in Brazil, due to its unique palatability and use as a raw material in the production of wines and juices, where the skins, seeds, and stems become industrial waste rich in antioxidant compounds and dietary fibers [7]. Wine production generates solid organic waste composed of seeds and grape skins that correspond to approximately 20 % of the weight of the fruit. This by-product is rich in fiber and antioxidants, and its use as a functional ingredient could promote a rational use [8,9].

Thus, the present project aims to develop biofilms of cassava starch matrix and different percentages of flour as a by-product of the wine industry, added with plasticizer glycerol, and evaluate the microscopic and mechanical properties of the systems.

Experimental

The films were produced by the casting method, and four formulations were studied, with variation in the percentage (0 %, 0.5 %, 2 %, and 4 %) of starch flour of grape residue 5 % and glycerol 20 % on starch was used for all formulations. The flour and water were homogenized with a magnetic stirrer for 10 min without heating. The solution was heated to 60 ºC for two minutes for homogenization. Then, the solution was placed in an ultrasonic bath at 60 ºC for five minutes with continuous dispersion. Then, glycerol was added to the solution and kept in agitation at 75 (±5) °C for 20 min. After reaching room temperature (21 ºC), the filmogenic solution was poured in proportionately to 0,236 g/cm^2 in plates and was dried for 24 h at 40 ºC.

Transmission optical microscopy (TOM; KONTROL IM100 with axle Z) was used to analyze the filler dispersion state in the starch matrix.

The films were characterized in terms of thickness, measuring eight random points of the sample with a digital micrometer and density based on their weight and thickness. The tensile test was performed according to ASTM 882-18 in texturometer TA.XTexpressC (Stable Micro Systems).

Results and Discussion

The thickness and density results are shown in Table 1. It is possible to observe that with the increase of the amount of flour in the systems, the thickness increases, and the density decreases. The presence of flour had little effect on the final weight of the samples. Thus, the change in density is related to the change in the volume of the sample, that is, an increase in thickness.

The increase in thickness is caused by the final appearance of the films, where the added flour resulted in micro reliefs at points where the flour grains were attached to the film. These reliefs caused the thickness to increase without significantly affecting the final weight, resulting in a decreased density.

Table 1 – Thickness and density of the film samples.

Sample	0 %	0.5 %	2 %	4 %
Thickness (mm)	0.116 ± 0.005	0.110 ± 0.009	0.121 ± 0.001	0.142 ± 0.004
Density (g/mm^3)	0.138 ± 0.007	0.132 ± 0.002	0.117 ± 0.008	0.108 ± 0.002

Through optical transmission microscopies (TOM) it was verified that the grape flour was well incorporated into the cassava starch matrix, forming continuous films and without evidence of voids at the particle/matrix interface, Fig. 1. This type of homogeneous structure is fundamental for the packaging development because they are more effective as a barrier to prevent the passage of oxygen, water vapor, and other gases, providing more protection against food spoilage and increasing its shelf life. It also indicates that the processing conditions were adequate. Biofilms with heterogeneous structures can be suitable sites for the growth of pathogenic bacteria, thus presenting a risk to public health.

It is possible to observe a compact structure, despite a heterogeneous appearance, caused by flour grains and small bubbles. No fissures were observed in the structure, indicating that the incorporation of the grains did not damage the films.

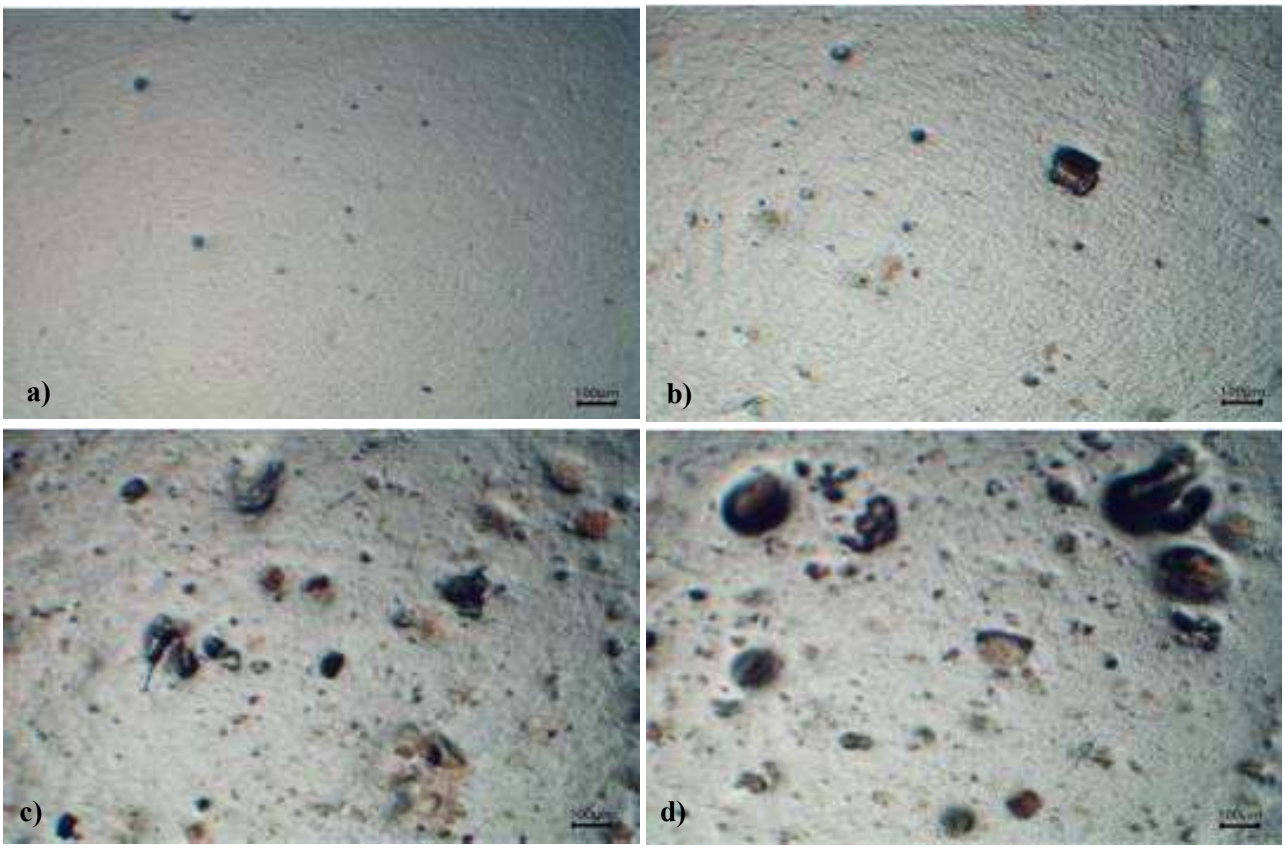

Figure 1 – Microscopy of biodegradable films with a) 0%, b) 0.5%, c) 2% and d) 4% of grape waste.

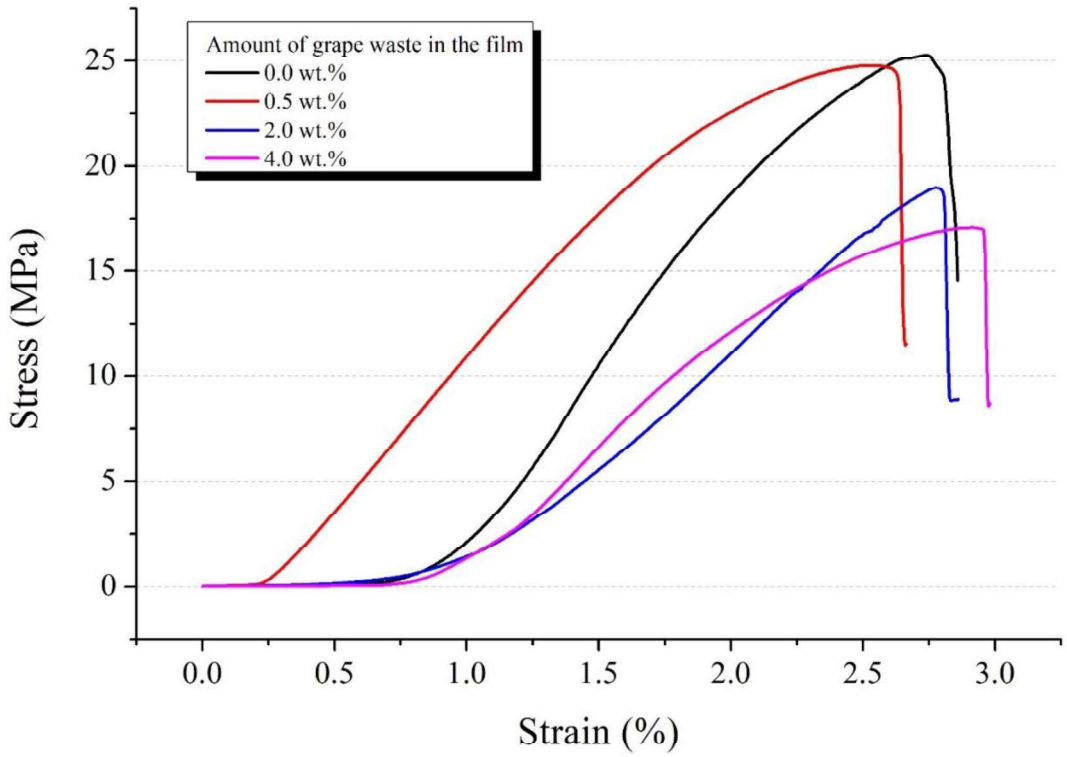

Figure 2 – Tensile test result of the grape flour biofilms systems and the pure starch biofilm matrix.

By the tensile test, according to Fig 2., considering the average values and comparing with the matrix without the addition of flour (0 %), the rupture stress, which is the maximum stress that a material can withstand before breaking, was very similar with the sample of 0.5 %. However, for the other systems with more flour (2 and 4 wt.%), the tension decreased 25% and 32% in relation to the pure matrix, respectively. This can be caused by the interaction between the chemical compounds found in grape flour with the molecules present in the biofilm interfering with the integrity of the polymer matrix, as well as the content of total sugars present in the fruits that can act as a plasticizer, weakening the intermolecular forces, reducing the resistance of the films [10].

Flour granules, especially the larger ones, can be a relevant factor in the mechanical performance of biofilms. The particles can act as defects and lead to stress build-up, triggering the crack propagation initiation point at the fracture. However, despite the failure stress having decreased, it was verified that the deformation increased with adding a greater amount of flour in relation to the pure matrix. And the biofilm with 0.5 wt.% of particles again maintained a similar result to the system without flour. The highest increase was for the biofilm sample with 4 wt.% flour, a 6% increase over the pure starch matrix. This indicates a good dispersion of the particles in the polymer, and the biofilms are more elastic as the flour is incorporated. However, the decrease in the rupture stress indicates they are less resistant.

Conclusions

The addition of grape residue showed an increase in thickness and a decrease in density in relation de pure matrix. It also significantly modified the rupture properties of the biofilms systems, making the biofilms less resistant to fracture, but their deformation increased with adding a greater amount of flour (4 wt.%). A small amount of flour (0.5 wt.%) does not significantly influence the mechanical properties of the matrix, but it can be relevant as an active component in food packaging. The microscopic structure indicated that the flour is well incorporated into cassava starch in all formulations, forming a continuous film without voids at the interface between polymer matrix and particles.

Acknowledgements

Authors are grateful for the funding support from FAPESC – Brazil (PAP 2021TR854) and CAPES - Brazil (PROAP/AUXPE) and Multi-User Facility infrastructure from Santa Catarina State University's Technological Sciences Center.

References

1. L. P. de Azevedo; et al. *Microplastics in the Ecosphere: Air, Water, Soil, and Food*. M. Vithanage; M. N. V. Prasad. Cap 28. p. 449-463, 2023.
2. A. L. M. P. Leite; C. D. Zanon; F. C. Menegalli. Carbohydrate Polymers, 157, 962–970, 2017. https://doi.org/10.1016/j.carbpol.2016.10.048
3. S. L. M. El Halal; et al. Carbohydrate Polymers, v. 133, p. 644–653, 2015. https://doi.org/10.1016/j.carbpol.2015.07.024
4. M. Caríssimi. Desenvolvimento e aplicação de filmes biodegradáveis a partir de amido de mandioca e microalga verde. Dissertação (Mestrado em Ciência e Tecnologia de Alimentos) - Universidade Federal do Rio Grande do Sul. 2017.
5. J. A. Batista. Desenvolvimento, caracterização e aplicações de biofilmes a base de pectina, gelatina e ácidos graxos em bananas e sementes de brócolos. Dissertação de Mestrado, Universidade Estadual de Campinas, Campinas, São Paulo. 2004.
6. S. Mali; et al. Carbohydrate Polymers, 60, 283-289, 2005. https://doi.org/10.1016/j.carbpol.2005.01.003

7. C. G. Otoni; et al. Comprehensive Reviews in Food Science and Food Safety, 16(5), 1151-1169. https://doi.org/10.1111/1541-4337.12281
8. R. A. Muhlack; R. Potumarthi; D. W. Jeffery. Waste Management, 72, 99–118, 2018. https://doi.org/10.1016/j.wasman.2017.11.011
9. A. Piovesana; M. M. Bueno; V. M. Klajn. Brazilian Journal of Food Technology, 16, 1, 68–72, 2013. https://doi.org/10.1590/S1981-67232013005000007
10. R.M.S. de Andrade. Desenvolvimento e caracterização de filmes biodegradáveis à base de resíduos de frutas e hortaliças. Dissertação de Pós-Graduação. Universidade Federal do Estado do Rio de Janeiro. Rio de Janeiro. 2014.

POROUS CHITOSAN BIOPOLYMER MEMBRANES BY ACETONE ADDITION AS A TUNABLE NON-SOLVENT COMPONENT

Angelo O. Silva[1], Alessandro R. Paulazzi, Ricardo S. Cunha[1], Cintia Marangoni[1], Dachamir Hotza[1] and Ricardo A.F. Machado[1]*

1 –Federal University of Santa Catarina (UFSC), Technological Center (CTC), Post-graduation Program in Chemical Engineering (PósENQ)
ricardo.machado@ufsc.br

Abstract - In this work, a chitosan porous membrane was synthesized by solvent evaporation technique using acetone as a non-solvent. The membrane was characterized by wettability (contact angle, swelling index), open porosity, crystallographic properties (XRD) and thermal analysis (DSC). The acetone concentration strongly affects the membrane features. Water contact angle values presented a moderate hydrophobic behavior ($\Theta > 80°$). Acetone promotes an increase in open porosity, swelling index, and a decrease in contact angle and crystallinity index. DSC analysis indicates a shift in degradation temperature between the precursor powder and chitosan membranes. However, no significant changes in Tg were noticed. Therefore, according to the intrinsic tunable effect of acetone addition, the membrane material obtained could be very promising to be further applied in membrane separation processes.
Keywords: *Chitosan. Porous Membranes. Acetone. Biopolymer.*
Fundings: CAPES; CNPq

Introduction

Chitosan materials have drawn growing attention as a promising renewable biopolymer soluble in aqueous acidic media [1,2]. The biggest advantages of biopolymers, such as chitosan, are non-toxicity, biocompatibility, and biodegradability. Also, different from the common synthetic polymers, the precursor raw materials come from renewable sources [3]. Therefore, chitosan has been increasingly used as a membrane precursor material for separation, concentration, and purification in different membrane applications [4].

The most common shaping route for chitosan membranes and films is denominated solvent, solution casting, or solvent evaporation [5]. This method consists of the first polymer dispersion in low concentrated organic acid solvents, especially acetic acid, following a drying step for complete solvent removal. The technique is limited to one specific material structure, to thin films usually deposited over a glass surface, and in the production of dense or low porous structures [5].

When a slow and gradual drying step is applied in the solution casting method, it is possible to obtain a chitosan material with a submicrometric pore size [6, 7]. Based on this, Sahebjamee *et al.* (2020) [8] developed porous structures of chitosan and other hydrophilic polymers by applying acetone as a non-solvent together in the dissolution process. Knowing that in certain solid loadings of chitosan exist a certain tolerance to amounts of organic solvents with a small carbon chain, their results produced a significant gain in porosity and surface area in only one condition tested. However, their work did not evaluate the effect of pure chitosan on the presence of acetone at different concentrations. Therefore, this work aims to develop a chitosan porous membrane synthesis by solvent evaporation technique using acetone as a non-solvent, producing a porous and hydrophobic material suitable for the membrane separation processes.

Experimental

Materials

The reagents used in all preparations, purifications, and characterizations are of analytical purity and were purchased from commercial sources and have not undergone prior purification. The synthesis of the membranes used medium molar mass commercial chitosan powder as a solid base material (Sigma-Aldrich, MM: 190-310 kDa, DD 75-85%), glacial acetic acid as an additive (Sigma-Aldrich), and acetone as a non-solvent (Exodo Científica, purity >99%). Deionized water (SPlabor) was used as a solvent in the production of membranes and to characterize contact angle and degree of swelling.

Membrane Synthesis

For the preparation of the membranes, the experimental route was based on Sahebjamee *et al.* (2020) [8]. First, samples with different compositions of chitosan content in mass fraction, in relation to total solvent mass, and different solvent volume ratios (water/acetone) were tested, as shown in Table 1.

Table 1 – Overview of Materials Used

Component	Function	Amount
Chitosan Powder	Matrix	1.0 wt%
Water (S1)	Solvent	Volume Ratio
Acetone (S2)	Non-Solvent	S1:S2 (1:0 – 8:1)
Acetic Acid	Additive	1.0 wt% in Water (S1)

The experimental preparation consists of four steps. First, a diluted solution of acetic acid was prepared in water at a fixed concentration of 1% (v/v). The second step consists of mixing all components: the desired amounts of acetone are added, and then the chitosan content is placed in the system; samples without the acetone addition were tested as a control. The third step consisted of magnetic stirring of the system at room temperature (25 ± 2 °C) until the solution was as homogeneous as possible. The last step is drying, which takes place at room temperature for 48 h in a fume hood with a relative humidity of ~60%. To facilitate the process of removing the dry membrane, a polyester terephthalate film (Mylar©) was glued with a double-sided adhesive tape and used on glass supports.

Membrane Characterization

The contact angle of the membranes was measured using a goniometer (Ramé-Hart model 250-F1) coupled with image processing software (DROPimage Advanced). The inserted volume of each drop on the membrane surface was approximately 10 μL, and 3 measurements for each sample were performed randomly to produce an average value. The Swelling Index (SI) determination was performed by immersing dry pre-weighed samples in distilled water at room temperature for 48 h. After immersion, the membranes were gently set on absorbent paper to remove excess and then weighed at saturation. The experiments were performed in triplicate, and the results are presented as mean value ± standard deviation. Eq 1 shows how SI (%) was calculated and analogously to Eq 1, the open porosity (P, in %) can be estimated by expanding Eq 1 into Eq 2, where Mw and Md are the masses (g) of the wet and dry membrane samples, respectively. ρH_2O is the density of water at room temperature (0.998 g.cm $^{-3}$) and ρ_{qui} is the density of chitosan powder (1.5 g cm-^{3}) given by the literature [9].

.

$$SI\ (\%) = \frac{M_w - M_D}{M_D} * 100 \quad (1)$$

$$P\ (\%) = \frac{\left[\frac{M_{w-}M_d}{\rho_{H2O}}\right]}{\left[\frac{M_{w-}M_d}{\rho_{H2O}}\right] + \frac{M_d}{\rho_{qui}}} * 100 \quad (2)$$

Membrane spectra were obtained by X-ray Diffractometry (XRD, Rigaku MiniFlex600) with a scintillation counter detector (Kβ filter), using CuKα radiation (λ = 1.5418 A°), and 40 kV. The samples of chitosan powder and membranes were analyzed in a range of 5-60°, following a step of 0.02° at a rate of 5°/min. Differential Scanning Calorimetry (DSC) measurements were performed in terms of degradation temperature (Tonset) and glass transition temperature (Tg). Solid samples with masses between 1 and 3 ± 1 mg were sealed in aluminum capsules and analyzed (Jade-DSC, Perkin Elmer). First, a heating and cooling curve was performed. The first run started with heating from 25 to 110 °C at 10 °C.min^{-1}, followed by cooling down to 25 °C at 10 °C.min^{-1}. The second run was performed with heating from 25 to 480°C at 10 °C.min^{-1}. The Tg of the materials was determined through the average value of the inflection region of the calorimetric curve, while the Tonset was defined as the initial temperature where the degradation peak of the samples begins.

Results and Discussion

Table 2 shows all the wettability properties (contact angle, swelling index, open porosity) of all membranes tested according to the variation in the volume ratio of water:acetone. The results show different values according to the presence of acetone and the volume of water:acetone ratio used.

Table 2 – Wettability Properties Obtained

Sample	Contact Angle (°)	Swelling Index (%)	Porosity (%)
1:0	86.19 ± 0.41	143.53 ± 24.17	67.36 ± 5.53
2:1	89.16 ± 3.46	163.02 ± 12.71	70.84 ± 1.88
3:1	99.34 ± 1.33	173.70 ± 40.21	70.88 ± 5.57
4:1	91.51 ± 2.37	247.11 ± 25.23	78.48 ± 2.19
5:1	88.17 ± 1.16	300.48 ± 19.53	81.77 ± 1.17
6:1	93.66 ± 0.64	237.65 ± 13.33	78.04 ± 1.22
7:1	100.01 ± 2.00	181.40 ± 17.69	72.88 ± 2.36
8:1	91.76 ± 0.58	164.99 ± 5.03	6719 ± 4.97

The water:acetone volume ratio employed promotes a maximum swelling index point. This value corresponds to 5:1 to 1.0 wt% of chitosan. This water uptake absorption capacity is related to the intrinsic hydrophilicity nature of the chitosan membrane [10]. Therefore, the present work shows that the increase in the swelling index is associated with the volume water:acetone ratio used may be associated with the increase in the open porosity of the system. The open porosity results show the same behavior as the swelling index results. Optimized acetone conditions produce a porosity percentage gain of 22.38% for 1.0 wt% of chitosan. These results demonstrate the importance of the presence of acetone in the production of the membrane microstructure and also reinforce the importance of optimizing the amount of acetone used for maximum porosity gain and better subsequent flow results.

XRD spectra for chitosan powder and the chitosan membranes containing 1 wt% chitosan as the volume water:acetone ratio increases are presented in Fig 1. It is possible to observe the crystallographic changes of chitosan powder for its conformation in membranes, and that all of the samples present semicrystalline polymer structures. [7, 11]. In the powder precursor sample, an amorphous peak centered at approximately 9° can be seen, and this peak shifts to approximately 15° in membrane conformations and also increases its width, becoming less noticeable.

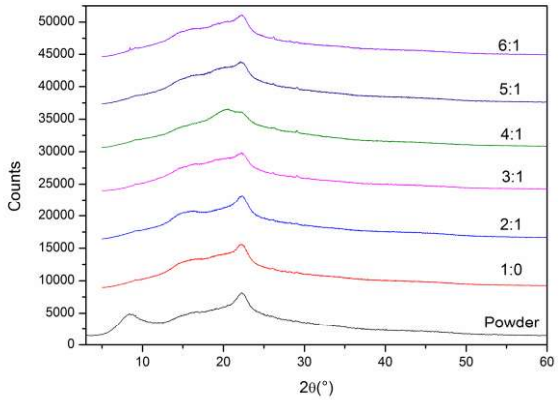

Figure 1 – XRD spectra for the membrane containing 1 wt% with the increase of water:acetone volume ratio.

According to Llanos, Vercik and Vercik (2015) [12], the modification of this first orthorhombic peak is related to the change in crystallite morphology in the chitosan polymer network connected with the loss of hydrogen bonds and deprotonation of amino groups. Fig 2. shows the thermograms of the membranes with 1.0 wt% chitosan according to the water:acetone volume ratio used. The thermograms were presented to demonstrate the thermal behavior of the membranes against a heating curve after a stage of thermal drying of the material.

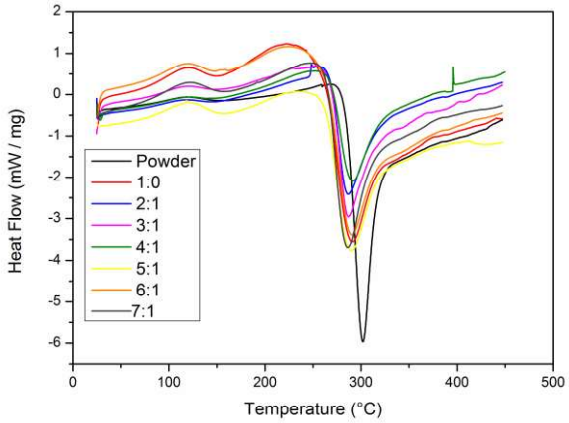

Figure 2 – DSC thermograms of the powder and membranes containing 1 wt% chitosan with different water:acetone solvent ratio.

In these thermograms, it is possible to identify the glass transition temperature (Tg) at the inflection point of each curves (~135°C), and the starting degradation temperature (Tonset) (~240°C) represented as the onset temperature of the exothermic peak, where the degradation of glucosamine units occurs [13]. The literature comments that the temperature of thermal degradation of chitosan is a function of the crystallinity change of the material [13]. Therefore, this alterations in Tonset might be associated with the crystallinity changes presented in the membrane development.

Conclusions

Chitosan porous membrane synthesis by solvent evaporation technique employing acetone as non-solvent was successfully performed. The synthesis route allowed to obtain membranes with high porosity, moderate hydrophobicity, and enhanced swelling index. Acetone was efficient as a porous agent and provide hydrophobicity in certain amounts. Its optimal volume ratio was 5:1. The crystallinity

index value has changed from the initial powder sample, but no strong alterations are observed between membrane composition systems. Tg remains constant in all membranes tested, but T_{onset} tends to be affected in relation to the acetone volume employed. The membrane material obtained is promising to be used in further membrane separation processes.

Acknowledgements
The authors are grateful to the Coordenação de Aperfeiçoamento de Pessoal de Nível Superior (CAPES, Brazil, finance code 01) and Conselho Nacional de Desenvolvimento Científico e Tecnológico (CNPq, Brazil) for financial support. Also, the authors are grateful to the Central Analisys of the Chemical Engineering Department at Federal University of Santa Catarina for the membrane characterization results.

References
1. U.G.T.M Sampath; Y.C. Ching; C.H. Chuah. Materials 2016, 9, 12, 1–32. https://doi.org/10.3390/ma9120991.
2. A.O. Silva; R.S. Cunha; D. Hotza; R.A.F. Machado. Carbohydrate Polymers 2021, 272, 118472. https://doi.org/10.1016/j.carbpol.2021.118472
3. M.E.A. Goosen. *Applications of chitin and chitosan.* Ed.; Lancaster: Technomic Publishing Company, 1996.
4. V. Vatanpour; B.Y. Gul; B. Zeytuncu; S. Korkut; G. Ilyasoglu; T. Turken; M. Badawi; I. Koyuncu; M.R. Saeb. Carbohydrate Polymers 2022, 281, 119041–119066. https://doi.org/10.1016/j.carbpol.2021.119041.
5. P. S. Bakshi; D. Selvakumar; K. Kardivelu; N.S. Kumar. International Journal of Biological Macromolecules 2020, 150, 1072–1083. https://doi.org/j.ijbiomac.2019.10.113
6. N. N. Rupiasih; M. Sumadiyasa; H. Suyanto; P. Windari. Journal of Physics: Conference Series 2017, 846, 1. https://doi.org/10.1088/1742-6596/846/1/012003.
7. N. N. Rupiasih; M. Sumadiyasa; I.K. Putra. IOP Conference Series: Materials Science and Engineering 2017, 196, 1. https://doi.org/10.1088/1757-899X/196/1/012039.
8. N. Sahebjamee; M. Soltanieh; S.M. Mousavi; A. Heydarinasab. Reactive and Functional Polymers 2020, 154, 104681. https://doi.org/10.1016/j.reactfunctpolym.2020.104681.
9. K. Picker-freyer; D. BRINK. American Association of Pharmaceutical Scientist Technology Journal 2006, 7, 3, 1-10. https://doi.org/10.1208/pt070375.
10. Z. Cui; E.S. Beach; P.T. Anastas. Green Chemistry Letters and Reviews 2011, 4, 1, 35–40. https://doi.org/10.1080/17518253.2010.500621.
11. M.K. Arantes; C.L. Kugelmeier; L. Cardozo-filho; M.R. Monteiro; C.R. Oliveira; H.J. Alves. Polymer Engineering and Science 2014, 1–08. https://doi.org/10.1002/pen.24038.
12. J. H. R. Llanos; L.C.O Vercik; A. Vercik. Journal of Biomaterials and Nanobiotechnology 2015, 06, 04, 276–291. https://doi.org/10.4236/jbnb.2015.64026.
13. L. S Guinesi; É.T.G Cavalheiro. Thermochimica Acta 2006, 444, 2, 128–133. https://doi.org/10.1016/j.tca.2006.03.003.

"BEYOND SYNTHESIS: HOW ECOTOXICOLOGY CAN HELP DEVELOP SUSTAINABLE POLYMERIC MATERIALS"

Marcelo Gryczak[1*], Tales S. Daitx[1], Douglas Gamba[1], Cesar L. Petzhold[1]

1 – Institute of Chemistry, Federal University of Rio Grande do Sul (UFRGS), Porto Alegre, RS, Brazil
marcelo.gryczak@ufrgs.br

Abstract - The article presents the importance of ecotoxicological evaluation in the design of new polymeric materials, ecotoxicology investigates the effects of chemical substances on ecosystems and living organisms, taking into account the interaction of these substances with the environment and their transport and transformation processes. Polymers, widely used in various industrial sectors, can cause significant environmental impacts, especially when improperly disposed. The study presents cases of the applicability of ecotoxicological evaluation in the development of new materials. The methodology of the case studies used was structured around: material, justification, bioindicators, parameters evaluated, and contribution to the development of the material. The examples used were the development of a composite LDPE/coal mining waste, a hydrogel from renewable sources, and a polymeric system for controlled release of fertilizer. The results highlight the relevance and effectiveness of implementing ecotoxicological evaluation in the design of new polymeric materials, allowing the conclusion that multidisciplinary studies with environmental perspectives are important in guiding the formulation of sustainable polymeric materials.
Keywords: *Polymers, ecotoxicology, environmental impact, sustainability*.

Introduction

Ecotoxicology is a science that investigates the effects of chemical substances on ecosystems and living organisms, taking into account their interaction with the environment and its processes of transport and transformation. It is therefore crucial for assessing the environmental risks associated with chemical compounds, as well as guiding environmental management and the development of new materials and substances with lower environmental impact [1].

Polymers, which are widely used in various industrial sectors, can cause significant environmental impacts, particularly when improperly disposed. Polymers in general are highly resistant to natural degradation and therefore remain in the environment for long periods of time, affecting the quality of soil, water, and air. In view of these significant environmental impacts, it is essential that sustainable solutions should be developed for the production, use, and disposal of polymeric materials [2].

Considering the environmental impacts that can be caused by certain polymers, it is essential to evaluate the behavior and its potential effects in different environmental conditions, being able to integrate the ecotoxicological evaluation in the development of these materials [3]. These studies are essential for guiding the research of new polymeric materials and improving the manufacturing of existing one. The results of ecotoxicological studies can be used to identify the best ways to dispose and manage polymeric materials in order to minimize their impact on the environment [4, 5]. Ecotoxicological studies in different environmental compartments and bioindicators are extremely important for understanding the exposure and effects of chemical substances in ecosystems. Since the dynamics of exposure is different in each environmental compartment, a preliminary understanding of the possible routes of contamination is necessary and, therefore, these

studies make it possible to evaluate the toxicity of pollutants in different organisms, from aquatic to terrestrial organisms [6].
The present study aims to analyze some examples of the applicability of ecotoxicological evaluation in the development of new materials in a polymer research group. To achieve this objective, case studies will be presented that demonstrate the relevance of adopting these practices in areas related to the conception of new materials.

Experimental

Regarding the methodological structure of this manuscript, we will present some case studies that were developed in the research group (SINPOL/UFRGS) with the aim of incorporating ecotoxicological evaluation into the development of new polymeric materials. Each case study will be structured as follows: title, justification, bioindicators, evaluated parameters, contribution to the material development and main publication.
Examples will be presented on the implementation of environmental behavior studies in the for the following materials: LDPE/coal mining waste composite, hydrogel from renewable sources, and polymeric system for controlled release of fertilizer.
With the methodological description, the overall results obtained from these studies will be presented in the next section, allowing for a more precise evaluation of the impact of ecotoxicological analyses on the development of these materials.

Results and Discussion

Table 1 presents the results of some case studies demonstrating the relevance and effectiveness of implementing ecotoxicological evaluation in the conception of new polymeric materials.

Table 1: Presentation of case studies.

Material: LDPE/coal mining waste composite
Justification: The research group sought to develop a system to mitigate the environmental impacts caused by coal mining waste, through the formulation of a polymeric composite.
Bioindicators: *Eisenia fetida* (avoidance behavior, feeding activity), *Collembolos* (mortality), *Vibrio fischeri* (bioluminescence).
Contribution: The present study confirmed the effectiveness of blocking the formation of mineral acid drainage by the Low Density Polyethylene (LDPE) matrix interface, as well as establishing the relationship between the matrix/reinforcement fraction and the desirable properties with the resulting environmental behavior.
Main publication: Gryczak, M., Wong, J. W., Thiemann, C., Ferrari, B. J., Werner, I., & Petzhold, C. L. (2020). Recycled low-density polyethylene composite to mitigate the environmental impacts generated from coal mining waste in Brazil. *Journal of environmental management*, *260*, 110149.
Material: Hydrogel from renewable sources
Justification: This was a study developed to understand the environmental behavior in the formulation of a hydrogel from renewable sources used in agriculture.
Bioindicators: *Zea mays* (growth and biomass balance), *Allium cepa* (root development), *Eisenia fetida* (avoidance behavior).
Contribution: The study showed that the use of compounds from renewable sources in the hydrogel formulation can have significant environmental impacts. The acidification of the soil resulting from the dragging of certain compounds resulted in a decrease in terrestrial biological activity. Therefore, the implementation of this study during the formulation of the hydrogel contributed to the reevaluation of the hydrogel composition, taking into account the ecotoxicological effects found.
Main publication: Study with intellectual protection.

Material: Polymer with controlled fertilizer release
Justification: This study was implemented to evaluate the applied efficiency of the NPK fertilizer release profile in a controlled release polymeric system.
Bioindicators: *Lactuca sativa* (index of germination and root development).
Contribution: In this study it was possible to evaluate the efficiency and applicability of the controlled release systems that were developed, tracing a profile of conditions in which they favored the highest performance of plant growth.
Main publication: Daitx, T. D. S., de Lima, V. S., Gryczak, M., Petzhold, C. L., Carli, L. N., & Mauler, R. S. (2020). Poly (hydroxybutyrate)-based systems behavior on the controlled release of NPK fertilizers. *Polymers for Advanced Technologies*, *31*(11), 2579-2587.

The case studies presented demonstrate the versatility in the implementation of ecotoxicological studies in the development of polymeric materials.
The first study and evaluation showed that it is possible to develop materials with greater environmental efficiency, reducing the impacts caused by mining waste, using a hydrophobic system. In the second, the formulation of a bio-hydrogel for use in agriculture was evaluated and through the implemented studies we identified compounds responsible for soil acidification and, based on this information, the hydrogel was reformulated to reduce its environmental impact. In the third study, the evaluated system allowed tracing a profile of conditions that favored the best performance of plant growth. This is important to understand the application of the developed material in relation to dose/response.
Ecotoxicological studies are needed to assess the potential impact of polymers and their degradation products on the environment and its biota. These studies help to identify the toxicological mechanisms and effects of exposure to polymers on different organisms and to determine safe exposure limits to minimize the environmental impact of these materials [7].

Conclusions

The case study examples presented in the article highlight the importance of ecotoxicological studies as a necessary characterization for the development of sustainable polymeric materials. It is evident that such studies allow the formulation of safer and more environmentally responsible materials.

Acknowledgements

CAPES for providing financial resources for the studies presented.

References

1. M. Gavrilescu; K. Demnerová; J. Aamand; S. Agathos; F. Fava. 2015. Emerging pollutants in the environment: present and future challenges in biomonitoring, ecological risks and bioremediation. New biotechnology, 32, 147-156. https://doi.org/10.1016/j.nbt.2014.01.001
2. L. Rigamonti; M. Grosso; J. Møller; V. Sanchez; S. Magnani; T. Christensen. 2014. Environmental evaluation of plastic waste management scenarios. Resources, Conservation and Recycling, 85, 42-53. https://doi.org/10.1016/j.resconrec.2013.12.012
3. I. Vikhareva; G. Aminova; A. Mazitova. 2021. Ecotoxicity of the adipate plasticizers: Influence of the structure of the alcohol substituent. Molecules, 26, 4833. https://doi.org/10.3390/molecules26164833
4. A. Panda; K. Dyadyura; J. Valíček; M. Harničárová; M. Kušnerová; T. Ivakhniuk; I. Pandová. 2022. Ecotoxicity Study of New Composite Materials Based on Epoxy Matrix DER-331 Filled with Biocides Used for Industrial Applications. Polymers, 14, 3275. https://doi.org/10.3390/polym14163275

5. T. Kobayashi; L. Nakajima. 2021. Sustainable development goals for advanced materials provided by industrial wastes and biomass sources. Current Opinion in Green and Sustainable Chemistry, 28, 100439. https://doi.org/10.1016/j.cogsc.2020.100439
6. L. Wolska; A. Sagajdakow; A. Kuczyńska; J. Namieśnik. 2007. Application of ecotoxicological studies in integrated environmental monitoring: possibilities and problems. TrAC Trends in Analytical Chemistry, 26, 332-344. https://doi.org/10.1016/j.trac.2006.11.012
7. Z. Yao; H. J. Seong; Y. S. Jang. 2022. Environmental toxicity and decomposition of polyethylene. Ecotoxicology and Environmental Safety, 242, 113933. https://doi.org/10.1016/j.ecoenv.2022.113933

REGENERATED CELLULOSE FILAMENTS OBTAINED FROM TEXTILE COTTON WASTE RECYCLING USING IONIC LIQUID

Beatriz B. Brito[1], Beatriz Krüger[1], Rita C. S. C. Valle[1], Cintia Marangoni[2] and Andrea C. K. Bierhalz[1]*

1 – Department of Textile Engineering, Federal University of Santa Catarina – Campus Blumenau, Blumenau, Brazil
andrea.krause@ufsc.br
2 – Department of Chemical Engineering and Food Engineering, Federal University of Santa Catarina, Florianópolis, Brazil

Abstract – Cotton fiber waste is abundant in the textile sector and due to its high cellulose content, is attractive to form regenerated cellulose filaments. This study aimed to obtain regenerated cellulose filaments using pre-consumption cotton waste as raw material and a system based on imidazolium ionic liquid and dimethyl sulfoxide (DMSO) as solvents. Filaments were obtained by wet spinning using water or ethanol as antisolvents and the degree of polymerization (DP), morphology, and mechanical properties were evaluated. Micrographs confirmed the complete dissolution of the cellulose in the ionic liquid/DMSO system and homogeneous regeneration. Compared to cotton waste, the DP was reduced by 95% and 76% for filaments regenerated with water and ethanol, respectively. The mechanical properties were not affected by the antisolvent. In general, it was demonstrated that the life cycle of cotton fiber can be increased by using ionic liquid technology.
Keywords: *Cotton fiber. Ionic liquids. Textile waste. Wet-spun filament. Regenerated cellulose.*
Fundings: Support Foundation of Santa Catarina State (FAPESC) Process n. 2021TR000327

Introduction

At the end of the 20th century, large brands in the textile industry began the fast fashion movement, a pattern of increasingly accelerated fashion development, leading to the excessive consumption of clothes and other textile articles [1]. The high demand intensified the manufacture of these items, generating a large amount of waste from the stages of the production process (pre-consumption waste) and the inevitable post-consumption disposal. The textile segment has come to be considered the second most polluting sector in the world, taking into account the volume of material discarded without prior treatment [2].

This scenario has driven the search for alternatives for recycling textile waste to reduce the amount of material disposed of in landfills or dumps and contribute to including textile waste in the reverse logistics chain [3]. One of the alternatives for the reuse of cellulosic residues, for example, is the development of artificial fibers using the processes of dissolution and regeneration of cellulose, such as viscose and lyocell [4]. However, these traditional processes use aggressive solvents that have environmental, economic, and social implications [5].

Given the limitations observed in the viscose and lyocell processes, new solvents, including ionic liquids (ILs), have been studied. The ILs have important properties in the direct dissolution of cellulose, which include thermal stability, low melting point, polarity, hydrophilicity, and viscosity, producing fibers with characteristics of great commercial interest [6].

The present work aimed to obtain regenerated cellulose filaments from the dissolution of cotton textile waste in the IL imidazolium 1-ethyl-3-methylimidazolium chloride [Emim]Cl, using dimethylsulfoxide (DMSO) as co-solvent. The influence of the use of deionized water and ethanol as

antisolvents in the regeneration step on the degree of polymerization and mechanical properties of the filaments was investigated.

Experimental

Materials

Fibers from cotton waste, from the industrial process of textile plushing, were used to obtain regenerated cellulose filaments. Ionic liquid 1-ethyl-3-methylimidazolium chloride ([Emim]Cl) (Sigma-Aldrich, USA) was used as a solvent. Dimethylsulfoxide P. A (DMSO) was used as co-solvent and ethanol P.A and deionized water as antisolvent.

Dissolving the cellulose and obtaining the regenerated cellulose filament

Dissolution of cellulose followed the procedure described by Liu et al. [7], with some modifications. Initially, cotton samples were dried at 105°C for 24 h to remove moisture. The cotton fibers (0.09 g) were dissolved in 3 g of ionic liquid at 110°C, under continuous magnetic stirring, with a heating oil bath [7]. Complete dissolution was observed by polarized light optical microscopy (ZEISS, AxioLab.A1 model). After dissolution, 1.5 g of DMSO was added to reduce viscosity.

The wet spinning process of the cellulose dissolved was performed using an infusion pump (Fresenius Kabi, Injectomat Agilia model) with an attached syringe of 10.5 mm internal diameter, at a rate of 45 mL/h. The solution was extruded directly into a bath of deionized water or ethanol at 25°C and kept at rest for 15 min for coagulation. Next, the regenerated cellulose filament was washed with plenty of deionized water to completely remove the residual solvent and co-solvent system and dried in an oven at 60 °C for further characterization.

Degree of polymerization (DP)

The degree of polymerization of cotton waste and regenerated cellulose filaments was determined according to the ASTM D1795-13 standard [8]. Initially, all samples were dried at a temperature of 105°C to remove moisture. Subsequently, 0.018 g of cotton waste and filament samples were weighed. Fractionated into small pieces, each sample was inserted into a 250 mL Erlenmeyer flask containing glass spheres and 15 mL of water. After 15 min of continuous stirring, 15 mL of cuproethylenediamine solution (CUEN) at 1 M was added. With the flask sealed, maintaining the system under an inert nitrogen atmosphere, the dissolution was carried out in an orbital shaker (NL-343-01, New Lab), at 25 °C, for 1 h. After complete dissolution, a 7.0 mL aliquot of the solution was transferred to the Cannon-Fenske capillary viscometer, and kept in a bath at 25 °C, to determine the flow time. The flow time of the CUEN solution, without the presence of cellulose, was also determined.

The degree of polymerization (DP) was determined from Eq. 1.

$$DP = [\eta].190 \quad (1)$$

Where η is intrinsic viscosity (dL/g), determined from Eq. 2.

$$\log\frac{\eta_{sp}}{C} = \log[\eta] + k.[\eta].C \quad (2)$$

In Eq. 2, η_{sp} is the specific viscosity (dL/g) determined by $\eta_{rel} - 1$. The relative viscosity (η_{rel}) was determined by the ratio between the solution flow times through the solvent, in seconds, using the same viscometer [8]; C is the polymer concentration (g/dL); η is the intrinsic viscosity (dL/g); and k is a constant (k = 0.13).

Morphological and mechanical characterization

The morphological characteristics of the surface and cross-section of the regenerated cellulose filaments were analyzed by scanning electron microscopy (SEM). The samples were fixed with carbon tape on the stubs and covered with a thin layer of gold using the LEICA metallizer equipment (EM SCD 500, Austria). The analysis was performed using a JEOL microscope (JSM-6390 LV, USA) with an accelerating voltage of 10 kV to 15 kV.

The mechanical resistance of the filaments was evaluated in terms of tensile strength, elongation at break, and tenacity, expressed in cN/Tex, according to the ASTM D2256/D2256M standard [9]. Test specimens with 150 mm in length were used. The tensile tests were carried out in a texturometer equipment (TA.XT Plus, Stable Micro Systems, United Kingdom), using a 50 N load cell, initial grip spacing of 10 cm, and cross-head speed of 2 mm/min. Ten replicates were used for each type of sample. The diameter of the filaments was measured with a digital micrometer (Digimess, Brazil), with 5 measurements along the length of the filament.

Results and Discussion

The dissolution kinetics of cellulose from cotton textile waste in imidazolium ionic liquid at 110°C was monitored for 150 min and the images are shown in Fig 1. It is possible to observe the effect of time on dissolution, considering that the amount of cotton fibers decreases with increasing dissolution time. The micrographs reveal that the cotton fibers were already dissolved in 90 min of dissolution. The presence of small particles still observed after cellulose dissolution was attributed to impurities of the cotton residue. These results indicate the dissolution potential of the ionic liquid [Emim]Cl, corroborating previous studies [10,11].

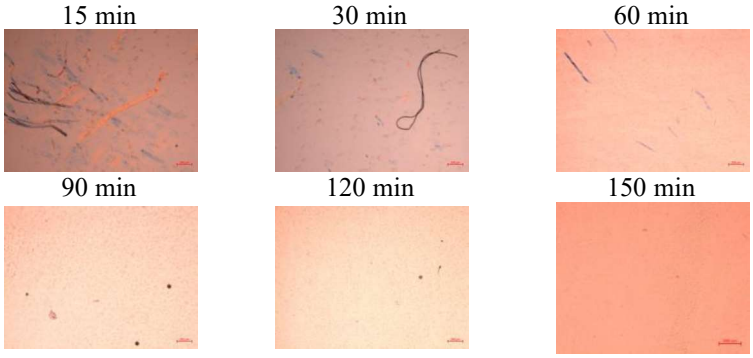

Figure 1 – Dissolution of cellulose using ionic 9liquid [Emim]Cl evaluated over time by optical microscopy.

The results of the degree of polymerization (DP) presented in Table 1 indicated a strong influence of the cellulose dissolution and regeneration process on this property. Filaments of regenerated cellulose showed a great reduction of DP in comparison with the cellulose from cotton waste. Regarding the antisolvent used for coagulation, filaments regenerated in ethanol showed less depolymerization (76%) when compared to filaments regenerated in water (95%). The potential of using water and ethanol as antisolvents was also verified in the study by Tan et al., who observed the performance in controlling the structure and properties of cellulose dissolved in imidazolium ionic liquid, with emphasis on ethanol, which promoted the aggregation of the cellulose chains [12].

Table 1 – Degree of polymerization of regenerated cellulose filaments in imidazolium ionic liquid [Emim]Cl

Material	Coagulant	Degree of polymerization (DP)
Regenerated cellulose	Water	177 ± 34
	Ethanol	847 ± 84
Cellulose of cotton fibers	-	3,587 ± 100

The morphology of the surface and cross-section of the cellulose filaments regenerated in water and ethanol, investigated by SEM, is shown in Fig 2. The micrographs indicate a smooth, dense, and homogeneous microstructure, with the absence of fibrous particles and pores. This result reveals the recycling potential of the cotton textile residue using the ionic liquid [Emim]Cl as solvent and DMSO as co-solvent in the dissolution of the cellulose, evidenced by the absence of undissolved fibers and a relatively uniform regeneration. The homogeneous and dense aspect of the cross-section of the regenerated cellulose filaments indicates that the regeneration process occurred homogeneously. Lee et al. reported similar results in obtaining regenerated cellulose filaments using imidazole ionic liquid as solvent and DMSO and DMF as co-solvents in dissolving cellulose [13].

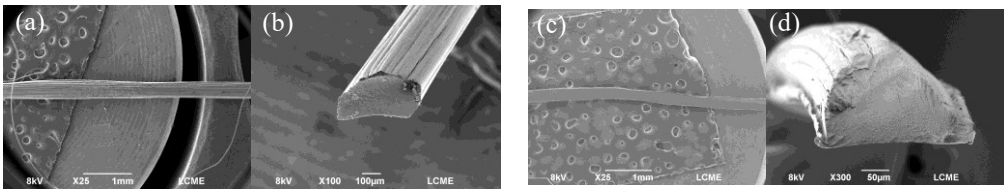

Figure 2 – SEM images of the surface and cross-section of cellulose filaments regenerated in water (a, b) and in ethanol (c, d).

Values for diameter, tensile strength, elongation at break, and tenacity of the regenerated cellulose filaments can be seen in Table 2. The results of the samples regenerated in water or ethanol did not show significant differences ($p < 0.05$). The values of tensile strength are within the results achieved in processes with ionic liquids (130-375 MPa) observed by Hauru et al. [14]. Commercial viscose fibers present tensile strength in the range between 180 and 234 MPa, while lyocell in the range of 315 to 423 MPa [15]. The results of previous studies indicate that the elongation, diameter, and tenacity values determined in the filaments regenerated in water and ethanol are of the same order [16,17]. It is important to point out that the mechanical properties of regenerated cellulose filaments are affected by the type of solvent and cellulose coagulant in dissolution processes using ionic liquids [4].

Table 2 – Diameter, tensile strength (σ), elongation at break (ε), and tenacity of the regenerated cellulose filaments in imidazolium ionic liquid [Emim]Cl

Antisolvent	Diameter (mm)	σ (MPa)	ε (%)	Tenacity (cN/Tex)
Water	0.24 ± 0.01	174.26 ± 26.59	6.18 ± 2.45	8.38 ± 1.07
Ethanol	0.20 ± 0.03	182.32 ± 34.11	5.03 ± 1.48	7.84 ± 2.13

Conclusions

The present study evaluated the potential of the system based on imidazolium ionic liquid [Emim]Cl and DMSO in the recycling of cotton textile waste, transforming it into a regenerated cellulose filament. It was observed that the solvent system was efficient in dissolving the cellulose, with a dissolution time of 90 min. The wet spinning technique, using water or ethanol as coagulants, produced homogeneous filaments, with a dense microstructure and without undissolved fibers and pores. The regeneration with ethanol resulted in lower depolymerization than those with water, but the mechanical properties were similar. The technology of ionic liquids (ILs) used in the recycling of textile residues revealed great potential in industrial application and in the environmentally appropriate disposal of these residues and in increasing the useful life cycle of the cotton fiber.

Acknowledgements

The authors thank the FAPESC (Process n. 2021TR000327) and CAPES (Financial code 001) for financial support and the Central Laboratory of Electronic Microscopy (LCME - UFSC) for technical support during SEM analysis.

References

1. J. A. S. Duarte. Dissertation, University of Lisbon, 2021
2. G. Hole; A. S. Hole Sustain. Product. Consum. 2020, 23, 42. https://doi.org/10.1016/j.spc.2020.04.005
3. T. Exchange, *Preferred Fiber & Materials Market Report 2021*, Textile Exchange, Texas, 2021
4. B. Medronho; B. Lindman Adv. Colloid Interface Sci. 2015, 222, 502. https://doi.org/10.1016/j.cis.2014.05.004.
5. A. Michud; M. Tanttu; S. Asaadi; Y. Ma; E. Netti; P. Kääriainen; A. Persson; A. Berntsson; M. Hummel; H. Sixta Text. Res. J. 2015, 86, 543. https://doi.org/10.1177/0040517515591.
6. J. M. Rieland; B. J. Love Resour. Conserv. Recycl. 2020, 155, 104678. https://doi.org/10.1016/j.resconrec.2019.104678.
7. Z. Liu; H. Wang; Z. Li; X. Lu; X. Zhang; S. Zhang; K. Zhou Mater. Chem. Phys. 2011, 128, 220. https://doi.org/10.1016/j.matchemphys.2011.02.062.
8. American Society for Testing and Materials (ASTM) in Proceedings of Standard Test Method for Intrinsic Viscosity of Cellulose, United State, 2021, 1-6.
9. American Society for Testing and Materials (ASTM) in Proceedings of Standard Test Method for Tensile Properties of Yarns by the Single-Strand Method, United State, 2021, p. 13.
10. B. Kosan; C. Michels; F. Meister. Cellulose, 2008, 15, 59. https://doi.org/10.1007/s10570-007-9160-x.
11. T. Uto; K. Yamamoto; J. I. Kadokawa J. Phys. Chem. B. 2018, 122, 258, https://doi.org/10.1021/acs.jpcb.7b09525.
12. X. Tan; L. Chen; X. Li; F. Xie Int. J. Biol. Macromol. 2019, 124, 314, https://doi.org/10.1016/j.ijbiomac.2018.11.138.
13. Y. J. Lee; S. J. S. G Lee.; S. W. Jeong; H. C. Kim; T. H. Oh; S. J. S. G Lee Fibers Polym. 2019, 20, 501, https://doi.org/10.1007/s12221-019-8335-z.
14. L. K. J. J. Hauru; M. Hummel; A. Michud; H. Sixta Cellulose, 2014, 21, 4471, https://doi.org/10.1007/s10570-014-0414-0.
15. X. Jiang; Y. Bai; X. Chen; W. Liu. J Bioresour. Bioprod. 2020, 5, 16, https://doi.org/10.1016/j.jobab.2020.03.002.
16. F. Fu; Y. Guo; Y. Wang; Q. Tan; J. Zhou; L. Zhang. Cellulose, 2014, 21, 2819, https://doi.org/10.1007/s10570-014-0297-0.
17. C. Olsson; G. Westman. J. Appl. Polym. Sci. 2013, 127, 4542–4548, https://doi.org/10.1002/app.38064.

SYNTHESIS OF NEW SUSTAINABLE POLYESTER-TYPE HYDROGELS FROM CHEMICAL RECYCLED POLY(ETHYLENE TEREPHTHALATE) APPLIED IN THE REMOVAL OF INDIGO CARMINE DYE

Daniela E. Schneider[1*], Tomás M. Simioni[1], César L. Petzhold[1], Tales S. Daitx[1*]

1 – Institute of Chemistry, Federal University of Rio Grande do Sul (UFRGS), Porto Alegre, RS, Brazil
danielaeduardaschneider@hotmail.com, tales.daitx@ufrgs.br

Abstract - In this work a chemical recycling of poly(ethylene terephthalate) was performed through the microwave glycerolysis reaction and their products were crosslinked to produce sustainable hydrogels for application on wastewater treatment of the textile industry. The depolymerization reaction was performed at 250 °C at different reaction times (5 min, 15 min and 30 min) and the depolymerization products were crosslinked with citric acid to produce hydrogels. All compounds were characterized by spectroscopy analysis and the results indicated the formation of products of interest. Additionally, the hydrogels were applied on the removal of indigo carmine dye from aqueous solutions demonstrating adsorption capacity in the range of 40-97% by a pseudo-first order mechanism, indicating that the contact time between the hydrogel and the dye is decisive for a greater efficiency of adsorption.

Keywords: *Chemical recycling, Dyes adsorption, Indigo carmine, PET recycling, Wastewater treatment.*

Introduction

Colored effluents are generated by various industries such as textile, cosmetics, paper, food, etc., and are highly toxic and present a risk to human health, aquatic ecology and the environment. Indigo carmine (IC) is one of the most popular dyes and is commonly used in the textile industry, especially in the dyeing of denim goods. In the denim textile industry approximately 3-12 g of IC is needed for coloring a pair of blue denim pants. Considering the use of IC in different areas of industry, around 40 ktons of the dye is produced annually based on the global demand. The presence of IC in the environment presents risks to human health when in contact with the body, as it can permanently damage the cornea, to the respiratory tract and the skin, causing severe irritation. In addition, contamination of surface water with the dye can increase turbidity and reduce the photosynthesis process, threatening aquatic ecosystems [1].

An alternative for the treatment of effluents from the textile industry is the use of adsorbent materials such as hydrogels, which are capable of adsorbing dyes and removing them from the effluent. Hydrogels can be produced from polymers and an alternative that arises is the use of industrial plastic waste, since the increase in its production and the difficulty to degrading this material leads to a large increase in the generation of plastic waste. Through chemical recycling, it is possible to transform these residues into monomers or macromonomers that can undergo reactions that lead to the preparation of materials such as hydrogels. Among polymeric waste, poly(ethylene terephthalate) (PET) is very promising since it is one of the most generated plastic waste and can undergo chemical recycling using various reagents. A PET chemical recycling reaction is solvolysis, which consists of the use of solvents to promote depolymerization, an example is glycerol, a by-product of the biodiesel-production, whose demand is growing in some countries [2].

In view of the above, the present work aims at the chemical recycling of PET via reaction with glycerol under microwave radiation (MW) and synthesizes a new class of sustainable polyester-type hydrogels using citric acid (CA) as a crosslinker. In addition, the materials obtained were structurally characterized and applied for the removal of the IC dye in aqueous medium.

Experimental

Depolymerization of poly(ethylene terephthalate)

Waste PET (wPET) was collected from discarded PET soft drink bottles. The wPET was cleaned with a soap solution rinsed with deionized water and dried. The material was cut manually into small pieces of approximately 50 mm^2. The depolymerization reaction was conducted through glycerolysis reaction in a 1:6.25 (wPET:glycerol) molar ratio under MW conditions at 250 °C and zinc acetate catalysis (1 wt.% percent of wPET). The reaction was carried out at three different times (5 min, 15 min and 30 min) and the samples were named as dPET05, dPET15 and dPET30, respectively. The recycled products (dPET) were analyzed without prior purification through Attenuated total reflectance Fourier-transform infrared (FTIR) and hydrogen nuclear magnetic resonance (^{1}H NMR) spectroscopies and index of hydroxyls using a titration method [3].

Synthesis and application of hydrogels

For the synthesis of hydrogels, two different proportions of CA were studied (10 and 20 mmol of crosslinker per gram of dPET). The reactions were carried out in an oil bath at 150 °C and tin (II) chloride catalysis (2 wt.% carboxyl content from CA) for 3 h and then the system pressure was reduced and the reactions continued until the material vitrified (about 2 h for 20 mmol of CA and 1 h for 10 mmol of CA). After synthesis, the obtained hydrogels were submerged in deionized water in the proportion of 40 mL for 0.5 g of hydrogel for 48 h to remove the soluble fraction and evaluate the water uptake capacity (W_u). Further the hydrogels were lyophilized and characterized by FTIR.

Adsorption experiments with IC dye were conducted to study the capacity of the hydrogels to remove anionic compounds from aqueous solutions. Therefore, 200 mg of hydrogel were immersed in 25 mL of an aqueous solution of IC with a concentration of 10 ppm. At specific time intervals (0, 15 min, 30 min, 1 h, 2 h, 3 h, 4 h, 5 h, 6 h, 7 h, 8 h, 9 h and 24 h), the residual dye concentration was measured by Ultraviolet-visible spectroscopy (UV-Vis) at λ_{max} = 610 nm.

Results and Discussion

Depolymerization of poly(ethylene terephthalate)

The depolymerization reactions of wPET (Fig. 1) were successfully conducted in all reaction times studied, generating a viscous liquid (dPET).

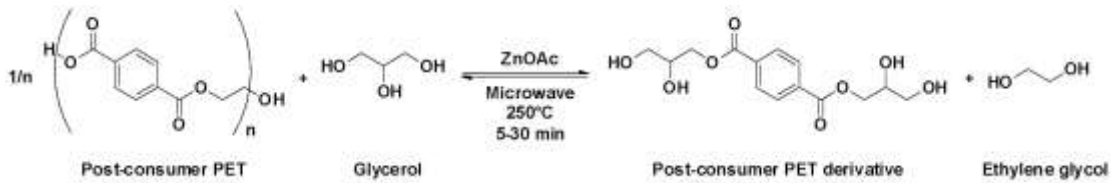

Figure 1. Glycolysis reaction of wPET under different microwave conditions.

For the samples dPET05, dPET15 and dPET30, the hydroxyl index was 313 ± 9, 292 ± 39 and 243 ± 31 mg KOH g^{-1}, respectively. The highest hydroxyl index obtained in 5 min of reaction may be related to a larger excess of unreacted glycerol, while for longer times (15 min and 30 min),

the conversion of the glycerolysis is higher, decreasing residual glycerin and, consequently the hydroxyl content. Furthermore, it was observed that the longer the MW radiation time, the less viscous and more yellowish the dPET. The more intense coloration may be due to the formation of the thermal degradation product of the glycerin present in excess and the decrease in viscosity may be related to a greater breakdown of the PET chains [4].

For ^{1}H NMR analysis, a sign related to the hydrogens of the aromatic ring, originating from the PET chain, is observed at 8.12 ppm. The characteristics signals of glycerol are in the region of 3.2 to 3.8 ppm and the signal at 3.4 ppm is characteristic of the hydrogens from ethylene glycol subproduct. This indicates the formation of the species of interest for all reaction times [4].

The FTIR analysis was performed for all reaction times and also for the wPET sample. In Fig. 3(a) we can observe the bands at 3300 cm^{-1} and 1040 cm^{-1} that indicate the presence of new O-H and C-O-H bonds, respectively. At 1729 cm^{-1} and 730 cm^{-1} there are signals of aromatic carboxylic esters, indicating the insertion of glycerol units in the PET chains, and the formation of the product (Fig.1) [4].

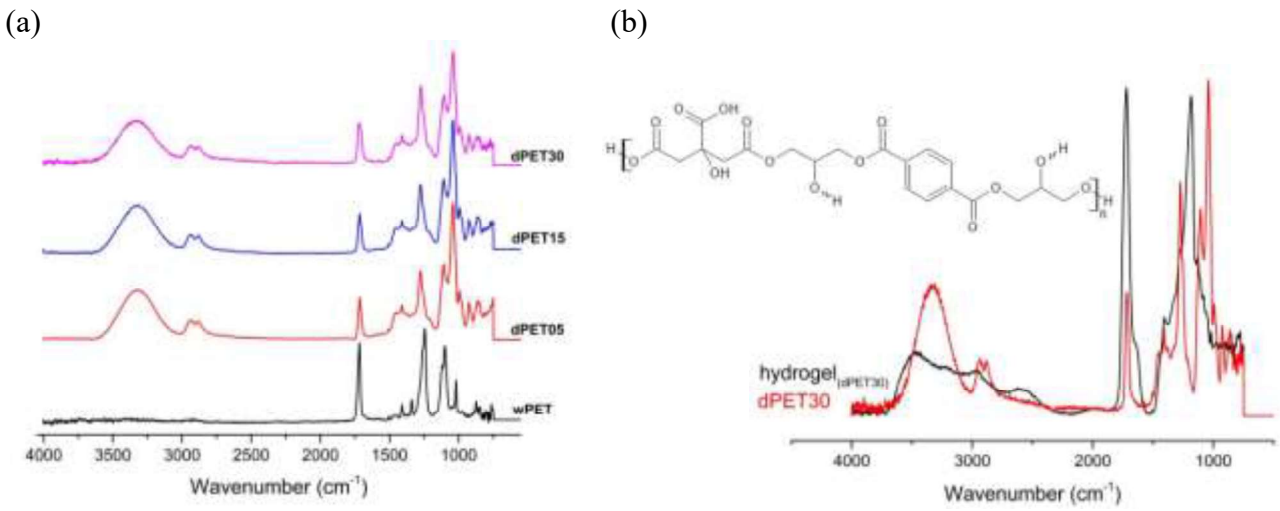

Figure 3. FTIR-ATR of wPET and dPET obtained from different reaction times (a), and hydrogel synthesized from dPET30 crosslinked with 20 mmol of citric acid (b).

Synthesis and application of hydrogels

Aiming at the synthesis in as few steps as possible, dPET were used in the preparation of hydrogels without previous treatment, since unreacted glycerol itself has hydroxyl groups that can also undergo crosslinking. For all dPET samples, the synthesis of hydrogels was possible through cross-linking with citric acid. Through the FTIR analysis it is possible to observe the decrease of the intensity of the hydroxyl band in approximately 3300 cm^{-1} in comparison with the respective dPET sample, which is an indication of the occurrence of crosslinking (Fig. 3(b)) [4].

The material obtained was previously washed, which consists of immersion in deionized water for 48 h at room temperature. In this step, it was possible to determine the swelling capacity (Eq. 1) of the hydrogels as well as their soluble content (Eq. 2) [5], as shown in Table 1:

$$Water\ uptake(W_u) = \frac{Wwet - Wdry}{Wwet} \times 100 \qquad (1)$$

$$Solubility\ index(S_i) = \frac{m_1 - m_2}{m_1} \times 100 \qquad (2)$$

where W_{wet} and W_{dry} are the weights of the wet and dry hydrogel, respectively, and m_1 is the dry hydrogel mass before washing and m_2 is the dry hydrogel mass after swelling.

Table 1. Results of W_u and S_i for the hydrogels dPET05-10 (05-10), dPET15-10 (15-10), dPET30-10 (30-10), dPET05-20 (05-20), dPET15-20 (15-20) and dPET30-20 (30-20).

Sample	05-10	15-10	30-10	05-20	15-20	30-20
W_u (%)	639 ± 85	310 ± 63	604 ± 78	1122 ± 148	550 ± 89	1442 ± 175
S_i (%)	30 ± 4.6	24.8 ± 20.5	29.5 ± 0.8	19.4 ± 0.9	38.2 ± 5.5	83.9 ± 7.5

It is observed that higher crosslinking content (20 mmol) gives the material a higher water uptake capacity and solubility. This is because CA introduces highly hydrophilic groups (-COOH) capable of interacting with water and promoting physical crosslink (ionic and weak hydrogen bond interactions). However, this effect leads to a lower mechanical resistance of the material and, consequently, its disintegration in the aqueous phase. On the other hand, at lower CA content the –COOH groups tend to react with the hydroxyl groups attaching to the carbon chains producing a greater number of active sites. These sites are able to adsorb dye molecules and therefore it is expected that a higher adsorption of IC for hydrogels produced with lower CA content in shorter reaction times. This result is observed experimentally, according to Table 2, the highest adsorption content of 97% was obtained for the dPET05-10 sample [5,6]. This result is very positive because the objectives of the work regarding the recycling of plastic waste and dye removal were achieved, almost completely removing the contaminant.

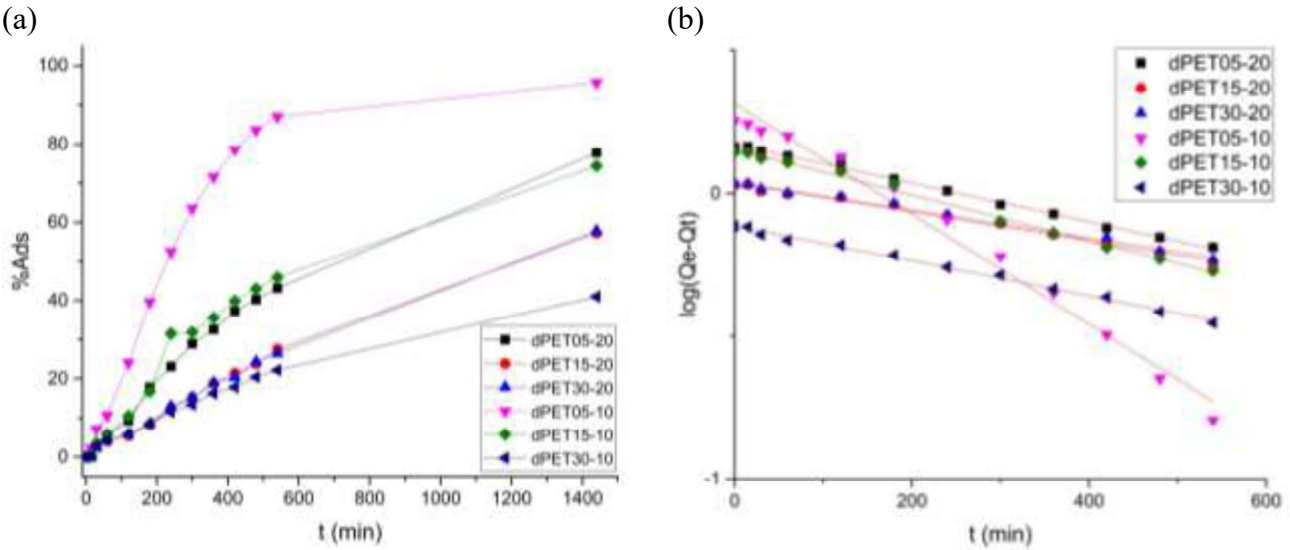

Figure 4. Capacity of IC adsorption (a) and pseudo-first order kinetic model for adsorption (b).

In order to understand the adsorption mechanism, the kinetic analysis was performed by applying the equation of the pseudo-first-order in the linearized form (Eq. 3) [5]:

$$\log(Q_e - Q_t) = \log Q_e - \frac{K_1}{2.303} t \qquad (3)$$

where Q_e and Q_t (mg g^{-1}) are the adsorption capacity of the material at the equilibrium and at time, respectively, and K_1 (min^{-1}) is the pseudo-first order rate constant.

The high correlation between the experimental data applied to the pseudo-first order kinetic equation indicates that the adsorption mechanism of the hydrogels follows this model for the IC dye (Fig. 4(b)). Also, the experimentally obtained $Q_{e(exp)}$ values presented in Table 2 are close to the

respective theoretical values ($Q_{e(cal)}$), which reinforces the correct application of the kinetic model. This means that the rate of change of solute adsorption with time is directly proportional to the difference in saturation concentration and the amount of dye adsorbed with time. Thus, it is indicated that the adsorption occurs by diffusion through the interface [5].

Table 2. Pseudo-first order kinetic parameters of IC dye adsorption and adsorption values for the hydrogels dPET05-10 (05-10), dPET15-10 (15-10), dPET30-10 (30-10), dPET05-20 (05-20), dPET15-20 (15-20) and dPET30-20 (30-20).

Sample	05-10	15-10	30-10	05-20	15-20	30-20
$Q_{e(exp)}$ (mg g^{-1})	1.6064	1.1095	0.6591	1.0849	1.0452	0.8623
$Q_{e(cal)}$ (mg g^{-1})	2.0573	1.4313	0.7691	1.4861	1.0899	1.0935
K_1 (min^{-1})	0.0044	0.0018	0.0014	0.0016	0.0012	0.0011
R^2	0.98419	0.99492	0.99502	0.9971	0.98866	0.99233
Adsorption 24h (%)	97 ± 1.7	74 ± 0.6	40 ± 2.6	76 ± 2.3	63 ± 4.4	56 ± 2.3

Conclusions

The chemical recycling of PET can be carried out quickly and efficiently through the glycerolysis reaction with MW radiation. The depolymerization product can be used directly in the preparation of hydrogels through crosslinking with citric acid. The adsorption of the indigo carmine dye was successful, reaching adsorption values of 97% for the sample with the shortest reaction time (5 min) and lowest crosslinking content (10 mmol g^{-1}), with an adsorption capacity of 1.6064 mg g^{-1}. The adsorption mechanism follows a pseudo-first order kinetics, which indicates that the adsorption occurs by diffusion through the interface. The material obtained in a sustainable way can be used in the effluent treatment for the removal of dyes, thus helping to reduce plastics waste and improve water quality.

Acknowledgements

The authors are grateful to Conselho Nacional de Desenvolvimento Científico e Tecnológico (CNPq) and Fundação de Amparo à Pesquisa do estado do Rio Grande do Sul (PRONEX/FAPERGS - Finance Code 16/2551-0000470-6) for financial support.

References

1. M. F. Chowdhury; S. Khandaker; F. Sarker; A. Islam; M. T. Rahman; M. R. Awual Journal of Molecular Liquids 2020, 318, 114061. https://doi.org/10.1016/j.molliq.2020.114061.
2. F. Zhang; F. Wang; X. Wei; Y. Yang; S. Xu; D. Deng; Y. Wang Journal of Energy Chemistry 2022, 69, 369-388. https://doi.org/10.1016/j.jechem.2021.12.052.
3. E. Fernandes; J. Vicente; R. Cruz; M. Nele; E. Nunes; R. Costa-Félix Polymer Testing 2014, 33, 16-20. http://dx.doi.org/10.1016/j.polymertesting.2013.10.015.
4. V. Gayathri; R. T. B. Sheyara; N. Devassy; D. Samanta Journal of Applied Polymer Science 2022, 139, 52474. https://doi.org/10.1002/app.52474.
5. H. T. Nguyen; F. A. Ngwabebhoh; N. Saha; T. Saha; P. Saha International Journal of Biological Macromolecules 2022, 222, 77-89. https://doi.org/10.1016/j.ijbiomac.2022.09.040.
6. C. Demitri; R. D. Sole; F. Scalera; A. Sannino; G. Vasapollo; A. Maffezzoli; L. Ambrosio; L. Nicolais Journal of Applied Polymer Science 2008, 110, 2453-2460. DOI 10.1002/app.28660.

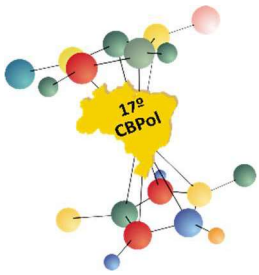

TGA MONITORING OF THE GLYCOLYSIS OF HIGH TENACITY POLYESTER FIBER FROM MOORING LINES

Elaine M. Senra[1*], Renan H.G. Almeida[1], Ana L. N. Silva[1,2], José C. C.S. Pinto[3] and Elen B. A. V. Pacheco[1,2]

1 – Instituto de Macromoléculas Professora Eloisa Mano, Universidade Federal do Rio de Janeiro (UFRJ), Rio de Janeiro, RJ, Brazil, elainemsenra@ima.ufrj.br*
2 – Escola Politécnica/Programa de Engenharia Ambiental, Universidade Federal do Rio de Janeiro (UFRJ), Rio de Janeiro, RJ, Brazil
3 – Programa de Engenharia Química/COPPE, Universidade Federal do Rio de Janeiro (UFRJ), Rio de Janeiro, RJ, Brazil

Abstract – This study analyzed the chemical recycling of high tenacity polyethylene terephthalate (PET_H) from decommissioned oil platforms. The PET fibers are from mooring lines, which form part of the solid waste generated at the end of a platform's lifespan and require proper disposal. PET glycolysis was performed as an alternative to reintroducing the material into the production chain. The degrading agent used was 400 molar mass polyethylene glycol (PEG400) and glycolysis was carried out at 205-210ºC in the presence of zinc acetate as catalyst. The raw material and product were characterized by Fourier-transform infrared spectroscopy (FTIR) and thermogravimetric analysis (TGA) and the reaction was monitored by TGA, with aliquots extracted at 20, 60, 120 and 180 minutes. The product was vacuum filtered at a temperature of 100°C. The TGA curves of the reaction samples show two thermal events: 1) values between 337 and 364°C; and 2) decrease of the PET_H degradation temperature, which was initially 439°C. The degradation temperature of PET_H decreased by up to 40-45°C during the glycolysis reaction. In the present study, glycolysis formed oligomers with ester groups, known as oligoesters, which are promising sources of raw material for the chemical industry.
Keywords: *Chemical recycling, glycolysis, PET, high tenacity PET, TGA*
Fundings: This study was funded by the Coordination for the Improvement of Higher Education Personnel (CAPES).

Introduction

Stationary offshore production units were designed and constructed to adapt to a field aimed at producing petroleum or gas for at least 15 to 20 years [1]. These offshore activities are eventually abandoned. Decommissioning includes environmental care and concern over suitable disposal of the solid waste produced. Among the materials decommissioned are mooring lines made of high tenacity polyethylene terephthalate (PET_H) [2], which exhibits higher molar mass than bottle grade PET and should be recovered to optimize its properties, thereby meeting Circular Economy principles. Different PET recycling methods have been studied [3,4], the most widely applied being mechanical recycling. However, chemical recycling (hydrolysis, alcoholysis, acidolysis, glycolysis and aminolysis) [5,6] has attracted the interest of industries and the scientific community. Among the main chemical treatments of PET, to date only glycolysis has reached commercial maturity [7]. Glycolysis is a PET transesterification reaction with excess glycol that occurs between 180 and 240°C, processed under 0.1–0.6 MPa of pressure or at ambient pressure in the presence of transesterification catalysts to produce monomers and olygomers. The oligomers and monomers formed from short-chain glycolosis agents, such as ethylene glycol, have a molar mass varying from 210 to 595 $g \cdot mol^{-1}$ [5]. Since the PEG400 glycolysis agent has a larger carbon chain than short-chain agents, they form a long-chain oligomer that can vary between 200 and 1380 $g \cdot mol^{-1}$ [5,8]. The main catalyst used in glycolysis reactions is zinc acetate [6,9].

Experimental

Materials

High-tenacity polyester fiber was obtained from a mooring line (mol.wt. 192 g mol^{-1}), and cut into approximately 1 cm pieces. Zinc acetate was used as the catalyst for PET depolymerization. Polyethylene glycol) (mol.wt. 400 g mol^{-1}) (PEG400) and zinc acetate were used as supplied.

Raw material and reaction product characterization

PET and PEG400 were characterized by attenuate total reflection Fourier-transform infrared spectroscopy (ATR-FTIR) (Perkin-Elmer Spectrum Version 10.4.2) and thermogravimetric analysis (TGA) (TA Instruments Q500). Analysis was conducted with 60 scans per second at 4.00 cm resolution. The raw material degradation temperature was determined as a function of weight loss with a rise in temperature by TGA in nitrogen purge gas, at a heating velocity of 10°C/min and temperature range of 30-700°C.

Oligoester synthesis

Oligoester was synthesized using PET_H glycolysis via the PEG400 glycolysis agent and zinc acetate as catalyst. The molar ratio of PET_H repeating unit to glycol was 1:5. To that end, 15g of PET_H and 156g of PEG400 were used. The catalyst was used at a mass ratio of 5% based on PET mass. The reaction was processed in a 1-L glass reactor under agitation, reflux condenser, inert gas, and temperature controller. Heating was carried out using a thermal mantle. First, the reactor was added with PEG400 and the catalyst, heated to a temperature of 100°C, then gradually added with fibers to avoid agglomeration in the reactor, under 40 rpm agitation. After the fiber was added, the reaction medium was heated to 205-210°C and agitation increased to 80-100rpm. Sample aliquots were removed at 20, 60, 120 and 180 min of reaction for TGA analysis. At the end of the reaction, the product formed was vacuum filtered at 100°C and characterized by ATR-FTIR.

Results and Discussion

Characterization of raw materials

First, the raw materials were characterized by ATR-FTIR. Fig. 1 shows the characteristic peaks of PET_H (Fig. 1a) and PEG 400 (Fig. 1b), whose main bands were highlighted for PET and PEG characterization. Fig. 1a shows the characteristic PET_H peaks, whose main bands are 2963cm^{-1} for symmetric stretching bands -CH_2 of 1712 cm^{-1} for the C=O group; between 1016 and 1240 cm^{-1} for the COOC group; 1504 cm^{-1} for C=C of the benzene ring and 650 and 900 cm^{-1} for aromatic C-H, results also observed in the literature [10,11]. Fig. 1b shows characteristic PEG 400 peaks and the following bands are highlighted: 3447 cm^{-1} for O-H stretching, 2865 cm^{-1} for -CH_3 stretching, and 1095 cm^{-1} for C–O–C symmetrical stretching [12,13]. The results of characterization analyses confirm the chemical structures of the raw materials used and were also applied to compare and discuss the results of the reactions carried out.

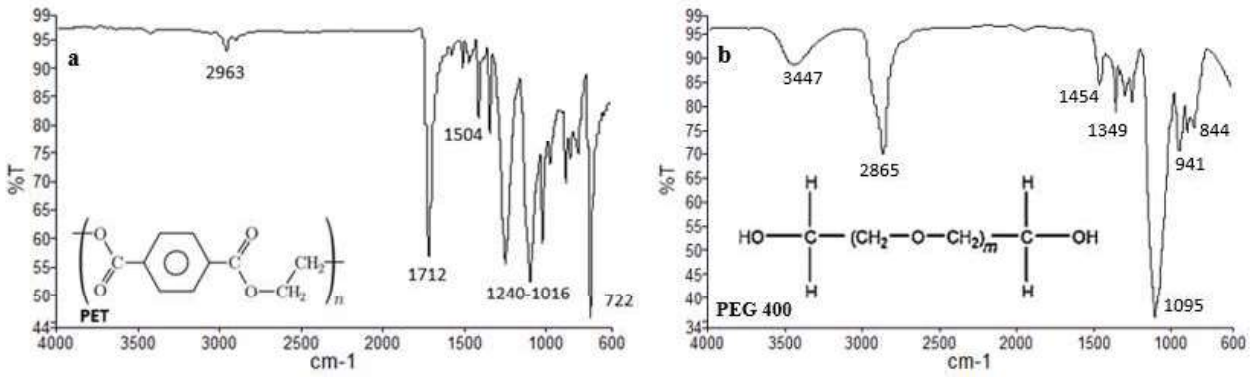

Figure 1. ATR-FTIR spectrum of : (a) PET_H and (b) PEG 400.

Fig. 2 shows the weight loss curve obtained by thermogravimetric analysis (TGA) and differential thermogravimetry (DTG) of PEG400 (Fig. 2a) and PET_H (Fig. 2b). The DTG curve (Fig. 2a) exhibits a maximum PEG400 degradation temperature of 343.6°C. Fig. 2b shows that maximum and minimum PET_H degradation occurred at 439.4 and 621.4°C, respectively.

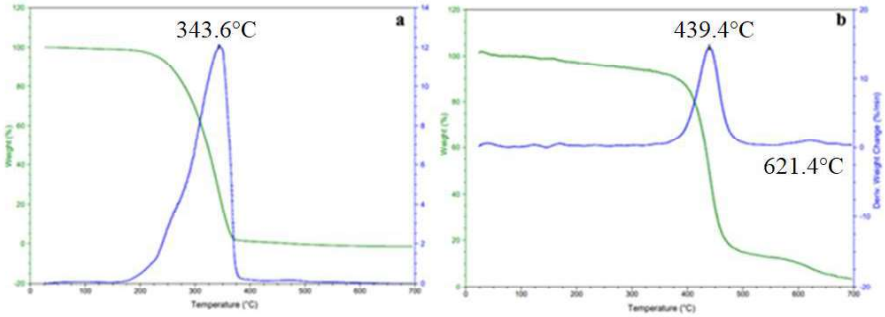

Figure 2. Thermogravimetric and differential thermogravimetry curves of PEG400 (a) and PET_H (b)

Oligoester Synthesis

It was difficult to chemically recycle PET_H fibers due to their larger size when compared to PET flakes or pellets, which are the most commonly recycled forms of PET [6,14]. When fiber is added to the reaction, the glycolysis agent is absorbed by the fiber and the reaction medium exhibits a very low liquid level, which hinders suitable homogenization of the solution for subsequent reaction. It was not possible, for example, to use lower proportions of glycolysis agents and PET, such as a PET/glycol molar ratio of 1:2, as observed in other studies [8,15], where PET was in the form of flakes. Adding PET_H fibers to the reaction medium at ambient temperature was also not favorable for glycolysis, since the fiber took longer to solubilize and the reaction medium remained heterogeneous for longer, which was 50 min for the medium to become homogeneous, when the fiber was no longer visualized. Adding PET_H to the reaction medium at a temperature of 80 to 100°C produced a better result, since the fibers dissolved faster in the medium and after 30 min, the reaction medium became homogeneous. Agitation in the medium was initially maintained at 40 rpm and once all the PET fiber was added, agitation increased to 80 to 100 rpm, thereby preventing the fibers from adhering to the internal reactor wall and the agitator. At the end of the reaction, the medium was cooled to 100°C and vacuum filtered.

Oligoester characterization

Oligoester formation using the glycolysis reaction was confirmed by ATR-FTIR analysis. The spectrum presented in Fig. 3 showed C=O stretching of around 1719 cm^{-1}, which is a band characteristic of ester bond formation in PET glycolysis [8]. Comparison of the curves in Fig. 1 shows some similarity with the FTIR spectrum of PEG (Fig. 1b), but the latter does not contain the band at 1719 cm^{-1}. The band around 3451 cm^{-1} is due to the free hydroxyl group present in glycolyzed PET oligoesters [16].

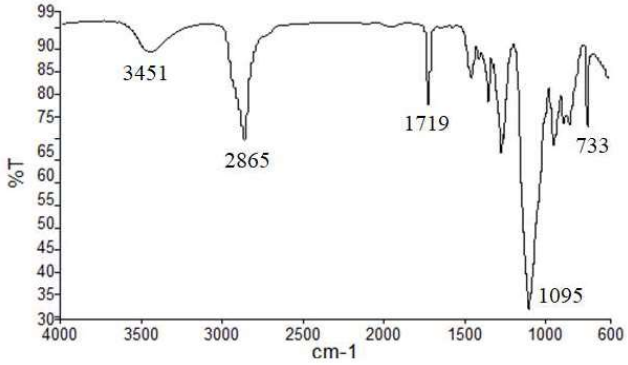

Figure 3. ATR-FTIR spectrum of glycolyzed PET (oligoester)

TGA was used to monitor the glycolysis reaction by observing the variation in maximum PET_H degradation temperature, caused by the glycolysis reaction [17]. Weight loss and maximum degradation temperatures are shown in Fig. 4a and 4b. Two degradation peaks were observed. The first thermal event occurred between 337 and 364°C, likely corresponding to PEG and the oligomers formed. The values of the first event were near those of PEG (343 °C) in the first 20 minutes of reaction, an expected result, since PEG is excessively used. At 180 minutes, the thermal degradation temperature increased by around 25°C. There are reports in the literature [18] of oligomers glycolized with glycol ethylene from PET obtained at a PEG temperature of 341°C. TGA analysis of the second degradation peaks indicates a decline of around 45°C in the first 60 minutes of reaction, compared to the original PET_H), in addition to a 40°C decrease after 20 and 180 minutes of reaction, suggesting possible PET degradation.

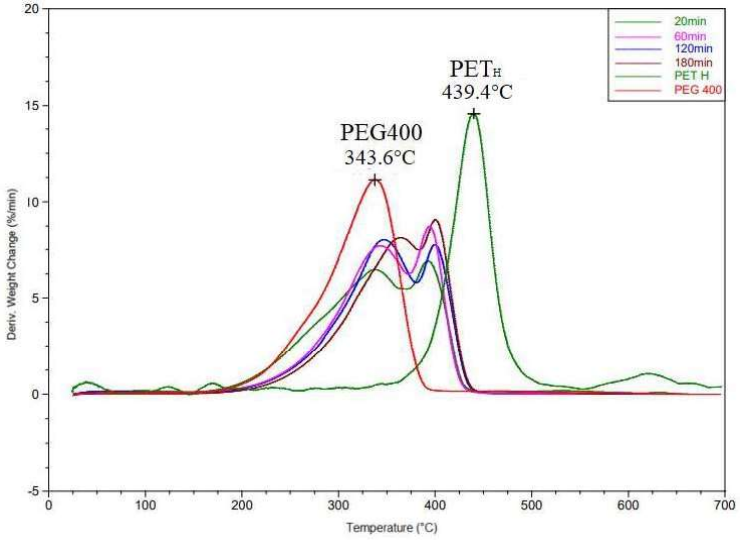

Figure 4. Differential thermogravimetry curves: PET_H, PEG400 and samples extracted at 20, 60, 120 and 180 min of reaction.

Table 1. Maximum degradation temperatures of the raw materials and samples of the reaction medium using thermogravimetric analysis.

Sample/Glycolysis time	First DTG peak (°C)	Second DTG peak (°C)
PET_H	-	439
PETG400	343	-
20 min	337	393
60 min	343	394
120 min	346	399
180 min	364	399

Conclusion

High tenacity PET fiber reacted with polyethylene glycol with a molar mass of 400, a result confirmed by ATR-FTIR and TGA. The synthesis of the PET oligoester was confirmed by ester bond formation observed by ATR-FTIR. The thermal analysis results demonstrated that the PET degradation peak decreased by 40-45 °C, confirming the reaction with polyethylene glycol.

Acknowledgements

The authors thank the Coordination for the Improvement of Higher Education Personnel (CAPES) for the scholarship awarded to Elaine Meireles Senra.

References

1. E.J. Techera, J. Chandler, Mar. Policy 2015, 59. https://doi.org/10.1016/J.MARPOL.2015.04.021.
2. D.P. Sudaia, M.B. Bastos, E.B. Fernandes, C.R. Nascimento, E.B.A.V. Pacheco, A.L.N. da Silva, Mar. Pollut. Bull 2018, 135. https://doi.org/10.1016/j.marpolbul.2018.06.066.
3. P. Sarda, J.C. Hanan, J.G. Lawrence, M. Allahkarami, J. Polym. Sci. 2022, 60. https://doi.org/10.1002/pol.20210495.
4. E. Barnard, J.J. Rubio Arias, W. Thielemans, Green Chem. 2021, 23. https://doi.org/10.1039/d1gc00887k.
5. B. Geyer, G. Lorenz, A. Kandelbauer, Express Polym. Lett. 2016, 10. https://doi.org/10.3144/expresspolymlett.2016.53.
6. A.B. Raheem;, Z.Z. Noor, A. Hassan, M.K.A. Hamid, S.A. Samsudin, A.H. Sabeen, J. Clean. Prod. 2019, 225. https://doi.org/10.1016/j.jclepro.2019.04.019.
7. S.M. Cakić, I.S. Ristić, D.T. Stojiljković, N.N. Nikolić, B. Todorović, N. V. Radosavljević-Stevanović, Polym. Bull. 2019, 76. https://doi.org/10.1007/s00289-018-2429-4.
8. S.M. Cakić, I.S. Ristić, M.M. Cincović, D.T. Stojiljković, C.J. János, C.J. Miroslav, J. V. Stamenković, Prog. Org. Coatings 2015, 78. https://doi.org/10.1016/j.porgcoat.2014.07.012.
9. A.M. Al-Sabagh, F.Z. Yehia, D.R.K. Harding, G. Eshaq, A.E. ElMetwally, Green Chem. 2018, 18. https://doi.org/10.1039/c6gc00534a.
10. E.M. Senra, A.E.F.A. da Silva, L.L.Y. Visconte, A.L.N. Silva, E.B.A.V. Pacheco, J. Polym. Environ. 2022. https://doi.org/10.1007/s10924-022-02471-9.
11. I. Acar, G. Güçlü, Polym. Eng. Sci. 2013, 53. https://doi.org/10.1002/pen.23491.
12. M.A. Marcos, D. Cabaleiro, M.J.G. Guimarey, M.J.P. Comuñas, L. Fedele, J. Fernández, L. Lugo, Nanomaterials 2018, 8. https://doi.org/10.3390/nano8010016.
13. M. Sahu, V.R.M. Reddy, B. Kim, B. Patro, C. Park, W.K. Kim, P. Sharma 2022, 15. https://doi.org/10.3390/ma15051708.
14. B. Shojaei, M. Abtahi, M. Najafi, Polym. Adv. Technol. 2020, 31. https://doi.org/10.1002/pat.5023.
15. V.S. MR Patel, JV Patel, Polym Int. 2006, 55. https://doi.org/10.1002/pi.
16. S.M. Cakić, I.S. Ristić, M. M-Cincović, N.Č. Nikolić, O.Z. Ilić, D.T. Stojiljković, J.K. B-Simendić, Prog. Org. Coatings 2012, 74. https://doi.org/10.1016/j.porgcoat.2011.11.024.
17. F. Chen, Q. Zhou, R. Bu, F. Yang, W. Li, Fibers Polym. 2015, 16. https://doi.org/10.1007/s12221-015-1213-4.
18. X. Zhou, C. Fang, Q. Yu, R. Yang, L. Xie, Y. Cheng, Y. Li, Int. J. Adhes. Adhes. 2017, 74. https://doi.org/10.1016/j.ijadhadh.2016.12.010.

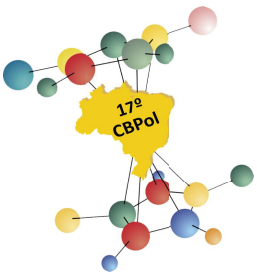

UV BLOCKING PROPERTIES OF POLYCAPROLACTONE-TRIOL-BASED POLYURETHANE FILMS INCORPORATED WITH CITRUS PEEL EXTRACTS

Jéssica S. Chaves[1], Roberta S. Rocha[1], Eduarda M. Lemes[1], Roberta C. Rieffel[2], Irene C. Kulkamp-Guerreiro[2], Karine M. Zepon[1,3] and Rachel F. Magnago[1,3]

1 – Laboratory of Active Materials, University of Southern Santa Catarina (UNISUL), Palhoça, SC, Brazil
rachelfaverzanimagnago@gmail.com
2 – Federal University of Rio Grande do Sul (UFRGS), Porto Alegre, RS, Brazil
3 – Laboratory of Biomaterials and Biomimetics, University of Southern Santa Catarina (UNISUL), Tubarão, SC, Brazil

Abstract - Polyurethane (PU) and citrus-PU (orange, lemon and tangerine) membranes were produced and evaluated for UV radiation blocker and thermal properties. The membranes were evaluated by thermogravimetry, by UV-Vis spectrophotometry and also the amount of resveratrol (RSV) and lipoic acid (ACL) were evaluated by an Agilente high-performance liquid chromatograph (model 1200 Infinity). Orange (Ora-PU), lemon (Lem-PU) and tangerine (Tan-PU) membranes showed that the membranes are thermally stable at temperatures up to 250 °C. Finally, Ora-PU, Lem-PU, and Tan-PU membranes blocked UV radiation reducing the decomposition of RSV and ACL, confirming their potential use as topical dressings.
Keywords: *Film; Polycaprolactone-triol; Polyurethane; Terpenes; UV blocker.*
Fundings: No funding.

Introduction

Non-toxic polymeric materials are widely used in medical, biomedical, and pharmaceutical fields for tissue engineering [1], implants [2], and drug delivery systems [3, 4]. Excellent UV protection in the 200 to 400 nm range was observed by Zhang et al. (2019) [5] in ultrathin PU films synthesized using lignin as hard segments and polycaprolactone glycol as soft segments coupled using hexamethylene diisocyanate (HDI). Barbosa et al. (2022) [6], for example, reported that the incorporation of limonene (1-methyl-4-(1-methyl phenyl)-cyclohexene) to chitosan films increased the barrier to light transmission, especially to UV radiation. Polyurethanes are among the most ubiquitous materials in the biomedical field whose use includes but is not limited to heart valves, intra-aortic balloons, guided bone regeneration, breast implants, and drug delivery systems. One factor that explains this widespread use is the presence of amide bonds in its structure (-NH-COO-). They are related to the amide bonds found in the chemical structure of the proteins. Besides, polyurethane properties can be tailored and tuned to achieve specific features important for biomedical devices, especially in drug delivery systems [4]. Limonene is one of the most abundant terpenes in nature and is commonly found in the peel of lemons [7], oranges and tangerine [8]. The therapeutic effects of limonene have been extensively studied and include but are not limited to anti-inflammatory, antioxidant, antinociceptive, anticancer, antidiabetic, antiviral, and gastroprotective activity [9]. Therefore, this study investigated the incorporation of oily citrus peel extracts into PCL-T and HDI-based polyurethane films, investigating their UV barrier effect.

Experimental

Polycaprolactone triol (PCL-T, 900 g.mol^{-1}, Sigma-Aldrich), 1,6-hexamethylene diisocyanate (HDI, Sigma-Aldrich), and limonene (CAS:5989-27-5, Sigma-Aldrich) were used as received.
The fruits Pear orange - *Citrus sinensis* peel, Ponkan mandarin - *Citrus reticulata* peel, and Tahiti lemon - *Citrus latifolia* peel were purchased from the State Supply Center in Florianópolis, Santa Catarina, Brazil. The peels were dried in an oven at 40 ºC and ground with a knife mill. Tetrahydrofuran (THF), calcium chloride, and hexane were obtained from Synth (Brazil).
The crushed orange, lemon, and tangerine peels were placed on filter paper, and oil extraction was performed using a soxhlet extractor. Accordingly, 250 mL of hexane was added to a 500 mL flat bottom flask that was then coupled to the soxhlet and refluxed for 24 h. After that, the solvent was removed using a rotary evaporator, and the obtained oil was weighed (Jayaprakasha et al., 2000). The limonene concentration of the extracts was determined by ultraviolet-visible spectroscopy (UV-VIS) using a validated method in the concentration range of 5 to 0.3 mg mL^{-1} with a correlation coefficient of 0.9906 at 260 nm. The calibration curve was constructed using five dilutions from a solution of 5 mg limonene and 4.5 g Tween-80 in phosphate-buffered saline. For each extracted oil, a solution was prepared with 0.25 mg mL^{-1} oil, 4.5 g Tween-80, and phosphate-buffered saline solution.
Pure PU and PU films containing the oily extracts obtained from orange (Ora-PU), lemon (Lem-PU), and tangerine (Tan-PU) peels were synthesized by polycondensation. Briefly, the PU was prepared round bottom flask with a drying tube was flamed with a Bunsen burner. Then a solution containing 1 g of PCL-T (900 g.mol^{-1}) in 4 mL THF was transferred to the flask under stirring in an oil bath between 50 ºC and 55 ºC. After 5 min of stirring, 0.37 g of HDI previously solubilized in 4 mL THF was added to the flask. The reaction medium was kept under stirring for 48 hours, and then 0.25 g of oil extracted from orange, lemon, or tangerine was added and kept for 15 min under stirring. In the end, the mixture was poured into a Petri dish and kept at room temperature until complete evaporation of the solvent (48 hours to 72 hours) [4].
The spectral transmittance of PU, Ora-PU, Lem-PU, and Tan-PU films was investigated using a UV-vis spectrophotometer (UV-vis; LGS 53, Bel Photonics, Brazil) in the UVB (280 - 315 nm), UVA (315 - 400 nm) and visible (400 - 700 nm) wavelength ranges. The transmittance reading was performed for each prepared film at specific intervals. For the stability test to UVA radiation, the actives resveratrol (RSV) and lipoic acid (ACL), sensitive to radiation activity, were used [10]. In the preparation of the samples, a concentration of 1000 µg/mL of actives (RSV and ACL) diluted in DMSO was used. For negative controls, RSV and ACL solutions in DMSO were used. Test samples and controls were distributed in 96-well plates and exposed to a source of UVA radiation in a mirrored chamber with four 30 W UVA lamps with radiation intensity 0.286 W.m^{-2}, arranged in parallel and suspended 42 cm from the samples. In the times of exposure to UVA radiation 0, 2, 4 and 8 hours, 50 µL of the samples were collected, and diluted in 1 mL of an acetonitrile solution containing 0.05% BHT, the samples were then homogenized and filtered in vials, therefore, the degradation of the RSV and ACL assets was evaluated by HPLC-UV, according to the methodology described by Davies et al. (2018). The quantification of RSV and ACL assets was performed on an Agilente high-performance liquid chromatograph, model 1200 Infinity, with automatic injector and diode array (DAD) and refractive index (RID) detectors, using a C18 column (150 x 4 .60 mm, 5 µm particle and 110 µm diameter) coupled to a C18 pre-column, at a temperature of 25°C and flow rate of 0.8 mL/min. The mobile phase used was composed of an acetonitrile solution and 0.01 M phosphoric acid (60:40, v/v). Chromatograms were obtained with a UV detector with a wavelength of 235 nm. To quantify the RSV and ACL assets, an analytical curve previously prepared was used, according to the methodology by Davies et al. (2018) [11]. Lipoic acid with R^2=0.9977 and Resveratrol with R^2=0.9993. The analysis was performed in

triplicate and statistically analyzed using the GraphPad Prism program, with analysis of variance and post hoc Dunnet tests. Results were expressed as mean and standard deviation.
Thermogravimetric analyses (TGA) were performed on a Linseis STA PT 1000 instrument from room temperature to 700 ºC, with a heating ramp of 10 ºC min^{-1} in a nitrogen atmosphere.

Results and Discussion

The yields of oil extraction from orange, tangerine, and lemon peels were 2,10 ± 0,19% (about shell weight), 3,60 ± 0,32% (about shell weight) e 5,20 ± 0,06% (concerning shell weight), respectively, these values being higher than those found by Ndayishimiye et al. (2017) [12] for *Citrus ichangensis* × *Citrus reticulata*. The limonene contents quantified by UV-vis from orange, tangerine, and lemon oil were 56 mg mL^{-1}, 71,42 mg mL^{-1} e 81,39 mg mL^{-1}, respectively, and these contents were similar to those reported by Shin et al. (2022) [8]. It is worth noting that the limonene absorption band at 260 nm comes from transitions $\pi \rightarrow \pi^*$ of connections C=C present in the cyclohex-1-ene ring and prop-1-en-2-il. Fig. 1(a) shows the visual appearance of PU, Ora-PU, Lem-PU, and Tan-PU films, while Fig. 1(b) shows the transmittance spectra of the films.

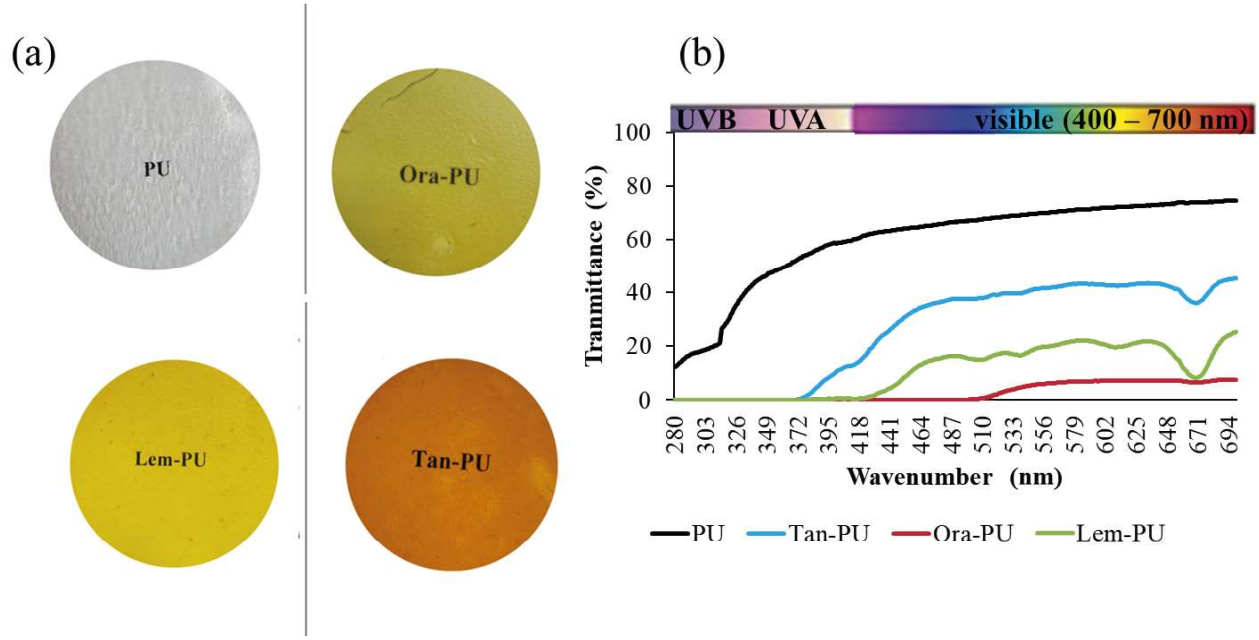

Fig. 1. (a) Visual appearance of PU, Ora-PU, Lem-PU and Tan-PU films obtained from the polycondensation reaction between PCL-T and HDI with citrus extracts, (b) Transmittance analysis of PU, Ora-PU, Lem-PU and Tan-PU films in the wavelength range of 280-700 nm

Fig. 1(a) shows that all films showed a uniform, homogeneous surface without bubbles (https://youtube.com/shorts/TAS49446AB4). In Fig. 1, the transmittance spectra revealed that the PU film transmits light in the UVB (280 - 315 nm), UVA (315 - 400 nm), and visible (400 - 700 nm) regions with a maximum transmittance of 74.5% at 700 nm. Films of Ora-PU, Lem-PU, and Tan-PU showed no transmittance in the UVB region, and the films Ora-PU e Lem-PU were able to block UVA radiation as well. For the film Tan-PU, UVA radiation was transmitted from 375 nm with a maximum of 45.5% transmittance at 700 nm.
PU film showed two stages of mass loss, the first attributed to the degradation of the urethane bond and the second related to the decomposition of PCL-T, membranes showed that the membranes are thermally stable at temperatures up to 250 °C.
Quantification results for RSV and LA were performed using a positive control (no barrier), PU, Ora-PU, Lem-PU and Tan-PU films for time 0, 2, 4 and 8 hours, as shown in Table 1.

Table 1. Percent non-degraded RSV and LA for positive control (no barrier), PU, Ora-PU, Lem-PU and Tan-PU films for times 0, 2, 4 and 8 hours in UVA.

Samples	Time			
	0 h	2 h	4 h	8 h
Control LA	100%	58,31±0,03%	55,06±0,01%	48,42±0,03%
PU	100%	74,27±0,02%	53,71±0,03%	41,78±0,02%
Ora-PU	100%	79,26±0,01%	79,95±0,02%	71,17±0,00%
Lem-PU	100%	73,88±0,01%	75,94±0,01%	73,50±0,01%
Tan-PU	100%	81,34±0,02%	69,86±1,05%	68,18±0,06%
Control RSV	100%	36,01±0,00%	12,44±0,00%	10,51±0,01%
PU	100%	38,11±0,03%	14,43±0,00%	9,62±0,00%
Ora-PU	100%	98,42±0,00%	91,89±0,01%	78,63±0,00%
Lem-PU	100%	75,78±0,07%	77,64±0,01%	58,88±0,03%
Tan-PU	100%	97,02±0,00%	86,61±1,74%	79,09±0,03%

In Table 1, it can be seen that both for the control and for the PU film, the degradation was greater than 50% for LA and ~90% for RSL, that is, the PU film does not block UVA radiation. All PU films prepared with citrus extracts blocked UVA radiation, keeping the LA and RSV intact between 74% to 98% up to 2 h, between 77% to 92% up to 4 h and 68% to 79% up to 8 h. In addition, the Ora-PU film was more efficient to maintain the integrity of LA for 2 h and 4 h, however for the total time of 8 h the best performance was observed for Lem-PU film. Similar result was observed for RSV, where Ora-PU was more efficient in the first 4 hours, however for the total time of 8 h the best result was observed for Tan-PU.

Antioxidants were kept in greater quantity and for a longer time under UVA radiation, thus decreasing or inactivating free radicals and/or reducing oxidative damage. Recently, studies have demonstrated that RSV has many biological activities, including cardioprotective, chemopreventive, neuroprotective, anti-inflammatory, and antioxidant effects. Likewise, LA is a potent antioxidant with reactive oxygen species scavenging activity, ability to repair other antioxidants (such as ascorbic acid, α-tocopherol and glutathione) under physiological and pathophysiological conditions in vivo, and can also chelate metals. LA can prevent aging caused by sun damage, aiding recovery from injuries, preventing skin inflammation and photocarcinogenesis caused by ultraviolet radiation [11]. In this way, films prepared with citrus peel extracts maintain LA and RSV activity.

Thermal stability evaluation of PU, Ora-PU, Lem-PU and Tan-PU films was performed by thermogravimetry (Fig. 2).

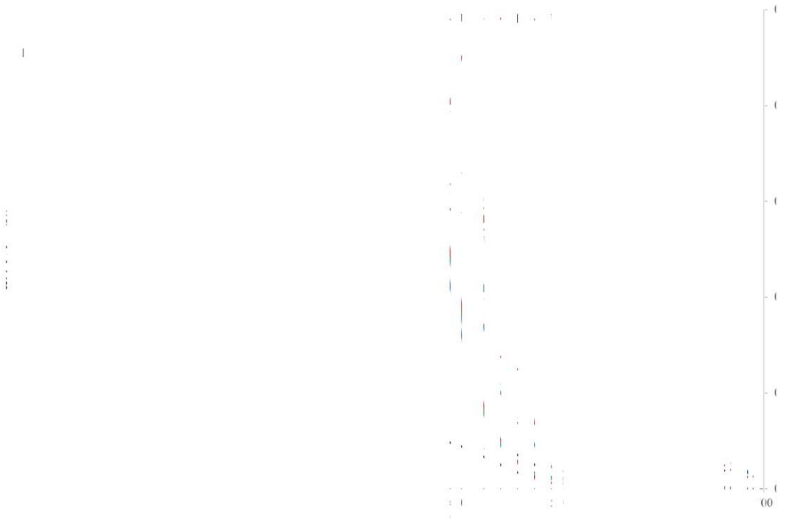

Fig. 2. Thermograms of (a) TGA and (b) DrTGA of PU (black line), Ora-PU (red line), Lem-PU (green line) and Tan-PU (blue line).

In Fig. 2, the PU film showed two stages of mass loss, the first attributed to the degradation of the urethane bond and the second related to the decomposition of PCL-T. The primary decomposition peak was observed between 250 °C and 365 °C, with maximum degradation temperature at 322 °C [4]. The citrus oil extracts' films showed higher thermal stability than the pure film. The main decompositions occur between 280 ºC and 490 ºC, with maximum degradation temperatures at 410 ºC, 405 ºC, and 402 ºC for Ora-PU, Lem-PU, and Tan-PU, respectively. In addition, no mass loss was observed for Ora-PU, Lem-PU, and Tan-PU films in the temperature range from 50 to 120 °C, related to the evaporation of unassociated water and limonene.

Conclusions

PU membranes were obtained by polycondensation reaction between PCL-T and HDI, with and without the addition of citrus extracts obtained from citrus fruit peels. Membranes with extracts were shown to block UVA and UVB radiation. The membranes showed thermal stability up to 250 ºC. The analytical method used to determine the percentage of RSV and LA showed that membranes with citrus extracts prevent the decomposition of RSV (Lem-PU maintained 74% in 8 h) and LA (Tan-PU maintained 79% in 8 h). Prepared films can be indicated for potential use as topical dressings.

Acknowledgements

The authors thank the support of the INSTITUTO ÂNIMA/UNISUL and PIBIC/CNPq scientific initiation scholarship.

References

1. H. Y. Mi; X. Jing; G. Yilmaz; B. S. Hagerty; E. Enriquez; L. S. Turng. Chemical Engineering Journal 2018, 348, 786. https://doi.org/10.1016/j.cej.2018.04.198
2. S. Y. Lee; S. C. Wu; H. Chen; L. L. Tsai; J. J. Tzeng; C. H. Lin; Y. M. Lin. BioMed Research International 2018. https://doi.org/10.1155/2018/3240571
3. N. Abbasnezhad; N. Zirak; M. Shirinbayan; S. Kouidri; E. Salahinejad; A. Tcharkhtchi; F. Bakir. Journal of Applied Polymer Science 2021, 138. https://doi.org/10.1002/app.50083
4. R. F. Magnago; A. C. Aguiar; I. F. Valezan; F. M. Moraes; A. L. Ziulkoski; F. D. P. Morisso; L. A. Kanis; K. M. Zepon. European Polymer Journal, 2022, 179. https://doi.org/10.1016/j.eurpolymj.2022.111533
5. Y. Zhang; J. Wang; X. Fang; J. Liao; X. Zhou; S. Zhou; F. Bai; S. Peng. Polymer 2019, 178. https://doi.org/10.1016/j.polymer.2019.121572
6. M. H. R. Barbosa; S. Á. Gonçalves; L. Marangoni Jr; R. M. V. Alves; R. P. Vieira. Journal of Food Measurement and Characterization 2022, 16, 2011. https://doi.org/10.1007/s11694-022-01337-x
7. A. Martínez-Abad; M. Ramos; M. Hamzaoui; S. Kohnen; A. Jiménez; M. C. Garrigós. Foods 2020, 9(10). https://doi.org/10.3390/foods9101493
8. S. D. Shin; C. S. Kim; J. H. Lee. Food Science and Technology 2022, 42. https://doi.org/10.1590/fst.95921
9. A. J. Vieira; F. P. Beserra; M. C. Souza; B. M. Totti; A. L. Rozza. In Chemico-Biological Interactions 2018, 283, 97. https://doi.org/10.1016/j.cbi.2018.02.007
10. C. B. Detoni; G. D. Souto; A. L. M. Silva; A. R. Pohlmann; S. S. Guterres. Photochemistry and Photobiology 2012, 88, 913. https://doi.org/10.1111/j.1751-1097.2012.01147.x
11. S. Davies; S. Jacobus; S. Stanisçuaski; I. C. Külkamp. Drug Analytical Research 2018, 2, 13. https://doi.org/10.22456/2527-2616.82578
12. J. Ndayishimiye; A. T. Getachew; B. S. Chun. Waste and Biomass Valorization 2017, 8, 1205. https://doi.org/10.1007/s12649-016-9697-8

CHEMICAL RECYCLING OF POLY(3-HYDROXYBUTYRATE-CO-3-HYDROXYVALERATE) (PHBV) SOLUTION BLOW SPUN FIBERS THROUGH HYDROLYSIS

Lucas G. Rabello[1,2*], Roberto C. C. Ribeiro[2], José C. Pinto[3] and Rossana M. S. M. Thiré[1]

1 – Programa de Engenharia Metalúrgica e de Materiais (PEMM/COPPE), Universidade Federal do Rio de Janeiro (UFRJ), Rio de Janeiro, RJ, Brazil
**lucas.g.rabello@coppe.ufrj.br*
2 – Centro de Tecnologia Mineral (CETEM), Rio de Janeiro, RJ, Brazil
3 – Programa de Engenharia Química (PEQ/COPPE), Universidade Federal do Rio de Janeiro (UFRJ), Rio de Janeiro, RJ, Brazil

Abstract - Polymeric micro-and nanostructured fibrous membranes have been gaining prominence worldwide in applications such as air filtering, food packaging, and tissue engineering due to their high surface area/volume ratio. In this sense, biodegradable polymers from renewable sources, such as poly(3-hydroxybutyrate-co-3-hydroxyvalerate)(PHBV), can potentially reduce the environmenta[1] impact generated by the massive disposal of fossil-based plastics[1]. However, the destination of this biodegradable material in post-consumer landfills or composting does not necessarily reduce the environmental damage[2]. Therefore, it is necessary to find ways to return this material to the chemical chain, such as chemical recycling through hydrolysis. In this context, the present work aimed to produce fibrous membranes by solution blow spinning (SBS) from solutions containing 4, 6, and 8 m/v% of PHBV and assess the polymer recyclability through hydrolysis. The fibrous membranes were subjected to hydrolytic reactions in aqueous solutions with pH values of 4, 7, and 10 at 40, 60, and 80 °C for three weeks based on a design of experiments (DoE). Additionally, the hydrolysis reactions' environmental impact was assessed through the factor proposed by Bernard *et al.* (2021)[3]. The membranes produced from 4 m/v% solutions provided the highest weight loss (68 wt%) in an aqueous solution (pH = 4 at 80 °C), exhibiting the lowest environmental impact during the chemical recycling process ($2x10^5$ °C.min), concerning the 8% fibers ($25x10^5$ °C.min). The analysis of variance (ANOVA) showed that the fiber diameter was the most significant factor during the recycling reactions, evidencing that materials should be designed to promote the principles of the circular economy. Finally, it can be concluded that PHBV-based nonwoven fibrous membranes can promote the principles of the circular economy if polymers are correctly designed.

References

1. L. Kaniuk; U. Stachewicz *ACS Biomater. Sci. Eng.* 2021, 7, 12, 5339–5362. https://doi.org/10.1021/acsbiomaterials.1c00757.
2. M. Guo; D. C. Stuckey; R. J. Murphy *Green Chem.* 2013, 15, 706-717. https://doi.org/10.1039/C2GC36546D.
3. E. Barnard; J.J. Rubio Arias; W. Thielemans *Green Chem.* 2021, 23, 3765–3789. https://doi.org/10.1039/d1gc00887k.

Fundings: CAPES, CNPq, and FAPERJ.

Keywords: *PHBV, fibers, solution blow spinning, hydrolysis, circular economy.*

COMPARISON OF MANUAL PROCESSES WITH NEW TECHNOLOGIES FOR SEPARATING AND REUSING PLASTICS FROM MUNICIPAL SOLID WASTE.

Manoel Lisboa da Silva Neto[1], Suely de Medeiros Onofrio Gama[1], Fabio José Esper[1], Hélio Wiebeck[1]

1 – Department of Materials Engineering, University of São Paulo (USP), São Paulo, SP, Brazil
manoel.lisboa@mlsn.com.br

Abstract - One of the problems in our society today is the amount of natural resources we are using and at the same time the amount of waste we are discarding in the environment. Brazil alone disposes about 80 million tons of urban solid waste annually. The average gravimetric composition of MSW(Municipal Solid Waste) is approximately 45% of organic waste, 14% of rejects and materials such as plastic, paper, metals and glass, which could be reused, promoting the circular economy and sustainability. The current manual solid waste sorting is very slow and inefficient in production and quality. Manual sorting is usually associated with sedimentation or flotation tanks, sometimes using cyclones or hydrocyclones. Large-scale segregation demands new technologies such as automated sorting units. Automated systems, Material Recovery Facilities (MRFs) allow a significant increase in productivity in addition to a much higher quality in the separation. The automated sorting systems are capable of processing up to 50t/h of mixed MSW. The process begins with the separation of the organic materials, followed by the separation by type of material, using technologies for separating parts with two-dimensional/three-dimensional (2D/3D) formats, light and heavy fractions, magnetic and non-magnetic metals, and plastics by optical reading via infrared. The use of NIR(Near-infrared spectroscopy) allows the separation of plastic by type of resins and colors, significantly facilitating the processes of recycling and reuse of these materials. These systems allow the separation of up to 7t/h, equivalent to 800 people doing manually. Artificial intelligence has been applied for quality control with the function of removing contamination, promoting better separation, which results in the production of very high-quality PCR(Post-Consumer Resin). As Brazil intends to recovery and mine solid waste from landfills or even dumps, these are the key technology to address the problem.

Keywords: *Recycling, Municipal Solid Wast, Sorting technology, MSW recovery, Material Recovery Facilities (MRFs)*

References,

1. ABRELPE, Panorama dos Resíduos Sólidos no Brasil 2020, https://abrelpe.org.br/panorama-2020/ Acesso em: 25 maio 2023.
2. BRASIL. Decreto n. 7.404, DE 23 DE DEZEMBRO DE 2010. Regulamenta a Lei no 12.305, de 2 de agosto de 2010. Diário Oficial da União, Brasília, 12 de janeiro de 2022. Disponível em:.Acesso em: 04 jun. 2022.
3. Tianchen Ji a , Huaiying Fang, Rencheng Zhang, Jianhong Yang, Lulu Fan, Yangyang Hu, Zhengxing Cai Low-value recyclable waste identification based on NIR feature analysis and RGB-NIR fusion,
4. Giovanni Gadaleta, Sabino De Gisi, Silvio M.C. Binetti, Michele Notarnicola, Outlining a comprehensive techno-economic approach to evaluate the performance of an advanced sorting plant for plastic waste recovery

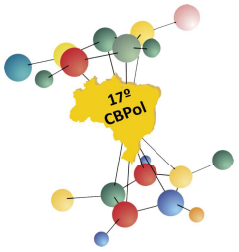

DEVELOPMENT OF A METHODOLOGY FOR EVALUATING BIODEGRADATION OF FLEXOGRAPHIC INKS

Letícia A. C. Laqua[1], Karina L. Andrade[1], Elisângela G. de Moraes[1], Joceane Azolin[1], Naionara A. Daronch[1], Leonardo de Apolinário[2], Elton da Silva[2], Camila Michels[1], Ricardo A. F. Machado[1]

1 – Department of Chemical Engineering and Food Engineering, Federal University of Santa Catarina (UFSC), Florianópolis, SC, Brazil.
corresponding author: leticia.costa@posgrad.ufsc.br
2 – Anjo Tintas Ltda., Criciúma, SC, Brazil.

Abstract – While progress and technological development have improved people's quality of life, they have also brought complications such as increased population growth, unwise use of resources, and increased waste generation. Among the most abundant solid residues, polymeric ones (plastics) stand out, which have low cost, are impermeable, flexible, and resistant to impacts, which justifies their wide use, becoming a worldwide concern. In this context, the flexographic printing ink in these polymeric packages also deserves attention and valuation of the contribution degree to the environmental impact generated by the disposal of these packages. Printing inks are quick-drying inks with resistance to temperature variation, composed of resins, solvents, pigments, and additives, which are incorporated into the formulation according to the final requirements of the packaging type. Thus, this work aimed to develop a methodology for evaluating the biodegradability of printing ink for flexible packaging. A method mentioned in the literature to evaluate polymer biodegradation was used to perform the test but with no records of use in inks. The test was performed in Oxitop; a pressure monitoring device developed to measure the biochemical oxygen demand (BOD). This test is based on calculating the theoretical oxygen demand (ThOD) required for the biodegradation of the test sample. The system has an agitation plate and six pressure sensors connected to glass vials. The test sample, activated sludge, and a medium with nutrients essential for the biological degradation of the material are stored. In this study, the activated sludge was collected from Casan's water treatment plant in Florianópolis SC and prepared according to the OECD Guidelines for the Testing of Chemicals. The sample analyzed refers to a paint composition often present in flexible packaging based on nitro-fumaric resin. The results showed that the method used is promising for evaluating the biodegradation of flexographic inks.

Fundings: The authors would like to acknowledge Anjo Tintas for the financial support and the Laboratório de Controle de Processos e Polimerização for making the laboratory available for the test.

Keywords: Flexographic ink; Polymeric packaging; Biodegradation; Oxitop.

DOES THE DEGRADATION LEVEL INTRODUCE BIASES IN MICROPLASTIC ANALYSIS? (SPOILER: YES…)

Ellen S. A. Duarte[1], Cristiane Vidal[2], Crislaine F. Bertoldi[1], Luiz F. L. Oliveira[3], Ramon Domingues[2], Kaique C. Silva[3], Maria C. Canela[3*], Andreia N. Fernandes[1], Cassiana C. Montagner[2***], Walter R. Waldman[4****]**

1 – Chemistry Institute, Federal University of Rio Grande do Sul (UFRGS), Porto Alegre, RS, Brazil

2 – Chemistry Institute, State University of Campinas (Unicamp), Campinas, SP, Brazil

3 – Science and Technology Center, State University of Northern Rio de Janeiro Darcy Ribeiro (UENF), Campos dos Goytacazes, RJ, Brazil

4 – Center for Sciences and Technology for Sustainability, Federal University of São Carlos, Sorocaba, SP, Brazil

*Corresponding authors: *mccanela@uenf.br, **andreia.fernandes@ufrgs.br, ***ccmonta@unicamp.br, ****walter@ufscar.br*

Abstract - Plastic pollution is ubiquitous, and microplastics are its most pervasive face. To better understand the extent of the microplastic impact, we need to monitor their distribution and assess their properties. For this purpose, a general protocol is to collect samples, disassemble and digest the matrix where the microplastic is, separate them by density, filter, and finally analyze them through visual features or spectroscopy. Regarding the digestion step, extra care must be taken to be sure that the advanced oxidation processes (AOP) do not also affect the microplastics. Several works in the literature have already validated AOP protocols for microplastic analysis, although primarily using pristine microplastics.[1,2] Since weathering plays a role in yielding decreased molar mass, modified surface, and increased crystallinity, we tested the validation of AOP against more environmentally relevant microplastics that were transformed through accelerated photodegradation. We treated pristine and artificially degraded samples of HDPE, PP, PET, and Nylon 6,6 with Fenton- and Persulfate-based AOP and checked the influences on the microplastic properties. The Fourier Transform Infrared spectroscopy (FTIR) showed that pristine samples were almost unaffected. In contrast, the degraded ones significantly changed, increasing or decreasing the carbonyl and hydroxyl intensity, according to the polymer. Also, even after thoroughly rinsing the samples, following the regular protocols, the spectra showed evidence of iron hydroxide for the Fenton treatment, indicating strong adherence to the microplastic surface, affecting further surface studies, like chemical sorption and biofilm formation. Degraded samples were fragmented during the AOP, whereas most of the pristine ones kept integrity. Most explanations lie in the degraded samples being sensitive to oxidation processes due to their decreased molar mass and increased surface polarity. Our main output is that the AOP changes degraded samples, so careful validation must be done to avoid bias.

References

1. Pfeiffer, F.; Fischer, E. K. *Front. Environ. Sci.* 2020, *8*, 572424. https://doi.org/10.3389/fenvs.2020.572424.
2. Fraissinet, S.; Pennetta, A.; Rossi, S.; De Benedetto, G. E.; Malitesta, C. *Marine Pollution Bulletin* **2021**, *173*,

Fundings: The authors acknowledge the contribution of Capes, CNPq, Fapesp, Faperj, Fapergs. and the Instituto Nacional de Ciências e Tecnologias Analíticas Avançadas (INCTAA).

Keywords: *Microplastics, digestion, degradation, FTIR, advanced oxidation processes*

EVALUATION OF PLASTIC DEGRADATION UNDER SEMI-CONTROLLED ENVIRONMENTAL CONDITIONS

Victor Z. Resende[1], Beatriz C. Vizioli[1] and Cassiana C. Montagner[1]*

1 – Environmental Chemistry Laboratory (LQA), Department of Analytical Chemistry, Chemistry Institute, University of Campinas (UNICAMP), Campinas, SP, Brazil ccmonta@unicamp.br

Plastic desired properties such as lightweight, low cost, low toxicity, stability, durability, mouldability, and resistance, among others, render them versatile for numerous applications in several economic sectors, but also particularly long-lasting after being discarded. Thus, plastics tend to accumulate and persist rather than decompose [1]. Due to inadequate waste management and disposal, plastic pollution constitutes an ever-increasing threat to human and environmental health [2]. Once in the environment, plastic degradation inevitably occurs due to several physical, chemical, and biological processes, yet our understanding is still very limited [3, 4]. This work aimed to evaluate the environmental degradation of commercial plastics such as ethylene-vinyl acetate copolymer (EVA) foam sheets, polyethylene (PE) disposable bags, polyethylene terephthalate (PET) textile fabrics, and polypropylene (PP) disposable masks. Three mesocosm systems (one aquatic and two terrestrial) were used to simulate semi-controlled environmental conditions. Unused plastic materials were cut into strips and randomly arranged in the mesocosms. Samples were collected monthly over a year, from November 2021 to October 2022. Prior to instrumental analysis, samples were carefully washed, air-dried for 24 hours, then photographed and weighed for visual and mass inspection. Plastic characterization was carried out using Attenuated Total Reflectance-Fourier Transform Infrared Spectroscopy (ATR-FTIR), Differential Scanning Calorimetry (DSC), and Thermogravimetric Analysis (TGA). Visual and mass inspection showed plastic fragmentation, biofilm formation and soil incrustation. Main monitored ATR-FTIR bands (C=O, C–O, O–H, S=O, among others) showed gradual increase, whereas DSC and TGA analyses showed specific patterns of crystallinity and degradation according to each type of mesocosm and plastic.

References

1. Li, P., Wang, X., Su, M., Zou, X., Duan, L., Zhang, H., *Bull. Environ. Contam. Toxicol.* 2021, 107, 577–584. https://doi.org/10.1007/s00128-020-02820-1
2. Ali, S.S., Elsamahy, T., Koutra, E., Kornaros, M., El-Sheekh, M., Abdelkarim, E.A., Zhu, D., Sun, J., *Sci. Total Environ.* 2021, 771, 144719. https://doi.org/10.1016/j.scitotenv.2020.144719
3. Liu, L., Xu, M., Ye, Y., Zhang, B., *Sci. Total Environ.* 2022, 806, 151312. https://doi.org/10.1016/j.scitotenv.2021.151312
4. Zhang, K., Hamidian, A.H., Tubić, A., Zhang, Y., Fang, J.K.H., Wu, C., Lam, P.K.S., *Environ. Pollut.* 2021, 274, 116554. https://doi.org/10.1016/j.envpol.2021.116554

Keywords: *environmental degradation; mesocosm systems; ATR-FTIR; DSC; TGA.*

GLYCOLYSIS OF PET BY MICROWAVE-ASSISTED HYDROTHERMAL METHOD USING A CLOSED SYSTEM

Ananda Ramires das Neves Stigger[1*], Tiago Vidaletti[1], Wesley Formentin[1], Mario Lucio Moreira[2] and Rosane Ligabue[1]

1 – Post-graduate Program in Materials Engineering and Technology (PGETEMA), Pontifical Catholic University of Rio Grande do Sul (PUCRS), Porto Alegre, RS, Brazil
**ananda.stigger@edu.pucrs.br*
2 – Post-graduate Program in Physics (PPGFís), Federal University of Pelotas (UFPel), Pelotas, RS, Brazil

Abstract – The polyethylene terephthalate (PET) is an excellent material with different applications, as bottes for example, but with a short lifetime (around 45% of PET world production in 2021 was single-se product). This generates a large waste amount (post-consumer PET) that, due to inadequate management, ends up in landfills and, consequently, in lakes, seas and oceans, causing damage to the environment and human health. Chemical recycling is one way transform PET waste into high added value compound, it is the most used commercially [1]. The obtained monomer is bis (2-hydroxyethyl) terephthalate (BHET), it is interesting industrially for being the monomer for the production of virgin PET, reducing the utilization of fossil feedstocks make more economy sustainable [2]. The present work evaluated the depolymerization of PET via microwave assisted hydrothermal (MAH) method using titanate nanotube (TNT) as catalyst in this process, this catalyst was described in the literature [3-5]. The microwave used as a close system, and it is possible to control the temperature and pressure of glycolysis reaction, the parameter evaluated was reaction time (1h, 1,5h and 2h) to obtained BHET monomer using virgin PET palletes. The PET conversion and selectivity in BHET were approximately 100% and 65,5%, respectively, in 2h of glycolysis, indicating that the MAH method proved to be promising for obtaining BHET from PET in times shorter than those used in conventional glycolysis.

References

1. PU, Mengyuan et al. A facile, alternative and sustainable feedstock for transparent polyurethane elastomers from chemical recycling waste PET in high-efficient way. **Waste Management**, v. 155, p. 137-145, 2023. https://doi.org/10.1016/j.wasman.2022.10.032.
2. SHIRAZIMOGHADDAM, Shadi et al. Chemical Recycling of Used PET by Glycolysis Using Niobia-Based Catalysts. **ACS Engineering Au**, 2023.
3. LIMA, Gabrielle R. et al. Titanate Nanotubes Modified With Zinc and Its Application in Post-Consumer PET Depolymerization. In: **Macromolecular Symposia**. 2019. p. 1800008.
4. LIMA, Gabrielle Ritter et al. Titanate nanotubes as new nanostrutured catalyst for depolymerization of PET by glycolysis reaction. **Materials Research**, v. 20, p. 588-595, 2017.
5. LIMA, Gabrielle Ritter et al. Evaluation of sodium/protonated titanate nanotubes catalysts in virgin and post consumer PET depolymerization. **Catalysis Letters**, v. 149, p. 1415-1426, 2019.

Fundings: CNPq and CAPES.
Keywords: Titanate Nanotube, glycolysis, microwave-assisted hydrothermal method, chemical recycling, PET.

INCORPORATION OF BIO-BASED MATERIALS IN COMERCIAL POLYMERS: STUDY OF POLY(BUTYLENE-ADIPATE-CO-TEREPHTHALATE)/WHEY PROTEIN ISOLATE BLENDS

Marina Fernandes Cosate de Andrade[1] e Ana Rita Morales[1*]

1 – School of Chemical Engineering, University of Campinas (UNICAMP), Campinas, SP, Brazil
morales@unicamp.br

Abstract - Proteins have been evaluated as a promising option for packaging materials due to their good oxygen barrier properties. The addition of proteins is an alternative for the partial replacement of polymers from petroleum using raw materials from a renewable source. The goal of this work was to study the blend of the thermoplastic whey protein isolate (WPIT) with a commercial petroleum polymer, poly(butylene adipate-co-terephthalate) (PBAT). Protein is not processable in its natural form and its denaturation and plasticization are necessary to transform it into a thermoplastic material. Plasticizers such as glycerol and polyethylene glycol (PEG) were studied to obtain WPIT. Blends were prepared using a torque rheometer and characterized for rheological properties by parallel plate and morphological properties by scanning electron microscopy. Raman spectroscopy showed that blends using glycerol presented well-defined WPIT domains with no adhesion to the PBAT matrix. This result was explained by the predominance of elastic components of WPIT and PBAT in process conditions as well as the viscosity ratio between components not favoring an improved dispersion and mixing. Another plasticizer for the protein, PEG, improved WPIT preparation as well as decreased the viscosity ratio between polymers and the elastic component of WPIT and PBAT. PEG blends presented homogeneous morphology, and reduced domain size. Besides, atomic force microscopy-based infrared spectroscopy showed that PEG blends presented both WPIT and PBAT in each phase, which is evidence of partial miscibility. Mechanical properties by tensile test and oxygen and water vapor permeability tests were conducted to evaluate the blend's performance. Blend (70/30) PBAT/WPIT showed a reduction of 20% in the oxygen permeability coefficient. Young's modulus as well as the water vapor permeability coefficient increased with the presence of WPIT.

References

1. M.F. Cosate de Andrade; M. Strauss; A.R. Morales *Journal of Polymers and the Environment* 2019, 27, 2131. https://doi.org/10.1007/s10924-019-01502-2
2. M.F. Cosate de Andrade; H. Loureiro; C.I.G.L. Sarantopóulos; A.R. Morales *Journal of Polymers and the Environment* 2021, 29, 3288. https://doi.org/10.21203/rs.3.rs-220062/v1
3. M.F. Cosate de Andrade, Ph.D. Thesis, University of Campinas, 2019.

Fundings: This work was financed by Conselho Nacional de Desenvolvimento Científico e Tecnológico (CNPq) and Coordenação de Aperfeiçoamento de Pessoal de Nível Superior – Brazil (CAPES) – Finance Code 001.

Keywords: *Polymer blends, Whey protein, Biopolymer, PBAT*

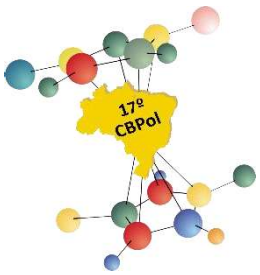

POLYAMIDE 6 TEXTILE RECYCLING: AN EVALUATION OF THE USE OF CARBODIIMIDE

Graziela S. Baccarin[1], Lucas H. Staffa[2] and Sandra A. Cruz[1]*

1 – Department of Chemistry (DQ), Federal University of São Carlos (UFSCar), São Carlos, SP, Brazil
gsbaccarin@estudante.ufscar.br
2 – Department of Materials Engineering (DEMa), Federal University of São Carlos (UFSCar), São Carlos, SP, Brazil

Abstract

The fabric remaining from the textile industry, but mainly related to clothing, is an important environmental and economic problem. On a global scale, in 2015, 92 million tons of fabric were discarded, and it is expected that by 2030 this number will increase to 148 million tons [1]. Concomitantly with consumption, there is the disposal that usually occurs in sanitary landfills, by incineration for conversion into energy, and inappropriately in dumps. An alternative to the disposal of waste from the textile industry is recycling [1,2]. This study intended to carry out the recycling of post-industrial polyamide 6 (PA6) waste in order to develop a material that can return to its original application. Thus, initially, fabric scraps were submitted to the press and milling process for shape adjustment and were chemically (FTIR), thermally (TGA, DSC), and rheologically (frequency sweep, amplitude sweep, and time sweep) analyzed. Subsequently, PA6 fabric waste was recycled by incorporating carbodiimide in different content to modulate its molar mass and molar mass distribution. This is a fundamental step for adapting and modulating the physicochemical, flow and mechanical properties. Results indicated that the carbodiimide molecule is essential for modulating the physicochemical and flow properties of polyamide 6, once it increases the PA6 molar mass, enabling the return of this material for its initial application and closing the life cycle loop. This study sheds light on the polyamide 6 fabric recycling viability, and it indicates that it is possible to use recycled fabric as raw material for the textile industry.

References.

1. S. Z. Kunchimion; M. Tausif; P. Goswami; V. Cheung *Journal of Polymer Research* 2019, 26, 162. https://doi.org/10.1007/s10965-019-1827-0
2. M. Jabbari; M. Skrifvars; D. Åkesson; M. J. Taherzadeh *Journal of Applied Polymer Science* 2016, 13. https://doi.org/10.1002/app.42829.

Fundings: This study was financed in part by the Coordenação de Aperfeiçoamento de Pessoal de Nível Superior - Brasil (CAPES) - Finance Code 001.

Keywords: *Polyamide 6, Carbodiimide, Textile recycling, Polymer recycling*, *Recycling*

POLYSACCHARIDES AND ECO-FRIENDLY PACKAGING: TRENDS AND INNOVATIONS

Ana Luísa de B. Oliveira, Giovany E. R. de Moraes, Huéberton B. Naves, Fabíola M. da Costa, Sidney Souza dos Santos, Fauze A. Aouada[1] and Márcia R. De Moura[*]

Grupo de Compósitos e Nanocompósitos Híbridos, GCNH, Department of Physics and Chemistry, São Paulo State University (UNESP), School of Engineering, Ilha Solteira, SP, Brazil
marcia.aouada@unesp.br

Considerable efforts have been dedicated to developing packaging food with eco-friendly characteristics to address the adverse effects in pollution resulting from irregular disposal of conventional packaging in the environment, whether terrestrial or aquatic[1,2]. Polysaccharide-based films materials, meet most of these requirements. However, due to its hydrophilic nature and unsatisfactory mechanical properties, structural stability is still an obstacle to overcome. To address this issue and be able to apply these materials as real packaging for food, just as conventional ones are applied. Nanocellulose has been incorporated into polysaccharide films to turn them more hydrophobic and enhance their mechanical properties[3]. In addition, the new materials prepared by the research group have greater biodegradability than conventional materials. Therefore, we propose investigating in reserch group a new and efficient protocol of packaging preparation eco-friendly that comprehensively examines the hidrophilic and mechanical properties and biodegradability during the storage and handling. The most used polysaccharides are: alginate, pectin, carboxymethylcellulose and hydroxypropylmethylcellulose. In this presentation, results will be presented and discussed to demonstrate that the technologies employed by the film preparation group using nanocelluloses result in films with improved properties and equivalent to traditional packaging. With a differential in relation to the greater biodegradability of the film, reducing the potential for pollution that the disposal of this material may cause, whether disposal in a terrestrial environment or an aquatic environment. These findings suggest that cellulose-based cryogels could offer an environmentally-friendly solution in pachaging insdustry.

Fundings: The authors thank the São Paulo Research Foundation (FAPESP) (Grants No. 2019/06170-1 and No. 2013/07296-2 CEPID) and CNPq (Grant No. 315513/2021-7). The Physics and Chemistry Department of the São Paulo State University (UNESP) and the PROPG are acknowledged for the financial support. This work was partially funded in by the Coordenação de Aperfeiçoamento de Pessoal de Nível Superior - Brazil (CAPES; Finance Code 001). This work was partially supported by Brazilian agencies MCTIC/CNPq (Grant #406973/2022-9) through INCT/ Polysaccharides (National Technology-Science Institute for Polysaccharides).

Keywords: Polysaccharide; Packaging; Nanocellulose; Biodegradability

References:

1. V. S. Dos Santos, et. al. Polymers, 2023, 15, 2244.
2. T. F. S. Saranti, et. al. Polymers, 2021, 13, 4298.
3. P.T.S. Melo, et.al. ACS Applied Materials & Interfaces, 2020, 12, 46661.

RECYCLING OF FACE SHIELD HEADBANDS BASED ON PP/SGF COMPOSITE: INFLUENCE OF REPROCESSING CYCLES ON RHEOLOGICAL AND MECHANICAL BEHAVIOR

Cindy M. Kawaushi, Jaqueline V. O. Silva, João Otavio G. O. Prado, Murilo M. Balarini, Vinícius P. Silva, Fernando Passareli, Lourival Varanda, Osvaldo F. Souza Jr, Osvaldo J. Corrêa, Juliano Marini*

Department of Materials Engineering (DEMa), Federal University of São Carlos (UFSCar), São Carlos, SP, Brazil
juliano.marini@ufscar.br

Abstract - Due to the COVID-19 pandemic, there was a significant increase in the production of personal protective equipment (PPE) and, consequently, in the generation of plastic waste (both during production and post-consumer) [1]. Several coordinated actions between the productive sector, government and public research institutions were developed in Brazil [2], such as the production and distribution of face shields for agents of the health sector who worked tirelessly on the front lines of fighting the pandemic. In this work, the recycling of face shield headbands (pre-use) based on polypropylene (PP) composite with 30 wt% of short glass fibers (SGF) was analyzed, through several reprocessing cycles (up to 10) in a twin-screw extruder. For each reprocessing cycle, the materials were injection molded and analyzed for rheological, mechanical (tensile and notched Izod impact tests), and heat deflection temperature (HDT) behavior. Fourier transform infrared spectroscopy (FTIR) and scanning electron microscopy (SEM) were used to evaluate PP degradation and fiber size decrease during reprocessing, respectively. Despite a continuous reduction in viscosity (and increase in melt flow index, MFI) with increasing number of cycles, the values of elastic modulus, yield stress and impact strength showed minimal variation up to the 7th reprocessing cycle (Fig. 1). After this cycle, there was a greater rate of variation in rheological and mechanical performance, correlated with greater degradation of PP and breakage of glass fibers.

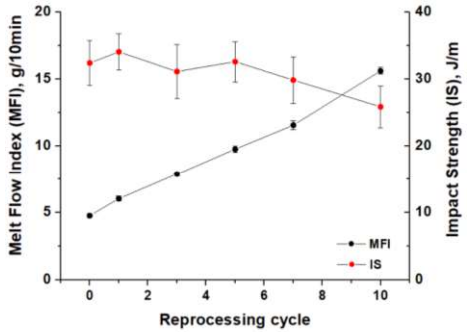

Figure 1 - MFI and IS as a function of the number of reprocessing cycles.

References

1. A. L. P. Silva et al. *Chemical Engineering Journal* 2021, *405*, 126683. https://doi.org/10.1016/j.cej.2020.126683
2. M. Panizzon, C. F. Costa, I. B. O. Medeiros *Revista de Administração Pública* 2020, *54*, 635. https://doi.org/10.1590/0034-761220200378

Keywords: *Recycling; face shield headbands; polypropylene composite; mechanical behavior; rheology.*

SUPERCRITICAL CO_2 FOAMING AND DEGRADATION BEHAVIOR OF PBAT/PLA BLENDS FOR ENHANCING LIGHTWEIGHT BIOPOLYMER

Guilherme M. R. Lima[1], M. F. Meindertsma[1], A. Mukherjee[1], D. Parisi[1], F. Picchioni[1], R. K. Bose[1*]

1 – Engineering and Technology Institute Groningen, University of Groningen (RUG), Nijenborgh 4, Groningen, Groningen, The Netherlands
r.k.bose@rug.nl

The development of lightweight biopolymer foams utilizing supercritical carbon dioxide ($scCO_2$) as a foaming agent holds great promise. $scCO_2$ offers numerous advantages, including low critical temperature and pressure as well as non-toxicity. Furthermore, blending biopolymers presents a valuable strategy for leveraging their mechanical properties, optimizing material characteristics, and effectively addressing individual limitations. It is imperative to have a thorough understanding of biodegradable polymer degradation to optimize material performance. During our investigation of biopolymers and their blends, we explored novel properties in solid materials and porous structures. To achieve this, we employed an extruder to blend polybutylene adipate terephthalate (PBAT) with polylactic acid (PLA), where PBAT acted as the carrier while PLA was added up to 15% in the blend. As part of our study, we assessed the degradation mechanisms of the PBAT/PLA blend by subjecting it to two aging chambers to evaluate its degradation behavior. The first chamber was a UV aging chamber with a radiation intensity of 130 $W \cdot m^{-1}$ and near-zero humidity, while the second chamber was a humidity cabinet maintained at 85 % humidity. These chambers allowed us to investigate the effects of photo and hydrolytic degradation on the blend. The blends with PLA ratios up to 5 % showed minimal impact on the final mechanical properties, while exceeding this threshold resulted in significant enhancements. Similarly, incorporating more than 5 % PLA into PBAT for foaming demonstrated notable changes in compression results and foam expansion. PBAT/PLA properties varied under UV or humidity exposure based on composition. Incorporating PLA into PBAT increased susceptibility to hydrolytic degradation, leading to significant changes in blend properties. However, higher PLA content in PBAT blends demonstrated potential resistance to photo-degradation, indicating improved durability.

1. Picchioni, F. *Polym. Int*. 2014, 63, 1394–1399, https://doi.org/10.1002/pi.4722.
2. S.P. Nalawade, F. Picchioni, L. Janssen, *Prog. Polym. Sci*. 31 (2006) 19–43, https://doi.org/10.1016/j.
3. Su, S.; Duhme, M.; Kopitzky, R., *Materials* 2020, 13, 4897. https://doi.org/10.3390/ma13214897

Keywords: *Biodegradable, Foam, Blend, CO_2, Degradation*

THE ROLE OF CARBODIIMIDE IN BIOPOLYMER RECYCLING AND ITS EFFECT ON FOOD SAFETY

Robert Paiva[1], Cristina Nerín[2], Magdalena Wrona[2], Sandra A. Cruz[1]

1- Department of Chemistry, Federal University of São Carlos (UFSCar), São Carlos, SP, Brazil
2- Department of Analytical Chemistry, University of Zaragoza, Zaragoza, Spain.
sandra.cruz@ufscar.br

ABSTRACT

The use of recycled polymers for food contact is a major challenge for the industry. Environmental protection policies, especially international ones, are moving towards (1) phasing out single-use plastics, (2) making disposable packaging 100% recycled, and (3) increasing the use of materials from renewable and compostable sources for quick disposal applications. Additionally, Polylactic acid (PLA) is a biopolymer commonly used in food packaging due to its good characteristics and compostability. In this work we studied the recyclability of PLA with the intention of using it in package in direct contact with food. The PLA samples were subjected to recycling process via extrusion using different content of carbodiimide. Rheological, thermal, and chemical analyses indicated that carbodiimide can increase the thermal stability and the molar mass of recycled PLA, allowing its return to the same production cycle. However, to this end, to evaluate the safety of the recycled material the analysis of the non-intentionally substances (NIAS) is required. The presence of contaminants associated with high shear rates and temperatures characteristics of the recycling process results in a formation of new molecules with low molar mass. These have greater migration potential contaminating the food and constitute a risk to consumers. High-resolution mass spectrometry with a tandem quadrupole-time of flight mass spectrometer was used for the identification of non-volatile compounds, and solid-phase microextraction gas chromatography-mass spectrometry, for volatiles compounds. The results indicated an increase in the formation of volatile and non-volatile compounds after the material has undergone the recycling process. However, the incorporation of carbodiimide reduces the formation of NIAS since this functional molecule was able to minimize the degradative effects. Thus, carbodiimide presents itself as a potential compound in recycling by promoting an increase in molar mass enabling the use of recycled PLA for food contact and reducing the formation of NIAS, increasing food safety.

References

1. M. Wrona; C. Nerín *Molecules* 2020, *25* https://doi.org/10.3390/molecules25030752
2. R. Paiva; M. Wrona; C. Nerín; I. Bertochi; L. Gavril; S.A. Cruz *Food Chem* 2021, *350*, 129250. https://doi.org/10.1016/j.foodchem.2021.129250.
3. J.N. Hahladakis; C.A. Velis; R. Weber; E. Iacovidou; P. Purnell *J Hazard Mater* 2018, *344*, 179–199 https://doi.org/10.1016/j.jhazmat.2017.10.014.

Fundings: FAPESP (2021/08224-1)

Keywords: *recycling, food safety, carbodiimide, PLA*

UPCYCLING BANANA PEELS: TRANSFORMING WASTE INTO BIOPLASTIC FILMS WITH SPECIAL PROPERTIES

Rodrigo D. Silva[1]*, Thályta F. Pacheco[2,3], Amanda D. de Santi[4], Fabiana Manarelli[5], Breno R. Bozzo[5], Michel Brienzo[6], Caio G. Otoni[7], Henriette M. C. Azeredo[1]*

1 – Embrapa Instrumentation, São Carlos, SP, Brazil
rodrigo.dsilva@gmail.com; henriette.azeredo@embrapa.br
2 – Biochemical Processes Laboratory, Embrapa Agroenergy, Brasília, DF, Brazil;
3 – Graduate Program of Microbial Biology, Institute of Biology, University of Brasília, Brasília, DF, Brazil
4 – Materials Engineering Department, São Carlos School of Engineering (EESC), University of São Paulo (USP), São Carlos, SP, Brazil
5 – Chemistry Department, Federal University of São Carlos (UFSCar), São Carlos, SP, Brazil;
6 – Institute for Research in Bioenergy (IPBEN), São Paulo State University (UNESP), Rio Claro, SP, Brazil
7 – Department of Materials Engineering (DEMa), Federal University of São Carlos (UFSCar), São Carlos, SP, Brazil

Abstract - Bananas, one of the most widely produced fruits globally, generate a substantial amount of peels during the commercial processing of their products. However, this byproduct is currently underutilized despite its significant potential for bioplastic production, which can effectively address environmental concerns associated with the use of conventional plastics. In this study, we propose simple pretreatments to directly convert bulk (whole) banana peels into bioplastic films. The influence of different variables on film performance was investigated, including the type of banana peels (unblanched *vs*. blanched), acid concentration in the pretreatment medium, and the carboxymethyl cellulose content in the films. The incorporation of CMC significantly improved the mechanical properties of the films. Additionally, by subjecting the banana peels to bleaching prior to drying and milling, their antioxidant activity was successfully preserved. Even after the pretreatment, the bioplastic films retained a substantial portion of the antioxidant activity of banana peels. Moreover, these films exhibited remarkable UV-blocking properties, making them a potential eco-friendly option for active food packaging applications. This work, therefore, presents a sustainable approach to upcycle banana peels, contributing to the development of a circular bioeconomy.

Fundings: FAPESP (#2017/22401-8, #2020/11104-5, #2021/05092-7). CNPq (#308777/2021-2, #304753/2022-0).

Keywords: *Banana peels. Bioplastic. Upcycling. UV-blocking. Antioxidant activity.*

ADSORPTION STUDY OF PHENATHRENE FROM AQUEOUS SOLUTION BY POLYMERIC RESINS CROSSLINKED WITH DIVINYLBENZENE

Rafael L. Pinto[1*], Mônica R. C. M. Calderari[1], Ezaine C. C. T. Santos[2] and Luciana C. Costa[2]

1 – Fernanda Coutinho Analytical Center (CAFC), Chemistry Institute, State University of Rio de Janeiro (UERJ), Rio de Janeiro, RJ, Brazil (rafaeldelimap@hotmail.com)
2 – Department of Pharmacy, Faculty of Biological and Health Sciences, State University of Rio de Janeiro (UERJ), Rio de Janeiro, RJ, Brazil

Abstract – Polycyclic aromatic hydrocarbons (PAHs) are a class of pollutants that deserve special attention due to their harmful properties to humans. Thus, there is a need to develop new analytical techniques to monitor PAHs present at low concentrations in aqueous media. In the current work, the ability to remove phenanthrene (PHE) (model HPA) from aqueous solutions by adsorption on different cross-linked polymeric resins (different monomeric compositions and morphological properties) was studied. In the study of adsorption kinetics, two resins were chosen that showed high removal efficiencies in preliminary tests. In general, the results obtained in the initial tests showed that most of the resins containing the Sty monomer or cross-linked with DVB showed satisfactory PHE removal values in water. The Freundlich model proved to be a better fit for the observed adsorption than the Langmuir model. The kinetic data were better fit by the pseudo-second-order reaction and Urano-Tachikawa models.

Keywords: *PAHs, phenanthrene, crosslinked polymeric resins, adsorption.*
Fundings: National Council for Scientific and Technological Development (CNPq), Research Support Foundation of the State of Rio de Janeiro (FAPERJ)

Introduction

PAHs are persistent organic pollutants (POPs), toxic, lipophilic, can bioaccumulate in aquatic species, and have a high potential for long-range transport in the environment. Published research on the harmful effects of these compounds on living organisms and public concern led the main international environmental protection agencies to include PAHs in the list of priority substances for monitoring [1–3]. Monitoring these compounds is also essential, as they serve as indicators of sources of pollution [4]. However, PAHs are present in aquatic systems at low concentrations. The currently available analytical methods for quantification cannot detect very low amounts of pollutants in aqueous media, requiring the adoption of techniques for separating and pre-concentrating these compounds [5]. Cross-linked polymeric resins have been reported in the literature for the removal of various organic and inorganic pollutants in aqueous media due to the advantages of these materials, such as high physical and chemical stability, high adsorption capacity and selectivity, the possibility of controlling the characteristics morphological characteristics (pore structure and specific area) and the ease of regeneration and reuse [6–8]. Following this line, the present work aims to apply reticulated polymeric resins that present monomeric compositions, morphological properties, and diverse polarities to remove PAH in water and study the kinetic mechanism of adsorption of the most efficient resins. Knowledge of these phenomena can significantly contribute to identifying the most suitable type of resin for removing the pollutant. In the future, these resins may be used as a solid phase in extraction and pre-concentration techniques.

Experimental

Preliminary adsorption study

Preliminary adsorption tests were carried out to verify the feasibility and effectiveness of PHE removal using cross-linked polymeric resins with different structures, polarities, and morphological properties as adsorbents. Based on the selection of the best resin(s), equilibrium studies and adsorption kinetics will be carried out. The experiments were carried out in batches, from the dispersion of 15 mg of resins in test tubes containing 5 mL of PHE solution (1.0 mg L^{-1}). Then, the tubes were placed on a Kline-type shaker and left under mechanical agitation for 30 min at room temperature. The solutions were analyzed by spectrofluorimetry ($\lambda_{ex}/\lambda_{em}$ = 250/364 nm). The study was carried out with ten resins previously synthesized and characterized. The tests were realized in triplicate. The morphological properties of these resins are described in Table 1.

Table 1 – Morphological properties of polymeric adsorbents used

Resin (with DVB)	S_{BET} (m^2 g^{-1})	V_{pore} (cm^3 g^{-1})	D_{pore} (A°)	Resin (with EGDMA)	S_{BET} (m^2 g^{-1})	V_{pore} (cm^3 g^{-1})	D_{pore} (A°)
DVB	447.9	0.91	105.7	EGDMA	7.8	0.03	291
CMS/DVB	29.4	0.10	120.9	CMS/EGDMA	6.3	0.03	256.2
GMA/DVB	19.9	0.15	193.9	GMA/EGDMA	9.3	0.03	113.4
MAA/DVB	60.7	0.05	69.9	MAA/EGDMA	7.4	0.03	170.7
Sty/DVB	175.2	0.62	174.1	Sty/EGDMA	61.5	0.02	30.6

CMS – chloromethylstyrene; DVB – divinylbenzene; EGDMA – ethylene glycol dimethacrylate; GMA – glycidyl methacrylate; MAA – methacrylic acid; Sty – styrene.
The resins used in this work have a monomer/crosslinker ratio (%) of 0/100 and 40/60

Batch adsorption experiments

Five test tubes were prepared for the adsorption equilibrium study, each containing 2 mg of resin and 40 mL of PHE solution at different concentrations (0.2–1.0 mg L^{-1}). The tubes were then shaken for 30 min at 25 °C and 200 rpm. The concentration of PHE in the solution was quantified by spectrofluorimetry.

Adsorption equilibrium data were analyzed using Langmuir and Freundlich models (in their linearized versions). For the adsorption kinetics study, sixteen test tubes containing 15 mg of resin were prepared, and then 5 mL of PHE solution was added at a concentration of 1.0 mg L^{-1}. The tubes were mechanically shaken in a shaker incubator at a speed of 200 rpm and a temperature of 25 °C. Samples were taken at predetermined intervals (1 to 10, 30, 60, 120, 180, 240, and 1440 min). Kinetic data were analyzed by kinetic reaction models (pseudo-first order, pseudo-second order, and Elovich) and diffusion models (external diffusion, Weber-Morris, and Urano-Tachikawa intraparticle diffusion) in their linearized versions.

Results and Discussion

Preliminary adsorption study

The resins containing styrene (Sty) or divinylbenzene (DVB) in their compositions increased the percentage of PHE removal initially present in the solution (Table 2).

Table 2 – Results of preliminary tests of resins for removal of PHE in aqueous medium

Resin (with DVB)	Removal (%)	Resin (with EGDMA)	Removal (%)
DVB	99.9	EGDMA	68.9
CMS/DVB	70.3	CMS/EGDMA	69.0
GMA/DVB	92.9	GMA/EGDMA	47.9
MAA/DVB	93.4	MAA/EGDMA	61.5
Sty/DVB	97.3	Sty/EGDMA	99.2

Analyzing the data individually, it is noted that the preliminary test of adsorption of PHE in an aqueous solution by DVB resin presented better removal efficiency (99.9%) when compared to the

other resins. The phenomenon of adsorption of PHE molecules by DVB resin particles is driven by hydrophobic interactions such as van der Waals forces and mainly by π–π interactions. The DVB resin also has a higher specific area (447.9 m^2 g^{-1}) (Table 1) when compared to the Sty/DVB resin and even the other resins. This fact contributes to a more significant interaction between the adsorbent sites and the adsorbate molecules. Thus, the DVB and Sty/DVB resins were selected for the batch adsorption study (equilibrium and kinetics) since these resins have a more apolar character and a more significant interaction with PHE.

Equilibrium modelling

The PHE adsorption isotherms on the DVB and Sty/DVB resins at 25°C showed that as the PHE concentration increased, the adsorption capacity of both resins increased significantly. The data obtained by the adsorption equilibrium isotherms are commonly used to analyze the interaction between the adsorbent (DVB and Sty/DVB resins) and adsorbate (PHE). Langmuir and Freundlich isotherm equations are typically used to describe liquid-solid phase adsorption. The Langmuir equation assumes that adsorption occurs on the surface of the solid and that the surface is covered in a monolayer. On the other hand, the Freundlich model assumes that multilayer adsorption is a process on a heterogeneous surface. Table 3 presents the calculated constants for both models.

Table 3 – Isothermal parameters for adsorption of phenanthrene in cross-linked polymeric resins at 25 °C

Isotherm models	Equation (linear form)	Coefficients	Resins	
			DVB	Sty/DVB
Langmuir	$\frac{C_e}{q_e} = \frac{1}{q_{max}K_L} + \frac{C_e}{q_{max}}$	r^2	0.9362	0.3648
		K_L (L mg^{-1})	0.07	0.07
		q_{max} (mg g^{-1})	277.78	263.16
Freundlich	$\ln q_e = \ln K_F + \frac{1}{n}\ln C_e$	r^2	0.9998	0.998
		K_F (mg g^{-1})	17.68	16.94
		n	1.03	1.02

r^2 – correlation coefficient; K_L – Langmuir constant related to the interaction between adsorbate and adsorbent interaction; q_{max} – maximum adsorption capacity; K_F – Freundlich adsorption capacity constant; n – constant related to the heterogeneity of the adsorbent surface

As shown in Table 3, the Freundlich model proved to be a better fit for the observed adsorption than the Langmuir model. In other words, the PHE adsorption process on the surface of DVB and Sty/DVB resins exhibited multilayer, not monolayer, behavior. The magnitude of the exponent 1/n between 0 and 1 and values of n greater than 1 indicate favorable conditions for adsorption.

Kinetic modelling

Reaction-base kinetic models

The polymers' sorption mechanism was investigated using pseudo-first-order, pseudo-second order, and Elovich kinetic models (Table 4).

The coefficients of determination (r^2) ranged from 0.879 to 0.996. According to the equation representing the pseudo-first-order model, the calculated maximum adsorption capacity at equilibrium (q_e, calc) disagreed with the values of the maximum experimental adsorption capacities (q_e,exp) for PHE solutions with initial concentrations of 1.0 mg L^{-1}.

On the other hand, using the equation of the pseudo-second-order model, it was possible to obtain better results. The pseudo-second-order kinetic constant (k^2) and the q_e calc were obtained from constructing the graph t/qt versus t. The values of the r^2 coefficients were 0.995 and 0.996 for DVB and Sty/DVB resins, respectively. Furthermore, the values of q_e, calc agreed with q_e,exp. The qe, calc values for the adsorption of PHE by DVB and Sty/DVB resins obtained in this work form 0.314 and 0.271 mg g^{-1}, respectively. These results indicate that the pseudo-second-order mechanism best predicts the adsorption process for both adsorbents. The pseudo-second-order model best

represents the kinetic data for most adsorptive systems, providing the best correlation for the systems studied throughout the entire process time. This model is the most suitable for experimental data in the initial stages of the adsorption process. Using the Elovich model, it was possible to obtain a linear relationship between q_t versus lnt over the adsorption period, obtaining r^2 coefficients of 0.974 and 0.951 for the DVB and Sty/DVB resins, respectively. These coefficient values are those obtained using the pseudo-second-order model equation. The Elovich equation does not predict any defined mechanism but helps describe adsorption on adsorbents with highly heterogeneous structures. This indicates that the Elovich model cannot be used to predict the adsorption kinetics of PHE in polymeric resins.

Table 4 – Parameters of the reaction kinetic models for the adsorption of PHE on DVB and Sty/DVB resins, at a concentration of 1.0 mg L^{-1} and a temperature of 25 °C

Reaction-base kinetic models	Equation (linear form)	Coefficients	Resins	
			DVB	Sty/DVB
Pseudo-first order	$\ln(q_e - q_t) = \ln q_e - k_1 t$	r^2	0.949	0.879
		k_1 (min^{-1}) (10^{-4})	1.748	1.603
		$q_{e,calc}$ (mg g^{-1})	0.138	0.098
		$q_{e,exp}$ (mg g^{-1})	0.311 ± 0.001	0.272 ± 0.001
Pseudo-second order	$\frac{t}{q_t} = \frac{1}{k_2 q_e^2} + \frac{t}{q_e}$	r^2	0.995	0.996
		k_2 (g mg^{-1} min^{-1})	5.976	7.825
		$q_{e,,alc}$ (mg g^{-1})	0.314	0.271
		$q_{e,exp}$ (mg g^{-1})	0.313 ± 0,002	0.273 ± 0.001
		h (mg g^{-1} min^{-1})	0.589	0.574
Elovich	$q_t = \left(\frac{1}{\beta}\right)\ln(\alpha\beta) + \left(\frac{1}{\beta}\right)\ln t$	$r^{2.}$	0.974	0.951
		α (mg g^{-1} min^{-1})	2.829	2.486
		β (mg g^{-1})	20,704	23,697

r^2 – correlation coefficient; k_1 – pseudo-first order rate constant; $q_{e,calc}$ – calculated sorption capacity; $q_{e,exp}$ – experimental sorption capacity; k_2 – pseudo-second order rate constant, h – initial adsorption rate; α – initial adsorption rate; β – desorption constant.

Diffusion-base kinetic models

Using the linear form of the Weber-Morris intraparticle diffusion model, it was possible to construct the curve graph by plotting q_t versus $t_{1/2}$. From the data obtained by the graph, the intraparticle diffusion constant (k_{id}) was determined (Table 5).

Table 5 – Parameters of kinetic diffusional models for the adsorption of PHE on DVB and Sty/DVB resins, at a concentration of 1.0 mg L^{-1} and a temperature of 25 °C

Diffusion-base kinetic models	Equation (linear form)	Parâmetros	Resin	
			DVB	Sty/DVB
External diffusion	$\ln\frac{C_t}{C_0} = -k_f\frac{A}{V}t \quad \frac{A}{V} = \frac{3m}{\rho d}$	r^2	0.948	0.880
Intraparticle diffusion (Weber-Morris)	$q_t = k_{id}\,t^{1/2} + C$	r^2	0.914	0.863
		k_{id} (mg g^{-1} min$^{-1/2}$)	0.048	0.042
Intraparticle diffusion (Urano-Tachikawa)	$-\log\left[1-\left(\frac{q_t}{q_e}\right)^2\right] = \left(\frac{4\pi^2 D_i}{2{,}3d^2}\right)t$	r^2	0.956	0.906
		Di (10^{-8}) (cm^2 s^{-1})	3.59	77.7

r^2 – correlation coefficient; k_{id} – intra-particle diffusion rate constant; Di – sum of pore and surface diffusion.

In the Weber-Morris intraparticle diffusion model, the line does not pass through the origin, indicating some degree of boundary layer control and that intraparticle diffusion is not the only step. Still, also

other processes can control the adsorption rate. The results showed that these graphs can present multilinearity, indicating that the adsorption occurs in two or more stages. In the Urano-Tachikawa intraparticle diffusion model, the adsorption rate is minimal and independent of stirring speed, so external diffusion is irrelevant compared to the overall adsorption rate. Through the linearization of the equation that represents this model, it was possible to construct the curve graph by plotting $-\log[1-(q_t/q_e)_2]$ versus t. Mean particle diameter (d) values for DVB and Sty/DVB resins are 5.93×10^{-3} and 2.84×10^{-2} cm, respectively. The Urano-Tachikawa intraparticle diffusion coefficient (Di) was obtained from the slope value of the graph line. The r^2 coefficients for the DVB and Sty/DVB resins were, respectively, 0.956 and 0.906, indicating a disagreement between this model and experimentally obtained data.

Conclusions

Preliminary batch adsorption tests allowed the individual evaluation of PHE removal efficiency in aqueous medium by ten polymeric resins with different structures, polarities, and morphological properties. Resins containing Sty monomer or cross-linked with DVB showed the highest PHE removal efficiency (99.9–70.3%) being attributed mainly to the greater number of π–π interactions between adsorbate and adsorbent. The study of adsorption kinetics in batches of DVB and Sty/DVB resins indicated that for both resins, the systems showed high PHE adsorption in the first minutes. The pseudo-second order model better represented the experimentally obtained data for the adsorption kinetics of the two studied systems. The values of $q_{e,exp}$ and $q_{e,calc}$ showed agreement. The k_2 constants obtained for both resins showed that the interaction adsorbate-adsorbent occurred quickly. Among the diffusional models, the one that best fitted the data obtained was the Urano-Tachikawa model, with an r^2 of 0.956 and 0.906 for the DVB and Sty/DVB resins, respectively.

Acknowledgements

The authors thank CAPES and CNPq for financial support.

References

1. Y-G. Gu; H-B. Li; H-B. Lu Ecological Engineering 2017, 101, 179–184. https://doi.org/10.1016/j.ecoleng.2017.02.007.
2. M. Liu; J. Feng; P. Hu; L. Tan; X. Zhang; J. Sun Ecological Engineering 2016, 95, 143–151. https://doi.org/10.1016/j.ecoleng.2016.06.045.
3. R. Sarria-Villa; W. Ocampo-Duque; M. Páez; M. Schuhmacher Science of the Total Environment 2016, 540, 455–465. https://doi.org/10.1016/j.scitotenv.2015.07.020.
4. N. Manousi; G. A. Zachariadis Molecules 2020, 25, 2182. https://doi.org/10.3390/molecules25092182.
5. M. Pogorzelec; K. Piekarska Science of the Total Environment 2018, 631–632, 1431–1439. https://doi.org/10.1016/j.scitotenv.2018.03.105.
6. G. Busca; S. Berardinelli; C. Resini; L. Arrighi, L. Journal of Hazardous Materials 2008, 160, 265–288. https://doi.org/10.1016/j.jhazmat.2008.03.045.
7. W. Kujawski; A. Warszawski; W. Ratajczak; T. Porębski; W. Capała; I. Ostrowska Separation and Purification Technology, 40, 123–132. https://doi.org/10.1016/J.SEPPUR.2004.01.013.
8. I. Vazquez; J. Rodriguez Iglesias; E. Maranon; L. Castrillon; M. Alvarez Journal of Hazardous Materials 2007, 147, 395–400. https://doi.org/10.1016/j.jhazmat.2007.01.019.

A NEW BIOPOLYURETHANE COATING BASED ON BIO OIL

Ítalo M. Costa[1], Pedro H.B.O. Nogueira[1], Vânya M. D. Pasa[1], and Renata C. S. Araujo[1]*

1 – Department of Chemistry, Federal University of Minas Gerais, Minas Gerais, MG, Brazil
marquesitalo@ufmg.br

Abstract - A polyurethane coating was developed using Eucalyptus pyrolysis oil as the polyol, a product obtained from the pyrolysis of wood, a type of lignocellulosic biomass. The Eucalyptus pyrolysis oil was chemically modified by means of two chemical reactions in sequence, glycidylation and opening of the oxirane ring. The reactions were carried out with the aim of promoting the chemical bonding of chains of a fatty acid, ricinoleic acid, to other compounds present in the composition of this mixture. The modified pyrolysis oil then underwent reaction with the MDI isocyanate to give rise to a polyurethane resin that was applied as a coating to protect the metallic surface of carbon steel. The results showed that the coating obtained from the modified pyrolysis oil did not have the strong unpleasant odor characteristic of its raw material, showed high thermal stability, excellent adhesion to carbon steel and excellent anticorrosive performance.

Keywords: B*iomass. Pyrolysis oil. Renewable. Polyurethane.*

Introduction

The growing world industrial production has been causing environmental problems such as global warming and problematic waste disposal. In addition, there is a great concern to obtain new materials considering the decarbonization processes. Therefore, researchers and industries have been looking for alternatives to the use of petrochemical products and raw materials from renewable sources have become an important solution to obtain environmentally friendly polymers.
Polyurethanes are polymers that allow the replacement of polyols by raw materials from renewable sources such as cellulose, lignin, vegetable oils, among others [1,2,3].
The synthesis of polymers from renewable resources is currently part of the efforts made in the search for sustainable polymers in a context of energy transition [4,5].

Experimental

In the present work, polyurethane coatings were developed using *Eucalyptus* pyrolysis oil as a polyol, a product obtained from the pyrolysis of the wood from this plant species. *Eucalyptus* pyrolysis oil was chemically modified through two chemical reactions and used in the synthesis of a polyurethane resin that was applied as a protective coating on carbon steel.
The *Eucalyptus* bio-oil was modified by chemical reactions, obtaining a new polyol, according to the sequence shown in figure 1.

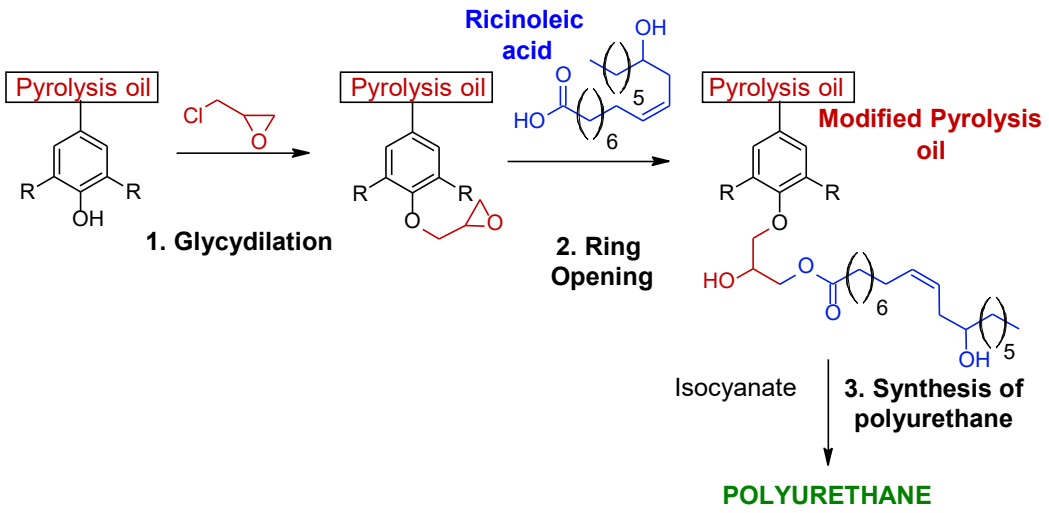

Figure 1 – Chemical modification of pyrolysis oil

The hydroxyl content of new biopoliol based on modified *Eucalyptus* was determined using ASTM E222-17. Polyurethane coatings were applied in carbon steel plates without any treatment (Figure 2). The coatings were characterized by thermal analysis (TG and DSC), infrared spectroscopy and impedance spectroscopy. Adhesion test was also performed, according to ASTM D3359-17.

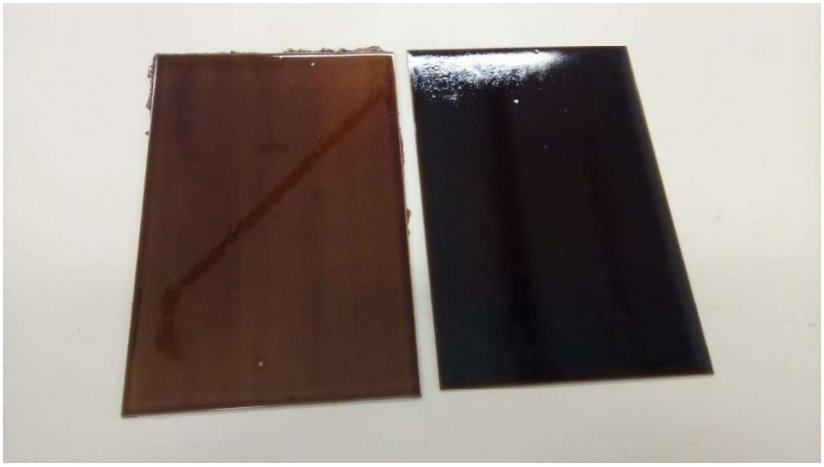

Figure 2 – Modified pyrolysis oil based polyurethane coatings.

Results and Discussion

The hydroxyl content was determined showing the value 374 mg KOH/g. This value is higher than the original biooil that had 174 mg KOH/g.
The thermogravimetric analysis of biopoliol and the PU based on this new biopoliol were showed in Figure 3. The thermal stability increased in PU showing the intial degradation up to 238 °C. In the DSC analysis a glass transition temperature (Tg) was determined at 21 °C, an important property to obtain flexible PU coating.

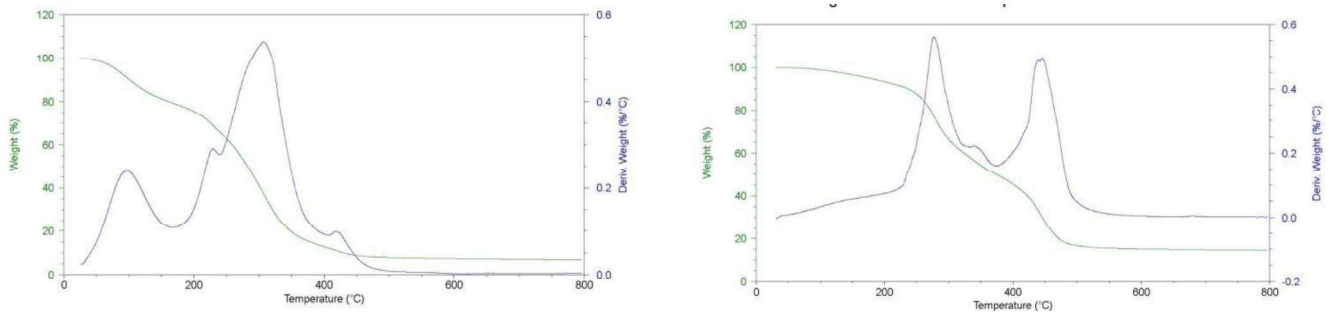

(a) (b)

Figure 3 – TG curves of new biopoliol (a) and PU coating based on new biopoliol

The Adhesion by tape test was carried out according to the ASTM D3359-17 adhesion test, the coating showed high adhesion (5A) with no peeling or removal during the test. That is an important result to PU coating act as a protector barrier.

The electrochemical impedance performed immediately and after 7 days of immersion in saline solution initially showed an impedance modulus of the order of 10^5 Ω and an increase to the order of 10^6 Ω on the seventh day. Impedance readings were also taken after subsequent cathodic polarization cycles which showed an increase in the capacitive character of the plates as shown by the Nyquist diagram in figure 4.

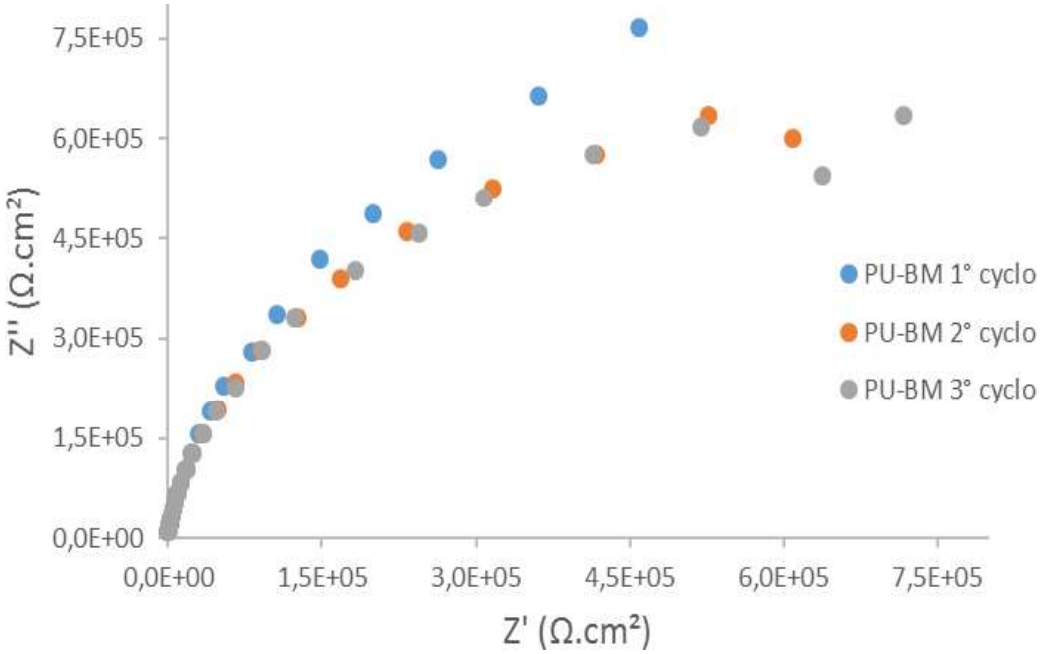

Figure 4 – Nyquist diagram for modified pyrolysis oil polyurethane.

Conclusions

A new polyol obtained from the modification of *Eucalyptus* bio-oil was used in the synthesis of polyurethane coatings. The coating produced exhibited high carbon steel adhesion, high thermal stability and good anti-corrosion protection capability.

Acknowledgements

To the Human Resources Program of the National Agency of Petroleum, Natural Gas and Biofuels – PRH-ANP, supported with resources from the investment of oil companies qualified in the P, D&I Clause of ANP Resolution No. 50/2015.

References

1. T. Mekonnen; T. Haile; M. Ly, Applied Surface Science 2021, 540, 148299. https://doi.org/10.1016/j.apsusc.2020.148299.
2. X. Ma; J. Chen; J. Zhu; N. Yan, Macromolecular Rapid Communications 2021, 42, 2000492. https://doi.org/10.1002/marc.202000492.
3. P. Paraskar; M. Prabhudesai; V. Hatkar; R. Kulkarni, Progress in Organic Coatings 2021, 156, 106267. https://doi.org/10.1016/j.porgcoat.2021.106267 .
4. Z. Wang; M. Ganewatta; C. Tang, Progress in polymer Science 2020, 101, 101197 https://doi.org/10.1016/j.progpolymsci.2019.101197.
5. K. Müller; C. Zollfrank; M. Schmid, Macromolecular materials and Engineering 2019, 304,1800760. https:// doi.org/ 10.1002/mame.201800760.

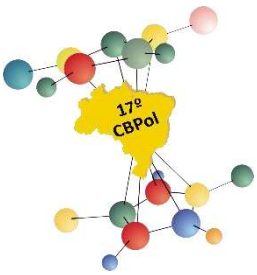

ANTIOXIDANT ACTIVITY AND THERMAL DEGRADATION OF BIOFILMS INCORPORATED WITH GRAPE RESIDUES

Bruna P. Zanfonato[1*], Rafael S. K. Zacarão[1], Nicole M. da Costa[1], Andréia Z. Dinon[1], Marcia B. Schuster[1],

1 – Department of Food Engineer and Chemical Engineer, Santa Catarina State University (UDESC), Pinhalzinho, SC, Brazil.
brunazanfonato159@gmail.com

Abstract - Reusing natural residues with functional properties is a promising way to improve the biopolymer characteristics. Thus, the objective of this work was to evaluate the antioxidant activity (AA) and thermal properties of biofilms made with cassava starch (5 wt.%) and different percentages of grape waste flour (0, 0.5, 1, 2, 4 wt. %). The films were prepared by casting method using an ultrasonic bath. The grape waste flour showed an AA of 92.02%, and the AA in the film increased as the flour percentage increased, reaching 66.74% for biofilms made with the addition of 4 wt. % of flour. The AA can be explained by the presence of polyphenolic compounds in the grape waste flour. However, the addition of grape waste flour decreased the thermal stability of the films compared to the pure starch film. Temperature of 5% weight loss for the films with flour is around 80 ºC and for de pure matrix is 108 °C. Grape waste flour in films has potential to curb oxidation in various products due to AA.

Keywords: *wine industry by-products; antioxidant activity; thermogravimetry.*

Fundings: Authors are grateful for the funding support from FAPESC – Brazil (PAP 2021TR854) and CAPES - Brazil (PROAP/AUXPE).

Introduction

The global consumption of plastics, including fibers and additives, has been consistently rising. In 2019, approximately 353 Mt of plastic waste were generated worldwide, with only about 55 Mt collected for recycling, while 22 Mt were discarded [1]. Packaging plays a crucial role in preserving and transporting products until they reach consumers, especially in maintaining the quality and freshness of food products [2].

Although petrochemical-based plastics are commonly used in food packaging, their non-renewable nature and extended degradation periods can carry on significant environmental threats [3,4]. As a result, there is a growing focus on materials derived from biodegradable polymers and natural elements from waste and food by-products [5].

Starch emerged as an alternative in the development of biodegradable polymer packaging due to its low cost and renewable sources. Additionally, researchers have explored incorporating various organic substances to enhance the quality of starch-based biofilm [6]. Diverse residues generated by industries present opportunities to develop natural and biodegradable packaging and, also to contribute with physicochemical properties. Within the wine industry, grape residues were about 50% of the total volume of raw material used for wine production [7]. Consequently, the need for proper disposal and minimizing environmental impact offers possibilities for reuse, which can promote sustainability and can prevent the contamination of soil and water [8,9,10]. Among the residues generated in the production of wine, berry, skin, and seeds can be highlighted. These residues

represent a promising source for extracting natural bioactive compounds and phenolic substances [7, 11].

Therefore, the main objective of this work was to develop biofilms using cassava starch and grape waste flour from the wine industry's residue. The antioxidant activity of grape waste flour and biofilms were evaluated. Additionally, the transfer of properties from the grape waste flour to cassava starch films was analyzed. The thermal degradation of the biofilms was also evaluated to assess their suitability for future applications.

Experimental

To produce the grape waste flour used in this work, Niagara's grape residues from the wine industry, containing bagasse, peels, and seeds, were dried in an oven with air circulation at 40 °C for 42 h and grounded in a knife mill to obtain a fine powder with granulometry smaller than 0.208 mm. The flour was analyzed for antioxidant activity by the DPPH method [12].

The polymeric films were produced by casting method. The film solution was prepared using 5 wt.% cassava starch in water and different concentrations of flour from grape residues (0, 0.5, 1, 2, and 4 wt.% based on starch dry weight). The solution was magnetic stirred for 10 min at room temperature, then submitted to the ultrasonic bath for 5 min at 60 °C. The glycerol, (20 wt.% on starch dry weight) was added to the solution, followed by magnetic stirring at 75 °C for 20 min. The filmogenic solution was poured into plastic plates proportionately to 0.236 g/cm^2, and film cure was realized in an oven at 40 °C for 24 h before the analysis.

For antioxidant activity (AA), a solution with 0.1 g of grape waste flour or 0.1 g of film and 2 mL of distilled water was prepared and agitated for 30 min at room temperature. An aliquot of 500 µL of supernatant was added to 2 mL of DPPH solution (0.06 mM). A control was also prepared without film sample. The absorbance (Abs) reading for triplicate was carried out in a spectrophotometer (K37-UVVIS/ KASVI) at 517 nm. A standard curve was prepared using gallic acid. Antioxidant activity was determined by Eq. 1.

$$\%AA = 100 * \left(1 - \frac{Abs\ Sample}{Abs\ Control}\right) \quad (1)$$

The thermogravimetry (TG) was performed using a TGA 55 instrument under a nitrogen atmosphere (N_2), with a flow rate at 40.0 mL/min. For the analysis, 10 mg of the film was heated from 25 °C to 600 °C at a heating rate of 10 °C/min.

Results and Discussion

The biofilms showed a crescent increase for AA with the increase in grape waste flour concentration (Fig. 1). The highest AA values were found for the grape waste flour residues (92.02%) and for biofilms produced with addition of 4 wt.% of grape waste flour (66.74%). Similar values of AA (91.7%) were also found in Niagara grape residues by Mourera et al. (2018) [13]. The film with 0.5 wt.% grape waste flour showed an expressive AA of 33.41%. The 4 wt.% sample has eight times more grape waste flour and only twice the AA compared to the 0.5 wt.% sample. The AA results can be explained by the presence of polyphenolic compounds in the grape waste flour and the interaction of them with the film. It can be possible that the use of an ultrasonic bath to prepare the films may have increased the extraction or interaction of polyphenolic compounds from the grape waste flour with the film and consequently its antioxidant properties. The AA of the films was determined by examining the antioxidant capacity of grape flour. Grapes, in general, contain high amounts of phenolic compounds, particularly flavonoids, which are major contributors to the fruit's antioxidant capacity. These compounds are present in the grape's skin and pomace, making the flour rich in them and giving it a high value for antioxidant activity [14].

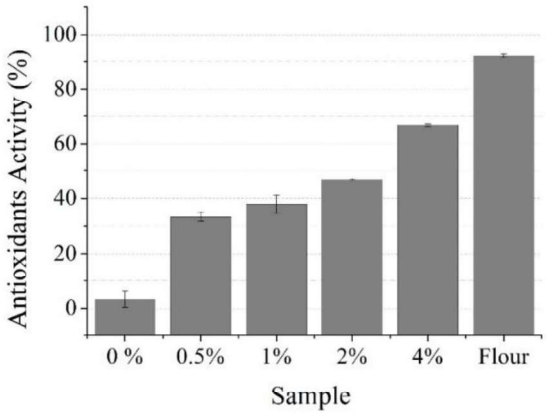

Figure 1 – Antioxidant activity for films and flour.

The flour from grape residues showed an IC50 (concentration when 50 % of the DPPH free radical is captured) of 17.036 µg/mL [14]. IC50 of 10.23 µg/mL and 7.49 µg/mL were found in grapes by Pesco et al. (2012) and Soares et al. (2008), respectively [15,16].

With the increase in antioxidant activity, the film shows a high potential for application, mainly in products that have a high rate of degradation by oxidation, such as food and some beverages [5], being able to reduce the rate of degradation or even avoid it, improving the product quality and increasing the shelf life.

The thermal degradation curve (Fig. 2) is similar in all samples, with multiple weight loss stages. There is a noticeable decrease in values between 50 and 150°C, indicating the loss of moisture and volatile elements in the film. At temperatures between 200 and 300°C, at second stage, a rapid slope can be observed in all films, which indicates the decomposition of organic materials, which may be starch, glycerol and some waste components. On temperature approximately between 300 and 400°C, it was observed the highest weight loss, indicating a degradation of starch components [6].

At temperatures of approximately 350°C it was possible to observe that the film with 4 wt.% showed the lowest weight loss compared to the other samples. The percentage difference in weight loss between films containing 4 wt.% was approximately 9,1% lower than the films without grape waste flour.

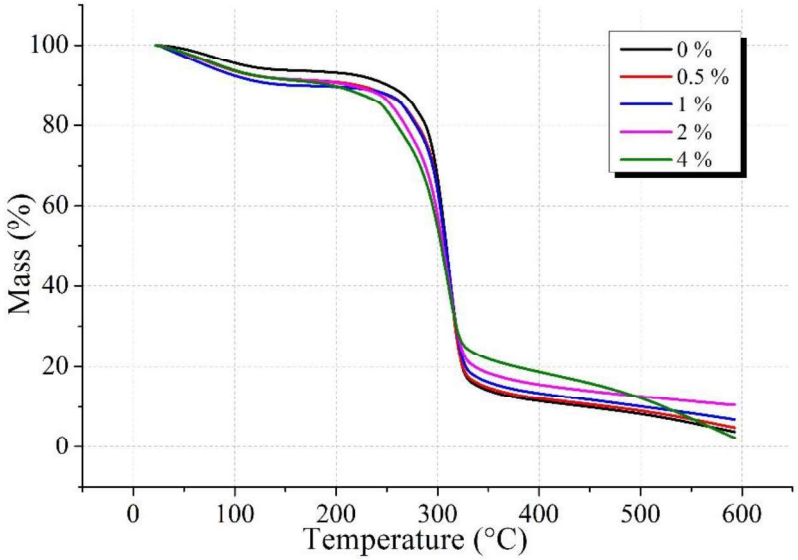

Figure 1 - Thermogravimetry curves of all samples studied.

The thermal decomposition temperature of 5% weight loss is the onset of decomposition temperature ($T_{5\%}$) and the temperature of maximum weight loss rate (T_{max}) is the peak temperature in derivative thermogravimetry (DTG) curve. According to Table 1, it was possible to observe that the 5% weight loss temperature ($T_{5\%}$) for the films with grape waste flour presented values of ~80 °C and for pure biofilm the value was 108 °C. The decrease on temperature, indicates a decrease of thermal stability for films with grape waste flour added. At temperatures close to 100°C, the carbonization of organic matter from the grape occurs [17], what can be the main reason for the weight loss observed. The films may experience hindrance in energy dissipation due to the presence of flour grains, which can lead to greater degradation at lower temperatures [18].

The degradation of pure glycerol occurs at temperatures close to 270 °C, where the bonds between glycerol and the polymer begin to break down. In contrast, the degradation of pure starch occurs at 317 °C. The starch degradation temperature is close to the highest degradation rate observed for all samples (~310 °C).

Table 1 – Thermogravimetry results.

Sample	$T_{5\%}$	T_{max}	Weight loss (%) of T_{max}
Starch	77 °C	317 °C	47
Glycerol	104°C	270 °C	52
0%	108 °C	313 °C	60
0.5%	82 °C	312 °C	60
1%	71 °C	312 °C	58
2%	84°C	309 °C	58
4%	81 °C	309 °C	57

Temperature of 5% weight loss ($T_{5\%}$), and maximum (T_{max}) weight loss.

The temperature where starch degradation occurs is where most of the mass is lost, as the films are primarily composed of starch. The interaction of glycerol with starch can delay glycerol degradation by increasing the temperature compared to pure plasticizer, which may explain the weight loss being accentuated in a narrower range of 290 to 310 °C, where degradation is possibly occurring for glycerol and starch, simultaneously.

The temperature of maximum weight loss (T_{max}) for all samples was similar. However, it is possible to observe a small decrease in weight loss at this point as the percentage of flour increases in the biofilms, with the lowest mass loss being 57 % and 58 % for 4 and 2 % of flour in the biofilm, respectively. Probably, the residual mass of degradation contains residues of inorganic matter, like ash and minerals, that did not degrade.

Conclusions

From the results presented, it is possible to state that the AA of the films increased with the increase in concentration of grape waste flour added to the films. The highest AA was found for films produced with 4 wt.% of flour. The significant increase in antioxidant activity, provided by the incorporation of the flour, allows the application of film in specific products subject to oxidation, thus reducing this characteristic that can cause losses to the product and even extend its shelf life.

As for the thermogravimetric properties, the flour addition caused a decrease in the thermal stability of the samples compared to the control film. However, the temperature of 5% weight loss observed for the films (~ 80 °C) probably does not compromise the application of this biofilm in the packaging industry. On the other hand, there were no significant differences on temperature of maximum mass loss, with values very close to the starch degradation temperature, the main component of the film.

The biofilms showed a high potential to use residues from the wine industry, reducing the amount of waste discarded, adding value to the same, and when incorporated into cassava starch biofilms, improving antioxidant activity and enhancing its application to specific demands, principally for foods and products susceptible to oxidation.

Acknowledgements
Authors are grateful for the funding support from FAPESC – Brazil (PAP 2021TR854), CAPES - Brazil (PROAP/AUXPE) and Multi-User Facility infrastructure from Santa Catarina State University's Technological Sciences Center.

References

1. OECD, *G*lobal Plastics Outlook: Economic Drivers, Environmental Impacts and Policy Options, OECD Publishing, Paris, 2022, https://doi.org/10.1787/de747aef-en.
2. R. Priyadarshi; J. W. Rhim; Innovative Food Science and Emerging Technologies 2020, -62, 102346. https://doi.org/10.1016/j.ifset.2020.1023486
3. S. Sid; et al., Trends in Food Science and Technology 2021, 115, 87-104, https://doi.org/10.1016/j.tifs.2021.06.026
4. A. Chamas; et al., ACS Sustainable: Chemistry and Engineering 2020, 8, 3494-3511, https://doi.org/10.1021/acssuschemeng.9b06635.
5. E. Jamróz; J. Tkaczewska; M. Kopec; A. C. Wójcik. Food Chemistry, 383, 132425. https://doi.org/10.1016/j.foodchem.2022.132425
6. E. J. G. Laureanti; et al., Journal of Applied Polymer Science 2021, 138, 50922. https://doi.org/10.1002/app.50922
7. D.P. Makris; et al. Journal of Food Composition and Analyses 2007, 20,125-132. https://doi.org/10.1016/j.jfca.2006.04.010.
8. M. A. Cardoso; et al., Revista Nacional de Gerenciamento de Cidades 2015, 03, 149-161, https://doi.org/10.17271/231884723192015
9. L. O. S. Martins; L. T. Silva; R. A. F. Livre de Sustentabilidade e Empreendedorismo 2017, 2, 142-166.
10. L. A. L. Querino; J. P. G. Pereira. Revista Monografia Ambientais 2016, 15, 404-415, https://doi.org/10.5902/2236130819452
11. M. Rubilar; et al. Agricultural and Food Chemistry 2007, 55, 10101-10109,
12. M. D. S. M. Rufino; et al. Comunicado Técnico. Empresa Brasileira de Pesquisa Agropecuária, julho, 2007.
13. D. C. S. Pesco; et al. VI Mostra Interna de Trabalhos de Iniciação Científica 2012, 5. 978-85-8084-413-9
14. S. Verruck; E. S. Prudencio; S. M da Silveira; Revista do Congresso Sul Brasileiro de Engenharia de Alimentos 2018, 4, 111. https://doi.org/10.5965/24473650412018111
15. L. P. Moureira; et al. Anais do 10º salão internacional de ensino, pesquisa e extensão 2018, 10.
16. M. Soares; et al. Revista Brasileira de Fruticultura 2008, 30, 59-64. https://doi.org/10.1590/S0100-29452008000100013
17. A. V. R. Salcedo; A. F. R. González; J. M. B. Burgos. Ingeniería y Desarrollo 2018, 36, 398-417. https://doi.org/10.14482/inde.36.2.10379
18. L. C. Klemann, mestre. Dissertação de mestrado. Universidade Federal de Santa Catarina. Joinville. 2018.

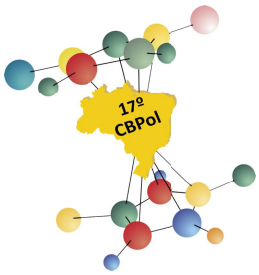

PROPERTIES OF PACKAGING FILMS FOR MEAT PRODUCTS WITH MALEIC ANHYDRIDE-BASED COMPATIBILIZER

Bruna Bonato Turriziani[1], Roniérik Pioli Vieira[2], Luís Marangoni Júnior[3], Rosa Maria Vercelino Alves[3*]

1 - Pos's graduation of the Institute of Food Technology, Campinas, São Paulo, Brazil.

2 - School of Chemical Engineering, University of Campinas, São Paulo, Brazil.

3 - Packaging Technology Center, Institute of Food Technology, Campinas, São Paulo, Brazil.

**rosa.cetea@gmail.com*

Abstract - The effect of 5 and 7% of PCA-MA (polyolefin compatibilizer additive with maleic anhydride) on the properties of two multilayer packaging materials (Polyethylene (PE)/PE/ adhesive (ad) / polyamide (PA)/ad/PE/PE and PE/ad/PA/ ethylene vinyl alcohol (EVOH/PA)/ad/PE, PA: polyamide used for meat products were studied. The incorporation of PCA-MA resulted in the reduction of the crystallinity index and consequently, a reduction in tensile strength and puncture resistance and higher water vapor permeability. Overall, although PCA-MA incorporation resulted in some loss of packaging properties, this additive can be considered an attractive alternative to facilitate the recycling process of these complex materials.

Keywords: *multilayer flexible packaging; recycling; polyamide; ethylene vinyl alcohol; polyethylene.*

Fundings: This study was partly financed by the Coordination for the Improvement of Higher Education Personnel – Brazil (CAPES) – Financial Code 001 and FAPESP for its support in the purchase of part of the equipment used in this study (Research Aid - Multiuser Equipment Program: Processes FAPESP no 2018/15759-6 and 2018/15758-0).

Introduction

Because packaging for meat products has different polymers they are usually incinerated or landfilled and for their recycling it is necessary the use of compatibilizer additives as maleic anhydride (MA) [1] to enhance the interactions between the different polymers and minimize agglomeration during the recycling process [2, 3, 4]. MA is reactive towards hydroxyl and amine groups, forming covalent and/or hydrogen bonds, resulting in enhancement of properties after recycling [5]. Then the aim of this study was to investigate the incorporation of 5 and 7% of maleic anhydride-based compatibilizer additive (PCA-MA) on the properties of two multilayer packaging materials used for the meat products.

Experimental

Materials: LDPE (low density polyethylene 219M, Dow, Argentina); LLDPE: linear low-density polyethylene 8051G, Dow, Argentina); adhesive Bynel 41E1352, Dow, USA; PAUltramid C40L, BASF, Germany; PCA-MA - polyolefin compatibilizer additive with maleic anhydride - Retain 3000, Dow, USA; EVOH - ethylene vinyl alcohol F171B, Kuraray, USA.

Coextrusion of the films: The multilayer films were coextruded in a pilot balloon extrusion line (Coex Extruder Dr Collin, model BL180/400, Germany), with two different compositions, PE/PE/ad/PA/ad/PE/PE (Film A) and PE/ad/PA/EVOH/PA/ad/PE (Film B), and 5% and 7% concentrations of compatibilizer additive with maleic anhydride were added to each structure.

Characterization of the films

X-ray diffraction (XRD): X-ray analyzer (X'Pert-MPD, Philips, Almelo, Netherlands) was employed for crystallinity evaluation and the XRD measurements of multilayer packaging films were operated with Cu Kα radiation (λ = 1.54 Å) at a scan rate of 0.033°/s (step = 0.04° and time per step = 1.2 s), with the accelerated voltage of 40 kV and the applied current of 40 mA, varying from 5 to 30°. The global crystallinity index (CI) of the films was estimated through the ratio

between the area under the peaks (crystalline regions) and the total area (crystalline and amorphous regions).

Tensile strength: tensile strength was determined using a universal testing machine (Instron, 5565-E2, USA) [6], operating with cell load 5 kN at 23 ± 2 °C and 50 ± 5% RH. Test speed was 500 mm min^{-1} and with initial grip separation of 50 mm in the machine direction (MD) and transverse direction (TD).

Puncture resistance: was determined using a universal testing machine (Instron, 5565-E2, USA), with a load cell of 5 kN operating in compression, using a 3.2 mm metal tip at a constant speed of 25 mm min^{-1} [7].

Water vapor transmission rate (WVTR): determined in an equipment with infrared sensor, PERMATRAN (MOCON, USA) [8] at 38 °C and 90% RH.

Oxygen transmission rate (OTR): determined in an OXTRAN equipment (MOCON, USA) [9], with the external side of the sample was in contact with the permeant gas (100% O_2) at 23 ºC and 75 ± 2% RH and the permeation area was 50 cm^2. The results were corrected for 1 atm permeant gas partial pressure gradient.

Results and Discussion

X-ray diffraction (XRD): Fig 1 presents the XRD patterns for Film A and Film B. The main polyethylene diffraction peaks, at 2θ = 21.5 and 24°, correspond to the (110) and the (200) crystal planes of its orthorhombic unit cell. These diffraction peaks have been commonly reported for both LDPE and LLDPE [10–13], differing in magnitude of their area relative to the different crystallinities. Overall, it was found that the XRD profiles did not undergo drastic changes, except for the minimal changes in the relative areas of the main identified peaks. Therefore, global crystallinity indices (CI) were estimated to provide a quantitative analysis.

The CI values for the samples of both films ranged from 24.3 to 28.3% (**Table 1**), and are in agreement with previously reported values for LDPE/LLDPE blends [27, 29]. These CI can be considered low due to the large proportion of LDPE in the outer layers of the samples evaluated. Additionally, the incorporation of the PCA-MA in these layers apparently provided a tendency to slightly reduce the CI for both film A and film B. However, for this sample, the incorporation of different proportions of PCA-MA resulted in a similar effect on CI.

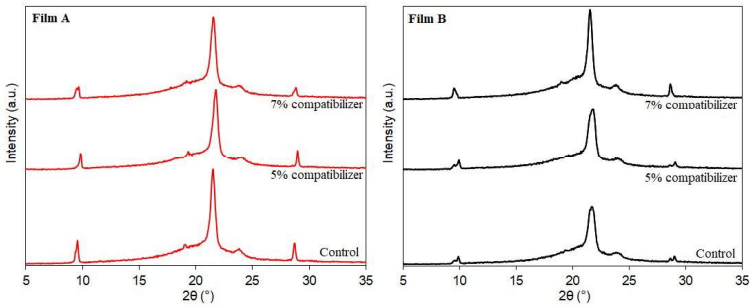

Figure 1. XRD of multilayer packaging films with different compatibilizer concentrations.

Table 1. Crystallinity index (%) of the packaging films.

Film A	CI (%)	Film B	CI (%)
Control	27.6	Control	28.3
5% compatibilizer	25.8	5% compatibilizer	26.7
7% compatibilizer	24.3	7% compatibilizer	26.6

Tensile strength: the incorporation of PCA-MA compatibilizer significantly reduced the TS of both films in both directions. The results for Film A, in MD and DT, ranged from 36.8 to 26.5 MPa, and from 31.5 to 26.7 MPa, respectively. For Film B, TS ranged from 32.8 to 28.2 MPa in MD, and from 28.7 to 24.9 in DT, as shown in Fig 2.

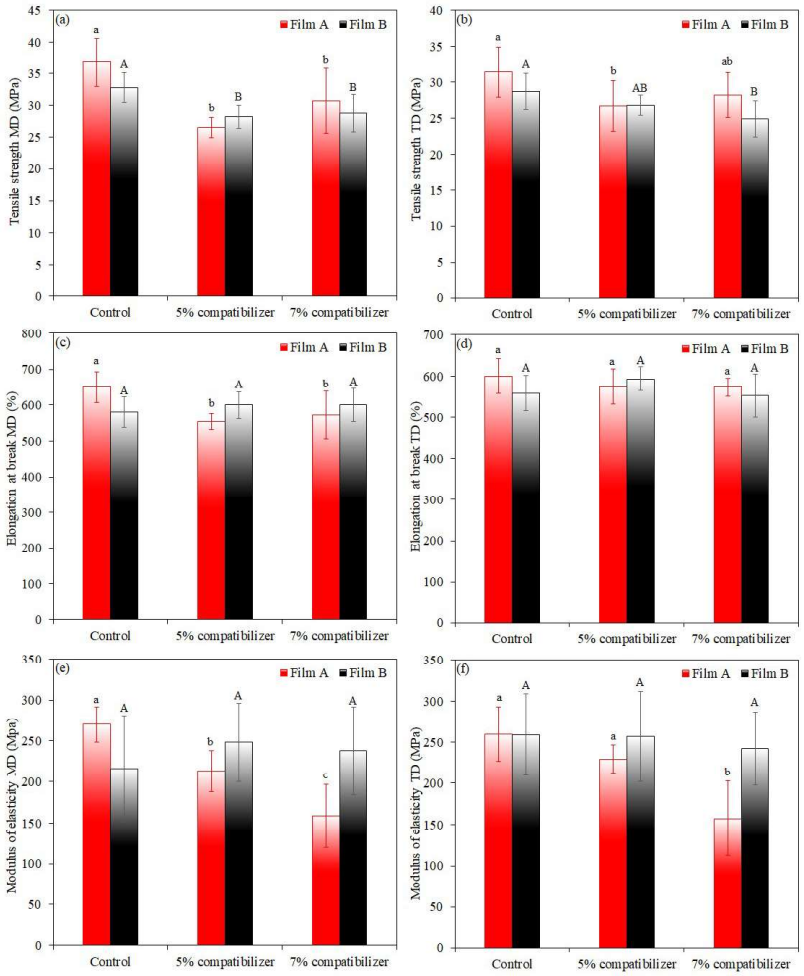

Figure 2. Tensile strength in MD (a), tensile strength in TD (b), elongation at break in MD (c), elongation at break in TD (d), modulus of elasticity in MD (e), and modulus of elasticity in TD (f) of multilayer packaging films with different compatibilizer concentrations.

Elongation at break (EB) of all samples were above 400%, which were typical values for films with PE and EVOH [14] and the incorporation of the compatibilizer did not significantly influence the EB of Film B in MD and TD, and for Film A only in TD (Fig 2 (c, d)). However, when 5% and 7% of compatibilizer were incorporated, there was a significant reduction of 14.7% and 12.1%, respectively, in the EB of Film A in MD. A similar reduction in EB as a function of maleic anhydride concentration was also observed for PE/PA blends [15]. A possible explanation for this behavior is that the fracture initiated in the PA layer can be transmitted to the other PE layers in a cohesive way, resulting in a reduction of EB [16]. However, interestingly this behavior was observed only in the MD of Film A. The ME results of Film B did not show a significant difference between the different samples in the two directions of the material, regardless of the concentration of compatibilizer used (Fig. 2 (e) and (f)). However, for Film A, the compatibilizer significantly reduced the ME considering the test in both directions. These small reductions in mechanical properties are probably caused by the intrinsic properties of PCA-MA, in addition to the correlation with the observed reductions in the crystallinity index, mentioned above. Similar behavior was also observed in the literature for polypropylene [18].

Puncture resistance: The puncture resistance and elongation at puncture results are shown in Fig. 3 (a) and (b), respectively. The control Film A had a puncture resistance of 23.8 N and elongation at puncture of 17.8 mm. These values are higher than those of the Film B counterpart (puncture resistance: 20.4 N; elongation at puncture: 15.4 mm). The higher value presented in Film A in relation to Film B can be attributed to the higher thickness of the polyamide layer. This polymer is widely used for meat products packaging because of its mechanical performance [17] and it is an important quality parameter for packaged products with spikes and bones, such as meat products.

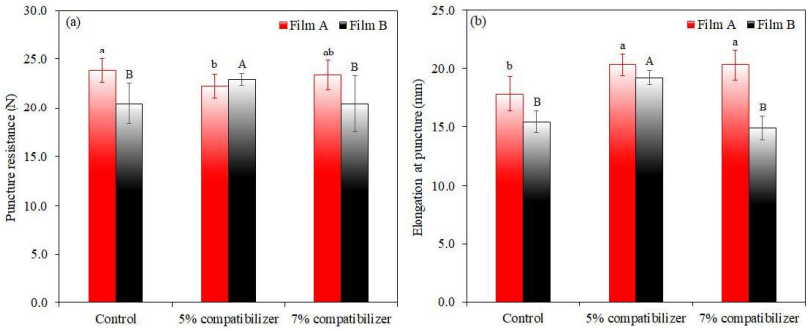

Figure 3. Puncture resistance (a) and elongation at puncture (b) of multilayer packaging films with different compatibilizer concentrations.

The incorporation of PCA-MA resulted in a slight reduction in puncture resistance and an increase in elongation at puncture. These results may be correlated with the slight reduction in crystallinity index (**Table 2**), and are similar to those found for polypropylene added with maleic anhydride [18]. In addition, the lower puncture resistance observed for Film A with 5% compatibilizer can be also correlated with the lower total thickness of this film, in relation to the control A (**Table 1**). However, for Film B with 5% compatibilizer, the values of puncture resistance and elongation at puncture were slightly higher than the other samples, showing no correlation with the crystallinity results. Finally, it is important to highlight that the changes in puncture performance are within the acceptable range by the industry, which is 25% [19].

Water vapor transmission rate (WVTR) and oxygen transmission rate (OTR): Regarding OTR, the results for control Films A and B were 43.84 ± 3.25 and 3.88 ± 0.48 mL m^{-2} day^{-1}, respectively. The lower OTR of Film B is attributed to the combined presence of PA and EVOH layers in the packaging. EVOH and PA are widely used to confer elevated oxygen barrier to multilayer packaging. Due to the hydrophilic nature of these polymers, they are generally applied as an intermediate layer between at least two layers of a hydrophobic material (inner and outer layer), such as polyethylene (PE) or polypropylene (PP) [20]. The incorporation of the compatibilizer additive did not result in significant changes in the OTR of Film A. However, a small increase in the OTR of Film B was observed with the incorporation of 5% of the compatibilizer. A small reduction in the oxygen barrier was also observed for PE/EVOH films compatibilized with LDPE-g-MA, and was attributed to a possible modification of the film morphology [21].

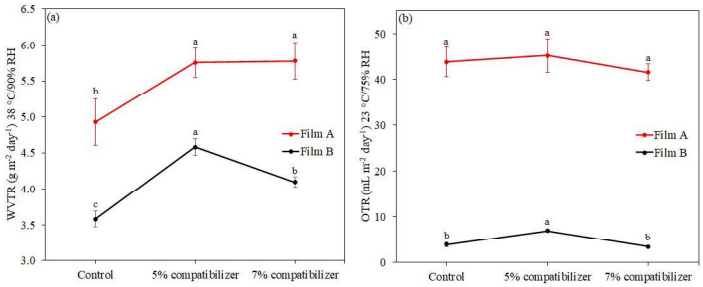

Figure 4. WVTR (a) and OTR (b) of multilayer packaging films with different compatibilizer concentrations.

Conclusions: The incorporation of PCA-MA provided a to slightly reduce the crystallinity index of the films, which may be also correlated with the reductions in tensile strength and puncture resistance. Additionally, an increase in the water vapor transmission rate was observed after the incorporation of PCA-MA, being related with the presence of hydrophilic groups of the compatibilizer and also the reduction in crystallinity. The oxygen transmission rate was little influenced by the compatibilizer. Overall, although the incorporation of PCA-MA resulted in some loss of property, this is a promising alternative to enable that flexible multi-material PE, PA and EVOH-based packaging are recyclable.

Acknowledgements
To the Center Technology Center and BRF S.A. for the analyses carried out in the laboratories for the development of this research and to Dow's Pack Studio for the production of alternative flexible packaging.

References

1. V. Lahtela, S. Silwal, T. Kärki Re-Processing of Multilayer Plastic Materials as a Part of the Recycling Process: The Features of Processed Multilayer Materials. Polym. 12. 2020.
2. M.C. Mulakkal; A. Castillo Castillo A, A. C.Taylor, et al (2021) Advancing mechanical recycling of multilayer plastics through finite element modelling and environmental policy. Resour Conserv Recycl 166:105371. https://doi.org/https://doi.org/10.1016/j.resconrec.2020.105371
3. N. F. Braga, A. M. LaChance, B. Liu, et al (2019) Influence of compatibilizer and carbon nanotubes on mechanical, electrical, and barrier properties of PTT/ABS blends. Adv Ind Eng Polym Res 2:121–125. https://doi.org/https://doi.org/10.1016/j.aiepr.2019.07.002
4. O Horodytska, FJ Valdés, A Fullana (2018) Plastic flexible films waste management – A state of art review. Waste Manag 77:413–425. https://doi.org/https://doi.org/10.1016/j.wasman.2018.04.0235.
5. J Maris, S Bourdon, J-M Brossard, et al (2018) Mechanical recycling: Compatibilization of mixed thermoplastic wastes. Polym Degrad Stab 147:245–266. https://doi.org/https://doi.org/10.1016/j.polymdegradstab.2017.11.001
6. ASTM-D882 (2018) Standard Test Method for Tensile Properties of Thin Plastic Sheeting. West Conshohocken. 12p.
7. ASTM-F1306 (2016) Standard test method for slow rate penetration resistance of flexible barrier films and laminates. 5
8. ASTM-F1249 (2020) ASTM INTERNATIONAL: Standard test method for water vapor transmission rate through plastic film and sheeting using a modulated infrared sensor. 7
9. ASTM-F1927 (2020) ASTM INTERNATIONAL: Standard test method for determination of oxygen gas transmition rate, permeability and performance at controlled relative humidity through barrier materials using a coulometric detector. 6
10. M Hamouya, A Mahir, MC Idrissi (2014) Natural Ageing of Stabilized and Unstabilized Ldpe Films: Xrd and Sem Analysis. Int J Res Eng Technol 03:210–215. https://doi.org/10.15623/ijret.2014.0312027
11. K Zhang, L Zhong, J Gao, et al (2019) Temperature dependence of crystalline structure and DC performance in LLDPE/HDPE blending material. IEEE Trans Dielectr Electr Insul 26:754–759. https://doi.org/10.1109/tdei.2018.007652
12. T Furukawa, H Sato, Y Kita, et al (2006) Molecular structure, crystallinity and morphology of polyethylene/ polypropylene blends studied by Raman mapping, scanning electron microscopy, wide angle X-ray diffraction, and differential scanning calorimetry. Polym J 38:1127–1136. https://doi.org/10.1295/polymj.PJ2006056
13. W Chen, B Qu (2004) LLDPE/ZnAl LDH-exfoliated nanocomposites: Effects of nanolayers on thermal and mechanical properties. J Mater Chem 14:1705–1710. https://doi.org/10.1039/b401790k
14. MW Spencer, L Cui, Y Yoo, DR Paul (2010) Morphology and properties of nanocomposites based on HDPE/HDPE-g-MA blends. Polymer (Guildf) 51:1056–1070. https://doi.org/https://doi.org/10.1016/j.polymer.2009.12.047

15. J Feng, G Zhang, K MacInnis et al (2019) Effect of compatibilizer on morphology and properties of HDPE/Nylon 6 blends. J Polym Sci Part B Polym Phys 57:281–290. https://doi.org/https://doi.org/10.1002/polb.24783
16. N Sallem-Idrissi, V Miri, A Marin et al (2012) The role of strain-induced structural changes on the mechanical behavior of PA6/PE multilayer films under uniaxial drawing. Polymer (Guildf) 53:5336–5346. https://doi.org/https://doi.org/10.1016/j.polymer.2012.09.027
17. AA Tyuftin, JP Kerry (2020) Review of surface treatment methods for polyamide films for potential application as smart packaging materials: surface structure, antimicrobial and spectral properties. Food Packag Shelf Life 24:100475. https://doi.org/https://doi.org/10.1016/j.fpsl.2020.100475
18. A Saffar, PJ Carreau, A Ajji, MR Kamal (2014) Development of polypropylene microporous hydrophilic membranes by blending with PP-g-MA and PP-g-AA. J Memb Sci 462:50–61. https://doi.org/https://doi.org/10.1016/j.memsci.2014.03.024
19. Y Lambert, G Demazeau, A. Largeteau et al (2000) Packaging for high-pressure treatments in the food industry. Packag Technol Sci 13:63–71. https://doi.org/10.1002/1099-1.
20. Marangoni Júnior L, Oliveira LMD, Bócoli PFJ, et al (2020) Morphological, thermal and mechanical properties of polyamide and ethylene vinyl alcohol multilayer flexible packaging after high-pressure processing. J Food Eng 276. https://doi.org/10.1016/j.jfoodeng.2020.109913
21. Rahnama M, Oromiehie A, Ahmadi S, Ghasemi I (2017) Oxygen-barrier films based on low-density polyethylene/ ethylene vinyl alcohol/ polyethylene-grafted maleic anhydride compatibilizer. Polyolefins J 4:137–147. https://doi.org/10.22063/poj.2016.1398

BIOCHAR DERIVED FROM BRAZILIAN-PINE FRUIT SHELL AND AGAROSE HYDROGEL COMPOSITES FOR ENVIRONMENTAL ANALYSIS

Alessandra Bitobrovec[1], Carlos A. F. dos Santos[1], Dayane Reina[1], Bruna F. P. Schmite[1], Adriano G. Viana[2], Ernandes T. Tenório Neto[3], Vanessa Egéa dos Anjos[1].

1 – Laboratory of Chemical Speciation and Environmental Chemistry (LEQQA), State University of Ponta Grossa (UEPG), Ponta Grossa, PR, Brazil
alebito@outlook.com
2– Laboratory of Spectroscopy, Characterization and Modeling (LESCAM), State University of Ponta Grossa (UEPG), Ponta Grossa, PR, Brazil
3– Laboratory of Multifunctional Polymeric Materials (LMPM), State University of Ponta Grossa (UEPG), Ponta Grossa, PR, Brazil

Hydrogels (HG) are promising materials to concentrate and remove trace contaminants from freshwater bodies[1]. They can be combined with biochar (BC), forming hydrogel composites with enhanced absorption efficiency. BC is an environmentally friendly and low-cost material prepared by the pyrolysis of different biomass, including plants and waste of food or animals[2]. Herein, we investigated the preparation and the properties of Agarose-based hydrogels with BC from the residue of Brazilian-pine fruit shell, which is widely consumed in southern Brazil. We prepared the BC by slow pyrolysis of the biomass at 800 °C under a reduced oxygen atmosphere. Composites were obtained by combining BC (1-3% g g^{-1}) and Agarose (2% g g^{-1}) in a disk-shaped mold with a thickness of 1.0 mm and diameter of 29 mm. The hydrogel-biochar composite (CP) showed an improved absorbent property that could be regenerated and reused. Through the sorption and desorption assays of Cr(III) and Cr(VI), we found that the composite with a lower mass of biochar (1.7%) was the best composition for chromium retention in pH 7.0, with three hours of contact time. In this case, the sorption values were 82±10% and 47±3% for Cr(III) and Cr(VI), respectively. The SEM images showed that the CP had interconnected pores contributing to the Cr sorption. Moreover, the FTIR spectra obtained before and after the sorption studies revealed that Cr species interact with -OH and C-O functional groups from the CP. After the concentration of Cr species onto the composite, the desorption was carried out with 1 mol L^{-1} HNO_3. Cr(III) was eluted with one extraction step, allowing the subsequent extraction of Cr(VI) with two steps. Our results indicate that the obtained CP using the residue of Brazilian-pine fruit shell is suitable for both the sorption and the differentiation of Cr species.

References

1. S. Perumal et al. *Chemosphere* 2022, *286*, 131760. https://doi.org/10.1016/j.chemosphere.2021.131760
2. S. Wijitkosum. *International soil and water conservation research* 2022, *10*, 335-341. https://doi.org/10.1016/j.iswcr.2021.09.006

Fundings: CAPES, CNPq, UEPG, C-Labmu.

Keywords: *Araucaria angustifolia, adsorbent, sorption, Cr(III), Cr(VI).*

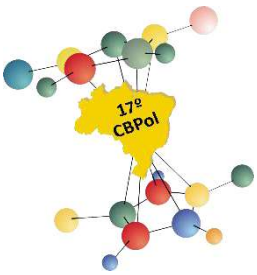

BIODEGRADABLE ACTIVE MATERIALS BASED ON STARCH AND BLACKBERRY DRY RESIDUE

Amanda Chezini[1], Ana B. Klosowski[2], Giovani A. Carvalho[1]; Juliana B. Olivato[1,2,3*]

1 – Post-graduation Program of Food Science and Technology, State University of Ponta Grossa (UEPG), Ponta Grossa, PR, Brazil
2 – Post-graduation Program of Pharmaceutical Sciences, State University of Ponta Grossa (UEPG), Ponta Grossa, PR, Brazil
3 – Department of Pharmaceutical Sciences, State University of Ponta Grossa (UEPG), Ponta Grossa, PR, Brazil.
**jbolivato@uepg.br*

Abstract - The production of non-biodegradable plastics has increased substantially, due to high consumption, low cost and market demand. The aim of this work was to produce a biodegradable starch-based material containing blackberry dry residue (BDR). The increase in the proportion of BDR resulted in more dense biodegradable materials, with lower water vapor permeability and lower water solubility. Scanning electron microscopy (FEG-SEM) analysis revealed that the surface of the Control samples (BDR0) had continuous and smooth characteristics, and with the inclusion of BDR, the surface of the material has become more heterogeneous. The total phenolic content of the biodegradable materials increased in higher concentrations and times in the aqueous medium, resulting in a maximum value of 38.47 ± 10.68 mg EAG/g for 48 hours of immersion in the sample with higher BDR concentration (BDR10). The inclusion of blackberry dry residues produced biodegradable materials with promising properties.

Keywords: *Byproduct; biodegradable materials; active packaging*.

Introduction

One of the main interests in applying natural polymers in the production of flexible packaging is precisely to replace the use of synthetic polymers, which drastically reduce the environmental problem and the accumulation of hard-to-degrade waste [1]. Over the past decade, many studies have been developed into the research and production of biodegradable films based on macromolecules, such as starch [2,3]. In addition, the use of starch offers advantages, such as its low cost, abundance, its renewable and biodegradable nature.

Active packaging, in addition to the functions common to all packaging, promotes the interaction of components present in the packaging with the packaged food, whose primary objective is to prolong the shelf life and maintain the quality of the products. The functional active packaging is crucial for the preservation of the food, since the added natural additives maintain their microbiological characteristics [4, 5]. Among the various types of active packaging, that which exerts an antioxidant effect is fundamental for the preservation of foodstuffs, avoiding degradation by oxidation of lipids [6, 7].

Biodegradable packaging dramatically reduces the use of synthetic polymers, and the application of bio-active compounds with antioxidant action will collaborate in a significant way with the preservation of food quality, combined with the reuse of industrial waste, important to industry, beneficial to society and valuable to the environment [8].

The purpose of this work was to develop an active packaging using starch and blackberry dry residues. The biodegradable active packaging was produced by thermopressing process and their mechanical, optical, barrier and structural properties were evaluated, as the controlled releases of phenolic compounds with antioxidant properties.

Experimental

Obtention and processing of dry blackberry residue (BDR)

BDR has been obtained after treatment of fruit in juice industries. The BDR was dried in an oven (60°C – 4 hours) and then ground into small particles.

Production and characterization of the active biodegradable materials

The production of active biodegradable materials was carried out by thermopressing (175°C / 1 atm) to obtain materials similar to trays. The trays were composed of cassava starch, glycerol (10 % w/v) and blackberry dry residues (BDR) (0, 2.5, 5 and 10 % w/w). All formulations were added of 100 mL of distilled water and 0.5 g of sodium benzoate as a preservative. The samples were coded as BDR followed by the concentration of residues in the formulation. The biodegradable active materials have been conditioned into B.O.D (25°C) and characterized for their mechanical, thermal, structural and barrier properties.

To determine the release content of total phenolic compounds from the biodegradable materials, the material was immersed in distilled water for up to 48 h at a 1:10 concentration, with 1g of sample and 10mL of water. 1 mL aliquots have been removed at time intervals: 0, 1, 2, 3, 4, 5, 6, 24 and 48 hours. Aliquots of 200 µL of each time were combined with 7 mL of distilled water, 500 µL of Folin-Ciocalteau reagent and after 30 s, added 2.5 mL of Na_2CO_3 10.6% (w/v). After 5 min of incubation at temperature of 50ºC, the absorbance was measured at λ = 715 nm in a reader SynergyTM H1 hybrid multi-mode chips with Gen5.2 software (BioTek®, USA). The results of the content of total phenolic compounds were expressed as equivalents of gallic acid (mg AG.g^{-1})

Results and Discussion

The thickness of biodegradable materials ranged from 2.816 to 2.972 mm, with no statistical difference observed between the samples. The color of the materials was expressed according to CIELAB. The L* result obtained for the BDR0 confirms the clarity of the sample, with the values close to 100. The BDR10 formulation, which has the highest percentage of BDR in its composition, had the lowest luminosity (L*) value, indicative of a darker profile. The a* coordinate has increased in higher concentrations of BDR for each formulation, indicating a redder color. The same trend was observed for opacity, with higher results for the BDR10 formulation.

The mechanical properties of the active materials are presented in Table 1. The results showed that the addition of BDR leads to reduced materials resistance. No expressive difference in the tensile

strength and elongation results between materials with the addition of BDR highlights a positive point, because an increase in the BDR proportions has not changed its resistance and flexibility.

Table 1 – Mechanical properties of the active biodegradable materials.

Formulations	Density (g/cm^3)	Tensile Strenght (MPa)	Elongation at break (%)	Young's Modulus (MPa)
BDR0	8.30 ± 1.42^{a}	1.57 ± 0.43^{a}	21.04 ± 5.38^{a}	9.70 ± 2.75^{a}
BDR2.5	8.42 ± 0.30^{a}	0.68 ± 0.35^{b}	15.17 ± 4.73^{a}	7.21 ± 2.29^{a}
BDR5	9.30 ± 0.49^{a}	0.54 ± 0.11^{b}	17.80 ± 2.65^{a}	4.36 ± 0.81^{b}
BDR10	12.08 ± 3.24^{b}	0.47 ± 0.13^{b}	14.95 ± 4.08^{a}	$5.17 \pm 1.07^{b,c}$

Different letters in the same column indicate statistical difference (Tukey's test, $p<0,05$).

The percentage of water solubility of the materials showed a variation from 30.83 to 40.24%. It can be observed that the addition of BDR reduced the solubility of the material which is directly related to the physicochemical composition of BDR (lignocellulosic fibers) which impacts the interaction between the materials and water [9].

Thermogravimetric analysis showed three degradation steps. Thee first stage of degradation occurred between 75 and 170°C and refers to the gradual loss of water. The second stage occurred between 27°C and 325°C and was related to the decomposition of starch (amylose + amylopectin). The third stage occurred between 375° and 500°C can be attributed to the oxidation of organic matter. In the biodegradable active materials dTG curves, the maximum degradation temperature was observed to be 312°C for BDR2.5, 310°C for BDR5 and 308°C for BDR10, values similar to those observed for the BDR0 sample and referent to the starch degradation. Increasing the fiber content in the formulations and/or hydrogen interactions between molecules can alter the thermal stability of materials [10], however this influence was not observed in this study.

Scanning electron microscopy images showed that the BDR0 formulation presented a compact and regular surface area, which was visually modified after the addition of BDR in concentrations of 2.5%, 5% and 10%. The material surface images showed that the control sample (BDR0) exhibited a continuous, smooth and homogeneous characteristic, with no pores, cracks or irregularities. With the increasing concentration of BDR, the surface of the material has become more heterogeneous and rougher, suggesting that the addition of higher BDR concentrations could modify the regularity of the polymer matrix.

Table 2 shows the results of the content of phenolic compounds as a function of the time of immersion in water, to simulate the controlled release into food. In these results, a higher percentage of phenolic compounds were released from the film over time, reaching values of 38.47 mg $EAG.g^{-1}$ for BDR10 at 48 hours. This test was carried out to evaluate the migration potential of the bioactive incorporated into the biodegradable packaging, resulting in an active system. In this way, the observed results were promising, proving the performance of the starch-based biodegradable materials incorporated with BDR as active packaging, with continuous and prolonged release of antioxidants.

Table 2 – Phenolic compounds content (mg AG.g^{-1}) released from the active biodegradable materials.

Time (hour)	BDR0	BDR2.5	BDR5	BDR10
0	8.68 ± 1.25	8.68 ± 0.62	17.43 ± 0.62*#	19.31 ± 2.25*#
1	10.56 ± 0.62	12.22 ± 0.72	22.64 ± 2.00*#	22.64 ± 2.00*#
2	11.81 ± 0.62	12.64 ± 0.72	23.06 ± 0.00*#	25.56 ± 2.25*#
3	12.22 ± 0.36	13.47 ± 0.36	23.27 ± 1.57*#	26.18 ± 3.30*#
4	12.85 ± 0.95	15.35 ± 0.95	25.14 ± 1.30*#	26.81 ± 1.08*#
5	13.68 ± 1.87	15.97 ± 0.95	25.97 ± 2.52*#	26.81 ± 1.25*#
6	14.52 ± 0.36	16.18 ± 1.25	25.97 ± 0.95*#	28.06 ± 0.62*#
24	14.52 ± 0.36	17.02 ± 1.30	30.14 ± 2.00*#	28.47 ± 0.95*#
48	16.18 ± 1.87	17.85 ± 1.80	32.43 ± 0.62*#	38.47 ± 10.68*#

*Statistical difference compared to BDR0 ($p<0.01$).
Statistical difference compared to BDR2.5 ($p<0.01$).

Conclusions

The use of blackberry dry residue in biodegradable active materials reduced its mechanical resistance, when compared to the sample without BDR (BDR0), however there was no difference in this parameter with the increase in the concentration of BDR incorporated in the materials. The SEM images of the sample BDR0 had a homogeneous surface, without roughness and, with the addition of BDR, the materials had a surface more heterogeneous. As a result, biodegradable materials were promising for food application, exhibiting structural integrity and lack of pores.

The antioxidant activity of the biodegradable materials with BDR proven to be higher in samples with greater BDR concentrations (BDR10) and highlight the role of samples as active packaging for the controlled and prolonged release of antioxidants.

Therefore, it is concluded that biodegradable materials incorporating blackberry dry residue from the food industry may be an alternative to obtaining active packaging, which prevents the oxidation of food, in addition to being a sustainable appeal and promoting the valorization of this by-product.

Acknowledgements

The authors would express their gratitude to the multiuser laboratories at State University of Ponta Grossa for their technical support, and Coordenação de Aperfeiçoamento Pessoal de Nível Superior and Fundação Araucária for their financial support.

References

1. J.B. Olivato; M.V.E. Grossmann; A.P. Bilck; F. Yamashita, L.M. Oliveira. *Polímeros-Ciência e Tecnologia* 2013, 23(1), 32. doi:10.1590/S0104-14282013005000017

2. L.C.M. Almeida; F.K. Carvalho; J.B. Olivato. Macromolecular Symposia 2022, 406(1). doi:10.1002/masy.202200013
3. T. Yi; M. Qi; Q. Mo et al. Processes 2020, 8(3). doi:10.3390/pr8030329
4. P. Veiga-Santos; C.K. Suzuki; K. F. Nery; M.P. Cereda; A.R.P Scamparini. LWT - Food Science and Technology 2008, 41(8), 1506. doi:10.1016/j.lwt.2007.09.011
5. T.B.V. Silva; T.F.M Moreira; A. Oliveira et al. Food Funct 2019, 10(12), 7697. doi:10.1039/c9fo01315f
6. A. C. Lopes; M.K. Barcia; T. B. Veiga; F. Yamashita; M.V.E. Grossmann; J. B. Olivato. Polym Adv Technol. 31, 10. doi:10.1002/pat.5130
7. C. R. Afonso; R.S. Hirano; A.L. Gaspar et al. International Journal of Biologic Macromolecules 2019, 132, 1262. doi:10.1016/j.ijbiomac.2019.04.052
8. J. C. F. Fidelis; A.R.G Monteiro; M.R.S. Scapim et al. Italian Journal of Food Science 2015, 27(4), 468. doi:10.14674/1120-1770/ijfs.v379
9. F. Debiagi; S. Mali; M.V.E. Grossmann, F. Yamashita. Ciência e Agrotecnologia 2010, 34(6), 1522. http://www.scielo.br/pdf/cagro/v34n6/24.pdf
10. M.A.V.T. Garcia; C.F. Garcia; A.A.G Faraco. *Starch/Staerke* 2020, 72(7-8), 1. doi:10.1002/star.201900270

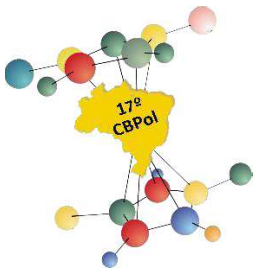

CELLULOSE HYDROGELS WITH LIGNIN BIOCHAR FOR REMOVAL OF HEAVY METAL IONS

Lucas. R. Gonçalves[1], Rafaela R. Ferreira[1], Alana G. Souza[1], Talles B. Costa[1], Rennan F. S. Barbosa[1] and Derval. S. Rosa[1]*

1 – Center for Engineering, Modelling and Applied Social Sciences, University Federal of ABC (UFABC), Santo André, São Paulo, SP, Brazil
dervalrosa@yahoo.com.br

Abstract – The presence of heavy metal ions in water represents an important risk to human health and other living beings. Due to this, the development of different techniques for the removal of these pollutants, such as adsorbent materials, has been shown to be necessary. In order to deal with these problems, cellulose hydrogels were synthesized with the addition of lignin biochar to remove heavy metals from contaminated water. The FTIR analysis showed that there were no significant structural changes in the hydrogels after the addition of Bc. The hydrogels exhibited good water absorption capacity, with the degree of swelling (DS) being greater than 290% for all samples. Finally, the cellulose-based hydrogel composites presented the following metallic affinity order: $Cu^{2+} > Cr^{6+} > Cd^{2+} > Zn^{2+} > Ni^{2+} > Mn^{2+}$.

Keywords: *Hydrogels; Cellulose; Biochar; Lignin; Heavy metals adsorption.*

Fundings: This research was financed by Fundação de Amparo à Pesquisa do Estado de São Paulo (FAPESP) (2020/13703-3, 2021/14714-1, 2022/01382-3, 2022/11133-0), Conselho Nacional de Desenvolvimento Científico e Tecnológico (CNPq) (308053/2021-4, 403934/2021-4), and Coordenação de Aperfeiçoamento de Pessoal de Nível Superior (CAPES) (Finance Code 001).

Introduction

The presence of pollutants in water is a worldwide problem, since thousands of humans and other living beings depend on its use for survival. The consumption of contaminated water can generate extremely dangerous effects, affecting the environment and the lives of the creatures that use it [1]. Exposure to heavy metals such as lead, cadmium, mercury and arsenic presents several risks to human health according to the WHO (World Health Organization), since in underdeveloped countries contact with these pollutants is still a real problem [2]. In view of the scope of this issue, several techniques have been developed for the removal of pollutants, mainly heavy metals, from effluents such as coagulation/flocculation, ion exchange, reverse osmosis, and membrane filtration. Because these processes have limitations such as low selectivity, high consumption of reagents and possible secondary contamination [1,3]. With this in mind, the adsorption method gains visibility due to its high efficiency, ease of operation and low waste generation. The possibility of producing low-cost and ecologically correct adsorbent materials is essential, since lignin and the biochar derived from its structure have the necessary characteristics for the treatment of tributaries [1].

The production of activated biochar from lignin for use as an adsorbent material has been gaining prominence in new studies. These carbon-rich materials are highly porous, have a large surface area (500 to 2000 m^2g^{-1}), are renewable because they are derived from biopolymers and have a functionalized phenolic structure [4]. Biochar is produced from the pyrolysis of biomass under

oxygen limitation in a controlled environment, during this process the volatilization of the water present in its composition occurs, giving rise to its porous structure. Due to their chemical and morphological characteristics, studies show that lignin-derived biochars have excellent performance in the immobilization of organic and inorganic pollutants, acting as adsorbents of pollutants in water [4,5].

The present study aims to report the synthesis process of cellulose hydrogels with the addition of lignin biochar and to evaluate their adsorption capacity and their selectivity for different heavy metal ions.

Experimental

1. Hydrogels synthesis

In this experiment, four cellulose hydrogels were produced: one pure (Cellulose) and three with the addition of biochar at different concentrations (Bc - 1%, Bc - 3%, and Bc - 5%). The preparation of the hydrogels involved dissolving urea and sodium hydroxide in water, followed by the addition of microcrystalline cellulose. The mixture was refrigerated at approximately -10 °C for 24 hours and then stirred when the solution was partially liquid. Biochar was added at different concentrations, and the solution was stirred for 30 minutes at approximately 900 rpm. After the addition of epichlorohydrin for crosslinking, the solutions were dried in an oven at 60 °C for 48 hours. The hydrogels were washed with water for 72 hours to remove epichlorohydrin residues and then dried again in an oven at 60 °C for 24 hours.

2. Characterization

Fourier transform infrared spectroscopy (FTIR) was conducted in a Frontier 94.942 equipment (PerkinElmer, USA) with attenuated total reflectance (ATR) accessory. The range from4000 to 400 cm^{-1} was evaluated with 32 scans, and a resolution of 4 cm^{-1}.

The degree of swelling of the hydrogels was determined by immersing ~0.1 g dry hydrogel fragments in distilled water, with mass measurements obtained at regular intervals within a period of one week (168 h). The experiments were performed at room temperature and the degree of swelling (DS) was calculated using Eq.1 [3], where m_s (t) is the swollen mass of hydrogel in a time t (g), and m (t = 0) is the dry hydrogel mass (g) [3].

$$DS = \frac{m_s(t) - m(t=0)}{m(t=0)} \; x \; 100 \qquad (1)$$

3. Selectivity

The affinity of cellulose-based hydrogels for Cu^{2+}, Zn^{2+}, Ni^{2+}, Cd^{2+}, Mn^{2+}, Cr^{6+} (0.05 mmol/L each) were performed using a dosage of 1.0 g/L. The sorption tests were conducted in a shaker incubator at room temperature and pH between 4.0 – 4.5. After 24 h, metal concentrations were determined by ion chromatography (940 Professional IC Vario, Metrohm). Removal efficiencies (%R) was determined by Eq.2, where C_0 is the metal initial concentration (mmol/L), and C_e is the metal concentration at equilibrium (mmol/L).

$$\%R = \frac{C_0 - C_e}{C_0} \; x \; 100 \qquad (2)$$

Results and Discussion

1. Fourier-transform infrared spectroscopy

FTIR analysis was performed to compare the composition of cellulose hydrogels without and with Bc to identify vibrational modes of bonds and the chemical groups and modifications of the materials. The spectra of all samples showed great similarity, as can be seen in Fig. 1. The 3338 cm^{-1} band was found for all hydrogel samples (Fig. 2-a) and is related to the presence of hydroxyl groups O-H characteristic of polysaccharides [6,7]. As these bonds are commonly found in the crystalline structure of cellulose, it can be said that the appearance of this peak indicates its presence in the three-

dimensional structure of hydrogels. The 2916 cm^{-1}, 2887 cm^{-1}, and 2848 cm^{-1} bands (Fig. 2-a) are related to the presence of C-H bonds, which are also normally found in polysaccharides, again indicating the presence of cellulose.

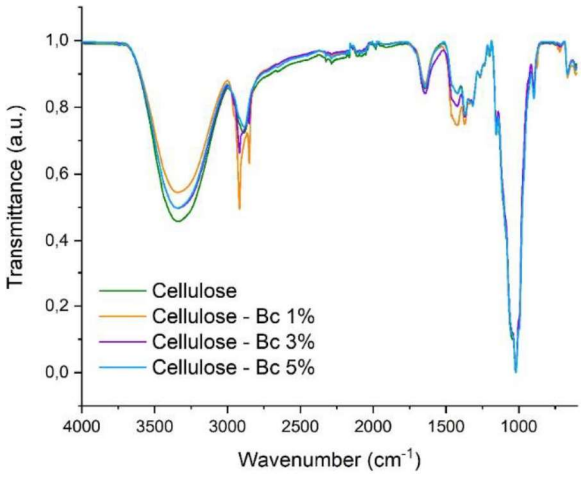

Figure 1 – Spectra of hydrogel samples.

Fig. 2-b shows a series of bands typically associated with cellulose present in the region comprised between peaks 1650 cm^{-1} and 890 cm^{-1}. The peaks 1644 cm^{-1}, 1370 cm^{-1}, 1315 cm^{-1}, 1265 cm^{-1}, 1200 cm^{-1}, 1154 cm^{-1}, 1020 cm^{-1}, and 896 cm^{-1} correspond to the stretching and bending vibrations of -CH2 and - CH, -OH and C-O bonds of cellulose [6–9]. Therefore, the spectra of the hydrogels were similar, without significant chemical changes related to the inclusion of Bc, not compromising the crosslinking process of the hydrogel. Thus, new functional groups are introduced into the structure, seeking to improve water absorption and interactions with a target contaminant [10].

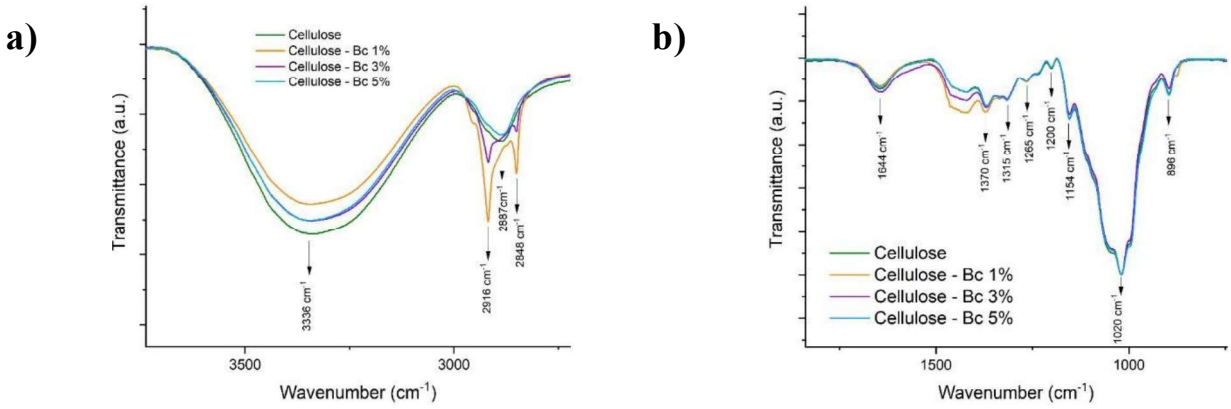

Figure 2 – Characteristic peaks found in two regions: a) 3500-2800 cm^{-1} and b) 1650-890 cm^{-1}.

2. Water absorption

Fig.3 shows the water absorption of the hydrogels produced, and it is possible to observe a rapid increase in mass in the first hours, that is, rapid diffusion of water into the interior of the material. After the initial 24 h, it is possible to identify a constant behavior (plateau), indicating material saturation and maintenance of balance with a slight increase (not expressive).

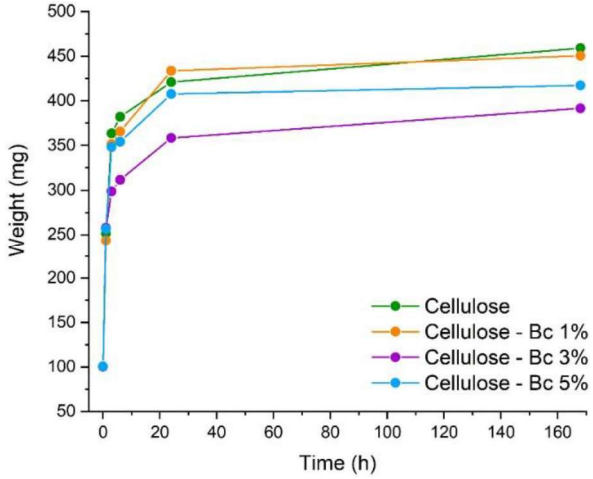

Figure 3 – Characteristic peaks found in two regions: a) 3500-2800 cm^{-1} and b) 1650-890 cm^{-1}.

The degree of swelling for the hydrogels produced, highlighting the pure hydrogel, without addition of Bc, with a high absorption capacity of 357.93%. The hydrogel with the addition of 1% of Bc presented a DS very close to the pure hydrogel, of 348.37%, while the other hydrogels with higher percentages of Bc, 3% and 5%, presented lower values of DS, 290.72% and 314.23%, respectively. The results indicated that for higher percentages of Bc the water absorption capacity of the hydrogel suffers a decrease. While for the Cellulose and Bc 1% samples the difference was only 9.56%, the difference of the Cellulose, Bc 3% and Bc 5% samples were, respectively, 67.21% and 43.7%. One hypothesis is that the addition of filler generally reduces the elasticity of the material and increases its stiffness, resulting in lower water absorption values [11]. This fact is directly related to the degree of crosslinking of the hydrogel, a parameter responsible for providing information about the stability between the chains of the polymeric network of the hydrogel and consequently the mechanical properties of the material, such as hardness, for example.

3. Ion selectivity

In effluent samples, heavy metals are found with other potentially toxic contaminants at varying concentrations, affecting their sorption efficiency due to competition for binding sites. From Figure 4, neat hydrogel, hydrogel composites, and biochar presented the following metallic affinity order: $Cu^{2+} > Cr^{6+} > Cd^{2+} > Zn^{2+} > Ni^{2+} > Mn^{2+}$.

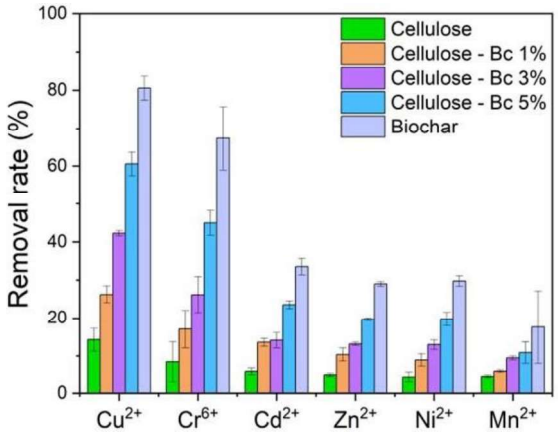

Figure 4 – Metal affinity of heavy metal ions (Cr^{6+}, Cd^{2+}, Ni^{2+}, Mn^{2+}, Zn^{2+}, and Cu^{2+}) by Bc, neat hydrogel, and hydrogel composites.

It is interesting to note that proposed hydrogel composites exhibited an increase in removal efficiency for Cu^{2+} (14.25% for Cellulose to 60.57% for Cellulose - Bc 5%) and Cr^{6+} (8.48% for Cellulose to 44.99% for Cellulose - Bc 5%), while biochar showed removal efficiency of 80.57 and 67.31% for Cu^{2+} and Cr^{6+}, respectively, under the same operational conditions. Regarding divalent cations (Zn^{2+}, Cd^{2+}, Ni^{2+}, and Mn^{2+}) uptake, a lower removal efficiency (less than 20%) was obtained for developed hydrogel composites, while for biochar there was a low removal percentage for Cd^{2+} (33.49%), followed by Zn^{2+} (28.99%), Ni^{2+} (27,73%), and Mn^{2+} (17.62%). The high removal of Cu^{2+} and Cr^{6+} by biochar and hydrogel composites may be related to its high specific surface area with numerous pores, besides a charged surface with many oxygens' functional groups. Thus, subsequent studies will be performed to investigate the kinetics and equilibrium sorption in a batch system, as well as toobtain breakthrough curves in a fixed-bed continuous system, aiming at a later application on an industrial scale.

Conclusions

The cellulose hydrogels produced with the addition of Bc did not show significant structural alterations according to the FTIR analysis, indicating a good dispersion of the Bc particles, favoring the adsorption of metallic ions, since there is the presence of a greater number of active sites on the surface of the material. The samples showed good absorption capacity, a fundamental characteristic for the functioning of the hydrogels, and the degree of swelling (DS) was greater than 290% for all of them. However, for higher concentrations of Bc, there was a decrease in DS, which can be explained by a possible increase in the degree of crosslinking. The addition of the 5% m/m concentration of Bc favored the sorption process, reaching a maximum removal for Cu^{2+} and Cr^{6+}. Therefore, it is possible to say that low-cost, environmentally friendly materials with potential application in contaminated water were obtained.

Acknowledgements

The authors thanks the UFABC and REVALORES Strategic Unit.

References

1. Y. Sun; T. Wang; X. Sun; L. Bai; C. Han; P. Zhang. Industrial Crops and Products 2021, 166, 113473. https://doi.org/10.1016/j.indcrop.2021.113473.
2. L. Järup. British Medical Bulletin 2003, 68, 167-182. https://doi.org/10.1093/bmb/ldg032.
3. J. Marciano; R. Ferreira; A. de Souza; R. Barbosa; A. Junior; D. Rosa. International Journal of Biological Macromolecules 2021, 181, 112-124. https://doi.org/10.1016/j.ijbiomac.2021.03.117.
4. N. Supanchaiyamat; K. Jetsrisuparb; J. Knijnenburg; D. Tsang; A. Hunt. Bioresoul Technology 2019, 570-581. https://doi.org/10.1016/j.biortech.2018.09.139.
5. J. Wan; L. Liu; K. Ayub; W. Zhang; G. Shen; S. Hu; X. Qian. Fuel 2020, 269, 117142. https://doi.org/10.1016/j.fuel.2020.117142.
6. V. Hospodarova; E. Singovszka; N. Stevulova. American Journal of Analytical Chemistry 2018, 9, 303-310. https://doi.org/10.4236/ajac.2018.96023.
7. M. Sadeghi Afjeh; G. Bageri Marandi; M. Zohuriaan-Mehr. Separation Science and Technology 2021, 56, 1195-1210. https://doi.org/10.1080/01496395.2020.1775254.
8. Z. Akl; E.Zaki; S.ElSaeed. ACS Omega 2021, 6, 34193-34205. https://doi.org/10.1021/acsomega.1c01559.
9. R. Domingues; P. Trugilho; C. Silva; I. De Melo; L. Melo; Z. Magriotis; M. Sánchez-Monedero. PLoS One 2017, 12, 1-19. https://doi.org/10.1371/journal.pone.0176884.
10. P. Vilela; C. Matias; A. Dalalibera; V. Becegato; A. Paulino. Journal of Environmental Chemical Engineering 2019, 7,103327. https://doi.org/10.1016/j.jece.2019.103327.
11. D. Sarmah; N. Karak. Journal of Applied Polymer Science 2020, 137, 1–12. https://doi.org/10.1002/app.48495.

COMPOSITE HYDROGEL BASED ON ALGINATE-G-POLY(ACRYLAMIDE)/CARBON NANOTUBES FOR SOLID PHASE EXTRACTION OF METALS FROM CORN CEREAL SAMPLES

Charlie Gomes[1*], Emilly Silva,[2] Mariana A. Vieira[1], André Fajardo[2]

1 - Laboratório de Metrologia Química (LabMequi), Universidade Federal de Pelotas (UFPel), Campus Capão do Leão, Pelotas-RS, Brazil.
2 - Laboratório de Tecnologia e Desenvolvimento de Compósitos e Materiais Poliméricos (LaCoPol), Universidade Federal de Pelotas (UFPel), Campus Capão do Leão Pelotas-RS, Brazil.
(*) charlieggomesii@gmail.com

Abstract - Composite hydrogels containing nanofillers are extensively applied in the sorption of different compounds from aqueous solutions; however, this ability is poorly exploited in the extraction and pre-concentration of analytes from complex matrices. As a contribution to this field, this study reports the synthesis of a composite hydrogel of alginate-g-poly(acrylamide) matrix filled with functionalized multi-walled carbon nanotubes (ALG-g-PAAM/MWCNT-f). This composite served as a solid-phase extractor (SPE) for the separation of Pb^{2+} and Cd^{2+} from a digested corn cereal sample before their analytical determination. After composite characterization, a series of experiments using low dosages of ALG-g-PAAM/MWCNT-f demonstrated that the composite has a higher sorption capacity for Pb^{2+} (5.1 mg/g) and Cd^{2+} (3.9 mg/g) under favorable experimental conditions. As demonstrated, the presence of the MWCNT-f benefited the SPE performance of the composite. The sorption of both cations followed pseudo-first-order kinetics, while the experimental data were well-fitted by the Freundlich isotherm. Also, ALG-g-PAAM/MWCNT-f showed selectivity for Pb^{2+}, and it is reusable up to 10 times without losing sorption performance. After sorption and extraction, both metals were completely recovered, facilitating their quantification by the MIP OES technique. In short, ALG-g-PAAM/MWCNT-f was an effective SPE for the separation and extraction of Pb^{2+} and Cd^{2+}, which can be beneficial for food control and safety.

Keywords: *Alginate; composite materials; sorption; food analysis; analytical methods.*

Fundings: The authors thank CNPq (Brazil) for financial support and PQ fellowship (Process 303125/2022-5) to A.R.F. This study was financed in part by CAPES/Proap (Brazil), Finance Code 001.

Introduction

The investigation and determination of metal species in food samples are essential to designate their level of contamination and monitor the ecological and health risks associated with them [1]. The complexity of some food matrices makes metal determination a non-trivial task, mainly because of some interfering substances [2]. The low concentration of metal ions in these samples and the low selectivity and sensitivity of analytical techniques are additional shortcomings. Alternatively, preconcentration processes are often required since they increase the concentration of these analytes before qualitative or quantitative analysis or detection. Although this benefit, the inclusion of a preconcentration step in an analytical routine may harm aspects such as cost and time. To abate these drawbacks, more feasible and efficient pre-concentration processes have been studied to facilitate the determination of metal ions in food samples. According to the literature, solid-phase extraction, filtration, and electrochemical methods are often utilized in the separation and preconcentration of metal species in different food samples. Among them, solid-phase extraction using sorbent materials has been applied as a powerful tool for separating various inorganic

products and analytes, showing stability and high reuse potential. Most recently, polymeric hydrogels gained attention as SPE mainly because of their chemical and physical characteristics [3]. Briefly, hydrogels are three-dimensional hydrophilic materials with a high capacity to absorb and retain large amounts of water. Overall, these soft materials possess highly functionalized networks offering many interaction sites for different solutes and analytes. Beyond the flexibility of composition and processing, hydrogel matrices can be associated with different (nano)fillers (e.g., magnetic and metal nanoparticles, MOFs, and carbon nanotubes), which results in materials with enhanced sorption performance and robustness for SPE applications. Despite this encouraging scenery, studies dealing with the development and application of composite hydrogels containing CNTs or MWCNT specifically for SPE uses are still limited. Furthermore, most studies reporting the sorbent properties of hydrogels containing these fillers are conducted in conditions far from those faced by the analysts that work with food samples, and selectivity is not verified [4]. To fill this gap, this study reports the synthesis of an original composite hydrogel of alginate grafted with poly(acrylamide) (ALG-g-PAAM) filled with MWCNT functionalized with carboxyl and hydroxyl groups (MWCNT-f) and exploited its use as SPE to separate/concentrate metal ions (Pb^{2+} and Cd^{2+}) from an as-digested food sample, as depicted in Fig. 1. Alginate (ALG) is a natural polysaccharide commercially extracted from brown algae and widely used to prepare sorbent materials due to the presence of many functional groups (–OH and –COOH groups mostly) on its backbone.

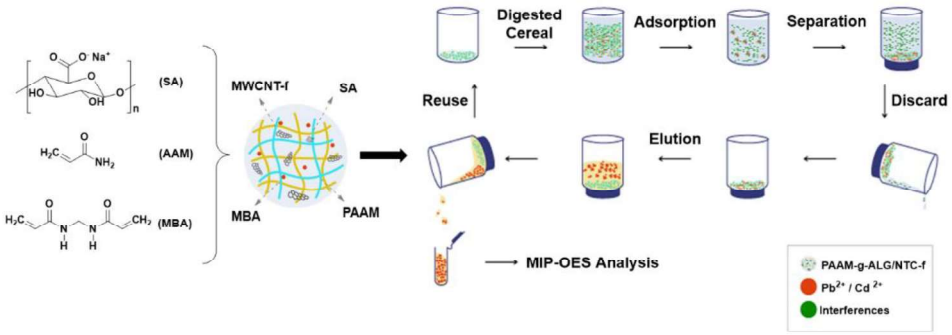

Fig. 1. Graphic summary of the experimental procedure done in study.

Experimental

Synthesis of the hydrogels: Hydrogels were synthesized via simultaneous radical graft polymerization of acrylamide monomers (AAM) onto the ALG backbone using *N*,*N*-methylene bisacrylamide (MBA) as the crosslinker. For this, ALG (500 mg) was added to a three-necked flask placed on a magnetic stirrer and solubilized in distilled water (40 mL). Then, a $K_2S_2O_8$ solution (20 mg in 5 mL of distilled water) was added to the reaction flask, which was sealed and purged with N_2 for 15 min. The temperature was increased and kept at 70 ºC using an oil bath. Next, AAM (250 mg) and MBA solution (20 mg in 5 mL of distilled water) were simultaneously added to the reaction mixture under stirring. After 60 min, the synthesized hydrogel was allowed to cool to room temperature. The completely hardened hydrogel particles were recovered, thoroughly washed with ethanol, and distilled water and then, oven-dried (40 °C for 10 h). The powdered hydrogel was sieved to obtain particle sizes around 200 µm (5/16 mesh) and stored away from moisture, heat, and light before use and characterization. This sample, labeled ALG-g-PAAM, was synthesized for comparative purposes. The composite hydrogel containing MWCNT-f was synthesized similarly; however, 10 mg of the filler was added to the reaction system and homogenized together with the ALG solution before the grafting/crosslinking step. Herein, the polymer:filler mass ratio was fixed at 1:0.13 based on previous experiments that pointed out the maximum dispersible amount of MWCNT-f. The composite (particle size around 200 µm) was labeled as ALG-g-PAAM/MWCNT-f.

Sorption experiments: These experiments were performed to investigate the ability of synthesized hydrogels to separate Pb^{2+} and Cd^{2+} ions from corn cereal samples, which were previously digested. The experimental procedures used to digest the cereal sample are described by Silva et al. [5]. The following general protocol was utilized in the sorption experiments: 10 mg of each hydrogel (ALG-g-PAAM or ALG-g-PAAM/MWCNT-f) was put in contact with 50 mL of the digested cereal solutions for 1 h. The set (hydrogels + solutions) was orbitally stirred (100 rpm) at room temperature during this while. To quantify the sorption of the two metals, aliquots were collected from the cereal solutions, filtered, and analyzed by MIP OES.

Results and Discussion

To evaluate the hydrogels formed, FTIR was performed to study the composition of the adsorbent, here in a more summarized way we will discuss only the hydrogels. Fig. 2(a) shows the FTIR spectra containing the hydrogels (ALG-g-PAAM and ALG-g-PAAM/MWCNT-f), the broadband in the region 3680–3100 cm^{-1} is due to the O–H stretching (–OH groups) overlapping the N–H stretching ($–NH_2$ groups). The sharpening of these bands compared to the ALG spectrum suggests that the grafting of the reaction consumed part of its –OH groups, which corroborates the literature. Characteristic bands of PAAM moieties at 1650 and 1454 cm^{-1} (C=O stretching of $–CONH_2$ groups and N–H bending of $–NH_2$ groups) and bands associated with the –COOH groups of ALG (at 1625 cm^{-1}) were also noticed. The FTIR spectrum of the composite hydrogel (ALG-g-PAAM/MWCNT-f) exhibited an increase in the intensity of the band associated with the O–H stretching (around 3440 cm-1) because of the –OH and –COOH groups of MWCNT-f. Additionally, the appearance of a band at 1735 cm^{-1} can be attributed to the C=O stretching of MWCNT-f. Finally, the sharpening of the band attributed to the C=O stretching of the –COOH groups of ALG indicates the interaction of these groups with the MWCNT-f by H-bond, probably. Indeed, the presence of hydrophilic groups on the surface of MWCNT-f showed to be crucial to disperse this filler throughout the ALG-g-PAAM matrix. Complementary to FTIR analysis, the maximum grafting degree for both hydrogels was around 325%, while the gel yield was close to 47%, respectively.

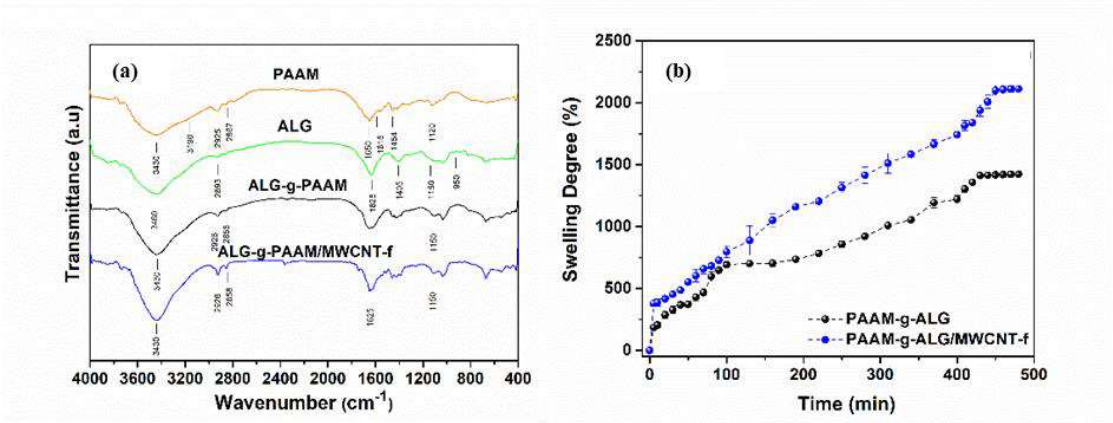

Fig. 2. (a) FTIR spectra of PAAM, Alg, PAAM-g-ALG, and PAAM-g-ALG/MWCNT-f. (b) Swelling kinetics of PAAM-g-ALG and PAAM-g-ALG/MWCNT-f at distilled water.

The swelling capacity of synthesized materials, shown in Fig. 2(b), is one of the most important parameters to understand their sorption capacity. As noticed, the hydrophilic nature of ALG and PAAM allowed both hydrogels to have high swelling degree rates at the beginning of the experiment. After 100 min, the liquid uptake rate for ALG-g-PAAM seems to slow down and the swelling achieves equilibrium around 400 min. The maximum swelling degree computed for this hydrogel was 1.425%, indicating that it can be classified as a superabsorbent hydrogel. Comparatively, the swelling curve of ALG-g-PAAM/MWCNT-f suggests that the liquid uptake follows different kinetics for this hydrogel. According to the experimental data, the swelling degree

rate for the composite increases until it achieves equilibrium (2,113%) at around 460 min. These discrepancies between the swelling capacity and kinetics observed for the ALG-g-PAAM and ALG-g-PAAM/MWCNT-f can be explained by the presence of the MWCNT-f in the composite.
The sorption tests were performed at different pHs, mainly due to the acid digestion of cereals, to show that the material resists very acidic pHs and high temperatures, showing the applicability of the hydrogel. To explain some properties of the compounds, the processes of sorption kinetics and isotherms were evaluated and the models that best suited the results obtained in this research were the pseudo-first order kinetics and the Freundlich sorption model for the isotherms, these data typically assumes that the sorption process occurs due to the complexation of one metal ion onto one unoccupied binding site on the surface of the hydrogels.

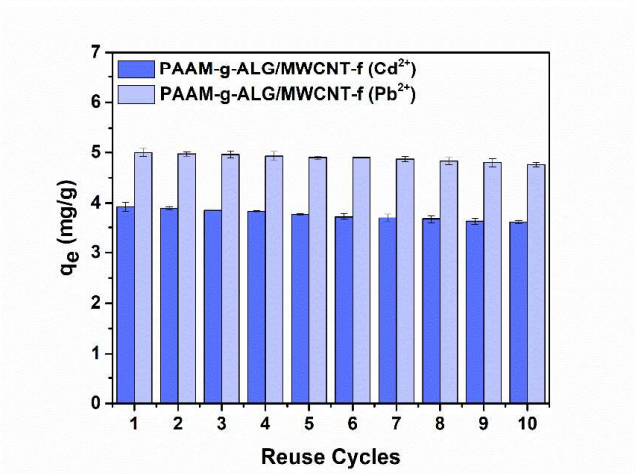

Fig. 3. Adsorption capacity at equilibrium for Cd^{2+} and Pb^{2+} by the PAAM-g-ALG/MWCNT-f hydrogel after consecutive cycles of sorption/desorption.

Desorption experiments were performed to investigate the release of sorbed metals by the hydrogel composite and its potential in consecutive reuse cycles. The reuse of the SPE material is desirable for practical and large-scale applications. To explain, both studies were only performed with the ALG-g-PAAM/MWCNT-f hydrogel since this sample showed superior performance to ALG-g-PAAM in all previous experiments. The authors believe that the composite hydrogel has a higher potential as an SPE material. The sorption capacity of ALG-g-PAAM/MWCNT-f hydrogel was (re)calculated after each sorption/desorption cycle for both metal ions. The results are shown in Fig. 3. The highest qe values were calculated for the sorption of Pb^{2+} ions highlighting the greater affinity of this metal by the composite hydrogel than the Cd^{2+} ions. After ten consecutive reuse cycles, the sorption capacity of ALG-g-PAAM/MWCNT-f for both metals showed a minimal impairment. At the last reuse cycle, the reduction of the sorption capacity did not exceed the margin of 10% compared to the first, which characterizes the remarkable reusability potential of this composite hydrogel. This feature encourages the use of this material as SPE for the separation and pre-concentration of analytes from food samples. Moreover, the sorbed metals were completely desorbed (100% recovered) from the post-used composite hydrogel after each reuse cycle using HNO_3 as the extracting solution. This acid protonates the binding sites on the surface of the hydrogel and disrupts their interaction with the sorbed metals releasing them into the extraction medium. After desorption, the regenerated hydrogels were directly washed with distilled water, collected, and dried, and, thereafter, reused in the next sorption cycle. In short, this is a simple and attractive operational approach compared to other materials ranked as potential SPE [4]. The complete desorption of the metals from the composite strengthens the suggestion that this material is efficient in separating the analytes from a complex matrix facilitating their further determination/quantification.

Conclusions

The separation of Pb^{2+} and Cd^{2+} ions from a digested cereal sample was studied under different conditions using two ALG-g-PAAM and ALG-g-PAAM/MWCNT-f hydrogels as SPE materials. Various experiments demonstrated that both hydrogels were efficient for this task, even under the harsh conditions used to digest the cereal sample. Comparatively, the presence of MWCNT-f enhanced the sorption capacity of the composite hydrogel, likely due to increasing the stability of the polymeric matrix and the increment of the binding sites for the metal ions. The composite hydrogel exhibited a heterogeneous morphology, superabsorbent behavior, and low sensitivity to external interferents, which can explain its enhanced performance compared to the pristine hydrogel. Kinetic experiments revealed ALG-g-PAAM/MWCNT-f (10 mg) allowed removing both metals (Pb^{2+} and $Cd^{2+)}$ completely (100%) in only 40 min via a surface sorption process. The sorbed metals were efficiently recovered from the composite using an HNO_3 extraction solution facilitating their further quantification by MIP OES. Besides, the post-used composite was reused in 10 sorption/desorption consecutive cycles with minimum impairment towards its sorption capacity. Also, it was verified that the sorption of Pb^{2+} occurs preferentially compared to $Cd^{2+.}$ In short, the composite hydrogel containing MWCNT-f can be ranked as a potential SPE material with simple operation and high efficiency to separate and preconcentrate these two metals from complex food matrices, such as the cereal sample. This study can be useful to other researchers that work on the analytical aspects of food chemistry and industry.

Acknowledgements

CTNano-UFMG (Brazil) is also thanked for the donation of MWCNT-f.

References

[1] D.H. Bonemann, A.O. de Souza, C.C. Pereira, E.Q. Oreste, A.S. Ribeiro, M.A. Vieira, Food Hydrocoll. 118 (2021) 106802. https://doi.org/10.1016/J.FOODHYD.2021.106802.

[2] E. Hakme, S. S. Herrmann, M. E. Poulsen, Brazilian Journal of Analytical Chemistry. 7 (2020). https://doi.org/10.30744/brjac.2179-3425.AR-36-2019.

[3] M. Czikkely, E. Neubauer, I. Fekete, P. Ymeri, C. Fogarassy, Water (Basel). 10 (2018) 1377. https://doi.org/10.3390/w10101377.

[4] T. Daşbaşi, Ş. Saçmaci, A. Ülgen, Ş. Kartal, Food Chem. 197 (2016) 107–113. https://doi.org/10.1016/J.FOODCHEM.2015.10.093.

[5] E. C.Silva, C.G. Gomes, C., M.A. Vieira, A.R. Fajardo, International Journal of Biological Macromolecules, in press (2023), https://doi.org/10.1016/j.ijbiomac.2023.124586.

DEVELOPMENT AND CHARACTERIZATION OF STARCH-BASED COMPOSITE FILMS CONTAINING BREWERS' SPENT GRAIN EXTRACT

Ana B. Klosowski[1], Patrícia M. Campos[1] and Juliana B. Olivato[1]*

1 – Department of Pharmaceutical Sciences, State University of Ponta Grossa (UEPG), Ponta Grossa, PR, Brazil
annablk@hotmail.com

Abstract – Starch-based films are eco-friendly, biodegradable and can be easily obtained by solvent casting method. Due to this, the aim of this study was to develop and characterize cassava starch films containing 5% of brewers' spent grain extract through physical, optical, mechanical and thermal properties, and % release of phenolic compounds. The films with extract were compared with control, being observed significative differences for the parameter of density, it was increased by extract (1.47±0.09 $g.cm^{-3}$). Furthermore, the tensile strength (6.73±2.37 MPa) and elongation at break (14.78±10.57%) decreased with the addition of extract. It was observed in SEM-FEG images a wrinkled surface. Both films presented high degradation temperatures (250-350 ºC) and it was observed 100% release of phenolic compounds within 4 hours. Therefore, the films developed are considered promising biodegradable materials for the release of bioactive compounds.

Keywords: *By-product, Cassava starch, Biodegradable films, Phenolic compounds, Solvent casting*

Introduction

Biodegradable materials have been the subject of great interest by the scientific community because they are degraded and metabolized by microorganisms present in the environment, thus avoiding accumulation and generating an environmental pollution problem [1]. One of the most prominent biodegradable polymers is starch. Starch is a natural and eco-friendly biopolymer that can be extracted of different sources, such cassava, rice and potato [2]. Furthermore, the starch presents advantages of low cost, being abundant and nontoxic, and especially the films with cassava starch have good flexibility and low water vapor permeability [3,4]. However, it is necessary to break the hydrogen bonds present in the starch to destroy the crystalline structure, transforming it into amorphous, facilitating its processing and improving properties related to mechanical strength and high hydrophilicity. One of the most used ways to help the film formation process is the use of plasticizers, such as glycerol [3]. The addition of plasticizer increases moisture absorption in the films, due to this, the use of reinforcing agents, such other polymers, is important to overcome the limitations of starch isolated [5]. An example of polymer is poly (vinyl alcohol) (PVA), which showed to increase the film flexibility and elongation at break, maintaining the biodegradable characteristics of material [6].

Brewers' spent grain (BSG) is the more abundant by-product of the brewing industry. It is currently used as animal feed, but its rich composition, mainly containing phenolic compounds, which can be used in different materials in pharmaceutical and food areas [7]. The main phenolic compounds found in the BSG extracts were the ferulic and p-coumaric acid, followed by caffeic, sinapic and syringic acids. Some properties of these compounds, such as antioxidant, anti-inflammatory and anticancer properties, make the by-product of the brewing industry the subject of much research. Thus, the present study aimed to obtain biodegradable and sustainable starch films as an alternative for incorporating brewers' spent grain extract.

Experimental

Films production

Samples were developed using the *solvent casting* technique. The components present in the formulation were (3% (%, w.v^{-1}) cassava starch, 20% (%, w.v^{-1}) of glycerol and poly (vinyl alcohol), both calculated in relation to cassava starch). These components were homogenized in q.s.p. 100 mL of water and heated until 90 ºC, with constant stirring, that it necessary to occur the gelatinization of starch. In the cooling step, the brewers' spent grain extract (5%, w.v^{-1}) was added and then, 50g of mixture was carefully transferred to the petri dish (150mm x15mm). In the last step, the formulations were dried in the oven (60ºC) until complete evaporation of solvent and formation of films. The films (control and with brewers' spent grain) were carefully removed from the petri dish and stored at room temperature (25±2ºC).

Characterisation of the cassava starch containing brewer's spent grain extract

Thickness and density of films

The thickness of films was measured with digital micrometer with resolution 0.001mm, through 10 random points. For the density, the films (2cmx2cm) were stored at 25 °C in a desiccator with $CaCl_2$ (0% RH) for 7 days and then weighed to determination of weight of films. The thickness, width and length were evaluated to perform the density calculation.

Apparent opacity

Apparent opacity was determined by means of colorimeter (HunterLab - USA) at a 10° angle and illuminant D_{65} (day light), according to Hunterlab methods (Hunter Associates Laboratory, 1997). Sample opacity (Y) was calculated as the ratio between the opacity of the sample placed under a black pattern (Y_B) and the opacity of the sample placed under a white pattern (Y_W). The opacity results (Y) were divided by the sample thickness and expressed in the arbitrary scale (0–1% μm^{-1}). The determinations were performed in triplicate.

Water solubility and Water vapor permeability (WVP)

In the determination of Water solubility, the samples were previously dried (7 days – 0% RH), weighed and immersed in 20mL of distilled water and remained in contact for 48 h. After this period, the excess of water was removed from the recipients and the samples were dried in a 105 °Coven for 3 h and then weighed again. The weight difference was used to determine the water solubility of the samples. The test was conducted in triplicate.

In the Water vapor permeability, the samples were stored at 25 ºC and 53% RH for 48 h. Each film sample was fixed in a circular opening of a permeation cell with 60 mm of internal diameter with silicone grease to ensure that the humidity migration occurred only through the film. The interior of the cell was filled with anhydrous $CaCl_2$ (0% RH), and the device was stored at 25 ºC in a desiccator to maintain a 75% RH gradient across the film. A sodium chloride saturated solution was used in the desiccator to provide 75% RH. The samples were weighed every 1 h for 9 h and at 24 h. Changes in the weight of the cell or mass gain (m) were plotted as a function of time (t). The slope of the line was calculated by linear regression ($r^2 > 0.97$), and the water vapor permeation ratio (WVPR).

Mechanical Properties

A universal mechanical testing machine (Shimadzu, Kioto, Japan) was used to determinate the tensile properties of the films. Tensile tests were based on American Society for Testing and Material Standard (ASTM) D882-91 (1996b). Ten samples of each formulation were cut in the machine direction (longitudinal), with 50 mm in length and 20 mm in width, and fit to the tensile grips. The cross head speed was set at 0.8 mm.s^{-1}, and the initial distance between the grips was 30 mm. Before the tests, the samples were conditioned at 25 ± 2 ºC and 53 ± 2% RH for 48 h. The tensile strength (MPa), elongation at break (%) and Young's modulus (MPa) were determined.

Scanning electron microscopic (SEM) analysis

A scanning electron microscope Tescan model Mira 3 was used to make observations of the fractured surface of the films. The samples were submerged in liquid nitrogen and then broken (cryogenic fracture). Before coating with a gold layer, the samples were stored at 25 ±2 ºC in a desiccator with $CaCl_2$ (0% RH) for 7 days. The coating was performed with a SputterCoater (Quorum SC7620). Images were taken of the fractured surface, with 1 kx of magnification.

Thermogravimetric analysis (TGA)

The thermogravimetric analysis was conducted using a PerkinElmer (STA 600) Simultaneous Thermal Analyzer. The samples were previously dried in desiccator with calcium chloride for 7 days and then heated from 20 to 500 °C, 10 °C.min^{-1}, under nitrogen flow (50 mL.min^{-1}). The maximum degradation temperatures were extracted from the dTG curves, obtained using Origin 9.0 software.

Release of phenolic compounds

The films, in dimensions 2cmx2cm, were previously dried in desiccator with calcium chloride for 7 days. After 7 days, the films were immersed in 10 mL of distilled water, at 25 ± 2 ºC, and aliquots of 1 mL were collected and replaced in 30 minutes, 1 hour, 2 hours, 3 hours and 4 hours. 200 µL of aliquots were added in the mixture of 7 mL of distilled water and 500 µL of Folin-Ciocalteau reagent. After 30 seconds, 2.5 mL of sodium carbonate (10.6%, % w.v^{-1}) were added. Then, the preparation was heated in water bath at 50 ºC for 5 minutes, and the absorbance was determined in spectrophotometer at λ=715 nm. The test was performed in triplicate.

Statistical analysis

The data were analyzed using the GraphPad Prism 9.0 software, for Student's t test (5% significance).

Results and Discussion

The results obtained, both for the control film and for the film with brewers' spent grain extract, showed no significant difference for thickness (0.007±0.018 cm for control and 0.009±0.035 cm for film with extract), apparent opacity (35.08±2.48 %.µm^{-1} for control and 35.86±1.85 %.µm^{-1} for film with extract), water solubility (67.26±3.76 % for control and 66.40±1.98 % for film with extract) and WVP (2.67x10^{-11}±0.043 g.seg^{-1}.m^{-1}Pa^{-1} for control and 4.21x10^{-11}±0.060 g.seg^{-1}.m^{-1}Pa^{-1} for film with extract).

The extract contributed to the increase of density of films, with value of 1.47±0.09 g.cm^{-3}, in contrast to the control film (1.28±0.04 g.cm^{-3}). The presence of glycerol may have interfered with the molecular organization, increasing the free volume. The apparent opacity is related with thickness of materials and both Control and BSG extract films has not presented significant difference, i. e., the opacity between films has not changed. This fact can be considered positive, since in case of commercialization, the films may have greater consumer acceptance.

The mechanical properties are shown in Table 1. Tensile strength and elongation at break were reduced in the 5% of brewers' spent grain composite films. The mechanical performance was adversely affected by the fractures and voids in the films surface, as evidenced in SEM images. This fact points to a positive effect of BSG in the mechanical performance of the starch films, resulting in less rigid and brittle materials to be used as biodegradable material. The distribution of the hydrophobic substance between the two phases of a polymeric matrix can occur. Consequently, different interactions of the extract with each polymer phase can modify the polymer chain interactions.

Table 1 – Tensile strength, elongation at break, and Young's modulus of the biodegradable starch films

Samples	Tensile strength (MPa)	Elongation at break (%)	Young's module (MPa)
Control	8.63±1.52^{a}	34.28±24.06^{c}	178.75±39.15^{e}
5% BSG	6.73±2.37^{b}	14.78±10.57^{d}	152.48±57.86^{e}

^{a,b,c,d,e} Means in the same column with different letters differ significantly (Student's t test; $p<0.05$)

In the thermogravimetric analysis (Figures 1A and 1B), the first step refers to weight loss under 130 °C which mainly caused by the volatilization of free water in the films. The second stage (130–200 °C) was due to the evaporation of bound water and glycerol [8]. The third step (250-350 ºC) corresponding the thermal degradation of many organic extractives, fats, waxes, alkaloids, glycosides present in the brewers' spent grain extract. The temperature around 300 ºC (Figure 1B) is related to the decomposition of starch (amylose + amylopectin) [9].

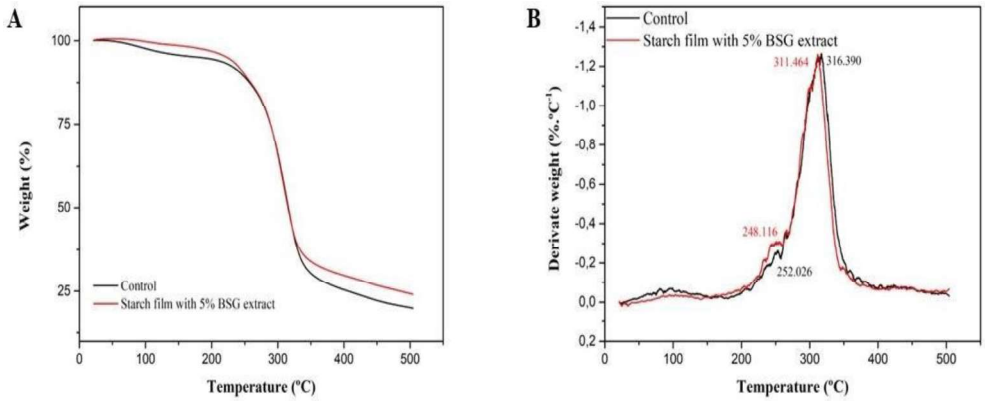

Figure 1 – TGA thermograms (A) and dTG graphs (B) of control and BSG extract starch films

In SEM analysis, it observed that when brewers' spent grain was added to the polymeric matrix, this became less homogeneous, with a more wrinkled surface fracture (Figure 2B), indicating a deficient phase compatibility. These results therefore confirm the results of mechanical properties.

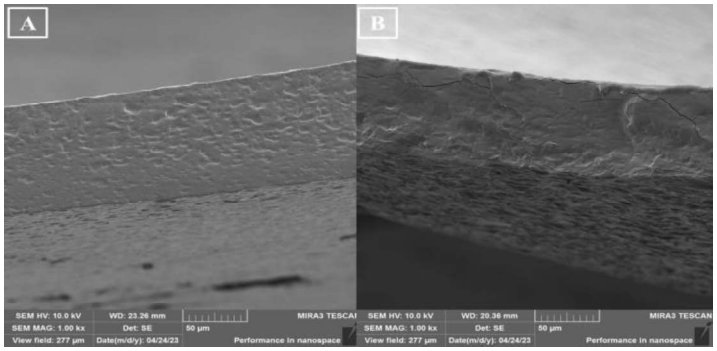

Figure 2 – FEG-SEM images for criofractures of control (A) and BSG extract starch films (B)

The release profile of phenolic compounds presented in the extract incorporated from the cassava starch films was evaluated in water (Figure 3). The results indicated that the phenolic compounds were stable in this media and able to be extracted from the materials after the solvent casting process, ocorring 100% of release these compounds within 4 hours.

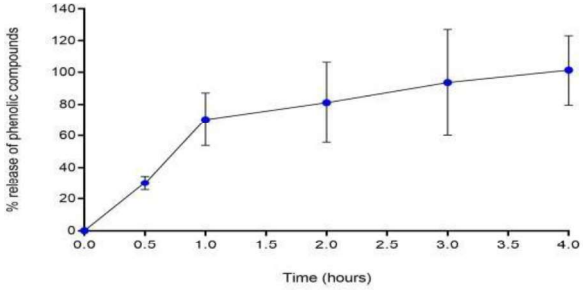

Figure 3 – Release profile of phenolic compounds total from starch biodegradable films in water for 4 hours

Conclusions

The starch films were successfully obtained, showing the release of the total amount of phenolic compounds within 4 hours. The resistance of the films was compromised with the addition of the extract, but depending on the application, more flexible and less resistant films are more interesting. Therefore, the developed films are considered promising materials for the incorporation and release of bioactive compounds.

Acknowledgements

The authors wish to thank the Koch Ltda for brewers' spent grain donation, the multiuser laboratories at State University of Ponta Grossa for their technical support, and CAPES for the financial support.

References

1. D. C. M. Ferreira; G. Molina; F. M. Pelissari Composites Part B: Engineering 2020, 183, 107682. https://doi.org/10.1016/j.compositesb.2019.107682
2. M. A. M. Akhir; S. A. Zubir; J. Mariatti Polymers for Advanced Technologies 2023, 34, 717–730. https://doi.org/10.1002/pat.5922
3. A.Thongmeepech; T. Koda; A. Nishioka Carbohydrate Polymers 2023, 306, 120618. https://doi.org/10.1016/j.carbpol.2023.120618
4. C.P.Y. Loo; N.M. Sarbon Food Bioscience 2020, 35, 100589. https://doi.org/10.1016/j.fbio.2020.100589
5. R.A.Shapii; S. H. Othman; R. K. Basha; M. N. Naim Nanotechnology Reviews 2022, 11, 1464–1477. https://doi.org/10.1515/ntrev-2022-0094
6. W.Janik; A. Wojtala; A. Pietruszka; G. Dudek; E. Sabura Polymers 2021, 13, 1–14. https://doi.org/10.3390/polym13162685
7. T. Bonifácio-Lopes; A.A. Vilas Boas; E.R. Coscueta; E.M. Costa; S. Silva; D. Campos; J.A. Teixeira; M. Pintado Food & Function 2020, 11, 8963–8977. https://doi.org/10.1039/D0FO01426E
8. Y. Fang; J. Fu; C. Tao; P. Liu; B. Cui International Journal of Biological Macromolecules 2020, 155, 1350–1358.https://doi.org/10.1016/j.ijbiomac.2019.11.110
9. A.C.Lopes; M.K. Barcia; T.B. Veiga; F.Yamashita; M.V.E. Grossmann; J.B. Olivato Polymers for Advanced Technologies 2021, 32, 779–788.https://doi.org/10.1002/pat.5130

DEVELOPMENT OF BIODEGRADABLE FILM OF THERMOPLASTIC STARCH AND YERBA MATE WASTE

Thaís F. Rodrigues[1]*, Jenifer Panizzon[1], Isabela Sant'Anna[2] and Vanusca D. Jahno[1]

1 – Graduate Program in Environmental Quality, Feevale University, Novo Hamburgo, RS, Brazil
thais.fatimarodrigues@gmail.com
2 – Chemical Engineering undergraduate student, Feevale University, Novo Hamburgo, RS, Brazil

Abstract - Biodegradable and bio-based polymers can be an alternative when it comes to reducing the impact on the environment, since it is possible to prepare bioplastics from starch, a natural polymer widely available and inexpensive and add organic waste, such as yerba mate, largely consumed in South America. Thus, the objective of this work was to develop thermoplastic starch films with yerba mate waste. The methodology was performed from a formulation containing starch, glycerol and deionized water, and added 20% yerba mate waste (YMW). Films were formed by casting at room temperature and oven drying, and characterized by visual, thermal, morphological, mechanical and chemical profile analysis. The results showed material surfaces homogenization due to the complete melting of the starch granules, high thermal stability and increased thickness with the addition of YMW. Also, it was possible to verify that the drying process can interfere in the mechanical properties of the films.

Keywords: *Biodegradable polymer. Bioplastics. Corn starch films. Organic waste.*

Introduction

Yerba mate (*Ilex paraguariensis* St. Hill. Aquifoliaceae) is a plant species widely used in the preparation of a beverage appreciated for its peculiar bitter taste and stimulating properties, known as chimarrão and tererê (in Portuguese) or mate (in Spanish), mainly in South American countries, including Brazil, Uruguay, Argentina, and Paraguay. It is estimated that 1 million people in South American countries consume about 1-2 L per day of mate infusion and for centuries, yerba mate was used by the native peoples of South America, especially the indigenous Guarani as a stimulant drink [1]. Brazil is the leading producer, with 880,000 tons of yerba mate produced in 2019, followed by Argentina with 837,000 tons and Paraguay with a production of 171,000 tons [2]. However, large amounts of waste are generated, both in the processing (drying, sapping and canching), and after the consumption of yerba mate products, requiring the development of different applications and technologies for this material [3]. In general, some studies have already assessed the potential uses of yerba mate waste (YMW), such as in the production of charcoal for the removal of organic contaminants from aqueous solution [4]; as an adsorbent material to remove methylene blue [5]; in the production of substrates for plant cultivation [6]; of medium density particleboards [7] and of briquettes and composites [8]. Therefore, using bio-based materials has relevance for their biodegradability, sustainability, and respect for the environment [9]. Starch blends are among the biobased and biodegradable bioplastics [10], in which thermoplastic starch (TPS) presents great potential due to its abundant supply, low cost, complete biodegradation and high biocompatibility [11, 12], and Brazil stands as a leader in research regarding the development of these films [13]. In this sense, the aim of the present work is to evaluate the use of yerba mate waste in the development of biodegradable films based on thermoplastic starch.

Experimental

Preparation of biodegradable films

TPS films were prepared using 70% soluble corn starch and 30% glycerol dissolved in deionized water, corresponding to 18 g of starch and 5.4 g of glycerol, in 600 mL of deionized water. The solution was kept at 70 ºC for 30 minutes with constant mechanical stirring at 70 rpm. Afterwards, it was poured and leveled on a Teflon® nonstick sheet. The formation of three films (≈175 mL each) by casting occurred at room temperature (on average 22,5 ºC and 58% relative humidity) for 48 hours. Another formulation was prepared under the same conditions and films were formed in an oven at 60 ºC for 8 hours. This way, two drying methods were compared. Films with the addition of 20% post-consumption yerba mate were prepared with 14.4 g of starch, 4.3 g of glycerol, and 3.6 g of yerba mate, in 600 mL of deionized water. The following procedures for gelatinization and drying were the same as for TPS. The YMW was dried at 100 °C, separated into different granulometries, and only the fractions smaller than 32 mesh were used for preparation and subsequent characterizations of the films.

Characterization of the prepared films and raw materials used

Visual analysis was performed from photographs and morphological analysis was performed on a Scanning Electron Microscope (SEM) by observing the top surface and cross section, with cryogenic fracturing, of the films. Samples were prepared with a thin layer of gold and the chemical profile was evaluated by analysis in the infrared region, in the range between 4000 cm^{-1} and 650 cm^{-1}, using a spectrophotometer, coupled to the Attenuated Total Reflection (ATR-FTIR) accessory. The thermogravimetric analysis was performed in a Simultaneous Thermal Analyzer (STA), in nitrogen gas atmosphere with a flow of 20 mL min^{-1}, with a heating rate of 10 ºC min^{-1} and a heating ramp between 15 ºC and 900 ºC. The thickness of the films was obtained from the average of ten random points, in triplicate, using a digital micrometer, with precision of 0.001 mm. The tensile strength (MPa) and elongation (%) properties were determined in a dynamometer, operating with a load cell of 5 kgf and speed of 50 mm min^{-1}. The analysis was performed on 10 test specimens, which were kept in a desiccator for 48 hours. All procedures and analysis were conducted at the Clean Technology Research and Development Center (CTL) and at the Advanced Studies in Materials laboratory, both at Feevale University.

Results and Discussion

Different drying procedures did not change the visual aspect of the films, as shown in Fig. 1a. Thus, it was observed in the TPS films a smooth, colorless, transparent surface with small bubbles, while the films with YMW showed transparency and brown hue with rough top surface and smooth bottom surface, due to the yerba mate particles not dissolving in the starch solution. The YMW chemical profile indicated a broad absorption band at 3298 cm^{-1} related to OH groups, present in cellulose molecules, lignin, water, and other compounds such as chlorogenic acid. 2921 cm^{-1} and 2850 cm^{-1} were assigned to CH stretching vibrations of the CH_2 and CH_3 groups. The region between 1800 and 1500 cm^{-1} was related to carbonyls of esters, amides, acids, and other compounds such as Xanthines and Saponines. Around 1733 cm^{-1}, the presence of acetyl and ester groups can be indicated for hemicellulose. The angular deformation (scissor vibration) of CH_2 and CH_3 were observed in the region between 1500 and 1250 cm^{-1}, while the stretching vibrations of the CO bond were assigned between 1300 and 1000 cm^{-1} [14, 15]. Both films showed functional groups mainly related to starch, however, an increase in the intensity of the bands was observed for the TPS films compared to the films with YMW. This may indicate a higher availability of OH groups in the TPS film, around 3289 cm^{-1} [16]. At approximately 2928 cm^{-1} it was associated with the CH_2 bond. The band at 1647 cm^{-1} was assigned to the bending vibration of H_2O. At 1336 cm^{-1}, 1150 cm^{-1} and 1077 cm^{-1} occurred the bending and stretching of COH, respectively. At 995 cm^{-1} a typical amylopectin bond vibration occurred [17, 18]. Fig. 1b presents all the FTIR spectra.

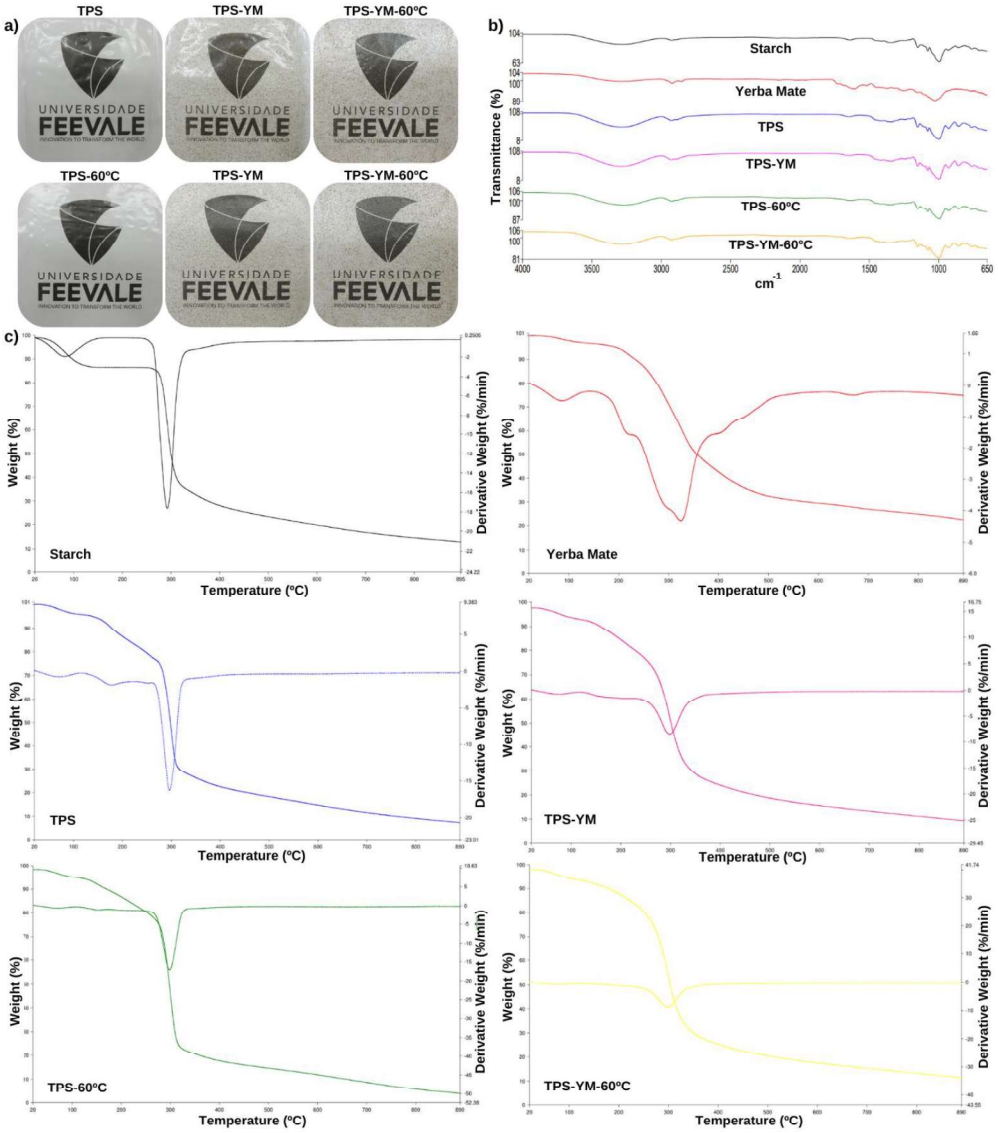

Figure 1 – Analysis of the films, starch and yerba mate: a) photographs, b) FTIR, c) TGA and DTG.

The thermogravimetric curve (TGA) and its derivative (DTG) as shown in Fig. 1c followed the expected pattern for starch films plasticized with glycerol [16]. The first thermal event was observed for all films and raw materials between 61.3 °C and 75.5 °C, related to water evaporation. The second stage of mass loss occurred for corn starch at T_{max} 293.0 ºC, this degradation temperature is higher than the films (between 149.6 ºC and 174.5 ºC) due to the gelatinization reaction that reduces the energy required to destroy the internal starch structure [19]. YMW showed mass loss between 215.5 ºC and 670.4 ºC, related to degradation of pectin, hemicellulose, cellulose, and lignin, respectively, over four steps [14]. The last thermal event of the films occurred between 298.4 ºC and 299.1 ºC, attributed to degradation of starch components [20, 21]. The TPS and TPS films with yerba mate waste showed similarities, with thermal stability of approximately 298 ºC. Regarding thickness and mechanical properties, the results are presented in Table 1.

Table 1 – Thickness and mechanical properties of the films.

Film	Thickness (mm)	Tensile strength (MPa)	Elongation at break (%)
TPS	0.08 ± 0.01	2.39 ± 0.18	59.62 ± 15.63
TPS-60ºC	0.09 ± 0.01	7.67 ± 3.93	3.62 ± 0.51
TPS-YM	0.26 ± 0.04	0.57 ± 0.09	33.97 ± 6.27
TPS-YM-60ºC	0.25 ± 0.02	0.88 ± 0.23	16.53 ± 6.86

The thickness of the films with YMW was higher than the TPS films, consistent with other studies [14, 17, 20]. There was variability in the mechanical properties of the films, and the results observed for TPS were similar to those in the literature. However, TPS-60°C showed opposite values to TPS, with an increase in tensile strength and reduction in elongation percentage. This pattern also occurred with the TPS-YM and TPS-YM-60ºC films, but both obtained mechanical properties lower than the control film, different from what has already been reported by other authors [16, 18, 22].

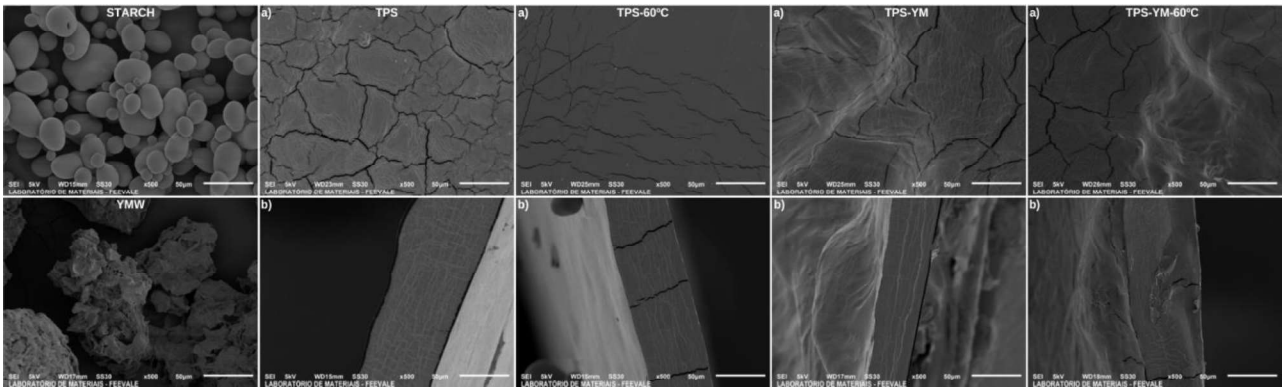

Figure 2 – SEM micrographs (500x) from starch, YMW, TPS and YMW films: a) top surface and b) cross section.

Fig. 2 presents the morphological analysis, indicating cracks on the surface of all films, which may be a consequence from sample preparation or electronic impact during scanning [17, 23]. It was observed that the surface of the TPS films were smooth compared to the films with YMW, which exhibited roughness [16]. In addition, no starch granules were visualized in the cross section, suggesting that complete gelatinization occurred [22]. Yerba mate waste showed irregular shape, varying in terms of forms and sizes [24], as does starch depending on its botanical origin and in the case of corn starch, the shape is polygonal [25].

Conclusions

Films with thermal stability (T_{max} ≈298 ºC) were obtained. An increment in elongation percentage was observed for films formed at room temperature and higher tensile strength values for films dried at 60 ºC. In conclusion, it was possible to develop TPS films using yerba mate waste, and applications in packaging and in the agricultural sector can be envisioned.

Acknowledgements

The authors gratefully acknowledge CAPES and CNPq for funding, and Feevale University for providing the infrastructure to conduct this study.

References

1. E. C. Morais; A. Stefanuto; G. A. Klein; B. C. Boaventura; F. Andrade; E. Wazlawik; P. F. Di Pietro; M. Maraschin; E. L. J. Silva. Journal of Agricultural and Food Chemistry 2009, 57, 8316-8324. https://doi.org/10.1021/jf901660g.
2. Department of Rural Economy - DERAL, 2020. Erva-Mate. Conjuncture Analysis – 2019/20 Crop. https://www.agricultura.pr.gov.br/sites/default/arquivos_restritos/files/documento/2019-12/erva-mate_2020.pdf.
3. J. T. Souza. Ph.D. Thesis. Federal University of Santa Maria, 2016.
4. M. Gonçalves; M. C. Guerreiro; M. L. Bianchi; L. C. A. Oliveira; E. I. Pereira; R. M. Dallago. Ciência e Agrotecnologia 2007, 31(5), 1386-1391. https://doi.org/10.1590/S1413-70542007000500017.

5. M. T. Veit; S. Bedin; G. C. Gonçalves; S. M. Palácio; M. R. Fagundes-Klen. Eclética Química 2016, 39(1), 227-243. https://doi.org/10.26850/1678-4618eqj.v39.1.2014.p227-246.
6. L. S. Krepki. M.Sc. Thesis. Federal University of Paraná, 2018.
7. A. B. Cunha; C. A. Carvalho; R. Buss; D. B. Waltrick; R. R. S. Barnasky; R. A. Hennel; R. Antunes. Scientia Forestalis 2019, 47, 124, 724-732. https://doi.org/10.18671/scifor.v47n124.14.
8. R. C. Rosa. M.Sc. Thesis. Federal University of Santa Maria, 2020.
9. U. Amin; M. U. Khan; Y. Majeed; M. Rebezov; M. Khayrullin; E. Bobkova; M. A. Shariati; I. M. Chung; M. Thiruvengadam. International Journal of Biological Macromolecules 2021, 183, 2184-2198. https://doi.org/10.1016/j.ijbiomac.2021.05.182.
10. European Bioplastics, 2022. Fact Sheet. What are bioplastics? https://docs.europeanbioplastics.org/publications/fs/EuBP_FS_What_are_bioplastics.pdf.
11. H. Cheng; L. Chen; D. J. McClements; T. Yang; Z. Zhang; F. Ren; M. Miao; Y. Tian; J, Jin. Trends in Food Science & Technology 2021, 114, 70-82. https://doi.org/10.1016/j.tifs.2021.05.017.
12. J. Zhang; F. Zou; H. Tao; W. Gao; L. Guo; B. Cui; C. Yuan; P. Liu; L. Lu; Z. Wu; Y. Fang. Industrial Crops & Products 2023, 194, 116358. https://doi.org/10.1016/j.indcrop.2023.116358.
13. J. R. V. Matheus; P. M. Farias; J. M. Satoriva; C. J. Andrade; A. E. C. Fai. International Journal of Biological Macromolecules 2023, 225, 658-672. https://doi.org/10.1016/j.ijbiomac.2022.11.129.
14. M. P. Arrieta; L. Peponi; D. López; M. Fernández-García. Industrial Crops and Products 2018, 111, 317-328. https://doi.org/10.1016/j.indcrop.2017.10.042.
15. M. C. A. Marcelo; D. Pozebon; M. F. Ferrão. Food Additives & Contaminants: Part A 2015, 32, 1215-1222, http://dx.doi.org/10.1080/19440049.2015.1050702.
16. A. López-Córdoba; S. Estevez-Areco; S. Goyanes. Carbohydrate Polymers 2019, 215, 377-387. https://doi.org/10.1016/j.carbpol.2019.03.105.
17. J. M. F. Pavoni; C. L. Luchese; I. C. Tessaro. International Journal of Biological Macromolecules 2019, 138, 693-703. https://doi.org/10.1016/j.ijbiomac.2019.07.089.
18. L. Dai; J. Zhang; F. Cheng. International Journal of Biological Macromolecules, 2019, 132, 897-905. https://doi.org/10.1016/j.ijbiomac.2019.03.197.
19. B. Wang; G. Zhang; S. Yan; X. Xu; D. Wang; B. Cui; A. M. A. El-Aty. International Journal of Biological Macromolecules 2023, 226, 580-587. https://doi.org/10.1016/j.ijbiomac.2022.12.084.
20. C. M. Jaramillo; T. J. Gutiérrez; S. Goyanes; C. Bernal; L. Famá. Carbohydrate Polymers 2016, 151, 150-159. https://doi.org/10.1016/j.carbpol.2016.05.025.
21. P. González-Seligra; L. Guz; O. Ochoa-Yepes; S. Goyanes. LWT 2017, 84, 520-528. https://doi.org/10.1016/j.lwt.2017.06.027.
22. R. L. Ceballos; O. Ochoa-Yepes; S. Goyanes; C. Bernal; L. Famá. Carbohydrate Polymers 2020, 244, 116495. https://doi.org/10.1016/j.carbpol.2020.116495.
23. A. Cano; A. Jiménez; M. Cháfer; C. Gónzalez; A. Chiralt. Carbohydrate Polymers 2014, 111, 543-555. https://doi.org/10.1016/j.carbpol.2014.04.075.
24. B. K. Vargas; E. G. Frota; L. F. Santos; J. P. Gutkoski; S. T. Lopes; C. D. Bertol; T. E. Bertolin. Food Bioscience 2021, 41, 100999. https://doi.org/10.1016/j.fbio.2021.100999.
25. X. Wang; C. K. Reddy; B. Xu. Food Chemistry 2018, 259, 81-88. https://doi.org/10.1016/j.foodchem.2018.03.121.

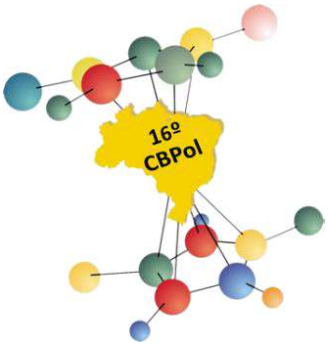

ECO-AUDIT ANALYSIS AND IMPACT OF DIFFERENT END-OF-LIFE FOR PLASTIC BOTTLES

Paulo R. Z. de Sá[1], Adriana M. C. de Souza[1], Patrícia S. Calvão [2]*

1 – Department of Materials Engineering, Centro Universitário FEI, São Bernardo do Campo, SP, Brazil

2 – Department of Metallurgical and Materials Engineering, University of São Paulo (USP), São Paulo, Brazil.

patycalvao@usp.br

Abstract – Due to the environmental crisis faced in recent decades arising from the mass production and consumption of various polymeric products, it is necessary to know the environmental impacts of each production stage of the production systems and to compare the environmental performance of each type of material, and seek more sustainable solutions for production processes. This research aims, through the Eco Audit tool found in the ANSYS GRANTA EduPack® software, to evaluate the environmental performance of bottles made of polypropylene (PP), high-density polyethylene (HDPE) and low-density polyethylene (LDPE), considering different types of discards (end-of-life). It can be concluded that among the bottle production life cycle stages, the most significant environmental burden is in the processes involving oil and gas extraction to polymerization. Regarding energy consumption and CO_2 emissions, incineration was the least advantageous final disposal, and recycling proved the most eco-sustainable. PP proved to be the most eco-sustainable polymer.

Keywords: *Eco-Audit, Embodied Energy, CO_2 Footprint, Plastic Bottles, End-of-life Alternatives.*

Introduction

In 2018, it was estimated that around 359 million tons of plastic were produced worldwide and that the number of plastic products has grown considerably after the last half of the 20th century. Studies indicate that about 30% of products are still in use. When considering post-consumption, the numbers indicate that only 9% of the total was recycled, 12% incinerated, and 79% accumulated in landfills, dumps, oceans, and forests, generating significant environmental impacts [1]. Commodity polymers such as PP, HDPE, and LDPE have been widely used in various products, emphasizing bottles and packaging [2]. Therefore, sustainable solutions must be found for these products' production processes and end-of-life, and that circular approaches must be adopted. It is necessary for producers to seek sustainable alternatives for their businesses and for consumers to be aware and make choices thinking about the environment [3].

To achieve a sustainable production of a product, it is necessary to know all the phases of its life cycle, evaluating how the technologies and materials used in the production can affect the environment and the ecosystem in which the production system of such product is inserted [4]. In this context, the Life Cycle Assessment (LCA) has gained much prominence in academia and research sectors in companies since it has proven to be an excellent tool for comparing products and understanding the possible environmental damage that each product, service, or technology generates, from its manufacture to its disposal.

According to NBR ISO 14040 (2001) [5], LCA is a technique that measures precisely all possible environmental impacts that a product, service, or technology generates from "cradle to grave," as it is commonly known. The methodology of a LCA must primarily contain the objective and scope of the study, Life Cycle Inventory Analysis, Life Cycle Impact Assessment and Life Cycle Interpretation [6]. It is a relatively laborious technique, mainly considering the Cycle Inventory Analysis where the data are collected and the specific calculation procedures of the studied product system are defined [7].

The objective of this research was to evaluate the environmental performance of PP, HDPE, and LDPE bottles using a more simplified methodology (Eco Audit) which aims to present data on the environmental impact of each stage in the production of bottles, not requiring a robust life cycle inventory and modeling. Eco-audit analyzes the five phases of a product's life (material, manufacturing, transport, use and disposal) and estimate which of these phases demands more energy (embodied energy) or has a larger carbon footprint [8].

Experimental

Eco audit analysis of plastic bottles was performed using ANSYS GRANTA EduPack® 2021 software. All stages of the life cycle analysis were investigated in Brazil. The bottle packaging materials chosen in the software were: Polypropylene (PP – homopolymer, low flow); High-density polyethylene (PE-HD – general purpose, extrusion); Low-density polyethylene (PE-LD – general purpose, extrusion). In the manufacturing stage, the production of 10,000 units of 60 g bottles by extrusion was examined. In this study, neither caps production nor package filling was considered.

For transport analysis, a 14 tonne (2 axle) truck covering a distance of 200 km was adopted. In the use stage, transport in a family car (gasoline) covering a distance of 6 km in one day was studied, using the plastic bottle for 120 days with a product life of 2 years. These inputs were the same for all materials. For the disposal phase, different possibilities were studied: landfill, recycle, combustion, downcycle and reuse (only once); it was considered that the material could be 100% recovered in all options.

Results and Discussion

Fig 1 and 2 show, respectively, the energy required and carbon emission (CO_2 footprint) in each life cycle phase of PP, HDPE, and LDPE bottles. In this case, it was considered the final disposal of the materials in a landfill.

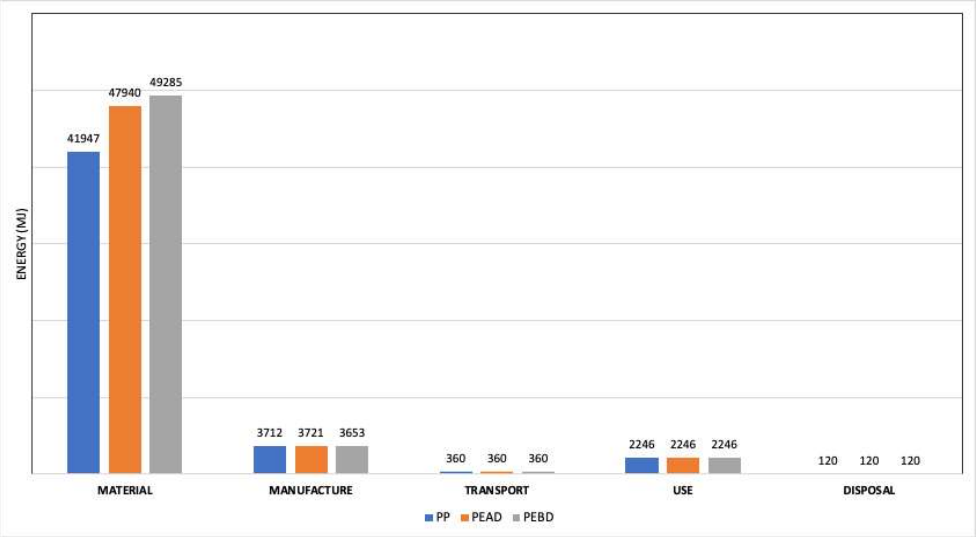

Figure 1 – Required energy at each life-phase for different plastic bottles materials (disposal in landfills).

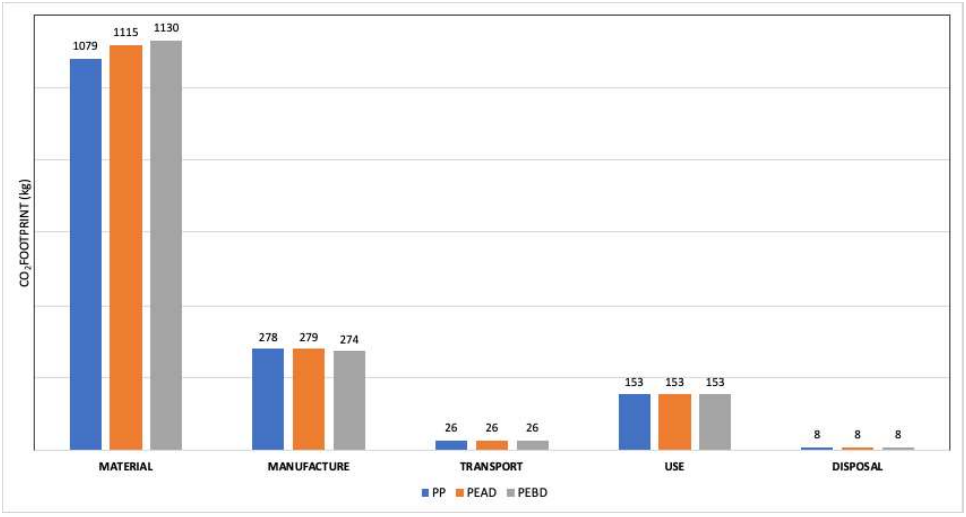

Figure 2 – Carbon emission at each life-phase for different plastic bottles materials (disposal in landfills).

For all materials studied, the higher energy is consumed in the material production phase (primary), involving oil and gas extraction to polymerization (Fig 1). The same behavior was observed in Fig 2 for carbon production (CO_2 footprint). Together, the manufacturing, transport, use, and disposal phases represent, on average, 14% of energy and 42% of the carbon footprint related to the production of the materials. LDPE requires more energy and emits more CO_2 during primary production compared to HDPE and PP.

Figure 3 shows the amount of water used in the primary production and manufacture (processing) of bottles and the average cost of virgin polymers (R$/kg). LDPE bottle production consumes more water compared to HDPE, which is also the material with the highest cost. On the other hand, PP presented a better comparative balance between cost and water use.

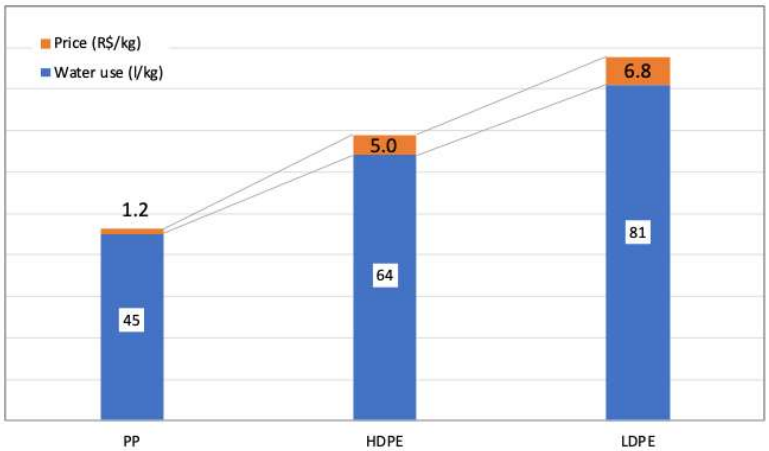

Figure 3 - Water consumption (primary production and processing) and cost of bottle materials.

Fig 4 shows the total energy consumed at all stages of the bottle's life cycle (material + manufacturing + transport + use) and the amount of energy that can be recovered in different end-of-life options: recycling, incineration, downcycling, and reuse. Fig 5 presents the same analysis for carbon emissions.

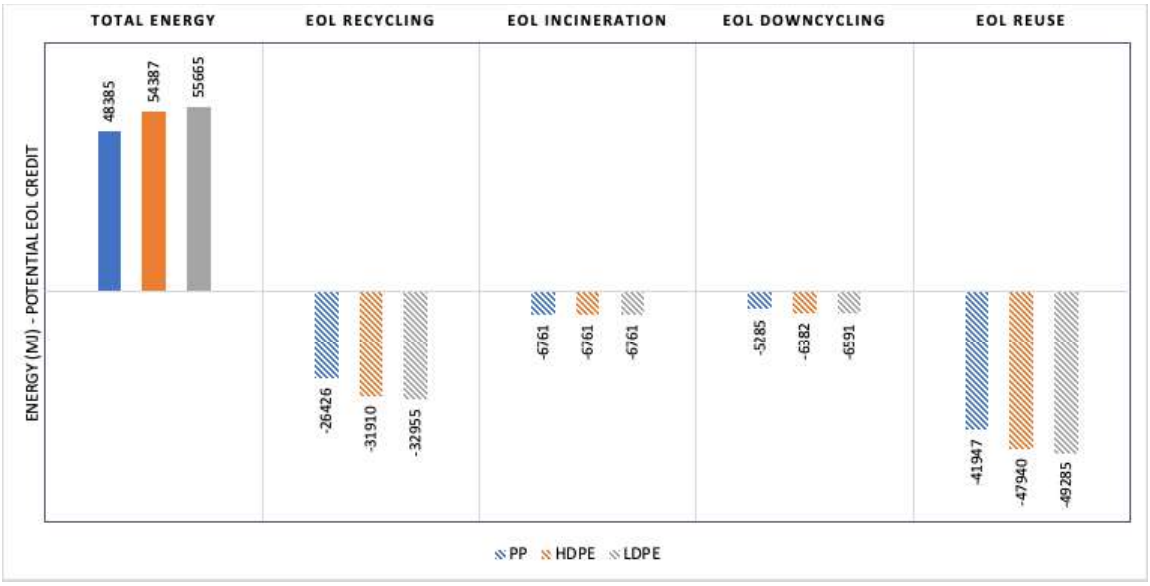

Figure 4 – Total energy compared with energy credit for different end-of-life (EoL) options for plastic bottles.

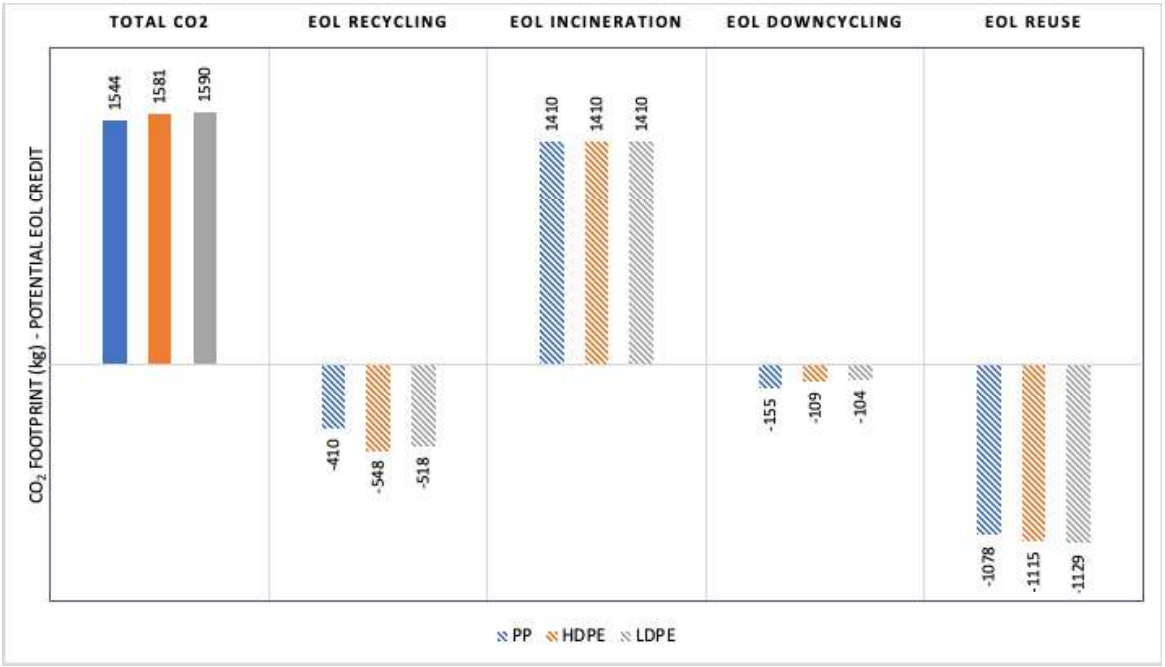

Figure 5 - Total carbon emission compared with carbon credit for different end-of-life (EoL) options for plastic bottles.

Recycling and reuse have a more significant credit potential for energy and CO_2 footprint compared to incineration and downcycling for all materials studied. It is important to highlight that albeit the reuse of plastic bottles has been studied, this practice is not recommended for some products. Moreover, water consumption in cleaning after using bottles should be considered for a more in-depth analysis.

For recycling, LDPE showed the highest energy recovery (Fig 4), while HDPE and PP showed 66% and 80% of their value, respectively. Regarding reuse, HDPE has the highest energy recovery, followed by PP and LDPE. Incineration is the worst type of final deposition since it emits high amounts of CO_2 into the environment (Fig 5), which values more significant than in the synthesis and manufacture of the material itself, although there is a recovery of thermal energy. In the case of recycling, HDPE has the highest recovery of CO_2 emissions, followed by LDPE and PP, while in terms of reuse, LDPE had the best performance, followed by HDPE and PP.

Conclusions

In this work, an Eco-audit analysis of PP, HDPE, and LDPE bottle packaging was conducted using the ANSYS GRANTA Edupack software. Energy waste and carbon footprint were adopted as sustainability indicators, and the end-of-life options for the products were also evaluated. It was observed that PP bottles have the best environmental performance compared to HDPE and LDPE ones. Comparing different types of end-of-life, it was observed that recycling and reuse are more environmentally favorable options for the three types of plastic bottles.

Acknowledgements

The author would like to thank Centro Universitário FEI for financial support and availability of the GRANTA Edupack (ANSYS) software.

References

1. A.E. Schwarz, T.N. Ligthart, D. Godoi Bizarro, P. De Wild, B. Vreugdenhi, T. van Harmelen, Waste Management 121 (2021) 331–342. https://doi.org/10.1016/j.wasman.2020.12.020.
2. Cleanup report – The international Coastal Cleanup. Ocean Conservancy's International Coastal Cleanup. Washington. 2020.
3. Autor desconhecido. Relatório da ONU sobre poluição plástica alerta sobre falsas soluções e confirma necessidade de ação global urgente. UNEP, Out. 2021.
4. V. Siracusa; C. Ingrao; A.Lo Giudice; C. Mbohwa; M. Dalla Rosa Food Research International 2014, 62, 151-161. https://doi.org/10.1016/j.foodres.2014.02.010.
5. ASSOCIAÇÃO BRASILEIRA DE NORMAS TÉCNICAS. NBR 14040: Gestão ambiental – Avaliação do ciclo de vida – Princípios e estrutura.
6. ASSOCIAÇÃO BRASILEIRA DE NORMAS TÉCNICAS. NBR 14044: Gestão ambiental — Avaliação do ciclo de vida — Requisitos e orientações. Rio de Janeiro, jun. 2009.
7. J. R. B. CHEHEBE. Análise do ciclo de vida de produtos: ferramenta gerencial da ISO 14000. Qualitymark, Rio de Janeiro: 2002.
8. M. Ashby, *Materials and the Environment: Eco-Informed Material Choice*. 2nd Ed., Butterworth-Heinemann, Oxford, 2013.

EFFLUENT CHEMICAL INDUSTRY WASTEWATER TREATMENT BY MEMBRANE DISTILLATION USING COMMERCIAL MEMBRANES

Léticia V. Aimi[1*], Regilene S. Silva[2], Cintia Marangoni[2] and Noeli Sellin[1]

1 – Graduate Program in Process Engineering, University of Joinville Region (UNIVILLE), Joinville, SC, Brazil
leticia.aimi@gmail.com
2 – Graduate Program in Chemical Engineering, Federal University of Santa Catarina (UFSC), Florianopolis, SC, Brazil

Abstract – This study investigated for the first-time water recovery from chemical industry wastewater by membrane distillation (MD) process using commercial polytetrafluoroethylene (PTFE) and polyvinylidene fluoride (PVDF) membranes. Effluent and membrane characterization techniques were used to evaluate the MD performance and membrane fouling properties. Both membranes showed removal efficiency of the DCMD (Direct Contact Membrane Distillation) system for Iodine, COD, and Conductivity parameters. Less fouling for the PTFE membrane was observed, and the fouling phenomenon was more evident for the PVDF membrane, which caused a decrease in its hydrophobicity. PTFE membrane showed better performance due to greater porosity and hydrophobicity when compared to PVDF membrane. However, the structure of the membranes and the permeate flux were not affected, indicating that commercial membranes are potential candidates for the industrial-scale deployment of MD, which can accelerate the commercialization process of MD in the chemical industry.
Keywords: *Water reclamation, DCMD, PTFE, PVDF, Chemical Industry.*

Introduction

Chemical industry wastewater involves organic and inorganic pollutants, which are highly toxic and carcinogenic. Without proper treatment, these non-biodegradable compounds severely threaten the environment. Current solutions to decrease the environmental impact of chemical industry wastewater include physical, chemical, and biotechnological processes. However, these applied techniques have limitations, such as low process efficiency, large amounts of sludge generation, and use of harmful chemicals. In this sense, to improve the quality of recovered water, the chemical sector must adopt innovative treatment technologies [1].

Membrane Distillation (MD) is an attractive technique for treating and reusing wastewater, especially the direct contact configuration [2]. It is a thermal separation technique where a microporous hydrophobic membrane acts as a physical barrier, allowing only vapor to pass through. In Direct Contact Membrane Distillation (DCMD), the effluent to be treated (process feed), as well as the recovered water (permeate), are in direct contact with the membrane. Mass transport is initiated by the evaporation of the feed liquid at the liquid-vapor phase boundary, and the vapor pressure gradient induces the diffusion of vapor molecules through the membrane pores. Condensation of the vapor occurs later on the permeate side [3]. The advantages of MD include efficiently removing high amounts of pollutants, employing a simple heat transfer mechanism, and can utilize low-grade waste heat [4].

The present work objective is to investigate the application of flat commercial PTFE and PVDF membranes in treating chemical industry wastewater with MD. Commercial membranes were analyzed for porosity, hydrophobicity, thickness, and composition. Experiments were carried out on

a laboratory scale, and the results of permeate flux, mass flow rate and physical-chemical characterization of the effluent are reported. Similar work has yet to be conducted to study the effects of DCMD specifically applied to chemical industry effluent treatment, so more research is needed.

Experimental

In this study, a commercial polymeric membrane of polytetrafluoroethylene (PTFE) (membrane solutions) and polyvinylidene fluoride (PVDF) (ISEQ00010 Merck Millipore) was used. The PTFE is flat and hydrophobic, with pore size of 0.22 μm, thickness of 170 μm, porosity of 75%, and polypropylene support. The PVDF membrane is flat and hydrophobic, with pore size of 0.20 μm, thickness of 118 μm, and porosity equal to 75%.

The chemical industry that supplied the sample treats in its effluent treatment station the wastewater originating in the production processes of iodine, cobalt, and selenium salts, as well as the water from the purges of the cooling towers and containment basins. The sample used was taken from a 100 m³ tank, which receives the wastewater and, through mechanical agitation, performs the equalization process. The samples were characterized before and after the DCMD experiments, the quantified parameters were: concentration of iodine, Chemical Oxygen Demand (COD) and conductivity. The physicochemical characteristics of the chemical industry effluent are shown in Table 1.

Table 1 - Physicochemical characteristics of the chemical industry wastewater.

Parameter	Chemical industry wastewater
Iodine (mg/L)	595.6
COD (mg/L)	1,500.0
Conductivity (μs/cm)	2,980.0

The MD unit comprises a feed tank, permeate tanks, a feed pump, permeate pumps, a thermal resistor, digital panel, a digital thermocryostatic bath, digital thermometers, and flat sheet membrane modules. The permeate flux J ($kg.m^{-2}.h^{-1}$) obtained during the operation is calculated using Eq. 1, where Δm are the permeate masses (kg), A is the effective membrane area (m^2), and Δt is the total operating time (h). The mass flow rate $\dot{m}$ ($g.h^{-1}$) corresponds to the ratio between the permeate mass (g) and the experiment time (h).

$$J = \frac{\Delta M}{A \times \Delta t} \quad (1)$$

$$\dot{m} = \frac{\Delta M}{\Delta t} \quad (2)$$

Membranes characterizations were analyzed using Attenuated Total Reflectance-Fourier Transform Infrared spectroscopy (ATR-FTIR) (IRSpirit–Shimadzu) with a diamond tip, 4 cm^{-1} resolution, and 32 scans. The Raman spectra were analyzed in an Anton Paar Cora 5200 Raman equipment with a laser excitation of 785 nm and analyzed from 100 to 2300 cm^{-1}. The hydrophobicity of the membranes was evaluated by analyzing the contact angle using the sessile drop method, performed on a Ramé-Hart goniometer, model 250-F1 (DROPImage Advanced software). The thickness of the membrane was determined using a digital caliper (MTX, 316119), 10 random measurements was performed on each membrane, and the volumetric porosity (%) of each membrane was determined by the gravimetric method. The membranes were characterized with the membranes intact and contaminated, making it possible to define the influence of the process on the material of the membranes.

Results and Discussion

The results obtained during the characterization of the effluents, presented in Table 2, demonstrate a removal efficiency of the DCMD system for both membranes in the Iodine, COD, and Conductivity parameters. The most significant values were achieved in the tests carried out with the commercial PTFE membrane, which is justified due to its characteristics concerning porosity and hydrophobicity and the final permeate flux, which is higher than that obtained in the test carried out with the commercial PVDF membrane.

Table 2 - Characterization of the effluents resulting from the tests carried out with the PTFE and PVDF membrane.

Parameter	PTFE		PVDF	
	Feed	Permeate	Feed	Permeate
Iodine (mg/L)	469.7	55.5	538.0	72.6
COD (mg/L)	114.0	292.0	562.0	434.0
Conductivity (µs/cm)	5250.0	87.5	2500.0	130.2

High permeate flux and mass flow rate were obtained for commercial PTFE and PVDF membranes over 4 h of DCMD operation applied to chemical industry wastewater (Fig. 1). The characteristics that allowed the high permeate fluxes were the adequate pore size, the high porosity, and the high hydrophobicity of the membranes. The high porosity of the membranes increased the area available for the evaporation of water molecules. Consequently, there was a more significant increase in permeate flux and mass flow rate. The commercial PTFE membrane showed a final permeate flux 4.97% higher than the commercial PVDF membrane, which is explained by the lower porosity and hydrophobicity of the PVDF membrane compared to the PTFE membrane. However, both membranes showed similar permeate fluxes at 4 h.

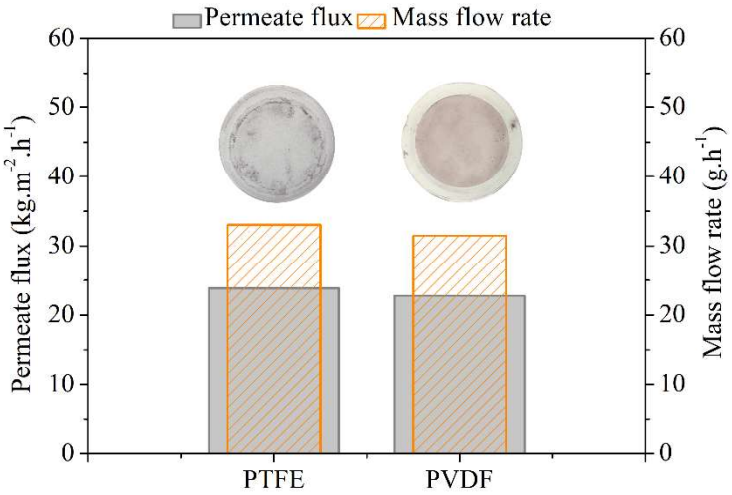

Figure 1 - Permeate flux and mass flow rate from DCMD experiments with PTFE and PVDF membranes.

To better understand these results, membrane characterizations were performed regarding ATR-FTIR, RAMAN, hydrophobicity, volumetric porosity, and thickness. The interaction of chemical industry wastewater with the surface of the membranes was determined using ATR-FTIR to obtain information about the functional groups on its surface. The spectrum of intact PTFE and PVDF membranes after use in the DCMD operation is represented in Fig. 2 a and b. The corresponding bands for the PTFE membrane peak are remarkably close to 1205 cm^{-1} and 1153 cm^{-1}, representing the asymmetric elongation vibration and the symmetric elongation vibration of binding to its C-F binding monomer, and the peak near 2998 cm^{-1}, refers to the CH bond associated with axial

strain vibrations. The wavenumber (cm^{-1}) from 1400 to 500 corresponds to the C-Halogen bond, which is present in the membrane structure of PVDF in the C-F form. All the peaks that are in this variation range are related to the structure of the membrane itself. That is, there was no change in the chemical structure of the membranes.

RAMAN spectra were also performed to verify possible changes in the structure of PTFE and PVDF membranes (Fig. 2 c and d). We observed firm absorption peaks at 816 cm^{-1}, 1160 cm^{-1}, 1210 cm^{-1}, 1330 cm^{-1}, and 1463 cm^{-1}, corresponding to the asymmetric and symmetric stretching peaks of C-F in the PTFE molecular structure. In the analysis of the RAMAN spectra, all PVDF membranes showed peaks at 611 cm^{-1}, 794 cm^{-1}, and 1430 cm^{-1}, characteristic of the α and β phase of PVDF. Thus, the results of the RAMAN spectra corroborate the ATR-FTIR analysis, indicating that these effluents could not change the structure of the membranes.

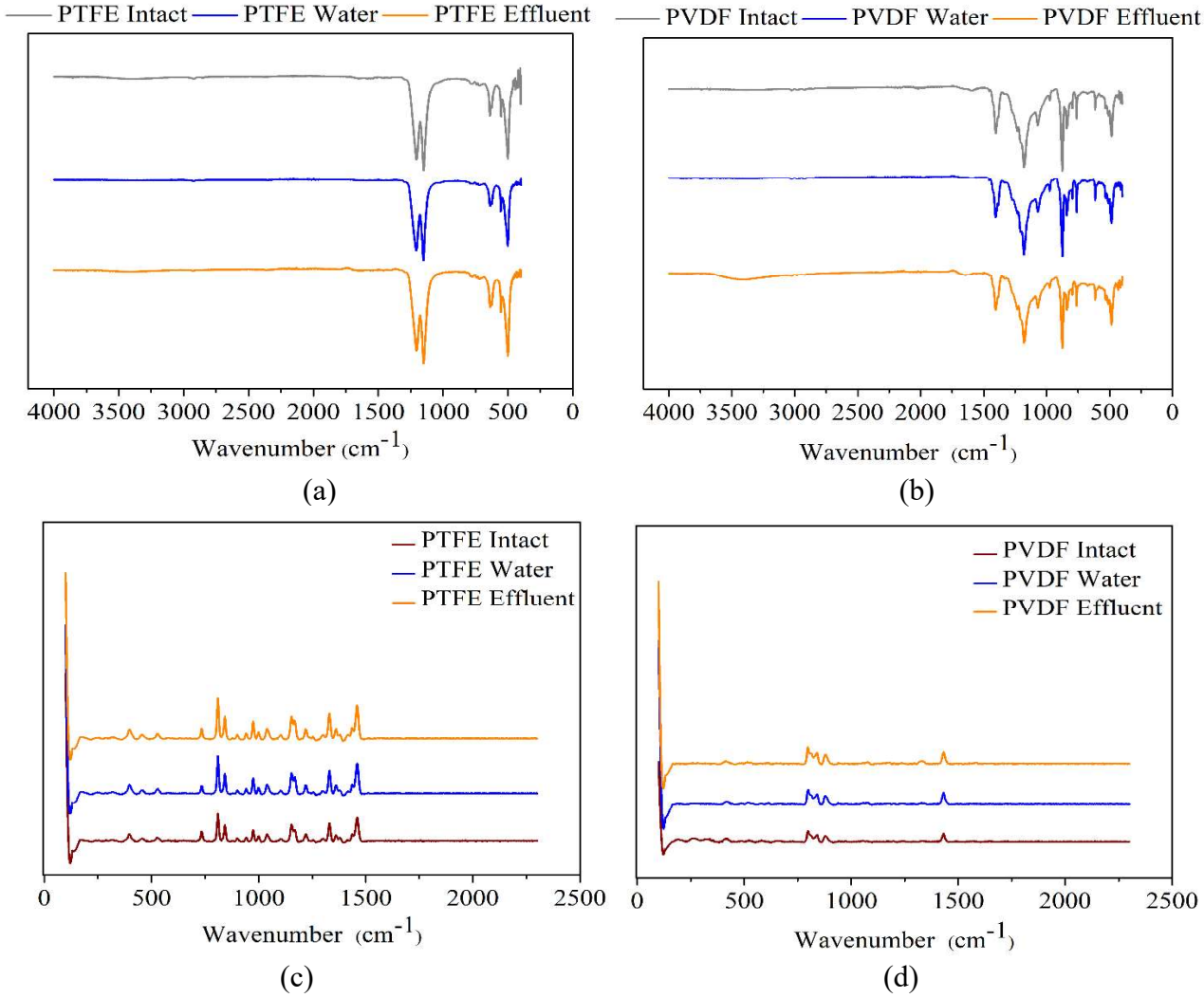

Figure 2 - ATR-FTIR (a and b) and RAMAN (c and d) spectra of commercial PTFE and PVDF membrane before and after DCMD experiments.

Table 3 shows intact and contaminated PTFE and PVDF membrane contact angle values. According to the results, it is observed that with all membranes, there was variation in the contact angle. Decreased contact angle on contaminated membranes can be attributed to fouling on the membrane surface. The PTFE membrane continued with an angle greater than 90º, indicating that there is still hydrophobicity of the membrane surface. While the decrease in the contact angle of the PVDF membrane made the membrane surface hydrophilic, indicating that there was a more

significant interaction of the effluent with this membrane, causing greater fouling, it has already been reported in the literature that the PVDF membrane is more subject to deposit and fouling phenomena. The fouling phenomenon originated from the deposition of effluent molecules on the surface and within the membrane's pores. Therefore, surface adsorption may be one of the reasons for the pore wetting induced by the pores of the PVDF membrane becoming hydrophilic. However, it is worth noting that there was no notable decrease in the permeate flux when compared to the PTFE membrane. Observing the results of thickness and porosity (Table 3), it is possible to conclude that the thickness and porosity of the membranes were little affected by their use in MD with the effluent.

Table 3 - Thickness, contact angle and porosity of commercial PTFE and PVDF membranes intact and after DCMD experiments.

Membrane	Thickness (µm)	Contact angle (°)	Porosity (%)
PTFE Intact	170 ± 0.010	119.10 ± 0.01	75 ± 0.007
PTFE Effluent	170 ± 0.009	107.80 ± 0.09	72 ± 0.003
PVDF Intact	118 ± 0.003	110.95 ± 0.001	68 ± 0.036
PVDF Effluent	118 ± 0.005	84.84 ± 0.09	66 ± 0.003

Conclusions

Based on the tests carried out, the potential for applying the DCMD process to treat real effluents from the chemical industry was proven. The reduction of iodine, conductivity, and COD contaminants was achieved using commercial flat PTFE and PVDF membranes. The PTFE membrane showed the best results in the DCMD process due to its average pore diameter, porosity, hydrophobicity, and low degree of liquid absorption. The PVDF membrane resulted in a lower permeate flux and reduction efficiency due to its final contact angle, which made its surface hydrophilic, causing more significant fouling and pore wetting. Several membranes are currently cited in the literature for the DCMD process, but their commercialization is still restricted. Although the MD process presents promising results in the treatment of effluents, more research must be carried out to enable its industrial implementation.

References

[1] K. Manzoor, S.J. Khan, M. Yasmeen, Y. Jamal, M. Arshad, J. Journal of Water Process Engineering 2022 102603. 10.1016/j.jwpe.2022.102603.

[2] R. de S. Silva, H. Ramlow, B. de C. Santos, H.B. Madalosso, R.A.F. Machado, C. Marangoni, Journal of Water Process Engineering 2021. https://doi.org/102339. 10.1016/j.jwpe.2021.102339.

[3] F. Ricceri, M. Giagnorio, G. Farinelli, G. Blandini, M. Minella, D. Vione, A. Tiraferri, Scientific Reports 2019. https://doi.org/10.1038/s41598-019-51167-z.

[4] A.F.S. Foureaux, V.R. Moreira, Y.A.R. Lebron, L.V.S. Santos, M.C.S. Amaral, Separation and Purification Technology 2020. https://doi.org/116251. 10.1016/j.seppur.2019.116251.

EVALUATION OF COMPOSTING AND VERMICOMPOSTING IN THE DEGRADATION OF HDPE FILMS

Jonas L. de Bitencourt[1,2,3], Ruth M.C. Santana[2], Edson L. Francisquetti[1], Mara Z. Andrade[1], Laura A. Souza[1].

1 –Instituto Federal de Ciência e Tecnologia do Rio Grande do Sul (IFRS), Campus Farroupilha, Farroupilha, RS, Brasil. jonas.bitencourt@farroupilha.ifrs.edu.br
2 – Universidade Federal do Rio Grande do Sul (UFRGS), RS, Brasil.
3 – Centro Universitário Uniftec, Bento Gonçalves, RS, Brasil.

Abstract - The gravimetric composition of a landfill consists of approximately 10% polymers, with plastic bags used to contain organic waste being a significant contributor. Exploring alternatives to mitigate the impacts resulting from the improper disposal of these residues is deemed necessary. The films used in these bags are durable and impermeable, which hinders the degradation of the enclosed organic fraction. Therefore, employing methods that facilitate the segregation of these materials enhances the lifespan of landfills, leading to positive environmental effects. This also allows for the valorization of organic waste through processes like composting and vermicomposting. This study aims to analyze the biodegradation and deterioration of HDPE films through the use of such methods. Vermicomposting employed annelids of the *Eisenia fetida* species to determine their efficiency in breaking down the polymeric material. The biodegradation of the polymeric materials was assessed through FTIR, tensile mechanical testing, and optical microscopy. The crystallinity of the materials was evaluated using DSC. The obtained results revealed material degradation and an efficiency increase in the vermicomposting environment compared to composting.

Keywords: *Biodegradation, Vermicomposting, Composting, Polyethylene, Eisenia fetida.*

Introduction

Synthetic polymers derived from petrochemicals have very low degradation rates and become an environmental problem when improperly discarded, posing a risk to ecosystem balance [1-3]. Global consumption of plastic bags is estimated at 0.5 to 1 trillion bags per year, or 1 to 2 million bags every minute [1]. In Brazil, it is estimated that about one and a half million plastic bags are distributed per hour in various commercial establishments such as shops and supermarkets. A small portion of these bags is recycled, while a significant amount ends up in landfills [4]. The high productivity and indiscriminate use of these bags, combined with improper disposal, have worsened environmental problems, especially in soil and water. It is estimated that about 10% of all organic waste collected in cities consists of single-use plastic bags, as it is common practice to use them to contain organic waste [5]. These bags are resistant and impermeable, which hinders the degradation of organic matter [6]. Given these circumstances, it is important to seek alternatives to mitigate the impacts resulting from the use of plastic bags as waste containers. Through composting and vermicomposting, these bags can be more easily separated in landfills. This allows for the valorization of organic waste while extending the lifespan of the landfill, reducing environmental impacts [7]. Composting is an exothermic aerobic biooxidation process of a heterogeneous organic substrate in solid state. It involves the production of carbon dioxide, water, mineral substances, and the stabilization of organic matter [8]. On the other hand, vermicomposting is a method for treating and valorizing the organic fraction of waste using species of earthworms [9]. These annelid animals are found in moist soils worldwide. They create tunnels and channels in the soil, where they reside and ingest plant residues along with significant amounts of soil. This ingestion results in the

production of humus, which is decomposed organic matter and is considered an excellent nutrient source for plant growth [9]. The research conducted in this study aims to analyze the biological degradation and breakdown of high-density polyethylene plastic bags in a composting environment and a vermicomposting environment, using Eisenia fetida earthworms.

Experimental

Structure of Vermicomposting and Composting

Two identical structures were used, one for composting and the other for vermicomposting. The structure consists of two digestion boxes measuring 60 x 42 cm and a leachate collection base. The total height of the structure is 78 cm, with a volume of 45 liters, as shown in Fig 1. In both containers, garden soil (without additives or fertilizers), fruits, vegetables, greens, dry leaves, and cow manure were added in the same quantities. Temperature, pH, and soil moisture measurements were taken using a measurement sensor, Smart brand, model 4.1 Soil Survey Instrument, ISO 9001:2000.

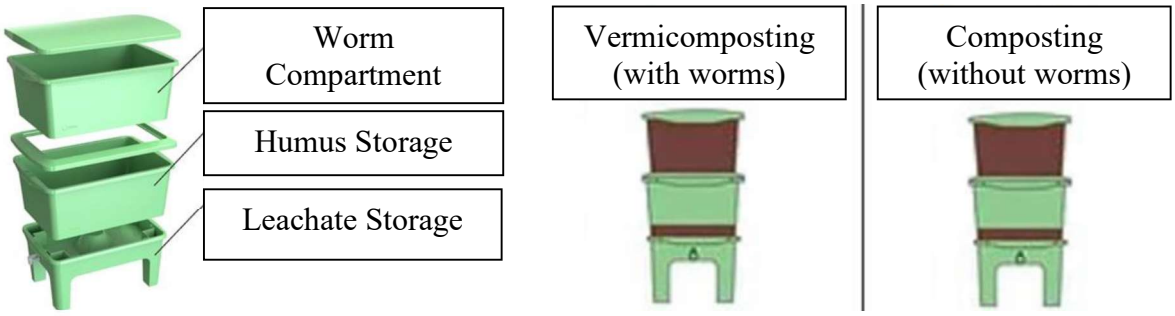

Figure 1 Structure Vermi/composting Humi. Source: https://composteirahumi.eco.br/

In the vermicomposting container, 942 adult worms of the species *Eisenia fetida* were added, as shown in Fig 2.

Figure 2 Minhocas *Eisenia fetida.*

Polymeric Samples

The samples, cut into strips measuring 20 x 5 cm, consist of an HDPE film collected from a supermarket, produced by Altaplast Embalagens, certified according to ABNT NBR 14937. The samples were collected in triplicate at 30, 60, and 90-day intervals.

Caracterization

The samples were analyzed using the following techniques: Fourier-transform infrared spectroscopy (FTIR) using a Perkin Elmer FT-IR spectrometer frontier with an attenuated total reflection (ATR) accessory; differential scanning calorimetry (DSC) using a Perkin Elmer DSC 6000 instrument; universal testing machine (tensile mechanical testing) using an Emic DL 20000 model; optical microscope (OM) using a 400X Series Digital Microscope.

Results and Discussion

The FTIR characterization was performed on the initial samples and after 30, 60, and 90 days of vermicomposting and composting. Fig 3 and Fig 4 show the FTIR spectra of the HDPE samples subjected to vermicomposting and composting, respectively.

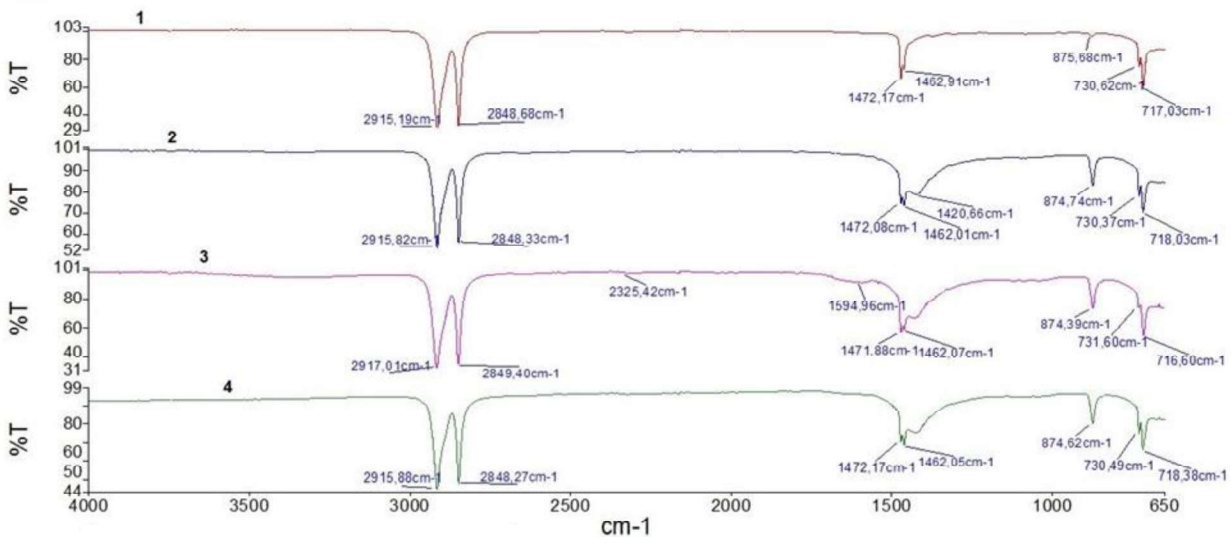

Figure 3 FTIR PEAD vermicomposting (1=0, 2=30, 3=60 e 4=90 days).

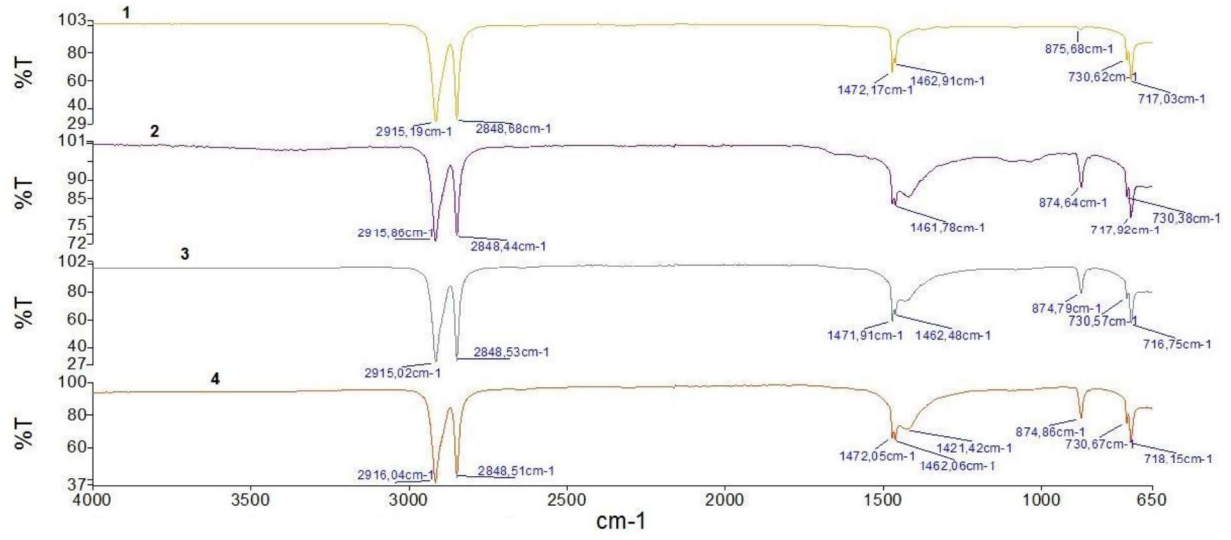

Figure 4 FTIR PEAD composting (1=0, 2=30, 3=60 e 4=90 days).

In the degradation of HDPE, the formation of carbonyl compounds and alkenes can be observed. In the spectra of 30, 60, and 90 days, this can be seen in the emergence of a peak in the 1420 cm-1 band, reflecting the formation of carbonyls, and the 874 cm-1 band indicating the formation of alkenes. Therefore, it can be inferred that degradation occurred in the polymeric chain of HDPE, both in vermicomposting and composting. Fig 5 presents the results of the tensile testing of the samples subjected to composting and vermicomposting.

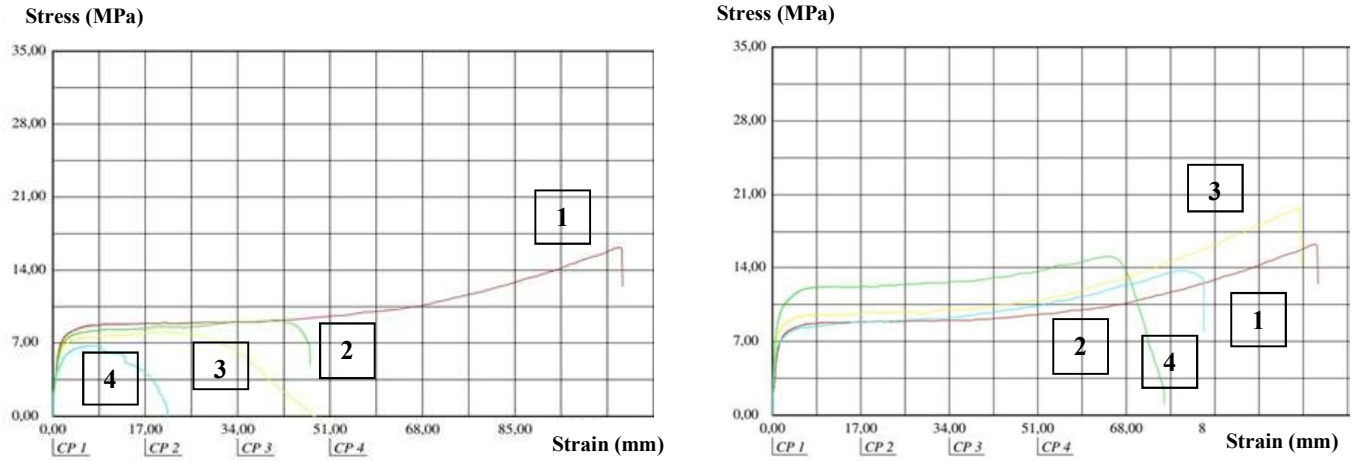

Figure 5 Tensile Testing of HDPE: Vermicomposting (left) and Composting (right) (1=0, 2=30, 3=60, and 4=90 days).

It can be inferred that the duration of vermicomposting and composting made the samples more fragile, with a lower modulus of elasticity. When analyzing the stress-strain graphs, a loss of mechanical properties can be observed in a large portion of the samples, with this effect being more pronounced in the vermicomposting samples. Significant reductions in maximum tensile stress (58.34%) and deformation (79.81%) are observed in the vermicomposting samples, while the yield stress remains stable. These results indicate significant changes in the mechanical properties after the vermicomposting process. In the composting process, the HDPE showed a 15.1% reduction in maximum tensile stress, an increase in yield stress, and a 20.7% reduction in deformation. Based on the data obtained from the DSC tests, Table 1 was prepared, showing the reductions in crystallinity of HDPE in relation to the method used, either vermicomposting or composting.

Table 1 Reduction in HDPE crystallinity.

Method	Material (days)	Ton	Tc	Tend	ΔHc	Ton	Tf	Tend	ΔHf	Xc (%)
Composting	HDPE 0	117,7	115,7	110,5	-117,9	120,1	127,4	130,1	107	**37**
	HDPE30	117,7	116	111,8	-128,8	120,5	128	130,5	126,8	**43,5**
	HDPE60	117,4	114,5	107,8	-132,9	121	129,9	132,7	113,3	**38,9**
	HDPE90	117,4	114,9	108,7	-120,1	121,1	129,5	132,4	106,3	**36,5**
Vermicompost.	HDPE 0	117,7	115,7	110,5	-117,9	120,1	127,4	130,1	107	**37**
	HDPE30	117,5	115,7	111	-82,2	120,9	128,3	130,9	87	**29,9**
	HDPE60	117,4	114,6	106,9	-105	120,9	130,2	133,3	99	**34**
	HDPE90	117,5	114,8	108	-95,2	120,6	128,9	131,6	89,1	**30,6**

There is a reduction in crystallinity observed only in the samples taken from vermicomposting. The 30-day sample showed a reduction of 7.1%, the 60-day sample showed a reduction of 3%, and the 90-day sample showed a reduction of 6.4%. These results corroborate with the findings from the mechanical tests, as a reduction in polymer crystallinity leads to a decrease in the elastic modulus.

On the other hand, the HDPE samples from composting showed small variations in the percentage of crystallinity, which was also observed in the mechanical tests with little variation in the material's elasticity. The images obtained by the optical microscope, Fig 6, highlight the change in the material's surface over time. It is possible to observe that more changes occurred in the surface of the samples subjected to vermicomposting. The tear in sample d, from vermicomposting, is a result of the passage of the annelid.

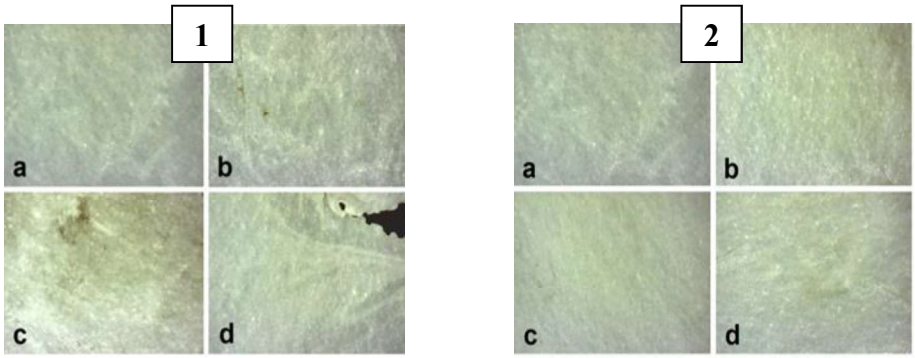

Figure 6 Optical microscopy (OM) HDPE vermicomposting (1), HDPE composting (2); after (a=0 day, b=30 days, c=60 days, d=90 days). Magnification scale 50X.

Conclusions

Based on the conducted tests, it can be concluded that degradation occurred in the polymeric films, with a notable effect in the vermicomposting process. In the case of HDPE samples, after 90 days, there was a decrease in maximum stress from 16.2 to 6.75 MPa, a reduction in elastic deformation from 104 to 21 mm, and a 6.4% decrease in crystallinity. In composting, after 90 days, there was a decrease in maximum stress from 16.2 to 13.75 MPa, a reduction in elastic deformation from 104 to 82.5 mm, and no significant reduction in crystallinity. FTIR analysis of both vermicomposting and composting samples revealed the formation of carbonyl compounds and alkenes, indicating polymer chain degradation. However, it can be concluded that vermicomposting showed higher efficiency in terms of biodegradation.

References

1. Romão, W.; Spince, M. A. S.; Paoli M. Poli(tereftalato de etileno), PET: Uma revisão sobre os processos de síntese, mecanismos de degradação e reciclagem. Polímeros: Ciência e Tecnologia. 2009,19:121 – 132.
2. Talvitie, Julia et al. Solutions to microplastic pollution–Removal of microplastics from wastewater effluent with advanced wastewater treatment technologies. Water research, v. 123, p. 401-407, 2017.
3. Usha, Rajamanickam; Sangeetha, T.; Palaniswamy, M. Screening of polyethylene degrading microorganisms from garbage soil. Libyan Agric Res Cent J Int, v. 2, n. 4, p. 200-4, 2011.
4. Brasil. MINISTÉRIO DO MEIO AMBIENTE (MMA). Gestão de resíduos orgânicos. 2010. http://www.mma.gov.br/responsabilidadesocioambiental/producao-e consumosustentavel/saco-e-um-saco/saibamais.
5. Brasil. SENADO FEDERAL (SF). Sacola plástica é uma das maiores vilãs do meio ambiente.2016. https://www12.senado.leg.br/noticias/materias/2016/04/19/sacola-plastica-e-uma-das- maiores-vilas-do-meio-ambiente.
6. CEMPRE. Compromisso Empresarial para Reciclagem. Cempre Review. 2019. https://cempre.org.br/wpcontent/uploads/2020/11/CEMPRE-Review2019.pdf.
7. Naddafi, K.; Zamanzadeh, M.; Azimi, A.A.; Omrani, G.A.; Mesdaghinia, A.R.; Mobedi, E., 2004. Effect of temperature, dry solids and C/N ratio on vermicomposting of wates activated sludge. *Pakistan Journal of Biological Science*, vol. 7, no. 7, pp. 1217-1220.

8. Domínguez, J., Edwards, C.A., Subler, S., 1997. A comparison of composting and vermicomposting. Biocycle 4, 57–59.
9. Eckhardt, D., Antoniolli, Z., Schiedeck, G., Santana, N., Redin, M., Domínguez, J., Josemar, R., Jacques, S.. (2016). Vermicompostagem como alternativa para o tratamento de resíduos nas propriedades rurais do Rio Grande do Sul. In: Manejo e conservação do solo e da água em pequenas propriedades rurais no sul do Brasil: práticas alternativas de manejo visando à conservação do solo e da água, Edition: Porto Alegre, Rio Grande do Sul, Brasil, Chapter: 6, Publisher: UFRGS – Universidade Federal do Rio Grande do Sul, Editors: Tales Tiecher, pp.87-99.

EVALUATION OF COMPOSTING AND VERMICOMPOSTING IN THE DEGRADATION OF PLA/TPS BLEND FILMS

Jonas L. de Bitencourt[1,2,3], Ruth M.C. Santana[2], Edson L. Francisquetti[1], Mara Z. Andrade[1], Laura A. Souza[1].

1 –Instituto Federal de Ciência e Tecnologia do Rio Grande do Sul (IFRS), Campus Farroupilha, Farroupilha, RS, Brasil. jonas.bitencourt@farroupilha.ifrs.edu.br
2 – Universidade Federal do Rio Grande do Sul (UFRGS), RS, Brasil.
3 – Centro Universitário Uniftec, Bento Gonçalves, RS, Brasil.

Abstract - A sanitary landfill contains approximately 10% of polymers in its composition, such as polyethylene bags used for containing organic waste. These bags possess impermeability and mechanical strength characteristics, causing organic matter to become trapped within, hindering its degradation. Consequently, this reduces the landfill's lifespan. Furthermore, improper disposal of polyethylene bags is observed, leading to a significant environmental issue as they are not recycled but rather contribute to pollution. In an effort to mitigate these problems, the methods of composting and vermicomposting are intended to be evaluated for decomposing bags made from a biodegradable blend of polylactic acid with thermoplastic starch (PLA/TPS). In vermicomposting, annelids of the Eisenia fetida species were utilized to assess their efficiency in decomposing PLA/TPS. Biodegradation of PLA/TPS was determined through Fourier-transform infrared spectroscopy (FTIR), tensile mechanical testing, and optical microscopy. The results obtained revealed degradation of PLA/TPS, as well as enhanced efficiency in the vermicomposting environment compared to composting.

Keywords: *Biodegradation, Vermicomposting, Composting, Eisenia fetida, Polylactic acid.*

Introduction

Polymers derived from petroleum exhibit slow rates of degradation. This, coupled with their large-scale production and improper disposal, poses a severe environmental problem that can disrupt ecosystem balance [1-3]. It is estimated that globally, 0.5 to 1 trillion plastic bags are consumed annually [1]. In Brazil, about one and a half million plastic bags are estimated to be distributed every hour in commercial establishments. A small fraction of these is recycled, with the majority ending up in landfills [4]. Roughly 10% of all collected organic waste in cities comprises single-use synthetic plastic bags, often used to contain organic refuse [5]. These bags are sturdy and impermeable, impeding organic material degradation [6]. Therefore, it's pertinent to seek alternatives to mitigate the environmental impacts arising from the use of plastic bags as waste containers. Over the past two decades, biodegradable materials have been developed, such as thermoplastic starches (TPS), polylactic acid (PLA), and their blends. However, these polymers still have limitations in terms of cost, mechanical and chemical resistance when compared to synthetic polymers. Moreover, the recycling of biodegradable polymers, according to The European Waste Framework Directive, should be carried out through composting [7]. This enables their segregation in landfills. Thus, organic waste can be valorized through composting and vermicomposting methods, consequently extending landfill lifespans and diminishing environmental impacts [8]. Composting is defined as the exothermic aerobic biooxidation of a heterogeneous solid-state organic substrate. This process yields carbon dioxide, water, mineral substances, and organic matter stabilization [9]. Conversely, vermicomposting is an approach for treating and valorizing the organic fraction of waste, employing specific earthworm species [10]. These worms produce humus, which is decomposed organic matter and an excellent nutrient source for plant development

[11]. The research undertaken in this study aims to analyze the biodegradation and alteration of PLA/TPS plastic bags in vermicomposting and composting environments.

Experimental

Vermicomposting and composting structures

The composting and vermicomposting structures utilized were identical in design. Their dimensions measured 60 centimeters in length, 42 centimeters in width, and 78 centimeters in height. The structure has a capacity of 45 liters and comprises two digestion chambers and a leachate collection base, as shown in Fig 1. Within these containers, equal quantities of topsoil (without additives or fertilizers), fruits, vegetables, leafy greens, dried leaves, and cow manure were added. Temperature, pH, and soil moisture measurements were conducted using a measurement sensor from the Smart brand, model 4.1 Soil Survey Instrument, ISO 9001:2000.

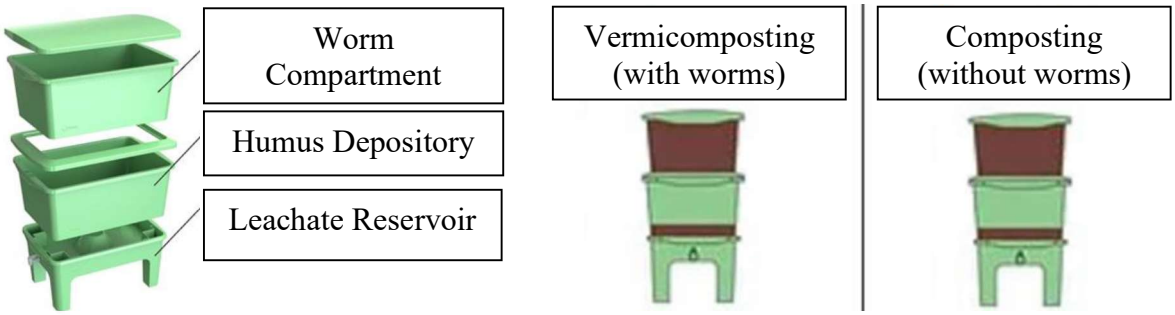

Figure 1 Structure Vermi/composting Humi. Source: https://composteirahumi.eco.br/

In the vermicomposting container, 942 adult worms of the species Eisenia fetida were added, Fig 2.

Figure 2 Earth worms Eisenia fetida.

Polymeric samples

The samples were cut into strips measuring 20 centimeters in length and 5 centimeters in width. The films are composed of PLA/TPS and were manufactured in Germany by the company Melitta Europa, certified under DIN EN 13432. The samples were collected in triplicate from both composting and vermicomposting structures at intervals of 30, 60, and 90 days.

Caracterization

The samples were analyzed using the following techniques: FTIR (Fourier Transform Infrared Spectroscopy) on a Perkin Elmer FT-IR spectrometer frontier with an attenuated total reflectance (ATR) accessory; DSC (Differential Scanning Calorimetry) on a Perkin Elmer DSC 6000 instrument; Universal Testing Machine for tensile mechanical testing, model Emic DL 20000; Optical Microscope (OM), model 400X Series Digital Microscope.

Results and Discussion

FTIR characterization was performed on the initial samples and after 30, 60, and 90 days of vermicomposting and composting. Fig 3 and Fig 4 display the FTIR spectra of the PLA/TPS samples subjected to vermicomposting and composting, respectively.

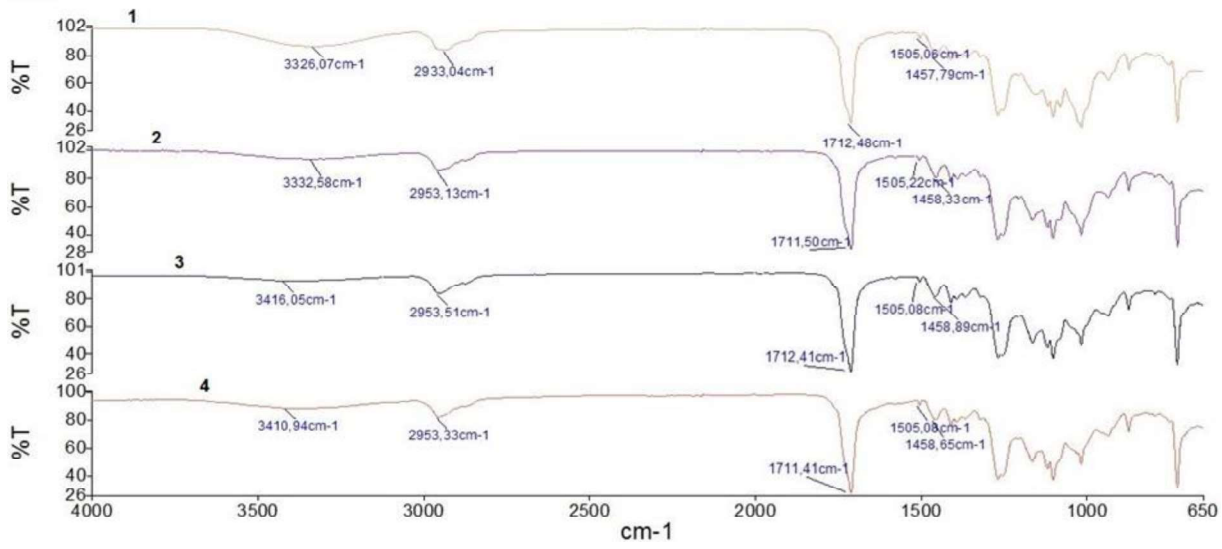

Figure 3 FTIR PLA/TPS vermicomposting (1=0, 2=30, 3=60 e 4=90 days).

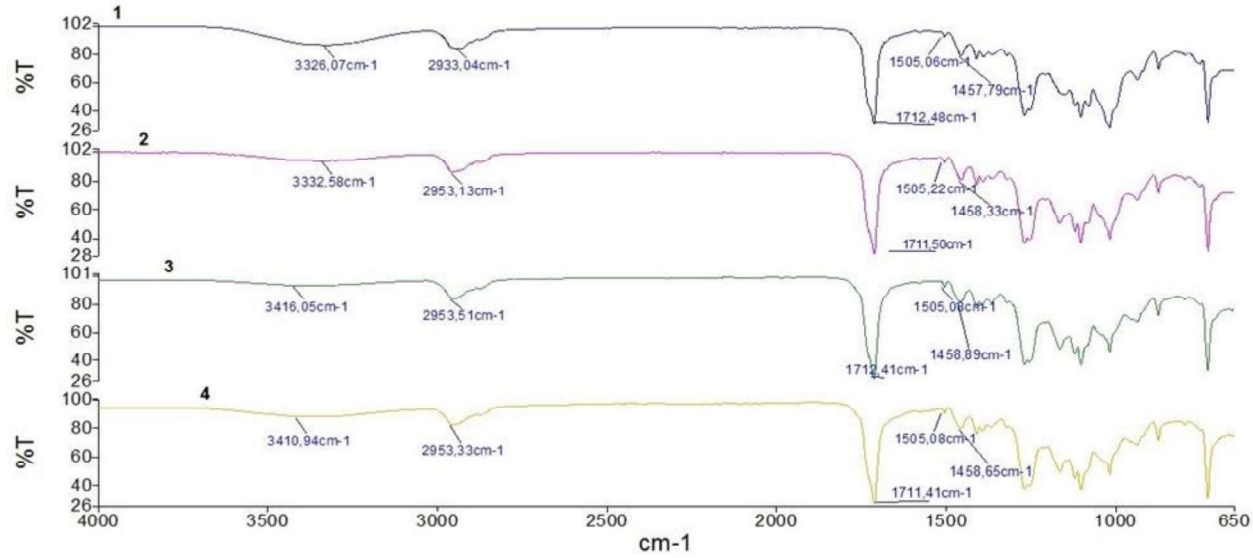

Figure 4 FTIR PLA/TPS composting (1=0, 2=30, 3=60 e 4=90 days).

Upon analyzing the spectra of PLA/TPS, changes were observed in the region of 3400 cm-1, where it can be seen that the initial sample had a more pronounced peak compared to the 30, 60, and 90-day samples. It can be concluded that degradation occurs through the disappearance of hydroxyl groups from the polymer chain, as indicated in the aforementioned region. This was observed in both the composting and vermicomposting samples. Fig 5 presents the results of the tensile tests conducted on the samples subjected to composting and vermicomposting.

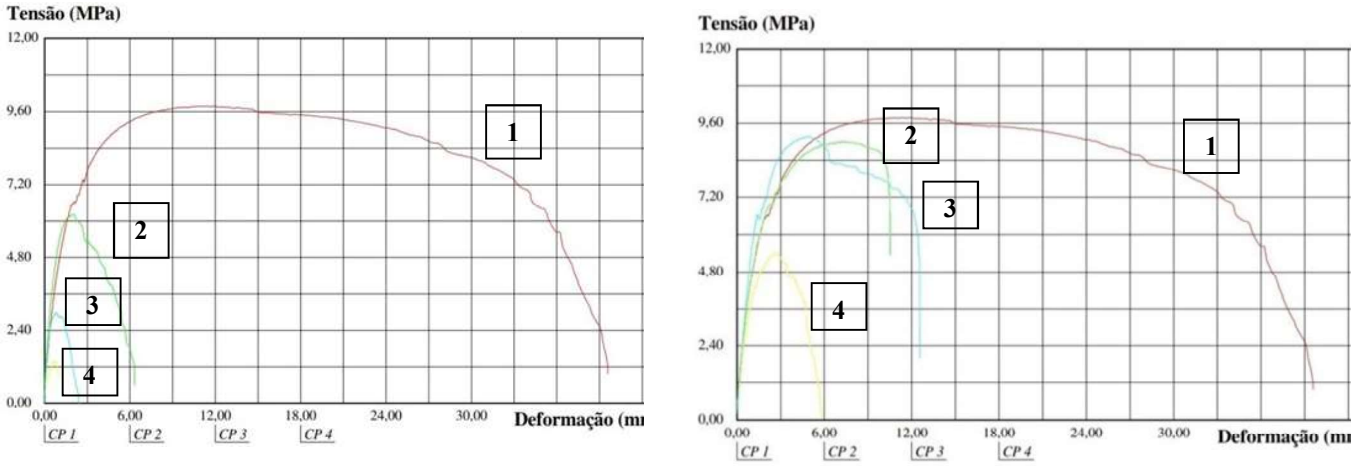

Figure 5 Tensile Testing of PLA/TPS Samples: Vermicomposting (left) and Composting (right) (1=0, 2=30, 3=60, and 4=90 days).

It can be inferred that the duration of exposure made the samples more fragile, resulting in a lower modulus of elasticity. By analyzing the graphs of the tensile tests, a loss of mechanical properties in the samples can be observed, with this effect being more pronounced in the vermicomposting samples. The PLA/TPS showed significant reductions in maximum stress (85.9%) and strain (97%) in the vermicomposting process. In composting, the PLA/TPS exhibited reductions in maximum stress (44.6%) and strain (76%). Based on these results, it can be concluded that significant changes occur in the mechanical properties of the materials after the vermicomposting process. The images obtained by the optical microscope, shown in Fig 6, clearly demonstrate the change in the material's surface over time. It is evident that there were more surface changes in the samples subjected to vermicomposting. The tear in sample d from the vermicomposting process is due to the passage of the annelid.

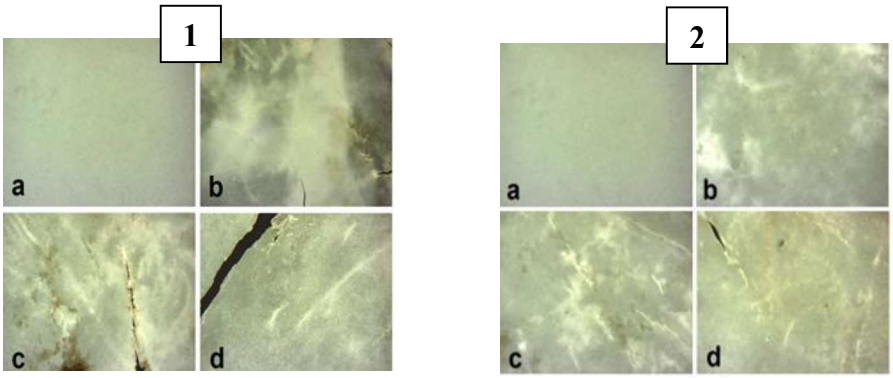

Figure 6 Optical Microscopy (OM) of PLA/TPS: Vermicomposting (1), Composting (2); after (a=0 days, b=30 days, c=60 days, d=90 days). Magnification scale 50X.

Conclusions

Based on the conducted tests, it can be stated that degradation occurred in the polymer films, with a notable emphasis on the vermicomposting process. In the case of PLA/TPS samples, after 90 days of vermicomposting, there was a decrease in maximum stress from 9.79 to 1.38 MPa and a reduction in elastic deformation from 39.5 to 1.2 mm. In composting, after 90 days, there was a decrease in maximum stress from 9.79 to 9.01 MPa and a reduction in elastic deformation from 39.5 to 9.5 mm. Through FTIR analysis, it was observed that hydroxyl groups in the polymer chain

disappeared, indicating material degradation in both vermicomposting and composting samples. However, it can be affirmed that vermicomposting demonstrated higher efficiency in terms of biodegradation.

References

1. Romão, W.; Spince, M. A. S.; Paoli M. Poli(tereftalato de etileno), PET: Uma revisão sobre os processos de síntese, mecanismos de degradação e reciclagem. Polímeros: Ciência e Tecnologia. 2009,19:121 – 132.
2. Talvitie, Julia et al. Solutions to microplastic pollution–Removal of microplastics from wastewater effluent with advanced wastewater treatment technologies. Water research, v. 123, p. 401-407, 2017.
3. Usha, Rajamanickam; Sangeetha, T.; Palaniswamy, M. Screening of polyethylene degrading microorganisms from garbage soil. Libyan Agric Res Cent J Int, v. 2, n. 4, p. 200-4, 2011.
4. Brasil. MINISTÉRIO DO MEIO AMBIENTE (MMA). Gestão de resíduos orgânicos. 2010. http://www.mma.gov.br/responsabilidadesocioambiental/producao-e-consumo-sustentavel/saco-e-um-saco/saibamais.
5. Brasil. SENADO FEDERAL (SF). Sacola plástica é uma das maiores vilãs do meio ambiente.2016. https://www12.senado.leg.br/noticias/materias/2016/04/19/sacola-plastica-e-uma-das- maiores-vilas-do-meio-ambiente.
6. CEMPRE. Compromisso Empresarial para Reciclagem. Cempre Review. 2019. https://cempre.org.br/wpcontent/uploads/2020/11/CEMPRE-Review2019.pdf.
7. Adamcová, Dana et al. SEM analysis and degradation behavior of conventional and bio-based plastics during composting. Acta Universitatis Agriculturae et Silviculturae Mendelianae Brunensis, v. 66, n. 2, p. 349-356, 2018.
8. Naddafi, K.; Zamanzadeh, M.; Azimi, A.A.; Omrani, G.A.; Mesdaghinia, A.R.; Mobedi, E., 2004. Effect of temperature, dry solids and C/N ratio on vermicomposting of wates activated sludge. *Pakistan Journal of Biological Science*, vol. 7, no. 7, pp. 1217-1220.
9. Domínguez, J., Edwards, C.A., Subler, S., 1997. A comparison of composting and vermicomposting. Biocycle 4, 57–59.
10. Chanu, Thongam & Sharma, Arun &Muralidhar, Ande& Prasad, J.K. & Patnaik, R.R.S.. Vermicompost Production Technology for Organic Aquaculture. Aquaculture Times (2017).
11. Eckhardt, D., Antoniolli, Z., Schiedeck, G., Santana, N., Redin, M., Domínguez, J., Josemar, R., Jacques, S.. (2016). Vermicompostagem como alternativa para o tratamento de resíduos nas propriedades rurais do Rio Grande do Sul. In: Manejo e conservação do solo e da água em pequenas propriedades rurais no sul do Brasil: práticas alternativas de manejo visando à conservação do solo e da água, Edition: Porto Alegre, Rio Grande do Sul, Brasil, Chapter: 6, Publisher: UFRGS – Universidade Federal do Rio Grande do Sul, Editors: Tales Tiecher, pp.87-99.

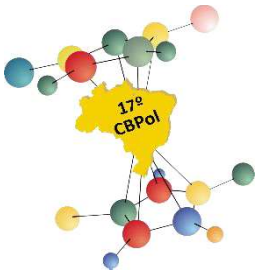

EVALUATION OF USING KRAFT LIGNIN-BASED BIOCHAR IN THE ADSORPTION OF METHYLENE BLUE DYE

Lázaro H. Pereira[1], José L. N. Gomes[1], Rayanne F. Araujo[2] and Francisco Avelino[2]

1 – Post graduation program in renewable energies (PPGER), Federa Institute of Ceará (IFCE), Maracanaú, CE, Brazil lazaro.henrique.pereira07@aluno.ifce.edu.br
2 – Department of Research, Extension and Production (DPEP), Federal Institute of Ceará (IFCE), Iguatu, CE, Brazil

Abstract – Kraft lignin is a residue from the pulp and paper industry. In addition to being a renewable resource, it has proven to be an excellent biosorbent for removing various groups of contaminants, including dyes, heavy metals, and drugs. The aim of this work was to evaluate the adsorptive performance of kraft lignin (KL) and kraft lignin biochar (KLB) for removing methylene blue (MB) from a simulated effluent. The production of KLB was carried out through thermal treatment and the adsorption tests were performed to evaluate the influence of the concentration of biosorbents, MB, pH, and ionic strength on the removal efficiency. The maximum removal efficiency obtained was 98% in the removal of MB, using 1 g L-1 of KLB in 5 mg L-1 of MB solution. Therefore, it can be concluded that the BLK produced through the thermal treatment of crude lignin has presented high efficiency in the removal of the dye, probably due to the increase in the number and size of the pores on the surface of the material.

Keywords: *Renewable resource, biosorbents, textile industry.*

Fundings: This work was funded by Fundação Cearense de Apoio ao Desenvolvimento Científico e Tecnológico (FUNCAP) under the grant number FUNCAP BP4-0172-00159.01.00/20.

Introduction

Kraft lignin (KL), a waste from the pulp and paper industry, is a biopolymer present in great abundance, in which about 50 million tons of waste containing lignin are generated annually, with high potential to be used in various applications, including the production of high-added value products [2]. The use of polymeric resins has been widely used in recent years, mainly due to their high adsorption capacity and the ease of recovery of phenolic compounds, besides low cost and easy regeneration [2]. The contamination of water resources has been much discussed due to the negative impacts on the environment, as well as the ecological disturbances to the aquatic biota and the damage to humans caused by the presence of various contaminants in the environment, such as drugs, pesticides and dyes from the industry textile [3]. Among the dyes present in the effluent of the textile industry, methylene blue (MB) is one of the most common. Its negative potential for water bodies is related to blocking the penetration of light into the aquatic body, harming living organisms, as for humans, its primary contact can cause eye burns, if ingested it produces a burning sensation and later vomiting [4]. In this context, the biochar produced from lignin is a very promising alternative, because through processes that modify the chemical structure of Kraft lignin, such as the temperature used in production and the pyrolysis time, they can favor the adsorption process of organic pollutants [5]. Thus, the objective of this work was to evaluate the adsorptive performance of KL and KL-based biochar (KLB) on the removal efficiency of methylene blue from a simulated effluent.

Experimental

Biochar production

Kraft lignin was gently donated by Suzano S/A. For the preparation of Kraft lignin biochar (KLB), a sample of 3 grams of KL was heated in a furnace at 500°C for 30 minutes at the heating rate of 5°C min^{-1} with a limited oxygen atmosphere. After cooling at room temperature, the material was macerated and stored in a suitable container for carrying out the next experiments.

pH at Point of Zero Charge (pH_{pzc})

The pH_{pcz} determination was carried out using 0.75 mg of each material in 125 ml erlenmeyer flasks, varying the pH from 2 to 10 in a solution of 25 ml of 0.1 mol L^{-1} NaCl. The pH of each point was adjusted with 0.01 mol L^{-1} NaOH and 0.01 mol L^{-1} HCl. After this process, the samples were placed under constant agitation at 100 rpm for 48 hours at 23 ± 2 °C. Then, the pH was measured in a pH-meter and the graphs were produced containing the relationship between the initial pH and the final pH of the adsorbents.

Adsorption experiments

The adsorption tests were carried out in 250 mL erlenmeyer flasks, varying the concentration of the two adsorbents, KL and KLB from 0.25 to 3 g L^{-1}. 25 ml of 5 mg L^{-1} MB solution was added to each flask. After this process, the erlenmeyer flasks were placed on a shaker at 120 rpm for 1 hour at 25°C . Then, the samples were centrifuged at 2,000 rpm for 10 minutes and the absorbance was measured in a UV-VIS spectrophotometer at 664 nm. For the adsorbate variation experiment, the MB variation from 2.5 to 10 mg L^{-1} was performed, in which case a fixed concentration of KL and KLB was selected. The tests were performed in triplicate and the contaminant removal efficiency was calculated using Eq. 1.

$$Removal\ efficiency\ (RE, \%) = \frac{C_0 - C_f}{C_0} x\ 100 \quad (1)$$

Where: C_0 is the initial concentration of MB before the adsorption tests and C_f is the final concentration of MB after the adsorption tests both in mg L^{-1}.

Ionic Strength (NaCl)

The ionic strength tests were performed varying the NaCl concentration from 0.001, 0.01 and 0.1 mol.L^{-1}. In this experiment, the optimized concentration of each adsorbent was used to determine the removal efficiency of MB from the effluents when NaCl was present.

Results and Discussion

pH at Point of Zero Charge (pH_{pzc})

The results referring to the pHpzc assay are shown in Fig 1 KL's pHpzc is 6.4, while KLB's is 9.4. This characterization reflects on the adsorption potential of the adsorbent at different pHs, because when changing the pH conditions of the solution, a negative or positive interference in the adsorption process may occur. At these pH_{PZC} values, the biosorbents will present a balance between the positive and negative charges on their surfaces, which will certainly affect their interaction with the contaminant depending on its polarity and surface charge as well.

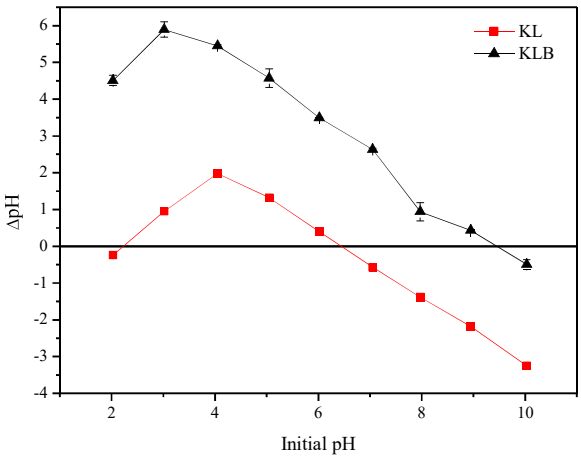

Figure 1 – Variation of ΔpH vs initial pH for KL and KLB.

Variation of adsorbents concentration

After the biochar production process, it was observed 50% weight loss in KL. The results referring to the removal efficiency of 5.0 mg L^{-1} MB varying the concentration of the adsorbents are shown in Fig 2 it can be observed that there was an increase in the removal efficiency of MB for KLB, since increasing the concentration of this adsorbent there was an increase in the removal efficiency as well. On the other hand, for KL, when its concentrations were increased, an inverse relationship occured, reducing the removal efficiency of MB. The optimized concentration chosen for KLB was 1 g L^{-1}, since at this concentration the average removal efficiency was 95%, whereas in relation to KL the optimized concentration was 0.25 g L^{-1}, since the lowest adsorbent concentration value showed the highest removal efficiency of MB with an average of 78%. In the study carried out with the biochar produced from bamboo, an efficiency of 98% was obtained in the removal of 50 mg L^{-1} of MB when using 16 g L^{-1} of the adsorbent. If compared with the biochar from kraft lignin, the removal efficiency of 98% was achieved when using 1 g L^{-1} of KLB to remove 5 mg L^{-1} of MB. In terms of proportion, to remove 50 mg L^{-1}, 10 g L^{-1} of the KLB biosorbent would be required, revealing that both adsorbents have similar efficiencies, however, KLB has a greater adsorption capacity [5].

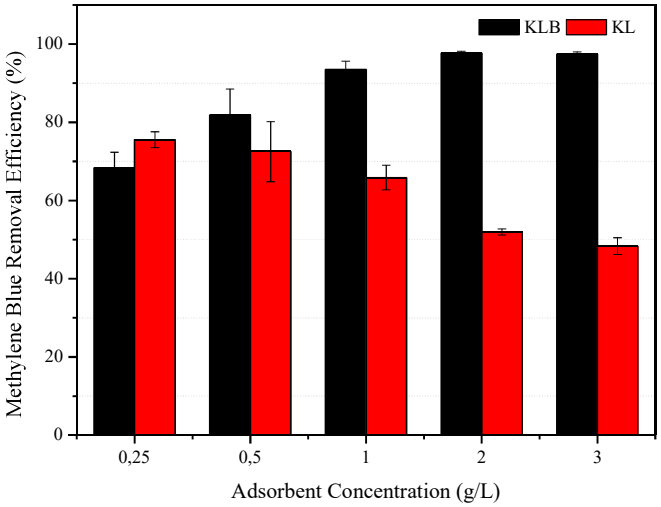

Figure 2 – Removal efficiencies of MB varying adsorbents concentration.

Variation of Methylene Blue concentration

In Fig 3, it is possible to observe that the removal efficiency of MB using the KLB decreased by increasing the concentration of the contaminant. On the other hand, in relation to the KL adsorbent it was observed that the increase in the concentration of the contaminant did not cause a significant reduction in the removal efficiency of MB. The reduction in MB removal efficiency probably occurred due to the saturation of the active sites present in the biosorbent, as well as the competition of MB molecules for these sites.

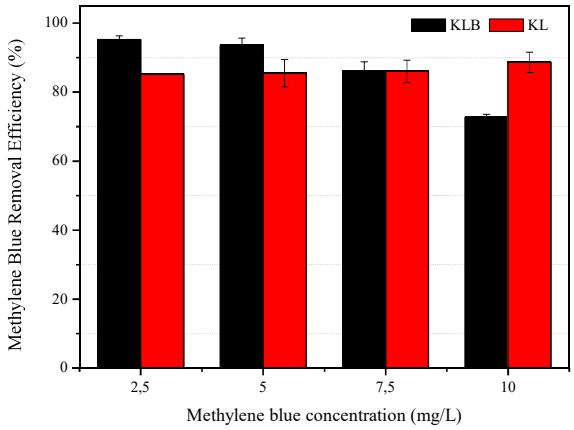

Figure 3 – Removal efficiencies of MB varying the contaminant concentration.

From the data obtained, it was possible to carry out the analysis of the pH variation of the methylene blue solution at 5 mg L^{-1}, in order to verify the variation in the removal efficiency of the contaminant in different pH ranges. The results obtained are shown in Fig 4 and Fig 5 and it can be seen from the analysis of the graphs that there was no significant change in the efficiency of removing the contaminant with the pH variation, suggesting that any effluents with pH in the analyzed range can be treated without any pH adjustments, which represents a desirable feature from the technological point of view.

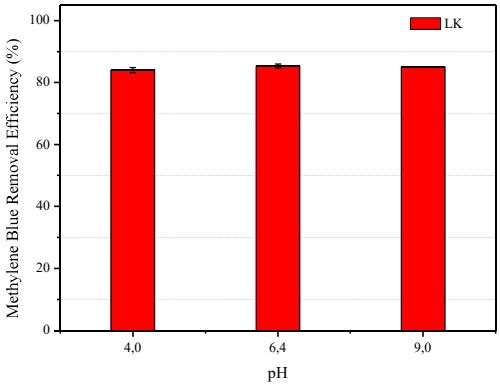

Figure 4 – Removal efficiencies of MB varying pH for KL

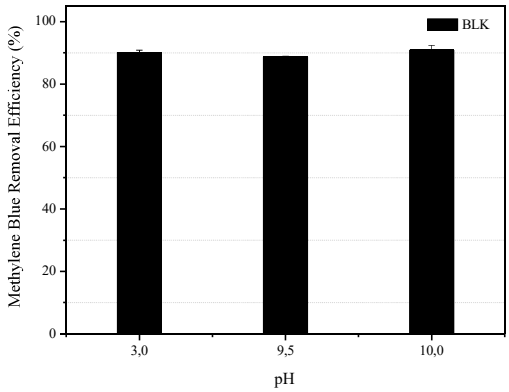

Figure 5 – Removal efficiencies of MB varying pH for KLB

Regarding the efficiency of MB removal in different salt concentrations, it is possible to observe in Fig 6 that when increasing the salt concentration, there was a decrease in the removal efficiency of MB ionic or both LKB and LK. This fact occurred more significantly for KLB, because the removal efficiency decreased from 90 % to 70 %, revealing that there is a relationship between the concentration of salts in the medium and the efficiency of removing the contaminant. This fact may initially occur due to the competition between MB and NaCl for active sites present in the adsorbent.

In addition, the presence of salt in the effluent from the textile industry directly influences the MB removal efficiency, as studies carried out have shown that solutions without the presence of salt obtained better dye removal efficiency [7].

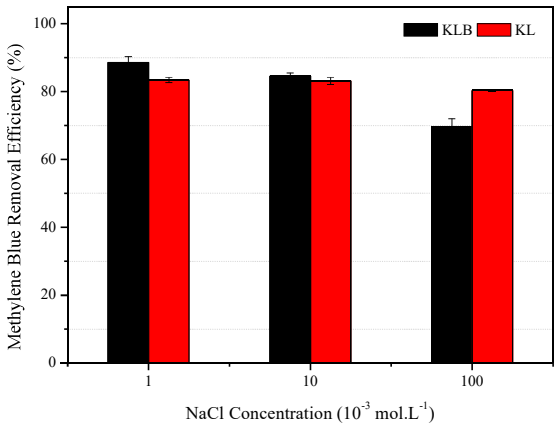

Figure 6 – Removal efficiencies of MB varying the ionic strength for KL and KLB.

Conclusions

In this work, a study was carried out about the effects of several parameters on the removal efficiency of MB, a substance present in the effluent of the textile industry, a sector of great development in the Brazilian industry. Excellent dye removal values with a concentration of 5 mg L^{-1} were achieved using 1 g/L of KLB, showing an efficiency of approximately 98 %. However, lower concentrations, such as 1 g L^{-1}, reached an efficiency of 94 %, resulting in almost the same removal efficiency using lower biosorbent concentration. Therefore, the use of a biosorbent produced from Kraft lignin to remove the methylene blue proved to be a sustainable alternative with great benefits, due to the high availability of this residue produced by the Kraft industry and its physical and chemical properties that favor the process of adsorption of contaminants.

References

1. S. Junior; A. Menezes; C. Ataíde **Journal of Analytical and Applied Pyrolysis** 2019, 144, 104720. https://doi.org/10.1016/j.seppur.2019.116083.

2. I. Mota; P. Pinto; Loureiro, J. Loureiro; A. Rodrigues **Separation and Purification Technology** 2020, 234, 116083, 2020. https://doi.org/10.1016/j.seppur.2019.116083

3. L. Araujo; S. Mazzetto; D. Lomanaco; F. Avelino **Journal of Biological Macromolecules** 2022, 220, 1267-1276. https://doi.org/10.1016/j.ijbiomac.2022.08.195.

4. T. Kurniawan; Z. Mengting; D. Fu; S. Yeap; H. Othman; R. Avtar; T. Ouyang **Journal of Environmental Management** 2020, 270, 110871. https://doi.org/10.1016/j.jenvman.2020.110871.

5. L. Constantin in Proceedings of 10th Uergs Integrated Teaching, Research and Extension Hall, Rio Grande do Sul, 2021, Vol. 1, 10.

6. N. Goetz; S. Kunst; F. Morisso; C. Oliveira; T. Machado **Materia** 2022, 27. https://doi.org/10.1590/1517-7076-RMAT-2022-0065.

7. A. Sousa in Proceedings of 30th Brazilian Congress of Environmental and Sanitary Engineering, Natal, 2019.

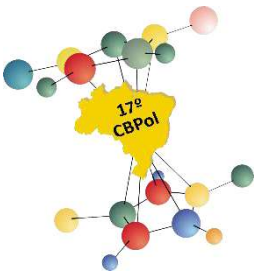

EXTRACTION, PURIFICATION AND APPLICATION OF BREWER'S SPENT GRAIN IN STARCH-BASED COMPOSITES

Georgia W. Ramos[1], Ana B. Klosowski[1], Aline C. Lopes[1]; Giovani A. Carvalho[2]; Juliana B. Olivato[1,2,3*]

1 – Post-graduation Program of Pharmaceutical Sciences, State University of Ponta Grossa (UEPG), Ponta Grossa, PR, Brazil
2 – Post-graduation Program of Food Science and Technology, State University of Ponta Grossa (UEPG), Ponta Grossa, PR, Brazil
3 – Department of Pharmaceutical Sciences, State University of Ponta Grossa (UEPG), Ponta Grossa, PR, Brazil.
**jbolivato@uepg.br*

Abstract - Lignocellulosic fibers from brewer's spent grain (BSG) can act as reinforcing agents, improving the resistance and rigidity of the starch-based polymer composites. Biodegradable composite materials were produced with cassava starch and BSG of the Pilsen and Weiss types, which have been subjected to alkaline and peroxide treatments. The inclusion of treated BSGs resulted in homogeneous matrices with the starch, without the presence of pores and/or cracks, as evidenced by the scanning electron microscopy images. The tensile strength of the composites was improved with the inclusion of BSB(P) and BSB(W), indicating the action of the materials as reinforcing agents. The BSG of the brewing industry incorporated into biodegradable films has provided promising properties to be a viable alternative to non-biodegradable polymeric packaging.

Keywords: *Byproducts; biodegradable materials; fibers; packaging*.

Introduction

The reuse of industrial process by-products in the production of biodegradable films has attracted increasing interest. In addition to adding value to these wastes, various functional compounds which may be present in by-products may be of interest to enhance the functional properties of polymeric materials. Biodegradable polymeric materials are a possibility to overcome the ecological issues associate with the residue accumulation in the environment because of the non-degradable plastics. Starch is a biopolymer with interesting properties: non-toxic, renewable, biodegradable, abundant and inexpensive. To improve the mechanical performance of starch-based materials, the addition of reinforcement materials is frequently used. In this way, lignocellulosic fibers act as reinforcing agents, improving the resistance and rigidity of the polymer composites [1,2].

Microbreweries in Campos Gerais - PR produce a significant number of by-products which are mainly intended for animal feed. Brewers' Spent Grains (BSG) represent 85% of the by-products of the brewery and consists of pulp and residues of barley husks, in addition to grains such as rice, corn and wheat, according to the composition of the beer. BSG composition contains fibers and proteins, generated in large quantities daily and at low cost, which makes reusing this material relevant [3,4]. Because of the large amount of material, it is necessary to find other ways to reuse

these wastes, in search of an economically viable alternative that is not harmful to the environment [5,6].

On this basis, the purpose of this work was to produce biodegradable films based on starch and BSG. BSG was used as a filler and tested in different proportions, using the BSG from Pilsen and Weiss beer production. The mechanical, structural and barrier properties of the films were evaluated, considering an alternative to the short life cycle packaging.

Experimental

Obtention and processing of BSG

BSG was supplied by Koch Bier (Ponta Grossa – PR), from two production processes: Pilsen beer and Weiss beer, which were collected immediately after the wort filtration. The BSG was subsequently dried in an oven (60°C – 24 hours) and then ground in a grinder. The particles were standardized in a sieved (46 mesh). Following that process, BSG went through a different process, as shown in Table 1.

Table 1 – BSG treatments

Samples	Treatment
BSI	BSG without treatment
BSM	20 g BSG in 300 mL of NaOH 10% (w/v), stirring at 60°C for 60 min, filtered
BSP	20 g BSG in 150 mL of NaOH 10% (w/v) and 150 mL of H_2O_2 12% (w/v), stirring at 60°C for 60 min, filtered and washed with distilled water
BSB	Treatment BSM + Treatment BSB

Production of the biodegradable materials

Biodegradable materials were produced with cassava starch (3%, w/w) by casting technique. The filmogenic solution was heated to 95°C, then poured into acrylic plates and dried in an oven for 8 h at 50°C. The BSG was added to the films at 3% (w/w) relative to starch, and glycerol was used as a plasticizer (20% w/w, relative to starch). The samples were coded as BSM, BSP and BSB, according to the treatment of the by-product, followed by P or W, which refers to BSG of Pilsen and Weiss beers, respectively. A Control formulation was produced without BSG. The biodegradable films were conditioned in B.O.D (25°C) and characterized for mechanical, structural and barrier properties according to ASTM (2010) [7,8] methods.

Results and Discussion

The results of thickness, density, and mechanical properties of starch-based materials with BSG are shown in Table 2. No significant difference was observed in the thickness and density of the films with the inclusion of BSG, independent of treatment. This indicates that the treatment applied to the BSG fibers has not affected the compaction of the chains and, therefore, the total solids per film area, which results in maintains the density and thickness of the materials.

BSP formulations, processed with hydrogen peroxide, have led to a reduction in film solubility. This was achieved by reducing the water-soluble content of BSG treated with H_2O_2, which

reduced the water solubility of the materials. This effect was observed mainly in the BSG from Weiss beer production (BSP (W)), resulting in 19,04% of water solubility (Table 2).

Scanning electron microscopy images showed good interfacial adhesion of BSG lignocellulosic fibers and starch-based polymeric matrix, without disruptions, cracks or pores on the film surface. Considering the BSG treatments, the samples without treatment (BSI) (P) showed a rough surface and the BSB (P) samples were smoother. This indicates that the treatments contribute to improve the affinity of the BSG lignocellulosic fibers with the matrix, making the material more homogeneous.

Table 2 – Thickness, density and mechanical properties of starch-based materials with BSG.

Formulations	Thickness (mm)	Density (g/cm³)	Tensile Strenght (MPa)	Elongation at break (%)	Young's Modulus (MPa)
Control	0.060±0.017^{a}	0,155±0.019 a	10.23±1.73^{b}	13.71±1,78^{a,b,c}	175.01±20.45^{a}
BSI(P)	0.080±0.030 ^{a}	0,070±0,038 a	3,98±0,30^{a,b}	12,34±1,73^{a,b,c}	167.12±33.98^{a}
BSM(P)	0.085±0.020 ^{a}	0.113±0.002 ^{a}	3.53^{a,b}	57.23^{d,e}	124.89^{a}
BSP(P)	0.060±0.015 ^{a}	0.127±0.021 ^{a}	5.23±0.63^{a,b}	10.88±4.28^{a,b,c}	178.37±35.06^{a}
BSB(P)	0.085±0.027 ^{a}	0.135±0.042 ^{a}	17.78±2.18^{c}	4.38±0.62^{a}	262.37±89.61^{a}
BSI(W)	0.075±0.020 ^{a}	0.149±0.010 ^{a}	1.98±0.22^{a}	83.84±10.96^{e}	185.03±23.75^{a}
BSM(W)	0.070±0.014 ^{a}	0.133±0.023 ^{a}	5.60±0.62^{a,b}	34.92±5.01^{c,d}	225.97±29.44^{a}
BSP(W)	0.070±0.021 ^{a}	0.159±0.009 ^{a}	5.57±1.13^{a,b}	33.08±3.45^{b,c,d}	146,49±18.43^{a}
BSB(W)	0.070±0.028 ^{a}	0.110±0.019 ^{a}	18.35±0.87^{c}	4.94±0.65^{a}	292.08±71.73^{a}

Different letters in the same column indicate statistical difference (Tukey's test, $p<0,05$).
The samples were coded as BSM, BSP and BSB, according to the treatment of the by-product, followed by P or W, which refers to BSG of Pilsen and Weiss beers, respectively. A Control formulation was produced without BSG.

BSB(P) and BSB(W) films resulted in increased tensile strength, highlighting the role of lignocellulosic fibers as reinforcement agents, making the films more resistant and indicates a promising commercial application of BSG subjected to alkaline and bleaching treatment. Other authors report that the inclusion of lignocellulosic fibers increases the tensile strength of the material, and reduces the flexibility of the polymeric chains, decreasing the deformation, which can be associated with an increase in the material's rigidity [9].

Water vapor permeability of the films is shown in Fig 1. The inclusion of BSM and BSP, for both Pilsen and Weiss, resulted in a higher WVP of the films, probably due to the hydrophilic nature of the lignocellulosic fibers in these treatments. The WVP for BSB of the type Pilsen (BSB(P) = 1.20 x 10^{-11} g/m.s.Pa) and Weiss (BSB(W) = 1.75 x 10^{-11} g/ m.s.Pa) recorded values similar to those observed in the Control sample (2.45 x 10^{-11} g/m.s.Pa). The combination of alkali treatment with immersion in hydrogen peroxide probably contributed to the removal of lignin and hemicellulose from the BSG, obtaining a purer material with better compatibility with the starch matrix. This result is consistent to that observed in the mechanical properties and microstructure of the films.

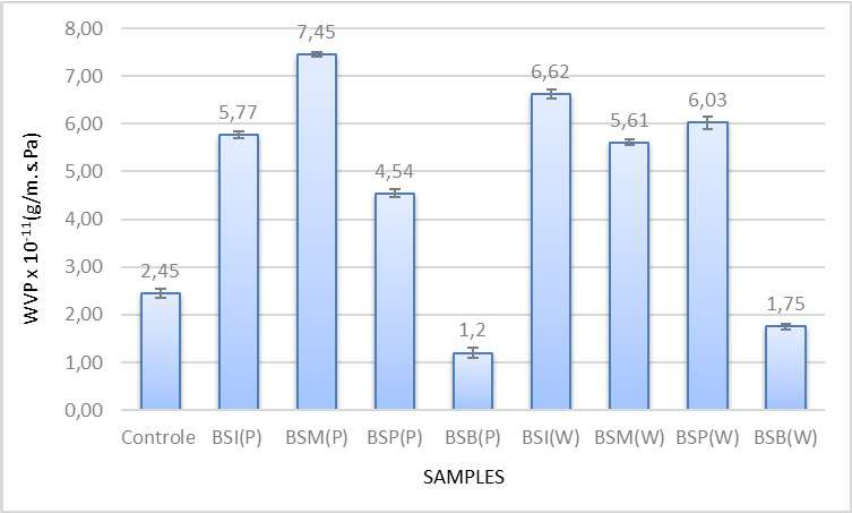

Figure 1 – Water vapor permeability (WVP) of the starch-based materials with BSG. The samples were coded as BSM, BSP and BSB, according to the treatment of the by-product, followed by P or W, which refers to BSG of Pilsen and Weiss beers, respectively. A Control formulation was produced without BSG.

Conclusions

BSGs of the Pilsen and Weiss types have been successfully subjected to alkaline and peroxide treatments. The inclusion of treated BSGs resulted in homogeneous matrices with the starch, without the presence of pores and/or cracks, as evidenced by the scanning electron microscopy images.

The tensile strength of the composites was improved with the inclusion of BSB(P) and BSB(W), indicating the action of the materials as reinforcing agents. The BSB(P) and BSB(W) films obtained the best characterization results for the films. So, the BSG treatment with alkaline solutions and hydrogen peroxide is therefore necessary and relevant in the improvement of the physicochemical characteristics of starch films containing lignocellulosic fibers of BSG. The BSG of the brewing industry incorporated into biodegradable films has provided promising properties to be a viable alternative to non-biodegradable polymeric packaging.

Acknowledgements

The authors would express their gratitude to Koch Ltda for BSG donation, the multiuser laboratories at State University of Ponta Grossa for their technical support, and Coordenação de Aperfeiçoamento Pessoal de Nível Superior and Fundação Araucária for their financial support.

References

1. L.C.M. Almeida; F.K. Carvalho; J.B. Macromolecular Symposium 2022, 406(1). doi:10.1002/masy.202200013
2. M.O. Reis; J. Zanela; J.B. Olivato; P.S Garcia; F. Yamashita; M.V.E. Grossmann. Journal of Polymers and the Environment 2014, 22(4). doi:10.1007/s10924-014-0674-7
3. E. Bravi; G. Francesco; V. Sileoni; G. Perretti; F. Galgano; O. Marconi. Antioxidants 2021, 10(2), 1. doi:10.3390/antiox10020165
4. P. Puligundla; C. Mok. Food Science and Biotechnology 2021, 30(3), 341. doi:10.1007/s10068-021-00900-4
5. A. A. Olajire. Journal of Cleaning Production 2020, 256. doi:10.1016/j.jclepro.2012.03.003

6. A. C. Fărcaş; S.A. Socaci; E. Mudura et al. Exploitation of Brewing Industry Wastes to Produce Functional Ingredients. In: *Brewing Technology*. InTech; 2017. doi:10.5772/intechopen.69231
7. American Society for Testing and Materials (ASTM) D 882-01: Standard Test Method for Tensile Properties of Thin Plastic Sheeting, 2002.
8. American Society for Testing and Materials (ASTM) E 96: Standard Test Methods for Water Vapor Transmission of Materials, 1995.
9. M. N. Castanho; K.S. Prado; J.M.F. Paiva. Polymer Composites 2022, 43(2), 811. doi:10.1002/pc.26412

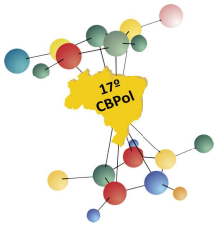

GREEN SYNTHESIS OF TITANIUM DIOXIDE NANOPARTICLES FOR APPLICATION IN PHOTOVOLTAIC DEVICES

Felipe S. C. Portes[1], Adhimar F. Oliveira[1] and Maria E. L. González[1]*

1 – Universidade Federal de Itajubá, Av BPS, 1303, Pinheirinho, Itajubá, MG 37500-903, Brazil
d2022004298@unifei.edu.br

Abstract - Energy demand is growing worldwide due to rapid population growth and technological advancements. An alternative is the conversion of solar radiation into electrical energy through photovoltaic devices. Considering such demand, this work presents the results of the synthesis and characterization of titanium dioxide nanoparticles ($NPsTiO_2$) produced by green synthesis, aiming at their application in thin film solar cells . Green synthesis is an emerging and prosperous process that does not generate environmental contamination and is cost-effective. The green synthesis of TiO_2 nanoparticles from plant extracts generates a reliable material for various applications, especially for optoelectronic devices. The synthesis was carried out using the extract of *Joannesia Princeps* fruit. The obtained $NPsTiO_2$ were characterized through ultraviolet-visible spectroscopy (UV-vis), thermogravimetric analysis (TGA), and X-ray diffraction (XRD). XRD pattern shows that the TiO_2 prepared by green synthesis was obtained in the anatase crystalline phase. The UV-vis spectrum of TiO_2 exhibited a semiconductor band of TiO_2 at 280 nm.. These results indicate that the obtained nanoparticles are a promising green alternative for low-cost photovoltaic device construction.

Keywords: *Titanium dioxide; Green synthesis; Photovoltaic devices.*

Introduction - Currently, photovoltaic technology involving wafer-based cells (traditional crystalline silicon or gallium arsenide), commercial thin-film cells (cadmium telluride, amorphous silicon, copper indium gallium selenide), and new thin-film technologies (perovskites, organic materials, quantum dots) are advancing with the advent of intense efforts [1]. Focusing on new thin-film technologies, titanium dioxide (TiO_2) is a material with excellent physicochemical properties that have shown increasing demand for the development of devices with potential technological [2] and environmental [3, 4] applications. This has been stimulated by its unique chemistry, such as the possibility of developing dye-sensitized solar cells [5], photocatalysts for water and air pollutant degradation [6], gas sensors, and photoluminescent materials [7]. TiO_2 has also shown great promise in transparent conductive oxide technology [8]. Rutile is a stable phase at high temperatures, while anatase and brookite are commonly found in natural and synthetic samples at the nanoscale. Heating and thickening processes lead to various transformations, such as anatase transforming into brookite and then into rutile, or brookite transforming into anatase and then into rutile. These transformation sequences indicate a close energy balance influenced by particle size. The surface enthalpies of the three polymorphs differ enough to allow for a crossover in thermodynamic stability, even under conditions that prevent thickening [9]. A third phase of TiO_2 is brookite, considered unstable [10]. The anatase phase of TiO_2 is well known for its chemical applications in the field of photochemistry in solar cells [11], photovoltaic cells, and photocatalytic processes that utilize semiconductor materials for the decomposition of organic materials in water or air [5]. Features such as the bandgap (3.0 eV for rutile and 3.2 eV for anatase), high refractive index, and high dielectric constant make TiO_2, preferably in its anatase polymorphic phase, an

attractive material for the construction of photoelectrodes for dye-sensitized solar cells (DSSCs). The high refractive index enhances UV radiation absorption due to efficient light scattering, while the high dielectric constant minimizes the recombination of photoexcited electrons through the electrostatic protection it provides. Regan and Gratzel (1991) produced mesoporous TiO_2 semiconductor films, predominantly in the anatase phase, with crystallite sizes of around 20 nm, a large surface area, and built a stable solar cell with an efficiency of approximately 11%, known as the Gratzel Cell [5]. The harnessing of free and abundant solar energy drives the research of new materials for optoelectronic devices. In this context, dye-sensitized solar cells are intensively investigated due to their high potential for electricity generation, combining cutting-edge technology with low-cost materials. However, the efficiency values are low, around 10% [12, 13]. The use of new materials is a crucial aspect in the study of DSSCs, where semiconductors like TiO_2 are frequently employed, and the differences in photovoltaic parameters are associated with two main factors: the energy gap, which varies for each oxide, and the particle size [14,15]. Another important factor related to the use of TiO_2 in DSSCs is the control of particle size. Different synthesis routes are described in the literature, such as co-precipitation, sol-gel, polymer precursor method, and hydrothermal method [9]. Among these methods, it is worth mentioning that the green synthesis method allows the production of TiO2 without using environmentally harmful reagents. Considering this concern, this work presents the results of the preparation and characterization of TiO_2 produced via green synthesis, based on the aqueous extraction of *Joannesia Princeps*'s fruit.

Experimental - To prepare the aqueous extract, 63.658g of Joannesia princeps fruit were previously hand-cut and dried at 70°C for 24 hours. The obtained extract was added to a beaker containing 20 mL of distilled water and subjected to an ultrasonic bath for 30 minutes at 50°C. Filtration was performed using a paper filter to separate the extract from the solid residue. This extract was characterized using Fourier-transform infrared spectroscopy (FTIR) in the range of 600-4000 cm^{-1} with a resolution of 4 cm^{-1}, utilizing an attenuated total reflectance (ATR) accessory on an IRTracer-100 instrument, and thermogravimetric analysis (TGA) on a TGA-50 instrument, both from SHIMADZU trademark. In addition, UV-vis analysis was carried out by a Cary 50 Bio instrument, from the Varian brand, for characterization and comparison with the titanium dioxide nanoparticles ($NPsTiO_2$) obtained through green synthesis.

The green synthesis of $NPsTiO_2$ was executed by using 70 mL of the previously obtained extract at a concentration of 50 g/L, and 6 mL of $TiCl_3$ (15%, Riedel-de-Haën) was added dropwise while the solution was heated to 50°C and stirred for 2 hours. After this period, the solution was stored in the refrigerator for 24 hours for sedimentation. In the subsequent process, the precipitate was washed with distilled water and centrifuged to remove impurities from the synthesis.

The $NPsTiO_2$ were characterized through TGA measurement. Subsequently, the $NPsTiO_2$ were calcined at a temperature of 500°C for a period of 4 hours in an oven. The calcined $NPsTiO_2$ UV-vis, and X-ray diffraction (XRD) using the X'Expert PRO equipment from Pan Analytical, in the 2θ range of 5° to 90°.

Results and Discussion

The FTIR spectrum of *Joannesia Princeps*'s fruit extract (Fig. 1a) displays OH bands (3221) cm^{-1}, C-O(H) at 1037 cm^{-1}, and functional groups capable of forming complexes with Ti3+ ions, the precursor of TiO2. The FTIR spectrum also reveals the presence of C=C double bonds in the extract. The residue obtained after thermogravimetric analysis indicates that the stable residue at 1000°C contains C=C and C≡C groups, suggesting the formation of stable cyclic species such as

benzene rings, as indicated by the presence of the phenyl pattern (1558, 1568, 1438) cm^{-1}. In Fig.

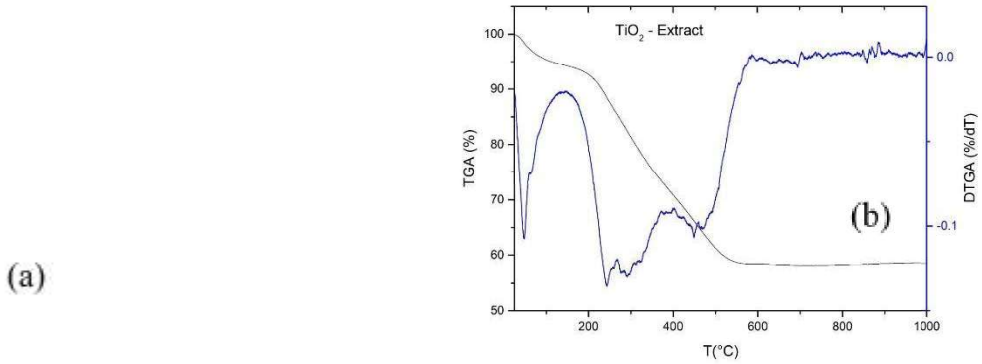

1b, the TGA of the extract together with TiO2 is presented. It is possible to observe a mass loss below 100ºC relative to humidity. Between 140 and 350ºC, the loss of volatile compounds takes place, and from 300 to 600ºC, the break of the main chain occurs. The two stages between 300 and 600 °C can be attributed to a different secondary metabolic present in the vegetal extract. After the TGA, it was found that approximately 58% of the material remained.

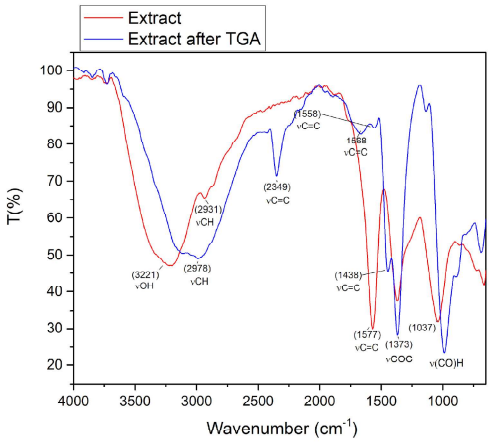

Figure 1 a) Ftir of extract and b) TGA of TiO2 with the extract.

Fig. 2a presents the results of the UV-Vis measurements of the extract and the extract together with TiO_2. At 280 nm, absorption can be attributed to the high-energy electronic transition (n-sigma* antibonding). In the XRD analysis of the TiO_2 NPs (Fig. 2b), which resulted from a calcination process conducted on the extract together with TiO_2, peaks corresponding to anatase TiO_2 can be observed, along with some contamination related to a residue from the extract.

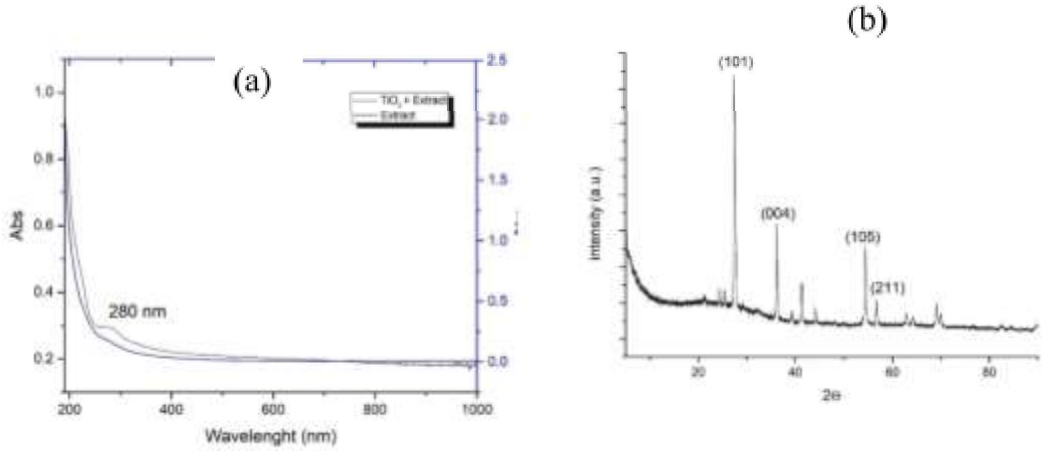

Figure 2: a) UV-Vis of the pure extract and the extract with TiO2 and b) XRD of the TiO2 nanoparticles

.

Conclusions

Titanium dioxide nanoparticles were synthesized through green synthesis using Joannesia Princeps fruit extract. The synthesis proved to be effective, producing titanium dioxide nanoparticles in the anatase phase. This methodology for preparing TiO_2 nanoparticles is important to avoid the use of expensive chemical reagents that can generate contamination when discarded. In future studies, it will be interesting to carry out calcination at higher temperatures, or to improve the washing process to reduce the contamination of nanoparticles by the extract, maintaining the anatase phase.

Acknowledgements - The authors would like to thank the Brazilian agencies CAPES, CNPq, and Fapemig (Finance Code APQ-02676-16 and APQ-00010-18) for financial support.

References

1. F. H. Alharbi and S. Kais; Renewable and Sustainable Energy Reviews, 2015, 43, 1073–1089. https://doi.org/10.1016/j.rser.2014.11.101
2. R. Parra, M. S. Góes, M. S. Castro, E. Longo, P. R. Bueno, and J. A. Varela; Chemistry of Materials, 2007, 20, 143–150. https://doi.org/10.1021/cm702286e
3. Z. Zafar, R. Fatima, and J.-O. Kim; Environmental Research 2021, 197, 111120. https://doi.org/10.1016/j.envres.2021.111120
4. M. Sedghi, R. Rahimi, and M. Rabbani; Inorganic Chemistry Communications, 2021, 126, 108486. https://doi.org/10.1016/j.inoche.2021.108486
5. Brian O'Regan and Michael Grätzel; Nature,1991, 353, 737-740. https://doi.org/10.1038/353737a0
6. Dorian A. H. Hanaor and Charles C. Sorrell; Journal of Materials Science, 2010, 46, 855-874. https://doi.org/10.1007/s10853-010-5113-0
7. M. Alfè, V. Gargiulo, M. Amati, V.-A. Maraloiu, P. Maddalena and S. Lettieri; Catalysts, 2021, 11, 795. https://doi.org/10.3390/catal11070795
8. N. Laidani, G. Gottardi, R. Bartali, V. Micheli, R. Brusa, S. Mariazzi; Handbook of Modern Coating Technologies, 2021, 15, 509-554. https://doi.org/10.1016/b978-0-444-63237-1.00015-2
9. X. Chen and S. S. Mao; Chemical Reviews, 2007, 107, 2891-2959. https://doi.org/10.1021/cr0500535
10. U. Diebold; Surface Science Reports, 2003, 48, 53-229 https://doi.org/10.1016/s0167-5729(02)00100-0
11. J. S. Lissau; Emerging Strategies to Reduce Transmission and Thermalization Losses in Solar Cells , M. Madsen, 2022
12. E. F. A. Carvalho and M. J. F. Calvete; Revista Virtual de Química, 2010, 2, 192-203. https://doi.org/10.5935/1984-6835.20100018
13. G. G. Sonai, M. A. M. Jr., J. H. B. Nunes, J. D. M. Jr., and A. F. Nogueira; Química Nova, 2015, 38, 1357-1365. https://doi.org/10.5935/0100-4042.20150148
14. D. Cahen, G. Hodes, M. Grätzel, J. F. Guillemoles, and I. Riess; The Journal of Physical Chemistry B, 2000, 104, 2053-2059. https://doi.org/10.1021/jp993187t
15. A.F. Oliveira, S.A.M. Silva, C.P. Rubinger, J. Ider, R.M. Rubinger, E.T.M. Oliveira, A.C. Doriguetto, H.B. de Carvalho, Materials Science and Engineering: B, 280, 2022, 115702. https://doi.org/10.1016/j.mseb.2022.115702

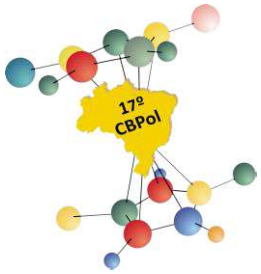

INFLUENCE OF DRYING CONDITIONS ON THE MELT FLOW INDEX OF POLYBUTYLENE SUCCINATE (PBS) AFTER LONG TIME STORAGE

Ilana A. Oliveira[1], Lucas N Horiuchi[2], Rosana L. L. Fialho [2], Joyce B Azevedo [1]

1- Institute of Science, Technology and Innovation, Federal University of Bahia (UFBA), Camaçari, BA, Brazil
ilanaoliveiraalmeida@gmail.com
2 – Graduate Program in Industrial Engineering, Federal University of Bahia (UFBA), Salvador, BA, Brazil

Abstract - Polybutylene succinate (PBS) is a biodegradable polymer that has good availability and attractive performance associated with a potential replacement of plastic, however it has limitations regarding storage time before processing. In this work, melt flow index (MFI) measurements were used to evaluate the influence of moisture in a PBS degraded by storage time. For this purpose, polymer samples were dried in an oven at a temperature ranging from 80 to 130°C. The results confirmed the PBS degradation condition, since the MFI of the sample without drying was 5 times greater than that indicated by the manufacturer. However, subjecting drying between 80 and 100°C, there is a reduction in the FI, which is possibly due to the presence of moisture in the samples and the consequent process of crystallization of the short chains. After 100°C, the polymer increases the melting index significantly, because of the accentuated degradation of the polymer by chain scission at higher temperatures.

Keywords: *Polybutylene succinate; Melt Flow Index; Drying; Storage.*

1.Introduction

The rapid increase in demand for low-cost materials has caused the consumption and production of polymers to have a significant increase in recent years. Consequently, there is an accumulation of improperly discarded polymeric waste. Within the industrial sectors, the biggest contributor to this problem is the packaging industry, which mainly uses polyolefins from non-renewable sources and at a lower cost [1]. This scenario has encouraged society and industry to encourage, research and use less impactful materials, such as biomaterials and biodegradable materials, in the most varied applications. Polymeric materials that have these characteristics have been an alternative to possible problems of disposal of conventional plastic waste. These polymers were used industrially for the first time in the 1980s in the production of films and other molded articles and since then constitute a market in constant growth [2, 3].

Among the biodegradable polymers with industrial prominence, polybutylene succinate (PBS) has good availability and attractive performance associated with a potential for replacing conventional plastics, making it possible to use it in several applications. However, the high price of PBS is an obstacle to increasing its use [4]. Another condition that limits the use of PBS are the conditions that cause its degradation.

PBS is an aliphatic, semicrystalline polyester with a glass transition temperature that can vary between -45 and -10ºC and its crystalline melting temperature is in the range of 90 to 120ºC [5]. Biodegradability and compostability contribute to the attractiveness of PBS.

Biodegradation of PBS chains is initiated by the hydrolysis of ester bonds, leading to the formation of water-soluble fragments with low molar mass. Small segments of PBS chains can be consumed by

microorganisms and finally transformed into environmentally friendly products, ie carbon dioxide, water and biomass [6,7].
One of the main forms of degradation of PBS is hydrolytic. Degradation by hydrolysis generates the decrease in PBS molar mass through chain scission and can be influenced mainly by temperature and polymer morphology. The amorphous areas are more easily penetrated by water than the crystalline ones, so the degradation has a higher rate in this region.
In this work, as it is a simple and fast method, the fluidity index was used to evaluate the presence of moisture in a PBS with a long storage time and therefore degraded. The molar mass reduction is a direct indication of the occurrence of breakage of bonds in the polymeric chain and the melt flow index measure, despite providing a relative value, is very informative in terms of variation of the molar mass of the polymer sample, being inversely proportional to the molar mass [8].

2.Experimental

In this work, a PBS trade name BioPBSTM FZ71 supplied by MCC Biochem was used. BioPBSTM is a soft and flexible semicrystalline polyester with excellent properties suitable for the injection process [9]. The storage time to which the polymer was submitted was of eighteen months, being twelve months longer than indicated by the manufacturer and therefore it was considered that this polymer was already degraded.
In addition to time, due to the sensitivity of polyesters to water, one of the main forms of PBS degradation is hydrolytic, which in turn is strongly influenced by temperature [10]. Therefore, the PBS was submitted to different drying conditions to evaluate the melt flow index.
The PBS samples were subjected to different temperatures between 80 and 130ºC in a digital sterilization and drying oven with air circulation and renewal, with a capacity of 150L, model EESCRA-150D by Vulcan. Moisture was related to the mass of the samples and the measurement was performed every 30 minutes until mass stabilization.
Once the drying time was established, the melt flow index of the samples was determined using a standardized plastometer at the Materials Development Laboratory at ICTI, based on the ISO–1133 standard with a temperature of 190°C and a weight of 2.16 kg.

3.Results and Discussion

Fig.1 presents the drying curve of the samples subjected to 100, 110 and 120°C. When subjected to 130°C, there was partial melting of the sample, making it impossible to calculate the humidity.

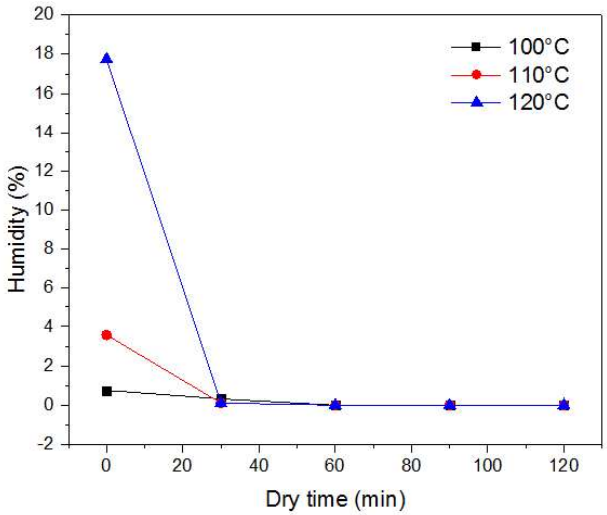

Figure 1. Moisture of PBS samples subjected to different drying conditions

It was verified through Fig. 1, that after 30 minutes all moisture was removed, regardless of temperature. Therefore, this time was adopted for drying the samples.
The melt flow index of PBS after long storage was determined in samples subjected to drying for 30 minutes at temperatures of 80, 90, 100, 110 and 120°C (Fig. 2). As expected, a high melt flow index fluidity was obtained for the PBS samples, reaching more than 5 times the value indicated for this property by the manufacturer [10].

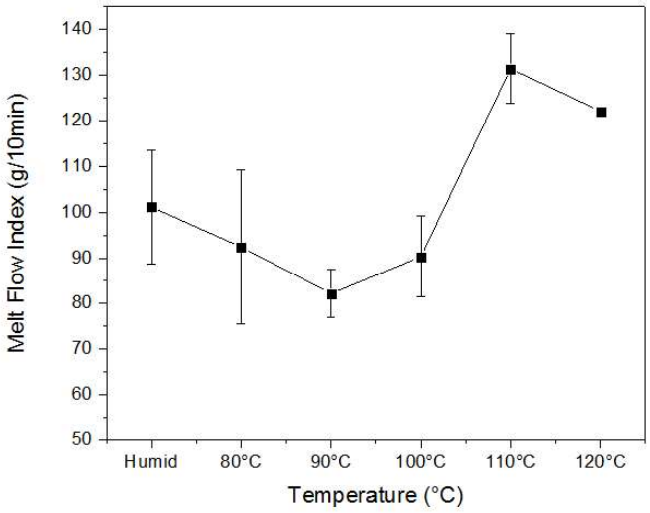

Figure 2. Melt flow index of PBS samples after long storage and different drying temperatures.

Considering the drying temperature in the degraded sample and comparing it with the so-called wet sample, it is observed that there is a reduction in the melt flow index in the samples dried at 80°C, 90°C and 100°C.
At 110 and 120ºC, an increase in the met flow index of 23 and 17% is observed when compared to the wet sample. One of the main forms of degradation of PBS is hydrolytic due to the sensitivity of polyesters to water. This type of degradation generates a decrease in the molar mass of PBS through chain scission and is influenced by temperature [10].
It is known that the increase in the melt flow index under standard conditions is an indirect indication of the decrease in molar mass [8]. Therefore, the increase of this property, at higher drying temperatures, is associated with degradation by PBS chain scission [10].
In the presence of moisture, PBS exhibits a crystallization behavior, very common to aliphatic and semi-crystalline biodegradable polymers. Studies indicate that the occurrence of crystallization is induced by the low molecular weight chains present in the degraded PBS. The amorphous regions of these semicrystalline polymers degrade preferentially, in relation to the crystalline ones, leading to chain scission and a reduction in the number of molecular tanglings in this region, in such a way, small chains are generated with the potential to rearrange themselves in crystalline form, increasing crystallinity of the polymer and thus reducing the melt flow index [11, 12].

Conclusions

After twelve months of storage, PBS shows severe degradation verified by melt flow index measurements. The drying procedure at temperatures up to 100°C is not efficient in removing moisture, which allows alignment of chains with lower molecular weight and reduction of the melt flow index. After 100°C, the melt flow index has a significant increase, indicating an accentuation in the degradation by breaking the PBS chains.

References

1. J. Sikora; L. Majewski; A. Puszka. Modern Biodegradable Plastics—Processing and Properties: Part I. Materials 2020, v. 13, n. 8, p. 1986. v. 13, n. 8, p. 1986. https://doi.org/10.3390/ma13081986.
2. A. K. MOHANTY; M. Misra; G. I. Hinrichsen. Biofibres, biodegradable polymers and biocomposites: An overview, 2000, v. 276, n. 1, p. 1-24.
3. D. Khodaei; C. Álvarez; A. M. Mullen. Biodegradable packaging materials from animal processing co-products and wastes: An overview, 2021, v. 13, n. 15, p. 2561. https://doi.org/10.3390/polym13152561.
4. S. Su, R. Kopitzky, S. Tolga, S. Kabasci. Polylactide (PLA) and its blends with poly (butylene succinate)(PBS): A brief review, 2019, Polymers, 11(7), 1193. https://doi.org/10.3390/polym11071193.
5. F. R. L. Castellões. Belo Horizonte, 2016.
6. M. L. Di Lorenzo; R. Androsch; M. C. Righetti. Low-temperature crystallization of poly(butylene succinate).European Polymer Journal, 2017, vol. 94, pp. 384–391. https://doi.org/10.1016/j.eurpolymj.2017.07.025.
7. S.A. Rafiqah; A. Khalina, A.S. Harmaen; I.A. Tawakkal,; K. Zaman; M. Asim; M.N. Nurrazi; C.H. Lee. Polymers, 2021, v. 13, n. 9, p. 1436. https://doi.org/10.3390/polym13091436
8. M. A. De Paoli, Marco Aurelio. Degradação e estabilização de polímeros. 2009.
9. BioPBS™ FZ71PM / FZ71PB Technical Data Sheet. Available in: https://productsandsolutions.pttgcgroup.com/filesproducts/pdf/packaging/TDS_FZ71PM_and_FZ71PB.pdf. Access: 15/03/2023.
10. E. P. Adamopoulou. Poly (butylene succinate): A promising biopolymer. 2013. Doctoral thesis. University of Piraeus (Greece).
11. Y.J. Phua, W.S. Chow, Z.A.M. Ishak. The hydrolytic effect of moisture and hygrothermal aging on poly (butylene succinate)/organo-montmorillonite nanocomposites. Polymer, 2011, v. 96, n. 7, p. 1194-1203. https://doi.org/10.3390/polym13091436.
12. R Muthuraj, M Misra, AK Mohanty. Hydrolytic degradation of biodegradable polyesters under simulated environmental conditions. Journal of Applied Polymer Science, 2015, v. 132, n. 27. https://doi.org/10.1002/app.42189.

INFLUENCE OF FEEDSTOCK COMPOSITION ON CHEMICAL RECYCLING OF PLASTIC WASTES VIA PYROLYSIS

Yasmin F. Siqueira[1], Débora M. V Miranda[2], Larissa L. A. Carvalho[1,2], Natasha K. Sitton[1,2], Regina F. Nonemacher[3], Ana P. Azeredo[3,4], Raquel S. Mauler[4], Luiz E. P. Borges[5] and José C. Pinto[1,2]*

1 – Programa de Engenharia de Processos Químicos e Bioquímicos, Universidade Federal do Rio de Janeiro, Rio de Janeiro, RJ, Brazil
2 – Programa de Engenharia Química / COPPE, Universidade Federal do Rio de Janeiro, Rio de Janeiro, RJ, Brazil
pinto@peq.coppe.ufrj.br
3 – Braskem S. A., Triunfo, RS, Brazil
4 – Instituto de Química, Universidade Federal do Rio Grande do Sul, Porto Alegre, RS, Brazil
5 – Seção de Engenharia Química, Instituto Militar de Engenharia, Rio de Janeiro, RJ, Brazil

Abstract - Pyrolysis is one of the polymer recycling techniques that has gained prominence in recent years, and the extrusion feeding process also arouses considerable interest in industries, since cascade processes (REX) can provide a globally effective solution for waste. Therefore, the present study investigated the influence of the feedstock composition on the performance of chemical recycling via thermal pyrolysis of post-consumer plastic wastes based on Linear Low-Density Polyethylene (LLDPE) under different conditions. The results indicated that modification of feed characteristics through REX can significantly affect the pyrolysis rates, affecting the production rates of the output streams and the composition of the products, depending on the co-feeding of additives. For example, the co-feeding of PP favored the increase of yields in all experimental conditions, and the co-feeding of peroxides caused the modification of the composition of the obtained products.
Keywords: Pyrolysis; Extrusion; REX; Plastics; LLDPE.
Fundings: This study was funded in part by Coordenação de Aperfeiçoamento de Pessoal de Nível Superior (CAPES). Conselho Nacional de Desenvolvimento Científico e Tecnológico (CNPq), Fundação Carlos Chagas Filho de Apoio à Pesquisa do Estado do Rio de Janeiro (FAPERJ) and Braskem.

Introduction

Thermoplastic materials, due to their low cost, lightweight, and high mechanical and chemical resistance, are widely used as substitutes for other materials such as steel, glass, and wood. Plastics play an important role in maintaining the quality and comfort of modern life. Therefore, these materials have become essential to human life, with new applications emerging every day. Thus, the production and consumption of plastic materials have experienced a significant increase in recent decades, and the trend is expected to continue growing in the near future [1-3].

In this scenario, the fundamental question arises regarding how to deal with plastic wastes, which are generated in large quantities. According to data from the World Bank, Brazil is the 4th largest producer of plastic wastes in the world, producing 11.3 million tons of plastic waste per year. Of this volume, 91% is collected, equivalent to 10.3 million tons annually, but only 1.28%, 145 thousand tons annually, are effectively recycled [4].

With the increasing environmental awareness, this issue has stimulated the emergence of management cultures for companies to comply with existing and developing regulations, as well as encouraging the transition from a traditional linear economy to a more circular economy, eliminating waste and reintegrating post-consumer polymers into the chemical chain.

Various techniques can be used for the reuse of post-consumer materials. In particular, the recycling of these materials can be done through mechanical, chemical, or energy processes, depending on the type of material to be recycled. According to WONG et al. [5], among the three mentioned recycling methods, chemical recycling aligns well with the principles of sustainable development, as it allows the discarded materials to return to their original compounds in a circular manner. Among the chemical recycling techniques, pyrolysis has gained particular prominence, because most polymeric wastes are compatible with this technique, constituting a good resource recovery strategy that can be developed in economically viable and sustainable processes [6].

Pyrolysis is an endothermic process that involves the thermal degradation of wastes in an atmosphere with partial or total absence of oxygen, avoiding direct combustion of the material [7]. This process typically generates gaseous, liquid, and residual solid products. Pyrolysis can also be conducted in the presence or absence of a catalyst. When the process is carried out without a catalyst, it is usually called thermal pyrolysis; otherwise, it is called catalytic pyrolysis [2].

The extrusion process has also gained considerable interest compared to other recycling methods, in terms of energy use and a range of environmental concerns during energy recovery [8]. This process can be used as an auxiliary technique for other recycling methods, allowing the polymer modification to improve the material characteristics. Moreover, if reactive extrusion (REX) processes are employed, the material is chemically modified, which can facilitate the recycling of wastes, adding value to the recycled material and increasing its acceptability in industries [9].

Based on the reasons mentioned above, the main objective of the present study was to investigate the influence of the feedstock composition on the performance of chemical recycling through thermal pyrolysis. The yields and compositions of the products obtained under different experimental conditions were evaluated, through manipulation of the reaction time and temperature. The polymers used in the investigation were polyolefins based on Linear Low-Density Polyethylene, (LLDPE) commonly used for production of commercial films and fibers.

Experimental

Materials

- Premier nitrogen with purity of 99.999%;
- Pellets of post-consumer LLDPE extruded at different conditions (identified as NExt and Ext);
- Pellets of post-consumer LLDPE extruded in presence of peroxide (RO_2) additive (identified as Ext+RO_2);
- Pellets of post-consumer LLDPE extruded in presence of polypropylene (PP) additive (identified as Ext.+PP).

The samples were processed and provided by Braskem, and their detailed characteristics will not be presented here for lack of space. Details of the extrusion operation cannot be disclosed for intellectual property reasons.

Methods

The experiments were conducted in a pyrolysis unit. In all cases, a fixed amount of 7 g of polymer (samples) was degraded at a pre-selected temperature (450 or 475 °C) and times (15, 30 and 45 min). The reaction system comprised a quartz reactor (internal diameter of 3 cm and height of 60 cm). The reactor was located inside two independent cylindrical electrical furnaces, used to control the reaction temperature, and were insulated with glass wool. Two thermocouples (“A” and “B”) were attached to the furnaces and used to provide temperature readings to the controller. A heating coil surrounded the quartz reactor and was used to preheat the nitrogen stream, used to maintain the reaction environment free of oxygen and to drag the generated gases. The nitrogen gas flow was kept constant in all trials (80 mL/min).

A cylindrical quartz melting pot (internal diameter of 2 cm and height of 12 cm) was used to place the polymer material inside the pyrolytic reactor. Before the start of the reaction, the melting pot was suspended by a wire above the furnace; after reaching the desired temperature, the melting pot

was placed into the reactor to initiate the pyrolysis reaction. The generated products were condensed with an electrostatic precipitator and the liquid fraction was stored in a glass flask. The final gas, liquid and solid mass fractions were quantified through regular mass balance computations. The liquid products were analyzed by GC–MS.

Results and Discussion

Yield Evaluation

A total of 16 experiments were conducted. Table 1 presents the adopted codes and the experimental conditions used to evaluate each sample, along with their respective yields.

Table 1 Samples yields obtained.

Code	Temperature (°C)	Time (min)	Condensable (%)	Gaseous (%)	Solid residue (%)
NExt.	450	15	4,98	2,28	92,74
NExt.	450	30	58,08	7,93	33,99
NExt.	450	45	49,94	6,68	43,38
NExt.	475	30	88,48	7,68	3,84
Ext.	450	15	20,09	3,56	76,35
Ext.	450	30	45,37	6,13	48,5
Ext.	450	45	71,47	8,70	19,83
Ext.	475	30	87,73	7,56	4,71
Ext.+RO_2	450	15	23,65	3,85	72,50
Ext.+RO_2	450	30	48,15	6,27	45,48
Ext.+RO_2	450	45	44,87	7,98	47,15
Ext.+RO_2	475	30	89,74	6,70	3,56
Ext.+PP	450	15	30,82	3,42	65,76
Ext.+PP	450	30	63,54	4,84	31,62
Ext.+PP	450	45	84,31	7,42	8,27
Ext.+PP	475	30	88,88	7,13	3,99

As expected, increasing the temperature led to higher yields of product fractions for all investigated samples [10]. The assays conducted at 475 °C consistently achieved conversions exceeding 87%. In contrast, assays conducted at a lower temperature (450 °C) and shorter reaction time (15 minutes) resulted in significantly lower conversions. The pyrolyzed samples were compared under the same experimental conditions to assess the influence of the extrusion feed step, with and without additives, on the yield. Fig 1 shows the condensable yields for each sample.

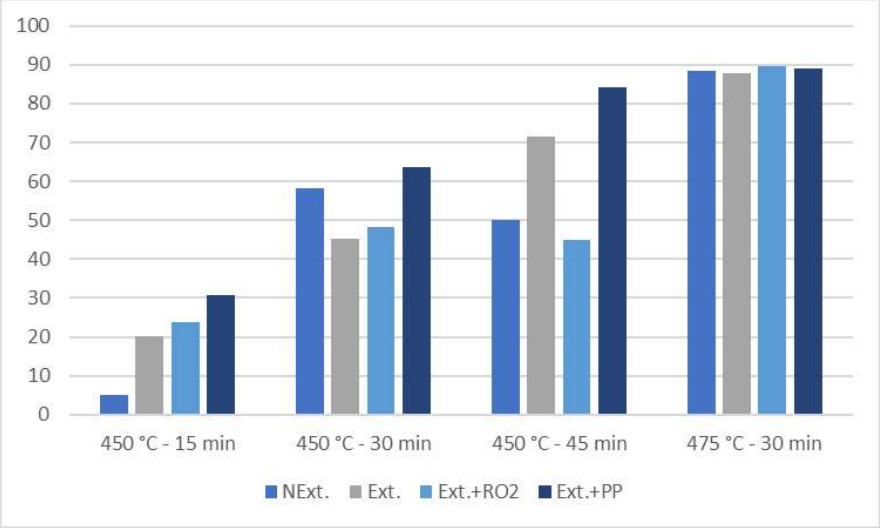

Figure 1 - Yields of Condensable Fractions Obtained in Pyrolysis of the Samples.

It was observed that the samples exhibited distinct behaviors. Firstly, the co-feeding of PP exerted a positive effect on increasing the yields under all conditions. This can be attributed to the fact that PP-based resins undergo degradation at lower temperatures compared to PE resins [10-11]. Therefore, the incorporation of PP benefits the yields by accelerating the reaction rates. Secondly, under lower conversion conditions, the extrusion operation was beneficial for increasing the yields in all considered cases. However, in the intermediate conversion regions, the effect of extrusion, as well as the REX with peroxide, on the yields of condensable fraction was less clear.

Evaluation of composition

The products from the liquid fraction were analyzed and will be compared under similar experimental conditions, as the objective is to evaluate the influence of extrusion on pyrolysis. Different experimental conditions can generate different products, so just one condition is sufficient to demonstrate whether the process affects the chemical composition of the products [2, 12-14]. The products were characterized using Gas Chromatography-Mass Spectrometry (GC-MS) analysis, using an HP5-ms capillary column manufactured by Agilent, model 19091S-433. The compounds were analyzed using the NIST (National Institute of Standards and Technology) library, based on the fragments generated in the mass spectrometer.

It can be observed in the Fig 2 that the samples exhibited distinct behaviors. The addition of peroxide during extrusion can modify the composition of the products, as an increase in the concentration of free radicals can trigger parallel reactions, resulting in an increase in the number and quantity of unsaturated products. Therefore, initially, this operation may be considered unfavorable. Additionally, the addition of PP also leads to changes in the concentration profiles due to the accelerated reaction progress, resulting in a higher presence of unsaturated compounds.

In the case of the NExt. and Ext. samples, the results were relatively similar, indicating that the extrusion step plays a less significant role in explaining the changes in the composition of the obtained products.

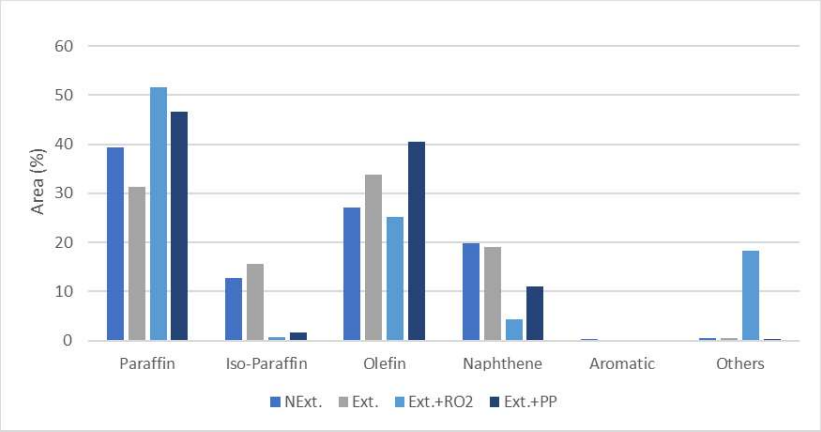

Figure 2 - PIONA analysis of the condensable fraction of pyrolysis products at the center point of the Samples.

Conclusions

The present study investigated the effect of the feedstock composition in the pyrolysis reaction of polyolefin resins (based on LLDPE, linear low-density polyethylene) derived from post-consumer waste. For this purpose, samples were subjected to pyrolysis at different temperatures (450 and 475°C) and reaction times (15 to 45 minutes). The results confirmed that the reaction temperature has a significant influence on pyrolysis, as increasing the temperature within a relatively narrow operating range significantly affects the yields of the product streams.

The collected information suggests that the effects of the feed composition have a greater influence on the performance of pyrolysis reactions, in terms of reaction rates and yields of the condensable

fraction,. Based on the obtained results and literature reports, it can be concluded that the composition of the post-consumer waste has a direct effect on the quality of the pyrolysis oils, particularly regarding the hydrocarbon matrix. The addition of additives such as peroxides or PP can change the chemical nature of the obtained products because the chemical composition of the feedstock greatly influences the progress of the reactions and the nature of the products obtained.

Acknowledgements
The authors thank CAPES, CNPq, FAPERJ, Braskem, SENAI, Petrobrás, and BNDES financial support and scholarships.

References

1. D. M. V. Miranda, Ph.D. Qualification, Federal University of Rio de Janeiro, 2019.
2. A. Duailibe; J. C. Pinto; J. J. S. Delgado in *Reciclagem química de resíduos plásticos – Tecnologias e Impactos*; E-papers, Ed.; 2019.
3. J. C. Pinto et al. in *Impactos Ambientais causados pelos Plásticos;* E-papers, Ed.; 2019; Vol. 2.
4. WWF. *Brasil é o 4o país do mundo que mais gera lixo plástico*. WWF Brasil. Available in: <https://www.wwf.org.br/?70222/Brasil-e-o-4-pais-do-mundo-que-mais-gera-lixo-plastico>. Accessed in: May 2023.
5. S. L. Wong et al.; *Current state and future prospects of plastic waste as source of fuel: A review*. Renewable and Sustainable Energy Reviews 2015, v. 50, p. 1167–1180. https://doi.org/10.1016/j.rser.2015.04.063.
6. D. M. Brás, M.Sc. Dissertation, NOVA University Lisbon, 2011.
7. M. M. Pedroza et al.; *Aproveitamento energético de resíduos sólidos urbanos em processo de Pirólise*. Revista Brasileira de Energias Renováveis 2017. http://dx.doi.org/10.5380/rber.v6i2.46577.
8. Y. Li et al.; *Improved properties of recycled polypropylene by introducing the long chain branched structure through reactive extrusion*. Waste Management 2018, v. 76, p. 172–179. https://doi.org/10.1016/j.wasman.2018.03.040.
9. G. H. Hu et al. in *Reactive Polymer Processing: Fundamentals of REX*. Reference Module in Materials Science and Materials Engineering. 2016. https://doi.org/10.1016/B978-0-12-803581-8.03365-8
10. D. L. Oliveira Jr., M.Sc. Dissertation, Federal University of Santa Maria, 2016.
11. K.-H. Lee in Thermal and catalytic degradation of waste HDPE; John Wiley & Sons Ed.; Feedstock recycling and pyrolysis of waste plastics, 2006, 129-160.
12. K. H. Lee; D. H. Shin, *Characteristics of liquid product from the pyrolysis of waste plastic mixture at low and high temperatures: Influence of lapse time of reaction*. Waste Management 2007, v. 27, n. 2, p. 168–176. https://doi.org/10.1016/j.wasman.2005.12.017
13. A. López et al. *Influence of time and temperature on pyrolysis of plastic wastes in a semi-batch reactor.* Chemical Engineering Journal, 2011, v. 173, n. 1, p. 62–71. https://doi.org/10.1016/j.cej.2011.07.037
14. H. A. Júnior, M.Sc. Dissertation, Federal University of Rio de Janeiro, 2017.

LIPASE NS-40116 INCORPORATED IN BACTERIAL CELLULOSE MODIFIED WITH ZEIN

Victória Fonseca Silveira[1*], Victória Mendes da Silva[2], Sandro Rogério Kumineck Junior[3], Michele Cristina Formolo Garcia[2], Ana Paula Testa Pezzin[3], Terezinha Maria Novaes de Oliveira[3], Andrea de Lima Schneider[1,2,3]

1 – Master program in Health and Environment, University of Joinville Region (UNIVILLE), Joinville, SC, Brazil, victoria.fonssecca@gmail.com
2 – Department of Chemical Engineering, University of Joinville Region (UNIVILLE), Joinville, SC, Brazil
3 - Master program in Process Engineering (MEP), University of Joinville Region (UNIVILLE), Joinville, SC, Brazil

Abstract - The immobilization of enzymes increases their stability and allows their reuse, and bacterial cellulose (BC), a material used in this technique. This work aimed to produce an enzymatic product to degrade oils and fats using BC as a matrix. BC membranes were produced by *Komagataeibacter hansenii*, and lipase was immobilized on the membranes (ex-situ method). Then the surface of the membranes was modified with a hydrophobic corn protein called zein. The membranes were characterized by TGA, FTIR, SEM analysis and a degradation test. TGA showed higher stability of the membranes with lipase and zein. The FTIR spectrum of pure BC membrane and zein-modified membrane were very similar because of the high zein coating. SEM analysis showed that zein-modified membranes with lipase presented smaller amounts of pores. Finally, using soy oil, lipase could degrade oil even after immobilization during the degradation test.
Keywords: *bacterial cellulose, zein, enzymes, lipase, immobilization*.
Fundings: The authors are grateful for the financial support of Capes and UNIVILLE for the project.

Introduction

Environmental pollution is an enormous obstacle faced by many countries. Improper disposal of pollutants compromises aquatic life, wildlife and humans [1]. Fats and oils are one of the primary contaminants in this scenario because they are used as feedstock in food, plastics and biofuels industries, for example. The presence of oils and fats in sewer systems causes pipe blockage [2]. Furthermore, their presence requires more flocculants in treatment stations and interferes with oxygen diffusion [3-4]. In this context, lipase enzymes are an option for the problem. They catalyze the breakdown of fats and oils, but their use as free enzymes in the environment can cause their inactivation by chemical, physical and biological factors [5-6]. Seeking to overcome these obstacles, studies have been conducted for the immobilization of enzymes in matrices to improve characteristics like activity, stability and reuse possibility [7]. A promising material for enzyme immobilization is bacterial cellulose (BC), an extracellular homopolysaccharide formed by glucopyranose units linked by β-(1,4) glycosidic bonds [8]. It is a biopolymer with interesting properties such as high water-holding capacity, biocompatibility and biodegradability [9,10]. BC can be used in oil-water separation; it is usually modified with hydrophobic substances for this application. A corn protein called zein is a material that can form a hydrophobic coating, resistant to microorganisms attacks and with excellent flexibility [11]. Due to its hydrophobicity, characteristic solubility, biocompatibility, biodegradability, abundance, origin of renewable resources and being recognized as safe (GRAS), zein is considered a versatile and promising food biopolymer [12]. Considering the current scenario,

this work aimed to develop a hydrophobic biomaterial to immobilize lipases, using BC as a matrix, for use in the degradation of vegetable oils.

Experimental

Synthesis of pure BC

The microorganism used was the bacterium *Komagataeibacter hansenii* ATCC 23769, stored in Petri dishes under refrigeration. In its activation and cultivation, a Mannitol Medium composed of mannitol (25 g· L^{-1}), peptone (5 g· L^{-1}), and yeast extract (3 g· L^{-1}) was autoclaved at 121 ºC for 20 min. The cells were activated in 500 mL Erlenmeyer bottles containing 100 mL of medium and pH 7.0, incubated at room temperature under static conditions for two days. After this period, the inoculum was transferred to the culture medium at a rate of 20% with initial optical density (O.D.) ranging from 0.9 to 1. This stage was conducted in Erlenmeyer bottles of 125 mL with 35 mL of culture medium, incubated in an oven at 30 °C in static condition for 12 days for the formation of hydrated blankets of BC.

Purification

The membranes were washed with water to remove the remaining culture broth and then treated with a 0.1 M NaOH solution in a thermal bath until 80˚C for 60 min to remove bacterial impurities and other contaminants. After this treatment, they were washed with distilled water until they reached pH 7, stored in distilled water and autoclaved to avoid contamination or drought in a greenhouse [13].

Lipase incorporation and modification with zein

The incorporation of the enzyme into the BC membrane was performed in 3 cycles, as shown in Fig 1. At the end of each cycle, the BC was washed with distilled water to remove excess enzymatic solution. Surface modification with Zein was performed, as shown in Fig 1.

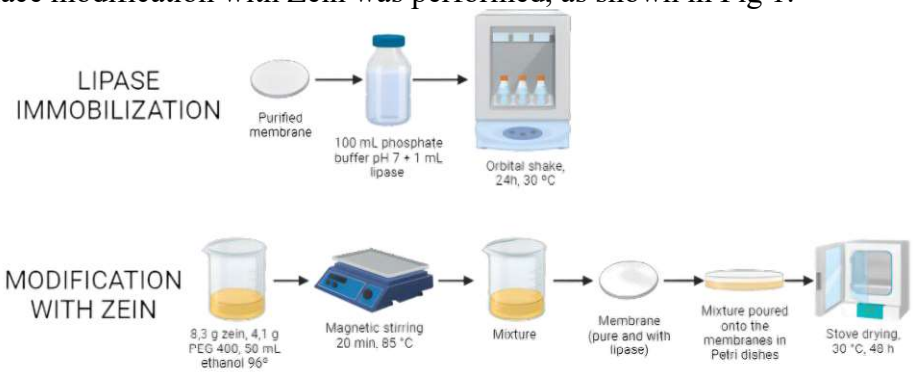

Figure 1 - Methodology scheme

Fourier Transform Infrared Spectroscopy (FTIR)

The characterization of the functional groups of the BC, BC/ENZ and BC/ENZ/ZE was carried out by Fourier Transform Infrared Spectroscopy (FTIR) in Perkin Elmer Frontier equipment. 32 scans were performed per sample, from 650 to 4000 cm^{-1}, with a resolution of 2 cm^{-1}, in attenuated total reflectance (ATR) mode.

Contact angle

The method used was the sessile drop, in which a drop of deionized water was deposited above the samples using a microsyringe. The drop was observed using a low magnification lens, and the contact angle was measured by a goniometer (Ramé-Hart Inst. Co. modelo 250-F1).

Oil degradation (acidity level)
For this test, membranes of BC/ENZ and BC/ENZ/ZE were used. All the membranes were put in 100 mL of citrate buffer pH 7 (0,05 M), and then 50 mL of ethyl ether was added to solubilize the soy oil 5,5% (w/v). This mixture was incubated under stirring at 150 rpm, 30 °C, for 90 min. After this time, titration was done with NaOH 1M to quantify fatty acids, using phenolphthalein as an indicator. The volume of NaOH spent in the titration was used to calculate the acidity level, as shown in Eq. 1 [14]. The test was done in triplicate for each sample.

$$Al = (NaOH\ mass/fatty\ mass) \quad (1)$$

Al = acidity level;
NaOH mass = quantity of NaOH used (g);
Fatty mass = quantity of fatty used (g).

Results and Discussion

Lipase incorporation and modification with zein
Through a macroscopic evaluation (Fig 2), it was possible to observe that the BC modified with zein (BC/ENZ/ZE) presented a yellowish color, forming a thin and homogeneous film on the surface of the BC, and also with a more brittle characteristic.

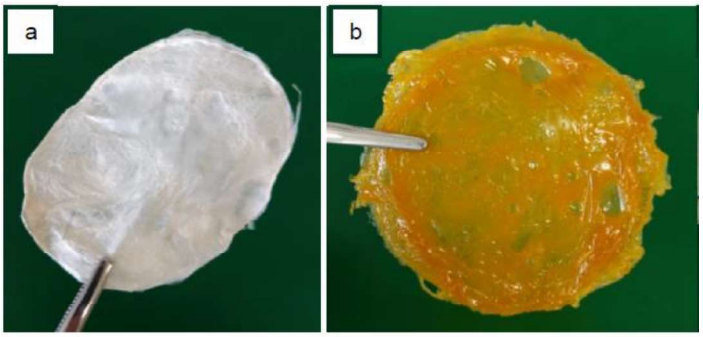

Figure 2 - Bacterial cellulose membrane (a) BC and (b) BC/ENZ/ZE

Fourier Transform Infrared Spectroscopy (FTIR)
The FTIR spectra of the ZE and CB/ZE samples showed amide bands A, I, and II identified at 3300 cm^{-1}, 1650 cm^{-1} and 1540 cm^{-1}, respectively, with amide A referring to the stretching of the N-H and O-H group of protein amino acids, amide I occur due to the C=O stretching of the amide group, and amide II is related to the vibrations of angular deformation of the N-H bond and stretching of the C-N bond [15].
In the CB/ENZ sample spectrum, the band at 1650 cm^{-1} related to amide I derived from lipase amino acids was observed. The band at 1530 cm^{-1} described in the literature and related to amide II shifted to 1545 cm^{-1} [16]. Due to the presence of the band at 1055 cm^{-1} referring to the vibration of the -C-O-C- bond of the CB pyranose ring, the characteristic lipase band at 1050 cm^{-1} referring to the deformation vibration of the primary amino group -NH_2 was not observed.

Contact angle
BC presented an angle of 45.2° and BC/ENZ an angle of 55°, showing that both are hydrophilic, a characteristic behavior of BC. While the BC/ENZ/ZE membrane presented an angle of 80°, showing that the samples became amphiphilic, therefore they are neither hydrophobic nor hydrophilic, which allows the BC to interact with the enzyme, the oil and the aqueous medium where it will be used. The ZE-only samples showed a contact angle of 93°, indicating they are hydrophobic [17]. The angles

were measured 4 times on each sample and then averaged. Fig 3 and Table 1 show the angles of samples BC, ZE, BC/ENZ and BC/ENZ/ZE.

Figure 3 - Contact angle of the BC samples (a) BC/ENZ/ZE;(b) BC/ENZ (c)

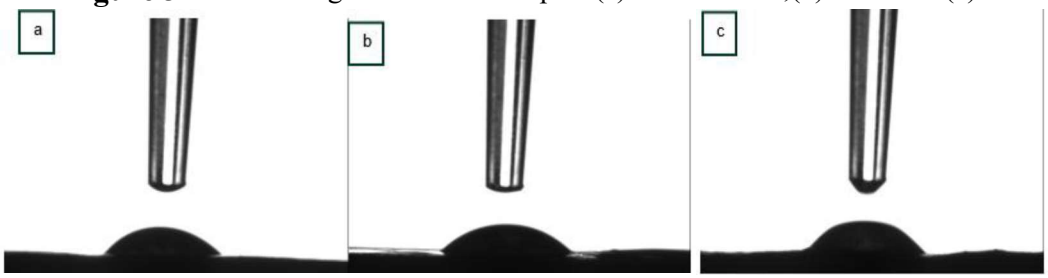

Table 1 - Values of the contact angles of the samples BC, ZE, BC/ENZ and BC/ENZ/ZE

Samples	Contact angle Mean ± SD	Classification
BC	45º ± 4,53	Hydrophilic
ZE	93° ± 4,05	Hydrophobic
BC/ENZ	55º ± 4,81	Hydrophilic
BC/ENZ/ZE	80º ± 3,66	Amphiphilic

Acidity level

Table 2 shows data from the soybean oil degradation test (acidity index). It is observed that even with the immobilization process, the lipase enzyme maintained the ability to hydrolyze soybean oil, with a more expressive value for the CB/ENZ/ZE sample (97%), which may be a result of the influence of the presence of zein, because it is also a protein.

Table 2 - NaOH mass average values and acid number for samples BC, BC/ENZ and BC/ENZ/ZE

Samples	Mass of NaOH(g) Average ± SD	Al (%) Average ± SD
BC	2,20 ± 0,1	45,57 ± 2,08
ZE	0,60 ± 0,06	12,50 ± 1,26
BC/ENZ	2,84 ± 0,27	58,80 ± 5,5
BC/ZE	0,85 ± 0,17	17,64 ± 3,60
BC/ENZ/ZE	3,20 ± 0	97,02 ± 3,6

Immobilization of lipase NS-40116 from *Thermomyces lanuginosus* was studied by Facin et al. [14] in polyurethane samples. Analysis of the hydrolysis capacity of vegetable oil showed that all samples reached maximum acidity (12 – 13%), that according to the authors, confirmed that the enzyme immobilized on the polyurethane support maintained its catalytic capacity [18]. Comparing with the results obtained in this work, it is observed that the values were higher even after the surface modification process of the BC membranes, which demonstrates the obtaining of a material that maintains the degradation characteristic of the enzyme. The BC/ZE and ZE alone samples showed the lowest acidity index, showing that this material has no property for oil degradation alone. This result corroborates the results found in the BC/ENZ/ZE samples.

Conclusions

By visual analysis, it was possible to observe that the intended modification occurred. The FTIR spectra showed characteristic bands of the pure materials in the respective modified samples.

However, the CB/ENZ/ZE sample did not show the BC bands, indicating that zein promoted a BC coating.
The acidity test showed that the enzyme was incorporated and remained active even after the modification process. BC/ENZ/ZE degraded the oil better than the other samples. The contact angle showed that the BC/ENZ/ZE sample was amphiphilic, allowing interaction at the water-oil interface and enabling oil degradation.

References

1. L. W. Yao; F. S. A. Khan; N. M. Mubarak; R. R. Karri; M. Khalid; R. Walvekar; E. C. Abdullah; S. Mazari; A. Shaukat; A. Ahmad; M. H. Dehghani, Journal of Molecular Liquids 2022, 354. https://doi.org/10.1016/j.molliq.2022.118849.
2. H. C. Huang; L. C. Chen; S. B. Lin; C. P. Hsu; H. H. Chen, Biosource Technology 2010, 101, 6084-6091. https://doi.org/10.1016/j.biortech.2010.03.031
3. A. A. Mendes; H. F. de Castro; E. B. Pereira, Química Nova 2005, 28 (2), 296 - 305. https://doi.org/10.1590/S0100-40422005000200022.
4. A. O. Alade; A. T. Jameel; S. A. Muyubi; M. I. A. Karim; Md. Z. Alam, IIUM Engineering Journal, 2011, 12 (4), 161 – 160. https://doi:10.31436/iiumej.v12i4.218.
5. F. W. Parques; G. A. Macedo, Química Nova, 2006, 29 (1), 93 - 99. https://doi.org/10.1590/S0100-40422006000100018.
6. S. Menocin; N. M. Domingues; D. M. G. Freire; J. V. Oliveira; M. D. Luccio; H. Treichel; D. de Oliveira, Food Science and Technology 2009, 29 (2), 440 - 443. https://doi.org/10.1590/S0101-20612009000200033.
7. A. Dantas, Masters Dissertation, Universidade Federal de Santa Catarina, 2017.
8. H. S. Barud, Masters Dissertation. Universidade Estadual Paulista, 2006.
9. E. Pecoraro; D. Manzani; Y. Messaddeq; S. J. L. Sidney, In: Monomers, polymers and composites from renewable resources. Elsevier, 2008. https://www.researchgate.net/publication/265727430_Chapter_17_Bacterial_Cellulose_from_Gluconacetobacter_xylinus_Preparation_Properties_and_Applications.
10. M. S. A. Camargo; A. P. Cercal; V. F. Silveira; K. C. B. Mancinelli; R. M. M. Gern; M. C. F. Garcia; G. P. Apati, A. L. D. S. Schneider, A. P. T. Pezzin Macromolecular Symposia 2020, 394, 2000149. DOI: 10.1002/masy.202000149.
11. R. Shukla; M. Cheryan, Industrial Crops and Products 2001, 13 (3), 171 - 192. https://doi.org/10.1016/S0926-6690(00)00064-9.
12. H. Zhang; Y. Zhao; X. Kang; H. Li; H. Mo, Food Science and Technology 2022, 42 (2). DOI 10.1590/FST.65522.
13. J. F. D. Costa; M. C. F. Garcia; G. P. Apati; H. D. S. Barud; A. L. D. S. Schneider; A. P. T. Pezzin Revista Matéria 2017, 22 (suppl1), e-11917. https://doi.org/10.1590/S1517-707620170005.0253.
14. E. A. Canesin; T. M. Amorin; A. F. F. Veroneze; R. M. Suzuki; V. V. S. Almeida; N. E. de Souza; E. G. Bonafé, Brazilian Journal of Food Research 2019, 10 (1), 77–92. DOI:10.3895/rebrapa.v10n1.5182.
15. E. Corradini. Thesis, Universidade de São Paulo, 2010.
16. T. K. A. Nguyen; B. N. Huynh; H. N. V. Thai; T. N. H. Tran; T. T. Truong; T. K. L. VU. Journal of Technical Education Science 2021, 67, 1–13, DOI 10.54644/JTE.67.2021.1083
17. C. Shuai; Z. Wang; H. Zhang; J. Jia; L. Huang; D. Wang; S. Chen; P. Feng. Materials Degradation 2022, 6, 87. https://doi.org/10.1038/s41529-022-00297-3.
18. B. R. Facin; A.Valério; D. Bresolin; G. Centenaro; D. D. Oliveira; J. V. Oliveira. Biocatalysis and Biotransformation 2018, 36, (5), 372–380. https://doi.org/10.1080/10242422.2018.1458842.

MECHANICAL PROPERTIES OF CELLULOSE FILAMENTS REGENERATED FROM COLORED COTTON WASTE USING IONIC LIQUID/COSOLVENTS SYSTEM

Aline F. Knihs[1], Larissa K. Aragão[1] Miguel A. Granato[1], Andrea C. K. Bierhalz[1] and Rita de C. S. C. Valle[1*]

1 – Department of Textile Engineering, Federal University of Santa Catarina – Campus Blumenau, Blumenau, Brazil
rita.valle@ufsc.br

Abstract - A considerable amount of dyed cotton from textile processes is disposed of in landfills, resulting in negative environmental impacts and unnecessary loss of natural resources. Thus, the purpose of this study was to evaluate the mechanical performance of regenerated cellulose filament dissolved in systems composed of ionic liquid (IL) 1-ethyl-3methylimidazolium chloride ([EMIN]Cl) and different proportions of the cosolvents dimethyl sulfoxide (DMSO) and dimethylformamide-N, N (DMF). The cotton residue was dissolved in [EMIM]Cl for 2.5 h at 110°C, and DMSO or DMF was added at proportions of 15, 30, and 50% (g cosolvent/ g IL). The filaments were evaluated regarding the degree of polymerization (DP) and mechanical properties. The use of 30% of DMSO resulted in filaments with higher DP and higher tensile strength. The mass fraction of 30% of DMF showed better mechanical properties than the other proportions.
Keywords: *Colored textile residue. Ionic liquid. Cosolvent. Regenerated cellulose fibers.*
Fundings: FAPESC Process n. 2021TR000327

Introduction

Cellulose is the most abundant biopolymer in the world, being a renewable and biodegradable source [1]. Therefore, this polymer has attracted increased interest in various fields, such as the textile industry. However, its processing is hampered due to its insolubility in water and common organic solvents [2]. As the solvents generally used for cellulose are toxic, aggressive to the environment and can cause derivatization of cellulose, new classes of solvents have been studied, such as ionic liquids (ILs) [3].

ILs are direct dissolution solvents of cellulose and can be defined as molten salts or even liquid electrolytes with melting points below 100 °C [4]. Imidazolium-based ILs are the most investigated, due to their high dissolution capacity, such as 1-allyl-3methylimidazolium chloride ([AMIM]Cl) and 1-ethyl-3-methylimidazolium chloride ([EMIM]Cl) [5]. During dissolution, the IL diffuses between the molecular chains of the cellulose and performs the breakdown of the intra- and intermolecular hydrogen bonds [6]. This diffusion is affected by the high viscosity of the ILs, which hinders the dissolution process as well as the regeneration of cellulose. To overcome this limitation, some polar aprotic organic solvents, such as dimethyl sulfoxide (DMSO) and dimethylformamide-N, N (DMF), are added as cosolvents to decrease the viscosity of the solution, without the precipitation of cellulose [7]. In addition to reducing viscosity, cosolvents facilitate cellulose dissolution at low temperatures, increase the efficiency of dissolution, allow a decrease in the use of IL's and, consequently, decrease the cost of the process [2,8]

In this work, a residue of dyeing cotton from the brushing textile process was used as source of cellulose. This residue is usually destined for landfills due to the presence of synthetic reactive

dyes. Thus, the objective of this work was to investigate the degree of polymerization and mechanical behavior of the wet-spun regenerated cellulose filaments using dissolution in chloride of 1-ethyl-3methyl imidazolium ([EMIN]Cl) and cosolvents DMSO and DMF in different proportions.

Experimental

The raw material for obtaining the regenerated cellulose is a 100% dyed cotton textile residue, from the brushing process of sweatshirts, donated by a company located in Santa Catarina, Brazil. The residue has green coloration and its trichrome is composed of reactive dyes of the azo class and vinyl sulfone. For the cellulose dissolution, were used the ionic liquid of the imidazole type 1-ethyl-3-methylimidazolium chloride ([EMIM]Cl) (Sigma-Aldrich) and the cosolvents Dimethyl sulfoxide P.A. (DMSO) (Anadrol) and Dimethylformamide-N,N P.A. (DMF) (Scientific Exodus).

Dissolution and Regeneration of Cellulose

For the cellulose dissolution, 0.09 g of previously dried green cotton was added to 3 g of [EMIM]Cl. The mixture was heated at 110°C in a glycerin bath and magnetically stirred for 2 h 20 min. Then, cosolvent DMSO or DMF was added at mass proportions of 15, 30 and 50% (g cosolvent/g IL) and the stirring was kept for additional 10 min. The filament was obtained by wet spinning technique, in which the dissolved cellulose was transferred to a syringe with an outlet diameter of 2 mm and connected to an infusion pump (Fresenius Kabi, model Injectomat Agilia). The spinning rate was 45 mL/h and the coagulation bath was composed of deionized water. After 15 min of coagulation, the filament was washed several times with deionized water until the ionic liquid was completely removed and then dried in an oven at 60 °C for 30 min.

Degree of Polymerization (DP)

The filament obtained was immersed in a solution of sulphuric acid (0.5 M) at 1% w/v in a water bath at 75 °C for 30 min. Then, the filaments were washed with deionized water until reaching neutral pH and dried in an oven at 45 °C for 12 h.

The mean degree of polymerization (DP) was determined by adapting ASTM D1795-13 [9], using cupriemethylenediamine (CUEN) as a solvent and a Cannon-Fenske capillary viscometer nº 75 at 25 °C.

Mechanical properties

The mechanical resistance of the regenerated fibers was evaluated in terms of tensile strength, elongation at break and Young's modulus by ASTM D2256/D2256M. Filaments samples with 150 mm long were analyzed in a texturometer (Stable Micro System, TA.TX Plus)), using a 50 N load cell, initial grip spacing of 10 cm, and cross-head speed of 2 mm/min. The comparison of means of 10 replicates was made by the Anova test with a significance level of 5 %, using the Statistica® 12 software.

Results and Discussion

The average diameters of filaments produced with from the cellulose dissolution with different IL/cosolvent mass fractions ranged from 207 μm to 259 μm. The use of cosolvent was essential for wet spinning processing, as it allowed to reduce the viscosity. It was noted that with the increase in the mass fraction of the cosolvent, the viscosity of the solution reduced. Fig 1 shows the aspect of the cotton waste used as cellulose raw material (a) and regenerated cellulose filaments (b). The green color of the textile waste was maintained in the formed filament, which would eliminate the need for dyeing processes. Macroscopically, it was not observed the presence of green dye in the ionic liquid/cosolvent bath after regeneration.

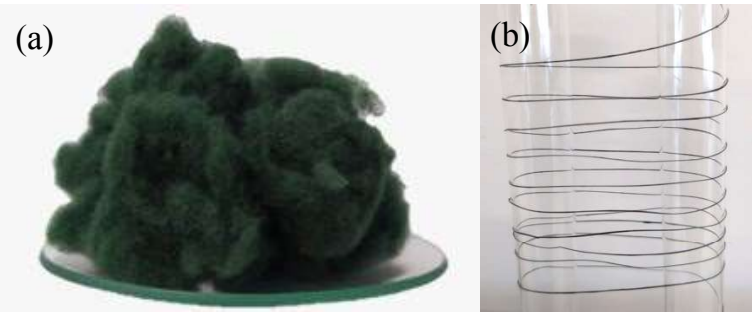

Figure 1 – Aspect of the textile cotton waste (a) and regenerated cellulose filament using cotton residue from the brushing process (b).

Degree of Polymerization (DP)

Fig 2 shows the results of the degree of polymerization of the regenerated cellulose samples after acid hydrolysis treatment. The acid treatment was used to facilitate the dissolution of the filament samples in CUEN solution. Due to the presence of dye, the conventional direct dissolution of the regenerated cellulose in CUEN is not achieved. However, the previous hydrolysis also contributes do depolymerization of cellulose.

The results indicate that the use of 30% DMSO (DMSO30) for cellulose dissolution resulted in filament with the highest DP (587). Regarding the filaments obtained with DMF, the DP is similar between the three mass fractions tested, presenting values between 391 and 438. Despite the acid hydrolysis treatment, the DP values of the regenerated filaments corroborate the DP of the commercial viscose (300-450) and the cellulose regenerated in [AMIM]Cl at 100 °C (550) [10].

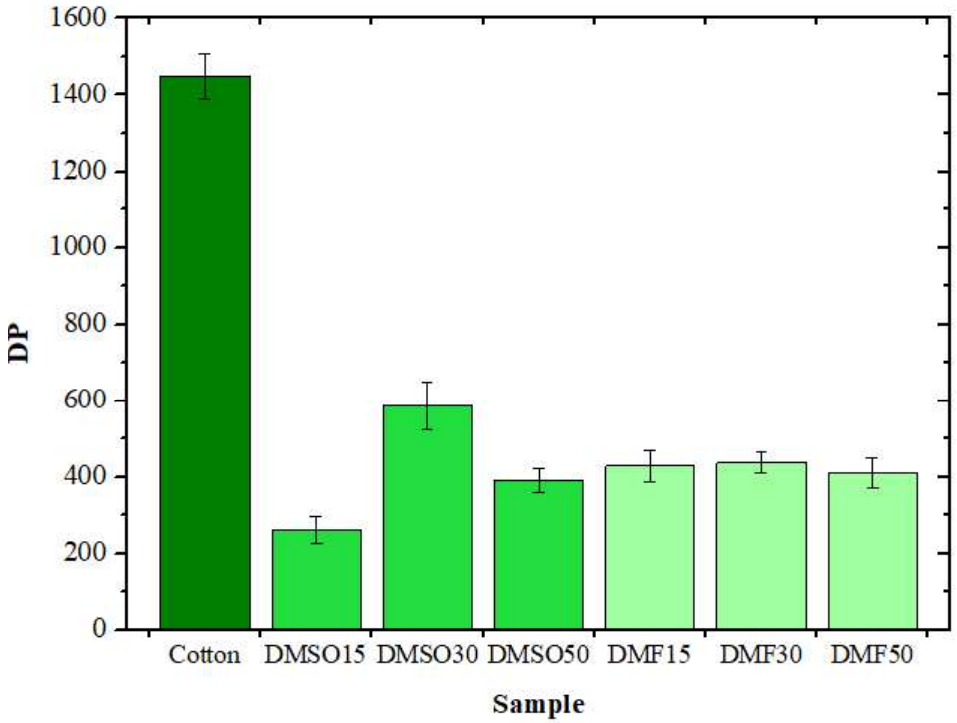

Figure 2 – Degree of polymerization of cotton residue and regenerated cellulose filaments obtained form dissolution with different proportions of cosolvent.

Mechanical properties

The results of the mechanical properties of the fibers regenerated from the brushing cotton residue, obtained from dissolution in [EMIM]Cl and cosolvents DMSO and DMF, are presented in Table 1.

It is noticed that the mass fraction of 30% for both cosolvents results in higher tensile strength when compared to the other mass fractions. It is also noted that DMSO cosolvent presented tensile strength values similar to the DMF cosolvent when compared to the same mass fractions. Studies found in the literature obtained tensile strength results similar to those of the present study [11,12]

Table 1 – Mechanical properties of regenerated filaments

Sample	Tensile strength (MPa)	Elongation at break (%)	Tenacity (cN/tex)	Young's modulus (GPa)
DMSO15	$193.65 \pm 25.89^{b,c}$	$6.90 \pm 1.72^{a,b}$	$8.99 \pm 2.48^{b,c}$	$17.14 \pm 1.28^{a,b}$
DMSO30	238.14 ± 24.02^{a}	$7.96 \pm 1.51^{a,b}$	$9.39 \pm 1.78^{b,c}$	17.39 ± 2.76^{a}
DMSO50	$198.34 \pm 38.17^{b,c}$	5.96 ± 1.56^{b}	5.87 ± 1.54^{c}	$12.32 \pm 2.70^{a,b}$
DMF15	185.35 ± 19.61^{c}	$6.72 \pm 2.18^{a,b}$	6.95 ± 2.26^{c}	$11.54 \pm 0.99^{a,b,c}$
DMF30	$228.33 \pm 22.02^{a,b}$	9.51 ± 2.43^{a}	13.09 ± 3.35^{a}	13.31 ± 1.19^{b}
DMF50	159.06 ± 21.77^{c}	$8.53 \pm 1.72^{a,b}$	$11.81 \pm 2.38^{a,b}$	10.76 ± 0.66^{c}

Results are presented as means ± standard deviation. Means followed by same letter in the same columns do not differ significantly $p < 0.05$.

The results of elongation at break indicated that this this property was little affected by the type and proportion of cosolvent. The values are slightly lower than those observed for Lyocell/NMMO fiber (11.2%) and the Lyocell/ NMMO fibers obtained using textile residues (14.1 %) [13]. The filament obtained with 30% of DMF presented the highest tenacity (13.09 cN/tex), which corresponds to a performance analogous to viscose (10 to 15 cN/tex) [14].

Young's modulus is related to the stiffness of the filament. The DMSO samples in the proportions of 15 and 30% presented a higher Young's modulus. Compared to commercial viscose fiber, the filaments obtained demonstrate Young's modulus twice as large [15].

Mechanical properties are influenced by the degree of polymerization. Overall, a higher DP results in better mechanical properties [10]. This correlates with the result obtained for the DMSO30 filament that presented the highest DP and, consequently, presented the highest tensile strenght Young's modulus.

Conclusions

This study demonstrated that cotton residues from the textile brushing process can be used as cellulose source for obtaining regenerated filaments with promising properties of industrial application. The green color of the cotton residue was also observed in the filament. The degree of polymerization was reduced compared to the residue, and the results were affected by cosolvent and proportion used. The mass fraction of 30% showed better results in both cosolvents. With the exception of tenacity, the DSMO cosolvent with 30% was found to be better than the same proportion of DMF cosolvent.

Acknowledgments

The authors thank the financial support of FAPESC (Process 2021TR000327) and CAPES (Finance Code 001).

References

1. N. Dissanayake, V.D. Thalangamaarachchige, S. Troxell, E.L. Quitevis, N. Abidi; Cellulose 2018, 6887–6900. https://doi.org/10.1007/s10570-018-2055-1
2. A. Xu, L. Chen, Y. Wang, R. Liu, W. Niu; Polymers 2019, 11(845), 14.

3. T.G. Paiva, M. Zanatta, E.J. Cabrita, C.E.S. Bernardes, M.C. Corvo; Journal of Molecular Liquids 2022 345, 117810. https://doi.org/10.1016/j.molliq.2021.117810
4. F. Hermanutz, M.P. Vocht, N. Panzier; *Macromolecular Materials and Engineering* 2019, 1800450, 1–8. https://doi.org/10.1002/mame.201800450
5. A. Xu, L. Cao, B. Wang; Carbohydrate Polymers 2015, 125, 249–254. https://doi.org/10.1016/j.carbpol.2015.02.045
6. T. Uto, K. Yamamoto, J.I. Kadokawa; Journal of Physical Chemistry B 2018, 122(1), 258–266. https://doi.org/10.1021/acs.jpcb.7b09525
7. F. Huo, Z. Liu, W. Wang; The Journal of Physical Chemistry 2013, 117, 11780–11792. https://doi.org/doi.org/10.1021/jp407480b
8. A.A. Shamsuri, K. Abdan, S.N.A.M. Jamil; E-Polymers 2021, 21(1), 869–880. https://doi.org/10.1515/epoly-2021-0086
9. ASTM D1795-13 - ASTM International. (2021)
10. R. De Silva, K. Vongsanga, X. Wang, N. Byrne; Cellulose 2015, 22(5), 2845–2849. https://doi.org/10.1007/s10570-015-0733-9
11. R. De Silva, N. Byrne; Carbohydrate Polymers 2017, 174, 89–94. https://doi.org/10.1016/j.carbpol.2017.06.042
12. C. Adu, C. Zhu, M. Jolly, R.M. Richardson, S.J. Eichhorn; Journal of Cleaner Production 2021, 280, 124503. https://doi.org/10.1016/j.jclepro.2020.124503
13. L.V. Haule, C.M. Carr, M. Rigout; Journal of Cleaner Production 2016, 112, 4445–4451. https://doi.org/10.1016/j.jclepro.2015.08.086
14. O.A. El Seoud, M. Kostag, K. Jedvert, N.I. Malek; Macromolecular Materials and Engineering 2020, 305(4), 1–21. https://doi.org/10.1002/mame.201900832
15. A. Michud, M. Tanttu, S. Asaadi, Y. Ma, A. Persson, E. Netti; Textile Research Journal 2016, 86. https://doi.org/10.1177/0040517515591774

METAL IONS REMOVAL EFFICIENCY USING GREEN CELLULOSE HYDROGEL ADSORBENT

Rafaela R. Ferreira[1], Carlos H. B. Franzin[1] and Derval S. Rosa[1]*

1 – Center for Engineering, Modeling, and Applied Social Sciences - CECS, Federal University of ABC (UFABC), Santo André, São Paulo 09210-580, Brazil
derval.rosa@ufabc.edu.br / dervalrosa@yahoo.com.br

.

Abstract – Effluent treatment remains a global challenge, especially in removing metallic ions present in wastewater, which represent a sererely threaten human health. Adsorption has proven to be an efficient approach to tackle this problem, and three-dimensional hydrogel has emerged as a promising material in this context. The aims of this paper is to develop cellulose (Hc) hydrogels by incorporation of montmorillonite (MMT) nanoclays cloisite 20A for the removal of toxic metallic ions. The hydrogels will be produced using a crosslinking agent, and different concentrations of MMT (3% and 5% by mass) will be tested. Analyzes of the chemical composition, morphology, and adsorption capacity of metallic pollutants will be carried out for both nanoclays and hydrogel systems. It is expected that this study will contribute to the advancement of effluent treatment, offering an efficient and sustainable solution for removing metallic contaminants, with benefits for public health and the environment.

Keywords: *Hydrogel; Cellulose; Nanoclays.*

Fundings: This research was financed by FAPESP (2022/01382-3, 2022/11133-0, 2021/14714-1, and 2020/13703-3), CNPq (308053/2021-4 and 403934/2021-4), and (CAPES) (Finance Code 001).

Introduction

The global scarcity of water resources is an urgent and worrying problem. Contamination of wastewater by metallic ions from industrial and agricultural sectors further aggravates the situation, bringing negative consequences for the environment and human health [1]. Faced with this alarming environmental scenario, several research studies have been conducted with the aiming of developing more efficient technologies and materials for the removal of toxic metallic ions from polluted waters. The most discussed and investigated techniques in this area are chemical precipitation, flotation, membrane filtration, ion exchange, biological methods, and adsorption [2]. In this context, the adsorption of metal ions has emerged as an efficient and low-cost technique for treating polluted waters [3].

Among adsorbent materials, three-dimensional cellulose-based hydrogels, especially when incorporated with nanoclays, have high adsorption capacity and favorable characteristics, such as ease of synthesis, application, and reusability [4]. In this study, it is proposed the development of a biodegradable cellulose (Hc) hydrogel containing nanoclays montmorillonite cloisite 20A®, in which the chemical, morphological and water absorption properties were evaluated in focus for a future application in removal water containing metal ions.

Experimental

1. Hydrogels synthesis

In this experiment, three cellulose hydrogels were produced: one of pure cellulose (HC) and two with the addition of clays at different concentrations (HC-MMT3% and HC-MMT5%). The preparation of the hydrogels involved dissolving urea and sodium hydroxide in water, followed by the addition of microcrystalline cellulose. The mixture was refrigerated at approximately -10 °C for

24 hours and then stirred when the solution was partially liquid. MMT was added at different concentrations, and the solution was stirred for 30 minutes at approximately 900 rpm. After the addition of epichlorohydrin for crosslinking, the solutions were dried in an oven at 60 °C for 48 hours. The hydrogels were washed with water for 72 hours to remove epichlorohydrin residues and then dried again in an oven at 60 °C for 24 hours.

2. Characterization

Fourier transform infrared spectroscopy (FTIR)

The functional groups were obtained using the FTIR technique (Frontier 94.942, PerkinElmer, USA) in the operation mode with attenuated total reflectance (ATR), using a range of 4000-500 cm^{-1}, spectral resolution of 4 cm^{-1}, and 32 scans.

Water absorption

The water absorption of the hydrogels was obtained by immersing 0.1 g of dry hydrogel pieces in 50 mL of ultrapure water. Samples were collected periodically from 0 to 24 h to weigh the mass of swollen hydrogels. At the end of the assay, the hydrogel solubility was measured to determine the weight loss. The degree of swelling (*DS*) were calculated by Eq.1 [5], where m_s (t) is the swollen mass of hydrogel in a time t (g), and m (t = 0) is the dry hydrogel mass (g).

$$DS = \frac{m_s(t) - m(t=0)}{m(t=0)} \, x \, 100 \qquad (1)$$

Scanning electron microscopy (SEM)

Morphology was obtained by SEM technique (FEI Quanta 250, Thermo Fisher Scientific, USA). Sample was covered with a thin layer of gold with a thickness of 25 nm (Sputtering Leica EM ACE200, Leica Microsystems, Germany). The micrographs were obtained under the conditions: current of 50 pA, voltage of 10 kV, and spot size of 4 nm.

Results and Discussion

Fig 1 (A) shows the infrared spectra for samples, HC sample (cellulose hydrogel): The spectrum shows a broad band between 3500 and 3200 cm^{-1}, with a peak at around 3300 cm^{-1}, indicating the presence of hydroxyl groups (OH). A low-intensity peak is also observed in the region from 2900 to 3000 cm^{-1}, related to the symmetric stretching of the C-H bonds. Furthermore, a weaker peak at 1650 cm^{-1} indicates the stretching of the C=O bond of the carbonyl group, and a strong peak around 1000 cm^{-1} represents the characteristic C-O-C glycosidic bond of the glucose molecule. There was also a weak band in the region from 1500 to 1250 cm^{-1}, corresponding to the CH_3 folding of the compounds' carbon chain. An enhancement of the signals is observed in all regions compared to the HC sample, especially for the 3 and 5% HC-MMT sample (cellulose hydrogel modified with 3 and 5% montmorillonite clay). It can be attributed to the successful interaction of montmorillonite clay with cellulose. Clay has distinctive characteristics in the FTIR spectrum, such as a band around 3400 cm^{-1} related to the OH groups present in its molecule, and peaks around 1020 cm^{-1} attributed to the vibration of the stretching of the Si-O bond in its structure [6].

One of the most significant and useful characteristics of hydrogels, which are evaluated in various aqueous solutions, is their ability to absorb and retain water in their network. The swelling behavior of the nanocomposite hydrogel with different percentages of MMT and pure hydrogel was examined in distilled water. The water absorption profiles of pure hydrogels and nanocomposites are shown in (Fig. 1B). The degree of swelling water capacities of the nanocomposite hydrogels HC-MMT3% (1320.4%) and HC-MMT5% (1199.3%) are lower than those of HC (1424.9%). The decrease in water absorption capacity by the addition of MMT hydrophobic nature due to its

organo-modification (with quaternary ammonium salt). On the other hand, the physical cross-linking effect of the clay layers in the hydrogel matrix can cause greater porosity of the hydrogel structure. The increase in porosity can lead to a rise in expansion affinity and, therefore, to an increase in the sorption capacity of metallic ions [7].

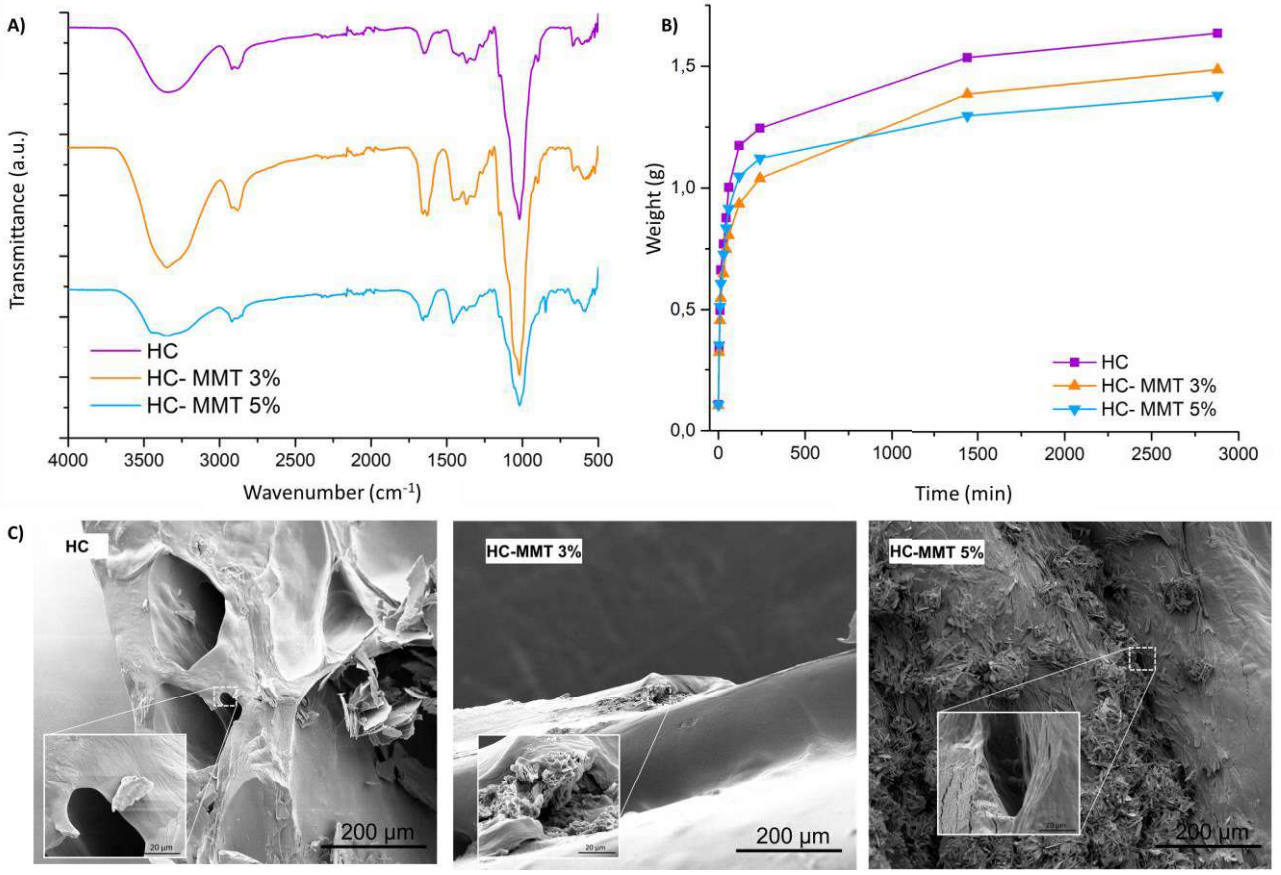

Figure 1 – A) The FTIR spectra of cellulose hydrogel without and with MMT; B) Water absorption of cellulose hydrogel without and with different MMT contents; C) SEM micrographs of the hydrogel samples.

The morphology of the synthesized hydrogels was evaluated using scanning electron microscopy (SEM) images of cross sections of crosslinked hydrogels, as illustrated in Fig 1 (C). The images revealed a characteristic three-dimensional (3D) pore structure, with interconnected pores, typical of natural polymeric hydrogels. This 3D porous structure with conductive pores is advantageous for sorption with metal ions. Furthermore, the hydrogel (HC) showed open hollow pores. Incorporation of HC-MMT3 and 5% into the matrix resulted in particle aggregation due to surface incorporation of these nanoparticles.

Conclusions

In summary, analysis of the infrared spectrum revealed that the cellulose hydrogel (HC) has hydroxyl groups (OH), C-H bonds, carbonyl groups (C=O) and the glycosidic bond C-O-C of glucose. Modification with montmorillonite clay (HC-MMT) enhanced signals in all regions, indicating a successful interaction between clay and cellulose. Scanning electron microscopy (SEM) showed a three-dimensional porous structure with interconnected pores in the hydrogels, while the incorporation of HC-MMT resulted in particle aggregation. The nanocomposites exhibited lower water absorption capacity due to the hydrophobic nature of the clay, but the physical interweaving

effect of the clay layers increased the porosity. In short, the addition of montmorillonite clay to the cellulose hydrogel altered its properties, affecting water absorption and possibly improving the sorption of metal ions.

Acknowledgements

The authors thank the technical support of the Multiuser Experimental Center of UFABC (CEM-UFABC), CECS (UFABC), and REVALORES for assistance. The authors also thank Ingredion Company for donation of the corn starches.

References

1. Al-Asadi, S.A.R., Al-Qurnawi, W.S., Al Hawash, A.B. et al. *Iraq. Appl Water Sci* 10, 103 (2020). https://doi.org/10.1007/s13201-020-01196-1
2. Ajiboye, T.O., Oyewo, O.A. & Onwudiwe, D.C. *J Inorg Organomet Polym* 31, 1419–1442 (2021). https://doi.org/10.1007/s10904-020-01803-3
3. Zaimee, M.Z.A.; Sarjadi, M.S.; Rahman, M.L. *Water* 2021, 13, 2659. https://doi.org/10.3390/w13192659
4. Teow, Yeit Haan, Li Ming Kam, and Abdul Wahab Mohammad. *Journal of environmental chemical engineering* 6.4 (2018): 4588-4597. https://doi.org/10.1016/j.jece.2018.07.010
5. Marciano, J. S., Ferreira, R. R., de Souza, A. G., Barbosa, R. F., de Moura Junior, A. J., & Rosa, D. S. (2021). *International Journal of Biological Macromolecules,* 181, 112-124. https://doi.org/10.1016/j.ijbiomac.2021.03.117
6. Hafezi, M., Khorasani, S. N., Khalili, S., & Neisiany, R. E. (2023). *International Journal of Biological Macromolecules*, 242, 124962. https://doi.org/10.1016/j.ijbiomac.2023.124962
7. Olad, A., Allami, Z., Hejazi, M. J., Eslamzadeh, M., Fathi, F., & Hezari, S. (2023). *Polymer Bulletin*, 1-22. https://doi.org/10.1007/s00289-023-04717-5

OIL SPILL RECOVERY FROM SEAWATER USING POST-CONSUMER POLYURETHANE FOAM HYDROPHOBIZED WITH PALMITIC ACID: A KINETIC STUDY

Keslei R. da Rocha[1*], Isadora C. B. do Nascimento[1], Osvaldo Chiavone Filho[1], Humberto N. M. de Oliveira[1]

1 – Department of Chemical Engineering, University of Rio Grande do Norte (UFRN), Natal, RN, Brazil
kesleirosendo@gmail.com

Abstract - This work modified polyurethane foam obtained from a post-consumer mattress with palmitic acid coating to increase hydrophobicity and oil affinity. Sorption tests were performed on a multicomponent system with seawater and diesel. The modification reduced approximately 184% of the seawater sorption, which indicates success in the polymer's surface hydrophobization. For Un-PC, the seawater sorption was best modeled by the pseudo-second-order kinetic model (R^2 = 0.99; SSR = 12.49), while the diesel sorption was best modeled by the logistic model (R^2 = 0.99; SSR = 13.53). For PA-PC, both seawater and diesel sorption data were best fitted using the logistic model (R^2 = 0.99; SSR = 0.48 and R^2 = 0.99; SSR = 5,97, respectively).

Keywords: *reuse of polymers, post-consumer mattress, surface modification, oil spill*

Fundings: This work is supported by the Brazilian National Agency of Petroleum, Natural Gas and Biofuels through the Human Resources Program PRH 44.1.

Introduction

Although unwanted, oil spills into the oceans can occur due to offshore drilling and transportation activities. When accidents with spills happen, the most immediate action is to fence the leak to prevent its propagation [1]. Then, different removal methods can be used to recover the oil spilled into the ocean. Incineration, pumping with a skimmer, and surfactant dispersants are traditionally used methods [1,2]. Alternative methods using high porosity structures to recover oils spilled have been used [3,4]. Polyurethane, for example, is a highly porous polymer commonly found in upholstery and mattresses [5]. Unfortunately, it is common to find post-consumer polyurethane mattresses discarded irregularly throughout large cities, increasing the need for study on reuse options. Although polyurethane foams obtained from semi-flexible mattresses are highly porous and can separate oils spilled in seawater, their selectivity for oil is low. This means that the foam absorbs both water and oils in high quantities. However, it is possible to change this behavior through surface modifications to increase the foams' selectivity for oils.

In this work, post-consumer polyurethane foams were coated with palmitic acid to increase selectivity for oils over seawater. The modification seeks to increase hydrophobicity and oil affinity. This opens the possibility of removing foams from the environment by recycling them through modification and subsequent reuse in recovering oils spilled in seawater.

Experimental

Post-consumer polyurethane foam was recovered from an irregular disposal area beside a highway. The label on the mattress indicates a density of 18 $kg \cdot m^{-3}$. Although dirty, there were no signs of

physical damage or visible compaction. The foam was washed with 70% ethanol and oven dried to constant mass. It was then cut into 1 cm³ cubes for modification and testing. All reagents used in this work were purchased from Synth, Brazil, and used as received.

Surface modification

The palmitic acid coating methodology was adapted from Li et al. [6] and Rocha et al. [7]: the foams cubes were immersed for 48 h in a 1 x 10^{-2} mol·L^{-1} of palmitic acid (PA) solution using anhydrous ethanol as solvent. Then, the cubes were dried in an oven at 60 °C resulting in the PA-PC foam.
Unaltered post-consumer foam (Un-PC) was used in the sorption tests and in the kinetics construction to compare results against the modified foam.

Sorption tests and kinetics

The sorption tests were performed according to the ASTM F726 and ASTM D95 [8,9] methodology. One-way analysis of variance was used to assess statistical significance using the Statistica 7 software. The kinetics were constructed and studied using the Origin 2016 software. All data was obtained at 23 °C ± 1 °C.
The kinetic models used were: pseudo-first-order - also known as Lagergren - (Eq. 1); pseudo-second-order - also known as Ho and McKay - (Eq. 2); Weber and Morris (Eq. 3); Logistic (Eq. 4) and Elovich (Eq. 5).

$$\frac{dq_t}{dt} = k_1(q_e - q_t) \quad (1)$$

$$\frac{dq_t}{dt} = k_2(q_e - q_t)^2 \quad (2)$$

$$q_t = K_d \cdot t^{\frac{1}{2}} + C \quad (3)$$

$$q_t = \frac{a}{(1 + b \cdot e^{-c \cdot t})} \quad (4)$$

$$\frac{dq_t}{dt} = \alpha \cdot e^{-\beta \cdot q_t} \quad (5)$$

Where: k1, k2, and Kd are the kinetic constants of Lagergren, HO & McKlay, and Weber & Morris, respectively; qe and qt are the amount of fluid sorbed at equilibrium and at the time t, respectively; t is time; a, b, and c are constants of the logistic model; α and β are constants of Elovich's model.

Results and Discussion

Sorption tests were performed on a multi-component system that simulate an oil spill. The results are compiled in Table 1. In the seawater (92%):(8%) diesel system, the Un-PC foam showed the highest sorption of diesel oil and seawater. Compared to PA-PC foam, Un-PC absorbed 184% more seawater and only 35% more diesel. Although the modified foam reduced the sorption capacity of diesel, it strongly reduced the sorption of seawater.
Two approaches are possible here. If the reservoir where the water/oil recovered by the foam can be emptied from below, the Un-PC foam can be an interesting option, even absorbing more water. Diesel will float since it is less dense than water and poorly soluble. In this way, it is possible to empty the lower part of the reservoir into the sea, as the lower layer is only composed of seawater (although traces of oil will be present). However, if the reservoir can only be emptied when returning to the mainland, choosing a foam with the characteristics of PA-PC is more appropriate, as it has better selectivity for oils and consequently will sorb less seawater.

Table 1: Sorption testes results for the multicomponent system seawater-diesel.

Sorption ($g \cdot g^{-1}$)	Seawater		Diesel	
	Un-PC	PA-PC	Un-PC	PA-PC
	$15.78^{a} \pm 0.51$	$5.56^{b} \pm 0.26$	$30.44^{A} \pm 1.86$	$22.54^{B} \pm 0.54$

Equal lowercase (seawater) and uppercase (diesel) letters on the same line indicate no statistical difference in the Tukey test with a significance level of 5%.

Fig. 1 shows the kinetic profiles of water and oil sorption using Un-PC foam in the seawater (92%):(8%) diesel multicomponent system. Table 2 presents the calculated parameters.

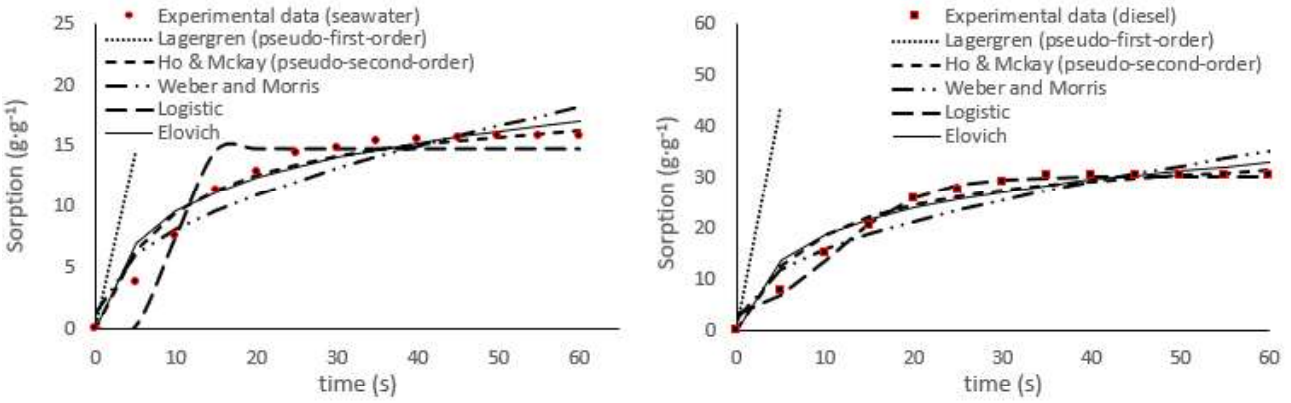

Figure 1. Kinetic profiles of water and oil sorption using Un-PC foam in the seawater (92%):(8%) diesel multicomponent system

Table 2: Calculated parameters for kinetic models.

Kinetics	Parameters	Seawater	Diesel
Pseudo-first-order	K1 ($g.g^{-1}.s^{-1}$)	0.13	0.16
	Qe ($g.g^{-1}$)	29.94	77.85
	R^2	0.92	0.92
	SRR	2393.33	27027.44
Pseudo-second-order	K2 ($g.g^{-1}.s^{-1}$)	0.0054	0.0028
	Qe ($g.g^{-1}$)	18.80	36.34
	R^2	0.99	0.99
	SRR	12.49	48.44
Elovich	α ($g.g^{-1}.\ s^{-1}$)	3.45	6.59
	β ($g.g^{-1}$)	0.23	0.12
	R^2	0.95	0.95
	SRR	19.47	73.56
Weber e Morris	Kd ($g.g^{-1}.\ s^{-0,5}$)	2.19	4.24
	C ($g.g^{-1}$)	1.18	2.13
	R^2	0.90	0.90
	SRR	32.32	117.43
Logistic	a ($g.g^{-1}$)	14.75	29.99
	b	8100.81	9.44
	c (s^{-1})	0.90	0.20
	R^2	0.90	0.99
	SRR	32.03	13.53

In the first 10 s, the Un-PC foam absorbed 50% of the oil available in the simulated spill. The oil recovery growth occurred until 20 s reaching 85% of the diesel initially available. Between 20 s and 35 s, recovery reached 99% and remained constant until the end of the test at 60 s. Similar behavior was observed for seawater sorption by Un-PC. Up to 20 s, seawater sorption occurred linearly, reaching about 13 $g \cdot g^{-1}$, then increasing slowly between 20 s and 35 s, reaching approximately 15 $g \cdot g^{-1}$. This value remained practically constant until the end of the test at 60 s.
The pseudo-second-order model for seawater and the logistic model for oil sorption were the kinetics that best described the sorption using Un-PC foams.

Fig. 2 shows the kinetic profiles of water and oil sorption using PA-PC foam in the seawater (92%):(8%) diesel multicomponent system. Table 3 presents the calculated parameters.

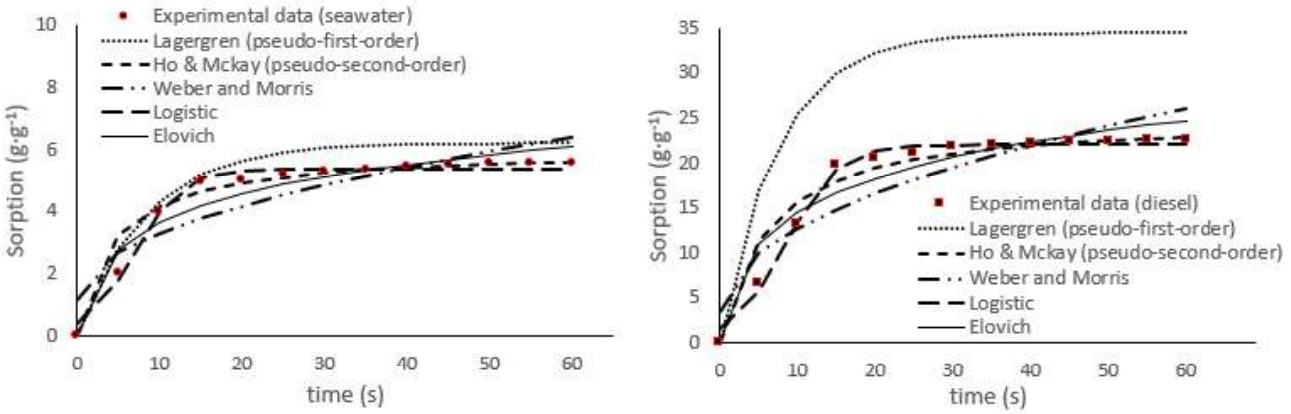

Figure 2. Kinetic profiles of water and oil sorption using PA-PC foam in the seawater (92%):(8%) diesel multicomponent system

Table 3: Calculated parameters for kinetic models.

Kinetics	Parameters	Seawater	Diesel
Pseudo-first-order	K1 ($g.g^{-1}.s^{-1}$)	0.12	0.13
	Qe ($g.g^{-1}$)	6.21	34.46
	R^2	0.96	0.89
	SRR	5.24	1670.76
Pseudo-second-order	K2 ($g.g^{-1}.s^{-1}$)	0.038	0.006
	Qe ($g.g^{-1}$)	5.98	25.17
	R^2	0.98	0.97
	SRR	1.66	35.93
Elovich	α ($g.g^{-1}.\ s^{-1}$)	1.75	6.09
	β ($g.g^{-1}$)	0.71	0.16
	R^2	0.97	0.93
	SRR	2.18	46.18
Weber e Morris	Kd ($g.g^{-1}.\ s^{-0,5}$)	0.67	2.91
	C ($g.g^{-1}$)	1.15	3.53
	R^2	0.81	0.83
	SRR	6.21	102.26
Logistic	a ($g.g^{-1}$)	5.36	22.01
	b	11.89	13.13
	c (s^{-1})	0.35	0.30
	R^2	0.99	0.99
	SRR	0.48	5.97

As observed for Un-PC, PA-PC recovered 50% of the oil initially spilled into the system in just 10 s of exposure. Up to 15 s, the sorption growth was practically linear. After that, growth occurred slowly until 50 s when there was stabilization without statistically relevant changes. At 60 s, the maximum recovery achieved was around 85%. For seawater, PA-PC sorbed linearly from the beginning until 15 s, strongly reducing water sorption from 20 s. The sorption capacity stability characterized by the pore's saturation occurs at 20 s for both seawater and diesel.

Among the kinetic models tested, the logistic was the one that best described the sorption behavior of both fluids. This fact can be attested by the coefficient of determination (R^2 = 0.99 for both fluids) and the Sum of the Square of Residues (SSR). For comparative purposes, the logistic model presented SSR = 0.48 and SSR = 5.97 against SSR = 5.24 and SSR = 1670.76 observed in the pseudo-first-order model for the kinetic data of seawater and diesel sorption, respectively. The higher the SSR, the further the models are from describing the experimental behavior.

Olivito et al. [10] synthesized bio-based polyurethane foams with cellulose and managed to absorb up to 65 $g \cdot g^{-1}$ of diesel in a distilled water-diesel system. Among the tested models, pseudo-second-order kinetics was the one that best modeled the diesel sorption data (R^2 = 0.99).

Conclusions

Polyurethane foams obtained from post-consumer mattresses can be potential alternative materials to recover oils spilled in seawater. With simple and low-cost modifications, it is possible to increase the selectivity of the foams, which in this work could absorb up to 22 times their own weight in oil in less than 35 seconds of exposure.

Acknowledgements

This work is supported by the Brazilian National Agency of Petroleum, Natural Gas and Biofuels through the Human Resources Program PRH 44.1.

References

1. S. A. Abernathy; J. K. Gilliam; P. J. Klouda, P. J. *Drilling and production discharges and oil spills in the marine environment*, U.S. Department of The Interior, Virginia, 1989.
2. D. Dave; A. E. Ghaly. Remediation Technologies for Marine Oil Spills: A Critical Review and Comparative Analysis. *American J. of Environmental Sciences*, v. 7, n. 5, p. 423–440, 2011.
3. H. Li; L. Liu; F. Yang. Hydrophobic modification of polyurethane foam for oil spill cleanup. *Mar. Pollut. Bull.*, v. 64, n. 8, p. 1648–1653, 2012.
4. T. J. Ko; J. H. Hwang; D. Davis; M. S. Shawkat, S. S. Han; K. L. Rodriguez; K. H. Oh; W. H. Lee; Y. Jung. Superhydrophobic MoS_2-based multifunctional sponge for recovery and detection of spilled oil. *Current App. Phys.*, v. 20, n. 2, p. 344–351, 2020.
5. A. C. Grotto; M. Hemkemeier; M. V. Rossato. Sustentabilidade no uso de poliuretano e reutilizações de aparas. *Res., Soc. and Develop.*, v. 9, n. 11, p. e99891110685, 2020.
6. B. Li; X. Liu; X. Zhang; J. Zou; W. Chai; Y. Lou. Rapid adsorption for oil using superhydrophobic and superoleophilic polyurethane sponge. *J. Chem. Tech. Biotec*., v. 90, n. 11, p. 2106–2112, 2015.
7. K. R. da Rocha; O. Chiavone-Filho; H. N. M. de Oliveira. A simple and efficient method of post-consumer polyurethane foam coating for oil spill sorption in seawater. *In: Open Science Researh III*, São Paulo, 2022, p. 2905-2913.
8. ASTM. F726-12 - Standard Test Methods for Sorbent Performance of Adsorbents. *ASTM International*, p. 1–6, 2012.
9. ASTM. D95-13 - Standard Test Method for Water in Petroleum Products and Bituminous Materials by Distillation. *Manual on Hydrocarbon Analysis, 6th Edition*, p. 545-545–3, 2013.
10. F. Olivito; V. Algieri; A. Jiritano; M. A. Tallarida; P. Costanzo; L. Maiuolo; A. de Nino. Bio-Based Polyurethane Foams for the Removal of Petroleum-Derived Pollutants: Sorption in Batch and in Continuous-Flow. *Polymers*, v. 15, n. 7, p. 1785, 2023.

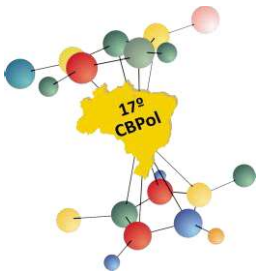

POST-CONSUMER PET/HDPE INJECTION AND EXTRUSION REPROCESSING

Luanda S. de Moraes[1]*, Viviana A. P. Maia Teixeira[1], Melissa M. dos Anjos[1], Guilherme S. L. Magalhães1[1], Diogo A. F. Coelho[2], Isac Martins Pereira[2]

1- Faculdade de Ciências Exatas e Engenharias, Universidade do Estado do Rio de Janeiro (UERJ-ZO), Rio de Janeiro, RJ, Brazil
luandasmoraes@gmail.com
2-Cogumelo Indústria e Comércio Ltda., Rio de Janeiro, RJ, Brazil

Abstract – The high demand for the synthesis of polymeric materials brings a reflection in the use of these post-consumer materials, especially Polyethylene Terephthalate (PET) applied on various products [1]. Aiming to reduce the impact of excessive disposal of these polymers, proposals for the development of new materials, whose composition enables their reuse, have become a priority [2]. The objective of this work was to produce post-consumer PET/HDPE polymeric blends for COGUMELO as a raw material option, which currently only recycles post-consumer HDPE. For the development of this work, post-consumer PET/HDPE polymeric blends were prepared in different proportions, which were processed through extrusion and injection. The results of the thermal and mechanical properties showed that the presence of PET in the blends, in different concentrations, had an impact on the increase of the indexes obtained in the thermal and mechanical analysis, in relation to the post-consumer HDPE matrix.
Keywords*: polymeric blends, post-consumer, reprocessing*
Fundings: FAPERJ – Fundação Carlos Chagas Filho de Amparo à Pesquisa do Estado do Rio de Janeiro.

Introduction

Plastic is present in contemporary life for its numerous positive characteristics, as it is a versatile, moldable, flexible, accessible, recyclable and resistant material, in addition to being able to be used in various applications, bringing practicality and improving the convenience of the goods and services offered [3]. However, it is imperative that recycling actions are carried out to prevent them, after consumption, from being improperly discarded in the environment, polluting and destroying various ecosystems, given the long time required for their degradation in nature. Polymeric materials such as High Density Polyethylene (HDPE) and Polyethylene Terephthalate (PET) represent two of the most consumed thermoplastic classes and are available in large quantities from domestic disposal, constituting a large portion of post-consumer plastic waste, mainly in the sector of packaging [4]. The modification of post-consumer PET and HDPE through the blending system, under appropriate conditions, can provide an alternative route for the commercialization of recycled materials, with satisfactory cost/performance, and in diverse and potential applications, that can range from domestic to engineering sectors. However, to date, the development of efficient processes for recycling post-consumer plastic mixtures by physical-mechanical methods has been very limited [5].

Experimental

Materials

To prepare the polymeric blends, the post-consumer PET and HDPE polymers were weighed and mixed in the proportions defined in Table 1, using a Mark1300 digital scale (BEL brand) and Sintered Ceramic Jar Mill (Marconi brand).

Table 1.Identification of blends.

Polymer	HDPE (%)	M1.1 (%)	M1.2 (%)	PET_{CR} (%)	PET_{IG} (%)	E1.1 (%)	E1.2 (%)
HDPE	100	50	50	-	-	40	40
PET CR	-	50	-	100	-	60	-
PET IG	-	-	50	-	100	-	60

Preparation of post-consumer PET/HDPE polymer blends

The polymeric materials were mixed in a Sintered Ceramic Jar Mill (Table 1), as well as the post-consumer PET and HDPE polymers, and, subsequently, processed in a Twin Screw Extruder (Extruder Mod. DCT 20-40/ TECK TRIL) in the molten state, in the temperature range of 140-240 ºC and rotation between 140-150 RPM.

Preparation of specimens for thermal tests

The polymeric blends produced from reprocessed post-consumer PET and HDPE (Table 1) were previously dried in a Drying and Sterilization Oven MA033 (Marconi brand) at 100ºC for 4 hours before use. Afterwards, they were pressed at 280ºC in a 15 TON Hydraulic Press (Marconi brand), separately in metallic form in the necessary dimensions (ISO 75-1 and 2) for application on the thermal resistance tests of HDT and VICAT.

Preparation of specimens for mechanical testing

The polymeric blends produced and the reprocessed post-consumer HDPE were heated in an oven at COGUMELO's laboratory to remove moisture. Then, they were injected in the temperature range of 100-200ºC, in the CESTARI injector at a speed of 500 RPM, for the production of specimens (60 x 60 x 430 mm) to be applied on the mechanical test of Vertical Deflection.

Thermal Characterization

The thermal resistance of polymer blends and reprocessed post-consumer PET and HDPE polymers was analyzed using HDT and VICAT tests (CEAST brand).

For the HDT test, specimens measuring 10 x 3 x 120 mm (ISO 180) were used, on which an effort was applied (APPLIED STRESS: 1820 kPa or 1.82 Mpa / SPAN or Free Span: 100 mm / Position: edge) under heating in a silicone bath.

In the VICAT test, specimens measuring 10 x 3 mm were used, heated in a silicone bath, subjected to a standardized vertical load of 10 N, penetrating exactly 1 mm into each sample, through a circular indenter with a cross section of 1 mm^2.

Mechanical Characterization

The determination of the Vertical Deflection of the samples was implemented using the equipment: load cell, dial indicator and digital stopwatch.

The measurement of the samples, arranged along the length (greatest measurement), was performed at a point along the midline between the supports, and with a dial indicator positioned halfway across the 300 mm free span, between the supports.

Results and Discussion

In the Vertical Deflection test, the samples were subjected to the application of a

concentrated load at a point along the midline of the specimen, between the supports, in a free span of 300 mm. In the HDT and VICAT analyses, the samples were tested under heating in oil. In this work, the use of Vertical Deflection, HDT and VICAT tests aimed to evaluate the influence of the presence of post-consumer PET in the blends in relation to thermal (HDT and VICAT) and mechanical (Vertical Deflection) stability.

The VICAT and HDT analyzes provided information on the thermal behavior of post-consumer polymer blends and reprocessed post-consumer PET and HDPE polymers (Table 2), with the thermal deflection temperature being obtained by the HDT test, determined through the decrease in the mechanical properties of the polymer, this value being a comparative data that defines the maximum service temperature of this material, Graphic 1 [6]. In the VICAT analysis, the softening temperatures of the material under heating were obtained, Graphic 2.

Table 2. VICAT and HDT analysis results.

SAM.	HDPE (100)	M1.1 *(50:50)	M1.2 *(50:50)	PET_{CR} (100)	PET_{IG} (100)	E1.1 *(40:60)	E1.2 *(40:60)
TEMP. (°C) VICAT	110,5	124,6	123,6	169,4	189,5	146,0	138,2
TEMP. (°C) HDT	66,6	77,0	87,0	146,8	NT	74,5	84,4

*Blends PET/ HDPE.
NT: Unable to test.

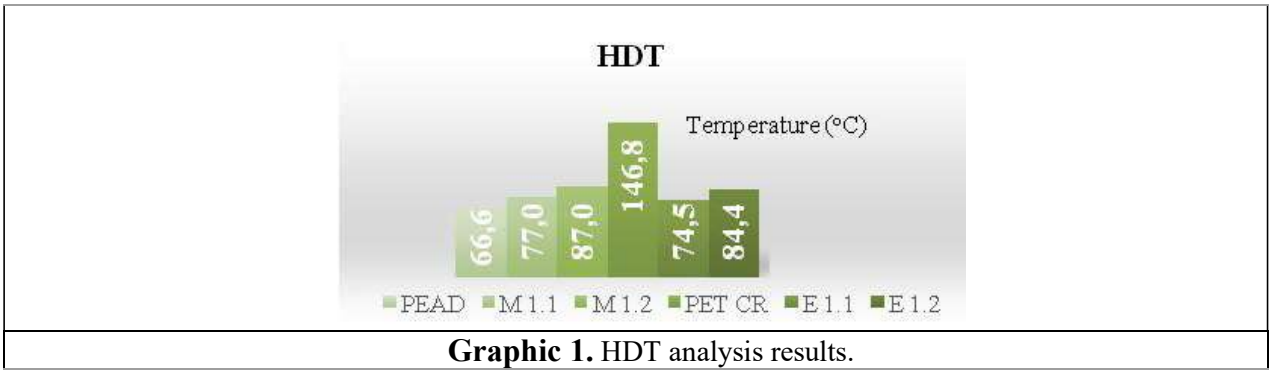

Graphic 1. HDT analysis results.

HDPE = PEAD.

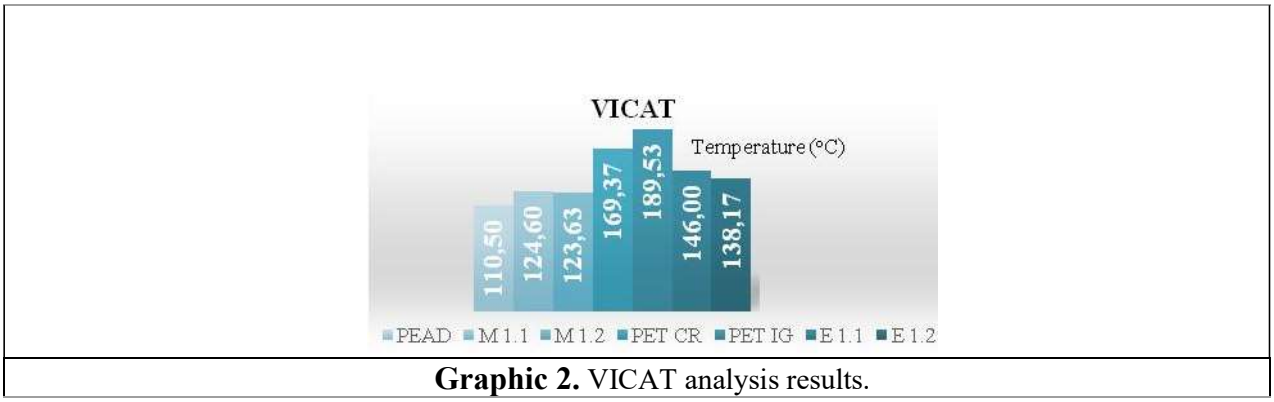

Graphic 2. VICAT analysis results.

HDPE = PEAD.

The Vertical Deflection analysis, on the other hand, provided information about the mechanical behavior of the polymer blends produced with post-consumer PET/HDPE, as well as post-consumer pure HDPE, which was used as a comparative criterion established for the mechanical test. It is observed that the smaller the arrow obtained, the better the mechanical performance of the material, becoming even more resistant. Data obtained for residual sag

corroborate this result (Graphics 3-4). The results are described in Tables 3 and 4.

Table 3. Results of Vertical Deflection in a free span of 300 mm, Charge (± 0,5 kg), Time (min).

SAMPLES			**HDPE COG.(100)**	**M1.1 (50:50)**	**M1.2 (50:50)**	**E1.1 (40:60)**	**E1.2 (40:60)**
LENGTH			**430 mm**				
POINT	Charge (± 0,5 kg)	Time (min)					
1	30	1	0,43	0,26	0,20	0,26	0,24
2	60	1	0,76	0,54	0,37	0,48	0,52
3	90	1	1,03	0,74	0,54	0,69	0,78
4	120	1	1,25	0,93	0,71	0,86	1,02
5	150	1	1,46	1,10	0,86	1,04	1,27

Table 4. Residual Arrow Results.

SAMPLES	**HDPE COG.(100)**	**M1.1 (50:50)**	**M1.2 (50:50)**	**E1.1 (40:60)**	**E1.2 (40:60)**
TIME(MIN.)	LENGTH: 430 mm				
15	0,41	0,31	0,19	0,20	0,41
20	0,39	0,30	0,18	0,19	0,39

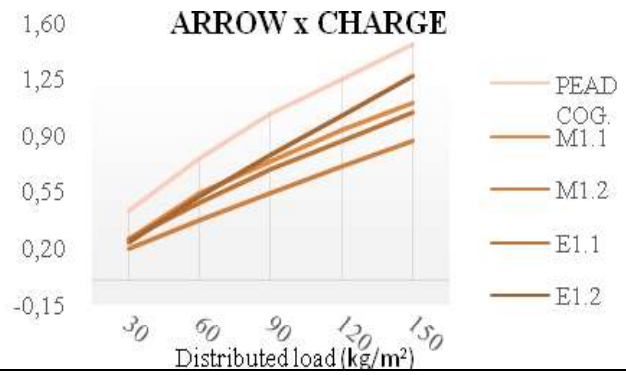

Graphic 3. Arrows after charging.

PEAD=HDPE.

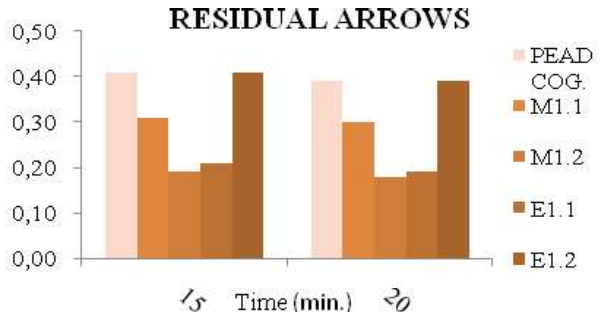

Graphic 4. Residual Arrows.

PEAD=HDPE.

Through the results obtained in the thermal analyses of VICAT and HDT, it was possible to observe the influence of the addition of post-consumer PET in polymeric blends based on HDPE, in which an increase in thermal resistance was observed when compared to the matrix of pure HDPE post-consumer. Similar to the thermal resistance results, this addition also raised the mechanical

resistance values, the growth in both being provided by the introduction of the molecular structure of PET in polymeric blends based on post-consumer HDPE. However, when we examine the presence of post-consumer HDPE in post-consumer PET-based blends, we observe a reduction in the values of thermal analyses.

Conclusions

The addition of post-consumer PET to post-consumer HDPE expanded the thermal and mechanical resistances of the material when compared to the values obtained for pure post-consumer HDPE. Such results were corroborated by the data obtained in the Vertical Deflection analysis, which also showed an increase in the mechanical resistance of the material, possibly provided by its molecular structure containing group benzene compounds responsible for the rigidity of the PET chain, giving the material greater thermal and mechanical resistance in the solid state.

Acknowledgements

The authors would like to thank FAPERJ and COGUMELO for the financial support and UERJ-ZO for making the Didactic & Materials Processing Research Laboratory (LDPPM) available.

References

1. I. M. E. Macedo; M. D. L. C. Souza; N. K. S. Shinohara; C. S. Santos; M. K. G. Silva. Brazilian Journal of Development 2020, 57704-57723. https://doi.org/10.34117/bjdv6n8-252.
2. S. K. Das; S. K. Eshkalak; A. Chinnappan; R. Ghosh; W. A. D. M. Jayathilaka; C. Baskar; S. Ramakrishna. Materials Circular Economy, 2021, 3, 9. https://doi.org/10.1007/s42824-021-00025-3.
3. Growth of PET recycling and the challenges of the sector. ABRE, 2020. Available at <https://www.abre.org.br/sustentabilidade/crescimento-da-reciclagem-do-pet-e-os-desafios-do-setor/>. Accessed on: March 08, 2023.
4. J. C. Caraschi; A. L. Leão. Acta Scientiarum, 2002, 24(6), 1599-1602. https://doi.org/10.4025/actascitechnol.v24i0.2462.
5. M. Pracella; L. Rolla; D. Chionna; A. Galeski. Macromolecular Chemistry and Physics 2002, 203, 1473. https://doi.org/10.1002/1521-3935(200207)203:10/11<1473::AID MACP1473>3.0.CO;2-4
6. G. A. S. Brito. *HDT and VICAT Thermal Resistance*. São Paulo, 2017.

REDUCTION, RECYCLING, AND REUSE OF POLYURETHANE MATTRESSES FOR RECOVERING OILS SPILLED IN SEAWATER: KINETICS AND SURFACE PHENOMENA STUDY

Keslei R. da Rocha[1*], Osvaldo Chiavone Filho[1], Humberto N. M. de Oliveira[1]

1 – Department of Chemical Engineering, University of Rio Grande do Norte (UFRN), Natal, RN, Brazil
kesleirosendo@gmail.com

Abstract - In this work, polyurethane foam obtained from a post-consumer mattress was modified with zinc oxide graft and coated with hexadecanoic acid to increase hydrophobicity and oil affinity. The characterizations confirmed the change in the surface structure with gains in the hydrophobization of the foam's surface. Sorption tests were performed on two multicomponent systems with seawater and diesel or 20W40 engine oil. The modification increased up to 950% the sorption capacity of 20W40 engine oil and a reduction of up to 72% in seawater sorption in the seawater-diesel system. In both systems, the sorptions of seawater and diesel oil or 20W40 engine oil were best modeled by pseudo-second-order and logistic kinetic models with $r^2 = 0.99$ for all cases.

Keywords: *reuse of polymers, post-consumer mattress, surface modification, oil spill*

Fundings: This work is supported by the Brazilian National Agency of Petroleum, Natural Gas and Biofuels through the Human Resources Program PRH 44.1.

Introduction

Oil is currently the primary source of energy in the world, along with coal. Its importance for the maintenance of global society is undeniable. Oil can be obtained on continents and islands (onshore) as well as under the oceans (offshore). Spills can occur in the oceans during well drilling, extraction, and transportation. When they occur, the first step is to contain the oil spread and then remove it [1].

Currently, incineration, pumping, and chemical dispersants are some of the methods used to remove oil spilled at sea [1,2]. Alternative methods have been developed to recover the spilled oils, such as sorption in porous polymeric structures [3,4], for example. Polyurethane is a highly porous polymer capable of absorbing fluids [3]. However, it has little selectivity and absorbs water and oil in high quantities. The main application of polyurethane is in the production of upholstery and mattresses [5]. Unfortunately, it is common to find polyurethane mattresses discarded in landfills or dumps after their useful life. Developing techniques for reducing, recycling, and reusing these foams is necessary to protect the environment.

In this work, the presence of post-consumer polyurethane foams in nature is reduced by recycling them through surface modifications so that they can be reused and applied to separate and recover oils spilled in seawater. One residue is used to remove another.

Experimental

Post-consumer polyurethane foam was recovered from an irregular disposal area beside a highway. The label on the mattress indicates a density of 18 $kg \cdot m^{-3}$. Although dirty, there were no signs of

physical damage or visible compaction. The foam was washed with 70% ethanol and oven dried to constant mass. It was then cut into 1 cm³ cubes for modification, characterization, and testing. All reagents used in this work were purchased from Synth, Brazil, and used as received.

Surface modification

Grafting with zinc oxide (ZnO) rods was performed in two stages, adapting the methodology of Li at al. [6] and Rocha et al. [7]. In the first step, a 1 mol·L^{-1} solution of potassium hydroxide was added dropwise to a 1 x 10^{-1} mol·L^{-1} solution of zinc acetate dihydrate until pH 11 was reached. Both solutions had methanol as solvent. The mixture was mechanically stirred at 510 rpm for 90 min and then centrifuged at 3500 rpm for 10 min. The supernatant was discarded and the precipitate was resuspended in distilled water. The foam cubes were submerged for 5 min in this suspension and then cured in a vacuum oven at 170 °C for 12 min. The soaking and curing procedures were repeated three times. In the second stage, the foams resulting from the first stage were submerged in a 3 x 10^{-3} mol·L^{-1} zinc nitrate hexahydrate and 3 x 10^{-3} mol·L^{-1} hexamethylenetetramine mixture. The mixture and the foams were kept in a water bath for 180 min at 90 °C. Finally, the foams were compressed and dried in an oven at 60 °C.

The foams grafted with ZnO were immersed for 48 h in a 1 x 10^{-2} mol·L^{-1} of hexadecanoic acid (HA) solution using anhydrous ethanol as solvent. Then, the cubes were dried in an oven at 60 °C resulting in the ZnO/HA-PC foam.

Characterizations, sorption tests, and kinetics

The sorption tests were performed according to the ASTM F726/D95 [8,9] methodology. The modifications were characterized by Scanning Electron Microscopy (SEM) + Energy Dispersion X-ray Spectroscopy (EDS) (Jeol, JSM - 6610LV, Japan), X-Ray Diffractometer (XRD) (Bruker, D8 Advance, USA), Fourier Transform Infrared Spectroscopy (FTIR) (Shimadzu, Iraffinity-1, Japan), and contact angle in a goniometer (Kruss, DSA 100, Germany). One-way analysis of variance was used to assess statistical significance using the Statistica 7 software. The kinetics were constructed and studied using the Origin 2016 software. All data was obtained at 23 °C ± 1 °C.

Results and Discussion

In Fig 1, it is possible to observe that the unaltered post-consumer foams (Un-PC) showed a smooth pore surface (Fig. 1, B). In contrast, the foams with the modification combining grafting and coating (ZnO/HA-PC) developed roughness (Fig. 1, D). In the highlight of Fig. 1-D, it is possible to notice the formation of zinc oxide sheets coated with hexadecanoic acid. The EDS identified the presence of carbon, nitrogen, and oxygen in both foams (as expected since these are fundamental elements of the polyurethane polymer). Zinc, as expected, was identified only in the foam grafted with this element (Fig. 1, C). Although calcium is not part of the original polymer composition, it was identified in both foams due to its addition as a "filler" in the expansion process. The contact angle test identified an increase of 10.5° after the combined modification. Although the increase was slight, it favored the gain in hydrophobization and oil affinity of the pore surface.

Fig. 2 shows the foams' diffractogram and spectrogram. The synodal curve in all cases was between the 10° and 20° positions (Fig. 2, left) showing a typical behavior of amorphous structures such as polyurethane, which is an amorphous polymer because it does not have a well-defined spatial order. The Zn peaks were not identified because the amount grafted onto the foams is lower than the detection limit of the employed technique.

The spectrograms for Un-PC and ZnO/HA-PC foams were similar (Fig. 2, right). The slight peak near 3338 cm^{-1} is typical for the N-H bond, while the peak near 2864 cm^{-1} characterizes the CH_2 group. The sequence of small peaks at 1713 cm^{-1}, 1528 cm^{-1}, and 1241 cm^{-1} is responsible for the C=O, N-H/C-H, and N-H/C-N bonds, respectively. Finally, the sharpest peak at 1100 cm^{-1} is

characteristic of the C-O-C bond. All those bonds are typical and expected in the polyurethane structure.

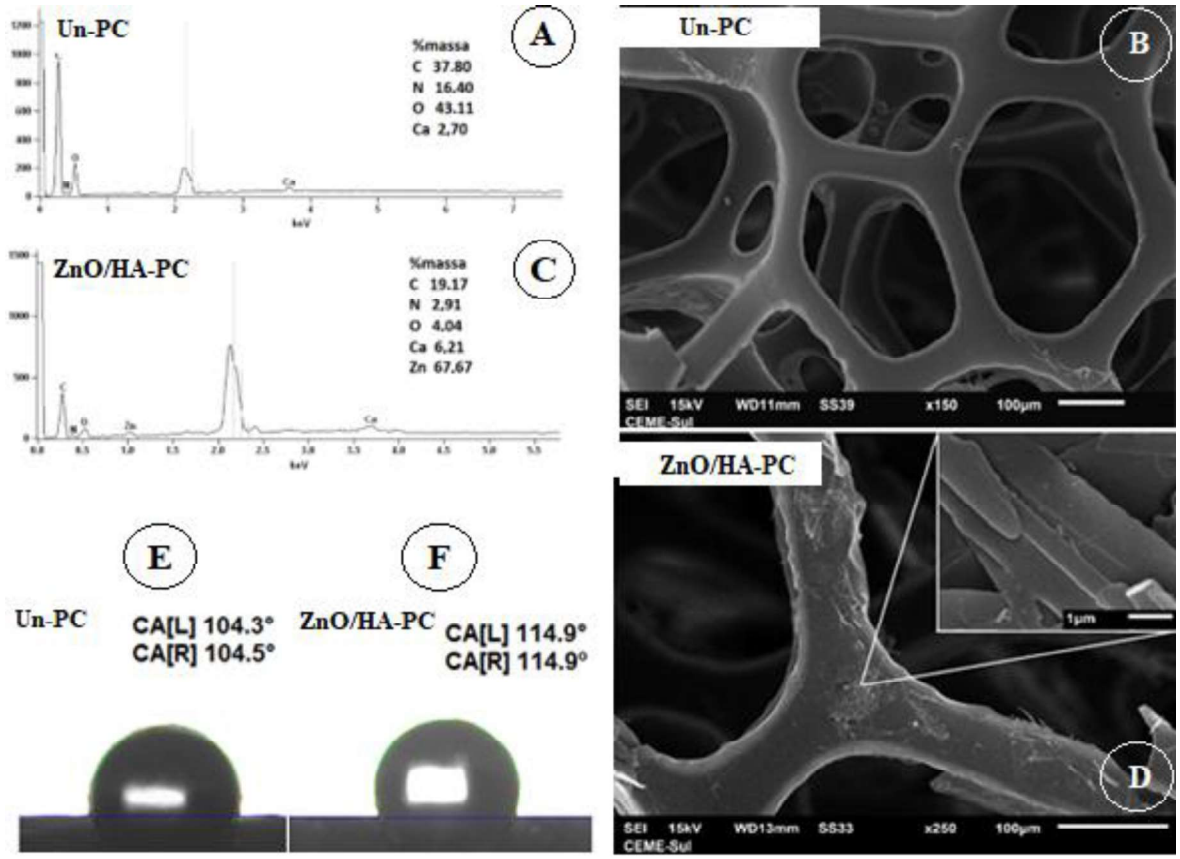

Figure 1. EDS, SEM, and contact angle before (A, B, and E respectively) and after (C, D, and F, respectively) ZnO grafting + HA coating.

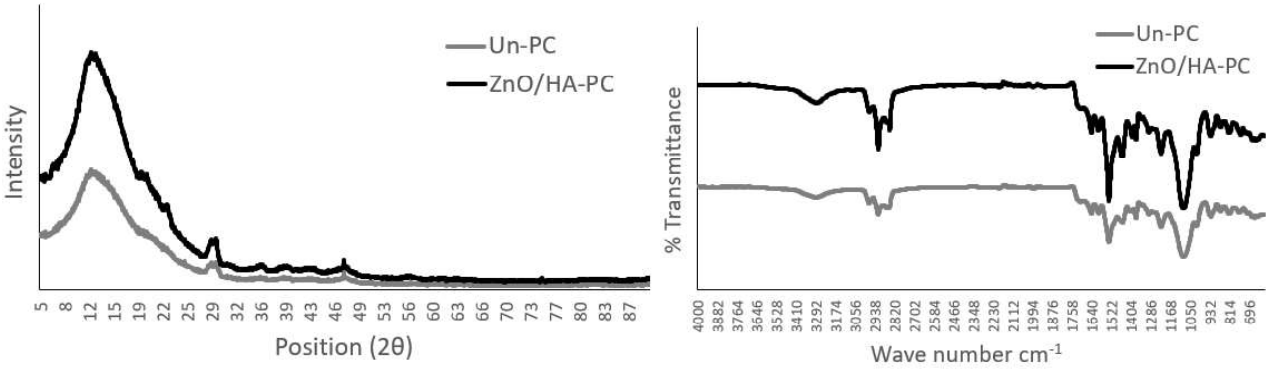

Figure 2. DRX and FTIR before (Un-PC) and after (ZnO/HA-PC) ZnO grafting + HA coating.

Sorption tests were performed on multi-component systems that simulate an oil spill. The results are compiled in Table 1. In the first system, seawater (92%):(8%) diesel oil, the Un-PC foam showed the highest sorption of diesel oil and seawater. Compared to ZnO/HA-PC foam, Un-PC absorbed 261% more seawater and only 20% more diesel fuel. Although the modified foam reduced the sorption capacity of diesel oil, it strongly reduced the sorption of seawater.

In the second system, seawater (92%):(8%) 20W40 engine oil, the ZnO/HA-PC foam showed the best results. There was an undesired increase in seawater sorption (compared to unaltered foam) but

also an outstanding 950% increase in 20W40 engine oil sorption. Un-PC foam was practically unable to sorb water or oil. Viscosity played a fundamental role when the two systems were compared. The viscosity of 20W40 engine oil (120 cSt) is about 30 times greater than the viscosity of diesel oil (4 cSt). In the system with diesel, both foams had an excellent performance in capturing the oil as it flowed easily into the pores. However, in the system with engine oil, the flow difficulty caused by the increase in viscosity made the ZnO/HA-PC foam modifications stop being coadjuvant and become the leading actor in attracting the oil to the inside of the pores.

Table 1. Sorption testes results on multicomponent systems seawater-diesel and seawater-20W40 engine oil.

Sorption ($g \cdot g^{-1}$)	Seawater		Diesel	
	Un-PC	ZnO/HA-PC	Un-PC	ZnO/HA-PC
	$15.78^{a} \pm 0.51$	$4.37^{b} \pm 0.20$	$30.44^{A} \pm 1.86$	$25.19^{B} \pm 0.99$
Sorption ($g \cdot g^{-1}$)	Seawater		20W40 engine oil	
	Un-PC	ZnO/HA-PC	Un-PC	ZnO/HA-PC
	$0.09^{b} \pm 0.00$	$0.45^{a} \pm 0.02$	$1.38^{B} \pm 0.04$	$14.50^{A} \pm 0.04$

Equal lowercase (seawater) and uppercase (oils) letters on the same line indicate no statistical difference in the Tukey test with a significance level of 5%.

Fig. 3 shows the kinetic profiles of sorption using ZnO/HA-PC foam in multicomponent systems seawater (92%):(8%) diesel oil and seawater (92%):(8%) 20W40 engine oil.

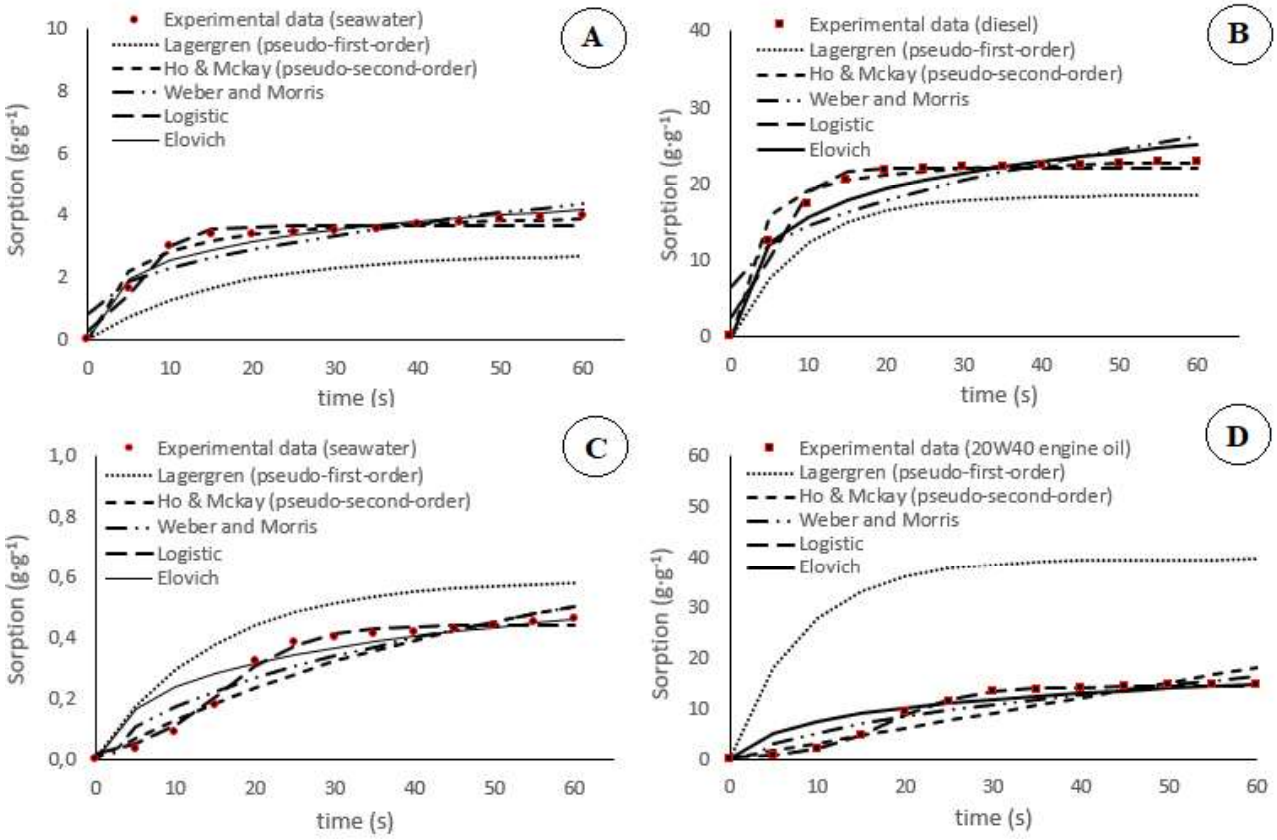

Figure 3. Kinetic profiles for water and oil sorption using ZnO/HA-PC foam in seawater (92%):(8%) diesel (A and B) and seawater (92%):(8%) 20W40 engine oil (C and D) multicomponent systems.

In the first multicomponent system, it is possible to observe a fast recovery of seawater and diesel oil. In 5 s, 45.5% of the initially spilled oil was already absorbed in the foam, and at 20 s, more than

82% had already been recovered (Fig. 3, B). From 20 s, the sorption remained with low growth stabilizing with approximately 87% of oil recovery at 60 s. Among the modeled kinetic models, the pseudo-second-order (HO & McLay) and logistic models were the ones that best described both the sorption behavior of seawater and diesel oil, both with $R^2 = 0.99$.
In the second multicomponent system, seawater and 20W40 engine oil sorption were slower due to the difficulty in fluid flow caused by the engine oil's higher viscosity. Up to 10 s, the sorption grew with a rectilinear profile. Between 10 s and 20 s, the sorption of seawater (Fig. 3, C) and engine oil (Fig. 3, D) increased exponentially. From 30 s, both fluids' sorption slowed until stabilization at 60 s, with the recovery of 55% of the engine oil initially spilled. As in the first system, the models that best described the sorption behavior of seawater and 20W40 engine oil were the pseudo-second-order model (HO & McLay) and the logistic one, both with $R^2 = 0.99$.

Conclusions

Polyurethane foams obtained from post-consumer mattresses can be potential alternative materials to recover oils spilled in seawater. With simple and low-cost modifications, it is possible to increase the selectivity of the foams, which in this work could absorb up to 25 times their own weight in oil in less than 30 seconds of exposure.

Acknowledgements

This work is supported by the Brazilian National Agency of Petroleum, Natural Gas and Biofuels through the Human Resources Program PRH 44.1.

References

1. S. A. Abernathy; J. K. Gilliam; P. J. Klouda, P. J. *Drilling and production discharges and oil spills in the marine environment*, U.S. Department of The Interior, Virginia, 1989.
2. D. Dave; A. E. Ghaly. Remediation Technologies for Marine Oil Spills: A Critical Review and Comparative Analysis. *American J. of Environmental Sciences*, v. 7, n. 5, p. 423–440, 2011.
3. H. Li; L. Liu; F. Yang. Hydrophobic modification of polyurethane foam for oil spill cleanup. *Mar. Pollut. Bull.*, v. 64, n. 8, p. 1648–1653, 2012.
4. T. J. Ko; J. H. Hwang; D. Davis; M. S. Shawkat, S. S. Han; K. L. Rodriguez; K. H. Oh; W. H. Lee; Y. Jung. Superhydrophobic MoS_2-based multifunctional sponge for recovery and detection of spilled oil. *Current App. Phys.*, v. 20, n. 2, p. 344–351, 2020.
5. A. C. Grotto; M. Hemkemeier; M. V. Rossato. Sustentabilidade no uso de poliuretano e reutilizações de aparas. *Res., Soc. and Develop.*, v. 9, n. 11, p. e99891110685, 2020.
6. B. Li; X. Liu; X. Zhang; J. Zou; W. Chai; Y. Lou. Rapid adsorption for oil using superhydrophobic and superoleophilic polyurethane sponge. *J. Chem. Tech. Biotec.*, v. 90, n. 11, p. 2106–2112, 2015.
7. K. R. da Rocha; O. Chiavone-Filho; H. N. M. de Oliveira. Post-consumer polyurethane foams hydrophobization through surface modifications for oil spill sorption. *Materials Research*, no prelo, 2023.
8. ASTM. F726-12 - Standard Test Methods for Sorbent Performance of Adsorbents. *ASTM International*, p. 1–6, 2012.
9. ASTM. D95-13 - Standard Test Method for Water in Petroleum Products and Bituminous Materials by Distillation. *Manual on Hydrocarbon Analysis, 6th Edition*, p. 545-545–3, 2013.

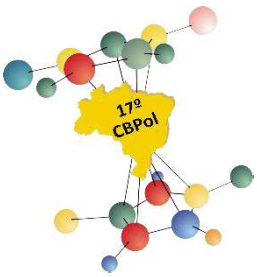

REMOVAL OF METHYLENE BLUE DYE FROM AQUEOUS SOLUTION USING POLYURETHANE FOAM SYNTHESIZED WITH ORANGE PEEL AS ADSORBENT

Ana P. P. Oliveira[1*], Isabela A. A. Fernandes[1], Tobias C. Negrão[1], Juliana R. Kloss[1] and Lucila A. A Coral[1]

1 – Academic Department of Chemistry and Biology (DAQBi), Federal University of Technology – Parana (UTFPR), Paraná, PR, Brazil anaoliveira.2001@alunos.utfpr.edu.br

Abstract - Synthetic dyes used in different industrial segments can pose a risk to the environment and health. Thus, several technologies and materials have been studied to remove these contaminants from wastewater, highlighting the use of pure polyurethane (PU) or synthesized with other materials (activated carbon, sodium alginate, graphene, and agro-industrial residues) as adsorbent, mainly due to its low cost, ease of preparation and removal capacity. This work aimed to study the removal of Methylene Blue (MB) dye using PU foam synthesized with different proportions of orange peel (OP, 7 % and 10 %) as adsorbent material in different time intervals (0.5, 1, 2, 3 and 4 h). Among the samples studied, the PU/OP10 presented the highest removal (58.2 %) and adsorption capacity (9.99 mg/g) of MB in 0.5 h. Therefore, presenting an improvement of these characteristics compared to the control PU, thus promoting the removal of contaminants concomitant with the reuse of agro-industrial residues.

Keywords*: Adsorption, Dyes, Polyurethane, Orange peel powder, Waste reuse.*

Introduction

Dyes, in general, are pollutants commonly found in wastewater from the paper, food, carpet, textile, rubber, plastic, pharmaceutical, and cosmetic industries, among others [1]. Wastewater-containing dye reduces dissolved oxygen (DO) levels and sunlight penetration, negatively impacting aquatic life [1,2]. As well, some dyes may have the potential to cause cancer and mutation [1,3]. Therefore, removing these contaminants becomes essential to preserve the environment, instigating researchers to study different techniques and materials that provide efficient alternatives for the removal of dyes and heavy metals [2].

Due to its ease of use and the availability of various natural adsorbents, adsorption is a common technique that has shown promise and effectiveness for removing contaminants from industrial effluents [4]. Among the adsorbent materials that have stood out in removing pollutants is polyurethane. This polymer is commonly synthesized through the reaction of a polyol with a diisocyanate, thus presenting itself as foam [5]. This material arouses interest as an adsorbent due to its chemical stability, biocompatibility, high mechanical strength, abrasion resistance, durability, high porosity, and low cost [2,5-6].

However, it is important to note that polyol is a petroleum derivative commonly used in the formulation of PU. This type of raw material has its use discouraged both by presenting a risk to the environment during its production and by advancing society's interests in using renewable raw materials. Renewable raw materials such as sunflower oil, palm oil, rapeseed oil, and agro-industrial waste, for example, are efficient alternatives to replace part of the polyol, improving the chemical

and physical properties of the PU [7]. Nevertheless, the polyol substituent must maintain or increases adsorption capabilities in the context of pollutant elimination. The orange peel, for example, is an agro-industrial waste that can remove numerous dyes such as Acid Violet 17, Direct Blue 86, Rhodamine B. Direct Yellow, Methylene Blue, and Remazol Brilliant Blue, among others [1]. This ability to remove dyes combined with its composition rich in lignin, hemicellulose, cellulose, limonene, and pectin, and the potential extraction of essential oils, can be an alternative to reduce the use of petrochemicals during the production of PU, as well as offer a nobler destination for the waste. In this context, this work aimed to investigate the removal capacity of methylene blue dye in an aqueous solution using polyurethane foam synthesized with powdered OP. In addition, the influence of different proportions of OP and time intervals in this capacity as been studied.

Experimental

Orange peel preparation

The orange peels, previously washed with detergent and water, were immersed in 2.5% sodium hypochlorite solution for 15 min to sanitize the material [8]. Subsequently, the peels were pre-dried at room temperature for 48 h. Given the time, the samples were dried in a laboratory oven (New Lab) at 50 ºC until constant mass. The dry material was crushed in a pan mill (Amef) in a rotation of 1120 rpm for 30 seconds per grinding cycle, which was repeated three times. The OP powder was crushed in a grinder and sieved in an electromagnetic sieve stirrer (Solotest) to obtain particles with a particle size of 100 mesh.

Synthesis of polyurethane/orange peel foams

The one-shot method was used for foaming (PU/OP), in which 4,4'-diphenylmethane diisocyanate (MDI) is added directly to polyol-polyester formulated with agitation manual. Thus, the powdered OP was mixed in the proportion of 7 % (PU/OP7) and 10 % (PU/OP10) to the polyol and stirred in a mechanical agitator (Fisatom, 713D) to MDI for 30 seconds at a rotation of 600 rpm. After 48 hours, the foams were ground in a pot mill (Amef) with a rotation of 1120 rpm for 30 seconds per grinding cycle (totaling 3 cycles). The powder obtained was sieved in an electromagnetic sieve stirrer to get particles with a particle size of 100 mesh and used as an adsorbent in the present study. The same procedure was performed for the PU foam without the orange peel, which was used as a control.

Adsorption study

The removal of methylene blue dye in an aqueous solution by the control PU, PU/OP7 and PU/OP10 was performed in a batch adsorption process in a shaker (Tecnal, TE-4200) at 25 °C. In this process, 1g/L of the adsorbent was added to the dye solution prepared in distilled water at 25 °C at a concentration of 20 mg/L [5]. Then, after specific time intervals (0.5, 1, 2, 3 and 4 h), the samples were centrifuged (Daiki, DT-4500) at 4000 rpm for 5 min and filtered with hydrophilic polytetrafluoroethylene (PTFE) syringe filter with a pore size of 0.22 μm. Subsequently, the concentration of the unabsorbed dye was determined at 664 nm with a UV-Vis spectrophotometer (Global Trade Technology).

Determination of the percentage removal of MB and adsorption capacity of foam after adsorption processes

The percentage removal and adsorption capacity were calculated by applying the following Eq. (1) and Eq. (2), respectively [9]:

$$\text{Re moval}(\%) = \frac{C_i - C_f}{C_i} x100 \quad (1)$$

$$q_t = \frac{C_i - C_f}{w} xV \quad (2)$$

where, C_i is initial MB concentration (mg/L); C_f is final MB concentration (mg/L); q_t is total adsorption capacity (mg/g); w is the weight of adsorbent (g), and V is the volume of MB solution (mL) [8].

Results and Discussion

Effect of the proportion of OP and time in percentage of removal of MB dye

Adsorption is a time-dependent process, and it is important to investigate how it influences the removal of the dye using pure PU, PU/OP7 and PU/OP10 (Fig. 1). It is possible to observe in Fig. 1 that the removal percentage of the MB dye was higher for the PU/OP10 (58.2 %) in the time of 0.5 h. In the study by Rosanti et al. [10], pure PO removed 38% of the MB dye in the same period. Similarly, the study by Baldez, Robaina and Cassela [11] showed removal of MB between 15 and 45 % when using pure PU as adsorbent material. Therefore, this inferior result demonstrates that PU synthesized with OP can increase this removal satisfactorily. In addition, it was observed that after this time there is a decay behavior of this removal up to 2 h, followed by an increase in time of 4 h. This behavior may be associated with adsorption at the sites of the first layer, promoting a decrease in removal (between 1 and 2 h) until all these sites are occupied. When the bonds of the dye molecules with the active site of the adsorbent in the first layer are finished, the next layer begins to have active sites filled, increasing the removal of the dyes in 4 h [12].

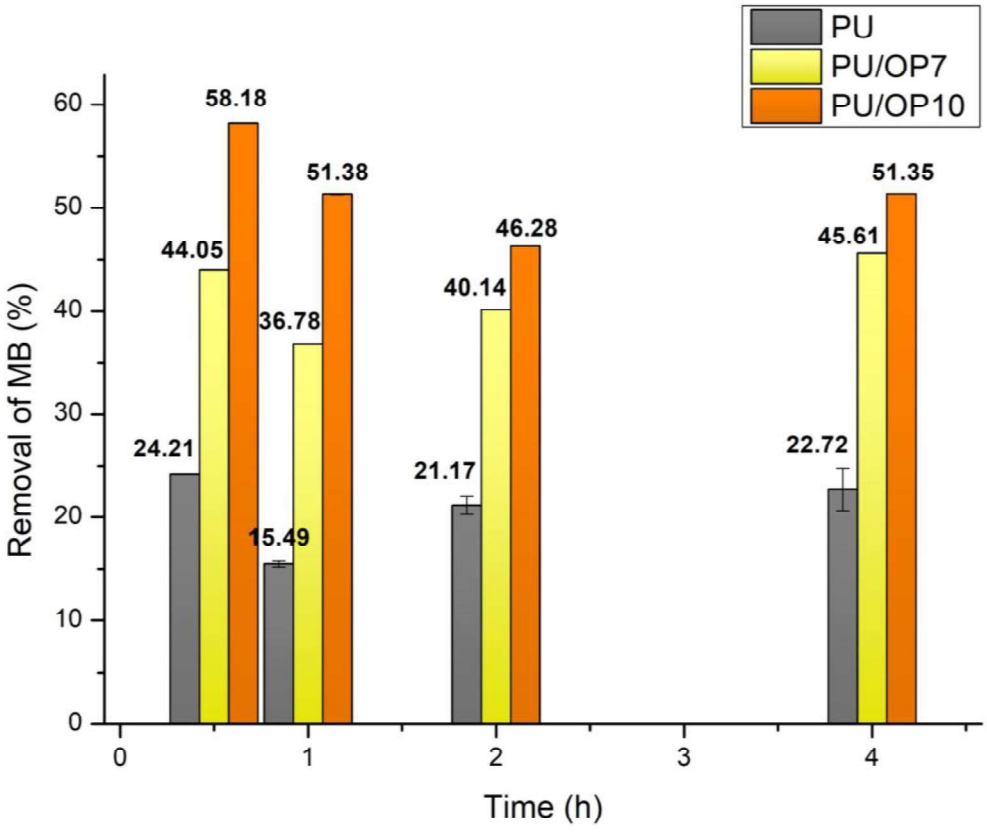

Figure 1 - Percentage of methylene blue dye removal using pure polyurethane foams and synthesized with orange peel in different proportions.

Note: MB: methylene blue; PU: polyurethane; PU/OP: polyurethane foams synthesized with orange peel.

Effect of the proportion of OP in adsorption capacity

The absorption capacity of the adsorbent was influenced by the proportion of substituent OP in the polyol (Table 1). In Table 1, it is possible to observe that the adsorption capacity proportionally increased with the addition of OP in the PU. Thus, among the samples, the PU/OP10 presented the highest adsorption capacity (9.99 mg/g) at 0.5 h. In the study by Goes et al. [13], the absorption capacity of MB dye (30 mg/L) by PU was 1.66 mg/g. Similarly, in the study by Sivaraj, Namasivayam and Kadirvelu [3], pure OP showed an adsorption capacity of Violet Acid dye 17 (20 mg/L) of 4 mg/g in 1 h. Therefore, the results demonstrate that adding the agro-industrial residue OP in the synthesis of PU promotes an improvement of the adsorption capacity, especially the proportion of 10% in relation to polyol.

Table 1 – Adsorption capacity of pure polyurethane foams and synthesized with orange peel.

Time (h)	Adsorption capacity (mg/g)		
	PU	**PU/OP7**	**PU/OP10**
0.5	3.83 ± 0.00	7.45 ± 0.14	9.99 ± 0.07
1	0.66 ± 0.01	4.59 ± 0.01	7.24 ± 0.12
2	0.98 ± 0.02	4.38 ± 0.11	5.53 ± 0.09
4	3.19 ± 0.05	7.28 ± 0.12	8.42 ± 0.10

Note: PU - pure polyurethane; PU/OP - polyurethane foams synthesized with orange peel.

Conclusions

The polyurethane foam synthesized with 10 % orange peel demonstrated the efficiency of removing methylene blue dye in aqueous solution compared to the control, presenting, consequently, the highest adsorptive capacity. This absorption capacity was influenced by the proportion of the substituent, being that the increase in the fraction of OP presented a direct relation with the increase of this capacity. In addition, the time also influenced the adsorption capacity, being sufficient in the time of 0.5 h. Thus, it was confirmed from the results that the use of orange peel as a partial substitute for polyol is an efficient alternative for removing the contaminant, reuse the residue and improvement of the adsorptive capacity of polyurethane foam. It is noteworthy that the absorption capacity can be improved due to the increase in porosity, surface area, the degree of distribution of chemical species, among others; so it is suggested that the next steps for this research seek to investigate the changes in the chemical and physical characteristics of the material, as well as to perform a kinetic study in order to understand the absorption mechanism and determine the dimension of the potential of PU/OP for removal of pollutants.

Acknowledgments

The authors acknowledge National Council for Scientific and Technological Development (CNPq) for the financial support.

References

1. M. R. Mafra; L. Igarashi-Mafra; D. R. Zuim; É. C. Vasques; M. A. Ferreira. Brazilian Journal of Chemical Engineering 2013, 30 (3), 667. https://doi.org/10.1590/S0104-66322013000300022.

2. K. L. Maurya; G. Swain; R. K. Sonwani; A. Verma; R. S. Singh. Bioresource Technology 2022, 351, 126999. https://doi.org/10.1016/j.biortech.2022.126999.

3. R. Sivaraj; C. Namasivayam; K. Kadirvelu. Waste Management 2001, 21 (1), 105. https://doi.org/10.1016/S0956-053X(00)00076-3.

4. Y. J. Vibhute; R. Jain. International Research Journal of Engineering and Technology 2021, 8 (7), 4457.
5. S. Farias, Ph.D. Thesis, Federal University of Santa Catarina, 2017.
6. M. Sultan. Environmental Chemistry Letter 2017, 15, 347. https://doi.org/10.1007/s10311-016-0597-8.
7. A. Gondaliya; M. Nejad. Molecules 2021, 26 (8), 2302. https://doi.org/10.3390%2Fmolecules26082302.
8. M. Ismail; J. Zhang. Outlooks on Pest Management 2004, 15, 29. https://doi.org /10.1564/15feb12.
9. S. Dey; S. R. Basha; G. V. Nabu; T. Nagendra. Cleaner Materials 2021, 1, 100001. https://doi.org/10.1016/j.clema.2021.100001.
10. A. D. Rosanti; Y. Kusumawati; F. Hidayat; A. Fadlan; A. R. K. Wardani; H. A. Anggraeni. Journal of The Turkish Chemical Society A 2022, 9 (1). 237. https://doi.org/10.18596/jotcsa.1003132.
11. E. E. Baldez; N. F. Robaina; R. J. Cassela. Journal of Hazardous Materials 2008, 159 (2-3), 580. https://doi.org/10.1016/j.jhazmat.2008.02.055.
12. M. M. Góes; M. Keller; V. M. Oliveira; L. D. G. Villalobos; J. C. G. Moraes; G. M. Carvalho. Industrial Crops and Products 2016, 85, 149. http://doi.org/10.1016/j.indcrop.2016.02.051
13. T. H. Dao; N. T. Nguyen; M. N. Nguyen; C. L. Ngo; N. H. Luong; D. B. Le; T. D. P. Polymers (Basel) 2020, 12 (7), 1554. https://doi.org/10.3390%2Fpolym12071554.

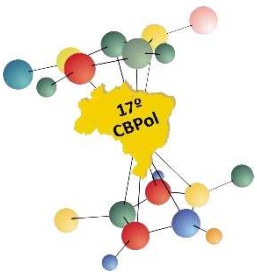

REMOVAL OF POTENTIALLY TOXIC METALS BY HYDROGELS CONTAINING MICROCELLULOSE WASTE FROM EUCALYPTUS SAWDUST

Talles B. da Costa[1], Rafaela R. Ferreira[1], Paulo H. Camani[1] and Derval dos S. Rosa[1]*

1 – Center for Engineering, Modeling, and Applied Social Sciences (CECS), Federal University of ABC (UFABC), Santo André, derval.rosa@ufabc.edu.br

Abstract - This work investigated the use of hydrogels based on corn starch reinforced with microcellulose (MC) prepared from eucalyptus sawdust wastes to remove potentially toxic metals (PTMs), such as copper (Cu^{2+}), zinc (Zn^{2+}), nickel (Ni^{2+}), manganese (Mn^{2+}), cadmium (Cd^{2+}), and hexavalent chromium (Cr^{6+}) from the sorption process. The MC presented the following metallic affinity order: $Cu^{2+} > Mn^{6+} > Ni^{2+} > Zn^{2+} > Cd^{2+} > Cr^{6+}$. Besides, incorporating MC fibers contribute to increased physicochemical properties with good interaction with corn starch. Cu^{2+} removal increased with high MC concentration in the starch hydrogel. The sorption affinity of Cu^{2+} has followed the order: MC > starch/MC-5% > starch/MC-3% > starch/MC-1% > starch/MC-0%. Thus, starch-containing cellulose microstructures are efficient alternatives to treat contaminated waters.

Keywords: Hydrogels; Microcellulose; Corn starch; Sorption; Potentially toxic metals.

Fundings: This research was financed by FAPESP (2022/11133-0, 2019/16301-6, 2022/01382-3, and 2020/13703-3), CNPq (308053/2021-4 and 403934/2021-4), and (CAPES) (Finance Code 001).

Introduction

Currently, the world faces difficulties related to the quantity of water due to industrial expansion, population growth, and urbanization intensification. PTMs are widely used in various industrial activities (e.g., electroplating, metallurgy, leather, and textile), and are often found in wastewater [1]. The presence of these metals in water resources is related to risks to human health and the environment. The sorption process is considered an alternative technology with a high potential for the removal of these metals at low concentrations. The application of advanced materials such as starch and microcellulose hydrogels can be an alternative to increase the sorption capacity of these metals [2-4].

This work evaluated the development of a biodegradable composite hydrogel based on corn starch-containing cellulose microstructures derived from eucalyptus wastes for the removal of PTMs (Cu^{2+}, Mn^{3+}, Ni^{2+}, Zn^{2+}, Cd^{2+}, and Cr^{6+}) from a synthetic aqueous medium.

Experimental

Microcellulose (MC) extraction

Cellulose isolation was carried out as described by Ferreira et al. [5]. The eucalyptus wastes were dried for 24 h. The samples were subjected to a solution of 3.2% *w/v* sodium chlorite and maintained under constant agitation at 70 °C for 2 h. After washing until neutral pH, the sample was subjected to an aqueous solution of 10% *w/v* sodium hydroxide and 10% *w/v* potassium hydroxide, under constant mechanical agitation at 25 °C for 2 h. The material obtained was washed until neutral pH. The MC was isolated by grinding the material in an aqueous medium at 5% *w/v*, using a

conventional blender for 30 min. Finally, it was combined with high-intensity ultrasound for 20 min, in pulses of 30 s with 5 s intervals in an ice bath.

Starch-based composite hydrogel synthesis

The starch-based hydrogels were synthesized according to the methodologies proposed by Camani et al. [4]. The hydrogels were prepared from starch Amisol 3408 containing 28% *w/w* amylose and 72% *w/w* amylopectin. Corn starch was dissolved in ultrapure water. After dissolving corn starch, sodium hydroxide was added. The mixtures were maintained under mechanical agitation at 40 °C for 3 h. Then, citric acid was added to form the crosslinking agent. Chemical crosslinking took place with the system under mechanical agitation at 40 °C for 17 h. The produced hydrogel was heated in a bath, stabilized at room temperature, and dried in an oven at 60 °C for 48 h. For the composite hydrogels, MC was added during the solubilization of starch in the concentrations of 1.0, 3.0, and 5.0% *w/w* (Starch/MC-1%, Starch/MC-3%, and Starch/MC-5%). Finally, the produced hydrogels were neutralized and dried again in an oven at 60 °C for 48 h.

Scanning electron microscopy (SEM)

Morphology was obtained by SEM technique (FEI Quanta 250, Thermo Fisher Scientific, USA). The sample was covered with a thin layer of gold with a thickness of 25 nm (Sputtering Leica EM ACE200, Leica Microsystems, Germany). The micrographs were obtained under the conditions: current of 50 pA, voltage of 10 kV, and spot size of 4 nm.

Laser diffraction spectroscopy (BetterSize)

To evaluate the particle size of MC, a BetterSize ST (Bettersize Instruments, China) was used, within a measurement range of 0.10 to 1000 μm.

Fourier transform infrared spectroscopy (FTIR)

The functional groups were obtained using the FTIR technique (Frontier 94.942, PerkinElmer, USA) in the operation mode with attenuated total reflectance (ATR), using a range of 4000-500 cm^{-1}, the spectral resolution of 4 cm^{-1}, and 32 scans.

Water absorption

The water absorption of the hydrogels was obtained by immersing 0.1 g of dry hydrogel pieces in 50 mL of ultrapure water. Samples were collected periodically from 0 to 24 h to weigh the mass of swollen hydrogels. At the end of the assay, the hydrogel solubility was measured to determine the weight loss. The degree of swelling (*DS*) and solubility (*%S*) were calculated by Equations (1) and (2), respectively.

$$DS = \frac{(m_t - m_i)}{m_i} \cdot 100 \quad (1)$$

$$\%S = \frac{(m_i - m_f)}{m_i} \cdot 100 \quad (2)$$

wherein, m_i is the initial dry mass of hydrogels (g), m_t is the swollen mass of hydrogels at time *t* (g), and m_f is the final dry mass of hydrogels (g).

Sorption assays

The affinity of MC for Cu^{2+}, Zn^{2+}, Ni^{2+}, Cd^{2+}, Mn^{2+}, Cr^{6+} (0.17 mmol/L each) and starch-based composite hydrogels for Cu^{2+} (1.0 mmol/L) were performed using a dosage of 10.0 g/L. The sorption affinity assays were conducted in a shaker incubator, under 200 rpm at room temperature (~ 25 °C) and pH between 4.0 – 4.5. After 24 h, PTMs concentrations were determined by ion

chromatography, IC (940 Professional IC Vario, Metrohm, Switzerland). Removal efficiencies (*%R*) were determined by Equation (3).

$$\%R = \frac{(C_0 - C_e)}{C_0} \cdot 100 \quad (3)$$

wherein, C_0 is the PTMs initial concentration (mmol/L) and C_e is the PTMs concentration at equilibrium (mmol/L).

Results and Discussion

Fig 1 shows the MC micrograph. The fibrous character is observed, in which the diameter is much smaller than the length of the fiber. The diameter observed in micrography of the MC sample varies between 7 – 20 µm. The presence of agglomerated regions is also noted, possibly due to hydrogen bonds after drying the sample for analysis or the presence of residual lignin.

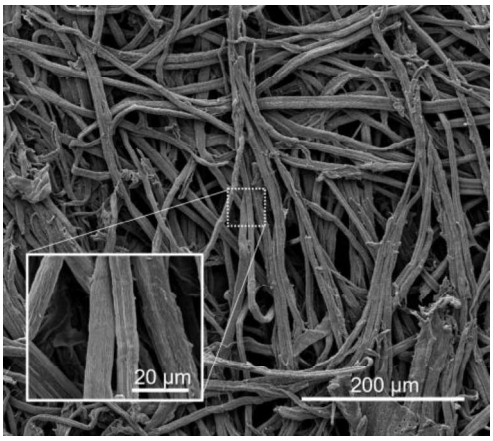

Figure 1 – Micrograph obtained by SEM of MC with 500x magnification.

BetterSize analysis was used to characterize the size distribution of MC particles. The size distribution curve is shown in Fig 2. The D_{90}, D_{50} and D_{10} values obtained were 14, 51 and 194 µm, respectively, with a Span of 3.6, indicating high fiber size dispersion. The $D_{4.3}$ and $D_{3.2}$ were 81.7 and 28.3 µm, respectively. The bimodal aspect of the distribution may be associated with a disturbance in the measurement by the difference in the dimension between diameter and length of the evaluated fibers. Another hypothesis is the heterogeneous in particle size distribution of these particles.

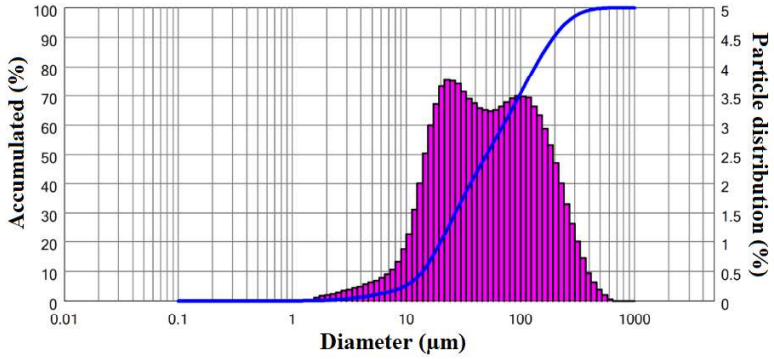

Figure 2 – Particle size distribution for MC obtained by BetterSize analysis.

In effluent samples, heavy metals are found with other potentially toxic contaminants at varying concentrations, affecting their sorption efficiency due to competition for binding sites. Thus, the performance of MC was investigated in synthetic wastewater with six coexisting ions (Cr^{6+}, Cd^{2+}, Ni^{2+}, Mn^{2+}, Zn^{2+}, and Cu^{2+}) at 0.17 mmol/L each (Fig 3). From Fig 3, MC presented the following metallic affinity order: $Cu^{2+} > Mn^{6+} > Ni^{2+} > Zn^{2+} > Cd^{2+} > Cr^{6+}$. It is interesting to note that the MC

exhibited a high removal efficiency for divalent cations (greater than 90%), while Cr^{6+} showed removal efficiency of around 30% under the same operational conditions. The high removal of divalent cation by MC may be related to its high specific surface area with numerous pores, besides to a negatively charged surface with many oxygens' functional groups.

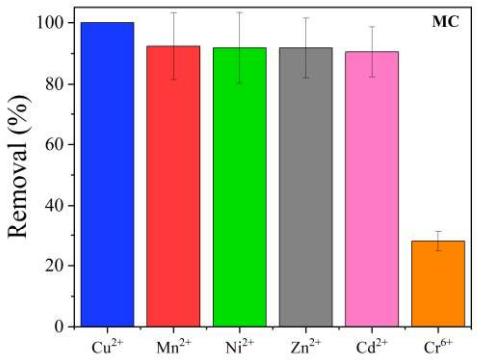

Figure 3 – Sorption affinity of PTMs ions (Cu^{2+}, Cd^{2+}, Mn^{2+}, Zn^{2+}, and Cr^{6+}) by MC.

Fig 4 (a) shows the FTIR spectra for MC, Starch/MC-0%, Starch/MC-1%, Starch/MC-3%, and Starch/MC-5%. A band around 3350 cm^{-1} and a less intense band at 2900 cm^{-1} are observed in all samples, characteristic of the symmetric stretching of the -O-H and -C-H bonds, present in MC and starch. The bands close to 895, 1025, and 1158 cm^{-1} are attributed to vibrations -C-H, elongation -C-O, and asymmetric vibration -C-O-C, of the MC chains, respectively [4,5]. Additionally, the bands around 1095, 1593, and 1731 cm^{-1} can be attributed to the presence of lignin and hemicellulose, which were not completely removed when obtaining the MC from the eucalyptus residue [5]. Fig 4 (a) also shows an increase in intensity at the 3280 cm^{-1} regions for Starch/MC-3% and Starch/MC-5% hydrogels, which could be associated with increased hydroxyls in the hydrogels since MC has this function group in its composition. It could indicate that hydrogels with a higher MC concentration might be more hydrophilic once the hydroxyl groups of that spectra are associated with water absorption. The wavenumber region between 1750 and 1450 cm^{-1} was shifted for high wavenumber, comparing the Starch/MC-0% hydrogel and composite hydrogels. Lastly, a peak at 1390 cm^{-1} had higher intensity and shifting for composite hydrogels containing 3.0 and 5.0% *w/w* MC.

From the observed water absorption results (Fig 4 (b)), all hydrogels showed considerable water absorption during the test. The pure starch composition showed approximately 89% of water absorption capacity. When incorporating the MC in the hydrogel, there was a reduction of absorption by up to 24%, which indicates that the microfibers probably increased the rigidity conformation of the hydrogel, resulting in less molecular chain mobility, diffusivity, and water retention within the pores and hydrogel volume. Additionally, during the water absorption tests, the hydrogel samples had high solubility in the aqueous medium without MC (close to 30.1%). This result indicates that the hydrogel without MC did not present a satisfactory physical performance for application in sorption tests. Adding MC to the starch hydrogel reduced the solubility in aqueous media to about 5%. Therefore, the addition of MC microstructure plays an important role in maintaining the network structure of the hydrogel.

The MC, starch-based hydrogel and hydrogels containing different MC concentrations (1.0, 3.0, and 5.0% w/w) were evaluated for Cu^{2+} sorption (Fig 4 (c)). The results indicate that there was a good affinity of Cu^{2+} for MC. However, MC has a high solubility in aqueous media (close to 32%), which makes its application difficult in the Cu^{2+} sorption process. Despite this, adding MC in the starch hydrogel polymeric matrix increased the Cu^{2+} sorption rates, reaching a maximum removal of about 52% for the starch/MC-5% sample.

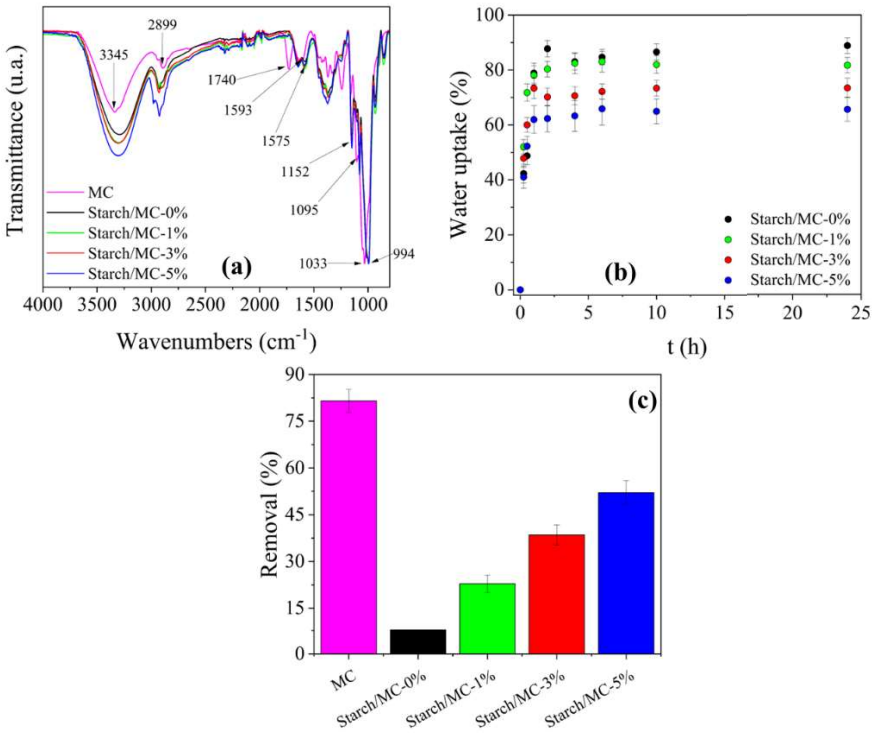

Figure 4 – FTIR spectra, water uptake (%), and removal efficiency of Cu^{2+} (%) for MC, corn starch-based hydrogel and hydrogels containing different MC concentrations (1.0, 3.0, and 5.0% *w/w*).

Conclusions

The present work demonstrated that starch-based composite hydrogel reinforced with MC is a promising biosorbent for application in the removal of PTMs (e.g., Cu^{2+}) in aqueous media. The results showed a direct effect of the addition of cellulose microstructure on the efficiency of the adsorptive process. The addition of the 5% *w/w* concentration of MC favored the process, reaching a maximum removal of about 52% for the starch/MC-5% hydrogel. In contrast, low water absorption was observed, that can be linked to decrease of chain mobility. Thus, to deeply understand the sorption process, additional studies will be carried out, including thermal, morphological, and chemical analyses.

Acknowledgements

The authors thank the technical support of the Multiuser Experimental Center of UFABC (CEM-UFABC), CECS (UFABC), and REVALORES for assistance. The authors also thank Ingredion Company for the donation of the corn starches.

References

1. M.A. Al-Ghouti; D.A. Da'Ana Journal of Hazardous Materials 2020, 393, 122383. https://doi.org/10.1016/j.jhazmat.2020.122383
2. F. Zia; K.M. Zia; M. Zuber; S. Kamal; N. Aslam Carbohydrate polymers 2015, 134, 784-798. https://doi.org/10.1016/j.carbpol.2015.08.034
3. A.D. Gupta; K.P. Rawat; V. Bhadauria; H. Singh Carbohydrate Polymers 2021, 269, 117763. https://doi.org/10.1016/j.carbpol.2021.117763
4. P.H. Camani; M.G.M. Gonçalo; R.F.S. Barbosa; D.S. Rosa Journal of Applied Polymer Science 2021, 138, 50863. https://doi.org/10.1002/app.50863
5. R.R. Ferreira; A.G. Souza; L.L. Nunes; N. Shahi; V.K. Rangari; D.S. Rosa Materials Today Communications 2020, 22, 100755. https://doi.org/10.1016/j.mtcomm.2019.100755

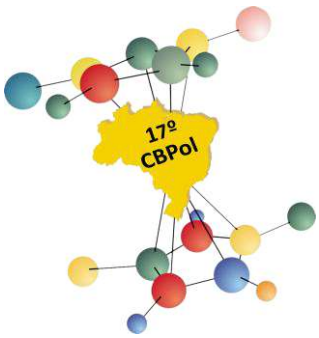

STUDY OF BIODEGRADATION OF A POLYELECTROLYTE COMPLEX: SPECTROSCOPIC AND MORPHOLOGICAL ASPECTS

Rafael F. P. da Rocha[1], Marcia P. M. da Costa[1], Antonio Carlos A. da Costa[2] and Ivana L. M. Ferreira[1*]

1 – Department of Chemical Processes, Rio de Janeiro State University (UERJ), Rio de Janeiro, RJ, Brazil
**ivanalmellof@gmail.com ; ivanamello@uerj.br*
2 – Department of Technologies of Biochemical Processes, Rio de Janeiro State University (UERJ), Rio de Janeiro, RJ, Brazil

Abstract – Since the degradation process of superabsorbent materials can influence the gradual release of substances, it is necessary to investigate this process. A polyelectrolyte complex (PEC) was prepared by mixing sodium alginate and chitosan solutions. The biodegradation process of this material was investigated through the characterization of the materials before and after burial in an Ultisol by Fourier-transform spectroscopy in the infrared region (FTIR), Raman spectroscopy and scanning electron microscopy (SEM). The results showed that the main alteration in the chemical composition was due to the breaking of the β-glycosidic bond, which altered to soil morphology from a leafy to fibrous structure, evidencing the fragmentation during biodegradation. Therefore, the results presented are valuable for understanding how the biodegradation of the PEC occurs, aiming at planning future strategies that can prolong the time of action of the material in soil.
Keywords: *biodegradation; alginate; chitosan; polyelectrolyte complex.*

Introduction

Polyelectrolytic complexes (PECs) are obtained from electrostatic interactions between two polyelectrolytes, namely polymers with opposite charges in their chains [1]. In this work, a PEC based on alginate (ALG) and chitosan (CHI) was used. Alginate is an anionic polysaccharide extracted mainly from brown seaweed [2], while chitosan is a cationic polysaccharide typically found in acid media, obtained through the deacetylation reaction of chitin [3], a polysaccharide extracted mainly from the shells of crustaceans [4]. Since the irrigation of agricultural crops is responsible for the highest percentage of water consumption in the world [5], the use of PECs or superabsorbent hydrogels capable of gradually retaining and releasing water or aqueous solutions is necessary [6, 7].
In this work, the effects of biodegradation of the polyelectrolytic complex were studied. For this, meticulous monitoring was carried to investigate possible chemical and morphological alterations of the materials during the biodegradation tests.

Experimental

Preparation of the polyelectrolyte complex (PEC)

The PEC was obtained from a previously prepared mixture of alginate and chitosan solutions [8]. After 24 hours of mixing, the PEC was washed and lyophilized.

Biodegradation assays

The PEC samples were buried in a clayey soil collected from a private property located in the municipality of Campos dos Goytacazes, in the northern region of the state of Rio de Janeiro, Brazil (latitude 21º14'55" S and longitude 41º19'23" W). The PEC samples were buried in individual polypropylene (PP) pots, with 800 grams of soil, at a depth of 5 cm [7]. The soil was irrigated daily and the samples were dug up daily until the fifth day, and thereafter weekly until the eighth week. Afterward, the samples were washed with deionized water, lyophilized, and characterized [9].

Characterization of the PEC samples before and after biodegradation assays

The PEC samples were characterized before and after the biodegradation tests by Fourier-transform spectroscopy in the infrared region (FTIR) and Raman spectroscopy, in order to observe possible changes in the chemical composition of the material, and scanning electron microscopy (SEM) to observe possible morphological changes in PEC samples during biodegradation.

Results and Discussion

In the biodegradation tests, it was possible to find intact PEC samples only up to two weeks (Fig. 1). Therefore, samples after this interval were washed and lyophilized. Between three and six weeks, the PEC samples were found without a defined form in the soil, i.e., as particulates. After six weeks, the samples were not found at all and were considered to be fully biodegraded.

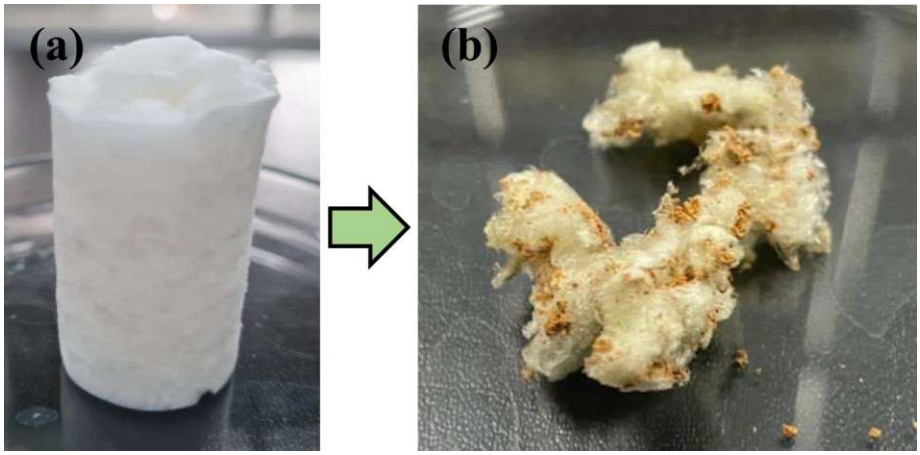

Figure 1 – PEC before burial in the soil (a) and after freeze-drying (b).

Fig. 2 shows a decrease in the transmittance intensity of some absorption bands of the PEC sample weeks after burial in relation to the sample before burial. These bands were located at 1152 cm^{-1} (stretching of the C-O-C bond of the pyranoside ring), at 1074 and 1018 cm^{-1} (stretching of the C-O bond of secondary alcohol) [10] and at 940 cm^{-1} (β-glycosidic bond) [11]. The decrease in these bands indicated that biodegradation occurred through the cleavage of these bonds [12]. Fig. 2 also shows an increase in the absorption of the band at 1275 cm^{-1}, referring to the stretching of the acetyl group [13], which is indicative of the increase in acetylated units, proportionally, in the PEC after two weeks of burial, in relation to the PEC before burial.

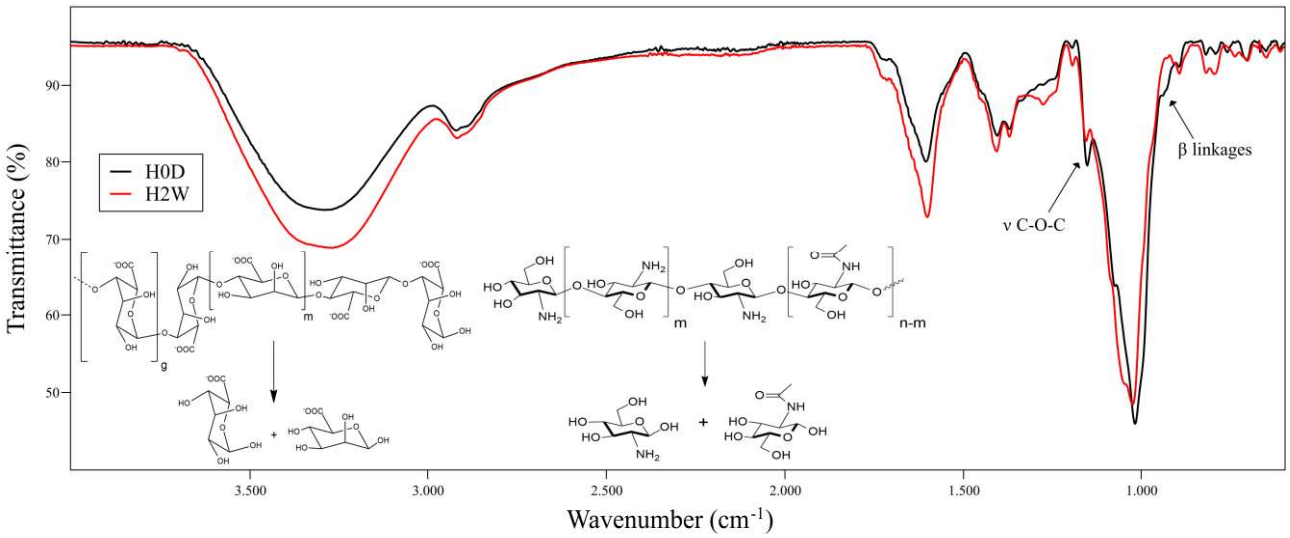

Figure 2 – PEC FTIR spectra before (H0D) and after two weeks of burial (H2W).

The results obtained by Raman spectroscopy (Fig. 3) indicated the lowest proportion of CH_3 and CH_2 groups (2941 and 2905 cm^{-1}), in addition to the breaking of glycosidic bonds (480 cm^{-1}) [14, 15], reinforcing the results obtained by FTIR.

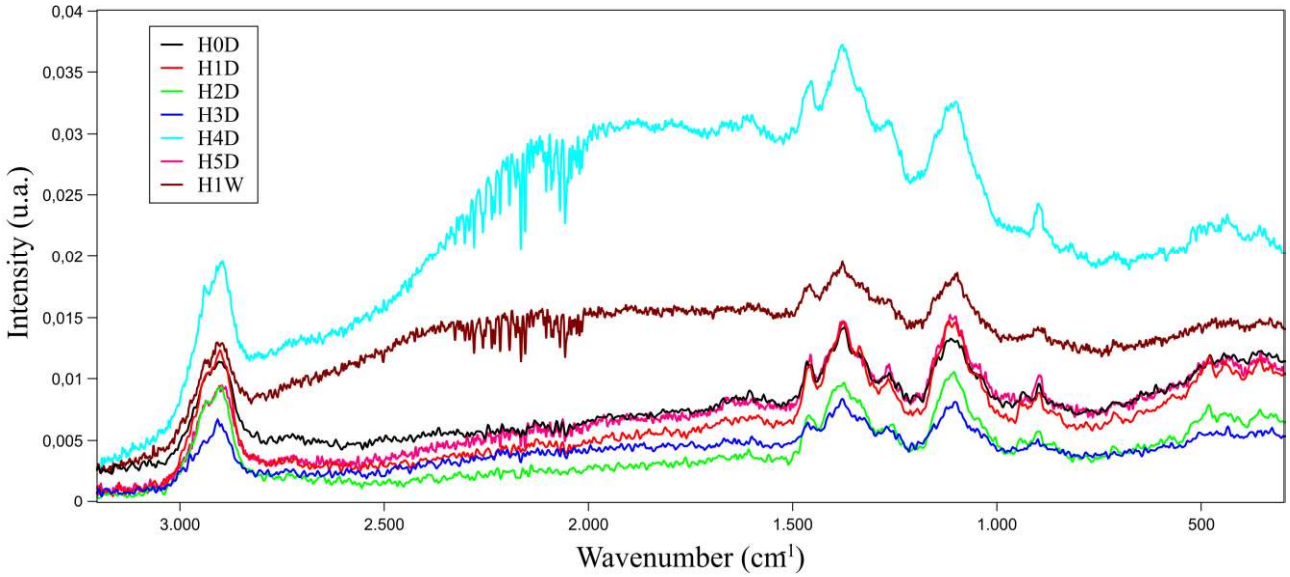

Figure 3 – Raman scattering spectra for the samples: H0D (before burial), H1D (after burial for 1 day), H2D (after 2 days), H3D (after 3 days), H4D (after 4 days), H5D (after 5 days) and H1W (after 1 week).

Fig. 4 shows the occurrence of a generalized change in the morphology of the PEC samples after biodegradation, such as roughness, fragmentation of the polymeric structure, and presence of fibrosity in the material.

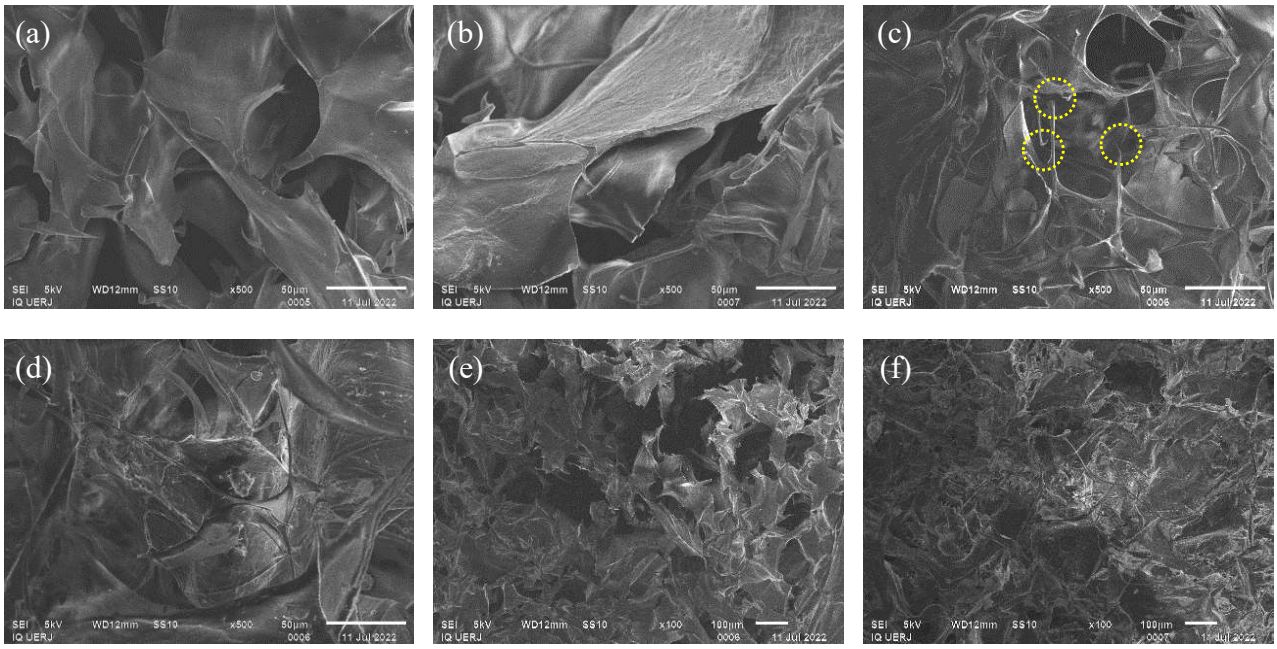

Figure 4 – SEM micrographs of samples: H0D (before burial) (a); H1D (after burial for 1 day) (b); H5D (after burial for 5 days) (c); H2W (after burial for 2 weeks) (d); H0D (e) and H2W (f) at 100x magnification. (a), (b), (c) and (d) with 500x magnification.

Conclusions

The biodegradation of the PEC prepared from sodium alginate was studied in clayey soil. Spectroscopic analyses (FTIR and Raman) revealed that the β-glycosidic bond is the main factor responsible for breaking the polymeric chains, even though the polyelectrolytes interact electrostatically. The morphological analysis (SEM) of the surface of the PEC revealed fragmentation of the polymeric structure and formation of fibrosity.

Acknowledgements

We thank the Carlos Chagas Filho Foundation for Research Support of the State of Rio de Janeiro (FAPERJ) and the National Council for Scientific and Technological Development (CNPq) for financial support. This study was also partly funded by the Office to Coordinate Improvement of Higher Education Personnel (CAPES), Finance Code 001.

References

1. M. He; L. Shi; G. Wang; Z. Cheng; L. Han; X. Zhang; C. Wang; J. Wang; P. Zhou; G. Wang International Journal of Biological Macromolecules 2020, 155, 1245-1251. https://doi.org/10.1016/j.ijbiomac.2019.11.092
2. N. M. Sanchez-Ballester; B. Bataille; I. Soulairol Carbohydrate Polymers 2021, 270, 118399. https://doi.org/10.1016/j.carbpol.2021.118399
3. M. Khajavian; V. Vatanpour; R. Castro-Muñoz; G. Boczkaj Carbohydrate Polymers 2022, 275, 118702. https://doi.org/10.1016/j.carbpol.2021.118702
4. S. M. Joseph; S. Krishnamoorthy; R. Paranthaman; J. A. Moses Carbohydrate Polymer Technologies and Applications 2021, 2, 100036. https://doi.org/10.1016/j.carpta.2021.100036
5. Agência Nacional de Águas, *Manual de usos consuntivos da água no Brasil*, ANA, Distrito Federal, 2019.
6. Saruchi; V. Kumar; H. Mittal; S. M. Alhassan International Journal of Biological Macromolecules 2019, 132, 1252-1261. https://doi.org/10.1016/j.ijbiomac.2019.04.023
7. A. M. Senna; V. R. Botaro Journal of Controlled Release 2017, 260, 194-201. https://dx.doi.org/10.1016/j.jconrel.2017.06.009

8. M. P. M. da Costa, Ph.D. Thesis, Universidade do Estado do Rio de Janeiro, 2018.
9. R. F. P. da Rocha, M.S. Dissertation, Universidade do Estado do Rio de Janeiro, 2023.
10. J. Ostrowska-Czubenko; M. Gierszewska-Druznska Carbohydrate Polymers 2009, 77, 590-598. https://doi.org/10.1016/j.carbpol.2009.01.036
11. G. A. Kloster; O. M. Londoño; K. R. Pirota; M. A. Mosiewicki; N. E. Marcovich Carbohydrate Polymer Technologies and Applications 2021, 2, 100083. https://doi.org/10.1016/j.carpta.2021.100083
12. V. Hasija; K. Sharma; V. Kumar; S. Sharma; V. Sharma Vacuum 2018, 157, 458-464. https://doi.org/10.1016/j.vacuum.2018.09.012
13. C. Y. Soon; Y. B. Tee; C. H. Tan; A. T. Rosnita; A. Khalina International Journal of Biological Macromolecules 2018, 108, 135-142. https://doi.org/10.1016/j.ijbiomac.2017.11.138
14. T. Schmid; A. Messmer; B. Yeo; W. Zhang; R. Zenobi Analytical and Bioanalytical Chemistry 2008, 391, 1907-1916. https://doi.org/10.1007/s00216-008-2101-1
15. A. Zając; J. Hanuza; M. Wandas; L. Dyminska Spectrochimica Acta Part A: Molecular and Biomolecular Spectroscopy 2015, 134, 114-120. https://doi.org/10.1016/j.saa.2014.06.071

SYTHESIS AND PROPERTIES OF POLYURETHANE COATINGS BASED ON BIOPOLYOLS: LIQUEFIED MACAÚBA ENDOCARP MIXED WITH CNSL

Lucius Stienissen[1], Pedro H. B. O. Nogueira[2], Renata C. S. Araújo[2]*

1 – Avans University of Applied Sciences, Chemistry department, Breda, The Netherlands
2 – Chemistry Department, Federal University of Minas Gerais (UFMG), Belo Horizonte, MG, Brazil
renatasa@ufmg.br

Abstract - The improvement of properties of coatings based on liquefied macaúba were studied by making a mixture with cashew nut shell liquid (CNSL) 1:1. These new coatings were more homogeneous, without pores. The thermal stability of the coatings did not change with different macaúba contents. However, the electrochemical impedance showed an increase in corrosion protection with increasing macaúba content, showing a maximum for the content of 30% of liquefied endocarp.
Keywords: *Polyurethane coatings, liquefied macaúba, cashew nut shell liquid, electrochemical impedance.*

Introduction

The growing global industrial production has been causing environmental problems such as global warming and the problematic disposal of waste. Therefore, researchers and industries have been looking for alternatives to the use of petrochemical products Biopolyols obtained from the liquefaction of macaúba endocarp were used in the synthesis of polyurethane coatings. The use of crude glycerol, despite decreasing the liquefaction yield, increased the thermal stability and the anticorrosive effect of the coatings. These coatings also showed pores and some phase segregation [1].
With the intention of improving the homogeneity and properties of these coatings based on liquefied endocarp, a blend was made with cashew nut shell liquid, which is also a material from a renewable source.

Experimental

Macaúba endocarp liquefaction
The endocarp liquefaction reaction was carried out at 130ºC for one hour. Different content of macaúba endocarp (0, 10, 20, 30, 30, 40 %) were used to study this influence on coatings properties.

Hydroxyl number
The hydroxyl content was determined from the acetylation of the samples and subsequent titration with NaOH (1.0 M) in potentiometric titrator. The procedure was based on the work of Hassan and Shukry [5].

Synthesis of coatings
The synthesis was carried out in one step, reacting a mixture of polyols and HDI (hexamethylene diisocyanate) at NCO/OH ratio = 1.1. For all contents of liquefied macaúba (0, 10, 20, 30 and 40%), the same weight of cashel nut shell liquid was mixed reacting with HDI and PUs were applied by spraying on carbon steel plates without any type of treatment.

Characterization of biopolyols and coatings
Biopolyols and coatings were characterized by thermogravimetry in TA equipment
TGA Q50, N_2 flow at 100 mL/min at a rate of 10°C/min up to 750°C. The absorption spectra in the infrared were obtained on the Perkin Elmer FTIR Frontier equipment by ATR in a range of 4000 to 550 cm^{-1}. The coatings were also characterized by electrochemical impedance performed in accordance to ASTM G3-14. In preparation for the impedance test, the coated plates were immersed in a 3.5% m/v NaCl solution for three days and, subsequently, the analyzes were carried out in the Autolab potentiostat from 0 to 100 kHz and 0.03V amplitude.

Results and Discussion

The thermogravimetric curves of coatings based on liquefied endocarp with different content and CNSL showed similar thermal stability. The fig. 1 showed curves of biocoatings with 0, 20 and 40% of liquefied macaúba. We can see Three main degradation events in DTG curves, characteristic of PUs degradation.

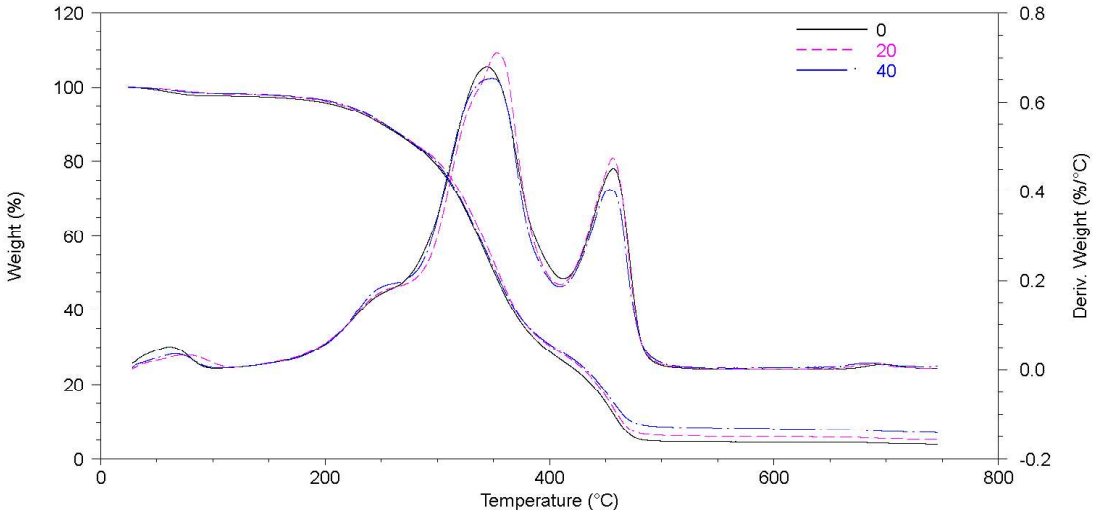

Figure 1 – TG curves for Biocoatings based on CNSL and liquefied macaúba in different contents.

Examples of IR spectra of the PU-coatings are shown in fig. 2. The spectra showed NH stretching bands at 3302 cm^{-1}, different types of CH bonds between 2800-2990 cm-1 and C=O bonds from urethane linkages at 1702 cm^{-1}. These stretching bands indicate the successful PUs synthesis. The coatings based only on liquefied macaúba endocarp showed an NCO band at 2280 cm^{-1} which did not occur in the coatings that were created with the CNSL.

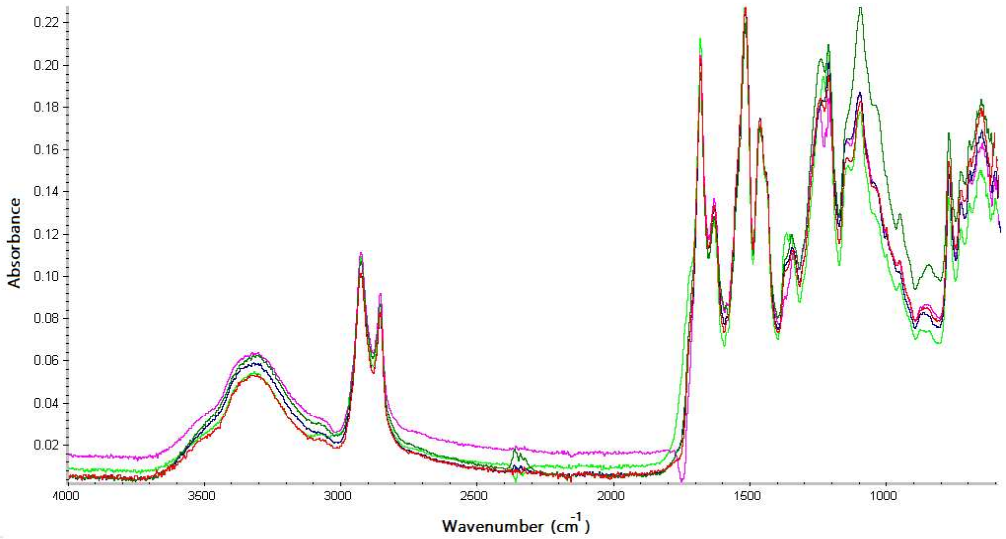

Figure 2 – FTIR spectra of polyurethane coatings based on a mixture of different content of liquefied macaúba endocarp (0, 10, 20, 30, 40%) and CNSL.

In the results obtained through electrochemical impedance spectroscopy, through the Nyquist diagrams (Fig. 3), it was observed that the applied polyurethane coatings containing 30% of liquefied macaúba in the blend showed a greater capacitive arc, which indicates a greater resistance to polarization. Such behavior was similar both in the initial test and after 24 hours of immersion, thus confirming that the coating obtained the best anticorrosive performance.

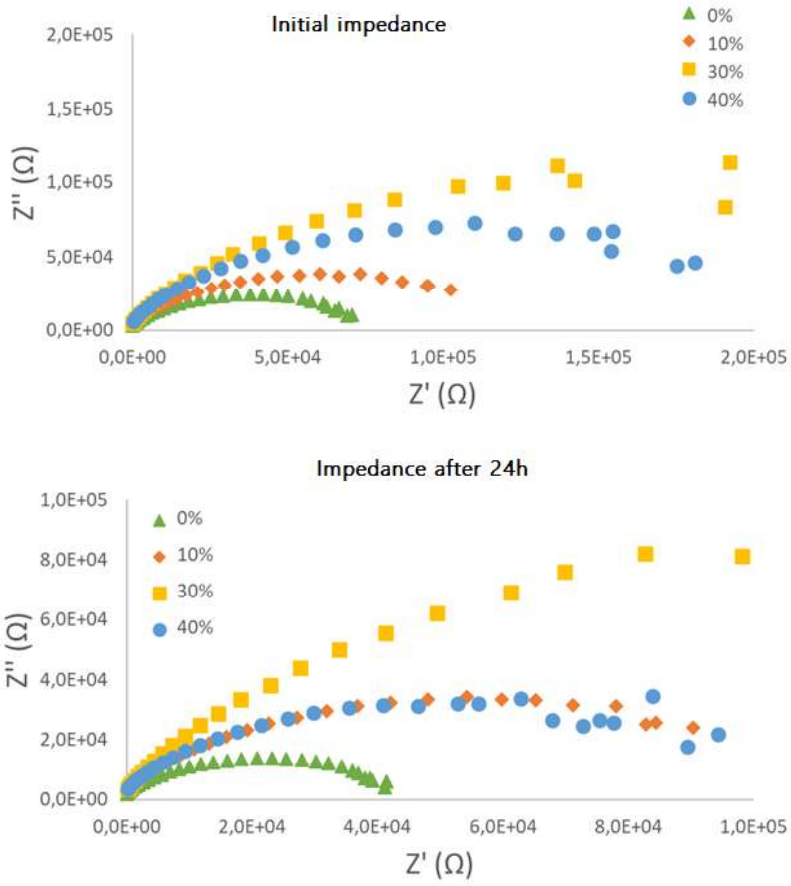

Figure 3 – Nyquist curves for PUs based on liquefied macaúba in different contents mixed with CNSL, with 0h and 24h immersed.

In the analysis of the Bode diagrams, both for the initial test and for the one carried out after 24 hours of immersion, the result is confirmed with the coating containing 30% w/w, obtaining the highest impedance modulus values.

Furthermore, all coatings showed similar behavior with respect to immersion time. Through the table 1and the bar graph (Fig. 4), it can be seen that after 24 hours of immersion in saline solution, all coatings had their impedance modules reduced. It happens that with the passage of time in immersion, the electrolyte diffuses through the pores of the coating and comes into contact with the metallic matrix, which increases the transfer of charge and mass due to the nucleation of small corrosion sites. However, it was observed that in the coating containing 40% m/m, the highest content studied, this drop was more pronounced. This fact may be due to the fact that a greater amount of biomass is present in the coating, phase separation increases the number of pores in the coating, making the diffusion of the electrolyte to the metallic matrix more efficient.

Table 1 – Values of impedance modulus performed at time zero and after 24 hours of immersion in saline solution

Impedance modulus performed at time zero and after 24 hours of immersion in saline solution.		
Macaúba content (%w/w)	**Initial impedance modulus (Ω)**	**Impedance modulus after 24h of immersion (Ω)**
0	57.177	46.653
10	122679	110323
30	338709	293053
40	204381	99911

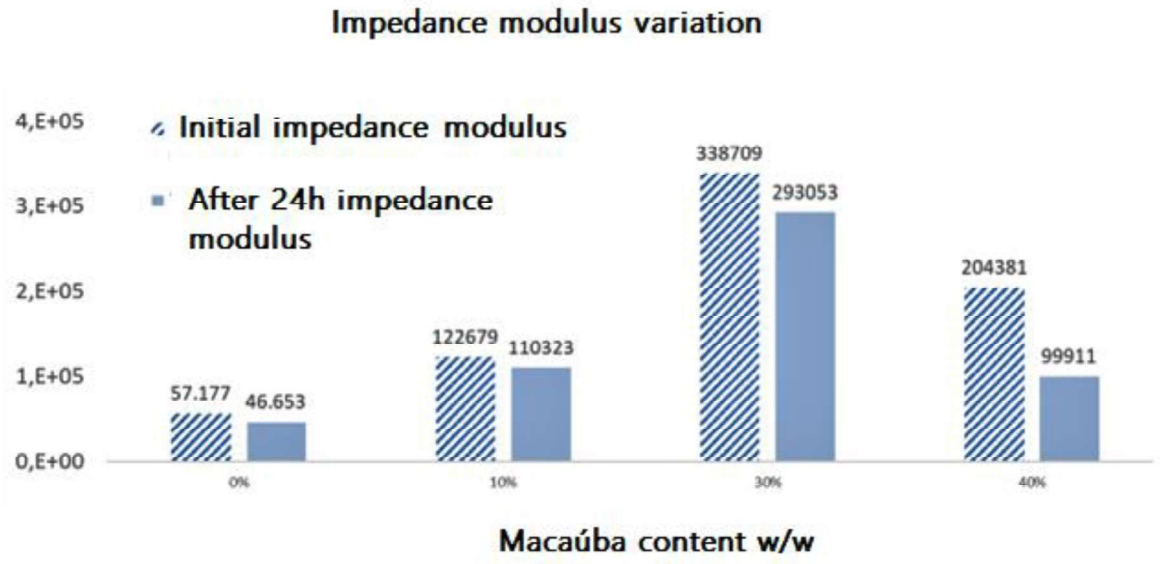

Figure 4 – Impedance modulus variation with time.

Conclusions

The usage of cashew nut oil during the curing process mixed the liquefied macaúba endocarp polyol with the HDI was better to create a homogeneous coating without phase segregation and pores. The produced coatings showed good adhesion, thermostability and anti-corrosive properties, which gives them potential as coatings for metal surfaces for commercial use.

Acknowledgements

To the Living Lab Biobased Economy project (Brazil - Netherlands) which provided the student Lucius Stienissen's internship at the Chemistry Department of UFMG.

References

1. R. V. Eijk, M. M. M. Ramos, P. H. B. O. Nogueira, R. C. S. Araújo, in Proceedings of 15th Congresso Brasileiro de Polímeros, Bento Gonçalves, 2019, 1166.
2. E. B. M. Hassan; N. Shukry, Industrial Crops and Products, 2008, 27(1), 33. https://doi.org/10.1016/j.indcrop.2007.07.004

THERMAL DECOMPOSITION OF DIFFERENT KRAFT LIGNINS THROUGH THERMOGRAVIMETRIC ANALYSIS

Thaiane A. Cruz[1], Jaqueline de O. Brotto[2], Mariana C. Pinto[1], Ricardo A. F. Machado[1], Ariovaldo Bolzan[1], Regina de F.P.M. Moreira[2], and Bruno F. Oechsler[1,*]

1. *Laboratory of Control and Polymerization Processes (LCP), Department of Chemical and Food Engineering (EQA), Federal University of Santa Catarina (UFSC), Florianópolis, SC, Brazil.*

*b.oechsler@ufsc.br

2. *Energy and Environment Laboratory (LEMA), Department of Chemical and Food Engineering (EQA), Federal University of Santa Catarina (UFSC), Florianópolis, SC, Brazil.*

Abstract – Lignin thermochemical conversion is becoming a promising pathway for the replacing of fossil resources in different applications, due to its structure composed of repeating units such as guaiacyl, syringyl, and p-hydroxyphenyl, whose thermal decomposition results in oxygenated aromatic compounds. Furthermore, the type of lignin can influence the composition of the final products obtained from pyrolysis and the comprehension of thermal decomposition stages would be useful to optimize the products selectivity and aromatic compound yield. This research aims to study the thermal pyrolysis behavior of two different kraft lignins (*Eucalyptus spp* and Pine Tree) using the ultimate analysis to determine the elemental composition and thermogravimetric analysis coupled with the deconvolution method to evaluate the thermal decomposition stages. The pyrolysis of the samples showed that the composition of lignin directly affects the thermal decomposition rates. Hardwood lignin produces more syringyl compounds than softwood lignin due to the higher presence of methoxyl groups, which can lead to a lower yield of aromatic products.

Keywords: *Kraft lignin, thermal pyrolysis, thermogravimetric analysis, softwood, hardwood.*

Fundings: CNPq (Conselho Nacional de Pesquisa e Desenvolvimento) and FAPESC (Fundação de Amparo à Pesquisa e Inovação do Estado de Santa Catarina).

Introduction

The pulp and paper sector produces streams with large amounts of lignocellulose, which consists of an abundant form of biomass with numerous possibilities as raw materials for the energy sector and the chemical industry due to its composition and availability. In industrial sites, lignin can be extracted from black liquor, a by-product of the cooking step, which is typically burned at recovery boilers. As well known, lignin presents an abundant natural phenolic structure and can be considered a renewable feedstock of phenolic and aromatic resources (basic building blocks of the chemical industry). In kraft pulping processes, lignin is readily available in large amounts, and its extraction from black liquor can reduced the bottlenecks associated with scale-up in recovery boilers [1]–[3].

Lignin is a complex three-dimensional amorphous polymer composed of three repeating units: p-hydroxyphenyl (H), guaiacyl (G), and syringyl (S). The proportions of these repeating units are highly variable and mainly depend on the type of lignocellulosic biomass, i.e., whether lignin was obtained from hardwood, softwood, or grasses. Depending on the lignin source, different ether (β-O-4, α-O-4) and carbon-carbon (β-1, β-5) linkages connect the repeating units. Softwood lignin (G-unit) has 43 – 50 % of ether linkages and more carbon-carbon bonds than hardwood lignins (S and G-units) which have 50 – 65 % of ether bonds. The density of these linkages depends on the amounts of repeating units in each lignin, and affects the thermal decomposition behavior and cracking product distribution [4], [5].

Pyrolysis is an efficient technology for the thermochemical conversion of lignin by the action of heat in an inert environment into bio-char, bio-gas, and bio-oil. During the thermal pyrolysis (Fig. 1), the lignin structures can be cleaved, producing several phenols and aromatic compounds with different functional groups, like carboxyl, carbonyl, and methoxy. When escaping from the benzene

ring, these groups form light gases (CH_4, CO_2) by thermal cranking, repolymerization, and aromatization. Following another pathway, lignin also generates bio-char with abundant functional groups through carbonization, in which the available functional groups can be further cracked with increasing temperature, producing light gases. In addition, the active aromatic species in bio-oil can be converted into bio-char through repolymerization [6], [7]. Therefore, this research aims to provide a broader view of the thermal pyrolysis behavior of two different types of kraft lignin from thermogravimetric analysis coupled with the deconvolution method. In addition, this work discusses the effect of repeating units and linkages amounts on stages of thermal pyrolysis, and, consequently, on the product distribution.

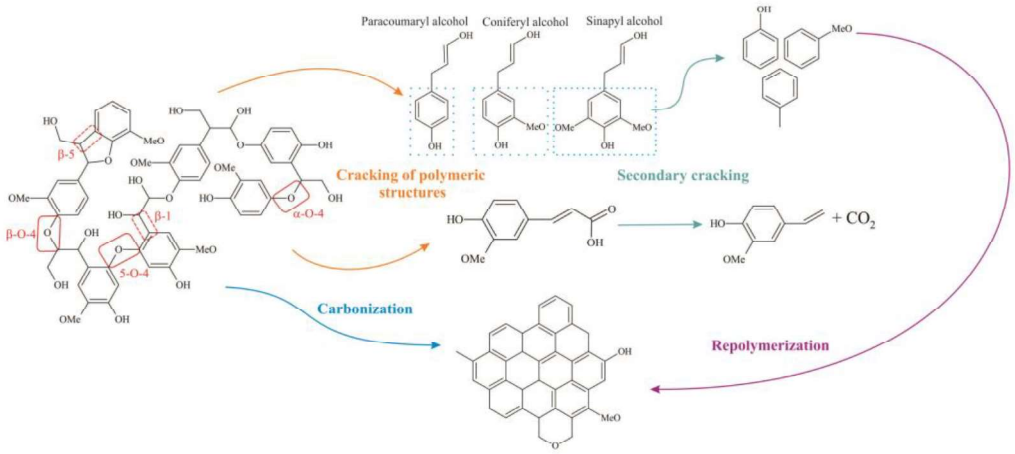

Figure 1: Pathways of thermal decomposition of lignin into pyrolysis products. The linkages marked by solid red squares are ether bonds and by red dot squares are condensed linkages. The blue dot squares are the repeating units of lignin: p-hydroxyphenyl, guaiacyl, and syringyl.

Experimental

Two samples of kraft lignin were used in experimental runs: *Eucalyptus spp* (lignin A), which was donated from International Paper, and the Pine Tree (lignin B) (CAS# 8068-05-1, cata# 471003) that was purchased from Sigma-Aldrich. These samples can be classified as hardwood and softwood lignins, respectively.

The ultimate analysis was carried out at the Laboratory of Analysis and Testing of coal and fuels in Criciúma-SC (SATC/LABSATC/LAEC) to determine the carbon (C), hydrogen (H), nitrogen (N), sulfur (S), oxygen (O) and ash content and was performed using a 2400 Series II CHNS/O analyzer (Perkin Elmer, USA) according to ASTM D5373-08.

The lignin pyrolysis was evaluated using a DTG-60 thermogravimetric analyzer (Shimadzu, Japan). For each experimental analysis, the sample (approximately 10 mg) was heated (from 25 to 900 °C) at 20°C/min under an inert flow of high-purity nitrogen gas (N2, 99.997%) at a flow rate of 100 mL min^{-1} [10]. The average DTG curve was built from the mass loss profiles (measured at duplicates), and the deconvolution method was applied to study the reactions that occurred during the pyrolysis of each lignin using OriginLab® Software.

Results and Discussion

Characterization

Table 1 lists the physicochemical properties and the elemental composition of the two Kraft Lignins samples. Hydrogen-to-carbon effective ratio (H/C_{eff}) was computed as shown in Table 1 to evaluate the relative hydrogen content of different feedstocks according to the number of O, C, and H moles in the sample. A higher ratio can suggest an increase in the amount of aromatic hydrocarbons in the bio-oil [8]. The percentage of methoxyl groups (OCH_3) was obtained based on the H and O contents as the footnote in Table 1 [9]. Similarly, the higher heating value (HHV) and low heating value

(LHV) were computed by equations in the footnote in Table 1, in which C, H, O, N, S, and ash are the mass fractions on a dry basis [10].

Compared to the pine tree sample (Lignin B), the eucalyptus sample (Lignin A) has higher amounts of C, H, S, and O, along with small N contents, indicating a higher quantity of methoxyl groups in the lignin A. However, lignin B has a higher H/C_{eff} ratio, meaning an easier conversion into aromatic hydrocarbons. The lower OCH_3 content in lignin B is desirable because produces a product with less acidity. The HHV and LHV of both samples suggest that lignin is an excellent energy source because can provide a high thermal yield in combustion processes. The physicochemical characterization shows similar results to the findings seen in other literature works [11], [12].

Table 1: Lignin physicochemical characterization.

Ultimate Analysis	Type of lignin		**Ultimate Analysis**	Type of Lignin	
	Eucalyptus *spp*	Pine Tree		Eucalyptus *spp*	Pine Tree
Carbon (C) [(a)]	56.4	49.36	Ash [(a)]	1.34	20.23
Hydrogen (H) [(a)]	5.91	4.82	H/C_{eff} [(c)]	0.38	0.42
Nitrogen (N) [(a)]	0.18	0.23	OCH_3 [(d)]	16.81	9.55
Sulfur (S) [(a)]	3.3	0.67	HHV [(e)] ($MJ.kg^{-1}$)	23.56	20.00
Oxygen (O) [(a, b)]	32.87	24.69	LHV [(f)] ($MJ.kg^{-1}$)	22.27	18.95

[a] Dry basis; [b] Calculated by the difference; [c] $H/C_{eff} = (H - 2O) / C$); [d] $OCH_3 = -18.5769 + 4.06580H + 0.345430O$; [e] $HHV\ (MJ.kg^{-1}) = 0.3491C + 1.1783H + 0.1005S - 0.1034O - 0.0151N - 0.0211Ash$ (3); [f] $LHV\ (MJ.kg^{-1}) = HHV\ (MJ.kg^{-1}) - 0.2183H$.

Evaluation of thermal decomposition

The thermogravimetry (TG) and derivative thermogravimetry (DTG) profiles of pyrolysis experiments at 20 °C/min for both lignins are presented in Fig. 2. The lignin thermal pyrolysis can be divided into three stages: the initial one associated to water evaporation (< 200 °C), the primary decomposition (200 – 500 °C), and carbonization stage (>500 °C). The first phase at < 200° (I) details part of the initial stage, where the sample presented dehydration. The main peaks (200 – 450 °C) occur in the second phase at 200 – 500° (II), indicating the final part of the initial stage and the first part of the second stage. In this step, lignin started to depolymerize into monomers, that were converted to methoxyphenols through the cleavage of ether and carbon-carbon bonds [4], [5], [7], [13]. At 400 – 600 °C, volatile compounds are released through reactions like depolymerization, demethoxylation, and the production of phenolic monomers is enhanced significantly due to the increase in the conversion of lignin. The third phase (III) represents the primary stage final part (500 – 600 °C) and the carbonization stage (600 – 900 °C), where happens the organization of benzene rings in a polycyclic structure, the aromatic ring secondary cracking, the removal of functional groups into char, and the char carbonization [4], [7].

At phase one, lignin B (A: 2.22%; B: 6.19%) lost more mass indicating a higher peak that was related to dehydration and depolymerization reactions that can produce G-type phenols. In contrast, lignin A lost more mass at phase II (A: 48.19%; B: 29.66%) possibly through depolymerization and repolymerization reactions of methoxyl groups. Moreover, hardwood lignin contains more ether bonds due to S-units, so one can see lower amounts of bio-char. However, lignin B has a higher condensation degree due to the G-unit and high carbon-carbon linkages, resulting in higher bio-char yield. Therefore, Lignin B is more susceptible to a second cracking of aromatic rings and rearrangement reaction at the third phase (A: 11.50%; B: 14.17%) thus leading to greater weight loss [3], [7], [14].

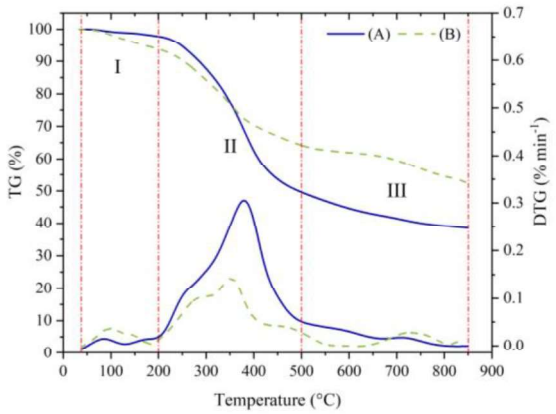

Figure 2: TG and DTG curves at 20 °C/min.

The deconvolution of DTG curves presented nine peaks during the temperature rise (Fig. 3). The first two peaks in both lignins represented the initial stage (< 200°C), where the weakly bonds at the functional groups are cleaved with the melting of lignin to form liquid intermediates. Peak one (A: 86 °C; B: 98 °C) can represent the water evaporation while the second peak (A: 171 °C; B: 143 °C) indicates the start of the ether linkages breakdown caused by the depolymerization reaction that forms the condensed lignin phase with a larger molecular weight [3], [7], [13].

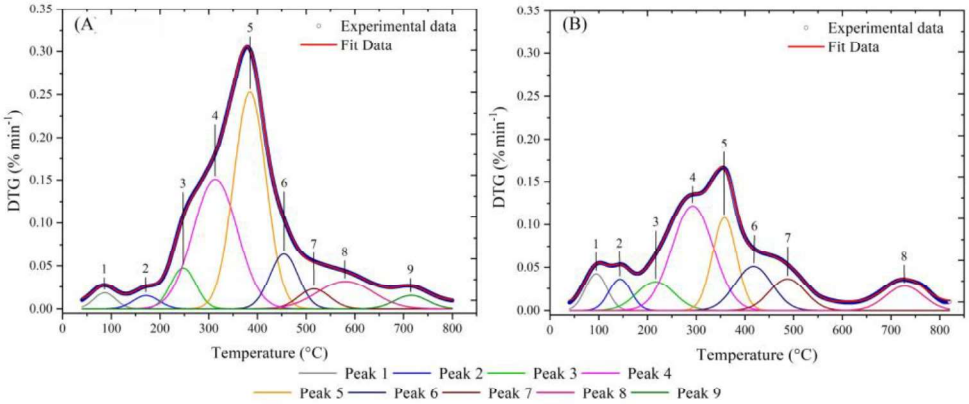

Figure 3: Deconvolution of DTG curves at a heating rate of 20°C/min: (A) Lignin A and (B) Lignin B

Peaks 3 and 4 between 200–350 °C represent the intermediate depolymerized into monolignols that can be converted to methoxyphenol through the cleavage of C-O and C-C bonds. Peak 3 (A: 247°C; B: 217 °C) represent the breaking of the most common linkage in lignin (β-O-4) and the reorganization of the chemical groups formed by breaking of the ether bonds, leading to the formation of oxygenated compounds such as CO, CO_2, and H_2O. Peak 4 (A: 313 °C; B: 292 °C) indicates a possible break of the bond between monomer units that provoke the release of phenolic compounds with a structure close to one of the monomer units (e.g. 4-vinylguaiacol) [13]. In lignin A, when the temperature reaches 385 °C at peak 5, the methoxy groups in the ortho position of the hydroxyl group become reactive and different types of fragmentation reactions result in the substitution of the methoxy group. However, these reactions tend to occur at a lower temperature in lignin B (357 °C) indicating that their bonds were easier to cleave due to the presence of fewer ether bonds than lignin A [4], [5].

At peak 6 (A: 455 °C; B: 418 °C), most of the initial bonds between monomer units have broken and severe gasification reactions started. At this stage, the substituent methoxyl groups were cleaved and hydroxyl or methylated groups bonded to the aromatic units, i.e., the major products formed in this stage like syringol can be converted into o-vanillin, guaiacol, and o-quinonemethide, meaning that the maximum yield of phenolic products can be achieved [3].

The second pyrolysis starts from peaks 7 and 8 in lignin A (516 °C; 579 °C) and at peak 7 in lignin B (488 °C). These peaks can be designated as reactions of demethylation, demethoxylation, and dehydrogenation that convert G-type compounds into catechol-type ones, alkyl-phenols, and aromatics. The presence of peaks 7 and 8 in lignin A can indicate a degradation of S-type to G-type units into other compounds such as methyphenol or can also represents the benzene rings broken down and conversion into no-condensable gases [3]. These peaks can also mean the start of the coke formation by the depolymerization process of the methyl groups. Peak 8 (728 °C) and Peak 9 (715 °C) in lignin B and lignin A, respectively, represent the coke formation, meaning that these peaks can be related to reconstruction, condensation, and polycondensation of the aromatic-ring structures [7].

Conclusions

Despite lignin being a natural source of phenolic compounds, the complexity of its structure should be considered when choosing the type of biomass for the pyrolysis processes. According to the results, softwood lignin started its decomposition at lower temperatures, which can be attributed to the presence of guaiacyl units. Hardwood lignin, however, needed higher temperatures to provide the decomposition of methoxyl groups that led to the transformation of S-unit phenol to G-unit phenol or another compound, justifying the lower amount of bio-char. The presence of OCH_3 directly influenced the pyrolysis reaction, indicating that the softwood lignin, due to its lower methoxy group content, can provide products with higher aromatic content. With the results presented in this study, the understanding of the lignin pyrolysis mechanism can be improved and used for future research on the composition of bio-oil, bio-gas, and bio-char.

References

1. A. Ház, M. Jablonský, I. Šurina, F. Kačík, T. Bubeníková, and J. Ďurkovič, Forests, 2019, vol. 10, no. 6, pp. 1–12. https://doi.org/10.3390/f10060483.
2. I. Hita, P. J. Deuss, G. Bonura, F. Frusteri, and H. J. Heeres, Fuel Process. Technol. 2018, vol. 179, pp. 143–153. https://doi.org/10.1016/j.fuproc.2018.06.018.
3. C. Chio, M. Sain, and W. Qin, Renewable and Sustainable Energy Reviews, 2019, vol. 107. Elsevier Ltd, pp. 232–249. https://doi.org/10.1016/j.rser.2019.03.008.
4. F. X. Collard and J. Blin, Renewable and Sustainable Energy Reviews, 2014, vol. 38. Elsevier Ltd, pp. 594–608. https://doi.org/10.1016/j.rser.2014.06.013.
5. S. Wang, G. Dai, H. Yang, and Z. Luo, Prog. Energy Combust. Sci. 2017, vol. 62, pp. 33–86, https://doi.org/10.1016/j.pecs.2017.05.004.
6. J. Yang, X. Wang, B. Shen, Z. Hu, L. Xu, and S. Yang. Renew. Energy, 2020, vol. 161, pp. 963–971. https://doi.org/10.1016/j.renene.2020.08.024.
7. X. Lu and X. Gu. BioMed Central, 2022. vol. 15, no. 1. https://doi.org/10.1186/s13068-022-02203-0.
8. H. Zhang, Y. T. Cheng, T. P. Vispute, R. Xiao, and G. W. Huber. Energy Environ. Sci. 2011, vol. 4, no. 6, pp. 2297–2307. https://doi.org/10.1039/c1ee01230d.
9. M. Jablonsky, M. Botkova, and J. Adamovska. Cellulose Chemistry Technology, 2015, vol. 49, no. 2, pp. 165–168.
10. J. C. G. da Silva, J. L. C. Pereira, S. L. F. Andersen, R. de F. P. M. Moreira, and H. J. José. Energy, vol. 210, 2020. https://doi.org/10.1016/j.energy.2020.118569.
11. M. Zhang, F. L. P. Resende, A. Moutsoglou, and D. E. Raynie. J. Anal. Appl. Pyrolysis, 2012, vol. 98, pp. 65–71. https://doi.org/10.1016/j.jaap.2012.05.009.
12. T. Ohra-Aho and J. Linnekoski. J. Anal. Appl. Pyrolysis, 2015, vol. 113, pp. 186–192. https://doi.org/ 10.1016/j.jaap.2014.12.012.
13. X. Chen et al. Fuel Process. Technol. 2019, vol. 196, no. August, p. 106180. https://doi.org/ 10.1016/j.fuproc.2019.106180.
14. H. Yang, K. Norinaga, J. Li, W. Zhu, and H. Wang. Fuel Process. Technol., 2018, vol. 181, pp. 207–214. https://doi.org/10.1016/j.fuproc.2018.09.022.

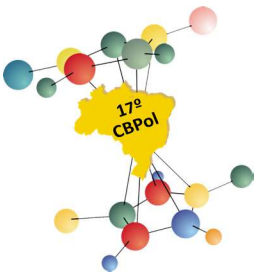

THERMAL DEGRADATION AND BIODEGRADABILITY OF POTATO STARCH FILMS WITH YERBA MATE EXTRACT AND MALIC ACID

Magali C. Casagranda[1]*, Renan B. da Silva[1] and Ruth M. C. Santana[1]

1 - Department of Materials Engineering, Federal University of Rio Grande do Sul (UFRGS), Porto Alegre, RS, Brazil
magalicanton@gmail.com

Abstract - Biodegradable potato starch-based films with 10% and 20% yerba mate extract concentrations were prepared by casting. The thermal degradation and biodegradability of the films obtained were studied, as well as the effect of the addition of malic acid to the composition. By TGA, it was found that the incorporation of yerba mate extract led to a decrease in the percentage of loss mass in the event with the highest degradation kinetics, a behavior amplified with the addition of malic acid. Formulations containing malic acid and yerba mate reached a higher temperature in the most intense mass loss event, suggesting an improvement in the thermal stability of the films, in addition to a higher degradation rate in the natural weathering and composting tests.
Keywords: *Starch films; potato starch; yerba mate; malic acid; thermal degradation; composting; natural weathering*

Introduction

In recent years, natural and biodegradable polymers have gained significant attention for the development of new eco-friendly materials capable of addressing the high consumption of non-renewable resources and the substantial amount of plastic waste generated [1]. Starch represents an interesting alternative due to its high degradation rate, having the potential to contribute to a significant reduction in waste volume and leading to a crucial environmental benefit [2].

The study of polymeric materials requires an efficient evaluation of their resistance to natural aging and biodeterioration by microorganisms since their exposure to the natural environment can modify both their appearance and properties. Additionally, the possibility of composting is important for the study of polymeric waste disposal. Furthermore, to determine their competitiveness and processability, it is essential to evaluate the temperatures supported by the material and its thermal degradation [2-3].

The incorporation of vegetal fibers into the polymeric matrix contributes to the modification of the material's properties and may also influence its degradation rate [4]. In this context, the addition of yerba mate, a plant of great importance to the southern region of Brazil, was studied as an extract. To enhance the material's thermal stability, the use of crosslinkers carboxylic acids such as malic acid (MA), which is a non-toxic and naturally occurring organic acid found in vegetables and fruits [5], was analyzed.

Experimental

Materials

Potato starch was supplied by Federal Institute of Rio Grande do Sul (IFRS). Glycerol P.A./ACS (NEON) was used as plasticizer and malic acid (DL) P.A. (Êxodo Científica) was used as crosslinking agent. Yerba mate (*Ilex paraguariensis*) extract was simulated using commercial yerba mate purchased at a local market in Porto Alegre, Brazil.

Preparation of the yerba mate extract
The yerba mate extract was prepared by infusing 3 g of sifted yerba mate in 100 g of distilled water at an initial temperature of 80 °C, under agitation [6-7]. After 5 minutes, the liquid was filtered and cooled to room temperature.

Preparation of the potato starch films
The polymeric matrix was developed by mixing 5 g of potato starch (PS) in glycerol (1 g) and distilled water (94 g). For samples containing yerba mate extract (YM), a fraction of distilled water was replaced by the desired concentration of extract (10 g and 20 g). The systems were homogenized under constant agitation at 100 °C until complete starch gelatinization. Subsequently, about 30 g of each filmogenic solution was poured into individual polymeric plates. After casting, the solutions were oven-dried at 30 °C for ~24 h under ventilation to form polymeric films. The same method was followed to prepare samples containing 0.5% malic acid (MA) (wt/vol), with a proportional decrease in the distilled water fraction. The samples produced are described in Table 1.

Table 1 – Composition of potato starch (PS) films with yerba mate extract (YM), with and without malic acid (MA).

Film specimen	Composition
PS	100% potato starch
PS10YM	Potato starch + 10% yerba mate extract
PS20YM	Potato starch + 20% yerba mate extract
MA	100% potato starch + 0.5% malic acid
MA10YM	Potato starch + 10% yerba mate extract + 0.5% malic acid
MA20YM	Potato starch + 20% yerba mate extract + 0.5% malic acid

Thermogravimetric analysis (TGA)
Thermogravimetric tests were performed using a *TA Instruments TGA Q50* equipment. Pieces of each film were heated from room temperature to 900 °C at a rate of 20 °C/min under nitrogen flow of 30 mL/min. From the plots of weight loss values versus temperature, the different degradation phases were obtained.

Natural weathering and composting
Three samples from each formulation (20 mm × 20 mm) were exposed to natural weathering from five and ten days on platforms built with an angle of 45° to the ground, in Porto Alegre, RS (Brazil), 30°04'23.9"S 51°06'52.2"W, according to D 1435- 99 standard.
The compost degradation was conducted based on G160-12 standard. Samples of each system (20 mm × 20 mm) were buried in containers with soil fertilized with organic compounds (humus) to a depth of approximately 20 mm. At the fifth and tenth days, three samples of each formulation were carefully removed from the soil, oven-dried and weighed on a precision scale. The loss of mass for both tests was calculated according to Eq. 1, where m_i and m_f are equivalent to the initial and final masses of the samples, respectively.

$$Loss\ of\ mass\ (\%) = ((m_i - m_f)/m_i) \times 100 \quad (1)$$

Results and Discussion
Thermogravimetric analysis (TGA) was carried out in order to analyze the thermal stability of the different starch-based films containing yerba mate extract (Fig. 1). While the thermal decomposition of potato starch takes place in two main stages, notably involving water evaporation (~ 120 °C) and decomposition of amylose and amylopectin (~ 320 °C) [6], the incorporation of yerba mate adds additional steps related to the degradation of pectins and hemicellulose (reportedly between 200 °C and 300 °C [1]), organic components present in the vegetal material. Within this

temperature range, the decomposition of the glycerol-rich phase also occurs. In all cases, this event is hidden by the intense peak observed in the same region [2], which corresponds to the largest drop in the TGA curve and represents the most intense mass loss.
By DTG (Fig. 1-b), a decrease in the peak of the highest degradation kinetics is visible in the samples containing yerba mate, proportional to the amount of extract added to the formulation. This is explained by the fact that this temperature range also corresponds to the degradation of cellulose in yerba mate, which is a less intense event compared to the main starch degradation step [2]. This behavior is replicated in samples containing malic acid (Fig. 1-d), although the addition of this agent is responsible for a significant decrease in the weight loss rate per Celsius degree.

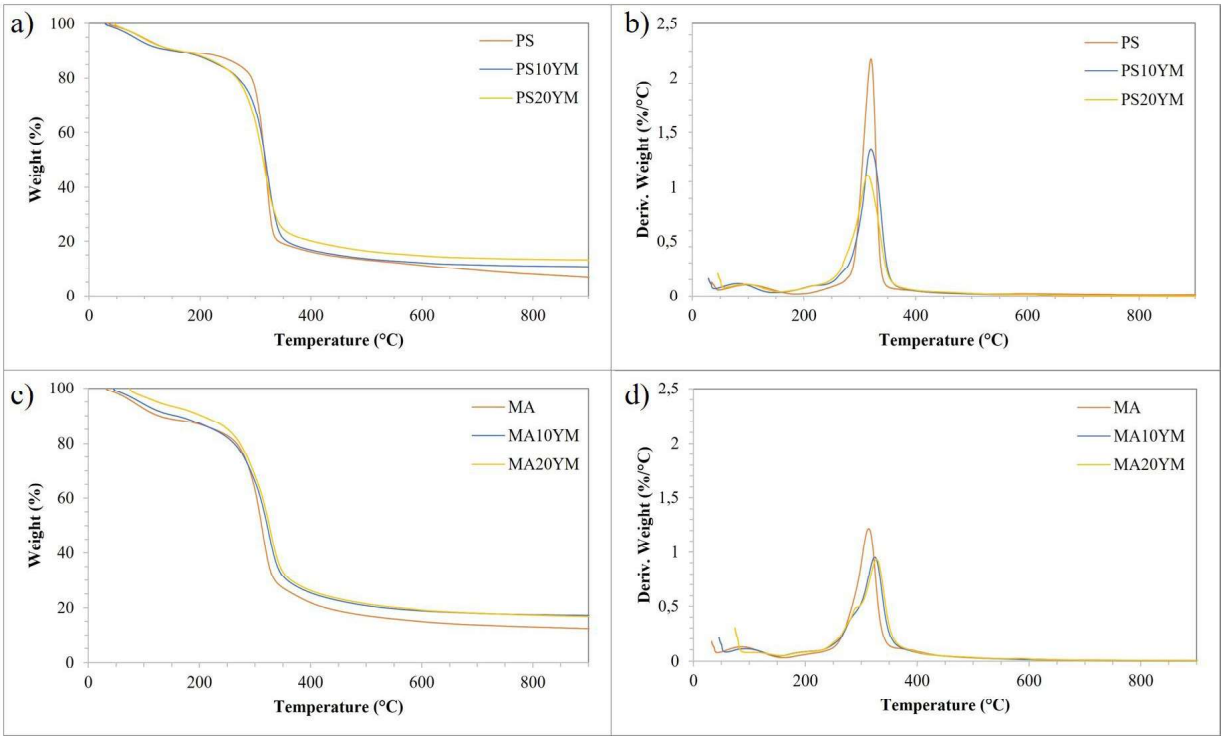

Figure 1 – (a) TGA curves for PS and PS/YM films; (b) DTG curves for PS and PS/YM films; (c) TGA curves for MA and MA/YM films; (b) DTG curves for MA and MA/YM films.

Table 2 presents the decomposition characteristics for the different films produced. Similar to Fig. 1, it can be observed that the percentage of mass loss at the main event decreases with increasing temperature for the samples containing malic acid and yerba mate. For pure PS, this stage occurs at approximately 319.91 °C and degrades 82.69% of the film's mass. In contrast, for the MA20YM sample, this stage eliminates 53.48% of the mass and takes place at approximately 327.23 °C. This implies that the addition of malic acid could improve the thermal degradation temperature, because the crosslinking present in this additive could strengthen the PS backbone chains and create strong linkages, thereby enhancing the thermal degradation temperature of the crosslinked films [5].
The remaining residues at the end of the process for films containing yerba mate are typically composed of aromatic rings, which exhibit stability in their ashes above 600 °C under a nitrogen atmosphere [7]. The high amount of residues in the malic acid films may also suggest the formation of strong crosslinkages between the acids and the potato starch chains [5].

Table 2 – Thermal decomposition characteristics of PS, PS/YM, MA and MA/YM film samples.

Sample	$\%m_1$	$\%m_2$	$\%m_3$	$\%m_4$	%ashes	T peak (°C)
PS	10.64	82.69	ND	ND	6.67	319.91
PS10YM	8.47	6.74	4.88	67.44	12.47	319.09

PS20YM	8.21	5.78	8.04	62.97	15.00	313.21
MA	10.03	4.91	57.34	13.72	14.00	313.40
MA10YM	8.28	5.46	17.05	50.34	18.87	323.97
MA20YM	4.18	5.91	17.13	53.48	19.30	327.23

%m: mass loss content at each stage of thermal decomposition.
T peak: temperature of greatest decomposition kinetics.
ND: not detectable.

In order to study the stability of the systems against degradation, natural weathering and composting tests were conducted for five and ten days. The temperatures in the city of Porto Alegre during the testing period ranged from 10 °C to 27 °C, presenting an average relative humidity between 70% and 95%. Fig. 2 provides a comparison of the percentage of remaining mass for all samples after the tests. All formulations exhibited a higher degree of mass loss during composting compared to natural ageing.

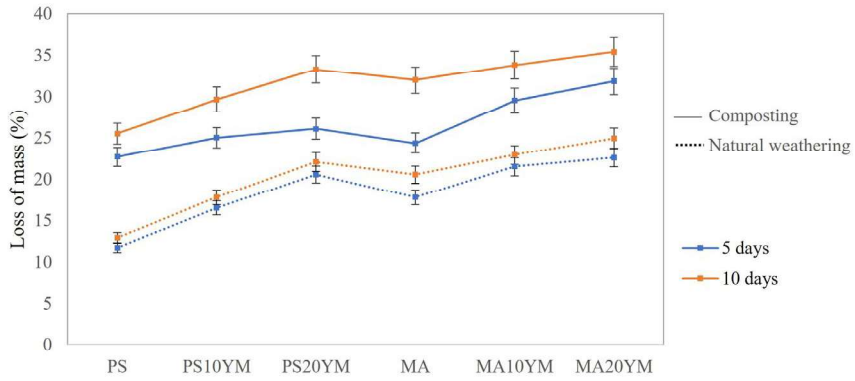

Figure 2 – Loss of mass by formulation as a function of composting time (continuous line) and weathering time (dashed line) for 5 days (blue line) and 10 days (orange line).

Vegetal compounds are easily degraded by microorganisms when buried in the soil [8]. In this sense, the incorporation of yerba mate may be responsible for increasing the rate of degradation of the material in the soil, since the addition of vegetal fibers can facilitate the hydrolysis process. This leads to the formation of small monomers and short chain oligomers that are available to microorganisms, resulting in a higher rate of decomposition [1-2]. Furthermore, some of the compounds of yerba mate had low molecular weight and, therefore, are more susceptible to degradation before starch [2].

The presence of lignin in yerba mate is capable of absorbing UV radiation, which accelerates the photodegradation of the samples when exposed to weathering [9]. Furthermore, the high hydrophilic character of vegetal compounds leads to a tendency to absorb atmospheric moisture, resulting in surface wear of the material through dilatation or delamination [10].

It is important to highlight that the addition of malic acid to the formulation is responsible for increasing the degradation rate of the material, resulting in a 35% weight reduction after 10 days of testing. This may indicate that malic acid acts as an anti-retrogradation agent for starch, inhibiting its recrystallization and leading to high moisture absorption, opposite to what is expected with the incorporation of these acids [11].

From Fig. 3, it is possible to compare the visual aspects of pure PS and MA20YM (lower and higher mass loss, respectively) at t_0 and after degradation tests. The absorption of UV radiation by lignin leads to a change in the coloration of the films, as can be observed in MA20YM, which had its color changed from greenish to transparent at the end of the weathering test. Compared to the PS film, the composting test showed the most significant variation in the appearance of the samples, with a thinning of the film with fractures that produced fragmentation and disintegration.

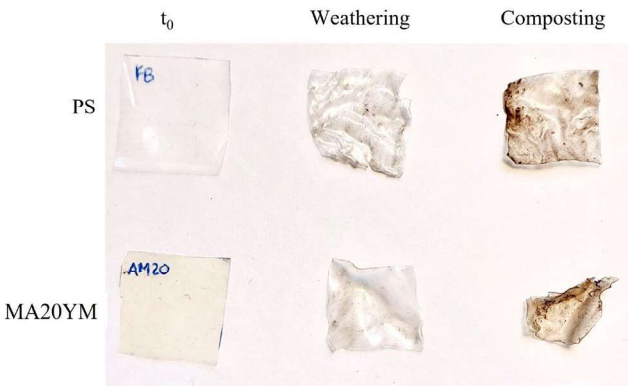

Figure 3 – Visual comparison between the samples PS and MA20YM after 10 days of natural weathering and composting, respectively.

Conclusions

Thermal analysis revealed a lower mass loss in the stage of highest degradation kinetics in the samples containing yerba mate, which is proportional to the amount of yerba mate extract added. This behavior became more apparent with the addition of malic acid to the yerba mate extract, indicating greater thermal stability in the films with this composition. The films with this formulation also exhibited higher mass loss in the biodegradation tests, suggesting that malic acid can act as an inhibitor of starch retrogradation, leading to increased moisture absorption in these samples. The faster degradation in soil of the starch-glycerol-yerba mate extract films makes them very promising to continue with new trends to preserve the environment.

Acknowledgements

The authors would like to thank to CAPES-PROEX for supporting the research, the Laboratory of Polymeric Materials (LaPol) from Federal University of Rio Grande do Sul (UFRGS) for the infrastructure provided and the Federal Institute of Rio Grande do Sul (IFRS) for donating the potato starch.

References

1. M. A. Arrieta et al. Industrial crops and products 2018, 111, 317-328. https://doi.org/10.1016/j.indcrop.2017.10.042
2. C. M. Jaramillo et al. Carbohydrate polymers 2016, 151, 150-159. https://doi.org/10.1016/j.carbpol.2016.05.025
3. X. Liu et al. Starch-Stärke 2012, 65, 48-60. https://doi.org/10.1002/star.201200198
4. K. G. Satyanarayana; G. G. C. Arizaga; F. Wypych. Progress in polymer science 2009, 34, 982-1021. https://doi.org/10.1016/j.progpolymsci.2008.12.002
5. N. Thessrimuang; J. Prachayawarakorn. Journal of polymers and the environment 2019, 27, 234-244. https://doi.org/10.1007/s10924-018-1340-2
6. Y. Liu et al. Materials 2019, 12, 699. https://doi.org/10.3390/ma12050699
7. E. Rayón et al. International journal of food properties 2015, 18, 1211-1222. https://doi.org/10.1080/10942912.2014.884578
8. T. Ohkita; S. H. Lee. Journal of applied polymer science 2006, 100, 3009-3017. https://doi.org/10.1002/app.23425
9. W. Yang et al. Industrial crops and products 2015, 77, 833-844. https://doi.org/10.1016/j.indcrop.2015.09.057
10. Z. N. Azwa et al. Materials & Design 2013, 47, 424-442. https://doi.org/10.1016/j.matdes.2012.11.025
11. M. B. K. Niazi; A. A. Broekhuis. European polymer journal 2015, 64, 229-243. https://doi.org/10.1016/j.eurpolymj.2015.01.027

THE ROLE OF ISOCYANATE IN THE PROPERTIES FOR RECYCLABLE POLYURETHANE FOAMS

Marys Lene B. Almeida[1*], Eliane Ayres[2], Mercês C. da Silva[3] and Rodrigo L. Oréfice[4]

1 – Department of Materials Engineering and Construction (DEMC), Federal University of Minas Gerais (UFMG), Belo Horizonte, Brazil
marysliz@yahoo.com.br
2 – Postgraduate program in Design (PPGD), State University of Minas Gerais (UEMG), Belo Horizonte, MG, Brazil,
3 – Institute of Integrated Engineering(IEI), Federal University of Itajubá (UNIFEI), Itabira, MG, Brazil
4 – Department of Metallurgical and Materials Engineering (DEMET), Federal University of Minas Gerais (UFMG), Belo Horizonte, Brazil

Abstract - Polyurethane foams were obtained from three aromatic isocyanates namely, toluene 2,4-diisocyanate, bifunctional 4,4′-methylene diphenyl diisocyanate, and poly(methylene diphenyl diisocyanate). In this work, the more suitable isocyanate has selected to produce foams able to be recycled through a process called vitrimerization. This process involves converting the permanent cross-linked thermosets into vitrimer polymers without depolymerization. The mechanochemical vitrimerization with the aid of a solid catalyst is considered a feasible method. Most of vitrimerization methods enables reprocessing of PU foams into films. In the mechanochemical method, the vitrimerized network can be foamed again by applying heat and small pressure. In a preliminary evaluation, carried out using SEM and TGA, the polymeric MDI seems to have giving rise to the appropriate foam, mainly because its good thermal stability. The vitrimerization experiments are ongoing and soon the findings will be reported.

Keywords: *Polyurethane foams, Isocyanates properties, Recyclable thermosets, Vitrimers.*

Fundings: The National Council for Scientific and Technological Development (CNPq). Referring to CNPq/MCTI-FNDCT CT-Petro Nº 43/2022 - Tecnologias para decomposição, tratamento e substituição do plástico. Grant/Award Number: 405414/2022-6.

Introduction

In general, polyurethanes (PU) are based on the exothermic reaction of polyisocyanates with polyol molecules, containing hydroxyl groups [1]. Relatively few basic isocyanates and a range of polyols of different molecular weights and functionalities are used to produce the whole spectrum of polyurethanes [1]. By itself, the polymerization produces a solid polyurethane. Foams are made by forming gas bubbles, in a process called blowing [1]. Several aromatic and aliphatic isocyanates are available, but about 95 percent of all polyurethanes are based on two of them. These are toluene diisocyanate (TDI) and diisocyanate diphenylmethane (MDI) and its derivatives [1]. TDI is almost always used as a mixture of the 2:4- and 2-6-isomers, usually the 80:20, and largely used for flexible foams [2]. The greatest outlet for MDI is in rigid foams, where it is employed as a complex mixture known as polymeric MDI [1, 2]. Pure MDI is a solid of melting point of 38 °C which is produced by separation from a polymeric MDI precursor [1]. There are three principal methods of PU foam preparation: (a) prepolymer; (b) semi-or quasi-prepolymer; and (c) one-shot [3]. The prepolymer process involves the reaction of a polyol with an excess of a diisocyanate prior to foaming. Foaming occurs by reaction of the prepolymer with water, with formation of urea linkages

and evolution of carbon dioxide, which acts as the blowing agent [3]. The semi-or quasi – prepolymer method utilizes the reaction of a diisocyanate with a portion of the polyol, resulting in a relatively low viscosity, low molecular weight polymer dissolved in a large excess of diisocyanate. Foaming is brought about by reacting the semi-prepolymer with the remainder of the polyol and water [3]. In the one-shot process the various foam components are mixed simultaneously [3]. The properties of PU foams are categorized based on the type of foam structure: open-cell structure or closed-cell structure [4]. In the open-cell structured foam the cell walls, or surfaces of the bubbles, are broken up and are filled up with air that fills up all the spaces in the material [4]. This makes the foam soft or weak [4]. In closed-cell foam, most of the cells or bubbles in the foam are not broken, and it is strong enough to resist major distortions [4]. On the other hand, thermosetting PU foams, cannot be recycled economically and efficiently due to their permanently crosslinked structures [5]. In order to circumvent this, researchers have increasingly focused on introducing dynamic covalent bonds to prepare PU foams containing covalent adaptable network (CAN) [5]. Such approach aims to combine the advantages of both type of polymers, thermoplastics and thermosets, and is known as vitrimeric behavior [6]. In polyurethanes with CAN-containing dynamic carbamate bonds, the chemical structure of isocyanate has a significant impact on the network rearrangement [6]. Gamardella et al. [7] demonstrated that among the reprocessable and recyclable poly(thiourethane) thermosets, that prepared from the aromatic isocyanate achieved the reorganization of the network faster than those prepared from the aliphatic isocyanate. Thus, this work aims to preliminary select the isocyanate to produce PU foam with promising thermal reprocessability by hard segments vitrimerization.

Experimental

The foams were prepared using the one-shot process with the amount of reagents entirely based on the previous work of our group [8]. In short, PPG 2000 (1.25 g) and Biopol® 411 (11.25 g), a polyol (ester) derived from castor oil, were mixtured with deionized water (0.4 g), tin catalyst (0.025 g), and silicone foam stabilizer (0.10 g). These reagents were under mechanical stirring at 1000 rpm for 2 min before the addition of TDI (11.65 g) and stirred for another 30 s when the foaming started. In the present work, TDI was replaced by pure MDI (Sigma –Aldrich SUK 256439) and polymeric MDI (Biopol® ISO, PolyUrethane - Ibirité, Brazil). The obtained foams were called as TDI foam, pure MDI foam and poly MDI foam, respectively. They were characterized by SEM (Hitachi 4000 Plus with backscattered electrons detector), FTIR (Thermo Scientific Nicolet™ 6700 Gold spectrophotometer in ATR mode) and TG (Exstar 7200, Seiko-SII Nanotechnology, Inc.).

Results and Discussion

The amide A, amide I, amide II and amide III bands are widely used in the spectroscopy study of polyurethane. The term "amide bands", which is taken from amide spectroscopy, is correct, because a urethane group differs from an amide group only by an additional oxygen atom [9]. Such bands were detected at 3304 cm^{-1} and, in the region called fingerprint region of the IR spectrum of PU, at 1700 cm^{-1}, 1522 cm^{-1} and 1182 cm^{-1}, respectively [9]. The absorption at 1042 cm^{-1} is attributed to C–O–C vibration of ether group and the presence of the band at 2270 cm^{-1} denotes residual free isocyanate groups (NCO) [10]. There are no significant differences between the spectra.

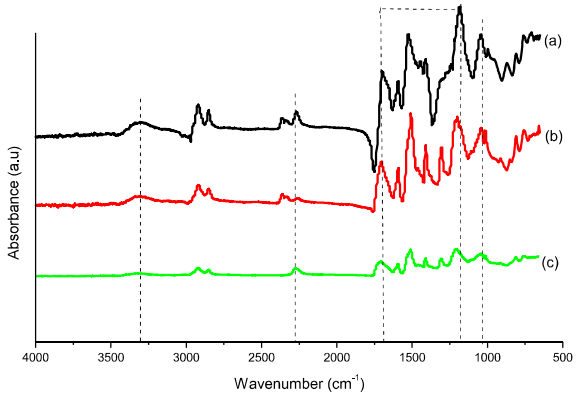

Figure 1 – FTIR spectra of: (a) TDI foam, (b) pure MDI foam and (c) poly MDI foam.

The morphology of the three foams was observed through SEM. Morphology of the foam reveals important information such as cell shape and domain size.

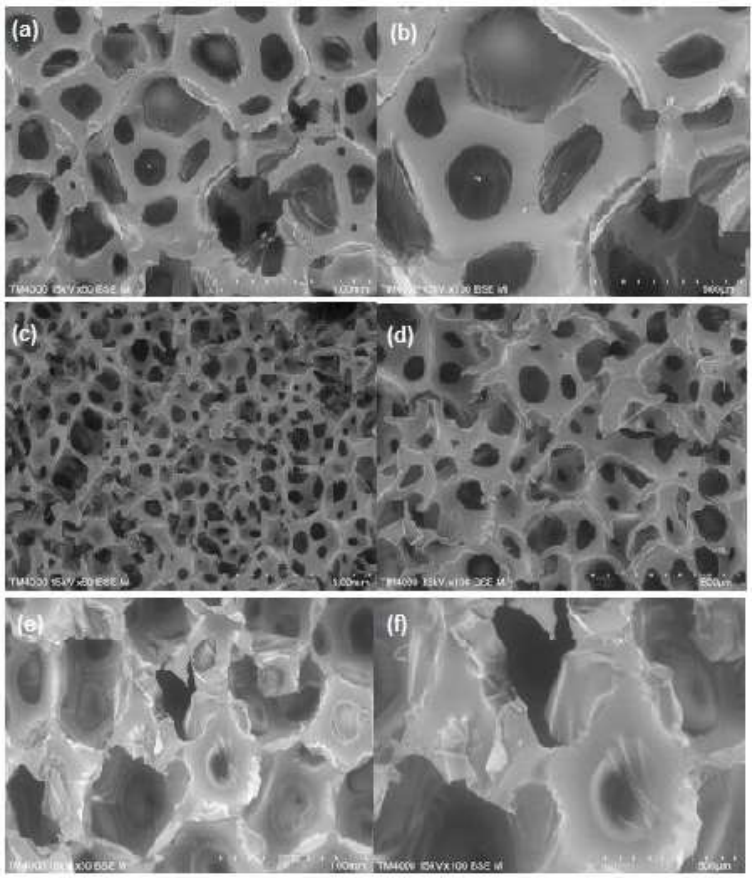

Figure 2 – SEM images of polyurethane foams: TDI foam (a and b), pure MDI foam (c and d) and poly MDI foam (e and f).

The texture is uniform in the case of pure MDI foam, with more well organized cell shapes than the other foam samples. Similar result was also observed by John et al. [11]. By comparing pure MDI foam with poly MDI foam, it is possible to see that the use of multifunctional polymeric MDI affects significantly the formation of the cellular morphology. Apparent density is so called because it is calculated from the volume of expanded cellular material that includes its cell cavities. Herein, cubic samples of known dimensions were weighed and the foam apparent density (ρ) was determined. The values in g cm^{-3} are 0.096±0.004, 0.0121±0.004 and 0.063±0.003 for TDI foam,

pure MDI foam and poly MDI foam, respectively. Bandegi et al [12] utilized the carbamate exchange reaction for the vitrimerization of thermoset rigid PU foams. Triazabicyclodecene (TBD) as organocatalyst was used for the vitrimerization in an environment-friendly mechanochemical process. The authors showed that the vitrimerized network could be foamed again by applying heat and small pressure. However, the initial foam has density of 0.01 g cm^{-3} and the density for the foam produced from the vitrimerized network is 0.56 g cm^{-3}. Thus, in a first exploratory study to obtain a foam from vitrimerized network, polymeric MDI might be selected.

The thermal stability of the foams was analyzed by TGA and the weight loss and the derivative curves are shown in Fig. 3. The first observation is a weight loss at around 100 °C, generally attributed to water evaporation. After this, all curves display two distinct regions of weight loss. The first one correlates with degradation of the hard segment, while the second one correlates with the degradation of the soft segment [13].

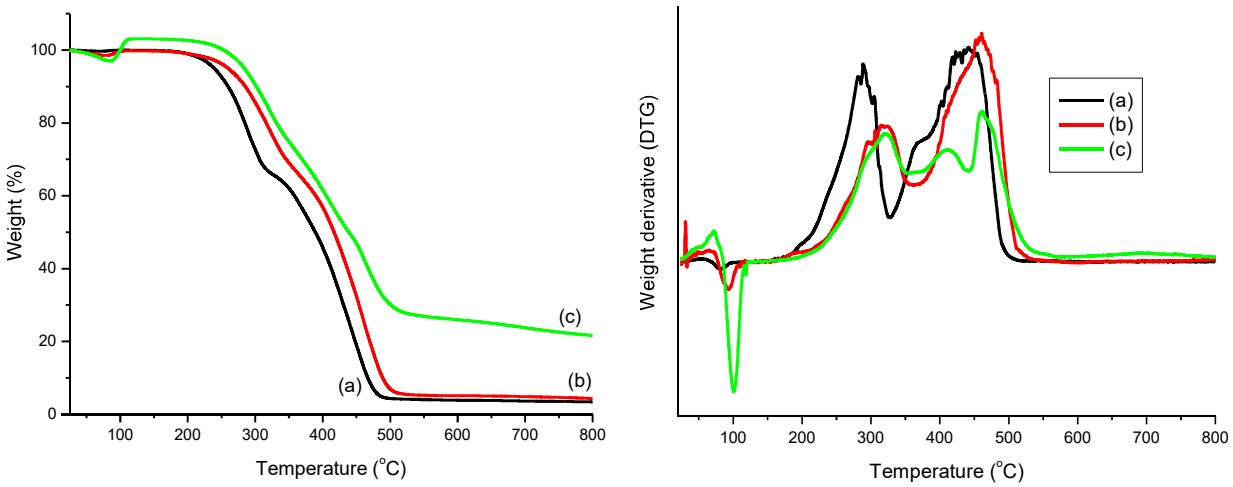

Figure 3 – TGA and DTG curves of the different PU foams: (a) TDI foam, (b) pure MDI foam and (c) poly MDI foam.

It's easily noticeable that foams based on MDI have more thermal stability than foam based on TDI, as well as poly MDI foam has more thermal stability than pure MDI foam. Foams obtained using MDI were rigid and the reaction was slower when compared to that of TDI [11]. It is obvious that the thermal stability of hard segment has a great influence on the thermal stability of soft segment [13]. The higher thermal stability of hard segment leaded to a higher degradation temperature of soft segment. In addition, the use of multifunctional polymeric MDI in fabrication of polyurethane foams affects significantly the formation of the cellular morphology [14]. Such observation is an accordance with SEM analysis, which showed pores that are more irregular. Possibly, there are more closed pores due to the high viscosity of the matrix resulting from the crosslinking reaction with polymeric MDI. In the poly MDI foam DTG curve the peak corresponding to degradation of the soft segment appears as a doublet, which reinforces the irregular morphology of the foam. In spite of this, polymeric MDI might be selected for producing a foam from vitrimerized network. Since high thermal stability is beneficial for the vitrimerization process.

Conclusions

Polyurethane foams were obtained with TDI, pure MDI or polymeric MDI for exploring the effect of isocyanate functionality on the properties such as cell morphology and thermal stability. The foam using polymeric MDI presented the lowest density. Due to this, polymeric MDI was considered a good candidate for producing vitrimer foam with the ability to foamed again after reprocessing. In addition, such polyurethane foam has greater thermal stability, which is beneficial for the vitrimerization process. The vitrimerization experiments are ongoing in our laboratory.

Acknowledgements
The authors are grateful to Minas Gerais State Research Support Foundation (FAPEMIG), Coordination for the Improvement of Higher Education Personnel (CAPES) and National Council for Scientific and Technological Development (CNPq).

References

1. G. Woods, *The ICI Polyurethanes Book*, Wiley–Blackwell, Hoboken, 1987.
2. J. M. Buist, R. Hurd and R. L. Stafford, in Advances in Polyurethane Technology, J. M. Buist & H. Gudgeon, Ed.; Maclaren and Sons Ltd (Elsevier Science Ltd.), London, 1968; 6, 187-249.
3. J. H. Saunders and K. C. Frisch, *Polyurethanes: Chemistry and Technology, Parte 2*, Interscience Publishers, New York, 1964.
4. A. S. Dutta, in *Recycling of Polyurethane Foams,* S. Thomas et al., Ed.; William Andrew Publishing, Maharashtra, 2018; 17-27. https://doi.org/10.1016/B978-0-323-51133-9.00002-4.
5. X. Z. Wang; M. S. Lu; J. B. Zeng; Y. Weng; Y. D. Li Green Chemistry 2021, 23(1), 307-313. https://doi.org/10.1039/D0GC03471A
6. J. Shi; T. Zheng; Y. Zhang; B. Guo; J. Xuo Polymer Chemistry 2021, 12(16), 2421-2432. https://doi.org/10.1039/D1PY00157D
7. F. Gamardella; S. De la Flor; X. Ramis; A. Serra Reactive and Functional Polymers 2020, 151, 104574. https://doi.org/10.1016/j.reactfunctpolym.2020.104574
8. M. B. L. Almeida; E. Ayres; M. C. da Silva; R. L. Oréfice Journal of Hazardous Materials 2018, 346, 285-295. https://doi.org/10.1016/j.jhazmat.2017.12.033
9. G. G. Suchkova;L. I. Maklakov Vibrational Spectroscopy 2009, 51(2), 333-339. https://doi.org/10.1016/j.vibspec.2009.09.002
10. I. Izarra; A. M. Borreguero; I. Garrido; J. F. Rodríguez; M. Carmona Polymer Testing 2021, 107268. https://doi.org/10.1016/j.polymertesting.2021.107268
11. J. John; M. Bhattacharya; R. B. Turner Journal of Applied Polymer Science 2002, 86(12), 3097-3107. https://doi.org/10.1002/app.11322
12. A. Bandegi; M. Montemayor; I. Manas-Zloczower Polymers for Advanced Technologies 2022, 33(10), 3750-3758. https://doi.org/10.1002/pat.5827
13. Y. M. Song; W. C. Chen; T. L. Yu; K. Linliu; Y. H. Tseng Journal of Applied Polymer Science 1996, 62(5), 827-834. https://doi.org/10.1002/(SICI)1097-4628(19961031)62:5<827::AID-APP15>3.0.CO;2-P
14. G. Sung; J. H. Kim Journal of Chemical Engineering 2017, 34, 1222-1228. https://doi.org/10.1007/s11814-016-0361-6

USE OF ACRYLONITRILE BUTADIENE STYRENE (ABS) WASTE FROM ELECTRICAL AND ELECTRONIC EQUIPMENT (WEEE) IN OBTAINING FILAMENTS FOR 3D PRINTING

Jonas Mantovani[1], Eveline Bischoff[1], Douglas A. Simon[1]*

1 – Instituto Federal do Rio Grande do Sul (IFRS), Farroupilha, RS, Brazil
**douglas.simon@farroupilha.ifrs.edu.br*

Abstract Waste from electrical and electronic equipment (WEEE) has been increasing rapidly due to its short lifespan. This study aims to assess the feasibility of producing a 3D printing filament from polymeric waste derived from CRT monitor and television casings. Spectroscopic characterization revealed differences in polymer identification compared to analysis results. The thermal and rheological properties were similar to virgin ABS. Extrusion of the waste ABS under the same conditions as virgin ABS was satisfactory, but post-extrusion cooling introduced high porosity. FDM printing with the recycled filament was efficient, but porosity was observed in the printed parts. Parts printed with the recycled filament exhibited lower mechanical properties, with a significant reduction in impact strength due to the voids. The filament produced from WEEE is suitable for 3D printing applications requiring good dimensional tolerance without high mechanical properties.

Keywords: *WEEE, Additive manufacturing, ABS, post-consumer waste*

Introduction

Currently, we live in a disposable society where the production of durable and reusable goods is not desired. In this context of exchange and disposal, waste generation continues to increase. Waste from electrical and electronic equipment (WEEE) has one of the highest growth rates due to the increasing popularity of electrical and electronic devices (EEE) and their accelerated obsolescence in the face of new technologies.

Recycling has emerged as a sustainable alternative to mitigate the negative effects of accumulating these wastes in the environment. Thermoplastic materials are easily recyclable, bringing cost savings to the industry by reducing the need for raw material acquisition [1].

With the growing competitiveness among companies, 3D printing has been widely adopted in industries due to improved processes, product quality, and cost and time reduction. The 3D printing process involves transforming a virtual 3D object into a physical object [2].

There are various types of additive manufacturing, but fused deposition modeling (FDM) is the most commonly used technique for constructing plastic parts with great geometric freedom, low equipment investment, and low consumable costs. FDM uses a thermoplastic polymer filament as the raw material for manufacturing parts, with the most commonly used materials being Acrylonitrile Butadiene Styrene (ABS) and Polylactic Acid (PLA) [2-4].

The properties of ABS have made it one of the most popular materials in the 3D printing process due to its good printability, precision, and dimensional stability. Additionally, the quality of parts printed with ABS using the FDM process can be controlled by adjusting various printing parameters such as infill type and density, printing orientation, layer height, printing temperature, printing speed, among others.

In this regard, this study will demonstrate the recycling capability of EEE waste, particularly ABS from polymer casings, to produce a filament for use in 3D printing using the FDM technique. The production potential of the filament through extrusion, the printability of this material in an open FDM printer, and the chemical, thermal, and rheological properties compared to commercial filament will be evaluated.

Experimental

Materials

The following materials were used for the experimental phase: ABS MG47F (manufactured by Sabic), with a melt flow rate of 5.6 g/10 min (230°C/3.8 kg), was used to produce the standard commercial filament. Waste from electrical and electronic equipment (EEE) originating from post-consumer electronic device casings, including CRT monitors, televisions, keyboards, and printers, which were damaged or obsolete. The waste was collected from a local repair shop located in Nova Prata-RS, Brazil.

Initially, the act of disassembling and segregating the polymer material from other composite materials, including metals, ceramics, electronic circuit components was executed. Only ABS housings were kept to subsequent steps.

Method

The waste was cleaned with water and neutral soap to remove impurities. The carcasses were broken into small pieces using a steel hammer, as seen in Figure 1. Fragments were dried for 48 hours in the shade and then packaged in clean plastic wrappers.

ABS fragments from WEEE were ground using a knife mill until reaching a size range of 1-5 mm. The flakes were then dried in an oven at 80 °C for 4 hours. Similarly, pure ABS pellets underwent the same drying process. Next, the ABS flakes were heated and extruded in an extruder with a 2.0 mm diameter matrix, using temperature ranges of 155-180 °C with a matrix temperature of 165 °C. The extruded filament was cooled in a water-filled bathtub, and its diameter was measured. Segments with diameters of 1.65-1.75 mm were selected for printing the CPs. The dried filament was then stored in a light-protected wrapper until used for printing.

The specimens were produced utilizing a Fused Deposition Modeling (FDM) printer, fabricated by Mastre Automação, and employing ABS filaments in conjunction with waste from Waste Electrical and Electronic Equipment (WEEE). The specimens were fabricated in accordance with the geometric specifications prescribed by the ASTM D638 — Type I standards for the analysis of tensile strength.

The test specimens were modeled using CAD software (Fusion 360) following the ASTM D638 standard. They were then exported to Ultimaker Cura software, version 5.0.1, in "stl" format. A printer specifically developed for this study was used to print the test specimens. Printing parameters are present in Table 1.

Figure 1 – Fragments of parts used for filament production.

Table 1 – Printing Parameters

Layer Height (mm)	0,2
Printing Temperature (º C)	185
Nozzle Diameter (mm)	0,4
Table Temperature (º C)	150
Perimeter Layers	5
Infill Percentage (%)	100
Printing Speed (mm/s)	60
Cooling Fan	Not Present
First Layer Speed (mm/s)	20

Characterization

Differential Scanning Calorimetry (DSC) analysis was conducted on the filament that was produced in order to determine the temperatures of melting (Tm) and glass transition (Tg). The aforementioned test was carried out utilizing Perkin Elmer DSC 6000 equipment in conformity to ASTM D3418. Each sample consisted of approximately 9 mg and was heated initially to 220 °C and allowed to stabilize for a duration of 3 minutes. Subsequently, the sample was cooled down to -30 °C and allowed to acclimatize for a period of 5 minutes, followed by a second heating up to 220 °C. The ramp for both heating and cooling was maintained at a constant rate of 20 °C/min, and the entire process was conducted in an environment of nitrogen.

For the mechanical tests, five specimens were printed for each sample, and a universal testing machine (EMIC, model DL200) with a 5000 N load cell was used. The specimens were tested at a crosshead speed of 10 mm/min according to the ASTM D638 standard. They were stretched until a 50 mm limit was reached.

Also, pure ABS and WEEE filaments printability were evaluated as weight and surface quality, as a qualitative measurement of roughness.

Results and Discussion

Differential Scanning Calorimetry

To investigate the thermal events that occurred during the heating and cooling of the r-ABS sample, differential scanning calorimetry was conduct. The results of which are presented in Figure 2, which includes both the cooling (depicted in blue) and second heating (depicted in red) curves. Our findings indicated that the r-ABS sample exhibited a single peak corresponding to the crystalline melting temperature (Tm), and a glass transition temperature (Tg) of approximately 102 °C, which is attributed to the acrylonitrile-styrene (SAN) phase of ABS. These observations confirmed the absence of a secondary polymer in the analyzed sample's composition.

In a similar study conducted by Harris et al. (2019) that focused on the thermal and mechanical properties of ABS, the authors found that Tm (ABS) was approximately 111.8 °C, and Tg was approximately 100.2 °C for pure ABS [3]. These results are analogous to the outcomes of our study.

Tensile Strength

The obtained results indicate similar Young's modulus for both recycled (r-ABS) and virgin ABS materials, as shown in Figure 3. The Young's modulus values were determined to be 534.3 MPa and 519.8 MPa for r-ABS and pure ABS, respectively. This suggests a comparable strength

between the materials, although the recycled material exhibits a slightly higher standard deviation. Further examination of the graphical representation highlights the superior properties of the recycled material.

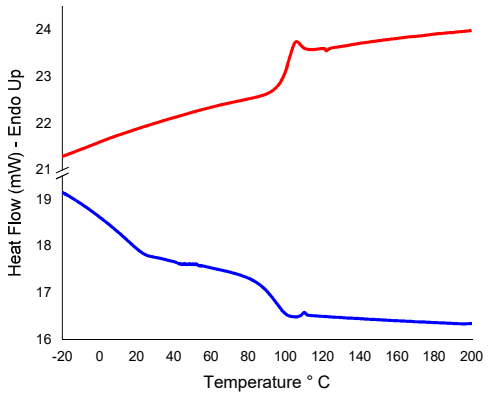

Figure 2 - DSC of the r-ABS sample being cooling in blue and second heating in red.

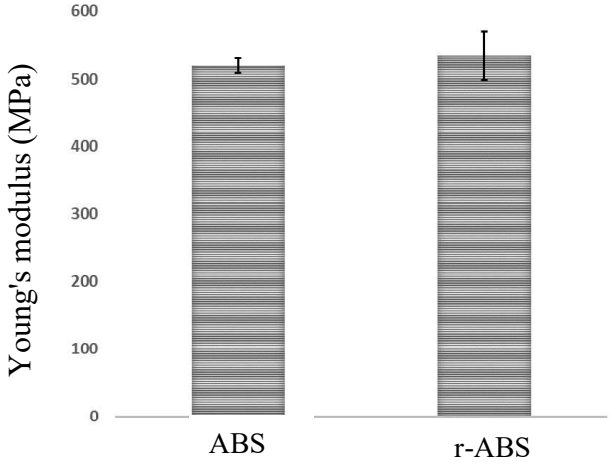

Figure 3 - Elasticity Modules for both recycled (r-ABS) and pure ABS materials

Figure 4 illustrates the average maximum breakage stress for ABS and r-ABS. The assessment of tension until rupture reveals similar outcomes for both materials, with no significant differences. The virgin ABS material demonstrated a maximum stress of 29 MPa, while r-ABS exhibited a value of 26 MPa.

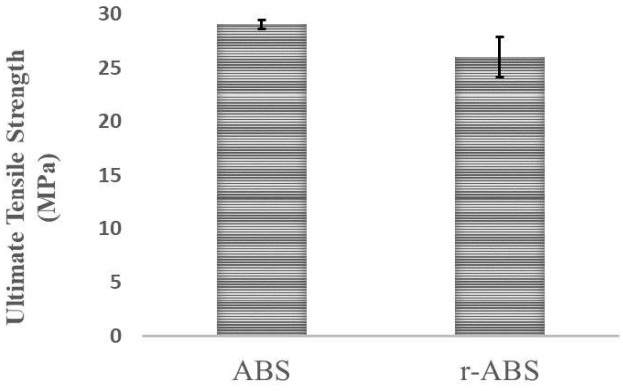

Figure 4 - Ultimate Tensile Strength of ABS and r-ABS.

These findings align with the research conducted by Fernandez-Vicente et al. (2016), which emphasized that higher fill density in FDM printing reduces voids and enhances tensile strength [5]. However, focusing solely on tensile properties without considering impact resistance may lead to the production of fragile products.

Conclusions

Through the present investigation, the potential of producing a filament for Fused Deposition Modeling (FDM) printing from recycled Acrylonitrile butadiene styrene (r-ABS), whose polymers were sourced from Waste Electrical and Electronic Equipment (WEEE), was evaluated. The preparation steps taken evince the ease with which collection, cleaning, and fragmentation can be carried out on a large scale, yielding high-quality flakes for filament production.

The manufacture of the r-ABS filament in a single-screw extruder was found to be feasible, devoid of major setbacks, but excessive porosity was observed in the recycled filament. Nevertheless, prints were achievable, exhibiting no consistent faults during the material deposition stage and without clogging in the printing nozzle, using parameters similar to those conventionally adopted for commercial ABS printing. Moreover, material adhesion to the printing table was more persistent during material deposition and was conveniently removable after cooling.

The results obtained suggest a similarity in the mechanical properties of recycling, making it a viable alternative to using virgin polymers in additive manufacturing applications.

Acknowledgements

This study was supported by the Instituto Federal de Educação, Ciência e Tecnologia do Rio Grande do Sul (IFRS).

References

1. A. Kasper; G. Berselli; B. Freitas; J. Tenório; A. Bernardes; H. Veit Waste Management 2011, 31, 12, 2536-2545. https://doi.org/10.1016/j.wasman.2011.08.013.
2. J. Lee; A. Jia; C. Chua Applied Materials Today 2017, 7, 120-133. https://doi.org/10.1016/j.apmt.2017.02.004
3. M. Harris; J. Potgieter; S. Ray; R. Archer; K. Arif Materials, 2019, 12, 4167. https://doi.org/10.3390/ma12244167
4. PACZEK, D. in Proceedings of 9th International Conference on Manufacturing Science and Education, Sibiu, Romania, 2019, Vol 1.
5. M. Fernandez-Vicente; W. Calle; S. Ferrandiz; A. Conejero 3D printing and additive manufacturing, 2016, 3, 183-192. https://doi.org/10.1089/3dp.2015.0036.

ABIOTIC DEGRADATION OF OXO-DEGRADABLE BAGS: POTENTIAL SOURCES OF MICROPLASTICS

Raimara de S. Gomes[1], Walter R. Waldman[2], and Andreia N. Fernandes[1]*

1 – Institute of Chemistry, Federal University of Rio Grande do Sul (UFRGS), Porto Alegre, RS, Brazil
*andreia.fernandes@ufrgs.br**
2 – Department of Physics, Chemistry, and Mathematics, Federal University of São Carlos (UFSCar), São Carlos, SP, Brazil

Biodegradable and oxo-degradable polymers were developed to limit human-induced plastic pollution.[1] In this study, we evaluated the microplastic fragmentation of commercial oxo-degradable bags compared to the conventional ones, both exposed to different abiotic experimental conditions. One conventional high-density polyethylene (HDPE) and three different HDPE oxo-degradable bags were selected. For the indoor degradation, the samples were cut into 6.5 x 6.5 cm and placed in an accelerated degradation box equipped with three mercury lamps (36 W) for 0-79 days, with blocks of 8 h of exposition followed by 16 h of a dark time. For the outdoor degradation, the samples were cut into 5.0 x 2.0 cm strips and exposed to the weather on two different slopes during 0-90 days of degradation. Structural modifications were evaluated through visual changes and chemical characterization using Fourier transform infrared spectroscopy (FTIR-ATR). For the indoor degradation, only HDPE conventional and 2/3 of the oxo-degradable bags showed visual change into slightly opaque and yellowish, both features increased with exposure time. 2/3 of oxo-degradable samples had small cracks that followed until fragmentation. Only one sample produced about 18 microplastic particles within 54 days and approximately 43 particles within 79 days. Furthermore, the longer the exposure time, the smaller the size of the fragmented particles. For the outdoor, only 2/3 of the oxo-degradable bags showed color change. As the exposure period increased, the conventional HDPE and 2/3 of the oxo-degradable samples showed color change and the presence of biofilms on the surfaces. Only one oxo-degradable sample had small cracks that followed until fragmentation. The FTIR spectra showed the development of the bands in the region from 1800 to 1650 cm^{-1} attributed to the carbonyl region[2] showing surface oxidation in all samples. We conclude that different commercial oxo-degradable bags presented fragmentation potentials, and therefore potentials for microplastic production.

1. J. Charles; G. R. Ramkumaar, *Asian Journal Chemistry* 2009, *21*, 4477.
2. A. Benítez; Sánchez, J. J.; Arnal, M. L.; Müller, A. J.; Rodríguez, O.; Morales, G. *Polymers Degradation and Stability* 2013, *98*, 2490. https://doi.org/10.1016/j.polymdegradstab.2012.12.011

Fundings: CNPQ, INCTAA, UFRGS, UFSCar.

Keywords: *Degradation, oxo-degradable, oxidation, microplastic*.

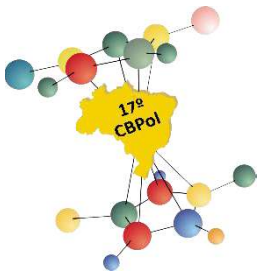

ACID HYDROLYSIS OF WASTE PET (POLYETHYLENE TEREPHTHALATE) AND PA (POLYAMIDE) MIX

Giovana G. Pomes, Helenir N. Ballin, Luciana Gaffo, Adonilson R. Freitas*

Center for Engineering and Exact Sciences (CECE), University of west of Paraná (UNIOESTE), Toledo, PR, Brazil
adonilson.freitas@unioeste.br

Abstract

The apparel industry has found in polymers a strong ally for the development of new fabrics and patterns. Taking that in account, there was an increase in the generation of non-biodegradable waste. And this problem has grown over time, with little attention has been devoted to this important class of materials and fabrics. Among the tissues widely consumed worldwide, PET (polyethylene terephthalate) and PA (polyamide) are the leaders. There is still no solution to this problem. The depolymerization of PET and PA by acid hydrolysis is already known in the literature but has been studied in isolation; in the present study, the mix of these polymers was investigated. The mix was refluxed in acid aquo solution for different intervals. The study was carried out using a factorial design 2^4 with the mass of PET, PA, pH and reaction time as input. The decrease in residual solid mass after the continuous reaction was used as the response. FTIR (Fourier transform infrared spectroscopy) was used to identify the components, due PET be we have only one already polyamide, might be more than one (Nylon 6; Nylon 6,6; Nylon 6,10; Nylon 6,12,). In this study, the FTIR-ATR, (spectroscopy in the infrared range by attenuated total internal reflection) was used. The ANOVA (variance analyses) showed that from four variables studied, only the concentration of polymers had a significance on the process and concentration of PET has great contribution. However, it was also found that PA decomposition was not as significant in isolation, suggesting a possible interaction with a byproduct of PET decomposition in the PA reaction. This type of synergistic effect contributes to the process. From the FTIR spectroscopy, characterized the material studied (PA), has been nylon 6,6.

References

1. Curti PS, Vidotti GJ, Rubira AF, Muniz EC.. Polym Deg Stab. 2003;**79**(2):325-331 https://doi.org/10.1016/S0141-3910(02)00296-3
2. D.C. Dragunski, A.R. Freitas, A.F. Rubira, E.C. Muniz. . Polym Deg Stab **67** (2000) 239–247 https://doi.org/10.1016/S0141-3910(99)00119-6
3. Freitas AR, Rubira AF, Muniz EC. Polym Deg Stab. 2008;**93**(3):601-607. https://doi.org/10.1016/j.molliq.2010.09.004
4. Freitas AR, Rubira AF, Muniz EC.. J Mol Liq. 2010;**157**(2):146-150. https://doi.org/10.1016/j.molliq.2010.09.004

Keywords: Hydrolysis, Acid, PET, PA, mix

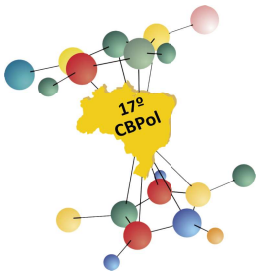

ACTION OF THE ANIONIC SURFACTANT SSO ON THE WATER VAPOR PERMEABILITY OF FILMS CONSISTING OF CASSAVA STARCH

Ingryd C. O. Medeiros[1], Lucas P. Soares[1], Ricardo H. L. Leite[2], Edna M. M. Aroucha[2] and Francisco Klebson G. Santos[1]*

1 – Department of Nature Science, Mathematics e Statistic, University Federal Rural of Semiarid (UFERSA), Mossoró, RN, Brazil klebson@ufersa.edu.br
2 – Department of Engineering and Technology, University Federal Rural of Semiarid (UFERSA), Mossoró, RN, Brazil

The environmental impacts caused by petrochemical plastics have intensified the search for biodegradable materials, such as biopolymers. One of the disadvantages of biopolymers, especially when their application is to obtain films for coating food, is their high hydrophilicity, which compromises their functions, such as a water vapor barrier. Many studies have been developed with the goal of changing the hydrophilicity of biopolymer films, using beeswax [1], carnauba wax [2], bentonite clay [3], among others. Surfactants have been used as conciliating agents between the polar and non-polar phases, mainly in lipid-added films. However, the action of surfactants on biopolymers has not been investigated in isolation yet. Based on this, this work aimed to evaluate the action of the ionic surfactant SSO (saponified sunflower oil) on the water vapor permeability (WVP) of cassava starch films. The films were prepared according to the methodology used in previous work [1]. Different levels of SSO, 1% and 3%, on a dry basis, were incorporated into cassava starch films during the gel formation process. The results showed the action of the surfactant, through the interaction with the amylose and amylopectin present in the films, reducing its WVP by up to 13%, making this ionic surfactant an important agent for reducing the hydrophilicity of cassava starch films. The results also showed that the surfactant had no significant effect on the solubility and optical properties of the films.

References

1. V. R. L. Oliveira; F. K. G. Santos; R. H. L. Leite; E. M. M. Aroucha; K. N. O. Silva. *Food Chemistry* 2018, 259, 55. https://doi.org/10.1016/j.foodchem.2018.03.101.
2. T. D. N. Xavier; V. R. L. Oliveira; R. H. L. Leite; E. M. M. Aroucha; F. K. G. Santos. *Revista Matéria* 2020, 25, 4. https://doi.org/10.1590/S1517-707620200004.1166.
3. M. K. S. Monteiro; V. R. L. Oliveira; F. K. G. Santos; E. L. Barros Neto; R. H. L. Leite; E. M. M. Aroucha; K. N. O. Silva. *Materials Science Forum* 2019, 958, 69. https://doi.org/10.4028/www.scientific.net/MSF.958.69.

Fundings: CNPq.

Keywords: *Biopolymer. Biofilm. Amylose. Amylopectin. hydrophilicity.*

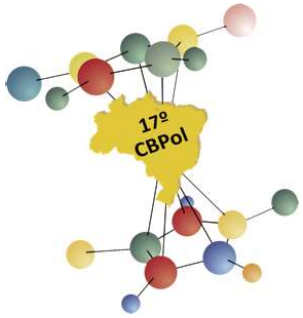

ADDITION OF TITANIUM DIOXIDE NANOPARTICLES IN ECOVIO® BIODEGRADABLE POLYMER FOR UV RADIATION BARRIER

Alexandra M. Bugiereck[1], Gustavo L. Colpani[1,2], Micheli Zanetti[1], Francieli Dalcanton[1], Luciano L. Silva[1], Márcio A. Fiori[1,2,3], Josiane M. M. de Mello[1,2]

1 – Post-Graduation in Technology and Innovation Management – PPGTI, Community University of the Region Chapecó (Unochapecó), Chapecó, SC, Brazil
alexandrambugiereck@unochapeco.edu.br
2 – Post-Graduation in Environments Sciences – PPGCA, Community University of the Region Chapecó (Unochapecó), Chapecó, SC, Brazil
3 – Physics Department – Technological Federal University of the Paraná (UTFPR), Pato Branco, PR, Brazil.

Abstract - The use of plastic produced from petroleum, has been environmental problems, due to its accumulation in the environment[1]. Therefore, research is being carried out on the use of biodegradable packaging, from renewable carbon sources. In these films it is possible to add properties and blocking ultraviolet (UV) radiation have great potential[2]. For this, titanium dioxide nanoparticles (TiO_2-NPs) can be used, which has the property of absorbing radiation. The objective of this study was to develop a polymeric film with blocks UV through the insertion of TiO_2-NPs in Ecovio®. The films were obtained by molding in solution, when pellets of the commercial polymer Ecovio® in Chloroform of 15:20 (polymer:solvent) were added to a beaker and NPs-TiO_2 at a concentration of 0.5%. Mixed for 2h they were poured into high density polymer plates and dried in an oven at 85°C for 24h. The specimens obtained were pressed under controlled conditions, for 30 min at 3 Tnf and 180ºC. The effectiveness of the barrier was carried out through the analysis of the film by Scanning Spectroscopy at a wavelength of 300-500 nm. The same was performed for pure Ecovio®. Evidence shows that pure Ecovio® has a low UV radiation barrier because it absorbs part of the light in the tested region, not completely transmitting the light beam that passes through the sample, but a sample containing 0,5% TiO_2-NPs increased the transmittance around 40% compared to the film without additive in the wavelength range of 320-290 nm evaluated, where the energy is responsible for food photodegradation which can cause discoloration and increased rancidity. It is concluded that the polymeric film obtained showed efficiency in blocking UV radiation, making it promising for biodegradable packaging production with UV radiation blocking, allowing an increase in the shelf life of products that suffer degradation due to this radiation.

References

[1]A.C. S. ALMEIDA. Aplicação de nanotecnologia em embalagens de alimentos. *Polímeros,* 2015, 25.
[2]P. KANMANI; J. RHIM. Properties and characterization of bionanocomposite films prepared with various biopolymers and ZnO nanoparticles. *Carbohydrate Polymers*, 2014, 106.

Fundings: PIBIC/CNPq, Unochapecó and FAPESC.
Keywords: *Biodegradable polymer packaging, anti-UV, photodegradation, NPs-TiO_2.*

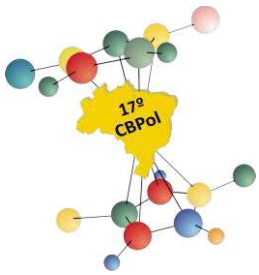

ADSORPTION OF CHLORPYRIFOS ON PHOTODEGRADED AND NON-PHOTODEGRADED MICROPLASTICS

Eric M. Silva[1*], Gabriela Z. Diaz[1], Kelven G. A. Conceição[1], Thais B. O. Costa[1], Diego Q. Melo[2], Lucila A. A. Coral[1] and Carla B. Vidal[1]

1 – Department of Chemistry & Biology, Federal University of Technology - Paraná (UTFPR), Curitiba, PR, Brazil

2 - Federal Institute of Education, Science, and Technology of Sertão Pernambucano (IFSertão), Petrolina, PE, Brazil

*ericmaciel@alunos.utfpr.edu.br

Abstract - The occurrence of microplastics in the environment highlights a warning about their impacts on the environment. Other agents, such as indiscriminately used pesticides, pose problems to the health of living organisms due to their toxicities. Thus, this study aimed to evaluate the adsorption capacity of photodegraded and non-photodegraded polyethylene terephthalate (PET) microplastics (MP) on the pesticide chlorpyrifos (CPF) removal, determining whether MPs can act as vectors, facilitating the contact of pesticides with aquatic organisms. MP accelerated photoaging was performed in a chamber containing UV-B fluorescent lamps. The MPs before and after aging were characterized using the point of zero charge (pzc) technique to determine the surface electrostatic potential, and scanning electron microscopy (SEM) to observe possible MPs morphological changes. Batch adsorption tests were carried out using 5 mg/L of initial CPF concentration, 0.2 g/L MP dosage at pH 7.0. High-performance liquid chromatography (HPLC) was employed to determine CPF concentration. The pHpzc values varied as follows: *in natura* PET (≈ 7.1), PET-1h (≈ 8.5), PET-4h (≈ 7.0), PET-6h (≈ 6.0), and PET-8h (≈ 6.3). SEM did not reveal significant morphological changes. The adsorption capacities (mg/g) decreased as the MPs underwent longer degradation times: *in-natura* PET (1.23) > PET-1h (0.99) > PET-4h (0.94) > PET-6h (0.88) > PET-8h (0.69). It is expected that hydrophobic interactions occur between the nonpolar chains of PET and the nonpolar compound CPF. With the increase in negative charges (observed in PET-6h and PET-8h), there was a disadvantage in the adsorption process. It was concluded that the photodegradation process interfered in the PET MPs adsorption capacities, indicating that degraded PET has reduced potential as a vector of contamination.

References

1. E. J. Meurer in *Fundamentos de Química do Solo*, E. J. Meurer Ed.; Biblioteca Setorial Da Faculdade de Agronomia da UFRGS, Porto Alegra, 2017.
2. W. A. Mannheimer, *Microscopia dos Materiais: Uma introdução*, E-papers Serviços Editoriais Ltda, Rio de Janeiro, 2002.
3. J. G. M. Vargas et al. *Microplástico: uso na indústria cosmética e impactos no ambiente aquático* 2022, 705-711. http://dx.doi.org/10.21577/0100-4042.20170870
4. D. M. Mitrano; P. Wick; B. Nowack *Placing nanoplastics in the context of global plastic pollution* 2021, 491-500. https://doi.org/10.1038/s41565-021-00888-2

Keywords: A*dsorption, photodegradation, pesticide, microplastic, PET.*

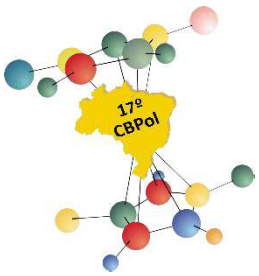

ADSORPTION OF THE ORGANOPHOSPHATE PESTICIDE ON PHOTODEGRADED POLYETHYLENE MICROPLASTICS

Gabriela Z. Diaz[1*], Eric M. Silva[1], Kelven G. A. Conceição[1], Giuliana B. Santana[1], Diego Q. Melo[2], Lucila A. A. Coral[1] and Carla B. Vidal[1]

1 – Department of Chemistry & Biology, Federal University of Technology - Paraná (UTFPR), Curitiba, PR, Brazil
2 - Federal Institute of Education, Science, and Technology of Sertão Pernambucano (IFSertão), Petrolina, PE, Brazil
* gabrieladiaz@alunos.utfpr.edu.br

Abstract - Microplastic particles (MPs) contamination poses an increasing threat to all ecosystems, potentially accompanied by other contaminants such as pesticides, which, if used indiscriminately, can pose health problems for humans and the environment. This study evaluated the effect of the pesticide chlorpyrifos adsorption on polyethylene microplastics subjected to photodegradation to simulate the effects of solar radiation. The photodegradation was conducted in a chamber equipped with UV-B fluorescent lamps at different exposure times (1, 4, 6, and 8h). The MPs before and after degradation were characterized in terms of surface electrostatic potential using the pH point of zero charge (pH_{PZC}) technique, and morphological changes were identified by scanning electron microscopy (SEM) technique. Adsorption tests were carried out at pH 7.0, with 10 mg/L of initial pesticide concentration and 0.2 g/L of MPs dosage. The aqueous solution's initial and final pesticide concentrations were determined using high-performance liquid chromatography (HPLC). The results indicated that photodegradation caused morphological alterations in the MPs by increasing cavities and roughness in the aged materials, as well as chemical changes, reflected in reducing pH_{PZC} values after aging. The adsorption tests revealed that the aged plastics had increased adsorption capacity, indicating that the polymer's photodegradation affected their ability to retain chlorpyrifos, meaning that these microplastics in the environment may have their toxic effects increased when exposed to weather conditions.

References

1. A. Herath; C. Reid; F. Perez; C. Pittman Jr.; T. E. Mlsna *Journal of Environmental Management* 2021, 296, 113186. https://doi.org/10.1016/j.jenvman.2021.113186
2. A. Mie; C. Rudén; P. Grandjean *Environmental Health* 2018, 17, 77. https://doi.org/10.1186/s12940-018-0421-y
3. C. Tavares; J. V. Gulmine; C. M. Lepienski; L. Akcelrud *Polymer Degradation and Stability* 2003, 81 (2), 367-373. https://doi.org/10.1016/S0141-3910(03)00108-3
4. L. Hlekelele; N. E. Nomadolo; K. Z. Setshedi; L. E. Mofokeng; A. Chettya; V. P. Chauke *RSC Advances* 2019, 9, 14531-14543. https://doi.org/10.1039/C9RA01666J
5. P. Agamuthu; S. Mehran; A. Norkhairah; A. Norkhairiyah *Waste Management & Research: The Journal for a Sustainable Circular Economy* 2019, 37(10): 987-1002. https://doi.org/10.1177/0734242X19845041

Keywords: *polyethylene, chlorpyrifos, adsorption, pesticide, microplastics*

A FACILE WAY TO RECYCLE EPOXY/CF RESIN COMPOSITES

Maikon S. Santos[1*], Larissa S. Montagna[1] and Fabio R. Passador[1]

1 – Department of Science and Technology, Polymer and Biopolymer Technology Laboratory (TecPBio), Federal University of São Paulo (UNIFESP), 330 Talim, São José dos Campos, São Paulo 12231-280, Brazil
maikon.stefan95@gmail.com

Abstract - Thermosetting composites of epoxy resin reinforced with carbon fiber (CF) are widely used in automotive applications mainly due to the several advantages offered by these materials [1]. However, in recent years, a growing increase in industrial waste from these composites has been observed, and consequently an urgent need for the correct disposal of these materials that have a high market value [2,3]. In this context, the present proposal aims to carry out the mechanical recycling of these thermosetting composites. The epoxy/FC wastes resulting from the production process of components in the automotive sector were collected, cut into small pieces using a grinder, and subsequently ground using a knife mill. Then, the granulometric separation of the resulting powder was carried out using a 10-mesh metal sieve to obtain smaller (< 45 μm) and larger (> 75 μm) particles. Then, the particles were characterized by scanning electron microscopy (SEM) and optical microscopy (OM). The mass yield of the milling process was determined by the difference between the final (after milling) and initial (before milling) mass. It was observed in the OM that the particles present different sizes and shapes with a large dispersion of the average particle size. In the SEM images, it was observed that the epoxy resin is well adhered to the carbon fiber. After the sieving process, it is noted the presence of few agglomerates and more dispersed carbon fibers. This technique made it possible to recover carbon fibers that can be used as reinforcement for the development of new composites with short fibers.

References

1. A. Muhammad, Md.R. Rahman, R. Baini, M.K.B. Bakri. *Advances in Sustainable Polymer Composites Woodhead Publishing Series in Composites Science and Engineering*, 2021, 185-20. https://doi.org/10.1016/B978-0-12-820338-5.00008-4
2. A. Jacob. *Reinforced Plastics*, 2014, 58, 1, 18-19. https://doi.org/10.1016/S0034-3617(14)70036-0
3. P.A.V. Donga, C. Azzaro-Pantel, A-L, Cadene. *Resources, Conservation & Recycling*, 2018, 133, 63–75. https://doi.org/10.1016/j.resconrec.2018.01.024.

Fundings: Capes.

Keywords: *Epoxy resin; Carbon fiber; Recycling; Thermosets, Composite Grinding.*

APPLICATION OF BACTERIAL CELLULOSE IN THE PRODUCTION OF A PAPER PACKAGING

Karina C. de Souza[1], Felipe C. S. Trindade[1], Viviane F. Caetano[2], Andréa F. S. Costa[3], Yeda M. B. de Almeida[2], Leonie A. Sarubbod[4], Gloria M. Vinhas[2]*

1- Center for Exact and Natural Sciences, Federal University of Pernambuco (UFPE), Recife, PE, Brazil;
2- Chemical Engineering Department, Federal University of Pernambuco (UFPE), Recife, PE, Brazil;
3- Agreste Region Academic Center, Federal University of Pernambuco (UFPE/CAA), Caruaru, PE, Brazil;
4- Catholic University of Pernambuco (UNICAP), Recife, PE, Brazil;
**gloria.vinhas@ufpe.br*

The Brazilian paper industry emerged from the eucalyptus monoculture generating severe consequences, such as the loss of biodiversity and many others. As an alternative to such questions, there is the production of bacterial cellulose (BC), which is a pure and non-toxic biopolymer. This study proposed an alternative production to conventional paper through the use of low cost BC in saline production medium. After producing the BC, 96.0 g were ground together with 100 mL of distilled water for 2 minutes until a paste was obtained. Then CaCO3, resin and Poly(vinyl acetate) were added. The final mixture was taken to the oven until it dried and formed the BC Paper film. As main results, BC Paper had a grammage of 139 g/m², and can be classified as "kraft" paper, which predominantly has a grammage between 70 and 180 g/m². In addition to being used as a raw material for the manufacture of corrugated cardboard and for paper bags, "kraft" paper can be used for direct wrapping of products or combined with other materials to obtain good mechanical resistance and protection against humidity. Due to its properties, BC has been produced, studied and indicated as a matrix for the development of new materials, such as, for example, in the manufacture of "green packaging". In Fig. 1-a and Fig. 1-c we have a pilot material called BC paper, which can be visually compared to bond paper (Fig. 1-b). In Fig. 1-d it is possible to observe a prototype of a packaging made from BC plus additives. The prototype using BC Paper obtained promising characteristics for use in sustainable packaging.

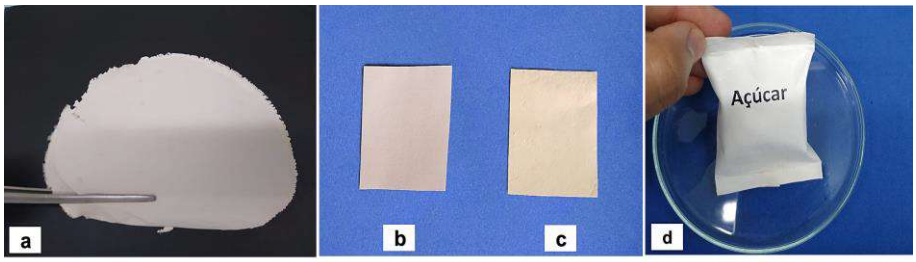

Figure 1- Plain Paper (b), BC Paper (a and c) and packaging prototype made from CB (d).

References

1. L. Kong; J. Zhao; J. Li; R. Lou; Y. Zhang *Journal of Cleaner Production* 2020, 277, 124018. https://doi.org/10.1016/j.jclepro.2020.124018.
2. M. Skočaj *Cellulose* 2019, 26, 6477. https://doi.org/10.1007/s10570-019-02566-y
3. E.S. Campos, *Curso Básico de Fabricação de Celulose e Papel*, Suzano, São Paulo, 2011.

Keywords: *Bacterial Cellulose, Papermaking, Packaging.*

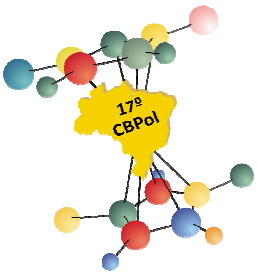

OBTENTION POLY (LACTIC ACID) (PLA)/ POLY (BUTYLENE ADIPATE-CO-TEREPHTHALATE) (PBAT) FIBERS BY ELECTROSPINNING FOR AIR FILTERS APPLICATION

Raul. P. da Silva[1], Gabriela B. Medeiros[2], Monica L. Aguiar[2], Edvani C. Muniz[1,3], Elisangela Corradini[1]*

1 – Post-graduation Program in Material Science and Engineering, Technological Federal University of Paraná (UTFPR), Londrina, PR, Brazil, ecorradinii@utfpr.edu.br
2 – Graduate Program of Chemical Engineering, Federal University of São Carlos (UFSCar), São Carlos, SP, Brazil
3 – Department of Chemistry, Federal University of Piauí, Campus Universitário Ministro Petrônio Portella, 64049-550, Teresina, Piauí, Brazil

Abstract – The air is a fundamental element for life on earth. Rapid urbanization and industrialization are releasing large amounts of pollutants (harmful gases, microorganisms, and particulate matter) into the atmosphere, leading to health hazards [1-3]. Air filtration is still the most promising technique for protection the air pollutants. Filters can be manufactured by several methods, one of them being the use of fibrous membranes obtained through electrospinning from polymeric solutions [4]. Electrospinning is the technique that combine the application of an electrostatic field to a moving fluid which will result in the formation fibers [5-6]. In this work, PLA/PBAT blends fibers were obtained by electrospinning solution in Dichloromethane/N,N-dimethylformamide (3/2, v/v) solutions. The morphology and the diameter of the fibers obtained were evaluated by scanning electron microscopy (SEM). The effects of process parameters and concentration in the diameter of the fibers and the process-yield were evaluated through an experimental design. Fiber diameters varied from 722 ± 316 nm to 1555 ± 644 nm. The variation of process parameters influenced in fibers morphology and fibers with smaller diameter were obtained at lower concentrations.

References

1. Y. Zhou; Y. Liu; M. Zhang; Z. Feng; D. Yu; K. Wang; *Nanomaterials* 2022, *12*(7), 1077; https://doi.org/10.3390/nano12071077.
2. D. Lv; M. Zhu; Z. Jiang; S. Jiang; Q. Zhang; R. Xiong; C. Huang; *Macromol. Mater. Eng.* 2018, 1800336. https://doi-org.ez48.periodicos.capes.gov.br/10.1002/mame.201800336
3. M. Zhu; J. Han; F. Wang; W. Shao; R. Xiong; Q. Zhang; H. Pan; Y. Yang; S. K. Samal; F. Zhang; C. Huang; Macromol. Mater. Eng. 2017, 302, 1600353.
4. Y. Guo; X. Wang; Y. Shen; K. Dong; L. Shen; A. A. A. Alzalab; *J Mater Sci 2022* 57, 58–104. https://doi-org.ez48.periodicos.capes.gov.br/10.1007/s10853-021-06575-w.
5. S. Khatsee, D. Daranarong, W. Punyodom, P. Worajittiphon, Applied Polymer 2018, 135, 46486. doi: 10.1002/app.46486.
6. J. Zhang; S. Gong; C. Wang; D.-Y. Jeong; Z. L. Wang; K. Ren; Macromolecular Materials and Engineering 2019, 304, 1900259. https://doi-org.ez48.periodicos.capes.gov.br/10.1002/mame.201900259.

Fundings: CNPq

Keywords: *Air Filter. Electrospinning. Polymeric Solutions. PLA/PBAT.*

BACTERIAL CELLULOSE PRODUCTION USING ERYTHRINA MULUNGU TEA AS A GROWTH MEDIUM

Girlaine S. Silva[1], Mariana A. Henrique[1], Fernanda V. Amorim[1], Severino A. Júnior[1], Glória M. Vinhas[1]

1 – Department of Materials Science, University of Pernambuco (UFPE), Recife, PE, Brazil

gloria.vinhas@ufpe.br

Abstract - Bacterial cellulose (BC) is a nanofibrillar extracellular polysaccharide that can be produced by several types of bacteria and has excellent characteristics, such as atoxicity, high crystallinity, high tensile strength, high water retention capacity, high purity, biocompatibility and biodegradability [1]. These characteristics provide the biopolymer with a wide range of applications in various industrial sectors such as food, cosmetics, medicine, among others [2]. The medium most used to produce BC is Hestrin, but due to its high cost, some alternative means with better cost-effectiveness have been used, with different carbon sources. In this work, the production of cellulose membranes was carried out using the bacteria Komagataeibacter hansenii and as a culture medium, tea from *Erythrina mulungu*, a plant characteristic of the caatinga that has several medicinal properties, and glucose as a source of carbon [3]. After the formation of the films, they were irradiated with gamma rays at a dosage of 25 kGy for effective sterilization. Then, they were dried in an oven at 45°C for 24 hours and then the characterizations were performed. The methods used to characterize the films were Fourier Transform Infrared Spectroscopy (FTIR), X-Ray Diffraction (XRD) and Thermogravimetric Analysis (TGA). Antimicrobial and antioxidant activity assays were also performed. As the main results showed, it was possible to verify that the BC membranes were perfectly formed through the innovative culture medium used, and its structure was confirmed through FTIR analysis. It was also observed through the XRD technique that the structure of the cellulose formed was less crystalline than the BC usually presents, however, with crystalline planes characteristic of type I cellulose. In the thermogravimetric analysis, three stages of degradation were observed, characteristic of the BC produced by conventional means, proving that the alternative medium of *mulungu* tea can be used to produce cellulose membranes.

References

1. A. Khalid; R. Khan; M. Ul-Islam; T. Khan; F. Wahid. Carbohydrate Polymers, 2017, 164, 214. http://doi.org/10.1016/j.carbpol.2017.01.061

2. J. Wang; J. Tavakoli; Y. Tang. Carbohydrate Polymers, 2019, 219, 63. https://doi.org/10.1016/j.carbpol.2019.05.008

3. R. M. Ramos; J. M. Feitosa; V. da Silva Lima; R. da Conceição Santos; A. M. de Oliveira; L. A. L. Soares; G. C. da Silva. Braz. J. of Develop., 2020, 6, 33140. https://doi.org/10.34117/bjdv6n6-026

Keywords: *Bacterial cellulose, Erythrina Mulungu, gamma radiation*

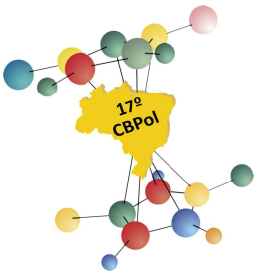

BIODEGRADABLE FILMS BASED ON CASSAVA STARCH AND RICE HUSK WITH IMPROVED PROPERTIES

Camila Horst[1], Bruno dos Santos Lima[1], Sílvia R. Grando[1], Simone H. Flores[2] and Tania M. H. Costa[1]*

1- Department of Chemistry, Universidade Federal do Rio Grande do Sul (UFRGS), Porto Alegre, RS, Brazil
camilahorst1@gmail.com
2- Department of Food Science and Technology, Universidade Federal do Rio Grande do Sul (UFRGS), Porto Alegre, RS, Brazil

The packaging is used to increase shelf life of food, to promote physical protection, among other benefits. Conventional packaging is responsible for a large part of the accumulation of garbage in urban centers, causing environmental and health damage. Due to this, biodegradable packaging has emerged as an alternative to minimize the environmental impact caused by packaging. A limiting factor for the large-scale use of these packages is their weak @mechanical, and physical-chemical properties. The agro-industrial wastes used as a filler show potential to improve these properties and increase the possibilities of applicability of biodegradable packaging. In this context, it was proposed the development of biodegradable films based on cassava starch with the addition of rice husk to improve the mechanical, thermal, and physical-chemical films properties. The films were prepared using the casting technique, adding cassava starch, and rice husks in amounts of 0 %, 20 %, 40 %, 50 %, and 60 % (in mass, based on the starch addition), samples CA0, CA20, CA40, CA50, and CA60, respectively. The films were characterized by water solubility, mechanical properties, and thermogravimetric analysis (TGA) techniques.The films obtained were intact, with good dispersion of rice husk. Rice husk additions influenced all the results obtained. Tensile strength had a maximum increase of 118%, and in Young's Modulus, the maximum increase was 364%. Rice husk additions also acted on the water solubility results, causing an average reduction of 50% in this parameter. Thermograms obtained in TGA demonstrate thermal degradation in three stages characteristic of plasticized starch films. The degradation rate showed a slight decrease in the samples with the addition of rice husk. The results show promising applicability for rice husk wastes, even as the possibility of the application as food packaging.

References:

1. A. Benjamin; J. Asante; E. Nyankson; D. Dodoo- Arhin; M. Oteng-Peprah; S. T. Azeko; A. S. Azeko; O. K. Oyewole; A. Yaya. *Polymer Composites. 2021.* 42:3216–3230. https://doi.org/10.1002/pc.26052
2. S. Varghese; H. Pulikklparambil; K. Promhuad; A. Srisa; Y. Laorensa; L. Jarupan; T. Nampitch; V. Chonhenchob; N. Harnkarnsujarit. *Polymer 2023, 15*, 648. https://doi.org/10.3390/polym15030648.
3. K. V. Aleksanyan. *Polymer 2023, 15*, 451. https://doi.org/10.3390/polym15020451.

Fundings: Fundação de Amparo à Pesquisa do Estado do RS (FAPERGS), Conselho Nacional de Desenvolvimento Científico e Técnológico (CNPQ) and Coordenação de Aperfeiçoamento de Pessoal do Nível Superior (CAPES).

Keywords: *Biodegradable films, rice husk, agro-industrial wastes, improve properties.*

BIODEGRADABLE POLYMER MATERIAL FROM MACROALGAE

Daniela P. Vieira[1], Fabio F. Neves[2] and Daniela Becker[1]

1 – Centro de Ciências Tecnológicas, Universidade do Estado de Santa Catarina (UDESC), Joinville, SC, Brazil
daniela.becker@udesc.br
2 – Centro de Educação Superior da Região Sul, Universidade do Estado de Santa Catarina (UDESC), Laguna, SC, Brazil

Abstract – Using red macroalgae in nature to produce polymer films has not yet been widely studied. *Kappaphycus alvarezzi*, macroalgae that contain the hydrocolloid carrageenan in its composition, which is a natural polymer, has prospects for use in non-food packaging and single-use objects. It is a biodegradable material that, when not chemically modified and not mixed with synthetic polymers, degradation is comparable to pure algae biomass in cold polar waters within 4.5-7 weeks. This research aims to evaluate the processing in the thermal and rheological properties of the material. The macroalgae were collected on a farm in the city of Palhoça/SC, and subsequently, the macroalgae were cleaned and desalinated. Grinding was performed using a knife mill and then dried in an oven at 40°C. The dried biomass was then processed in a Haake rheometer at a temperature of 110 °C at 200 rpm for 10 minutes in a 75/25 water/algae ratio. The processed biomass had a rubbery appearance after processing. Thermogravimetry analyses carried out in a nitrogen atmosphere showed a residue of 35% in the processed biomass and 42% in the virgin biomass. Both showed degradation at 177 °C and 182 °C, respectively, with the processed biomass losing water at 100 ° C. In the DSC analysis, the glass transition temperature of the processed and virgin biomass was 27°C and 22°C, respectively. The Melt Flow Index at 110°C the material did not show a viscous regime necessary for the validity of the analysis. The results indicate that the processing of macroalgae biomass in the presence of water alters its thermal and rheological behavior.

1. SAHA, Dipjyoti; BHATTACHARYA, Suvendu. Hydrocolloids as thickening and gelling agents in food: a critical review. Journal of food science and technology, v. 47, p. 587-597, 2010. https://doi.org/10.1007/s13197-010-0162-6.
2. SCHMIDTCHEN, Ludwig et al. Processing technologies for solid and flexible packaging materials from macroalgae. Algal Research, v. 61, p. 102300, 2022. https://doi.org/10.1016/j.algal.2021.102300.
3. U. Braeckman, et al., Degradation of macroalgal detritus in shallow coastal Antarctic sediments, Limnol. Oceanogr. 64 (4) (2019) 1423–1441. https://doi.org/10.1002/lno.11125.

Keywords: B*iodegradable polymer material, Kappaphycus alvarezzi, polymer from macroalgae.*

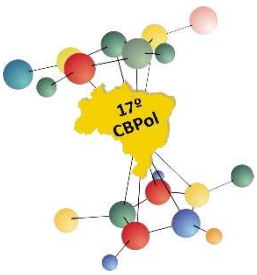

BIODEGRADATION OF MODIFIED POLY(ETHYLENE TEREPHTHALATE) FILMS UNDER ANAEROBIC CONDITIONS

João G. M. de Avellar[1], Dayanna K. M. de Oliveira [1], Gisely Alves da Silva[2], Renan R. O. de Souza[1], Jorge V. F. L. Cavalcanti[2], Yeda M. B. de Almeida[1], Maria de Los Angeles P. Fernandez[2] and Glória Maria Vinhas[1]

1 – Postgraduate Program in Material Science (PGMtr), Federal University of Pernambuco (UFPE), Recife, PE, Brazil
gloria.vinhas@ufpe.br
2 – Department of Chemical Engineering (DEQ), Federal University of Pernambuco (UFPE), Recife, PE, Brazil

Abstract - Due to the impacts caused by the increasing generation of plastic waste, alternatives to reduce the durability and resistance to degradation of these materials are explored by the scientific community. However, it is still necessary to broaden the studies about the effectiveness of the biodegradation of marketable plastics. The purpose of the study was to evaluate the biodegradability, under anaerobic conditions, of poly(ethylene terephthalate) (PET). This material is the film commercialized by the company Terphane called PETbio. The polymeric films were submerged in sludge from Sewage Treatment Plants, placed in digesters. The quantification of biodegradation was done through the evaluation of the biogas by gas chromatography. Regarding the characterization of the films, they were submitted to Scanning Electron Microscopy, Thermogravimetry, Differential Scanning Calorimetry and Fourier Transform Infrared Spectroscopy. Furthermore, analyses of the microorganisms present in the medium were performed. The results showed an increase in the anaerobic population and a decline in aerobic organisms, while methane gas production reached its peak at the end of the first month and continued to decline afterwards. At six months, under the study conditions, there was no statistical difference in biodegradation between the negative control films (PET) and the PETbio films.

References

1. J. A. C. Streit, Ph.D Thesis, University of Brasília, 2022.
2. B. Rani-Borge; A. U. Faria; A. Campos; S. P. C. Gonçalves; S. M. M. Martins-Franchetti. *Polímeros* 2016, 26(2), 161–167. https://doi.org/10.1590/0104-1428.2127
3. S. Selke; R. Auras; T. A. Nguyen; E. Castro Aguirre; R. Cheruvathur; Y. Liu, Y. Evaluation of Biodegradation-Promoting Additives for Plastics. *Environmental Science & Technology*, 2015, 49(6), 3769–3777. https://doi.org/10.1021/es504258u
4. T. G. Fonseca; Y. M. B. Almeida; G. M. Vinhas. *Polímeros*, 2014, 24(5), 567–571. https://doi.org/10.1590/0104-1428.1583
5. S. V. Canevarolo Jr. in *Ciência dos Polímeros*, ArtLiber Ed.; Câmara Brasileira do Livro, São Paulo, 2006.

Keywords: *PET, PETbio, biodegradation, anaerobiose.*

BIOPOLYMER-BASED TIO_2 FOR ENVIRONMENTAL REMEDIATION PROCESSES

Rodrigo P. Feitosa[1*], Joziel A. Oliveira[1], Francisca P. Araújo[2], Alan Í. Moraes[1], Luzia M. C. Honorio[3], Idglan S. Lima[1], Marcelo B. Furtini[1], Edson C. Silva-Filho[1], Josy A. Osajima[1]

1 - Federal University of Piauí (UFPI), Teresina, PI, Brazil
rooprado@ufpi.edu.br
2 - Rural Federal University of Pernambuco (UFRPE), Recife, PE, Brazil
3 - Federal University of Paraíba (UFPB), Areia, PB, Brazil

Abstract - The research aims to develop effective environmental remediation systems to address pollution and contamination [1]. A promising approach is to combine heterogeneous photocatalysis with titanium dioxide (TiO_2) and natural polymers to enhance the photocatalytic properties of the material for improved pollutant degradation and microbial elimination [2]. TiO_2 was synthesized with a biopolymer derived from the mesocarp of babassu coconut using the sol-gel method [3]. The obtained material was characterized using X-ray diffraction (XRD), N_2 adsorption-desorption, and diffuse reflectance spectroscopy (DRS). Photocatalytic tests were performed using methylene blue dye (MB) at a concentration of 12.0×10^{-6} mol L^{-1}, with a catalyst dosage of 0.5 g L^{-1}. Toxicity tests were conducted on the dye solution after the photocatalytic process to confirm the absence of toxic by-products. XRD analysis revealed that the material exhibited an anatase crystalline phase. N_2 adsorption-desorption showed a material with a type IV isotherm and an H_2 hysteresis characteristic of mesoporous materials. Material band gap energy was calculated using the Kubelka-Munk function, resulting in Eg = 3.19 eV. The photocatalytic tests demonstrated a dye discoloration rate of 69.3% for MB. The toxicity test indicated that no toxic by-products were generated during the photocatalytic process.

References

1. Araujo, F. P., Trigueiro, P., Honório, L. M. C., Oliveira, D. M., Almeida, L. C., Garcia, R. P., Lobo, A. O., Cantanhêde, W., Silva-Filho, E. C., & Osajima, J. A.. International Journal of Biological Macromolecules 2020, 165, 2813–2822. https://doi.org/10.1016/j.ijbiomac.2020.10.132.
2. Araujo, F. P., Honorio, L. M. C., Lima, I. S., Trigueiro, P., Almeida, L. C., Fechine, P. B. A., Santos, F. E. P., Peña-Garcia, R., Silva-Filho, E. C., & Osajima, J. A.. Ceramics International 2020, 46(10), 15534–15543. https://doi.org/10.1016/j.ceramint.2020.03.100.
3. Lopes, A. C. B., Araújo, F. P., Morais, A. I. S., de Lima, I. S., Honório, L. M. C., Almeida, L. C., Peña Garcia, R., Silva-Filho, E. C., Furtini, M. B., & Osajima, J. A.. Materials 2022, 15(13), 4559. https://doi.org/10.3390/ma15134559.

Keywords: *biopolymer, babassu mesocarp, TiO_2, methylene blue, environmental.*

CARBOXYMETHYL CELLULOSE/MORINGA OLEIFERA SEED HUSK ADSORBENTS FOR THE TREATMENT OF UNDERGRADUATE LABORATORY WASTE

Marleidy P. Callisaya[1], Denise F. S. Petri[1], Cristiane Finzi-Quintão[2], Pedro Vitoriano de Oliveira[1], Dairon P. Fuentes[1]

1 – Institute of Chemistry, University of São Paulo (USP), São Paulo, SP, Brazil marleidy@usp.br
2 – Chemical Engineering, Universidade Federal de São João del Rey (UFSJ), São João del Rey, MG, Brazil

Abstract - Given the scenario of waste generation in research and teaching laboratories, which leads to increasing contamination and environmental risks, this study presents an efficient biobased alternative for the treatment of these wastes. The combination of carboxymethyl cellulose (CMC), a cellulose ether of great importance and application in the industry, with the seed husk of *Moringa oleifera* (SM), CMC/SM25 cryogels (25% of SM mass in relation to CMC) were produced, aiming to treat laboratory wastes with a high concentration of metal ions. They were crosslinked by esterification reaction with citric acid. Scanning electron microscopy (SEM) images evidenced the porous morphology of the cryogels (Fig. 1). CMC/SM25 showed an average compression of 70.5 ± 2.7 kPa, mean apparent density (ρap) of 84.5 ± 3.8 kg/m^3, swelling degree (SD) of 35.4 ± 4.2 g_{water}/g and gel content of 77.3 ± 0.3%. Thermogravimetric analysis (TGA) presented an increased degradation temperature of CMC-SM25 (330.39°C) in comparison to pure CMC cryogels (321.15°C). CMC/SM25 cryogels (~100 mg) were packed into columns coupled to a peristaltic pump to keep the flow rate at 0.3 mL/min. The laboratory waste was dark brown (Fig. 1) and contained Cr^{6+}, Mn^{2+}, Co^{2+}, Fe^{3+}, Ni^{2+}, Cu^{2+}, Zn^{2+}, Sr^{2+}, Hg^{2+}, and Pb^{2+} ions, at pH 1. The CMC/SM25 adsorbents were highly efficient. They removed 100% of Hg^{2+}, Pb^{2+}, Fe^{3+}, Cr^{6+}, and Cu^{2+}. For Mn^{2+}, Co^{2+}, Ni^{2+}, and Zn^{2+} the removal was ~90%, and for Sr^{2+} it was 77%, turning the waste lighter (Fig. 1).

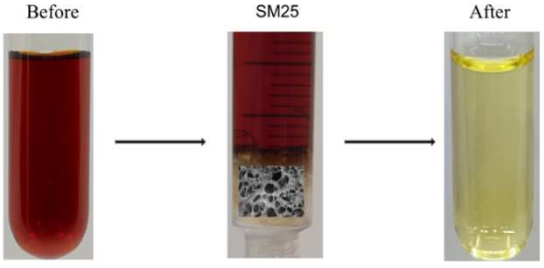

Figure 1 – The dark brown laboratory waste turned lighter due to the adsorption of metal ions on CMC-SM25 adsorbents.

Keywords: *carboxymethyl cellulose, biomass, adsorption, heavy metals*

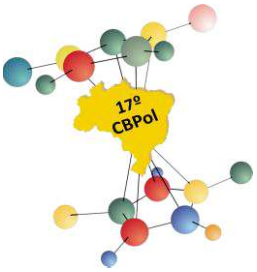

CASSAVA GUM HYDROGEL FOR ADSORPTION OF ORGANIC DYE

Joziel A. Oliveira[1], Josiel S. Lima[1], Rodrigo P. Feitosa[1], Emerson A. C. Moura[1], Ana C. A. Evangelista[1], Idglan S. Lima[1], Albert S. Silva[1], Ariane M. S. Nascimento[1], Francisco E. P. Santos[1], Edvani C. Muniz[1], Edson C. Silva-Filho[1] and Josy A. O. Furtini[1]

1 - Interdisciplinary Laboratory of Advanced Materials (LIMAV), Federal University of Piauí, 64049-550 Teresina-PI, Brazil.
jozielmateriais@gmail.com

Abstract Polysaccharides have been widely used for organic dye adsorption applications due to their high surface area and adsorption capacity [1-2]. These materials are biodegradable, renewable, and abundantly available in nature. Cassava gum is rich in starch, which is a polysaccharide capable of forming hydrogels, characterized by a three-dimensional network of polymers capable of retaining and releasing substances without damaging their structure [3]. Laponite is used because of its high adsorption capacity, which proves to be a promising material for pollutant removal when associated with cassava gum hydrogel. Thus, this study aims to produce cassava gum hydrogel with laponite for use in the adsorption of methyl blue dye. Through the X-ray diffraction (XRD) characterization technique, interactions between the cassava gum hydrogel and laponite were observed, leading to a semicrystalline to amorphous transition. The composite material formed by hydrogel and laponite obtained a higher efficiency in removing methyl blue dye, approximately 94% removal. The adsorption kinetics study showed that it occurs through chemisorption.

References

1. S. Sharma; G. Sharma; A. Kumar; T. S. AlGarni; Mu. Naushad; Z. A. ALOthman; F. J. Stadler Journal of Hazardous Materials 2022, 421, 126729. https://doi.org/10.1016/j.jhazmat.2021.126729.
2. H. Rodrigues Sousa; I. S. Lima; L. M. L. Neris; A. S. Silva; A. M. S. Santos Nascimento; F. P. Araújo; R. F. Ratke; D. A. Silva; J. A. Osajima; L. R. Bezerra; E. C. Silva-Filho Molecules 2021, 26, 2680. https://doi.org/10.3390/molecules26092680.
3. B. Zhu; D. Ma; J. Wang; J. Zhang; S. Zhang Macromolecules 2016, 89, 599-604. https://doi.org/10.1016/j.ijbiomac.2016.05.029.

Fundings: CAPES, CNPq, and FAPEPI

Keywords: *Polysaccharides, adsorption, and dye removal.*

CHARACTERIZATION OF POST-INDUSTRIAL PET WASTE FOR USE IN THE TEXTILE INDUSTRY

Thaiane N. da Silva [1]*, Daniela H. Tejada [2], Ana Maria F. de Sousa [1], Ana Lucia N. da Silva[2], Adriano A. Passos[3]

1- Programa de Pós-graduação em Engenharia Química (PPGEQ), Rio de Janeiro State University (UERJ), Rio de Janeiro, RJ, Brazil
thaianenolasco@gmail.com.br
2- Instituto de Macromoléculas Professora Eloisa Mano (IMA), Rio de Janeiro Federal University (UFRJ), Rio de Janeiro, RJ, Brazil
3- Instituto Senai de Inovação (ISI), University City of the Federal University of Rio de Janeiro, Rio de janeiro, RJ, Brazil

Abstract - There has been a significant increase in global consumption in recent years, with an emphasis on the textile industry. However, while the consumption of these products is widely discussed, little attention is paid to the waste generated during production and after consumption. Motivated by this theme, this study compares PET fiber derived from post-industrial (PET-PI) waste to recycled PET fiber (PET-C) obtained commercially (Fig 1.). The PET-PI was first purge with sodium carbonate, and then the fiber's properties were investigated using DSC, TGA, FTIR, and SEM analyses. The SEM reveals fiber surfaces that are deformed-free. In the case of FTIR, the obtained spectra were coherent and comparable to PET fiber studies [1], with bands in the same wavelength regions, indicating that the sodium carbonate treatment did not degrade the polymer. Regarding TGA, there are no differences between the Tonset and Tmax values of PET-PI before and after the treatment, confirming the FTIR findings that no degradation occurred during material purging with sodium carbonate under various conditions. Using DSC, the crystallinity of the fiber was determined, revealing that commercial PET-C is less crystalline than PET-PI. In addition, it was observed that the purge treatment decreased the PET-PI crystallinity. Therefore, the preliminary results obtained indicate that PET-PI has the potential to be introduced into the textile industry, promoting the opportunity to reintroduce the waste in order to produce environmentally friendly, sustainable products.

Figure 1- Post-industrial PET fiber waste and recycled PET commercial fiber.

References

1. J-R. Riba; R. Cantero; T. Canals; R. Puig Circular economy of post-consumer textile waste: Classification through infrared spectroscopy. Journal of Cleaner Production 2020, 272, 123011. https://doi.org/10.1016/j.jclepro.2020.123011.

Fundings: The authors would like to thank the National Council for Scientific and Technological Development (CNPq)- (309461/2021-9) and (307889/2022-0), CAPES, Senai Cetiqt (ISI), UFRJ (IMA) and UERJ;

Keywords: *post-industrial waste, synthetic fiber, and textile.*

CHARACTERIZATION OF THE FRACTION OF SOLID LIGNOCELLULOSIC RESIDUES OBTAINED AFTER ENZYMATIC HYDROLYSIS AND EVALUATION OF ITS POTENTIAL APPLICATIONS IN POLYMERIC MATERIALS

Luana A. de Queiroz[1]*, Daniel Pasquini[1] and Patrisia de O. Rodrigues[1]
1 – Institute of Chemistry, Federal University of Uberlândia, Uberlândia, MG, Brazil
luanaalves538@gmail.com

Abstract – Biomass has several applications such as biofuels, chemical compounds, polymers, resins, dispersants, solvents, films, among others [1]. The implementation of biorefineries based on lignocellulosic biomass for the conversion of waste into value-added products may be interesting mainly in the ethanol production chain from sugarcane. One of the possibilities would be to explore the production of cellulose nanocrystals (CNC) from the residues obtained after the enzymatic hydrolysis (RHE) of sugarcane bagasse (SCB). The objective of this study is to produce and characterize these RHE and verify if these materials have the necessary characteristics to produce CNC. Three SCB pre-treatments were carried out: PT1) 170°C, 1.5% NaOH, 30 min, bagasse:NaOH ratio 15:1; PT2) 0.4% NaOH, 70°C, 3h; followed by 0.5% of H_2SO_4, 140°C, 15min; and PT3) steam explosion, 190°C, 15min, followed by 1.0% NaOH, 100°C, 60min, bagasse:NaOH ratio 10:1. The pre-treated pulps were submitted to enzymatic hydrolysis with enzymatic cocktail produced by LNBR, at pH 5.0, 50°C, 72h. The pulps and RHE obtained were characterized by FTIR, MEV, chemical composition, DRX and TGA. PT3 showed greater mass loss (57.48%) but PT1 showed greater delignification (75.97%). The RHE contents were 30.6%, 21.96% and 41.06% for PT1, PT2 and PT3, respectively. After converting the polysaccharides during hydrolysis, the RHE showed lignin content of 26.31%(PT1), 30.915(PT2) and 26.81%(PT3). The FTIR spectra demonstrate the variation in the chemical composition in the different steps, corroborating the chemical characterization. It was observed by TGA that the RHE presented a decrease in the initial degradation temperature, but greater stability at elevated temperatures. The RHE presented a higher crystallinity index than the bagasse but lower than the pulps. As expected, SEM images show that RHE are more fragmented particles. We can conclude that the RHE can be used in the production of CNC, however there is a need to remove the residual lignin which is very high.

References:

1. J. Araki; M. Wada; S. Kuga; T., Okano. *Colloids and Surfaces A: Physicochemical and Engineering Aspects* 1998, 142, 75. https://doi.org/10.1016/S0927-7757(98)00404-X

Fundings: The authors thank the FAPEMIG, CAPES, CNPQ, and FINEP for their financial support.

Keywords: sugarcane bagasse, pulping, enzymatic hydrolysis, cellulose nanocrystals.

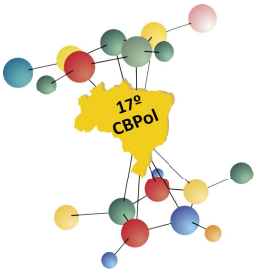

COMPOSITION ANALYSIS, RECYCLING AND *REDESIGN* PROPOSAL OF DISPOSABLE FACE MASKS

Larissa B. Nardini[1], Lais R. de Lima[1] and Sandra A. Cruz[1]

1 - Chemistry Department, Federal University of São Carlos (UFSCar), São Carlos, SP, Brazil
larissanardini@estudante.ufscar.br

The context of the COVID-19 pandemic, marked by the spread of the SARS-CoV-2 virus, has led to an emerging demand for disposable masks. Their use in public has become one of the most effective methods of preventing transmission of the virus. However, the high demand and improper disposal of masks are fueling plastic pollution and having a negative impact on the environment. Given this scenario, recycling of this personal protective equipment (PPE) has becomes an attractive alternative to mitigate these impacts. In this work, samples of disposable masks were analyzed by Fourier-transform infrared spectroscopy and differential exploratory calorimetry to identify the polymers that make up the masks. Thus, it was possible to affirm that most of them are made up by four different polymers, and one metallic component. The main body of the mask is made of polypropylene, while the side strap is composed of polyester and polyurethane, the latter of which may be without and with crosslinks. The wire, commonly found in disposable masks to fix it to the nose, is a polyethylene-coated metal. This composition makes the large-scale recycling process difficult, because these polymers have very distinct physical-chemical properties and behaviors. Currently, in view of all the problems associated with the difficult recyclability of some products, the concept of redesign has been debated. The redesign of a product for recycling may require reducing the diversity of polymeric materials used, reviewing the use and choice of additives, reconsidering multilayer films and rethinking additional items such as caps, labels, among others. Thus, in this work, commercial disposable masks were thoroughly evaluated with regard to their composition and the difficulty of their recyclability was verified. The combination of several incompatible and often infusible materials - such as PU with crosslinks - makes the recycling process costly and leads a material with low final quality. Therefore, a proposal to redesign the disposable mask was considered, and it is the determining factor to enable recycling and produce a material with greater added value.

1. C. Crespo; G. Ibarz; C. Saenz; P. Gonzalez; S. Roche *Waste and Biomass Valorization* 2021, 12, 6423–6432. https://doi.org/10.1007/s12649-021-01476-0
2. D. Battegazzore; F. Craveiro; A. Frache *Polymers* 2020, 12 (11), 2726.; https://doi.org/10.3390/polym12112726
3. J. Lange *ACS Sustainable Chem. Eng.* 2021 , 9 , 47 , 15722–15738;https://doi.org/10.1021/acssuschemeng.1c05013
4. J. Akindoyo; M. Beg; S. Ghazali; M. Islam; N. Jeyaratnam; A. Yuvaraj *RSC Adv.* , 2016,6 , 114453-114482 https://doi.org/10.1039/C6RA14525F

Fundings: National Council for Scientific and Technological Development (CNPq)
Keywords: *disposable mask, recycling, redesign.*

DEVELOPMENT AND CHARACTERIZATION OF BACTERIAL CELLULOSE REINFORCED WITH COCONUT FIBER

Karina C. de Souza[1], Dayanna K. M. de Oliveira [1], João G. M. de Avellar[1], Felipe C. S. Trindade[1], Camila N. Carneiro[1], Felipe P. da C Gomes[2], Yeda M. B. de Almeida[2], Gloria M. Vinhas[2]*

1- Center for Exact and Natural Sciences, Federal University of Pernambuco (UFPE), Recife, PE, Brazil;
2- Chemical Engineering Department, Federal University of Pernambuco (UFPE), Recife, PE, Brazil;
**gloria.vinhas@ufpe.br*

Bacterial cellulose (BC) is a biopolymer that is extremely versatile, it can be worked and molded in its pure form or processed and added with filler materials in order to obtain new composites. As an example, have a coconut fiber (CF) that is very resistant, but also elastic and can play an important role as a reinforcement material for the BC matrix. In this regard, very natural fibers, basically cellulose, hemicellulose and lignin, have become increasingly popular in the manufacturing industry, as they are sustainable materials that can be converted into useful products [1]. With the aim of developing new materials from natural fibers, this study examines the creation of BC composite film reinforced with CF. The filmogenic solution (BC and CF) was prepared in proportion 2:1 and then placed in a mold (A = 58 cm²), at 65 ºC until drying for 24 hours. The material was characterized by Fourier transform infrared spectrometry (FTIR). The pure BC was also characterized for comparative purposes. The FTIR analysis (Fig. 1) confirmed the existing functional groups in CF that overlapped those in BC, for the most part. However, the band close to 1736 cm^{-1} was attributed to the symmetrical stretching C=O of carbonyl groups evident in hemicelluloses and lignin, present only in coconut fibers [2]. In general, this study provides new perspectives for the application of ecologically correct natural fiber composites in the field of engineering and the manufacturing of products.

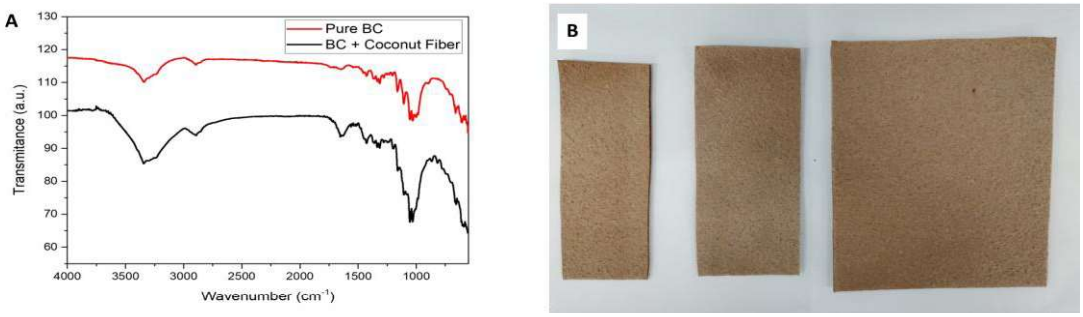

Figure 1- A: FTIR of pure BC and BC + Coconut fiber. B: Composite film of BC reinforced with CF.

References

1. M.A. Azman, M.R.M. Asyraf, et al. Polymers (Basel). 2021, 13(12):1917. doi: 10.3390/polym13121917.

2. R. Siakeng, M. Jawaid, et al. Alkali treated coir/pineapple leaf fibres reinforced PLA hybrid composites: Evaluation of mechanical, morphological, thermal and physical properties, 2020, 717–730, vol 14. doi.org/10.3144/expresspolymlett.2020.59

Keywords: Bacterial Cellulose; Coconut Fiber; Packaging; BC

DEVELOPMENT OF A STARCH-BASED POLYMER BLENDED WITH PET RECYCLING BY-PRODUCTS FOR THE SLOW RELEASE OF FERTILIZER

Esteban Gerling[1*], Daniela E. Schneider[1], Marcelo Gryczak[1], Cesar L. Petzhold[1] and Tales S. Daitx[1*]
1 – Institute of Chemistry, Federal University of Rio Grande do Sul, Porto Alegre, RS, Brazil
estebangerling@outlook.com, tales.daitx@ufrgs.br

Abstract - The objective of this work is producing polymeric blends based on starch and a derivative of the depolymerization reaction of poly(terephthalate of ethylene) (PET) to be applied on the slow release of urea [1, 2]. For this, the PET derivative (dPET) was obtained by glycerolysis reaction under microwave conditions and catalysis of zinc acetate [3]. The reaction was carried out at 250 ºC with 1:3 PET-glycerol ratio, in times of 5, 15 and 30 min, generating the by-products of interest. Thereafter, the blends were produced by casting process, where starch and dPET were mixed with a proportion of 35:65 w:w and with 5, 10 and 20% of urea. The suspensions were mixed in ultrasonic bath for 2 min for homogenization and were heated up to 85 ºC for 30 min. The blends were characterized by thermogravimetric analysis and in relation to their water absorption capacity, release of urea and toxicological analysis. In general, the blends showed good thermal stability and absorbed between 110-650% of water in 24 h. The slow release of urea in water was carried out with ultraviolet-visible spectroscopy at 420 nm, utilizing the Ehrlich reaction methodology [4]. The aqueous solutions samples were taken in 1, 7 and 14 days of interaction with blends. Through the results, it was observed that at first occurs a fast release of urea passing through a phase of reabsorption of this urea in solution and then a slow-release profile was verified, possibly due to partial diffusion of urea in the hydrogel, releasing about 30% urea in 7 days and 45% in 14 days. In additional, no harmful toxicological effects have been observed and the blends promoted corn and onion growth. Based on the aforementioned results, the developed blends showed a great potential for the slow release of urea in water.

References

1. L. Chen; Z. Xe; X. Zhuang; X. Chen; X. Jing *Carbohydrate Polymers* 2008, *72*, 342. https://doi.org/10.1016/j.carbpol.2007.09.003
2. T. S. Daitx, V. S. Lima, M. Gryczak, C. L. Petzhold, L. N. Carli, R. S. Mauler *Polymers Advanced Technologies* 2020, *31*, 2579. https://doi.org/10.1002/pat.4985
3. S. Cavalcante; D. Vieira; I. Melo *Proceedings* 2019, *41*, 78. https://doi.org/10.3390/ecsoc-23-06650
4. D. S. Gamarano, I. M. Pereira, A. C. Mottin, E. Ayres *Macromolecular Symposia*, 2022, 406, 2200043. https://doi.org/10.1016/j.carbpol.2007.09.003

Fundings: The authors are grateful to Conselho Nacional de Desenvolvimento Científico e Tecnológico (CNPq), Coordenação de Aperfeiçoamento de Pessoal de Nível Superior (CAPES), Fundação de Amparo à Pesquisa do estado do Rio Grande do Sul (PRONEX/FAPERGS - Finance Code 16/2551-0000470-6) and Programa de Pós-Graduação em Ciência dos Materiais (PPGCIMAT/UFRGS) for financial support.

Keywords: *Chemical recycling, Food Security, PET, Sustainability, Urea.*

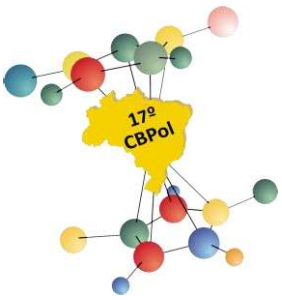

DEVELOPMENT OF CHITOSAN HYDROGELS WITH CARBON NANOTUBES FOR ADSORPTION OF COPPER IONS FROM INDUSTRIAL EFFLUENTS

Camila M. Dias[1], Mayara F. Castro[1], Júlia A. G. Oliveira[1], Lucas B. Moço[1] and Djalma Souza[1*]
1 – Advanced Materials Laboratory (LAMAV), State University of the North Fluminense Darcy Ribeiro (UENF), Campos dos Goytacazes, RJ, Brazil
djsouza@uenf.br

Abstract - Present in the composition of a large portion of industrial effluents, copper is a heavy metal highly harmful to human health and the environment. Among the treatments applied in effluent recovery, the adsorption technique is superior due to its efficiency, simplicity and low cost. Chitosan hydrogels were prepared with mass ratios of carbon nanotubes at 0.1%, 0.2%, and 0.3%. The hydrogels were obtained in the form of spheres using the alkaline coagulation technique, and the adsorption capacity of the developed adsorbents was studied using a copper sulfate solution (0.07g/mL). The morphological characterization of the adsorbent was carried out by scanning electron microscopy, which confirmed the adequate morphological formation for adsorption. The adsorption capacity was studied based on the data obtained from UV-visible spectroscopy, which showed a copper ion loading of up to 15 mg/g for the hydrogels with higher carbon nanotube content. Langmuir and Freundlich adsorption isotherms were also applied. It was concluded that the Freundlich isotherm model fitted better to the kinetic data of the samples, indicating that the adsorption occurs in a monolayer on the heterogeneous surface of the samples. Based on the results obtained, it was concluded that the formulation of chitosan hydrogel with carbon nanotubes is a favorable option to be used as a copper ion adsorbent.

References

1. Ahmed, M.J., Hameed, B.H., Hummadi, E.M. *Carbohydrate Polymers,* 2020, 247. https://doi.org/10.1016/j.carbpol.2020.116690
2. Jing, G.; Wang, L.; Yu, H.; Amer, W.A.; Zhang, L. *Colloids and Surfaces a: Physicochemical and Engineering Aspects*, 2013, 416, 86-94. https://doi.org/10.1016/j.colsurfa.2012.09.043
3. Dev, V.V., Nair, K.K., Baburaj, G., Krishnan, K.A. *Colloid and interface Science Communications*, 2022, 49. https://doi.org/10.1016/j.colcom.2022.100626

Fundings: The authors would like to thank Faperj, CAPES and UENF for the resources provided for the development of this research.

Keywords: *Chitosan, carbon nanotube, hydrogels, adsorption, copper ions.*

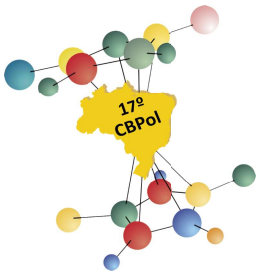

DEVELOPMENT OF SUSTAINABLE PRODUCTS WITH RECYCLED POLYMER COMPOSITES AND SILICA PARTICLES FROM FOUNDRY SAND

Alexsandro Foyth[1], Ronaldo Rodrigues[1], Leandro Speckhan[1], Bruno Senn[1], Palova S. Balzer[2]

1 – Department Automotive, Schulz S. A., Joinville, SC, Brazil, alexsandro.foyth@schulz.com.br
2 – Joinville Region University (UNIVILLE), Joinville, SC, Brazil, palovabalzer@univille.br

Abstract –Solid and semi-solid waste, according to ABNT 10,004 of 2014, results from industrial, domestic, hospital, commercial, agricultural, services and sweeping activities. Among the most produced waste are polymeric materials, which according to the study carried out by the World Wide Fund for Nature (WWF), Brazil produces 11 million tons of plastic waste per year. Another waste generated in large proportions is sand discarded from the foundry industry (ADF). In 2020, according to the Brazilian Foundry Association (ABIFA), more than 3 million tons were generated. With the aim of enabling the use of these residues in substitution of the base of pallets made of wood for a company in the foundry area of the city of Joinville, plates with recycled polymeric material from a recycling company in the municipality of Joinville were processed via cold compression. northern region of Santa Catarina and composites of this recycled material with 10 and 20% ADF from the green sand process. The plates obtained were machined in the shape of a specimen for tensile, compression, impact and hardness tests. For comparison, wooden boards of the same material as the base of the pellet were machined. It was verified that between the pure recycled polymeric material and the composites, the formulation with 10% of ADF presented the best results, mainly in relation to resistance to flexion and compression. Comparing the composite with 10% ADF with wood, the compressive strength of the composite was 52% higher than that of wood. Similar behavior was also verified in the resistance to impact, the composite with 10% presented resistance 38% greater than the wood. With this result, a pellet base was designed based on the piece produced with wood, and molded by cold compression. It was found that the replacement of wood by the developed composite is feasible for application, being currently applied in the field, reducing the maintenance of these parts. In addition to reusing polymeric material and ADF waste, it avoids the consumption of wood, promotes the circular economy, values waste and reduces costs regarding the disposal of the materials involved.

References.

1. Brazilian Association of Technical Sandards. Classification of Industrial solid waste. NBR 10004. Rio de Janeiro, 2004.
2. R. L. P. Carnin.; V. C. Battisti; L. D. B. Misanda Filho; Abifa 2021. 47, https://www.abifa.org.br/revista41/#p=47
3. World Wide Fund for Nature (WWF) https://www.wwf.org.br/?70222/Brasil-e-o-4-pais-do-mundo-que-mais-gera-lixo-plastico, accessed on jan,2019.

Fundings: Acknowledgment Schulz S.A. and University of Joinville Region (Univille).

Keywords: Waste, Recycling, Discarded Foundry Sand, Polymer Composite, Cold Compression.

EFFECT OF CELLULOSE ACETATE ADDITION ON THE BARRIER PROPERTIES OF BROKEN BEAN FLOUR FILMS

Daiane Nogueira[1], Juliana M. Latorres[1], Natasha M. Spindola[1], Vilásia G. Martins[1]

1 – School of Chemistry and Food Engineering, Federal University of Rio Grande (FURG), Rio Grande, RS, Brazil
daianenoguer@gmail.com

To minimize the impact of non-biodegradable packaging, different materials and combinations of these have been studied for the development of biodegradable films. However, the barrier properties of these films are still unsatisfactory for their application as food packaging. Thus, this study aimed to evaluate the barrier properties of broken bean flour films added with cellulose acetate. Control bean flour films (F1) were obtained by the casting method, at a concentration of 5% (w/v) of red bean flour and 30% (w/w) of glycerol. To prepare the blend (F2), the same filmogenic solution as F1 was mixed with the cellulose acetate solution in a 90:10 ratio. The films were characterized according to their thickness, water vapor permeability (WVP) and solubility (S). Statistical analysis of the thickness data showed that there was no difference between samples F1 and F2. This was expected due to the patterning of solids in the filmogenic solution deposited on the plates. The analysis of the results for WVP showed that after the formation of the blend with cellulose acetate, the film property did not improve, since the results were statistically equal, being 21.636 g.mm/h.m².kPa (F1) and 20.778 g.mm/h.m².kPa (F2). The S results also showed no significant difference between the F1 and F2 samples (24.9% and 24.3%, respectively). The results found showed that the addition of 10% of the cellulose acetate solution (1%) did not promote the expected improvement in the properties of the films. This may have occurred due to the low concentration of acetate in the final composition of the film. In view of this, we can conclude that new tests with higher proportions of cellulose acetate in relation to the filmogenic bean flour solution should be carried out.

References

1. D. Nogueira; N. M. Spindola; J. M. Latorres; J. A. V. Costa; V. G. Martins. *Polymer Engineering and Science* 2022, 62, 1070 - 1080. https://doi.org/10.1002/pen.25907.

2. Y. Liu; S. Ahmed; D. E. Sameen; Y. Wang; R. Lu; J. Dai; S. Li; W. Qin. *Trends in Food Science & Technology* 2021, 112, 532-546. https://doi.org/10.1016/j.tifs.2021.04.016.

Fundings: This study was financed in part by the Coordenação de Aperfeiçoamento de Pessoal de Nível Superior - Brasil (CAPES) - Finance Code 001". Also this work was supported by the Serrapilheira Institute (grant number Serra – 1709-20275).

Keywords: *broken bean, biodegradable films, acetate cellulose, food packaging, barrier properties.*

EFFECT OF CORN ZEIN ON THE PHYSICAL PROPERTIES OF BEAN FLOUR FILMS

Daiane Nogueira[1], Juliana Machado Latorres[1], Natasha M. Spindola[1] and Vilásia Guimarães Martins[1]

1- Laboratory of Food Technology, School of Chemistry and Food Engineering, Federal University of Rio Grande, 96203-900, Rio Grande, RS, Brazil.
vilasiamartins@gmail.com

The uncontrolled use of synthetic packaging has been associated with several environmental problems and has generated positive discussions about the use of environmentally friendly packaging. Natural polymers in packaging development are a promising alternative to solve the environmental problems associated with petroleum-based synthetic packaging. However, the physical properties of these packaging materials are unsatisfactory compared to currently commercialized packaging, limiting their application. This study aims to evaluate the effect of corn zein atomization on the physical properties of bean flour films. Bean flour films were produced by the casting technique at a concentration of 5% (w/v) flour and 30% glycerol (w/w). Subsequently, an ultrasonic atomization technique was used to deposit a 5% zein solution (ethanol - 80%) on the surface of the bean flour films. Then, films F1 (bean flour films) and F2 (bean flour films with zein) were characterized for thickness (mm), mechanical properties of the tensile strength (TS (MPa)) and elongation at break (E (%)), and water vapor permeability (WVP (g.mm/d.m².kPa)). The thickness of films F1 and F2 showed significant differences ($p<0.05$) and varied between 0.199 and 0.234 mm, respectively. Similarly, significant differences ($p<0.05$) were observed between F1 and F2 for TS (MPa) and E (%). F2 had higher TS (7.9 MPa) and lower E (11.29%) compared to F1, which had TS (5.79 MPa) and lower E (23.58%). For WVP, film F2 exhibited better water barrier property (27.75 g.mm/d.m².kPa) compared to film F1 (21.27 g.mm/d.m².kPa). These results suggest that atomization of corn zein constitutes a promising alternative to improve the properties of biodegradable packaging produced from bean flour.

References

1. D. Nogueira; N. M. Spindola; J. M. Latorres; J. A. V. Costa; V. G. Martins *Polymer Engineering and Science 2022*, *62*, 1070 - 1080. https://doi.org/10.1002/pen.25907.

2. O. Rompothi, P. Pradipasena, K. Tananuwong, A. Somwangthanaroj, T. Janjarasskul *Carbohydrate Polymers*. *2017*, *157*, 748-756. https://doi.org/10.1016/j.carbpol.2016.09.00.

3. C. D. Ferreira, V. Ziegler, I. S. Lindemann, J. F. Hoffmann, N. L. Vanier, M. Oliveira *Food Chemistry2 018*, *246*, 473-480. https://doi.org/10.1016/j.foodchem.2017.11.118.

Fundings: This study was financed in part by the Coordenação de Aperfeiçoamento de Pessoal de Nível Superior - Brasil (CAPES) - Finance Code 001". Also this work was supported by the Serrapilheira Institute (grant number Serra – 1709-20275).

Keywords: *sustainable packaging; biomaterials; black bean; ultrasonic atomization.*

ENHANCING SUSTAINABLE PACKAGING POTENCIAL: INVESTIGATION OF HIGH CALCIUM CARBONATE CONTENT VIA INJECTION MOLDING AS AN ALTERNATIVE TO FOSSIL-BASED PLASTICS

Franciele Saorin1*, Bruna L. Jatzek1, Marcia P. P. dos Santos1, María A. Restrepo2, Guilherme Silva3 and Rafael Justus3

1 - Cencoderma Instituição de Pesquisa e Desenvolvimento de Cosméticos Ltda, São José dos Pinhais, Paraná, Brazil
franciele.saorin@grupoboticario.com.br
2 – Okeanos Group, LLC, Colombia
3 – Aptar do Brasil Embalagens Ltda, Jundiaí, São Paulo, Brazil

Abstract – The article highlights the use of calcium carbonate (CaCO3), commonly used as a filler to enhance some polymers application properties, particularly in the context of sustainable alternatives to fossil-based plastics, specifically for applications that claim to be more sustainable. The study compares the Okeanos™ BC09 compound and polypropylene (PP) blends with 100wt% PP packaging for cosmetic packaging. Fourier Transform Infrared (FTIR) confirms CaCO3 absorption, while Differential Scanning Calorimetry (DSC) shows no thermal events for CaCO3, and Thermogravimetric Analysis (TGA) indicates delayed thermal degradation. Impressively, despite a 58% weight increase, the innovative BC09 compound packaging demonstrated a significant 20.5% reduction in carbon footprint, as measured by Life Cycle Assessment (LCA), without compromising processability and productivity. This indicates a promising avenue for environmentally friendlier packaging solutions.

Keywords: *Calcium Carbonate, Sustainable Packaging, Cosmetics, Fossil-based Plastic Alternative, LCA.*

Introduction

Emerging in the mid-19th century, the era of polymers took its first steps. This epoch has unfolded continuously, interconnected with advancements spanning myriad facets of human achievement. From the domains of automotive, electronics, and medicine to the pivotal realm of packaging, its impact remains profound [1]. Greenhouse gas emissions (GHG) from plastic's production and consumption are predicted to double by 2060 (3.8 Gigatonnes CO2 equivalent) from 2019 (1.6 Gigatonnes CO2 equivalent). This suggests a substantial growth in emissions if current trends continue [2]. Calcium carbonate (CaCO3), a renewable and abundant material found in sources like limestone, seafood residues, and eggshells, is commonly used to reinforce mechanical properties of polymer matrices due to its cost-effectiveness and biocompatibility [3,4]. While most studies focus on using CaCO3 as reinforcement, Okeanos™ introduces a

unique concept, employing CaCO3 as the main element in a material inspired by eggshells, aimed at partially replace non-renewable plastic in packaging. This material, known as BC09, blends CaCO3 with polyolefin for cohesion. To create packaging, this blend is mixed with polyethylene (PE) or polypropylene (PP) resins, adaptable for processes like injection, extrusion, and blowing molding.
This article compares cosmetic packaging made of a blend of CaCO3 and PP to 100wt% PP packaging, assessing processability, dimensional analysis, characterization, and LCA. The goal is to showcase that utilizing high CaCO3 percentages in packaging can offer an alternative to reduce the carbon footprint and lessening reliance on non-renewable resources.

Experimental

Materials and Methods

The CaCO3 used in this research was BC09 compound obtained from Okeanos LLC, Brazil and the PP used was H301 obtained from Braskem, Brazil.

Sample Preparation

Samples were prepared using a Haitian SA160t injection molding machine. The sample was placed in the injector's feed zone without prior treatment. Various CaCO3 concentrations were tested to maximize incorporation. Refer to Table 1 for formulations used.

Table 1 Composition of formulations used in this study

Sample	BC09 concentration		CaCO3 expected concentration	BCO9 addition	PP H301 addition
	CaCO3	HDPE + additives			
DS#1	-	-	-	-	100wt%
DS#2	70wt%	30wt%	10wt%	15wt%	85wt%
DS#3	70wt%	30wt%	40wt%	57wt%	43wt%
DS#4	70wt%	30wt%	51wt%	73wt%	27wt%

Processability and Dimensional Analysis

Table 2 shows the processing conditions used to produce the samples from BC09 compound and PP H301. Sample DS#1 is the standard. After the processing, analysis of process performance was conducted using 10 samples to assess measurements of weight, total height, and screw diameter, using a standard caliper Mitutoyo Like 1.

Table 2 Injection molding machine parameters

Parameter	100% PP H301 DS#1	15% BC09 + 85% PP H301 DS#2	57% BC09 + 43% PP H301 DS#3	73% BC09 + 27% PP H301 DS#4
Zone 1 (ºC)	230	175	175	175
Zone 2 (ºC)	225	190	190	190
Zone 3 (ºC)	220	190	190	190
Zone 4 (ºC)	220	190	190	190
Zone 5 (ºC)	210	190	190	190
Cooling time (s)	9	12	12	12
Holding time (s)	2.42	2.2	2.2	2.2
Screw speed (mm/s)	50	45	45	45
Cycle time (s)	22.24	22.97	22.9	22.92

Characterization techniques
Structural changes were measured via Fourier Transform Infrared Spectroscopy (FTIR) using a Nicolet iS50 spectrometer in ATR mode (4000 to 650 cm–1, 32 scans, 4 cm–1 resolution). Dynamic thermal behavior was assessed via heat flow DSC on a TA Instruments Discovery DSC250 (10°C/min, 5.95 mg). Thermogravimetric analysis (TGA) was performed with a TGA Q500 instrument, heating the sample to 800°C (10 °C/min, 11.76 mg).

LCA
Conducted LCA using SimaPro 9.1.1 with Ecoinvent 3.4 database via 20-year GWP method (IPCC 2013). Assumed IMA-NA 20164 study for calcium carbonate as benchmark, factoring in Brazil's energy grid change. Limited by single cradle-to-gate analysis study for "Calcium Carbonate, ground, fine treated, 3 microns." Resin production data solely from Ecoinvent database.

Results and Discussion
Processability Analysis
During processing, samples DS#2, DS#3 and DS#4 filled mold cavity easily. Additionally, during process in barrel there was a 31% temperature reduction in samples DS#2, DS#3, and DS#4 compared to sample DS#1, leading to decreased energy consumption. Despite a 25% increase in cooling time, the overall injection cycle remained unchanged, preserving mold productivity. Additionally, it is believed that the cooling time could even be reduced in long term studies. Graphs 1, 2 and 3 illustrate 3 important measurements: weight, internal height, and screw diameter, respectively. Sample DS#1, comprising the standard packaging made entirely of 100% PP H301, had established LSL (Lower Specification Limit), target, and USL (Upper Specification Limit) values.

Graph 1

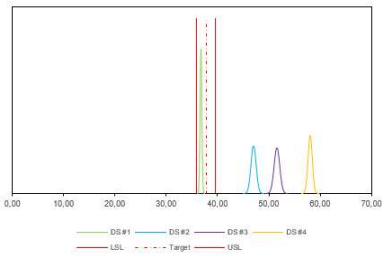

Weight

Graph 2

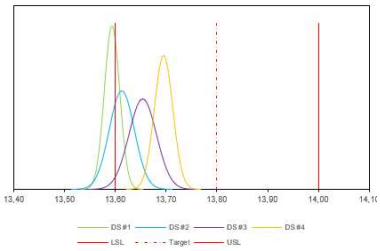

Internal Height

Graph 3

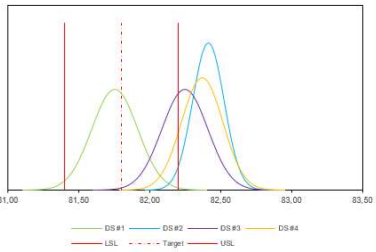

Screw Diameter

The weight increases in graph 1 shows proportionality to the rise in BC09 concentration, due to the high density of CaCO3 when compared to PP. In Graph 2, it is evident that the internal height of DS#1 yielded results below LSL. However, as the concentration of BC09 increased, the results fell within the target. This outcome can be attributed to the BC09 shrinkage rate being reduced compared to PP, thereby mitigating the deviation. The screw diameter depicted in graph 3 also falls outside the LSL, due to shrinkage rate, when measured in samples DS#2, DS#3 and DS#4. However, there appears to be no correlation between this deviation and the increase in concentration. Given that there was no impact on functionality, all concentrations received approval from usability perspective. With the aim of enabling packaging with the greatest reduction in fossil-based plastic, characterization and LCA analysis continued with the highest expected concentration of 51% CaCO3 in the final package, identified as sample DS#4, compared to DS#1.

Characterization techniques

The qualitative FTIR analysis in the mid-infrared spectrum is depicted in Figure 1, highlighting the absorption traits of PP H301. Figure 2 illustrates the interaction between polyolefin and CaCO3.

Figure 1

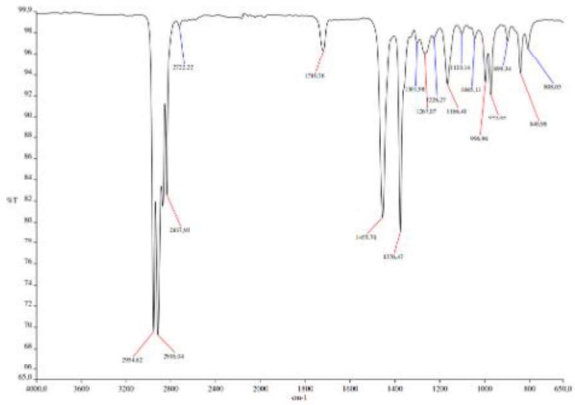

FTIR the mid-infrared spectrum sample DS#1

Figure 2

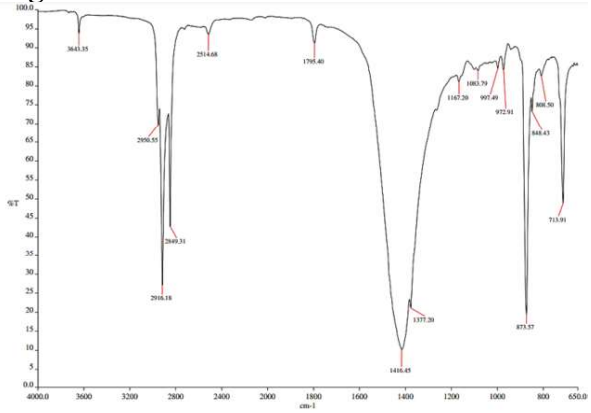

FTIR the mid-infrared spectrum sample DS#4

Fig 3 illustrates that the crystalline melting temperature reported in DSC aligns with the findings from studies conducted on PP H301 [5]. Fig 4 shows that two thermal events were observed when the sample DS#4 was heated, at 128°C and 162°C ($T_{\Delta max}$), indicating melting characteristics. During sample cooling, two thermal events were observed at 116°C and 119°C (Tpc), indicating crystallization characteristics. The melting temperatures at 128°C and 162°C indicate the presence of linear low-density polyethylene (LLDPE) and PP, respectively. No thermal events occur for CaCO3 in the conditions and measured range used.

Figure 3

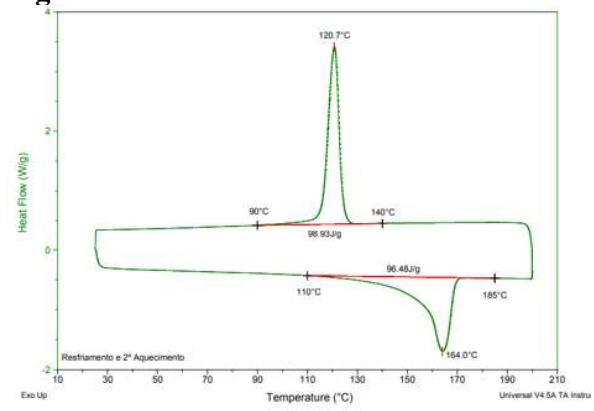

DSC curves sample DS#1

Figure 4

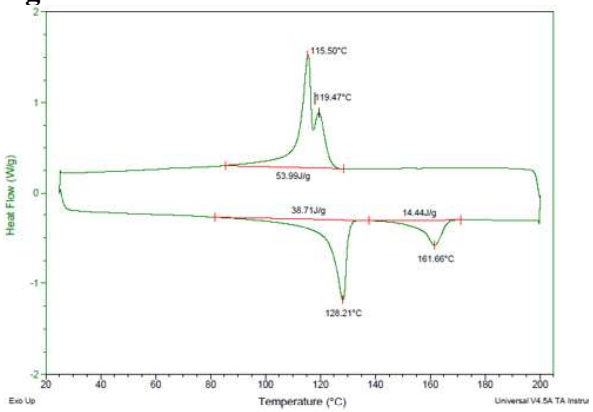

DSC curves sample DS#4

Thermogravimetric (TG) and Derivative thermogravimetry (DTG) of sample DS#1 illustrates in Fig 5 the beginning of thermal degradation occurred at 430ºC with maximum degradation around 460ºC. Fig 6 shows 3 thermal degradation events, illustrated:

(1) Mass reduced by 48.0% from 33°C to 550°C, mainly polymer loss.

(2) Mass decreased by 22.2% from 550°C to 800°C, due to carbonate decomposition. The presence of carbonate leads to a delay in thermal degradation, which means a stabilization effect.

(3) 29.8% mass as inorganic waste at 800°C, due to metallic oxides, fillers, calcium.

Figure 5

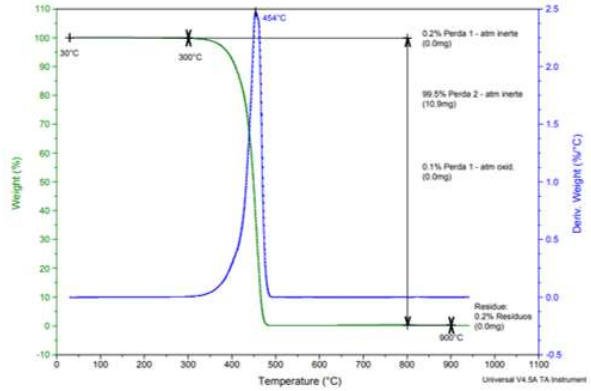

TGA analysis sample DS#1

Figure 6

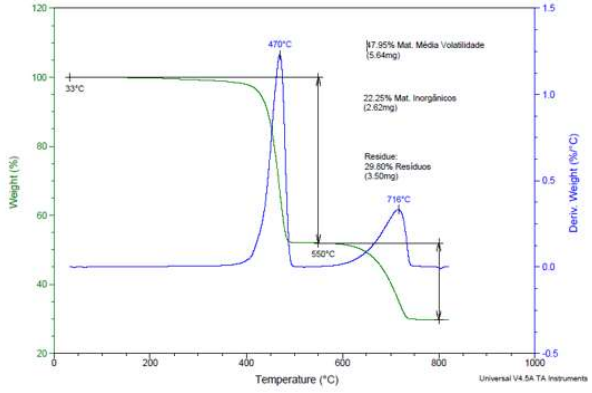

TGA analysis sample DS#4

LCA

When comparing samples DS#1 and DS#4 using the Life Cycle Assessment tool, the results indicate that by replacing packaging DS#1 with packaging DS#4, there is a projected carbon emission reduction of 20.5%, despite a weight increase of about 58%. This translates to a decrease in CO_2 equivalent emissions.

Conclusions

This study successfully demonstrates the feasibility of decreasing the fossil-based polypropylene concentration in cosmetic packaging produced through injection molding. This reduction of 20.5% in CO_2 equivalent emissions, compared to packaging using 100wt% fossil-based polypropylene, is achieved without compromising processability and productivity. There are two potential pathways for future studies: one involves designing a new injection mold that maintains structural integrity and visual impact, featuring thinner walls, possible due to lower shrinkage rate of CaCO3 that avoid warping, leading to a reduction in packaging mass and, consequently, greater sustainability benefits. The second pathway involves substituting fossil-derived polypropylene with bio-based polyolefins, aligning with environmentally friendly practices.

Acknowledgements

The authors would like to thank Grupo Boticário, Okeanos and Aptar for the resources allocated to this research project.

References

1. P. B. Patel; A. K. Gupta; R. S. Niranjan; A. K. Chandra; G. Pandey. Materials Today: Proceedings 2023, https://doi.org/10.1016/j.matpr.2023.08.072.

2.OECD (Organisation for Economic Co-operation and Development) (https://www.oecd.org/environment/plastics/increased-plastic-leakage-and-greenhouse-gas-emissions.htm). Accessed 08/24/23.

3. G. Golakiya, Ms.C. Thesis, University of Saskatchewan, 2022.

4. E. A. Almanza, H. H. Cocoletzi, E. R. Rosas, M. C. González, H. R. Lim, K. S. Khoo, V. Singh. Chemosphere 2022, 288, https://doi.org/10.1016/j.chemosphere.2021.132550.

5. B. S. R. Sá, Ms.C. Thesis, Universidade Tecnológica Federal do Paraná – UTFPR, 2019.

ENZYMATIC SYNTHESIS OF ALLYL-(METH)ACRYLATE MONOMERS FOR BIODEGRADABLE THIOL-ENE BASED POLYMERS

João V. C. Santin[1], Tamara Agner[1], Cristian de O. Romera[1], Pedro H. H. de Araújo[1] and Claudia Sayer[1]*

1 – Department of Chemical Engineering and Food Engineering (EQA), Federal University of Santa Catarina (UFSC), Florianópolis, SC, Brazil claudia.sayer@ufsc.br

Abstract - The use of oil derived polymers is widespread in modern society due to the current high availability and low cost of both the source material and final product. However, these materials are characteristically non-renewable resources and the resulting polymers are very rarely degradable and often not recyclable. Vegetable oils are employed in monomer synthesis and polymerization to create renewable materials, and the esterification of these oils can be a straightforward path to improve degradability. The green trend can be furthered by monomer synthesis and polymerization being carried out through green pathways, using enzymes as a catalyst for esterification and later polymer degradation, and photoinitiated thiol-ene addition as the polymerization mechanism. This study uses enzymatic esterification of undec-10-enoic acid, derived from castor oil, with both 2-hydroxyethyl acrylate and 2-hydroxyethyl methacrylate[1] to produce two asymmetric diene monomers in a solvent-free system at 50 ºC. Bulk thiol-ene photopolymerization of both monomers with a dithiol or a tetrathiol, as well as free radical homopolymerization, yielded solid cross-linked polymers, ranging between 12% and 92% gel content. FTIR analysis showed leftover thiol groups in methacrylate samples that had 1:1 stoichiometric proportion of thiol to double bond functional groups, indicating the prevalence of propagation in such systems. As such, polymerization of thiol-ene-methacrylate systems does seem to occur in two stages[2], and thiol addition is likely selective towards the allylic double bond, while acrylate systems show concurrent process and lower selectivity[3]. Presence of ester groups in the polymer backbone enables its biodegradation, which was verified in an enzymatic medium (*Candida antartica* lipase B) by measuring mass loss over 28 days, reaching losses between 10 and 70%, with the semicrystalline structure and highly cross-linked matrix slowing down degradation[4].

References:

1. C. de O. Romera; D. de Oliveira; P. H. H. Araújo; C. Sayer *Ind. Eng. Chem. Res*. 2019, *58*, 21044-21055. https://doi.org/10.1021/acs.iecr.9b02386.
2. T. Y. Lee; Z. Smith; S. K. Reddy; N. B. Cramer; C. N. Bowman *Macromolecules* 2007, *40*, 1466-1472. https://doi.org/10.1021/ma062494b.
3. N. B. Cramer; C. N. Bowman *Journal of Polymer Science* 2001, *39*, 3311-3319. https://doi.org/10.1002/pola.1314.
4. B. Laycock; M. Nikolić; J. M. Colwell; E. Gauthier; P. Halley; S. Bottle; G. George *Biotechnology Letters* 2017, *71*, 144-189. https://doi.org/10.1016/j.progpolymsci.2017.02.004.

Fundings: We thank Coordenação de Aperfeiçoamento de Pessoal de Nível Superior (CAPES) and Conselho Nacional de Desenvolvimento Científico e Tecnológico (CNPq) for the financial support.

Keywords: *Enzymatic synthesis; Photopolymerization; Thiol-ene-(meth)acrylate systems; Polymer biodegradation.*

EVALUATION OF ENVIRONMENTAL IMPACTS AND PRODUCTION PROCESSES OF CHITOSAN DERIVED FROM SHRIMP EXOSKELETONS

Marcelo B. O. Silva[1*], Sueli A. Oliveira[1] and Derval S. Rosa[1]

1 – Center for Engineering, Modelling and Applied Social Sciences (CECS), Federal University of ABC (UFABC), Santo André - SP, Brazil
marcelo.bruno@ufabc.edu.br

Abstract - The increasing interest in sustainable development has led to a growing focus on biodegradable polymers, with chitosan being a prominent candidate due to its derivation from chitin, the second most abundant biopolymer in nature. Chitosan offers high biocompatibility and versatility, enabling its application in diverse fields such as biomedicine, packaging, cosmetics, agriculture, water treatment, and electronics. This study investigates the production of chitosan from crustacean shell waste by utilizing the residual exoskeletons of shrimp (*Farfantepenaeus brasiliensis*). The chitosan production process involves demineralization, deproteinization, depigmentation, and deacetylation of chitin. However, producing chitosan from shrimp waste can potentially generate environmental impacts. This study compares different deacetylation methods: conventional heating (D-H) and microwave radiation with different power levels (D-M1, D-M2, and D-M3). The energy consumption per gram of chitosan produced is assessed for each deacetylation method, revealing values of 382.1 KJ/g, 14.3 KJ/g, 8.7 KJ/g, and 8.9 KJ/g for D-H, D-M1, D-M2, and D-M3, respectively. The deacetylation degree was 76%, 85%, 55%, and 88% for the D-H, D-M1, D-M2, and D-M3 samples, respectively. The results demonstrate that the application of microwave energy shows greater efficiency, reducing energy consumption and processing time compared to conventional heating methods. Environmental impact assessment using the *ReCiPe Midpoint H* method reveals that potential terrestrial ecotoxicity, global warming, non-carcinogenic human toxicity, and land use are the identified categories with the greatest relative environmental impact. The deacetylation method D-M3, utilizing microwave radiation at a power of 500 W, exhibits the lowest potential for environmental impact due to its higher efficiency. The application of microwave energy for deacetylation demonstrates improved efficiency and reduced environmental impact compared to conventional heating methods. The findings provide valuable insights for optimizing chitosan production processes, enhancing sustainability in waste valorization, and directing future research toward developing greener technologies in biopolymer production.

References

1. B. Fatima *IntechOpen* 2020 https://doi.org/10.5772/intechopen.89708.
2. I. Muñoz; C. Rodríguez; D. Gillet; B. M. Moerschbacher *The International Journal of Life Cycle Assessment* 2018, 23(5), 1151–1160 https://doi.org/10.1007/s11367-017-1290-2
3. S. Kou; L. M. Peters; M. R. Mucalo *International Journal of Biological Macromolecules* 2021, 169, 85–94 https://doi.org/10.1016/j.ijbiomac.2020.12.005

Fundings: This research was supported by the São Paulo Research Foundation (2020/13703-3) and Coordination for the Improvement of Higher Education Personnel (88887.529486/2020-00).

Keywords: *environment, microwave radiation, deacetylation, crustacean, chitin*

EVALUATION OF THE INFLUENCE OF COLORATION ON THE YIELD OF PET DEPOLYMERIZATION BY HYDROLYSIS

Adriel M. Almeida[1], Rodrigo L. Oréfice[2], Eliane Ayres[3], Mary L. Braga[4], Mercês C. Silva[1].

1- Institute of Integrated Engineering (IEI), Federal University of Itajubá (UNIFEI), Itabira, MG, Brazil, mercescoelho@unifei.edu.br
2- Department of Metallurgy and Materials Engineering (DEMET), Federal University of Minas Gerais, Belo Horizonte, MG, Brazil, .
3- Graduate Design Program (PPGD), Universidade do Estado de Minas Gerais (UEMG), Belo Horizonte, MG, Brazil, .
4- Department of Materials and Construction Engineering (DEMC), Federal University of Minas Gerais, Belo Horizonte, MG, Brazil,

Polymeric materials are obtained from non-renewable petroleum sources, therefore, these sources are subject to future scarcity, considering that the current consumption is more intense than their obtaining cycle. However, these polymerized materials present themselves as a major environmental problem, especially PET (polyethylene terephthalate), a highly resistant, durable, and versatile plastic that is widely used in packaging for beverages, food, and other products. However, it is extremely slow to decompose, leading to significant environmental problems. Millions of tons of PET are discarded annually, contributing to ocean pollution, ecosystem degradation, and the release of greenhouse gases during its production and disposal1,2. Based on these facts, the objective of this paper is to address the chemical recycling of PET using the hydrolysis method. Initially, hydrolysis was performed on plastics of different colors (transparent and green) to compare their yields and analyze about the interference of additives to the process. The hydrolysis was conducted in an alkaline solution using a solution of Sodium Hydroxide (NaOH) with a concentration of 10 mol/L. The synthesis was carried out in a double reaction flask by adding the NaOH solution to the PET waste, with a particle size of less than 1 cm². Then the system was heated to 118 ± 5 °C for 2 hours, and 50% v/v sulfuric acid was added until the pH reached 1. After cooling, the product was filtered1. The result of this study will be evaluated by means of Fourier transform infrared spectroscopy (FTIR), thermogravimetry (TGA) and the mass obtained from its precursors terephthalic acid (PTA) and ethylene glycol (EG).

References.

1. LACERDA, Carlos Eduardo de Oliveira. RECICLAGEM QUÍMICA DO POLI(TEREFTALATO DE ETILENO) - PET PÓS - CONSUMO VIA HIDRÓLISE. 2019. Tese (Doutorado) - UNIVERSIDADE FEDERAL DE PERNAMBUCO, Recife, 2019.
2. GEYER, B.; LORENZ, G.; KANDELBAUER, A. Recycling of poly(ethylene terephthalate) – A review focusing on chemical methods. Express Polymer Letters, v. 10, n. 7, p. 559- 586, 2016.

Fundings: CNPq/MCTI-FNDCT CT-Petro No 43/2022 Processo: 405414/2022-6
Keywords: *Environmental Problems, Chemical Recycling, PET (Polyethylene Terephthalate), Hydrolysis, Monomers.*

EVALUATION OF THERMAL BEHAVIOR IN POLYMERIC BLENDS OF EXPANDED POLYSTYRENE (EPS) AND WASTE TIRE RUBBER (WTR)

Antonio J. Andrade Junior, Silma S. Barros, Emerson F. Silva* and Clodoaldo Saron

Department of Materials Engineering (DEMAR), Engineering School of Lorena (EEL), University of São Paulo (USP), São Paulo, Lorena, SP, Brazil, emersonsilva1071@usp.br

Abstract - Waste management in an environmentally sustainable way is a difficult goal to achieve, especially considering the volume of waste produced each year, many of which are disposed of irregularly[1]. Recycling is a more appropriate form of disposal, using waste to produce new materials with potential for use and trade. Two materials that are commercially produced on a large scale and were recycled in this study were expanded polystyrene (EPS) and waste tire rubber (WTR). EPS is mainly used in protective packaging for electronic products and is difficult to reuse due to its low density[2]. Tires also have high consumption, with 1.5 billion tires discarded per year, which may increase with vehicle demand and could reach 5 billion by 2030[3]. The study produced blends of recycled polystyrene (PS) with WTR with the presence and absence of the compatibilizing agent styrene-butadiene-styrene (SBS) to promote the reuse of waste and transforming it into a new material to be evaluated. The thermal properties of the materials were evaluated from two analyses, the thermogravimetric analysis (TGA) and the dynamic mechanical analysis (DMA). It was observed that both the PS/WTR and PS/SBS/WTR samples showed an increase in thermal stability in presence of WTR content, indicated by the increase at the onset of decomposition and the maximum rate of thermal decomposition temperature, the result was more effective in the compatibilized samples[4,5]. The presence of rubber and compatibilizer resulted in increased thermal stability, reduction in the glass transition (Tg) and increased elastic energy storage of the blend.

References

1. I. Tsuchimoto; Y. Kajikawa *Sustainability* 2022, 14, 16340. https://doi.org/10.3390/su142416340.
2. S. C. Ugwu; C. M. Obele *World Journal of Advanced Engineering Technology and Sciences* 2023, 8, 315-329. https://doi.org/10.30574/wjaets.2023.8.1.0057
3. P. Grammelis; N. Margaritis; P. Dallas; D. Rakopoulos; G. Mavrias *Energies* 2021, 14, 571. https://doi.org/10.3390/en14030571.
4. C. B. B. Luna; E. M. Araújo; D. D. Siqueira; D. D. S. Morais; E. A. Santos Filho; M. V. L. Fook *Journal of Elastomers & Plastics* 2020, 52, 3-28. https://doi.org/10.1177/0095244318819213
5. K. Bedjaoui; R. Krache; A. M. Fernández; M. Guessoum *Materials Research Express* 2019, 6, 105334. http://dx.doi.org/10.1088/2053-1591/ab38e7

Keywords: *Polymeric Blend. Expanded polystyrene. Waste Tire Rubber. Recycling. Thermal Decomposition.*

Fundings: National Council for Scientific and Technological Development - CNPq (Proc. 309583/2020-9) and FAPESP (Proc. 2020/14318-6)

FULL FACTORIAL EXPERIMENTAL DESIGN ON EXTRACTION PROCESS OF TAMARIND SEED GUM (*Tamarindus indica* L.)

Thainara M. Silverio[1]; Jordanna G. A. Matos[1]; João V. W. Silveira[1*].

[1] *Institute of Science and Technology, Federal University of the Jequitinhonha and Mucuri Valleys (UFVJM), Diamantina, MG, Brazil.*
joao.silveira@ufvjm.edu.br

Abstract - The processing of tamarind pulp *(Tamarindus indica L.)* produces residues such as seeds, bark and fibers, which remain underused. Therefore, taking advantage of fruit residues in the development of new products is a technological alternative that can bring economic benefits to producers and positively impact the environment, leading to more diversified products. A byproduct that is less known and explored is the tamarind gum, a neutral polysaccharide biopolymer derived from the endosperm of tamarind seeds, in which it has functions of stabilization, emulsification, thickening, coagulation, water retention and film formation. For gum extraction, different temperatures (50, 60 and 70 ºC), pH (4, 7 and 10) and mass ratio (0.015; 0.020 and 0.025) were used for a 2^3 full factorial design. The resulting gum was dried in a circulation at 50 °C for 24 h, obtaining an average yield of 0.019 g gum/g seed. The processing is strongly dependent on the pH extraction media.

References

1. E. R. I. K. Alpizar Reyes et al., Ph.D. Thesis, Autonomous Mexico State University, 2018.
2. K. C. Ferreira, M.Sc. Thesis, Goiás Federal University, 2018.
3. C.M. Martins, Ph.D. Thesis, Federal University of Santa Catarina, 2022.

Fundings: ICT-UFVJM, CNPq and FAPEMIG (APQ-03106-21).

Keywords: *Sustainability; Polysaccharides; By-products.*

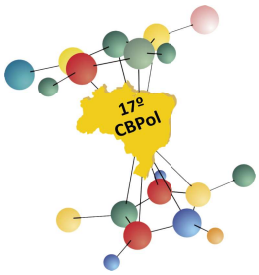

INFLUENCE OF DYES AND ADDITIVES USED IN POLYETHYLENE TEREPHTHALATE (PET) BOTTLE CAPS ON CHEMICAL RECYCLING VIA PYROLYSIS.

Natasha K. Sitton[1,2], Larissa L. A. Carvalho[1,2], Yasmin F. Siqueira[1], Mateus M. Barbio[2], Débora M. V. Miranda[2], Jamilly A. S. Barros[2], Márcio Nele[1,2] and José Carlos C. S. Pinto[1,2].

1 – School of Chemistry (EQ), Chemical and Biochemical Process Engineering Program (EPQB), Federal University of Rio de Janeiro (UFRJ), Rio de Janeiro, RJ, Brazil.
kelber@eq.ufrj.br
2 – Chemical Engineering Program (PEQ), Alberto Luiz Coimbra Institute for Graduate Studies and Engineering Research (COPPE), Federal University of Rio de Janeiro (UFRJ), Rio de Janeiro, RJ, Brazil.

Abstract - Many plastics have a short, one-time use, quickly becoming waste and accumulating in unwanted places[1]. For these materials to continue being used, it is necessary to develop chemical recycling techniques, such as pyrolysis, transforming plastic waste into raw material[2]. Thus, the objective of this work is to characterize PET bottle caps, analyze the products generated in the pyrolysis of the caps and verify whether the addition of dyes and other additives influence the generated product. Therefor, the caps were separated and ground and characterized by Fourier transform infrared spectroscopy, where it was verified that the blue bottle caps (BBC) are made of high density polyethylene (HDPE) and the purple bottle caps (PBC) are made of polypropylene (PP). Pyrolysis was carried out in a small reactor (7g), where the mass balance of the BBC was as HDPE (90% condensable, 10% gas and 0.1% solid residue) and the PBC as PP (80% condensable, 20% gas 0.2% solid residue). The analysis of the condensed fraction was performed by gas chromatography coupled to mass spectrometry, showing that most of the formed compounds are paraffins and olefins. Analysis was performed by X-ray fluorescence spectrometry, noting that all analyzed samples contained nickel and other metals used as catalysts to produce polymers. The colored materials had a large amount of titanium, which wasn't observed in the virgin materials. Titanium, among other metals, were not present in the condensed fraction, remaining only in the solid residue. Based on the above, it can be concluded that the generated products are like virgin polymers, and the condensed fraction contains less metallic contaminants than the raw material and can be added to existing chains for chemical recycling in the market.

References:

1. A. Ahamed., *et al*. Journal of Cleaner Production. 2021, *278*, 123956. https://doi.org/10.1016/j.jclepro.2020.123956
2. J. C. Pinto., *et al*. *Impactos Ambientais Causados pelo Plástico*, Ed.; e-papers, Rio de Janeiro, 2012. ISBN 978-85-7650-341-5

Fundings: AmBev and Braskem.

Keywords: *Pyrolysis, bottle caps, contaminant analysis.*

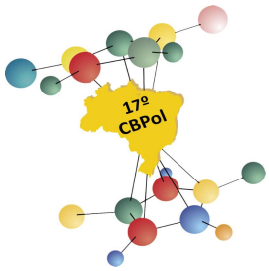

INTEGRATION OF TEXTILE WASTE IN THE PRODUCTION CHAIN STUDY OF EPOXY MATRIX COMPOSITES

Diego F.Guerra[1*], Mara Z. Andrade[1], Ana P. Bilck[1], Edson L.Francisquetti[1]

1 Department of Science and Materials Engineering, Instituto Federal de Educação, Ciência e Tecnologia do Rio Grande do Sul (IFRS), Farroupilha, RS, Brazil

**diegofeguerra@gmail.com*

The textile sector has experienced significant growth, reaching an estimated revenue of R$194 billion in 2021 [1]. However, it is concerning to note that approximately 170,000 tons of textile waste, such as fabric scraps, are improperly discarded in Brazil [2]. The objective of this study is to find a way to integrate textile waste into the production chain by using an epoxy polymer matrix to obtain a composite material. Initially, we evaluated the efficiency of resin catalysis. Four samples were prepared, each containing 10 g of epoxy resin (ER), to which we added 0.07 g (R1), 0.105 g (R2), 0.140 g (R3), and 0.175 g (R4) of catalyst (C). Sample R2 had the amounts of ER and C recommended by the resin manufacturer. We used a DSC 6000 (differential scanning calorimetry) Perkin Elmer instrument to determine the gel time and peak curing of the samples. The heating program consisted of an isothermal hold at 20°C for 30 minutes (to designate the gel time) and a heating ramp of 20°C/min up to 180°C (to determine the total curing time) in an N2 atmosphere at 20 mL/min, with a sample mass of 10 mg. The gel times obtained were 9, 18, 18, and 16 minutes, respectively, for R1, R2, R3, and R4. The gel times of R2, R3, and R4 are similar to those found by Abreu et al. [3]. The gel time was determined by observing a variation in the baseline during the isothermal hold. The total curing time was determined by observing the endothermic event at 179°C. Sample R1 did not exhibit complete curing, even though an endothermic peak at 100°C was observed, which was confirmed by the ΔH value, being 20% lower than the others. The results found are similar to those found by Costa et al. [4]. This indicates that any of the samples could be used for the continuation of the study. However, to confirm this choice, a tensile test was performed according to ASTM 638 standards. The results indicated that samples R3 and R4 showed a rupture stress 28% higher than sample R2. According to studies conducted by Abreu et al. [3], this increased strength can be attributed to the increase in entanglement density due to the availability of the catalyst, resulting in enhanced mechanical strength. It was also observed that R3 and R4 exhibited similar impact resistance. Based on these results, R3 is economically more viable for the continuation of the study, aiming to obtain composites with the addition of textile waste.

References

1.https://www.abit.org.br/noticias/industria-textil-e-de-confeccao-faturou-r-194-bilhoes-em-2021 Acesso em: 01/11/22.
2.https://consultoriamult.com.br/blog/residuos-da-industria-textil/#:~:text=Com%20isso%2C%20h%C3%A1%20uma%20grande,reaproveitamento%20e%20reutiliza%C3%A7%C3%A3o%20dos%20res%C3%ADduos.Acessoem: 01/11/22.
3. DE ABREU, Mariane MSP et al. in Proceedings of 9th Brazilian Congress of Polymers - 9th CBPol.ampina Grande-Br, 2007.
4. COSTA, Michelle L.; REZENDE, Mirabel C.; PARDINI, Luiz C. *Métodos de estudo da cinética de cura de resinas epóxi. Polímeros*, v. 9, p. 37-44, 1999. https://doi.org/10.1590/S0104-14281999000200011

Keywords: epoxy resin, textile waste. gel time, curing time, composites

LOW COST HETEROGENEOUS CATALYST FOR BIODIESEL PRODUCTION

Otávio Mariotto Silva[1], Andréia Fátima Zanette[1]*

1 – Department of Power Engineering, São Paulo State University (UNESP), Rosana, SP, Brazil
*andreia.zanette@unesp.br

Abstract

The world's dependence on fuels to maintain social and economic development motivates a significant increase in demand from the energy sector. As a sustainable alternative to vehicular diesel, we can mention biodiesel. Biodiesel can be obtained through the transesterification reaction where the transformation of fatty acids occurs, which react with alcohols with the aid of a catalyst, resulting in esters. The objective of this work is to evaluate the main parameters that directly influence the production of biodiesel in a process with continuous flow, using macauba oil and methanol as reagents and calcium oxide from the calcination of chicken eggshell as a heterogeneous catalyst. For the production of the catalyst, chicken eggshells were washed, dried, crushed and then placed in a muffle furnace at 1000°C for 5 hours for calcination. The catalyst produced was analyzed by Scanning Electron Microscopy (SEM) to characterize the catalyst surface (Fig 1). The transesterification reactions followed a 2^{4-1} fractional factorial design with four variables: temperature (50 to 60°C), flow rate (0.8 to 1.6 ml/min), catalyst concentration (2 to 10%) and molar ratio (1:6 to 1:12.) with triplicate in the central point. From the effect of each of the variables, it can be concluded that the transesterification yield is maximized in the following condition: temperature of 60°C, oil:methanol molar ratio of 1:12, catalyst concentration of 2% and flow rate of 0.8 ml/min. Under these conditions, the yield obtained was 97.78% in esters.

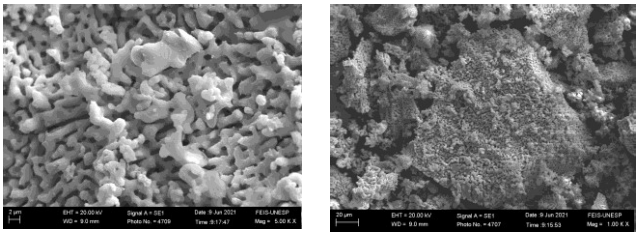

Figure 1 – Scanning Electron Microscopy of calcined eggshell.

References:

1. L. Castro; A. Barañamo; C. Pinheiro; L. Menini; P. Pinheiro. *Green Processing and Synthesis 2019, 8: 235–244.* https://doi.org/10.1515/gps-2018-0076
2. F. Yasar. *Fuel 2019, 255, 115828.* https://doi.org/10.1016/j.fuel.2019.115828.
3. A. Arumugam; V. Ponnusami. *Renewable Energy 2019, 131, 459-471.* https://doi.org/10.1016/j.renene.2018.07.059.

Fundings: The authors thank FAPESP (grant no. 2017/15399-7) for the financial support.

Keywords: *Biodiesel. Low cost heterogeneous catalyst. Macauba oil.*

In silico ANALYSIS POLYURETHANASE FROM *Serratia liquefaciens* WITH DIFFERENT POLYURETHANE MONOMERS AND TETRAMERS

Cleonice A. Salgado[1], Júnio G. Silva[2], Felipe A. de Almeida[3] and Maria C. D. Vanetti[1*]

1 – Department of Microbiology, Universidade Federal de Viçosa (UFV), Viçosa, MG, Brazil;
** Corresponding author: mvanetti@ufv.br;*
2 – Department of Chemistry, Universidade Federal de Minas Gerais (UFMG), Belo Horizonte, MG, Brazil; E-mail
3 – Instituto de Laticínios Cândido Tostes (ILCT), Empresa de Pesquisa Agropecuária de Minas Gerais (EPAMIG), Juiz de Fora, MG, Brazil;

Enzymes contribute to the biodegradation process of plastic polymers, so investigating enzyme-substrate interactions helps understand the molecular mechanisms of the biodegradation process. This work aimed to build nine monomers and nine tetramers of polyurethane (PU) and perform molecular docking with the modeled and validated structure of the polyurethanase from *Serratia liquefaciens* L135. The three-dimensional structures of PU monomers and tetramers were built and optimized by Spartan'14 version 1.1.8. Molecular docking was performed using the Molegro Virtual Docker® software, and the catalytic site was restricted to a sphere with a radius of 30 Å. The *in silico* approach, using molecular docking, allowed selection of the best substrate conformation for the enzyme activity according to the energy values. The more negative the binding energy and hydrogen bond values, the stronger the enzyme-substrate interactions. The *in silico* results showed that the nine monomers showed favorable interactions with the polyurethanase with binding energy values ranging from -84.75 to -121.71 kcal mol^{-1}. Tetramers showed less favorable interactions due to repulsive steric interactions attributed to their long chains, with binding energy values ranging from 24.26 to -45.50 kcal mol^{-1}. The higher binding energies of these PU monomers and tetramers may be due to higher hydrogen bonding interactions with polyurethanase ranging from -9.03 to -3.26 kcal mol^{-1}. Furthermore, the distance amino acid residue S207, part of the polyurethanase catalytic triad, ranged from 2.0 to 16.2 Å from the carbamate and ester groups of all PUs. The proximity is essential, as this amino acid residue is responsible for the hydrolytic action of polyurethanase. Therefore, polyurethanase from *S.liquefaciens* is a good candidate for *in vitro* investigation to mitigate environmental pollution by PUs.

Keywords: *Polyurethane pollution, Bioremediation, Enzyme, Molecular docking.*

Acknowledgment: *CNPq, CAPES, FAPEMIG.*

MECHANICAL PROPERTIES OF LDPE AND LDPE/PP BLENDS AFTER STRUCTURAL CHANGE BY HIGH SHEAR RATE

Emerson F. Silva*, Antonio J. A. Junior, and Clodoaldo Saron

Department of Materials Engineering(DEMAR), Engineering School of Lorena (EEL), University of São Paulo (USP), São Paulo, Lorena, SP, Brazil, emersonsilva1071@usp.br

Abstract – The separation of polymers is a fundament step during mechanical recycling of thermoplastic since the mixture of different polymers lead to the formation of immiscible polymer blends with depreciated mechanical properties. However, the separation of polymers is often unviable due to the combination of different polymers in the same products such as multilayer films. Low-density polyethylene (LDPE) and polypropylene (PP) are the main polymers, considering the global consume of the thermoplastics. Thus, in present study the aim was to evaluate the changes in mechanical properties of LDPE and LDPE/PP blends due to the probable structural change and molecular combination caused by mechanical processing under high shear rate, which can be a way to the compatibilization of complex mixtures of polymer waste during mechanical recycling. Virgin LDPE and LDPE/PP blend containing PP at 30 wt% (LDPE/PP30) were thermomechanically processed in an internal mixer MH-600 under atmosphere of nitrogen, maintaining a rotation at 4500 rpm by 30, 60 and 90s after polymer melting. Afterward, the materials were processed by injection molding for preparation of tensile specimens and analyzed in equipment EMIC DL2000, according to the standard practice ASTM D638[1]. It was verified significant changes in Young modulus, tensile strength and elongation at break of LDPE and PEBD/PP30 blend as a function of the processing time, which there is an increase in values of these properties in PEBD/PP30 blend when compared to the LDPE. Thus, the mechanical processing under high shear rate can be used to compatibilization of complex polymer mixture in mechanical recycling[2].

References

1. ASTM D638, Standard test method for tensile properties of plastics, Barr Haror Drive, West Cosnhohocken, USA, 2013
1. S. S. Saikrishnan; D. Jubinville; C. Tzoganakis; T. H. Mekonnen *Polym. Degrad. Stabil.*, v. 182, p. 109390, 2020. https://doi.org/10.1016/j.polymdegradstab.2020.109390

Fundings: National Council for Scientific and Technological Development - CNPq (Proc. 309583/2020-9) and FAPESP (Proc. 2020/14318-6).

Keywords: Recycling, LDPE, Shear Rate, Blends, Compatibilization.

MICROSPHERES OF NATURAL POLYMER PROMOTE LESS IMPACT ON THE ENVIRONMENT

Márcio F. J. Junior[2], Rafaela P. Cunha[1], Suzanna R. C. A. Sousa[1], Rita K. Silva[1], Christiane S. A. Sá[3], Késia K. O. S. Silva[1]

1 – Postgraduate Program in Textile Engineering, Federal University of Rio Grande do Norte (UFRN), Natal, Brazil
kesia.souto@ufrn.br
2 – Department of Textile Engineering (DET), Federal University of Rio Grande do Norte (UFRN), Natal, Brazil
3 – Postgraduate Program in Mechanical Engineering, Federal University of Rio Grande do Norte (UFRN), Natal, Brazil

Abstract - Among the different environmental decontamination processes under development, the use of natural polymers for the production of new materials has proven to be efficient for effluent treatment proposals. In this study, the natural polymer chitosan (QTS) was obtained from shrimp residues from fishing industries in the State of Rio Grande do Norte, aiming at a better use of this raw material that is discarded in nature, as well as the minimization of solid waste. Microspheres were produced from chitosan, with adsorptive properties for use in the treatment of effluents from textile industries, with minimization of environmental contaminants, through monitoring of environmental parameters of UV-Vis color, turbidity, pH, temperature and conductivity electrical, also having potential use in the removal of metallic cations from these effluents. All samples showed removal efficiency greater than 82%, regardless of the concentrations of the reagents used in the formation of the microspheres. High efficiency, above 91%, in removing color using 0.40% (w/v) of microspheres was observed in one of the samples after 48 hours of treatment. At times greater than 48 hours of treatment, a decrease in efficiency values was observed, due to the desorption of the dye with the microspheres. The use of natural polymers in the formulations studied brings an important advantage: they can be degraded by microorganisms present in the aquatic environment, resulting in environmentally less toxic products compared to those of synthetic origin. Therefore, polymeric microspheres act to reduce the toxic effects caused by heavy metals and dyes, promoting the renewal and preservation of the ecosystem.

References

1. E. Colombo; W. Li; S. Bhangu; M. Ashokkumar. *RSC Advances*, 2017, *31*, 19373. https://doi.org/10.1039/C7RA01227F.
2. J. Quinones; O. Brüggemann; C. Covas. *International Journal of Nanoparticle Research*, 2018; 2:3. https://doi.org/10.28933/ijnr-2017-12-1201.
3. C. Sá; R. Ladchumananandasivam; C. Rossi; R. Silva; W. Camboim; A. Zille; J. Padrão; K. Silva. 1. *Textile Research Journal*, 2022, *92*, 2643. https://doi.org/10.1177/00405175211007518.
4. R. Yang; H. Li; M. Huang; H. Yang; A. Li. *Water Research*, 2016, *95*, 59. https://doi.org/10.1016/j.watres.2016.02.068.
5. E. Brillas; C. Martínez-Huitle. *Applied Catalysis B: Environmental*, 2015, *166–167*, 603. https://doi.org/10.1016/j.apcatb.2014.11.016.

Fundings: This work has been supported by the following Brazilian research agencies: CAPES, CNPq, and FAPERN.

Keywords: *natural polymer, textile effluent; microspheres; chitosan; adsorption.*

MODIFICATION OF WHEY PROTEIN ISOLATE WITH SURFACTANT AND PLASTICIZER

Jhenifer S. Lopes[1], Marina F. Cosate de Andrade[1], Ana R. Morales[1]*

1 – School of Chemical Engineering, University of Campinas (UNICAMP), Campinas, SP, Brazil
morales@unicamp.br

Abstract - This work describes the modification process of whey protein isolate (WPI) with the surfactant cetylpyridinium chloride (CPC) as well as its combination with the plasticizer polyethylene glycol (PEG). The samples were named considering the composition (parts of PEG and/or CPC per 100 parts of WPI (phr)) and were prepared by dilution in deionized water and then subjected to thermal treatment, drying, lyophilization and milling. The rheological properties of the samples were studied by rheometry of parallel plates (deformation amplitude of 1.0%., distance between the plates of 1 mm, and angular frequency range of linear viscoelasticity from 0.01 to 500 rad/s at 160 ºC). As example of the results, the behavior for the sample 100PEG/75CPC and the complex viscosity for some samples are presented in Fig 1. The rheological behavior showed the predominance of the elastic component (G') in relation to the viscous one (G") for all samples. The formulations 0PEG/100CPC and 100PEG/75CPC presented lower values of complex viscosity at low shear rate. This behavior indicates that the original intramolecular interactions of the protein remained present or even that new interactions between the components were formed in such a way that the elastic behavior was predominant in the material.

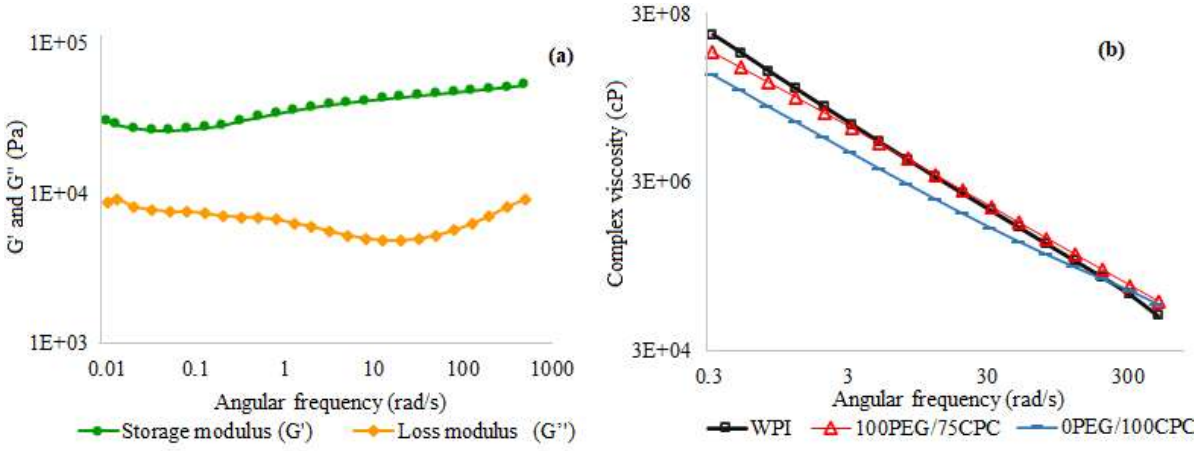

Figure 1- (a) Rheological behavior for 100PEG/75CPC sample; (b) Complex viscosity for some samples.

References

1. J.L.Lopes, MsC Dissertation, University of Campinas, 2023.

Fundings: Coordination for the Improvement of Higher Education Personnel – Brazil (CAPES) – Financing code 001.

Keywords: *proteins; whey protein isolate; cetylpyridinium chloride; polyethylene glycol.*

PLASTICIZATION OF CITRUS PULP: INFLUENCE OF WASHING METHODOLOGY AND GLYCEROL CONCENTRATION

Marina S. Paula[1], George F. Nunes[1], Caio G. Ottoni[1] and Silvia H. P. Bettini[1]

1 – Department of Materials Engineering (DEMa), Federal University of São Carlos (UFSCar), São Carlos, SP, Brazil
marinasp@estudante.ufscar.br

Abstract - The problem of inadequate disposal of post-consumer materials has been a topic of discussion for some time. In this regard, this study proposes alternatives to minimize environmental impacts from two different ways. The first one relates to conventional plastics, which have a lifespan incompatible with their degradation time. The second one concerns agro-industrial residues, also known as Food-Loss Waste, which has energy potential in its biomass. Through a biorefinery process, these residues are reintroduced into the circular economy and transformed into materials, thereby increasing their lifespan [1]. This work produces plasticized citrus pulp from orange residues obtained from juice-producing companies [2]. Additionally, two different washing methods are tested to extract sugar and other components of these residues. Washing method A involves using 99% ethyl alcohol in two long immersion cycles, while method B employs a freeze-dryer to remove water from the frozen waste. Furthermore, glycerol is incorporated as a plasticizing agent to improve the processability of the residue in tree different concentrations [3]. Next, each of these waste materials is fed into a co-rotating twin-screw extruder, maintaining the parameters for both washings and three different concentrations of glycerol, resulting in six different filaments of renewable origin. Finally, to evaluate the properties obtained in each of the biodegradable filaments, mechanical tensile strength tests and chromatographic chemical tests are conducted to analyze the components extracted from the residue and present in the washing alcohol. Through these tests, better mechanical properties were observed for the materials subjected to washing method A, and the presence of some components such as sugars and oils in the washing water justified this behavior.

References

1. C. Gomide, H. M. C. Azeredo, B. D. Mattos, M. Beaumont, D. S. Correa, O. J. Rojas. The Food–Materials Nexus: Next Generation Bioplastics and Advanced Materials from Agri-Food Residues. *Advanced Materials*, 2021, *33*, 2102520. https://doi.org/10.1002/adma.202102520.
2. J. E. Motezuki; S. H. P. Bettini; V. H Carvalho; L. C. Costa, B.R. Patent 10 2018 076487-0. 2018; *INPI*. 2018.
3. J. E. Motezuki. Ph.D. Thesis, Federal University of São Carlos, 2018.

Fundings: FAPESP – 2022/12341-6

Keywords: A*gro-industrial residues, Circular economy, Thermoplastic fibers, Filaments of renewable origin.*

PLASTIC PYROLYSIS VAPORIZATION

Laura P. da M. Costa[1*], Julián García Cárdenas[1], Amanda L. T. Brandão[2] and José Carlos Pinto[1]

1 – Programa de Engenharia Química, COPPE, Universidade Federal do Rio de Janeiro, Cidade Universitária, 68502 Rio de Janeiro, Brazil
laura@peq.coppe.ufrj.br
2 – Departamento de Engenharia Química e de Materiais, Pontifícia Universidade Católica do Rio de Janeiro (PUC-Rio), Gávea, 38097 Rio de Janeiro, Brazil

Abstract - Chemical recycling of plastics is currently being pursued as one of the most promising technologies to reduce post-consumer plastic's ecological and social impact. The technology can simultaneously process different post-consumer plastic types in an inert atmosphere, resulting in a liquid stream rich in hydrocarbons, low molecular weight gases, and a smaller char fraction. This is frequently simulated using lump approaches. However, even the works using more complex reaction networks do not consider a thermodynamic equilibrium between the liquid phase, containing lower molecular weight products, and the gas phase. In this work, we simulate the vapor-liquid equilibria (VLE) based on the ideal gases, the Peng-Robinson (PR) equation of state (EOS), and the Perturbed Chain Statistical Associating Fluid Theory (PC-SAFT) EOS. The kinetic reactions are simulated using a kinetic Monte Carlo (kMC) method similar to a previous methodology employed by our group. We show that, for polyolefins, the VLE is essential to obtain the diesel-, naphtha-, and wax-fractions obtained in the literature; and that different methodologies do not only lead to different simulation times but also the advantages and disadvantages of each.

References

1. F. Tumakaka; J. Gross; G. Sadowski *Fluid Phase Equilibria 2005, 228*, 89-98. https://doi.org/10.1016/j.fluid.2004.09.037.
2. L. P. da Mata Costa; A. L. Brandão; J. C. Pinto *Journal of Analytical and Applied Pyrolysis 2022, 167,* 105683. https://doi.org/10.1016/j.jaap.2022.105683.
3. R. E. Harmon; G. SriBala; L. J. Broadbelt; A. K. Burnham *Energy & Fuels 2021 35.8,* 6765-6775. https://doi.org/10.1021/acs.energyfuels.1c00342.

Fundings: Laura P. da M. Costa thanks Conselho Nacional de Desenvolvimento Científico e Tecnológico (CNPq) and CAPES for the doctoral scholarship.

Keywords: *kMC, VLE, pyrolysis, recycling, flash*

POLYMERS COMBINED WITH GEOLOGICAL MATERIAL AS A HUMAN LEGACY IN EARTH'S RECORD

Fernanda A. Santos[1]*, Angelo R. S. Oliveira[2], Giovana R. Diório[1], Carlos C. F. Guedes[1], Gerson Fernandino[3], Paulo C. F. Giannini[4], Rodolfo J. Angulo[1] , Maria Cristina de Souza[1] and Maria Aparecida F. César-Oliveira[2]*

1 – Department of Geology, Federal University of Paraná (UFPR), Curitiba, PR, Brazil
2 – Department of Chemistry, Federal University of Paraná (UFPR), Curitiba, PR, Brazil
mafco@ufpr.br; fernanda.avelars@gmail.com
3 – Interdisciplinary Department, Federal University of Rio Grande do Sul (UFRGS), Imbé, RS, Brazil
4 – Institute of Geosciences, University of São Paulo (USP), São Paulo, SP, Brazil

Abstract – There is a possibility that synthetic organic polymers might be preserved in the geological record when plastic is combined with denser material, such as rocks, pebbles, and sand. In this sense, novel plastic debris with a rock-like appearance has been reported worldwide in the marine environment. We reported the first plastic rock occurrences in Brazil in a remote site (Trindade Island, SE Atlantic Ocean). In addition to a geological approach, 16 samples were selected for chemical analyses through Fourier Transform Infrared Spectroscopy (FTIR) and Thermogravimetric Analysis (TGA) to identify the type of insoluble plastic resin present. Considering the visual isotropic resemblance of plastic in the deposits and its physical aspects, the selected samples were separated into two sets according to colors identified in melted occurrences. The profile of the spectra was compatible with that of pure polyethylene (PE) and polypropylene (PP) samples. The FTIR spectra presented some characteristic signals of high-density polyethylene (HDPE), low-density polyethylene (LDPE), and linear low-density polyethylene (LLDPE) spectra, such as the relatively intense bands at 717 and 730 cm^{-1} and in the region of 1464 and 1471 cm^{-1}. However, it is also possible to observe low-intensity signals in the 800 to 1200 cm^{-1} range, which is the fingerprint of the PP spectra, as well as the band at 1377 cm^{-1} which for PP is more intense than that in 1455 cm^{-1}. The most relevant information obtained through the TGA, conducted in an oxidizing atmosphere (synthetic air), referred to the low levels of inorganic substances found in both samples, which showed almost complete thermal degradation at 1000 ºC. The identification and analysis of plastic rocks in marine environments, such as these occurrences, indicate the potential preservation of synthetic organic polymers in sedimentary columns when combined with lithic materials. These findings contribute to our understanding of plastic pollution and its impact on geological systems. Thus, it is crucial to investigate the chemical composition of plastic debris, the main sources and alternatives to mitigate this type of pollution.

References:

1. F. A. Santos *et al. Marine Pollution Bulletin* 2022, 182, 114031. https://doi.org/10.1016/j.marpolbul.2022.114031.
2. M. R. Jung *et al. Marine Pollution Bulletin* 2018, 127, 704-16. https://doi.org/10.1016/j.marpolbul.2017.12.061.

Fundings: To LECOST/UFPR, Marinha do Brasil, CNPq, and CIRM for their financial support (557141/2009-5, 457714/2013-1, and 442865/2015-5. To FINEP, RBTB, MCTI, LEQUIPE/UFPR and DQUI/UFPR for the equipments used for chemical analyses. FAS acknowledges CAPES for providing a scholarship (88882.382069/2019-01). RJA acknowledges Fundação Araucária for providing a senior grant (45725) and CNPq fellowship (302913/2018–1 and 315663/2018-9).
Keywords: *plastic rocks, polyethylene, polypropylene, marine pollution, plastiglomerates.*

POLYURETHANES BIODEGRADATION BY *Staphylococcus warneri* ISOLATED FROM THE GUT OF LARVAE OF *Galleria mellonella*

Cleonice A. Salgado[1], Pedro M. P. Vidigal[2], and Maria C. D. Vanetti[1*]

1 – Department of Microbiology, Universidade Federal de Viçosa (UFV), Viçosa, MG, Brazil;
** Corresponding author: mvanetti@ufv.br;*
2 – Núcleo de Análise de Biomoléculas, Universidade Federal de Viçosa (UFV), MG, Brazil.

Polyurethanes (PUs) are plastic polymers found in many everyday products, occupying a sixth place among the most used plastics in the world. With high production and use, much PU waste accumulates as a pollutant in all ecosystems. Microorganisms have become a promising alternative to mitigate this environmental challenge. The searching for microorganisms of the gut microbiota of larvae for plastic degradation seems to be an attractive strategy. Therefore, this work aimed to isolate bacteria from the gut of the *Galleria mellonella* larvae with the potential to biodegrade PUs. A Gram-positive bacterium with the biodegradation potential of Impranil® PU was isolated. The DNA of this bacterium was extracted, sequenced, assembled, and annotated. The bacterium was identified as *Staphylococcus warneri* and was named strain UFV_01.21. *S. warneri* could use Impranil® as the only carbon source, in addition to biodegrading 58% and 96% of Impranil® in minimal medium and Luria Bertani broth, respectively, after six days of incubation, at 30 ºC. Impranil® and poly[4,4'-methylenebis(phenyl isocyanate)-alt-1,4-butanediol/di(propylene glycol)/polycaprolactone] (PCLMDI) films were used for biodegradation tests by *S. warneri*. It was verified that this isolate could form biofilms on the surface of these PUs, reaching 10^8 CFU/Impranil disk and 10^6 CFU/cm^2 of PCLMDI. In addition, by scanning electron microscopy, it was possible to observe cracks, pores, and roughness on the surface of these polymers, characterizing the biodegradation process. This is the first work that reports the potential of *S. warneri* to biodegrade PUs and confirms that the gut of larvae is a promising source of isolation of microorganisms capable of biodegrading plastic polymers.

Keywords: *Polymer, Bioremediation, Gut microbiota, Larvae.*

Acknowledgment: *NuBioMol-UFV, NMM-UFV, CNPq, CAPES, FAPEMIG.*

PREPARATION OF NEW SUSTAINABLE HYDROGELS FROM CHEMICAL RECYCLED POLY(ETHYLENE TEREPHTHALATE) AND APPLICATION ON THE REMOVAL OF CRYSTAL VIOLET DYE

Tomás M. Simioni[1*], Daniela E. Schneider[1], Cesar L. Petzhold[1] and Tales S. Daitx[1*]

Institute of Chemistry, Federal University of Rio Grande do Sul (UFRGS), Porto Alegre, RS, Brazil
tomassimioni6@gmail.com, tales.daitx@ufrgs.br

Abstract - Nowadays single use plastics have become a problem to society and alternatives for the use of these materials are emerging [1]. This work aims to recycle post-consume poly(ethylene terephthalate) (wPET) through glycerolysis reaction with 1:6.25 (wPET:glycerol) molar ratio under zinc acetate catalysis in microwave at 250 °C and different reaction times (5, 15 and 30 min). Afterwards, the recycled products (dPET) were transformed into hydrogels through reaction with citric acid and the materials were evaluated in relation to retain the crystal violet (VC) dye, aiming an application on wastewater treatment. The synthesis of hydrogels was performed using 10 and 20 mmol of citric acid/g of dPET under tin (II) chloride catalysis in an oil bath at 150 °C for 3 h followed by a step of vacuum until the hydrogel became rigid. The hydrogels were characterized by Fourier-transform infrared (FTIR) and hydrogen nuclear magnetic resonance (^{1}H NMR) spectroscopies and in relation to its capacity to absorb water and adsorb VC [2]. The results indicated that the dPET was successful obtained and the hydrogels were efficiently formed. For ^{1}H NMR, signs related to both aromatic portion derived from PET and alkyl portion derived from glycerol are observed, and in the FTIR, a large band at 3300 cm^{-1} related to O-H bond was observed [3]. When hydrogels were formed, the intensity of this band was decreased, indicating the cross-linking between the acidic portion of citric acid and the hydroxyls of dPET. In relation to the water absorption capacity, a range of 310-1442% was observed, where the highest values were obtained from samples with more content of citric acid. Regarding the VC adsorption, removals between 57-90% were obtained, where the best performances being observed for samples with longer reaction time in the depolymerization, indicating the hydrogels utility on wastewater treatment [3].

References

1. B. Shojaei; M, Abtahi; M. Najafi *Polymers for Advanced Technologies* 2020, *31*, 2912-2938. https://doi.org/10.1002/pat.5023

2. F. G. Mendonça; I. R. S. Menezes; I. F. Silva; R. M. Lago *New Journal of Chemistry* 2021, *45*, 2410. https://doi.org/10.1039/d0nj06138g

3. M. Garg; N. Bhullar; B. Bajaj; D. Sud *New Journal of Chemistry* 2021, *45*, 4938. https://doi.org/10.1039/d0nj05758d.

Fundings: The authors are grateful to Conselho Nacional de Desenvolvimento Científico e Tecnológico (CNPq) and Fundação de Amparo à Pesquisa do estado do Rio Grande do Sul (PRONEX/FAPERGS - Finance Code 16/2551-0000470-6) for financial support.

Keywords: *Chemical recycling, Crystal violet, Dyes adsorption, PET recycling, Wastewater treatment.*

PREPARATION OF SODIUM ALGINATE HYDROGELS FOR ADSORPTION OF COPPER IONS FROM INDUSTRIAL WASTEWATER

Lucas B. Moço[1], Camila M. Dias[1], Julia A. G. de Oliveira[1] and Djalma Souza[1]*

1 – Advanced Materials Laboratory, State University of Northern Fluminense Darcy Ribeiro, Campos dos Goytacazes, RJ, Brazil
djsouza@uenf.br

Abstract - Removal of heavy metals such as copper from industrial wastewater is a very important task due to the negative effects on human health and living organisms in the environment. For that purpose, hydrogels were prepared from sodium alginate reticulated with Ca^{+2} and Mg^{+2} ions and carbon nanotubes were added to act as adsorbent agent. Sodium alginate was dissolved (5% w/v) in water (pH 7) for 6 hours on magnetic stirring and samples contend 0, 0,01, 0,02 and 0,03 % wt. of carbon nanotubes was prepared. Sodium alginate spheres with carbon nanotubes were obtained by dripping the dissolved solution using a peristaltic pump. Reticulation was performed in solution containing $CaCl_2$ (5% w/v) and $MgCl_2$ (5% w/v), this reaction took the period of 1 hour under magnetic stirring to be completed. Hydrogels obtained were lyophilized for 24 hours. Scanning electron microscopy analysis showed that there is adhesion between the carbon nanotubes and the sodium alginate matrix and the existence of a rough surface with cavities, which contributed to the adsorption process. In terms of swelling degree, it was observed that the addition of nanotubes contributed to an increase in the adsorption capacity of the hydrogel, resulting in a swelling of around 600% within 40 minutes for the sample containing 0.03% carbon nanotubes. It was observed that the addition of carbon nanotubes contributed to improvement of the adsorption of copper ions. The hydrogel containing 0.03% wt. carbon nanotubes achieved a maximum adsorption capacity of 3.25 mg of copper ions per gram of adsorbent. The results showed that sodium alginate hydrogel containing carbon nanotubes can be applied efficiently in the removal of copper ions from contaminated industrial wastewater.

References

1. S. A. Al-Saydeh, M. H. El-Naas, S. J. *Zaidi. Journal of Industrial and Engineering Chemistry,* 2017, vol. 56, 35-44. https://doi.org/10.1016/j.jiec.2017.07.026
2. E. M. Ahmed. *Journal of Advanced Research*, 2015, vol. 6(2), 105-121. https://doi.org/10.1016/j.jare.2013.07.006
3. G. Jing, L. Wang, H. Yu, W. A. Amer, L. Zhang. *Colloids and Surfaces A: Physicochemical and engineering Aspects.* 2013, vol. 416, 86-94. https://doi.org/10.1016/j.colsurfa.2012.09.043
4. Y.-H. Li, Y. Zhu, Y. Zhao, D. Wu, Z. Luan. *Diamond and Related Materials*, 2006, vol. 15, 90-94. https://doi.org/10.1016/j.diamond.2005.07.004

Fundings: The authors would like to thank CAPES and FAPERJ for the financial support.

Keywords: *Sodium alginate, carbon nanotubes, hydrogels, cooper ions adsorption, heavy metals*.

PRODUCTION AND CHARACTERIZATION OF BIODEGRADABLE ACTIVE FILMS FOR COSMETIC APPLICATIONS

Flávia R. Ludka[1], Ana B. Klosowski[1], Francisca J. A. Vieira[2], Giovani A. Camargo[2], Juliana B. Olivato[1, 2, 3]*

1 – Post-graduation Program of Pharmaceutical Sciences, State University of Ponta Grossa (UEPG), Ponta Grossa, PR, Brazil
2 – Post-graduation Program of Food Science and Technology, State University of Ponta Grossa (UEPG), Ponta Grossa, PR, Brazil
3 – Department of Pharmaceutical Sciences, State University of Ponta Grossa (UEPG), Ponta Grossa, PR, Brazil.
**jbolivato@uepg.br*

Abstract – The reuse of industrial wastes is an alternative for sustainability. Brewers' spent grain (BSG) is a by-product rich in phenolic compounds with antioxidant action, and its use in cosmetic products to maintain skin health is interesting [1–3]. This work aimed to develop biodegradable films based on cassava starch and poly (vinyl alcohol), added of BSG extract. The total content of phenolic compounds and antioxidant activity ($ABTS^{\bullet+}$ and $DPPH^{\bullet}$) were performed in the BSG extract, and the mechanical, structural and barrier properties, as well as the release kinetics of total phenolic compounds from the biodegradable films was evaluated. The antioxidant activity of BSG extract evaluated by the ABTS•+ method showed IC50 of 2.0 ± 0.6, meanwhile the antioxidant activity by the DPPH• method showed the result of 196.0 ± 18.6. The total phenolic content for the extract was 310.1 ± 62.6 mg GAE/g. Higher proportions of BSG extracts resulted in denser films, with more heterogeneous and rougher surface, suggesting that higher concentrations of extract interfered in the regularity and homogeneity of the polymeric matrix. The mechanical performance and water vapor permeability of the biodegradable films was not significantly influenced by the inclusion of the BSG extract. An increase in the content of phenolic compounds released by the films was observed over time, reaching values of 163.3 ± 20.9 mg GAE/mL for films with 3 % (w/w) of BSG extract and 165.7 ± 23.6 GAE/mL for the films with 5% (w/w) of BSG extract, at the end of 4 hours, in aqueous media. BSG extract resulted in biodegradable films with promising physicochemical properties and antioxidant potential, which can represent an alternative to be applied as antiaging skin masks.

References

1. Bravi E, De Francesco G, Sileoni V, Perretti G, Galgano F, Marconi O. Brewing by-product upcycling potential: Nutritionally valuable compounds and antioxidant activity evaluation. Antioxidants. 2021 Feb 1;10(2):1–19.
2. Macias-Garbett R, Serna-Hernández SO, Sosa-Hernández JE, Parra-Saldívar R. Phenolic Compounds From Brewer's Spent Grains: Toward Green Recovery Methods and Applications in the Cosmetic Industry. Vol. 5, Frontiers in Sustainable Food Systems. Frontiers Media S.A.; 2021.
3. Almeida LCM, Carvalho FK, Olivato JB. Production and Characterization of Starch/PVA Blends with Bioactive Compounds from Malt Bagasse. Macromol Symp. 2022 Dec 1;406(1).

Keywords: *Brewers' spent grain; biodegradable materials; antioxidants; starch; phenolic compounds.*

PRODUCTION AND PHYSICAL-CHEMICAL ANALYSIS OF WOOD, PET, AND HDPE ECO-COMPOSITES FOR COATINGS

Syme R. S. Queiroz[1], Vera L. D. da Silva[1], Wander A. P. Costa[1], Patrick Moreira Lima[1], Liz S. Queiroz[2], Nilton C. A. Queiroz[1] and Rosemary M. P. Coutinho[1]

1 – Department of Education, Natural Resources, Infrastructure and Design (DERIN), Federal Institute of Pará (IFPA), Belém, Pa, Brazil

syme.souza@ifpa.edu.br

2 – Santa Catarina de Sena School, Belém, Pa, Brazil

Abstract - Wood is a product present in almost all stages of civil construction buildings such as coating. The major preoccupation occurs when we must reconcile the use of wood with its sustainability. Residue from domestic packaging of Polyethylene Terephthalate - PET and High-Density Polyethylene - HDPE have become a worldwide concern and any alternative to minimize this impact contributes to the improvement of the environment. Thus, composites were produced with powder of the sawing from five wood species used in the metropolitan region of Belém city, PET powder, and HDPE powder (wood/PET and wood/HDPE) in polyester resin matrix in the proportions of 10% and 15% of each filler in relation to the volume of resin for analysis of physical-chemical properties, Fig 1. The composites were obtained through a handmade process, with lamination hand layup at room temperature, 25°C. The results showed better mechanical performance in the flexural of both composites in relation to the polyester resin matrix, however, there was a reduction in density and hardness values that may be related to poor interaction between matrix and reinforcement.

Figure 1 – Composites: a) Resin/*Piptadenia Moniliformes* (timborana)/PET and b) Resin/*Piptadenia Moniliformes* (timborana)/ HDPE.

1. A. S. Gonçalves; C. F. Gererdo; S. C. A. França; D. C. Bastos; S. F. Santos. *Revista Univap - revista.univap.br São José dos Campos-SP-Brasil, v. 26, n. 51, 2020.* https://revista.univap.br/index.php/revistaunivap/article/view/2430
2. J. F. Pereira; M. C. C. Mattos; F. G. R Filho; S. F. Santos. *Revista Univap - revista.univap.br São José dos Campos-SP-Brasil, v. 26, n. 51, 2020.* https://revista.univap.br/index.php/revistaunivap/article/view/2423
3. A. Porras, A. Maranon, i. A. Ashcroft. pgs 66-73. 2015. www.elsevier.com/locate/compositesb.
4. M. F. G. H. Goll; J. S. Venzon; A. A. Vegini; J. R. Eleotério; L. B. B. Tavares. revista Matéria, v.23, n.4, 2018. https://www.scielo.br/j/rmat/a/jKHgMVBn7tdFYbJj4fFFwyH/?format=pdf&lang=en

Keywords: *Composite, Wood, PET, HDPE.*

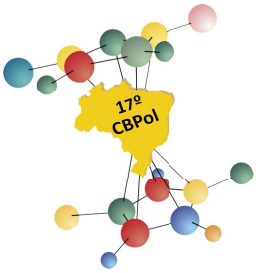

PRODUCTION AND REUSE OF KOMBUCHA WASTE FOR CELLULOSE PRODUCTION FROM DIFFERENT PLANTS EXTRACT

Pâmela B. F. G. S. Luna[1], Karina C. Souza[1], Rhodivam L. M. Feitosa[1*], Daniella S. C. Andrade[1], Dayanna K. M. Oliveira[1], Fernanda S. Silva[2], Alexciana P. Melo[2] and Glória M. Vinhas[2]

1 – Materials Science Program, Federal University of Pernambuco (UFPE), Recife, PE, Brazil
rhodivam.lucas@ufpe.br
2 – Department of Chemical Engineering, Federal University of Pernambuco(UFPE), Recife, PE, Brazil

Abstract - Kombucha tea is beverage consumed worldwide, and it was used for the first time in Asia due to its therapeutic properties. Traditionally, it is made using the infusion of black tea (*Camellia sinensis*), but other teas can be used to prepare it. Fermentation is performed in a static system and has two phases: a liquid called nutrient broth and a solid floating cellulosic phase called SCOBY. These two phases have microorganisms (a symbiotic association of bacteria and yeasts) and cellulose producing acetic bacterium. Bacterial cellulose (BC) in this process is considered a residue. Several studies have shown alternative materials to produce kombucha, and Brazil has a large amount of plant species, with pharmacological properties. So, the main purpose of this study is to produce kombucha using different plant extracts from different environments, mainly the northeast biome of Brazil and evaluate the effect of tea composition on cellulose production. Antimicrobial properties were evaluated through the halo inhibition test; thermal properties through thermogravimetric analysis (TGA); microstructure through scanning electron microscopy (SEM) and optical microscopy; crystallinity through X-ray diffraction (DRX) and cellulose functional groups through FTIR. The main results show that the structural, morphological and thermal characteristics of BC produced in different teas infusions have nanofibrillar properties and structure similar to BC produced in high cost biotechnological process in Hestrin and Schramm (HS) and bacteria of the gender *Gluconacetobacter*. Besides antioxidant compounds present in tea maximize the application of cellulose residue due to its excellent antibacterial properties.

Keywords: *residue, kombucha, bacterial cellulose, SCOBY, plants extracts.*

References

1. R.M.D. Coelho ; A.L. Almeida; R.Q.G. Amaral; R.N. Mota; P.H.M. Sousa. *International Journal of Gastronomy and Food Science* 2020, *22*, 100272. https://doi.org/10.1016/j.ijgfs.2020.100272.

2. E. Leonarski; K. Cesca; E. Zanella; B.U. Stambuk; D. Oliveira; P. Poletto. *LWT* 2021, *135*, 110075. https://doi.org/10.1016/j.lwt.2020.110075.

3. V.P. Ribeiro; A.C. Arruda; M.A. El-salam; J.K. Bastos. *Pharmaceutical Biology* 2018, *56*, 253. https://doi.org/10.1080/13880209.2018.1454480.

4. R. Jayabalan; R.V. Malbasa, E.S. Loncar; J.S. Vitas; M. Sathishkumar. *Comprehensive Reviews in Food Science and Food Safety* 2014, *13, 538.* https://doi.org/10.1111/1541-4337.12073

5. K.E. Emiljanowicz; E.M. Pańczyk. *Critical Reviews in Food Science and Nutrition* 2019, 1 https://doi.org/10.1080/10408398.2019.1679714.

RECYCLING MDF WASTE AS A NEW COMPOSITE MATERIAL AS AN ALTERNATIVE FOR INDUSTRY

Ruan D. B. Liberato[1,2*], Marcos R. Guilherme[2], Andrelson W. Rinaldi[2]

1 – Post-Graduation Mechanic Engeneering (PEM), Rinaldi Research Group (RRG), State University of Maringá (UEM), Maringá, PR, Brazil pg403728@uem.br
2 – Rinaldi Research Group, State University of Maringá (UEM), Maringá, PR, Brazil

Abstract - MDF, a raw material widely used in industries and construction, is a material internationally known as ecologically correct, since for its manufacture it is not used native trees, but reforested woods, such as pine and eucalyptus. However, even with this approach, its incorrect disposal becomes harmful to the environment, due to the resins used in the manufacturing process of the material. A material seen as class I by NBR 10.004/2004, this is a product with several problems when recycling is taken into account; it cannot be used as fuel under burning conditions, and the correct disposal of the residues of this material becomes a problem for companies. Taking into account this difficulty of disposal, a study of recycling of the material was necessary, with the focus to return this waste back to the industry as a new material, which could become a product with higher added value, with different characteristics of the original material, but with a recycling cycle in which the waste itself can return to the same line of recycling. Furthermore, this study presents promising results when empirically compared to the original material. In the initial tests, for proof of concept, the material showed higher resistance to damping when compared to traditional MDF, besides allowing the use of finishing techniques such as sanding. These characteristics were achieved from the insertion of certain proportions of polymers in the material, which were previously studied and evaluated. And the results led to the formation of a composite material with great potential to be explored.

References

1. **A. C. Cassilha; C. L. Podlasek; E. F. Casagrande Junior; M. C. Silva; S. N. F. Mengatto in Revista Educação & Tecnologia, 2003.**
2. **A O. Policarpo, G. R. Corrêa: *Ligno: a composite material with wood residue. 2019*, INSS 2318-6968. https://doi.org/10.5151/ped2018-8.2_ACO_14.**
3. **C. A. Correa, C. N. P. Fonseca, S. Neves, C. A. Razzino, E. Hage: *Termoplastics Wooden Composites in Forest* Products Journal, Vol. 52, n.06.**
4. **G. R. Corrêa, Post-Graduation. Dissertation, State University of Minas Gerais, 2004.**
5. **Hexion Inc. U.S. Patent 7803855B2, 2007.**

Fundings: CNPQ, CAPES and UEM.

Keywords: *Recycling. MDF. Industry. Resins. Sustainability.*

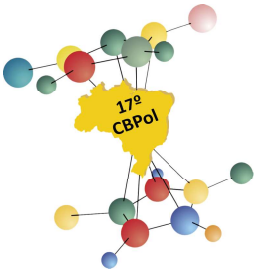

RECYCLING OF AEROSPACE COMPOSITES: NEW COMPOSITES OF PROTECTIVE POLYETHYLENE FILM REINFORCED WITH CF/PAEK WASTE

Ingrid C. L. Oliveira[1], Larissa S. Montagna[1], Fabio R. Passador[1].

1 – Polymer and Biopolymer Technology Laboratory (TecPBio), Department of Science and Technology, Federal University of São Paulo (UNIFESP), São José dos Campos, SP, Brazil
ingrid.christiny@unifesp.br

The aerospace sector stands out for the use of high-performance materials. However, some of these materials are polymer matrix composites with carbon fiber, which are usually discarded after use[1]. In the aerospace sector, poly(aryl-ether-ketone)(PAEK) reinforced with carbon fiber (CF) composites are being used as substitutes for thermoset matrix composites. In addition, PAEK/CF prepregs are transported and stored wrapped in a protective film composed of polyethylene (PE), which are discarded and incinerated during the preparation of the laminates. Resulting in the loss of technology, resources, and all the energy incorporated into the product[2]. Thus, this study aimed to investigate the feasibility of mechanical recycling of protective film waste and CF/PAEK composite waste. The methodology involved the grinding of protective film waste and CF/PAEK waste. The CF/PAEK particles were characterized using optical microscopy and scanning electron microscopy (SEM), and particle size was determined. After then, a blend of neat low-density polyethylene (LDPE), maleic anhydride-grafted linear low-density polyethylene (LLDPE-*g*-MA), and a protective film (50/3/47) was prepared using twin-screw extrusion. Composites were prepared using the same equipment and parameters, with the compatibilized blend g as the polymer matrix and adding 5, 10, and 15 wt% of CF/PAEK particles. Standardized test specimens were prepared by injection molding. The compositions were characterized by their mechanical properties, including tensile test, Izod impact resistance, and Shore D hardness. It was possible to observe an increase in the elastic modulus proportional to the content of CF/PAEK particles added. As well as an increase in Shore D hardness and Izod impact resistance.

References

1. Ibarra, R.M. Chapter 20: Recycling of thermosets and their composites. Thermosets (Second Edition) Structure, Properties, and Applications. 639-666, 2018. https://doi.org/10.1016/B978-0-08-101021-1.00020-4
2. Ashby MF. Chapter 4-End of first life: a Problem or a Resource? Materials and the environment (Third Edition) eco-informed material choice. Elsevier, 2021, pp. 65–85. DOI: 10.1016/B978- 0-12-821521-0.00004-9

Fundings: The authors thank FAPESP (Process 2020/12530-3) for financial support.

Keywords: *Thermoplastic composites, poly(aryl-ether-ketone), carbon fiber, recycling.*

REMEDIATION OF HEAVY METAL CONTAMINATED WATER ASSOCIATED WITH THE COLLAPSE OF MINING DAMS IN MINAS GERAIS BY USING A NANOCOMPOSITE-BASED POLYURETHANE FOAM

Philipe Augusto Pocidonio Silva[1] and Rodrigo Lambert Oréfice[1]*

1 – Department of Metallurgical, Materials Engineering, Federal University of Minas Gerais (UFMG), Av. Antônio Carlos, 6627 - Campus da UFMG, Pampulha, Belo Horizonte, MG, Brazil.
*rorefice@demet.ufmg.br

Abstract - The exponential increase in population and rapid development of various industries have increased water consumption in the last five decades [1], and it is predicted that by 2025, half of the world's population will live in water-scarce areas [2]. Mining dam failures in Brumadinho and Mariana in Brazil have caused water contamination in Paraopeba and Doce rivers with heavy metals[3–6], worsening the regional scenario. To mitigate this contamination, eco-friendly bio-based castor oil polyurethane foams (PUF), containing a cellulose-halloysite green nanocomposite were prepared[7]. These new adsorbents, with 0% weight of nanocomposite (PUF-0), 5% weight of nanocomposite (PUF-5), and 10% weight of nanocomposite (PUF-10) were produced. Sequentially they were morphologically analyzed, through scanning electron microscopy and X-ray tomography, and the adsorption capacity of the foams in pH=2 and pH=6.5 for manganese, nickel, and cobalt ions was investigated by using Ultraviolet-Visible spectroscopy [8]. An increase of 5.47 times in manganese adsorption capacity was found after only 30min in contact with a solution having this ion at pH=6.5 for PUF-5 and 11.38 times for PUF-10 when both were compared with PUF-0. Mn adsorption efficiency was 68.17% at pH=2 for PUF-5 and 100% for PUF-10 at pH=2 after 120h, while for the control foam, PUF-0, the adsorption efficiency was only 6.90%. The adsorption of cobalt and nickel was also evaluated and enhanced for foams that contained the nanocomposite. Thus, these results project a vast horizon for tailoring and improving the adsorption of toxic ions in bio-based polyurethane foams that extend the use of polyurethane foams beyond the well-documented application of this type of foam in collecting non-polar hazardous substances.

References

1. Prasad, P. S.; Gomathi, T.; Sudha, P. N.; Deepa, M.; Rambabu, K.; Banat, F.: Biosilica/Silk Fibroin/Polyurethane biocomposite for toxic heavy metals removal from aqueous streams. *Environmental Technology and Innovation*, 2022, 28, 102741. http://doi:10.1016/j.eti.2022.102741.
2. Organization, W. H.: *Drinking-water* Available online: https://www.who.int/news-room/fact-sheets/detail/drinking-water#:~:text=In 2017%2C 71%25 of the,at least a basic service. (accessed on Jan 4, 2021).
3. Ariana, R.: *A amarga realidade das águas do Rio Doce* Available online: https://www.cetem.gov.br/antigo/images/palestras/2015/mariana/07-ricardo-renata.pdf.
4. Instituto Brasileiro do Meio Ambiente e dos Recursos Naturais Renováveis - IBAMA: *Laudo Técnico Preliminar*;
5. Carvalho, M. S. de; Ribeiro, K. D.; Moreira, R. M.; Almeida, A. M. de: Concentração de metais no rio Doce em Mariana, Minas Gerais, Brasil. *Acta Brasiliensis*, 2017, 1, 37. http://doi:10.22571/actabra13201758.
6. Soares, A. L. C., Ph.D. Thesis, Federal University of Minas Gerais,2021.
7. Silva, P. A. P.; Oréfice, R. L.: Bio-sorbent from castor oil polyurethane foam containing cellulose-halloysite nanocomposite for removal of manganese, nickel and cobalt ions from water. *Journal of Hazardous Materials*, 2023, 131433. http://doi:10.1016/j.jhazmat.2023.131433.
8. Malik, M.; Chan, K. H.; Azimi, G.: Quantification of nickel, cobalt, and manganese concentration using ultraviolet-visible spectroscopy. *RSC Advances*, 2021, 11, 28014–28028. http://doi:10.1039/d1ra03962h.

Fundings: CAPES, FAPEMIG and CNPq the Brazilian research funding agencies.

Keywords: *Bio-based polyurethane, cellulose-halloysite, nanocomposite, Manganese Nickel and Cobalt removal, Wastewater treatment*

REMEDIATION POTENTIAL OF CONTAMINED SOILS BY LUBE OIL USING SODIUM POLYACRILATE

Thaina B. Rissati [1], Carla V. L. Pereira [1], Juan A. Q. Kuno[2], Sebastian I. P. Jorquera[2], Henrique S. M. Lopes[2], Patricio H. M. Albornoz[2] and Maira de L. Rezende[1]*

1 – Tecnologia em Polímeros, Faculdade de Tecnologia de Sorocaba (Fatec), Sorocaba, SP, Brazil
2 – Área Minería y Metalurgia, Universidad Tecnológica de Chile (INACAP), Iquique, Tarapacá, Chile
maira.rezende@fatec.sp.gov.br

Abstract

Contamination of soils and groundwater by petroderivatives has caused growing concern, due to its improper disposal, leading to serious environmental impacts [1, 2]. The present study aims to evaluate the efficacy of the superabsorbent polymer Sodium Polyacrylate (PAS), extracted from disposable diapers, as an alternative for the remediation of contaminants from lubricating oil in soil. Studies have been emphasizing the application of superabsorbent polymers, such as PAS, in soil remediation, due to its great absorption power of aqueous solutions, which can also be considered as an alternative for remediation of soils contaminated by mining activities [3-6]. Lubricating oils are often used in large machines, whose activity in the mining environment is extremely frequent. Thus, when dumped in soil, contamination by potentially toxic metals occurs, which can reach and pollute groundwaters [2]. In this work, contamination of soil by lubricating oil in systems were simulated, containing alternating layers of sand, soil and polymer, in order to evaluate how these soils can be affected by the oil runoff. All extracts were submitted to organic matter, pH, moisture, swelling capacity and Fourier Transform Infrared Spectroscopy (FTIR) analyses. FTIR results showed that the superabsorbent polymer is effective in the remediation of lubricating oil up to certain concentrations.

References

1. C. P. Devatha; A. V. Vishal; J. P. C. Rao. *Applied Water Science* 2019, *9*, 89. https://doi.org/10.1007/s13201-019-0970-4
2. J. Pichtel. *Applied and Environmental Soil Science* 2016, http://dx.doi.org/10.1155/2016/2707989.
3. Y. Zhang; H. Xi; T. Wei. *Water Air Soil Pollut* 2023, *234*, 196. https://doi.org/10.1007/s11270-023-06219-6.
4. D. K. Dehkordi; S. A. Shamsnia. *Clean Soil Air Water* 2020, 2000068. https://doi.org/10.1002/clen.202000068
5. N. Özbakan; B. Evirgen. Proceedings of CSEE'22, 2022, 185. DOI: 10.11159/icgre22.185.
6. M. A. Fayek; M. A. Abdel-Mohsen; S. I. Laz; S. M. El-Sayed. Plant Archives 2020, 20, 723.

Keywords: *sodium polyacrylate, superabsorbent polymer, soil, oil, remediation.*

SEPARATION AND IDENTIFICATION OF POLYMERS BY SELECTIVE DISSOLUTION AND PRECIPITATION TECHNIQUE AND FTIR FOR MULTILAYER PACKAGING RECYCLING

Nathan K. Carvalho[1]*, Amanda de S. M. de Freitas[1] and Ana P. Lemes[1]

1 – Department of Science and Technology, Federal University of São Paulo (UNIFESP), São José dos Campos, SP, Brazil
*nathan.carvalho@live.com

Abstract - Environmental problems related to waste accumulation have encouraged recycling, especially of polymeric materials, such as multilayer packaging, which is hardly recycled because of consisting of distinct materials in each layer[1-3]. Furthermore, knowing the polymers that compose the films is essential to make their recycling feasible[4]. The purpose of this work was to identify the polymers that compose three different postconsumer multilayer packaging by the techniques of selective dissolution and precipitation, optical microscopy (OP) and Fourier transformed infrared spectroscopy (FTIR). The packages were sanitized with neutral soap and water and cut into 1 cm^2 pieces. The samples were stirred in a solvent system of toluene at 110 °C for 4 h with a polymer-to-solvent mass ratio of 1:30. After heated filtration, the system was allowed to cool to room temperature, and then acetone was combined with the filtered solution with a solvent-to-antisolvent ratio of 1:4 by mass. Following stirring for 15 min, the precipitated solids were filtered out. The two solid fractions for each packaging were washed with water, dried in an oven overnight at 70 °C, and analyzed by OP and FTIR. Images showed that the first solid fractions (FSF) were composed of films which were not dissolved by toluene, whereas the second solid fractions (SSF) consisted of irregular forms in the majority, resulted from the precipitation process. FTIR spectra of FSF showed characteristic bands of ethylene vinyl alcohol copolymer and poly(ethylene terephthalate) for two packages, and ethylene vinyl alcohol copolymer and polyamide for the third one. As for SSF, the presence of polyethylene and ethylene vinyl acetate copolymer was indicated in all three packages. Therefore, selective dissolution and precipitation technique was crucial to separate some layers of the packages based on solubility. Polymers identification will be further explored by differential scanning calorimetry in order to confirm FTIR analysis.

References

1. C. T. M. Soares et al. *Resour Conserv Recycl* 2022, 176, 105905. https://doi.org/10.1016/j.resconrec.2021.105905.
2. V. Lahtela et al. *Polymers* 2020, 12, 2517. https://doi.org/10.3390/polym12112517.
3. A.-S. Bauer et al. *Foods* 2021, 10, 2702. https://doi.org/10.3390/foods10112702.
4. T. W. Walker et al. *Science Advances* 2020, 6, eaba7599. https://doi.org/10.1126/sciadv.aba7599.

Fundings: This study was financed in part by the Coordenação de Aperfeiçoamento de Pessoal de Nível Superior – Brasil (CAPES) – Finance Code 001 and also by grant #2022/00282-5, São Paulo Research Foundation (FAPESP).

Keywords: *recycling, multilayer packaging, selective dissolution, FTIR.*

STUDY OF POLYURETHANE FOAMS BASED ON WASTE COOKING OIL USING PYROLISIS CARBON AS FILLER

Guilherme A. Marques[1], Henry R. H. Abreu[1], Daniel B. Rezende[1], Camila N. C. Corgozinho[2].and Renata C. S. Araujo[2]*

1 – Chemical Engineering Department, Federal University of Minas Gerais, Belo Horizonte, MG, Brazil
2 - Chemistry Department, Federal University of Minas Gerais, Belo Horizonte, MG, Brazil
renatasa@ufmg.br

Abstract – The use of waste in the synthesis of materials is important to avoid the use of virgin raw materials and environmental degradation. In this work, in addition to the use of residual frying oil, pyrolysis charcoal obtained from materials from an association of recyclable waste pickers [1] was used. Polyurethane foams based on waste cooking oil were synthesized modifying the residual oil by epoxidation and ring opening, obtaining a polyol. The PU foams were synthesized using 0, 1, 2 e 4% of carbon from two sources: pyrolysis product and commercial activated carbon. The main objective was the use these materials as adsorbents, comparing just the foam and the set foams and carbon [2]. The foams obtained was homogeneous presenting as rigid materials, as showed in Fig. 1. The foams were characterized by infrared spectroscopy, thermogravimetric analysis and density. The thermal stability of PU foams with activated carbon were higher than pyrolysis carbon and the lower stability was observed for foam without carbon. As the carbon content decrease, the stability decreased. The density showed a little increase in foams based on carbon varying from 0,020 to 0,029 g/cm^3. An essay using blue methylene was performed to study the adsorptions showing the presence of carbon as an important addictive.

Figure 1 – Polyurethane foams based on waste cooking oil and pyrolysis and actived carbon as filler.

References.

1. J. O. Freitas, A. F. G. Almeida, D. B. Rezende, C. N. C. Corgozinho, R. C. S. Araújo, in Proceedings of 5th Congresso Sulamericano de Resíduos Sólidos e Sustentabilidade, Gramado, Brasil, 2022. http://dx.doi.org/10.55449/conresol.5.22.IV-014
2. R. Selvasembian, W. Gwenzi, N. Chaukura,, S. Mthembu, *Journal of Hazardous Materials,* 2021, 417, 125960.

Keywords: *Polyurethane foams, waste cooking oil, pyrolysis carbon, adsorption.*

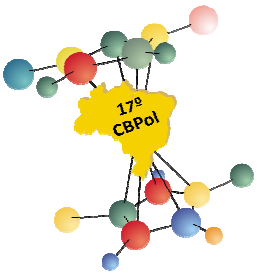

STUDY OF THE ADSORPTION OF CHROME AND DYES BY POLYMERIC MATRIXES

Nicole A. A. de Oliveira[1,2*], Fernando S. de Lima[1], Heber E. Andrada[2], Eduardo F. Molina[2]

1 – Laboratory of Chemistry and Manufactured Products,Technological Research Institute of the State of São Paulo, São Paulo, SP, Brazil nicoleao@ipt.br
2 – Department of Chemistry, University of Franca, Franca, SP, Brazil

Abstract – Over the years, concern for the environment has increased, researchers around the world seek sustaintable production alternatives and methodologies to reduce the environmental impacts caused by the industry. Dyes and metals have been the subject of several studies, since they have high toxicity for both fauna and flora, whether aquatic or terrestrial, and in some cases they can be cumulative in the food chain. Among the various industries, tanneries have a high potential for pollution, since they use both toxic metals and dyes in their production environment[1,2].
Adsorption, oxidative processes, membrane separation, among others, are methods studied for this purpose. The adsorption process is a methodology that offers a high efficienct of purification and removal of contaminants for both high and low concentrations; the operational easiness and the low cost of implementation are great attractions of this technique[3,4]. The use of polymers as adsorbents is a feasible route, however little studied with a view to film deposition or surface modification, as well as much of the literature that deals with adsorption focuses a lot on the foundation of the phenomenon[5,6]. This study arose due to the amount of waste generated by the leather-footwear industry and its classification as hazardous waste - class 1, mainly due to the presence of chromium. With this in mind this work evaluates the removal of hexavalent chromium and Azo dyes by polyurea membranes. The results obtained so far have suggest that the polyurea membrane is capable of removing the evaluated pollutants.

References

1. C. A. Costa, Master's Dissertation, Federal University of Rio Grande do Sul, 2000.
2. M. Dakiky; M. Khamis; A. Manassra; M. Mereb; *Advances in Environmental Research*, 2022, 533, 1093-0191. http://dx.doi.org/10.1016/S1093-0191(01)00079-X
3. J. L. Tambosi, Doctor's Thesis, Federal University of Santa Catarina, 2008.
4. P. Del Vecchio, Dissertation, Federal University of Rio Grande do Sul, 2016
5. C. Housmans; M. Sferrazza; S. Napolitano; *Macromolecules*, 2014, 47, 3390-3393. http://dx.doi.org/10.1021/ma500506r
6. P. Gin; N. Jiang; C. Liang; T. Taniguchi; B. Akgun; S.K. Satija; M.K. Endoh; T. Koga; *Physical Review Letters*, 2012, 22, 265501. https://doi.org/10.1103/PhysRevLett.109.265501

Fundings: This study was financed in part by the Coordenação de Aperfeiçoamento de Pessoal de Nível Superior - Brasil (CAPES) - Finance Code 001.

Keywords: *Polyurea, chromium, dyes*

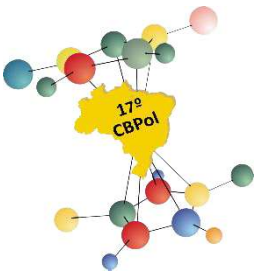

STUDY OF THE BIODEGRADATION OF CASSAVA STARCH PACKAGING WITH THE ADDITION OF TOMATO PEELS (LYCOPENE): A SUSTAINABLE APPROACH FOR REDUCING ENVIRONMENTAL IMPACT

Anômora A.R.S. Cotta[1,2], Laura F. Fonseca[1], Sorais V. Borges[2], Bruna S. Nascimento[2], Alexandre A.C. Cotta[3], Marali V. Dias[1,2]

1 – Graduate Program in Biomaterials Engineering., Federal University of Lavras (UFLA), Lavras, MG, Brazil
arianerochido@gmail.com
2 – Graduate Program in Food Engineering, Federal University of Lavras (UFLA), Lavras, MG, Brazil
3 - Graduate Program in Physical Engineering, Federal University of Lavras (UFLA), Lavras, MG, Brazil

Abstract

The growing negative impact of synthetic packaging on the environment and human health has led to the search for sustainable alternatives. In this context, biodegradable packaging made from natural polymers emerges, aiming to provide safe, healthy, and chemical-free food while reducing environmental impact. A recent study focused on the biodegradation of packaging made from cassava starch with the addition of tomato peel (lycopene), with the goal of deepening knowledge about the degradation process and evaluating its performance over time [1]. The packaging used consisted of modified cassava starch with different concentrations of total solids, incorporating tomato peel. The biodegradation process was assessed using a specific methodology, which involved burying the samples in the soil for approximately 18 days, with periodic removal every 6 days for monitoring [2]. After this period, the packaging was subjected to Fourier Transform Infrared Spectroscopy (FTIR) analysis and visual evaluation. During the biodegradation assessment, various visual changes were observed in the packaging composed of cassava starch and tomato peel, such as cracks, holes, fissures, size reduction, color change, and the presence of microbial colonies. These changes indicate the weakening of the polymeric chains and evaporation of the plasticizer from the polymeric matrix [2]. FTIR analysis revealed a gradual reduction in peak intensity, suggesting weakening and breaking of chemical bonds [3]. The presence of tomato peel significantly accelerated the degradation process, as confirmed by infrared spectroscopy analysis. These packages exhibit biodegradable characteristics and stand out as a sustainable alternative to reduce the environmental impact of conventional packaging, replacing non-biodegradable plastic materials.

References

1. S. Kumar, A. Mukherjee, J. Dutta. *Trends in Food Science & Technology*, v. 97, p. 196–209, 2020.
2. P. C. Silva, A. C. S. Oliveira, L. A. S. Pereira, M. Valquíria, G. R. Carvalho, K. W. E. Miranda, J. M. Marconcini, J. E. Oliveira. *Polymer Composites*, v. 41, p. 858–870, 2020.
3. S. Lv, Y. Zhang, J. Gu, H. Tan. *Journal of Environmental Management*, v. 228, p. 223–231, 2018.

Keywords: *Biodegradable Packaging, Active Packaging, Degradation and Biodegradation of Packaging.*

STUDY OF THE CONTAMINATION OF SAMPLES OBTAINED VIA PYROLYSIS OF VIRGIN POLYMERS AND PLASTIC WASTE RICH IN POLYOLEFINS

Jamilly A. S. Barros[1*], Laura P. M. Costa[1], Débora M. V. de Miranda[1], Larissa L. A. Carvalho[2], Yasmin F. Siqueira[2], Natasha S. Kelber[2], Mateus M. Barbio[2], José C. C. S. Pinto[1]

1 – Polymer Engineering Laboratory (Engepol), Chemical Engineering Program, COPPE, Federal University of Rio de Janeiro (UFRJ), Rio de Janeiro, RJ, Brazil
jamilly@peq.coppe.ufrj.br
2 – Polymer Engineering Laboratory (Engepol), Department of Chemical Engineering, School of Chemistry, Federal University of Rio de Janeiro (UFRJ), Rio de Janeiro, RJ, Brazil

Due to the complexity and diversity of polyolefin plastic waste streams and the inherent non-selective nature of the pyrolysis chemistry, the chemical decomposition of plastic waste is still not fully understood [1]. Accurate data of feedstock and products that also consider impurities is, in this context, quite scarce. In view of this, the search for new technologies for the treatment of this plastic waste has become a necessity of great energies [2,3]. The pyrolysis process is a promising alternative for recycling plastics [4]. The main objective of this work was to develop an experimental study on the thermochemical recycling via pyrolysis of different virgin and contaminated waste-derived polyolefin feedstocks (i.e., low-density polyethylene (PEBDL), polystyrene (PS) and high density polyethylene (PEAD), along with an investigation of the decomposition mechanisms based on the detailed composition of the pyrolysis oils. For each experiment, 7 g of sample, N_2 gas flow of 100 $mLmin^{-1}$ and 500 °C temperature were used. Liquid and gaseous samples were observed by gas chromatography for analysis of the present compounds. The results of the mass balance showed a high content of condensable followed by volatiles and solids, corroborating the creation of databases that make this process possible as a technique for characterizing mixtures of plastics and polymeric residues. In short, the study presented a sustainable alternative for the treatment of this waste in the context of the circular economy.

References

1. A. R. D. Monteiro; D. M. V. Miranda; J. C. Pinto; J. Soto. Macromolecular Reaction Engineering 2022. https://doi.org/10.1002/mren.202200037.
2. J. Pinto, A. Magrini; C. Melo. Impactos ambientais causados pelos plásticos - Uma discussão abrangente sobre os mitos e os dados científicos. 2 ed. Rio de Janeiro, E-papers, 2012.
3. H. C. Genuino; M. P. Ruiz; H. J. Heeres; S. R. A. Kersten. Waste Management 2023, 156, 208-215. https://doi.org/10.1016/j.wasman.2022.11.040.
4. A. Al-Rumaihi; M. Shahbaz; G. Mckay; H. Mackey; T. Al-Ansari. Renewable and Sustainable Energy Reviews 2022, 167, 112715. https://doi.org/10.1016/j.rser.2022.112715.

Fundings: CNPq, FAPERJ and Braskem.

Keywords: *Advanced Chemical Recycling; Pyrolysis; solid waste and Chemical compounds.*

STUDY OF THE PROPERTIES OF A COMPOSITE OF EXPANDED POLYSTYRENE WITH MDF

Jaqueline P. Pagnonceli[1], Júlia M. O. Callegari[1], Paulo R. de Souza[2], Adonilson R. Freitas[1] and Luciana Gaffo[1]*

1 – Chemistry, State University of West Parana (Unioeste), Toledo, PR, Brazil
lugaffo@yahoo.com.br
2 – Physics Department, Federal University of Santa Maria (UFSM), Santa Maria, RS, Brazil

The solid waste of plastic materials in the world reach number that reach millions of tons in recent decades, a large part of which is discarded improperly, harming the environment. Some of these residues are polystyrene (PS), which is a thermoplastic polymer and expanded polystyrene (EPS), produced by the polymerization of PS monomer, subjected to an expansion process. The objects produced from EPS are of very brief use, being quickly discarded. Another residue that has been the subject of study is leftover Medium Density Fibeboard (MDF) from furniture industries, usually burned for energy production, but depending on the conditions, it can release toxic substances into the environment. The use of these two materials, through the formation of composites, was the object of study in this work. Composites were prepared by solubilizing the EPS in chloroform and slowly adding the MDF. The already pasty material was placed in molds for drying. Different EPS/MDF ratios and different granulometries for MDF were used. Some characteristics and properties of the obtained composites were studied by scanning electron microscopy (SEM) and by tensile strength test. The results showed that the composites that presented the best homogeneity were those prepared using MDF with 32 mesh. The 1:1 mass ratio, EPS:MDF, in addition to having the best visual characteristics, was also the one that showed the greatest homogeneity in the SEM micrographs. The tensile strength test has not yet been carried out for samples with this proportion, and the best results so far have been presented by composites prepared in a 2:1 proportion (EPS:MDF). A very interesting result is that these composites absorb fat of animal origin, but do not absorb water. More experiments will be carried out to verify the absorption of water and oils or fats by these composites.

References

1. C. W. Zhang; R. J. Yang; X. M. Li; D. Yi *Chinese Journal of Polymer Science* 2016, *34*, 688. https://doi.org/10.1016/j.conbuildmat.2017.12.197.
2. J. W. Gomes; G. S. Godoi; L. G. M. De Souza; L. G. V. M. De Souza *Polímeros* 2017, *27,* 48. https://doi.org/10.1590/0104-1428.1915.
3. T. Masri, H. Ounis, L. Sedira, A. Kaci, A. Benchabane *Construction and Building Materials* 2018, *164*, 410. https://doi.org/10.1016/j.conbuildmat.2017.12.197.

Fundings: This work was supported by CNPq, CAPES and Fundação Araucária.

Keywords: *expanded polystyrene, EPS, MDF, composite.*

SYNTHESIS AND CHARACTERIZATION OF NANOCELLULOSE FROM INDUSTRIAL LAUNDRY

Fernanda M. F. Galvão[1], Felipe M. F. Galvão[2], Suzanna R. C. A. de Sousa[1], Prof. Dr. José H. O. do Nascimento[1,2] and Prof.ª Dr.ª Amanda M. D. Leite[1,3]

1 - Graduate Program in Textile Engineering (PPGET), Federal University of Rio Grande do Norte (UFRN), Natal, RN, Brazil
2 - Graduate Program in Chemical Engineering (PPGEQ), Federal University of Rio Grande do Norte (UFRN), Natal, RN, Brazil
3 – School of Science and Technology, Federal University (EC&T) of Rio Grande do Norte (UFRN), Natal, RN, Brazil
amanda.melissa.leite@ufrn.br

Abstract - Textiles have been concomitants of human civilization for thousands of years. Its industries are characterized as one of the main economic activities, surpassing values of billions of dollars per year. On the other hand, it is also one of the industries that most pollutes and harms the environment, with high energy consumption and uncontrolled waste generation. Conceptually clean production seeks to integrate continuous use with deterrent environmental approaches to processes, products and services, aiming to increase efficiency and minimize environmental risks. Due to the complexity of solid waste and effluents generated during the processing process, industrial laundries gain prominence and have a high polluting potential. Thus, the main objective of this research is to synthesize and characterize cellulose nanocrystals via acid hydrolysis, varying time and temperature of solid waste generated by drying machines, resulting from the jeans improvement process. Acid hydrolysis was performed using diluted sulfuric acid due to its low capacity to depolymerize cellulose in the concentrated fraction, analyzing treatment conditions for the isolation of cellulose nanocrystals, comparing at different temperatures (30˚C, 45˚C, 60˚C) and time (30, 45, 60 minutes) at the 60% concentration. The suspensions after hydrolysis were characterized by the techniques of Zeta Potential, X-ray Diffraction (XRD), Atomic Force Microscopy (AFM), Scanning Electron Microscopy (SEM), Fourier Transform Infrared Spectroscopy (FTIR), Thermogravimetric Analysis and Differential Scanning Calorimetry (TGA/DSC) and Particle Size. The microstructural and morphological results prove that nanocellulose can be obtained from residues from industrial dryers without the need for pre-treatment at 60% at 60˚C and time of 30 min. Making its synthesis and subsequent application of cellulosic films feasible.

Keywords: *Textiles; Jeans; Residue; Nanocellulose*

SYNTHESIS OF A RENEWABLE MONOMER DERIVED FROM 10-UNDECENOIC ACID

Juliana S. Zanatta[1], Letícia K. H. Patricio[1], Victor L. Spiess[1], Tamara Agner[1], Claudia Sayer[1] and Pedro H. H. de Araújo[1*]

1 – Department of Chemical Engineering and Food Engineering (EQA), Federal University of Santa Catarina (UFSC), Florianópolis, SC, Brazil pedro.h.araujo@ufsc.br

Abstract – The development of environmentally conscious and sustainable new materials follows Goal 12 of the United Nations´ 17 Sustainable Development Goals which emphasizes the importance of environmental sustainability[1]. In this context, the main objective of this work is the synthesis of a 100 % renewable biobased monomer (3-hydroxypropylundec-10-enoate) from 10-undecenoic acid (10-UA, 0.1 mol) by different esterification reactions using 1,3-propanediol (0.13 mol). In Steglich esterification, 4-dimethylaminopyridine is the nucleophilic catalyst (0.01 mol), and N,N'dicyclohexylcarbodiimide (0.1 mol) is the coupling agent. The reaction was carried out at room temperature for 18 h under magnetic stirring in dichloromethane (100 mL)[2]. In Fischer esterification, p-toluenesulfonic acid (0.009 mol) is the catalyst. Toluene (120 mL) was added to a round bottom flask equipped with a magnetic stirrer and a Dean-Stark apparatus and the reaction was performed at 135 °C for 5 h[3]. After the specified reaction times, the solvents were evaporated under reduced pressure, and liquid-liquid extraction was performed with sodium carbonate solution (1 M). Then, the crude product of each reaction was purified by column chromatography filled with silica gel using ethyl acetate and hexane as eluents in ratios of 30:70 and 50:50, respectively. The crude and purified products were submitted to proton nuclear magnetic resonance spectrometry analysis. Steglich esterification had a global conversion of the monomer of 96.3 % and a monomer selectivity of 83.3%, while Fischer esterification resulted in 99.1% and 72.1%, respectively. Therefore, the 3-hydroxypropylundec-10-enoate monomer was obtained with high selectivity in both synthetic routes. In the next step, this monomer, which is sourced exclusively from renewable resources, will be used to produce novel biopolymers.

References

1. K. Henderson; M. Loreau *Ecological Modelling* 2023, *475*, 110164. https://doi.org/10.1016/j.ecolmodel.2022.110164.
2. L. Raghunanan; S. S. Narine *ACS Sustainable Chem. Eng.* 2016, *4*, 693-700. https://doi.org/10.1021/acssuschemeng.5b01708.
3. P. B. Cardoso; T. O. Machado; P. E. Feuser; C. Sayer; M. A. R. Meier; P. H. H. de Araújo *European Journal of Lipid Science and Technology* 2018, *120*, 1700212. https://doi.org/10.1002/ejlt.201700212.

Fundings: We thank Conselho Nacional de Desenvolvimento Científico e Tecnológico (CNPq) and Coordenação de Aperfeiçoamento de Pessoal de Nível Superior (CAPES) for the financial support.

Keywords: *Renewable monomer, Steglich esterification, Fischer esterification, 10-Undecenoic acid.*

THE INFLUENCE OF SALT (*NaCl*) ON THE PYROLYSIS OF POLYPROPYLENE AND MARINE LITTER (REAL WASTE)

Yasmin F. Siqueira[1], Débora M. V Miranda[2], Larissa L. A. Carvalho[1], Natasha K. Sitton[1], Mateus Marques Barbio[1], Laura Pires da Mata Costa[2], Jamilly A. S. Barros[2], Luiz E. P. Borges[3] and José C. Pinto[1,2]*

1 – Programa de Engenharia de Processos Químicos e Bioquímicos, Universidade Federal do Rio de Janeiro, Rio de Janeiro, RJ, Brazil
2 – Programa de Engenharia Química / COPPE, Universidade Federal do Rio de Janeiro, Rio de Janeiro, RJ, Brazil
pinto@peq.coppe.ufrj.br
3 – Seção de Engenharia Química, Institut Militar Engenharia, Rio de Janeiro, RJ, Brazil

Abstract - Plastic materials are essential for human life and provide sustainable solutions for society. The current challenge, therefore, revolves around the management of plastic wastes, which constitute one of the major concerns of current society. Studies indicate that every minute, an amount equivalent to the contents of a garbage truck ends up "leaking" into the oceans, totaling approximately 8 million tons of plastic per year. For this reason, various technologies can be employed to reintroduce plastic wastes into the chemical chain. Pyrolysis is one of the polymer recycling techniques that has gained prominence in recent years because most polymeric wastes is compatible with this technique. For these reasons, the present study investigated the effect of salt on the pyrolysis process and product compositions. The aim was to simulate the marine environment, which contains approximately 3.5% *NaCl* (sodium chloride), to determine if a high concentration of salt would exert any significant impact on the process. Duplicate experiments were conducted using 10% commercial *NaCl* in polypropylene (PP) and real marine wastes, at an operating temperature of 500 °C. Thermal degradation provided high liquid yields in both cases, with increased amounts of solids in presence of *NaCl*, as expected. For the marine wastes, higher yields of volatiles and small amounts of solids (around 5 wt%) were obtained, which can be attributed to the presence of organic contaminants and inorganic fillers and contaminants (including salt) present from the marine environment. Regarding the composition of the products, it was characterized that the condensable liquid streams obtained from PP and PP/*NaCl* were rich in long-chain hydrocarbons and that the salt did not exert significant influence on the nature of the formed products, which is good for processing of marine wastes.

References

1. A. Duailibe; J. C. Pinto; J. J. S. Delgado in Reciclagem química de resíduos plásticos – Tecnologias e Impactos; E-papers, Ed.; 2019.
2. S. C. Kosloski-Oh, et al. Materials Horizons 2021, 8, 1084-1129. https://doi.org/10.1039/D0MH01286F.

Fundings: This study was funded in part by Coordenação de Aperfeiçoamento de Pessoal de Nível Superior (CAPES). Conselho Nacional de Desenvolvimento Científico e Tecnológico (CNPq), Fundação Carlos Chagas Filho de Apoio à Pesquisa do Estado do Rio de Janeiro (FAPERJ), Petrobras and Braskem.
Keywords: *Pyrolysis; Chemical recycling; Polypropylene; NaCl; Marine wastes.*

THE REFLUX INFLUENCE ON CHEMICAL RECYCLING OF VIRGIN AND WASTE POLYETHELENE PYROLYSIS

Larissa L. de A. Carvalho[1,2], Natasha K, Sitton[1,2], Yasmin F. Siqueira[1], Mateus M. Barbio[2] Débora M. V de Miranda[2], Jamilly Andressa S. Barros[2], Márcio Nele[1,2] and José Carlos Pinto[1,2].

[1] Universidade Federal do Rio de Janeiro, Escola de Química, Programa de Engenharia de Processos Químicos e Bioquímicos. [2] Universidade Federal do Rio de Janeiro, COPPE, Programa de Engenharia Química.
e-mail: lalmeida@peq.coppe.ufrj.br

Since its production and large-scale commercialization in the 1950s, more than 9 gigatons of plastic materials have been produced. Many of these materials have short life cycles, strongly contributing to the impressive fact that more than 70% of all plastic material produced in the world has already been discarded, and only 9% was recycled [1, 2]. Polyethylene is the mostly used plastic for packaging, which has commonly a single use, being a considerable a problem for mechanical recycling when in its flexible form [3]. Chemical recycling has gained prominence due to its potential of transforming the plastic carbon chain into smaller molecules with high added value. In this context, this work studies the pyrolysis of virgin polyethylene and flexible plastic waste rich in polyethylene, with the aim of understanding the influence of the reflux temperature on the polymer chain breaking. For this, a semi batch quartz reactor, inertized with 80mL.min^{-1} of nitrogen was inserted into an oven with two temperature zones. The first zone is where the pyrolysis occurs and it was maintained at 500 °C for all reactions, the second one is the top reflux zone and was set into different temperatures from off to 500°C. Reaction times were measured until the complete reaction, mass balances were calculated, and the condensable and gaseous products were characterized by chromatography. The results show that the decrease in reflux temperature led to longer retention times of pyrolysis gases inside the pyrolysis zone, increasing the total time for complete reaction and generating condensable products with lower boiling points thus forming increasingly lighter products. The study showed that manipulating the reflux temperature can orientate the chains size of the products aligned with the chemical industry necessity, promoting the circular economy of plastic waste.

References

1. PLASTICSEUROPE. Plastics - the Facts 2022.
2. MIRANDA, D. M. V. DE. Reciclagem química via Pirólise e Avaliação do Ciclo de Vida (ACV) de resíduos plásticos. Exame de Qualificação. Rio de Janeiro: Universidade Federal do Rio de Janeiro, jul. 2019.
3. AHAMED, A. et al. Life cycle assessment of plastic grocery bags and their alternatives in cities with confined waste management structure: A Singapore case study. Journal of Cleaner Production, v. 278, p. 123956, jan. 2021.

Fundings: CNPq, FAPERJ, Petrobras and Braskem.
Keywords: Chemical Recycling, Pyrolysis, Reflux, Plastic Waste, Polyethylene.

THE USE OF NATURAL POLYMER AS STRATEGIES TO IMPROVE THE PROPERTIES OF ZnO

Benjamim S. G. Rubim[1], Idglan S. Lima[1], Edson C. Silva-Filho[1], Marcelo B. Furtini[1], Josy A. Osajima[1]

1 – Interdisciplinary Laboratory of Advanced Materials (LIMAV), Federal University of Piaui (UFPI), Teresina, PI, Brazil
benjamimsgr97@outlook.com

The zinc oxide (ZnO) incorporated with a natural polymer through an environmentally friendly synthesis process [1,2] is one of the strategies to improve some properties of materials. This study aimed to synthesize ZnO using a sol-gel method, incorporating a natural polymer, and investigate its photocatalytic and antimicrobial properties to determine its potential for use in cementitious materials. The synthesized material was characterized using X-ray diffraction (XRD), while its photocatalytic activity was assessed by measuring its performance in degrading methylene blue dye under visible light. The characterization analysis confirmed the successful formation of ZnO nanoparticles and the presence of natural polymer within its matrix. Furthermore, the photocatalytic tests demonstrated effective degradation of the methylene blue dye, indicating the material's ability to function as a photocatalyst in the visible light spectrum. This research offers valuable insights for developing environmentally friendly treatments to enhance the durability and performance of construction materials while ensuring the well-being of both humans and the environment.

References

1. Constantino, J. C., Garcia, D. C., Palhares, H. G., Houmard, M., & Figueiredo, R. B.. Construction and Building Materials 2020, 250, 118732. https://doi.org/10.1016/j.conbuildmat.2020.118732.
2. Araujo, F. P., Trigueiro, P., Honório, L. M., Furtini, M. B., Oliveira, D. M., Almeida, L. C., ... & Osajima, J. A.. Dalton Transactions 2020, 49(45), 16394-16403. https://doi.org/10.1039/D0DT01128B.

Fundings: CAPES, CNPq, FAPEPI

Keywords: *ZnO, polymer, photocatalysis.*

USE OF LIGNIN-BASED HYDROGEL EXTRACTED FROM THE PEEL OF TINGUI (*Magonia pubescens A. St. -Hil.*) FOR DYE ADSORPTION

Bianca M. Benevides[1], Caroline P. X. Andrade[1], Débora V. Franco[1] and João V. W. Silveira[1*]

1 – Institute of Science and Technology, Federal University of Jequitinhonha and Mucuri Valleys (UFVJM), Diamantina, MG, Brazil
joao.silveira@ufvjm.edu.br

Abstract - The tingui or timbó (*Magonia pubescens* A. St. -Hil.) is a tree native from the Brazilian Cerrado. Its fruit was widely used in the last century, by the local rural population, for animal diseases treatment, fishing and the manufacture of soap. Its fruit has a resistant shell rich in lignin that can serve as a source for hydrogel production. The lignin was extracted from the fruit peel using the soda extraction method. The hydrogel was prepared using poly (methyl vinyl ether-co-maleic acid) and characterized. Methylene blue cationic dye and the indigo blue anionic dye were used, and a 2^3 full factorial experimental design was employed for adsorption tests. The pH, ionic force and adsorbent to solution ratio were analyzed as variable factors. The hydrogel obtained promising results in the adsorption of both dyes, adsorbing up to 84% of the cationic dye and up to 90% of the anionic dye. The hydrogel is effective in the adsorption of dyes, however a dependence of the pH on the stability of the hydrogel was observed, having a better performance in acidic pH.

References

1. F. Chen; et al. Facile preparation of cross-linked lignin for efficient adsorption of dyes and heavy metal ions. https://doi.org/10.1016/j.reactfunctpolym.2019.104336.
2. J. Domínguez-Robles; et al. Lignin-based hydrogels with “super-swelling” capacities for dye removal. https://doi.org/10.1016/j.ijbiomac.2018.04.044.
3. P. E. R. Carvalho. Espécies Arbóreas Brasileiras. Embrapa Informação Tecnológica, Brasília, 2010; Vol. 4, 529-534.
4. Y. Meng; et al. Lignin-based hydrogels: A review of preparation, properties, and application. https://doi.org/10.1016/j.ijbiomac.2019.05.198.

Fundings: ICT-UFVJM, CNPq and FAPEMIG (APQ-03355-18).

Keywords: *Lignocellulosic materials. Experimental design. Methylene blue. Indigo blue. Timbó.*

Utilizing Polyurethane Waste in the Production of Rigid Foams: Characterization and Properties

Matheus S. Pimentel[1*], Laís B. Borba[1], Maria Elena L. Gonzalez[2] , Marilia Sonego[1] , Mirian L. M. Melo[1]

1 –Institute of Mechanical Engineer (IEM), Federal University of Itajubá(UNIFEI), Itajubá, MG, Brazil

*matheu.1110@unifei.edu.br

2 – Institute of Physics and Chemistry(IFQ), Federal University of Itajubá(UNIFEI), Itajubá, MG, Brazil

This study focuses on the characterization of rigid polyurethane foam derived from powdered polyurethane waste and a methylene diphenyl diisocyanate (MDI) based resin. The waste material was obtained from the mechanical recycling of refrigerators. Various foam compositions were produced using the Extreme Vertices Mixture Design of Experiment (DOE) approach, incorporating waste concentrations ranging from 10% to 30%. Water was utilized as a blowing agent and to facilitate the foaming process, with a range of 20% to 40%.The foam samples were subjected to characterization through Thermogravimetric Analysis (TGA), and the apparent density and compression properties were evaluated following ASTM standards D1622 and D1621, respectively. The thermal behavior showed no significant variation among different compositions, all samples including the waste itself showed a peak of degradation at approximately 330~345ºC, followed by a gradual mass decline.The influence of waste concentration on the foam's density and compression properties was evident. As the waste content increased, the density notably increased, ranging from an average of 0.228 g/cm³ for lower waste concentrations to 0.425 g/cm³ for higher concentrations. Similarly, compression strength displayed a significant change, with lower waste concentrations exhibiting an average strength of 23.5 MPa, while higher concentrations reached 109.2 MPa and a more brittle behavior. Interestingly, the center point composition demonstrated a compression strength of 122.8 MPa.Overall, this study highlights the impact of waste concentration on the properties of rigid polyurethane foam, particularly regarding density and compression strength and thermal degradation. The developed rigid foam shows promising potencial for construction applications, providing a more sustainable disposal method for PU waste.

1. A. Kemona, M. Piotrowska *Polymers* 2020, 12, 1752 https://doi.org/10.3390/polym12081752
2. K. H. Choe, D. S. Lee, W. J. Seo, W. N. Kim, *Polymer* 2004, 36, 368–373 https://doi.org/10.1295/polymj.36.368
3. ASTM International. (2020). ASTM D1622-20 – Standard Test Method for Apparent Density of Rigid Cellular Plastics
4. ASTM International. (2017). ASTM D1621-16 – Standard Test Method for Compressive Properties of Rigid Cellular Plastics.
5. D. Bresolin, A. Valério, D. de Oliveira *et al. J Polym Environ* 2018, 26, 2467–2475 https://doi.org/10.1007/s10924-017-1138-7
6. L. Jiao, H. Xiao, Q. Wang, J. Sun *Polymer Degradation and Stability* 2013, 98, 2687-2696 .http://dx.doi.org/10.1016/j.polymdegradstab.2013.09.032
7. D. Rosu, N. Tudorachi, L. Rosu *Journal of Analytical and Applied Pyrolysis* 2010, 89, 152-158 https://doi.org/10.1016/j.jaap.2010.07.004
8. M. Li, M. Du, F. Wang, B. Xue, C. Zhang, H. Fang *Construction and Building Materials* 2020, 259, 119797 https://doi.org/10.1016/j.conbuildmat.2020.119797

Keywords: *Polyurethane, rigid foam, density, compression, tga*

XEROGEL OF LIGNOCELLULOSE EXTRACTED FROM COFFEE HUSKS AND CALCIUM PEROXIDE FOR THE CONTROLLED RELEASE OF O_2

Anna Clara D. Vilas Boas[1*], Camila G. Chiaregato[1], Denise F. S. Petri[1]

1 – Institute of Chemistry, University of São Paulo (USP), São Paulo, SP, Brazil
annadrumond@usp.br

Brazil is the largest coffee producer in the world. Coffee processing generates great amounts of waste, including coffee husks (CF) (Fig. 1a). This work aimed to obtain lignocellulose from CF with minimal cost and environmental impact. CF were washed with water at 50 ºC for 1 h and then treated with commercial sodium hypochlorite (2% v/v NaClO) at 50 °C for 2 h. The product obtained was a white gel like material (Fig. 1b). The exact content regarding holocellulose and lignin in the CF and the white gel is under progress. The gel was freeze dried, which led to the formation of cryogels without the necessity of using any crosslinking agent (Fig. 1c). In similar way, the gel was also oven dried in absence of a crosslinking agent, yielding films with high stability in the pH range from 1 to 11 (Fig. 1d). This behavior makes the gel a suitable matrix for the incorporation of CaO_2 microparticles for the controlled release of O_2 [1]. For this purpose, 143.7 mg of CaO_2 was added to 4.6 g of the gel and then oven dried at 100 °C for 2 h. This led to the formation of a xerogel containing CF lignocellulose and CaO_2 microparticles, coded as Xgel-CaO_2 (Fig. 1e), presenting slower O_2 release in aqueous media than pure CaO_2. Xgel-CaO_2 mitigated the burst effect by reducing the initial velocity of O_2 release from 0.82 ± 0.04 mg L^{-1} (pure CaO_2 microparticles) to 0.115 ± 0.003 mg L^{-1} (Fig. 1f).

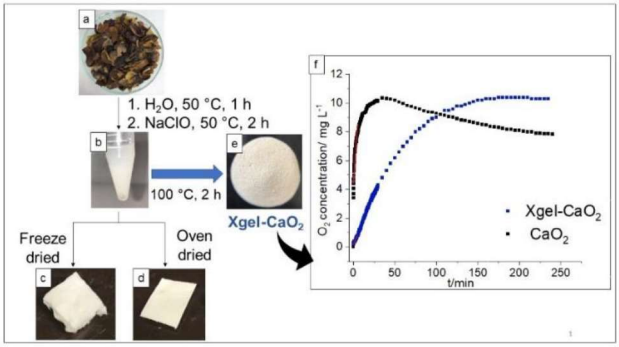

Figure 1– (a) Crude CF, (b) gel formed after washing CF with water at 50 °C for 1 h and treating with 2% v/v NaClO at 50 °C for 2 h, (c) cryogel and (d) film obtained after freeze or oven drying the white gel, (e) xerogel (Xgel-CaO_2) and (f) kinetics of O_2 release from pure CaO_2 microparticles and Xgel-CaO_2.

References

1. C. G. Chiaregato; O. D. Bernardinelli; A. Shavandi; E. Sabadini; D. F. S. Petri. *Carbohydrate Polymers* 2023, *316*, 121029. https://doi.org/10.1016/j.carbpol.2023.121029

Keywords: *Coffee husks, lignocellulose, xerogel, calcium peroxide, oxygen release*

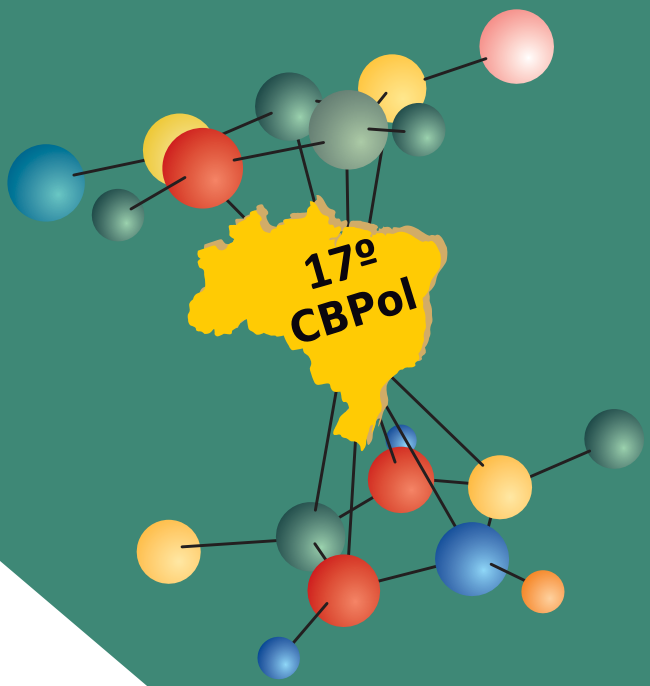

Biomedical applications of polymers

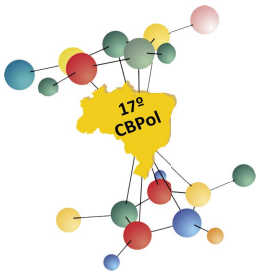

Biomaterials & Nanotechnology: the challenge in modifying nanoparticle surfaces

Marcia Margarete Meier

Department of Chemistry, Santa Catarina State University (UDESC), Joinville, SC, Brazil
marcia.meieri@udesc.br

Abstract - New materials must be developed to meet the demands of the modern society. The synthesis of new materials is one such strategy. Another important strategy is to change the characteristics of traditional materials, especially by incorporating nanoparticles into polymers. These nanoparticles can act as reinforcements, carriers of bioactive molecules, or stimuli-responsive bioactive structures.
In most of these situations, it is necessary to modify the surface of the nanoparticles to generate materials with specific characteristics for a given application.
For example, when using nanoparticles, as reinforcements, combined with polymer materials, it is often necessary to modify the nanoparticle surface to facilitate their dispersion in a polymeric matrix and even form a covalent bond with the polymer chains.
In this presentation, we will discuss the strategies adopted at the Interdisciplinary Polymer Center (NIPOL) aimed at modifying the surface of cellulose nanocrystals (CNC) to make it compatible with methacrylate polymers and poly (lactic acid). The impact of this surface modification on the generated composites will be demonstrated, covering challenging aspects such as characterizing and quantifying the surface modification of the CNC.
Furthermore, there are situations in which nanoparticles or nanostructured polymers are responsible for providing bioactivity. In this context, the results of the surface modification of nanohydroxyapatite, nanosilica and bacterial nanocellulose membranes will be presented and its performance will be described.

Fundings: FAPESC-2021TR654, FAPESC-2021TR1222

Keywords: *biopolymer, nanoparticle, surface, cellulose*

NATURAL POLYMERS: DEVELOPMENT OF ADVANCED MATERIALS AND DELIVERY SYSTEMS

Mariana Agostini de Moraes

1 – Department of Chemical Engineering, Federal University of São Paulo (Unifesp), Diadema, SP, Brazil
mamoraes@unifesp.br; marianaademoraes@hotmail.com

Abstract – Natural polymers are macromolecules found in renewable sources, which present biodegradability and can be used to prepare eco-friendly materials in several shapes, such as films, micro or nanoparticles and hydrogels, depending on the focused application. Moreover, the functional groups present in the natural polymers allow for chemical modifications, which expands the main field of applications of natural polymers-based materials [1]. The natural polymers are gaining increasing attention on the last years, mainly for advanced materials and drug release systems due to their biocompatibility and low immunological rejection [2]. Also, the release of the drug or bioactive compound from the natural polymer matrix can be modulated by several strategies, such as the use of co-encapsulation [3] or multi-layer systems [4], as well as applying crosslinking strategies or functionalization of the molecule. In this keynote, the development of several advanced materials using natural polymers will be explored, analyzing the relationship between structure and properties of the materials, as well as the influence of the drug on the final material.

References

1. J. Joye, I. and Julian McClements, D. *Curr. Top. Med. Chem.* 2015, *16*, 1026–1039. https://doi.org/10.2174/1568026615666150825143130
2. A. Mahmood et al. International Journal of Molecular Sciences 2022, 23, 1415. https://doi.org/10.3390/ijms23031415
3. A. Gonçalves, F. Rocha, B. N. Estevinho International Journal of Biological Macromolecules 2023, 224, 1217-1227. https://doi.org/10.1016/j.ijbiomac.2022.10.207
4. M. Pacheco et al. International Journal of Biological Macromolecules 2020, 152, 803-811. https://doi.org/10.1016/j.ijbiomac.2020.02.140

Fundings: The authors thank to FAPESP (#2020/08212-0 and #2016/17555-3) for financial support.

Keywords: *biopolymers, films, hydrogels, microparticles, bioactive compounds*

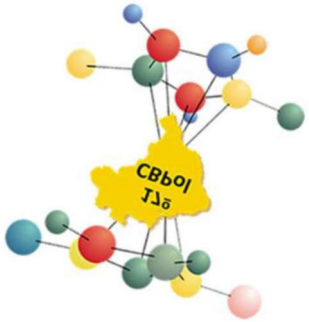

RECENTLY DEVELOPED POLYMERIC BIOMATERIALS AT GMPC/UEM AND LIMAV/UFPI

Edvani C. Muniz[1,2,3]

1 – Grupo de Materiais Poliméricos e Compósitos – GMPC
Departamento de Química – Universidade Estadual de Maringá
Av. Colombo, 5790 – Zona Sete - 87020-900 – Maringá – PR

2 – Programa de Pós-graduação em Ciência e Engenharia de Materiais - PPGCEM
Universidade Tecnológica Federal do Paraná
Av. dos Pioneiros, 3131 - Jardim Morumbi - 86036-370 - Londrina - PR

3 – Laboratório Interdisciplinar de Materiais Avançados - LIMAV
Departamento de Química - Universidade Federal do Piauí
Campus Universitário Ministro Petrônio Portella
Bairro Ininga - 64049-550 - Teresina – PI

In this keynote, some recent results obtained in the last 5 years in our research groups in the development of polymeric materials with potential application in the medical, pharmaceutical and tissue engineering areas will be presented. The materials are mainly those related to polymeric biomaterials, aiming at: i) the controlled release of drugs [1]; ii) bactericidal action [1,2]; iii) substrates for cell growth [3]; materials with virucidal action to combat the SARS-Cov 2 virus, related to the recent coronavirus pandemic, and for wound healing [4]. The polymeric materials that will be presented are prepared mainly through three-dimensional matrices (hydrogels) made from the formation of polyelectrolyte complexes between anionic/cationic polymers of chemically modified (or not) polysaccharides and through the electrospinning technique. Various methodologies for obtaining matrices of different geometries (cylindrical, spherical, irregular particles, thin films, nanofibers, etc.) of different sizes (macro, micro and nanometric scales) will be shown and discussed.

References:

[1] Oliveira, R. W. G., et al., Films composed of white angico gum and chitosan containing chlorhexidine as an antimicrobial agent. Int. J. Biol. Macromol. 235, 2023, 123905, DOI: 10.1016/j.ijbiomac.2023.123905

[2] Souza, P.R, et al., Poly(ethylene terephthalate) films coated with antimicrobial gelatin/ chondroitin sulfate polyelectrolyte multilayers containing ionic liquids. Progr. Org. Coatings, 170, 2022, 106997, DOI: 10.1016/j.porgcoat.2022.106997

[3] Bonkovoski, L.C. et al., Cytocompatible drug delivery devices based on poly[(2-dimethylamino) ethyl methacrylate]/chondroitin sulfate polyelectrolyte complexes prepared in ionic liquids. J. Drug Deliv. Sci. Tech. 63, 2021 - 102520, DOI: 10.1016/j.jddst.2021.102520

[4] Cestari, M. el al., Silk fibroin nanofibers containing chondroitin sulfate and silver sulfadiazine for wound healing treatment. J. Drug Deliv. Sci. Tech. 70, 2021 – 103221, DOI: 10.1016/j.jddst.2022.103221

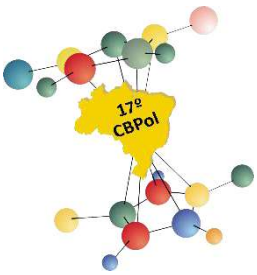

DEVELOPMENT OF CHITOSAN-BASED NANOPARTICLES FOR DOUBLE ENCAPSULATION OF 5-FLUOROURACIL AND METHOTREXATE

José Ribamar P. Junior*, Aline T. dos Santos, Eric P. Bandeira e Judith P. de A. Feitosa
Department of Organic and Inorganic Chemistry, Federal University of Ceará (UFC), Fortaleza, CE, Brazil
junior_sousa11@hotmail.com

Abstract - In this work, we develop nanoparticles based on chitosan, using the ionotropic gelation technique, for double encapsulation of methotrexate and 5-fluorouracil. The obtained nanoparticles were characterized by FTIR and dynamic light scattering. The yield of the reactions varied between 30 and 40%. Drug encapsulation efficiency was 12% for MTX and 17.4% for 5-FU. The FTIR spectrum of the nanoparticles showed the characteristic bands of the starting material. The nanometric size. The diameter of the nanoparticles obtained by dynamic light scattering were 146 and 440 nm for the drug-free and drug-containing systems, respectively. The zeta potential of both systems was above +27 mV, showing stability of the system in solution. Thus, the systems showed promising characteristics for future anticancer applications.
Keywords: *Chitosan, Nanoparticles, Ionic gelation, 5-Fluorouracil, Methotrexate.*

Introduction

According to data from the World Health Organization (WHO) published in 2020, diseases such as Alzheimer's, cancer, heart attacks and strokes are responsible for most deaths worldwide. Among the these cancer stands out, and has become a serious threat to human health, already being considered a public health problem worldwide [1]. It is estimated that in 2040 there will be 30.2 million cases of cancer, against 18.1 million in 2020.

In the Brazilian scenario, according to the National Cancer Institute (INCA), 704 thousand new cases of cancer are expected per year in the 2023-2025 triennium.

The main difficulty faced in the treatment of cancer is the metastasis phase. In more advanced cases, tumor removal is not as effective, due to the rapid spread of cells in the metastasis phase, which makes it possible for a new tumor to appear after surgery.

Currently, there are several types of treatments for cancer, such as: surgery, chemotherapy, radiotherapy and biological therapies (hormonal or immunological)[2]. One of the most used treatments is chemotherapy. Among the chemotherapy agents, 5-fluorouracil (5-FU)[3], methotrexate[4], paclitaxel [5] and doxorubicin[6] are the most used. However, despite its good efficacy, these drugs have several adverse reactions, such as: nausea, hair loss, liver damage and kidney damage. Some studies report that the combined use of drugs can attenuate these adverse reactions [7]

5-FU is a similar pyrimidine that acts through the irreversible inhibition of thymidylate synthase. It is constantly used in the treatment of malignant neoplasms, mainly those located in the colon, ovary, liver, lung, skin and breast.[8] Methotrexate is an antineoplastic drug, acting as a competitive inhibitor of dihydrofolate reductase necessary for DNA synthesis. However, it has some limitations in its application.[9] Chitosan (CH) is a cationic polysaccharide derived from chitin. It is a biodegradable and non-toxic polymer when administered orally. By presenting these characteristics, it is favorable to its application to produce usable particles in controlled release systems.

Experimental

Materials

Chitosan (77% deacetylation degree) was purchased from Polymar. Glacial acetic acid (CH_3COOH) was obtained from Synth. The reagents used: sodium hydroxide (NaOH) (Synth), 5-fluorouracil ($C_4H_3N_2FO_2$) (Sigma-Aldrich), Methotrexate ($C_{20}H_{22}N_8O_5$) (Sigma-Aldrich) sodium tripolyphosphate ($Na_5P_3O_{10}$) (Sigma-Aldrich), polyethylene glycol 1,450 $g.mol^{-1}$ (Sigma-Aldrich). To prepare the phosphate buffer: sodium hydrogenphosphate dihydrate ($Na_2HPO_4 \cdot 2H_2O$), potassium dihydrogenphosphate (KH_2PO_4) were obtained from Sigma-Aldrich. A dialysis membrane with a cut-off molar mass of 10,000 $g.mol^{-1}$ was used.

Nanoparticles production

Nanoparticles (NPs) were prepared following the methodology proposed by Samy et al., 2020.[10] The chitosan solution (CH) was prepared using a 0.5% (v/v) acetic acid solution. The sodium tripolyphosphate (TPP) solution was prepared in distilled water and the polyethylene glycol was solubilized in the TPP solution. The TPP/PEG solution was dropwise to the chitosan solution, with a flow rate of 1 $mL.min^{-1}$ with the aid of a peristaltic dosing pump. After the addition, the solution was under magnetic stirring (600 rpm) for 45 min. After then, the system was centrifuged at 6000 rpm for 30 min. The CH:TPP:PEG ratio used was 5:1:30. At the end of centrifugation, the supernatant of the system was dialyzed against distilled water and subsequently freeze-dried. Obtaining the free-drug nanoparticles.

MTX and 5-FU encapsulation

Double encapsulation was performed in two steps. In the first step, MTX was solubilized in 0.1 mol/L phosphate buffer (pH= 7.4) and dripped into the initial CH solution. The system was centrifuged and the supernatant dialyzed against distilled water. To NP with MTX was obtained after freeze-dried.
In the second step, for the encapsulation of 5-FU, the lyophilized NP with MTX was dispersed in an aqueous solution of 5-FU and remained under stirring for 24 h. After then, the system was centrifuged at 10,000 RPM for 15 min, and the precipitate freeze-dried to obtain NP with MTX and 5-FU double encapsulation.

Infrared absorption spectroscopy (FTIR)

The FT-IR spectra of the materials were obtained on KBr pellets using the Shimadzu IR Trace-100 spectrophotometer in the region from 400 to 4000 cm^{-1}.

Encapsulation efficiency

The encapsulation efficiency of MTX and 5-FU were using the solvent extraction method. Distilled water was the solvent, due to the high affinity of the drug with the solvent. 5 mg of nanoparticles were weighed and then dispersed in 10 mL of solvent. The system was stirred for 24 h and then centrifuged for 30 min at 10,000 rpm. The supernatant was analyzed in a UV-Vis spectrophotometer to quantify the drug present (5-Fu and MTX) in the sample. Thus, determining the Encapsulation Efficiency and the Drug Loading of the system. The drug calibration curves are in Eq. 1 and Eq. 2 for MTX and 5-FU, respectively.

$$y = 47.922x + 0{,}0087 \ (R^2=0{,}9998) \quad (1)$$
$$y = 53.571x + 0.0022 \ (R^2=0{,}9999) \quad (2)$$

where: y = absorbance and x = drug concentration in ppm.

Dynamic Light Scattering (DLS)

The mean diameter of the nanoparticles, the polydispersity index (PDI) and the zeta potential were determined by dynamic light scattering, using the Nano Zetasizer equipment from Malvern® model ZS 3600, with a 633 nm laser reader, operated at an angle of 173°.

Results and Discussion

Yield and encapsulation efficiency

The yield of obtaining nanoparticles was 33% for the system with drug-free nanoparticles. In the MTX and 5-FU encapsulation steps, the yield was 31 and 42%, respectively.
Encapsulation efficiency of 12.0% ± 1.3 was reached for MTX and of 17.4% ± 0.3 for 5-FU.

Infrared absorption spectroscopy (FTIR)

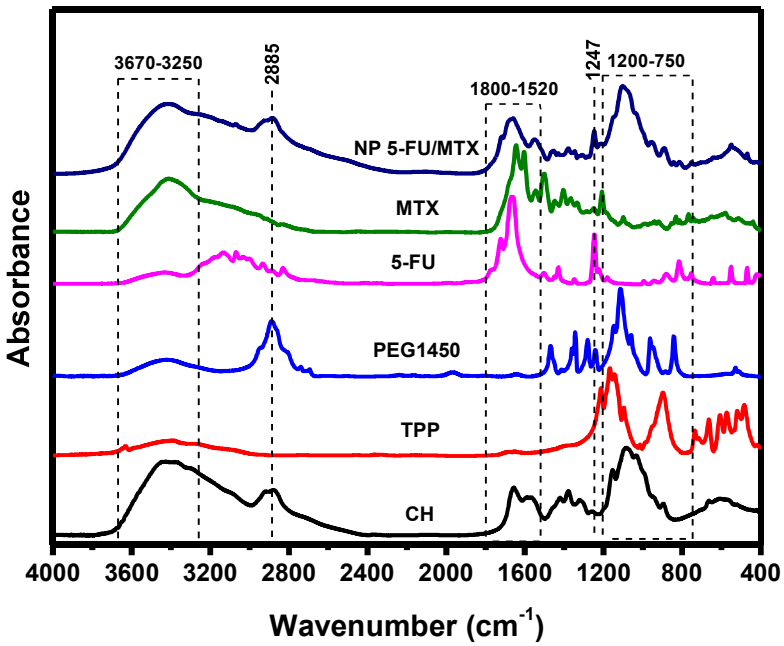

Figure 1 – FTIR spectrum in the range of 4000-400 $cm^{-1}$of chitosan, sodium tripolyphosphate, PEG 1450, MTX, 5-FU and the nanoparticle with double encapsulation.

Fig 1 shows the presence of characteristic bands of all starting materials in the nanoparticulate system. At 3420 cm^{-1} the presence of the band of strong intensity attributed to the stretching of the O-H and N-H bond present in the CH. At 2885 cm^{-1} a band attributed to symmetric and asymmetric stretching of C-H bonds [11]. The strong band in the region between 1800 and 1520 cm^{-1} is an overlap of the bands attributed to stretching of the C=O bond, present in CH, 5-FU also in MTX structure.[12-14] At 1247 cm^{-1} it is possible to observe the presence of a weak intensity band, which is attributed to the stretching of the single bond between C-N present in the 5-FU. In the FTIR spectrum of nanoparticles with 5-FU/MTX, in the region between 1200 cm^{-1} and 750 cm^{-1} several bands from the starting materials were observed.

Dynamic light scattering (DLS)

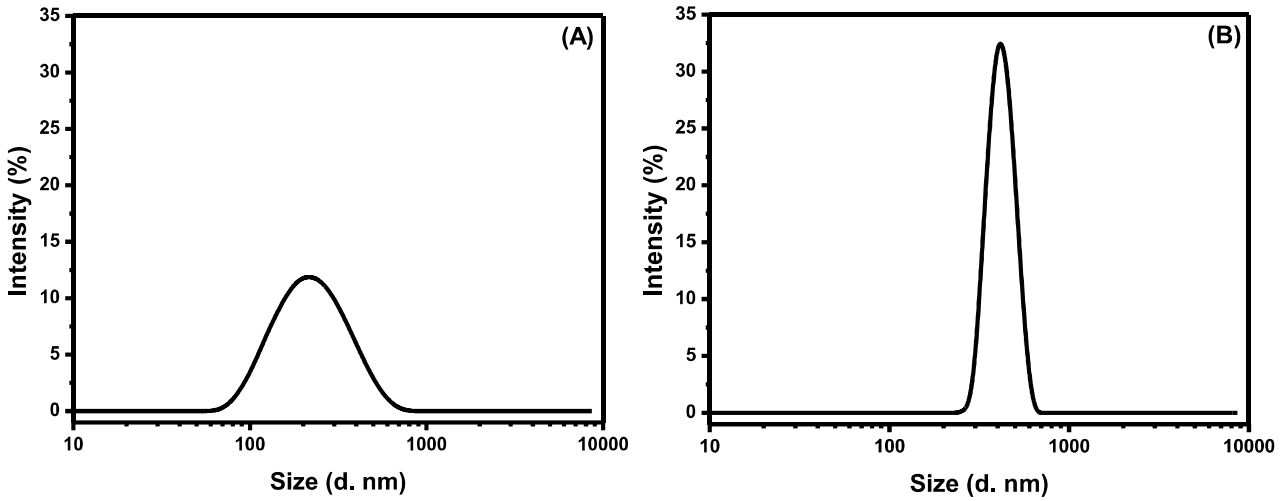

Figure 2 – Size distribution x intensity of: (A) drug-free nanoparticle; (B) NP MTX/5-FU.

In Fig. 2 the size distribution of the two systems presented a unimodal profile. Comparing the systems, the drug-free nanoparticle had a smaller diameter than the system with double encapsulation. This is due to the molar mass of MTX and 5-FU, 454 $g.mol^{-1}$ and 130 $g.mol^{-1}$, respectively.
Table 1 shows the diameter, polydispersion index and zeta potential of the nanoparticles. The NP diameter increased from 146 nm to 440 nm, along with the increase in PDI, rising from 0.214 to 0.380. The zeta potential followed the same trend, increasing from +27 to +31 mV, making the system more stable in solution.

Table 1 – Size, PDI and Zeta Potential of nanoparticles.

Sample	Size (d. nm)	PDI	Zeta Potential (mV)
NP	146 ± 2	0.214 ± 0.009	+27 ± 1
NP MTX/5-FU	440 ± 27	0.380 ± 0.001	+31 ± 1

Conclusions

Nanoparticles of MTX/5-FU were produced with a yield of 42%, with encapsulation efficiency of 12% and 17% for the encapsulation of MTX and 5-FU, respectively. The FTIR spectrum of the nanoparticles showed characteristic bands of the starting materials. The diameter of the systems were 146 and 440 nm for the systems without and with drugs. The zeta potential of the system was positive, which is ideal for systems targeting anticancer activity.
Therefore, these characteristics make the nanoparticulated system double encapsulated a potential anticancer application. thus, the nanoparticle can be studied later in *in vitro* assays against cancer cells, to evaluate its effect.

Acknowledgements
Acknowledgment to CNPq, FUNCAP, CAPES, INOMAT, INCT-Polysaccharides and UFC.

References

1. L. Sun et al., Asian Journal of Pharmaceutical Sciences 2017, 12, 418–423, doi: 10.1016/j.ajps.2017.04.002.
2. M. M. El-Hammadi, Á. V. Delgado, C. Melguizo, J. C. Prados, J. L. Arias, International Journal of Pharmaceutics 2017, 516, 61–70, doi: 10.1016/j.ijpharm.2016.11.012.
3. I. Khan, K. Saeed, I. Khan, Arabian Journal of Chemistry 2019, 12, 908–931, doi: 10.1016/j.arabjc.2017.05.011.
4. D. H. Hanna, A. A. Hamed, G. R. Saad, International Journal of Biological Macromolecules 2023, 240, 124396, doi: 10.1016/j.ijbiomac.
5. S. Ezrahi, A. Aserin, N. Garti, Advances in Colloid and Interface Science 2019, 263. 95–130, doi: 10.1016/j.cis.2018.11.004.
6. Y. Zhao, D. Y. Alakhova, X. Zhao, V. Band, E. V. Batrakova, and A. V. Kabanov, Nanomedicine 2020, 24, 102124, doi: 10.1016/j.nano.2019.102124.
7. C. Bailly, International Immunopharmacology 2019, 77, 105967, doi: 10.1016/j.intimp.2019.105967.
8. S. Khan, A. Madni, H. Shah, N. Jan, A. Shafiq, A. Basit, N. Rai, A. Ali, M. M. Khan, International Journal of Biological Macromolecules 2022, 222, 497–508, doi: 10.1016/j.ijbiomac.2022.09.196.
9. R. Verma, V. Singh, B. Koch, and M. Kumar, Colloids and Surfaces B: Biointerfaces 2023, 226, 113308, doi: 10.1016/j.colsurfb.2023.113308.
10. M. Samy, S. H. Abd El-Alim, A. E. G. Rabia, A. Amin, and M. M. H. Ayoub, International Journal of Biological Macromolecules 2020, 156, 783–791, doi: 10.1016/j.ijbiomac.2020.04.112.
11. A. Pawlak and M. Mucha, Thermochimica Acta 2003, 396, 153-166, https://doi.org/10.1016/S0040-6031(02)00523-3.
12. M. Rajaei, H. Rashedi, F. Yazdian, M. Navaei-Nigjeh, A. Rahdar, and A. M. Díez-Pascual, Journal of Drug Delivery Science and Technology 2023, 82, 104307, doi: 10.1016/j.jddst.2023.104307.
13. G. Radha, S. Raghunandhakumar, S. Balakumar, Journal of Drug Delivery Science and Technology 2023, 80, 104184, doi: 10.1016/j.jddst.2023.104184.
14. S. A. Ghumman, A. Mahmood, S. Noreen, A. Aslam, B. Ijaz, A. Amanat, R. Kausar, H. Hameed Arabian Journal of Chemistry 2023, 16, 2, 104463 doi: 10.1016/j.arabjc.2022.104463.

GELATIN-ALGINATE-BASED FILMS CONTAINING 1,4-ANHYDROUS-4-SELENE-D-THALITOL (SETAL) AS AN APPROACH FOR THE TREATMENT OF ATOPIC-DERMATITIS

Andressa Baptista Nörnberg[1]*, Guilherme T. Voss[2], Ethel A. Wilhelm[2], André R. Fajardo[1]

1 - Laboratório de Tecnologia e Desenvolvimento de Compósitos e Materiais Poliméricos (LaCoPol), Universidade Federal de Pelotas (UFPel), Pelotas-RS, Brazil
2 - Laboratório de Pesquisa em Farmacologia Bioquímica (LaFarBio), Universidade Federal de Pelotas (UFPel), Pelotas-RS, Brazil.
(*) andressanornberg@outlook.com.br

Abstract: This study investigates the encapsulation of 1,4-anhydro-4-seleno-d-thalitol (SeTal), a bioactive seleno-organic compound, in gelatin and alginate (Gel-Alg) polymeric films as a strategy for improving the treatment and attenuation of atopic dermatitis (AD) like symptoms in a mouse model. Hydrocortisone or vitamin C were encapsulated with SeTal in the Gel-Alg films, and their synergy was investigated. All the prepared film samples were able to encapsulate and release SeTal in a controlled manner. A series of in-vivo/ex-vivo experiments were performed using mice sensitization with dinitrochlorobenzene, which induces AD-like symptoms. Long-term topical application of the loaded Gel-Alg films attenuated disease symptoms and pruritus, with suppression of the levels of inflammatory markers, oxidative damage, and the skin lesions associated with AD. Moreover, the loaded films showed superior efficiency in attenuating the symptoms analyzed compared to hydrocortisone cream, a traditional AD treatment.

Keywords: *Skin diseases; 1,4-anhydro-4-seleno-D-talitol; hydrocortisone; vitamin C; biomaterials.*

Founding: The authors thank to CNPq (429859/2018-0, 312747/2020-9), FAPERGS (PqG 21/2551-0001943-3 and 21/2551-0002162-4), CAPES, the Independent Research Fund Denmark (Danmarks Frie Forskningsfond; DFF-7014-00047) and the Novo Nordisk Foundation (NNF13OC0004294 and NNF20SA0064214) for financial support.

Introduction

Atopic dermatitis (AD) is a well-known chronic inflammatory skin disease in which the patient experiences intense itching and recurrent eczematous lesions. The current treatments for this disease focus on restoring epidermal barrier function, with first-line therapies including topical corticosteroids. However, growing concerns regarding the use of this drug class among patients and medical professionals are resulting in decreased treatment compliance, which worsens AD control and patient welfare [1]. Accordingly, new agents are sought for the treatment and attenuation of AD symptoms as alternatives to corticosteroids.

In a previous study, we demonstrated the potential of SeTal (1,4-anhydro-4-seleno-D-talitol) to reduce inflammatory mediators associated with AD-type skin lesions induced by 2,4-dinitrochlorobenzene (DNCB) in mice [2]. To broaden our understanding of this compound and gain insight into its potential, herein we investigated the use of biopolymeric films composed of gelatin (Gel) and sodium alginate (Alg) loaded with SeTal as a local treatment for AD-like lesions. The use of these films as vehicles for the controlled release of SeTal is advantageous because it facilitates administration, increases compound bioavailability, and enables long-term treatment. The encapsulation of SeTal in a Gel-Alg film, in addition to overcoming the problems related to the rapid

release and loss of SeTal when applied to exudative lesions, due to the high solubility in water of this compound, also presents attractive properties for the preparation of biomaterials for application topical drugs on the skin. Blending Gel with Alg followed by crosslinking with low amounts of a carbodiimide allows the generation of materials with enhanced stability, mechanical and bioadhesive properties to be prepared [3].

Here, we also examined the potential additive effects of SeTal and other pharmacological agents used to treat AD symptoms, by also evaluating Gel-Alg films containing SeTal together with hydrocortisone (HC) or vitamin C (VitC). Despite concerns regarding the topical use of this corticosteroid, encapsulation of HC in a polymeric delivery device is an efficient alternative for controlling its systemic absorption, thereby limiting adverse side effects [4]. On the other hand, VitC is a powerful natural antioxidant that plays a pivotal role in various structural and functional skin processes. In this study, all prepared films were extensively characterized using a variety of analytic techniques, with systematic in-vitro/in-vivo/ex-vivo experiments used to evaluate their performance in the treatment and attenuation of AD-like symptoms in an animal model.

Experimental

Preparation of Gel-Alg films: The films (loaded or unloaded) were prepared by a conventional solvent casting method, with the composition of each sample detailed in Table 1. Experimentally, Gel was first solubilized in water (50 mL) at 60 °C for 1 h, after which Alg was added to this solution. The Gel:Alg mass ratio was fixed at 10:1 based on previous experiments. After homogenization, glycerol was added to the Gel-Alg solution, with stirring continued at 30 °C for another 30 min. *N*-(3-dimethylaminopropyl)-*N'*-ethylcarbodiimide hydrochloride (EDC) was then added to the solution while being vigorously stirred for 15 min prior to being poured into a Petri dish. Solvent casting followed by heating in an oven at 40 °C for 24 h led to a film, which was peeled from the Petri dish and stored in a dissector. The film samples loaded with SeTal, SeTal/HC, and SeTal/VitC were similarly prepared, with pre-determined amounts of the drug compounds added to the filmogenic solution with magnetic stirring for 30 min prior to the solvent-casting step. Based on previous experiments, the amounts of these compounds were adjusted to around 1 w/w% based on the total mass of biopolymer.

Table 1. Composition of the prepared Gel-Alg films.

Film	Gel (mg)	Alg (mg)	Glycerol (μL)[a]	EDC (mg)	SeTal (mg)	HC (mg)	VitC (mg)
Gel-Alg	900	90	100	5	-	-	-
Gel-Alg/SeTal	900	90	100	5	10	-	-
Gel-Alg/SeTal/HC	900	90	100	5	10	10	-
Gel-Alg/SeTal/VitC	900	90	100	5	10	-	10

[a] This volume refers to 126 μg of glycerol.

In-vivo and ex-vivo assays: Animal experiments were approved by the Committee for Care and Use of Laboratory Animals of the Universidade Federal de Pelotas (Brazil) (CEEA 4294-2015) according to the National Institutes of Health guidelines for the care and use of laboratory animals (65NIH Publications No. 8023, revised 1978). The experimental protocol for the *in vivo* experiments is summarized in Fig. 1. The mice were subjected to behavioral testing on the last day of the experimental protocol (day 30), after which the animals were euthanized and their backs, ears, and spleens were removed for further analysis. The effects of topically applying Gel-Alg, Gel-Alg/SeTal, Gel-Alg/SeTal/HC, and Gel-Alg/SeTal/VitC in cooperation with the control group were evaluated on skin lesion severity, scratching behavior, and back skin thickness.

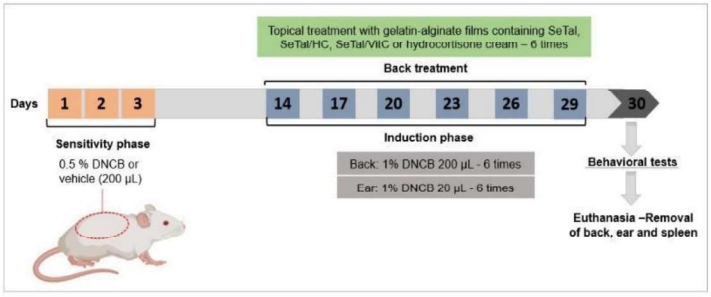

Fig. 1. Summary of the experimental protocol used to develop AD-like skin lesions in DNCB-sensitization mice.

Results and Discussion

Characterization of the Gel-Alg films

The chemical nature of the films was studied by FTIR spectroscopy with representative spectra presented in Fig. 2(a). The spectra of the Gel-Alg films exhibited major bands typically associated with the biopolymers used to prepare it, with those from Gel dominating, as it is present in excess. The band between 3600–3000 cm^{-1} is believed to reflect the high number of hydroxyl and amine groups, as well as the large number of H-bonds among the functional groups of Gel, Alg, and glycerol (the plasticizer). The shoulder-type band at 1689 cm^{-1} is assigned to amide C=O stretching formed through the crosslinking process. As reported by Staroszczyk et al. [5], EDC mediates the formation of iso-peptide bonds between amino groups and activated carboxylic groups of glutamic or aspartic acid residues in Gel. Since carboxylic groups are also available on the Alg backbone, we propose that amide bonds are also formed between the Gel and Alg chains. The spectrum of the film containing SeTal (Gel-Alg/SeTal) is similar to that of the bare film, indicative of weak interactions between this molecule and the polymer matrix, though the bands associated with C–H, C–O, and C–C vibration modes were more intense in the spectrum of Gel-Alg/SeTal compared to Gel-Alg, with these ascribed to contributions from the functional groups of SeTal. The spectrum of Gel-Alg/SeTal/HC exhibited a small band at 1742 cm^{-1} and a shoulder-type band at 1625 cm^{-1} assigned to the C=O and C=C stretching of HC. The more intense bands in the 1500–1200 cm^{-1} range are also attributed to HC, confirming the presence of this compound in the film. The spectrum of the film containing VitC exhibited the characteristic bands of Gel-Alg/SeTal with the additional bands observed at 3528, 1741, and 863 cm^{-1} assigned to the O–H, C=O, and C–C ring stretching vibrations of VitC. These findings confirm that VitC had been stably entrapped in the film. Moreover, these spectroscopic data indicate that both the SeTal and VitC in the Gel-Alg/SeTal/VitC films are physically entrapped in the polymer matrix, with no evidence of any chemical interactions.

The structures of the encapsulated compounds (SeTal, VitC, and HC) were determined by XRD. The data presented in Fig. 2(b), shows that Gel-Alg exhibits only a broad halo at around $2\theta \approx 20.3°$ in its XRD pattern, confirming the amorphous nature of this material. No significant changes were observed when the XRD pattern of the bare film was compared with those obtained from the drug-containing films (SeTal, SeTal/VitC, and SeTal/HC). The absence of diffraction peaks from these crystalline compounds (Fig. 1b) indicates that they undergo structural transitions to amorphous states during encapsulation. Thus, intermolecular interactions among SeTal, VitC, and HC with polymeric matrix appear to limit the crystallization of these compounds, which is advantageous in terms of drug solubility and release (cf. previous reports [6]).

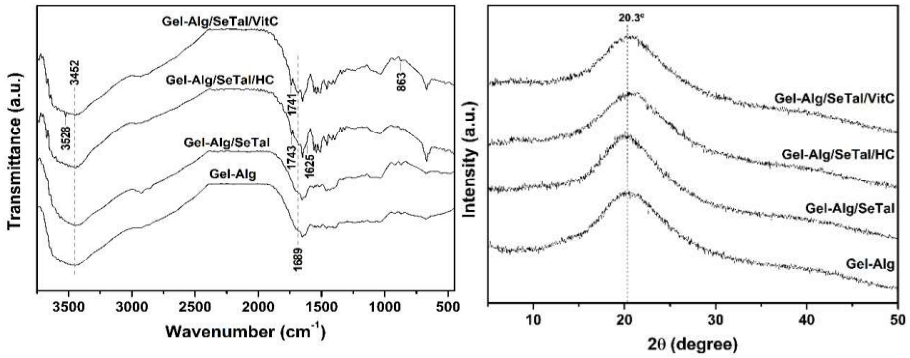

Fig. 2. (a) FTIR spectra and (b) XRD patterns of Gel-Alg, Gel-Alg/SeTal, Gel-Alg/SeTal/HC, and Gel-Alg/SeTal/VitC.

Effect of the prepared films on the clinical signs of AD-like skin lesions

DNCB has been used to induce AD-like skin conditions in mice. This small molecule of the hapten class penetrates the skin barrier and intact epidermis of mice to initially cause an acquired immune response. Repeated exposure leads to the development of an AD-like state [7]. DNCB induction causes anaphylaxis and the appearance of AD-like skin lesions, including thicker skin, dryness, swelling, edema, and erythema. The effects of topical application of Gel-Alg, Gel-Alg/SeTal, Gel-Alg/SeTal/HC and Gel-Alg/SeTal/VitC on skin lesion severity, itching behavior and back skin thickness can be observed in Fig. 3. One-way ANOVA followed by Tukey's post-hoc test revealed that DNCB significantly increased skin severity scores [$F_{6.42} = 45.79$, $p < 0.0001$], scratching behavior [$F_{6.42} = 420.3$, $p < 0.0001$] and back thickening [$F_{6.42} = 32.76$, $p < 0.0001$] compared with the control group, consistent with DNCB inducing an AD-like phenotype. Topical treatment with film loaded with Gel-Alg ($p < 0.0001$), Gel-Alg/SeTal ($p < 0.0001$), Gel-Alg/SeTal/HC ($p < 0.0001$) and Gel-Alg/SeTal/VitC ($p < 0.0001$) reduced the severity of DNCB-induced skin damage, scratching behavior, and back thickening. Gel-Alg/SeTal, Gel-Alg/SeTal/HC and Gel-Alg/SeTal/VitC films also significantly improved clinical and behavioral parameters compared to those detected with HC cream. DNCB-induced stimulation resulted in typical allergic responses including itching, erythema, skin thickening, edema, excoriation, and scaling typical of AD, and films improved these symptoms and pruritus.

AD induces a variety of immune responses, with the spleen being responsible for the production of immune cells, as well as other bodily functions [8]. Consequently, we measured spleen length and mass on day 30 to assess for splenomegaly, an indicator of immunologic abnormality [9]. This exposure to DNCB causes a significant increase in mouse spleen length [$F_{6.42} = 14.83$, $p < 0.0001$] and mass [$F_{6.42} = 39.26$, $p < 0.0001$], and this treatment with Gel-Alg ($p < 0.001$), Gel-Alg/SeTal ($p < 0.0001$), Gel-Alg/SeTal/HC ($p < 0.0001$) and Gel-Alg/SeTal/VitC ($p < 0.05$), as well as HC cream ($p < 0.01$), reducing these changes in the sensitization of animals with DNCB. The Gel-Alg/SeTal/HC film more effectively modulated these parameters than the HC cream. HC is a synthetic analog of cortisol and long-term administration is known to result in suppression of the hypothalamic-pituitary-adrenal (HPA) axis and adrenocorticotropic hormone, which leads to adverse effects including adrenal atrophy. In turn, changes in the HPA axis affect the immune system and inflammatory pathways [10], as observed in our study through changes in the spleens of animals sensitized with DNCB. Thus, the encapsulation of HC in the Gel-Alg film reduced the adverse effects of topical HC, while the incorporation of SeTal further improved its effects.

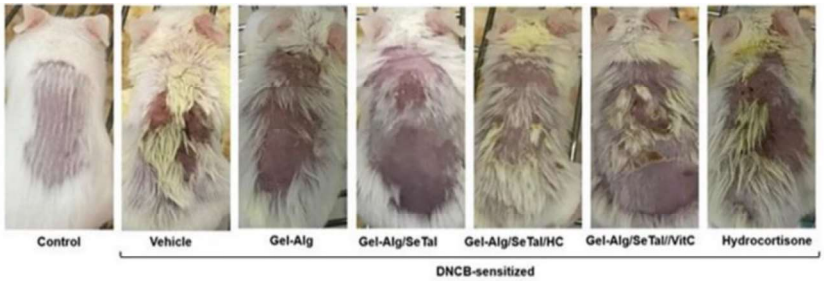

Fig. 3. Effects of topical treatment with various films (Gel-Alg, Gel-Alg/SeTal, Gel-Alg/SeTal/HC, and Gel-Alg/SeTal/VitC), as well as hydrocortisone cream on atopic-dermatitis-like (AD-like) symptoms in mice induced by DNCB, photographic images of dorsal skin.

Conclusions

Films of Gel and Alg were prepared and loaded with different compounds (SeTal, HC, and/or VitC) to serve as biomaterials for treating and attenuating symptoms of AD. Characterization analyses confirmed the presence of the compounds in the film matrices. A series of *in vivo/ex vivo* studies showed that films loaded with SeTal, HC, and/or VitC have beneficial effects on multiple parameters used to evaluate AD in a DNCB-induced model. These films were more efficient at treating or attenuating key disease parameters compared to the positive control (HC cream). Therefore, encapsulating SeTal with HC and/or VitC in a biopolymer film of Gel-Alg appears to be a promising alternative therapy for the long-term treatment of AD. Furthermore, these biopolymer films also reduced adverse effects associated with corticosteroids, such as HC. These films may also provide beneficial effects on other skin diseases.

References

[1] E. Axon; J. R. Chalmers; M. Santes; M. J. Ridd; S. Lawton; S. M. Langan; D. J. C. Grindlay; I. Muller; A. Roberts; A. Ahmed; H. C. Williams; K. S. Thomas. BMJ Open. 2021, 11, e046476. https://doi.org/10.1136/bmjopen-2020-046476.

[2] G. T. Voss; R. L. de Oliveira; M. J. Davies; W. B. Domingues; V. F. Campos; M. P. Soares; C. Luchese; C. H. Schiesser; E. A. Wilhelm. J. Trace Elem. Med. Biol. 2021, 67, 126795. https://doi.org/10.1016/j.jtemb.2021.126795.

[3] B. Cohen; O. Pinkas; M. Foox; M. Zilberman. Acta Biomater. 2013, 9, 9004. https://doi.org/10.1016/j.actbio.2013.07.002.

[4] G. T. Voss; M. S. Gularte; R. L. de Oliveira; C. Luchese; A. R. Fajardo; E. A. Wilhelm. Mater. Sci. Eng. C. 2020, 114, 111074. https://doi.org/10.1016/j.msec.2020.111074.

[5] C. Pena Serna; J. F. Lopes Filho, Food Technol. Biotechnol. 2015, 53. https://doi.org/10.17113/ftb.53.03.15.3725.

[6] M. Moghadam; M. S. Seyed Dorraji; F. Dodangeh; H. R. Ashjari; S.N. Mousavi; M.H. Rasoulifard, Eur. J. Pharm. Sci. 174 (2022) 106191. https://doi.org/10.1016/j.ejps.2022.106191.

[7] K. Saito, O. Takenouchi, Y. Nukada, M. Miyazawa, H. Sakaguchi, Toxicol. Vitr. 2017, 40, 11. https://doi.org/10.1016/j.tiv.2016.12.005.

[8] G.-H. Moon, Y. Lee, E.-K. Kim, K.-H. Chung, K.-J. Lee, J.-H. An, Nutrients. 2021, 13, 2448. https://doi.org/10.3390/nu13072448.

[9] S.-C. Han, G.-J. Kang, Y.-J. Ko, H.-K. Kang, S.-W. Moon, Y.-S. Ann, E.-S. Yoo, BMC Immunol. 2012, 13, 44. https://doi.org/10.1186/1471-2172-13-44.

[10] E. Kasahara, M. Inoue, Redox Rep. 2015, 20, 1. https://doi.org/10.1179/1351000214Y.0000000107.

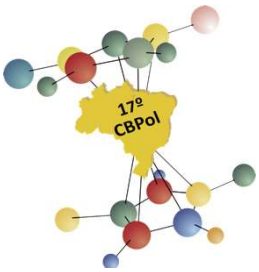

IN VITRO RELEASE AND *IN VIVO* PHARMACOKINETICS OF PRAZIQUANTEL LOADED IN PMMA-CO-DEAEMA SMART MICROPARTICLES

Emiliane D. Pereira[1]*, Luciana d. S. Dutra[1], Thamiris F. Paiva[2], Larissa L. d. A. Carvalho[3], Guilherme F. Ornellas[1], and José C. Pinto[1,3]

1 – Programa de Engenharia Química (PEQ-COPPE), Universidade Federal do Rio de Janeiro (UFRJ), RJ, Brazil

2 – Instituto SENAI de Inovação em Biossintéticos e Fibras (SENAI CETIQT), RJ, Brazil

3 – Programa de Engenharia de Processos Químicos e Bioquímicos (EQ), Universidade Federal do Rio de Janeiro (UFRJ), RJ, Brazil

emiliane@peq.coppe.ufrj.br

Abstract - Among neglected diseases around the world, schistosomiasis (caused by *Schistosoma mansoni*) is an important public health problem. This disease is treated through the oral administration of praziquantel (PZQ) and despite being a common pediatric disease, the treatment is with a large bitter- tasting tablet, which makes it difficult for patients' compliance. To allow more appropriate doses, improve taste acceptance for children and drug release at acidic pH, the drug PZQ was loaded on poly (methyl methacrylate) – co – (diethylamino)ethyl methacrylate) – PMMA-co-DEAEMA microparticles. The drug-loaded microparticles were characterized in vitro through dissolution tests and *in vivo* through pharmacokinetic analyses. The in vitro dissolution studies revealed a good PZQ release profile in an acidic medium, reaching values close to 100 % in less than 3 h. The *in vivo* pharmacokinetic analyses were conducted using an oral dose of 60 mg/kg. The microparticles showed to be an efficient release system, reaching an area under the curve (AUC) of 1063 ± 390 h.ng/mL.

Keywords: *praziquantel; drug polymer systems; PMMA-co-DEAEMA; microparticles; in vitro study; in vivo pharmacokinetics*

Fundings: Banco Nacional de Desenvolvimento Econômico e Social (Brasil)—PEQ-19391.

Introduction

Praziquantel (PZQ) is the drug of choice for the treatment of Schistosomiasis, a neglected disease considered the second-most important disease in tropical and subtropical areas (both in socioeconomic and public health terms), caused by a parasite called *Schistosoma mansoni* [1]. Although schistosomiasis is a common pediatric disease, the treatment is in the form of bitter-tasting, large tablets, which are usually split to provide a dose compatible with the child's weight, that makes difficult to treatment compliance [2]. To mask the taste of PZQ and allow more appropriate doses for children, polymer encapsulation is a very promising alternative. Among the many polymers that can be used for drug delivery systems, the copolymers of poly(methyl methacrylate) (PMMA) have been widely studied, since PMMA is a bio-inert material with many advantages such as low toxicity, highly compatibility with many drugs, and resistance to chemical hydrolysis [3]. A promising co-monomer for PMMA is 2-di(ethylamino)ethyl methacrylate

(DEAEMA), since with this it is possible to developed smart pH-responsive copolymer. The PMMA-co- DMAEMA smart copolymer can be used to improve the absorption of PZQ, as can be seen in the studies of [4] PAIVA et al. [5], ALVES et al. [6] and Pereira et al. [7] in which it was possible to produce pH-sensitive particles containing PZQ focusing the drug release preferentially in the acidic portions of the gastrointestinal tract. From this information, the main objective of the present work was to imprison praziquantel in the PMMA-co-DEAEMA matrix in the form of microspheres to mask the taste and odor of the drug evaluating the *in vitro* release and the *in vivo* pharmacokinetics of PZQ loaded in PMMA-co-DEAEMA microparticles.

Experimental

1. Materials

Methyl methacrylate (MMA) (purity of 99.5 wt% - stabilized with 100 ppm of tert-butylcathecol), DEAEMA (purity of 99 wt% and stabilized with 1500 ppm of hydroquinone monomethyl ether) were provided by Sigma Aldrich (St. Louis, MO, USA). Racemic mixture of PZQ was donated by Farmanguinhos (Rio de Janeiro, Brazil) with a minimum assay of 99 wt%. Azobisisobutyronitrile (AIBN) purity of 99 wt% and provided by Akzo Nobel, Arnhrm (The Netherlands) was used as a free-radical initiator. Hydrochloric acid (HCl), poly(vinyl alcohol) (PVA, with a minimum purity of 98 wt.%, a degree of hydrolysis of 88%, and a weight average molar mass of 2.5×10^4 g/mol), sodium dodecyl sulfate (SDS) Vetec (Rio de Janeiro, Brazil). Monobasic sodium phosphate monohydrate was provided by Vetec (Rio de Janeiro, Brazil), with minimum purity of 98 wt% and containing 2 wt% of water. Sodium phosphate dibasic anhydrous was provided by Vetec (Rio de Janeiro, Brazil) with minimum purity of 99 wt%. All chemicals were used as received, without any further purification. Ultra-pure water (obtained by reverse osmosis - Gehaka, Master System MS 2000, São Paulo, Brasil) was used as the dispersion medium for polymerization reactions.

2. Preparation of Smart PMMA-co-DEAEMA Microparticles Loaded with PZQ

All samples were prepared and analyzed in triplicates to observe reproducibility, which was always better than 5%.

To load PZQ and produce smart microparticles the in situ free-radical suspension polymerization, following the procedure described in the literature [5] was used. The aqueous phase was prepared with 1 wt% of PVA in relation to deionized water, and the organic phase was prepared with 30 wt% of PZQ, 1 wt% of AIBN, and 30 wt% of DEAEMA in relation to monomer MMA. The aqueous and organic phases ratio was equal to 70:30 and the polymerization reaction was carried out in a 1-L jacketed borosilicate glass reactor. The temperature used was 80ºC conducted under constant agitation of 1000 rpm (mechanical stirrer - model Eurostar Power Control, IKA, Germany), for 120 min. The reaction product was filtered with qualitative paper filter (80 g; porosity: 2.0 micra) and washed with deionized water using a vacuum filtration system. For the *in vitro* and *in vivo* tests, microparticles with diameters smaller than 106 μm were separated using granulometric sieves equipped with an electromagnetic agitator (model VP-01, Bertel, São Paulo, Brazil). The obtained particles will be referred to as PMMA-co-DEAEMA.

3. Characterizations

As the materials were analyzed in triplicates, the results are presented as averages of the obtained values. The particle size distributions were analyzed through dynamic light scattering (Mastersizer 2000, Malvern Instruments, Malvern, UK). The entrapment efficiency was determined through UV–VIS spectrometry (model Multiskan Go, ThermoScientific, Vantaa, Finland). For that, the polymer microparticles were weighed, dispersed in methanol, and left under magnetic stirring for 24 h. The material was filtrated using a syringe filter, Chromafil XTRA PET (25 mm–0.20 μm), and

the supernatant was analyzed through UV–VIS at 263 nm. *In vitro* dissolution test was performed using a dissolution tester (Ethik Tech- nology, São Paulo, Brazil) to verify the release rates of PZQ. Two different media were tested, one simulating the behavior in the gastric environment (aqueous HCl 0.1 M solution containing 0.2 wt% sodium lauryl sulfate) [8] and the other simulating the behavior in the intestinal environment (phosphate buffer pH 6.8). The dissolution tests were conducted in triplicates, using amounts of PMMA-co-DEAEMA microparticles corresponding to 0.66 g/L of PZQ and USP apparatus 2, operated at 37 ◦C under constant stirring of 50 rpm for a period of 3 h. The *in vivo* pharmacokinetic tests followed the rules of the ethical principles in animal experimentation adopted by the National Council for the Control of Animal Experimentation (CONCEA), the protocol used was reviewed and approved by the committee on ethics in animal use (CEUA) of CIEnP (Centro de Inovação e Ensaios Pré- Clínicos), under the numbers 217/01 and addenda 001 and 264/00 and is filed at CIEnP. This study was carried out by CIEnP, to do that it was used healthy rats of the *Rattus norvegicus* species and Sprague Dawley lineage from the breeding vivarium of CIEnP. The samples were prepared with final concentration of 60 mg/mL using glass vials, 2 wt% of Cremophor in an aqueous solution as a vehicle. The administration was by oral route (gavage), and the dose used was 60 mg/kg.

Results and Discussion

1. Particle Size Distribution

Figure 1A show PMMA-co-DEAEMA's size distribution, as can be seen the average diameter was equal to 28.7 ± 3 μm.

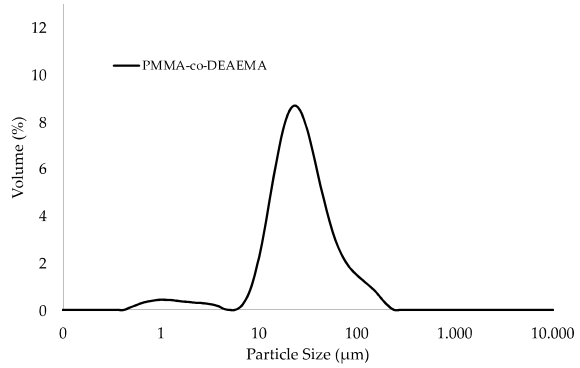

Figure 1 – PMMA-co-DEAEMA size distribution

It must be pointed out that the size of microparticle can be achieved through the manipulation of reaction operation parameters, such as type of surfactant, agitation, and the ratio between the dispersed and continuous phases. The average size obtained result is considered very good, since the smaller the particle size, less pronounced diffusional resistance, and consequently higher drug delivery efficiency [9] Besides that, particles smaller than 200 μm can improve the palatability of oral suspensions, reducing the feeling of roughness in the mouth [10]. Nonetheless, the analysis showed a high polydispersity, and wide particle size distribution can affect the release profile, since particles of different sizes will probably result in different rates of diffusion.

2. Dissolution

Prior to the dissolution study, the entrapment efficiency (EE) was calculated using UV-Vis spectroscopy. According to the analysis, the EE was equal to 96 ± 6 %. Figure 2 shows the release profiles of PZQ in the two different media. As can be seen, the release in the acid medium reaches almost 100% of PZQ released in the 3 hours interval, and the release in buffer solution (pH 6.8) does not reach 40% of PZQ released. That behavior confirms that the addition of the cationic comonomer makes the copolymer particles sensitive to pH modification. It is believed that the

protonation of the diethylaminoethyl groups takes place at acidic pH, resulting in hydrophilic structures that lead to more efficient swelling of copolymer matrix by water and higher rates of drug release in acidic aqueous environment.

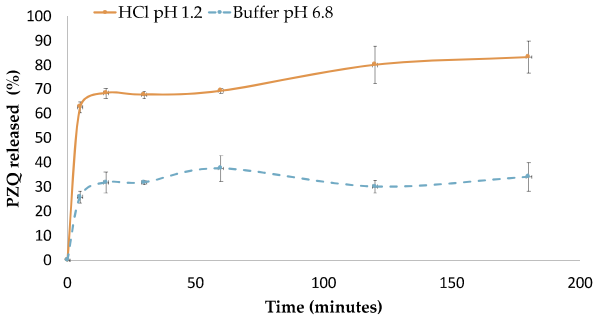

Figure 2 – PZQ release profile of smart microparticles using two different media: HCl - simulating the behavior in the gastric environment and Phosphate Buffer - simulating the behavior in the intestinal environment

3. Pharmacokinetic Studies

The obtained results showed that encapsulated PZQ was released from the polymer microspheres and absorbed in the gastrointestinal tract. The pharmacokinetic parameters are listed in Table 1 and PZQ plasma concentration profiles are shown in Figure 3.

As observed, PZQ in its free form reached maximum concentration (near 400 ng/L) after 15 min of oral administration and the smart microparticles based on PMMA-co-DEAEMA achieved significantly higher plasma concentrations (C_{max} = 1007 ± 83 ng/mL). That confirm the promising potential of using these polymer materials for drug entrapment and delivery. Additionally, bioavailability can also be evaluated through the area under the curves (AUC), which were statistically similar for free PZQ and smart microparticles.

Table 1. Pharmacokinetic parameters of animals treated with the evaluated polymer matrices (confidence level of 95%)

Parameters [1]	**Free PZQ**	**PMMA-co-DEAEMA**
C_{max} (ng/mL)	432 ± 98	1007 ± 83
AUC_{last} [2] (h.ng/mL)	1012 ± 424	1063 ± 390
AUC_{INF_obs} [3] (h.ng/mL)	1302 ± 525	1677 ± 384
K_e (1/h) [3]	0.25 ± 0.08	0.34 ± 0.08
T_{max} (h)	0.25	0.33 ± 0.08
$T_{1/2\beta}$ (h) [3]	3.64 ± 1.46	2.24 ± 0.46

[1] C_{max} (maximum concentration); AUC (area under the curve); K_e (elimination constant); T_{max} (time to reach maximum concentration); $T_{1/2\beta}$ (elimination half-life). Data expressed as mean ± confidence interval of mean.
[2] Last point collected after 8 h.
[3] Calculated with help of an exponential interpolator.

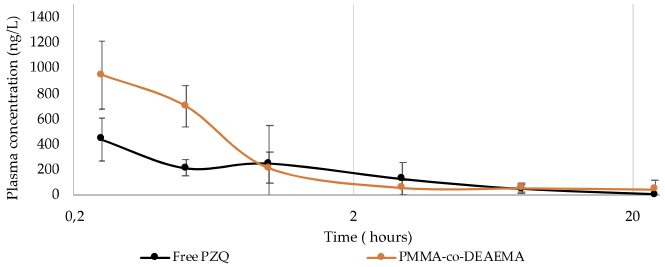

Figure 3 – PZQ release profile

Conclusions

The present study evaluated *in vitro* and *in vivo* release rates of loaded praziquantel (PZQ) in smart microparticles. The employed polymerization technique was efficient in producing polymer microparticles, presenting a small particle size, average 28.7 ± 3 μm and allowing the entrapment of PZQ with efficiencies near 100%. The obtained results showed that the smart PMMA-co-DEAEMA released close to 100 % of PZQ in less than 3 h. The *in vivo* pharmacokinetic analyses were conducted using free PZQ as the control group to compare to smart microparticles. This study showed that smart microspheres provided better absorption profile than the free form, displaying 2.2 times higher Cmax average value (1007 ± 83 ng/mL) than that obtained for PZQ in the free form (432 ± 98 ng/mL). Based on all these positive and encouraging results, the polymer matrix based on PMMA-co-DEAEMA showed to be very promising for the preparation of a new pharmaceutical product.

Acknowledgements

The authors thank CAPES (Coordenação de Aperfeiçoamento de Pessoal de Nível Superior), CNPq (Conselho Nacional de Desenvolvimento Científico e Tecnológico), FAPERJ (Fundação Carlos Chagas Filho de Amparo à Pesquisa do Estado do Rio de Janeiro) for supporting this work and providing scholarships, BNDES (Banco Nacional de Desenvolvimento Econômico e Social -Brasil) and Fiocruz (Fundação Oswaldo Cruz).

References

1. WHO Schistosomiasis. Available online: https://www.who.int/news-room/fact-sheets/detail/schistosomiasis (accessed on May, 25th, 2023).
2. M. Münster, MSc Dissertation, Heinrich-Heine-Universität Düsseldorf: Düsseldorf, Germany, 2018.
3. Y. Gao; J. Zhang; J. Liang; D. Yuan; W. Zhao; Eur. Polym. J. 2022, 175, 111379. https://doi.org/10.1016/j.eurpolymj.2022.111379.
4. A. Bratek-Skicki; Recent Advances and Challenges. Appl. Surf. Sci. Adv. 2021, 4, 100068. https://doi.org/10.1016/j.apsadv.2021.100068.
5. T.F. Paiva; J.B. Alves; P.A. Melo; J.C. Pinto; Macromol. React. Eng. 2019, 13, 1900028. https://doi.org/10.1002/mren.201900028.
6. J. B. Alves; T.F. Paiva; V.M. Salim; H. C. Ferraz; J.C. Pinto; SPE Polym. 2021, 2, 110–121. https://doi.org/10.1002/pls2.10037.
7. E. D. Pereira; L. S. Dutra; T. F. Paiva; L.L.A. de Carvalho; H.V.A. Rocha; J.C. Pinto; Materials 2023, 16, 3382. https://doi.org/10.3390/ma16093382
8. ANVISA. Farmacopéia Brasileira; Agência Nacional de Vigilância Sanitária: Brasília, Brazil, 2010.
9. S. A. Kulkarni; S. -S. Feng; Pharm. Res. 2013, 30, 2512–2522. https://doi.org/10.1007/s11095-012-0958-3.
10. Kimura, S., Uchida, S., Kanada, K., & Namiki, N. Int. J. Pharm., 2015 484,156–162. doi:10.1016/j.ijpharm.2015.02.

3D PRINTING OF POLY(Ɛ-CAPROLACTONE) METHACRYLATED/ SILANIZED-NANO-HYDROXYAPATITE RESIN BASED: SYNERGY IN MORPHOLOGY AND FUNCTIONALIZATION

Thiago Nunes Palhares[1], João F. P. Lovo[2], Gabriela C. Rodrigues[1], Alessandra L. Poli[1], Izaque A. Maia[3], Claudio Y. Morassuti[3], Jorge V. L. da Silva[3] and Carla C. Schmitt[1]

carla@iqsc.usp.br

1- São Carlos Institute of Chemistry – University of São Paulo (IQSC-USP), São Carlos, SP, Brazil

2- São Carlos School of Engineering University of São Paulo(EESC-USP), São Carlos, SP, Brazil

3- Division of Technology for Production and Health (DITPS), Renato Archer Information Technology Center (CTI)

Abstract – Additive manufacturing technology has been widely employed in the field of tissue engineering to create implants with a variety of shapes, sizes, and mechanical characteristics(1). Within this context, it can be used to produce three-dimensional structures known as scaffolds, which serve as support for the growth of cells and tissues(2,3). In this study, photosensitive polycaprolactone (PCL) resins were developed, a biocompatible and bioabsorbable polymer, with the incorporation of methacrylate groups. To enhance its properties, bioceramic fillers were added, hydroxyapatite (HAp), which also presents bioactivity in bone and dental tissues. Furthermore, the surface of the hydroxyapatite was treated with 3-aminopropyltrimethoxysilane (APTES) to promote greater interaction between the polymeric matrix and the inorganic filler. The developed resins were characterized by their mechanical and physical-chemical properties and were used for printing scaffolds, whose porosity and architecture were evaluated.

References:

1. S. Naghieh; M. R. K. Ravari; M. Badrossamay; E. Foroozmehr; M. Kadkhodaei *J Mech Behav Biomed Mater* 2016, *59*, 241. https://doi.org/10.1016/j.jmbbm.2016.01.031
2. J. Zhang; P. Xiao *Polym Chem* 2018, *9*,1530. https://doi.org/10.1039/C8PY00157J
3. S. Eshraghi; S. Das *Acta Biomater* 2012; *8*,3138. . https:// 10.1016/j.actbio.2012.04.022

Fundings:
.CAPES, CNPq, FAPESP.

Keywords:
Tissue engineering, 3D printing, photopolymerization, polycaprolactone, silanization.

ALGINATE/HYDROXYAPATITE FILMS WITH ANTIMICROBIAL PROPERTY AS A WOUND DRESSING

Marcela P. Bernardo[1,2*], Daniel Pasquini[1], Luiz H.C. Mattoso[2]
1 – Institute of Chemistry, Federal University of Uberlândia, Uberlândia, MG, Brazil
marcelapiassib@gmail.com
2 – National Nanotechnology Laboratory for Agribusiness. Embrapa Instrumentation, São Carlos, SP, Brazil

Abstract – Human skin, the body's largest organ, is essential for physical protection, sensory touch, and thermoregulation.[1] Wounds are described as skin integrity and function disruptions and may be caused by different factors, such as burns, mechanical trauma, and diseases.[2] Wound dressings exercise an essential function in supporting wound healing.[3] They provide a physical barrier between the wound and the external environment to prevent further damage or infection.[4] Considering the lack of wound dressing materials able to deliver antimicrobial agents and promote adequate healing of tissues, a wound dressing based on alginate and hydroxyapatite (HA) composite film is proposed. Alginate and alginate/hydroxyapatite (1%, w/w) composite films were obtained by continuous casting method and crosslinked with copper. X-ray diffraction (XRD) measurements were conducted on a Shimadzu XRD 6000 diffractometer, over the 2θ range of 10–70°, 1° min^{-1}. The water vapor permeability (WVP) of films was determined by ASTM E96 with modifications. The antimicrobial activity of the films was tested against *Escherichia coli* (ATCC 11229) and *Staphylococcus aureus* (ATCC 6538) as per the disc diffusion test methodology. Alginate exhibited a broad peak around 23°, characteristic of amorphous alginate.[5] The addition of hydroxyapatite to the alginate matrix affected the crystalline structure of the polymer: the broad reflection of alginate decreased and the characteristic peaks of HA become evidenced, indicating the interaction between HA and alginate on the composite. Water vapor permeability (WVP) is a fundamental property of wound dressings because the moisture content on the wound is essential for tissue healing. WVP of the composite films were higher in relation to pure alginate film, therefore the composite alginate films are more adequate for wound healing applications since an ideal environment for wound healing can be created. In addition, alginate/HA composite film displayed antimicrobial activity against both studied bacteria.

References:

1. Munhoz, D. R.; Bernardo, M. P.; Malafatti, J. O. D.; Moreira, F. K. V.; Mattoso, L. H. C.; *Int. J. Biol. Macromol.* 2019, *141*, 504. [https://doi.org/10.1016/j.ijbiomac.2019.09.019]
2. Abbafati, C. et al.; *Lancet* 2020, *396*, 1135. https://doi.org/10.1016/S0140-6736(20)31404-5
3. Bakhsheshi-Rad, H. R.; Hadisi, Z.; Ismail, A. F.; Aziz, M.; Akbari, M.; Berto, F.; Chen, X. B.; *Polym. Test.* 2020, *82*, 106298. https://doi.org/10.1016/j.polymertesting.2019.106298
4. Zhang, M.; Zhao, X.; *Int. J. Biol. Macromol.* 2020, *162*, 1414. [https://doi.org/10.1016/j.ijbiomac.2020.07.311
5. Salimi, E.; *Carbohydr. Polym.* 2021, *267*, 118236. https://doi.org/10.1016/j.carbpol.2021.118236

Fundings: The authors are thankful for financial support from FAPESP (grant n° 2018/07860-9) and CNPq/FAPEMIG (grant n° 150371/2023-3 and BPD-00165-22)

Keywords: wound healing, polymer composite, hydroxyapatite, tissue engineering.

COMPOSITE MEMBRANES OF POLY (GLYCEROL SEBACATE) WITH CALCIUM PHOSPHATES FOR BONE TISSUE REGENERATION

João F. Gomes-Neto[1], Carla S. Riccardi[1].

1 – Department of Bioprocess and Biotechnology, Sao Paulo State University (UNESP), Botucatu, SP, Brazil.
joao.f.gomes@unesp.br

Bone fractures occur frequently in the world population, reaching about 8.9 million cases in 2022, for example. As a result, new biomaterials such as titanium derivatives and its alloys, bioceramics, biopolymers, and composite materials are being developed. Bone tissue is a specialized connector that undergoes mineralization processes with calcium phosphates in the form of hydroxyapatite. Regeneration of bone tissue is a biological process controlled by progenitor cells capable of forming new osteoblasts. In this study, we investigated poly (glycerol sebacate) (PGS), a synthetic material with great osteogenic potential that has attracted more attention in the field of tissue regeneration (e.g., bone tissue) due to its good biocompatibility and high elasticity. This polymer can be designed to achieve mechanical properties and degradation rates targeted to a specific application, and has a chemically cross-linked structure that allows elastic recovery after impacts. The focus of this work is to investigate the physical, chemical and biological properties of PGS in its dense and porous form with the addition of calcium phosphates for bone regeneration. PGS was synthesized by prepolymerization of glycerol and sebacic acid in microwave followed by curing at 150°C for 24 hours. By modified protocols from the literature, the simulated body fluid (SBF) method was used to deposit calcium phosphates on PGS. The test samples were characterized for their structural and chemical properties by attenuated total reflectance Fourier transform infrared spectroscopy (ATR-FTIR), water vapor permeability, degree of swelling, and hydrolytic degradation. The tests have shown that the structurally modified PGS with the addition of calcium phosphates has great potential for use in bone tissue regeneration. Therefore, the chosen synthesis and chemical modification strategies were effective in producing a promising biomaterial that is cost-effective, biocompatible, bioresorbable and can be used for bone tissue development.

References

1. T. J. de Villiers & S. R. Goldstein. *Climacteric 2022*, *25:1*, 1-3. https://doi.org/10.1080/13697137.2021.1965408.
2. Datta, H. K., Ng, W. F., Walker, J. A., Tuck, S. P. & Varanasi, S. S. *J Clin Pathol 2008;61*:577–587. doi:10.1136/jcp.2007.048868.
3. Murphy, C. M., O'Brien, F. J., Little, D. G. & Schindeler, A. *European Cells & Materials 2013. 26*, 120-132. doi:10.22203/eCM.v026a09.
4. Gadomska-Gajadhur, A., Wrzecionek, M., Matyszczak, G., Pietowski, P. Wiechaw, M. & Ruskowski, P. *Organic process research & development 2018. 22*, 1793. doi: 0.1021/acs.oprd.8b00306.
5. Aydin, H. M., Salimi, K., Rzayev, Z. M. & Piskin, E. *Biomater. Sci. 2013. 1*, 503. doi:10.1039/c3bm00157a.
6. Tas, A. Cuneyt. *Biomaterials 2000. 21*, 1429-1438. doi:10.1016/s0142-9612(00)00019-3.

Fundings: CAPES – Coordenação de Aperfeiçoamento de Pessoal de Nível Superior

Keywords: *biopolymers, osteogenic potential, tissue regeneration, poly (glycerol sebacate), calcium phosphates.*

DEVELOPMENT OF COPOLYMER FILAMENT FOR 3D PRINTING BASED ON POLY(L-LACTIC ACID-CO-TRIMETHYLENE CARBONATE)

Gabriela A. Dias[1] and Sérgio H. Pezzin[1]

1 – Department of Chemistry, Santa Catarina State University (UDESC), Joinville, SC, Brazil
gabriela.alinedias@gmail.com

Abstract – The polymer poly-L-lactic acid (PLLA) has biomedical applications due to its biocompatibility and resorption. However, its hydrolysis releases lactic acid, resulting in an intense inflammatory reaction due to the pH decrease at the implantation site.[1] To mitigate this effect, the use of copolymer poly(l-lactic acid-co-trimethylene carbonate) (PLLA-PTMC) is proposed as a biocompatible material with a mild inflammatory response.[2] Currently, additive manufacturing is gaining ground in the biomedical field through three-dimensional printing (3D), enabling the production of customized prosthetics for each patient.[3] In order to enable 3D printing of absorbable parts with a mild inflammatory reaction, the production of filaments from PLLA-PTMC pellets (Resomer LT706S, Evonik) was tested through extrusion. The parameters were divided into 3 conditions: 170°C/without prior dehumidification, 170°C/with dehumidification, and 190°C/with dehumidification. The extrusion was carried out in a single-screw mini-extruder at 14 RPM, and the dehumidification was performed in an oven for 1 hour at 60°C. The temperature of 170°C was selected based on the differential scanning calorimetry (DSC) analysis, and the temperature of 190°C followed the proposal of Marchewka.[4] After extrusion of the 170°C/without dehumidification group, it was observed that the filament had roughness and imperfections, confirming the need for dehumidification in the other groups. The temperature of 170°C was not efficient, showing small defects along the filament attributed to partial polymer fusion. The temperature of 190°C yielded the best result, a homogeneous filament without imperfections. Then, a type V test specimen (ASTM D638) was printed on a 3D printer (Ender-3 PRO, Creality) using the 190°C filament. It was performed with a heated bed at 40°C, a nozzle temperature of 190°C, and a speed of 10 mm/s. The printed piece showed no defects or deformities, concluding that the filament is viable for 3D printing.

References

1. P. C. Lívia; M. F. de A. B. Carlos; A. N. T. N. Adriana; R. F. de B. Rodrigo; U. J. P. G. Marcelo; G. M. José; L. S. Rafael; M.C. D. Mônica; *Materials*, 2019, 12, n. 7, p. 1186, 2019. https://doi.org/10.3390/ma12071186
2. F. Tiziana; M. Torbjörn; F. Anna *American Chemical Society (ACS)*, 2019, 20, n. 3, p.1346-1361. http://dx.doi.org/10.1021/acs.biomac.8b01739.
3. D. E. G. Kasper; V.B. Bas; S. V. Jukka; *Biomacromolecules*, 2019, 21, n. 2, p. 366-375 http://dx.doi.org/10.1021/acs.biomac.9b01272.
4. M. Jakub; L. Jadwiga; *The international Journal of Advanced Manufacturing Technology*, 2020, 106, p. 4933-4944 https://doi.org/10.1007/s00170-020-04981-z

Keywords: 3D printing, Copolymers, Poly-lactic acid, Poly-trimethylene carbonate

EXTRUSION OF POLYCAPROLACTONE AND F18 BIOACTIVE FILLER COMPOSITES

Thiago A. Augusto[1*], Murilo C. Crovace[1,2,3] and Lidiane C. Costa[1,2,4]

1 – Graduate Program in Materials Science and Engineering (PPGCEM), Federal University of São Carlos (UFSCar), São Carlos, SP, Brazil
2 – Department of Materials Engineering (DEMa), UFSCar, São Carlos, SP, Brazil
3 – Bioactive Materials Laboratory (LMBio), UFSCar, São Carlos, SP, Brazil
4 – Center of Characterization and Development of Materials (CCDM), UFSCar, São Carlos, SP, Brazil
**Corresponding author: augusto.a.thiago@gmail.com*

Abstract

Polymer composites with bioactive fillers have great potential in biomedical applications due to the combination of mechanical and bioactive properties. Polycaprolactone (PCL) is a low melting temperature bioabsorbable polymer, while F18 is a bioactive glass with good processability, which favors its spinning from melt. So far, there has not been an investigation into composites of these materials obtained through extrusion. In order to study their properties, PCL 3D printing filaments with up to 12.5 wt% continuous and discontinuous fillers (powder and short fiber) of F18 were extruded and analyzed by differential scanning calorimetry, thermogravimetry and parallel plate rheology. For comparison, conventional glass fillers were also used. Manufacturing was successful, including the extrusion through a crosshead die for coating of glass fiber bundle. Composites with bioactive fillers showed lower thermal stability (up to 62°C below the decomposition temperature of neat PCL, 419°C), possibly because the ions released by these fillers are catalysts for chain scission reactions during melt processing [1]. Conventional powder and short fibers had a nucleating effect (increase of up to 7.9% in the degree of crystallinity compared to neat PCL), while bioactive powder restricted the ordering (decrease of up to 7.1% in the degree of crystallinity). Short and continuous bioactive fibers tend to lower the melting temperature (from 64°C to 59°C), a phenomenon attributed to matrix degradation. Short fibers raised the viscosity of the polymer more than the powder. However, by filtering the fillers, it is observed that short fibers and mainly the powder reduce the viscosity of the matrix, possibly due to the reduction of the molar mass. The results indicate that these composites are promising in the development of scaffolds through additive manufacturing.

References

[1] E. H. Backes et al., *J. Compos. Sci. 2019, 3(2)*, 52.

Fundings: This study carried out with financial support by the Coordenação de Aperfeiçoamento de Pessoal de Nível Superior – Brasil (CAPES) – Finance Code 001. Scholarship process no 88887.464623/2019-00.

Keywords: bioactive filler, bioactive glass fiber, biomedical composite

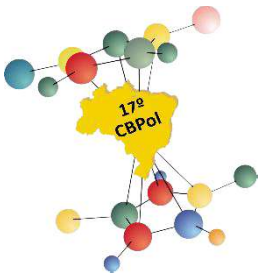

INFLUENCE OF DEGRADATION OF PLA/ZNO BIOCOMPOSITES ON SCAFFOLD CELL VIABILITY

Felippe Marega[1], Larissa Klok[2], Teresa T. Steffen[2], Samarah Harb[1], Henrique R. Sabedra[2], Daniela Becker[2] Luiz A. Pesssan[1] and Lidiane Costa[1] *

1 – Department of Materials Engineering (DEMa), Federal University of São Carlos (UFSCar), São Carlos, SP, Brazil
Felippe.m.marega@gmail.com
2 – Department of Mechanical Engineering, State University of Santa Catarina (Udesc), Joinville, SC, Brazil

The incorporation of zinc oxide (ZnO) into poly (lactic acid) (PLA) is a promising strategy for the manufacture of bioactive scaffolds for bone tissue application[1]. However, the degradation of the PLA matrix stimulated by the release of Zn^{2+} ions during processing is an obstacle to the application of this composite, since the acidic products resulting from degradation and the fast release of ions decrease cell viability in the culture medium[2]. Here, we functionalized ZnO with maleic anhydride using plasma, and subsequently fabricated the PLA-ZnO composites (5 and 10 wt% ZnO), aiming to control the ion release and degradation. This study analyzed whether plasma functionalization with maleic anhydride of ZnO particles (ZnO_MA) for 5 and 15 minutes effectively controls PLA degradation and, consequently, maintain the biocompatibility of the scaffolds. The material processing occurred through an internal mixer coupled with a torque rheometer at 175°C and 60 rpm for 5 min, with 5% and 10% ZnO. Afterward, scaffolds were manufactured by 3D printing. Thermogravimetric analysis (TGA) was used to evaluate the thermal stability of the composites and cell viability assay (WST-1) was performed to analyze mesenchymal stem cells proliferation of the scaffolds. TGA analysis showed that PLA/ZnO_MA biocomposites present an onset degradation temperature close to PLA, and 30 °C higher than the PLA-ZnO without plasma treatment. From the biological analysis, the samples containing raw ZnO decreased cell viability, with 10% ZnO being cytotoxic (≤ 70%); while the incorporation of ZnO_MA maintained the biocompatibility of the PLA. The cytotoxicity of PLA/ZnO composite is a consequence of the low pH caused by the release of acidic degradation products of PLA and the intense release of Zn^{2+} ions. We demonstrated that the ZnO plasma functionalization with maleic anhydride has excellent potential in controlling PLA degradation, therefore enabling cell proliferation.

References

1. Kołodziejczak-Radzimska, A.; Jesionowski, T. Zinc Oxide—From Synthesis to Application: A Review. Materials 2014, 7, 2833-2881. https://doi.org/10.3390/ma7042833.
2. Dutta, Tanushree, et al. Surface Engineered ZnO-Humic/Citrate Interfaces: Photoinduced Charge Carrier Dynamics and Potential Application for Smart and Sustained Delivery of Zn Micronutrient. ACS Sustainable Chemistry & Engineering, ,2019 l7,12. https://doi.org10.1021/acssuschemeng.9b01917.

Fundings: This study was financed in part by the Coordenação de Aperfeiçoamento de Pessoal de Nível Superior - Brasil (CAPES) - Finance Code 001. This study was financed by FAPESP (19/27415-2)
Keywords: *PLA; Zinc Oxide; Scaffold; Cellular Viability*

MECHANICAL CHARACTERIZATION OF HYDROGELS ENVISIONING ITS APPLICATION IN NEURAL NICHE

Eduardo H Backes[1-2*], Leonardo A. Pinto[2], Luiz A Pessan[1-2], Marimélia A Porcionatto[3-4]

1 – Department of Materials Engineering (DEMa), Federal University of São Paulo, São Carlos, SP, Brazil
2 – Graduate Program in Materials Science and Engineering, Federal University of São Carlos, São Carlos, SP, Brazil
3- Department of Biochemistry, Universidade Federal de São Paulo, Sao Paulo, São Paulo, Brazil,
4- Laboratory of Molecular Neurobiology, Universidade Federal de São Paulo, São Paulo, Brazil
**backes@ufscar.br*

Abstract

Hydrogel networks, composed of cross-linked polymers in a three-dimensional (3D) structure, can absorb and retain substantial quantities of water. The adjustable characteristics and adaptable manufacturing techniques of hydrogel materials have facilitated their utilization in various biomedical and engineering fields. These applications encompass tissue engineering, regenerative medicine, wastewater treatment, and soft robotics. With the advent of additive manufacturing, hydrogels have been used along with cells to develop bioinks and to manufacture bioprinted structures with a series of functions such as maintaining the phenotype and/or differentiation, envisioning disease modeling, and tissue engineering. For that, some properties are necessary: biocompatibility, biodegradation in a controlled manner, adequate rheological properties that allow printing, and mechanical properties like those of the tissue you want to recreate. Therefore, this study assessed different biocompatible hydrogels, aiming to recreate the neural niche for disease modeling. The systems were composed of gelatin methacrylate (GelMA), gelatin/GelMA, gelatin/GelMa/alginate (Al) and Gellan Gum (GG)/GelMa. The hydrogels developed were characterized by mechanical properties, biodegradation and cell viability (live-dead). The mechanical properties were assessed under a compression regime, and the specimens were cast into a Petri dish and further stamped with a punction to fabricate reproducible samples. The biodegradation was analyzed by evaluating their mass variation when exposed to PBS solution under different time points, and finally, their biocompatibility was determined by live-dead assay. By tailoring the hydrogel compositions, they presented compressive modulus from 5-10 kPa, biodegradation from several days to months and high biocompatibility (viability higher than 80%).

References

1. R. Ibañez; R.I. do Amaral; R.J.F.C., Reis; R.L., Marques; A.P., Murphy; C.M. ; O'Brien, F.J *Polymers* 2021, *13*, 2510. https://doi.org/10.3390/polym13152510.
2. V.H.M. Mouser; F.P.W. Melchels; J. Visser; W.J.A. Dhert; D. Gawlitta; J. Malda *Biofabrication* 2016, *8*. https://doi.org/10.1088/1758-5090/8/3/035003

Fundings: This work was supported by The São Paulo Research Foundation (FAPESP), grant numbers 2016/19084-8, 2018/12605-8, 2020/05289-2, 2020/13742-2, 2020/06153-7, 2021/14327-8; Coordination for the Improvement of Higher Education Personnel (CAPES), financial code 001; and National Council for Scientific and Technological Development (CNPq), grant number 309679/2018-4.
Keywords: *biofabrication, bioprinting, hydrogel, tissue engineering.*

SYNTHESIS, CHARACTERIZATION AND ANTIMICROBIAL PROPERTIES OF CHITOSAN-SILVER NANOPARTICLES FOR COATING MEDICAL DEVICES

Marcos A. Polinarski[1,2*], Manuela N. Ladeira[3], Phuong Nguyen-Tri[2], Juliana B. Wenzel[3], Helton José Alves[1]

1 – Laboratory of Materials and Renewable Energies, Department of Engineering and Exact Sciences, Federal University of Paraná (UFPR), Palotina, PR, Brazil marcospolinarski@ufpr.br
2 – Laboratory of Advanced Materials for Energy and Environment, Department of Chemistry, Biochemistry and Physics, University of Québec in Trois-Rivères, Trois-Rivières, QC, Canada.
3 – Federal University of Paraná (UFPR), Toledo, PR, Brazil

Microbial colonization and biofilm formation is one of the biggest concerns related to indwelling and implantable medical devices (e.g., Central Venous Catheter), that cause a threat to the health and the life of patients [1]. Due to the rise of resistance of specific bacterial strains towards antibiotics, there is an urgent need to develop technologies that can adequately protect against those pathogens [2]. Chitosan, a chitin-derived biopolymer, has been widely used to synthesize antimicrobial films and coatings, especially in the presence of inorganic metals, such as silver, due to its oligodynamic effect when in nanoparticles (NPs) form [3]. Combining silver and chitosan in a single material is one strategy to prevent biofilm formation. This work aimed to synthesize Chitosan-Silver nanoparticles (CS-AgNPs) to be used as an antimicrobial coating in medical devices. For the synthesis, chitosan and silver nitrate solution were combined in different ratios (2:1; 4:1; 6:1 (w/w)) and heated until boiled for 6 hours. The formed solution was characterized by Dynamic Light Scattering, UV-Vis spectra, and Scanning Electron Microscopy, and it has its antimicrobial and antibiofilm properties verified against *Staphylococcus aureus* by the Minimum Inhibitory Concentration method and biofilm formation assay, adapted from [4]. The synthesis was successfully performed, resulting in nanoparticles with a distribution size smaller than 100 nm. The presence of NPs was also confirmed by UV-vis absorption spectra, where the characteristic plasmon band at 415 nm indicates the presence of silver NPs. The combination of Chitosan and Silver resulted in a synergistic antimicrobial effect against *S. aureus*, with the capacity to inhibit and eradicate biofilm formation when coated in a polyurethane catheter surface at the 2:1 ratio. The material synthesized in this work can be seen as a promising strategy for an antimicrobial coating to prevent biofilm formation and bacterial infections caused by medical devices.

References

1. **Teixeira Santos, M. Lima, L. C. Gomes, F. J. Mergulhão.** ***Iscience*** **2021,** ***24*****(12), 103480 https://doi.org/10.1016/j.isci.2021.103480**
2. **R. Yeasmin, H. Zhang, H. Zhang, J Zhu.** ***Progress in Organic Coatings 2022, 182*****, 107615. https://doi.org/10.1016/j.porgcoat.2023.107615**
3. **M. A. Polinarski, A. L. Beal, F. E. J. B. Wenzel, G. R. Burin, G. I. Muniz, H. J. Alves.** ***Particle & Particle Systems Characterization 2021*****,** ***38*****(4), 2100009. https://doi.org/10.1016/j.porgcoat.2023.107615**
4. **S. Mulla, A. Kumar, S. Rajdev.** ***Advances in Microbiology 2016*****,** ***6*****(02), 73. 10.4236/aim.2016.62007**

Fundings: We thank to Araucária Foundation, the State Superintendence of Science, Technology and Higher Education of Paraná, and BIOPARK Educação for the financial help through a scholarship.

Keywords: *Biofilm, Central Venous Catheter, Bio-Composite, Bacterial Adhesion, Synergistic effect.*

SYNTHESIS OF POLYMERIC RESVERATROL PRODRUGS

Liege P. S. Reinert[1], Katiusca W. Miranda[1] and Sérgio H. Pezzin[1]*

1 – Center of Technological Sciences, Santa Catarina State University (UDESC), Joinville, SC, Brazil
sergio.pezzin@udesc.br

Abstract - In recent decades, resveratrol has gained importance due to its impressive range of biological activities, however, its true potential as a drug is restricted by its low bioavailability [1]. To minimize this pharmacokinetic problem, we studied a way to modify the chemical structure of the resveratrol molecule by synthesizing polymeric microparticles from the trans-resveratrol molecule, via condensation with carboxylic acids, obtaining new polyesters with potential use as prodrugs [2]. Resveratrol is a polyphenol obtained from renewable sources, such as grape skins, and has esterifiable hydroxylases [3]. Studies on the chemical composition of resveratrol polyesters obtained by condensation with sebacic and adipic acid dichlorides, ^{1}H and ^{13}C nuclear magnetic resonance (NMR) and infrared (FTIR) spectroscopy indicated that the syntheses were successful. Thermogravimetry (TG) indicated a degradation behavior in two steps, suggesting the degradation of the aliphatic region (sebacate and adipate region), followed by the decomposition of the aromatic rings (resveratrol region), while differential exploratory calorimetry (DSC) showed that thermoset resveratrol polyesters with Tg in the range between 43 and 77 ºC have been synthesized. Obtaining dense polymeric microparticles with a smooth surface was confirmed by means of microscopic analysis. The study of the *in vitro* hydrolytic degradation process in phosphate buffer pH 7.4, indicated that the polymers undergo a degradation of second order kinetics ($k= 1.69 \times 10^{-2}$ $m\%^{-1}$ s^{-1}) until the third week, passing to a first order degradation (1.25×10^{-3} s^{-1}) after this period. This result, together with studies by TG and DSC, suggest that there are less crosslinked domains that are more easily hydrolyzed and responsible for the first stage of mass loss, while more crosslinked domains (in greater proportion) are apparently more resistant to the hydrolytic process.

References

1. E.A. Oganesyan; I.I. Miroshnichenko; N.S. Vikhrieva; A.A. Lyashenko; S.Y. Leshkov *Pharmaceutical Chemistry Journal* 2010, *44*, 25-27. https://doi.org/10.1007/s11094-010-0401-1
2. A. Prudencio; N.D. Stebbins; M. Johnson; M. Song; B.A. Langowski; K.E. Uhrich. *Journal of Bioactive and Compatible Polymers* 2014, *29*, 208-220. https://doi.org/10.1177/0883911514528410
3. M.J. Acerson; M.B. Andrus *Tetrahedron Letters* 2014, *55*, 757-760. https://doi.org/10.1016/j.tetlet.2013.12.019

Fundings: FAPESC (2021TR928) and CAPES-DS.

Keywords: *Resveratrol, Polymeric prodrug, Microparticles, Controlled release, Bioavailability.*

ANTIMICROBIAL ACTIVITY OF SILVER NANOPARTICLES PRODUCED BY GREEN SYNTHESIS FROM ENDOPHYTIC FUNGI PENICILLIUM SPP

Laisa A. P. L. Garcia[1] Marcelo Assis[3] and Cristina P. Sousa[1, 2, 4]

1 – Laboratory of Microbiology and Biomolecules, Department of Morphology and Pathology (UFSCar), São Carlos, SP, Brazil
2 – Laboratory of Microbiology and Biomolecules, (LaMiB)Department of Morphology and Pathology (UFSCar), São Carlos, SP, Brazil
3 – Center for Development of Functional Materials (CDMF), and Chemistry Department (UFSCar), São Carlos, SP, Brazil
4 – Graduate Program of Biotechnology PPGBiotec (UFSCar), São Carlos, SP, Brazil
Correspondent author - prokarya@ufscar.br

Abstract

The increase in bacterial resistance to antimicrobials has become a major problem for public health in recent decades. Endophytic fungi, that lives in mutualistic association with plants, are a rich source of bioprospecting for such bioactive compounds. The objective of the present project was to synthesize silver nanoparticles through green synthesis, an ecologically sustainable approach that uses biological organisms as biofactories to the production of metallic nanoparticles. The utilization of metallic nanoparticles can be applied in the study of the control of resistance to traditional antimicrobials using inhibition as prevention of microbial diseases. The endophytic filamentous fungi *Penicillium* spp., isolated from *Polygala* spp., a plant collected in Brazil, were used in the biosynthesis of silver nanoparticles. The synthesis of AgNPs were conducted utilizing the *Penicillium* spp. fermentation broth with 1 mL de $AgNO_3$ (1mM). To conduct the characterization of AgNPs the 1,5 mL of reactional solution was submmited to the UV-Vis (200 and 800 nm) in 72, 144 and 216 h incubation, and fermentation broth without $AgNO_3$ as control. Subsequently, the nanoparticles were submitted to evaluative assays to test their antimicrobial, effects. The nanoparticles presented inhibition of *Escherichia coli* and *Staphylococcus aureus*, with better results for the Gram negative bacterium. The results show that the green synthesis is a good method to produce metallic nanocomposites utilizing endophytic *Penicillium* spp.

Key words: *Penicillium spp., endophytes, green synthesis, metallic nanoparticles, $AgNO_3$, microbial inhibition*

Experimental

The use of polimers as metallic nanoparticles is an important and innovative tool, since the generated data can achieve better results when the subject is the study of the microbial resistance to traditional antimicrobials.This protocol can impact directly the resistance as a major public health concern, giving new highlight into the microbial diseases.

To proceed with the development of the endophyte, *Penicillium* spp. was submmited to the fermentation broth that was cultivated in BDA, in the absence of light at 28°C, during 10 days incubation (Fig. 1).

The synthesis of AgNPs, was done utilizing 100 mL of fermentation broth with 1 mL of $AgNO_3$, to final concentration of 1 mM. The silver ions were reducted as visualized by color reactional change. The characterization of AgNPs was made utilizing UV-Vis in CDMF, Chemistry Department. The reactional solution was submmited to double beam spectrophotometry, operating in 200 and 800 nm in 72, 144 and 216 h of incubation time. Fermentation broth without AgNO3 was used as the negative control. The evaluation of AgNPs antimicrobial activity were made using the diffusion method in solid media. To do the characterization of AgNPs (CDMF/UFSCar) 1,5 mL of reactional solution was submmited to the UV-Vis (200 and 800 nm) in 72, 144 and 216 h incubation, and fermentation broth without $AgNO_3$ as control (Verassami et al., 2011).

To conduct the bioguided tests, we used the batcterial pathogens *Escherichia coli* and *Staphylococcus aureus* as Gram + and -, respectively. The bacterial padronization was made using spectophotometer at 620 nm and an OD between 0,08 e 0,10.

Results and discussion

Figure 1 show the studied organism, *Penicillium* spp. In this picture, it can be seen the morphologic colony characteristic of the fungi. Table 1 shows the antimicrobial effect of AgNPs against *E. coli* and *S. aureus,* that were similar, but higher to *S. aureus* with the identified inhibition zones.

Figure 1. *Penicillium* spp. typical microbial morphology, growing in BDA plate dish.

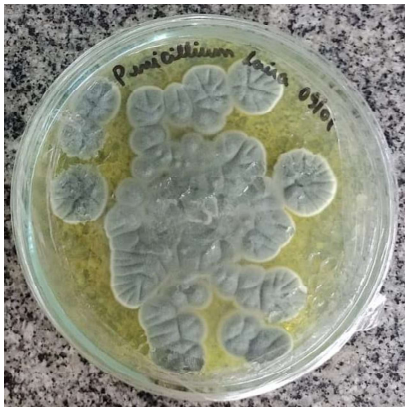

Figures 2 and 3 shows the UV-vis spectre for the tested samples. AgNPs have unique optical properties due to superficial plasmon ressonance.

Figura 2. UV-vis spectre with pic near 450 nm in the reactiona solutions, indicating the presence of silver nanoparticles. Control solution showed one pic near 200 nm indicating the presence of reductor molecules in the broth fermentation.

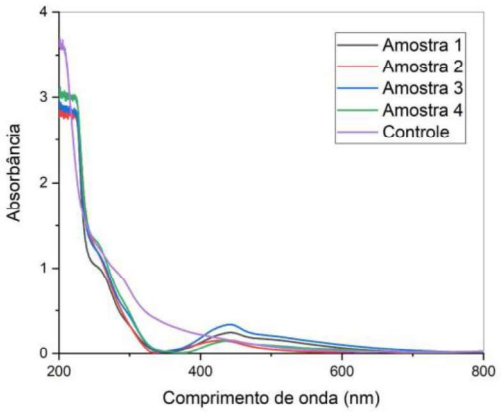

Figure 3 shows the UV-vis spectre with results from sample 3 in different incubation times. It can be seen that was a considerable pic after 72 hours of incubation. However, after 144 hours, the pic presented a little growth indicating that the synthesis was approching the end time.

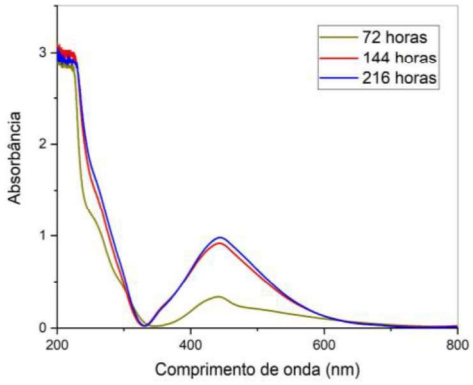

Figure 3. UV-vis spectre results from sample 2 in different incubation times.

Based on literature (Halkai et al., 2017), it is expected that the NPs synthetised from the *Penicillium* spp. fermentation broth presents morphology with 16-40 nm and spherical aspect.

The results presented in Table 1 shows the presence of halos numbers and data is similar to work conducted by Jaidev and Narasimha (2010).

Table 1. Nanoparticles inhibition zones (mm) sinthetized by *Penicillium* spp. broth fermentation against *E. coli* and *S. aureus.*

Samples	***E. coli***	***S. aureus***
AgNPs	1	2-4
AgNO3	1	1
Fermentation broth (- control)	-	-

In Figure 4 it is showed the inhibition halos against *Escherichia coli*. DA MOTA et al., (2018) worked with Gram negative bacteria and these authors results are similar to this presented here.

The Figure 4 shows the bioguided test with inhibition halos. Plates with *E. coli* in the a) AgNPs reactional solution, b) tetraciclin, c) AgNO3 and d) fermentation broth.

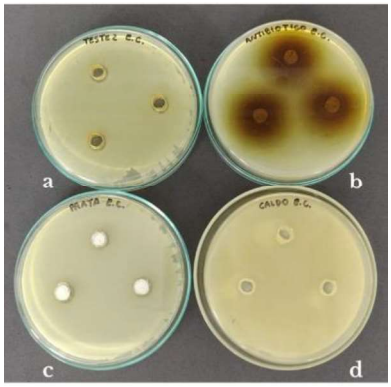

Source: Authors

In the figure 5, the results show the evaluation of AgNPs with charcteristic results. These data present some difference from Bogas et al., 2022.

Figure 5. *S. aureus* plates with (a) AgNPs reactional solution (b) tetraciclin, (c) AgNO3 solution and (d) fermentation broth.

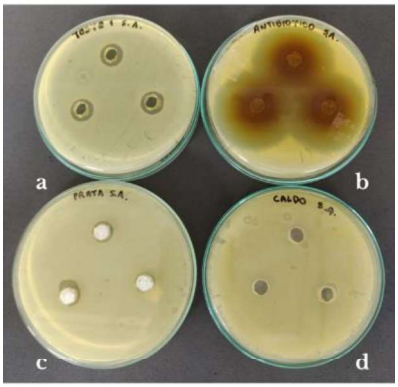

Source: Authors

There was no inhibition halo formation in the fermentation broth plate (a) and the tetraciclin (b). In the others tests the inhibition halo was present.

As can be seen in Figures 2 and 3, the plates with the AgNPs showed inhibition halos for both pathogens, with better results for S. aureus. On the other hand, the plates with AgNO3 (1 mM) had a small inhibition halo and the plates with fermentation broth presented no halo, as expected.

Conclusion

The extracellular syntesis of AgNPs from *Penicillium* fermentation broth was done succesfully.

The antimicrobial activity of nanoparticles presented activity against *E. coli* and S. *aureus.* The green synthesis can provide good results and an ecologically sustainable approach that uses biological organisms as biofactories in the production of metallic nanoparticles.

Acknowledgements

We thank FAPESP for grants numbers 2016/13423-5 and 2022/12836-5

References

R. Veerasamy, et al. Journal of saudi chemical society 2011, 15, 2, 113-120. https://doi.org/10.1016/j.jscs.2010.06.004

K. Halkai, K. Rahul et al. Journal of clinical and diagnostic research 2017 11. doi: 10.7860/JCDR/2017/29434.10681

L. R; Jaidev, G. Narasimha. Colloids and surfaces B: Biointerfaces 2010, 81, 430-433. 10.1016/j.colsurfb.2010.07.033

A. C. Bogas; S. H. Rodrigues; M. O. Gonçalves; M. Assis; E. Longo; Sousa. C.P. Frontiers in Nanotechnology, 2022, 10.3389/fnano.2022.823236.

CHITOSAN/GELATIN 3D PRINTED ANTIFUNGAL HYDROGELS

Camila L. Reginatto[1]*, Manoela A. M. Mace[2], Fernanda S. Moreira[1], Alexandre M. Fuentefria[2], Rosane M.D. Soares[1]

1- Polymeric Biomaterials Lab (Poli-Bio), Department of Organic Chemistry, Universidade Federal do Rio Grande do Sul (UFRGS), Porto Alegre, RS, Brazil
2- Department of Clinical Analysis, Federal University of Rio Grande do Sul (UFRGS), Porto Alegre, RS, Brazil

reginatto13@gmail.com

Abstract – 3D printing of hydrogels is a new strategy for encapsulating cells and drugs, allowing the manufacture of biomaterials for biomedical applications, ranging from organs and tissues to drug release devices and sensors. Chitosan is a well-known hydrogel that is widely used as a support for controlled drug release. Still, it has low mechanical properties that can be enhanced by adding gelatin to obtain a viscoelastic material capable of forming a scaffold by 3D printing. Crosslinking the chitosan/gelatin hydrogel with genipin, a biomolecule extracted from the jenipapo plant, improves its mechanical properties and stabilizes the material. Adding imidazolium-based ionic liquids containing fluconazole promotes antifungal activity in the material.

Keywords: *3D Printing, Chitosan, Gelatin, Genipin, Antifungal properties*

Fundings: CAPES, UFRGS

Introduction

The ability to print customizable three-dimensional structures has placed 3D printing in the tissue engineering scenario, allowing the production of three-dimensional supports that assist in cell proliferation and tissue reconstruction. Besides, it acts as a mechanical support during tissue reconstruction, remodeling and allowing drug delivery directly to the site. In addition, the designed supports are scaffolds and can be customized in shape, dimension, and porosity. [1] Bio-printing is more prominent than other techniques due to the possibility of manufacturing biological synthetic structures in a three-dimensional matrix. Thus, biological microenvironments can be created that can facilitate cell-cell and cell-matrix interactions. The great advantage of using hydrogels is their macromolecular structure. Because they are composed of polymeric chains that have the property of expanding their volume when immersed in water, they do not dissolve due to the presence of intermolecular interactions and/or cross-linking. In this way, they can maintain the structure of the solvent in their three-dimensional structural network, which can also contribute to the transport of oxygen and nutrients when used, for example, in tissue engineering [2]. Chitosan is a cationic copolymer composed of two monomers, D-glucosamine and N-acetyl-D-glucosamine.[3] In addition to being biocompatible, hypoallergenic, and biodegradable, it can also be used as a drug-carrying hydrogel, acting as a biomaterial for tissue engineering.[4] Although it has low mechanical properties, the chitosan chain presents the existence of amino ($-NH_2$) and hydroxyl (-OH) groups, which are typically used to react with crosslinking agents to promote crosslinking, thus improving the mechanical properties of the chitosan hydrogel. [5] Another versatile polymer is gelatin, obtained through processes involving the denaturation of collagen, which occurs through acidic or basic cleavage of intermolecular and intramolecular covalent bonds. Due to its chemical structure,

numerous functional groups pendant along the gelatin chain allow the molecule to undergo functionalization, such as the use of a drug, or even something more straightforward, such as a crosslinking reaction, to improve the material's mechanical properties. To improve the mechanical properties and stability of chitosan/genipin hydrogels, this project aimed to develop 3D-printed hydrogels and promote a post-crosslinking process, adding genipin as a chemical reagent. The incorporation of antifungal was assisted by adding ionic liquids, based on its ability to solubilize the flucozanol and promote a synergistic effect with the drug, which can increase its antifungal capacity.[6]

Experimental

Chitosan-gelatin hydrogels

For hydrogel preparation, chitosan 3% (w/v) was dissolved in lactic acid and gelatin, and 12% (w/v) was dissolved in PBS; both were stirred for 30 min at C for 30 min. Before forming the chitosan-gelatin blend, the pH was increased to 6.0 by adding 0.5 M NaOH.

Chitosan Gelatin with ionic liquids (E_8 or E_{15})

To prepare the hydrogel with ionic liquids, 2 mL of ionic liquid [C_{12}MIM]Br, denominated E_8, and [C_{16}MIM]Br, denominated E_{15}, was added to the gelatin preparation. For the preparation, 1.2 g of gelatin type B was mixed by magnet stirring with 2 mL of ionic liquid plus 8 mL PBS at 40°C for 30 min. The chitosan hydrogel was prepared with 0.3 g of chitosan and dissolved in 10 mL of lactic acid 3% (v/v) under magnetic stirring for 40 min. The bioink hydrogel was prepared chitosan/gelatin-ionic liquid in (1:2) ratio (w/w).

3D printed parameters

- Printing speed: 20%
- Print flow: 100%
- Temperature in the extrusion nozzle: 30°C
- Piston descent speed: 60%

Crosslinking Degree (%)

The crosslinking reaction was carried out after the printing process. The printed scaffold was immersed in an alcoholic genipin solution at 1.0, 0.5 and 0.25% (w/v) for 30 min at room temperature. Then, the crosslinked scaffolds were washed with water/ethanol solution.

Results and Discussion

Twelve 3D-hydrogels were obtained according to Table 1. The same method was applied to hydrogels containing the imidazolium ionic liquids E_8 and E_{15}. The hydrogels can be visualized in Figure 1. The changes in the colour is promoted by the covalent bond between chitosan amine groups and the genipin, which forms a chromophore group.

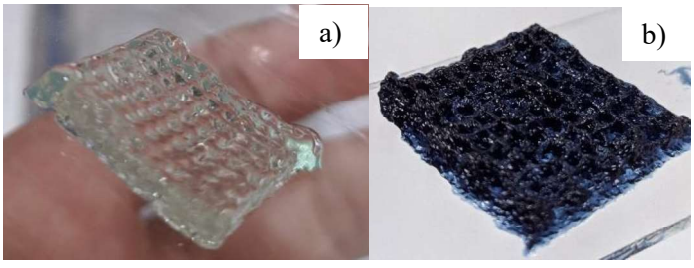

Figure 1. (a) 3D-Hydrogel chitosan/gelatin (b) 3D-Hydrogels after crosslinking.

Table 1. Chitosan/Gelatin hydrogel formulations for 3D printing

Hydrogel	Gelatin (ratio)	Chitosan (ratio)	Ionic Liquid (mL)	Genipin (% w/v)
CHI/GEL	2	1	-	-
CHI/GEL 0.25 GEN	2	1	-	0.25
CHI/GEL 0.5 GEN	2	1	-	0.5
CHI/GEL 1.0 GEN	2	1	-	1.0
CHI/GEL E8	2	1	2	-
CHI/GEL E8 0.25 GEN	2	1	2	0.25
CHI/GEL E8 0.5 GEN	2	1	2	0.5
CHI/GEL E8 1.0 GEN	2	1	2	1.0
CHI/GEL E15	2	1	2	-
CHI/GEL E15 0.25 GEN	2	1	2	0.25
CHI/GEL E15 0.5 GEN	2	1	2	0.5
CHI/GEL E15 1.0 GEN	2	2	2	1.0

The FTIR-ATR analysis revealed that hydrogels exhibited characteristic bands of gelatin and chitosan. Notably, we observed the corresponding band related to stretching the N-H bond of secondary amide at 3300 cm^{-1}, characteristic of the gelatin molecule. The same functional group also shows an apparent band at 1650 cm^{-1}, characteristic of the stretching of the C=O bond. From 3300 to 3500 cm^{-1}, the stretching band of the primary amine N-H and the bending of the primary amine N-H bond at 1550 cm^{-1} can be observed, corresponding to the chitosan chemical structure. The addition of ionic liquids did not cause displacement or the appearance of bands, and the crosslinking reaction promoted by the genipin was not visualized in the FTIR spectra. This behavior probably is due to the low concentration of genipin in the solution, which avoided the detection of characteristics bands in the FTIR-spectra.

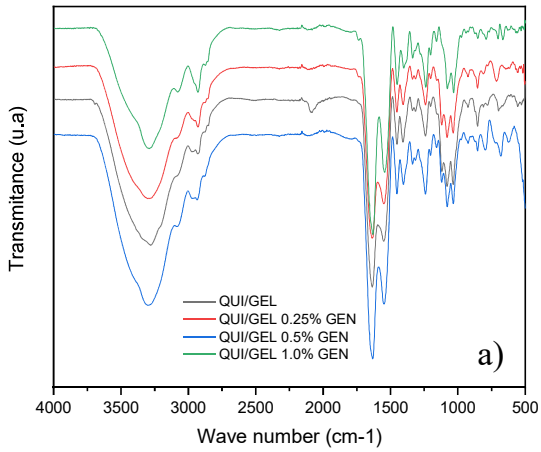

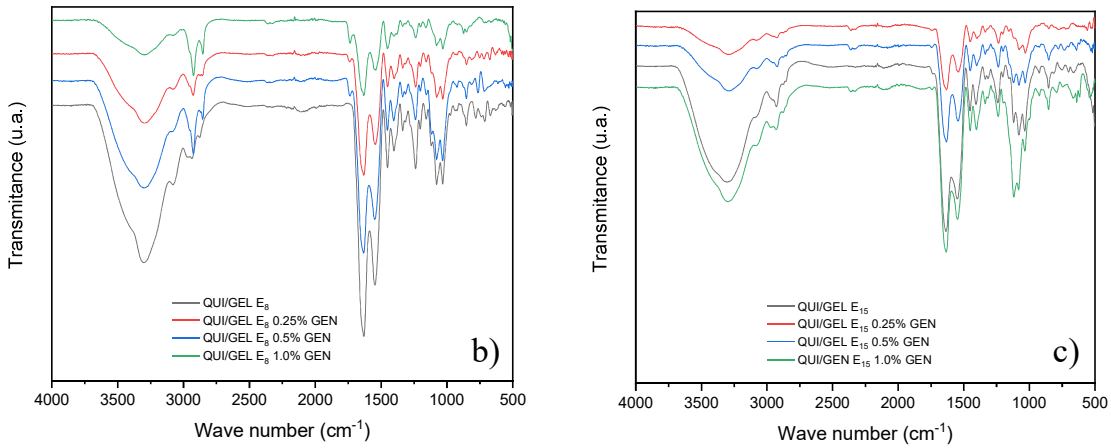

Figure 2. FTIR-ATR (a) Chitosan/Gelatin (CHI/GEL) and CHI/GEL with genipin (1.0; 0.5 and 0.25% w/v) (b) Hydrogel Chitosan/gelatin E_8 (CHI/GEL E_8) and (c) Chitosan/Gelatin E_{15} (CHI/GEL E_{15}) and CHI/GEL E_{15} with genipin (1.0; 0.5 and 0.25% w/v).

The swelling results are shown in Figure 3. Crosslinked hydrogels' swelling degree (%) was 550% compared to initial dry weight, whereas the crosslinked hydrogels presented a 490% swelling. It was observed that a higher genipin concentration led to a lower swelling degree. Besides that, the crosslinking provided more resistance to the hydrogel without solubilizing.

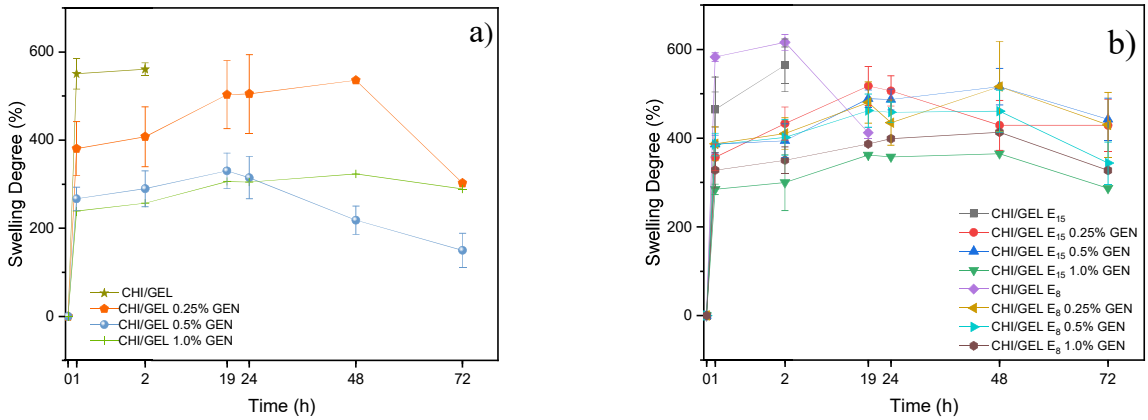

Figure 3. Swelling degree (%) of 3D hydrogels (a) Hydrogel CHI/GEL and hydrogel CHI/GEL crosslinked with genipin (1.0; 0.5 and 0.25%), (b) Hydrogels with ionic liquids, CHI/GEL E_8 and CHI/GEL E_{15}, (1.0; 0.5 and 0.25%).

A disk-diffusion assay was performed with the drug fluconazole to evaluate the efficiency of the hydrogels in releasing the ionic liquid containing fluconazole against *Candida albicans*. The methodology was adapted from the CLSI document M44-A2. Discs containing 25 µg of fluconazole were used for the control group. *C. albicans* was cultivated on Petri dishes containing Sabouraud Dextrose Agar with Chloramphenicol in a 1x106 UFC/mL concentration. The hydrogel samples remained in contact with the culture medium incubated for 48 hours at 35°C. The blank hydrogels (Chi/Gel) did not present an inhibition zone against *Candida albicans*. In contrast, the hydrogels containing E_8 ionic liquid exhibited a significant inhibition zone against C. albicans (20 mm), demonstrating that the developed material could release the drug into the medium. However,

the inhibition zones of the hydrogel containing E_{15} ionic liquid were not evident, but an antifungal effect was observed due to the inhibition of yeast growing in the hydrogel.

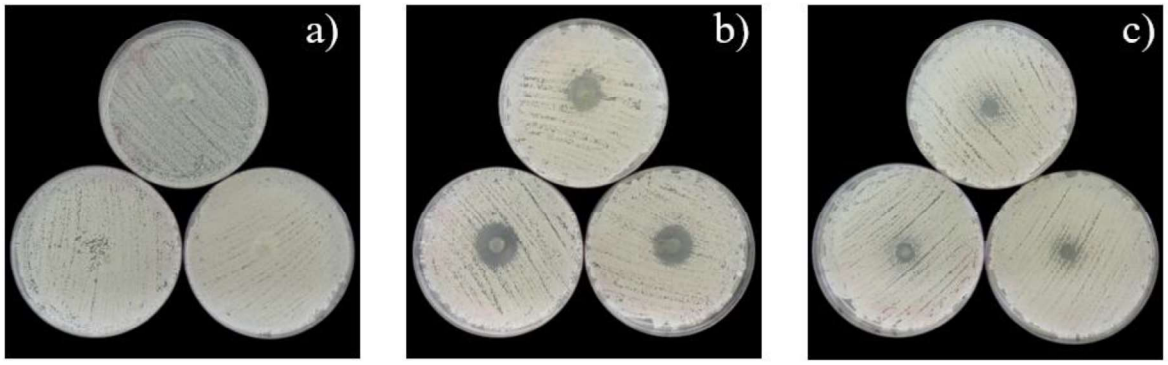

Figure 4. Adapted disk diffusion test of hydrogels: (a) CHI/GEL, (b) CHI/GEL E_8 and (c) CHI/GEL E_{15}.

Conclusions

We developed Chitosan/Gelatin 3D printed hydrogels with antifungal activity in the present work. The addition of genipin was effective as a crosslinking agent, showing an effect on swelling properties. Besides, the incorporation of ionic liquids did not affect the printability of the hydrogels.

The developed hydrogel demonstrated the ability to inhibit fungal growth on its surface, and hydrogels with ionic liquid in their composition were able to form an inhibition zone against *C. albicans*.

Acknowledgements

We acknowledge the financial support by Brazilian agencies CAPES and CNPq.

References

1. T. S. Jang, H. Do Jung, H. M. Pan, W. T. Han, S. Chen, and J. Song, "3D printing of hydrogel composite systems: Recent advances in technology for tissue engineering," *Int. J. Bioprinting*, vol. 4, no. 1, 2018

2. M. W. Tibbitt and K. S. Anseth, "Hydrogels as extracellular matrix mimics for 3D cell culture," *Biotechnol. Bioeng.*, vol. 103, no. 4, pp. 655–663, Jul. 2009

3. J. M. Unagolla and A. C. Jayasuriya, "Hydrogel-based 3D bioprinting: A comprehensive review on cell-laden hydrogels, bioink formulations, and future perspectives," *Appl. Mater. Today*, vol. 18, Mar. 2020

4. M. Helena Monteiro do Nascimento and C. Bertachini Lombello, " Hidrogéis a base de ácido hialurônico e quitosana para engenharia de tecido cartilaginoso," vol. 26, no. 4, pp. 360–370, 2016

5. M. C. G. Pella, M. K. Lima-Tenório, E. T. Tenório-Neto, M. R. Guilherme, E. C. Muniz, and A. F. Rubira, "Chitosan-based hydrogels: From preparation to biomedical applications. Carbohydrate Polymers, 196, 233–245, 2018.

6. C. Lárez Velásquez, A. Rivas, and I. Santos Ocanto, "Obtención de Genipina a partir de frutos de caruto (Genipa americana L.) del llano venezolano," vol. 9, no. 2, pp. 75–86, 2014

COATING SCAFFOLDS "Mg FOAMS" SURFACES WITH COLLAGEN SOLUTIONS TO EVALUATE CORROSION VELOCITY IN A SIMULATED ENVIRONMENT OF PHYSIOLOGICAL CONDITIONS

Mario Dayvid Carbajal Ccoyllo[1], Ana María Angulo Sotelo[1], Gloria Patricia Fernández-Morales[2], María Verónica Carranza-Oropeza [1]

1 – Faculty of Chemistry and Chemical Engineering, National University of San Marcos *(UNMSM), Lima, Lima, Perú.*
mario.carbajal@unmsm.edu.pe
2 – Faculty of Industrial Engineering, Pontifical Bolivarian University (UPB), Medellín, Antioquia

Abstract

AZ31 magnesium alloys have become an important alternative in orthopedic applications due to their biocompatibility, biodegradability, mechanical properties and promotion of bone regeneration making this temporary device suitable to avoid a new surgical intervention as well as pain and discomfort. However, the inherent corrosion rate of magnesium must be reduced, for this we propose to coat with different concentrations of collagen solutions (0, 16 and 64% w/w) the surfaces of these AZ31 alloys which we call *scaffolds* "Mg sponges", Beforehand, surface activations (alkaline activation and hydrofluoric activation) were performed to ensure the coating with the collagen solution and finally we evaluated the corrosion rate by means of the hydrogen evolution method in a simulated physiological conditions environment (SBF). Quantitative and qualitative study techniques such as atomic absorption spectroscopy (AA), with which we determined the magnesium concentration in the SBF solution, and scanning electron microscopy with atomic analysis (SEM/EDS) were used for the analysis of results to describe morphologically and elementally the surfaces before and after corrosion. The tests showed that the *scaffolds*, "Mg foams", corrode more for those samples having alkaline activation and no collagen coating, corrode less for those samples having hydrofluoric activation and coated with 16% (w/w) collagen and corrode minimally for those samples having hydrofluoric activation and coated with 64% (w/w) collagen.

Key words: *AZ31 magnesium, collagen, scaffolds, corrosion, physiological conditions.*

Funding: Projects with internal funding from National University of San Marcos - PCONFIG 2019 - C19070351

Introduction

Magnesium and its alloys have been the subject of study for many decades since the early 1878 for their potential uses in the field of biomaterials [1]. Magnesium itself is a light metal with very convenient characteristics such as low density, high strength, high buffering capacity, low heat capacity, negative electrochemical potential, non-toxicity, and above all it is an essential element in the biological functions of human beings [2, 3]. The use of Mg and its alloys is basically based on a Young's modulus similar (about 45 GPa) to that of human bone (15-30 GPa), which can reduce stress protection during load transfer at the bone-implant interface, and on its density which is 1.79 g/ cm^3, very close to that of human bone (1.75 g/cm^3) [4]. Titanium is the most used material in orthopedic implants over time, however, its use has been discussed because of its failures such as loosening after implantations and corrosion products that compromise related tissues [5]. As a result, magnesium has been proposed as a substitute for titanium as an orthopedic implant material due to its mechanical, chemical and biological qualities; many researchers have conducted studies that support this for decades [6-9]. Surface modification methods such as surface activation and coatings on magnesium-based materials have proven to be efficient in controlling the rate of degradation [7, 9, 10]. In this research, chemical surface treatments

such as alkaline and hydrofluoric surface treatments are proposed as they show promising results [10], and coating on collagen as it is abundantly found as a structural protein in the body [11], plays the role of a major component of the extracellular matrix (ECM) in addition to its biodegradation, biocompatibility and non-cytotoxicity properties, easily modified to produce materials as desired using its functional groups [12]. Importantly, the results of slowing down the corrosion rate of the "magnesium foams" ensure that this biomaterial remains for the necessary time required for bone regeneration and that when it finally culminates it can degrade completely without internal or external affectation.

Experimental Part

i) *Preparation of the Mg foam simples*

The cylindrical samples with dimensions of 7 mm in diameter and 60 mm in height, have a porosity percentage of 75 ± 2% and a specific surface area of 0.04354 cm^2/mg. These were cut into 12 pieces with dimensions of 7 mm in diameter and 10 mm in height approximately, then they were immersed in ultrasonic bath at 40°C for 10 minutes in acetone, then in chemically pure absolute ethanol and finally in distilled water. Finally, they were left to dry at ambient conditions in a fume hood for 1 hour.

ii) *Surface activation: a) in alkaline medium and b) with hydrofluoric acid.*

Samples of already cleaned "magnesium foam" scaffolds were immersed in boiling 5 M $KOH_{(ac)}$ solution for 15 minutes, then dried with cold air inside a fume hood for 1 hour and finally stored for 7 days inside a desiccator at ambient temperature and relative humidity conditions of 25 ± 3°C and 73 ± 5%, respectively. In a group of six, 50% of the samples already treated with 5 M $KOH_{(ac)}$ were immersed in prepared 40% (w/w) $HF_{(ac)}$ solution and then incubated in a water bath at 60°C for 30 minutes. The samples were then dried with cold air in a fume hood for 1 hour and finally stored in a desiccator for 7 days.

iii) *Coating with different concentrations of collagen.*

The concentrated solution of collagen 80%(w/w) used was mouse tail type I, (Sigma Aldrich, USA) from which the following solutions were prepared 0% (w/w) ,16% (w/w) and at 64% (w/w), the different magnesium elections samples were immersed in these concentrations for a time of 1 minute, then allowed to dry for a time of 15 minutes at temperature and relative humidity of 25 ± 3°C and 73 ± 5%, respectively, for each sample three repetitions were carried out.

iv) *Corrosion evaluation by the hydrogen evolution method.*

Each sample was immersed in simulated body fluid (SBF) solution for 24h. The physiological temperature was 37 ± 1°C, while the atmospheric pressure was kept constant at 760 mmHg. The pH of the SBF solution was regulated using 1M HCl and 1M NaOH in order to maintain the physiological pH of 7.4± 0.3, the system was armed to collect the volume of hydrogen gas by volumetric method and the measurement of the volume of hydrogen displayed in the burette was started every hour for 24 hours.

v) *Characterization of the coated surface.*

The characterization of the coated surfaces of the *scaffolds* "magnesium foams" was performed using a scanning electron microscope (SEM) models Prisma E of the TermoFisher brand with microanalysis detector (EDS) and the Quanta200 FEI. For atomic absorption, the Shimadzu AA-7000 Atomic Absorption Spectrometer was used.

vi) Statistical analysis of data

For the data analysis a 2x3 factorial experiment design was used which consists of six treatments with two, randomly obtaining 12 runs. This type of experiment was chosen to test the effect of different collagen concentrations (C0=0%, C1=16% and C2=64%), surface activation media (alkaline (OH) and hydrofluoric (HF)) and the interaction of both on corrosion rates.

Results and discussions

The tests showed that AZ31 magnesium alloys corrode more for those samples with alkaline activation and without collagen coating and where a higher volume of hydrogen gas is released (see Fig. 1). a,b,c) the before and after corrosion evaluation, they corrode a little and the volume of hydrogen gas evolved is less for those samples that have hydrofluoric activation and coated with 16% (w/w) of collagen and they corrode minimally for those samples that have hydrofluoric activation and coated with 64% (w/w) of collagen and therefore there is almost no hydrogen gas release (see Fig.1 d,c,e) before and after corrosion evaluation; their average corrosion rates being 7.92 ± 0.25,1.22 ± 0.02 and 0.89 ± 0.22 mm/year respectively. It is also demonstrated through ANOVA analysis that there is a significant effect of the collagen concentration on the corrosion rate which, at the same time, this effect is modulated by the type of surface activation used.

Figure 1

SEM images of the coated surface of the "Magnesium foams" *scaffolds* before and after corrosion evaluation

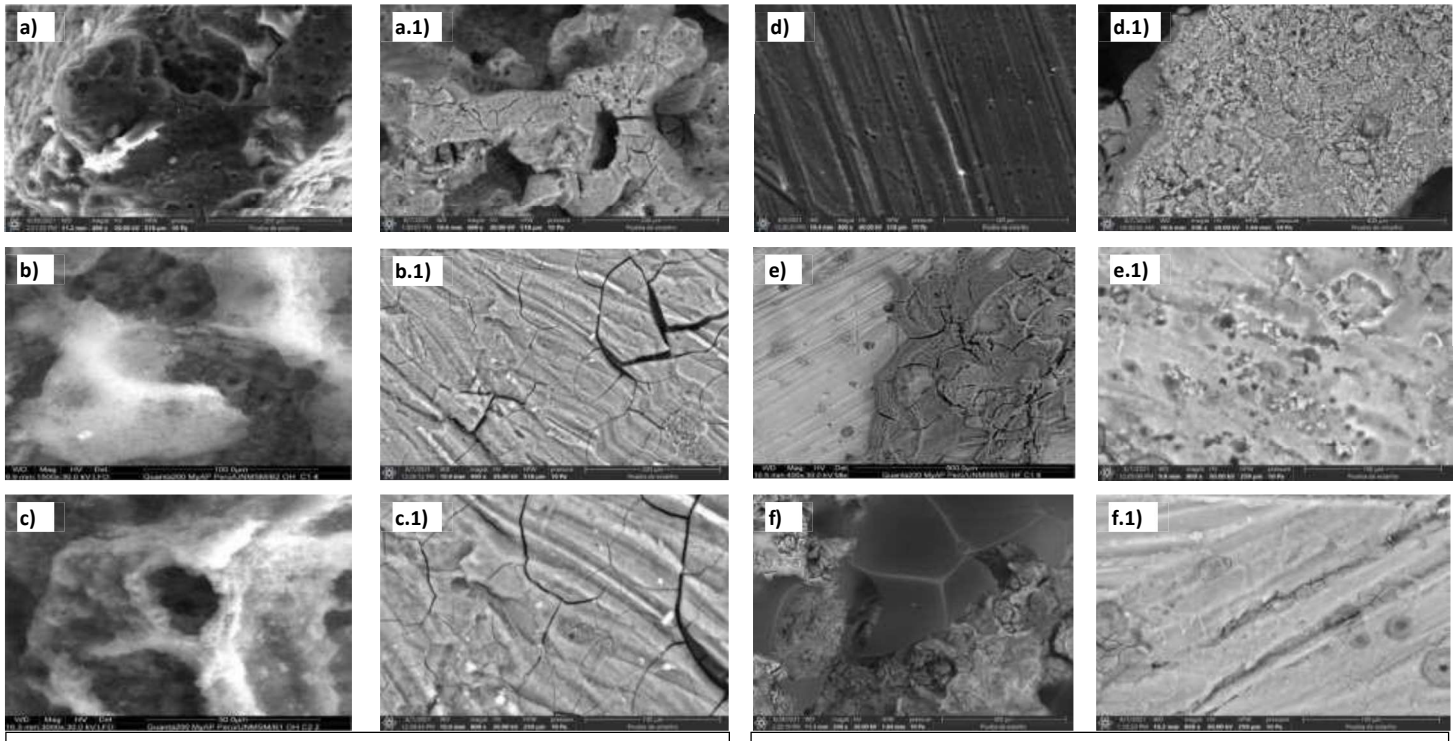

Figures a), b), c) have alkaline activation and coated with 0%(w/w) ,16%(w/w) and 16%(w/w) collagen respectively prior to corrosion evaluation.

Figures a.1), b.1), c.1) have alkaline activation and coated with collagen at 0%(w/w) ,16%(w/w) and 16%(w/w) respectively after corrosion evaluation.

Figures d), e), f) have hydrofluoric activation and coated with 0%(w/w) ,16%(w/w) and 16%(w/w) collagen respectively prior to corrosion evaluation.

Figures d.1), e.1), f.1) have fluoride activation and coated with collagen at 0%(w/w) ,64%(w/w) and 64%(w/w) respectively after corrosion evaluation.

Conclusions

The results of the tests performed indicate that a collagen coating was formed on the surface of the Mg sponge, which improved the corrosion resistance of the alloy in SBF solution. Surface activation in 40 (w/w%) HF is feasible in the generation of highly protective coatings against magnesium degradation in physiological media, and should be considered for future applications of magnesium as a temporary metallic implant. This simple chemical conversion treatment confers to the coating good protective properties in the physiological environment. The optimal conditions for corrosion abatement are to perform a fluoride surface modification and subsequent coating with collagen at a concentration of 64%(w/w), pH=7.4 ± 0.3, immersion time of 1 min, drying time of 15 min and temperature of 37 ± 1°C. Collagen coatings at lower concentration and with alkaline surface modification do not provide sufficient protection against substrate corrosion, which originated the imminent alkalinization of the medium and an increase in corrosion rate.

Acknowledgments

To our advisors, PhD. María Verónica Carranza Oropeza and PhD. Gloria Patricia Fernández Morales, for their time, teachings, dedication and patience invested in our persons in the realization of this research, particularly to Mg. Eder Clidio Vicuña Galindo, for his advice in the approach and interpretation of the statistical analysis, to PhD. Francisco Tarazona Vázquez, director of the Chemical Engineering Department of the University of Engineering and Technology-UTEC for providing us with the test laboratories.

Bibliographic references

[1] F. Witte. The history of biodegradable magnesium implants: A review 2010, 6(5), 1680-1692. https://doi.org/10.1016/j.actbio.2010.02.028

[2] G. Song. Corrosion electrochemistry of magnesium (Mg) and its alloys 2011; 3-65. https://doi.org/10.1533/9780857091413.1.3

[3] H. A. Briceño; L. F Cáceres; J. C. Joya; J. D. Barajas; F. Viejo; A. E. Coy. Aleaciones de magnesio: Una alternativa potencial en la fabricación de implantes biomédicos 2014, Revista Colombiana de Materiales, (5), 256-261.

[4] Y. Yang; W. Yang; C. He; E. Dianyu.; F. Qi; D. Xie; L. Shen; S. Peng; C. Shuai. Mg bone implant: Features, developments and perspectives 2020, 185, 108259. https://doi.org/10.1016/j.matdes.2019.108259

[5] S. Kumar; M. Nehra; D. Kedia; N. Dilbaghi; K. Tankeshwar; K. Kim. Nanotechnology-based biomaterials for orthopaedic applications: Recent advances and future prospects 2020, 106, 110154. https://doi.org/10.1016/j.msec.2019.110154.

[6] L. Ma; J. Niu. In vitro biocorrosion and biocompatibility of AZ31 modified with magnesium phosphate coating by chemical deposition 2019, 14, 208-214. https://doi.org/10.1016/j.surfin.2018.12.

[7] P. Xiong; J. Yan; P. Wang; Z. Jia; W. Zhou; W. Yuan; Y. Cheng; Y. Liu; Y. Cheng; D. Chen; Y. Zheng. A pH-sensitive self-healing coating for biodegradable magnesium implants 2019, 98, 160-173. https://doi.org/10.1016/j.actbio.2019.04.045

[8] C. Wang; H. Fang; X. Qi; C. Hang; Y. Sun; Z. Peng; W. Wei; Y. Wang. Silk fibroin film-coated MgZnCa alloy with enhanced in vitro and in vivo performance prepared using surface activation 2019, 91, 99-111. https://doi.org/10.1016/j.actbio.2019.04.048

[9] M. Yazdimamaghani; M. Razavi; D. Vashaee; K. Moharamzadeh; A.R. Boccaccini; L. Tayebi. Porous magnesium-based scaffolds for tissue engineering 2017, 71, 1253-1266. https://doi.org/10.1016/j.msec.2016.11.027

[10] J. Wang; J. Tang; P. Zhang; Y. Li; J. Wang; Y. Lai; L. Qin. Surface modification of magnesium alloys developed for bioabsorbable orthopedic implants: A general review 2012, 100B(6), 1691-1701. https://doi.org/10.1002/jbm.b.32707

[11] L. Li; L. Cui; R. Zeng; X. Chen; Y. Zheng; M. B. Kannan. Advances in functionalized polymer coatings on biodegradable magnesium alloys – A review 2018, 79, 23-36. https://doi.org/10.1016/j.actbio.2018.08.030

[12] W. Wagermaier; P. Fratzl. Collagen 2016. https://doi.org/10.1016/b978-0-12-803581-8.01493-4

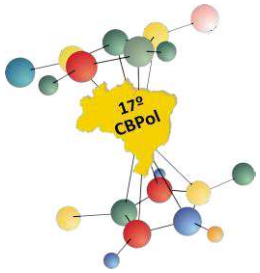

CONTROLLED RELEASE AND CELL VIABILITY OF MEGLUMINE ANTIMONIATE INCORPORATED INTO POLYMERIC MATRICES OF PEG 4000

Gabriel S. Nascimento[1], Laura Cardoso Campideli[1], Lucas Resende Dutra Sousa[2], Paula Melo de Abreu Vieira[3] Ângela Leão Andrade[1], Bruno Mendes Roatt[3], Viviane Martins Rebello dos Santos[1], Kátia Monteiro Novack[1,4*]

1 – Department of Chemistry, Federal University of Ouro Preto (UFOP), Ouro Preto, MG, Brazil
2- School of Pharmacy, Phytotechnology Laboratory, Federal University of Ouro Preto (UFOP), Ouro Preto, MG, Brazil
3-Center for Research in Biological Sciences, Laboratory of Morphopathology, Federal University of Ouro Preto, Ouro Preto, MG, Brazil
4-REDEMAT-Post Graduation of Materials Engineering, Federal University of Ouro Preto, Ouro Preto,MG, Brazil
knovack@ufop.edu.br

Abstract - Leishmaniasis is a globally neglected disease caused by the bite of hematophagous insects infected with the parasite Leishmania. In Brazil, the disease mainly manifests as cutaneous leishmaniasis. Over the years, one of the primary therapies has been the administration of pentavalent antimonials such as Glucantime®. However, the high toxicity and severe symptoms of this treatment lead many patients to abandon it. Thus, the use of polymers, such as PEG 4000, has gained prominence for its ability to reduce adverse effects and toxicity. Therefore, this study describes the analysis of the Zeta potential, controlled drug release, as well as the standard concentration curve. Consequently, the use of PEG 4000 and PEG 4000 Acetylated becomes a safe option for formulations aimed at the treatment of leishmaniasis. Cytotoxicity was determined and PEG 4000 and PEG 4000 Acetylated were not cytotoxic.

Keywords: *Antimoniate, Glucantime, controlled release, cell viability, Leishmaniasis*

Introduction

Leishmaniasis is a disease caused by protozoa of the Leishmania genus and is transmitted by hematophagous insects. Among them, Leishmania braziliensis (LT) is endemic in 76 countries and in the American continent, with Brazil being responsible for 90% of registered cases in Latin America. The main antiparasitic used in Brazil is meglumine antimoniate (Glucantime), Fig. 1, which is injectable. Due to the toxicity of antimony, a daily dose of the vaccine is recommended, and its side effects include nausea, vomiting, fever, fainting, among others [1]. Due to the various effects of antimony, many patients abandon the treatment, complicating their health and, in extreme cases, leading to death. To avoid the side effects, further research incorporates biodegradable polymers into the medication, encapsulating the same polymer and releasing the antimoniate into the patient's body. It is essential to mention PEG 4000 when it comes to polymers in the clinical and pharmaceutical industry, as it is the most widely used and is considered the safest for the human body. Furthermore, it is used due to its compatibility with medications, melting point,high hydrophilicity, chemical inactivity, the possibility to enhance other medications' solubility,and increase their half-lives [2,3]. Its use occurs when incorporated into other medications, suchas a capsule, transporting the medication and providing controlled release in the body. In medications with a high toxicity rate and, consequently, a large number of side effects, the process of incorporatingthe medication into polyethylene glycol can provide relief and reduction of side effects in the patient's

body [4]. PEG 4000 can be applied as bioactive pharmaceutical product, which means it can potentially increase the efficacy of medications and produce target specificity, unlike conventional pharmaceutical formulations. Therefore, when used in medication formulations, the doses and administration frequencies can be reduced, consequently mitigating the adverse effects caused by high doses and resulting in successful therapy. Additionally, the use of modified polymers exhibits specific actions and characteristics, such as the reduction of adverse effects, the ability to act directly on specific tissues or organs, and the reduction of the medication quantity while maintaining a concentration sufficient for effective therapeutic action without being destroyed before reaching the desired site. Therefore, applying PEG-4000 and acetylated PEG 4000, Fig.2, for treating leishmaniasis becomes a likely safe [5]. This study describes the analysis of zeta potential, controlled drug release, standard concentration curve, and cell viability.

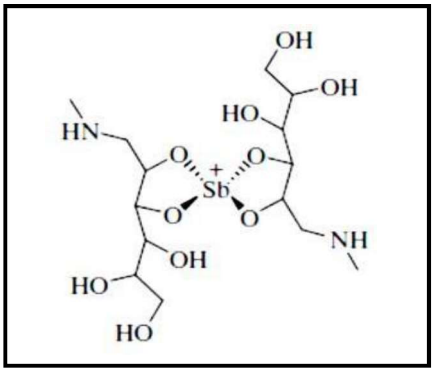

Figure 1: Chemical structure of Meglumine Antimoniate

General Considerations

Synthesis of acetylated PEG 4000 (P2)

In a round bottom flask, 2.00 g of PEG 4000 solubilized in 10.00 mL of dichloromethane and a solution with 5.00 mL of acetic anhydride and 5.00 mL of acetic acid were added. The reaction was maintained at a temperature of 40 ºC for 30 min. Upon completion of the reaction, the mixture was poured into a beaker with 100.00 mL of ice water. The modified PEG 4000 solidified and was separated by simple filtration. Solvent evaporation was made in a stove for 40 ºC and 1.00 g of a dry White film was obtained·

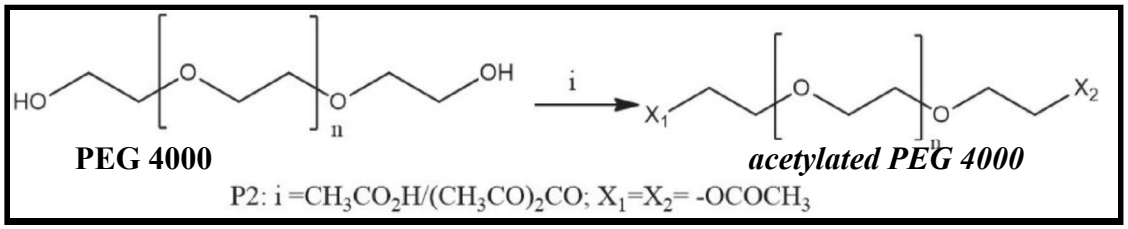

Figure 2: Synthesis of acetylated PEG 4000

Determination of Zeta Potential

The Zeta potential of the samples was determined by electrophoretic mobility using a Zetasizer. The samples were diluted in water and then placed in a capillary cell. Triplicate measurements were performed for four different samples. The results were expressed in millivolts (mV).

Incorporation of Meglumine Antimoniate in PEG 4000 and derivatives

In order to obtain the polymeric benznidazole particles, 1.20 g of polymer and 0.40 g of benznidazole were added to a beaker with 6.00 mL of acetone at approximately 30 °C. This system was kept mixing until complete dissolution. In a beaker containing 40.0 mL of water at approximately 70 °C, 0.48 g of polyvinyl alcohol were dispersed, stirring slowly until complete dissolution. The aqueous phase was poured into the organic phase. The mixture was subjected to agitation at 500 rpm for 4 h at 35 °C. Then, the products were taken to the oven at 40 °C for 24 h to evaporate the acetone. After this time, the particles were obtained.

Buffer Solution of pH 7.3

In the controlled release, one buffer solution of pH 7.3 was used to mimic the blood pH. In one beaker, 6.8 g of KH_2PO_4 was solubilized in 250 mL of MiliQ water. In another beaker, 1.4 g of NaOH was solubilized in 175 mL of MiliQ water. After both were solubilized, they were mixed, and the volume was made up with MiliQ water to 1000 mL. The solution was then poured into an amber glass container, labeled, and stored in a refrigerator. The pH was measured in a pH meter BEL ENGINEERING.

Standard Curve

The standard curve was performed by preparing solutions containing the ketoconazole drug and a pH 7.3 buffer solution at increasing concentrations (10 µg/mL, 20 µg/mL, 30 µg/mL, 40 µg/mL, and 50 µg/mL) in 10 mL volumetric flasks. Each solution was analyzed in UV-Vis spectrophotometer GENESYS 10S at the wavelength of 217 nm according to the recommendations by.

Controlled Release

For controlled release, absorbance readings were taken using a UV spectrophotometer, adopting the drug's wavelength of 217 nm as described in the literature. Solutions of the drug incorporated into the polymer were prepared with a concentration of 0.5 µg/mL in 10 mL volumetric flasks. The first reading was taken at time 0 (zero), and subsequent readings were taken at 30-minute intervals until 8 hours had elapsed. The solutions were prepared using a pH 7.3 buffer solution.

Cell Viability

Murine L929 fibroblasts, cultivated in RPMI 1640 medium (Sigma®), were distributed in 96-well plates at a density of 5 x 10^4 cells per well and then incubated at 37°C with 5% CO_2 for 24 hours. The cells were treated with samples dissolved in RPMI medium supplemented with 2% DMSO at concentrations ranging from 1000.00 to 7.81 µg/mL. Cell viability was assessed using the sulforhodamine B (SRB) assay [6]. After 24 and 48 hours of incubation, the medium was removed, and the cells were fixed with 20% trichloroacetic acid for 1 hour at 4°C. The plates were washed with distilled water and allowed to dry. Subsequently, the fixed cells were stained for 30 minutes with 0.1% SRB dissolved in 1% acetic acid. The plates were rewashed with 1% acetic acid and dried, and 200 µL of 10 mM TRIS buffer (pH 10.5) were added to solubilize the dye at room temperature for 30 minutes. The absorbance of the samples was read on a spectrophotometer at 490 nm, and the values were expressed as a percentage of cell viability using GraphPad Prism software 8.0.1.

Results and Discussion

Zeta Potential

The analysis of Zeta Potential indicates the surface charge of the sample, thus determining the stability of the particles [7]. High values of Zeta Potential (positive or negative) indicate that particles tend to repel each other (Table1). Zeta Potential values between -30 mV and +30 mV indicate

instability in the system, while other values indicate stability [2]. Table 1 presents the Zeta Potential values of the PEG 4000 samples, acetylated PEG 4000, and their respective drug incorporations. It can be observed that the values for PEG 4000 and its derivative are below 30 mV. However, the steric stabilization of PEG 4000 and its derivatives is provided by the surface groups of PEG, which is sufficient for stabilization. In comparison to the incorporations made with the drug, a significant variation is observed. This is due to the influence of the functional groups of the drug when incorporated into the polymeric matrices.

Table 1: Zeta potential of PEG4000 and derivades

Sample	Zeta Potential (mV)
PEG 4000	-5,13
PEG 4000 Acetylated	-14,30
PEG 4000 incorporated with Meglumine Antimoniate	+1,61
PEG 4000 Acetylated incorporated with Meglumine Antimoniate	+3,68

Controlled Release

Based on the release curve obtained at a wavelength of 217 nm, it is observed that initially there was a significant release of the drug until it reached its therapeutic range. Subsequently, the release stabilized and remained slow and constant. Therefore, the drug incorporated into PEG 4000 or PEG 4000 Acetylated exhibited a release profile, as shown in Fig. 3, displaying continuous release [2].

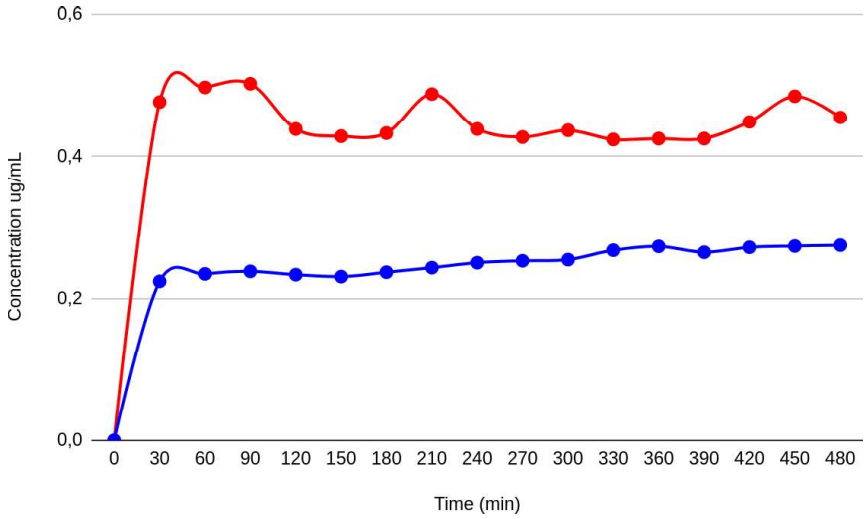

Figure 3: Release curve of PEG 4000 (blue) acetylated PEG 4000 (red) with incorporated meglumine antimoniate at pH 7.3.

Cell Viability

The administration of the drug can cause adverse effects. Thus, the developed acetylated PEG 4000 polymers are an alternative to reduce the toxicity of this antiprotozoal, as they reduce the drug's lipophilicity due to the polar terminal functional groups of acetylated PEG 4000. The cytotoxicity assay performed with sulforhodamine B indicated this low toxicity of the developed polymer. The tested concentrations of PEG 4000 Acet + Meglumine Antimoniate (1000 µg/mL) were considered nontoxic to fibroblasts (Fig. 4), according to ISO2009—10993-5, as the cell viability was higher than 70%. The concentration of 1000 µg/L was considered toxic as it was below 70%. The other concentrations of the samples were above the threshold, and thus considered nontoxic. In the 48-hour test, all concentrations were shown to be nontoxic. The fact of the absence of

toxicity may suggest a tendency not to observe the adverse effects experienced by patients when undergoing treatment with the non-incorporated medication.

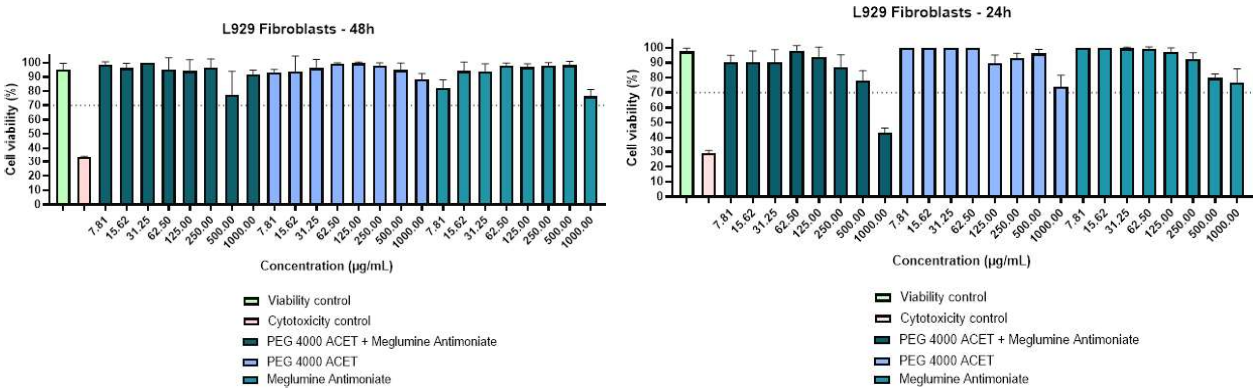

Figure 4: Cell viability assay

Conclusion

The release demonstrated efficiency, indicating a controlled release from the drug incorporated into acetylated PEG 4000, thereby increasing the therapeutic efficacy of the drug and reducing its toxicity. Furthermore, the Zeta Potential of the pure PEG 4000 and acetylated PEG 4000, as well as the drug incorporated into the polymeric matrices, exhibited values lower than |30| mV, indicating that these polymers had low electrostatic charge. Cytotoxicity was determined, and PEG 4000 and acetylated PEG 4000 were not cytotoxic.

Acknowledgements

The authors are thankful to the Federal University of Ouro Preto (UFOP) and the Conselho Nacional de Desenvolvimento Científico e Tecnológico (CNPq).

References

1. Santos, V. M. R.; Novack, K. M.; de Sousa, D. V. M.; Oliveira, S. R.; Donnici, C. L.; Polímeros 2015, 25, 19.

2. Santos, V. M. R.; Novack, K. M.; Silveira, B. M.; and Rosa, J. S.; Macromol. Symp. 2014, 343, 78.

3. Azevedo, M. L. S.; Silveira, B. M.; Novack, K. M.; and Dos Santos, V. M. R.; Macromol. Symp. 2018, 381, 1800145.

4. SCHAFFAZICK, S. R. et al. Caracterização e estabilidade físico-química de sistemas poliméricos nanoparticulados para administração de fármacos. Química Nova, v. 26, n. 5, p. 726–737, 2003.

5. Villanova JCO, Oréfice R L, Cunha AS (2010) Aplicações farmacêuticas de polímeros. Polímeros 20: 51–64, 2010. doi: 10.1590/S0104-14282010005000009.

6. Bokesch, H., Kenney, S., Boyd, M. R., 1990. New colorimetric cytotoxicity assay for anticancer-drug screening. J. Natl. Cancer. Inst., 82, 1107-1112. Vogel R, Pal, AK, Jambhrunkar S, Pragnesh P, Thakur SS, Reátegui E, Parekh HS, Saá P, Stassinopoulos A, Broom MF. (2017) Resolution Single Particle Zeta Potential Characterisation of Biological Nanoparticles using Tunable Resistive Pulse Sensing. Scientific Reports, 7: 1-13.

7. Alves TVG. Obtenção e caracterização de hidrogéis de poliacrilamida-co-metilcelulose como sistemas carreadores de cloridrato de propranolol (2011) Dissertação (Mestrado em Ciências Farmacêuticas) - Universidade Federal do Pará, Instituto de Ciências da Saúde, Belém.

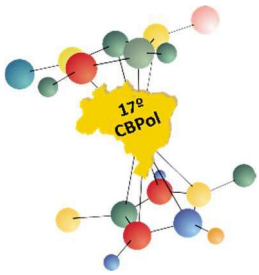

DESIGN AND PHARMACEUTICS ANALYSIS OF *in situ* FILM-FORMING SOLUTIONS CONTAINING POMEGRANATE PEEL EXTRACT FOR MASTITIS PROPHYLAXIS

Geanne A. Paula[1], Rita C. G. de Melo[2], Lílian G. Carreira[3*] and Janaina C. O. Villanova[2]

1 – Faculty of Pharmaceutical Sciences, Paulista State University "Júlio de Mesquita Filho" (UNESP), Araraquara, SP, Brazil

2 – Laboratory of Pharmaceutical Product Development, Center for Exact, Natural and Health Sciences - CCENS, Federal University of Espírito Santo (UFES), Alegre, ES, Brazil.

3 – Department of Rural Engineering, Center of Agricultural and Engineering Sciences - CCAE, Federal University of Espírito Santo (UFES), Alegre, ES, Brazil.

lilian.carreira@ufes.br

Abstract - Bovine mastitis is an inflammation of the mammary gland of cows responsible for major economic losses to dairy producers. Infection by microorganisms resistant to antimicrobials contributes to the high prevalence of mastitis. The objective of this work was to prepare polymeric film-forming solutions (FFS) for delivery pomegranate peel extract (PPE) at the teats of cows aiming prophylaxis of mastitis. FFS containing different polymers and PPE (1.25 to 3.75% w/w) were prepared and the solutions and films formed were submitted to tests for pharmaceutical evaluation. FFS containing poly(vinyl alcohol) (18.0 and 20.0% w/w), alone or associated with sodium polyacrylate (0.5 and 0.75% w/w), showed an adequate degree of fluidity and capacity filmogenic. The incorporation of PPE reduced the pH and increased the viscosity, but maintained the good results of the physical-chemical quality parameters of the films, so that these formulations were considered adequate for the intended purpose.

Keywords: *Bovine mastitis, polymeric films, poly(vinyl alcohol), sodium polyacrylate.*

Introduction

Bovine mastitis is a pathology that needs great attention. It is an inflammatory process established in the mammary gland of the animals, which may result from many ethiologic factors including infections by Gram-positive and Gram-negative microorganisms [1]. This condition impairs the quantity and quality of the milk produced, which in most cases becomes unfit for consumption and must be discarded. In addition to the loss of milk disposal and treatment of the animal, in some situations the cattle need to be sacrificed, which further increases the loss of the producer [1]. Bovine mastitis is considered a public health problem, since humans can eat foods that contain residues of antimicrobials used to treat it. Also, humans can eat in natura foods or his derivatives that contain the microorganisms that cause mastitis too, causing food infections [2].

One of the interests of the drug development area is the replacement of synthetic drugs by compounds from natural sources, especially in the class of drugs intended to combat or control microbial infections [3]. This happens because microorganisms increasingly improve their resistance mechanisms against antimicrobials used in pharmacotherapy [1]. Medicinal plants are promising alternatives to synthetic drugs. Vegetable derivatives of *Punica granatum* Linn, popularly known in Brazil as pomegranate, are used as antimicrobials, due to the richness of bioactive compounds in extracts or essential oils from different parts of the fruit, such as ellagic acid, gallic acid and punicalagin. Studies point to the effectiveness of pomegranate peel extracts (PPE) obtained in different polar solvents in inhibiting the growth of *Staphylococcus aureus*, one of the main microorganisms found in clinical findings of bovine mastitis [1, 4].

The application of film-forming polymeric solutions containing PPE on animal teats represents an innovative and alternative way to administer active ingredients for the prophylaxis of bovine mastitis at pre or pos-dipping. After milking and teat sanitization, the polymeric solutions dry and the films are formed *in situ*, remaining in place until they are removed with water, before the next milking. Film-forming solution (FFS) is a liquid or semi-solid system intended for topical application, where the solvent will quickly evaporate, forming a transparent, adhesive and flexible film [5]. Polymeric films forming a thin and transparent membrane and depending on the type of matrix formed, they can remain in place for a longer time and promote sustained drug release. Furthermore, they can act as a protective barrier against external agents and, as the solvent evaporates, they have good stability [6, 7].

The objective of this work was to prepare FFS based on poly(vinyl alcohol) alone or associated with sodium carboxymethylcellulose, pullulan, or sodium polyacrylate, aiming the topical administration of crude dry PPE with a view to form film *in situ* to prophylaxis of bovine mastitis by spraying. To this end, different formulations were prepared and the pharmaceutical quality parameters of interest were evaluated.

Experimental

Preparation of blends and polymeric films

The qualitative and quantitative compositions of the blends are given in Table 1 and were defined from modifications in the formulation proposed by Nishikawa *et al*. [8]. In all, 8 formulations were prepared.The low molar mass poly(vinyl alcohol) (PVA) (13,000 - 23,000 kDa) was completely solubilized in part of the water in a magnetic stirrer (FISATOM, model 752A, Brazil) under heating until 75º C. Then, the other polymers were added in their solid form, keeping stirring until complete dispersion and homogenization. Preservatives and chelating agents (potassium sorbate and EDTA, respectively) were dissolved in a sufficient amount of water, and were added in solutions under stirring without heating. Grain alcohol was incorporated after cooling. Finally, the plasticizer (propylene glycol) was incorporated under constant agitation. In the previously selected blends, the PPE was incorporated directly, through levigation, without heating, in the proportions of 1.25, 2.5 and 3.75% w/w.

Table 1 – Qualitative and quantitative composition of pure blend formulations

	FFS A	FFS B	FFS C	FFS D	FFS E	FFS F	FFS G	FFS H
	Proportion (% w/w)							
PVA	18.0	20.0	18.0	20.0	12.0	12.0	15.0	15.0
Na-CMC	-	-	-	-	0.5	0.75	0,5	-
Pullulan	-	-	-	-	-	-	-	5.0
Sodium polyacrylate	-	-	0.5	0.75	-	-	-	-
EDTA	0.1	0.1	0.1	0.1	0.1	0.1	0.1	0.1
Potassium sorbate	0.15	0.15	0.15	0.15	0.15	0.15	0.15	0.15
Propylene glycol	6.0	6.0	6.0	6.0	6.0	6.0	6.0	6.0
Grain alcohol	10.0	10.0	10.0	10.0	10.0	10.0	10.0	10.0
Purified water	65.75	63.75	65.25	63.0	71.25	71.0	68.25	63.75

Analysis of film forming solutions

The blends were evaluated macroscopically to describe the parameters of color, transparency, homogeneity, presence of bubbles, insoluble solids and apparent viscosity. The pH was determined by direct potentiometry, using a benchtop device for pH determination (DIGIMED, DM-22, Brazil), by immersing the electrode in a beaker containing a sample of each blend. Finnally, the viscosity of the formulations was measured using a BROOKFIELD digital rotational viscometer (model LV-DV2T, USA), with a small sample adapter, using an S4-31 spindle (experimentally determined), at a speed of 25 rpm and torque varying between 20 and 90%. Measurements of pH and viscosity were

performed in triplicate, at room temperature, and results were presented as mean and standard deviation.

Film preparation

The filmogenic capacity of the blends was preliminarily evaluated on the skin, by depositing approximately 125 mg in a pre-delimited area of the forearm and the time for total drying and formation of the films was timed. Visual analysis done as described above was performed.

For the analysis of the pharmaceutical quality parameters, films were formed by casting solvent technique on glass plates using an adapted accessory, with a thickness control of 0.75 mm. Once the blends were applied, the plates were left exposed to air for drying, and the films were cut into 2 x 2 cm dimensions. The thickness of dry films was evaluated using an external digital micrometer (MITUTOYO, model MDC-25PX, Japan). For this, 10 randomly selected points were measured in each film, in a total of 10 films of each formulation. The average weight was determined by individually weighing 10 films of each formulation using a MARTE analytical balance (model AD200, Brazil). Residual moisture was defined by measuring the water loss of samples submitted to drying by infrared radiation, in a moisture analyzer (SHIMADZU, model MOC63u, Philippines), where each film was placed in the equipment and heated to 105° C, until achieve mass balance. Analysis on the films were performed in triplicate and the results expressed as mean and standard deviation.

Results and Discussion

Formulations FFS E, F and G, containing sodium carboxymethylcellulose (Na-CMC) underwent gelling, forming an extremely viscous structured vehicle, and were excluded from the study. Na-CMC is a polymer consisting of a large number of hydroxyl and carboxyl groups, which substantially increase its swelling capacity [9]. In some products this characteristic is desired, as in solid dosage forms. For FFSs, however, which must remain fluid until they are applied to the skin, the structure of the vehicle is a disadvantage. FFS H, containing pullulan, was also excluded from the study due to the occurrence of phase separation.

FFS formulations must be homogeneous, free of lumps, with a shiny appearance and pleasant sensory when applied [10, 11]. Among the formulations prepared with synthetic polymers, formulations A, B, C and D, containing PVA at 18 and 20% w/w, alone or associated with sodium polyacrylate at 0.5 and 0.75% w/w, were transparent, homogeneous and without suspended or precipitated particles. The FFS do not dripped onto the skin and the films did not break during removal. The FFS showed good filmogenic capacity, spreading and completely covering the skin, continuously. The same aspect was observed from films prepared onto glass plates. These solutions gave rise to intact, soft and flexible films, with a pleasant texture and easy to remove from the skin and from to the glass plate, desirable characteristics for use as a pharmaceutical dosage form [5, 10, 12].

After preliminary analysis, the pure blends FFS A, FFS B, FSS C and FFS D were selected for the incorporation of PPE at concentrations of 1.25% (FFS A1, B1, C1 and D1), 2.5% (A2, B2, C2 and D2) and 3.75% (A3, B3, C3 and D3) w/w. All the characteristics observed in the pure films were maintained, except for the color, which became amber-yellow, typical of PPE. The color intensity increased with increasing extract concentration in the formulation, as shown in Figure 1. The drying time of these formulations on the skin ranged from 23 to 42 min, with only FFS A3, B, C1, D and D2 showing an average drying time greater than 30 min.

Viscosity is an important FFS parameter, since the formulations cannot be excessively viscous, which makes application and drying difficult, and they must not be too fluid, so that they do not flow before forming films at the application site [11, 12]. Table 2 brings the viscosity values obtained for the FFS, as well as the other results of the physical-chemical characterization.

Figure 1 – a) Representative image of the polymeric blends before and after the addition of PPE; b) Representative image of pure films and with different concentrations of extract, formed on the glass plate.

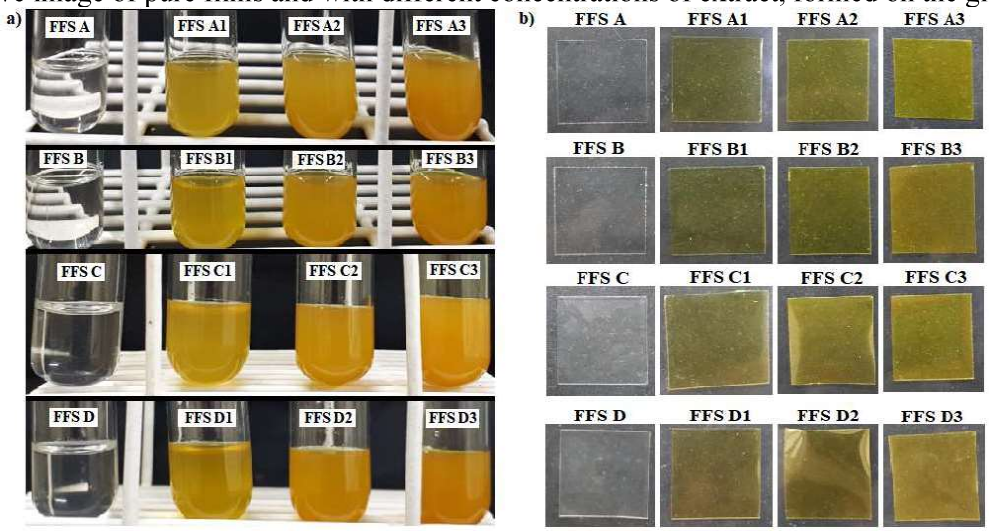

Table 2 – Result of the physicochemical evaluation of the FFS and formed films

	Viscosity (cP)	pH	Average weight (mg)	Thickness (µm)	Residual moisture (%)
FFS A	277.2 (± 5.2)	6.06 (± 0.03)	44.30 (± 0.015)	113.7 (± 0.039)	12.63 (± 2.69)
FFS A1	289.6 (± 7.2)	5.80 (± 0.09)	56.00 (± 0.024)	137.8 (± 0.054)	10.99 (± 3.47)
FFS A2	342.8 (± 4,2)	5.70 (± 0.04)	68.40 (± 0.019)	165.0 (± 0.043)	14.98 (± 3.59)
FFS A3	415.2 (± 6.7)	5.49 (± 0.14)	89.69 (± 0.012)	113.2 (± 0.015)	14.87 (± 2.36)
FFS B	431.2 (± 3.7)	6.12 (± 0.04)	43.30 (± 0.016)	110.6 (± 0.040)	17.15 (± 3.71)
FFS B1	497.6 (± 12.8)	5.81 (± 0.05)	48.10 (± 0.008)	118.8 (± 0.021)	13.26 (± 1.25)
FFS B2	510.4 (± 8.2)	5.69 (± 0.04)	59.50 (± 0.022)	155.3 (± 0.053)	12.42 (± 1.14)
FFS B3	536.8 (± 11.3)	5.48 (± 0.01)	48.50 (± 0.009)	124.5 (± 0.032)	14.65 (± 2.72)
FFS C	324.8 (± 7.9)	7.05 (± 0.07)	31.40 (± 0.002)	82.5 (± 0.006)	15.52 (± 1.19)
FFS C1	325.2 (± 3.17)	6.26 (± 0.13)	54.0 (± 0.014)	140.8 (± 0.032)	11.82 (± 0.20)
FFS C2	374.4 (± 3.2)	5.81 (± 0.18)	52.0 (± 0.028)	128.4 (± 0.064)	10.33 (± 2.19)
FFS C3	407.6 (± 12.8)	5.81 (± 0.02)	52.40 (± 0.017)	128.6 (± 0.038)	10.15 (± 2.36)
FFS D	438.0 (± 7.3)	6.94 (± 0.07)	45.4 (± 0.009)	109.9 (± 0.019)	13.08 (± 0.71)
FFS D1	544.0 (± 5.7)	6.23 (± 0.18)	40.90 (± 0.006)	103.7 (± 0.008)	11.91 (± 0.28)
FFS D2	557.2 (± 1.4)	6.05 (± 0.02)	44.90 (± 0.004)	114.1 (± 0.025)	12.10 (± 0.81)
FFS D3	616.0 (± 4.9)	5.85 (± 0.01)	53.60 (± 0.004)	127.3 (± 0.009)	8.47 (± 0.14)

Viscosity is one of the most significant rheological parameters that need to be considered during the preparation of *in situ* polymeric film forming solutions because the factor affects the drying time of the film [13, 14]. Formulations of pure blends with a higher proportion of polymers showed higher viscosity, results consistent with the literature, since there is a greater degree of crosslinking at a higher concentration of polymers [15]. It can also be observed that the incorporation of PPE increased the viscosity of the blends and that the values were higher in the formulations with a higher proportion of extract, probably due to the greater amount of solid material present. Moderate viscosity is a preferable flow characteristic for in situ FFS because high or low viscosity results in failure to spread, breakage or non-uniform film formation [15, 16]. The possibility of the existence of interactions between the phenolic compounds present in the extract and the polymeric chains will be researched using appropriate techniques. The addition of PPE in the formulation promoted a decrease in the pH values of the pure blends. The pH value observed for a pure extract solution in water at 10% w/w was 3.48 [16], which justifies the pH reduction observed in the formulations with extract.

The close average thickness and weight values between the different formulations allow inferring that there is no relationship between these parameters and the concentration of polymer or extract present, and the low values of standard deviation observed, desirable in any studies that compare repetitions of the same test, are an indicator that there is reproducibility in the preparation technique and homogeneity in the formulation obtained [17].

The percentage of free residual water present in the films varied between 8.47 and 17.14%. Despite the great influence of free water content on attributes such as mechanical strength, flexibility and tackiness of polymeric films, there are no specifications in the literature for comparing these parameters.

Conclusions

The formulations containing Na-CMC were very viscous, while in the FFS containing pullulan there was phase separation, and therefore, both were excluded from the study after a preliminary evaluation. The FFS obtained from PVA at concentrations of 18.0 and 20.0% w/w, alone or associated with sodium polyacrylate (0.5 and 0.75% w/w), showed an adequate degree of fluidity, with filmogenic capacity and formation of intact, soft and flexible films. The incorporation of PPE promoted a reduction in pH and an increase in viscosity, but maintained the good results of the physical and chemical quality parameters of the formed films. For this reason, FFS A, B, C and D, with different concentrations of extracts, are considered suitable vehicles for the intended purpose.

Acknowledgements

The authors thank FAPES (Universal TO #03/2021 and PICJr #09/2019), CAPES (funding code 001) and CNPq.

References

1. T. S. Lopes; P. S. Fontoura; A. Oliveira; F. A. Rizzo; S. Silveira; A. F. Streck. *R. Vet. Sci*. 2020, *131*(1), 186.
2. T. F. Procópio; M. C. Moura; E. F. L. Bento; T. Soares; L. C. B. B. Coelho; R. P. Bezerra; R. A. Mota; A. L. F. Porto; P. M. G. Paiva; T. H. Napoleão. *Microbiologyopen*. 2019, *8*(11), 1.
3. N. N. Costa; L. F. Lopes; D. F. Ferreira; E. M. L. Prado; J. A. Severi; J. A. Resende; F. P. Careta; M. C. P. Ferreira; L. G. Carreira; S. O. L. Souza; M. A. P. Cotrim; T. Boeing; S. F. Andrade; R. L. Oréfice; J. C. O. Villanova. *Mater. Sci. Eng*. 2020, *109*, 110643.
4. T. B. Machado. *Biomed. J. Sci. Technol. Res.* 2019, *13*(4), 10092.
5. K. Kathe; H. Kathpalia. *Asian J. Pharm*. 2017, *12*(6), 487.
6. J. B. Taksande; M. Gupta; R. V. Trivedi; K. J. Wadher. M. J. Umekar. *J. Appl. Pharm. Res*. 2016, *4*(3), 8.
7. J. Suksaeree; P. Maneewattanapinyo; K. Panrat; W. Pichayakorn; C. Monton. *J. Polym. Environ*. 2021, *29*(10), 3174.
8. D. D. O, Nishikawa; V. Zague; R. P. Vieira; T. M. Kaneko; M. V. R. Velasco; A. R. Baby. *Rev. de Ciênc. Farm. Básica e Apl*. 2007, *28*(2).
9. H. Bosch, MSc. Dissertation, Federal University of Fluminense, 2016.
10. J. A. Oshiro Junior; L. M. Shiota; L. A. Chiavacci. *Matéria - Rio De Janeiro.* 2014, 24.
11. M. H. Alkurd, MSc. Dissertation, University of Mississippi, 2019.
12. T. T. D. Tran; P. H. L. Tran. *Pharmaceutics*. 2019, *11*(6), 290.
13. A. K. Umar; M. Butarbutar; S. Sriwidodo; N. Wathoni. *Drug Des. Devel. Ther*. 2020, *14,* 2909.
14. B. Dhimmar; R. Pokale; M. Rahamathulla; U. Hani; M. Y. Alshahrani; S. Alshehri; F. Shakeel; P. Alam; R. A. M. Osmani; A. B. Patil. *Polymers.* 2023, *15*, 1003
15. Z. A. Sadeq; E. Ghazy; Z. Salim. *Int. J. Pharm. Res*. 2020, *12*(4).
16. T. M. Silva, MSc. Dissertation. Federal University of Espírito Santo, 2021.
17. S. Karki; H. Kim; S. J. Na; D. Shin; K. Jo; J. Lee. *Asian J. Pharm*. 2016, *11*(5), 559.

DEVELOPMENT OF BACTERIAL CELLULOSE INCORPORATED WITH ESSENTIAL OILS FOR WOUND TREATMENT

Sandro Rogério Kumineck Junior[1*], Victória Fonseca Silveira[2], Denise Abatti Kasper Silva[1], Michele Cristina Formolo Garcia[3], Giannini Pasiznick Apati[3], Andréa Lima dos Santos Schneider[2,3], Ana Paula Testa Pezzin[1], Flares Baratto-Filho[1]

1 – Master program in Process Engineering (MEP), University of Joinville Region (UNIVILLE), Joinville, SC, Brazil Joinville, SC, Brazil
sandrorkjunior98@gmail.com
2 – Master program in Health and Environment, University of Joinville Region (UNIVILLE), Joinville, SC, Brazil
3 – Department of Chemical Engineering, University of Joinville Region (UNIVILLE), Joinville, SC, Brazil

Abstract - Bacterial cellulose (BC) is promising for application as wound dressing because it is non-toxic, non-allergenic and maintains moisture in the wound. Although BC does not have antimicrobial activity, its structure allows the incorporation of antimicrobial compounds such as essential oils (EOs). This study aims to associate BC membranes with rosemary, clove, eucalyptus, ginger, lavender and lemongrass EOs to obtain wound dressings. The Gas Chromatography–Mass Spectrometry and Fourier Transform Infrared Spectroscopy analyses showed characteristic compounds of EOs in the incorporated membranes. The Scanning Electron Microscopy indicated that the EOs filled the membrane pores and coated the cellulose fibers. The incorporation of EOs into BC improved the antimicrobial properties of the biomaterial, highlighting the samples incorporated with clove, ginger and lemongrass EOs.
Keywords: *Bacterial cellulose, essential oils, wound dressings.*
Fundings: The authors are grateful for the financial support of FAPESC and UNIVILLE for the project.

Introduction

Traditional methods of treating chronic wounds include dressings that can interfere with the healing process since constant dressing changes are made, causing pain and discomfort to the patient and delaying tissue reconstitution [1]. As an alternative to traditional dressings, a new generation of functional dressings has been developed seeking to prevent infections and improve wound healing, with properties such as maintenance of wound moisture, removal of exudates and antimicrobial control. In that regard, biopolymer-based dressings may be a good choice for treating these wounds [1, 2]. Thus, bacterial cellulose (BC) stands out because it is biodegradable, has high purity, high mechanical resistance, biocompatibility and has a reticulated structure that serves as a barrier against pathogenic microorganisms. BC has a structure similar to the skin's extracellular matrix, creating and maintaining a humid environment for the wound due to its high hydrophilicity and also serving as a barrier against UV radiation [3]. However, BC alone cannot inhibit the growth of pathogenic microorganisms, which reduces its effectiveness as a dressing for contaminated wounds. Nonetheless, antimicrobial agents can be incorporated into its structure to improve its biological properties. In this sense, essential oils (EOs) become a good option for this purpose due to their antimicrobial, antioxidant, and anti-inflammatory properties, arising from the presence of bioactive compounds such as phenols and terpenes in its structure. In addition, EOs are advantageous over synthetic antimicrobial agents because they are widely available natural compounds with low toxicity [4, 5], making the material promising for application in tissue regeneration. In that regard, some EOs that can be used for the production of biocomposites includes rosemary (REO), clove (CEO), eucalyptus (EEO), ginger (GEO), lavender (LEO) and lemongrass (LGEO)[5]. In addition to their antimicrobial properties, these EOs stimulate tissue regeneration, strengthen the immune

system, exert a healing effect on individual organs and systems (respiratory and digestive organs, nervous and circulatory systems) [6]. In this context, the present work aims to develop a BC dressing incorporated with the aforementioned EOs.

Experimental

Production and characterization of materials

BC membranes were synthesized by the bacterium *Komagataeibacter hansenii* (ATCC 23769) in a culture medium adapted from Hestrin and Schramm [7], incubated at 30 °C in static condition for 12 days. Afterwards, the BCs were purified with a 0.1 M NaOH solution at 80 °C for 1 h. Subsequently, the membranes were washed with distilled water repeatedly until the pH 7. Then, the BC membranes were sterilized and submitted to the incorporation processes. Following the methodology adapted from Albuquerque [8], BC membranes were immersed in 150 mL of ethanol at 60 °C for 10 min. Afterward, each BC was immersed in a solution containing 3.0 g of EO in 20 mL of ethanol and heated at 60 °C until the solution evaporated. Finally, the BCs incorporated with the EOs were lyophilized and stored for analysis of incorporated EO content by Gas Chromatography-Mass Spectrometry (GC-MS), High Resolution Scanning Electron Microscopy (SEM), Fourier Transform Infrared Spectroscopy (FTIR) and antimicrobial activity.

Results and Discussion

The main components of EOs detected by GC-MS in the samples are presented in Table 1.

Table 1 - Main components of EOs detected by GC-MS.

Components	Sample	Concentration (%)	Sample	Concentration (ppm)
Eucalyptol	**REO**	72.222	**BC/R**	4,640
Camphor		13.366		258.133
α-pinene		4.105		6,164
Eugenol	**CEO**	86.809	**BC/C**	76,860
β-caryophyllene		11.397		nd
Eucalyptol	**EEO**	89.303	**BC/E**	4,220
Limonene		8.259		4,120
Ar-curcumene	**GEO**	2.215	**BC/G**	364,440
Zingiberene		3.651		102,840
β-sesquiphelandrene		1.484		232,440
Neral		6.882		117,360
Geranial		9.536		151,200
β- caryophyllene		10.709		93,240
Linalool	**LEO**	45.298	**BC/L**	126,880
Linalyl acetate		35.844		126,980
Neral	**LGEO**	30.292	**BC/LG**	60,360
Geranial		41.572		85,680

*nd = not detected.

The compound with the highest concentration in REO and EEO was eucalyptol. The concentrations in ppm of the BC/R and BC/E compounds were low concerning the other samples, which may be due to the greater volatilization of these EOs and their components during incorporation into the BC. For CEO, eugenol, the major compound of clove [9]; and β-caryophyllene were identified. The incorporated sample maintained a high concentration of eugenol; however, β-caryophyllene was not identified. The GEO showed the greatest variety in its composition, where β-caryophyllene, neral and geranial (citral) were identified with the highest percentage. The compounds with the highest concentrations in BC/G were ar-curcumene and β-sesquiphelandrene, possibly due to greater

volatilization of the other compounds during incorporation. LEO and LGEO presented two major compounds each: linalool and linalyl acetate, and neral and geranial, respectively. The BC/LG sample kept geranial as the compound with the highest concentration, and BC/L had a very close concentration between its two compounds, suggesting a greater volatilization of linalool. The chemical composition of essential oils is quite variable, as it depends on the EOs extraction method and time, type and concentration of solvents, the species involved, the climatic conditions and the soil where the plant was grown, among others [10].

The FTIR spectra presented the main bands obtained from the samples of BC, EOs, and incorporated BCs. The BC sample showed high-intensity bands at 3344 cm^{-1}, attributed to the axial stretching of hydroxyl groups present in organic compounds [11]. Other bands referring to the presence of OH groups were observed at 1205 and 664 cm^{-1}, referring to in-plane binding and out-of-plane angular deformation, respectively [3]. Bands referring to the C-H bonds of methyl groups were observed at 2896 and 895 cm^{-1} due to stretching and angular deformation, respectively [12]. Furthermore, several bands attributed to the stretching of C-O groups were observed, such as those at 1336, 1161, 1055 and 1032 cm^{-1} [12]. Moreover, the band at 1641 cm^{-1} stands out, which, in the case of BC, refers to the angular deformation of water, demonstrating its hydrophilicity [3]. In the incorporated samples, several bands related to EOs appeared, such as the C-H stretching band in vinyl groups at 3088 cm^{-1}, attributed to the presence of linalool and linalyl acetate in the BC/L sample [13]; around 1735 cm^{-1}, referring to the stretching of C=O groups for BC/R, BC/L and BC/LG samples, derived from camphor, linalyl acetate and citral (neral and geranial), respectively [13]; around 1675 cm^{-1} for BC/G and BC/LG, attributed to citral [14]. Bands referring to the eugenol of the BC/C sample were observed at 3515 and 1511 cm^{-1}, attributed to the stretching of O-H bound to benzene and stretching of C=C of the aromatic ring, respectively [15]. Bands were observed at 985 cm^{-1}, referring to out-of-plane symmetric deformation of CH_2, which, in the case of samples incorporated with rosemary and eucalyptus, can be attributed to the presence of eucalyptol[16].

The morphologies of pure BC and incorporated BCs were observed by SEM (Fig. 1).

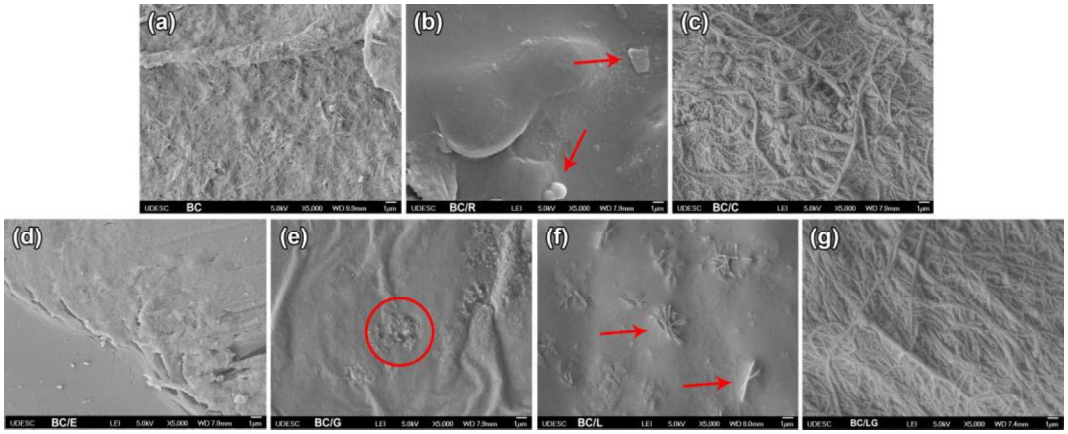

Figure 1 - SEM micrographs (a) BC, (b) BC/R, (c) BC/C, (d) BC/E, (e) BC/G, (f) BC/L and (g) BC/LG.

The micrograph of pure BC (Fig. 1a) shows the typical structure of this material, consisting of tangled nano and microfibrils arranged randomly and with pores [17]. The BC/R (Fig. 1b) presented a more homogeneous and smooth surface, demonstrating that the EO filled the membrane pores. Similar morphology to that of BC/R was observed for samples of BC/G (Fig. 1e), with regions of greater roughness, and BC/L (Fig. 1f), where fibers can be seen at different points. BC/C (Fig. 1c) and BC/LG (Fig. 1g) samples maintained the tangled fiber structure of pure BC, however, with greater thickness and roughness. In this case, the EOs might have coated the BC fibers. Finally, the BC/E (Fig. 1d) presented a region resembling the BC/R, BC/G and BC/L samples with a homogeneous surface; however, it also has a region with greater roughness. These two regions are

separated by an interface with irregularities, which may be related to the difference in BC membrane thickness in these regions. The interaction between BC and added materials can occur by the hydrogen bonds between the hydroxyls of the BC with the added materials [18], which causes a decrease in porosity and roughness [19]. This behavior was observed for BC/L, where an interaction between the linalool hydroxyl and the BC hydroxyls may have occurred. The same was not observed for BC/C, where the interaction between BC and eugenol hydroxyl maintained the fibrillar morphology of the sample. The other samples do not have hydroxyls in the structure of their main components, where the interaction may have happened by physical adherence. In addition, the evaporation of EOs during the preparation of samples for analysis may have caused a collapse of the pores of the membranes, which explains the samples that presented a smoother surface.
Fig. 2 shows the antimicrobial activity results obtained for REO (R), CEO (C), EEO (E), GEO (G), LEO (L) and LGEO (LG) at 15%; and for BC samples incorporated with the EOs against *C. albicans, E. coli* and *S. aureus*.

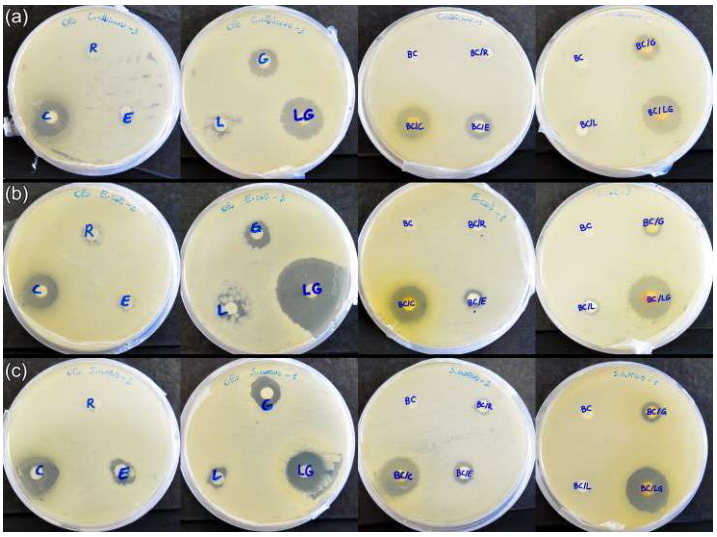

Figure 2 - Antimicrobial of the samples for (a) *C. albicans*, (b) *E. coli* and (c) *S. aureus*.

REO did not show inhibitory action against the microorganisms. The BC/R had inhibition halos with a mean diameter of 8.67 mm against *S. aureus* (Fig. 2c), suggesting a lower absorption of EO by the filter paper used in the test concerning the amount absorbed by the BC. EEO and LEO samples showed irregular halos for *E. coli* and *S. aureus,* and there was no inhibition of *C. albicans*. Conversely, the BC/E sample had inhibition zones against all test microorganisms. The BC/L sample maintained antimicrobial activity against *E. coli* but with a decrease in the inhibition zone from approximately 14 mm to 7.25 mm. The BC/R and BC/E samples showed a similar concentration of eucalyptol in their composition; however, the antimicrobial activities were different, which may be related to the different morphologies of these samples. On the other hand, CEO, GEO and LGEO showed inhibitory effects for all test microorganisms, with halos. With few exceptions, the membranes incorporated with these EOs had a slight decrease in the average diameter of the inhibition zones, suggesting minor incorporation or less diffusion of the microbial agents in these incorporated BCs. The literature proves the inhibitory action of these oils against *C. albicans, E. coli* and *S. aureus* [20–22]. The components of EOs, such as phenols and terpenes, have hydroxyl groups that affect the cells of microorganisms by several mechanisms, which include disturbance of the enzymatic system, damage to the genetic material of the microorganism and reactions with the phospholipid membrane, resulting in the release of cell constituents and consequent death of microorganisms [4]. Thus, considering the compounds identified in the GC-MS, it is possible to state that the compounds with the greatest antimicrobial power were eugenol, present in CEO, and citral, present in GEO and in greater quantity in LGEO.

Conclusions

The effectiveness of the incorporations was confirmed by GC-MS and FTIR analyses, which identified the compounds of the EOs in the incorporated BCs. CEO and LGEO coated the cellulose fibers, maintaining a morphology more similar to the original, while the other EOs infiltrated the pores of the cellulose membrane, filling them and giving the samples a more distinct morphology. CEO, GEO and LGEO showed the best antimicrobial activities due to the presence of eugenol and citral mainly. These characteristics were maintained after incorporation into BC. Based on the results obtained, it is possible to affirm that incorporating EOs in BC membranes is promising due to the good characteristics inherent to cellulose and the ease of application of the methodology.

References

1. J. Boateng,; O. Catanzano. Journal of Pharmaceutical Sciences, 2015, 104, 3653–3680. https://doi.org/10.1002/jps.24610.
2. S. Gustaite; *et al.* Colloids and Surfaces A: Physicochemical and Engineering Aspects, 2015, 480, 336–342. https://doi.org/10.1016/j.colsurfa.2014.08.022.
3. H. S. Barud, Ph.D. Thesis, Universidade Estadual Paulista, 2010.
4. S. Casalini; M. G. Baschetti. Journal of The Science of Food and Agriculture, 2022, 103. https://doi.org/10.1002/jsfa.11918.
5. I. Liakos; *et al*. Journal of Materials Chemistry B, 2015, 3, 1583-1589. https://doi.org/10.1039/C4TB01974A.
6. E. Schmidt; *et al;*. Natural Product Communications, 2010, 5, 1365-1368. https://doi.org/10.1177/1934578X1000500906.
7. S. Hestrin; M. Schramm. The Biochemical Journal, 1954, 58, 345-352. https://doi.org/10.1042/bj0580345.
8. R. M .B. Albuquerque. Master's. Dissertation, Universidade Católica de Pernambuco, 2019.
9. N. Hasheminejad; F. Khodaiyan; M. Safari. Food Chemistry, 2019, 275, 113-122. https://doi.org/10.1016/j.foodchem.2018.09.085.
10. A. Ali; J. J. Cottrell; F. R. Dunshea. Metabolites, 2022, 12, 1016. https://doi.org/10.3390/metabo12111016.
11. A. Ricci; *et al.* Applied Spectroscopy Reviews, 2015, 50, 407–442. https://doi.org/10.1080/05704928.2014.1000461.
12. É. Pecoraro; *et al.* Monomers, Polymers and Composites from Renewable Resources, 2007, 369-383. https://doi.org/10.1016/B978-0-08-045316-3.00017-X.
13. E. Truzzi; *et al.* Phytochemical Analysis, 2021, 32, 907-920. https://doi.org/10.1002/pca.3034.
14. G. Antonioli; *et al.* Food Chemistry, 2020, 326, 126997. https://doi.org/10.1016/j.foodchem.2020.126997.
15. V. V. Kopp. Master's. Dissertation, Universidade Federal do Rio Grande do Sul, 2020.
16. A. Dzimitrowicz; *et al.* Arabian Journal of Chemistry, 2019, 12, 4795–4805. https://doi.org/10.1016/j.arabjc.2016.09.007.
17. M. Fernandes; *et al.* Microbial Biotechnology, 2019, 12, 650–661. https://doi.org/10.1111/1751-7915.13387.
18. N. Shah; *et al.* Carbohydrate Polymers, 2013, 98, 1585–1598. https://doi.org/10.1016/j.carbpol.2013.08.018.
19. E. Jahed; *et al.* Reactive and Functional Polymers, 2017, 117, 70-80. https://doi.org/10.1016/j.reactfunctpolym.2017.06.008.
20. N. Rahimifard; *et al.* Biomedical and Pharmacology Journal, 2015, 1, 43-46.
21. P. K. Sharma; V. Singh; M. Ali. Pharmacognosy Journal, 2016, 8, 185-190. http://doi.org/10.5530/pj.2016.3.3.
22. A. Ahmad; A. Viljoen. Phytomedicine, 2015, 22, 657–665. https://doi.org/10.1016/j.phymed.2015.04.002.

FABRICATION AND CHARACTERIZATION OF VANILLIN CROSSLINKED CHITOSAN FILMS WITH MODULATED MECHANICAL PROPERTIES AND SURFACE TOPOGRAPHY FOR CELLULAR ATTACHMENT

Rafael L. C. G. da Silva[1*], Denise F. S. Petri[1]

1 – Chemistry Department, University of São Paulo (USP), São Paulo, SP, Brazil
rafaelcruz@iq.usp.br

Chitosan is a polysaccharide widely used as a scaffold for cell adhesion and proliferation. However, it is unclear how some scaffold's physical features like topography and nanomechanical properties might affect the cellular behavior. In this work, we propose a simple methodology for the production of vanillin crosslinked chitosan scaffolds with different mechanical properties and surface topography via the incorporation of Polydimethyl siloxane (PDMS) oil/water emulsions of controlled size. Vanillin was successfully grafted onto the chitosan backbone, resulting in increased crosslinking between chitosan chains. PDMS emulsions were then produced and incorporated into the modified chitosan solution. The casting of the precursor solution led to the formation of films with increased roughness and lower Young's modulus in comparison to the dried films in the absence of PDMS emulsions. The PDMS-incorporated crosslinked films showed large surface heterogeneity, which influenced C2C12 cells attachment differently.

Keywords: *Chitosan scaffolds, Mechanical properties, Cell mechanotransduction.*
Fundings: FAPESP 2020/05632-9 / BEPE FAPESP 2021/13925-9

Introduction

Tissue engineering has emerged as a promising alternative to conventional approaches, such as prosthetics and tissue transplantation, commonly used in regenerative medicine [1]. The underlying principles of this field involve the integration of cells, scaffolds, and growth factors to develop innovative materials capable of repairing damaged tissues and organs, and potentially even replacing them in the future [1,2]. Generally, an appropriate scaffold needs to possess specific physical and chemical properties that can effectively stimulate the processes of cell adhesion, migration, proliferation, and differentiation [3,4]. For a scaffold to be effective in tissue engineering, it is crucial that its chemical composition promotes suitable wettability and affinity for cell proteins responsible for adhesion while ensuring controlled degradation [5] and minimizing adverse immune responses [6]. The use of natural compounds has emerged as an alternative to synthetic materials in the production of new scaffolds [7,8]. Chitosan is a naturally occurring polysaccharide formed by β (1 → 4) glycosidic bonds between 2-acetamido-2-deoxy-D-glycopyranose (GlcNAc) and 2-amino-2deoxy-D-glycopyranose (GlcN) units and can be obtained by deacetylation of chitin, the second most abundant natural polysaccharide after cellulose.

In addition to its abundance, chitosan also presents exceptional biocompatibility, low toxicity and the presence of reactive chemical groups in its structure, which guarantees the

possibility of further modifications, both chemical and biological [9]. For these reasons, chitosan has been considered one of the main biopolymers with medical applications, mainly in the field of regenerative medicine. Many studies have evaluated its application in the production of scaffolds for the growth and regeneration of different tissues, including: skin, bone, cartilage and nerves [10].

Additionally, physical attributes of cellular scaffolds such as nanotopography and mechanical properties are also known to significantly impact cellular behavior [7]. Several parameters such as migration, gene expression, signaling and polarization can be drastically altered through the production of scaffolds with different rigidity and topographic patterns printed on their surface [11]. Biological materials might exhibit a complex structure at both micro- and nano-scale levels, and are generally soft, presenting values of Young's modulus from tens of Pa to several MPa. Owing to this, the biomechanical characterization of these materials normally requires both force and displacement at micro- and nano-scale resolutions [11].

AFM measurement methods provide a variety of tools for evaluating properties at the nanoscale by measuring local interactions between the tip of a microcantilever and the surface being analyzed, which guarantees the analysis of surface morphology in three dimensions with a resolution of a few nanometers. In addition, the technique allows for analysis in a liquid medium and does not require specific sample preparation methods, which makes it excellent for the study of biological samples and hydrogels. Fig 1 presents a scheme for obtaining mechanical properties of a soft material via AFM. An indentation force (F) is applied to the sample surface through the tip of a flexible cantilever with a known elastic constant (k). The microscope's piezoelectric scanning system monitors the movement of the base of the cantilever (z) as the probe tip advances to different depths within the surface (δ), producing a small deflection of the probe tip. An optical system, consisting of a laser beam and a photodetector determines how much the cantilever deflects from its original value (d). Equations 1 and 2 present the calculations of depth (δ) and indentation force (F), respectively.

$$\delta = z - d \quad (1)$$

$$F = kd \quad (2)$$

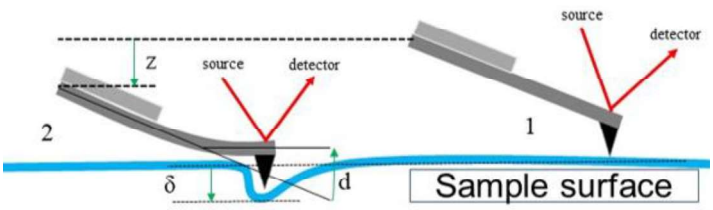

Figure 1- Scheme of application of the AFM technique for the quantification of mechanical properties of soft materials.

Different models of force-indentation curves (F-δ) can be adjusted to estimate elastic properties of materials. The Hertzian model assumes that the contact between two elastic bodies is a smooth, curved surface and that the deformation and stress caused by the contact can be described by a set of equations. These equations take into account the geometry of the contact surface, the elastic properties of the materials involved, and the amount of force applied.

The main challenge of this study consists in the development of a simple procedure for the creation of crosslinked chitosan scaffolds with surface topography features and modulable mechanical properties. Changes in surface roughness and mechanical properties of the produced scaffolds will be consistently evaluated using atomic force microscopy applying the Hertzian model of contact. Afterwards, the cellular behavior of C2C12 rat muscle cells will be evaluated for the different systems produced.

Experimental

Fig 2 presents a scheme of all the steps followed for the production of chitosan scaffolds. In step 1, a chitosan solution (1% w/w in 50 mM acetic acid) was prepared with the addition of vanillin (20% in relation to the chitosan mass) as the crosslinking agent, under magnetic stirring for 24 hours. Zou et al [12] demonstrated that the formation of the Schiff's bases can occur between the chitosan primary amines and the vanillin aldehyde.

In step 2, two oil-water (O/W) emulsions were prepared. In the first emulsion, the oil phase was composed of a mixture between polydimethyl siloxane (PDMS) and its curing agent at a proportion of 10:1, whereas in the second emulsion the oil phase was composed of hexane. Both dispersions were produced in the final volumetric fraction of 0.05 with respect to the aqueous phase which was composed of polysorbate 20 at its CMC (80 mM) and lauryl alcohol (40 mM), which acted as a coemulsifier.

In step 3, the emulsions were be dripped into the previously crosslinked chitosan solution under vigorous magnetic stirring, at room temperature, until complete dispersion. In step 4, the colloidal systems were deposited in silicon molds and left to dry at room temperature. It was expected that after solvent evaporation the PDMS emulsion pattern could leave protuberances on the surface of the produced scaffolds. In the case of the system containing the n-hexane emulsion, it was expected that the hexane molecules had completely evaporated from the casting solution, producing cavities on the surface of the dried scaffolds. PDMS emulsions had their size distribution characterized using optical microscopy and their surface charge was accessed by measuring their zeta potential. Surface modifications and mechanical properties of the dried films (before and after incorporation of the emulsions) were followed using mainly AFM technique.

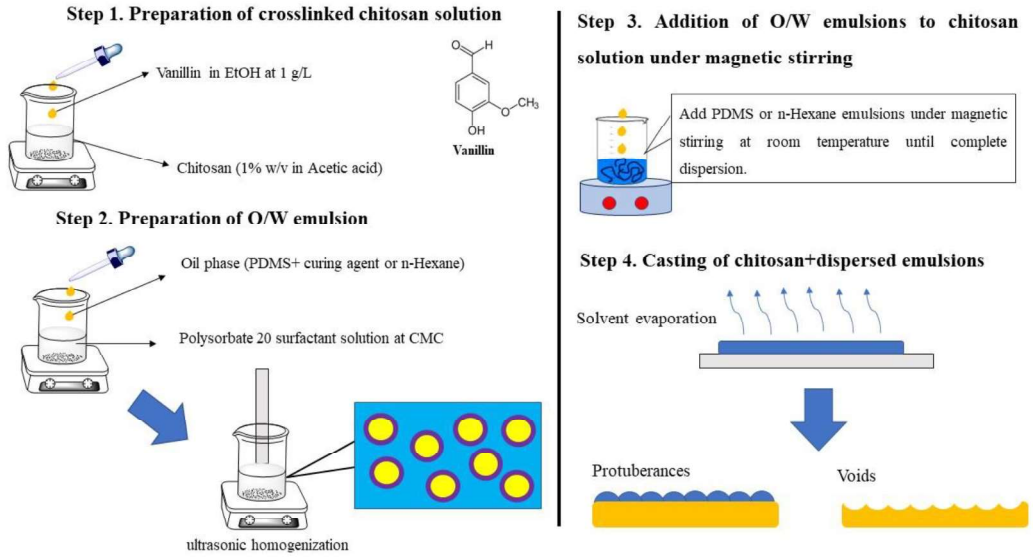

Figure 2- Schematic representation of all steps followed for the production of chitosan scaffolds.

Results and Discussion

Qualitative evidences of the grafting of vanillin to the chitosan backbone were obtained by ATR-FTIR and 1H NMR spectroscopies of the dried films. The crosslinking between chitosan chains was quantitatively evaluated by immersing the films in water and following their swelling degree (SD) and gel contents (GC). The GC increased from 57 to 69.8 % upon adding vanillin to the chitosan backbone whereas the SD decreased from 29.4 to 23.2%, which indicates that the

grafting of the natural aldehyde leads to an increase the number of joint points between chitosan chains.

The production of Tween 20 stabilized PDMS emulsions was followed using optical microscopy (Fig 3B). These emulsions presented a broad size distribution in the micrometric range of 1 to 9 μm (Fig 3A), with the most frequent size within 2 to 3 μm and an average negative zeta potential of 12 mV. Fig 3B shows an SEM image of PDMS domains immobilized in dried crosslinked chitosan films. The broad size distribution of PDMS domains could still be observed as well as the first evidence of surface modification by the incorporation of the emulsions.

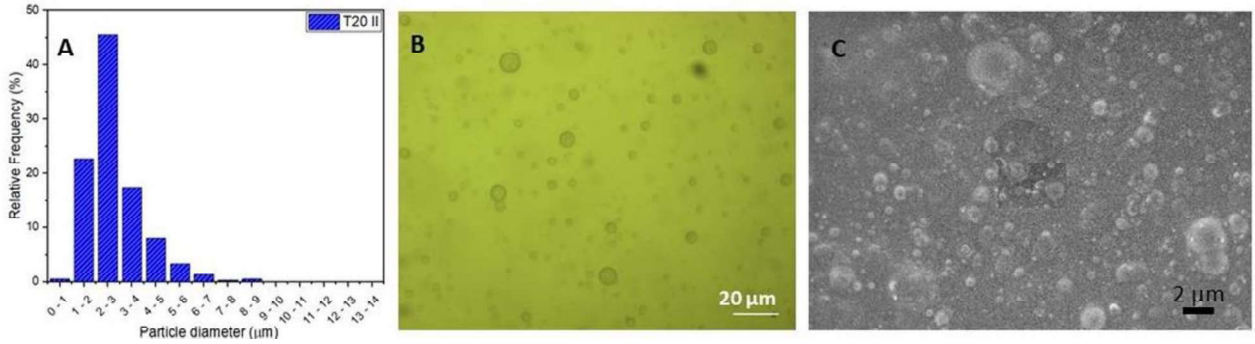

Figure 3 – Size distribution of Tween 20 stabilized PDMS emulsions (A), Optical microscopy of Tween 20 stabilized PDMS emulsions in water (B), PDMS domains immobilized in dried crosslinked chitosan films.

Figs 4A and B show the process of surface modification of chitosan films upon the immobilization of PDMS emulsions. The arithmetic average roughness (Ra), which indicates the average difference between peaks and valleys in the AFM images, invreased from 1.19 to 53.99 nm upon inserion of the PDMS domains. This process can be better seen at the lower 3D AFM images. On the other hand, the force-volume mapping of the two different systems sowed an overall decrease to the average Young`s modulus of the crosslinked chitosan films from 3.18±0.27 GPa (CV= 9%) to 1.38±0.6 GPa (CV=48%). The higher coefficient of variation obtained for the population of force-indentation curves after PDMS emulsions incorporation indicated a greater level of dispersion around the mean value for such system, which in its turn is a reflex of regions with greater or lesser concentrations of emulsions on the film surface, leading to a higher heterogeneity of elasticity modulus. Such heterogenity seemed to influence the attachment of C2C12 rat muscle cells to the surface of the modified material once regions fully covered with cells contrasted with regions were very little population could be detected, as presented in the confocal microscopy image in Fig 4C.

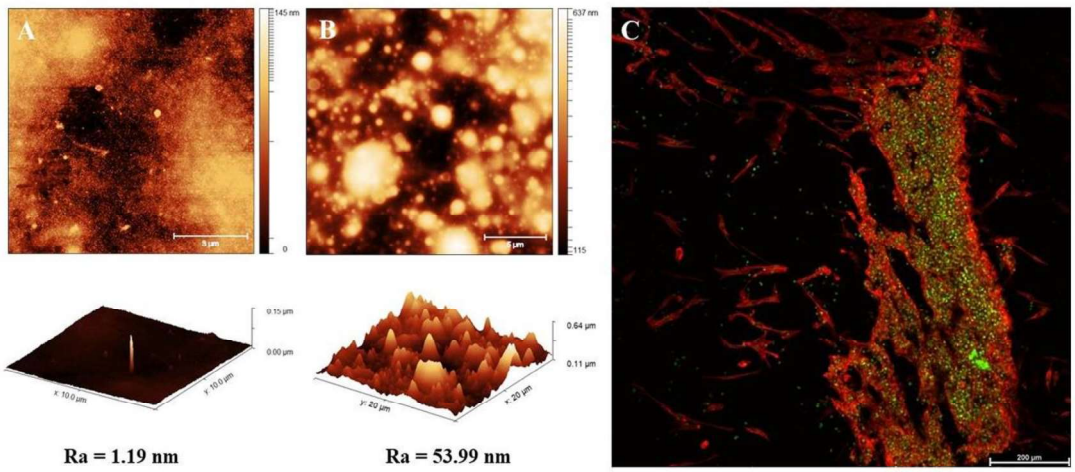

Figure 4 – AFM images of vanillin crosslinked chitosan films in the absence (A) and in the presence of PDMS surface domains (B). Confocal microscopy of C2C12 rat muscle cells adhered to crosslinked chitosan film with PDMS domains on its surface (C).

Conclusions

Vanillin was successfully grafted to the backbone of chitosan, as indicated by structural changes using ATR-FTIR and NMR techniques, which led to a subsequent increase in the crosslinking between chitosan chains. The incorporation of PDMS emulsions into the crosslinked films induced surface topography modifications, resulting in an increase in the average surface roughness, as well as a decrease in the material mechanical properties, measured via the mapping of force-indentation curve maps. Finally, the attachment of C2C12 rat muscle cells to the surface of the modified chitosan film was evaluated using confocal microscopy, which revealed regions fully covered with cells contrasting with regions where very little population could be detected. These findings suggest that the surface modification process has a significant impact on cell attachment and could be used to develop new biomaterials with improved properties for tissue engineering applications. Overall, this study provides important insights into the modification of chitosan films with PDMS emulsions, with potential applications in the development of new biomaterials for tissue engineering and related fields.

Acknowledgements

The authors acknowledge FAPESP processes number 2020/05632-9 and 2021/13925-9 for the financial support.

References

1. Ikada, Y.; J R Soc Interface, 3, 2006 – 589-601. https://doi.org/10.1098/rsif.2006.0124
2. Lanutti, J.; Reneker, D.; Ma, T.; Tomasko, D.; Farson, D.; Mater Sci Eng C, 27, 2007 – 504- 509. https://doi.org/10.1016/j.msec.2006.05.019
3. Semeano, A. T.; Glaser, T.; Ulrich, H. Petri, D. F. S. Scaffolds for Embrionic Stem Cells Growth and Differentiation, in Working with Stem Cells, Ulrich H. and Negares, P. D. Ed., Springer, 2016.
4. Zhang, K., Wang, S., Zhou, C.; Bone Res, 6, 2018 – 1–15. https://doi.org/10.1038/s41413-0180032-9
5. De Masi, A.; Tonazzini, I.; Masciullo, C.; Mazzena, R.; Chiellini, F.; Puppi, D.; Cecchini, M.; Biophys Rev, 11, 2019 – 807 – 815. https://doi.org/10.1007/s12551-019-00591-6
6. Bitar, K. N.; Zakhem, E.; Biomed Eng Comput Biol, 6, 2014 – 13- 20. https://doi.org/10.4137/BECB.S10961
7. Jahangirian, H.; Ghasemian, L. E; Rafiee-Moghaddam, R.; Webster, T. J.; Int J Nanomedicine, 13, 2018 – 5953 – 5969. https://doi.org/10.2147/IJN.S127683
8. Ha, T.; Minh, T.; Nguyen, D.; Minh, D.; in J Tissue Eng Regen M, Ed., Andrades, J. A., 2013, 5772 - 55668.
9. De Assis Gonsalves, A.; Araujo, C. R. M.; Soares, N. A.; Goulart, M. O. F.; De Abreu, F. C. Diferentes Estrategias Para A Reticulaqao De Quitosana. Quim. Nova 2011, 34 (7), 1215–1223. https://doi.org/10.1590/S0100-40422011000700021.
10. Shi, C.; Zhu, Y.; Ran, X.; Wang, M.; Su, Y.; Cheng, T.; J Surg Re, 133, 2006- 185–92. https://doi.org/10.1016/j.jss.2005.12.013
11. Efremov, Y. M.; Okajima, T.; Raman, A. Measuring Viscoelasticity of Soft Biological Samples Using Atomic Force Microscopy. Soft Matter 2020, 16 (1), 64–81. https://doi.org/10.1039/c9sm01020c.
12. Zou, Q.; Li, J.; Li, Y. Preparation and characterization of vanillin-crosslinked chitosan therapeutic bioactive microcarriers. International Journal of Biological Macromolecules, v. 79, p. 736–747, 2015. https://doi.org/10.1016/j.ijbiomac.2015.05.037

FLUORESCENCE INTERACTION STUDIES BETWEEN CURCUMIN AND PIPERINE: TARGETING INCORPORATION INTO POLYMERIC NANOCARRIERS

Ângela G. L. L. Andrade[1*], Camila F. F. Marin[1] Alexandre L. Parize[1]
1 – Department of Chemistry, Santa Catarina Federal University (UFSC), Florianópolis, SC, Brazil
angela.lechinski@gmail.com

Abstract – Curcumin (CUR), a yellow hydrophobic polyphenolic compound, often used in cooking, has been explored in pharmacological applications for demonstrating interesting anti-inflammatory, antimicrobial, anticancer, antioxidant, and healing properties. The widespread use of CUR presents a major obstacle, due to its low water solubility and short circulating half-life, limiting its bioavailability. In the literature, the number of studies that aim to evaluate the spectroscopic effects of the association of CUR with other molecules that can improve its solubility in aqueous media is still limited. Thus, the present study proposes a spectroscopic characterization of CUR in different percentages of water/acetonitrile (0 to 100% v/v) by the absorption and emission spectroscopy to evaluate the effects of piperine (PIP) on the process of self-aggregation of CUR. The fluorimetric method employed was preceded by electronic absorption analysis to determine the maximum absorption of each percentage. In general, the increase in water percentages promoted a sharp decrease in the intensity of absorption and emission for CUR and mixtures, favoring the self-aggregation of molecules. In addition, these previous results indicate that PIP acts to reduce the processes of self-aggregation of CUR, that is, acting as a solubility promoter. Therefore, an interesting candidate to be used together with CUR in polymer micelles of the Pluronic® type for use in dressings, which provide a more liposoluble microenvironment, which can accommodate poorly soluble compounds such as CUR with greater efficiency, thus favoring, its use in the biomedical field.
Keywords: Curcumin, piperine, fluorescence, absorption, emission.

Introduction

Curcumin (CUR) is a yellow hydrophobic polyphenolic compound, often used in cooking, and is extracted from a tropical plant of the ginger family, originating in South Asia [1]. When inserted into an aqueous medium, CUR presents two very important balances, namely the 1,3 diketo/keto-enol balance (keto-enol; D/CE) (Figure 1) and the process of self-aggregation into dimers, when two CUR molecules form self-aggregates through association [2].

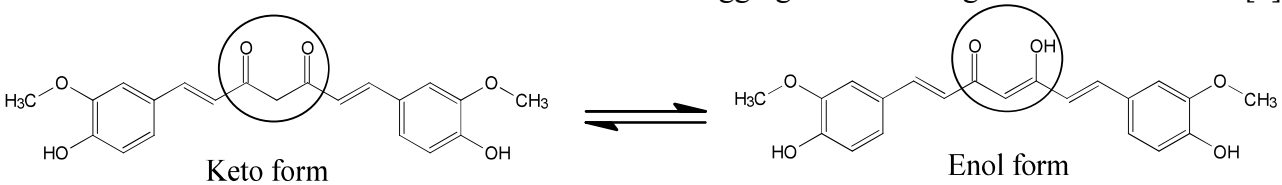

Figure 1 – Keto-enol tautomerism of CUR. Adapted from Pereira, C.I. (2022) [3].

The typical characteristics of the aggregation of these monomers and dimers can be analyzed through their spectroscopic properties, through the observation of the splitting of the absorption band, spectral shift, decrease in absorption at the maximum wavelength of the monomer, and additional band formation at other wavelengths [3]. Thus, in acidic or neutral aqueous solution, CUR has intense

absorption between 410 and 430 nm with a maximum wavelength (λmax) at 421 nm and a weak absorption in the region between 260 and 280 nm, due to the π→π* transitions [4].

By interesting biological activities and prophylactic effects for human health, such as anti-inflammatory, antioxidant, antitumor, antimicrobial, and antifungal activity, enabling its application as an active ingredient in the treatment of various diseases, CUR has attracted much interest in the scientific Community. However, CUR is difficult to solubilize in an aqueous medium, a fact that limits its bioavailability. In this way, the use of solubility-promoting agents becomes an interesting and attractive alternative [5].

Piperine (PIP) is an alkaloid present in black pepper (*Piperis nigrum*), which is one of those responsible for the spicy taste in the Piper species. According to studies, it can enhance the absorption of several active compounds, such as CUR, promoting greater bioavailability of the active, orally or transdermally. Thus, its use in formulations with CUR is favored, to obtain synergistic action in a specific treatment [6].

The incorporation of formulations with synergistic action such as CUR and PIP in nanocarriers such as polymeric micelles is also an effective alternative to overcome deficiencies associated with CUR, improving its therapeutic abilities and stability. Therefore, triblock copolymers based on Pluronic®, such as F-127, are used for drug encapsulation and delivery [7]. Therefore, the objective of this study is to evaluate the behavior of CUR in the presence of piperine (PIP), in aqueous medium, and water-acetonitrile mixtures. In this scenario, this preliminary study is fundamental to defining the best conditions for the future incorporation of the CUR/PIP mixture in polymeric micelles based on pluronic F-127.

Experimental

Experimental methodology

Solutions with different percentages of water and acetonitrile 99,9% (Sigma Aldrich) (ACN) were prepared by measuring separately the fractions of each solvent that were then combined. The solutions ranged from 0 to 100% water and acetonitrile. The ACN/H_2O percentages being: 100/0, 90/10, 85/15, 80/20, 75/25, 70/30, 60/40, 50/50, 40/60, 30/70, 20/80, 10/90 and 0/100. UV-Vis and fluorescence analyzes were performed for these ACN/H_2O percentages for CUR (Sigma Aldrich) (1 $\mu mol \cdot L^{-1}$) with PIP 92% (Sigma Aldrich (1 $\mu mol \cdot L^{-1}$)) solutions.

Fluorimetric titration

From CUR in 70%ACN/30%H_2O (1.0 $\mu mol \cdot L^{-1}$) and stock solutions of PIP 70%ACN/30%H_2O ($1x10^{-4}$ $mol \cdot L^{-1}$; $2.0x10^{-4}$ $mol \cdot L^{-1}$; $2.5x10^{-4}$ $mol \cdot L^{-1}$; $3.0x10^{-4}$ $mol \cdot L^{-1}$ and $3.5x10^{-4}$ $mol \cdot L^{-1}$), the CUR titration was performed. It started with 1.4 mL of the CUR solution, followed by successive additions of 150 µL of the PIP solutions. The fluorescence spectrum was followed from 441 to 800 nm, using λ_{exc} = 421 nm, excitation/emission slits = 10/10. Then, the calculation of the Stern-Volmer equation was carried out (Eq. 1):

$$\frac{F_0}{F} = 1 + K_{SV}[Q] \qquad [1]$$

Being F_0 and F the fluorescence intensity in the absence and presence of the quencher, [Q] the concentration of the quencher and Ksv is the association constant.

Characterization

UV-Vis spectroscopic analyzes were carried out using Kasuabi B-500 equipment with optical fiber. Fluorimetric analyzes were carried out in Cary Varian Eclipse equipment at the Laboratory of Catalysis and Interfacial Phenomena (LACFI) for the proportions of acetonitrile and water studied.

Results and Discussion

The spectral absorption of curcumin (CUR) in different percentages of water-acetonitrile (v/v) is shown in Figure 2 (a). It is observed that the increase in the percentage of water in the samples generates a sharp decrease in the intensity of the CUR spectra. This behavioral trend is related to the aggregation of CUR [8]. Samples with a higher percentage of acetonitrile (ACN) showed higher absorption intensities. Thus, for the CUR with 100% ACN, λ_{max} was obtained at 419 nm. The molar absorptivity (ε) at 419 nm was 59.8×10^3 $L \cdot mol^{-1} \cdot cm^{-1}$, which is following the literature [4]. It is also observed that the percentage with the addition of 10% of H_2O, presented a slightly higher intensity of absorption compared to 100% ACN.

By incorporating piperine (PIP) into the system, it can be seen that the spectral behavior of the CUR maintained the tendency of decay in the intensity of the spectra with the increase in the percentage of water. However, the addition of PIP (Figure 2 (b)) resulted in a more accentuated decrease in spectral absorption between each percentage of water, remaining close to zero for the percentages below 20% of ACN, with also a decrease in the width of the bands formed, when compared to the absorption spectrum of the CUR alone. For 100% ACN, the molar absorptivity (ε) at 420 nm was 68.1×10^3 $L \cdot mol^{-1} \cdot cm^{-1}$, indicating that the addition of PIP led to a slight increase in the probability of electronic transition.

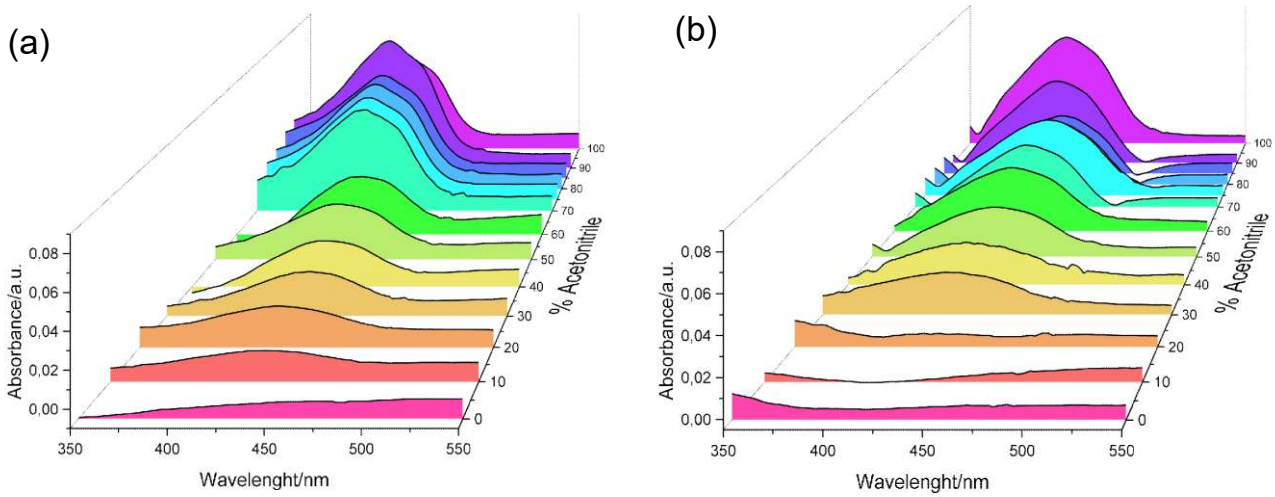

Figure 2 – Absorption spectrum (a) CUR and (b) CUR-PIP.

The interaction study of CUR and PIP in mixtures in percentages of water-acetonitrile is presented in Figure 3. The spectral emission profiles of CUR (Figure 3 (a)) follow a similar tendency to the absorption spectra of the compound. However, there are practically no differences in width. For percentages rich in water, emission extinction is observed. In studies available in the literature, it is reported that the fluorescence emission of CUR in high percentages of water is related to three conditions: (i) decrease in molar absorptivity; (ii) water molecules acting as a quenching agent of the monomeric form of CUR in state of electronic excitation; and (iii) the formation of non-fluorescent self-aggregating species of CUR [3,9].

Still, for the spectrum with only CUR, maximum emission was observed at 526 nm for 100% solvent. Percentages below 70% of ACN are practically extinct. The fluorescence spectrum of CUR and PIP (Figure 3(b)), showed a high emission intensity at 100% ACN with maximum emission at 517 nm. The addition of 10% of water provided an intense decrease in fluorescence emission, while the other percentages showed almost non-existent emission.

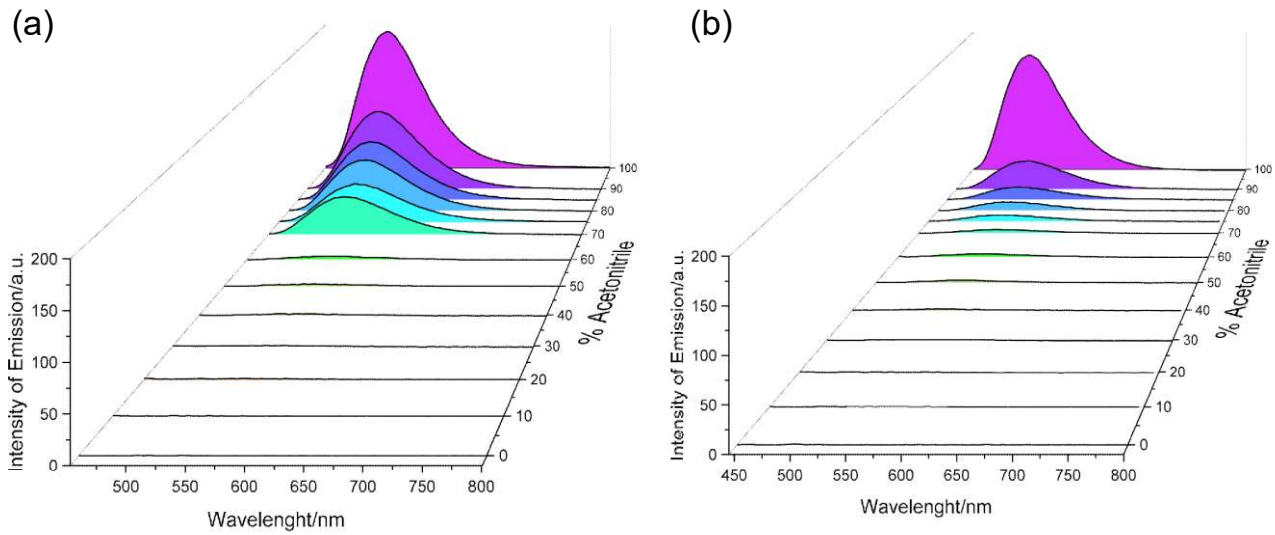

Figure 3 – Emission spectrum (a) CUR and (b) CUR-PIP.

In Figure 4 (a), the emission of CUR is observed in increasing variations of PIP concentration. The emission intensity decreases with the increase in the concentration of PIP in the medium, corroborating the previously analyzed studies, indicating that CUR interacts with PIP. It is also noted that the increase in PIP concentration generates precipitation.

Assuming a static fluorescence quenching mechanism, between CUR and PIP, we can apply the Stern-Volmer equation (Eq. 1) to the influence of the quenching agent. In Figure 4 (b), we have the formation of a straight line that correlates the concentration of the quenching agent [S] and the fluorescence intensity - (F_0/F), which presents a linear increase as a function of the increase in concentration. The value of the Stern-Volmer constant (Ksv) is 713 ± 44 $L \cdot mol^{-1}$ with $R^2 = 0.992$.

In general, the increase in the percentage of water leads to a sharp decrease in the absorption and emission spectra of CUR and mixtures, favoring the self-aggregation of molecules in the medium [9]. It is observed that there was an interaction of CUR with PIP, however, larger studies need to be carried out to evaluate this interaction and its impact.

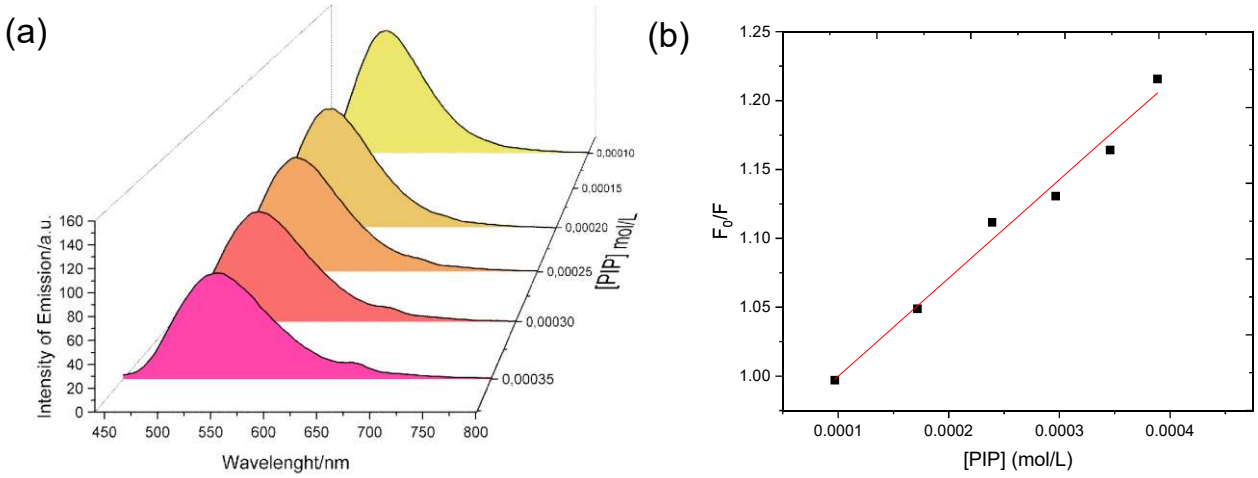

Figure 4 – (a) Emission spectrum of CUR (1µmol·L^{-1}) varying PIP concentration at 70%ACN/30%H_2O and (b) Graphic representation of CUR fluorescence suppression by PIP.

Conclusions

The absorption spectra of the CUR and the mixtures containing PIP described a tendency towards a decrease in the formation of electronic absorption bands and fluorescence emission with the increase in the percentage of water in the medium. The spectra with only CUR suggest better results for percentages of up to 30% of water in the medium, in which the formation of self-aggregates can be better controlled. Similar results were observed for mixtures of CUR with PIP. Concerning the emission spectra only for the CUR, a marked reduction was observed with the increase in the percentage of water, obtaining practically the extinction of the fluorescence for the highest percentages. In the presence of PIP, however, all percentages of water generated emission spectra close to zero, with a region of intense emission being observed only for 100% solvent. By fluorimetric titration, it is observed that CUR and PIP interact to reduce the fluorescence emission of CUR. The Stern-Volmer constant obtained indicates good efficiency in suppressing CUR fluorescence in the presence of PIP.

From the present study, it is intended to insert the CUR-PIP in biocompatible polymeric systems (micelles originated by Pluronic® F127) for use in bandages, aiming for biomedical applications. It is expected that in the aqueous environment, the hydrophilic portion from the most external region of the micelles and the hydrophobic portion present in the center of the micelle in which the drug will be incorporated, promoting its stability and favoring an improvement in its delivery, increasing the absorption over the skin. It is also estimated that the formation of these micellar systems in an aqueous solution makes it possible to observe the shift in the keto-enol equilibrium, providing a more significant interaction between the drug and copolymer.

Acknowledgments

Thanks for the financial support of the CAPES – Financial code 001; CNPq (for A.L.P. for his PQ fellowship (Process 305112/2022–8) and Laboratory of Catalysis and Interfacial Phenomena (LACFI) for kindly allowing the use of fluorimeter.

References

1. M. Ilangovan, et al. Industrial Crops and Products, 2018, 112, 556. https://doi.org/10.1016/j.indcrop.2017.12.042
2. N. K. Bhatia, et al. RSC Advances, 2016, 6, 105, 103275. https://doi.org/10.1039/C6RA24256A
3. C. I. D. Pereira, et al. Dyes And Pigments, 2022, 197, 109887. https://doi.org/10.1016/j.dyepig.2021.109887
4. D. Patra, C. Barakat. Spectrochim Acta Parte A Mol Biomol Spectrosc, 2011, 79, 1034. https://doi.org/10.1016/j. saa.2011.04.016
5. T. Jiang, W. Liao, C. Charcosset. Food Res. Int. 2020, *132*, 109035. https://doi.org/10.1016/j.foodres.2020.109035
6. S. Chen, Li, et al. Food Hydrocoll. 2020, *99*, 105334. https://doi.org/10.1016/j.foodhyd.2019.105334.
7. R. Ganguly, et al. Journal of Molecules Liquids. 2020, 314, 113591. https://doi.org/10.1016/j.molliq.2020.113591
8. K. Priyadarsini, Molecules, 2014, 19, 12, 20091. https://doi.org/10.3390/molecules191220091
9. C. F. Freitas, et al. Photochem Photobiol, 2016, 92, 790. https://doi.org/10.1111/ php.12645

HUMAN IMMUNOGLOBULIN G ADSORPTION WITH DIFFERENT RATES OF STIRRING ONTO FIBROIN MICROPARTICLES

Antônio A. O. Santana Júnior[1], Cláudio P. Pinheiro[1*], Igor T. L. Bresolin[1] and Mariana A. Moraes[1]

1 – Chemical Engineering Department, Federal University of São Paulo, Diadema, SP, Brazil
claudiopinheiro11@hotmail.com

Abstract - The antibody immunoglobulin G (IgG) is employed for many different medicinal purposes. It is necessary to employ high purity IgG for these applications, which requires employing purification chromatographic methods based on adsorption. However, it is crucial to first conduct research to determine how IgG interacts with the adsorbent before utilizing chromatographic methods. Additionally, there are no studies that analyze IgG adsorption by fibroin in the literature. As a result, the objective of this study was to assess how well human IgG adhered to fibroin microparticles while changing the rotation rate from 20 to 40 rpm. Using the atomization process, the microparticles were produced from a fibroin solution. The average diameter of the microparticles was 108.5 m. At 30 rpm, the adsorption capacity was 704.29 mg g^{-1}. The adsorption capacity found in this study is higher than that reported for other adsorbents in the literature.
Keywords: *Atomization, rotation rate, Bath Adsorption, Zeta potential*.

Introduction

Immunoglobulins are glycoproteins that perform several important functions by interacting with various cell bodies, where protection is a major concern. Mammalian immunoglobulins are divided into five classes based on their structure and biological properties: IgA, IgD, IgE, IgM, and IgG, with the latter being the most common [1, 2].

Adsorption techniques are often used to obtain IgG, since many proteins may have surface charges derived from their amino acids. In addition, the pH of the medium affects the surface charge of proteins, providing an easy way to tune the adsorption properties of solutes. Therefore, protein adsorption and desorption can be performed by changing the pH or ionic strength of the eluent [3].

Silk fibroin is a polymer that can be used as an ion exchange matrix [4]. Fibroin is a natural polymer obtained from silkworm cocoons *Bombyx mori* and spider webs *Nephila clavipes*. Fibroin consists of two chains, one with a high molecular weight of approximately 325 kDa and the other with a low molecular weight of approximately 25 kDa. Sericin also exists in the cocoon, which has the function of combining fibroin filaments and protecting the cocoon [5]. Due to the existence of weak acids and bases, fibroin is an amphoteric matrix that exchanges ions, and the pH of the medium can govern the flow of ions. As a result, fibroin is a matrix that depends on the pH [6].

Despite fibroin having a high capacity for dye adsorption, there are no studies that examine IgG adsorption by fibroin in the literature. Therefore, the main goal of our work was to confirm the ideal circumstances for the IgG adsorption process in fibroin microparticles. With the help of the study's findings, it will be feasible to investigate novel uses for microparticles that take into consideration the medium in which they are placed as well as enhance IgG purification methods that may be used in the pharmaceutical industry.

Experimental

Material

Bombyx mori silkworm cocoons were provided by Bratac (Londrina, Brazil). Octapharma's (Austria) high purity human Immunoglobulin G (IgG) antibody (Octagam) was employed. Analytical grade compounds were employed.

Fibroin solution preparation

Silkworm cocoons were treated with 600 mL of an aqueous sodium carbonate solution (Na_2CO_3) containing 1 g L^{-1} of sodium carbonate for every 50 g of cocoon for 90 minutes at a constant temperature of 85°C. Every 30 minutes, the Na_2CO_3 solution was replaced, and the sericin-free fibroin was then thoroughly rinsed with distilled water. The fibroin was then dried for 24 hours at room temperature. Sericin-free fibroin strands were broken apart. 100 mL of a ternary solution of calcium chloride ($CaCl_2$), ethanol (CH_3CH_2OH), and water (H_2O) (in a molar ratio of 1:2:8) were added to each 10 g of fibroin, and the resulting suspension was kept at 85° C for 90 minutes. In distilled water, the 10% (w v^{-1}) fibroin saline solution was dialyzed for 3 days, at 10 °C, in a volumetric ratio of 1:15 (fibroin:water). The dialysis water was changed every 24 h.

Preparation of the silk fibroin microparticles

Using ethanol as a coagulant, the microparticles were created by atomization. An atomizing nozzle with a diameter of 0.5 mm (Labmaq, Brazil), a peristaltic pump TE-BP-01 Mini (Tecnal, Brazil), and a compressor type OP8,1/30II (Pressure, Brazil) make up the atomization system. The coagulant solution was being stirred while the atomizing nozzle was 14 cm above it. Pumping was done using compressed air at a pressure of 1 bar and a flow rate of 0.045 L h^{-1} for the silk fibroin solution. The microparticles were then agitated for 10 min after 30 minutes of resting. Using a sample of 272 data points and a Primo Star microscope from Zeiss (Germany) with 10 x objectives, the average size of the material was determined.

FTIR-ATR Spectroscopy

The experiment was conducted using a Fourier transform infrared spectrophotometer (FTIR) from the Agilent Cary 360 (Agilent, USA), with a 400–4000 cm^{-1} scanning range, a spectral resolution of 4 cm^{-1}, and 128 scans.

Zeta potential

The analysis was performed with ten suspensions of 10 mL of ultrapure water with 0.1 g of microparticles, each suspension had a different pH (2 to 11). The analysis was performed with the Malvern Zetasizer Nano Zs90 equipment.

Adsorption isotherms with different stirring rates

The tests were conducted in 2 mL Eppendorf® tubes with 0.4 mL of the suspension (25% v v^{-1}) of fibroin microparticles equilibrated in MOPS buffer, pH 8, 25 °C, and the stirring rate from 20 rpm to 40 rpm was investigated in order to get the adsorption isotherms. To achieve end-over-end agitation, a Revolver-type tube rotator (Thermo Scientific, USA) was employed. The immunoglobulin solution was added after the microparticles at a concentration ranging from 0.5 to 25 mg mL^{-1}. Based on earlier adsorption kinetics tests, the tubes were shaken for a full hour. The supernatant was then separated from the liquid by centrifuging the flasks for 5 min at 2300 rpm. Reading the absorbance at 280 nm in a UV-VIS spectrophotometer model UV-1280 was used to quantify immunoglobulins.

The adsorption capacity was obtained by Equation 1. Langmuir-Freundlich (Equation 2) model were fitted to the experimental data using the iterative method of Levenberg-Marquardt using Origin® software (Microcal, USA).

$q_e=(C_0 - C_e)V/m$ (1)

$q_e=q_{mLF}(C_e)^n/[K_{d(LF)}+(C_e)^n]$ (2)

where q_e is adsorption capacity (mg g^{-1}), C_0 and C_e are the initial and equilibrium concentrations of IgG in the liquid phase (mg L^{-1}), respectively; m is the mass of adsorbent (g) and V is the volume of the solution (L), q_{mLF} is the maximum adsorption capacity of the Langmuir-Freundlich model (mg g^{-1}), $K_{d(LF)}$ (mol L^{-1}) is the Langmuir-Freundlich constant, n is the heterogeneity factor.

All experiments were performed in triplicate.

Results and Discussion

The infrared spectra of fibroin microparticles is shown in Fig 1. The β-sheet conformation is shown to be connected with the absorption bands for Amide I around 1620 cm^{-1} and the band for Amide II near 1515 cm^{-1}, whereas the α-helix conformation is shown to be linked with the absorption band for Amide III near 1230 cm^{-1}. The same peaks were also attained for fibroin microparticles produced using a hexafluoropropanol-methanol coagulant solution [7)] and silk fibroin scaffolds produced by treatment with ethanol [8].

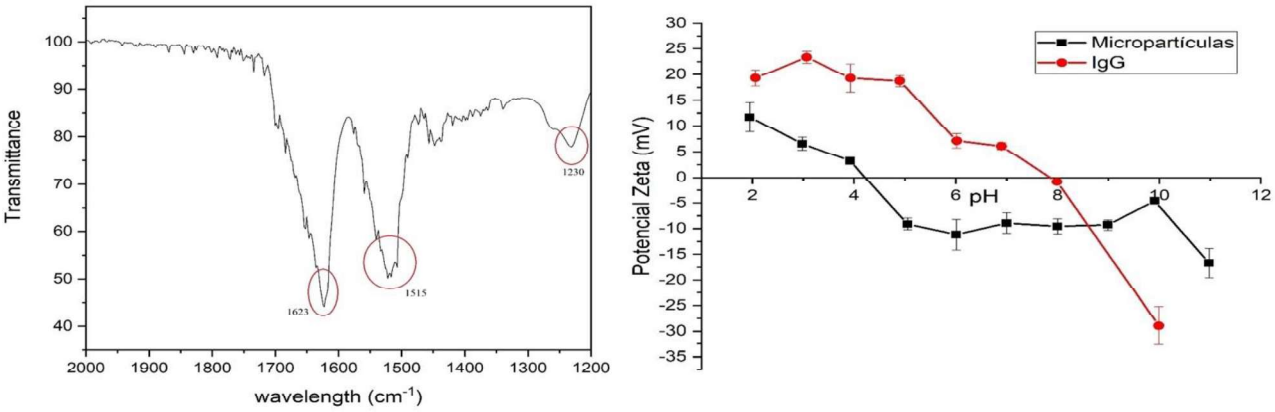

Figure 1 – FTIR-ATR Spectroscopy of fibroin microparticles and Zeta potential analysis of fibroin microparticles and IgG

It is feasible to identify the pH at which the charge of the microparticles and the IgG are equal to zero by using the Zeta Potential analysis to calculate the surface charges of the IgG and the fibroin microparticles, according to the pH fluctuation. Figure 1 illustrates the outcomes. When the pH was between 2 and 4, the fibroin microparticles assumed a positive charge, and when the pH was between 5 and 11, they assumed a negative charge. This behavior revealed that the isoelectric point of the microparticles is between pH values 4 and 5, which is consistent with the literature [9]. Deprotonation of carboxyl groups occurs at higher pHs while protonation of amino groups ($-NH_2$) occurs at lower pHs.

The immunoglobulin G utilized has an isoelectric point close to 8. IgG demonstrated a positive charge between pH 2 and 7 and a negative charge between pH 8 and 10. Microparticles have a positive charge between pH 4 and pH 8, whereas IgG has a negative charge. This area is thus anticipated to have the best adsorption properties.

The average diameter of the microparticles was 108.5 ± 53.4 µm.

Effect of rotation

As demonstrated in Fig 2, the q_e values increased as the agitation rate increased from 20 rpm to 30 rpm, however there was a decrease from 30 rpm to 40 rpm because the greater agitation may have denaturized the IgG. IgG is by far the most prevalent immunoglobulin and has a number of subclasses, some of which are more stable than others [10].

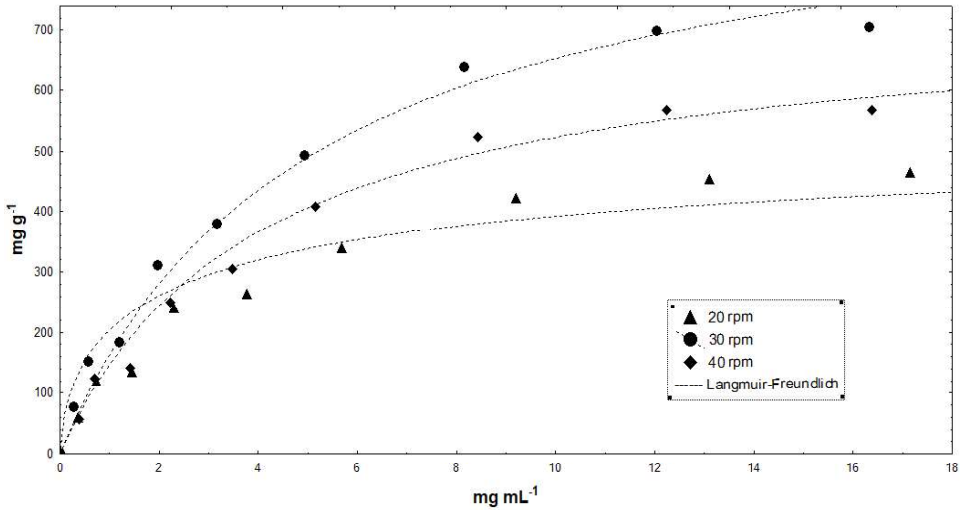

Figure 2 – Adsorption of IgG onto fibroin at different agitation rates, with MOPS buffer, pH 8 and 25 °C.

The rotational speed of 30 rpm had the highest adsorption capacity (704.29 mg g^{-1}), followed by 40 rpm (544.4 mg g^{-1}) and 20 rpm (415.5 mg g^{-1}). The adsorption capacity found in this study is higher than that reported for other adsorbents in the literature. Furthermore, there are currently no studies that assess the potential of the fibroin as a matrix for human IgG adsorption.

The Langmuir-Freundlich model yielded values for n that were all less than 1, indicating that the adsorption of one molecule had no effect on the adsorption of another, demonstrating negative cooperativity. The highest value for χ^2 was 760.7, and the R^2 for all isotherms was more than 0.98. For 20, 30, and 40 rpm, the values obtained for q_{mLF} were 880.7, 1050.7, and 902.5 mg g^{-1}, respectively.

Conclusions

At pH 8, 25 °C, and 30 rpm, and MOPS buffer, fibroin was able to achieve an adsorption capacity of 704.29 mg g^{-1}. Additionally, the adsorption capacity obtained in this study is higher than that reported for other adsorbents in the literature. Consequently, with the successful completion of the project, it will be feasible to investigate novel fibroin microparticle uses and enhance IgG purification methods.

Acknowledgements

The authors are grateful for the financial support from FAPESP (process 2018/15539-6) and grant received from CAPES (PDPG program) and FAPESP (grant 2022/05336-6).

References

1. M. Daëron, International reviews of immunology 1997, 16(1-2), 1-27. https://doi.org/10.3109/08830189709045701
2. A. C. M. Passaro; T. M. Mozetic; J. E. Schmitz; I. J. da Silva Jr; T. D. Martins; I. T. L. Bresolin Chemical Product and Process Modeling 2019, 14(4), 20190077. https://doi.org/10.1515/cppm-2019-0077
3. B. K. Nfor; T. Ahamed; G. W. van Dedem; L. A. van der Wielen; E. J. van de Sandt; M. H. Eppink; M. Ottens Journal of Chemical Technology & Biotechnology 2008, 83(2), 124-132. https://doi.org/10.1002/jctb.1815
4. M. Kucharska; J. Grabka Talanta 2010, 80(3), 1045-1051. https://doi.org/10.1016/j.talanta.2009.09.032

5. E. Wenk; H. P. Merkle; L. Meinel Journal of controlled release 2011, 150(2), 128-141. https://doi.org/10.1016/j.jconrel.2010.11.007
6. S. Kapoor; S. C. Kundu Acta biomaterialia 2016, 31, 17-32. https://doi.org/10.1016/j.actbio.2015.11.034
7. A. Nisal; R. Sayyad; P. Dhavale; B, Khude; R. Deshpande; V. Mapare; P. Venugopalan Scientific reports 2018, 8(1), 7235. https://doi.org/10.1038/s41598-018-25643-x
8. Y. Hu; Q. Zhang; R. You; L. Wang; M. Li Advances in Materials Science and Engineering 2012. https://doi.org/10.1155/2012/185905
9. S. Rastogi; B. Kandasubramanian Environmental Science and Pollution Research 2020, 27, 210-237. https://doi.org/10.1007/s11356-019-07280-7
10. G. Vidarsson; G. Dekkers; T. Rispens Frontiers in immunology 2014, 5, 520. https://doi.org/10.3389/fimmu.2014.00520

IMMOBILIZATION OF LACCASES ON STY-DVB COPOLYMERS CONTAINING DIAZONIUM GROUPS

Adilson Muniz de Araujo[1], Ezaine Cristina Corrêa Torquato dos Santos[1], Stefany dos Santos Silva de Souza[1], Rafael de Lima Pinto[2], Mônica Regina da Costa Marques Calderari[2], Luciana da Cunha Costa[1]*

1 – Department of Pharmacy, Faculty of Biological and Health Sciences, State University of Rio de Janeiro (UERJ), Rio de Janeiro, RJ, Brazil1
2 - Fernanda Coutinho Analytical Center (CAFC), Chemistry Institute, State University of Rio de Janeiro (UERJ), Rio de Janeiro, RJ, Brazil
luciana.cunha.costa@uerj.br

Abstract – Laccases are glycoproteins that can catalyze oxidation reactions of several pollutants. This Study focuses on preparing biocatalysts by immobilizing Trametes versicolor laccase on diazotized Styrene-Divinylbenzene copolymers, aiming application in the degradation of nonylphenol. Styrene-divinylbenzene was prepared by aqueous suspension polymerization. These copolymers were submitted to nitration, reduction, and diazotization reactions to insert diazonium groups on these supports. These modifications reactions were accompanied by FTIR spectroscopy. The copolymers containing nitro, amino, and diazonium groups and unmodified copolymers were put in contact with laccase solution on citrate-phosphate buffer pH5, 20 mM to prepare heterogeneous biocatalysts. The characterization of the copolymer showed a porous material, reaching a specific surface area of 175.2 m^2 g^{-1} and a pore volume of 0.62 cm^3 g^{-1}. The copolymers containing amino and diazonium groups showed percentages of immobilization yield.

Keywords: *Laccase, styrene-divinylbenzene copolymers, heterogeneous biocatalyst, diazonium groups*

Fundings: Research Support Foundation of the State of Rio de Janeiro (FAPERJ)

Introduction

Laccases are extracellular monomeric glycoproteins in the multicopper oxidase family isolated mainly from higher fungi [1]. These enzymes have been the subject of research mainly due to their ability to catalyze the oxidation of various substrates and their wide application in different industrial sectors, such as biofuels, biosensors, and organic synthesis, among others [2]. Enzymatic immobilization aims to enable the reuse of enzymes in other cycles, improving the cost-benefit ratio and providing stability to changes in pH and temperature [3]. Melo et al. (2017) [4] showed that microspheres of glycidyl methacrylate-co-ethylene glycol dimethacrylate (GMA-EDGMA) containing diazonium groups are adequate supports to laccase. Diazonium groups also can be introduced on styrene-divinylbenzene (Sty-DVB) copolymers through nitration and reduction reactions of benzene rings. These monomers cost less than glycidyl methacrylate and ethylene glycol dimethacrylate monomers. Sty-DVB copolymers containing diazonium groups have been investigated as supports of complexing groups for metals of environmental concern. However, these materials have not been sufficiently investigated as supports for laccases. This work aims at a

comparative study of the immobilization of laccase from *Trametes versicolor* onto Sty-DVB containing nitro, amino, and diazonium groups, besides unmodified copolymers.

Experimental

Synthesis of Sty-DVB copolymers

The Sty-DVB copolymer was prepared by aqueous suspension polymerization. The aqueous phase consisted of polyvinyl alcohol (PVA) and NaCl (1.5% m/v to the volume of distilled water). The organic phase was composed of the initiator Azobisisobutyronitrile (AIBN) (1% to the sum of the number of moles of monomers), Sty (0.12 mol), and DVB (0.18 mol) and the diluent n-heptane (degree of dilution of 100% v/v, to the volume of monomers). The organic phase: aqueous phase ratio was 1:3 v/v. The reaction was conducted in a tribulated flask with a mechanical stirrer and a thermostatic bath for 24 hours, using a stirring speed of 200 rpm and a temperature of 80 ºC. At the end of the reaction, the particles obtained were isolated through vacuum filtration, washed with distilled water, ethanol, and acetone, and dried at 60 ºC in an oven for 24 hours. The Sty-DVB copolymer was characterized by determining the apparent density, optical microscopy, SEM, and determination of specific area, volume, and pore diameter by ASAP.

Chemical modification of the Sty-DVB copolymer

The Sty-DVB copolymer has been chemically modified to insert diazonium groups into its structure. The polymer was pre-swelled in 1,2-dichloroethane (82 ml) for the nitration reaction for 24 hours. The nitration reaction was carried out using a mixture of HNO_3 (51.3 mL) and H_2SO_4 (60.5 mL) for 4 hours at 60°C, under stirring at 100 rpm. The polymers were separated by vacuum filtration, washed with distilled water, ethanol, and methanol, and dried in an oven at 60ºC for 24 hours. For the reduction reaction, the nitrated copolymer (7 g) was kept in contact with a solution composed of absolute ethanol (17.5 mL), anhydrous SnCl2 (172.536 g), and HCl (196 mL). The mixture was purged with N_2 for 5 minutes. The reaction was carried out under slow stirring at 100 rpm at 90°C for 24 hours. At the end of the reaction, the beads were washed with 2 mol/L NaOH solution, water, ethanol, and methanol and dried at 50 ºC in an oven. The reduced copolymer was maintained in contact with dioxane (30 ml) for 30 minutes before the diazotization reaction. The diazotization reaction was carried out using aqueous HCl solution and $NaNO_2$ solution under stirring at 100 rpm and monitoring the temperature (0–5 °C). The diazotized copolymer was filtered, washed with a small volume of distilled water, and stored under refrigeration. These reactions were followed by FT-IR spectroscopy.

Immobilization of Trametes Versicolor laccases on copolymers

All copolymers were submitted to contact with laccase solution to prepare heterogeneous biocatalysts. In other words, this step employed unmodified copolymers besides copolymers with nitro, amino, and diazonium groups. These materials were pre-treated with 20 mM citrate-phosphate buffer pH 5 at 5°C and gently stirred in an orbital shaker for 1 hour. At the end of the period, the support was filtered under refrigeration. Soon after, an enzymatic laccase solution was prepared in a 20 mM citrate-phosphate pH5 buffer (2mg/ml). Then each copolymer was placed in contact with the enzymatic solution. Control of the enzymatic solution was also prepared and maintained under the same conditions for comparison purposes. Enzyme immobilization was performed at 5°C, 100 rpm for 24h. Aliquots were collected at times: 0, 15', 30', 45', 60', and 1440' to monitor the occurrence of immobilization through enzymatic kinetics. The laccase activity was monitored spectrophotometrically using substrate oxidation of 2,2'-azino-bis(3-ethylbenzoathiazoline-6-sulfonic acid) (ABTS) (436 nm) [5].

Results and Discussion

A copolymer combining DVB crosslinking agent and Sty comonomer was synthesized by aqueous suspension polymerization. The apparent density, specific surface area, pore volume, and average pore diameter data obtained for the particles are presented in Table 1.

Table 1. Apparent density, specific surface area, volume and average pore diameter data for Sty-DVB copolymers

	D_{ap} (gcm^{-3})	S ($m^2 g^{-1}$)	V_p ($cm^3 g^{-1}$)	D (Ă)
Sty-DVB	0.22 ± 0.010	175.2	0.62	174,1

D_{ap}: apparent density; S: specific surface area; V_p: Pore volume; D: Mean pore diameter.

Optical (a) and scanning electron (b) microscopies can be seen in Figure 1. These data indicate that the copolymer Sty-DVB is a mesoporous material with an average pore diameter of 17.4 nm. This data was confirmed by N_2 adsorption-desorption curve, which showed a type IV isotherm (Figure 2).

Figure 1. Optical Microscopy and Scanning Electron Microscopy for Sty-DVB Copolymers

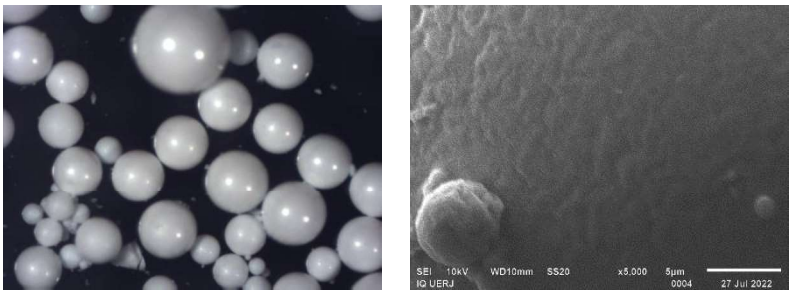

(a) (b)

Figure 2. N_2 adsorption-desorption isotherms of Sty-DVB copolymer

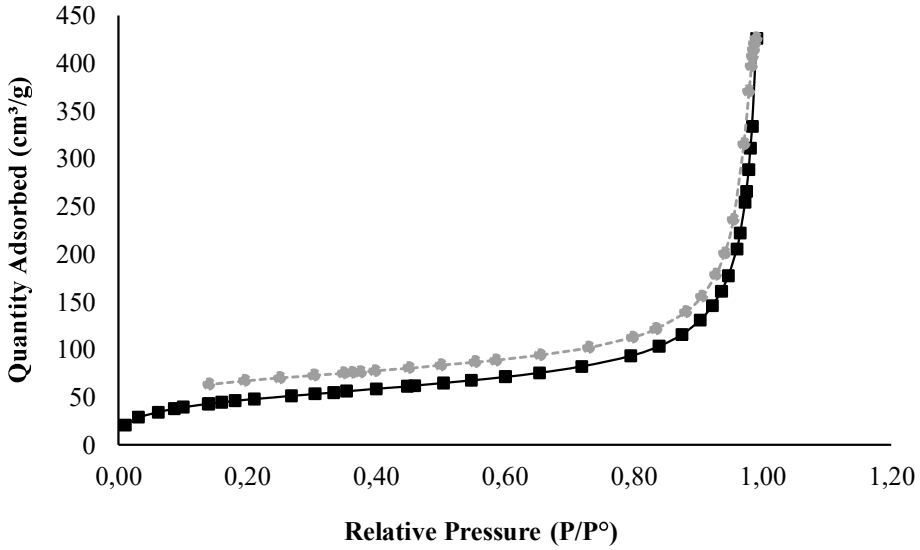

Sty-DVB copolymer was submitted to nitration, reduction, and diazotation reactions to introduce new functional groups on the polymeric structure. These modifications were accompanied by FTIR spectroscopy. The nitration reaction was confirmed by bands at 1523 and 1348 cm^{-1}, attributed to asymmetric and symmetric axial deformation of the NO_2 group. The reduction of these groups was confirmed by the significative reduction of bands attributed to nitro groups besides a considerable

broadening in the band around 3426 cm^{-1} signaled as asymmetric stretching of the amino group [6, 7].

Figure 3 shows comparative curves relating the immobilization yield as a function of time (60 minutes) for Sty-DVB copolymer after reactions to introduce nitro, amino, and diazonium groups on the polymeric structure. The yield of laccase immobilization at the end of the contact time was: 30.1%, 92.3%, 97.9%, and 98.6%, respectively, for the unmodified copolymer, a copolymer with NO_2 groups, NH_2 groups, and diazonium groups. This result indicates the need for polar functional groups in the polymeric matrix for better enzyme interaction. Probably the immobilization of laccase on modified supports probably involves non-specific interactions between functional groups and enzymes. More specifically van-der-Waals interactions and hydrogen bonds between these functional groups and amino acid side chains of enzymes.

Figure 3. Comparative immobilization yield of laccases on different supports: Sty-DVB and Sty-DVB copolymers containing nitro, amino and diazonium groups.

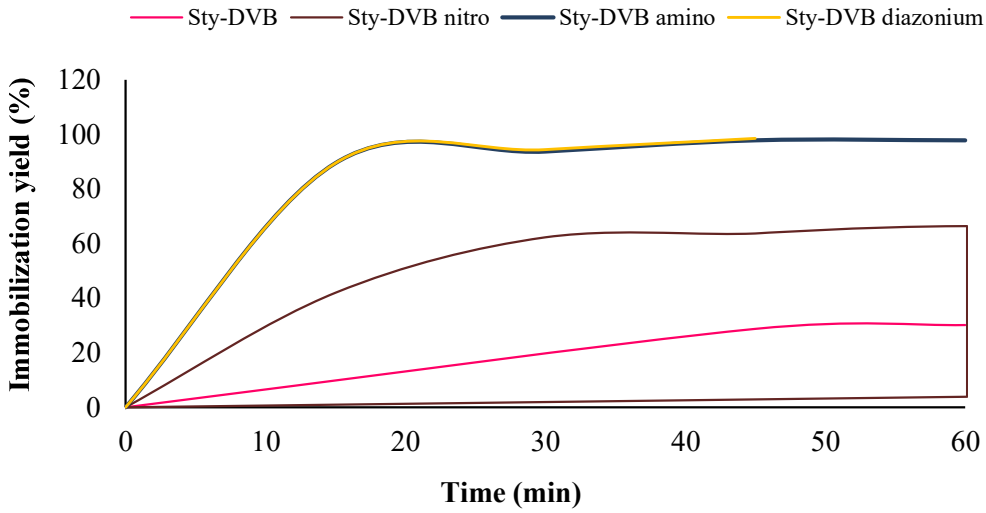

Conclusions

A low degree of immobilization yield was observed for the unmodified Sty-DVB copolymer. However, introducing nitro, amino, and diazonium groups in these copolymers increased immobilization yield. For the copolymers containing amino and diazonium groups, immobilization yields 97.9% and 98.6%, respectively. The immobilization of laccase on copolymers containing nitro, amino, and diazonium groups involves van-der-Waals interactions and establishing hydrogen bonds with amino acid side chains of enzymes.

Acknowledgements

Research Support Foundation of the State of Rio de Janeiro (FAPERJ)

References

1. M. Alcalde; D. M. Mate; Microbial Biotechnology 2016, 10, 1457–1467. https://doi.org/10.1111/1751-7915.12422.

2. L. A. R. Montoya; et al.; Journal of Molecular Liquids 2015, 212, 30–37. https://doi.org/10.1016/j.molliq.2015.08.040

3. M. Fernández-Fernández; et al.; Biotechnology Advances 2013, 31-8, 1808-1825. https://doi.org/10.1016/j.biotechadv.2012.02.013

4. C. F. Melo; et al.; Journal of the Brazilian Chemical Society 2017, 28-11, 2192-2201. https://doi.org/10.21577/0103-5053.20170070

5. A. H. Miller, Ph.D. Thesis, Paulista State University, 2020.

6. R. M. Silverstein; F. X. Webster; D. J. Keimle. Identificação Espectrofotométrica de Compostos Orgânicos., Ed. LTC – gen, 2005.

7. D. L. Paiva; G. M. Lampman; G. S. Kriz. Introduction to Spectroscopy., Ed. Brooks/cole – Thomson Learning, 2001.

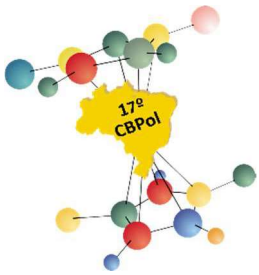

PHYSICAL-CHEMICAL ANALYSIS OF PVA-BASED POLYMERIC FILMS BY ADDITION OF POMEGRANATE EXTRACT

Bruno C. Manhães[1], Geanne A. Paula[2], Janaina C. O. Villanova[3], Lilian C. Carreira[1*]

1 – Department of Rural Engineering, Center for Agricultural and Engineering Sciences - CCAE, Federal University of Espírito Santo (UFES), Alegre, ES, Brazil.

2 – Faculty of Pharmaceutical Sciences, Paulista State University "Júlio de Mesquita Filho" (UNESP), Araraquara, SP, Brazil.

3 – Laboratory of Pharmaceutical Product Development, Center for Exact, Natural and Health Sciences - CCENS, Federal University of Espírito Santo (UFES), Alegre, ES, Brazil.

lilian.carreira@ufes.br

Abstract - The aim of this study was to evaluate physical-chemical properties of PVA-based water-soluble polymeric films containing pomegranate peel extract (PPE) for the treatment of bovine mastitis. Sixteen formulations were prepared varying polymeric compositions and PPE concentrations. TGA and DSC analyses were performed to study the material behavior, FTIR spectroscopy was performed to examine chemical interactions, and XRD was applied to analyze crystalline structure and physical stability. The results demonstrated that any significant disturbances in the films, and an increase in the amorphous phase with increasing PPE proportion as well. Stability was verified of all films as the PPE concentration. Thus, it is possible to infer that the films maintained their chemical and physical stability when used in combination with the pomegranate peel extract.

Keywords: *PVA-based films, pomegranate peel extract (ECR), bovine mastitis treatment, physical-chemical properties, polymeric formulations*

Introduction

Bovine mastitis, which causes inflammation of the mammary gland of dairy cattle, is a major obstacle for the livestock industry worldwide [1]. It reduces milk production and quality, increases expenses, and may require disposal of both milk and animals. Furthermore, the disease involves pathogens that can pose a risk to public health [2,3]. It´s considered a complex disease, depending on several factors such as the environment in which the animal is kept, the type of microorganism involved, and the characteristics of the animal. Therefore, many studies have been conducted to find the best possible solution for the problem [3].

Pomegranate (*Punica granatum*) has been studied as a potential solution to reduce the damage caused by mastitis. This fruit is known for its various medicinal properties, including anti-inflammatory, antimicrobial, and antioxidant actions. Several studies have explored the antimicrobial effects of pomegranate, and it has been traditionally used by different cultures worldwide to combat many microbiological diseases, such as throat infections, ulcers, salmonellosis, urinary tract infections, and cavities [4]. Given that mastitis is a multifaceted condition, pomegranate is being evaluated for its overall antimicrobial properties to combat this disease.

The mastitis treatment should be simple to apply and maintain, with consistent effectiveness for dairy cattle natural grazing environments to ensure adequate protection against external factors. One promising solution is the use of film-forming systems (FFS) devices based in polymers capable of incorporating pomegranate extract, offer a variety of application options and can provide a reliable protective coating [5]. Thus, the combination of pomegranate extract (PPE) with an efficient and

effective treatment system becomes a promising option among treatments for bovine mastitis, and further studies are necessary to understand the applicability of this combination.

Experimental

The films that were prepared using the compositions described in Tables 1 and 2 belongs a previous work developed by Paula [6], based on modifications to the formulation proposed by Nishikawa *et al* [14].

Table 1 – Percentual Composition of formulations A and B.

Components	Quantity (%m/m)							
	A	**A1**	**A2**	**A3**	**B**	**B1**	**B2**	**B3**
PVA	18,0	18,0	18,0	18,0	20,0	20,0	20,0	20,0
Poly(sodium acrylate)	-	-	-	-	-	-	-	-
EDTA	0,1	0,1	0,1	0,1	0,1	0,1	0,1	0,1
Polyproprilene glycol	6,0	6,0	6,0	6,0	6,0	6,0	6,0	6,0
Potassium sorbate	0,15	0,15	0,15	0,15	0,15	0,15	0,15	0,15
Grain alcohol	10,0	10,0	10,0	10,0	10,0	10,0	10,0	10,0
Purified water QSP	100,0	100,0	100,0	100,0	100,0	100,0	100,0	100,0
PPE	-	1,25	2,5	3,75	-	1,25	2,5	3,75

Table 2 – Percentual Composition of formulations C and D.

Components	Quantity (%m/m)							
	C	**C1**	**C2**	**C3**	**D**	**D1**	**D2**	**D3**
PVA	18,0	18,0	18,0	18,0	20,0	20,0	20,0	20,0
Poly(sodium acrylate)	0,5	0,5	0,5	0,5	0,75	0,75	0,75	0,75
EDTA	0,1	0,1	0,1	0,1	0,1	0,1	0,1	0,1
Polyproprilene glycol	6,0	6,0	6,0	6,0	6,0	6,0	6,0	6,0
Potassium sorbate	0,15	0,15	0,15	0,15	0,15	0,15	0,15	0,15
Grain alcohol	10,0	10,0	10,0	10,0	10,0	10,0	10,0	10,0
Purified water QSP	100,0	100,0	100,0	100,0	100,0	100,0	100,0	100,0
PPE	-	1,25	2,5	3,75	-	1,25	2,5	3,75

After preparing the samples in different formulations of polymer blends and PPE, the films obtained, and pomegranate extract were evaluated using the following tests.

X-Ray Diffraction (XRD)

The samples were evaluated in a Rigaku x-ray diffractometer (40kV and 15 mA – Cu-kα radiation) in a 2θ angle range from 5º to 80º and a scan rate of 10º/min.

Fourier-transform infrared spectroscopy (FTIR)

The spectra of PPE and the films were obtained using a Bruker spectrophotometer. It was performed 32 scans in the range of 4000-400 cm^{-1} using the attenuated total reflectance (ATR) technique.

Thermogravimetric Analysis (TGA) and Differential Scanning Calorimetry (DSC)

The TGA and DSC analysis for all the samples were obtained using a Setaram equipment. TGA and DSC data for PPE were obtained through a single heating cycle in a range of 25ºC to 200ºC. For the films, the first heating cycle was carried out of 25ºC to 200ºC, followed cooling to room temperature. Subsequently, a second heating cycle was performed from to 25ºC until 400ºC, both subjected to a heating/cooling rate at 10ºC/min under nitrogen atmosphere.

Results and Discussion

This study expands upon research developed by De Paula [6], which analyzed pharmacological properties and antimicrobial activity of proposed polymeric films. C formulation was identified as

the most promising sample, so this report focuses on the results for FTIR, XRD, TGA and DSC results for this formulation.

The PPE and C formulations FTIR spectra are presented at Fig. 1. The results for PPE showed a broad band in the region between 3600 and 3200 cm^{-1}, corresponding to the axial vibration of -OH , bands at 1700 to 1610 cm^{-1} related to the axial deformation vibration of C=O and amide I, and bands between 1000 and 1200 cm^{-1}, that is characteristic of angular deformation vibration of glycosidic linkage -C-O-C and angular deformation vibration of -C-O. These analyses can be compared and validated according to what was observed by [7], who studied the possibility of producing polymeric films based on PVA, PAA, and pomegranate extract.

For C formulation films, it was observed that although the intensity of the bands at 1700-1610 cm^{-1} decreased, the absence of complete disappearance or significant shift of the main PVA bands in the spectra containing the extract, suggests that chemical interactions occurred between the extract and the polymeric matrix, but did not result in significant changes in the chemical structure of the components involved.

Figure 1 – FTIR spectra of the PPE and C formulation films

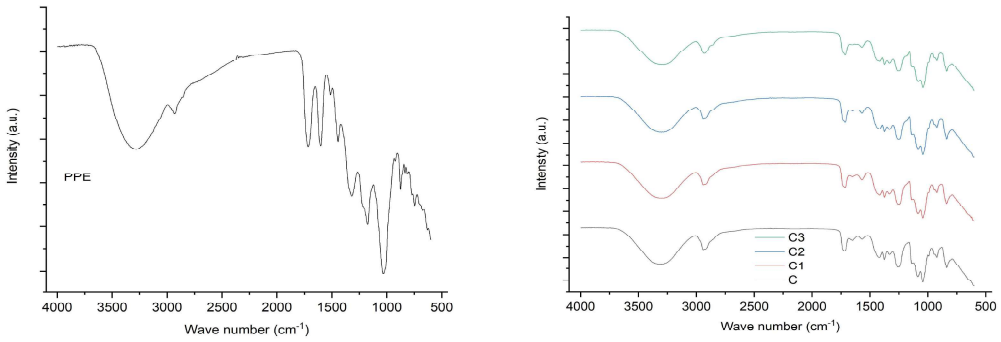

The analysis of the PPE diffractometric profile shows a broad peak near 22º. At polymeric sample without PPE, it was possible to observe an intense peak at 19.7°, which is characteristic of PVA and associated with a crystallographic plane of the crystalline phase. A lower intensity peak is observed at 40.9°, related to PVA amorphous phase [8]. It is important to noted that when ECR is incorporated (Fig 2-b), there is a reduction in the signal's intensity and a slight broadening at the base of the diffractograms, which may be attributed to a reduction in the percentage of PVA crystallinity phase due to interactions with PVA and phenolic groups present in the PPE. The reduction of the crystalline phase directly interferes in the polymeric chain's organization, resulting in disorder and reducing intermolecular interactions, leading to increased molecular mobility [9].

The PPE thermogram initially displayed a weight gain phenomenon and that can be attributed to gas absorption and by the fact that the PPE extract is completely dried, a process that removes water from its composition. Therefore, there are no inherent losses due to water evaporation that are commonly in the beginning of the procedure, only those to the related material's own degradation. However, at films thermgram, it was possible to observe a first slight decline that starts near 100°C, which is associated to water loss. In addition, a second pronounced decline can also be observed between 250 and 320°C, which represents the polymeric material degradation [10]. Additionally, it should be noted that increasing in the PPE proportion at the samples leads to a slight reduction in the initial degradation temperature. This is because the structure of PPE contains phenolic agents which, when incorporated into the polymer matrix molecules, cause the formation of structures with a lower crystallinity degree when compared to the pure polymer. As a result, the degradation process begins more easily and requires less energy to complete [11]. These results corroborated those found for the XDR analysis.

Figure 2 – XRD pattern of the PPE and C formulation films

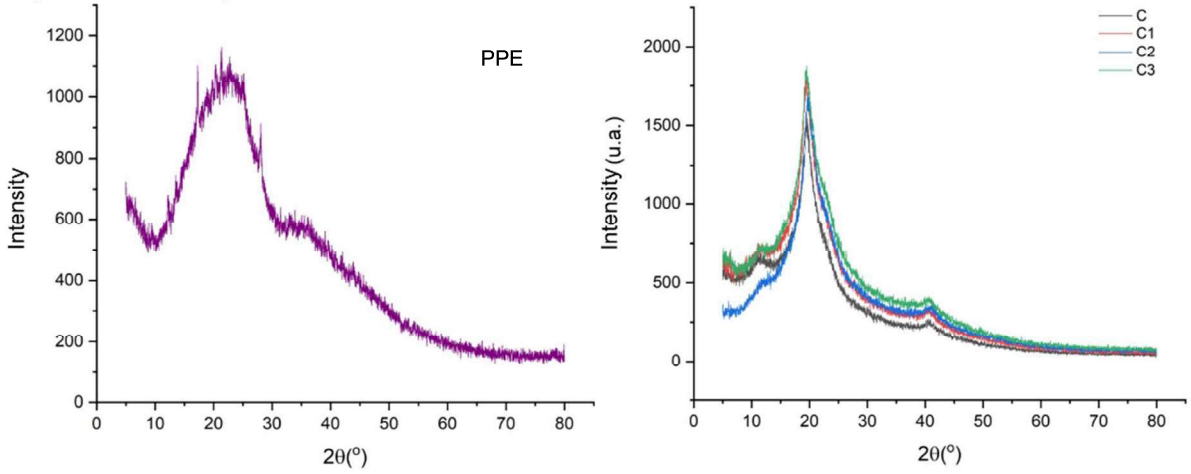

Figure 3 – Thermograms of PPE and C formulation films

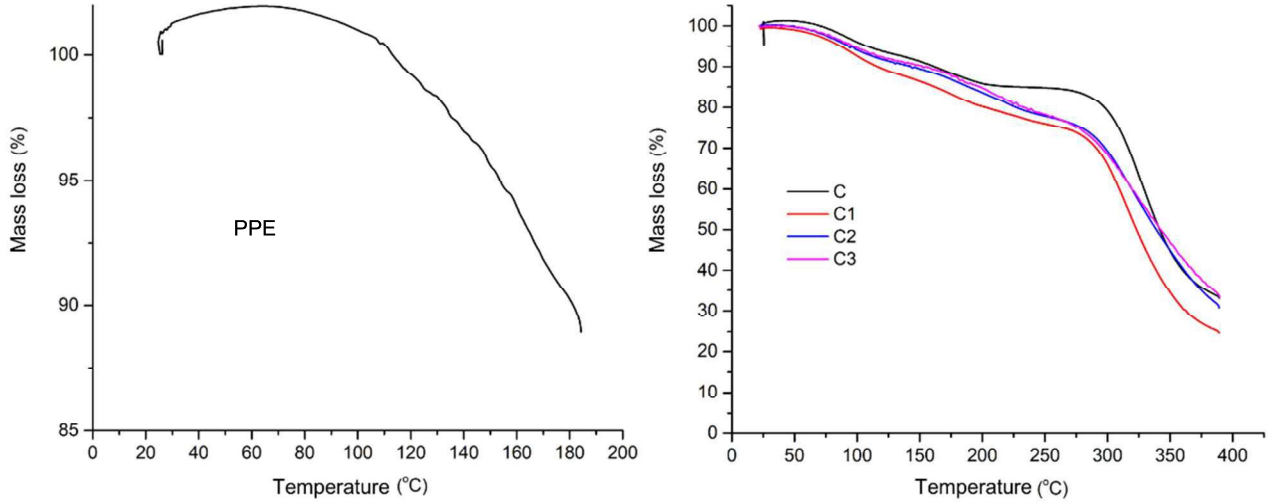

The DSC curve for the PPE shows a single thermal event at around 250°C. The DSC curve for the film without PPE addition shows two thermal events. The first occurring at around 200°C and the second at around 325°C. According to studies [12, 13], the crystalline melting temperature (T_m) of PVA occurs in a range at 198.5°C and 202.7°C. So, it can be inferred that the first thermal event observed is associated with T_m of PVA. The occurrence of the second thermal event can be associated to degradation of polymeric matrix, which is corroborated to TGA results. In addition, the thermal analysis of films containing PPE revealed an expansion of peak base, an intensity reduction, and a slight shift to lower temperatures for all PPE content. These changes were attributed to aromatic groups presents on the extract, which are relatively large and less mobile. This hindered an orderly alignment of polymer matrix chains, and this effect was more pronounced with increasing extract concentration due to the weakening intermolecular bonds in the disordered polymer structure [11]. Although, even with a reduced melt temperature for material fusion, it remains significantly higher than both ambient temperature and the site of application temperature, which ensures the material's functional integrity.

Figure 4 – DSC curves of PPE and C formulation films

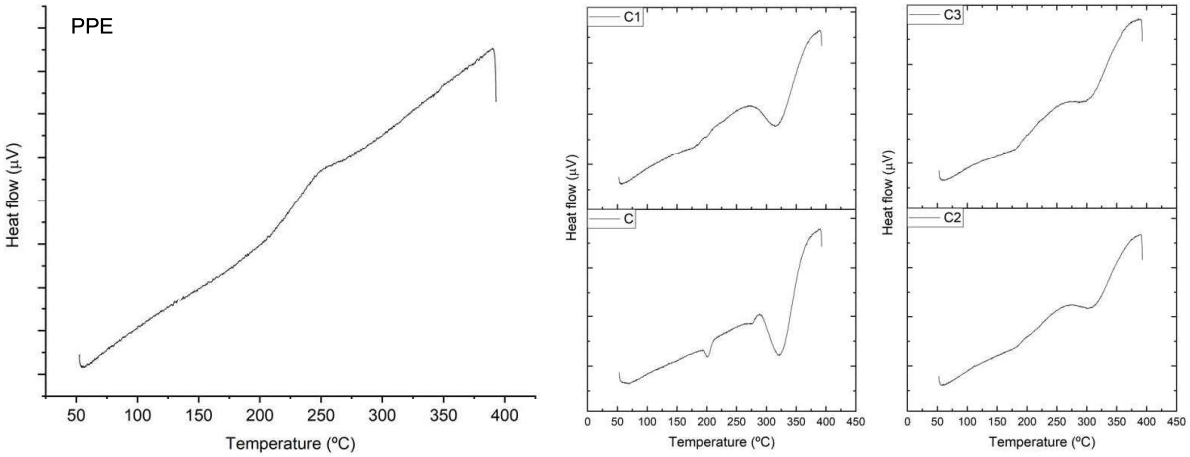

Conclusions

According to the results, the pomegranate extract incorporating allowed for the creation of intact and stable films for the intended purpose. The FTIR analysis showed no significant disturbances in the curves, indicating good interaction and preservation of the PPE properties. XRD patterns revealed that the presence of phenolic agents in the extract broadened the base and reduce the intensity of the characteristic PVA peak, increasing the amorphous phase and hindering the crystalline structural organization. The phenolic agents present at PPE extract were also responsible for slightly shifting the degradation temperature and crystalline melting (T_m) present in the TGA and DSC tests. Therefore, it can be inferred that the films maintained their chemical and physical stability when used in combination with the pomegranate peel extract.

References

1. L. H. Silva; C. Primieri. Mastite bovina: Revisão bibliográfica 2020, 3, 2.
2. B. C. Lopes; M. de P. Manzi; H. Langoni. Etiologia das mastitis: Pesquisa de micro-organismos da classe mollicutes. 25, 41. https://doi.org/10.35172/rvz.2018.v25.41.
3. S. M. Coser; M. A. Lopes; G. M. Costa *Mastite bovina: Controle e prevenção,* Universidade Federal de Lavras, Ed.; Lavras, 2012; n. 93, 1-30.
4. C. H. Degáspari; A. P. Dutra. Propriedades fitoterápicas da romã (*Punica granatum L*) 2011, 12, 27237. http://dx.doi.org/10.5380/acd.v12i1.27237.
5. D. C. P. Santana, Master Degree. Thesis, Universidade do Sul de Santa Catarina, 2020.
6. G. A. de Paula, Final Project. Thesis, Universidade Federal do Espírito Santo, 2022.
7. N. N. Costa, Master Degree. Dissertation, Universidade Federal do Espírito Santo, 2021.
8. M. Teodorescu; M. Bercea; S. Morariu. Biothecnology Advances 2018, 37, 008. https://doi.org/10.1016/j.biotechadv.2018.11.008
9. F. P. Brita *et al.* Revista Eletrônica de Materiais e Processos 2011, 13, 1809-8797.
10. A. de Campos, Doctorate Degree. Thesis, Universidade Estadual Paulista "Julio de Mesquita Filho", 2008.
11. L. Akcelrud. *Fundamentos da ciência dos polímeros*, Manole Ed.; 2007.
12. J. Jose; F. Shezad; A. M. Al-Harthi. Polymer bulletin 2014, 71.
13. S. R. Sudhamani; M. S. Prasad; K. U. Sankar. Elsevier 2003, 17, 3. https://doi.org/10.1016/S0268-005X(02)00057-7.
14. D. O. Nishikawa. Revista. de Ciências Farmacêuticas Básicas e Aplicadas 2007, 28, 2.

POLY(VINYL ALCOHOL) MEMBRANES OBTAINED BY ELECTROSPINNING CONTAINING 5-AMINOLEVULINIC ACID FOR PHOTODYNAMIC THERAPY OF SKIN CANCER

Vanessa F. da Silva[1], Maria Bernadete Riemma Pierre[2], Luiz Guilherme A. de Paula[1] and Marcos L. Dias[1]*

1 – Instituto de Macromoléculas Eloisa Mano, Universidade Federal Rio de Janeiro (UFRJ), Rio de Janeiro, RJ, Brazil
vanessa.silva@nano.ufrj.br
2 - Faculdade Farmácia, Universidade Federal do Rio de Janeiro, Rio de Janeiro, RJ, Brazil

Abstract - Photodynamic therapy (PDT) is an effective technique in the topical treatment of skin cancer, and has been successful using 5-aminolevulinic acid (5-ALA) as a photosensitizing agent (FS). However, its penetration into thick tumor tissues is hindered due to the high hydrophobicity. So, the electrospinning technique was used to obtain polymeric membranes of poly(vinyl alcohol) to convey the prodrug in the treatment of non-melanoma skin cancer. The most suitable membrane has fibers with thicknesses up to 250 nm, and was electrospun with 0.1 mL/h flow rate, 18 kV and 11 cm distance between collector and needle. The membranes were cross-linked by glutaraldehyde vapor for 6 hours under vacuum in a desiccator, with hydrochloric acid as a catalyst, in order to reduce their water solubility. Both membranes with and without crosslinking were subjected to SEM, FT-IR and TGA, for material characterization.

Keywords: *electrospinning, skin cancer, 5-aminolevulinic acid, poly(vinyl alcohol).*

Introduction

Photodynamic Therapy (PDT) is a topical treatment that combines visible light with a photosensitizing molecule to eliminate cells. Photosensitizers (FS) are substances that generate reactive oxygen species (ROS) when they absorb energy at a specific wavelength [1]. PDT is particularly effective in treating tissue wounds associated with Cutaneous Leishmaniasis, ocular degeneration, and tumors. In Brazil, skin cancer is the most common type of cancer, but despite its frequency, it is also one of the pathologies with a high cure rate.

One extensively studied photosensitizer is 5-aminolevulinic acid (5-ALA), which has been researched since the 1990s. It is referred to as a prodrug because it stimulates the synthesis of Protoporphyrin IX (PpIX) [2]. This natural molecule is essential in our cells for the production of the heme group of hemoglobin during the Porphyrin pathway. However, unlike PpIX, 5-ALA is hydrophilic and cannot penetrate the stratum corneum, the outermost protective barrier of the skin. Therefore, high doses of topical 5-ALA are required to achieve significant concentrations of PpIX, often resulting in pain for patients [3]. Consequently, in the last decade, numerous studies have focused on developing safe and effective methods to enhance the diffusion of the prodrug.

In this project, nanofibers were chosen as the delivery system due to their ability to increase the dissolution rate of the drug and carrier, resulting in a controlled drug release. The electrospinning technique was employed to form the nanofibers, which relies on the application of a potential gradient between the polymer solution and the metal collector. This electric field disrupts the surface tension of the solution, causing it to stretch into a cone shape known as the Taylor Cone [1]. Eventually, the surface tension is broken, and a polymeric jet is generated between the needle and the collector. Electrospinning requires a high voltage source, needle, syringe, infusion pump, metallic collector,

and two electrodes. Therefore, the key parameters for electrospinning are voltage, flow rate of the polymeric solution, and the distance between the needle and the collector.
The chosen polymer for drug diffusion was poly(vinyl alcohol) (PVA), which is a synthetic, biocompatible, and non-toxic polymer that readily degrades in aqueous media. PVA and 5-ALA possess significant hydroxyl content, making them compatible due to their hydrophilic nature. The production of PVA involves the polymerization of vinyl acetate monomers to form poly(vinyl acetate) (PVAc), followed by the hydrolysis of the acetate groups, resulting in a polymer chain with pendant hydroxyl groups [4]. PVA exhibits excellent processability and is suitable for the formation of hydrogels, fibers, and films. It possesses desirable properties such as elasticity, thermal stability, chemical resistance, and mechanical strength, making it widely employed in biomedical applications.

Experimental

Materials

PVA (M_w = 30,000 to 70,000) and a hydrolysis grade of 87% to 90% was purchased from Sigma-Aldrich in powder form. 5-ALA was also purchased from Sigma-Aldrich (molecular weight, 167.6 g/mol). Glutaraldehyde 25% and acetate buffer solution with a pH of 5 and a concentration of 0.1 molar were prepared by the laboratory staff using glacial acetic acid and sodium acetate trihydrate.

Electrospun membranes of PVA/5-ALA

A 20% w/v solution of PVA was prepared by dissolving PVA in a buffer solution with pH 5 at 80 °C for 3 hours. After this period, the solution was stirred for 24 hours at room temperature. The solution containing 5-ALA was produced by adding the prodrug at a concentration of 1 wt%, in relation to the mass of the polymer, after 24 hours of polymer stirring. After addition of ALA, the mixture remained another half hour of stirring for total compatibility between the polymer and the drug. [5]
In this work, the electrospinning apparatus consisted of a high-voltage power supply (Glassman High Voltage PS/FC 6p02.0-11, USA), an infusion pump (KDScience, USA), a needle with an inner diameter of 0.8 mm (22G), and a grounded metal collector. The solution was injected using 5 mL plastic syringes and independently pushed at flow rates of 0.1 mL/h. Under the processing conditions, the voltage varied between 18 kV, the distance between needle and grounded metal collector was 11 cm, and the temperature and humidity were kept between 20-22°C and 50-60%, respectively.

Crosslinking of membranes

The electrospun membranes were cross-linked with Glutaraldehyde (Glu) vapour for 6 hours, using Hydrochloric Acid (HCl) as a catalyst in a 3:1 (Glu:HCl) ratio, and a dissecator, to enhance a sealed and vacuum environment [6].

Characterizations

The membranes obtained by electrospinning were characterized using scanning electron microscopy (SEM), which allowed evaluating the morphology of the fibers in terms of the presence of defects, average fiber diameter, and porosity. For the SEM analyses, the membranes were coated with gold using a metallizer. The fiber diameter was quantified using ImageJ software.
Fourier-transform infrared spectroscopy (FTIR) with an ATR accessory in the range of 4000 to 400 cm^{-1} was performed to observe the relative bands of functional groups of polymer and drug.
Thermogravimetric analysis (TGA) was used to characterize the thermal stability profile of the membranes, including the initial temperature and the temperature of maximum weight loss rate. The samples were heated from 25°C to 700°C at a rate of 10°C/min under a nitrogen flow of 60 mL/min.

Results and Discussion

Figure 1 displays scanning electron microscopy (SEM) images of the PVA, PVA/5-ALA, cross-linked PVA, and cross-linked PVA/5-ALA samples. The samples labeled with the suffix "-ret"

indicate that they were cross-linked using glutaraldehyde vapor. The SEM images were taken at a magnification of 50,000x and exhibited uniform and defect-free fibers in all samples. The PVA sample (Figure 1A) exhibited an average diameter of (137 ± 72) nm, while the PVA/5-ALA sample (Figure 1B) has an average diameter of (112 ± 75) nm. In the case of the PVA-ret sample (Figure 1C), the average diameter is (123 ± 52) nm. The final cross-linked PVA/5-ALA sample displayed fibers with a slightly larger standard deviation, with an average diameter of (164 ± 80) nm. These results suggest that the fibers are homogenous and reproducible, with mean diameters below 250 nm.

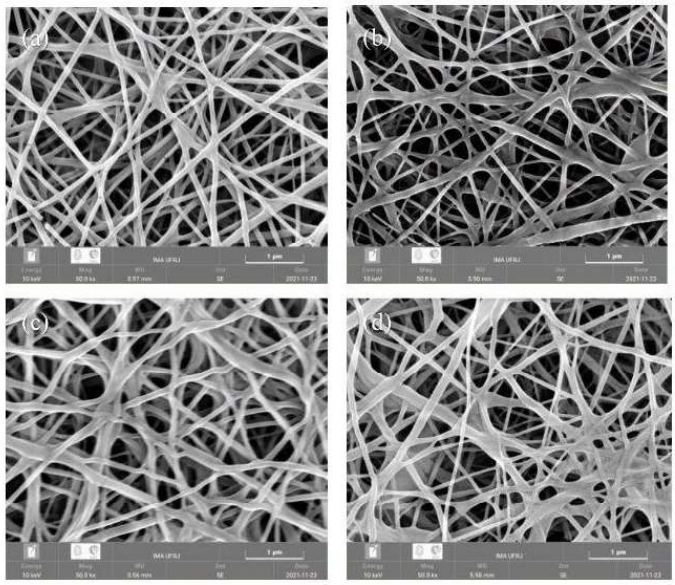

Figure 1. SEM images of electrospun (a) PVA, (b) PVA-5ALA, (c)PVA-ret, (d) PVA/5ALA-ret

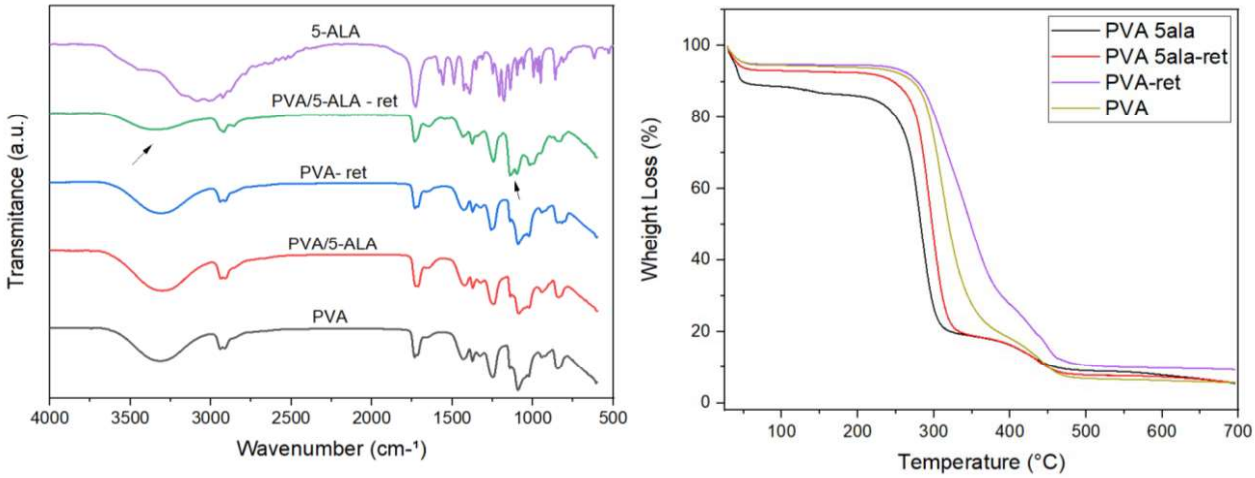

Figure 2. (a) FTIR spectra, and (b) TGA analysis of PVA samples PVA, PVA-5ALA, PVA-ret, and PVA/5ALA-ret.

The FTIR-ATR spectra are presented in Figure 2A that refers to the addition of 5-ALA in PVA membranes and its crosslinking. Analyzing the addition of ALA, it is inferred a significant increase in the bands at 3300cm^{-1} and 1700cm^{-1} that corresponds to the increase in the number of hydroxyls (-OH) and carbonyls (C=O). In the case of the PVA/5-ALA-ret sample, as indicated by the arrows in Figure 2A, a distinct band appears at 1100 cm^{-1}, which corresponds to the presence of the acetate bond resulting from the crosslinking process [7]. Additionally, there is a significant decrease in the

intensity of the band at 3300 cm-¹, which represents consumption of the hydroxyl groups due to the crosslinking.

The TGA analysis presented in Figure 2B clearly shows that when 5-ALA was added to fibers, its thermal stability decreases. The PVA/5-ALA-ret sample had two weight loss events with different T_{onset} temperatures, common to PVA, the first at 273.6°C and the second at 402.9°C, with a final degradation temperature of 474.4°C.

Conclusions

This work successfully achieved the fabrication of monolithic fibers of PVA/5-ALA as confirmed by the SEM analysis. SEM images demonstrated homogeneous fiber structures and a mean diameter below 250 nm. The FTIR analysis confirms the successful crosslinking of the membranes, as indicated by the presence of the acetate absorption band and the decrease in the intensity of the band associated with exposed hydroxyl groups. This confirms the chemical changes that occur during the crosslinking process and provides evidence of the modified composition of the membranes. Additionally, the TGA analysis plays a crucial role in understanding the effects of the drug on the thermal stability of the PVA. The results indicate that the addition of the drug leads to a decrease in the thermal stability. However, the subsequent crosslinking process significantly improves the thermal stability of the membranes. This can be attributed to the increased crosslinking within the polymer chains, which enhances the overall structural integrity and stability of the membranes. Considering these findings, it can be inferred that the properties of the nanofibers, as observed through these analyses, make them suitable for membrane applications. The successful crosslinking and improved thermal stability highlight the potential of these nanofibers in various membrane-based applications.

Acknowledgements

Thanks to CNPq for funding this research

References

1. Rossin et al. Química Nova 2020 43(5), 613-622. http://dx.doi.org/10.21577/0100-4042.20170524

2. Torezan, L.; Niwa, A. B. M.; Neto, C. F. Anais Brasileiros de Dermatologia [online]. 2009, 84(5) 445-459. https://doi.org/10.1590/S0365-05962009000500002.

3. Champeau et al. Journal of Photochemistry & Photobiology, B: Biology, 2019, 197. https://doi.org/10.1016/j.jphotobiol.2019.111544

4. Chiellini, E., Corti, A., D'Antone, S. & Solaro, R. Biodegradation of poly(vinyl alcohol) based materials. *Prog. Polym. Sci.* **28**, 963–1014 (2003)

5. Yoo et al. Internacional Journal of Nanomedicine, v.7, 1997-2005, 2012. https://doi.org/10.2147%2FIJN.S30298

6. Shaikh et al. Biofabrication, 2012, 4(2), 1-21. http://dx.doi.org/10.1088/1758-5082/4/2/025002

7. Hulupi M. & Haryadi H., Materials Today: Proceedings, 2019, 13(1), 199-204. https://doi.org/10.1016/j.matpr.2019.03.214.

PRODUCTION AND CHARACTERIZATION OF BIODEGRADABLE WOUND DRESSINGS CONTAINING ZEOLITE SILVER PARTICLES

Aline C. Lopes[1*] and Juliana B. Olivato[1]

1 – Department of Pharmaceutical Sciences, State University of Ponta Grossa (UEPG), Ponta Grossa, PR, Brazil
line_lopes123@hotmail.com

Abstract – Zeolite silver (ZeAg) particles with antimicrobial activity were added to biodegradable wound dressings based on starch and brewer's spent grain (BSG). Four samples of biodegradable wound dressings (0, 0.5, 1 and 2% (w/v) of ZeAg particles) were obtained by thermopressing method and analyzed concerning their morphology, thickness, density, solubility, water vapor permeability (WVP), water solubility and absorption indexes (WSI/WAI), and mechanical properties. The dressings had a rough appearance and brownish colors due to the addition of BSG. There was no significant difference between the samples in the thickness, density, solubility, WVP and WSI tests. SEM images showed a high number of pores in the surface of dressings. Regarding WAI test, the dressing with the addition of 0.5% ZeAg particles obtained significant increase of the water absorption in relation to the other samples. The wound dressings with addition of 2% of ZeAg showed significant higher values in elongation at break, tensile strength and elastic modulus, as a consequence of the reinforcement role of the particles. Therefore, the biodegradable materials with ZeAg particles are considered promising for the application as a biodegradable wound dressing.

Keywords: *Starch, Brewers' spent grain, Wound dressings, Zeolite, Silver ions.*

Introduction

Biopolymers of natural origin are promising due their characteristics of biocompatibility, non-toxicity, processability and availability, in addition to being biodegradable, such as starch [1]. Starch-based polymeric materials have some disadvantages such as their high permeability to water vapor and low mechanical performance, forming brittle materials. To overcome these limitations, the use of lignocellulosic fibers as reinforcement in starch-based polymeric materials becomes a promising alternative. These materials are inexpensive and biodegradable, in addition to increasing the resistance of polymeric matrices [2]. Brazil presents a territory where high amounts of lignocellulosic agro-industrial residues are produced. Brewers' spent grain (BSG) is the more abundant by-product of the brewing industry. It is currently used as animal feed, but due its rich composition, it can be also used in pharmaceutical and food applications [3,4].

One of the many biomedical applications of natural polymers is in the area of tissue immunity, serving as raw material in the production of biodegradable dressings. These materials must protect the injury until the healing process is completed [5]. Dressings with the addition of antimicrobials are efficient in healing infected and exudative wounds, with high absorption capacity due to their structure with high porosity, in addition to avoiding microbial contamination at the wound site [6]. An example is the use of silver compounds (Ag to treat infections in open wounds, burns and ulcers. However, they have some difficulties related to the release of Ag+ ions [7], and the use of materials that act as particle carriers seems to circumvent this problem, and zeolites stand out in this function [8]. Zeolites are natural or synthetic microporous minerals and are formed by silicon and aluminum molecules with ion exchange capacity, being used as catalysts, adsorbents, molecular sieve and dehydration and rehydration of materials [9].

Therefore, the purpose of this work was to produce biodegradable wound dressings based on starch and BSG including different proportions of zeolite and silver particles. The structural, barrier

and mechanical properties of the biodegradable materials were evaluated, considering an alternative to obtaining biodegradable polymers for biomedical purposes.

Experimental

Zeolite and silver particles production

The obtention of ZeAg particles is shown in the Fig 1.

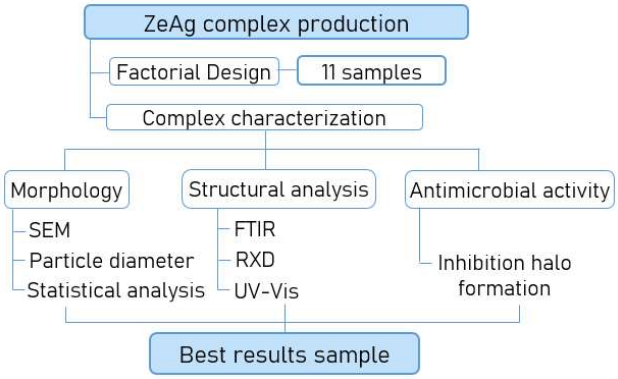

Figure 1 – Obtention of ZeAg particles.

Wound dressings production

Four samples were tested to obtain the wound dressings, by using *thermopressing* method. The components of the formulations were cassava starch (85% $w.v^{-1}$), glycerol (9% $w.v^{-1}$), BSG (5% $w.v^{-1}$) and different concentrations of the ZeAg particles (0, 0.5, 1 and 2% $w.v^{-1}$). These components were mixed in 100 mL of water and was manually stirred. Subsequently, the mixtures were weighed, obtaining approximately 100 g of each formulation and this amount was transferred to the previously heated thermopress (175°C / 1 atm), for 18 minutes. The formulations were stored at 25±2ºC until the analysis.

Characterization of the biodegradable wound dressings

Scanning electron microscopic (SEM) analysis

A scanning electron microscope Tescan model Mira 3 was used to make observations in the surface of the dressings. Before coating with a gold layer, the samples were stored at 25 ±2 ºC in a desiccator with $CaCl_2$ (0% RH) for 7 days. The coating was performed with a SputterCoater (Quorum SC7620). Images were taken of the surface, with 1 kx of magnification.

Thickness and density of wound dressings

The thickness of films was measured with digital micrometer with resolution 0.001mm, through 5 random points. For the density, the films (2cmx2cm) were stored at 25 °C in a desiccator with $CaCl_2$ (0% RH) for 7 days and then weighed to determination of weight of films. The thickness, width and length were evaluated to perform the density calculation.

Water Solubility and Water vapor permeability (WVP)

For the water solubility test the samples were previously dried in a desiccator containing $CaCl_2$ (0% RH) for 7 days. After this period, they were weighed and immersed in distilled water (30:1 ratio – water:sample) for 48 hours at 25 °C. Excess water was removed and the material was dried in an oven at 105 °C until a constant mass, which is used as the final mass of the samples to calculate the water solubility of the materials. The determinations were performed in triplicate. The WVP was determined by the gravimetric method with adaptations from the American Society for Testing and Material (ASTM E-96-95, 1996).

Water Absorption and Water Solubility Index (WSI and WAI)

The water absorption index (WAI) and the water solubility index (WAI) were determined according methodology of Anderson et al. (1969) [10] with some modifications. Were placed in a centrifuge tube, previously weighed, approximately 2.5 g of sample and 30 mL of water. The tubes were shaken for 30 minutes on a mechanical shaker, then centrifuged at 3000 rpm for 5 minutes. The supernatant liquid was carefully transferred to a Petri dish and placed in an oven at 105°C until constant weight. The remaining material from the centrifuge tube (gel) was weighed and the WAI (g water/g solid) calculated was calculated by the ratio between the mass of the gel and the mass of the sample. WSI was calculated by the ratio between the mass of the evaporation residue and the initial mass of the sample.

Mechanical Properties

A universal mechanical testing machine (Shimadzu, Kioto, Japan) was used to determinate the tensile properties of the films. Tensile tests were based on American Society for Testing and Material Standard (ASTM) D882-91 (1996) [11]. The tensile strength (MPa), elongation at break (%) and Young's modulus (MPa) were determined.

Statistical analysis

The data were expressed as mean and standard deviation, followed by ANOVA analysis and Tukey,s test, with 5% variance ($p < 0.05$).

Results and Discussion

The different wound dressing formulations presented the visual appearance shown in Fig 2. The brownish coloration is due to the addition of 5% BSG in the formulations (Fig 2B, 2C and 2D). The materials presented a highly porous surface with malleability and resistance right after the process.

Figure 2 – Biodegradable wound dressings. (A) Control sample, (B) 0.5% of ZeAg, (C) 1% of ZeAg, (D) 2% of ZeAg.

In SEM analysis, it was observed that sample with 0,5% of ZeAg (Fig 3B), showed a high number of pores throughout the surface area, leaving the material irregular, which can be attributed to the evaporation of water from the formulation during sample thermal processing. This porous aspect leads to a greater capacity for water and liquids absorption, due to the presence of cavities, which becomes an ideal characteristic in obtaining dressings that act on exudative wounds. The other samples showed homogeneity and regularity on their surfaces.

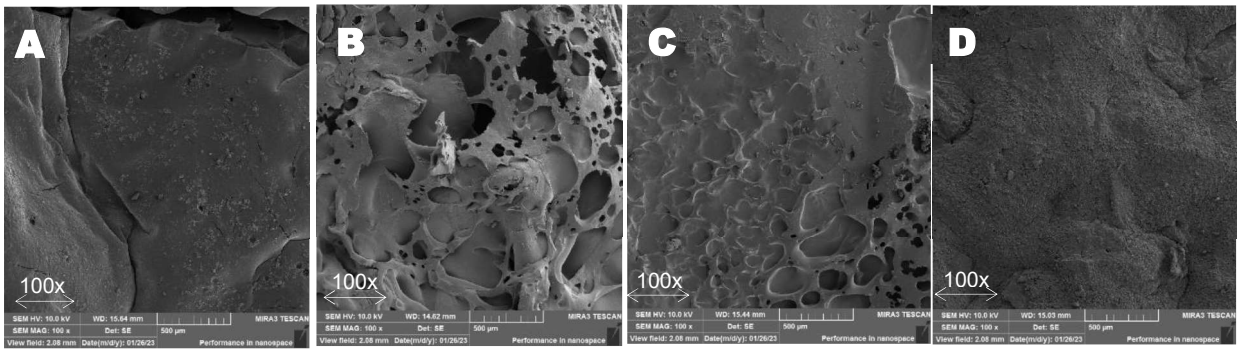

Figure 3 – SEM images for biodegradable wound dressings. (A) Control sample, (B) 0.5% of ZeAg, (C) 1% of ZeAg, (D) 2% of ZeAg.

The results obtained, both for the control and for the dressings with ZeAg, showed no significant difference for thickness, density, water solubility, WVP and WSI. Regarding WAI test, the formulation of 0.5% ZeAg showed significant higher value (4,274±0,495) in comparison with the other samples (2,864± 0,098 for the control, 2.341 ± 0.09 to ZeAg 1% and 2.315 ± 0.104 to ZeAg 2%). In accordance with SEM images, this formulation shows the higher presence of pores on the surface, which may have exposed the hydrophilic groups of the polymer and resulted in greater absorption of water.

The mechanical properties are shown in Table 1. Tensile strength and elongation at break have been significantly increased in the 1 and 2% of ZeAg formulations. The rigidity represented by Young's module were affected with 2% of ZeAg complex, leading to reinforcement of the biodegradable material. These results points to a positive effect of ZeAg particles in the mechanical performance of the biopolymers dressings, resulting in more resistant materials to be used in biomedical applications. Several articles show the influence of zeolites on mechanical properties of starch films [12, 13].

Table 1 – Tensile strength, elongation at break, and Young's modulus of the biodegradable wound dressings.

Samples	Tensile strength (MPa)	Elongation at break (%)	Young's module (MPa)
Control	0.667 ± 0.106^{a}	12.658 ± 7.257^{a}	14.199 ± 3.794^{a}
ZeAg 0.5%	0.572 ± 0.266^{a}	19.201 ± 4366^{a}	10.428 ± 0.029^{a}
ZeAg 1%	2.459 ± 0.130^{b}	$27.675 \pm 4.401^{a,b}$	12.155 ± 1.846^{a}
ZeAg 2%	2.836 ± 0.464^{b}	32.494 ± 7.856^{b}	32.820 ± 0.593^{b}

^{a,b} Samples with different letters in the same column are different (Tukey's test, $p<0.05$).

Conclusions

The biodegradable wound dressings materials were successfully obtained mechanical properties were improved with the addition of the ZeAg particles in concentrations above 1% which showed a significant increase in resistance and rigidity, in addition to increasing the elongation of the materials. Thus, the tests carried out in this work demonstrate that the biodegradable polymeric materials developed have the potential to be used as a dressing aimed at application in exudative wounds. However, it is necessary to carry out additional tests aimed at increasing the performance of its antimicrobial properties and evaluating its cytotoxicity.

Acknowledgements

The authors would express their gratitude to the multiuser laboratories at State University of Ponta Grossa for their technical support, and Coordenação de Aperfeiçoamento Pessoal de Nível Superior and Fundação Araucária for their financial support.

References

1. J. Lei; L. Sun; P. Li; C. Zhu; Z. Lin. Heal. Sci. J. 2019, 13, 1–8. doi:10.21767/1791-809X.1000662.
2. M. Silva; W. Silva; A. Pereira. Brazilian Journal of Development 2020, 6, 86238-86250. doi:10.34117/bjdv6n11-155.
3. L. A. Kubaski; P. B. Ito. Graduation's Thesis - Universidade Tecnológica Federal do Paraná, 2017.
4. D. N. Florindo. (Graduation's Thesis - Universidade Tecnológica Federal do Paraná, 2017.
5. V. C. Souza; J. Villarroel-Rocha; M. J. G. de Araújo; K. Sapag; S. B. C. Pergher. Perspectiva, Erechim 2019, 43, 85-97. http://doi.org/11336/114930.
6. Z. Obagi; G. Samiani; A. Grada; V. Falanga. Surg Technol Int. 2019, 10, 50-57.
7. G. P. Barbosa. Materials Science and Engineering C 2016, 60, 246-254. https://doi.org/10.1016/j.msec.2015.11.034.
8. M. Servatan; P. Zarrintaj; G. Mahmodi; S-J. Kim; M. Ganjali; M. Saeb. Drug Discovery Today 2020, 25, 4. https://doi.org/10.1016/j.drudis.2020.02.005.
9. P. H. Yassue-Cordeiro; C. H. Zandonai; C. F. da Silva; N. R. C. Fernandes-Machado. Polímeros, 2014, 25, 492–502. doi:10.1590/0104-1428.2059.
10. R.A. Anderson. et al. Gelatinization of corn grits by roll-and extrusion-cooking. Cereal Science Today 1969, 14, 4-7. https://doi.org/10.1002/star.19700220408.
11. American Society for Testing and Materials – ASTM. D882-91: Standard Test Methods for Tensile Properties of Thin Plastic Sheeting. Philadelphia: ASTM, 1996. (Annual Book of ASTM Standards).
12. A. F. Santos. Master's Thesis. Universidade Tecnológica Federal do Paraná, 2014.
13. D. Bendahou. et al. Industrial Crops and Products 2015, 72, 107-118. https://doi.org/10.1016/j.indcrop.2014.12.055.

PVA/CHITOSAN FIBERS PRODUCED BY ELECTROSPINNING: STRUCTURAL, THERMAL, MORPHOLOGICAL, ANTIBACTERIAL AND CYTOTOXYC PROPERTIES

Jéssica L. Andrade[1,2], Daniela M. F. Oliveira[1]

1- Programa de Pós-Graduação em Química, Universidade Estadual de Maringá (UEM), Maringá, PR, Brazil
2- Departamento Acadêmico de Química, Universidade Tecnológica Federal do Paraná (UTFPR), Campo Mourão, PR, Brazil
jessicaandrade@utfpr.edu.br

Abstract
Poly(vinyl alcohol) (PVA) is a polymer widely used in several sectors due to its solubility in water and non-toxicity. Chitosan (CS) is a biopolymer, biocompatible with excellent antimicrobial activity. PVA/CS blends are promising materials. In present study, PVA/CS fibers at different mass compositions (100/0, 99/01, 95/05, 90/10, 85/15 and 80/20) were prepared by electrospinning technique. SEM images showed nanofibers with uniform morphology, homogeneous dispersion of CS into PVA matrix, and good interfacial adhesion between the polymeric constituents. The results also evidenced intermolecular interactions between two polymers in the blends. PVA/CS fibers exhibited inhibition action against gram-negative (*E. Coli*) and gram-positive (*S. Aureus*) bacteria, but they were non-cytotoxic for fibroblasts cells, indicating be suitable for tissue engineering applications.

Keywords: *Poly(vinyl alcohol); Chitosan; electrospinning; scaffolds; antibacterial activity.*

Introduction

Hybrid polymer materials, as the polymeric blends, always attracted considerable attention because they can combine efficiently the advantages of both components and adjust its properties for the desired application. Poly(vinyl alcohol) (PVA) is a non-toxic and water-soluble polymer [1]. Thus, it has found widespread applications, as food packaging [2], and in the biomedical field as in drug delivery system, wound dressings and skin tissue engineering [3, 4]. Chitosan (CS) is cationic linear polysaccharide consisting of poly-β-(1-4)-D-glucosamine units obtained by partial deacetylation of chitin, the second most abundant biopolymer after cellulose, and the major component of crustaceous, insects and fungi [4, 5]. CS has been aroused great interest due its significant antimicrobial properties and unique biological properties, such as non-toxicity, biocompatibility and biodegradability [2, 5]. However, CS has some limitations in its applications, due low mechanical strength, rigid structure and high production cost. One way to overcome these disadvantages is to blending it with synthetic polymers as PVA. PVA/CS in fibers morphology, prepared by electrospinning have exhibited excellent properties as the ability of physical gelation due to inter and intra-molecular hydrogen bonding [6]. Besides that, for fiber blends, the addition of CS to PVA has a thickener effect, increasing the viscosity and giving rise to uniform nanofibers [4]. Electrospinning, is a practical technique to produce polymers nanofibers, with relative low-cost and simplicity. The electrospinning process consists of the application of a strong electrostatic field to a viscous polymer solution held in a needle. Above a given threshold voltage, the electrostatic force overcomes the polymer droplet surface tension, and the resulted jet is ejected from the needle tip toward a collecting [7]. Due to the nanostructured architecture produced by such a process, the nanofibers are suitable to be applied tissue engineering as scaffold [4]. In present study, PVA/CS

fibers at different compositions were prepared by electrospinning technique, aiming to develop a suitable biopolymeric platform for cell growth. A comprehensive investigation of the structural, thermal properties, morphology, antibacterial and cytotoxic activity of these materials was done.

Experimental

2.1. Preparation of PVA/CS fibers

PVA and CS solutions were prepared separately. PVA solution (12% w/v) was prepared in distilled water, using a magnetic stirrer and mild heating of 45 °C for 4 hours. CS solution (2% w/v) was prepared in acetic acid solution (2 wt.%) and stirred for 4 hours. To prepare PVA/CS fibers at different compositions (% weight), both PVA and CS solutions were mixed and stirred for 8 hours at room temperature (~25 °C), for complete homogenization. The mass ratio between PVA/CS was varied in 100/0 (pure PVA), 99/01, 95/05, 90/10, 85/15 and 80/20.

2.2. Characterization of PVA/CS fibers

PVA/CS fibers were characterized by ATR-FTIR spectroscopy (BrukerVertex 70Z spectrometer) and X-ray diffraction (XRD) (Bruker D2 Phaser XRD diffractometer). The percent crystallinity (Xc%) of the fibers was measured as a ratio of the crystalline peak area to the total area from XRD as follows **Equation 1** [7]:

$$Xc\ (\%) = \frac{A_c}{(A_c + A_a)}\ x\ 100 \quad \textbf{(1)}$$

In which A_c corresponds to the peak area of crystalline phase; A_a is the area of amorphous phase and Xc (%) is the percent crystallinity.

The thermal properties of PVA/CS fibers (6.0 mg) were investigated by simultaneous thermogravimetry/differential scanning calorimetry (TG/DSC) STA 6000 Perkin Elmer (UTFPR/Medianeira), using alumina sample holders, with heating rate of 10 °C min^{-1}, under a flow of O_2 (white martins, 5.0 purity) at 20 mL min^{-1}, by heating from 50 to 600 °C. Scanning electron microscopy (SEM) was obtained in a FEI Quanta 250 microscope. The hydrophilicity of the fibers surfaces was analysed from contact angles (θ_c) measures, determined from the captured image of the drop-fabric contact at 22 °C using a Cam-Plus contact angle meter (Tantec, Denmark). The results were reported as a mean of three measurements (n = 3) ± SD.

2.3. Antibacterial activity and Cell viability

The antibacterial action of PVA/CS fibers was evaluated against Gram-negative *Escherichia coli (E. Coli)* and Gram-positive *Staphylococcus aureus (S. Aureus)* stains, using the disc-diffusion method. The *in-vitro* cytotoxicity of PVA/CS fibers was investigated for health fibroblast cells (ATCC L929) after 24 hours of incubation, and by MTT method.

Results and Discussion

Fig. 1(a) shows FTIR spectrum of pure PVA (100/0) fiber, which exhibits absorption bands at 3600-3000 cm^{-1}, characteristics of O-H stretching; between 2980 and 2876 cm^{-1} and a shoulder at 2850 cm^{-1}, that can be attributed to C-H symmetric and asymmetric stretching [8, 9]; and also bands around 1756, 1676 and 1560 cm^{-1}, that are associated to stretching of acetate groups (COO^-), residues of poly (vinyl acetate) [10]. The absorption bands observed between 1500-1176 cm^{-1}, are attributed to the angular deformation of C-H bond, coming from the CH_2 group of the polymeric chain. The intense bands at 1150 and 980 cm^{-1} are associated to the stretching of C-C and C-O bond in structure of PVA, and the bands with low and medium intensity below 980 cm^{-1} are attributed to the scissor-like stretch of CH_2 [11]. The spectra of PVA/CS fibers displayed similar bands of pure PVA, however with the emergence of some bands such as at 3000 cm^{-1}, characteristic of combined stretching vibration of the hydroxyl O-H and amine/amide group N-H, from chitosan, as well as the intramolecular hydrogen bonds [3,12,13].

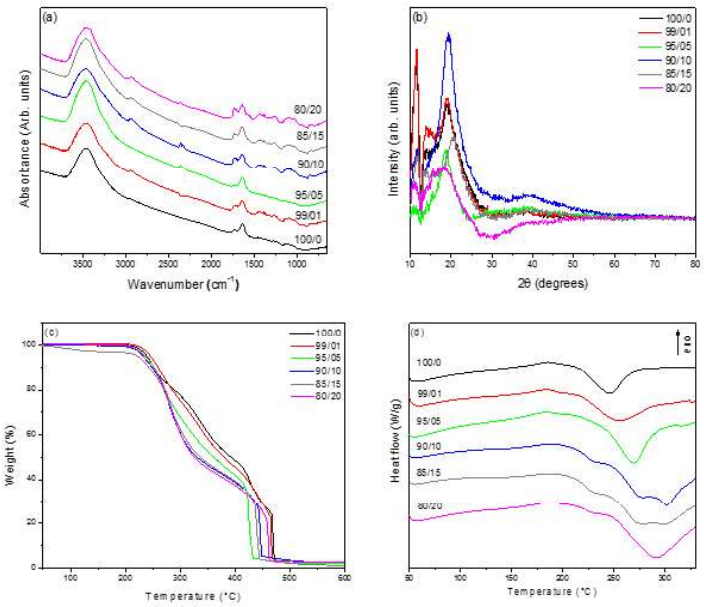

Figure 1. **(a)** ATR/FTIR spectra; **(b)** XRD diffractograms; **(c)** TG and **(d)** DSC curves, obtained for PVA/CS fibers.

Table 1. Crystalline peak center position (2θ); percent crystallinity (X_c%); melting temperature (T_m), and contact angle, measured for PVA/CS fibers.

	Fibers			
	2θ	**X_c (%)**	**T_m (°C)**	**contact angle (degree)**
100/0	19.1	74.1	246	104.5 ± 2.4
99/01	18.8	74.4	255	92.7 ± 7.7
95/05	18.8	59.6	269	92.7 ± 4.3
90/10	19.2	69.9	275	95.7 ± 1.0
85/15	20.5	78.6	275	95.9 ± 1.2
80/20	18.5	59.3	292	96.0 ± 7.6

Fig 1(b) shows X-ray diffractograms obtained for PVA/CS fibers. PVA exhibits a more intense peak centered at 2θ= 19.1°, corresponding to (101) crystal plane [14], and a halo at 40.0° belong to (111) crystal plane, demonstrating its semi-crystalline structure. PVA/CS blends showed smoothly deviations in Bragg angles and lower crystallinity than pure PVA (**Table 1**), indicating that PVA and CS probably have interactions that affect the structural arrangement of polymer chains.

Fig 1(c) shows TG curves obtained for PVA/CS fibers. The thermal degradation of pure PVA occurs in three steps, and is caused by the water evaporation and polymer chains thermal degradation [15]. PVA/CS fibers showed behaviour similar to pure PVA, however the mains step of thermal degradation, between approximately 250-400 °C, was slightly shifted to lower temperatures. **Fig 1(d)** shows DSC curves of PVA/CS fibers, which exhibit a widening in the melting peak with increasing CS contents in the blends. Melting temperatures (T_m) presented in **Table 1** demonstrate an increase in T_m for all PVA/CS blends compared to pure PVA, probably due to strong intermolecular hydrogen bonding interactions between PVA and CS, that can restrict the flexibility of PVA chain, requiring more energy for PVA/CS blends melting [16] and due to the T_m of crystalline domains of CS, since CS is a semi-crystalline polymer.

SEM images obtained from PVA/CS fibers (**Fig. 2)** show elongated and uniform nanofibers with regular arrangement (beads-free) until 15% CS. Considering that all images are obtained with the same magnification, it is noted that the average diameter of the nanofibers

decrease with the increase of CS content. The contact angle estimated to the fibers (**Table 1**) varied from 104.5 ± 2.4 (100/0) to 92.7 ± 4.3 (99/01 and 95/05), demonstrating that the presence of CS in PVA matrix slightly decreases the hydrophobic character of fiber surfaces, enhancing its characteristics for applications as scaffolds in tissue engineering.

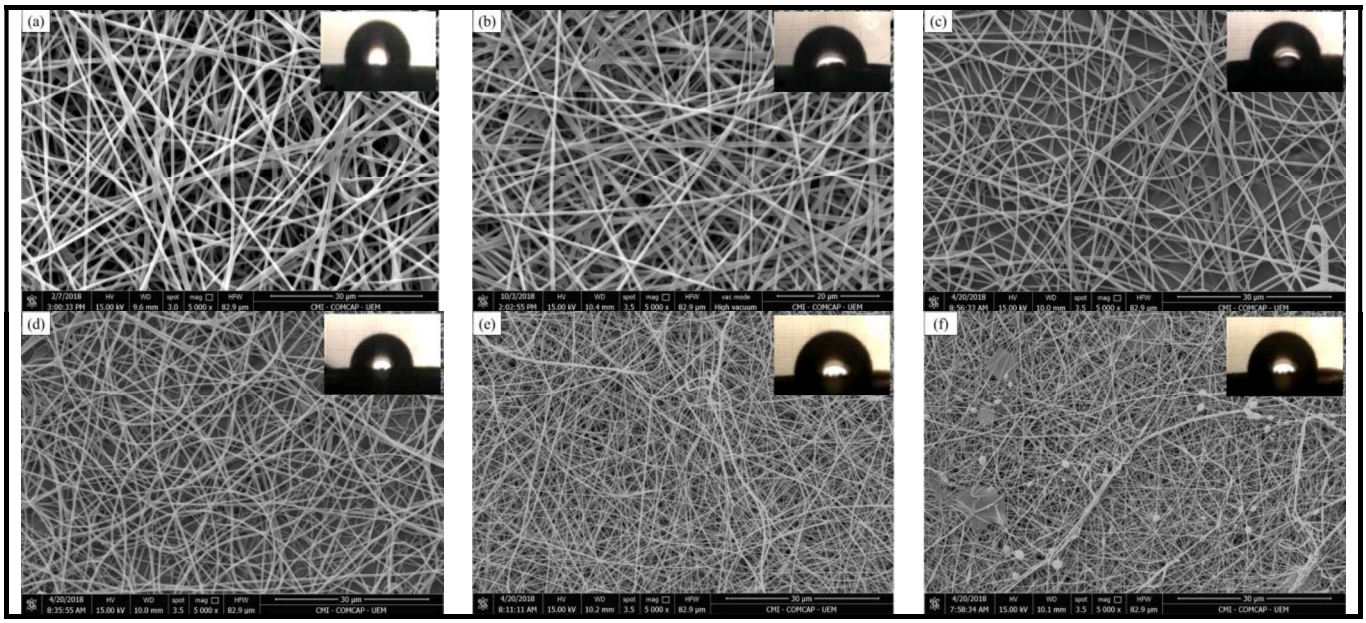

Figure 2. SEM micrographs of PVA/CS fiber surfaces with different compositions: (a) 100/0, (b) 99/01, (c) 95/05, (d) 90/10, (e) 85/15 and (f) 80/20. Magnification 5000x and scale bar 30 μm. The insets show the corresponding contact angle measurements on the surfaces.

The antibacterial efficacy of PVA/CS fibers against *E. Coli* are show in **Fig. 3(a)** and **(b)**, and against *S. Aureus* in **Fig. 3(c)** and **(d)**. It is observed a narrow inhibitory zone around all PVA/CS fibers, especially for 95/05 sample against *S. Aureus*. This antibacterial action of PVA/CS fibers is assigned to Chitosan, which has a well-established antimicrobial activity in the literature [5]. The antibacterial activity of CS is attributed to deleterious interaction with protonated amino groups of CS with the negative charges at bacteria surface [4], that decrease the bacterium membrane permeability, resulting in inhibition of the growth bacterial [2]. The *in-vitro* cytotoxicity of PVA/CS fibers was evaluated for fibroblast cells by indirect MTT assay (**Fig. 3(e)),** and the results indicated a cell viability between 78 and 100% compared to the control, demonstrating that our PVA/CS fibers are not cytotoxic for healthy fibroblast cells.

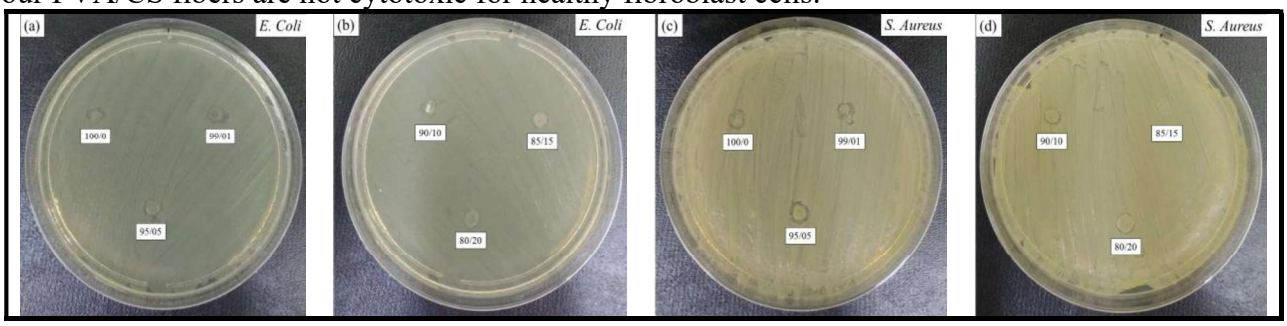

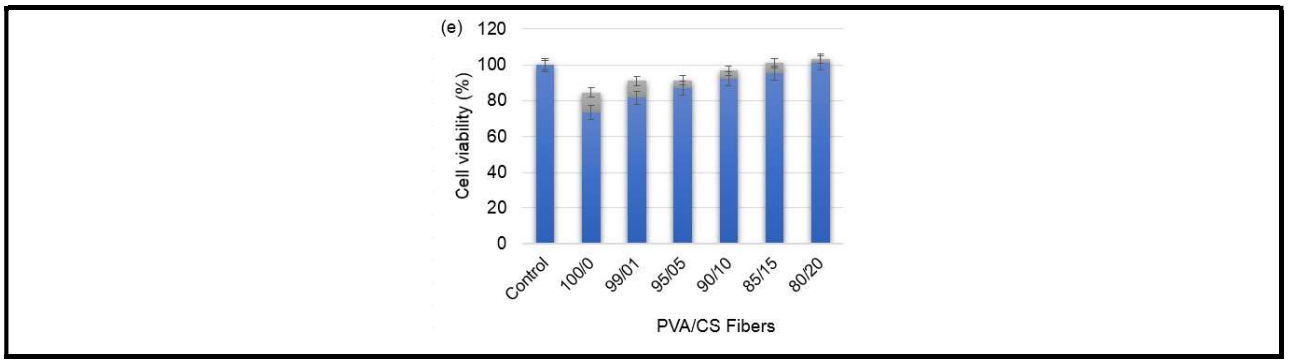

Figure 3. Images of agar plates and inhibition zone for (a) and (b) *E. Coli*; (c) and (d) *S. Aureus,* both in contact with PVA/CS fibers. (e) Fibroblast cells viability by MTT assay in presence of PVA/CS fibers after 24 hours of incubation.

Conclusions

PVA/CS fibers with different CS contents were successfully prepared by electrospinning method. The results indicated a good interfacial adhesion, and the presence of intermolecular interactions between two polymers in the blends, beyond uniform distribution of CS into PVA matrix. In addition, it we verified that the melting temperature of PVA in the blends was affected by presence of CS. PVA/CS exhibited elongated, continuous and uniform nanofibers until 15% of CS. Contact angles measure on fiber surfaces demonstrated the hydrophobic character of the fibers, required for use as scaffolds. PVA/CS fibers showed potential antibacterial against gram-negative and gram-positive bacteria, and does not show any cytotoxicity for health fibroblast cells, being promising materials to be used as scaffolds in tissue engineering.

Acknowledgements

This study was financially supported by CNPq (Processes n. 405381/2016-6 and n. 302503/2021-6), and CAPES agency for the PhD fellowship destinated to J. L. Andrade. The authors are grateful to "COMCAP/UEM" for supplying some equipments, UTFPR campi Campo Mourão by financial support in the participation of the congress, UTFPR campi Medianeira and Londrina by TGA, DSC and XRD analysis, and to Professor Dr. Elza Kimura from Department of Pharmacy of UEM university for her cooperation with the cell viability tests.

References

1. *Encyclopedia of Polymer Science & Technology*, John Wiley & Sons, 1969; v. 14, 149-199.
2. G. Dudek; R. Turczyn; K. Konieczny. Separation and Purification Technology 2020, 234, 116094.
3. J. Sriupayo et al. Polymer 2005, 46, 5637-5644.
4. E. F. Reis et al. Materials Research 2006, 9, 185-191.
5. G. Attia; M. F. H. A. El-kader. International Journal of Eletrochemical Science 2013, 8, 5672-5687.
6. S. Sheik et al. International Journal of Biological Macromolecules 2018, 116, 45-53.
7. H. Abral, et al. Journal of Materials Research and Technology 2020, 9, 2477-2486.
8. Y. Tsuchiya; K. Sumi. Journal of Polymer Science Part A-1: Polymer Chemistry 1969, 7, 3151-3158.
9. A. C. Alavarse et al. Materials Science and Engineering C 2017, 77, 271-281.
10. X. Zhang, et al. International Journal of Biological Macromolecules 2020, 142, 551-558.
11. I. S. Elashmawi; A. A. Menazea. Journal of Materials Research and Technology 2019, 8, 1944-1951.
12. H. LEE et al. Carbohydrate Polymers 2020, 232, 115771.
13. A. El-shamy; H. S. Zayied. Synthetic Metals 2020, 259, 116218.
14. S. Ram; T. K. Mandal. Chemical Physics 2004, 303, 121-128.
15. S. Kumar et al. Journal of Applied Polymer Science 2009, 115, 3056-3062.
16. S. Kumar et al. Carbohydrate Polymers 2019, 205, 559-54.

ROTARY JET SPUN MEMBRANE BASED ON POLY(E-CAPROLACTONE), HYDROXYAPATHITE AND SILVER NANOPARTICLES

Gabriella Monteiro Alves[1] *, Daniel Komatsu[2], Cecília A. C. Zavaglia[3], Felipe Zavaglia[3], Cleudmar Amaral de Araújo[4], Stella Aparecida de Andrade Pinto[5,6], Marco V. Chaud[7], Eliana A. R. Duek[1,2,3]

1- Federal University of São Carlos (UFSCar), São Carlos, SP, Brazil
2- Pontifical Catholic University of São Paulo (PUC), Sorocaba, SP, Brazil
3- State University of Campinas (UNICAMP), Campinas, SP, Brazil
4- Federal University of Uberlândia, Center for Exact Sciences and Technology, Center for Projects and Mechanical Systems, Uberlândia, MG, Brazil
5- Faculdade São Leopoldo Mandic, Campinas, SP, Brazil
6- Hermínio Ometto Foundation (FHO), Araras, SP, Brazil
7- Laboratory of Biomaterials and Nanotechnology - UNISO. Sorocaba, SP, Brazil

E-mail: gabriellamontalves@gmail.com

Abstract

In this study, a membrane was obtained based on Poly(e-caprolactone) (PCL), Hydroxyapatite (HAp), and Silver Nanoparticles (AgNP). It was characterized using Fourier Transform Infrared Spectroscopy (FTIR) and Scanning Electron Microscopy (SEM). In the FTIR spectrum of the PCL+AgNP membrane, it was not possible to observe the characteristic absorption band of AgNP. This could be due to the low concentration of AgNP that was impregnated on the surface of the membrane. In the micrograph, it is possible to observe that the blasting of AgNP onto the membrane surface did not alter the morphology of the membranes.

Keywords: *Membrane, Rotary jet spinning, Poly(e-caprolactone), Hydroxyapatite and Silver Nanoparticle.*

Fundings: Conselho Nacional de Desenvolvimento Científico e Tecnológico (CNPq).

Introduction

Polymers are excellent candidates for the development of a membrane with bactericidal/virucidal characteristics. Poly(e-caprolactone) (PCL) has properties that favor the use of the physical technique (Rotary jet spinning) to obtain polymeric fibers [3-6]. Rotary jet spinning is a physical technique for obtaining polymeric fibers in micrometric and nanometric scales. This technique stands out as an alternative to electrospinning, for obtaining fibers without depending on the conductivity of the solution. So, it is a versatile technique where polymeric emulsions or suspensions are used. Furthermore, rotary jet spinning technique presents a higher production rate in relation to the electrospinning [2-4]. Hydroxyapatite (HAp) has been widely used as a biocompatible ceramic in many areas of medicine, but mainly for contact with bone tissue, due to its resemblance to mineral bone. Finally, to add bactericidal characteristics to rotary jet spun membrane, Silver Nanoparticle (AgNP) was sputtering on the rotary jet spun membrane surface [8-9].

Experimental

The PCL solution was prepared adding 3g of PCL in 16 ml of chloroform. After PCL solubilization was added 1%, 2%, 4% and 8% of HAp (Hap weight/PCL weight) and the PCL membranes were obtained by the Rotary jet spinning. The solutions were poured into the reservoir and kept rotating at 3,500 rpm. After obtaining the rotary jet spun membranes, AgNP was sputtered on its surface using the spray method. Subsequently, the samples were submitted to FTIR and SEM

analyses. In the FTIR analysis, the samples of rotospun PCL, pure hydroxyapatite and silver nanoparticle were analyzed in a Spectrum 65 model spectrophotometer (Perkin Elmer), in ATR module, each sample was scanned 64 times in the absorption spectrum of 4500 - 500 cm $^{-1}$. Scanning electron microscopy (SEM) was performed on the fiber surface. The images were taken using a JEOL electronic microscope, model JSM – IT 200. A voltage of 3.0 kV was used.

Results and Discussion

The Fig. 1 illustrates the FTIR spectra of rotary jet spinning membrane with different concentrations of HAp and AgNP. The sample of pure PCL membrane shows absorption band at 2940 cm^{-1} and 2860 cm^{-1} corresponding to the asymmetric and symmetric stretching vibrations of the CH_2 group, respectively. The absorption band at 1720 cm^{-1} corresponds to the stretching vibration of the carboxylic bond (–C=O). The absorption band at 1240 cm^{-1} corresponds to asymmetrical stretching of the C–O–C bond the absorption band at 1170 cm^{-1} corresponds to symmetrical stretching of the C–O–C bond. Furthermore, the bands at 1460 cm^{-1} and 1370 cm^{-1} are due to –CH bending of $–CH_3$ (symmetrical) and bending vibrations in the OH, respectively.

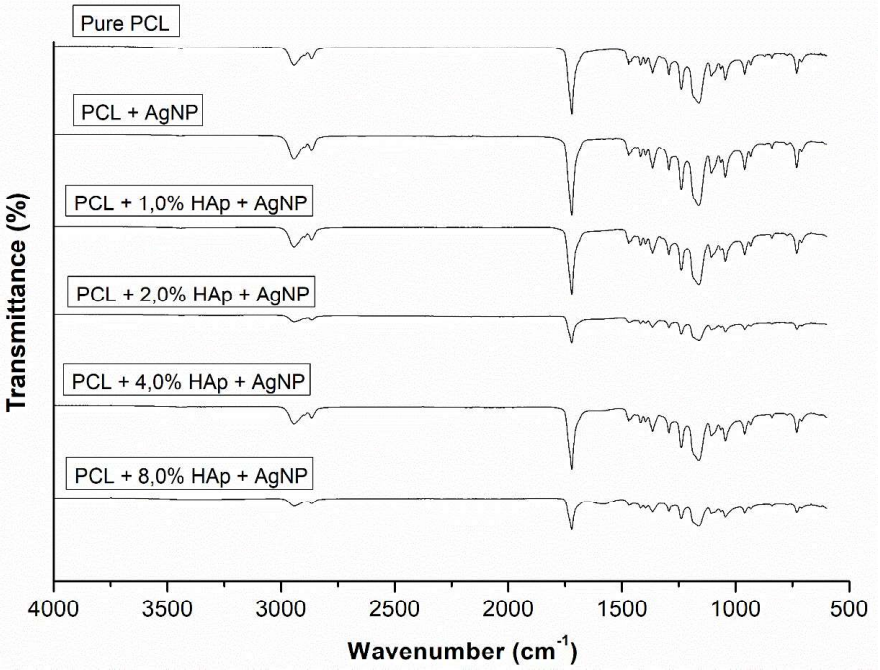

Fig. 1. FTIR spectra of rotary jet spinning membrane with different concentrations of HAp and AgNP.

After impregnating AgNP on the surface of PCL+HAp membranes, the spectra showed changes in absorption band intensities. In this case, it was observed that the absorption band at 2946 cm^{-1} (asymmetrical stretching of the CH_2 group) and 2863 cm^{-1} (at the symmetrical stretching of the CH_2 group) showed a reduction in intensity. In addition to these, the absorption band at 1726 cm^{-1} (carboxylic bond stretching (–C=O)) and 1167 cm^{-1} (symmetrical C–O–C bond stretching) also showed a reduction in intensity. Thus, the reduction in the intensity of the absorption band may be related to the change in the vibration profile of these bonds, due to the presence of AgNP.

The Fig. 2 shows SEM images of rotary jet spun membranes. In 43x increase, was possible to observe an enlargement along the wire, in the oval shape, is observed for all samples. With increasing the concentration of HAp, the amount of this oval shape in the rotary jet spun membranes increases. This could happen due to the difficulty of polymeric chains to flow during the rotary jet spinning process, since the presence of HAp preventing the sliding of one polymer chain over another when stretched at the exit of the capillary orifice as a jet. In 250x increase, it is possible to observe that the increase in the concentration of HAp makes the surface of the fiber rougher and with a greater presence of holes. In this case, during the exit of the PCL solution from the capillary orifice the HAp particles can pierce the polymer surface and lodges inside the formed wire. After spraying up the AgNP on the surface of rotary jet spun membrane, the presence of AgNP does not change the

morphology of membranes (PCL+HAp).

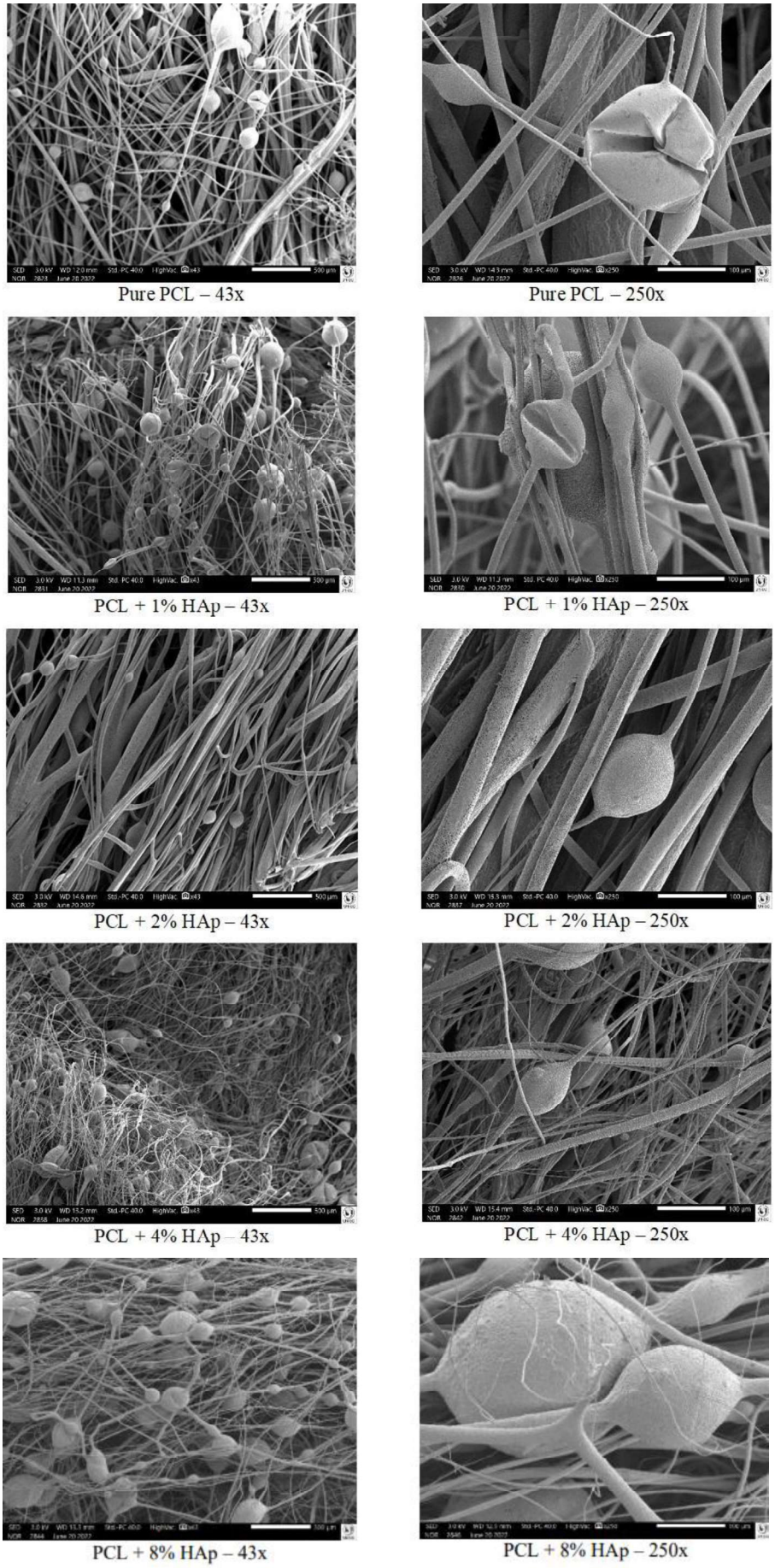

Fig. 2. SEM images of rotary jet spun membranes.

Conclusions

The results showed low interaction between the PCL and HAp. After AgNP was sputtered on the rotary jet spun membrane surface (PCL+HAp), again low interaction between the PCL, AgNP and HAp chains is observed. SEM images showed that the presence of HAp makes the surface of the fiber rougher and with a greater hole than pure PCL membrane.

Acknowledgements

To CNPq for granting the scientific initiation scholarship.

References

1. AHMAD, A.; MUKHERJEE, P.; SENAPATI, S.; MANDAL, D.; KHAN, M. I.; SASTRY, M. Extracellular biosynthesis of silver nanoparticles using the fungus Fusarium oxysporum. Colloids and Surfaces B: Biointerfaces, v. 28, p. 313–318, 2003. https://doi.org/10.1016/S0927-7765(02)00174-1.

2. ANDRADE, P. F. Preparação e caracterização de nanopartículas de prata e de nanocompósitos poliméricos antimicrobianos. 2013. 182 f. Tese (Doutorado em ciências) – Instituto de Química, Universidade Estadual de Campinas, Campinas, 2013.

3. BADROSSAMAY a,b,1, Engineering hybrid polymer-protein super-aligned nanofibers via rotary jet spinning. Biomaterials, v. 35, n. 10, p. 3188–3197, 2014. https://doi.org/10.1016/j.biomaterials.2013.12.072.

4. BADROSSAMAY, M. R. *et al*., Nanofiber Assembly by Rotary Jet-Spinning. Nationales Institutes of health, v. 86, n. 3, p. 2257–2261, 2010. https://doi.org/10.1021/nl101355x.

5. HU, J. *et al*., Drug-loaded emulsion electrospun nanofibers: Characterization, drug release and in vitro biocompatibility. RSC Advances, v. 5, n. 121, p. 100256– 100267, 2015. https://doi.org/10.1039/C5RA18535A.

6. HUSSEINY, S. M.; SALAH, T. A.; ANTER, H. A. Biosynthesis of size-controlled silver nanoparticles by Fusarium oxysporum, their antibacterial and antitumor activities. Beni-Suef University Journal of Basic and Applied Sciences, v. 4, n. 3, p. 225–231, 2015. https://doi.org/10.1016/j.bjbas.2015.07.004.

7. KAUR, A; KUMAR, R. Enhanced bactericidal efficacy of polymer stabilized silver nanoparticles in conjugation with different classes of antibiotics. RSC Advances, v. 9, p. 1095-1105, 2019. https://doi.org/10.1039/C8RA07980C.

8. KHARAGHANI *et al*., Electrospun antibacterial polyacrylonitrile nanofiber membranes functionalized with silver nanoparticles by a facile wetting method. European Polymer Journal, v. 108, p. 69-75, 2018. https://doi.org/10.1016/j.eurpolymj.2018.08.021.

WET-SPUN FILAMENTS BASED ON ALGINATE AND CHITOSAN WITH DRUG RELEASE

Lucas S. Silva[1] and Andrea C. K. Bierhalz[1]*

1 – Department of Textile Engineering, Federal University of Santa Catarina (UFSC), Santa Catarina, SC, Brazil
andrea.krause@ufsc.br

Abstract – Natural polymers such as alginate and chitosan has received increased interest for biomedical applications because of its biodegradability, biocompatibility, and non-toxicity. This study aimed to develop alginate filaments, through the wet spinning technique using coagulation bath containing calcium chloride at concentrations of 10% (w/v). After spinning process, the filaments were coated with a chitosan solution at a concentration of 2.5% (w/v). Sodium diclofenac (SD) was incorporated in the alginate matrix before coating or in the chitosan coating. The morphology of the filaments was more homogeneous in the presence of the chitosan coating and with SD incorporated in the chitosan. The water absorption capacity increased in the presence of coating, but the mass loss in 7 and 14 days was lower than filament without coating. The release kinetic in water demonstrated that the incorporation of the SD in alginate matrix before coating results in a higher amount of SD released and that this takes longer to reach equilibrium.
Keywords: *Wet spinning, medical textiles, drug release, biopolymers.*

Introduction

Since ancient Egypt, the most used method to unite edges of wounds caused by trauma or surgical incisions is a suture. Tendons, hair, intestine of animals, and natural fibers such as silk and linen were used. Currently, a large number of materials for sutures are available, with a wide range of characteristics [1].

Suture materials are classified mainly based on two factors: according to degradability into absorbable or non-absorbable, and according to their source into natural or synthetic. The sutures can also be coated, dyed, and structured in monofilament or multifilament [2].

Absorbable sutures are used for invasive sutures and are characterized by gradually losing their resistance until completely absorbed by the body. Absorbable suture of catgut, for example, is made from the sheep's intestine and has been associated with hypersensitivity reactions and infections [3]. Considering that suture materials must be biocompatible, biodegradable, and induce a minimal inflammatory response, polymers of natural origin are good candidates for their development.

Sodium alginate is a salt of alginic acid, a linear polysaccharide found in brown algae and produced by some species of bacteria. This polymer is composed of repeating units of α-L-guluronic acid (G) and β-D-mannuronic acid (M), linked by glycosidic bonds. One of the most important characteristics of alginate is its ability to form strong gels in the presence of divalent ions, such as calcium. Sodium alginate can maintain a physiologically moist environment and has been widely used for wound healing applications [4].

Another polymer of great interest for biomedical applications is chitosan. This polysaccharide is biocompatible, non-toxic, has antimicrobial properties, and a cationic character, giving it a wide range of applications involving the formation of polyelectrolyte complexes (PECs) with anionic polymers, such as alginate [5].

A strategy to obtain differentiated suture materials capable of effectively contributing to the regeneration process is the incorporation of therapeutic compounds in their structure, such as anti-inflammatory drugs and antibiotics. In this sense, the present study aimed to obtain wet-spun filaments based on alginate coated with chitosan and containing sodium diclofenac (SD). The drug SD was incorporated in alginate before chitosan coating and together with chitosan coating, and the kinetic release *in vitro*, morphology, and water absorption capacity and mass loss of these structures was compared.

Experimental

Materials

The polymers used to obtain the filaments were medium viscosity sodium alginate and chitosan obtained from shrimp shell with a degree of deacetylation ≥ 75% and molecular weight of 190-375 kDa, both from Sigma-Aldrich (USA). The crosslinking agent used in the coagulation bath was calcium chloride and the dissolution of chitosan was performed using acetic acid, both analytical grade products. As a drug model, was used the anti-inflammatory sodium diclofenac (Sigma-Aldrich, USA).

Production of filaments

To obtain the filaments, sodium alginate solution was initially prepared in deionized water at concentrations of 2% (w/v) under magnetic stirring at room temperature (25°C). Next, the coagulation bath solution was prepared, which consisted of dissolving calcium chloride in deionized water at a concentration of 10% (w/v). Using a Fresenius Kabi infusion pump model Injectomat Agilia (Germany) and a 60 mL syringe, the solution was extruded at a constant flow rate of 60 mL/h through a needle 2 mm in diameter and 4 mm in length, directly into the coagulation bath.

The cross-linked filaments were manually collected from the bath, extended around cylindrical support, and then washed with distilled water to remove excess calcium chloride. Subsequently, the filaments were extended with the aid of universal supports, where they remained for 24 hours until complete drying.

For chitosan coating, alginate filaments previously prepared and dried were completely immersed in 10 mL of a chitosan solution (2.5% w/v) dissolved in acetic acid (2% v/v). The filaments were removed from the bath and again extended to dry at room temperature.

The filaments containing the sodium diclofenac (SD) were obtained in two different ways: dispersed in alginate and dispersed in chitosan. For both cases, 25 mg of diclofenac per g of alginate was added to the polymeric solution. The drug was added to the sodium alginate solution before wet spinning and to the chitosan solution before the filament coating process. The processs for production of the filaments with SD was the same as already described.

Morphology

The morphology of the filament's surface was analyzed from images taken with field emission gun - scanning electron microscopes (FEG-SEM) (TermoFisher Scientific, model Quattro S).

Water absorption capacity and mass loss

The water absorption capacity of the filaments was determined, in triplicate, by immersing 5 cm long samples in 10 mL of deionized water at 25°C. After 24 hours, the filaments were removed and gently pressed between two sheets of filter paper to remove excess water, and then weighed for determining wet mass. The water absorption capacity (WAC) was obtained from Eq. 1, where M_w is the mass of wet sample and M_d is the mass of the sample before immersion (dry mass).

$$WAC = \frac{M_w - M_d}{M_d} \times 100 \qquad (1)$$

For mass loss determination, samples at the same conditions were kept immersed in water for 7 days and 14 days. After these periods, the samples were removed and dried in an oven at 100°C until constant mass. The mass loss (ML) was calculated from Eq. 2, where Mi is the mass before immersion and Mf is the mass after immersion and drying.

$$ML = \frac{M_i - M_f}{M_f} \times 100 \qquad (2)$$

Release kinetic

For the analysis of SD release, 20 cm long filaments samples were immersed in flasks containing 10 mL of deionized water, which were kept under stirring at 90 rpm and 37ºC in an orbital shaker. At time zero, the filaments were immersed in water, and after a predetermined time interval, an aliquot was removed from the flask for absorbance measure in the Micronal AJX-1900 spectrophotometer, at a wavelength of 275 nm. The aliquot was then placed back in the flask and the test was performed at different time intervals until equilibrium was reached.

Results and Discussion

Macroscopically, the filaments obtained by the wet spinning technique presented a homogeneous and uniform appearance. Under the processing conditions used, it was possible to continuously obtain 8 m of filament for each batch of 60 mL of polymeric solution. Regarding the microscopic aspect, the samples showed differences, as can be seen in the FEG-SEM images in Fig 1.

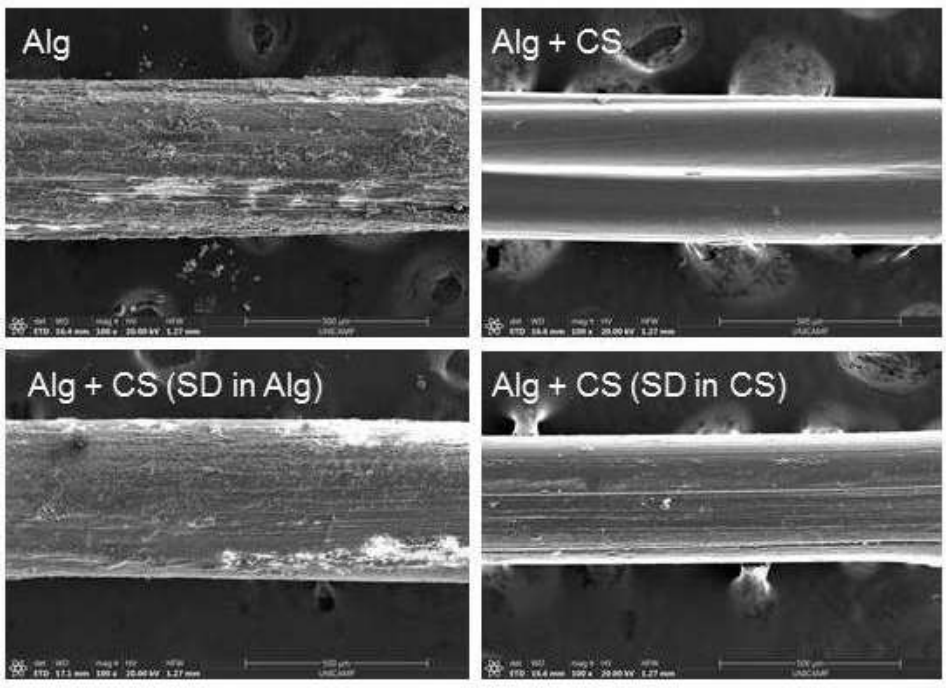

Figure 1 – FEG-SEM images of the filaments of alginate (Alg), alginate coated with chitosan (Alg + CS), and alginate coated with chitosan containing sodium diclofenac (SD) added in alginate and in CS.

The pure alginate filament (Alg) showed a surface without fractures or pores, but with the presence of particles attributed to calcium. Although an intensive washing was carried out after coagulation, an amount adhered to the surface remained. In the filament coated with chitosan (Alg + CS), the surface becomes smoother, and the calcium particles are no longer visible. For the filament containing the drug added to the alginate solution (SD in Alg), the presence of particles on the surface is also observed and can be attributed to the drug that may have diffused from the alginate core to the chitosan layer during the coating process. In image of the filament with the drug added in the chitosan solution (SD in CS), the heterogeneity is smaller. Although the same mass of drug was added to both solutions, only a few part of the chitosan solution is transformed into a coating, which justifies the smaller apparent amount of SD.

The results of water absorption capacity (WAC) (Table 1), indicated that, compared to the control filament (Alg), the presence of the chitosan coating promoted an increase in WAC. This result is due to the hydrophilicity of chitosan and the fact that the cross-linked alginate structure is in the inner part of the filament. The incorporation of the SD drug in the chitosan coating (SD in CS) showed an increase of the WAC in relation to the filament Alg + CS, which can be attributed to the reduction of interactions between chitosan and alginate because of the drug incorporation and also due to its hydrophilicity. For applications involving suture, low WAC values are desired because high swelling can compromise the mechanical resistance and security of the knots. In general, the results obtained are considered satisfactory. Azam et al. [6], for example, obtained water absorption values for alginate filaments (1 to 1.5%) in the order of 200%. In the study of Cruz [7], chitosan filaments with a concentration of 2.0% and 2.5% had a degree of swelling that varied between 350% and 550%

Table 1– Water absorption capacity (WAC) and mass loss (ML) of the filaments.

Sample	WAC (%)	ML 7 d (%)	ML 14 d (%)
Alg (control)	22.9 ± 3.9	46.0 ± 0.2	49.7 ± 0.9
Alg + CS	37.9 ± 4.8	24.9 ± 2.7	28.3 ± 1.1
Alg + CS (SD in Alg)	38.8 ± 0.8	30.6 ± 2.8	33.1 ± 2.1
Alg + CS (SD in CS)	55.2 ± 7.8	22.6 ± 2.4	24.1 ± 3.9

Filament mass loss was similar at 7 and 14 days. The highest mass loss was observed for the pure alginate filament. This result correlated well to the FEG-SEM images that indicate the presence of particles on the surface. These particles may have been removed when in contact with the water. Despite having higher WAC, the filaments coated with chitosan (Alg + CS) had a mass reduction of almost 50% compared to the uncoated sample. The formation of polyelectrolyte complexes between alginate and chitosan tend to form more stable structures in liquid media.

The release kinetics of SD from the filaments in contact with water at 37°C are presented in Fig 2.

When SD is dispersed in the chitosan coating (SD in CS), release equilibrium was reached in about 40 minutes, with a maximum release of 2.6 mg of the drug for each gram of filament. On the other hand, the filament with SD dispersed in alginate obtained a maximum release of 7.4 mg of the drug for each gram of filament. In addition to the greater mass of SD released, equilibrium was reached at around 70 minutes.

The slower release of the SD when it is present inside the fiber is already expected, since it has the outer layer of chitosan as a barrier, making it difficult to diffuse it in the medium. This type of filament can be used in applications where a more prolonged release is sought, aiming at the diffusion of the drug in the organism for a long period of time.

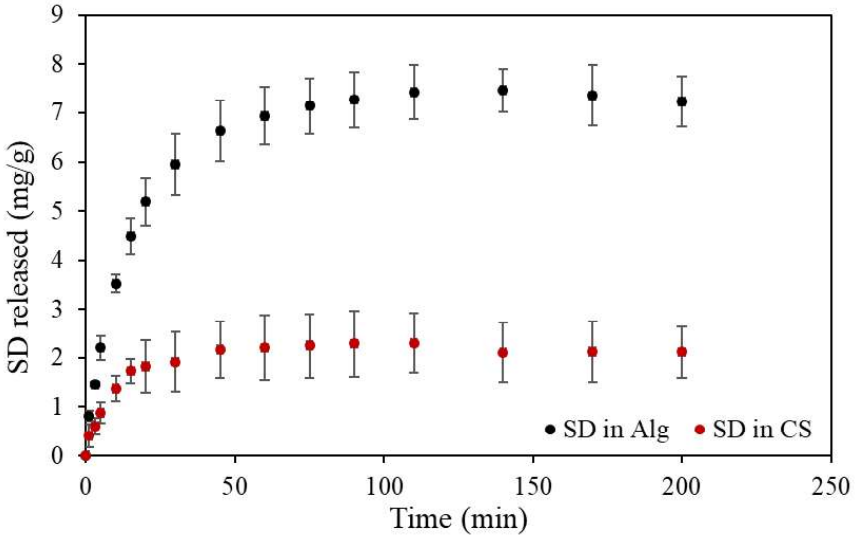

Figure 2 – FEG-SEM images of the filaments.

Conclusions

The study demonstrated that macroscopically uniform alginate filaments can be obtained by the wet spinning technique using a coagulation bath with $CaCl_2$. The microstructure of the filament becomes more homogeneous with the application of a chitosan coating. The presence of the coating promotes increased water absorption capacity and reduced mass loss. These results were satisfactory considering an application such as suture. The *in vitro* release assays at 37°C indicated that the incorporation of the SD drug in the alginate matrix with subsequent chitosan coating results in a higher amount released and a longer time to reach equilibrium. In general, alginate filaments coated with chitosan and containing SD in the inner part of the structure have potential for subsequent studies aiming at biomedical applications.

Acknowledgements

The authors thank the CAPES for financial support.

References

1. A. C. Medeiros; I. Araújo-Filho; M. D. F. Carvalho Journal of Surgical and Clinical Research 2016, 7, 11437. https://doi.org/10.20398/jscr.v7i2.11437.
2. A. Faris, L. Khalid, M.Hashim, S. Yaghi, T. Magde, W. Bouresly, Z. Hamdoon, A.T. Uthman, H. Marei, N. Al-Rawi International Dental Journal 2022, 72, 005. https://doi.org/10.1016/j.identj.2022.02.005.
3. V. Barbakadze; M. Merlani; L. Gogilashvili; L. Amiranashvili; A. Petrou; A. Geronikaki; A. Ćirić, J. Glamočlija; M. Soković Antibiotics 2023, 12, 12020285. https://doi.org/10.3390/antibiotics12020285.
4. A. Froelich; E. Jakubowska; M. Wojtyłko; B. Jadach; M. Gackowski; P. Gadziński; O. Napierała; Y. Ravliv; T. Osmałek Pharmaceutics 2023, 15, 1142. https://doi.org/10.3390/pharmaceutics15041142
5. P. S. Bakshi; D. Selvakumar; K. Kadirvelu; N. S. Kumar International Journal of Biological Macromolecules 2019, 150, 113. https://doi.org/10.1016/j.ijbiomac.2019.10.113.
6. F. Azam; F. Ahmad; S. Ahmad; M. S. Zafar; Z. Ulker Polymers 2022, 14, 14214707. https://doi.org/10.3390/polym14214707.
7. R. C. A. L. Cruz, Ph.D. Thesis, Universidade Federal de Campina Grande, 2016.

BIOPOLYMERIC FILMS FOR CONTROLLED RELEASE OF HYDROCORTISONE: POTENTIAL DEVICES FOR MANAGING CHRONIC SKIN CONDITIONS

Matheus S. Gularte[1]*, Guilherme T. Voss[2], Ethel A. Wilhelm[2] and André R. Fajardo[1]

1 – Centro de Ciências Químicas e Farmacêuticas (CCQFA), Federal University of Pelotas (UFPel), Pelotas, RS, Brazil. (*) omatheusgularte@gmail.com

2 – Centro de Ciências Químicas e Farmacêuticas (CCQFA), Federal University of Pelotas (UFPel), Pelotas, RS, Brazil

Abstract

Atopic dermatitis (AD) is the most common chronic inflammatory skin disease with nasty effects on the psychosocial well-being of patients. Typically, glucocorticoids, such as hydrocortisone (HC), are the primary pharmacologic drugs used to treat AD and its symptoms. However, long-term treatment with HC is often accompanied by severe adverse effects [1]. So, this study reports the encapsulation of HC in polymeric films based on gelatin (Gel) and gelatin/starch (Gel/St) and investigates their potential to treat and attenuate 2,4-Dinitrochlorobenzene (DNCB)-induced AD-like symptoms in BALB/c mice model. The prepared films were characterized by different techniques, which indicated that HC was physically entrapped into the polymer matrices. In vitro experiments indicate that the HC release process occurs in a controlled manner (up to 48 h) for both films. Regarding the in vivo experiments, HC-loaded films (Gel@HC and Gel/St@HC), unloaded films (Gel and Gel/St), and HC cream (1%) (as reference) were applied topically on the back of the DNCB-sensitized animals and skin severity scores and scratching behavior was determined. Ex-vivo experiments were done to quantify inflammatory and/or biochemical parameters. As assessed, the topical application of the biopolymeric films (loaded or not with HC) improved the inflammatory parameters, while a lower corticosterone level was observed for the animals treated with Gel and Gel@HC films. In summary, the HC-loaded films showed superior efficiency to treat/attenuating the analyzed parameter than the HC cream (1%). Further, no death or sign of toxicity was observed in animals exposed to HC-loaded films. Thus, the encapsulation of HC in biopolymeric films seems to be a promising alternative for the treatment of injuries caused by chronic skin diseases that require prolonged use of glucocorticoids [2].

References

[1] A. Heratizadeh; *Curr. Opin. Allergy Clinic. Immun.* 2016, 16, 458464.
[2] G. T. Voss; M. S. Gularte; R. L. de Oliveira; C. Luchese; A. R. Fajardo; E. A. Wilhelm; *Materials Science and Engineering: C* 2020, 114, 111074.

Keywords: *Hydrocortisone, Chronic skin disease, Gelatin, Starch, Drug delivery.*

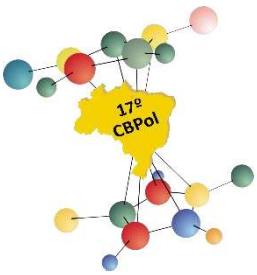

CERIUM OXIDE NANOPARTICLE DEPOSITION ON PLA/TCP SCAFFOLDS VIA ACTIVE SCREEN PLASMA

Luis Guilherme S. Rosa[1], Daniela Becker[1], Luis César Fontana[1], Eduardo H. Backes[2], Lidiane C. Costa[2], Luiz A. Pessan[2], Samarah V. Harb[2]

1 – Department of Materials Engineering, Santa Catarina State University (UDESC), Joinville, SC, Brazil
luis.rosa0521@edu.udesc.br
2 – Department of Materials Engineering (DEMa), Federal University of São Carlos (UFSCar), São Carlos, SP, Brazil

Abstract – PLA (polylactic acid) scaffolds present an alternative for metallic bone implants in the biomedical field, because of their biocompatibility and good mechanical properties. However, its low hydrophilicity and low surface energy make bone growth around the scaffold's implemented area difficult. To overcome such limitations, surface treatments like plasma can be applied. Plasma is a macroscopic neutral partially ionized gas, consisting of neutral particles, ions, and electrons moving randomly in space. It is possible to create a low-pressure plasma in laboratory by applying an external electric field to accelerate the electrons and consequently ionize the particles by electron-neutral collisions. Plasma surface modification is an efficient and low-pollutant technique alternative to traditional wet-chemical methods. Nevertheless, the high temperature of the plasma system can be harmful to PLA and other polymers. To avoid sample excessive heating, a configuration known as active screen is used, consisting of a metallic cage positioned inside the reactor, where the polymer sample is protected from the plasma's hotter regions. The present work aimed to successfully modify a PLA/β-TCP (Polylactic acid/ β-tricalcium phosphate) scaffold surface using active screen argon plasma to create reaction sites to further deposit cerium oxide nanoparticles onto its surface. These nanoparticles are known for their ability to scavenge reactive oxygen species that derive from metabolic reactions, which can interfere with bone cell growth around the scaffold. The scaffolds were exposed to the plasma and then submerged in an aqueous and ethanolic cerium oxide solution (0,1% m/v) for 10 minutes. Thermogravimetric analysis and Fourier-Transform Infrared (FTIR) were used to verify the presence of the nanoparticles. However, it was not possible to detect cerium oxide nanoparticles on the scaffold's surface, probably because of the solution's poor stability or the inability of the argon plasma to create reaction sites.

Fundings: The authors acknowledge the financial support provided by CAPES, FAPESC and FAPESP.

Keywords: *PLA scaffold, cerium oxide nanoparticles, plasma, active screen, surface modification.*

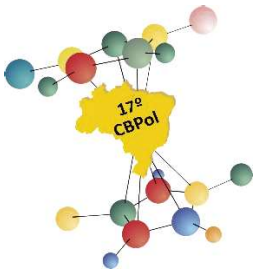

CHARACTERIZATION OF PBAT NANOFIBERS WITH ANTIMICROBIAL ESSENTIAL OIL PRODUCED BY SOLUTION BLOW SPINNING

Larissa K. M. Gomes[1*], Ermeson D. S. Silva[2] , Grazielle R. de Cerqueira[1], Michelle F. de Andrade[1], Gloria Maria Vinhas[1], Edvânia T. Teófilo[3], Carolina L. Morelli[1] and Yêda M. B. de Almeida[1]

1 – Science Materials Program, Federal University of Pernambuco (UFPE), Recife, PE, Brazil

**larissa.maia@ufpe.br*

2 – Department of Materials Engineering (DEMa), Federal University of São Carlos (UFSCar), São Carlos, SP, Brazil

3 – Materials Engineering Course, Federal University of Cariri, Juazeiro do Norte, CE, Brazil

Abstract – Solution Blow Spinning (SBS) is a promising technology for manufacturing polymeric fiber mats that can be used in various biomedical applications such as bioactive scaffolds, wound dressings, and new devices for controlled drug delivery [1,2,3]. Cinnamon essential oil (CE) derived from (C. Cassia) has demonstrated antimicrobial properties [4]. Thus, in this work, nanofiber mats of Poly (butylene adipate co-terephthalate) - (PBAT) incorporated with CE were produced by SBS, and their antimicrobial activity against *Escherichia coli* and *Staphylococcus aureus* was tested. The nanofiber mats were produced from solutions containing 15 and 20% w/v of PBAT pellets dissolved in chloroform. The effects of adding 20% of CE of PBAT weight on the fiber morphology and structural properties of the obtained mats were studied. The spun mats were characterized for their morphological properties (by SEM), thermal properties (by TGA and DSC), diffractometric properties (by XRD), spectroscopic properties (by FTIR), and antimicrobial properties (agar diffusion). SEM studies showed that most fibers had a cylindrical, smooth, and intertwined morphology for all compositions. Average nanofibers diameters were 242 ±51 and 314 ±67 nm for solutions with 15 and 20% w/v of pure PBAT, respectively. The diameter of the nanofibers increased after the addition of CE, being of 323±72 and 461±159 nm for solutions mentioned before. The addition of CE reduced the glass transition temperature (Tg), melting point (Tm), crystallization temperature (Tc) and crystallinity of PBAT because of its plasticizing effect. XRD studies showed that the incorporation of CE was not sufficient to induce any new phase formation in PBAT. FTIR and Principal Component Analysis (PCA) studies confirmed the presence of CE in the PBAT nanofibers. The nanofiber mats demonstrated antimicrobial action, with mean inhibition halos ranging from 2.6 to 2.1 ± 0.1 mm for E. coli and 1.4 to 1.6 ± 0.2 mm for S. aureus.

References

1..R. Liu; X. Xu; X. Zhuang; B. Cheng. *Carbohydrate Polymers*,101,2014, 1116-1121,https://doi.org/10.1016/j.carbpol.2013.10.056

2. E.L.G. Medeiros; A.L Braz.; I.J. Porto; A. Menner; A. Bismarck; A. R. Boccaccini;… J.J. Blaker. *ACS Biomater. Sci. Eng*., 2016, 2,1442–1449. https://doi.org/10.1021/acsbiomaterials.6b00072

3.M. A Souza; J. E. Oliveira; E.S. Medeiros; G.M. Glenn; L.H.C Mattoso. *J. Nanosci. Nanotecnologia*, 2015, 15, 5628–5636, https://doi.org/10.1166/jnn.2015.9692

4. D.F. Firmino, D.F;. T.T.A Cavalcante ; G. A. Gomes; N. C. S Firmino; L. D. Rosa ; M. G. De Carvalho , *5 Sci World J.* 2018;1-9. https://doi.org/10.1155/2018/7405736

Keywords: *SBS; Nanojfibers; PBAT; Cinnamomum cassia oil; Antimicrobial activity.*

CHITOSAN/Zn^{2+}-CURCUMIN OR Cu^{2+}-CURCUMIN ANTIMICROBIAL MEMBRANES FOR PHOTODYNAMIC THERAPY

Luana A. S. Braga[1*], Maria E. L. González[1] and Adhimar F. Oliveira[1]

1 – Institute of Physics and Chemistry, Federal University of Itajubá, Itajubá, MG, Brazil
luanasbraga@unifei.edu.br

Abstract – The antimicrobial activity of the curcumin associated to photodynamic therapy is a promising treatment to skin wounds. Metal curcumin complexes increase the antimicrobial properties and bioavailability of curcumin and decreased metal toxicity. This work aims to synthesize metal complexes of curcumin with zinc and copper as antimicrobial agent in chitosan membranes to photodynamic therapy. The synthesis was carried out in a ratio 1:1 curcumin: metal ion (Zn^{2+} and Cu^{2+}) at reflux for 1 hour at 80°C, using ethanol as solvent. The complexes were dried and analyzed by FTIR, UV-Vis spectroscopy, SEM-EDS, DSC, TGA and XRD techniques. In addition, a study of the antimicrobial activity associated with photodynamic therapy was carried out. Preliminary results indicate that the synthesis of Zn^{2+} and Cu^{2+} curcumin complexes was possible. The XRD (Fig 1a) shows comparatively the crystalline pattern of the complexes and of the curcumin. The MEV images in the Fig 1a, show the different morphology of Zn^{2+} and Cu^{2+} curcumin complexes.

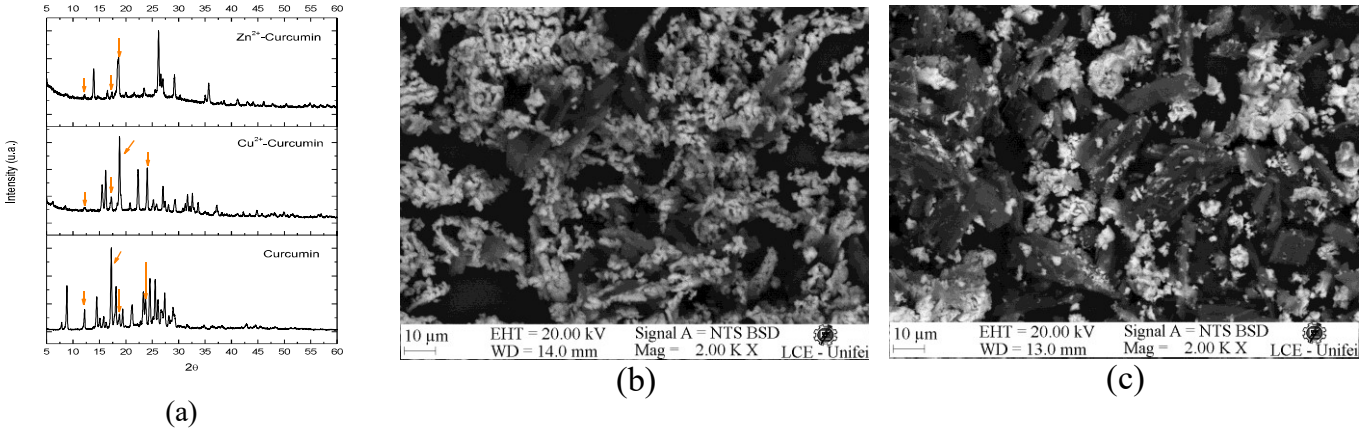

(a) (b) (c)

Figure 1. XDR pattern Curcumin and Zn^{2+}, Cu^{2+}-Curcumin complexes (a) MEV Cu^{2+}-Curcumin (b); Zn^{2+}-Curcumin (c)

References

1. C. P. B. Vieira; T. M. E. Araújo. Prevalence and factors associated with chronic wounds in older adults in primary care. *Rev Esc Enferm USP*. 2018; 52:e03415. DOI: http://dx.doi.org/10.1590/S1980-220X2017051303415.
2. K. I. Priyadarsini. The Chemistry of Curcumin: From Extraction to Therapeutic Agent. *Molecules* 2014, 19, 20091-20112; https://doi.org/10.3390/molecules191220091.
3. S. Prasad; D. DuBourdieu; A. Srivastava; P. Kumar; R. Lall. Metal–Curcumin Complexes in Therapeutics: An Approach to Enhance Pharmacological Effects of Curcumin. *Int. J. Mol. Sci.* 2021, 22, 7094. https://doi.org/10.3390/ijms22137094.

Keywords: *chitosan, curcumin complexes, antimicrobial activity, photodynamic therapy.*

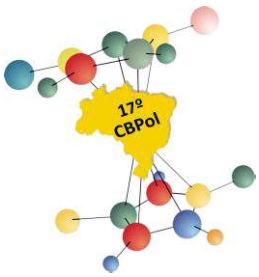

CONTROLLED RELEASE FROM POLY-3-HYDROXYALKANOATE MICROPARTICLES CONTAINING NANOMAGNETITE

Mayara F. Castro[1*], Rubén J. S. Rodriguez[1], Jose Gregório C. Gomez[2]
1 – State University of the North Fluminense Darcy Ribeiro (UENF), Campos dos Goytacazes, RJ, Brazil
mayarafreitascastro@gmail.com
2 – University of São Paulo (USP), São Paulo, SP, Brazil

Abstract - Controlled release in cancer treatments offers a promising approach to enhance the efficacy of medications, reduce side effects and personalize treatment. One of the challenges is the formulation of magneto-responsive materials designed for release an active component at a predictable programmed rate to achieve One of the challenges is the formulation of magneto-responsive materials designed to release an active component at a predictable programmed rate to achieve a great level of serum concentration. Nanomagnetite (Fe_3O_4) stands out as a notable choice for controlled release formulations due to its high saturation magnetization and biocompatibility. Various polymer components are used, including polyhydroxyalkanoates (PHAs), due to their biocompatibility and biodegradability. This research aimed the development and characterization of the formulations for the controlled release of an anticancer drug, etoposide, from poly-3-hydroxybutyrate (P(3HB)) and poly-3-hydroxybutyrate-*co*-3-hydroxyhexanoate (P(3HB-*co*-3HHx)) microparticles containing Fe_3O_4. Nanomagnetite was synthesized using the coprecipitation method and analyzed through X-Ray Diffraction (XRD) and Vibrating Sample Magnetometry (VSM), yielding superparamagnetic nanoparticles with an average crystal size of 10.09 nm and a saturation magnetization of 69.57 umu/g. The particles were formulated using the simple emulsion method, where the organic phase (PHAs, chloroform, nanomagnetite, and etoposide) was emulsified in an aqueous phase (polyvinyl alcohol solution) at a temperature of 10ºC, mechanical stirring at 200 rpm, and ultraturrax at 13,500 rpm. Scanning Electron Microscopy (SEM) images revealed that the formed particles were spherical with an average size of 3.4 µm (P(3HB)) and 8.23 µm (P(3HB-*co*-3HHx)). The systems utilizing P(3HB) and P(3HB-*co*-3HHx) exhibited a triggered release effect (24.1% and 17.9%, respectively) induced by an oscillating external magnetic field (0.2 T and 116 Hz) after 168 hours.

References

1. E. Kiliçay; M. Demirbilek; M. Türk; E. Güven; B. Hazer; E. B. Denkbas. *European Journal of Pharmaceutical Sciences* 2011, 44, 310-320. https://doi.org/10.1016/j.ejps.2011.08.013.
2. M. F. Castro; T. T. Mendonça; L. F. Silva; J. G. C. Gomez; R. J. S. Rodriguez. *Internation Journal of Biological Macromolecules* 2021, 166, 448-458. https://doi.org/10.1016/j.ijbiomac.2020.10.203
3. E. Erdal; D. Kavaz; M. Şam; M. Demirbilek; M. E. Demirbilek; N. Sağlam; E. B. Denkbaş. *Journal of Biomedical Nanotechnology* 2012, 8(5), 800-808. https://doi.org/10.1166/jbn.2012.1431
4. F. Fabris; K. H. Tu; C. A. Ross; W. C. Nunes. *Journal of Applied Physics.* 2019, 126, 173905. https://doi.org/10.1063/1.5125595.

Fundings: The authors thanks FAPERJ and CAPES for their financial support.

Keywords: *Vectorized and controlled release, Polyhydroxyalkanoates, etoposide, nanomagnetite*.

CONTROLLING THE DEGRADATION OF PLA/ZNO COMPOSITE THROUGH FILLER SURFACE MODIFICATION

Daniel Aparecido Lopes Vieira da Cunha[1], Daniela Becker[4], Felippe Migliato Marega[1], Larissa Aline Klok[4], Luiz Antonio Pessan[1,2], Teresa Tromm Steffen[4] and Lidiane Cristina Costa[1,2,3*]

1 – Federal University of São Carlos, Graduate Program in Materials Science and Engineering, São Carlos, SP, Brazil
danielcunha@estudante.ufscar.br
2 – Federal University of São Carlos, Department of Materials Engineering, São Carlos, SP, Brazil
3 – Center for Characterization and Development of Materials, Federal University of São Carlos (UFSCar), São Carlos, SP, Brazil
4 – Department of Mechanical Engineering, State University of Santa Catarina (UDESC), Joinville, SC, Brazil

The composites of poly(lactic acid) and zinc oxide (PLA/ZnO) are considered highly promising materials for the fabrication of scaffolds for tissue engineering. However, the presence of ZnO fillers promotes significant degradation of the polymeric matrix during processing, caused by the release of Zn^{+2} ions that attack the ester bond of PLA, leading to chain polymer breakage and degradation[2]. One alternative to reduce the release of Zn^{+2} ions is to perform surface modification of the filler. In this work, the surface of ZnO was modified with L-lactic acid via plasma and by physical mixing. A portion of plasma-functionalized fillers was vacuum-filtered in distilled water to assess the influence of unreacted monomers on polymer degradation. Composites were processed using an internal mixer coupled with a torque rheometer (175ºC/60 rpm/5 min). The degradation control was also analyzed through parallel plate rheometry using a permanent regime condition and thermogravimetry (TGA). The viscosity versus shear rate curves revealed the occurrence of control of PLA degradation, with an increase in viscosity of approximately 75% for plasma-modified PLA/ZnO over unmodified PLA/ZnO. Such results are similar to the data obtained by torque rheometry. Also, it was found that the excess L-lactic acid present in the composites with unwashed fillers promoted greater control of PLA degradation compared to those with washed fillers. PLA/ZnO composites modified by physical mixing showed degradation control comparable to that exhibited by plasma functionalized ones. TGA analysis showed that surface-modified PLA/ZnO composites exhibited higher decomposition onset temperatures than unmodified PLA/ZnO, providing evidence of increased thermal stability with treatment. We demonstrate that surface modification via plasma and by direct mixing of ZnO with L-lactic acid has potential for controlling the degradation of PLA. This enables the production of scaffolds with high structural quality, making them suitable for tissue engineering applications.

References

1. A. Kołodziejczak-Radzimska; T. Jesionowski. Zinc Oxide—From Synthesis to Application: A Review. Materials, 2014, 7, 2833-2881. https://doi.org/10.3390/ma7042833.
2. S. Ghaffari; M. Sarrafzadeh; Z. Fakhroueian; M. Khorramizadeh. Functionalization of ZnO nanoparticles by 3-mercaptopropionic acid for aqueous curcumin delivery: synthesis, characterization, and anticancer assessment. Materials Science and Engineering: C, 2017, 79, 465-472. https://doi.org/10.1016/j.msec.2017.05.065.

Fundings: This study was financed by the Coordenação de Aperfeiçoamento de Pessoal de Nível Superior (CAPES) – Finance Code 001; Conselho Nacional de Desenvolvimento Científico e Tecnológico (CNPq) – Finance Code 141052/2021-0; and Fundação de Amparo à Pesquisa do Estado de São Paulo (FAPESP) – Finance Code 19/27415-2.
Keywords: *PLA; Zinc Oxide; Scaffold; Plasma Surface Treatment; Surface Treatment.*

DEVELOPMENT AND CHARACTERIZATION OF 3D PRINTED BIOCOMPOSITES BASED ON PLA/PBAT/BIOSILICATE®

Fernanda A. Credo[1], Daniel A. L. V. Cunha[1], Rubens E. Santos[2], Murilo C. Crovace[1] and Lidiane C. Costa[1,2*]

1 – Department of Materials Engineering (DEMa), Federal University of São Carlos (UFSCar), São Carlos, SP, Brazil
fernanda.alice@estudante.ufscar.br
2 – Center for Characterization and Development of Materials (CCDM), Federal University of São Carlos (UFSCar), São Carlos, SP, Brazil

Polymeric composite materials with bioactive ceramic fillers have great potential for application in tissue engineering, especially in the manufacturing of scaffolds. Adding bioactive glass to the melt mixture can degrade Polylactic acid (PLA) due to the release of calcium ions. Strategies to prevent degradation include the investigation of polymeric blends. In this work, custom scaffolds were fabricated using additive manufacturing with the Ecovio® blend (45% PLA and 55% poly(butylene-adipate-co-terephthalate) (PBAT)) and Biosilicate® in different proportions (1% to 10%). The composites were obtained through a Haake internal mixer (170°C/60rpm/5min) and the formulations were 3D printed using a temperature reduction method to control the viscosity due to the filler addition. The processing temperature ranged from 165°C (pure Ecovio®) to 138°C (Ecovio® with 10% Biosilicate®). The printed scaffolds were analyzed by Scanning Electron Microscopy, revealing an adequate distribution of the bioactive filler. Measurements showed that the particles had average sizes of 23 to 27 μm, close to the incorporated size of 20 μm. However, samples with 5% and 10% bioactive glass showed larger clusters up to 120 μm. From the Differential Scanning Calorimetry curves, a high crystallinity of PLA was determined in the prints (11-24%), likely influenced by the thermal flow during processing and the decrease in molar mass. Furthermore, composites with the bioactive filler showed a glass transition around 50°C, characteristic of PLA, and another around 36°C, possibly indicating a transesterification reaction during degradation. Results from Thermogravimetric Analysis revealed that the addition of Biosilicate® to the PLA/PBAT blend reduced the initial decomposition temperature from 315°C to 225°C with 10% biofiller. The maximum decomposition temperature of PLA decreased by approximately 100°C with increasing filler content, mainly affecting the PLA phase of the blend.
In conclusion, the printed scaffolds can be successfully produced using the PLA/PBAT blend, effectively controlling the degradation of PLA.

References

1. Backes EH, Pires LdN, Costa LC, Passador FR, Pessan LA. Analysis of the Degradation During Melt Processing of PLA/Biosilicate® Composites. *Journal of Composites Science.* 2019; 3(2):52. https://doi.org/10.3390/jcs3020052.
2. Sanchez, L.C., Beatrice, C.A.G., Lotti, C. et al. Rheological approach for an additive manufacturing printer based on material extrusion. *Int J Adv Manuf Technol 105*, 2403–2414 (2019). https://doi.org/10.1007/s00170-019-04376-9.

Keywords: *Ecovio; Blend PLA/PBAT; Biosilicate®; 3D Printed; Scaffold.*

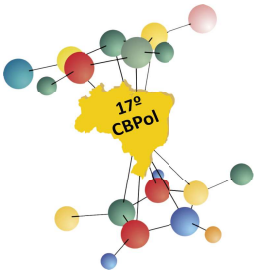

DEVELOPMENT OF BIOMATERIALS REINFORCED WITH BIOMIMETIC COMPONENTS AND SCAFFOLD PRODUCTION VIA 3D PRINTING APPLIED TO BONE TISSUE ENGINEERING

Luan Vieira Brito de Campos[1], Ana Lúcia Nazareth da Silva[2], Alexandre M. Rossi[3], Livia Rodrigues de Menezes[4] Eduardo La Marca da Silva[5] Renan Henriques Gonçalves de Almeida[6]

1 – Department Of Polymer Science And Technology - Institute Of Macromolecules Professora Eloisa Mano (IMA), Federal University of Rio de Janeiro (UFRJ), Rio de Janeiro, RJ, Brazil (luan.campos@ima.ufrj.br)
2 – Department Of Polymer Science And Technology - Institute Of Macromolecules Professora Eloisa Mano (IMA), Federal University of Rio de Janeiro (UFRJ), Rio de Janeiro, RJ, Brazil (ananazareth@ima.ufrj.br)
3 – Department of Condsensed Matter, Applied Physics and Nanoscience, Centro Brasileiro de Pesquisas Físicas (CBPF), Rio de Janeiro, RJ, Brazil (rossi@cbpf.br)
4 – Department Of Polymer Science And Technology - Institute Of Macromolecules Professora Eloisa Mano (IMA), Federal University of Rio de Janeiro (UFRJ), Rio de Janeiro, RJ, Brazil (liviarmenezes@ima.ufrj.br)
5 - Department Of Polymer Science And Technology - Institute Of Macromolecules Professora Eloisa Mano (IMA), Federal University of Rio de Janeiro (UFRJ), Rio de Janeiro, RJ, Brazil (eduardolamarca@eq.ufrj.br)
6 - Department Of Polymer Science And Technology - Institute Of Macromolecules Professora Eloisa Mano (IMA), Federal University of Rio de Janeiro (UFRJ), Rio de Janeiro, RJ, Brazil (eduardolamarca@eq.ufrj.br)

Abstract - Tissue engineering is a very promising area in the realization of successful treatments related to loss, defects and injuries in human body tissues. The methods and materials used today may not be efficient in achieving satisfactory clinical results due to limitations in mechanical properties, complex geometric shape, and scalability of the production process. In graft-based bone tissue engineering, a high-performance material is critical to the success of a tissue regeneration strategy, and the main trends in the field are to produce grafts with customized geometric shape, interconnected porous structure, with physical composition, chemistry and biomimetic components that enhance biological performance and regeneration of complex bone tissues. Three-dimensional (3D) printing can produce customized grafts and prostheses that are highly desirable for bone tissue engineering. The present work aims to compare different biocomposites using hydroxyapatite as biomimetic filler and their thermo-mechanical, rheological and biocompatibility characteristics. The methodology includes drying, weighing, extrusion, pelletization, filament production for 3D printing, and the fabrication of final parts based on 3D models of real-life injuries. The ongoing analysis plan encompasses a range of tests, including porosity assessment, density determination, molecular weight analysis, thermo-mechanical evaluations, melt flow index determination, SEM-EDS, cytotoxicity assessments, and both in vitro and in vivo biological studies.

References.

1. DUBINENKO, Gleb et al. Highly filled poly (l-lactic acid)/hydroxyapatite composite for 3D printing of personalized bone tissue engineering scaffolds. Journal of Applied Polymer Science, v. 138, n. 2, p. 49662, 2021.

2. AGUILAR-RABIELA, Arturo E. et al. Integration of Mesoporous Bioactive Glass Nanoparticles and Curcumin into PHBV Microspheres as Biocompatible Composite for Drug Delivery Applications. Molecules, v. 26, n. 11, p. 3177, 2021.

3. VYAS, Cian et al. 3D printing of silk microparticle reinforced polycaprolactone scaffolds for tissue engineering applications. Materials Science and Engineering: C, v. 118, p. 111433, 2021.

4. SADHASIVAM, Balaji; RAMAMOORTHY, Devi; DHAMODHARAN, Raghavachari. Scale-up of non-toxic poly (butylene adipate-co-terephthalate)-Chitin based nanocomposite articles by injection moulding and 3D printing. International Journal of Biological Macromolecules, v. 165, p. 3145-3155, 2020.

Fundings: Polimex Bioplásticos (www;polimex.eco.br)
Keywords: *Biocomposite, Scaffold, Bone tissue, Hydroxyapatite, Calcium phosphate, 3D printing*

DEVELOPMENT OF BIOPOLYMERIC SYSTEMS FOR ENCAPSULATION OF BARBATIMÃO EXTRACT

Jose Gregorio Fontainez Garrido[1], Fabiana Perrechil [2] and Mariana Agostini de Moraes [2]*

1 – Graduate Program in Engineering and Material Science, Federal University of São Paulo (UNIFESP), São Paulo, SP, Brazil.
2 – Department of Chemical Engineering, Federal University of São Paulo (UNIFESP), São Paulo, SP, Brazil.
mamoraes@unifesp.br

Abstract - Microencapsulation of bioactive compounds is a set of processes in which active substances are coated with a wall material, being protected from the external environment. It is a technology that can be applied in several areas, such as medicine, pharmaceuticals and cosmetics, and the study of the release profile of encapsulated compounds is essential to determine possible applications. Barbatimão is a native plant from the Brazilian Cerrado and its therapeutic use is widespread in popular medicine due to its astringent properties, being used as healing and anti-inflammatory agent. Barbatimão bark extracts (*Stryphnodendron adstringens*) can be encapsulated before application to protect the bioactive compounds and promote a gradual release over long periods of time. These systems can be prepared from natural raw materials and renewable sources, such as lipids and natural polymers, presenting biodegradable and biocompatible properties and showing a wide range of applications. Thus, the objective of this study is to develop biopolymeric systems for the encapsulation of barbatimão extract, in order to preserve its bioactive properties. Therefore, alginate microparticles produced from ionic gelation technique were developed and the methods of incorporation of barbatimão extract in the microparticles were evaluated. Two methods were used for barbatimão extract incorporation into the alginate microparticles: addition of the extract to the alginate solution before the preparation of the microparticles and adsorption of extract in the microparticles. The alginate microparticles exhibited a spherical shape and were dispersed individually, with a mean diameter of 36.57 ± 6.96 μm and an aspect ratio of 1.03 ± 0.23. The incorporation of the extract in the sodium alginate solution before preparing the microparticles showed low values of encapsulation efficiency, while the adsorption process led to higher values of incorporation of the extract into the microparticles. In this way, the methodology of incorporation of the extract by adsorption was chosen for the next steps of the project. Systems with greater encapsulation efficiency of the active compound will be applied to control the release of barbatimão extract.

References.

1. Q. Liu; H. Liu; Y. Fan *Microscopy Research and Technique* 2017, *80*, 312-320. https://doi.org/10.1002/jemt.22606.
2. K. Numata; S. Yamazaki; N. Naga *Biomacromolecules* 2012, *13,* 1383-1389. https://doi.org/10.1021/bm300089a.
3. A. C. Pássaro; T. Mozetic; J. E. Schmitz; I. J. Da Silva; T. D. Martins; I. T. L. Bresolin. *Chemical Product and Process Modeling* 2019, *14*, 12–16. https://doi.org/10.1515/cppm-2019-0077.

Fundings: FAPESP n°2018/15539-6 and CAPES finance code 001.

Keywords: *microparticles, barbatimão, biopolymers, bioactive compounds, controlled release.*

DEVELOPMENT OF CITRAL NANOEMULSIONS COATED WITH N-SUCCINYL CHITOSAN FOR THE TREATMENT OF ORAL MUCOSAL DISEASES

Layla Schlichting[1*], Rodrigo Henrique Saatkamp[1] and Alexandre Luis Parize[1]

1 – Department of Chemistry, Federal University of Santa Catarina (UFSC), Florianópolis, SC, Brazil
**layla.schlichting@posgrad.ufsc.br*

Abstract – Oral mucosal diseases are relatively common and are characterized by the appearance of blisters, ulcers or painful wounds in the oral cavity, affecting the quality of life of patients[1]. The use of biocompatible and biodegradable compounds such as chitosan (QTS) and citral, which have antimicrobial activity, has been reported in the literature for a wide range of applications, but they have limitations in terms of solubility in water. The aim of this study is to elaborate a nanoemulsion (NE) with citral, functionalized with N-succinyl chitosan (NQTS), with a focus on topical application in wounds in the oral mucosal region, where the polymer will act in the greater mucoadhesion of the system, enhancing the drug effect, accelerating the healing process. The o/w NEs were prepared with lecithin and P123 loaded with avocado oil and citral via the spontaneous emulsification technique[2]. NEs were coated with QTS and NQTS for comparison. The chemical modification of chitosan[3] was confirmed by Fourier Transform Infrared Spectroscopy with the appearance of a characteristic amide C=O band at 1655cm^{-1} and a secondary amide band at 1558cm^{-1}, in addition to the band at 1721 cm^{-1} associated with acid C=O carboxylic. Thermogravimetric analysis showed distinct degradation profiles, in addition to having more water loss for NQTS, indicating its greater affinity for water. By Differential Scanning Calorimetry, different glass transition temperatures were seen for QTS and NQTS. Elemental analysis data (CHN) suggest a degree of substitution greater than 50%. The result obtained with the dynamic light scattering technique showed that the methodology[2] using lecithin and P123 as surfactants resulted in a monodisperse system with a droplet size smaller than 200 nm for the NEs. The results show that a nanoemulsion loaded with citral coated with NQTS was obtained, which presents promising characteristics for the treatment of diseases in the oral mucosa.

References:

1. Gao, H.; Wu, N.; Wang, N.; Li, J.; Sun, J.; Peng, Q. *International Journal of Biological Macromolecules* 2022, 222, 3178–3194. https://doi.org/10.1016/j.ijbiomac.2022.10.090.
2. Bouchemal, K.; Briançon, S.; Perrier, E.; Fessi, H. *International Journal of Pharmaceutics* 2004, 280 (1), 241–251. https://doi.org/10.1016/j.ijpharm.2004.05.016.
3. Thao, N. T. T.; Wijerathna, H. M. S. M.; Kumar, R. S.; Choi, D.; Dananjaya, S. H. S.; Attanayake, A. P. *International Journal of Biological Macromolecules* 2021, *193*, 1823–1834. https://doi.org/10.1016/j.ijbiomac.2021.11.015.

Fundings: CNPQ/CAPES.
Keywords: *nanoemulsions, citral, chitosan, healing, oral mucosa.*

DEVELOPMENT OF CRYOGEL SYSTEMS FOR BIOMEDICAL APPLICATIOINS

Pedro Henrique Sá Alves[1]*, Beatriz Luci Fernandes[2] and Clayton Fernandes de Souza[1,2]

1 – School of Education and Humanities, Chemistry Undergraduate Course, Pontifícia Universidade Católica do Paraná (PUCPR), Curitiba, Paraná, Brazil

2 – Health Technology Graduate Program, Pontifícia Universidade Católica do Paraná (PUCPR), Curitiba, Paraná, Brazil

hdsa.pedro@gmail.com

The use of hydrocolloids to obtain three-dimensional systems has been gaining prominence in tissue engineering, generating substrates, such as scaffolds, with high surface area and adsorption. With advance of cell therapy, there are an increasing of studies related to produce and evaluate cell growing in materials like aerogels and cryogels, exploring these systems herewith new techniques, including 3D-bioprinting. To produce these systems, biopolymers, including polysaccharides and proteins, are the most common raw materials, capable to form viscous solutions until rigid hydrogels. Based on this context, this study aimed to develop systems based on fucogel-FC, gellan-GL, commercial gelatin-CG and hydrolyzed collagen-HC for 3D bioprinting and cryogels for biomedical applications. The hydrogel solutions were prepared in concentration 2wt% with different proportions of the biopolymers. Firstly, to investigate hydrogel behavior during bioprinting process, the flow behavior was simulated with the aid of the syringe, varying the internal diameter of the needle tip. In the second step, to produce the cryogel systems, the hydrogels were deposited in petri dishes, frozen and lyophilized. The materials were characterized by integrity after the printing flow, composition by infrared spectroscopy (FTIR), morphology by scanning electron microscopy (SEM) and stability in different pH. The results obtained with the simulated tests of extrusion in a 3D-bioprinter, was possible modulate the morphology of the hydrogels, maintaining the structural integrity, forming suitable supports for cell growth. By FTIR analysis, was observed different functional groups (-OH, -COOH, -NH, -COC) in structured scaffold. Additionally, the morphology of the cryogels systems showed micro-porosities between 70 and 80 μm with high heterogeneity and good stability in different pH media. The results of morphology, composition and stability, indicated that the hydrogel and cryogel has a high potential to be explored in different conditions for cell growth, thinking in biomedical applications.

References

1. E.B.Yahya; A. A. Amirul; A.K. H.P.S; N. G. Olaiya; M.O. Iqbal; F. Jummaat; A.S. A.K.; A.S. Adnan *Polymers* 2021, 13, 1612. https://doi.org/10.3390/polym13101612
2. J. Huang; J. Xiong; D. Wang; J. Zhang; L. Yang; S. Sun; Y. Liang. *Gels* **2021**, *7*, 144. https://doi.org/10.3390/gels7030144
3. A. Iglesias-Mejuto; C.A. García-González *Polymers* **2022**, *14*, 1211. https://doi.org/10.3390/polym14061211

Keywords: *Hydrogels, cryogel, 3D-bioprinting, polysaccharides, proteins.*

DEVELOPMENT OF MEMBRANES BASED ON KAPPA-CARRAGEENAN AND MICROFIBRILLATED CELLULOSE

Pedro Henrique de Sa Alves[1*], Beatriz Luci Fernandes[2] and Clayton Fernandes de Souza[1,2]

1 – School of Education and Humanities, Chemistry Undergraduate Course, Pontifícia Universidade Católica do Paraná (PUCPR), Curitiba, Paraná, Brazil

2 – Health Technology Graduate Program, Pontifícia Universidade Católica do Paraná (PUCPR), Curitiba, Paraná, Brazil

hdsa.pedro@gmail.com

Occlusive dressings are typically unicellular materials that provide a scaffold structure for tissue engineering. These supports can generate functional and bioactive surfaces with porous structures as well mechanical properties for healing process of the skin. Some biopolymers, e.g., the bacterial cellulose is extensive explored for this application. However, the BC works only a physical barrier of the injured surface, not avoiding totally against infections. Thus, inclusion of bioactive additives is interesting to effective healing process. Therefore, the aim of this work was incorporate on BC matrix, the kappa-carrageenan (KC), a natural polysaccharide extracted from red algae of the *Rodophyceae*, as bioactive additive to produce the scaffold system. To this, the BC was mechanically defibrillated and characterized whit Fourier Transform Infrared (FTIR). The purification of KC, 1g was suspended in 50mL phosphate buffer at 65ºC and 85ºC, stirred for 5h, elevated the temperature at 85ºC, and then centrifuged and precipitated with ethanol and dried in an oven at 25 ºC for 72h. After, the BC (0,4g) was dissolved in deionized water (20 mL) and stirred for 10 min, elevated the temperature at 80ºC and was added KC, the resulting solution was dried in a oven at 60 ºC for 48h. The BC and KC mixtures were prepared in the ratios of 1:1, 2:1, and 4:1, resulting in thicknesses between 0.07mm to 0.01mm, respectively. Morphologically, the composites of BC and KC showing a better uniformity compared to the control membrane with only BC. However, the inclusion of KC indicates less mesh like surface compared with BC membrane. The results showed the viability of production of BC and KC composites by casting method, allowing the inclusion of a bioactive biopolymers, such as Kappa-carrageenan, thinking to produce a biomaterial for biomedical field.

References

1. Edson Hipólito Júnior, Alan G. Gonçalves, Miguel D. Noseda, Maria Eugênia R. Duarte, Fábio S. Murakami, Diogo R.B. Ducatti, Semi-synthesis of N-alkyl-kappa-carrageenan derivatives and evaluation of their antibacterial activity, Carbohydrate Research, Volume 499, 2021, 108234, ISSN 0008-6215, https://doi.org/10.1016/j.carres.2021.108234.
2. Velásquez P, Montenegro G, Valenzuela LM, Giordano A, Cabrera-Barjas G, Martin Belloso O. k-carrageenan edible films for beef: Honey and bee pollen phenolic compounds improve their antioxidant capacity. Food Hydrocoll [Internet]. 2022;124:107250. Available from: https://www.sciencedirect.com/science/article/pii/S0268005X21006664

Keywords: *Kappa-carrageenan; Healing membranes; Bacterial cellulose;*

DEVELOPMENT OF PMMA-BASED BONE CEMENT LOADED WITH QUATERNIZED POLYETHYLENEIMINE (QPEI)

Carmen Raiza Aires Soares Preza[1]; Liliane Maria Ferrareso Lona[2]
1 – Department of Materials and Bioprocesses Engineering, Campinas State University (UNICAMP), São Paulo, SP, Brazil
raizaaires@hotmail.com
2 – Departamento de Processos Químicos (DPQ), Campinas State University (UNICAMP), São Paulo, SP, Brazil
liliane@feq.unicamp.br

Abstract - The prevalence of surgical site infections in hospital environments is consistently increasing (INPA, 2022). The use of PMMA-based bone cement for filling and stabilizing bone defects or fixing prostheses is a widely adopted practice in orthopedics. However, bone cement may carry a risk of infectious complications, leading to unfavorable clinical outcomes. Therefore, alternative approaches are being sought to minimize the spread of infectious agents. Biocidal polymers are polymeric materials that incorporate additives or chemical substances into their structure to prevent or inhibit the growth of microorganisms. Among these substances, quaternized polyethyleneimine (QPEI) stands out as a cationic polymer with excellent antimicrobial properties (Lan *et al*., 2019). QPEI is derived by quaternizing the amino groups of polyethyleneimine (PEI). The objective of this study is to develop a bone cement loaded with QPEI, with the aim of preventing bacterial colonization and reducing the incidence of surgical site infections and prosthesis-related complications. Bone cement formulations with the addition of QPEI were prepared and evaluated through chemical, mechanical, thermal, morphological, and biocide tests to assess the material's performance. Structural and chemical analysis of QPEI demonstrated its technological viability. The Br and I content obtained through X-ray fluorescence analysis confirms the functionalization with alkyl groups. Furthermore, the resistance to axial compression of the specimens was tested with varying concentrations of QPEI in the formulation, revealing that an increased amount of quaternized polyethyleneimine leads to a reduction in the material's compressive strength. The development of QPEI-loaded PMMA-based bone cements exhibited technological performance in accordance with normative standards.

References

1. Instituto Nacional De Pesquisas Da Amazônia. *Manaus: Editora INPA 2022*, 39 p.: il. color. ISBN: 978-65-5633-025-9.
2. Lan, T.; Guo, Q.; Shen, X. *Journal of Biomaterials Science 2019*, 30:14, 1243-1259. https://doi.org/10.1080/09205063.2019.1627650.

Keywords: *surgical site infections; PMMA-based bone cement; quaternized polyethyleneimine; antimicrobial properties; chemical composition*

DEVELOPMENT OF TPS/PVA/NCC FILMS FOR THE RELEASE OF COPPER OXIDE NANOPARTICLES - POTENTIAL APPLICATION AS TRANSDERMAL DRESSINGS

Amanda de S. M. de Freitas[1], Nathan K. Carvalho[1*], Marystela Ferreira[2] and Ana Paula Lemes[1]

1 – Institute of Science and Technology (ICT), Federal University of São Paulo (UNIFESP), São José do Campos, SP, Brazil
2 - Science and Technology Center for Sustainability (CCTS), Federal University of São Carlos (UFSCar), Sorocaba, SP, Brazil
*nathan.carvalho@live.com

Abstract - There is a constant search to create alternatives to replace traditional dressings by biodegradable materials[1]. Furthermore, it is desired that these materials present good performance properties, low cost, easy processing, and the possibility of controlled release of actives[2]. In this sense, transdermal dressings of thermoplastic starch (TPS) with different percentages (10, 20, 30 and 40%) of polyvinyl alcohol (PVA) and reinforced with 2.5; 5.0 and 10% of cellulose nanocrystals (NCC) were optimized by casting technique. The synthesis and characterization of copper oxide nanoparticles (NPCuO) was also carried out. The nanobiocomposites film with the best properties for application were additivated with NPCuO, aiming to study the controlled release of these nanoparticles by the dressing. The final material developed (T/P/10NCC/NPCuO) was extensively characterized, with measurements of thickness, swelling capacity in PBS buffer, tensile test. In addition, solubility, water vapor permeation, and the cytocompatibility of the developed films were studied. Results showed that the nanobiocomposites presented thickness of ± 0.097 mm, being suitable for application in dressings, which ranges from 0.05 to 0.1 mm[1]. The material also presented swelling capacity of approximately 249% in PBS buffer, allowing the absorption of wound exudates. The elongation at rupture of 16.53%, thus showing a flexibility that allows the application in articulable areas of the skin. Added to this, the film presented solubility in PBS of 25%, and water vapor permeability rate of 1.36 $g.mm^{-2}.kPa^{-1}.day^{-1}$, results within the expected standards of commercial dressings with capacity to release actives. Cytocompatibility tests proved that the material allows cell proliferation for up to 48 hours. Due to the characteristics of the optimized film, this was considered a promising material for application as a transdermal dressing.

References:
1. P.L. da Silva, A.M.M. Gomes, N.M.P.S. Ricardo, T.F. Machado, Quim. Nova 2016, 39, 450. http://dx.doi.org/10.5935/0100-4042.20160043.
2. A. Das, S. Bhattacharyya, R. Uppaluri, C. Das, Int. J. Biol. Macromol. 2020, 155, 260. https://doi.org/10.1016/j.ijbiomac.2020.03.185.

Fundings: This work was financed in part by the Coordination for the Improvement of Higher Education Personnel - Brazil (CAPES) - Financing Code 001. FAPESP projects 2019/15976-0 (APL) and 2020/12659-0 (MF). CNPq grants 313989/2018-4 (APL) and 301955/2019-0 (MF).
Keywords: *starch, cellulose nanocrystals, copper oxide nanoparticles, sustained release, transdermal dressings*

ENCAPSULATION OF INDOCYANINE GREEN PHOTOSENSITIZING AGENT IN POLYGLOBALIDE NANOPARTICLES FOR COMBINED CANCER PHOTOTHERAPY

Julia L. Oliveira[1], Tamara Agner[1], Claudia Sayer[1], Karina Cesca[1], Ana Paula I. S. Boemo[1]*

1 – Department of Chemical Engineering and Food Engineering, Federal University of Santa Catarina (UFSC), Florianópolis, SC, Brazil
ana_immich@ufsc.br

Abstract - Phototherapy has low invasiveness, insignificant toxicity, reduced side effects, and a lack of drug resistance in cancer treatments [1]. The encapsulation of photosensitizing agents is a useful tool to overcome some limitations since in addition to reducing the time that the photosensitizer takes to accumulate in the tumor [2], it also increases the accumulation power in strategic points of the cancer cell and presents greater penetration and retention in tumor tissue [3]. This work aims to encapsulate the hydrophilic photosensitizing agent Indocyanine Green (ICG) in polyglobalide (PGL) nanoparticles (NPs). PGL was synthesized via enzymatic polymerization (Novozym 435, Candida antarctica B lipase immobilized on porous support) in solution at 65ºC. The encapsulation method was the Double Emulsion solvent evaporation technique. The first emulsion (water-in-oil) was prepared by mixing 0.5mL of an aqueous ICG solution (2.5mg/mL) to the organic phase of PGL (1.01g PGL in 10.18mL of dichloromethane - DCM) under magnetic stirring, followed by ultrasound emulsification (VC-505 Ultrasonic Processor, Sonics Materials) at 70% amplitude for 5 min (10s on/ 5s off). This first emulsion was then added to 112mL of PVA aqueous solution (0.5 wt%) and emulsified by ultrasound at 70% amplitude for 12min (10s on/ 5s off) to form the second emulsion (water-in-oil-in-water). Then, the DCM was fully evaporated and the particle size and polydispersity index (PDI) of NPs were analyzed by Dynamic Light Scattering (Zetasizer Nano-S, Malvern Instruments). The Encapsulation Efficiency (EE) was determined by ultraviolet-visible spectroscopy (UV-Vis U-1900 Hitachi) from the non-encapsulated ICG in the supernatant. Different formulations and experimental conditions were evaluated, and in the optimal ones, NPs with less than 300nm and PDI < 0.2 (narrow size distribution) were obtained. The EE of ICG in PGL NPs was 87,68±0,01 %. Then, the double emulsion technique proved to be an efficient strategy to encapsulate ICG in PGL nanoparticles.

References

1. A. Boonman, M. Cuypers, G. Leusink, J. Naaldenberg, H. Bloemendal. *Lancet Oncol*, 2022, 23(4): e174-e183. https://doi.org/10.1016/S1470-2045(21)00694-X.
2. M. Patel, A. Prabhu. *Int J Pharm*. 2022, 25;618:121697. https://doi.org/10.1016/j.ijpharm.2022.121697.
3. J. . Vardy, A. Liew, A. Warby, A. Elder, I. Keshet, R. Devine, C. Ouliaris, C. Renton, M. Tattersall, H. Dhillon. *Support Care Cancer* 2022, 30(4):3503-3512. https://doi.org/10.1007/s00520-022-06804-1.

Fundings: The authors would like to thank the financial support provided by the Coordenação de Aperfeiçoamento de Pessoal de Nível Superior (CAPES) and the Conselho Nacional de Desenvolvimento Científico e Tecnológico (CNPq).

Keywords: *Polymeric Nanoparticles; Encapsulation; Cancer phototherapy.*

ENCAPSULATION OF PHOTOPROTECTIVE COMPOUNDS INTO STARCH PARTICLES

Letícia Miranda[1], Luciana Dutra[2*], Martina C. C. Pinto[2], Rafael C. Lima[1], Marcio Nele[1,2], José Carlos Pinto[1,2]

1 - Programa de Engenharia de Processos Químicos e Bioquímicos / EQ, Universidade Federal do Rio de Janeiro, Cidade Universitária, Rio de Janeiro, RJ, Brazil
2 - Programa de Engenharia Química, COPPE, Universidade Federal do Rio de Janeiro, Rio de Janeiro, RJ
ldutra@eq.ufrj.br

Abstract - Skin cancer is the most common of all cancers worldwide. In this way, it is mandatory to adopt an adequate routine for sun protection, including the use of sunscreen lotion. However, despite the proven effectiveness of numerous chemical filters, many of them are also known for their allergenic and carcinogenic potential effects, which may be mitigated by exploring some encapsulation routes. Thus, the present work describes the encapsulation of photoprotective actives on starch nanoparticles for cosmetic applications, exploring the in situ inverse miniemulsion technique. More specifically, this work evaluates the influence of such ultraviolet (UV) hydrophilic and hydrophobic filters (such as filtrasol and octocrylene) on the particle size distribution and morphology of starch beads. It also evaluates the encapsulation efficiency and the sun protection factor (SPF) of the loaded nanoparticles in sunscreen formulations. The studied UV filters did not affect the miniemulsion reticulation of starch chains, enabling the synthesis of distinct loaded nanoparticles. The addition of the filters shifted the particle size distribution to larger diameters, which is still acceptable for cosmetic formulations. Furthermore, starch latices were easily incorporated into sunscreen lotion formulations. The encapsulation efficiency and sun protection factors are still being evaluated. It was possible to observe that the filters were satisfactorily encapsulated by the in situ miniemulsion polymerization technique. Therefore, the use of in situ polymerization to produce starch nanoparticles loaded with UV filters is promising, presenting scientific, technological, and health relevance.

References

1. M. S. Chang, R. I. Hartman, N. Trepanowski, E. L. Giovannucci, H. Nan, X. Li, American Journal of Epidemiology 2022, 191, 10.
2. American Cancer Society, Key Statistics for Melanoma Skin Cancer, https://www.cancer.org/cancer/melanoma-skin-cancer/about/key-statistics.html, accessed: March, 2023.
3. J. D'Orazio, S. Jarrett, A. Amaro-Ortiz, T. Scott, Int J Mol Sci 2013, 14, 6.
4. INCA, "Câncer de pele não melanoma". Language: Portuguese, https://www.inca.gov.br/tipos-de-cancer/cancer-de-pele-nao-melanoma, accessed: March, 2021.

Keywords: *encapsulation, photoprotective active, nanoparticles, starch.*

ENGINEERING HIGHLY POROUS 3D ARCHITECTURES BASED ON NANOCELLULOSE THROUGH *IN VIVO* BIOFABRICATION

Ana Carolina Aguiar[1*], Filipe V. Ferreira[1], Liliane M.F. Lona[1]

1 – School of Chemical Engineering, University of Campinas (UNICAMP), Campinas, SP, Brazil.
**carolinadeaguiar96@gmail.com*

Three-dimensional (3D) biomaterials based on bacterial cellulose (BC) hold tremendous potential for biomedical applications due to their exceptional mechanical resistance, flexibility, biocompatibility, and water adsorption capacity. In this study, we developed multifunctional platforms using a straightforward biofabrication method. The culture medium containing *Komagataeibacter medellinensis* bacteria was confined using superhydrophobic particles (specifically polytetrafluoroethylene - PTFE), resulting in the formation of liquid marbles. Following an incubation period, the PTFE particles were removed, yielding highly porous BC capsules. This methodology enables the fabrication of capsules with diverse shapes, sizes, thicknesses, and even compartmentalization (*e.g.*, capsule within a capsule) (Fig. 1). Encouraging results are presented, highlighting the influential process variables governing capsule formation, including culture medium volume, incubation time, humidity, and temperature. In summary, we introduce a multifunctional device prepared through an *in vivo* bioprocess with vast potential for advanced applications, such as drug release systems and tissue engineering.

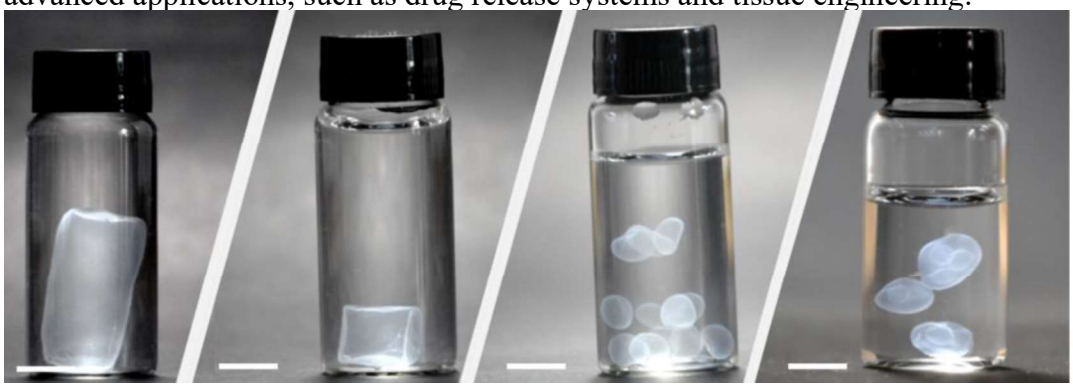

Figure 1. Bacterial cellulose capsules obtained from the biosynthesis process. Scale bar 1 cm.

References

1. Greca, L. G., Lehtonen, J., Tardy, B. L., Guo, J., & Rojas, O. J. (2018). Biofabrication of multifunctional nanocellulosic 3D structures: a facile and customizable route. Materials Horizons, 5(3), 408–415.

2. Kim, J., Shin, S., & Hyun, J. (2021). Controlled production of soft magnetic hydrogel beads by biosynthesis of bacterial cellulose. Journal of Industrial and Engineering Chemistry, 100, 260–269.

Fundings: grant 2021/00980-1 and 2021/09341-1, São Paulo Research Foundation (FAPESP).

Keywords: *Biofabrication, Nanocellulose. Drug release systems.*

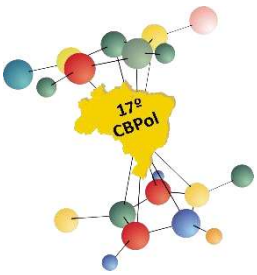

EVALUATION OF THE ANTIBACTERIAL ACTIVITY OF CHLORHEXIDINE ASSOCIATED WITH CASSAVA GUM HYDROGEL

Idglan S. Lima[1], Albert S. Silva[1], Ariane M.S. Nascimento[1], Luis H. Oliveira[1], Alan I.S. Morais[1], Francisco E. P. Santos[1], Josy A. Osajima[1], Edvani C. Muniz[1] and Edson C. Silva-Filho[1]

1 - Interdisciplinary Laboratory of Advanced Materials (LIMAV), Federal University of Piauí, 64049-550 Teresina-PI, Brazil.

i.dglan@hotmail.com

Abstract - The use of polysaccharides in the production of new materials for biomedical applications has become an attractive approach, mainly due to the abundance of these polysaccharides in nature and their biodegradable nature [1]. However, the antimicrobial properties of substances such as chlorhexidine (CLX) poses a significant challenge [2-4]. This challenge arises from the increasing number of pathogenic bacteria that are constantly a problem due to the rise in antibiotic resistance [5]. Therefore, the objective of this study was to synthesize cassava gum hydrogels as a protective vehicle for chlorhexidine digluconate. Characterizations using X-ray diffraction (XRD) and Differential Scanning Calorimetry (DSC) confirmed the incorporation of CLX into the hydrogel matrix. Antibacterial activity against Gram-positive (*Staphylococcus aureus*) and Gram-negative strains (*Escherichia coli)* showed satisfactory results for hydrogels containing 0.5% CLX, which exhibited a 100% antibacterial effect. The toxicity results using *Artemia salina* demonstrated that the material did not exhibit cytotoxicity, thereby enabling the use of the hydrogel as a drug delivery agent.

References

1. Lima, I.S. de; Ferreira, M.O.G.; Barros, E.M.L.; Rizzo, M. dos S.; Santos, J. de A.; Ribeiro, A.B.; Anteveli Osajima Furtini, J.; C. Silva-Filho, E.; Estevinho, L.M. *Int J Mol Sci* 2023, *24*, doi:10.3390/ijms24032210.
2. Ribeiro, J.S.; Sanz, C.K.; Münchow, E.A.; Kalra, N.; Dubey, N.; Suárez, C.E.C.; Fenno, J.C.; Lund, R.G.; Bottino, M.C. *Dental Materials* 2022, *38*, 1507–1517, doi:10.1016/J.DENTAL.2022.07.002.
3. Meng, N.; Zhou, N.L.; Zhang, S.Q.; Shen, J. *Int J Pharm* 2009, *382*, 45–49, doi:10.1016/J.IJPHARM.2009.08.004.
4. Ferreira, M.O.G.; de Lima, I.S.; Morais, A.Í.S.; Silva, S.O.; de Carvalho, R.B.F.; Ribeiro, A.B.; Osajima, J.A.; Silva Filho, EC. *J Drug Deliv Sci Technol* 2019, *49*, 375–382, doi:10.1016/J.JDDST.2018.12.003.
5. Hou, J.; Long, X.; Wang, X.; Li, L.; Mao, D.; Luo, Y.; Ren, H. *J Hazard Mater* 2023, *442*, 130042, doi:10.1016/J.JHAZMAT.2022.130042.

Fundings: CAPES, CNPq, and FAPEPI

Keywords: *Biomaterials, polysaccharides, and biological activity.*

GREEN TECHNIQUES FOR MODIFYING CASSAVA STARCH TO IMPROVE FEASIBILITY IN PRINTED BONE SCAFFOLDS PRODUCTION

Samile B. de Aguiar[1] and Bianca C. Maniglia[1]*

1 – Institute of Chemistry, University of São Paulo (USP), São Carlos, SP, Brazil
*biancamaniglia@iqsc.usp.br

Recent 3D printing advances enable the development of precise and complex porous scaffolds for bone tissue regeneration. These mimic bone tissue, facilitating osteoinductive cell growth [1]. Natural polymer-based hydrogel scaffolds, including starch, offer biodegradability and biocompatibility advantages [1]. However, native starch hydrogels have rheological and mechanical limitations. Green techniques like thermal treatments (dry heating - DHT, and heat moist - HMT) enhance functionality in various starch sources [1,2]. This study presents a pioneering investigation into the application of these physical technologies for modifying cassava starch. The aim is to enhance the printability and biodegradability of its hydrogels, with a specific focus on their utilization in the 3D printing of scaffolds (Fig 1). HMT was done in the starch (30% moisture content) at 100 ºC for 1, 2, 3, and 4 h) and DHT (10% moisture content) at 130 ºC for 1, 2, 3, and 4 h. The mechanical properties and printability of the starch hydrogels (10 % wt) were evaluated. Scaffolds based on these hydrogels were printed (BioedPrinterV4, BioEdTech - Brazil) and freeze-dried, and their biodegradability and swelling were evaluated. Increasing the modification time directly increases the impact on the evaluated parameters. HMT shows superior efficiency to DHT in achieving effects. In general, both technologies improved hydrogel printability, while modified starch-based scaffolds exhibited reduced swelling and biodegradability, enhancing their potential as bone scaffolds.

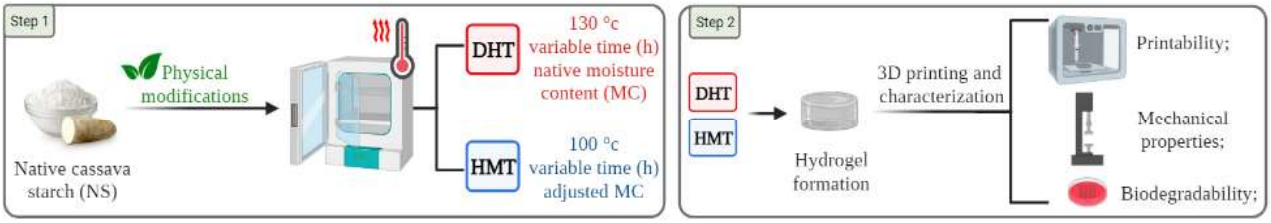

Figure 1. Schematic representation of methodology used in this work.

References
1. B. C. Maniglia; D. C. Lima; M. D. M. Junior; P. Le-Bail; A. Le-Bail; P. E. D. Augusto *Food Research International* 2020, 128. https://doi.org/10.1016/10.1016/j.foodres.2019.108803.
2. Y. Cahyana; E. Wijaya; T. S. Halimah; H. Marta; E. Suryadi; D. Kurniati *Food Chem* 2019, 274. https://doi.org/10.1016/j.foodchem.2018.09.004.

Fundings: FAPESP (2020/08727-0) and CAPES.

Keywords: *Cassava starch; physical and "green" modifications; DHT; HMT; 3D printing; bone scaffolds.*

IMPROVEMENT OF THE MECHANICAL PROPERTY AND COEFFICIENT OF FRICTION OF THE HIGH-DENSITY POLYETHYLENE/HYDROXYAPATITE NANOPARTICLE COMPOSITE (HDPE/HA) BY ADDING THE ERUCAMIDE-MONTMORILLONITE (EU/MMT) NANOCOMPOSITE

Rodrigo Gaio[1], Letícia Bavaresco Cima[3], Micheli Zanetti[1], Luciano Luiz Silva[1], Josiane Maria Muneron de Mello[1,2], Thiago André Carniel[4], Abel André Candido Recco[5], Éverton Rafael Breitenbach[4], Gustavo Lopes Colpani[1,2], Márcio Antônio Fiori[1,2,6*]

1 – Post-Graduation Program in Technology, Management and Innovation (PPGTI), Community University of Chapecó Region (Unochapecó), Chapecó, SC, Brazil.
2 – Post-Graduation Program in Environment Science (PPGCA), Community University of Chapecó Region (Unochapecó), Chapecó, SC, Brazil.
3 – Chemical Engineering Department, Community University of Chapecó Region (Unochapecó), Chapecó, SC, Brazil.
4 – Mechanical Engineering Department, Community University of Chapecó Region (Unochapecó), Chapecó, SC, Brazil.
5 – Physics Department (CCT), State University of Santa Catarina (UDESC), Joinville, SC, Brazil.
6 – Physics Department (DAFIS-PB), Federal Technological University of Paraná (UTFPR), Pato Branco, PR, Brazil.
marciofiori@utfpr.edu.br

Abstract - Polymeric composites containing hydroxyapatite have been applied for the manufacture of bone joint prostheses due to the advantages offered by the polymeric matrices, such as chemical stability, non-toxicity and good mechanical properties, and because of the biocompatibility of hydroxyapatite, which favors the osseointegration process. For these composites, one of the great challenges has been to reduce the coefficient of friction of their surfaces, with the main objective of increasing the mechanical resistances when applied as joint prostheses and, therefore, increasing the useful life of the elements manufactured with these materials. Considering these challenges, this work aimed to obtain and characterize a composite made of High-Density Polyethylene (HDPE) and Hydroxyapatite (HA) with a nanocomposite made of erucamide and montmorillonite (EU/MMT). The incorporation of the nanocomposite aimed to make the HDPE matrix compatible with the EU, considering that the EU is applied to reduce the friction coefficient of the polymer. In this process, it was considered that montmorillonite is a compatibilizer of erucamide molecules with the hydroxyapatite and HDPE phases. In the studies, the effects of the nanocomposite concentration on the friction coefficient and on the mechanical properties when subjected to tensile and bending stresses were evaluated. Thermal analysis, infrared spectroscopy, and analysis with scanning electron microscopy and atomic force microscopy were applied to carry out more detailed studies regarding the properties of the EU/MMT nanocomposite and the surface characteristics of the specimens. The results indicated that it is possible to reduce of 29.7% the friction coefficient of the HDPE/HA composite with the use of the nanocomposite, without impairing the mechanical properties. These results enhance the use of HDPE/HA as a material that can be applied to the manufacture of bone joints, even replacing traditional polymeric composites for this purpose.

Keywords: *HDPE/Hydroxyapatite composites, EU/MMT nanocomposite, HDPE/Hydroxyapatite-EU/MMT composite, Erucamide, Erucamide/Hydroxyapatite.*

STUDY OF THE CONTROLLED RELEASE OF VITAMIN B12 AND CYTOTOXICITY ASSAYS OF HYDROGELS BASED ON XANTHAN GUM

Francielle Lopes[1], Adrielle C. Reis[1], Kátia S. Paludo[2], Michele K. Lima-Tenório[1], Adriano G. Viana[1*]
1 – Chemistry Departament, Ponta Grossa State University (UEPG), Ponta Grossa, PR, Brasil
adrianoviana@uepg.com
2 – Biology Departament, Ponta Grossa State University (UEPG), Ponta Grossa, PR, Brasil

Abstract – Polymers of natural origin are being widely used in the development of controlled drug release systems[1], where devices such as hydrogels (HGs)[2] stand out. The presence of ionizable functional groups in the matrix of HGs gives these materials different swelling behaviors, especially in response to the pH of the system, thus enabling them to be applied in controlled drug release studies[3]. Thus, in this work, four different formulations of HGs were developed using 50.0 mg of the naturally anionic polysaccharide xanthan gum[4], previously modified with glycidyl methacrylate[5], and different amounts of the spacer agent *N'N'*-dimethylacrylamide (DMA; 70 - 250 mL), aiming to study the release of vitamin B12 (VB12) in a simulated gastrointestinal system[6]. For the synthesis of HGs the methodology of radical polymerization was used. From the synthesized HGs, two of them showed pH-responsiveness, highlighting the formulation called XG4 (250 mL of DMA), which was chosen for VB12 release assays. This HG was carried with 3.10 ± 0.97 μg of VB12 g^{-1} of dryed HG and released about 35% of VB12 at pH 1.2, reaching equilibrium in 2 h and 45% of VB12 at pH 6.8, reaching equilibrium in 7 h (Fig 1A). Such results demonstrate that this HG would be a suitable device for the controlled release of the drug, especially in the intestinal environment. *In vitro* cytotoxicity assays were also performed on HGs according to ISO 10993-5, using albino 3T3-Swiss cells (Fig 1B). As it is possible to verify by the MTT and neutral red (NR) assays, the materials presented non-toxic and biocompatible characteristics, essential properties for their applications for *in vivo* drug carriers.

Figure 1. Gastrointestinal release of VB12 to XG4 (A). Cytotoxicity assays for HGs (B).

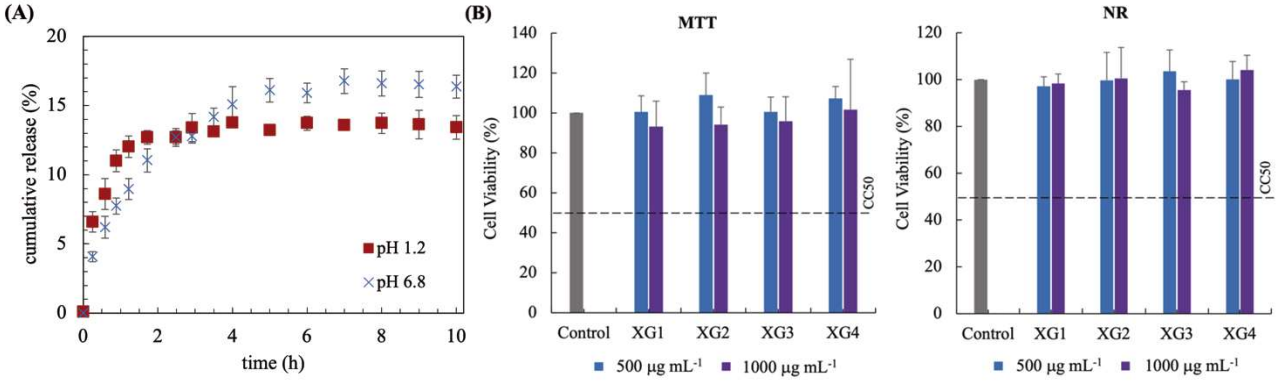

References
1. E. M. Ahmed *Journal of Advanced Research* 2015, 6, 105–121. https://doi.org/10.1016/j.jare.2013.07.006
2. C. Li; et al. *Acta Pharmaceutica Sinica B* 2019, 9, 6, 1145-1162. https://doi.org/10.1016/j.apsb.2019.08.003
3. S. Mehra; et al. *Polymer chemistry* 2021, 12, 2404 – 2420. https://doi.org/10.1039/D0PY01729A
4. J. Patel; et al. *The Royal Society of Chemistry* 2020, 10, 27103-27136. https://doi.org/10.1039/D0RA04366D
5. A. V. Reis; et al. *Journal of Organic Chemistry* 2009, 74, 10, 3750-3757. https://doi.org/10.1021/jo900033c
6. European Pharmacopoeia (Ph. Eur.), 11th Edition, 2023.

Fundings: CAPES (88887.499540/2020-00)

Keywords: *xanthan gum, vitamin B12, hydrogel, controlled drug release, cytotoxicity*

TANNIN DERIVAVITE POLYMER AS VENUE FOR NEW BIOMATERIALS

Paulo C. F. da Câmara[1,3], Alessandro F. Martins[2], Rosangela C. Balaban[1] and Matt J. Kipper[3]

1 – Laboratory of Petroleum Research, LAPET, Institute of Chemistry, Federal University of Rio Grande do Norte, UFRN, 59078-970 Natal, RN, Brazil paulocfcamara@gmail.com
2 – Laboratory of Materials, Macromolecules and Composites, Federal University of Technology, Apucarana, PR 86812-460, Brazil
3 – Department of Chemical and Biological Engineering, Colorado State University, Fort Collins, CO 80523, USA

Abstract – Tanfloc (TN), an amino-functionalized condensed polyphenol, a few years back have basically been used for complexation of heavy metal in water treatments [1]. However, this polycation has peculiarities such as biocompatibility, low toxicity and hydrophilicity that draws attention to be used as scaffolds or in surface modification for biomedical applications [2]. In recent years, TN-based materials have expanded from polyelectrolyte complexes to layer-by-layer deposition to bio-functionalize surfaces such as titania nanotubes [3]. Hence, the aim of this work was to gather the latest publications around TN and discuss its features for bioengineering. Fig 1 schematize how TN have been combined with other macromolecules to produce nanofibers, hydrogels and other biomaterials that promote cell response, antibacterial activity, blood compatibility, endothelialization, conferring remarkable functions for biomedical implants and regenerative medicine.

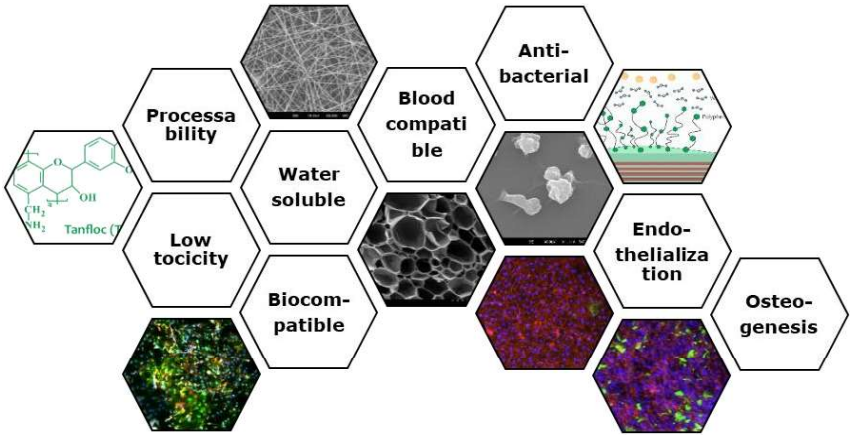

Figure 1. Multiple uses of tannin derivative polymer (Tanfloc) in bioengeneering.

References

1. Facchi et. all. International Journal of Biological Macromolecules 2017, 103, 129-138, http://dx.doi.org/10.1016/j.ijbiomac.2017.05.033.
2. Câmara et. all. RSC Advances 2019, 9, 25836-25846, https://doi.org/10.1039/C9RA03903A.
3. Sabino et. all. Carbohydrate Polymers 2021, 251, 117079, https://doi.org/10.1016/j.carbpol.2020.117079.
4. Bezerra et. all. Materials Today Communications 2021, 26, 101883, https://doi.org/10.1016/j.mtcomm.2020.101883.

Keywords: *Tissue engineering; Tannins; Biomolecules; Cytocompatibility; Hemocompatibility.*

USING BURITI (MAURITIA FLEXUOSA L.) OIL TO OBTAIN POLYURETHANES

Thátila W. V. de Sousa 1*, Fernando S. Reis [3], Ewerton G. Vieira [2], José E. M. de Matos [1,3]

1 - Materials Science and Engineering Graduate Program, Federal University from Piauí, Teresina, PI, Brazil.
2 – Federal Institute of Education, Science and Technology of Maranhão, Buriticupu, MA, Brazil.
3 - Chemistry Department, Federal University from Piauí, Teresina, PI, Brazil.

thatila.vieira@ufpi.edu.br

Abstract - Plant-derived polyurethanes (PU) have been highlighted in studies related to the therapy/replacement of bone tissue [1]. Among the vegetable oils used for this purpose, buriti (Mauritia Flexuosa L.) oil is an excellent candidate for the manufacture of these materials since it is an oil rich in bioactive compounds, such as carotenoids, tocopherols, and fatty acids, which have antioxidant and anti-inflammatory properties [1,2]. This research aimed to synthesize polyurethanes using buriti oil as a source of polyol, in addition to incorporating hydroxyapatite (HA) in the polymeric matrix. The monoacylglyceride (MAG) was obtained with the reaction between buriti oil and glycerol in the presence of the catalyst LiOH [3]. The obtained polyurethanes were characterized by Fourier Transform Infrared Spectroscopy (FTIR), X-Ray Diffraction (XRD), and Scanning Electron Microscopy (SEM). The characterizations confirm the formation of polyurethanes and the incorporation of hydroxyapatite in the polymeric matrix.

References:

1. P. M. Paraskar; M. S. Prabhudesai; V. M. Hatkar & R. D. Kulkarni *Progress in Organic Coatings* 2021, *156*, 106267. https://doi.org/10.1016/j.porgcoat.2021.106267.
2. F. S. Lima; L. F. L. Matos; I. K. C. Pacheco; F. S. Reis; J. Pierot; J. V. Camara; J.M.E. Matos; A. B. Ribeiro; W. L. Moura; A. C Fialho *Polímeros: ciência e Tecnologia* 2022, *32*, e2022003. https://doi.org/10.1590/0104-1428.210018.
3. I. K. C. Pacheco; F. S. Reis; C. E. S. Carvalho; J. M. E. Matos; N. M. Argolo Neto; S. A. F. Baeta; K. R. Silva; H. V. Dantas; F. B. Sousa; A. C. V. Fialho *Biomedical Materials* 2021, *16*, 065006. https://doi.org/10.1088/1748-605X/ac1f9e.

Fundings: FAPEPI - Research Support Foundation of the State of Piauí

Keywords: *Biomaterials, polyurethane, vegetable oil.*

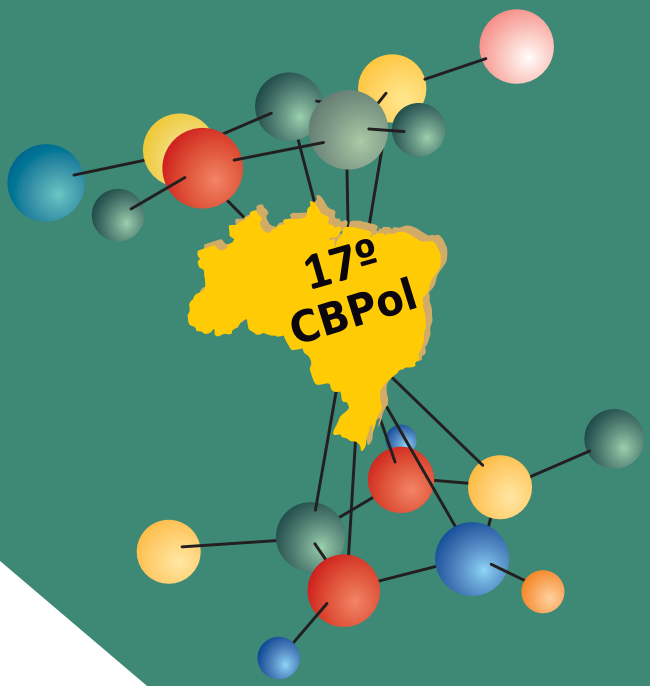

Polymers in agriculture and special industrial applications

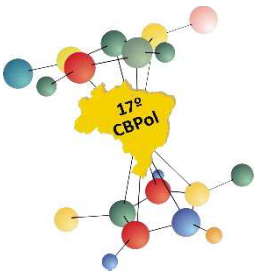

POLYSACCHARIDE-BASED MATERIALS FOR ENHANCED EFFICIENCY FERTILIZERS: PERSPECTIVES FOR THE SUSTAINABLE DEVELOPMENT GOALS

Roselena Faez

Laboratório de Materiais POliméricos e Biossorventes (LAB-MPB), Departamento de Ciências da Natureza, Matemática e Educção (DCNME), Iniversidade Federal de São Carlos (UFSCar), Araras, SP, Brazil
faez@ufscar.br

Abstract - The global challenge of sustainably feeding a growing population leads us to explore innovative solutions in agriculture. This talk focuses on a promising approach to employing polysaccharide-based materials in enhanced efficiency fertilizers (EEFs) to align with the Sustainable Development Goals (SDGs). EEFs, known to improve nutrient uptake, reduce fertilizer runoff, and minimize environmental impacts, hold immense potential for advancing sustainable agricultural practices. In this context, we will explore how we can take advantage of the chemical versatility of polysaccharides to develop EEFs with superior properties. However, the road to large-scale adoption of polysaccharide-based EEFs is challenging. Thus, existing limitations and ongoing research areas will also be addressed, illuminating opportunities for innovation and improvement. Additionally, accelerating the adoption of these innovative fertilizers for a more sustainable and prosperous future for agriculture will require collaborative efforts involving interdisciplinary researchers, policymakers, and industry stakeholders. In conclusion, emphasis will be placed on the key role of polysaccharide-based materials in advancing sustainable agriculture and achieving the SDGs.

Fundings: This study was financed in part by the Conselho Nacional de Desenvolvimento Científico e Tecnológico (CNPq) and Fundação de Amparo à Pesquisa do Estado de São Paulo (FAPESP, process number 19/02535-5).

Keywords: *Biopolymer, chitosan, starch, cellulose, algae-based polymer.*

SYNTHESIS AND APPLICATIONS OF GLYCO-AMPHIPHILES

Sami Halila

Insert here the author(s) affiliation(s). Write the e-mail of the author to whom correspondence should be addressed.
Example:
1 – Centre de Recherches sur les Macromolécules Végétales
CNRS – Univ. Grenoble Alpes – France, sami.halila@cermav.cnrs.fr

Abstract - Carbohydrates are Ubiquitous in Nature and consist a huge feedstock of renewable and biodegradable materials. Moreover, they cover most of the living cells and are now recognized as major actors in many biological processes by interacting with various carbohydrate-binding proteins such as lectins, growth factors, enzymes and so on. As a result, carbohydrates present many opportunities for intervention in disease diagnosis and therapy. However, carbohydrates are scarcely found alone since they are linked to lipids (glycolipids, glycosphingolipids) forming the cell wall, to proteins (glycoproteins, proteoglycans) inducing 3D conformation and increasing stability and others. Despite the elegant carbohydrate chemistries devised by glycochemists, an effective and modular synthetic approach that meets the ever increasing interest in the preparation of functional carbohydrate derivatives is needed. Over the last decade, a continuous effort has been devoted to my research for the use of chemo-, stereo- and site-selective modification of the reducing-end of carbohydrates without the use of protecting groups in the spirit of click chemistry for the production of functional carbohydrate derivatives and mainly glyco-amphiphiles with self-assembly properties in bulk or in solution.
During my talk, I will focus my presentation on the synthetic strategies allowing the modification of the reducing end of low-molecular weight carbohydrates by integrating hydrophobic segments leading to glyco-amphiphiles. Next, I will show how glyco-amphiphiles have been applied in various fields including self-assembly in solution (nanoparticles, gels) and with an opening on liquid crystal based-biosensor taking advantages on interaction with pathogenic carbohydrate-binding proteins.

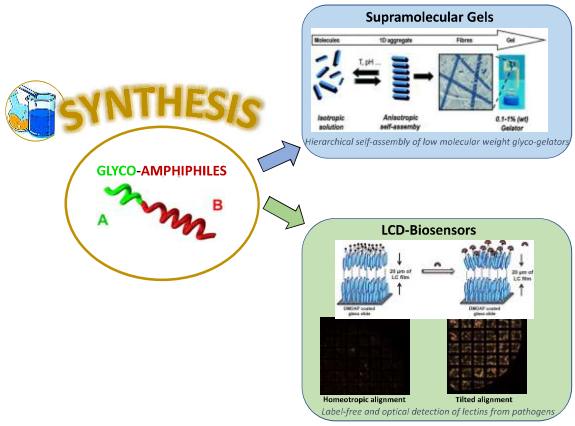

BACTERIAL CELLULOSE FILMS FOR BIODEGRADABLE PACKAGING WITH ESSENTIAL OILS

Stefani R. Z. Teixeira[1], Michele C. F. Garcia[2], Denise A. K Silva[1], Ana P. Kurek[1], Andréa L. D. S. Schneider[1,2] and Ana P. Testa Pezzin[1]*

1 – Master program in Process Engineering (MEP), University of Joinville Region (UNIVILLE), Joinville, SC, Brazil
Joinville, SC, Brazil
anapezzin@yahoo.com.br
2 – Department of Chemical Engineering, University of Joinville Region (UNIVILLE), Joinville, SC, Brazil

Abstract - This work aimed to evaluate the effect of essential oils (EOs) of clove, cinnamon, basil and oregano as additives in bacterial cellulose matrix for application in food packaging. BC membranes were synthesized by the bacteria *Komagataeibacter hansenii* and incorporated into EOs using ethanol as a solvent. The membranes were characterized by Fourier transform infrared spectroscopy (FTIR), thermogravimetric analysis (TGA), antimicrobial activity and soil biodegradation. FTIR analyses confirmed the incorporation of EOs into BC membranes. The thermal stability of the incorporated membranes was superior to pure BC. All samples showed antibacterial potential, except BC incorporated with the essential oil (EO) of basil. The fungal analysis was performed by visually evaluating the appearance of filamentous fungi on the surface of the pieces of bread. Soil biodegradation tests have proven the biodegradability of the incorporated membranes.
Keywords: *Active packaging, bacterial cellulose, essential oil.*
Fundings: The authors are grateful for the financial support of FAPESC and UNIVILLE for the project.

Introduction

Packaging is relevant in the food industry in product protection and conservation, information and convenience to the consumer [1]. In times when food consumption is high, competitiveness among companies is frequent, and it is necessary to create and innovate to gain prominence in this market. Among these are the innovations in food packaging associated with mechanical resistance, barrier properties and gases and aromas, ensuring consumer safety and practicality [2]. New packaging additives have been developed to provide active protection to the product. Active packaging was officially defined as "packaging with active additives that are mainly intended to extend the expiration date and maintain/improve the condition of packaged foods" [3]. In developing new additives, it is essential to consider that plastic packaging consumption produces large waste that accumulates in landfills [4]. The problem with incorrect disposal of plastics generates several environmental problems, such as flooding in large cities and pollution, among others [5]. Due to the large amount of food packaging produced and later discarded each year, the tendency is the use biodegradable polymers as potential substitutions to non -biodegradable petrochemical polymers [6]. A biopolymer targeted by various research is cellulose, the most abundant in nature and essential in the global economy [7]. The BC is synthesized purely, free from other plant molecules, and its purity does not require a high cost of extraction, purification processes and the use of environmentally hazardous chemicals [8]. The BC consists of a translucent and gelatinous film formed by cellulose microfibrils produced by various microorganisms [9]. Its physical and

mechanical properties are related to its nano and well-linked microfibrils, creating an extensive surface area with spacing that allows a large amount of liquid to retain [10]. Therefore, essential oils (EOs) are additives widely used in the food industry and in packaging to prolong the shelf life. EOs has antifungal, antioxidant, antiviral, antitoxic, antiparasitic, antibiotic and antiseptic properties [11]. Thus, an alternative to be evaluated is a packaging composed of BC with promising and poorly studied EOS incorporated into their matrix for specific actions. To this end, this work addressed the use of BC for application in biodegradable food packaging (active packaging). Clove, cinnamon, basil and oregano EOs were incorporated to develop active packaging to possibly be biodegradable and even extend the life of the food shelf.

Experimental

Obtaining BC and incorporation of essential oils (EOs)

The synthesis of BC membranes was performed by the *Komagataeibacter hansenii* bacteria ATCC 23769 cultivated in manitol (MM). Cultivation and purification followed methodology presented in previous works [12]. The incorporation of EOs into the membranes was performed according to Albuquerque [13]. Briefly, excess water from the membranes with paper towels were removed, after the membranes were immersed at 150 mL of 99% ethanol and heated at 60 °C for 10 min. After removal of excess ethanol, the membranes were incorporated with a 20 mL ethanolic solution containing 3.0 g of each EO and heated in a greenhouse at 60 °C for 10 min. In the end, the incorporated membranes were dried in greenhouse at 50 °C to constant mass.

Membranes Characterization

The membranes were characterized for infrared spectroscopy with Fourier transform (FTIR-ATR), thermogravimetric analysis (TGA), antimicrobial activity of the membrane and biodegradation in ASTM G160-98 soil.

Results and Discussion

Obtaining the BC and incorporation of the essential oils (EO)

After cultivation, the BC membranes had an average thickness of 0.25 mm and a gelatinous appearance, as reported in the literature [14]. The membranes were previously immersed in an ethanol solution, promoting the replacement of water molecules inside the membrane. After the membranes were transferred to an ethanolic solution containing and dissolved (15% m/m), the diffusion was accelerated as a function of heating in a 60 °C heating for 10 min.

Infrared spectroscopy with Fourier Transform - FTIR

FTIR analysis was performed to prove the presence of EO in the BC membranes. The BCs prominent bands and characteristic connections were found in the pure BC membrane. The FTIR spectrum of the clove had characteristic bands corresponding to the stretch of the vibration of the hydroxyl group (O-H) linked to benzene [15], the stretch C = C and the stretching of the aromatic ring [16]. The cinnamon EO FTIR spectrum presented the C = C stretch referring to the aromatic ring, a C-OH alcohol, alkanes CH_2 that face oscillation between aromatic rings = CH for flexion absorption on the plane, the ester C-O-C aromatic ring, C-OH stretching vibration of phenolic groups, C-OH deformation vibration and aromatic rings absorption = CH [17]. Already in the BC with the incorporation of basil EO, the bands attributed to the stretching vibrations of the aromatic ring- C = C- [18], and the band that represented the curvature C- H of alcene/aromatic groups [19]. With CB incorporated with oregano OE, the bands found indicated the presence of the carbonyl group (C = O), the unsaturations of the benzene ring and one of the rings itself. These bands are from p-ciman, thymol and Y aromatic hydrocarbons, and Y hydrocarbons -terpinene, in addition to the clove phenolic composed in the composition of the EO-OR [20].

Thermogravimetric analysis (TGA)

The thermal degradation profile of the pure BC membrane presented 3 main events of mass loss provided for in the literature [21]. In comparison, BC, with the incorporation of EOs, presented 4 main mass loss events, one of them being the mass loss related to the percentage of incorporated. The 1st stage of mass loss occurred between 30 and 150 °C, referring to water loss of samples (2.6 to 5.5%) [22]. And simultaneously, the evaporation of the EOS, in the 2nd stage, between 116 and 172 °C with a mass loss between 8.4 and 10.5% corresponding to volatilization of the volatile compounds of the oil [23]. The 3rd stage and most intense is attributed to the degradation of cellulose, including the depolymerization and decomposition of glucose units, which occurred in T_{onset3} 321 °C and T_{PEAK3} of 349 °C, with 73.8% mass loss for pure BC sample, the fact also evidenced by Lima et al. [21]. The presence of the oil did not change the degradation temperature of the films in question, as they all behaved similarly.

Antibacterial activity of the incorporated membranes

The antibacterial activity of the samples with EOS was evaluated against the Staphylococcus aureus and *Escherichia coli* bacteria. The inhibition halos (mm) of microbial growth refers to the BC incorporated. The BC-Or membrane showed a 13.33 mm inhibition halo, followed by CB-C with 9.33 mm and CB-C-C-CE with a 5.67 mm halo. *E. coli* BC-Or also stood out among the others with 11.33 mm of inhibition halo, followed by CBCR (6.67 mm), CBCA (5.33 mm). BC with basil showed no antimicrobial activity [24]. He studied antimicrobial activity in cellulose acetate films with 15% oregano, and obtained 10 mm of inhibition halo for both *E. coli* and *S. aureus*.

Soil biodegradation

Membranes with approximate masses with an average standard deviation of 0.014 were buried in composed soil and removed after 1, 15 and 30 days from the biodegradation test. Fig 1 shows the loss of membrane mass during the test. During the 30 days of study, there was a subtle mass reduction. Arancibia et al. [25] studied the biodegradation of soy protein films with citronella additive, the films were kept on soil exposed to atmospheric conditions for 6 months, and it was possible to observe in 1 month a wrinkling of the films and for a period of conditioning longer (3 months), the wrinkling was more pronounced. The film's surface has changed, particularly in movies stored for 6 months. Given the above, it is suggested for future work to perform the biodegradation test for a more extended period to prove the complete biodegradability of the films.

Evaluation of the antifungal activity of membranes used on the surface of bread slices

Antifungal analysis was performed visually, and the appearance of filamentous fungi was the end of the evaluation of each membrane. The accompaniment was daily, with a photographic record. In Fig 2, the bread and their respective membranes incorporated after 4 days of maturity of the bread were observed. On this day, the appearance of filamentous fungi on the surface of the slices of bread was beginning. However, the membranes remain fungal-free, except for pure BC, which already demonstrates the beginning of fungal growth on its surface.

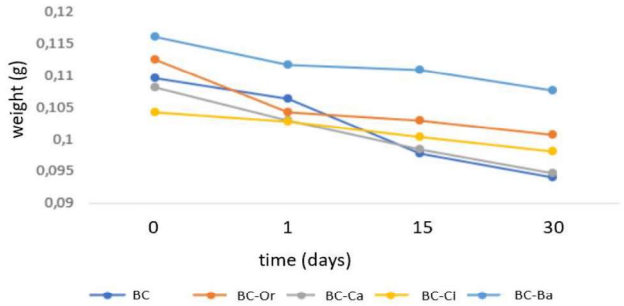

Figure 1-Mass of pure BC, BC with oregano EO (BC-ROR), clove (BC-CA), cinnamon (BC-CI), basil (BC-BA) after 1, 15 and 30 days of soil exposure.

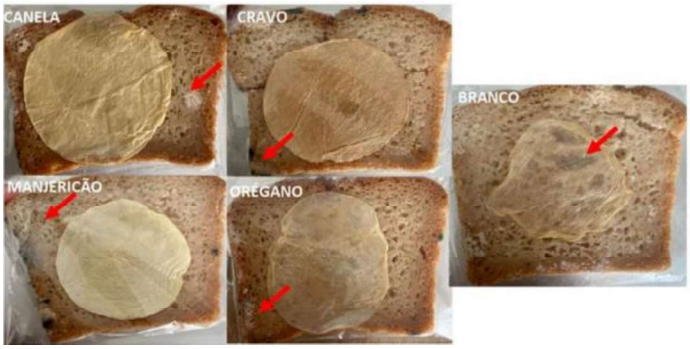

Figure 2- Antifungal analysis of samples applied to bread after 04 days of maturity.

After 10 days of bread maturity, there is the appearance of filamentous fungi in the pure BC, BC-C, BC-B-BA membranes, and the BC-BA sample stands out for having greater fungal growth in this period of time, while in the BC-C-C-C-C-CE membranes only growth begins. But the BC-Or membrane remains free of fungi to the 14-day bread-salary period, when the beginning of fungal growth was observed.

Conclusions

BC membranes have been promising for use as active packaging with natural additives. FTIR analyses proved EOS incorporated into the BC membranes, and TGA analysis showed better thermal stability for incorporated samples.

The BC-Or membrane demonstrated more effective antibacterial action, followed by membranes incorporated with (clove, cinnamon and oregano) which also demonstrated satisfactory effects. As for the visual growth analysis of filamentous fungi, it was realized that the EOS has efficient antifungal action, as they extended the shelf life of packed bread within 10 days without molding. The films incorporated with the EOs were influential in the function the study determined, and the incorporation methodology used with ethanol, performing polarity exchange, actually favored the incorporation of EOs in the membrane.

References

1. E. Fasano *et al*. Food Control 2012, 27 (1), 132–138. https://doi.org/10.1016/j.foodcont.2012.03.005.
2. A. P. M. Landim *et al*. Polímeros 2016, 26, 82–92. https://doi.org/10.1590/0104-1428.1897.
3. K. G. Zinoviadou; K. P. Koutsoumanis; C. G. Biliaderis Meat Science 2009, 82 (3), 338–345. https://doi: 10.1016/j.meatsci.2009.02.004.
4. L. Avérous Journal of Macromolecular Science, Part C: Polymer Reviews 2004, 44 (3), 231–274. https://doi.org/10.1081/MC-200029326.

5. A. C. T. Nunes, Dissertação, Pontifícia Universidade Católica do Rio de Janeiro (PUC-Rio), 2018.
6. D. Puglia; E. Fortunati; J. M. Kenny. *Multifunctional Polymeric Nanocomposites Based on Cellulosic Reinforcements*. Elsevier, Amsterdam, 2016, 205–252.
7. P. Carreira *et al*. Bioresource Technology 2011, 102 (15),7354 - 7360. https://doi.org/10.1016/j.biortech.2011.04.081
8. P. Cazón; M. Vázquez Food Hydrocolloids 2021, 113, 106530. https://doi.org/10.1016/j.foodhyd.2020.106530.
9. G. F. Picheth *et al.* International Journal of Biological Macromolecules 2017, 104, 97–106. https://doi.org/10.1016/j.ijbiomac.2017.05.171.
10. M. Poletto; H. L. Ornaghi Jr, (Eds.). *Cellulose - Fundamental Aspects and Current Trends*. InTechOpen, London, 2015.
11. T. Huang, *et al.* Polymers 2019, 11 (3), 560. https://doi.org/10.3390/polym11030560.
12. S. R. Z. Teixeira *et al*. Materials Research 2019, 22 (suppl. 1), e20190054. http://dx.doi.org/10.1590/1980-5373-MR-2019-0054.
13. R. M. B. Albuquerque, Dissertação, Universidade Católica de Pernambuco (UNICAP), 2019.
14. D. O. S. Recouvreux, Tese, Universidade Federal de Santa Catarina (UFSC), 2008.
15. S. PENG, *et al*. Journal of Food Protection 2015, 78 (1), 22 - 30. https://doi: 10.4315/0362-028X.JFP-14-246.
16. T. Wang *et al*. Journal of Inclusion Phenomena and Macrocyclic Chemistry 2011, 71, 207–213. https://doi.org/10.1007/s10847-011-9928-3.
17. Y. Li; D. Kong; H. Wu Industrial Crops and Products 2013, 41, 269–278. https://doi.org/10.1016/j.indcrop.2012.04.056.
18. G. Dhoot. *et al.* Polymer 2009, 50 (6), 1470–1482. https://doi.org/10.1016/j.polymer.2009.01.026.
19. W. Sajomsang *et al*. Carbohydrate Polymers 2012, 89 (2), 623–631. https://doi.org/10.1016/j.carbpol.2012.03.060.
20. S. F. O. Pontes, Tese, Universidade Federal de Viçosa (UFV), 2013.
21. L. R. Lima *et al*. Química Nova 2015, 38 (9), 1140-1147. https://doi.org/10.5935/0100-4042.20150131.
22. D. Mondal *et al*. Carbohydrate Polymers 2013, 96 (1), 57–63. https://doi.org/10.1016/j.carbpol.2013.03.064.
23. A. C. F. Portella, *et al.* Química Nova 2014, 37 (5), 844-849. https://doi.org/10.5935/0100-4042.20140136.
24. R. M. F. Magalhães, Dissertação, Universidade Federal de Goiás (UFG), 2012.
25. M. Y. Arancibia *et al.* Food Control 2014, 44, 7–15. https://doi.org/10.1016/j.foodcont.2014.03.025.

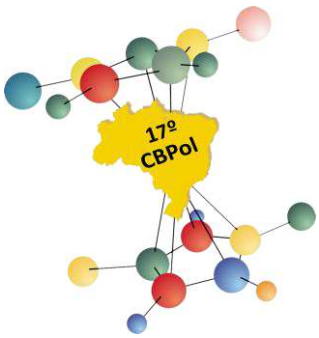

BIODEGRADATION OF POLYELECTROLYTE COMPLEXES IN ULTISOL CONDITIONING: PHYSICOCHEMICAL AND MICROBIOLOGICAL MONITORING

Rafael F. P. da Rocha[1], Marcia P. M. da Costa[1], Antonio Carlos A. da Costa[2] and Ivana L. M. Ferreira[1*]

1 – Department of Chemical Processes, Rio de Janeiro State University (UERJ), Rio de Janeiro, RJ, Brazil
**ivanalmellof@gmail.com ; ivanamello@uerj.br*
2 – Department of Technologies of Biochemical Processes, Rio de Janeiro State University (UERJ), Rio de Janeiro, RJ, Brazil

Abstract – In this work, the influence of biodegradation of a polyelectrolyte complex (PEC) based on alginate (ALG) and chitosan (CHI) on the fertility of an Ultisol was evaluated. In addition, pH and soil moisture were monitored in order to observe the potential of PEC as soil conditioner. The physical, chemical and microbiological properties of the soil were analyzed before and eight weeks after the PEC samples were buried, by the company LaborSolo (Londrina, PR). The results showed that burying the PEC for eight weeks did not significantly alter soil fertility, with leaching being the main factor responsible for the reduction of some levels of macro and micronutrients. Soil pH remained in a range considered not harmful for PEC stabilization, while soil moisture with PEC was higher than moisture without PEC until the end of the eight weeks. These results demonstrate that PEC inclusion is promising for the conditioning of clayey soil.
Keywords: *biodegradation; alginate; chitosan; ultisol conditioning; soil monitoring.*

Introduction

Alginate (ALG) is an anionic polysaccharide produced in sodium form by brown algae, mostly [1], while chitosan (CHI) is a cationic polysaccharide obtained by the deacetylation reaction of chitin [2], generally obtained from the shells of crustaceans [3]. The material formed by the electrostatic interactions between the two polyelectrolytes is called a polyelectrolyte complex (PEC) [4].
In this work, soil from the northern region of the state of Rio de Janeiro was used. Of the total area of the region, 48.91% (156,657 hectares) corresponds to clayey soil. Since PEC based on ALG and CHI has already been used for the gradual release of glyphosate [6], a herbicide widely used on soybean crops, it is of paramount importance to study the impacts of this material on the soil, as well as its potential as a soil conditioner.

Experimental

Preparation of polyelectrolyte complexes (PECs)

ALG and CHI solutions were prepared in previously determined concentrations. After preparation, the polysaccharide solutions were mixed for 24 hours, washed with deionized water and

lyophilized. For the preparation of PEC, the volumetric ratio was maintained at 1:1, pH at 6 and temperature at 50 ºC [7].

Soil burial assays

The prepared PEC samples were buried in soil for eight weeks at a depth of 5 cm and irrigated daily [8, 9]. The soil used was taken from a private property located in the municipality of Campos dos Goytacazes, in the northern region of the state of Rio de Janeiro, Brazil (latitude 21º14'55" S and longitude 41º19'23" W).

Soil monitoring

The soil's physical, chemical and microbiological characteristics were evaluated before and after the PEC burial tests, in order to know more about the soil, and its microbiota, and to observe whether the biodegradation of PEC would influence soil fertility.
Over the eight weeks of testing, the soil was monitored in relation to pH and moisture. Soil pH monitoring aims to verify whether pH is responsible for the destabilization of polymeric chains. For this, 10 g of soil was removed and 25 mL of 0.01 mol L^{-1} $CaCl_2$ aqueous solution was added. The solution was stirred and the pH was read in the supernatant solution [10]. Soil moisture was determined using the greenhouse method [11] and was calculated according to Eq. 1.

$$U\ (\%) = (m_{water}/m_{dry\ soil}) \times 100\% \qquad (1)$$

Where: U (%) is the calculated soil moisture, m_{water} is the mass of water present in the soil and $m_{dry\ soil}$ is the mass of soil after drying in an oven.

Results and Discussion

Table 1 presents the results obtained from the microbiological analysis of the soil before and eight weeks after the PEC samples were buried.

Table 1 – Microbiological analysis of soil with and without PEC.

Soil	Bacteria ($\mu g/cm^3$)	Beneficial fungi ($\mu g/cm^3$)	Potentially pathogenic fungi ($\mu g/cm^3$)	F:B ***	Fungal spores ($indiv./cm^3$)
Without PEC	10094	11	N.D.*	0.001	N.D.
With PEC **	677041	100	204	0.0001	270489

*N.D. = Not detected; ** after burial for eight weeks; *** Fungi:Bacteria ratio.

It was possible to observe a significant increase in the number of bacteria and fungi in the soil after eight weeks of testing. This increase indicated that biodegradation was taking place with daily irrigation.
Table 2 reports the results obtained from the physical analysis of the soil, confirming that it is a clayey soil.

Table 2 – Results of soil physical analysis with and without PEC samples.

Soil	Soil texture	Composition		
		Sand (%)	Silt (%)	Clay (%)
Without PEC	Clay	18	22	60
With PEC*	Clay	30	16	54

* eight weeks after burial.

Table 3 presents the results obtained by the chemical analysis of the soil, before and after eight weeks of testing.

Table 3 – Soil chemical analysis with and without PEC samples.

Soil	**Anionic macronutrients (mg/dm^3)**			**Cationic macronutrients (cmol$_c$/dm^3)**			
	Mehlich 1 Phosphorus	**Mehlich 3 Phosphorus**	**SO_4^{2-}**	**Ca^{2+}**	**Mg^{2+}**	**K^+**	**Na^+**
Without PEC	5.37	0.11	12.16	1.39	2.04	0.08	0.02
With PEC**	4.01	N.D.*	29.71	1.41	1.46	0.07	0.07

Soil		**CEC*** (cmol$_c$/dm^3)**		**Micronutrients (mg/dm^3)**				
	Organic matter (g/dm^3)	**pH 7.0**	**Effective**	**B**	**Cu^{2+}**	**Fe^{2+}**	**Mn^{2+}**	**Zn^{2+}**
Without PEC	6.34	7.06	3.53	0.38	0.41	143.18	150.97	1.51
With PEC**	4.23	6.36	3.01	0.42	0.26	115.62	117.11	1.11

* N.D. = Not detected; ** eight weeks after burial; *** Cation Exchange Capacity (CEC).

The results showed, in general, a decrease in levels of macro and micronutrients, such as phosphorus, Mg^{2+}, Fe^{2+}, Mn^{2+}. However, there was an increase in some micronutrients, such as SO_4^{2-}, Ca^{2+}, Na^+ and B. The CEC decreased after eight weeks of testing, indicating a decrease in soil fertility, but it was not highly significant. The decrease in some levels of macro and micronutrients is possibly related to leaching, which occurred through daily irrigation until the end of the eight weeks, while the consumption of organic matter is related to the increase in the microbiota.

The results obtained for soil pH and moisture (Fig. 1) demonstrated that the pH did not change significantly, remaining between the pKa of carboxyl groups and amino groups, of the alginate and chitosan chains, respectively [12, 13]. Thus, it was not responsible for the collapse of the material. The soil moisture results showed that the presence of PEC made the soil wetter compared to the soil without PEC. The highest moisture obtained was recorded after seven days of testing, where the soil with PEC was 7% moister than the soil without it. Higher soil moisture with PEC was maintained until the end of the eight weeks of testing, demonstrating the potential of PEC based on sodium alginate and chitosan as a clayey soil conditioner [14].

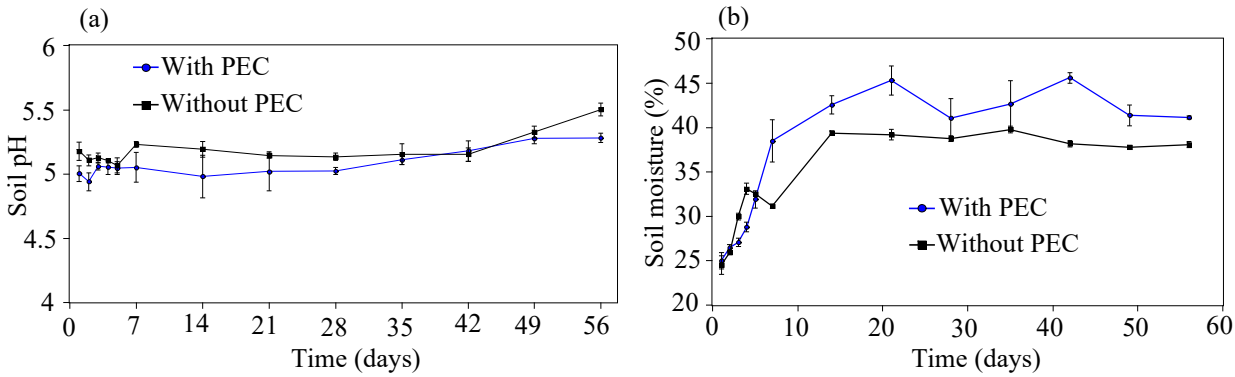

Figure 1 – Soil monitoring, with and without PEC, in relation to variations in: pH (a) and moisture (b) during the test period.

Conclusions

We can conclude that PEC based on alginate and chitosan has promise as a clayey soil conditioner. The biodegradation of PEC did not significantly alter soil fertility, while increasing its moisture and keeping it higher than that of the soil without PEC until the end of the eight weeks. By determining the pH of the soil during the biodegradation test of the PEC samples, it was possible to conclude that the pH of the soil did not influence the stabilization of the material.

Acknowledgements

We thank the Carlos Chagas Filho Foundation for Research Support of the State of Rio de Janeiro (FAPERJ) and the National Council for Scientific and Technological Development (CNPq) for their financial support. This study was also partly funded by the Office to Coordinate Improvement of Higher Education Personnel (CAPES), Finance Code 001.

References

1. N. M. Sanchez-Ballester; B. Bataille; I. Soulairol Carbohydrate Polymers 2021, 270, 118399. https://doi.org/10.1016/j.carbpol.2021.118399
2. M. Khajavian; V. Vatanpour; R. Castro-Muñoz; G. Boczkaj Carbohydrate Polymers 2022, 275, 118702. https://doi.org/10.1016/j.carbpol.2021.118702
3. S. M. Joseph; S. Krishnamoorthy; R. Paranthaman; J. A. Moses Carbohydrate Polymer Technologies and Applications 2021, 2, 100036. https://doi.org/10.1016/j.carpta.2021.100036
4. M. He; L. Shi; G. Wang; Z. Cheng; L. Han; X. Zhang; C. Wang; J. Wang; P. Zhou; G. Wang International Journal of Biological Macromolecules 2020, 155, 1245-1251. https://doi.org/10.1016/j.ijbiomac.2019.11.092
5. Empresa Brasileira de Pesquisa Agropecuária, *A produção da soja e do milho como um caminho para o desenvolvimento do agronegócio da região norte fluminense*, EMBRAPA, Rio de Janeiro, 2021.
6. M. P. M. da Costa; K. Rabelo; I. L. M. Ferreira; M. T. M. Cruz Journal of Applied Poylmer Science 2022, 139, 51776. https://doi.org/10.1002/app.51776
7. M. P. M. da Costa, Ph.D. Thesis, Universidade do Estado do Rio de Janeiro, 2018.
8. A. M. Senna; V. R. Botaro Journal of Controlled Release 2017, 260, 194-201. https://dx.doi.org/10.1016/j.jconrel.2017.06.009
9. R. F. P. da Rocha, M.S. Dissertation, Universidade do Estado do Rio de Janeiro, 2023.

10. Empresa Brasileira de Pesquisa Agropecuária, *Manual de métodos de análise de solo*, EMBRAPA, Distrito Federal, 2017.
11. Associação Brasileira de Normas Técnicas, *NBR 6457: amostras de solo: preparação para ensaios de compactação e ensaios de caracterização: método de ensaio*, ABNT, Rio de Janeiro, 2016.
12. M. Wolf; E. B. Tambourgi; A. T. Paulino Colloids and Surfaces A: Physicochemical and Engineering Aspects 2021, 609, 125679. https://doi.org/10.1016/j.colsurfa.2020.125679
13. L. F. W. Vleugels; S. Ricois; I. K. Voets; R. Tuinier Food Hydrocolloids 2018, 81, 273-283. https://doi.org/10.1016/j.foodhyd.2018.02.049
14. V. Hasija; K. Sharma; V. Kumar; S. Sharma; V. Sharma Vacuum 2018, 157, 458-464. https://doi.org/10.1016/j.vacuum.2018.09.012

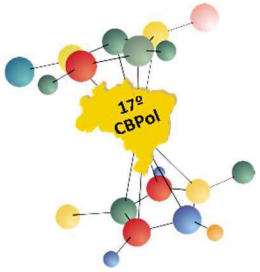

COTTON FABRIC FUNCTIONALIZED WITH CHITOSAN AND NEEM SEED OIL AIMING REPELLENT TEXTILE APPLICATIONS

Quesli Martins[1], Cristiane da Costa [1] and Andrea C. K. Bierhalz[1]*
1 – Department of Textile Engineering (DET), Federal University of Santa Catarina (UFSC), Blumenau, SC, Brazil.
andrea.krause@ufsc.br

Abstract: Textiles functionalized with active insecticide/repellent compounds have a potential to prevent disease-transmitting insect bites. A sustainable and effective approach is the combination of neem seed oil (NSO), which acts as a repellent and insecticide, and chitosan (CS), which forms a coating on cotton fibers, allowing for a prolonged and controlled release of the oil. In this study, a 100% cotton fabric was impregnated with different combinations of NSO and CS to investigate the color change in the fabric and the release kinetics of NSO from the fabrics to aqueous media. It was found that the impregnation of solutions containing only NSO caused changes in color and whiteness, with greater variation and less uniformity than the combination of CS + NSO in the same solution. Samples impregnated only with NSO released more oil than those impregnated with NSO and CS in two steps. In general, the results indicate that the combination of NSO and CS is promising in the development of textiles for the prevention of vector-borne diseases.
Keywords: *Textile functionalization; Insect repellent fabric; Chitosan; Neem Oil; Extended release.*

Introduction

The global spread of vector-borne diseases represents an alarming challenge, affecting millions of people annually. The industry and research in the textile field have shown a growing interest in the functionalization of textile substrates with repellents and insecticides as an effective form of protection against insect vectors [1-2]. These functional textiles can be used in several sectors, offering a safe and convenient form of prevention, reducing exposure to vectors, and, consequently, reducing the risk of contracting diseases [3].

The demand for more sustainable and safer solutions has driven the search for natural active agents and biopolymers for textile functionalization, such as neem seed oil and chitosan. Neem seed oil, extracted from the neem tree (*Azadirachta indica*), is known for its insecticidal and repellent properties [4]. In addition, this compound has low toxicity to humans and the environment [5]. On the other hand, chitosan, derived from the chitin found in crustaceans, has antimicrobial, biodegradable, and biocompatible characteristics [6]. Although chitosan does not have repellent and insecticidal properties by itself, it can interact with other compounds and form coatings or films on the surface of fabrics, mainly cellulosic substrates.

The combination of neem seed oil and chitosan in the functionalization of textile substrates presents potential for synergistic advantages. While neem oil can act as a repellent and insecticide, chitosan tends to contribute to the adhesion and formation of a coating on the fabric fibers, enhancing the controlled release of the oil and prolonging its effectiveness. Understanding the functionalization mechanisms and the properties of the resulting fabrics allows for exploring new application possibilities and contributing to the development of more efficient and ecologically correct textile products.

Thus, this study aims to obtain a 100% cotton textile substrate treated with a combination of neem seed oil and chitosan coating. The effect of the presence of the oil and/or chitosan coating was compared in terms of color change and oil release kinetics.

Experimental

Materials

As a textile substrate, was used a 100% cotton fabric (CO) of 120 g/m² and 180 threads/inch, in white color (optical white), and a taffeta structure. The materials used for functionalization were crude neem

vegetable oil (cold-pressed seeds of *Azadirachta indica*) provided by Passiflora (Brazil), chitosan of medium molecular weight and degree of deacetylation between 75-85% (Sigma-Aldrich, USA), Tween 80 (Exodus Científica, Brazil) as a stabilizer/surfactant. For the impregnation bath solution, anhydrous citric acid (Neon, Brazil) was used as a crosslinking agent, and anhydrous monobasic sodium phosphate (Lafan, Brazil) as a catalyst.

Preparation of impregnation solutions

The impregnation of the substrates was carried out using three different types of solutions: aqueous solutions containing neem seed oil (NSO) and surfactant, chitosan solutions at 0.5% (w/v) containing NSO and surfactant, and chitosan solutions at 0.5 % (w/v) containing only surfactant. To prepare the aqueous solutions, NSO and surfactant (Tween 80) were combined in a 1:3 mass ratio using a 5% (w/v) concentration of Tween 80 in 20 mL of deionized water.

Chitosan solution (CS) was prepared by dissolving 0.1 g chitosan in 20 mL of 1% (v/v) of aqueous acetic acid solution under magnetic stirring at 500 rpm and 25 °C. After dissolution for 30 min, 5% (w/v) of Tween 80 was added to the chitosan solution, and the mixture was stirred for additional 10 minutes. For chitosan-neem solution (CS-NSO), NSO was added to the chitosan emulsion with Tween 80 previously prepared, at a mass proportion of 1:3 oil-surfactant ratio under stirring for another 2 minutes.

Impregnation

The fabric samples with 1 g, previously washed, were immersed in a 20 mL solution of NSO, CS, or CS-NSO containing 0.5% (w/v) of monobasic sodium phosphate and 1% (w/v) of citric acid, for 30 minutes. Then, the impregnation process was carried out using a laboratory Foulard, adjusted for a pick-up between 90% and 100% (4.8 rpm, 1.4 bar). The samples were dried at 60 °C for 3 minutes and subsequently cured at 120 °C for 2 minutes in an oven with air circulation and renewal.

Fig 1 illustrates the combinations of types of solutions for fabric impregnation. NSO + 0.5% CS samples were prepared in two steps: first, the NSO solution was applied on cotton fabric, followed by the CS 0.5% solution impregnation.

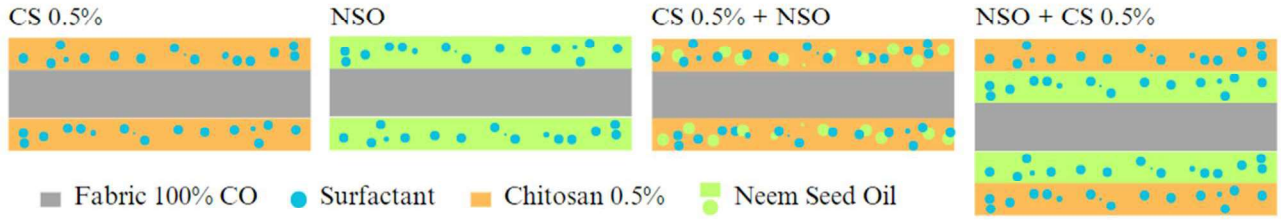

Figure 1 – Scheme of the types of solutions for impregnation.

The pick-up of the samples was determined by weighing the fabric before and after impregnation through Foulard, in dry and wet states, respectively.

Colorimetry

The colorimetric parameters and whiteness degree (Berger whiteness) of the cotton fabric after impregnations were evaluated using the Datacolor 500® reflectance spectrophotometer in CIELab color space using the D65 illuminant and with a 10º observer angle using 6 mm aperture.

In CIELab system, L* is the color lightness (L* = 0 for black and L* = 100 for white), a* is the green (-)/red (+) axis, and b* is the blue (-) /yellow (+) axis. The total color difference (ΔE), calculated by Eq. 1, was used to compare untreated (control) and fabrics treated with CS, NSO and CS-NSO, where ΔL*, Δa*, and Δb* are the difference between the L*, a*, and b* values, respectively, of the cotton fabric before and after the treatment.

$$\Delta E = \sqrt{\Delta L^2 + \Delta a^2 + \Delta b^2} \qquad (1)$$

NSO release kinetics in water

The kinetic release of the NSO from the fabric was evaluated *in vitro* using an aqueous media. Samples with 2 cm² were immersed in a flask containing 10 mL of deionized water. The system was maintained at a constant temperature of 25°C and stirred at 150 rpm in a New Lab model NL-343-01 shaker incubator. At predetermined time intervals, 3 mL aliquots of the solution were removed and analyzed by UV-Vis spectroscopy (model AJX-1900, Micronal) at a wavelength of 209 nm. The obtained absorbance was used to calculate the concentration of oil released in the water, based on the oil calibration curve previously obtained ($y = 1.716x + 0.0144$, $R^2 = 0.9972$). After each time measurement, aliquots were returned to the original solution to ensure that the system volume did not change.

Results and Discussion

After the preparation process, the obtained solutions were visually homogeneous, presenting a milky yellow color. However, it was observed that the aqueous NSO solution presented a phase separation during the period of fabric immersion and the NSO tended to accumulate on the surface of the solution. Consequently, differences in fabric appearance after treatment were observed.

When visually analyzing the samples before and after the impregnation of the solutions, Fig 2, it is evident the presence of spots in the samples impregnated with the NSO suspension, that result in an undesired effect on the appearance of the fabric. On the other hand, in the samples treated with CS solutions, a visual uniformity in terms of color, indicating a more homogeneous impregnation and an aesthetically pleasing result.

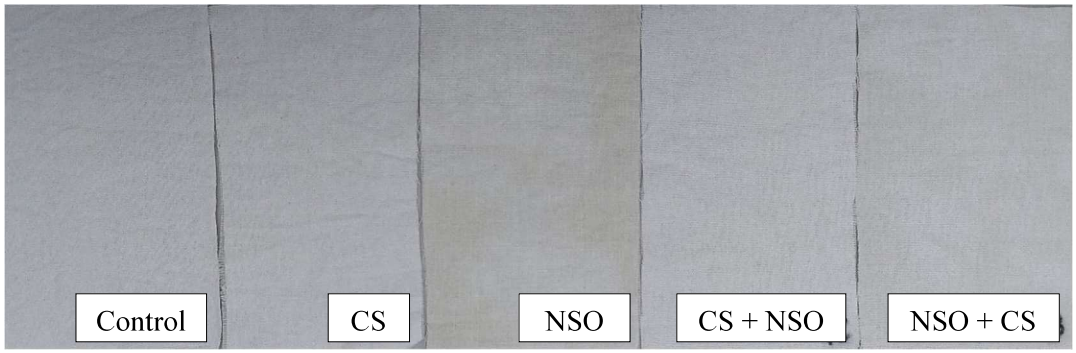

Figure 2 – Visual comparison of samples before and after impregnation of solutions in daylight.

These differences were quantified by color and the whiteness measurements using the fabric without impregnation as the control group. Table 2 shows the values obtained for each of the parameters of the CIELab system (L*, a*, b*) and the result obtained for the total color difference (ΔE).

Table 2 – Variations in color parameters for different combinations of CS 0.5% and NSO.

Sample	L*	a*	b*	ΔE	Nota ΔE
Control	89.9	2.44	-14.41	-	-
CS + NSO	89.60 ± 0.21	1.23 ± 0.12	-11.29 ± 0.35	3.36 ± 0.36	3
NSO + CS	88.73 ± 0.27	-0.05 ± 0.09	-7.56 ± 0.93	7.38 ± 0.93	2 - 1.5
NSO	88.41 ± 0.49	0.8 ± 0.59	-9.14 ± 2.36	5.73 ± 2.44	3 - 2
CS	90.07 ± 0.08	1.38 ± 0.11	-12.14 ± 0.36	2.52 ± 0.36	3.5

The impregnated samples showed lower values of a* and higher values of b*, indicating a more greenish and yellowish color, characteristic of NSO [5], when compared to the untreated fabric. Furthermore, the influence of the presence of NSO on the reduction of ligthness (L*) of the color can be observed.

Regarding the ΔE (total color difference) of the control sample, the ABNT NBR ISO 105-A05:2007 standard provides a classification in the color change in grayscale, where 5 is the best classification

and 1 is the worst. Based on this pattern and the results obtained, impregnation with the aqueous solution of NSO resulted in higher rates of color difference, indicating greater variation than the control. Another important factor is the standard deviation of these samples, which was greater than those impregnated with CS. This deviation refers to a non-uniform oil coverage on the textile surface, causing stains, while the samples impregnated with CS showed less deviation and greater uniformity in the finish, corroborating with visually observed in Fig 2.

Table 3 - Variations in the whiteness degree for different combinations of CS and NSO.

Sample	Whiteness Berger	Δ Berger
Control	143.62	-
CS + NSO	128.43 ± 1.64	-15.19 ± 1.63
NSO + CS	109.41 ± 5.13	-34.21 ± 5.13
NSO	114.9 ± 11.56	-28.72 ± 11.56
CS	134.04 ± 1.62	-9.58 ± 1.61

The whiteness values presented in Table 3 are consistent with the color parameter results. Despite the slight increase in ligthness observed in the CS samples (Table 2), all samples showed a reduction in ligthness as they acquired a yellowish color, especially those impregnated with NSO solution. Overall, it is evident that the impregnations altered the color and whiteness of the substrates.
Fig 3 presents the results of the release kinetic of the NSO from cotton fabric to aqueous media at 25°C.

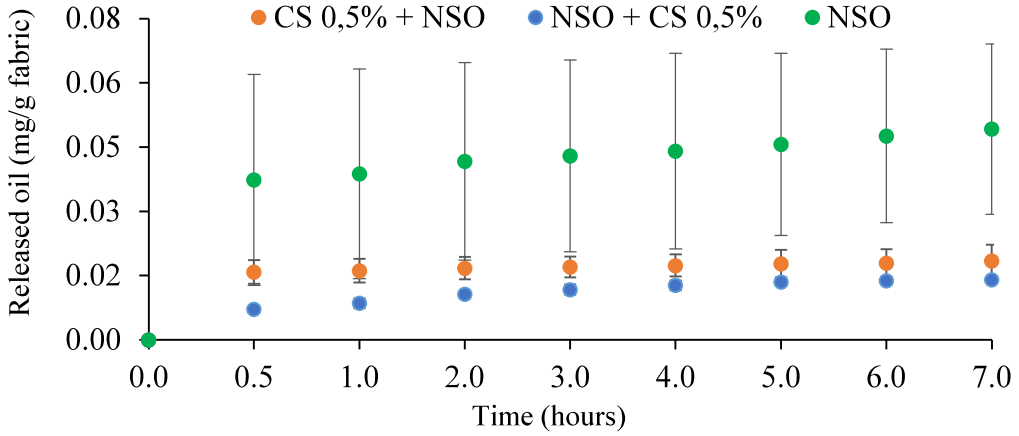

Figure 3 - NSO releases kinetics in comparison with CS release.

The results obtained confirm that NSO is released from substrates when in contact with water. The release profiles of the three analyzed samples showed similar behavior.
The sample impregnated in two steps (NSO + CS) showed the lowest amount of oil released. On the other hand, the sample impregnated only with oil (NSO) had the highest amount released. During the period evaluated, all samples showed slight growth in their release profiles.
In samples impregnated only with NSO, the oil was directly dispersed in liquid form in an aqueous solution containing surfactant, keeping the oil particles suspended in the solution. Although this facilitates release, this fact revealed a heterogeneous distribution of oil on the fabric surface due to the heterogeneous nature of the NSO solution during the dipping process. This characteristic is responsible for the observed variation in oil release.
The slower release in samples containing chitosan may be related to the possibility of chemical interaction between chitosan and cotton, which results in greater adhesion to the fabric.
Regarding the difference in release between samples impregnated with chitosan and oil, in samples impregnated in only one step (CS + NSO), the oil is dispersed in the polymeric matrix, that is, the release occurs from the coating to liquid media. In the samples with NSO + CS, the oil needs to

migrate from the fabric surface through the chitosan coating, due to the two-step impregnation process, which results in a slower release of the oil.
Considering an application such as fabric with repellent functionality, a slower release is desirable as it may result in a prolonged effect. However, it is important to emphasize that this study was carried out in a liquid medium, simulating rigorous release conditions, which results in higher release rates than in a gaseous medium. The release of the active principle must be sufficient to promote the desired repellent/insecticide effect, which can only be evaluated through i*n vivo* tests. Based on the results obtained so far, it can be inferred that the application of the NSO solution would not allow repeated use after washing, due to the rapid release observed in aqueous media. This test serves as a preliminary assessment of the behavior of textile substrates as carriers of the active agent. Therefore, additional analyzes are necessary to evaluate the system's resistance to washing and to determine the moment in which the complete depletion of the active principle will occur.

Conclusions

This study investigated the functionalization of cotton fabrics using neem seed oil (NSO) and chitosan (CS). Impregnation of fabrics with NSO resulted in changes in color and whiteness degree, with greater color variation and less uniformity in samples with the direct application of the NSO aqueous solution to the use of the CS solution. Samples impregnated only with NSO released more than those impregnated with NSO and CS in two steps since the oil particles are free on the surface. The results indicate that the combination of NSO and CS can be a promising approach for the development of functional textiles aiming prevention of vector-borne diseases. More analyzes are needed to evaluate the resistance to washing and determine the time of exhaustion of the active principle and improve the performance and durability of these materials, promoting advances and contributing to the production of textile products that are safer, more efficient, sustainable, and effective in protecting against transmitted diseases. by vectors.

Acknowledgements

The authors thanks to the Coordenação de Aperfeiçoamento de Pessoal de Nível Superior (CAPES) and Fundação de Amparo à Pesquisa do Estado de Santa Catarina (FAPESC) for financial support, and Passiflora Óleos for neem seed oil donation.

References

1. N. Singh; A. Madhu; P. D. Venkatraman in *The Textile Institute Book Series,* S. ul-Islam, A. Majumdar, B. Butola, Ed.; Woodhead Publishing, 2023; 509-334.
2. P. P. Chavan; P. Pandit in *The Textile Institute Book Series*, S. ul-Islam, B. S. Butola, Ed.; Woodhead Publishing, 2020; 335-357.
3. G. Natarajan; T. P. Rajana; S. Das; Journal of Natural Fibers 2022, 19:11, 4350-4367. https://doi.org/10.1080/15440478.2020.1857895
4. R. Roychoudhury in *Ecofriendly Pest Management for Food Security*, Omkar, Ed.; Academic Pres, Lucknow, 2016; 545-558.
5. S. Chatterjee; S. Bag; D. Biswal; D. S. Paria; R. Bandyopadhyay; B. Sarkar; A. Mandal; T. K. Dangar; Acta Tropica 2023, 240, 106858.
6. A. Elamri; K. Zdiri; M. Hamdaoui; O. Harzallah; Chitosan: A biopolymer for textile processes and products, Textile Research Journal 2023, 93 (5-6):1456-1484.

ENCAPSULATION OF COPAIBA ESSENCIAL OIL AND JOJOBA VEGETABLE OIL IN BIOPOLYMERIC NANOPARTICLES

Raphael F. S. Baraldi[1], Cristiane da Costa [1]

I - Department of Textile Engineering, Federal University of Santa Catarina (UFSC), Campus Blumenau, SC, Brazil
raphael.baraldi@grad.ufsc.br

Abstract - Essential and vegetable oils are widely employed across industries for their antioxidant, anti-inflammatory, healing, and moisturizing traits. This study aimed to develop nanoparticles with copaiba essential oil (CEO) and jojoba vegetable oil (JVO), using the emulsification/ionic gelation method. This process involves the interaction of positive ions from chitosan with negative ions from sodium alginate, forming a stable 3D network or gel. Nanocapsules in the diameter range 147-312 nm were obtained for the studied systems. Nanocapsules of chitosan/alginate, encapsulating JVO exhibited a good polydispersity index (PDI) with values around 0.25 and smaller particle diameter (Dp), when compared with nanoparticles containing CEO. In terms of encapsulation efficiency (EE), CEO samples achieved better results compared to JVO samples, with EE values up to 90%. The prepared of nanocapsules are promising for application in functional textiles.

Keywords: Nanocapsules; biopolymer; encapsulation efficiency; alginate; chitosan.
Fundings: CNPq/PIBIC, CNPq/Process 425402/2018-5T

Introduction

Essential and vegetable oils (E/VOs) are widely used in various fields such as cosmetics, food, textile, agricultural, medicine, and therapy. In the textile industry, E/VOs have been used to obtain antimicrobial, repellent, flavored, medical and skin care textiles [1]. One vegetable oil with a wide range of benefits is jojoba vegetable oil (JVO), which has anti-inflammatory properties, antioxidant action, antiviral activity, analgesic activities, among others [2]. On the other hand, copaiba essential oil (CEO) has interesting characteristics including analgesic, antiparasitic, larvicidal, antibacterial, and anti-inflammatory actions [3]. However, the instability of essential and vegetable oils under normal conditions poses a barrier to be overcome, which makes the nanoencapsulation of oils to prevent oxidative degradation so interesting [4]. In addition, the incorporation of nanoencapsuled compounds can result in textile products with greater washing durability, better fixation, lower toxicity, prolonged release and activity [1].

One of the most promising methods for oil nanoencapsulation is the ionic gelation method. This method involves a chemical process in which the positive ions from one solution interact with the negative ions from another solution, forming a stable three-dimensional network or gel [5].

Sodium alginate is a polysaccharide capable to form gels and can be used in the ionic gelation method [6]. The gel formation is initiated in the presence of the Ca2+ cation from Calcium Chloride (CaCl2), and this model is known as the "egg-box" model [5]. Chitosan can also be added to this process through the strong electrostatic interaction between the amino groups of chitosan and

the carboxylic groups of sodium alginate [7]. Such addition helps in stabilizing the surface charges and assists in reinforcing and preventing the degradation of the nanocapsule [8].

This work aimed to study the encapsulation of copaiba essential oil and jojoba vegetable oil in sodium alginate and sodium alginate/chitosan nanoparticles, produced using the emulsification/ionic gelation technique. The samples were characterized based on their size, polidispersity, and encapsulation efficiency.

Experimental

Materials

All the equipment and reagents used can be observed in Table 1.

Table 1 – The equipment and reagents used, as well as their respective company.

Commercial name	Company
Tween 80	Êxodo Científica
Sodium alginate	Êxodo Científica
Chitosan	Êxodo Científica
Jojoba oil	Ferquímica
Copaiba oil	Ferquímica
Calcium Chloride	ACS Química
Acetic Acid	CRQ Química
Ultrasonic Homogenizer	U.S. Solid
UV-M51	Bel Engineering
TC-10.000	Daiki
DLS	Malvern NanoS

Preparation of polymeric nanoparticles

To prepare the nanoparticles, first 10 mL of an aqueous solution with 1.0% w/v Tween 80, were mixed with 0.2 g of JVO or CEO under magnetic stirring for 5 min, followed by sonication for 18 min using an ultrasonic homogenizer with pulse parameters of 60 s on/30 s off, maximum amplitude of 40%, and performed in an ice bath to prevent heating of the solution. Then, 6 mL of sodium alginate were slowly added to the prepared oil dispersion under gentle agitation, followed by sonication using the same parameters. Subsequently, the obtained dispersion was dropped into 15 mL of $CaCl_2$ solution for the CEO/Alg-1, CEO/Chi-1, JVO/Alg-1, and JVO/Chi-1 samples, or into 21 mL of $CaCl_2$ solution for the CEO/Alg-2, CEO/Chi-2, JVO/Alg-2, and JVO/Chi-2 samples, under gentle agitation, followed by sonication under the same parameters. Finally, for the CEO/Chi-1, CEO/Chi-2, JVO/Chi-1, and JVO/Chi-2 samples, the dispersion was dropped into 6 mL of chitosan solution 1.0% v/v dissolved in 2.0% v/v acetic acid, followed by sonication under the same parameters. The samples were then placed in amber vials, cataloged, and stored in a refrigerator at an average temperature of 4 °C for further characterization.

Characterization

The encapsulation efficiency (EE), by indirect method was used to determine the amount of encapsulated oil. 1 mL of the nanoparticle dispersion was centrifuged in an Eppendorf tube for 15 min at 10,000 rpm using a mini centrifuge. After this, an aliquot of the supernatant was collected, diluted in ethanol, and transferred to a quartz cuvette. The absorbance was measured at 208 nm for JVO and 224 nm for CEO using an UV-vis spectrophotometer, with all samples being triplicated.

The EE value was calculated using Eq. 1, where the oil concentrations were obtained using the calibration curves Yjojoba = 7.029x + 0.003 for JVO and Ycopaiba = 13.071x + 0.302 for CEO, where Y is the absorbance found at 224 nm for CEO and 208 nm for JVO, and X is the concentration of the oil.

$$\%EE = \frac{Oil\ concentration_{Initial} - Oil\ concentration_{Supernatant}}{Oil\ concentration_{Initial}} \quad (1)$$

The particle size and size distribution (PDI) of the samples were determined by dynamic light scattering (DLS), at 25 °C, without prior dilutions. All measurements were carried out in triplicate.

Results and Discussion

The dispersions of both oils appeared homogeneous with a translucent white color.
The values of average particle diameter (Dp) and polydispersity index (PDI) of the nanoparticles can be observed in Table 2.

Table 2 – Average particle size (Dp) and polydispersity (PDI) of the prepared nanoparticles

Symbology	Md PDI	Md Dp
CEO/Alg-1	0.404 ± 0.018	184 ± 3
CEO/Alg-2	0.426 ± 0.013	241 ± 1
CEO/Chit-1	0.496 ± 0.019	241 ± 5
CEO/Chit-2	0.459 ± 0.026	313 ± 11
JVO/Alg-1	0.258 ± 0.037	148 ± 4
JVO/Alg-2	0.245 ± 0.002	156 ± 3
JVO/Chit-1	0.350 ± 0.037	195 ± 3
JVO/Chit-2	0.284 ± 0.007	184 ± 2

Polydispersity index values in the range of 0.1 to 0.25 indicate a narrow size distribution with low colloidal instability, while PDI values above 0.5 indicate a broad distribution [9]. Therefore, it can be noticed that the JVO samples, especially those without chitosan, exhibited a lower polydispersity around 0.25 (excluding the JVO/Chit-1 sample), compared to the CEO samples, which had a PDI around 0.44.

Small nanocapsules were obtained for all formulations, with average diameters in the range 147-312 nm. It can be observed that the average diameter (Dp) of the JVO samples was smaller compared to the CEO samples, except for the CEO/Alg-1 sample. This result may be due to the differences in the oils composition which leads to different interactions with the polyelectrolytes sodium alginate and chitosan. Comparing nanoparticles with only alginate and those with alginate and chitosan, it can be noticed that the particle diameter always increased after chitosan addition, showing the formation of a second layer in the nanocapsule's shell

The values obtained for encapsulation efficiency are presented in Figure 1. High encapsulation efficiencies were obtained for both alginate and alginate/chitosan nanoparticles encapsulating copaiba oil. Samples with CEO achieved approximately double the EE% compared to JVO samples. This result is due to the complexity of vegetable oils, which contain a variety of lipids and bioactive compounds, making efficient encapsulation challenging. Additionally, lower affinity and unfavorable interactions between the vegetable oil and the encapsulation material may have compromised the effectiveness of the process [10]. The fact that JVO samples had the smallest

average particle diameter results may be also linked to their low EE%, meaning that the oil did not enter the nanocapsules, resulting in smaller particle sizes compared to the others.

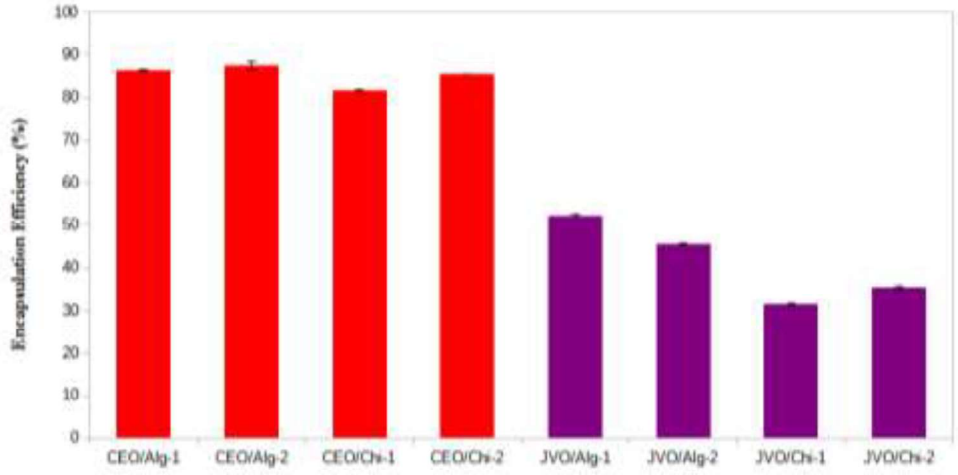

Figure 1 – Encapsulation efficiency of CEO (red bars) and JVO (purple bars) in the prepared nanoparticles.

Conclusion

The results obtained in this study demonstrate the effectiveness of nanoencapsulation of copaiba essential oil and jojoba vegetable oil. All the studied formulations resulted in capsules in the submicrometric range, with Dp values from 147 to 312 nm. Nanoparticles with copaiba oil samples showed great encapsulation efficiency, with the CEO/Alg-2 sample reaching a value of 89.03%. On the other hand, the encapsulation efficiency for samples with jojoba oil was considerably lower representing approximately half of the values obtained in copaiba oil samples. This disparity may be related to the lower affinity between the compounds present in the jojoba vegetable oil and the polymers used for encapsulation. However, further in-depth studies and tests are required to identify the underlying causes of this lower encapsulation efficiency.

In summary, nanoencapsulation offers opportunities to improve the functionalities provided by essential and vegetable oils, but the complex characteristics of oils and variable properties, can affect the encapsulation process. With ongoing efforts in this area, oil nanoencapsulation has the potential to play a significant role in the textile industry, enabling the production of functional textiles with natural components.

Acknowledgements

This work was supported by the Coordenação de Aperfeiçoamento de Pessoal de Nível Superior - Brasil (CAPES) and Conselho Nacional de Desenvolvimento Científico e Tecnológico – Brasil (CNPq).

References

1. S. Ghayempour, M. Montazer, R. M. Mahmoudi International Journal of Biological Macromolecules 2016, 93. doi: 10.1016/j.ijbiomac.2016.08.076.
2. H. A. Gad; A. Roberts; S. H. Hamzi; H. A. Gad; I. Touiss; A. E. Altyar; O. A. Kensara; M. L. Ashour Polymers 2021, 13(11), 1711. https://doi.org/10.3390/polym13111711.

3. A. B. F. de Lima; S. M. B. Leite; B. A. I. da Silva; E. I. L. Tenente; S. A. M. dos Santos; E. M. da S. Assunção; E. de S. Maciel; W. S. de Souza; I. N. Kaneko; C. A. da Costa; J. de O. Monteschio Research, Society and Development 2020, 9(10), e7649109078. https://doi.org/10.33448/rsd-v9i10.9078.
4. R. Delshadi; A. Bahrami; A. G. Tafti; F. J. Barba; L. L. Williams Trends in Food Science and Technology 2020, 104. https://doi.org/10.1016/J.TIFS.2020.07.004.
5. C. Hu; W. Lu; A. Mata; K. Nishinari; Y. Fang International Journal of Biological Macromolecules 2021, 177, 578–588. https://doi.org/10.1016/J.IJBIOMAC.2021.02.086.
6. A. Ahmad; N. M. Mubarak; F. T. Jannat; T. Ashfaq; C. Santulli; M. Rizwan; A. Najda; M. Bin-Jumah; M. M. Abdel-Daim; S. Hussain; S. Ali Processes 2021, 9. https://doi.org/10.3390/PR9010137.
7. D. Bedade; Y. B. Sutar; R. S. Singhal Food Chemistry 2019, 275. https://doi.org/10.1016/J.FOODCHEM.2018.09.090.
8. L. Segale; L. Giovannelli; P. Mannina; F. Pattarino Scientifica 2016, 5062706. https://doi.org/10.1155/2016/5062706.
9. C. D. Ferreira, I. L. Nunes; *Nanoscale Research Letters 2019*, *14*(1), 9. https://doi.org/10.1186/s11671-018-2829-2
10. J. F. Masiero, J. E. Barbosa, L. O. Macedo, A. de Souza, M. N. Yukuyama, G. J. Arantes, N. A. Bou-Chacra; *Industrial Crops and Products 2021*, *170*, 113838. https://doi.org/https://doi.org/10.1016/j.indcrop.2021.113838

THE EFFECT OF HUMIDIFICATION WITH SALINE SOLUTION ON IMPEDANCE MEASUREMENTS OF ELETROSPUN PVC/CNT MEMBRANES

Marcio Briesemeister[1], John A Gomez-Sanchez[2], Pedro Bertemes Filho[2] and Sérgio Henrique Pezzin[1]

1 – Materials Science and Engineering Program, Santa Catarina State University (UDESC), Joinville, SC, Brazil
2 - Electrical Engineering Program, Santa Catarina State University (UDESC), Joinville, SC, Brazil
marcio.brie@gmail.com

Abstract - The advancement of electrospinning technology, combined with the versatility and low cost of PVC, favored the expansion of the use of the material for a wide variety of applications: air/water filtration systems, energy, and corrosion protection [1]. Mechanical resistance, adjustable hydrophobicity, and high porosity are characteristics that can be highlighted in electrospun PVC mats [1], and the combination of the material with other functional nanofillers, such as carbon nanotubes (CNTs), can further expand its field of use [2]. The present study aims to evaluate the influence of humidification with saline solution on the electrical impedance spectrum of electrospun PVC/CNT membranes. For this, membranes containing up to 3 wt% of CNTs were electrospun from solutions in THF/DMF and characterized by FE-SEM and TEM to analyze the morphology of the membranes and verify the dispersion of CNTs inside the nanofibers. Finally, dry, and wet membranes were subjected to electrical impedance spectroscopy measurements in the range of 10 Hz to 5 MHz. For dry membranes, no significant differences were found in impedance results as a function of CNTs concentration. On the other hand, for those humidified with saline solutions there was a reduction in the impedance modulus from 8.7%, for neat PVC membrane, to 93.7%, for PVC/CNT 3% composites, demonstrating that the impedance modulus decreases exponentially with the concentration of CNTs. This behavior may be related to the hydrophilic characteristic of the nanotubes used, due to some degree of oxidation of the CNTs, thus increasing the interaction with water, and providing a greater ionic transport through the composite. TEM images show that most nanotubes are inside the fibers and oriented along them, while SEM micrographs showed membranes with homogeneous distribution of fibers with surface porosity.

References:

1. L. Quoc Pham, M.V. Uspenskaya, R.O. Olekhnovich, R.A. Olvera Bernal. *Fibers*, 9 (2021), p. 12. https://doi.org/10.3390/fib9020012.
2. L. Liu, W. Xu, Y. Ding, S. Agarwal, A. Greiner, G. Duan. *Composites Communicatio*, 22 (2020), p. 100506. https://doi.org/10.1016/j.coco.2020.100506.

Fundings: Thanks to FAPESC for the financial support (2021TR928), UNIEDU for scholarship (18243), and the Multi-User Facility infrastructure from CCT/UDESC.

Keywords: *Electrospun nanofibers; Polyvinylchloride; Carbon nanotubes; Electrical impedance spectroscopy; saline solution*

EFFECTS OF A CHITOSAN/GELATIN AND POMEGRANATE (*PUNICA GRANATUM* L.) PEEL EXTRACT COATING ON THE PHYSICOCHEMICAL AND SHELF-LIFE OF PAPAYA (*CARICA PAPAYA* L.) FRUITS

Mirella Romanelli V. Bertolo*, Cristiane T. Moreira and Stanislau Bogusz Junior

University of São Paulo (USP), São Carlos Institute of Chemistry (IQSC), São Carlos, SP, Brazil
mirella.bertolo@usp.br

Abstract - Papaya is a fruit cultivated in tropical regions and appreciated worldwide due to its high nutritional value and economic potential, despite its short shelf-life and high susceptibility to fungal diseases [1]. One alternative to extend the shelf-life of papaya is the use of polymeric edible coatings, based on natural polymers like chitosan and gelatin and containing phenolic compounds to confer antioxidant activity [2]. The aim of this study was to develop a chitosan/gelatin-based (C/G) coating containing pomegranate peel extract (PPE) and evaluate the improvements brought by its application on the shelf-life of papaya fruits. The coating (CPPEG) was prepared by dipping an ethanolic solution (60%, v/v) of PPE in a 2% (w/w) chitosan solution (in 1% w/w lactic acid), followed by mixing with a 1% (w/w) gelatin solution (1:1) at 45 °C. The final concentration of PPE in the coating was 4 mg g^{-1}. The papaya fruits were coated with 1 mL of CPPEG for 10 s (n = 10), dried at room temperature, and stored at 16 °C and 65% of relative humidity. A control group of uncoated papayas was also evaluated. CPPEG was able to decrease the weight loss of the fruits after 15 days of storage (23.29 ± 7.62% for the uncoated papayas and 13.71 ± 4.24% for the coated ones); the coated fruits showed significantly equal values of hardness (4.56 ± 2.98 N), pH (6.08 ± 0.22) and total soluble solids (8.73 ± 1.19%) than the uncoated fruits, indicating that the coating was able to maintain the physicochemical properties of papayas. Moreover, the ripening of the coated fruits was visually delayed. Thus, the coating developed in this study has promising properties to be used in maintaining the physicochemical quality and extending the shelf life of papayas.

References

1. Y. Zhou; L. Hu; Y. Chen; L. Liao; R. Li; H. Wang; Y. Mo; L. Lin; K. Liu. *LWT* 2022, *171*, 114134. https://doi.org/10.1016/j.lwt.2022.114134.
2. M. R. V. Bertolo; L. D. Dias; J. G. Oliveira Filho; F. Alves; C. A. Marangon; V. C. A. Martins; M. D. Ferreira; V. S. Bagnato; A. M. G. Plepis; S. Bogusz Junior. *Food Packaging and Shelf Life* 2022, *34*, 100986. https://doi.org/10.1016/j.fpsl.2022.100986.

Fundings: FAPESP grant: 2019/18748-8.

Keywords: *papaya, chitosan, gelatin, pomegranate, coatings.*

FUNCTIONALIZATION OF TEXTILE SUBSTRATE WITH CONDUCTIVE POLYMER

Ludimilla B. Ferreira[1], Pedro Bachmann[1], Cláudia Merlini[2] and Fernanda Steffens[1]*

1 – Textile Engineering Postgraduate Program (PGETEX), Federal University of Santa Catarina (UFSC), Blumenau, SC, Brazil ludimillabarbosa18@gmail.com

2 – Special Coordination of Material Engineering, Federal University of Santa Catarina (UFSC), Blumenau, SC, Brazil

Abstract – Smart textiles have been studied as materials capable of sensing and responding to external stimuli and, in very intelligent systems, adapting to the environment.[1,2] The use of textile structures is of great interest due to their characteristics such as conformability, flexibility, and comfort offered to the user. Given the above, there is a tendency to develop smart textiles that can be applied as wearable devices and that offer technological solutions to the user in order to take advantage of the movements generated during the use of clothes and accessories to supply and conduct an electric current that can be used in electronic devices.[2-4] Thus, this present study aims to develop a conductive textile from the functionalization of the surface of two knitted fabrics – Jersey and Rib in cotton and viscose- and to evaluate its conductivity. During the studies, polymerization conditions were made using polypyrrole (PPy) and $FeCl_3$ in different concentrations respecting the molar ratio of 2:1 [$FeCl_3$: PPy], as presented in previous works[5,6]. In the visual analysis, it was observed that the samples produced with ¼ of concentration presented little residue on the surface and less rigidity when compared to the other conditions produced. Another point observed, the time of 1 hour of polymerization, showed greater adhesion of the polymer to the surface, presenting the most effective functionalization condition. In the conductivity analysis, the 4-point technique was used and it was possible to observe that the functionalized knitted fabrics were shown to be conductive in all conditions studied, presenting conductivities of 0.06 S/cm and 0.04 S/cm for viscose Jersey and cotton Rib knitted fabric, respectively. This study has great potential to develop smart textiles in which conductivity is an important differential and opens up new possibilities for wearable technology.

Keywords: *Smart textile; polypyrrole; weft knitted fabric.*

References

1. N. D. Yilmaz. *Smart Textiles*. 1. ed. Hoboken: John Wiley & Sons, Inc., 2018.
2. G. Chen; Y. Li; M. Bick; J. Chen. *Chemical Reviews* 2020, 120. https://doi.org/10.1021/acs.chemrev.9b00821.
3. H. Gauche; F. R. Oliveira; C. Merlini; A, P. Hiller; A. P. G. V. Souto; I. D. Cabral; F. Steffens. *Journal of Natural Fibers* 2020, 19. https://doi.org/10.1080/15440478.2020.1821288.
4. M. Tokarska; M. Orpel. *Textile Research Journal* 2019, 89. https://doi.org/10.1177/0040517518763978
5. C. Merlini; S. D. A. S. Ramôa; G. M. O. Barra. *Polymer Composites* 2013, 34. https://doi.org/10.1002/pc.22448.
6. C. Merlini; R. S. Almeida; M. A. D'Ávila; V. H. Schreiner; G. M. O. Barra. *Materials Science & Engineering* 2014, 179. https://doi.org/10.1016/j.mseb.2013.10.003.

FUNCTIONAL POROUS MATERIALS FROM LIGNOCELLULOSE

Denise F. S. Petri[1]*

1 – Institute of Chemistry, University of São Paulo (USP), São Paulo, SP, Brazil dfsp@iq.usp.br

Abstract - Lignocellulose is the primary component of many biomasses, including sugarcane bagasse (SB) and kapok fibers (KF). Lignocellulose contains cellulose, hemicellulose, and lignin, and can be assembled with the aid of citric acid and polydopamine (PDA) to create functional porous materials. Recently, we combined SB microparticles with KF, which are hydrophobic hollow fibers extracted from the seeds of *Ceiba speciosa*. Such combination led to filters able to demulsify O/W emulsion wastes from a local lithium grease manufacturer. The mechanism proposed involved the ion-exchange of Li+ by H+ on the SB surface, whereas the oil phase adsorbed on the KF surface. PDA coated SB microparticles were outstanding adsorbents towards Cr(IV) ions; under optimized operational conditions, the adsorption capacity was 1417.04 mg/g. Electrostatic interactions and ion-dipole interactions, evidenced by X-ray photoelectron spectroscopy (XPS), drove the efficient adsorption process. The spent adsorbents were successfully incorporated into cements, which presented mechanical properties similar to the pure cement and no leaching of Cr(VI) was observed, indicating that this is a sustainable strategy to handle with the spent adsorbents. SB microparticles combined with chitosan or carboxymethyl cellulose via esterification with citric acid provided low-cost filters to treat the wastewater of undergraduate laboratory containing 17 metal ions at pH 1. The charges on the polysaccharides and on SB microparticles played an important role on the metal ions selective adsorption. These are some examples to show that combining lignocellulose with other low impact reactants opens a myriad of new functional materials (Figure 1).

Figure 1 – Examples of functional lignocellulosic materials for treatment of laboratory and industrial waste.

Fundings: FAPESP (2018/13492-2) and CNPq (304017-2021) are gratefully acknowledged.

Keywords: *lignocellulose, biomass, adsorption, demulsification, polydopamine*

POLYETHERIMIDE MEMBRANES FOR SEPARATION OF SYNTHETIC EFFLUENT

Pamela T. V. da Silva[1*], Vanessa N. Medeiros[1], Renê A. da Paz[1], Bruna A. Araújo1, Rafael A. Dias[1], Edcleide M. Araújo[1].

1 – Academic Unit of Materials Engineering (UAEMa), Federal University of Campina Grande (UFCG), Campina Grande, PB, Brazil
*pamela_thainara@hotmail.com

Abstract - Currently, the world uses membrane technology for wastewater treatment, desalination, gas separation, and effluent treatment as an attractive process for water quality. The class of organic (polymeric) membranes is widely used in water treatment, where the final study leads to one for removing specific organic contaminants and resistance to biological treatment, preventing the reach of these compounds to the environment and the water consumed by humans. This research aims to develop membranes varying the proportion of polyetherimide (PEI) with solvent (90/10, 85/15, and 80/20) obtained by the phase inversion method for water treatment with synthetic dyes. Flow measurements and contact angle characterized the membranes to determine their hydrophilicity through the sessile drop method, permeate quality analysis, and atomic force microscopy (AFM). With the analysis of the red dye used as a synthetic effluent, it was possible to obtain promising results, with a turbidity reduction rate of the permeate greater than 90%. In the AFM analysis, the roughness parameters were visualized, verifying the influence of the polymer content on the surface morphology. Parts of the AFM images suggest a sign of increased surface pore diameter. The contact angle measurements corroborate the results obtained by the flow measurement, confirming the surface hydrophilicity.

Fundings: The authors thank UFCG, CAPES, CNPq, and FAPESQ/PB for financial support.

Keywords: *membrane, polyetherimide, synthetic effluent.*

SYNTHESIS OF POLYANILINE ON PLASMA TREATED CARBON FIBER TEXTILE FOR SUPERCAPACITOR APPLICATIONS

Wilma de Medeiros[1], Luis Cesar Fontana[2] and Carla Dalmolin[1]*

1 – Department of Chemistry, Santa Catarina State University (UDESC), Joinville, SC, Brazil
carla.dalmolin@udesc.br
2 – Department of Physics, Santa Catarina State University (UDESC), Joinville, SC, Brazil

Abstract - The chronic depletion of fossil fuel sources and vital environmental pollution issue demand for systems or devices using green and renewable energy, aiming sustainability and reducing dependence on the non-renewable sources. So, research has been intensified to build efficient materials, as conducting polymers, for power sources and charge accumulation devices. Polyaniline (Pani) is widely studied due its easy synthesis, good chemical and thermal stabilities, high electric conductivity and reversive oxidation / reduction processes. However, interaction between Pani and the carbon substrate used as current collector interferes on the efficiency of the final electrode. So, the present work has the objective of evaluate the effect of the plasma functionalization of carbon fiber textile (CF), with the intention to promote conjugated covalent bonds between the substrate and the polymeric chain, intensifying their interaction and electron transfer. The applied methodology was based on exposition of CF to Ar/N_2 plasma, to promote reactive groups on its surface and creating anchors to the grow of the polymeric chain in the following interfacial synthesis of Pani. For comparison purposes, Pani electrodes were produced using CF without any treatment or CF with previous adsorbed aniline. The morphological characterization, by Scanning Electron Microscopy (SEM), allied with X-Ray Photoelectron Spectroscopy (XPS), showed modifications on the fiber rugosity and the insertion of polar and N-functional groups on its surface. Eventually, the electrochemical Properties of the electrode were evaluated by Cyclic Voltammetry (CV) and Electrochemical Impedance Spectroscopy (EIS). The results showed lower impedance and higher peak and capacitive currents for the electrode whose CF was treated by Ar/N_2 when compared with electrodes with CF without treatment or with adsorbed aniline.

Fundings: FAPESC, CAPES, CNPq.

Keywords: *Polyaniline, Carbon fiber textile, Supercapacitors, Plasma*

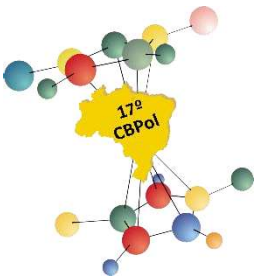

ANTIOXIDANT PERFORMANCE OF NATURAL ANTIOXIDANT-LOADED GELATIN FILMS PRODUCED BY SOLUTION CASTING METHODS

André M. Silva[1,2], Liliane S. F Leite[1], Luiz H. C. Mattoso[1] and Francys K V Moreira[2,*]

[1]National Nanotechnology Laboratory for Agriculture (LNNA), Embrapa Instrumentation, São Carlos (SP), Brazil.
[1]Multifunctional Packaging group (GEF[m]), Department of Materials Engineering (DEMa), Federal University of São Carlos (UFSCar), São Carlos (SP), Brazil. [*]francys@ufscar.br

Abstract - This work was aimed at evaluating the antioxidant capacity of biodegradable gelatin films loaded with tannic acid (TA) and citric acid (CA). Both TA and CA are natural, non-toxic, and cheap antioxidant compounds, so their potential in active packaging have grown over the last years. TA- and CA-loaded gelatin films were prepared by bench casting (BC) at 35 ºC and continuous solution casting (CSC) at 120 ºC to evaluate the effect of casting conditions on the antioxidant performance of the ensuing films. From the DPPH scavenging method, it was observed that the TA-loaded gelatin films had a superior antioxidant activity than those containing CA. In addition, the antioxidant activity of TA was even more pronounced in the films produced by CSC rather than by BC, presenting Ec_{50} equal to 0.1 g/L and 4 g/L, respectively. CSC is a suitable technique to hasten the production of biodegradable active packaging from gelatin and natural antioxidants.
Keywords: *Biodegradable packaging, DPPH, casting, active packaging.*
Fundings: FAPESP (Project nº 2022/13428-8); CNPq Universal (Project nº 407288/2021-0).

Introduction

Over the last decades, research into new biodegradable films has focused on incorporating bioactive agents to extend the shelf-life of food products while reducing the amount of non-biodegradable plastic used in packaging [1]. Gelatin films, for instance, can serve as a carrier medium for bioactive additives with the purpose of adding antioxidant, bactericidal and pH-responsive functions to products [2]. Gelatin is a water-soluble protein obtained from hydrolysis of collagen, the most abundant protein in nature. Some key features of gelatin films beyond their intrinsic biodegradability include low O_2 permeance, but moderate one to moisture, good mechanical properties, and high optical transparency [2-4].

In a previous study, tannic acid (TA) was compounded with gelatin by bench casting (BC) to successfully create new eco-friendly antioxidant films [5]. TA are plant-derived polyphenolic compounds that have received much attention due to their low cost and multifunctionalities, such as antioxidant capacity, broad antimicrobial activity, and cross-linking effect on polymers such as gelatin [6-9]. However, TA can under oxidation and lose antioxidant activity depending on how it is exposed to O_2 and heat in aqueous environments [5]. Thus, it is utmost importance to evaluate the effect of processing conditions on the antioxidant performance of TA-loaded gelatin films, especially when produced by solution casting techniques.

This work aimed to investigate the correlation between casting conditions and antioxidant properties of TA-loaded gelatin films produced by solution casting. Temperature was varied by conducting BC at 35 ºC and by producing films using a pre-pilot continuous solution casting (CSC) method at 120 ºC [10]. TA was further compared with citric acid (CA) regarding the potential of ensuing antioxidant films with gelatin. CA is one the most traditional organic acids used in the food industry mainly as

an acidulant, flavoring, and antioxidant in the preparation of different products [11-13]. The molecular structures of both antioxidant agents are depicted in Fig. 1.

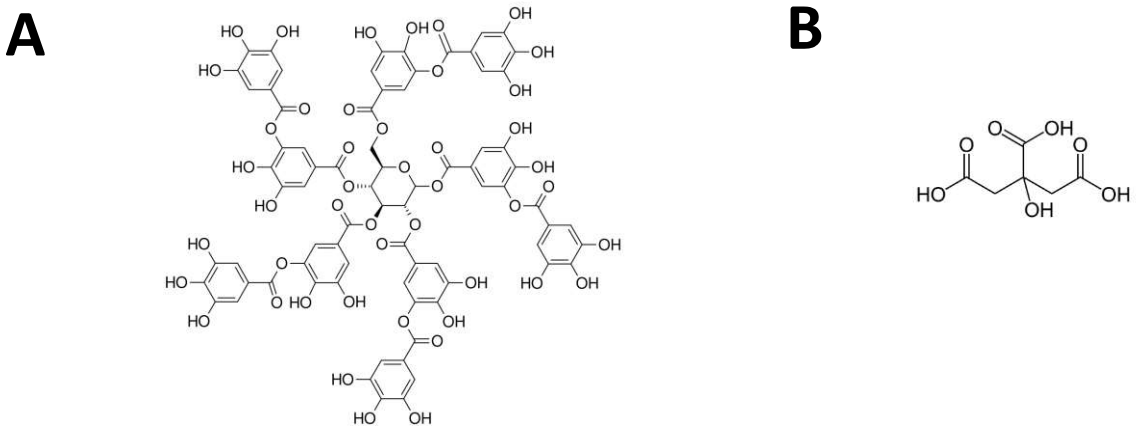

Figure 1: Molecular structure of (A) tannic acid [14] (B) citric acid [15].

Experimental

Materials

Powdered bovine gelatin (Bloom Strength-280) was provided by Gelco Gelatinas do Brasil Ltda (Pedreiras, SP). Tannic acid (TA) was purchased from Sigma-Aldrich (USA). Citric acid was purchased from ACS Científica (Brazil). Glycerol (CAS No. 56-81-5) was used as a plasticizer in all samples. All solutions were prepared with ultrapure water obtained from a Milli-Q system.

Preparation of film-forming solutions (FFS)

Aqueous gelatin/TA and gelatin/CA solutions were produced by mixing 30% (w/w) of gelatin, 25% (w/w) of glycerol followed by heating in a water bath under mechanical stirring for 20 min at 70 - 80 °C. Then, the antioxidant agents were added at 3% (w/w, gelatin mass basis) to the solutions using a mechanical stirrer for 10 min [5].

Bench (BC)

FFS were bench cast on steel plates (D = 40 cm) and dried in an air-circulating oven at 35 ºC for 24 h. Afterwards, films were peeled off from the plates and stored in plastic bags prior to use.

Continuous solution casting (CSC)

FFS were processed by CSC on a KTF-S labcoater casting machine (Werner Mathis AG, Switzerland), using a doctor blade to conveyor height of 1.2 mm, conveyor speed of 12 cm/min and drying temperature at 120 °C [10]. Films were peeled off from the conveyor and stored in plastic bags prior to use.

Determination of antioxidant activity

Antioxidant activity was determined for each film using the standard DPPH free radical scavenging method, as described elsewhere [15 - 18].

Results and Discussion

Fig. 2 shows the results of the DPPH scavenging tests carried out for gelatin films containing TA and CA at 3% (w/w). It is possible to observe a clear difference between the proposed casting methods.

The most effective reductions in DPPH absorbance were achieved with the CSC-films, particularly those loaded with TA.
BC and CSC differ not only concerning temperature, but also with respect to the drying time. For BC, the drying time FFS was about 24 h, which may have led to a substantial oxidation of TA due to its prolonged exposure in an aqueous medium even at low temperature [5]. Yet for CSC, the drying time was drastically cut down to 16 min [11]. The results indicate that CSC did not degrade TA at a high extent, even processing the FFS at 120 ºC.
An important parameter that can be obtained from the curves shown in Fig. 2 is the Ec_{50} (sample concentration capable of reducing the initial concentration of DPPH by 50%). According to the results, the Ec_{50} of TA-loaded gelatin films produced by BC and CSC were 4 g/L and 0.1 g/L, respectively, denoting the feasibility of CSC in preserving the antioxidants properties of TA.

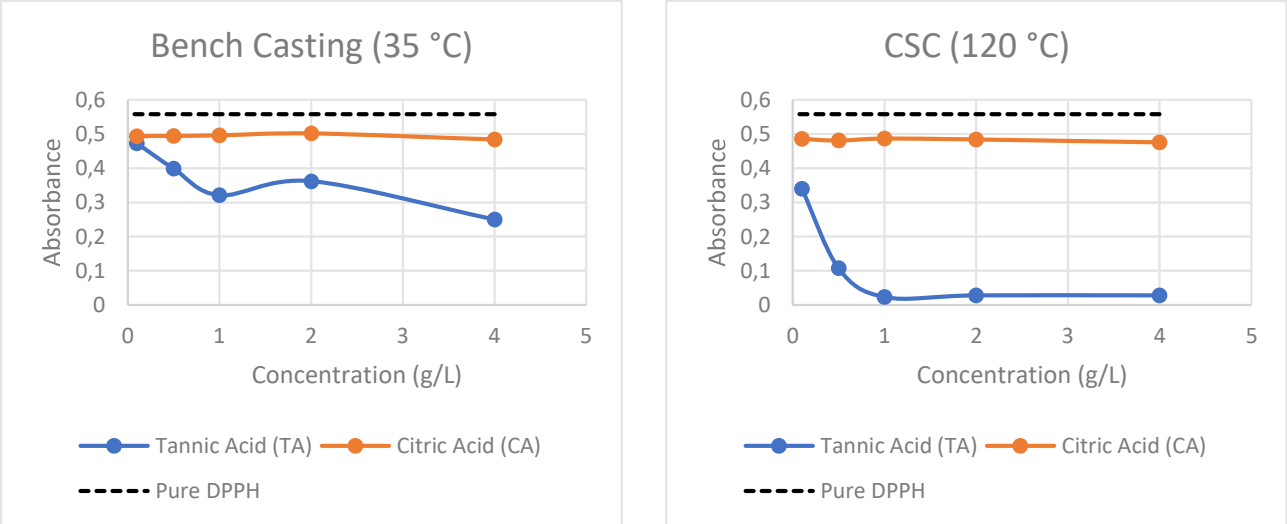

Figure 2: DPPH absorbance variation as a function of antioxidant (TA or CA)-loaded gelatin film concentration (g/L). Pure DPPH absorbance (A = 0.558) was added as a reference for null antioxidant activity.

It is also verified from Figure 2 that the TA-loaded gelatin films exhibited a significantly higher antioxidant activity than those loaded with CA, this latter presenting an ineffective result by the proposed method with no EC_{50} found in the studied concentration rage. A possible explanation for this result is that the main antioxidant mechanism of CA is based on its chelating effect on metal ions that catalyze oxidation reactions instead of scavenging free radicals. On the other hand, TA is a sterically hindered polyphenolic antioxidant, as illustrated in Fig. 1, that reacts directly with DPPH or any other free radical in a similar manner to primary antioxidants used in polymers (Irganox® and so on).

Conclusions

Biodegradable gelatin films containing TA displayed antioxidant performance that are highly superior to films containing CA. In addition, the films produced from the CSC method containing tannic acid showed the highest antioxidant activity among the tested films, with an Ec_{50} of 0.1 g/L, evidencing the superior viability of this method over BC and confirming the antioxidant activity of tannic acid at high processing temperatures. Therefore, the scaled-up production of antioxidant films for packaging using the CSC method is a potential alternative due to its various commercial advantages when compared to BC.

Acknowledgements

The authors gratefully acknowledge the financial support provided by the São Paulo Research Foundation (FAPESP) (grant number 2022/13428-8), Coordination of Superior Level Staff

Improvement - Brasil (CAPES) - Finance Code 001, National Network of Laboratories for Nanotechnology (SisNANO), and CNPq Universal Program (Project nº 407288/2021-0).

References

[1] S. Sivakanthan, S. Rajendran, A. Gamage, T. Madhujith, and S. Mani, "Antioxidant and antimicrobial applications of biopolymers: A review," *Food Research International*, vol. 136, p. 109327, Oct. 2020, doi: 10.1016/J.FOODRES.2020.109327.

[2] X. Zhang *et al.*, "Lignocellulosic nanofibrils as multifunctional component for high-performance packaging applications," *Mater Today Commun*, vol. 31, Jun. 2022, doi: 10.1016/j.mtcomm.2022.103630.

[3] A. Rohman, A. Windarsih, Y. Erwanto, and Z. Zakaria, "Review on analytical methods for analysis of porcine gelatine in food and pharmaceutical products for halal authentication," *Trends Food Sci Technol*, vol. 101, pp. 122–132, Jul. 2020, doi: 10.1016/J.TIFS.2020.05.008.

[4] J. P. Santos, V. M. Esquerdo, C. M. Moura, and L. A. A. Pinto, "Crosslinking agents effect on gelatins from carp and tilapia skins and in their biopolymeric films," *Colloids Surf A Physicochem Eng Asp*, vol. 539, no. September 2017, pp. 184–191, 2018, doi: 10.1016/j.colsurfa.2017.12.018.

[5] L. S. F. Leite *et al.*, "Effect of Tannic Acid and Cellulose Nanocrystals on Antioxidant and Antimicrobial Properties of Gelatin Films," *ACS Sustain Chem Eng*, 2021, doi: 10.1021/acssuschemeng.1c01774.

[6] P. Dalev *et al.*, "Biodegradation of chemically modified gelatin films in a simulated natural environment," *Biotechnology and Biotechnological Equipment*, vol. 15, no. 2, pp. 116–123, 2001, doi: 10.1080/13102818.2001.10819142.

[7] I. Gülçin, Z. Huyut, M. Elmastaş, and H. Y. Aboul-Enein, "Radical scavenging and antioxidant activity of tannic acid," *Arabian Journal of Chemistry*, vol. 3, no. 1, pp. 43–53, Jan. 2010, doi: 10.1016/J.ARABJC.2009.12.008.

[8] J. Guo, L. Ge, X. Li, C. Mu, and D. Li, "Periodate oxidation of xanthan gum and its crosslinking effects on gelatin-based edible films," *Food Hydrocoll*, vol. 39, pp. 243–250, 2014, doi: 10.1016/j.foodhyd.2014.01.026.

[9] M. do L. L. R. Menezes *et al.*, "Effect of tannic acid as crosslinking agent on fish skin gelatin-silver nanocomposite film," *Food Packag Shelf Life*, vol. 19, no. March 2018, pp. 7–15, 2019, doi: 10.1016/j.fpsl.2018.11.005.

[10] L. S. F. Leite, C. M. Ferreira, A. C. Corrêa, F. K. V. Moreira, and L. H. C. Mattoso, "Scaled-up production of gelatin-cellulose nanocrystal bionanocomposite films by continuous casting," *Carbohydr Polym*, vol. 238, no. January, p. 116198, 2020, doi: 10.1016/j.carbpol.2020.116198.

[11] W. Zhang, S. Roy, E. Assadpour, X. Cong, and S. M. Jafari, "Cross-linked biopolymeric films by citric acid for food packaging and preservation," *Adv Colloid Interface Sci*, vol. 314, p. 102886, Apr. 2023, doi: 10.1016/J.CIS.2023.102886.

[12] B. S. Börekçi, G. Kaban, and M. Kaya, "Citric acid production of yeasts: An overview," *Eurobiotech Journal*, vol. 5, no. 2. De Gruyter Open Ltd, pp. 79–91, Apr. 22, 2021. doi: 10.2478/ebtj-2021-0012.

[13] A. R. Angumeenal and D. Venkappayya, "An overview of citric acid production," *LWT - Food Science and Technology*, vol. 50, no. 2, pp. 367–370, Mar. 2013, doi: 10.1016/J.LWT.2012.05.016.

[14] Tannic acid. https://en.wikipedia.org/wiki/Tannic_acid
[15] Citric acid formula. https://www.softschools.com/formulas/chemistry/citric_acid/329/
[16] W. Brand-Williams, M. E. Cuvelier, and C. Berset, “Use of a Free Radical Method to Evaluate Antioxidant Activity,” 1995.
[17] M. Do *et al.*, “Metodologia Científica: Determinação da Atividade Antioxidante Total em Frutas pela Captura do Radical Livre DPPH Introdução”.
[18] C. Sanchez-Moreno, “Review: Methods used to evaluate the free radical scavenging activity in foods and biological systems,” *FOOD SCIENCE AND TECHNOLOGY INTERNATIONAL*, vol. 8, no. 3, pp. 121–137, Jun. 2002, doi: 10.1106/108201302026770.

CHITOSAN FILMS FOR THE STABILIZATION OF ENZYMES IN AQUEOUS SOLUTIONS

Larisa F. da Cruz[1], Amanda G. Polizeli[1], Mirlene P. Vitorino[2], Heveline Enzweiler[3] and Alexandre T. Paulino[1,2,4*]

1 - Postgraduation Program in Food Science and Technology, Santa Catarina State University (UDESC), Pinhalzinho, SC, Brazil
2 - Postgraduation Program in Applied Chemistry, Santa Catarina State University (UDESC), Joinville, SC, Brazil
3 - Department of Food and Chemical Engineering, Santa Catarina State University (UDESC), Pinhalzinho, SC, Brazil
4 - Department of Chemistry, Santa Catarina State University (UDESC), Joinville, SC, Brazil
**Email: alexandre.paulino@udesc.br.*

Abstract

Chitosan-co-GLU/eucalyptus residue composite films were synthesized, characterized, and tested for the stabilization of enzymes in aqueous solutions, using lactase as enzyme model. Point of zero charge, Fourier-transformed infrared spectrometry, thermal analysis, and scanning electron microscopy confirmed the film structures. The following experimental conditions assisted in avoiding enzymatic degradation: i) enzyme/buffer solution ratio of 0.0057, ii) pH 5.6, iii) membrane mass greater than 50 mg and iv) temperature from 10 to 45ºC. Some polymeric materials serve as supports for the enzyme immobilization and matrices for the stabilization of soluble free enzyme in solution. Overall, food industrial reactor walls covered with thin chitosan films could be strategies for using free lactase in the production of dairy foods.

Keywords: *Film. Chitosan. Lactase. Stabilization.*

Introduction

Lactase is an enzyme of the family of β-D-galactosidases (β-D-galactohydrolase EC 3.2.1.23) that is extracted from different sources, such as plants, animals, microorganisms (bacteria, yeasts [*Kluyveromyces lactis* or *fragilis*] and fungi [*Aspergillus oryzae*]) [1]. In the food industry, lactase is essential to the manufacturing of lactose-free dairy products, as a large and growing number of individuals are unable to digest this carbohydrate [2]. The use of lactase in the treatment of dairy effluents is also a promising strategy for the hydrolysis and recovery of whey [3]. Thus, this enzyme has considerable market potential due to the diversity of products that can be produced without lactose and possibility of using this enzyme in novel food and environmental technologies [4].

The low stability of lactase under operational conditions involving variations in temperature and pH limits the applications of this enzyme. Moreover, consumption in the reaction medium hinders the recovery and reuse of the enzyme, which constitutes a challenge that further diminishes the application of lactase in the food industry [1]. Thus, studies on the forced degradation of lactase in aqueous solutions are conducted to determine and predict possible degradation mechanisms under conditions of operational stress [5] and assist in finding ways to enhance enzymatic stability to make the application of enzymes feasible under different real-life situations in the food industry.

Therefore, the aim of this work was to synthesize, characterize and test chitosan composite films in the stabilization of lactase in aqueous solutions containing different enzyme/buffer solution ratios at different temperatures and pH values.

Experimental

Synthesis of chitosan films

Initially, known amounts of chitosan were dissolved in a beaker containing diluted acetic acid, followed by the addition of glutaraldehyde and, when the aim was to prepare the film composite, eucalyptus residue. The solution was transferred to small, duly cleaned Petri dishes, which were subsequently placed in a forced-air oven (Fanem® Orion 515) at 60°C for 24 h for complete chemical reticulation. After the formation of thin, chemically reticulated films, the polymeric materials were placed into a desiccator for 24 h prior to the lactase stability studies.

Characterization of chitosan films

The point of zero charge on the polymeric structure of the film was determined by immersing 100 mg of dry material in 25 mL of NaCl (0.1 g L^{-1}) with initial pH ($pH_{initial}$) ranging from 2 to 12 (adjusted by the addition of HCl or NaOH 0.1 mol L^{-1}). After 24 h of contact, the final pH (pH_{final}) of the solutions was measured. Fourier-transformed infrared (FT-IR) spectra were recorded in a PerkinElmer Frontier spectrometer with attenuated total reflectance (ATR). The operating conditions were wavenumber between 500 and 4000 cm^{-1}, 32 scans per minute and resolution of 4 cm^{-1}. The thermogravimetric analysis (TGA) was performed in the PerkinElmer STA 6000 analyzer. Differential scanning calorimetry (DSC) was performed in the Netzsch DSC 200 F3 analyzer. These analyses were conducted by placing the samples in alumina pans and heating the system between 30 and 600°C at a rate of 10°C min^{-1}. The entire process was performed in a nitrogen atmosphere with a flowrate of 20 mL min^{-1}. For scanning electron microscopy (SEM), the polymeric films were placed in distilled water for 24 h, freeze-dried for 12 h, coated with a thin layer of gold and photographed using the JEOL equipment, model JSM-6701F.

Lactase stability assays

Different masses of the dry films (50, 100 or 200 mg) were separately introduced to 15 mL of three different buffer solutions (acetate buffer solution 0.10 mol L^{-1} with pH 4.0, acetate buffer solution 0.10 mol L^{-1} with pH 5.6 or phosphate buffer solution 0.10 mol L^{-1} with pH 6.8). Soluble lactase was then added with different enzyme/buffer solution ratios (0.00575, 0.0230, 0.04025, 0.0575 and 0.07475) to each of the recipients. The flasks were then kept in a shaker incubator (Solab, SL-221) with stirring at 140 rpm and different temperatures (10, 20, 37 and 45°C). Aliquots of the aqueous solutions with the enzyme were collected at time intervals between 0 and 120 min for the quantification of the protein content using UV-Vis spectrophotometry (Spectroquant Prove 600, Merck) at a wavelength of 595 nm. The enzyme concentration was estimated using calibration curve for bovine serum albumin (BSA).

Results and Discussion

Film of chitosan

A chitosan-co-GLU film and chitosan-co-GLU/eucalyptus residue composite film were effectively synthesized, as shown in Figure 1.

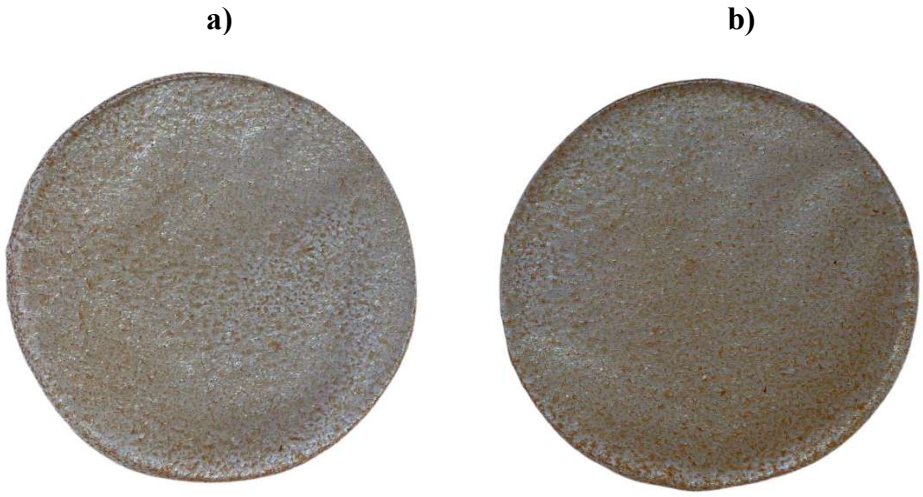

Figure 1 – Photographs of chitosan-co-GLU film (a) and chitosan-co-GLU/eucalyptus residue composite film (b).

The two films had a similar appearance. However, the composite one was stronger because eucalyptus residue has a high quantity of cellulose (~30 % of total mass) and lignin (~30 % of total mass). Moreover, the composite polymeric film contains a greater quantity of chemical groups on its surface that can interact with enzymes in solutions and modulate enzymatic stability. However, the presence of wood fibers in polymeric structures tends to diminish the porosity of the final material, compromising the intra-pore immobilization process, which occurs by diffusion and intermolecular interactions [6]. Only the composite membrane was used in the stabilization studies of β-D-galactosidase in an aqueous solution due to its greater durability in the reaction medium.

Characterization of chitosan films

The point of zero charge on the surface of the chitosan-co-GLU films and chitosan-co-GLU/eucalyptus residue composite films was 4.82 and 4.37, respectively. This means that protonated glucosamine (NH_3^+) and carboxyl (COOH) groups would be found on the surface of the solid support and in the structure of the enzyme at pH lower than 4.82 and 4.37, which practically coincides with the isoelectric point of β-D-galactosidase (4.50), whereas deprotonated amine (NH_2) and carboxyl (CH_3COO^-) groups would be found on the surface of the solid material and in the structure of the enzyme at pH higher than 4.82 and 4.37. These groups were confirmed in the polymer structures by means of absorption bands visualized by FTIR. The thermogravimetric analysis curves revealed two thermal decomposition stages. The first occurred between 80 and 140°C and was due to the loss of moisture from the hydrophilic three-dimensional networks [7]. The second occurred between 230 and 330°C and was due to the breaking of glycosidic bonds in the polymeric networks [6]. From differential scanning calorimetry were confirmed the thermogravimetry results. The scanning electron microscopy images have shown a slightly porous, less compact morphology on the surface of the chitosan-based film and a rougher, more rigid morphology on the surface of the chitosan-based composite films containing eucalyptus residue.

Lactase degradation/stability profiles

A reduction in the degradation of lactase was found with the increase in the mass of the composite film in the reaction medium. As the film practically does not absorb water to the point of changing the concentration of the enzyme in the reaction medium, the composite material clearly stabilized the enzyme during the operational procedure compared to the experiment with no film

(control). Even low quantities of film were sufficient to inhibit enzymatic degradation. The enzyme/buffer solution ratio practically did not affect biodegradation at values higher than 0.0057. Indeed, lactase degradation was similar at higher ratios comparing the absence of the film (control) to the presence of 50 mg of composite film. The increase in the enzyme/buffer solution ratio (maintaining the buffer volume constant) increased the quantity of enzyme in the medium, which also increased the saturation capacity of the film surface due to the occurrence of electrostatic interaction forces. The β-D-galactosidase degradation profiles at pH 4.0 were similar. No significant enzymatic degradation occurred in either the absence (control) or presence of the composite film in the medium, demonstrating that the polymer material exerted no influence on the enzymatic degradation process at this pH. Moreover, greater catalytic activity of the enzyme was found at this pH because its isoelectric point (4.5) is higher than the pH of the aqueous medium. Thus, the optimal pH range for the activity of lactase used in reaction systems includes pH 4.5, as described in the literature [3]. Practically no degradation of the enzyme occurred at 10 to 20°C. This is an interesting finding; as enzymatic immobilization processes would avoid the sorption of degraded particles with low catalytic activity on the surface of solid support structures. As lactase naturally has high activity at temperatures lower than room temperature, the presence of the polymeric film in the reaction medium did not generate substantial effects to the point of altering the enzymatic degradation profile. At higher temperatures (37 and 45°C), however, the presence of the composite film in the medium preserved the enzyme in comparison to the studies in the absence of the film (control). At both temperatures (37 and 45°C), higher concentrations of the enzyme were found in the media containing the composite film.

Conclusions

Chitosan films are solid matrices with potential to stabilize free soluble lactase in aqueous solutions. The intermolecular interactions that occurred at the film/enzyme/solution interface favored the approximation of the enzyme to the surface of the polymer material, which diminished the degradation of the enzyme in the operational medium. This phenomenon assisted in the maintenance of the activity of lactase. Thus, the enzyme could be reused for longer periods in lactose hydrolysis processes and under pH and temperature conditions that would otherwise denature or degrade the protein. As a conclusion, food industrial reactor walls covered with thin chitosan films could be strategies for using free lactase in the production of dairy foods with high efficiency.

Acknowledgements

CNPq (Grant number: 313064/2022-9), FAPESC (Grant numbers: 2021/TR791 and 2023/TR331), CAPES (Finance Code 001) and UDESC

References

[1] F.M. Almutairi; M. Monier; R.A.S. Alatawi; A.S. Alhawiti; H.H. Al-Rasheed; T.M. Almutairi; N.H. Elsayed. Reactive and Functional Polymers 2022, 172, 105159.
[2] A.B. Argenta; A.De.P Nogueira; A. Scheer. International Dairy Journal 2021, 117, 105007.
[3] T.L. Albuquerque; M. Sousa; E. Gomes; N.C. Silva; C.A.C.G. Neto; L.R.B. Gonçalves; R. Fernandez-Lafuente; M.V.P. Rocha. International Journal of Biological Macromolecules 2021, 191, 881–898.
[4] M.S. Melchiors; M. Piovesan; V.R. Becegato; V.A. Becegato; E.B. Tambourgi; A.T. Paulino. Journal of Environmental Management 2016, 182, 574 – 580.
[5] M. Király; B.D. Kiss; P. Horváth; L. Drahos; A. Mirzahosseini; G. Pálfy; I. Antal; K. Ludányi.

Biotechnology Reports 2021, 30, e00637.
[6] A.G. Souza; C.T. Cesco; G.F. Lima; E.E.S. Artifon; D.S. Rosa; A.T. Paulino. International Journal of Biological Macromolecules 2019, 140, 33–42.
[7] A.T. Paulino; A.G.B. Pereira; A.R. Fajardo; K. Erickson; M.J. Kipper; E.C. Muniz; L.A. Belfiore; E.B. Tambourgi. Carbohydrate Polymers 2012, 90, 1216–1225.

EFFECT OF NANOCLAY ADDITION IN POLY(LACTIC ACID) (PLA)/POLY(BUTYLENE ADIPATE-CO-TEREPHTHALATE) (PBAT) BLENDS IN AGROINDUSTRY SECTOR APPLICATION

Renan Henriques G. de Almeida[1*], David Gonçalves Pena[2], Elisson Brum D. da Rocha[3], Ana Maria F. de Sousa[3], Elen B. A. Vasques Pacheco[1] Ana Lúcia N. da Silva[1,4],

1 – Institute of Macromolecules (IMA), Federal University of Rio de Janeior (UFRJ), Rio de Janeiro, RJ, Brazil
renan.henriques@ima.ufrj.br
2 – School of Chemistry (EQ), Federal University of Rio de Janeior (UFRJ), Rio de Janeiro, RJ, Brazil
3 – Institute of Chemistry, State University of Rio de Janeiro (UERJ), Rio de Janeiro, RJ, Brazil
4 - Environmental Engineering Program (PEA), Federal University of Rio de Janeiro (UFRJ), Rio de Janeiro, RJ, Brazil

Abstract -. Poly(lactic acid) (PLA) has good processability and high mechanical resistance, but due to its low toughness, it is normally used in blends with poly(adipate-cobutylene terephthalate) (PBAT). With the aim of improving the interaction between the PLA and PBAT phases, the blends were processed by reactive extrusion, at different experimental conditions, using maleic anhydride (MA) and dicumyl peroxide (DCP).. The processing conditions of PLA/PBAT (70/30, wt.%) with /bentonite clay (100% organophilized) was evaluated based on thermal and rheological properties. The TGA analysis showed a decrease in thermal stability of PLA phase , but when increasing the screw speed, maintaining the low level of the feed rate, an increase in PBAT phase thermal stability was observed. As expected, the MFI analysis showed a decrease in flow behaviour in systems with clay. The DSC analysis showed that clay filler presented a nucleating effect in the PLA/PBAT blends. This effect was more pronounced in composites processed at lower feed rate, independently the screw speed analysed. The morphology showed a reduction on the PLA drop diameter when bentonite was added into PLA/PBAT blends, suggesting a compatibilizing effect of the clay between the polymeric phases.

Keywords: *Biopolymers, Polymers Blends, Poly(lactic acid), Poly(butylene adipate-co-terephthalate).*

Fundings: This study was financed in part by the Coordenação de Aperfeiçoamento de Pessoal de Nível Superior - Brasil (CAPES) - Finance Code 001.

Introduction

The growing search for the sustainable use of natural resources and the environment has led to an increase in interest in the development of biodegradable polymers (from natural sources) in the last 20 years. Poly(lactic acid) (PLA) is the most used biopolymer thanks to its good processability, high mechanical strength and stiffness. However, it has low toughness at room temperature and low heat deflection temperature in relation to conventional polymers [1].

The blend of poly(lactic acid) (PLA) with poly(adipate-cobutylene terephthalate) (PBAT) has been widely used to balance the properties of PLA, since PBAT has high elongation at break and low elastic modulus, but its mixture is thermodynamically immiscible, which compromises the material's performance. In order to improve the miscibility, a reactive in situ extrusion using maleic anhydride and dicumyl peroxide can be employed [2].

Based on this, this work aims to determine the optimal processing condition to produce the composite based on PLA / PBAT / bentonite clay 100% organophilized (organoclay – OC). The nanoclay was added to act as a coating in controlled release systems. Previous results was analysed by thermal, rheological and morphological behaviour.

Experimental

Material

The biopolymers PLA Ingeo^{tm} 4043D frow NatureWork and PBAT ecoflex F Blend C1200 from BASF were used along with the additives for reactive extrusion, which are the maleic anhydride (grade M188) and dicumyl peroxide (grade 329541) both purchased from Sigma Aldrich and the bentonite clay 100% organophilized donated by CLARIANT.

Methodology

Determination of optimal processing parameters

The determination of the optimum processing condition for PLA/PBAT 70/30 wt. % blend (reactive extrusion *in situ* using 2 phr of maleic anhydride and 1 phr of dicumyl peroxide in relation to PLA mass) was determined using a 2^n (n = process variables) factorial design. The systems were produced in a twin-screw corrotational extruder, with the following process variables: screw speed (S), feed rate (FR) and clay content (C). The temperature profile set in the extrusion process was 90 – 190 ºC. The organoclay (OC) was added into the polymer matrix (PLA/PBAT) in 3 wt.% content.

Table 1 shows the design matrix used.

Table 1 – Design matrix of PLA/PBAT/OC composites

Process conditions (S/FR/C)	Screw speed (rpm)	Feed rate (kg.h^{-1})	Clay content (wt. %)
200S/2.50FR/0C	200	2.50	0
200S/5.05FR/0C	200	5.05	0
300S/2.50FR/0C	300	2.50	0
300S/5.05FR/0C	300	5.05	0
200S/2.50FR/3C	200	2.50	3
200S/5.05FR/3C	200	5.05	3
300S/2.50FR/3C	300	2.50	3
300S/5.05FR/3C	300	5.05	3

Characterization of samples

The thermogravimetric analysis (TGA) of the samples was used to evaluate the thermal stability of the composite. and the maximum degradation temperature (T_{MAX}) of PLA and PBAT. They were performed on a TA instrument TG analysis model Q500 analysis instrument, in a nitrogen atmosphere, with a heating rate of 10°C/min over a temperature range of 25-700°C.

The flow behaviour was analysed by Melt flow index (MFI), in a DYNISCO polymer test (MOD. LMI 4000), following ASTM D1238-13, with temperature and weight conditions being 190°C and 2160g respectively.

Differential scanning calorimeter (DSC) analysis was also performed on the systems produced to monitor the glass transition temperature (Tg), crystalline melting temperature (Tm), crystallization temperature (Tc,). A Model Q2000 DSC analysis Ta instrument was used for the test, under nitrogen atmosphere and in cycles with the following conditions: (i) Fast cooling down to -60 °C (quench); (ii) Heating from -60 to 210°C (10°C/min); (iii) Isothermal for 1 min; (iv) Fast cooling down to -70 °C (quench); (v) Heating from -70 to 210°C (10°C/min) and (vi) Cooling down to -70°C (10°C/min).

DSC analysis was also used to obtain the degree of crystallization of the PLA phase of the systems, based on the first heating, using Eq. 1.

$$\chi c = 100 \, X \, \frac{\Delta Hm - \Delta Hc}{\Delta HPLA^{\infty}} \qquad (1)$$

Where χc is the degree of crystallinity of the PLA phase, ΔHm the enthalpy of fusion, ΔHc is the enthalpy of crystallization and ΔH_{PLA}^{∞} is the enthalpy of fusion of 100% crystalline PLA (93 J/g) [3].

The morphology of the neat PLA and the samples 200S/2.50FR/0C and 200S/5.05FR/3C was investigated by studying cryogenic fractured surfaces using a scanning electron microscope (SEM), FEI Quanta 400, accelerating voltage of 500X. The fractured samples were coated with gold particles before the experiment.

Results and Discussion

Figure 1 shows the TGA curves (and the DTG) for all the PLA/PBAT/OC systems. Table 2 presents the data from the TGA curves.

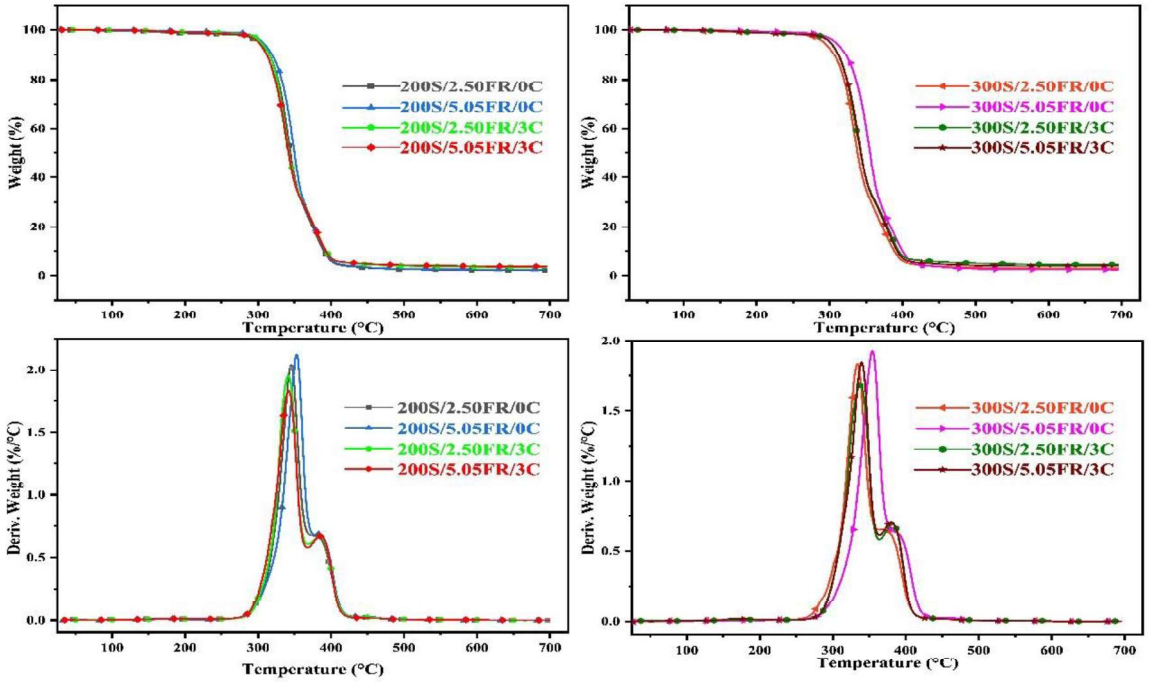

Figure 1 – TGA curves of the PLA/PBAT/OC systems.

Table 2 – TGA results of PLA/PBAT/OC systems

Sample	$T_{MAX\,1}$ (°C) (PLA)	$T_{MAX\,2}$ (°C) (PBAT)
200S/2.50FR/0C	342	375
200S/5.05FR/0C	349	382
300S/2.50FR/0C	334	371
300S/5.05FR/0C	354	382
200S/2.50FR/3C	338	380
200S/5.05FR/3C	339	381
300S/2.50FR/3C	338	382
300S/5.05FR/3C	339	380

S = screw speed; FR = feed rate and C = organoclay content

The results of the TGA (Table 2. and Fig.1.) were analysed considering T_{MAX1} (PLA) and T_{MAX2} (PBAT). It is possible to notice that the addition of clay leads to a reduction in the thermal stability

of the material, as it can catalyse the degradation process through the strongly acidic sites generated during the thermal degradation of the intercalating agent [4]. Furthermore, its ability to reduce the material's sensitivity to processing is also observed, an effect evidenced by the non-variation of T_{MAX1} and T_{MAX2}. It is also noted that the systems produced without adding clay, lower feed rates cause higher degradation during processing, however, increasing the screw speed from 200 to 300 rpm does not change its thermal stability.

Regarding MFI Analysis (Table 3.), it can be observed that the systems produced with 3 wt. % of clay presented a smaller variation in viscosity (8%); while those obtained without the nanoclay showed a variation of 22%, which indicates that the composites produced are less sensitive to processing conditions and present greater uniformity among themselves, corroborating the TGA analysis. It is also noted that higher feed rates and lower screw speed tend to have higher MFI values. Probably, such conditions allow the occurrence of degradation processes of the polymeric matrix during processing.

Table 3 – MFI results of the PLA/PBAT/OC systems

Sample	MFI (g/10 min)
200S/2.50FE/0C	16,08 ± 0,82
200S/5.05FE/0C	19,30 ± 0,60
300S/2.50FE/0C	11,60 ± 0,40
300S/5.05FE/0C	19,50 ± 0,76
200S/2.50FE/3C	10,48 ± 0,18
200S/5.05FE/3C	11,60 ± 0,40
300S/2.50FE/3C	11,10 ± 0,38
300S/5.05FE/3C	9,60 ± 0,40

S = screw speed; FR = feed rate and C = organoclay content

The DSC results (Table 4. and Fig. 2.) showed that the addition of clay lead to the occurrence of only one peak of Tm, a higher Tc (cooling) value and a higher crystallinity degree (PLA phase), which suggests the effect of clay as a nucleating agent. It is also notice that the composites produced with a lower rate feed showed greater crystallinity. For all the analysed samples can be seen that there was no variation in Tg values of PLA and PBAT.

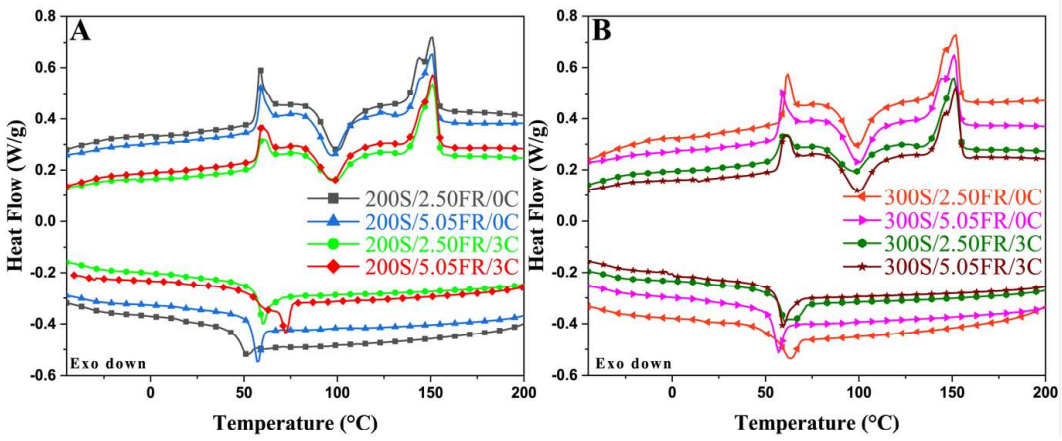

Figure 2 – DSC curves of the samples extruders using screw speed of 200 rpm (A) and 300 rpm (B)

Table 4 – DSC results of the PLA/PBAT/OC systems

Sample	Tg (°C) (PBAT)	Tg (°C) (PLA)	Tm 1 (°C)	Tm 2 (°C)	Tc (°C) (1st heating)	Tc (°C) (cooling)	Degree of crystallinity (%)
200S/2.50FR/0C	-27,57	58,85	144	151	100	52	0,23

200S/5.05FR/0C	-29,58	59,56	145	151	98	57	0,70
300S/2.50FR/0C	-29,13	60,01	146	152	100	63	0,74
300S/5.05FR/0C	-29,42	59,69	115	151	100	57	1,22
200S/2.50FR/3C	-28,51	60,2	-	151	99	60	4,51
200S/5.05FR/3C	-30,7	59,94	-	151	98	72	1,92
300S/2.50FR/3C	-29,22	59,18	-	151	98	60	5,17
300S/5.05FR/3C	-29,76	59,73	146	152	100	59	0,49

S = screw speed; FR = feed rate and C = organoclay content

The SEM micrographs (Fig. 3.) showed that PBAT phase was dispersed in the PLA matrix by drop form. The addition of clay lead to a better PBAT phase distribution, reducing the drop diameter. Possibly thanks to a better interaction between the two phases. This behavior suggest a compatibilizing effect of clay between PLA and PBAT phases

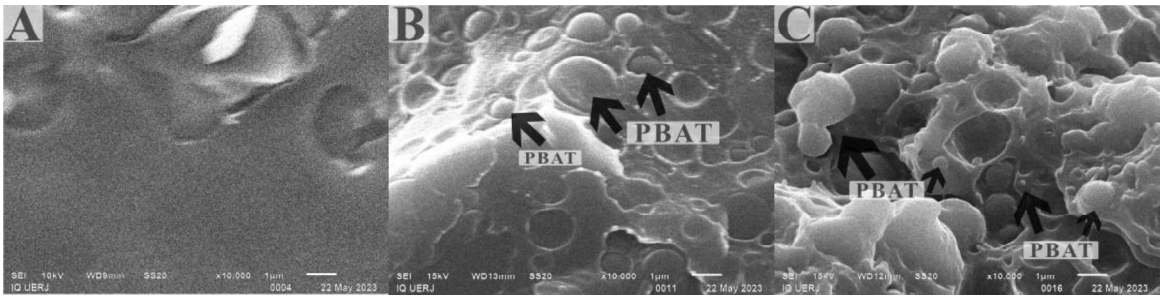

Figure 3 – Micrographs of Neat PLA (A), 200S/2.50FR/0C (B) and 200S/5.05FR/3C (C)

Conclusions

From TGA analysis, it was observed that the addition of bentonite clay to PLA/PBAT blend led to a reduction in the thermal stability of the blend.

The MFI data showed that the addition of clay filler to PLA/PBAT blends restricted the flow behaviour of the melt, resulting in systems with higher viscosity. Beyond this, it was noticed a tendency to increase the flow behavior when higher feeding rates and lower screw speed conditions were applied during processing. Probably due to the occurrence of a degradation process of the polymeric matrix on these processing conditions.

From DSC analysis, it was observed that clay acts as a nucleating agent, leading to an increase in crystallinity degree and crystallinity temperature (Tc). This corroborated SEM micrographs, which was observed smaller size of PBAT phase, favouring to crystallization process.

Acknowledgements

We would like to thank the Institute of Macromolecules Professor Eloisa Mano (IMA), the Nucleus of Excellence in Recycling and Sustainable Development (NERDES) and the Conselho Nacional de Desenvolvimento Cientíco e Tecnológico - CNPQ (307889/2022 and 309461/2021-9) for all the support offered.

References

1. X. Chen; Z. Zeng; Y. Ju; M. Zhou; H. Bai; Q. Fu Polymer 2023, 266, 125620. https://doi.org/10.1016/j.polymer.2022.125620
2. V. C. S. Barbosa; A. M. F. de Sousa; A. L. N. da Silva Polímeros 2022, 32(3), e2022033. https://doi.org/10.1590/0104-1428.20220018
3. V. C. S. Barbosa, MSC. Dissertation, Federal University of Rio de Janeiro, 2022.
4. G. C. V. Iulianelli; P. J. O. Sebastião; M. I. B. Tavares; F. A. dos Santos Materials Science and Applications 2015, 6, 860-868. http://dx.doi.org/10.4236/msa.2015.610088

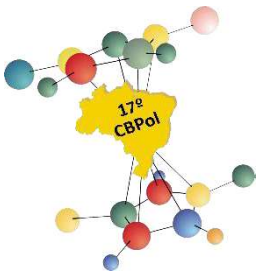

EFFECT OF STORAGE CONDITIONS ON THE MECHANICAL RESISTANCE OF HIGH-DENSITY POLYETHYLENE AS GASOLINE-ETHANOL BLEND PACKAGING

Thainá Braz Hank[1*], Neli Branco de Miranda[2], Dilamara Riva Scharf[2], Luiz Felipe Ribeiro dos Santos[1], Johnny De Nardi Martins[1]

1 – Center of Technology, Exact Sciences and Education, University of Santa Catarina (UFSC), Blumenau, SC, Brazil
thaina.hank@ufsc.br
2 – Department of Chemical Engineering, University of Blumenau (FURB), Blumenau, SC, Brazil

Abstract
In order to oversee fuels in Brazil, the National Agency of Petroleum, Biofuels, and Natural Gas uses high-density polyethylene (HDPE) containers. The fuel, due to environmental conditions, can cause changes in the mechanical properties of HDPE, as reported in previous studies with gasoline-ethanol blend. Therefore, there is a need to investigate the integrity of containers exposed to gasoline-ethanol blend during inspection. This work investigated the effect of two storage conditions, refrigerator (R) and storage room (SR), on the mechanical resistance of HDPE to gasoline-ethanol blend (E31) for four and eight months. After storage, the following order of yield stress was obtained: 4-R > 8-R ~ 8-SR ~ 4-SR, and for 8-R, 4-SR, and 8-SR, there was a decrease in the tensile modulus. The FT-IR data showed an indication of the presence of carbon double bonds only on the inner surface of HDPE bottle after four months of storage in the SR.
Keywords: High-density polyethylene, Biofuel, Storage, Compatibility, Gasoline-ethanol blend.

Introduction

Owing to the need for a reconfiguration of energy consumption towards sources which result in lower pollutant emissions, it is expected that several countries increase their consumption of bioethanol in the next few years [1]. New studies on the compatibility between polymeric materials and gasoline-ethanol blends are relevant not only in the Brazilian context, but also for better understanding of a future that will be present in countries that adopt policies based on bioethanol.

Aiming to ensure the quality of liquid fuels sold in Brazil, the National Agency of Petroleum, Natural Gas, and Biofuels (ANP) acquired polymeric packaging for collecting fuels in inspection. A technical study was conducted validating the need for packaging with specific requirements, such as the manufacturing material, wall thickness, and volume [2]. The ANP also uses instructions contained in NBR 14883[3], a standard that suggests which recipients can be used for the storage of petroleum derivatives in Brazil, to verify the requirements demanded in the process of purchasing these packages [4]. NBR 14883 is quite like ASTM D4057, however it does not consider the specificities of the fuel marketed in the national territory [3,5].

The composition of gasoline sold in Brazil, blended with ethanol, raises doubts about the compatibility of the polymeric recipients suggested by NBR 14883. In addition, there is no scientific basis for determining the appropriate conditions and time for storing gasoline-ethanol blends in the high-density polyethylene (HDPE) containers purchased by the ANP suggested by NBR 14883.

Few studies have reported changes in the yield elongation, yield stress, and glass-to-rubber transition of HDPE when exposed to gasoline-ethanol blends, which can compromise the integrity of

the packaging and the fuel. On this context this work studied the effect of two storage conditions, refrigerator (R) and storage room (SR), on the mechanical resistance of HDPE to gasoline-ethanol blend (E31) for four and eight months [6,7].

Experimental

The bottles made of HDPE, shown in Figure 1, were donated by ANP for the study. They hold one liter of fuel. The walls have a minimum thickness of 1.5 mm and weigh around one hundred grams each. Some properties of the HDPE packaging are shown in Table 1.

Table 1 – Characteristics of HDPE packaging.

Properties		Technique
Melting point	132 °C	DSC
Crystallinity Degree	52,2 %	DSC
Degradation range temperature	464 – 508 °C	TGA
Degradation peak temperature	494 °C	TGA
Color	Yellow	Visual

The gasoline-ethanol blend was donated by the University of Blumenau (FURB), where the study was mainly conducted. Some of the physico-chemical characteristics of the control fuel are shown in Table 2.

Table 2 – Physico-chemical characteristics of the gasoline-ethanol blend before storage.

Properties		Method
Density at 20 ºC	744,85 kg/m³	NBR 14065:2013
Sulfur	41,561 mg/kg	ASTM D5453:2019a
Aspect	Clean and free of impurities	NBR 14954:2021
Color	Yellow	NBR 14954:2021
Anhydrous ethanol content	31 % vol.	NBR 13992:2015

After being filled with one liter of gasoline-ethanol blend, the recipients were divided into two storage conditions with monitored temperature, for 4 and 8 months. Half of the bottles were kept in a refrigerator, at an average temperature of 7.5°C±0.2 for the first 4 months and 6.6°C±0.8 for the total of 8 months. In the storage condition in the warehouse, the bottles that remained for 4 months were exposed to an average temperature of 17.7°C±2.7 and 17.9°C±2.7 for a total of 8 months.

At the end of the storage time, the packages were laser-cut following the direction of the larger dimension with a Nippon NP 1080, in the dimensions of type 2 specimens specified in ASTM D638[8], as shown in Figure 1.

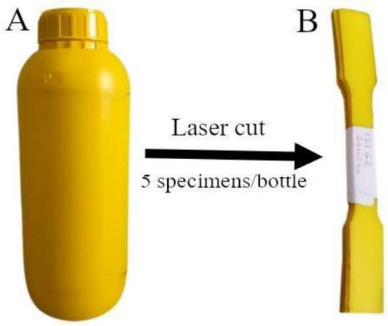

Figure 1 – A) HDPE packaging used by ANP. B) Type 2 test specimens cut from the packaging.

Five specimens from each packaging were subjected to tensile strength tests using an Instron EMIC machine with a load cell capacity of 500 kgf and a testing speed of 10 mm/min. The median values from the five stress-strain curves for each packaging were calculated. The tensile modulus of the HDPE of each packaging was calculated using the slope coefficient from linear range of elastic region of respective median curve.

The analysis of the functional groups of HDPE was done after the material's spontaneous drying. A Perkin Elmer Frontier Infrared Spectrophotometer and the ATR method were used from 4000 to 400 cm^{-1}.

Results and Discussion

We observed in the stress-strain curve, displayed in Figure 2, that the HDPE of the bottles stored in all conditions had a decrease in yield stress after the storage time. The HDPE which held the yield stress was the one from the bottle stored in the refrigerator for four months, with 18 MPa compared to the 19 MPa from the control bottle. Then, for the bottles stored for eight months in the refrigerator, four and eight months in the storage room, the yield stress was 17 MPa.

The variation in yield stress of the polymer when the storage conditions were compared over time suggests that storing the packaging containing this gasoline-ethanol blend in the refrigerator delays the decrease in yield stress in the short term, but over time tends to reach the absolute variation as observed in the storage room. In the storage room, regarding yield stress, four months were enough to reach an "equilibrium" in the interaction between the material and the fuel due to the slight variation compared to the result obtained for the HDPE stored for eight months.

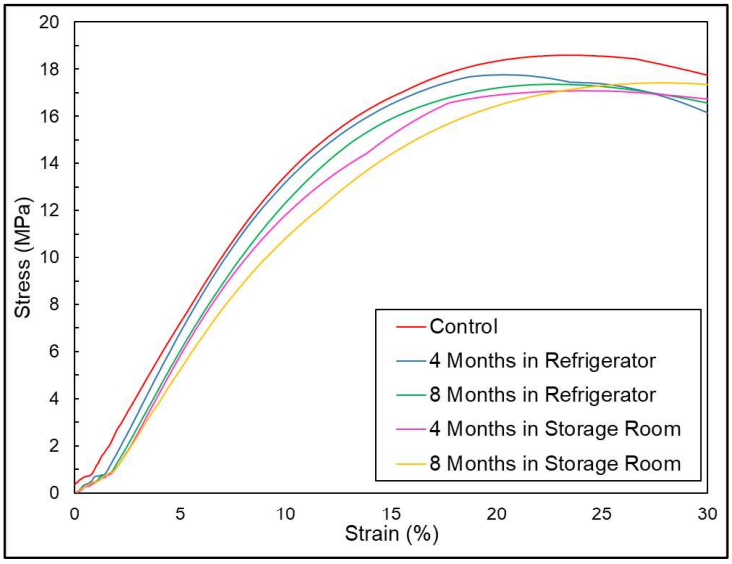

Figure 2 – Stress-strain curves of HDPE of bottles: control, four months after E31 storage in refrigerator, eight months in refrigerator, four months in storage room and eight months in storage room.

The HDPE in contact with the gasoline-ethanol blend for four months in the refrigerator had 161 MPa of tensile modulus as displayed in Table 3, an increasing of 11 MPa compared to the control bottle. After eight months of storage in the refrigerator, the tensile modulus was 148 MPa, similar to 150 MPa obtained from control. Regarding the HDPE stored in the storage room for four and eight months, we found 146 and 109 MPa of tensile modulus, respectively. When comparing the two conditions, a decreasing trend in the tensile modulus of the HDPE kept in the storage room was observed. This suggests that the higher temperature of the storage room had an influence on the decrease observed for the tensile modulus, mainly after four months of storage fuel.

Table 3 – Tensile modulus of HDPE of bottles: control, storage E31 in refrigerator and storage room, for four and eight months.

Storage time (Months)	Storage condition (ºC)	Tensile modulus (MPa)
0 (Control)	-	150
4	Refrigerator (7.5±0.2)	161
4	Storage room (17.7±2.7)	146
8	Refrigerator (6.6±0.8)	148
8	Storage room (17.9±2.7)	109

The infrared absorption bands present on the inside and outside face of the HDPE bottle were shown in Figure 3 where differences could be observed. The broad band present in the region of 3300 cm^{-1} was more pronounced on the external face of the packaging, which may indicate retention of ethanol present in the stored fuel. Another possibility was the appearance of hydroxyl groups due to thermal aging of the HDPE [9].

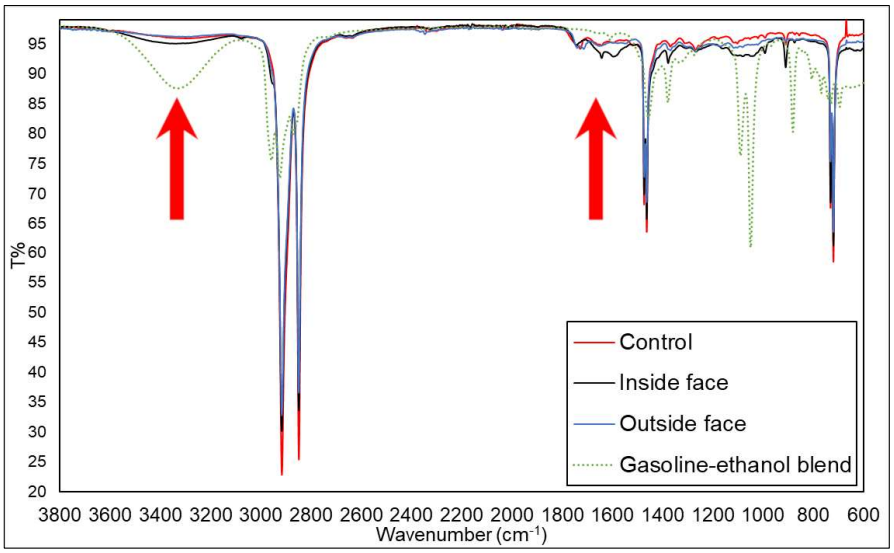

Figure 3 – ATR-FTIR analysis of HDPE bottles: control, inside face, outside face of HDPE and gasoline-ethanol blend after four months in storage room.

The region between 1500-1800 cm^{-1} had changes suggesting the presence of carbon double bonds, mostly inside the bottle, and carbonyl groups on both surfaces, indicating degradation processes in the material. Therefore, the gasoline-ethanol blend affected HDPE in a heterogeneous way through the thickness of the packaging after four months of storage in the storage room.

Conclusions

The tensile tests showed that the HDPE bottles had lower yield stress when exposed to the blend gasoline-ethanol in both conditions. The refrigerator condition delayed the loss of yield stress compared to the bottles stored in the storage room, but over the eight months, it reached the same yield stress value as the HDPE in the storage room.

The HDPE had a different behavior in the tensile modulus after four months of exposure to the fuel, whereas in the refrigerator condition, the tensile modulus increased and in the storage room, it decreased. This behavior was not stated after eight months, as the improvement in the first months was lost, bringing the tensile modulus of the HDPE in the refrigerator closer to the control. In the storage room, there was a continuous loss of tensile modulus up to the end of the storage time. When comparing the infrared absorption bands present on the internal and external surfaces of the HDPE

bottle after four months of storage of the gasoline-ethanol blend in the storage room, a difference was observed in the region of hydroxyl groups, which may be associated with the presence of ethanol from the fuel still retained in the HDPE or the appearance of hydroxyl groups resulting from the thermal aging of the polymer. Another difference was the indication of the presence of carbon double bonds on the inner surface of the bottle.

Acknowledgements
The authors would like to thank UFSC and FURB for their partnership in the development of this work, and ANP for donating the inspection packaging.

References

1. IEA (2022), World Energy Investment 2022, OECD Publishing, Paris, https://doi.org/10.1787/7a0d89ff-en.
2. Agência nacional do petróleo, gás natural e biocombustíveis (2022), *Edital N° Pregão 35/2022*, Governo federal do Brasil, accessed 20 October 2022, http://www.comprasnet.gov.br/acesso.asp?url=/edital-323031-5-00035-2022
3. Associação brasileira de normas técnicas. (2021). *Petróleo, derivados de petróleo e biocombustíveis – Amostragem manual* (NBR 14883). Retrieved from https://www.abntcatalogo.com.br/pnm.aspx?Q=R2ZCUzM4WWxUREkyZUpVVkg2OWZlT2VPUnY0U2graWp3ek1RcnAxL240ST0=
4. Feitosa, N. (2022). *Webinar Norma Brasileira para Amostragem - Rumo à Excelência Analítica* [Webinar]. Instituto brasileiro de petróleo e gás. https://youtu.be/grfm7elb6d0
5. American society for testing and materials. (2022). *Standard Practice for Manual Sampling of Petroleum and Petroleum Products* (D4057). Retrieved from https://www.astm.org/d4057-22.html
6. Z. Jiangfang; C. Xuehong. Journal of Elastomers & Plastics 2021, 53, 3-13. https://doi.org/10.1177/0095244319891206.
7. M. Kass; C. Janke; T. Theiss; S. Pawel; J. Wolf; W. Koch. SAE International Journal of Fuels and Lubricants 2014, 7, 457-470. https://doi.org/10.4271/2014-01-1465.
8. American society for testing and materials. (2022). *Standard Test Method for Tensile Properties of Plastics* (D638). Retrieved from https://www.astm.org/d0638-22.html
9. C. Campanale; I. Savino; C. Massarelli; V. Uricchio. Polymers 2023, 15, 911. https://doi.org/10.3390/polym15040911

EFFECTS OF INTERACTIONS OF β-D-GALACTOSIDASE WITH CHITOSAN FILMS AND EVALUATION BY FACTORIAL DESIGN

Larisa F. da Cruz[1], Amanda G. Polizeli[1], Mirlene P. Vitorino[2], Heveline Enzweiler[3] and Alexandre T. Paulino[1,2,4*]

1 - Postgraduation Program in Food Science and Technology, Santa Catarina State University (UDESC), Pinhalzinho, SC, Brazil
2 - Postgraduation Program in Applied Chemistry, Santa Catarina State University (UDESC), Joinville, SC, Brazil
3 - Department of Food and Chemical Engineering, Santa Catarina State University (UDESC), Pinhalzinho, SC, Brazil
4 - Department of Chemistry, Santa Catarina State University (UDESC), Joinville, SC, Brazil
**Email: alexandre.paulino@udesc.br.*

Abstract
Effects of interactions of β-D-galactosidase with chitosan films were studied by applying a central composite rotatable factorial design. The interactions increased the enzyme stability in solution between 0 and 60 min, with the most stability decrease occurring in assay 14 (80.03%). Assay 4 stood out between 60 and 120 min, with 42.05% protein concentration decrease. Significance was found for the linear enzyme/buffer ratio, linear temperature, and quadratic pH ($p < 0.05$) in the interval between 0 and 60 min of study. In the interval between 60 and 120 min, there was significance ($p < 0.12$) for linear temperature, the temperature-enzyme/buffer ratio interaction and the interaction between linear pH and linear enzyme/buffer ratio. Effects of the experimental variables on the stabilization of β-D-galactosidase in solution after interactions with chitosan films were effectively described, indicating that food industrial reactors covered with such biomaterials could be a strategy for the hydrolysis of lactose during milk-producing processes.

Keywords: *Polysaccharide. Polymer matrix. Stability. Experimental design.*

Introduction

β-D-Galactosidase is a glycoside hydrolase secreted by microorganisms, plants, and animals. It is widely used for the conversion of lactose into glucose and galactose [1,2]. β-D-galactosidase is the main enzyme used for the processing of dairy products with low- or zero-lactose content. The focus of the dairy industry that produces these types of products is lactose-intolerant individuals [3]. However, the denaturation and degradation of the free enzyme in solution is a disadvantage during industrial processes [3]. Thus, studies that describe interactions between β-D-galactosidase and solid supports constitutes a strategy for circumventing problems associated with the hydrolysis of lactose in industrial reactors [4]. Polymeric materials and composites synthesized by chemical or physical reticulation are part of a set of solid supports for studies on the immobilization, stabilization, and degradation of enzymes in aqueous solutions due to their physicochemical properties [5]. Such materials include those based on chitosan, pectin, gum Arabic, guar gum and other polysaccharides [6]. Intermolecular interactions that occur on the surfaces of biopolymer-based solid supports offer greater stability of enzymes in operational media with abrupt changes in temperature and pH when compared to the free enzyme [5]. It is therefore possible to conduct forced degradation studies with enzymes in aqueous media to determine enzyme degradation routes

under different conditions of operational stress [7]. Therefore, the aim of the present work was to apply experimental planning using a 2^3 central composite rotatable design for evaluating the stabilization of β-D-galactosidase in aqueous solution containing a chitosan-based composite film. Different operational conditions were defined and evaluated in the experimental planning (variations in temperature, pH, aqueous enzyme/buffer solution ratio and interaction time).

Experimental

Synthesis of chitosan films

Initially, known amounts of chitosan were dissolved in a beaker containing diluted acetic acid, followed by the addition of glutaraldehyde and, when the aim was to prepare the film composite, eucalyptus residue. The solution was transferred to small, duly cleaned Petri dishes, which were subsequently placed in a forced-air oven (Fanem® Orion 515) at 60°C for 24 h for complete chemical reticulation. After the formation of thin, chemically reticulated films, the polymeric materials were placed into a desiccator for 24 h prior to the β-D-galactosidase stability studies.

Enzyme partitioning assays between solution and film surface

The β-D-galactosidase content in solution after different contact times is an indicative of the presence of nondegraded full enzyme macromolecules. A relation between the initial and final enzyme concentrations can indicate the partitioning of the compound between solution and polymeric film surface, as there was no relevant immobilization in the biomaterial structure. β-D-galactosidase partitioning experimental assays between solution and film surface were conducted by varying the enzyme/buffer solution ratio, temperature, and pH of the aqueous solutions to evaluate the variables that would be later used in the experimental design. Some experimental conditions used in the present study were based on assays previously conducted by our research group [8]; in which the authors suggested that pH 5.6 and a temperature of 37 °C are desirable for studying the immobilization and activity of β-D-galactosidase obtained from *Kluyveromyces lactis*. For all assays, control experiments without the chitosan film were conducted with the same experimental conditions and variables. From these initial test studies, some conditions were established for the experimental design of the current study.

Experimental planning

Experimental planning with a 2^3 central composite rotatable design was used to evaluate the effects of temperature, pH and enzyme/buffer solution ratio during the β-D-galactosidase stability studies in an aqueous medium containing a chitosan-based film. Six axial points and three repetitions of the central point were used, totaling 17 assays. The axial points were used for the determination of the degrees of freedom and evaluation of the quadratic equations. The dependent variable was enzyme concentration (mg mL^{-1}) with loss percentages determined in two steps: from 0 to 60 and 60 to 120 min. The respective intervals were chosen for understanding the effects of variables at different times by using p-values of 0.12 and 0.05, respectively. These significances were fixed at each condition to estimate the effects on real-world processes, in which commonly take place enzyme inactivation. The independent variables were temperature (X1), pH (X2) and enzyme/buffer ratio (X3). Table 1 displays the variables selected to study the effects of temperature, pH, and enzyme/buffer ratio in the stability of β-D-galactosidase in solution.

Table 1 – Independent variables with respective levels used in experimental planning with 2^3 central composite rotatable design.

		Levels				
Variables	Code	-1.68	-1	0	1	1.68
Temperature (°C)	(X1)	29.0	32.2	37.0	41.8	45.0
pH	(X2)	4.40	4.90	5.60	6.30	6.80
Enzyme/buffer solution ratio	(X3)	0.14	0.58	1.22	1.86	2.30

Results and Discussion

Enzyme partitioning assays between solution and polymeric film surface

The enzyme partitioning assays enabled the determination of favorable experimental conditions for the studies, which are important to assist in diminishing the loss of enzymes in real industrial processes. The best experimental variables for β-D-galactosidase partitioning in aqueous medium containing the chitosan composite film were i) enzyme/buffer ratio of 0.0057, ii) pH 5.6, iii) film mass of 50 mg, and iv) temperature lower than 37 °C, as shown in Fig. 1.

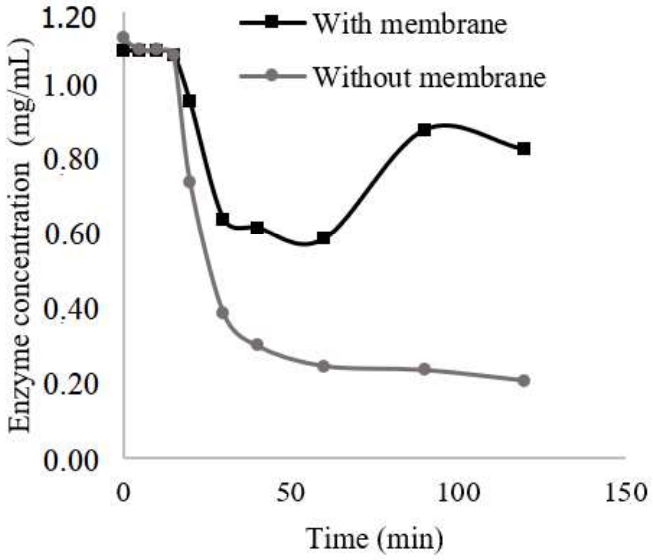

Fig. 1 – β-D-galactosidase content in aqueous solution with and without chitosan composite film. Experimental conditions: pH 5.6, enzyme/buffer ratio of 0.0057 and temperature of 37 °C.

Under the experimentally optimized conditions, the presence of the chitosan film in the aqueous solution was essential to avoiding enzyme activity and concentration loss. It took place due to weak intermolecular and intramolecular interactions on the surface and in the pores of the film, leading to the stabilization of β-D-galactosidase. This stabilization increased the quantity of enzyme in the reaction medium, enabling its reuse, with a subsequent reduction in the cost of industrial processes involving the application of β-D-galactosidase in the production of dairy products. The pre-established experimental conditions enabled the determination of the levels to be used in the factorial design, confirming 50 mg of biopolymeric film as a standard quantity for all experiments.

Experimental planning

The results of the experimental planning with a 2^3 central composite rotatable design, in the interval from 0 to 120 min, are presented in Table 2. These results were separately presented in two-

time intervals due to need of having two significance levels for the factorial design considered in this work.

Table 2 – Results of experimental planning with 2^3 central composite rotatable design, in the interval from 0 to 120 min. Independent variables: temperature (X1), pH (X2) and enzyme/buffer ratio (X3).

Assays	**Independent variables**			**Quantity of enzyme (%) between 0 and 120 min**	
	X1	X2	X3	0~60	60~120
1	32.2	4.9	0.58	28.01	15.85
2	41.8	4.9	0.58	52.74	21.60
3	32.2	6.3	0.58	34.21	16.01
4	41.8	6.3	0.58	54.62	42.05
5	32.2	4.9	1.86	35.12	26.42
6	41.8	4.9	1.86	68.20	-5.150
7	32.2	6.3	1.86	67.83	33.05
8	41.8	6.3	1.86	79.23	22.37
9	29.0	5.6	1.22	17.41	24.20
10	45.0	5.6	1.22	58.26	-2.160
11	37.0	4.4	1.22	12.99	0.370
12	37.0	6.8	1.22	6.080	21.75
13	37.0	5.6	0.14	6.330	10.24
14	37.0	5.6	2.30	80.03	21.54
15	37.0	5.6	1.22	55.02	14.66
16	37.0	5.6	1.22	61.39	9.040
17	37.0	5.6	1.22	64.32	4.980

The enzyme loss rates determined in the assays containing the chitosan composite film ranged from 6.08 to 80.03% between 0 and 60 min and from -5.15 (or zero) to 42.05% in the interval from 60 to 120 min. Negative degradation values can be associated to loss of mass due to desorption of enzyme weakly immobilized in the first times of contact. Overall, the enzyme loss results with negative values could be considered as zero. Slight response variations were identified at the central points, indicating the good repeatability of the experiment. The interval between 0 and 60 min was that in which a greater loss rate was found due to the influence of the variables of the process, with the greatest decrease occurring in assay 14 (80.03% protein loss). Assay 4 stood out in the interval between 60 and 120 min, with 42.05% protein loss. Thus, a higher decrease occurred in the initial time interval, indicating a greater loss rate in the first minutes of the experiment. Considering the application of β-D-galactosidase in an aqueous solution to produce products by the dairy industry, it is important to monitor the enzyme decrease rate in the first moments of lactose hydrolysis to minimize losses in the industrial process. Thus, the polysaccharide film could be a useful option for the stabilization of enzymes in a reaction medium, enabling their reuse and diminishing the cost of the process.

Conclusions

The factorial design was of the utmost importance, as it enabled the determination of the best operational conditions for the use of β-D-galactosidase in solutions containing a chitosan composite film with the aim of avoiding enzymatic inactivation. Thus, such studies are useful for enabling the application of free β-D-galactosidase for the hydrolysis of lactose in industrial processes with high efficiency and low concentration loss. This could enable increasing the benefit/cost ratio of the production of dairy products with a low lactose content or even zero-lactose dairy products.

Acknowledgements

CNPq (Grant number: 313064/2022-9), FAPESC (Grant numbers: 2021/TR791 and 2023/TR331), CAPES (Finance Code 001) and UDESC

References

[1] M. Wolf; L.A. Belfiore; E.B. Tambourgi; A.T. Paulino. International Dairy Journal, 2019, 92, 77-83.
[2] J.R. Xavier; K.V. Ramana; R.K. Sharma. Journal Food Biochemistry 2018, 42, e12564.
[3] A. Shafi; Q. Husain. Materials Today Communications 2022, 32, 103828.
[4] F.M. Almutairi; M. Monier; R.A.S. Alatawi; A.S. Alhawiti; H.H. Al-Rasheed; T.M. Almutairi; N.H. Elsayed. Reactive and Functional Polymers, 2022, 172, 105159.
[5] M. Wolf; A.T. Paulino. International Journal of Biological Macromolecules 2019, 986-997.
[6] M.J. Paz; S. Serafini; H. Enzweiler; L.J. Visioli; A.T. Paulino. In: A. Lichtfouse, E., Muthu, S.S., Khadir (Ed.), Environmental Footprints and Eco-Design of Products and Processes, Springer, 2022: pp. 131–146.
[7] M. Király; B.D. Kiss; P. Horváth; L. Drahos; A. Mirzahosseini; G. Pálfy; I. Antal; K. Ludányi. Biotechnology Reports, 2021, 30, e00637.
[8] D.C. Hanauer; A.G. de Souza; M.A. Cargnin; B.C. Gasparin; D.S. Rosa; A.T. Paulino. Journal of Industrial and Engineering Chemistry, 2021, 97, 368-382.

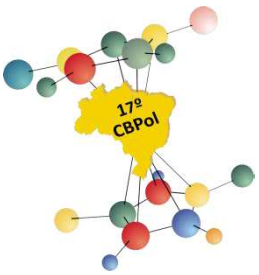

FTIR AND AFM CHARACTERIZATION OF ZEIN/LIGNIN NANOPARTICLES AS GEOPROPOLIS CARRIERS FOR THE TREATMENT OF AGROECOLOGICAL SEEDS

Gisele de C. Ferreira[1*], Roberta R. M. de Freitas[2], Jhones L. de Oliveira[2], Anderson P. E. Santo[2] and Leonardo F. Fraceto[2]

1 – Center for Engineering, Modeling and Applied Social Sciences, Universidade Federal do ABC (UFABC), Santo André, SP, Brazil campos.gisele@ufabc.edu.br
2 – Institute of Science and Technology of Sorocaba (ICTS), Universidade Estadual Paulista (UNESP), Sorocaba, SP, Brazil

Abstract
It seeks to expand the natural applications that have efficient activity against phytopathogens that bring greater productivity to agricultural crops. Two formulations of zein/lignin nanoparticles were characterized in terms of shape, size (nm) and dispersivity using the optical techniques of spectroscopy in the infrared region by Fourier Transform (FTIR) and atomic force microscopy (AFM). The results obtained by FTIR of the two formulations as well as their components separately demonstrated the presence of chemical interactions between the components of the formulations, as well as specific chemical groups used for production. Images obtained by AFM showed that all formulations presented spherical nanoparticles and with a greater frequency of size between 40 and 60 nm for formulations containing geopropolis compared to the formulation without geopropolis 80 – 100 nm. All results suggest that the proposed combination is suitable for the application performed and can be used for seed treatment as soon as more studies determine efficient and safe dosages against specific phytopathogens.

Keywords: *Natural products. Stingless bee. Nanotechnology*

Fundings: CAPES, UNESP, UFABC.

Introduction

Brazil is one of the countries that produces the most raw materials of animal and vegetable origin in the world, however, its permissive legislation regarding synthetic inputs used in agriculture represents an imminent socio-environmental risk [1,2]. In this context, the search for natural products that can be safely used as biopesticides is growing, however, it is necessary that these products are efficient against organisms and microorganisms resistant to conventional pesticides [3].

In order to develop a suspended polymeric formulation, composed of renewable materials and containing an active ingredient from Brazilian biodiversity, for application in the treatment of agroecological seeds and, in the sense of combining nanotechnology with propolis, in order to improve the solubility characteristics of the bioactive components, the materials zein, lignin and geopropolis from Mandaçaia (Melipona quadrifasciata) were gathered. The antisolvent precipitation method [4] was applied, where zein and geopropolis, soluble in alcohol, are suspended in an aqueous solution containing lignin. Zein, the main endospermal protein of corn (Zea mays), stands out for its technological properties of solubility, as it is efficient in encapsulating hydrophobic compounds. In addition, it improves the release of liposoluble substances and promotes protection

against ultraviolet (UV) rays of bioactive compounds susceptible to photodegradation [5]. Lignin was chosen as a stabilizer for the colloidal suspension formed by zein and geopropolis extract, since it can react with hydrophilic and hydrophobic components of both zein and geopropolis, due to its amphiphilic nature [6].

Previous results, obtained using the dynamic light scattering technique, with samples of zein/lignin formulations containing geopropolis, the same ones used in the present study, demonstrated that two (F and G) among six samples had the best hydrodynamic diameter characteristics (nm), polydispersion index, Zeta potential (mV) and pH, over 85 days. Furthermore, the encapsulation efficiency was greater than 99.8% m/m for the six analyzed samples [7]. With this, the present study aims to characterize the F and G samples regarding the chemical groups involved in the preparation reaction of the polymeric formulation, by FTIR and regarding the morphology of the nanoparticles, size (nm) and dispersivity that will be evaluated by images obtained.

Experimental

Materials

All reagents used were analytical grade and deionized water purified by Milli-Q system, Millipore (Bedford, MA, USA). Proprietary absolute ethyl alcohol (P.A.) and potassium bromide (KBr) obtained from Labsynth were used. Alkali lignin and zein reagents (low sulfonate) were obtained from Sigma-Aldrich (Saint Louis, MO, USA).

Samples

Two samples of raw geopropolis from Mandaçaia bees (*Melipona quadrifasciata*), obtained from meliponiculturists in the region of Itapetininga, in the state of São Paulo, were identified as F come from the urban area of Itapetininga and G from the urban area of Tatuí. The samples were collected in August 2021 and sent, under refrigeration and protected from air, light and heat, to the Environmental Nanotechnology laboratory of the Institute of Science and Technology of Sorocaba (ICTS/UNESP).

Procedures

Geopropolis samples were extracted with 80% ethyl alcohol solution [8]. For the preparation of the formulation, the antisolvent precipitation method [4] was used, with modifications. Where, 12 mL of 2% m/m zein solution was added to 3 mL of 10% m/m geopropolis extract for 15 minutes, then 30 mL of 1% m/v lignin solution was added and the mixture was stirred for 30 minutes. After this period, the mixture was rotary evaporated to a final volume of 30 mL.

Infrared spectra were obtained by transmittance in the spectral range of 4000 - 400 cm −1, with 64 scans. Each sample was prepared in a KBr pellet at a mass ratio of 99:1.

Images were obtained using the atomic force microscopy technique, Basic AFM (Nano surf, EasyScan2), with a contact module using the Tap A1G cantilever for scanning the samples. For sample preparation, a 10,000 - fold dilution of the prepared formulations was performed.

Results and Discussion

The FTIR spectrum reflects information about the chemical bonds of functional groups. Therefore, FTIR spectra were used to investigate potential interactions between zein, lignin and geopropolis extracts F and G. Next, in Fig. 1, the infrared absorption spectra of geopropolis F and G samples, zein/lignin nanoparticles with geopropolis F and G and the physical mixtures will be presented.

Figure 1 - Infrared spectra of geopropolis extract, and zein/lignin nanoparticles with geopropolis extracts

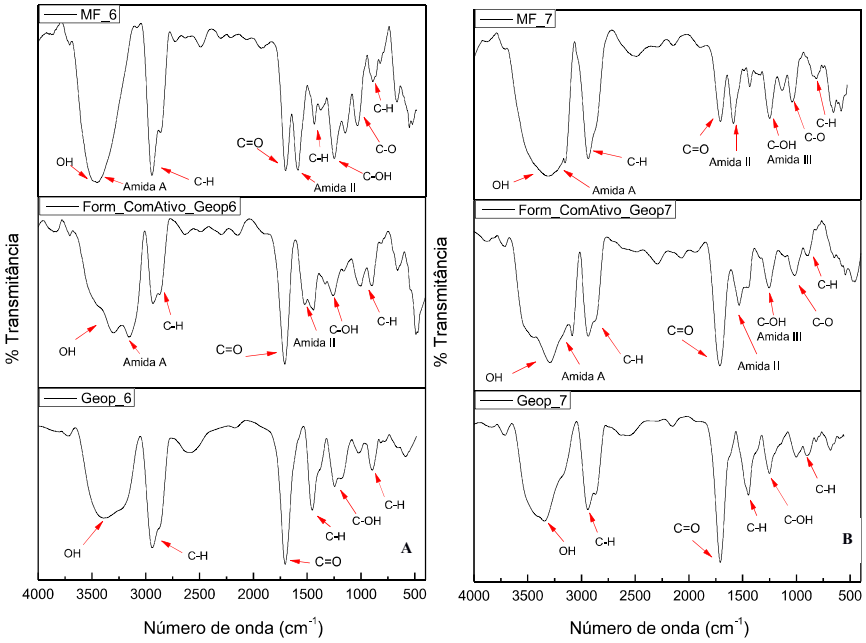

(A) - Geop_6 - extract of geopropolis F; Form_ComAtivo_Geop 6 - geopropolis F nanoparticle formulation; MF_6 - physical mixture of zein, lignin and geopropolis F components; (B) - Geop_7 - geopropolis G; Form_ComAtivo_Geop 7 - geopropolis G nanoparticle formulation; MF_7 - physical mixture of zein, lignin and geopropolis G components. **Source:** elaborated by the author

Observing the FTIR spectra of geopropolis F and G (Fig. 1) it is possible to verify the similarity between them. Both extracts come from the same Mandaçaia stingless bee species, which may explain this similarity between the spectra. The first band observed in both was at approximately 3300 $cm^{-1,}$ referring to the elongation vibration of hydroxyl groups (OH of phenolic compounds) [9]. The bands at approximately 2920 cm^{-1} are attributed to the C-H stretching vibration of the methylene group. The band at 1698 cm^{-1} corresponds to the C=O stretching vibration, correlated with the antioxidant capacity [10]. The band at 1460 cm^{-1} may be related to CH3, CH2, flavonoids and aromatic rings, where the vibrations would be the bending vibration (δ) of C-H and the stretching vibration of aromatics. The peak at approximately 1230 cm^{-1} is associated with phenolic resins [11,12]. The peak of ~ 879 cm^{-1} can be attributed to α-type glycosidic bonds present in carbohydrates of glycosylated polyphenols [13].

In the spectra for the physical mixture and the active formulation, both for geopropolis F and for geopropolis G, it is possible to observe an overlap and displacement of some characteristic bands of their components. However, in physical mixtures, a higher concentration of peaks is observed, that is, less overlap. In formulations with active compound, the spectra showed characteristic peaks of zein, lignin and geopropolis, which corroborates the results of encapsulation efficiency and confirms the chemical interaction between the components.

The images obtained by AFM are shown in Fig. 2. These allowed the observation of the spherical shape of the nanoparticles in the zein/lignin formulations without geopropolis (F0), zein/lignin and geopropolis F (F6) and zein/lignin and geopropolis G (F7).

Figure 2 - AFM of formulation samples without and with active F and G

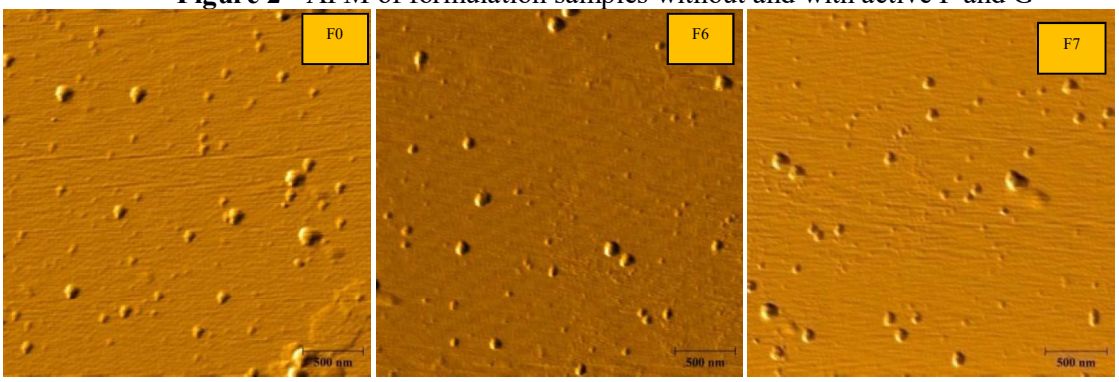

F0 – formulation without geopropolis; F6 – formulation with geopropolis F; F7 – formulation with geopropolis G. **Source:** elaborated by the author

Another possible aspect to be observed from F0, F6 and F7 (Fig. 2) is the size of the nanoparticles in the three different formulations. Therefore, the diameter sizes (nm) of the nanoparticles were measured using the Image J software, and the values obtained are represented in the histograms (Fig. 3).

Figure 3 - Size distribution of nanoparticle formulations without and with geopropolis

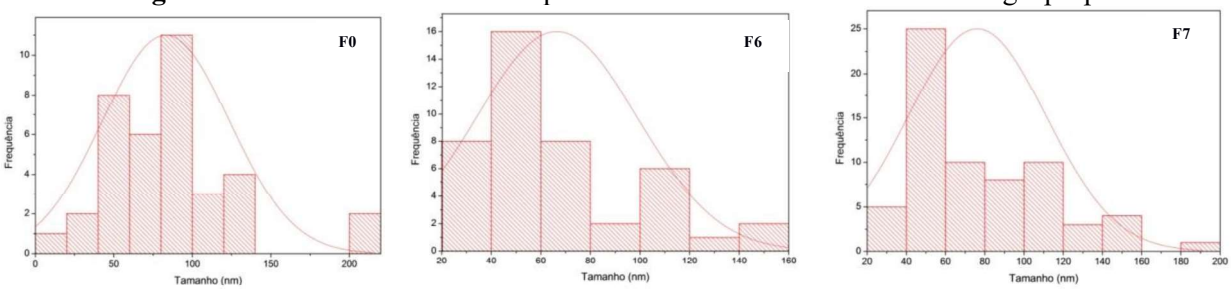

F0 - formulation without active; F6 - formulation with geopropolis F; F7 - formulation with geopropolis G. **Source**: elaborated by the author

The tendency of polydisperse systems is evidenced by observing the histograms. Nanoparticles with sizes between 40 and 60 nm showed a higher frequency for F6 and F7 while for F0, the highest frequency observed was for nanoparticles with sizes between 80 and 100 nm. This demonstrates a possible effect of smaller particle sizes in the presence of geopropolis.

Conclusions

Spectra in the infrared regions of the extracts showed vibrations of hydroxyls and aromatic compounds, characteristic of phenolic compounds, naturally and mostly present in geopropolis. In addition, spectra of nanoparticles containing geopropolis provided results that point to the chemical interaction of zein, lignin and geopropolis components.

Images obtained by AFM showed spherical nanoparticles and a higher frequency of smaller nanoparticles (40-60 nm) when the formulations had geopropolis in the composition. These results corroborate that the choice of formulation was suitable for the proposed application. In addition to the treatment of arable seeds, formulations incorporated with geopropolis can be applied in post-harvest technologies, in the coating of fruits and vegetables, as well as in the grain storage sector, replacing synthetic fungicides.

Acknowledgements

This work was carried out with the support of the Coordination for the Improvement of Personnel Higher Education – Brazil (CAPES) – Financing Code 001.

References

(1) Freitas, B. M. C.; Bombardi, L. M. The National Irrigation Policy and the Use of Pesticides in Brazil: Contamination and Poisoning in Ceará. *GEOgraphia*2018, *20* (43), 86–100. https://doi.org/10.22409/GEOgraphia2018.v20i43.a27213.

(2) Bombardi, L. M. *A Geography of Agrotoxins Use in Brazil and Its Relations to the European Union*; Portal de Livros Abertos da USP, 2019. https://doi.org/10.11606/9788575063590.

(3) Dayan et al. Natural products in crop protection. *Bioorg. Med. Chem.*2009, *17* (12), 4022–4034. https://doi.org/10.1016/j.bmc.2009.01.046.

(4) Hu, K.; McClements, D. J. Fabrication of Surfactant-Stabilized Zein Nanoparticles: A PH Modulated Antisolvent Precipitation Method. *Food Res. Int.*2014, *64*, 329–335. https://doi.org/10.1016/j.foodres.2014.07.004.

(5) Wang et al. Preparation, stability, antioxidative property and in vitro release of cannabidiol (CBD) in zein-whey protein composite nanoparticles. *LWT*2022, *162*, 113466. https://doi.org/10.1016/j.lwt.2022.113466.

(6) Ni, S.; Bian, H.; Zhang, Y.; Fu, Y.; Liu, W.; Qin, M.; Xiao, H. Starch-Based Composite Films with Enhanced Hydrophobicity, Thermal Stability, and UV-Shielding Efficacy Induced by Lignin Nanoparticles. *Biomacromolecules*2022, *23* (3), 829–838. https://doi.org/10.1021/acs.biomac.1c01288.

(7) Ferreira, G. C.; Pereira, A. E. S.; Fraceto, L.F. Geopropolis encapsulation efficiency in a zein and lignin based nanosystem for agricultural applications. In XXI Meeting of Surfaces and Nanostructured Materials, Río Cuarto, 2022, Vol. 1, 380

(8) Park, Y. K.; Ikegaki, M.; Abreu, J. A. da S.; Alcici, N. M. F. ESTUDO DA PREPARAÇÃO DOS EXTRATOS DE PRÓPOLIS E SUAS APLICAÇÕES. *Food Sci. Technol.*1998, *18*, 313–318. https://doi.org/10.1590/S0101-20611998000300011.

(9) Oliveira, R. N.; Mancini, M. C.; Oliveira, F. C. S. de; Passos, T. M.; Quilty, B.; Thiré, R. M. da S. M.; McGuinness, G. B. FTIR Analysis and Quantification of Phenols and Flavonoids of Five Commercially Available Plants Extracts Used in Wound Healing. *Matér. Rio Jan.*2016, *21*, 767–779. https://doi.org/10.1590/S1517-707620160003.0072.

(10) Moţ, A. C.; Silaghi-Dumitrescu, R.; Sârbu, C. Rapid and Effective Evaluation of the Antioxidant Capacity of Propolis Extracts Using DPPH Bleaching Kinetic Profiles, FT-IR and UV–Vis Spectroscopic Data. *J. Food Compos. Anal.*2011, *24* (4–5), 516–522. https://doi.org/10.1016/J.JFCA.2010.11.006.

(11) Shakoury, N.; Aliyari, M. A.; Salami, M.; Emam-Djomeh, Z.; Vardhanabhuti, B.; Moosavi-Movahedi, A. A. Encapsulation of Propolis Extract in Whey Protein Nanoparticles. *LWT*2022, *158*, 113138. https://doi.org/10.1016/J.LWT.2022.113138.

(12) Surek, M.; Cobre, A. de F.; Fachi, M. M.; Santos, T. G.; Pontarolo, R.; Crisma, A. R.; Felipe, K. B.; Souza, W. M. de. Propolis Authentication of Stingless Bees by Mid-Infrared Spectroscopy and Chemometric Analysis. *LWT*2022, *161*, 113370. https://doi.org/10.1016/J.LWT.2022.113370.

(13) Kazemi, F.; Divsalar, A.; Saboury, A. A. Structural Analysis of the Interaction between Free, Glycated and Fructated Hemoglobin with Propolis Nanoparticles: A Spectroscopic Study. *Int. J. Biol. Macromol.*2018, *109*, 1329–1337. https://doi.org/10.1016/J.IJBIOMAC.2017.11.143.

PECTIN EDIBLE FILM OBTAINED FROM ORANGE PEEL: FABRICATION AND APPLICATION TO EXTEND THE SHELF LIFE OF MINIMALLY PROCESSED APPLES

Monique A. P. Cotrim[1], Marina R. F. de Ferraz[1] and Eliane Ayres[1]*

1 – Escola de Design, State University of Minas Gerais (UEMG), Belo Horizonte, MG, Brazil
eliane.ayres.pu@gmail.com

Abstract – Brazil is the leading orange juice producer worldwide, generating tons of fruit residue and waste annually. To help minimize the environmental burden of the orange juice industry, a promising alternative is to repurpose this waste into new sustainable materials. In the present work, orange peels were used to extract pectin, which was used to produce edible film formulations aiming to extend the shelf life of fresh-cut apple. The addition of $CaCl_2$ to the formulation reduced edible film sensitivity to water and resulted in a lower browning index (BI) when applied to apples. Fruit without coating became brown rapidly and presented the highest browning index among evaluated samples.

Keywords: *Orange peel, pectin, edible film, minimally processed apples*

Fundings: FAPEMIG Edital Nº 002/2018 - Programa Pesquisador Mineiro - PPM XII. Grant/Award Number: PPM-00609-18 and Edital 08/2022 - PIBIC/FAPEMIG/UEMG.

Introduction

Brazil is the leading orange juice producer worldwide [1]. Around half of the feed used in industrial orange juice production ends up as residue, the majority of that composed of peels [1]. One alternative to minimize such environmental impact is to use waste and byproducts as precursors to develop sustainable materials [2]. About 30% of raw orange peels is pectin [2], which is a polysaccharide mixture containing methylated ester of D-galacturonic acid units [2] that have excellent film-form properties, and so can be used in the manufacturing of edible films [3-5]. Edible films can extend food shelf-life and help to reduce the use of conventional non-biodegradable packaging [3]. This class of packaging can be ingested or converted into simple compounds harmless to the environment if discarded [6]. In addition to that, it can be used as an alternative to fulfill the commercial demand for minimally processed food (fresh-cut fruit), extending its shelf life and keeping its nutritional value [7]. Edible films should have low cost, be made of readily available material, and have adequate barrier properties [4]. In this context, the present work investigated the extraction of pectin from orange peel, the production of edible films, and its application on fresh-cut apples aiming to expand fruit shelf life. FTIR spectra results confirmed the successful obtention of pectin from orange peel. Pectin edible films were characterized by FTIR, moisture content, and solubility in water. The effect of pectin film on fresh-cut apples was evaluated by calculating the Browning index.

Experimental

Materials

Orange peels were manually removed from "Serra D´água" (*Citrus Sinensis*) oranges bought in a local market (Belo Horizonte, Brazil). Fresh apples (Fuji) were bought in a local shop (Belo

Horizonte, Brazil). Fuji apple was chosen for this study due to commercial demand and the rapid browning of its tissue after cutting [8]. $CaCl_2$ (Synth, Brazil), Glycerol (Synth, Brazil), Ethanol 96% (Synth, Brazil), Citric Acid (Engenharia das Essências, Brazil) were used as received without further purification.

Pectin extraction

Pectin was extracted by the "hot water method" reported by Benassi *et al* [9]. Dried orange peels were added to an aqueous citric acid solution (pH 1,5) with a liquid/solid ratio (LSR) equal to 20. The mixture was kept under magnetic stirring at 70 °C for 1h. After that, the mixture was filtered, and ethanol (96%) was added to the remaining liquid (1:1 v/v). After 24 h, precipitated pectin was filtered, washed with ethanol (96%), centrifugated, and dried at ambient temperature. The dried material was milled into powder using a grinder (IKA A10, IKA Labortechnik, Germany).

Film preparation

Pectin films were prepared by the solution cast method, as reported in the literature [10]. 4 g of pectin was dissolved in 170 mL of deionized water (DI). Glycerol was added at 20% (w/w, based on pectin) as plasticizer. Then, 30 mL of a 1% $CaCl_2$ solution was added, and the resultant solution kept under magnetic stirring for 20 min at 70 ˚C. One formulation without $CaCl_2$ was also prepared, using an equivalent amount of DI in place of $CaCl_2$ solution. The film-forming solution (FFS) was cooled down at room temperature, casted on a plastic petri dish and dried at ambient temperature.

Application of FFS solution on fresh-cut apple

Fresh-cut pieces of apples were individually immersed for 60´s in the Pectin/Glycerol FFS (PEC/Gly) and Pectin/Glycerol/$CaCl_2$ FFS (PEC/|Gly/$CaCl_2$). The coated fruits were air-dried and then kept at ambient temperature [8]. Fruits without film were used as control and stored at the same conditions.

FTIR

The chemical structure of extracted pectin and pectin films was investigated by FTIR (Nicolet 6700, Thermo Scientific) using an ATR accessory, at absorption mode, at a range of 4000-500 cm^{-1}, with 4 cm^{-1} resolution.

Film water sensitivity: moisture content and water solubility

Samples of 2 cm x 2 cm were dried in an oven at 105 ◦C until constant weight. At least tree samples were evaluated for each formulation. To evaluate moisture content samples were weighed on an analytical scale (±0.0001 g) before and after drying. The moisture content was calculated by Eq. 1:

$$MC(\%) = \frac{W_1 - W_2}{W_1} \times 100 \quad (1)$$

Where W_1 is the initial weight, W_2 is the film weight after drying.

To evaluate water solubility dried film samples were immersed into 20 mL of water at ambient temperature for 6 h. The liquid was filtered, and the remaining solid was dried at 105 °C until a constant weight was obtained. The solubility in water was calculated by Eq. 2:

$$S(\%) = \frac{W_1 - W_2}{W_1} \times 100 \quad (2)$$

Where W_1 is the initial weight, W_2 is the remaining dry matter weight.

Effect of films on Apple shelf life: Browning Index (BI)

The effect of film application on prolonging apple shelf life was investigated by the Browning Index (BI) as suggested in the literature [7]. It was used a spectrophotometer (Konica Minolta CM-600D) in reflectance mode, using the CIE color space parameters L*, a*, and b*. illuminant/angle D65/10˚ with a 30 mm measurement opening controlled by Spectra Magic NX Software. The browning index (BI) was calculated according to Eq.3 [7]:

$$BI = 100 \times \frac{(X - 0.31)}{0.172} \quad (3)$$

Where X was calculated by Eq.4:

$$X = \frac{(a^* + 1.75L^*)}{5.64L^*} + a^* - 3.02b^* \quad (4)$$

Four slices of apple were used for the color test, with eight readings per analysis (3 readings per slice), during 0, 1, 2, 3, 4, 20, and 24h. Samples were stored at ambient temperature without any additional cover.

Results and Discussion

The FTIR spectra of neat pectin, PEC/Gly film, and PEC/Gly/$CaCl_2$ shown in Fig.1 do not present a significant change among them, as reported previously in the literature [5]. It was observed a broad band around 3300 cm^{-1} attributed to the hydroxyl groups in pectin, as well as absorbed water [5]. The presence of a peak at 1745 cm^{-1}, that is characteristic of methoxycarbonyl absorption, and a peak at 1630 cm^{-1} attributed to carboxyl absorption [11], could be an indication that the pectin obtained was High Methoxyl pectin (HM) [11]. Pectin can be classified into two categories according to the degree of methyl esterification (DE). Low Methoxyl (LM) when DE<50%, and High Methoxyl (HM) when DE>50% [9, 11]. Wang et al [11] reported that HM and LM pectin present subtle differences in FTIR absorbance. According to the authors, HM pectin has characteristic peak at 1750 and 1630 cm^{-1}, while in LM pectin the carboxyl absorbance peak is at a lower wavenumber (1604 cm^{-1}). According to the literature [9] the pectin extraction method adopted in the present work results in HM pectin. Sayah et al [12] also reported that using citric acid to extract pectin, as used in the present work, resulted in HM pectin. LM pectin has different properties that LM pectin. For instance, LM jellifies slower than HM pectin [9].

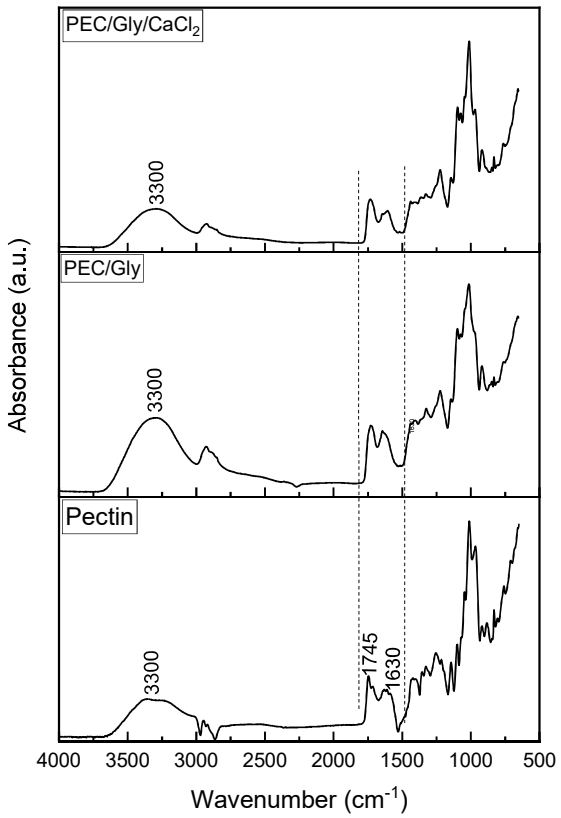

Figure 1. FTIR spectra (Neat pectin, PEC/Glycerol, PEC/Glycerol/$CaCl_2$).

The sensitivity of films to water was evaluated by moisture content and solubility in water [5]. Pectin is a hydrocolloid that can hold a large amount of water [4]. Such behavior can be explained by the presence of numerous hydroxyl groups in pectin that favor the interaction with water molecules due to hydrogen bonds, leading to water diffusion into and through the material [2]. According to the literature [13], a high-water solubility is an important factor in edible films considering that it should easily dissolve in the mouth. As presented in Table 1, developed pectin films without $CaCl_2$ possess high sensitivity to water. Water solubility is around 89%, and moisture content 23%. The addition of $CaCl_2$ contributed to reducing the film solubility to 85.70% and moisture content to 19.78%. This could be due the formation of a more compact structure, due to ionic linkages between calcium ions and galacturonic acid units of pectin, which is described as the "egg-box" model [11]. Zhang *et al* [5] reported a similar result (87.53%) for pectin/thymol films cross-linked with $CaCl_2$. The authors also reported that cross-linking with $Fe3^+$ and Cu^{2+} reduced the water solubility of the films to 23.57 and 23.46%. Hari *et al* [10] reported lower values of moisture content and solubility in water for crosslinked pectin with Ca^{2+}, being 14.2% and 31.8%, respectively. Such differences could be due to variations in pectin structures due to species, ripping stage, and storage conditions [11].

Table 1. Moisture sensitivity of developed edible films.

Water sensitivity	PEC/Gly film	PEC/Gly/$CaCl_2$ film
Moisture Content (%)	23.9 ± 0.0075	19.78 ± 0.0058
Solubility in water (%)	89.21±0,0188	85.70 ± 0.0172

Data represent the mean ± standard deviation.

When an apple is peeled off and/or is sliced, its color rapidly changes to brown, reducing minimally processed fruit shelf life. This happens due to polyphenol oxidases releasing after damage to cell tissue [7, 14]. As shown in Fig.2, the uncoated slices presented higher browning index values during the storage time of 24 h. Coated apple slices took longer to increase the BI index. After 24 h, samples coated with PEC/$CaCl_2$ presented the lowest BI index, indicating that the film formulation was efficient in delay browning of fresh cut apples. Sólis-Contreras et al [7] investigated three formulations of edible films (Citric acid/Chitosan/Cinnamon oil; Glycerol/Cinnamon oil/Guar Gum; Glycerol/Cinnamon oil/Guar Gum/Corn Starch) for fresh cut apples and reported that all of them had a similar BI value, while uncoated apples showed the highest BI.

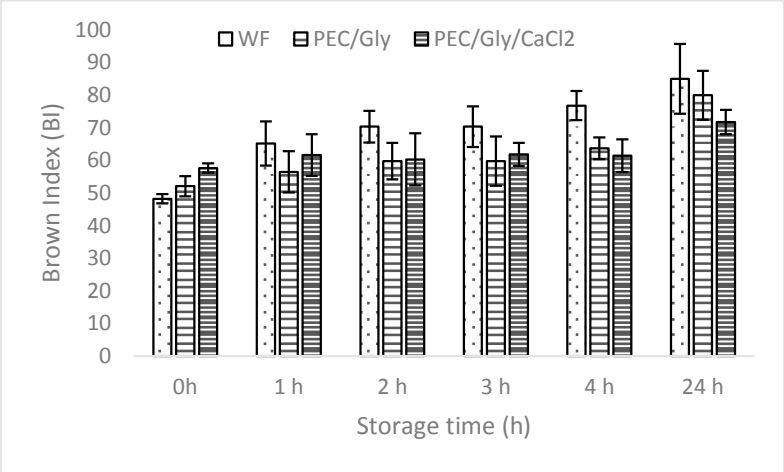

Figure 2. The brown index (BI) of Fuji apple slices coated (with PEC and PEC/$CaCl_2$) and not treated (WF) at hour 0, and after 1, 2, 3, 4, 20, and 24 hours of storage at ambient temperature. Values indicate the means ± standard deviations.

Conclusions

Pectin was obtained from orange peel and successfully used to produce edible films. The addition of $CaCl_2$ reduced edible film moisture content and solubility in water. When applied to fresh-cut apples it delayed, and diminished the browning process compared with uncoated fruit, indicating its potential use in extending the shelf life of minimally processed apples.

Acknowledgements

The authors are grateful to Minas Gerais State Research Support Foundation (FAPEMIG), Coordination for the Improvement of Higher Education Personnel (CAPES) and National Council for Scientific and Technological Development (CNPq).

References

1. M.P.Jiménez-Castro; L. S. Buller; A. Zoffreo; M. T. Timko; T. Forster-Carneiro. Journal of Environmental Chemical Engineering, 2020, 8, 104035. https://doi.org/10.1016/j.jece.2020.104035
2. A. I. Quilez-Molina; G. Mazzon; A. Athanassiou; G. Perotto. Materials Today Communications , 2022, 32, 103871. https://doi.org/10.1016/j.mtcomm.2022.103871.
3. A. Sood; C.S. Saini. Food Hydrocolloids, 2022, 123, 107135. https://doi.org/10.1016/j.foodhyd.2021.107135
4. W. A. Asfaw; K. D.Tafa; N. Satheesh. Heliyon, 2023, 9, e13724. https://doi.org/10.1016/j.heliyon.2023.e13724
5. W. Zhang; J. Cao; W. Jiang. Food Hydrocolloids, 2022, 128, 107594. https://doi.org/10.1016/j.foodhyd.2022.107594
6. F. L. Seixa; F. R. B. Turbiani; P. G. Salomão; R. P. Souza; M.L. Gimenes. Chemical Engineering Transactions, 2013, 32, 1693-1698. https://doi:103303CET1332283
7. G. A.Solís-Contreras; M. C. Rodríguez-Guillermo; M. L.Reyes-Veja; C. N. Aguilar; O. N. Rebolloso-Padilla; J. Corona-Flores; L.A.A. Soriano-Melgar; X. Ruelas-Chacon. Foods, 2021, 10, 597. https://doi.org/10.3390/ foods10030597
8. M.A. Rojas-Grau; M.S. Tapia; F.J. Rodrıiguez; A.J. Carmona; O. Martin-Belloso. Food Hydrocolloids, 2007, 21, 118-127. https://doi:10.1016/j.foodhyd.2006.03.00
9. L. Benassi; I. Alessandri; I. Vassalini. Molecules, 2021, 26, https://doi.org/10.3390/molecules26061766
10. K. D. Hari; C. V. Garcia, G.H. Shin, J.T Kim. Polymers, 2021, 13, 2403. https:// doi.org/10.3390/polym1315242403
11. H. Wang; S. Fei ; Y. Wang; L. Zanc; J. Zhu; Carbohydrate Polymers, 2020, 231, 115673. https://doi.org/10.1016/j.carbpol.2019.115673
12. M. Y. Sayah; R. Chabir; H. Benyahia; Y. R.Kandri; F. O. Chahdi; H.Touzani; F. Errachidi. Plos One, 2016, 0161751. https://doi:10.1371/journal.pone.0161751
13. S. Namratha; V. Sreejit; R. Preetha. International Journal of Food Science and Technology, 2020, 55, 1497–1505. http://doi:10.1111/ijfs.14550
14. C. Fagundes; R. D. M. C. Amboni, A. R. Monteiro. Journal of Food Processing and Preservation, 2013, 37, 405-412. https:// doi:10.1111/j.1745-4549.2011.00660.x

Performance assessment of bacterial cellulose films from Kombucha in conservation of strawberries *in natura*

Evelin T. B. Serpa[1], Renata Leme[1], Suelen C. A. Sacardo[1], Henrique S. M. Lopes[1], Paulo Bálsamo[1] and Maira de L. Rezende[1]*

1 – Technological College of Sorocaba (Fatec) - Sorocaba, SP, Brazil
**maira.rezende@fatec.sp.gov.br*

Abstract - Biopolymers emerge as an important and sustainable alternative for the development of eco-friendly packaging. In this work, bacterial cellulose (BC) was obtained from Kombucha, an ancient, fermented beverage valued for its health benefits, which fermentation occurs naturally, taking several days to complete. Three different commercial packaging were compared to a BC film from Kombucha, as a conservation method for strawberries *in natura*. Materials were investigated pre and post use, regarding its structure, thermal properties, and crystallinity, and strawberries were analyzed by its mass loss and visual aspect. Regarding conservation method investigated, synthetic polymers (PE, PP and PVC) showed significant lower mass loss when compared to BC and to Control sample. Water vapor permeability (WVP) of these films is lower when compared to BC, promoting lower moisture loss, which preserves the fruit moisture, texture and weight for longer periods and, when compared to commercial packaging, its performance is inferior, which can be justified by the greater absorption of water by the BC. Thus, it is possible to infer that its performance may be higher when used in dry food packaging. Another promising application for the BC membrane is in membranes for dermal dressings in the medical field.
Keywords: bacterial cellulose, biopolymer, kombucha, strawberries, films.
Fundings: São Paulo Research Foundation (FAPESP) n° 2022/08431-0

Introduction

Nowadays, plastics films are one of the main materials used to preserve food, being an important segment in food production [1]. However, large production and consumption of plastic packaging has brought several problems, such as improper use and disposal, resulting in negative environmental impacts, including water and soil pollution [2]. Approximately one third of domestic waste consists of packaging and about 80% of it is short-term packaging, which reduces the useful life of landfills, its most common destination [3]. Therefore, biopolymers emerge as an important and sustainable alternative for the development of eco-friendly packaging [4], [5]. In this segment, bacterial cellulose stands out as a biopolymer that results from the metabolism of a cell growth cycle, which are derived from biological sources, such as microorganisms, plant biomass and agro-waste. Being obtained naturally by the ecosystem increases their importance in relation to their biodegradability, since they can be easily degraded by microorganisms found in the environment. [6], [7]. In this work, bacterial cellulose (BC) was obtained from Kombucha, an ancient, fermented beverage valued for its health benefits, which fermentation occurs naturally, taking several days to complete. Obtention consists in a biofilm, known as SCOBY (Symbiotic Culture of Bacteria and Yeasts), composed of bacteria and yeasts, added to a substrate of green or black tea, sucrose and kept in a place without light, resulting in the formation of a new BC membrane that floats in the liquid [8]. BC is a linear polymer, with molecular structure identical to cellulose from plants. It is produced by aerobic bacteria and has

physical-chemical properties suitable for various applications [9], [10], obtained from a symbiotic culture (SCOBY) of bacteria *Gluconacetobacter* in a suitable culture medium [11]. This bacterium is considered purer than plant-derived celluloses, i.e., related to the absence of hemicelluloses and lignin, and has a distinct fibrous structure, with unique properties, such as high porosity, nanofibrillar structure, ability to retain water, crystallinity, and higher degree of polymerization, as well as high mechanical and tensile strength [12]. Here, three different commercial packaging were compared to a BC film from Kombucha, as a conservation method for strawberries *in natura*. Materials were investigated pre and post use, regarding its structure, thermal properties, and crystallinity, and strawberries were analyzed by its mass loss and visual aspect.

Experimental

Four samples were investigated and compared in this work, Bacterial Cellulose (BC) from Kombucha and three commercial packaging from Polypropylene (PP), Polyethylene (PE) (according to the manufacturer it is an 80% HDPE/20% LLDPE blend) and Polyvinyl chloride (PVC). Kombucha bacterial cellulose was obtained by fermenting green tea rich in sugar with the addition of SCOBY, under conditions with room temperature and shelter from light. After 5 days, BC film presented an appropriate thickness to be removed from the liquid-air interface. BC film was then washed in distilled water and treated with sodium hydroxide solution, at 80°C for 1 hour. After treatment, BC film was washed again in distilled water, dried for 72 hours at 35 °C and then stored for further analysis. Fourier Transform Infrared Spectroscopy (FTIR) analysis was performed in a Perkin Elmer Frontier equipment with Attenuated Total Reflection (ATR) accessory, from 4000 to 400 cm^{-1}, 4cm^{-1} of resolution and 16 scans. Differential Scanning Calorimetry (DSC) analysis was conducted in a TA Instruments DSC25 equipment with RCS90 cooling system, from room temperature to melting of each polymer, under a heating rate of 10°C/min. Samples masses were about 2-4mg placed in an aluminum pan. Enthalpy of melting and melting temperature were obtained by TRIOS™ software. Strawberries were tested by its mass loss up to 11 days, under two different conditions, at room temperature and under typical refrigeration, both with the presence of each film for conservation (BC, PP, PE and PVC) and without the film (Control). After weighing, strawberries' visual aspects were analyzed.

Results and Discussion

Fig. 1 presents FTIR spectra (a) and thermal analysis of DSC (b) for all samples prior to the strawberry test. Since all commercial polymers tested present similar monomers, several bands in the spectra are similar, varying only in shape and/or intensity. All samples presented methyl or methylene (C-H_n) absorption bands near 2920-2850 cm^{-1} region, sharper for PE and PVC [13]. PE also presented characteristic alkane bands at 1472 and 1462 cm^{-1}, clearly observed at Fig. 1 (a). At 1458 cm^{-1}, PP presented a characteristic band of alkane, according to the authors [14], which is also observed here, blue shifted in comparison to the PE spectra. Additionally, PVC presented a characteristic band at 698-638 cm^{-1} region, related to C-Cl bond [15]. BC sample showed characteristic bands of cellulose at 3345 cm^{-1}, associated to -OH elongation. At 2925 and 2854 cm^{-1} regions, typical -CH bonds were observed. Band located at 1647 cm^{-1} was attributed to C=O group, suggesting the production of organic acids, such as acetic acid, derived from kombucha fermentation. Bands located at 1428 cm^{-1} and 1312 cm^{-1} are typical for cellulose -CH_2 and -CH or -COO groups, respectively, and 1168 to 1000 cm^{-1} are associated to the elongation of –COC and -CO groups. Also, bands located at 668, 604, 550 cm^{-1} correspond to the presence of sugars [16]–[18].

Commercial polymers melting temperatures (T_m), glass transition temperature (T_g), crystallinity index (X_C) and enthalpy of melting (ΔH_m) are presented in Fig. 1 (b), prior to the strawberry test. PVC presented typical amorphous curve under DSC analysis, with no detected melting peak and T_g at 61.60 °C, lower than the observed by others (86 °C) [19]. PP and PE melting temperatures are similar to those observed by [19] and both enthalpy of melting (ΔH_m) peaks are in agreement to

literature findings, with only PE presenting higher ΔH_m of 146.91 J/g, compared to the observed (97 J/g) [20]. BC sample showed an endothermic event close to 100°C, referring to the loss of water from the biofilm. The absence of other events suggests that the bacterial cellulose is amorphous and thermally stable, as no further thermic event was observed [16], [17], [21] Crystallinity indexes (X_C) were calculated by Eq. 1, according to [22] and are expressed as a percentage value in Fig. 1 (b) for semicrystalline polymers.

$$Xc = \frac{\Delta Hm}{\Delta Hm0} \cdot 100\% \quad (1)$$

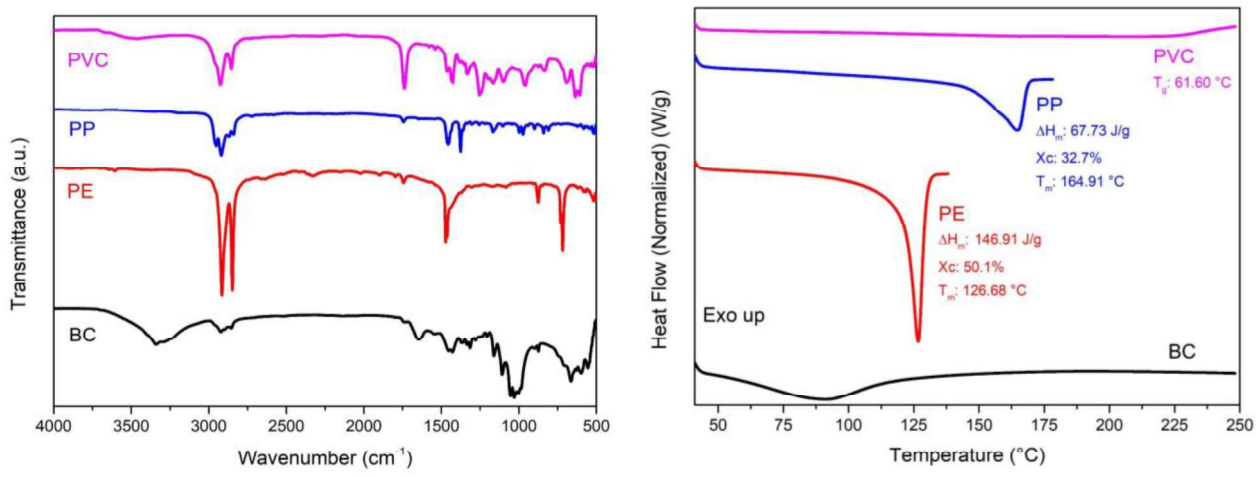

(a) (b)

Figure 1 - FTIR spectra (a) and DSC analysis (b) of all samples.

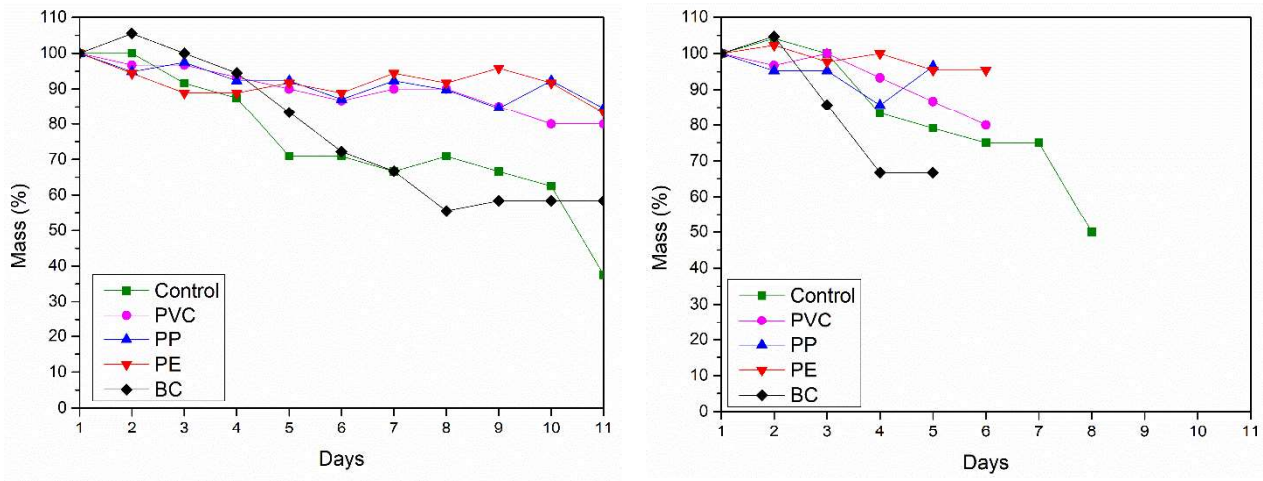

(a) (b)

Figure 2 - Strawberries mass loss up to 11 days of analysis. Fig. 2 (a) shows the behavior of fruit conditioned in a refrigerator and Fig. 2 (b) at room temperature.

Fig. 2 presents strawberries' mass loss. It is possible to observe that Control sample presented the highest mass loss rate during the storage, as expected, followed by BC, PVC, PE and PP. Under refrigeration, strawberries lasted significant longer, but mass loss were greater, considering the same period. This observation is related to the longer conservation of strawberries under refrigerated conditions combined to higher moisture loss [23]–[25]. Regarding conservation method investigated, synthetic polymers showed significant lower mass loss when compared to BC and to Control sample.

Water vapor permeability of these films is lower when compared to BC, promoting lower moisture loss, which preserves the fruit moisture, texture and weight for longer periods [26]–[29]. However, BC increased the durability of strawberries compared to Control sample and its high biodegradability should be considered in the development of several types of packaging.

Conclusions

The results obtained in this work allow us to conclude that the BC packaging provides greater conservation when compared to fruits that were exposed directly in the environment. However, when compared to commercial packaging, its performance is inferior, which can be justified by its greater absorption of water, being possible to conclude that its performance may be higher when used in dry food packaging. Further studies should be performed in addressing other promising applications for BC, such as membranes for dermal dressings in the medical field.

Acknowledgements

The authors would like to thank São Paulo Research Foundation (FAPESP) n° 2022/08431-0.

References

[1] J. D. C. G. M. GONÇALVES, "Resíduos sólidos e contaminação dos solos: percepção dos alunos da EJA da escola estadual de Ouro Velho. – PB.," UNIVERSIDADE FEDERAL DE CAMPINA GRANDE, Sumé, 2017.

[2] M. D. C. ALMEIDA, "Alternativas do uso de sacolas plásticas ecologicamente sustentáveis para o meio ambiente," UNIVERSIDADE TECNOLÓGICA FEDERAL DO PARANÁ, Medianeira, 2018.

[3] M. da E. Ministério do Meio Ambiente, *Consumo sustentável: Manual da educação.* 2005.

[4] O.-W. Lau and S.-K. Wong, "Contamination in food from packaging material," 2000. [Online]. Available: www.elsevier.com/locate/chroma

[5] F. Gu, J. Guo, W. Zhang, P. A. Summers, and P. Hall, "From waste plastics to industrial raw materials: A life cycle assessment of mechanical plastic recycling practice based on a real-world case study," *Science of the Total Environment*, vol. 601–602, pp. 1192–1207, Dec. 2017, doi: 10.1016/j.scitotenv.2017.05.278.

[6] G. P. Udayakumar *et al.*, "Biopolymers and composites: Properties, characterization and their applications in food, medical and pharmaceutical industries," *Journal of Environmental Chemical Engineering*, vol. 9, no. 4. Elsevier Ltd, Aug. 01, 2021. doi: 10.1016/j.jece.2021.105322.

[7] P. R. Yaashikaa, P. Senthil Kumar, and S. Karishma, "Review on biopolymers and composites – Evolving material as adsorbents in removal of environmental pollutants," *Environ Res*, vol. 212, Sep. 2022, doi: 10.1016/j.envres.2022.113114.

[8] R. Jayabalan and V. Y. Waisundara, "Kombucha as a functional beverage," in *Functional and Medicinal Beverages: Volume 11: The Science of Beverages*, Elsevier, 2019, pp. 413–446. doi: 10.1016/B978-0-12-816397-9.00012-1.

[9] H. M. C. Azeredo, H. Barud, C. S. Farinas, V. M. Vasconcellos, and A. M. Claro, "Bacterial Cellulose as a Raw Material for Food and Food Packaging Applications," *Frontiers in Sustainable Food Systems*, vol. 3. Frontiers Media S.A., Feb. 18, 2019. doi: 10.3389/fsufs.2019.00007.

[10] M. Garrido-Romero, R. Aguado, A. Moral, C. Brindley, and M. Ballesteros, "From traditional paper to nanocomposite films: Analysis of global research into cellulose for food packaging," *Food Packag Shelf Life*, vol. 31, Mar. 2022, doi: 10.1016/j.fpsl.2021.100788.

[11] S. Chakravorty, S. Bhattacharya, A. Chatzinotas, W. Chakraborty, D. Bhattacharya, and R. Gachhui, "Kombucha tea fermentation: Microbial and biochemical dynamics," *Int J Food Microbiol*, vol. 220, pp. 63–72, Mar. 2016, doi: 10.1016/j.ijfoodmicro.2015.12.015.

[12] H. Zhang *et al.*, "Complete genome sequence of the cellulose-producing strain Komagataeibacter nataicola RZS01," *Sci Rep*, vol. 7, no. 1, Dec. 2017, doi: 10.1038/s41598-017-04589-6.

[13] J. Wu, T. Chen, X. Luo, D. Han, Z. Wang, and J. Wu, "TG/FTIR analysis on co-pyrolysis behavior of PE, PVC and PS," *Waste Management*, vol. 34, no. 3, pp. 676–682, Mar. 2014, doi: 10.1016/j.wasman.2013.12.005.

[14] C. Fan, Y. Z. Huang, J. N. Lin, and J. Li, "Microplastic constituent identification from admixtures by Fourier-transform infrared (FTIR) spectroscopy: The use of polyethylene terephthalate (PET), polyethylene (PE), polypropylene (PP), polyvinyl chloride (PVC) and nylon (NY) as the model constituents," *Environ Technol Innov*, vol. 23, Aug. 2021, doi: 10.1016/j.eti.2021.101798.

[15] M. Saleem Khan, R. A. Qazi, and M. S. Wahid, "Miscibility studies of PVC/PMMA and PS/PMMA blends by dilute solution viscometry and FTIR," 2008. [Online]. Available: http://www.academicjournals.org/AJPAC
[16] F. Sederavičiūtė, P. Bekampienė, and J. Domskienė, "Effect of pretreatment procedure on properties of Kombucha fermented bacterial cellulose membrane," *Polym Test*, vol. 78, Sep. 2019, doi: 10.1016/j.polymertesting.2019.105941.
[17] Z. Li *et al.*, "The use of bacterial cellulose from kombucha to produce curcumin loaded Pickering emulsion with improved stability and antioxidant properties," *Food Science and Human Wellness*, vol. 12, no. 2, pp. 669–679, Mar. 2023, doi: 10.1016/j.fshw.2022.07.069.
[18] V. M. Bergottini and D. Bernhardt, "Bacterial cellulose aerogel enriched in nanofibers obtained from Kombucha SCOBY byproduct," *Mater Today Commun*, vol. 35, Jun. 2023, doi: 10.1016/j.mtcomm.2023.105975.
[19] D. Sorolla-Rosario, J. Llorca-Porcel, M. Pérez-Martínez, D. Lozano-Castelló, and A. Bueno-López, "Study of microplastics with semicrystalline and amorphous structure identification by TGA and DSC.," *J Environ Chem Eng*, vol. 10, no. 1, Feb. 2022, doi: 10.1016/j.jece.2021.106886.
[20] L. Cafiero, D. Fabbri, E. Trinca, R. Tuffi, and S. Vecchio Ciprioti, "Thermal and spectroscopic (TG/DSC-FTIR) characterization of mixed plastics for materials and energy recovery under pyrolytic conditions," *J Therm Anal Calorim*, vol. 121, no. 3, pp. 1111–1119, Sep. 2015, doi: 10.1007/s10973-015-4799-2.
[21] H. S. Barud *et al.*, "Thermal characterization of bacterial cellulose-phosphate composite membranes.," 2007.
[22] S. V. Canevarolo Jr., *Polymer Science: A Textbook for Engineers and Technologists*. 2020.
[23] C. Shrivastava *et al.*, "Digital twins for selecting the optimal ventilated strawberry packaging based on the unique hygrothermal conditions of a shipment from farm to retailer," *Postharvest Biol Technol*, vol. 199, May 2023, doi: 10.1016/j.postharvbio.2023.112283.
[24] M. C. N. Nunes, J. K. Brecht, S. A. Sargent, and A. M. M. B. Morais, "Effects of delays to cooling and wrapping on strawberry quality (cv. Sweet Charlie)," 1995.
[25] V. H. Tournas and E. Katsoudas, "Mould and yeast flora in fresh berries, grapes and citrus fruits," *Int J Food Microbiol*, vol. 105, no. 1, pp. 11–17, Nov. 2005, doi: 10.1016/j.ijfoodmicro.2005.05.002.
[26] Z. Dong *et al.*, "Characterization of new active packaging based on PP/LDPE composite films containing attapulgite loaded with Allium sativum essence oil and its application for large yellow croaker (Pseudosciaena crocea) fillets," *Food Packag Shelf Life*, vol. 20, Jun. 2019, doi: 10.1016/j.fpsl.2019.100320.
[27] M. L. Iglesias Montes, V. P. Cyras, L. B. Manfredi, V. Pettarín, and L. A. Fasce, "Fracture evaluation of plasticized polylactic acid / poly (3-HYDROXYBUTYRATE) blends for commodities replacement in packaging applications," *Polym Test*, vol. 84, Apr. 2020, doi: 10.1016/j.polymertesting.2020.106375.
[28] L. Bastarrachea, S. Dhawan, and S. S. Sablani, "Engineering Properties of Polymeric-Based Antimicrobial Films for Food Packaging," *Food Engineering Reviews*, vol. 3, no. 2. pp. 79–93, Jun. 2011. doi: 10.1007/s12393-011-9034-8.
[29] Y. Wen *et al.*, "Development of intelligent/active food packaging film based on TEMPO-oxidized bacterial cellulose containing thymol and anthocyanin-rich purple potato extract for shelf life extension of shrimp," *Food Packag Shelf Life*, vol. 29, Sep. 2021, doi: 10.1016/j.fpsl.2021.100709.

SYNTHESIS AND CHARACTERIZATION OF FATTY AMIDES WITH POTENTIAL FOR BIOLUBRICANT

Paola Stradolini da Silva[1]* and Cesar Liberato Petzhold[1]
1 – Department of Organic Chemistry, Federal University of Rio Grande do Sul (UFRGS), Porto Alegre, RS, Brazil
paolastradolini@gmail.com

Abstract - Biolubricants are considered a potential alternative for the lubricant industry, to reduce the use of the world reserves of fossil fuels sources and the environmental impact. This work aims to obtaining fatty amides through transamidation of different fatty acids, stearic acid (SA), oleic acid (OA) and castor oil (CO) with diethanolamine (DEA), to evaluate the effect of the presence/absence of unsaturation, and hydroxyl group in a carbon chain of the same size (C18). The fatty amides were characterized by nuclear magnetic resonance (NMR), Fourier transform infrared (FTIR), size exclusion chromatography (SEC), thermogravimetry (TGA), differential scanning calorimetry (DSC) and dynamic viscosity (η). The fatty amide obtained from the reaction of DEA with castor oil showed lower melting point, higher thermal oxidative stability and higher viscosity index, characterizing the presence of unsaturation and hydroxyl group are important for obtaining better lubricating properties.

Keywords: *Biolubricant, Fatty acid, Sustainable sources, Vegetable oil.*

Introduction

Lubricants has an important role in industry, for the proper functioning and prolonging the useful life of the machinery, as it reduces the friction and wear [1]. Due to the increase in energy consumption worldwide, increases the need to technologies focused on development of sustainable sources to replace the use of fossil sources. Biolubricants have been studied as a proposal to minimize the impact on the environment as well as on the dependence of fossil sources in the industry [2-3].

There are several types of fatty acids, which can be saturated, unsaturated, polyunsaturated, with short or long carbon chains, in addition to being able to have a higher content of hydroxyls (as is the case of ricinoleic acid), not to mention the chemical modifications that can insert epoxide rings, higher content of hydroxyls, organic compounds to increase the carbonic chain, variation of the index of acidity, as well the polarity of the molecule, etc. All with the aim of promoting the optimization of properties for a certain purpose. Vegetable oils formed by fatty acids are the raw material usually the most used to produce biolubricants, due to the properties, such as a low pour point, a good oxidative stability and low viscosity variation with heating, which guarantees a high viscosity index, being important for good biolubricants [4].

Therefore, this work presented an evaluation of the application of fatty amides as potential for biolubricant from the modification of different fatty acids with diethanolamine, one saturated fatty acid (stearic acid), one unsaturated fatty acid (oleic acid) and a triglyceride formed by the ricinoleic fatty acid which in addition to being unsaturated has the differential of having a hydroxyl in its structure. With this, it will be possible to evaluate the influence of unsaturation and polar groups in obtaining the desirable properties for a good lubricant [5].

Experimental

Transamidation of fatty acids and vegetable oil

Approximately 0.1 mol of fatty acid or vegetable oil and 0.35 mol of diethanolamine (DEA) were added to a 250 mL round bottom flask, fixed to the magnetic stirrer at a speed of 300 rpm, for 12 h

at a temperature of 130 ºC, Fig 1. The fatty amide was washed with a saturated sodium chloride solution and extracted with diethyl ether. The organic phase was dried over anhydrous sodium sulfate (Na_2SO_4), and then filtered and placed on a rotary evaporator [6].

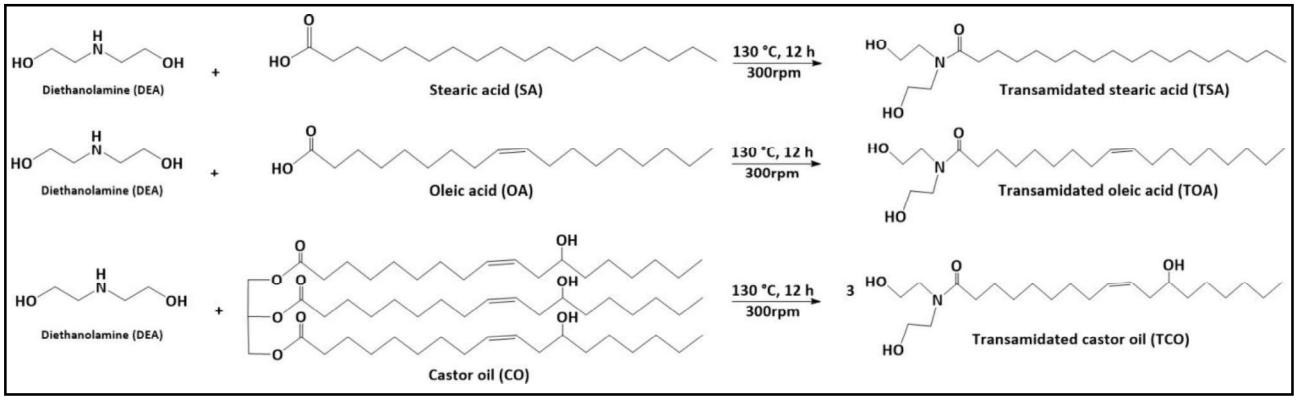

Figure 1. Synthetic routes for obtaining fatty amides from fatty acids and vegetable oil.

Nuclear magnetic resonance

^{1}H NMR was performed to monitor changes in stearic acid, oleic acid and castor oil from the synthetic routes shown in Fig. 1, a Bruker 400 MHz spectrometer was used.

Fourier transform infrared

The spectra were obtained using the Nicolet 6700 – Thermo equipment, in attenuated total reflection (ATR) mode with germanium crystal, and 4 cm^{-1} resolutions, operating in the range of 4000-500 cm^{-1}.

Size exclusion chromatography

The analysis was performed to evaluate the molecular weight of the fatty amides.

Thermogravimetry

The thermogravimetric analysis was used to investigated the oxidative stability of the compounds by the initial temperature T_{onset} and the maximum temperature of degradation T_{peak}, in an SDT Q600 TA Instruments equipment, using an aluminum plate.

Differential scanning calorimetry

The analysis was carried out in an inert atmosphere, in a standard plate, in the temperature range from – 70 to 100 °C, at a rate of 20 °C.min^{-1}. The pour point is a very important parameter when it is treated to lubricants, and can be estimated by determination of the melting point by DSC (Q2000 TA Instruments [7].

Dynamic viscosity

The dynamic viscosities were obtained from rheology analysis (ARES-G2 TA Instruments) at 40 °C and 100 °C and the viscosity index (VI) according ASTM D2270.

Results and Discussion

Nuclear magnetic resonance

The ^{1}H NMR spectraof stearic acid (SA), oleic acid (OA), castor oil (CO) and their respective fatty amides, from transamidations with diethanolamine (DEA), are shown in Fig. 2. Methynic hydrogen (a) signals corresponding to the glycerol portions of triglycerides are seen in the 5.2-5.3 ppm region, and 4.1-4.3 ppm methylene hydrogens (b) in the CO spectrum. These signals are not seen in the other spectra because they do not have the glycerol moieties attached. The signals of hydrogens attached to the vinyl carbons (c) of the double bond (C9 and C10) present in the spectra of CO, OA and their respective fatty amides, TCO and TOA are seen in the 5.5 ppm region, but are not seen in the spectra of SA and TSA, since SA is a saturated fatty acid. Once the reactions occur with the DEA, new signals at 3.4-4.0 ppm were observed related to the hydrogens attached to OH groups (d).

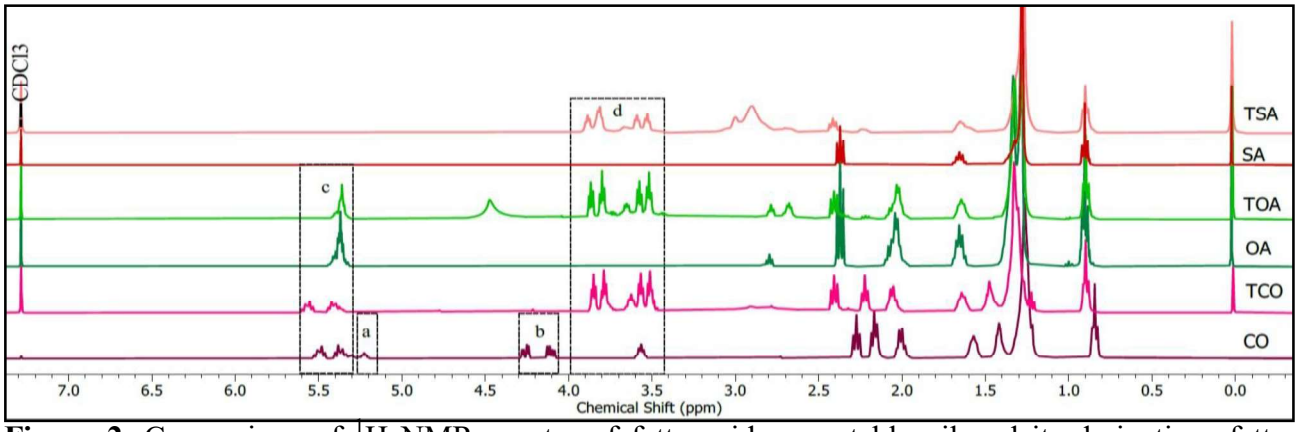

Figure 2. Comparison of ^{1}H NMR spectra of fatty acids, vegetable oil and its derivatives fatty amides.

Fourier transform infrared

The FTIR spectra of stearic acid (SA), oleic acid (OA), castor oil (CO) and their respective fatty amides, from transamidations with diethanolamine (DEA), are shown in Fig. 3. The bands observed in the regions 3411 cm^{-1} and 1052 cm^{-1} refer to the stretching and deformation vibrations of the hydroxyl group (-OH), respectively. They come from the alcohol and the hydroxyl group present in the C12 of CO, because of that they are seen in all spectra, except in SA and OA. The spectra of SA, OA and CO have bands in the regions 1713 cm^{-1} and 1451 cm^{-1} refer to the stretching and deformation vibrations of the ester (-CO), at the same time the spectra of TSA, TOA and TCO have bands in the regions 1629 cm^{-1} and 1451 cm^{-1} refer to the stretching of amide (- C=O) and amine (-CN-).

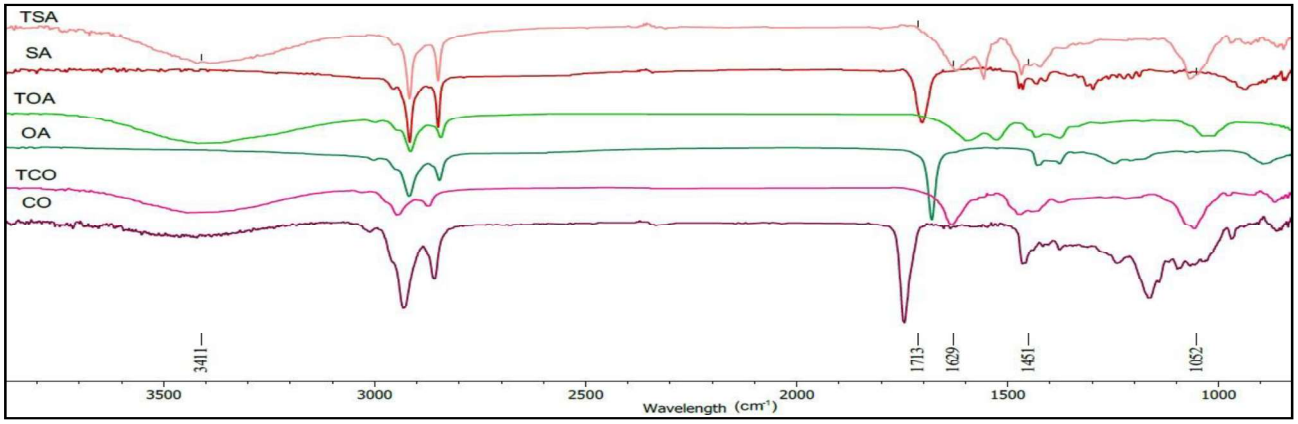

Figure 3. Comparison of FTIR spectra of fatty acids, vegetable oil and its derivatives fatty amides.

Size exclusion chromatography

The results are presented in table 1. As expected, a higher molecular weight was observed for TCO and a lower molecular weight for TSA, presenting lower values in relation to their respective fatty acids and vegetable oil.

Table 1. Average molecular weights and dispersity from fatty acids, vegetable oil and its derivatives fatty amides.

Sample	Mn (g.mol^{-1})	Mw (g.mol^{-1})	Đ
TSA	358	376	1.0
AS	341	359	1.0
TOA	755	790	1.0
AO	870	962	1.1
TCO	821	844	1.0
CO	1036	1316	1.2

Thermogravimetry

The first weight loss process until 150° C is due to the volatilization of the humidity and volatile compounds followed by the chain degradation of the fatty amides. The results indicated a similar behavior stability of TSA and TOA, while TCO presented higher stability. The temperatures T_{onset} and T_{peak} are showed in table 2, the TGA and DTG curves are seen in Fig 4.

Table 2. Values of T_{onset} and T_{peak} from the TGA and DTG curves of derivatives fatty amides.

Sample	T_{onset} (° C)			T_{peak} (° C)		
	First	Second	Third	First	Second	Third
TSA	108	366	460	112	372	469
TOA	112	366	473	119	369	484
TCO	100	402	499	134	439	528

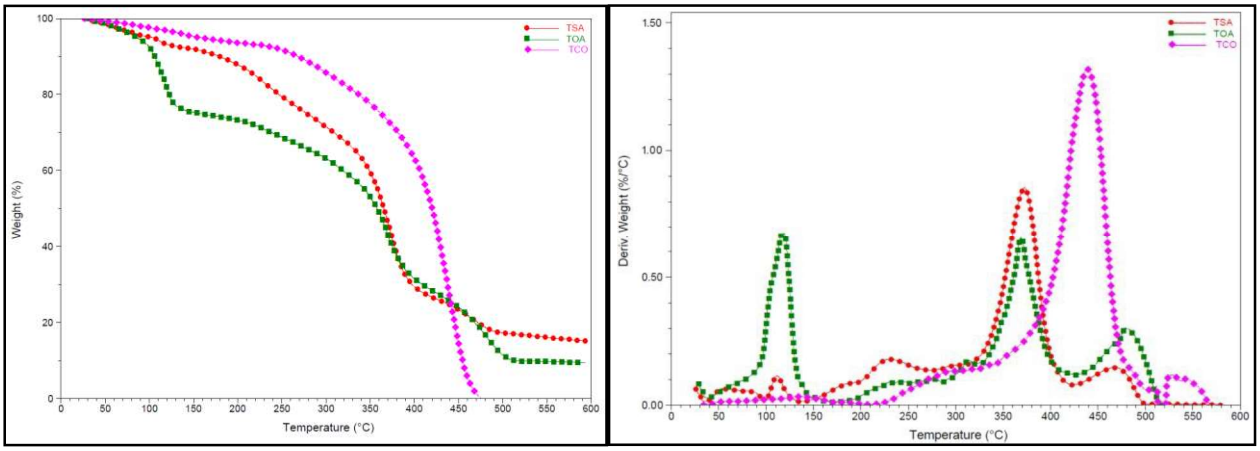

Figure 4. On the left TGA curves and on the right DTG curves from derivatives fatty amides.

Differential scanning calorimetry

The results presented in Fig 4 showed an endothermic peak (a melting point) about 51.7 ºC for TSA and three endothermic peaks about -64 ºC, - 18 ºC and 17ºC for TOA, while TCO do not show a melting point on the range temperature which the analysis occurred. This suggests that the TCO has a pour point below - 60 °C.

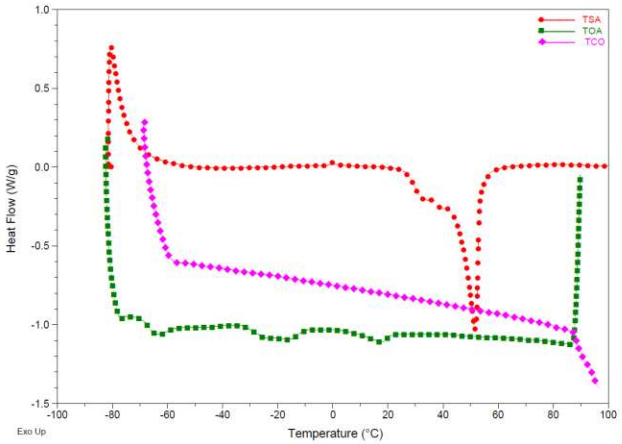

Figure 5. DSC second heating curves from derivatives fatty amides ($20^{o}C.min^{-1}$).

Dynamic viscosity

The results are summarized in table 3. TCO showed a high VI value about 514 cP, meanwhile TOA showed a lower VI, about 48 cP and TSA being solid at room temperature, with melting point (T_m) being above 70 ºC (as shown in the DSC), it was not possible to measure at 40 ºC, and at 100 ºC the equipment failed to measure.The higher the VI, the better the lubrication performance, which means greater viscosity stability in the face of temperature variations.

Table 3. Dynamic viscosity and viscosity index of derivatives fatty amides.

Sample	Dynamic viscosity (cP)		Viscosity Index [a]
	40 ºC	100 ºC	
TSA[b]	-	-	-
TOA	1061	37	48
TCO	590	290	514

a) Determined considering a unitary density of the products;
b) solid at room temperature.

Conclusions

The viscosity index (VI), melting point and oxidative stability of castor oil fatty amide (TCO) were better than TSA and TOA results. Therefore, they indicate that the presence of unsaturation and polar groups as hydroxyl act in obtaining more desirable properties of a biolubricant. Therefore, TCO fatty amide is more suitable for application as a biolubricant.

Acknowledgements

The authors thank the support of the Coordination for the Improvement of Higher Education Personnel (CAPES) and the Institute of Chemistry at the Federal University of Rio Grande do Sul.

References

1. J. Salimon, N. Salih, E. Yousif. European Journal of Lipid Science and Technology. 2010, 112, 519–530. https://doi.org/10.1002/ejlt.200900205.
2. A. Campanella, E. Rustoy, A. Baldessari, M.A. Baltanás. Bioresource Technology. 2010, 101, 245–254. https://doi.org/10.1016/j.biortech.2009.08.035.
3. R. K. Elango; K. Sathiasivan; C. Muthukumaran; V. Thangavelu; M. Rajesh; K. Tamilarasan. Microchemical Journal, **2019**, 145, 1162. https://doi.org/10.1016/j.microc.2018.12.039.
4. S. Khan, P. Das, M. A. Quadir, M. Thaher, S. N. Annamalai, C. Mahata, A. H. Hawari, H. A. Jabri. Science of the Total Environment, 2022, 847, 157648. http://doi.org/10.1016/j.scitotenv.2022.157648.
5. N. Annissa; WIDAYAT, Widayat. *MATEC Web of Conferences,* **2018**, 156.
6. J-M. Pin; M. Misra; A. K. Mohanty. Macromolecular Rapid Communication, 2019, 40, 1900093. https://doi.org/10.1002/marc.201900093.
7. I. M. Cavalcante; N. R. D. C. Rocha; D. H. A. De Brito; A. P. D. Schuller; J. F. Câmara Neto; S. M. De Morais; F. M. T. Luna; M. T. G. F. Schanz; M. E. Maier; N. M. P. S. Ricardo. J. Am. Oil Chem. Soc. **2019**, 96 (1), 75-82. https://doi.org/10.1002/aocs.12160.

THE INFLUENCE OF IONIZING RADIATION ON THE PHYSICAL PROPERTIES OF POLYESTER MULTIFILAMENTS

Camila G. Melo [1], Leonardo G. de A. e Silva[1], Jorge M. Rosa[2], Maria da C. C. Pereira[1]

1 – Instituto de Pesquisas Energéticas e Nucleares, IPEN - CNEN, São Paulo, SP, Brasil
camila.gomes.melo@hotmail.com
2 – Faculdade de Tecnologia SENAI Antoine Skaf, São Paulo, SP, Brasil

Abstract – The polyester fibers stand out among the fibers used in the textile industry, due to their numerous factors that make them attractive in terms of cost-effectiveness. The interaction of ionizing radiation with the polyester substrate allows the formation of reactive species capable of stimulating structural modifications of the fiber and, consequently, altering its properties. In this sense, the present work proposes to analyze the influence of ionizing radiation on the physical properties of PES multifilaments. PES multifilament samples were exposed to Cobalt-60 gamma ionizing radiation, with doses ranging from 50 kGy to 200 kGy. The physical properties of tensile strength and elongation were verified. Gamma irradiation treatment proved to be effective in increasing the elongation and strength of the PES multifilament.
Key words: *elongation, ionizing radiation polyester, tenacity textile.*
Financing: IPEN - CNEN/SP

Introduction

In the 1920s, the concept of polymer served as the basis for the subsequent development of numerous products of synthetic origin obtained from petroleum, such as polyester. Due to its diversity, it is used in numerous sectors such as automotive, civil construction, packaging, medical equipment, consumer products, among others [1 – 3].

In the textile sector, numerous synthetic fibers were developed, such as polyethylene terephthalate (PET), known in Brazil as polyester (PES), whose production rose exponentially in the 1980s, currently making up 2/3 of the total products sold in the sector [4, 5]. The Brazilian panorama of consumption, in tons, of PES multifilaments in the last 5 years is shown in Fig. 1 [6].

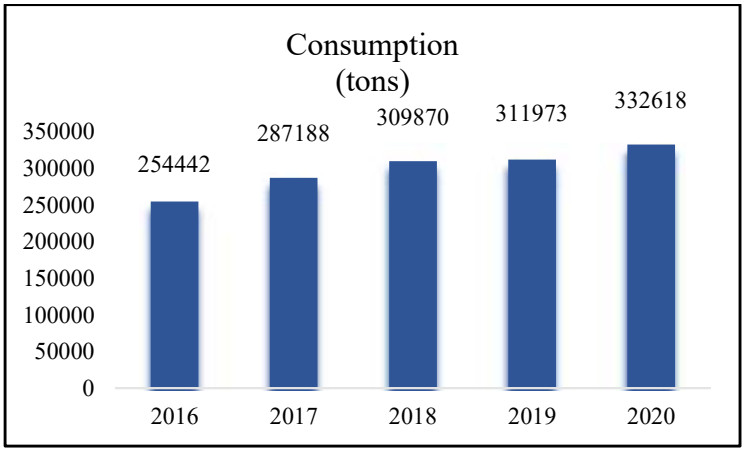

Figure 1. Overview of PES consumption from the years 2016 to 2020 [6].

In general, polymeric materials can be synthesized or adapted for numerous purposes, through processes such as ionizing radiation, whose interaction with polymeric materials allows changes in physical-chemical properties of interest to numerous areas, such as textiles. In this sense, the present work proposes to analyze the influence of ionizing radiation on the physical properties of PES multifilaments [7, 8].

Experimental

Samples of PES multifilament (192/40 Dtex) were exposed to gamma ionizing radiation through the Colbalt 60 Multipurpose Irradiator (IM – 60 Co), located at the Centro de Tecnologia de Radiação (CETER-IPEN), whose analysis took place by comparing samples without treatment and those irradiated with doses that varied between 50 kGy and 200 kGy. The physical properties of tensile strength, called toughness (cN tex^{-1}), and elongation (%) were verified using the STATIMAT 4U equipment by Textechno, located at the Faculdade de Tecnologia do SENAI "Antoine Skaf".

Results and discussion

The figures below represent the observed relationships between absorbed dose and elongation (Fig. 2), and between absorbed dose and tenacity (Fig. 3), of PES multifilament samples.

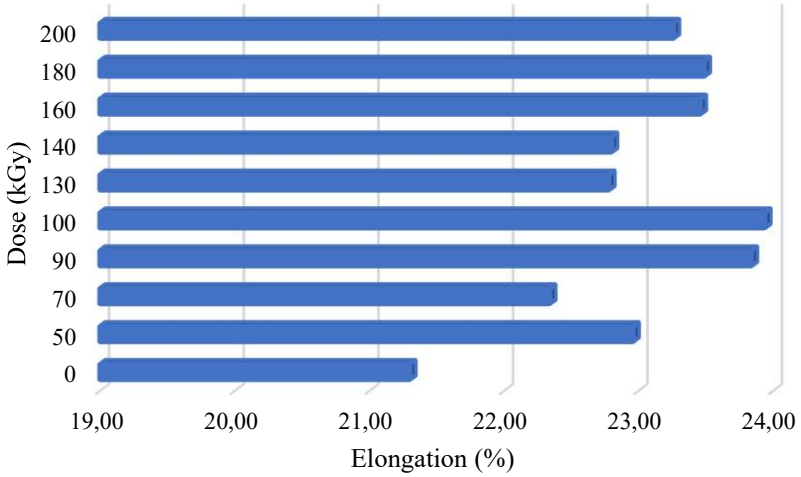

Figure 2. Elongation of the PES multifilament as a function of the absorbed dose.

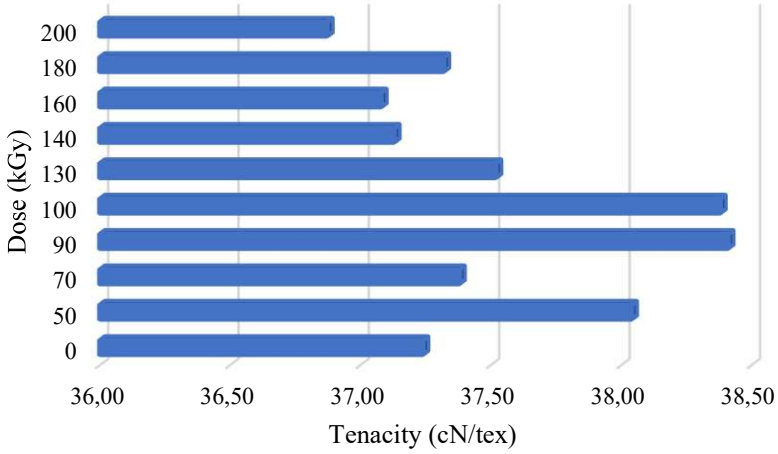

Figure 3. Tenacity of PES multifilament as a function of absorbed dose.

The samples showed a non-linear increase in the elongation of the PES multifilaments, reaching a maximum of 23.94% at 100 kGy, in other words, it elongated more than 10% compared to the untreated sample. The yarn tenacity increased up to a dose of 130 kGy, whose maximum value of 38.41 cN tex^{-1} was obtained at 90 kGy. Thereafter, there was a drop in toughness with the lowest toughness observed at 200 kGy. Due to the fact that the warp threads are exposed to attrition and tension, resulting from the comb hitting the weft thread in in weaving, for example, the elongation and resistance of the thread to breakage become important characteristics for a smaller number of breaksof and the consequent increase in weaving efficiency.

This elongation behavior was also observed by Gisbert et al. [9], when analyzing the effect of the electron beam in 100% PES tissues, whose maximum elongation was reached at 100 kGy. In a study carried out in 1989, Fadel, Abdel-Zaher and El-Messiery [10] when examining the effects of neutron fluences on the mechanical properties of polyester, they found that the minimum value of tensile strength corresponded to a maximum value of elongation, but that at fluences greater than 10 N $cm^{2\ -1}$ a slow decrease in both properties.

The mechanical properties of PES have been linked to changes in the crystallinity of the fiber, in which the higher the irradiation doses, the greater the degree of crystallization, resulting in the rearrangement of molecules and reduction of amorphous zones in the fiber [9, 11].

Conclusion

The cobalt-60 gamma irradiation process proved to be effective in altering the physical properties of elongation and tenacity of the analyzed polyester multifilament. After treatment, the sample increased elongation by around 12%, contributing to the increase in breaking strength and consequently increased efficiency in weaving machines.

Acknowledgements

We would like to thank the Instituto de Pesquisas Energéticas e Nucleares (IPEN) and the Comissão Nacional de Energia Nuclear (CNEN) for financial support and the Faculdade de Tecnologia SENAI for providing the necessary resources for the development of this work.

References

1. Ahani M, Khatibzadeh M, Mohseni M. Studying the thermodynamic parameters of disperse dyeing of modified polyethylene terephthalate sheets using hyperbranched polymeric additive as a nanomaterial. J Ind Eng Chem [Internet]. 2013;19(6):1956–62. Available from: http://dx.doi.org/10.1016/j.jiec.2013.03.003
2. Manich AM, Bosch T, Carilla J, Ussman MH, Maillo J, Gacén J. Thermal Analysis and Differential Solubility of Polyester Fibers and Yarns. Text Res J [Internet]. 2016;73(4):1–23. Available from: https://doi.org/10.1177/004051750307300410
3. Silva RS, Bianchini VK. Estudo sobre custos ecológicos no tingimento de tecido utilizado em linha automativa. Química Têxtil. 2021;141:6–17.
4. Townsend T. 1B - World natural fibre production and employment. In: Handbook of Natural Fibres: Second Edition [Internet]. Elsevier Ltd; 2020. p. 15–36. Available from: http://dx.doi.org/10.1016/B978-0-12-818398-4.00002-5
5. Henry B, Laitala K, Klepp IG. Microfibres from apparel and home textiles: Prospects for including microplastics in environmental sustainability assessment. Sci Total Environ [Internet]. 2019;652:483–94. Available from: https://doi.org/10.1016/j.scitotenv.2018.10.166
6. ABRAFAS. Fibras Manufaturadas: Estatisticas [Internet]. 2021. Available from: https://www.abrafas.org.br/estatisticas-anuais
7. Raju A, Rao BS, Madhukar K, Reddy KR, Sadhu V, Chouhan R. Effect irradiation on physicochemical and mechanical properties of polymers and polymer blends [Internet]. Green

Sustainable Process for Chemical and Environmental Engineering and Science: Green Composites: Preparation, Properties and Allied Applications. Elsevier Inc.; 2022. 147–163 p. Available from: http://dx.doi.org/10.1016/B978-0-323-99643-3.00011-5
8. Naikwadi AT, Sharma BK, Bhatt KD, Mahanwar PA. Gamma Radiation Processed Polymeric Materials for High Performance Applications: A Review. Front Chem. 2022;10(March):1–15.
9. Gisbert J, Bonet MA, Díaz P, Montava I, Monllor P. Electron beam effect on poly (ethylene terephthalate) fibres. Int J Cloth Sci Technol. 2012;24(4):211–20.
10. Fadel MA, Tera FM, Abdel-Zaher N, El-Messiery MA. Possible control of the mechanical properties of nylon-6, dralon and polyester polymers by neutron irradiation. Polym Degrad Stab. 1989;23(3):209–16.
11. El-Zahhar AA, Yassien KM, El-Bakary MA. Study on the thermal and structural properties of gamma-irradiated polyethylene terephthalate fibers. J Polym Eng. 2020;40(2):129–35.

ACTIVE FILMS WITH JAMBOLAN EXTRACT (*SYZYGIUM CUMIN*) BASED ON ALGINATE/XANTHAN: CHARACTERIZATION AND ANTIOXIDANT ACTION

Anderson C. Bezerra (PG)[1*], Isis L.C. Peralta[1], Andrelina M.P. Santos(PQ)[2], Ana Maria Q. López(PQ)[1]**

1 -Student of the "Graduate Program in Chemistry and Biotechnology", Institute of Chemistry and Biotechnology, Federal University of Alagoas (UFAL)- anderson.campos@ifal.edu.br , ** amql@qui.ufal.br; 2 –Laboratory of Bioprocesses, Federal University of Pernambuco (UFPE)*

Abstract - This study aimed to evaluate film-forming blends of alginate and xanthan containing aqueous extracts of Jambolan (or *Syzygium jambolanum* L) (EABV). In addition, thickness, moisture, water solubility, color, opacity, antioxidant capacity (DPPH radical scavenging) and total phenol concentration of the films were analyzed. The solubility of the films was not altered with theaddition of different extract volumes (EABV) (Table 2), although the other physical and optical characteristics were affected. There was a significant increase in moisture and greater opacity, with brown tones (lower EABV concentrations) and blue-green tones in the films with higher EABV concentrations (Figure 1). Films containing higher concentrations of extract showed visible color changes from pink to blue in different pH buffers. The EABV inserted in biofilms increased the visible light barrier property. Despite the increase total phenolics in concentration and antioxidant capacity, the increasing incorporation of EABV did not change the thickness of thefilms (Table 1). The results showed that EABV can be successfully added to alginate/xanthan films and can be used to obtain active packaging in order to evaluate product shef-life by pH variation food spoilage.

Table 2. Content of total phenolic compounds and free radical scavenging activity of alginate/xanthan films incorporated with different concentrations of EABV.

Films	Sodium Alginate (%)	Xantan (%)	Glycerol (%)	EABV (%)	Phenolics (mg/g de filme)	Sequestration DPPH (%)
Control	1,5	0,75	0,2	0,0	0,00 ± 0,00	0,00 ± 0,00
1%EABV	1,5	0,75	0,2	1,0	3,42 ± 0,08	42,57 ± 1,30
2%EABV	1,5	0,75	0,2	2,0	4,23 ± 0,04	51,37 ± 0,75
4%EABV	1,5	0,75	0,2	4,0	4,60 ± 0,05	52,77 ± 0,66
5%EABV	1,5	0,75	0,2	5,0	4,14 ± 0,27	50,72 ± 1,09
8%EABV	1,5	0,75	0,2	8,0	5,24 ± 0,23	55,23 ± 1,26

Table 1. Physical characteristics of alginate/xanthan added with EABV extract.

Films	Thickness(mm)	Humidity (%)	Solubility in H_2O (%)
Control	0,062±0,008	15,20± 1,96	100
1% EABV	0,061±0,005	28,67± 2,10	100
2% EABV	0,052±0,005	29,34± 1,32	100
4% EABV	0,068±0,007	30,58± 0,14	100
5% EABV	0,065±0,009	33,09± 0,47	100
8% EABV	0,070±0,007	35,06±0,57	100

Figure 1. Alginate/xanthan films added with different proportions of aqueous extract of widow's earring (EABV).

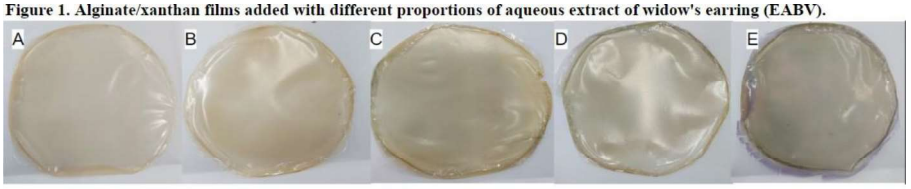

A=1%EABV, B=2%EABV, C=4%EABV, D=5%EABV, D=8%EABV.

References

ALIZADEH-SANI, M. et al. pH-sensitive (halochromic) smart packaging films based on natural food colorants for the monitoring of food quality and safety. Trends in Food Science & Technology, v. 105, p. 93–144, nov. 2020.

TAHIR, H. E. et al. Smart films fabricated from natural pigments for measurement of total volatile basic nitrogen (TVB-N) content of meat for freshness evaluation: A systematic review. Food Chemistry, v. 396, p. 133674, dez. 2022.

Keywords: *Biodegradable polymers; food pigment; food quality monitoring; unconventional fruits; phenolic compounds*

ALGINATE-BASED HYDROGEL FOR ENCAPSULATION OF PLANT-GROWTH-PROMOTING BACTERIA

Eduarda Guerlinguer[1]*, Lais Priscila Karas[1], Helyemari Valentim Althaus[1], Cristiane Colodel[1], Nicoly de Simas[1], Ernandes Taveira Tenório-Neto[2], Rafael Mazer Etto[1], Michele Karoline Lima-Tenório[1,2], Carolina Weigert Galvão[1]

1 – Microbial Molecular Biology Laboratory, State University of Ponta Grossa (UEPG), Ponta Grossa, PR, Brazil
eduarda_guerlinguer@hotmail.com
2 – Laboratory of Multifunctional Polymeric Materials, State University of Ponta Grossa (UEPG), Ponta Grossa, PR, Brazil

Hydrogels (HG) have attracted attention in the scientific field due to their capacity to absorb fluids, particularly water, and their ability to enclose and release active substances[1,2]. They are a sustainable choice in agriculture as they can encapsulate plant-growth-promoting bacteria (PGPB), an eco-friendly fertilizer that fixes nitrogen, solubilize nutrients and/or produce fitohormones[3]. In this context, the present work aims to analyze the survival of bacteria encapsulated in alginate-based hydrogels at different storage times. The sodium alginate was chemically modified using glycidyl methacrylate (GMA) and then crosslinked by an ultrasound-induced radicalar approach with N, N-dimethylacrylamide (DMAAm), and sodium acrylate to obtain the hydrogels. The HG was dialyzed in distilled water until reaching chemical equilibrium, dried (40 ºC) and posteriorly autoclaved for bacteria encapsulation. Scanning electron microscopy (SEM) showed the hydrogels' internal porous structure characteristic of such material. The autoclaved HG showed the maximum swelling degree in bacteria culture medium after 32 hours, reaching 113,32 $g.g^{-1}$ by an anomalous transport mechanism. The encapsulated *Azospirillum brasilense* AbV5/6 survived into HG after the drying process and 30 days of storage, keeping around 10^8 CFU/g of HG, independently of the hydrogel shape (grainy or thin film). The bacteria-loaded hydrogels are stored at room temperature and without light to evaluate bacterial viability over extended periods. Our results indicate that the obtained material has a great potential to encapsulate and release bacteria probably due to its 3D polymer network and property to allow water diffusion.

References

1. Y. Bashan; et al. Plant and Soil 2014, 378. https://doi.org/10.1007/s11104-013-1956-x.
2. M. K. Lima-Tenório; et al. Carbohydrate Polymers 2023, 308. https://doi.org/10.1016/j.carbpol.2023.120631.
3. J. J. Perez; et al. Carbohydrate Polymers 2018, 202. https://doi.org/10.1016/j.carbpol.2018.07.084.

Fundings: CNPq, Fundação Araucária and CAPES
Keywords: *Azospirillum spp., biofertilizer, sustainable agriculture.*

ANALYSIS THE INFLUENCE OF THE DRYING METHOD ON THE BACTERIAL CELLULOSE MEMBRANES PROPERTIES

Julie A. P. Cavalcante[1], Karina C. de Souza[2], Ângela M. M. Santos[2], Felipe C. S. Trindade[2], Luciano C. Almeida[2] Glória M. Vinhas[2], Severino A. Júnior[1]

1 – Department of Fundamental Chemistry (DQF), Federal University of Pernambuco (UFPE), Recife, PE, Brazil
julie.cavalcante@ufpe.br
2 – Department of Chemical Engineering (DEQ), Federal University of Pernambuco (UFPE), Recife, PE, Brazil

Abstract –

Bacterial cellulose membranes have been produced and used in a wide range of applications, from the food and pharmaceutical sector to the biomedical area. This material has a 3D structure composed largely of water and nanometric fibers, which are formed according to the growth of the bacteria used [1]. According to the chosen drying method, the structural and morphological properties are directly affected [2,3], as the fiber packaging can be modified in each process, and this aspect interferes with the application [4]. The objective of this work was to produce bacterial cellulose membrane through the cultivation of Gluconacetobacter hansenii in Hestrin and Schramm standard medium, with four different drying techniques: oven (BCOD), room temperature, freezer and ultra-freezer combined with lyophilization) and consequently at different temperatures. The physical-chemical, morphological, and structural properties of the produced bacterial cellulose membranes were evaluated by Fourier transform infrared spectroscopy (FTIR), X-ray diffraction (XRD), scanning electron microscopy (SEM), BET surface area and thermogravimetric analysis (TGA). The results showed that the four drying techniques affected the structure and final properties of BC. Although, ultra freezer drying with lyophilization (FD) showed better porosity, and freezer drying (RD) showed better crystallinity, oven drying (OD) resulted in films with a different color from the others and with good cohesion between the fibers, and at room temperature (ED) also showed good crystallinity with standard coloration and good cohesion between the polymeric fibers. Therefore, for each type of application, a drying technique can be used, as a way of optimizing the production process of bacterial cellulose membranes.

Keywords: *Bacterial Cellulose. Drying. Temperature. Properties.*

References

1. L. Bao *et al. Materials Science and Engineering C* 2021, 122. https://doi.org/10.1016/j.msec.2021.111922.
2. M. P. Illa, C. S. Sharma, M. Khandelwal. *Journal of Materials Science* 2019, 54(18), 12024–12035. https://doi.org/10.1007/s10853-019-03737-9.
3. E.I. Kashcheyeva, et al *Polymers* 2022, 14, 18. https://doi.org/10.3390/polym14183899.

A NEW METHOD FOR DETERMINATION OF GLYCEROL IN BIODIESEL USING CELLULOSE MONOLITH SORPTIVE STIR BAR

Pablo H. S. Martins[1], Poliana Ricci[1], Rosana M. N. Assunção[1,2] and Anizio M. Faria[1,2]*

1 – Institute of Chemistry, Federal University of Uberlândia, Uberlândia, MG, Brazil
2 – Institute of Exact and Natural Sciences of Pontal, Federal University of Uberlândia, Ituiutaba, MG, Brazil
anizio@ufu.br

Abstract – Glycerol is a co-product of the transesterification process in biodiesel synthesis, and its presence in biodiesel (0.020 % w/w) is a big problem for combustion engines. The official methods for quantification of glycerol in biodiesel require specific, high cost and toxic reagents, opposing the purpose of biofuels.[1,2] So, this work aimed at a simple, efficient, reagent-free, solvent-free, and low-cost method for free glycerol determination in biodiesel. The proposed methodology involves stir bar sorptive extraction (SBSE) of glycerol from biodiesel followed by high-performance liquid chromatography (HPLC) analysis. Sorptive stir bars were prepared with commercial cellulose acetate by dissolving it in dimethylformamide using octanol as a non-solvent. After the phase separation, octanol was removed via solvent exchange. Deacetylation of cellulose acetate monoliths (CAM) using a 0.25 mol/L NaOH solution yielded cellulosic monolith stir bars (CM). Optimization of glycerol extraction from fortified methyl oleate was achieved by the SBSE method using CM stir bars, considering factors such as contact time, desorption time and temperature, eluent, and stir bar length. The optimized conditions involved a 15-minute contact time between a 10-mm CM stir bar and biodiesel sample, followed by glycerol desorption in deionized water at 70 °C for 15 min. Under these conditions, HPLC analysis exhibited 86% glycerol recovery, statistically comparable to the official method. In conclusion, the developed SBSE-HPLC method using cellulose monolith sorptive stir bars was efficient, simple, cost-effective, and environmentally eco-friendly, making it suitable for routine analysis in biodiesel quality control processes.

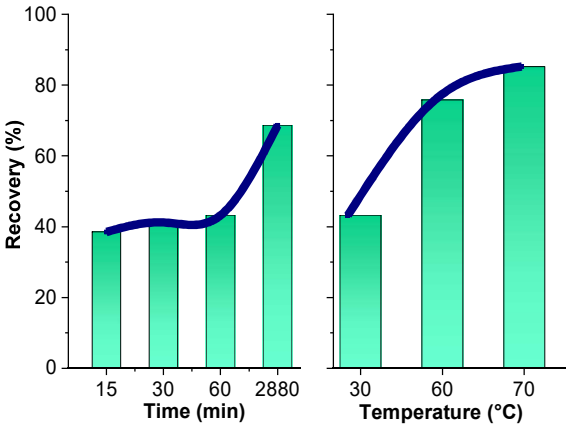

Figure 1 – Glycerol recovery (%) from methyl oleate under different desorption (a) time and (b) temperature using the SBSE method with cellulose monolith stir bar.

References

1. AOCS Ea 6-94, Determination of Crude Glycerin, Titrimetric Method; AOCS: Urbana, IL, 1994.
2. M. R. Monteiro; A. R. P. Ambrozin; L. M. Lião; A. G. Ferreira *Talanta* 2008, *77*, 593-605. https://doi.org/10.1016/j.talanta.2008.07.001.

Fundings: FAPEMIG APQ-1901-22, FINEP 01.13.0371.00

Keywords: *Monolithic cellulose, stir bar sorptive extraction, glycerol, biodiesel, HPLC.*

ANGICO GUM HYDROGEL: INFLUENCE OF POLYSACCHARIDE PURIFICATION ON WATER ABSORPTION AND TOXICITY

Albert S. Silva[1] , Idglan S. de Lima[1] , Ariane M. S. S Nascimento[2], Joyce A. Borges[2], Rodrigo P. Feitosa[1], Emerson A. C. Moura[3], Ana C. A. Evangelista[3], Edvani C. Muniz[1,2], Josy A. O. Furtini[1,2], Edson C. Silva-Filho[1,2]
1 - Postgraduate Program in Materials Science and Engineering - PPGCM, Federal University of Piaui (UFPI), Teresina, PI, Brazil
2 - Postgraduate Program in chemistry- PPGQ, Federal University of Piaui (UFPI), Teresina, PI, Brazil
3- Federal University of Piaui (UFPI), Teresina, PI, Brazil
albert@ufpi.edu.br

Superabsorbent hydrogels have great technological potential due to their water retention capacity hundreds of times, which guarantees their application in important areas such as agriculture [1]. The objective of this work was the synthesis of angico gum hydrogels from purified and non-purified polysaccharides. Unpurified polysaccharides were used in their natural form, while purified ones were precipitated in ethyl alcohol [2]. Tests of water absorption capacity and toxicity against *Artemia salina* were performed [3]. Both materials showed close results for water absorption capacity, with values greater than 200 times their dry mass, indicating that the purification of the polysaccharide does not interfere with the swelling capacity of the hydrogels. Furthermore, no toxicity was observed against *Artemia salina*. The results suggest that the synthesis of angico gum hydrogels can be performed without the polysaccharide purification step, maintaining its desired properties and reducing a step in the synthesis process, thus promoting a lower process time and cost for larger scale applications.

References

1. H. Rodrigues, I.S. Lima, L.M.L. Neris, A.S. Silva, A.M.S. Santos Nascimento, F.P. Araújo, R.F. Ratke, D.A. Silva, J.A. Osajima, L.R. Bezerra, E.C. Silva-Filho, Superabsorbent Hydrogels Based to Polyacrylamide/Cashew Tree Gum for the Controlled Release of Water and Plant Nutrients, Molecules. 26 (2021) 2680. https://doi.org/10.3390/molecules26092680.
2. SILVA, André G. da; RODRIGUES, Judith F.; PAULA, Regina Célia M. de. Composição e propriedades reológicas da goma do angico (Anadenanthera Macrocarpa Benth). Polímeros, v. 8, p. 34-40, 1998. https://doi.org/10.1590/S0104-14281998000200006
3. B.N. Meyer, N.R. Ferrigni, J.E. Putnam, L.B. Jacobsen, D.E. Nichols, J.L. McLaughlin, Brine shrimp: A convenient general bioassay for active plant constituents, Planta Med. 45 (1982) 31–34. https://doi.org/10.1055/s-2007-971236.

Fundings: CAPES, CNPq and FAPEPI

Keywords: *Hydrogel, polysaccharide, crosslinking.*

ANTIOXIDANT ACTIVITY OF BOVINE GELATIN FILMS ADDED OF A LIPID EXTRACT FROM OLIVE GROWING RESIDUES

Fernanda S.G. Brazeiro[1], Catarina M. Moura[2] and Vilásia G. Martins[1]

1– Laboratory of Food Technology, Federal University of Rio Grande (FURG), Rio Grande, RS, Brazil
vilasiamartins@gmail.com

3 - Food Engineering, Federal University of Pampa (UNIPAMPA), Bagé, RS, Brazil

New technologies are being created to reduce the impact of synthetic packaging on the environment. One alternative to substitute synthetic materials is the production of biodegradable films that, once incorporated with additives with characteristics such as antioxidants, become active packaging. The present research has the purpose to evaluate the antioxidant activity (AA) of biodegradable films made with bovine gelatin (BG) incorporated with lipid extract from olive oil waste. The concentrations of the extract used were 0% control film (BG), 10% (GB10), 20% (BG20), and 30% (BG30). For AA, two different methods were used, ABTS radical capture and DPPH free radical scavenging. It was noticed that as the extract concentration increased, there was an increase in the AA of the films by both methods, being for GB10 (98.65% e 39.57%), BG20 (98.92% and 46.65%) and highest AA for BG30 (98.99% and 54.43%), all of them higher than control films (59.36% and 38.30%), for DPPH and ABTS, respectively. The increase in the AA of the films is due to the high content of total phenols present in the extract, then the films with a higher amount of extract had higher antioxidant activity. Therefore, active films containing antioxidant compounds have great potential to reduce degradative processes such as lipid oxidation.
.

Keywords: *additives, active packaging, sustainable packaging*.

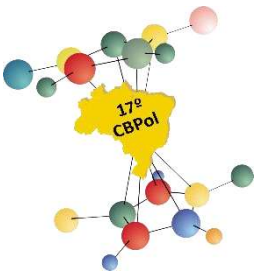

ANTIOXIDANT ACTIVITY OF SODIUM ALGINATE FILMS FUNCTIONALIZED WITH PURPLE ONION PEEL AND BLUE FLOUR EXTRACT

Luan G. Santos[1], Vilásia G. Martins[1*]

1 – Laboratory of Food Technology, School of Chemistry and Food Engineering, Federal University of Rio Grande, Rio Grande, RS, Brazil
[*]E-mail: vilasiamartins@gmail.com

Polysaccharide-based films (e.g., sodium alginate) are a sustainable alternative to reduce the environmental impacts caused by non-biodegradable materials derived from petroleum. The incorporation of plant extracts rich in phenolic compounds in biopolymeric films helps in the development of active packaging that prevents oxidation and extends the shelf-life of food products. The aim of this study was to produce alginate films incorporated with purple onion peel (PO) and blue flower (BF) extracts and evaluate their antioxidant potential against ABTS and DPPH radicals. The extracts were obtained with 60% ethanol (v/v), with the PO in a ratio of 1:20 (g/mL) for 1 h in a shaker at 25 ºC, while the BF used an ultrasound at 350 W, 45 ºC and 30 min in a proportion of 1:80 (g/mL). The filmogenic solution was obtained by mixing sodium alginate (2%), glycerol (40%), and distilled water at 70 ºC for 1 h. Separately, the solution was incorporated with 30% (v/v) of the PO and BF extracts, obtaining the films by the casting method at 40 ºC for 24 h, denominated as POF and BFF, respectively. A control film (CF) was obtained under the same conditions without the addition of extract. The films were evaluated for their content of phenolic compounds and capture of ABTS and DPPH radicals. The CF, POF, and BFF films showed phenolic content of 0.36, 26.19, and 4.91 mg EAG g^{-1}, respectively. When evaluating the antioxidant activity of functionalized films, it was observed that POF presented values 4.9 and 7.58 times greater than BFF for ABTS and DPPH radicals, respectively. Therefore, this study shows that sodium alginate films can be functionalized with PO and BF extracts, and the films incorporated with PO have greater bioactive potential due to their higher content of phenolic compounds.

Fundings: This study was financed in part by the Coordenação de Aperfeiçoamento de Pessoal de Nível Superior - Brasil (CAPES) - Finance Code 001 and Conselho Nacional de Desenvolvimento Científico e Tecnológico (CNPq). This research was developed within the scope of the Capes-PrInt Program (Process # 88887.310848/2018-00).

Keywords: *Biodegradable Packaging. Active packaging. Food preservation.*

APPLICATION OF PAAM/CMC-NANOCLAY NANOCOMPOSITES TO IMPROVE THE SOIL PROPERTIES

Uilian G. Yoneawa[1], Erika T. Ganda[1], Fabrício C. Tanaka[1], Marcia R. de Moura[1] Marcelo C. M. T Filho[2] and Fauze A. Aouada[1]*

1 – Department of Physics and Chemistry, São Paulo State University (Unesp), Ilha Solteira, SP, Brazil.
fauze.aouada@unesp.br
2 – Department of Plant Protection, Rural Engineering, and Soils, São Paulo State University (Unesp), Ilha Solteira, SP, Brazil

The objective of this work is to evaluate the hydrophilic property of the nanocomposite hydrogels (H-NC) and their effect on soil properties. H-NC were synthesized from polyacrylamide, carboxymethylcellulose and different concentrations of nanoclay (0, 10, and 20% w/v).[1,2] The hydrophilic behavior and soil properties were analyzed with respect to degree of swelling (DS), kinetic parameters, water retention capacity (WRC) in the soil, moisture cycle, and drying. Finally, the effects of H-NC on values of pH of the soil solution were also analyzed. DS results in soil solution and distilled water demonstrate that the addition of nanoclay decreases the hydrophilicity of the polymer matrix in both swelling media studied. This effect was more pronounced in soil solution medium, reducing around 15.2, 13.0, and 10.5 g/g (in relation to distilled water medium) for the hydrogels containing 0, 10, and 20% nanoclay, respectively. Probably, the mono, di and trivalent cationic ions, extracted from the soil, interacts with anionic groups present in polymeric chains and/or nanoclay structures reducing the elasticity of the nanocomposite chains. The kinetic parameters, obtained from Ritger-Peppas model, showed that the water mechanism followed preferentially the anomalous transport, and the water absorption increased by increasing nanoclay concentration. The WRC results on soil were 28.4 ± 0.4%, 47.0 ± 0.9%, 45.8 ± 0.7% and 45.6 ± 0.6% for the control (without hydrogel), and the hydrogel composed by 0, 10, and 20% nanoclay, respectively. Additionally, even after four cycles of soil moisture and drying, the containers containing the H-NC still demonstrate excellent WRC when compared to the control. From analysis of pH of the soil solution, it was possible to conclude that the presence of H-NC contributes for adjusting the pH of the medium, acting a buffer material. Therefore, it is evident that the H-NC synthesized in this work are promising materials to improve soil quality, with possible application in agriculture as a soil conditioner.

References

1. D. W. S. Nascimento; et al., *Journal of Nanoscience and Nanotechnology* 2016, *16*, 1-7. https://doi.org/10.1166/jnn.2017.12664.
2. A. W. Filho; et. al., *Polymers* 2022, *14*, 4564. https://doi.org/10.3390/polym14214564.

Fundings: São Paulo Research Foundation (FAPESP) (2018/18697-1; 2013/07296-2), National Council for Scientific and Technological Development (CNPq) (MCTIC Grant #406973/2022-9 through INCT/Polysaccharides – National Technology-Science Institute for Polysaccharides; MRM 315513/2021-7; FAA 312414/2018-8; 316174/2021-1). This study was financed in part by the Coordenação de Aperfeiçoamento de Pessoal de Nível Superior – Brasil (CAPES) – "Finance Code 001".

Keywords: *hydrogel, nanocomposite, nanoclay, soil, agriculture*.

BABASSU MESOCARP HYDROGEL FOR MACRONUTRIENT RELEASE

Ariane M. Nascimento[1], Albert S. Silva[1], Joyce A. Borges[1], Érico R. Dias[1], Idglan S. Lima[1], Heldeney R. Sousa[2], Edvani C. Muniz[1], Josy A. Osajima[1], Edson C. Silva-Filho[1]*

Incorporate the author(s) affiliation(s). Write the e-mail of the author to whom the correspondence should be addressed. Example:
1 – Interdisciplinary Laboratory of Advanced Materials (LIMAV), Federal University of Piaui (UFPI), Teresina, PI, Brazil
edsonfilho@ufpi.edu.br
2 - Federal Institute of Piaui (IFPI), Teresina, PI, Brazil

The search for strategies to maximize production and reduce costs is being pursued in the field of agriculture. Babassu mesocarp as a biodegradable polymer aims to minimize the environmental impact. Thus, superabsorbent hydrogels based on polysaccharides are being used as controlled soil and macronutrient fertilizers. The synthesis of babassu mesocarp hydrogel with and without phosphate was performed. The hydrogel was characterized by spectroscopy in the Infrared Region with Fourier transform and its capacity to swell at different pHs, its controlled release of macronutrients and its toxicity test against *Artemia saline* were studied. HMB showed characteristic vibration of the acrylamide monomer around 1670 cm^{-1}, and the starch bands were masked by the polyacrylamide bands and the phosphate incorporated into the polymeric matrix. The swelling study shows that the hydrogels exhibited an expansion capacity (~ 30,000 times). The release of phosphate began 30 min after contact with the medium and remains constant after 24 hours in solution and does not demonstrate toxicity. Superabsorbent hydrogels have shown promise in delivering macronutrients.

References

1. H. Sousa; I. Lima; E. Silva-Filho. *Journal of Molecular Liquids* 2023, *373*, 121463. https://doi.org/10.1016/j.molliq.2023.121463.
2. I. S. Lima, Ph.D. Thesis, Federal University of Piaui, 2023.
3. A. Ferreira; A. Fajardo; E. Muniz. *Carbohydrate polymers* 2021, *266*, 118116. https://doi.org/10.1016/j.carbpol.2021.118116.

Fundings: We thank CNPq, Capes, Piaui Research Foundation (FAPEPI).

Keywords: *Agriculture, polymer, toxicity*

Biodegradation evaluation in the soil of an enhanced efficiency fertilizer composed of poly(vinyl alcohol) and starch microspheres

Rodrigo Ragazzi dos Santos[1], Renato Nallin Montagnolli[2] and Roselena Faez[1]*

1- Laboratory of Polymeric Materials and Biosorbents (LAB-MPB), Department of Natural Science, Mathematical and Education (DCNME), Federal University of São Carlos (UFSCar), Araras, SP, Brazil. E-mail: faez@ufscar.br
2 - Laboratory of Agricultural and Molecular Microbiology (LAMAM), Department of Natural Science, Mathematical and Education (DCNME), Federal University of São Carlos (UFSCar), Araras, SP, Brazil. E-mail: renatonm@ufscar.br

Abstract - Enhanced efficiency fertilizers (EEFs) are an alternative for applying the necessary nutrients, attenuating losses, and promoting more sustainable agriculture. The challenge is to develop EEFs materials that degrade after fulfilling their function. Then, it is essential to understand how the biodegradation process occurs in soil and what factors influence it. We evaluate the EEFs produced by a double cover, i.e., a spray drying (starch-nutrients) to obtain microspheres and the melt-processing (PVA/microspheres) in an internal mixing chamber (Haake Rheocord) followed by the hot-pressed to get 10 mm pastilles. The biodegradation (Bartha respirometry method for 100 days) in the soil of PVA/microspheres was allied to chemical (FTIR), thermal (DSC), and morphological (SEM) characterization. After biodegradation, we observed an increase in the C=O band, ~ 1640 cm^{-1} [1]. Besides, there was an increase in the T_g of all materials. Furthermore, starch-based material showed a higher CO_2 release and a mycelial coverage on the material's surface. The results indicate that the PVA biodegradation process started and was positively influenced by the starch presence.

References:

1. Ben Halima, N. Poly(vinyl alcohol): Review of its promising applications and insights into biodegradation. *RSC Advances*, v. 6, n. 46, p. 39823–39832, 2016. DOI: 10.1039/c6ra05742j.

Keywords: sustainable agriculture; spray drying; degradable polymer.

CHEMICALLY MODIFIED CELLULOSE NANOFIBRILS AS A MACRONUTRIENT-CARRYING VEHICLE

Sahmira Bianchi[1], Débora França[1] and Roselena Faez[1]*

1 – Laboratory of Polymeric Materials and Biosorbents (LAB-MPB), Department of Natural Science, Mathematical and Education (DCNME), Federal University of São Carlos (UFSCar), Araras, SP, Brazil
faez@ufcsar.br

Abstract - Most of the nutrients used to meet the plant's nutritional needs are lost through volatilization and leaching. Enhanced efficiency fertilizers (EEF) emerge as an alternative to improve nutrient uptake. Besides, it is important to anchor the nutrients on biobased and biodegradable materials [2]. Cellulose nanofibrils (CNF) are a structural component of cellulose, are biodegradable, biocompatible with the nutrients used in EEF, have adaptable chemical surface and measure 10-100 nm in width. Here, we used ultrasonic defibrillated anionic (CNF_{ANI}, oxidation mediated by 2,2,6,6-tetramethylpiperidine1-oxyl) or cationic (CNF_{CAT}, etherization by 2,3epoxypropyltrimethylammonium chloride) surface-modified CNF [3,4] and added equimolar $(NH_4)_2HPO_4$ to the surface charges. Finally, the CNF/$(NH_4)_2HPO_4$ suspensions were spray-dried to obtain microspheres (Fig 1). The thermal, structural, and morphological characterizations showed that doubling the amount of salt in the CNF_{CAT} microspheres affects the nutrient release mechanism. Furthermore, the nutrients released into water confirmed that the CNF surface charge influences the CNF/$(NH_4)_2HPO_4$ interaction. After a week, the CNF_{ANI} and CNF_{CAT} released 27.7 and 74.5% of NH_4^+ and 37.2 and 5.9% of PO_4^{3+}, respectively. We conclude that after this period, the ions continued to interact with the surface charge of CNF, slowing the nutrient release.

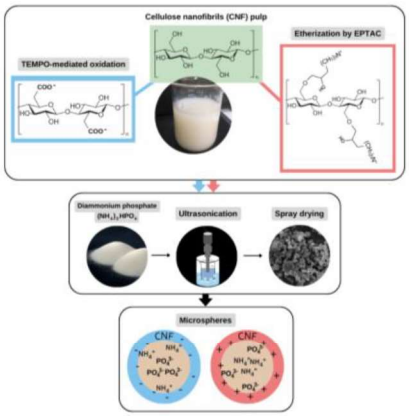

Modified CNF microspheres production

References

1. S. Salimi; R. Sotudeh-Gharebagh; R. Zarghami; S. Y. Chan & K. H. Yuen. *ACS Susteinable Chemistry & Engineering* 2019, *7*, 15800-15827. https://doi.org/10.1021/acssuschemeng.9b02744.
2. T. Saito; S. Kimura; Y. Nishiyama & A. Isogai. *Biomacromolecules* 2007, *8*, 2485-2491. https://doi.org/10.1021/bm0703970.
3. H. Sehaqui; A. Mautner; U. P. de Larraya; N. Pfenninger; P. Tingaut & T. Zimmermann. *Carbohydrate polymers* 2016, *135*, 334-340. https://doi.org/10.1016/j.carbpol.2015.08.091.

Fundings: This study was financed in part by the Conselho Nacional de Desenvolvimento Científico e Tecnológico (CNPq) and Fundação de Amparo à Pesquisa do Estado de São Paulo (FAPESP, process number 17/24595-4 and 19/02535-5).
Keywords: *Biopolymer. Enhanced Efficiency Fertilizers. Cellulose Nanofibrils. Chemical Modification. Ultrasonication.*

DEVELOPMENT, CHARACTERIZATION, AND APPLICATION OF BIOFILM IN BRAZIL NUT USING PECTIN EXTRACTED FROM ORANGE ALBEDO FROM MARABÁ/PA JUICE INDUSTRIES

Suzane S. S. Rodrigues[2], Vera L. D. da Silva[1], Syme R. S. Queiroz[1], Rosemary M. P. Coutinho[1]* and Silvana N. de Melo [2]

1 – Department of Chemistry, Federal Institute of Education, Science and Technology of Pará (IFPA), Belém, PA, Brazil rosemary.coutinho@ifpa.edu.com.br
2 – Food department, State University of Para (UEPA), Belém, PA, Brazil

Abstract - The food industry generates large amounts of waste daily, causing environmental and social problems. In this context, the research aimed to utilize pectin extracted from orange peel albedo, a by-product of the food industry, to produce a biofilm and test its application on peeled Brazil nuts. The samples were selected based on size, ripeness, and intact appearance, excluding those with apparent damage. Pectin extraction was carried out in 10% citric acid following the methodology proposed by Canteri (2010) and cited by Trevisoli (2014). The biofilms were produced using the Casting method with water as the solvent. Four formulations (F_1, F_2, F_3, and F_4) were created with different concentrations of pectin (30%, 40%, 50%, and 60% dry mass) in 100 mL of distilled water, along with 8% (w/v) glycerol, under agitation and heating at 80 °C for 2 hours. The films were kept at room temperature for 120 hours and characterized regarding visual aspects, acid solubility, thickness, moisture content, density, water vapor permeability, water absorption, grammage, soluble solids content, pH, and mass loss. The moisture content ranged from 12.33% to 23.67%, and water vapor permeability values ranged from 0.23 to 0.26 g/cm². Formulations F_3 and F_4 showed lower mass loss, corresponding to grammage values of 0.02 to 0.05 g/cm². Acid content ranged from 3.63 to 4.96, while soluble solids content ranged from 1.50 to 2.40 °Brix. The analyzed biofilms showed mass loss of less than 3% compared to the initial weight and dissolved completely in water. The results indicated that formulations F_3 and F_4, with higher pectin concentrations, produced thicker and less dense films with good acid solubility. The nuts with biofilm exhibited lower mass loss and higher soluble solids content, indicating an extended shelf life. The biofilms completely degraded within 15 days. The research achieved its objective, demonstrating the feasibility of producing and characterizing biofilms using pectin from orange

peel albedo. The biofilms exhibited favorable properties such as acid solubility and resistance. Formulations F_3 and F_4 stood out, showing potential for edible packaging. The application of the biofilm on peeled Brazil nuts resulted in reduced conversion of reserve tissues into soluble sugars, indicating improved food preservation.

Keywords: *Pectin; plasticizer; Brazil nuts, Biofilm*

References

1. ALVES, Mayke. Os tipos de laranja populares no Brasil e cheios de benefícios para a saúde. *Agro 2.0*, 2020. Disponível em: https://agro20.com.br/tipos-laranja/. Acesso em 01 de outubro de 2022
2. Angles, M. N.; Dufresne, A.; *Macromolecules* 2000, 33, 8344.
3. AOAC. ASSOCIATION OFFICIAL ANALYTICAL CHEMISTIS. Official Methods of Analysis of AOAC International.18th. ed.Gaithersburg: AOAC, 2010.
4. CANTERI, M. H. G.; MORENO, L.; WOSIACKI, G.; SCHEER, A. P. Pecta: da matéria-prima ao produto fal. *Polímeros*, v. 22, p. 149-157, 2012.
5. Cruz, W. F. Aplicação e avaliação de biopolímeros de amido e gelatina como revestimento em materiais de embalagens, Tese apresentada à Faculdade de Engenharia de Alimentos da Universidade Estadual de Campinas. p.99 - 100 2018.
6. TREVISOLI, T.R. Caracterização da farinha de casca de poncã e otimização da extração de pectina. 2014. 48f. Trabalho de Conclusão de Curso (Curso Superior de Engenharia de Alimentos), Departamento de Alimentos, Universidade Tecnológica Federal do Paraná. Campo Mourão, 2014.

DEVELOPMENT OF BIODEGRADABLE MICROCAPSULES CONTAINING *BACILLUS AMYLOLIQUEFACIENS* BS01 FOR BIOLOGICAL CONTROL

Éder Ramin de Oliveira[1], Letícia Cuebas[1], Iron Amoreli de Figueiredo Ribeiro[2], Gilson Paulo Manfio[2], Eduardo Roberto de Almeida Bernardo[2], Derval dos Santos Rosa[1*]

1 – Center for Engineering, Modeling, and Applied Social Sciences (CECS), Federal University of ABC (UFABC), Santo André, Brazil.
**dervalrosa@yahoo.com.br*
2 – Research and Development (R&D), Agrivalle Brasil, Indaiatuba, Brazil.

Abstract - Microbiological control methods are efficient, sustainable, non-polluting, and low-cost alternatives for the management of agricultural pests and diseases. However, microorganisms are relatively sensitive to formulation ingredients and environmental conditions during storage and field application, which impact upon efficiency and shelf life of products. In this context, biodegradable microparticles of *Bacillus amyloliquefaciens* BS01 were developed by the emulsion method using sodium alginate gelling in different concentrations (3.5 and 5% wt) and stirring rates (1000 and 1500 rpm), focusing on particle size optimization. Fig 1 represents the methodology employed. Microparticles were evaluated by particle size (laser diffraction), morphology (SEM), UV protection, and antagonistic effect. Spherical cross-linked microparticles obtained (minimum diameter of 47 µm) showed high cell viability, efficient UVB radiation protection, and were effective in controlling the fungi *Sclerotinia sclerotiorum* and *Rhizoctonia solani* under *in vitro* assay conditions. Our results support further development of the technology towards a novel industrial process.

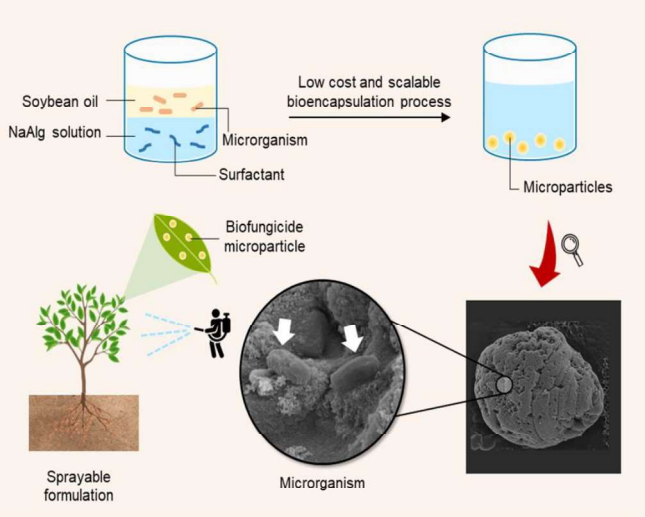

Fig 1 - Methodology used and images of the encapsulated bacterial cells.

Funding: The authors thank the financial support provided by Fundep (Project nº 27178) and Agrivalle Brasil.
Keywords: *encapsulation; alginate microparticles; microbial biological control agents; Bacillus amyloliquefaciens.*

DEVELOPMENT OF BIOPOLYMERIC BEADS FOR APPLICATION IN THE CONTROLLED RELEASE PROCESS OF POTASSIUM IN THE SOIL

Aline Fernandes de Oliveira[1]*, Cristian Berto da Silveira[1] and Valdir Soldi[2]

1 – Department of Fishery Engineering and Biological Sciences, State University of Santa Catarina, Laguna, SC, Brazil. aline.oliveira@udesc.br
2 – Department of Chemistry, Federal University of Santa Catarina (UFSC), Florianópolis, SC, Brazil

Potassium is a nutrient of great importance for agriculture, and its availability in the soil is a limiting factor in plant development, but it is an easily leached nutrient due to its high solubility in water.

In this work, beads were developed from carboxymethylcellulose (CMC) and sodium alginate (SA) biopolymers aiming at application in the process of controlled release of potassium in the soil.

The beads were prepared through the extrusion/solidification method, with polymeric solutions of CMC/AS 50/50 composition, and with the addition of potassium in the forming solution. The solution was dropped into a calcium chloride solution (2% m/v) and the beads resulting from two periods of time in contact with the crosslinking solution were evaluated: 30 and 360 minutes.

The determination of the amount of nutrient incorporated in the beads was carried out through a digestion process and the results indicated the incorporation of 0.208 mg and 0.211 mg of potassium per mg of crosslinked beads for 30 and 360 minutes, respectively.

The incorporated nutrient release process was evaluated through leaching columns, containing 2 kg of sandy soil, for the reference sample (potassium incorporated directly into the soil) and for the beads, in triplicate. The leached water was collected and the released potassium content was determined by flame spectrophotometry.

As a result of the leaching process, the reference sample releases approximately 92% of potassium in the first five leachings, while for the beads the release was 43% (crosslinked for 30 minutes) and 37% (crosslinked for 360 minutes).

The nutrient release results showed a controlled release of potassium which prevented nutrient loss by leaching, while making the nutrient available for a longer time in the soil and making it more available to plants.

Keywords: biopolymers, beads, controlled release, soil, potassium

DEVELOPMENT OF CROSSLINKED BIOFILMS FOR APPLICATION IN CONTROLLED NUTRIENT RELEASE SYSTEMS

Cristian Berto da Silveira[1] *, Aline Fernandes de Oliveira[1] and Valdir Soldi[2]

1 – Department of Fishery Engineering and Biological Sciences, State University of Santa Catarina, Laguna, SC, Brazil. cristian.silveira@udesc.br
2 – Department of Chemistry, Federal University of Santa Catarina (UFSC), Florianópolis, SC, Brazil

One of the biggest problems found in the process of fertilization of large areas is the loss of nutrients by leaching. Potassium, for example, is a nutrient of great importance for plants, and its availability in the soil is a limiting factor in their development, but it is an easily leached nutrient. To remedy this problem, the development of controlled nutrient release systems can be a viable alternative to control potassium release.

The main objective of this work was the development of biofilms from the polysaccharides carboxymethylcellulose (CMC) and sodium alginate (SA), for application in controlled potassium release processes.

Films were prepared by dissolving amounts of CMC/AS (50/50) at a concentration of 2% (w/v). Potassium (240 mg) as well as crosslinking agents (calcium or EDC (1-ethyl-3-(3-dimethylaminopropyl)carbodiimide) were incorporated into the film-forming solution. The mechanical and morphological properties were evaluated, as well as water absorption and swelling tests.

The potassium release process was evaluated through leaching columns, containing 2 kg of sandy soil, for the reference sample (240 mg of potassium incorporated directly into the soil) and for the films, in triplicate. released potassium was determined by flame spectrophotometry.

The results showed that about 93% of the potassium incorporated directly into the soil was released by the fourth leaching. For the same amount of potassium initially incorporated, the cross-linked films in solution with EDC and calcium, presented in the same period a release of 40 and 55% of the nutrient, respectively.

The results showed that crosslinked films developed from CMC/AS showed a gradual release of potassium, which prevents the loss of the nutrient by leaching, while making the nutrient available for a longer time to the plant.

Keywords: sodium alginate, carboxymethylcellulose , controlled release, potassium, soil.

DEVELOPMENT OF POROUS FIBROIN MEMBRANES AND APPLICATION AS A POTENTIAL ADSORBENT FOR REMOVAL OF ORGANIC DYES

Gabriel Y. Ottaiano[1], Antonio O. S. Junior[1], Caroline Bertagnolli[2] and Mariana A. de Moraes[1]*

1 – Department of Chemical Engineering, Federal University of São Paulo (Unifesp), Diadema, SP, Brazil
mamoraes@unifesp.br
2 – Hubert Curien Pluridisciplinary Institute – University of Strasbourg (Unistra), Strasbourg, France

Abstract – One of the main challenges that humanity currently faces and will struggle within the next decades is environmental pollution, which together with climate change threatens the environment and quality of life on Earth in an irremediable manner. In this work, the aim is to investigate the use of fibroin membranes to adsorb pollutant composite material such as organic dyes. Fibroin is a protein extracted from the silkworm cocoon that shows excellent biodegradability properties and adsorption capacity, and it represents a potential natural adsorbent for various contaminants. The fibroin porous membranes were tested and, for comparison purposes, a regenerated dense fibroin membrane was tested under the same conditions for adsorption. Briefly, the silk cocoon sericin was removed by washing the cocoons with a sodium carbonate solution (0.5% w/v). Following this, the fibroin was solubilized in a ternary solution of calcium chloride, ethanol and water (1:2:8) to form a 10% fibroin solution. For the porous membrane, the fibroin solution was poured into water at a ratio of 1:100 and stirred to create a foam, which was collected, compressed repeatedly and stored in ethanol for one day, then washed with water and freeze-dried. For the regenerated membrane, the fibroin was dialyzed for three days to remove salt, poured in petri dishes and dried at room temperature. Then, the membranes were immersed in ethanol and dried again. For the adsorption tests, methylene blue, crystal violet and methyl orange were used as model dyes. Approximately 1.5 mL of dye solution at different dye concentrations was placed in contact with the membranes. For low concentrations of dye, adsorption was above 90% at pH near to neutral. The fibroin membranes, therefore are an interesting alternative in what concerns the adsorption of dyes and considering the adsorbent's biodegradability.

References

1. G. Nogueira; R. Weska; W. Vieira Jr.; B. Polakiewicz; A. Rodas; O. Higa. M. Beppu *Jornal of Applied Polymer Science* 2009, 617-623. https://doi.org/10.1002/app.30627.

Fundings: Grant #2021/14018-5, São Paulo Research Foundation (FAPESP).

Keywords: *Biopolymeric membranes; Wastewater treatment; Adsorption; Fibroin.*

DEVELOPMENT OF STARCH/XANTHAN GUM/NANOEMULSION OF CINNAMON ESSENTIAL OIL BASED FILM FOR EDIBLE COATING

Maíra de A. Peixoto[1] and Vanusca D. Jahno[1]

1 – Feevale University, Graduate Program in Environmental Quality, Novo Hamburgo, RS, Brazil
mairapeixoto@hotmail.com

Abstract – In recent years, the use of edible coatings to preserve the quality and reduce the spoilage of fruits during the post-harvest period has increased because they can minimize water loss, control the internal gas atmosphere, and decrease fruit respiration rate. Polysaccharides such as starch and xanthan gum may be used as coating materials. Nanoemulsions have been employed to improve the properties of coatings. The objective of this study was to develop an edible coating based on starch with addition of cinnamon oil nanoemulsion to coat fruits and enhance their shelf life. Three formulations were tested. A 2% (w/v) starch coating solution was prepared by dissolving starch in distilled water with 20% glycerol (w/starch dry weight). Another solution was prepared as described previously, adding 0,1% of xanthan gum to its composition. In the last formulation, 1% (v/v) of cinnamon oil nanoemulsion was added to the starch – xanthan gum solution. The nanoemulsion was produced by adding cinnamon essential oil and Tween 80 to distilled water. The nanoemulsion was characterized for its mean particle size. All formulations were characterized for their film surface morphology using scanning electron microscopy (SEM), thermogravimetric analysis and FTIR spectroscopy. Strawberries were coated with a starch – xanthan gum solution and a starch – xanthan gum – nanoemulsion solution. Nanoemulsions with particle sizes below 200 nanometers were obtained and successfully incorporated into the polymeric films. The film composed of starch and xanthan gum were exhibited a homogeneous surface morphology as the starch film. However, the film with the nanoemulsion showed a distinct microstructure surface. Strawberries covered with the solution containing the cinnamon nanoemulsion showed the lowest mass loss. It was possible to develop a formulation for a polymeric film using only biodegradable compounds. Moreover, the development of these films has proven viable alternative for producing edible coatings for fruits.

References

1. T. F. S. Saranti; P. T. S. Melo; M. A. Cerqueira; F. A. Aouada; M. R. de Moura *Polymers* 2021, *13*, 4298. https://doi.org/10.3390/polym13244298.
2. H. Eom; Y. Chang; E. Lee; H. Choi; J. Han *LWT – Food Science and Technology* 2018, *516-522*, 97. https://doi.org/10.1016/j.lwt.2018.07.044.
3. J. G. Oliveira Filho; B. R. Albiero; I. H. Calisto; M. R. V. Bertolo; F. C. A. Oldoni; M. B. Egea; S. Bogusz Junior; H. M. C. de Azeredo; M. D. Ferreira *International Journal of Biological Macromolecules* 2022, *812-823*. https://doi.org/10.1016/j.ijbiomac.2022.08.049.
4. T. Odetayo; S. Tesfay; N. Z. Ngobese *Food Science & Nutrition* 2022, *10*, 2149-2167. https://doi.org/10.1002/fsn3.2557.

Fundings: CNPq.
Keywords: Edible Coating. Starch. Xanthan Gum. Nanoemulsion. Polymeric Film.

EFFECT OF HYDROLYSIS ON THE QUANTIFICATION OF SULFONATED POLYACRYLAMIDE BY SEC-UV

*Cecília C. R. Gonçalves[1], Angela C. P. Duncke[1], Luis Maqueira Espinosa[1], Eduardo Creatto[1], Jones Limberger[1], Aurora Pérez-Gramatges[1]**
[1]Department of Chemistry, Pontifical Catholic University of Rio de Janeiro, PUC-Rio, Rio de Janeiro, Brazil
aurora@puc-rio.br

Polyacrylamides (PAM) are widely used in the petroleum industry as rheological modifiers. Its quantification in production water (PW) is important for optimizing the process and for controlling wastewater disposal.[1] Its quantification via size exclusion chromatography with UV Vis detection (SEC-UV) can eliminate interfering substances from a complex matrix and provides a low detection limit. However, the hydrolysis of PAM under reservoir conditions can affect the quantification of the polymer in PW.[2] The conversion of the amide the functional group to carboxylate could affect the UV-Vis detection and/or the hydrodynamic volume of the polymer. Sulfonated polyacrylamide (PAM-AMPS) is used to increase resistance to hydrolysis and allow its application at high temperatures, despite literature reports that hydrolysis still occurs in reservoir conditions[3]. Therefore, the aim of this work was to evaluate the possible effects of PAM-AMPS hydrolysis on the chromatographic behavior of this polymer, and the implications for its quantification in produced water. For that, sulfonated polyacrylamide was submitted to alkaline hydrolysis in different conditions and afforded polymers with different hydrolysis degree (HD). The resulting partially hydrolyzed sulfonated polyacrylamides were analyzed through ^{13}C NMR, FTIR, and back-titration, and HD ranging from 7 to 30% were observed, with the three employed techniques providing statistically equivalent HD values. The hydrodynamic properties of the hydrolyzed polymers were studied by DLS, and the results were correlated with the analytical responses obtained by UV- Vis and SEC-UV. The results showed that polymer hydrolysis affects its UV-Vis absorption as well as its quantification by SEC-UV, with errors of up to 30%. These findings were atribuited to (i) the exchange of the chromophore, which leads to changes in the absorptivity of the polymer, and (ii) the enhance in the ionophilicity that alters polymer conformation and consequently, the environment experienced by the absorbing chromophores.

1. S. Jouenne *Journal Of Petroleum Science And Engineering 2020.* http://doi.org/10.1016/j.petrol.2020.107545.
2. K. C. Taylor and H. A. Nasr-El-Din Hisham *Journal Of Petroleum Science And Engineering* 1994. http://doi.org/10.1016/0920-4105(94)90003-5.
3. H. V.P. Vieira, P.F. Oliveira, J. A. Costa, L.A. Oliveira, L.S. Mota and C. R. E. Mansur *Journal of Applied Polymer Science* 2021. http://doi.org/10.1002/app.51301.

Fundings: CNPq, CAPES, FAPERJ and Equinor

Keywords: *polyacrylamide, hydrolysis degradation, polymer quantification, EOR, SEC-UV*

ELECTROCHEMICAL PROPERTIES OF POLYANILINE SYNTHETIZED ON PLASMA TREATED CARBON FIBER TEXTILE FOR SUPERCAPACITOR APPLICATIONS

André Felipe Deziderio Borges[1], Carlos Eduardo de Jesus[1*], Luis Cesar Fontana[2] and Carla Dalmolin[1]

1 – Department of Chemistry, Santa Catarina State University (UDESC), Joinville, SC, Brazil
carloseduardo092003@gmail.com
2 – Department of Physics, Santa Catarina State University (UDESC), Joinville, SC, Brazil

Abstract – Demand for cleaner and more renewable energies than fossil fuels, robust and efficient energy storage systems are needed, capable of storing energy produced in excess and distributing it when production falls below of demand. To meet this demand, existing battery technologies are insufficient and it is necessary to develop energy accumulators that accept charge and discharge surges and at the same time have a high storage capacity. In this context, supercapacitors, particularly those based on a pseudocapacitive effect, have stood out in the scientific community as promising alternatives. The current work presents the results of the electrochemical performance of polyaniline coated carbon fiber electrodes. The surfaces of the carbon fiber samples were functionalized by plasma generated in a cathode cage, with the intent of creating covalent bonds between the active electrode and the current collector, with the objective of improving electrochemical performance. A new methodology for the deposition of polyaniline films over carbon fiber was developed, consisting of the previous deposition of a thin layer of aniline over the fibers, through physical vapor deposition, followed by plasma functionalization and, finally, the growth of polyaniline films through the electrodeposition process. The chemical, physical and electrochemical properties of the polyaniline electrodeposited over the fibers were evaluated. It was observed a significant improvement in the electrochemical performance of the electrodes obtained through the methodology developed in this work, that is, with previous deposition of a thin film of aniline and functionalization in pulsed plasma (100 kHz) of N_2/Ar, generated in a cathode cage, that resulted in an increase of about 40% in the peak current of the oxidation process of the polyaniline in relation to the control sample.This result came together with an increase of the electric double layer capacitance of these electrodes and of an increase in the mass of dopant absorbed. The results obtained qualify the methodology developed in this work for the deposition of polyaniline films over carbon fibers and, consequently, for the application of these electrodes as electric double layer capacitors with pseudocapacitive effect.

Fundings: FAPESC, CAPES, CNPq.
Keywords: *Polyaniline, Carbon fiber textile, Supercapacitors, Plasma*

ENCAPSULATION OF THE UREA FERTILIZER IN LIGNIN NANOCAPSULES

Renato C. T. Porto[1], Patrícia Z. Uchôa[1], Jean C. Hoepfner[2], SamantaFinsterbuch[2], Sérgio H. Pezzin[1]

1 – Chemistry Department, Center of Technological Sciences, Santa Catarina State University, Joinville, Brazil.
pzuchoa@gmail.com
2 – Center of Technological Sciences, Santa Catarina State University, Joinville, Brazil.

Abstract – Russia's war with Ukraine brought global consequences in relation to input consumption, due to import restrictions, one of the most affected products in Brazil was agricultural fertilizer. From this perspective, this work carried out a study of urea encapsulation in lignin nanocapsules in order to enhance its use by reducing product losses. Lignin is a natural, biodegradable, biocompatible polymer that does not cause soil or water contamination, in addition to being a residue from the paper industry. The nitrogen present in urea, on the other hand, has some difficulty penetrating the soil, due to UV radiation, leaching losses, among others, causing the need for constant application. Lignin nanocapsules were produced by the antisolvent method together with urea and characterized by thermal and microscopic analyses, in addition to controlled release and degradation stability. The nanocapsules produced have sizes between 390 nm and with Tg 127°C, a considerable increase compared to lignin. At an encapsulation efficiency of 60%, the release of the urea occurs in a slow and controlled manner for 22 days at pH 7.

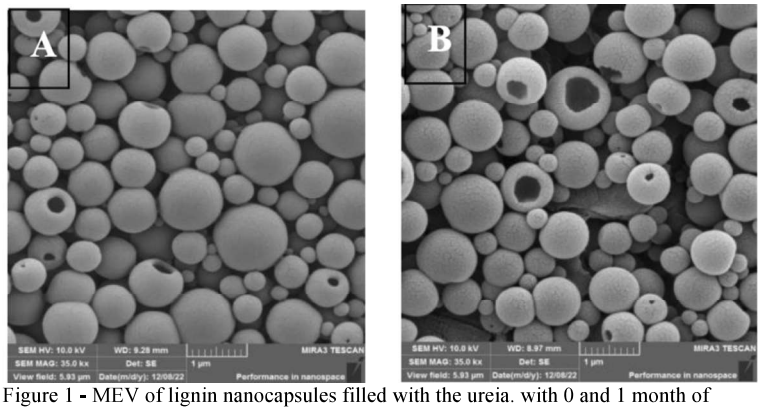

Figure 1 - MEV of lignin nanocapsules filled with the ureia. with 0 and 1 month of shelflife (A and B respectively).

1. YEARLA, S. R.; PADMASREE, K. Exploitation of subabul stem lignin as a matrix in controlled release agrochemical nanoformulations: a case study with herbicide diuron. Environ. Sci. Pollut. Res., v.23, p.18085 – 18098, 2016.
2. LI, H.; DENG, Y.; LIANG, J.; DAI, Y.; LI, B.; REN, Y.; QIU, X.; LI, C. Direct preparation of hollow nanospheres with kraft lignin: A facile strategy for effective utilization of biomass waste. BioResources., v. 11, p. 3073–3083, 2016.

Fundings: FAPESC, CAPES and NÓRIO – Nanotechnology.

Keywords: nanocapsules, lignin, encapsulation, urea fertilizer, controlled release

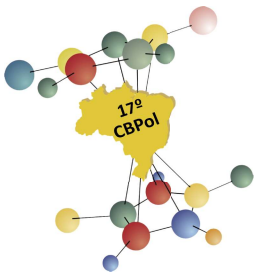

ETHYL HYDROXYETHYL CELLULOSE (EHEC) FILMS CONTAINING ALFA-TOCOPHEROL: EFFECTS ON STABILITY, RELEASE IN VITRO AND PROPERTIES OF THE FILM

Greice M. Zickuhr[1], Juliana P. Dreyer[2], Leandro G. Nandi[2], Rafael F. N. Quadrado[3], André R. Fajardo[3], Larissa N. Carli[1] and Ismael C. Bellettini[1]*

1 – Centro Tecnológico, de Ciências Exatas e Educação, Federal University of Santa Catarina (UFSC), Blumenau, SC, Brazil. (*) ismael.bellettini@ufsc.br
2 – Departamento de Química, Federal University of Santa Catarina (UFSC), Florianópolis, SC, Brazil
3 – Laboratório de Tecnologia e Desenvolvimento de Compósitos e Materiais Poliméricos (LaCoPol), Federal University of Pelotas (UFPel), Pelotas, RS, Brazil

Abstract - The use of antioxidant compounds, such as α-tocopherol, in the production of active packaging is one of the ways to minimize or delay lipid oxidation, one of the main factors leading to early food degradation. Cellulose-derived ethers, such as ethyl hydroxyethyl cellulose (EHEC), may be an alternative to produce biodegradable polymeric films to control the release of active compounds in food products.[1,2] Thus, the objective of this work was to obtain EHEC films with antioxidant properties by incorporating nanoparticles (NP) of ethyl hydroxyethyl cellulose/dodecanoic acid (EHEC-C12) containing α-tocopherol in their formulation. The α-tocopherol was encapsulated at concentrations of 1–3% (w/w), and the NPs were incorporated into EHEC films, as well as 2% (w/w) of non-encapsulated α-tocopherol. Particle sizes of 722 ± 209 nm and 665 ± 213 nm were observed by dynamic light scattering for NPs modified with 10 and 20% dodecanoic acid, respectively, and polydispersion index < 0.30. The incorporation of α-tocopherol into the films did not change the barrier or thermal properties of EHEC. However, the degradation temperature of α-tocopherol increased from 200 to 263 ºC, after embedment in the films. The nanoencapsulation favored a more homogeneous dispersion of α-tocopherol in the polymeric matrix slightly influencing the mechanical properties. The incorporation of α-tocopherol into the films also increased its stability under ambient conditions for 72 days, and under UV radiation (λ = 254 nm) for 6 h. Fast α-tocopherol release profiles were observed from the films when immersed in absolute ethanol, with 50% being released in the first 15 min of the assay. Pure EHEC films did not show antioxidant properties, but with the incorporation of different proportions of NP, an increase in the antioxidant capacity of the films was observed.

References

1. A. Dey; S. Neogi. *Trends in Food Science and Technology* 2019, 90, 26-34. https://doi.org/10.1016/j.tifs.2019.05.013.

2. S.M. Martelli; C. Motta; T. Caon; J. Alberton; I.C. Bellettini; A.C.P. do Prado; P.L.M. Barreto; V. Soldi. *Food Science and Technology* 2017, 77, 21-29. https://doi.org/10.1016/j.lwt.2016.11.026.

Keywords: *Ethyl hydroxyethyl cellulose, α-tocopherol, Polymeric nanoparticles, Active packages, Antioxidant properties*.

EVALUATION OF THE INFLUENCE OF OXYPROPYLATED CELLULOSE NANOFIBRILS ON THE MECHANICAL AND MORPHOLOGICAL PROPERTIES OF POLYURETHANE FOAM

Rafael. S. Duarte[1], Aparecido J De Menezes[2], Mário Henrique A. Lima[2], Mercês C. Silva*[1].

1- Institute of Integrated Engineering (IEI), Federal University of Itajubá (UNIFEI), Itabira, MG, Brazil, mercescoelho@unifei.edu.br

2- Graduate Program in Materials Science- PPGCM/UFSCar, Federal University of São Carlos (UFSCar), Sorocaba, SP, Brazil

The oxypropylation of biomasses, which consists of the polymerization of poly(propylene oxide) chains from OH groups of lignocellulosic materials, has been employed as a strategy for the synthesis of new polyols for the polyurethane industry [1]. In the present work, cellulose nanofibrils (CNFs) obtained from the defibrillation of cellulose fibers previously functionalized via oxypropylation reaction in the molar ratio [OHcellulose]/[Propylene Oxide] equal to 1:0.3[2] and named CNFs103 were used. Through the acetylation reaction with 14% v/v acetic anhydride solution in the presence of pyridine, followed by titration with 2 mol.L-1 NaOH solution and Thermogravimetry (TGA) obtained the hydroxyl index (IOH) and moisture content of the sample equal to 780 mg KOH g-1 and 4%, respectively. A polyol blend of 2,5g of this sample with 97,5 g of castor oil-derived biopolyol 411 (IOH 311 mg KOH g-1)[3] was employed in the synthesis of polyurethane foam from 4,4-diphenylmethane diisocyanate polymer (MDIp), H_2O as expander, surfactant Tegostab, N, N Dimethylcyclohexylamine and triethylamine as catalysts. The same formulation was used to elaborate a foam containing 100% of the commercial biopolyol that presented density of 27.76 g cm-3, while the samples containing the polyol blend presented density of 28.70 g cm-3. Analyses using Fourier transform infrared spectroscopy (FTIR), compression tests, scanning electron microscopy are underway to evaluate the effect of CNFs103 sample on the structural, morphological and strength properties of polyurethane foam.

References.

1. WU, M et al. Preparation of rigid polyurethane foam from lignopolyol obtained through mild oxypropylation. Royal Society of Chemistry, 12, 21736, 2022. DOI: 10.1039/d2ra02895f.
2. LIMA, M. et al. Functionalized Cellulose Nanofibrils Obtained from Cellulose Oxypropylated. Chemistry Africa, 2023.
3. SANTOS, O.H.S et al. Synthesis and performance of different polyurethane foams as oil sorbents. Journal of Applied Polymer Science 134 (41), 45409, 2017.

Fundation: FAPEMIG - PROJETO 00038-22.
Keywords: *Hybrid polyol, Polyurethane foam, Oxypropylation.*

GENERATION OF 3D PRINTING FILAMENTS FOR CONTROLLED RELEASE FERTILIZER UTILIZING PLA, UREA, AND ROCK POWDER

Gabriella N. Chagas[1,2*], Marceli N. Conceição[2], Roberto C. C. Rossana M. S. M. Thiré[1]
(Times New Roman 10, bold, centered paragraph, single space)

1 – Programa de Engenharia Metalúrgica e de Materiais (PEMM/COPPE), Universidade Federal do Rio de Janeiro, RJ, Brazil
*gabriella.chagas@coppe.ufrj.br
2 – Centro de Tecnologia Mineral (CETEM), Rio de Janeiro, RJ, Brazil

Abstract - Excessive fertilization stands as a significant contributor to ecological predicaments in the realm of agriculture. A prospective solution to address this issue lies in the application of controlled release fertilizer (CRF) [1,2]. Regrettably, the majority of instances involving CRFS necessitate the inclusion of solvents during their manufacturing process [3]. Within this framework, the objective of the work was to produce filaments for 3D printing consisting of PLA, urea and potassium rock powder for application in agricultural artifacts with controlled fertilizer release system via extrusion and without using solvents. The filaments were manufactured by extrusion varying the urea concentration (5 and 10 % m/m), mineral filler (0 and 10 % m/m) and processing temperatures (130 to 190 °C). The filaments were investigated by TGA, SEM, FTIR, and nutrient release test in distilled water. The results indicated that the addition of rock powder helped trap urea in the CRFS during the extrusion step, making the release of the nitrogen fertilizer more efficient when compared to the material without mineral filler, resulting in a filament with better printability. It was possible to produce printable filaments from a solution of PLA, urea and mineral filler, with release of nitrogen fertilizer (1.6 to 70.9 mg/L of urea in distilled water) during the evaluated period of 30 days. Finally, the materials produced proved to be a promising and environmentally friendly alternative for use in agricultural artifacts with nutrient release control.

References (Times New Roman 10, bold) – Follow the examples in Times New Roman 10, single space line, justified paragraph, 1 column.

1. P. Vejan et al., *Journal of Controlled Release* 2021, 339, 0168-3659, https://doi.org/10.1016/j.jconrel.2021.10.003.
2. Y. Li. Et al., *Progress in Organic Coatings*, 2018, 119, 0300-9440, https://doi.org/10.1016/j.porgcoat.2018.02.013.
3. K. Lubkowski et al., *J. Agric. Food Chem*., 2015, 63, 2597. https://doi.org/10.1021/acs.jafc.5b00518

Fundings: This study was financed in part by the Coordenação de Aperfeiçoamento de Pessoal de Nível Superior - Brasil (CAPES) - Finance Code 001.

Keywords: *3D printing, biopolymers, controlled-release, agriculture, rock powder.*

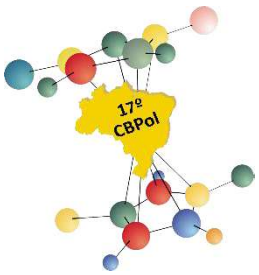

NANOCOMPOSITE HYDROGELS OF CASHEW TREE GUM WITH LAPONITE TO CONTROL WATER RELEASE

Jhaemely G. V. Silva[1*], Albert S. Silva[1], Josy A. Osajima[1], Edvani C. Muniz[1], Edson C. Silva-Filho[1], Francisco E. P. Santos[1]

1 – Federal University of Piauí (UFPI), Piauí, PI, Brazil
jhaemely_silva@ufpi.edu.br

Abstract – The use of superabsorbent hydrogels in agricultural applications contributes to sustainable development because they can function as soil conditioners, storing larger volumes of water and reducing irrigation waste through the control of water release [1]. To investigate the swelling capacity and rheological properties of the hydrogels, superabsorbent nanocomposite hydrogels based on polyacrylamide, laponite, and cashew tree gum were synthesized using polymerization reaction. The results demonstrate normal modes that confirm the formation of hydrogels by FTIR and the presence of laponite in the nanocomposites' crystalline network by XRD. Based on rheological experiments, the presence of laponite in the hydrogels increased the material's resistance. With the swelling test, it was determined that an increase in pH from 4 to 7 favored the swelling of the hydrogels; however, the swelling capacity decreases with an increase in the amount of laponite because the addition of an inorganic load to the hydrogel matrix increases the density of crosslinking, resulting in a decrease in water absorption [2]. In the toxicity test, it was feasible to confirm that *Artemia salina* nauplii mortality was low in both nanocomposite hydrogels, and that the materials containing the highest concentration of cashew tree gum did not exhibit mortality in the bioassay. The results suggest that superabsorbent nanocomposite hydrogels with a higher cashew tree gum concentration and laponite addition are suitable for agricultural production.

References

1. Rukchonlatee, S., Siriphannon, P. Facile Preparation of Montmorillonite/Crosslinked Chitosan Containing Potassium Nitrate Nanocomposites as Eco-Friendly Slow-Release Fertilizers. J Polym Environ (2023). https://doi.org/10.1007/s10924-023-02815-z.
2. Rodrigues Sousa, H.; Lima, I.S.; Neris, L.M.L.; Silva, A.S.; Santos Nascimento, A.M.S.; Araújo, F.P.; Ratke, R.F.; Silva, D.A.; Osajima, J.A.; Bezerra, L.R.; Silva-Filho, E.C. Superabsorbent Hydrogels Based to Polyacrylamide/Cashew Tree Gum for the Controlled Release of Water and Plant Nutrients. Molecules 2021, 26, 2680. https://doi.org/10.3390/molecules26092680.

Fundings: A UFPI, FISMAT, CAPES and LIMAV.

Keywords: Nanocomposite hydrogels, Rheological properties, Laponite and Cashew tree gum.

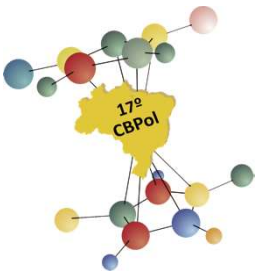

IN-SITU POLYMERIZED PEBAX®/POLYDOPAMINE BLEND MEMBRANES WITH HIGH CO_2/N_2 SELECTIVITY.

Ariele dos Santos Pirola [1], Paula Sacchelli Pacheco [1], Sônia Faria Zawadski[2] and Daniel Eiras [1]*

Insert here the author(s) affiliation(s). Write the e-mail of the author to whom correspondence should be addressed. Example:
1 – Graduate Program of Materials Science and Engineering (PIPE/UFPR). Federal University of Parana. Brazil
eiras@ufpr.br

2 – Graduate Program of Chemistry (PPGQ/UFPR). Federal University of Parana. Brazil.

Abstract - The objective of this work was to produce Pebax®/polydopamine blends by *in -situ* polymerization and apply these blends to produce membranes for gas separation. The blends were produced by *in-situ* polymerization of polydopamine using air as oxidant and sodium hydroxide to control the pH of the reaction medium. Different concentrations of dopamine hydrochloride were used to prepare the membranes and solvent mixtures with different ethanol/water ratios were used to dissolve Pebax® and prepare de membranes. Flat sheet membranes were tested for gas permeation, DSC, TGA, WAXD, SEM and FTIR. Visual inspection was used to identify the presence of polydopamine in the membranes. The results show that there is an optimal concentration of dopamine hydrochloride (1mg/mL) that produces the best CO_2/N_2 ideal selectivity (α=100, P=114 Barrer). DSC and WAXD results indicate that polydopamine has great influence on the crystallization of Pebax®, reducing the melting and crystallization temperatures of PA blocks and increasing the melting temperature of PEO blocks. The results of permeation tests indicate that the presence of polydopamine reduces the diffusion coefficient of Pebax® by reducing the segmental mobility of PEO blocks and possibly the fraction free volume. Compared to the trade-off, Pebax®/PDA membranes surpasses the upperbound for CO_2/N_2 separation.

References

1. J. Liebscher, R. Mrówczyński, H. A. Scheidt, C. Filip, N. D. Haìdade, R. Turcu, A. Bende, S. Beck, *Langmuir* **2013**, *29*, 10539. https://dx.doi.org/10.1021/la4020288
2. H. M. Lee, I. S. Youn, M. Saleh, J. W. Lee, K. S. Kim, *Physical Chemistry Chemical Physics* **2015**, *17*, 10925. https:// 10.1039/c5cp00673b
3. G. Dong, J. Zhang, Z. Wang, J. Wang, P. Zhao, X. Cao, Y. Zhang, *ACS Appl Mater Interfaces* **2019**, *11*, 19613. https://10.1021/acsami.9b02281
4. Y. Liu, X. Li, Y. Qin, R. Guo, J. Zhang, *J Appl Polym Sci* **2017**, *134*, https://10.1021/acsami.9b02281 10.1002/app.44564.

Fundings: Coordenação de Aperfeiçoamento de Pessoal de Nível Superior (CAPES), by the financial support of this project under the grant 37759299168/CAPES-PRINT738088P, and Conselho Nacional de Desenvolvimento Científico e Tecnológico (CNPq) for financial support under the grants 420696/2018-0 and 440036/2019-4.
Keywords: *Pebax, polydopamine (PDA), in-situ polymerization, CO_2 separation, polymer blends.*

PEBAX®/ZIF-67 MIXED MATRIX MEMBRANES FOR CO_2/N_2 SEPARATION.

Paula S. Pacheco [1*], Sônia Faria Zawadzki [2] and Daniel Eiras [1]

1 – *Graduate Program of Materials Science and Engineering (PIPE/UFPR). Federal University of Parana. Brazil*
paula.sacchelli@gmail.com

2 – *Graduate Program of Chemistry (PPGQ/UFPR). Federal University of Parana. Brazil.*

Abstract -. In this study, PEBAX/ZIF-67 mixed matrix membranes (MMMs) were fabricated to investigate their permeability and selectivity properties for gas separation applications. PEBAX, a commercially available copolymer, served as the continuous phase in the MMMs. ZIF-67 (zeolitic imidazolate frameworks) was synthesized in methanol using the solvothermal method with different concentrations of nanoparticles (1%, 3%, and 5%), followed by drying at varying temperatures to evaluate its impact on membrane performance. The nanoparticles were characterized by SEM, WAXD, and BET. The MMMs were produced in two steps, starting with dissolving PEBAX in an ethanol/water solution (70/30) followed by adding the different concentrations of ZIF-67 that were already dispersed in a solution by ultrasonic bath. The solution was then poured into petri dishes and dried in a vacuum oven at 40 °C for 48 hours to completely evaporate the solvent. Permeation tests were conducted at 10 and 15 bar for single gases (N_2 and CO_2) in a constant pressure cell with variable volume at 35 °C. SEM images revealed ZIF-67 particles with an approximate diameter of 200 nm, while WAXD results exhibited characteristic peaks corresponding to the SOD (sodalite) structure of ZIF-67. For neat PEBAX, CO_2 permeability increased with pressure, while N_2 permeability remained constant. The ideal CO_2/N_2 selectivity also rose with pressure, reaching 67 (CO_2 permeability = 132 ± 3.5 Barrer) at 15 bar. The effect of ZIF-67 particles varied with pressure and composition. At 10 bar, CO_2/N_2 selectivity decreased for all compositions compared to neat PEBAX. However, at 15 bar, the membrane with 1 wt% ZIF-67 exhibited higher selectivity than neat PEBAX, surpassing Robeson's upper bound for MMMs.

References

1. S. Feng, M. Bu, J.Pang, W. Fan, L.Fan, H. Zhao, G. Yang, H. Guo, G. Kong, H. Sun, Z. Kang, D. Sun, Journal of Membrane Science **2020**, 593, 117404. https://doi.org/10.1016/j.memsci.2019.117404

2. X. Guo, T. Xing, Y. Lou, J. Chen, Journal of Solid State Chemistry **2016**, 235. https://doi.org/10.1016/j.jssc.2015.12.021

3. S. Meshkat, S. kaliaguine, D. Rodrigue, Separation and Purification Technology **2019**, 235, 116150. https://doi.org/10.1016/j.seppur.2019.116150

4. N. Liu, J. Cheng, W. Hou, X. Yang, J. Zhou, Journal of Applied Polymer Science **2021**, 138, 50553. https://doi.org/10.1002/app.50553

Fundings: Conselho Nacional de Desenvolvimento Científico e Tecnológico (CNPq) for financial support under the grants 420696/2018-0 and 440036/2019-4.

Keywords: *Gas separation membranes, PEBAX, ZIF-67, mixed matrix membranes.*

PHOTOSTABILITY STUDY OF ANGICO GUM HYDROGEL

Josy A. Osajima[1,2], Albert S. Silva[1],Marcelo B. Furtini[1], Edson C. S. Filho[1,2], Edvani C. Muniz[1,2]*
1 - Postgraduate Program in Materials Science and Engineering - PPGCM, Federal University of Piaui (UFPI), Teresina, PI, Brazil
2 - Postgraduate Program in chemistry- PPGQ, Federal University of Piaui (UFPI), Teresina, PI, Brazil
josyosajima@ufpi.edu.br

Hydrogels are polymeric materials formed by the reaction of one or more types of monomers and have a molecular chain formed by physical or chemical crosslinks [1]. Despite the environmental appeal around the accumulation of polymeric materials in the environment, it is necessary to consider that degradation is only sometimes the result desired by industries because, depending on how polymer-based parts are used, these reactions may bring financial losses [2]. Studying photostability is important to understand how angico hydrogel behaves against UV light before use in environmental conditions. Thus, this study aimed to investigate the photostability of angico hydrogel against ultraviolet (UV) radiation for agricultural applications. Angico hydrogels were synthesized via crosslinking and characterized by viscometry. The photostability study was carried out in an irradiation box with temperature control, and samples were taken at predetermined times for up to 2 hours. The hydrogels were placed in a reactor to irradiate all sides equally. The source light was a 125 W mixed mercury vapor lamp without a bulb, and the UV radiation intensity was 5.6 mW/m². The analysis was in triplicate. Through the test, an increase in viscosity was observed as a function of the time of exposure to light due to the formation of species with higher molar mass. In conclusion, exposing the hydrogel to UV radiation promoted crosslinking reactions, thus increasing its viscosity.

References

1. SHAN, Shuang et al. High-performance hydrogel adsorbent based on cellulose, hemicellulose, and lignin for copper (II) ion removal. Polymers, v. 13, n. 18, p. 3063, 2021.
2. RABELLO, Marcelo; DE PAOLI, Marco-Aurelio. Aditivação de termoplásticos. São Paulo: Artliber, 2013.

Keywords: *Hydrogel, polysaccharide, crosslinking.*

PHYSICOCHEMICAL PERFORMANCE OF AN ECO-FRIENDLY AGRICULTURAL COMMERCIAL PRODUCT: EVALUATION OF PHEROGEN® INTERACTION ON SOY LEAVES UNDER SIMULATED ENVIROMENTAL CONDITIONS

Letícia Fonseca Balcewicz[1], Heloise Ribeiro de Barros[2], Izabel Cristina Riegel Vidotti Miyata[1]

1 – Grupo de Pesquisa em Macromoléculas e Interfaces (GPMIn), Department of Chemistry, Federal University of Paraná (UFPR), Curitiba, PR, Brazil leticiafonseca@ufpr.br
2 – Provivi do Brasil, Campinas, SP, Brazil

Abstract - The demand for sustainability in agriculture motivates the development of products to replace the use of chemical insecticides such as the use of pheromones in encapsulated formulations with controllable release to interrupt the reproductive cycle of pests. Soybean leaves have a hydrophobic character and crop protection agents (CPA) must be able to adhere to leaves surfaces to be efficient[1]. In this context, a physicochemical study of the CPA product Pherogen®, a formulation of encapsulated pheromone in polymeric microcapsules developed by the company Provivi, was conducted aiming optimization of its performance in soybean plantations. Pherogen® was first characterized by Scanning Electron Microscopy which showed different adhesion behaviors of the microcapsules depending on the substrate. The contact angle (CA) of green and dry leaves was measured to determine the wettability of the substrates by the product and calculate the work of adhesion. Three liquids of different polarities were used to measure CA to further characterize surface free energy on soy leaves[2]. The physicochemical study revealed that Pherogen® has better adhesion on dry leaves and matured green leaves from reproductive stages, due to hydrophilic characteristics. Currently, volatiles released from the Pherogen® application are being characterized and submitted to a kinetic study. This investigation will provide details about key chemical features involved in the application of the product on soybean crops and is important to improve the efficiency of Pherogen® and optimize its use economically.

References:

1. H. Kang; P.M. Graybill; S. Fleetwood; J.B. Boreyko; S. Jung *PLoS one* 2018, *13*, e0202900. https://doi.org/10.1371/journal.pone.0207425.
2. C.E.P. da Silva; M.A.S. de Oliveira, F.F. Simas, I.C. Riegel-Vidotti *Food Hydrocolloids* 2020, *100*, 105394. https://doi.org/10.1016/j.foodhyd.2019.105394.

Fundings: Fundação de Estudos e Pesquisas Agrícolas e Florestais (FEPAF) and Provivi.

Keywords: *Crop protection agents, pheromones, polymeric microcapsules, soybean, wettability.*

POLYANILINE COATING ON COPPER AND ITS CORROSION PROTECTION IN ACID MEDIUM

Pedro José de Souza Medeiros[1*] and Carla Dalmolin[1]

1 – Department of Chemistry, Santa Catarina State University (UDESC), Joinville, SC, Brazil
pedro.medeiros@edu.udesc.br

Abstract - Copper (Cu) is widely used in industrial applications such as process equipment, and electrical and electronic devices. Apart from high electrical and thermal conductivity and excellent formability, Cu also exhibits good corrosion resistance; however, it corrodes in variety of aggressive environments. Copper protection against corrosion is usually carried out by an inhibitor, using organic compounds mainly benzotriazoles and aminotriazole as well as its derivatives. Apart from the good protective properties of inhibitors in various corrosive environments, they are quite toxic; hence, application of conducting polymers could be considered as a possible environmental-friendly procedure in corrosion protection of Cu. In this work, polyaniline (Pani) coating on Cu was studied in order to verify its corrosion resistance and electrochemical properties for a conducting cable. Pani was obtained by interfacial polymerization in its acid form, emeraldine salt. For dissolution in n-methyl-pyrrolidone (NMP), the powder were treated in alkaline (ammonia) medium – 1.0 mol/L – for 30 min, to form the emeraldine base. A solution of Pani in its alkaline form (emeraldine base) in NMP – 0,03 mg/mL – was used for deposition on the Cu surface by drop casting. Coated cables were dried at 60 °C for 24h and then stored at room temperature, protected from light. Electrochemical characterization was performed using a 3-electrode cell, where Cu/Pani cables were the working electrodes, Ag/AgCl was used as reference electrode and Pt as counter-electrode. In cyclic voltammetry (CV) and electrochemical impedance spectroscopy (EIS) were made in acid medium, HCl 0.1 mol/L. CV showed the electrochemical profile expected for Pani and EIS showed an improvement on the corrosion resistance of Cu, verified by the increase in the charge transfer resistance of the electrode.

Fundings: FAPESC.

Keywords: *Polyaniline; Coatings; Corrosion; Conducting Polymers*

POLY(TMPTA-*CO*-EDMA-*CO*-MAA) MOLECULARLY IMPRINTED WITH N-NITROSODIMETHYLAMINE AS A MONOLITHIC SORBENT FOR DISPOSABLE PIPETTE EXTRACTION

Allyson L. R. Santos[1] and Anizio M. Faria[1,2]*

1 – Institute of Chemistry, Federal University of Uberlândia (UFU), Uberlândia, MG, Brazil
leandroallyson@hotmail.com
2 – Institute of Exact and Natural Sciences of Pontal, Federal University of Uberlândia (UFU), Uberlândia, MG, Brazil

Abstract – N-nitrosodimethylamine (NDMA) is a carcinogenic subproduct spontaneously formed in some drugs, such as ranitidine and valsartan.[1] The small amount of NDMA formed in the presence of several other molecules in the drug requires specific methods for its isolation and subsequent determination in these drugs.[2] This study proposes the development of a monolithic organic polymeric device with the NDMA molecularly imprinted for the selective extraction of NDMA from different commercial drugs, with subsequent determination by high-performance liquid chromatography (HPLC). For this, the *in situ* polymerization of trimethylolpropane triacrylate (TMPTA), methacrylic acid (MAA), and ethylene glycol dimethacrylate (EDMA) was used with 2,2-azobisisobutyronitrile (AIBN) as a radical initiator and different porogenic solvents for the formation of a polymeric monolith organic inside a micropipette tip.[3] Different concentrations of NDMA were evaluated as a template for the molecularly imprinted polymer monolith. The best conditions for the preparation of a highly porous monolith of poly(TMPTA-co-EDMA-co-MAA) molecularly imprinted with NDMA were obtained at 60 °C for 20 h, using isopropanol and polyethyleneglycol-1000 as porogenic solvents and the ratio TMPTA:MAA:EDMA:porogen 4:2:14:80, w/w/w/w. Poly(TMPTA-co-EDMA-co-MAA) monoliths were morphologically and structurally characterized. The monoliths showed 65.8 % of total porosity, with a BET-specific surface area of 81.4 m^2/g and a total pore volume of 0.24 cm^3/g. In the infrared spectra of poly(TMPTA-co-EDMA-co-MAA), the disappearance of the signal at 1630 cm^{-1}, attributed to the stretching of the C=C bond of the monomers, and the signal broadening from 1000 to 1550 cm^{-1} were observed. NDMA molecularly imprinted was obtained from a 0.5mmol/L of NDMA solution. The extraction of NDMA from drugs is in the study, using the disposable pipette extraction method with NDMA molecularly imprinted poly(TMPTA-co-EDMA-co-MAA).

References

1. F. S. Aldawsari;Y. M. Alshehry; T. S. Alghamdi *J. Food Drug Anal.* 2021, *29*, 39. https://doi.org/10.38212/2224-6614.1133.
2. H. Lim; Y. Oh; H. Shin *J. Pharm. Biomed. Anal.* 2020, *189*, 113460. https://doi.org/10.1016/j.jpba.2020.113460.
3. F. Maya; B. Paull *J. Sep. Sci.* 2019, *42*, 1564. https://doi.org/10.1002/jssc.201801126.

Fundings: FAPEMIG APQ-1901-22, FINEP 01.13.0371.00

Keywords: *Molecularly imprinted polymer, NDMA, polymethacrylate, polymerization in situ.*

PRODUCTION OF WOOD PLASTIC COMPOSITE USING EUCALYPTOS WITH VULCANIZED NATURAL RUBBER

Felipe R. Rodrigues[1], Diego Silva de Melo[2], Michael J. Silva[2], Rodrigo A. Bispo[1], Sergio A. M. da Silva[3]

1 – Department of Physics and Chemistry, Paulista State University (UNESP), Ilha Solteira, SP, Brazil
fr.rodrigues@unesp.br
2 – Department of Energy Engineering, Paulista State University (UNESP), Rosana, SP, Brazil
3 – Department of Civil Engineering, Paulista State University (UNESP), Ilha Solteira, SP, Brazil

Abstract - The wood industry has been one of the main demotivators for the production of wood panels, mainly due to the use of carcinogenic resins in these panels, which will be recurrent for a little over 70 years [1,2]. Based on this situation, and with the intention of producing a wood-polymer composite panel, this study seeks to obtain a particleboard composite from eucalyptus waste using vulcanized natural rubber (VNR) as a binding agent. Panels were produced using 100 phr of natural rubber (NR) as reference material and two different concentrations of eucalyptus residue, 100 phr and 200 phr (Table 1). To obtain the first conductive polymeric nanocomposites, the mass of all the starting materials was measured, including natural rubber (NR), stearic acid and zinc oxide. Subsequently, the breakdown of the NR molecules is carried out through a cylinder mixer. After this process, stearic acid and zinc oxide are added, after this process, a minimum of 4 hours is waited in order to enhance the activation process. After the stipulated time, the mixture is returned to the mixer, the MBTS, TMTD and sulfur are weighed on the scale and mixed into the mixture. Subsequently, the samples were assigned to the rheometric test to determine the optimal curing time. Finally, they are placed in a hydraulic press heated to a temperature of 150°C. SEM analysis indicated that the eucalyptus particles are homogeneously distributed and that the VNR coated these particles, demonstrating good interaction between the phases. In order to evaluate the influence of VNR as a binder in particleboard composites, mechanical tests in tensile and compression modes were conducted. According to the results, as eucalyptus residue concentration was increased, the material became stiffer due to a decrease in stress at rupture and an increase in strain at rupture. According to the TG/DTG analysis, the particleboard composites presented the characteristic thermal decomposition events of VNR, as well as degradation of the cellulose that forms the eucalyptus particles. Both particleboard samples present good stability thermal. Due to this, the samples have excellent potential for use in the civil and construction industries.
Keywords: Vulcanized natural rubber; Eucalyptus; Composite; Wood, Plastic.

Table 1 – Quantity of materials for the production of panels

Components	VNR	Panel-1	Panel-2
Vulcanized Natural Rubber (VNR)	100.00	100.00	100.00
Zinc oxide	4.00	4.00	4.00
Stearic acid	2.00	2.00	2.00
Sulfur	1.50	1.50	1.50
Dibenzothiazol disulfide (MBTS)	1.00	1.00	1.00
Tetramethylthiuram disulfide (TMTD)	0.50	0.50	0.50
Eucalyptus	0	100	200

References

1. Zhou, X.; He, P.; Peng, W.; Lü, F.; Shao, L.; Zhang, H. Upcycling of real-world HDPE plastic wastes into high-purity methane and hierarchical porous carbon materials: influence of plastics additives. Journal of Environmental Chemical Engineering, v. 11, I. 2, p. 2213-3437, Jan. 2023. https://doi.org/10.1016/j.jece.2023.109327.
2. PlasticsEurope, Plástics – the facts 2021, in, 2021.

STUDY OF THE THERMAL STABILITY OF A GRANULATED ORGANOMINERAL FERTILIZER BASED ON LIGNOCELLULOSIC RESIDUE BY THERMOGRAVIMETRIC ANALYSIS

Henrique A. Sobreira[1*]; Marcos V. Ferreira[1]; Anizio M. Faria [1,2]; Rosana M. N. Assunção[1,2]

1 – Institute of Chemistry, Federal University of Uberlândia (UFU), Uberlândia, MG, Brazil
henrique@iftm.edu.br
2 – Institute of Exact and Natural Sciences of Pontal, Federal University of Uberlândia (UFU), Uberlândia, MG, Brazil

Abstract - Organomineral fertilizers are produced by incorporating mineral fertilizers into lignocellulosic-based residues, offering an alternative to improve the quality and productivity of agricultural inputs. Understanding the interactions within the components of the granulated organomineral fertilizer is crucial to contribute to its efficacy. The objective of this study was to evaluate the thermal stability of a lignocellulosic residue-based granulated organomineral fertilizer (GOF) through thermogravimetric analysis (TGA). The decomposition curves of the ammonium monophosphate (MAP), lignocellulosic residues, and GOF were compared. The results from Fig. 1 revealed that the decomposition of MAP occurs in three distinct stages. In the first event, MAP decomposes into ammonia, phosphoric acid, and water, with a mass loss of 9.8% at an onset temperature of 189 °C. Subsequently, a second decomposition event related to the release of water and pyrophosphoric acid takes place. With increasing temperature, a third decomposition reaction occurs, where pyrophosphoric acid decomposes into water and phosphorus pentoxide, resulting in a total mass loss of 63.5%. For the GOF, a similar decomposition pattern was observed, with the first stage involving the release of a greater amount of volatile substances, such as water, that come from the lignocellulosic-based residues. The second decomposition event, starting at a temperature of 178 °C, corresponds to the degradation of ammonia and ammonium monophosphate, similar to the MAP curve. The total mass loss was 33.2%. GOF exhibited higher thermal stability than the lignocellulosic-based residues, demonstrating an increase of approximately 30 °C in the second decomposition stage. Additionally, the presence of the lignocellulosic base in the GOF prevented its complete decomposition, increasing its thermal stability, but did not prevent the initial decomposition of the ammonium phosphate. These characteristics can contribute to the efficacy of GOF in providing nutrients to plants over long periods.

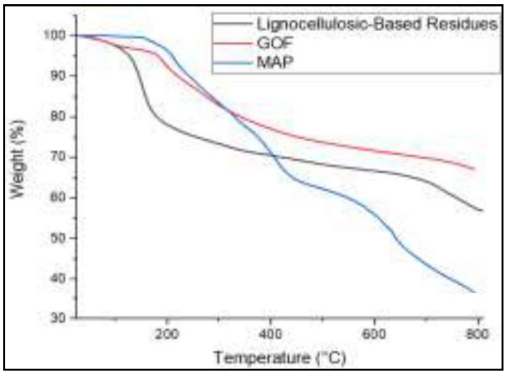

Figure 1 – Thermogravimetric curves for the lignocellulose base, GOF, and MAP.

References

1. N. Vollmer; R. *Ayers International Journal of Self Propagating High-Temperature Synthesis, 2012, 21, 4.* https://doi.org/10.3103/S1061386212040073.

Keywords: *Organomineral fertilizer, Lignocellulosic residue, Thermogravimetric analysis.*

SUPERABSORBENT HYDROGELS BASED ON ALGINATE/POLYACRYLATE AND POLYACRYLAMIDE AS WATER RETAINER

Natalia Pettinelli[1], Constanza Sabando[1], Johanna Castaño[2] and Saddys Rodríguez-Llamazares[1]*

1 – Centro de Investigación de Polímeros Avanzados, Edificio Laboratorio CIPA, Concepción, Chile

s.rodriguez@cipachile.cl

2 – Department of Chemical Engineering, Universidad de Concepción, Concepción, Chile

Abstract

Water-retention hydrogels based on synthetic polymers, such as polyacrylate and polyacrylamide, show advantages related to their high-water absorption capacity (300–500 g/g in water).[1] However, the effectiveness of them is hampered, among others, by their non-degradability. Combining superabsorbent synthetic polymers with polysaccharides such as sodium alginate (Alg) can balance water absorption and retention properties and biodegradability.[2] Superabsorbent hydrogels based on alginate-graft-polyacrylamide (Alg-*g*-PAm), alginate-graft-potassium polyacrylate (Alg-*g*-PAc) and alginate-graft-poly(acrylamide-co-potassium acrylate) (Alg-*g*-PAc-co-Am) were prepared by free-radical copolymerization in aqueous media, using N,N-methylene-bisacrylamide as crosslinker and potassium persulfate as initiator. Divalent ions were also incorporated into the formulation to result in the hydrogel formation. The effect of type of synthetic polymer: polyacrylate, polyacrylamide and poly(acrylate-*co*-acrylamide) grafted onto sodium alginate backbones on the hydration properties and biodegradability of hydrogels prepared with a weight ratio of 4:1, Alg: synthetic monomer was investigated. Fourier transform infrared spectroscopy revealed that the synthetic monomer was grafted onto Alg. Surface morphology of the hydrogels was assessed by scanning electron microscopy (SEM). The swelling capacity ranged from 60 to 400 g/g in tap water and depended on the synthetic monomer grafted. Biodegradation studies of the hydrogels were carried out by soil burial test, and weight loss was observed above 60% in 30 days. Different degradation stages were also evaluated using SEM. In conclusion, the superabsorbent hydrogels exhibited high water retention capacity and biodegradability, making them efficient water-saving materials for agricultural applications.

References:

1. L. Chang; L. Xu; Y. Liu; D. Qiu. *Polymer Testing* 2021, *94*, 107021. https://doi.org/10.1016/j.polymertesting.2020.107021.
2. K. Saruchi; Kumar, V.; H. Mittal, H.; S. M. Alhassan. *International Journal of Biological Macromolecules* 2019, *132*, 1252-1261. 10.1016/j.ijbiomac.2019.04.023.

Fundings: Fondef ID21I10108, CIPA, ANID Regional, GORE BIO BIO, R17A10003

Keywords: *Alginate, polyacrylamide, polyacrylate, Water retention, Biodegradation*

SYNTHESIS AND CHARACTERIZATION OF CASHEW GUM (Anacardium occidentale L) HYDROGELS CONTAINING MODIFIED PHOSPHATES

Joyce A. Borges[1], Albert S. Silva[1], Ariane M. S. Nascimento[1], Idglan S. Lima[1], Edvani C. Muniz[1], Josy A. Osajima[1], Edson C. Silva-Filho[1]

1 – Laboratório Interdisciplinar de Materiais Avançados (LIMAV), Universidade Federal do Piauí,64049-550, Teresina – PI, Brasil.

joyceab@ufpi.edu.br

Abstract: Hydrogels are polymeric materials that can be obtained from natural polymers, such as cashew tree gum (CG). CG is a natural exudate obtained from the *Anacardium occidentale L.*, which is widely found in the northeast region of Brazil and, due to its biocompatible, low cost and handling, has been widely studied [1,3]. Ceramic materials such as hydroxyapatite, a calcium phosphate, can be added to CG hydrogels, whose surface can be modified with silane agents that allow the formation of more efficient materials [2]. The objective of this work was the synthesis and characterization of cashew tree gum hydrogels containing phosphates modified with the silane agent 3-aminopropyltriethoxysilane (APTES). The materials were characterized by X-ray diffraction and FTIR, and the ecotoxicity test against *Artemia saline* was performed. The characterizations confirmed the formation of hydrogels. The ecotoxicity test of these materials against *Artemia salina* was performed at different concentrations and, at the end of the test, the amount of live nauplii was greater than 70%, indicating that the hydrogels did not present toxicity at the concentrations studied.

References

1 M. KSO. Abreu; M. Silva; D. S. Abreu; A. R. Ritcher; R. C. M. Paula; V. R. L. Constatino; I. F. Vasconcelos; F. GS. de Oliveira; A. S. de Melo; M. A. Correa; I. CN. Diógenes. Colloids and Surfaces A: Psycochemical and Engineering Aspects. 2023, 656, 130307. https://doi.org/10.1016/j.colsurfa.2022.130307;

2 O. G. Cisneros-Pineda; W. H. Kao; M. I. Loria-Bostarrachea; Y. Veranes-Pantoja; J. V. Cauich-Rodríguez; J. M. Cervantes-UC. Materials Science and Engineering C. 2014, 40, 101016. https://doi.org/10.1016/j.msec.2014.03.064;

3 H. R. Sousa; I. S. Lima; L. M. L. Neris; A. S. Silva; A. M. S. S. Nascimento; F. P. Araújo; R. F. Ratke; D. A. Silva; J. S. Osajima; L. R. Bezerra; E. C. Silva-Filho. Molecules. 2021, 26, 103390. https://doi.org/10.3390/molecules26092680;

Fundings: We thank CNPq, Capes, Piaui Research Foundation (FAPEPI).

Keywords: *Hydrogel, cashew tree gum, toxicity*

SYNTHESIS OF ANIONIC SCALE INHIBITOR WITH DENDRITIC STRUCTURE BY AZA-MICHAEL ADDITION OF ETHYLENEDIAMINE TO α,β-UNSATURATED COMPOUNDS

Chun T. Huang[1]*, Adriane A. S. Santos[2], Fernanda C. Vargas[2] and Cesar L. Petzhold[1]

1 – Department of Organic Chemistry, Federal University of Rio Grande do Sul (UFRGS), Porto Alegre, RS, Brazil
chun.te.huang@outlook.com
2 – Research, Development, and Innovation (RD&I), Dorf Ketal Brasil LTDA, Nova Santa Rita, RS, Brazil

Abstract - The Campos Basin is one of the major oil-producing regions in Brazil and has several pre-salt fields. These reservoirs are located beneath layers of salt and are considered extremely challenging but highly promising for oil exploration and production. During offshore exploration activities in ultra-deepwater and other harsh environments, scale formation is a significant issue encountered in the upstream oil and gas industry. In this work, the field water chosen for study has a scaling tendency for both the most common inorganic scales in the oil and gas industry, deposition of $CaCO_3$ (calcite) and $BaSO_4$ (barite). However, this problem can be effectively addressed through the injection of scale inhibitors. We herein reported the synthesis and characterization of a series of anionic molecules with dendritic structures. These structures were synthesized through the aza-Michael reaction using ethylenediamine as a starting material. The investigation of the reaction involved different approaches, including conventional thermal heating and microwave irradiation. The application of microwave irradiation significantly speeds up the process, enhancing the synthetic utility of this methodology for the preparation of these types of derivatives. The formation of dendritic structures was confirmed by ^{1}H NMR. Furthermore, the influence of the anionic functional group (phosphonic, carboxylic and sulfonic) on both the efficiency of scale inhibition and the brine compatibility was investigated and compared with the commercially available ethylenediamine tetramethylene phosphonic acid (EDTMP) using standard bottle test. Commercial EDTMP proved to be the most effective inhibitor for barite scale, but it exhibited limited compatibility with brine solutions. In contrast, although all synthesized scale inhibitors showed better brine compatibility compared with EDTMP, they failed to effectively inhibit barite at a dosage of 2.5 ppm of active acid. This inefficiency persisted even when combining carboxylic and sulfonic dendritic molecules physically or utilizing a molecule containing both functional groups.

References

1. R. Bisatto; V. M. Picoli; C. L. Petzhold *Journal of Petroleum Science and Engineering* 2022, *213,* 110331. https://doi.org/10.1016/j.petrol.2022.110331.

Fundings: This work was supported by Coordenação de Aperfeiçoamento de Pessoal de Nível Superior, Brazil (CAPES). The authors acknowledge the PPGCIMAT (Programa de Pós-Graduação em Ciência dos Materiais) from UFRGS (Universidade Federal do Rio Grande do Sul) and DORF KETAL BRASIL LTDA company for the support on analysis.

Keywords: *Scale inhibitor, dendrimer, Michael addition, calcium carbonate, barium sulphate.*

SYNTHESIS OF BIOCHAR-HYDROGEL COMPOSITE AS ECO-FRIENDLY ALTERNATIVE FOR AGRICULTURAL APPLICATIONS WITH CONTROLLED WATER ABSORPTION AND NUTRIENTS RELEASE

Marcela S. Frizzo[1*], Natália Pettinelli[2], Johanna Castaño[3], Saddys Rodríguez[4], Gonzalo Recio[5]

1,5 – Facultad de Ingeniería, Arquitetura y Diseño, Universidad San Sebastián (USS), Concepción, Chile
marcela.frizzo@gmail.com
2,4 – Centro de Investigación de Polímeros Avanzados (CIPA), Concepción, Chile
3- Facultad de Ingeniería Química, Universidad de Concepción, Chile

Abstract – For a very long time have existed two significant problems in agricultural techniques, that are the excessive irrigation and the ineffectiveness of quick fertilizer[1]. Therefore, several attempts have been made to increase the effectiveness of quick fertilizer. Superabsorbent hydrogels have been applied to improve water and nutrient retention in agricultural soils as suggested[2,3]. However, the high costs and negative environmental effects of these polymeric soil additives prevent their widespread use on big farms. Thus, solutions are urgently needed to optimize the hydrogel application. Biochar, which is a cost-effective pyrolysis product, has been applied as a soil amendment for soil fertility reservation. This work present different alginate/acrylamide mass ratios hydrogel with interpenetrated networks, and alginate/Ca^{2+} molar ratios ions, that form a physically cross-linked network with the alginate. The best relation between Al and AM was 4:1; and alginate and AL: Ca^{2+} 1:1. For the synthesis of the composite was mixed 5% (w/w) modified biochar with calcium, potassium, and phosphorous with alginate (AL) and acrylamide (AM) hydrogels. The physic-chemical properties of the composite, such as absorption and retention of water and nutrient liberation, were characterized. Modified biochar-hydrogel composite presents a significant swelling capacity (8569 ± 835% water was absorbed after 24 h), retention (presenting a loss of water about 18% in 14 days of environment exposition) and calcium, potassium and phosphorous nutrients release of (29, 10, 50 ppm in 6 days). The results revealed the biochar-hydrogel composite is a promising soil amendment regarding economic benefit and environmental footprint.

1. T.S. Du, S.Z. Kang, J.H. Zhang, W.J. Davies, Deficit irrigation and sustainable water-resource strategies in agriculture for China's food security, J. Exp. Bot. 66 (8) (2015) 2253–2269, https://doi.org/10.1093/jxb/erv034.

2. S. Kim, G. Iyer, A. Nadarajah, J.M. Frantz, A.L. Spongberg, Polyacrylamide hydrogel properties for horticultural applications, Int. J. Polym. Anal. Char. 15 (5) (2010) 307–318, https://doi.org/10.1080/1023666X.2010.493271.

3. S. Mohammadi-Khoo, P.N. Moghadam, A.R. Fareghi, N. Movagharnezhad, Synthesis of a cellulose-based hydrogel network: characterization and study of urea fertilizer slow release, J. Appl. Polym. Sci 133 (5) (2016), https://doi.org/10.1002/app.42935.

Fundings: Fondo de Fomento al Desarrollo Científico y Tecnológico (FONDEF)

THE USE OF CASSAVA GUM (*Manihot esculenta*) HYDROGEL FOR STORAGE AND RELEASE OF MACRONUTRIENTS IN AGRICULTURAL

Edson C. Silva-Filho[1], Idglan S. Lima[1], Albert S. Silva[1], Ariane M.S. Nascimento[1], Joyce A. Borges[1], Francisco E. P. Santos[1], Josy A. O. Furtini[1] and Edvani C. Muniz[1]

1 - Interdisciplinary Laboratory of Advanced Materials (LIMAV), Federal University of Piauí, 64049-550 Teresina-PI, Brazil.

edsonfilho@ufpi.edu.br

Abstract - Hydrogels (hydro-retaining polymers) are being explored as viable options for processing and releasing macronutrients in agriculture. However, commercial hydrogels are entirely composed of synthetic materials derived from petroleum [1]. Hydrogels produced from natural materials emerge as an alternative to resolve this problem [2,3]. This research aimed to synthesize superabsorbent hydrogels from cassava gum and polyacrylamide for macronutrient release. The material was characterized by X-ray Diffraction (XRD) and Scanning Electron Microscopy (SEM). The characterizations confirmed the formation of the hydrogel and the presence of phosphate in its matrix. The hydrogel was studied for its capacity of controlled release of macronutrients and its toxicity test against *Artemia salin*e. After 30 minutes of contact with the medium, the hydrogels began to release phosphate, maintaining a constant rate after 24 hours in solution. Furthermore, no toxicity of the hydrogels was observed. The synthesis of hydrogels with phosphate incorporation into the polymer matrix occurred satisfactorily, resulting in a promising material for the controlled release of macronutrients.

References:

1. A. Abbasi, F. Khatoon, S. Ikram. Int J Biol Macromol. 231 (2023) 123240. https://doi.org/10.1016/J.IJBIOMAC.2023.123240.

2. H. Rodrigues Sousa, I. Sá Lima, L. Matheus Lima Neris, A. Santos Silva, A. Maria Silva Santos Nascimento, F. Pereira de Araújo, R. Felippe Ratke, J. Anteveli Osajima, R. Loiola Edvan, C. Kauany da Silva Azevedo, B. Henrique Vilsinski, E. Curti Muniz, E. C. Silva-Filho. J Mol Liq. 376 (2023) 121463. https://doi.org/10.1016/J.MOLLIQ.2023.121463.

3. H. Rodrigues Sousa, I. Sá Lima, L. Matheus Lima Neris, A. Santos Silva, A. Maria Silva Santos Nascimento, F. Pereira Araújo, R. Felippe Ratke, D. Alves Silva, J. Anteveli Osajima, L. Rocha Bezerra, E. Cavalcanti Silva-Filho, molecules (2021). https://doi.org/10.3390/molecules26092680.

Fundings: CAPES, CNPq and FAPEPI

Keywords: *Hydrogel, Release, and Polysaccharide.*

USE OF POLYSULFIDES FROM INVERSE VULCANIZATION AS STRATEGIC MATERIALS FOR AGRICULTURE

Stella F. Valle[1*], Amanda S. Giroto[1], Nicolai D. Jablonowski[2], and Caue Ribeiro[1]

1 – Embrapa Instrumentação, São Carlos, SP, Brazil. 2 – Forschungszentrum Jülich GmbH, Jülich, Alemanha.
**stellafvalle@gmail.com*

Abstract - Sulfur (S) is a vital nutrient for plant growth, often managed with elemental sulfur (S_8) application as a pellet or as a matrix to carry other essential fertilizers. Despite its advantage as an abundant low-cost residue, S_8 tends to form brittle and non-uniform matrices, and its difficult processability is a challenge.[1] Moreover, since plants can only absorb sulfate, the recovery of S_8-S by crops depends on its biological oxidation in soil, which is significantly slow and limiting to the fertilizer efficiency.[2,3] Polysulfides (PolyS) are easily processible and versatile S-rich materials obtained with the inverse vulcanization of S_8.[4] This sustainable one-pot method is based on the stabilization of polymeric S-chains with small amounts of alkenes, without solvent use and byproduct formation.[5] Herein, PolyS was studied as a multifunctional matrix for the fine dispersion of phosphorus (P) in controlled-release fertilizer (CRF) composites. Solubility control of P fertilizers is important to minimize losses and environmental impacts. At the same time, matrix systems can also favor the dissolution of sources with low solubility like phosphate rocks. PolyS has an agronomic role as a S fertilizer, with superior oxidation to sulfate than S_8. Thus, it is an ideal substitute to conventional polymeric or S_8-based CRF matrices. Results showed that PolyS oxidation favored P solubilization with its local acidity, while the polymeric barrier avoided a fast P release. Moreover, soybean cultivation with the composites reached increased plant biomass and S use efficiency than with a commercial reference. Overall, the PolyS proved to be an interesting CRF matrix for a more sustainable and efficient S and P delivery to plants.

References

1. Griebel, J. J., Glass, R. S., Char, K. & Pyun, J. *Prog. Polym. Sci.* 2016, 58, 90–125. https://doi.org/10.1016/j.progpolymsci.2016.04.003.
2. Degryse, F., Ajiboye, B., Baird, R., Silva, R. C. & Mclaughlin, M. J. *Soil Sci. Soc. Am. J.* 2016, 80, 294–305. https://doi.org/10.2136/sssaj2015.06.0237.
3. Scherer, H. W. *Eur. J. Agron.* 2001, 14, 81–111. https://doi.org/10.1016/S1161-0301(00)00082-4.
4. Chung, W. J. et al. *Nat. Chem.* 2013, 5, 518–524. https://doi.org/10.1038/nchem.1624.
5. Worthington, M. J. H., Kucera, R. L. & Chalker, J. M. *Green Chem.* 2017, 19, 2748–2761. https://doi.org/10.1039/C7GC00014F.

Keywords: *Polysulfide; Composite; Controlled-release fertilizer; Sulfur; Phosphate.*

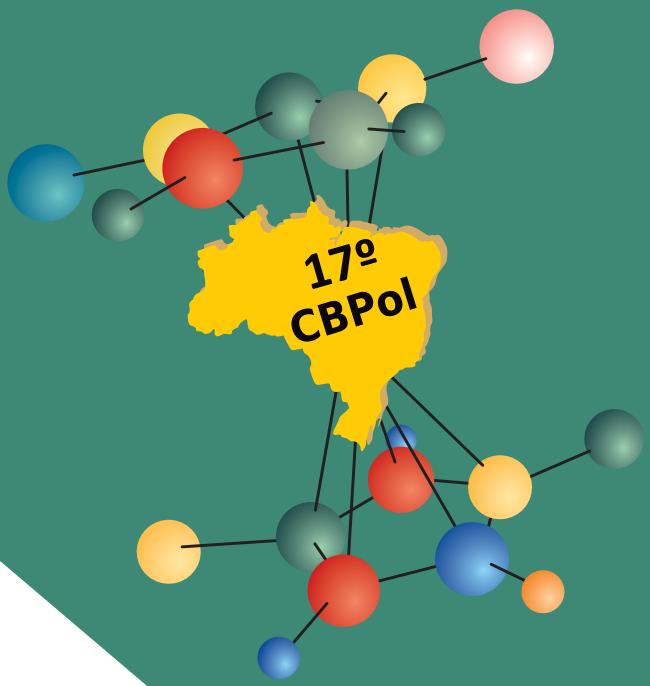

Innovation and management involving polymers and education

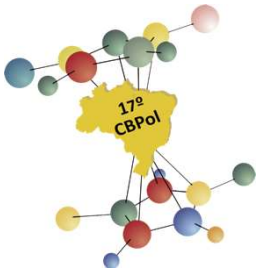

CIRCULAR ECONOMY TRENDS ABOUT THE REUSE OF SYNTHETIC FIBER WASTE FROM THE OIL INDUSTRY

Daniela Hurtado Tejada[1], Thaiane Nolasco da Silva[2], Ana Maria Furtado de Sousa[2], Ana Lucia Nazareth da Silva[1,3], Suzana Borschiver[1]

1 – Rio de Janeiro Federal University, Universidade Federal do Rio de Janeiro, Programa de Engenharia Ambiental, Rio de Janeiro, RJ, Brazil
2 – Rio de Janeiro State University, Graduate Program in Chemical Engineering, Rua São Francisco Xavier 524 – Maracanã, Rio de Janeiro, RJ, Brazil
3 – Rio de Janeiro Federal University, Universidade Federal do Rio de Janeiro, Instituto de Macromoléculas Professora Eloisa Mano (IMA/UFRJ), Rio de Janeiro, RJ, Brazil

Abstract – Oil and Gas and textile industries have significant potential to contribute to environmental improvements across their entire supply chain, allowing the achievement of sustainable development goals. Implementing a circular economy promotes natural resource conservation, reuse, and recycling of textiles, and is a means of achieving sustainability. The purpose of this research is to investigate and analyze the most recent circular economy trends concerning oil and gas industry synthetic fiber waste reuse. The Scopus database was used to conduct a literature review, and the first 50 articles from 2021 to 2023 were chosen. Following an examination of the articles, the trends are classified into thematic axes. According to the findings, most of the articles are focused on the use of synthetic fiber to cement and mortar reinforcement, followed by using recycled synthetic fiber to reinforce polymers. Recycled polyester and polypropylene fibers are the most mentioned on the articles.
Keywords: *circular economy, textile industry, synthetic fiber*

Introduction

The textile industry, like any other, can help to reduce environmental impacts by implementing projects that reduce natural resource depletion, water and energy consumption, water pollution during dyeing processes, greenhouse gas emissions, and post-consumer waste generation [1-2]. Examples of challenges include reducing water consumption in cotton t-shirts [3] and jeans [4] productions. Total greenhouse gas emissions from textile production exceed those from all international travel and maritime shipping combined [5]. Similarly, the demand for sustainability has produced both opportunities and difficulties for the future of oil and gas industry, exploring different areas such as offshore wind resources, biofuels, and carbon capture and storage [11]. Furthermore, fossil fuels such as oil and natural gas are used to manufacture synthetic textile fiber, which contributes to greenhouse gas emissions [6]. The textile industry, for example, consumes approximately 342 million barrels of oil per year [5].

In terms of textile production, synthetic fibers account for 62.3% of total textile production (51.5% of total polyester), natural fibers account for 31.5%, and artificial fibers account for 6.2% [7]. As a result, the textile industry offers opportunities for

improvement in terms of lowering environmental impacts, and many companies within the industry are already taking action.

Under the circular economy, the "take-make-waste" model should be replaced by a "system where materials are not lost after use but remain in the economy" [8]. The three pillars of the circular economy, according to [9], are "eliminate waste and pollution, keep products and materials in use, and regenerate natural systems." In addition, the circular economy emphasizes closed-loop systems such as reusing, repairing, refurbishing, remanufacturing, recycling, and sharing products and materials [10] as illustrated in Figure *1*. According to regulations such as the European Green Deal and the Circular Economy Strategy, implementing a circular economy in the textile industry is a driver for sustainability [2], as it promotes natural resource conservation, textile reuse, and material recycling [9].

Figure 1 – Main loops of a circular economy

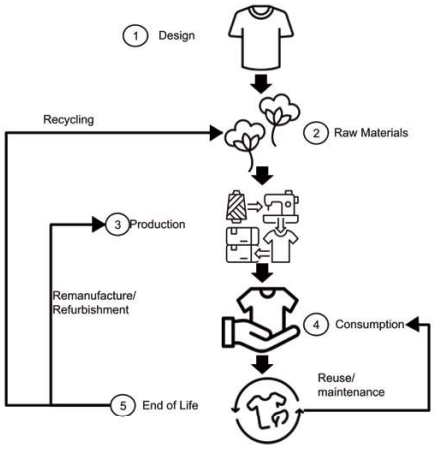

The purpose of the current study is to investigate the most recent circular economy trends in the textile industry. It is structured as follows. Section 2 corresponds to experimental, where the methodology is explained. Section 3 corresponds to Results and Discussion. And finally, section 4 corresponds to conclusions.

Experimental

Scopus was chosen as the research platform for the study of circular economy trends about the reuse of synthetic fiber waste from the oil industry, implementing the next research strategy shown in Figure 2:

Figure 2 - Research Strategy

(TITLE-ABS-KEY ("mooring rope*" OR "anchor rope*" OR "polyester mooring rope*" OR "polyester mooring line*" OR "polyester mooring system*" OR "synthetic fiber mooring" OR "synthetic fibre mooring rope*" OR "FPSO mooring" OR "FPSO mooring system" OR "floating production, storage and offloading mooring system" OR "floating production, storage and offloading mooring" OR "nylon mooring rope*" OR "HMPE mooring rope*") OR TITLE ("synthetic fiber*" OR "synthetic fibre*" OR "polyester fiber*" OR "polyester fibre*" OR "HMPE fiber*" OR "HMPE fibre*" OR "nylon fiber*" OR "nylon fibre*" OR "polypropylene fiber*" OR "polypropylene fibre*" OR "Polyethylene fiber*" OR "polyethylene fibre*" OR "aramid fiber*" OR "aramid fibre*" OR "polyamide fiber*" OR "polyamide fibre*" OR "High Modulus Polyethylene fiber*" OR "High Modulus Polyethylene fibre*") AND TITLE (recycling OR recycled OR refurbish OR refurbished OR remanufacturing OR remanufactured OR recovering OR recovered OR "other application*" OR recyclability OR reusability OR circular OR circularity)) AND PUBYEAR > 2020

Results and Discussion

The research for the years 2021, 2022 and 2023 yielded 76 documents (scientific papers). Figure 3 depicts the number of documents by year. China, India, Italy, and the United Kingdom are the major players in terms of document production by country.

Figure 3 - Documents by year related to circular economy trends about of reuse of synthetic fiber waste

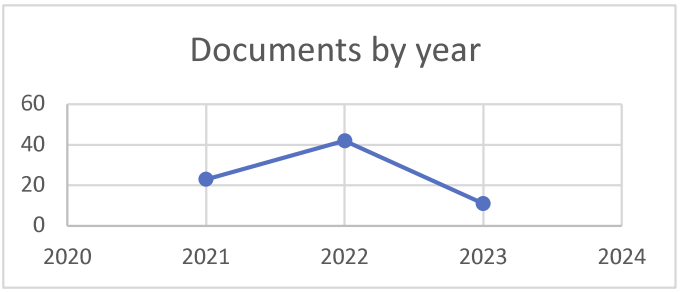

Fifty of the seventy-six documents found were chosen for analysis, which were classified according to the application and the type of raw material, as shown in Table 1.

Table 1 - Articles classified by application and raw material.

Theme	*Scope of the study*	*Number of documents*
Type of application	*Construction (concrete, mortar or other construction elements reinforcement)*	23
	Reinforcing polymers	4
	Development of Sustainable and Functional textiles	3
	Floor paving tiles application	1
	Soil improvement	3
	Reinforcement for Packaging Applications	1
	Depolymerization	1
	Reuse	1
Type of raw material	*Recycled nylon fibers*	7
	Recycled polypropylene fiber	9
	Recycled polyester fibers	10
	High Density Polyethylene Fiber	1
	Recycled Polyethylene Fibres	2
	Recycled PET	3
	Recycled aramid fiber	1

According to Table 1, the use of recycled synthetic fiber in construction corresponds to 71% of the applications. Followed by reinforcing polymers, with 14%. Therefore, the

most trending applications correspond to the use of recycled synthetic fiber in cement reinforcement, mortar reinforcement, and recycled concrete reinforcement with recycled synthetic fibers. According to [13], in order to improve the compressive strength and nonlinear behavior of the concrete, recycled polypropylene fibers are utilized. Moreover, [14] says masonry constructions' seismic performance is improved when waste nylon fibers are added to the mortar as reinforcement and concrete reinforcement with synthetic fiber can "increase the roughness of the crack surface and reduce the crack permeability [15]. The use of recycled synthetic fiber in the production of fresh concrete is particularly attractive due to the low cost of the raw materials and environmental protection [12].

According to the results, it is expected that polymer reinforcement with synthetic fiber becomes a trending application. Concerning the type of raw material, recycled polypropylene fibers and recycled polyester fiber, with 28% each one, were the most referenced, followed by recycled nylon fiber with 24%.

Although the reuse of synthetic mooring lines, specifically, is not broadly researched, there are studies about biocatalytic depolymerization of waste polyester mooring lines from oil and gas offshore platforms [16], and a study about the reuse of waste polyester mooring line [17]. Thus, the reuse of synthetic fiber would contribute to the reduction of plastic waste and to a circular economy in the oil and gas industry.

The next processes are mentioned on the articles: compression molding technique to produce composite materials from industrial plastic wastes reinforced with recycled nylon fibers [18]. Plus, room-temperature solid-state shear milling method to break the cross-linking bonds of waste polyurethane foam [19]. Plasma assisted dyeing to produce multichromic polyester textiles [20]. Extrusion blending to reinforce recycled polyethylene with waste polyester fiber [21]. And injection molding machine to manufacture fibers, made of recycled polyethylene, that are used as a reinforcement for structural concrete [22].

Conclusions

According to the research strategy applied, among the most evident trends, the use of recycled synthetic fiber in the construction area is outstanding. Concrete reinforcement and mortar reinforcement are the most mentioned among construction applications. The literature review revealed that recycled synthetic fibers can still meet high performance and durability standards when used as cement reinforcement.

Furthermore, polymer reinforcement with recycled synthetic fiber is expected to be another relevant trend among applications. Concerning raw material, recycled polyester fiber and recycled polypropylene fibers are the most referenced among the studies analyzed, followed by recycled nylon fiber.

Acknowledgements

The authors would like to thank the Conselho Nacional de Desenvolvimento Científico e Tecnológico (CNPq), and Coordenação de Aperfeiçoamento de Pessoal de Nível Superior (CAPES).

Ana Maria F. de Sousa and Ana Lúcia Nazareth da Silva have received research support from Conselho Nacional de Desenvolvimento Científico e Tecnológico – CNPQ (309461/2021-9) and CNPQ (307889/2022-0), respectively.

The authors would like to thank the financial support from the Human Resources Program of the National Agency of Petroleum, Natural Gas and Biofuels – PRH-ANP, supported with funds from investment by oil companies qualified in the P, D&I Clause of ANP Resolution No. 50/2015.

References

1. de Oliveira Neto, G. C., Correia, J. M. F., Tucci, H. N. P., Librantz, A. F. H., Giannetti, B. F., & de Almeida, C. M. V. B. (2022). Sustainable Resilience Degree assessment of the textile industrial by size: Incremental change in cleaner production practices considering circular economy. *Journal of Cleaner Production*, *380*(July). https://doi.org/10.1016/j.jclepro.2022.134633
2. Papamichael, I., Voukkali, I., Loizia, P., Rodrıguez-Espinosa, T., Pedreño, J. N., & Zorpas, A. A. (2023). Textile waste in the concept of circularity. *Sustainable Chemistry and Pharmacy*, *32*(January), 100993. https://doi.org/10.1016/j.scp.2023.100993
3. National Geographic. (2013, 0m24s). *How Your T-Shirt Can Make a Difference*. Retrieved from Youtube: https://www.youtube.com/watch?v=xEExMcjSkwA
4. The World Bank Group. (2019). *How Much Do Our Wardrobes Cost to the Environment?* Retrieved from The World Bank: https://www.worldbank.org/en/news/feature/2019/09/23/costo-moda-medio-ambiente
5. Ellen MacArthur Foundation. (2017). *A new textiles economy: Redesigning fashion's future*. Retrieved from Ellen MacArthur Foundation: http://www.ellenmacarthurfoundation.org/publications
6. European Environemnt Agency. (2021). *Plastic in textiles: towards a circular economy for synthetic textiles in Europe.* Retrieved from European Environemnt Agency: https://www.eea.europa.eu/publications/plastic-in-textiles-towards-a/file
7. MODEFICA, FGVces, REGENERATE. (2020). *Fios da Moda: Perspectiva Sistêmica Para Circularidade*. Retrieved from MODEFICA: https://pesquisas.modefica.com.br/fios-da-moda/
8. United Nations Environment Programme. (2020). *Sustainability and Circularity in the Textile Value Chain.* Retrieved from United Nations Environment Programme: https://www.oneplanetnetwork.org/sites/default/files/unep_sustainability_and_circularity_textile_value_chain_1.pdf
9. Ellen MacArthur Foundation. (2021). *The Jeans Redesign Guidelines.* Retrieved from Ellen MacArthur Foundation: https://emf.thirdlight.com/link/az03k410stb7-6azlt5/@/preview/1?o
10. Khajuria, A., Atienza, V. A., Chavanich, S., Henning, W., Islam, I., Kral, U., … Li, J. (2022). Accelerating circular economy solutions to achieve the 2030 agenda for sustainable development goals. *Circular Economy*, *1*(1), 100001. https://doi.org/10.1016/j.cec.2022.100001
11. World Economic Forum. (2023). Oil and Gas: Oil, Gas, Climate and the Environment. Obtenido de World Economic Forum: https://intelligence.weforum.org/topics/a1Gb0000000LOnGEAW/key-issues/a1Gb00000015Q8qEAE
12. Rao, M. M., Patro, S. K., & Basarkar, S. S. (2022). Mechanical and Post-Cracking Performance of Recycled High Density Polyethylene Fiber Reinforced Concrete. Journal of The Institution of Engineers (India): Series A, 103(2), 519–530. https://doi.org/10.1007/s40030-022-00625-5
13. Najaf, E., Orouji, M., & Zahrai, S. M. (2022). Improving nonlinear behavior and tensile and compressive strengths of sustainable lightweight concrete using waste glass powder, nanosilica, and recycled polypropylene fiber. Nonlinear Engineering, 11(1), 58–70. https://doi.org/10.1515/nleng-2022-0008
14. Ranjan, N., Banerjee, S., Nayak, S., & Das, S. (2023). Exploring applicability of recycled nylon fiber reinforced mortar in joints and plaster to enhance the bond strength, in-plane and

out-of-plane capacity of masonry structures. *Journal of Building Engineering*, *72*(April), 106744. https://doi.org/10.1016/j.jobe.2023.106744

15. Li, M., Chai, J., Zhang, X., Qin, Y., Ma, W., Duan, M., & Zhou, H. (2023). Quantifying the recycled nylon fibers influence on geometry of crack and seepage behavior of cracked concrete. *Construction and Building Materials*, *373*(February), 130853. https://doi.org/10.1016/j.conbuildmat.2023.130853

16. de Castro, A. M., Carniel, A., Menezes, S. M., Chinelatto Júnior, L. S., de Honorato, H., Lima, A. P., & Chaves, E. G. (2022). Biocatalytic depolymerization of waste polyester mooring lines from oil and gas offshore platforms made of poly(ethylene terephthalate) (PET). *Journal of Chemical Technology & Biotechnology*, *97*(3), 709–718. https://doi.org/10.1002/JCTB.6955

17. Gage, C. R., Liagre, P. F., Heyl, C. N., & Del Vecchio, C. (2021). Dropped Polyester Mooring Line Qualification for Reuse. *Proceedings of the Annual Offshore Technology Conference*. https://doi.org/10.4043/31052-MS

18. Owen, M. M., Achukwu, E. O., Romli, A. Z., Abdullah, A. H. Bin, Ramlee, M. H., & Shuib, S. Bin. (2023). Thermal and mechanical characterization of composite materials from industrial plastic wastes and recycled nylon fibers for floor paving tiles application. *Waste Management*, *166*(January), 25–34.

19. Duan, R., Wei, L., Coates, P., Kelly, A., Wang, C., Chen, B., … Lu, C. (2023). Reinforcing mechanically reclaimed polyurethane foam wastes-based elastomer with modified recycled polyester fibers. *Journal of Polymer Science*, *n/a*(n/a). https://doi.org/https://doi.org/10.1002/pol.20230166

20. Althumayri, K., Alqarni, S. A., Alamrani, N. A., Alnoman, R. B., Abualnaja, M. M., Sayqal, A., & El-Metwaly, N. M. (2022). Immobilization of chalcone chemosensor into plasma-pretreated recycled polyester fibers toward multi-stimuli responsive textiles for detection of ammonia. *Journal of Molecular Liquids*, *367*, 120432. https://doi.org/10.1016/j.molliq.2022.120432

21. Su, J., Jiang, Z., Fang, C., Yang, M., Wu, L., & Huang, Z. (2022). The Reinforcing Effect of Waste Polyester Fiber on Recycled Polyethylene. *Polymers*, *14*(15). https://doi.org/10.3390/polym14153109

22. Sainz-Aja, J. A., Sanchez, M., Gonzalez, L., Tamayo, P., Del Angel, G. G., Aghajanian, A., … Thomas, C. (2022). Recycled Polyethylene Fibres for Structural Concrete. *Applied Sciences (Switzerland)*, *12*(6), 1–20. https://doi.org/10.3390/app12062867

Clay-Based Polymeric Nanocomposites: Bibliometric and Visual Analysis of Research Trends Using VOSviewer

Robson S. Costa[1]*; Mario O. Menezes[2], Esperidiana A.B. Moura[1]

[1] IPEN- Instituto de Pesquisas Energéticas e Nucleares, Centro de Química e Meio Ambiente, 2242 Prof. Lineu Prestes, Av., São Paulo, SP, 05508-000, São Paulo, Brazil.
corresponding: rscosta@usp.br

[2] IPEN- Instituto de Pesquisas Energéticas e Nucleares, Centro do Reator de Pesquisas, 2242 Prof. Lineu Prestes, Av., São Paulo, SP, 05508-000, São Paulo, Brazil.

Abstract - This study reviews the advantages, limitations, and current issues of clay-based polymeric nanocomposites. These composites offer improved properties at low filler loading, including superior mechanical, physical, and chemical characteristics such as gas and liquid barrier properties. The study highlighted the diverse applications of clay in various fields and the fluctuation in research interest over the years. Although research on these nanocomposites has increased steadily from 1958 to 2014, a decline has been observed from 2015 to 2021. The study serves as a valuable reference for researchers and identifies topics that have advanced in this research area. Despite significant progress in synthetic methods and the use of engineering polymers, understanding the enhancement mechanisms in nanocomposites remains a challenge.

Keywords: *Bibliometric, scientific production, Clay-Based Polymeric Nanocomposites, VOSviewer, Web of Science (WoS)*

Introduction

Clay/polymer nanocomposites represent a prime example of nanotechnology. Smectite-type clays have been shown to greatly enhance the mechanical and engineering properties of the resulting material without compromising its optical properties. Nanoscale clay structure modifications have led to novel material properties that can be applied commercially. In fact, the first commercial application of clay/nylon-6 nanocomposites was as timing belt covers for Toyota cars in collaboration with Ube in 1991 [1]. Modification of clay minerals has been necessary to optimize their applications, with the polymer surface modification method identified as an effective approach [2]. There are two main methods for polymer surface modification including the physical adsorption method which can alter the nature of clay mineral surfaces and the chemical grafting approach that can enhance interaction with polymer [2], [3]. Bibliometric analysis using VOSviewer software remains a useful technique for decision-making in research topics and identifying important literature in the field [4], [5]. The present study aims to show trends in research over the years on the production of polymeric clay nanocomposites and their applications in various other fields from 1958 to 2021. The bibliometric analysis results provided the types of journals, publication topics, the country of origin of researchers, and the particular journals where the publication was published.

Clay-based polymeric nanocomposite

Clay-based polymeric nanocomposite, which is a combination of clay and polymeric material, is being studied extensively in scientific research. The utilization of nanocomposites in industries is expanding due to their outstanding mechanical, thermal, and electrical properties. Clay-based polymeric nanocomposites are created to enhance the product's characteristics and properties. The addition of nanofillers such as clay into the polymeric matrix in small quantities significantly enhances the mechanical strength and durability of the composite. These nanocomposites have shown improved properties such as stiffness, thermal stability, reduced gas permeability, increased radiation shielding, and flame resistance. Therefore, researchers are focusing on developing [3], [6] nanocomposites with improved characteristics to meet the growing demand in various industries.

Bibliometric analysis and VOSviewer

Bibliometric analysis and VOSviewer are powerful tools used in data science for analyzing and visualizing the relationships between various articles, authors, and journals. By conducting bibliometric analysis, researchers can identify the most cited articles in a particular field, the most influential authors, and the impact of a journal in the academic community. This information can help researchers understand the research trends in their field and identify potential collaborators [4]. On the other hand, VOSviewer is a software tool designed to generate visual representations of bibliometric maps, co-authorship networks, and keyword co-occurrence associations. With VOSviewer, researchers can visualize the relationships between different articles, authors, and keywords in their field [7], [8].

Methods

This study analyzed scientific publications about clay-based polymeric nanocomposites using bibliometric analysis. A total of 14,786 articles, including original research and reviews, published in english between 1991 and 2021, were obtained from the Web of Science (WoS) [10]. For data collection, the Publish or Perish reference manager application was used, and "search expressions" were conducted as indicated in Table 1.

Table 1 - The use of "search expressions" for article selection in WOS.

Date	Search Expressions	Filters	Number of Articles Found
02/02/2022	((ALL=(clay*)) AND ALL=(Pol?mer*)) AND ALL=(nanocomposite*)	all fields	14,786

The study analyzed 14,786 documents on clay-based polymeric nanocomposites retrieved from the WoS database. At least 5 documents and 23 citations per author were used to ensure specificity in the analysis. The data was analyzed using VOSviewer, which generated bibliometric maps, co-authorship networks, and keyword co-occurrence associations. Network, density, and overlay visualizations were used to present data mapping articles. The study highlighted the use of bibliometric analysis and VOSviewer as powerful tools in visualizing scientific literature. Microsoft Excel, Zotero and WoS were used for grammar checks, article reviews, and citations. The study highlighted the relationships between authors, articles, and journals in the context of clay-based polymeric nanocomposites.

Results and Discussion

Advancements in clay-based polymeric nanocomposites research

The research papers on the periodic database have been arranged based on their year of publication. The graph illustrated in Figure 1 demonstrates the development of clay-based research from 1958 to 1990, covering research areas such as clay/polymer composites. The research on clay/polymer composites experienced a significant increase from 18 articles in 1988 to 51 in 1990.
The graph illustrated in Figure 2 demonstrates the development of clay-based research from 1991 to 2021, covering research areas such as clay-based polymeric nanocomposites. The research on clay-based polymeric nanocomposites experienced a significant increase from 85 articles in 2000 to

955 in 2013. However, there has been a gradual decline in research activity in this field since 2015, with a total of 480 articles in 2021[8], [9].

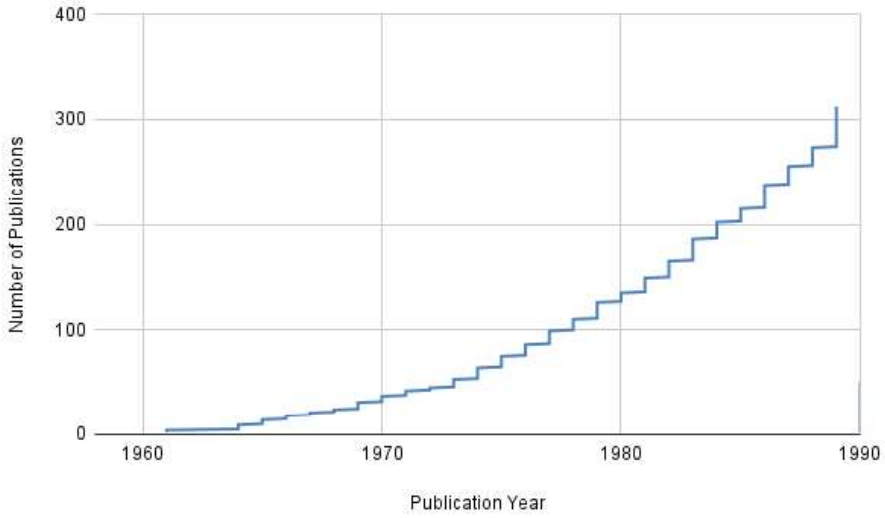

Figure 1 - Level of development of research on clay/polymer composites.

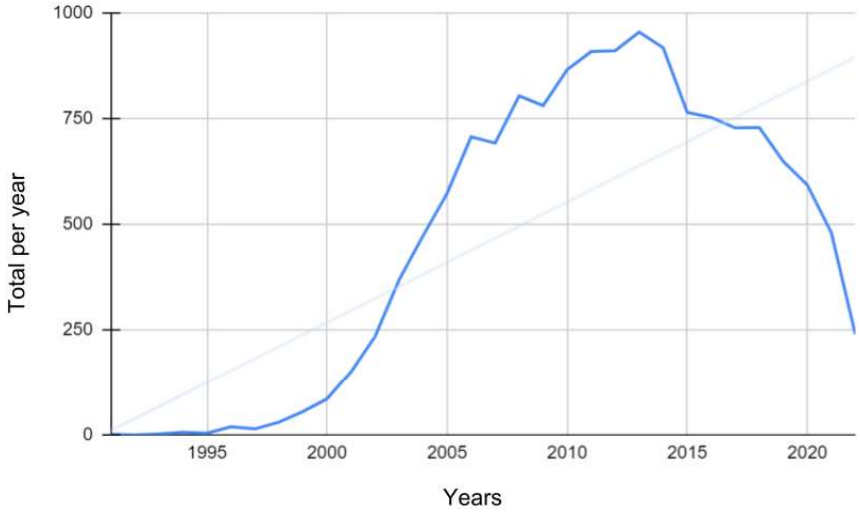

Figure 2 - Level of development of research on clay-based polymeric nanocomposite.[1]

Figures 1 and 2 illustrate the developmental landscape of this research field, showcasing significant advances in chronological order, including:

- 1980 - Toyota began work on exfoliating clay in nylon-6, which led to the history of clay/polymer nanocomposites;
- 1991 - Toyota and Ube collaborated to use clay/nylon-6 nanocomposites as timing belt covers for Toyota cars;
- 2001 - General Motors and Basell applied clay/polyolefin nanocomposites as a step assistant component for GMC Safari and Chevrolet Astro vans. These nanocomposites were later applied in the doors of Chevrolet Impalas;

[1] ((ALL=(clay*)) AND ALL=(Pol?mer*)) AND ALL=(nanocomposite*) – 14,493 – main collection of WoS, website of Science; Access in 15/08/2022;

- 2014 - Polyolefin/clay nanocomposites are manufactured using melt, solution, and in situ polymerization techniques. In situ polymerization yields fully exfoliated nanocomposites with excellent dispersion. The research identified in this study focuses on the utilization of clay-supported catalysts, such as Ziegler-Natta, metallocene, and late transition metal catalysts;
- 2016-The researchers examined the moisture barrier properties of polymer/clay and polymer/graphene nanocomposites. They identified models that predict the decrease in water vapor permeability, taking into account factors such as tortuosity, geometry, platelet stacking, orientation, polymer chain confinement, and plasticization;
- 2017- Data analysis revealed that nanocomposite hydrogels utilized in cartilage tissue engineering offer a favorable microenvironment for cell proliferation and tissue generation, resembling the ECM. Injectable hydrogels, despite their limited mechanical strength, are preferred due to their minimal invasiveness. Various NCH systems are employed in the field of cartilage tissue engineering;
- 2019 - This year, several studies have addressed the significance of advancing water purification technologies, including the development of polymer-clay composite membranes;
- 2020 - The benefits of using 2D platelet/disk-shaped fillers, like nanoclays, to enhance gas barrier properties, mechanical properties, and thermal stability of polymers were highlighted.

The use of Vosviewer in studying clay-based polymeric nanocomposites visualization is the topic area.

The VosViewer app served as the reference manager for collecting research data. Out of the 11,885 keywords found, 1,058 were selected regarding the production and use of clay in polymeric composites. The research on clay-based polymeric nanocomposites was grouped into 9 clusters, with Cluster 1 consisting of 374 items and the remaining clusters decreasing in quantity. Each cluster is color-coded for easy identification in Table 2 [9].

Table 2 - Most frequently used keywords in articles.

Nº	Keyword	Occurrences	Nº	Keyword	Occurrences
1	mechanical-properties	3546	11	intercalation	976
2	clay	2820	12	nanoparticles	789
3	behavior	2576	13	polypropylene	765
4	morphology	2550	14	layered silicate nanocomposites	763
5	nanocomposites	2236	15	exfoliation	755
6	montmorillonite	2206	16	polymers	707
7	composites	1674	17	degradation	664
8	clay nanocomposites	1440	18	films	628
9	polymer	1309	19	performance	620
10	silicate nanocomposites	1221	20	dispersion	583

Conclusions

This bibliometric study provided a comprehensive overview of research on clay-based polymeric nanocomposites, highlighting key factors in their development. The use of smectite-type clays as fillers in polymers was found to be crucial in improving mechanical and engineering properties while maintaining optical properties. The study reviewed three main methods for producing clay/polymer nanocomposites: in situ polymerization, solution-induced intercalation, and melt processing. Ongoing research aims to enhance their mechanisms and nanostructure. Clay-based polymeric nanocomposites have shown potential as replacements for traditional fiber-reinforced composites. The study presented the developmental landscape of the clay-based polymeric nanocomposites research field, highlighting significant advances from 1980 to 2020. Furthermore, the study emphasized the importance of developing effective and innovative CPNs for removing emerging pollutants under real-world conditions.

Acknowledgements
It was supported by the Brazilian agencies FAPESP (2018/22214-6), CAPES, CNPq. The first author was financed by the Coordenação de Aperfeiçoamento de Pessoal de Nível Superior - Brasil (CAPES) - Finance Code 88887.475077/2020-00

References

[1] F. Gao, "Clay/polymer composites: the story", *Mater. Today*, vol. 7, nº 11, p. 50–55, nov. 2004, doi: 10.1016/S1369-7021(04)00509-7.

[2] R. Babu Valapa, S. Loganathan, G. Pugazhenthi, S. Thomas, e T. O. Varghese, "Chapter 2 - An Overview of Polymer–Clay Nanocomposites", em *Clay-Polymer Nanocomposites*, K. Jlassi, M. M. Chehimi, e S. Thomas, Orgs., Elsevier, 2017, p. 29–81. doi: 10.1016/B978-0-323-46153-5.00002-1.

[3] P. Anadão, "Polymer/ Clay Nanocomposites: Concepts, Researches, Applications and Trends for The Future", *Nanocomposites - New Trends Dev.*, set. 2012, doi: 10.5772/50407.

[4] R. Costa e E. Moura, "A Bibliometric Analysis of the Strategy and Performance Measurement of the Polymer Matrix Nanomaterials Development Scenario Globally, and the Participation of Brazil", 2020, p. 329–342. doi: 10.1007/978-3-030-36628-5_31.

[5] N. J. van Eck e L. Waltman, "Software survey: VOSviewer, a computer program for bibliometric mapping", *Scientometrics*, vol. 84, nº 2, p. 523–538, 2010, doi: 10.1007/s11192-009-0146-3.

[6] M. Kotal e A. K. Bhowmick, "Polymer nanocomposites from modified clays: Recent advances and challenges", *Prog. Polym. Sci.*, vol. 51, p. 127–187, dez. 2015, doi: 10.1016/j.progpolymsci.2015.10.001.

[7] H. Sastranegara, *VOSviewer: a tool for bibliometric analysis*. 2021.

[8] A. Fauziah, "A Bibliometric Analysis of Nanocrystalline Cellulose Production Research as Drug Delivery System Using VOSviewer", *Indones. J. Multidiciplinary Res.*, vol. 2, nº 2, Art. nº 2, 2022, doi: 10.17509/ijomr.v2i2.43341.

[9] E. J. Rinia, Th. N. van Leeuwen, H. G. van Vuren, e A. F. J. van Raan, "Comparative analysis of a set of bibliometric indicators and central peer review criteria: Evaluation of condensed matter physics in the Netherlands", *Res. Policy*, vol. 27, nº 1, p. 95–107, maio 1998, doi: 10.1016/S0048-7333(98)00026-2.

[10] A. Nandiyanto e D. F. Al Husaeni, "A bibliometric analysis of materials research in Indonesian journal using VOSviewer", *J. Eng. Res.*, vol. 9, dez. 2021, doi: 10.36909/jer.ASSEEE.16037.

USE OF ASSOCIATION RULES FOR EVALUATION OF STRESS CRACKING IN POLYMERS

Lucas M. Hallmann[1,2*], Edson L. Francisquetti[2] and Ruth M. C. Santana[1]

1 - Departamento de Materiais, Laboratório de Materiais Poliméricos (LAPOL), Universidade Federal do Rio Grande do Sul (UFRGS), Porto Alegre, RS, Brasil
lucas.hallmann@farroupilha.ifrs.edu.br
2 – Departamento de Materiais, Instituto Federal de Educação, Ciência e Tecnologia do Rio Grande do Sul (IFRS), Farroupilha, RS, Brasil

Abstract: This article discusses the application of data science techniques to the study of Environment Stress Cracking (ESC) in materials science, specifically in high-density polyethylene. ESC is a phenomenon where a slow and cumulative transfer of energy from a wetting agent or fluid applied to a surface causes a fracture due to the inability of the structure to absorb the energy fully. This article argues that data science techniques, particularly rule-based machine learning, can provide valuable insights into the factors and patterns of interaction involved in ESC. The study used data collected from bodies of PEAD subjected to the ASTM D1693 method, with fluids including Igepal CO-630, Monoethylene Glycol, neutral commercial detergent, Sodium Hypochlorite, and Hydrogen Peroxide. The variables observed in the experiment were fluid, pH, melting point, sample description, sample type, thickness, weight, absorption, bottle area, start and end time, total time, and fracture. After data collection, the authors used Python programming language and libraries such as Pandas, Numpy, Scikit-learn, MLxtend, Matplotlib, Plotly, and Seaborn to preprocess and analyze the data. The rule-based machine learning technique was applied to identify regular occurrences within the dataset, and the correlation between the variables was analyzed to understand the influence of factors on ESC. The authors conclude that the use of data science techniques provides a novel and replicable approach to analyzing ESC in polymers, which can help researchers gain a deeper understanding of this phenomenon without spending excessive time on manual analysis.

Keywords: High-Density Polyethylene, Rule-Based Machine Learning, Environment Stress Cracking

Introduction

The scientific investigation follows a systematic and methodical process for observing and understanding a phenomenon, with the use of tools to assist in the evaluation of the process and work with the data collected in the experimental phase. Data science is essential for exploratory data analysis and consolidation, but its application is still strongly linked to the fields of computing and statistics. It is important to use digital technologies for the collection, production, and sharing of information, as the demand to develop deep analytical skills can subtract time from research [1,2].

So, analyzing Environment Stress Cracking in polymers such as high-density polyethylene through the lens of data science becomes an interesting alternative. This approach, besides differing from conventional statistical analysis, can be replicated and shared without requiring the researcher to rework their analysis. Considering that a

phenomenon is the result of factors acting under the same circumstance, producing the same result, if we analogously consider these factors as variables and their way of acting as a pattern of interaction, this situation is no different from an abstraction of mining association rules, included in frequent pattern mining, an area widely explored in Knowledge Discovery in Databases (KDD) [1,3].

In materials science, Environment Stress Cracking (ESC) is a phenomenon where a stress applied to a surface in contact with a wetting agent or fluid transfers energy to an area of that surface, slowly and cumulatively, to the point that the structure cannot absorb the energy fully, causing a rupture. This phenomenon occurs through repetitive mechanical stress, not chemical attack. Brittle fracture is characteristic of this rupture condition [4–6].

Considering this scenario, where research is immersed in data, we seek to demonstrate an alternative use of some data science techniques in the field of materials science, specifically to the study of Environment Stress Cracking that occurs in polymers such as the target of the study, high density polyethylene.

Experimental

Initially we started by obtaining the data used in the study. The way to perform the ESC test was based on the ASTM D1693 standard, using the folded strip method. In this test, specimens with dimensions recommended by the standard are taken from the flask. These are bent and placed on a U-shaped profile support. These specimens were taken from HDPE blown bottles. As for the fluids, Igepal CO-630, Monoethylene Glycol were used as standardized representatives, and commercial neutral detergent, Sodium Hypochlorite and Hydrogen Peroxide were used as representatives of domestic fluids. The samples were immersed in the fluids in baths at 50 ºC, for the time necessary for the samples to show damage [7,8].

The parameters observed in the experiment were: fluid, pH, melting point, sample description, sample type, thickness (a, b, c), perceived thickness, weight (initial, final and variation), absorption (in case of occurrence), flask area, date and time (initial and final), total time, fracture (direction, time and intensity). With the exception of the total time variable, all variables are categorical (nominal) [1].

After completing the observation stage of the experiment and obtaining the data, we started the data treatment stage. For use in the analysis, after some data transformations, the following variables were used: fluid, pH, melting point, sample type, thickness perception, absorption, total time, direction, fracture type and intensity (Fig. 1). The Python programming language was used together with Jupyter Notebook and the libraries Pandas, Numpy, Scikit-learn, MLxtend, Matplotlib, Plotly, Seaborn, all in their stable versions.

	nome	ph	ponto_fusao	tipo_amostra	espessura_percepcao	peso_resultado	sentido_fratura	tipo_fratura	intensidade_fratura
count	90	90	90	90	90	90	90	90	90
unique	5	3	2	6	2	3	4	4	5
top	Igepal	neutro	positivo	curva superior	grossa	absorveu	Transversal	Não ocorreu	zero
freq	18	54	54	15	47	69	37	35	35

Figure 1 - Overview of the base used in the analysis, in Dataframe format

Two techniques were used to analyze this data, one aiming to search for patterns to understand the fracture behavior and the other to understand the influence of factors (variables) on each other, i.e., the search for a correlation between them. The first of the techniques used is the use of association rules (rule-based machine learning), also called market basket analysis, which aims to locate regular occurrences within a dataset, in rules

of the type if A (antecedent) then B (consequent). As a recurrent problem of applying this approach, we have the creation of several rules, and to separate the most significant ones, we count on statistical indexes of minimum support, minimum confidence and lift [9].

In a simplified way, we can understand support as the percentage of times that A and B occur in the base (Eq. 1). Confidence, on the other hand, represents the percentage of occurrence of B in all those of A (Eq. 2). The lift, on the other hand, calculates the chance of B occurring, if A occurs, considering the popularity of B (Eq. 3). When the lift is greater than 1, it reinforces the occurrence of the pattern. Thus, relating these indices to the Dataset itemsets, we can obtain rules (or behaviors) of great importance (relevance) [10,11].

$$supp(A) = (\#A \text{ in } B) / (\#B) \quad \textbf{(1)}$$

$$conf(A=>B) = supp(A \text{ union } B) / supp(B) \quad \textbf{(2)}$$

$$lift(A=>B) = supp(A \text{ union } B) / (supp(A)*supp(B) \quad \textbf{(3)}$$

So, we started working with the result dataset using the Apriori algorithm from the MLxtend library, aiming to search for regular itemsets. Some of the results obtained can be seen in Fig. 2. These results were obtained using a support of 0.3 (30%).

```
    itemset support >= 0.3
0.  (absorveu, positivo)
1.  (grossa, absorveu)
2.  (neutro, positivo)
3.  (absorveu, zero, 11, integro, nao ocorreu)
4.  (nao ocorreu, 11)
5.  (grossa, transversal)
6.  (microfissura, baixa)
```

Figure 2 - Itemset found with 0.3 support

Following the analysis, once we know the Itemset with the most interesting results, we implement the "*association_rules*" of the "*mlxtend.frequent_rules*" package, passing the Itemset as a parameter along with the Dataset, so we can look for frequent patterns and consequently understand the behavior presented during the experiment. In Fig. 3 you can examine some results obtained with this action.

	antecedents|consequents|	support|confidence|lift		
0	(microfissura)=>(baixa)	0.31	0.87	2.71
1	(integro)=>(zero, absorveu, 11, nao ocorreu)	0.31	0.80	2.71
2	(grossa, positivo)=>(absorveu)	0.42	0.80	2.57
3	(absorveu, 11, zero)=>(nao ocorreu)	0.31	1.00	2.57
4	(transversal)=>(grossa)	0.32	0.78	1.50
5	(neutro)=>(positivo)	0.44	0.66	1.11

Figure 3 - Some results obtained in the search for association rules

It is noticeable that some of the results of Itemset are somehow reflected in the search for rules, and after this action, we must consider whether the rules found are important to the context of the experiment. The interpretation of the obtained results should not be taken literally, but interpreted by the researcher within a specific context [11].

Results and Discussion

A possible reading of the result of rule 0 (Fig. 3), would be: "there is each micro-crack type fracture, it will be classified as a low intensity fracture with a minimum possibility of occurrence of 87%" or a less obvious rule, as the number 2: "in samples of thick thickness, exposed to fluids with positive melting point fluid absorption occurs 80% of the time". These are some of the countless possible interpretations of the many different rules generated by the use of the association rules technique.

It is also possible to concatenate other techniques and refine the understanding, such as using a correlation matrix displayed in a heatmap (Fig. 4):

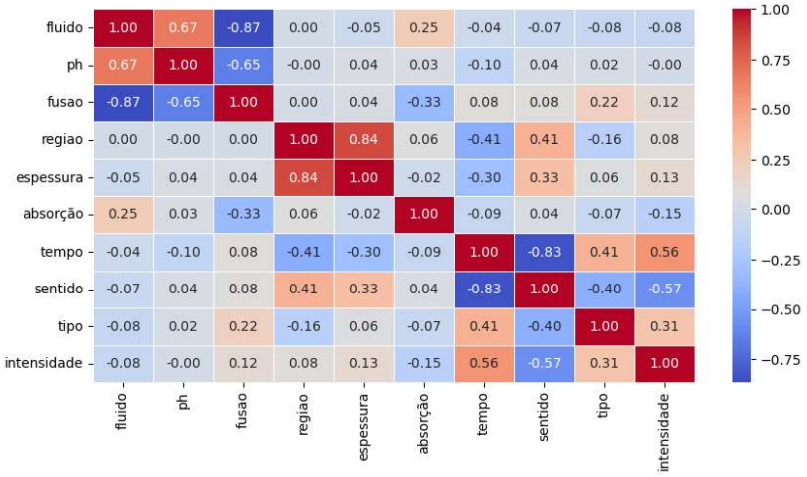

Figure 4 - Correlation matrix using Pearson's method, in the same Dataset used for the association rules.

We can see that we have a strong correlation between variables such as the thickness of the sample and the region from which it was taken, where this can imply in cross-sectional fractures in 78%, considering the inference between the patterns obtained in the association rules together with the correlation shown in the matrix.

Conclusions

Using unusual approaches to understanding a phenomenon can open new paths, especially when it comes to replicating and sharing techniques. Feeding an already created database, which can be shared among several researchers online, as well as the programming codes used for data analysis, saves time and avoids rework. This also allows for explicit assimilation of the technique and its execution, facilitating replication.

In the case of polymer behavior, it is possible to have very valuable insights by crossing the responses of the approaches and building knowledge, as for example when we realize that the region of the flask determines the direction of rupture more than the wall thickness, although transverse fractures are common in thicker samples. This kind of detail would perhaps go unnoticed if only traditional approaches to analysis were used.

Acknowledgements

The authors thank the Laboratory of Polymeric Materials at UFRGS and Materials Department of IFRS (campus Farroupilha) for supporting the research and CAPES and CNPq for the aid granted.

References

1. Rodrigues AA, Dias GA. Estudos sobre visualização de dados científicos no contexto da Data Science e do Big Data. Pesquisa Brasileira em Ciência da Informação e Biblioteconomia (PBCIB) [Internet]. 2017 Jun 30 [cited 2023 Apr 12];219–28. Available from: https://pbcib.com/index.php/pbcib/article/view/34774/
2. Brito A da C, Tenorio MB. Habilidades primárias para trabalhar com ciência de dados e big data. Revista Alomorfia [Internet]. 2019 [cited 2023 Apr 10];3:01–12.

Available from: https://www.alomorfia.com.br/index.php/alomorfia/article/view/10/6
3. Goldschmidt R, Passos E. Data Mining: um guia prático. 1st ed. Vol. 4. Rio de Janeiro: Elsevier Editora Ltda; 2005.
4. Reddy D V, Butul B. A COMPREHENSIVE LITERATURE REVIEW OF LINER FAILURES AND LONGEVITY [Internet]. 1999 [cited 2023 Apr 25]. Available from: https://archive.epa.gov/region5/waste/clintonlandfill/web/pdf/cl_044.pdf
5. Scheirs J. Compositional and failure analysis of polymers: a practical approach. John Wiley & Sons; 2000.
6. Queiroz G de C. Resistência dos polietilenos ao stress cracking ambiental (ESC - environmental stress cracking) [Internet]. 2006 Jan [cited 2023 Apr 22]. Available from: https://ital.agricultura.sp.gov.br/arquivos/cetea/informativo/v18n1/v18n1_artigo3.pdf
7. ASTM International. Standard Test Method for Environmental Stress-Cracking of Ethylene Plastics. D1693 [Internet]. 2020;15:1–11. Available from: www.astm.org,
8. Hallmann LM, Francisquetti EL, Santana RMC. Avaliação do tensofissuramento em frascos soprados de PEAD com fluídos domissanitários. In: 24 Cbecimat [Internet]. Águas de Lindóia; 2022 [cited 2023 May 8]. Available from: https://www.monferrer.com.br/METALLUM/CBECIMat2022/PROGRAMA-AF.pdf
9. Borgelt C, Kruse R. Induction of Association Rules: Apriori Implementation. In: Physica H, editor. Compstat [Internet]. Heidelberg: Physica-Verlag HD; 2002 [cited 2023 May 9]. p. 395–400. Available from: https://link.springer.com/chapter/10.1007/978-3-642-57489-4_59
10. Agrawal R, Imieliński T, Swami A. Mining association rules between sets of items in large databases. In: Proceedings of the 1993 ACM SIGMOD international conference on Management of data - SIGMOD '93 [Internet]. New York, New York, USA: ACM Press; 1993 [cited 2023 May 9]. p. 207–16. Available from: https://rakesh.agrawal-family.com/papers/sigmod93assoc.pdf
11. Al-Maolegi M, Arkok B. An Improved Apriori Algorithm for Association Rules. International Journal on Natural Language Computing [Internet]. 2014 Feb [cited 2023 May 9];3. Available from: https://arxiv.org/abs/1403.3948

AN EXPERIENCE OF DEVELOPMENT OF HDPE/NATURAL FIBER COMPOSITES IN HIGH SCHOOL TO PROMOTE RECYCLING

Arlete G. A. Pinto[1], Bruna B. G. Silva[2] and Alex S. Sirqueira[3]*

1 – Colégio Estadual Janete Mandarino, Rio de Janeiro, RJ, Brazil
2- SESC Jacarepaguá, Rio de Janeiro, RJ, Brazil
3 – Laboratório de Estatística e Matemática Aplicada (LEMA), UERJ, RJ, Brazil
alex.sirqueira@uerj.br

Abstract - In Brazil, there is a lack of interaction between engineering and exact sciences courses with high school education, which has led to a lack of interest among secondary school students in careers such as Engineering. To address this issue, actions that stimulate abstract reasoning and increase exposure to fundamental subjects like mathematics, physics, and chemistry are needed. This work presents the results of junior scientific initiation activities carried out by a high school student. The proposal was to incorporate research in the field of recycling into the students' daily activities, aiming to develop critical thinking and analytical skills. After selecting two students from public schools located in different regions of Rio de Janeiro, the composites were processed in the polymer processing laboratory at UERJZO. The developed composites were made from waste materials such as coconut fiber, sisal, and corn cob. This stage of the project sparked great interest among the students, fueling their scientific curiosity and analytical approach. The mechanical properties of tensile strength, density, hardness, impact, and Vicat were evaluated. For the students, it was a unique opportunity, and the actions were disseminated in their schools. The second stage of the project involves the development of selective collection actions in schools.

References

1. SAMPAIO, M.S. Obtenção e caracterização de compósitos de polietileno com fibras naturais. 2019. 62 f. Projeto final da graduação (Bacharel em Engenharia Química) - Universidade Federal do Rio de Janeiro, Rio de Janeiro, RJ, 2019.
2. Sirqueira, Alex S.; SANTOS, M. C. C.. Escolaridade e educação ambiental na região da extrema Zona Oeste do Rio de Janeiro. REVISTA TECNOLOGIA E SOCIEDADE (ONLINE), v. 55, p. 136-148, 2023.

Fundings: FAPERJ.

Keywords: *Recycling, Composite, High School, Environment education, mechanical properties*

CHALLENGES AND OPPORTUNITIES FOR PLASTIC RECYCLING DURING THE COVID-19 PANDEMIC: A CASE STUDY IN SÃO PAULO STATE, BRAZIL

Lais R. Lima[1*]; Rafaela F. Gutierrez[2]; Amanda L. Generoso[1]; and Sandra A. Cruz[1]

1 – Federal University of São Carlos - UFSCar, São Carlos, São Paulo, 13565-905, Brazil.

2 – University of Toronto, Toronto, Canada.

laisroncalho@gmail.com

Abstract - Brazil was one of the country most affected for the COVID-19 pandemic and faced one of the worst public health crises in its history in the period of 2020 to 2021. The crisis raised concerns primarily about the cross-contamination risks associated with waste management. The waste pickers, who are still very vulnerable in the Brazilian reality, were directly impacted by social isolation at the beginning of the pandemic. This work addressed the impact of the peak period of the pandemic on waste pickers organized in three cooperatives located in different municipalities in the State of São Paulo. The gravimetric data and the invoicing of each cooperative were evaluated, more specifically in terms of plastic materials, since these are one of the most important materials for the income generation of the cooperatives. The achievements arising from opportunities in the face of a shortage of raw materials around the world, with emphasis on polymer materials, were also highlighted.

References

1. A. M. M. Azevedo; J. Gutberlet; S. D. Araújo; F. H. Duarte *Ambiente & Sociedade* 2022, *25*, 1–25. https://doi.org/10.1590/1809-4422asoc20210088r1vu2022l2oa.
2. H. L. Corrêa; D. G. Corrêa *Frontiers in Sustainability* 2021, *2*, 1–9. https://doi.org/10.3389/frsus.2021.644309.
3. L. R. Lima; R. F. Gutierrez; S. A. Cruz *Circular Economy and Sustainability* 2022, *2*, 903–913. https://doi.org/10.1007/s43615-021-00130-0.

Fundings: São Paulo Research Foundation.

Keywords: *waste management, waste pickers cooperatives, recycling.*

POLYMERS AND PEPTIDES: WORLDWIDE TECHNOLOGICAL INTEREST

Tatiana A. Campos[1], Juan P.B. Roa[2] and Rodrigo M. Verly[1]*

1 – Department of Chemistry (DeQui), Federal University of Vales do Jequitinhonnha e Mucuri (UFVJM), Diamantina, MG, Brazil tatiana.andrade@ufvjm.edu.br
2 – Institute of Science and Technology, Federal University of Vales do Jequitinhonnha e Mucuri (UFVJM), Diamantina, MG, Brazil

Abstract - The polymer sector is versatile and capable of serving several applications, including the structuring of systems containing other types of molecules, including peptides [1,2]. In order to understanding the technological development of the sector of polymers associated with peptides, an evaluation was made in the search system of the European Patent Office (EPO), which lists more than 140 million patent documents from different countries as a sampling strategy. what are the main industries related to the sector. The exploratory research was based on the terms "peptide" and "polymer" in all fields of the Espacenet [3] platform and was conducted for evaluation in the entire scope of the platform defined as a global evaluation and also specifically in Brazil until the year 2022, including the main sectors related to the International Patent Classification (IPC) [3]. The results show that considering all patents involving peptides, 38% are related to Polymers, reaching a total of about 227 thousand different patent families, of which 140.5 thousand (62%) are protected under the patent cooperation treaty (PCT), in an accumulated of around 880 thousand publications. The main countries are: United States (16 %), European Patent Office (12%), Japan (10%), China (9%) and Canada (8%). Brazil appears in 8th position with 3% with 26.8 thousand publications. Research data indicate that 56% of the documents meet human needs; 39%, Chemistry and metallurgy; 5% related to physics and less than 1% related to the performing operations sector; transporting. The results demonstrate the great technological interest in the association of polymeric materials with peptides and point out that this is a technological development market with a great perspective of internationalization, especially in the area of classification A61 - human necessities - health; life-saving; amusement medical or veterinary science; hygiene. The work points out that the association has great potential for the internationalization of the technologies developed.

1. Bhatia, S. Natural Polymer Drug Delivery Systems: Nanoparticles, Plants, and Algae, Springer International Publishing; Gurgaon, 2016; 95-118. DOI 10.1007/978-3-319-41129-3
2. A. George; P.A. Shah; P.S. Shrivastav Natural biodegradable polymers based nano-formulations for drug delivery: A review. Int J Pharm. 2019; https://doi.org/10.1016/j.ijpharm.2019.03.011
3. EPO – EUROPEAN PATENT OFFICE. Espacenet Resource Book 1.44.1, 2023. https://www.epo.org/searching-for-patents/technical/espacenet.html#tab-1

Keywords: *Technological Information, Espacenet, peptide, polymer*

Platinum Sponsor

KRONA TUBOS E CONEXÕES

Palladio Sponsor

CREA-SC

Gold Sponsor

INSTRON

TA Instruments

Silver Sponsor

UNION

Zwick / Roell

Senior Sponsor

nano

PerkinElmer For the Better

NETZSCH Proven Excellence.

ReoTerm

SHIMADZU Excellence in Science

Master Sponsors

Anton Paar

Plásticos Máquinas Técnicas Ltda.

DOW

HSENSOR

KCEN

ROYAL SOCIETY OF CHEMISTRY

Junior Sponsors

CCDM DEMa/UFSCar

IOTO INTERNATIONAL

GRUPO WORTEX

Support

abtb

CAPES

fapesc

INCT Polissacarídeos

Joinville e Região Convention & Visitors Bureau

Plástico virtual

RHEIN

UDESC

univille

UNIVERSIDADE FEDERAL DE SANTA CATARINA

UFRGS UNIVERSIDADE FEDERAL DO RIO GRANDE DO SUL

UTFPR UNIVERSIDADE TECNOLÓGICA FEDERAL DO PARANÁ